Helga Kolb • Eduardo Fernandez • Ralph Nelson

Webvision

The Organization of the Retina and Visual System

Last Updated: May 28, 2020

University of Utah Health Sciences Center
Salt Lake City (UT)

University of Utah Health Sciences Center, Salt Lake City (UT)

Copyright: © 2022 Webvision

All copyright for chapters belongs to the individual authors who created them. However, for non-commercial, academic purposes, images and content from the chapters portion of Webvision may be used with a non-exclusive rights under a Attribution, Noncommercial 4.0 International (CC BY-NC) Creative Commons license. Cite Webvision, http://webvision.med.utah.edu/ as the source. Commercial applications need to obtain license permission from the administrator of Webvision and are generally declined unless the copyright owner can/wants to donate or license material. Use online should be accompanied by a link back to the original source of the material. All imagery or content associated with blog posts belong to the authors of said posts, except where otherwise noted.

NLM Citation: Kolb H, Fernandez E, Nelson R, editors. Webvision: The Organization of the Retina and Visual System [Internet]. Salt Lake City (UT): University of Utah Health Sciences Center; 1995-.

Understanding the organization of the vertebrate retina has been the goal of many talented visual scientists during the past 100 years. With Cajal's (1892) anatomic descriptions of the cell types that constitute the retina in a number of vertebrate species, and with an early understanding of the role of visual purple in photochemistry in combination with psychophysical studies of adaptation and color vision, we had in the sixties the rudiments of an understanding of how the retina might be organized and functioning.

To go further, though, we were beginning to need detailed information of neural circuits that underlie these functions. It was the advent of electron microscopy, microelectrode recording techniques, and pharmacology that then allowed us an era of very rapid advancement. The purpose of this Electronic Tutorial is to summarize these recent advances and to describe our present understanding, based primarily on anatomic investigations, of the Neural Organization of the Mammalian Retina. As time goes on we have been inviting other authors to write chapters on their speciality concerning the retina or other visual pathways. A great addition has been a section on Psychophysics of Vision which we hope will be of general information to all interested in learning the basics of visual perception.

Table of Contents

About the Editors ix

Introduction xiii

Foundations 1

Gross Anatomy of the Eye 3
Helga Kolb

Simple Anatomy of the Retina 11
Helga Kolb

Anatomy and Physiology of the Retina 35

The Retinal Pigment Epithelium 37
Olaf Strauss

Photoreceptors 59
Helga Kolb

Outer Plexiform Layer 91
Helga Kolb

Inner Plexiform Layer 109
Helga Kolb

Morphology and Circuitry of Ganglion Cells 123
Helga Kolb

Visual Responses of Ganglion Cells 151
Ralph Nelson

Melanopsin-expressing, Intrinsically Photosensitive Retinal Ganglion Cells (ipRGCs) 201
Dustin M. Graham and Kwoon Y. Wong

The Anatomy and Physiology of Direction-Selective Retinal Ganglion Cells 241
Jinyue Liu

Glial Cells of the Retina 255
Helga Kolb

The Architecture of the Human Fovea 265
Helga Kolb, Ralph F. Nelson, Peter K. Ahnelt, Isabel Ortuño-Lizarán, and Nicolas Cuenca

Retinal Circuits 315

Circuitry for Rod Signals through the Retina 317
Helga Kolb

Cone Pathways through the Retina 337
Helga Kolb

Roles of Amacrine Cells 355
Helga Kolb

AII Amacrine Cells 397
Mahnoosh Farsaii and Victoria P. Connaughton

Midget pathways of the primate retina underlie resolution and red green color opponency 417
Helga Kolb

S-Cone Pathways ... 443
Helga Kolb

Feedback Loops in the Retina ... 455
Helga Kolb

Myriad roles for gap junctions in retinal circuits ... 467
Stuart Trenholm and Gautam B. Awatramani

Neuroactive Substances in the Retina ... 515

Neurotransmitters in the Retina ... 517
Helga Kolb

$GABA_C$ Receptors in the Vertebrate Retina ... 539
Haohua Qian

Glycine Receptor Diversity in the Mammalian Retina ... 553
Silke Haverkamp

Role of Dopamine in Retinal Function ... 567
Elka Popova

Phototransduction and Photoreceptor Synaptic Pathways ... 629

Phototransduction in Rods and Cones ... 631
Yingbin Fu

S-Potentials and Horizontal Cells ... 669
Ido Perlman, Helga Kolb, and Ralph Nelson

Glutamate and Glutamate Receptors in the Vertebrate Retina ... 725
Victoria Connaughton

Bipolar Cell Pathways in the Vertebrate Retina ... 751
Ralph Nelson and Victoria Connaughton

Retinal Neurogenesis: Early stages in the Development of Neurons and Pathways ... 799

Development of Cell Types and Synaptic Connections in the Retina ... 801
Josh Morgan and Rachel Wong

Formation of Early Retinal Circuits in the Inner-Plexiform Layer ... 825
Kevin Ford and Marla Feller

Development of Retinal Ganglion Cell Dendritic Structure and Synaptic Connections ... 847
Ning Tian

Evolution of the Vertebrate Eye ... 865

Evolution of Phototransduction, Vertebrate Photoreceptors and Retina ... 867
Trevor D Lamb

Neural Basis of Color Perception ... 979

Color Vision ... 981
Peter Gouras

Visual Behavior ... 1023

Principles of Vision 1025
Michael Kalloniatis and Charles Luu

Visual Acuity 1049
Michael Kalloniatis and Charles Luu

Temporal Resolution 1075
Michael Kalloniatis and Charles Luu

Light and Dark Adaptation 1089
Michael Kalloniatis and Charles Luu

The Perception of Color 1103
Michael Kalloniatis and Charles Luu

The Perception of Space 1131
Michael Kalloniatis and Charles Luu

The Perception of Depth 1145
Michael Kalloniatis and Charles Luu

Brain Visual Areas 1155

The Primary Visual Cortex 1157
Matthew Schmolesky

Repair and Regeneration of Visual Neurons 1189

Cellular Remodeling in Mammalian Retina Induced by Retinal Detachment 1191
Steven K. Fisher, Geoffrey P. Lewis, Kenneth A. Linberg, Edward Barawid, and Mark R. Verardo

Regeneration in the Goldfish Visual System 1233
Sam Nona

Regeneration in the Visual System of Adult Mammals 1267
Yves Sauve and Frederic Gaillard

Fetal Tissue Allografts in the Central Visual System of Rodents 1307
Frederic Gaillard and Yves Sauve

Electrophysiology: The Study of Light-Evoked Field Potentials 1347

Visually Evoked Potentials 1349
Donnell Creel

The Electroretinogram: ERG 1379
Ido Perlman

Clinical Electrophysiology 1421
Donnell J. Creel

Visual and Auditory Anomalies Associated with Albinism 1481
Donnell J. Creel

Diseases of the Eye and Retina 1519

Retinal Degeneration, Remodeling and Plasticity 1521
Bryan William Jones, Robert E. Marc, and Rebecca L. Pfeiffer

Age-Related Macular Degeneration (AMD) 1561
Gregory S. Hageman, Karen Gehrs, Lincoln V. Johnson, and Don Anderson

Diabetic retinopathy and a novel treatment based on the biophysics of rod photoreceptors and dark adaptation: Diabetic retinopathy and its treatment 1607
Geoffrey B. Arden and David J. Ramsey

The Science Behind Myopia 1655
Brittany J. Carr and William K. Stell

Crystalline Lens and Cataract 1699
Joah F. Aliancy and Nick Mamalis

Intraocular Lenses for Cataract Surgery 1717
Jason Nguyen and Liliama Werner

What is glaucoma? 1733
David Križaj

Visual Prosthesis 1773

Introduction to Visual Prostheses 1775
Eduardo Fernandez and Richard Normann

Retinal Prostheses 1801
Ethan D. Cohen

Facts and Figures Concerning the Human Retina 1825

Facts and Figures Concerning the Human Retina 1827
Helga Kolb

About the Editors

Dr. Helga Kolb

Dr. Helga Kolb was born and educated in England receiving B.Sc., M.Sc. and Ph.D. degrees from the University of Bristol. Her first position in eye research was at the Institute of Ophthalmology, Judd Street, London. In 1966, Dr. Kolb emigrated to the USA. She took up positions in eye research in the Wilmer Institute, Johns Hopkins University, The National Eye Institute, Bethesda and the National Institute of Neurological Diseases and Stroke, Bethesda. Eventually Helga settled with her husband Richard Normann in the beautiful mountain west at the University of Utah, Salt Lake City, Utah. She is presently Professor Emeritus of Ophthalmology and Visual Science at the John Moran Eye Center, University of Utah. Her research interests include light and electron microscopy and immunostaining of the retina with emphasis on retinal neurocircuitry. Many of her important contributions to retinal research have been with her long time collaborators, Dr. Ralph Nelson and Dr. Nicolas Cuenca. In 1993 she was honored with the Proctor Medal award by the Association for Research in Vision and Ophthalmology (ARVO), in 2000 with the Von Sallmann award and in 2002 with the "Margaret Pittman Lectureship award" from the National Institutes of Health. In recognition of her contribution to vision research over the years, in 2011, she and her husband, Dick Normann, were awarded the Doctor Honoris Causa degrees from Miguel Hernandez Universidad de Elche, Spain.

Dr. Helga Kolb: helga.kolb@hsc.utah.edu

Dr. Eduardo Fernandez

Dr. Eduardo Fernandez was born in Elda (Spain) in 1962. Received the M.D. degree from the University of Alicante (Spain) in 1986 and the Ph. D. degree in Neurosciences with honors from the University of Alicante in 1990. His collaboration with Dr. Helga Kolb, began with a stay from 1990 to 1991 under a postdoctoral fellowship of the Spanish Government (FPI program). During that time he worked on the synaptic organization of the turtle retina and on the neural transmitter modulation of 2nd messenger systems in retinal cells. He is currently Associate Professor at the University Miguel Hernandez (Spain) and Director of the Foundations of Vision and Artificial Vision Division of the Institute of Bioengineering of the University Miguel Hernandez (Alicante, Spain). In the last years he has been using histological as well as electrophysiological techniques to understand how mammalian retinal cells and the circuitry within the retina can manage and code visual information. He is also actively working on the development of a visual neuroprosthesis for the profoundly blind.

Dr. Eduardo Fernandez: e.fernandez@umh.es

Dr. Ralph Nelson

Dr. Ralph Nelson was born in Hartford Connecticut. He received his B.A. in Biophysics from Amherst College in 1967 and his Ph.D. in Biophysics from Johns Hopkins University in 1972. He currently heads the Neural Circuitry Unit at The National Institutes of Neurological Disorders and Stroke, National Institutes of Health, Bethesda Maryland. While at Johns Hopkins, he studied conductance mechanisms responsible for light responses of retinal bipolar cells and in his postdoctoral studies at the National Institutes of Health he pioneered the use of intracellular recording and dye-marking of retinal neurons in the mammalian retina. Together with

Helga Kolb he has made major contributions towards the understanding of ON and OFF pathways and the neural processing of rod and cone signals in the mammalian retina. Dr. Nelson's laboratory is currently investigating the relationship of receptors on retinal neurons to processing of visual information in retinal neural circuits, and has begun to explore zebrafish as a model system for such studies.

Dr. Ralph Nelson: NelsonR@ninds.nih.gov

Introduction

Our eyes are marvelous sense organs that allow us to appreciate all the beauty of the world we live in, to read and gain knowledge, and to communicate our thoughts and desires to each other through visual expression and visual arts.

Vision is the most fundamental of our senses and it is perhaps the greatest tragedy of all when blindness robs us of this modality. Although all parts of the eye are important for perceiving a good image, the most vital layer for vision is the retina. The retina is essentially a piece of brain tissue that gets direct stimulation from the outside world's lights and images.

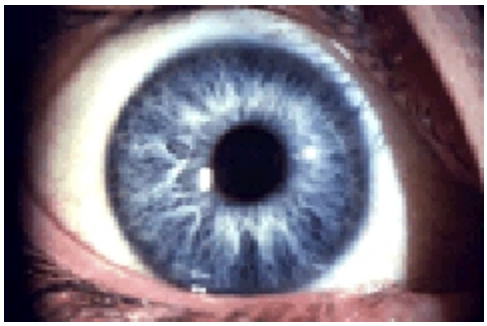

Understanding the organization of the vertebrate retina has been and is still the goal of many talented visual scientists over the years. Ramon y Cajal in the 19th century already presented the first comprehensive anatomic descriptions of the neural cell types that constitute the retina in a number of vertebrate species. There then followed an understanding of the role of visual purple in photochemistry and important psychophysical studies on image formation, light and dark adaptation and color vision.

To go further, though, we were beginning to need detailed information of neural circuits that underlie these functions. It was the advent of electron microscopy, microelectrode recording techniques, immunostaining and pharmacology in the 20th century that then allowed us a very rapid advancement of knowledge on the organization of the retina and visual system. The purpose of this Electronic Tutorial is to summarize our present understanding of the field, based primarily on anatomical and physiological investigations. As time goes on we have been inviting other authors to write chapters on their speciality concerning the retina and higher visual pathways. We also attempt to add clinical research findings in cell biology and genetics of retinal diseases. A great addition has been a section on **Psychophysics of Vision** which we hope will be of general information to all interested in learning the basics of visual perception.

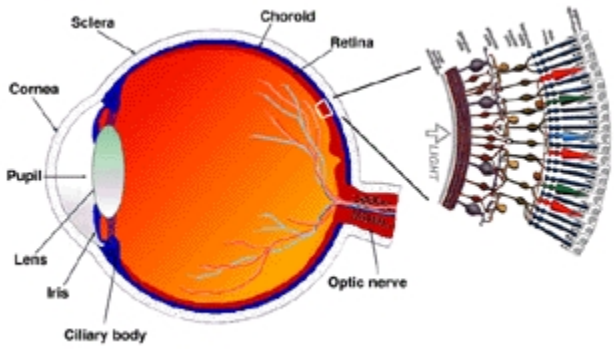

We have tried to present material at the cutting edge of the present knowledge, but in a simple way that is accessible to both students, professional and non-expert people.

If you have questions, suggestions for improvements, or other useful comments, do not hesitate to contact us at the addresses listed in About the Editors.

Foundations

Gross Anatomy of the Eye

Helga Kolb

Created: May 1, 2005; Updated: May 1, 2007.

Overview

When looking into someone's eyes, we can easily see several structures (Fig. 1):

- A black-looking aperture, the **pupil**, that allows light to enter the eye (it appears dark because of the absorbing pigments in the retina).
- A colored circular muscle, the **iris**, which is beautifully pigmented and gives us our eye color (the central aperture of the iris is the pupil). This circular muscle controls the size of the pupil so that more or less light, depending on conditions, is allowed to enter the eye. Eye color, or more correctly, iris color, is due to variable amounts of eumelanin (brown/black melanins) and pheomelanin (red/yellow melanins) produced by melanocytes. More eumelanin is found in brown-eyed people, and more pheomelanin is found in blue- and green-eyed people. The *melanocortin-1 receptor* (*MC1R*) gene is a regulator of eumelanin production and is located on chromosome 16q24.3. Point mutations in the *MC1R* gene affect melanogenesis. The presence of point mutations in the *MC1R* gene alleles is a common feature in light-skinned and blue- and green-eyed people (1, 2).
- A transparent external surface, the **cornea**, that covers both the pupil and the iris. This is the first and most powerful lens of the optical system of the eye and allows, together with the crystalline lens, the production of a sharp image at the retinal photoreceptor level.
- The "white of the eye", the **sclera**, which forms part of the supporting wall of the eyeball. The sclera is continuous with the cornea. Furthermore, this external covering of the eye is in continuity with the dura of the central nervous system.

The Eyeball

When we remove the eye from the orbit, we can see that the eye is a slightly asymmetrical sphere with an approximate sagittal diameter or length of 24 to 25 mm and a transverse diameter of 24 mm. It has a volume of about 6.5 cc.

A cross-sectional view of the eye shows (Fig. 2):

- Three different layers:
  1. The external layer, formed by the **sclera** and **cornea**.
  2. The intermediate layer, divided into two parts: anterior (**iris** and **ciliary body**) and posterior (**choroid**).
  3. The internal layer, or the sensory part of the eye, the **retina**.
- Three chambers of fluid: **anterior chamber** (between cornea and iris), **posterior chamber** (between iris, zonule fibers and lens), and the **vitreous chamber** (between the lens and the retina). The first two chambers are filled with aqueous humor, whereas the vitreous chamber is filled with a more viscous fluid, the vitreous humor.
- The sagittal section of the eye also reveals the lens, which is a transparent body located behind the iris. The lens is suspended by ligaments (called zonule fibers) attached to the anterior portion of the ciliary body. The contraction or relaxation of these ligaments, as a consequence of ciliary muscle actions, changes the shape of the lens, a process called **accommodation** that allows us to form a sharp image on the retina.

Light rays are focused through the transparent cornea and lens upon the retina. The central point for image focus (the visual axis) in the human retina is the **fovea**. Here a maximally focused image initiates resolution of the finest detail and direct transmission of that detail to the brain for the higher operations needed for

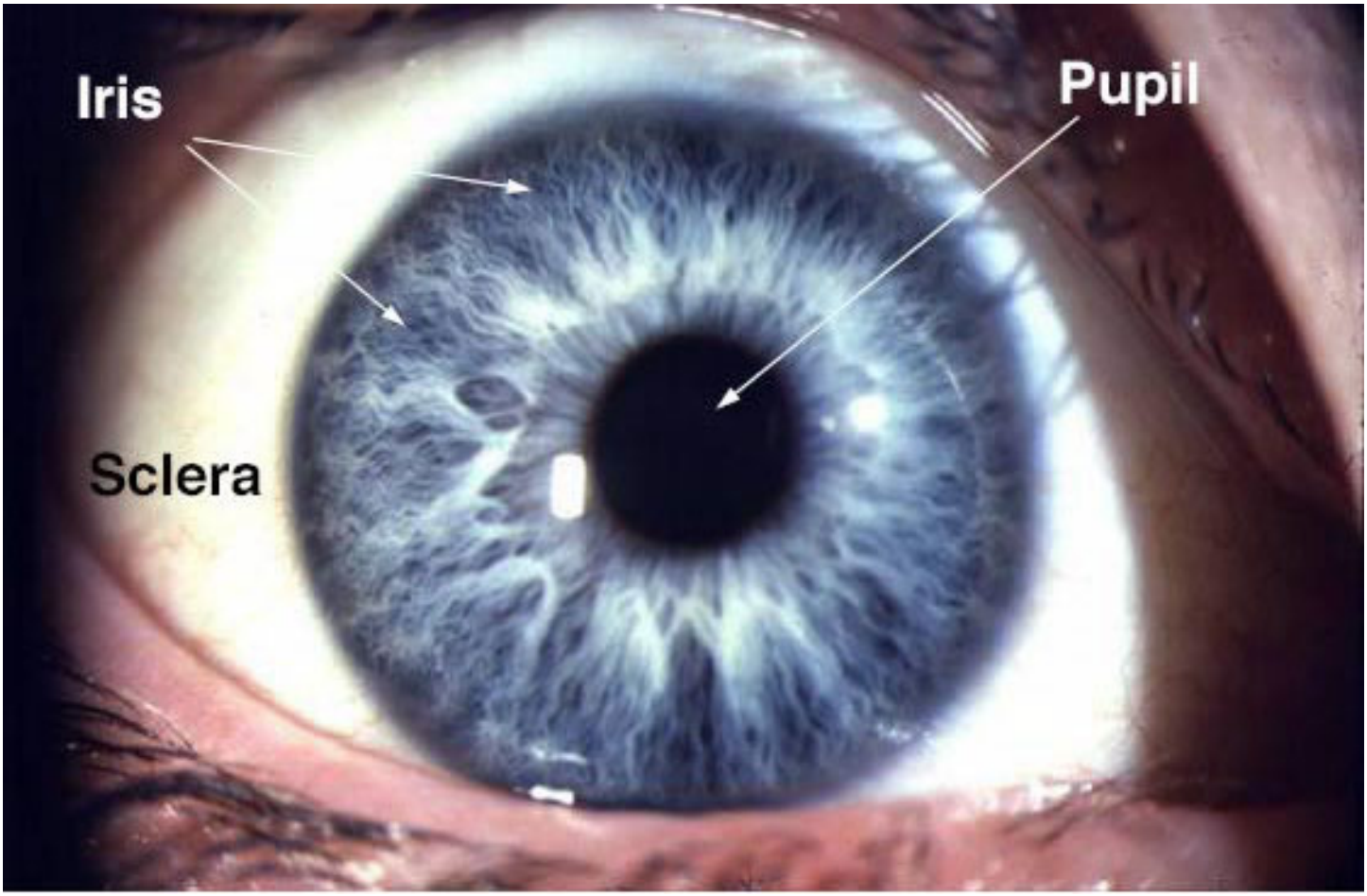

Figure 1. View of the human eye.

perception. The optic axis is slightly closer to the nasal area and projects closer to the optic nerve head. The optic axis is the longest sagittal distance between the front or vertex of the cornea and the furthest posterior part of the eyeball. The eye is rotated around the optic axis by the eye muscles. Instead of a fovea, some vertebrate retinas have another specialization of the central retina, known as an **area centralis** or a visual streak.

Extraocular Muscles

Each eyeball is held in position in the orbital cavity by various ligaments, muscles, and fascial expansions that surround it (Fig. 3). Inserted into the sclera are three pairs of muscles (six muscles altogether). Two pairs are rectus muscles that run straight to the bony orbit of the skull, orthogonal to each other (the superior rectus, the inferior rectus, the lateral rectus, and the medial rectus muscles). Another pair of muscles, the oblique muscles (superior oblique and inferior oblique), are angled, as the name implies, obliquely. These muscles, named **extraocular muscles**, rotate the eyeball in the orbits and allow the image to be focused, at all times, on the fovea of the central retina.

Development of the Eye

The retina is a part of the central nervous system and an ideal region of the vertebrate brain to study, because similar to other regions of the central nervous system, it **derives from the neural tube** (Fig. 4). The retina is formed during development of the embryo from **optic vesicles** outpouching from two sides of the developing neural tube. The primordial optic vesicles fold back in upon themselves to form the **optic cup**, with the inside of

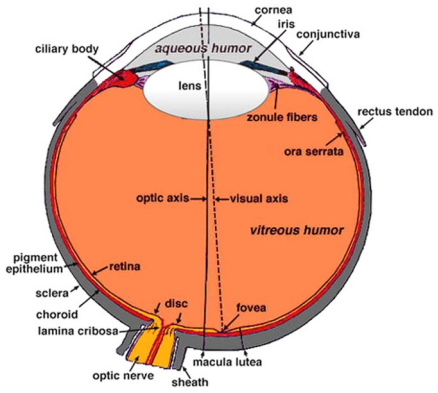

Figure 2. Sagittal section of the adult human eye.

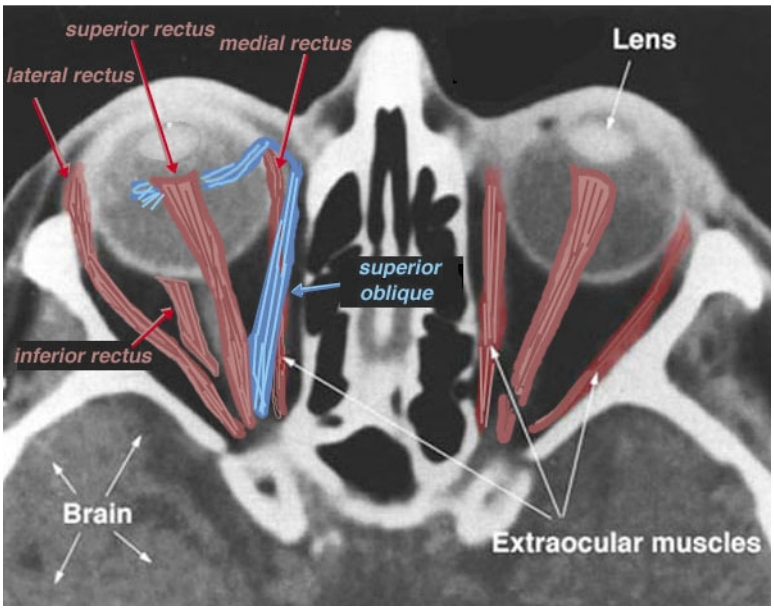

Figure 3. CT horizontal transverse scan.

the cup becoming the retina and the outside remaining a single monolayer of epithelium, known as the retinal pigment epithelium. Initially, both walls of the optic cup are one-cell thick, but the cells of the inner wall divide to form a neuroepithelial layer many cells thick—the retina (see the movie of the morphogenesis).

Sensory retinal development begins as early as the optic vesicle stage, with the migration of cell nuclei to the inner surface of the sensory retina. Additional retinal development is characterized by the formation of more layers, arising from cell division and subsequent cell migration. The retina develops in an inside-to-outside manner: ganglion cells are formed first, and photoreceptors cells become fully mature last.

Additional changes in retinal morphology are accomplished by simultaneous formation of multiple, complex intercellular connections. Thus, by 5 months of gestation, most of the basic neural connections of the retina have been established (Fig. 5) (4).

The functional synapses are made almost exclusively in the two plexiform layers, and the perikarya of the nerve cells are distributed in the three nuclear layers.

Photoreceptor cell maturation begins with the formation of outer segments (OS) containing visual pigment from multiple infoldings of the plasma membrane of each cell. Outer segment formation proceeds, and the eye becomes sensitive to light at about 7 months of gestation.

The final portion of the sensory retina to mature is the fovea, where the ganglion cell layer thickening begins during midgestation. The outer nuclear layer is also wider here than elsewhere in the retina and consists almost entirely of developing cone cells. The ganglion cell nuclei migrate radially outward in a circle, leaving the fovea free of ganglion cell nuclei. Cell-cell attachments persist, however, and foveal cone cells alter their shape to accomodate the movement of ganglion cells. Foveal development continues with cell rearrangements and alteration in cone shape until about 4 years after birth (5, 6).

Surface membranes cover the eye cup and develop into lens, iris, and cornea, with the three chambers of fluid filled with aqueous and vitreous humors (Fig. 6).

Preview

In the following chapters, we will describe in greater detail the individual nerve cells that make up the retina and the functional pathways into which these neurons are organized. Eventually, we will progress to a stage where we can understand the summary diagrams (Fig. 7 and Fig. 8) that show the function and wiring of the two best understood mammalian retinas—the cat and primate retinas.

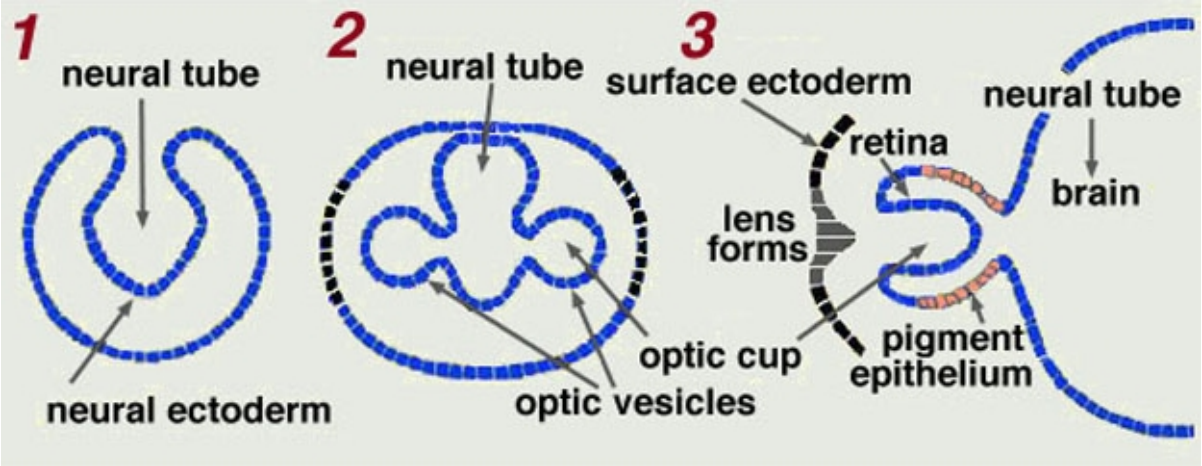

Movie 1. A morph of development of the eye.

Download video

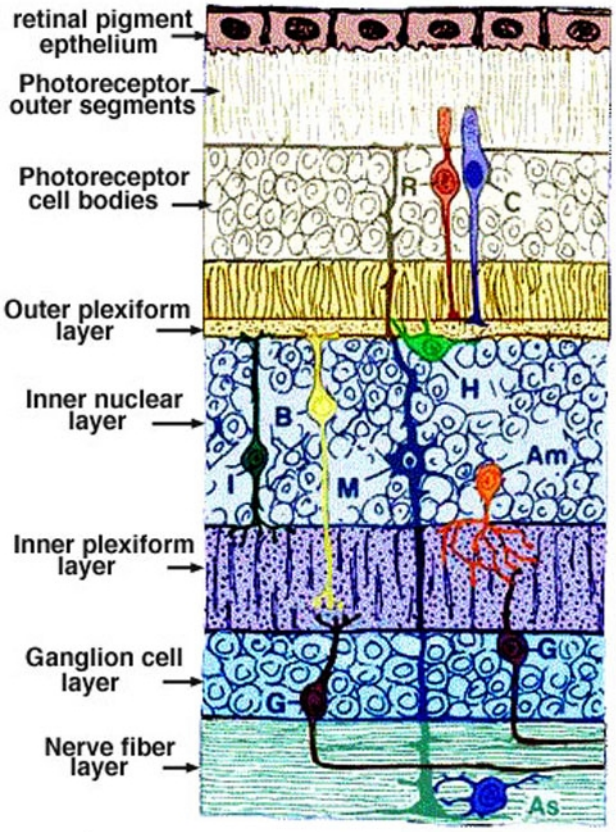

Figure 5. Schema of the layers of the developing retina around 5 months of gestation. (Modified from Ogden (3).)

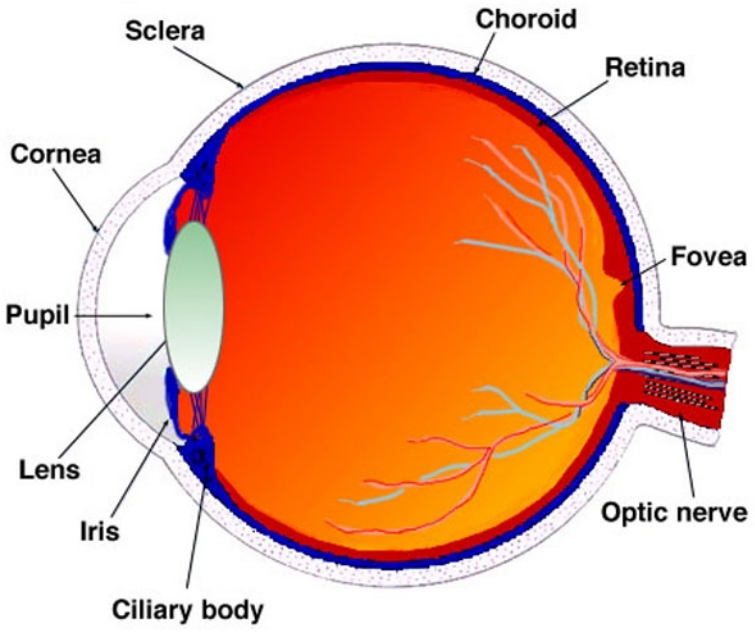

Figure 6. Near-axial (near-horizontal) section of the adult human eye.

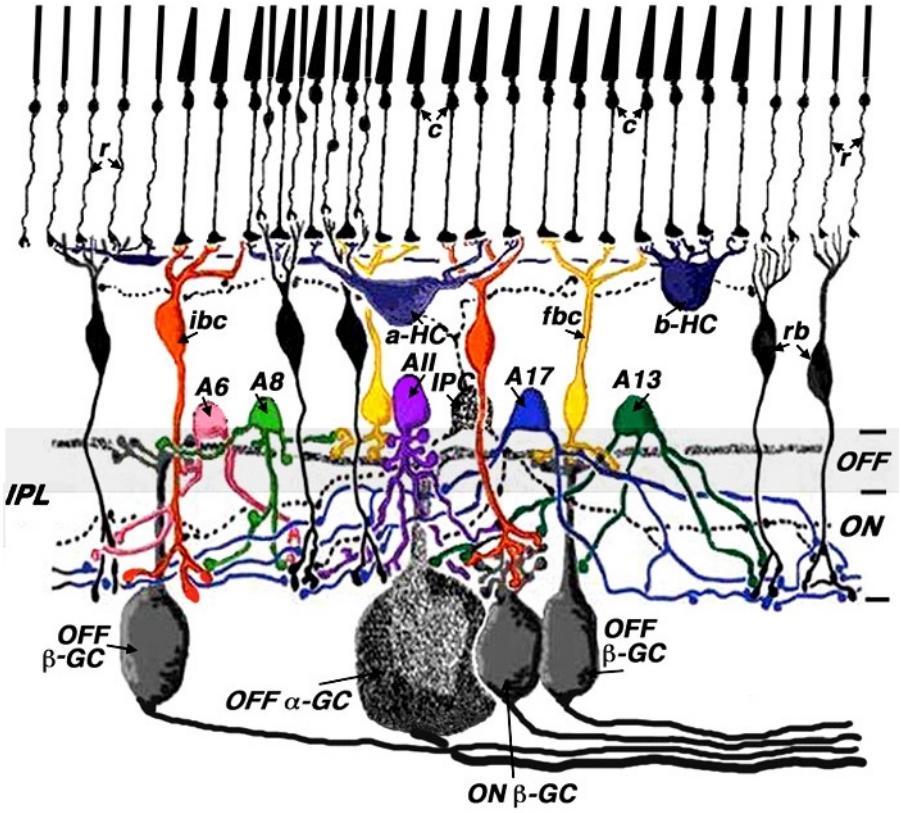

Figure 7. Diagrammatic scheme of the cat retina

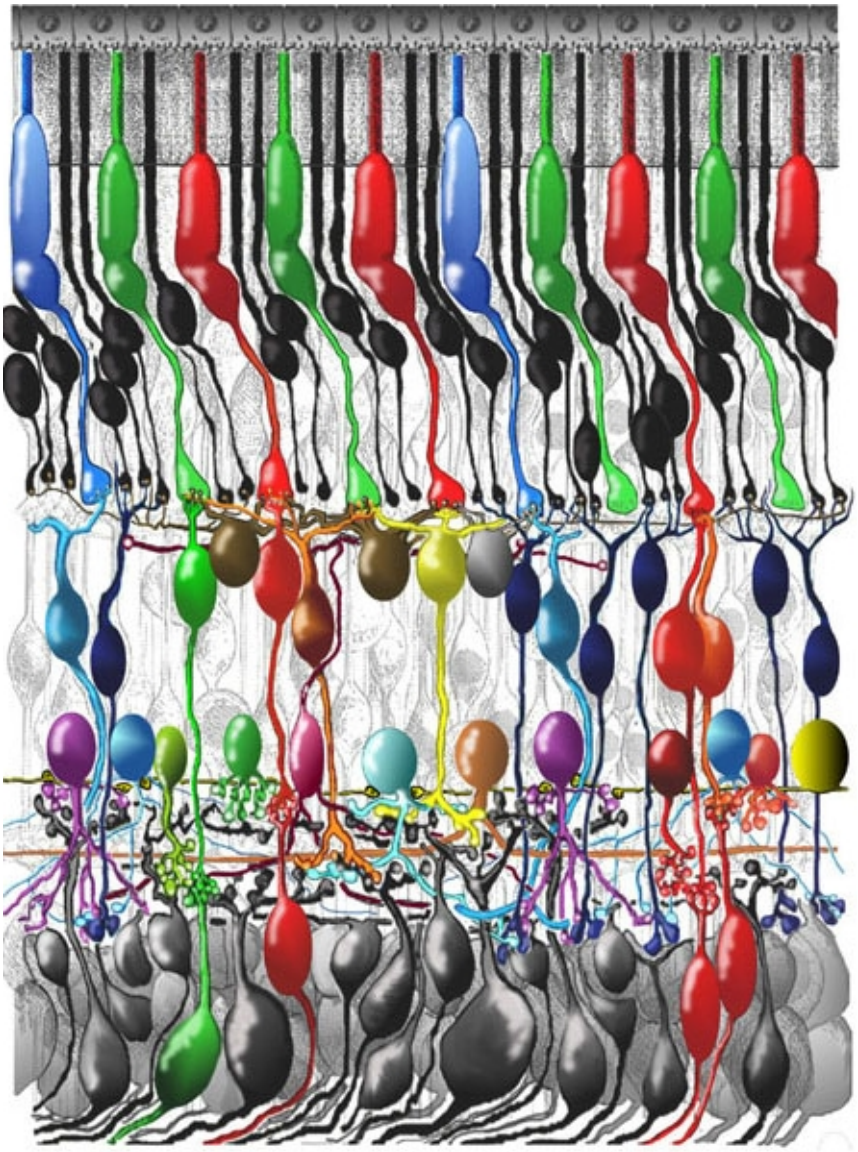

Figure 8. Scheme of the human retina.

References

1. Metzelaar-Blok JAW, ter Huurne JA, Hurks HM, Keunen JE, Jager MJ, Gruis NA. Characterization of melanocortin-1 receptor gene variants in uveal melanoma patients. Invest Ophthalmol Vis Sci. 2001;42:1951–1954. PubMed PMID: 11481256.
2. Valverde P, Healy E, Jackson I, Rees JL, Thody AJ. Variants of the melanocyte-stimulating hormone receptor gene are associated with red hair and fair skin in humans. Nat Genet. 1995;11:328–330. PubMed PMID: 7581459.
3. Ogden TE. Retina: basic science and inherited retinal disease. Vol. 1. St. Louis: The CV Mosby Co.; 1989.
4. Mann I. The development of the human eye. New York: Grune and Stralton; 1964.
5. Hendrickson AE, Youdelis C. The morphological development of the human fovea. Ophthalmology. 1984;91:603–612. PubMed PMID: 6462623.
6. Curcio CA, Hendrickson AE. Organization and development of the primate photoreceptor mosaic. Prog Ret Ret. 1991;10:89–120.

Simple Anatomy of the Retina

Helga Kolb, PhD[1]

Created: May 1, 2005; Updated: January 31, 2012.

1. Overview

When an ophthalmologist uses an ophthalmoscope to look into your eye he sees the following view of the retina (Fig. 1).

In the center of the retina is the optic nerve, a circular to oval white area measuring about 2 x 1.5 mm across. From the center of the optic nerve radiate the major blood vessels of the retina. Approximately 17 degrees (4.5-5 mm), or two and half disc diameters to the left of the disc, can be seen the slightly oval-shaped, blood vessel-free reddish spot, the fovea, which is at the center of the area known as the macula by ophthalmologists (Fig. 1). An animation of the view from iris to retina can be seen in movie 1.

A circular field of approximately 6 mm around the fovea is considered the central retina while beyond this is peripheral retina stretching to the ora serrata, 21 mm from the center of the retina (fovea). The total retina is a circular disc of between 30 and 40 mm diameter (1-3).

The retina is approximately 0.5 mm thick and lines the back of the eye. The optic nerve contains the ganglion cell axons running to the brain and, additionally, incoming blood vessels that open into the retina to vascularize the retinal layers and neurons (Fig. 2). A radial section of a portion of the retina reveals that the ganglion cells (the output neurons of the retina) lie innermost in the retina closest to the lens and front of the eye, and the photosensors (the rods and cones) lie outermost in the retina against the pigment epithelium and choroid. Light must, therefore, travel through the thickness of the retina before striking and activating the rods and cones (Fig. 2). Subsequently the absorbtion of photons by the visual pigment of the photoreceptors is translated into first a biochemical message and then an electrical message that can stimulate all the succeeding neurons of the retina. The retinal message concerning the photic input and some preliminary organization of the visual image into several forms of sensation are transmitted to the brain from the spiking discharge pattern of the ganglion cells.

A simplistic wiring diagram of the retina emphasizes only the sensory photoreceptors and the ganglion cells with a few interneurons connecting the two cell types such as seen in figure 3.

When an anatomist takes a vertical section of the retina and processes it for microscopic examination it becomes obvious that the retina is much more complex and contains many more nerve cell types than the simplistic scheme (above) had indicated. It is immediately obvious that there are many interneurons packed into the central part of the section of retina intervening between the photoreceptors and the ganglion cells (Fig. 4).

All vertebrate retinas are composed of three layers of nerve cell bodies and two layers of synapses (Fig. 5). The outer nuclear layer contains cell bodies of the rods and cones, the inner nuclear layer contains cell bodies of the bipolar, horizontal and amacrine cells and the ganglion cell layer contains cell bodies of ganglion cells and displaced amacrine cells. Dividing these nerve cell layers are two neuropils where synaptic contacts occur (Fig. 5).

The first area of neuropil is the outer plexiform layer (OPL) where connections between rod and cones, and vertically running bipolar cells and horizontally oriented horizontal cells occur (Figs. 6 and 7).

Author Affiliation: 1 Moran Eye Institute, University of Utah School of Medicine, Salt Lake City; Email: Helga.kolb@hsc.utah.edu.

Corresponding author.

The second neuropil of the retina, is the inner plexiform layer (IPL), and it functions as a relay station for the vertical-information-carrying nerve cells, the bipolar cells, to connect to ganglion cells (Figs. 8 and 9). In addition, different varieties of horizontally- and vertically-directed amacrine cells, interact in further networks to influence and integrate the ganglion cell signals. It is at the culmination of all this neural processing in the IPL that the message concerning the visual image is transmitted through ganglion cells to the brain along the optic nerve.

2. Central and peripheral retina compared

Central retina close to the fovea is considerably thicker than peripheral retina (compare Figs. 10A with 10B). This is due to the increased packing density of photoreceptors, particularly the cones, and their associated bipolar and ganglion cells in central retina compared with peripheral retina.

Central retina is cone-dominated retina whereas peripheral retina is rod-dominated. Thus in central retina the cones are closely spaced and the rods fewer in number between the cones (Figs. 10A and 10B).

The outer nuclear layer (ONL), composed of the cell bodies of the rods and cones, is about the same thickness in central and peripheral retina. However in the peripheral retina the rod cell bodies outnumber the cone cell bodies while the reverse is true for central retina. In central retina, the cones have oblique axons displacing their cell bodies from their synaptic pedicles in the outer plexiform layer (OPL). These oblique axons, with accompanying Müller cell processes, form a pale-staining fibrous-looking area known as the Henle fibre layer. The latter layer is absent in peripheral retina.

The inner nuclear layer (INL) is thicker in the central area of the retina compared with peripheral retina, due to a greater density of cone-connecting second-order neurons (cone bipolar cells), smaller-field and more closely-spaced horizontal cells, and amacrine cells concerned with the cone pathways (Fig. 10). As we shall see later, cone-connected circuits of neurons are less convergent in that fewer cones impinge on second order neurons, than rods do in rod-connected pathways.

A remarkable difference between central and peripheral retina can be seen in the relative thicknesses of the inner plexiform layers (IPL), ganglion cell layers (GCL) and nerve fibre layers (NFL) (Figs. 10A and 10B). This is again due to the greater numbers and increased packing-density of ganglion cells needed for the cone pathways in the cone-dominant foveal retina as compared the rod-dominant peripheral retina. The greater number of ganglion cells means more synaptic interaction in a thicker IPL and greater numbers of ganglion cell axons coursing to the optic nerve in the nerve fibre layer (Fig. 10A).

3. Müller glial cells

Müller cells are the radial glial cells of the retina (Fig. 11). The outer limiting membrane (OLM) of the retina is formed from adherens junctions between Müller cells and photoreceptor cell inner segments. The inner limiting membrane (ILM) of the retina is likewise composed of laterally contacting Müller cell end feet and associated basement membrane constituents.

The OLM forms a barrier between the subretinal space, into which the inner and outer segments of the photoreceptors project to be in close association with the pigment epithelial layer behind the retina, and the neural retina proper. The ILM is the inner surface of the retina bordering the vitreous humor and thereby forming a diffusion barrier between neural retina and vitreous humor (Fig. 11).

Throughout the retina the major blood vessels of the retinal vasculature supply the capillaries that run into the neural tissue. Capillaries are found running through all parts of the retina from the nerve fibre layer to the outer plexiform layer and even occasionally as high as in the outer nuclear layer. Nutrients from the vasculature of the choriocapillaris behind the pigment epithelium layer supply the delicate photoreceptor layer.

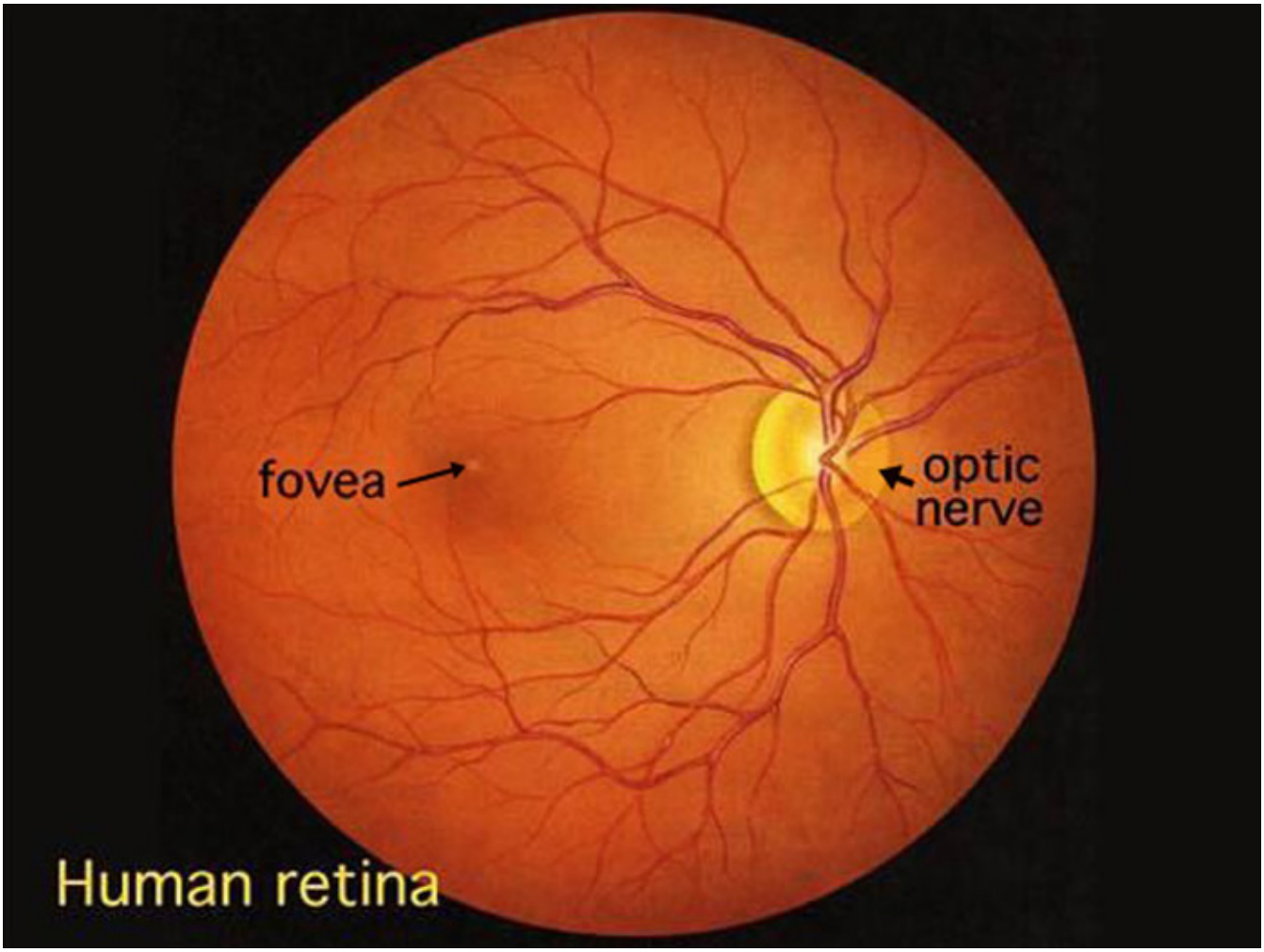

Figure 1. A view of the retina seen through an ophthalmoscope.

Movie 1. An animation from the iris to the retina.
Download video

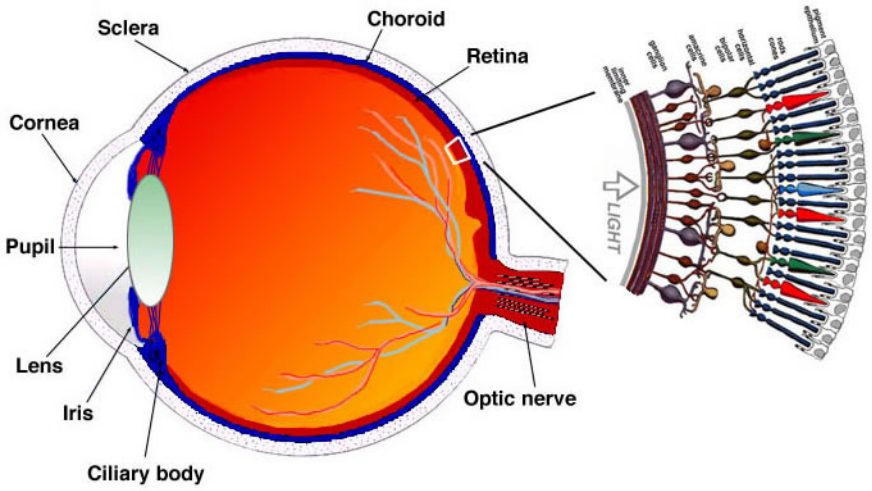

Figure 2. A drawing of a section through the human eye with a schematic enlargement of the retina.

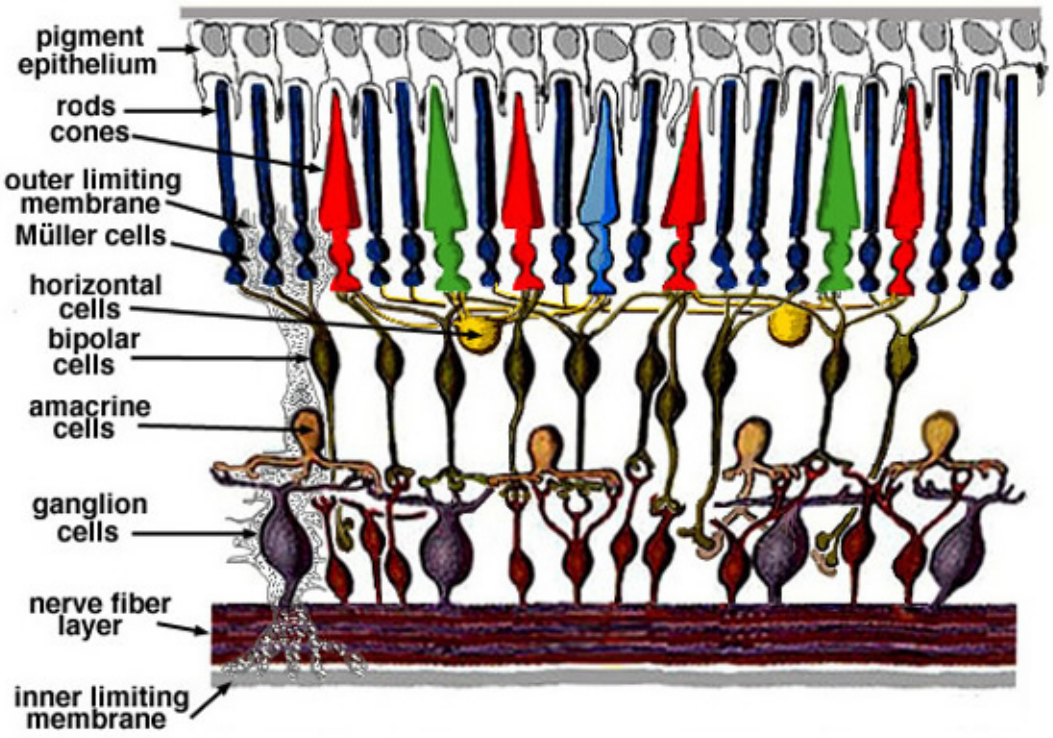

Figure 3. Simple diagram of the organization of the retina.

4. Foveal structure

The center of the fovea is known as the foveal pit (1) and is a highly specialized region of the retina different again from central and peripheral retina we have considered so far. Radial sections of this small circular region of retina measuring less than a quarter of a millimeter (200 μm) across are shown below for human (Fig. 12A) and for monkey (Fig. 12B).

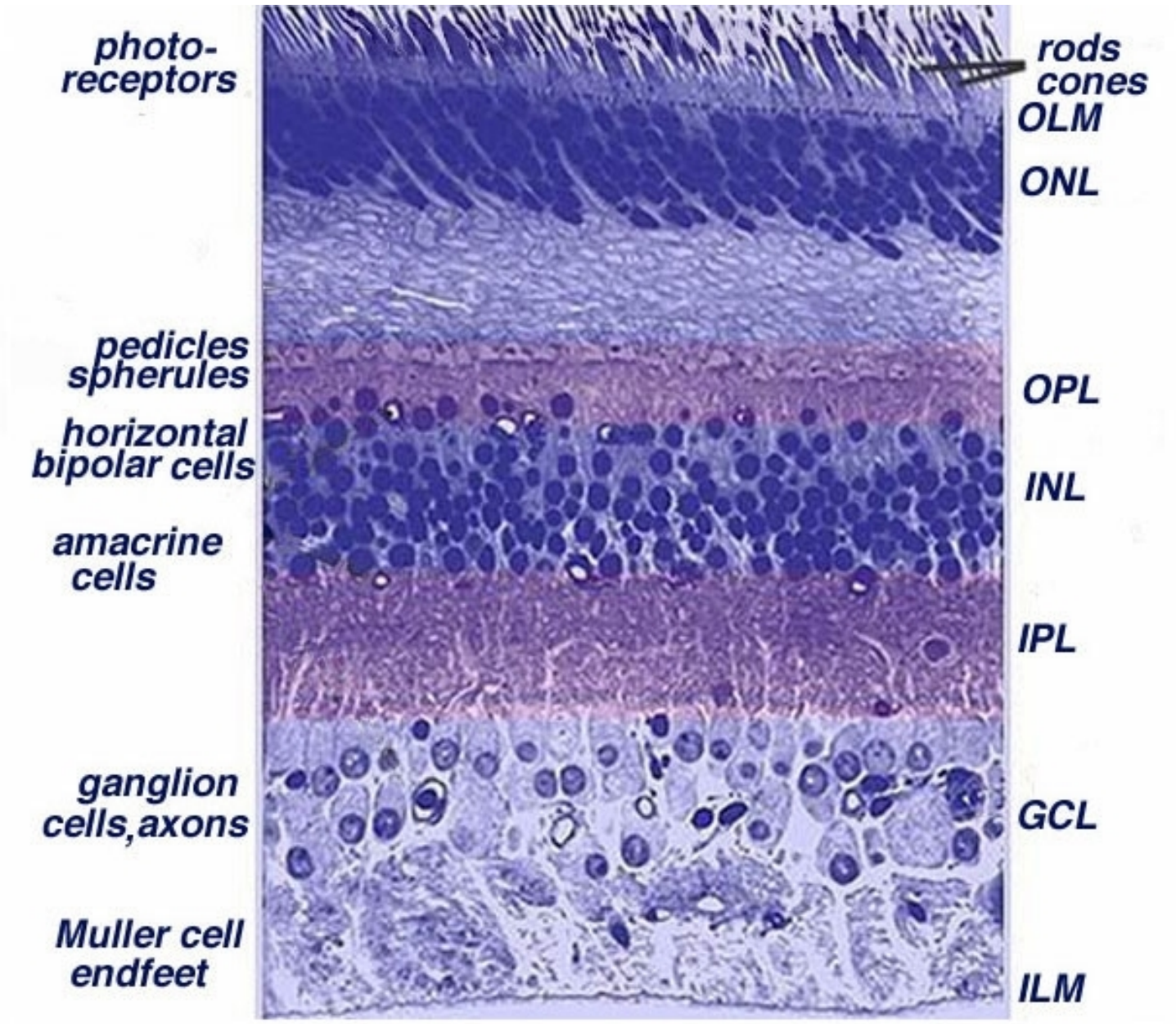

Figure 4. Light micrograph of a vertical section through central human retina.

The foveal pit is an area where cone photoreceptors are concentrated at maximum density with exclusion of the rods, and arranged at their most efficient packing density which is in a hexagonal mosaic. This is more clearly seen in a tangential section through the foveal cone inner segments (Fig. 13).

Below this central 200 μm diameter central foveal pit, the other layers of the retina are displaced concentrically leaving only the thinnest sheet of retina consisting of the cone cells and some of their cell bodies. Radially distorted but complete layering of the retina then appears gradually along the foveal slope (right and left sides of Figs. 12a and 12b) until the rim of the fovea is made up of the displaced second- and third-order neurons related to the central cones. Here the ganglion cells are piled into six layers so making this area, called the foveal rim or parafovea (1), the thickest portion of the entire retina.

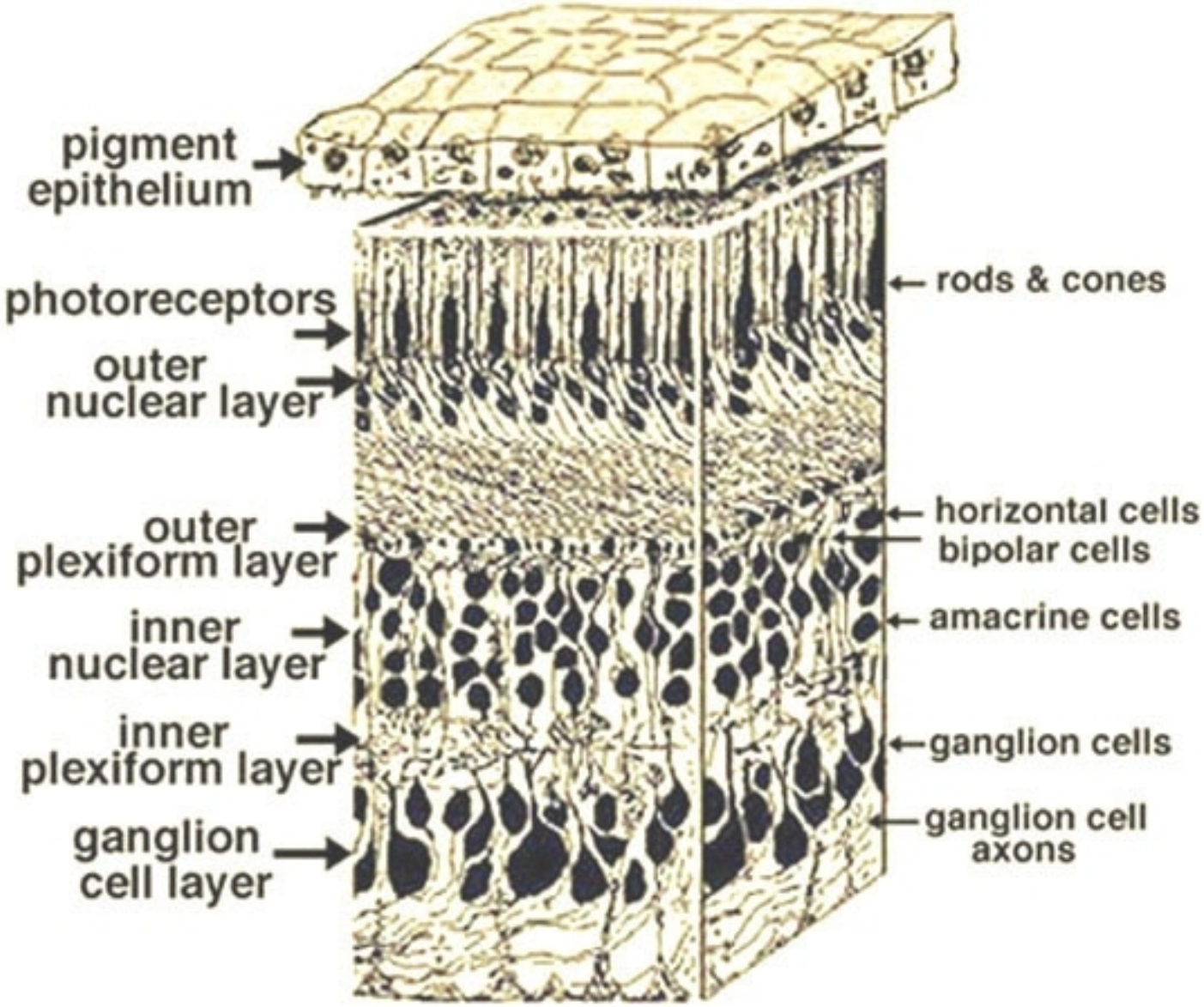

Figure 5. 3-D block of a portion of human retina.

5. Macula lutea

The whole foveal area including foveal pit, foveal slope, parafovea and perifovea is considered the macula of the human eye. Familiar to ophthalmologists is a yellow pigmentation to the macular area known as the macula lutea (Fig. 14).

This pigmentation is the reflection from yellow screening pigments, the xanthophyll carotenoids zeaxanthin and lutein (4), present in the cone axons of the Henle fibre layer. The macula lutea is thought to act as a short wavelength filter, additional to that provided by the lens (5). As the fovea is the most essential part of the retina for human vision, protective mechanisms for avoiding bright light and especially ultraviolet irradiation damage are essential. For if the delicate cones of our fovea are destroyed, we become blind.

The yellow pigment that forms the macula lutea in the fovea can be clearly demonstrated by viewing a section of the fovea in the microscope with blue light (Fig. 15). The dark pattern in the foveal pit extending out to the edge of the foveal slope is caused by the macular pigment distribution (6).

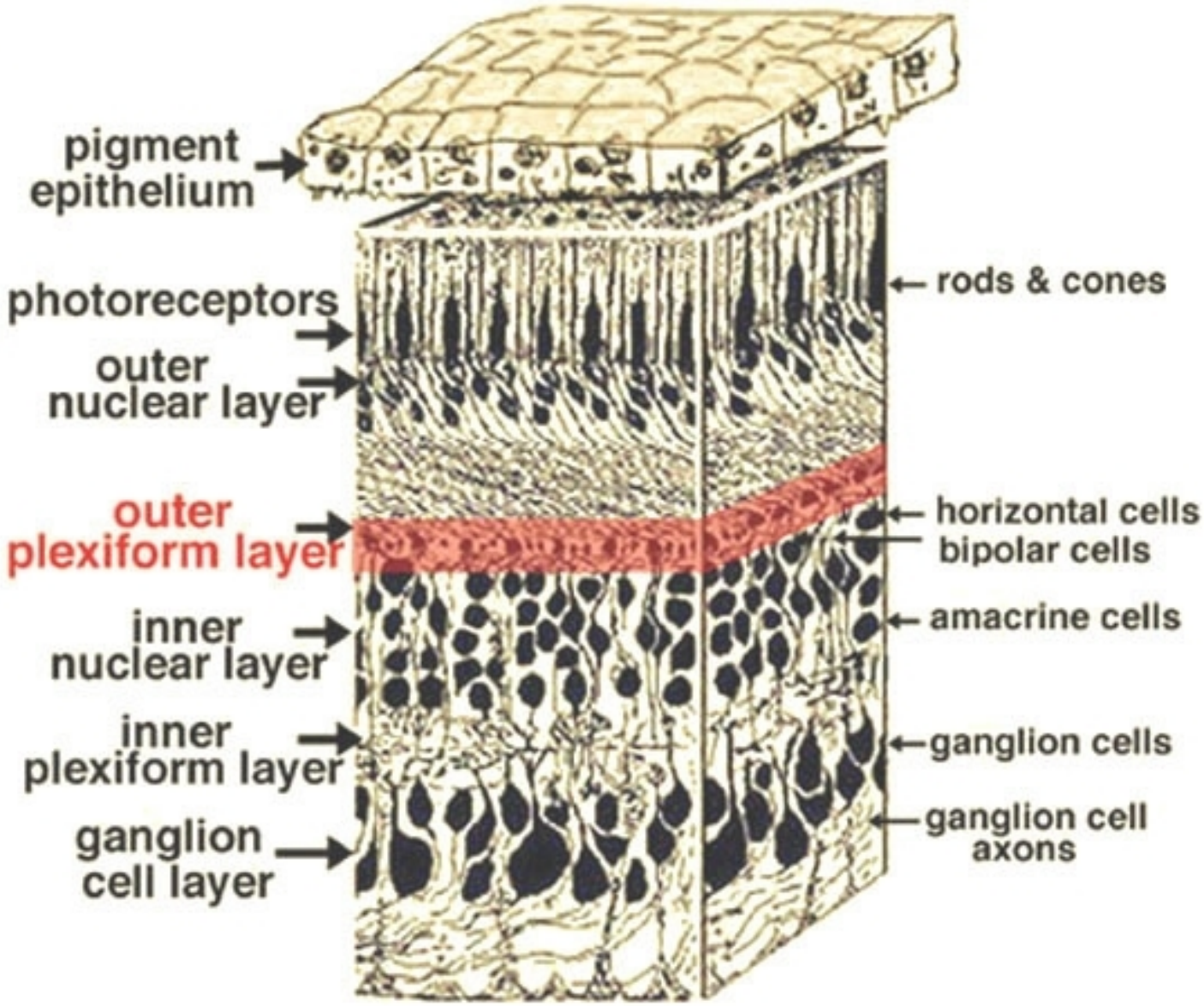

Figure 6. 3-D block of retina with the outer plexiform layer (OPL) highlighted in red. .

If one were to visualize the foveal photoreceptor mosaic as though the visual pigments in the individual cones were not bleached, one would see the picture shown in Figure 16 (lower frame) (picture from Lall and Cone, 1996). The short-wavelength sensitive cones on the foveal slope look pale yellow green, the middle wavelength cones, pink and the long wavelength sensitive cones, purple. If we now add the effect of the yellow screening pigment of the macula lutea we see the appearance of the cone mosaic in Figure 16 (upper frame). The macula lutea helps enhance achromatic resolution of the foveal cones and blocks out harmful UV light irradiation (Fig. 16 from Abner Lall and Richard Cone, unpublished data).

6. Blood supply to the retina

There are two sources of blood supply to the mammalian retina: the central retinal artery and the choroidal blood vessels. The choroid receives the greatest blood flow (65-85%) (7) and is vital for the maintainance of the outer retina (particularly the photoreceptors) and the remaining 20-30% flows to the retina through the central

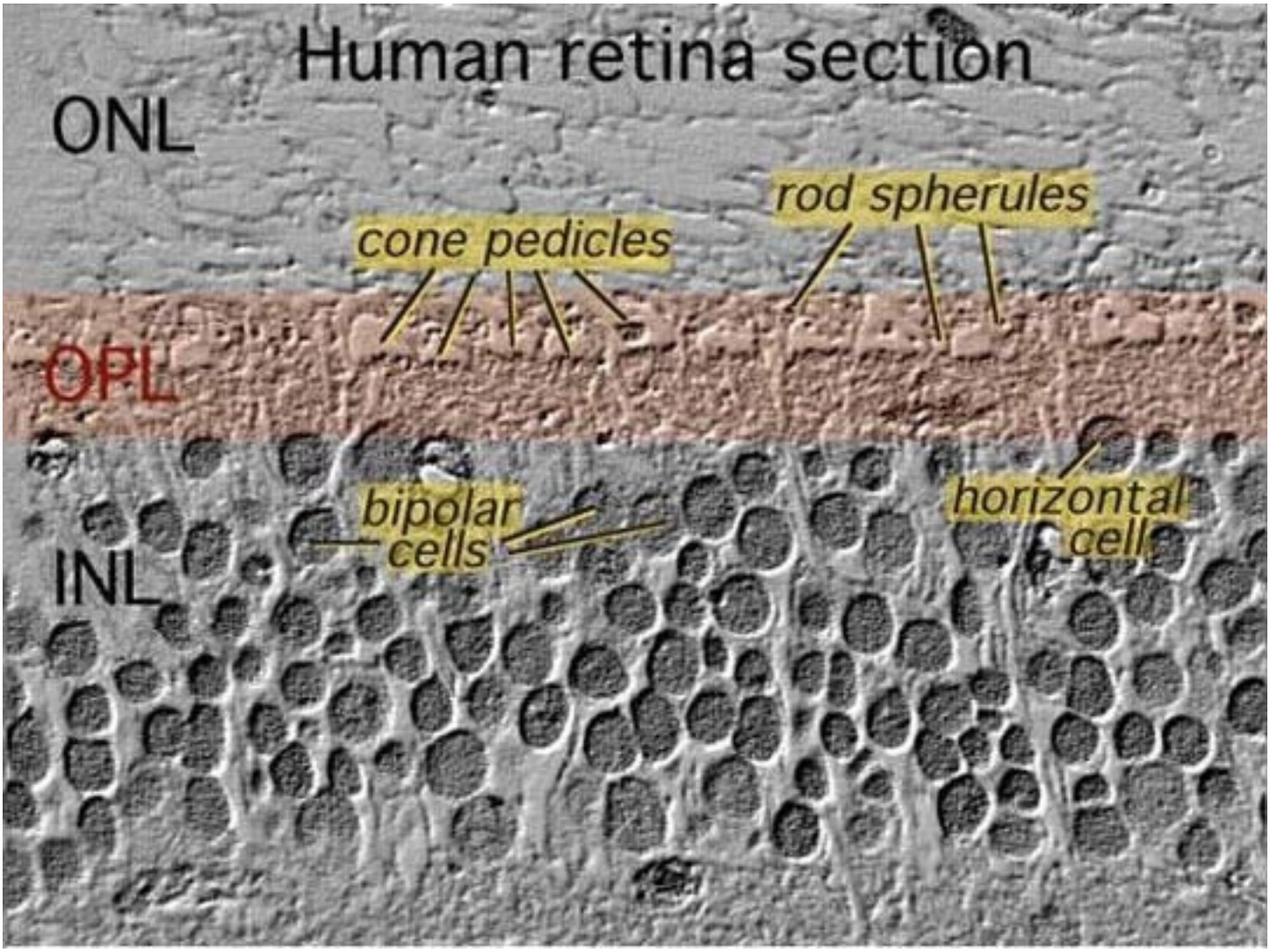

Figure 7. Light micrograph of a vertical section through the outer plexiform layer (OPL). Cone pedicles and rod spherules are the synaptic terminals of cones and rods. The outer nuclear layer (ONL) contains the cell bodies of rods and cones. The inner nuclear layer (INL) contains the cell bodies of horizontal cells, bipolar cells, and amacrine cells.

retinal artery from the optic nerve head to nourish the inner retinal layers. The central retinal artery has 4 main branches in the human retina (Fig. 17).

The arterial intraretinal branches then supply three layers of capillary networks i.e. 1) the radial peripapillary capillaries (RPCs) and 2) an inner and 3) an outer layer of capillaries (Fig. 18A). The precapillary venules drain into venules and through the corresponding venous system to the central retinal vein (Fig. 18B).

The radial peripapillary capillaries (RPCs) are the most superfical layer of capillaries lying in the inner part of the nerve fiber layer, and run along the paths of the major superotemporal and inferotemporal vessels 4-5 mm from the optic disk (8). The RPCs anastomose with each other and the deeper capillaries. The inner capillaries lie in the ganglion cell layers under and parallel to the RPCs. The outer capillary network runs from the inner plexiform layer to the outer plexiform layer thought the inner nuclear layer (8).

As will be noticed from the flourescein angiography of Figure 17, there is a ring of blood vessels in the macular area around a blood vessel- and capillary-free zone 450-600 μm in diameter, surrounding the fovea. The macular vessels arise from branches of the superior temporal and inferotemporal arteries. At the border of the avascular zone the capillaries become two-layered and finally join as a single layered ring. The collecting venules are

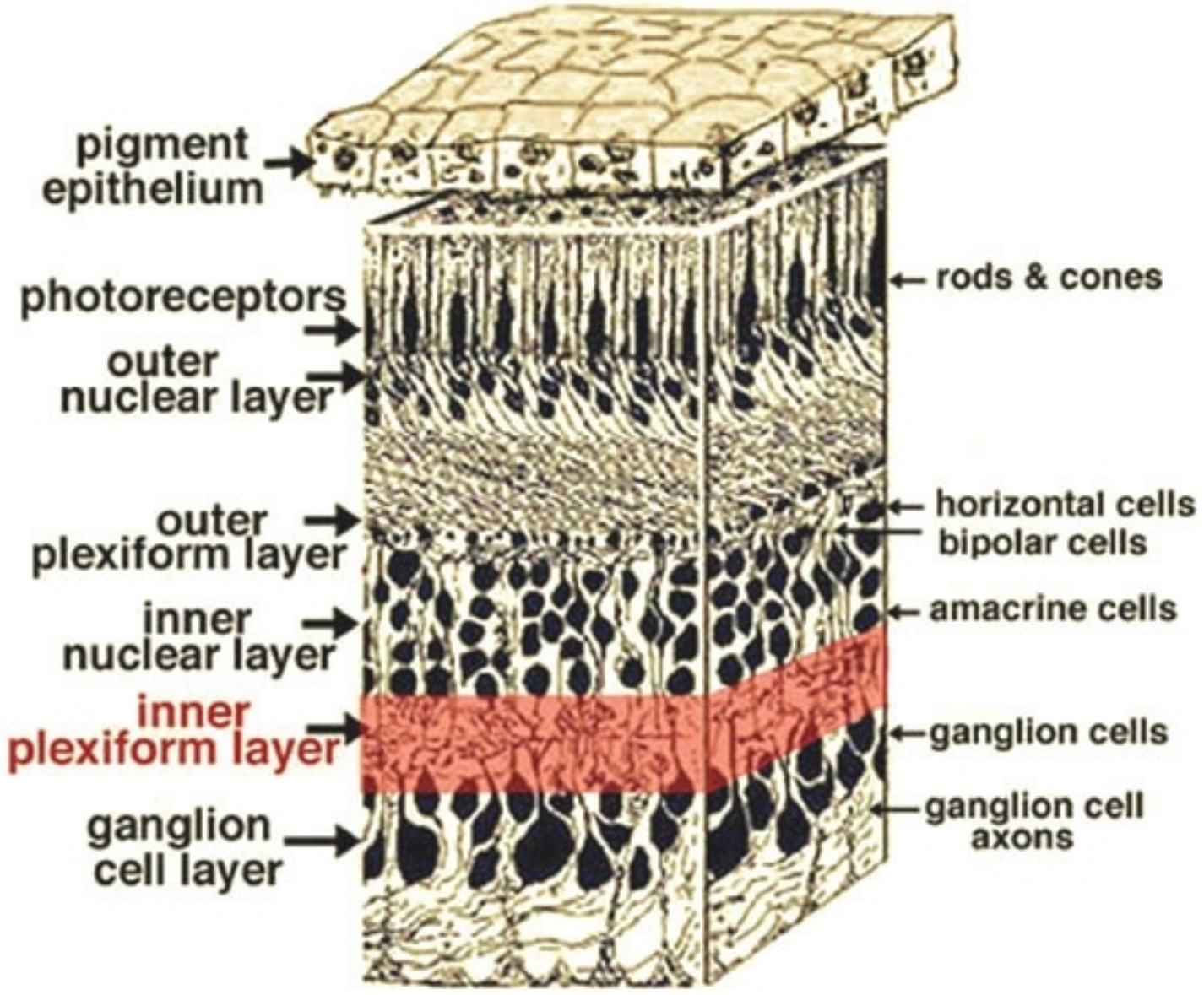

Figure 8. 3-D block of retina with the inner plexiform layer (IPL) highlighted in red.

deeper (posterior) to the arterioles and drain blood flow back into the main veins (Fig. 19). In the rhesus monkey this perimacular ring and blood vessel free fovea is clearly seen in the beautiful drawings made by Max Snodderly's group (9) (Fig. 20).

The choroidal arteries arise from long and short posterior ciliary arteries and branches of Zinn's circle (around the optic disc). Each of the posterior ciliary arteries break up into fan-shaped lobules of capillaries that supply localized regions of the choroid (10). The macular area of the choroidal vessels is not specialized like the retinal blood supply is (8). The arteries pierce the sclera around the optic nerve and fan out to form the three vascular layers in the choroid: outer (most scleral), medial and inner (nearest Bruch's membrane of the pigment epithelium) layers of blood vessels. This is clearly shown in the corrosion cast of a cut face of the human choroid in figure 21A (8). The corresponding venous lobules drain into the venules and veins that run anterior towards the equator of the eyeball to enter the vortex veins (Fig. 21b). One or two vortex veins drain each of the 4 quadrants of the eyeball. The vortex veins penetrate the sclera and merge into the ophthalmic vein as shown in the corrosion cast of figure 21B (8).

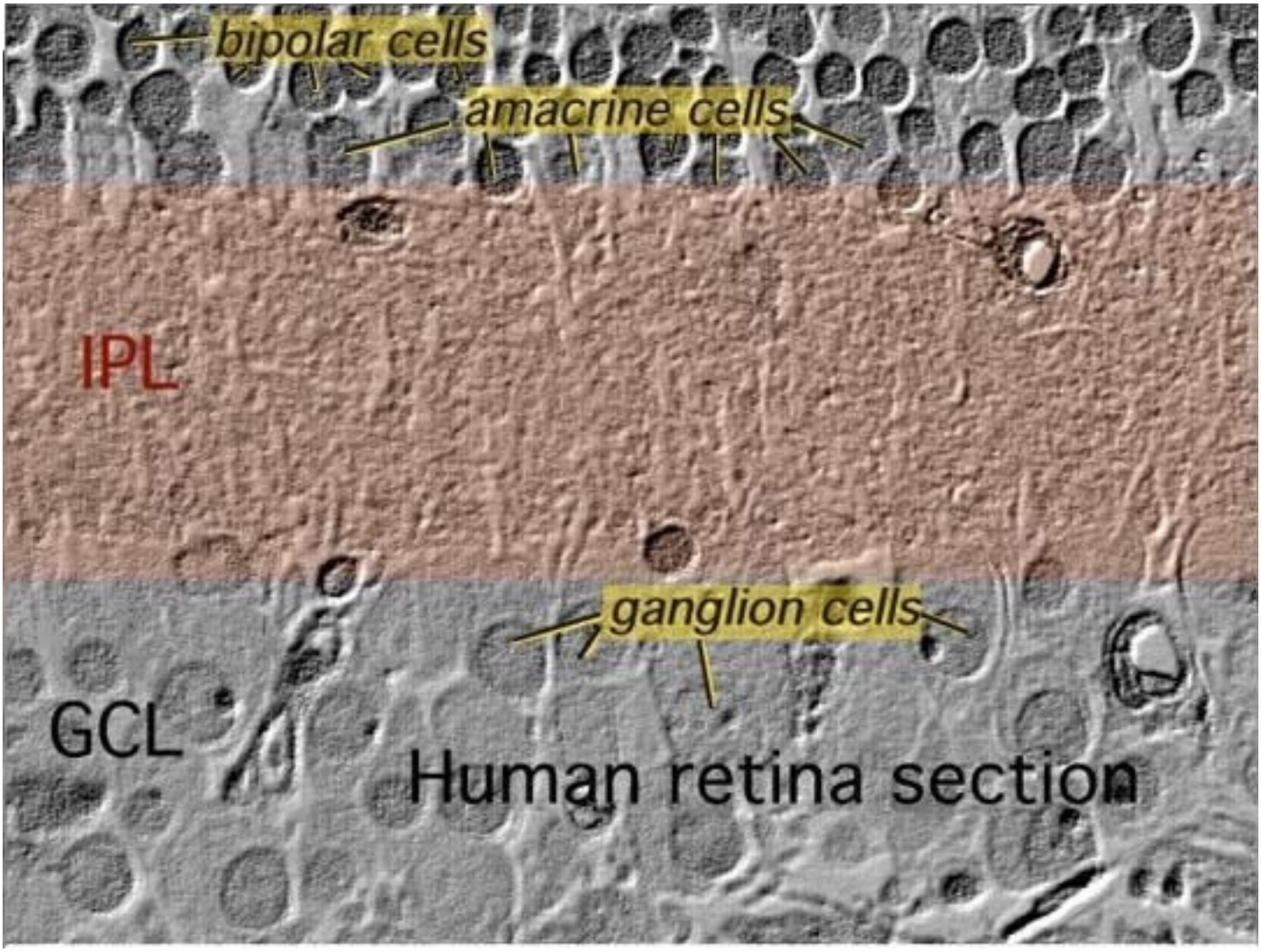

Figure. 9. Light micrograph of a vertical section through the inner plexiform layer (IPL), highlighted in red. Amacrine cells and bipolar cells lie above the IPL. Ganglion cells form the ganglion cell layer (GCL) which lies just below the IPL. Processes from all 3 cell types interconnect within IPL circuitry.

7. Degenerative diseases of the human retina

The human retina is a delicate organization of neurons, glia and nourishing blood vessels. In some eye diseases, the retina becomes damaged or compromised, and degenerative changes set in that eventually lead to serious damage to the nerve cells that carry the vital messages about the visual image to the brain. We indicate four different conditions where the retina is diseased and blindness may be the end result.

Age related macular degeneration is a common retinal problem of the aging eye and a leading cause of blindness in the world. The macular area and fovea become compromised due to the pigment epithelium behind the retina degenerating and forming drusen (white spots, Fig. 22) and allowing leakage of fluid behind the fovea. The cones of the fovea die causing central visual loss so we cannot read or see fine detail.

Glaucoma (Fig. 23) is also a common problem in aging, where the pressure within the eye becomes elevated. The pressure rises because the anterior chamber of the eye cannot exchange fluid properly by the normal aqueous outflow methods. The pressure within the vitreous chamber rises and compromises the blood vessels of the optic

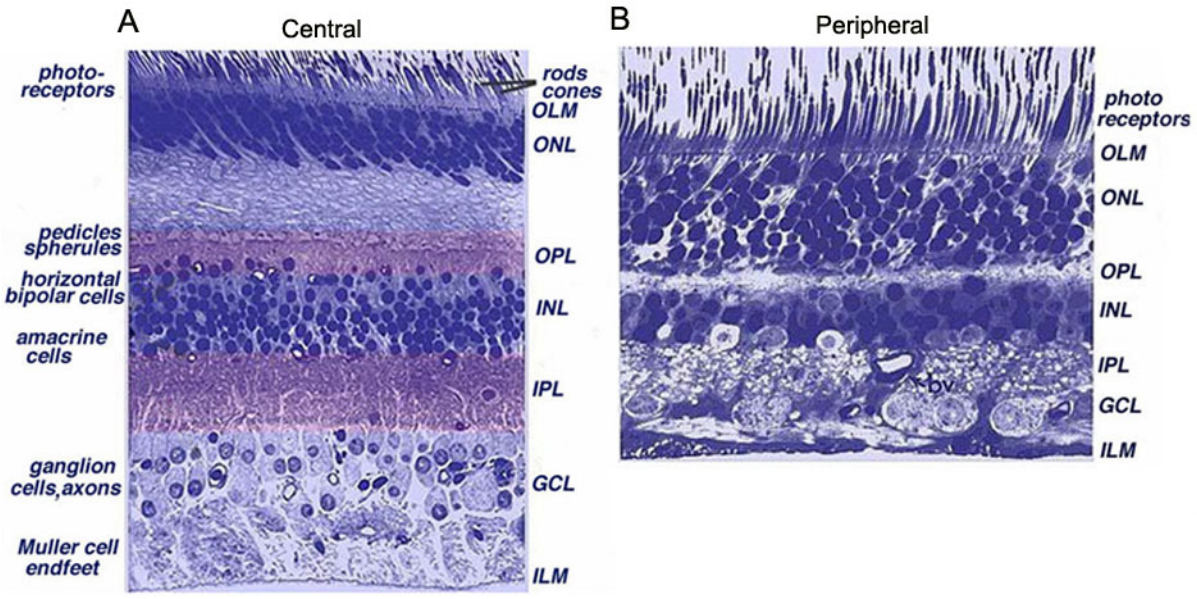

Figure 10. Different structure of central and peripheral human retina. *A*. In central retina the inner and outer plexiform layers (IPL, OPL) are thicker than in peripheral retina. The inner nuclear and ganglion cell layers (INL, GCL) contain more cells, but of smaller diameter. *B*. Peripheral retina is thinner overall than central retina, though cells are larger in diameter, most layers are thin. The outer nuclear layer (ONL) is densely populated with rods. OLM, outer limiting membrane; ILM, inner limiting membrane.

nerve head and eventually the axons of the ganglion cells so that these vital cells die. Treatment to reduce the intraocular pressure is essential in glaucoma.

Retinits pigmentosa (Fig. 24) is a nasty hereditary disease of the retina for which there is no cure at present. It comes in many forms and consists of large numbers of genetic mutations presently being analyzed. Most of the faulty genes that have been discovered concern the rod photoreceptors. The rods of the peripheral retina begin to degenerate in early stages of the disease. Patients become night blind gradually as more and more of the peripheral retina (where the rods reside) becomes damaged. Eventually patients are reduced to tunnel vision with only the fovea spared the disease process. Characteristic pathology is the occurrence of black pigment in the peripheral retina and thinned blood vessels at the optic nerve head (Fig. 24).

Diabetic retinopathy is a side effect of diabetes that affects the retina and can cause blindness (Fig. 25). The vital nourishing blood vessels of the eye become compromised, distorted and multiply in uncontrollable ways. Laser treatment for stopping blood vessel proliferation and leakage of fluid into the retina, is the commonest treatment at present.

About the Author

The biosketch for Helga Kolb appears in the Webvision section About the Editors.

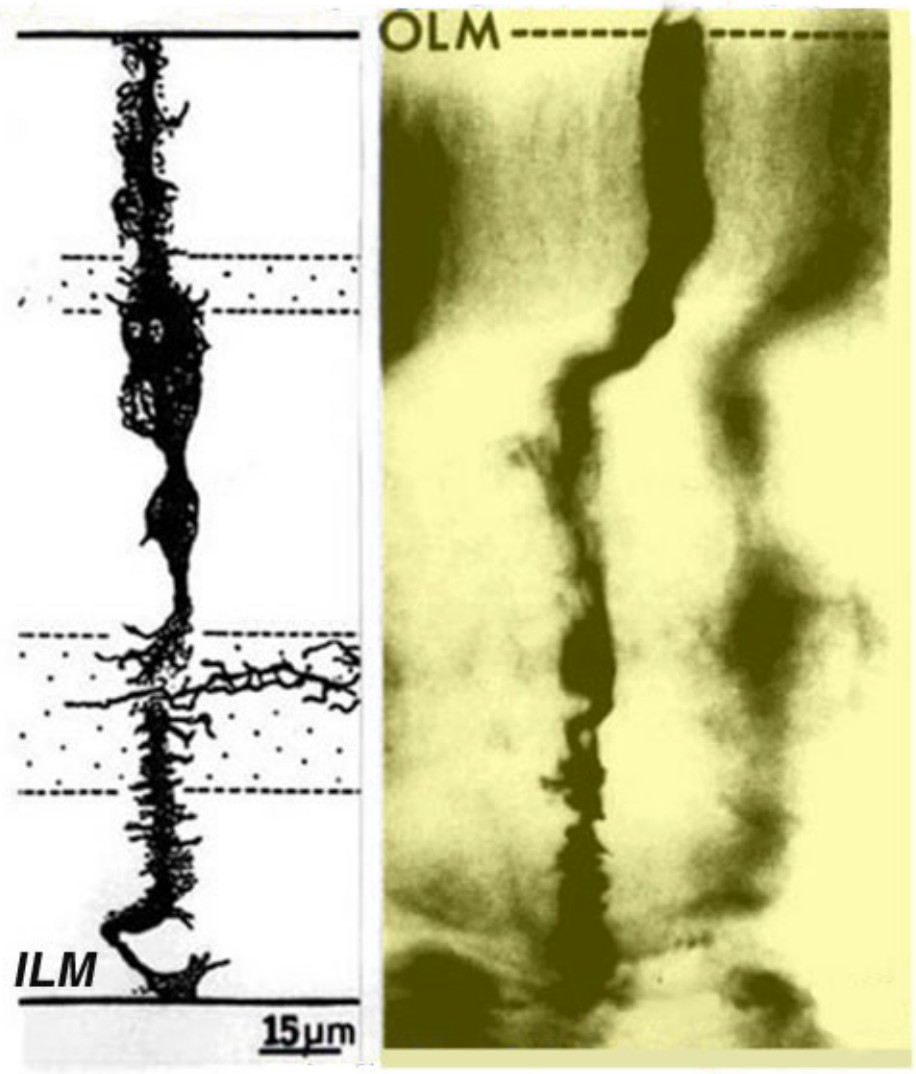

Figure 11. Vertical view of Golgi-stained Müller glial cells. OLM, outer limiting membrane; ILM, inner limiting membrane.

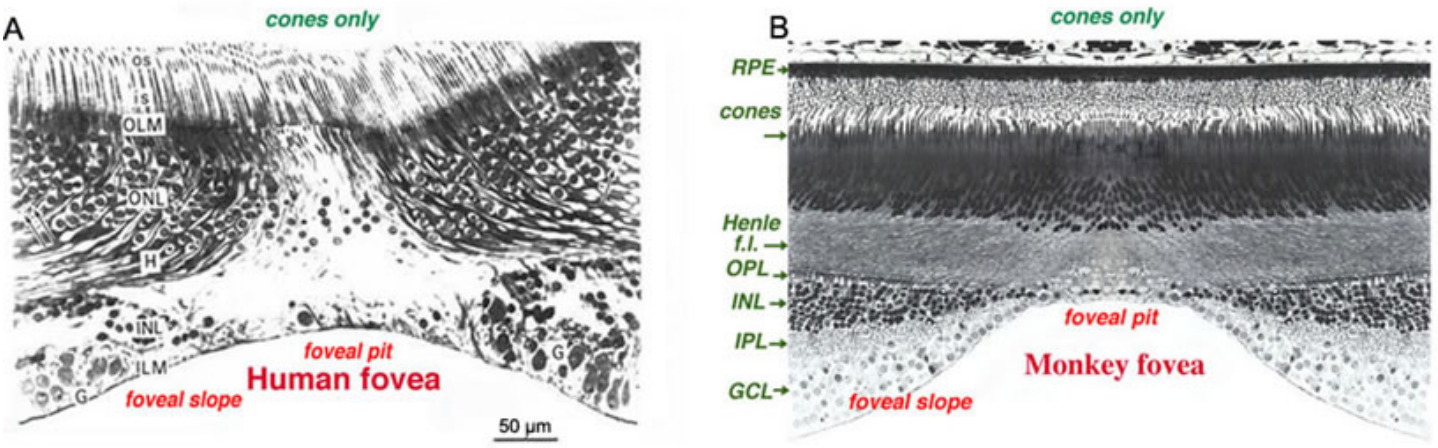

Figure 12. Foveal regions of primate retinas. *A*. Vertical section of the human fovea from Yamada, 1969 (11). os, outer segments; is, inner segments; OLM, outer limiting membrane; ONL, outer nuclear layer; H, Henle fibers; INL, inner nuclear layer; ILM, inner limiting membrane; G, ganglion cells. *B.* Vertical section of monkey fovea from Hageman and Johnson, 1991 (12). RPE. Retinal pigment epithelium; Henle f.l., Henle fiber layer; OPL, outer plexiform layer; INL, inner nuclear layer; IPL, inner plexiform layer; GCL, ganglion cell layer.

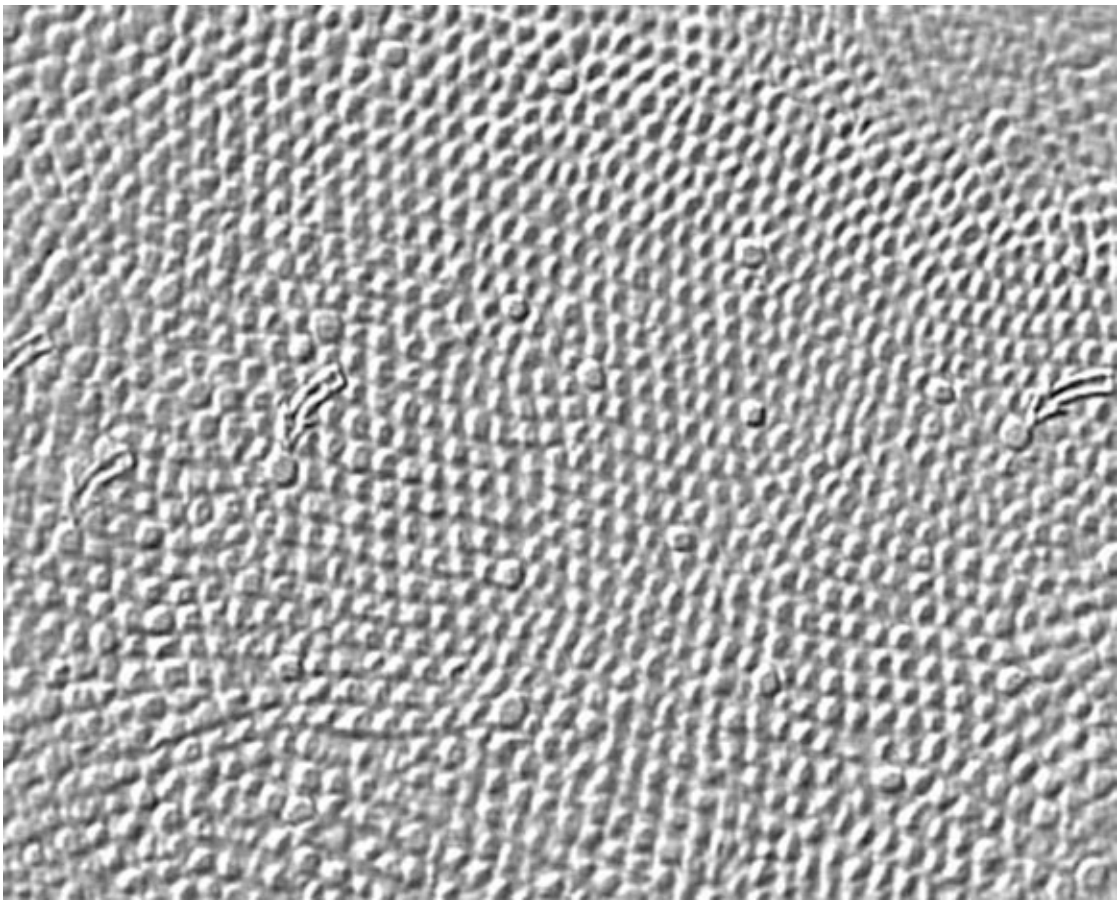

Figure 13. Tangential section through the human fovea. Reproduced from Ahnelt, Kolb and Pflug (1987) (13).

Figure 14. Ophthalmoscopic appearance of the retina to show the macula lutea (yellow area around the fovea).

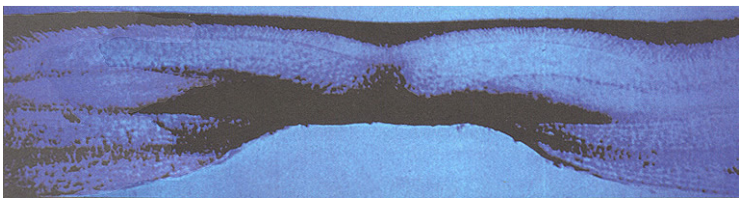

Figure 15. Vertical section through the monkey fovea to show the distribution of the macula lutea (black). From Snodderly et al., 1984 (6).

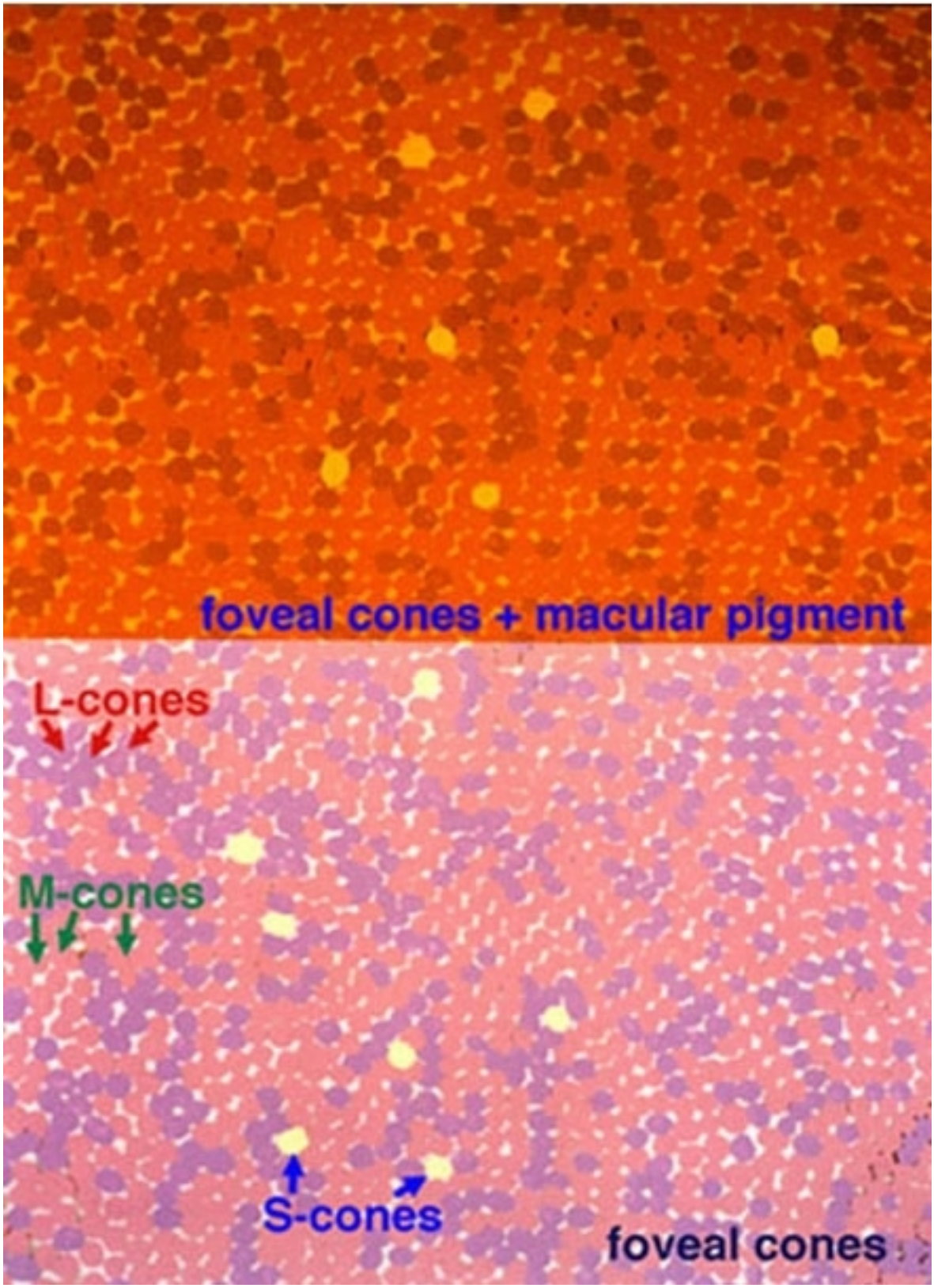

Figure 16. Appearance of the cone mosaic in the fovea as seen with (above) and without (below) the macula lutea screening pigment. The image is courtesy of Abner Lall (Howard University) and Richard Cone (Johns Hopkins University).

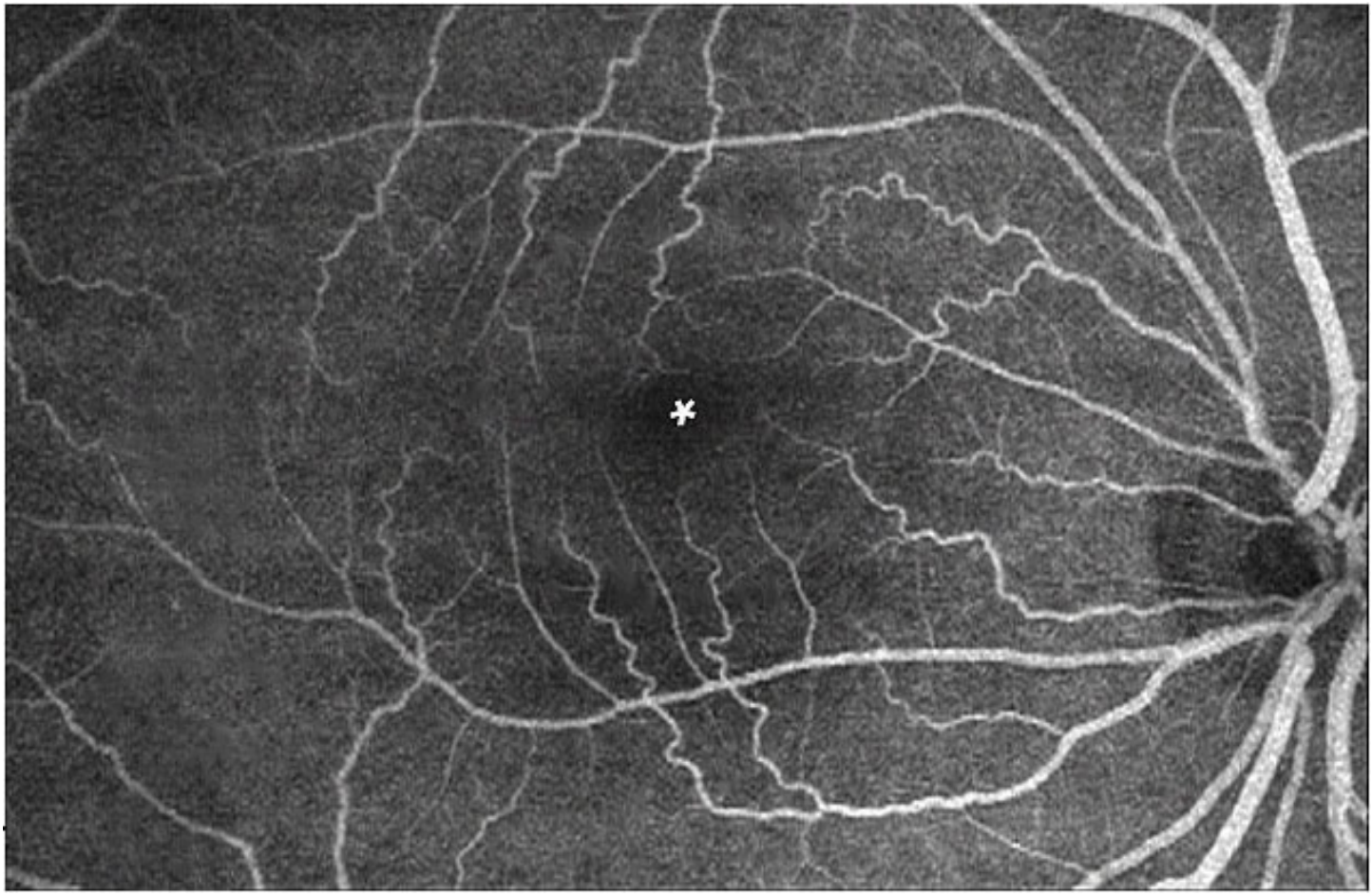

Figure 17. Fundus photograph showing fluorescein imaging of the major arteries and veins in a normal human right eye retina. The vessels emerge from the optic nerve head and run in a radial fashion, curving toward and around the fovea (asterisk in photograph). The image is courtesy of Isabel Pinilla, Spain.

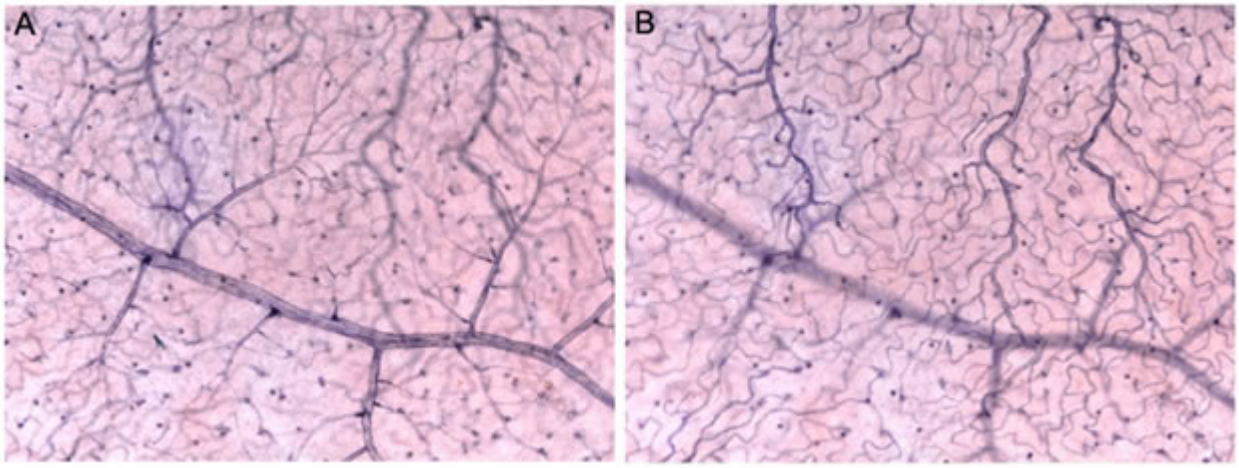

Figure 18. Microvasculature of the retina. *A*. Flatmount view of a rat retina stained with NADPH-diaphorase at the level of focus of a major artery and arterioles. *B*. Flatmount view of a rat retina stained with NADPH-diaphorase at the level of focus of a major vein and venules. The images are courtesy of Toby Holmes, Moran Eye Center.

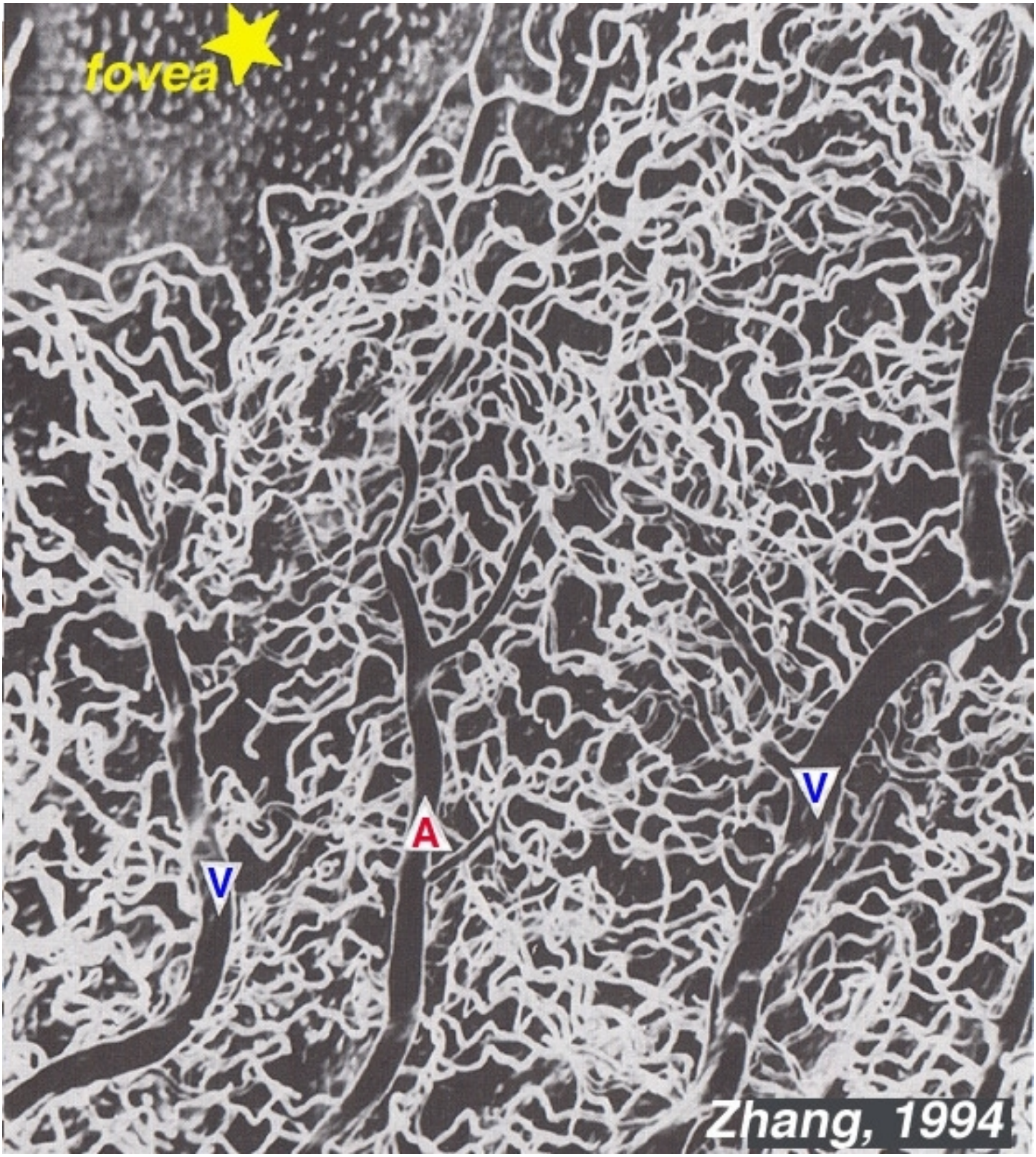

Figure 19. The macular vessels of the monkey eye form a ring around the avascular fovea (star). A, arteriole; V, venule. The illustration is from Zhang, 1994 (8).

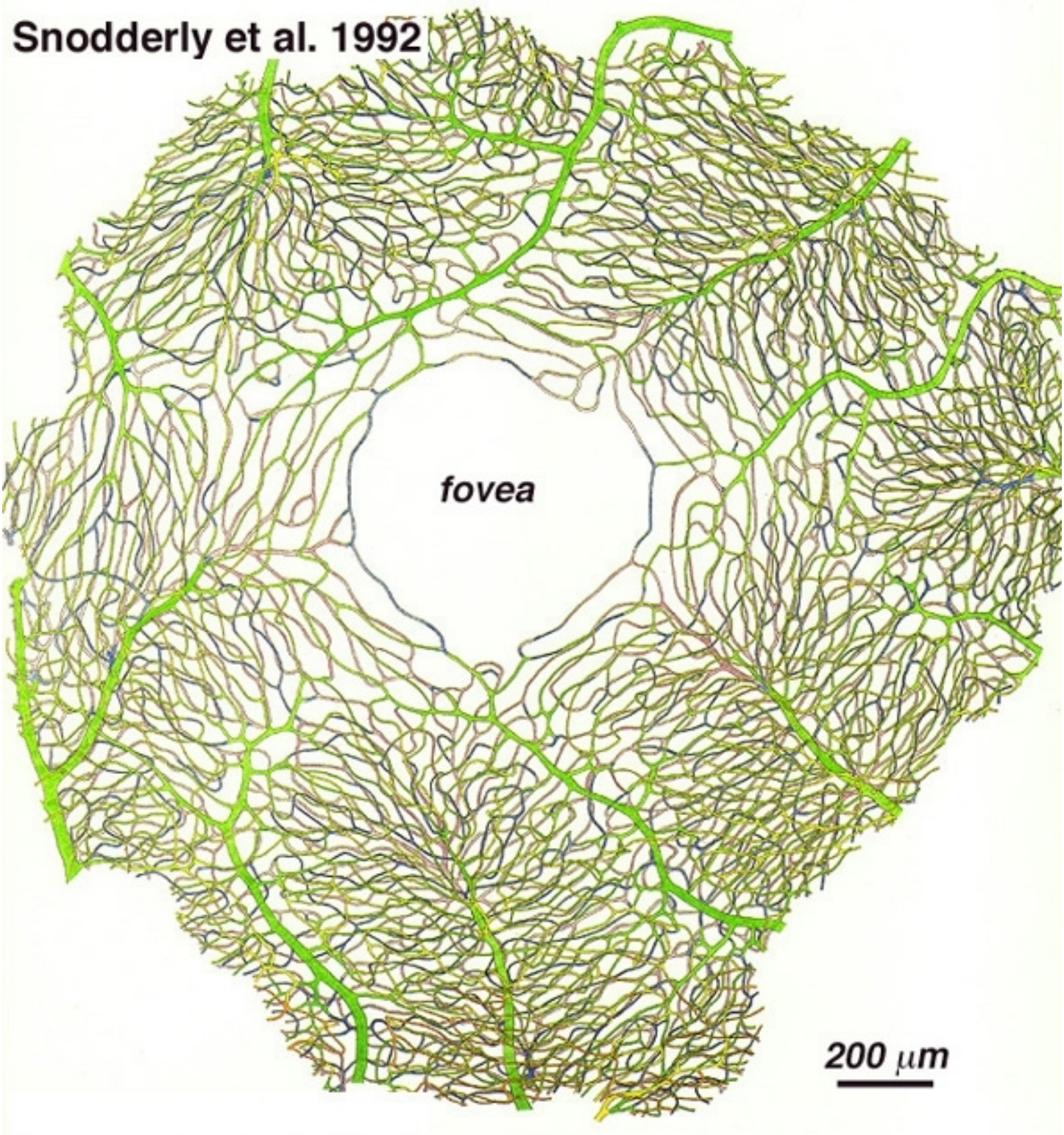

Figure 20. Diagram of the retinal vasculature around the fovea in the rhesus monkey derived from more than 80 microscope fields. The figure is from Snodderly et al., 1992 (9).

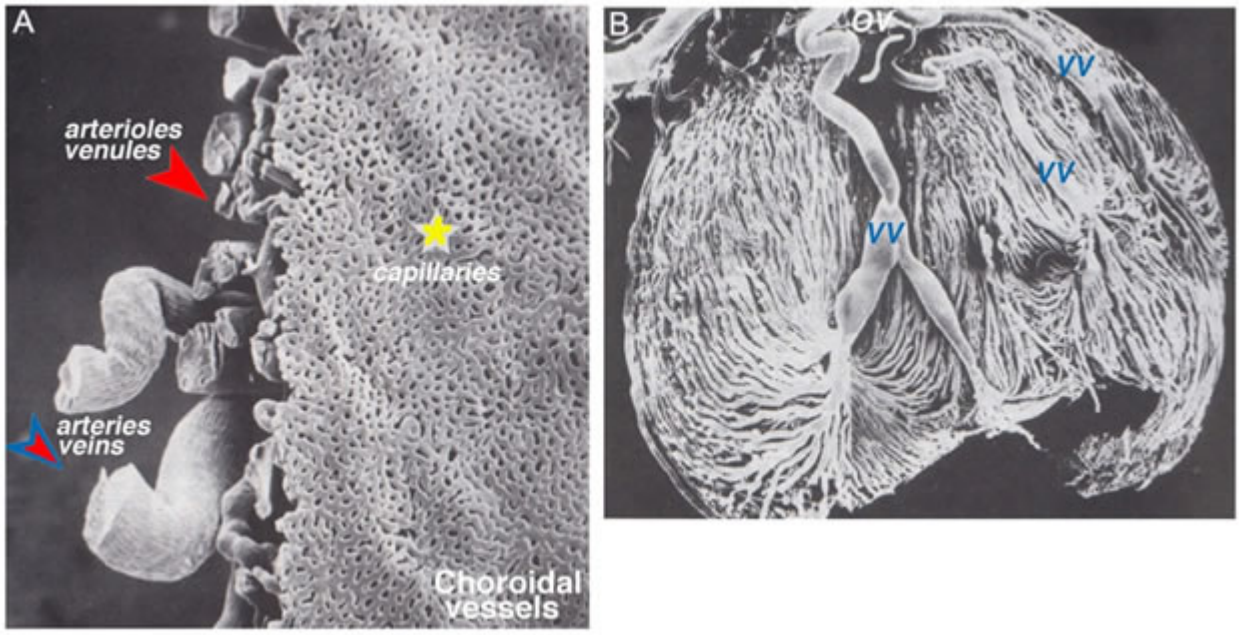

Figure 21. Corrosion casts of the vasculature of the human eye. *A*. The three vascular layers in the choroid: outer arteries and veins (red/blue arrow), medial arterioles and venules (red arrow), and inner capillary bed (yellow star). *B*. Cast of the upper back of the human eye with the sclera removed. The vortex veins (VV) collect the blood from the equator of the eye and merge with the ophthalmic vein (OV). The illustrations are from From Zhang 1994 (8).

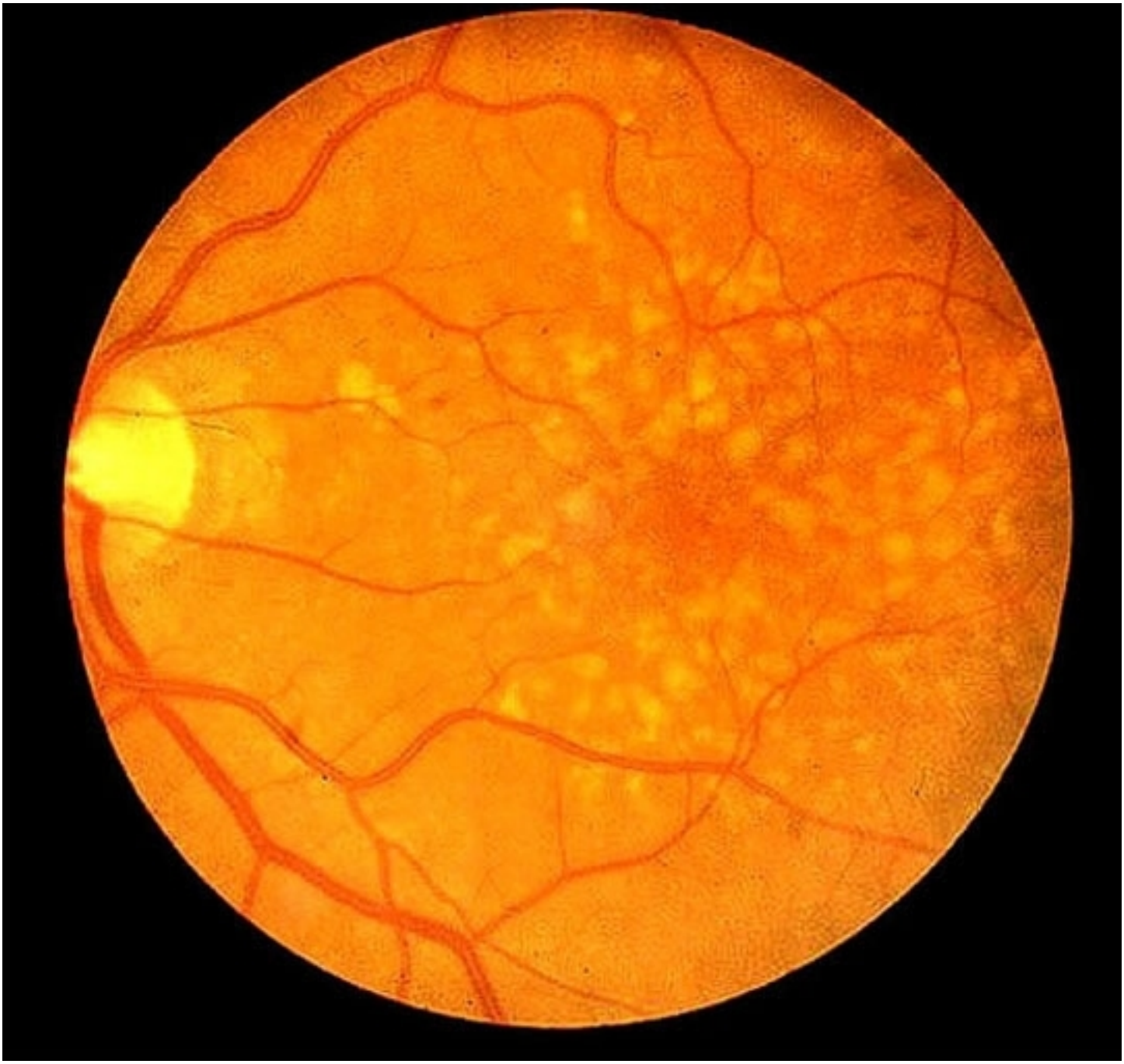

Figure 22. A view of the fundus of the eye and of the retina in a patient who has age-related macular degeneration.

Figure 23. A view of the fundus of the eye and of the retina in a patient who has advanced glaucoma.

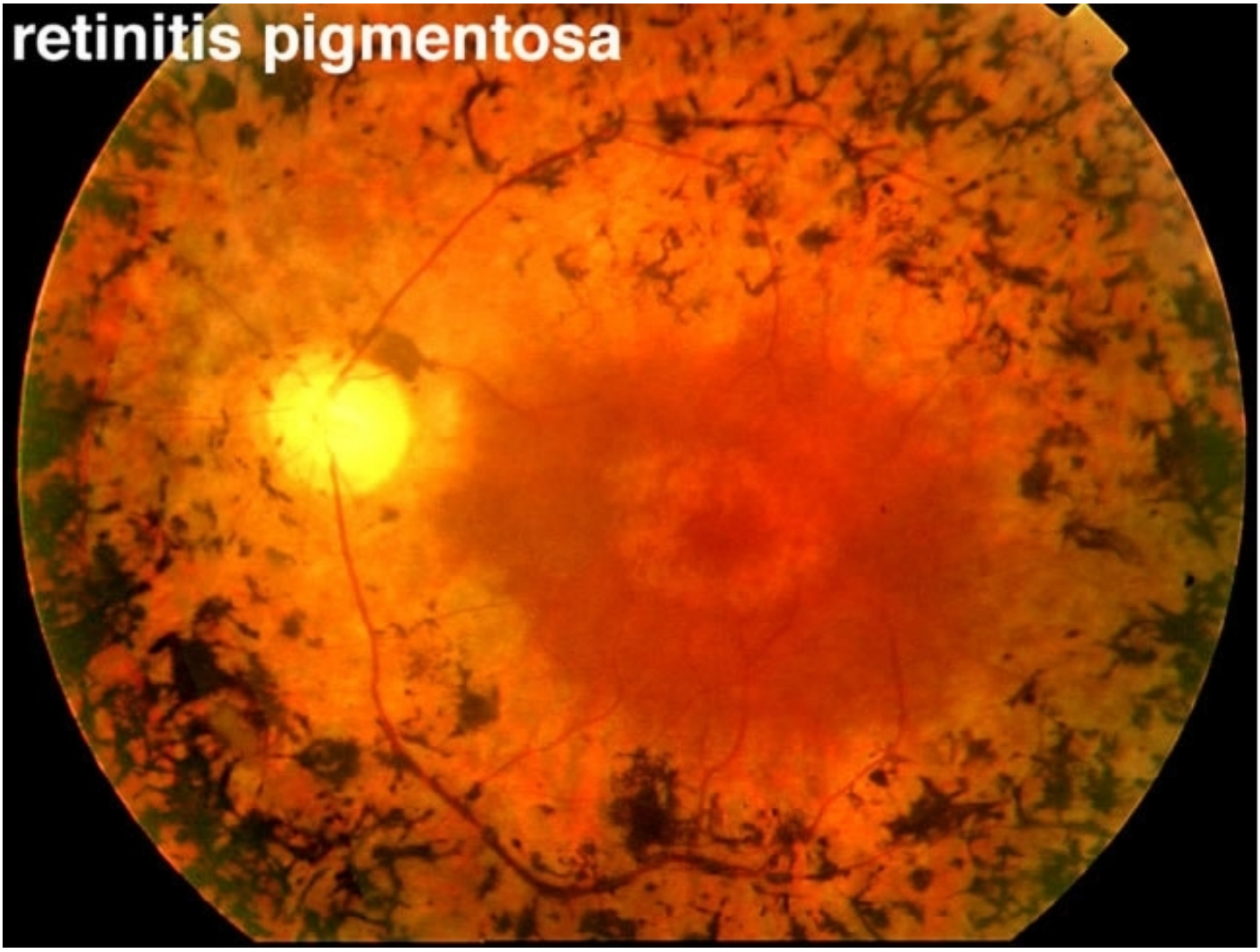

Figure 24. A view of the fundus of the eye and of the retina in a patient who has retinitis pigmentosa.

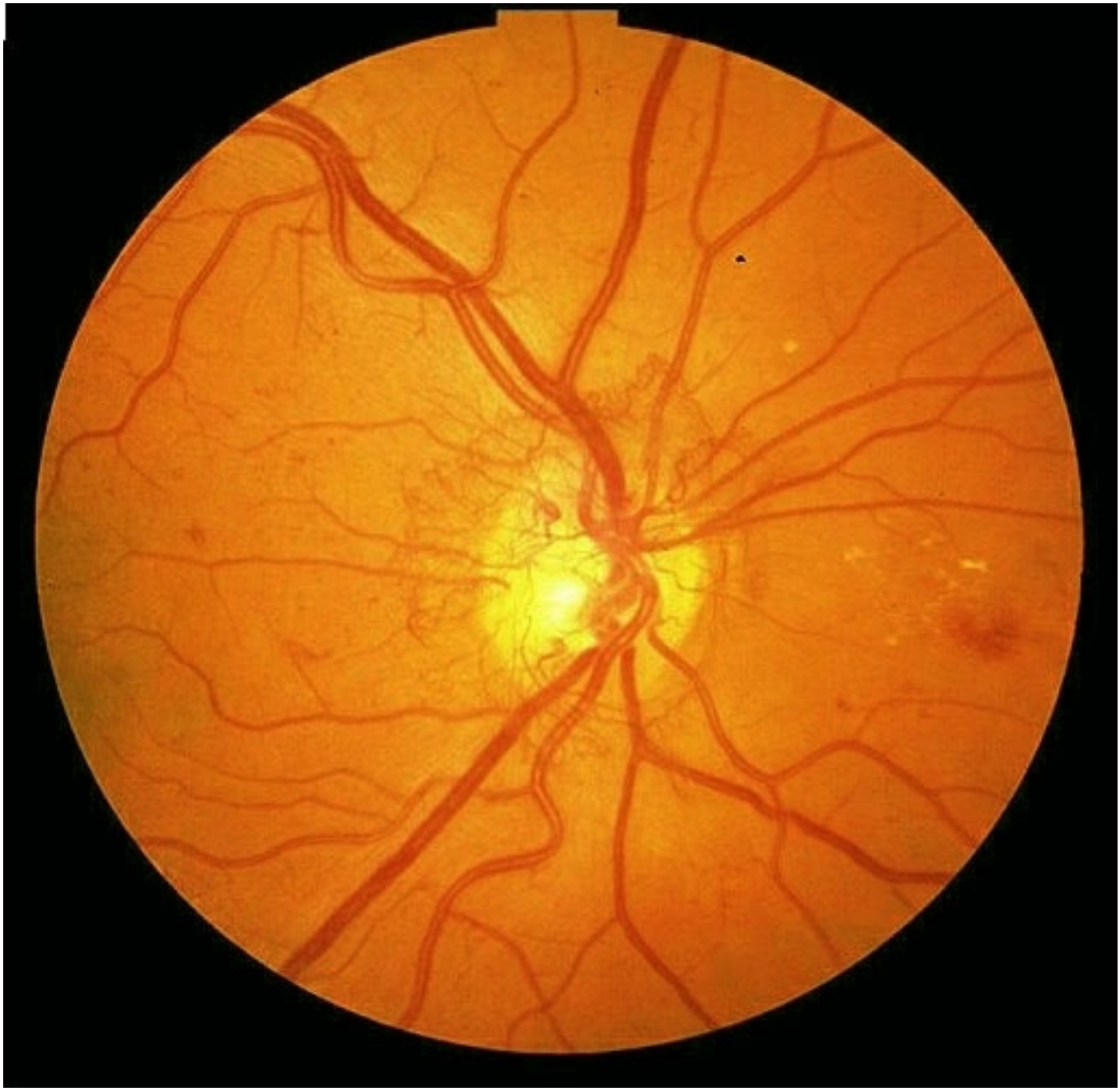

Figure 25. A view of the fundus of the eye and of the retina in a patient who has advanced diabetic retinopathy.

References

1. Polyak, S.L., *The Retina*1941, Chicago: University of Chicago.
2. Kolb, H., *The neural organization of the human retina.*, in *Principles and practice of clinical electrophysiology of vision*, J.R. Heckenlively and G.B. Arden, Editors. 1991, Mosby Year Book: St. Louis. p. 25-52.
3. Van Buren, J.M., *The retinal ganglion cell layer : a physiological-anatomical correlation in man and primates of the normal topographical anatomy of the retinal ganglion cell layer and its alterations with lesions of the visual pathways*1963, Springfield, Ill.: Charles C. Thomas. x, 143 p.
4. Bone R.A., Landrum J.T., Tarsis S.L. *Preliminary identification of the human macular pigment.* .Vision Res. 1985;25(11):1531–5. PubMed PMID: 3832576.

5. Rodieck, R.W., *The vertebrate retina; principles of structure and function*. Series of books in biology. 1973, San Francisco,: Freeman. x, 1044 p.
6. Snodderly D.M., Auran J.D., Delori F.C. *The macular pigment. II. Spatial distribution in primate retinas.* .Invest Ophthalmol Vis Sci. 1984;25(6):674–85. PubMed PMID: 6724837.
7. Henkind, P., R.I. Hansen, and J. Szalay, *Ocular circulation*, in *Physiology of the human eye and visual system*, R.E. Records, Editor. 1979, Harper & Row: Hagerstown, Md. p. 98-155.
8. Zhang H.R. *Scanning electron-microscopic study of corrosion casts on retinal and choroidal angioarchitecture in man and animals.* .Progress in Retinal and Eye Research. 1994;13(1):243–270.
9. Snodderly D.M., Weinhaus R.S., Choi J.C. *Neural-vascular relationships in central retina of macaque monkeys (Macaca fascicularis).* .J Neurosci. 1992;12(4):1169–93. PubMed PMID: 1556592.
10. Hayreh S.S. *Segmental nature of the choroidal vasculature.* .Br J Ophthalmol. 1975;59(11):631–48. PubMed PMID: 812547.
11. Yamada E. *Some structural features of the fovea centralis in the human retina.* .Arch Ophthalmol. 1969;82(2):151–9. PubMed PMID: 4183671.
12. Hageman, G.S. and L.V. Johnson, *The photoreceptor-retinal pigmented epithelium interface.*, in *Principles and practice of clinical electrophysiology of vision*, J.R. Heckenlively and G.B. Arden, Editors. 1991, Mosby Year Book: St. Louis. p. 53-68.
13. Ahnelt P.K., Kolb H., Pflug R. *Identification of a subtype of cone photoreceptor, likely to be blue sensitive, in the human retina.* .J Comp Neurol. 1987;255(1):18–34. PubMed PMID: 2434534.

Anatomy and Physiology of the Retina

The Retinal Pigment Epithelium

Olaf Strauss, PhD[1]

Created: January 26, 2011.

1. Introduction

The simplest light detecting organs are composed of two cell types: the light sensitive photoreceptor and the pigmented cell. Both cell types appear in conjunction in every eye of the animal kingdom from insects, mollusca to higher vertebrates (1). Functional interaction of both the pigmented cell and the photoreceptor cells is essential for visual function (2-5). Already beginning with the embryonic development the functional differentiation of the photoreceptor layer and the retinal pigment epithelium (RPE) depend on each other (6, 7). When the communication between the developing RPE and the developing neuronal retina is interrupted the RPE is able to form a multilayered retina-like structure by itself (8).

The RPE and the neural retina co-differentiate during development of the eye. Parts of the RPE/photoreceptor interaction such as importing the vitamin A derivitive, retinal, its metabolism and recycling are initiated before vision starts, and serve as differentiation signals for both tissues (9, 10). Furthermore, analyses of hereditary types of retinal degeneration reveal a strong dependence of the RPE on the photoreceptors and vice versa. For example, mutations in genes which are expressed in the photoreceptor cells can lead to a primary RPE disease with loss of photoreceptors occurring secondarily. Or, on the other hand, mutations in genes which are expressed in the RPE can lead to primary photoreceptor degeneration. Thus the ability of the photoreceptor cell to detect light depends on its interaction with the pigmented cell.

In the vertebrate eye the RPE is located between the light-sensitive outer segments of the photoreceptors and blood supply of the choroid. It is a hexagonally packed, tight-junction, connected, single sheet of cells containing pigment granules (Figures 1 and 2, PG) and organelles for digestion of photoreceptor outer segment membranes into phagosomes (Figure 2, Phagosomes, Ph). With its apical membrane and processes (Figure 1, ap), it faces the subretinal space which is occupied by an extracellular matrix specialized to enable interaction between the RPE and the light sensitive outer segments of the photoreceptors (Figures 1 and 2, os, ROS) (11-14). With its basolateral membrane, the RPE is in contact with the highly specialized multilayered Bruch's membrane (Figures 1 and 2, BM) which also represents an interaction matrix for the RPE with blood flow in the fenestrated vessels of the choroid (the choriocapillaris, CC; Figures 1 and 2) (15).

Figure 3 shows a summary drawing of the pigment epithelium and its functional attributes that will be discussed in the following chapter. Pigment epithelial functions are: light absorption, epithelial transport, spatial ion buffering, visual cycle, phagocytosis, secretion and immune modulation.

2. Absorption of light

At a first glance, light absorption is the most obvious function of the RPE. The cells are heavily pigmented and cover the inner surface of the bulbus. As in a camera, this improves the quality of the optical system of the eye by absorbing scattered light. For a long time this function was believed to be the only one by the RPE. Now we know of a great many other functions of the RPE (see above, Figure 3).

In the human eye, light is focused by a lens onto the cells of the macula resulting in a strong concentration of photo-oxidative energy in the retina (16-18). Furthermore, the choroid is a tissue which shows a higher specific blood perfusion than the kidney (19-22). But, the oxygen extraction by the retina during the passage through the

Author Affiliation: 1 Department of Ophthalmology, University of Regensburg, Germany; Email: strauss@eye-regensburg.de.

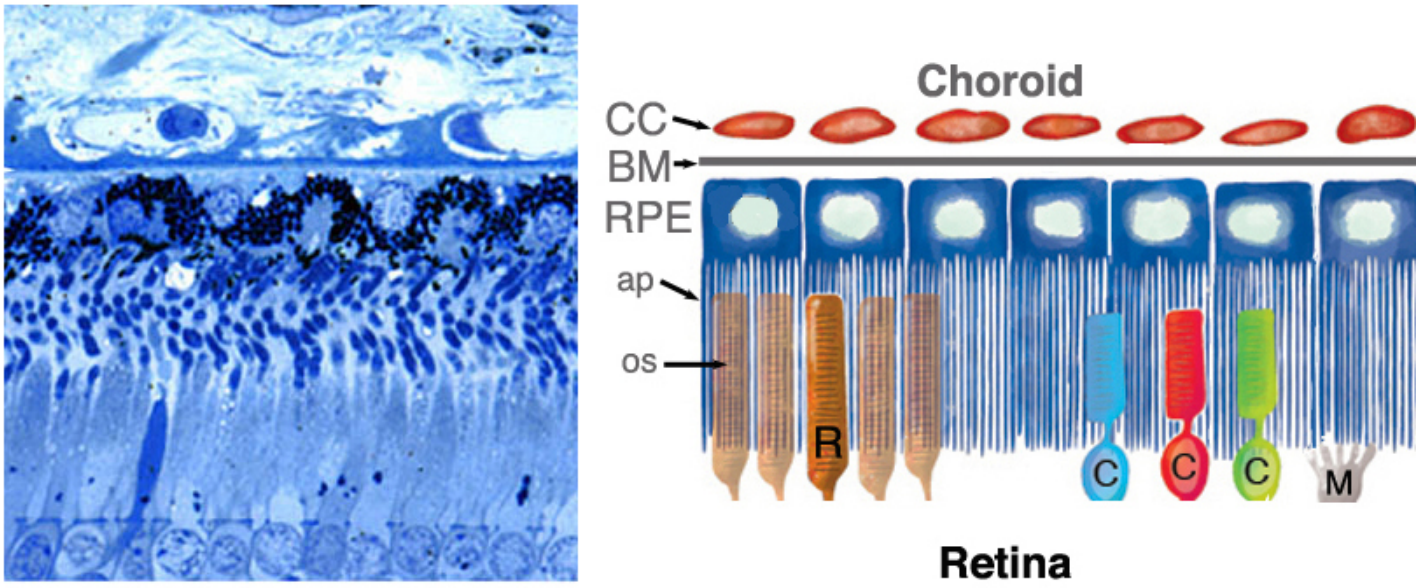

Figure 1. Light micrograph of the human retinal pigment epithelium (left) with the choroid above and the retina below. Cartoon of the retinal pigment epithelium (RPE) (right) aligned alongside the micrograph. CC, Choriocapillaris; BM, Bruch's membrane; RPE. retinal pigment epithelium; ap, apical processes; os, outer segments; C, cones. R, rods.

choroid is relatively low. The venous blood from the choroid still shows an oxygen saturation of more than 90%. Thus the RPE is exposed from the retinal side to a strong photo-oxidative energy and from the blood side by an overflow of oxygen. Photo-oxidation leads to damage of the photoreceptor outer segment tips so they need a constant renewal process from their base (see Photoreceptors, Webvision) (described below in section 6). The renewal process however involves the phagocytosis of destroyed and shed photoreceptor outer segments by the RPE. This adds a strong load of free radicals in addition to the high photo-oxidative environment. Thus the RPE has to be capable of maintaining the structural integrity of the retina by an efficient defense against free radicals, photo-oxidative exposure and light energy (16-18).

For this purpose the RPE has several lines of defense and the first line is the melanosomes or pigment granules (17). Depending on the light-dark cycle, they move inside the cytoplasm to the apical processes under light conditions. The light absorption by the melanosomes heats up of the RPE/choroid complex to temperatures above 40^{o} C (23, 24). It is possible that the high perfusion of the choroid serves to transport away the heat from the retina. Further lines of defense are high concentrations of non-enzymatic and enzymatic anti-oxidants and the ability of the cells to repair damaged lipids, proteins and DNA. In man, these mechanisms provide protection of the photoreceptor/RPE/choroid complex and maintenance of the structural integrity of this complex for decades. However, it is known that the human retina accumulates lipofuscin (an end product of phagosome breakdown) during its life-time, beginning at a young age. This accumulation debilitates the RPE cells and their lines of defense become weaker over time (17, 25-29). It is believed that a reduced capability to absorb light and to compensate for oxidative damage are important factors initiating the chain of events leading to the onset of age-related macular degeneration in the older population (see Age-Related Macular Degeneration, Webvision).

3. Epithelial transport

The RPE forms a tight-junction epithelium located between the blood flow of the choroid and the outer segments of the photoreceptors. There are tight junction between the lateral surfaces of the hexagonal epithelial sheet (Fig. 2, TJ) (4, 30, 31). In this way the RPE forms a part of the blood/retina barrier. The barrier function of a tight epithelium implies an efficient isolation of the inner retina from systemic influences at the choroidal side.

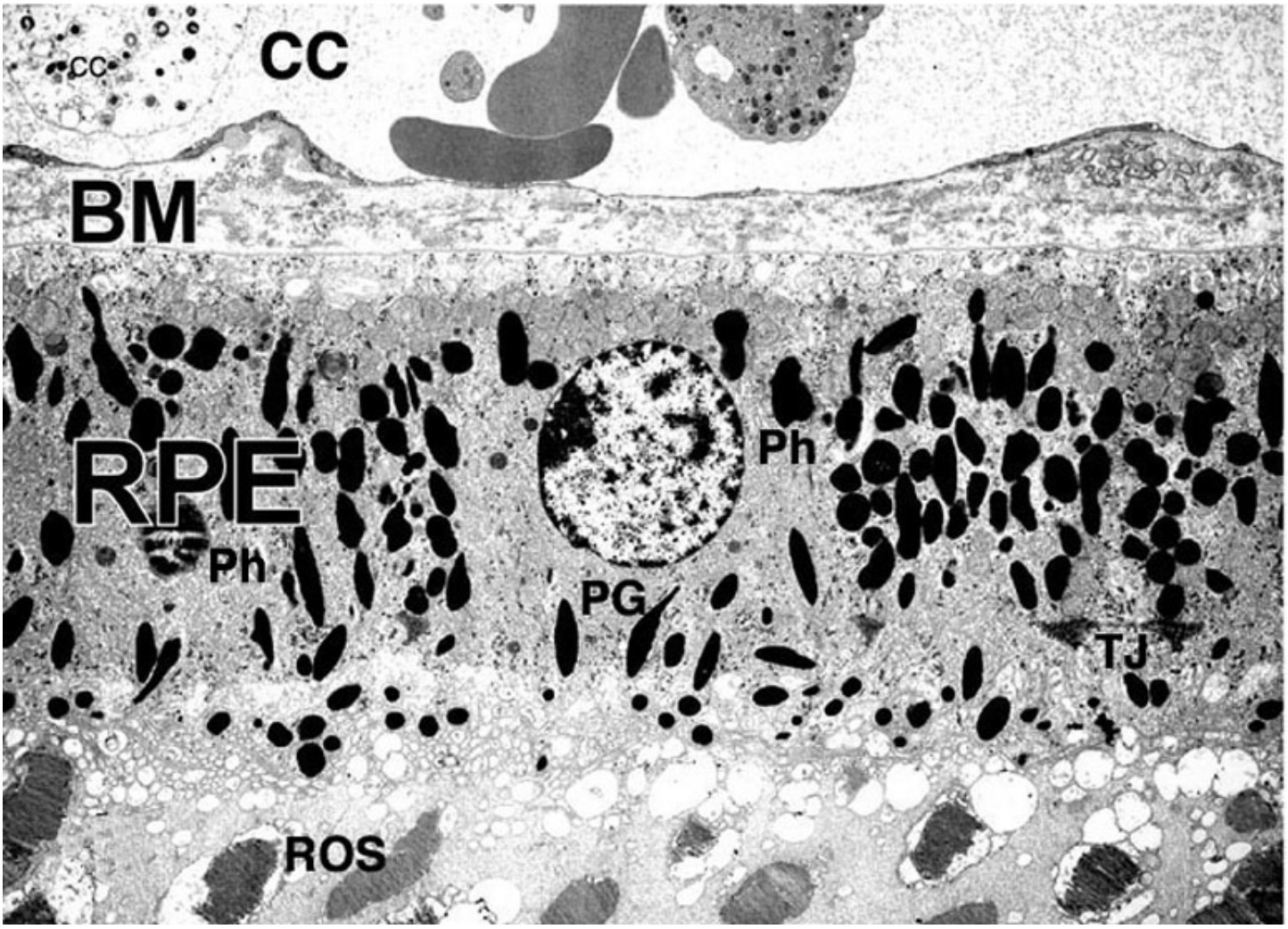

Figure 2. Transmission electron micrograph of the RPE cells and the RPE-choroid interface in a normal human donor eye. cc, choriocapillaris; BM, Bruchs membrane; RPE, retinal pigment epithelium; ROS, rod photoreceptor outer segments; Ph, phagosomes; PG, pigment granules; TJ, tight junctions.

This is of importance for the immune privilege of the eye (see section 8) and for a highly selective transport between the blood and the subretinal space. This epithelial transport serves to supply nutrients to the photoreceptors (transport from the blood to the retinal side), control the ion homeostasis in the subretinal space and to eliminate water and metabolites from retinal tissue (transport from the retinal to the blood side).

Transport from the blood side to the retina

The photoreceptors are highly specialized cells which need the supply of essential metabolites. These are glucose for energy metabolism, retinal for the visual cycle of the opsins, and ω-3 fatty acids for specialized phospholipids to compose the membranes of photoreceptors which are highly enriched by ω-3 fatty acids. All these nutrients are taken up by the RPE and are transported to the photoreceptors. To transport glucose the RPE expresses the glucose transporters GLUT1 and GLUT3 in both the apical and basolateral membrane (32, 33). GLUT3 serves for the basic transport whereas GLUT1 is responsible for an inducible transport system to meet metabolic needs. The transport of retinal starts with uptake of retinol from the blood and is then transferred into the visual cycle of retinal which is described below (Section 5). To transport ω-3 fatty acids, the RPE preferentially takes up 22:6ω3 fatty acid in a concentration dependent manner (34, 35). Inside the RPE the compound is incorporated

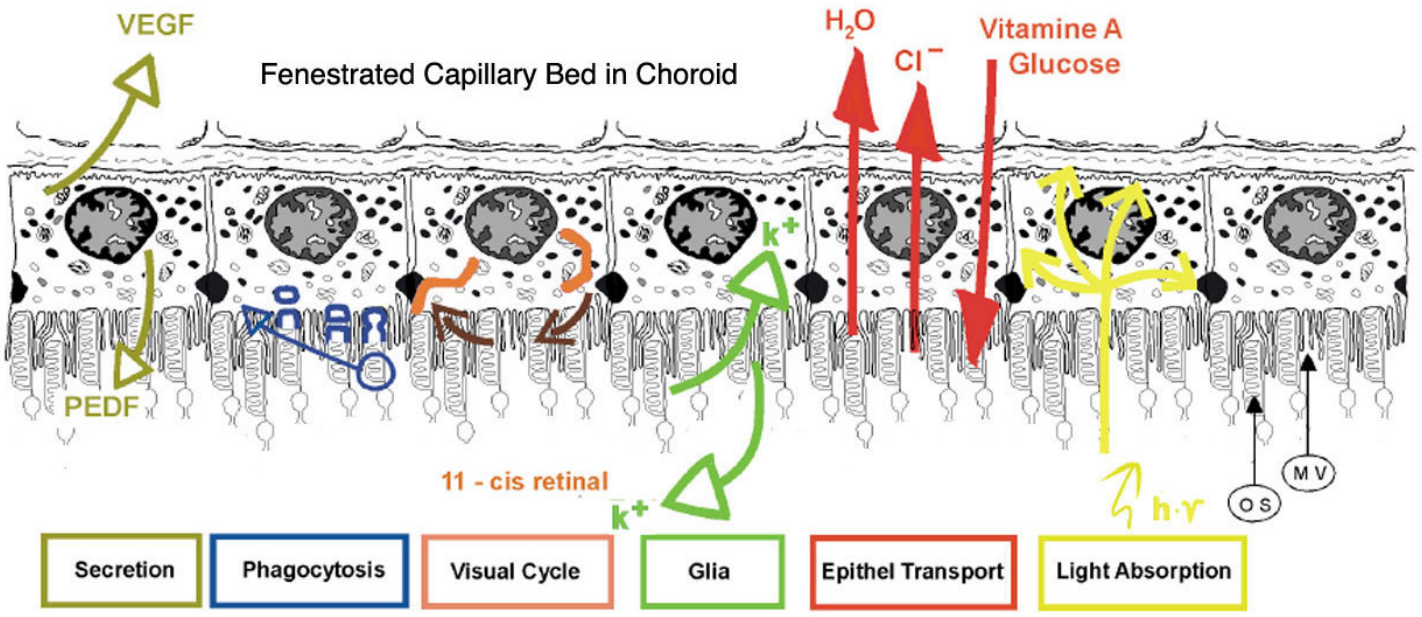

Figure 3. Summary diagram of the major functions of the RPE from Strauss, 2005 (2).

into glycerolipids for synthesis, storage and subsequent delivery in a recycling process involving the phagocytotic process (see Section 6).

Transport from the subretinal space to the blood side

Mainly water, ions and metabolic end products are transported from the retinal side to the blood side (4, 30, 31, 36, 37). The retina is the tissue with the highest cell density in the human body. The photoreceptors, neurons and glial cells, have a high metabolic turn-over rate leading to production of metabolic water which accumulates in the retina. In addition, intraocular pressure drives a movement of water from the anterior eye towards the retina where it accumulates. Furthermore, a large part of the metabolic activity of retinal cells results in the production of lactic acid. Up to 19 mM lactic acid concentration has been reported in the subretinal space (38).

Water is eliminated from subretinal space by active transport by the RPE. The transportation rate was estimated to range from 1.4 to 11 µl x cm^{-2} x h^{-1} (39-41). This transport of water is driven by a transepithelial transport of Cl^- from subretinal space to the blood side through the RPE (Figure 4A). The Cl^- transport is an active transport driven by the activity of the apically localized Na^+/K^+-ATPase which uses the energy of ATP to transport 3 Na^+ in exchange for 2 K^+ against concentration gradients out of RPE cells. The K^+ ions which are transported into the cytoplasm recycle through apically localized Kir7.1 inward rectifier K^+ channels into the subretinal space (42). This results in a gradient for Na^+ into the RPE cell which has a low intracellular Na^+ concentration. The recycling of K^+ back into the subretinal space through inward rectifier K^+ channels enhances the transport efficiency by the Na^+/K^+-ATPase because it decreases the gradient for K^+ across the apical membrane of the RPE (43). The reason why the Na^+/K^+-ATPase is apically located is not clear. As will be explained below in Section 4, it probably serves to maintain the ion homeostasis in the subretinal space by spatial buffering of ions. The Cl^-driven transport of water establishes an adhesion force between the RPE and the neuronal retina which is removed by blocking the Na^+/K^+-ATPase with Ouabain (44).

The transportation pathway begins with an uptake of Cl^- from subretinal space, across the apical membrane of the RPE cells. Driven by the gradient for Na^+ which is established by the Na^+/K^+-ATPase, Cl^- is taken into the cell across the apical membrane by the activity of the $Na^+/K^+/2Cl^-$ co-transporter (4, 30, 36, 45). Since K^+ recycles back through apical inward rectifier channels into the subretinal space and Na^+ is transported out of the

cell by the Na^+/K^+-ATPase, the transport activity of the $Na^+/K^+/2Cl^-$ co-transporter results mainly in an accumulation of Cl^- inside RPE cells. Depending on the species, the intracellular Cl^- activity ranges from 20 – 60 mM (46-48). Since the basolateral membrane has a large Cl^- conductance the Cl^- which accumulates in the intracellular space of the RPE leaves the cell across the basolateral membrane to the blood side. This results in a basolateral negative transepithelial potential ranging between 5 -15 mV (30, 31).

A crucial step in this transport pathway is the basolateral membrane conductance for Cl^-. Thus mechanisms which regulate the efflux pathway across the basolateral membrane regulate the overall epithelial transport of Cl^- across the RPE. For this purpose, different types of Cl^- channels, which differ in their activation mechanisms to link Cl^- conductance to different second-messenger pathways of RPE cells, are localize in the basolateral membrane. A basic transportation rate seems to be provided by the ClC-2 Cl^- channel (49).

In a knock-out mouse model for ClC-2 Cl^- channels, an absence of a transepithelial potential is observed and the mice become blind, showing a phenotype comparable to that of Retinitis pigmentosa (49). Another basolateral Cl^- channel might be CFTR (cystic fibrosis transmembrane regulator) which enables a cAMP-dependent modulation of the Cl^- transport across the basolateral membrane (50, 51) and a Ca^{2+}-dependent Cl^- channel which enables a regulation of the transport by changes in intracellular Ca^{2+}. The molecular identity of this Cl^- channel is possibly bestrophin-1 (52).

As mentioned above the metabolic activity results in large concentrations of lactic acid in the subretinal space. Lactic acid is eliminated from subretinal space by the RPE (37, 53) (Figure 4B). Uptake of lactic acid occurs across the apical membrane of the RPE by the mono-carboxylate transporter-1 MCT1 and the release of lactic acid to the blood side across the basolateral membrane occurs via the activity of the mono-carboxylate transporter-3 (MCT3). The transport of lactic acid requires an efficient pH regulation and an adaptation of the volume transport because a large amount of transported water is metabolic water. The pH regulation of the RPE cells involves the activity of Na^+ coupled, secondary active transport mechanisms of the apical membrane of the RPE (54, 55). H^+ ions are removed from the cytoplasm by the Na^+/H^+-exchanger and HCO_3^- is accumulated in the cytosol by the transport activity of the $Na^+/2HCO_3^-$ co-transporter (56). At the basolateral membrane of the RPE, a HCO_3^-/Cl^- exchanger interferes with control of intracellular HCO_3^- by the apical $Na^+/2HCO_3^-$ co-transporter. At high pH the RPE transports HCO_3^- from subretinal space to the blood side. At low pH the basolateral HCO_3^-/Cl^- exchanger is stimulated, which increases the intracellular HCO_3^- concentration and HCO_3^- released to the subretinal space across the apical membrane by the activity of the Na^+/HCO_3^- co-transporter, which runs then in the reverse mode.

The involvement of the HCO_3^-/Cl^- exchanger at the basolateral membrane links the water transport to the pH regulation and therefore to the transport of lactic acid (46, 47, 56-62). At resting conditions, the HCO_3^-/Cl^- exchanger in the basolateral membrane reduces the transportation rate of Cl^- across the basolateral membrane, and therefore, the transepithelial transport of volume, because a small amount of Cl^-, which leaves the cell through basolateral Cl^- channels, is transported back into the intracellular space by the activity of the HCO_3^-/Cl^- exchanger. At low pH the HCO_3^-/Cl^- exchanger transports Cl^- out of the cell to take up HCO_3^- for pH regulation, which in turn leads to increase of Cl^- and volume transport. This is supported by the pH sensitivity of basolateral ClC-2 Cl channel which increases its activity by a decrease of extracellular pH. The fact that the transport of volume is linked to the HCO_3^- transport is used in the treatment of macular edema. Application of inhibitors of carbonic anhydrase increases the speed of volume resorption by the RPE (62, 63). The transport of osmolytes across the RPE from subretinal space to the blood side establishes an osmotic driving force for water across the RPE.

The RPE is a tight epithelium which means that the transport of water cannot occur through any paracellular transportation route. All transported volume has to take the transcellular route. For this purpose the RPE expresses aquaporine-1 water channels which are localized in both the basolateral and the apical membrane of

the RPE (64, 65). However it has also been suggested that the mono-carboxylate transporters are able to transport water.

4. Spatial buffering of ions

As described above, the RPE maintains the ion homeostasis of the subretinal space by epithelial transport of ions. However, the light-dependent changes of the photoreceptor activity and the activity of the second order neurons lead to very fast changes in the subretinal space, which requires a fast and capacitative compensation by the RPE (66). If these changes were not compensated for, the overall excitability of the photoreceptors and the neurons would quickly change and proper signal transduction of visual information would not be possible. The normal transepithelial transport of ions would be too slow to compensate quickly enough for these changes.

Other mechanisms based on the activity of voltage-dependent ion channels add to the basic transepithelial transport of ions. In this process the compensation for changes in the subretinal K^+ concentration and retinal volume are most important. In the dark cGMP-gated cation channels are open in the outer segments of photoreceptors. The influx of Na^+ and Ca^{2+} through these channels is counterbalanced by an outflow of K^+ at the inner segment. These ionic currents represent the so called dark current (67). When light falls onto photoreceptor outer segments, the cGMP-dependent cation channels are closed and the K^+ outflow at the inner segment becomes smaller. At the same time Na^+/K^+-ATPase at the inner segment takes up K^+ into the photoreceptor. This results in a reduction of the K^+ concentration in the subretinal space from 5 mM to 2 mM (4, 66). This decrease is compensated for by the RPE. The mechanism is based on the fact that the ion conductance of the apical membrane of the RPE is dominated by a K^+ conductance (36). The light-induced decrease in the subretinal K^+ concentration leads to hyperpolarization of the apical RPE membrane. This in turn leads to activation of inward rectifier K^+ channels generating an efflux of K^+ into the subretinal space, and to an increase of the subretinal K^+ concentration back to normal values (68). For this purpose the RPE expresses Kir7.1 channels located in the apical membrane of the RPE (69). Kir7.1 channels were found to display a rather mild rectification but show increased conductance when extracellular K^+ is decreased. This makes these K^+ channels the ideal candidates for this function (42, 70). This compensatory pathway enables fast reactions of the RPE to either decreases or increase in the subretinal K^+ concentration.

A model, which has been developed by LaCour, explains the compensation of K^+ concentration changes by epithelial transport with a rather small transepithelial K^+ transport from subretinal space to the blood side under control conditions (68, 71). The major part of K^+ which is taken up across the apical membrane, via the activity of the $Na^+/K^+/2Cl^-$ co-transporter, recycles back into subretinal space through apical K^+ channels. A smaller part leaves the cell across the basolateral membrane to the blood side. In the case of a decrease of the subretinal K^+ concentration, apical membrane conductance for K^+ increases. This leads to an increases in the proportion of K^+ which recycles back to the subretinal space and, subsequently, to further decrease in the transepithelial transport of K^+ by the RPE. In the situation where the subretinal K^+ concentration increases, the apical membrane conductance decreases due to inactivation of Kir7.1 channels and due to depolarization of the apical membrane. Now a smaller proportion of K^+ which is taken up across the apical membrane can recycle back to the subretinal space. This increases the amount of K^+ which is transported across the RPE to the blood side. Due to the fast coupling of K^+ concentration with apical transmembrane potential, and ion conductance, the RPE is able to respond to changes in the subretinal K^+ concentration as fast as they occur.

When the retina is stimulated by light, a small and transient change in the extracellular volume in the retina is observed (36, 72). These changes are compensated for by Müller glia cells in the inner retina and by the RPE at the outer retina. Again the compensation mechanism is a fast reaction which adds to the sustained transepithelial transport by the RPE, in this case the transport of water. The fast coupling is again enabled by voltage-dependent modulation of ion transport. As described above the transport of water into the RPE is driven by a transepithelial transport of Cl^- which is linked to the transport of HCO_3^- and lactate. The light-dependent

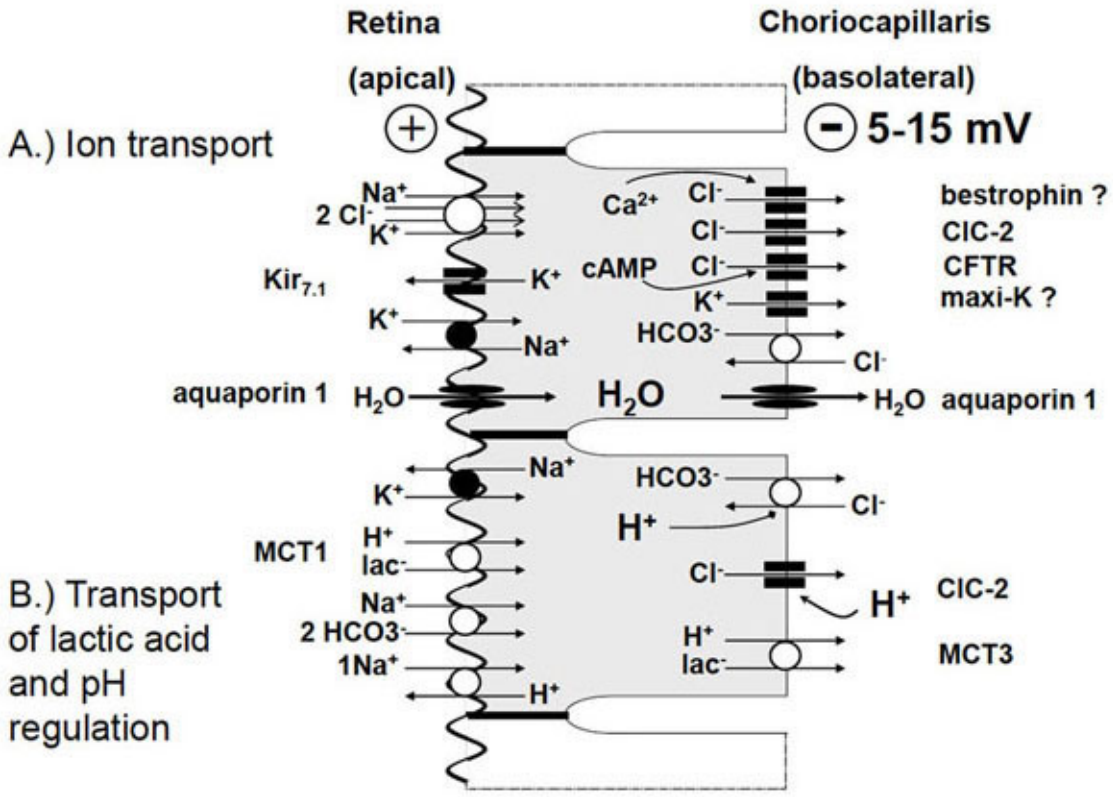

Figure 4. Epithelial transport and pH regulation in RPE cells. A. Transepithelial transport of ions across the RPE: Cl^- is predominantly transported from the subretinal space to the choriocapillaris. This transport drives water through aquaporins from the subretinal space to the choriocapillaris. The driving force for epithelial transport is provided by the apically located Na^+/K^+-ATPase. K^+ transported by the ATPase recycles through the apical membrane and facilitates establishment of a Na^+ gradient into the cell. The Na^+ gradient serves to drive uptake K^+ and Cl^- on the apical side resulting in a high intracellular Cl^- activity. Cl^- is extruded from the cell on the basolateral side through Cl^- channels. The efficiency Cl^- extrusion from the cell is reduced by activity of a Cl^-/HCO_3^- exchanger which transports Cl^- back into the cell. B) Transport of lactic acid and pH regulation: Lactic acid is removed from the subretinal space by the lac-/H^+ cotransporter. Through the basolateral membrane lactic acid leaves the cell using a different subtype of lac-/H^+ cotransporter. The necessary pH regulation occurs using a Na^+/H^+ exchanger and a Na^+/HCO_3^- exchanger in the apical membrane and a Cl^-/HCO_3^- exchanger at the basolateral membrane. The activity of Cl^-/HCO_3^- exchanger is supported by basolateral Cl^- channels which result in a cycling of Cl^- across the basolateral membrane. In the case of intracellular acidification the Cl^-/HCO_3^- exchanger is inhibited whereas Cl^- channels are activated. This increases the net water transport. Abbreviations: ClC-2, voltage-dependent Cl channels of the ClC family; CFTR, cystic fibrosis transmembrane conductance regulator; Kir7.1, inwardly rectifying K^+ channel 7.1; maxi-K, large conductance Ca^{2+}-dependent K^+ channel; MCT1, monocarboxylate transporter 1; MCT3, monocarboxylate transporter 3. From Strauss, 2005 (2).

modulation of water transport is based on the fact that the apical Na^+/HCO_3^- co-transporter is electrogenic. This means that this transportation activity is not electroneutral because it does not transport an equivalent amount of positive and negative charges (56, 73-75). The light-dependent hyperpolarisation of the apical membrane reduces the transport rate of Na^+/HCO_3^- co-transporter which in turn leads to intracellular acidification. As described above the water transport can be enhanced by intracellular acidification which leads to an increased efflux of Cl^- across the basolateral membrane of the RPE.

5. Visual Cycle

Vision starts with the absorption of a photon by the chromophore of rhodopsin, 11-cis retinal (67, 76-78). After absorption of a photon 11-cis retinal has changed its conformation into all-trans retinal and rhodopsin becomes meta-rhodopsin in a defined time before its activity is terminated by phosphorylation. After additional reaction

steps, rhodopsin is able to exchange all-trans retinal for 11-cis retinal and it can be activated again by a photon. Thus all-trans retinal needs to be re-isomerized to ensure a sufficient delivery of 11-cis retinal for all visual needs and proper visual function (1, 79). Since photoreceptors do no express a re-isomerase for all-trans retinal, the re-isomerization takes place in the RPE. For this purpose all-trans retinal is delivered to the RPE, re-isomerised to 11-cis retinal and delivered back to photoreceptors. This process is called the visual cycle of retinal (80-82, see Phototransduction, Webvision]. The visual cycle for rods occurs via the RPE (Figure 5). The visual cycle for cones is less clear. It can be that part of the cone all-trans retinal is recycled by the RPE and part is recycled by Müller glia cells.

The visual cycle of rods starts in the discs in the outer segments where all-trans retinal is transferred from the intradiscal space to the cytosolic space of the rod outer segment by an ATP-driven flippase ABCR or ABCA4 (ATP-binding cassette protein). This step involves the reaction of all-trans-retinal with phosphatidylethanolamine to N-retinylidine-phosphatidylethanolamine. In the next step all-trans retinal is reduced to all-trans retinol by a membrane bound retinol-dehydrogenase and is delivered to the subretinal space where it is loaded to IRBP (interstitial retinal binding protein), a carrier protein, and transported to the RPE. After uptake into the RPE all-trans retinol is transferred to CRBP (cellular retinol binding protein) which delivers all-trans retinol to a protein complex of several enzymes. This complex consists of LRAT (lecithin:retinol transferase), RPE65 (RPE protein with 65 kDa) and RDH5 (11-cis-retinol dehydrogenase). The three enzymes catalyze the three step reaction from all-trans retinol to 11-cis retinal: esterification of retinol by adding an aycl-group (LRAT), re-isomerisation to 11-cis using the energy from ester-hydrolysis (RPE65) and oxidation to 11-cis retinal (RDH5). The reaction is accelerated by CRALBP (cellular retinylaldehyde-binding protein) which is also part of the enzyme complex and to which 11-cis retinal is immediately transferred. From CRALBP 11-cis retinal is released to IRBP and transported back to photoreceptors. The exact mechanisms by which all-trans retinol enters the RPE and by which 11-cis retinal leaves the RPE are not clear.

The visual cycle fulfills an essential task of maintaining visual function and needs therefore to be adapted to different visual needs such as vision in darkness or lightness (1, 79). For this, functional aspects come into play: the storage of retinal and the adaption of the reaction speed. Basically vision at low light intensities requires a lower turn-over rate of the visual cycle whereas during light the turn-over rate is much higher. In the transition from darkness to light suddenly, large amount of 11-cis retinal is required. This comes not directly from the visual cycle but from several retinal pools of retinal binding proteins which are connected to each other by the transportation and reaction steps of the visual cycle. The first pool is the amount of 11-cis retinal which is in the rod outer segments. When the level of this pool is reduced, then the refilling of this pool is started by uptake of retinal from the next pool: the IRBP in the subretinal space. A drop in the retinal level of this pool is refilled from CRALBP which can be refilled from RPE65. With the connected pools for 11-cis retinal the changes in illumination can quickly be adapted. Thus, the RPE plays a crucial role in visual function, in the light adaptation. RPE65 plays a double crucial role in the visual cycle (83, 84). On one hand it catalyses the re-isomerization reaction at light conditions. In the dark it functions as a retinol binding protein and represents an important retinol pool for the visual cycle. RPE65 combines both essential functions for adaptation of the visual cycle: storage and enzyme reaction.

6. Phagocytosis of photoreceptor outer membranes

As mentioned above the light-sensitive photoreceptor outer segments (POS) goes through a constant destruction due to photo-oxidative damage. To maintain vision, the POS are constantly renewed by shedding the destroyed tips of the POS and by phagocytosis of the POS by the retinal pigment epithelium (3, 4, 85-89). This is a diurnally regulated process which takes place in the morning and is triggered by light (86-88, 90-93). It takes approximately eleven days to renew the whole length of the photoreceptor outer segment. Night active or day active animals show the same diurnal rhythm of phagocytosis (94). In this process the proper length of the photoreceptor outer segments is maintained by a coordinated activity of phagocytosis and POS shedding. The

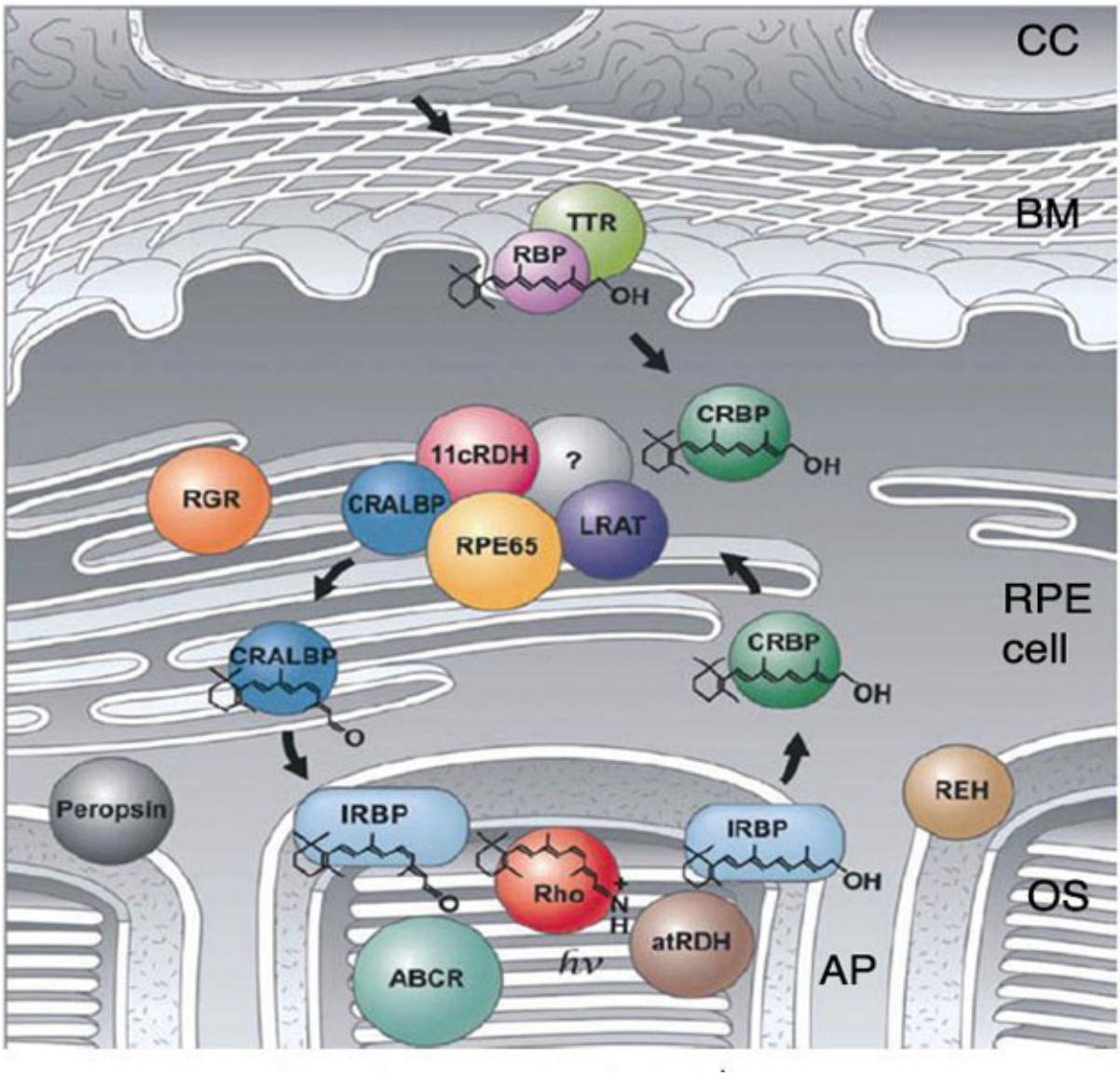

Figure 5. The visual cycle as adapted from Thompson and Gal (81). Light transduction starts with photon absorption by rhodopsin. The process of light absorption underlies the stereochemical change of 11-cis retinal into all-trans retinal. All-trans retinal is metabolized into all-trans retinol and transported to the RPE. In the RPE retinol is re-isomerized to 11-cis retinal and then redelivered to the photoreceptors. The regeneration seems to follow two pathways. One occurs through an as yet unidentified enzyme thought to function as an isomerohydrolase. The second pathway involves a light-dependent pathway using the RPE-retinal G-protein coupled receptor which isomerises all-trans retinal to 11-cis retinal, following light absorption. Abbreviations: CC, choidocapillaris; BM, Bruchs membrane; OS, outer segments; AP, apical processes; IRBP, interstitial retinal binding protein; CRBP, cellular retinol binding protein; CRALBP, cellular retinaldehyde binding protein; atRDH, all-trans retinol dehydrogenase; 11cRDH, 11cis retinol dehydrogenase; LRAT, lecithin retinol acyltransferase; RPE65, RPE specific protein with MD 65 kD; RGR, RPE-retinal G-protein coupled receptor; RBP/TTR, retinol-binding protein/transthyretin complex.

process is not only regulated by the circadian rhythm but also by coordination between the RPE and the photoreceptors.

Primarily three receptors have been identified to be involved in the regulation of phagocytosis of POS by the RPE (Fig. 6, above): CD36, receptor-tyrosinekinase c-mer (MerTK) and $\alpha_V\beta_5$ integrin (95-102). Basically CD36 is required for the process of POS internalization, MerTK is required to activate the phagocytosis and $\alpha_V\beta_5$ integrin is required for binding of POS, and for the initiation of the phagocytosis in the diurnal state. The interplay between these receptors ensures regulated and coordinated POS phagocytosis. The relevance of these

receptor molecules in the cell membrane was unraveled in the phenotypes of different knock-out animals. A loss of MerTk leads to human Retinitis pigmentosa and to a comparable type of retinal degeneration in the Royal College of Surgeons (RCS) rat which represents the oldest animal model for inherited retinal degeneration [100-102]. The loss of β5-integrin leads to a loss of circadian regulation of phagocytosis with a subsequent late onset of lipofuscin accumulation in the RPE (97-99).

It is not known what signaling molecule enables the communication between the RPE and the photoreceptors at the start of phagocytosis. It may be that the presence of the shed POS is sufficient to initiate the phagocytosis (103). The first step in this process is the binding of POS to the RPE through the αVβ5 integrin. The secreted glycoprotein milk fat globule-EGF8 (MFG-8), which is expressed by the RPE and can activate αVβ5 integrin, seems to be an important activator of diurnal stimulation of phagocytosis (104-106). Activation of the integrin produces an intracellular signaling cascade which involves focal adhesion kinase (FAK) (98). FAK is able to phosphorylate MerTK which can now be activated. The activation mechanism for MerTK is not clear. The natural ligand for MerTK is a protein called Gas6 (growth-arrest-specific protein 6). Gas6 is found in the retina and is strongly expressed by the RPE (107). Thus it can be that the Gas6 is an autocrine stimulator of phagocytosis by the RPE.

However a recent publication suggested that probably another ligand for MerTk is playing a role. In this publication it was shown that the tubby and tubby-like proteins, which are found in photoreceptors, can bind to MerTK and represent "eat-me" signals for the process of phagocytosis by RPE cells (and also for macrophages) (108). Activation of MerTK results in an intracellular signaling cascade which involves the generation of inositol-1,4,5-trisphosphate (InsP3) and a subsequent increase in intracellular free Ca^{2+}. The phagocytosis by itself is enabled by the phagocytosis receptor CD36.

7. Secretion

The RPE is an epithelium which closely interacts with photoreceptors on one side but must also be able to interact with cells on the blood side of the epithelium, such as endothelial cells or cells of the immune system. In order to communicate with the neighboring tissues the RPE is able to secrete a large variety of factors and signaling molecules. It secretes ATP, fas-ligand (fas-L), fibroblast growth factors (FGF-1, FGF-2, and FGF-5), transforming growth factor-β (TGF-β), insulin-like growth factor-1 (IGF-1), ciliary neurotrophic factor (CNTF), platelet-derived growth factor (PDGF), vascular endothelial growth factor (VEGF), lens epithelium-derived growth factor (LEDGF), members of the interleukin family, tissue inhibitor of matrix metalloprotease (TIMP) and pigment epithelium-derived factor (PEDF) (2).

In the healthy eye some of these factors are constantly released and help to maintain the structural integrity of the neighboring tissues. PEDF is for example a neurotrophic factor which is secreted to the apical/retinal side of the RPE to stabilize the neuronal retina by prevention of apoptosis (109-111). VEGF and TIMP are secreted to the basolateral side of the RPE and are required to stabilize the fenestrated structure of the endothelium of the choroid (112). Other factors are activated when the retina or the RPE are exposed to pathological conditions such as hypoxia or metabolic stress. In order to enable a finely regulated secretory activity of the RPE in health and disease the RPE expresses a number of Ca^{2+}-dependent regulatory mechanisms (113) (Figures 7 and 8). If the regulation of secretion fails under certain pathologies then the RPE will promote proliferative diseases such as choroidal neovascularisation.

The main trigger of secretory activity in the RPE is an increase in intracellular free Ca^{2+} second-messengers. In order to regulate secretion specific for the different factors, the RPE expresses a large number of different ion channels or transporters which increase intracellular free Ca^{2+}. As in many other secretory tissues such as the beta-cells of the pancreas or neuroendocrine cells, the RPE expresses voltage-dependent Ca^{2+} channels of the neuroendocrine subtype. The latter are composed of the $Ca_V1.3$ subtype (114-116). In the RPE the L-Type channel is regulated by either cytosolic tyrosine kinases, such as src-type kinase, or by receptor tyrosine kinase,

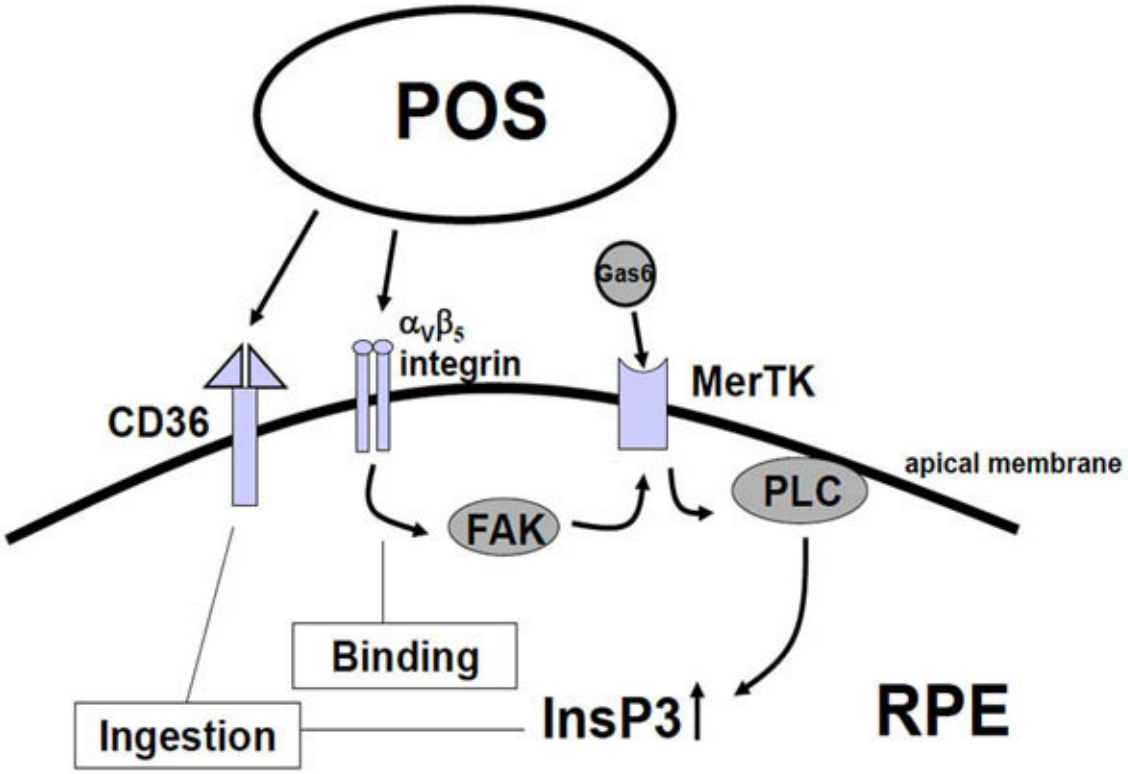

Figure 6. Phagocytosis.The figure shows the molecules involved in the initiation of photoreceptor outer segment phagocytosis. The initiation starts with binding of photoreceptor outer segment membranes. The event of binding is transduced into an intracellular signal, a rise in intracellular InsP3, which in turn leads to ingestion of the bound photoreceptor outer segment membranes. Binding is likely mediated by integrins and signal transduction occurs through the receptor tyrosine kinase MerTK. Ingestion involves the macrophage receptor CD36. Coordinated signal transduction occurs through integrin and MerTK interaction through the focal adhesion kinase. Abbreviations: CD36, macrophage phagocytosis receptor; FAK, focal adhesion kinase; Gas6, Growth-arrest-specific protein 6; InsP3, inositol-1,4,5-trisphosphate; MerTK, receptor tyrosine kinase c-mer; PLC, phospholipase C; POS, photoreceptor outer segment. From Strauss, 2005 (2).

such as the FGF receptor FGFR-2 (117-119). Since a large number of factors are known to increase secretion by the RPE acting via tyrosine kinase, the L-type channel regulates of number of different factors.

Another Ca^{2+} channel, which is thought to be involved in the regulation of growth-factor secretion by the RPE, is the TRPV2 channel (transient-receptor-potential channel, vanilloid subtype) (120). Activation of this channel leads to an increased secretion of VEGF by the RPE. It seems that mainly the IGF-1 stimulated VEGF is increased by a signal cascade involving the activation of TRPV2. This ion channel is an interesting candidate for understanding some clinical observations. TRPV2 channels can be activated by heat. And heat-dependent activation of TRPV2 channels can stimulate the secretion of VEGF. Laser treatment which causes an increase in the temperature of the RPE is often used in the treatment of degenerations such as AMD or diabetic retinopathy. This same laser treatment most probably causes an increase in the secretion of growth-factors from the RPE and it may be that TRPV2 activation is permitting this secretion.

8. Immune privilege of the eye

The inner eye represents an immune privileged space which is disconnected from the immune system of the blood stream (121-123). The immune privilege is supported by the RPE in two ways. First, it represents a mechanical and tight barrier which separates the inner space of the eye from the blood stream. Second, the RPE

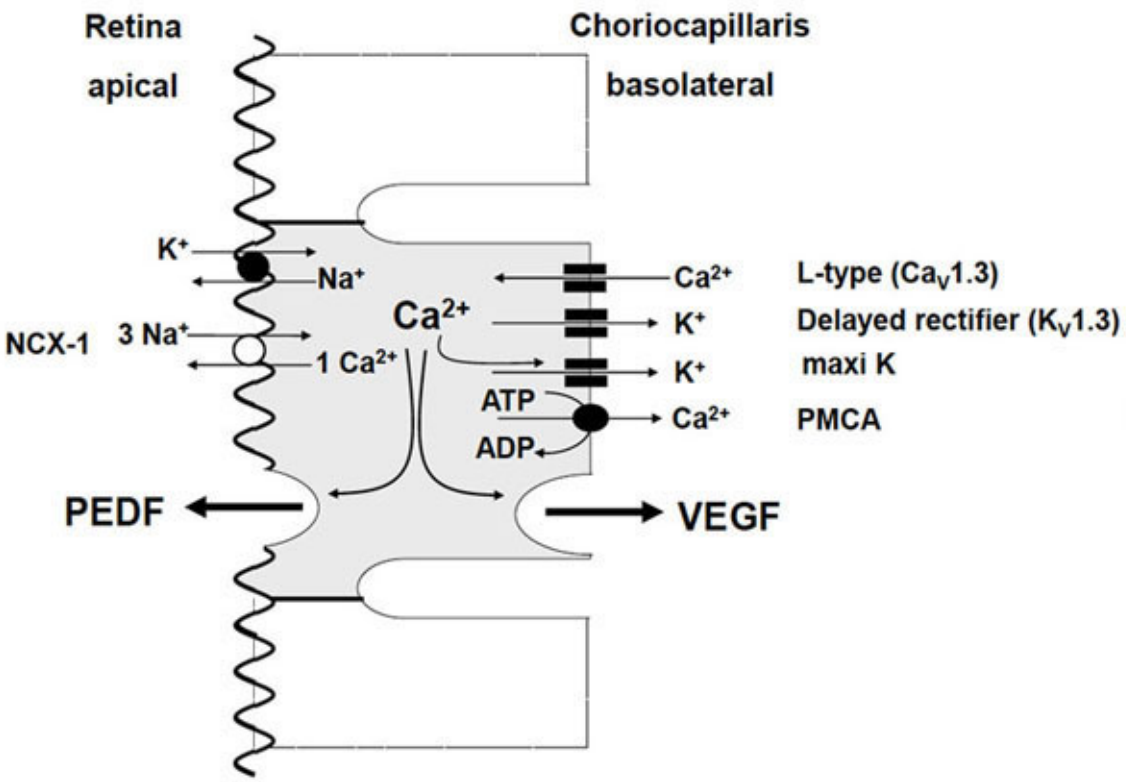

Figure 7. In the healthy eye the RPE secretes the neurotrophic factor PEDF into the subretinal space at the apical side of the RPE. The angiogenic factor, VEGF is secreted from the basolateral side into the extracellular matrix where it stabilizes the endothelium of the choriocapillaris and helps to keep it fenestrated. RPE cells express the neuroendocrine subtype of L-Type Ca2+ channels. Activation of these channels increases intracellular free Ca2+ which triggers the release of growth factors. This is terminated by either deactivation of L-type channels via activation of delayed rectifier K+ channels and hyperpolarization of the cell or by transport mechanism which decrease intracellular free Ca2+ such as Ca2+ ATPase or Na+/Ca2+ exchanger. Abbreviations: Delayed rectifier (KV1.3), outwardly delayed rectifying K+ channel composed of KV1.3 subunits; L-Type (CaV1.3), L-type Ca2+ channel of the neurendocrine subtype defined by the CaV1.3 or α1D subunit; maxi-K, large conductance Ca2+-dependent K+ channel; NCX-1, cardiac sodium calcium exchanger-1; PEDF, pigment epithelium-derived factor; PMCA, plasma membrane calcium-ATPase; VEGF, vascular endothelial growth factor. From Strauss 2005 (2).

is able communicate with the immune system in order to silence immune reaction in the healthy eye or, on the other hand, to activate the immune system in the case of disease (Figure 8). For these purposes the RPE can secrete immune modulatory factors such as interleukin-8 (IL-8) (124), complement factor H (CFH) (125, 126) or monocyte chemotactic protein-1 (MCP1) (127). Also the RPE is able to react to different factors of immune signaling cascades by expressing corresponding receptors. The receptors are MHC receptors (128, 129), toll-like receptors (130) or receptors for signaling molecules such as tumor-necrosis factor- α(TNF-α) (131).

The knowledge that the RPE is able to interact with the immune system has gained an increasing interest lately. Many types of retinal degeneration seem to be associated with an insufficiency to silence the immune reactions, for example, in age-related macular degeneration (See Age-Related Macular Degeneration (AMD), Webvision). On the other hand, an understanding of the immune privilege of the RPE is going to be helpful in the treatment of retinal degenerations by injected peptides, gene-therapy via viruses or in approaches using transplantation.

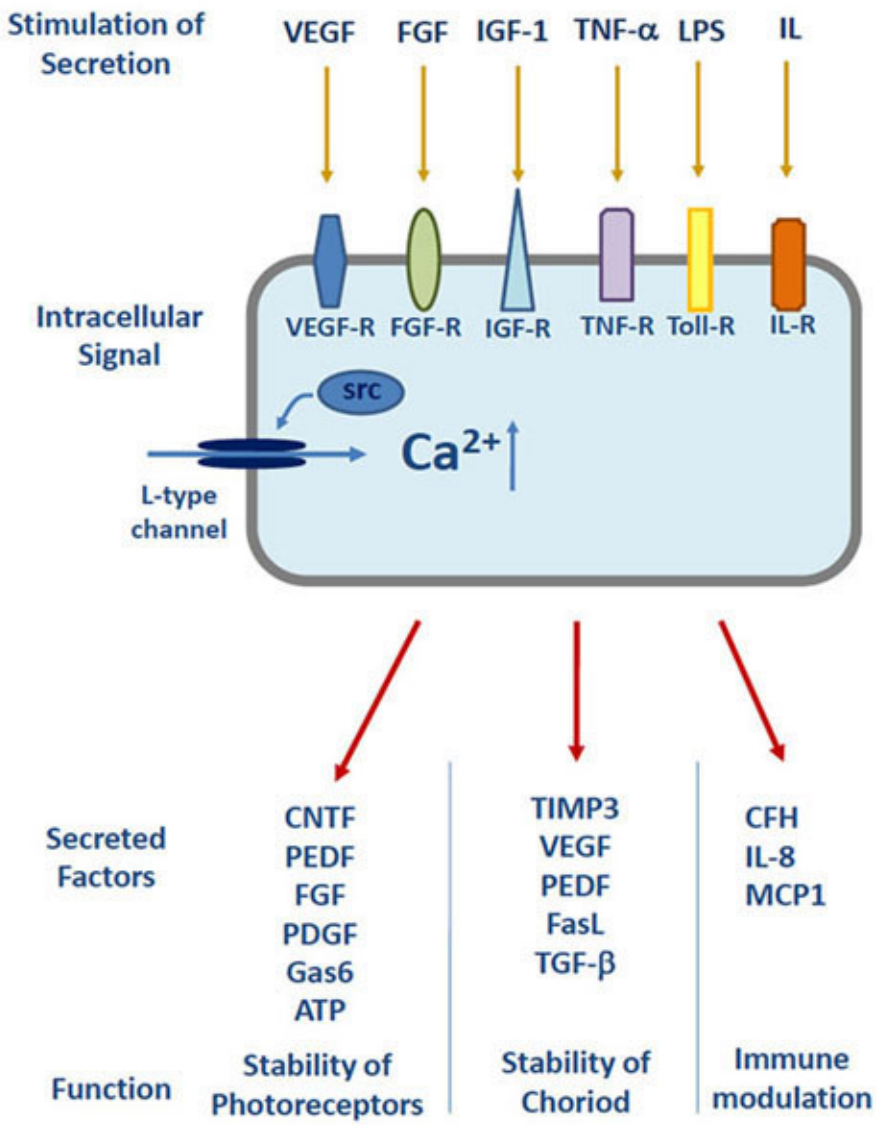

Figure 8. Growth-factor signalling in the RPE. Stimulation of secretion by the RPE and summary of the secreted molecules by their functional role. Trigger for secretion are Ca^{2+}-channels of the RPE. Abbreviations: ATP, Adenosine triphosphate; CFH, complement Factor H; CNTF, ciliary neurotrophic factor; FASL, CD95 apoptosis receptor ligand; FGF, fibroblast growth factor; IL, interleukin; IGF-1, insulin-like growth factor-1; LPS, lipopolysaccharides; PEDF, pigment epithelium-derived factor; PDGF, platelet-derived growth factor; TIMP3, tissue inhibitor of metallo matrix proteases; VEGF, vascular endothelial growth factor; TGF-β, transforming growth factor-β. Receptors: FGF-R, fibroblast growth factor receptor; IGF-R, insulin-like growth factor receptor; IL-R, interleukin receptor; MCP-1, monocyte chemotactic protein 1; TNF-R, tumor necrosis factor receptor; Toll-R, toll-like receptors; VEGF-R, vascular endothelial growrc, src-type intracellular tyrosine kinase. Adapted from Strauss, 2009 (133).

About the Author

Olaf Strauss is a Berliner, educated in Berlin until receiving his doctorate in Zoology and Physiology in 1990 and the habilitation in 1999 from the Berlin Freie University. After five years as a professor in Experimental Ophthalmology, UKE, Hamburg, he took up a position in Experimental Ophthalmology at the University Hospital, Regensburg. He is presently Professor in Experimental Ophthalmology at the University of Regensburg. His research interests have always been on understanding the function of the retinal pigment epithelium. Two major areas of research on the RPE are of interest: secretion and phagocytosis. His work has focused on the Ca^{2+}-dependent regulation by ion channels and cytosolic Ca^{2+} stores. Recent work focuses on the interaction of bestrophin-1 with voltage-dependent Ca^{2+} channels in Best's vitelliforme macular dystrophy and on the systemic influence on retinal function by the renin-angiotensin system.

References

1. Lamb TD, Collin SP, Pugh EN Jr. Evolution of the vertebrate eye: opsins, photoreceptors, retina and eye cup. Nat Rev Neurosci. 2007;8:960–76. PubMed PMID: 18026166.
2. Strauss O. The retinal pigment epithelium in visual function. Physiol Rev. 2005;85:845–81. PubMed PMID: 15987797.
3. Bok D. The retinal pigment epithelium: a versatile partner in vision. J Cell Sci Suppl. 1993;17:189–95. PubMed PMID: 8144697.
4. Steinberg RH. Interactions between the retinal pigment epithelium and the neural retina. Doc Ophthalmol. 1985;60:327–46. PubMed PMID: 3905312.
5. Sparrow JR, Hicks D, Hamel CP. The retinal pigment epithelium in health and disease. Curr Mol Med. 2010;10:802–23. PubMed PMID: 21091424.
6. Marmorstein AD, Finnemann SC, Bonilha VL, Rodriguez-Boulan E. Morphogenesis of the retinal pigment epithelium: toward understanding retinal degenerative diseases. Ann N Y Acad Sci. 1998;857:1–12. PubMed PMID: 9917828.
7. Rizzolo LJ. Polarity and the development of the outer blood-retinal barrier. Histol Histopathol. 1997;12:1057–67. PubMed PMID: 9302567.
8. Fessler F. Zur Entwicklungsmechanik des Auges. Arch Entw Mechan. 1920;46:169–201.

9. McCaffery P, Lee M., Wagner M. E., Sladek N. E., Dräger U. C. Asymmetrical retinoic acid synthesis in the dorsoventral axis of the retina. Development. 1992;115:371–382. PubMed PMID: 1425331.
10. Mendelsohn C, Ruberte E., Le Meur M., Morris-Kay G., Chambon P. Developmental analysis of the retinoic acid-inducible RAR-b2 promoter in transgenic animals. Development. 1991;113:723–734. PubMed PMID: 1668276.
11. Gonzalez-Fernandez F, Healy JI. Early expression of the gene for interphotoreceptor retinol-binding protein during photoreceptor differentiation suggests a critical role for the interphotoreceptor matrix in retinal development. J Cell Biol. 1990;111:2775–84. PubMed PMID: 1703544.
12. Hollyfield JG. Hyaluronan and the functional organization of the interphotoreceptor matrix. Invest Ophthalmol Vis Sci. 1999;40:2767–9. PubMed PMID: 10549633.
13. Pepperberg DR, Okajima TL, Wiggert B, Ripps H, Crouch RK, Chader GJ. Interphotoreceptor retinoid-binding protein (IRBP). Molecular biology and physiological role in the visual cycle of rhodopsin. Mol Neurobiol. 1993;7:61–85. PubMed PMID: 8318167.
14. Uehara F, Matthes MT, Yasumura D, LaVail MM. Light-evoked changes in the interphotoreceptor matrix. Science. 1990;248:1633–6. PubMed PMID: 2194288.
15. Guymer R, Luthert P, Bird A. Changes in Bruch's membrane and related structures with age. Prog Retin Eye Res. 1999;18:59–90. PubMed PMID: 9920499.
16. Beatty S, Koh H, Phil M, Henson D, Boulton M. The role of oxidative stress in the pathogenesis of age-related macular degeneration. Surv Ophthalmol. 2000;45:115–34. PubMed PMID: 11033038.
17. Beatty S, Boulton M, Henson D, Koh HH, Murray IJ. Macular pigment and age related macular degeneration. Br J Ophthalmol. 1999;83:867–77. PubMed PMID: 10381676.
18. Winkler BS, Boulton ME, Gottsch JD, Sternberg P. Oxidative damage and age-related macular degeneration. Mol Vis. 1999;5:32. PubMed PMID: 10562656.
19. Alm A, Bill A. Blood flow and oxygen extraction in the cat uvea at normal and high intraocular pressures. Acta Physiol Scand. 1970;80:19–28. PubMed PMID: 5475327.
20. Alm A, Bill A. The oxygen supply to the retina. I. Effects of changes in intraocular and arterial blood pressures, and in arterial P O_2 and P CO_2 on the oxygen tension in the vitreous body of the cat. Acta Physiol Scand. 1972;84:261–74. PubMed PMID: 5015191.
21. Alm A, Bill A. The oxygen supply to the retina. II. Effects of high intraocular pressure and of increased arterial carbon dioxide tension on uveal and retinal blood flow in cats. A study with radioactively labelled microspheres including flow determinations in brain and some other tissues. Acta Physiol Scand. 1972;84:306–19. PubMed PMID: 4553229.
22. Alm A, Bill A. Ocular and optic nerve blood flow at normal and increased intraocular pressures in monkeys (Macaca irus): a study with radioactively labelled microspheres including flow determinations in brain and some other tissues. Exp Eye Res. 1973;15:15–29. PubMed PMID: 4630581.
23. Auker CR, Parver LM, Doyle T, Carpenter DO. Choroidal blood flow. I. Ocular tissue temperature as a measure of flow. Arch Ophthalmol. 1982;100:1323–6. PubMed PMID: 7103818.
24. Parver LM. Temperature modulating action of choroidal blood flow. Eye (Lond). 1991;5(Pt 2):181–5. PubMed PMID: 2070878.
25. Boulton M, Dayhaw-Barker P. The role of the retinal pigment epithelium: topographical variation and ageing changes. Eye. 2001;15:384–389. PubMed PMID: 11450762.
26. Boulton M (1991) Ageing of the retinal pigment epithelium. In: Osborne NN, Chader GJ (eds) Progress in retinal research. Pergamon Press, Oxford, New York, pp. 125-51
27. Schutt F, Davies S, Kopitz J, Holz FG, Boulton ME. Photodamage to human RPE cells by A2-E, a retinoid component of lipofuscin. Invest Ophthalmol Vis Sci. 2000;41:2303–8. PubMed PMID: 10892877.
28. Ben-Shabat S, Parish CA, Vollmer HR, Itagaki Y, Fishkin N, Nakanishi K, Sparrow JR. Biosynthetic studies of A2E, a major fluorophore of retinal pigment epithelial lipofuscin. J Biol Chem. 2002;277:7183–90. PubMed PMID: 11756445.
29. Delori FC, Goger DG, Dorey CK. Age-related accumulation and spatial distribution of lipofuscin in RPE of normal subjects. Invest Ophthalmol Vis Sci. 2001;42:1855–66. PubMed PMID: 11431454.

30. Miller SS, Steinberg RH. Active transport of ions across frog retinal pigment epithelium. Exp Eye Res. 1977;25:235–48. PubMed PMID: 304010.
31. Miller SS, Steinberg RH. Passive ionic properties of frog retinal pigment epithelium. J Membr Biol. 1977;36:337–72. PubMed PMID: 302862.
32. Ban Y, Rizzolo LJ. Regulation of glucose transporters during development of the retinal pigment epithelium. Brain Res Dev Brain Res. 2000;121:89–95. PubMed PMID: 10837896.
33. Sugasawa K, Deguchi J, Okami T, Yamamoto A, Omori K, Uyama M, Tashiro Y. Immunocytochemical analyses of distributions of Na, K-ATPase and GLUT1, insulin and transferrin receptors in the developing retinal pigment epithelial cells. Cell Struct Funct. 1994;19:21–8. PubMed PMID: 8069944.
34. Bazan NG, Gordon, W. C., Rodriguez de Turco, E. B. (1992) Docosahexaenoic acid uptake and metabolism in photoreceptors: retinal conservation by an efficient retinal pigment epithelial cell-mediated recycling process. Neurobiology of Essential Fatty Acids:295-306
35. Bazan NG, Rodriguez de Turco EB, Gordon WC. Docosahexaenoic acid supply to the retina and its conservation in photoreceptor cells by active retinal pigment epithelium-mediated recycling. World Rev Nutr Diet. 1994;75:120–3. PubMed PMID: 7871812.
36. Hughes BA, Gallemore RP, Miller SS (1998) Transport mechanisms in the retinal pigment epithelium. In: Marmor MF, Wolfensberger TJ (eds) The retinal pigment epithelium. Oxford University Press, New York, Oxford, pp. 103-134
37. Hamann S. Molecular mechanisms of water transport in the eye. Int Rev Cytol. 2002;215:395–431. PubMed PMID: 11952236.
38. Adler AJ, Southwick RE. Distribution of glucose and lactate in the interphotoreceptor matrix. Ophthalmic Res. 1992;24:243–52. PubMed PMID: 1436983.
39. Edelman JL, Miller SS. Epinephrine stimulates fluid absorption across bovine retinal pigment epithelium. Invest Ophthalmol Vis Sci. 1991;32:3033–40. PubMed PMID: 1657816.
40. Hughes BA, Miller SS, Machen TE. Effects of cyclic AMP on fluid absorption and ion transport across frog retinal pigment epithelium. Measurements in the open-circuit state. J Gen Physiol. 1984;83:875–99. PubMed PMID: 6330281.
41. Tsuboi S. Measurement of the volume flow and hydraulic conductivity across the isolated dog retinal pigment epithelium. Invest Ophthalmol Vis Sci. 1987;28:1776–82. PubMed PMID: 3667149.
42. Hughes BA, Takahira M. Inwardly rectifying K^+ currents in isolated human retinal pigment epithelial cells. Invest Ophthalmol Vis Sci. 1996;37:1125–39. PubMed PMID: 8631627.
43. Hu JG, Gallemore RP, Bok D, Lee AY, Frambach DA. Localization of NaK ATPase on cultured human retinal pigment epithelium. Invest Ophthalmol Vis Sci. 1994;35:3582–8. PubMed PMID: 8088949.
44. Frambach DA, Roy CE, Valentine JL, Weiter JJ. Precocious retinal adhesion is affected by furosemide and ouabain. Curr Eye Res. 1989;8:553–6. PubMed PMID: 2743794.
45. Miller SS, Edelman JL. Active ion transport pathways in the bovine retinal pigment epithelium. J Physiol. 1990;424:283–300. PubMed PMID: 1697344.
46. Joseph DP, Miller SS. Apical and basal membrane ion transport mechanisms in bovine retinal pigment epithelium. J Physiol. 1991;435:439–63. PubMed PMID: 1722821.
47. La Cour M. Cl^- transport in frog retinal pigment epithelium. Exp Eye Res. 1992;54:921–31. PubMed PMID: 1381683.
48. Wiederholt M, Zadunaisky JA. Decrease of intracellular chloride activity by furosemide in frog retinal pigment epithelium. Curr Eye Res. 1984;3:673–5. PubMed PMID: 6609051.
49. Bosl MR, Stein V, Hubner C, Zdebik AA, Jordt SE, Mukhopadhyay AK, Davidoff MS, Holstein AF, Jentsch TJ. Male germ cells and photoreceptors, both dependent on close cell-cell interactions, degenerate upon ClC-2 Cl^- channel disruption. Embo J. 2001;20:1289–99. PubMed PMID: 11250895.
50. Blaug S, Quinn R, Quong J, Jalickee S, Miller SS. Retinal pigment epithelial function: a role for CFTR? Doc Ophthalmol. 2003;106:43–50. PubMed PMID: 12675485.

51. Weng TX, Godley BF, Jin GF, Mangini NJ, Kennedy BG, Yu AS, Wills NK. Oxidant and antioxidant modulation of chloride channels expressed in human retinal pigment epithelium. Am J Physiol Cell Physiol. 2002;283:C839–49. PubMed PMID: 12176741.
52. Hartzell HC, Qu Z, Yu K, Xiao Q, Chien LT. Molecular physiology of bestrophins: multifunctional membrane proteins linked to best disease and other retinopathies. Physiol Rev. 2008;88:639–72. PubMed PMID: 18391176.
53. Hamann S, Kiilgard JF, la Cour M, Prause JU, Zeuthen T. Cotransport of H^+, lactate, and H_2O in porcine retinal pigment epithelial cells. Exp Eye Res. 2003;76:1–12. PubMed PMID: 12634113.
54. Keller SK, Jentsch TJ, Janicke I, Wiederholt M. Regulation of intracellular pH in cultured bovine retinal pigment epithelial cells. Pflugers Arch. 1988;411:47–52. PubMed PMID: 2832823.
55. Keller SK, Jentsch TJ, Koch M, Wiederholt M. Interactions of pH and K^+ conductance in cultured bovine retinal pigment epithelial cells. Am J Physiol. 1986;250:C124–37. PubMed PMID: 3942203.
56. la Cour M. pH homeostasis in the frog retina: the role of Na+:HCO3- co-transport in the retinal pigment epithelium. Acta Ophthalmol (Copenh). 1991;69:496–504. PubMed PMID: 1750318.
57. la Cour M, Lin H, Kenyon E, Miller SS. Lactate transport in freshly isolated human fetal retinal pigment epithelium. Invest Ophthalmol Vis Sci. 1994;35:434–42. PubMed PMID: 8112991.
58. Bialek S, Miller SS. K^+ and Cl^- transport mechanisms in bovine pigment epithelium that could modulate subretinal space volume and composition. J Physiol. 1994;475:401–17. PubMed PMID: 8006825.
59. Botchkin LM, Matthews G. Chloride current activated by swelling in retinal pigment epithelium cells. Am J Physiol. 1993;265:C1037–45. PubMed PMID: 8238297.
60. Hamann S, la Cour M, Lui GM, Bundgaard M, Zeuthen T. Transport of protons and lactate in cultured human fetal retinal pigment epithelial cells. Pflugers Arch. 2000;440:84–92. PubMed PMID: 10864001.
61. Wolfensberger TJ, Dmitriev AV, Govardovskii VI. Inhibition of membrane-bound carbonic anhydrase decreases subretinal pH and volume. Doc Ophthalmol. 1999;97:261–71. PubMed PMID: 10896339.
62. Linsenmeier RA, Padnick-Silver L. Metabolic dependence of photoreceptors on the choroid in the normal and detached retina. Invest Ophthalmol Vis Sci. 2000;41:3117–23. PubMed PMID: 10967072.
63. Marmor MF. Control of subretinal fluid: experimental and clinical studies. Eye. 1990;4:340–344. PubMed PMID: 2199242.
64. Hamann S, Zeuthen T, La Cour M, Nagelhus EA, Ottersen OP, Agre P, Nielsen S. Aquaporins in complex tissues: distribution of aquaporins 1-5 in human and rat eye. Am J Physiol. 1998;274:C1332–45. PubMed PMID: 9612221.
65. Stamer WD, Bok D, Hu J, Jaffe GJ, McKay BS. Aquaporin-1 channels in human retinal pigment epithelium: role in transepithelial water movement. Invest Ophthalmol Vis Sci. 2003;44:2803–8. PubMed PMID: 12766090.
66. Steinberg RH, Linsenmeier RA, Griff ER. Three light-evoked responses of the retinal pigment epithelium. Vision Res. 1983;23:1315–23. PubMed PMID: 6606894.
67. Baylor D. How photons start vision. Proc Natl Acad Sci U S A. 1996;93:560–5. PubMed PMID: 8570595.
68. la Cour M. The retinal pigment epithelium controls the potassium activity in the subretinal space. Acta Ophthalmol Suppl. 1985;173:9–10. PubMed PMID: 3002115.
69. Shimura M, Yuan Y, Chang JT, Zhang S, Campochiaro PA, Zack DJ, Hughes BA. Expression and permeation properties of the K^+ channel Kir7.1 in the retinal pigment epithelium. J Physiol. 2001;531:329–46. PubMed PMID: 11230507.
70. Hughes BA, Takahira M. ATP-dependent regulation of inwardly rectifying K^+ current in bovine retinal pigment epithelial cells. Am J Physiol. 1998;275:C1372–83. PubMed PMID: 9814987.
71. la Cour M, Lund-Andersen H, Zeuthen T. Potassium transport of the frog retinal pigment epithelium: autoregulation of potassium activity in the subretinal space. J Physiol. 1986;375:461–79. PubMed PMID: 2432225.
72. Huang B, Karwoski CJ. Light-evoked expansion of subretinal space volume in the retina of the frog. J Neurosci. 1992;12:4243–52. PubMed PMID: 1331360.

73. Kenyon E, Maminishkis A, Joseph DP, Miller SS. Apical and basolateral membrane mechanisms that regulate pH_i in bovine retinal pigment epithelium. Am J Physiol. 1997;273:C456–72. PubMed PMID: 9277343.
74. Lin H, Kenyon E, Miller SS. Na-dependent pH_i regulatory mechanisms in native human retinal pigment epithelium. Invest Ophthalmol Vis Sci. 1992;33:3528–38. PubMed PMID: 1334478.
75. Lin H, Miller SS. pH_i regulation in frog retinal pigment epithelium: two apical membrane mechanisms. Am J Physiol. 1991;261:C132–42. PubMed PMID: 1858851.
76. Okada T, Ernst OP, Palczewski K, Hofmann KP. Activation of rhodopsin: new insights from structural and biochemical studies. Trends Biochem Sci. 2001;26:318–24. PubMed PMID: 11343925.
77. Hofmann KP. Signalling states of photoactivated rhodopsin. Novartis Found Symp. 1999;224:158–75discussion 175-80. PubMed PMID: 10614051.
78. Baylor DA, Burns ME. Control of rhodopsin activity in vision. Eye. 1998;12(Pt 3b):521–5. PubMed PMID: 9775212.
79. Lamb TD, Pugh EN Jr. Dark adaptation and the retinoid cycle of vision. Prog Retin Eye Res. 2004;23:307–80. PubMed PMID: 15177205.
80. Baehr W, Wu S. M., Bird A. C., Palczewski K. The retinoid cycle and retina disease. Vis Res. 2003;43:2957–2958. PubMed PMID: 14611932.
81. Thompson DA, Gal A. Vitamin A metabolism in the retinal pigment epithelium: genes, mutations, and diseases. Prog Retin Eye Res. 2003;22:683–703. PubMed PMID: 12892646.
82. Thompson DA, Gal A. Genetic defects in vitamin A metabolism of the retinal pigment epithelium. Dev Ophthalmol. 2003;37:141–54. PubMed PMID: 12876835.
83. Xue L, Gollapalli DR, Maiti P, Jahng WJ, Rando RR. A palmitoylation switch mechanism in the regulation of the visual cycle. Cell. 2004;117:761–71. PubMed PMID: 15186777.
84. Jin M, Li S, Moghrabi WN, Sun H, Travis GH. Rpe65 is the retinoid isomerase in bovine retinal pigment epithelium. Cell. 2005;122:449–59. PubMed PMID: 16096063.
85. Strauss O, Stumpff F, Mergler S, Wienrich M, Wiederholt M. The Royal College of Surgeons Rat: an animal model for inherited retinal degeneration with a still unknown genetic defect. Acta Anat (Basel). 1998;162:101–11. PubMed PMID: 9831756.
86. LaVail MM. Rod outer segment disc shedding in relation to cyclic lighting. Exp Eye Res. 1976;23:277–80. PubMed PMID: 987920.
87. LaVail MM. Circadian nature of rod outer segment disc shedding in the rat. Invest Ophthalmol Vis Sci. 1980;19:407–11. PubMed PMID: 7358492.
88. LaVail MM. Outer segment disc shedding and phagocytosis in the outer retina. Trans Ophthalmol Soc U K. 1983;103(Pt 4):397–404. PubMed PMID: 6380008.
89. Kevany BM, Palczewski K. Phagocytosis of retinal rod and cone photoreceptors. Physiology (Bethesda). 2010;25:8–15. PubMed PMID: 20134024.
90. Green CB, Besharse JC. Retinal circadian clocks and control of retinal physiology. J Biol Rhythms. 2004;19:91–102. PubMed PMID: 15038849.
91. Besharse JC, Defoe DM (1998) Role of the retinal pigment epithelium in photoreceptor membrane turnover. In: Marmor MF, Wolfensberger TJ (eds) The retinal pigment epithelium. Oxford University Press, Oxford, pp. 152-172
92. Besharse JC, Hollyfield JG. Turnover of mouse photoreceptor outer segments in constant light and darkness. Invest Ophthalmol Vis Sci. 1979;18:1019–24. PubMed PMID: 478775.
93. Besharse JC, Hollyfield JG, Rayborn ME. Photoreceptor outer segments: accelerated membrane renewal in rods after exposure to light. Science. 1977;196:536–8. PubMed PMID: 300504.
94. Bobu C, Hicks D. Regulation of retinal photoreceptor phagocytosis in a diurnal mammal by circadian clocks and ambient lighting. Invest Ophthalmol Vis Sci. 2009;50:3495–502. PubMed PMID: 19234351.
95. Finnemann SC, Silverstein RL. Differential roles of CD36 and alphavbeta5 integrin in photoreceptor phagocytosis by the retinal pigment epithelium. J Exp Med. 2001;194:1289–98. PubMed PMID: 11696594.

96. Ryeom SW, Sparrow JR, Silverstein RL. CD36 participates in the phagocytosis of rod outer segments by retinal pigment epithelium. J Cell Sci. 1996;109(Pt 2):387–95. PubMed PMID: 8838662.
97. Finnemann SC, Bonilha VL, Marmorstein AD, Rodriguez-Boulan E. Phagocytosis of rod outer segments by retinal pigment epithelial cells requires alpha(v)beta5 integrin for binding but not for internalization. Proc Natl Acad Sci U S A. 1997;94:12932–7. PubMed PMID: 9371778.
98. Finnemann SC. Focal adhesion kinase signaling promotes phagocytosis of integrin-bound photoreceptors. Embo J. 2003;22:4143–4154. PubMed PMID: 12912913.
99. Nandrot EF, Kim Y, Brodie SE, Huang X, Sheppard D, Finnemann SC. Loss of Synchronized Retinal Phagocytosis and Age-related Blindness in Mice Lacking {alpha}v{beta}5 Integrin. J Exp Med. 2004;200:1539–1545. PubMed PMID: 15596525.
100. D'Cruz PM, Yasumura D, Weir J, Matthes MT, Abderrahim H, LaVail MM, Vollrath D. Mutation of the receptor tyrosine kinase gene Mertk in the retinal dystrophic RCS rat. Hum Mol Genet. 2000;9:645–51. PubMed PMID: 10699188.
101. Gal A, Li Y, Thompson DA, Weir J, Orth U, Jacobson SG, Apfelstedt-Sylla E, Vollrath D. Mutations in MERTK, the human orthologue of the RCS rat retinal dystrophy gene, cause retinitis pigmentosa. Nat Genet. 2000;26:270–1. PubMed PMID: 11062461.
102. Feng W, Yasumura D, Matthes MT, LaVail MM, Vollrath D. Mertk triggers uptake of photoreceptor outer segments during phagocytosis by cultured retinal pigment epithelial cells. J Biol Chem. 2002;277:17016–22. PubMed PMID: 11861639.
103. Teirstein PS, Goldman AI, O'Brien PJ. Evidence for both local and central regulation of rat rod outer segment disc shedding. Invest Ophthalmol Vis Sci. 1980;19:1268–73. PubMed PMID: 7429763.
104. Mallavarapu M, Finnemann SC. Neural Retina and MerTK-Independent Apical Polarity of alphavbeta5 Integrin Receptors in the Retinal Pigment Epithelium. Adv Exp Med Biol. 2010;664:123–31. PubMed PMID: 20238010.
105. Nandrot EF, Chang Y, Finnemann SC. Alphavbeta5 integrin receptors at the apical surface of the RPE: one receptor, two functions. Adv Exp Med Biol. 2008;613:369–75. PubMed PMID: 18188966.
106. Nandrot EF, Anand M, Almeida D, Atabai K, Sheppard D, Finnemann SC. Essential role for MFG-E8 as ligand for alphavbeta5 integrin in diurnal retinal phagocytosis. Proc Natl Acad Sci U S A. 2007;104:12005–10. PubMed PMID: 17620600.
107. Karl MO, Kroeger W, Wimmers S, Milenkovic VM, Valtink M, Engelmann K, Strauss O. Endogenous Gas6 and Ca^{2+} -channel activation modulate phagocytosis by retinal pigment epithelium. Cell Signal. 2008;20:1159–68. PubMed PMID: 18395422.
108. Caberoy NB, Zhou Y, Li W. Tubby and tubby-like protein 1 are new MerTK ligands for phagocytosis. EMBO J. 2010;29:3898–910. PubMed PMID: 20978472.
109. Cayouette M, Smith SB, Becerra SP, Gravel C. Pigment epithelium-derived factor delays the death of photoreceptors in mouse models of inherited retinal degenerations. Neurobiol Dis. 1999;6:523–32. PubMed PMID: 10600408.
110. Ogata N, Wang L, Jo N, Tombran-Tink J, Takahashi K, Mrazek D, Matsumura M. Pigment epithelium derived factor as a neuroprotective agent against ischemic retinal injury. Curr Eye Res. 2001;22:245–52. PubMed PMID: 11462162.
111. Becerra SP, Fariss RN, Wu YQ, Montuenga LM, Wong P, Pfeffer BA. Pigment epithelium-derived factor in the monkey retinal pigment epithelium and interphotoreceptor matrix: apical secretion and distribution. Exp Eye Res. 2004;78:223–34. PubMed PMID: 14729355.
112. Witmer AN, Vrensen GF, Van Noorden CJ, Schlingemann RO. Vascular endothelial growth factors and angiogenesis in eye disease. Prog Retin Eye Res. 2003;22:1–29. PubMed PMID: 12597922.
113. Wimmers S, Karl MO, Strauss O. Ion channels in the RPE. Prog Retin Eye Res. 2007;26:263–301. PubMed PMID: 17258931.
114. Rosenthal R, Strauss O. Ca^{2+}-channels in the RPE. Adv Exp Med Biol. 2002;514:225–35. PubMed PMID: 12596924.

115. Catterall WA. Structure and regulation of voltage-gated Ca^{2+} channels. Annu Rev Cell Dev Biol. 2000;16:521–55. PubMed PMID: 11031246.
116. Striessnig J. Pharmacology, structure and function of cardiac L-type Ca^{2+} channels. Cell Physiol Biochem. 1999;9:242–69. PubMed PMID: 10575201.
117. Rosenthal R, Thieme H, Strauss O. Fibroblast growth factor receptor 2 (FGFR2) in brain neurons and retinal pigment epithelial cells act via stimulation of neuroendocrine L-type channels (Ca(v)1.3). Faseb J. 2001;15:970–7. PubMed PMID: 11292657.
118. Strauss O, Mergler S, Wiederholt M. Regulation of L-type calcium channels by protein tyrosine kinase and protein kinase C in cultured rat and human retinal pigment epithelial cells. Faseb J. 1997;11:859–67. PubMed PMID: 9285484.
119. Strauss O, Buss F, Rosenthal R, Fischer D, Mergler S, Stumpff F, Thieme H. Activation of neuroendocrine L-type channels (alpha1D subunits) in retinal pigment epithelial cells and brain neurons by pp60(c-src). Biochem Biophys Res Commun. 2000;270:806–10. PubMed PMID: 10772906.
120. Cordeiro S, Seyler S, Stindl J, Milenkovic VM, Strauss O. Heat-sensitive TRPV channels in retinal pigment epithelial cells: regulation of VEGF-A secretion. Invest Ophthalmol Vis Sci.51:6001–8. PubMed PMID: 20539001.
121. Ishida K, Panjwani N, Cao Z, Streilein JW. Participation of pigment epithelium in ocular immune privilege. 3. Epithelia cultured from iris, ciliary body, and retina suppress T-cell activation by partially non-overlapping mechanisms. Ocul Immunol Inflamm. 2003;11:91–105. PubMed PMID: 14533028.
122. Streilein JW, Ma N, Wenkel H, Ng TF, Zamiri P. Immunobiology and privilege of neuronal retina and pigment epithelium transplants. Vision Res. 2002;42:487–95. PubMed PMID: 11853765.
123. Wenkel H, Streilein JW. Evidence that retinal pigment epithelium functions as an immune-privileged tissue. Invest Ophthalmol Vis Sci. 2000;41:3467–73. PubMed PMID: 11006240.
124. Relvas LJ, Bouffioux C, Marcet B, Communi D, Makhoul M, Horckmans M, Blero D, Bruyns C, Caspers L, Boeynaems JM, Willermain F. Extracellular nucleotides and interleukin-8 production by ARPE cells: potential role of danger signals in blood-retinal barrier activation. Invest Ophthalmol Vis Sci. 2009;50:1241–6. PubMed PMID: 19029040.
125. Kim YH, He S, Kase S, Kitamura M, Ryan SJ, Hinton DR. Regulated secretion of complement factor H by RPE and its role in RPE migration. Graefes Arch Clin Exp Ophthalmol. 2009;247:651–9. PubMed PMID: 19214553.
126. Chen M, Forrester JV, Xu H. Synthesis of complement factor H by retinal pigment epithelial cells is down-regulated by oxidized photoreceptor outer segments. Exp Eye Res. 2007;84:635–45. PubMed PMID: 17292886.
127. Austin BA, Liu B, Li Z, Nussenblatt RB. Biologically active fibronectin fragments stimulate release of MCP-1 and catabolic cytokines from murine retinal pigment epithelium. Invest Ophthalmol Vis Sci. 2009;50:2896–902. PubMed PMID: 19151387.
128. Jorgensen A, Wiencke AK, la Cour M, Kaestel CG, Madsen HO, Hamann S, Lui GM, Scherfig E, Prause JU, Svejgaard A, Odum N, Nissen MH, Ropke C. Human retinal pigment epithelial cell-induced apoptosis in activated T cells. Invest Ophthalmol Vis Sci. 1998;39:1590–9. PubMed PMID: 9699548.
129. Liversidge J, McKay D, Mullen G, Forrester JV. Retinal pigment epithelial cells modulate lymphocyte function at the blood-retina barrier by autocrine PGE2 and membrane-bound mechanisms. Cell Immunol. 1993;149:315–30. PubMed PMID: 8330312.
130. Kindzelskii AL, Elner VM, Elner SG, Yang D, Hughes BA, Petty HR. Toll-like receptor 4 (TLR4) of retinal pigment epithelial cells participates in transmembrane signaling in response to photoreceptor outer segments. J Gen Physiol. 2004;124:139–49. PubMed PMID: 15277575.
131. Oh H, Takagi H, Takagi C, Suzuma K, Otani A, Ishida K, Matsumura M, Ogura Y, Honda Y. The potential angiogenic role of macrophages in the formation of choroidal neovascular membranes. Invest Ophthalmol Vis Sci. 1999;40:1891–8. PubMed PMID: 10440240.
132. Thompson DA, Gal A. Vitamin A metabolism in the retinal pigment epithelium: genes, mutations, and diseases. Prog Retin Eye Res. 2003;22:683–703. PubMed PMID: 12892646.

Strauss O. The role of retinal pigment epithelium in visual functions. Ophthalmologe. 2009;106:299–304. PubMed PMID: 19343352.

Photoreceptors

Helga Kolb, PhD[1]

Created: May 1, 2005; Updated: February 28, 2012.

Two or three types of cone photoreceptor and a single type of rod photoreceptor are present in the normal mammalian retina. Some non-mammalian retinas have even more cone types (see later).

1. Light microscopy and ultrastructure of rods and cones

In vertical sections of retina prepared for light microscopy with the rods and cones nicely aligned, the rods and cones can be distinguished rather easily.

Cones are robust conical-shaped structures with cell bodies situated in a single row just below the outer limiting membrane (OLM) and with inner and outer segments protruding into the subretinal space towards the pigment epithelium (Fig. 1, Fig. 2). In foveal retina, where only cones are concentrated, their cell bodies are layered in oblique columns below the outer limiting membrane. Rods, on the other hand, are slim rod-shaped structures with their inner and outer segments filling the area between the larger cones in the subretinal space and stretching to the pigment epithelium cells. Rod cell bodies make up the remainder of the outer nuclear layer below the cone cell bodies. Apical processes from the pigment epithelium envelop the outer segments of both rods and cones (not always clear in histological sections).

The higher magnification afforded by the electron microscope allows better resolution of rod and cone photoreceptors.

Ultrathin sections viewed in an electron microscope (Fig. 2, Fig. 3) show rods and cones from human and squirrel retinas (1). The photoreceptor consists of 1) an outer segment, filled with stacks of membranes (like a stack of poker chips) containing the visual pigment molecules such as rhodopsins, 2) an inner segment containing mitochondria, ribosomes and membranes where opsin molecules are assembled and passed to be part of the outer segment discs, 3) a cell body containing the nucleus of the photoreceptor cell and 4) a synaptic terminal where neurotransmission to second order neurons occurs.

Outer and inner segments of rods (i.s.) are generally thinner than those of cones in mammalian retinas. For example, the rod inner segments are 2 μm and the cone inner segments are about 6 μm in diameter in peripheral human retina. In the fovea, however, where there are only cone photoreceptors, the most central cones are even thinner than the average rod at about 1.5 μm diameter. Inner segment regions of both rods and cones are filled with long thin mitochondria. At the top of the inner segment a thin cilium joins the inner and outer segments of the rods and cones (Fig. 3 and see movie 1).

2. Outer segment generation

It is from the base of the cilium that membrane evaginations and invaginations occur to produce the outer segment (o.s.) or the important visual pigment-bearing portion of the photoreceptor. Outer segments of both the rods and cones arises from outpouching (Fig. 4) of the photoreceptor cell plasma membrane at this point (see below) (2). An animation of outer segment generation appears in movie 2.

Author Affiliation: 1 Moran Eye Institute, University of Utah School of Medicine, Salt Lake City; Email: Helga.kolb@hsc.utah.edu.

Corresponding author.

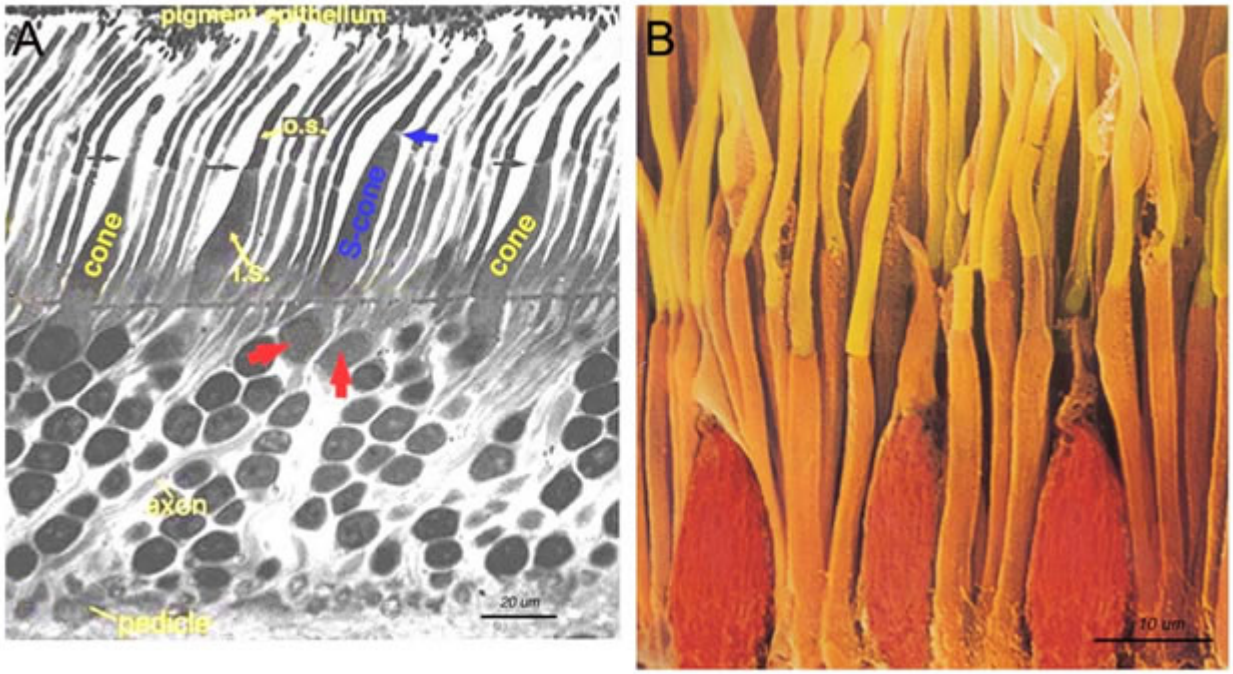

Figure 1. Primate rods and cones. *A*. Semi-thin section of human outer retina to show the rods and cones. Short-wavelength S-cones (blue cones) are commonly found occurring next to a neighboring longer-wavelength cone (red arrows). *B*. Scanning electron micrograph of the rods and cones of the primate retina. The image is adapted from one by Ralph C. Eagle of Photo Researchers, Inc.

These expanding membrane plates (Fig. 5) become detached as free floating discs inside the outer segment membrane in the case of the rods. In the case of the cones though, the outer segment discs remain attached to the outer segment membrane.

So the outer segment is a structure filled entirely with discs of folded double membranes in which are embedded the light sensitive visual pigment molecules (Fig. 6).

The opsin molecule, which binds the chromophore 11-cis retinal to form the visual pigment, is manufactured in the Golgi apparatus of the inner segment and presented to the outer membrane at the cilium, via fusion areas using G-proteins (3, 4).

In contrast, the other part of the visual pigment molecule in the outer segment discs which is retinal (vitamin A product), is provided to the discs from the pigment epithelium via carrier molecules (retinal binding proteins, IRBP) within the interphotoreceptor matrix of the subretinal space (Fig. 7) (5, 6). This is further covered in the chapter The Retinal Pigment Epithelium by Olaf Strauss.

3. Visual pigments and visual transduction

Vertebrate photoreceptors can respond to light by virtue of their containing a visual pigment embedded in the bilipid membranous discs that make up the outer segment. The visual pigment consists of a protein called opsin and a chromophore derived from vitamin A known as retinal. The vitamin A is manufactured from beta-carotene in the food we eat, and the protein is manufactured in the photoreceptor cell (see above). The opsin and the chromophore are bound together and lie buried in the membranes of the outer segment discs (Fig. 8).

About 50% of the opsin is within the bilipid membrane connected by short protein loops outside. Each molecule of rhodopsin consists of seven of these transmembrane portions surrounding the chromophore (11-cis retinal) in the lipid bilayer (Fig. 9). The chromophore apparently lies horizontally in the membrane and is bound at a lysine residue to helix seven (7, 8) (Fig. 9). Each outer segment disc, of course, contains many thousands of visual

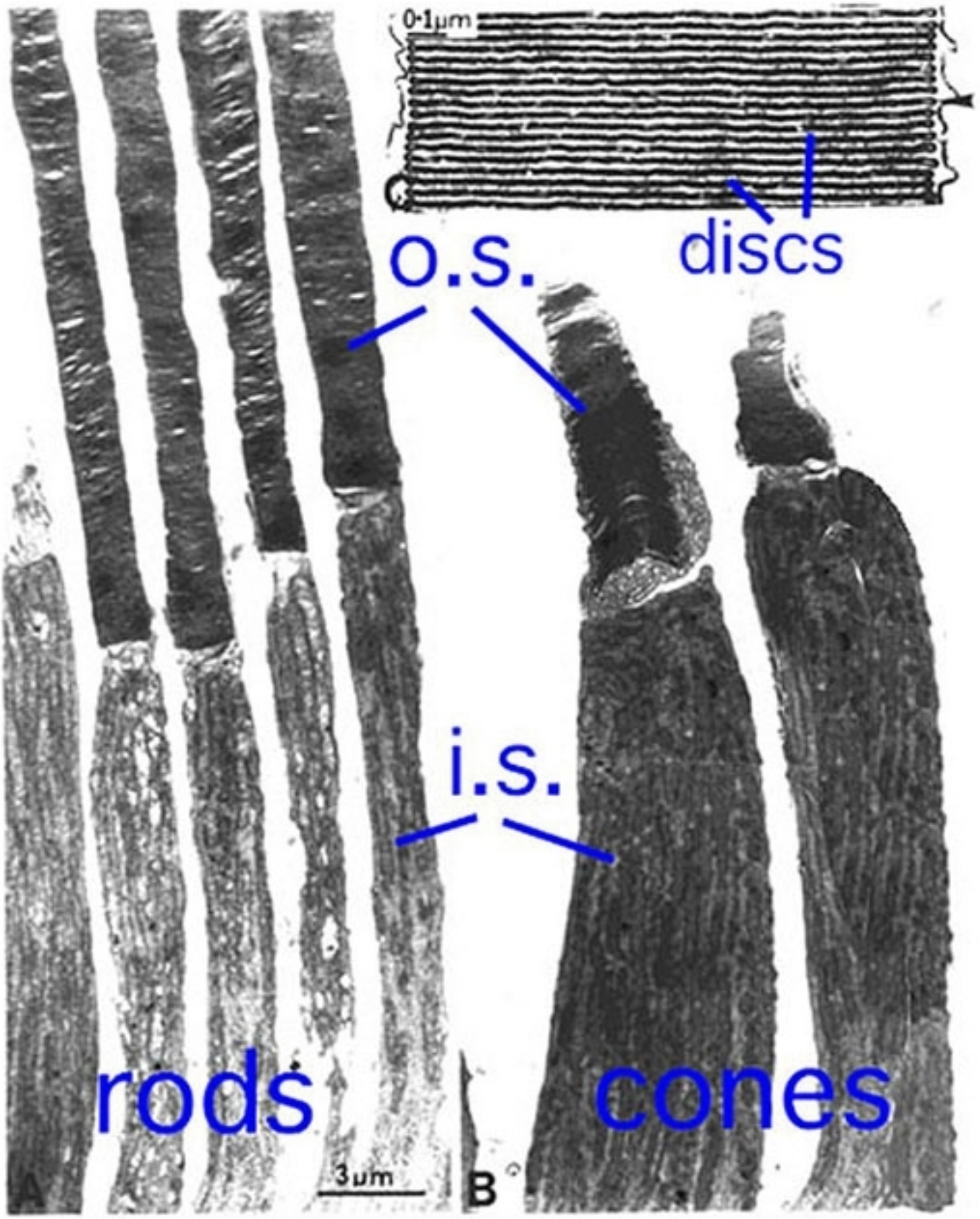

Figure 2. Low magnification EM image of monkey rods and cones with an enlargement of the outer segment discs.

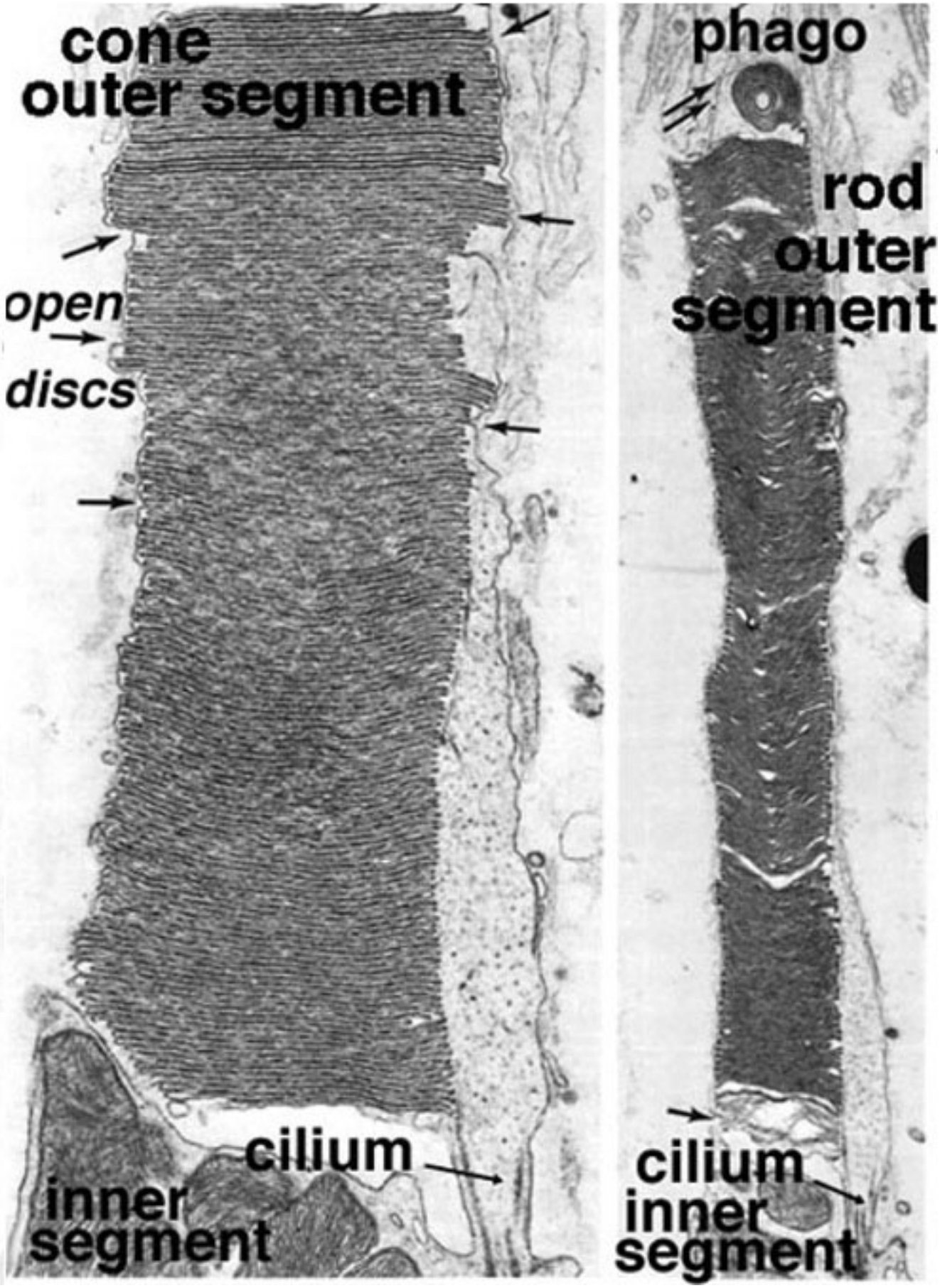

Figure 3. High magnification EM images of cone and rod outer segments in the ground squirrel retina. Phago, phagosome. The illustration is from Anderson and Fisher, 1976 (1).

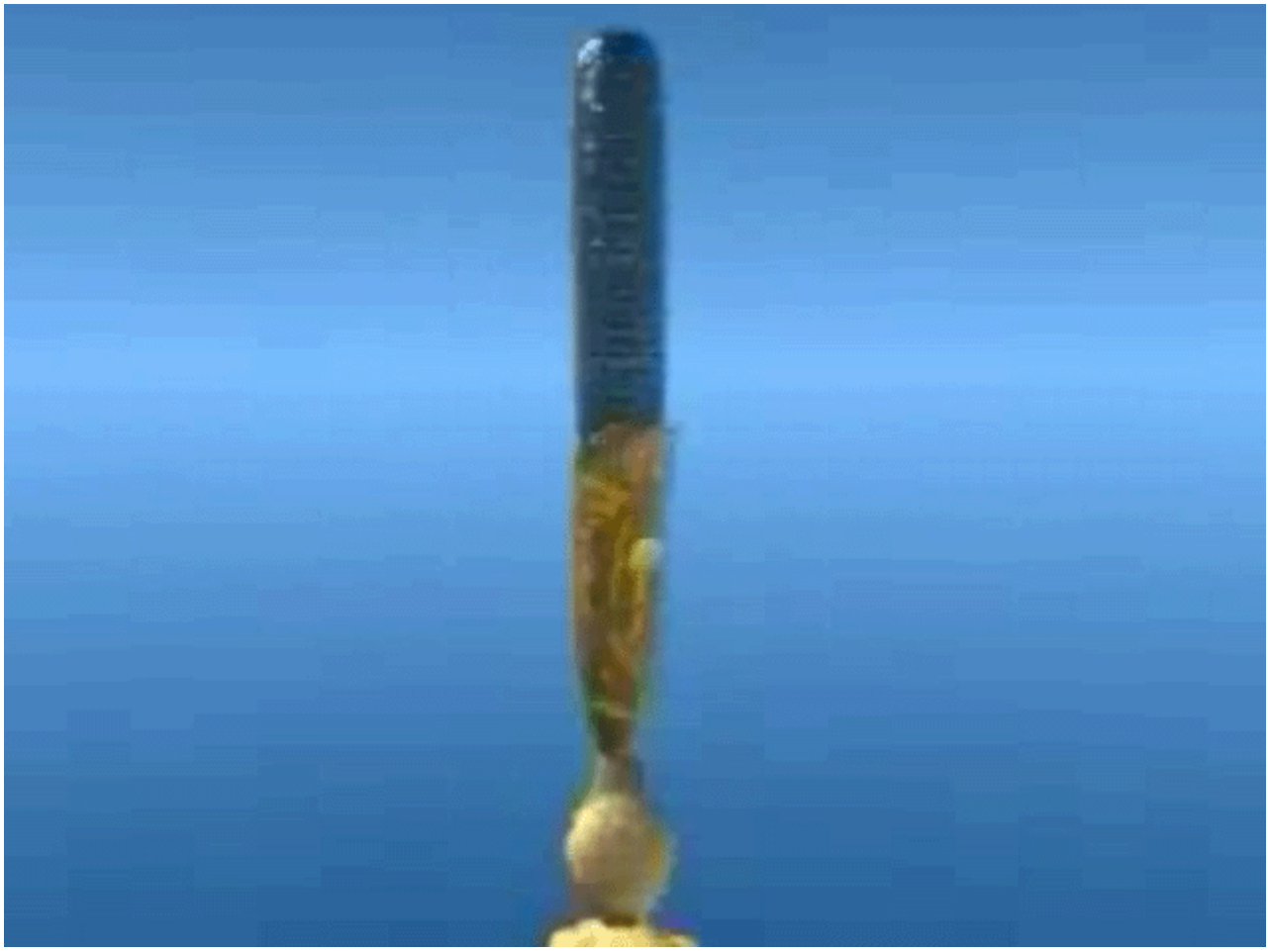

Movie 1. A photoreceptor with emphasis on the inner and outer segments and the disc structures within the outer segment. Movie made by Carlos Rozas (Canal Web, Chile).

Download video

pigment molecules. Upon absorption of a photon of light, the retinal isomerizes from the 11-cis form to the all-trans form which starts conformational changes in the molecule resulting in bleaching. Several intermediaries are formed in bleaching among them metarhodopsin II which activates the G-protein transducin and a further cascade of events summarized below (7, 9) and in the Webvision chapter Phototransduction in Rods and Cones by Yingbin Fu.

Light transduces the visual pigment via the following enzyme cascade: photons - rhodopsin - activated rhodopsin (metarhodopsin II) - a GTP binding protein (transducin) - an enzyme hydrolyzing cGMP (cGMP-phosphodiesterase) - closes a membrane bound cGMP-gated cation channel. The Webvision chapter on Phototransduction explains the details of this process.

In the dark, steady current flows into the open channels, carried mainly by Na^+ ions, constituting a "dark current" that partially depolarizes the photoreceptor cell (Fig. 10). Thus, the depolarized photoreceptor releases neurotransmitter (the amino acid glutamate) from its synaptic terminals onto second-order neurons in the dark. On light stimulation the rhodopsin molecules are isomerized to the active form, the above cascade ensues, leading to closure of the cation channels of the photoreceptor membrane, stopping the dark current and causing the photoreceptor cell membrane to hyperpolarize and cease neurotransmitter release to second-order neurons (Fig. 10) (10-13).

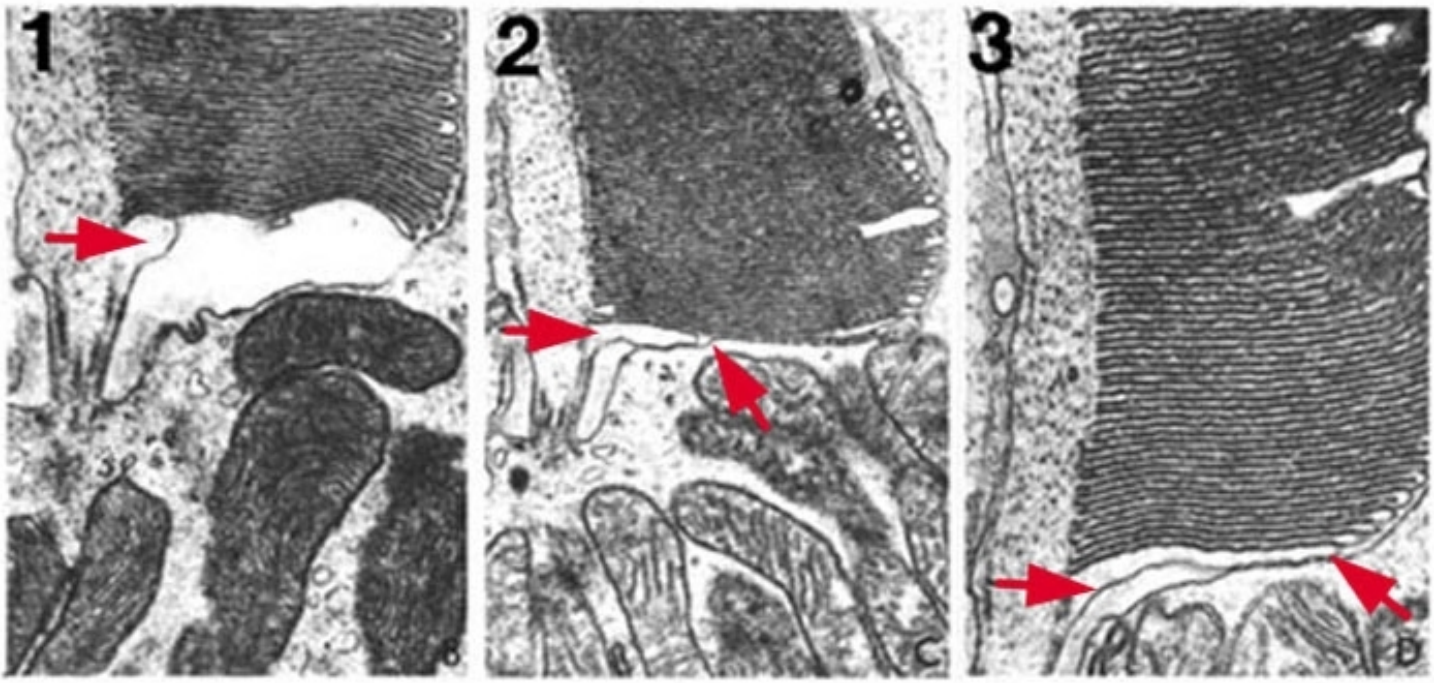

Figure 4. Photoreceptor outer segments are generated at the cilium (red arrows). The illustration is adapted from Steinberg, Fisher and Anderson, 1980 (2).

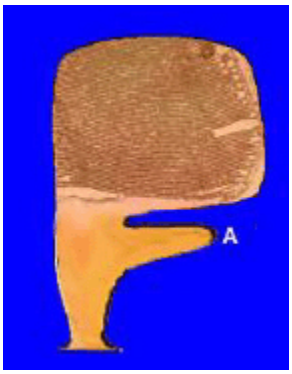

Movie 2. An animation of the outer segment generation.

Download video

The "dark current" is composed mainly of the influx of the Na^+ component (80%) however, a Ca^{2+} component (15%) and a Mg^{2+} component (5%) are also present (13). In darkness there must be a mechanism to remove Ca^{2+} as well as the excess Na^+, and it is thought to be done so through a sodium/calcium exchanger in the membranes of the outer segment of the photoreceptor. Ca^{2+}, once thought to be the second messenger in linking the rhodopsin photoisomerization to the membrane events is now known to have a secondary but important regulatory role in phototransduction. Although it does not directly participate in the transduction cascade it does improve the signaling capability of the rods in speeding the recovery after illumination and down regulating of the rods sensitivity in steady illumination (13). The latter effect is a mechanism for light adaptation. For it must be remembered that a photoreceptor cell does not simply detect light. It can also adapt to environmental light. For example cone photoreceptors can adapt so that our visual system can see from the dim shadows under a tree to objects in bright sunlight snow, a shift of light intensity of 7-9 log units of light intensity (14). Rod photoreceptors, thought at one time not to light adapt, are now known to adapt over a range of 2 log

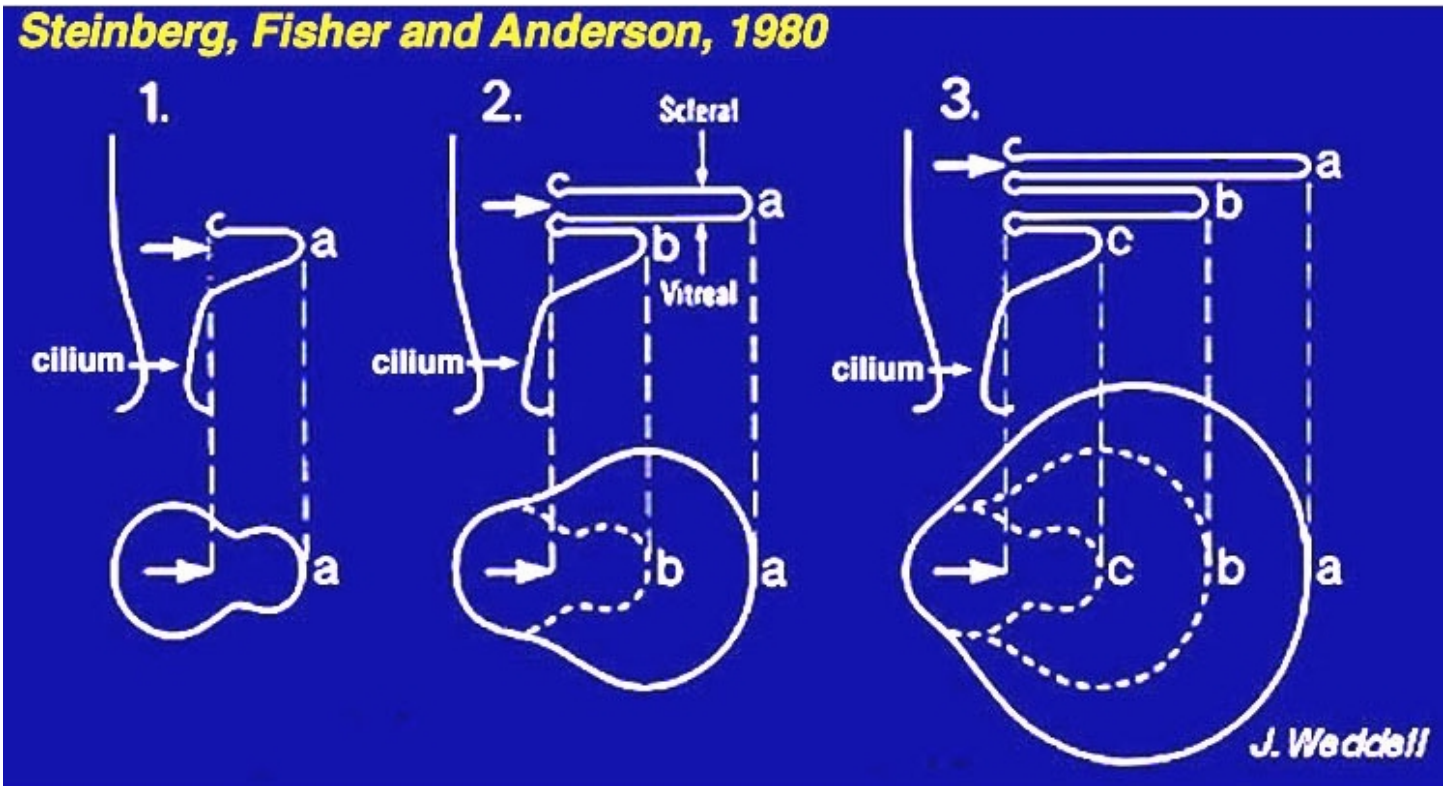

Figure 5. Diagram of outer segment generation. The schema is from Steinberg, Fisher and Anderson, 1980 (2).

units of background intensity and combined with a network adaptation through the whole visual system, allows as much as 5 log units of background intensity adaptation in rod driven vision (13). An animation of phototransduction appears in movie 3.

4. Phagocytosis of outer segments by pigment epithelium

The stacks of discs containing visual pigment molecules in the outer segments of the photoreceptors are constantly renewed. New discs are added at the base of the outer segment at the cilium as discussed above. At the same time old discs are displaced up the outer segment and are pinched off at the tips and engulfed by the apical processes of the pigment epithelium (Fig. 11, Fig. 12). These discarded, spent discs become known as phagosomes in the pigment epithelial cells. They are then broken down by lysis. Photoreceptor outer segment discs are phagocytosed by the pigment epithelium in a diurnal cycle. There is a burst of disc shedding at light on in the morning, judged by increased numbers of phagosomes in the pigment epithelium shortly thereafter (15). An animation of phototransduction appears in movie 4.

Cone outer segments differ from rod outer segments in several respects. Firstly, they are shorter and more conical with a wider base and tapering shape compared with those of rods. Secondly, as mentioned above, their discs are connected to the plasma membrane throughout the extent of the outer segment, and thus they are open to extracellular space. Apical processes of the pigment epithelium phagocytize chunks of cone outer segments, just as they do the rod outer segments, but at a different time in the diurnal cycle compared with rods i.e. at light off-set compared light-onset (15-19).

5. Different types of cone photoreceptor

As we have seen from the morphological appearances described above, two basic types of photoreceptor, rods and cones, exist in the vertebrate retina (Fig. 13). The rods are photoreceptors that contain the visual pigment -

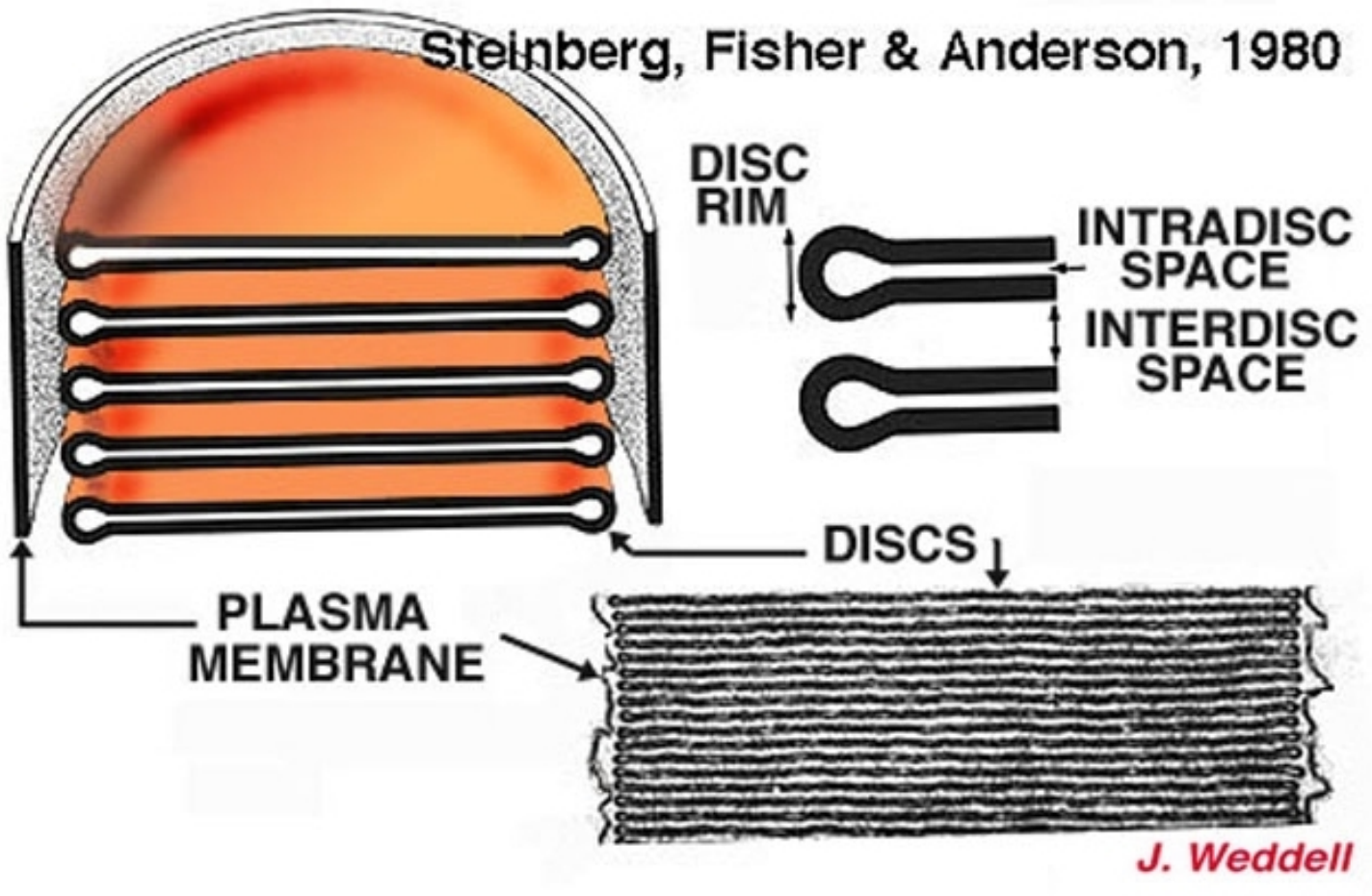

Figure 6. Drawing and micrograph of rod outer segment discs. The illustration is from Steinberg, Fisher, and Anderson, 1980 (2).

rhodopsin and are sensitive to blue-green light with a peak sensitivity around 500 nm wavelength. Rods are highly sensitive photoreceptors and are used for vision under dark-dim conditions at night. Cones contain cone opsins as their visual pigments and, depending on the exact structure of the opsin molecule, are maximally sensitive to either long wavelengths of light (red light), medium wavelengths of light (green light) or short wavelengths of light (blue light). Cones of different wavelength sensitivity and the consequent pathways of connectivity to the brain are, of course, the basis of color perception in our visual image.

Three different cone mechanisms can be detected in behavioral, psychophysical and physiological testing (Fig. 14A). These mechanisms are the basis of so called trichromatic vision which most humans have. Where only one or two visual pigment bearing types of cone are present the vision is said to be monochromatic or dichromatic.

Most mammalian species are dichromatic containing as well as rods only middle and short wavelength sensitive cones in their retinas. Primates and humans, birds, reptiles and fish are trichromatic, tetrachromatic and some even pentachromatic (within the latter three vertebrate phyla).

Thus long, medium and short wavelength cones have been demonstrated to exist in human retina by photometric, psychophysical and molecular biological methods: L-cones (red) are known to be maximally sensitive to wavelengths peaking at 564nm, M-cones (green) at 533nm and S-cones (blue) at 437nm respectively (Fig14A) (20).

Normal human color vision depends on the three cone mechanisms. This adds an additional dimension to color vision over those of dichromatic mammals, creating reds and greens rather than just long wavelength (red) and

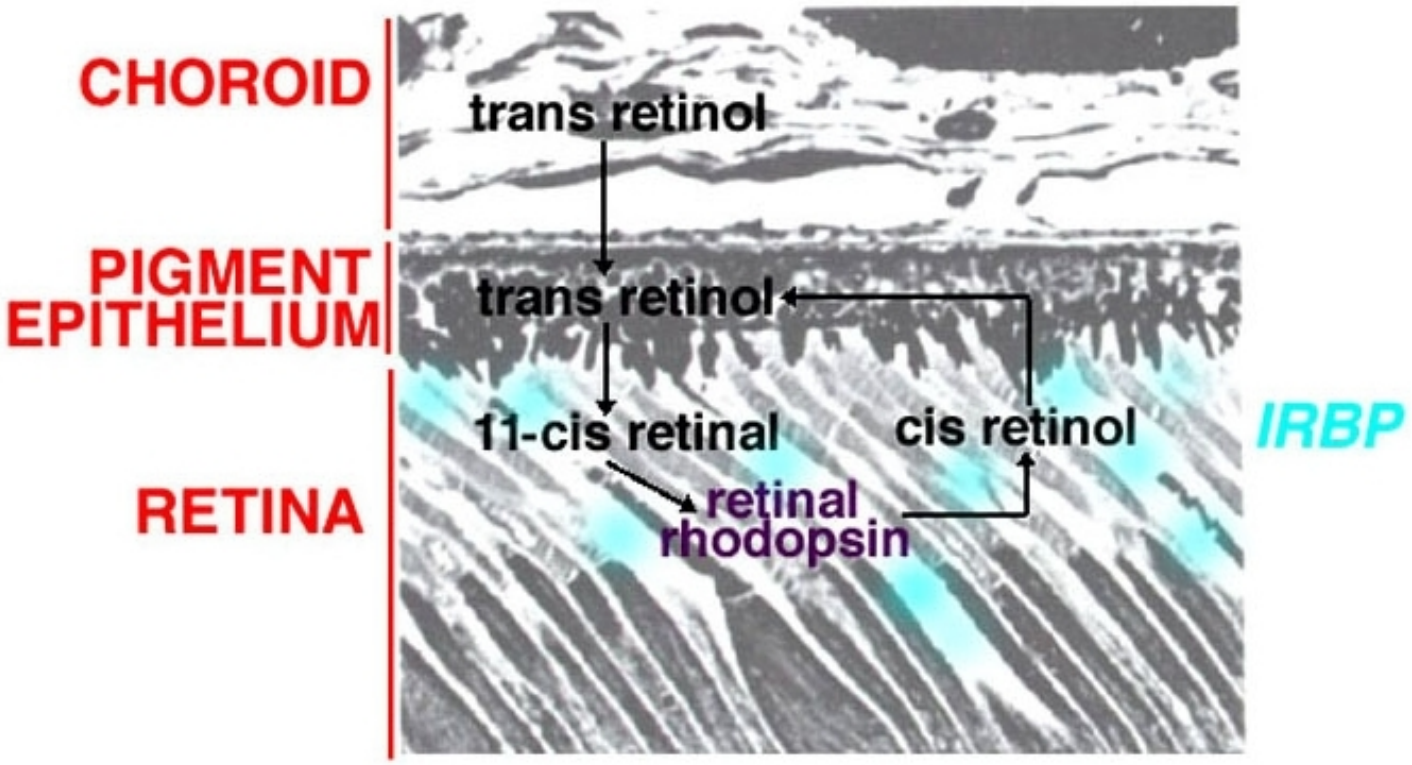

Figure 7. The location of interphotoreceptor retinal binding proteins (6) lies between the pigment epithelium and the photoreceptor outer segments. This region is know as the interphotoreceptor matrix..

short wavelength (blue). To do, this nature splits the long-wave system into two similar systems with slightly different spectral sensitivities with relatively similar opsins (Fig. 14B). One cone opsin is most sensitive to yellow-green and the other to yellow-red. This splits the brightest and yellow part of the visible spectrum into two color bands, one green and the other red. This red-green system works in parallel with that for blue-yellow.

Figure 14B shows the subtle difference in the molecular structure of the red and green cone photopigments compared with either the blue-cone pigment or the rhodopsin rod pigment (21).

To understand color vision and how the colored visual message is processed in the retina we need to be able to start with a morphological distinction of the three (or more) cone types, so they can then, hopefully be identified with any color specific connections they make, i.e. connections to bipolar, horizontal cell and finally ganglion cells of the retina. Fortunately, certain vertebrate species have distinctly different morphological cone types in their retinas and it has recently become possible to correlate these morphologies with spectral sensitivity. Now we can distinguish short, medium and long wavelength cones in retinas of some fish, frogs, birds, and reptiles (turtles) based on distinct morphological differences. Turtle retinas for example have colored oil droplets in their different spectral types of cone which identify them rather readily (Fig. 15, Fig. 16) (22, 23).

However, primate and human retinas still contain cone types which look essentially the same morphologically, but here too with anatomical techniques we are beginning to be able to see at least a difference between the short wavelength cone and the two longer wavelength cones. Specialized histochemical techniques (24), dye uptake studies (25) or use of antibodies specific for visual pigments (26) have allowed identification of the different spectral types of cone in most mammalian species now. In primate retina antibodies against visual pigments stain outer segments of the L/M-cones together or the S-cones only.

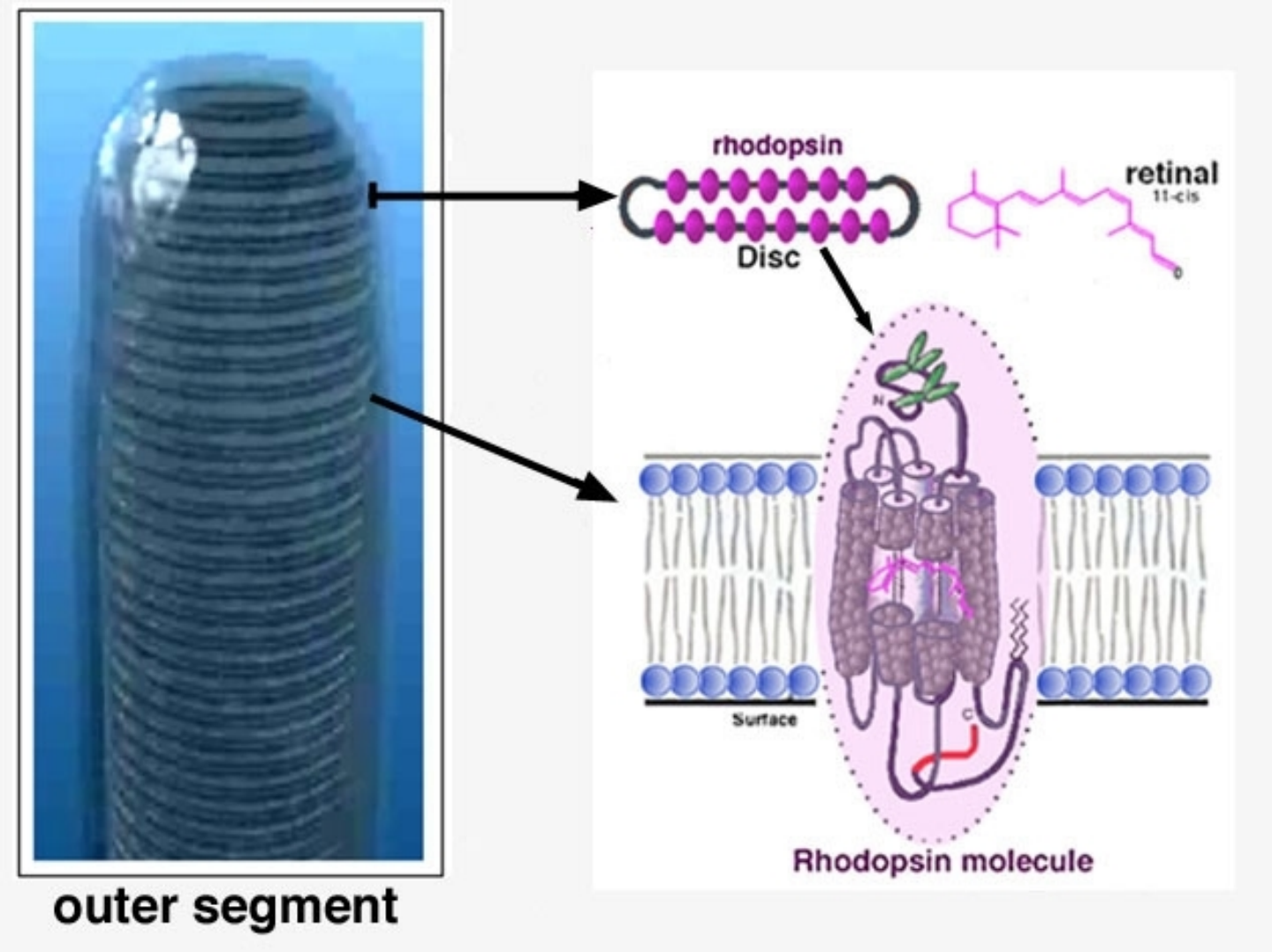

Figure 8. Schematic diagram of rhodopsin in the outer segment discs.

In Figure 17, in anti-visual pigment antibody stained tissue, the S-cones stand out as the cones that are not stained because the antibody recognizes only L- and M-cone visual pigment. i.e. the brown stained cone profiles are L- and M-cone types while the unstained profiles surrounded by blue circles are the S-cones (27).

6. Morphology of the blue or S-cones

Careful morphological studies have enabled us to distinguish the short wavelength specific (blue) cone from the medium and long wavelength specific cones in the human retina even without special antibody staining techniques (28).

Thus, we now know that S-cones have longer inner segments that project further into subretinal space than do the longer wavelength cones (Fig 18). S-cone inner segment diameters do not vary much across the entire retina, thus they are fatter in the foveal area but thinner in the peripheral retina than longer wavelength cones. These S-cones also have smaller and morphologically different pedicles than the other two wavelength cones (29). Furthermore, throughout the retina, the S-cones have a different distribution and do not fit into the regular hexagonal mosaic of cones typical of the other two types.

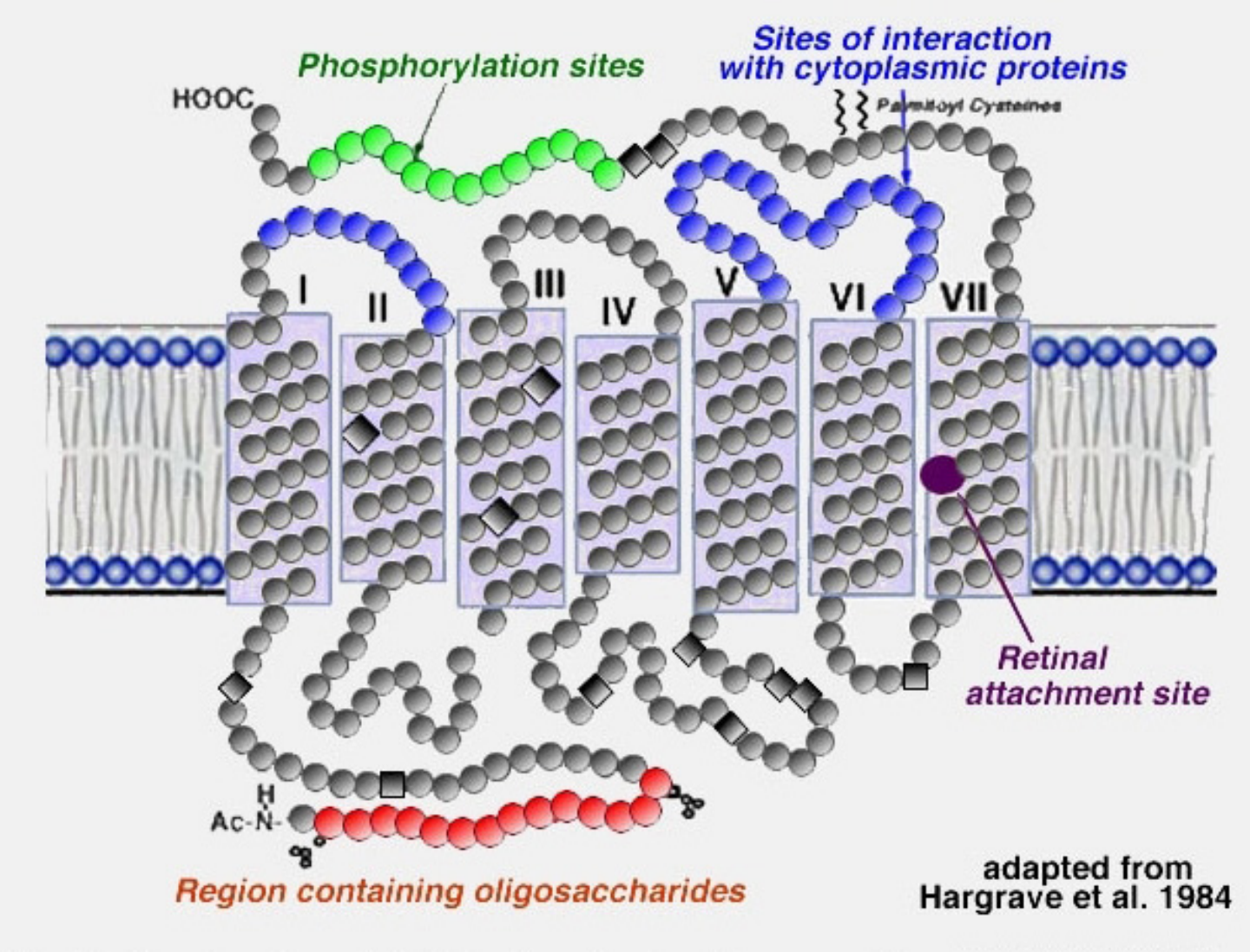

Figure 9. Structural model of rhodopsin showing seven transmembrane domains and the attachment site for retinal. The figure is adapted from Hargrave et al, 1984 (8)

This is illustrated in the tangential section of the foveal cone mosaic (Fig. 19) where the hexagonal packing is distorted in many places by a larger-diameter cone (arrowed cones) breaking up the perfect mosaic into irregular subunits. The larger-diameter cones are S-cones. These cones have their lowest density in the foveal pit at 3-5% of the cones, reach a maximum density of 15% on the foveal slope (1 degree from the foveal pit) and then form an even 8% of the total population elsewhere in the retina (28).

Analogous information concerning relative distributions of the M- and L-cones in the human retina is not easily available because we cannot tell them apart by morphological features or even by anti-visual pigment staining. In the monkey retina, Marc and Sperling (24), performed a colored light-dependent histochemical staining technique on freshly excised monkey eyes. They found that L-cones (red) occur as about 33% of the cones throughout the retina, while M-cones (green) peak in the fovea at 64% and vary between 52% and 59% elsewhere in the retina. However, others have found the L-cones to outnumber the M-cones in fovea and perifoveal psychophysical testing paradigms (30). Laser interferometry techniques (31, 32), measuring the distribution of the red and green cones in the living human fovea, show there to be considerable variation amongst individuals. Some have an equal distribution of L- and M-cones, but others have a larger number of red cones even up to the ratio of 16 L-cones:1 M-cone. Both Roorda and Williams and Hofer et al's (31, 32) data in

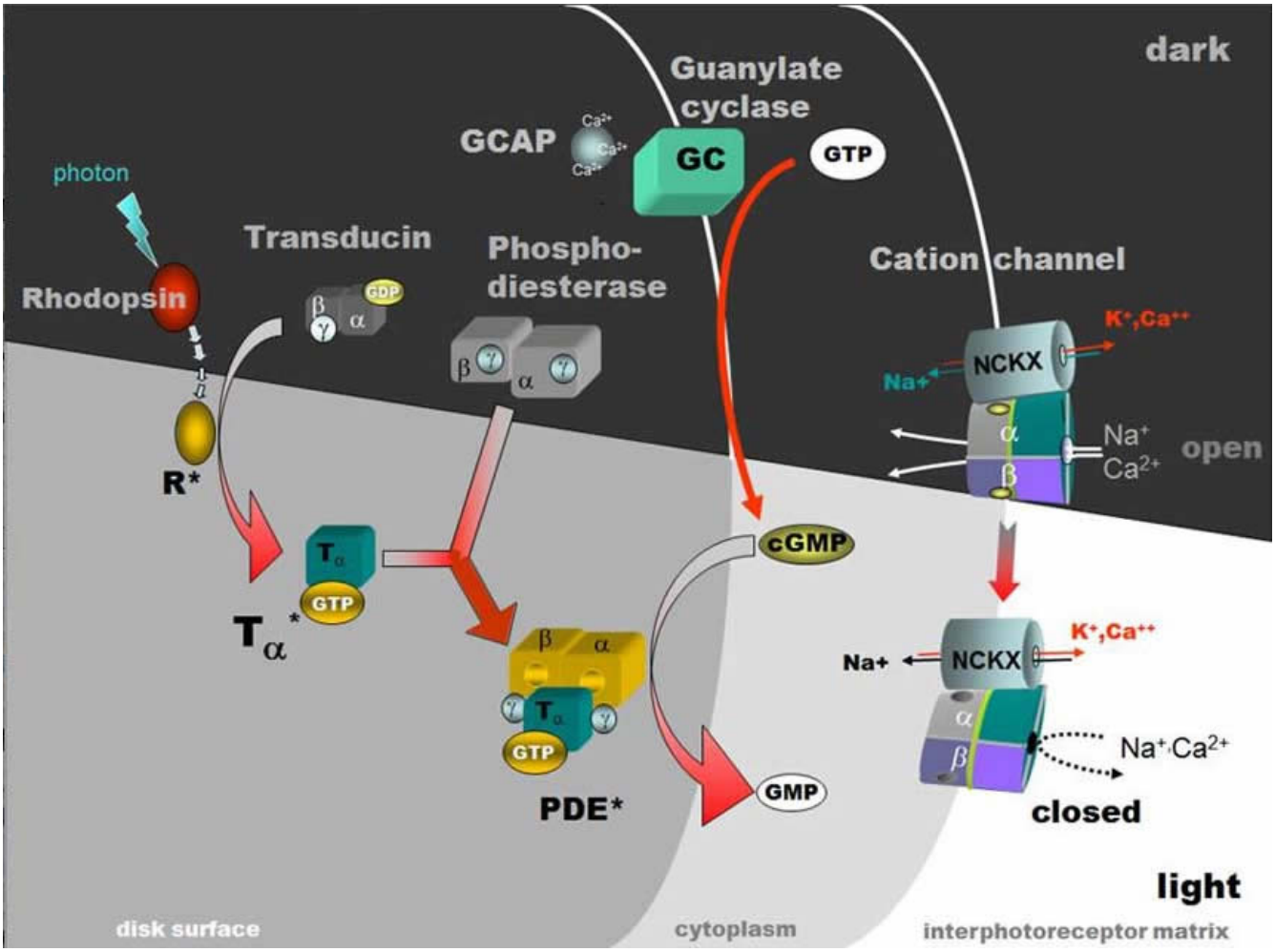

Figure 10. Activation of rhodopsin by light and the phototransduction cascade. Light transduces the visual pigment via the following enzyme cascade: photons – rhodopsin – activated rhodopsin (R^+) (metarhodopsin II) – a GTP binding protein ($T\alpha^*$) (transducin) – an enzyme hydrolyzing cGMP (cGMP-phosphodiesterase, PDE*) – closes membrane bound cGMP-gated cation channel (lower right). The illustration is courtesy of Wolfgang Baehr..

human and Mollon and Bowmaker (33) in monkey fovea show an irregular and patchwork nature of the L- and M-cone distribution (see chapter on midget pathways, Figure 5).

7. Densities of rods and cones in the human retina

It is important for our understanding of the organization of the visual connections for us to know the spatial distribution of the different cell types in the retina. Photoreceptors, we know, are organized in a fairly exact mosaic. As we saw in the fovea, the mosaic is a hexagonal packing of cones. Outside the fovea, the rods break up the close hexagonal packing of the cones but still allow an organized architecture with cones rather evenly spaced surrounded by rings of rods. Thus in terms of densities of the different photoreceptor populations in the human retina, it is clear that the cone density is highest in the foveal pit and falls rapidly outside the fovea to a fairly even density into the peripheral retina (Fig. 20, Fig. 21) (34, 35). There is a peak of the rod photoreceptors in a ring around the fovea at about 4.5 mm or 18 degrees from the foveal pit. The optic nerve (blind spot) is of course photoreceptor free (see below).

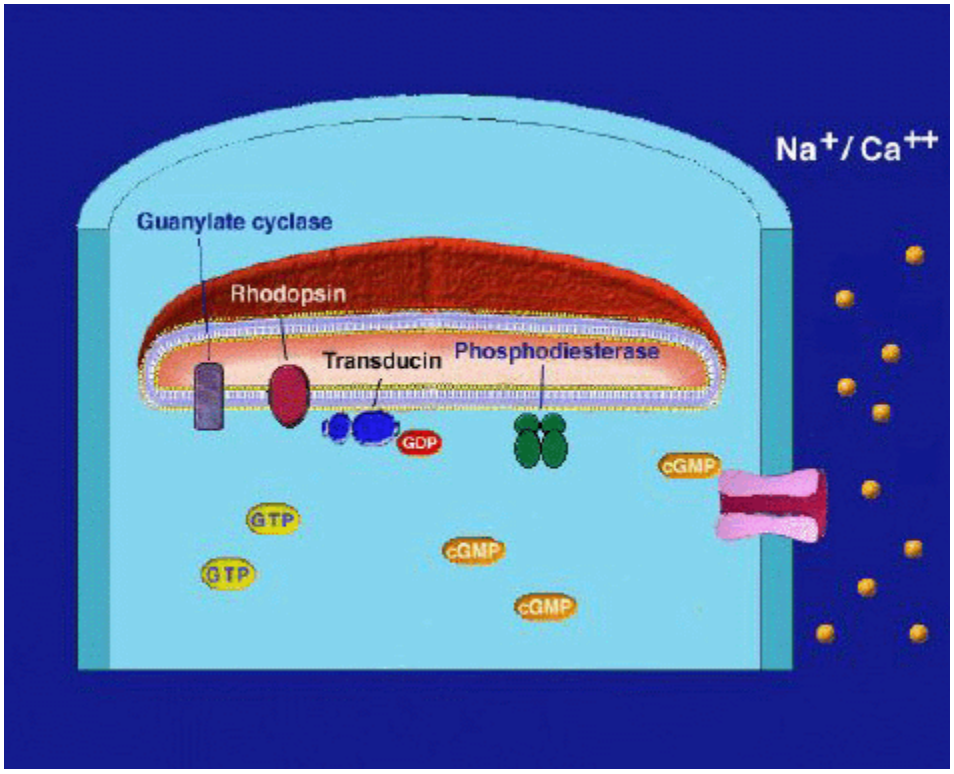

Movie 3. An animation of photo transduction.

Download video

8. Rods and Night Vision

Rods convey the ability to see at night, under conditions of very dim illumination. Animals with high densities of rods tend to be nocturnal, whereas those with mainly cones tend to be diurnal. The nature of dim light is important both to physicists and to biologists. In 1905 Einstein proposed that light propagated only in discrete irreducible packets or quanta (36). This explained the non-classical features of the 'photoelectric effect', a process by which light facilitates the release of electrons from metal surfaces, described by Heinrich Hertz in 1887 (37). Rods are so sensitive that they actually detect single quanta of light, much as do the most sensitive of physical instruments. In 1942 Selig Hecht argued that human rods must be capable of detecting individual light quanta because light flashes so dim that only 1 in 100 rods were likely to absorb a quantum were yet reliably seen by careful observers (38). A century after the original discovery of the photoelectric effect it has become possible to record directly the minute electrical voltages in rods induced by absorption of individual light quanta. An excellent example is shown in the suction electrode recordings of monkey rods by Schneeweis and Schnapf (39) (Fig. 22). Each dot in the figure below represents delivery of a very dim pulse of light containing only a few quanta. Voltage responses appear to come in 3 sizes: none, small, and large, representing the detection of 0, 1 or 2 quanta in each flash. The granularity of response to dim light stimuli is evident.

Rod sensitivity appears to be bought at a price, however, since rods are much slower to respond to light stimulation than cones. This is one reason why sporting events such as baseball become progressively more difficult as daylight fails. Both electrical recordings and human observations suggest that signals from rods may arrive as much as 1/10 second later than those from cones under lighting conditions where both can be simultaneously activated (40).

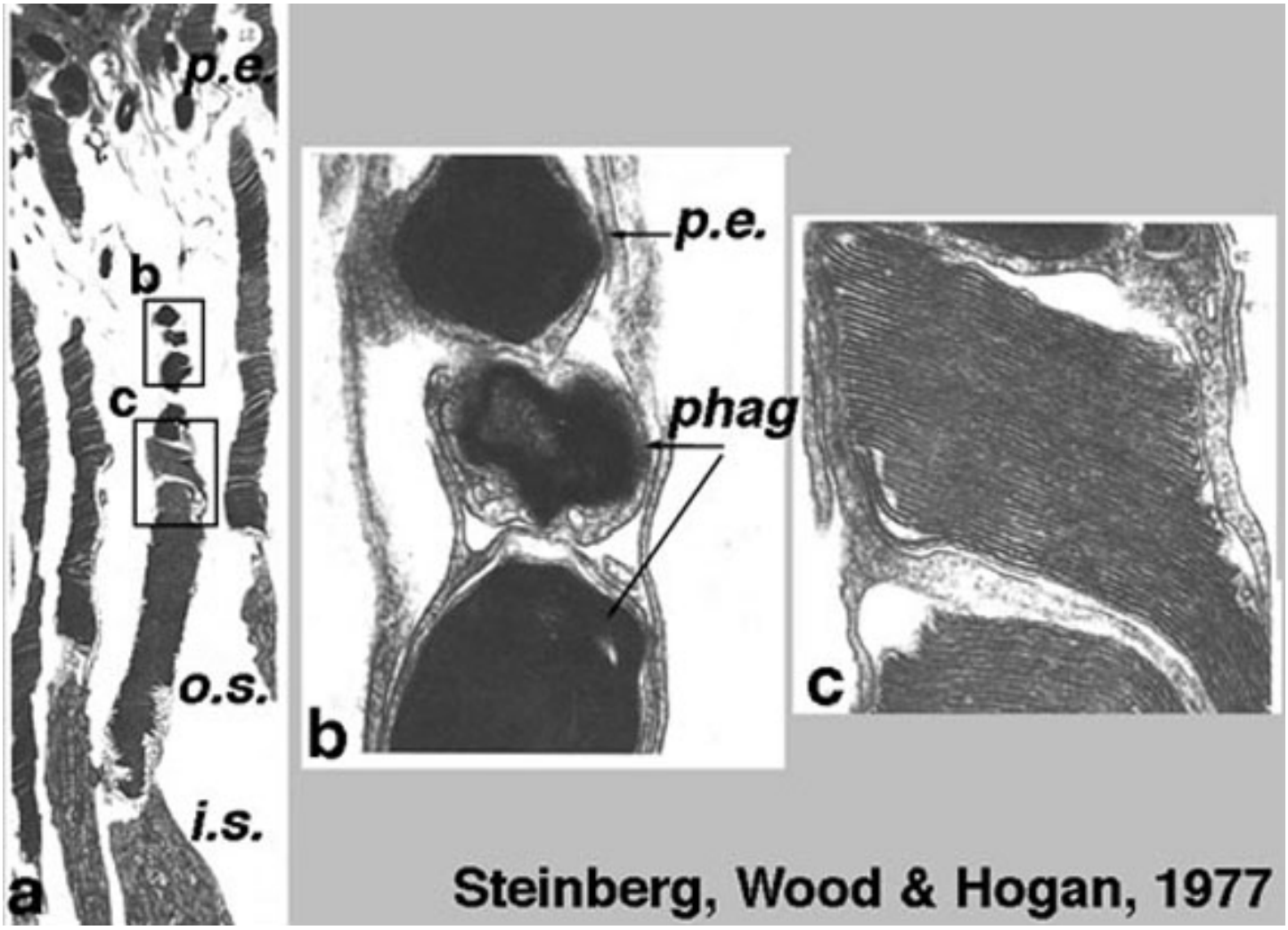

Figure 11. Section through an RPE cell to show stages of outer segment phagocytosis. p.e., pigment epithelium; phag, phagosome. The illustration is from Steinberg, Wood and Hogan, 1977 (18).

9. Ultrastructure of rod and cone synaptic endings

The job of the photoreceptor cell in the retina is to catch quanta of light in the visual pigment-containing membranes of the outer segment and pass a message, concerning numbers of quanta of light and sensitivities to the different wavelengths, to the next stage of integration and processing at the outer plexiform layer. The way in which quanta are transformed into electrical signals is developed in the Webvsion chapter on Phototransduction.

The information transmitting end of the cone cell is known as the pedicle and of the rod cell as the spherule. Cone pedicles are large, conical, flat end-feet (8-10 µm diameter) of the cone axon that lie more or less side by side on the same plane at the outer edge of the outer plexiform layer (OPL) (Fig. 23A, Fig. 23B). The more numerous rod spherules, in contrast, are small round enlargements of the axon (3-5 µm diameter) or even extensions of the cell body. They lie packed between and above the cone pedicles (Fig. 23A, Fig. 23B). The synaptic endings of both photoreceptor types are filled with synaptic vesicles. At their synapses to second-order neurons (bipolar and horizontal cells), both rod spherules and cone pedicles exhibit dense structures known as synaptic ribbons pointing to the postsynaptic invaginated processes (asterisks in Fig. 24). In the cone pedicle approximately 30 of these ribbons occur and are associated with 30 "triads" of invaginated processes (29). In the rod spherule 2 ribbons are associated with 4 invaginated second-order neurites while the cone pedicle delivers information to over a hundred second-order neurons (Fig. 23B).

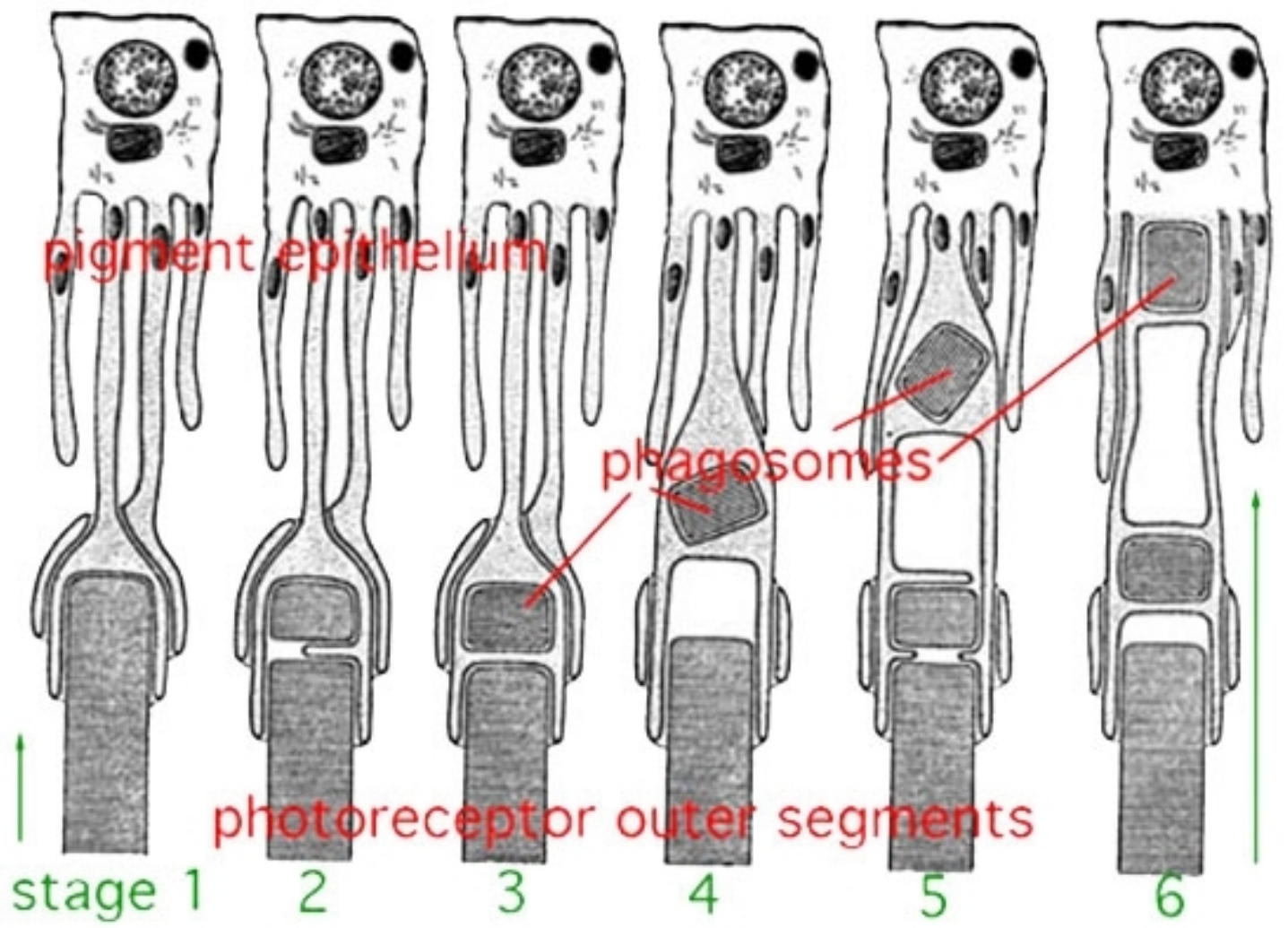

Figure 12. Diagrammatic representation of disc shedding and phagosome retrieval into the pigment epithelial cell.

The cone "triad" of invaginated second-order processes consists typically of a central element which is a dendritic terminal of an invaginating bipolar cell (IBC), and two lateral elements which are dendritic terminals of horizontal cells (HC) (Figs. 24, 25, and 27). In addition, other varieties of bipolar cell have dendrites making synaptic contacts on the under surface of the cone pedicle at what were first called flat contacts (FBC) (41-43) (Fig. 27), but then were better characterized and defined by Lasansky (44) as basal junctions (Fig. 26).

Rods spherules have only two synaptic ribbons associated with two lateral elements that are horizontal cell axon terminals (HC) and two central invaginating dendrites of rod bipolar cells (Fig. 28) (35) (41-43). There are no basal junctions on rod spherules.

10. Interphotoreceptor contacts at gap junctions

There also appears to be a pathway for crosstalk between cones and between cones and rods in the human retina. Cone pedicles have small projections from their sides or bases that pass to neighboring rod spherules and cone pedicles. Where these projections, called telodendria, meet they have a specialized junction known to be typical of electrical synaptic transmission. These are minute gap junctions (Fig. 29) (45, 46).

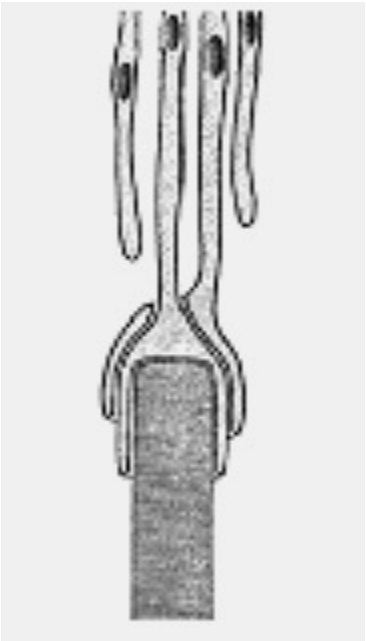

Movie 4. An animation of the phagocytosis.

Download video

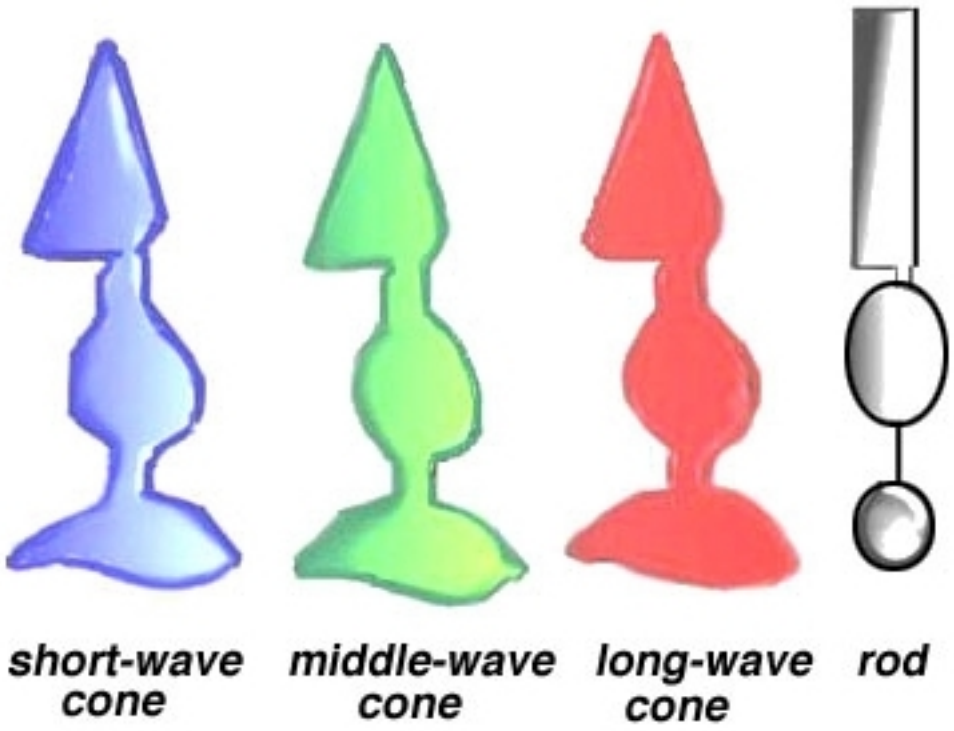

Figure 13. Photoreceptor types. There are four photoreceptor types in the human retina. Short-wavelength cones (blue), medium-wavelength cones (green), long-wavelength cones (red) and rods..

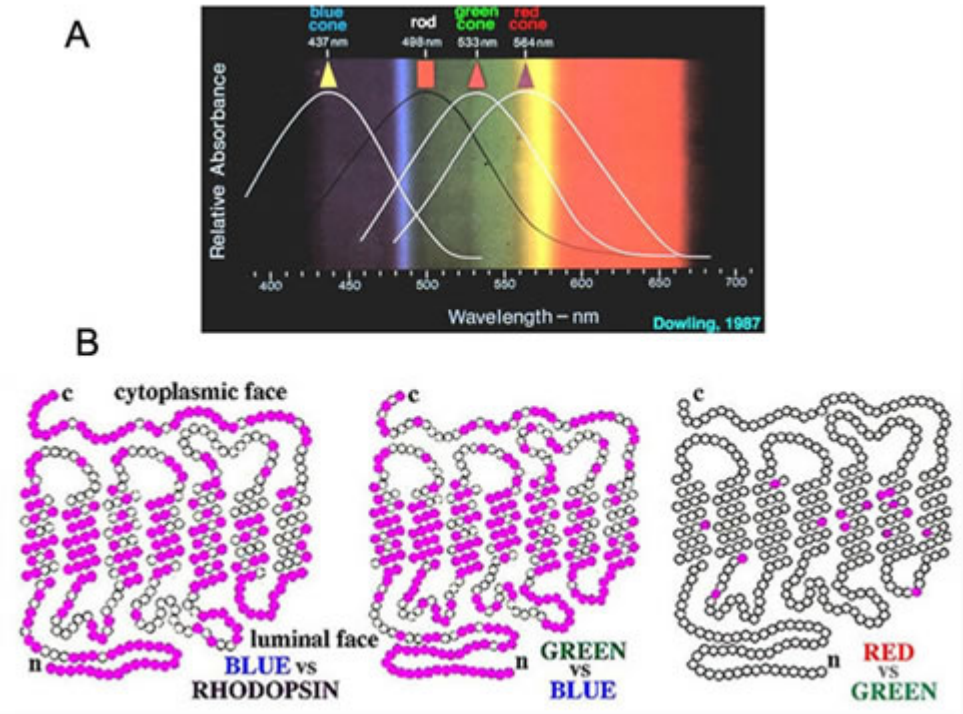

Figure 14. Opsin molecules: different spectra and different amino acid sequences. *A.* Light Spectra and visual pigment absorbance. The peak spectral sensitivities of the 3 cone types and the rods in the primate retina first published by Brown and Wald, 1963 (49). The illustration is from Dowling, 1987 (50). *B.* The closely related molecular structures of cone opsins. The blue-cone opsin compared with rhodopsin (left). The blue-cone opsin compared with the green-cone opsin (center). A comparison of red and green-cone opsins (right) reveals only minimal differences. The pink filled circles represent amino acid substitutions between compared opsins. The open circles indicate identical amino acids. The illustration is adapted from Nathans et al., 1986 (21).

As many as 3-5 gap junctions occur on a single rod spherule from neighboring cone telodendria, and a single cone pedicle can have as many as 10 contacts to neighboring rods. Pedicles of S-cones do not have as many telodendrial gap junctions with either neighboring rods or cones (29) and thus, this cone type remains relatively isolated in the cone mosaic, and, as we shall see later, remains isolated to the ganglion cell level too, due to connections with a specific 'S-cone bipolar cell'.

Direct interactions between different functional classes of photoreceptors were not anticipated based on any known or theoretical needs of the visual system. In fact such connections would appear to degrade spatial resolution, and, potentially, color perception by mixing signals from photoreceptors at different locations or with different photopigments. Nonetheless, in agreement with anatomical findings, mammalian cones appear to carry rod signals. The slow wave forms of rod signals are easily distinguished from the rapid wave forms of cone signals in voltage recordings from single cones. Examples of voltage responses from monkey cones are illustrated in Figure 30 (39). Voltage records resulting from red and green stimuli balanced to produce equal peak responses are illustrated.

Both records exhibit the same initial peak hyperpolarization in response to the brief stimulus, however the green stimulus (solid trace) also evokes a slower hyperpolarizing phase after the initial response which the red stimulus (dotted trace) does not (Fig. 30). This latter electrical wave has the characteristics of a rod signal. Such signals have also been observed in cat cones (47). One theory of the utility of this arrangement is that it allows rods to utilize neural pathways devoted to both cones and rods in sending visual information to the inner plexiform layer. Cone pathways may be tuned to faster temporal characteristics than rod pathways, and so by utilizing both pathways, rods may transmit a wider bandwidth of temporal information. There is evidence for two rod pathways with different dynamic signatures in perceptual experiments (48). Although the functional role of

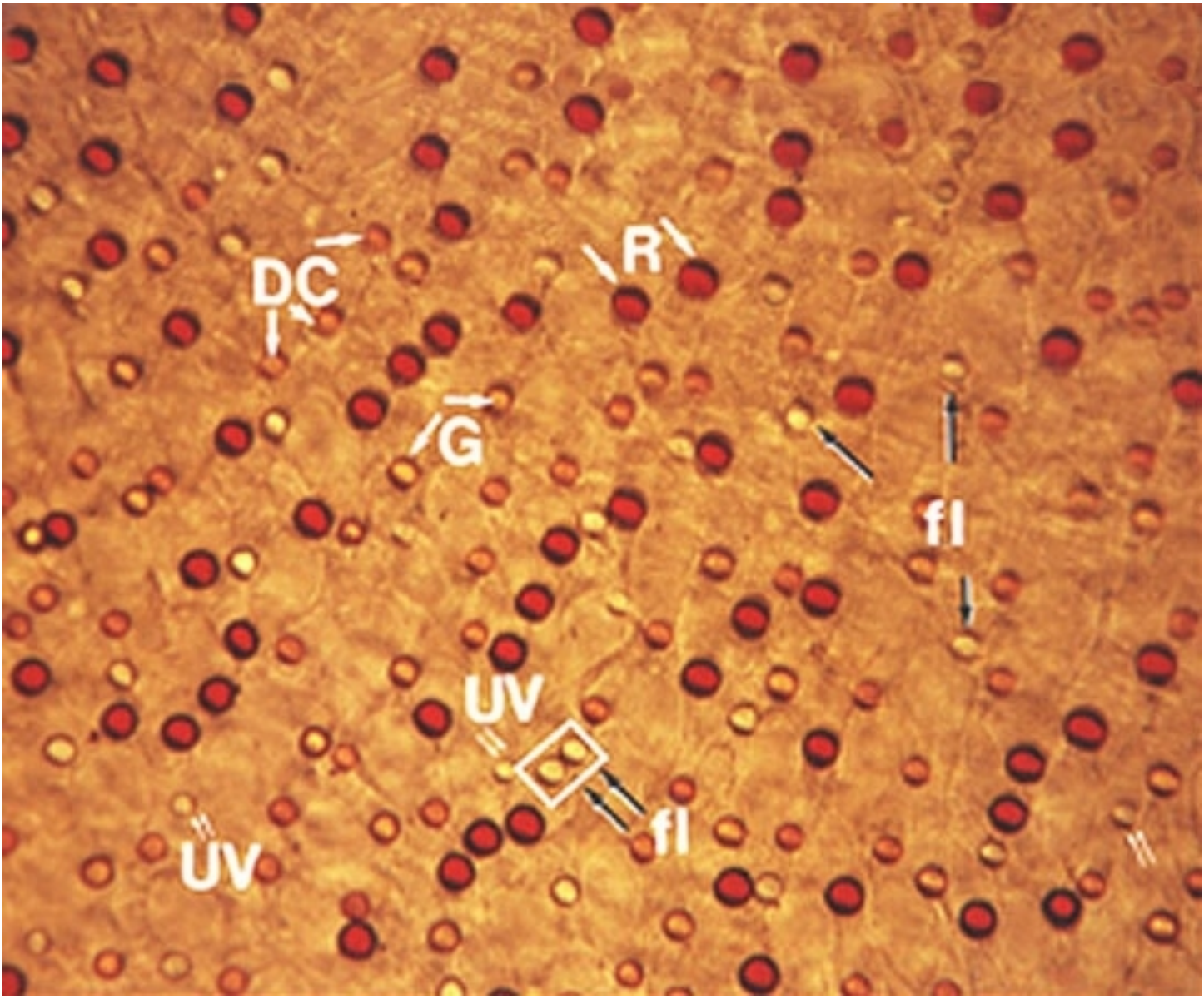

Figure 15. Turtle cone oil droplets. DC, double cone with orange oil droplet; B, green cone with yellow oil droplet; R, red cone with red oil droplet; fl, blue cone with a fluorescent oil droplet; UV, ultraviolet absorbing cone with a clear small oil droplet.

interreceptor junctions is still a matter of debate, they perhaps serve as a philosophical warning to studies of biological sensory systems: Not even the receptor cells themselves stand in isolation of the activity and influence of neighboring neurons.

About the Author

The biosketch for Helga Kolb appears in the Webvision section About the Editors.

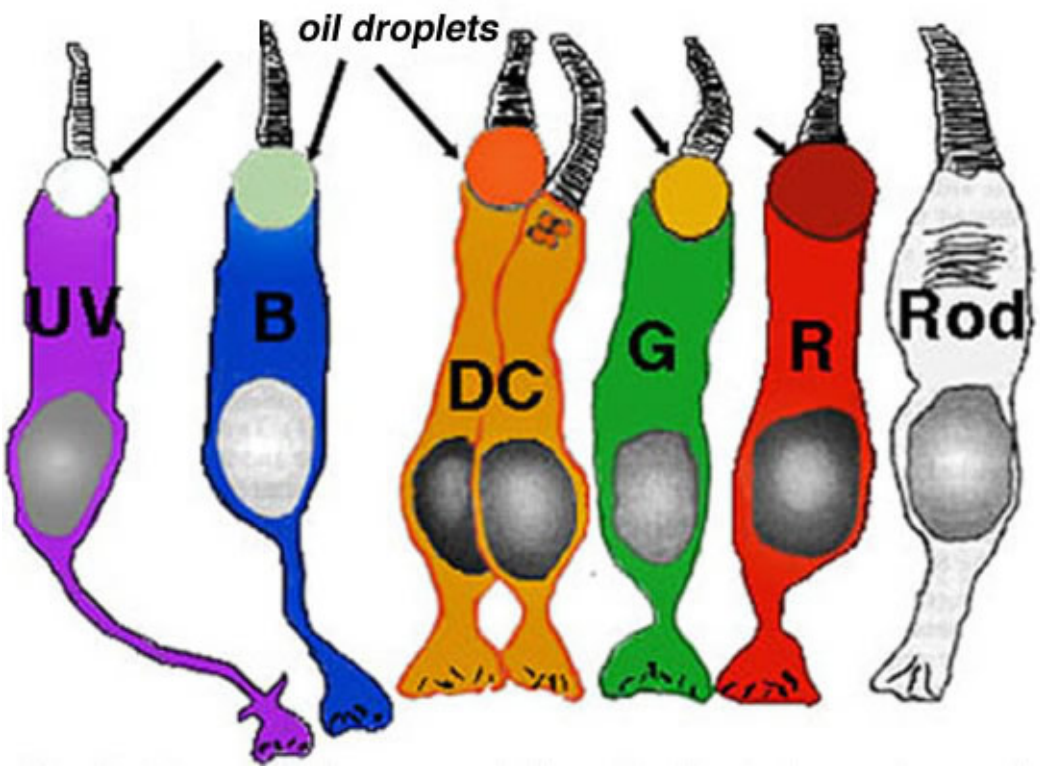

Figure 16. Diagramatic representation of turtle photoreceptors and their associated oil droplets. UV, UV cone; B, blue cone; DC, double cone; G, green cone; R, red cone; Rod, rod (no oil droplet).

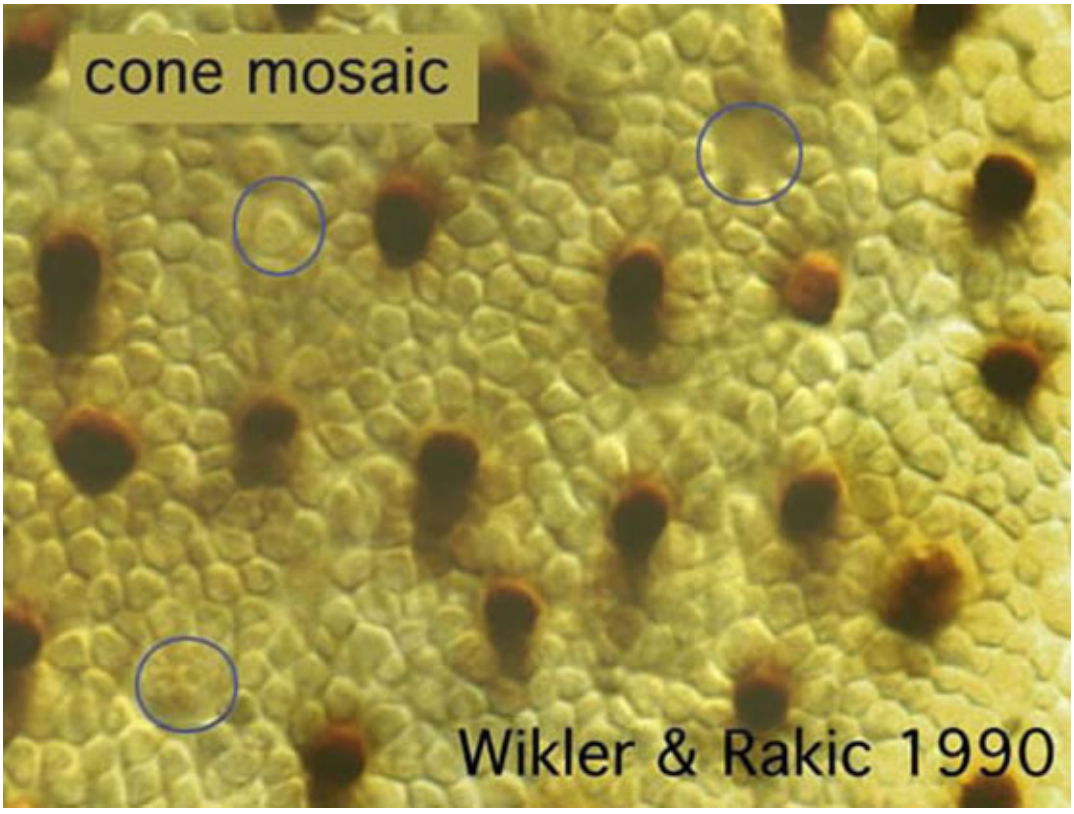

Figure 17. Primate cone mosaic as revealed by anti-cone opsin immunostaining. Cones that do not stain brown are blue cones (blue circles). The illustration is from Wikler and Rakic, 1990 (27).

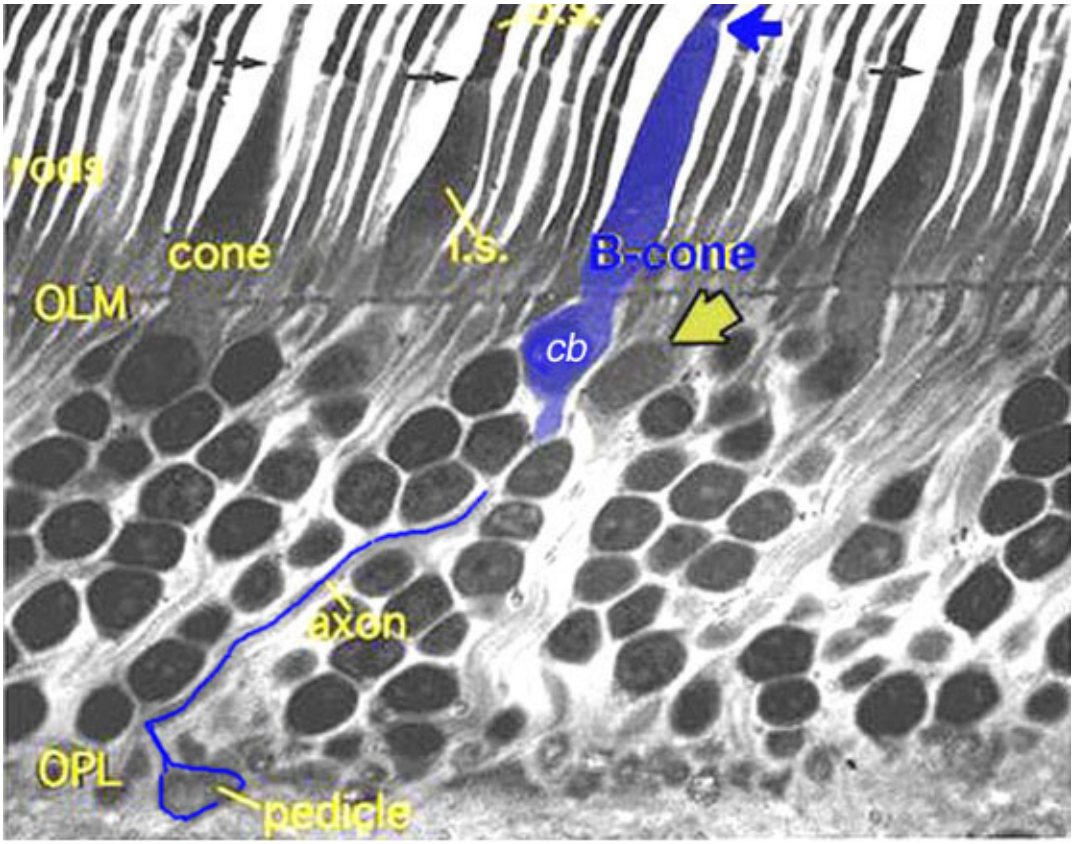

Figure 18. Vertical section of human retina to show the differences between L/M cones and S-cones (blue or B-cones). o.s., cone outer segments; i.s. cone inner segment; cb, cell body; OLM, outer limiting membrane; OPL, outer plexiform layer.

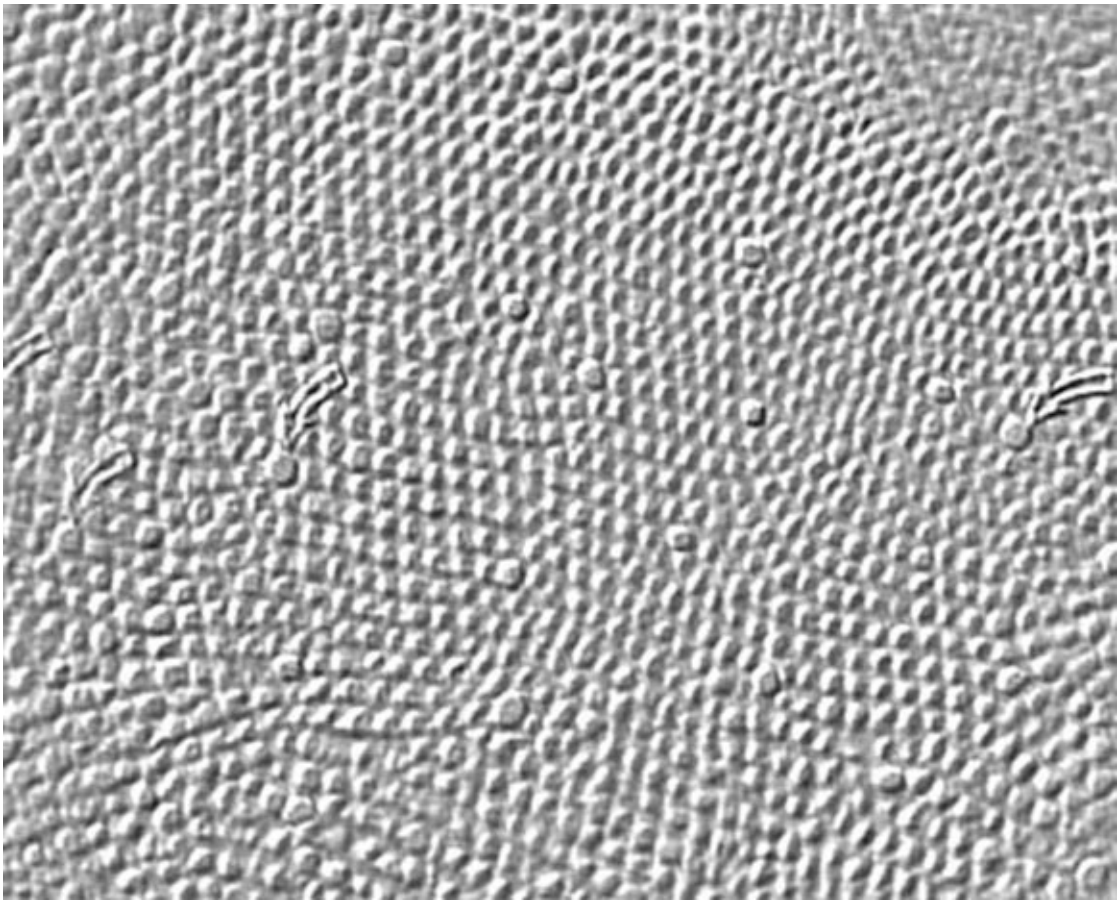

Figure 19. Tangential section through the human fovea. The larger cones (arrows) are blue cones. The figure is from Ahnelt, Kolb and Pflug, 1987 (28).

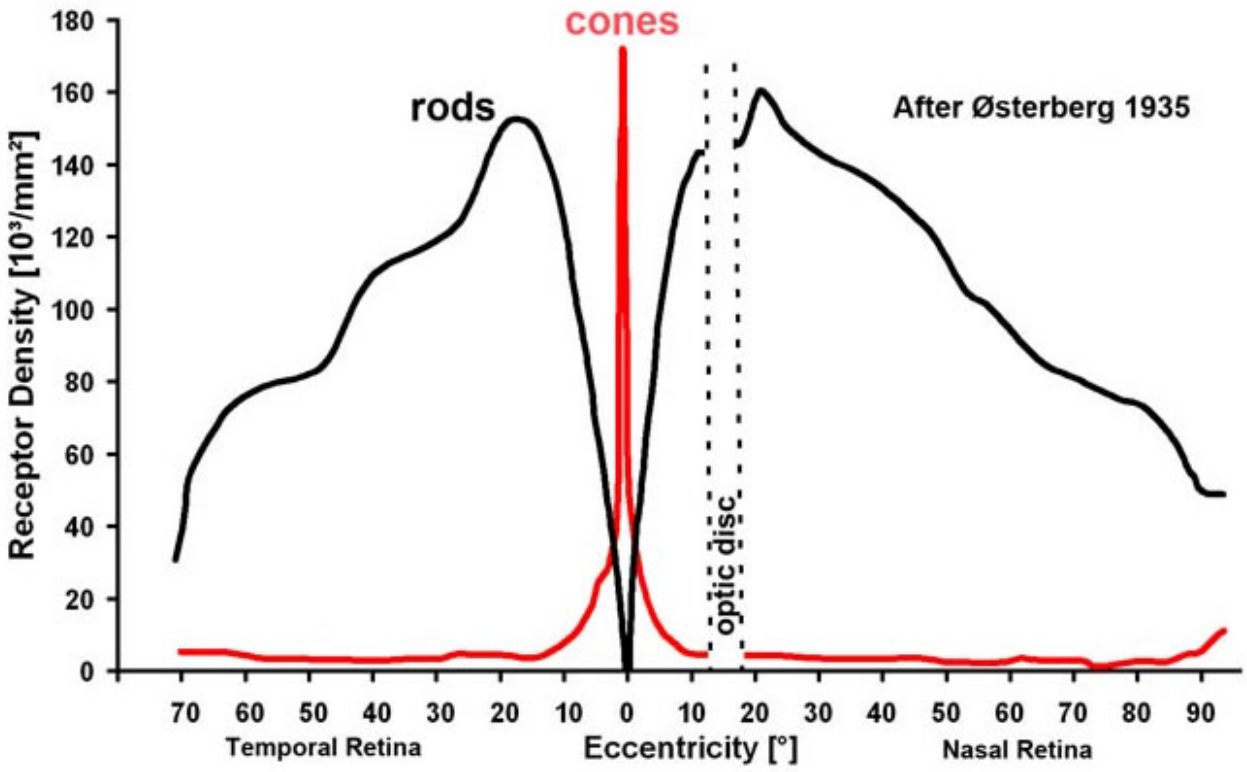

Figure 20. Graph to show rod and cone densities along the horizontal meridian. The illustration is adapted from Østerberg, 1935 (35).

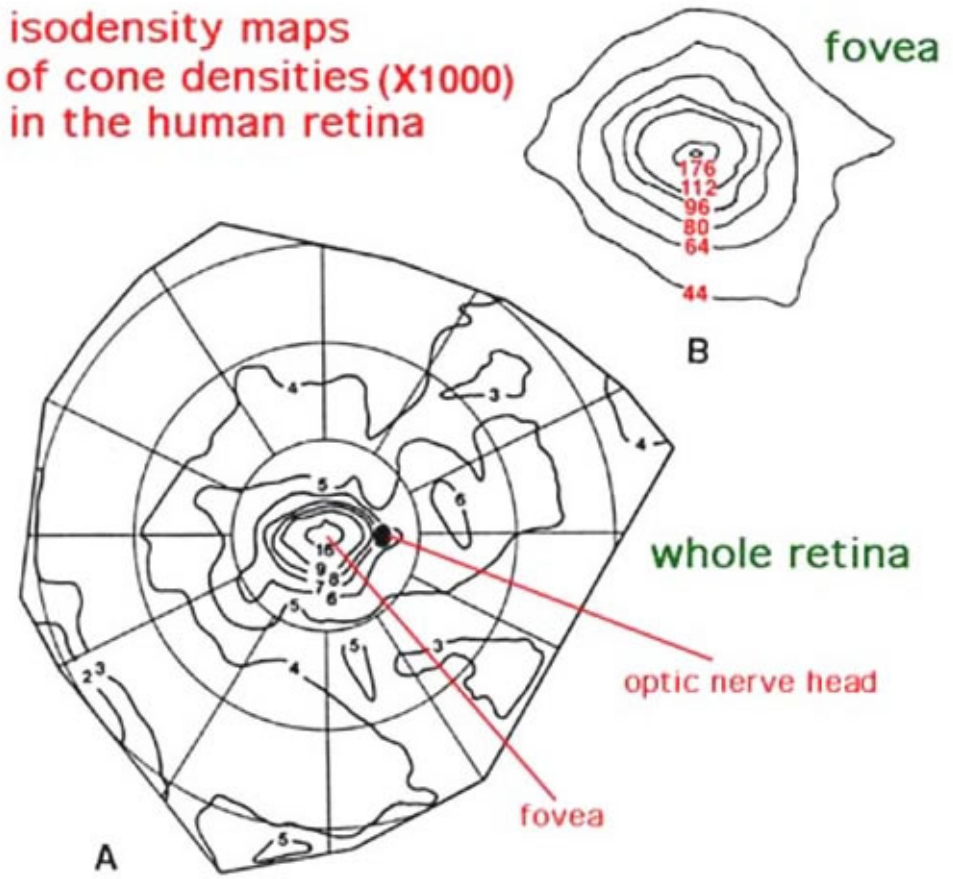

Figure 21. Cone densities in human retina as revealed in whole mount (*A*). The foveal area is enlarged in *B*. Adapted from Curcio et al, 1987 (34).

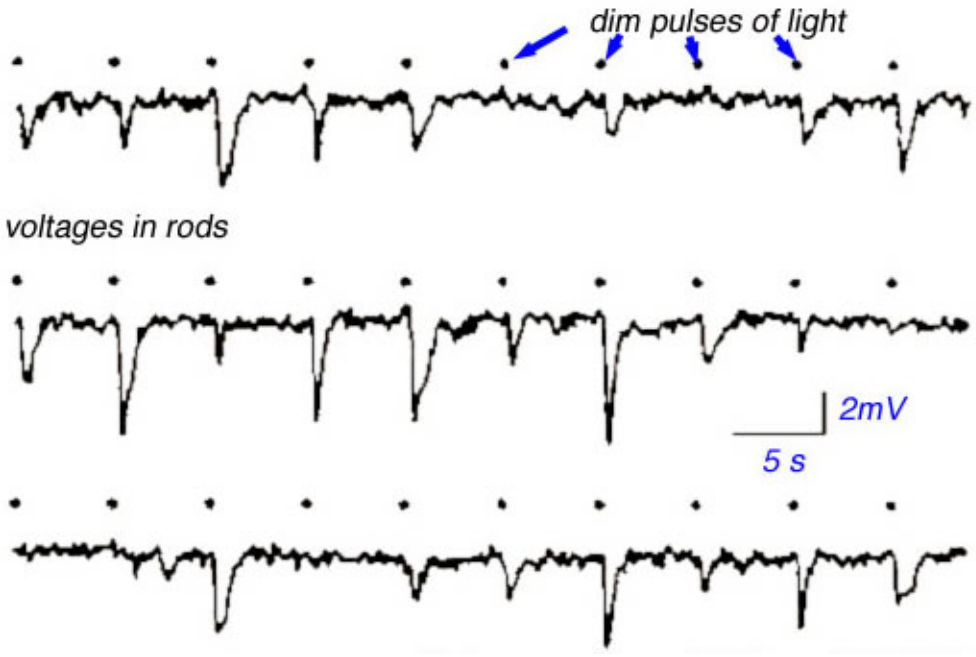

Figure 22. Photovoltages recorded in monkey rods. The illustration is from Schneeweis and Schnapf, 1995 (39).

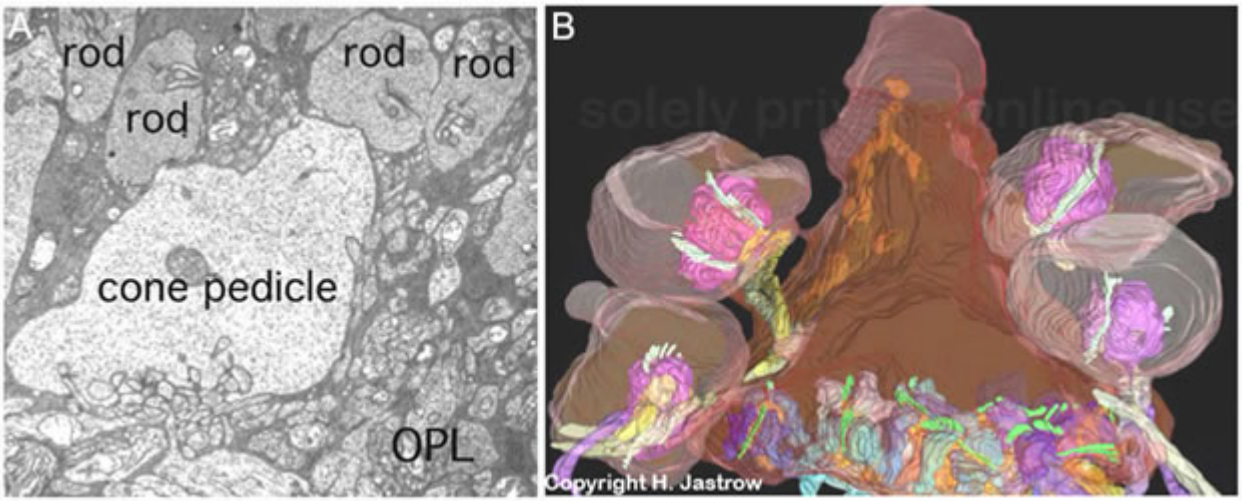

Figure 23. Ultrastructure of the cone synaptic pedicle. *A*. EM picture of cone pedicle and rod spherules in cat retina. *B*. Reconstruction from electron microscopy of a cone pedicle (center) surrounded by rod spherules. The illustration in *B* is courtesy of Holger Jastrow, Department of Anatomy and Cell Biology, University of Mainz, Germany.

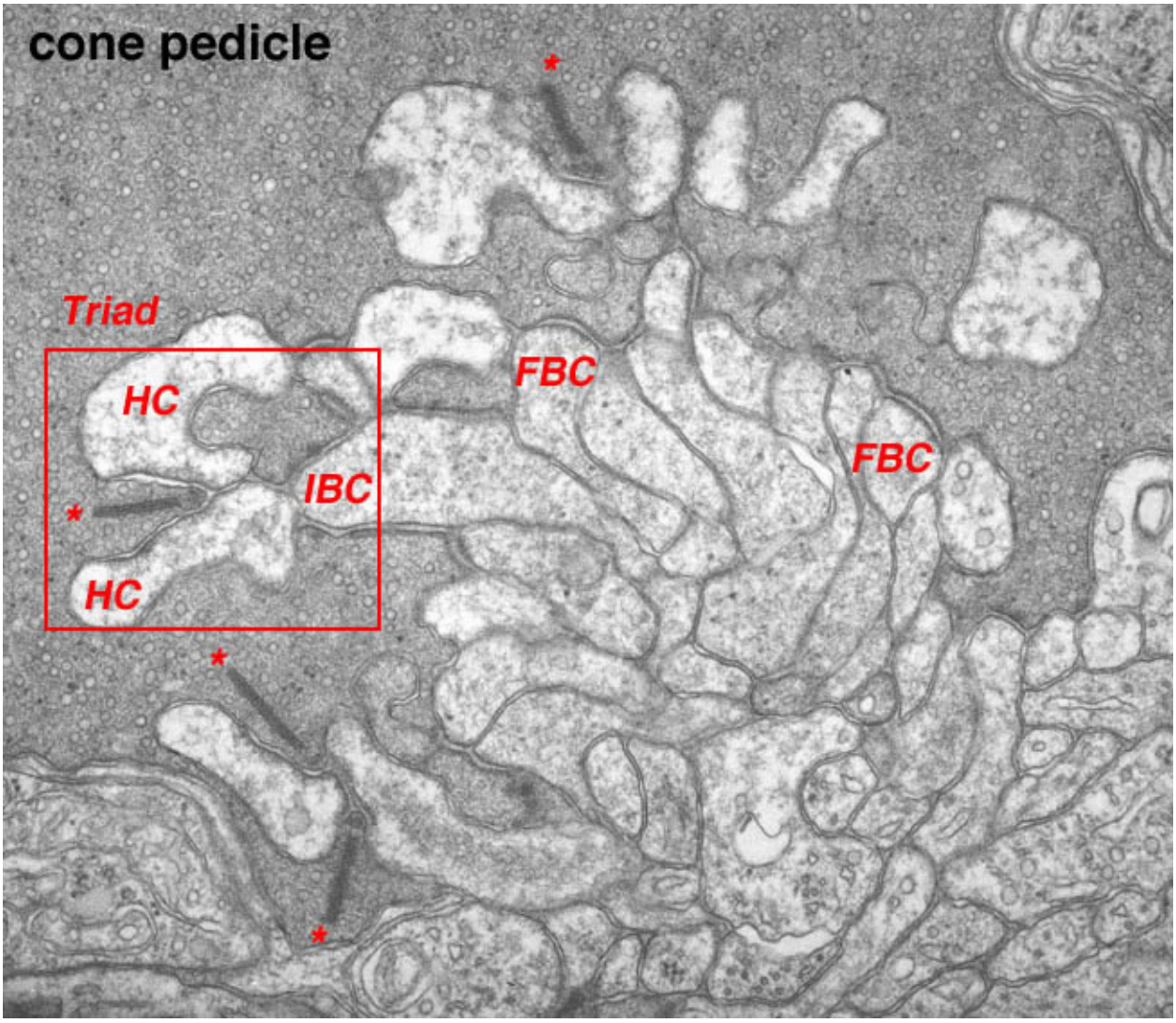

Figure 24. Electron micrograph of a cone pedicle in the turtle retina. The triad synapse is outlined in red. This is composed of 2 horizontal cell (HC) dendrites and an invaginating cone bipolar (IBC) dendrite. FBC: flat bipolar contacts. The picture is courtesy of Arnaldo Lasansky, NIH.

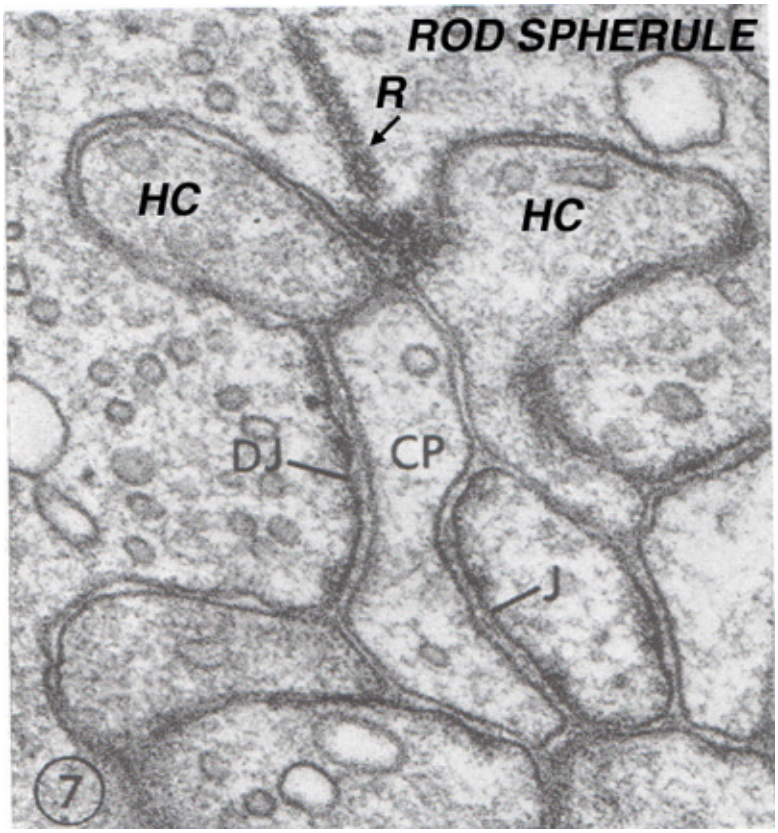

Figure 25. Electron micrograph of a rod spherule in the monkey retina. R, ribbon; HC, horizontal cell processes; DJ, distal junction; CP, central process; J. Junction. The figure is from Lasansky, 1972 (51).

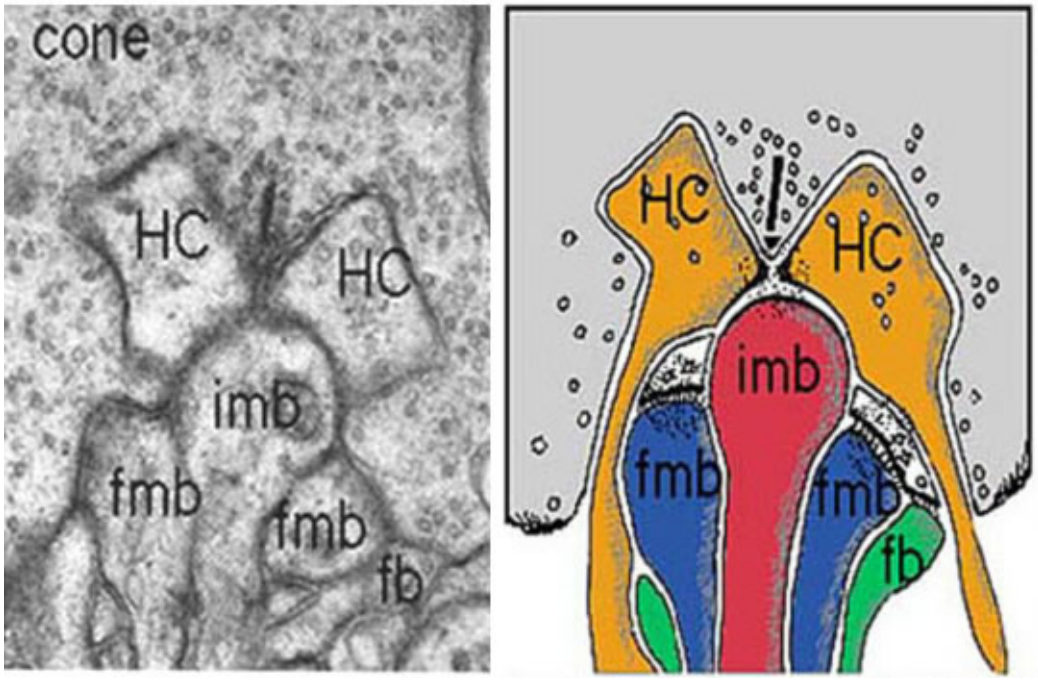

Figure 27. Electron micrograph of a cone triad and a drawing to show bipolar contacts in human. imb, invaginating midget bipolar dendrite; fmb, flat midget bipolar dendrite; HC, horizontal cell dendrite; fb, flat diffuse bipolar dendrite.

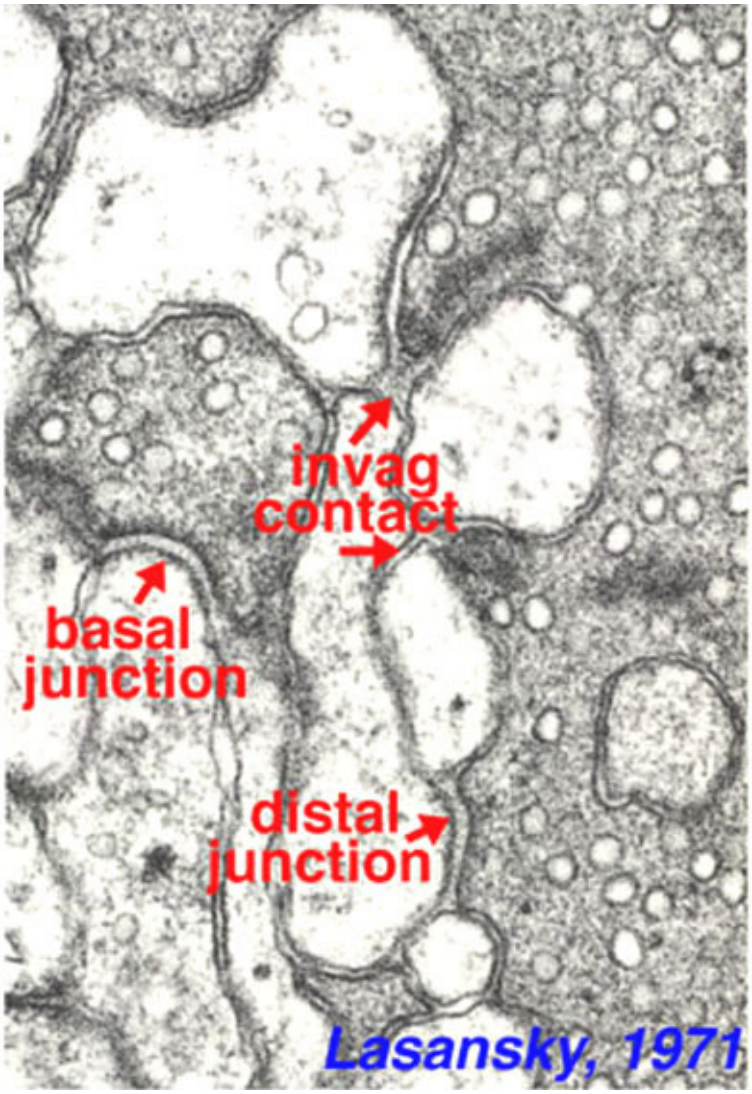

Figure 26. Electron micrograph of a turtle cone pedicle and types of bipolar synaptic contacts (junctions) at the ribbon synapse. The figure is from Lasansky, 1971 (44).

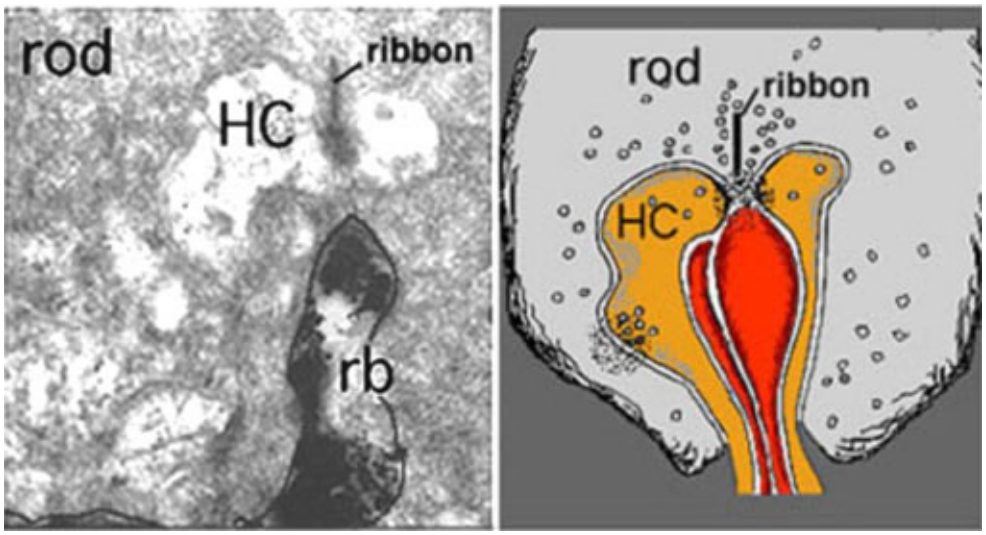

Figure 28. Electron micrograph and drawing of a rod triad in monkey. rb, rod bipolar dendrite; HC, horizontal cell axon terminal processes.

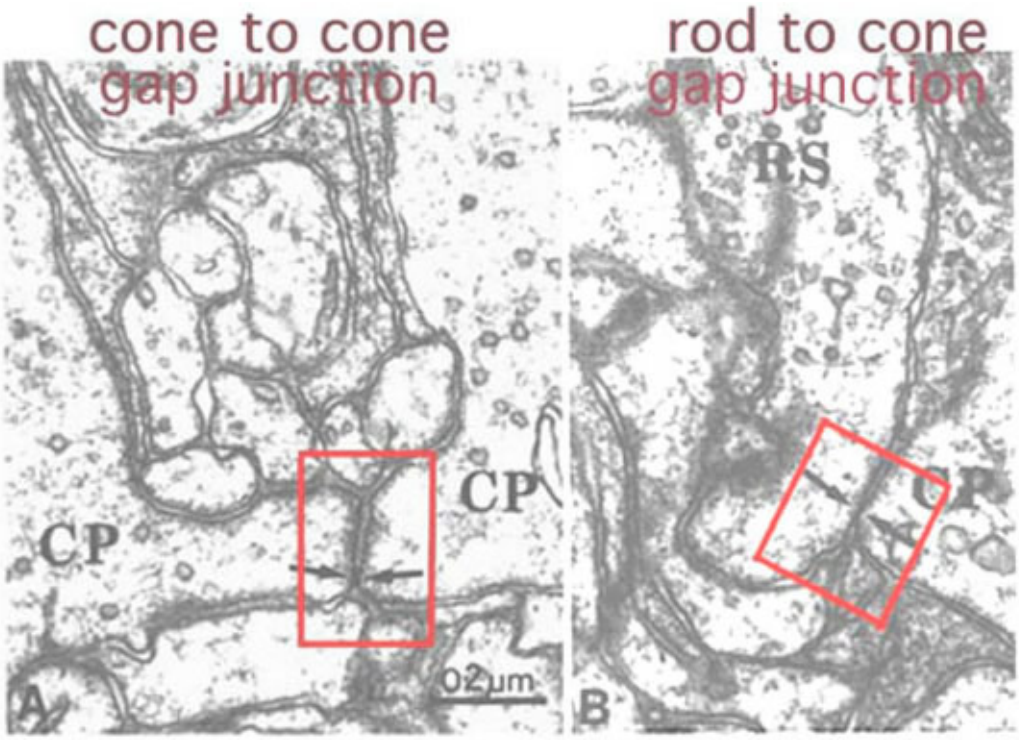

Figure 29. Tiny "kissing" gap junctions between two cones (left) and between rods and cones (right). The electron micrograph is courtesy of Avery H Nelson, NIH (45).

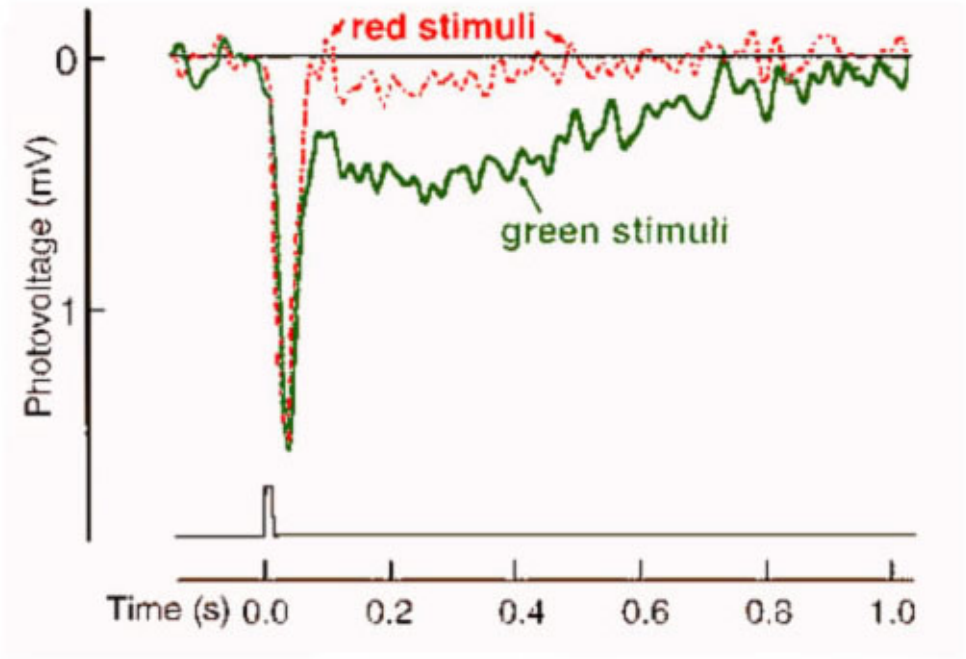

Figure 30. Voltage recording from a monkey cone with red and green stimuli balanced to elicit equal peak amplitudes. The green stimulus (solid trace) also evokes a slower hyperpolarizing phase after the initial response which the red stimulus (dotted trace) does not. The slow electrical wave has the characteristics of a rod signal. The illustration is from Schneeweis and Schnapf, 1995 (39).

References

1. Anderson D.H., Fisher S.K. *The photoreceptors of diurnal squirrels: outer segment structure, disc shedding, and protein renewal.* .J Ultrastruct Res. 1976;55(1):119–41. PubMed PMID: 1263298.
2. Steinberg R.H., Fisher S.K., Anderson D.H. *Disc morphogenesis in vertebrate photoreceptors.* .J Comp Neurol. 1980;190(3):501–8. PubMed PMID: 6771304.
3. Deretic D.et al. *rab8 in retinal photoreceptors may participate in rhodopsin transport and in rod outer segment disk morphogenesis.* .J Cell Sci. 1995;108(Pt 1):215–24. PubMed PMID: 7738098.
4. Papermaster D.S., Schneider B.G., Besharse J.C. *Vesicular transport of newly synthesized opsin from the Golgi apparatus toward the rod outer segment. Ultrastructural immunocytochemical and autoradiographic evidence in Xenopus retinas.* .Invest Ophthalmol Vis Sci. 1985;26(10):1386–404. PubMed PMID: 2931395.
5. Adler A.J., Martin K.J. *Retinol-binding proteins in bovine interphotoreceptor matrix.* .Biochem Biophys Res Commun. 1982;108(4):1601–8. PubMed PMID: 6891215.
6. Chader G.J. *Interphotoreceptor retinoid-binding protein (IRBP): a model protein for molecular biological and clinically relevant studies. Friedenwald lecture.* .Invest Ophthalmol Vis Sci. 1989;30(1):7–22. PubMed PMID: 2643589.
7. Hargrave P.A., McDowell J.H. *Rhodopsin and phototransduction: a model system for G protein-linked receptors.* .FASEB J. 1992;6(6):2323–31. PubMed PMID: 1544542.
8. Hargrave P.A.et al. *Rhodopsin's protein and carbohydrate structure: selected aspects.* .Vision Res. 1984;24(11):1487–99. PubMed PMID: 6533983.
9. Archer S., Hope A., Partridge J.C. *The molecular basis for the green-blue sensitivity shift in the rod visual pigments of the European eel.* .Proc Biol Sci. 1995;262(1365):289–95. PubMed PMID: 8587887.
10. Fu, Y., *Phototransduction in Rods and Cones*, in *Webvision: The Organization of the Retina and Visual System*, H. Kolb, E. Fernandez, and R. Nelson, Editors. 2010: Salt Lake City (UT).

11. Kawamura, S., *Photransduction, excitation and adaptation.*, in *Neurobiology and clinical aspects of the outer retina*, M.B.A. Djamgoz, S.N. Archer, and S. Vallerga, Editors. 1995, Chapman & Hall: London; New York. p. 105-131.
12. Stryer L. *Visual excitation and recovery.* .J Biol Chem. 1991;266(17):10711–4. PubMed PMID: 1710212.
13. Yau K.W. *Phototransduction mechanism in retinal rods and cones. The Friedenwald Lecture.* .Invest Ophthalmol Vis Sci. 1994;35(1):9–32. PubMed PMID: 7507907.
14. Normann, R.A., I. Perlman, and P.E. Hallet, *Cone photoreceptor physiology and cone contributions to colour vision.*, in *The perception of colour* P. Gouras, Editor. 1991, Macmillan Press Ltd.: London. p. 146-162.
15. Young R.W. *The renewal of rod and cone outer segments in the rhesus monkey.* .J Cell Biol. 1971;49(2):303–18. PubMed PMID: 19866760.
16. Besharse J.C. *Chapter 3 The daily light-dark cycle and rhythmic metabolism in the photoreceptor—Pigment epithelial complex.* .Progress in Retinal Research. 1982;1(0):81–124.
17. LaVail M.M. *Rod outer segment disk shedding in rat retina: relationship to cyclic lighting.* .Science. 1976;194(4269):1071–4. PubMed PMID: 982063.
18. Steinberg R.H., Wood I., Hogan M.J. *Pigment epithelial ensheathment and phagocytosis of extrafoveal cones in human retina.* .Philos Trans R Soc Lond B Biol Sci. 1977;277(958):459–74. PubMed PMID: 16301.
19. Young R.W. *Visual cells and the concept of renewal.* .Invest Ophthalmol Vis Sci. 1976;15(9):700–25. PubMed PMID: 986765.
20. Gouras P. *Chapter 8 Color vision.* .Progress in Retinal Research. 1984;3(0):227–261.
21. Nathans J., Thomas D., Hogness D.S. *Molecular genetics of human color vision: the genes encoding blue, green, and red pigments.* .Science. 1986;232(4747):193–202. PubMed PMID: 2937147.
22. Ammermüller J., Kolb H. *Functional architecture of the turtle retina.* .Progress in Retinal and Eye Research. 1996;15(2):393–433.
23. Kolb, H. and L.E. Lipitz, *The anatomical basis for colour vision in the vertebrate retina.*, in *The perception of colour.*, P. Gouras, Editor. 1991, Macmillan Press Ltd.: London. p. 128-145.
24. Marc R.E., Sperling H.G. *Chromatic organization of primate cones.* .Science. 1977;196(4288):454–6. PubMed PMID: 403607.
25. DeMonasterio F.M., Schein S.J., McCrane E.P. *Staining of blue-sensitive cones of the macaque retina by a fluorescent dye.* .Science. 1981;213(4513):1278–81. PubMed PMID: 7268439.
26. Szel A., Diamantstein T., Rohlich P. *Identification of the blue-sensitive cones in the mammalian retina by anti-visual pigment antibody.* .J Comp Neurol. 1988;273(4):593–602. PubMed PMID: 3209737.
27. Wikler K.C., Rakic P. *Distribution of photoreceptor subtypes in the retina of diurnal and nocturnal primates.* .J Neurosci. 1990;10(10):3390–401. PubMed PMID: 2145402.
28. Ahnelt P.K., Kolb H., Pflug R. *Identification of a subtype of cone photoreceptor, likely to be blue sensitive, in the human retina.* .J Comp Neurol. 1987;255(1):18–34. PubMed PMID: 2434534.
29. Ahnelt P., Keri C., Kolb H. *Identification of pedicles of putative blue-sensitive cones in the human retina.* .J Comp Neurol. 1990;293(1):39–53. PubMed PMID: 2312791.
30. Cicerone C.M., Nerger J.L. *The relative numbers of long-wavelength-sensitive to middle-wavelength-sensitive cones in the human fovea centralis.* .Vision Res. 1989;29(1):115–28. PubMed PMID: 2773329.
31. Hofer H.et al. *Organization of the human trichromatic cone mosaic.* .J Neurosci. 2005;25(42):9669–79. PubMed PMID: 16237171.
32. Roorda A., Williams D.R. *The arrangement of the three cone classes in the living human eye.* .Nature. 1999;397(6719):520–2. PubMed PMID: 10028967.
33. Mollon J.D., Bowmaker J.K. *The spatial arrangement of cones in the primate fovea.* .Nature. 1992;360(6405):677–9. PubMed PMID: 1465131.
34. Curcio C.A.et al. *Distribution of cones in human and monkey retina: individual variability and radial asymmetry.* .Science. 1987;236(4801):579–82. PubMed PMID: 3576186.
35. Østerberg G. *Topography of the layer of rods and cones in the human retina.* .Acta ophthalmol. 1935;13(S6):11–103.

36. Einstein A. *On a Heuristic Viewpoint Concerning the Production and Transformation of Light.* .Annalen der Physik. 1905;17(6):132–148.
37. Hertz H. *Ueber den Einfluss des ultravioletten Lichtes auf die electrische Entladung.* .Annalen der Physik. 1887;267(8):983–1000.
38. Hecht S., Shlaer S., Pirenne M.H. *Energy, Quanta, and Vision.* .J Gen Physiol. 1942;25(6):819–40. PubMed PMID: 19873316.
39. Schneeweis D.M., Schnapf J.L. *Photovoltage of rods and cones in the macaque retina.* .Science. 1995;268(5213):1053–6. PubMed PMID: 7754386.
40. MacLeod D.I. *Rods cancel cones in flicker.* .Nature. 1972;235(5334):173–4. PubMed PMID: 4551230.
41. Dowling J.E., Boycott B.B. *Organization of the primate retina: electron microscopy.* .Proc R Soc Lond B Biol Sci. 1966;166(2):80–111. PubMed PMID: 4382694.
42. Kolb H. *Organization of the outer plexiform layer of the primate retina: electron microscopy of Golgi-impregnated cells.* .Philosophical Transactions of the Royal Society, London, B. 1970;258:261–283.
43. Missotten, L., *The ultrastructure of the human retina*1965, Brussel: Arscia Uitgaven. 184 p.
44. Lasansky A. *Synaptic Organization of Cone Cells in the Turtle Retina.* .Philosophical Transactions of the Royal Society of London. B, Biological Sciences. 1971;262(844):365–381.
45. Nelson, R., et al., *Spectral Mechanisms in Cat Horizontal Cells*, in *Neurocircuitry of the retina : a Cajal memorial*, A. Gallego, Editor. 1985, Elsevier: New York. p. 109-121.
46. Raviola E., Gilula N.B. *Intramembrane organization of specialized contacts in the outer plexiform layer of the retina. A freeze-fracture study in monkeys and rabbits.* .J Cell Biol. 1975;65(1):192–222. PubMed PMID: 1127010.
47. Nelson R. *Cat cones have rod input: a comparison of the response properties of cones and horizontal cell bodies in the retina of the cat.* .J Comp Neurol. 1977;172(1):109–35. PubMed PMID: 838876.
48. Sharpe L.T., Stockman A., MacLeod D.I. *Rod flicker perception: scotopic duality, phase lags and destructive interference.* .Vision Res. 1989;29(11):1539–59. PubMed PMID: 2635479.
49. Brown P.K., Wald G. *Visual Pigments in Human and Monkey Retinas.* .Nature. 1963;200:37–43. PubMed PMID: 14074625.
50. Dowling, J.E., *The retina: an approachable part of the brain.* 1987, Cambridge (MA): Belknap Press of Harvard University Press.
51. Lasansky A. *Cell junctions at the outer synaptic layer of the retina.* .Invest Ophthalmol. 1972;11(5):265–75. PubMed PMID: 4112852.

Outer Plexiform Layer

Helga Kolb

Created: May 1, 2005; Updated: May 1, 2007.

A certain degree of integration of the visual message takes place at the first synapse in the retina, in the outer plexiform layer. Here cone pedicles and rod spherules are synaptic upon various bipolar cell and horizontal cell types. In addition, as mentioned in the previous section, cone pedicles pass electrical messages between each other and between rod spherules so that a small amount of rod and cone signal mixing occurs at this layer (1, 2).

Two important synaptic interactions that occur at the outer plexiform layer are:

1. the splitting of the visual signal into two separate channels of information flow, one for detecting objects lighter than background and one for detecting objects darker that background
2. the instillation of pathways to create simultaneous contrast of visual objects

In the first synaptic interactions, the channels of information flow are known as the basis of successive contrast, or ON and OFF pathways, respectively, whereas the second interaction puts light and dark boundaries in simultaneous contrast and forms a receptive field structure, with a center contrasted to an inhibitory surround. We shall see how these two necessary, visual information processes are created by synaptic interactions at the outer plexiform layer.

Techniques That Have Been Used to Understand Neural Pathways in the Retina

By using various anatomical techniques, the morphologies of individual neurons that make up the retina and contribute processes for synaptic interaction in the plexiform layers have been discovered and described over the years. The most important technique among these is a specific neural stain named after a famous early Italian neuroanatomist, Camillo Golgi (1885), who lived at the end of the last century (3). This staining method was used most extensively and with extraordinary success by the great Spanish anatomist, Ramon y Cajal (1892) (Fig. 1) (4).

In fact, the monumental studies of Ramon y Cajal form the basis of neuroanatomy for the vertebrate nervous system in general and the retina in particular. One of Cajal's drawings of nerve cells in the retina stained by Golgi techniques (4) is shown in Fig. 2. In this one figure from Cajal's book on the vertebrate retina, we see photoreceptors, bipolar cells, horizontal cells, and some amacrine cell types. Cajal pointed out that photoreceptors-bipolar cells-ganglion cells were involved in passing rod or cone information through the vertical pathways, and that horizontal and amacrine cells were involved in lateral interactions. He introduced the idea that synaptic connections were set up between specific cell types in the plexiform layers by virtue of nerve cells' dendrites and axons costratifying precisely to ensure that the correct presynaptic cell talked to the correct postsynaptic cell.

In 1941, Stephen Polyak authored landmark books concerning the organization of the primate retina and visual system and was the man most responsible for applying the Golgi stain to monkeys and chimpanzees (5). Even today, we continue to use the Golgi method in research on cat, monkey, and human retinas (6-12).

Some of the cells we have described since Cajal and Polyak are shown in Fig. 3. It becomes immediately obvious that our drawings of Golgi-stained cells differ from those of Cajal, in that we have drawn complete cells from a surface or wholemount view looking into the retina mounted flat. Being able to prepare wholemounts of retinas was a great advance for our understanding of the morphologies of nerve cells in the retina becauser it allowed us to see complete dendritic tree spreads of stained cell, which were often truncated in the sectioned retinas that Cajal and Polyak studied. Thus, we have been able to add significant numbers of new cell types to the original

descriptions. Also, with the advent of electron microscopy, histochemical and immunocytochemical staining, and electrophysiological single-cell recording and staining, we can now direct these techniques at elucidating neural circuits in the retina in a way not available to our predecessors. All of the descriptions of cells and circuits that follow in this chapter come from experiments over the years using a combination of these techniques but always with the morphological data from Golgi staining as a basis.

Bipolar Cells

In human retina, 11 different bipolar cell types are revealed by Golgi staining (10, 12-14). Ten are for cones, and one type is for rods (Fig. 4).

Human retina, like most mammalian retinas, is rod dominated outside of the fovea. Therefore, rod bipolar cells form the numerically superior part of the bipolar population in human retinas.

The rod bipolar is typically a stout bipolar, with a cell body situated middle to high in the inner nuclear layer and producing a tuft of dendrites entering the OPL and reaching up to different levels between cone pedicles to reach the stacked rod spherules (Fig. 5 and Fig. 6).

The rod bipolar dendritic terminals end one to a rod spherule as the central invaginating dendrite (shown by electron microscopy in Fig. 5 and Fig. 6) (7). In the central retina, rod bipolar dendritic trees are small (15 μm across), and 15–20 rods are contacted. In the peripheral retina, the dendritic tree is 30 μm across and contacts 40–50 rods.

Ten different types of cone bipolar are present in human retina. Seven of them are concerned with converging information from many cones. They are known as diffuse-cone bipolar types (DBs). Three cone bipolar types are concerned only with single-cone contacts in a one-to-one relationship. These are known as midget bipolars, and blue-cone-specific types.

Some of the diffuse-cone bipolars are very wide field (giant) in dendritic spread (70–100 μm) and connect with as many as 15–20 cones (8). Little is known concerning the wide-field cells and and their role in retinal processing. These cells need further exploration. Commonly, the smaller diffuse bipolar cells collect information from 5 to 7 cones in the central retina and from 12 to 14 cones in the peripheral retina. The midget bipolar cells contact single cones, but there are two different varieties of them per cone. Thus, cones of the fovea have output to two midget bipolar cells, and of course, some still output to the diffuse bipolar cells as well. The two types of midget bipolar differ in their contact with the cone pedicle (Fig. 7).

The invaginating midget bipolar type (IMB) connects with the cone pedicle as central invaginating dendrites (Fig. 7, red profiles) at ribbon synapses in the cone pedicles (7). Flat midget bipolar cells (FMBs) contact the cone pedicle by means of semi-invaginating, wide-cleft basal junctions (Fig. 7, green profiles). Often, FMB dendrites make two contacts with the cone pedicle on either side of the central invaginating dendrite from the other midget bipolar cell (7).

A cone bipolar cell that is thought to be specific for the short-wavelength cones, or blue cones (S-cones), has been described in monkey (10, 15) and in human retina (12). This blue S-cone bipolar (Fig. 8) typically contacts one cone heavily, by several dendrites converging on that particular cone pedicle as central elements at the ribbons; thus, it is essentially another type of midget bipolar cell, but it differs from regular IMBs and FMBs in having also two or more wispy dendrites contacting either another cone pedicle or ending blindly in the OPL (see the later chapter on S-cone pathways). There is also a type of giant, bistratified cone bipolar cell in primate retina (Fig. 8, GBB) that has been proposed to be involved in the blue-cone system, because its axonal branching level in the IPL corresponds exactly to the dendritic branching levels of the bistratified blue/yellow ganglion cell of the S-cone pathways through the retina (see the later chapter on the S-cone pathways) (16).

Figure 1. Picture of Cajal.

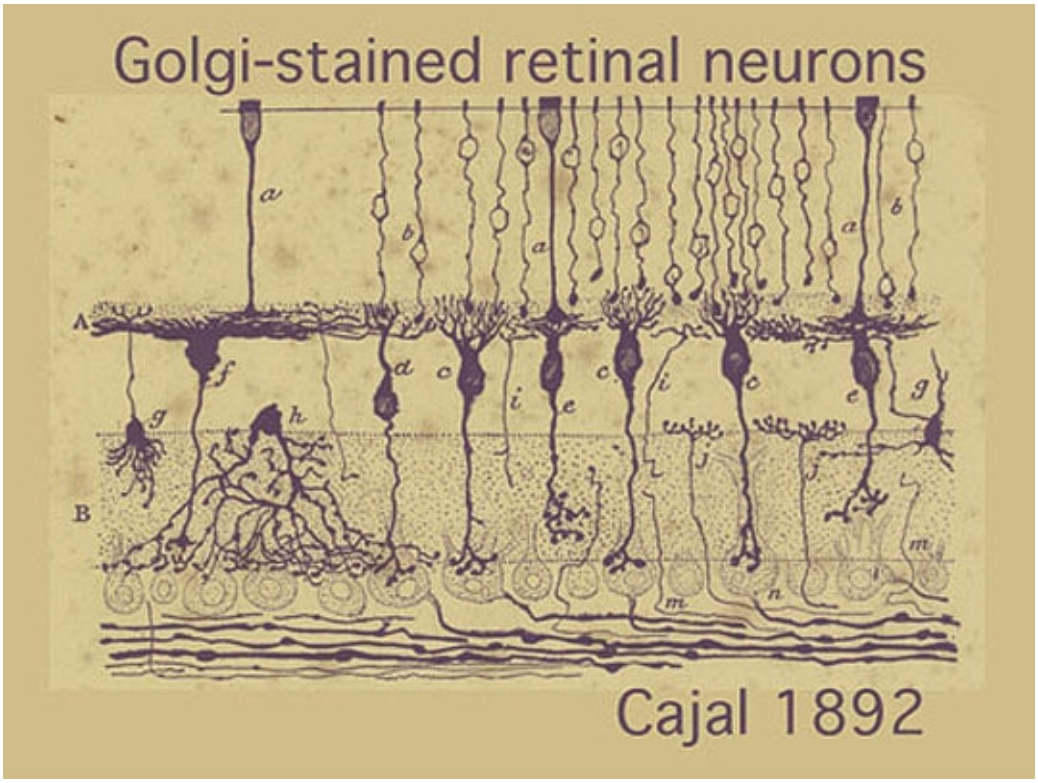

Figure 2. Cajal's drawing.

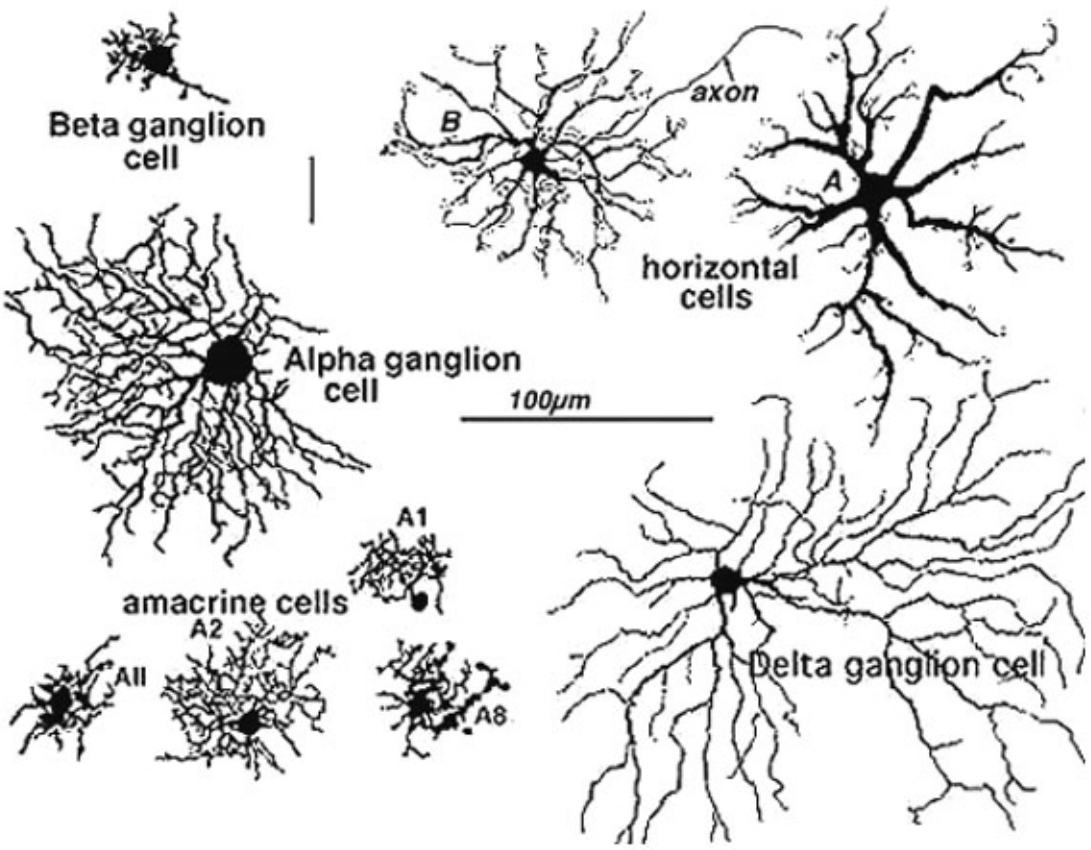

Figure 3. Golgi-stained neurons of cat retina.

The remaining diffuse bipolar types in primate retinas (Fig. 8) are analogous to cone bipolar cells of other mammalian retinas in contacting clusters of cone pedicles, as mentioned above. Similar to the midget bipolar cells, though, these diffuse types also differ in their types of synaptic contacts with cone pedicles, being either flat-contacting types (making basal junctions with cone pedicles) or invaginating and ribbon-contacting types, or even being types that mix these types of contacts (17) (see also Kolb and Nelson (18) for a review on photoreceptor to bipolar contacts in the vertebrate retina).

Horizontal Cells

All mammalian retinas have two types of horizontal cell (HC) as the laterally interconnecting neurons in the outer plexiform layer (14). The cat has been studied extensively as a model mammalian retina, and the two types, known as A-type and B-type, are illustrated in Fig. 9 (19). The A- and B-type HCs are very similar in appearance in the rabbit retina as well.

The A-type HC is a large, sturdy cell with radiating dendrites covering a dendritic field of 150–250 μm, depending on area of retina (all neurons of the retina are small in dendritic expanse in the central or foveal retina and increase in dendritic tree size with eccentricity from the central area). The B-type HC in the mammalian retina differs from the A-type in having a smaller, bushier (in general) dendritic tree (75–150 μm in diameter) and bearing an axon that travels 300 μm or more before ending in a huge, expansive axon terminal tree. The dendrites of both A-type and B-type HCs end in cone pedicles, whereas the axon terminals of the B-type HCs end in rod spherules (Fig. 9) (19).

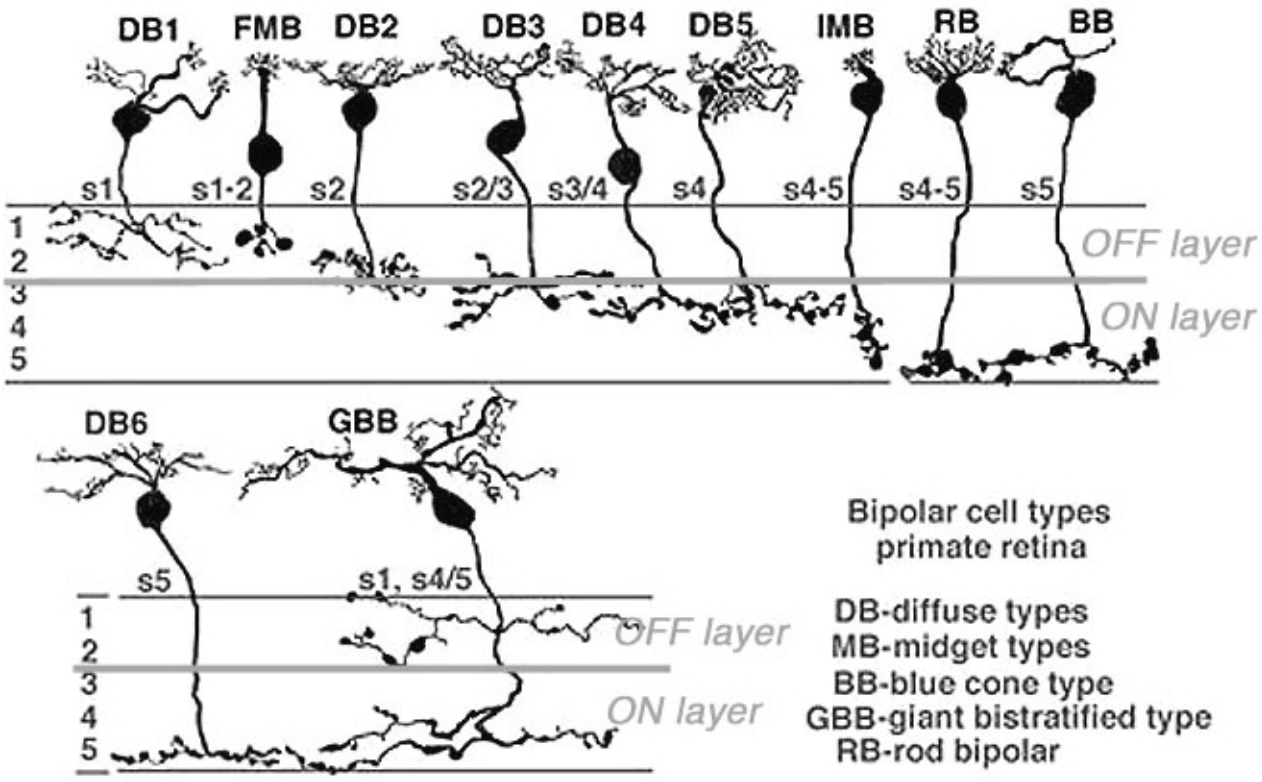

Figure 4. Bipolar cell types in human retina.

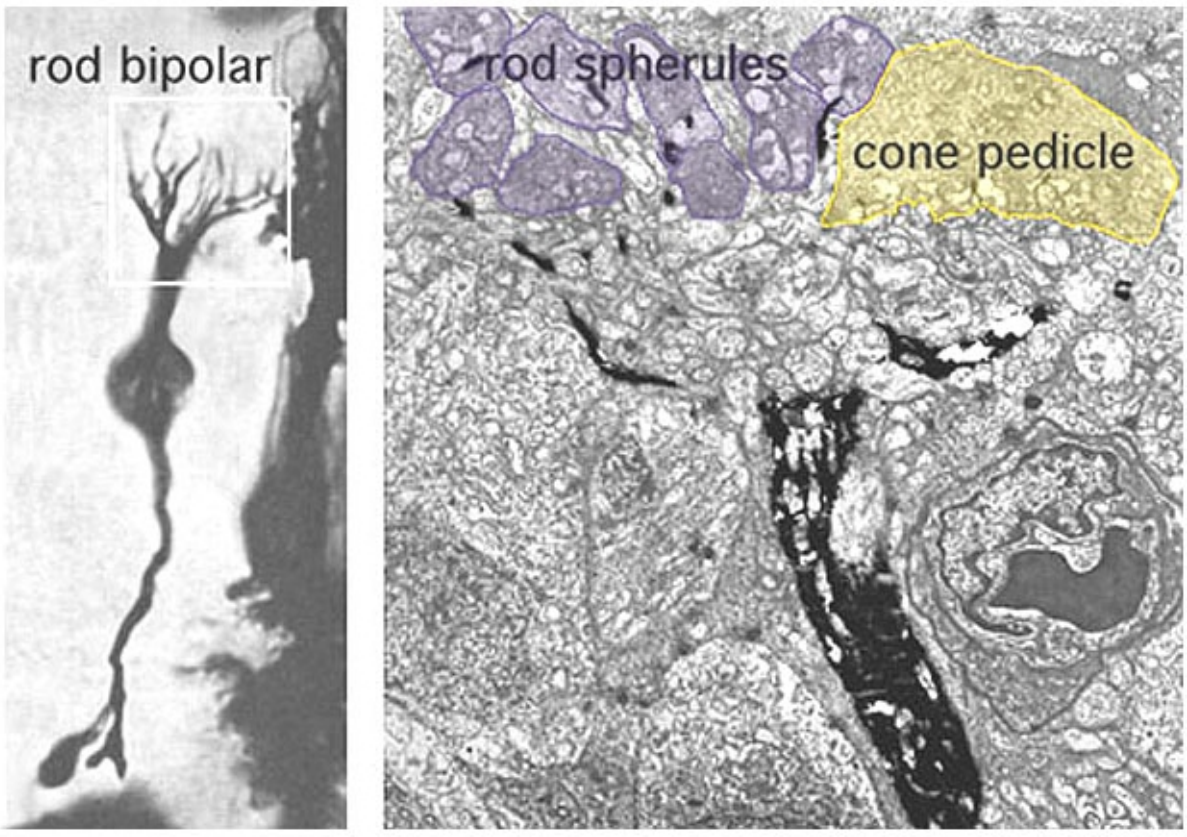

Figure 5. Rod bipolar cell at low magnification.

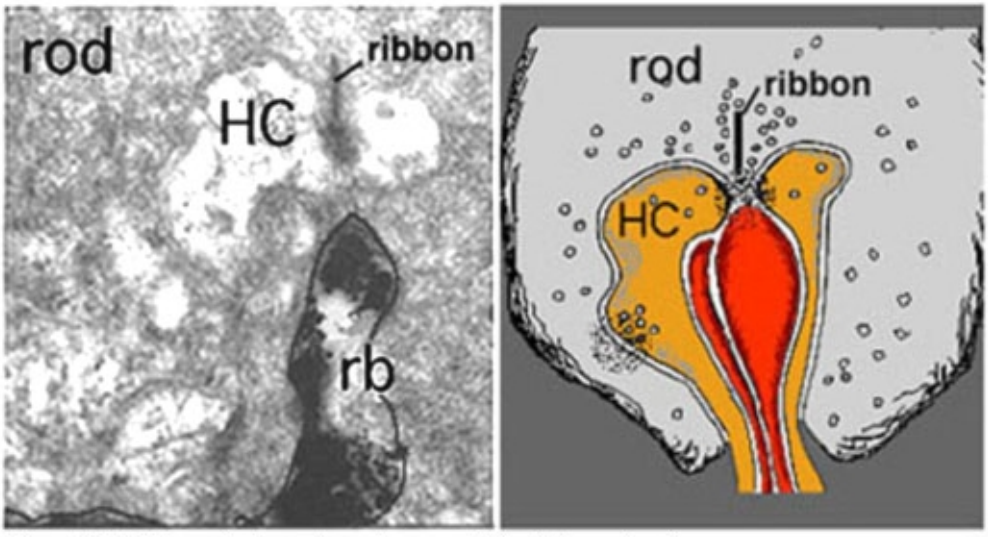

Figure 6. EM and drawing of a rod triad (monkey). rb, rod bipolar dendrite; HC, horizontal cell axon terminals.

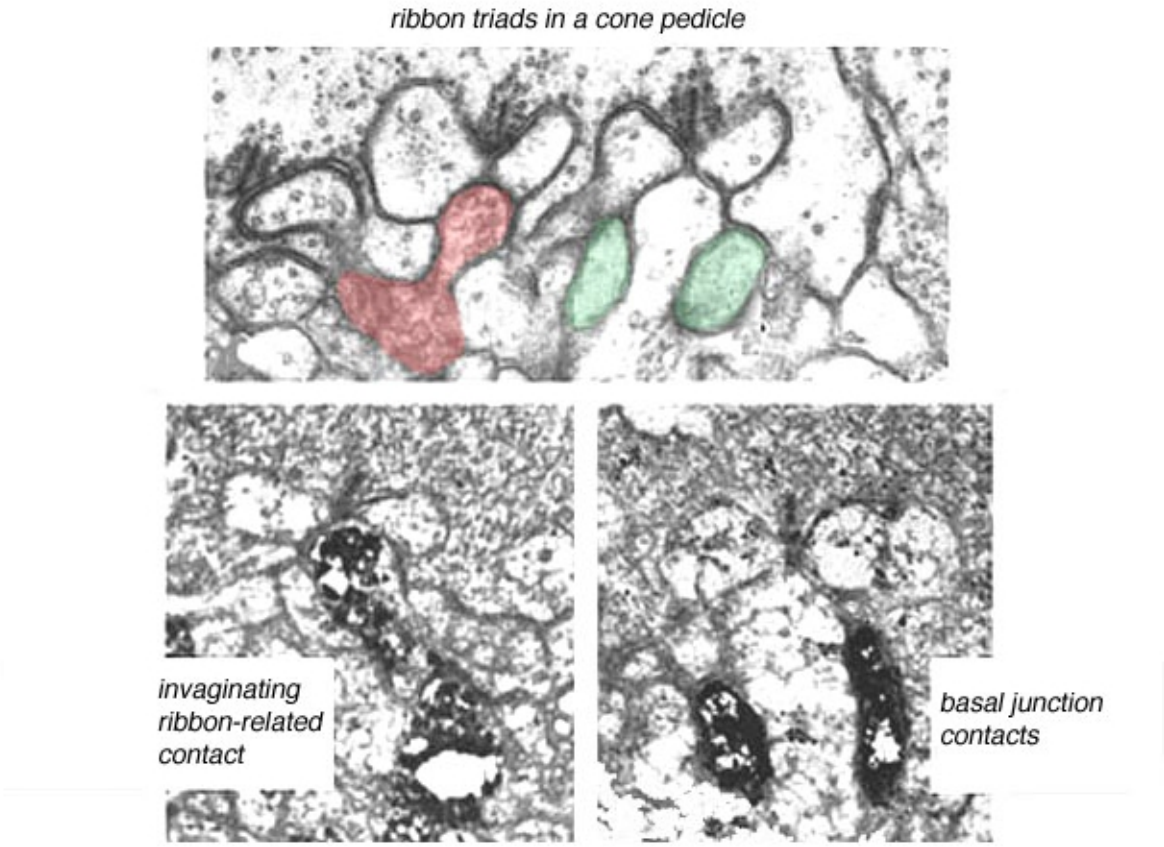

Figure 7. Midget bipolar cell contacts.

Primates, although obviously mammals, have been thought of as somewhat different in their HC make-up compared with cats. Originally, there was thought to be only one HC type, called an HI, that looked like a miniature version of the cat B-type HC (5). In 1980, we described a second type of HC in the rhesus monkey retina and called it the HII type (20). Most recently, we have been able to distinguish a third type, the HIII type,

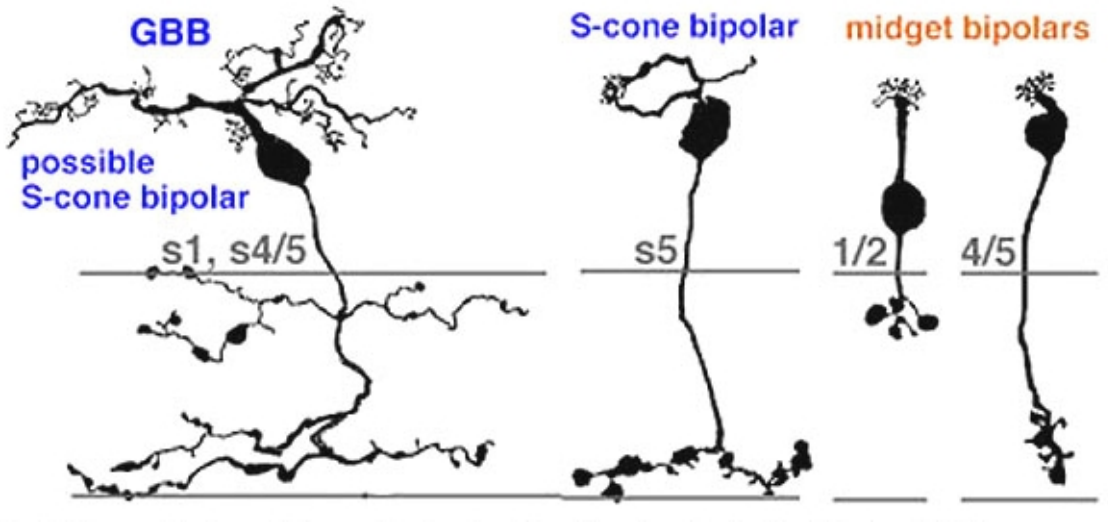

Figure 8. S-cone bipolar cell types of primate retina.

of HC in the human retina (21). Light micrographs and drawings of Golgi-stained examples of these three types are illustrated in Fig. 10 and Fig. 11.

HI is the classic HC of primate retina (5). It is a small-field cell (15-μm-diameter dendritic tree in the fovea, 80–100-μm in the periphery) with stout dendrites, giving rise to distinct clusters of round or donut-shaped terminals contacting cones as lateral elements of the ribbon synapses (Fig. 12).

In peripheral retina, the HI cells have much bigger dendritic trees, and their radiating dendrites contact as many as 18 cones. The HI cell has a single, thick axon that passes laterally in the outer plexiform layer to terminate more than 1 mm away in a thickened axon terminal stalk that bears a fan-shaped profusion of lollipop-like terminals. HI axon terminals end in rod spherules as lateral elements of the ribbon synapses (Fig. 13) (7).

HIII cells are similar in appearance to HI cells, but everywhere in the retina, HIII cells are one-third bigger in dendritic tree size and typically, particularly in the peripheral retina, asymmetrical in shape (one or two dendrites are much longer than others). The clusters of terminals contact cones in the same manner as the HI cell terminals, and because of their bigger field size, they contact more cone pedicles (9–12 in the foveal retina, 20–25 in the peripheral retina). The axon of the HIII has not been conclusively followed to a terminal yet, so we know nothing of the nature of the photoreceptor type it contacts, although we suspect it is a mixture of rods and cones.

HII cells are more spidery and intricate in dendritic field characteristics than either of the other types (20). Their terminals are not clearly seen as clusters approaching cone pedicles, but they are known to end in cone pedicles (20, 22, 23). HII cells also bear an axon, but this is quite different from that of the other two HC types. It is short (100–200 μm), curled instead of straight, and has contacts to cone pedicles by means of small, wispy terminals.

Recent findings from electron microscopic studies of Golgi-stained HCs of the human retina show that there is some color-specific wiring going on for the three cell types (Fig. 14) (22, 23).

Thus, HIs contact medium- and long-wavelength cones primarily, but with a small number of contacts to any short-wavelength cones in the dendritic field. HII cells contact short-wavelength cones, directing major dendrites to these cones in their dendritic fields where they occur and contacting with lesser numbers of terminals of other types of non-short-wavelength cone. The HII cells axon contacts short-wavelength cones only. HIII cells have large dendritic terminals in medium- and long-wavelength cones, seemingly avoiding short-

wavelength cones in their dendritic tree (23). Thus, a wiring diagram can be made (Fig. 15) that summarizes our present understanding of the spectral connections of the three HC cell types of the primate retina.

ON and OFF Center Pathways and Center Surround Organization of the Retina

We know that a photoreceptor neurotransmitter (which is glutamate, see Dowling (24) and Massey (25) for reviews) is released in the dark in the vertebrate retina (26). Thus, the photoreceptor, whether it be rod or cone, is in a depolarized state in the dark. On light stimulation, the photoreceptor responds with a hyperpolarization; transmitter release ceases, but the postsynaptic bipolar cells respond with either hyperpolarization or depolarization of their membranes. The hyperpolarizing type of bipolar cell is called an OFF-center cell, whereas the depolarizing bipolar cell is called an ON-center cell (27, 28).

The origin of these two important ON-center and OFF-center channels is determined by the types of synaptic contacts that these bipolars make with cone pedicles or rod spherules. Thus, the type of bipolar cell making invaginating contacts (several cone bipolar types, among them the IMB type and the rod bipolar type) responds to light with an inverted sign compared with the photoreceptor. They give depolarizing responses to light and are thought to be stimulated via metabotropic glutamate receptors, specifically mGluR6, and signal via a G protein cascade (29, 30) (see chapters on rod and cone pathways). These depolarizing bipolar cells have an APB-sensitive glutamate receptor (Fig. 16 and Fig. 17) (31).

On the other hand, the type of bipolar cell that makes contact with the photoreceptor at a basal junction responds to light just like the photoreceptor by hyperpolarizing (see above). The hyperpolarizing types are driven via ionotropic (iGluR) AMPA-kainate glutamate channels in their synapses with photoreceptors (33). Hyperpolarizing (basal junction-contacting) bipolar cells are the start of OFF-center channels, and the depolarizing (invaginating, ribbon-related) bipolar types are the start of ON-center channels throughout the whole retina and visual system. In a later chapter, we find out that only excitatory channels are present at the level of information transfer between cone bipolar cells and ganglion cells in the inner plexiform layer. Therefore, the status of the signal transmitted by the ganglion cell to the brain is essentially determined by the nature of the cone bipolar contacting it, which in turn is determined by its photoreceptor synapse.

In submammalian species, intracellular recordings from the cones have indicated that they receive a feedback inhibitory message from horizontal cells (see a movie of the intracellular recordings of a cone and bipolar cells) (33). In fish retinas, there is morphological evidence that the horizontal cell lateral elements at the triad synapse produce spinules at which feedback signaling occurs to the cone (see Djamgoz and Kolb (34) for a review). In mammalian cones, there is no unequivocal morphological evidence for this feedback synapse, but some kind of feedback is expected at this site (see above).

Horizontal cell lateral elements, i.e., horizontal cell dendrites, have vesicles within them that could be directed at the cone membrane. This arrangement of horizontal cell dendrites on either side of the ribbon synapse in the triad, with the bipolar cell dendrites forming the central or basal junction position, is very important (Fig. 18). A small local circuit is formed here, that influences the flow of information throughout the whole retina.

We know that a photoreceptor neurotransmitter is released in the dark in the vertebrate retina. Thus, the photoreceptor, whether it be rod or cone, is in a depolarized state in the dark. On light stimulation, the photoreceptor reacts with a hyperpolarization; transmitter release ceases, but the postsynaptic bipolar cells respond with either hyperpolarization or depolarization of their membranes. The horizontal cells respond with a hyperpolarization as well, but a feedback synapse from the horizontal cell to the photoreceptor is also thought to occur. The feedback signal sums information from a network of horizontal cells connected over a wide spatial area of the outer plexiform layer. Thus, this large spatial area influences the photoreceptor and the bipolar cell to

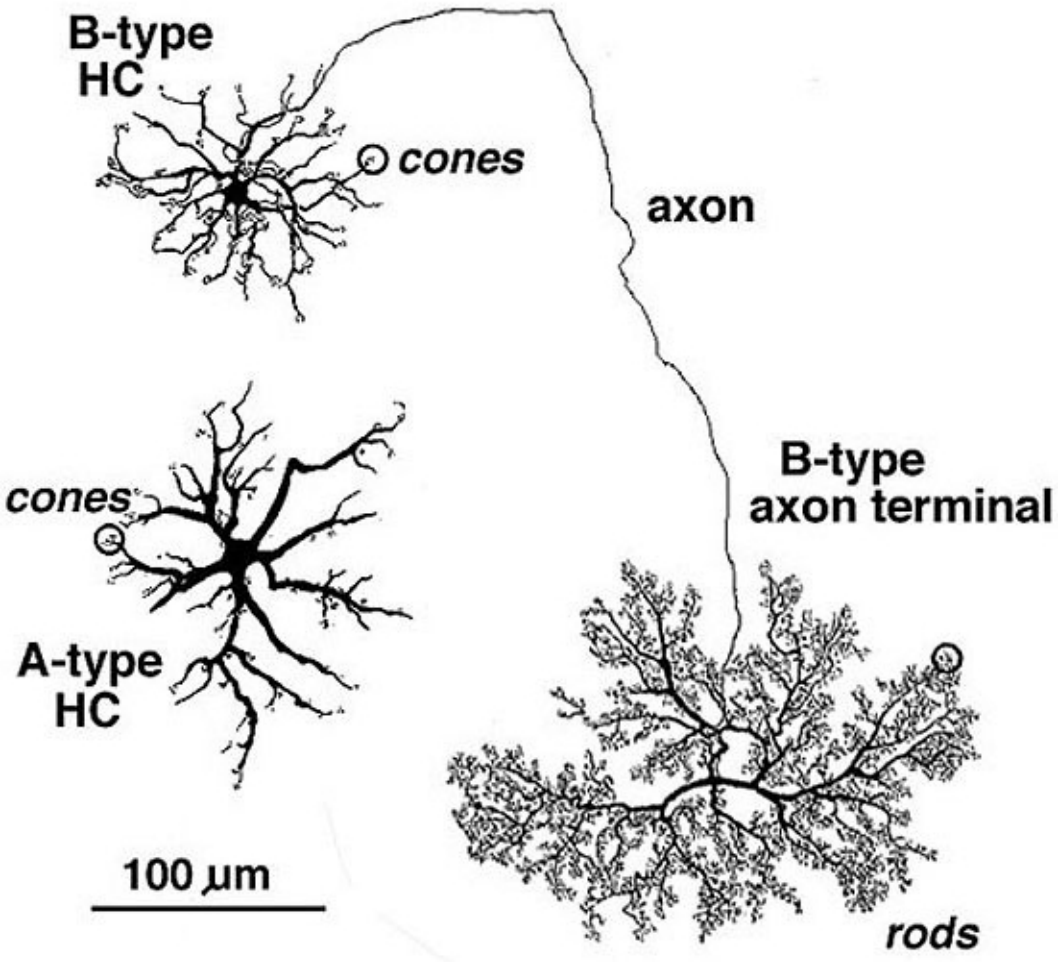

Figure 9. Horizontal cells in cat retina.

include a response coming from a surround region of retina. This local circuit provides the bipolar cell with a center-surround organization.

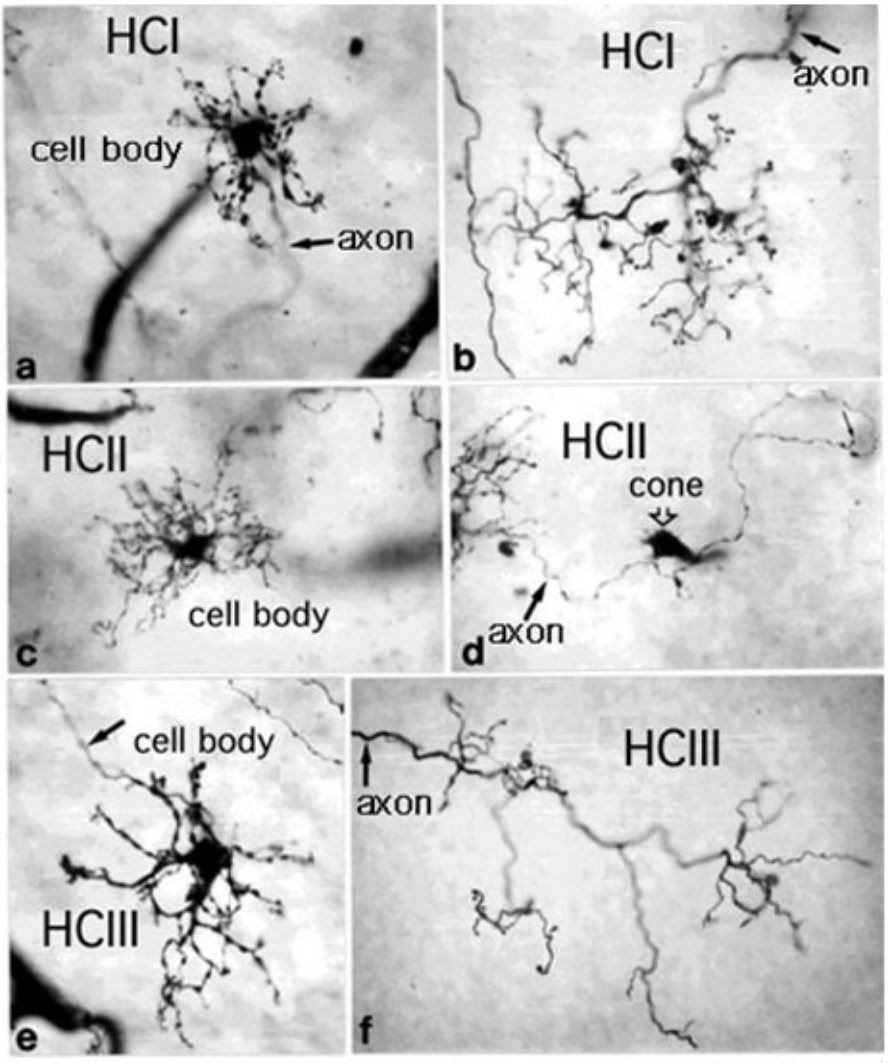

Figure 10. Light micrograph of human horizontal cells.

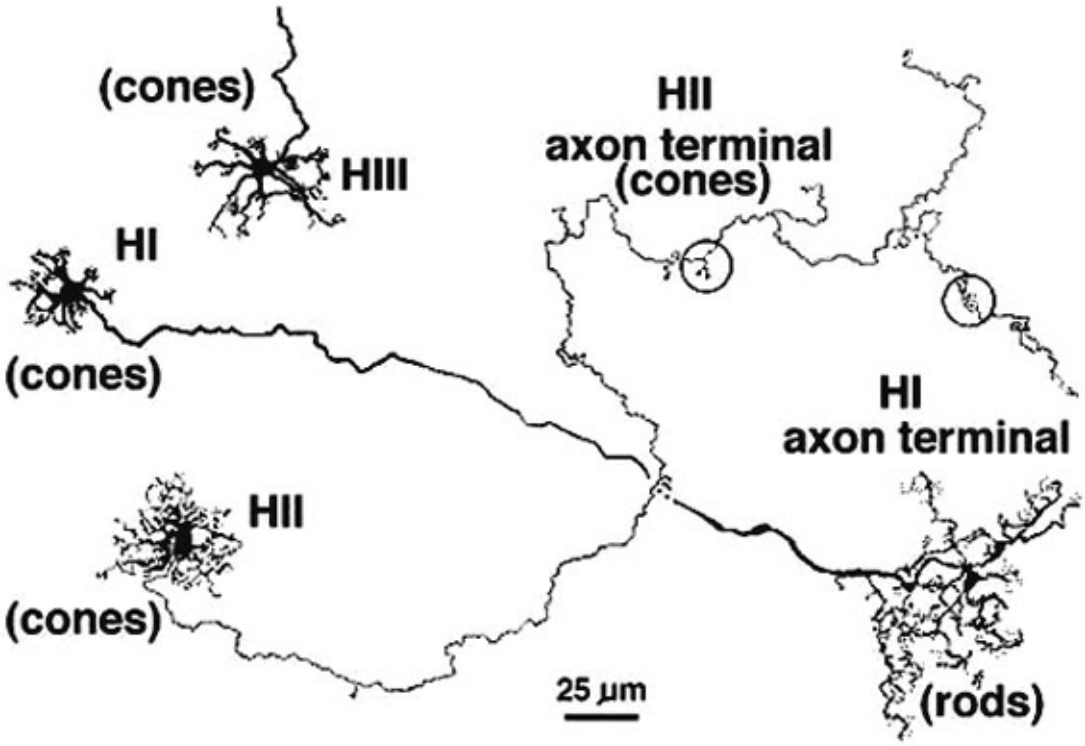

Figure 11. Drawings of monkey horizontal cells.

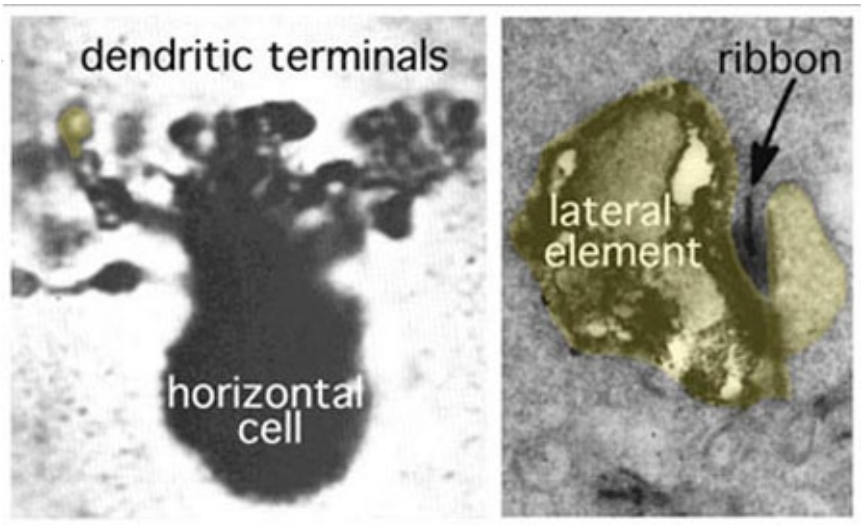

Figure 12. HI horizontal cell of primate retina.

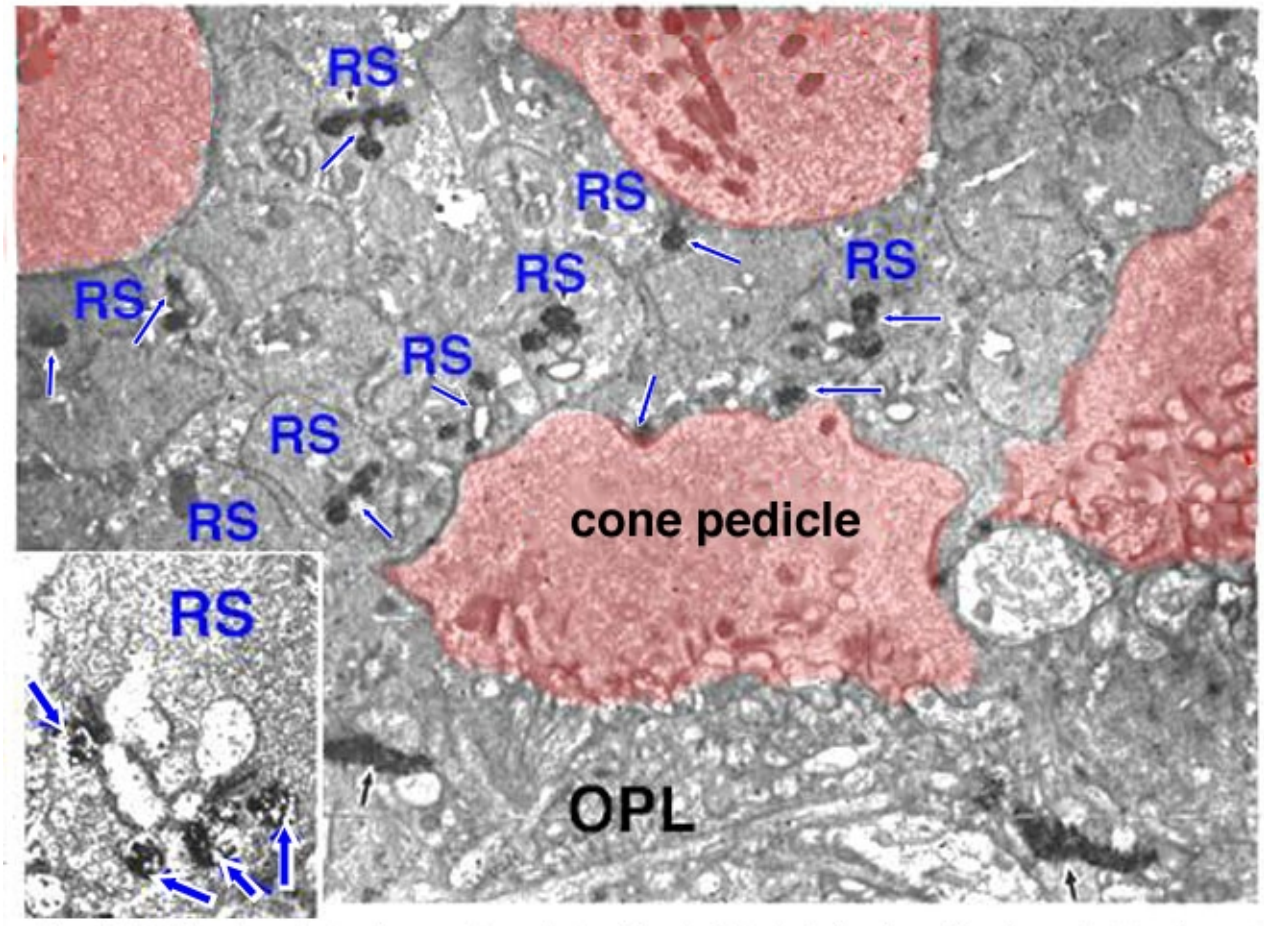

Figure 13. HI horizontal cell terminals.

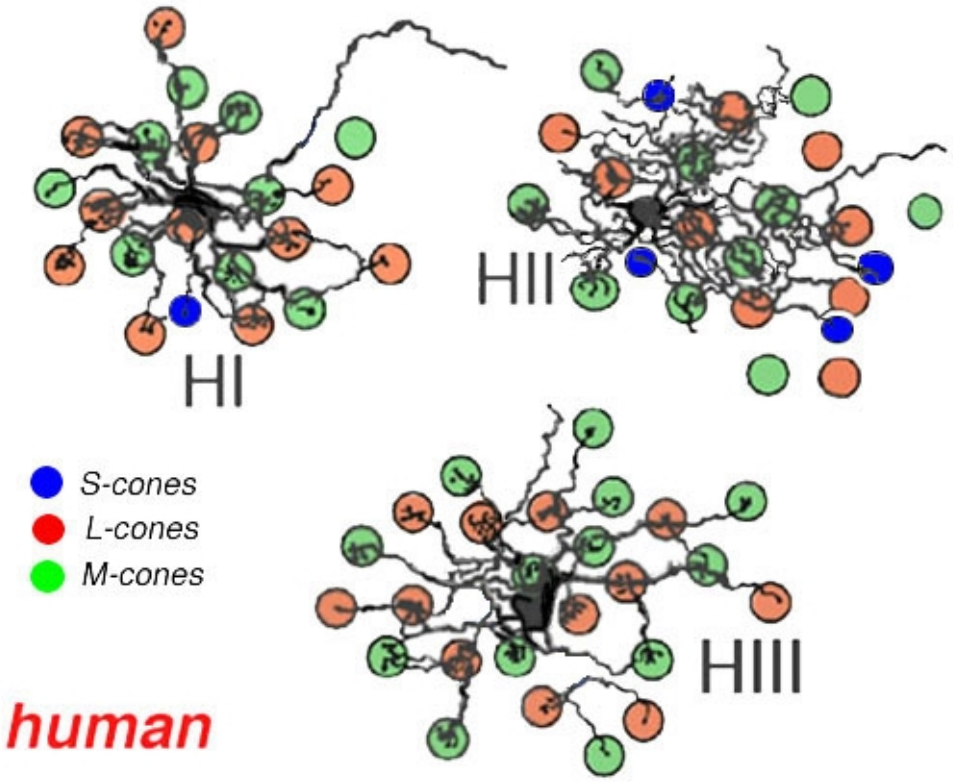

Figure 14. Three cell types of horizontal cells in human retina.

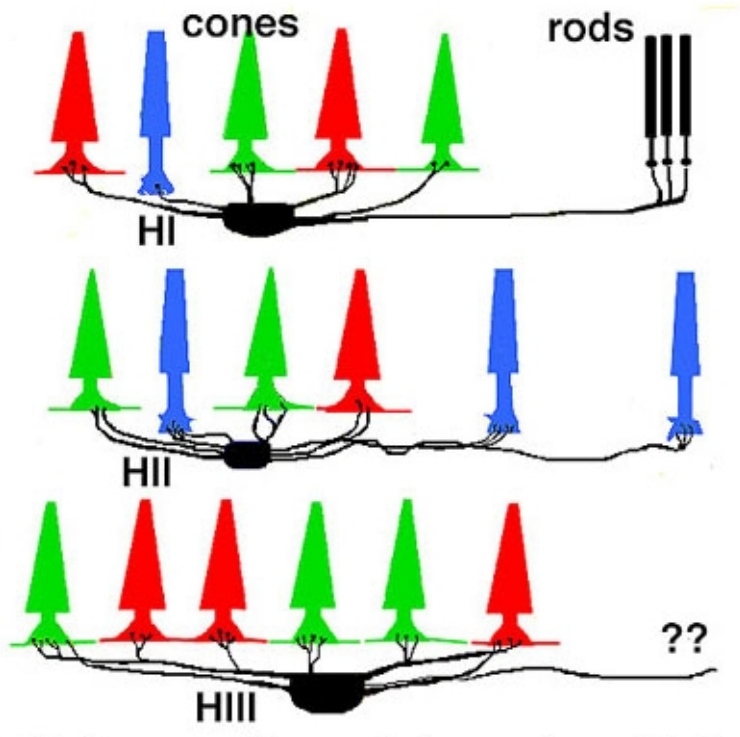

Figure 15. Summary of the spectral connections of the three HC types of the primate retina.

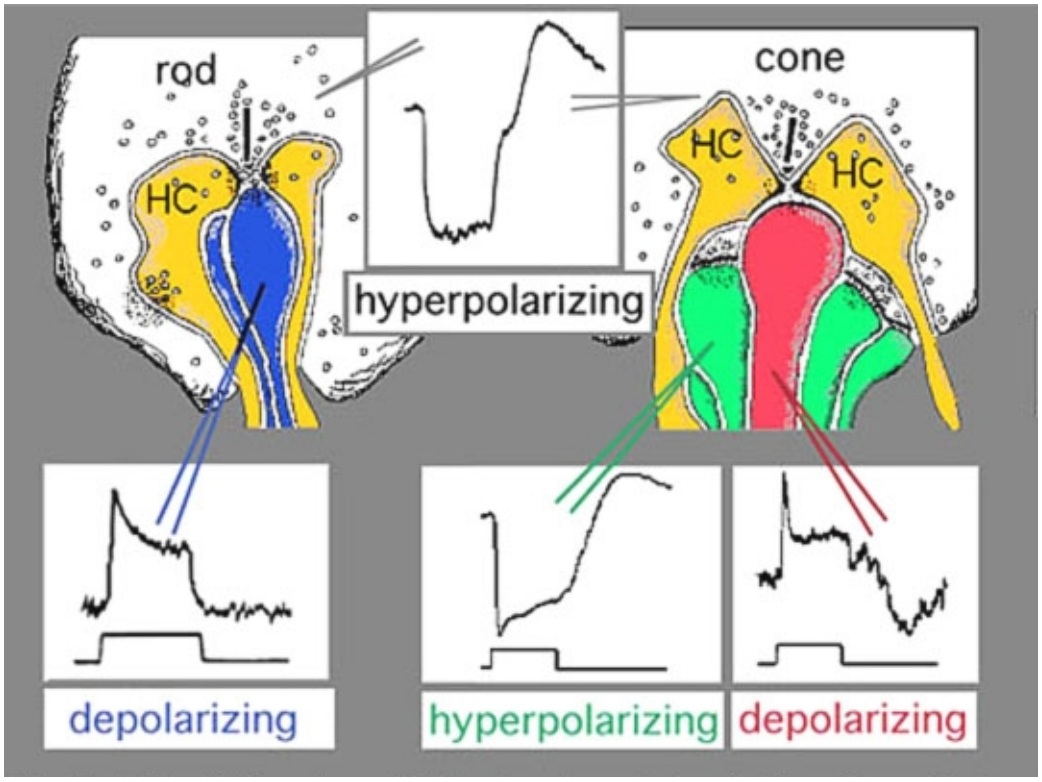

Figure 16. Origin of ON-center and OFF-center channels.

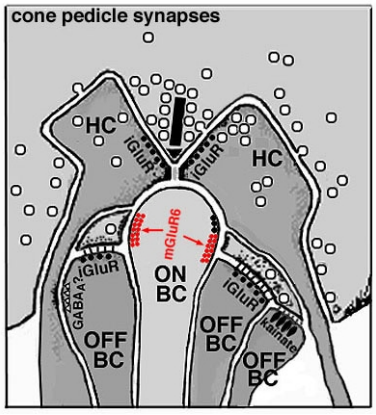

Figure 17. Drawing of the organization of the photoreceptor synapse showing the different glutamate receptors that are presently known to be on the various postsynaptic dendrites.

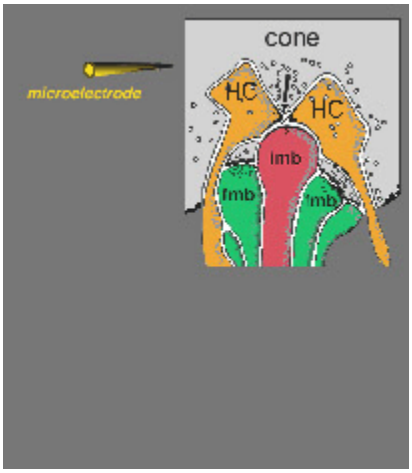

Movie 1. A movie of the intracellular recordings of a cone and bipolar cells.

Download video

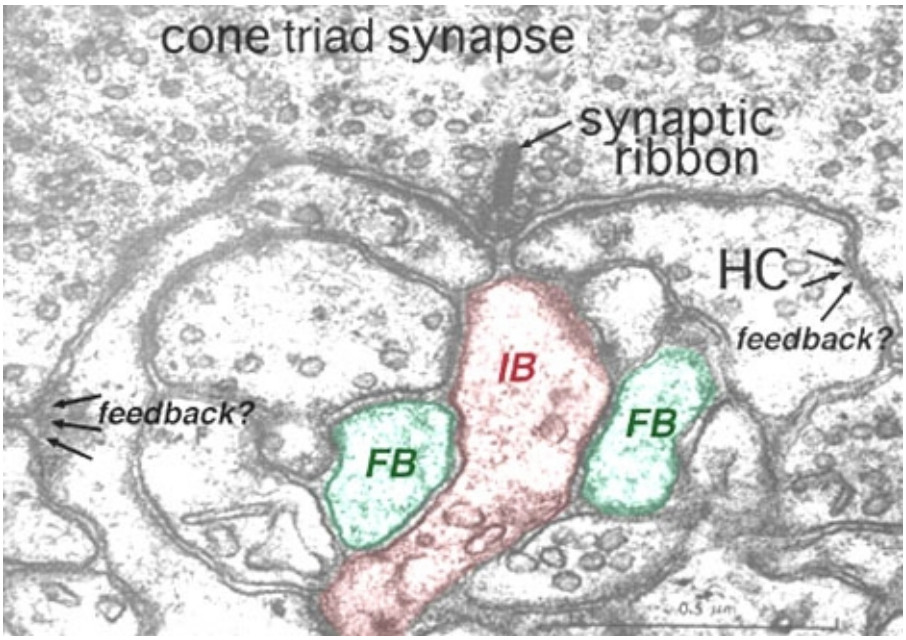

Figure 18. Electron micrograph of synaptic contacts in a cone pedicle triad synapse. Possible feedback synapses in horizontal cells are shown.

References

1. Kolb H. The organization of the outer plexiform layer in the retina of the cat: electron microscopic observations. J Neurocytol. 1977;6:131–153. PubMed PMID: 856949.
2. Nelson R. Cat cones have rod input: a comparison of the response properties of cones and horizontal cell bodies in the retina of the cat. J Comp Neurol. 1977;172:109–136. PubMed PMID: 838876.
3. Golgi C. Sulla fina anatomie degli organi centrali del sistemi nervosa. 1885; Calderini.
4. Cajal SR. The Structure of the Retina. 1892. In: Thorpe SA, Glickstein M, translators. Springfield (IL): Thomas, 1972.
5. Polyak SL. The Retina. Chicago: The University of Chicago Press; 1941.

6. Boycott BB, Dowling JE. Organization of the primate retina: light microscopy. Phil Trans R Soc B. 1969;255:109–184.
7. Kolb H. Organization of the outer plexiform layer of the primate retina: electron microscopy of Golgi-impregnated cells. Phil Trans R Soc B. 1970;258:261–283.
8. Mariani AP. A diffuse, invaginating cone bipolar cell in primate retina. J Comp Neurol. 1981;197:661–671. PubMed PMID: 6262388.
9. Mariani AP. Giant bistratified bipolar cells in monkey retina. Anat Rec. 1983;206:215–220.
10. Mariani AP. Bipolar cells in monkey retina selective for the cones likely to be blue-sensitive. Nature. 1984;308:184–186. PubMed PMID: 6199677.
11. Kolb H, Nelson R, Mariani A. Amacrine cells, bipolar cells and ganglion cells of the cat retina: a Golgi study. Vision Res. 1981;21:1081–1114. PubMed PMID: 7314489.
12. Kolb H, Linberg KA, Fisher SK. Neurons of the human retina: a Golgi study. J Comp Neurol. 1992;31:147–187.
13. Boycott BB, Wassle H. Morphological classification of bipolar cells of the primate retina. Eur J Neurosci. 1991;3:1069–1088. PubMed PMID: 12106238.
14. Mariani AP. Multiaxonal horizontal cells in the retina of the tree shrew, Tupaia glis. J Comp Neurol. 1985;233:553–563. PubMed PMID: 3980782.
15. Kouyama N, Marshak DW. Bipolar cells specific for blue cones in the macaque retina. J Neurosci. 1992;12:1233–1252. PubMed PMID: 1556594.
16. Kolb H, Goede P, Roberts S, McDermott R, Gouras P. Uniqueness of the S-cone pedicle in the human retina and consequences for color processing. J Comp Neurol. 1997;386:443–460. PubMed PMID: 9303428.
17. Hopkins JM, Boycott BB. Synapses between cones and diffuse bipolar cells of a primate retina. J Neurocytol. 1995;24:680–694. PubMed PMID: 7500123.
18. Kolb H, Nelson R. The organization of photoreceptor to bipolar synapses in the outer plexiform layer. In: Djamgoz MBA, Archer SN, Vallerga S, editors. Neurobiology and clinical aspects of the outer retina. London: Chapman and Hall; 1995. p. 273–296.
19. Kolb H. The connexions between horizontal cells and photoreceptors in the retina of the cat: electron microscopy of Golgi-preparations. J Comp Neurol. 1974;155:1–14. PubMed PMID: 4836060.
20. Kolb H, Mariani A, Gallego A. A second type of horizontal cell in the monkey retina. J Comp Neurol. 1980;189:31–44. PubMed PMID: 6766145.
21. Kolb H, Fernandez E, Schouten J, Ahnelt P, Linberg KA, Fisher SK. Are there three types of horizontal cell in the human retina? J Comp Neurol. 1994;343:370–386. PubMed PMID: 8027448.
22. Ahnelt P, Kolb H. Horizontal cells and cone photoreceptors in primate retina: a Golgi-light microscope study of spectral connectivity. J Comp Neurol. 1994;343:387–405. PubMed PMID: 8027449.
23. Ahnelt P, Kolb H. Horizontal cells and cone photoreceptors in human retina: a Golgi-electron microscopic study of spectral connectivity. J Comp Neurol. 1994;343:406–427. PubMed PMID: 8027450.
24. Dowling JE. The retina: an approachable part of the brain. In: Cambridge (MA): The Belknap Press, Harvard University Press; 1997.
25. Massey SC. Cell types using glutamate as a neurotransmitter in the vertebrate retina. Prog Retinal Res. 1990;9:399–425.
26. Trifonov YA. Study of synaptic transmission between the photoreceptor and the horizontal cell using electrical stimulation of the retina. Biofizika. 1968;10:673–680.
27. Werblin FS, Dowling JE. Organization of the retina of the mudpuppy, *Necturus maculosus*. II. Intracellular recording. J Neurophysiol. 1969;32:339–355. PubMed PMID: 4306897.
28. Werblin F. Synaptic connections, receptive fields, and patterns of activity in the tiger salamander retina. Invest Ophthalmol Vis Sci. 1991;32:459–483. PubMed PMID: 2001922.
29. Nawy S, Jahr CE. Suppression by glutamate of cGMP activated conductance in retinal bipolar cells. Nature. 1990;346:269–271. PubMed PMID: 1695713.
30. Dhingra A, Lyubarsky A, Jiang M, Pugh EN Jr, Birnbaumer L, Sterling P, Vardi N. The light response of ON bipolar neurons requires Gαo. J Neurosci. 2000;20:9053–9058. PubMed PMID: 11124982.

31. Slaughter MM, Miller RF. 2-Amino-4-phosphonobutyric acid: a new pharmacological tool for retina research. Science. 1981;211:182–184. PubMed PMID: 6255566.
32. Slaughter MM, Miller RF. An excitatory amino acid antagonist blocks cone input to sign-conserving second-order retinal neurons. Science. 1983;219:1230–1232. PubMed PMID: 6131536.
33. Baylor DA, Fuortes MGF, O'Bryan PM. Receptive fields of cones in the retina of the turtle. J Physiol. 1971;214:265–294. PubMed PMID: 5579638.
34. Djamgoz MBA, Kolb H. Ultrastructural and functional connectivity of intracellularly stained neurones in the vertebrate retina: correlative analyses. Microscopy Res Techniques. 1993;24:43–66.

Inner Plexiform Layer

Helga Kolb

Created: January 1, 2001; Updated: March 30, 2007.

Bipolar, Amacrine, and Ganglion Cells Interact in the Inner Plexiform Layer

The axonal endings of bipolar cells bring information from the outer plexiform layer (OPL) to the neuropil of the inner plexiform layer (IPL) (Figure 1). Here bipolar cells talk to different varieties of functionally specialized amacrine cells and to dendrites of the various ganglion cells. The neuropil is a confusing network of interconnecting profiles that, to be understood, has to be investigated at the higher magnification afforded by the electron microscope (over the light microscope) (Figure 2) and with knowledge gained from Golgi-staining for morphology and intracellular electrophysiology for function of individual cells in the network.

Ultrastructure of the Neuropil of the Inner Plexiform Layer

A view of a small part of the neuropil of the inner plexiform layer is shown in the electron micrograph (Figure 3). Bipolar cell axon terminals (Figure 3, red profiles) are vesicle-filled profiles, containing irregular, long mitochondria and neurotubules. Their synapses are typified by a small synaptic ribbon pointing into a wedge with two post synaptic profiles (known as a dyad) at the apex (Figure 4, red dots in bipolar cell profiles) (1). Amacrine cell dendrites are also vesicle filled and have round mitochondria and sometimes neurofilaments as well as neurotubules. Amacrine profiles vary between being very small cross-sections through thin straight tubes and being larger varicosities budding off the dendrites.

Typically, amacrine cells synapse upon other profiles (bipolar axons, amacrine cells, or ganglion cell dendrites) in the enlarged varicosities at what is known as a conventional synapse: the synapse consists of synaptic vesicles clustered at a pre- and post-membrane density (Figure 4, yellow dots in amacrine profile) (1). Ganglion cell dendrites (Figure 3, yellow profiles) are recognizable as profiles lacking synaptic vesicles but containing ribosomes, neurotubules, and filaments. Ganglion cell dendrites are seen to be postsynaptic to bipolar ribbon synapses and amacrine conventional synapses. Bipolar cells are also postsynaptic to many amacrine synapses. Often amacrine cells make what are called reciprocal synapses to the bipolar cell axons from which they receive ribbon synapses (Figure 4, yellow dots).

This reciprocal synapse is in essence a feedback synapse to the bipolar cell axon in the inner plexiform layer, with the same strategic importance as the horizontal cell dendrite making a feedback synapse at the photoreceptor ribbon synapse, in the outer plexiform layer. It will be remembered that such a local circuit in the outer plexiform layer was thought to provide the bipolar cell response with a center-surround organization. It has been suggested that another surround mechanism coming from the amacrine cells could be added at this reciprocal (feed-back) synapse in the inner plexiform layer.

Different Morphological Types of Amacrine and Ganglion Cells

It is clear that there are many different kinds of amacrine cell and ganglion cell branchings in the IPL of the human retina. From Golgi-staining studies, we know that there are at least 25 different amacrine cell types in the monkey and human retinas (2, 3). Some drawings of different amacrine cells as seen after Golgi-staining in wholemounts of human retina are shown in Figure 5.

The amacrine cells are classified into different types based on morphological characteristics of dendritic tree size, such as small, medium, and large branching characteristics (i.e., tufted, varicose, linear, beaded, and radiate) and, most importantly, on the stratification of their dendrites in the IPL (2, 3). The neuropil of the IPL was arbitrarily

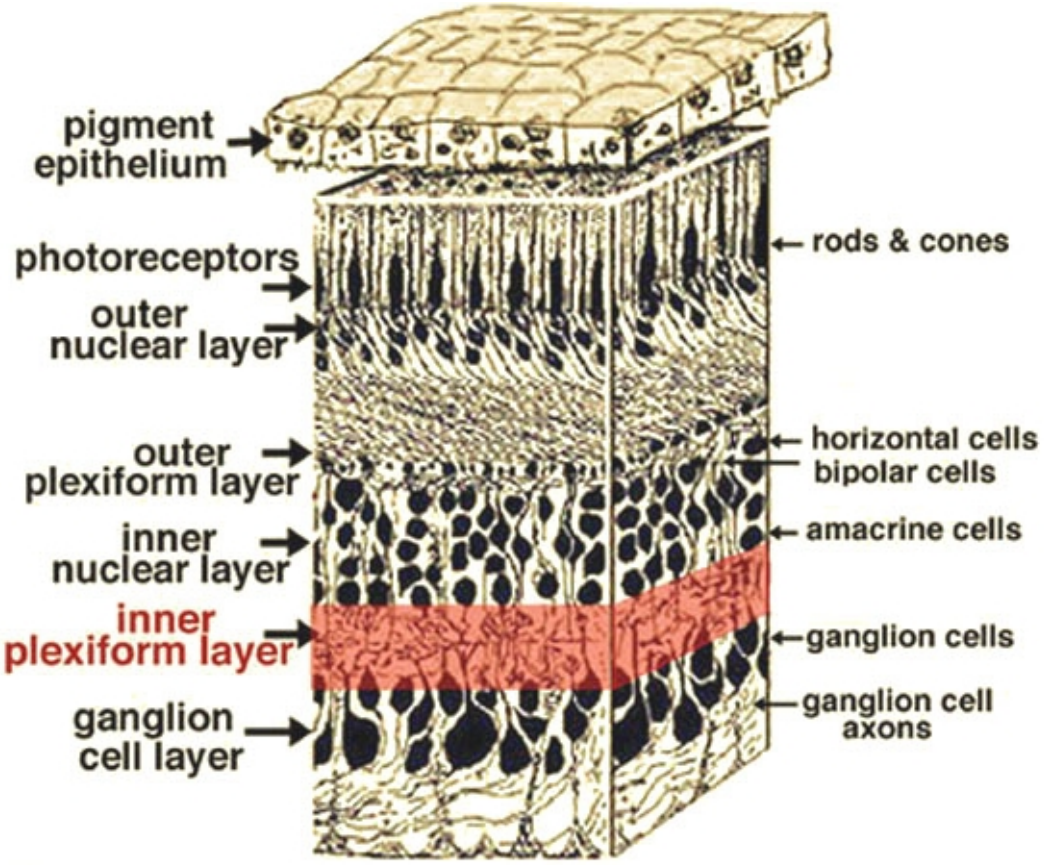

Figure 1. 3-D block of retina with the inner plexiform layer highlighted (red).

divided into five strata by Cajal (4), because he appreciated the fact that cells branching in disparate strata could **not** make synaptic interactions, whereas those that costratified could. This five-strata, descriptive classification scheme has been used by morphologists since that time to classify retinal cells on their dendritic branching level. See, for example, that in Figure 6, some amacrine cells have dendrites in strata 1 and 2 (called broadly stratified types; Figure 6, cell 8) or strata 1 and 5 (called bistratified types; Figure 6, cell 1), stratum 1, or any of the five strata (called monostratified; Figure 6, cell 13) or dendrites through all strata 1 to 5 (called diffuse types; Figure 6, cells 12 and 14).

In Figure 6, the amacrine cells have been stained by the Golgi procedure which, as we have seen, is very good for showing the isolated complete shape and size of a nerve cell. Newer techniques are also providing valuable information on cell shapes and sizes: techniques such as using intracellular staining through a microelectrode, and immunocytochemistry to stain cells with antibodies to their neurotransmitter or synthesizing enzymes.

These are some different amacrine cell types stained by injection of dyes through a microelectrode inserted into the cell body. The cells that look like exploding fireworks are called "starburst" cells and are known to use acetylcholine as their neurotransmitter (Figure 7) (5-7).

Another type of amacrine cell, thought to contain serotonin as a neurotransmitter, has been stained by the same technique (Figure 8) (8).

Using similar morphological techniques of Golgi staining, immunocytochemisry, and intracellular staining, the ganglion cells of the retina have been classified into various different types (Figure 9, Figure 10). As many as 25 different types exist in mammalian and human retinas, a few of which are shown in both sectioned view (Figure 9) and wholemount view (Figure 10). As with the amacrine cells, ganglion cells are classified onto the different

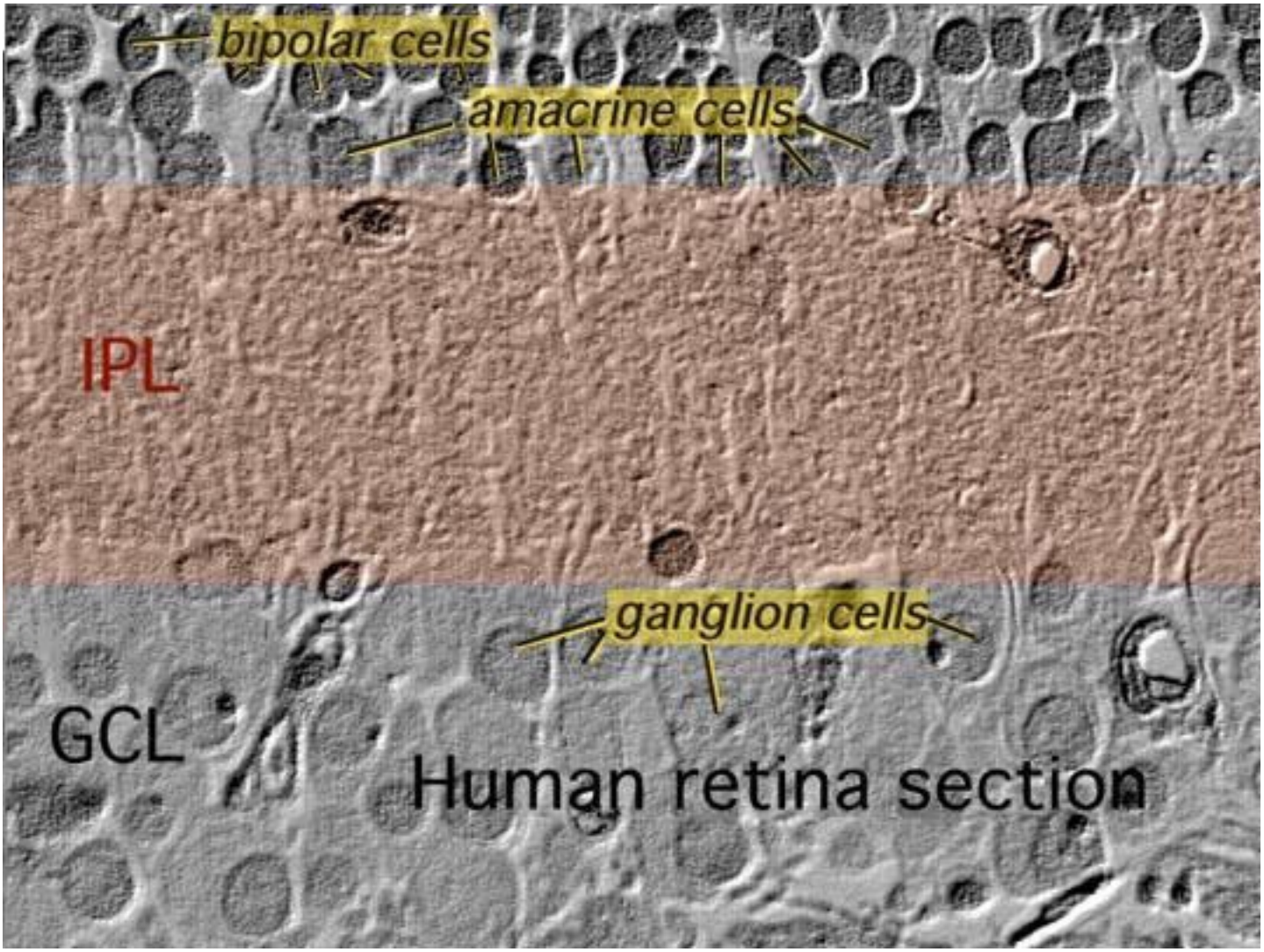

Figure 2. Light micrograph of a vertical section of the human retina to show the inner plexiform layer (IPL).

types by cell body size, dendritic tree spread, branching patterns (e.g., radiate or tufted), and branching level in the five strata of the IPL. In both cat and human retinas, ganglion cells can be from small to large, diffuse, bistratified, and various monostratified, large-field types with different stratification levels in the inner plexiform layer.

Both amacrine and ganglion cells increase in dendritic tree span with eccentricity from the fovea. The very smallest dendritic fields for all cells types being possessed by cells of the fovea or area centralis are shown in Figure 11 for the common ganglion cells of the cat retina (alpha and beta types). The same ganglion cell types are ten times the size in dendritic tree spread in peripheral retina (9, 10). For this reason, classification of amacrines and ganglion cells has to always take eccentricity from the fovea into account and compare cells in similar areas of retina to be sure that they are indeed different cell types.

In the human retina, the commonest ganglion cell types are the parasol and the midget ganglion cells, shown in Figure 12 (3, 11-13). They are also known as P cells (midget ganglion cells), because of their projection to the parvocellular layers, and M cells (parasol ganglion cells), because of their projection to the magnocellular layers of the lateral geniculate nucleus (14). We shall return to these ganglion cell types in a later chapter.

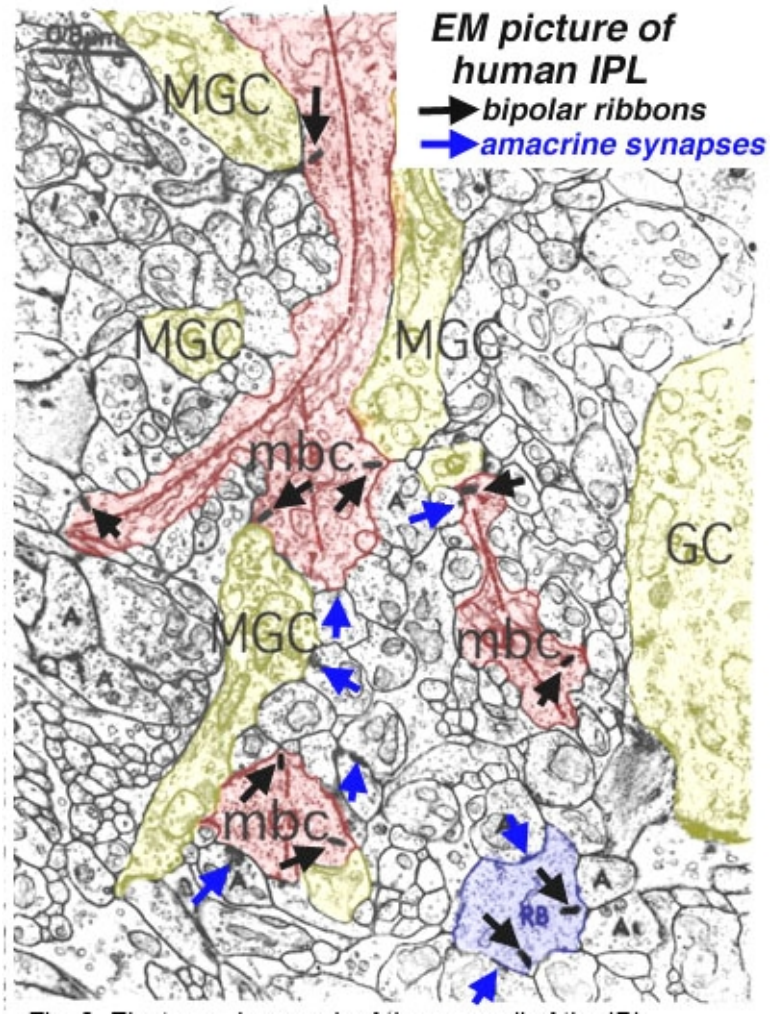

Figure 3. Electron micrograph of the neuropil of the IPL.

Stratification of Amacrine and Ganglion Cells in Relationship to Bipolar Cell Axons

One may ask why amacrine cells and ganglion cells should be classified on stratification level of their dendrites, particularly if they look the same in other respects, such as field size, cell body size, and dendritic morphology. It was already clear to Cajal (4) 100 years ago that dendrites of amacrine and ganglion cells and axons of bipolar cells were arranged to costratify in some meaningful manner. The meaning of costratifications and orderly arrangements of branching levels, other than the obvious of making sure certain cell types made synapses with certain other cell types, escaped him though.

We had to wait for 70 years before the answer was found in the physiological responses of the different nerve cells of the retina. In the 1970s, it became possible to make intracellular recordings from the neurons of the retina with dye-filled glass microelectrodes. Physiologists were able to record both the response of the impaled cell to light and to fill the cell with a fluorescent dye, such as Lucifer, to see what type of cell it was (Figure 13, left) (see the animation of the ionotophoresis of Lucifer dye into a ganglion cell via a microelectrode and see the animation of the physiological recording procedure).

In the 1950s and 1960s, it became apparent from ganglion cell recordings in the mammalian retina that the visual message leaving the retina was in the form of ganglion cell axon spike discharges that occurred either

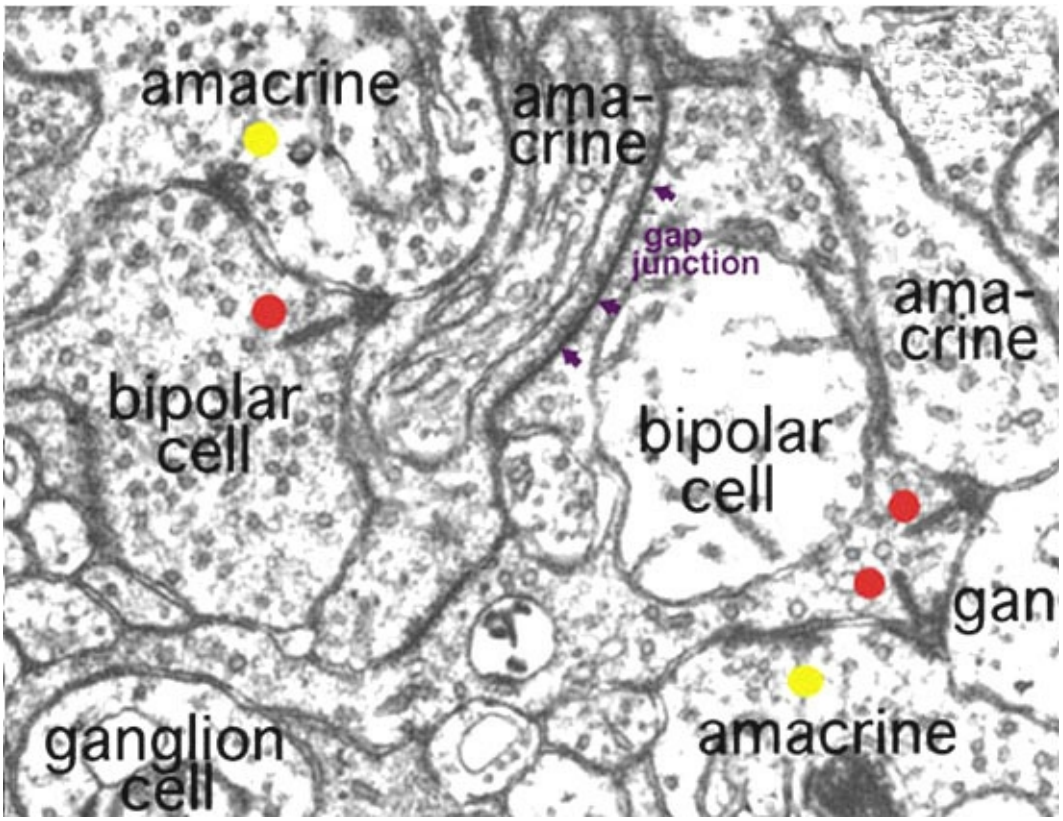

Figure 4. Electron micrograph of reciprocal synapses in the IPL.

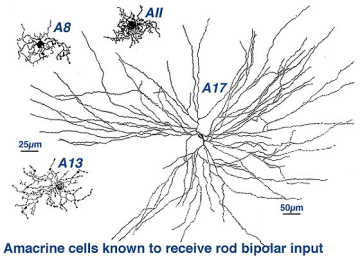

Figure 5. Amacrine cells in human retina.

when a spot of light stimulated the retina (ON discharge to light) or when the spot of light was turned off (OFF discharge). Ganglion cells were responding to either one or the other of the change of state of light. The one group was stimulated by the light brighter than background and the other by light darker than background (15, 16). Next came intracellular recordings from the five basic cell types in a mudpuppy retina, which revealed that cells preceding ganglion cells also fell into the two physiological types, i.e., bipolar and amacrine cells could give ON or OFF discharges (17, 18). Knowing now that bipolar cells could be ON- or OFF-center to a spot of light (they could have the opposite response in a surround concentrically around their central receptive field; mentioned in the chapter on the outer plexiform layer and dealt with in detail in later chapters on circuitry for rod and cone signals), it was reasonable to suggest that OFF-center bipolar chains excited OFF ganglion cells, and that ON-center bipolar cell chains excited ON ganglion cells. The typical bipolar cell types that might form the bipolar chains driving ganglion cells of the primate retina are shown in Figure 14.

These bipolar cells, as described in the previous section on the outer plexiform layer, make different types of synapses with cone pedicles and rod spherules. Some types make basal contacts on the surface of the cone

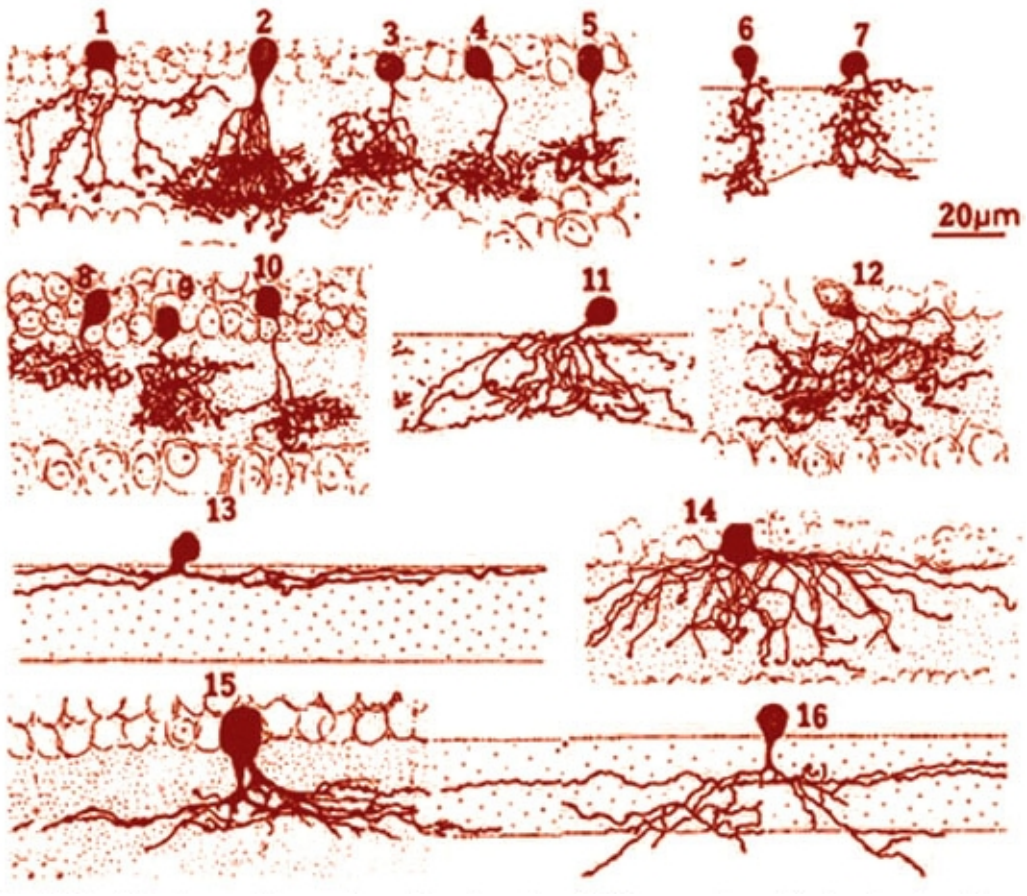

Figure 6. Stratification of amacrine cells in human retina.

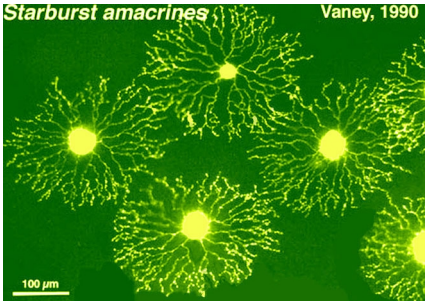

Figure 7. Starbust amacrine cells.

pedicles, and others make invaginating contact to end close to the synaptic ribbons in both rod spherules and cone pedicles.

It is now thought that bipolar cells respond to light just like the photoreceptor, with a slow hyperpolarization when the bipolar dendrite is in the basal junction position. In contrast, the other type of contact, invaginating to the ribbon synapse, causes the bipolar to respond to light with an inverted sign compared with the photoreceptor. It gives a slow depolarizing response. Thus, the nature of the postsynaptic membrane channels on the cone bipolar cell dendrite is the important designator of the response sign the bipolar will have. The hyperpolarizing bipolar types are the start of OFF-center channels, and the depolarizing types are the start of ON-center channels through the retina.

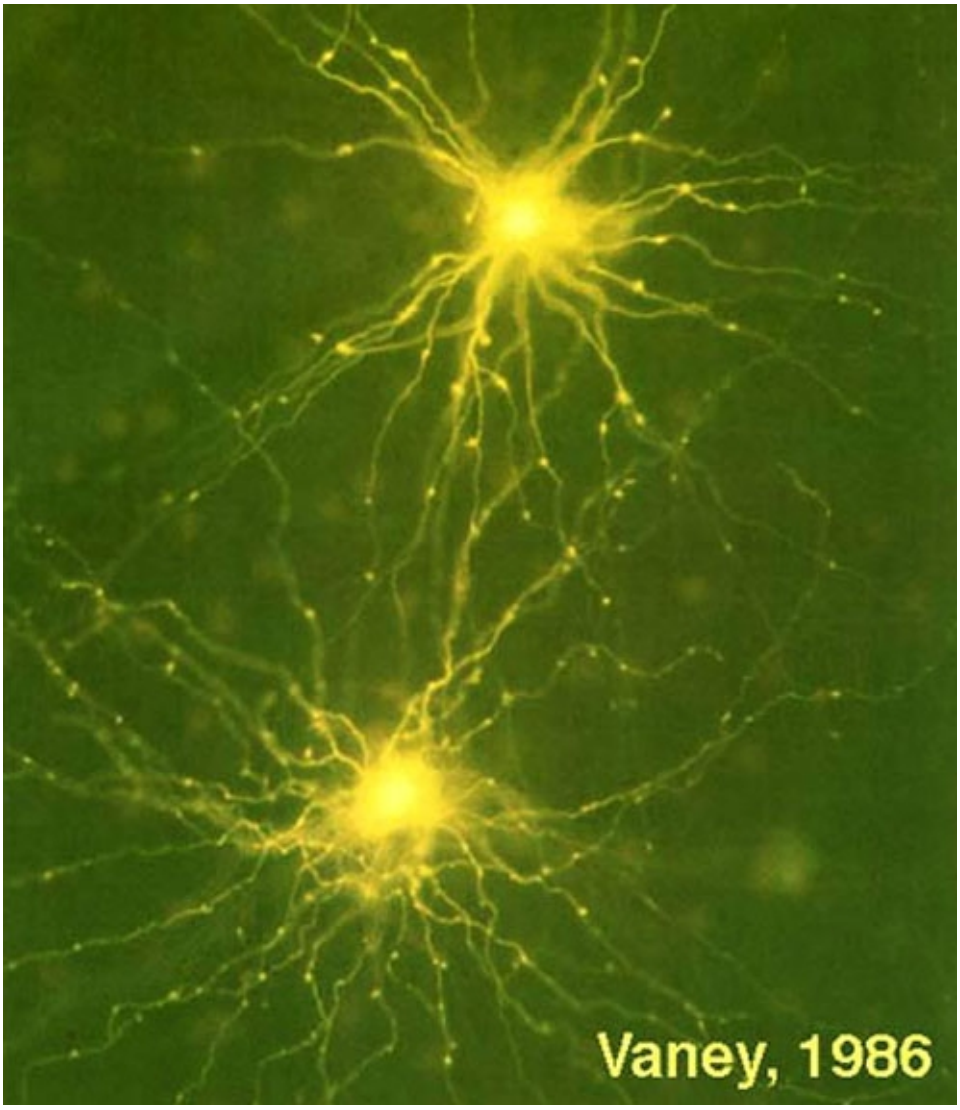

Figure 8. Serotonin-containing amacrine cells.

The bipolar cells shown in Figure 14 will be noticed to have different axonal ending levels in the inner plexiform layer, e.g., DB1 has an axon ending in the stratum 1 neuropil close to the amacrine cell layer of the inner nucelar layer, while imb has an axon ending at the opposite side of the inner plexiform layer in straum 5 against the ganglion cell bodies. It seems obvious now, but it took a lot of painstaking serial section recontruction to show (19, 20) that DB1 and imb made contacts only with ganglion cells that had dendritic stratification in the same neuropil as the respective bipolar axonal terminals. At the level of information transfer between bipolar cells and ganglion cells in the IPL, only excitatory channels are present (21), so the type of signal transmitted to the ganglion cell, as either ON- or OFF-center, is essentially determined by the bipolar cells contacting it (Figure 15).

To keep the ON and OFF channels separate through the ganglion cells to the brain, the inner plexiform layer is divided into two functionally discrete sublaminae, called **a** (the two strata below the amacrine cell bodies) and **b** (the other three strata stretching to the ganglion cell bodies) (22). Interactions are only allowed between basal-contacting cone bipolar types and one set of ganglion cells in sublamina **a**, whereas invaginating-contacting cone bipolar cells can interact only with another set of ganglion cells branching in sublamina **b** (see above). Gouras (1971) (23) was the first to suggest that this specificity of bipolar-to-ganglion-cell contacts underlay ON-center and OFF-center midget ganglion cell responses in monkey. Later, Nelson et al. (24) conclusively proved this

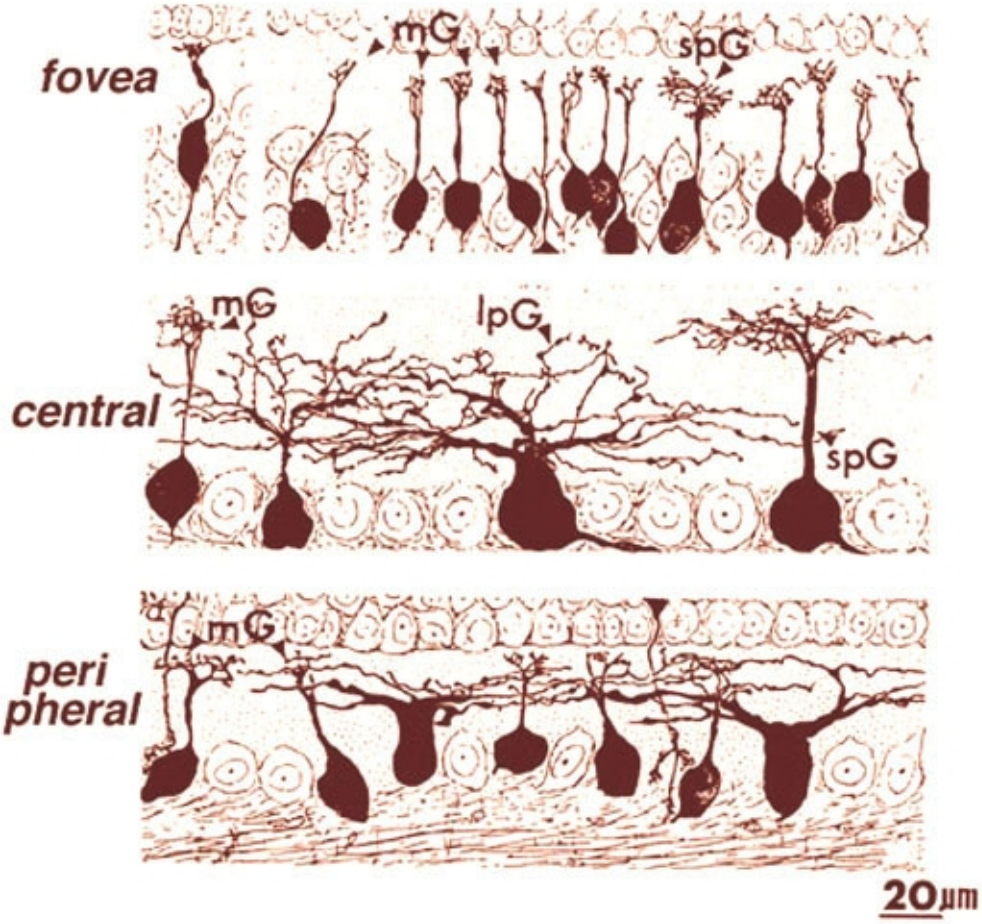

Figure 9. Sectioned view of ganglion cells.

hypothesis by means of intracellular recording and marking experiments in ganglion cells of cat (Figure 16) (see the animation of the physiological recording of ON and OFF beta ganglion cells).

Figure 16 shows the intracellular recordings made from two different ganglion cells of Nelson and coauthors' study (24). One cell proves to be ON-center, giving a burst of spikes riding on a depolarization of the membrane as soon as the light flash goes on. In contrast, the other cell is OFF-center, giving a hyperpolarization to the membrane when the light flash is on, but a burst of spikes riding on the depolarization when the light flash is over. The ON-center ganglion cell has dendrites restricted to branching in sublamina **b** and has synaptic input from invaginating types of bipolar cell. The OFF-center cell has dendrites reaching higher to branch only in sublamina **a** and gets synapses from basal junction contacting types of bipolar cell.

There is a definite functional architecture to the inner plexiform layer of the mammalian retina and, in fact, to all vertebrate retinas. Stratification of the neuropil is formed by specific levels of branching of bipolar, amacrine, and ganglion cells so that specialized circuits of interactions are set up. In addition, there has, during the course of evolution, been an imposition of a broad division of the two halves of the inner plexiform layer into the top half, allowing only interactions for the OFF-center ganglion cell pathways and in the bottom half, only for the ON-center ganglion cell pathways. Bipolar and ganglion cells are chiefly responsible for the bisublaminar organization, but amacrine cells, particularly if they are of the sustained physiological types, are also drawn in. However, many amacrine cells are diffuse or bistratified and serve to connect the ON- and OFF-center neuropils, whereas still others stratify in such a manner at the border between the two functional neuropils, to receive both ON and OFF inputs to drive them. Such amacrine cells may be in the majority in the vertebrate retina and are thought to be involved more in temporal facets of retinal performance. They may be important for fast transfer

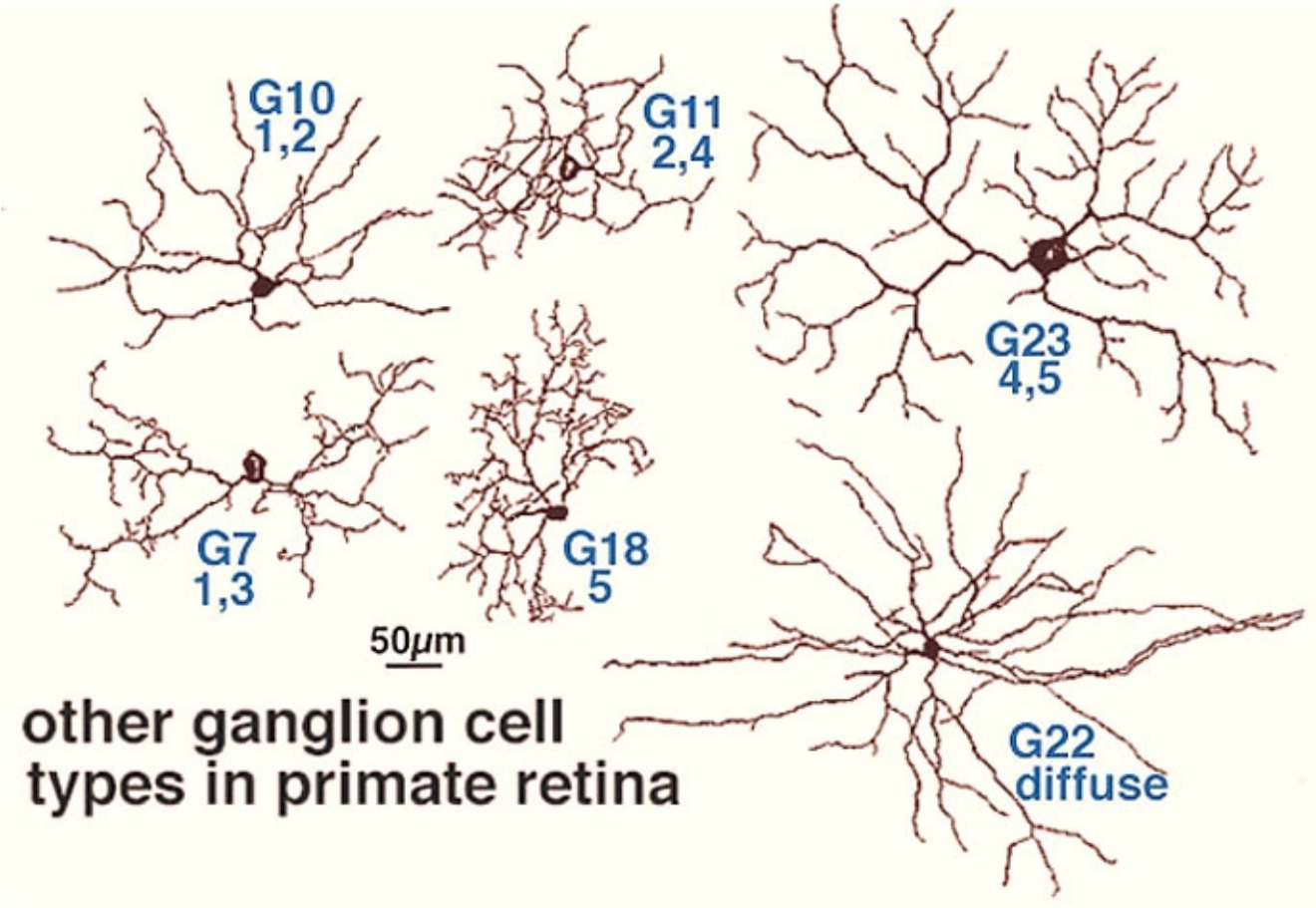

Figure 10. Wholemount view of Golgi-stained ganglion cells in primate retina.

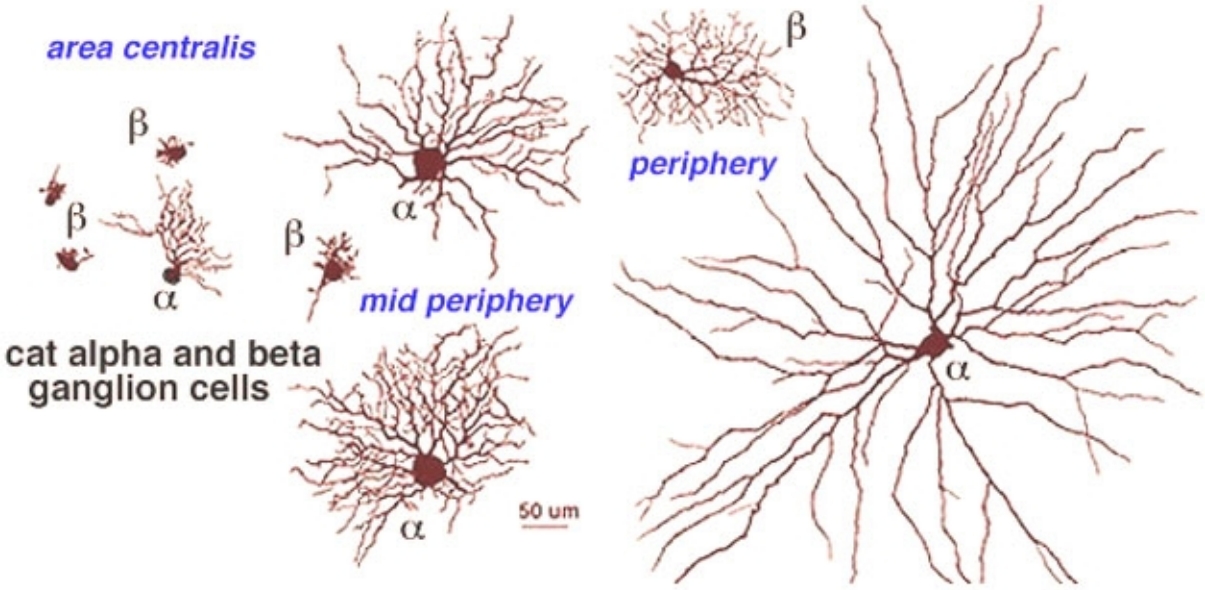

Figure 11. Cat ganglion cells.

of information, i.e., for speeding up signals The role of some of these amacrine cells will become clearer in later chapters.

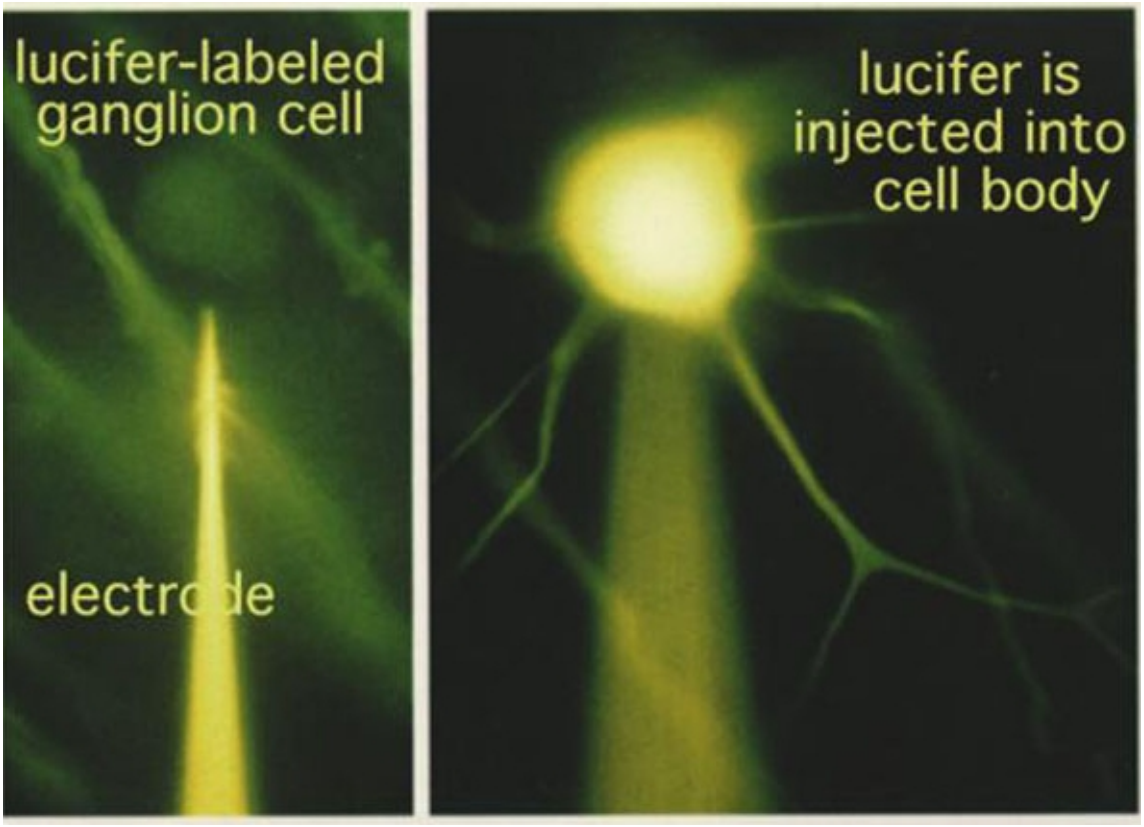

Figure 12. Primate ganglion cells.

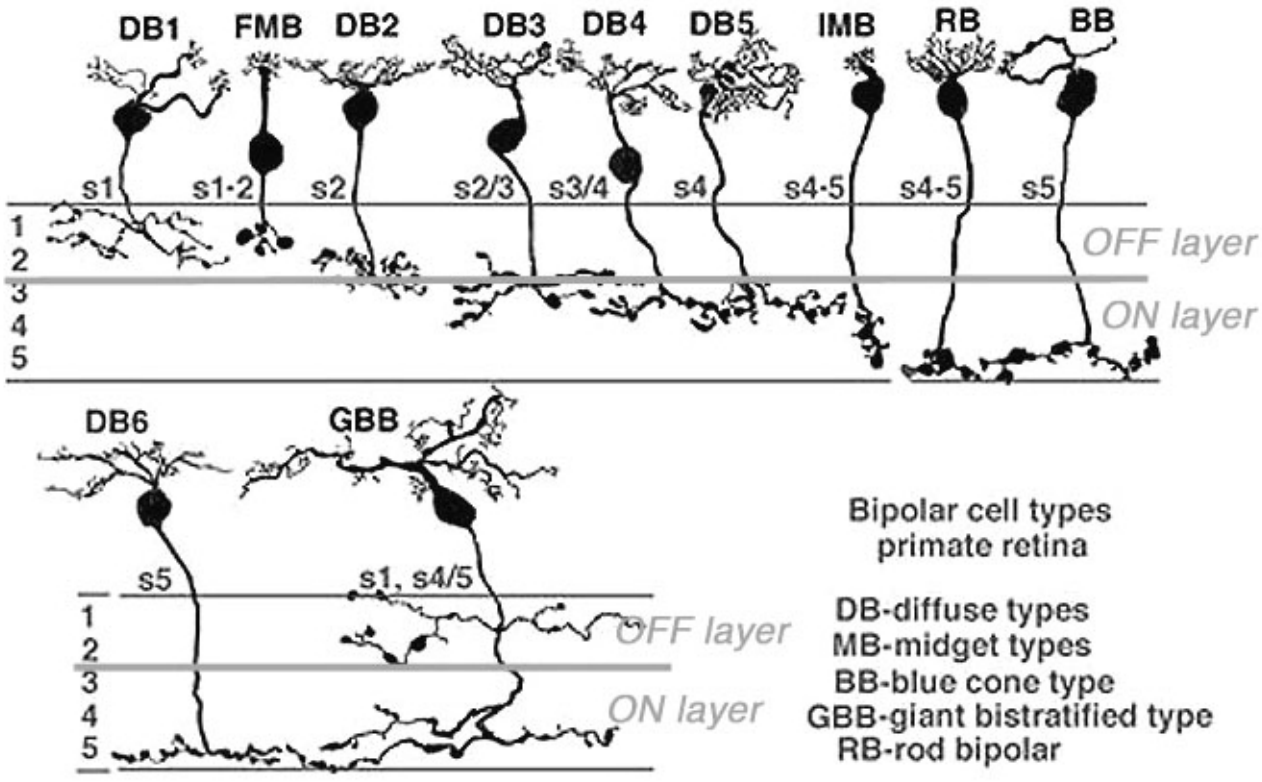

Figure 13. Experimental procedure for impaling ganglion cell in the retina.

Movie 1. An animation of the iontophoresis of Lucifer dye into a ganglion cell via a microlectrode.
Download video

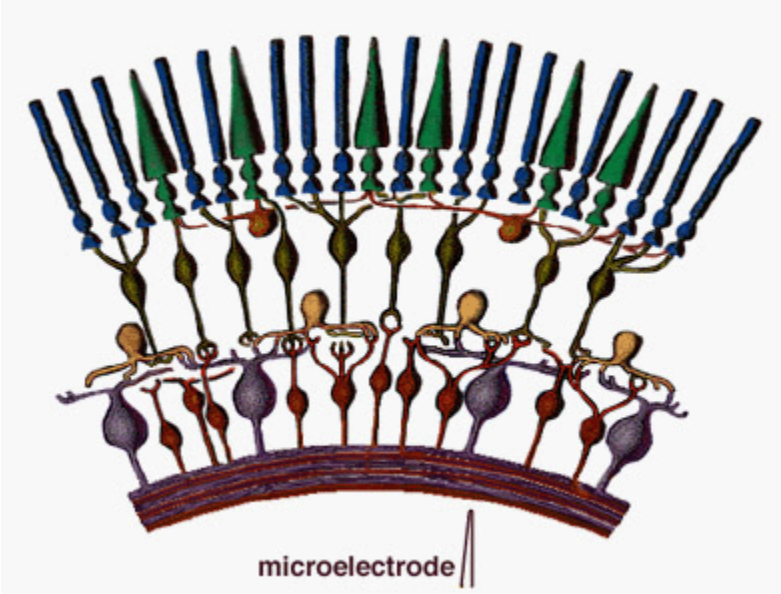

Movie 2. An animation of the physiological recording procedure.
Download video

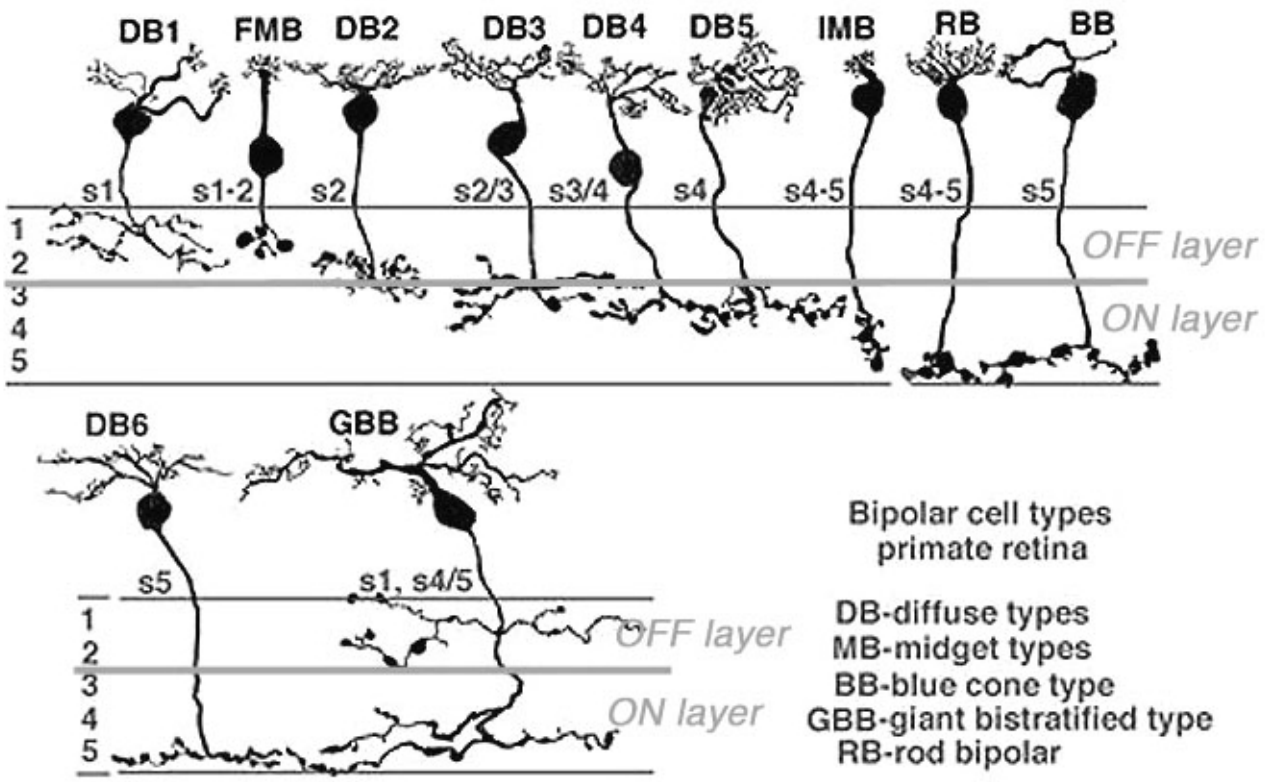

Figure 14. Bipolar cell types in human retina (from Golgi staining).

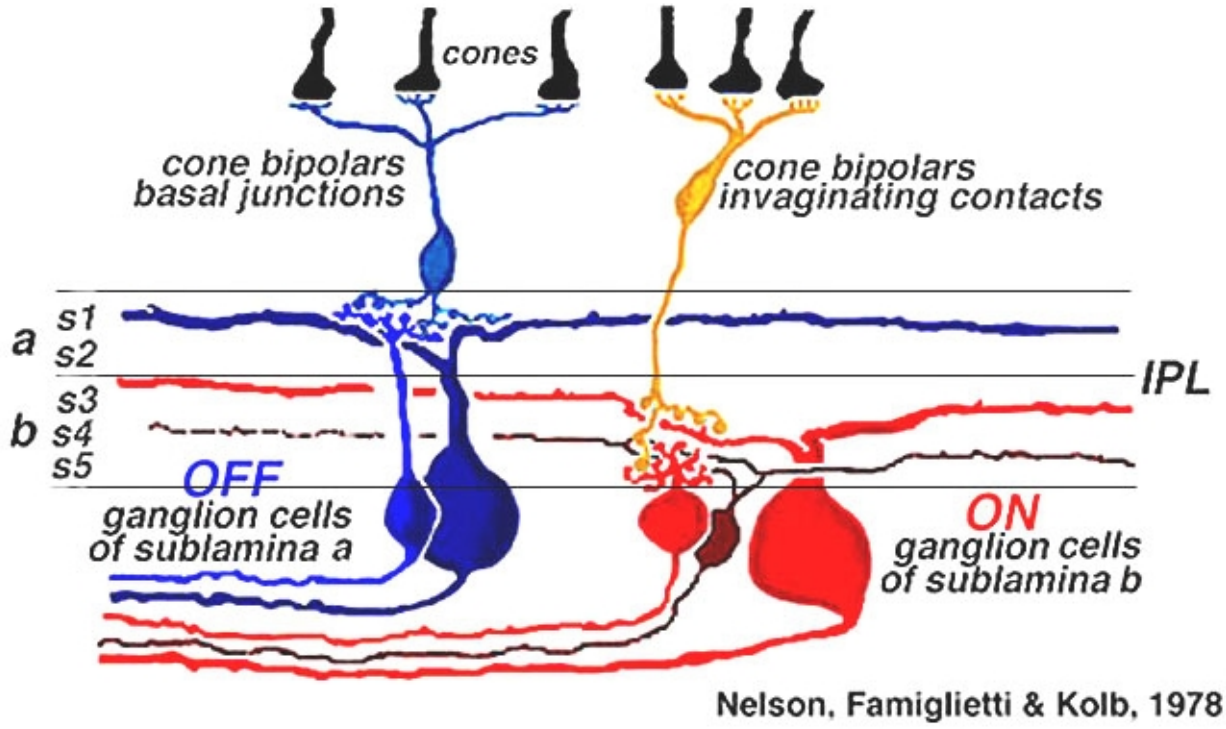

Figure 15. Organization of ON- and OFF-center ganglion cells.

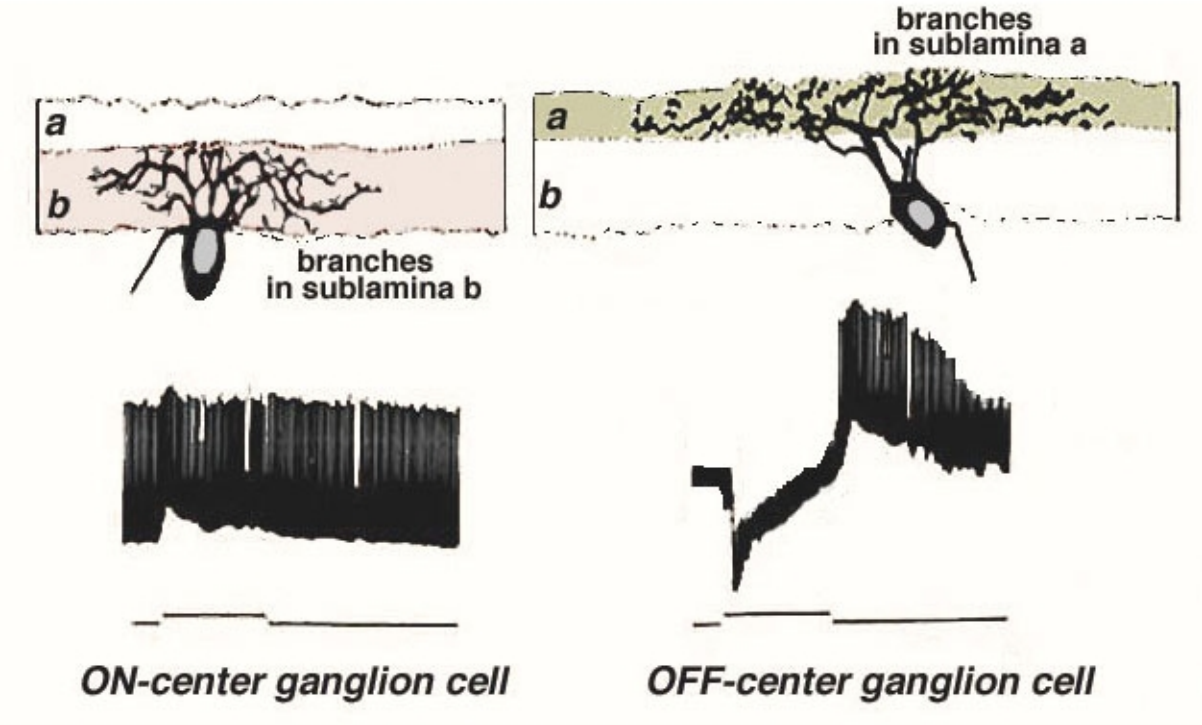

Figure 16. Intracellular recordings of ON-center and OFF-center ganglion cells.

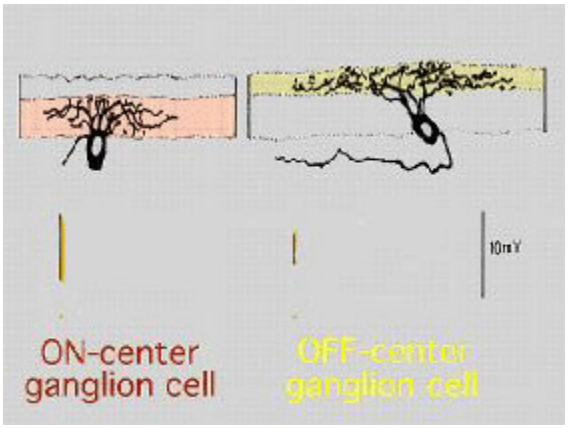

Movie 3. An animation of the physiological recording of ON and OFF beta ganglion cells.
Download video

References

1. Dowling JE, Boycott BB. Organization of the primate retina: electron microscopy. Proc R Soc Lond B Biol Sci. 1966;166:80–111. PubMed PMID: 4382694.
2. Mariani AP. Amacrine cells of the rhesus monkey retina. J Comp Neurol. 1990;301:382–400. PubMed PMID: 2262597.
3. Kolb H, Linberg KA, Fisher SK. The neurons of the human retina: a Golgi study. J Comp Neurol. 1992;318:147–187. PubMed PMID: 1374766.
4. Cajal SR. In: Thorpe SA, Glickstein M, translators. The structure of the retina. 1892. Springfield (IL): Thomas; 1972.

5. Famiglietti EV. 'Starburst' amacrine cells and cholinergic neurons: mirror-symmetric ON and OFF amacrine cells of rabbit retina. Brain Res. 1983;261:138–144. PubMed PMID: 6301622.
6. Masland RH. Amacrine cells. Trends Neurosci. 1988;11:405–410. PubMed PMID: 2469207.
7. Vaney DI. The mosaic of amacrine cells in the mammalian retina. Prog. Ret. Res. 1990;9:49–100.
8. Vaney DI. Morphological identification of serotonin-accumulating neurons in the living retina. Science. 1986;233:444–446. PubMed PMID: 3726538.
9. Boycott BB, Wassle H. The morphological types of ganglion cells of the domestic cat's retina. J Physiol. 1974;240:397–419. PubMed PMID: 4422168.
10. Kolb H, Nelson R, Mariani A. Amacrine cells, bipolar cells and ganglion cells of the cat retina: a Golgi study. Vision Res. 1981;21:1081–1114. PubMed PMID: 7314489.
11. Polyak SL. The retina. Chicago: University of Chicago Press; 1941.
12. Rodieck RW, Binmoeller KF, Dineen J. Parasol and midget ganglion cells of the human retina. J Comp Neurol. 1985;233:115–132. PubMed PMID: 3980768.
13. Dacey DM. The mosaic of midget ganglion cells in the human retina. J Neurosci. 1993;13:5334–5355. PubMed PMID: 8254378.
14. Shapley R, Perry VH. Cat and monkey retinal ganglion cells and their visual functional roles. Trends Neurosci. 1986;9:229–235.
15. Kuffler SW. Discharge patterns and functional organization of mammalian retina. J Neurophysiol. 1953;16:37–68. PubMed PMID: 13035466.
16. Enroth-Cugell C, Robson JG. The contrast sensitivity of retinal ganglion cells of the cat. J Physiol. 1966;187:517–552. PubMed PMID: 16783910.
17. Werblin FS, Dowling JE. Organization of the retina of the mudpuppy, Necturus maculosus. II. Intracellular recording. J Neurophysiol. 1969;32:339–355. PubMed PMID: 4306897.
18. Kaneko A. Physiological and morphological identification of horizontal, bipolar and amacrine cells in goldfish retina. J Physiol. 1970;207:623–633. PubMed PMID: 5499739.
19. Kolb H. The inner plexiform layer in the retina of the cat: electron microscopic observations. J Neurocytol. 1979;8:295–329. PubMed PMID: 490185.
20. Kolb H, DeKorver L. Midget ganglion cells of the parafovea of the human retina: a study by electron microscopy and serial section reconstructions. J Comp Neurol. 1991;303:617–636. PubMed PMID: 1707423.
21. Raviola E, Raviola G. Structure of the synaptic membranes in the inner plexiform layer of the retina: a freeze-fracture study in monkeys and rabbits. J Comp Neurol. 1982;209:233–248. PubMed PMID: 7130454.
22. Famiglietti EV, Kolb H. Structural basis for ON- and OFF-center responses in retinal ganglion cells. Science. 1976;194:193–195. PubMed PMID: 959847.
23. Gouras P. The function of the midget system in primate color vision. Vis Res. 1971;3:397–410. PubMed PMID: 5293881.
24. Nelson R, Famiglietti EV, Kolb H. Intracellular staining reveals different levels of stratification for on-center and off-center ganglion cells in the cat retina. J Neurophysiol. 1978;4:472–483.

Morphology and Circuitry of Ganglion Cells

Helga Kolb

Created: May 1, 2001; Updated: April 4, 2007.

General Morphology

Ganglion cells are the final output neurons of the vertebrate retina. The ganglion cell collects the electrical messages concerning the visual signal from the two layers of nerve cells preceding it in the retinal wiring scheme. A great deal of preprocessing has been accomplished by the neurons of the vertical pathways (photoreceptor to bipolar to ganglion cell chain), and by the lateral pathways (photoreceptor to horizontal cell to bipolar to a macrine to ganglion cell chain), before presentation to the ganglion cell, and so it represents the ultimate signaler to the brain of retinal information. Ganglion cells are larger on average than most preceding retinal inter neurons and have large diameter axons capable of passing the electrical signal, in the form of transient spike trains, to the retinal recipient areas of the brain many millimeters or centimeters distant from the retina. The optic nerve collects all of the axons of the ganglion cells, and this bundle of more than a million fibers (in humans, at least) then passes information to the next relay station in the brain for sorting and integrating into additional information-processing channels.

Cajal (1), in his monumental work on Golgi staining of the vertebrate retina, was able to classify many different varieties of ganglion cell based on form (dendritic morphology), extent (cell body and dendritic tree size), and number of sub layers in which they arborize (stratification levels in the inner plexiform layer). He considered the retina to be remarkably uniform across all vertebrates, differing only in respect to rod and cone specializations for **the visual sense of the animal**. Looking at Cajal's (1) drawings of dog ganglion cells as compared with the frog ganglion cell, for example, the former seem simpler in form than the latter cells (see Fig. 1 and Fig. 2), but we actually now know that there is a common evolutionary path taken by different ganglion cell types so that different morphological and functional classes are similar throughout the species. For example, the large ganglion cells, with open radiate branching patterns, process fast, transient impulse trains and, in all vertebrate retinas, are concerned with motion detection and alerting the animal to threatening, moving visual imagery, wherease small bushy ganglion cell types are concerned with processing small stationary, fine detail in tonically activated messages in all species.

In the 1940s, Polyak (2) produced a phenomenal description of the Golgi-impregnated neurons of the primate retina and therein he gave us a good classification of ganglion cell types (see chapter on Midget Pathways). So by the 1960s, we had a fairly extensive description and classification of the ganglion cells in mammalian and monkey retinas, but all the data were based on vertical sections of stained ganglion cells (1-6). The advent of a technique to perform Golgi staining on whole mount retinas allowed a reinterpretation of many of the earlier classifications, because now we could see the entire dendritic tree of a ganglion cell. The whole mounts could also be compared with images of intracellularly injected cells after physiological recordings (Fig. 3 and Fig. 4, and see the animation of the iontophoresis of Lucifer dye into a ganglion cell via a microlectrode).

A particularly successful morphological classification scheme was proposed by Boycott and Wassle (7). Three main classes of physiological response type were correlated with three morphological classes of ganglion cell in cat retina. Thus, the alpha, beta, gamma and delta morphological ganglion cell types were considered to be the equivalents of the Y, X, and W types of the physiology (reviewed in 7-11) (Fig. 5). By comparison with Cajal's drawings, it was clear that alpha and beta types were already described (see Cajal drawing of dog and ox retinal ganglion cells) and another 10 or more of Cajal's (1) types were lumped under the umbrella of gamma and delta groups.

By 1978, we knew that alpha and beta cells of Boycott and Wassle (7) could be subdivided into separate subtypes, depending on whether they branch in sublamina **a** or sublamina **b** of the inner plexiform layer (12) (see chapter

on Inner Plexiform Layer). Sublamina **a** contained dendrites of cells with physiologically defined OFF-center receptive fields and sublamina **b** dendrites of cell with ON-center receptive fields (13). A new classification of Golgi-stained ganglion cells (14) could now relate both alpha and beta cells to the functionally important sublamina scheme and further, described many new types of cells including and going beyond the gamma and delta cells. The 20 cell types over and above the alpha, beta, and gamma cells were named from G4 to G23 in order of cell body size and dendritic form (i.e., from smallest types, G4 to largest types at G23) (14).

Alpha and Beta Ganglion Cell Types of Mammalian Retinas

Alpha and beta ganglion cells of the cat retina are arranged in regular, superimposed bi-level mosaics across the whole retina (15, 16). Both OFF-center (branching in sublamina **a**) and ON-center (branching in sublamina **b**) varieties of alpha and beta cells are arranged in a closely packed pattern with minimal overlap of their peripheral dendrites. ON and OFF varieties are always paired as shown in the Wassle and coauthors elegant papers (15, 16) (Fig. 6 and Fig. 7), and between an ON/OFF pair there is sampling of almost the same retinal space (Fig. 7).

Both cell types have their smallest dendritic tree sizes at the area centralis of the cat retina (equivalent to the fovea of primate retinas) and radiate out from this central point with gradually expanding circular dendritic trees. To maintain the low overlap ratio of their dendritic trees, the cells with larger fields are consequently spaced at greater intervals from each other, i.e., density of the cells/mm^2 of retina is inversely proportional to distance from the area centralis. This is shown in Fig. 8, where the increase of ganglion cell size as shown with distance from the area centralis (a.c.): peripheral alpha and beta retinal ganglion cells are 10-fold larger than their area centralis relatives.

Non-Alpha and Non-Beta Ganglion Cell Types in Mammalian Retinas

It has been estimated that between 50% and 60% of all ganglion cells in the cat retina are cells other than alpha and beta types (17, 18). Alpha cells form 3% and beta cells 45-50%. A Golgi study by Kolb and coauthors (14) indicated that 21 different morphological types of ganglion cell were of the non-alpha/non-beta cells classes (some of them are shown in Fig. 9, and others are shown in the human ganglion cell section). The G3 was the equivalent of the gamma cell of Boycott and Wassle (7) (Fig. 5). G3 may be a concentrically organized type of W cell (9, 18), and according to Kolb and coauthors (14), comes in ON- and OFF-sublaminal branching subtypes. G19 cells equivalent to delta cells of Boycott and Wassle (7) (Fig. 5) probably also come in the ON- and OFF subtypes (19-21). Diffuse wide-field G4 and monostratifying G18 cells are probably equivalent to two different OFF-tonic cells and G15 to an ON-directional cell (22). G19, which is similar to one type of delta cell of Boycott and Wassle (7), may be an ON-tonic cell, whereas G22 is almost certainly an ON/OFF phasic type (22). The newly described Q cell of Troy et al (23). may also be the physiological correlate of an ON-delta morphological type. Ganglion cells with the morphology of G21 and G23 are labeled by retrograde transport of tracers from brain visual centers: G21 from the accessory optic system (24). The speculation is that G21 is a directionally selective ganglion cell, because cells of the accessory optic system are reported to be directionally selective (25). A ganglion cell type that could be a G23 type has been labeled from retrograde markers injected into the retinal recipient zone (RRZ) in the pulvinar (26) and has been named the epsilon cell. However, the staining of epsilon cells has never been good enough to be sure which Golgi type it really is.

Other ganglion cell types that have been reported using tracer or other staining techniques than the Golgi method include the medium-gamma cells, g1 and g2 cells (not clear which Golgi types these are) (27), Neuropeptide Y immunoreactive (NPY-IR) cells (28), ganglion cells of the geniculate wing (29), and indoleamine-containing ganglion cells likened to delta cells (21, 30).

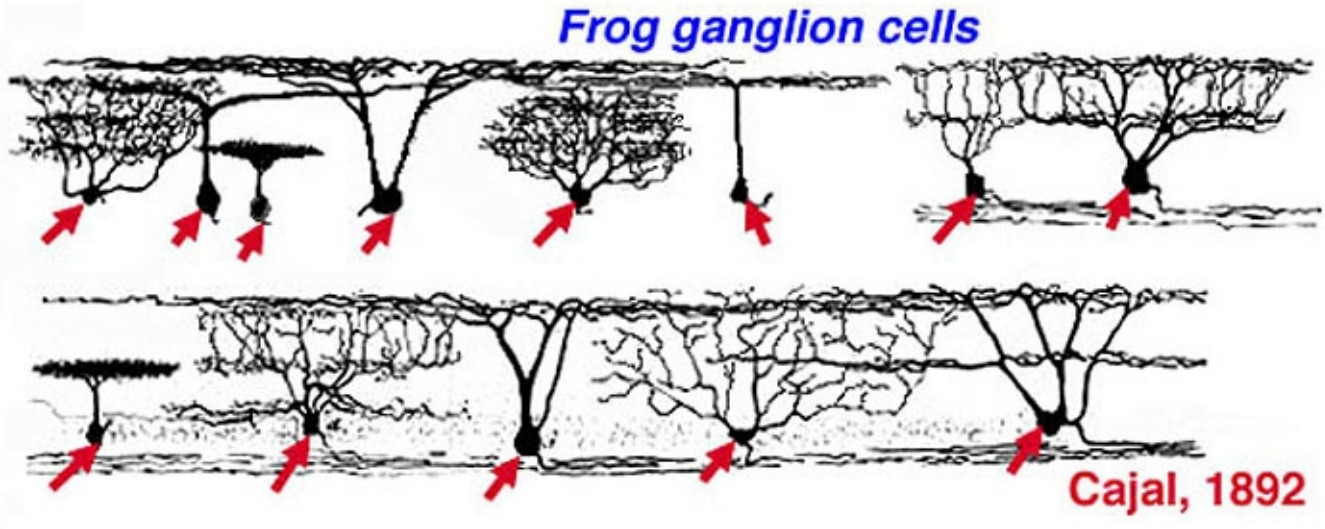

Figure 1. Cajal's drawing of ganglion cells of the frog's retina.

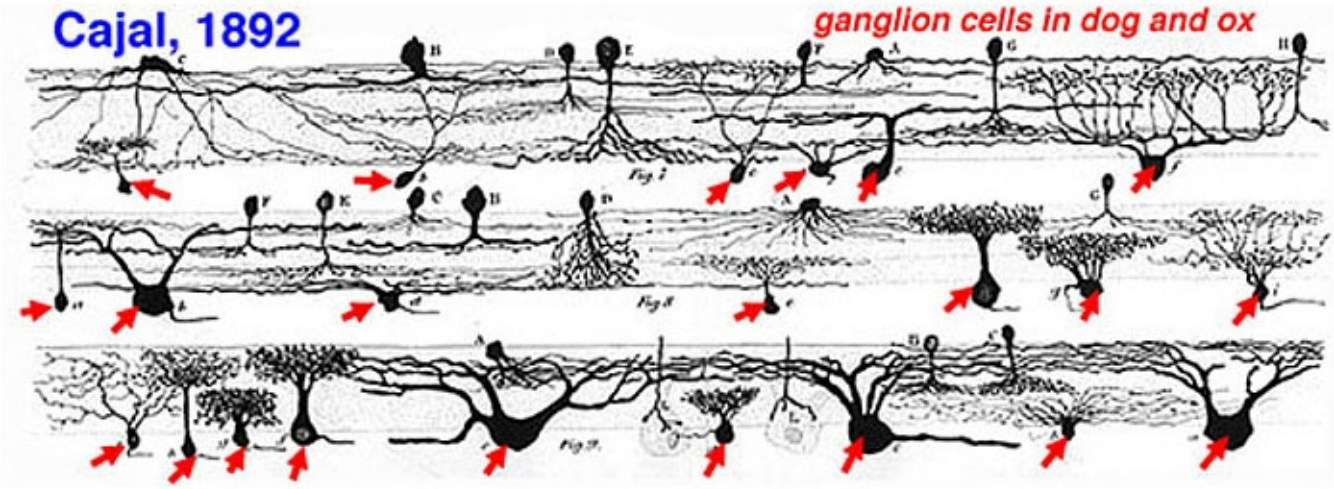

Figure 2. Cajal's drawing of ganglion cells of ox and dog retinas.

Convergence of Photoreceptors and Second-Order Neurons to Cat Retinal Ganglion Cells

The organization of the cat retina with a concentration of small-field beta cells in the area centralis allows the lowest convergence ratio of cone photoreceptors to ganglion cells. This is presumed to be the substrate for the high-acuity pathways. The human (primate) retina culminates this trend with the development of the midget system and the photoreceptor to ganglion cell pathway to a one-to-one relationship of course (see chapter on midget pathways).

An electron microscope analysis, of two area centralis beta cells in the cat, showed that each ganglion cell received input from three or four cone bipolars which, in turn, received input from four to eight cones (15, 16, 31) (Fig. 10). Another OFF-center beta ganglion cell has been calculated to have 14 definite bipolar cell axon terminals inputting the dendrites (Fig. 11, four bipolar axons shown in red, arrows). Thus, this type of ganglion

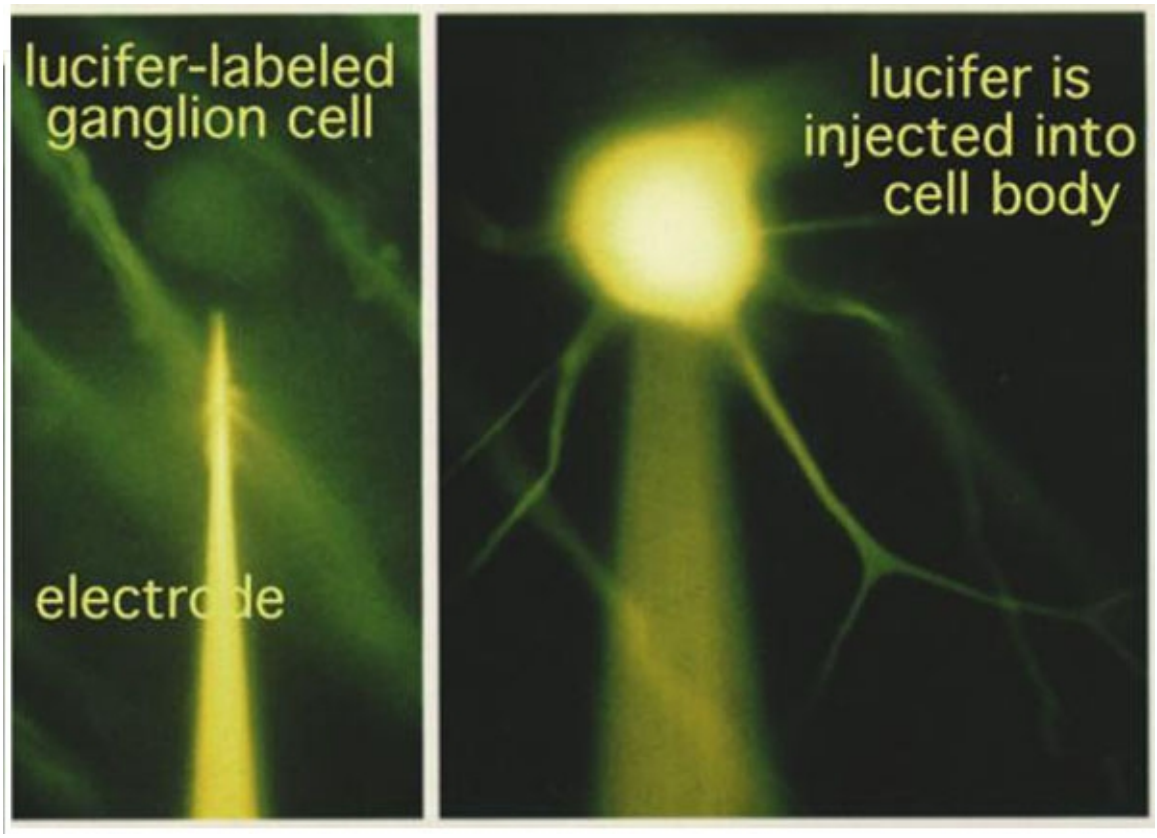

Figure 3. Experimental procedure for impaling ganglion cells and injecting lucifer dye in the retina. (Courtesy of Josef Ammermuller.)

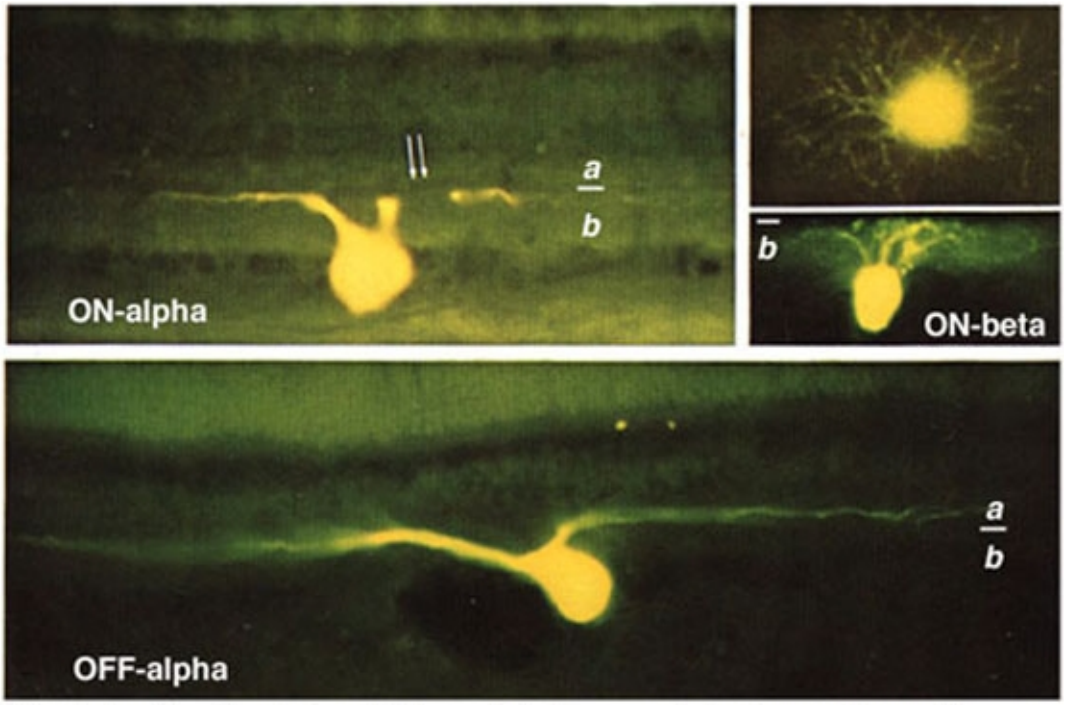

Figure 4. Lucifer-injected and intracellularly recorded cat ganglion cells.

cell would have convergence of approximately 100 cones through the 14 bipolar cells of two subtypes (see Fig. 12 and Fig. 13, small-field (yellow) and large-field (red) types of cone bipolar).

Movie 1. An animation of the iontophoresis of Lucifer dye into a ganglion cell.
Download video

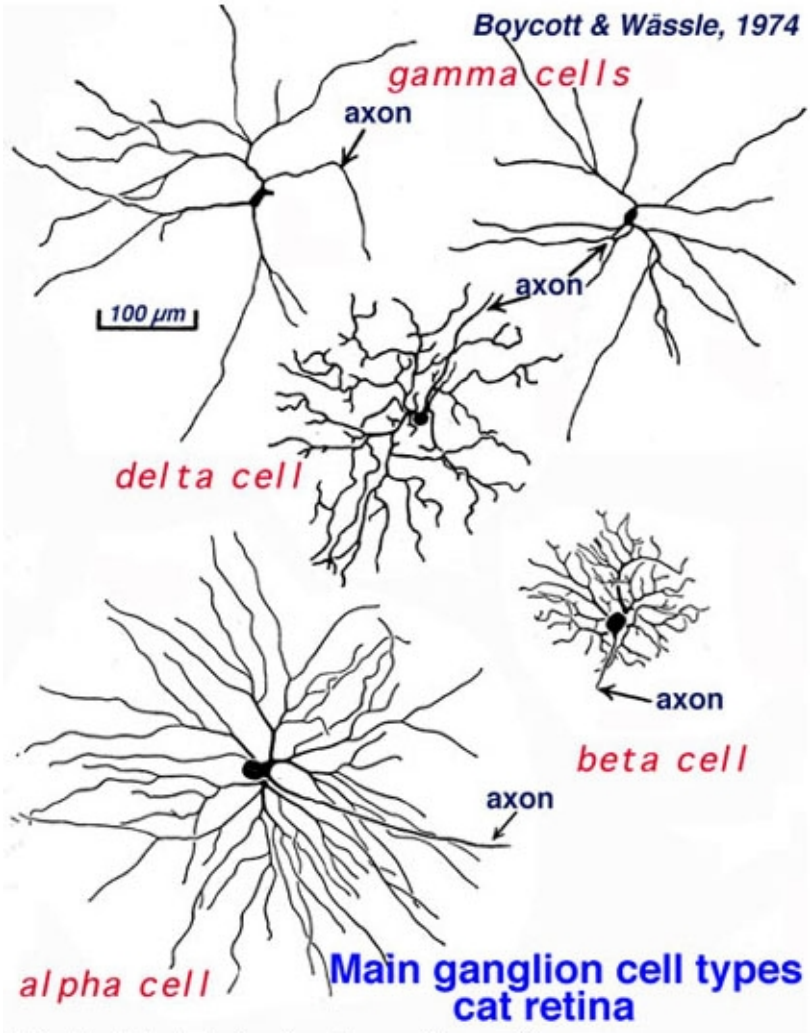

Figure 5. Golgi-stained cat ganglion cells.

It is also calculated that about 14 AII amacrine cells (Fig. 13, purple cells) would also have input, thereby converging 4200 rods through 280 rod bipolar cells to the 14 AII cells of input (Fig. 18). In addition, 28 to 41

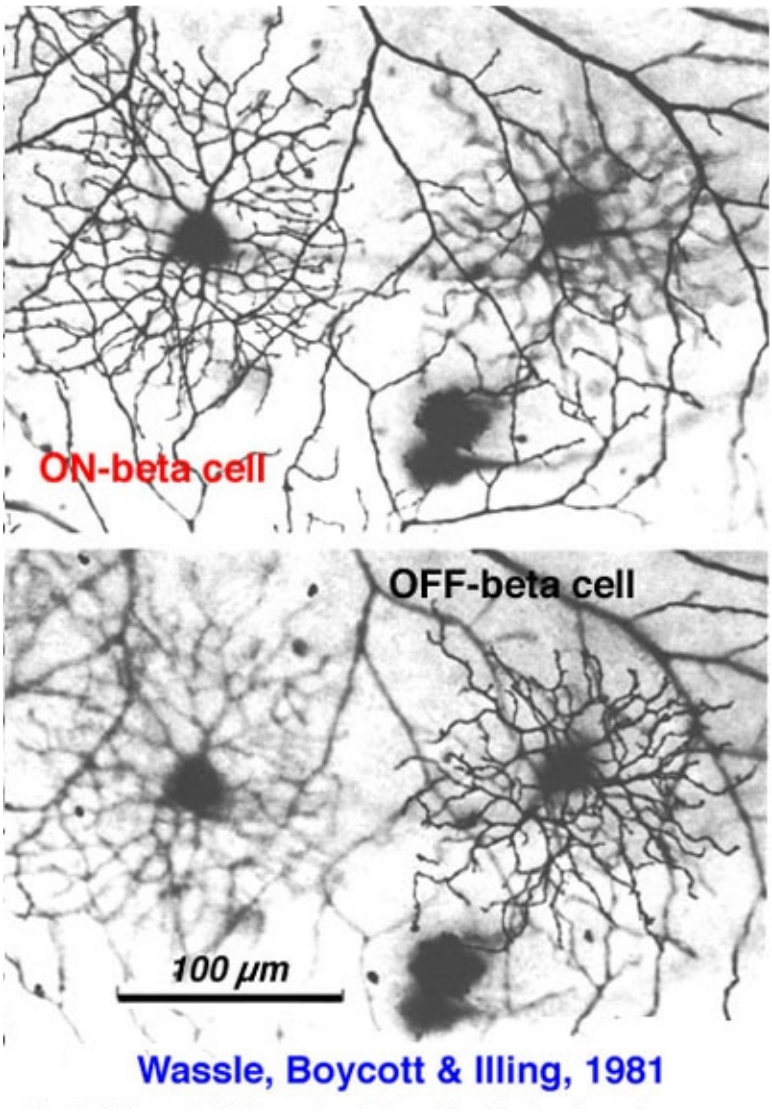

Figure 6. ON- and OFF-center beta cells of cat retina shown at different planes of focus.

other amacrine cells probably have synapses, allowing even more convergence over a greater laterally spreading area than the ganglion cells dendritic tree diameter would have.

In the same vein, we have information on convergence of bipolar cells and amacrine cells upon both ON-center and OFF-center alpha ganglion cells (32, 33). In the model of the OFF-center alpha cell seen in Fig. 14 and Fig. 15, cone bipolar synapses, from only one type of OFF-center cone bipolar (cb2 type, red dots), form 20% of the total synaptic input, and the rest of the input is from various kinds of amacrine cells. A minimum of 142 bipolar cells, 256 AII amacrine cells, and 1,011 other amacrine cells, together, provide between 6,000 and 10,000 synapses on the dendritic tree of this OFF-center alpha ganglion cell. With a potential cone convergence of 5-15 cones per bipolar cell, it is possible that 15,000 cones could ultimately be involved in the capture area of this type of ganglion cell.

In the case of the rod system, the convergence of preceding neurons to the ganglion cell is enormous, i.e., calculated by Sterling et al. (34) to be 75,000 rods through 5,000 rod bipolar cells to 250 AII amacrine cells to a single alpha cell (Fig. 11). The other amacrine cell input and their corresponding convergences are not capable of being assessed at the present time. Interestingly though, physiological measures of receptive field center sizes of

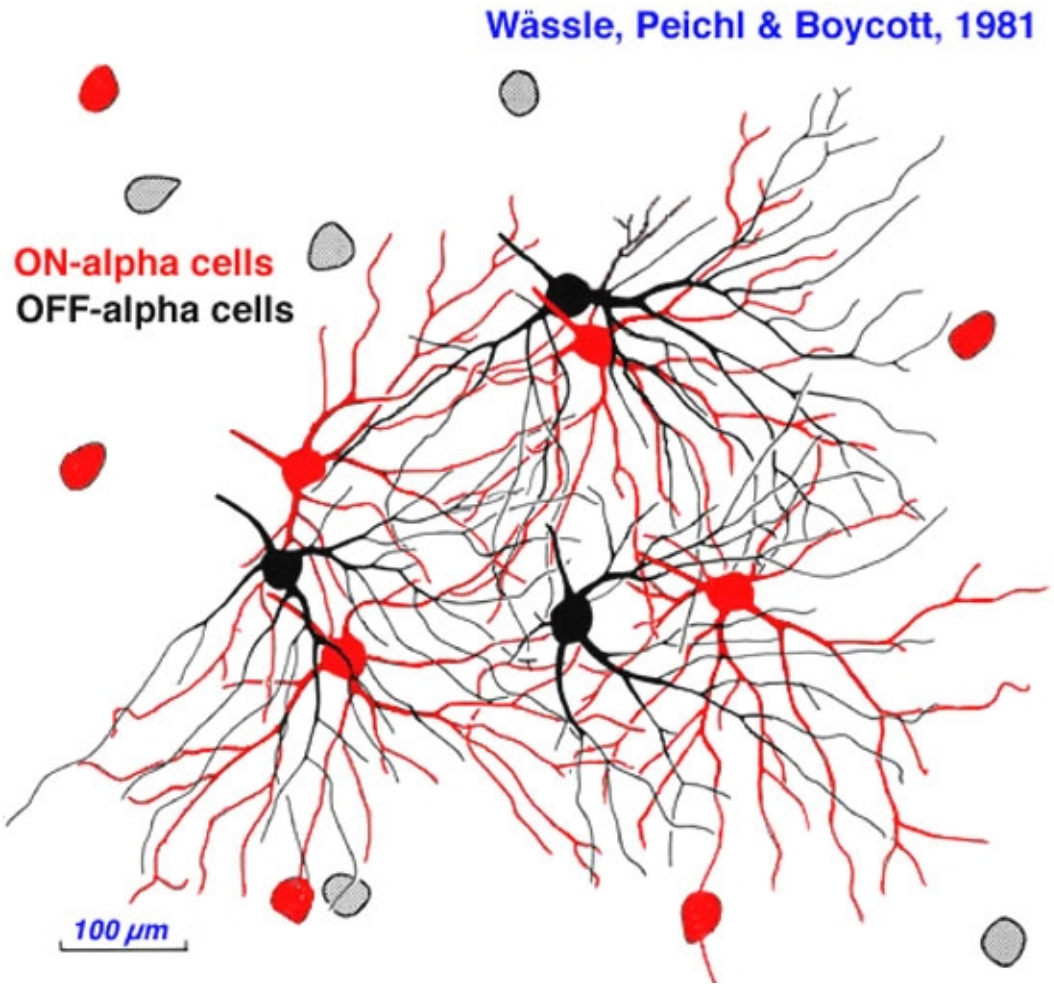

Figure 7. HRP-filled ON- and OFF-center alpha cell mosaics in cat retina.

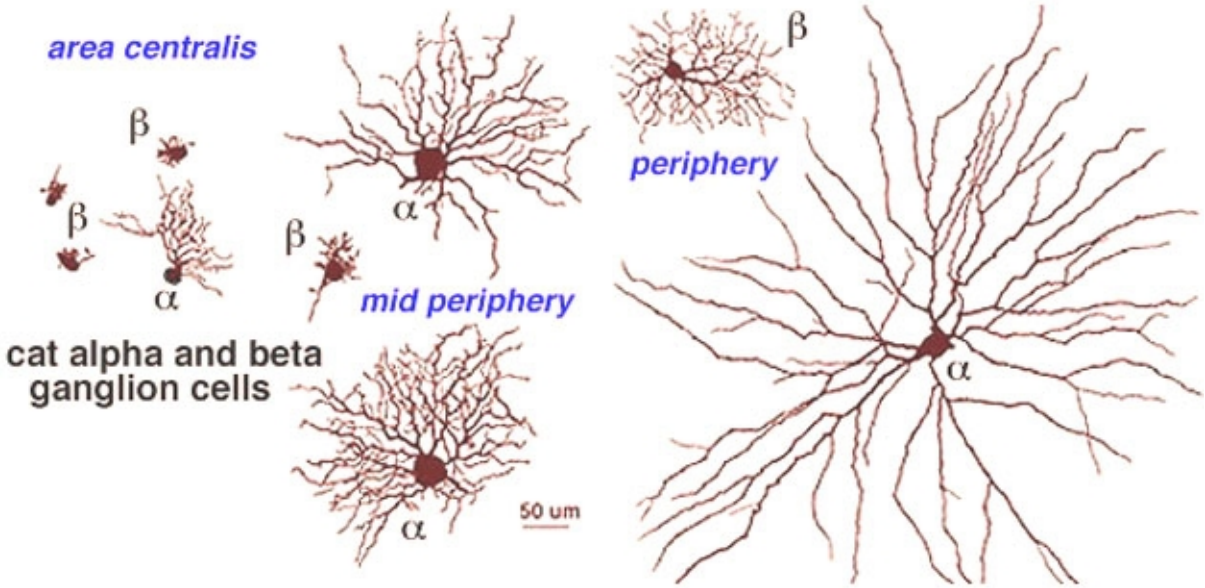

Figure 8. Cat ganglion cells (Golgi-stained wholemount views).

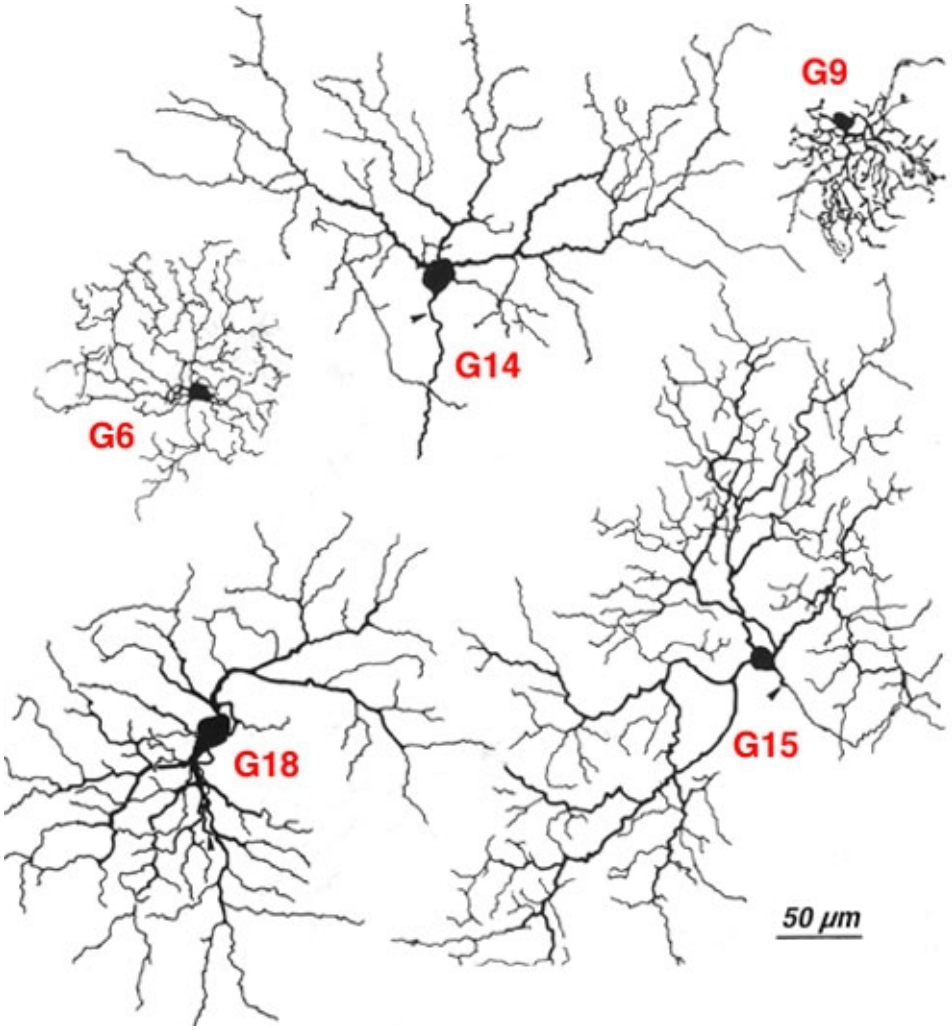

Figure 9. Some of non-alpha/non-beta ganglion cells of cat retina.

alpha cells are not much larger than their dendritic tree sizes (21, 35) (see below), despite enormous convergence and very wide lateral interactive potential.

Identity of Amacrine Cell Types Inputing Cat Alpha and Beta Ganglion Cells

As shown in the summary diagrams (Fig. 17 and Fig. 18), recent evidence suggests that several different morphological types of amacrine cells, as well as bipolar cell types, have synaptic input to the OFF-beta and OFF-alpha ganglion cells.

AII amacrine cells are particularly evident to both OFF-center ganglion cell types (Fig. 17 and Fig. 18, AII) and as mentioned above (see Fig. 13 and Fig. 15, previous section). AII cells are known to be glycinergic (36, 37). A small-field, bistratified amacrine cell with morphological characteristics complementary to the AII known as A8 (14) (see chapter on roles of amacrine cells) has been studied for transmitter content (37) and in intracellular recordings and marking (38). A8 is considered a glycinergic cell (37). It synapses in sublamina a upon tufted dendrites and dendritic varicosities typical of the OFF-beta ganglion cell (Fig. 17, A8). However, these A8 amacrine profiles have not been seen to input large-diameter, OFF-alpha ganglion cell dendrites (Fig. 18). A13 cells are considered GABAergic cells (37) and known to be postsynaptic to rod and cone bipolars and make

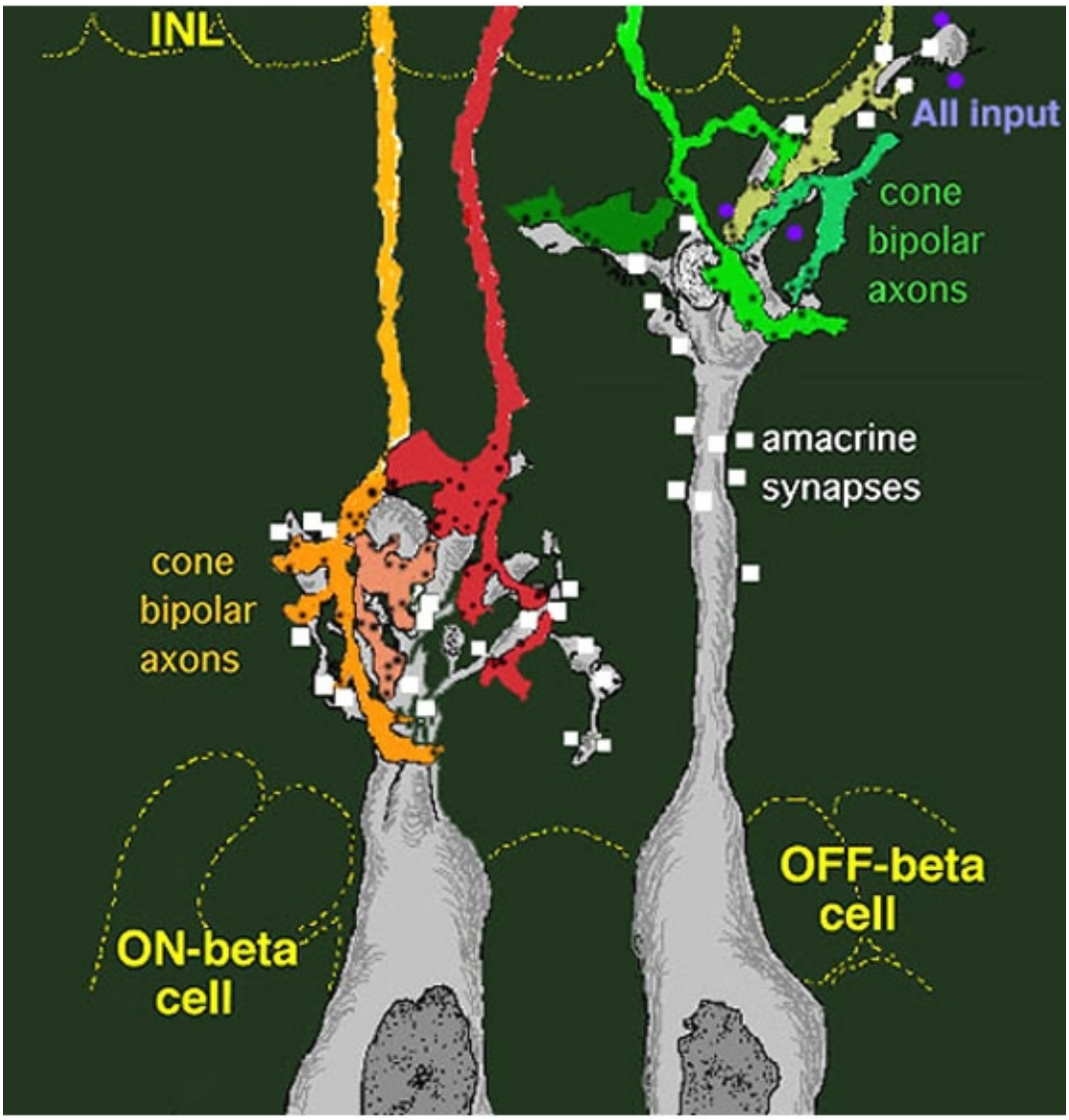

Figure 10. Reconstructions from electron microscopy of ON- and OFF-center beta cells of cat area centralis.

synapses with the cell body and primary dendrites in sublamina **a** and **b** of both ganglion cell types as well (33, 38) (Fig. 17 and Fig. 18, A13).

Small amacrine cells marked as A2/3 are shown on the summary diagrams (Fig. 17 and Fig. 18, A2/3). Poucho and Goebel (37, 39) have clearly subdivided types A2, A3 and A4 by their neurotransmitter content. Thus, A2 is probably GABAergic, whereas A3 and A4 are apparently medium-intensity glycinergic. Because only A2 and A3 cell types branch in strata 1 and 2 while A4 branches deeper in stratum 3, it is more likely that the former two cells are the candidates for synaptic input to the OFF-alpha and OFF-beta cells. Freed and Sterling (40) propose that glycinergic A4 amacrines are presynaptic to ON-center alpha cells: it is thus possible then that A3 are glycinergic counterpart amacrines reserved for the OFF-center variety of ganglion cell.

Some of the amacrine profiles synapsing upon the OFF-alpha ganglion cell have the morphology of A19 amacrine cells (32, 41, 42) (Fig. 18, A19, arrows). They are large-field with large-diameter dendrites tapering to fine, long processes covering 500 µm or more of field. Like most wide-field amacrine cells of the mammalian retina, A19 cells are thought to be GABAergic (37) and ON-OFF in physiology (32). They run in lower sublamina **a** in S2 co-stratifying with OFF-center alpha cell dendrites. A19 cells have been characterized, by their content of neurotubules and their gap junctions to other A19s (41, 42). Moreover, HRP-injected A19 cells have

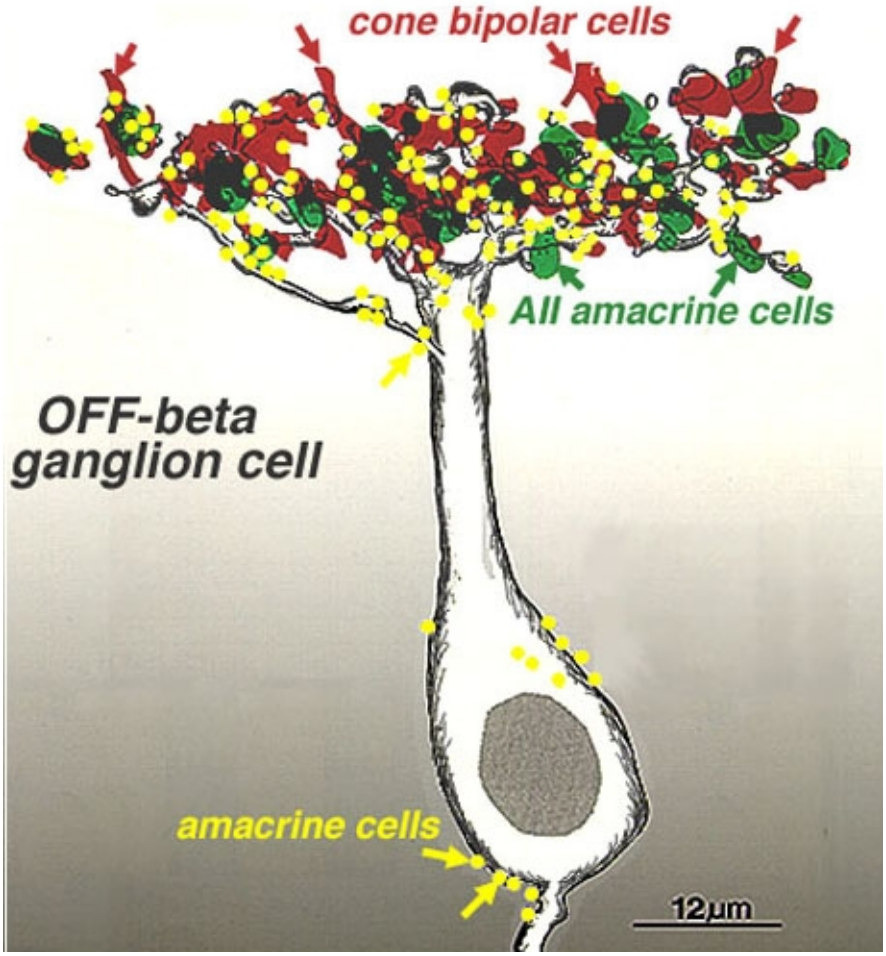

Figure 11. Reconstruction from electron microscopy of an HRP-filled OFF-center beta cell in cat retina.

been seen to run along and across large-diameter alpha cell dendrites in sublamina **a**, making intermittent synapses (32).

Among the many wide-field amacrine synapses upon OFF-center alpha cells, some are probably from acetylcholine containing or "starburst" amacrine cells (43-45) (Fig. 18, ACh, stippled cell). Vardi and co-workers (46) showed, by lucifer filling alpha ganglion cells and immunocytochemically staining cholinergic amacrine cells, that the latter amacrine's distal varicose dendrites run in bundles and loops along and across alpha cell dendrites in strata 2 and 3 of the inner plexiform layer, having ample opportunity for synaptic interaction. There is also convincing evidence for physiological effects of acetylcholine upon Y ganglion cells (47-49) and evidence that alpha cell dendrites contain ACh receptor sites (50). Thus, it seems probable that the two cholinergic amacrine cell types contributing to **a** and **b** sublaminae in cat retina are providing synaptic inputs to OFF- and ON-center alpha ganglion cells, respectively.

Primate Ganglion Cells

There are at least 18 different morphological types of ganglion cell in the human retina. All but three of these correspond to cells in the cat retina and have, where possible, been given the same G number. Some of the cat types have not been seen in human retina but undoubtedly they are there. Special names are reserved for P and M ganglion cells that are specific to the human high visual acuity and color-processing systems. They are thought to be specialized evolutionary correlates of beta and alpha cells, respectively (51) and comprise the major input to the geniculo-striate areas (52-55). Thus, P cells are considered to be mostly midget ganglion cells

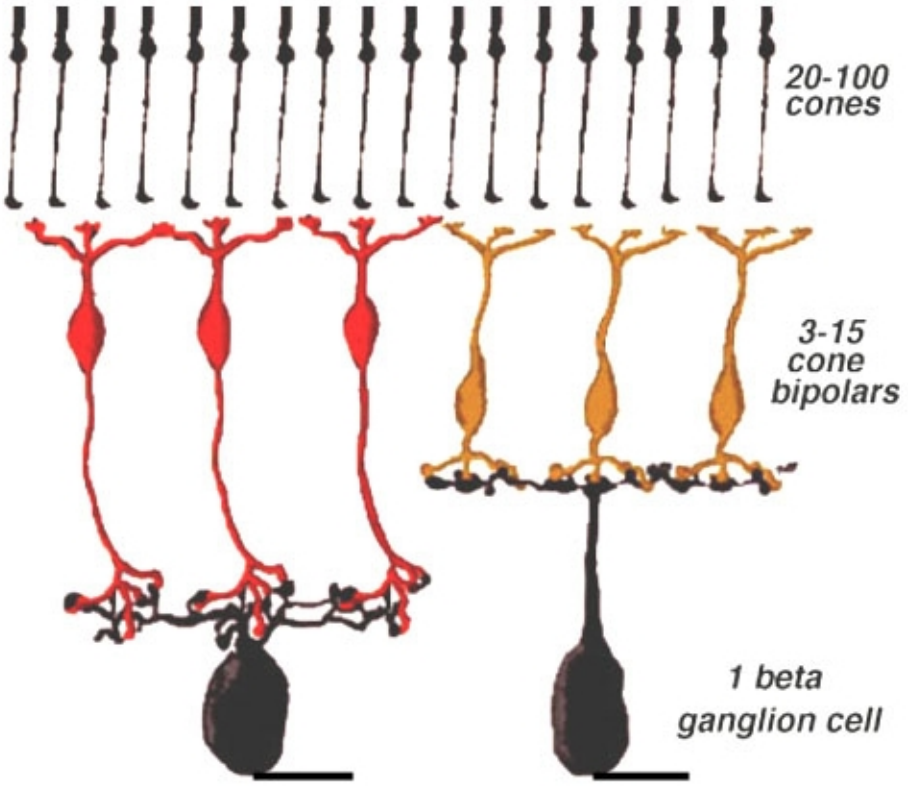

Figure 12. Convergence of cones and bipolar cells upon ON- and OFF-center beta cells.

and equivalent to beta cells of cat and project to the **P**arvocellular layers of the LGN. M cells, on the other hand, probably equivalent to alpha cells of cat and project to the **M**agnocellular layers of the LGN (Fig. 19 and see the animation of two Golgi-stained P cells in the human retina).

Polyak (2) first described the midget ganglion cells and considered them to form the majority of the ganglion cell types of monkey central retina. More recent retrograde staining studies indicate that ganglion cells—with medium-size cell bodies and the smallest dendritic trees, putting them into a "midget" category of cell—comprise 80% of the ganglion cell population in the monkey retina, and these cells project to the parvocellular layers of the LGN (53). The question then arises as to how many cell types correspond to these parvocellular projecting ganglion cells. Polyak (2) described midget ganglion cells quite clearly as the ganglion cells with the smallest dendritic trees, never much exceeding the diameter of their cell body, which is 9-12 μm. It is clear that the cells of the fovea meet this criterion (Fig. 19.1). However, outside of the fovea and beyond 3 mm of eccentricity, the midget ganglion cells can have dendritic tree sizes as large as 100 μm (56-58).

Physiologically, we suspect, by virtue of their being single-cone-connected via their exclusive connection to single midget bipolar cells in the foveal area (59, 60) that P cells are the opponent chromatic units, or the Type 1 cells of Weisel and Hubel of the LGN (61, 62). Outside of the fovea, where they clearly are receiving input from more than one midget bipolar cell by virtue of their increased dendritic tree size, midget ganglion cells or P cells may become broader band (63). We suspect that the P cells always receive input through midget bipolar cells but probably from more than one midget bipolar cell. In peripheral retina, the P cell dendritic trees become large enough for axons of three to five midget bipolar cells to have input. It remains to be seen whether chromatic specificity can remain under these conditions.

There is general agreement that the magnocellular-projecting ganglion cells are the parasol cells that Polyak described (1). Although some of Polyak's giant cells are by cell body size and dendritic tree size characteristics

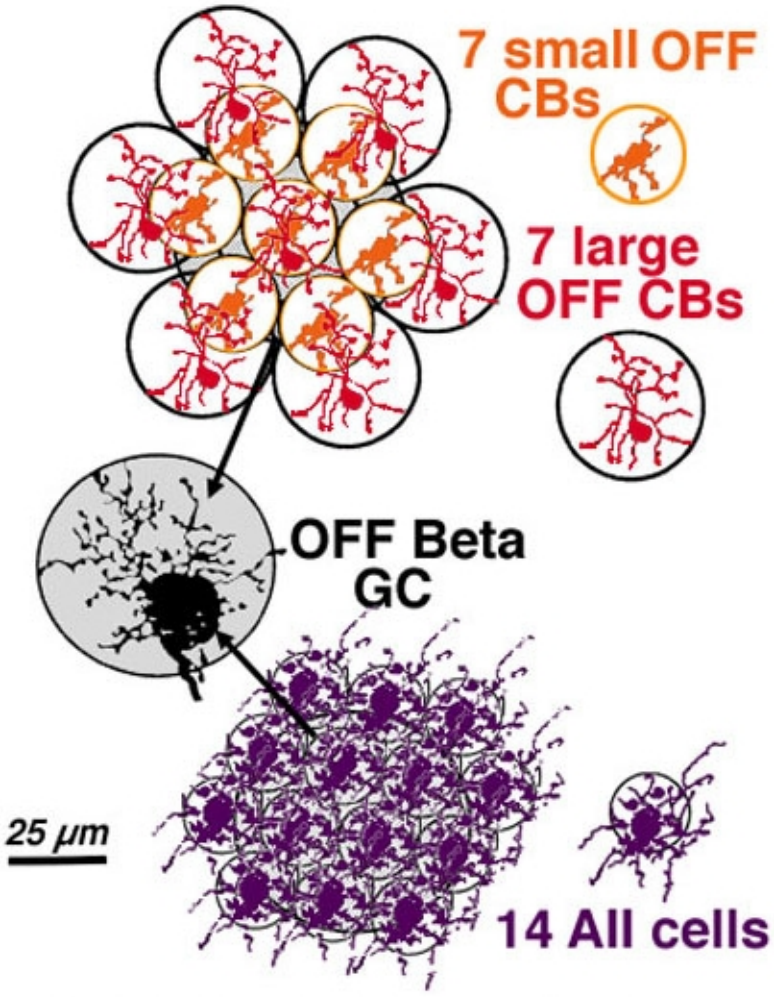

Figure 13. Model of the two cone bipolar types and AII amacrine cell inputs to the dendritic tree of an OFF-beta cell.

undoubtedly are the equivalent of Golgi-stained M cells in the far peripheral retina (57, 58, 64) and of the large-bodied, multibranched, reduced silver-stained cells of Silveira and Perry (65).

The other ganglion cells in human that are not in the geniculo-striate projections correspond to some of those retrogradely filled in Perry and co-workers studies (53, 54) of cells projecting to the midbrain (Fig. 20, Fig. 21, Fig. 22, Fig. 23). Two of these varieties in macaque retina may be G22 and G23 cells (Fig. 23). The G19 is equivalent to the cell in cat retina that has been stained by intracellular dye-injection and is apparently monoamine accumulating (30) (Fig. 22). Ganglion cells with complex receptive field characteristics such as directional selectivity (DS) may be present in human retina, too. Thus, G11 (Fig. 24) is a bistratified cell that could correspond to the rabbit ON-OFF DS cell and G22 (Fig. 23) to an ON directionally selective cell (66). Ganglion cells selective for orientation and uniformity could correspond to G8 (Fig. 24) and G17 (Fig. 22), respectively, in human retina (66). Several of the concentric sluggish cells of the rabbit are also seen in human Golgi-stained counterparts, for example G3 and G20 could be an ON-center varieties and G7 and G4 OFF-center varieties (67) (Fig. 21, Fig. 22, Fig. 23, Fig. 24).

Only two physiologically recorded and stained monkey ganglion cells have been reported thus far. One is the little understood biplexiform ganglion cell (68, 69) (Fig. 25), which gives a sustained ON-center physiology, representative of its direct input from rod photoreceptors. We will return to this fascinating ganglion cell type later (see below). The other ganglion cell that has been recorded from in monkey is the blue/yellow opponent ganglion cell projecting to the parvocellular layers of LGN (70) (see chapter on S-cone pathways).

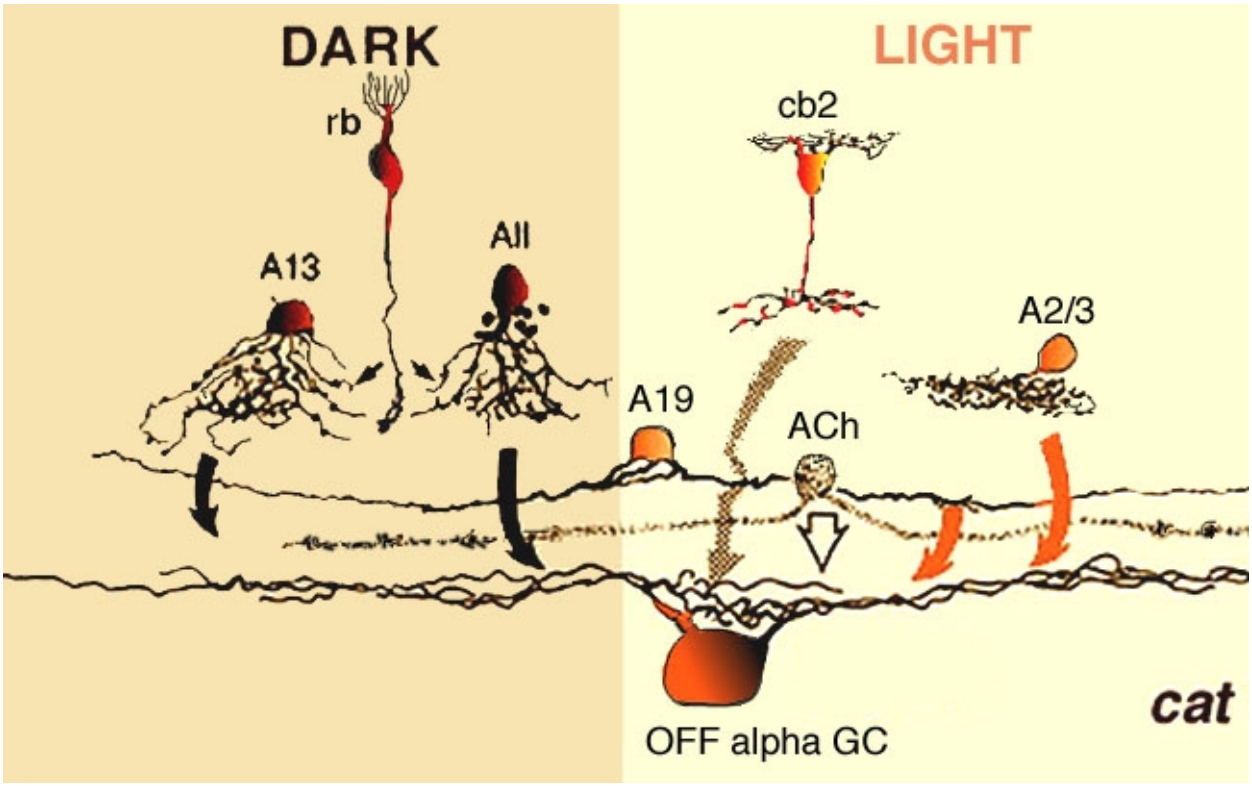

Figure 18. Probable input neurons to OFF-alpha cells of cat retina.

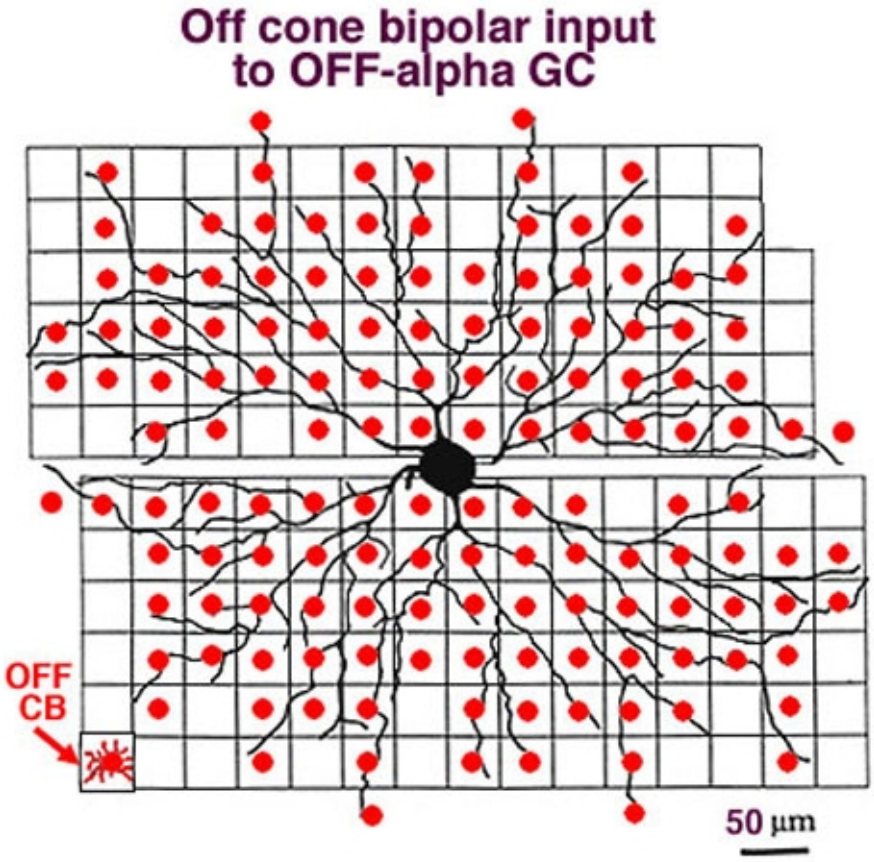

Figure 14. Model of numbers of cone bipolar cells inputing an OFF-center alpha cell.

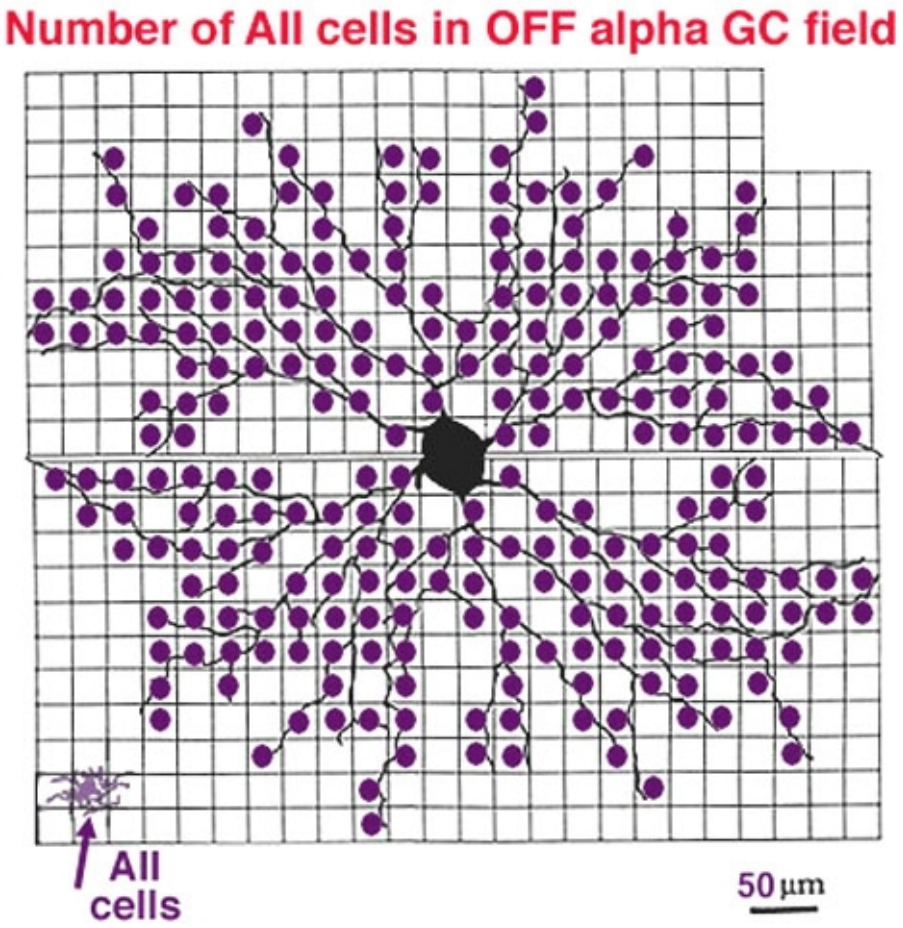

Figure 15. Model of the number of AII amacrine cells inputing the dendritic tree of an OFF-alpha cell.

Rabbit Ganglion Cells

The rabbit retina has been extensively studied because it is a more accessible retina in respect to isolation, staining, and recordings than some other mammalian retinas. The retina can be isolated and kept alive for hours of experimental study with simple perfusion techniques. Rabbit retina was originally studied for the property of directional selectivity in ganglion cells. Because this retina has a visual streak specialization, it was found quite early on (71) that many of the the ganglion cells were sensitive to motion and direction of the movement of visual stimuli.

Interestingly, there has never been a systematic classification of the different types of rabbit ganglion cell based on a morphological technique like the Golgi. However, the intracellular staining and physiological approaches have yielded a very nice functional classification scheme that supercedes the need for a Golgi study nowadays.

Ganglion cells equivalent to ON and OFF-alpha types in cat are also seen in rabbit (19, 67). They have both a similar physiology and dendritic field size and shape, although in rabbit their cell bodies may not be quite as large in size as in cat retina. Equivalent beta cell types in rabbit are a little more equivocal. Cells that respond with the linear, brisk sustained concentric receptive field organization that come in ON- and OFF-center pairs are seen in rabbit, and their appearance is rather similar to peripheral beta cells of cat. They have, however, smaller cell body sizes, again like the alpha cell comparison (67). Because no cell with the exact same morphology as a central beta cell, even on the visual streak of rabbit retina, has been seen (67), some suggest that there is no real equivalent of the beta cell in rabbit (20). The question remains an open one, because the rabbit

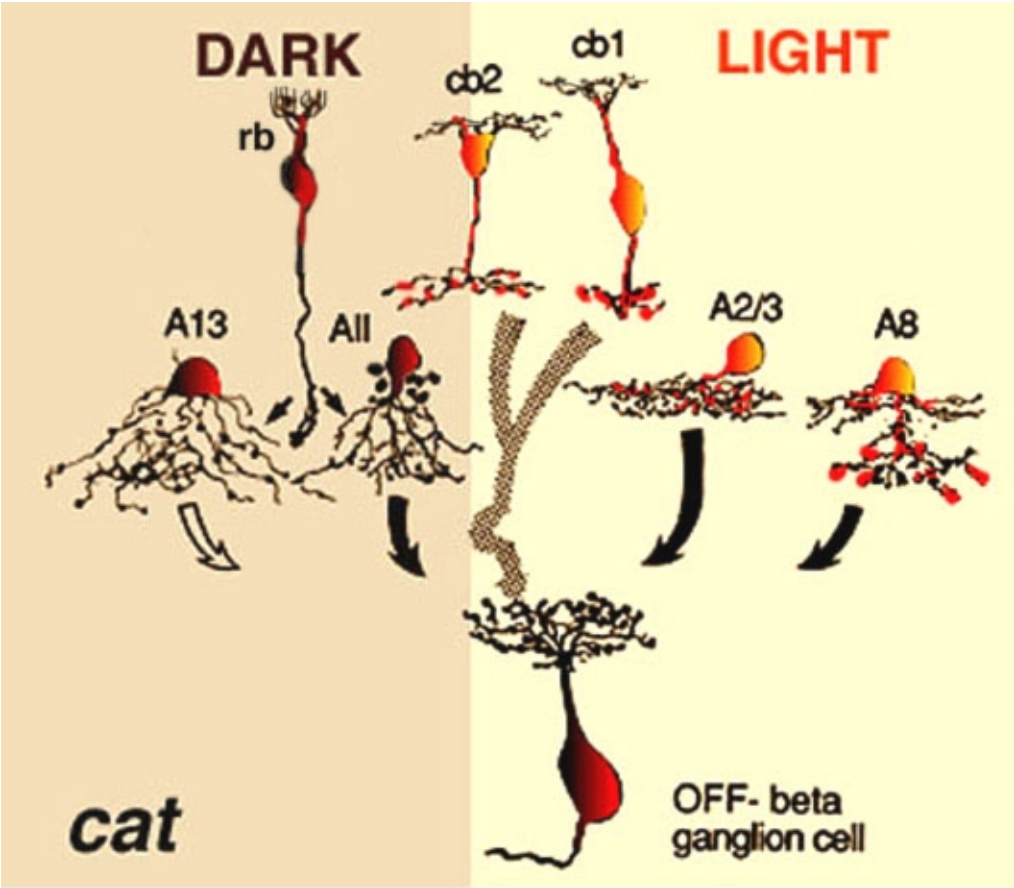

Figure 17. Probable input neurons to OFF-beta cells of cat retina.

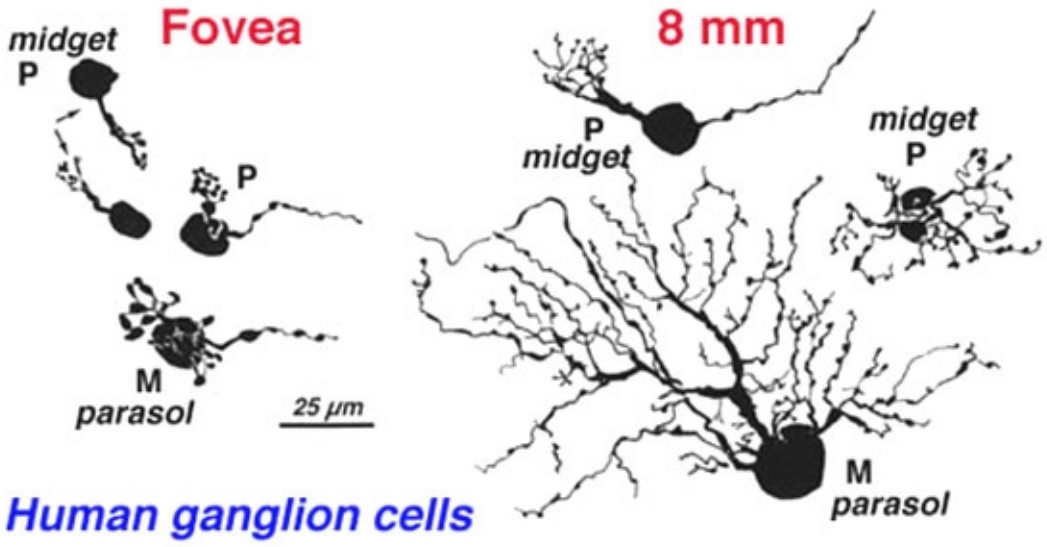

Figure 19. Ganglion cell types involved in geniculate-striate pathways of human retina.

visual system has a different organization than the cats, with a horizontal streak in the retina, no binocular overlap of the visual fields, and projections to visual centers in the tectum rather than the geniculo-striate.

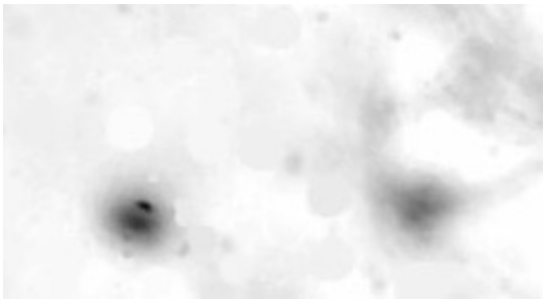

Movie 2. A focus series of two Golgi-stained P cells in the human retina.

Download video

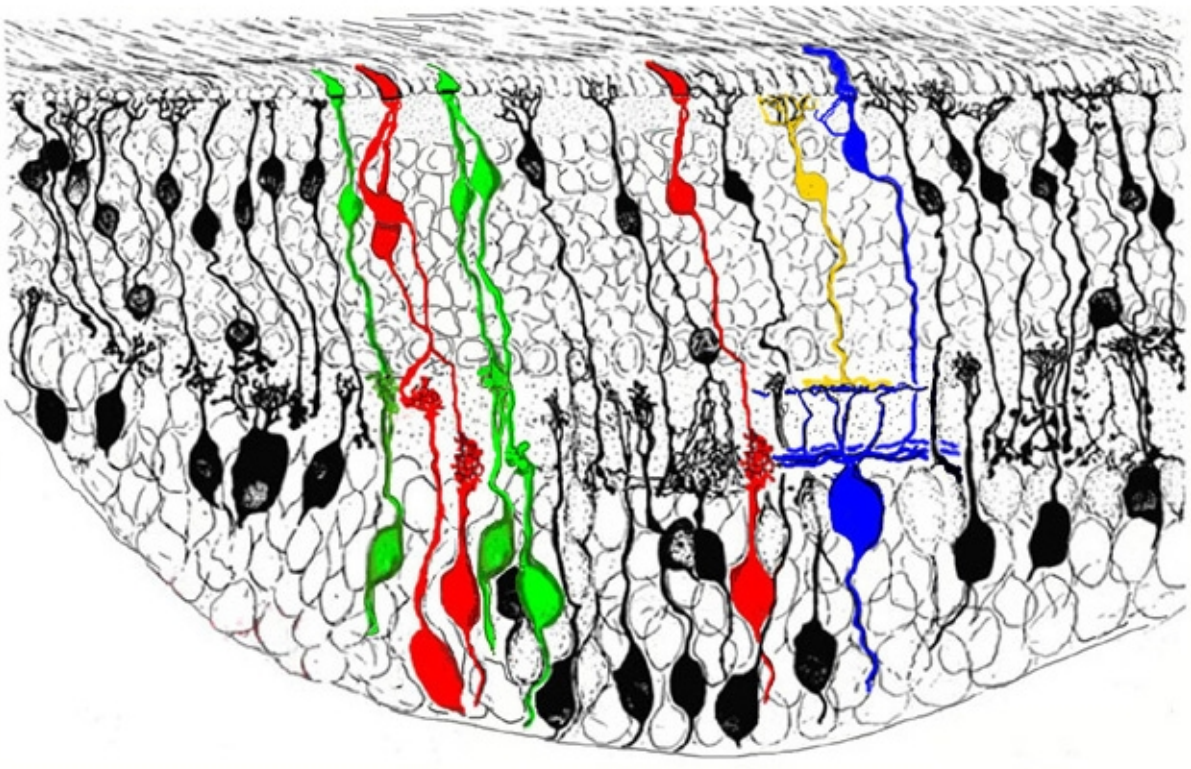

Figure 19.1. The commonest ganglion cells types of the primate fovea are the P cells, or midget ganglion cells, and the bistratified blue-on/yellow-off ganglion cell.

Other ganglion cells of rabbit, with concentric receptive field physiology but more sluggish response patterns, are also demonstrated in Amthor and co-authors' work (67). Many of these types are similar to the non-alpha/non-beta cell types of the cat in morphology. However, the correlation between the ganglion cell physiology of the two species is difficult to make at the present time. Some comparisons between the ganglion cells of the human retina and those of the rabbit have been attempted (64). Interestingly, a great many more similarities exist between ganglion cell types of the ground squirrel and rabbit retinas (72).

The more unusual feature detectors of the rabbit retina are the motion-sensitive, orientation- and direction-sensitive ganglion cells (66). The bistratified ON-OFF directional selective (DS) ganglion cells of the rabbit retina have attracted a lot of attention, mainly because many aspects of the circuitry have been elucidated (Fig. 26). For example, the acetylcholine containing amacrine cells, also called starburst cells, are the major input cells (73-76)

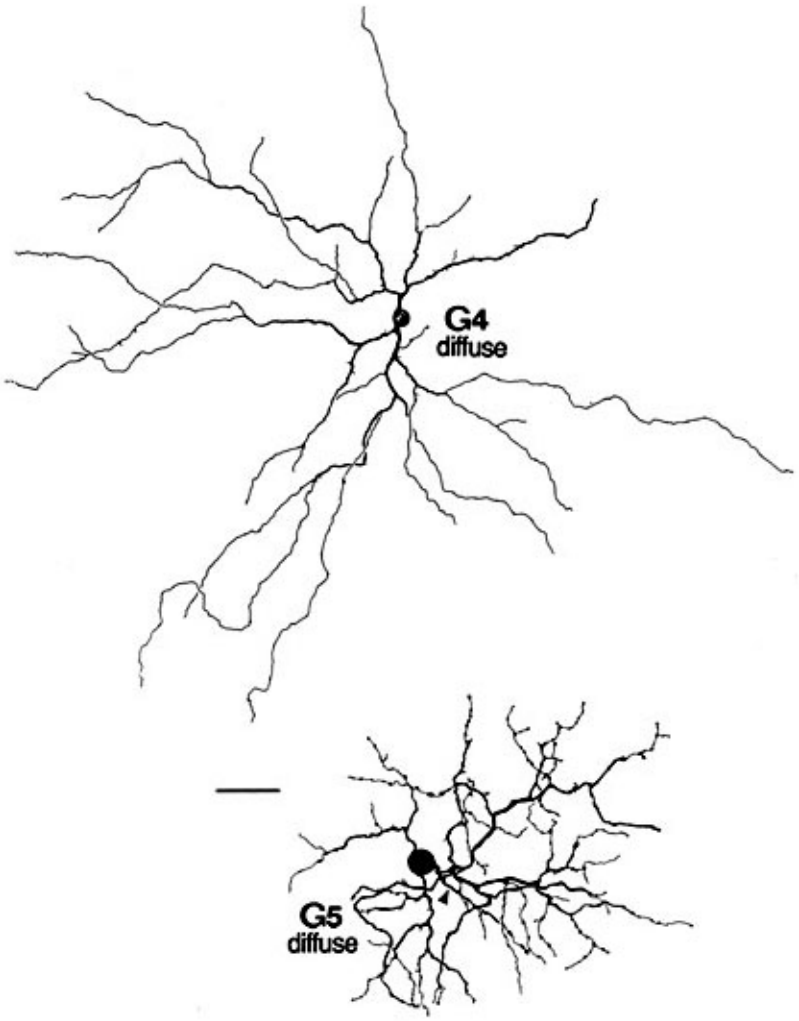

Figure 20. G4 and G5 ganglion cells of human retina.

(see chapter on roles of amacrine cells). The effects of antagonists of acetylcholine have been known for a long time to eliminate directional selectivity in the rabbit retina, and amacrines containing GABA are also known to be involved (77, 78). The fascinating aspect of the ON-OFF directionally selective ganglion cells of rabbit is that they are bistratified and have the two layers of their dendrites oriented orthogonal to each other (see Fig. 26). The orientation of the outer dendritic tree (i.e., the OFF layer of dendrites) is favored to be with the preferred direction of the cells response to a moving target (66).

The other type of directionally selective cell in rabbit is the ON-center type, and its single layered dendritic tree in sublamina **b** (ON layer of the inner pleiform layer) is not as obviously oriented with the preferred direction (Fig. 27). Other ganglion cell types that are prominent and well characterized in Amthor and co-workers (66) in the rabbit retina include orientation selective, local edge detectors and uniformity detectors (suppressed by contrast) (Fig. 28 and Fig. 29). It is particularly interesting that each of the different types of ganglion cells have a distinctly different morphology, primarily concerning the substructure of their dendrites. Many of them have another feature in common in that they typically show an orientation of the whole dendritic tree away from the cell body in an asymmetric pattern (see Fig. 26, Fig. 27, Fig. 28, Fig. 29). All the details of these morphologies can be found in the elegant papers of Amthor et al. (66, 67), and the reader is encouraged to look there.

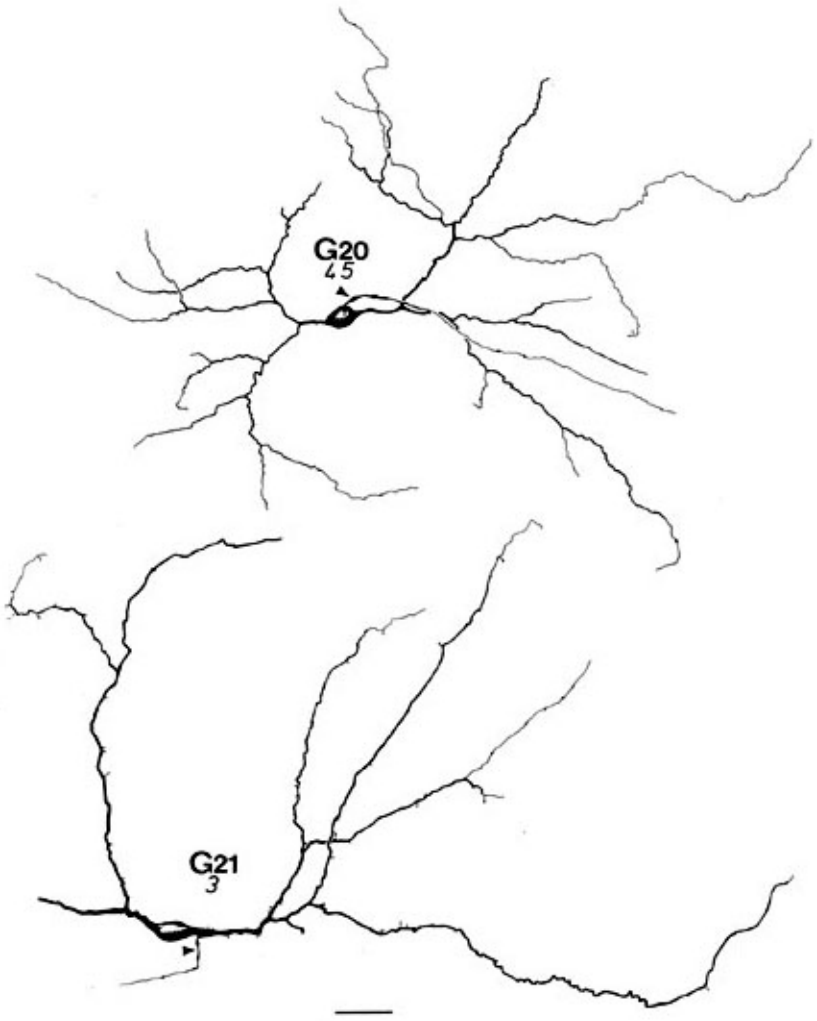

Figure 21. G20 and G21 cells of human retina.

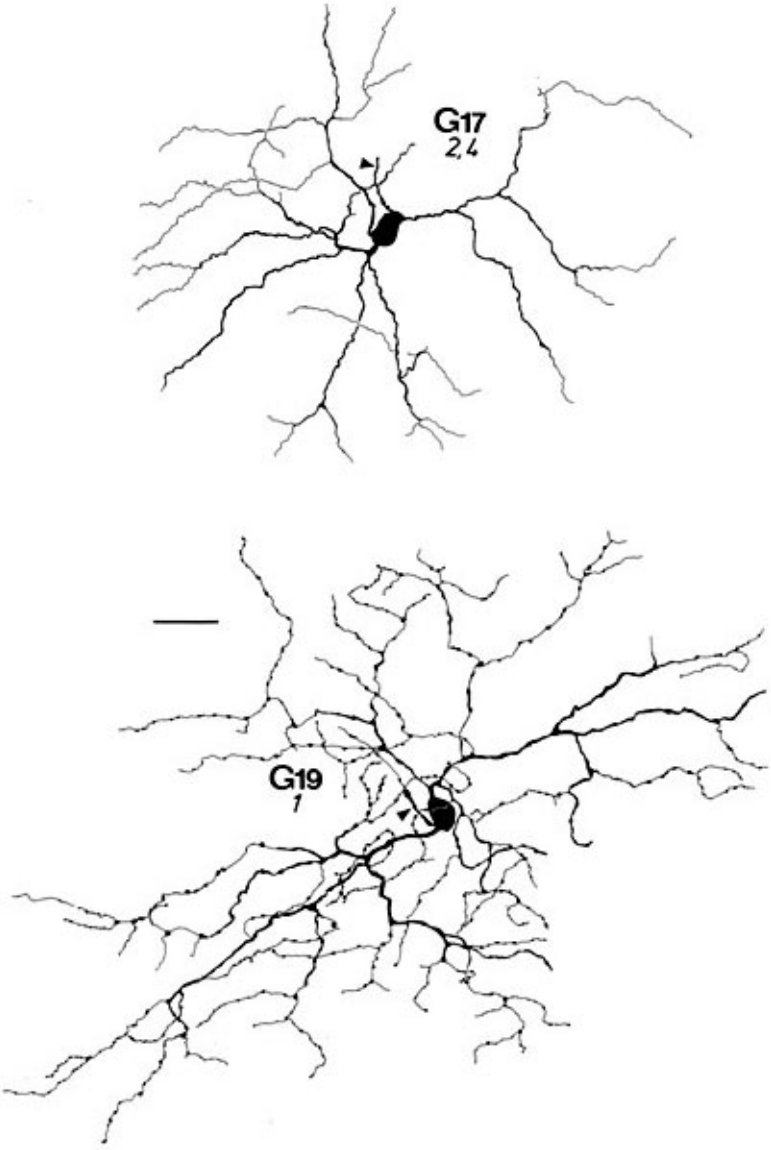

Figure 22. G17 and G19 cells of human retina.

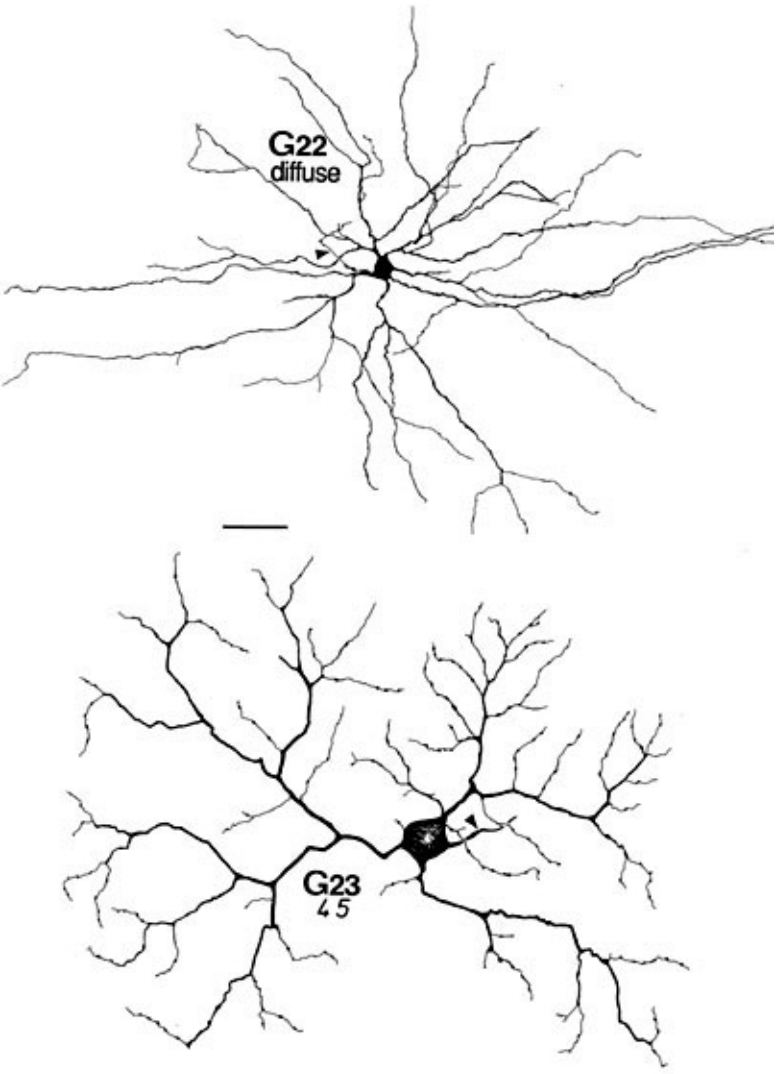

Figure 23. G22 and G23 cells of human retina.

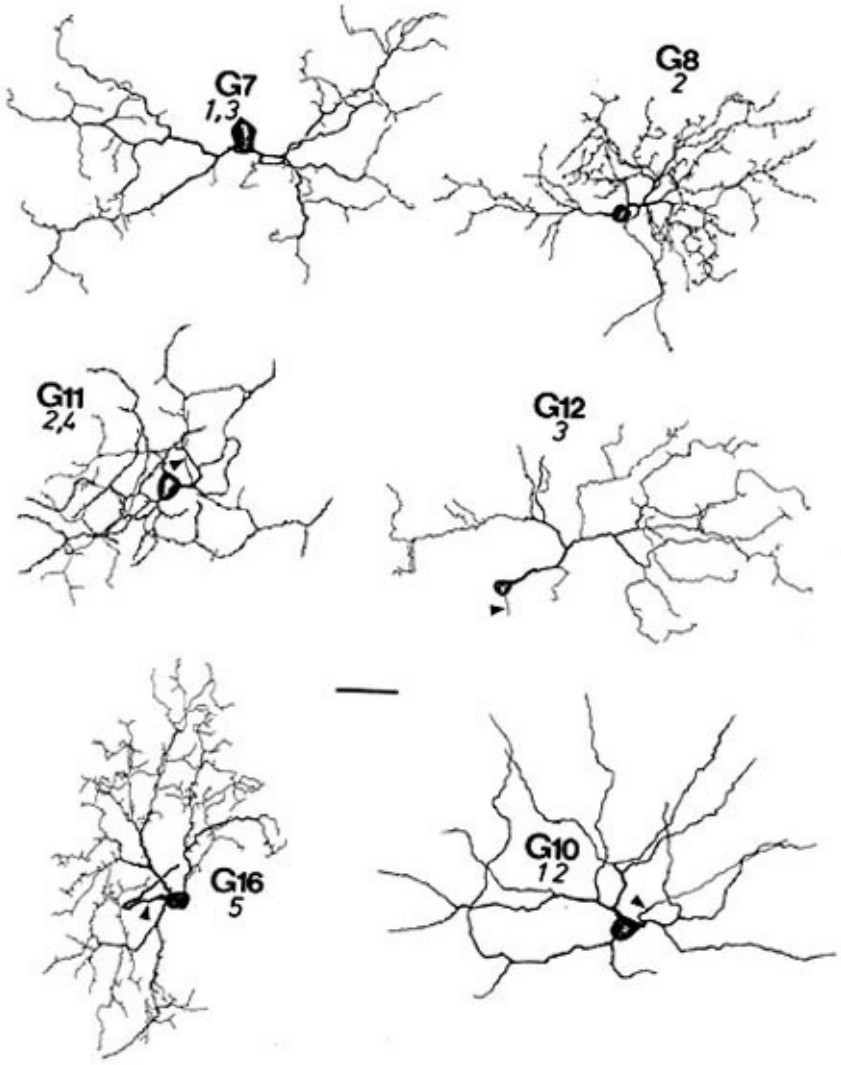

Figure 24. Smaller-field ganglion cells of human retina.

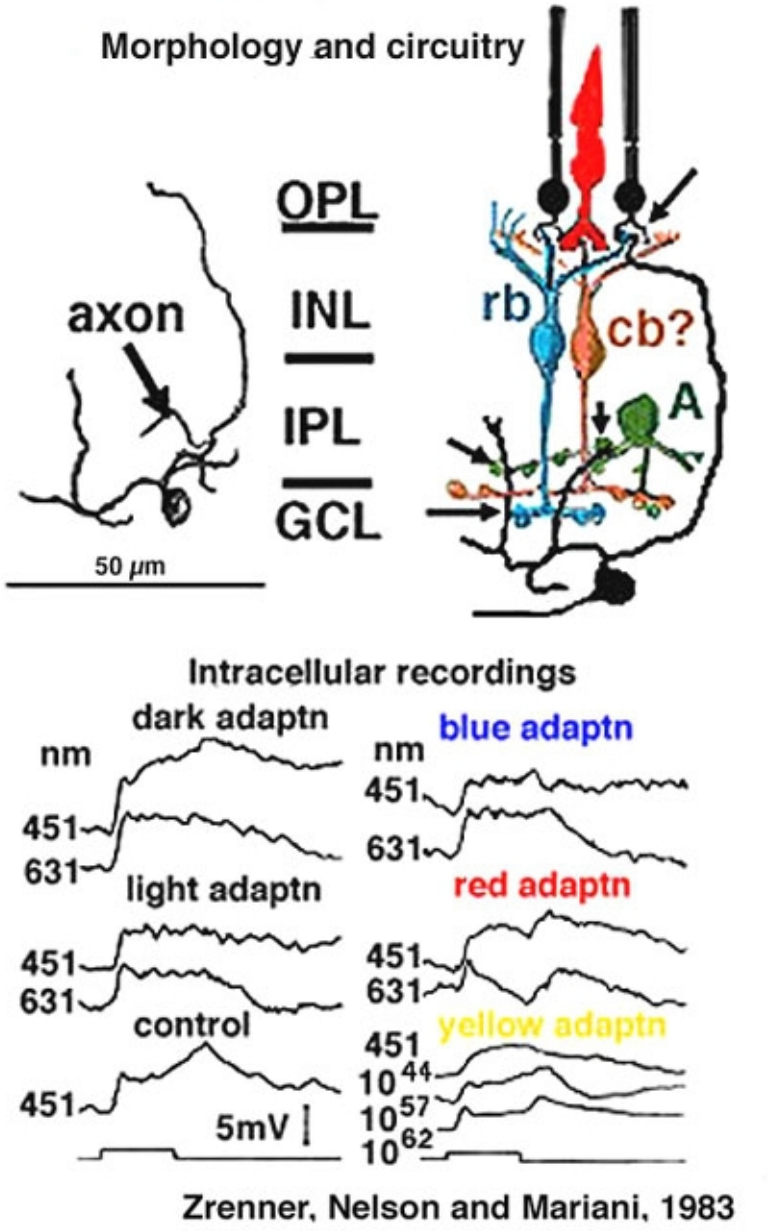

Figure 25. Biplexiform ganglion cell of the monkey retina.

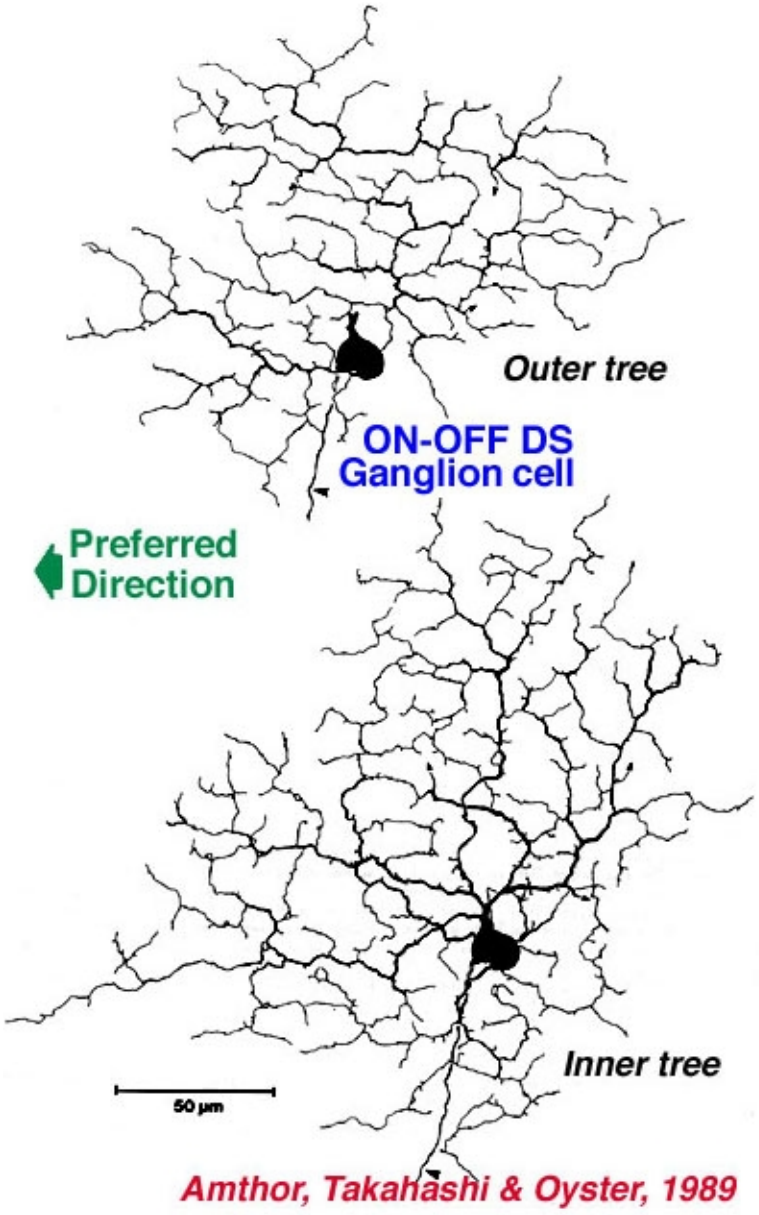

Figure 26. ON-OFF directionally selective ganglion cell of rabbit retina.

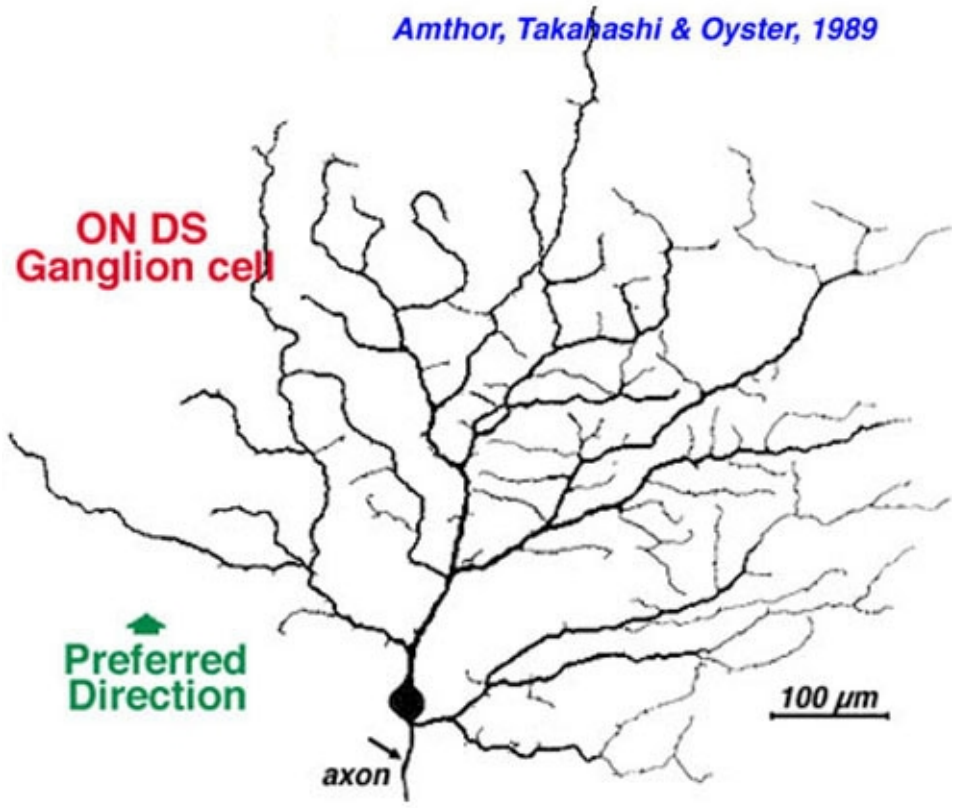

Figure 27. ON-directionally selective ganglion cell of rabbit retina (66).

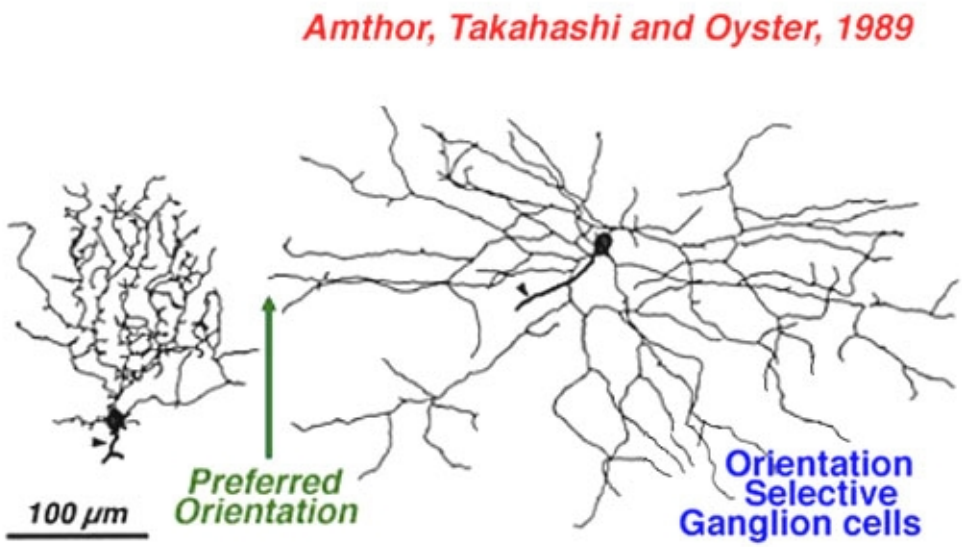

Figure 28. Direction- and orientation-selective ganglion cells of rabbit retina.

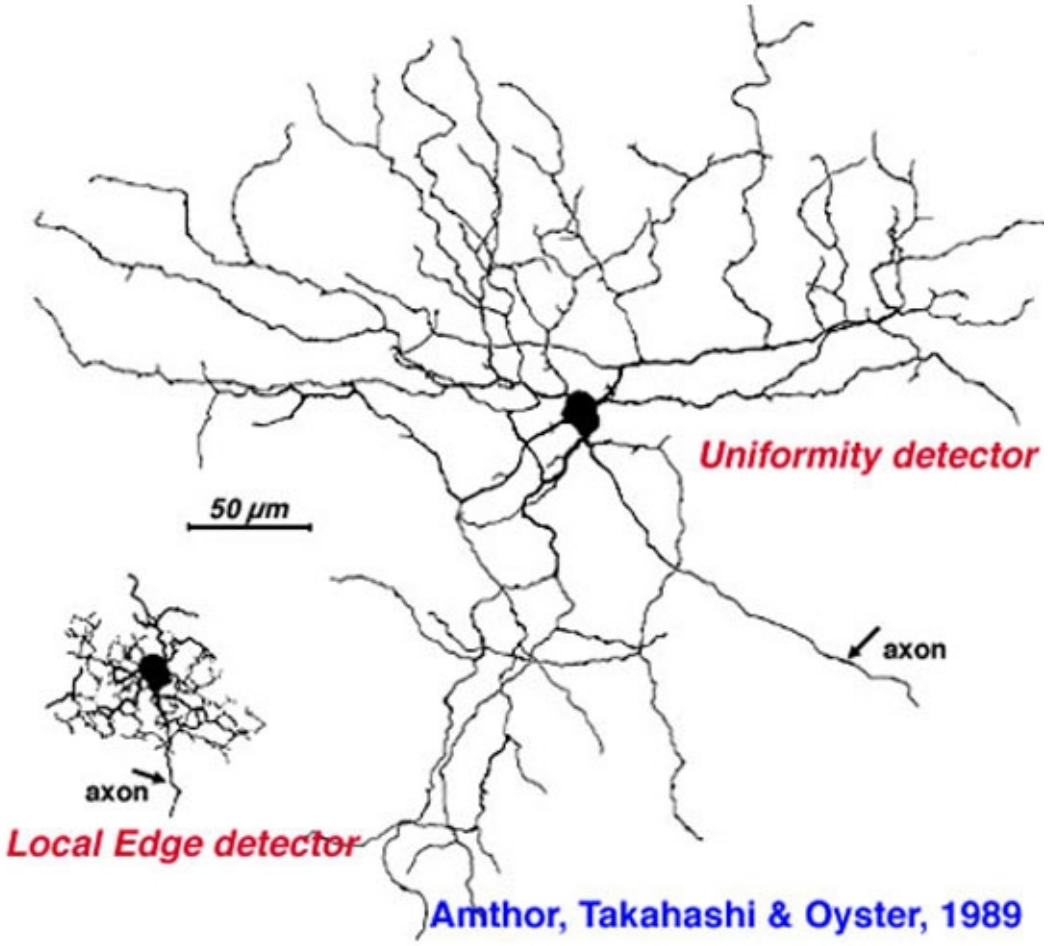

Figure 29. Uniformity detector and local edge detector ganglion cells of rabbit retina.

References

1. SR Cajal. In: Thorpe SA, Glickstein M, translators. 1892. The structure of the retina. Springfield (IL): Thomas. 1972.
2. Polyak SL. The retina. Chicago: University of Chicago; 1941.
3. Boycott BB, Dowling JE. Organization of the primate retina: light microscopy. Philos Trans. R. Soc. B. 1969;255:109–184.
4. Brown JE, Major D. Cat retinal ganglion cell dendritic fields. Exp Neurol. 1966;15:70–78. PubMed PMID: 5934665.
5. Leicester J, Stone J. Ganglion, amacrine and horizontal cells of the cat's retina. Vision Res. 1967;7:695–705. PubMed PMID: 4181430.
6. Shkolnik-Yarros EG. Neurons of the cat retina. Vision Res. 1971;11:7–26. PubMed PMID: 5575855.
7. Boycott BB, Wassle H. The morphological types of ganglion cells of the domestic cat's retina. J Physiol. 1974;240:397–419. PubMed PMID: 4422168.
8. Cleland BG, Levick WR. Brisk and sluggish concentrically organised ganglion cells in the cat's retina. J Physiol. 1974;240:421–456. PubMed PMID: 4421622.
9. Cleland BG, Levick WR. Properties of rarely encountered types of ganglion cells in the cat's retina. J Physiol. 1974;240:457–492. PubMed PMID: 4420300.
10. Enroth-Cugell C, Robson JG. The contrast sensitivity of retinal ganglion cells of the cat. J Physiol. 1966;187:517–552. PubMed PMID: 16783910.

11. Levick WR, Thibos LN. Receptive fields of cat ganglion cells: classification and construction. Prog Retinal Res. 1983;2:267–320.
12. Famiglietti EV, Kolb H. Structural basis of "On-" and "Off-" centre responses in retinal ganglion cells. Science. 1976;194:193–195. PubMed PMID: 959847.
13. Nelson R, Famiglietti EV, Kolb H. Intracellular staining reveals different levels of stratification for On-and Off-centre ganglion cells in cat retina. J Neurophysiol. 1978;41:472–483. PubMed PMID: 650277.
14. Kolb H, Nelson R, Mariani A. Amacrine cells, bipolar cells and ganglion cells of the cat retina: a Golgi study. Vision Res. 1981;21:1081–1114. PubMed PMID: 7314489.
15. Wassle H, Peichl L, Boycott BB. Morphology and topography of on- and off-alpha cells in the cat retina. Proc R Soc Lond B Biol Sci. 1981;212:157–175. PubMed PMID: 6166012.
16. Wassle H, Boycott BB, Illing R-B. Morphology and mosaic of on- and off-beta cells in the cat retina and some functional considerations. Proc R Soc Lond B Biol Sci. 1981;212:177–195. PubMed PMID: 6166013.
17. Fukuda Y, Stone J. Retinal distribution and central projections of Y-, X- and W-cells of the cat's retina. J Neurophysiol. 1974;37:749–772. PubMed PMID: 4837773.
18. Stone J, Fukuda Y. Properties of cat retinal ganglion cells: Comparison of W-cells with X- and Y-cells. J Neurophysiol. 1974;37:722–748. PubMed PMID: 4600539.
19. Peichl L, Buhl EH, Boycott BB. Alpha ganglion cells in the rabbit retina. J Comp Neurol. 1987;263:25–41. PubMed PMID: 2444630.
20. Wassle H, Boycott BB. Functional architecture of the mammalian retina. Physiol Rev. 1991;71:447–480. PubMed PMID: 2006220.
21. Wassle H, Voigt T, Patel B. Morphological and immunocytochemical identification of indoleamine-accumulating neurons in the cat retina. J Neurosci. 1987;7:1574–1585. PubMed PMID: 3553450.
22. Fukuda Y, Hsiao C-F, Watanabe M, Ito H. Morphological correlates of physiologically identified Y-, X-, and W-cells in cat retina. J Neurophysiol. 1984;52:999–1013. PubMed PMID: 6520634.
23. Troy JB, Schweitzer-Tong DE, Enroth-Cugell Ch. Receptive-field properties of Q retinal ganglion cells of the cat. Vis Neurosci. 1995;12:285–300. PubMed PMID: 7786850.
24. Farmer SG, Rodieck RW. Ganglion cells of the cat accessory optic system: morphology and retinal topography. J Comp Neurol. 1982;205:190–198. PubMed PMID: 7076892.
25. Grasse KL, Cynader MS. Electrophysiology of medial terminal nucleus of accessory optic system in the cat. J Neurophysiol. 1982;48:490–504. PubMed PMID: 7119859.
26. Leventhal AG, Keens J, Tork I. The afferent ganglion cells and cortical projections of the Retinal Recipient Zone (RRZ) of the cat's 'Pulvinar Complex'. J Comp Neurol. 1980;194:535–554. PubMed PMID: 7451681.
27. Leventhal AG, Rodieck RW, Dreher B. Central projections of the cat retinal ganglion cells. J Comp Neurol. 1985;237:216–226. PubMed PMID: 4031122.
28. Hutsler JJ, White CA, Chalupa LM. Neuropeptide Y immunoreactivity identifies a group of gamma-type retinal ganglion cells in the cat. J Comp Neurol. 1993;336:468–480. PubMed PMID: 8263231.
29. Pu M, Berson DM, Pan T. Structure and function of the retinal ganglion cells innervating the cat's geniculate wing: An in vitro study. J Neurosci. 1994;14:4338–4358. PubMed PMID: 8027783.
30. Dacey DM. Monoamine-accumulating ganglion cell type of the cat's retina. J Comp Neurol. 1989;288:59–80. PubMed PMID: 2794138.
31. Kolb H. The inner plexiform layer in the retina of the cat: electron microscopic observations. J Neurocytol. 1979;8:295–329. PubMed PMID: 490185.
32. Freed MA, Pflug R, Kolb H, Nelson R. ON-OFF amacrine cells in cat retina. J Comp Neurol. 1996;364:556–566. PubMed PMID: 8820883.
33. Kolb H, Nelson R. Off-alpha and off-beta ganglion cells in the cat retina. II. Neural circuitry as revealed by electron microscopy of HRP stains. J Comp Neurol. 1993;329:85–110. PubMed PMID: 8454727.
34. Sterling P, Freed MA, Smith RG. Architecture of rod and cone circuits to the on-beta ganglion cell. J Neurosci. 1988;8:623–642. PubMed PMID: 2828567.
35. Nelson R, Kolb H, Freed M. Off-alpha and Off-beta ganglion cells in cat retina. I. Intracellular electrophysiology and HRP stains. J Comp Neurol. 1993;329:68–84. PubMed PMID: 8454726.

36. Kalloniatis M, Marc RE, Murry RF. Amino acid signatures in the primate retina. J Neurosci. 1996;16:6807–6829. PubMed PMID: 8824321.
37. Pourcho RG, Goebel DJ. A combined Golgi and autoradiographic study of 3(H)glycine-accumulating amacrine cells in the cat retina. J Comp Neurol. 1985;233:473–480. PubMed PMID: 2984258.
38. Kolb H, Nelson R. Hyperpolarizing, small-field, amacrine cells in cone pathways of cat retina. J Comp Neurol. 1996;371:415–436. PubMed PMID: 8842896.
39. Pourcho RG, Goebel DJ. Neuronal subpopulations in cat retina which accumulate the GABA agonist (3H)muscimol: a combined Golgi and autoradiographic study. J Comp Neurol. 1983;219:25–35. PubMed PMID: 6619330.
40. Freed MA, Sterling P. The ON-alpha ganglion cell of the cat retina and its presynaptic cell types. J Neurosci. 1988;8:2303–2320. PubMed PMID: 3249227.
41. Kolb H, Nelson R. Neural architecture of the cat retina. Prog. Ret. Res. 1984;3:21–60.
42. Kolb H, Nelson R. (1985) Functional neurocircuitry of amacrine cells in the cat retina. In: Gallego A, Gouras P, editors. Neurocircuitry of the retina: a Cajal memorial. New York: Elsevier Press. pp. 215-232.
43. Famiglietti EV. 'Starburst' amacrine cells and cholinergic neurons: mirror-symmetric ON and OFF amacrine cells of rabbit retina. Brain Res. 1983;261:138–144. PubMed PMID: 6301622.
44. Tauchi M, Masland RH. The shape and arrangement of the cholinergic neurons in the rabbit retina. Proc R Soc Lond B Biol Sci. 1984;223:101–119. PubMed PMID: 6151180.
45. Vaney DI. The mosaic of amacrine cells in the mammalian retina. Prog. Ret. Res. 1990;9:49–100.
46. Vardi N, Masarachia PJ, Sterling P. Structure of the starburst amacrine network in the cat retina and its association with alpha ganglion cells. J Comp Neurol. 1989;288:601–611. PubMed PMID: 2808752.
47. Ikeda H. Transmitter action at cat retinal ganglion cells. Prog. Ret. Res. 1985;4:1–32.
48. Schmidt M, Humphrey MF, Wassle H. Action and localization of acetylcholine in the cat's retina. J Neurophysiol. 1987;58:997–1015. PubMed PMID: 3694255.
49. Straschill M, Perwein J. The inhibition of retinal ganglion cells by catecholamines and g-aminobutyric acid. Pflugers Arch. 1969;312:45–54. PubMed PMID: 5388469.
50. Kaneda M, Hashimoto M, Kaneko A. Neuronal nicotinic acetylcholine receptors of ganglion cells in the cat retina. Jpn J Physiol. 1995;45:491–508. PubMed PMID: 7474530.
51. Leventhal AG, Rodieck RW, Dreher B. Retinal ganglion cell classes in the old world monkey: morphology and central projections. Science. 1981;213:1139–1142. PubMed PMID: 7268423.
52. Perry VH, Cowey A. The morphological correlates of X- and Y-like retinal ganglion cells in the retina of monkeys. Exp Brain Res. 1981;43:226–228. PubMed PMID: 7250268.
53. Perry VH, Oehler R, Cowey A. Retinal ganglion cells that project to the dorsal lateral geniculate nucleus in the macaque monkey. Neuroscience. 1984;12:1101–1123. PubMed PMID: 6483193.
54. Perry VH, Cowey A. Retinal ganglion cells that project to the superior colliculus and pretectum in the macaque monkey. Neuroscience. 1984;12:1125–1137. PubMed PMID: 6483194.
55. Shapley R, Perry VH. Cat and monkey retinal ganglion cells and their visual functional roles. Trends Neurosci. 1986;9:229–235.
56. Dacey DM. The mosaic of midget ganglion cells in the human retina. J Neurosci. 1993;13:5334–5355. PubMed PMID: 8254378.
57. Rodieck RW, Binmoeller KF, Dineen JT. Parasol and midget ganglion cells of the human retina. J Comp Neurol. 1985;233:115–132. PubMed PMID: 3980768.
58. Watanabe M, Rodieck RW. Parasol and midget ganglion cells of the primate retina. J Comp Neurol. 1989;289:434–454. PubMed PMID: 2808778.
59. Calkins DJ, Schein SJ, Tsukamoto Y, Sterling P. M and L cones in macaque fovea connect to midget ganglion cells by different numbers of excitatory synapses. Nature. 1994;371:70–72. PubMed PMID: 8072528.
60. Kolb H, DeKorver L. Midget ganglion cells of the parafovea of the human retina: A study by electron microscopy and serial section reconstructions. J Comp Neurol. 1991;303:617–636. PubMed PMID: 1707423.

61. Gouras P. Identification of cone mechanisms in monkey ganglion cells. J Physiol. 1968;199:533–547. PubMed PMID: 4974745.
62. Wiesel TN, Hubel DH. Spatial and chromatic interactions in the lateral geniculate body of the rhesus monkey. J Neurophysiol. 1966;29:1115–1156. PubMed PMID: 4961644.
63. Gouras P, Zrenner E. Color coding in primate retina. Vision Res. 1981;21:1591–1598. PubMed PMID: 7336591.
64. Kolb H, Linberg KA, Fisher SK. The neurons of the human retina: a Golgi study. J Comp Neurol. 1992;318:147–187. PubMed PMID: 1374766.
65. Silveira LCL, Perry VH. The topography of magnocellular projecting ganglion cells (M-ganglion cells) in the primate retina. Neuroscience. 1991;40:217–237. PubMed PMID: 1711175.
66. Amthor FR, Takahashi ES, Oyster CW. Morphologies of rabbit retinal ganglion cells with complex receptive fields. J Comp Neurol. 1989;280:97–121. PubMed PMID: 2918098.
67. Amthor FR, Takahashi ES, Oyster CW. Morphologies of rabbit retinal ganglion cells with concentric receptive fields. J Comp Neurol. 1989;280:72–96. PubMed PMID: 2918097.
68. Mariani AP. Biplexiform cells: ganglion cells of the primate retina that contact photoreceptors. Science. 1982;216:1134–1136. PubMed PMID: 6177044.
69. Zrenner E, Nelson R, Mariani A. Intracellular recordings from a biplexiform ganglion cell in macaque retina, stained with horseradish peroxidase. Brain Res. 1983;262:181–185. PubMed PMID: 6301632.
70. Dacey DM, Lee BB. The 'blue-on' opponent pathways in primate retina originates from a distinct bistratified ganglion cell. Nature. 1994;367:731–735. PubMed PMID: 8107868.
71. Barlow HB, Levick WR. The mechanism of directionally selective units in the rabbit's retina. J Physiol. 1965;178:477–504. PubMed PMID: 5827909.
72. Linberg KA, Suemune S, Fisher SK. Retinal neurons of the California ground squirrel, Sperophilus beecheyi: A Golgi study. J Comp Neurol. 1996;365:173–216. PubMed PMID: 8822165.
73. Famiglietti EV. Starburst amacrine cells in cat retina are associated with bistratified, presumed directionally selective, ganglion cells. Brain Res. 1987;413:404–408. PubMed PMID: 3607491.
74. Famiglietti EV. Synaptic organization of starburst amacrine cells in rabbit retina: analysis of serial thin sections by electron microscopy and graphic reconstruction. J Comp Neurol. 1991;309:40–70. PubMed PMID: 1894768.
75. Masland RH. Amacrine cells. Trends Neurosci. 1988;11:405–410. PubMed PMID: 2469207.
76. Masland RH, Mills JW, Cassidy C. The functions of acetylcholine in the rabbit retina. Proc R Soc Lond B Biol Sci. 1984;223:121–139. PubMed PMID: 6151181.
77. Daw NW, Ariel M. Effect of synaptic transmitter drugs on receptive fields of rabbit ganglion cells. Vision Res. 1981;21:1643–1648. PubMed PMID: 6278756.
78. Wyatt HJ, Daw NW. Specific effects of neurotransmitter anatagonists on ganglion cells in rabbit retina. Science. 1976;191:204–205. PubMed PMID: 1857.

Visual Responses of Ganglion Cells

Ralph Nelson

Created: May 1, 2001; Updated: April 10, 2007.

Overview

Ganglion cells are the final output neurons of the vertebrate retina. Ganglion cells collect information about the visual world from bipolar cells and amacrine cells (retinal interneurons). This information is in the form of chemical messages sensed by receptors on the ganglion cell membrane. Transmembrane receptors, in turn, transform the chemical messages into intracellular electrical signals. These are integrated within ganglion-cell dendrites and cell body, and "digitized", probably in the initial segment of the ganglion-cell axon, into nerve spikes. Nerve spikes are a time-coded digital form of electrical signaling used to transmit nervous system information over long distances, in this case through the optic nerve and into brain visual centers.

Ganglion cells are also the most complex information processing systems in the vertebrate retina. It is a general experimental truth that an organism as a whole cannot behaviorally respond to visual stimuli that are not also detectable by individual ganglion cells. Different cells become selectively tuned to detect surprisingly subtle "features" of the visual scene, including color, size, and direction and speed of motion. These are called "trigger features". Even so, signals detected by ganglion cells may not have a unique interpretation. Equivalent signals might result from an object changing brightness, changing shape, or moving. It is up to the brain to determine the most likely interpretation of detected events and, in the context of events detected by other ganglion cells, take appropriate action.

Ganglion cell axons terminate in brain visual centers, principally the lateral geniculate nucleus and the superior colliculus. Ganglion cell axons are directed to specific visual centers depending on the visual trigger features they encode. The optic nerve collects all the axons of the ganglion cells. In humans, this optic nerve bundle contains more than one million axons.

History of Electrical Recordings

In 1967, Ragnar Granit and H. Keffer Hartline (1) shared the Nobel prize in physiology and medicine for the first electrical recordings of light responses from individual ganglion cells of the vertebrate retina. In this, both laureates acknowledged the earlier seminal influence of Edgar D. Adrian, winner of the 1932 Nobel prize in physiology and medicine. Adrian pioneered the measurement of impulse discharges from individual peripheral nerve axons and was principally responsible for the discovery that nerve fibers transmit signals in the form of a temporal sequence of "all or none" impulses. Granit (2) also noted the influence of the anatomist Santiago Ramon y Cajal, winner of the 1906 Nobel prize, in illustrating a complex retinal circuitry worthy of physiological investigation.

Hartline (3, 4) pushed experimental technology of the 1930s to its limits in obtaining extracellular recordings of individual ganglion cells. There were no solid state electronics. Special purpose, "direct coupled" vacuum tube amplifiers were designed. There were no oscilloscopes or computers for display and storage of signals. String galvanometers were used; a pencil of light played from a tiny mirror, minutely vibrating in a magnetic field, onto moving photographic film to document electrical events. There were no microelectrodes; ganglion cell axon bundles were teased off the retinal surface with dissecting tools and lifted onto a coarse cotton-wick electrode, such as earlier used for massed potential recordings. Ultimately, this technique proved too difficult to pursue and left no legacy. It remained for Granit (2) to introduce microelectrodes for such recordings, which greatly facilitated the ease of data collection. Granit also made the first ganglion cell recordings from a mammalian retina, the cat retina. This retina, as pursued by his students and others, has been a staple of visual electrophysiology. Yet the experimental designs and approaches provided by Hartline continue to be used. So

many of his findings, such as the multiplicity of ganglion cell response types, have proved accurate, such that the succeeding field of ganglion cell electrophysiology sometimes appears almost as a footnote to his work (Fig. 1 and Fig. 2).

ON and OFF Responses

Hartline's electrical recordings of single optic nerve fiber responses revealed "discharges of impulses", or "action potentials" in response to light stimulation. The discharge patterns were, however, diverse (5). Three unique patterns of light response were described (Fig. 3).

"ON" type fibers responded with a transient burst to light onset and a sustained elevated discharge rate throughout the photic stimulation (Fig. 3). "ON-OFF" fibers responded with discharge bursts at the onset and cessation of light stimuli but were otherwise quiet. "OFF" fibers were quiet until the stimulus light was turned off, whereupon they responded with a sustained burst of impulses. The situation was far different from fibers in the optic nerve of the invertebrate *Limulus polyphemus*, which Hartline also studied. There, all fibers responded with ON-type discharges. The result implied that a relatively high degree of visual processing occurred within the vertebrate retina, and that visual information was filtered by retinal circuitry into a number of subcategories. The exact number of such categories is still difficult to define exactly but now would easily number a dozen (6, 7). Because of the diverse categories of responses found in retinal ganglion cells, these cells are sometimes thought of as "feature detectors" (8).

ON- and OFF-type signal detection remains as the most significant subdivision among visual features extracted by ganglion cells. Combined morphological and physiological studies of individual ON- and OFF-type ganglion cells revealed different inner plexiform layer stratification patterns (9, 10, 11) and suggested a basis in retinal circuitry for these types (Fig. 4). The dendrites of OFF-type ganglion cells branch in the inner plexiform layer zone close to the amacrine cell bodies. Here they come in synaptic contact with the axon terminals of OFF-type bipolar cells. The dendrites of ON-type ganglion cells branch in the inner plexiform layer zone close to the ganglion cell bodies. Here they make synaptic contact with the axon terminals of ON-type bipolar cells (10). Dendritic trees of ON-OFF cells typically arborize in both zones of the inner plexiform layer, presenting a "bistratified" appearance (12).

Receptive Field

Hartline introduced the "nearly definable" concept of "receptive field" to describe the spatial properties of retinal ganglion cells. He used "spot mapping" to define such fields, a technique still widely used. Cells were found to respond to relatively dim spots when the stimulus was positioned in the "center" of the receptive field, but brighter stimuli were required as the spots were moved away from this region. An example of the spot mapping technique, taken from Kuffler (13) shows the reduction in response vigor as stimulus spots are displaced from the center (Fig. 5). Hartline concluded that ganglion cell receptive fields were fixed in space and immobile, typically did not extend beyond 1 mm in diameter, and were graded in sensitivity over this region. Receptive fields were much larger than expected of individual photoreceptors, suggesting signal processing and integration through retinal circuitry.

Evidently, circuitry was the source of a spatial weighting function, shaped so that sensitivity diminished radially with distance from the "receptive field center". Hartline also noted other features suggestive of hidden complexity in this simple concept. Response wave forms tended to become more transient and less sustained as spots were displaced (Fig. 5). Subtle movements, on the order of a few μm, much smaller than the receptive field itself, could evoke vigorous discharges, a kind of ganglion cell "hyperacuity effect" (see also ref. 14).

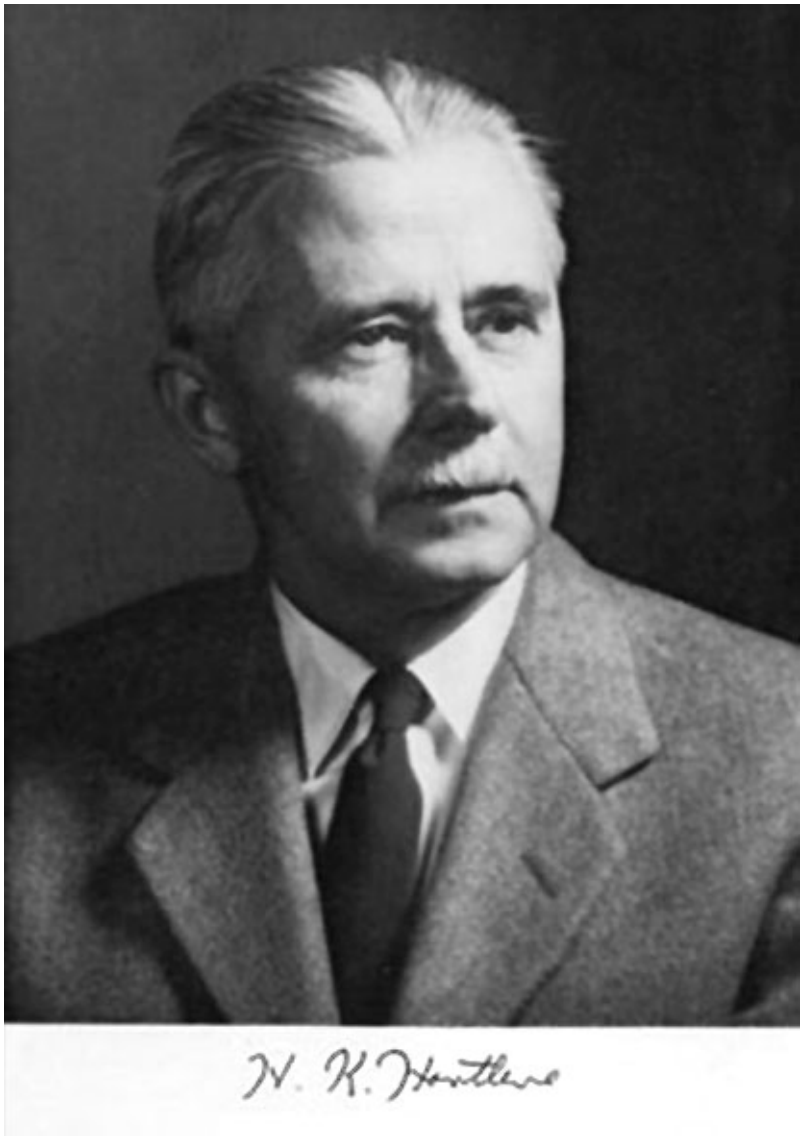

Figure 1. Haldan Keffer Hartline, 1967 Nobel Laureate.

Centers and Surrounds

Although Hartline went on to study lateral inhibition of receptive fields in the *Limulus* retina and his laboratory made other valuable contributions to neurobiology and vision, discovery of lateral inhibitory interactions in vertebrate ganglion cells and the concept of "antagonistic surround" is generally credited to Stephen Kuffler.

As noted by Hartline, not only strength of response,but also a change in form of response occurs as stimuli are moved across ganglion cell receptive fields. Kuffler (13) noted a particularly abrupt change in form, from onset excitation for stimulation in the center of the field to offset excitation for stimulation in the receptive field periphery. An example is illustrated in Fig. 6. In Fig. 6a, a spot, centered near the electrode tip, evokes a burst of impulses at stimulus onset. In Fig. 6b, the spot is displaced by 0.5 mm, where it evokes no impulses at onset but a burst of impulses at offset. In Fig. 6c, an intermediate spot position is found where both actions are evoked by the stimulus. The example (Fig. 6) shows properties of a classic ON-center, receptive field, with OFF surround. Conversely, OFF-center cells, which are excited at stimulus offset by central stimulation, have regions in the peripheral receptive field where ON excitation is evoked. This is the classic center-surround receptive field organization of ganglion cells (see the animation of the center and surround receptive field organization of a beta

Figure 2. Ragnar Granit, 1967 Nobel Laureate.

ganglion cell). Such organization was further examined with intracellular recording techniques. These techniques revealed not only the ganglion cell impulses but also the slow changes in ganglion cell membrane potential, which modulate the impulse rate.

Torstein Wiesel, 1981 winner of the Nobel prize in physiology and medicine, provides an example of such an intracellular recording in Fig. 7, which allows further features of the surround response to be seen. In Fig. 7a, a small spot of light depolarizes the membrane of the cell and evokes a vigorous burst of impulses. This is an ON-center cell. In Fig. 7b, the stimulus is an annulus, a ring of light designed to stimulate the receptive field surround but not the center. Impulses are silenced during stimulus presentation, but a burst appears at annulus offset. This is a classic surround pattern. A hyperpolarization of the membrane occurs while the annulus is ON and impulses are silenced. This is a feature of the response hidden from extracellular recording methods. The surround stimulus actively inhibits the cell by hyperpolarizing its membrane. Finally, the response to the large spot stimulus (Fig. 7c) should not be neglected. The large spot, like the small spot (Fig. 7a), evokes a membrane depolarization and sustained burst of impulses. But the depolarization is smaller and the burst less vigorous. The net impact of the center-surround receptive-field structure is that ganglion cells "prefer" small spots to large

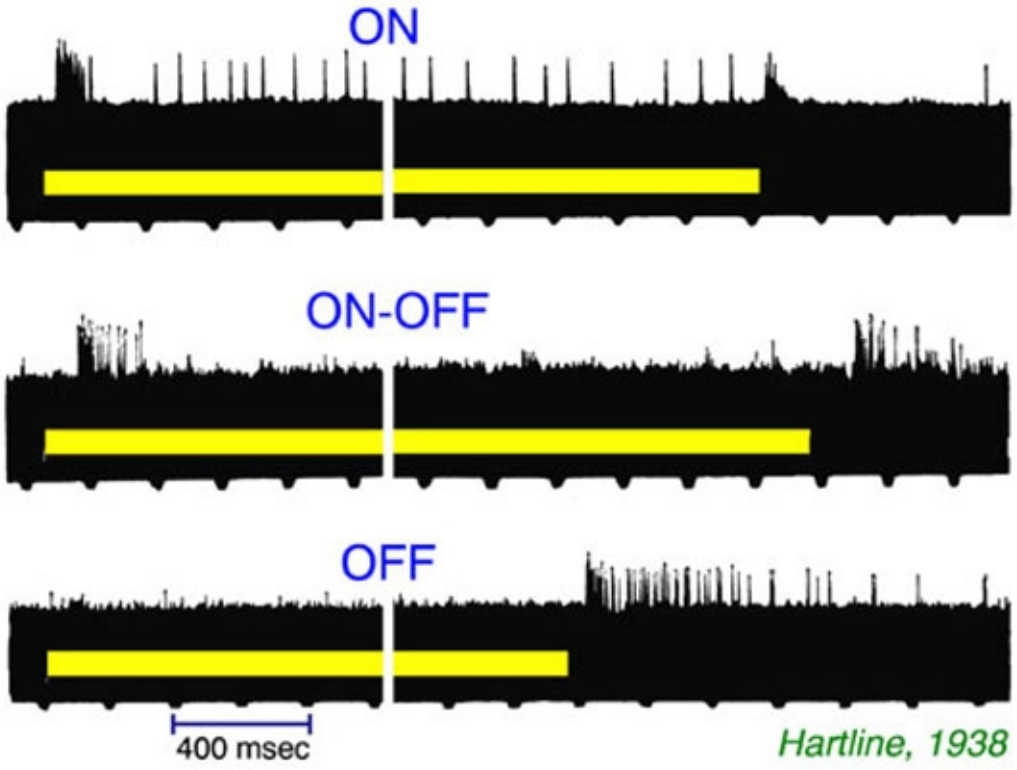

Figure 3. ON, OFF, and ON-OFF ganglion cells. After Hartline (87).

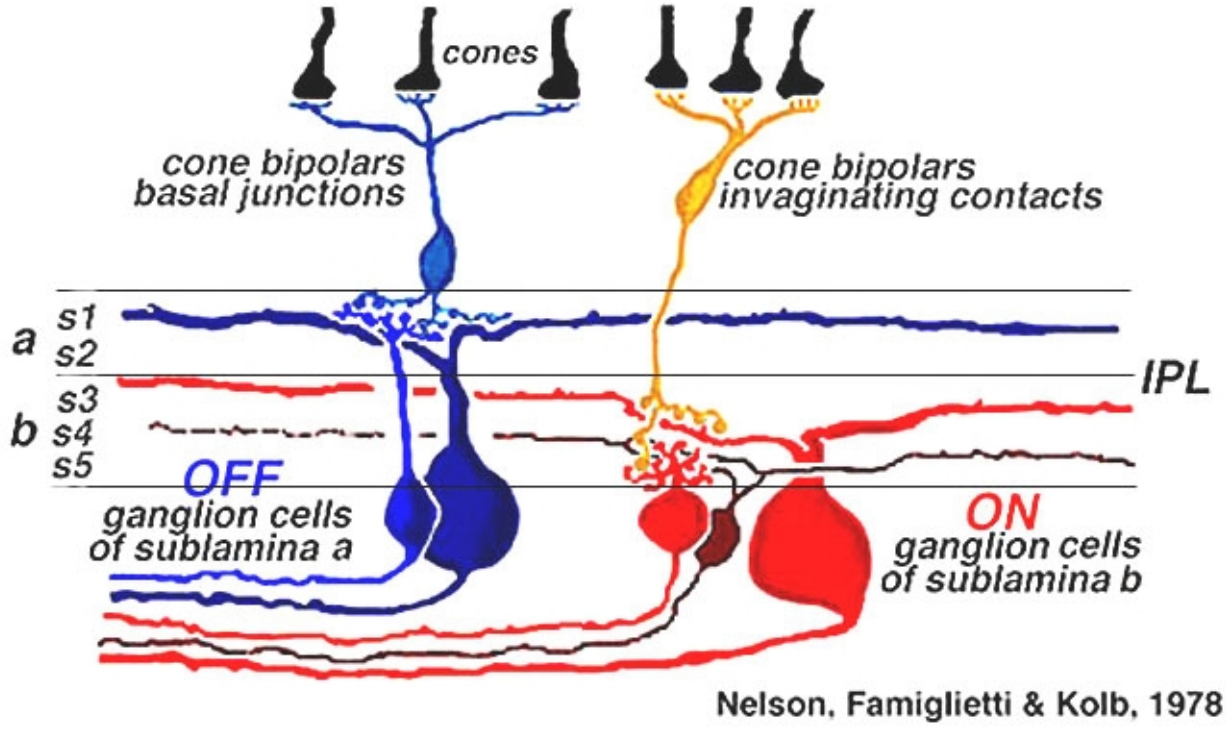

Figure 4. Organization of ON- and OFF-center ganglion cells into sublaminas a and b.

spots! Size selectivity is a unique and telltale characteristic of ganglion cell physiology. To summarize, ganglion cell center-surround interaction is a multifaceted phenomenon.

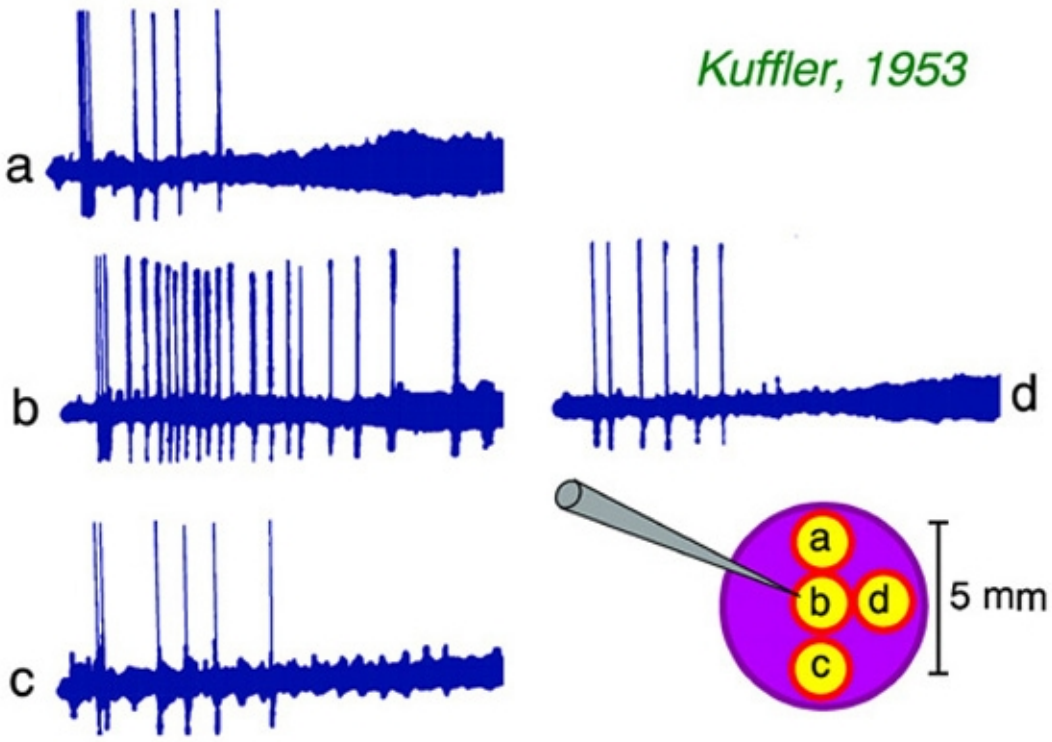

Figure 5. Spot mapping of cat retinal ganglion cell receptive-field center (13).

Features of ganglion cell center-surround interactions include:

- Change from sustained to transient center response as stimuli are displaced from the center.
- Excitatory responses evoked to opposite stimulus phase with surround stimulation.
- Active inhibition of the center response with surround stimulation.
- A maximal response can be evoked only with an optimally sized spot ("spatial tuning").

The question arises whether the four phenomena listed above represent a single mechanism or several. Evidence tends to suggest the latter, because there are many cases where some of these phenomena are present but not others. The most ubiquitous and characteristic feature is the last, however—spatial tuning. Although cells that do not fit into the ON- or OFF-center categories, such as the true ON-OFF center cells as described by Hartline (Fig. 3b), still exhibit spatial tuning.

Contrast Sensitivity Functions and the Difference of Gaussians Receptive Field Model

The characteristic spatial tuning of ganglion cell receptive fields is reflected in peaked contrast sensitivity functions (Fig. 8). Each vertebrate ganglion cell is "tuned" (responds best) for objects of a different size. Among the population of ganglion cells, a wide range of sizes is covered, perhaps corresponding to the wide range of object sizes in the visual image. This tuning reflects in part the variable dendritic span in ganglion cells (as elaborated below). Dendritic span is one of the factors allowing ganglion cells to collect visual signals over a broad reach of visual space. Receptive field centers and dendritic fields can be similar in size (15) (Fig. 9). But dendritic field span in itself does not provide for a decline in sensitivity as stimulus sizes become large. Surrounds are required. Tuning can be modeled as a result of center-surround interaction. In the OFF-center cell of Fig. 9, ON-excitatory surround responses are evoked by slit stimuli placed near the edge of the dendritic field (16).

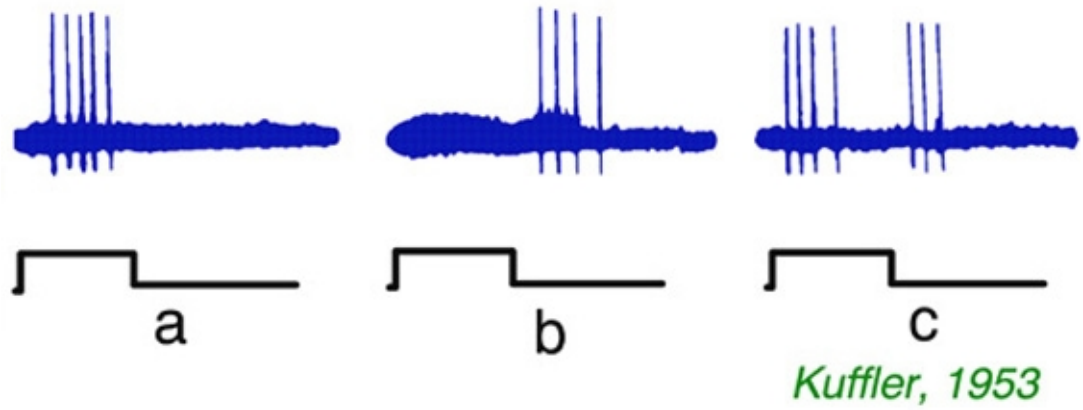

Figure 6. Opposed center and surround responses in cat ganglion cell (13).

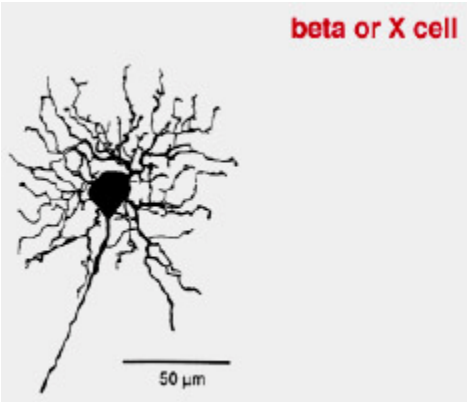

Movie 1. An animation of the center and surround receptive field organization of a beta ganglion cell.
Download video

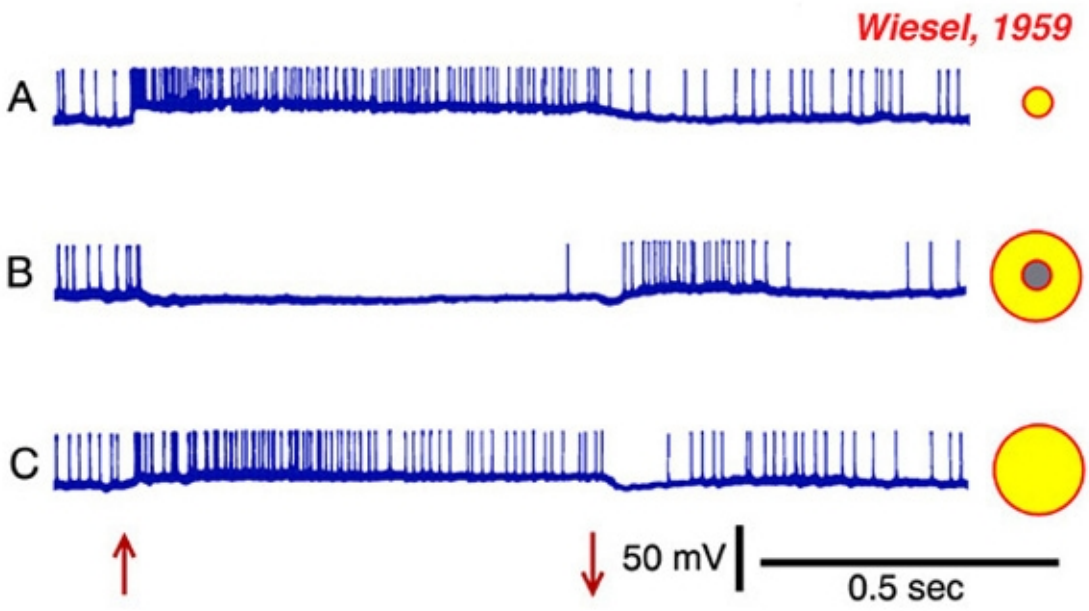

Figure 7. Changes in ganglion cell membrane potential accompanying center and surround responses (93).

Contrast sensitivity functions are a receptive field characterization generated, not using spots or slits of light, but by broad-field stimuli consisting of spatial sine waves. These appear as patterns of alternating, fuzzy-edged, light and dark bars covering all of visual space. "Contrast" is the difference in brightness between the light and dark phases of the pattern. In this receptive field characterization, contrast is reduced until the ganglion cell just barely responds to the introduction of such a stimulus into a featureless field. This is the threshold. The process is then repeated for patterns with different bar widths, or "spatial frequencies" (the reciprocal of the number of bright- and dark bar-pairs per unit distance). The sensitivities (the reciprocals of contrast thresholds) are plotted as a function of spatial frequency. The net result is a curve (Fig. 8), which demonstrates that in ganglion cells there is an optimal spatial frequency of stimulation. Patterns of this frequency can be observed with the highest sensitivity and lowest contrast. In Fig. 8, this frequency is about 0.6 cycles per degree, which scales to a bright-dark bar pair every 350 μm on the retinal surface, or a bright bar width of half this distance (175 μM).

Contrast sensitivity is one measure of size selectivity in ganglion cells. Another measure is "hyperacuity". This is the ability to detect movements within the ganglion cell receptive field. Cat ganglion cells can detect image displacements as small as 1' of arc (about 4 μm on the retinal surface or a movement of about 3 cm at 100 m distance). These displacements are much smaller than one might expect based on receptive field center sizes (which are typically several hundred μm in diameter on the retinal surface) or contrast sensitivity functions (14). Both contrast sensitivity measures and hyperacuity measures have the appeal that they may be applied equally as well to the sensitivity of a whole organism as to a single cell. Comparisons of organism performance to ganglion cell performance generally leads to the conclusion that organisms cannot detect visual stimuli that are not detected at least equally well by ganglion cells.

Peaked contrast sensitivity functions can be successfully modeled as a linear subtraction of two concentric, opposed receptive-field mechanisms (Fig. 10). In a well-studied version, of this model both the center ($W_c(r)$) and the surround ($W_s(r)$) are given Gaussian sensitivity profiles, with greatest sensitivity in the center of the receptive field and a smooth, steep decay of sensitivity away from the center (17). The center mechanism predominates for centrally located stimuli, because it is stronger at this location, but the surround mechanism prevails for peripheral stimulation because the surround radius (r_s) is greater than the center radius (r_c). These radii affect the rates at which sensitivity declines as stimuli are moved away from the center. This model is often referred to as the DOG (Difference of Gaussians) model. The curved line fitting the data in Fig. 8 was generated by a DOG model.

X and Y Receptive Fields

One of the assumptions of the DOG model (18) is that ganglion cells linearly add signals from both center and surround mechanisms for all points in space. This suggested that ganglion cells be tested for spatial linearity. Some cells (X-cells) pass the test, whereas others (Y-cells) do not, despite the fact that all receptive field data are well represented by the DOG model.

In Fig. 11, impulse firing rate is shown for different positions (or spatial phase) of the sine wave stimulus with respect to the receptive field center. To change the spatial phase, the pattern is shifted right and left by incremental amounts. For the X-cell (Fig. 9A), when the pattern is positioned so that the transition from light to dark passes directly through the center of the field, a "null response" is produced. Introduction of the stimulus produces no effect on firing rate. The tendency of the bright bars to excite the cell is exactly compensated by the tendencies of the dark bars to reduce the firing rate. For the Y-cell (Fig. 9B), no such stimulus position can be found. There is always a residual response, in this case the "null phase" results in transient increases in firing at both introduction and removal of the stimulus. The test is a particularly severe one for linearity. Not only is perfect spatial summation required, but the form of response to light increments must be exactly the opposite to the form of response to a light decrement for effects to exactly cancel. Y-cells may have linear spatial summation,

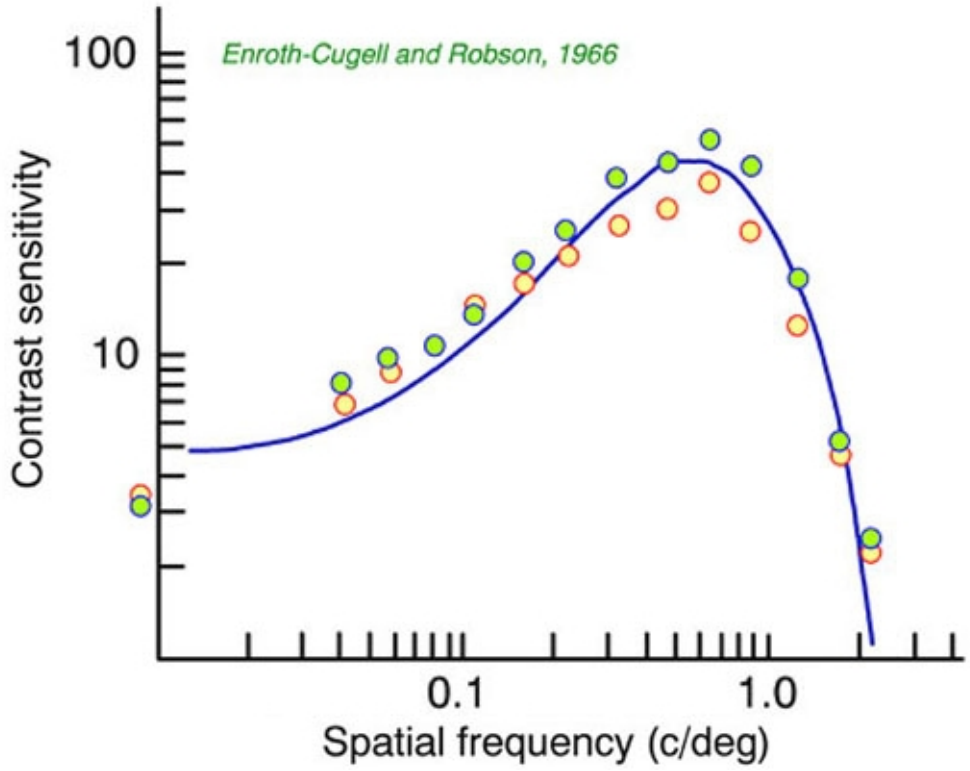

Figure 8. Contrast sensitivity function of cat retinal ganglion cell. Green and yellow symbols are the data generated with vertical and horizontal patterns, respectively, showing a symmetry of size sensitivity (18).

but evidently increment and decrement wave forms are not sufficiently symmetric for signals to cancel. This failure of linearity in Y-cells is thought to be attributable to inputs from non-linear subunits (19).

X- and Y-cells are differentiated in other ways as well. X-cells are numerous and have rather narrow receptive fields, and in cat retina are used for highest acuity vision. These are morphologically the "beta" cells of cat retina. Y-cells are rather sparsely distributed and have wide receptive fields. These are morphologically the "alpha" cells of the cat and most likely serve a visual alerting function. They are sometimes named according to the shape of the response wave form to steps of light. Y-cells are called "brisk transient" cells, and X-cells are called "brisk sustained" cells (20). Y-cells are also distinguished from X-cells by larger axon diameters and quicker conduction times from retina to the thalamic visual centers of the brain. These sets of cells initiate two separate and parallel pathways for transfer of visual information to brain visual centers (21). Morphological features and the distribution of X/beta, Y/alpha ganglion cells are discussed below.

Directionally Selective Ganglion Cells

Computing the direction of motion for a moving objector scene is the most complex information processing task performed by vertebrate retinas. Directionally selective retinal ganglion cells respond to stimuli moving in a preferred direction and are inhibited by stimuli moving in the opposite or null direction. The preferred direction is independent of the nature of the object, which can be either bright or dark, a simple object such as a small spot, or a complex object, such as a drifting grating (22). Because of center-surround inhibition, however, like other ganglion cells, directionally selective cells respond best to small spots. In addition to a preferred direction of movement these cells have preferred speeds of movement, some prefer slow movements, whereas others prefer rapid movements. They most commonly exhibit true ON-OFF receptive field centers when mapped with stationary spots, although not all cells with ON-OFF centers are directionally selective. Less frequently encountered types are ON-center when mapped with stationary spots (23) or OFF-center (24). This type of

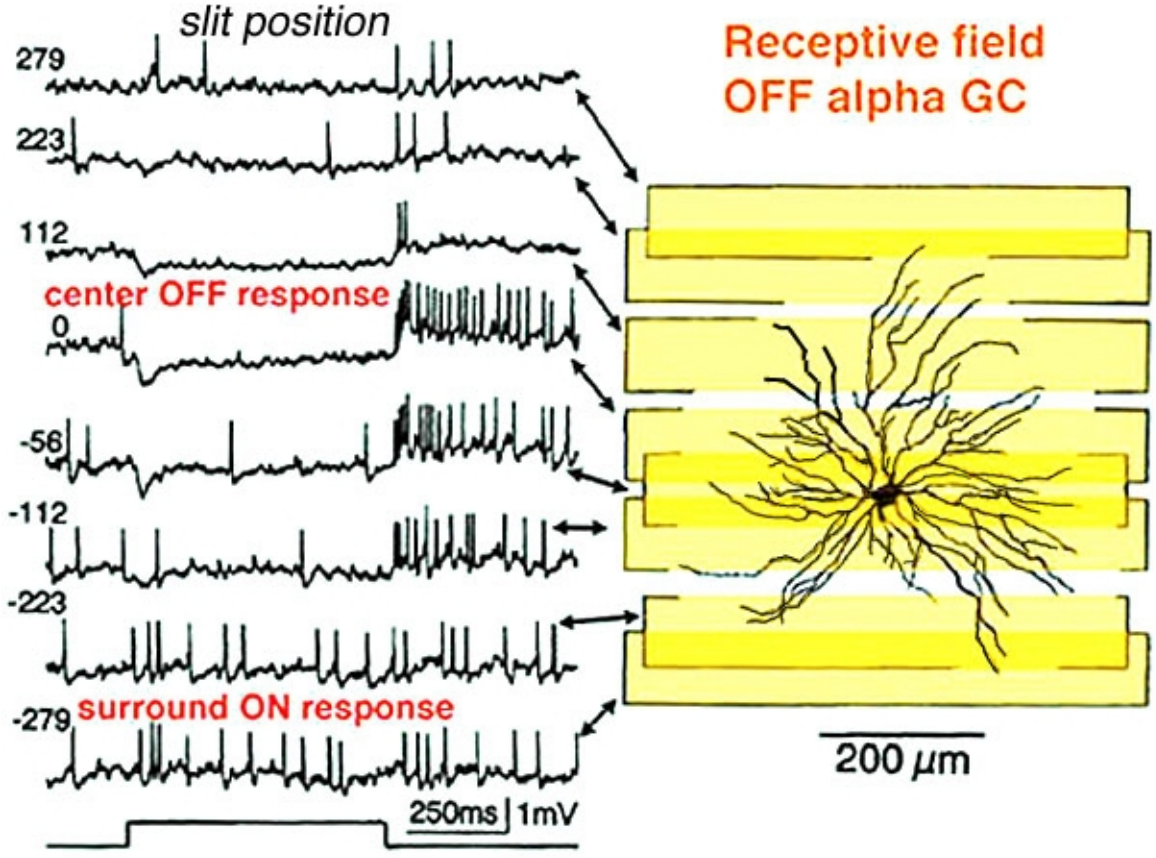

Figure 9. Relationship of dendritic and receptive field in an intracellularly stained, cat OFF-center ganglion cell (16).

response is encountered in many vertebrate retinas including birds (25, 26), reptiles (26-28), some mammals (22, 29), fish (30, 31), and amphibians (32), but is rather rare in cat (6) or primate retinas (33).

In Fig. 12, small spots of light are moved into the field of an ON-OFF type rabbit directionally selective ganglion cell from different points of the compass. When the spot is moved up from the bottom, a vigorous spike discharge occurs. When the spot is moved down from the top, no response occurs.

Modeling Directional Selectivity

The amazing feat of signal extraction found in directional selectivity, performed by a remarkably few retinal neurons, has sparked sustained interest in modeling this system, starting with the discoverers (34). Such attempts have generally met with failure (35), but here are some of the givens and some of the approaches: 1) it is generally believed that retinal interneurons are not themselves directionally selective (32), except perhaps in turtle retina (27, 36, 37); 2) models must yield the same preferred direction for both dark and bright spots. Originally, it was thought that the contrast invariance of directionally selective cells was attributable to the common ON-OFF type physiology (38) and interactions between signals of the ON and OFF pathways. The discovery of both ON-type and OFF-type directionally selective cells with contrast invariance suggests that this is not the case. The persistence of directionally selective responses under pharmacological blockade of the ON component also suggests that cooperation of both ON and OFF bipolar pathways may not be required. In ON-OFF cells, both pathways yield the same preferred directions, however (39); 3) there is evidence of preferred direction facilitation (40) as well as null direction inhibition; 4) there is little evidence that directionally selective ganglion cells themselves exhibit morphological polarization (12, 15, 24, 41, 42).

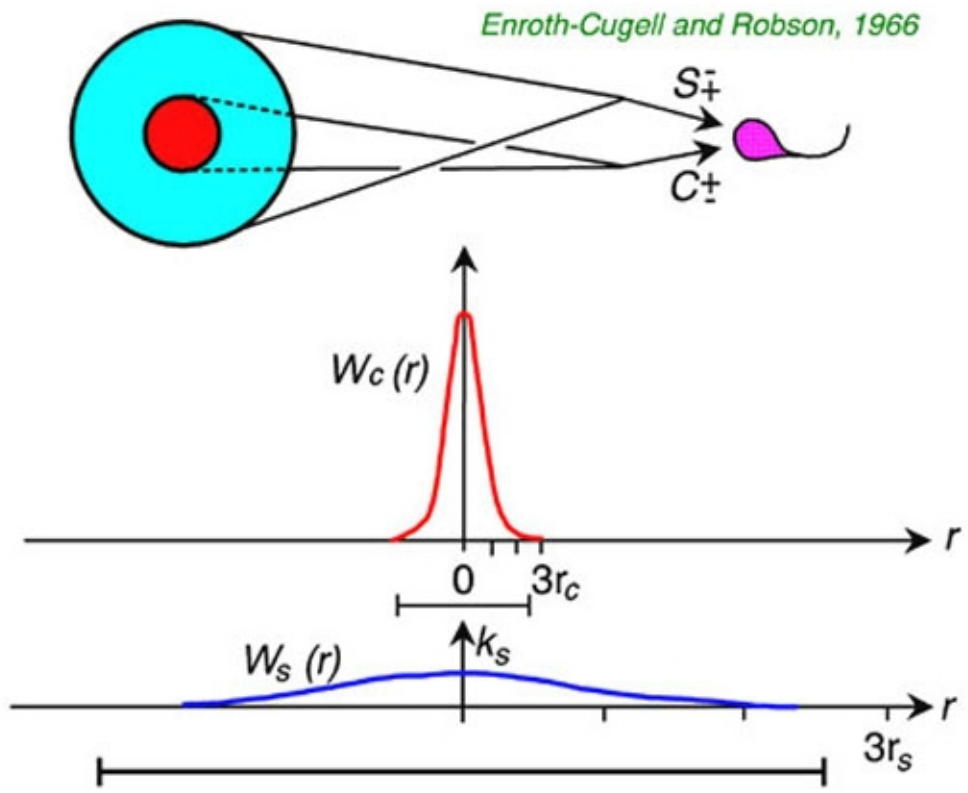

Figure 10. Difference-of-Gaussians Receptive Field Model (18).

Directionally selective ganglion cells, stained after microelectrode recordings, have a distinctive dendritic morphology with many apparently closed, or nearly closed, loops, giving the appearance of anastimosing dendrites (Fig. 13, Fig. 14). ON-OFF directionally selective ganglion cells are bistratified in the inner plexiform layer (Fig. 13), whereas ON-type directionally selective cells are monostratified, close to ganglion cell bodies (Fig. 14). None of these morphological features hints at the orientation of the null/preferred axis, however.

Some form of morphological polarization of presynaptic interneurons is a common feature of models of directionally selectivity: 1) Intrinsic neurons with axons. Originally the axon bearing horizontal cells of mammals were suggested as providing the directional arrow in the retina (29). Because ON and OFF pathways have not yet diverged at the horizontal cell level of signal processing, contrast invariance would be explained. However, bipolar cells were not found directionally selective (32). Association amacrine cells with intraretinal axons have been been found in pigeons (43). With appropriate connectivity, these might be the substrate of directional selectivity. Unfortunately, such cells do not appear to be common to most species. 2) Functional polarization of presynaptic amacrine cell dendrites. Starburst amacrine cells are cholinergic and excitatory and appear to release acetylcholine primarily at dendritic tips. An excess innervation by such amacrine cells on one side of the directionally selective cell might result in preferred direction excitation. Ablation of these cells with lasers, or pharmacological blockade of acetylcholine, have failed to abolish directional selectivity, though (35).

Pharmacology of Directional Selectivity

Some pharmacological agents abolish, or partially abolish, directional selectivity. The most classic of these is picrotoxin, a convulsant, and blocker of receptors for the inhibitory neurotransmitter gamma-aminobutyric acid (GABA). Both $GABA_A$- and $GABA_C$-type receptors, the latter very common in the retina, are blocked by picrotoxin.

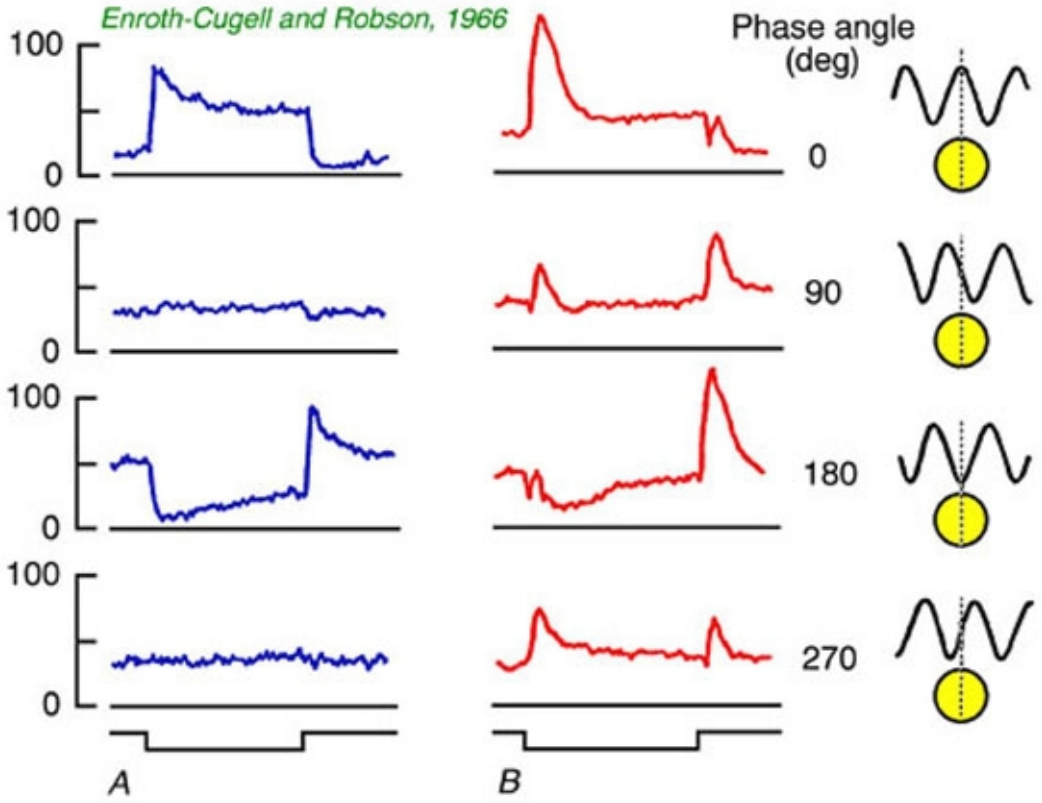

Figure 11. The null test for linear summation within X- and Y-type receptive fields (18).

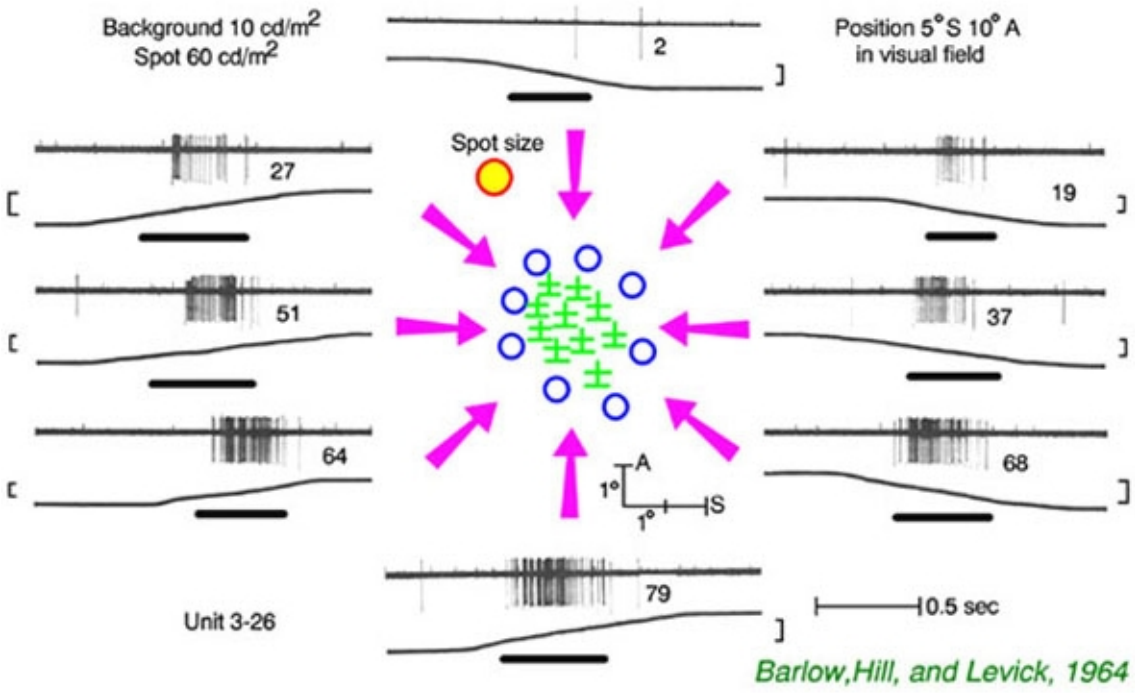

Figure 12. Responses of directionally selective ganglion cell to objects with different directions of motion (23).

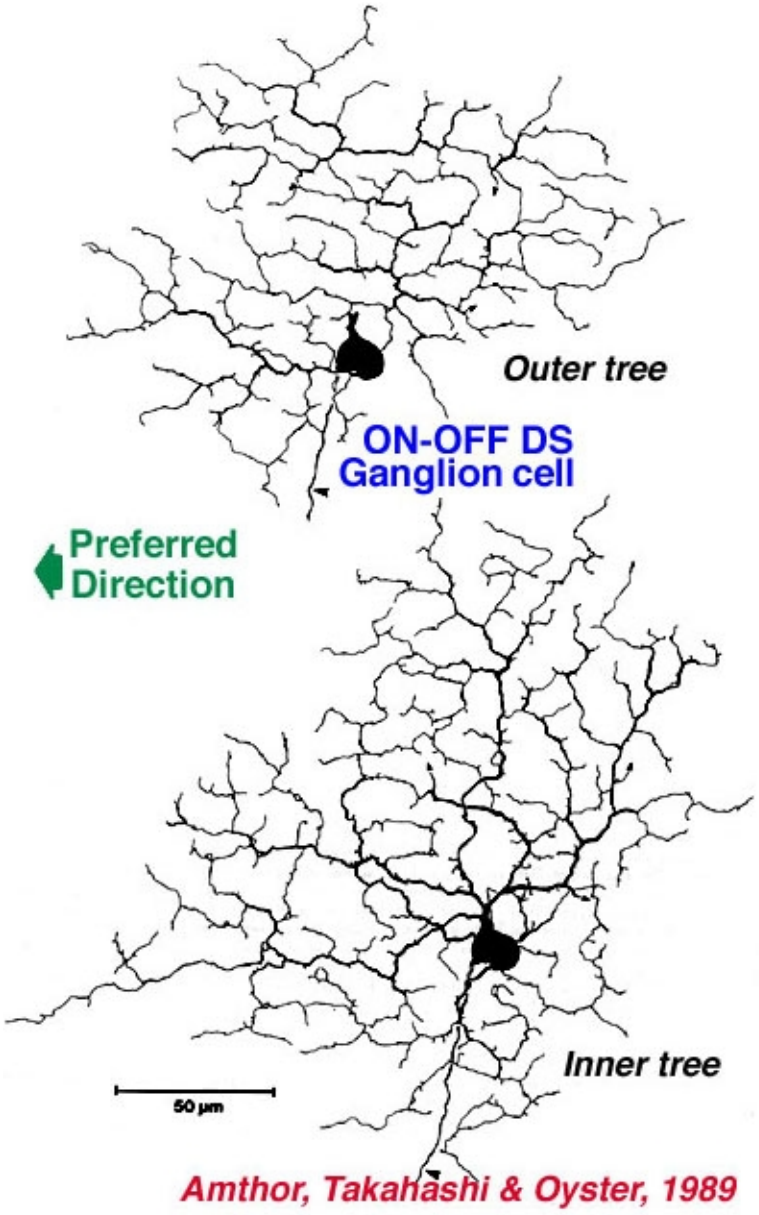

Figure 13. ON-OFF directionally selective ganglion cell of rabbit retina.

Fig. 15A illustrates the static receptive field properties of an ON directionally selective cell in rabbit retina. This cell responds to spots moving toward the lower left (Fig. 15B, P) but not the upper right (Fig. 15B, N). No responses are seen to bars of light, regardless of the direction of motion. This indicates a particularly strong surround antagonism suppressing responses to large stimuli. Picrotoxin abolishes both directional selectivity and size specificity. In these experiments (44), strychnine— another convulsant and blocker of the inhibitory neurotransmitter glycine—did not have these effects. This suggested that GABA was selectively important in neural circuitry underlying the generation of directionally selective responses. The $GABA_A$-selective antagonist SR95531 blocks directional responses, suggesting that this particular subtype of GABA receptor is critical to the process (39).

The neurotransmitter acetylcholine is a potent excitatory agent for directionally selective ganglion cells (45). It is released by presynaptic cholinergic "starburst" amacrine cells and provides excitation at both onset and offset of the stimulus. Blockade of cholinergic input (46, 47), or ablation of cholinergic amacrine cells, reduces but does not abolish directional selectivity (35). The metabotropic glutamate receptor agonist *APB* blocks the ON

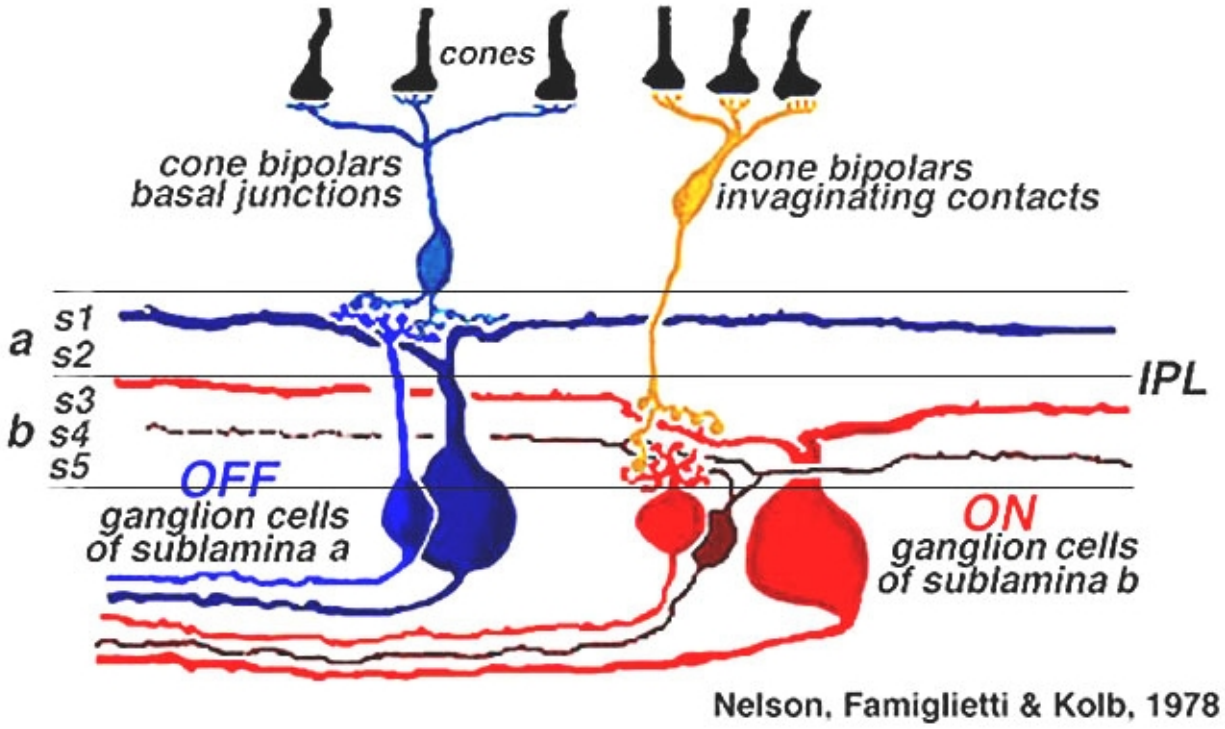

Figure 14. ON directionally selective ganglion cell of rabbit retina (12).

component of all responses in ON-OFF type directionally selective cells (39, 46). However, the OFF component of directional responses remains. *N*-Methyl-D-aspartate (NMDA) receptor agonists do not block directionally selective responses, and by implication directionally selective ganglion cells contain excitatory NMDA response components, which are non-directional (46). Interestingly, the AMPA-kainate receptor antagonist NBQX potently blocks directional selectivity in both ON-OFF and ON-type cells, leaving vigorous responses to movement in all directions (Fig. 16). Thus, a non-NMDA glutamate receptor may be selectively involved in the directionally selective mechanism, possibly as an excitatory (bipolar) input to a GABAergic interneuron (46).

Color and Spectral Responses

Ganglion cells respond to colored stimuli in one of two ways: color opponent responses and luminance responses. The patterns are similar to those of horizontal cells, which occur in chromatic and luminance types. Color opponent ganglion cells are found principally in vertebrates, which behaviorally can discriminate color. Goldfish are an animal model with color vision and have provided much information on the way in which vertebrate retinas process color. In this animal, it was first realized that individual cones express only one each of three genomically available cone photopigment types (colloquially, red, green, or blue cones; technically, long (L), mid (M), or short (S) wavelength types). This supported at least part of Thomas Young's (48) 19th century "trichromatic" theory of color vision. Neural retina does not preserve the purity of this spectral trilogy, however. Signals are both added and subtracted to form luminance and color opponent channels, respectively. Color opponency was a color vision theory of the 19th century physiologist Ewald Herring (49). Retina operationally combines both ideas from Young and Herring in processing spectral information.

In Fig. 17, white light is broken into spectral colors with a monochrometer and flashed on the retinal surface while recording ganglion cell discharges. Short-wavelength lights (400-560 nm, blue or green) excite the cell, evoking impulse discharges. Long-wavelength stimuli (570-700 nm, red) inhibit discharges during presentation but evoke discharges at offset. This is a classic color opponent pattern of the RG (red/green) type (50). There is also a symmetrical type excited by red stimuli and inhibited by green.

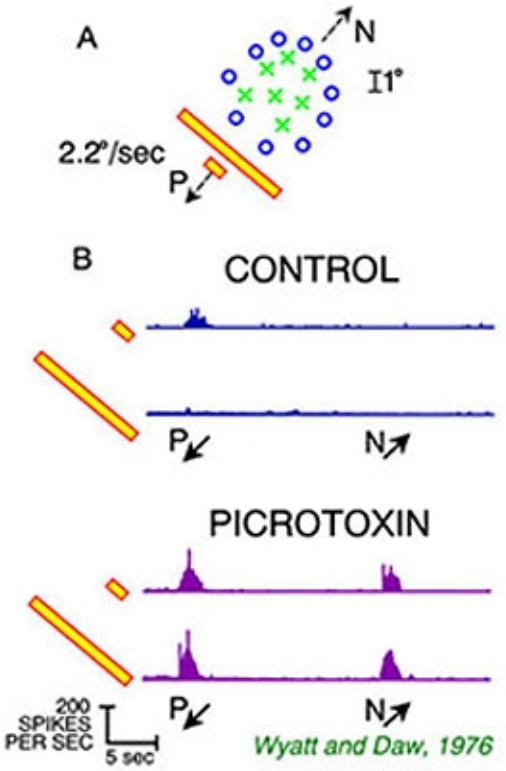

Figure 15. The GABA antagonist picrotoxin blocks directional selectivity in ON directionally selective ganglion cells. After Wyatt and Daw (44).

In cells with input pathways arising from more than one spectral class of cone, the relative strength of different cone inputs can be modified by colored backgrounds (50). This is called "selective chromatic adaptation". In the cell of Fig. 17, red backgrounds reduce the strength of OFF inhibitory responses, allowing green ON excitatory responses to be seen at long wavelengths. Conversely, green backgrounds reduce the strength of ON responses and allow red OFF responses to be seen at short wavelengths. Modification of spectral properties by colored backgrounds is often used to evaluate cone inputs, even in the absence of color opponent signals.

Cats, like many other large mammals aside from primates, are often thought to be color blind. Present evidence suggests that cats can distinguish blue from colors of longer wavelength (51), but that their color acuity is much worse than primates (52). Ganglion cells in cat retina are primarily of the luminosity type. Fig. 18 provides an example of this type of cell. Spectral curves always peak at 556 nm, characteristic of the cat's red cones, regardless of attempts to shift the sensitivity toward longer or shorter wavelengths with selective chromatic adaptation. Very rarely, color opponent cells are seen in cat. In Fig. 19 is an example of a cell excited by blue stimuli and inhibited by red. In cat retina such cells may account for only 1% of the ganglion cell population, all with blue ON excitation and red OFF inhibition (20, 51).

Color and Receptive Fields

Color opponent ganglion cells can have centers and surrounds, each with separate color opponent properties. A common type in goldfish retina is the double opponent ganglion cell. In this type, each color mechanism in the receptive field center is opposed by a mechanism of the same color type but opposite sense in the surround (53). Spectral properties of a goldfish ganglion cell with a red OFF-center, red ON-surround in combination with a

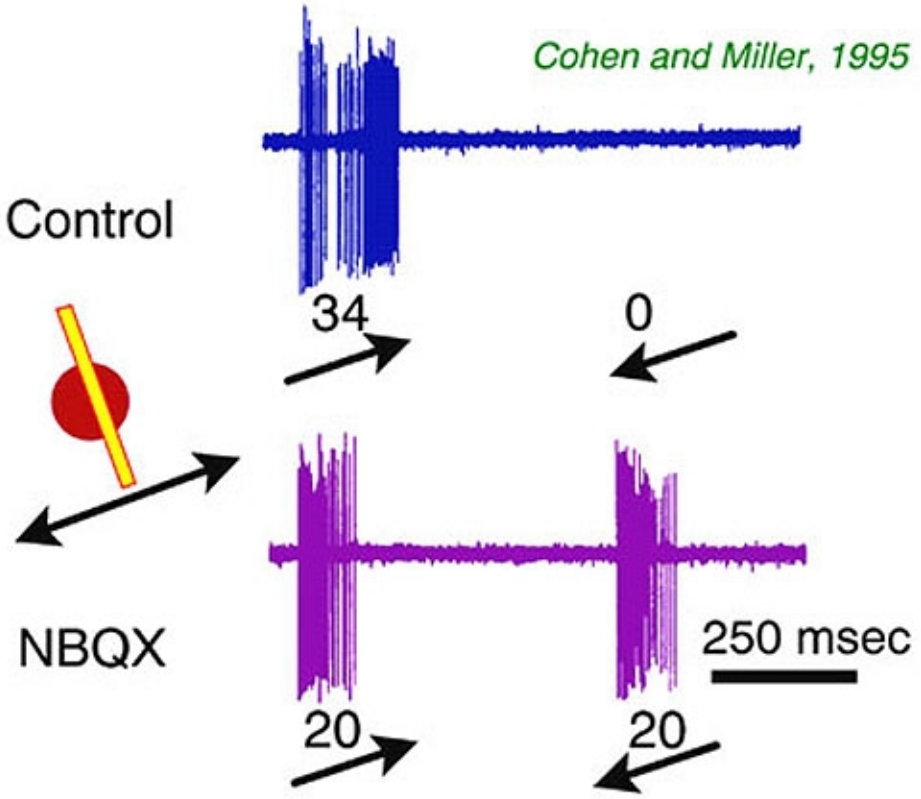

Figure 16. The AMPA-kainate antagonist NBQX (10 μM) blocks directional selectivity in ON-OFF directionally selective ganglion cell. After Cohen and Miller (46).

green ON-center, green OFF-surround appears in Fig. 20. This type of cell is thought to excel at "simultaneous color contrast"—the ability to detect color changes at borders.

Color opponency is not the only way in which cone signals are processed in the retina. In Fig. 21 is an example of synergistic addition of blue and red cone signals in the surround mechanism of a cat OFF-center ganglion cell. It is apparent then, that ganglion cells may combine cone signals in a myriad of ways. In the twilight-hunting cat, signal detection may be more important than color discrimination. Adding signals from different cone mechanisms may increase signal amplitudes across the spectrum. Multiple cone types may thus serve at least two roles, discrimination of color and increased spectral coverage.

Tonic and Phasic Ganglion Cells of Primate Retina

Primate retinal ganglion cells occur in two broad categories, "tonic" and "phasic", as described by Gouras (36). Tonic cells respond to light stimuli in a steady maintained manner. Receptive field centers are extremely small, about 15 μm on the retinal surface (~4' of arc, about 10 cm at 100-m distance). Tonic cells are often called "midgets" because they probably represent recordings of midget ganglion cells described by Polyak (54) (see below). They occur with a density distribution across the retina comparable to, anatomically, midget cells (55). The tiny receptive field centers match well the anatomical sizes of these tiny cells. The optic nerve conduction velocities of tonic fibers are slow (~2 m/s) (56). As a group, these cells are also often referred to as the "parvocellular pathway" or "P" cells. This is because the tonic fibers terminate in the parvocellular layer ofthe lateral geniculate nucleus of the thalamus.

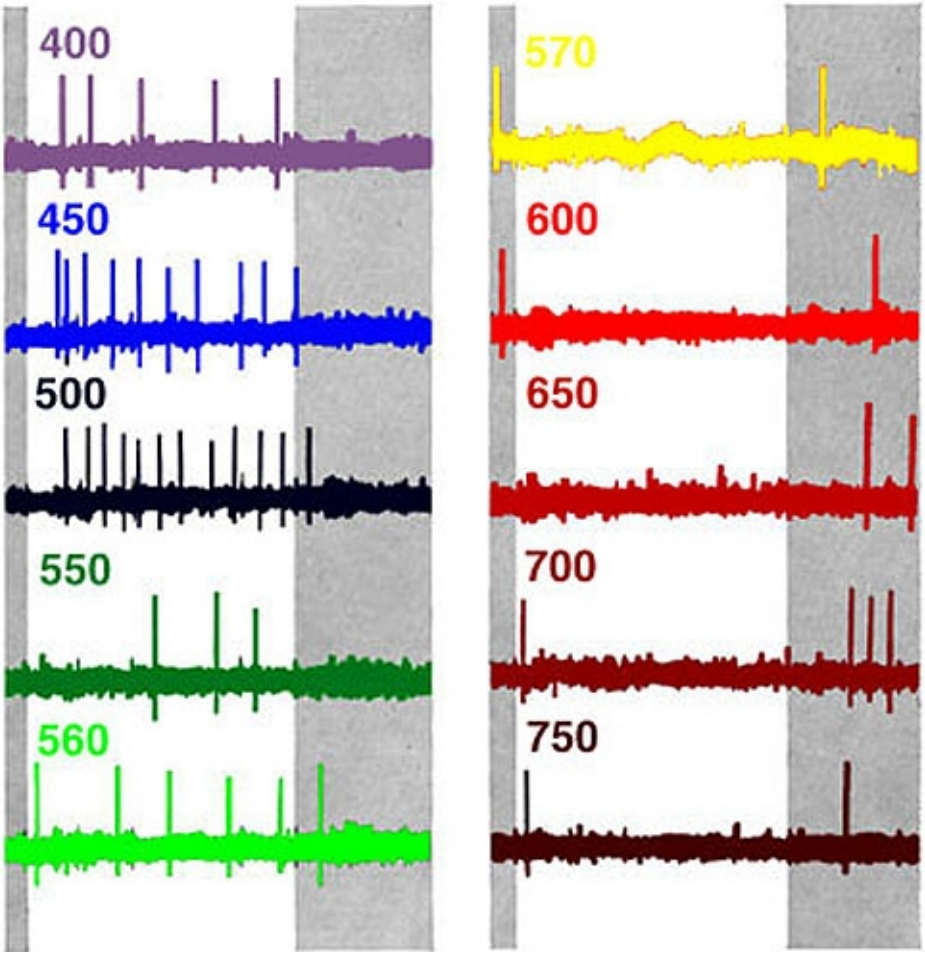

Figure 17. Impulse discharges of ganglion cells in goldfish retina. Half-second stimuli (white) are different wavelengths (left). Short wavelength (blue or green excite the cell; long wavelength stimuli (red) inhibit it). From MacNichol (94).

Phasic responses originate with morphologically larger ganglion cell types with fast optic nerve fiber conduction velocities (~4 m/s) (56). Microelectrode staining of such cells shows that they are "parasol" types (57). ON-types branch low in the inner plexiformlayer (sublamina **b**), whereas OFF-types branch high in the innerplexiform layer (sublamina **a**), following the classic branching pattern for ON- and OFF-center cells (10, 57). Phasic cells are often referred to as the "magnocellular" or "M-cell" pathway because their fibers terminate in the magnocellular layer of the lateral geniculate nucleus of the thalamus. Near the fovea, receptive fields of phasic cells are two to three times larger than those of tonic cells and may be 10 times larger in peripheral retina.

Tonic cells of the parvocellular pathway respond best to stimuli with high contrast and fine grain, whereas phasic cells respond to stimuli with very weak contrast, covering larger areas (58).

Color Properties of Primate Ganglion Cells

Tonic cells occur in three spectral types: red-center, green-center, and blue-center cells. Stimuli consisting of small spots evoke spectral responses consistent with the action of only a single spectral type of cone in each case. Surround responses are also spectrally selective and are generated only from spectral types of cone not found in the center responses (33). Tonic cells are spectrally opponent types, but the opponent signals are distributed in different regions of space.

Phasic cells combine red and green cone signals synergistically in both center- and opponent-surround mechanisms of the receptive field. These cells are luminosity types and are not generally color opponent,

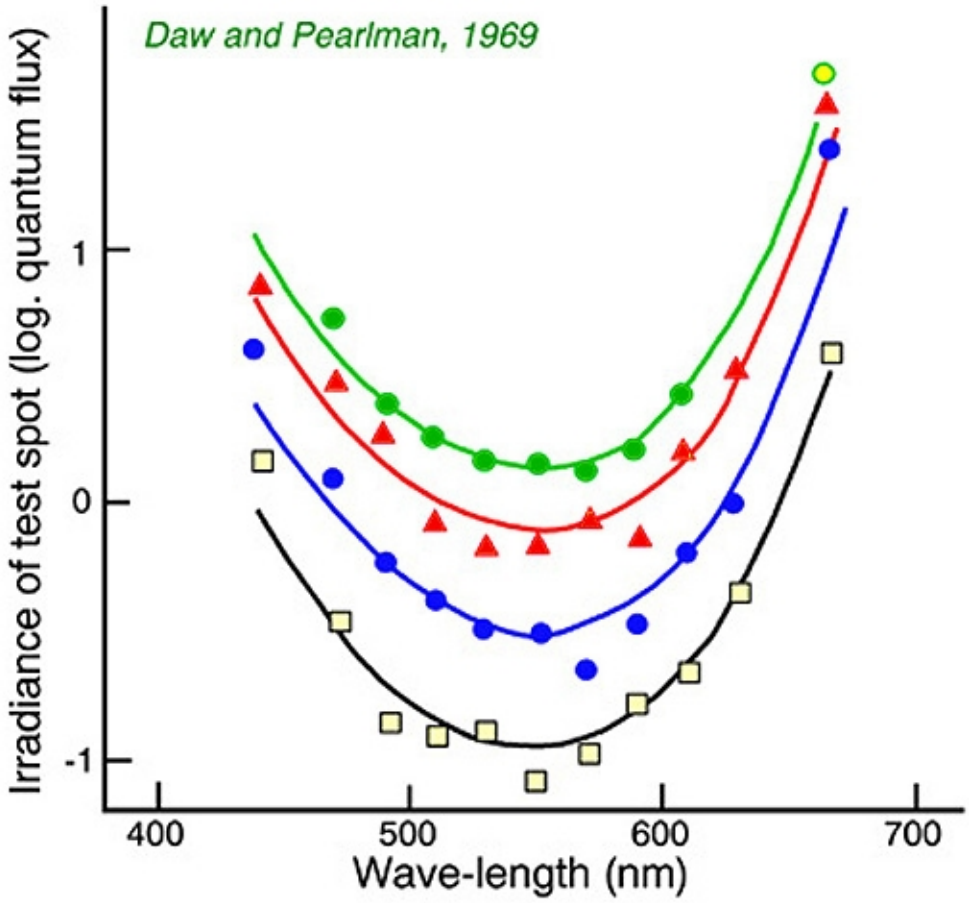

Figure 18. Spectral sensitivities of cat ganglion cell under conditions of selective chromatic adaptation. White background (squares), blue background (blue circles), red background (red triangles), and green background (green circles). After Daw and Pearlman (95).

although in some cases an imbalance of the strength of spectral mechanisms in center and surround generates some opponent characteristics (33).

A classic tonic ganglion cell with green ON-center and red OFF-surround responses appears in Fig. 22. Small green spots (540 nm, 0.02°) excite the cell, evoking a maintained discharge. Large red spots (640 nm, 2°) inhibit impulse firing, but excitation occurs when the red stimulus is turned OFF. This is a chromatically opponent receptive field surround mechanism. In Fig. 23 are spectral sensitivities of three different tonic cells for small spots. Spectral sensitivities are not altered by selective chromatic adaptation (33), indicating that each center mechanism behaves as if it were driven by a single spectral class of cone. At the top of the figure is a blue-sensitive tonic cell. The 650 Fresnel peak on the light frequency axis corresponds to about 450 nm, the peak of blue-sensitive cones. Similarly, the middle panel (Fig. 23) illustrates a green-center tonic cell, and the lower panel, a red-center tonic cell. It is important to realize that tonic cells come in OFF- as well as ON-center varieties. Thus, there are at least six different center mechanisms for this concentric color opponent class of cell. Blue OFF-center types appear to be particularly rare, however (33). Some surround mechanisms in tonic cells combine more than one cone mechanism. When the different color properties of surrounds are considered, there are a total of 12 spectral categories for this class. Reid and Shapley (59), however, found only one spectral class of cone in tonic cell surrounds.

Impulse discharges of a phasic ganglion cell (Fig. 24) exhibit an initial transient burst followed by a sustained discharge for small spots, and only a transient ON burst for large spots, as delayed antagonistic surround

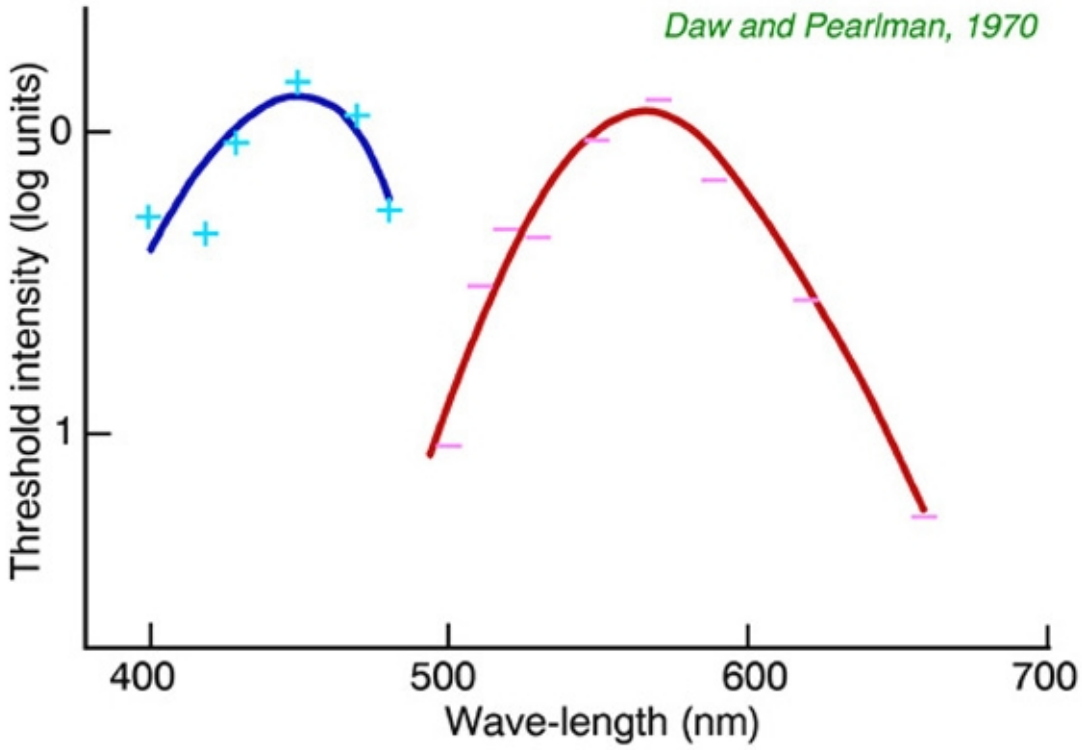

Figure 19. Blue ON, red OFF color opponent cat ganglion cell recorded on white background. (+/blue) spectral sensitivity of ON excitation, (−/red) spectral sensitivity of OFF excitation. After Daw and Pearlman (51).

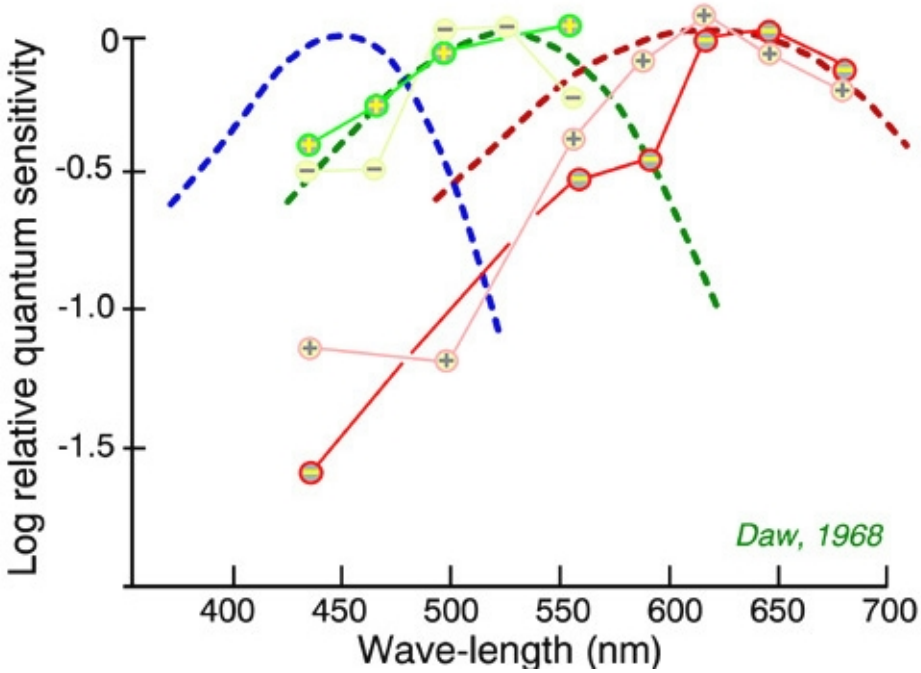

Figure 20. Red OFF center double opponent color cell of the goldfish retina. Center responses, yellow symbols; surround responses, gray symbols; excitation, +; inhibition, −. Dotted lines are red, green, and blue photopigment absorption spectra for comparison to sensitivities of receptive field mechanisms. After Daw (96).

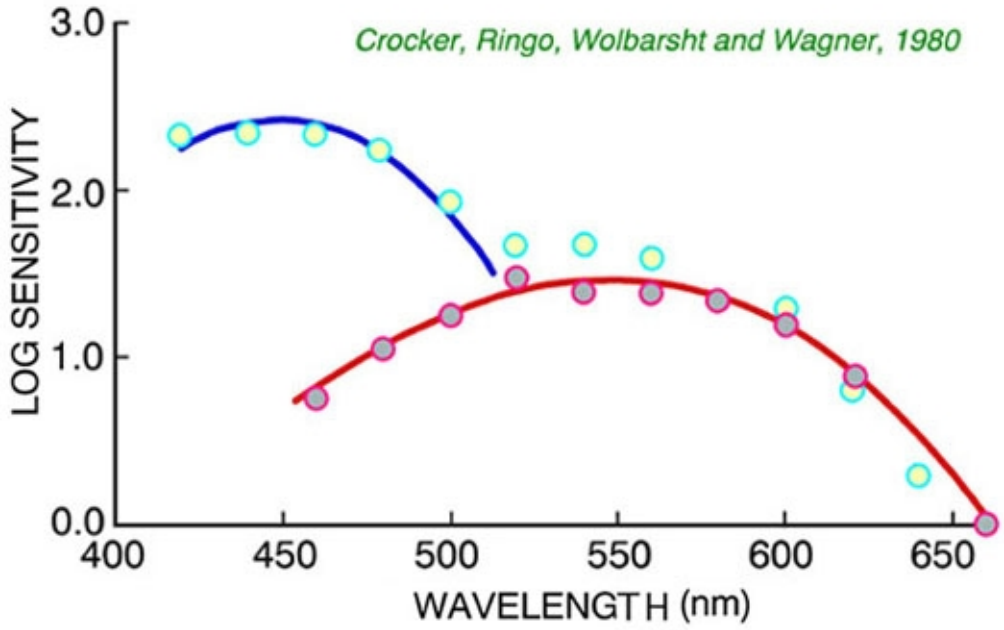

Figure 21. Synergistic action of red and blue cone signals in receptive field surround of cat OFF-center cell. Red-gray symbols, center OFF responses; blue-yellow circles, surround ON responses. Bright yellow light was required to bring out the blue mechanism. After Crocker et al. (97).

responses, induced by the large stimulus, inhibit the sustained response component. Large red spots evoke a particularly brisk OFF discharge from the receptive field surround. The cell is spectrally a luminosity type, with excitatory center responses to all wavelengths of stimulation. Both red and green cone signals sum synergistically to produce the center responses of primate phasic ganglion cells (Fig. 25). Red background lights will selectively desensitize the red cone signal components, revealing the green cone component of the center response; likewise, blue background lights selectively desensitize the green cone signal component, revealing red cone contributions to the center response.

Intracellular recordings from phasic ganglion cells in isolated monkey retina (Fig. 26) confirm that these responses originate in parasol-type ganglion cells (Fig. 27). The phasic, parasol response is chromatically a luminosity type. Vigorous responses are evoked by alternating bright and dark periods (Fig. 26a) but not by alternating blue and yellow colors (Fig. 26b), or magenta and green colors (Fig. 26c) balanced for brightness. Phasic cells sense luminance changes but not color changes (57).

There are also color opponent ganglion cells in primate retina with color opponent centers but no surround (class 2: color opponent, non-concentric) (33). These occur in both blue-yellow and red-green opponent types. The receptive fields are rather large, similar to phasic cells. Opposed spectral mechanisms fully overlap within this large receptive field center (33). No antagonistic surround mechanisms is found. Dacey and Lee (57) have recorded and stained a candidate for one of these types, a blue-yellow opponent cell. Morphologically, it is a small, bistratified ganglion cell.

Unlike the phasic cell (Fig. 26), this blue-excited cell is able to respond to color changes, being excited by a change from yellow-to-blue stimuli of equal luminance (Fig. 28c). As a bistratified type, it is clearly not a midget ganglion cell. Dacey and Lee (57) plausibly argue that the cell receives OFF-type red and green bipolar cell input onto its outer, OFF-layer dendritic tree and ON-type blue bipolar cell input onto its inner, ON-layer dendritic tree. Dacey and Lee (57) also describe a small, peripheral, monostratified ganglion cell responding to red-green

color changes but not to the magenta-green color changes designed to excite blue-sensitive ganglion cells. As yet, foveal and para foveal midget cells have not been marked by microelectrode staining techniques.

Rod Signals in Retinal Ganglion Cells

In addition to information about color, ganglion cells also transmit to the brain a monochromatic, non-color-containing signal from rods. Rods detect visual stimuli at very low light levels, including visual threshold. Their true sensitivity is rarely tested in a typical urban environment, but imagine a moonless rural night without street lights. Shapes and forms are fuzzy, colorless, and slowly perceived. This is rod vision. Such visual environments are often termed "scotopic", in contrast to brighter "photopic" environments where shape, color, and movement are readily seen. In photopic environments, cones are active. Amazingly, individual ganglion cells transmit both sorts of information, a sort of multiplexing of signals with very different characteristics, although it is only with a "mesopic" visual environment, with intermediate levels of ambient illumination, that both signals may be simultaneously present.

Rod and cone signals are found mixed in the major X- and Y-type ganglion cells (beta and alpha morphological types) in cat retina (60), and such signals are always found to be of the same polarity as the center mechanism for cone signals. Rod and cone signals are clearly mixed in the phasic type ganglion cells of the primate magnocellular pathway (61, 62). Whether tonic cells of the parvocellular pathway contain significant rod input remains controversial. Recent studies suggest that such input is either weak or absent (63) and may be absent entirely in blue-center cells. The M-cell/magnocellular pathway appears likely to be the principal conduit for transferring visual information to the primate brain under conditions of dim illumination (64). This point, however remains controversial (65). In goldfish retina, only ganglion cells with red cone-dominated center mechanisms contain rod signals (66). However, no such selective cone association has been reported in primate (62).

Rod Signals Are Delayed

Rod signals develop more slowly than cone signals. Reaction times driving automobiles or playing sports out of doors is slower at night. This is because rod signals are characteristically slow, and it is this photoreceptor system that is active at night or with dim illumination.

In Fig. 29, extracellular spikes from a primate ON-center retinal ganglion cell can be seen composed of two distinct clusters with different delays. With yellow backgrounds, only short latency spikes are generated in response to a brief flash, regardless of wavelength or stimulus brightness. These are cone signals. Under dark-adapted conditions and threshold stimulation, only long latency spikes occur. These are rod signals. Under dark adaptation and with somewhat brighter red stimuli, which begin to stimulate cones, a mixed response can be seen composed of both short latency cone components (arrow) and long latency rod components. In Fig. 30, rod and cone responses are seen in intracellular recordings of a cat OFF-center ganglion cell. Responses to flickering red (647 nm) stimuli arise mainly from red cones, whereas those from blue (441 nm) stimuli arise only from rods. Superposition of responses allows easy comparison of the timing of rod and cone signals with each flicker cycle. Rod ON hyperpolarizations evoked by the blue stimulus are distinctly delayed as compared with cone ON hyperpolarizations evoked by the red stimulus. The different delay is also apparent with the excitatory impulses evoked at the offset phase of each cycle.

In a series of flicker responses evoked by different brightnesses of blue-light stimuli, there is a characteristic shortening of phase delay with brighter stimuli. This reflects a shift from rod to cone activation in the ganglion cell signal. In Fig. 31, bright stimulus, cone-dominated flicker appears in the left column of flicker responses, whereas dim stimulus, rod-dominated flicker appears in the right column. The change in delay of ON-inhibition in this OFF alpha ganglion cell is readily apparent when the two columns are compared. In fact, on the right, rod flicker response is so slow that the excitatory OFF response of the preceding flicker cycle appears in the very

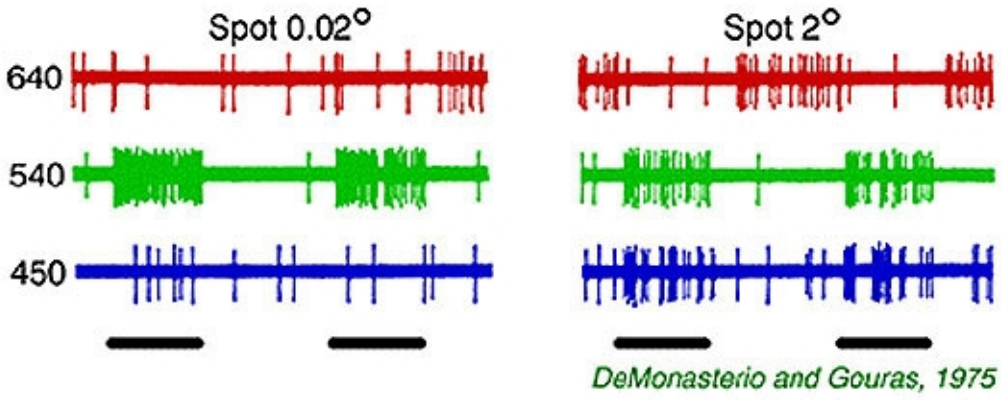

Figure 22. Spectral responses of tonic ganglion cell in rhesus monkey retina. Stimulus wavelength in nm is given to the left of impulse discharge responses. The light stimulus is ON during the black bars at the bottom of the figures. This cell is a green ON-center ref OFF-surround unit. After De Monasterio and Gouras (33).

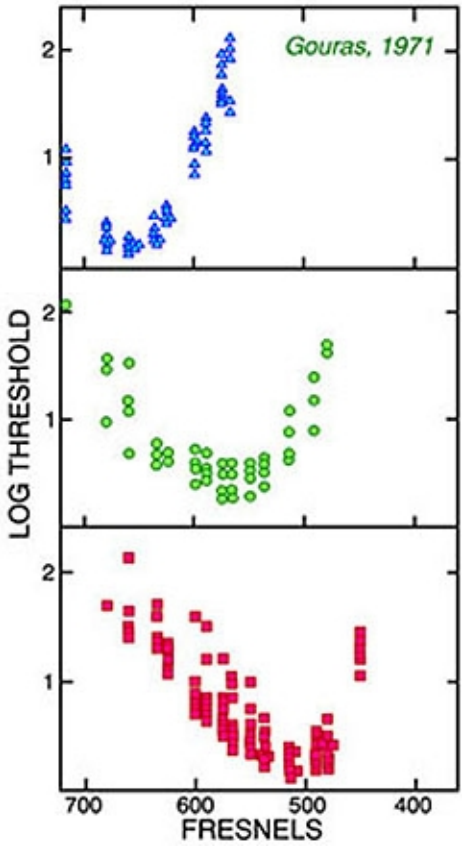

Figure 23. Spectral sensitivities for small spots of red (bottom), green (mid), and blue (above) sensitive tonic cells. Center responses appear to be driven in each case only by a single spectral class of cone. After Gouras (98).

middle of the current ON stimulation cycle. Response contradicts stimulus, an example of how perception might be at variance with reality. A superimposed horizontal cell response behaves similarly in this brightness series, although overall, it responds a little more slowly than the ganglion cell. Flicker cycles from an AII amacrine cell for dim stimuli are also shown. Many AII amacrines lack significant cone system signals, so that only very slow

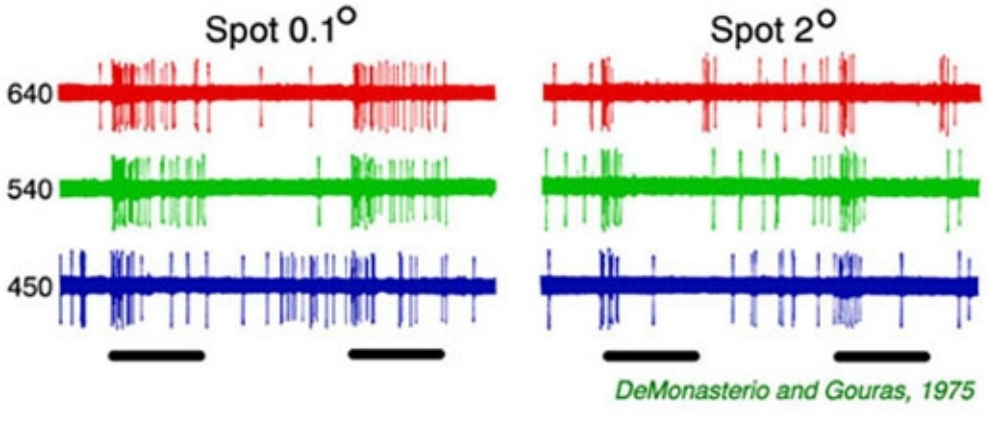

Figure 24. Spectral responses of phasic ganglion cell in rhesus monkey retina. Stimulus wavelength in nm given to left of impulse records. The light stimulus is ON during the black bars at the bottom of the figure. This cell is spectrally a luminosity type with ON-center and OFF-surround responses. After De Monasterio and Gouras (33).

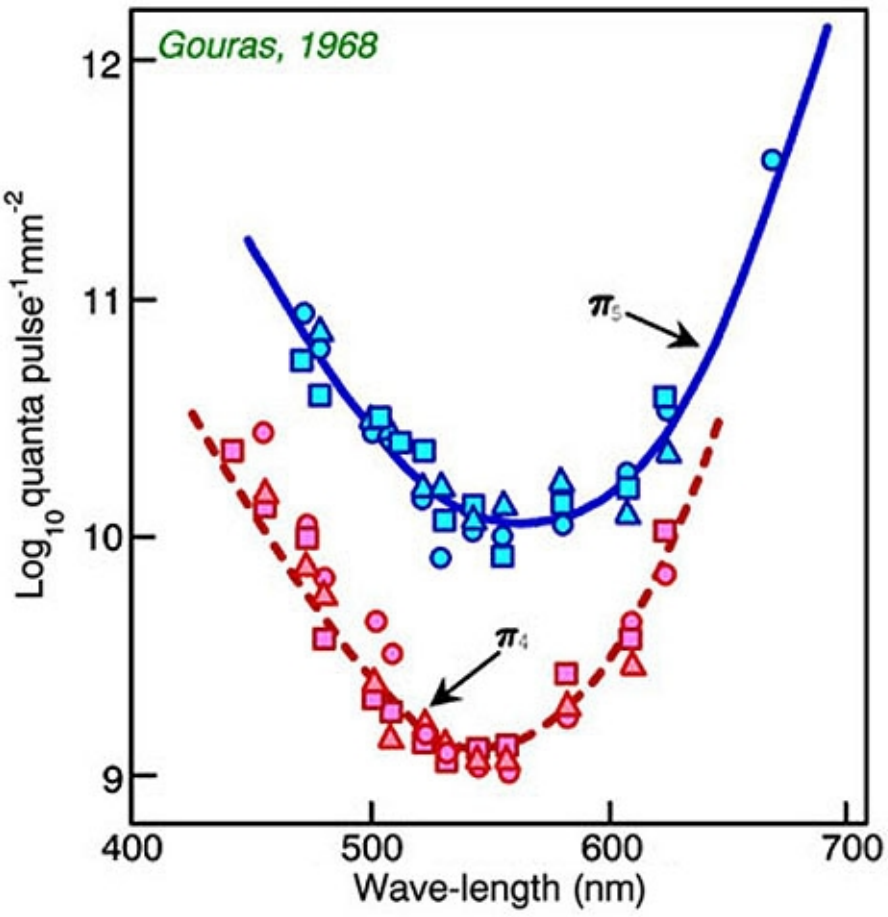

Figure 25. Spectral sensitivities of three phasic ganglion cells in rhesus monkey retina. Closed symbols, blue adapting light; open symbols, red adapting light. Shift in sensitivity peaks demonstrates red and green cone signals combining synergistically. After Gouras (55).

rod flicker can be observed. The rod responses of this AII cell are delayed 65-70 msec compared with bright-light cone responses seen in ganglion cells or horizontal cells.

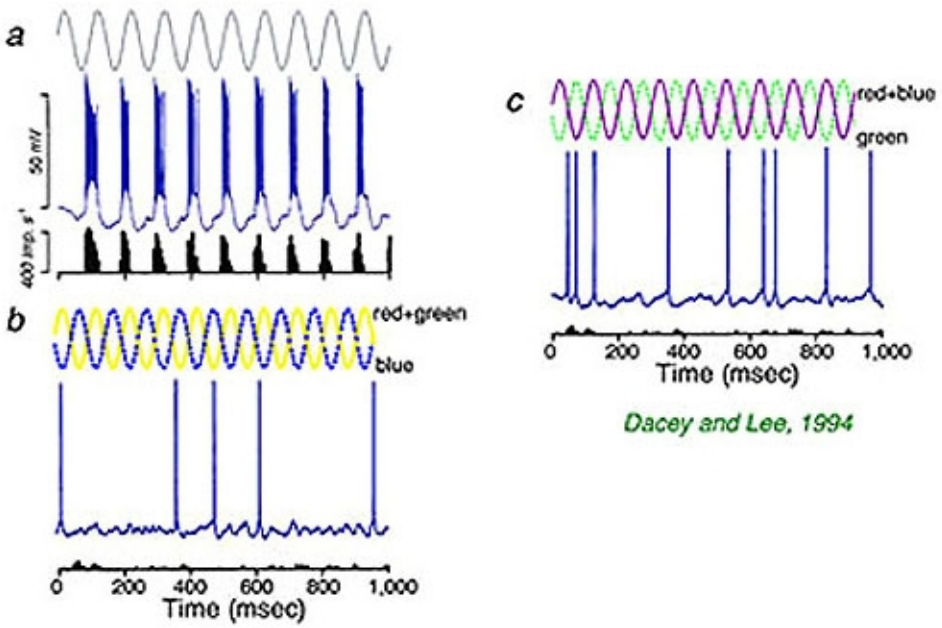

Figure 26. Intracellular recording of OFF-center phasic ganglion cell from monkey retina. The cell responds vigorously to alternating light and dark stimuli (a) but not to alternating colored stimuli with brightness of colors matched (b and c). After Dacey and Lee (57).

There is often a minimum amplitude in such flicker *versus* stimulus intensity series. This occurs because at brightness levels where rod and cone signals are both present, they are far enough out of phase with each other to mutually cancel. An example is seen in the 4.33 horizontal cell trace (Fig. 31). Flicker amplitudes for both dimmer and brighter stimuli are actually larger. The OFF-alpha ganglion cell appears also to have minimal, if not absent, flicker, near this stimulus brightness. This counterintuitive effect can be subjectively perceived. Certain flicker stimuli can be seen if they are bright or dim, but not if of intermediate intensity (67).

Rod system delays occur in specialized retinal circuitry devoted to rods. The retina has developed a set of neurons and synapses especially tuned for processing visual signals under dim lighting conditions. These may include specialized synapses between rods and bipolar cells, as well as specialized sets of rod amacrine cells. These cells are tuned to the longer integration times of rods.

In Fig. 32, turtle ganglion cell impulses are evoked by electric current injection directly into the rods and cones themselves. The delay to onset of the first impulse discharge in underlying ganglion cells is measured. This technique separates circuitry delays from delays in photoreceptor transductive machinery. OFF discharge latency (the time between cessation of hyperpolarizing current injection into a photoreceptor and the first ganglion cell impulse) was found to be about 100 msec when electrically stimulating red cones, but longer (150 msec) when stimulating rods. Interestingly, ON-discharges evoked by red cone stimulation (time from hyperpolarizing current onset to first spike) were also slow (170 msec), suggesting a slower pathway for ON cone information as well, possibly through a metabotropic glutamate pathway in such cone bipolar cells.

Detection of Light Quanta by Retinal Ganglion Cells

Retinal ganglion cells have no true threshold for detection of dim stimuli (68). When many responses are averaged, signals can be seen for light stimuli as dim as desired, and this includes stimuli so dim that only a few physical quanta of light are delivered to the surface of the eye at the cornea. Of course, in total darkness, retinal ganglion cells still exhibit a maintained but variable spontaneous firing rate, and it is against this background noise that quantal responses must be detected.

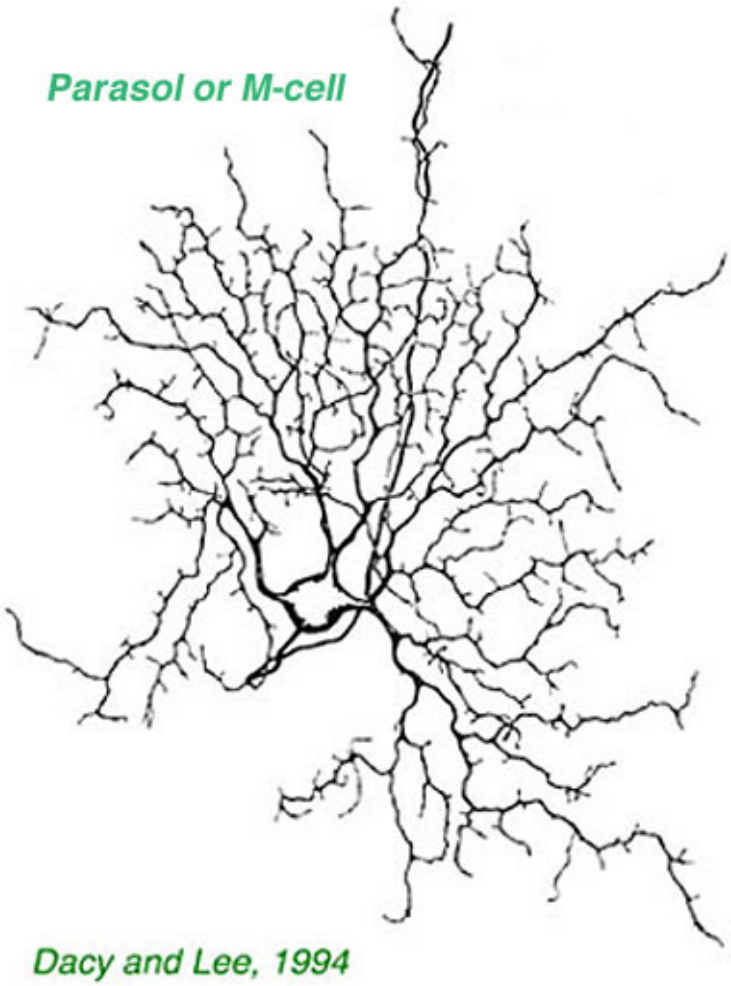

Figure 27. Drawing of a stained parasol cell in the monkey retina. Cells like this produce phasic, luminosity-type responses. The cell is 210 x 270-μm in width. After Dacey and Lee (57).

A post-stimulus time histogram (PHST) averages the number of nerve spikes fired over time for many repetitions of a stimulus. It is a useful tool for detecting small signals. This is seen in Fig. 33 for a brief, dim stimulus, which delivers on average only five quanta to the cornea each flash. Owing to optical losses, perhaps only one of these quanta is effectively absorbed in a rod and transduced into neural activity. Even so, on average, a substantial burst in mean firing rate occurs. Through analysis of data such as these, Barlow et al. (68) concluded that a single quantum absorption resulted in the firing of two to three extra ganglion cell nerve impulses. Cross-correlations in firing patterns of adjacent cells under conditions of dim illumination agree with this estimate and suggest that the time course of increased firing probability for a single quantum absorption may last about 50 msec or more, and that several adjacent ganglion cells detect the event (69).

Because of fluctuations in spontaneous background firing, single quantal events might not be readily detected in a single cell. However, three to four quantal absorptions within the cell's receptive field would be easily noticed in the discharge pattern.

Receptive Field Alterations with Rod Vision

In retinal ganglion cells, separate rod and cone pathways converge. One might expect then, during dark adaptation, as input signals to ganglion cells shift from cone-related to rod-related pathways, that receptive field properties of ganglion cells might change. The changes are, in fact, rather subtle and require careful probing with

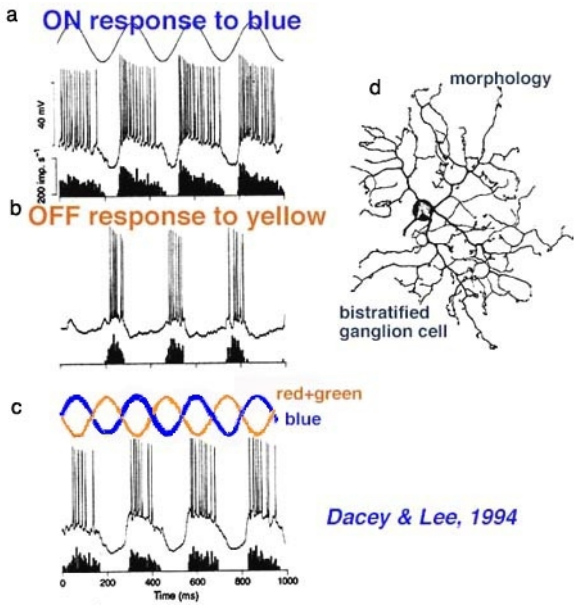

Figure 28. Blue-ON, yellow-OFF chromatic ganglion cell in monkey retina. a. Alternating blue and dark stimuli evoke ON responses. b. Alternating yellow and dark stimuli evoke OFF responses. c. Alternating blue and yellow colors matched in brightness evoke blue-ON, yellow OFF responses. d, e, f. Morphological appearance of the small, bistratified ganglion cell from which blue-sensitive responses were recorded. After Dacey and Lee (57).

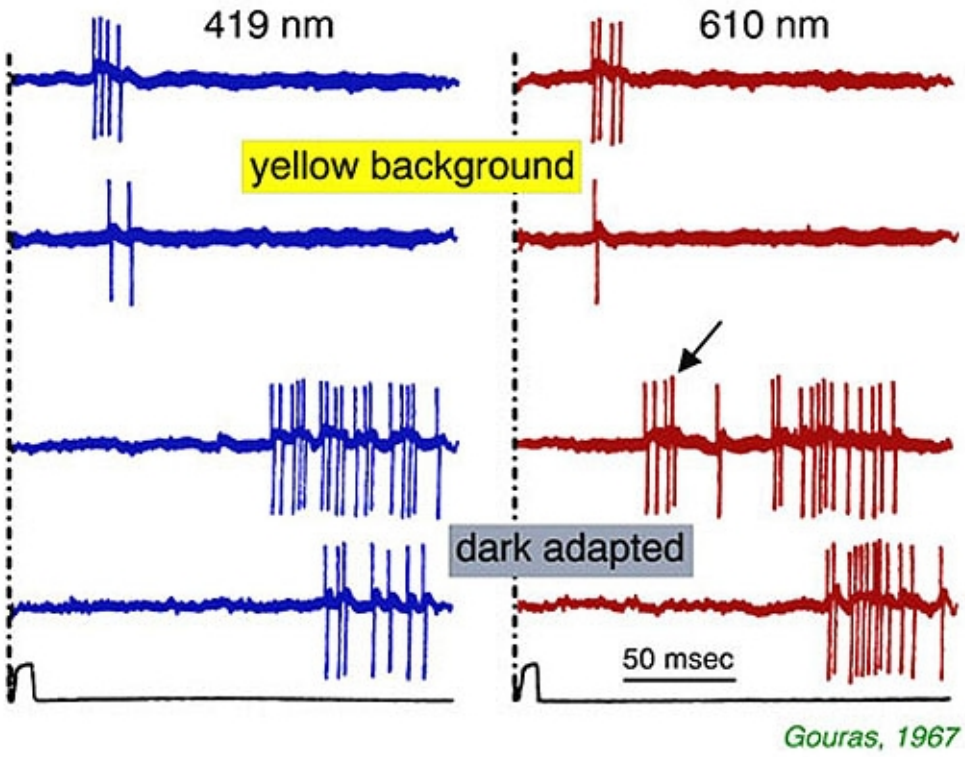

Figure 29. Threshold and near-threshold responses of primate ON-center ganglion cells with rod-favoring blue (419 nm) and cone-favoring red (610 nm) stimuli under dark-adapted and bright-background conditions. Extracellular records, from Gouras (61).

physiological stimuli and pharmacological tools. The size of receptive field center mechanisms frequently increases. Receptive field surround responses are often less vigorous. The pharmacology of light responses

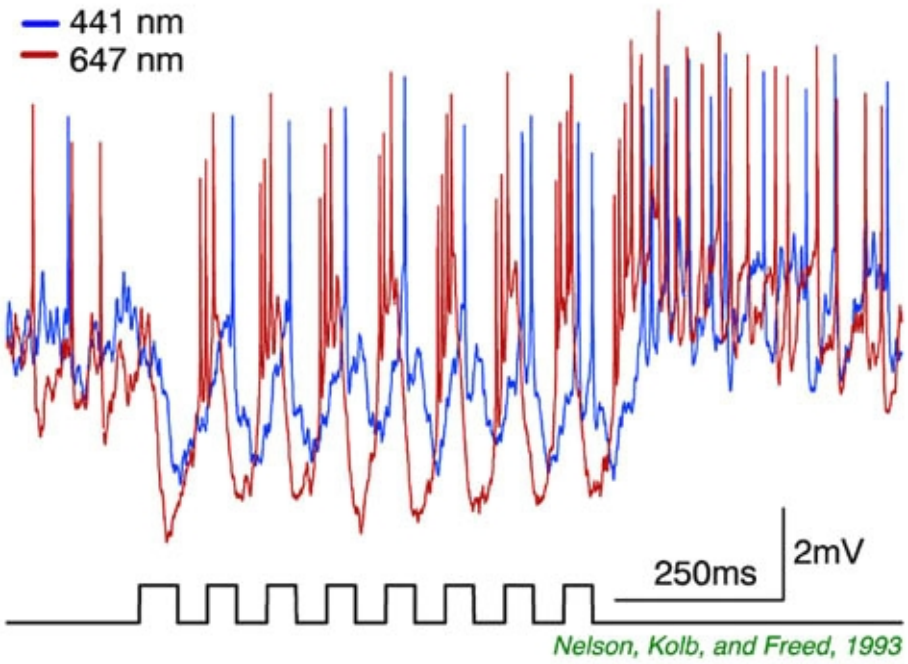

Figure 30. Near-threshold intracellular responses of cat ganglion cell to cone-favoring red (647 nm) and rod-favoring blue (441 nm) flickering stimuli. After Nelson et al. (16).

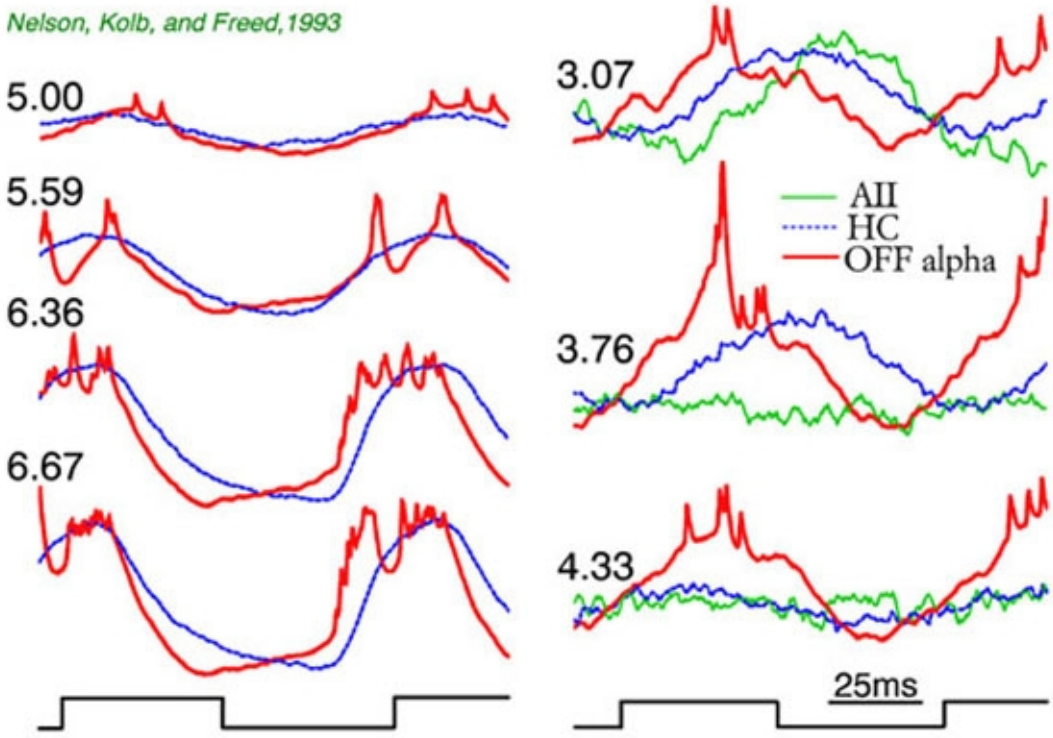

Figure 31. Phase differences in rod and cone flicker responses. Intensity response series for blue (441 nm) flickering stimuli in an OFF-center ganglion cell (OFF-alpha), a horizontal cell (HC), and an AII amacrine cell (AII). The ON-center AII amacrine response is inverted for comparison with the other OFF-center cells. In the right column, gain has been increased to better display the lower amplitude rod signals. Stimulus brightness is given in log quanta μm-2 sec-1 next to each trace. Reproduced from Nelson et al. (16).

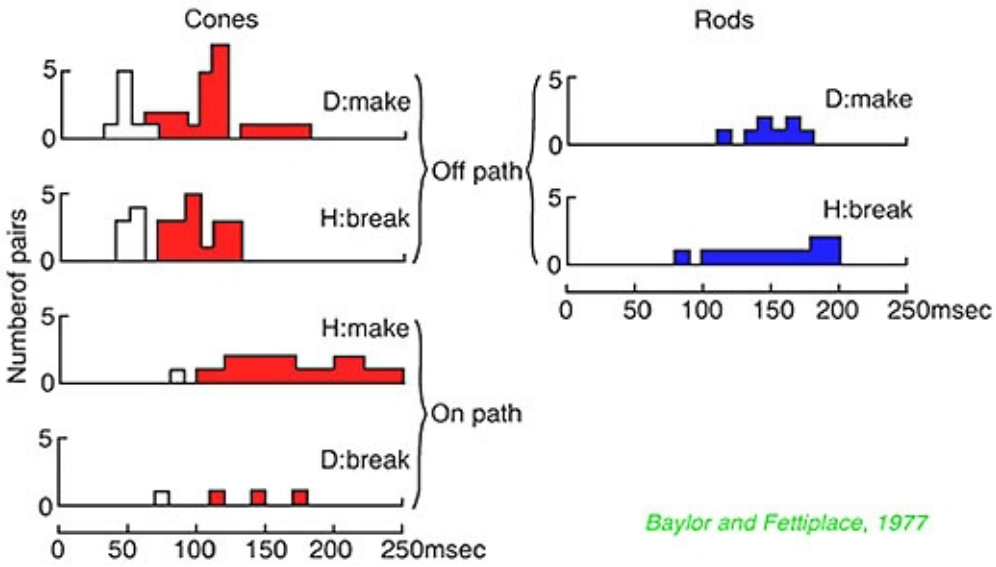

Figure 32. Turtle ganglion-cell mean impulse latencies for three synaptic pathways from photoreceptors to ganglion cells: OFF responses from red cones (red), OFF responses from rods (blue), and ON responses from red cones. Electrical currents injected directly into rods or cones generated responses. OFF responses were measured from the offset of hyperpolarizing steps (break) or the onset of depolarizing steps (make), and conversely for ON responses. Hatched cells could not be driven antidromically, fired only one impulse, and may be amacrine cells. Current pulses were 400-900 msec long. Reproduced from Baylor and Fettiplace (99).

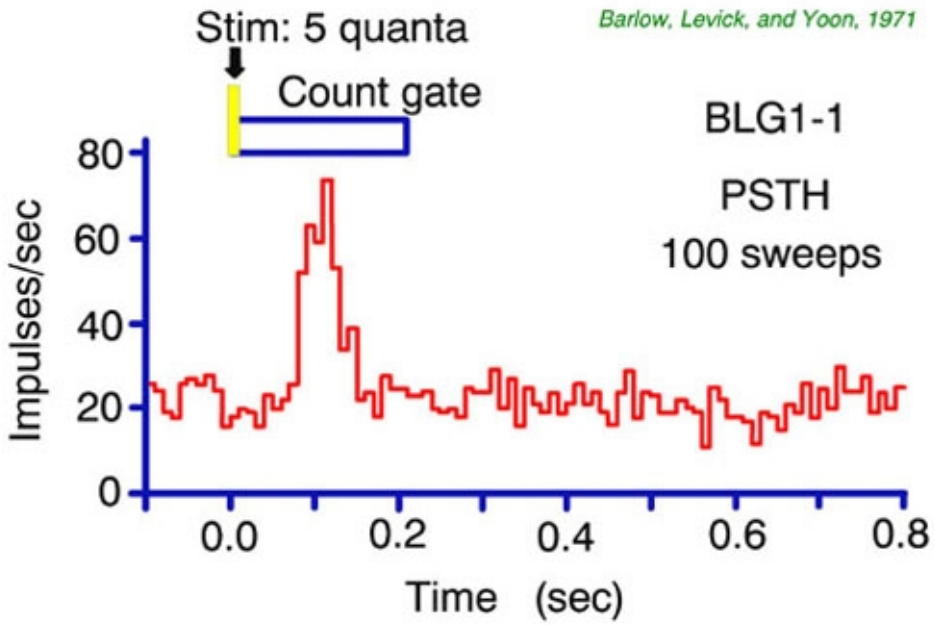

Figure 33. Post Stimulus Time Histogram (PSTH) of a cat ON-center ganglion cell response to a very dim stimulus, delivering only five quanta of light to the cornea in a 10-msec flash. The "Count Gate" is a 200-msec long interval in which impulse responses were counted, either in the dark or after the dim flash. Reproduced from Barlow et al. (68).

changes. All of these effects result from changes in the dominant retinal circuitry pattern driving ganglion cells as the retina adjusts to dim lighting conditions.

Changes in cat OFF-type ganglion cell center size during light and dark adaptation appear in Fig. 34, where response discharge rates for small-spot probes are mapped across the receptive field center. Under conditions of moderate light adaptation (mesopic, red), a narrowly peaked profile is observed, signifying a localized receptive field center. With dark adaptation, the profile spreads out (scotopic, blue) as the center becomes larger and more diffuse. Along with changes in center size, there is a change in response waveform. Under mesopic conditions, OFF excitation is brisk, transient, and of short latency. Under scotopic conditions, a more protracted, longer latency response occurs (similar to delays described above). In rabbit retina (7), dark-adapted ganglion cell center mechanisms shrunk as much as 30% during light adaptation (mean, 12%).

Surround strength diminishes during dark adaptation. In Fig. 35, responses of an OFF-center rabbit retinal ganglion cell are followed through a prolonged period in the dark. After a brief (10-min) interval, a large-spot stimulus evokes a weak ON discharge from the surround mechanism and a strong OFF discharge from the center mechanism. An annular stimulus, more selective for the surround mechanism, evokes a strong ON discharge from the surround and a relatively weak OFF discharge from the center (red). Following an extensive 30-min period of dark adaptation, the ON-surround discharges disappear from responses evoked by either stimulus (blue).

Loss of surround response can be reversed by pharmacological intervention (Fig. 35). Introduction of a cyclic AMP analogue (CPT-cAMP) into the perfusion media of this dark adapted ganglion cell restores surround responses (magenta). In additional experiments (70), strychnine, an antagonist of the inhibitory neurotransmitter glycine, was also found to restore surround responses to dark-adapted ganglion cells. It appears that surround responses are actively inhibited in dark-adapted retina by activation of glycinergic circuitry, probably from rod-dominated amacrine cells. This glycinergic amacrine release appears modulated by the intracellular messenger cAMP.

A shift in the pharmacological sensitivities of ganglion cell center mechanisms also occurs during dark adaptation, particularly for OFF-center cells in cat retina. These responses become sensitive to agents active at metabotropic glutamate receptors, normally associated with ON-type bipolar cells, and to agents selective for receptors to the inhibitory neurotransmitter glycine. Such sensitivities are not seen in the light-adapted state.

OFF discharges of a cat Y-type ganglion cell appear unaffected by the metabotropic glutamate agonist APB in the light-adapted state (Fig. 36), an expected result as cone signals (and perhaps mesopic rod signals) are transferred to such cells primarily through OFF cone bipolar cells. These use ionotropic glutamate receptors (kainate or AMPA) in synaptic transmission, which are unaffected by APB. APB does effectively block ON inhibition in the dark-adapted state. Rod bipolars are ON-type bipolars sensitive to APB. So this result likely means that ON-type rod bipolar cells are the primary signal pathway for transferring visual signals from rods to these OFF-center ganglion cells during dark adaptation. Rod bipolars do not contact OFF-center ganglion cells directly, but through inhibitory amacrine cells, such as the glycinergic AII amacrine cell. In agreement with this circuit for dark-adapted signaling, strychnine blocks ON inhibition in an OFF-center X-type ganglion cell (Fig. 37), but only in the dark-adapted state. Light responses of ON-center cells are effectively blocked by APB in both light- and dark-adapted states.

APB may not effectively block rod signals in **all** ganglion cell types however. DeVries and Baylor (71) showed, in rabbit retina, that rod responses in "brisk" ganglion cells were eliminated by APB, but rod responses of "directionally selective" or "sluggish" ganglion cell types were not. Rod signals that could not be blocked in these ganglion cells may use a pathway through rod-cone photoreceptor gap junctions into the APB-resistant OFF cone bipolar pathway.

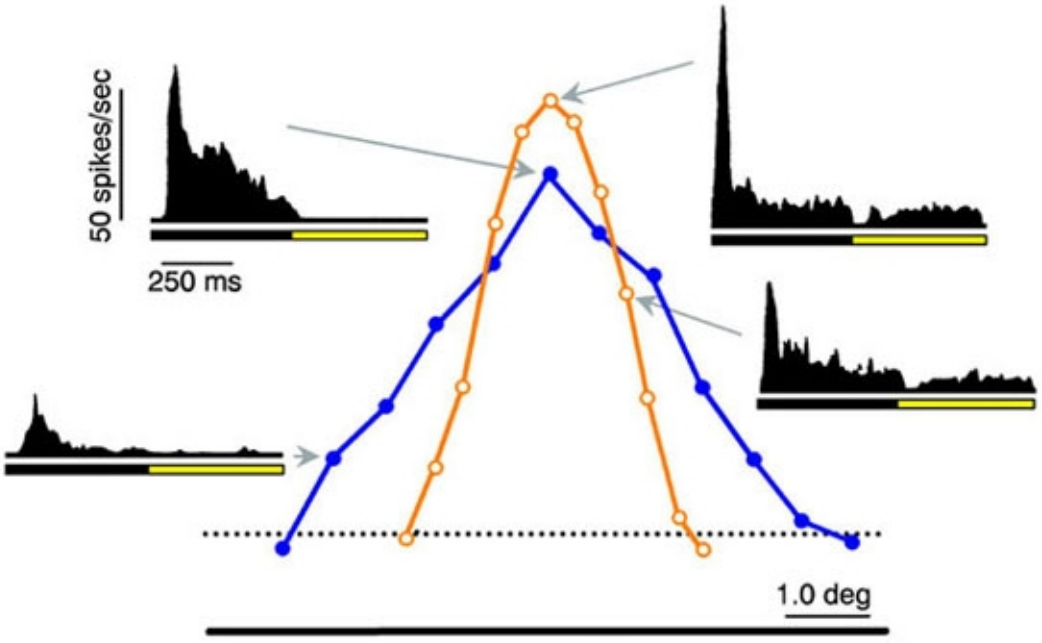

Figure 34. Ganglion cell receptive field centers increase in size during dark adaptation. Responses are more sustained. The profiles are small-spot response amplitudes from different positions within the OFF-center receptive field. Open symbols (red) recorded on mesopic (intermediate intensity) backgrounds. Closed symbols (blue), recorded in fully dark-adapted state. Post stimulus time histograms shown for indicated points (arrows). Repetitive stimulus was OFF for 500 msec (black bar, shown first) then ON for 500 msec (yellow bar, shown last). After Peichl and Wässle (100).

Spatial Distribution of Ganglion Cell Fields

Ganglion cells transmit visual information to the brain as a concert of individual signals arising from multiple cells representing different points in space. Information about visual objects is thus shared in parallel pathways from many ganglion cells. The arrangement of ganglion cells on the retinal surface is not spatially random. Each cell type is distributed in an ordered mosaic. Within each mosaic, cells tend to be spaced apart so as not to occupy a neighboring cell's territory (72). Characteristically, the "nearest neighbor distances" are greater than would be expected of a random distribution. Cells of different types may be closely spaced, however. The mosaics of different cell types are said to be independent. Receptive and dendritic fields of cells within a mosaic partially overlap (Fig. 39).

Neighboring ON- and OFF-center alpha cells position themselves in space in characteristic ways (Fig. 38). In the mosaic of ON-center cells, neighbors do not approach each other closely, maintaining an "arms length" spacing, close enough to "shake hands" with the distal dendrites of neighboring ON cells, but rarely closer. A similar spacing occurs among OFF-center cells. ON- and OFF-center cells appear mutually indifferent to each other's presence and may approach closely without an exclusionary zone. These cell types are said to occupy independent lattices (72). ON and OFF Y-cells are thought to illustrate general relationships within and among lattices.

Receptive fields and dendritic fields are similarly spaced. Multielectrode arrays allow simultaneous recording of all ganglion cell light responses in a patch of retina, characterization of trigger features, and mapping of receptive fields (7). Such studies show that receptive fields of ganglion cell types having common trigger features approach each other only at the edges. When spatial profiles are fit with two-dimensional Gaussian functions, receptive

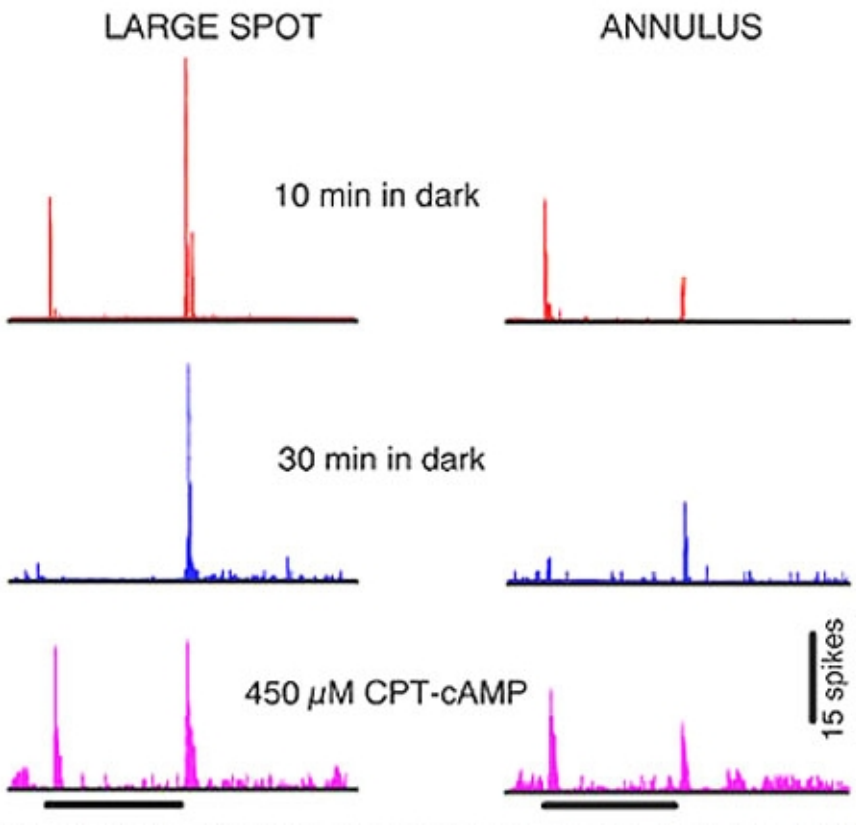

Figure 35. Ganglion cell receptive field centers increase in size during dark adaptation. Responses are more sustained. The profiles are small-spot response amplitudes from different positions within the OFF-center receptive field. Open symbols (red), recorded on mesopic (intermediate intensity) backgrounds. Closed symbols (blue), recorded in fully dark-adapted state. Post stimulus time histograms shown for indicated points (arrows). Repetitive stimulus was OFF for 500 msec (black bar, shown first) then ON for 500 msec (yellow bar, shown last). After Peichl and Wässle (100).

field centers are typically 2 Gaussian radii apart. In this arrangement, summation of sensitivities from all cells of a given type leads to a flat sensory surface (7).

Ganglion Cell Mosaics and Spatial Resolution

The lattice spacing of ganglion cell receptive field centers may limit certain forms of visual acuity, according to the Nyquist limit (7, 73). To unambiguously define the spatial grain of a periodic pattern, grating, or spatial sine wave, at least two cellular detectors are required, spaced closely enough that if one is at the peak of brightness of a repeating pattern, the other is at the trough. If multiple peaks and troughs occur in the space intervening between the two closest cells, signals will, of course, be detected in both but cannot unambiguously be associated with any single spatial periodicity. In fact, excitation patterns similar to those produced by low frequency patterns (wide spacing of peaks and troughs) may be produced by high spatial frequency patterns. This is called spatial aliasing. DeVries and Baylor (7) argue that spatial integration within the ganglion cell receptive field acts as a spatial low-pass filter to attenuate signals from very high spatial frequencies, preventing detection, so that such ambiguities do not arise.

Spatial resolution of ganglion cells and the spacing of receptive field centers appears approximately equal (7, 73). Given this observed relationship, the spatial low-pass filtering action of ganglion cell receptive fields would appear to attenuate periodic patterns at or above the Nyquist limit by about a factor of five or more (Fig. 40B), thus reducing the likelihood of detecting potentially confusing higher spatial frequencies with potential for aliasing. The ability to resolve regularly repeating spatial patterns, such as spatial sine waves, is a good proxy for

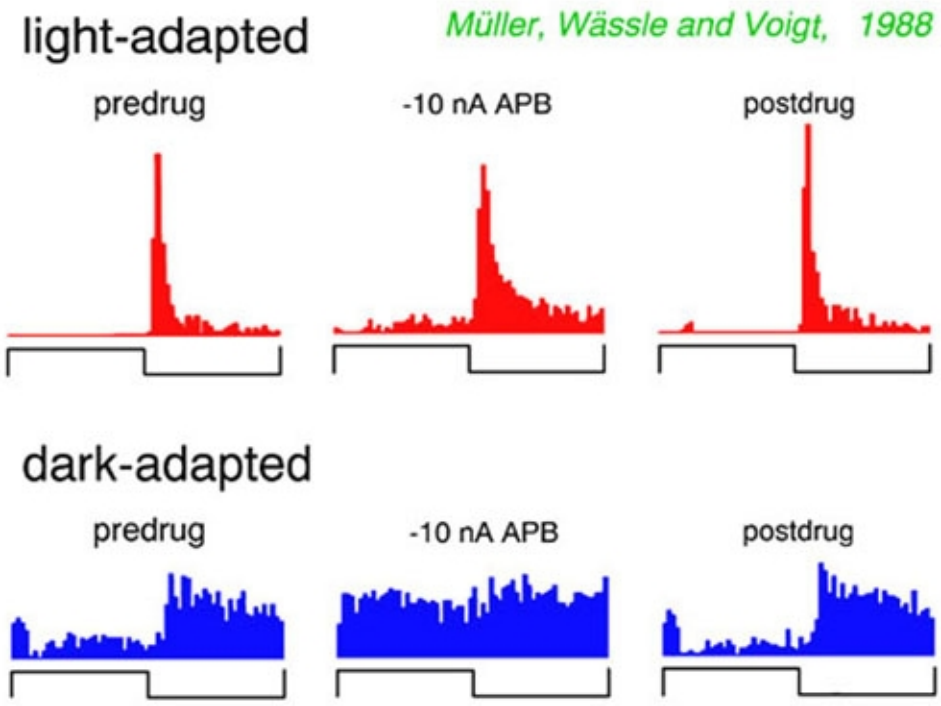

Figure 36. An excitatory metabotropic glutamate agonist selective for ON-center bipolar cells (2-amino-4-phosphonobutyrate, APB) blocks light responses of an OFF-center Y-type cat ganglion cell in the dark-adapted, but not the light-adapted, state. APB was applied electrophoretically from a nearby micropipette filled with the substance. Spot stimulus is congruent with the center mechanism. Upward deflection of the stimulus trace indicates light ON. The stimulus is repetitive, 512 msec ON, followed by 512 msec OFF. After Müller et al. (85).

spatial resolution in general, because all spatial patterns can be represented, in Fourier fashion, by sums of orthogonal spatial sine waves.

Arguments concerning ganglion cell spacing and visual system spatial performance are constrained by several caveats. First visual space is covered by many cell mosaics. One must carefully consider which mosaic might be limiting for the task at hand, or if any one mosaic need be. Second, as discussed previously, stimulus movements much finer than any retinal cell mosaic spacing can be detected by ganglion cells, if not precisely localized (14). This is referred to as visual hyperacuity (74). Finally, it is well to recall that older style video cameras achieved high spatial resolution without any mosaic of discrete detectors. "Newvicon" tubes used a single photosensitive surface, scanned by a single electron beam. Spatial resolution was excellent. If the visual system were supplied data about the velocity of image motion, even a single cell might, in principle, attain spatial resolution unconstrained by Nyquist mosaic limits.

Correlated Firing of Neighboring Ganglion Cells

Ganglion cell fields partially overlap in visual space. Ganglion cells, moreover, share an overlapping neural substrate composed of retinal interneurons and circuitry. Synchronous chemical synaptic signals from individual amacrine and bipolar cells are distributed onto multiple ganglion cells. Such signals may spread among these presynaptic elements through mutual interconnections by electrical junctions. Finally, ganglion cells themselves intercommunicate through electrical junctions. So although ganglion cells eagerly stake out their own individual turf in a spatial anatomical sense, the physiological signals they transmit are often plagiarized from common sources, resulting in highly correlated firing patterns among neighboring cells.

Such cross-correlations in firing pattern may be significant centrally, where signals converge on common neurons in the brain centers. Synapses that are simultaneously activated tend to be mutually strengthened. Such

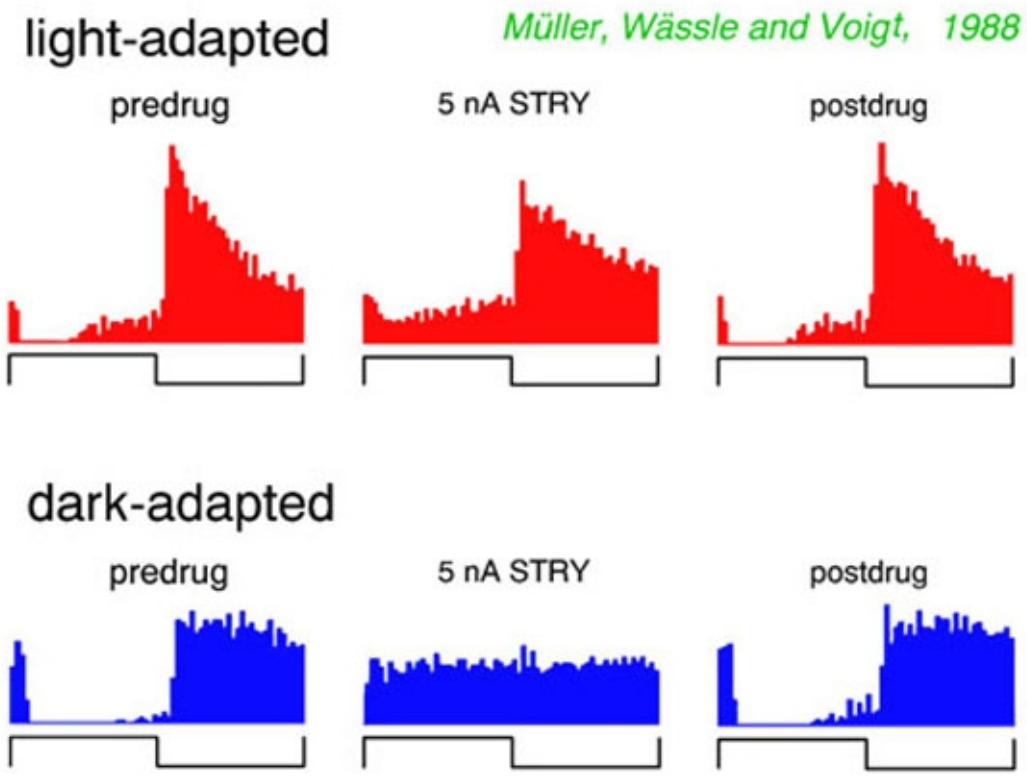

Figure 37. An agonist of the inhibitory neurotransmitter glycine (strychnine, STRY) blocks OFF-center light responses of an X-type ganglion cell in the cat retina, but only in the dark-adapted state. Strychnine was applied electrophoretically from a nearby micropipette filled with the antagonist. Small-spot stimuli are selective for the center mechanism. Upward deflection of the stimulus trace indicates light ON. The stimulus is repetitive, 512 msec ON, followed by 512 msec OFF. After Müller et al. (85).

synapses are often called "Hebian" and are thought to be reinforced by calcium entry through simultaneously active synapses. Calcium enters through synapses containing the glutamatergic NMDA receptor. The physiological effect is referred to as long term potentiation (LTP), wherein synaptic currents become larger with repeated stimulation.

Cross-correlations are generated from simultaneous recording of two ganglion cell spike trains. Impulses from the first cell set the zero time around which impulse firing rate histograms for the second cell are generated. The histogram is accumulated for every impulse fired by the first cell. When two neighboring ON-center cells are so paired, a large central peak in firing rate for the second ON cell is seen (Fig. 41, red, left). A similar pattern is seen when two OFF cells are recorded (Fig. 41, blue right). In both cases, increased firing rate represents an increased likelihood that if one cell fires, the other will also. Impulse generation in the two cells is not independent. The cells share common excitatory inputs sources and are likely to be simultaneously excited. There is symmetry about the zero time axis. This is consistent with the idea that the cells share one or more common excitatory inputs, and that either one may respond first.

When an OFF cell and an ON cell are simultaneously recorded, the situation is different. There is a large central trough in the firing rate from the second cell (Fig. 14, center, magenta). When one cell fires a spike, the other is inhibited from firing, regardless of whether it is the ON cell that fires or the OFF. There appear to be common, spontaneously active inputs for both cells, inhibitory for one while excitatory for the other. Symmetry about the time zero axis suggests that in fact two symmetric inputs are required: one inhibiting the ON cell while exciting the OFF cell, and the other exciting the ON cell while inhibiting the OFF cell. Physiologically, ON and OFF ganglion cell mosaics are not independent then. Mutual inputs are found. Such inputs occur, however, only for

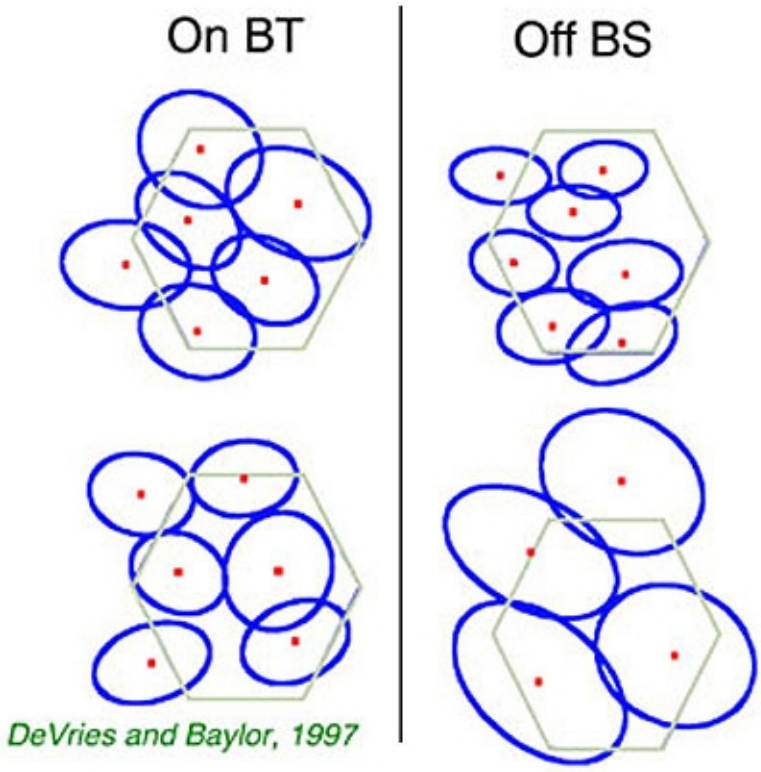

Figure 39. Gaussian receptive field borders of neighboring, simultaneously recorded, rabbit retinal ganglion cells. Mosaics of ON brisk transient cells (On BT) or OFF brisk sustained cells (Off BS) are spaced about 2 Gaussian radii apart. Elliptical profiles (blue) are at 1 Gaussian radius from receptive-field centers (red squares). The gray hexagon outlines the borders of the multi-electrode recording array. After DeVries and Baylor (7).

cells with overlapping, or partially overlapping, receptive fields, as is also the case for paired ON or paired OFF cells (75).

In the illustration (Fig. 41), the events induced the altered firing probability to last 10 msec or less. These were described as arising from spontaneously active inputs, best observed in moderately light-adapted preparations (75). As progressively dimmer backgrounds were used, other cross-correlations with longer durations (50 msec or longer) were observed. These were associated with quantum detection by rods (69). Finally, shorter duration events were also observed and appeared associated with direct electrical interconnections between neighboring cells of the same center response polarity (76). There appear to be multiple mechanisms of different temporal duration leading to synchronization of firing among neighboring cells.

Among the multiple mechanisms of different temporal duration leading to synchronization of firing among neighboring cells, even some of the longer duration cross-correlations between neighboring ganglion cells appear also to be mediated by electrical junctions.

Three cross-correlation patterns of different durations were identified among salamander ganglion cells, narrow (0-1 msec), medium (10-50 msec), and broad (50-100 msec). Broad correlations were blocked by cadmium chloride-containing medium, but narrow and medium correlations were not (Fig. 42). Cadmium chloride blocks calcium-dependent synaptic transmission, making it very likely that both narrow and medium time correlations were mediated by other means, such as electrical junctions. Direct electrical connections among ganglion cells may mediate narrow correlations, similar to cat retina, whereas medium correlations may result from electrical coupling between amacrine and ganglion cells. Waves of slow potentials passing through the amacrine layer may stimulate multiple ganglion cells by this mechanism. The cadmium-sensitive broad correlations appear to result, at least in part, from photoreceptor photon noise (77), as in the cat.

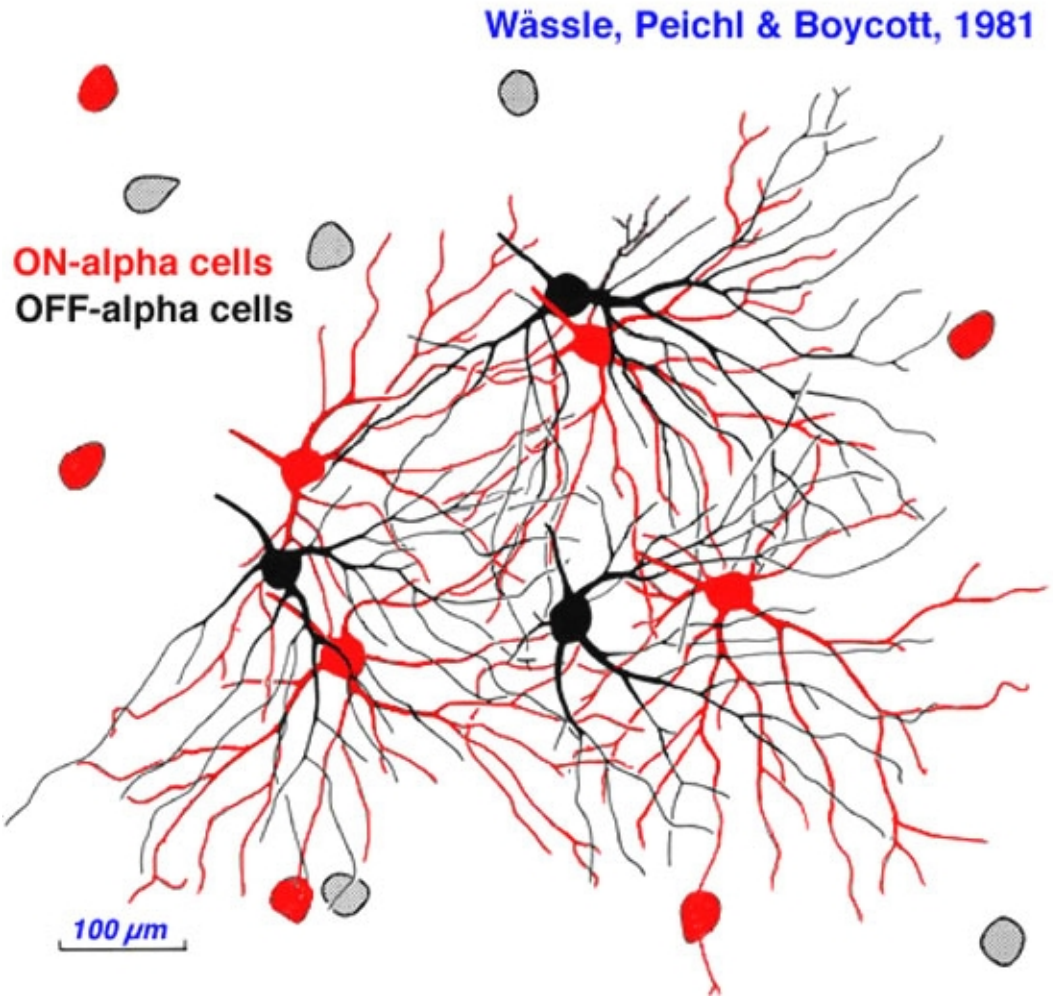

Figure 38. HRP-filled ON- and OFF-center alpha cell mosaics in cat retina.

Only time-invariant background stimulation was used in the previous two studies. When localized flashing stimuli are used, a further cross-correlation pattern emerges. Oscillatory firing patterns become entrained among cells responding to a contiguous stimulus.

Ganglion cells develop a high frequency (~100 Hz) oscillatory firing pattern when presented with localized bright stimuli. This is seen in autocorrelation functions (black, Fig. 43). These functions show that the probability of a second ganglion cell impulse depends, in a periodic way, on the firing of a previous impulse in the same cell. If stimuli are spatially separate (left, Fig. 43), the oscillatory firing patterns in the two cells are independent. However, if the stimulus covers the area between the two cells, oscillatory patterns in each cell become entrained with each other. This is seen in an oscillatory cross-correlation function in the two cells firing patterns for this stimulus (right, Fig. 43). This is a long-range effect. The two ganglion cells need not have overlapping receptive fields. It is a longer distance phenomenon than reported for other cross-correlation patterns in ganglion cell firing. It likely involves gap junctions among ganglion or amacrine cells (78).

Neurotransmitter Receptors and Synaptic Currents

Ganglion cells are tiny, information processing, neural machines. They extract features of the visual world, encode them in frequency-modulated spike trains, and send them coursing along optic nerve axons to various visual brain centers. The first step in this process is the binding of amacrine and bipolar cell neurotransmitters onto specialized receptor proteins embedded in ganglion cell dendritic membrane. These receptor molecules are

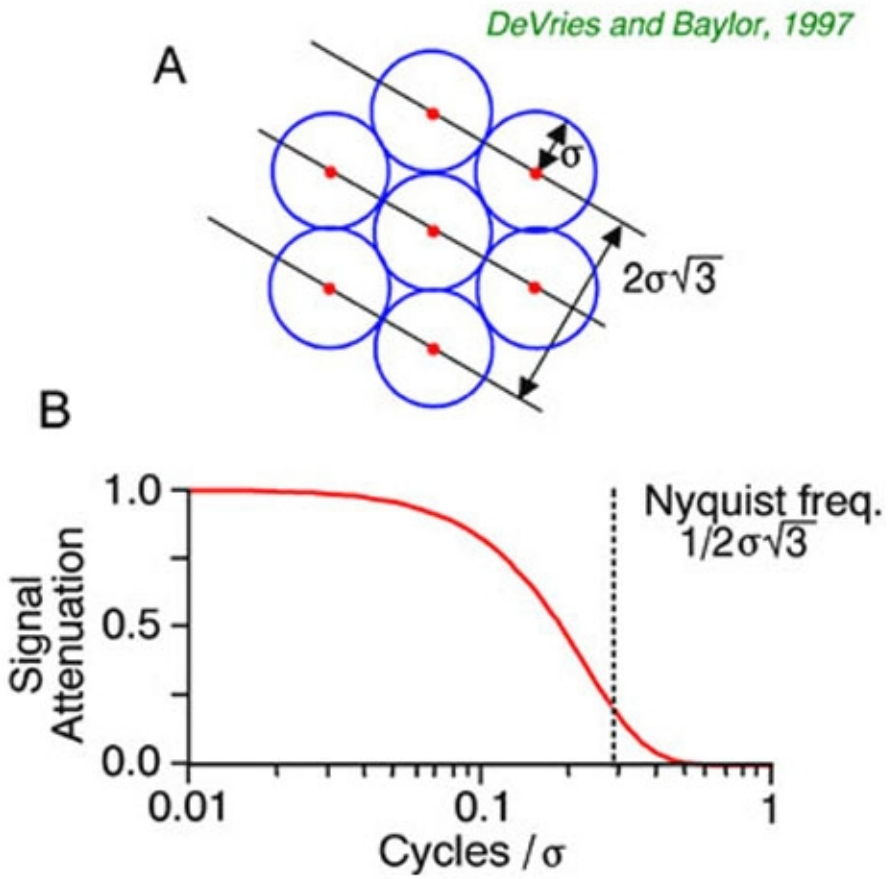

Figure 40. Spatial resolution of a ganglion cell mosaic. A. Receptive field centers are found spaced approximately one Gaussian radius (Greek sigma) apart. Presumptive hexagonal packing of receptive fields on the surface leads to to the indicated Nyquist frequency limit. B. Spatial integration within the receptive field attenuates high spatial frequencies and limits aliasing. After DeVries and Baylor (7).

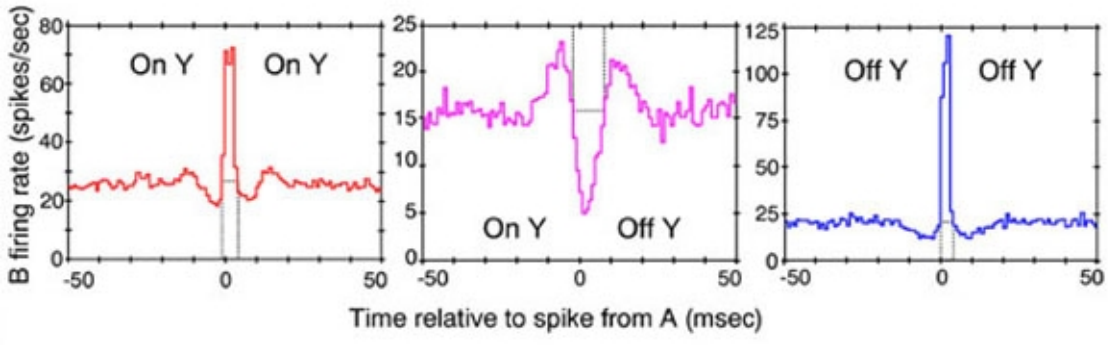

Figure 41. Correlations in the firing pattern of simultaneously recorded, neighboring Y-cells in cat retina. Firing rate histograms are generated for cell B, referenced to the points in time (0 msec) when cell A fires an impulse. Patterns are generated from spontaneous activity in the presence of a steady mesopic background. After Mastronarde (75).

concentrated at sites of synapses with amacrine and bipolar cells. Once the neurotransmitter is bound, ion-selective channels, a kind of micropore in the subsynaptic membrane, open. Charged ionic species rush through these channels, driven by electrochemical gradients. As a consequence, current flows into the cell, altering

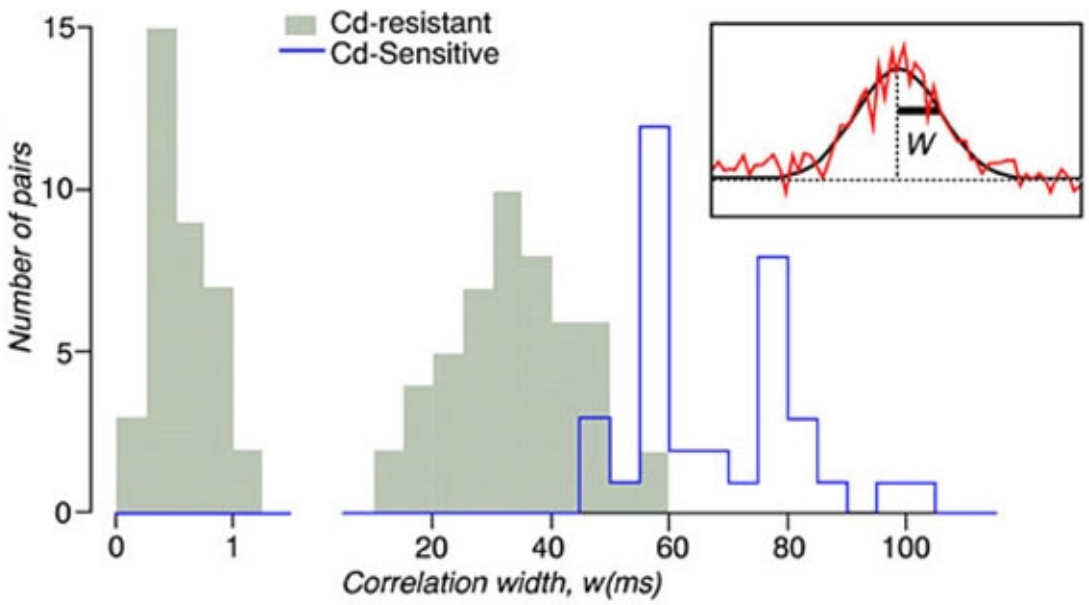

Figure 42. Both chemical and long time scale electrical interactions contribute to cross-correlations among retinal ganglion cells. Cross-correlations generated from recordings with multielectrode arrays in salamander, fit by Gaussians of standard deviation W (inset), are categorized as to the time scale of the correlation (W) and as to cadmium sensitivity. After Brivanlou et al. (77).

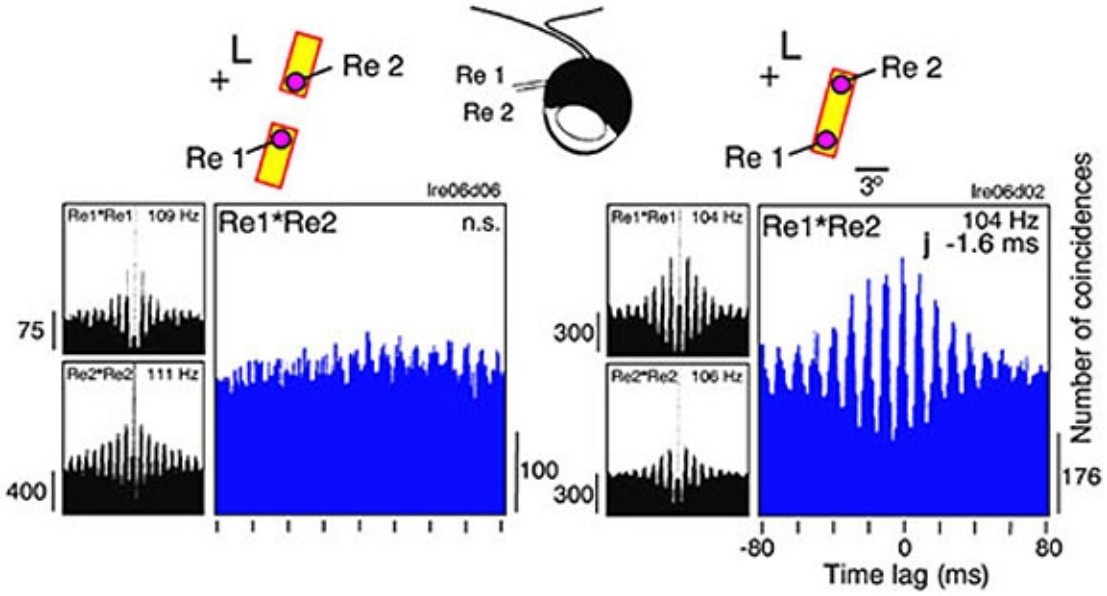

Figure 43. When stimuli cover the area between ganglion cells, oscillatory patterns become entrained. Re1 and Re2 denote two ON-type retinal ganglion cells with receptive fields separated by 6 degrees. Autocorrelation functions (black) and cross-correlation functions (blue) are shown for spatially separate (left) and spatially contiguous (right) stimuli in cat retina. After Neuenschwander and Singer (78).

membrane potential. These synaptic currents, through a complex interplay of dendritic structure and other potential-sensitive ion channels (79), alter ganglion cell firing rates and convey visual signals to the brain.

There are eight synaptic ion channel associated retinal neurotransmitter receptors. Such receptors are referred to as "ionotropic". Glutamate, the most common excitatory neurotransmitter, activates three distinct channels: AMPA-type channels, kainate-type channels, and NMDA-type channels. Acetylcholine is another excitatory neurotransmitter active at nicotinic receptors. Excitatory receptors are associated with channels selective for positively charged ionic species, monovalent or divalent cations. When open, they allow positive charges to enter neurons, depolarizing them and exciting impulse firing. GABA and glycine are inhibitory ionotropic neurotransmitters. GABA activates two distinct ionotropic receptor types: the bicuculline-sensitive $GABA_A$ receptor and the bicuculline-insensitive $GABA_C$ receptor. Bicuculline is a convulsant, and a common blocker of GABA inhibitory action. GABA and glycine open channels selective for the negatively charged chloride anion, which hyperpolarizes neurons and inhibits impulse firing. In teleost fish retinas, a further inhibitory, chloride-selective channel present in bipolar cells has been found activated by glutamate. All of these ionotropic receptors are heteropolymers composed typically of five subunits. There are multiple alleles of these subunits, allowing for considerable heterogeneity in receptor composition and details of function.

Retinal ganglion cells respond to all common excitatory or inhibitory retinal neurotransmitters. When neurotransmitters are applied to the solution that bathes ganglion cells, membrane currents are induced. AMPA, kainate (Fig. 44) or NMDA evoke excitatory currents in both ON- and OFF-type cat beta cells (80). NMDA currents are of the typical "conditional" sort, dominant only if cells are depolarized first by other excitatory neurotransmitters, or in the absence of extracellular magnesium (Fig. 45). Extracellular acetylcholine also excites retinal ganglion cells (80-84).

When the bath is applied, inhibitory retinal neurotransmitters GABA and glycine potently evoke inhibitory currents in ganglion cells. GABA receptors in cat beta cells are of the "A" type. These responses can be largely blocked by the GABA-antagonist bicuculline. Strychnine effectively blocks glycine-evoked currents (80).

Ganglion cell membranes appear to be broadly tuned to receive signals from many neurotransmitter systems. Rather than being neurotransmitter selective, they limit input of information from amacrine and bipolar cells by selective synaptic connections. Thus, it is important to study the properties of responses evoked by natural photic stimulation to determine which of the available transmitter systems in the retinal inner plexiform layer are actually used. In extracellular impulse recordings, metabotropic glutamate receptors were shown important for the ON-center circuit in cat alpha and beta ganglion cells, whereas both these receptors and glycine receptors were found important for OFF alpha and beta cells (85). To determine whether either of these systems operates directly on the ganglion cell itself, it is necessary to measure light-evoked conductance changes in intracellular ganglion cell recordings.

Central illumination of an ON-center ganglion cell depolarizes the cell membrane. Much of the normally inside-negative resting potential is lost. The action excites nerve impulse activity. There is an increase in membrane conductance with a reversal potential near 0 mV, typical of an open ion channel selectively permeable to cations. This synaptic mechanism causes light responses to increase in amplitude as the cell is hyperpolarized by extrinsic current. The picture is consistent with the activation of ionotropic glutamate receptors permeable to sodium, potassium, and perhaps calcium ions (86, 87). In the cat ON-beta ganglion cell (Fig. 46), reversal potentials were found to shift to more negative values over the time course of the response. This appears to result from delayed activation of inhibitory synaptic currents with negative reversal potentials. Such inhibition arises in part from the receptive field surround but also may be intrinsic to the center mechanism. A simple circuit involving excitatory ionotropic glutamate impingement from narrow field bipolar cells, and a more protracted GABAergic and/or glycinergic input from broader field amacrine cells, serves to model such results. ON-center ganglion cells may receive tonic inhibitory input in the dark as well (86) (Fig. 47).

Central illumination of OFF-center ganglion cells hyperpolarizes the cell membrane. The normally inside-negative cell potential increases in magnitude. This action reduces nerve impulse activity and causes the cell to become quiet. Concomitantly, there is an increase in membrane conductance with a reversal potential more

negative than the resting potential. This is typical of the opening of channels selectively permeable to the chloride anion (86). A simple circuit involving narrow-field GABA- or glycine-releasing amacrine cells, which are themselves excited by light, serves to model the OFF-center response.

The neural circuits of ON- and OFF-center ganglion cells appear asymmetric. One might have expected the activity of OFF-center cells to be diminished in the light principally through loss of excitatory input from OFF-center bipolar cells. Yet, it is amacrine inhibition that appears key to the physiology of these cells. There is evidence of excitatory input from bipolar cells at stimulus offset. At this point in time, there is a burst of action potentials driven by excitatory, depolarizing synaptic input. This appears to be the role for glutamate released from OFF bipolar cells onto OFF-center ganglion cells. There may also be a low level of dark excitation of these cells contributed by OFF-center bipolar cell input (86). There is, as yet, little evidence concerning synaptic mechanisms involved in the excitatory surround responses of these cells.

Ganglion Cells That Are Involved in the Circadian Clock

Certain large-field, sparsely-branching ganglion cell types are known to project to the hypothalamic suprachiasmatic nucleus (SCN) in the brain (Fig. 49). The latter nucleus is the primary circadian oscillator in mammals and is essentially the biological clock, allowing reseting of bodily functions to local time. The ganglion cells involved in entraining the circadian clock project from the eye to the SCN via the retinohypothalamic tract (RHT) (Fig. 48). They apparently contain the neuropeptide pituitary adenylate cyclase activating polypeptide (PCAP), as well as glutamate. They receive input in the inner plexiform layer from amacrine cells and cone bipolar cell axons (88). These ganglion cells are now known to contain a photoreceptive pigment—melanopsin—in their dendrites, proximal axons, and cell membranes and are thus intrinsically photreceptive. In other words, they do not need the input of rods and cones to activate them to light; they can signal, luminance levels at least, independently of the photoreceptor bipolar chain of input (89, 90). The responses of these melanopsin ganglion cells are slow, sluggish depolarizations in contrast to the faster hyperpolarizing responses of rods and cones (Fig. 50). They are probably the equivalent ganglion cells to those described by Barlow and Levick (91) as luminance units in 1969 and described by Pu (92) in 1999, both in cat retina. The action spectrum of the melanopsin ganglion cells appears to be attributable to an opsin-like pigment, but it is most sensitive at 484 nm compared with rods at 500 nm and cones at 510 (green cones) and 359 nm (UV cones) in the mouse (89) (Fig. 50).

The melanopsin ganglion cels are also thought to be involved in the pupillary light reflex for they also project to the lateral geniculate nucleus through the olivary pretectal nucleus (OPN) and on to the Edinger Westaphal nucleus (EW) for control of the pupillary light reflex (Fig. 48, light blue pathway).

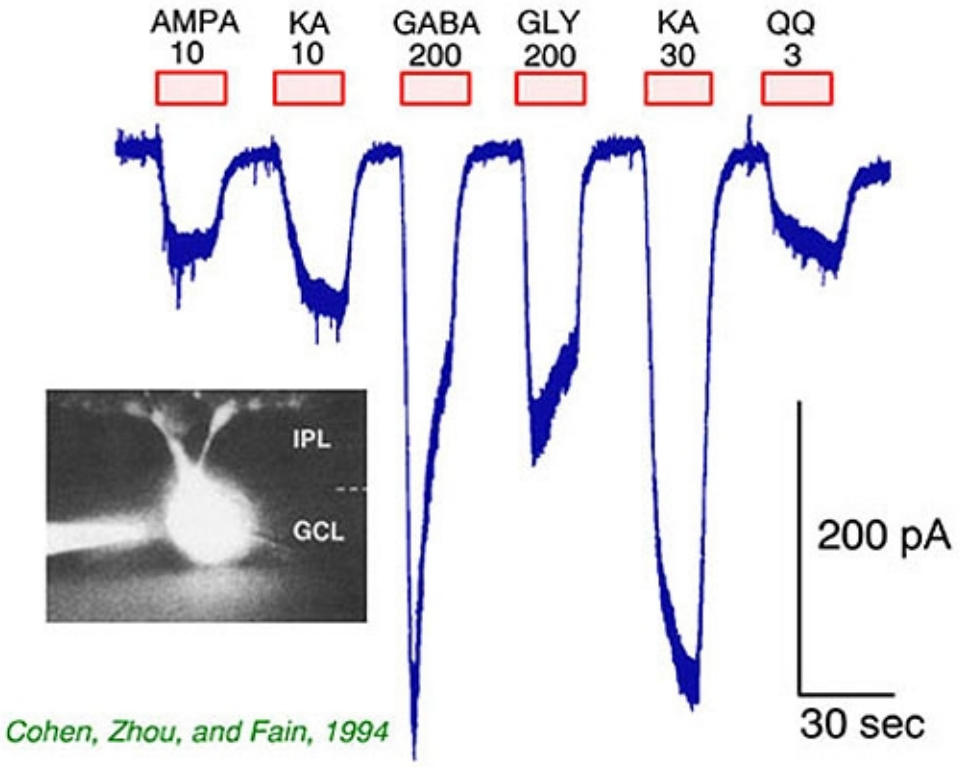

Figure 44. Membrane currents evoked by excitatory or inhibitory neurotransmitters applied to a cat OFF beta type ganglion cell. The cell (seen in the inset together with recording electrode) was studied in a retinal slice. GABA and glycine (GLY) activate inhibitory neurotransmitter receptors. AMPA (alpha-amino-3-hydroxy-5-methylisoazole-4-propionic acid), kainic acid (KA), and quisqualic acid (QQ) activate glutamatergic excitatory receptors. Numbers give doses in mM. Release of endogenous neurotransmitter has been blocked by cobalt. After Cohen et al. (80).

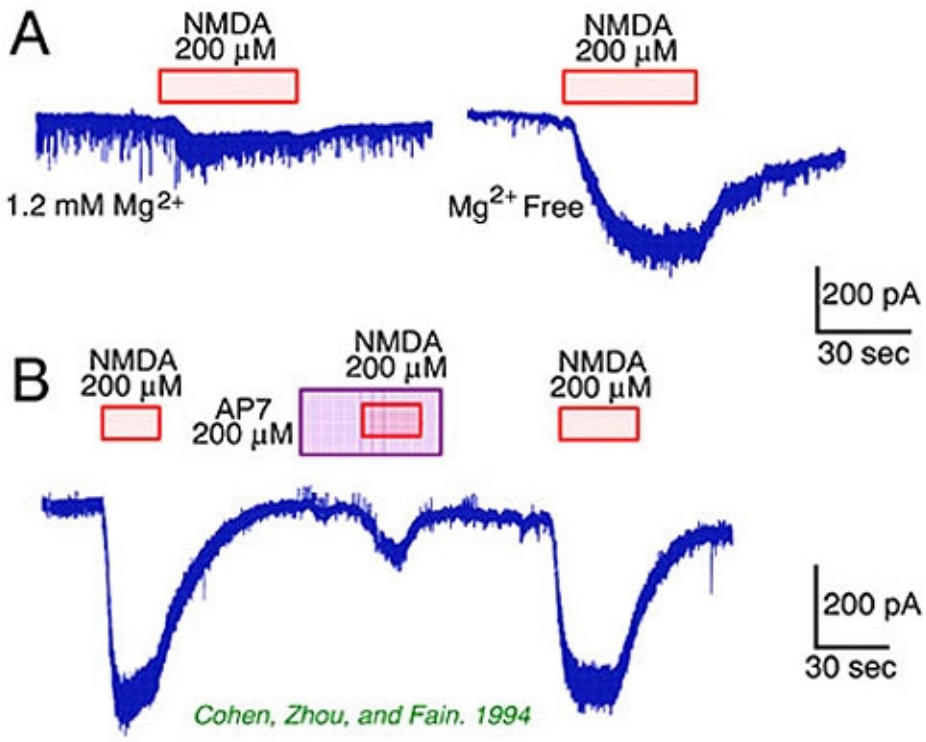

Figure 45. N-methyl-D-Aspartate (NMDA) activates an excitatory glutamate receptor in a cat ON beta ganglion cell (A) or OFF beta ganglion cell (B). Responses are conditional on either the absence of magnesium ions in the medium (A) or depolarized membrane potentials. They can be reversibly blocked (B) by the NMDA receptor antagonist 2-amino-7-phosphonoheptanoic acid (AP7). After Cohen et al. (80).

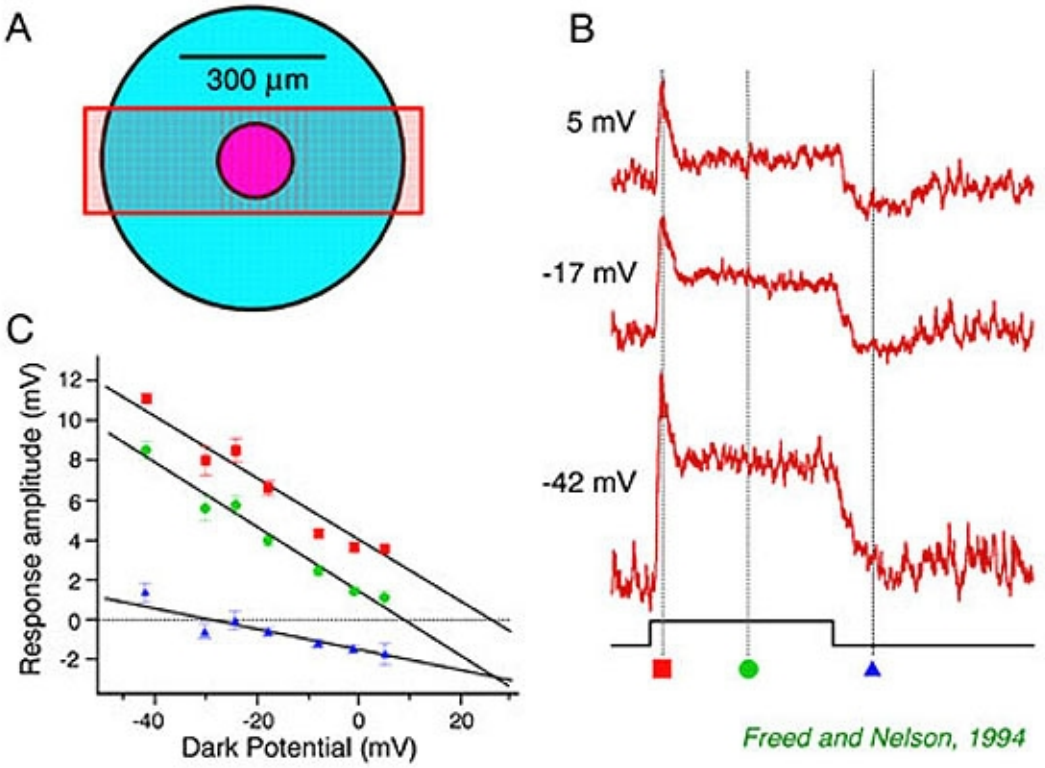

Figure 46. Properties of light-evoked synaptic voltages in ON-center cat beta ganglion cell. A. Slit stimulus covers the center (inner circle) and part of the surround (outer circle) of the receptive field. B. Depolarizing, excitatory responses become larger and more sustained as the ganglion cell is hyperpolarized by extrinsic current. C. Reversal potential of the light responses becomes progressively more negative over time but always exceeds the dark potential. After Freed and Nelson (87).

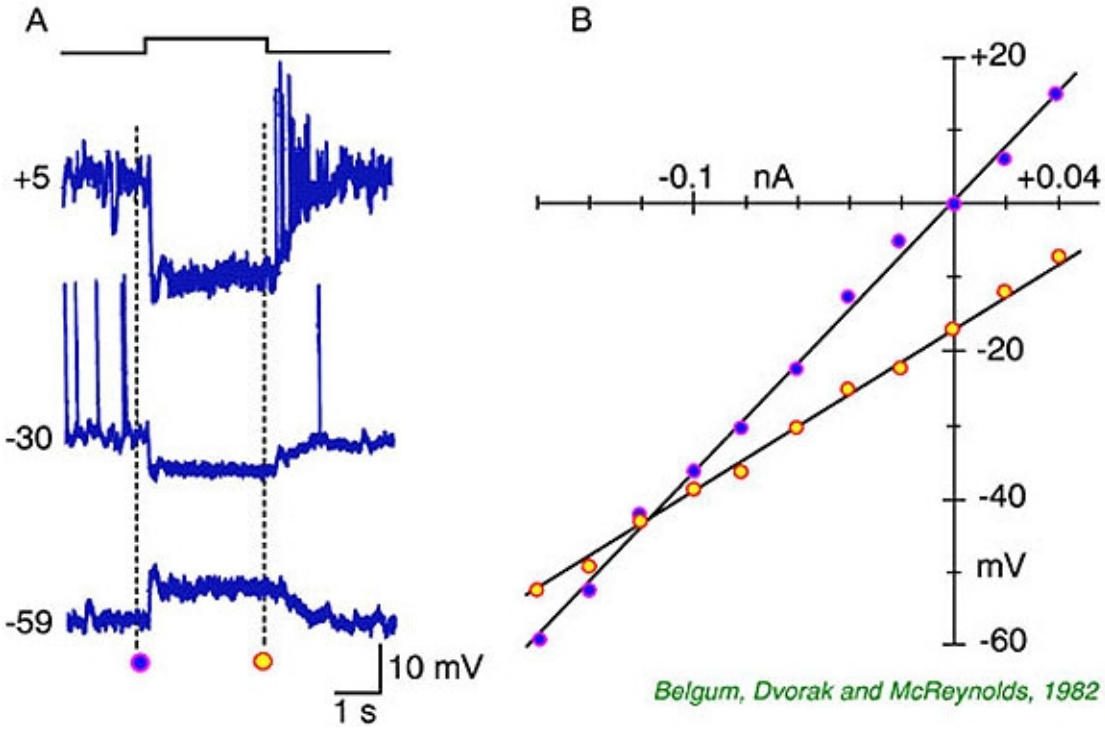

Figure 47. Properties of light-evoked synaptic voltages in OFF-center mudpuppy ganglion cell. A. Hyperpolarizing, inhibitory responses become larger as the cell is depolarized by extrinsic current. B. Reversal of the light response occurs at voltages more negative than the dark potential. After Belgum et al. (86).

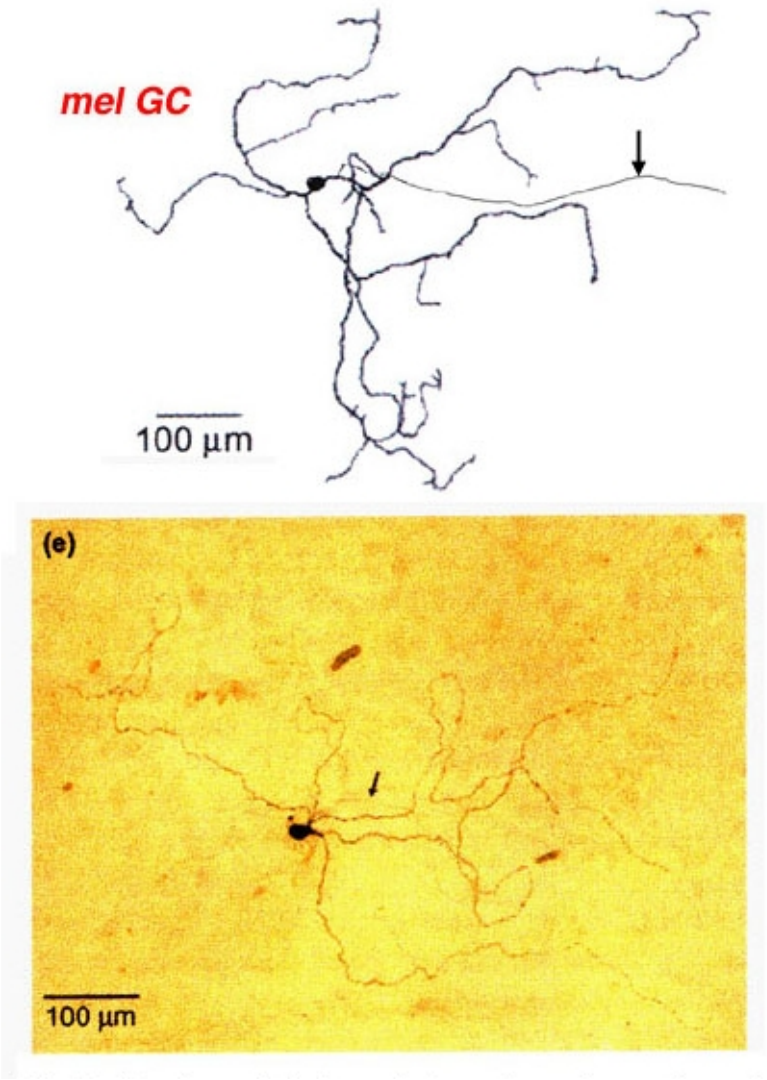

Figure 49. Drawing and photograph of a melanopsin ganglion cell in whole-mount mouse retina. The axon is indicated by an arrow. After Berson (89).

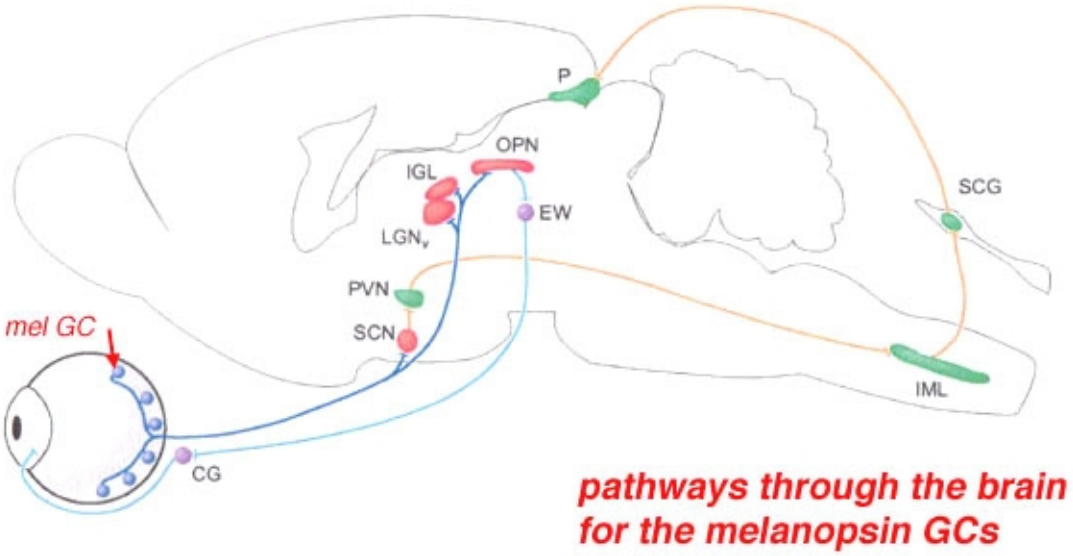

Figure 48. Diagram of the pathways taken by melanopsin ganglion cells to the brain. The pathway is to the suprachiasmatic nucleus (SCN) via the retinohypothalamic tract (blue) and on to the pituitary to regulate melatonin release. This circuit drives the circadian oscillator. A second pathway is through the lateral geniculate nucleus to the olivary pretectal nucleus (OPN) and to the Edinger Westaphal nucleus (EW) for control of the pupillary light reflex (light blue). After Berson (89).

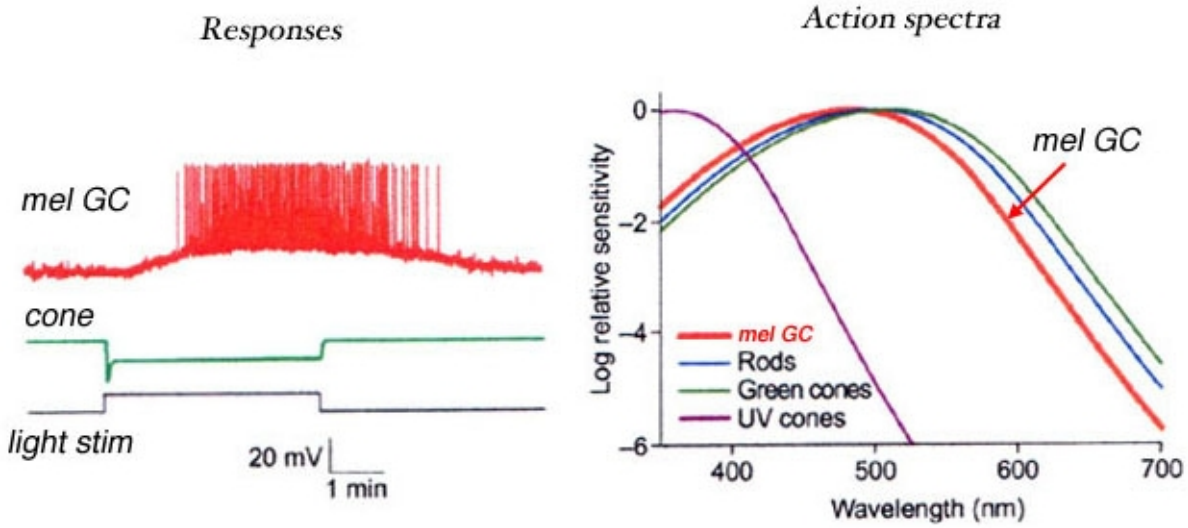

Figure 50. The physiological responses of melanopsin ganglion cells to light. The response on the left shows the melanopsin cell's slow onset, steady-state depolarizing spiking that occurs to a light flash as compared with the slow but faster onset hyperpolarization of the green cones in the mouse retina. The action spectra to the right show the melanopsin ganglion cell to have a peak sensitivity to light of 484 nm, compared with the rods and other cone types in the mouse. After Berson (89).

References

1. Hartline HK. Visual receptors and retinal interaction. Science. 1969;164:270–278. PubMed PMID: 5776637.
2. R. Granit. Sensory mechanisms of the retina. London: Oxford University Press; 1947.
3. Hartline HK. The receptive fields of optic nerve fibers. Am J Physiol. 1940;130:690–699.
4. Hartline HK. The effects of spatial summation in the retina on the excitation of the fibers of the optic nerve. Am J Physiol. 1940;130:700–711.
5. Hartline HK. The response of single optic nerve fibers of the vertebrate eye to illumination of the retina. Am J Physiol. 1938;121:400–415.
6. Cleland BG, Levick WR. Properties of rarely encountered types of ganglion cells in the cat's retina. J Physiol. 1974;240:457–492. PubMed PMID: 4420300.
7. DeVries SH, Baylor DA. Mosaic arrangement of ganglion cell receptive fields in rabbit retina. J Neurophysiol. 1997;78:2048–2060. PubMed PMID: 9325372.
8. Lettvin JY, Maturana HR, McCulloch WS, Pitts WH. What the frog's eye tells the frog's brain. Proc Inst Radio Eng N Y. 1959;47:1940–1951.
9. Amthor FR, Takahashi ES, Oyster CW. Morphologies of rabbit retinal ganglion cells with concentric receptive fields. J Comp Neurol. 1989;280:72–96. PubMed PMID: 2918097.
10. Nelson R, Famiglietti EV, Kolb H. Intracellular staining reveals different levels of stratification for On-and Off-centre ganglion cells in cat retina. J Neurophysiol. 1978;41:472–483. PubMed PMID: 650277.
11. Peichl L, Wässle H. Morphological identification of on- and off-centre brisk transient (Y) cells in cat retina. Proc R Soc Lond B Biol Sci. 1981;212:139–156. PubMed PMID: 6166011.
12. Amthor FR, Takahashi ES, Oyster CW. Morphologies of rabbit retinal ganglion cells with complex receptive fields. J Comp Neurol. 1989;280:97–121. PubMed PMID: 2918098.
13. Kuffler SW. Discharge patterns and functional organization of mammalian retina. J Neurophysiol. 1953;16:37–68. PubMed PMID: 13035466.
14. Shapley R, Victor J. Hyperacuity in cat retinal ganglion cells. Science. 1986;231:999–1002. PubMed PMID: 3945816.
15. Yang G, Masland RH. Direct visualization of the dendritic and receptive fields of directionally selective retinal ganglion cells. Science. 1992;258:1949–1952. PubMed PMID: 1470920.
16. Nelson R, Kolb H, Freed M. Off-alpha and Off-beta ganglion cells in cat retina. I. Intracellular electrophysiology and HRP stains. J Comp Neurol. 1993;329:68–84. PubMed PMID: 8454726.
17. Rodieck RW. Quantitative analysis of cat retinal ganglion cell response to visual stimuli. Vision Res. 1965;5:583–601. PubMed PMID: 5862581.
18. Enroth-Cugell C, Robson JG. The contrast sensitivity of retinal ganglion cells of the cat. J Physiol. 1966;187:517–552. PubMed PMID: 16783910.
19. Shapley RM, Victor JD. Nonlinear spatial summation and the contrast gain control of cat retinal ganglion cells. J Physiol. 1979;290:141–163. PubMed PMID: 469742.
20. Cleland BG, Levick WR. Brisk and sluggish concentrically organised ganglion cells in the cat's retina. J Physiol. 1974;240:421–456. PubMed PMID: 4421622.
21. Cleland BG, Dubin MW, Levick WR. Sustained and transient neurones in the cat's retina and lateral geniculate nucleus. J Physiol. 1971;217:473–496. PubMed PMID: 5097609.
22. Barlow HB, Hill RM. Selective sensitivity to direction of movement in ganglion cells of the rabbit retina. Science. 1963;139:412–414. PubMed PMID: 13966712.
23. Barlow HB, Hill RM, Levick WR. Retinal ganglion cells responding selectively to direction and speed of image motion in the rabbit. J Physiol. 1964;173:377–407. PubMed PMID: 14220259.
24. Jensen RJ, DeVoe RD. Comparisons of directionally selective with other ganglion cells of the turtle retina: intracellular recording and staining. J Comp Neurol. 1983;217:271–287. PubMed PMID: 6193149.

25. Holden AL. Responses of directional ganglion cells in the pigeon retina. J Physiol. 1977;270:253–269. PubMed PMID: 903893.
26. Maturana HR, Frenc S. Directional movement and horizontal edge detectors in the pigeon retina. Science. 1963;142:977–979. PubMed PMID: 14069232.
27. Ammermuller J, Muller J, Kolb H. The organization of the turtle inner retina. II. Analysis of color-coded and directionally selective cells. J Comp Neurol. 1995;358:35–62. PubMed PMID: 7560276.
28. Kittila CA, Granda AM. Functional morphologies of retinal ganglion cells in the turtle. J Comp Neurol. 1994;350:623–645. PubMed PMID: 7890834.
29. Michael CR. Receptive fields of single optic nerve fibers in a mammal with an all-cone retina. II. Directionally selective units. J Neurophysiol. 1968;31:257–267. PubMed PMID: 4301175.
30. Cronly-Dillon JR. Units sensitive to direction of movement in goldfish optic tectum. Nature. 1964;203:214–215. PubMed PMID: 14207259.
31. Jacobson M, Gaze RM. Type of visual response from single units in the optic tectum and optic nerve of the goldfish. Q J Exp Physiol. 1964;49:199–209.
32. Werblin FS. Response of retinal cells to moving spots: Intracellular recording in Necturus maculosus. J Neurophysiol. 1970;33:342–350. PubMed PMID: 5439341.
33. De Monasterio FM, Gouras P. Functional properties of ganglion cells of the rhesus monkey retina. J Physiol. 1975;251:167–195. PubMed PMID: 810576.
34. Barlow HB, Levick WR. The mechanism of directionally selective units in the rabbit's retina. J Physiol. 1965;178:477–504. PubMed PMID: 5827909.
35. He S, Masland RH. Retinal direction selectivity after targeted laser ablation of starburst amacrine cells. Nature. 1997;389:378–382. PubMed PMID: 9311778.
36. Borg-Graham L. Conductance changes are greater from preferred versus null responses in directionally-selective retinal ganglion cells. Soc Neurosci Abstr. 1997;23:2360.
37. Criswell MHCellular mechanisms of movement detection and directionality in the turtle retina [dissertation]. Bloomington (IN): Indiana University; 1997.
38. Dowling JE. Organization of vertebrate retinas. Invest Ophthalmol. 1970;9:655–680. PubMed PMID: 4915972.
39. Kittila CA, Massey SC. Effect of ON pathway blockade on directional selectivity in the rabbit retina. J Neurophysiol. 1995;73:703–712. PubMed PMID: 7760129.
40. Grzywacz NM, Amthor FR. Facilitation in ON-OFF directionally selective ganglion cells of the rabbit retina. J Neurophysiol. 1993;69:2188–2199. PubMed PMID: 8350138.
41. Amthor FR, Oyster CW, Takahashi ES. Morphology of ON-OFF direction-selective ganglion cells in the rabbit retina. Brain Res. 1984;298:187–190. PubMed PMID: 6722555.
42. Yang G, Masland RH. Receptive fields and dendritic structure of directionally selective retinal ganglion cells. J Neurosci. 1994;14:5267–5280. PubMed PMID: 8083735.
43. Mariani AP. Association amacrine cells could mediate directional selectivity in pigeon retina. Nature. 1982;298:654–655. PubMed PMID: 7099261.
44. Wyatt HJ, Daw NW. Specific effects of neurotransmitter antagonists on ganglion cells in rabbit retina. Science. 1976;191:204–205. PubMed PMID: 1857.
45. Daw NW, Ariel M. Effect of synaptic transmitter drugs on receptive fields of rabbit ganglion cells. Vision Res. 1981;21:1643–1648. PubMed PMID: 6278756.
46. Cohen ED, Miller RF. Quinoxalines block the mechanism of directional selectivity in ganglion cells of the rabbit retina. Proc Natl Acad Sci U S A. 1995;92:1127–1131. PubMed PMID: 7862647.
47. Grzywacz NM, Tootle JS, Amthor FR. Is the input to a GABAergic or cholinergic synapse the sole asymmetry in rabbit's retinal directional selectivity? Vis Neurosci. 1997;14:39–54. PubMed PMID: 9057267.
48. Young T. On the theory of light and colours. Philos Trans R Soc Lond B Biol Sci. 1802;92:20–71.
49. Hering E. Grundzuge einer theorie des Farbensinnes Sitzungsber. k. Akad. Wissensch, Math-naturwissensch. Cl. Wein. 1875;70:169.

50. Wagner HG, MacNichol EF, Wolbarsht ML. Thee response properties of single ganglion cells in the goldfish retina. J Gen Physiol. 1960;43:45–62.
51. Daw NW, Pearlman AL. Cat colour vision: evidence for more than one cone process. J Physiol. 1970;211:125–137. PubMed PMID: 5500987.
52. Loop MS, Bruce LL, Petuchowski S. Cat color vision: The effect of stimulus size, shape and viewing distance. Vision Res. 1979;19:507–513. PubMed PMID: 483578.
53. Daw NW. Goldfish retina: organization for simultaneous color contrast. Science. 1967;158:942–944. PubMed PMID: 6054169.
54. Polyak SL. The retina. Chicago: University of Chicago Press; 1941.
55. Gouras P. Identification of cone mechanisms in monkey ganglion cells. J Physiol. 1968;199:533–547. PubMed PMID: 4974745.
56. Gouras P. Antidromic response of orthodromically identified ganglion cells in monkey retina. J Physiol. 1969;204:407–419. PubMed PMID: 4980966.
57. Dacey DM, Lee BB. The 'blue-on' opponent pathways in primate retina originates from a distinct bistratified ganglion cell. Nature. 1994;367:731–735. PubMed PMID: 8107868.
58. Kaplan E, Shapley RM. The primate retina contains two types of ganglion cells, with high and low contrast sensitivity. Proc Natl Acad Sci U S A. 1986;83:2755–2757. PubMed PMID: 3458235.
59. Reid RC, Shapley RM. Spatial structure of cone inputs to receptive fields in primate lateral geniculate nucleus. Nature. 1992;356:716–718. PubMed PMID: 1570016.
60. Enroth-Cugell C, Hertz BG, Lennie P. Convergence of rod and cone signals in the cat's retina. J Physiol. 1977;269:297–318. PubMed PMID: 894595.
61. Gouras P. The effects of light-adaptation on rod and cone receptive field organization of monkey ganglion cells. J Physiol. 1967;192:747–760. PubMed PMID: 4964632.
62. Wiesel TN, Hubel DH. Spatial and chromatic interactions in the lateral geniculate body of the rhesus monkey. J Neurophysiol. 1966;29:1115–1156. PubMed PMID: 4961644.
63. Lee BB, Smith VC, Pokorny J, Kremers J. Rod inputs to macaque ganglion cells. Vision Res. 1997;37:2813–2828. PubMed PMID: 9415362.
64. Purpura K, Kaplan E, Shapley RM. Background light and the contrast gain of primate P and M retinal ganglion cells. Proc Natl Acad Sci U S A. 1988;85:4534–4537. PubMed PMID: 3380804.
65. Merigan WH, Maunsell JHR. How parallel are the primate visual pathways. Annu Rev Neurosci. 1993;16:369–402. PubMed PMID: 8460898.
66. Raynauld J-P. Goldfish retina: sign of the rod input in opponent color ganglion cells. Science. 1972;177:84–85. PubMed PMID: 5041783.
67. MacLeod DIA. Rods cancel cones in flicker. Nature. 1972;235:173–174. PubMed PMID: 4551230.
68. Barlow HB, Levick WR, Yoon M. Responses to single quanta of light in retinal ganglion cells of the cat. Vision Res. 1971;3:87–101. PubMed PMID: 5293890.
69. Mastronarde DN. Correlated firing of cat retinal ganglion cells. II. Responses of X- and Y- cells to single quantal events. J Neurophysiol. 1983;49:325–349. PubMed PMID: 6300341.
70. Jensen RJ. Involvement of glycinergic neurons in the diminished surround activity of ganglion cells in the dark-adapted rabbit retina. Vis Neurosci. 1991;6:43–53. PubMed PMID: 1851036.
71. DeVries SH, Baylor DA. An alternative pathway for signal flow from rod photoreceptors to ganglion cells in mammalian retina. Proc Natl Acad Sci U S A. 1995;92:10658–10662. PubMed PMID: 7479860.
72. Wässle H, Peichl L, Boycott BB. Morphology and topography of on- and off-alpha cells in the cat retina. Proc R Soc Lond B Biol Sci. 1981;212:157–175. PubMed PMID: 6166012.
73. Wässle H, Boycott BB. Functional architecture of the mammalian retina. Physiol Rev. 1991;71:447–480. PubMed PMID: 2006220.
74. Westhiemer G. The spatial sense of the eye. Invest Ophthalmol Vis Sci. 1979;18:893–912. PubMed PMID: 478780.
75. Mastronarde DN. Correlated firing of cat retinal ganglion cells. I. Spontaneously active inputs to X- and Y-cells. J Neurophysiol. 1983;49:303–324. PubMed PMID: 6300340.

76. Mastronarde DN. Interactions between ganglion cells in cat retina. J Neurophysiol. 1983;49:350–365. PubMed PMID: 6300342.
77. Brivanlou IH, Warland DK, Meister M. Mechanisms of concerted firing among retinal ganglion cells. Neuron. 1998;20:527–539. PubMed PMID: 9539126.
78. Neuenschwander S, Singer W. Long-range synchronization of oscillatory light responses in the cat retina and lateral geniculate nucleus. Nature. 1996;379:728–733. PubMed PMID: 8602219.
79. Fohlmeister JF, Miller RF. Mechanisms by which cell geometry controls repetitive impulse firing in retinal ganglion cells. J Neurophysiol. 1997;78:1948–1964. PubMed PMID: 9325363.
80. Cohen ED, Zhou ZJ, Fain GL. Ligand-gated currents of alpha and beta ganglion cells in the cat retinal slice. J Neurophysiol. 1994;72:1260–1269. PubMed PMID: 7528793.
81. Kaneda M, Hashimoto M, Kaneko A. Neuronal nicotinic acetylcholine receptors of ganglion cells in the cat retina. Jpn J Physiol. 1995;45:491–508. PubMed PMID: 7474530.
82. Lipton SA, Aizenmann E, Loring RH. Neural nicotinic acetylcholine responses in solitary mammalian retinal ganglion cells. Pflugers Arch. 1987;410:37–43. PubMed PMID: 3684508.
83. Masland RH, Ames A. Responses of acetylcholine of ganglion cells in an isolated mammalian retina. J Neurophysiol. 1976;39:1220–1235. PubMed PMID: 993829.
84. Schmidt M, Humphrey MF, Wässle H. Action and localization of acetylcholine in the cat's retina. J Neurophysiol. 1987;58:997–1015. PubMed PMID: 3694255.
85. Müller F, Wässle H, Voigt T. Pharmacological modulation of the rod pathway in the cat retina. J Neurophysiol. 1988;59:1657–1671. PubMed PMID: 3404200.
86. Belgum JH, Dvorak DR, McReynolds JS. Sustained synaptic input to ganglion cells of mudpuppy retina. J Physiol. 1982;326:91–108. PubMed PMID: 7108811.
87. Freed MA, Nelson R. Conductances evoked by light in the ON-beta ganglion cell of the cat retina. Vis Neurosci. 1994;11:261–269. PubMed PMID: 8003453.
88. Belenky MA, Smeraski CA, Provencio I, Sollars PJ, Pickard GE. Melanopsin retinal ganglion cells receive bipolar and amacrine cell synapses. J Comp Neurol. 2003;460:380–393. PubMed PMID: 12692856.
89. Berson DM. Strange vision: ganglion cells as circadian photoreceptors. Trends Neurosci. 2003;26:314–320. PubMed PMID: 12798601.
90. Foster RG. Shedding light on the biological clock. Neuron. 1998;20:829–832. PubMed PMID: 9620688.
91. Barlow HB, Levick WR. Changes in the maintained discharge with adaptation level in the cat retina. J Physiol. 1969;202:699–718. PubMed PMID: 5789945.
92. Pu M. Dendritic morphology of cat retinal ganglion cells projecting to suprachiasmatic nucleus. J Comp Neurol. 1999;414:267–274. PubMed PMID: 10516596.
93. Wiesel TN. Recording inhibition and excitation in the cat's retinal ganglion cells with intracellular electrodes. Nature. 1959;183:264–265. PubMed PMID: 13622769.
94. MacNichol EF. Three-pigment color vision. Sci Am. 1964;211:48–56.
95. Daw NW, Pearlman AL. Cat colour vision: One cone process or several? J Physiol. 1969;201:745–764. PubMed PMID: 5767891.
96. Daw NW. Colour-coded ganglion cells in the goldfish retina: extension of their receptive fields by means of new stimuli. J Physiol. 1968;197:567–592. PubMed PMID: 5666170.
97. Crocker RA, Ringo J, Wolbarsht ML, Wagner HG. Cone contributions to cat retinal ganglion cell receptive fields. J Gen Physiol. 1980;76:763–785. PubMed PMID: 10822503.
98. Gouras P. The function of the midget cell system in primate color vision. Vision Res. 1971;3:397–410. PubMed PMID: 5293881.
99. Baylor DA, Fettiplace R. Transmission from photoreceptors to ganglion cells in turtle retina. J Physiol. 1977;271:391–424. PubMed PMID: 200736.
100. Peichl L, Wässle H. The structural correlate of the receptive field centre of alpha ganglion cells in the cat retina. J Physiol. 1983;341:309–324. PubMed PMID: 6620182.

Melanopsin-expressing, Intrinsically Photosensitive Retinal Ganglion Cells (ipRGCs)

Dustin M. Graham, Ph.D.[1,*] and Kwoon Y. Wong, Ph.D.[2,†]

Created: August 1, 2008; Updated: November 2, 2016.

1. Introduction

For the greater part of 150 years it was assumed that the mammalian retina contained only two classes of photoreceptors, rods and cones. However, a flurry of studies in the late 1990s and early 2000s demonstrated the existence of a third class of mammalian photoreceptors that differs greatly from rods and cones. It utilizes a different photopigment, is much less sensitive to light, responds to light far more slowly, and has far lower spatial resolution, characteristics that fit with its primary function of signaling ambient light levels (irradiance) to the brain. Most surprisingly, these photoreceptors are retinal ganglion cells (RGCs), and thus, have the unique ability to communicate directly with higher visual centers of the brain. These intrinsically photosensitive retinal ganglion cells (ipRGCs) are a rare subpopulation of ganglion cells (<5%) whose primary role is to signal light for largely subconscious, non-image-forming visual reflexes, such as pupillary constriction, neuroendocrine regulation, and synchronizing daily ("circadian") physiological rhythms to the light/dark cycle ("circadian photoentrainment"). Recent research has revealed additional roles for ipRGCs in conscious visual perception, including brightness discrimination and contrast detection. Many visual behaviors under ipRGC control are remarkably tonic, and require prolonged integration of ambient light levels. The unique properties of ipRGCs make them well suited for regulating such behaviors.

2. History and discovery

As a graduate student in 1923, Clyde Keeler made a number of interesting observations from mice that had severe outer retinal degeneration (1, 2). Though they lacked most of their rod and cone photoreceptors, and were considered functionally blind, these mice were still able to constrict their pupils in response to light (3), leading Keeler to deduce that some other photoreceptive cells must be lurking in the retina. But an alternative, more parsimonious explanation for these pupil reflexes was that they were driven by the small number of surviving cone photoreceptors, and so the existence of non-rod non-cone photoreceptors remained uncertain. Seven decades later, Russell Foster and colleagues engineered mice that lacked all rods and cones, which displayed not only robust pupillary light reflexes, but also maintained the ability to shift their circadian rhythms in accordance with shifting light cycles, and to suppress nocturnal pineal melatonin secretion in response to light pulses (4, 5). [Recent work detected a very small number of ultraviolet cones in these mice (6), but they were unlikely to be stimulated by the 509 nm stimuli used in the Foster studies.] These processes disappeared, however, when animals had their eyes removed, strongly supporting Keeler's prediction of a novel ocular photoreceptor (7). But it wasn't until the discovery of a new light-sensitive molecule (or opsin), from an unlikely source, that Keeler's prediction would prove true.

Author Affiliations: 1 Nature Publishing Group, One New York Plaza, Suite 4500, New York NY 10004-1562; Email: dustinmichaelgraham@gmail.com. 2 Department of Ophthalmology & Visual Sciences, Department of Molecular, Cellular & Developmental Biology, University of Michigan, Ann Arbor, MI 48105.; Email: kwoon@umich.edu.

Corresponding author.

* See 'About the authors'

† See 'About the authors'

Iggy Provencio and colleagues, studying the photosensitive skin cells ("dermal melanophores") of frogs, cloned a novel opsin-like molecule which they proposed was responsible for the redistribution of skin pigment in response to light (8). Orthologues of this putative opsin, which Provencio et al. called melanopsin, were also found to be expressed in a small subset of RGCs in mouse (Figure 1A) and human retinas (8-10), and additional work found that melanopsin-containing cells send their axons to the suprachiasmatic nucleus (SCN), the site of the mammalian central circadian clock (11, 12).

These findings suggested that these RGCs could be the mysterious third photoreceptor type Keeler had predicted almost 80 years earlier. They express a putative opsin, potentially allowing them to directly respond to light, and they send axon projections to a brain target known to be involved in two of the visual reflexes observable in rodless/coneless mice, i.e. circadian photoentrainment and photic suppression of pineal melatonin release. However, definitive proof that these melanopsin-containing, SCN-projecting RGCs could directly sense light was still lacking. Combining tracer injections into the SCN with electrophysiology, David Berson and colleagues tested the hypothesis that SCN-projecting RGCs are photoreceptive. They made whole-cell recordings from RGCs retrogradely labeled by the tracers (Figure 1B), and found that these cells were indeed able to respond to light in the presence of a cocktail of drugs that eliminated all rod and cone signaling in the retina (Figure 1C, *top*) (13). Even after mechanical isolation from the rest of the retina, these cells were still photosensitive (Figure 1C, *bottom*), leaving to rest all doubts that the labeled RGCs were true photoreceptors (13). Immunohistochemistry performed after whole-cell recording confirmed the presence of melanopsin in these SCN-projecting cells (14). The morphology and distribution of these SCN-projecting ipRGCs are illustrated in Figure 2.

3. Melanopsin

We now know that the ability of ipRGCs to respond directly to light is indeed due to expression of melanopsin. The melanopsin gene (opn4) has been found in many mammalian species, e.g. mice, monkeys, and humans (9). Hydrophobicity analysis of melanospin's amino-acid sequence predicted a 7-transmembrane structure, common to all G protein-coupled receptors (Figure 3A, B) (8). Interestingly, melanopsin shares higher homology with the rhabdomeric opsins (r-opsins) of invertebrate photoreceptors than with the ciliary opsins (c-opsins) of vertebrate photoreceptors, suggesting that melanopsin could signal light through a different phototransduction mechanism than that used in vertebrate rods and cones (Figure 3C) (8) (see "Phototransduction" below).

Although the first studies of ipRGCs implicated melanopsin as the photopigment in these cells, a role for a group of blue-light-absorbing flavoproteins known as cryptochromes could not be initially ruled out (15). Cryptochromes function as photopigments in plants and invertebrate animals, and early studies favored their functioning as retinal photopigments in the mammalian circadian system (16, 17). However, subsequent work provided overwhelming evidence that melanopsin is the photopigment in ipRGCs. When the melanopsin gene was deleted via transgenic techniques in mice ("melanopsin-knockout mice"), RGCs retrogradely labeled from the SCN no longer could respond directly to light (18). In addition, animals missing the melanopsin gene showed deficiencies in multiple visual reflexes such as pupillary constriction and photoentrainment (18-22). Despite this evidence, there were still controversies regarding melanopsin's ability to function as a photopigment. For example, it remained possible that melanopsin is not the ipRGC photopigment, but is instead an isomerase essential for the proper functioning of the ipRGC photopigment. These doubts were firmly extinguished with a series of experiments whereby the melanopsin gene was heterologously expressed in multiple cell types that are normally insensitive to light. When made to express melanopsin, these cells were able to robustly respond to light, indicating melanopsin's ability to function as a bona fide photopigment (23-25).

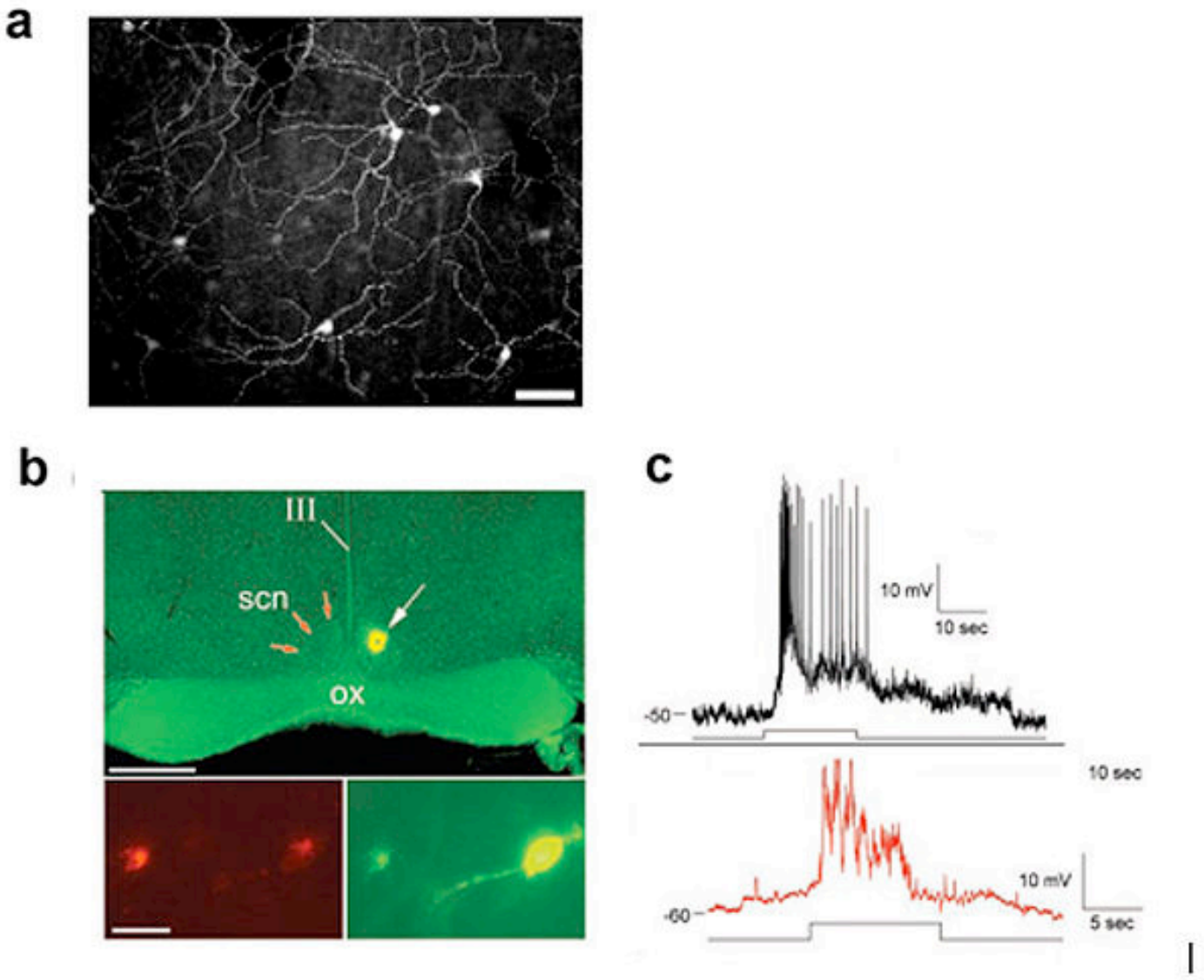

Figure 1. Discovery of ipRGCs. (A) Melanopsin immunostaining of ganglion cells in the whole-mount mouse retina. Adapted from Provencio et al. 2002 (10). (B) Injection of a fluorescent tracer into the suprachiasmatic nucleus (SCN) above the optic chiasm (ox) in a rat (top panel) and subsequent retrograde labeling of RGCs (lower left panel, red staining). The retrolabeled cell on the right was whole-cell-recorded and filled with the fluorescent dye Lucifer Yellow (lower right panel, yellow staining). (C) Whole-cell patch-clamp recordings of retrolabeled rat RGCs showing responses to light under synaptic blockade (black trace), and after mechanical isolation (red trace). Adapted from Berson et al. 2002 (13).

4. Phototransduction

As seen in Figure 4, the intrinsic light response of ipRGCs differs dramatically from those of rods and cones. Most notable, is the difference in response polarity: the direct photoresponse of ipRGCs is depolarizing, whereas rods and cones hyperpolarize to light. In addition, ipRGCs are much less sensitive to light than the classical photoreceptors, and signal with far slower kinetics (Figure 4A) (13, 26). IpRGCs are also capable of very long-lasting light responses, faithfully encoding stimulus energy over relatively long periods of time (Figure 4C). This feature sets ipRGCs apart from all other mammalian RGCs, which cannot stably represent ambient light levels in this fashion (27-29). Another remarkable feature of ipRGC physiology is the ability of their dendrites (which contain melanopsin) to respond directly to light (13). Combined with their large overlapping dendritic fields, the entire ipRGC population creates what Provencio and colleagues called a “photoreceptive net” (10). These

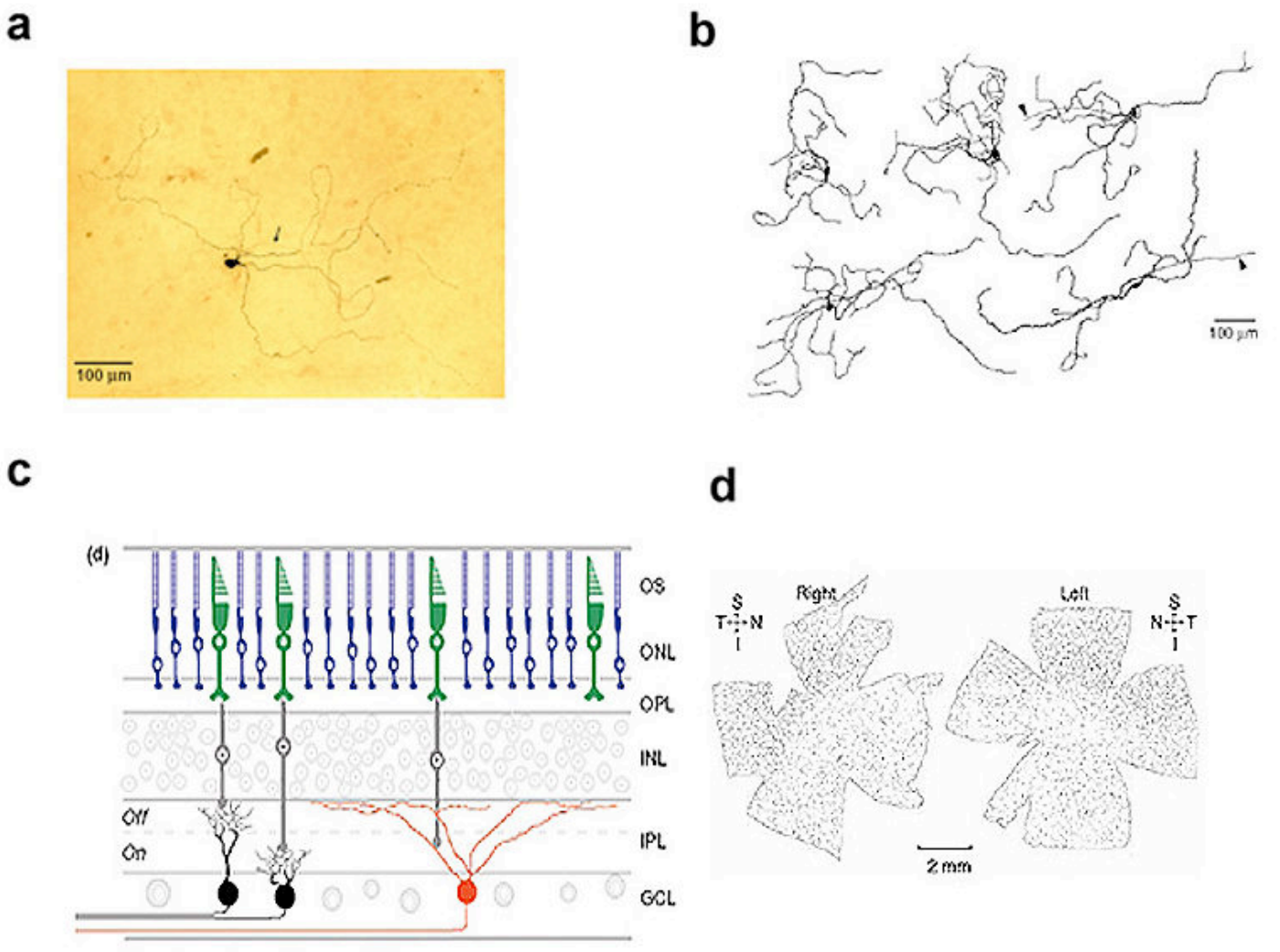

Figure 2. Morphological characteristics and distribution of SCN-projecting ipRGCs. (A) Photomicrograph of a typical SCN-projecting ipRGC filled with intracellular dye during whole-cell recording. Adapted from Berson 2003 (18). (B) Camera lucida drawing of multiple SCN-projecting ipRGCs stained with intracellular dye. Adapted from Berson et al. 2002 (13). (C) Schematic drawing comparing the dendritic spread and termination patterns of SCN-projecting ipRGCs with those of typical conventional (i.e. non-intrinsically photosensitive) ganglion cells. Adapted from Berson 2003 (18). (D) Whole-mount retinas stained for melanopsin showing overall distribution of ipRGCs throughout the retina. Adapted from Hattar et al. 2002 (14).

characteristics of ipRGCs are no doubt tailored to their role in signaling diffuse ambient light levels over many hours for tonic, non-image-forming visual behaviors such as photoentrainment and pupillary reflex. A further distinction of ipRGCs is their action spectrum (i.e. wavelength-sensitivity function), due to the utilization of melanopsin as their photopigment. IpRGC photoreception is most sensitive to light at around 480 nm (13, 30, 31), significantly different (≥20 nm) from the best wavelengths for stimulating rods and cones (Figure 4B).

As noted earlier, animal photoreceptors come in two basic flavors: rhabdomeric (found mainly in invertebrates), and ciliary (vertebrate rods and cones being most notable). A defining feature of rhabdomeric and ciliary photoreceptors is the distinct biochemical cascades both cell classes use to transduce light energy into an electrical signal the brain can interpret. Rods and cones use a cascade involving cyclic guanosine monophosphate (cGMP) as a second messenger (Figure 5B) (32, 33). The response to light is a decrease in cGMP levels which closes cGMP-gated cation channels, causing the plasma membrane to hyperpolarize. This is in stark contrast to rhabdomeric photoreceptors which use a phosphoinositide signaling cascade involving the

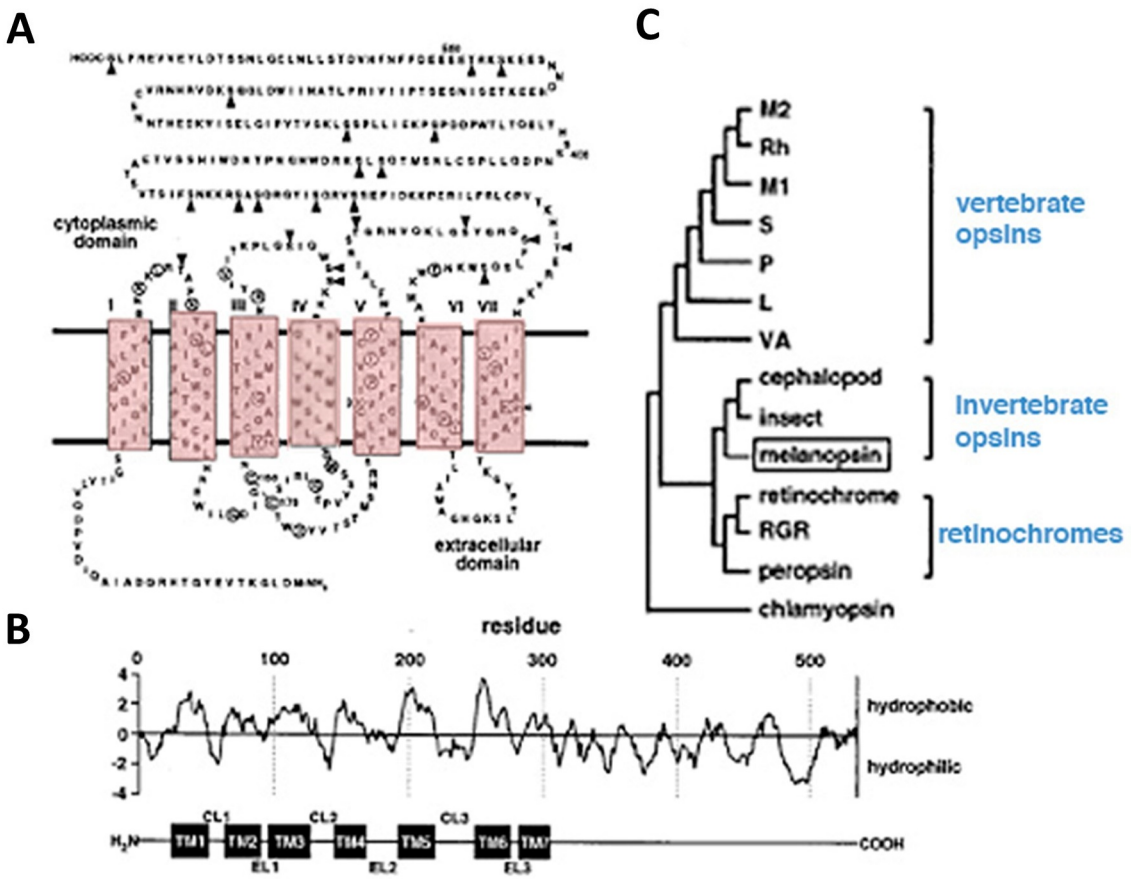

Figure 3. The melanopsin gene. (*A*) Deduced amino-acid sequence and predicted secondary structure of melanopsin. The 7 shaded regions indicate transmembrane domains. (B) Hydropathy analysis for secondary structure prediction. (*C*) Phylogenetic tree comparing melanopsin to representative opsins of vertebrate and invertebrate species. From chicken: L, long-wavelength-sensitive opsin; M1, blue-like middle-wavelength-sensitive opsin; M2, green-like middle-wavelength-sensitive opsin; P, pineal opsin; Rh, rhodopsin; and S, short-wavelength-sensitive opsin. From Atlantic salmon: VA, vertebrate ancient opsin. Adapted from Provencio et al. 1998 (8).

enzyme phospholipase C (PLC) and breakdown of the membrane lipid phosphatidylinositol bisphosphate (PIP2) (Figure 5A), leading to the opening of cation channels and membrane depolarization (34, 35). In addition, although both phototransduction cascades are G protein-mediated, the specific G proteins required are different. Ciliary photoreceptors require transducin, a member of the Gi/o family of G proteins, whereas rhabdomeric photoreceptors use a G protein of the Gq/11 family (Figure 5).

Just like rod and cone photopigments, melanopsin uses *11-cis*-retinal as the light-absorbing chromophore, and light-induced isomerization of *11-cis*-retinal to *all-trans*-retinal is the first step in the phototransduction process (36, 37). However, melanopsin's relatively high homology with invertebrate opsins, and the depolarizing intrinsic light response of ipRGCs, suggest these neurons may use a rhabdomeric phototransduction cascade distinct from the rod and cone ciliary cascade. Early pharmacological studies of ipRGCs could not confirm this hypothesis, most likely due to the whole-mount retina preparation employed. The combination of photosensitive ipRGC dendrites buried deep within the inner plexiform layer (IPL, where synapses are formed among bipolar, amacrine and ganglion cells) and a glial membrane sheath covering the retinal surface, created a significant diffusion barrier for pharmacological agents, especially hydrophobic drugs commonly used to study transduction mechanisms. To overcome this hurdle, David Berson and colleagues recorded from mechanically dissociated ipRGC somas to facilitate pharmacological manipulation. Isolated ipRGCs survive remarkably well in culture, generating robust light responses for up to 6 days. Using this system, Berson et al. showed that ipRGC

phototransduction utilizes a rhabdomeric-like phosphoinositide cascade, requiring a member (or possibly members) of the Gq/11 family of G proteins and the effector enzyme phospholipase C (PLC) (Figure 6) (38) (but see(39)). In addition, the presence of specific Gq/11 and PLC isoforms was confirmed in ipRGCs using single-cell RT-PCR and immunocytochemistry, consistent with the pharmacological findings (38). Genetically knocking out the β4 isoform of PLC nearly eliminated the intrinsic light response of ipRGCs (40).

In rhabdomeric photoreceptors, breakdown of PIP2 by PLC generates two by-products: a membrane-bound component called diacylglycerol (DAG), and inositol-triphosphate (IP3), which is free to move about the cytosol (34). DAG can be broken down within the membrane into polyunsaturated fatty acids (PUFAs), which have been shown to directly open Drosophila photoreceptors' Transient Receptor Potential (TRP) channels (41). IP3, on the other hand, can cause release of Ca^{2+} from intracellular stores, which can lead to the opening of so-called "store-operated channels" in the plasma membrane. In Drosophila photoreceptors the downstream mechanism linking PIP2 breakdown to TRP channel opening is still unclear, although a membrane-associated pathway is likely (42). In ipRGCs, the light-gated cation channels are also TRP channels, specifically, TRPM6 and TRPM7 (40), and data strongly suggest that the cytosolic IP3 pathway is not required for phototransduction, similar to Drosophila photoreceptors (Figure 7) (38). Intracellular application of high concentrations of IP3 neither induced a current, nor did it occlude light responses in ipRGCs (Figure 7A), although it did modulate certain response properties, suggesting a non-essential secondary role for IP3 and intracellular Ca^{2+}. Likewise, ipRGC phototransduction survived blockade of IP3 receptors with intracellular heparin, or intracellular Ca^{2+} store depletion using thapsigargin (Figure 7A). Only after extended exposure to very high (10mM) concentrations of the general Ca^{2+} chelator BAPTA, does one see significant attenuation of phototransduction (38), although this is probably a side effect of clamping resting intracellular Ca^{2+} levels so low that enzymes such as PLC are no longer able to function (43). The most compelling evidence that ipRGC phototransduction does not require the cytosolic IP3 branch is that excised patches of ipRGC membrane (both outside-out and inside-out) remained autonomously photosensitive (Figure 7B), ruling out a vital role for highly diffusible cytosolic components (38). Based on these findings, all the necessary components for ipRGC phototransduction appear to be within, or tightly coupled to, the plasma membrane.

The exact channel-gating mechanism downstream of PLC activation is still not clear. Application of DAG or PUFAs, either to isolated ipRGC somas or to excised patches of ipRGC membrane, failed to evoke a current or to block light responses (Figure 8A-D). An alternative hypothesis, and one in line with a membrane-associated transduction cascade, is that the breakdown of PIP2 itself (as opposed to production of DAG or PUFAs) is the critical signal that opens the light-gated TRP channels in ipRGCs. There is evidence that PIP2 can either open or close a variety of ion channels, including the light-gated channels in Drosophila photoreceptors (44, 45). As a preliminary test of this hypothesis, Berson et al. pharmacologically interfered with PIP2 synthesis using wortmannin. This drug inhibits phosphoinositide 4-kinase (PI4-K), the synthetic enzyme for phosphatidylinositol 4-phosphate (PIP), which is an essential precursor of PIP2. According to the hypothesis, wortmannin should slow the termination of the photocurrent at light offset by delaying the restoration of resting levels of PIP2 and, hence, the closure of the light-gated channels. Indeed, when wortmannin was included in the recording pipette solution, response shutoff was dramatically delayed (Figure 8E). Further and more direct evidence, however, is needed to resolve the gating mechanism of the light-modulated channels in ipRGCs.

Following light exposure, *all-trans*-retinal in a rod, cone or ipRGC photopigment must be isomerized back to *11-cis*-retinal to make the photopigment photoexcitable again (46). For rhodopsin, this re-isomerization requires the adjacent retinal pigment epithelium (RPE), while cone pigments rely on Müller glial cells in addition to the RPE (47). In contrast, photoexcited melanopsin appears to retain *all-trans*-retinal and isomerize it to *11-cis*-retinal upon subsequent photon absorption, in a process called photoreversal (48-52). Thus, melanopsin can function as both photopigment and photoisomerase, similar to some invertebrate photopigments, and ipRGCs remain directly light-sensitive when RPE enzymes that synthesize *11-cis*-retinal are genetically or

pharmacologically inhibited (53, 54). Nevertheless, without these enzymes, the melanopsin-based light response of ipRGCs is attenuated, suggesting that melanopsin function depends on the RPE to some extent (37, 55).

5. Synaptic input

Although ipRGCs can function as photoreceptors, they nevertheless receive intraretinal synaptic input from rod/cone-driven circuits. Electron microscopy revealed synaptic contacts made by amacrine and bipolar cells onto melanopsin-immunopositive processes in the IPL (56). Thus, ipRGCs respond to light not only directly through melanopsin, but also indirectly through synaptically mediated input from rods and cones (27, 30, 57-59). Both the intrinsic light response and the extrinsic, rod/cone-driven light response are remarkably tonic and can signal light continuously for at least 10 hours (28). Moreover, the receptive fields for both response components are coextensive with each ipRGC's dendritic field (27). However, these components are drastically different in two important ways. Firstly, whereas the intrinsic photoresponse is very sluggish, the extrinsic response is as rapid as the light responses of conventional RGCs (Figure 9) (27). The intrinsic response integrates photons over many seconds, while the extrinsic response enables ipRGCs to track rapid changes in light intensity (26, 27, 60). Secondly, the intensity thresholds for rod input, cone input and melanopsin phototransduction are vastly different, roughly 7 log photons cm^{-2} s^{-1}, 9 log photons cm^{-2} s^{-1} and 11 log photons cm^{-2} s^{-1}, respectively (30, 58). The different dynamic ranges of synaptic input and intrinsic photoreception enable ipRGCs to encode light intensities spanning at least 9 orders of magnitude (30).

Using whole-cell voltage-clamp recordings combined with pharmacology, investigators demonstrated that SCN-projecting ipRGCs have spontaneous inhibitory and excitatory synaptic inputs in the dark, and that they express receptors for glutamate, GABA and glycine (27, 57). Light stimulation increases both excitatory glutamatergic input and inhibitory GABA/glycinergic input, which are presumably mediated by bipolar and amacrine cells, respectively (27). Both inputs evoke primarily ON light responses, although comparatively weak OFF responses can also be seen under some conditions (27, 58, 61). This predominating ON-channel input was surprising because SCN-projecting ipRGC dendrites are found mainly in the distal half of the IPL, which had been assumed for decades to be the "OFF" sublamina where RGCs receive input only from OFF bipolar cells but not ON bipolars (62, 63). ON bipolar cells use two unconventional strategies to release glutamate onto the dendrites of SCN-projecting mouse ipRGCs in the "OFF" sublamina. Some ON bipolar cells' axons extend lateral protrusions that contain synaptic vesicles (Figure 10A), whereas others possess *en passant* (in passing) synaptic vesicles within their axonal shafts (64). Distally stratifying ipRGCs are also present in rabbit, marmoset and macaque retinas, and they likewise receive unconventional ON bipolar input in the "OFF" sublamina (Figure 10C) (65, 66).

The mammalian retina contains about a dozen types of bipolar cells and over 30 types of amacrine cells (67, 68). In mice, the ON bipolar cells that use axonal side branches to contact "OFF"-sublamina ipRGC dendrites appear to be type-6 cone bipolar cells (Figure 10A) (64). Trans synaptic viral tracing has shown that these "OFF"-sublamina ipRGC dendrites are also directly postsynaptic from dopaminergic amacrine cells which costratify with these ipRGC dendrites (69). As will be discussed in detail in "Adaptation, neuromodulation, and circadian control", ipRGCs receive modulatory input from dopaminergic amacrine cells (70, 71). Trans synaptic viral tracing also revealed that proximally stratifying mouse ipRGCs with dendrites in the "ON" sublamina (see "Morphological and physiological diversity") are directly postsynaptic from type-8 ON cone bipolar cells and another type of monostratified amacrine cell (Figure 10B) (69). In rabbits and primates, distally stratifying ipRGCs are contacted by a type of calbindin-positive ON cone bipolar cell (Figure 10C) (65) and DB6 ON cone bipolars (Figure 10D) (66), respectively. Besides receiving direct ON cone bipolar input, ipRGCs also receive ON rod bipolar input, albeit polysynaptically just like for all other mammalian RGCs (59, 66). Specifically, ipRGCs receive ON rod bipolar input through AII amacrine cells making gap junctions onto ON cone bipolar cells, which then synapse on ipRGCs. Another putative pathway that affects ipRGCs may be added by centrifugal fibers entering the retina. These centrifugal fibers are known to be histaminergic (72) and they have an effect on

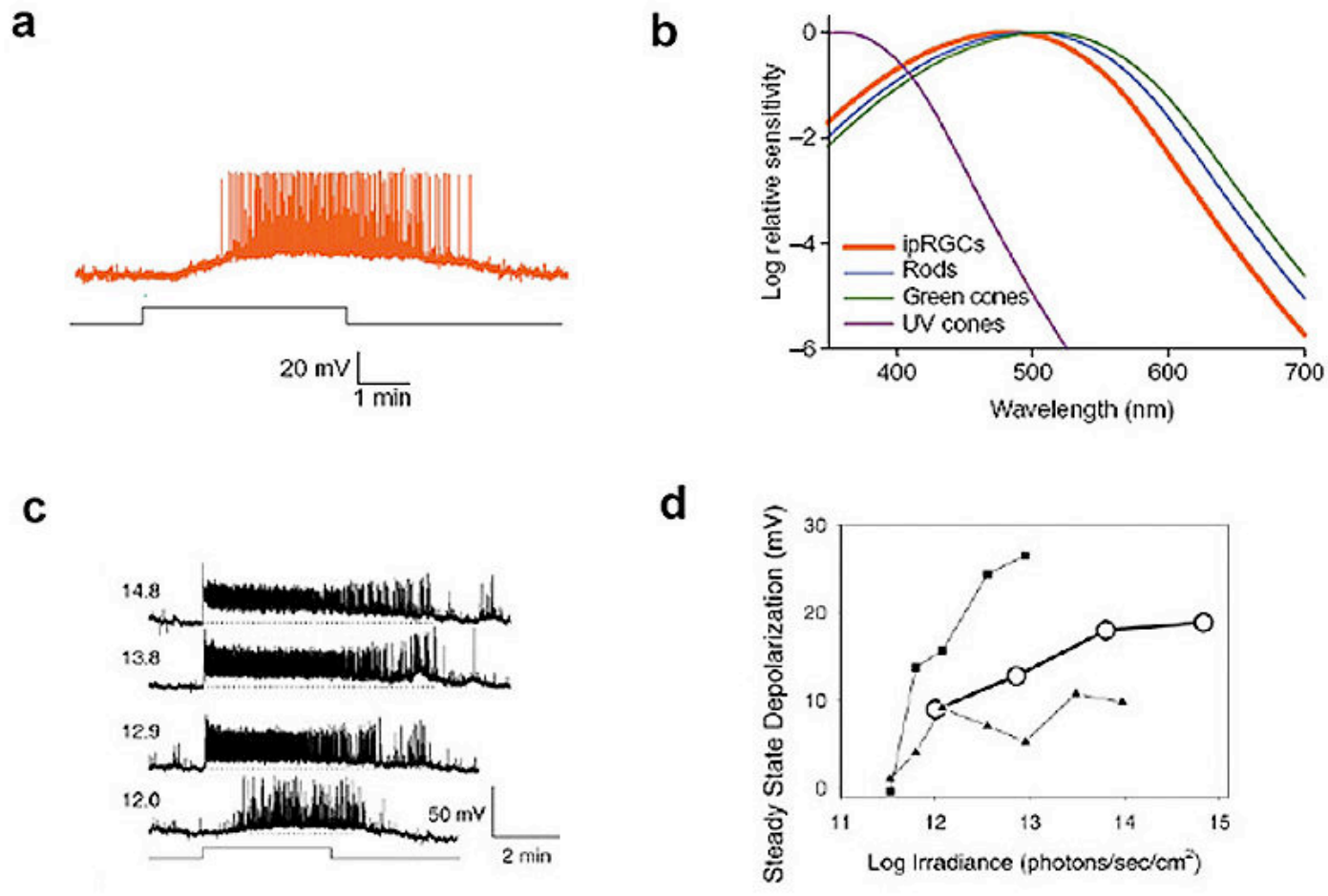

Figure 4. Physiological characteristics of intrinsic photosensitivity in ipRGCs. All recordings were made in the presence of rod/cone signaling blockers. (A) Current-clamp recording from a rat ipRGC showing a depolarizing light response with spiking and slow kinetics. (B) Comparison of action spectra for rat rods and cones with that of rat ipRGCs. Adapted from Berson 2003 (18). (C) Whole-cell recording from a rat ipRGC showing changes in response amplitude and kinetics with increasing levels of illumination. (D) Plot of steady-state response amplitude versus light intensity for 3 separate rat ipRGCs. Adapted from Berson et al. 2002 (13).

dopaminergic amacrine cells in mouse retina through H1 receptors (73). The synaptic input to "OFF"-stratifying ipRGCs is summarized in Figure 11.

6. Intraretinal synaptic output

Besides receiving intraretinal synaptic input, ipRGCs mediate intraretinal synaptic output. For many decades, RGCs were thought to function strictly as retinal output neurons, signaling only to higher visual centers of the brain. But there is electron microscopy evidence that RGC dendrites are presynaptic in catfish (74), and more recent work by Douglas McMahon and coauthors yielded evidence that ipRGCs signal to a subpopulation of dopaminergic amacrine cells (DA cells). Dopamine released by DA cells diffuses throughout the retina and reshapes the functional properties of retinal circuits according to current lighting conditions and time of day, and thus allows the retina to be a more dynamic system (75). DA cells come in three flavors showing transient, sustained and null responses to light (76). The light responses of the transient DA cells were eliminated by L-AP4, which blocks rod/cone signaling to ON bipolar cells (Figure 12A). By contrast, the sustained DA cells remained light-responsive in the presence of L-AP4 (Figure 12B), or in rod/cone degenerate retinas (77). In the presence of L-AP4, the sustained DA cells' light responses peaked at a wavelength near 480nm (Figure 12C),

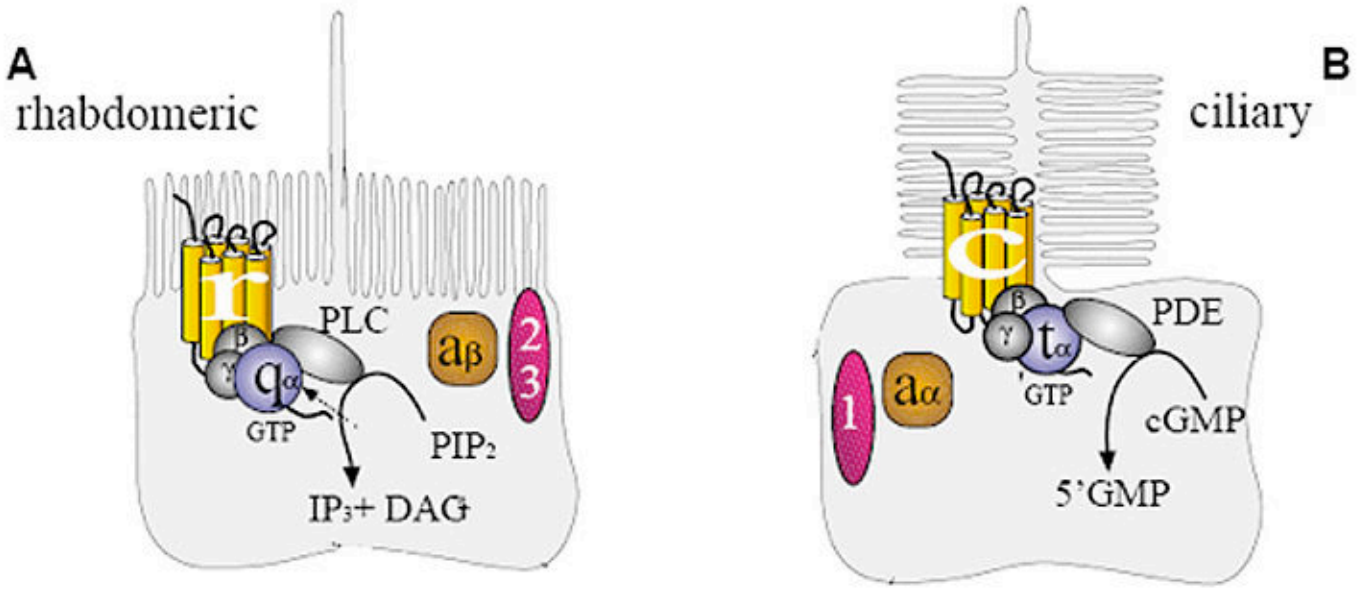

Figure 5. Schematic representation of the phototransduction cascades in (A) rhabdomeric photoreceptors and (B) ciliary photoreceptors. Adapted from Arendt 2003 (32).

matching very well with a melanopsin-based input (76, 77). In melanopsin-knockout mice, blocking ON bipolar input with L-AP4 abolished all DA cells' light responses, confirming that the L-AP4-resistant photoresponse originates from ipRGCs (78).

In addition, staining for cFos, an immediate early gene used to mark activated neurons, showed that roughly the same percentage of DA cells were activated by sustained light in rod/cone degenerate retinas as retinas injected with L-AP4 (Figure 13) (77). Knocking out melanopsin suppressed light-induced dopamine release (79). These observations strongly suggest that sustained DA cells receive input from ipRGCs. Both DA cells and SCN-projecting ipRGCs have dendrites stratifying in the outermost sublayer of the IPL, raising the possibility that these ipRGC dendrites signal directly to the DA dendrites (69, 70). Another plausible transmission route has been suggested by the observation that some ipRGCs extend axon collaterals toward the IPL (Figure 14) (80). In support of the latter possibility, blocking voltage-gated Na^+ channels (which are present in RGC axons) with tetrodotoxin suppressed ipRGC signaling to DA cells (81). Antagonizing AMPA/kainate receptors also disrupted ipRGC output to DA cells (78), suggesting ipRGCs signal to DA cells by releasing glutamate in a Na^+ spike-dependent manner.

IpRGC signaling to sustained DA cells can account for the light-induced secretion of dopamine in rat retinas with severe rod/cone degeneration (82, 83) (but see(84)). Because dopamine is known to play myriad modulatory roles throughout the retina, intraretinal output from ipRGCs to DA cells could influence image-forming retinal circuits, and several studies have reinforced this possibility. Using a non-invasive field-potential recording technique called the electroretinogram, Mark Hankins and Rob Lucas found that prolonged nocturnal light exposure altered the photoresponse kinetics of ON bipolar cells in human subjects (Figure 15). This effect exhibited a remarkably long integration time and was most optimally induced by 483 nm light, implicating a melanopsin-based mechanism (85). The same researchers later observed diurnal rhythms in the amplitude and kinetics of the mouse electroretinogram, which were abolished upon knocking out melanopsin (86). Additional evidence for ipRGC regulation of retinal function came from a study by Ouria Dkhissi-Benyahya et al. examining clock gene expression in rods and cones. In wild-type mice, the expression of these clock genes

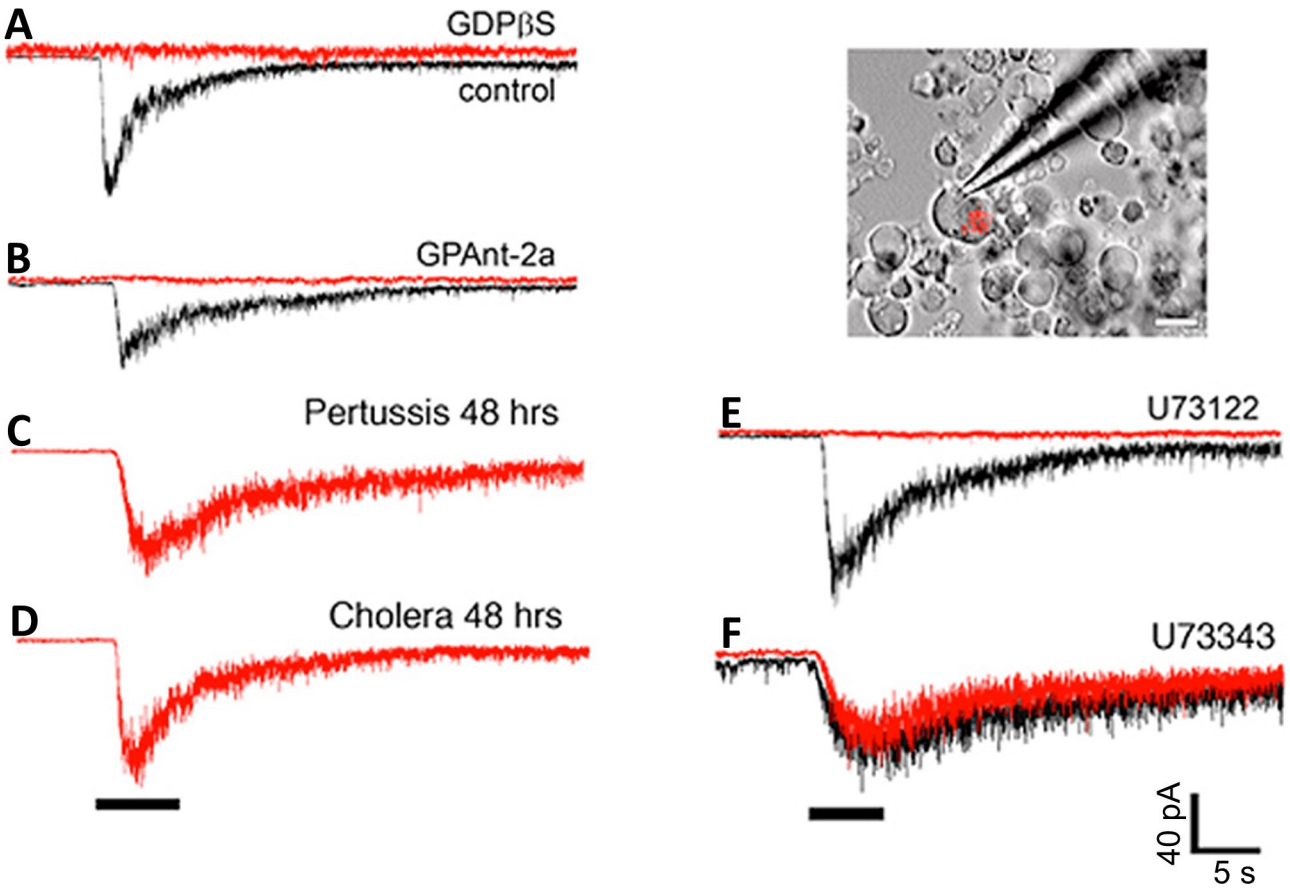

Figure 6. Invertebrate-like phosphoinositide phototransduction cascade in ipRGCs, elucidated through whole-cell recordings from dissociated rat ipRGCs. (A) GDPβS, a general G protein blocker, completely abolished the light response in ipRGCs (red trace), indicating a G protein-coupled cascade. (B) The specific Gq/11 family G protein blocker GPAnt-2a completely blocked the light response in ipRGCs (red trace), while 48-hour incubation in toxins disrupting (C) Gi/o-family G protein signaling and (D) Gs-type G protein signaling did not block the light response. (E) Consistent with a Gq/11- and PLC-mediated cascade, the PLC blocker U73122 completely blocked the light response (red trace), while the inactive analog U73343 (F) had no effect, indicating the effect of U73122 is specific. Inset is a picture of an isolated rat ipRGC in culture during a typical patch-clamp recording; red dots within the cell are due to the tracer dye retrogradely transported from the SCN. Adapted from Graham et al. 2008 (38).

(which are thought to drive circadian rhythms within the retina) exhibits a daily rhythm, but when melanopsin was knocked out, this rhythm was dampened substantially (79).

Ca^{2+} imaging suggested an additional potential pathway for intraretinal signaling by ipRGCs. Under normal physiological conditions, about 3% of ganglion cell layer (GCL) cells in rodless coneless mouse retinas showed increases in Ca^{2+} dye signals in response to light, but in the presence of the gap junction blocker carbenoxolone, this percentage dropped to ~1%, leading the authors to propose that ipRGCs propagate their light responses to amacrine cells in the GCL ("displaced amacrine cells") via gap junctions (87). But this conclusion was challenged by subsequent research showing that carbenoxolone has various non-specific effects, and can abolish light-driven increases in Ca^{2+} signals even in mechanically dissociated ipRGCs (88). Nonetheless, tracer dye coupling between ipRGCs and displaced amacrines had been observed (89), and so gap-junction-mediated intraretinal signaling by ipRGCs remained a possibility. A recent study showed that rat ipRGCs indeed transmit their melanopsin-based light responses to displaced amacrine cells (90). Whole-cell recordings were made from >2,000 randomly targeted displaced amacrine cells to search for cells exhibiting spiking, sustained ON light responses, and 154 such cells were encountered. Surprisingly, all of them were still photosensitive during bath

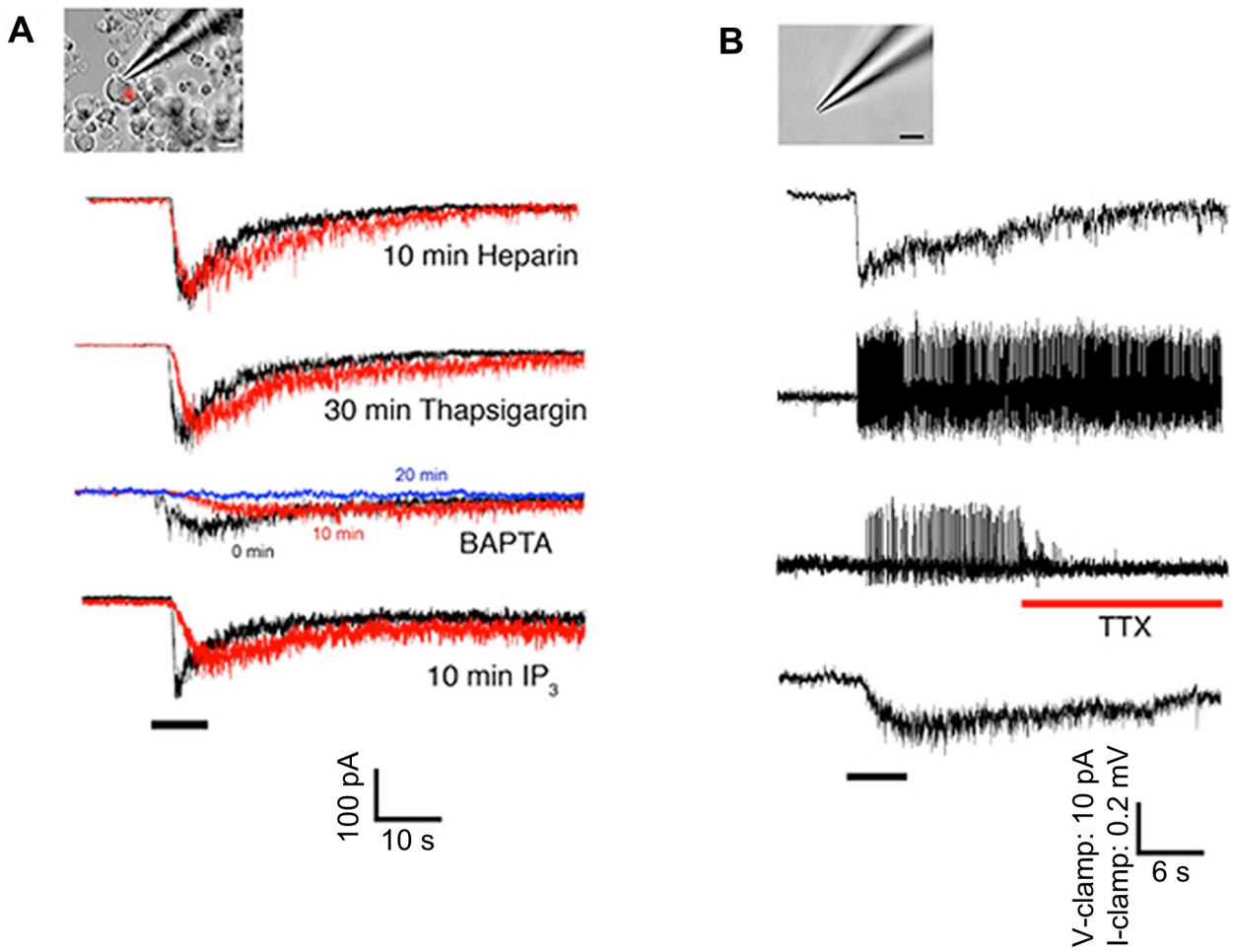

Figure 7. Evidence for a membrane-associated phototransdcution cascade in ipRGCs. (A) Whole-cell patch-clamp recordings from dissociated rat ipRGCs. Voltage-clamp traces showing control light responses (black traces) and light responses after 10-minute (red traces) and 20-minute (blue trace) application of various agents to block the cytosolic IP3-related branch of the phosphoinositide signaling cascade. (B) Light responses from excised patches of ipRGC membrane. Top two traces are voltage-clamp (top trace) and current-clamp (second from top trace) recordings from an inside-out patch of ipRGC membrane. The bottom two traces are current-clamp (second from bottom trace) and voltage-clamp (bottom trace) recordings from outside-out patches of ipRGC membrane. Note the cessation of spiking activity in response to applied TTX (second to bottom trace) indicating the spikes are due to voltage-gated Na+ channels. Stimulus light timings are indicated by the horizontal black bars. Adapted from Graham et al. 2008 (38).

application of L-AP4, DNQX and D-AP5, which fully block rod/cone signaling to the inner retina. In the presence of these drugs, all 154 amacrines gave sluggish depolarizing light responses resembling ipRGCs' intrinsic light responses, but they lost all photosensitivity after the addition of the gap junction blocker meclofenamic acid, indicating that ipRGCs signal to these amacrines via gap junctions (90).

7. Morphological and physiological diversity

The SCN-projecting rat and mouse ipRGCs appear to be morphologically homogeneous, suggesting they constitute a single cell type (but see(91)). All such cells have somas medium in size among GCL neurons and sparse dendrites terminating in the outermost sublayer ("S1") of the IPL, corresponding to the main plexus of melanopsin-immunoreactive dendrites (Figure 16A-C, G) (12-14). However, a number of studies from the early 2000s implicated the existence of multiple types of ipRGCs. For example, there is an additional plexus of melanopsin-positive dendrites in the innermost sublayer ("S5") of the IPL (10). Ca^{2+} imaging and "blind"

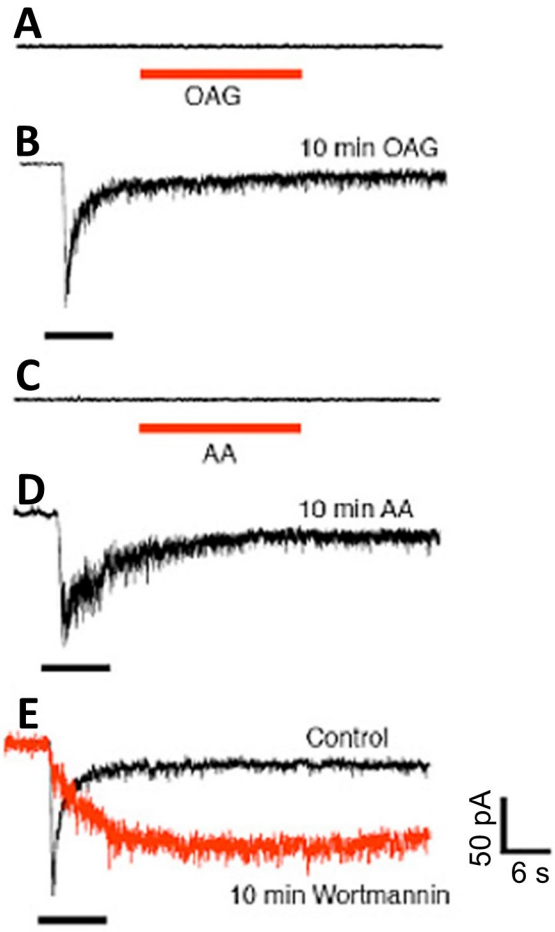

Figure 8. Possible gating mechanism for the light-modulated channels in ipRGCs. (A) The DAG analogue OAG did not induce a current in ipRGCs when applied from a puffer pipette, (B) nor did it block the light response after prolonged bath application at high concentrations. (C) The polyunsaturated fatty acid arachidonic acid (AA) did not induce a current in ipRGCs when applied via puffer pipette, (D), nor did it block the light response when bath-applied for prolonged periods. (E) Wortmannin significantly delayed post-illumination ipRGC response recovery (red trace) compared with control cells (black trace), suggesting PIP2 breakdown itself may be the gating mechanism of the light-modulated channels in ipRGCs. Adapted from Graham et al. 2008 (38).

multielectrode-array extracellular spike recording also revealed diverse melanopsin-mediated light responses in the GCL (31, 87). Using various fluorescent labeling techniques, subsequent work revealed the existence of at least at least five morphological types of melanopsin-expressing ipRGCs in the mouse retina. The SCN-projecting type originally described by David Berson is now called "M1", whereas the new types are called M2, M3, M4 and M5 (69, 92, 93). Examples of mouse M2 cells are shown in Figure 16D-F, H. By whole-cell-recording from a large sample of randomly selected RGCs, all five morphological types of ipRGCs were also found in the rat (94); representative examples are shown in Figure 17. Among these ipRGC types, M1 is the only one that stratifies exclusively in S1 of the IPL. M3 is the only bistratified type, extending dendrites toward both S1 and S5. The remaining ipRGC types are all monostratified in S5, with M2 having relatively sparse dendrites, M4 having denser and radiate dendrites similar to the previously described alpha cell (95, 96), and M5 having the densest dendrites covering the smallest fields (Figure 17).

The five types of ipRGCs exhibit diverse physiological properties, suggesting they perform different functions. In both mouse and rat, the five ipRGC types spike spontaneously at different frequencies (58, 94). The various types of mouse ipRGCs also differ significantly in various basic biophysical properties such as membrane resistance,

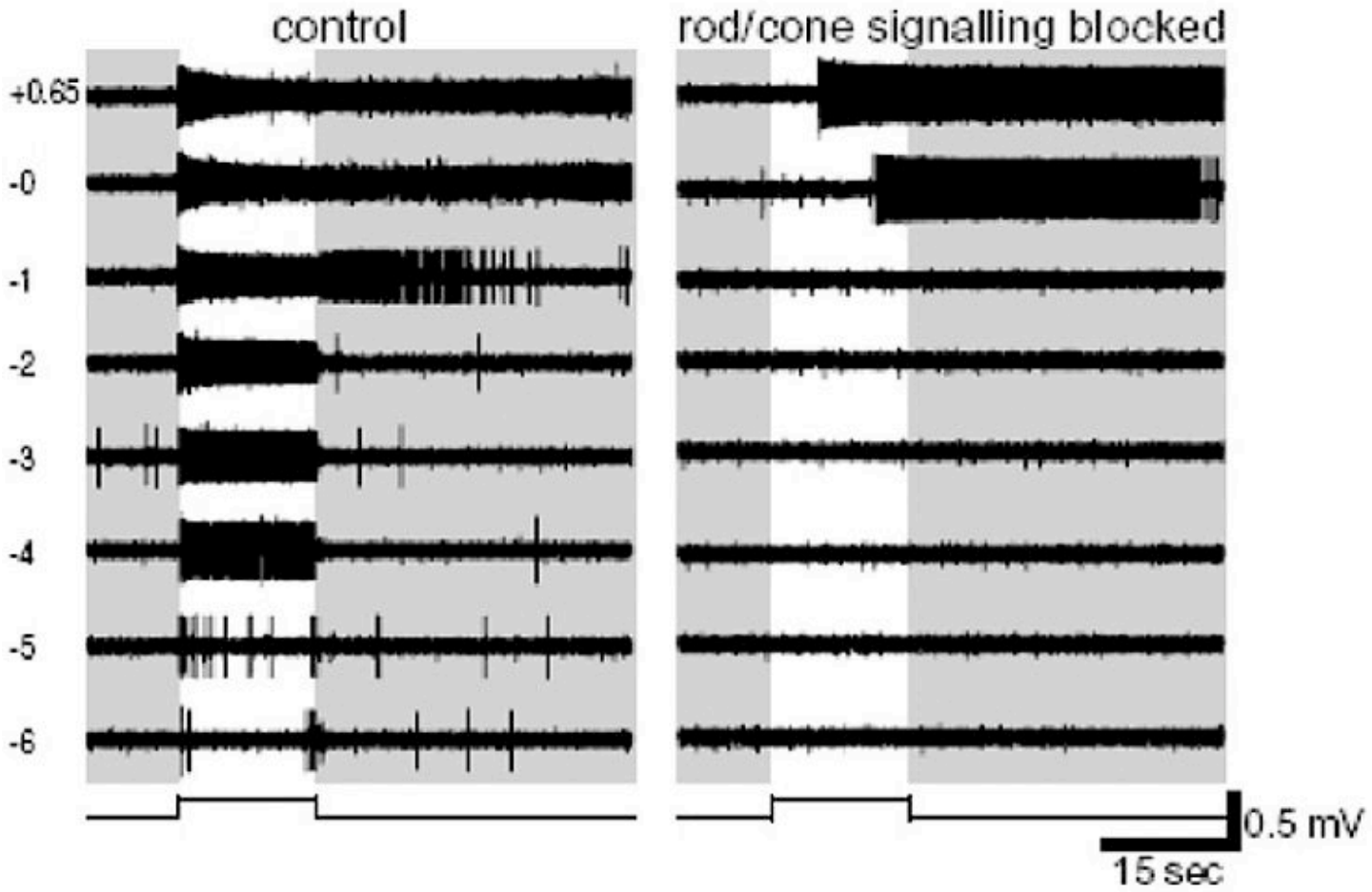

Figure 9. Extracellular spike recording of a rat ipRGC using an electrode in a multielectrode array. Note how the long-lasting and relatively insensitive intrinsic melanopsin-driven component becomes obvious at increasing illumination levels (left traces) and can easily be isolated using pharmacological blockade of rod/cone-driven input (right traces). Adapted from Wong et al. 2007(27).

membrane capacitance, Na^+ spike waveform, Na^+ spike threshold, and voltage-gated Ca^{2+} and K^+ currents (97, 98). Under dark-adapted conditions, the five mouse ipRGC types respond fairly similarly to full-field light, generating sustained depolarizing responses that last for the duration of the light (58). Under light-adapted conditions, however, M1's and M2's cone-driven full-field light responses are significantly different, with the former's responses being far more transient and much lower in amplitude (61). Diversity was also observed in the various cell types' responses to moving lights, and to light spots of different sizes, even under dark-adapted conditions. All five cell types responded more strongly to moving lights than to static lights; however, different cell types appeared tuned to different speeds of motion (Figure 18A).

Furthermore, whereas M1's receptive field consists of just an ON-center region, the non-M1 ipRGCs' receptive fields display ON-center/OFF-surround antagonism, so that a large light spot illuminating the entire receptive field induces a weaker response than a smaller spot covering just the center region (Figure 18B) (58). Under conditions blocking rod/cone signaling, the five types of rat and mouse ipRGCs generate melanopsin-based light responses that differ in kinetics, amplitude, and threshold, with M1 cells' intrinsic photoresponses being the fastest, largest, and most sensitive (Figure 19) (58, 93-95, 97).

Besides mice and rats, many other species that have been examined also possess multiple morphological and/or physiological types of ipRGCs, although it is unknown whether these other species also have five ipRGC types. In primates including humans, only two morphological types of melanopsin-expressing RGCs have been documented (Figure 20). Both cell types have giant somas and sparse, monostratifying dendrites. The outer-

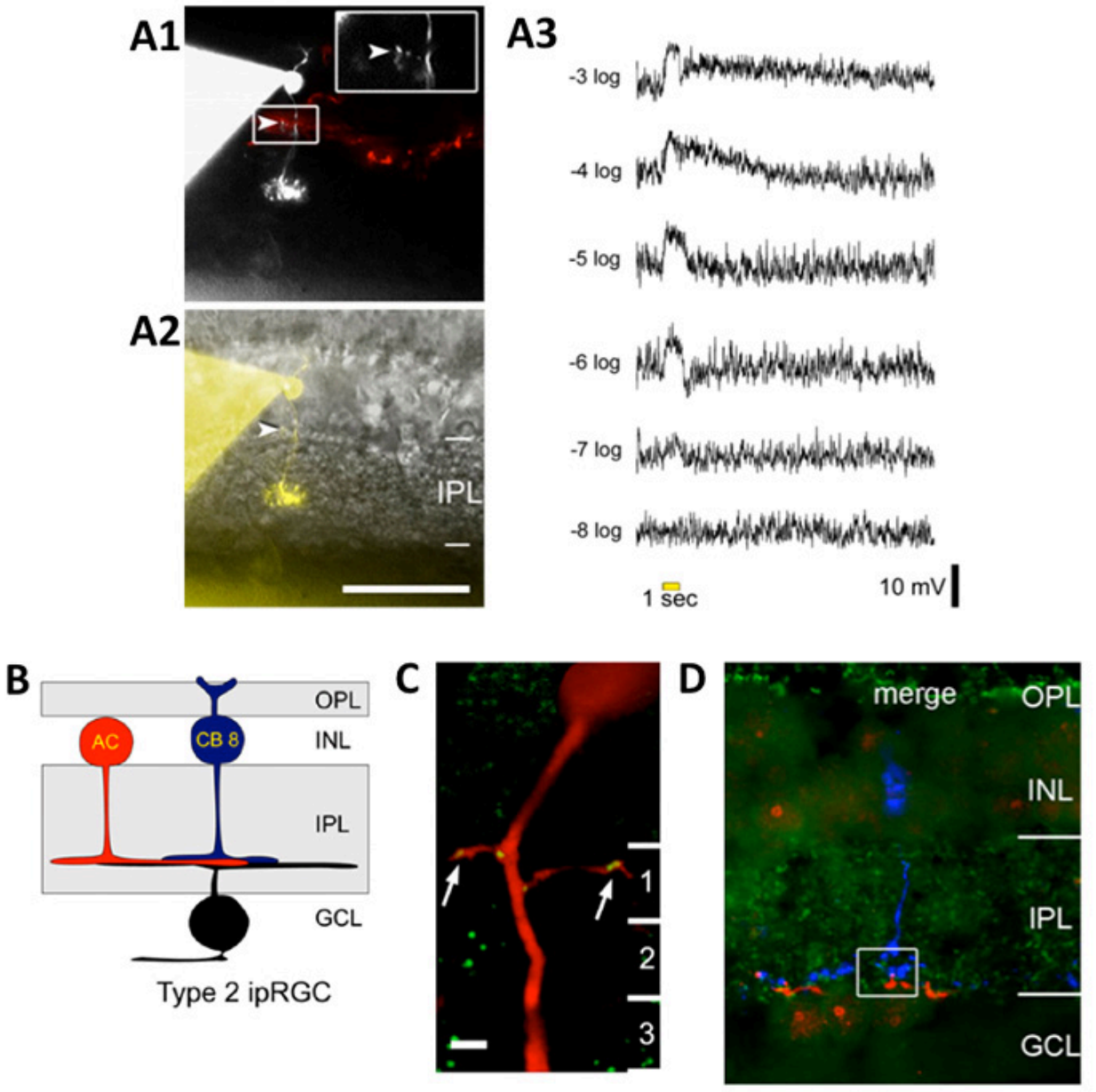

Figure 10. Examples of bipolar and amacrine cell types known to be presynaptic to ipRGCs. (A) In mice, type-6 ON cone bipolar cells extend lateral axonal branches in S1 of the IPL, where they contact the distal dendrites of ipRGCs. A1 & A2: Intracellular fill using the fluorescent dye HyLite488. A1 shows the staining in white, and the Red Fluorescent Protein (RFP)-labeled dendrites of dopaminergic amacrine cells (which serve as a marker for S1) in red. A2 shows the same bipolar cell in an infrared image of the retinal slice. The axonal protrusion (arrowhead) is near the outermost limit of the IPL. A3: Current-clamp light responses from a type-6 ON cone bipolar cell that possessed an ectopic axon terminal in S1. Adapted from Dumitrescu et al. 2009 (64). (B) Type-8 ON cone bipolar cells and an amacrine cell type monostratifying in S5 are presynaptic to M2-type ipRGCs in mice. Adapted from Viney et al. 2007 (69). (C) In rabbits, calbindin-positive ON cone bipolar cells are presynaptic to ipRGC dendrites in S1. *Red*, calbindin antibody staining. *Yellow*, RIBEYE antibody staining of synaptic ribbons. Adapted from Hoshi et al. 2009 (65). (D) In macaques, DB6 ON cone bipolar cells contact ipRGCs. *Blue*: CD15 antibody staining of a DB6 cell. *Red*: melanopsin antibody staining. Adapted from Grünert et al. 2011 (66).

stratifying type stratifies in S1 whereas the inner-stratifying type stratifies in S5, and so they could be homologous to the M1 and M2 types found in rodents (30, 66, 99-101). The dendritic fields of the outer-

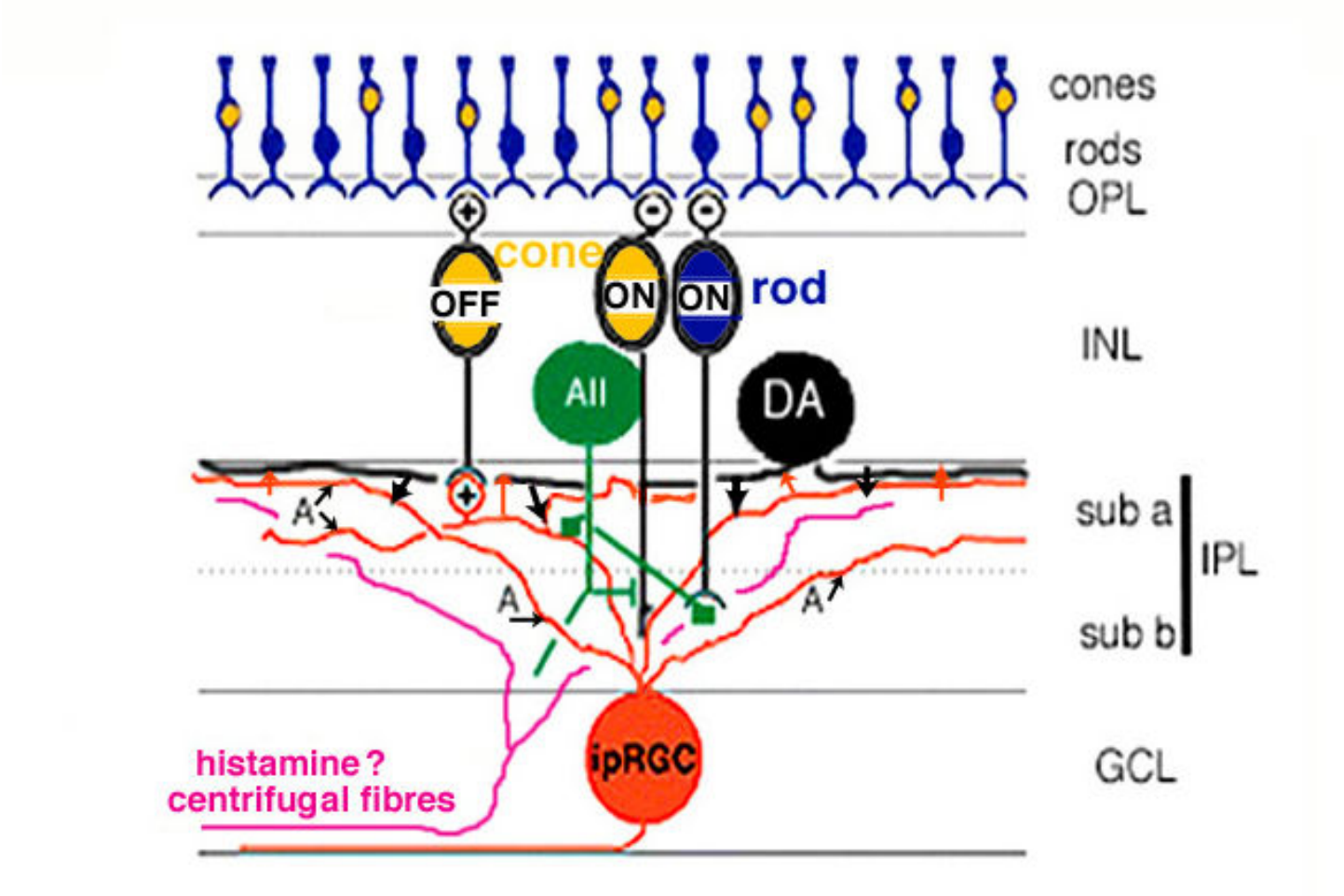

Figure 11. Presumptive synaptic connection scheme for M1-type, SCN-projecting ipRGCs. OPL, outer plexiform layer; INL, inner nuclear layer; IPL, inner plexiform layer; GCL, ganglion cell layer; OFF, OFF cone bipolar cell (yellow); ON, ON rod (blue) and ON cone bipolar cell (yellow); A, amacrine cell input; ipRGC, intrinsically photosensitive retinal ganglion cell (orange); AII, rod amacrine cell (green); DA, dopaminergic amacrine cell (black); centrifugal fibers (pink) enter the retina and have influence on dopaminergic amacrine cells, which in turn modulate ipRGCs by releasing dopamine.

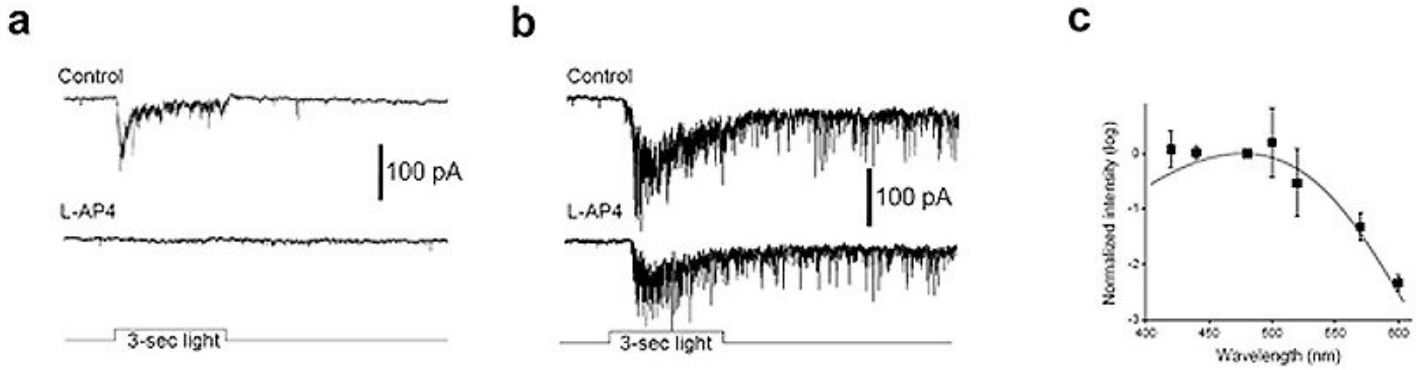

Figure 12. Physiological evidence for a melanopsin-based input to mouse dopaminergic amacrine cells (DA cells). Whole-cell voltage-clamp recordings from a transient DA cell (A) and a sustained DA cell (B). Notice how the application of L-AP4, an agent used to block rod/cone-driven photoresponses from ON bipolar cells, completely eliminated the light response of the transient DA cell (A), whereas it had little effect on the sustained DA cell (B). Panel C shows a fitted plot of L-AP4-resistant responses to varying wavelengths of light, showing a peak near 480 nm, the λ_{max} for stimulating melanopsin. Adapted from Zhang et al. 2008 (77).

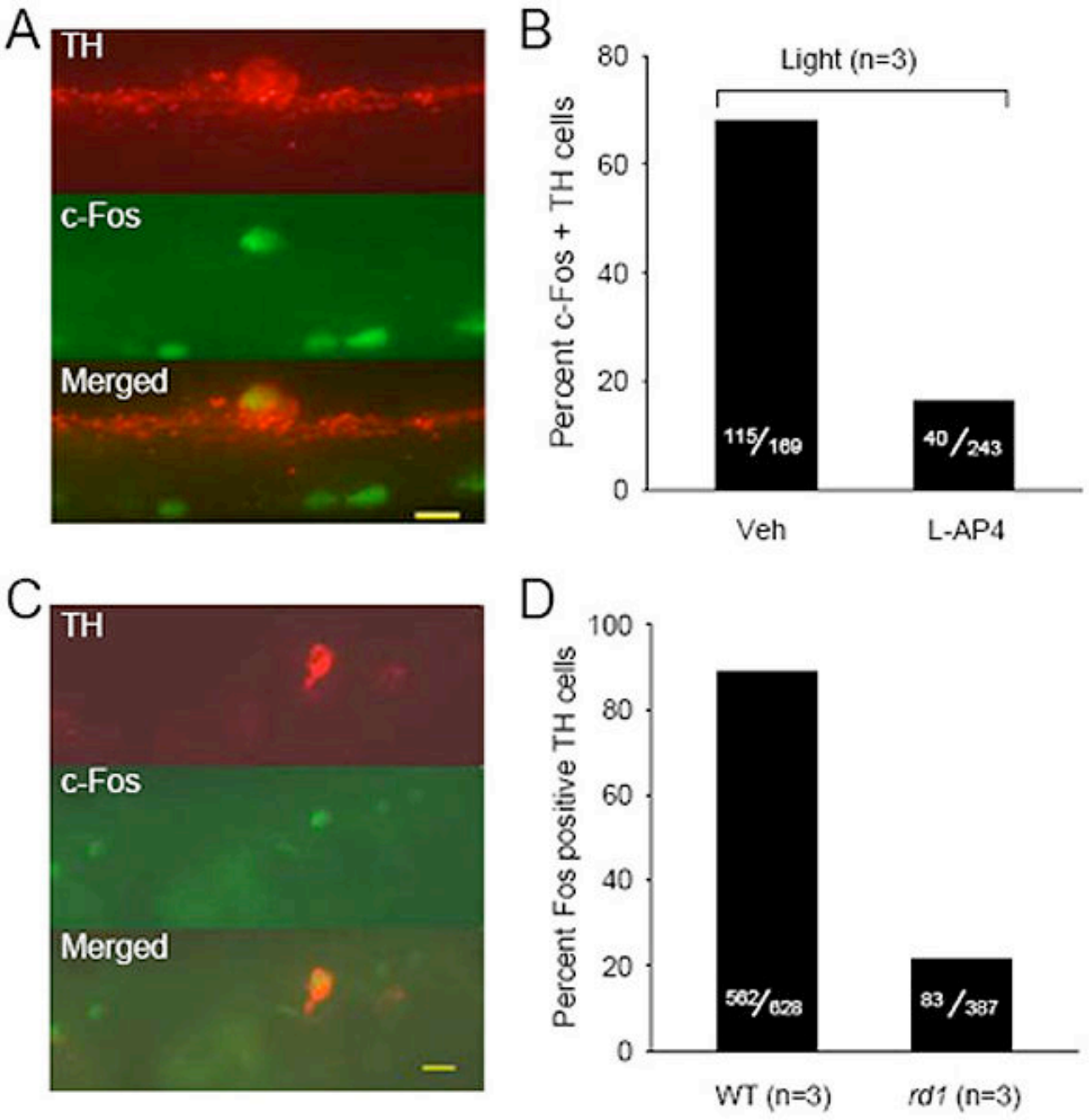

Figure 13. Light-induced cFos staining in retinas with rod/cone input blocked pharmacologically, and in retinas with no rods and virtually no cones. (A, B) Mouse retinas injected with L-AP4 or just the vehicle. A: Example staining illustrating that even with rod/cone input blocked using L-AP4, some dopaminergic amacrine cells (DA cells) showed light-driven expression of the immediate early gene cFos, an indicator of neural activity. Red: tyrosine hydrolase staining of DA cells. Green: cFos staining. B: Summary results for all DA cells examined. The vehicle-injected retinas showed ~70% of DA cells were activated by light, but with the drug L-AP4 injected, roughly 20% of the DA cells were cFos-positive, indicating only a small number of DA cells are potentially contacted by ipRGCs. (C, D) Results from uninjected wild-type and retinal degenerate (rd1) mice. C: Example staining in rd1 retinas. D: Wild-type (WT) animals had roughly 90% of DA cells with light-evoked cFos staining, whereas in rd1 mice roughly 20% of DA cells stained for cFos, matching very well with the L-AP4 experiment (panel B). Adapted from Zhang et al. 2008 (77).

stratifying cells tile the retina with little overlap, but they overlap substantially with the dendritic fields of the inner-stratifying cells, suggesting they constitute two distinct cell types (99). The receptive fields of both outer- and inner-stratifying primate ipRGCs consist only of an ON-center region, and both cell types appear to

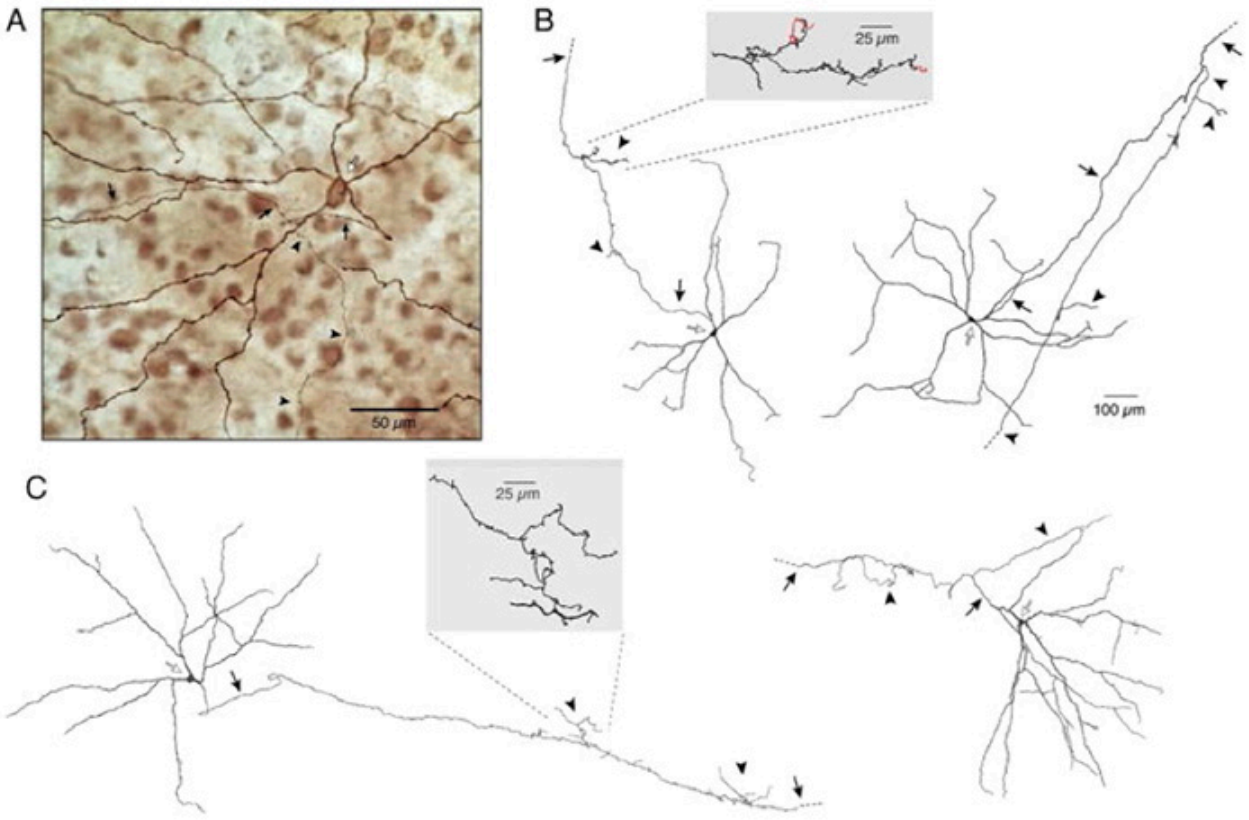

Figure 14. Primate ipRGCs possess axon collaterals. (A) An outer-stratifying melanopsin-positive cell from a macaque. The axon (*black arrows*) extends thin collaterals (*arrowheads*). (B) Tracings of two inner-stratifying macaque ipRGC. *Arrows*, axons. *Arrowheads*, axon collaterals. (C) Tracings of two inner-stratifying human ipRGCs. *Arrows*, axons. *Arrowheads*, axon collaterals. Adapted from Joo et al. 2013 (80).

generate remarkably similar rod-driven, cone-driven and melanopsin-mediated light responses (Figure 21) (30). Moreover, both types project to the lateral geniculate nucleus and olivary pretectal nucleus (see "Central Projections" below for further information) (30, 102). Thus, functional differences between the outer- and inner-stratifying primate ipRGCs remain elusive, although there is anatomical evidence that they receive different synaptic inputs (99, 101).

8. Central Projections

Using a transgenic mouse line whose ipRGCs express the marker enzyme β-galactosidase, Samer Hattar et al. visualized the axons of M1-type ipRGCs and characterized their projections throughout the brain. As expected for cells that regulate non-image-forming visual behaviors, Hattar and colleagues found M1-type ipRGCs sent dense projections to the SCN, the intergeniculate leaflet (IGL), and the olivary pretectal nucleus (OPN) (Figure 22A–C) (103). The SCN and IGL are parts of the circadian system, while the OPN mediates the pupillary light reflex. In addition to these expected sites, the same study discovered a number of other central targets. Within the hypothalamus, M1 cells sent axonal fibers to the ventral portion of the subparaventricular zone, a region controlling the autonomic nervous system. Rostrolateral to the SCN, a number of scattered fibers reach the lateral and ventrolateral preoptic areas, which influence release of reproductive hormones from the pituitary

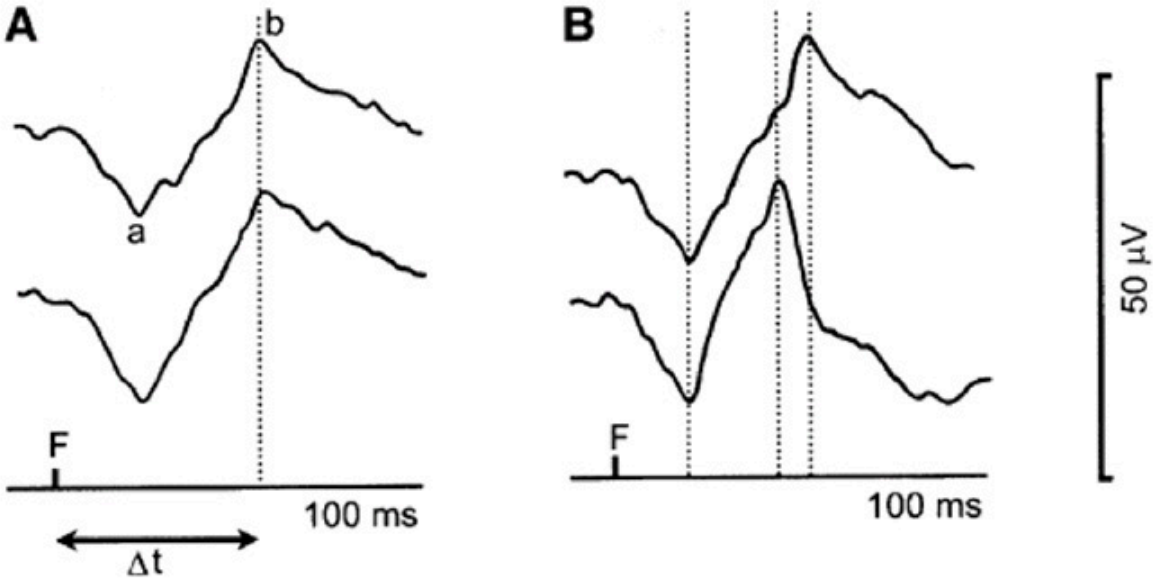

Figure 15. Electroretinograms recorded from a human subject. Each sweep lasted 100 ms, with a flash presented at "F". "a" denotes the a-wave, which arises from the hyperpolarizing light response of photoreceptors; "b" denotes the b-wave, which reflects the depolarizing light response of ON bipolar cells. (A) The upper recording was made at 9 PM, after which the subject was kept in darkness until performing the lower recording at 3 AM. The timings of the a- and b-waves were unchanged. (B) After recording the upper trace at 9 PM, a 15-min 471-nm light was presented to the subject at 11 PM and the bottom trace recorded at 3 AM. Notice that the 15-min light accelerated the b-wave. Adapted from Hankins & Lucas 2002 (85).

(103). The brain targets identified in this study are summarized in Figure 22D. These central projections suggest that M1 cells regulate a diverse array of non-image forming visual functions.

More recently, using a more sensitive Cre-based melanopsin reporter mouse line to label all five ipRGC types, Hattar and colleagues detected pronounced ipRGC projection to two additional visual nuclei: the dorsal division of the lateral geniculate nucleus (LGN), which is the primary thalamic relay site of retinal input to the visual cortex, and the superior colliculus (SC), a sensorimotor nucleus that detects novel visual stimuli (Figure 22E, F). Retrograde and anterograde labeling has shown that primate ipRGCs also project to both the LGN and SC (30, 100). These findings suggest that in addition to their well-known role in regulating subconscious visual reflexes, ipRGCs may contribute to conscious visual perception, a possibility that has received strong support from electrophysiological and behavioral studies (see "Behavioral aspects of ipRGC function" below).

9. Adaptation, neuromodulation, and circadian control

IpRGC photosensitivity displays various forms of plasticity. The gain of melanopsin phototransduction is influenced by background light level and prior lighting history. IpRGCs' light responses are also modulated by neuromodulators released endogenously within the retina. Moreover, these neurons' photoresponse amplitude depends on the time of day, suggesting it is under circadian control. All three aspects of ipRGC plasticity are considered in this section.

The image-forming visual system can operate over a wide spectrum of ambient light intensities covering more than ten orders of magnitude. While much of this range is due to the existence of two separate photoreceptor

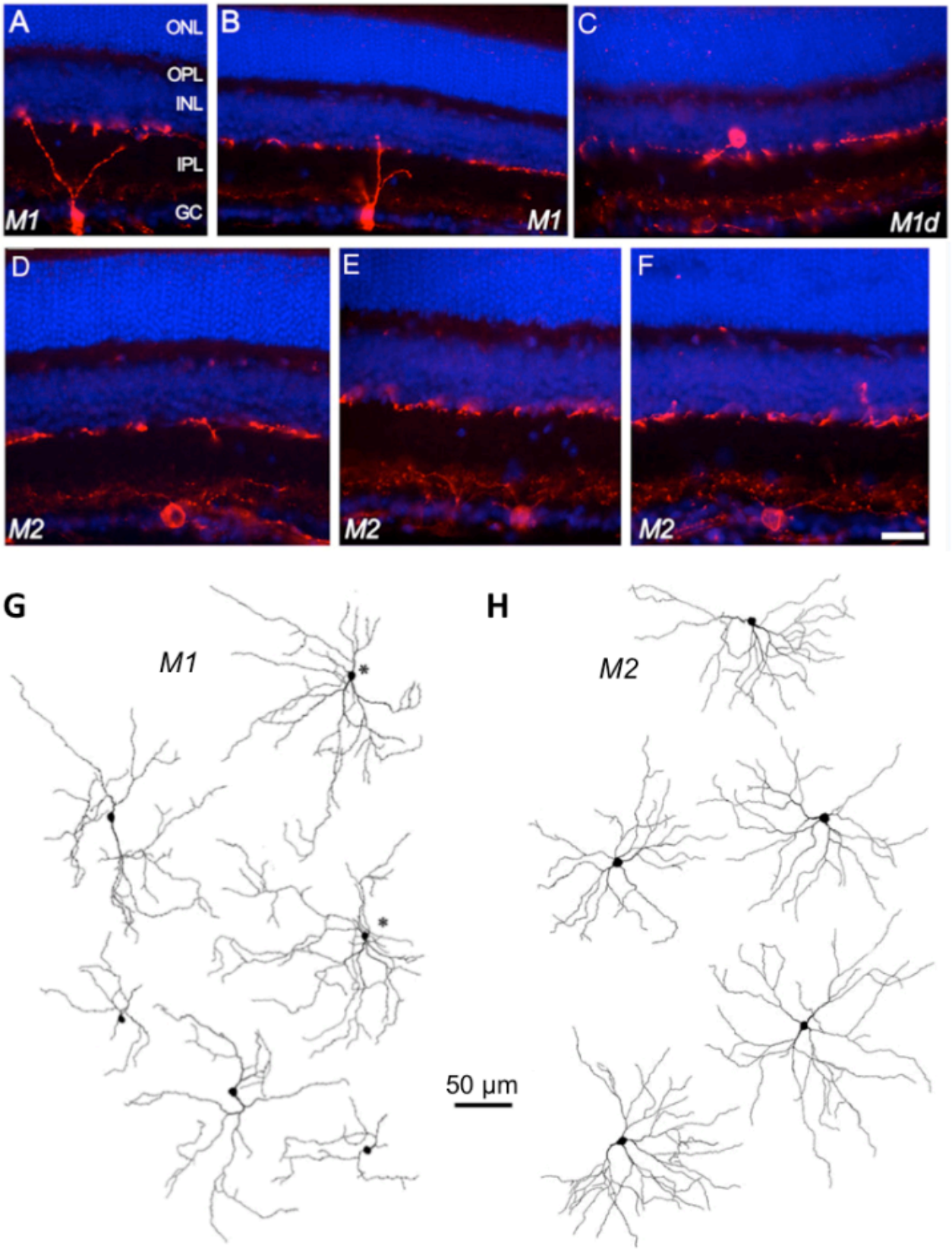

Figure 16. Morphologies of M1-type and M2-type mouse ipRGCs. (A-F). The morphologies of M1 and M2 cells as seen in vertical sections of immunostained (melanopsin, red; DAPI, blue) mouse retinas. Notice the different stratification levels of their dendrites. (G & H) Drawings of immunostained melanopsin ganglion cells in mouse retinal wholemount. G: Tracings of M1 cells. The cells marked with asterisks had somas displaced to the inner nuclear layer. H: Tracings of M2 cells. Scale bar: 500 µm. Adapted From Berson et al., 2010 (154).

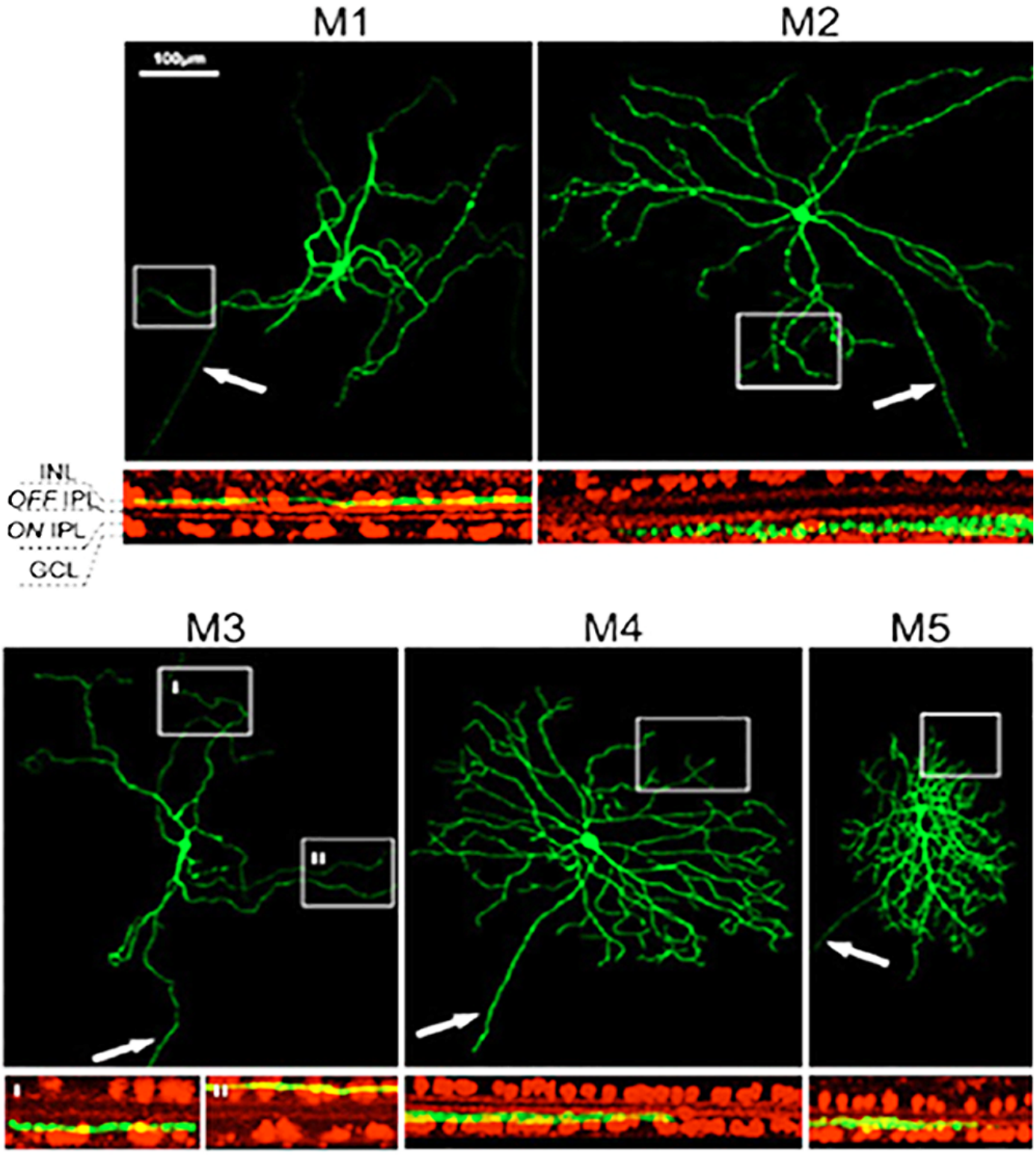

Figure 17. Morphologies of the five types of rat ipRGCs. *Top row*: z-projected confocal images showing intracellular dye fills of the five ipRGC types. Arrows denote axons. *Bottom row*: Rotated views of the regions outlined by rectangles in the above z-projections, showing the stratification patterns of distal dendrites. The choline acetyltransferase (ChAT) bands (*red*) serve as markers for the S2 and S4 sublayers of the IPL. Adapted from Reifler et al. 2015 (94).

systems (rods and cones) that operate over different light intensity ranges, some of the capacity is due to the ability of both rods and cones to change their sensitivity to light, a process called adaptation (104). When

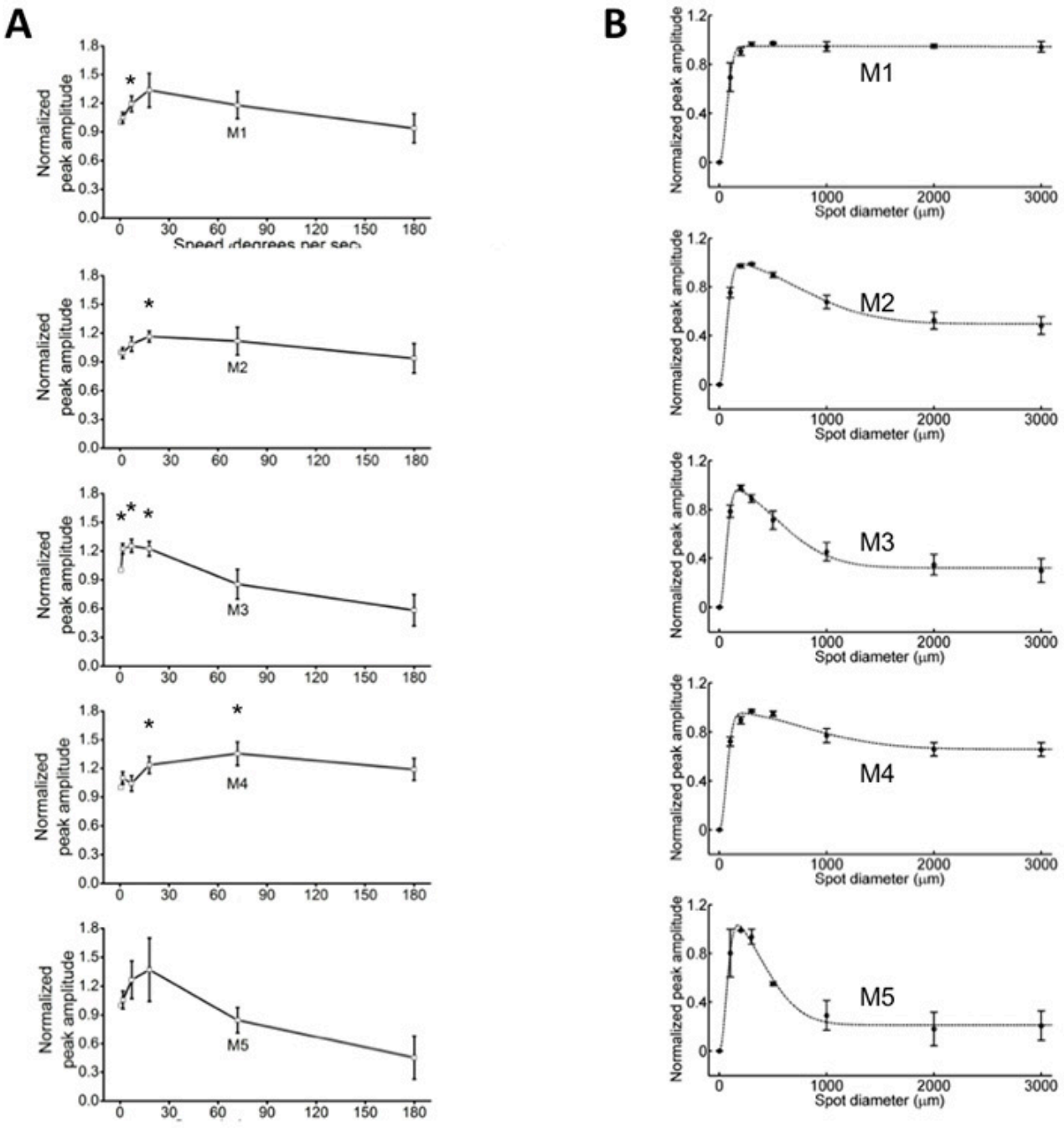

Figure 18. Mouse ipRGCs' responses to motion and receptive field organization. (A) A light bar was drifted over the receptive fields of mouse ipRGCs at different speeds and peak response amplitudes measured. The five cell types responded best to different speeds of motion. (B) Light spots of various diameters centered within the receptive field were presented to the five types of ipRGCs. For M1 cells, response amplitude increased as the spot diameter increased to 300 μm, beyond which no further amplitude change was observed, indicating the absence of an antagonistic surround in the receptive field. But for M2 – M5 cells, response amplitude declined as the spot diameter exceeded a certain value, indicative of a suppressive OFF surround. Adapted from Zhao et al. 2014 (58).

presented with a constant background light, rods and cones generate an initial peak response which relaxes during the steady illumination, indicating desensitization to the light over time. This desensitization allows the photoreceptors to increase their dynamic range, so they can respond to light intensities that would otherwise be saturating. This is termed "light adaptation". Conversely, when placed back into a dark environment, rods and

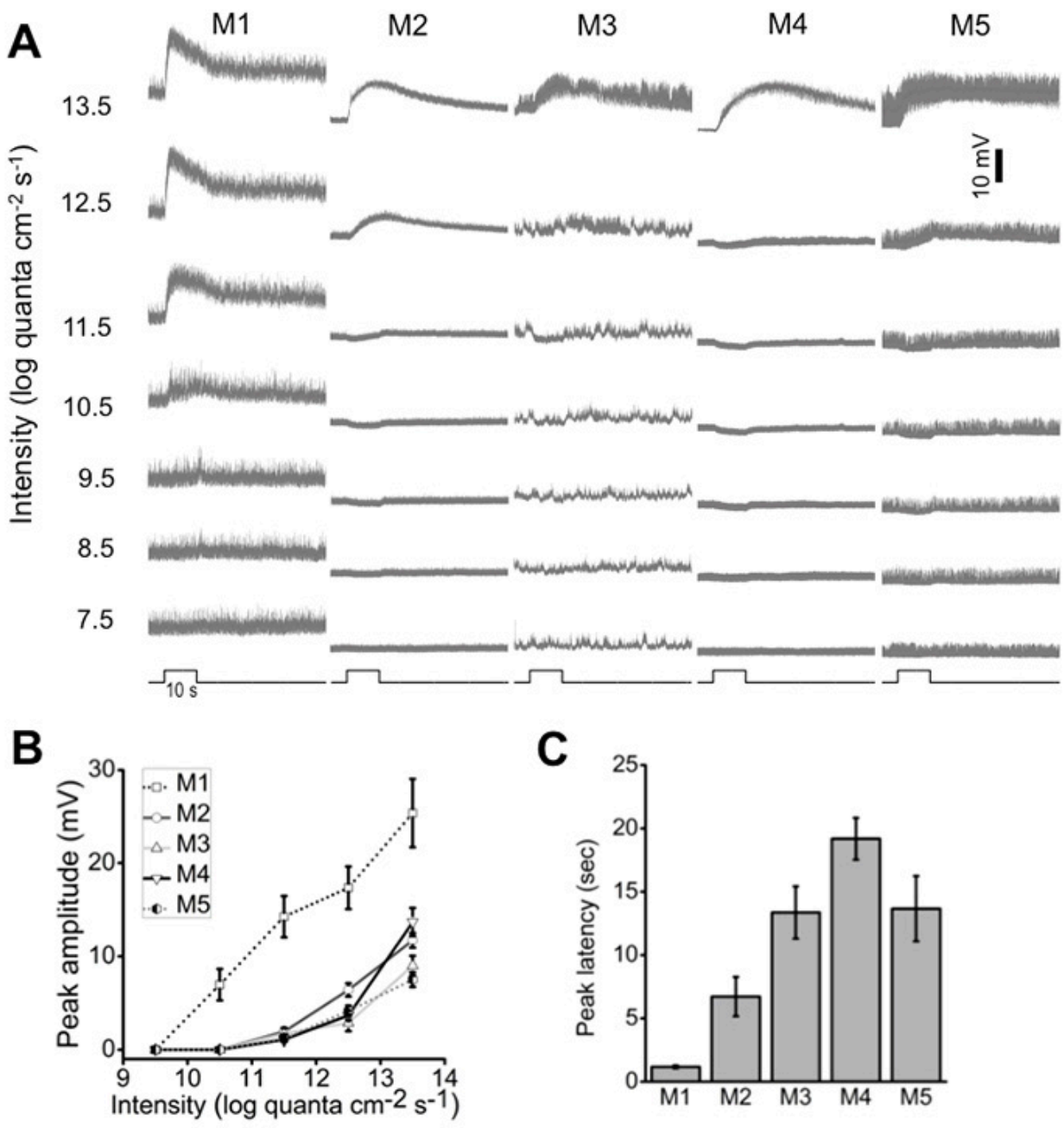

Figure 19. The five types of mouse ipRGCs generate diverse intrinsic photoresponses, recorded during rod/cone signaling blockade. (A) The averaged intrinsic light responses of the five cell types. The *gray* regions indicate S.E.M. (B) At all light intensities, M1 cells generate larger intrinsic light responses than the other four ipRGC types. (C) Peak latencies for the five cell types' responses to the 13.5 log quanta cm^{-2} s^{-1} stimulus (top recordings in panel A). Adapted from Zhao et al. 2014 (58).

cones gradually regain their sensitivity, a process called "dark adaptation". Both light and dark adaptation are a direct consequence of changes in the phototransduction cascade. While rods have a relatively limited ability to adapt to background illumination, saturating at high light levels, cones exhibit an almost infinite capacity to adapt to light levels (105, 106).

Due to their role in stable representations of absolute light levels, and their unusually tonic response properties, it was initially not clear whether ipRGCs' intrinsic photosensitivity would display similar adaptation

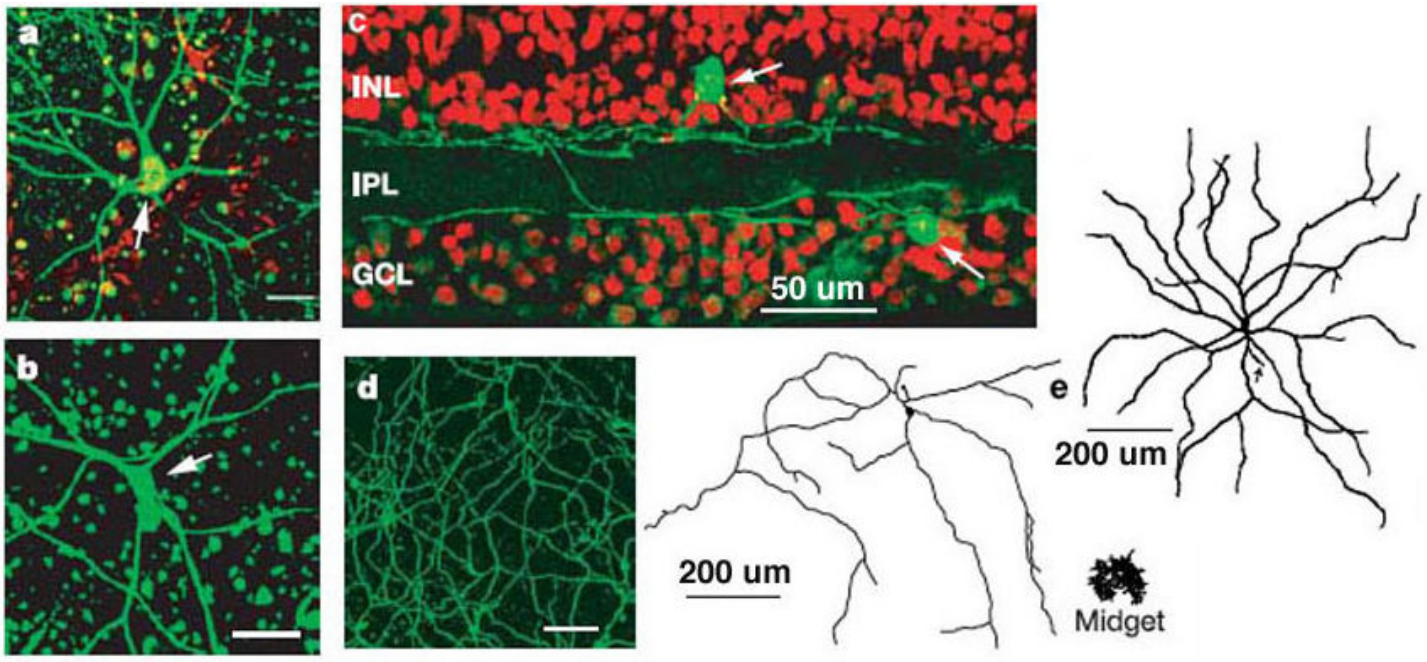

Figure 20. The morphology of melanopsin-expressing ganglion cells in monkey and human retinas. (A) A melanopsin-immunopositive human ganglion cell (green) as seen in peripheral retina wholemount. (B) A macaque melanopsin-immunopositive ganglion cell. Scale bars are both 50 μm. (C) Dendrites of melanopsin-immunopositive ganglion cells running in S1 and S5 of the inner plexiform layer. (D) Melanopsin-immunopositive ganglion cells in peripheral retina. Scale bar, 200 μm. (E) Drawings of two melanopsin-immunopositive ganglion cells in the peripheral retina (left and right cells). A peripheral midget ganglion cell (center) is drawn for size comparison in this part of peripheral retina. Adapted from Dacey et al., 2005 (30).

mechanisms as rods and cones. David Berson and colleagues found that when ipRGCs were exposed to a nearly saturating background light, these cells gradually became desensitized, while responses to a brighter pulse of light on top of the background light became larger over time (Figure 23).

Background light also accelerated photoresponse kinetics, so that the response to a light pulse peaked faster, and also decayed faster toward to the baseline after cessation of the pulse. These are hallmarks of light adaptation. Furthermore, when previously light-adapted ipRGCs were left in the dark for increasing periods of time, their responses to the same light stimulus intensity increased, a clear indication of dark adaptation (Figure 24) (107). Although Wong *et al.*2005 (107) found that ipRGCs light-adapt and dark-adapt much slower than do the classical photoreceptors, subsequent work revealed two important similarities between ipRGC and rod/cone adaptations: for all three photoreceptor classes, the flash sensitivity *vs.* background intensity relationship can be described by the Weber-Fechner law, and light adaptation is at least partly mediated by Ca^{2+} (108). These similarities are somewhat surprising, considering that ipRGCs use a phototransduction cascade that differs drastically from rods' and cones' (see the "Phototransduction" section above).

In addition to the above acute adaptational effects on ipRGCs' intrinsic photosensitivity, prolonged exposure to light or darkness significantly modulates melanopsin mRNA levels. In rats maintained in constant darkness, melanopsin expression rose progressively for at least 5 days, whereas those kept in constant light became nearly completely devoid of melanopsin mRNA after 7 days (109).

As mentioned earlier in the "Intraretinal synaptic output" section, dopamine is an important neuromodulator that has widespread influences on retinal function. Thus, not surprisingly, it has been shown to modulate ipRGCs. Dopamine and an agonist for D1-class dopamine receptors were found to acutely attenuate the intrinsic light responses of dissociated ipRGCs (71). Moreover, prolonged application of a D2-class dopamine agonist

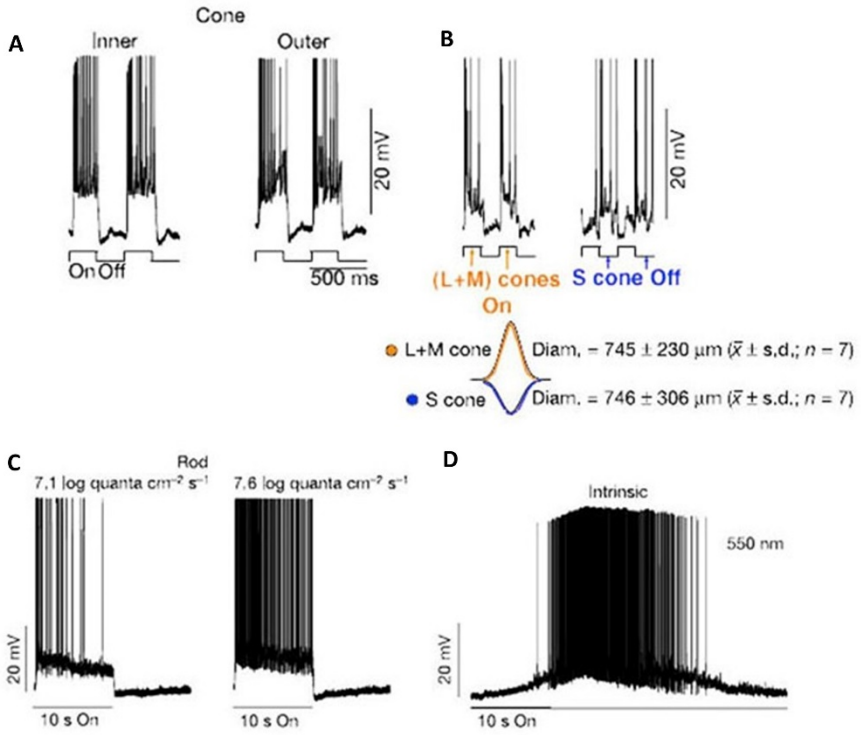

Figure 21. Intracellular recordings of primate ipRGCs' light responses. (A) Primate ipRGCs depolarize to a light that stimulates all cone types. (B) When stimuli selective for specific cone types are used, primate ipRGCs show ON responses to L+M cone input (*yellow*) but OFF responses to S-cone input (blue). The receptive field has coextensive "blue OFF" and "yellow ON" regions with no surround inhibition, as shown in the difference-of-Gaussians plot at the bottom. (C) Primate ipRGCs give a strong ON response to rod-selective light steps. Responses to two light intensities are shown. (D) After blocking rod/cone input with drugs, the slow, excitatory, sustained, intrinsic response to light is revealed. Adapted from Dacey et al., 2005 (30).

enhanced the mRNA levels of melanopsin and pituitary adenylyl cyclase-activating peptide (PACAP), a peptide present in ipRGCs (110). Adenosine, which appears to rise at night and during prolonged darkness (111), has been reported to shorten the duration of ipRGCs' intrinsic photoresponses, but unlike dopamine, it does not significantly reduce the peak amplitude of these responses (112). Melatonin, which is also released primarily at night, has been reported to modulate the rod/cone-driven light responses of M4-type rat ipRGCs (113). Finally, there is indirect evidence that cholecystokinin released from amacrine cells modulates retinal input to the central circadian clock (114).

IpRGCs are well known to mediate photoentrainment of the central circadian clock (see "Behavioral aspects of ipRGC function). But there is evidence that these RGCs are themselves under circadian regulation. In both light/dark ("LD") and constant dark ("DD") conditions, melanopsin mRNA levels in rat retinas display a daily rhythm. This rhythm disappeared in rod/cone degenerate rats, suggesting it is driven by the retinal circadian clock rather than the SCN's central circadian clock (115). Multielectrode-array extracellular recording indeed demonstrated a statistically significant increase in the amplitude of rat ipRGCs' intrinsic photoresponse early in the subjective night compared to all the other circadian times examined (116), although this increase was much smaller than the amplitude of the circadian rhythm in melanopsin mRNA expression (115). The synaptically driven light response of M4 ipRGCs also exhibits circadian variation (113).

10. Behavioral aspects of ipRGC function

Daily rhythms in mammalian physiology and behavior, collectively called circadian rhythms, are controlled by a tiny cluster of cells in the SCN of the hypothalamus. SCN neurons possess a transcription/translation-based

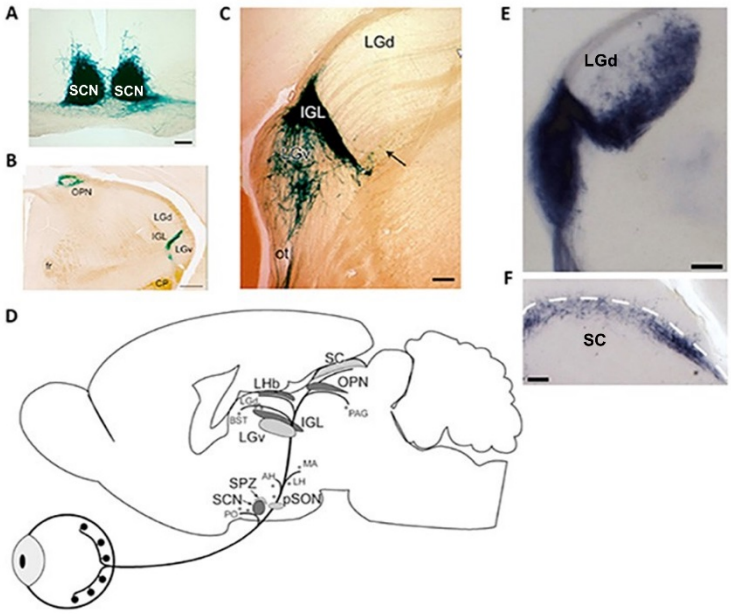

Figure 22. Axonal projections of mouse ipRGCs. (A-D) X-gal staining of axonal projections from M1 cells in tau-LacZ mice. A; M1 cells send a very dense projection to the suprachiasmatic nuclei (SCN) located in the hypothalamus, consistent with their known role in regulating photoentrainment of the central circadian clock, located in the SCN. B: Staining showing M1 projections to the intergeniculate leaflet (IGL) and the olivary pretectal nucleus (OPN). Cerebral peduncle (CP) and fasciculus retrofelxus (fr) are also shown. C: Close-up view of staining in the IGL, the ventral region of the lateral geniculate nucleus (LGv), and a few stained fibers in the dorsal lateral geniculate nucleus (LGd). The optic tract (ot) is also shown. D: Summary of the M1 ipRGC targets revealed in this study. AH, anterior hypothalamic nucleus; BST, bed nucleus of the stria terminalis; IGL, intergeniculate leaflet; LGd, lateral geniculate nucleus, dorsal division; LGv, lateral geniculate nucleus, ventral division; LH, lateral hypothalamus; LHb, lateral habenula; MA, medial amygdaloid nucleus; OPN, olivary pretectal nucleus; PAG, periaqueductal gray; PO, preoptic area; pSON, peri-supraoptic nucleus; SC, superior colliculus; SCN, suprachiasmatic nucleus; SPZ, subparaventricular zone. Adapted from Hattar et al. 2006 (103). (E & F) Axons of M1 – M5 ipRGCs revealed by alkaline phosphatase labeling in Opn4Cre/+; Z/AP mice, showing substantial projection to image-forming visual nuclei. E: Staining in the lateral geniculate nucleus (LGN). A comparison with panel C shows that the LGv and LGd are far more heavily innervated in this mouse line, presumably due to axons from one or more of the non-M1 ipRGC types. F: Staining in the superior colliculus (SC). Adapted from Ecker et al. 2010 (93).

molecular clock that allows them to autonomously regulate activity patterns in near 24-hour rhythms, which ultimately lead to daily changes in behaviors such as sleep/wake cycles and rhythms in core body temperature. However, the circadian clock is not tuned perfectly to 24 hours, and in order to adjust to changes in the animals' environmental light/dark phases, the SCN must be reset periodically so that circadian rhythms are synchronized (or "entrained") to the light/dark cycle. Light is by far the most potent circadian entrainment cue, and ipRGCs are the primary cells that carry this signal since eliminating these neurons abolished photoentrainment in mice (117-119). Melanopsin-knockout animals have relatively normal circadian rhythms, and do not display any overt dysfunction in their ability to entrain to light. However, light pulses induced significantly smaller phase shifts in these animals' circadian rhythms (Figure 25), revealing a crucial role for melanopsin signaling (20, 21). On the other hand, rods are essential for photoentrainment to dim light (120, 121), whereas cones are important for proper responses of the photoentrainment system to short-duration light pulses (122, 123).

The SCN signals through various neural circuits to coordinate circadian rhythms throughout the body. In one of these circuits, the SCN regulates secretion of the sleep-promoting hormone melatonin from the pineal gland into the bloodstream: SCN → paraventricular nucleus of the hypothalamus → intermediolateral nucleus of the spinal

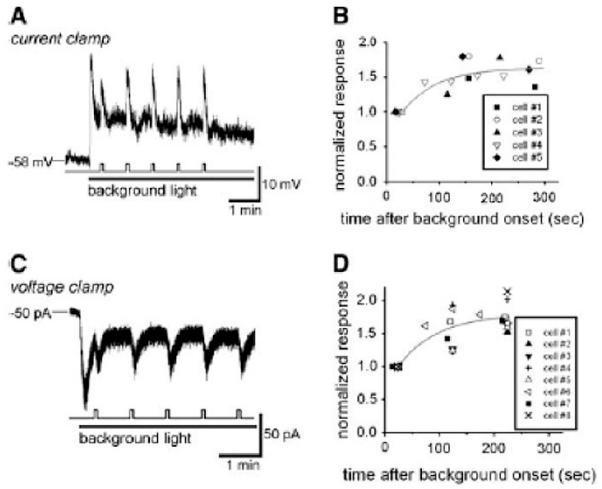

Figure 23. Evidence for light adaptation in ipRGCs. All recordings were made in the presence of rod/cone signaling blockers to isolate the intrinsic light response. (A) Current-clamp recording from a rat ipRGC with test pulses superimposed on an adapting background light. The cell decreased its sensitivity to the background light over time and was able to generate a larger response to the test pulse towards the end of the recording compared to the response to the same test pulse right after onset of the background light. (B) Summary data for current-clamp recordings from five ipRGCs subjected to the panel A experiment. (C) Voltage-clamp recording using same conditions as in panel A showing similar adaptation to the background light, demonstrating that voltage change is not required for light adaptation. (D) Summary data for voltage-clamp recordings from eight ipRGCs subjected to the panel C experiment. Adapted from Wong et al. 2005 (107).

cord → superior cervical ganglion → pineal gland (124). As a result of this SCN regulation, melatonin is released from the pineal only during subjective night. Upon exposure to sufficiently intense light, however, ipRGC input acutely suppresses this release of melatonin (125-127). Because ipRGCs remain photosensitive in the absence of rods and cones, rodless coneless mice and some blind patients continue to exhibit this non-image-forming visual response (Figure 26) (5, 128, 129).

IpRGCs are also responsible for light-evoked constriction of the pupil. Projections of ipRGC axons to the OPN, the retino-recipient site responsible for the pupillary light reflex, make them likely candidates for regulating this response. Indeed, melanopsin-knockout animals had diminished pupillary light reflexes at high irradiance levels (Figure 27A, B) (18). In addition, melanopsin-knockout mice without functional rods or cones were completely unable to constrict their pupils in response to light (Figure 27C) (19, 22). Furthermore, killing ipRGCs using various methods dramatically attenuated the pupillary light reflex (117, 119).

Numerous additional non-image-forming photic responses have been reported to be at least partly mediated by ipRGCs. These include acute suppression of the nocturnal locomotor activity of mice ("negative masking") (130), light-induction of sleep ("photosomnolence") (131-134) and maintenance of light-induced sleep in mice (135), modulation of cognitive performance in humans (136, 137), enhancement of alertness in humans (138), antidepressant effect in rats (139) and humans (140), light-induced exacerbation of headache in humans (141), photophobia and light avoidance in mice (142, 143), light-dependent relaxation of blood vessels (144), and stimulation of the secretion of follicle-stimulating hormone (FSH) in women (145).

In addition, there is emerging evidence that melanopsin contributes to visual perception, which is probably mediated by ipRGC projection to the LGN and/or SC (30, 58, 93, 95, 146). Some blind patients with severe outer retinal degeneration but relatively normal ipRGCs possess a rudimentary ability to detect the presence of intense blue light (129), and fully sighted humans as well as mice appear to depend partly on melanopsin for brightness discrimination (147). Mice lacking rod/cone photoreception (but with intact melanopsin photoreception) were able to distinguish a computer screen displaying black and white stripes from a uniform gray screen of an equal

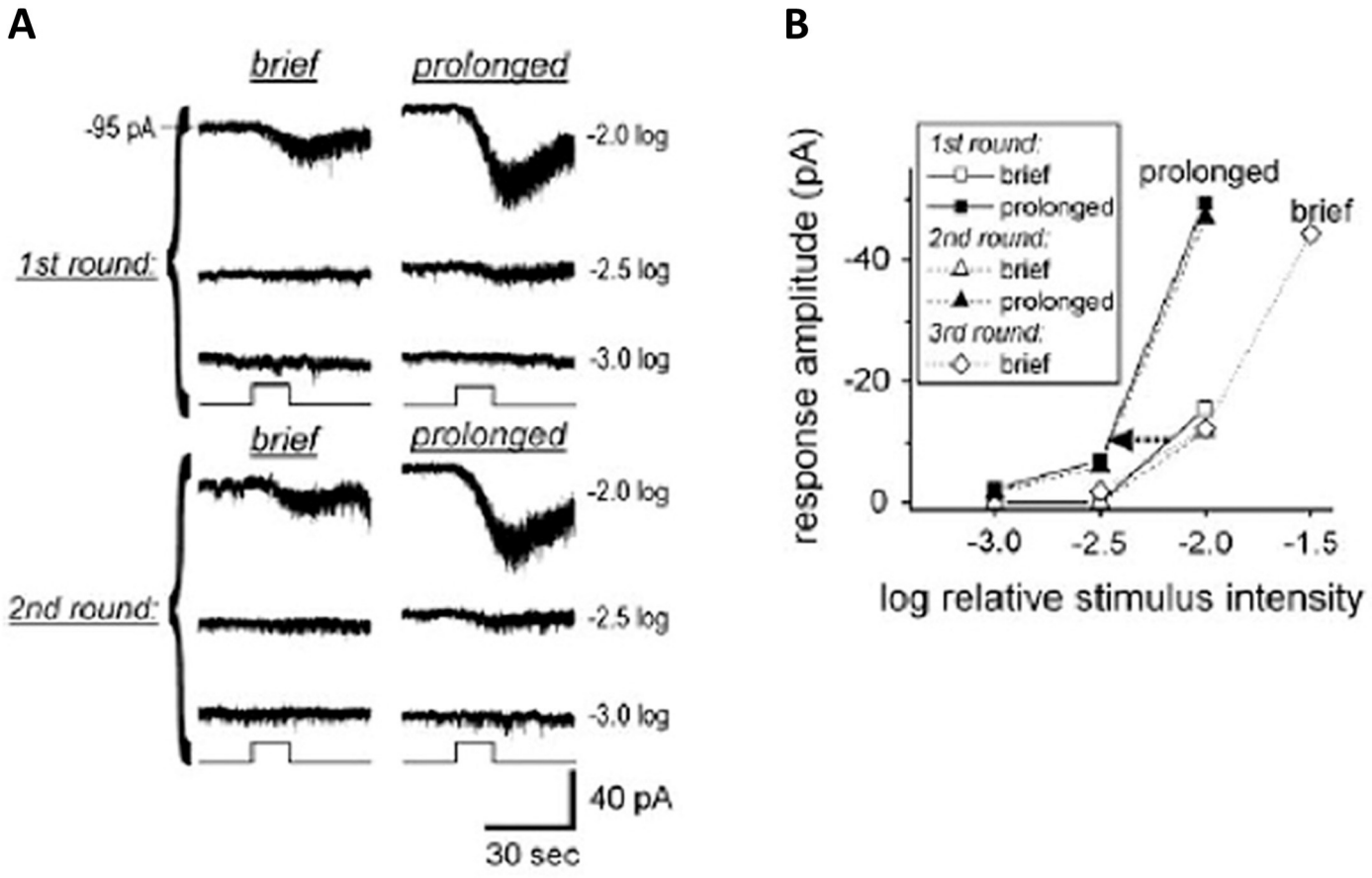

Figure 24. Evidence for dark adaptation in ipRGCs. All recordings were made in the presence of rod/cone signaling blockers. (A) Voltage-clamp recordings from a rat ipRGC responding to different light intensities after multiple rounds of brief and long periods of dark adaptation. Notice that for each light intensity, the cell consistently generated a larger response after longer periods of being in the dark. (B) Summary data from all cells tested. Adapted from Wong et al. 2005 (107).

mean intensity, suggesting melanopsin is sufficient for a certain degree of pattern vision (93). There is also preliminary psychophysical evidence that melanopsin directly contributes to color vision in humans, challenging the trichromatic theory (148). Most recently, mice lacking melanopsin were shown to have behavioral deficits in contrast sensitivity (96).

IpRGCs are likely to perform additional image-forming visual functions because under conditions preserving synaptic input, primate ipRGCs receive color-opponent (blue OFF, yellow ON) input from cones (Figure 21B), implicating a capacity for color discrimination (30). Furthermore, with the exception of M1 cells, all the other four types of mouse ipRGCs have receptive fields with antagonistic ON-center, OFF-surround regions (Figure 18B), suggesting these cells perform spatial analysis (58, 95). Finally, the five types of mouse ipRGCs are tuned to different speeds of motion (Figure 18A), raising the possibility that they contribute to motion analysis (58).

11. Roles in development

Melanopsin expression begins before birth (149) and ipRGCs become photosensitive earlier than either rods or cones (31, 150). One function for this early emergence of melanopsin-based photosensitivity is negative phototaxis, which causes mouse pups as young as P6 (postnatal day 6) to turn away from bright light (142). Melanopsin has also been shown to regulate the early development of retinal neurons, retinal blood vessels and retinogeniculate circuits. In wild-type mice reared under normal light/dark conditions, embryonic hyaloid vasculature regresses and the retinal vasculature starts to form during early postnatal days. But in melanopsin-

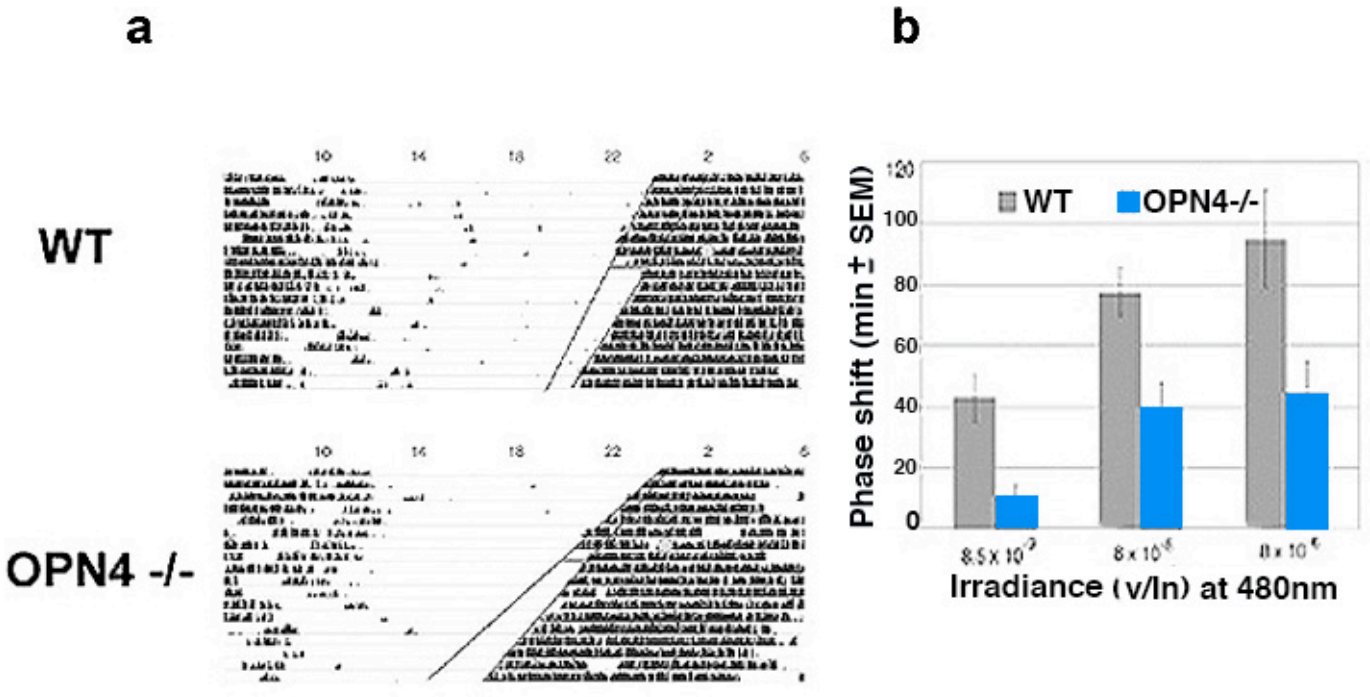

Figure 25. (A) The circadian rhythms of wild-type mice (WT) are more sensitive to phase-shifting light pulses than for melanopsin-knockout animals (OPN4 -/-). In this experiment, mice were kept in sound- and light-proof boxes with no outside indication of time of day. The tick marks indicate rotations of a running wheel present in the cages, and the animals are said to be awake and active during persistent times of wheel-running activity. Under these conditions the animals are "free-running", which means the rhythm of running and sleeping is determined solely by their internal circadian clock, and not outside cues. The magnitude of phase-shifting is measured as the shift in the rhythm of wheel running activity in the days following a pulse of light (gray circles) presented during the so-called "subjective" night phase (period of high wheel-running activity). A comparison of the gray horizontal bars in panel A, representing the degree of change in the wheel-running rhythm, demonstrates the wild-type animal's wheel-running rhythm was shifted further to the right (longer gray horizontal bar) by the light pulse than was the melanopsin-knockout animal's rhythm. B: A comparison of the degree of phase shift by the three light intensities for wild-type (grey) versus melanopsin-knockout animals (blue). Adapted from Panda et al. 2002 (20).

knockout mice or mice dark-reared from late gestation, the regression of the hyaloid vasculature was delayed and the retinal vasculature overgrew (Figure 28A, bottom row). Furthermore, the number of RGCs and amacrine cells increased (Figure 28B, blue). These observations suggest that during late gestation, melanopsin-mediated light detection activates a signaling pathway that suppresses the number of GCL neurons and regulates the timing of vasculature development (151).

As mentioned in the "Intraretinal synaptic output" section above, ipRGCs signal not only to the brain but also within the retina. Intraretinal signaling by ipRGCs is already apparent by P4. Besides participating in ion regulation (152), such early signaling also controls the temporal properties of retinal waves. Retinal waves are spontaneous bursts of action potentials that propagate across RGCs during early postnatal development, and they contribute to the refinement of retinogeniculate projections. In wild-type mice, light increases the duration of each burst of spikes, and afferent axons from ipsilateral and contralateral retinas terminate in largely distinct parts of the dorsal LGN. In melanopsin-knockout mice, however, this effect of light on burst duration was absent, and ipsilateral and contralateral retinal inputs to the dorsal LGN became less segregated (153).

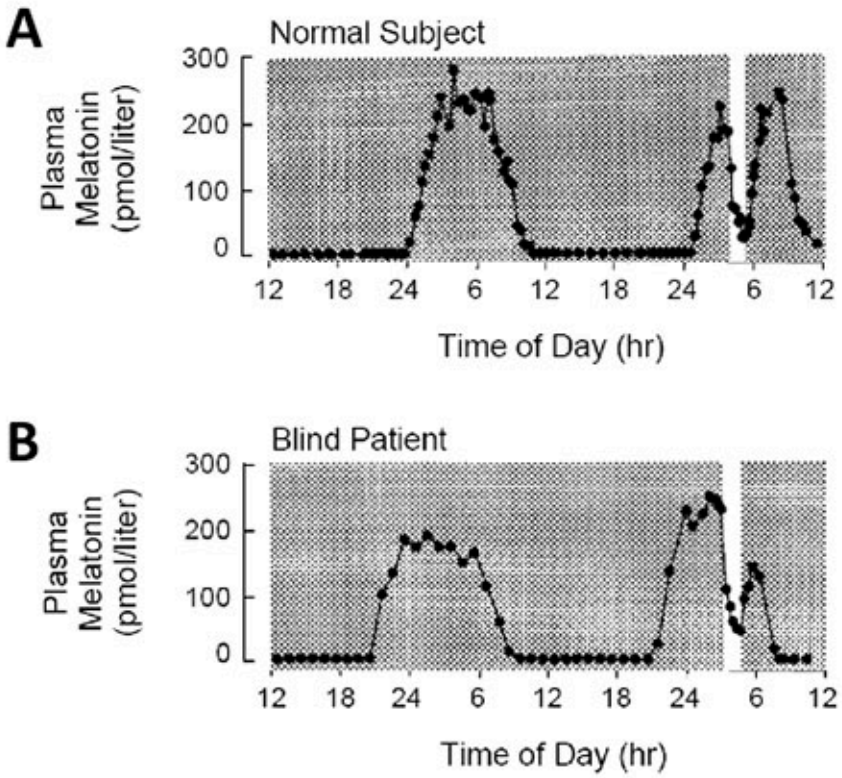

Figure 26. Photic suppression of nocturnal pineal melatonin secretion in humans. A normal, sighted subject (A) and a blind subject (B) were kept in a dim (< 15 lux) environment for 48 hours. A ~10,000 lux light pulse lasting 90 – 100 min (*white vertical bars*) was presented during the second subjective night. In both subjects, plasma melatonin levels were acutely suppressed by the light pulse. Adapted from Czeisler et al. 1995 (128).

12. Conclusions

IpRGCs are mammalian photoreceptors whose morphological and physiological characteristics seem well suited for their primary role as light detectors for non-image forming visual reflexes. Because they were discovered so recently, many mysteries remain, and an untold number of functions for this rare and special type of ganglion cell should not be overlooked. Their invertebrate-like phototransduction cascade makes them unique among known vertebrate photoreceptors, and provides a window into possible mechanisms of the evolution of the retina. In addition to their intrinsic melanopsin-driven photosensitivity, ipRGCs receive rod and cone synaptic input and thus may provide the brain with different information in series, separated by complex spatial and temporal dynamics. Although they drive a number of tonic behaviors, requiring accurate representation of ambient light levels of long periods of time, ipRGCs can adapt to both light and darkness. They have an ability to communicate back to the retina, possibly changing the functional properties of image-forming retinal circuitry. Emerging evidence suggests that ipRGCs can also directly contribute to conscious visual perception. Finally, these RGCs regulate the early development of the retina and the retinogeniculate pathway. As the years catch up with this relatively young field of ganglion-cell photoreceptors, it is beginning to look like many RGC types are photoreceptive and perform diverse functional roles.

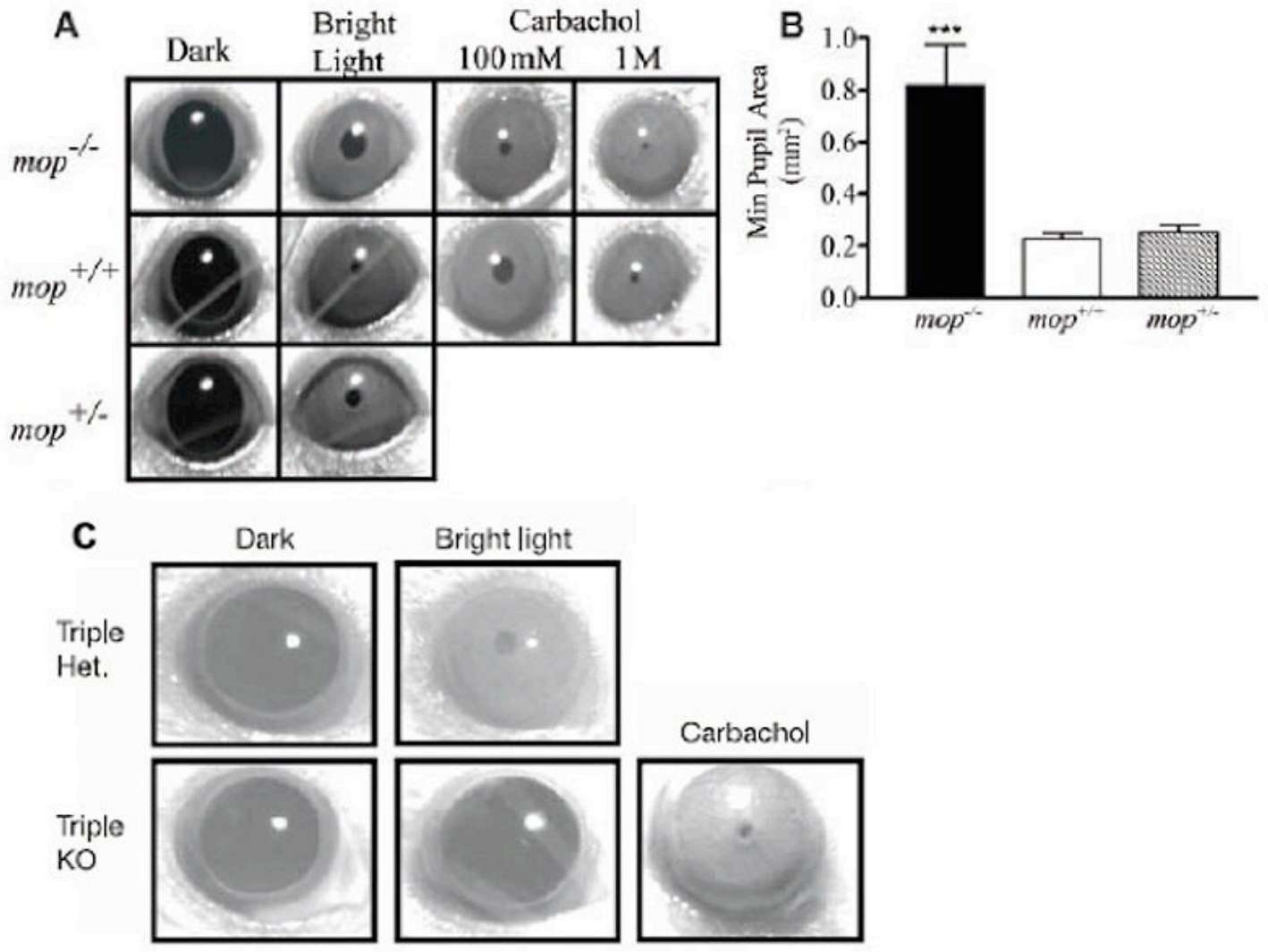

Figure 27. IpRGCs mediate light-evoked pupillary constriction. (A) Melanopsin-knockout mice (mop-/-) showed a defect in their ability to fully constrict their pupils in response to bright white light compared to wild-type animals (mop+/+), while the effect of the drug carbachol (which acts directly on the muscles that constrict the pupil) had the same effect in both melanopsin-knockout and wild-type animals suggesting the defect was due to ipRGC signaling. (B) Summary data on pupil constriction for all melanopsin-knockout and wild-type animals in response to bright light. Adapted from Lucas et al. 2003 (18). (C) Animals with no functioning rods or cones, and missing the melanopsin gene (Triple KO) completely lost the ability to constrict their pupils in response to light, indicating a requirement for melanopsin-based signaling in ipRGCs as well as signaling via synaptic input from rods and cones. Adapted from Hattar et al. 2003 (22).

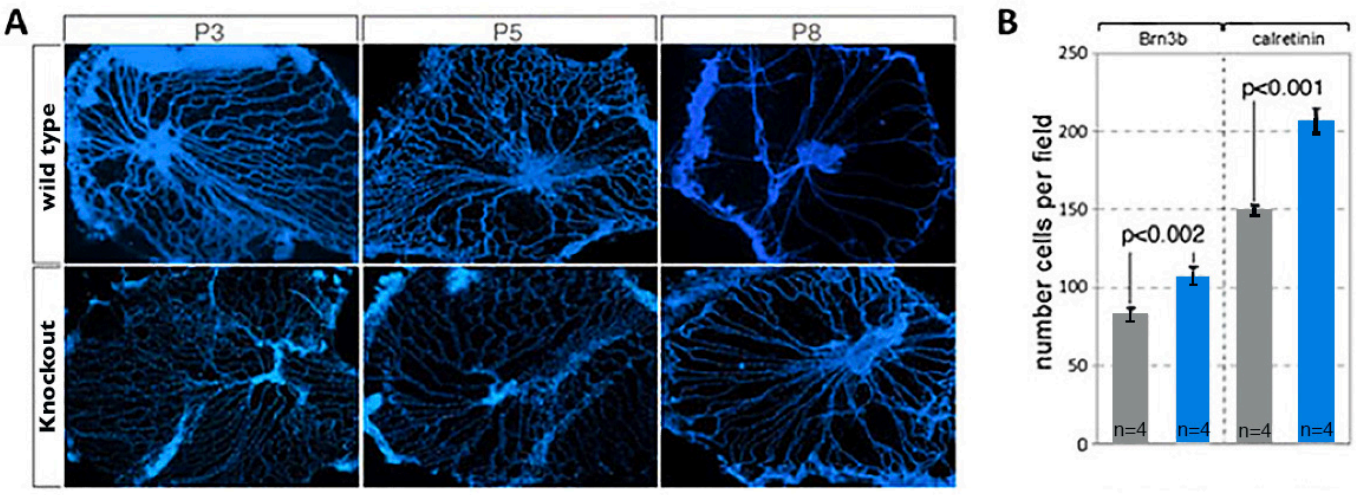

Figure 28. Eliminating melanopsin alters the development of hyaloid blood vessels and retinal neurons. (*A*) Hyaloid vessels persist at P8 in melanopsin-knockout mice. *Top row*: Whole-mount retinas obtained from wild-type mice at P3, P5 and P8. *Bottom row*: Whole-mount retinas from melanopsin-knockout mice at P3, P5 and P8. (*B*) Quantification of Brn3b-positive RGCs and calretinin-positive amacrine cells in wild-type (grey) versus melanopsin-knockout mice (blue) Adapted from Rao et al. 2013 (151).

About the authors

Dr. Kwoon Wong grew up in Hong Kong, when it was still a British colony. His undergraduate major at the University of Texas at Austin was biochemistry, and as he started his PhD career at Harvard he was convinced that he wanted to study cancer biology. But an immensely satisfying rotation in Prof. John Dowling's lab lured Kwoon into the world of neurophysiology, and he has been studying the visual system ever since. For his PhD thesis, he studied glutamate receptors and transporters at the photoreceptor-bipolar cell synapse in fish retinas. Then, at the 2002 Society for Neuroscience conference, he saw Prof. David Berson's fascinating symposium presentation on melanopsin-expressing ganglion cells, a novel class of retinal photoreceptors involved in non-image-forming visual behaviors. Awestruck by this talk, Kwoon decided to do his postdoctoral work with Prof. Berson at Brown. During Kwoon's six years in the Berson lab, he investigated melanopsin ganglion cells' light responses and synaptic circuits. Since Jan 2010, he has been an Assistant Professor at the University of Michigan, where he has continued to study these exotic ganglion cells.

Dr. Dustin M. Graham was born and raised in Pleasanton, California and received his Ph.D. in Neuroscience from Brown University. He began his research career at Santa Clara University in the lab of Dr. David Tauck, studying neural pathways of learning and memory in the pond snail Lymnaea stagnalis. His interests turned to the retina while working with Dr. Ralph Nelson at the National Institutes of Health. There he helped develop a rapid labeling technique to delineate morphological subtypes of retinal neurons in zebrafish. As a graduate student, Dustin studied mammalian circadian rhythms and the newly discovered melanopsin ganglion cell activity in Dr. David Berson's lab. He focused on the phototransduction cascade in ipRGCs, and developed a dissociation and culturing procedure to identify and record light responses from isolated ipRGCs. Dustin has since completed research fellowships in the Department of Psychology, University of Virginia, and in the Department of Neurobiology & Behavior, Stony Brook University, NY. He is currently an editor in the Nature Publishing Group, New York, NY.

References

1. Keeler C.E., Sutcliffe E., Chaffee E.L. Normal and "Rodless" retinae of the house mouse with respect to the electromotive force generated through stimulation by light. Proc Natl Acad Sci U S A. 1928;14(6):477–84. PubMed PMID: 16577134.
2. Van Gelder R.N. Non-visual photoreception: sensing light without sight. Curr Biol. 2008;18(1):R38–9. PubMed PMID: 18177714.
3. Keeler C.E. Iris movements in blind mice. Am J Physiol. 1927;81:107–112.
4. Freedman M.S., Lucas R.J., Soni B., von Schantz M., Munoz M., David-Gray Z., Foster R. Regulation of mammalian circadian behavior by non-rod, non-cone, ocular photoreceptors. Science. 1999;284(5413):502–4. PubMed PMID: 10205061.
5. Lucas R.J., Freedman M.S., Munoz M., Garcia-Fernandez J.M., Foster R.G. Regulation of the mammalian pineal by non-rod, non-cone, ocular photoreceptors. Science. 1999;284(5413):505–7. PubMed PMID: 10205062.
6. Semo M.a., Coffey P., Gias C., Vugler A. Retrograde Melanopsin signaling increases with age in retinal degenerate mice lacking rods and the majority of cones. Investigative ophthalmology & visual science. 2016;57(1):115–125. PubMed PMID: 26780315.
7. Klein D.C., Weller J.L. Rapid light-induced decrease in pineal serotonin N-acetyltransferase activity. Science. 1972;177(4048):532–3. PubMed PMID: 5050487.
8. Provencio I., Jiang G., De Grip W.J., Hayes W.P., Rollag M.D. Melanopsin: An opsin in melanophores, brain, and eye. Proc Natl Acad Sci U S A. 1998;95(1):340–5. PubMed PMID: 9419377.

9. Provencio I., Rodriguez I.R., Jiang G., Hayes W.P., Moreira E.F., Rollag M.D. A novel human opsin in the inner retina. J Neurosci. 2000;20(2):600–5. PubMed PMID: 10632589.
10. Provencio I., Rollag M.D., Castrucci A.M. Photoreceptive net in the mammalian retina. This mesh of cells may explain how some blind mice can still tell day from night. Nature. 2002;415(6871):493. PubMed PMID: 11823848.
11. Gooley J.J., Lu J., Chou T.C., Scammell T.E., Saper C.B. Melanopsin in cells of origin of the retinohypothalamic tract. Nat Neurosci. 2001;4(12):1165. PubMed PMID: 11713469.
12. Hannibal J., Hindersson P., Knudsen S.M., Georg B., Fahrenkrug J. The photopigment melanopsin is exclusively present in pituitary adenylate cyclase-activating polypeptide-containing retinal ganglion cells of the retinohypothalamic tract. J Neurosci. 2002;22(1):RC191. PubMed PMID: 11756521.
13. Berson D.M., Dunn F.A., Takao M. Phototransduction by retinal ganglion cells that set the circadian clock. Science. 2002;295(5557):1070–3. PubMed PMID: 11834835.
14. Hattar S., Liao H.W., Takao M., Berson D.M., Yau K.W. Melanopsin-containing retinal ganglion cells: architecture, projections, and intrinsic photosensitivity. Science. 2002;295(5557):1065–70. PubMed PMID: 11834834.
15. Berson D.M. Phototransduction in ganglion-cell photoreceptors. Pflugers Arch. 2007;454(5):849–55. PubMed PMID: 17351786.
16. Kavakli I.H., Sancar A. Circadian photoreception in humans and mice. Mol Interv. 2002;2(8):484–92. PubMed PMID: 14993400.
17. Van Gelder R.N., Gibler T.M., Tu D., Embry K., Selby C.P., Thompson C.L., Sancar A. Pleiotropic effects of cryptochromes 1 and 2 on free-running and light-entrained murine circadian rhythms. J Neurogenet. 2002;16(3):181–203. PubMed PMID: 12696673.
18. Lucas R.J., Hattar S., Takao M., Berson D.M., Foster R.G., Yau K.W. Diminished pupillary light reflex at high irradiances in melanopsin-knockout mice. Science. 2003;299(5604):245–7. PubMed PMID: 12522249.
19. Panda S., Provencio I., Tu D.C., Pires S.S., Rollag M.D., Castrucci A.M., Pletcher M.T., Sato T.K., Wiltshire T., Andahazy M., Kay S.A., Van Gelder R.N., Hogenesch J.B. Melanopsin is required for non-image-forming photic responses in blind mice. Science. 2003;301(5632):525–7. PubMed PMID: 12829787.
20. Panda S., Sato T.K., Castrucci A.M., Rollag M.D., DeGrip W.J., Hogenesch J.B., Provencio I., Kay S.A. Melanopsin (Opn4) requirement for normal light-induced circadian phase shifting. Science. 2002;298(5601):2213–6. PubMed PMID: 12481141.
21. Ruby N.F., Brennan T.J., Xie X., Cao V., Franken P., Heller H.C., O'Hara B.F. Role of melanopsin in circadian responses to light. Science. 2002;298(5601):2211–3. PubMed PMID: 12481140.
22. Hattar S., Lucas R.J., Mrosovsky N., Thompson S., Douglas R.H., Hankins M.W., Lem J., Biel M., Hofmann F., Foster R.G., Yau K.W. Melanopsin and rod-cone photoreceptive systems account for all major accessory visual functions in mice. Nature. 2003;424(6944):76–81. PubMed PMID: 12808468.
23. Melyan Z., Tarttelin E.E., Bellingham J., Lucas R.J., Hankins M.W. Addition of human melanopsin renders mammalian cells photoresponsive. Nature. 2005;433(7027):741–5. PubMed PMID: 15674244.
24. Panda S., Nayak S.K., Campo B., Walker J.R., Hogenesch J.B., Jegla T. Illumination of the melanopsin signaling pathway. Science. 2005;307(5709):600–4. PubMed PMID: 15681390.
25. Qiu X., Kumbalasiri T., Carlson S.M., Wong K.Y., Krishna V., Provencio I., Berson D.M. Induction of photosensitivity by heterologous expression of melanopsin. Nature. 2005;433(7027):745–9. PubMed PMID: 15674243.
26. Do M.T., Kang S.H., Xue T., Zhong H., Liao H.W., Bergles D.E., Yau K.W. Photon capture and signalling by melanopsin retinal ganglion cells. Nature. 2009;457(7227):281–7. PubMed PMID: 19118382.
27. Wong K.Y., Dunn F.A., Graham D.M., Berson D.M. Synaptic influences on rat ganglion-cell photoreceptors. J Physiol. 2007;582(Pt 1):279–96. PubMed PMID: 17510182.
28. Wong K.Y. A retinal ganglion cell that can signal irradiance continuously for 10 hours. J Neurosci. 2012;32(33):11478–85. PubMed PMID: 22895730.
29. Barlow H.B., Levick W.R. Three factors limiting the reliable detection of light by retinal ganglion cells of the cat. J Physiol. 1969;200(1):1–24. PubMed PMID: 5761942.

30. Dacey D.M., Liao H.W., Peterson B.B., Robinson F.R., Smith V.C., Pokorny J., Yau K.W., Gamlin P.D. Melanopsin-expressing ganglion cells in primate retina signal colour and irradiance and project to the LGN. Nature. 2005;433(7027):749–54. PubMed PMID: 15716953.
31. Tu D.C., Zhang D., Demas J., Slutsky E.B., Provencio I., Holy T.E., Van Gelder R.N. Physiologic diversity and development of intrinsically photosensitive retinal ganglion cells. Neuron. 2005;48(6):987–99. PubMed PMID: 16364902.
32. Arendt D. Evolution of eyes and photoreceptor cell types. Int J Dev Biol. 2003;47(7-8):563–71. PubMed PMID: 14756332.
33. Fu Y., Yau K.W. Phototransduction in mouse rods and cones. Pflugers Arch. 2007;454(5):805–19. PubMed PMID: 17226052.
34. Hardie R.C. Phototransduction in Drosophila melanogaster. J Exp Biol. 2001;204(Pt 20):3403–9. PubMed PMID: 11707492.
35. Hardie R.C., Raghu P. Visual transduction in Drosophila. Nature. 2001;413(6852):186–93. PubMed PMID: 11557987.
36. Walker M.T., Brown R.L., Cronin T.W., Robinson P.R. Photochemistry of retinal chromophore in mouse melanopsin. Proc Natl Acad Sci U S A. 2008;105(26):8861–5. PubMed PMID: 18579788.
37. Fu Y., Zhong H., Wang M.H., Luo D.G., Liao H.W., Maeda H., Hattar S., Frishman L.J., Yau K.W. Intrinsically photosensitive retinal ganglion cells detect light with a vitamin A-based photopigment, melanopsin. Proc Natl Acad Sci U S A. 2005;102(29):10339–44. PubMed PMID: 16014418.
38. Graham D.M., Wong K.Y., Shapiro P., Frederick C., Pattabiraman K., Berson D.M. Melanopsin ganglion cells use a membrane-associated rhabdomeric phototransduction cascade. J Neurophysiol. 2008;99(5):2522–32. PubMed PMID: 18305089.
39. Chew K.S., Schmidt T.M., Rupp A.C., Kofuji P., Trimarchi J.M. Loss of gq/11 genes does not abolish melanopsin phototransduction. PLoS One. 2014;9(5):e98356. PubMed PMID: 24870805.
40. Xue T., Do M.T., Riccio A., Jiang Z., Hsieh J., Wang H.C., Merbs S.L., Welsbie D.S., Yoshioka T., Weissgerber P., Stolz S., Flockerzi V., Freichel M., Simon M.I., Clapham D.E., Yau K.W. Melanopsin signalling in mammalian iris and retina. Nature. 2011;479(7371):67–73. PubMed PMID: 22051675.
41. Chyb S., Raghu P., Hardie R.C. Polyunsaturated fatty acids activate the Drosophila light-sensitive channels TRP and TRPL. Nature. 1999;397(6716):255–9. PubMed PMID: 9930700.
42. Acharya J.K., Jalink K., Hardy R.W., Hartenstein V., Zuker C.S. InsP3 receptor is essential for growth and differentiation but not for vision in Drosophila. Neuron. 1997;18(6):881–7. PubMed PMID: 9208856.
43. Hardie R.C. Inhibition of phospholipase C activity in Drosophila photoreceptors by 1,2-bis(2-aminophenoxy)ethane N,N,N',N'-tetraacetic acid (BAPTA) and di-bromo BAPTA. Cell Calcium. 2005;38(6):547–56. PubMed PMID: 16140375.
44. Hardie R.C. TRP channels in Drosophila photoreceptors: the lipid connection. Cell Calcium. 2003;33(5-6):385–93. PubMed PMID: 12765684.
45. Suh B.C., Inoue T., Meyer T., Hille B. Rapid chemically induced changes of PtdIns(4,5)P2 gate KCNQ ion channels. Science. 2006;314(5804):1454–7. PubMed PMID: 16990515.
46. Hubbard R., Kropf A. The action of light on rhodopsin. Proceedings of the National Academy of Sciences. 1958;44(2):130–139. PubMed PMID: 16590155.
47. Wang J.S., Kefalov V.J. The cone-specific visual cycle. Prog Retin Eye Res. 2011;30(2):115–28. PubMed PMID: 21111842.
48. Mure L.S., Rieux C., Hattar S., Cooper H.M. Melanopsin-dependent nonvisual responses: evidence for photopigment bistability in vivo. J Biol Rhythms. 2007;22(5):411–24. PubMed PMID: 17876062.
49. Emanuel A.J., Do M.T. Melanopsin tristability for sustained and broadband phototransduction. Neuron. 2015;85(5):1043–55. PubMed PMID: 25741728.
50. Koyanagi M., Kubokawa K., Tsukamoto H., Shichida Y., Terakita A. Cephalochordate melanopsin: evolutionary linkage between invertebrate visual cells and vertebrate photosensitive retinal ganglion cells. Curr Biol. 2005;15(11):1065–9. PubMed PMID: 15936279.

51. Davies W.I., Zheng L., Hughes S., Tamai T.K., Turton M., Halford S., Foster R.G., Whitmore D., Hankins M.W. Functional diversity of melanopsins and their global expression in the teleost retina. Cell Mol Life Sci. 2011;68(24):4115–32. PubMed PMID: 21833582.
52. Matsuyama T., Yamashita T., Imamoto Y., Shichida Y. Photochemical properties of mammalian melanopsin. Biochemistry. 2012;51(27):5454–62. PubMed PMID: 22670683.
53. Doyle S.E., Castrucci A.M., McCall M., Provencio I., Menaker M. Nonvisual light responses in the Rpe65 knockout mouse: rod loss restores sensitivity to the melanopsin system. Proc Natl Acad Sci U S A. 2006;103(27):10432–7. PubMed PMID: 16788070.
54. Tu D.C., Owens L.A., Anderson L., Golczak M., Doyle S.E., McCall M., Menaker M., Palczewski K., Van Gelder R.N. Inner retinal photoreception independent of the visual retinoid cycle. Proc Natl Acad Sci U S A. 2006;103(27):10426–31. PubMed PMID: 16788071.
55. Zhao X., Pack W., Khan N.W., Wong K.Y. Prolonged inner retinal photoreception depends on the visual retinoid cycle. J Neurosci. 2016;36(15):4209–17. PubMed PMID: 27076420.
56. Belenky M.A., Smeraski C.A., Provencio I., Sollars P.J., Pickard G.E. Melanopsin retinal ganglion cells receive bipolar and amacrine cell synapses. J Comp Neurol. 2003;460(3):380–93. PubMed PMID: 12692856.
57. Perez-Leon J.A., Warren E.J., Allen C.N., Robinson D.W., Brown R.L. Synaptic inputs to retinal ganglion cells that set the circadian clock. Eur J Neurosci. 2006;24(4):1117–23. PubMed PMID: 16930437.
58. Zhao X., Stafford B.K., Godin A.L., King W.M., Wong K.Y. Photoresponse diversity among the five types of intrinsically photosensitive retinal ganglion cells. J Physiol. 2014;592(Pt 7):1619–36. PubMed PMID: 24396062.
59. Weng S., Estevez M.E., Berson D.M. Mouse ganglion-cell photoreceptors are driven by the most sensitive rod pathway and by both types of cones. PLoS One. 2013;8(6):e66480. PubMed PMID: 23762490.
60. Walch O.J., Zhang L.S., Reifler A.N., Dolikian M.E., Forger D.B., Wong K.Y. Characterizing and modeling the intrinsic light response of rat ganglion-cell photoreceptors. J Neurophysiol. 2015;114(5):2955–66. PubMed PMID: 26400257.
61. Schmidt T.M., Kofuji P. Differential cone pathway influence on intrinsically photosensitive retinal ganglion cell subtypes. J Neurosci. 2010;30(48):16262–71. PubMed PMID: 21123572.
62. Nelson R., Famiglietti E.V. Jr, Kolb H. Intracellular staining reveals different levels of stratification for on- and off-center ganglion cells in cat retina. J Neurophysiol. 1978;41(2):472–83. PubMed PMID: 650277.
63. Famiglietti E.V. Jr, Kolb H. Structural basis for ON-and OFF-center responses in retinal ganglion cells. Science. 1976;194(4261):193–5. PubMed PMID: 959847.
64. Dumitrescu O.N., Pucci F.G., Wong K.Y., Berson D.M. Ectopic retinal ON bipolar cell synapses in the OFF inner plexiform layer: contacts with dopaminergic amacrine cells and melanopsin ganglion cells. J Comp Neurol. 2009;517(2):226–44. PubMed PMID: 19731338.
65. Hoshi H., Liu W.L., Massey S.C., Mills S.L. ON inputs to the OFF layer: bipolar cells that break the stratification rules of the retina. J Neurosci. 2009;29(28):8875–83. PubMed PMID: 19605625.
66. Grunert U., Jusuf P.R., Lee S.C., Nguyen D.T. Bipolar input to melanopsin containing ganglion cells in primate retina. Vis Neurosci. 2011;28(1):39–50. PubMed PMID: 20950505.
67. Kolb H., Nelson R., Mariani A. Amacrine cells, bipolar cells and ganglion cells of the cat retina: a Golgi study. Vision Res. 1981;21(7):1081–1114. PubMed PMID: 7314489.
68. Masland R.H. Cell populations of the retina: the Proctor lecture. Invest Ophthalmol Vis Sci. 2011;52(7):4581–91. PubMed PMID: 21712414.
69. Viney T.J., Balint K., Hillier D., Siegert S., Boldogkoi Z., Enquist L.W., Meister M., Cepko C.L., Roska B. Local retinal circuits of melanopsin-containing ganglion cells identified by transsynaptic viral tracing. Curr Biol. 2007;17(11):981–8. PubMed PMID: 17524644.
70. Vugler A.A., Redgrave P., Semo M., Lawrence J., Greenwood J., Coffey P.J. Dopamine neurones form a discrete plexus with melanopsin cells in normal and degenerating retina. Exp Neurol. 2007;205(1):26–35. PubMed PMID: 17362933.

71. Van Hook M.J., Wong K.Y., Berson D.M. Dopaminergic modulation of ganglion-cell photoreceptors in rat. Eur J Neurosci. 2012;35(4):507–18. PubMed PMID: 22304466.
72. Gastinger M.J., O'Brien J.J., Larsen N.B., Marshak D.W. Histamine immunoreactive axons in the macaque retina. Invest Ophthalmol Vis Sci. 1999;40(2):487–95. PubMed PMID: 9950609.
73. Frazao R., McMahon D.G., Schunack W., Datta P., Heidelberger R., Marshak D.W. Histamine elevates free intracellular calcium in mouse retinal dopaminergic cells via H1-receptors. Invest Ophthalmol Vis Sci. 2011;52(6):3083–8. PubMed PMID: 21310914.
74. Sakai H.M., Naka K., Dowling J.E. Ganglion cell dendrites are presynaptic in catfish retina. Nature. 1986;319(6053):495–7. PubMed PMID: 2418365.
75. Dowling, J.E., The retina: an approachable part of the brain. revised edition ed. 2012, Cambridge, MA: The Belknap Press of Harvard University Press.
76. Zhang D.Q., Zhou T.R., McMahon D.G. Functional heterogeneity of retinal dopaminergic neurons underlying their multiple roles in vision. J Neurosci. 2007;27(3):692–9. PubMed PMID: 17234601.
77. Zhang D.Q., Wong K.Y., Sollars P.J., Berson D.M., Pickard G.E., McMahon D.G. Intraretinal signaling by ganglion cell photoreceptors to dopaminergic amacrine neurons. Proc Natl Acad Sci U S A. 2008;105(37):14181–6. PubMed PMID: 18779590.
78. Zhang D.Q., Belenky M.A., Sollars P.J., Pickard G.E., McMahon D.G. Melanopsin mediates retrograde visual signaling in the retina. PLoS One. 2012;7(8):e42647. PubMed PMID: 22880066.
79. Dkhissi-Benyahya O., Coutanson C., Knoblauch K., Lahouaoui H., Leviel V., Rey C., Bennis M., Cooper H.M. The absence of melanopsin alters retinal clock function and dopamine regulation by light. Cell Mol Life Sci. 2013;70(18):3435–47. PubMed PMID: 23604021.
80. Joo H.R., Peterson B.B., Dacey D.M., Hattar S., Chen S.K. Recurrent axon collaterals of intrinsically photosensitive retinal ganglion cells. Vis Neurosci. 2013;30(4):175–82. PubMed PMID: 23834959.
81. Prigge C.L., Yeh P.T., Liou N.F., Lee C.C., You S.F., Liu L.L., McNeill D.S., Chew K.S., Hattar S., Chen S.K., Zhang D.Q. M1 ipRGCs Influence Visual Function through Retrograde Signaling in the Retina. J Neurosci. 2016;36(27):7184–97. PubMed PMID: 27383593.
82. Morgan W.W., Kamp C.W. Dopaminergic amacrine neurons of rat retinas with photoreceptor degeneration continue to respond to light. Life Sci. 1980;26(19):1619–26. PubMed PMID: 7382733.
83. Vugler A.A., Redgrave P., Hewson-Stoate N.J., Greenwood J., Coffey P.J. Constant illumination causes spatially discrete dopamine depletion in the normal and degenerate retina. J Chem Neuroanat. 2007;33(1):9–22. PubMed PMID: 17223011.
84. Cameron M.A., Pozdeyev N., Vugler A.A., Cooper H., Iuvone P.M., Lucas R.J. Light regulation of retinal dopamine that is independent of melanopsin phototransduction. Eur J Neurosci. 2009;29(4):761–7. PubMed PMID: 19200071.
85. Hankins M.W., Lucas R.J. The primary visual pathway in humans is regulated according to long-term light exposure through the action of a nonclassical photopigment. Curr Biol. 2002;12(3):191–8. PubMed PMID: 11839270.
86. Barnard A.R., Hattar S., Hankins M.W., Lucas R.J. Melanopsin regulates visual processing in the mouse retina. Curr Biol. 2006;16(4):389–95. PubMed PMID: 16488873.
87. Sekaran S., Foster R.G., Lucas R.J., Hankins M.W. Calcium imaging reveals a network of intrinsically light-sensitive inner-retinal neurons. Curr Biol. 2003;13(15):1290–8. PubMed PMID: 12906788.
88. Bramley J.R., Wiles E.M., Sollars P.J., Pickard G.E. Carbenoxolone blocks the light-evoked rise in intracellular calcium in isolated melanopsin ganglion cell photoreceptors. PLoS One. 2011;6(7):e22721. PubMed PMID: 21829491.
89. Muller L.P., Do M.T., Yau K.W., He S., Baldridge W.H. Tracer coupling of intrinsically photosensitive retinal ganglion cells to amacrine cells in the mouse retina. J Comp Neurol. 2010;518(23):4813–24. PubMed PMID: 20963830.
90. Reifler A.N., Chervenak A.P., Dolikian M.E., Benenati B.A., Li B.Y., Wachter R.D., Lynch A.M., Demertzis Z.D., Meyers B.S., Abufarha F.S., Jaeckel E.R., Flannery M.P., Wong K.Y. All spiking, sustained ON

displaced amacrine cells receive gap-junction input from melanopsin ganglion cells. Curr Biol. 2015;25(21):2763–73. PubMed PMID: 26441349.
91. Baver S.B., Pickard G.E., Sollars P.J., Pickard G.E. Two types of melanopsin retinal ganglion cell differentially innervate the hypothalamic suprachiasmatic nucleus and the olivary pretectal nucleus. Eur J Neurosci. 2008;27(7):1763–70. PubMed PMID: 18371076.
92. Schmidt T.M., Taniguchi K., Kofuji P. Intrinsic and extrinsic light responses in melanopsin-expressing ganglion cells during mouse development. J Neurophysiol. 2008;100(1):371–84. PubMed PMID: 18480363.
93. Ecker J.L., Dumitrescu O.N., Wong K.Y., Alam N.M., Chen S.K., LeGates T., Renna J.M., Prusky G.T., Berson D.M., Hattar S. Melanopsin-expressing retinal ganglion-cell photoreceptors: cellular diversity and role in pattern vision. Neuron. 2010;67(1):49–60. PubMed PMID: 20624591.
94. Reifler A.N., Chervenak A.P., Dolikian M.E., Benenati B.A., Meyers B.S., Demertzis Z.D., Lynch A.M., Li B.Y., Wachter R.D., Abufarha F.S., Dulka E.A., Pack W., Zhao X., Wong K.Y. The rat retina has five types of ganglion-cell photoreceptors. Exp Eye Res. 2015;130:17–28. PubMed PMID: 25450063.
95. Estevez M.E., Fogerson P.M., Ilardi M.C., Borghuis B.G., Chan E., Weng S., Auferkorte O.N., Demb J.B., Berson D.M. Form and function of the M4 cell, an intrinsically photosensitive retinal ganglion cell type contributing to geniculocortical vision. J Neurosci. 2012;32(39):13608–20. PubMed PMID: 23015450.
96. Schmidt T.M., Alam N.M., Chen S., Kofuji P., Li W., Prusky G.T., Hattar S. A role for melanopsin in alpha retinal ganglion cells and contrast detection. Neuron. 2014;82(4):781–8. PubMed PMID: 24853938.
97. Schmidt T.M., Kofuji P. Functional and morphological differences among intrinsically photosensitive retinal ganglion cells. J Neurosci. 2009;29(2):476–82. PubMed PMID: 19144848.
98. Hu C., Hill D.D., Wong K.Y. Intrinsic physiological properties of the five types of mouse ganglion-cell photoreceptors. J Neurophysiol. 2013;109(7):1876–89. PubMed PMID: 23343892.
99. Jusuf P.R., Lee S.C., Hannibal J., Grunert U. Characterization and synaptic connectivity of melanopsin-containing ganglion cells in the primate retina. Eur J Neurosci. 2007;26(10):2906–21. PubMed PMID: 18001286.
100. Hannibal J., Kankipati L., Strang C.E., Peterson B.B., Dacey D., Gamlin P.D. Central projections of intrinsically photosensitive retinal ganglion cells in the macaque monkey. J Comp Neurol. 2014;522(10):2231–48. PubMed PMID: 24752373.
101. Neumann S., Haverkamp S., Auferkorte O.N. Intrinsically photosensitive ganglion cells of the primate retina express distinct combinations of inhibitory neurotransmitter receptors. Neuroscience. 2011;199:24–31. PubMed PMID: 22044923.
102. Dacey D.M., Peterson B.B., Robinson F.R., Gamlin P.D. Fireworks in the primate retina: in vitro photodynamics reveals diverse LGN-projecting ganglion cell types. Neuron. 2003;37(1):15–27. PubMed PMID: 12526769.
103. Hattar S., Kumar M., Park A., Tong P., Tung J., Yau K.W., Berson D.M. Central projections of melanopsin-expressing retinal ganglion cells in the mouse. J Comp Neurol. 2006;497(3):326–49. PubMed PMID: 16736474.
104. Perlman I., Normann R.A. Light adaptation and sensitivity controlling mechanisms in vertebrate photoreceptors. Prog Retin Eye Res. 1998;17(4):523–63. PubMed PMID: 9777649.
105. Fain G.L., Matthews H.R., Cornwall M.C., Koutalos Y. Adaptation in vertebrate photoreceptors. Physiol Rev. 2001;81(1):117–151. PubMed PMID: 11152756.
106. Knox B.E., Solessio E. Shedding light on cones. J Gen Physiol. 2006;127(4):355–8. PubMed PMID: 16567463.
107. Wong K.Y., Dunn F.A., Berson D.M. Photoreceptor adaptation in intrinsically photosensitive retinal ganglion cells. Neuron. 2005;48(6):1001–10. PubMed PMID: 16364903.
108. Do M.T., Yau K.W. Adaptation to steady light by intrinsically photosensitive retinal ganglion cells. Proc Natl Acad Sci U S A. 2013;110(18):7470–5. PubMed PMID: 23589882.
109. Hannibal J., Georg B., Hindersson P., Fahrenkrug J. Light and darkness regulate melanopsin in the retinal ganglion cells of the albino Wistar rat. J Mol Neurosci. 2005;27(2):147–55. PubMed PMID: 16186625.

110. Sakamoto K., Liu C., Kasamatsu M., Pozdeyev N.V., Iuvone P.M., Tosini G. Dopamine regulates melanopsin mRNA expression in intrinsically photosensitive retinal ganglion cells. The European journal of neuroscience. 2005;22(12):3129–36. PubMed PMID: 16367779.
111. Ribelayga C., Mangel S.C. A circadian clock and light/dark adaptation differentially regulate adenosine in the mammalian retina. J Neurosci. 2005;25(1):215–22. PubMed PMID: 15634784.
112. Sodhi P., Hartwick A.T. Adenosine modulates light responses of rat retinal ganglion cell photoreceptors througha cAMP-mediated pathway. J Physiol. 2014;592(Pt 19):4201–20. PubMed PMID: 25038240.
113. Pack W., Hill D.D., Wong K.Y. Melatonin modulates M4-type ganglion-cell photoreceptors. Neuroscience. 2015;303:178–88. PubMed PMID: 26141846.
114. Shimazoe T., Morita M., Ogiwara S., Kojiya T., Goto J., Kamakura M., Moriya T., Shinohara K., Takiguchi S., Kono A., Miyasaka K., Funakoshi A., Ikeda M. Cholecystokinin-A receptors regulate photic input pathways to the circadian clock. FASEB J. 2008;22(5):1479–90. PubMed PMID: 18073333.
115. Sakamoto K., Liu C., Tosini G. Classical photoreceptors regulate melanopsin mRNA levels in the rat retina. J Neurosci. 2004;24(43):9693–7. PubMed PMID: 15509757.
116. Weng S., Wong K.Y., Berson D.M. Circadian modulation of melanopsin-driven light response in rat ganglion-cell photoreceptors. J Biol Rhythms. 2009;24(5):391–402. PubMed PMID: 19755584.
117. Hatori M., Le H., Vollmers C., Keding S.R., Tanaka N., Buch T., Waisman A., Schmedt C., Jegla T., Panda S. Inducible ablation of melanopsin-expressing retinal ganglion cells reveals their central role in non-image forming visual responses. PLoS One. 2008;3(6):e2451. PubMed PMID: 18545654.
118. Goz D., Studholme K., Lappi D.A., Rollag M.D., Provencio I., Morin L.P. Targeted destruction of photosensitive retinal ganglion cells with a saporin conjugate alters the effects of light on mouse circadian rhythms. PLoS One. 2008;3(9):e3153. PubMed PMID: 18773079.
119. Guler A.D., Ecker J.L., Lall G.S., Haq S., Altimus C.M., Liao H.W., Barnard A.R., Cahill H., Badea T.C., Zhao H., Hankins M.W., Berson D.M., Lucas R.J., Yau K.W., Hattar S. Melanopsin cells are the principal conduits for rod-cone input to non-image-forming vision. Nature. 2008;453(7191):102–5. PubMed PMID: 18432195.
120. Altimus C.M., Guler A.D., Alam N.M., Arman A.C., Prusky G.T., Sampath A.P., Hattar S. Rod photoreceptors drive circadian photoentrainment across a wide range of light intensities. Nat Neurosci. 2010;13(9):1107–12. PubMed PMID: 20711184.
121. Lall G.S., Revell V.L., Momiji H., Al Enezi J., Altimus C.M., Guler A.D., Aguilar C., Cameron M.A., Allender S., Hankins M.W., Lucas R.J. Distinct contributions of rod, cone, and melanopsin photoreceptors to encoding irradiance. Neuron. 2010;66(3):417–28. PubMed PMID: 20471354.
122. Dkhissi-Benyahya O., Gronfier C., De Vanssay W., Flamant F., Cooper H.M. Modeling the role of mid-wavelength cones in circadian responses to light. Neuron. 2007;53(5):677–87. PubMed PMID: 17329208.
123. Dollet A., Albrecht U., Cooper H.M., Dkhissi-Benyahya O. Cones are required for normal temporal responses to light of phase shifts and clock gene expression. Chronobiol Int. 2010;27(4):768–81. PubMed PMID: 20560710.
124. Larsen P.J., Enquist L.W., Card J.P. Characterization of the multisynaptic neuronal control of the rat pineal gland using viral transneuronal tracing. Eur J Neurosci. 1998;10(1):128–45. PubMed PMID: 9753120.
125. Brainard G.C., Hanifin J.P., Greeson J.M., Byrne B., Glickman G., Gerner E., Rollag M.D. Action spectrum for melatonin regulation in humans: evidence for a novel circadian photoreceptor. J Neurosci. 2001;21(16):6405–12. PubMed PMID: 11487664.
126. Thapan K., Arendt J., Skene D.J. An action spectrum for melatonin suppression: evidence for a novel non-rod, non-cone photoreceptor system in humans. J Physiol. 2001;535(Pt 1):261–7. PubMed PMID: 11507175.
127. Vartanian G.V., Li B.Y., Chervenak A.P., Walch O.J., Pack W., Ala-Laurila P., Wong K.Y. Melatonin Suppression by Light in Humans Is More Sensitive Than Previously Reported. J Biol Rhythms. 2015;30(4):351–4. PubMed PMID: 26017927.

128. Czeisler C.A., Shanahan T.L., Klerman E.B., Martens H., Brotman D.J., Emens J.S., Klein T., Rizzo J.F. 3rd. Suppression of melatonin secretion in some blind patients by exposure to bright light. N Engl J Med. 1995;332(1):6–11. PubMed PMID: 7990870.
129. Zaidi F.H., Hull J.T., Peirson S.N., Wulff K., Aeschbach D., Gooley J.J., Brainard G.C., Gregory-Evans K., Rizzo J.F. 3rd, Czeisler C.A., Foster R.G., Moseley M.J., Lockley S.W. Short-wavelength light sensitivity of circadian, pupillary, and visual awareness in humans lacking an outer retina. Curr Biol. 2007;17(24):2122–8. PubMed PMID: 18082405.
130. Mrosovsky N., Hattar S. Impaired masking responses to light in melanopsin-knockout mice. Chronobiol Int. 2003;20(6):989–99. PubMed PMID: 14680139.
131. Lupi D., Oster H., Thompson S., Foster R.G. The acute light-induction of sleep is mediated by OPN4-based photoreception. Nat Neurosci. 2008;11(9):1068–73. PubMed PMID: 19160505.
132. Morin L.P., Studholme K.M. Separation of function for classical and ganglion cell photoreceptors with respect to circadian rhythm entrainment and induction of photosomnolence. Neuroscience. 2011;199:213–24. PubMed PMID: 21985934.
133. Altimus C.M., Guler A.D., Villa K.L., McNeill D.S., Legates T.A., Hattar S. Rods-cones and melanopsin detect light and dark to modulate sleep independent of image formation. Proc Natl Acad Sci U S A. 2008;105(50):19998–20003. PubMed PMID: 19060203.
134. Tsai J.W., Hannibal J., Hagiwara G., Colas D., Ruppert E., Ruby N.F., Heller H.C., Franken P., Bourgin P. Melanopsin as a sleep modulator: circadian gating of the direct effects of light on sleep and altered sleep homeostasis in Opn4(-/-) mice. PLoS Biol. 2009;7(6):e1000125. PubMed PMID: 19513122.
135. Muindi F., Zeitzer J.M., Colas D., Heller H.C. The acute effects of light on murine sleep during the dark phase: importance of melanopsin for maintenance of light-induced sleep. Eur J Neurosci. 2013;37(11):1727–36. PubMed PMID: 23510299.
136. Vandewalle G., Gais S., Schabus M., Balteau E., Carrier J., Darsaud A., Sterpenich V., Albouy G., Dijk D.J., Maquet P. Wavelength-dependent modulation of brain responses to a working memory task by daytime light exposure. Cereb Cortex. 2007;17(12):2788–95. PubMed PMID: 17404390.
137. Vandewalle G., Collignon O., Hull J.T., Daneault V., Albouy G., Lepore F., Phillips C., Doyon J., Czeisler C.A., Dumont M., Lockley S.W., Carrier J. Blue light stimulates cognitive brain activity in visually blind individuals. J Cogn Neurosci. 2013;25(12):2072–85. PubMed PMID: 23859643.
138. Viola A.U., James L.M., Schlangen L.J., Dijk D.J. Blue-enriched white light in the workplace improves self-reported alertness, performance and sleep quality. Scand J Work Environ Health. 2008;34(4):297–306. PubMed PMID: 18815716.
139. Iyilikci O., Aydin E., Canbeyli R. Blue but not red light stimulation in the dark has antidepressant effect in behavioral despair. Behav Brain Res. 2009;203(1):65–8. PubMed PMID: 19379775.
140. Meesters Y., Dekker V., Schlangen L.J., Bos E.H., Ruiter M.J. Low-intensity blue-enriched white light (750 lux) and standard bright light (10,000 lux) are equally effective in treating SAD. A randomized controlled study. BMC Psychiatry. 2011;11:17. PubMed PMID: 21276222.
141. Noseda R., Kainz V., Jakubowski M., Gooley J.J., Saper C.B., Digre K., Burstein R. A neural mechanism for exacerbation of headache by light. Nat Neurosci. 2010;13(2):239–45. PubMed PMID: 20062053.
142. Johnson J., Wu V., Donovan M., Majumdar S., Renteria R.C., Porco T., Van Gelder R.N., Copenhagen D.R. Melanopsin-dependent light avoidance in neonatal mice. Proc Natl Acad Sci U S A. 2010;107(40):17374–8. PubMed PMID: 20855606.
143. Matynia A., Parikh S., Chen B., Kim P., McNeill D.S., Nusinowitz S., Evans C., Gorin M.B. Intrinsically photosensitive retinal ganglion cells are the primary but not exclusive circuit for light aversion. Exp Eye Res. 2012;105:60–9. PubMed PMID: 23078956.
144. Sikka G., Hussmann G.P., Pandey D., Cao S., Hori D., Park J.T., Steppan J., Kim J.H., Barodka V., Myers A.C., Santhanam L., Nyhan D., Halushka M.K., Koehler R.C., Snyder S.H., Shimoda L.A., Berkowitz D.E. Melanopsin mediates light-dependent relaxation in blood vessels. Proc Natl Acad Sci U S A. 2014;111(50):17977–82. PubMed PMID: 25404319.

145. Danilenko K.V., Sergeeva O.Y. Immediate effect of blue-enhanced light on reproductive hormones in women. Neuro Endocrinol Lett. 2015;36(1) PubMed PMID: 25789589.
146. Brown T.M., Gias C., Hatori M., Keding S.R., Semo M., Coffey P.J., Gigg J., Piggins H.D., Panda S., Lucas R.J. Melanopsin contributions to irradiance coding in the thalamo-cortical visual system. PLoS Biol. 2010;8(12):e1000558. PubMed PMID: 21151887.
147. Brown T.M., Tsujimura S., Allen A.E., Wynne J., Bedford R., Vickery G., Vugler A., Lucas R.J. Melanopsin-based brightness discrimination in mice and humans. Curr Biol. 2012;22(12):1134–41. PubMed PMID: 22633808.
148. Horiguchi H., Winawer J., Dougherty R.F., Wandell B.A. Human trichromacy revisited. Proc Natl Acad Sci U S A. 2013;110(3):E260–9. PubMed PMID: 23256158.
149. Tarttelin E.E., Bellingham J., Bibb L.C., Foster R.G., Hankins M.W., Gregory-Evans K., Gregory-Evans C.Y., Wells D.J., Lucas R.J. Expression of opsin genes early in ocular development of humans and mice. Exp Eye Res. 2003;76(3):393–6. PubMed PMID: 12573668.
150. Sekaran S., Lupi D., Jones S.L., Sheely C.J., Hattar S., Yau K.W., Lucas R.J., Foster R.G., Hankins M.W. Melanopsin-dependent photoreception provides earliest light detection in the mammalian retina. Curr Biol. 2005;15(12):1099–107. PubMed PMID: 15964274.
151. Rao S., Chun C., Fan J., Kofron J.M., Yang M.B., Hegde R.S., Ferrara N., Copenhagen D.R., Lang R.A. A direct and melanopsin-dependent fetal light response regulates mouse eye development. Nature. 2013;494(7436):243–6. PubMed PMID: 23334418.
152. Berkowitz B.A., Roberts R., Bissig D. Light-dependant intraretinal ion regulation by melanopsin in young awake and free moving mice evaluated with manganese-enhanced MRI. Mol Vis. 2010;16:1776–80. PubMed PMID: 20808732.
153. Renna J.M., Weng S., Berson D.M. Light acts through melanopsin to alter retinal waves and segregation of retinogeniculate afferents. Nat Neurosci. 2011;14(7):827–9. PubMed PMID: 21642974.
154. Berson D.M., Castrucci A.M., Provencio I. Morphology and mosaics of melanopsin-expressing retinal ganglion cell types in mice. J Comp Neurol. 2010;518(13):2405–22. PubMed PMID: 20503419.

The Anatomy and Physiology of Direction-Selective Retinal Ganglion Cells

Jinyue Liu, B. A.[1,*]

Created: August 20, 2015.

1. Introduction

The ability to detect moving objects in the visual scene is fundamental to our daily survival. It originates within the sensory organ, the retina, where a significant proportion of retinal ganglion cell (RGC) responses is dedicated to detecting motion in different directions (Figure1).

The first evidence for such retinal computation was established in the rabbit retina by Barlow and colleagues in the 1960s. By moving small spots of light across parts of the receptive field of a direction-selective RGC (DSGC), they showed that a moving stimulus can elicit strong spiking of action potentials in one direction (henceforth referred to as the preferred direction) but not in the opposite, or null, direction (Figure 2) (1).

In fact, there are different types of DSGCs and they can be segregated based on two criteria. First, they either respond to both light onset and offset (ON-OFF), or just to the former (ON). Second, they prefer different directions of motion. These functional characteristics give rise to four types of ON-OFF DSGCs and three types of ON DSGCs. The ON-OFF DSGCs (ooDSGCs) each detect motion in one of four cardinal axes while the ON DSGCs detect movement in the dorsal, ventral and nasal directions (2) (Figure 3).

Since then, advances in mouse genetics has enabled the study of analogous DSGC populations in the mouse retina, and also led to the discovery of an OFF DSGC type that detects upward motion in the visual scene (3). These new tools complement existing technologies like electron microscopy and dye-filling techniques by allowing specific types of RGCs to be genetically labeled and manipulated. This facilitates the search for morphological correlates of their physiological function. In the following segments, I shall describe the morphology and physiological properties that underlie the direction-selective responses of each DSGC type.

2. ON-OFF DSGCs (ooDSGCs)

ooDSGC morphology and electrophysiological responses

ooDSGCs are the most extensively studied population of direction-selective RGCs, in part due to their more frequent occurrence. They have bistratified dendrites, laminating in both the ON and OFF sublaminae of the inner plexiform layer (IPL) within the retina (Figure 4) (4). Within each sublamina, the dendrites co-laminate with those of interneurons, namely glutamatergic bipolar cells that provide the main source of excitatory input, and starburst amacrine cells (SAC) which provide largely inhibitory input.

A stimulus entering the receptive field of an ooDSGC in its preferred direction will elicit the most robust action potential spiking and little or no response in the null direction (Figure 5) (5). This directional preference persists regardless of changes in the size, shape, contrast or trajectory of the moving stimulus (1).

Author Affiliation: 1 Department of Molecular and Cellular Biology and Center for Brain Science, Harvard University, Cambridge, MA 02138;Program in Neuroscience, Harvard Medical School, Boston, MA; Email: jinyueliu@fas.harvard.edu.

Corresponding author.

* See 'About the author'

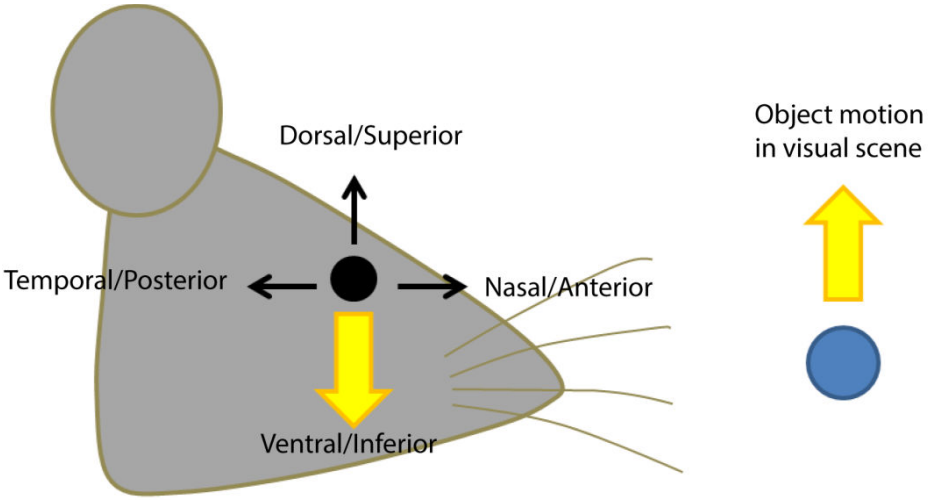

Figure 1. Cardinal axes of the visual field of a mouse. DSGCs in the retina respond best to motion in one of these directions. Due to inversion of light by the lens, the direction of movement of an object in the visual scene corresponds to movement in the opposite direction along the retinal plane. In the example, a DSGC that detects ventral motion responds best to an object moving upwards in the visual scene.

Mechanisms of direction selectivity in ooDSGCs

There are potentially three mechanisms by which direction-selective responses in ooDSGCs can be generated. Interaction with their presynaptic interneurons can produce 1) stronger excitation in the preferred direction or 2) stronger inhibition in the null direction. 3) Postsynaptic integration of excitation and inhibition within the ooDSGC can also give rise to robust response in the preferred but not the null direction. In order to address these possibilities, an understanding of the components of the direction-selective circuit is first needed.

Starburst amacrine cells are a key component of the ooDSGC direction-selective circuit

Since SAC dendrites interact extensively with those of ooDSGCs (6, 7) (Figure 6), SACs were thought to be key mediators of the direction-selective responses of ooDSGCs. Indeed, ablating SACs in mouse retinas abolishes direction-selective responses in ooDSGCs (Figure 7) (8).

SACs provide asymmetric inhibitory input onto ooDSGCs

In fact, SACs are a key source of inhibitory input for ooDSGCs (9). Using paired patch-clamp recordings, it was shown that depolarizing a SAC located on the null side of an ooDSGC elicits inhibition in that ganglion cell (Figure 8). On the other hand, SACs on the preferred side contribute relatively little inhibition.

Excitatory input, namely cholinergic input from SACs and glutamatergic input from bipolar cells, lack direction selectivity, implying that asymmetric SAC inhibition is the primary mechanism for generating direction-selective responses in ooDSGCs (9, 10).

How is this asymmetric wiring between SACs and ooDSGCs established? Direction selectivity is present before eye opening at two postnatal weeks, so visual experience does not seem to be necessary for establishing the circuit (11). A clue came from performing paired recordings of SACs and ooDSGCs in transgenic mice over postnatal development (12). SAC-ooDSGC connections on both the null and preferred sides of the ooDSGC are of equal strength during the first postnatal week, but only those made by null-side SACs strengthen significantly over the second postnatal week. Such developmental sculpting gives rise to a circuit where inhibitory currents from null-side SACs are larger while excitatory currents from SACs on either side are similar (Figure 9).

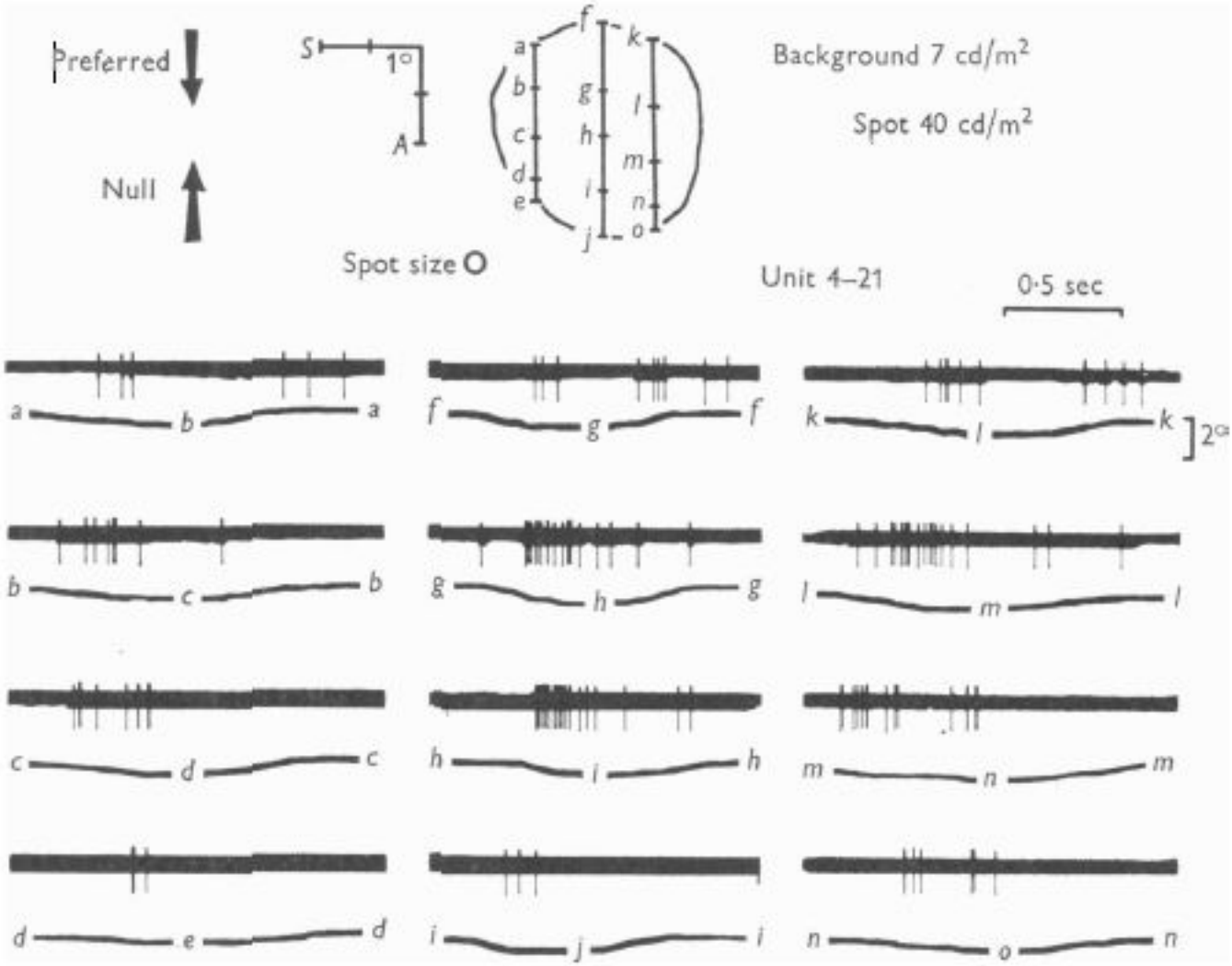

Figure 2. Small spots of light were moved across parts of the receptive field of a DSGC as indicated by the alphabetic letters (top) and spiking responses were recorded from the cell (bottom). Each tick along the horizontal time axis is an action potential. The cell is more responsive when the spot moves downwards (for example g to h or l to m) rather than upwards (for example h to g or m to l). From Barlow and Levick, 1965 (1).

Structural basis for the asymmetric inhibitory SAC input onto ooDSGCs

A landmark experiment by Briggman and colleagues (13) provided a structural basis for this functional asymmetry. By correlating physiological responses of each ooDSGC with structural evidence from serial block-face electron microscopy of putative synapses on these same cells, they showed that the SACs on the null side of ooDSGCs make more inhibitory synapses onto ooDSGC dendrites compared to SACs on the preferred side. In particular, individual SAC dendrites that are oriented antiparallel to the null direction of the ooDSGC contribute to the majority of these inhibitory synapses (Figure 10). Hence, an increase in the number of SAC-ooDSGC inhibitory synapses, rather than the strength of individual ones, accounts for the direction-selective responses of ooDSGCs.

Individual SAC dendrites are direction-selective

Each SAC can wire to multiple ooDSGCs and contribute to their direction-selective responses. This is possible because each SAC dendrite is an independent direction-selective unit (14) (Figure 11). When a stimulus is presented in a centrifugal direction, moving from its cell body out to the distal tips, the SAC dendrite inhibits the

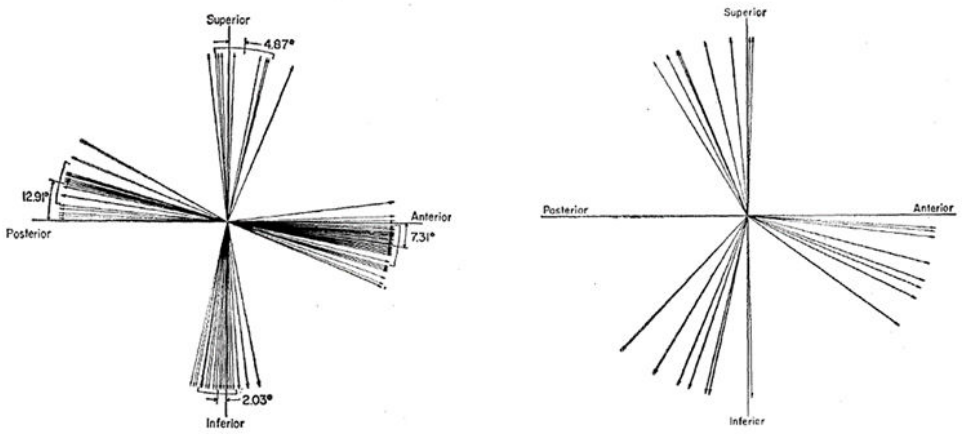

Figure 3. DSGCs can be classified into discrete types based on their functional properties. Distributions of directional preferences reveal four types of ooDSGCs (left) and three types of ON-DSGCs (right). Each vector indicates preferred direction of one DSGC. Axes represent the visual field. From Oyster and Barlow, 1967 (2).

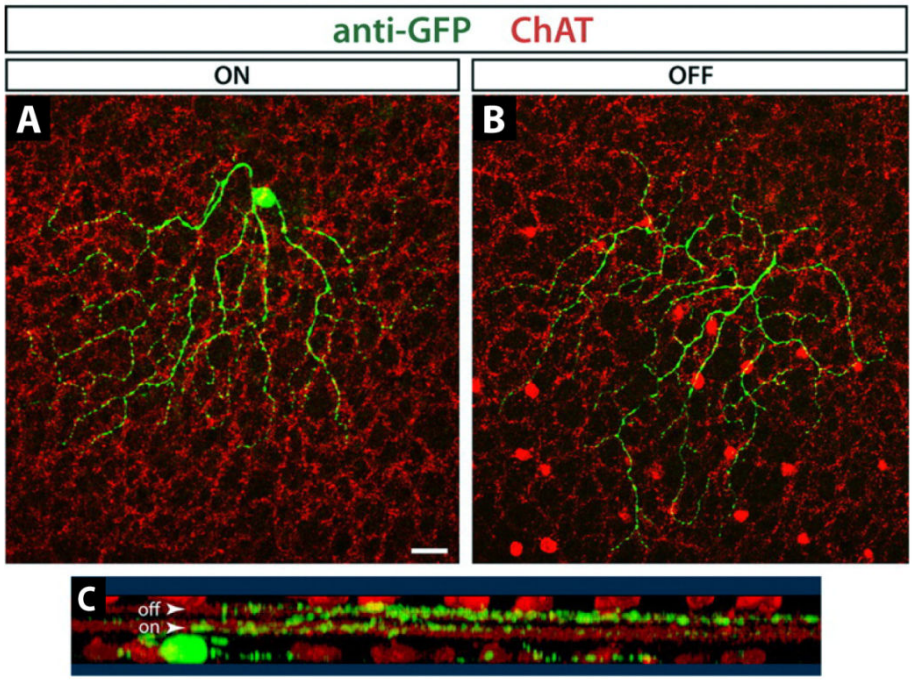

Figure 4. Morphology of an ooDSGC revealed by GFP labelling in a transgenic mouse line. (A-E) En face views of the ON (A) and OFF (B) dendritic arbors and their co-stratification with the ON and OFF SAC plexus (in red) respectively, indicated by immunostaining to choline acetyltransferase, a SAC marker. (C) Rotated view of the ooDSGC to illustrate its bistratified dendrites and colamination with SACs. Adapted from Kay et al., 2011(4).

ooDSGC that it connects to. Therefore, each SAC dendrite responds best to motion in the opposite direction relative to that preferred by its postsynaptic ooDSGC (Figure 12).

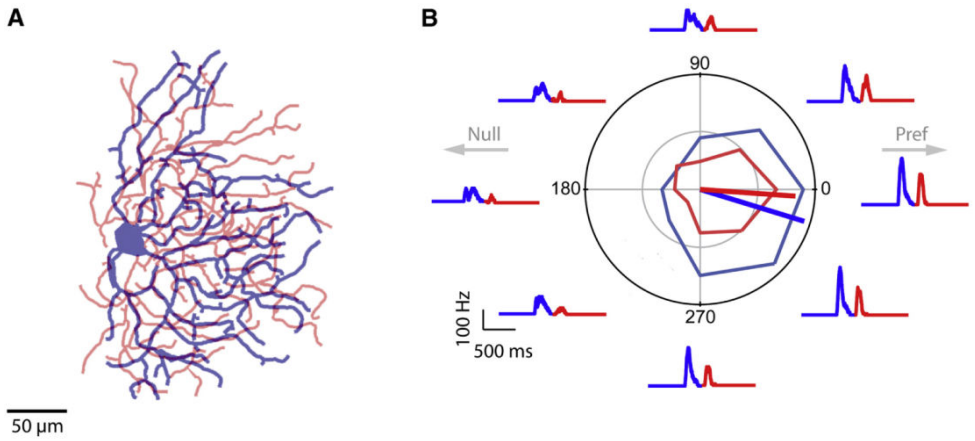

Figure 5. (A) Reconstruction of the ON (blue) and OFF (red) dendritic arbors of an ooDSGC. (B) ON (blue) and OFF (red) responses of an ooDSGC (similar to that in A) to a spot of light moving in eight directions across its receptive field. Distance from origin of the polar plot indicates spike rates. Preferred direction is indicated by the vector and the extent of the preference by its length. Surrounding traces are spike rate histograms in each direction. From Trenholm et al., 2011 (5).

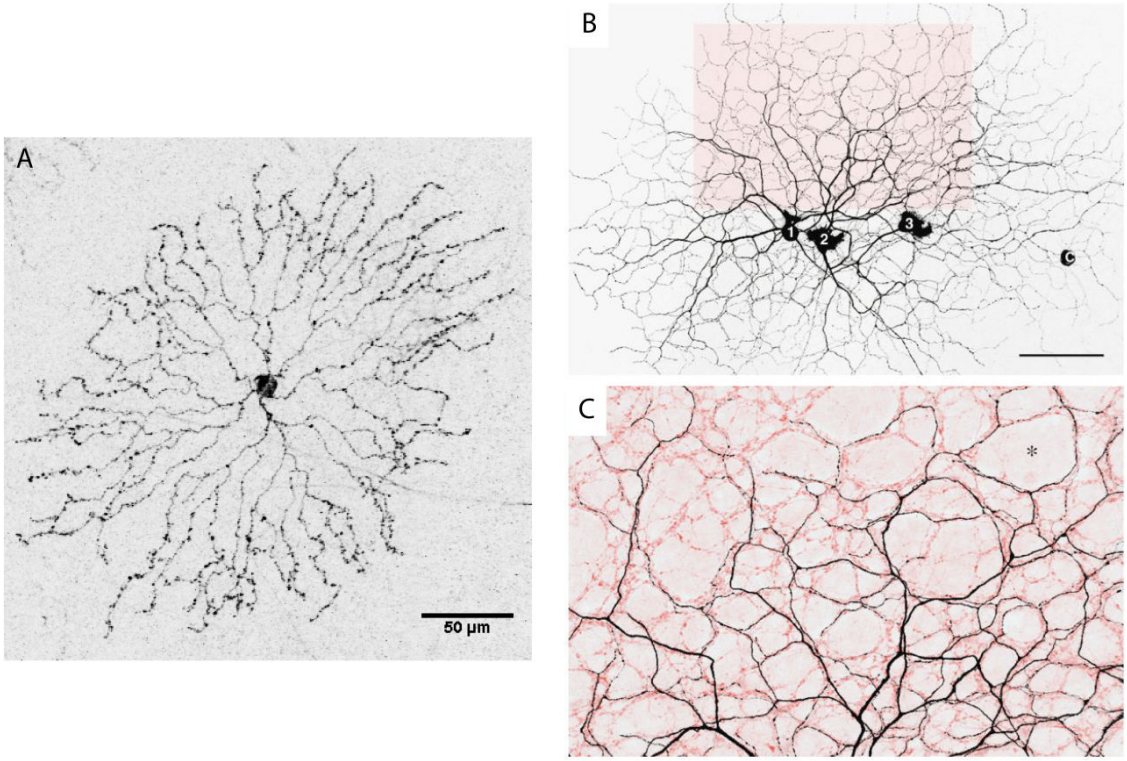

Figure 6. (A) A starburst amacrine cell (SAC) in the mouse retina. As the name suggests, it has radially symmetric dendrites. (B-C) The dendrites of SACs cofasiculate with ooDSGC dendrites in the rabbit retina. (B) The dendritic morphologies of three ooDSGCs as revealed by neurobiotin injections. (C) High-magnification view of highlighted region in (B), showing the ON dendritic plexi of SACs in red and ooDSGCs in black. The close interaction between the dendrites of these two cell types form a series of lacunae, or gaps, one of which is marked by the asterisk. (B-C) are from Vaney and Pow, 2000 (7).

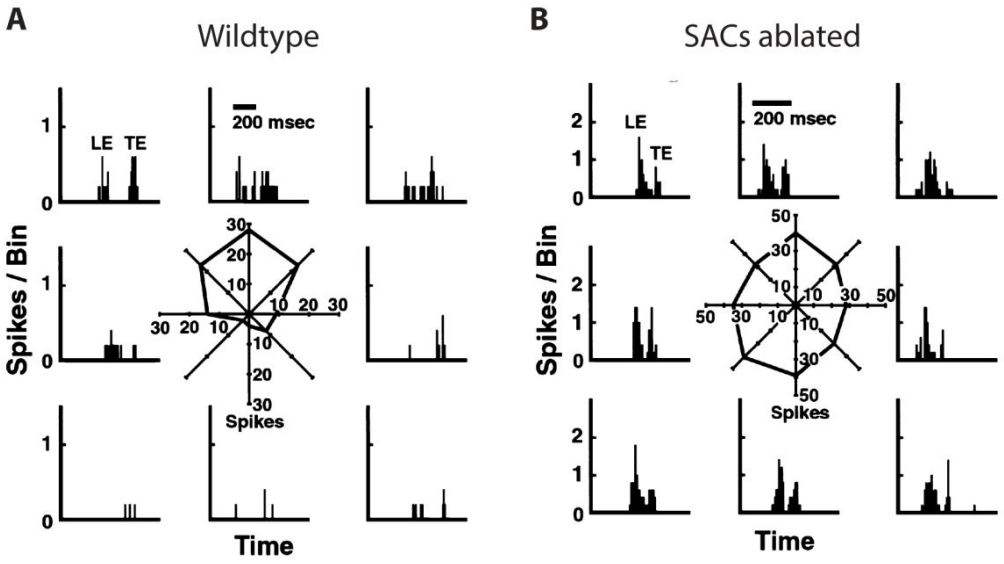

Figure 7. Responses of ooDSGCs in wildtype mouse retinas (A) or SAC-ablated retinas (B) to a moving bar. Polar plots are a sum of responses from four trials in eight directions. Surrounding traces are representative responses from a single ooDSGC. The cell fires when the bar enters (leading edge, LE) and leaves (trailing edge, TE) its receptive field. Normal ooDSGCs respond most strongly for bars moving in their preferred direction, while ooDSGCs in SAC-ablated retinas respond similarly in all directions. From Yoshida et al. 2001 (8).

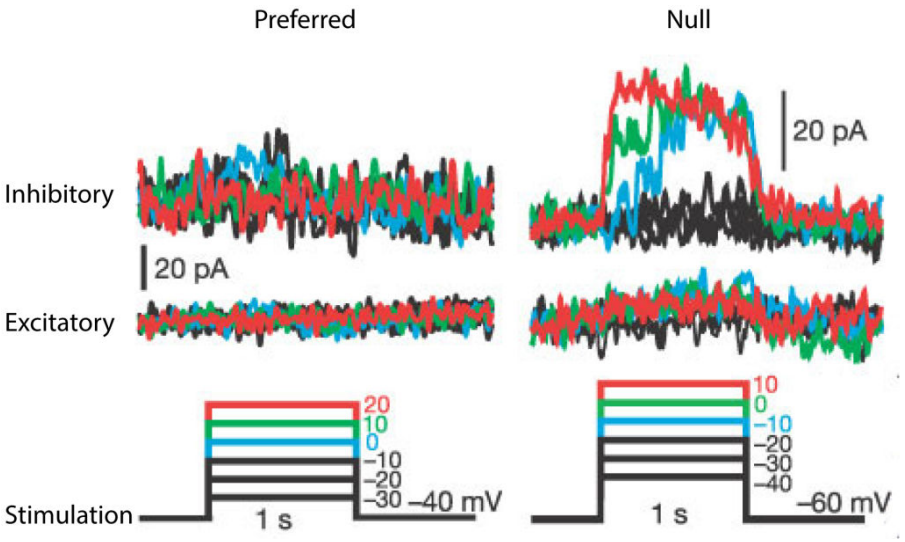

Figure 8. Inhibitory and excitatory currents recorded from ooDSGCs when neighboring SACs on their preferred or null side are stimulated with depolarizing voltage steps. Stimulation and corresponding responses are color coded. Depolarization of SACs on the null side, and not those on the preferred side, elicits inhibitory currents. There is a lack of excitatory inputs from SACs on either side. Adapted from Fried et al., 2002 (9).

3. ON DSGCs

Response properties of ON DSGCs

A separate class of direction-selective RGCs responds only to light increments. Called ON DSGCs, they detect stimuli moving in one of three directions: dorsal, ventral and nasal, with a slight offset from the horizontal and

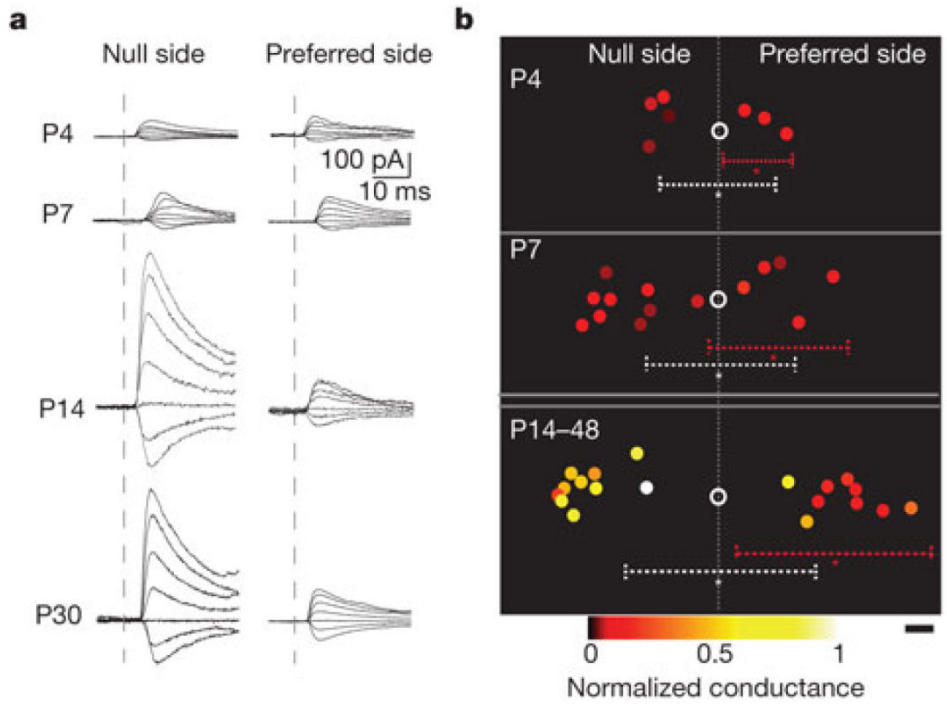

Figure 9. (a) Postsynaptic GABAergic currents measured from ooDSGCs in response to depolarizations of neighboring SACs on the null or preferred sides at postnatal days 4, 7, 14 and 30. (b) Relative positions of the cell bodies of the ooDSGCs and interacting SACs. Open circles in the middle represent ooDSGCs. Filled circles represent SACs, color-coded for whole-cell GABAergic conductance strength (normalized across all ages) elicited in the postsynaptic ooDSGC. Dashed lines represent average dendritic arbor diameter of the ooDSGC (white) and SACs (red), and asterisks, the average cell body locations. From Wei et. al., 2011 (12).

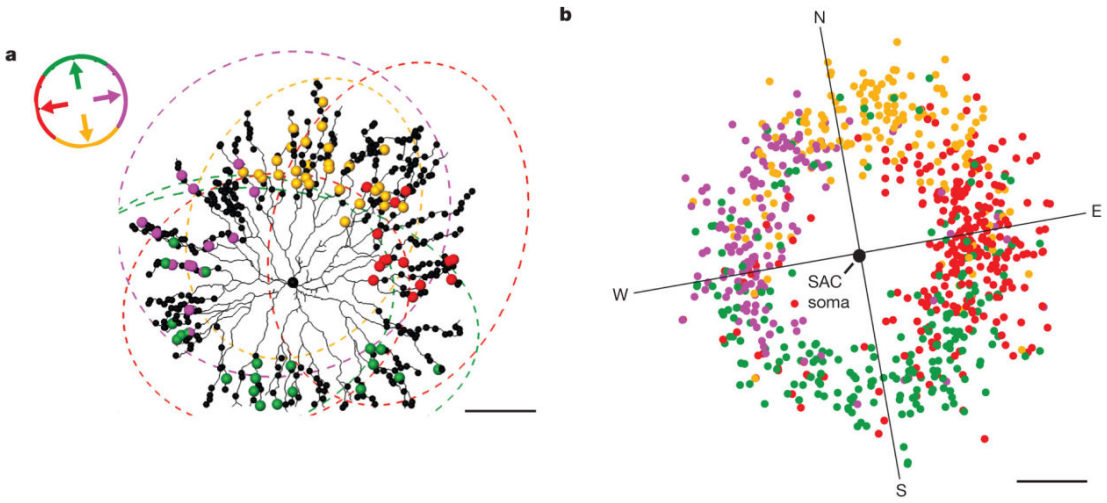

Figure 10. (a) An OFF SAC and its putative output synapses along the distal tips (black dots). The dendritic trees of nearby ooDSGCs are outlined in color-coded dashed ellipses and their preferred directions indicated in the top-left. The SAC-ooDSGC synapses are similarly color-coded. Although the dendritic trees of single ooDSGCs and SACs can overlap extensively, ooDSGCs mostly connect to individual SAC dendrites that are oriented along their null direction. For instance, southward-pointing SAC dendrites tend to make synapses onto ooDSGCs preferring northward direction. (b) Output synapse locations of 24 SACs overlaid on one another. From Briggman et al., 2011 (13).

vertical axes (Figure 3) (1, 15, 16). Each direction is encoded by two types of ON DSGCs with different response properties: one has sustained spike responses while the other has transient responses (Figure 13).

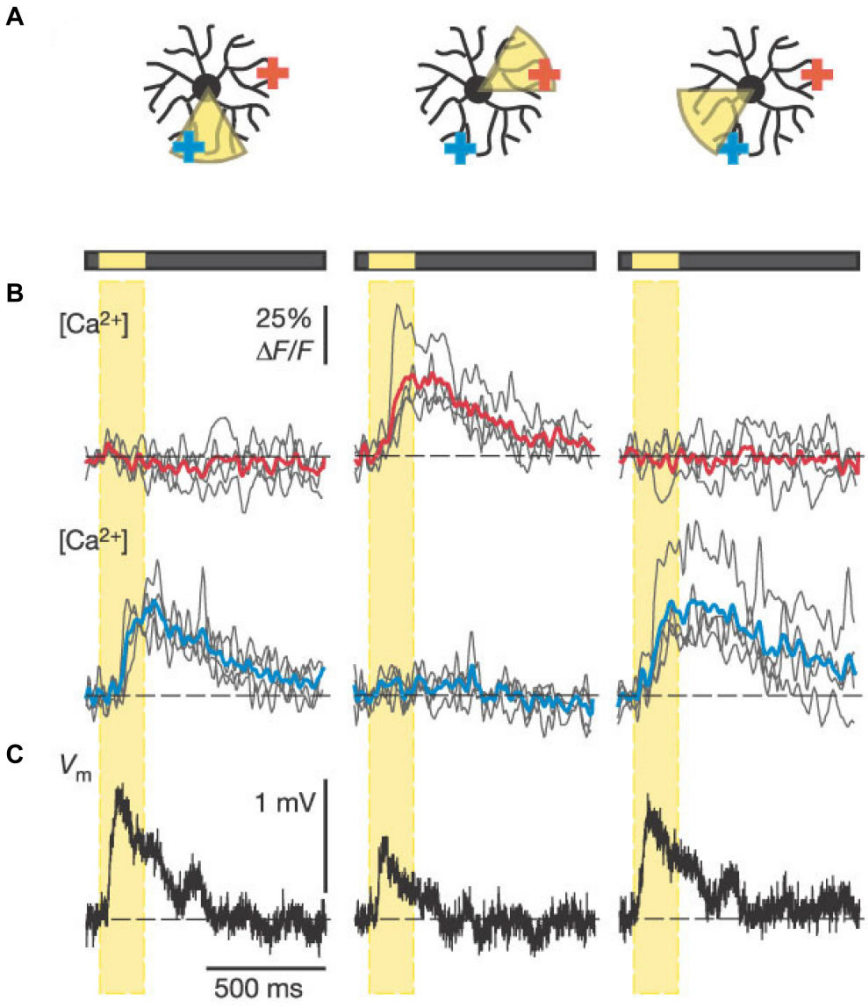

Figure 11. Local stimulation of SAC dendrites evokes calcium signals which are required for neurotransmitter release. (A) Sectors of the dendritic field of a SAC are being illuminated (in yellow) at random while dendritic calcium concentrations [Ca^{2+}] are being measured locally at two sites within its dendritic arbor. Stimulation sites and corresponding Ca^{2+} traces are color-coded in blue and red. While the cell is depolarized (C, membrane voltage V_m) regardless of the site of illumination, calcium signals are only evoked when the recording site is illuminated. In the instance shown on the left, illumination over the blue cross elicits an increase in [Ca^{2+}] at the blue cross but not at the red cross. From Euler et al., 2002 (14).

Morphology of ON DSGCs

As their functional properties suggest, ON DSGC dendrites ramify in just the ON sublamina within the IPL, co-stratifying with the dendritic plexus of ON SACs (Figure 14). Occasional processes to the OFF sublamina have been observed (15, 17). However, the morphologies of sustained and transient ON DSGCs differ in various aspects. First, sustained ON DSGCs have more terminal dendrites arising perpendicularly from their parent dendrites. Second, transient ON DSGCs show tracer coupling to non-SAC amacrine cells while sustained ones do not (18, 19).

Mechanism of direction selectivity in ON DSGCs

The direction-selective responses of ON DSGCs, just like their bistratified counterparts, are generated by asymmetric inhibition from ON SACs on their null side. This was shown by expressing channelrhodopsin in SACs, photostimulating them, and recording responses from their postsynaptic, ON DSGCs (20). Stimulating null-side SACs elicited more inhibitory currents than those on the preferred side while cholinergic input was

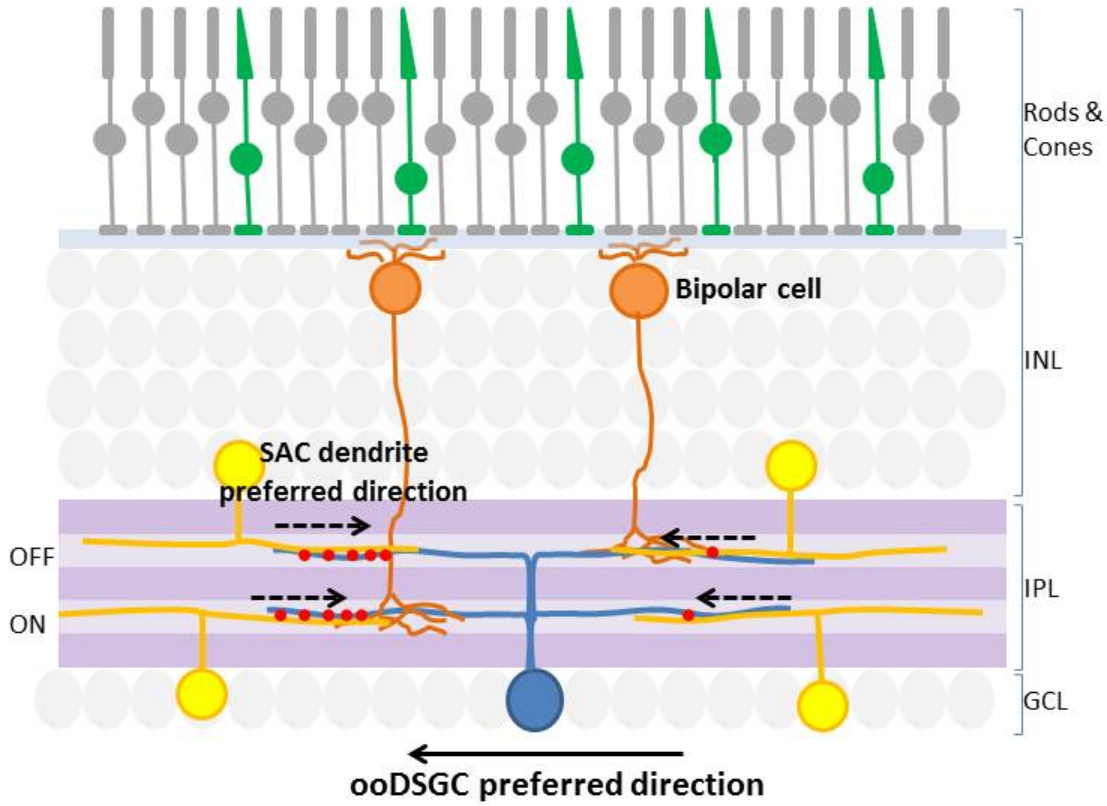

Figure 12. Schematic of a retinal cross-section illustrating the ooDSGC direction-selective circuit. In this model, the ooDSGC (in blue) prefers direction to the left (solid arrow). SAC dendrites are in yellow, with their preferred direction marked by the dashed arrows. SAC dendrites preferring motion direction opposite to that of the ooDSGC make more inhibitory synapses (red dots) onto the ooDSGC. INL, inner nuclear layer; IPL, inner plexiform layer; GCL, ganglion cell layer. OFF, OFF sublamina of the IPL containing the dendrites of OFF SACs. ON, ON sublamina of the IPL containing the dendrites of the ON SACs.

symmetric throughout. Glutamatergic input from ON bipolar cells are not direction-selective either (21). ON-DSGCs, however, respond better to slower stimuli compared to ooDSGCs (22).

4. OFF DSGCs

The latest DSGC type to be discovered is an OFF DSGC in the mouse retina (3). Called J-RGCs for their enriched expression of junctional adhesion molecule B (JAM-B), they have remarkably asymmetric dendrites that point ventrally and laminate within the outermost sublamina of the IPL (Figure 15).

These ventrally asymmetric J-RGCs respond to upward motion in the visual scene. Interestingly, a small fraction of J-RGCs residing in the most dorsal and ventral parts of the retina have symmetric dendritic arbors and are not direction-selective (Figure16) (3, 23). Such remarkable correlation between the dendritic structure and their direction-selective responses is unprecedented.

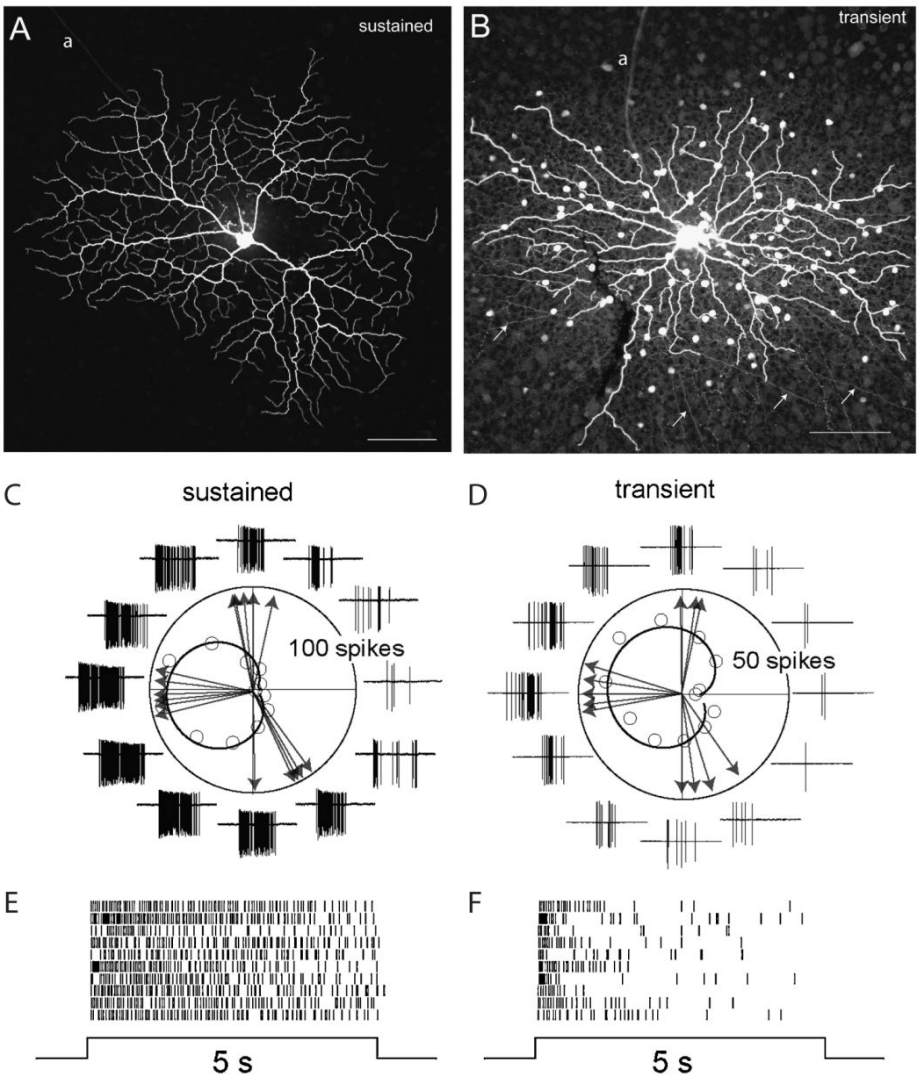

Figure 13. Dendritic morphologies of sustained (A) and transient (B) ON DSGCs in the rabbit retina. 'a' marks the axon. (C, D) Responses to a moving bar in 12 directions from multiple ON DSGCs reveal three subtypes within each type of ON DSGC. Each arrow represents the preferred direction of one cell. Traces around the polar plot are responses from a single ON DSGC; its mean number of spikes in each direction is indicated with open circles. (E, F) Responses to a stationary spot of light at the receptive field of sustained (E) and transient (F) ON DSGCs. Each row of ticks represents action potential spikes from one cell. From Kanjahan and Sivyer, 2010 (19).

The mechanism by which J-RGCs generate their direction selectivity remains unclear. It is probably very different from the SAC-mediated circuit that the ooDSGCs and ON DSGCs utilize, since J-RGCs do not co-laminate with SACs. Finding out the interneuron types that interact with J-RGC dendrites will be a key step towards elucidating its direction-selective circuit.

5. Conclusion

The DSGCs covered above make up most of the direction-selective ganglion cell types but are, by no means, exhaustive. With more extensive functional analyses, additional DSGC types may be revealed (24). Further structural analysis at both the dendritic and synaptic level will also shed light on the precise mechanisms that create direction-selectivity. It will be equally intriguing to understand how these direction-selective computations from the retina are integrated at higher brain centers.

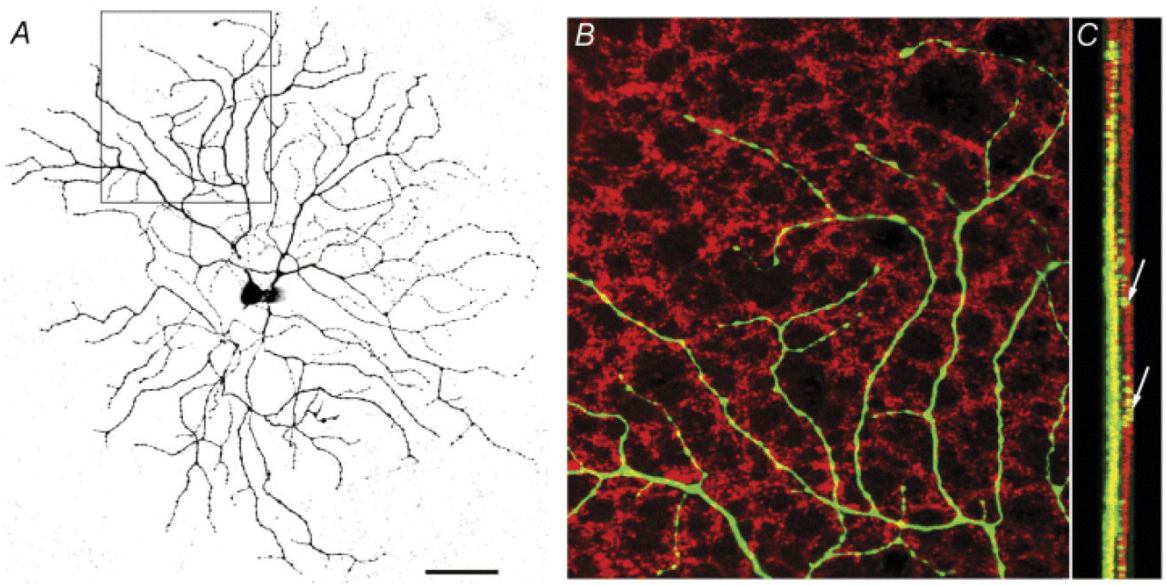

Figure 14. Morphology of an ON DSGC in the mouse retina. (A) En face view. Scale = 50μm. (B) Cofasiculation of ON DSGC dendrites (in green) with the ON SAC processes (in red). (C) Rotated view of the cell in B reveals tight co-stratification of ON DSGC dendrites with those of ON SACs (in yellow). Arrows point to the occasional processes that stray to the OFF SAC plexus. From Sun et al., 2006 (15).

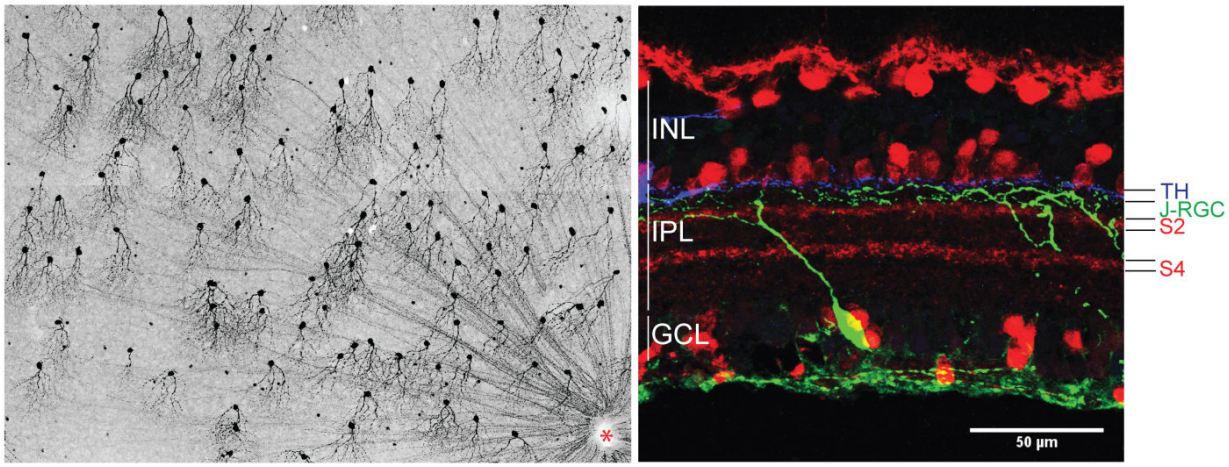

Figure 15. Left, retinal whole mount showing en face views of J-RGCs and their axons radiating from the optic nerve (asterisk). Right, J-RGC lamination (in green) in a retinal cross section. J-RGCs laminate above the processes of OFF SACs (in red, labeled s2) and below those of dopaminergic amacrine cells (in blue, labeled TH for tyrosine hydroxylase). Left, unpublished observations. Right from Liu and Sanes 2014 (25).

About the author

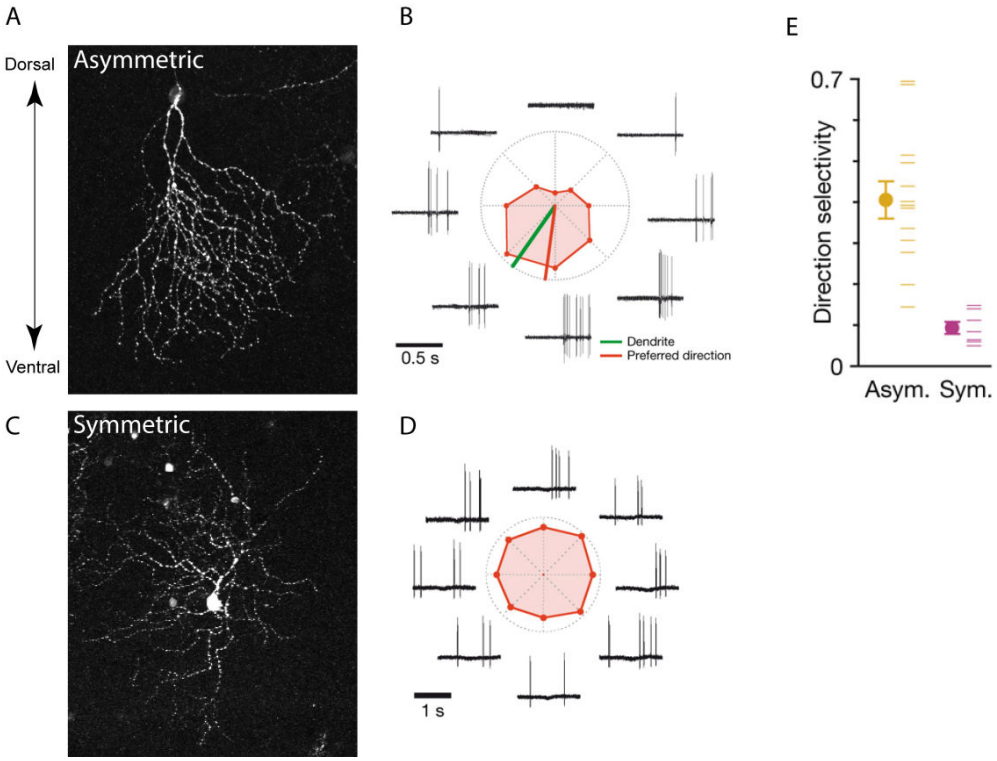

Figure 16. En face views of ventrally asymmetric (A) and symmetric (C) J-RGCs. (B, D) Responses to a small dot moving in 8 directions for asymmetric and symmetric J-RGCs respectively. Average responses are displayed as a polar plot. Surrounding traces are responses in each direction. The bold red line is the vector sum of responses in all directions and represents the preferred stimulus direction. The green line is the direction of the dendritic arbor. (E) Degree of direction selectivity for asymmetric and symmetric J-RGCs, ranging from 0 (least direction-selective) to 1. Each mark represents one cell. A from Liu and Sanes, 2014 (25). B, D and E are from Kim et al., 2008 (3).

Jinyue Liu grew up in Singapore and ventured to the University of Cambridge, UK, for her Bachelor's degree (BA hons) in natural sciences. She was supported by a National Science Scholarship from the Agency for Science, Technology and Research (A*STAR, Singapore). At Cambridge, Jin worked with Prof. William Harris on the role of metabolism in the differentiation of retinal progenitor cells. She is currently a Ph.D. candidate at Harvard University and is engaged in research to understand the mechanisms underlying development and circuitry of retinal ganglion cells, in Josh Sanes' lab. Email address: jinyueliu@fas.harvard.edu

References

1. Barlow H.B., Levick W.R. The mechanism of directionally selective units in rabbit's retina. The Journal of Physiology. 1965;178(3):477–504. PubMed PMID: 5827909.
2. Oyster C.W., Barlow H.B. Direction-Selective Units in Rabbit Retina: Distribution of Preferred Directions. Science. 1967;155(3764):841–842. PubMed PMID: 6019094.
3. Kim I.-J., Zhang Y., Yamagata M., Meister M., Sanes J.R. Molecular identification of a retinal cell type that responds to upward motion. Nature. 2008;452(7186):478–482. PubMed PMID: 18368118.
4. Kay J.N., De la Huerta I., Kim I.-J., Zhang Y., Yamagata M., Chu M.W., Meister M., Sanes J.R. Retinal ganglion cells with distinct directional preferences differ in molecular identity, structure and central projections. The Journal of Neuroscience. 2011;31(21):7753–7762. PubMed PMID: 21613488.
5. Trenholm S., Johnson K., Li X., Smith R.G., Awatramani G.B. Parallel Mechanisms Encode Direction in the Retina. Neuron. 2011;71(4):683–694. PubMed PMID: 21867884.

6. Famiglietti E.V. Dendritic Co-stratification of ON and ON-OFF directionally selective ganglion cells with starburst amacrine cells in rabbit retina. The Journal of Comparative Neurology. 1992;324(3):322–335. PubMed PMID: 1383291.
7. Vaney D.I., Pow D.V. The dendritic architecture of the cholinergic plexus in the rabbit retina: Selective labeling by glycine accumulation in the presence of sarcosine. The Journal of Comparative Neurology. 2000;421(1):1–13. PubMed PMID: 10813769.
8. Yoshida K., Watanabe D., Ishikane H., Tachibana M., Pastan I., Nakanishi S. A Key Role of Starburst Amacrine Cells in Originating Retinal Directional Selectivity and Optokinetic Eye Movement. Neuron. 2001;30(3):771–780. PubMed PMID: 11430810.
9. Fried S.I., Munch T.A., Werblin F.S. Mechanisms and circuitry underlying directional selectivity in the retina. Nature. 2002;420(6914):411–414. PubMed PMID: 12459782.
10. Park S.J.H., Kim I.-J., Looger L.L., Demb J.B., Borghuis B.G. Excitatory Synaptic Inputs to Mouse On-Off Direction-Selective Retinal Ganglion Cells Lack Direction Tuning. The Journal of Neuroscience. 2014;34(11):3976–3981. PubMed PMID: 24623775.
11. Chan Y.-C., Chiao C.-C. Effect of visual experience on the maturation of ON–OFF direction selective ganglion cells in the rabbit retina. Vision Research. 2008;48(23–24):2466–2475. PubMed PMID: 18782584.
12. Wei W., Hamby A.M., Zhou K., Feller M.B. Development of asymmetric inhibition underlying direction selectivity in the retina. Nature. 2011;469(7330):402–406. PubMed PMID: 21131947.
13. Briggman K.L., Helmstaedter M., Denk W. Wiring specificity in the direction-selectivity circuit of the retina. Nature. 2011;471(7337):183–188. PubMed PMID: 21390125.
14. Euler T., Detwiler P.B., Denk W. Directionally selective calcium signals in dendrites of starburst amacrine cells. Nature. 2002;418(6900):845–852. PubMed PMID: 12192402.
15. Sun W., Deng Q., Levick W.R., He S. ON direction-selective ganglion cells in the mouse retina. The Journal of Physiology. 2006;576(1):197–202. PubMed PMID: 16901944.
16. Yonehara K., Ishikane H., Sakuta H., Shintani T., Nakamura-Yonehara K., Kamiji N.L., Usui S., Noda M. Identification of Retinal Ganglion Cells and Their Projections Involved in Central Transmission of Information about Upward and Downward Image Motion. PLoS ONE. 2009;4(1):e4320. PubMed PMID: 19177171.
17. Dhande O.S., Estevez M.E., Quattrochi L.E., El-Danaf R.N., Nguyen P.L., Berson D.M., Huberman A.D. Genetic Dissection of Retinal Inputs to Brainstem Nuclei Controlling Image Stabilization. The Journal of Neuroscience. 2013;33(45):17797–17813. PubMed PMID: 24198370.
18. Hoshi H., Tian L.-M., Massey S.C., Mills S.L. Two distinct types of ON directionally selective ganglion cells in the rabbit retina. The Journal of Comparative Neurology. 2011;519(13):2509–2521. PubMed PMID: 21618235.
19. Kanjhan R., Sivyer B. Two types of ON direction-selective ganglion cells in rabbit retina. Neuroscience Letters. 2010;483(2):105–109. PubMed PMID: 20678546.
20. Yonehara K., Balint K., Noda M., Nagel G., Bamberg E., Roska B. Spatially asymmetric reorganization of inhibition establishes a motion-sensitive circuit. Nature. 2011;469(7330):407–410. PubMed PMID: 21170022.
21. Yonehara K., Farrow K., Ghanem A., Hillier D., Balint K., Teixeira M., Jüttner J., Noda M., Rachael L. Neve, K.-K. Conzelmann, and B. Roska, The First Stage of Cardinal Direction Selectivity Is Localized to the Dendrites of Retinal Ganglion Cells. Neuron. 2013;79(6):1078–1085. PubMed PMID: 23973208.
22. Sivyer B., Van Wyk M., Vaney D.I., Taylor W.R. Synaptic inputs and timing underlying the velocity tuning of direction-selective ganglion cells in rabbit retina. The Journal of Physiology. 2010;588(17):3243–3253. PubMed PMID: 20624793.
23. Kim I.-J., Zhang Y., Meister M., Sanes J.R. Laminar Restriction of Retinal Ganglion Cell Dendrites and Axons: Subtype-Specific Developmental Patterns Revealed with Transgenic Markers. The Journal of Neuroscience. 2010;30(4):1452–1462. PubMed PMID: 20107072.
24. Helmstaedter M., Briggman K.L., Turaga S.C., Jain V., Seung H.S., Denk W. Connectomic reconstruction of the inner plexiform layer in the mouse retina. Nature. 2013;500(7461):168–174. PubMed PMID: 23925239.

25. Liu, J. and J.R. Sanes, Development of dendrites in a direction-selective ganglion cell in the mouse retina Society for Neuroscience Annual Meeting. 2014:725.01.

Glial Cells of the Retina

Helga Kolb

Created: May 1, 2001; Updated: April 17, 2007.

Three basic types of glial cell are found in the human retina: Muller cells, astroglia, and microglia. All were described for the retina by Cajal (1) more than 100 years ago in 1892.

Muller Cells

Muller cells are the principal glial cell of the retina. They form architectural support structures stretching radially across the thickness of the retina and are the limits of the retina at the outer and inner limiting membrane, respectively. A complete understanding of the shape of a Muller cell is best seen after Golgi staining, as shown originally by Cajal (1) below (Fig. 1).

Muller cell bodies sit in the inner nuclear layer and project irregularly thick and thin processes in either direction to the outer limiting membrane and to the inner limiting membrane. Muller cell processes insinuate themselves between cell bodies of the neurons in the nuclear layers and envelope groups of neural processes in the plexiform layers. In fact, retinal neural processes have direct contact, without enveloping Muller cell processes, only at their synapses.

A single progenitor cell gives rise to both Muller cells and retinal neurons (2), although apparently in two phases. The earliest phase neurons born at the apical margin of the neuroepithelium, adjacent to the pigment epithelium, produces primary neurons consisting of cone cells, horizontal cells, and ganglion cells. The second phase of cells, also born at the apical margins, produces Muller cells and rod photoreceptors, bipolar cells and amacrine cells (3). All of the developing neurons and the Muller cells have to migrate inward to their final position, and it is thought that the Muller cell processes and trunks guide much of the neuron migrations and direct the neurite differentiations (Fig. 2).

The junctions forming the outer limiting membrane are between Muller cells and other Muller cells with photoreceptor cells as sturdy desmosomes' coronial adherents. In some species, gap junctions (specialized membrane associations and channels that allow passage of small molecules and ions) or tight junctions are part of these Muller cell junctions (4) but not so in mammalian species, where no dye coupling has ever been observed (3, 5). The surface of the Muller cell facing the pigment epithelium and subretinal space is expanded by many projections of the Muller cell membrane, known as apical villi. The inner limiting membrane, on the other hand, is formed by the conical endfeet of the Muller cell, but no specialized junctions are seen here. Muller cells also form endfeet on the large retinal blood vessels at the inner surface of the retina. The surface of the Muller cell membrane facing the vitreous is covered with a mucopolysaccharide material and thus forms a true basement membrane.

Muller cells contain glycogen, mitochondria, and intermediate filaments that are immunoreactive for vimentin and to some extent to glial fibrillary acidic protein (GFAP). The latter filaments are normally in the inner half of the Muller cells and their endfeet, but after trauma to the retina, such as retinal detachment, both vimentin and GFAP are massively upregulated and found throughout the cell (see below) (6, 7) (Fig. 3).

Muller cells have a range of functions, all of which are vital to the health of the retinal neurons. Muller cells function in a symbiotic relationship with the neurons (for an excellent review, see Reichenbach and Robinson (3)). Thus, Muller cell functions include:

1. Supplying end products of anaerobic metabolism (breakdown of glycogen) to fuel aerobic metabolism in the nerve cells.
2. They mop up neural waste products, such as carbon dioxide and ammonia, and recycle spent amino acid transmitters.

3. They protect neurons from exposure to excess neurotransmitters, such as glutamate, using well-developed uptake mechanisms to recycle this transmitter. They are particularly characterized by the presence of high concentrations of glutamine synthase.
4. They may be involved in both phagocytosis of neuronal debris and release of neuroactive substances such as GABA, taurine, and dopamine.
5. They are thought to synthesize retinoic acid from retinol (retinoic acid is known to be important in the development of the eye and the nervous system) (8).
6. They control homeostasis and protect neurons from deleterious changes in their ionic environment by taking up extracellular K^+ and redistributing it.
7. They contribute to the generation of the electroretinogram (ERG) b-wave (4, 9), the slow P3 component of the ERG (10), and the scotopic threshold response (STR) (11). They do so by regulation of K^+ distribution across the retinal vitreous border, across the whole retina, and locally in the inner plexiform layer of the retina (see figure below from Reichenbach and Robinson (3), adapted from Newman (12)) (Fig. 4).

Astrocytes

Astrocytes are not glial cells of the retinal neuroepithelium but enter the developing retina from the brain along the developing optic nerve (13, 14). They have a characteristic morphology of a flattened cell body and a fibrous series of radiating processes. Intermediate filaments fill their processes, and thus they stain dramatically with antibodies against GFAP (15). Astrocyte cell bodies and processes are almost entirely restricted to the nerve fiber layer of the retina. Their morphology changes from the optic nerve head to the periphery: from extremely elongated near the optic nerve to a symmetrical stellate form in the far peripheral retina (15) (Fig. 5 and Fig. 6).

In Golgi and immunocytochemical staining, they look like cell bodies with fibrous tangles aligned along the ganglion cell axons coursing through the nerve fiber layer. In distribution, astrocytes reach their peak on the optic nerve head and have a fairly uniform decline in density in radiating rings from the nerve head. They are not present in the avascular fovea or ora serrata (Fig. 7).

Thick and thin astrocytes have been distinguished on the basis of staining with antibodies to GFAP (16). Thus, astrocytes are arranged over the surface of the ganglion cell axon bundles as they course into the optic nerve head, forming a tube through which the axons run. Gap junctions and zonula adherens junctions have been described between astrocytic processes in cat retina (17).

The blood vessels running in and among the ganglion cell bundles are also covered by both processes and even an occasional cell body of an astrocyte. The function of astrocytes enveloping ganglion cell axons and the relationship to blood vessels of the nerve fiber layer suggest they are axonal and vascular glial sheaths and part of a blood-brain barrier. Similar to Muller cells, they are known to contain abundant glycogen, and they may form a nutritive service in providing glucose to the neurons. In addition, they probably serve a role in ionic homeostasis in regulating extracellular potassium levels and metabolism of neurotransmitters like GABA (Fig. 8).

Microglial Cells

The third glial cell type is supposedly of mesodermal origin and thus, strictly speaking, are not neuroglial as the astrocytes and Muller cells are. They enter the retina coincident with the mesenchymal precursors of retinal blood vessels in development (14). Microglial cells are ubiquitous in the human retina, being found in every layer of the retina.

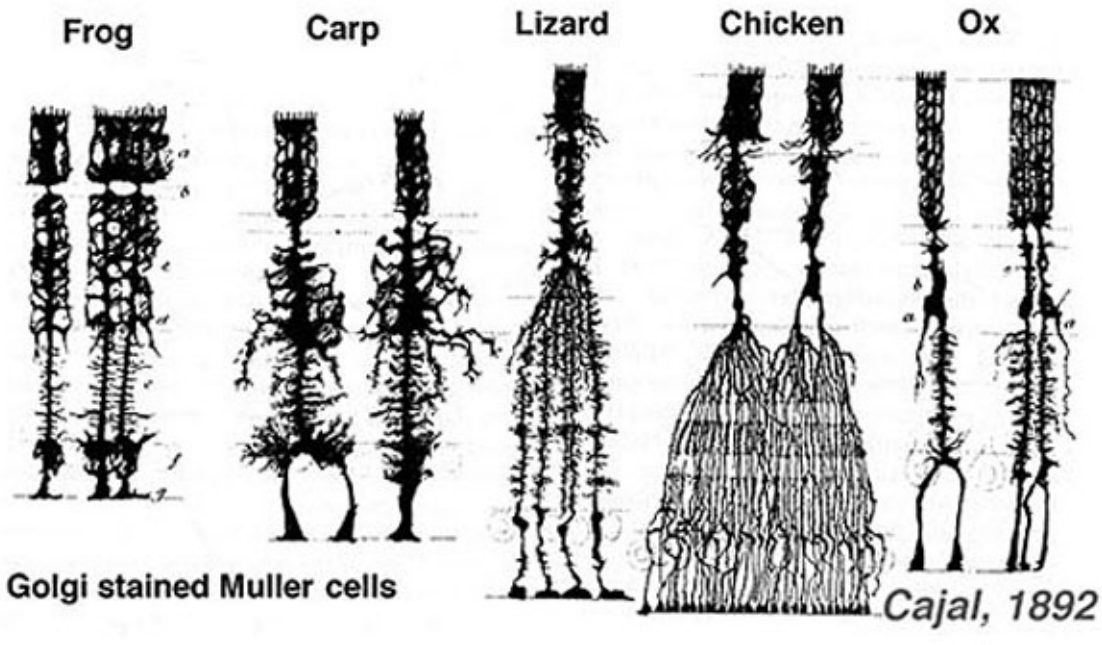

Figure 1. Golgi-stained Muller cells. From Cajal (1).

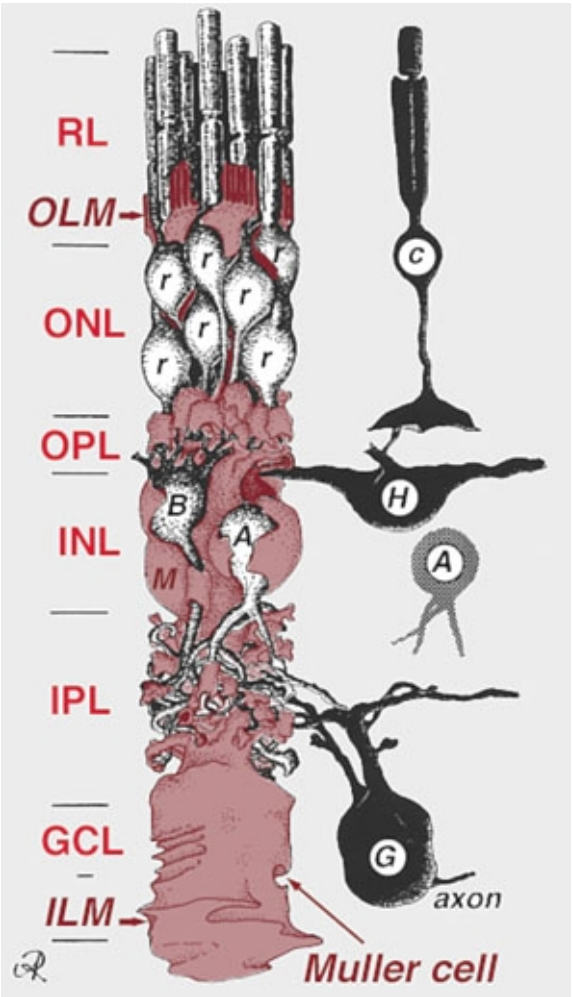

Figure 2. 3-D schematic drawing of the relationship between Muller cell and other retinal neurons.

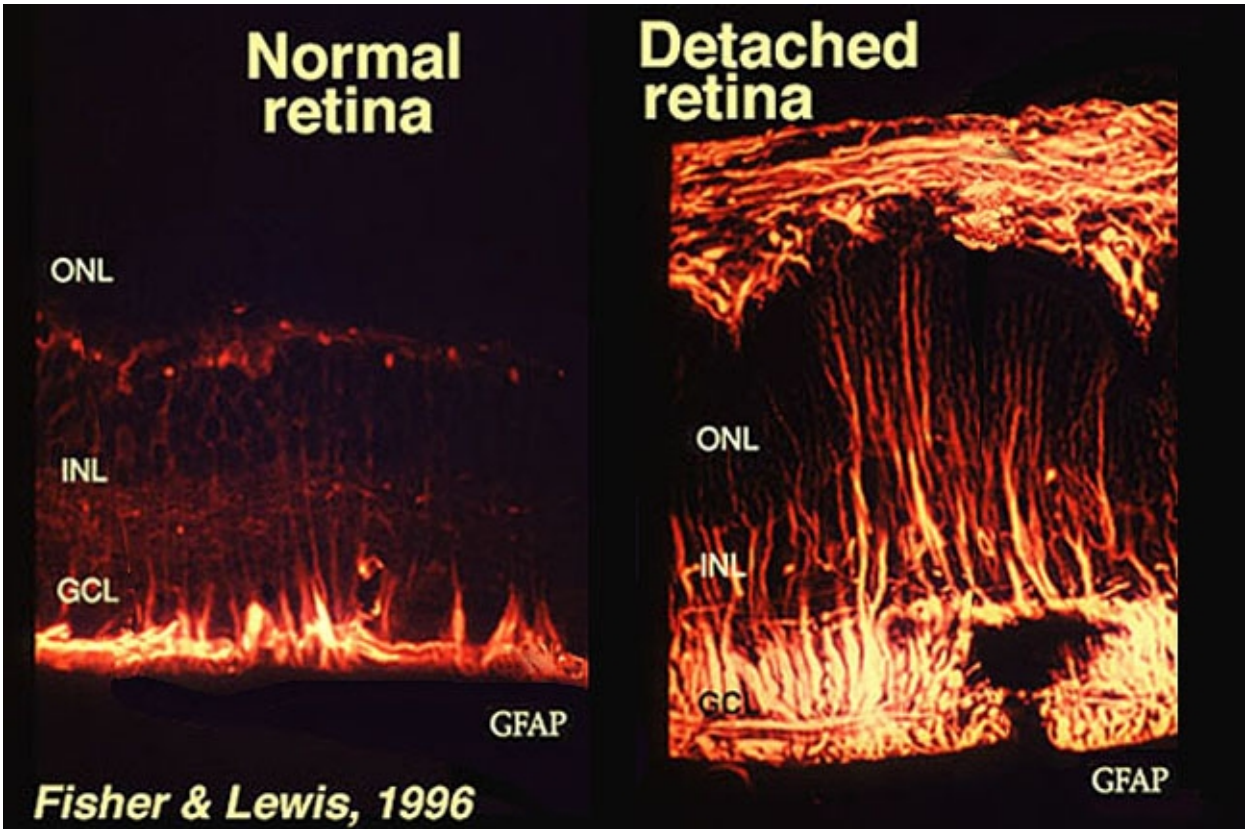

Figure 3. GFAP immunoreactivity in Muller cells. From Fisher and Lewis (7).

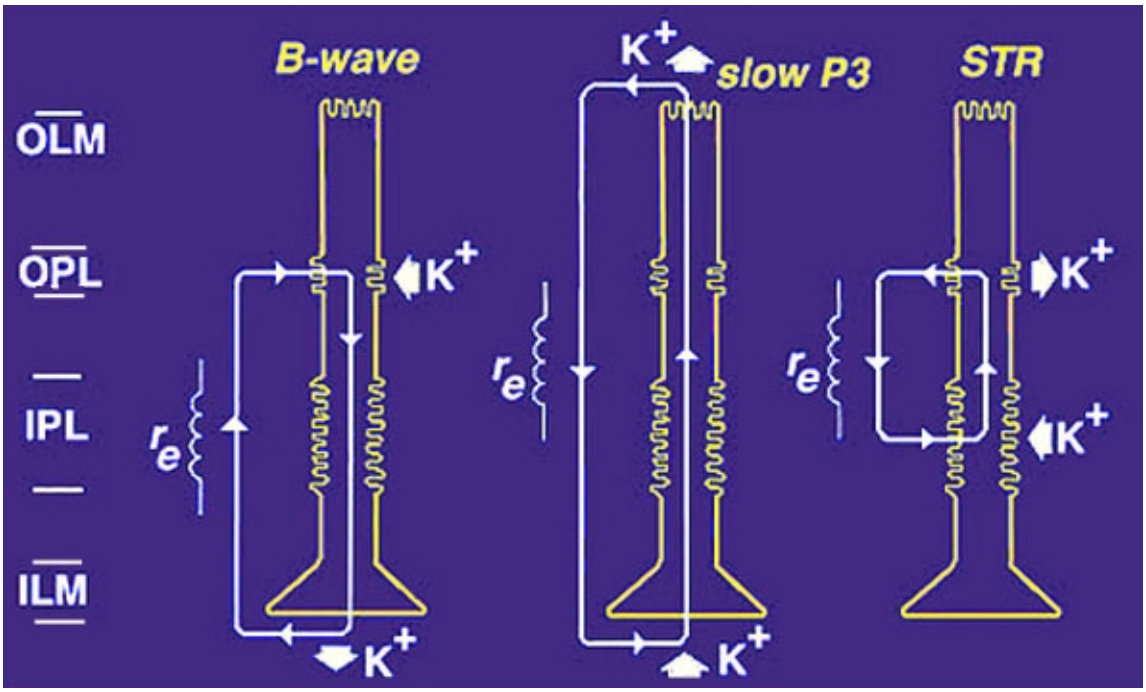

Figure 4. Regulation of K^+ by Muller cells in Muller cells.

In Golgi-stained retina, they look like strange, multipolar forms with small cell bodies and irregular short processes. In fact, in Golgi preparations they have sometimes been mistaken for nerve cells, particularly when they lie in a nuclear layer with a single orientation of their processes in the plexiform layer (Fig. 9).

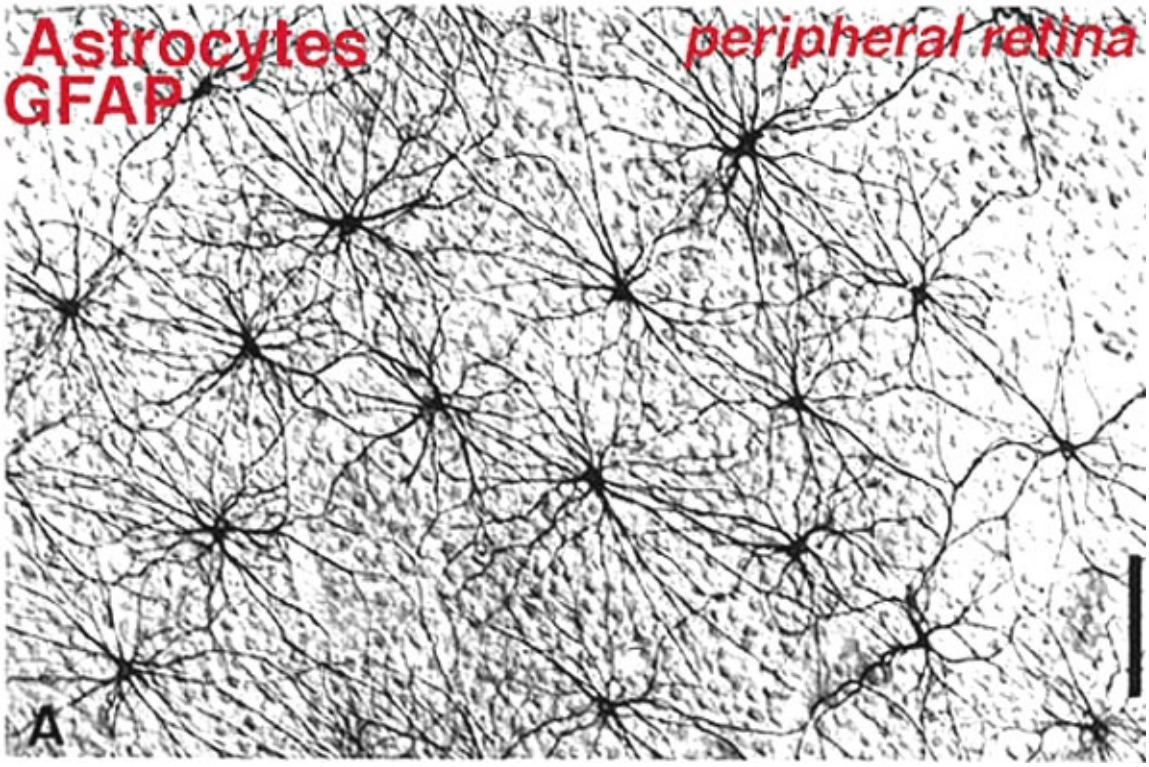

Figure 5. Astrocytes in peripheral retina.

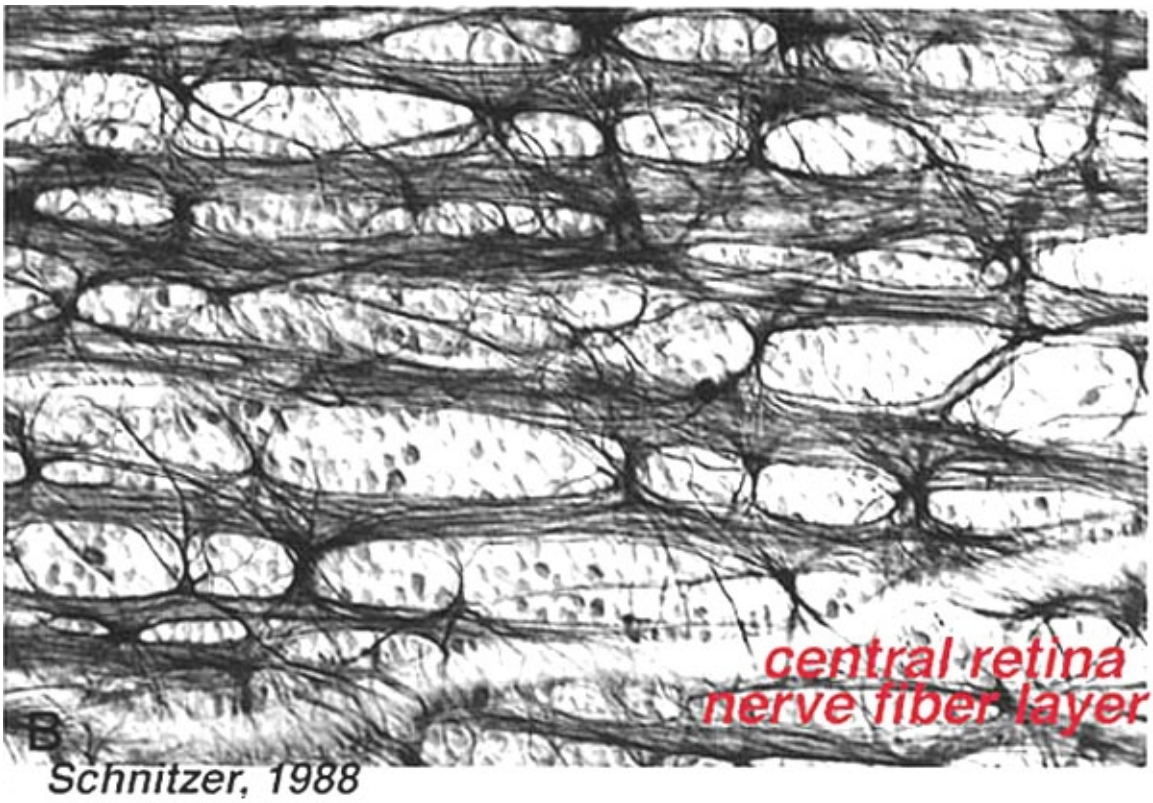

Figure 6. Astrocytes in central retina. From Schnitzer (15).

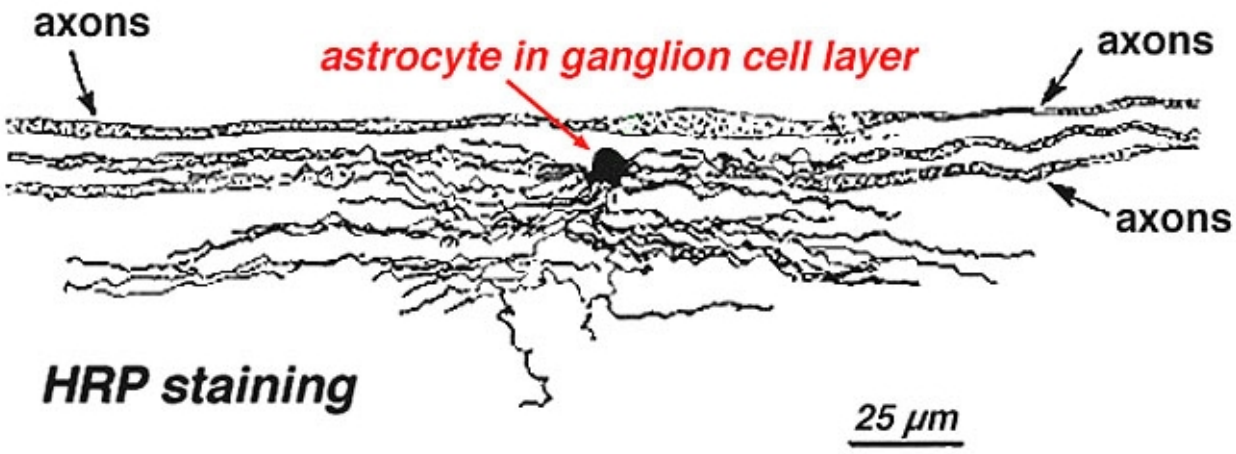

Figure 7. HRP staining of astrocytes in the ganglion cell layer.

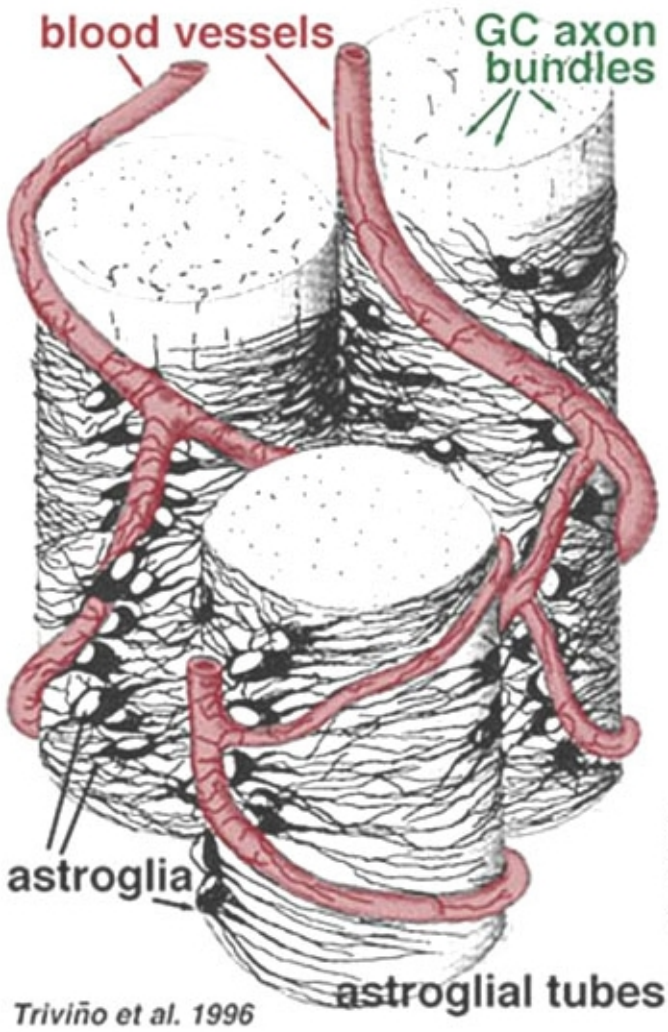

Figure 8. 3-D block of astrocytes arranged over the surface of ganglion cell axon bundles. From Trivino et al. (16).

Microglial cells may be of two types. One form is thought to enter the retina at earlier stages of development from the optic nerve mesenchyme and lie dormant in the retinal layers for much of the life of the retina. The other form of microglia appear to be blood-borne cells, possible originating from vessel pericytes (18, 19). Both types can be stimulated into a macrophagic function on trauma to the retina, and then they engage in phagocytosis of degenerating retinal neurons (Fig. 10).

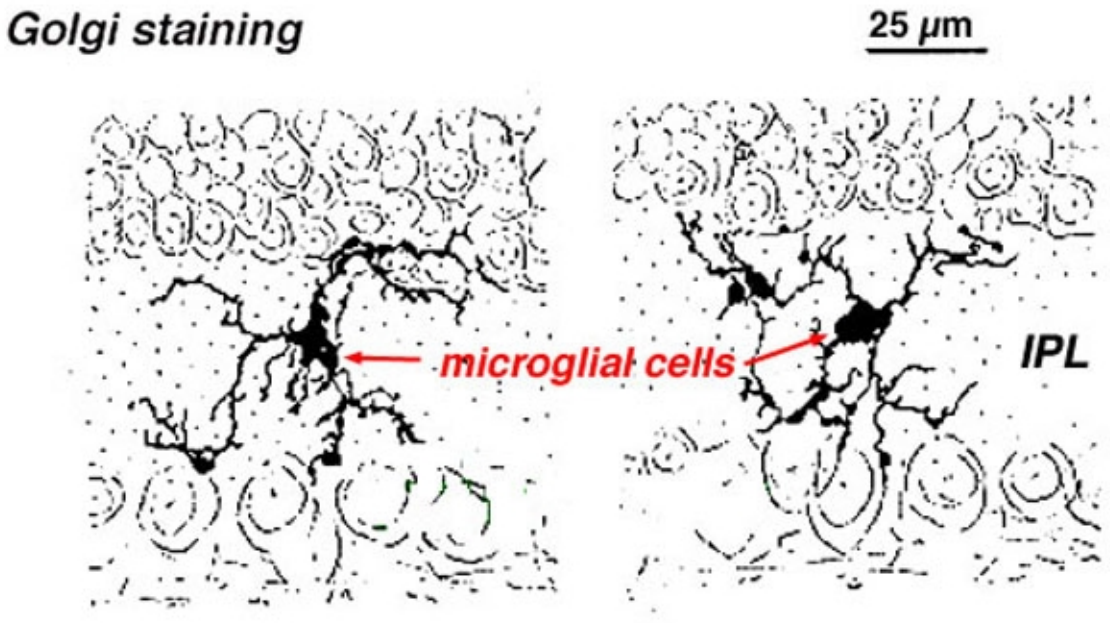

Figure 9. Golgi staining of microglial cells.

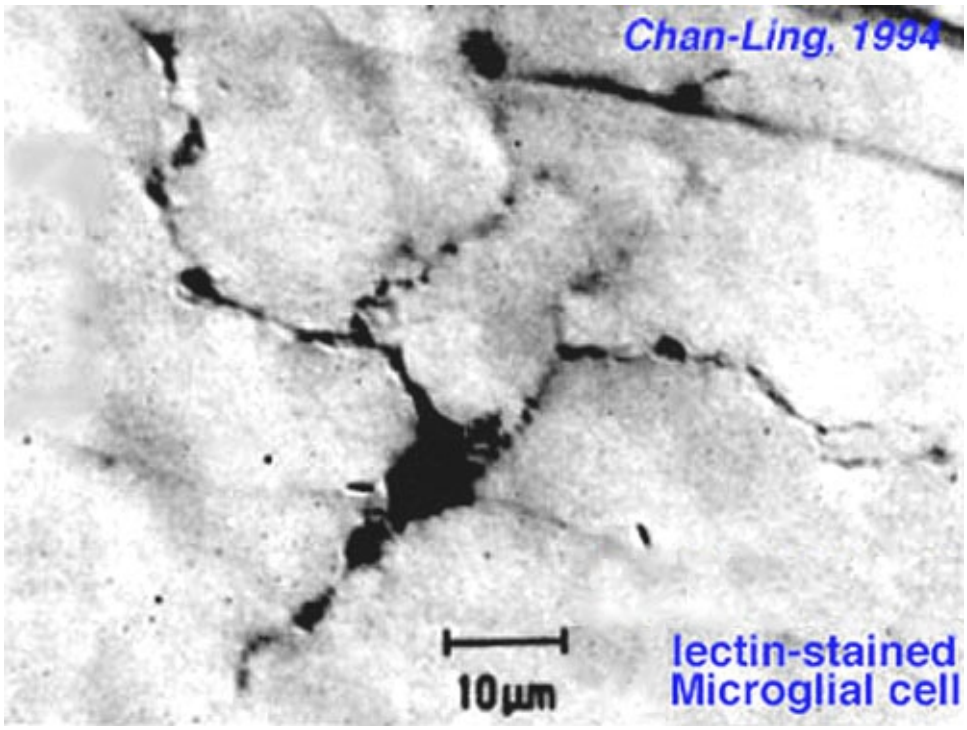

Figure 10. Lectin-stained microglial cell. From Chan-Ling (14).

References

1. Cajal SR. In: Thorpe SA, Glickstein M, translators. 1892. The structure of the retina. Springfield (IL): Thomas; 1972.
2. Turner DL, Cepko CL. A common progenitor for neurons and glia persists in rat retina late in development. Nature. 1987;328:131–136. PubMed PMID: 3600789.

3. Reichenbach A, Robinson SR. The involvement of Müller cells in the outer retina. In: Djamgoz MBA, Archer SN, Vallerga S, editors. Neurobiology and clinical aspects of the outer retina. London: Chapman & Hall; 1995. p. 395-416.
4. Miller RF, Dowling JE. Intracellular responses of the Muller (glial) cells of the mudpuppy retina: their relation to b-wave of the electroretinogram. J Neurophysiol. 1970;33:323–341. PubMed PMID: 5439340.
5. Robinson SR, Hampson ECGM, Munro MN, Vaney DI. Unidirectional coupling of gap junctions between neuroglia. Proc. Austr. Neurosci. Soc. 1993;3:167.
6. Guerin CJ, Anderson DH, Fisher SK. Changes in intermediate filament immunolabeling occur in response to retinal detachment and reattachment in primates. Invest. Ophthal. Vis. Sci. 1990;31:1474–1482. PubMed PMID: 2387680.
7. Fisher SK, Lewis GP. Photoreceptors and beyond: cellular and molecular effects of retinal detachment.2nd Great Basin Visual Science Symposium, II, University of Utah Press. 1995.
8. Edwards RB. Biosynthesis of retinoic acid by Müller glial cells: a model for the central nervous system? Prog. Ret. Eye Res. 1994;13:231–242.
9. Newman EA, Odette LL. Model of electroretinogram b-wave generation: a test of the K+ hypothesis. J Neurophysiol. 1984;51:164–182. PubMed PMID: 6319623.
10. Karwoski CJ, Proenza LM. Relationship between Muller cell responses, a local transretinal potential, and potassium flux. J Neurophysiol. 1977;40:244–259. PubMed PMID: 845622.
11. Frishman LJ, Steinberg RH. Light-evoked increases in [K+]o in proximal portion of the dark-adapted cat retina. J Neurophysiol. 1989;61:1233–1243. PubMed PMID: 2746323.
12. Newman EA. Electrophysiology of retinal glial cells. Prog. Ret. Res. 1989;8:153–172.
13. Stone J, Dreher Z. Relationship between astrocytes, ganglion cells and vasculature of the retina. J Comp Neurol. 1987;255:35–49. PubMed PMID: 3819008.
14. Chan-Ling T. Glial, neuronal and vascular interactions in the mammalian retina. Prog. Ret. Eye Res. 1994;13:357–389.
15. Schnitzer J. Astrocytes in mammalian retina. Prog. Ret. Res. 1988;7:209–232.
16. Trivino A, Ramirez JM, Salazar JJ, Ramirez AI, Garcia-Sanchez J. Immunohistochemical study of human optic nerve head astroglia. Vision Res. 1996;36:2015–2028. PubMed PMID: 8776468.
17. Stone J, Makarov F, Hollander H. The glial ensheathment of the soma and axon hillock of retinal ganglion cells. Vis Neurosci.12:273–279. PubMed PMID: 7786848.
18. Boycott BB, Hopkins JM. Microglia in the retina of monkey and other mammals; its distinction from other types of glia and horizontal cells. Neuroscience. 1981;6:679–688. PubMed PMID: 6165924.
19. Gallego A. Comparative studies on horizontal cells and a note on microglial cells. Prog. Ret. Res. 1986;5:165–206.

The Architecture of the Human Fovea

Helga Kolb, Ph.D.,[1,*] Ralph F. Nelson, Ph.D.,[2,†] Peter K. Ahnelt, Ph.D.,[3,‡] Isabel Ortuño-Lizarán, Ph.D.,[4,§] and Nicolas Cuenca, Ph.D.[4,‖]

Created: February 7, 2020; Updated: May 20, 2020.

Abstract

We summarize the development, structure, different neural types and neural circuitry in the human fovea. The foveal pit is devoid of rod photoreceptors and of secondary and tertiary neurons, allowing light to directly stimulate cones and give us maximal visual acuity. The circuitry underlying the transmission to the brain occurs at the rim of the fovea. The predominant circuitry is concerned with the 'private' cone to midget bipolar cell and midget ganglion cell pathways. Every cone drives two midget bipolar cells and two midget ganglion cells so that the message from a single cone is provided to the brain as a contrast between lighter signals (ON pathways) or darker signals (OFF pathways). The sharpening of this contrast message is provided by horizontal-cell feedback circuits and, in some pathways by amacrine circuitry. These midget pathways carry a concentric color and spatially opponent message from red and green cones.

Blue cones are sparse, even largely missing in the foveal center while occurring at somewhat higher density than elsewhere in the cone mosaic of the foveal slope. Signals from blue cones have different pathways to ganglion cells. The best understood is through an ON-type blue-cone-selecting bipolar cell to a non-midget, small bistratified ganglion cell. An OFF-center blue midget bipolar is known to be present in the fovea and connects to a blue OFF midget ganglion cell. Another OFF blue message is sent to a giant melanopsin ganglion cell that is present in the foveal rim area, but the circuitry driving that is less certain and possibly involves an intermediate amacrine cell. The H2 horizontal cells are thought to be feedback neurons primarily of the blue cone system.

Amacrine cells of the fovea are mostly small-field and glycinergic. The larger field GABAergic amacrines are present but more typically surround the fovea in a ring of processes, with little or no penetration into the foveal center. Thus, the small field glycinergic amacrines are important in some sort of interplay with the midget bipolar–midget ganglion cell channels. We have anatomical descriptions of their synaptology but only a few have been recorded from physiologically. Both OFF pathway and ON pathway amacrines are present in the fovea.

Introduction

The central point of the visual field ahead of us is the image falling on the fovea in the human retina. This is the area of our visually sensitive retina where the cone photoreceptors are tightly packed, where rod photoreceptors are excluded and where all intervening layers of the retina are pushed aside concentrically to allow light to reach

Author Affiliations: 1 Department of Ophthalmology and Visual Sciences, University of Utah (emeritus); Email: helga.kolb@hsc.utah.edu. 2 National Institute of Neurological Disorders and Stroke, NIH, Bethesda MD; Email: nelsonr@ninds.nih.gov. 3 Department of Physiology and Pharmacology, Medical University of Vienna; Email: peter.ahnelt@meduniwien.ac.at. 4 University of Alicante, Spain; Email: isortliz@ua.es; Email: cuenca@ua.es.

Corresponding author.

* About the authors

† About the authors

‡ About the authors

§ About the authors

‖ About the authors

the densely packed sensory cones with minimum scatter from overlying tissues. The fovea is where focusing on fine detail in the image is perfected, allowing us to read, discriminate colors well and sense three-dimensional depth.

General features of the fovea

Looking at the retina lining the back of the eyeball in a human, we can see the clear landmark of the optic nerve head (papilla) and radiating blood vessels (Figure 1). Temporal to the optic nerve head at a distance approximately 2.5 optic nerve (disk) diameters at roughly 3.4 mm distance lies a dark brown-yellowish area (Figure 1), in the center of which is the tiny circular fovea. The position of the fovea can be seen clearly in the retina illustrated in Figure 2A. This eye was treated with RNA-later for preservation, allowing for a clear view of a yellow macula lutea area and including the brown central point, (foveal pit) (Figure 2A).

The area called the macula by ophthalmologists is a circular area around the foveal center of approximately 5.5 mm diameter (Figure 2B) The macula lutea with the yellow pigmentation extends across the fovea into the parafoveal region and a little beyond. This area is about 2.5 mm in diameter (Figure 2B). The actual fovea is about 1.5 mm in diameter and the central fovea consists of a foveal pit (umbo) that is a mere 0.15 mm across (Figure 2B). This foveal pit is almost devoid of all layers of the retina beneath the cone photoreceptors. On the edges of the foveal pit the foveal slope is still mainly devoid of other layers but some cell bodies of retinal interneurons, bipolar and horizontal cells and even some amacrine cell processes are becoming evident. By the 0.35 mm diameter circular area the first ganglion cell bodies, the retinal neurons sending signals to the brain, are beginning to appear. All the central fovea that measures 0.5 mm across is avascular (FAZ).

The avascular nature of the central fovea is depicted in Figure 3. A human retina wholemount has the blood vessels immunostained with antibodies against Collagen IV and is photographed by stacked images in a confocal microscope. It is absolutely clear that the smallest capillaries even, do not intrude into the foveal center (Figure 3, f) of 500 μm diameter, thereby known as the avascular zone.

In vertical section of the human retina from the optic nerve head through the foveal pit and beyond (Figure 4), it is clear where the fovea is located relative to the nerve head (on). Figure 4 (a) is a confocal image after immunostaining with antibodies that are specific for cone photoreceptors [arrestin antibodies for cones, green; cytochrome C antibodies for mitochondria, blue; and for Müller glial cells and RPE, antibodies against cytoplasmic retinaldehyde binding protein (CRALBP), red]. In comparison is seen an optical coherence tomography (OCT) picture in Figure 4 (b) of exactly the same area of human retina. In both images it is clear that the second and third order neurons of the inner nuclear and ganglion cell layers respectively are not present in the foveal pit.

In the foveal pit the only neurons are cone photoreceptors, all with slim inner segments, packed cell bodies, up to 6 layers deep reaching to the floor of the foveal pit (Figure 5, green cells). However, there are many expanded-looking Müller glia surrounding these cones (Figure 5, red profiles). A central bouquet of cones has their synaptic pedicles ending at the foveal pit floor (Figure 5, green spots, arrows), whereas the cones surrounding them stretch their axons (known as Henle fibers) and presynaptic pedicles away from the center of the foveal pit to the foveal slope area (Figure 5, green spots form a continuous line, arrows). The lack of blood vessels in the central pit can be seen by the absence of the blue circular profiles there (Figure 5, bv).

O'Brien and colleagues (1) very elegantly illustrated the cone axons radiating out from the foveal pit forming the Henle fiber layer and terminating in distant pedicles in a whole mount monkey retina (Figure 6). The picture would be very similar in a human retina. The Henle fiber layer is a combination of outward radially directed axons of the cones, and where rods begin to appear, also rod axons, and Müller cell processes. It is interesting to note in Figure 5 that the pedicles of the very central bouquet of cones are widely spaced ending on the foveal pit

floor. We know from Figure 5 that these central bouquet cone pedicles are separated by voluminous Müller cell elements.

Development of the fovea

Understanding how the primate fovea develops from fetal to adult stage of the retina has been a very difficult task in vision research. This has, of course been due to the difficulty of obtaining retinas from human pre-birth and baby eyes. Even fetal monkey material has been scarce to obtain. Dr. Anita Hendrickson (Figure 7) at the University of Washington, Seattle, spent most of her career pursuing this subject of retinal research, and has contributed almost all we know.

The earliest fetal retinas examined (2) were from a week-22 eye. The fovea is not recognizable at this stage, because the central region of the retina, where the fovea will develop, consists primarily of several layers of ganglion cell bodies and inner nuclear layer cells (INL), presumably amacrine and bipolar cells (Figure 8, a). A single layer of developing cones stretches from outer plexiform layer (OPL) to pigment epithelium and choroid (Figure 8, a, right inset). A hint of a developing cone pedicle is seen (Figure 8, right red arrow) but there is no sign of outer segments of cones (Figure 8, right, apposing red arrowheads). By fetal week 28, an indentation of the retina at the thickest ganglion cell layer appears and can be considered the earliest sign of the foveal pit (Figure 8, b, P). The inner nuclear layer has become thinner and appears pushed out of the pit (P) but a kind of split is occurring in the middle of the INL known as the transient layer of Chievitz (TC, Figure 8, c) (3). By fetal week 37 (Figure 8, c) a pronounced foveal pit is evident (P), the ganglion cells are thinned to 2 or 3 deep and the TC area in the INL appears like a sheared, radially projecting area of probable Müller cell fibers. Through the latter two fetal stages, where the foveal pit is becoming obvious, the cones are still immature, arranged in a single layer and have no visible outer segments (Figure 8, b and c). However, there is the first suggestion of the cone axons being tilted away from their cell bodies to form the early Henle fiber layer.

It is interesting to closely examine the cone photoreceptors in the fetal 35-to-37-week retinas as illustrated by Hendrickson and coauthors (2). Figure 9 shows how immature the cones of the foveal pit are compared with those of the cones at some distance from the fovea (Figure 9. 2 mm from fovea). At the foveal pit area, the cones are just stubby cells with a synaptic pedicle, little to no lengthened inner segment and zero outer segments (Figure 9, fovea). By 800 μm to 2 mm from the developing foveal pit, the cones become elongated vertically and have definite cone pedicles. Most cell bodies descend away from the external limiting membrane and have elongating axons that are angled away from the foveal pit, forming the early Henle fiber layer. Inner segments are long, but the outer segments are still not formed. (Figure 9, 800 μm and 2 mm).

At birth of the human baby the retina in the eye is looking recognizably foveate (Figure 10, a). The foveal pit now contains a very thin, only one layer thick, ganglion cell layer, a thin inner plexiform layer (IPL) but a prominent inner nuclear layer (INL) (Figure 10, a). The cones are now evident as straight vertical cones with synaptic pedicles, cell bodies and inner segments. There are probably developing cone outer segments too (not easy to see at this magnification). But the pit is still several cell layers thick with only the cones on the foveal slope beginning to angle away from the pit. Further out on the foveal slope the cone Henle fiber layer is obvious now (Figure 10, a). By 15 months after birth, the baby retina has a definite fovea and even the central cones are angling out to the foveal slope. Inner and outer segments are well developed in the pit and no other layers of the retina are here anymore (Figure 10, b and c). By 13 years the fovea is completely developed (Figure 10, d) (2).

What forces could cause this remarkable transformation of an evenly thick multi-cell, layered retina to become concavely dimpled, buckled up and stretched outwards to form a single layered pit at the fovea and a high sided sloping tissue with the highest concentration of cell layers at the foveal rim. The developmental effort is to ensure that a central area of the retina is concentrated with the slimmest packed cones with no obstruction of incoming light by secondary and tertiary cell layers.

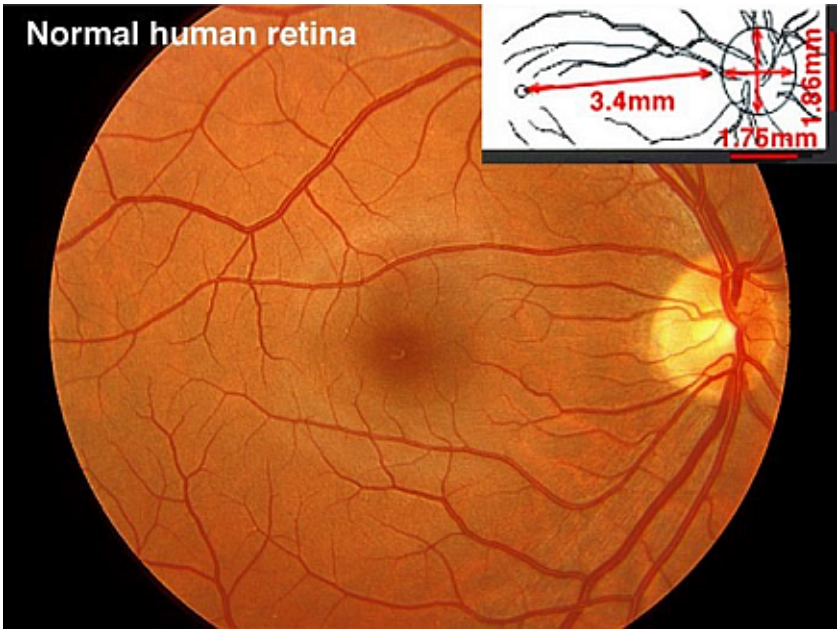

Figure 1. The normal human retina fundus photo shows the optic nerve (right), blood vessels and the position of the fovea (center).

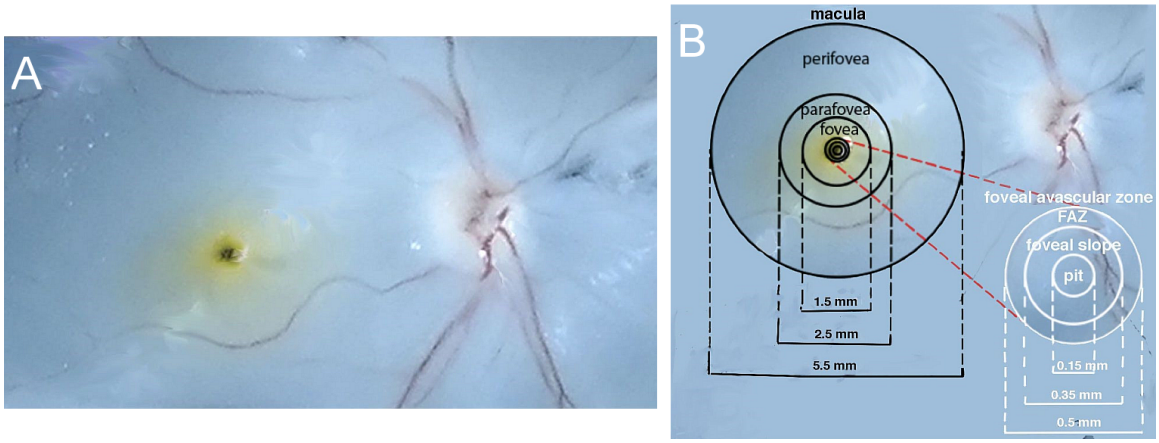

Figure 2. (A) An isolated human retina shows the optic nerve (right), blood vessels and the fovea (center) with surrounding macula lutea (yellow). Cuenca et al, prepublication. (B) A map of the whole macular area to show the dimensions of the foveal pit, foveal avascular zone, parafovea, perifovea, and the limits of the macula. Inset shows the dimensions of the foveal avascular zone, which is the fovea we are discussing here. Cuenca et al, prepublication.

The most recent investigations on this developmental phenomenon in the human (primate) retina provide evidence that the radial retinal glia - the Müller cells and possibly the astrocytes of the ganglion cell layer - are instrumental in this process (4). The Müller cells of the foveal pit are closely associated with the cone fibers and together they make up the Henle fibers layer (Figure 11A, red profiles). Bringmann and colleagues suggest that the Müller cells exert tractional forces onto cone axons fibers by a vertical contraction of the central most Müller cells and cones so they become elongated and very thin (Figure 11, B, blue arrows). After widening of the foveal pit by elimination of astrocytes in the pit and ganglion cell layers, the Henle fibers are forced, by horizontal contraction of their surrounding Müller cell processes in the outer plexiform layer, to pull the cone and then rod photoreceptor centrifugally away from the pit (Figure 11, B, orange arrows).

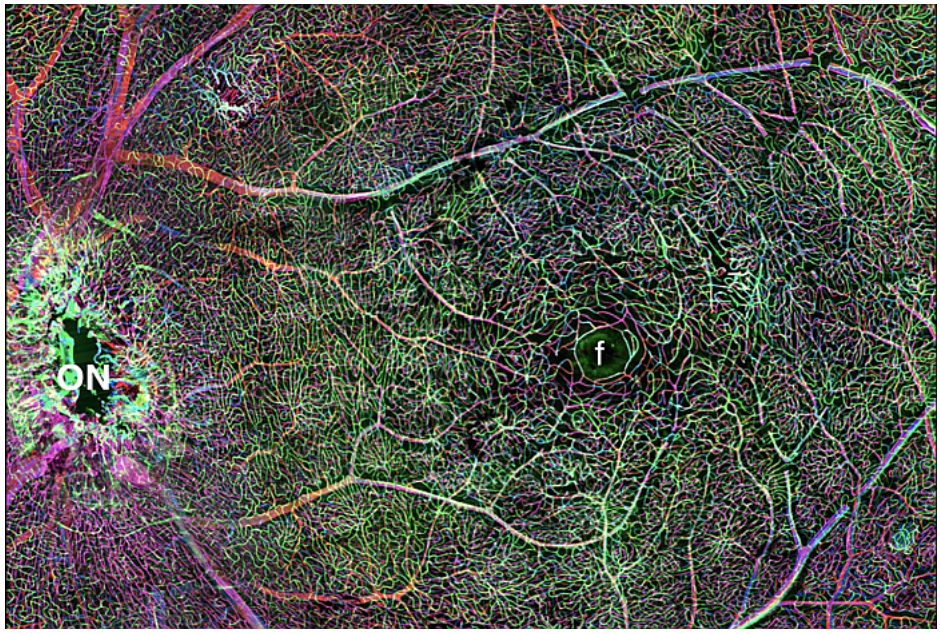

Figure 3. Wholemount of human retina with blood vessels immunostained with Collagen IV. The confocal microscopy of stacked images clearly shows the optic nerve head (ON) and all the blood vessels to the smallest capillaries. The capillaries surround the fovea (f), but do not enter it, thereby making the fovea avascular.

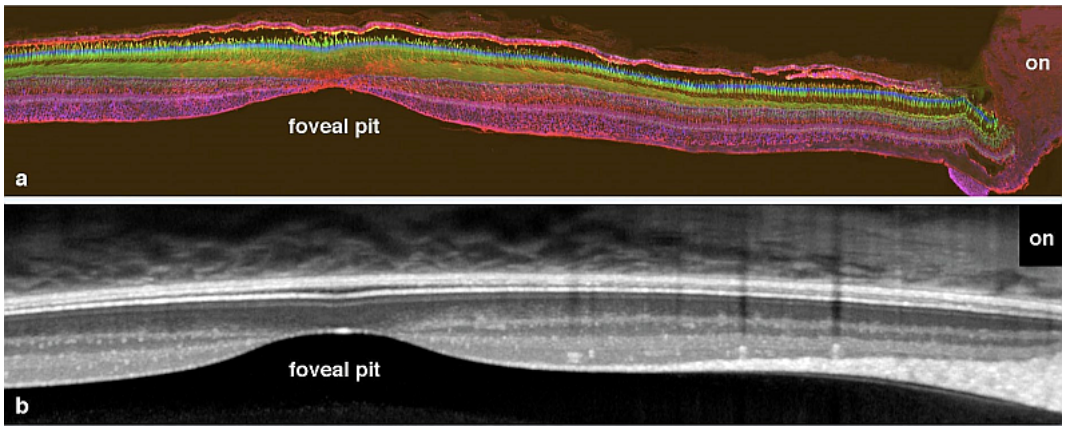

Figure 4. (a) An immunostained human retina section covering the optic nerve (ON) and the foveal pit. Cones, anti-arrestin (green); pigment epithelial and Müller cells, anti CRALPB (red) (109); mitochondria, anti-cytochrome C (blue). (b) An OCT image of the same retinal area in a normal human subject. The second and third order neurons of the retinal inner nuclear and ganglion cell layers respectively are not present in the foveal pit. Adapted from Cuenca, Ortuño-Lizarán and Pinilla 2018 (110).

The mosaic of cones in the fovea

The term "foveal cone mosaic" generally refers to the strikingly regular patterns of condensed cone inner and outer segments with largely triangular crystalline organization, which nevertheless includes non-randomly distributed discontinuities (5, 6). The less familiar and less understood part of foveal cones is the further course towards their synaptic terminals. It includes a two-step transition. From a two-dimensional mosaic for image reception it is rearranged into to a three-dimensional somata tiling, which then again spreads out to establish the concentric monolayered pedicle meshwork (7-9).

The mature human fovea consists of 3 spectral types of cone: red or long wavelength sensitive cones, L-cones; green or medium wavelength cones, M-cones; and blue or short wavelength cones, S-cones. These three types of

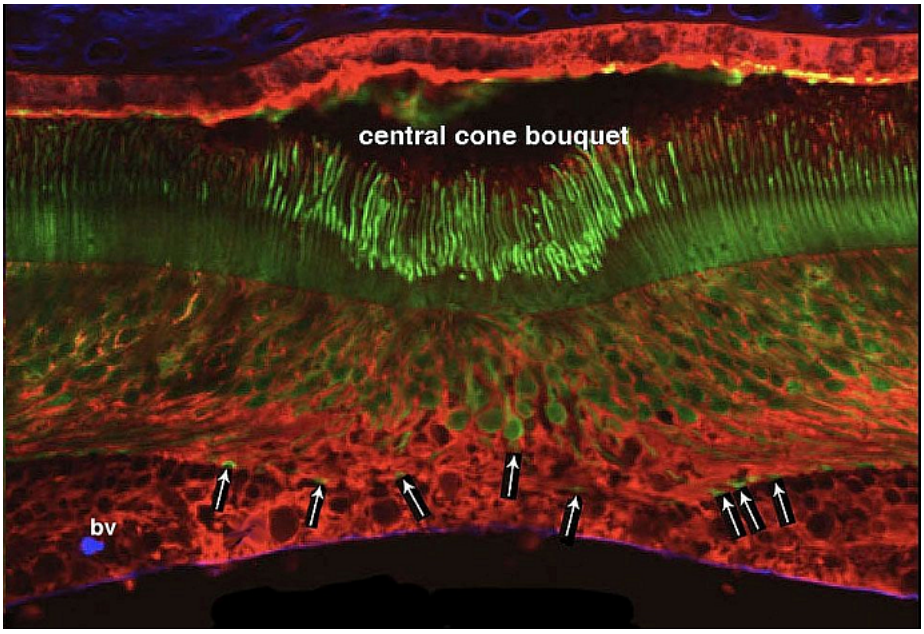

Figure 5. Vertical section of the human fovea immunostained with antibodies to cone arrestin (green), CRALBP (red) and Collagen IV (blue).

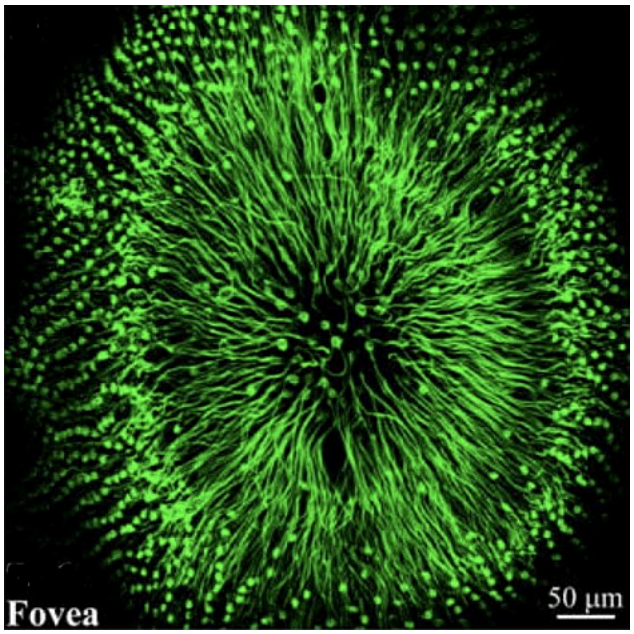

Figure 6. A wholemount monkey fovea immunostained with cone arrestin. The axons of the cones radiate out to a ring of cone pedicles. Central bouquet cone axons stay in the foveal pit. From O'Brien et al., 2012 (1).

cone are tightly packed and at their most concentrated (up to 200,000/mm^2 in the fovea (8, 10) (see Webvision Facts and Figures). Rods are not present in the foveal pit, appearing first halfway into the foveal slope, beyond the 300 µm diameter area (see Figure 2B).

It is extremely difficult to get a horizontal section through the central fovea particularly including the central bouquet of cones because of the concave nature of the fovea. Figure 12 (a) manages to get such a view of a horizontal slice through the inner segments of the cones of a human fovea (7). The tiniest central cones in the center of the photograph (Figure 12 a) are very slim at 2.5-3 µm in diameter and become progressively larger as

Figure 7. A young Anita Hendrickson at her microscope. From her obituary in 2017 (111).

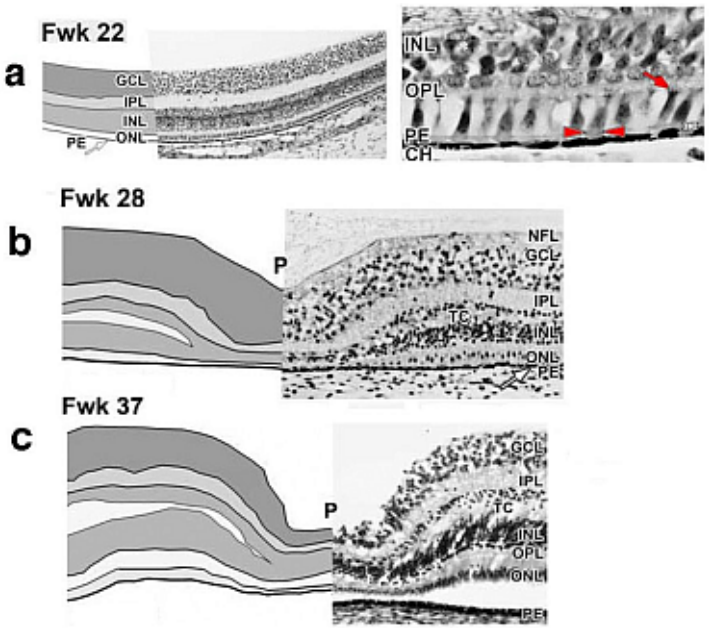

Figure 8. Foetal human retina at (a) foetal week (Fwk) 22, (b) Fwk 28, and (c) Fwk 37. The foveal position is not noticed at week 22 but in later weeks becomes dimpled as ganglion cells become displaced out radially from the developing foveal pit. In the beginning the retina is thick, multilayered and cones are undeveloped with no outer segments or visual pigment (a: right enlarged photo, red arrow heads point to a cone nucleus, a stubby inner segment, and a developing cone pedicle). From Hendrickson et al., 2012 (26).

they move along a radial gradient from the central bouquet. It is noticeable that the cones are not uniformly distributed in a hexagonal mosaic. Small patches of cones are hexagonal and then the patch is interrupted and shifts the surrounding patches slightly (Figure 12 a). Ahnelt and coauthors (11) noticed that these shifts in the mosaic usually were associated with the position of a slightly larger diameter cone. They proposed that these larger cones were the short wavelength cones, the S-cones, and described their morphological differences from the surrounding, more common L- and M-cones (11).

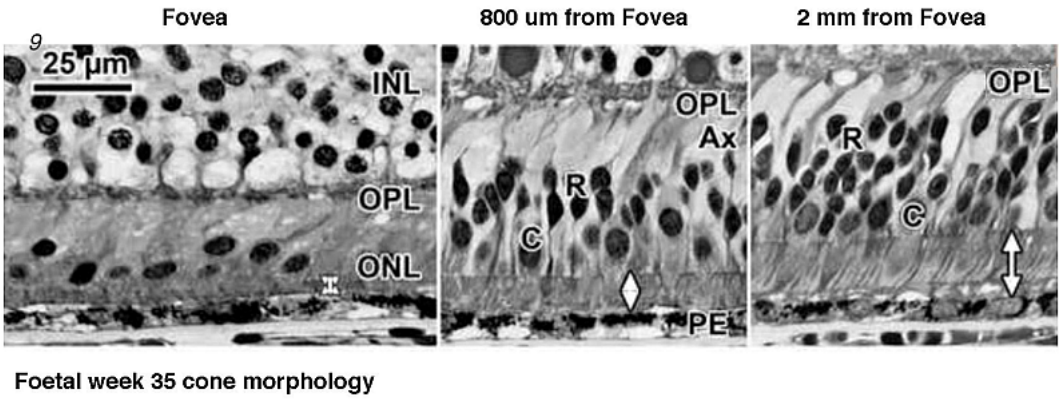

Figure 9. Sections of the retina of a human foetus at 25 weeks gestation. The cones of the fovea are still undeveloped with no outer segments, and a synaptic area with no axon. From 800 µm to 2 mm from the foveal center there are clear elongated inner segments but still no outer segments. The slanting of the cone axons out radially is beginning to be evidence of a developing Henle fiber layer. From Hendrickson et al., 2012 (26).

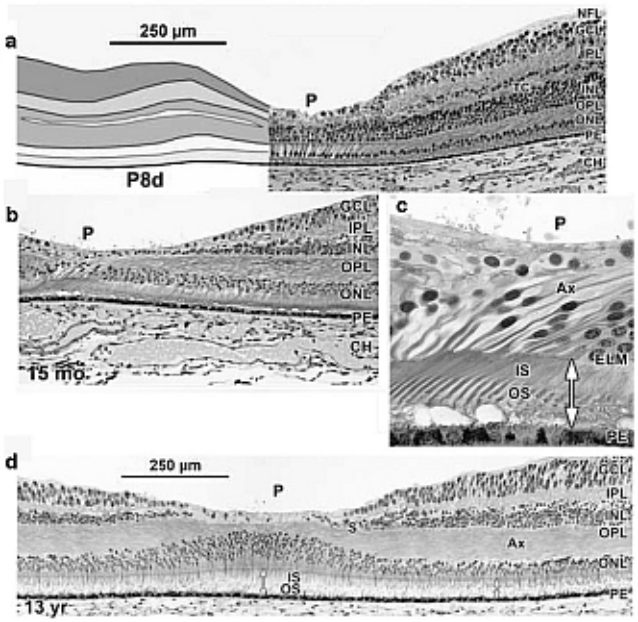

Figure 10. The foveal retina sections of a human from (a) postnatal 8 days (P8d), through (b) 15 months, to fully formed (d) 13 years. (c) At 15 months the cones are thin, have outer segments and squash together and, except for the central bouquet, send axons radially outwards as the Henle fiber layer. Second order neurons and ganglion cells are pushed along the foveal slope to form a pile of ganglion cell bodies at the foveal rim. From Hendrickson et al., 2012 (26).

S-cones are relatively rare in the retina compared with the much more dominant L- and M- cones. The S-cones are, however, ubiquitous in all vertebrate retinas, with the exception of cetaceans (12). As far as other mammals are concerned S-cones are commonly paired with L-cones to give them a dichromatic color sense. These L-cones vary in spectral peak, and the more mid-spectral types are called M-cones. In old world monkeys and apes, and in man an L-opsin gene duplication and further mutation produced an extra mid-spectral L-cone opsin subtype, M-cone opsin. The combination of L-cones, M-cones and S-cones provides trichromacy. This trichromacy allows discrimination of green, yellow and blue/purple hues.

There are differences in the genetic structure and locus of the S-cone visual pigment compared with the M- and L-cone pigments (13), yet the S-cones always form a consistent 8-10% of the mammalian cone photoreceptor population (14, 15). In primates and humans of course, the S-cones are rather scarce in the foveal pit. Some

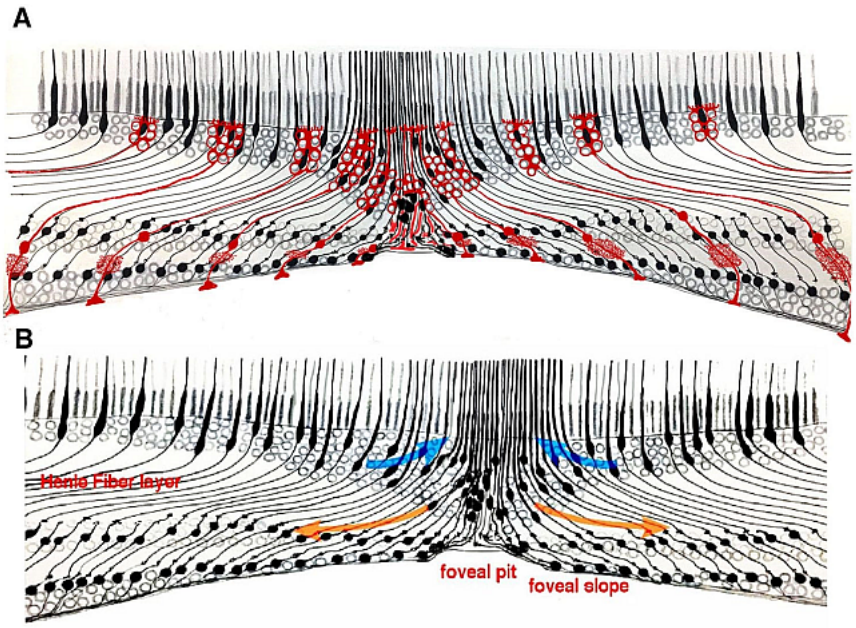

Figure 11. (A) A human fovea drawing to show that the Henle fiber layer consists of cone photoreceptor axons as well as envelopingMüller cells and fibers (red). B) Drawing to show the central foveal cone bouquet of thin and closely packed cones in the foveal pit. The cone axons on the foveal slope move radially out with the Müller cells to form the Henle fiber layer and end in pedicles that make connection with bipolar cells at some distance from the foveal pit. Blue arrows show the vertical squeezing and packing of the cones in the foveal pit and orange arrows show the displacement horizontally of the foveal cone axons, during development of the adult fovea.

authors suggest that there is a so-called blue cone blind spot (16). However, S-cones peak in number on the foveal slope of the human retina and here form about 12% of the population. Figure 12 (b) shows the peak S-cone distribution on the foveal slope in a human retina as identified by the larger size and arrangement in the mosaic breaking up the regular hexagonal pattern distribution of the other cone types. In Figure 12 (c) the S-cones have been colored in for clarity.

Since these earlier identifications of foveal S-cones on morphological criteria (11), antibodies against the S-cone pigments in the cone outer segments have been developed and are able to positively identify the S-cones in the overall population by immunocytochemical methods. In figure 13, the human foveal pit (FP) and foveal slope are immunostained with an S-cone antibody and illustrate the S-cones as black spots and angled black cone outer segments. In the foveal pit only a few S-cones appear interspersed in the mosaic of highest density (Figure 13). However, their proportion increases in surrounding areas and are at their highest density on the foveal slope (Figure 13 brown spots, top and right-hand side).

Figure 14 illustrates immunostaining in vertical section and the scarcity of S-cones in the foveal pit compared to the increase in number of this population of cones on the foveal slope, of a human retina. A map of the S- cone distribution in another human fovea is shown in Figure 15. The lighter to darker blue shading indicates less dense to denser S- cone presence. Note in both images (Figs. 14 and 15) there are very small numbers of S-cones in the foveal pit.

It has been rather easy to identify S-cones in the human fovea and the rest of the retina by these immunocytochemical techniques where S- cones can be visualized and distinguished from the surrounding L- or M-cones. Figure 16 shows a spectacular confocal image of the cones in near peripheral human retina by immunolabeling with cone arrestin, and by the HJ455 antibody to S-cones, that shows up the S-cone opsin both in the outer and inner segments.

Sadly, the L-cones and M-cones are not distinguishable on immunostaining techniques because their visual pigments are so close in structure. There is presently no antibody developed to separately mark them into L- or M- cone types. So, to identify L- and M-cones in the human fovea we must go to other more sophisticated techniques. Psychophysical measurements have suggested that L- cones usually outnumber M-cones by 2:1 in the human fovea (17). Microspectrophotometry of all cones in small patches of cones in the fovea of monkeys, has revealed that L- and M-cones occur in about equal proportion (18).

Newer techniques, introduced by Roorda and Williams (19), use adaptive optics to make direct measurements of spectral sensitivity of foveal cones in the living human eye (Figure 17). They found that humans varied greatly in the proportions of L-cones to M-cones: some individuals have almost equal proportions while others have a higher proportion of L-cones, even to the extreme of 16 L-cones to every M-cone (Figure17, BS). While the sparser S-cones are spaced regularly, the L- and M-cones lie randomly in the mosaic meaning that clusters of cones of the same spectral type will occur together as suggested from Mollon and Bowmaker's paper (18). Roorda and coauthors (20) concluded that L- and M-cones are in a random distribution in the foveal center (21). Nevertheless, the human subjects HS and BS in Figure 17 would seem intuitively to have a different perception of color. But both subjects were reported to have normal color vision (19). A single cone is achromatic, and its stimulation doesn't result in color vision unless there is comparison to stimulation of a neighbouring cone with different opsin (22). This comparison is done by retinal and brain neural circuitry (see later section on horizontal cell roles in spectral antagonism). Some elegant recent human adaptive optics studies and psychophysical reporting found that 79% of targeted cones in the foveal center, tested for color perception, correctly identified the color (hue) (22). Interestingly, others, using similar techniques of adaptive optics and human reports of hue for single cone stimulation with colored light in the fovea, found a considerable proportion of cones produced only white sensations (21).

The architecture of foveal fibres of Henle and pedicles

The process of centrifugal displacement by the Henle layer affects cone pedicles in different ways, depending on their eccentricity (Figure 18).

In the central bouquet of cones in the foveal pit, the pedicles appear to stay in place (Figure 18). In serial semithin (Figure 19, a) and electron microscopic (Figure 19, b) sections, a few roundish pedicles can be found at the foveal floor (Figure 19, a-c, circles). They are isolated from each other, thus lacking any connections to other cones via telodendria. Still they are contacted by dendritic processes running horizontally from a few interneurons (presumably bipolar and horizontal cells) from the foveal slope or even those neurons lying embedded in voluminous Müller cell processes (Figure 19 b-c, red circles around pedicles).

From the outer central cones, Henle fibers of short length terminate in peculiar tadpole-like pedicles (Figure 18, Figure 19, d-e). They too are largely isolated from neighboring terminals and are characteristic of the cone pedicles until about 1° or 288 µm out (23). Beyond this zone – still almost entirely established by cone terminals only – the pedicles make up a patchy mosaic (Figure 19, f-g). These terminals elaborate telodendrial networks that end on neighboring cone pedicles at gap junction connections (1, 24). This pedicle mosaic tends to establish radial arrays yet is locally influenced by interspersed glia (Figure 19, g).

The cones of the foveal pit project vertically downwards (Figure 20, a). As the concentrated central cones have to extend their axons radially out of the pit they, together with Müller cells, become the Henle fibers. The cone axons become longer and longer as they project onto the foveal slope and into the parafovea (Figure 20, b, 200-400 µm long). From then on, further out into the perifovea, the axons begin to shorten and by 3 mm eccentricity from the foveal pit axons are essentially no length at all (Figure 20, c-d, 4000 µm periphery). The Henle fiber layer is over as is the macula lutea (Figure 2A, Figure 2B).

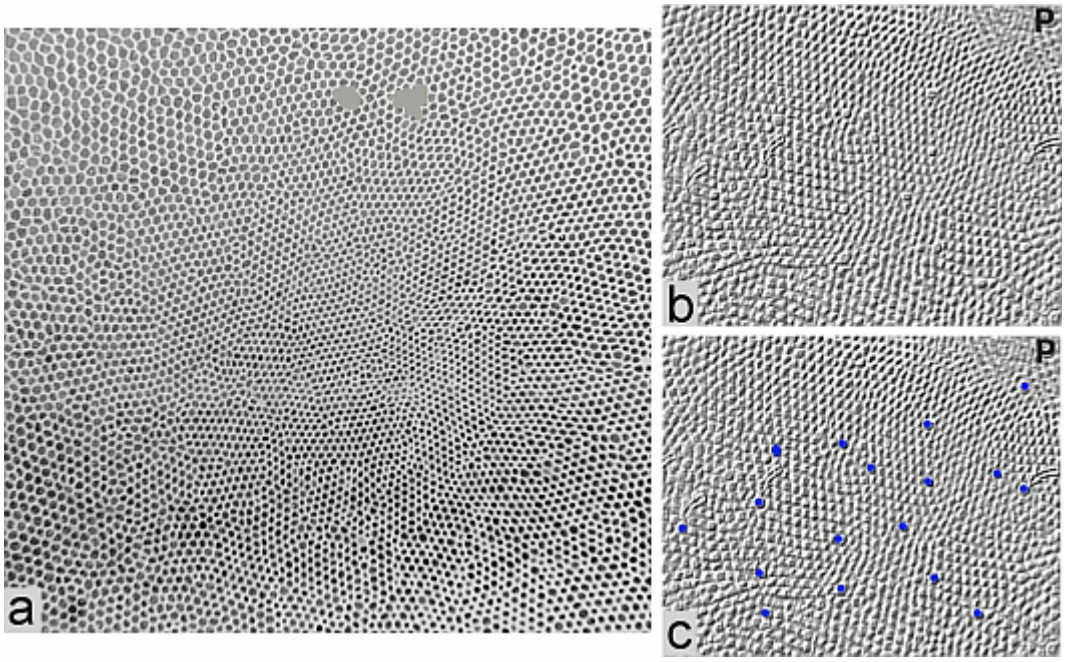

Figure 12. (a) A horizontally sectioned and stained human retina at the foveal pit and rod free area. (b) A whole-mount photograph of the foveal slope of a human retina. **P** (upper right corner) is the foveal pit. The larger S-cone profiles break up the mosaic of cones into disjointed groups of closely packed smaller profile cones [arrows in (a, b)]. (c) The larger S-blue cones in (b) are colored in as blue. From Ahnelt et al., 1987 (11).

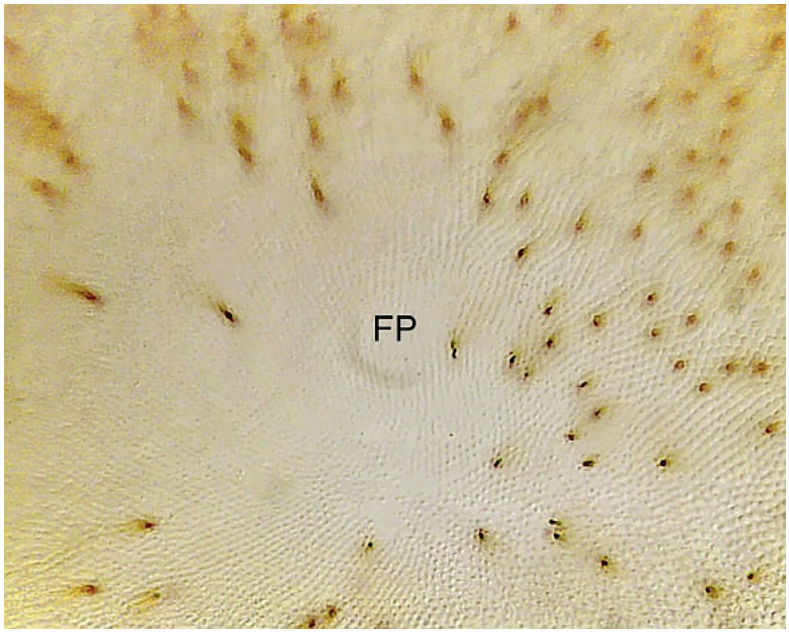

Figure 13. The foveal pit (FP) and part of the foveal slope are immunostained with an S-cone opsin in a human retina.

Substructure of the foveal cone architecture

S-cones and M/L-cones differ in the time course of mitotic differentiation and expression of opsins. According to Xiao and Hendickson (25), S-opsin and various synaptic proteins are detectable at fetal week 11, while various synaptic and transduction proteins appear in M/L cone subclasses before their opsin visual pigments are detected at fetal week 13 (26). It is clear that S-cones develop in a different mosaic than M/L-cones. Ahnelt and

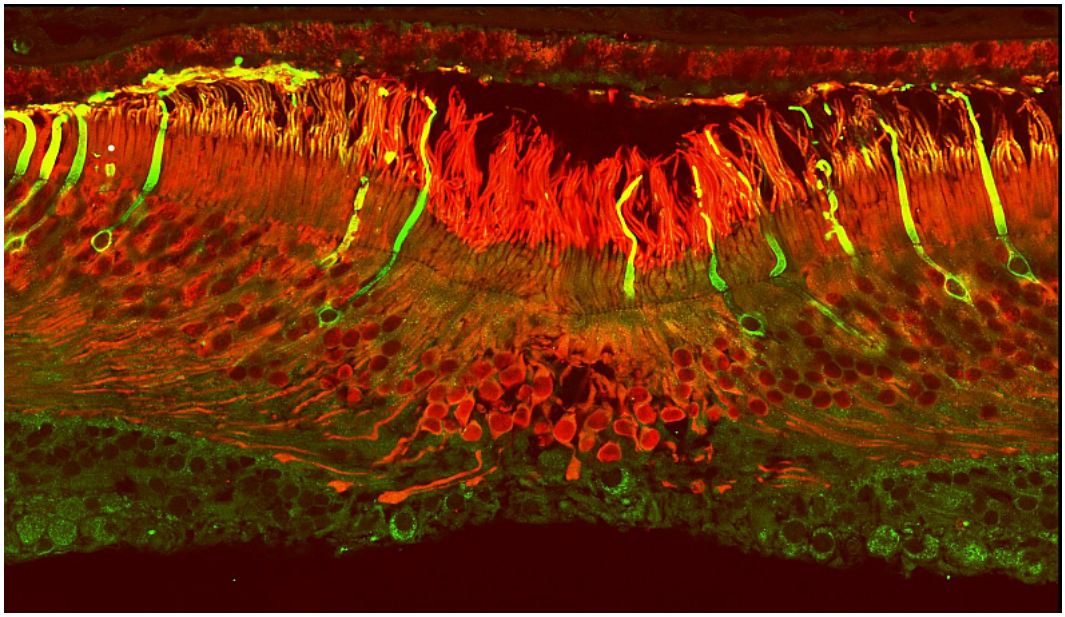

Figure 14. Vertical section of a human foveal pit immunostained with antibodies against cone arrestin for all cones (red), and JH455, which labels S-cones (green). Few S-cones are found in the foveal pit.

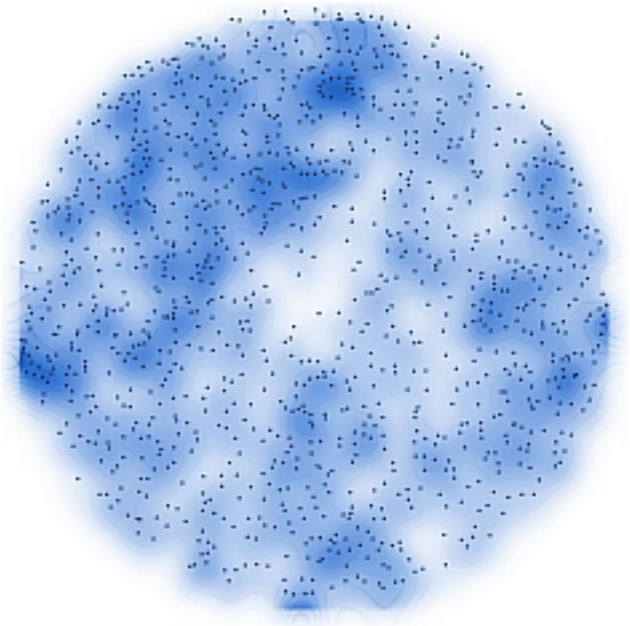

Figure 15. Every S-cone is labelled with S-cone opsin antibody in a human fovea. The more intense blue shading indicates greater densities of S-cones in the foveal slope where they reach 12% of the cone population.

coworkers (7) have noted that cones likely to be short wavelength sensitive tend to occur in irregular positions in both, foveal and peripheral areas. Figure 21A shows an opsin labeled S-cone (asterisk) positioned between seemingly linear series of unlabeled M/L-cone inner segments. Thus in the foveal all-cone mosaic, S-cones appear to interrupt the linear beads of L/M cone-cell inner segments and clearly do not belong to the mosaic of M- and L-cones (6).

The S-cones form a random mosaic like the M/L cones except at the foveal slope area where they are at highest concentration. Here they approach a non-random distribution (25).

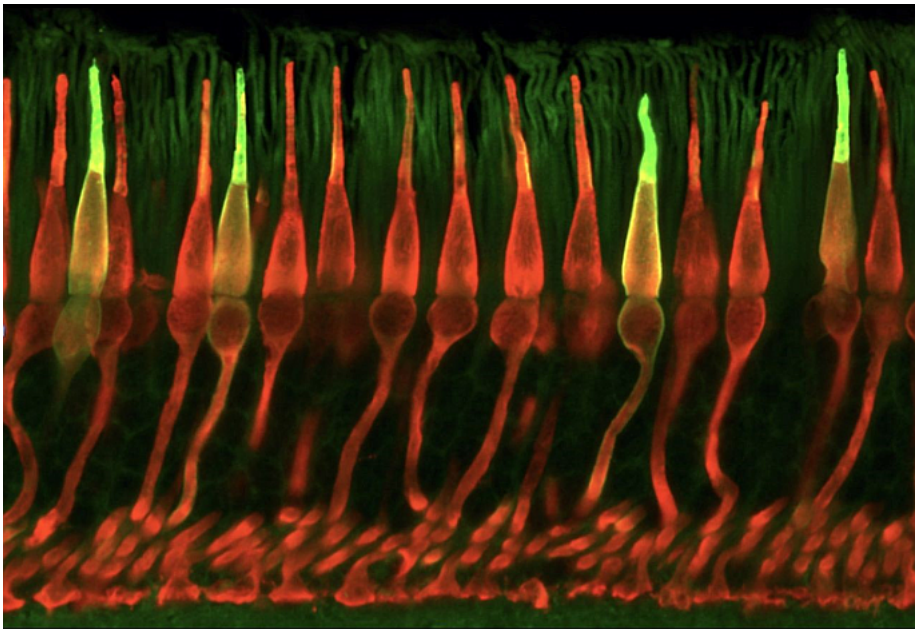

Figure 16. Near peripheral retinal human cones stained with HJ455 antibody that identifies the S-cones (green) amongst the arrestin (red) labeled cones.

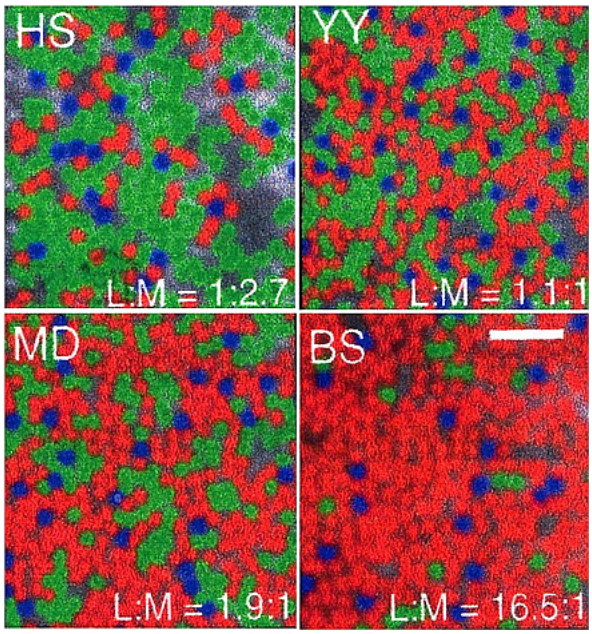

Figure 17. Method of adaptive optics shows mosaics of L (red), M (green) and S (blue) cones in four human subjects with normal color vision. The ratio of S to L and M cones is constant, but that of L to M cones varies from 2.7:1 (L:M) to 16.5:1 (L:M). Adapted from Roorda and Williams, 1999 (19).

Figure 21B shows a schematic summary (7) of cone arrangement in the mosaic of the foveal slope area where the S-cones develop first and reach the non-random mosaic arrangement (25, 27). Three L/M cone patches are exemplified with false colors (yellow, dark blue green and light green). These have migrated downward from an initial position near the external limiting membrane (ELM) to form bead-like arrangements of M/L cone cell bodies in the depths of the outer nuclear layer (ONL). Their axons (Henle fibers) emerge from the cone nuclear layer and radiate centrifugally towards their pedicles. At the intersection of the L/M patches sits an S-cone always with its cell body, unmigrated, up at the outer limiting membrane. Figure 21B left top, indicates the

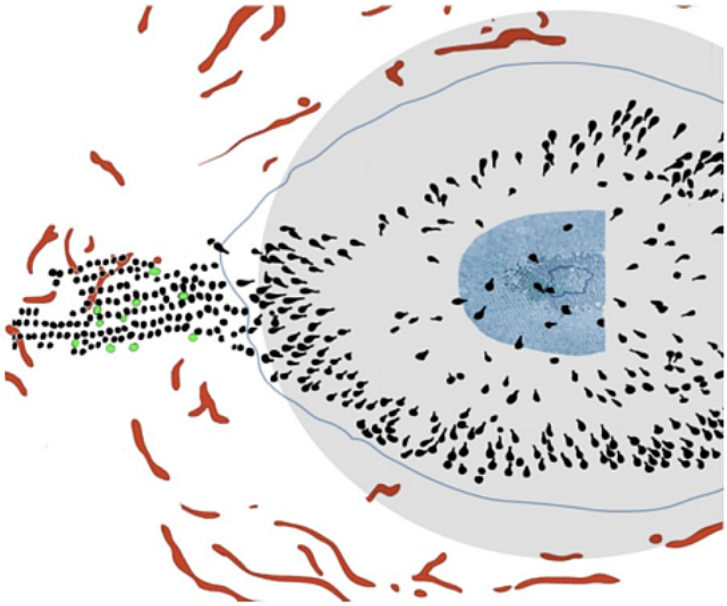

Figure 18. Foveal pit in blue and the foveal slope to the foveal edge in grey. Cone pedicles lack telodendria in the foveal pit. Pedicles with increasing eccentricity along the slope have tadpole-like shape. More peripherally cone pedicles are round in shape and have telodendrial interconnections. The transition coincides with the appearance of capillaries (red) and microglia (green spots). The thin blue line denotes the elliptical course of the external limiting membrane sectioned at the foveal slope at 1 degree (300 µm eccentricity).

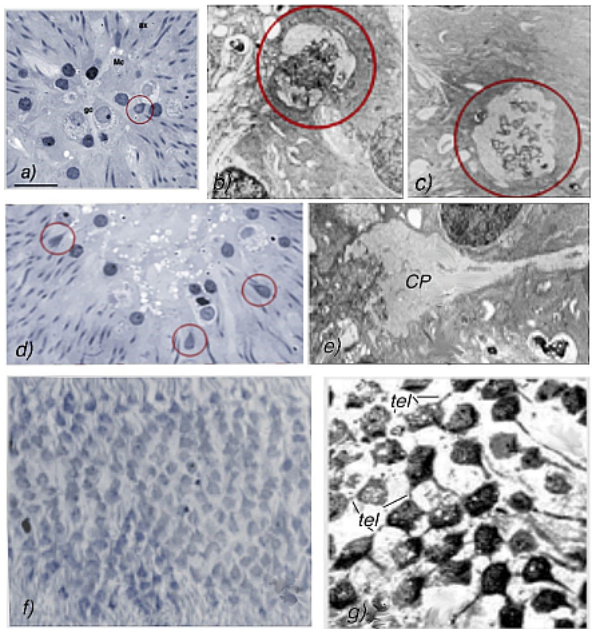

Figure 19. LM and EM appearances of cone pedicles. (a), (b) and (c) are isolated pedicles of the foveal pit (red circles). There are large Müller-cell processes and neural processes running to the cone pedicles. (d) and (e) show tadpole-like cone pedicles on the foveal slope. (f) Pedicles at the first capillary zone are arranged in curved, bead-like series. (g) Higher magnification shows the telodendrial network between most cone pedicles in (f). (a) is from Ahnelt, 1998 (112), ganglion cell (gc), Müller cell (Mc), cone axon (ax), scale bar 50 µm. (g) is from Ahnelt and Pflug 1986 (113).

original position (transparent ovals) of M/L cell bodies before mosaic condensation and their presumed path (tapered rays) to their adult positions.

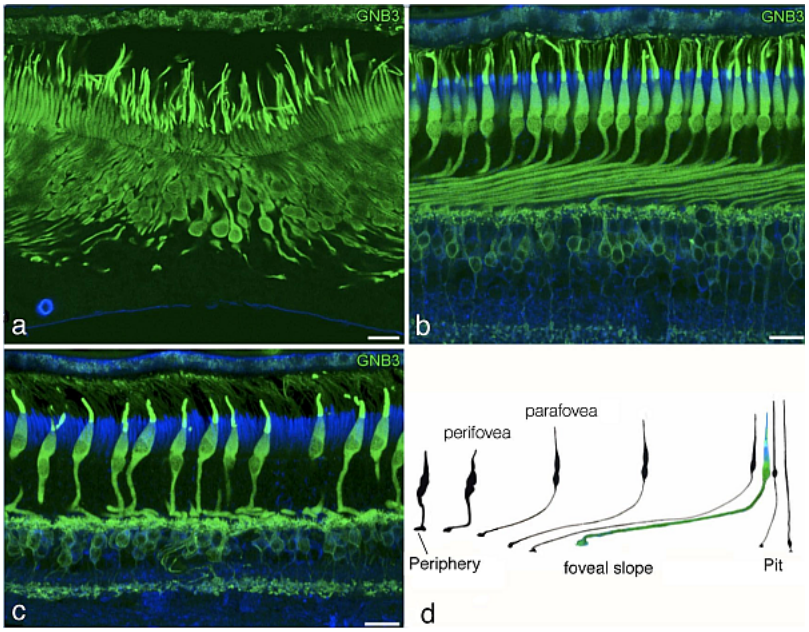

Figure 20. Cone morphology in the foveal pit (a), foveal slope (b) and peripheral retina (c). Cones and ON bipolar cells are immunostained with GNB3 (green). Drawing (d) shows the cone morphologies in the different areas. An S-cone (blue-green) is shown in comparison with the M/L-cone types.

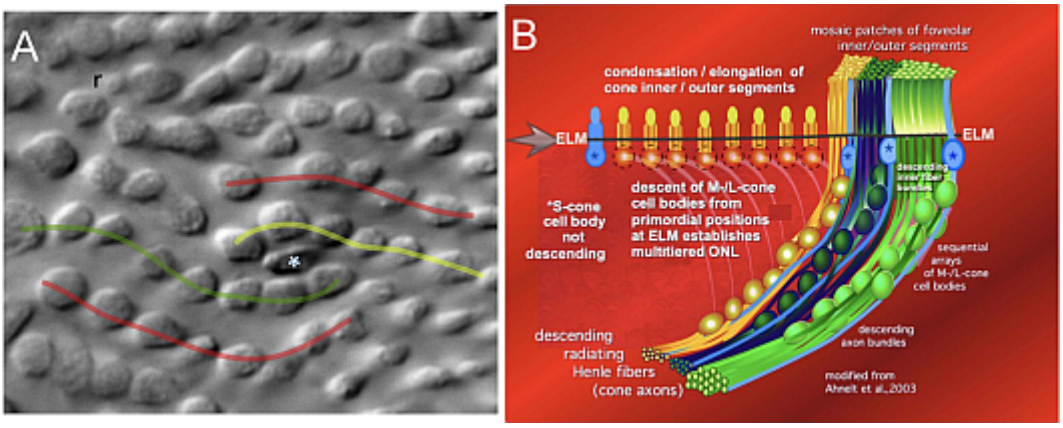

Figure 21. (A) Human cone inner segment mosaic on the foveal slope. Note the first rod (r), and the bead-like arrangement (colored lines) of the M- and L-cones circumventing an S-cone labeled by an S-opsin antibody (asterisk). (B) The transformation of the foveal cone mosaic groups (yellow, dark green, light green) by condensation of their inner/outer segments to vertical sequences of beaded cell bodies and descending, radiating axons in the Henle fiber layer. At left, the original position of the yellow group's cell bodies (line of ovals) before mosaic condensation is indicated, as well as their eventual path (curved lines) to their adult positions. Apparently, S-cones (blue) do not participate in this process, as their cell bodies stay close to the ELM (external limiting membrane, large arrow). Adapted from Ahnelt et al, 2004 (7).

Horizontal cells of the fovea

As we have illustrated in Figure 2B, the whole fovea is roughly 1.5 mm across and so any cell found within 750 µm of the foveal center is considered a foveal associated cell. It has been hard to get good staining of horizontal cells (HC) of the fovea but some Golgi impregnated human retinas in our possession did allow us to see a few within the 750 µm of eccentricity around the central foveal pit (Figure 22) (28).

The closest to the foveal center, which is of course cell free except for cone photoreceptors and some dendrites running up to synapse with the central cones, would be the HC at 200 μm from the foveal center (Figure 22, top cell). These horizontal cells are elongated and arranged concentrically in a circle around the foveal center and on the far edge of the foveal pit. The area could still be in the avascular zone. Note the dendrites are reaching quite far to contact central cones. The cells are axon bearing, but morphologically it is difficult to judge of which type. The cells at 350 μm (Figure 22) are much smaller than the foveal edge HC but now recognizable as H1, H2 and H3 cell types (28). The smallest are the H1 cells that appear to contact about 4-5 cones, judging by their dendritic clusters. H2 cells are wirier and more irregular than H1 and H3 cells but have quite closely packed and profuse dendrites (Figure 22). These H2 cells would be reaching into the foveal slope area, where we know there is the highest density of S-cones, to contact the latter cone type. H3 cells may also be reaching into the foveal slope but we know from previous data they do not receive synapses from S-cones (29, 30). There are no evident axons on these Golgi stained horizontal cells (Figure 22, 350 μm), which probably reflects understaining.

The three horizontal cells at 500 μm from the foveal center (Figure 22) would also be foveal HCs but in an area where blood vessels occur and the first rod photoreceptors are present. As can be seen they are a little larger in dendritic field size (Figure 22). The H1 cell contacts 6 cones and the H3 about 8-9 cones (Figure 22). H1 and H2 types here have axons (small arrows in Figure 22), which will expand into axon terminals in contact with rods in the case of H1, and with S-cones in the case of H2 cells (31).

By confocal microscopy the central human fovea can be seen to contain parvalbumin immunoreactive horizontal cells (Figure 23, a-b; green cells under the cone pedicles). Parvalbumin identifies H1/H3 horizontal cell types and it is likely that the Golgi staining at the 200 μm distance from the central foveal pit is therefore of these types. They are elongated and not closely packed. Their dendrites would be reaching to contact central foveal bouquet cones (Figure 23, b). In contrast, the H1s of the foveal slope are closely packed with vertically squashed cell bodies and small bushy dendrites reaching to the closely packed cone pedicles at the ends of the Henle-fiber-layer cone axons (Figure 23, c). These HCs are clearly the same as those in the Golgi preparations at 300-500 μm (Figure 22).

The H2 cells of the human retina are known to be particularly associated with the S-cone (blue) photoreceptors (see Webvision chapter on S-cone pathways). We know that H2 cells stain with antibodies to calbindin in the human retina as compared to parvalbumen staining for H1/H3 cells. Figure 24 (white arrows) shows a few calbindin positive HCs (red cells, arrows) on the foveal slope in human retina. In addition to the H2 cells with cell bodies close to the OPL, there are diffuse cone bipolar cells contacting several cones, and amacrine cells stained with calbindin. These red, diffuse bipolar cells have cell bodies lower in the inner nuclear layer and long slanted single apical dendrites as compared to the red H2 cells. Note in this section of human fovea the first rods are present on the foveal slope and the first rod bipolar cells are staining for the antibody to PKC (Figure 24, green cells).

Horizontal cells of the vertebrate retina are known to have important roles in sharpening and scaling of responses from photoreceptors through the subsequent retinal pathways to influence the ganglion cell output (32). At the first level of the outer plexiform layer, horizontal cells are involved in feedback of signal from surrounding cones to each individual cone's receptive field. This surround input is expanded well beyond the horizontal cell's dendritic connectivity field by virtue of gap junctions that join the dendrites of many horizontal cells of the same type together. i.e. in human retina the H1-H1 cells would be joined in gap junctions and the H2 cells would likewise be joined to other H2 cells (See the Webvision chapter Myriad roles for gap junctions in retinal circuits). This large feedback effect provokes an expanded region of antagonistic signal compared with the central cone signal. In the case of M- or L-cones the antagonistic surround is a mixed M- and L-cone signal. In other words, individual M- and L-cones do not show classic spectral opponency just mixed M- / L-cone surround antagonism (33). The feedback in the case of an S-cone would come from H2 cells, whose contacts include surrounding M- and L-cones. Indeed S-cones have been recorded from in monkey retina and found to

have blue–yellow spectral opponency as well as center-surround organization (34, 35). Presumably spatial opponency would be transmitted from the M- and L-cones to their respective bipolar cell connections, and in the case of the S-cone, a true spectral opponency has been proven to be transmitted as well (34). No recordings have been made in foveal cones to really see if an M- or L-cone has a spectrally opponent surround like that of (albeit peripheral) S-cones (35).

Midget bipolar cells of the fovea

A long time ago the great Spanish anatomist, Santiago Ramón y Cajal described the neurons of the different vertebrate retinas as seen by sectioned Golgi-stained material. He noted many different types of bipolar cells in the various species and that there were particularly tiny dendritic spreads for some bipolar cells in the bird retina (36). He suggested that these bipolar cells contacted single cones.

In 1941, Stephen Polyak (Figure 25) published books on the neural cell types revealed by Golgi and other silver methods in monkey and human retinas and brain. In central monkey and human retinas Polyak observed and illustrated several types of bipolar cells, but he was very concentrated on the remarkably small dendritic tops of some types that he construed as contacting single cones. He named these bipolar cells, midget bipolar cells (mbc).

Figure 26 shows Polyak's original drawing of these midget bipolar cells and larger dendritic field size bipolar cells that would appear to contact several cones (Figure 26, imb, fmb and dfb). Polyak also drew and commented briefly that the midget bipolar cells appeared to be of two varieties, one that had a long axon to the inner plexiform layer, and the other a much shorter axon ending higher in the inner plexiform layer. At the same time, there were midget ganglion cells that had small dendritic trees that came in the two varieties possibly reaching to the axon terminals of the two types of midget bipolar cells (Figure 26, mgcs).

Some years later, we set out to see whether Polyak was correct in assuming midget bipolar dendrites synapsed only with one cone pedicle (37, 38) using the technique of performing electron microscopy on Golgi impregnated cells located by light microscopy (39). It turned out that, indeed midget bipolar cells contacted a single cone, but unexpectedly, there were two types of midget bipolar cells each having different synaptic connections with their cone pedicles (Figure 27). One type, that we called flat midget bipolar cells, had a particularly horizontally orientated and flattened dendritic top and made contacts with the cone pedicle on either side of the central dendrite at the synaptic ribbon triad of processes (Figure 27, a-c). The other type of midget bipolar that we called an invaginating midget bipolar cell had a spikey dendritic top with small finger like projections (tiny arrow, Figure 27, d) that contacted the cone pedicle as the central element of the ribbon triad of processes (Figure 27, e-f).

By careful examination of our Golgi stained monkey and human retinas we could occasionally observe that the two Golgi stained midget bipolar cells types converged on the same cone (40) (Figure 27, g).

Confocal imaging of the human foveal slope and rim can distinguish the two types of midget bipolar cell by using different immunostains. Figure 28 illustrates the GNB3 stained cones, Henle fibers and the invaginating midget bipolar cells (in green) contacting single cone pedicles and sending axonal endings to the lower (more vitread) strata of the inner plexiform layer to end close to the multitiered ganglion cell layer of predominantly midget ganglion cells. GNB3 is a G-protein subunit common to both cones and ON bipolar cells (41). The invaginating midget bipolar cells are also reaching into the foveal center to contact the central isolated cones of the cone bouquet (Figure 28, c, inset).

In contrast, Figure 29 shows a section of the human fovea immunostained with recoverin antibodies (red) known to reveal flat midget bipolar cells specifically (42), as well as photoreceptors (43). These flat midget bipolar cells are contacting each a single cone pedicle and their axons are angled with the foveal slope direction

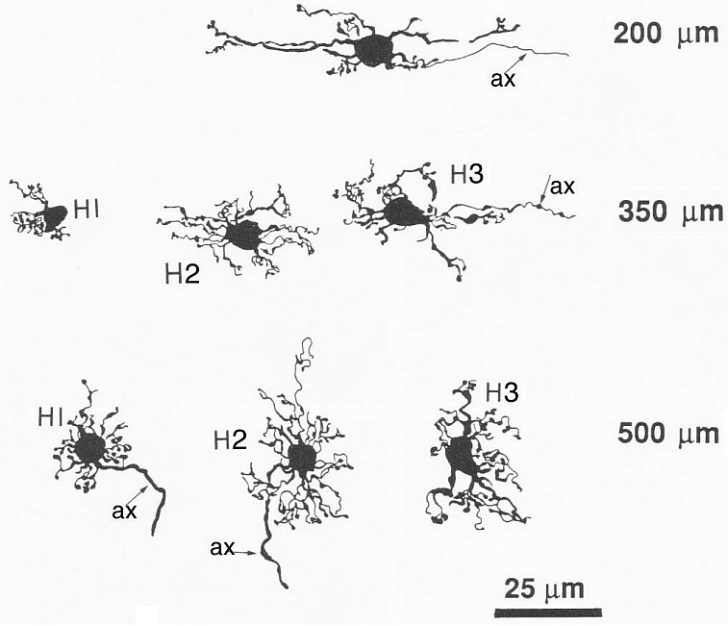

Figure 22. The shape and size of horizontal cells in the human fovea (Golgi staining). The smallest HCs are in the avascular zone edge of the foveal slope (350 µm). The closest HCs stained on the inner foveal slope (200 µm) are stretched out, with dendrites following the circular foveal pit circumference and reaching into the central bouquet of cones. From Kolb et al., 1994 (28).

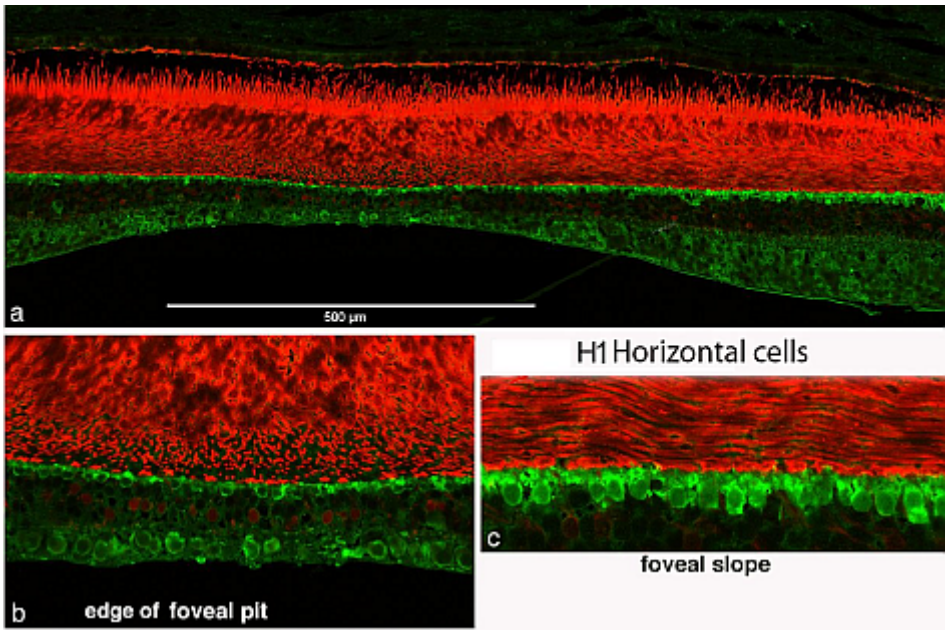

Figure 23. Vertical section of the human fovea cut along the edge of the foveal pit. H1 horizontal cells are immunostained with anti-parvalbumin (green) and cone photoreceptors with recoverin (red). H1 cells are very crowded together in the foveal slope.

to their axon terminals ending high (more sclerad) in the outer strata of the IPL. The more isolated cone pedicles of the foveal pit (Figure 29, b, inset) are clearly being contacted by these flat midget bipolar cells too.

So, we understand now that each foveal cone photoreceptor synapses with two midget bipolar cells. We also now know that there are four or five other types of cone bipolar cells (Figure 26, dfb) that overlap to contact many cones in primate retina, as in other vertebrate retinas (see Webvision chapter on Outer Plexiform Layer). Midget

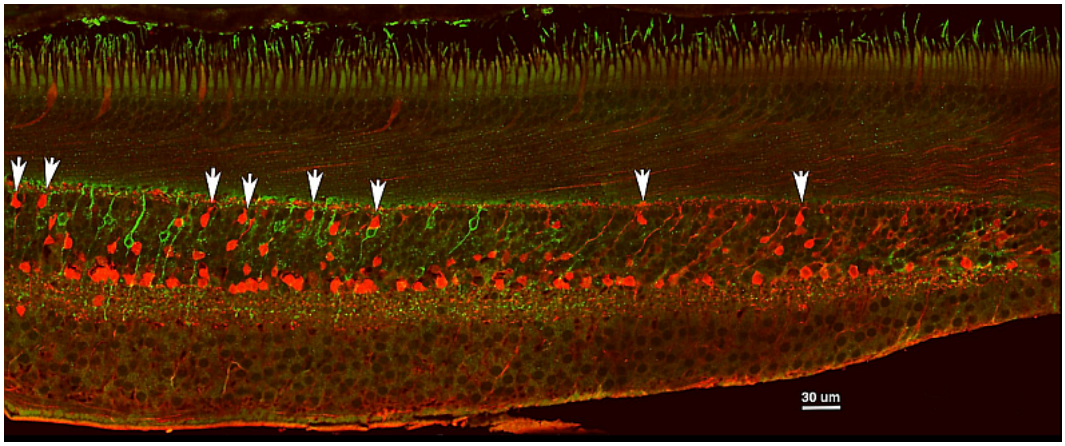

Figure 24. Human foveal slope area immunolabeled with antibodies against calbindin (red) that marks H2 horizontal cells, some bipolar and some amacrine cell types. H2 cells are marked with arrows. The first rod bipolar cells on the foveal slope are labeled with PKC-alpha antibodies (green).

bipolar cells are only found in primate and bird retinas though, and these are the only retinas that have a fovea. Hence the very special nature of the foveal midget system in high visual acuity and color processing.

Midget ganglion cells and the midget system for red L- and green M-cones in the fovea

We have seen how every cone of the foveal area contacts two types of midget bipolar cell which in turn contact a midget ganglion cell each. The flat midget bipolar cell (fmb) contacts the type of midget ganglion cell that reaches high into the IPL, while the invaginating midget bipolar (imb) cell contacts the type of midget ganglion cell that has dendrites in the lower IPL close to its cell body in the ganglion cell layer, as was first suggested by Polyak's drawing (Figure 26). Figure 30 illustrated this finding for Golgi stained midget bipolar cells (mBC) and ganglion cells (mGCs) as seen in the human fovea itself and at 2 mm distance from the fovea i.e. in perifovea. In the fovea where rods are absent (Figure 30, a, foveal cone mosaic) the midget bipolar cells and midget ganglion cells have very small axon terminals and dendrites respectively (less than 10 μm span) and in one image can be seen to stain clasped together (Figure 30, c left cell couple). In the perifovea the cones are now separated by rings of rods (Figure 30, b, receptor mosaic) and the related mb axon terminals and mGC dendrites are slightly wider spread (10-12 μm) (Figure 30, d).

We have been able to reconstruct the midget bipolar and midget ganglion cell synaptic connections by serial section electron microscopy in the fovea and perifovea, in order to see whether there is indeed a one to one relationship (44, 45). Figure 31 shows some sample micrographs from flat-midget-ganglion-cell (mgc) contacts with flat midget bipolar cells (fmb) in the foveal slope (rod free area) and both types of bipolar to ganglion cell contacts in the perifoveal (as in the area of Figure 30, b). All our EM images show all ribbon contacts from one mbc axon to dendrites of a single mGC in the perifoveal material. Typically, there is an amacrine cell companion at the postsynaptic dyad (Figure 31, a-d). Frequently the amacrine cells make reciprocal (feedback) synapses to the midget bipolar terminal, and occasionally to the midget GC involved as well (Figure 31, d). The amacrines are probably of at least two types involved in these synaptic exchanges (see later section on amacrines of the fovea).

The reconstructions of the EM serial photographs are shown in Figure 32 (44, 45). The reconstructed perifoveal invaginating and flat midget bipolar cells with their respective ganglion cells showed almost exclusive interaction between a bipolar axon and a ganglion cell dendritic tree. There were 2 or so ribbon synapses that could have been directed to another ganglion cell dendrite in the 4 pairs of cells reconstructed (Figure 32, Perifovea). In the

Figure 25. Steven Polyak circa 1940.

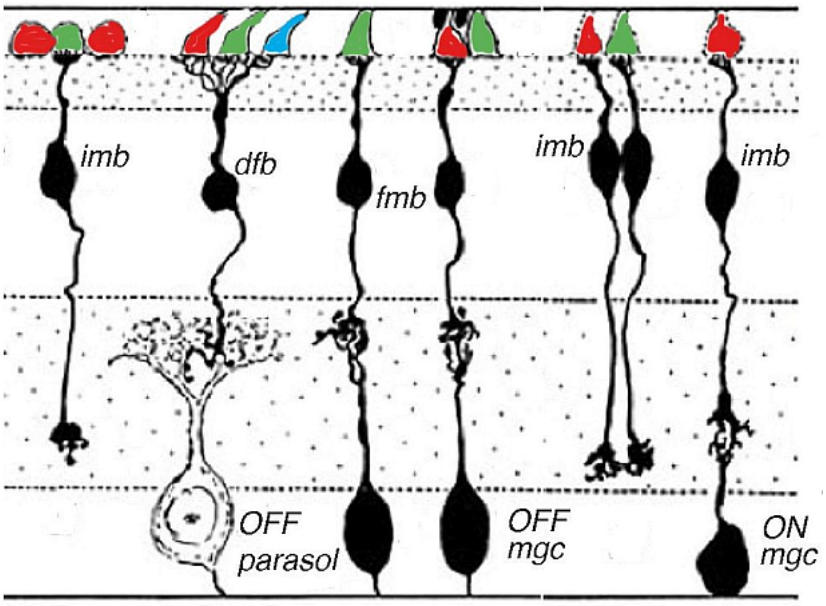

Figure 26. Original drawings of Polyak (90). Bipolar cells and ganglion cells of the central retina. We now know that the invaginating midget bipolar cells (imb) and flat midget bipolar cells (fmb) are physiologically different. Polyak described midget ganglion cells (mgc) as of two types, which we now know are OFF mgc and ON mgc. These connect to fmbs and imbs respectively. Large field bipolar cells (dfb) and parasol ganglion cells were also described by Polyak. The cone spectral types have been colored in by the present authors.

case of the reconstruction of midget bipolar cells and midget ganglion cells of the fovea (Figure 32, Fovea at 570 μm) we determined that there were 3 imbcs to 2 mgcs (Figure 32, fovea, very left-hand cells) and 2 imbcs to a single midget GC (Figure 32, Fovea, right side). However, the limits of our series of the reconstruction probably mean that we missed some adjoining mGCs in this tightly packed neuropil of very small dendritic and axonal profiles. We suggested (46) that each midget bipolar type directed the majority of its synapses to a single midget ganglion cell top, but some synapses probably got shared with a neighboring midget ganglion cell too.

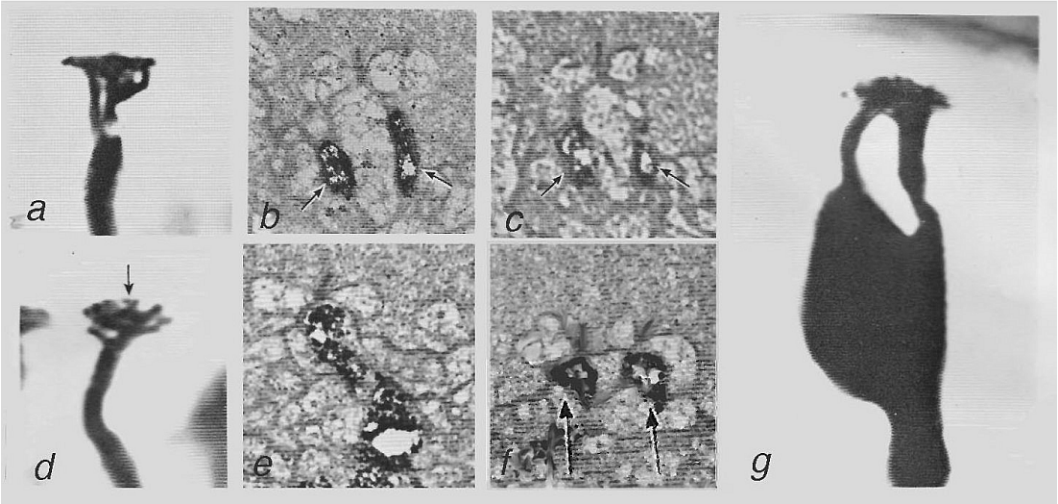

Figure 27. Golgi-stained midget bipolar cells in central monkey retina. (a) shows the flat dendritic top of a flat midget bipolar. (b) and (c) electron micrographs (EMs) show the dendritic terminals contacting a single cone at basal junctions. (d) shows the spikey top of an invaginating midget bipolar and (e) and (f) EMs show dendritic terminals making ribbon contacts with a single cone. (g) Golgi-stained pair of midget bipolar cells contacting the same cone pedicle. From Kolb, 1970 (37).

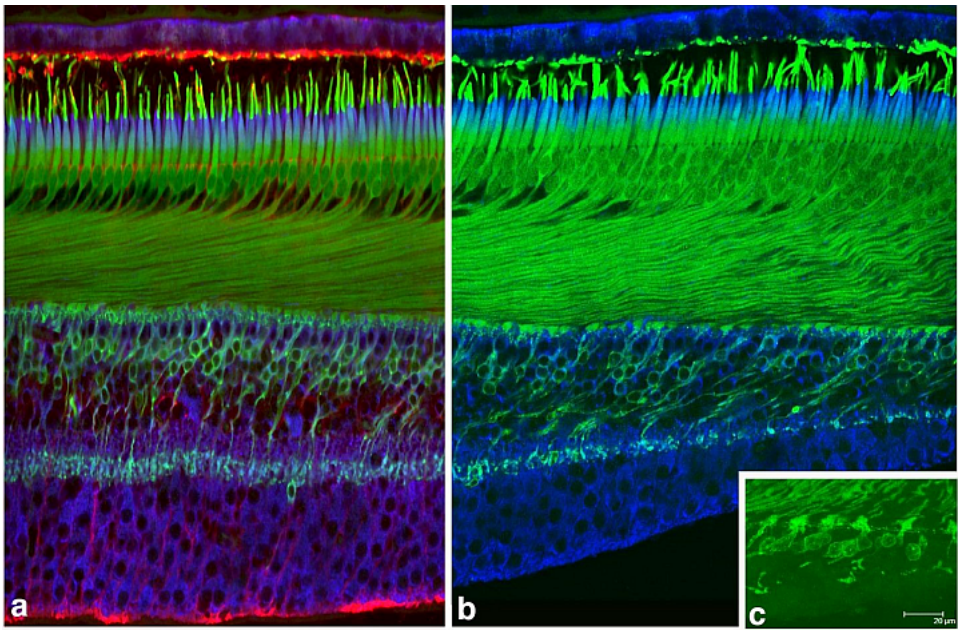

Figure 28. Vertical sections of the foveal rim (a) and the foveal slope (b) to show invaginating midget bipolar cells (imb) contacting cone pedicles of the radiating Henle fiber axons of the foveal cones. The inset (c) shows the imb cells reaching to contact foveal pit cones. Antibodies are against GNB3 (green) for cones and imb cells, CRALBP (red) marks Müller cells and pigment epithelial cells, and Cytochrome C stains mitochondria (blue).

In sum, the relationship between cones and their midget ganglion cells appears to be one cone to two midget bipolar cells and two midget ganglion cells in the foveal and perifoveal regions of the human retina. The same applies to macaque and new world monkey retinas (47).

Our understanding of the significance of every cone photoreceptor having two bipolar and two ganglion cell channels through the primate retina became clear in the 1970s when it was proved unequivocally that the IPL was divided into an OFF-center neural processing in the upper half of the IPL and an ON-center neural processing in the lower half of the IPL (48) (see Webvision chapter on Inner Plexiform Layer). The bipolar cells

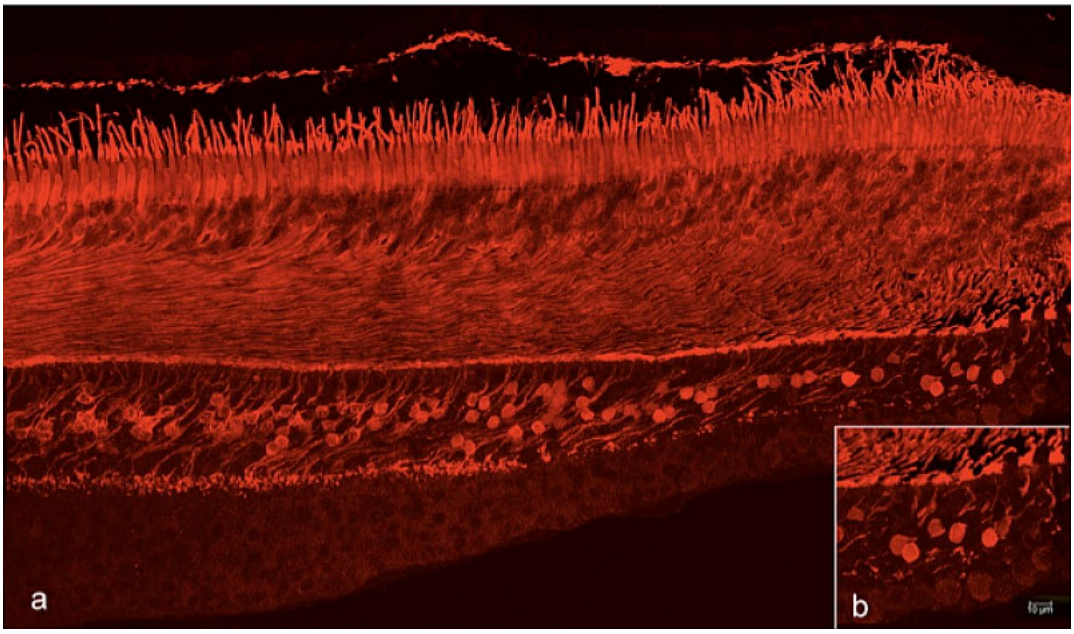

Figure 29. Vertical section of the human fovea slope (a) immunostained with antibodies to recoverin, showing cones, and flat midget bipolar cells (fmb) connecting to single cone pedicles. Inset (b) shows the fmb cells stretching into the foveal pit to make cone contacts.

that make central ribbon-related contacts give ON center (depolarizing signals to light flashes) while the bipolar cells with flat (superficial junction) contacts with the cone pedicles give OFF center (hyperpolarizing signals to light flashes). So, the invaginating midget bipolar cells are ON center and connect with the lower-IPL-branching ON-center midget ganglion cells (Figure 32, Figure 33). In contrast the flat midget bipolar cells are OFF center and connect exclusively with the OFF-center midget ganglion cells of the upper IPL (Figure 32, Figure 33). The messages from a single cone can be transmitted to the brain via exclusive (private) channels for either brighter than background light (ON center message) or darker than background light (OFF center message). Figure 33 shows diagrammatically these private pathways for the midget system in the fovea and the perifovea.

This ON and OFF segregation of the light signal to the two parallel pathways is basic to the organization of light perception of both intensity and hue in the retina and brain (49). In the human fovea and perifovea the private midget pathways dominate the architecture probably forming about 80% of the neural channels. The density of the midget bipolar cells and their midget ganglion cells bodies stacked 6-8 cells deep on the edge of the fovea can be seen in Figure 24, Figure 28, and Figure 29. Furthermore, as we saw in the mapping of cone spectral types in the fovea (19), the vast majority are red L-cones or green M-cones in the fovea and elsewhere in the retina. And these red/green cone pathways are thought to be using the midget bipolar and midget ganglion cell systems to ensure private lines for high acuity function as well as hue (see Webvision chapter on Midget Pathways).

The one-cone-to-two-ganglion-cell midget pathways break down beyond 10 degrees from the fovea in the retina. Outside of the fovea the midget system is multicone connected (50-52).

It is well established that the midget chain of neurons for M- and L-wavelength detection in the midget ganglion cells has a spectrally opponent center-surround organization (Figure 34) (53, 54), reviewed in (55). Thus, midget ganglion cells of central retina (not fovea though), when recorded from electrophysiologically, have the smallest receptive fields, and are organized as L-cone ON or OFF center, and M-cone ON or OFF center. Each midget ganglion cell type has a larger surround of the opposite polarity and of the opponent color (Figure 34). The centers of the midget ganglion cells in peripheral retina, as Chichilnisky's group have elegantly shown (50), are comprised of a predominant numerical cone type, say L-or M-cones, but many more M-, L-, and even S-cones in the larger surround receptive fields. This suggests a more mixed spectral input to surrounds. The retinal

pathways making opponent color surrounds are still not clearly understood for the red and green midget ganglion cells although the predominant theory is that HC feedback at the outer plexiform layer makes for a center surround organization in the bipolar cells (34, 56). Dennis Dacey's group (57) have recently measured the strength and opponent color of the surrounds in peripheral midget ganglion cells and using a difference of Gaussian receptive field model predicted the color opponent surround that is recorded. But as stated above the midget bipolar cells of the **fovea** have not been recorded from to understand whether the midget bipolar is already color opponent due to horizontal cell feedback.

There are also more diffuse channels mixing red and green cone signals in the fovea. Figure 24, in the horizontal cell section, showed a diffuse type of cone bipolar cell called db3 that immunostains with calbindin in the fovea. Its axon terminals are seen positioned in the center of the IPL (Figure 24). The diagram of Figure 35 illustrates ON and OFF pairs of diffuse bipolar cells with contacts to ON and OFF parasol ganglion cells (also shown in Polyak's drawing of the foveal bipolar and ganglion cells in Figure 26 and see later drawings of wide-field bipolar cells). Parasol ganglion cells are thought to be achromatic (53) but motion sensitive (58). See more details of glutamate channels of the two ON and OFF bipolar connections (59) and types of bipolar cells in vertebrate retinas in the Webvision chapter on Bipolar Cell Pathways in the Vertebrate Retina by Nelson and Connaughton.

Counts of midget ganglion cells in the fovea

As we have seen above, the high acuity red and green channels in the retina are processed through parallel single-channel midget bipolar cells and midget ganglion cells to the brain. These high acuity circuits mean that every cone of the fovea will transmit an ON and an OFF signal via two midget bipolar cells and two midget ganglion cells. Every cone in the fovea must have at least two ganglion cells to contact. Are there enough ganglion cells in the foveal slope and foveal rim to ensure these parallel pathways in human retina? Curcio and Allen's (10) quantitative counts on human retinas indicate that there are.

Maps of the ganglion cell numbers counted at every 400 μm from the foveal pit (Figure 36, a, foveal pit is black) show the peak ring of ganglion cell (GC) bodies (Figure 36 orange patchy red ring) at about 800 μm to 1 mm from the central pit. There are large numbers of GCs up to this ring, consistent with the increasing piling up of GC bodies into 6 rows deep at maximum. This piling up of the GCs is clearly seen in the previous confocal images of the foveal rim of human retinas (Figure 24, Figure 28).

The cone densities are highest in the foveal pit and rod free area (Figure 36, b) and the Henle fiber lengths (cone axons) allow the foveal cones to reach the midget and other cone bipolar cells, which are also eccentrically directed to final connections with the midget and a few other GC types (see later section on blue or S-cone pathways). The counts reveal that between 2 and 3 GCs are present in the foveal area for each cone photoreceptor (10).

Things are different in peripheral retina where single cones have input to midget cone bipolar cells with several dendritic clusters for up to 3 cones per bipolar, and many midget bipolar cells converge onto a single midget ganglion cell with a wide dendritic tree (46). The one-cone-to-two-ganglion-cell channel is not available for high acuity vision in the periphery.

A demonstration of single cones mapping onto single midget ganglion cells with either ON or OFF light responses was elegantly demonstrated in the fovea of a **living** monkey retina by William's group (60). Using their signature methodology of adaptive optics to image the cones (as in Figure 17), spatial white noise stimulation of central foveal cones, and responses of ganglion cells with calcium signaling, this team of researchers was able to relate a single cone to its ON or OFF centered midget ganglion cell at the foveal rim 300-400 μm distance (Figure 37, ON mgcs circled in red and OFF mgcs in green).

In this way this team of researchers was able to map the distribution of the midget ganglion cells in a ring around the fovea at between 300 and 400 μm from the cones central to their receptive fields. Interestingly the

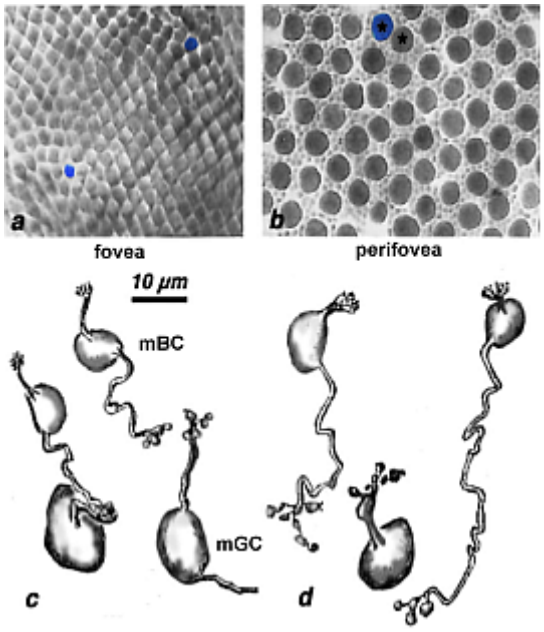

Figure 30. Midget ganglion cells and midget bipolar cells of the fovea (c), and of the perifovea (d) from Golgi-stained human retina. The photoreceptor mosaics (a, b) are above the Golgi-stained cells of (c) and (d). Blue cones are indicated in both mosaics. Midget ganglion cells (mGC), midget bipolar cells (mBC). From Kolb and Marshak, 2003 (46).

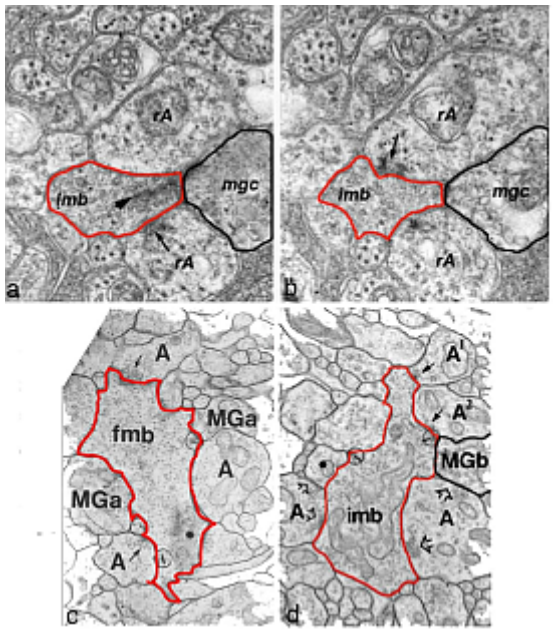

Figure 31. EM of flat (fmb) and invaginating (imb) midget bipolar cells making ribbon synapses on midget ganglion cells (mgc, MGa, MGb). (a) and (b) are from the human fovea and (c) and (d) from the parafovea. A: amacrine cells make synapses on the midget bipolar cell axon terminals. rA is a reciprocal amacrine cell synapse. From Kolb and Marshak, 2003 (46).

ganglion cells with deep cell bodies closer to the outer plexiform layer were closer to the central fovea i.e that 300 μm ring, whereas ganglion cells in the superficial ganglion cell layer were between 400 and 500 μm from the central cones, so that one point in space at the ganglion-cell layer represents more than one point in visual space. This all reflects the Henle axon layer and the pulling of the inner retinal cells obliquely away from the center with the superficial cells being pulled further out radially in development (see section of development of the fovea).

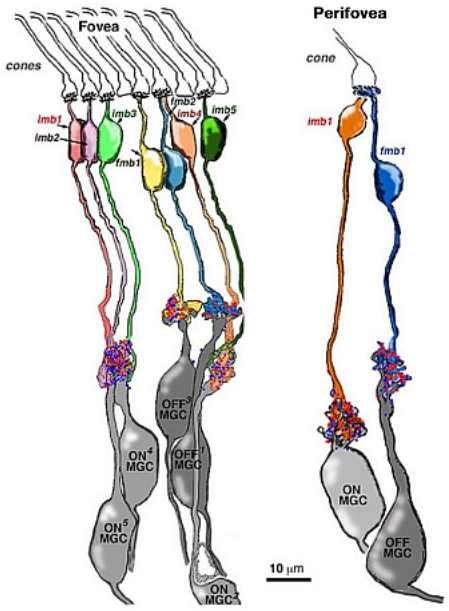

Figure 32. Drawing of reconstructed human midget ganglion cells with their cone input as routed through midget bipolar cells. Fovea: 5 midget ganglion cells get input from 7 midget bipolar cells. Perifovea: there is a strictly 1:1 relationship between ganglion cells and bipolar cells. One cone provides input to 2 mbcs and 2 MGCs in all areas of retina outside the fovea. From Kolb and Marshak, 2003 (46).

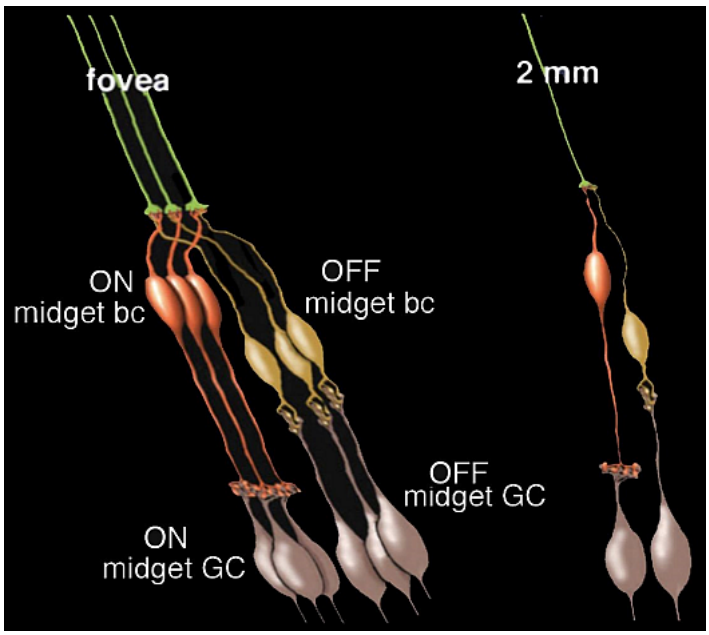

Figure 33. Diagrammatic scheme of the private wiring pattern of the midget system in the fovea and perifovea (at 2 mm). One cone – 2 midget bc's (one ON, one OFF) – 2 midget GC (one ON, one OFF).

Blue S-cone pathways in the fovea

So far, we have dealt with the architecture of the predominant cone spectral and high acuity pathways in the fovea namely the midget pathways for the green M-cones and red L-cones. What of the blue S-cone pathways? As we have seen above the S-cones have a small presence in the foveal cone mosaic (3% of cones generally) but

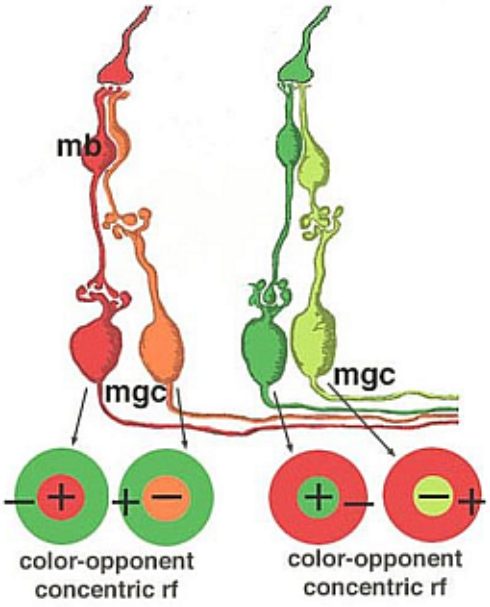

Figure 34. L/M midget ganglion cells have concentric and spectrally opponent receptive fields (rf). An L-cone (red cone) will feed an L-off and an L-on signal through its 2 midget bipolar cells (mb) to 2 midget ganglion cells (mgc). The mgcs will be either red ON center (+) or red OFF center (-) and have a green opponent surround either OFF (-) or ON (+). The M-cone (green cone) is similarly wired through mb cells and mgcs to generate spectrally opponent center surround organizations.

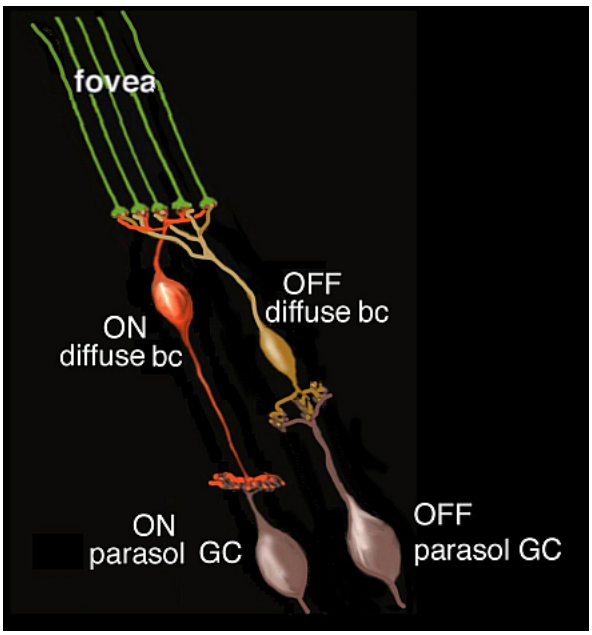

Figure 35. Diagrammatic scheme of the wiring pattern of the diffuse bipolar cell (bc) and parasol ganglion cell (GC) system in the fovea. Each cone (either L, M, or S type) will provide input to two diffuse bcs (ON and OFF types) and two parasol GCs (ON and OFF types).

reach their peak number for the whole retina at 12% of cones in foveal slope and rim at approximately 1 degree of eccentricity (Figure 13, Figure 14, Figure 15).

Mariani (61) described from a Golgi staining study of rhesus monkey retina, a bipolar cell that appeared to be selective for cone types that he proposed were the blue or S-cones. These cone bipolar cells were not midget per se. They appeared to be contacting 1-3 cones situated far apart and their axon terminals were always in the ON

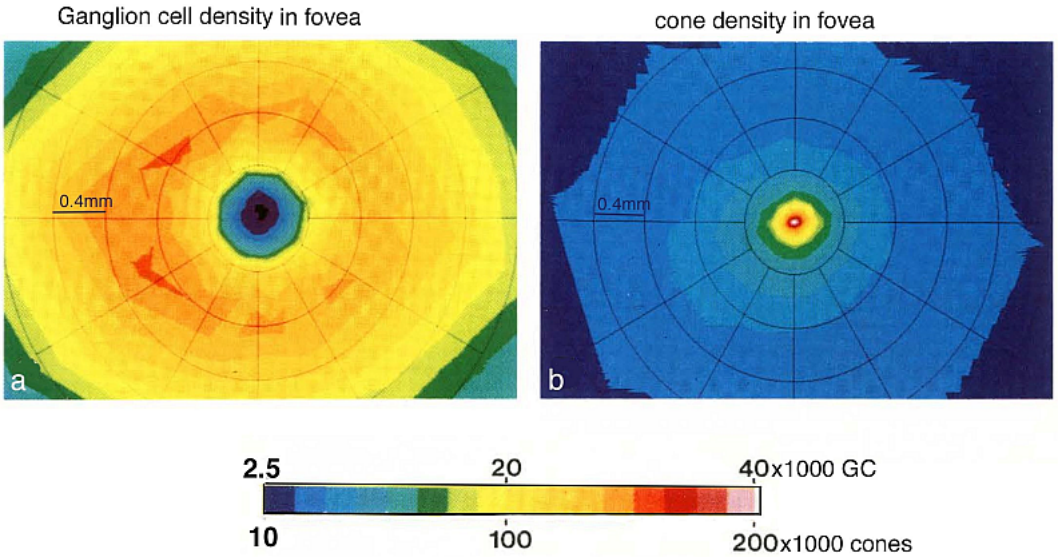

Figure 36. Computer generated heat maps of density counts of (a) ganglion cells, and (b) cones in a human fovea. Ganglion cells are at a minimum in the foveal center (black spot) and peak (red/orange) in a ring about 1 mm from the foveal center. (b) Cones peak at the highest numbers (white spot) in the foveal center and fall off to lower densities radiating out to the edge of the fovea. Color coding bar below gives cell density per mm^2 times a thousand. From Curcio and Allen, 1990 (10).

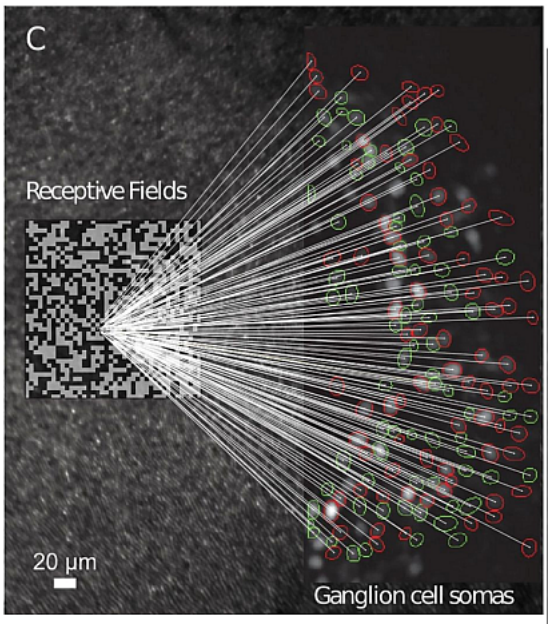

Figure 37. Using adaptive optics to image the cones in monkey fovea and stimulating with spatial white-noise checkerboards allows responses of ganglion cells to be seen by calcium signaling. Thus, a single cone can be followed to its ON- or OFF-center midget ganglion cell at the foveal rim 200-400 µm distant. ON, red and OFF, green. From MacGregor et al., 2018 (60).

layer deep in the IPL neuropil (Figure 38, A). Axon terminals were rather wide-spread compared with the restricted narrow axon terminals of M- or L-cone connecting midget bipolar cells of the central retina. Kouyama and Marshak (62) later confirmed that this type of bipolar was selective for S-cones by an immunostaining light microscope study. The cells were selectively immunoreactive for glycine-extended precursors of cholecystokinin. Later an electron microscope study of the fovea with serial sections and reconstructions (63) showed that this type of S-cone bipolar (Figure 38, A) was probably an ON center type due to its invaginating synapses with the

S-cone (not shown in Figure 38), and its axonal terminal ending deep in the IPL neuropil to contact the lower branches of a small bistratified ganglion cell (Figure 38, B-C, Figure, 39).

In the nineties Dacey and Lee (64) first described the morphology and the intracellular responses of the small bistratified ganglion cell as blue ON and yellow OFF. Figure 39 shows this blue-ON yellow-OFF bistratified ganglion cell stained with neurobiotin and recorded for light response and receptive field structure in the monkey peripheral retina (34). The bistratified cells of the fovea are presumed to have a similar dendritic tree but much smaller of course. The estimate from Calkins and coauthors (63) was that this ganglion cell type on the foveal rim, where they are at their highest numbers, forms 3% the ganglion cell population.

Apparently, humans can discriminate blue–yellow gratings of about 7–14 cycles/degree (16, 65-67). This limit corresponds to the Nyquist limit for the densest region of the S cone mosaic at 1° eccentricity (16, 68). The B–Y ganglion cell mosaic would support discrimination of the finest blue–yellow grating. These ON blue, yellow OFF GCs project to the koniocellular layers of the lateral geniculate body in the brain. It is now accepted that this blue-yellow ganglion cell circuit is the major pathway from blue S-cones to signal the brain about blue hue discrimination (34).

So far in this chapter only an ON center bipolar and ganglion cell for the S-cones have been described. Are there any OFF-center S-cone pathways? An OFF S-cone midget bipolar making basal junctions with the blue cone pedicle near the triad ribbon synapses, like in red and green midget bipolar cells, has been reconstructed by serial section electron microscopy in the monkey fovea (Figure 40; A, A) (69, 70). Its axon terminal contacts the small dendritic tree of a midget ganglion cell (69-71) (Figure 40; B, B).

Very recently S-cone OFF type of responses have been recorded from S-OFF midget ganglion cells (mgc) in the monkey macular area (70). This S-OFF mgc had a blue-OFF center and blue-ON surround organization. Its receptive field was interpreted by the authors to have a role in edge detection similar to L/M mgcs (70). Previously in monkey lateral geniculate nucleus, S-OFF responses had been recorded (72). To date there is no evidence for a matching S-ON **midget** ganglion cell in primate retina.

In 2005 Dacey and colleagues reported on "giant" ganglion cells that gave blue S-cone OFF responses in monkeys (73). These ganglion cells are intrinsically photoreceptive ON-types (iPRGCs) due to melanopsin photopigment in their membranes but also they are driven by both rod and L/M cone inputs in their ON responses (see Webvision chapter on Melanopsin-Expressing, Intrinsically Photosensitive Retinal Ganglion Cells). The overall cone input is S-cone OFF and M/L-cone ON, with a coextensive receptive field organization. In human retina multielectrode array studies also showed the ON responses of iPRGCs integrated rod and cone signals with intrinsic melanopsin photosensitivity. The human melanopsin signals came in at least three photoresponse variants (74). The morphologies of the "giant" melanopsin ganglion cells are shown in Figure 41.

These cell types are many times larger in both cell body size and dendritic field diameter than the bistratified S-ON, yellow-OFF ganglion cell described above (Figure 39). The giant cells have dendritic trees covering 1 mm in area (Figure 41, a, c). There are two stratification types of giant melanopsin ganglion cells. One of the giant melanopsin cell types (outer type) stratifies in stratum S1 right under the amacrine cell layer. The other (inner type) has dendrites running in S5 just above the ganglion cell layer (Figure 41, b) (73). The dendritic trees of "giant" melanopsin types are rather large in the fovea too (500-1000 μm diameter), forming a distinct ring of cells around the fovea (Figure 42). The "giant" S-OFF melanopsin GCs project to the parvo and magnocellular layers of the lateral geniculate nucleus (73). Furthermore, there is now thought to be to be a third type of ip-melanopsin cell in the human retina and all are densely distributed in perifoveal retina (74, 75).

The question arises as to what bipolar or amacrine cell would have input to S-cone-OFF, L/M-cone-ON melanopsin cells, particularly those that branch in the lower or inner IPL. The S-OFF midget bipolar cell could contact the outer giant melanopsin cell, but it is so far only known to contact the S-cone OFF midget ganglion cell. Most of the diffuse cone bipolar cells of the primate retina have contacts with an S-cone in their dendritic

coverage of the overlying cones, as summarized by Dacey (34) (Figure 43). These types of bipolar have not been recorded from to know how much OFF- S-cone signal would come through in their possible input to the outer type giant melanopsin ganglion cell dendritic trees (i.e. from DB1 and DB2 in Figure 43). Those bipolar cells with minority S-cone contacts that branch in the area of the inner types of giant melanopsin ganglion cells would potentially have minimal S-cone ON input but **not** S-cone OFF input (Figure 43). For these reasons the S-cone OFF signal in the giant melanopsin ganglion cells is now theorized to be via an intervening inhibitory amacrine cell circuit from the ON blue bipolar (B, B, Figure 43) to the dendrites of the melanopsin GCs (76, 77). An S-cone amacrine circuit from S-ON bipolar cells to M1 melanopsin iPRGCs has been found in dense reconstructions of monkey perifovea (77).

There is one last cone bipolar cell that has been all but ignored in the human retina. This is a giant bistratified bipolar cell that was described first by Mariani (78) in monkey retina and later by Kolb and coauthors (79) in a Golgi study of human retina. This bipolar type has the widest dendritic span of all cone bipolar cells, exceeding 50 µm in the central retina and as much as 100 µm in the periphery. The dendrites are searching for occasional cones to contact as would be expected if they were synapsing with the occasional S-cone in the dendritic field spread. The contacts are basal junctions, typically associated with OFF-bipolar physiology. The wide spreading axon terminal stratifies in both stratum 1 and stratum 5 of the IPL viz, right in the same strata of the dendritic spreads of the ON-layer and OFF-layer giant melanopsin ganglion cells (Figure 44). This giant bipolar has recently been mentioned in a paper on synaptic connectivity to melanopsin-containing ganglion cells in primate retinas (80). Putative and confirmed S-cone bipolar cells and their S-cone driven ganglion cells for the human fovea are illustrated in the summary diagram of Figure 44.

Amacrine cells of the fovea

There are about 30 different amacrine cell types in the human retina (79). All those with small dendritic spreads are known to use glycine as a neurotransmitter, while the larger field amacrine cells use GABA as a transmitter. It is assumed that all the medium to larger field GABAergic amacrine cells would be at their densest and form a ring around the fovea much like the larger field ganglion cell types as in Figure 42. Densities and distributions of amacrine cells are very difficult to assess, except with mixtures of immunostains for different putative amino-acid or peptide neurotransmitters, enzymes for pathways involved in catecholamine synthesis, or characteristic calcium-binding proteins. So, it has been a challenge to categorize the different amacrine cell populations particularly among the small-field amacrine cells that are crowded together in the fovea and tile the retinal IPL. Larger field amacrines are more widely spaced but have considerable overlap of their dendritic fields.

Data concerning amacrine cells in human retina, and fovea in particular, are very scarce. Golgi studies have revealed the different types of amacrine cell in the monkey and human retinas (79, 81) and immunostaining studies have given us details of acetylcholine containing amacrines (starburst cells) (82), dopamine containing amacrine cells (61), peptides (83) and AII amacrines (84-87) (see Webvision chapter on Roles of Amacrine Cells). The paper by Rodieck and Marshak (82) gives the only quantification we have for starburst amacrine cells which contain acetylcholine in the human retina (Figure 45). Clearly, they peak in density at the fovea between 0- and 2-mm eccentricity. The two types of starburst cells are plotted separately in Figure 45, i.e. amacrine cells in the ganglion cell layer (GCL) and those in the amacrine cell layer (ACL). The ACL starburst cells are not counted any closer than 1.5 mm eccentricity. However, the ACL cells are always lower in number compared with the GCL-occurring cells in all areas of retina, i.e. foveal, temporal, nasal, upper and lower quadrants (Figure 45).

Amacrine cells with small dendritic fields are well characterized and classified into different types in human retina (79). As mentioned above all these different small field cells are glycinergic. Although they haven't been so demonstrated in human retina, they have in mouse retina by immunostaining in the thy1-GFP-O mouse retina (88, 89) (Figure 46). These cells are clearly recognizable across species and are seen in human and monkey retina

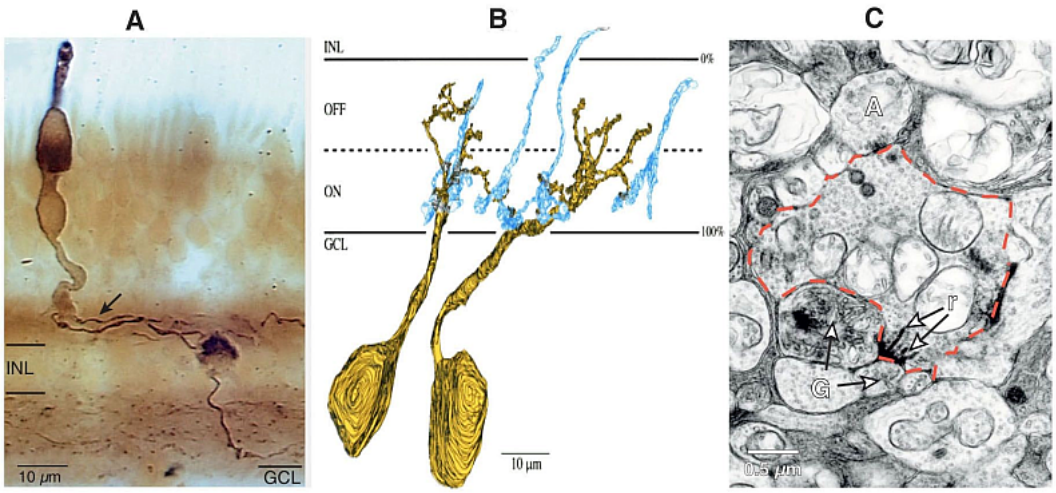

Figure 38. (A) A blue cone bipolar stained with anti-cholecystokinin contacts a blue cone, immunostained with an antibody to S-opsin. (B) A pair of small bistratified ganglion cells (yellow) are contacted at their lower dendrites in the ON layer of the IPL by blue cone bipolar cell axons (blue profiles). Reconstructions of serial sections in EM of the fovea in monkey retina. (C) EM of a section of the blue cone bipolar cell axon (red dashed outline) in the series to show its ribbon contacts (arrows) to the dendrites of the small bistratified ganglion cell (G). From Calkins et al. (63), 1998; and Dacey et al., 2014 (34).

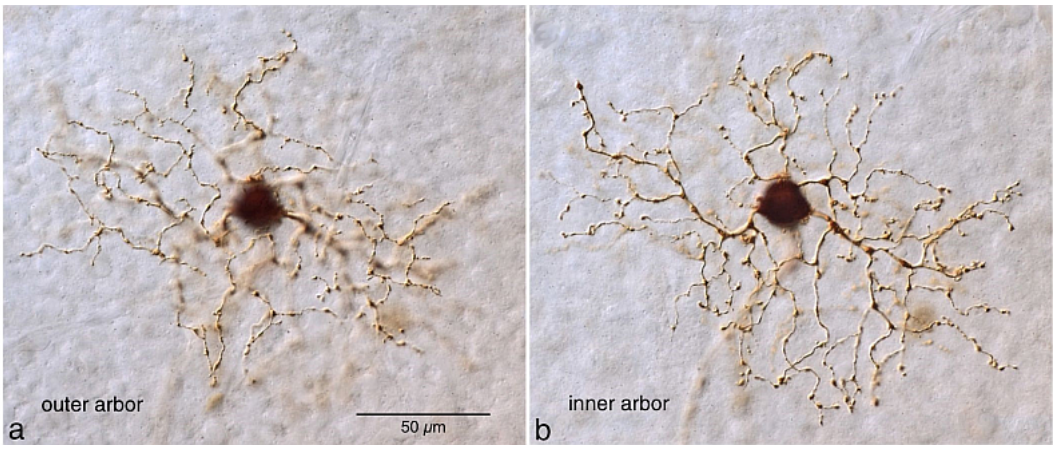

Figure 39. Neurobiotin, intracellularly filled, small bistratified ganglion cell in monkey retina. (a) The outer dendritic tree is in focus while (b) the inner dendritic tree is in focus. The cell responded to blue S-cone stimulation with an ON response and to yellow stimulation of L and M cones with an OFF response. Both receptive fields were coextensive. From Dacey et al., 2014 (34).

too. We are presuming and have evidence on some of these small field cells that they are most frequent in and near the fovea.

Kolb and coauthors Golgi study of small field amacrine cells (79) was done on whole mount preparations so a vertical section view of some of these small field amacrines has to come from Polyak's book (90). See Webvision chapter on Roles of Amacrine Cells to see more details of Polyak's Golgi staining of amacrine cells. In Figure 46 he shows a small-field amacrine that stratifies in the top strata (number P8), another type in the middle strata (number P9) and third type in the lower strata (number P10) of the IPL neuropil. These are quite possibly the same as the glycinergic amacrine cells seen in mouse retina (89) (Figure 46 C, D and E). Cells A and B and F (Figure 46) were not described by Polyak but one or more were described by more recent authors (79, 84, 85, 91-94). See more details in the Webvision chapter on Roles of Amacrine Cells.

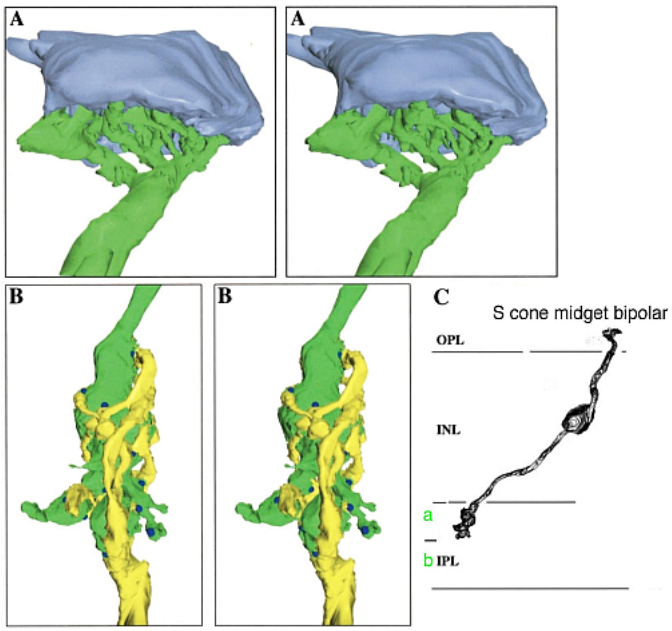

Figure 40. Reconstruction picture from EM series of a midget bipolar cell in monkey fovea. The dendritic top (green) contacts a single S-cone pedicle (blue) with many flat contacts (A, A), while its axon terminal in sublamina ***a*** of the IPL is synaptic upon a midget ganglion cell's dendritic tree (B, B) (yellow). A drawing of the complete S-cone midget is seen in (C). A, A and B, B are stereo pairs. If you can fuse the images, they appear 3-dimensional. From Klug et al., 2003 (69).

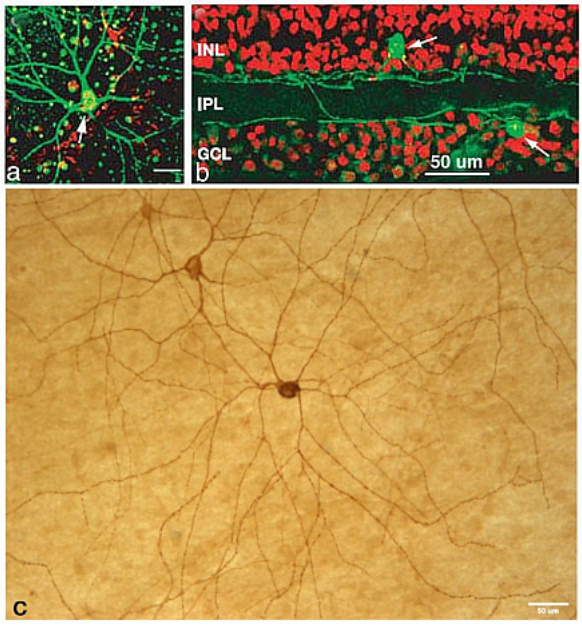

Figure 41. (a) A giant melanopsin-IR ganglion cell of peripheral human retina (green). (b) inner and outer melanopsin-IR ganglion cells in vertical section with dendrites in S5 and S1 of the IPL respectively. From Dacey et al., 2005 (73). (c) Giant melanopsin cells immunostained with melanopsin antibody in peripheral human retina. Their dendritic trees cover one mm area of retina.

A great many small field amacrine cells are stained with calbindin from the foveal rim into the foveal slope, as we have seen in Figure 24. Figure 47 (a) shows calbindin immunoreative (CB-IR) cells close to the fovea and in the foveal pit (Figure 47; a, c; green and orange cells). The orange amacrine cells co-label mixed calbindin and calretinin (CR) immunoreactivity. Some calbindin cells do not co-label with calretinin (green cells) and some calretinin cells do not co-label with calbindin (red cells). Thus, there are at least 3 different types of small field

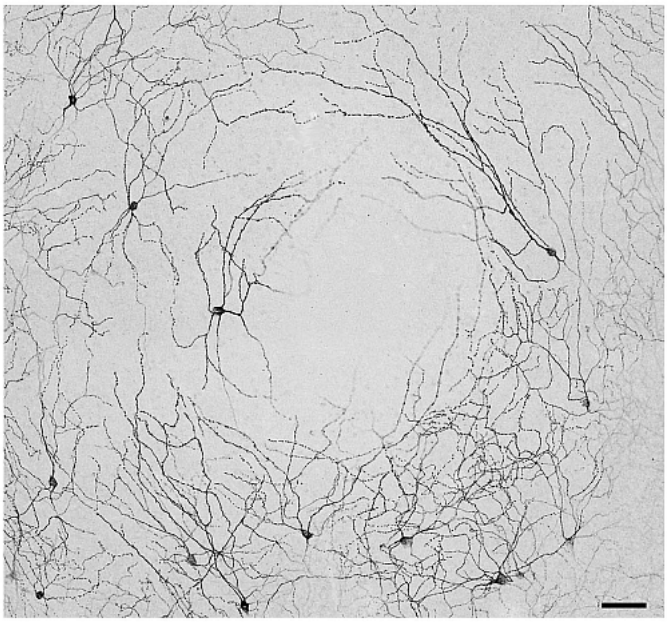

Figure 42. Melanopsin-expressing cells in the human foveal region. A single image from a stack of images is shown. The dendritic processes of the foveal cells wrap around the foveal pit. Scale bar = 100 µm. From Nasir-Ahmad et al., 2019 (114).

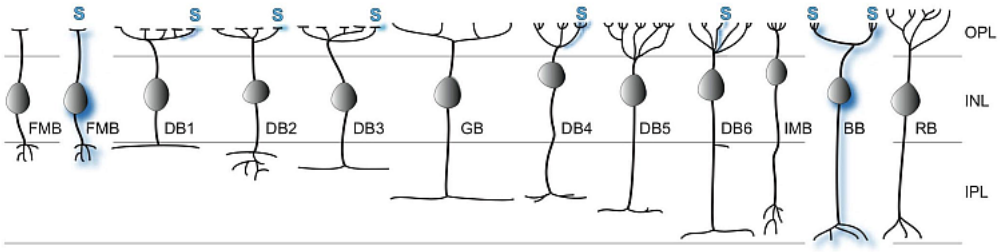

Figure 43. Schematic that illustrates the bipolar cell types of the primate retina currently known to have S-cone connectivity, indicated by S and blue shading. A subset of flat midget bipolar cells (FMB), and the blue cone bipolar (BB) make selective connections with S-cones. DB1, DB2, DB3, DB4, and DB6 bipolar cells, like other diffuse types, receive input primarily from L- and M-cones, but also make consistent but sparse S-cone connections. From Dacey et al. 2014 (34).

cell in the fovea. Probably they are equivalent to cells A, E and F in Figure 46. In addition, there are 2 cell types in Figure 47, in the monkey fovea, viz. one that colocalizes parvalbumin (PV) and calretinin (CR) (white arrows, Figure 47, b) and one solely PV-IR (green cells; Fig. 47, b). We know that A in Figure 46 is the well-known AII amacrine cell that is a cross over bistratified cell well documented to receive rod bipolar cell input and transmit rod signals to ON cone bipolar cells via gap junctions and to OFF cone bipolar cells and OFF ganglion cells via glycinergic synapses (84, 95-97) (see Webvision chapter on AII Amacrine Cells).

AII cells would not be expected to occur right in the rod-free fovea of the human retina but only to occur as the rods and rod bipolar cells appear on the foveal slope. AII amacrines are well known to be calbindin-IR, calretinin-IR and glycine-IR (85-87). AII amacrine cells reach their peak density of 10,500 cells/mm^2 at 1 mm from the foveal center. The cells of Figure 47 (c) right in the foveal pit and immediate foveal slope are CR –IR but not CR/CB-IR and therefore we suggest they are not the AII amacrine cells (Figure 47, arrow head points to a cell body, and small double arrows point to many CR dendrites) (85). The same conclusion can be drawn from a recent immunostained human retina shown in Figure 48.

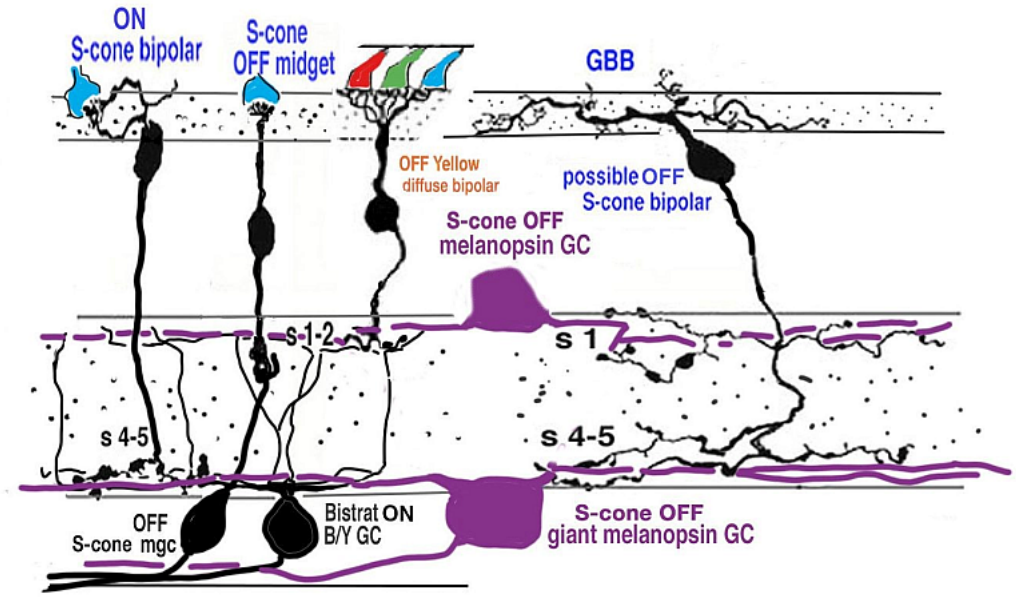

Figure 44. Drawing of the neurons involved in transmitting S-cone signals through the retina. The ON S-cone bipolar cell and the S-cone OFF midget bipolar cell are known to contact bistratified ON blue/yellow ganglion cells (Bistrat ON B/Y GC) and OFF S-cone midget ganglion cells (OFF S-cone mgc) respectively. The OFF yellow diffuse bipolar cells (dfb) contact all spectral cone types, and possibly contact the bistratified ON B/Y GC to provide OFF yellow opponency. The inner giant melanopsin GC could receive some ON input from the S-cone bipolar cells, but a dominant OFF S-cone input is not fully explained yet. An S-cone amacrine cell selective for ON-S-cone bipolar cells (not shown) likely provides S-cone OFF input to the outer giant melanopsin M1 GC. A giant bistratified bipolar cell (GBB, possible OFF S-cone bipolar) is theorized by us to be available to both inner and outer giant intrinsically photosensitive melanopsin ganglion cells.

The foveal retina (Figures 48, a-b) is compared to peripheral retina (Figure 48, c) in this double stained section for glycine (green cells) and CR (red cells). CR-IR amacrine cells are in the foveal pit area but are not double stained AII cells. AII cells are seen on the foveal slope (Figure 48, a-b) as double stained cells (yellow cells). They are very common in the peripheral retina (Figure 48, c, yellow cells). In all areas of retina there are still some pure CR-IR amacrine cells that are not AII cells (Figure 48, c, red cell bodies). These CR-IR amacrines do not appear to stain for glycine (probably for some technical staining reasons) in our human material. Green cells in the foveal pit and periphery that immunostain for glycine are mostly cone bipolar cells in Figure 48 a-c.

Our detailed EM study (85) showed that the CR-IR amacrine cells of the foveal slope closest to the foveal pit occurred internal to the first rod spherule and rod bipolar (Figure 49, a, arrow 4, 350 µm from the foveal pit). Cells at position arrows 3 and 1, 2 were amacrine cells that occurred at the same position that the first rod bipolar cells entered the IPL neuropil. They were a mixed group of CA-IR amacrine cells, many with AII characteristics i.e. input from rod bipolar axons and gap junctions with diffuse ON center bipolar cell types. In the foveal region we and others have never seen invaginating midget cone bipolar cells getting gap junction contacts from an amacrine cell (44, 46, 63, 69). Thus, we conclude that AII amacrine cells have nothing to do with the midget system in the foveal retina at least. We also conclude a different small field amacrine cell from AII cells, that is CR-IR, occurs in central, rod-free fovea. Recent studies by Lee and coauthors (86) and Strettoi et al. (98) come to a different conclusion.

The question is what type of amacrine cell is the CR-IR cell of our foveal study (Figure 49, cell 4 at 350 µm from the foveal center). Light microscopy suggest this CR-IR cell has a tristratified or diffuse dendritic tree with fine dendrites throughout the IPL (Figure 49 b, A curved arrow). The electron microscope study of the cells at 350 µm from the foveal center indicated that the CR-IR processes were receiving ribbon input from OFF midget bipolar cells and fed reciprocal synapses to the same bipolar terminal (Figure 50, a-b). The CR-IR amacrine

received input from a bipolar cell's axon terminal in the lower IPL neuropil, therefore from an ON center bipolar (Figure 50, c). This was likely an ON midget bipolar but an ON diffuse bipolar axon terminal could not be ruled out (Figure 50, d), because this study is looking at neuropil with many stained processes from multiple stained cells. The CR-IR amacrines also made clear synapses upon a large ganglion cell process that was almost certainly an ON-center midget ganglion cell (Figure 50, c and d). In the fovea the CR-IR amacrine cell seems to be driven by OFF and ON midget bipolar cells and make reciprocal synapses upon the OFF bipolar type at least, and crossover inhibitory synapses upon ON midget ganglion cells (Figure 50 a, b, c, d, and summarized in e).

Besides the CR-IR putative small field diffuse amacrine cell, there are at least two other small field, glycinergic amacrine cells that are probably part of the foveal and midget bipolar-midget ganglion cell system of transmission of cone specific pathways. These are the A8 bistratified cell (79, 92) which can be stained with synuclein antibodies (93, 94) and a small field glycinergic amacrine equivalent to Figure 46, E, A3 or knotty type 2 cells, which can be marked with Parvalbumen immunoreactivity (91, 99) (see Webvision chapter on Roles of Amacrine Cells). An additional small field glycinergic cell described in rat, mouse and macaque monkey retina is immunoreactive to the vesicular glutamate transporter 3 (100). This vGluT3 cell is likely found in human retina too. Its dendritic tree lies between the two cholinergic amacrine types' branching levels, where it receives input from bipolar cells and from other amacrine cells. The axon terminals of OFF diffuse cone bipolar types DB3 and ON diffuse cone bipolar DB5 (see Figure 43) run within the vGluT3 dendritic tree, so it is possible that vGluT3 cells are driven by both ON and OFF light responses and that they transmit this response to (at least) OFF ganglion cells (100, 101). In mouse retina, this amacrine cell selectively targets suppressed-by-contrast ganglion cells (102). It remains to be seen whether a glutamatergic amacrine cell is present in human fovea.

Furthermore there is at least one wide-field CR immunoreactive GABAergic amacrine that has dendrites coursing through the IPL on the foveal slope and even crossing the foveal pit floor (85, 86). This wide field A19 cell, immunostains for GABA, CB and CR (85). There is indirect evidence that the perifoveal blue-cone amacrine, perhaps the human A12, is GABAergic (77, 79).

Other wide-field amacrine cells are certainly present around the fovea at high density, as are all amacrine and ganglion cell types. Figure 51 shows the distribution of dopaminergic amacrine cells immunostained with tyrosine hydroxylase at the human fovea. These cells are at quite high concentration here and have a meshwork of dendrites forming a nest of processes around the foveal rim (Figure 51). The few dopaminergic synaptic beads in the foveal slope and pit (Figure 51, green spots) are probably synapsing upon small field A8 cell types, the CR immunoreactive small, diffuse amacrine. These are the same CR-IR amacrines we immunostain in the foveal center (Figure 48, Figure 49) (85). Dopaminergic amacrine cells synapse on AII amacrine cells in perifovea and peripheral retina (Figure 52) and on the stratum 1 melanopsin ganglion cell (103). Dopamine amacrine cells are also GABAergic and reach their highest concentration at the 4 mm ring around the foveal center where the highest concentration of rods is found (Figure 51) (104).

Summary

The diagram in Figure 53 summarizes the different neural types and their circuitry in the human fovea. The central foveal pit is devoid of second and third order neurons because of the close packing of the cone photoreceptors and the pushing out radially of these circuits to drive ganglion cells piled up at the outer edge of the foveal slope and thence passing visual messages to the visual centers in the brain. The cone mosaic in the foveal pit and throughout the rod free zone through the foveal slope is the basis of our visual acuity. We know that the human visual system is capable of acuity of 1 min of arc or 60 cycles/degree of visual angle. One degree of visual angle is thought to cover approximately 280-300 μm of retinal distance. The center of the fovea is about one degree across thus allowing visual discrimination of 1 min of arc i.e. the center to center spacing (3 μm) of the cones of the central mosaic in the foveal pit.

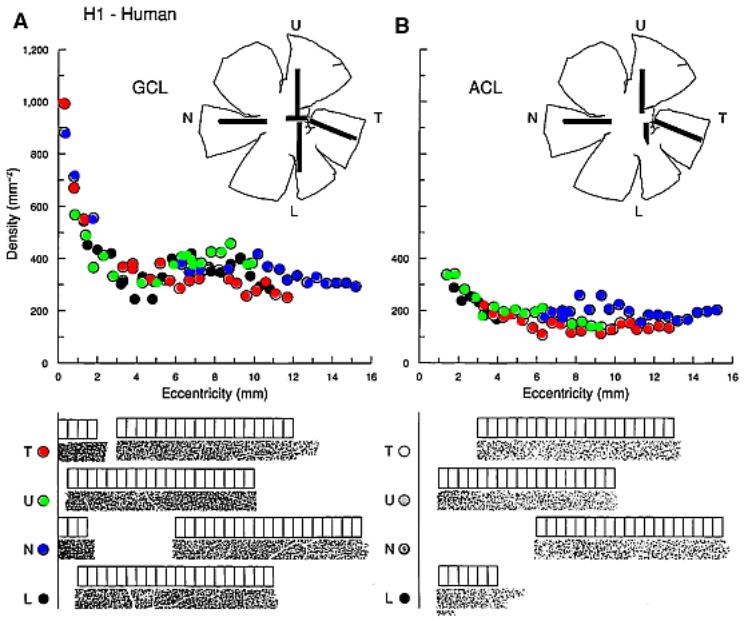

Figure 45. The counts of acetylcholine containing amacrine cells (starburst cells) in the human retina with eccentricity from the fovea. Strips counted for stained cells in nasal (N), temporal (T), upper (U) and lower (L) retina are shown for starburst cells in the ganglion cell layer (GCL) (A), and in the amacrine cell layer (ACL) (B). More cells lie in the GCL. Actual cell counts (dots) are shown in the lower panels. Clearly GCL starburst cells are at a peak density at the fovea. From Rodieck and Marshak, 1992 (82).

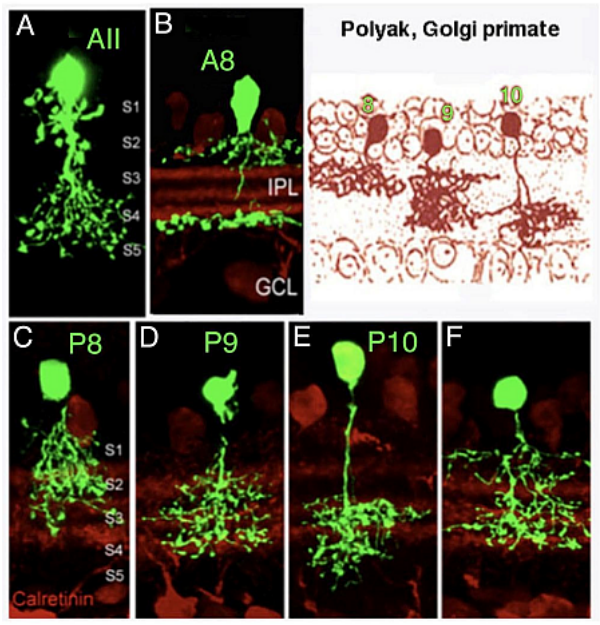

Figure 46. Glycine staining of amacrine cells expressing GFP (green fluorescent protein) in the thy1-GFP-O mouse (88). AII (A) and A8 (B) cells are well known crossover glycinergic amacrine cells in mammalian retina. Other small field amacrine cells (C-F) branch at different strata of the IPL, and all have been described in the human retina. Polyak's (#8, #9, #10) drawings are shown in the right inset drawing and compared to counterparts in mouse retina (C-E, P8, P9, P10). From Wässle et al., 2009 (89); Polyak, 1941 (90).

The central fovea with no superficial cell bodies and neural circuitry allows light to directly stimulate cones and give us this maximal visual acuity, but the circuitry underlying the transmission of this acuity to the brain must occur at the rim of the fovea. The rim of the fovea is where the ganglion cells are piled 6 to 7 deep (Figure 53) and is the foveal area containing all the intervening cells and connectivity to drive those ganglion cells. The

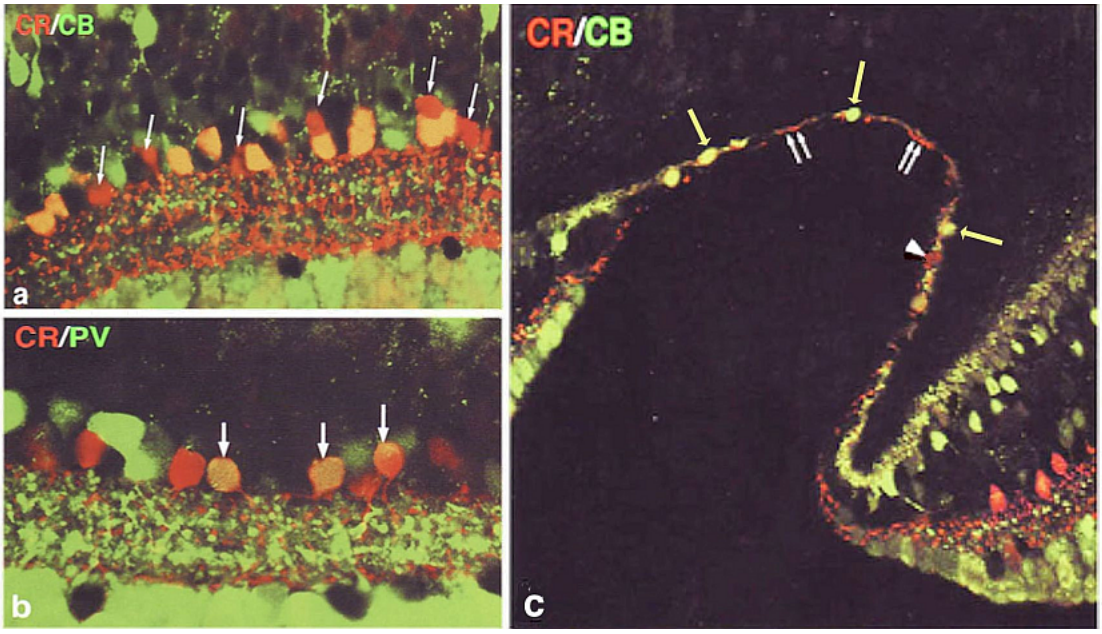

Figure 47. Immunostained central monkey retina, double staining with calretinin (CR, red) and calbindin (CB, green) or parvalbumin (PV, green). (a) Many amacrines double stain (yellow) with CR and CB (AII cells) but some are CR alone (white arrows). (b) Many amacrine cells double stain with CR and PV (arrows, yellow) but some are PV alone or CR alone. (c) In the foveal slope and pit, some amacrine cells are CR alone (red cell bodies and processes, double arrows and arrowhead). CR cells are on the foveal slope (right hand side). CB cells (green) are also in the foveal pit (green arrows), but they could be CB bipolar cells. From Kolb et al., 2002 (85).

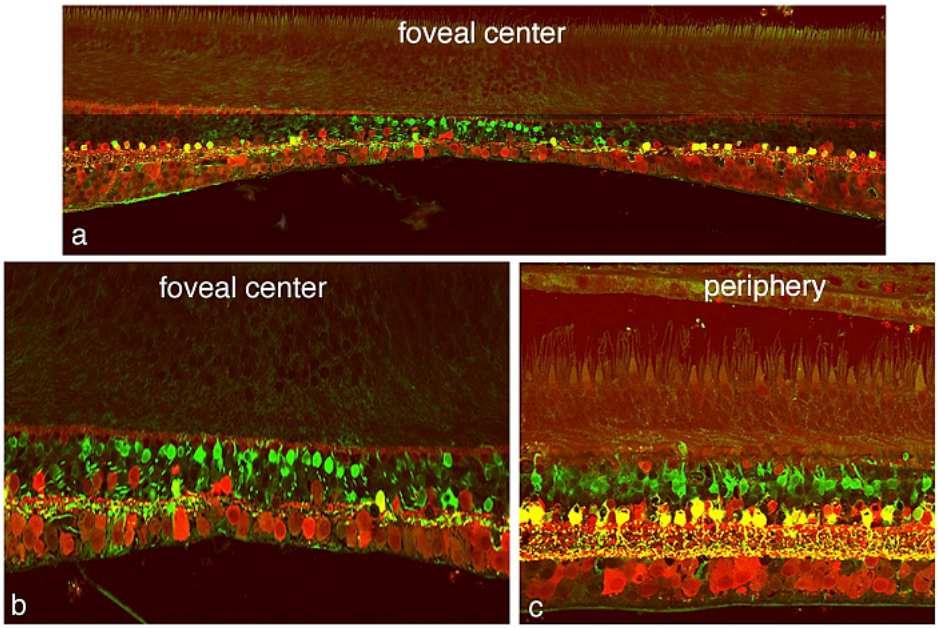

Figure 48. Fovea of the human retina immunostained for calretinin (CR red) and glycine (green). (a) Just at the beginning of the foveal slope, the amacrine cells and ganglion cells are labeled solely with CR, while bipolar cells label for glycine. Some double labeled (yellow) amacrine cells begin to appear on the outer foveal slope. (b) is an enlargement of the foveal center. (c) Shows that many amacrine cells in peripheral retina double label for CR and glycine (yellow). They are probably AII amacrine cells. Some bipolar cells label for glycine, while ganglion cells label for CR solely.

predominant circuitry is concerned with the private cone to midget bipolar and midget ganglion cells. Every cone drives two midget bipolar cells and two midget ganglion cells so that the message from a single cone is provided to the brain as a contrast between lighter signals (ON pathways) or darker signals (OFF pathways)

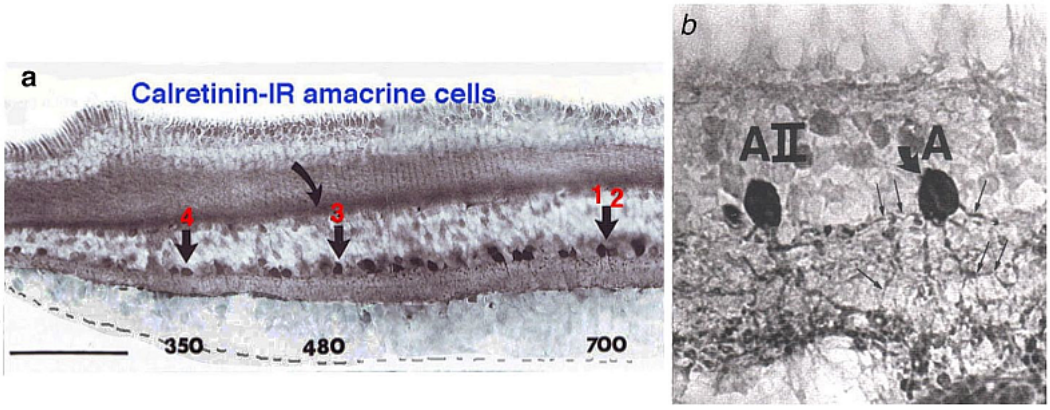

Figure 49. (a) Vibratome section of half a fovea of monkey retina immunostained for calretinin (CR-IR). The distance from the fovea is expressed in µm. At 480 µm the first rod spherules appear (curved arrow). At 350 µm there are no rod spherules or rod bipolar cells. (b) Cryostat of the CR-IR material outside of the fovea where it is clear that one CR-IR cell is an AII amacrine cell (lobular appendages and distal dendrites in lower IPL), while the other amacrine (A, curved large arrow) has an array of fine dendrites with synaptic boutons passing down through the entire IPL (fine arrow) either in a tristratified or diffuse branching pattern. From Kolb et al., 2002 (85).

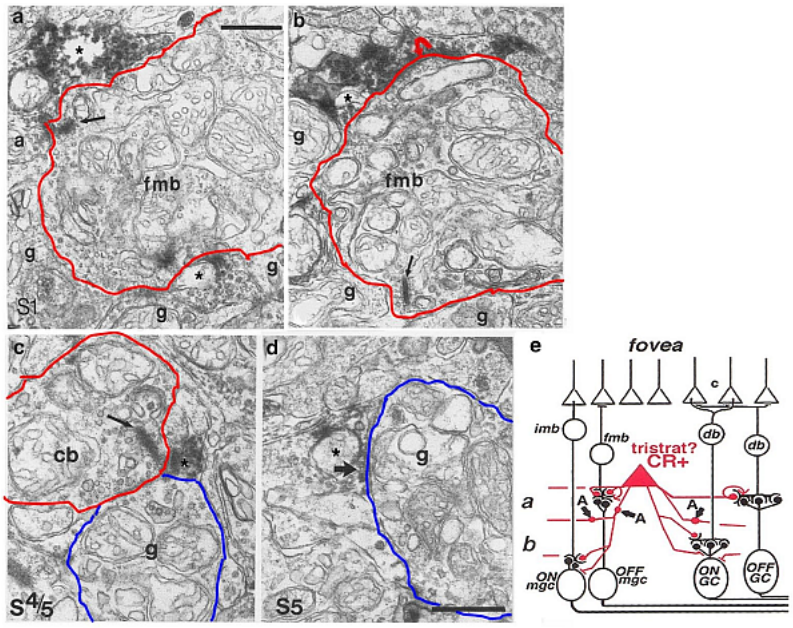

Figure 50. EM of CR-IR profiles (black, asterisk) in stratum 1 (a, b) and deep in the IPL in stratum 4/5 (c, d). The CR-IR profiles are postsynaptic to ribbons of flat bipolar cells, most of which are flat midget bipolar cells (fmb) and make reciprocal synapses (red arrow). In (c, d) CR-IR profiles are post-synaptic to bipolar cells, most of which are invaginating midget bipolar cells (imb) and presynaptic to ganglion cells, most of which are ON center midget ganglion cells (mgcs). Scale bar = 0.5 µm. (e) Summary diagram of the circuitry of the CR-IR amacrine cell of the fovea. From Kolb et al., 2002 (85).

(Figure 53). The sharpening of this contrast message is provided by horizontal-cell feedback circuits and, in some pathways by amacrine circuitry. The human retina with 3 spectral types of cone means that many of these midget pathways will carry a concentric color opponent message (Figure 53). For example, a red cone will transmit to a midget bipolar cell and a midget ganglion cell a red ON center, green OFF surround or a red OFF center and a green ON surround. The same occurs for the green cone message to midget bipolar cells and midget ganglion cells (Figure 53, red and green neurons). In these red and green color pathways, the H1 horizontal cell is thought to play a role via feedback mechanisms to give the midget bipolar and midget ganglion cells the concentric opponent message (Figure 53). A current model of color vision channels in the human fovea,

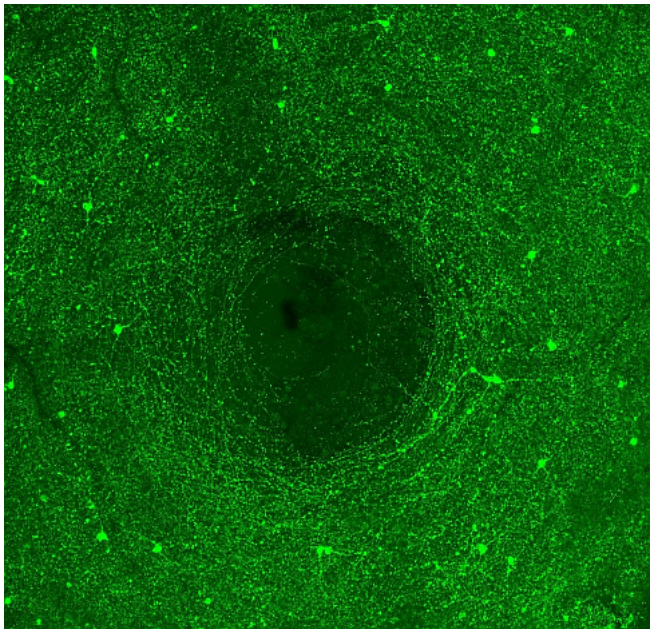

Figure 51. Wholemount of the fovea in a human retina that is immunostained for tyrosine hydroxylase. The stained dopaminergic amacrine cells are numerous and have a meshwork of dendrites surrounding the fovea. Some fine dendrites penetrate the foveal slope and surround the foveal pit.

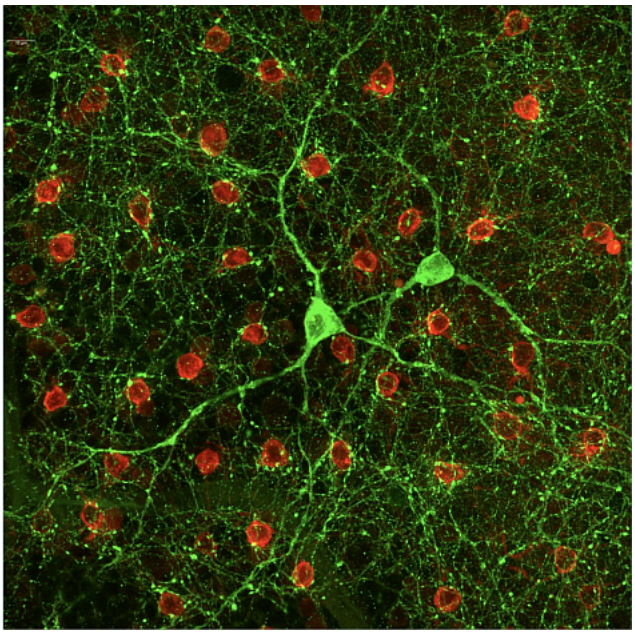

Figure 52. Wholemount human retina immunostained for tyrosine hydroxylase (Th, green) and Calretinin (CR, red). The Th-IR cells are dopamine cells and exhibit rings of synaptic profiles around the CR-IR cell bodies of AII amacrine cells in this case.

however, suggests that the red and green cone midget systems are not channels for color hue, but are primarily chromatic edge and visual acuity channels (70).

Signals from blue cones in the foveal slope have different pathways, in the case of ON center blue signals, to a non midget small bistratified ganglion cell (Figure 53) via the lower tier of dendrites. The upper tier of dendrites receives red and green cone OFF input from a diffuse cone bipolar type (Figure 53, yellow/orange cells). An OFF-center blue midget bipolar cell is known to be present in the fovea and connect to a blue-OFF midget

ganglion cell (Figure 53). Another OFF blue message is sent to giant melanopsin ganglion cells that are present in the foveal ring area, but the circuitry driving these is uncertain and possibly involves an intermediate amacrine cell (not drawn in Figure 53). The H2 horizontal cells are thought to be feedback neurons of the blue cone system providing a concentric color-opponent organization of blue cones (35), nonetheless there is no concentric opponent visual message for the bistratified blue-driven ganglion cell types (Figure 53, blue and yellow opponent fields are coextensive), unlike the red and green cone midget ganglion cells.

Apart from the midget system that dominates the fovea, there is a presumed non-color channel (i.e. luminosity channel) in the fovea via the diffuse bipolar cells that get input from several cones of different spectral type and carry that non-color-specific message about light to a large field ganglion cell type known as a parasol ganglion cell (Figure 53, grey cells with receptive field structure in grey). Parasols also come in ON center and OFF center varieties, and are thought to have a center–surround organization concerning light and dark although they may have an imbalance of the strength of spectral mechanisms in center and surround (51, 105). These cells respond strongly to a sequence of slits consecutively displaced along a fixed direction, but much more poorly to a sequence of randomly positioned slits. This is evidence of tuning for motion (58).

Amacrine cells of the fovea are mostly small field and glycinergic. The larger field amacrines are present but more typically surround the fovea in a ring of processes, with little or no penetration into the foveal center (Figure 53). Thus, the small field glycinergic amacrines are important in some sort of interplay with the midget bipolar cell – midget ganglion cell channels (Figure 53, A8, CR and PV cells). We have anatomical descriptions of their synaptology but only the A8, P8 (called A2 in cat retina) (106) and PV cells have been recorded from. All have cone driven responses. Some are OFF center (A2, A8), and some are ON center (PV cells). All have been hypothesized to have a role in the generation of antagonistic surrounds of ganglion cells, but this remains to be proven. Foveal midget ganglion cells appear to receive little direct synaptic inhibition (107).

In sum, the fovea is a small but vital area of the central retina, unique in neural circuits, and molecular expression (108). The foveal cones themselves have evolved a sustained response characteristic, suited to standing contrast, that differs from peripheral cones (107). Foveal midget ganglion cells show virtually no synaptic inhibition, as compared to peripheral midgets (107). The fovea appears to have evolved in development from a central mound of cells as seen, for instance, in cat area centralis, to a virtually neuron-free pit, to concentrate cone photoreceptors into a dense array to be maximally sensitive to the smallest stimuli, and further, displace all ensuing circuitry into an exquisitely organized small surrounding rim of real estate in the retina foveal slope. If this small area is damaged by looking at the sun, by inherited cone atrophies or degenerated by age related macular degeneration (AMD), or even underdeveloped, as happens in albino people (see Webvision chapter on albinism), our eyesight becomes very poor.

Acknowledgements

P.A., N.C., I.O.-L. and R.F.N. thank H.K. for initiating and organizing this project, in part arising from long and fruitful collaboration among our laboratories. P.A thanks collaborators at the Medical University of Vienna and elsewhere, in particular Christian Schubert, Martin Glösmann and Dietmar Pum. Eduardo Fernandez obtained part of the human donor tissue. P.A work was supported by grants from the Austrian Science Fund (FWF)and EC-grant QLK6-CT-2001-00279. N.C. work was supported by the Spanish government, MINECO-FEDER-BFU2015-67139-R, RETICS-FEDER-RD16/0008/0016 and FPU14/03166. Generalitat Valenciana-FEDER, IDIFEDER/2017/064 and Prometeo-2016/158. R.F.N. work was supported by the Intramural Research Program of the National Institute of Neurological Disorders and Stroke, National Institutes of Health, Bethesda MD.

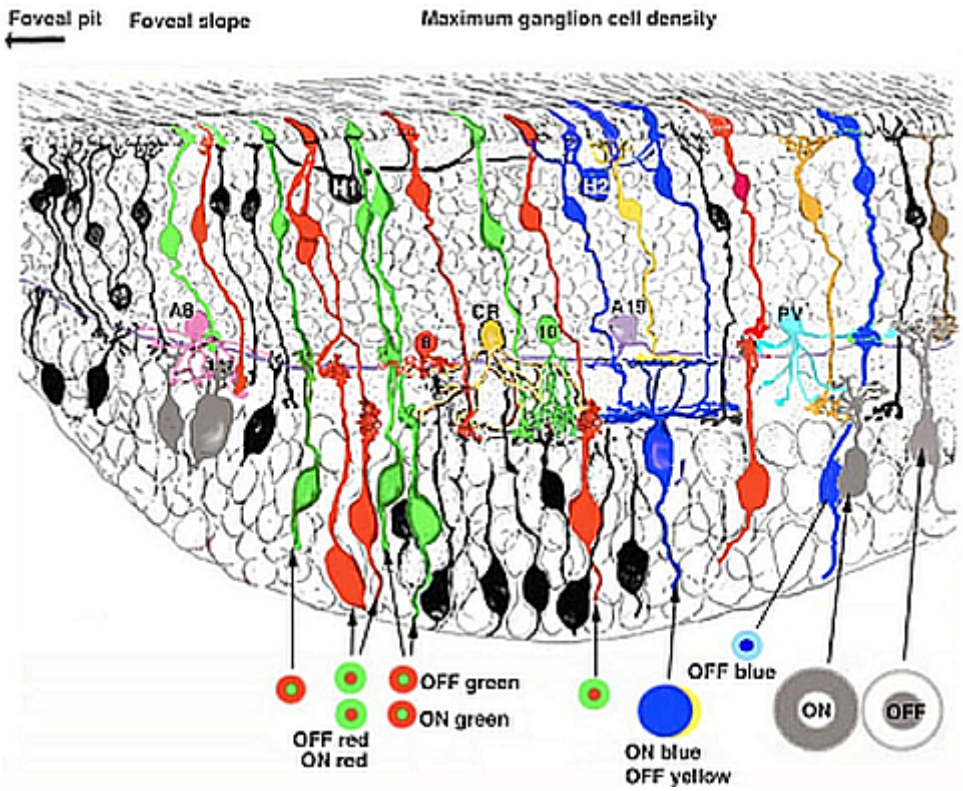

Figure 53. Summary diagram of the neural architecture of the human fovea, adapted from an original drawing of Polyak (1941) (90). The cone pedicles are closely abutting in the foveal OPL where ON and OFF midget cone bipolar cell dendrites contact them. ON and OFF midget bipolar cells contact ON and OFF midget ganglion cells in the inner retina providing M- and L-cone-connected private channels (red and green cells). The S-cone midget system (small blue cells) is only an OFF midget bipolar-ganglion cell channel, but the S-ON channel is via a blue-selective bipolar cell and a bistratified B/Y ganglion cell chain. A diffuse bipolar cell (yellow) provides OFF L/M cone input. Diffuse cone bipolar cells (brown and orange cells) contact the parasol ganglion cells (grey cells). Various small field amacrine cells are indicated as A8, P8, CR, P10, A19 and PV. H1 and H2 horizontal cells are indicated as feedback neurons for the M and L-cone (H1) and for the S-cone (H2) pathways.

About the authors

Helga Kolb, **Ph.D.** is the originator and chief editor of Webvision. She was born in England and educated with degrees from Bristol University. Helga has been in eye research since 1961, at first doing electrophysiology at the Institute of Ophthalmology, Moorfields Eye Hospital, and then emigrating to the USA. At the Wilmer Institute, Baltimore, in John Dowling's lab, along with Brian Boycott she continued work in anatomy of the retina concentrating on understanding the neurons and wiring of the monkey retina. Later at the NEI, and the NINDS, Bethesda**,** she collaborated with Peter Gouras and Ralph Nelson on joint physiology and electron microscopy of retinal neurons to understand the connections of cell types involved in light, dark and color pathways in cat and monkey retinas. On moving to Utah, Helga continued collaborative projects with Ralph Nelson and started new collaborations with various postdocs in her lab from Europe and China mainly. Thus, Peter Ahnelt and Nicolas Cuenca aided and abetted studies of the monkey and human retina, before going on to their stellar careers in Austria and Spain respectively. All of us have been fascinated with the organization of the human fovea and this chapter represents our collaboration over the years.

Ralph F. Nelson, **Ph.D.** received his B.A. in Biophysics from Amherst College and his Ph. D. in Biophysics from Johns Hopkins University. At Johns Hopkins, under the preceptorship of John Dowling, he studied conductance

mechanisms responsible for light responses of retinal bipolar cells. In his postdoctoral studies at the National Institutes of Health in Dr. Peter Gouras' lab, he formed a close collaboration with Helga Kolb in pioneering a type of study in which the light responses of retinal neurons were tightly interpreted in terms of synaptic connectivity. This group was the first to show that separation of bipolar/ganglion cell connections into two layers within the IPL underlaid the ON-center and OFF-center responses of the retina and whole visual system. Ralph Nelson's laboratory is the Neural circuitry Unit of the Basic Neurosciences Program at the National Institute of Neurological Diseases and Stroke, NIH, Bethesda. His recent studies are on the neural circuitry for image processing in zebrafish retina.

Dr. Peter Ahnelt, Ph.D. was born in Bernstein, Austria. He received his Ph.D. in Biology at the University of Vienna in 1980. His foremost interest was the identification of color specific cone photoreceptors in ground squirrel retinas at the Dept. of General and Comparative Physiology, Medical University of Vienna (MUW). In 1984/85 he worked as a post-doc in Helga Kolb's lab at the University of Utah, identifying two spectral subtypes of human cone photoreceptors based on morphological and topographic criteria. Further studies at the U of U, revealed patterns of color-specific connections between human cone and horizontal cell subtypes. As associate professor at the MUW, in collaboration with Jan Nora Hokoc, Eduardo Fernandez, and Martin Glösmann he worked on understanding the various evolutionary and ecological trends underlying mammalian/primate photoreceptor mosaic organization. When retinal OCT imaging was advancing in labs such as Wolfgang Drexler's, Peter made correlations of OCT signal profiles with retinal sublayers. More recently, Peter is interested in the role of Fractalkine in microglial activation in a retinitis pigmentosa mouse model.

Isabel Ortuño-Lizarán, Ph.D. is from Elda, Alicante, Spain and studied for a Biotechnology degree in the Polytechnic University of Valencia, Spain. After, she received a master's degree in Neurosciences at the University of Valencia, she recently finished a doctorate degree (2019) at the University of Alicante, under the supervision of Dr. Nicolás Cuenca. Her research has been mainly focused on studying the human retina and foveal organization in Cuenca's lab. She has also been working on understanding the visual impairment in Parkinson's disease using human retinas and examining the melanopsin ganglion cell density and degeneration rates with the disease progress.

Nicolás Cuenca, Ph.D. was born in Elda, Alicante, Spain. He has a B.Sc. Degree in Biological Sciences from the University of Valencia, Spain and a Ph.D. Degree from the University of Alicante, Spain. He carried out postdoctoral studies at the Department of Physiology, University of Utah (USA) in Helga Kolb's laboratory. Currently, Nicolas is Full Professor in the Department of Physiology, Genetics and Microbiology at the University of Alicante. His research is dedicated to the understanding the functional organization of the mammalian retina. He has extensive expertise in the field of retinal connectivity, morphology and functional correlations, and is an expert in confocal microscopy of immunostained retinas. Nicolas has won many awards

throughout Europe for his photography of immunostained retinas. Presently he is studying the disruption of the retinal architecture including blood vessels and glial cells in inherited retinal degenerations. He is concentrated on therapeutic treatments using animal models for retinitis pigmentosa, glaucoma and macular degeneration. His team is aiming to slow down the progression of neurodegenerative diseases, through the use of cell transplant, antiapoptotics, gene therapy and antioxidant drugs. All are welcome to visit his imaging website at www.retinalmicroscopy.com.

References

1. O'Brien J.J., Chen X., MacLeish P.R., O'Brien J., Massey S.C. Photoreceptor coupling mediated by connexin36 in the primate retina. Journal of Neuroscience. 2012;32(13):4675–4687. PubMed PMID: 22457514.
2. Hendrickson, A., D. Possin, L. Vajzovic, and C.A. Toth, *Histologic development of the human fovea from midgestation to maturity.* American journal of ophthalmology. 2012; 154(5):767-778. e2.
3. Hendrickson A.E., Yuodelis C. The morphological development of the human fovea. Ophthalmology. 1984;91(6):603–612. PubMed PMID: 6462623.
4. Bringmann A., Syrbe S., Görner K., Kacza J., Francke M., Wiedemann P., Reichenbach A. The primate fovea: Structure, function and development. Progress in retinal and eye research. 2018;66:49–84. PubMed PMID: 29609042.
5. Curcio C.A., Sloan K.R. Packing geometry of human cone photoreceptors: variation with eccentricity and evidence for local anisotropy. Visual neuroscience. 1992;9(2):169–180. PubMed PMID: 1504026.
6. Pum D., Ahnelt P.K., Grasl M. Iso-orientation areas in the foveal cone mosaic. Visual neuroscience. 1990;5(6):511–523. PubMed PMID: 2085468.
7. Ahnelt, P., C. Schubert, and E. Anger, *Macular Photoreceptor Organization. Modular substructuring–a consistent feature along all foveal cone elements*, in *The Macula Diagnosis, Treatment and Future Trends*. 2004, Springer: Vienna.
8. Curcio C.A., Packer O., Kalina R.E. A whole mount method for sequential analysis of photoreceptor and ganglion cell topography in a single retina. Vision research. 1987;27(1):9–15. PubMed PMID: 3303679.
9. Schein S.J. Anatomy of macaque fovea and spatial densities of neurons in foveal representation. Journal of Comparative Neurology. 1988;269(4):479–505. PubMed PMID: 3372725.
10. Curcio C.A., Allen K.A. Topography of ganglion cells in human retina. Journal of comparative Neurology. 1990;300(1):5–25. PubMed PMID: 2229487.
11. Ahnelt P.K., Kolb H., Pflug R. Identification of a subtype of cone photoreceptor, likely to be blue sensitive, in the human retina. Journal of Comparative Neurology. 1987;255(1):18–34. PubMed PMID: 2434534.
12. Peichl L., Behrmann G., Kröger R.H. For whales and seals the ocean is not blue: a visual pigment loss in marine mammals. European Journal of Neuroscience. 2001;13(8):1520–1528. PubMed PMID: 11328346.
13. Nathans J., Piantanida T.P., Eddy R.L., Shows T.B., Hogness D.S. Molecular genetics of inherited variation in human color vision. Science. 1986;232(4747):203–210. PubMed PMID: 3485310.
14. Kolb, H. and L. Lipitz, *The anatomical basis for colour vision in the vertebrate retina*, Volume 6: The perception of colour, in *Vision and Visual Dysfunction*, P. Gouras, Editor. 1991, Macmillan Press Ltd,: London. p. 128-145.
15. Marc R.E., Sperling H.G. Chromatic organization of primate cones. Science. 1977;196(4288):454–456. PubMed PMID: 403607.
16. Williams D.R., MacLeod D.I., Hayhoe M.M. Punctate sensitivity of the blue-sensitive mechanism. Vision research. 1981;21(9):1357–1375. PubMed PMID: 7314519.
17. Cicerone C.M., Nerger J.L. The relative numbers of long-wavelength-sensitive to middle-wavelength-sensitive cones in the human fovea centralis. Vision research. 1989;29(1):115–128. PubMed PMID: 2773329.
18. Mollon J., Bowmaker J. The spatial arrangement of cones in the primate fovea. Nature. 1992;360(6405):677. PubMed PMID: 1465131.

19. Roorda A., Williams D.R. The arrangement of the three cone classes in the living human eye. Nature. 1999;397(6719):520. PubMed PMID: 10028967.
20. Roorda A., Metha A.B., Lennie P., Williams D.R. Packing arrangement of the three cone classes in primate retina. Vision research. 2001;41(10-11):1291–1306. PubMed PMID: 11322974.
21. Hofer H., Singer B., Williams D.R. Different sensations from cones with the same photopigment. Journal of Vision. 2005;5(5):5–5. PubMed PMID: 16097875.
22. Schmidt B.P., Boehm A.E., Foote K.G., Roorda A. The spectral identity of foveal cones is preserved in hue perception. Journal of vision. 2018;18(11):19–19. PubMed PMID: 30372729.
23. Drasdo N., Fowler C. Non-linear projection of the retinal image in a wide-angle schematic eye. The British journal of ophthalmology. 1974;58(8):709. PubMed PMID: 4433482.
24. Ahnelt P., Pflug R. Telodendrial contacts between foveolar cone pedicles in the human retina. Experientia. 1986;42(3):298–300. PubMed PMID: 3956685.
25. Xiao M., Hendrickson A. Spatial and temporal expression of short, long/medium, or both opsins in human fetal cones. Journal of Comparative Neurology. 2000;425(4):545–559. PubMed PMID: 10975879.
26. Hendrickson A., Zhang C. Development of cone photoreceptors and their synapses in the human and monkey fovea. Journal of Comparative Neurology. 2019;527(1):38–51. PubMed PMID: 28074469.
27. Cornish E.E., Hendrickson A.E., Provis J.M. Distribution of short-wavelength-sensitive cones in human fetal and postnatal retina: early development of spatial order and density profiles. Vision research. 2004;44(17):2019–2026. PubMed PMID: 15149835.
28. Kolb H., Fernandez E., Schouten J., Ahnelt P., Linberg K.A., Fisher S.K. Are there three types of horizontal cell in the human retina? Journal of Comparative Neurology. 1994;343(3):370–386. PubMed PMID: 8027448.
29. Ahnelt P., Kolb H. Horizontal cells and cone photoreceptors in primate retina: a Golgi-light microscopic study of spectral connectivity. Journal of Comparative Neurology. 1994;343(3):387–405. PubMed PMID: 8027449.
30. Ahnelt P., Kolb H. Horizontal cells and cone photoreceptors in human retina: A Golgi-electron microscopic study of spectral connectivity. Journal of Comparative Neurology. 1994;343(3):406–427. PubMed PMID: 8027450.
31. Ahnelt, P.K. and H. Kolb, *Short-wavelength-sensitive cones: morphology and color-specific connections*, in *Colour Vision Deficiencies XII*. 1995, Springer. p. 285-297.
32. Drinnenberg, A., F. Franke, R.K. Morikawa, J. Jüttner, D. Hillier, P. Hantz, A. Hierlemann, R.A. da Silveira, and B. Roska, *How diverse retinal functions arise from feedback at the first visual synapse.* Neuron. 2018; 99(1):117-134. e11.
33. Verweij J., Hornstein E.P., Schnapf J.L. Surround antagonism in macaque cone photoreceptors. Journal of Neuroscience. 2003;23(32):10249–10257. PubMed PMID: 14614083.
34. Dacey D.M., Crook J.D., Packer O.S. Distinct synaptic mechanisms create parallel S-ON and S-OFF color opponent pathways in the primate retina. Visual Neuroscience. 2014;31(2):139–151. PubMed PMID: 23895762.
35. Packer O.S., Verweij J., Li P.H., Schnapf J.L., Dacey D.M. Blue-yellow opponency in primate S cone photoreceptors. Journal of Neuroscience. 2010;30(2):568–572. PubMed PMID: 20071519.
36. Cajal, S.R.y., *The structure of the retina*. 1933/1972, Translated by S. Thorpe and M. Glickstein: Charles C. Thomas Publisher.
37. Kolb H. Organization of the outer plexiform layer of the primate retina: electron microscopy of Golgi-impregnated cells. Philosophical Transactions of the Royal Society of London. B, Biological Sciences. 1970;258(823):261–283. PubMed PMID: 22408829.
38. Kolb H., Boycott B., Dowling J. A second type of midget bipolar cell in the primate retina. Philos Trans R Soc Lond B Biol Sci. 1969;255:177–184.
39. Stell W.K. Correlation of retinal cytoarchitecture and ultrastructure in Golgi preparations. The Anatomical Record. 1965;153(4):389–397. PubMed PMID: 4160117.

40. Boycott B.B., Dowling J.E. Organization of the primate retina: light microscopy, with an appendix: a second type of midget bipolar cell in the primate retina. Philosophical Transactions of the Royal Society of London. Series B, Biological Sciences. 1969;255(799):109–184.
41. Ritchey E.R., Bongini R.E., Code K.A., Zelinka C., Petersen-Jones S., Fischer A.J. The pattern of expression of guanine nucleotide-binding protein β3 in the retina is conserved across vertebrate species. Neuroscience. 2010;169(3):1376–1391. PubMed PMID: 20538044.
42. Milam A.H., Dacey D.M., Dizhoor A.M. Recoverin immunoreactivity in mammalian cone bipolar cells. Visual neuroscience. 1993;10(1):1–12. PubMed PMID: 8424920.
43. Zang J., Neuhauss S.C. The Binding Properties and Physiological Functions of Recoverin. Frontiers in molecular neuroscience. 2018.:11. PubMed PMID: 30618620.
44. Kolb H., Dekorver L. Midget ganglion cells of the parafovea of the human retina: a study by electron microscopy and serial section reconstructions. Journal of Comparative Neurology. 1991;303(4):617–636. PubMed PMID: 1707423.
45. Marshak D.W., Yamada E.S., Bordt A.S., Perryman W.C. Synaptic input to an ON parasol ganglion cell in the macaque retina: a serial section analysis. Visual neuroscience. 2002;19(3):299–305. PubMed PMID: 12392179.
46. Kolb H., Marshak D. The midget pathways of the primate retina. Documenta Ophthalmologica. 2003;106(1):67–81. PubMed PMID: 12675488.
47. Jusuf P.R., Martin P.R., Grünert U. Synaptic connectivity in the midget-parvocellular pathway of primate central retina. Journal of Comparative Neurology. 2006;494(2):260–274. PubMed PMID: 16320234.
48. Nelson R., Famiglietti E. Jr, Kolb H. Intracellular staining reveals different levels of stratification for on-and off-center ganglion cells in cat retina. Journal of Neurophysiology. 1978;41(2):472–483. PubMed PMID: 650277.
49. Nelson R., Kolb H. ON and OFF pathways in the vertebrate retina and visual system. The visual neurosciences. 2004;1:260–278.
50. Field G.D., Gauthier J.L., Sher A., Greschner M., Machado T.A., Jepson L.H., Shlens J., Gunning D.E., Mathieson K., Dabrowski W. Functional connectivity in the retina at the resolution of photoreceptors. Nature. 2010;467(7316):673. PubMed PMID: 20930838.
51. Kling A., Field G., Brainard D., Chichilnisky E. Probing Computation in the Primate Visual System at Single-Cone Resolution. Annual review of neuroscience. 2019.:42. PubMed PMID: 30857477.
52. Telkes I., Lee S.C., Jusuf P.R., Grünert U. The midget-parvocellular pathway of marmoset retina: A quantitative light microscopic study. Journal of Comparative Neurology. 2008;510(5):539–549. PubMed PMID: 18683219.
53. Gouras P. Identification of cone mechanisms in monkey ganglion cells. The Journal of physiology. 1968;199(3):533–547. PubMed PMID: 4974745.
54. Gouras P., Zrenner E. Color coding in primate retina. Vision Research. 1981;21(11):1591–1598. PubMed PMID: 7336591.
55. Dacey D.M., Packer O.S. Colour coding in the primate retina: diverse cell types and cone-specific circuitry. Current opinion in neurobiology. 2003;13(4):421–427. PubMed PMID: 12965288.
56. Dacey D., Packer O.S., Diller L., Brainard D., Peterson B., Lee B. Center surround receptive field structure of cone bipolar cells in primate retina. Vision research. 2000;40(14):1801–1811. PubMed PMID: 10837827.
57. Wool L.E., Crook J.D., Troy J.B., Packer O.S., Zaidi Q., Dacey D.M. Nonselective wiring accounts for red-green opponency in midget ganglion cells of the primate retina. Journal of Neuroscience. 2018;38(6):1520–1540. PubMed PMID: 29305531.
58. Manookin, M.B., S.S. Patterson, and C.M. Linehan, *Neural mechanisms mediating motion sensitivity in parasol ganglion cells of the primate retina.* Neuron. 2018; 97(6):1327-1340. e4.
59. Slaughter M.M., Miller R.F. 2-amino-4-phosphonobutyric acid: a new pharmacological tool for retina research. Science. 1981;211(4478):182–5. PubMed PMID: 6255566.

60. McGregor J.E., Yin L., Yang Q., Godat T., Huynh K.T., Zhang J., Williams D.R., Merigan W.H. Functional architecture of the foveola revealed in the living primate. PloS one. 2018;13(11):e0207102. PubMed PMID: 30485298.
61. Mariani A.P. Bipolar cells in monkey retina selective for the cones likely to be blue-sensitive. Nature. 1984;308(5955):184. PubMed PMID: 6199677.
62. Kouyama N., Marshak D. Bipolar cells specific for blue cones in the macaque retina. Journal of Neuroscience. 1992;12(4):1233–1252. PubMed PMID: 1556594.
63. Calkins D.J., Tsukamoto Y., Sterling P. Microcircuitry and mosaic of a blue–yellow ganglion cell in the primate retina. Journal of Neuroscience. 1998;18(9):3373–3385. PubMed PMID: 9547245.
64. Dacey D.M., Lee B.B. The'blue-on'opponent pathway in primate retina originates from a distinct bistratified ganglion cell type. Nature. 1994;367(6465):731. PubMed PMID: 8107868.
65. Mullen K.T. The contrast sensitivity of human colour vision to red-green and blue-yellow chromatic gratings. The Journal of physiology. 1985;359(1):381–400. PubMed PMID: 3999044.
66. Sekiguchi N., Williams D.R., Brainard D.H. Efficiency in detection of isoluminant and isochromatic interference fringes. JOSA A. 1993;10(10):2118–2133. PubMed PMID: 8229351.
67. Stromeyer C. III, Kranda K., Sternheim C. Selective chromatic adaptation at different spatial frequencies. Vision research. 1978;18(4):427–437. PubMed PMID: 664322.
68. Curcio C.A., Allen K.A., Sloan K.R., Lerea C.L., Hurley J.B., Klock I.B., Milam A.H. Distribution and morphology of human cone photoreceptors stained with anti-blue opsin. Journal of Comparative Neurology. 1991;312(4):610–624. PubMed PMID: 1722224.
69. Klug K., Herr S., Ngo I.T., Sterling P., Schein S. Macaque retina contains an S-cone OFF midget pathway. Journal of Neuroscience. 2003;23(30):9881–9887. PubMed PMID: 14586017.
70. Patterson S.S., Kuchenbecker J.A., Anderson J.R., Bordt A.S., Marshak D.W., Neitz M., Neitz J. An S-cone circuit for edge detection in the primate retina. Scientific Reports. 2019;9(1):11913. PubMed PMID: 31417169.
71. Wool L.E., Packer O.S., Zaidi Q., Dacey D.M. Connectomic identification and three-dimensional color tuning of S-OFF midget ganglion cells in the primate retina. Journal of Neuroscience. 2019;39(40):7893–7909. PubMed PMID: 31405926.
72. Wiesel T.N., Hubel D.H. Spatial and chromatic interactions in the lateral geniculate body of the rhesus monkey. Journal of neurophysiology. 1966;29(6):1115–1156. PubMed PMID: 4961644.
73. Dacey D.M., Liao H.-W., Peterson B.B., Robinson F.R., Smith V.C., Pokorny J., Yau K.-W., Gamlin P.D. Melanopsin-expressing ganglion cells in primate retina signal colour and irradiance and project to the LGN. Nature. 2005;433(7027):749. PubMed PMID: 15716953.
74. Mure L.S., Vinberg F., Hanneken A., Panda S. Functional diversity of human intrinsically photosensitive retinal ganglion cells. Science. 2019;366(6470):1251–1255. PubMed PMID: 31806815.
75. Hannibal J., Christiansen A.T., Heegaard S., Fahrenkrug J., Kiilgaard J.F. Melanopsin expressing human retinal ganglion cells: Subtypes, distribution, and intraretinal connectivity. Journal of Comparative Neurology. 2017;525(8):1934–1961. PubMed PMID: 28160289.
76. Miyagishima K.J., Gruenert U., Li W. Processing of S-cone signals in the inner plexiform layer of the mammalian retina. Visual neuroscience. 2014;31(2):153–163. PubMed PMID: 24016424.
77. Patterson S.S., Kuchenbecker J.A., Anderson J.R., Neitz M., Neitz J. A Color Vision Circuit for Non-Image-Forming Vision in the Primate Retina. Current Biology. 2020. PubMed PMID: 32084404.
78. Mariani A.P. Giant bistratified bipolar cells in monkey retina. The Anatomical Record. 1983;206(2):215–220. PubMed PMID: 6846872.
79. Kolb H., Linberg K.A., Fisher S.K. Neurons of the human retina: a Golgi study. Journal of comparative neurology. 1992;318(2):147–187. PubMed PMID: 1374766.
80. Jusuf P.R., Lee S.C., Hannibal J., Grünert U. Characterization and synaptic connectivity of melanopsin-containing ganglion cells in the primate retina. European Journal of Neuroscience. 2007;26(10):2906–2921. PubMed PMID: 18001286.

81. Mariani A.P. Amacrine cells of the rhesus monkey retina. Journal of comparative neurology. 1990;301(3):382–400. PubMed PMID: 2262597.
82. Rodieck R., Marshak D. Spatial density and distribution of choline acetyltransferase immunoreactive cells in human, macaque, and baboon retinas. Journal of Comparative Neurology. 1992;321(1):46–64. PubMed PMID: 1613139.
83. Marshak D.W. Peptidergic neurons of the macaque monkey retina. Neuroscience Research Supplements. 1989;10:S117–S130. PubMed PMID: 2574431.
84. Kolb H., Famigilietti E. Rod and cone pathways in the inner plexiform layer of cat retina. Science. 1974;186(4158):47–49. PubMed PMID: 4417736.
85. Kolb H., Zhang L., Dekorver L., Cuenca N. A new look at calretinin-immunoreactive amacrine cell types in the monkey retina. Journal of Comparative Neurology. 2002;453(2):168–184. PubMed PMID: 12373782.
86. Lee S.C., Weltzien F., Madigan M.C., Martin P.R., Grünert U. Identification of AII amacrine, displaced amacrine, and bistratified ganglion cell types in human retina with antibodies against calretinin. Journal of Comparative Neurology. 2016;524(1):39–53. PubMed PMID: 26053777.
87. Wässle H., Grüunert U., Chun M.N., Boycott B.B. The rod pathway of the macaque monkey retina: identification of AII-amacrine cells with antibodies against calretinin. Journal of Comparative Neurology. 1995;361(3):537–551. PubMed PMID: 8550898.
88. Feng G., Mellor R.H., Bernstein M., Keller-Peck C., Nguyen Q.T., Wallace M., Nerbonne J.M., Lichtman J.W., Sanes J.R. Imaging neuronal subsets in transgenic mice expressing multiple spectral variants of GFP. Neuron. 2000;28(1):41–51. PubMed PMID: 11086982.
89. Wässle H., Heinze L., Ivanova E., Majumdar S., Weiss J., Harvey R.J., Haverkamp S. Glycinergic transmission in the Mammalian retina. Frontiers in molecular neuroscience. 2009;2:6. PubMed PMID: 19924257.
90. Polyak, S.L., *The retina*. 1941, Chicago: Chicago University Press.
91. Klump K.E., Zhang A.-J., Wu S.M., Marshak D.W. Parvalbumin-immunoreactive amacrine cells of macaque retina. Visual neuroscience. 2009;26(3):287–296. PubMed PMID: 19435546.
92. Kolb H., Nelson R. Hyperpolarizing, small-field, amacrine cells in cone pathways of cat retina. Journal of Comparative Neurology. 1996;371(3):415–436. PubMed PMID: 8842896.
93. Lee S.C., Meyer A., Schubert T., Hüser L., Dedek K., Haverkamp S. Morphology and connectivity of the small bistratified A8 amacrine cell in the mouse retina. Journal of Comparative Neurology. 2015;523(10):1529–1547. PubMed PMID: 25630271.
94. Neumann S., Haverkamp S. Characterization of small-field bistratified amacrine cells in macaque retina labeled by antibodies against synaptotagmin-2. Journal of Comparative Neurology. 2013;521(3):709–724. PubMed PMID: 22821706.
95. Bloomfield S.A., Xin D., Osborne T. Light-induced modulation of coupling between AII amacrine cells in the rabbit retina. Visual neuroscience. 1997;14(3):565–576. PubMed PMID: 9194323.
96. Dacheux R.F., Raviola E. The rod pathway in the rabbit retina: a depolarizing bipolar and amacrine cell. Journal of Neuroscience. 1986;6(2):331–345. PubMed PMID: 3950701.
97. Nelson R. AII amacrine cells quicken time course of rod signals in the cat retina. Journal of Neurophysiology. 1982;47(5):928–947. PubMed PMID: 6177841.
98. Strettoi E., Masri R.A., Grünert U. AII amacrine cells in the primate fovea contribute to photopic vision. Scientific reports. 2018;8(1):16429. PubMed PMID: 30401922.
99. Bordt A.S., Hoshi H., Yamada E.S., Perryman-Stout W.C., Marshak D.W. Synaptic input to OFF parasol ganglion cells in macaque retina. Journal of Comparative Neurology. 2006;498(1):46–57. PubMed PMID: 16856174.
100. Haverkamp S., Wässle H. Characterization of an amacrine cell type of the mammalian retina immunoreactive for vesicular glutamate transporter 3. Journal of comparative neurology. 2004;468(2):251–263. PubMed PMID: 14648683.

101. Johnson J., Sherry D.M., Liu X., Fremeau R.T. Jr, Seal R.P., Edwards R.H., Copenhagen D.R. Vesicular glutamate transporter 3 expression identifies glutamatergic amacrine cells in the rodent retina. Journal of comparative neurology. 2004;477(4):386–398. PubMed PMID: 15329888.
102. Lee S., Zhang Y., Chen M., Zhou Z.J. Segregated glycine-glutamate co-transmission from vGluT3 amacrine cells to contrast-suppressed and contrast-enhanced retinal circuits. Neuron. 2016;90(1):27–34. PubMed PMID: 26996083.
103. Liao H.W., Ren X., Peterson B.B., Marshak D.W., Yau K.W., Gamlin P.D., Dacey D.M. Melanopsin-expressing ganglion cells on macaque and human retinas form two morphologically distinct populations. Journal of Comparative Neurology. 2016;524(14):2845–2872. PubMed PMID: 26972791.
104. Mariani A.P., Kolb H., Nelson R. Dopamine-containing amacrine cells of rhesus monkey retina parallel rods in spatial distribution. Brain research. 1984;322(1):1–7. PubMed PMID: 6518360.
105. De Monasterio F., Gouras P. Functional properties of ganglion cells of the rhesus monkey retina. The Journal of physiology. 1975;251(1):167–195. PubMed PMID: 810576.
106. Kolb H., Nelson R., Mariani A. Amacrine cells, bipolar cells and ganglion cells of the cat retina: a Golgi study. Vision Res. 1981;21(7):1081–1114. PubMed PMID: 7314489.
107. Sinha, R., M. Hoon, J. Baudin, H. Okawa, R.O. Wong, and F. Rieke, *Cellular and circuit mechanisms shaping the perceptual properties of the primate fovea.* Cell. 2017; 168(3):413-426. e12.
108. Peng, Y.-R., K. Shekhar, W. Yan, D. Herrmann, A. Sappington, G.S. Bryman, T. Van Zyl, M.T.H. Do, A. Regev, and J.R. Sanes, *Molecular classification and comparative taxonomics of foveal and peripheral cells in primate retina.* Cell. 2019; 176(5):1222-1237. e22.
109. Saari J.C., Bunt-Milam A.H., Bredberg D.L., Garwin G.G. Properties and immunocytochemical localization of three retinoid-binding proteins from bovine retina. Vision research. 1984;24(11):1595–1603. PubMed PMID: 6398562.
110. Cuenca N., Ortuño-Lizarán I., Pinilla I. Cellular characterization of OCT and outer retinal bands using specific immunohistochemistry markers and clinical implications. Ophthalmology. 2018;125(3):407–422. PubMed PMID: 29037595.
111. Curcio C.A., Provis J., Wong R., Neitz M. Obituary: Anita Hendrickson, PhD. The Journal of comparative neurology. 2019;527(1):11–12.
112. Ahnelt P.K. The photoreceptor mosaic. Eye. 1998;12(3b):531–540. PubMed PMID: 9775214.
113. Ahnelt P.K., Pflug R. Telodendrial contacts between foveolar cone pedicles in the human retina. Experientia. 1986;42(3):298–300. PubMed PMID: 3956685.
114. Nasir-Ahmad S., Lee S.C., Martin P.R., Grünert U. Melanopsin-expressing ganglion cells in human retina: Morphology, distribution, and synaptic connections. Journal of Comparative Neurology. 2019;527(1):312–327. PubMed PMID: 28097654.

Retinal Circuits

Circuitry for Rod Signals through the Retina

Helga Kolb

Created: May 1, 2001; Updated: September 1, 2009.

Rods

Rod photoreceptors and rod-connected nerve cells through the retina are responsible for pathways concerned with night vision and increased sensitivity of our visual system under what is called scotopic conditions (conditions of very little ambient light). Most vertebrates have a preponderance of rod photoreceptors in their retinas and such animals are very good at hunting and movement at night because of their very sensitive scotopic visual systems. Some animals are even completely nocturnal and have lost some of their cone types and their cone system neurons.

Humans, of course, are highly visual vertebrates and function mostly with their cone systems for color and high acuity form vision. However, the rod system is also important for our capacity to move around and function in scotopic conditions. If our rods or rod system neurons become diseased and degenerated we become night blind as happens to unfortunate people who have a disease called retinitis pigmentosa.

When looking at the mosaic of human photoreceptors it becomes apparent that the human retina is actually rod-dominated numerically. That is, rod photoreceptors out-number cone photoreceptors by orders of magnitude and the consequent second- and third-order neurons recruited for processing rod-driven vision outnumber the cone pathways neurons everywhere but in the central fovea (Fig. 1).

Rods peak in density in a ring approximately 5mm (18o) from the center of the fovea (human (1); rhesus monkey (2)). Rods are present in greater numbers than cones from 2 mm from the fovea to the far periphery. As can be seen in Fig. 2, the rods always form a nice hexagonal packing around the cones and separate the cones from each other.

Rod Bipolar Cells

As was pointed out in a previous section, only one morphological type of bipolar cell has been found to make connections with the rod photoreceptors. The rod bipolar collects input from between 15 and 30 rod spherules in the outer plexiform layer (Fig. 3).

Electron microscope investigation of Golgi-impregnated rod bipolar cells first showed that the rod bipolar dendrite penetrates into the rod spherule to make an invaginating ribbon related type of contact (3) (Fig. 4). This invaginating contact is known to bear metabotropic glutamate receptors in the bipolar dendrite membrane (Fig. 5). The receptor was proved to be mGluR6 by Numura and coauthors (4) and Vardi and Morigawa (5) using immunocytochemistry against the cloned mGluR6 receptor. Since then the mGluR6 receptor is thought to trigger a second messenger cascade involving GalphaO, transducin molecules, to act on voltage gated Ca channels (6, 7).

Both Golgi impregnation of single rod bipolar cells (Fig. 6) and immunocytochemical staining of rod bipolar cell populations with protein kinase C (PKC) (Fig. 7) show the characteristic morphology of the rod bipolar cell type in mammalian retina (8, 9). The immunocytochemical staining and confocal microscopy is now the most illustrative way of seeing the rod bipolar cells in mammalian retinas (Cuenca personal communication) (Fig. 7). As can be seen in this stunning micrograph (which incidentally won the first place award in science photos at the Spanish Congress of Neuroscience, 2009) rod bipolar cells (red) send dendrites to the rod spherules in the outer plexiform layer (green) to end at synaptic ribbons therein (blue) and axons to the inner plexiform layer where they terminate deep, close to the ganglion cell bodies, as narrow-field, clumpy axon terminals (red).

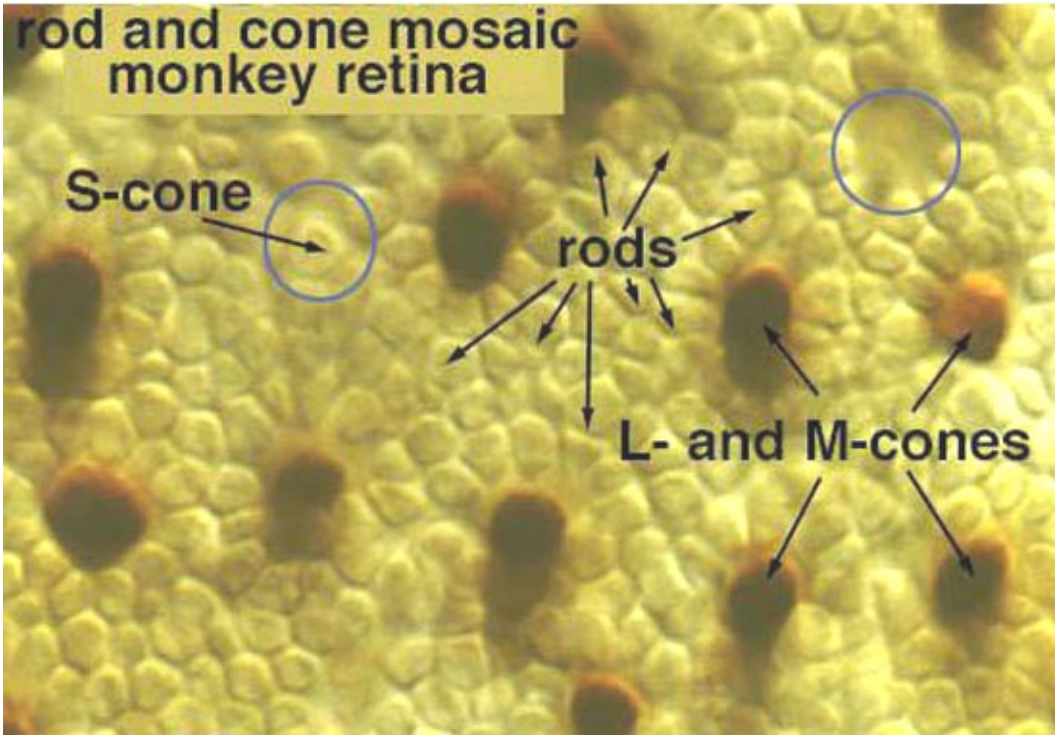

Figure 1. Light micrograph of the primate photoreceptors.

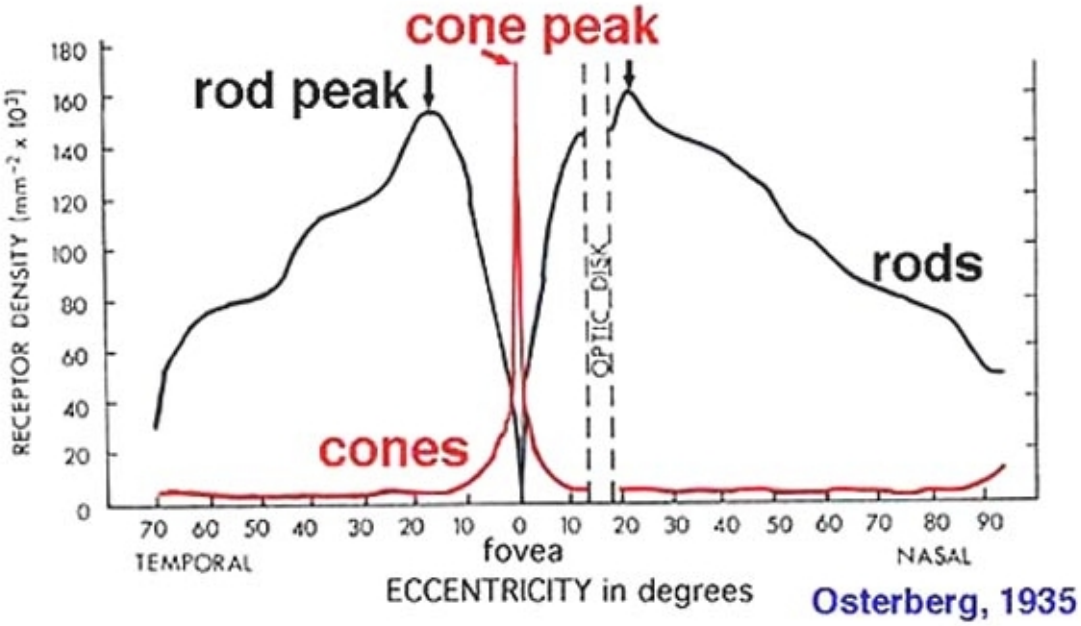

Figure 2. Graph to show rod and cone densities along the horizontal median.

Electron microscopy of the rod bipolar cell axons in the inner plexiform layer shows that they make ribbon synapses only upon amacrine cell profiles. A ganglion cell dendrite is not seen to be postsynaptic to rod bipolar cell axons (10, 11). This allows for both divergence of the rod signal and collection (convergence) of signals from many rods and rod bipolars, by means of these amacrine cells, before synaptic output to ganglion cells. Most commonly the output of the rod bipolar ribbon is to a dyad of amacrine cell processes, one of which is known as

AII and the other as A17, a reciprocal amacrine (see below). The AII is characterized by making gap junctions with neigboring cone bipolar or other AII profiles. The A17 is characterized by always making a return synapse known as a reciprocal synapse to the rod bipolar axon terminal (Fig. 8 and Fig. 9).

Rod Amacrine Cells

Two amacrine cells are key in the rod pathway circuitry through the mammalian retina (see above). The one is a small-field, bistratified cell given the name AII in its original description, to compare with the other amacrine common at the rod bipolar ribbon dyad, known as AI (10). Since then the AII label has stuck to the rod amacrine but the AI label has been dropped in favor of calling the cell the A17 or reciprocal amacrine. The small AII amacrine is probably the commonest amacrine cell in the mammalian retina (512,000 total in cat retina) followed by the A17 cell (between 170,000 and 230,000 cells in rabbit) (12) (Fig. 10).

Two other amacrine cells are known to be involved in the rod pathways but to a lesser extent that AII and A17. These cells are A8 and A13 (above). But they are more strongly driven by the cone system in that greater numbers of cone bipolar cells have synapses upon them than rod bipolar cells. We shall, therefore, consider them in great detail in the chapter on cone driven pathways through the retina. However one amacrine cell, A18, is definitely involved in the pathways of the rod system by virtue of influencing both AII and A17 amacrine cells. So we will describe A18 cells in detail in this chapter.

AII Amacrine Cells

AII amacrines are fascinating, small-field amacrines that have a seminal role in the rod pathways, and in linking the rod and cone pathways so that the rod signals can also use the cone bipolar pathways to ganglion cells. The narrow-field bistratified rod amacrine cell, AII, is primarily postsynaptic to rod bipolar axon terminals in lower sublamina **b** of the IPL (30% of its input (13)). Its major output is from its lobular appendages upon ganglion cells that have dendrites only in sublamina **a** (8, 14) (Fig. 11).

The AII also passes rod-driven information to a cone bipolar cell that makes contact with ganglion cells of sublamina **b**. It does so through large gap junctions with these cone bipolar axons before they in turn make their ribbon synapses to those ganglion cells (black spots on AII primary dendrites to pink cb axon). A little OFF-center cone bipolar input is provided to the AII lobular appendages by cb1 and cb2 cone bipolar cells in sublamina **a** (19% of input (13)) (yellow cb profiles). AII amacrine cells are also coupled across the retina in a weak electrical syncytium by virtue of their gap junctions between their dendrites in sublamina **b** (gj, lower right) (14-16) (Fig. 12).

We know from the intracellular recordings done in cat retina that ganglion cells with dendrites in sublamina **a** respond to light with a hyperpolarizing or OFF-center response and that ganglion cells with dendrites in sublamina **b** respond with a depolarizing or ON-center response (17).

We also know that rod bipolar cells respond to light with a center-depolarizing (ON-center) responses (18), and by virtue of their deep penetrating axon terminals to sublamina **b** we expect them to carry rod ON-center signals to the next order neurons i.e. either ganglion cell or amacrine cell of that neuropil. Since rod bipolar cells do not synapses directly with ganglion cells we expect the rod bipolar cell to have output at ribbon synapses instead to center depolarizing (ON-center) amacrine cells. And this is in fact what has been discovered from intracellular recordings in cat and rabbit retinas. AII amacrine cells respond to light with a depolarizing response (ON center response) in their centers (18) (Fig. 13).

Thus the center-depolarizing (ON-center) AII cell make a sign-inverting synapse upon the center-hyperpolarizing (OFF-center) type of ganglion cell to contribute rod signals to the center response of the receptive field of that ganglion cell. (Amacrine cells in general are known to be inhibitory neurons using

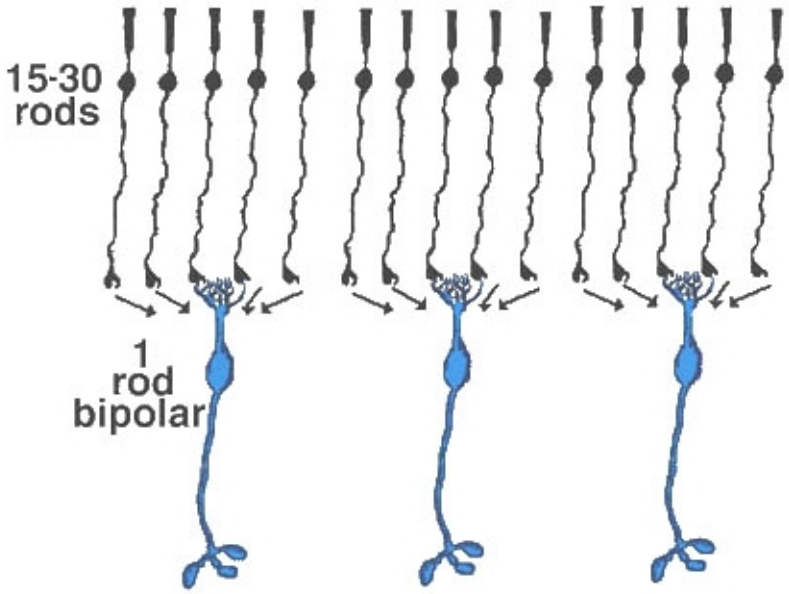

Figure 3. Convergence of rod pathways.

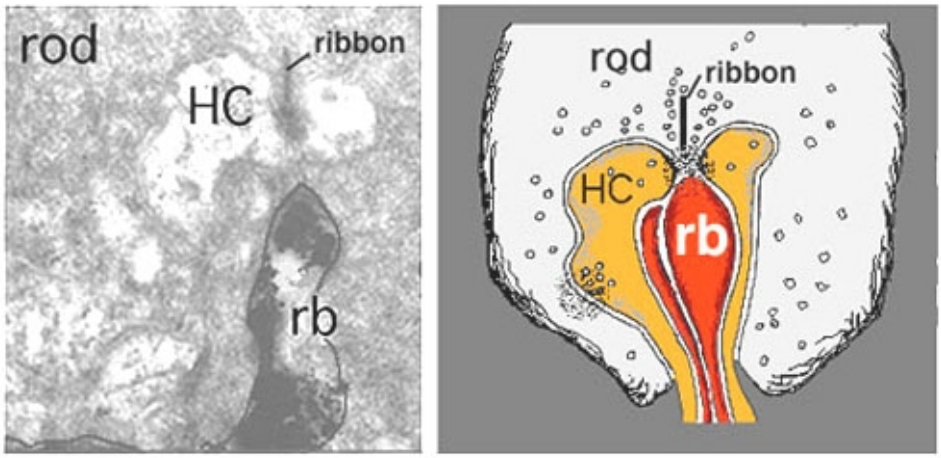

Figure 4. Electron micrograph and drawing of a rod spherule.

common inhibitory neurotransmitters of the CNS like glycine and GABA). AII amacrine cells are glycinergic (19). The AII uses the gap junction with the sublamina **b** type of cone bipolar (cb5 in Fig. 13) to pass center-depolarizing (excitatory) input to the center-depolarizing ganglion cell with which the cone bipolar has synapses (cb5 to ON-center beta GC, Fig. 13). By this division of function within the small dendritic field of the AII amacrine cell, rod signals can be ensured of reaching both ON- and OFF-center types of ganglion cells (Fig. 14).

A17 Amacrine Cells

A17 cells are very wide-field diffusely branching amacrine cells types. Their fine dendrites pass through the IPL to end running in the lower sublamina **b**, receiving synapses at intervals denoted by their beads from rod bipolar axon terminals (Fig. 15).

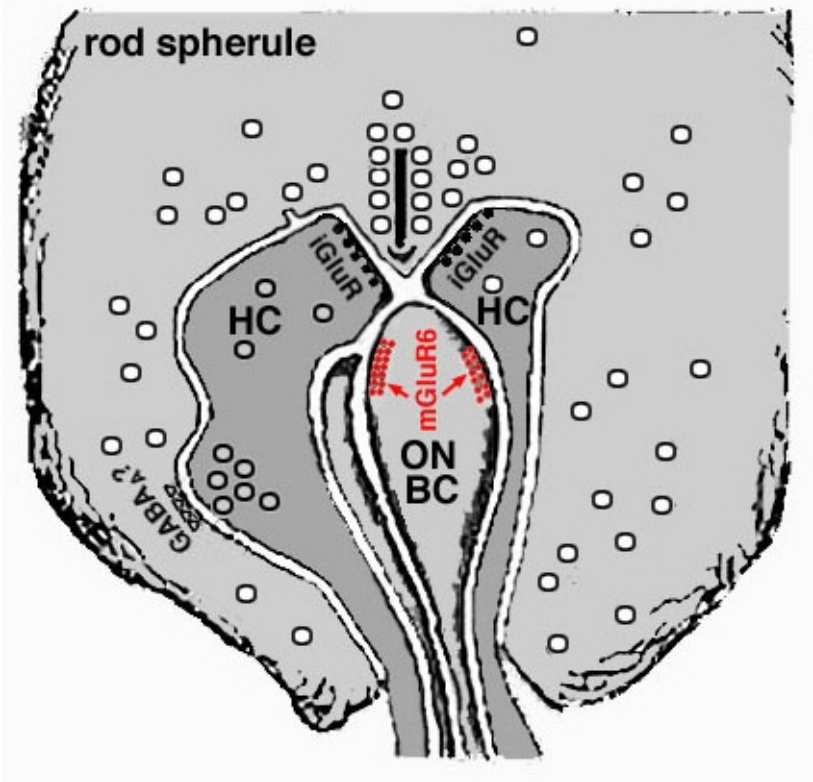

Figure 5. The present understanding of the receptor molecules thought to be present at the rod to bipolar and horizontal cell dendrites in the mammalian retina.

A single A17 amacrine cell receives synaptic input from approximately 1000 rod bipolar cells. Interestingly A17 cells do not appear to make synapses upon other amacrine or ganglion cells, instead they merely interconnect rod bipolar cells by reciprocal synapses. The A17 thus has a completely different receptive field area over which it collects rod signals than its narrow-field partner at the dyad, the AII amacrine cell. Presumably the A17 is an integrating unit that helps set sensitivity levels over a very large area of rod photoreceptors and rod bipolar cells (20).

Like the AII amacrine cell A17 cells respond to light flashes with a center depolarizing response (20). Its ON-center response reflects the rod generated ON-center message (18). But unlike the AII, the A17 cell's output is only known to be reciprocal synapses to the rod bipolar from which it receives input (20) (Fig. 16).

A17 cells are very sensitive at low light intensities and may play a role in converging and amplifying rod signals from large areas of retina. A17 is known to accumulate serotonin in rabbit retina (12) but is thought to be a GABAergic neuron in terms of neurotransmission, in all mammalian retinas (21).

Dopamine Containing (A18) Cells of the Retina

A18 is a wide-field amacrine with extensive dendritic branching in the stratum next to the amacrine cell bodies, i.e. S1 of sublamina **a**. The A18 is known to be a dopaminergic amacrine cell and the whole population of these cells in the retina can be revealed by immunostaining to the synthesizing enzyme of dopamine, tyrosine hydroxylase (above). A18 has thin dendrites and axon like processes that run for hundreds of microns (Fig. 17).

The fine terminals of these processes surround cell bodies and dendrites of amacrine cells AII, A8, A17 and possibly A13 cells (22-24). The A18 thereby synapses in profusion upon the two major and some of the minor amacrines of the rod pathways. In addition, the A18 receives many synapses from other amacrine cells and some few synapses from a cone bipolar cell type, as yet not positively identified, but possibly the type known as a giant

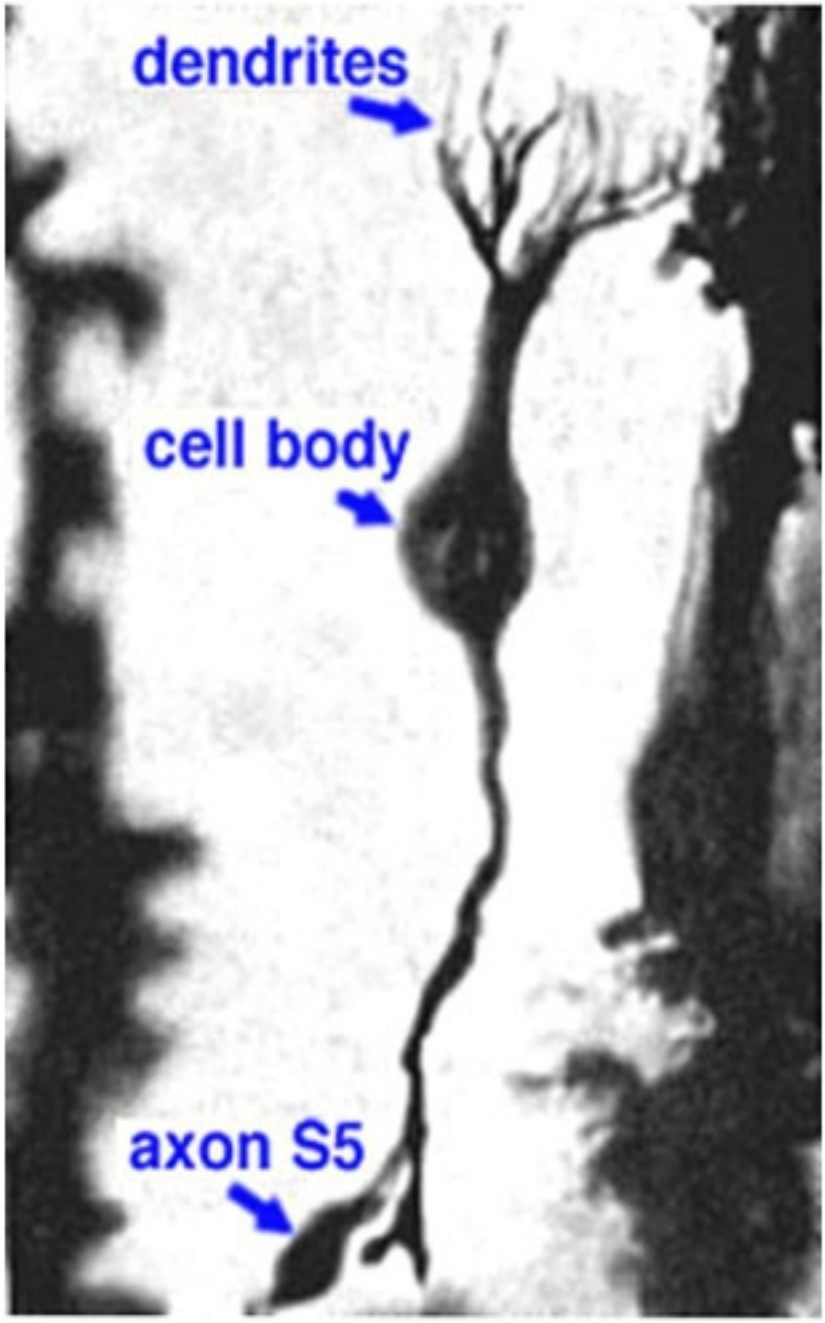

Figure 6. Golgi impregnation of rod bipolar cells.

bistratified cone bipolar cell (25). Recently it has also been discovered that deep axon-like processes of the A18 amacrine passing in S5 of sublamina **b** make synapses directly upon rod bipolar axon terminals (23). A18 has not yet been studied by intracellular recordings, but equivalent dopaminergic amacrine cells in other species are known to be transient-sustained, center-depolarizing in response type (26) (Fig. 18).

It is thought that the dopaminergic A18 cell has an effect upon the rod AII amacrine to uncouple the syncytium of AIIs across the retina and to uncouple the AII amacrine from the cone bipolar cell of sublamina **b** (27, 28). This could have the effect of increasing receptive field sizes of ganglion cells under scotopic conditions, providing added sensitivity to the rod system messages in the ganglion cells. Dopaminergic amacrine cells are also thought to function in the circadian cycle of the shift from dark to light conditions, and in modulating the adaptational state of the whole retina.

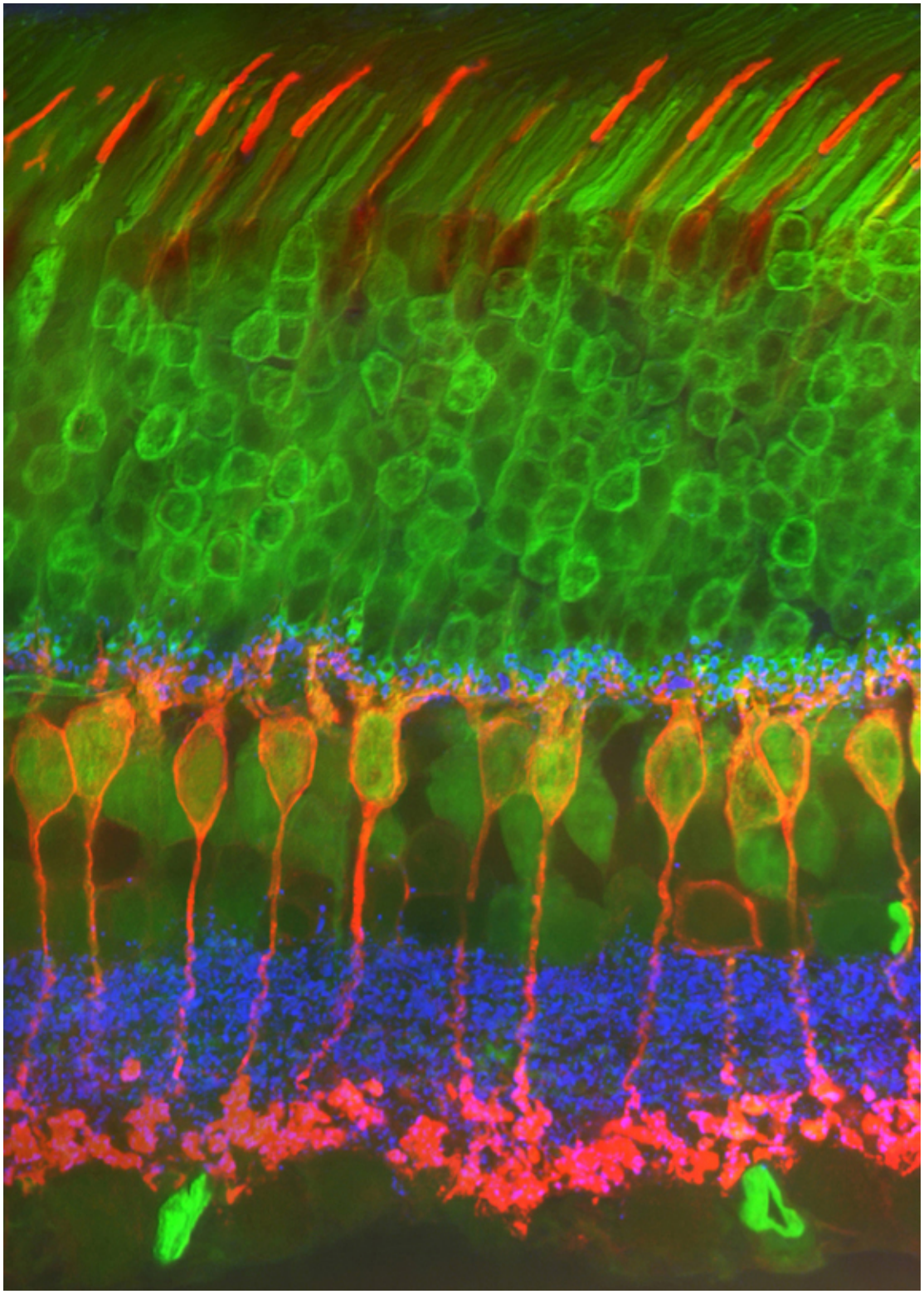

Figure 7. PKC immunostaining of rod bipolar cells (orange/red) in transgenic GFP mouse (green). Other immunostaining is bassoon for synaptic ribbons (blue) in the OPL and for GABA in the terminals packing the IPL (blue). Cone outer segments are stained for transducin (red). (From Nicolas Cuenca personal communication).

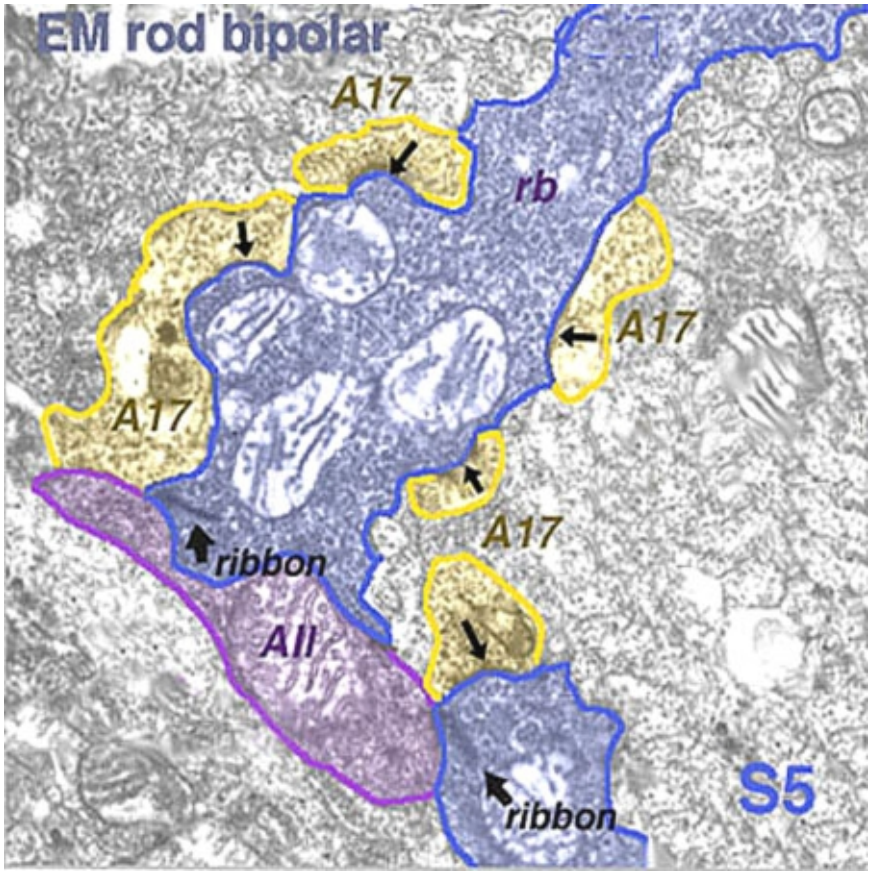

Figure 8. Electron micrograph of a rod bipolar axons.

The Rod Pathway Is Convergent to Increase Sensitivity

Rod pathways involve huge convergences and divergences of cell contacts. The pathway starts with many rods converging information to the rod bipolar cell in the OPL. Rod responses are carried to the next stage of processing in the IPL where divergence occurs to several different amacrine cell types, the most important of which are the AII and the A17 cells. Rod bipolar cells do not contact ganglion cells directly. Instead they contact amacrine cells which spread out the rod information before converging on ganglion cells. One other cell type is also influential upon the rod pathways. This is the dopaminergic amacrine, A18.

The huge convergence of the rod system in the cat retina has been calculated by Sterling and coauthors (29, 30) and Kolb and Nelson (8). Thus about 1500 rods have input to a single small-field ON-beta ganglion cell via 100 rod bipolars, 5 AII amacrine cells and 4 cone bipolar axons. In the case of a large-field OFF-alpha ganglion cell, 75,000 rods drive 5000 rod bipolars and 250 AII amacrine cells before converging on the ganglion cell (Fig. 19).

In terms of divergence of the rod system, we know that a single rod photoreceptor passes information to 2 rod bipolar cells, thence through 5 AII amacrines to 8 cone bipolar cell axons to drive 2 ON-beta cells (29, 30). So it is, that divergent and then convergent circuitry provides pooling and amplification of the rod signal in very low light levels to allow our visual system to be sensitive to a single quantum of light (31).

Summary Diagram of the Rod System of the Mammalian Retina

Combining the physiological responses we now understand for the neurons of the rod system in the cat retina, with their anatomical connections, we can construct a summary diagram of the likely pathway for scotopic vision though the human retina (Fig. 20) (see the animation of the rod circuits).

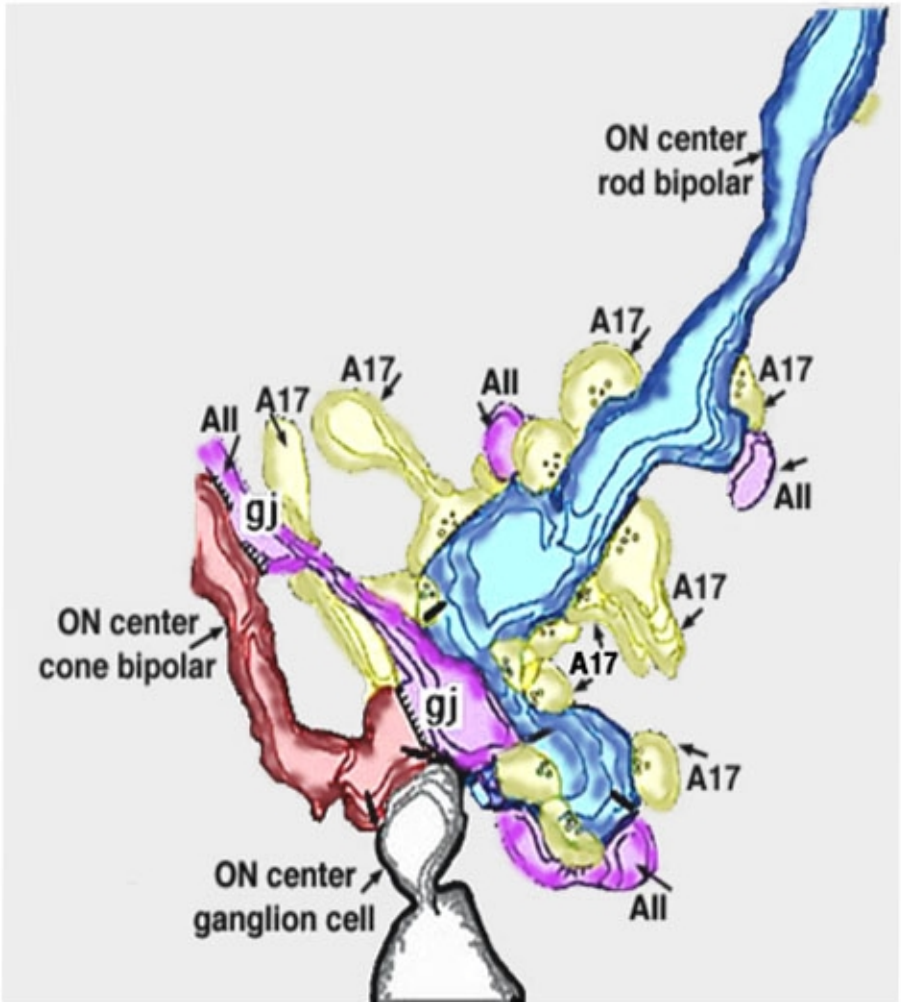

Figure 9. 3-D view of a rod bipolar axon terminal.

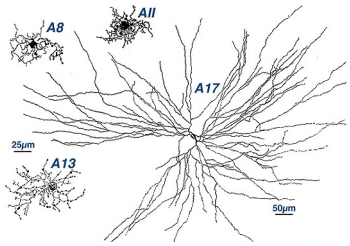

Figure 10. Rod amacrine cells of human retina.

Signals from hyperpolarizing rod photoreceptors depolarize rod bipolar cells. Rod bipolar cells synapse upon two depolarizing amacrine cells, the wide-field A17 and the small bistratified AII amacrine cells. Rod signals reach OFF-center ganglion cells (a-type beta GC) via chemical synaptic input from the AII amacrine cell lobular appendages (boxed region a). ON-center ganglion cells (b-type beta GC) receive rod signals, via AII amacrine cell electrical synapses at gap junctions to cone bipolar cells (ibc, boxed region b). The latter cone bipolars stimulate the ON-center ganglion cells by excitatory chemical synapses. Dopaminergic amacrine cells (Fig. 20, *DA*) influence the rod pathways by chemical synapses in the IPL upon AII and A17 amacrine cells and via an internuncial GABA-ergic interplexiform cell (see later section for more details on interplexiform cells), which in turn synapses upon rod bipolar cells in the OPL.

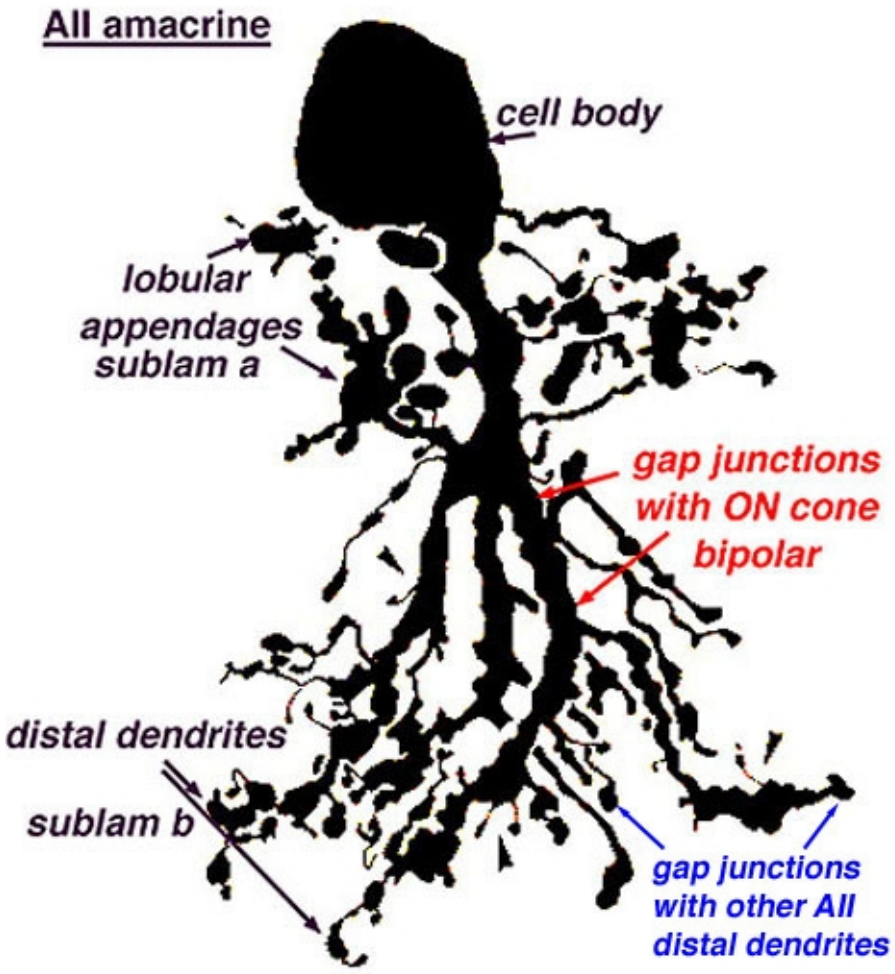

Figure 11. AII amacrine cell.

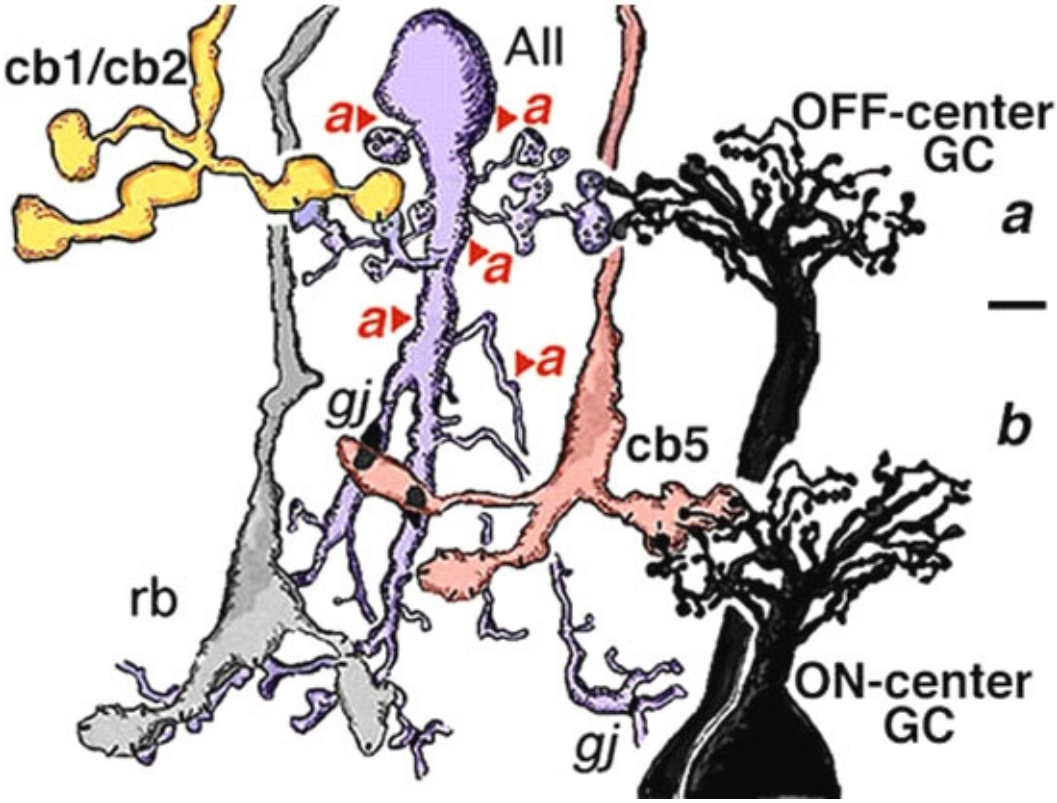

Figure 12. Circuitry for AII amacrine cells.

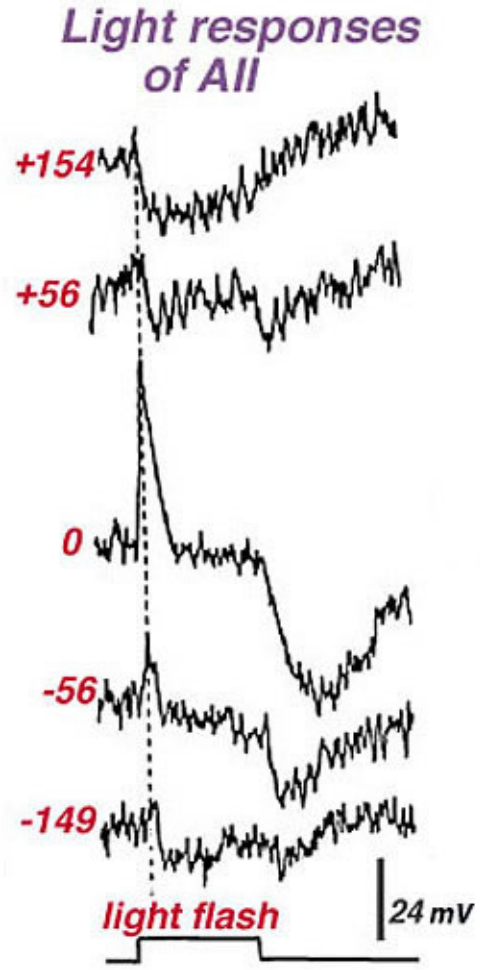

Figure 13. Intracellular recordings of AII amacrine cells.

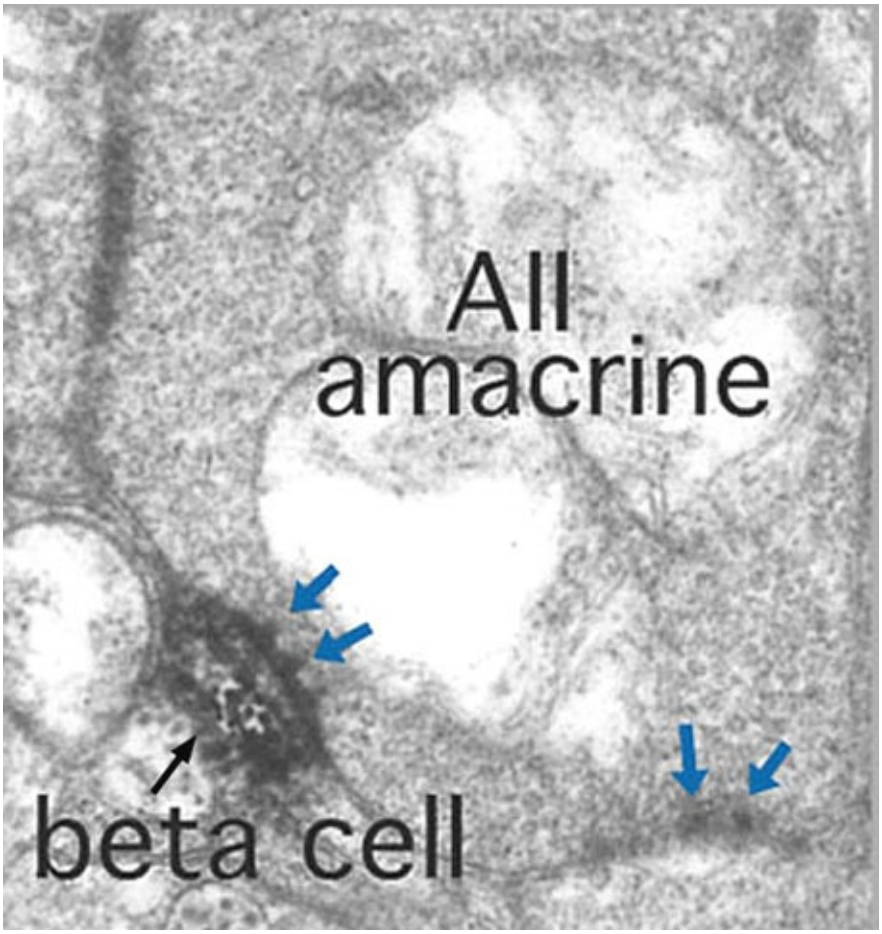

Figure 14. Electron micrograph of a synapse in an AII amacrine cell.

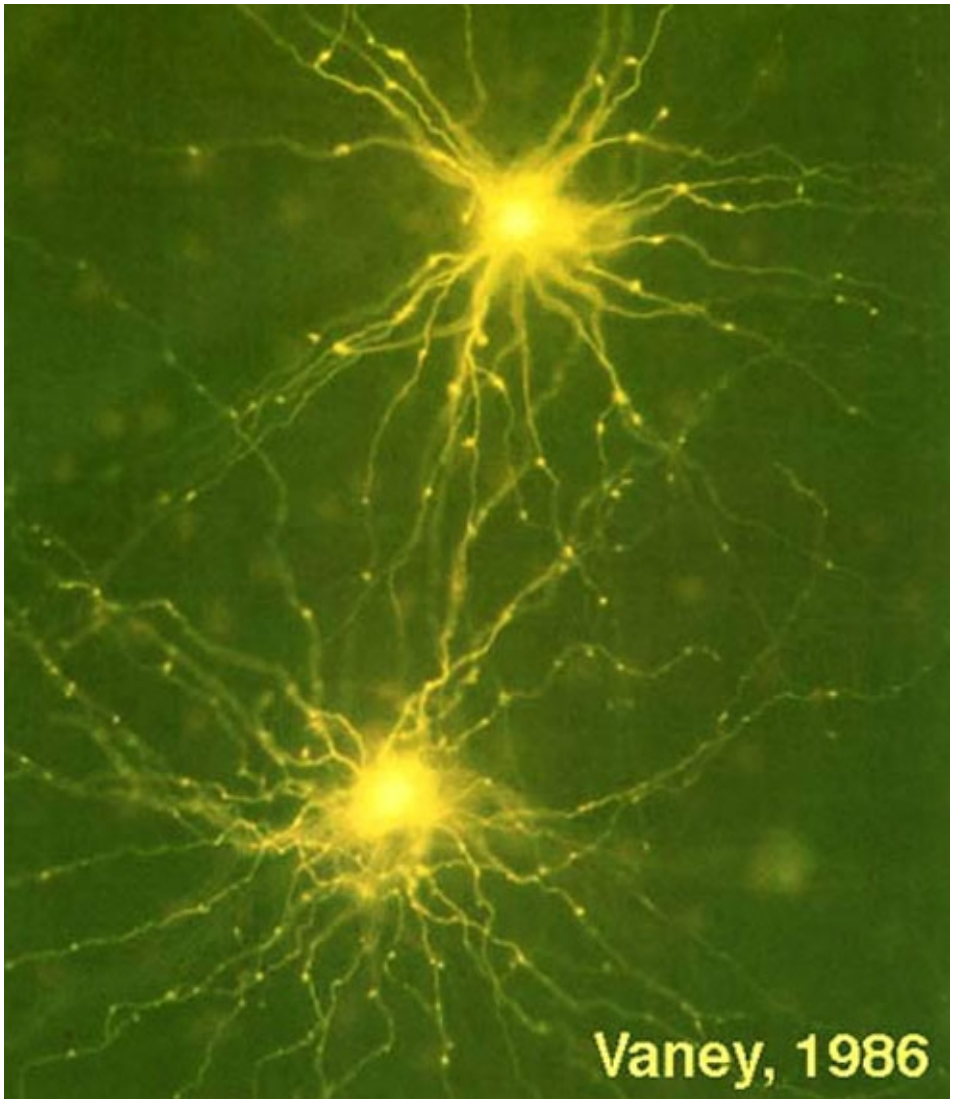

Figure 15. Serotonin-containing amacrine cells stained with Lucifer yellow in whole-mount rabbit retina.

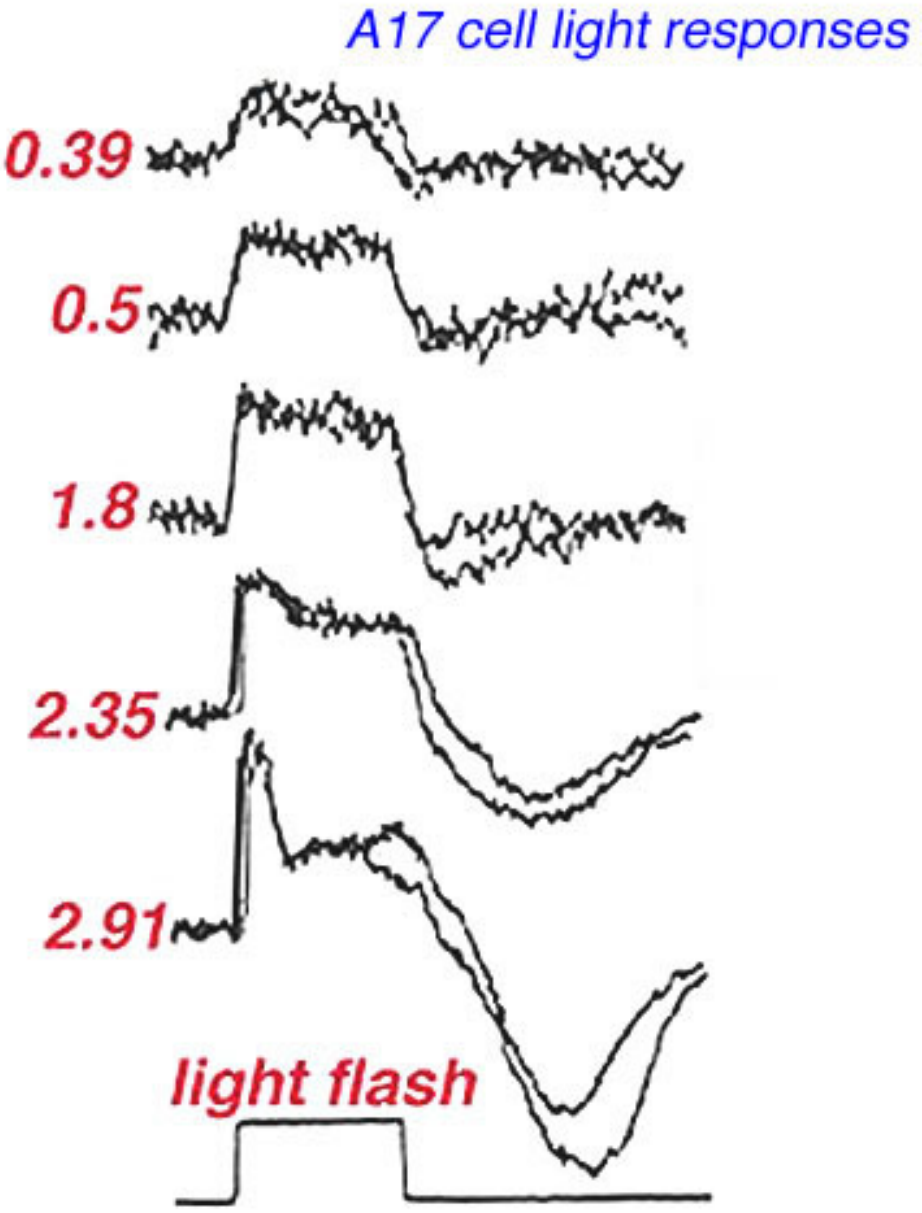

Figure 16. Intracellular recordings of AI7 amacrine cells.

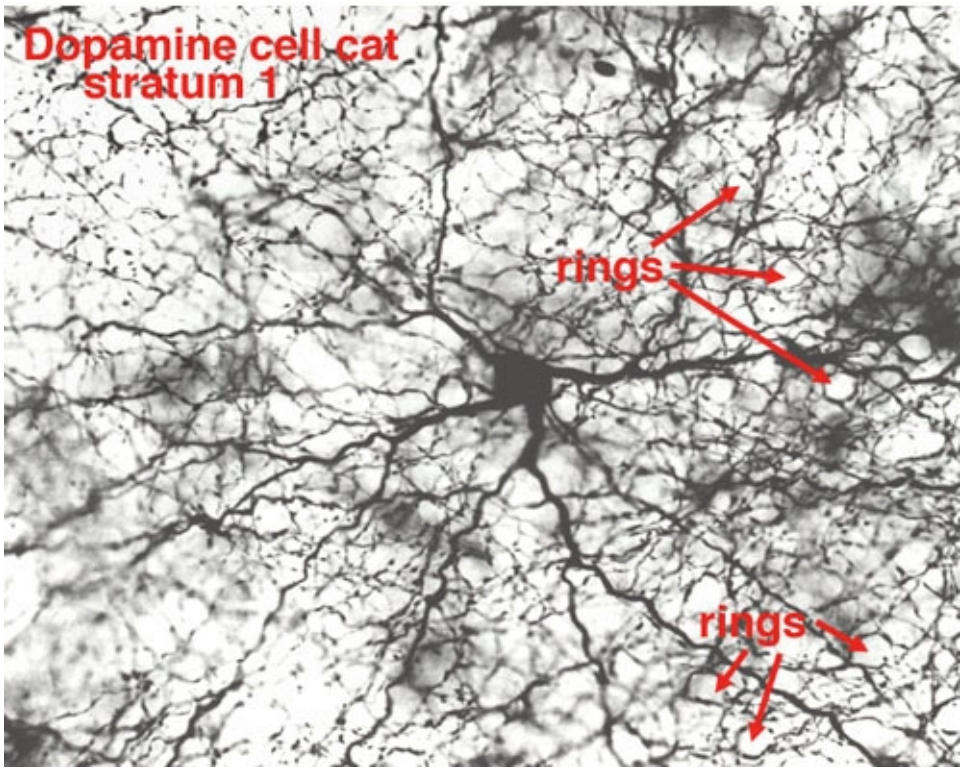

Figure 17. A18 amacrine cell.

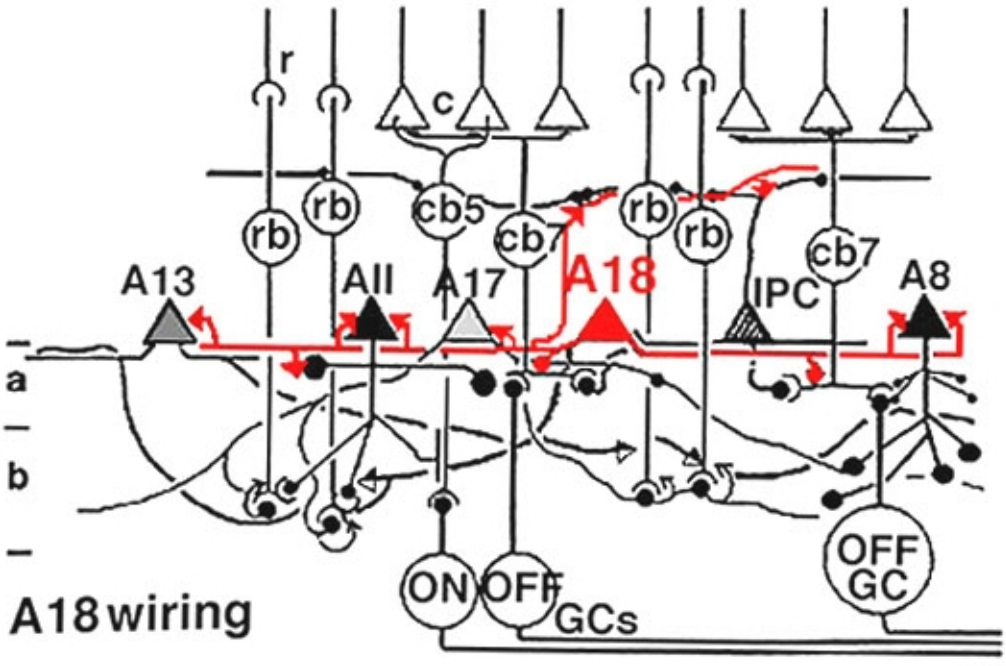

Figure 18. Wiring diagram of A18 amacrine cells.

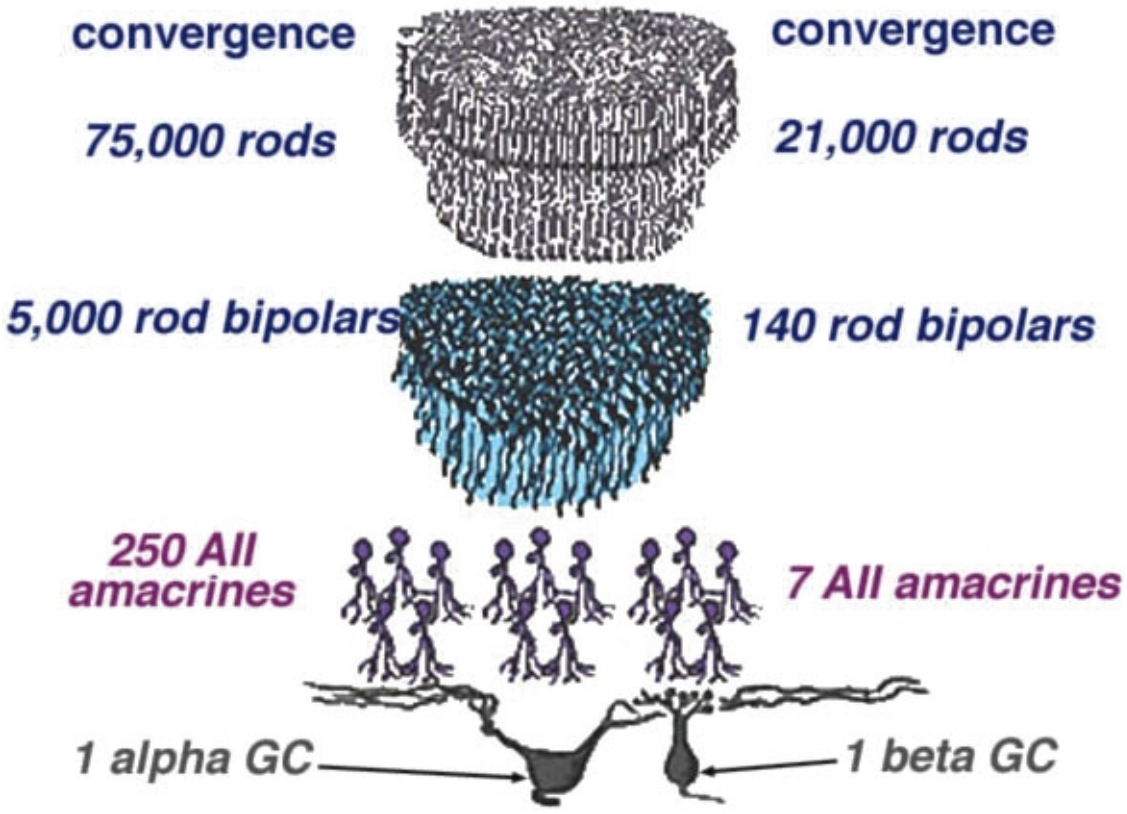

Figure 19. Convergence of rods, rod bipoloar, and AII amacrine cells to alpha and beta cells of cat retina.

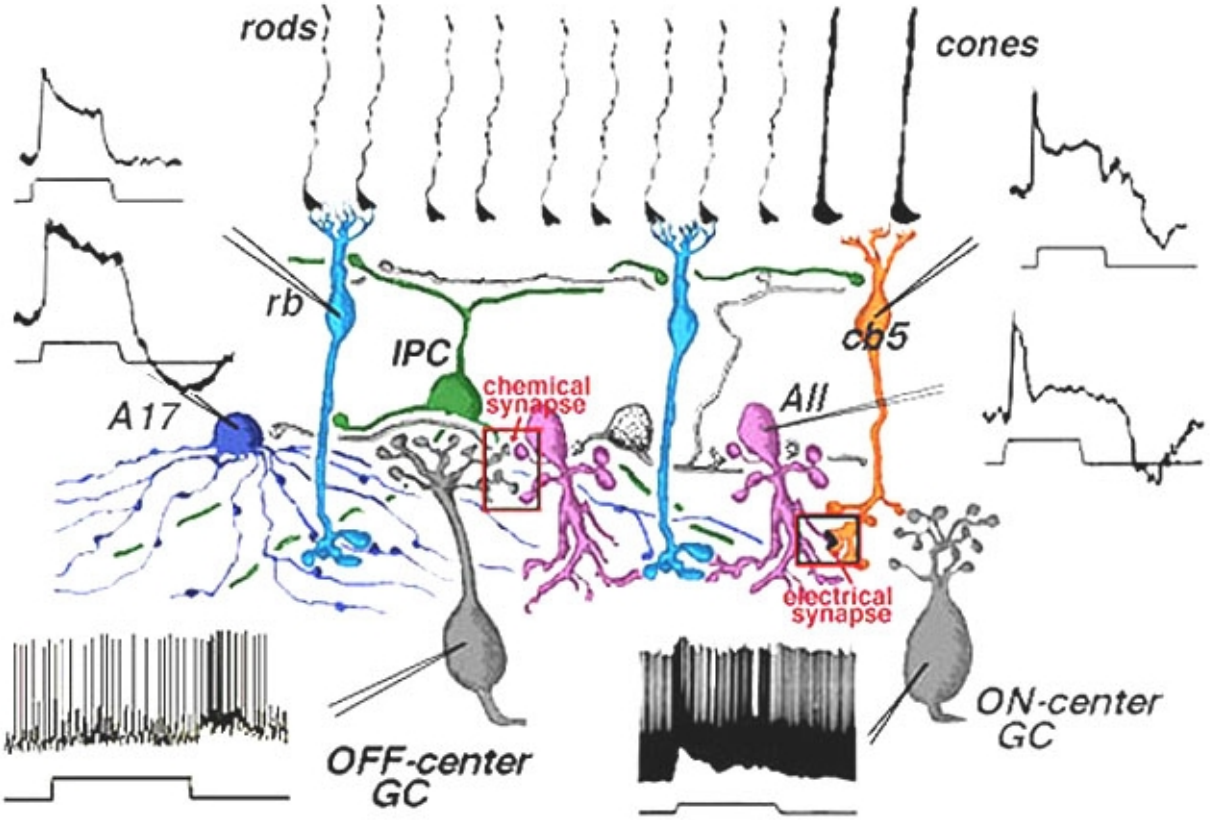

Figure 20. Summary diagram of the neurons and their responses involved in rod-driven pathways.

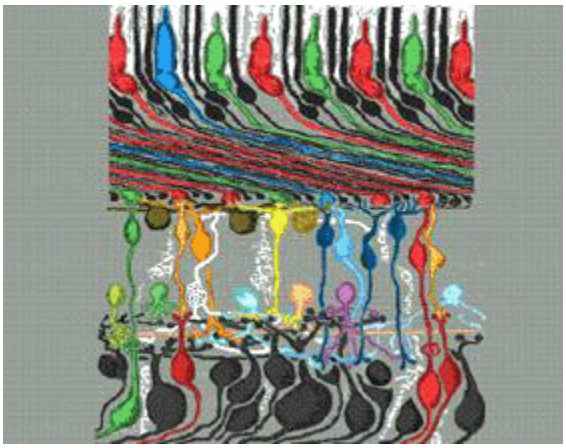

Movie 1. An animation of the rod circuits.

Download video

References

1. Østerberg G. Topography of the layer of rods and cones in the human retina. Acta Ophthal. 1935. suppl. 6.:1–103.
2. Mariani AP, Kolb H, Nelson R. Dopamine-containing amacrine cells of rhesus monkey retina parallel rods in spatial distribution. Brain Res. 1984;322:1–7. PubMed PMID: 6518360.

3. Kolb H. Organization of the outer plexiform layer of the primate retina: electron microscopy of Golgi-impregnated cells. Phil Trans R Soc B (Lond.). 1970;258:261–283.
4. Numura A, Shigemoto R, Nakamura Y, Okomoto N, Mizumo N, Nakanishi S. Developmentally-regulated postsynaptic localization of a metabotropic glutamate receptor in rat rod bipolar cells. Cell. 1994;77:361–369. PubMed PMID: 8181056.
5. Vardi N, Morigawa K. ON cone bipolar cells in rat express the metabotropic receptor mGluR6. Vis Neurosci. 1997;14:789–794. PubMed PMID: 9279006.
6. Nawy S. The metabotropic receptor mGluR6 may signal through Go, but not phosphodiesterase, in retinal bipolar cells. J Neurosci. 1999;19:2938–2944. PubMed PMID: 10191311.
7. Dhingra A, Lyubarsky A, Jiang M, Pugh EN, Birnbaumer L, Sterling P, Vardi N. The light response of ON bipolar neurons requires Gao. J Neurosci. 2000;20:9053–9058. PubMed PMID: 11124982.
8. Kolb H, Nelson R. Off-alpha and off-beta ganglion cells in the cat retina. II. Neural circuitry as revealed by electron microscopy of HRP stains. J Comp Neurol. 1993;329:85–110. PubMed PMID: 8454727.
9. Grünert U, Martin PR, Wässle H. Immunocytochemical analysis of bipolar cells in the Macaque monkey retina. J Comp Neurol. 1994;348:607–627. PubMed PMID: 7530731.
10. Kolb H, Famiglietti EV. Rod and cone pathways in the inner plexiform layer of the cat retina. Science. 1974;186:47–49. PubMed PMID: 4417736.
11. Kolb H. The inner plexiform layer in the retina of the cat: electron microscopic observations. J Neurocytol. 1979;8:295–329. PubMed PMID: 490185.
12. Vaney DI. The mosaic of amacrine cells in the mammalian retina. Prog Ret Res. 1990;9:49–100.
13. Strettoi E, Raviola E, Dacheux RF. Synaptic connections of the narrow-field, bistratified rod amacrine cell (AII) in the rabbit retina. J Comp Neurol. 1992;325:152–168. PubMed PMID: 1460111.
14. Famiglietti EV, Kolb H. A bistratified amacrine cell and synaptic circuitry in the inner plexiform layer of the retina. Brain Res. 1975;84:293–300. PubMed PMID: 1111833.
15. Nelson R. AII amacrine cells quicken the time course of rod signals in the cat retina. J Neurophysiol. 1982;47:928–947. PubMed PMID: 6177841.
16. Vaney DI. Patterns of neuronal coupling in the retina. Prog Ret and Eye Res. 1994;13:301–355.
17. Nelson R, Famiglietti EV, Kolb H. Intracellular staining reveals different levels of stratification for on-center and off-center ganglion cells in the cat retina. J Neurophysiol. 1978;41:427–483.
18. Dacheux RF, Raviola E. The rod pathway in the rabbit: a depolarizing bipolar and amacrine cell. J Neurosci. 1986;6:331–345. PubMed PMID: 3950701.
19. Pourcho RG, Goebel DJ. A combined Golgi and autoradiographic study of 3(H)glycine-accumulating amacrine cells in the cat retina. J Comp Neurol. 1985;233:473–480. PubMed PMID: 2984258.
20. Nelson R, Kolb H. A17: a broad-field amacrine cell of the rod system in the retina of the cat. J Neurophysiol. 1985;54:592–614. PubMed PMID: 4045539.
21. Pourcho RG, Goebel DJ. Neuronal subpopulations in cat retina which accumulate the GABA agonist (3H)muscimol: a combined Golgi and autoradiographic study. J Comp Neurol. 1983;219:25–35. PubMed PMID: 6619330.
22. Pourcho RG. Dopaminergic amacrine cells in the cat retina. Brain Res. 1982;252:101–109. PubMed PMID: 7172014.
23. Kolb H, Cuenca N, Wang H-H, DeKorver L. The synaptic organization of the dopaminergic amacrine cell in the cat retina. J Neurocytol. 1990;19:343–366. PubMed PMID: 2391538.
24. Voigt T, Wässle H. Dopaminergic innervation of AII amacrine cells in mammalian retina. J Neurosci. 1987;7:4115–4128. PubMed PMID: 2891802.
25. Hokoc JN, Mariani AP. Tyrosine hydroxylase immunoreactivity in the rhesus monkey retina reveals synapses from bipolar cells to dopaminergic amacrine cells. J Neurosci. 1987;7:2785–2793. PubMed PMID: 2887643.
26. Ammermüller J, Kolb H. The organization of the turtle inner retina I. On- and off-center pathways. J Comp Neurol. 1995;358:1–34. PubMed PMID: 7560272.

27. Hampson ECGM, Vaney DI, Weiler R. Dopaminergic modulation of gap junction permeability between amacrine cells in mammalian retina. J Neurosci. 1992;12:4911–4922. PubMed PMID: 1281499.
28. Jensen RJ, Daw NW. Effects of dopamine and its agonists and antagonists on the receptive field properties of ganglion cells in the rabbit retina. Neurosci. 1986;17:837–855.
29. Sterling P, Cohen E, Freed M, Smith RG. Microcircuitry of the ON-beta ganglion cell in daylight, twilight, and starlight. Neurosci Res Suppl. 1987;6:S269–S285. PubMed PMID: 3317147.
30. Sterling P, Freed MA, Smith RG. Architecture of rod and cone circuits to the On-beta ganglion cell. J Neurosci. 1988;8:623–642. PubMed PMID: 2828567.
31. Hecht S, Schlaer S, Pirenne MH. Energy, quanta and vision. J Gen Physiol. 1942;25:819–840. PubMed PMID: 19873316.

Cone Pathways through the Retina

Helga Kolb

Created: May 1, 2001; Updated: July 1, 2009.

Circuitry for Cone Signals

Cone photoreceptors are the sensors of bright light and different wavelengths of light in the retina. They are sensitive in photopic (bright light) conditions and come in several types according to the structure of the visual pigments or opsins in their outer segment regions. In dichromatic animal species there are two types of visual pigments in two types of cone (most mammals): cones sensitive to blue light and cones sensitive to red-green light. In trichromatic animal species (some primates and man) there are three types of cone according to their visual pigments (see chapter on photoreceptors). These are long wavelength (red), medium wavelength (green) and short wavelength (blue) sensitive cones (Fig. 1).

The circuitry whereby cone signals pass through the retina to the ganglion cells is rather different from that of the rod pathways. The first difference is at the outer plexiform layer. The cones synapse upon **various** cone bipolar types rather than on a single type like the rod system. Thus at the outer plexiform layer a choice of pathways is already installed for the cone system. As we have already mentioned (section on the OPL), cone bipolars come in varieties distinguished by the size of their dendritic field (midget, diffuse, and large-field diffuse) and by their different types of synaptic contact with the cone pedicles i.e. invaginating-ribbon synapses, semi-invaginating basal junctions or non-ribbon related basal junctions (see section on OPL).

Vertebrate photoreceptors are in a depolarized state in darkness and are hyperpolarized by light (1). Thus it is thought that the neurotransmitter glutamate is released continuously in the dark and is suppressed by light (Fig. 2).

Different glutamate receptor types appear on depolarizing ON- and hyperpolarizing OFF-center bipolar cells (2). The OFF-bipolar receptor appears to be related to the AMPA-kainate type and so is a common, excitatory, ionotropic glutamate receptor (iGluR). In contrast the ON-type bipolar cells have metabotropic receptors (mGluR) that bind selectively the glutamate agonist APB (or AP4, 2-amino-4-phosphonobutyrate), and are insensitive to AMPA-kainate ligands. Application of APB selectively hyperpolarizes their membrane potentials and suppress the light-responses of ON-center bipolar cells (3, 4). The receptor at the ON-bipolar cell is now thought to be mGluR6 (5, 6). Receptor-activated G-proteins, originally thought to mimic the cyclic-GMP cascade occurring in photoreceptors are the underlying mechanism of transduction in ON-center bipolar cells (7, 8). Most recently, good evidence has been provided for a subunit of the transducin molecule, GalphaO, to be the second messenger in the ON-center bipolar cell activation pathway (9, 10).

Thus, we know that the cone bipolar types that make central ribbon contacts or narrow-cleft, semi-invaginated contacts have the metabotropic glutamate receptors (Fig. 3) and will be ON-center (center-depolarizing) types (ON BC), while cone bipolar cells that make wide-cleft basal junctions (OFF BC) will have the ionotropic glutamate receptors (Fig. 3) and will respond to light like the photoreceptor itself, i.e. will be OFF-center (centre-hyperpolarizing) types (11) (see movie of the intracellular recordings).

Some years ago it was demonstrated by electron microscopy and 3-D reconstruction of cone bipolar profiles in the inner plexiform layer of the cat retina, that these bipolar axons make most of their ribbon output synapses to ganglion cell dendrites (12) (Fig. 4 and Fig. 5).

Bipolar cell axons that terminated in sublamina **a** of the inner plexiform layer (closer to the amacrine cell bodies) made ribbon synapses exclusively with dendrites of ganglion cells that had dendrites in this sublamina. In fact, such bipolar cell axons did not even reach down far enough to contact ganglion cells in sublamina **b** of

the IPL. The ganglion cells branching in sublamina **a** were known from Nelson and coworkers findings (13) to give OFF-center responses to light flashes.

Conversely the cone bipolar cells with axons in sublamina **b** of the inner plexiform layer (closer to the ganglion cell bodies) made ribbon synapses only upon the dendrites of ganglion cells that branch in sublamina **b**. Again, Nelson et al. (13) had shown that such ganglion cells were ON-center in response to light flashes (Fig. 6) (see the movie of the intracellular recordings).

In the human retina the common cone bipolar cells are, like the cat, classified not only by the nature of their synapses with cone pedicles, but also by which sublamina of the IPL their axons terminate in. Thus, some of the cone bipolar types send axons to sublamina **a** (fb types) and others to sublamina **b** (ib types) of the IPL.

We expect that like the cat, human cone bipolar cells with axons in sublamina **a** will connect to OFF-center (center-hyperpolarizing) ganglion cells and bipolar cells with axons in sublamina **b** will connect to ON-center (center-depolarizing) ganglion cells (Fig. 7).

Thus a major difference in the circuitry of the cone compared the rod pathways in the mammalian retina is that cone bipolar cells make direct synapses with ganglion cell dendrites, without the need for intermediate amacrine cell circuitry as occurs in the rod pathway (see previous chapter). The cone pathways are, therefore, both more direct and more narrow-field and convergent than the rod pathways. Fewer cones converge onto cone bipolars than rod to rod bipolars and then only a relatively small number of cone bipolar cells converge onto their ganglion cells. The ultimate in low convergence ratio is the midget system in the human and primate retina, which we shall deal with separately in another section (Fig. 8).

Cone Pathways Mediate Successive Contrast (ON and OFF Pathways)

Cone pathways in mammalian and human retinas run as two parallel streams of information directly from the cone photoreceptor to the ganglion cell through the straight pipe-line, the cone bipolar cell. What is the reason for two parallel channels for the cone system when the rod system had only one? The answer is that this organization allows one channel to provide information to the ganglion cell concerning brighter than background stimuli (the ON-center channel) and the other, darker than background stimuli (the OFF-center channel) as first demonstrated by Kuffler (14) in 1953 from recordings of ganglion cells in the cat retina.

As we have seen above the anatomical substrate for the origins of these two important ON-center and OFF-center channels in the bipolar cell is in the types of synaptic contacts cone bipolar cells make with cone pedicles in the mammalian retina (see above) (11, 12, 15). The hyperpolarizing bipolar types are the start of OFF-center channels and the depolarizing types are the start of ON-center channels through the retina (Fig. 9.).

The ribbon synapse of the cone bipolar cells to the ganglion cell dendrites in the IPL, is considered to be an excitatory synapse and so, the type of signal in the ganglion cell, (either ON- or OFF-center) is essentially determined by the nature of the cone bipolar cells contacting it. Thus the complete circuit to carry the message concerning brightness and darkness through the retina in the cat is shown below (Fig. 10) (see an animation of the cone circuits.).

Cones hyperpolarize to light but two bipolar channels, one carried by a depolarizing bipolar (orange cell and light response) and the other by a hyperpolarizing bipolar (yellow cell and light response), split the original cone signal into lightness or ON-center and darkness or OFF-center. These bipolar responses are transmitted directly to ganglion cells architecturally separated to the different sublaminae of the inner plexiform layer, resulting in one channel of ganglion cells with dendrites in proximal retina (sublamina **b**) becoming ON-center and the other types with dendrites only in distal retina (sublamina **a**) becoming OFF-center.

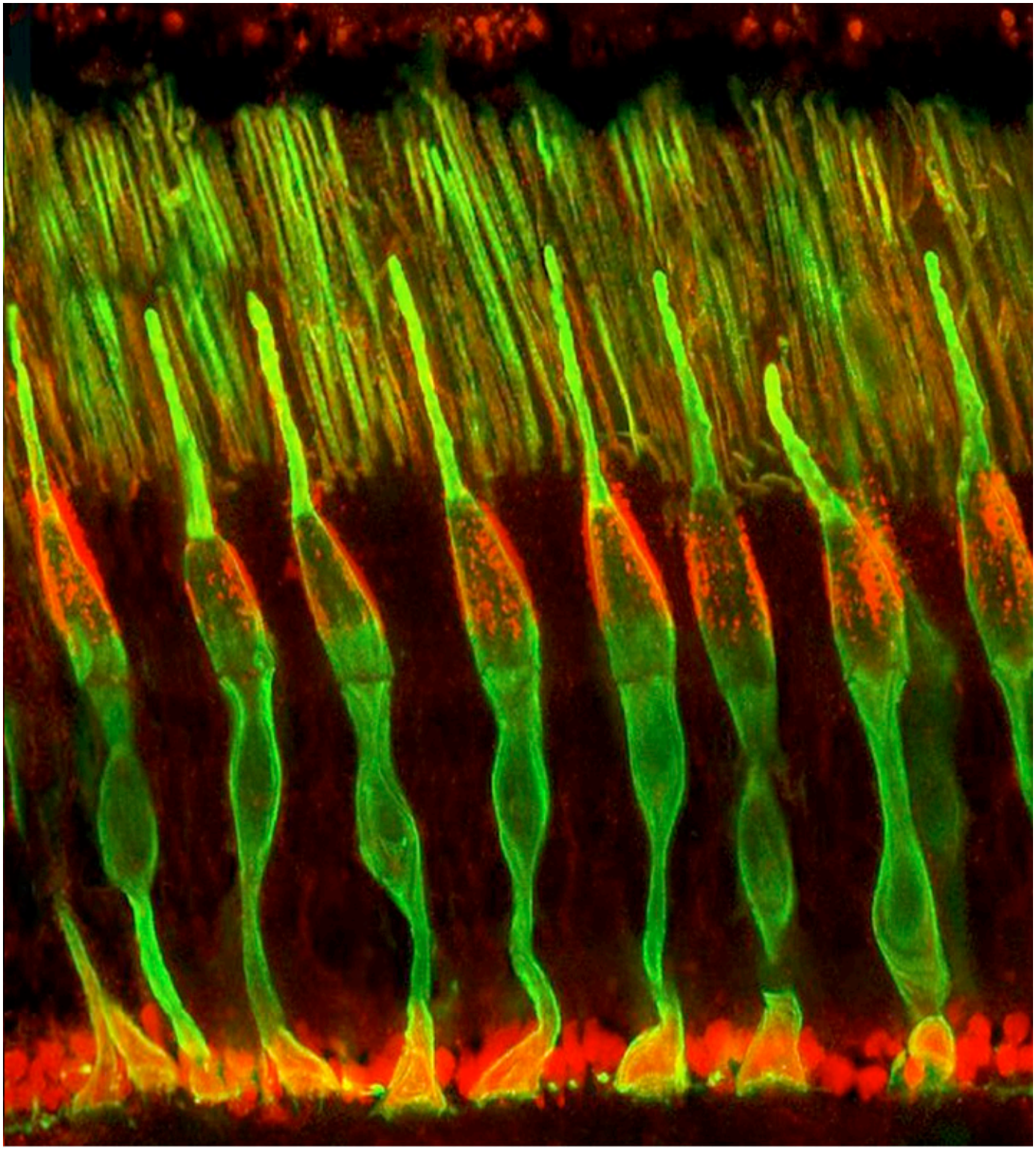

Figure 1. Confocal micrograph to show the cones of the monkey retina. Monkey retinal sections were triple immnunolabeled with antibodies against alpha-synuclein in red, and arrestin and rhodopsin in green to show the entire morphology of cones (green, elongated cells) from the outer segment to their axon terminals (pedicles), and rod outer segments (top green lines) and rod axon terminal (spherules, red dots). (Courtesy of Professor Nicolas Cuenca, University of Alicante, Spain).

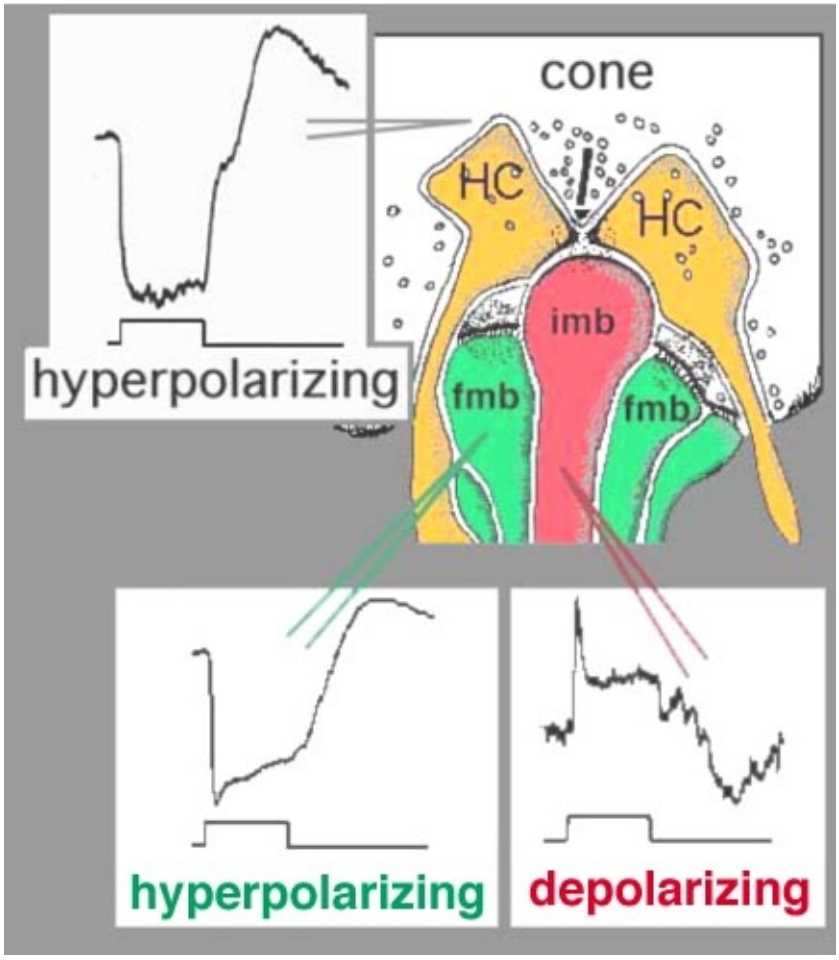

Figure 2. Schematic drawing of the cone synapses to bipolar and horizontal cells.

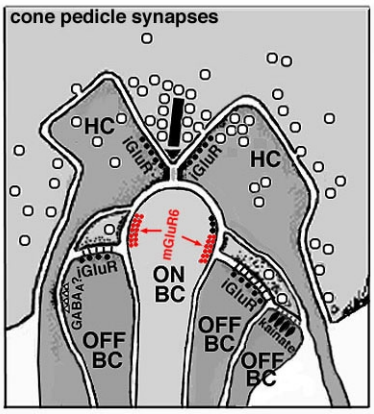

Figure 3. Drawing of the organization of the photoreceptor synapse showing the different glutamate receptors that are presently known to be on the various postsynaptic dendrites.

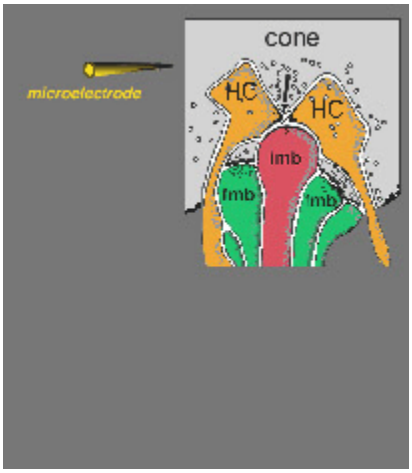

Movie 1. A movie of the intracellular recordings.

Download video

Cone Pathway Circuits Mediate Simultaneous Contrast (Center-Surround Receptive Fields)

Information concerning the overall brightness or darkness of the image is of primary importance for visual sensation, but putting these two informations in simultaneous contrast to each other greatly improves the resolution of the image.

Simultaneous contrast is achieved by lateral inhibition where a dark boundary inhibits a light area or vice versa. In the retina, an important finding by Hartline (16) from frog optic nerve recordings first described retinal ganglion cell receptive fields as concentric with a response of opposite sign to the center found in a surround of the receptive field (Fig. 11).

It is thought that horizontal cells at the OPL provide, through a mechanism of lateral inhibition, a surround arranged around the receptive field center of firstly the photoreceptor itself and then the bipolar cell contacting the photoreceptor (17-19). The wiring responsible appears to start at the small local circuit we saw in the cone triads at the ribbon synapses (see the chapter on the outer plexiform layer) (Fig. 12).

Thus, the negative feedback synapse of the horizontal cell to the cone photoreceptor at the ribbon triad synapse allows the larger receptive field of the horizontal cell network (horizontal cells are coupled in a syncytium across the retina by electrical synapses between neighboring cells. Like horizontal cells are coupled to each other) to provide a surround to the narrow central cone response (20). This concentric organization is then transmitted to the bipolar cells making contact with the cone (21) and thence to the ganglion cell that the cone bipolar cell contacts (see the movie of the mechanism of lateral inhibition on a stimulated cone).

The diagram in Fig. 13 summarizes the architecture for center surround organization by means of horizontal cell to cone bipolar cell circuits in the cone bipolar system of the mammalian retina. The center pathway is created by the cone to bipolar to ganglion cell through-channel, while the injection of horizontal cell information provides an antagonistic surround to the center: an OFF-surround for the ON-center channel (horizontal cell and orange bipolar, left hand pathway) and an ON-surround for the OFF-center channel (horizontal cell and yellow bipolar, right hand pathway (19, 22) (see the animation of the formation of surrounds for cone bipolar and ganglion cells).

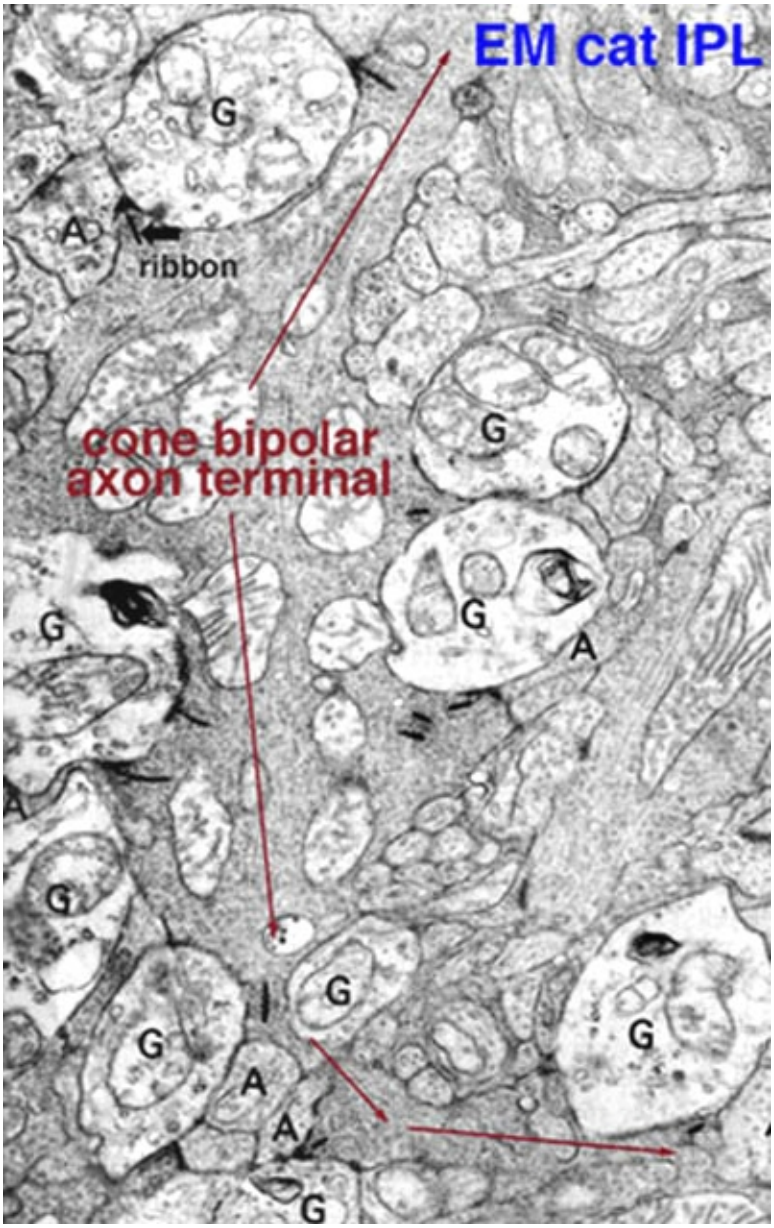

Figure 4. Electron micrograph of a cone bipolar axon terminal

In mammalian retinas, surround responses are not as strong a component of bipolar cell receptive field as they are in cold-blooded vertebrate bipolars (11). Compare for instance the bipolar responses from a Turtle retina (23) with those of a cat retina (11) in Fig. 14 and Fig. 15.

We know from intracellular and extracellular recordings of cat and monkey ganglion cells (14, 24-27) that the commonest mammalian ganglion cells have a strong center surround organization. Thus, it is possible that additional surround antagonism to the bipolar driven center response of a ganglion cell, is constructed by certain, as yet not fully understood, amacrine cell networks in the inner plexiform layer (Fig. 16).

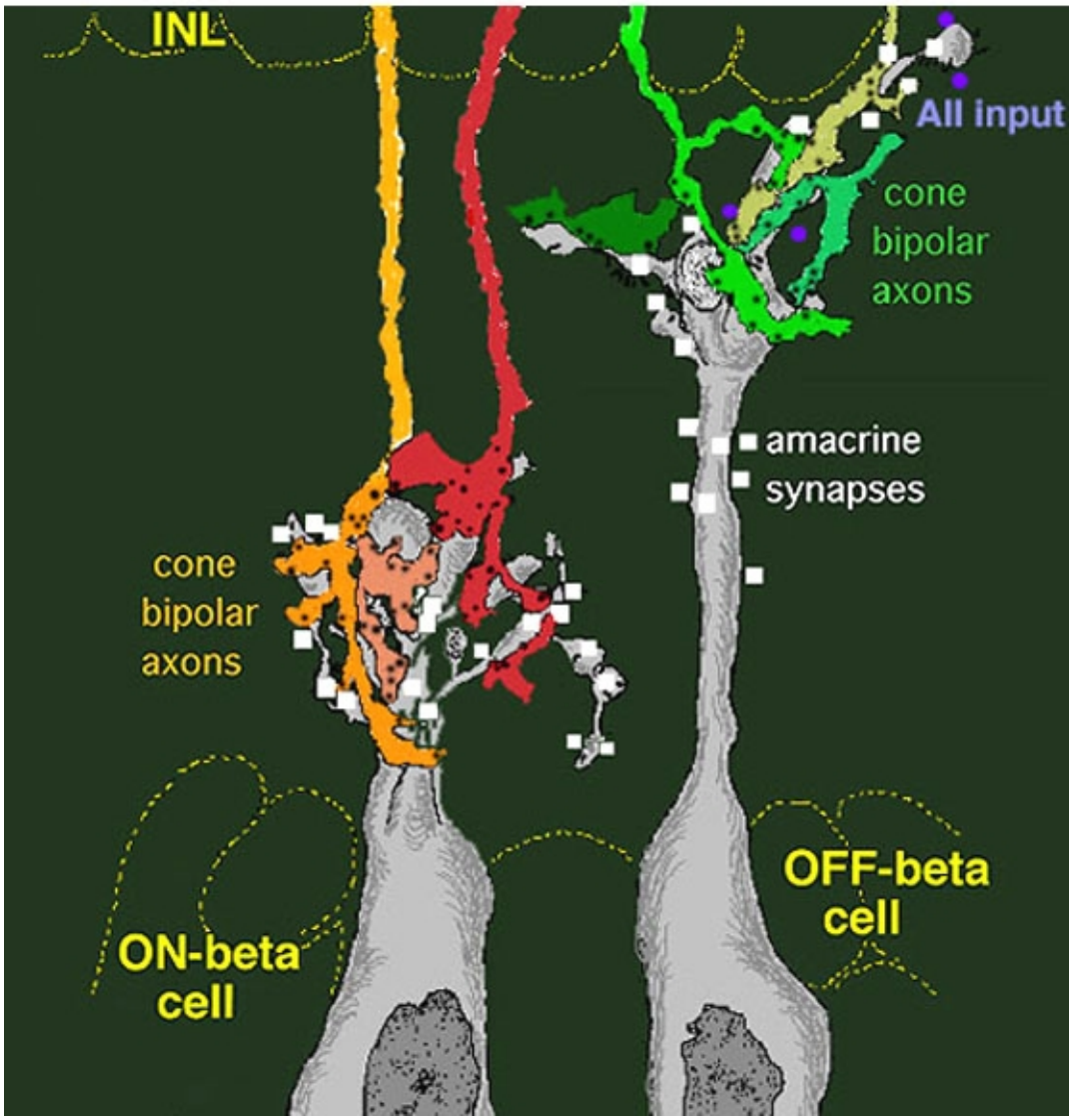

Figure 5. Reconstructions from electron microscopy of ON- and OFF- center beta cells of cat area centralis.

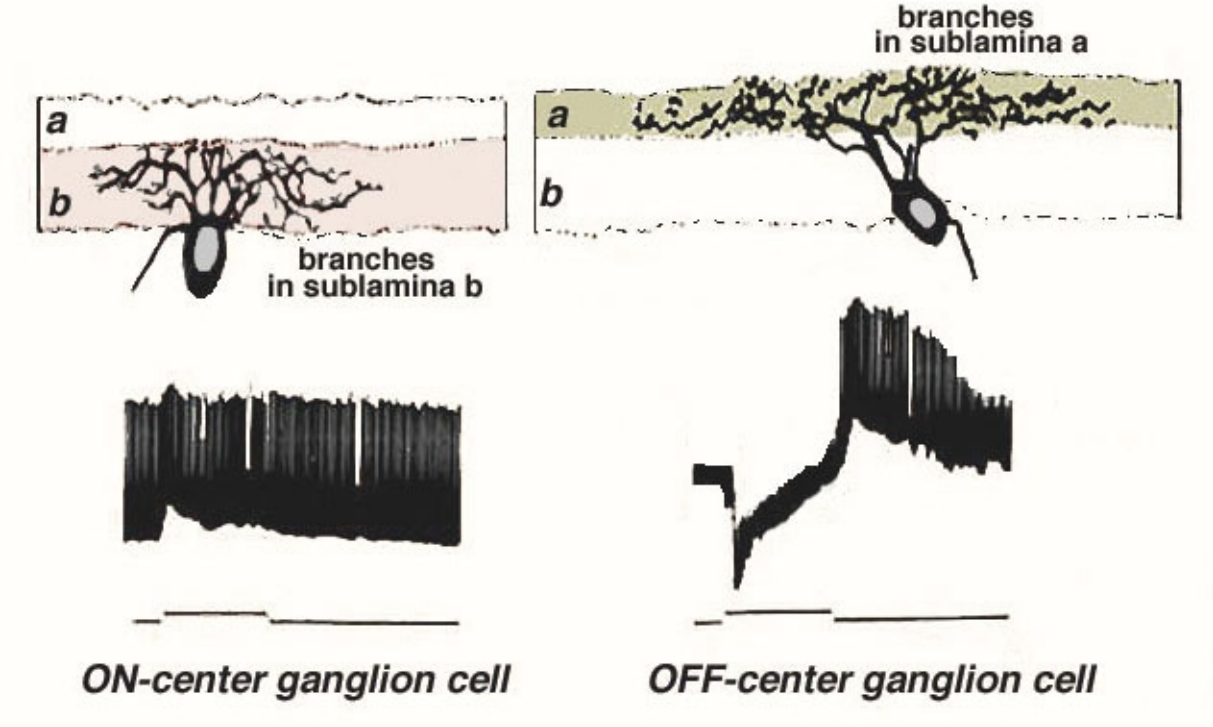

Figure 6. Intracellular responses of ON-center and OFF-center ganglion cells.

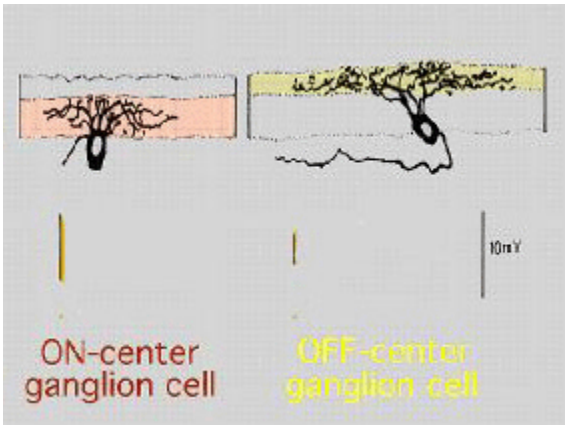

Movie 2. A movie of the intracellular recordings.

Download video

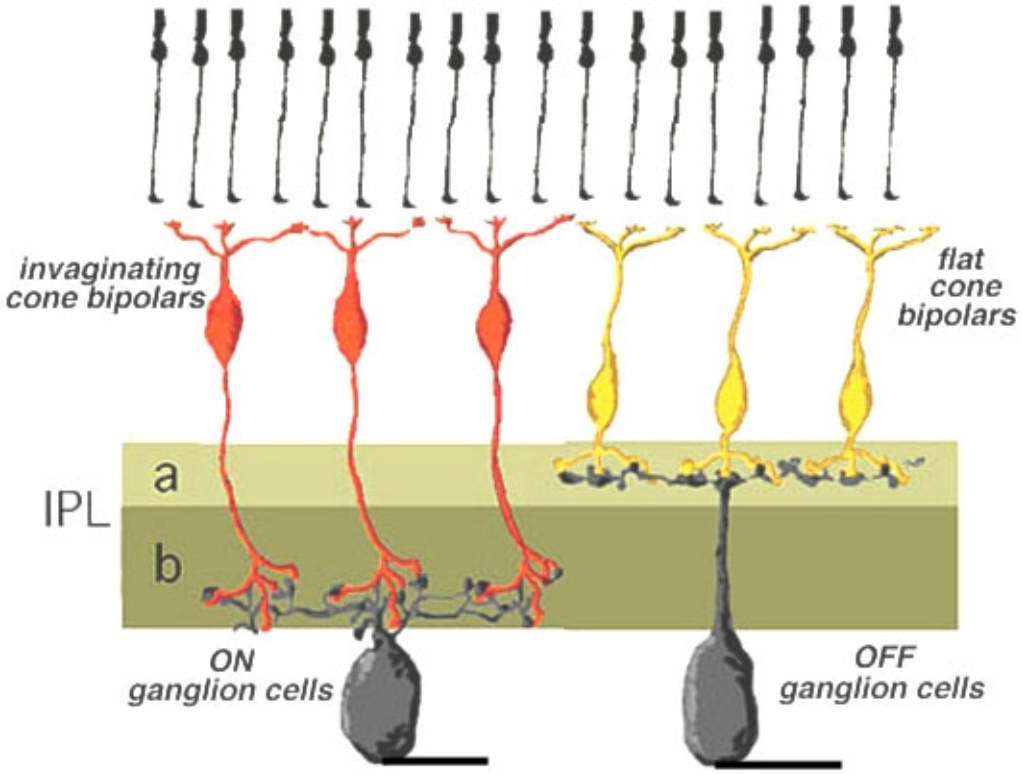

Figure 7. Schematic drawing of the cone bipolar subtypes.

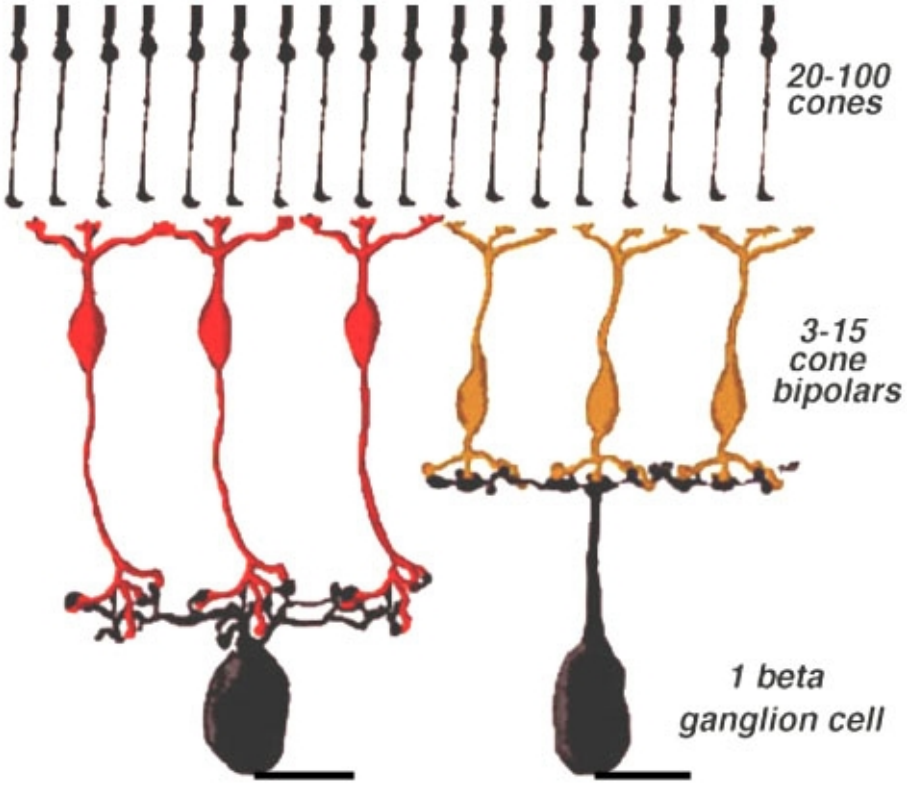

Figure 8. Convergence of cones and bipolar cells upon ON- and OFF- center beta cells.

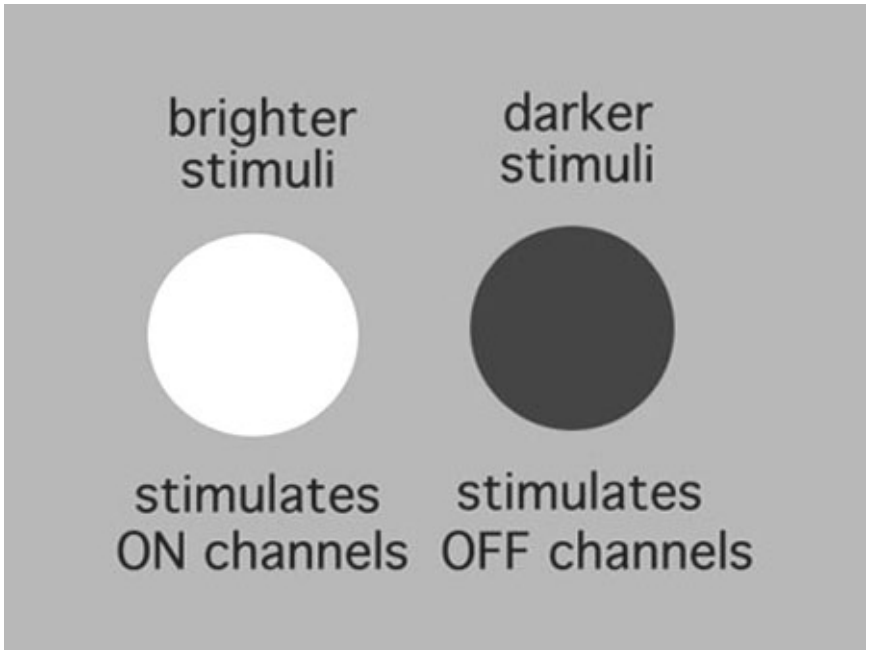

Figure 9. Stimuli for ON and OFF center channels.

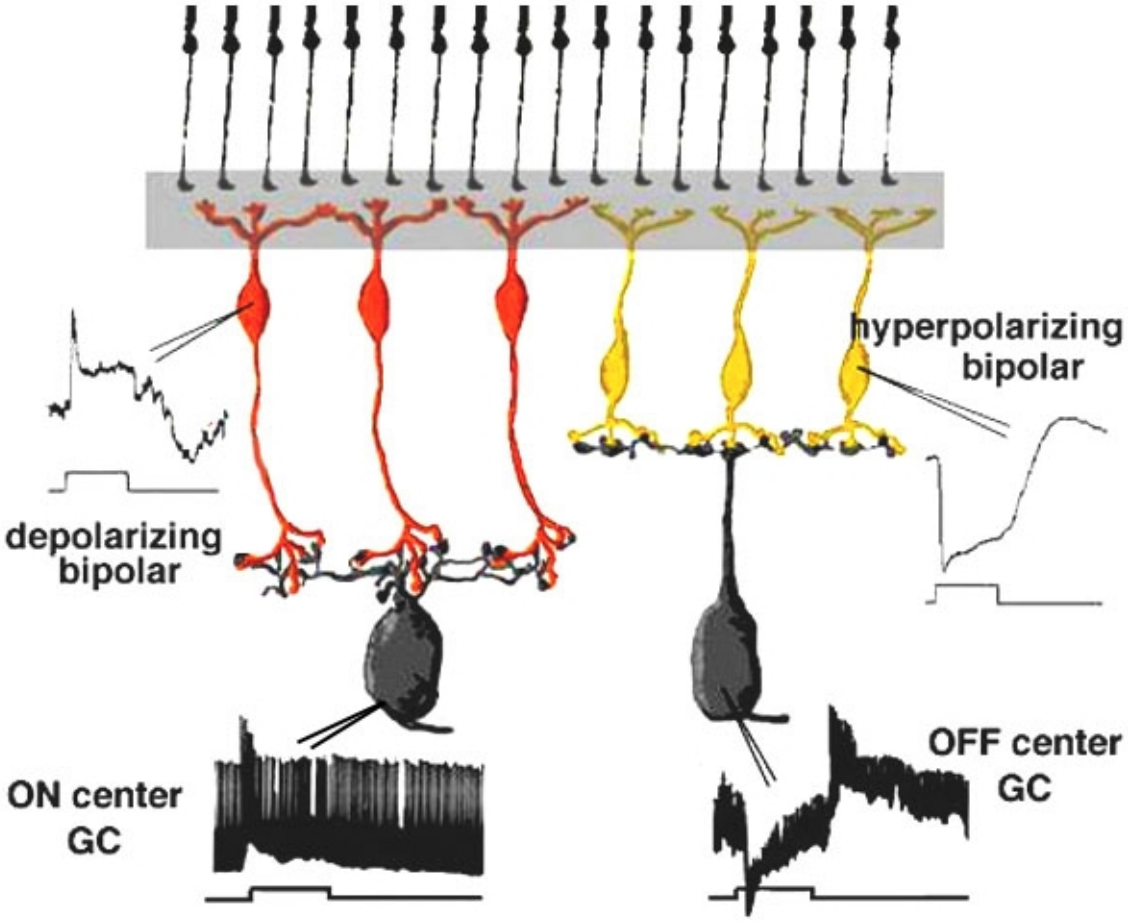

Figure 10. Circuits concerning brightness (left) and darkness (right) processing through the retina.

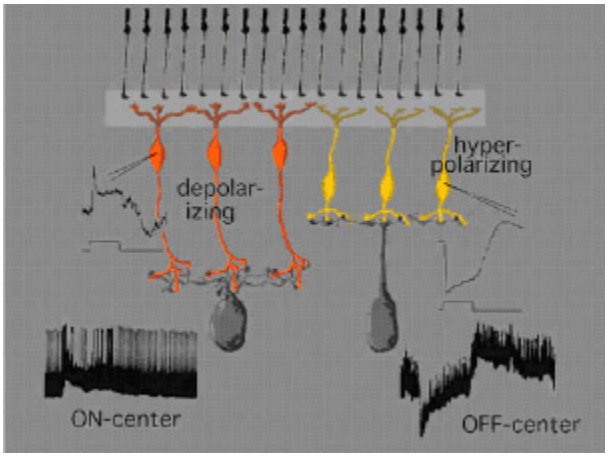

Movie 3. An animation of the cone circuits.

Download video

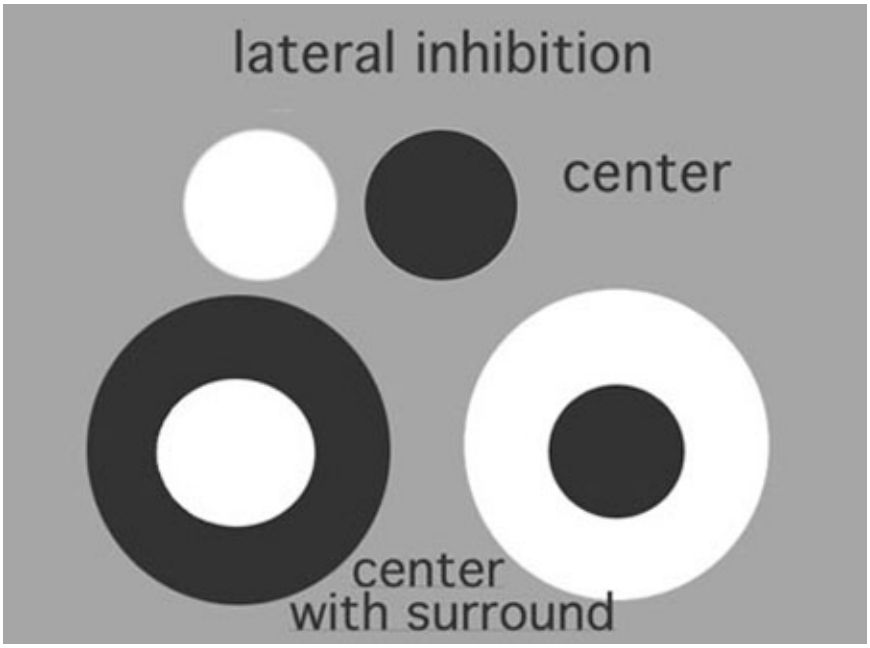

Figure 11. Center-surround receptive fields.

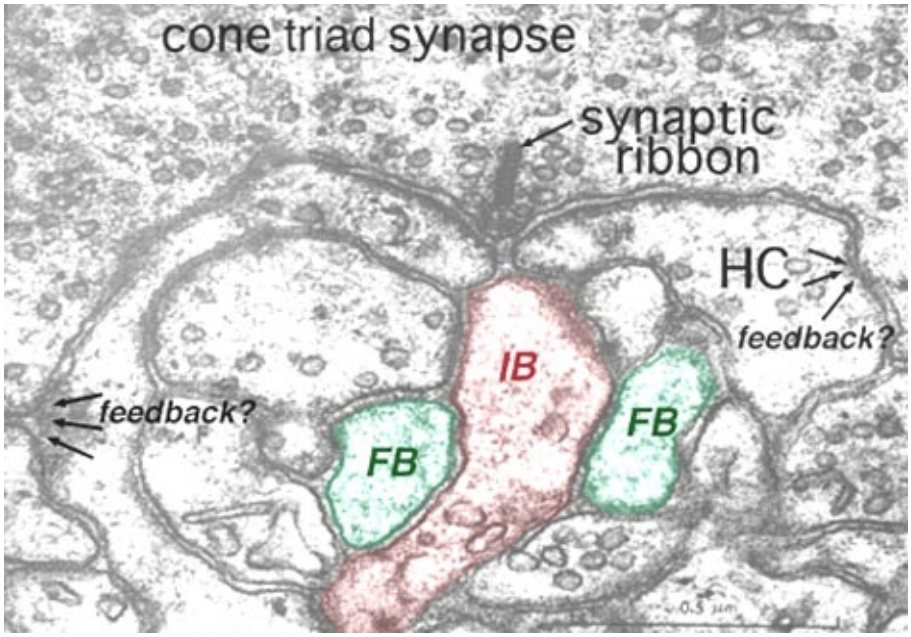

Figure 12. Electron micrograph of a cone triad (59 K jpeg image)

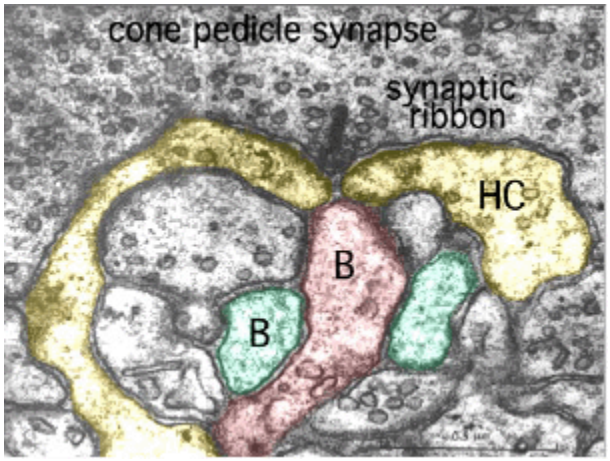

Movie 4. A movie of the mechanism of lateral inhibition on a stimulated cone.

Download video

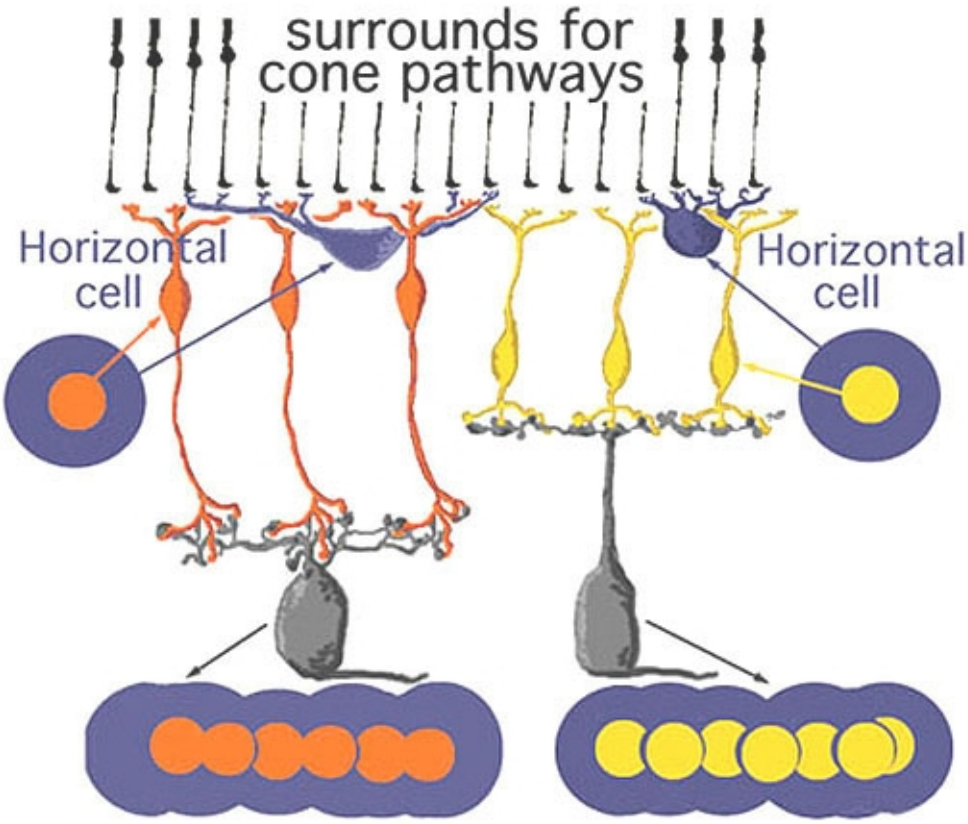

Figure 13. Diagram of organization of center-surround circuits using horizontal cell circuitry.

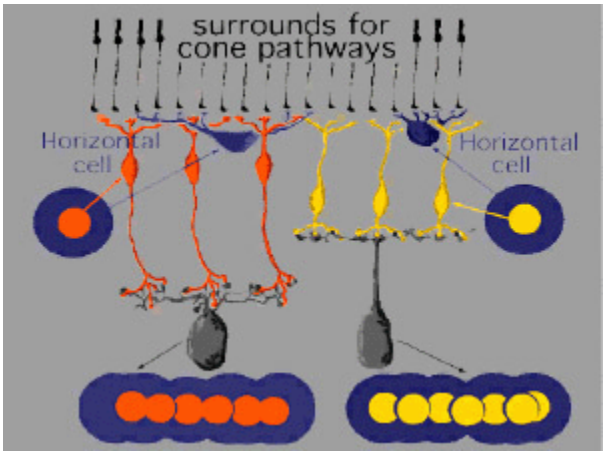

Movie 5. An animation of the formation of surrounds for cone bipolar and ganglion cells.
Download video

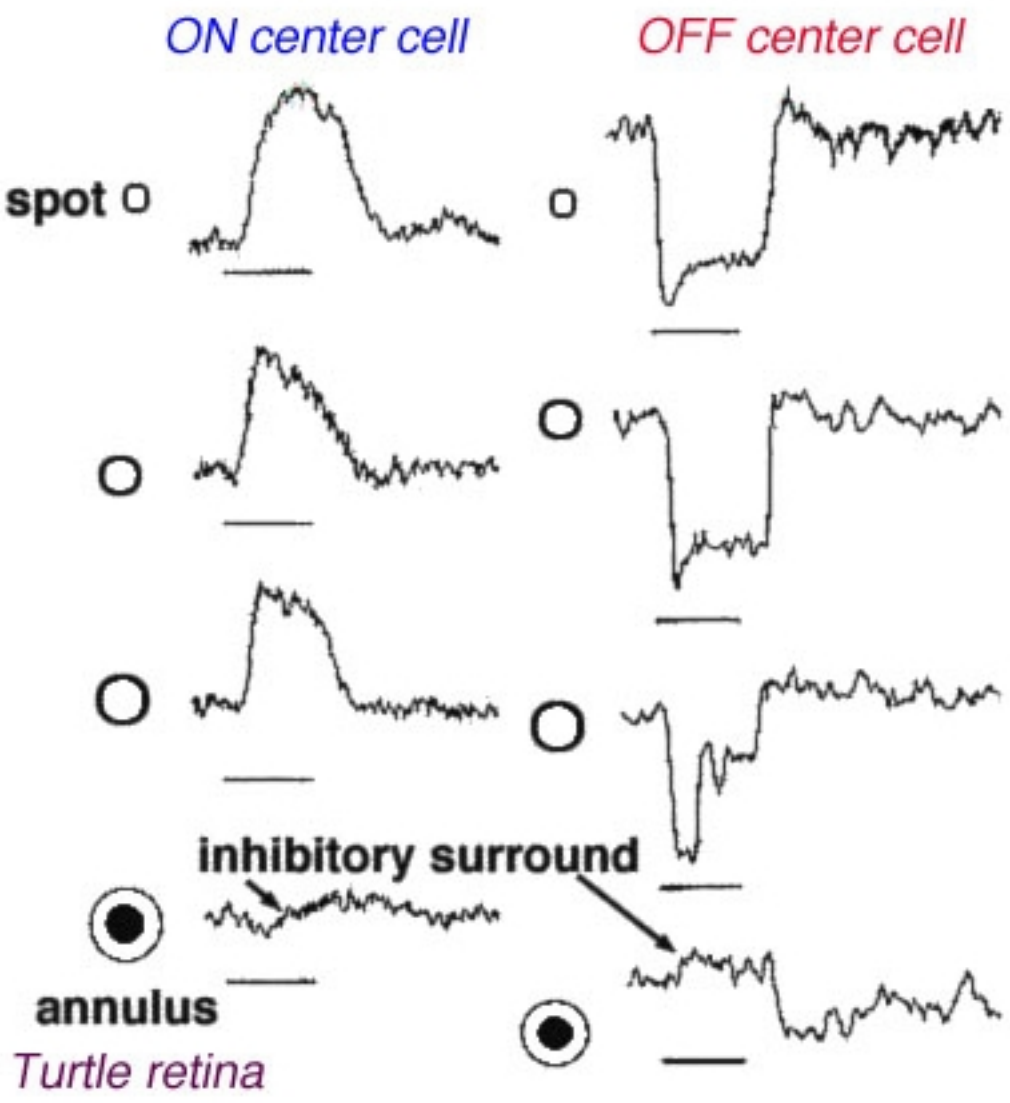

Figure 14. Bipolar cell recordings in turtle retina.

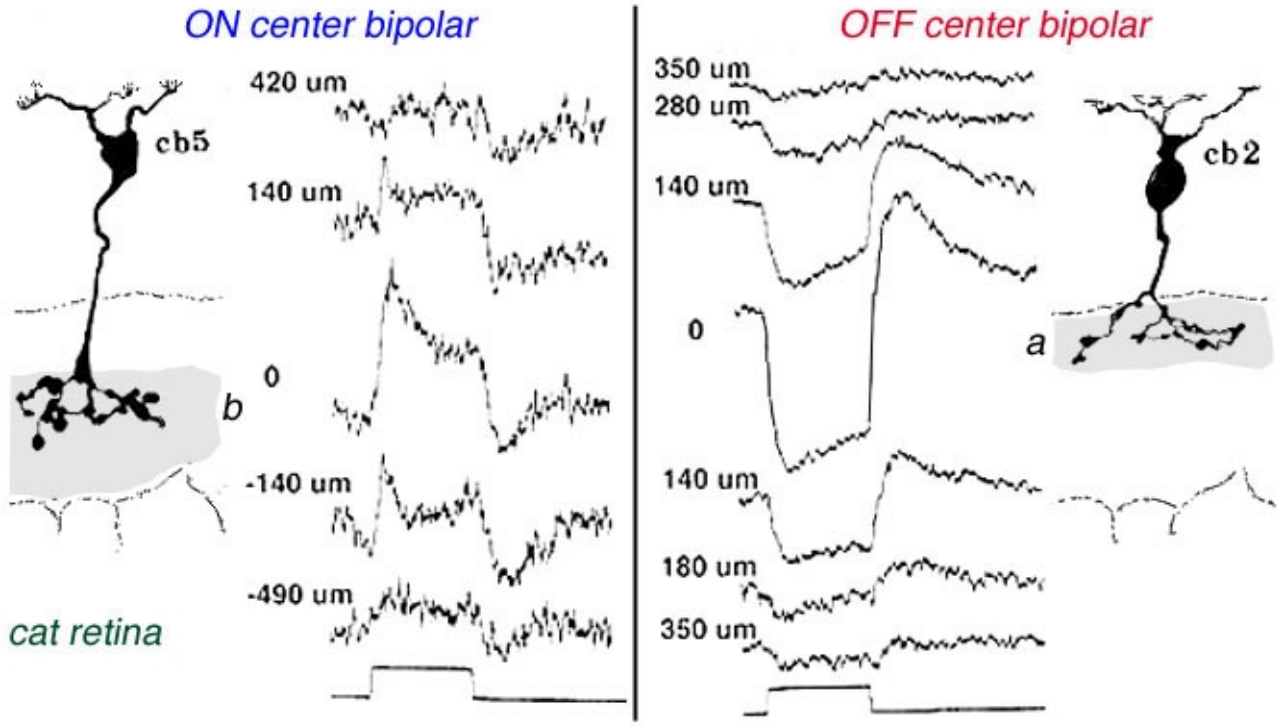

Figure 15. Bipolar cell recordings in cat retina.

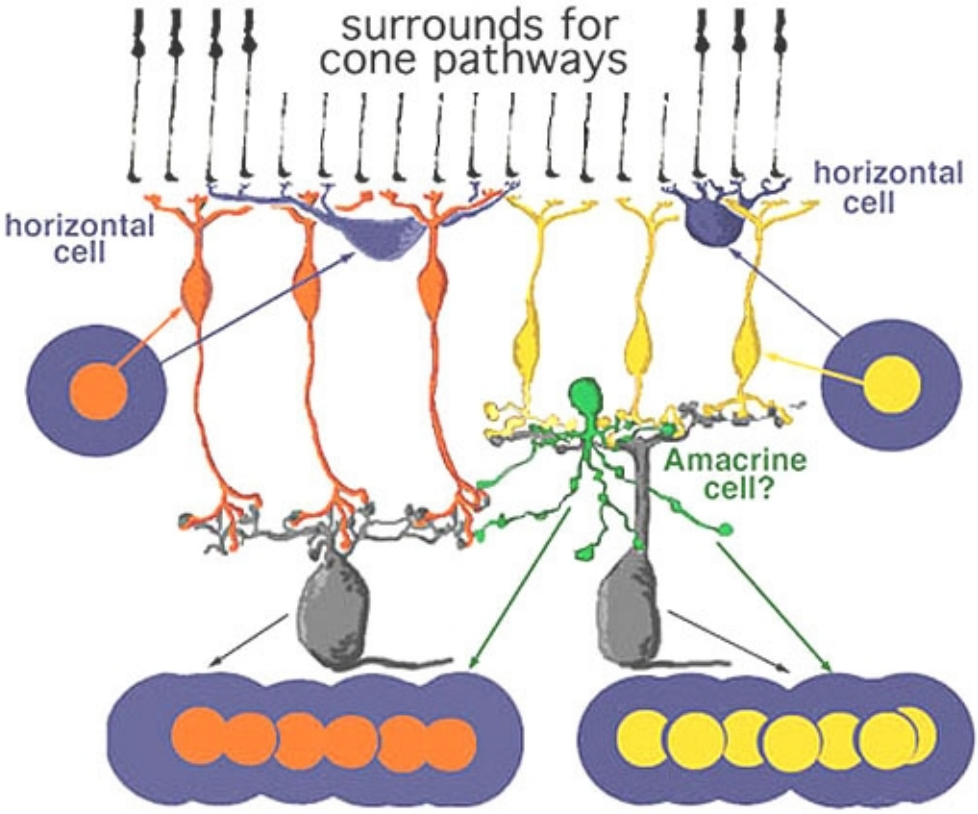

Figure 16. Diagram of the organization of center-surround circuits using both horizontal cells and amacrine cells.

References

1. Trifonov YA. Study of synaptic transmission between the photoreceptor and the horizontal cell using electrical stimulation of the retina. Biofizika. 1968;10:673–680.
2. Miller RF, Slaughter MM. Excitatory amino acid receptors of the retina: Diversity and subtype and conductive mechanisms. Trends Neurosci. 1986;9:211–213.
3. Nawy S, Copenhagen DR. Multiple classes of glutamate receptor on depolarizing bipolar cells in retina. Nature. 1987;325:56–58. PubMed PMID: 3025746.
4. Slaughter MM, Miller RF. 2-amino-4-phosphonobutyric acid: A new pharmacological tool for retina research. Science. 1981;211:182–184. PubMed PMID: 6255566.
5. Numura A, Shigemoto R, Nakamura Y, Okomoto N, Mizumo N, Nakanishi S. Developmentally-regulated postsynaptic localization of a metabotropic glutamate receptor in rat rod bipolar cells. Cell. 1994;77:361–369. PubMed PMID: 8181056.
6. Vardi N, Morigawa K. ON cone bipolar cells in rat express the metabotropic receptor mGluR6. Vis. neurosci. 1997;14:789–794. PubMed PMID: 9279006.
7. Nawy S, Jahr CE. Supression by glutamate of cGMP activated conductance in retinal bipolar cells. Nature. 1990;346:269–271. PubMed PMID: 1695713.
8. Shiells RA, Falk G. Glutamate receptors of rod bipolar cells are linked to a cyclic GMP cascade via a G-protein. Proc Biol Sci. 1990;242:91–94. PubMed PMID: 1706097.
9. Dhingra A, Lyubarsky A, Jiang M, Pugh EN, Birnbaumer L, Sterling P, Vardi N. The light response of ON bipolar neurons requires Gao. J Neurosci. 2000;20:9053–9058. PubMed PMID: 11124982.
10. Nawy S. The metabotropic receptor mGluR6 may signal through Go, but not phosphodiesterase, in retinal bipolar cells. J Neurosci. 1999;19:2938–2944. PubMed PMID: 10191311.
11. Nelson R, Kolb H. Synaptic patterns and response properties of bipolar and ganglion cells in the cat retina. Vision Res. 1983;23:1183–1195. PubMed PMID: 6649437.
12. Kolb H. The inner plexiform layer in the retina of the cat: electron microscopic observations. J Neurocytol. 1979;8:295–329. PubMed PMID: 490185.
13. Nelson R, Famiglietti EV, Kolb H. Intracellular staining reveals different levels of stratification for on-center and off-center ganglion cells in the cat retina. J Neurophysiol. 1978;41:427–483.
14. Kuffler SW. Discharge patterns and functional organization of mammalian retina. J Neurophysiol. 1953;16:37–68. PubMed PMID: 13035466.
15. Cohen E, Sterling P. Demonstration of cell types among cone bipolar neurons of cat retina. Philos Trans R Soc Lond B Biol Sci. 1990;330:305–322. PubMed PMID: 1982357.
16. Hartline HK. The receptive fields of optic nerve fibers. Am J Physiol. 1940;130:690–699.
17. Baylor DA, Fuortes MGF, O'Bryan PM. Receptive fields of the cones in the retina of the turtle. J. Physiol. 1971;214:265–294. PubMed PMID: 5579638.
18. Kaneko A. Physiological and morphological identification of horizontal, bipolar and amacrine cells in goldfish retina. J Physiol. 1970;207:623–633. PubMed PMID: 5499739.
19. Werblin FS, Dowling JE. Organization of the retina of the mudpuppy, Necturus maculosus. II. Intracellular recording. J Neurophysiol. 1969;32:339–355. PubMed PMID: 4306897.
20. Naka K-I. Neuronal circuitry in the catfish retina. Invest. Ophthal. 1976;15:926–935.
21. Toyoda J-I. Membrane resistance changes underlying the bipolar cell response in the carp retina. Vision Res. 1972;12:283–294.
22. Werblin FS. Synaptic connections, receptive fields, and pattens of activity in the tiger salamander retina. Invest Ophthal Vis Sci. 1991;32:459–483. PubMed PMID: 2001922.
23. Ammermüller J, Kolb H. The organization of the turtle inner retina I. On- and off-center pathways. J Comp Neurol. 1995;358:1–34. PubMed PMID: 7560272.
24. Enroth-Cugell C, Robson JG. The contrast sensitivity of retinal ganglion cells of the cat. J Physiol. 1966;187:517–552. PubMed PMID: 16783910.

25. Gouras P. Identification of cone mechanisms in monkey ganglion cells. J Physiol. 1968;199:533–547. PubMed PMID: 4974745.
26. Levick WR, Thibos LN. Receptive fields of cat ganglion cells:classification and construction. Prog Ret Res. 1983;2:267–320.
27. Shapley R, Perry VH. Cat and monkey retinal ganglion cells and their visual functional roles. Trends Neurosci. 1986;9:229–235.

Roles of Amacrine Cells

Helga Kolb

Created: May 1, 2005; Updated: April 30, 2007.

General Characteristics

Amacrine cells of the vertebrate retina are interneurons that interact at the second synaptic level of the vertically direct pathways consisting of the photoreceptor-bipolar-ganglion cell chain. They are synaptically active in the inner plexiform layer (IPL) and serve to integrate, modulate, and interpose a temporal domain to the visual message presented to the ganglion cell. Amacrine cells are so named because they are nerve cells thought to lack an axon (1). Today, we know that certain large-field amacrine cells of the vertebrate retina can have long "axon-like" processes, which probably function as true axons in the sense that they are output fibers of the cell (see a later section on dopaminergic amacrine cells). However, these amacrine axons remain within the retina and do not leave the retina in the optic nerve, as do the ganglion cell axons (Fig. 1).

Since the time of Cajal, we have known that amacrine cells come in all shapes, sizes, and stratification patterns. Since those days, many more morphological subtypes have and continue to be described from additional Golgi studies, intracellular recordings, and immunocytochemical staining. Thus, we presently have a classification of amacrine cells consisting of about 40 different morphological subtypes (Fig. 2).

It is useful and most easily understandable to group the amacrine cell types into the general descriptors of narrow-field (30-150 µm), small-field (150-300 µm), medium-field (300-500 µm) and wide-field (>500 µm) based on a measurement of their dendritic field diameters (2). Then, the next most important criterion of classification involves knowing the stratification of the cells. It is generally agreed now that the IPL can be subdivided into five equi-thickness strata or sublayers (1) into which amacrine, bipolar, and ganglion cell processes can be assigned. All of these cell types are now classified primarily on the stratum or strata of the IPL in which their dendrites or axons are located. This is because, as mentioned in previous chapters, the IPL of vertebrate retinas can be divided into areas of neuropil, where specific cells are put into synaptic contacts and form circuits only with cells earmarked for a particular functional role.

Many varieties of amacrine cell are monostratified (restricted to a single stratum), whereas others are bi- or tri-stratified. When amacrine or ganglion cell processes pass through all the strata of the IPL from distal to proximal or *vice versa*, they are called diffuse cells. Superimposed upon Cajal's five strata subdivision of the IPL is a sublaminar division of the IPL. The first two strata, 1-2, are known as sublamina **a** of the IPL, whereas strata 3-5 are known as sublamina **b** by this scheme (3). It will be remembered from previous chapters that sublamina **a** contains bipolar axons and ganglion cell connections that lead to OFF-center ganglion cell physiology, whereas sublamina **b** contains bipolar to ganglion cell connections resulting in ON-center ganglion cell physiology (4).

Fig. 3 shows drawings of some small field amacrine cells of the monkey retina as seen in vertical sections. Small-field cells like these can be well visualized in section because their dendritic trees are contained within the depth of the section. However, large-field cells are not so well described in the section where their dendrites get cut off.

It was only when whole-mount preparations, from Golgi staining (5, 6) or immunocytochemical staining (7), were attempted that we could classify such cells. Then the full extent of their dendritic trees, which can be up to 1 mm in spread, could be visualized (see Fig. 4a) and a whole new understanding of amacrine cells became available.

A new technique of intracellular staining by a photochemical method has been developed In Richard Masland's group as an alternative to the unreliable Golgi technique (8). Amacrine cells of the rabbit retina are labeled with the nuclear stain DAPI and then selected, single-nuclei are irradiated by a narrow beam of light to drive DAPI to the oxidation of non-fluorescent dihydrorhodamine-123 to the fluorescent rhodamine-123. The complete cell

body and the dendritic tree are thus revealed under viewing in the fluorescence or confocal microscopes. By this method, 30 or so different varieties of amacrine cell can be photographed and drawn in full detail in the rabbit retina. Twenty-two varieties of amacrine cell have been seen in Golgi preparations in cat and primate retinas, so either some have been missed that were seen in rabbit, or else they are not as well deveoped in these less complex mammalian retinas. In any event, the narrow-field and medium-field types revealed by MacNeil and Masland's work (8) are shown in Fig. 4b and Fig. 4c. Another five different, wide-field, monostratified types were also encountered in rabbit retina by this method (not illustrated). They correspond closely to the wide-field types seen in monkey, cat, and human (2, 9, 10).

Amacrine Cell Circuitry as Revealed by Electron Microscopy

Kidd (11) and later Dowling and Boycott (12) were the first to identify the three types of profiles that contribute to the IPL by electron microscopy. The electron micrograph (Fig. 5) shows the cytological criteria on which we now recognize bipolar, amacrine, and ganglion cell profiles in the neuropil. Thus bipolar cell axonal endings are recognized by being filled with synaptic vesicles and having a ribbon-shaped density (red spots) pointing to two postsynaptic profiles (amacrine and ganglion). Amacrine profiles are also filled with synaptic vesicles but make synapses characterized by membrane densities at which the vesicles are particularly clustered (yellow spots). Ganglion cell profiles are recognized as being only postsynaptic to either bipolar axons or amacrine processes, containing no vesicles but instead a content of neurotubules, ribosomes, and glycogen granules.

Amacrine cell synapses are frequently seen to be reciprocal to bipolar ribbon input, i.e., the amacrine returns a synapse in the vicinity of the ribbon input synapse (arrowheads). Most amacrine cells are inhibitory neurons in the vertebrate retina, containing the common inhibitory neurotransmitters GABA or glycine. GABAergic amacrine cells, in particular, typically make reciprocal synapses with bipolar cells. A17 is the most well studied of the GABAergic reciprocal amacrine cells in the retina, and we shall return to this cell later.

We have learned much concerning the synaptic relationships of certain narrow-field amacrine cells as well as bipolar and small ganglion cell types, such as midget ganglion cells of the primate retina, from reconstructions of serial-section electron micrographs. The circuitry of the AII amacrine cell in the cat retina was first appreciated by this means (13, 14). However, with the advent of intracellular dye injection of electron-dense materials (horseradish peroxidase, HRP, or the photo reduction of Lucifer yellow) after physiological recordings or the development of electron-dense immunostains for electron microscopy, neurocircuitry was made easier for us. We could look at amacrine cells and their synaptic inputs by study of fewer sections, and it was not as critical to photograph every single section in a series. The amacrine cell of interest would always be clearly marked black and easily found in the synaptic neuropil. It is from this technique that we have learned most about amacrine cells and their circuitry in the mammalian retina. The remainder of this chapter will describe the morphology, circuitry, and intracellular responses of the amacrine cells that are most completely understood at present.

A2: Narrow-field, Cone Pathway Amacrine Cell

A2 is a narrow-field amacrine with a 20-60-µm-wide dendritic tree composed of multi-branched, beaded, and appendage-bearing dendrites, mostly confined to stratum 2 of the IPL (Fig. 6).

Intracellular recordings from A2 cells (formerly called A4) indicate that these cells give true slow potential, hyperpolarizing response to light (OFF-center) at all positions of the slit in their receptive fields, and they have no sign of an inhibitory surround (15).

A2 cells receive bipolar input from OFF-center types of cone bipolar cell of sublamina **a** and make reciprocal synapses to these bipolar axons. A2 amacrine cells then synapse upon OFF-center ganglion cell dendrites of sublamina **a**. The A2 cell makes an inhibitory synapse upon these ganglion cells, because it is thought to be a GABAergic cell type (16).

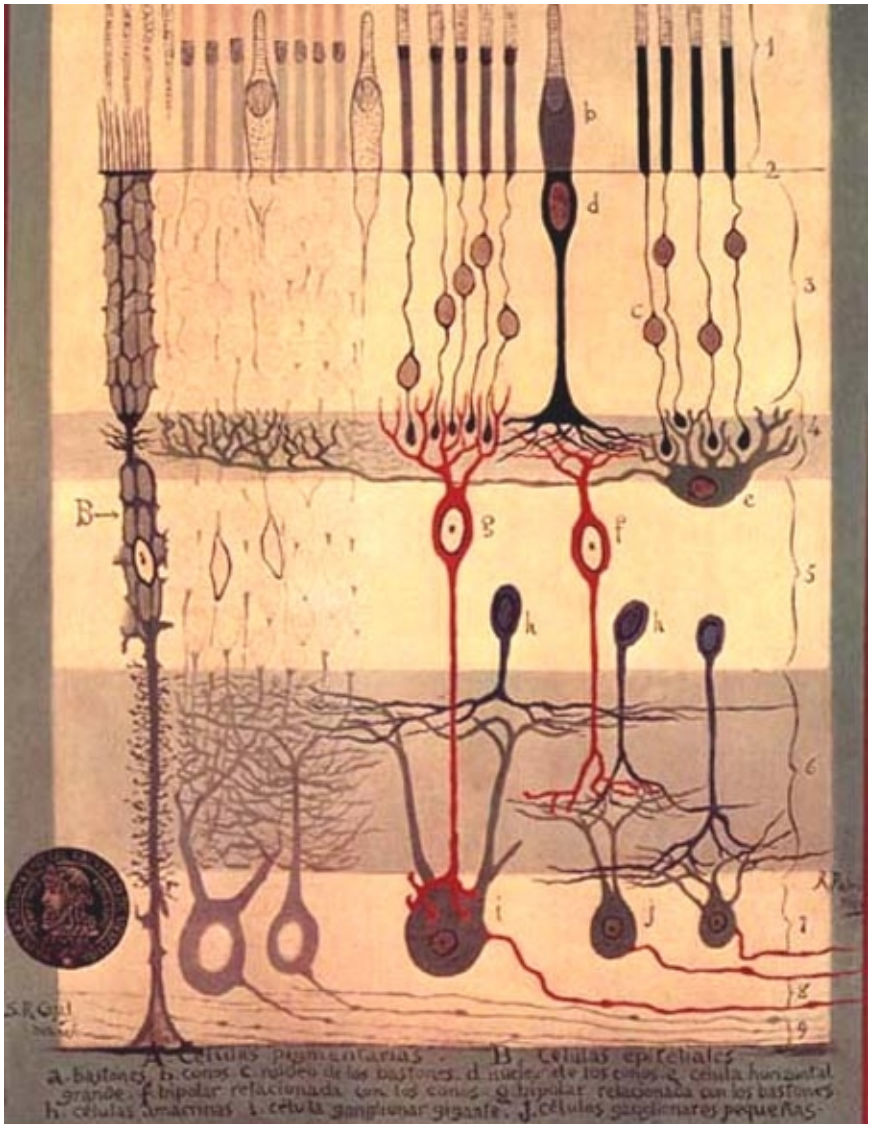

Figure 1. Drawing of the retina made by Cajal.

A possible role is in disinhibition of the ganglion cells' center responses. Alternatively, A2 cells, despite being small-field types, might have a role in the generation of antagonistic surrounds of ganglion cells (17). A2 cells receive a great many amacrine inputs to their dendritic trees, which could be from wider field cells than they are are themselves, so giving them a much larger receptive field size than their actual dendritic tree size would indicate (Fig. 7).

AII: A Bistratified Rod Amacrine Cell

In Fig. 8 are shown four examples of the best-studied amacrine of all in the vertebrate retina: the AII "rod amacrine" of the mammalian retina. These cells have been recorded from by microelectrodes, and dyes have been iontophoresed into the cell after the intracellular recordings (18). The AII cell was first described from Golgi staining and electron microscopic examination (13, 19).

AII is a narrow-field amacrine (dendritic tree diameter typically 30-70 μm) with a bistratified morphology: the mitral-shaped cell body gives off a single, stout apical dendrite, and a cluster of lobular appendages (round blobs just below the cell body) (Fig. 9) arise from the main dendrite in sublamina **a** of the IPL. The finer "arboreal

Figure 2. Picture of Camillo Golgi.

dendrites" (20) penetrate down into sublamina **b** to end close to the ganglion cell layer. In the human retina, such an AII amacrine cell is seen in a surface view of a wholemount.

In cat and rabbit retinas, from which AIIs have been recorded, the AII cell is a rod-dominated depolarizing (ON-center) cell (18, 21, 22). Thus, in the center of its receptive field the cell gives a transient depolarizing response with a pronounced sustained plateau (ON-center) and a long, drawn-out hyperpolarization after light off. By 140 μm to either side of the center, the response to a light flash is now an inverted response, indicating a hyperpolarizing surround (OFF-surround) (18) (Fig. 10).

Electron microscopy has shown that the AII is primarily postsynaptic to rod bipolar axon terminals in lower sublamina **b** of the IPL (30% of its input) (23). Its major output is upon ganglion cells that have dendrites only in sublamina **a**, i.e., AII cell lobular appendages synapse upon OFF-center a and b ganglion cells (17) (Fig. 11).

The AII also passes rod-driven information through the ON-center cb5 cone bipolar to ON-center a and b ganglion cells by means of gap junctions (Fig. 12, black spots on AII primary dendrites to pink cb axon). A little OFF-center cone bipolar input is provided to the AII lobular appendages by cb1 and cb2 OFF-center cone bipolar cells in sublamina **a** (19% of input) (Fig. 12, yellow cb profiles) (23).

Thus, AII cells do carry some cone pathway components to their ON-center responses, which could come from excitatory input from ON-center cb5 at the gap junctions or from the direct cb1 or cb2 synapses, which would have to be inhibitory, in this case. AII amacrine cells are also couple across the retina in a weak electrical syncytium by virtue of their gap junctions between their arboreal dendrites in sublamina **b** (Fig. 12, gj, lower right; see an animation of the wiring pattern) (13, 18, 24).

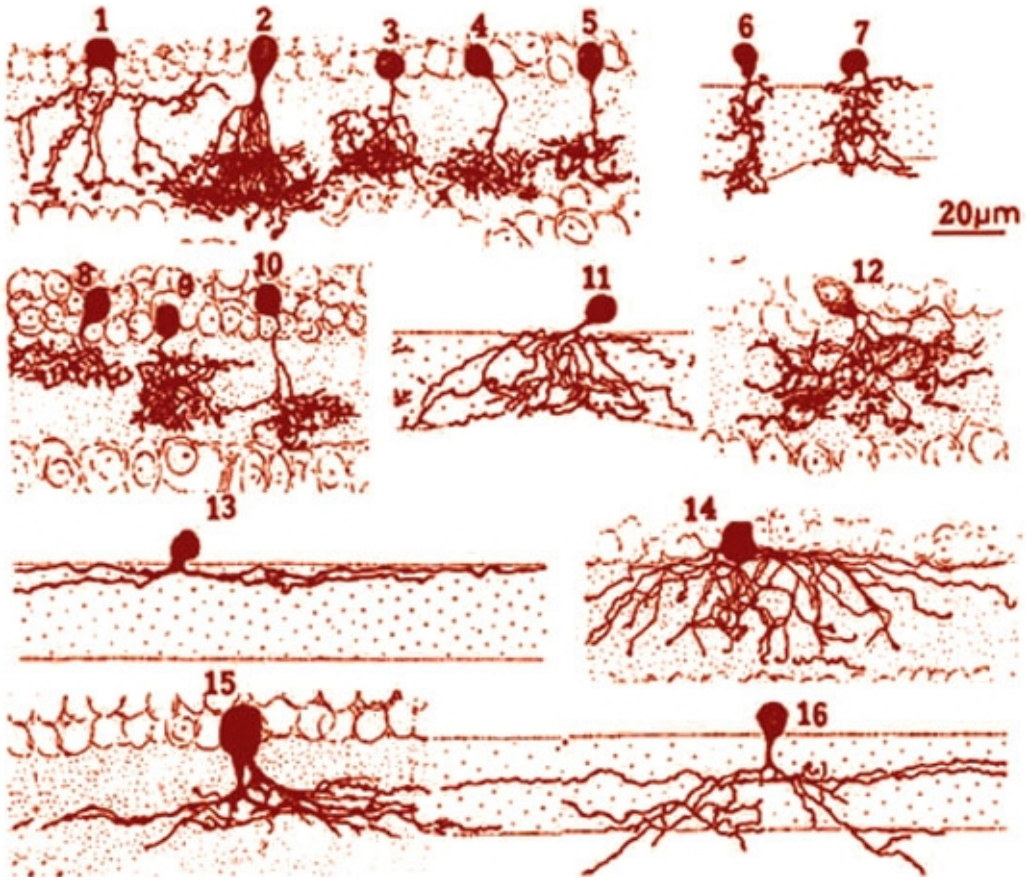

Figure 3. Stratification patterns of small and medium-field amacrine cells in primate retina. From Polyak (81).

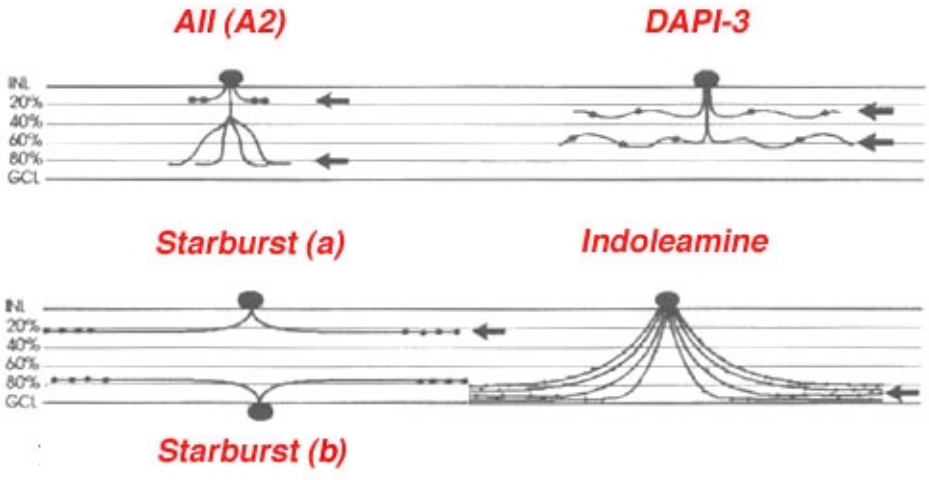

Figure 4a. Golgi-stained, wide-field amacrine cells as seen in whole-mount retina of the cat. Amacrines are classified by number and strata of the IPL in which they branch.

The dopaminergic amacrine cell provides a considerable number of synapses to the AII cell, either directly upon its cell body or upon its lobular appendages (Fig. 11, A, red arrowheads) (25, 26). Dopamine cells are thought to have a function in the inner retina to uncouple AII amacrine cells from both their contacts with the depolarizing cone bipolar and the AII amacrine coupled network (24, 27). As much as 51% of the input to AII amacrine cells is from various other amacrine cells though, and most of these inputs occur in the central part of the cells'

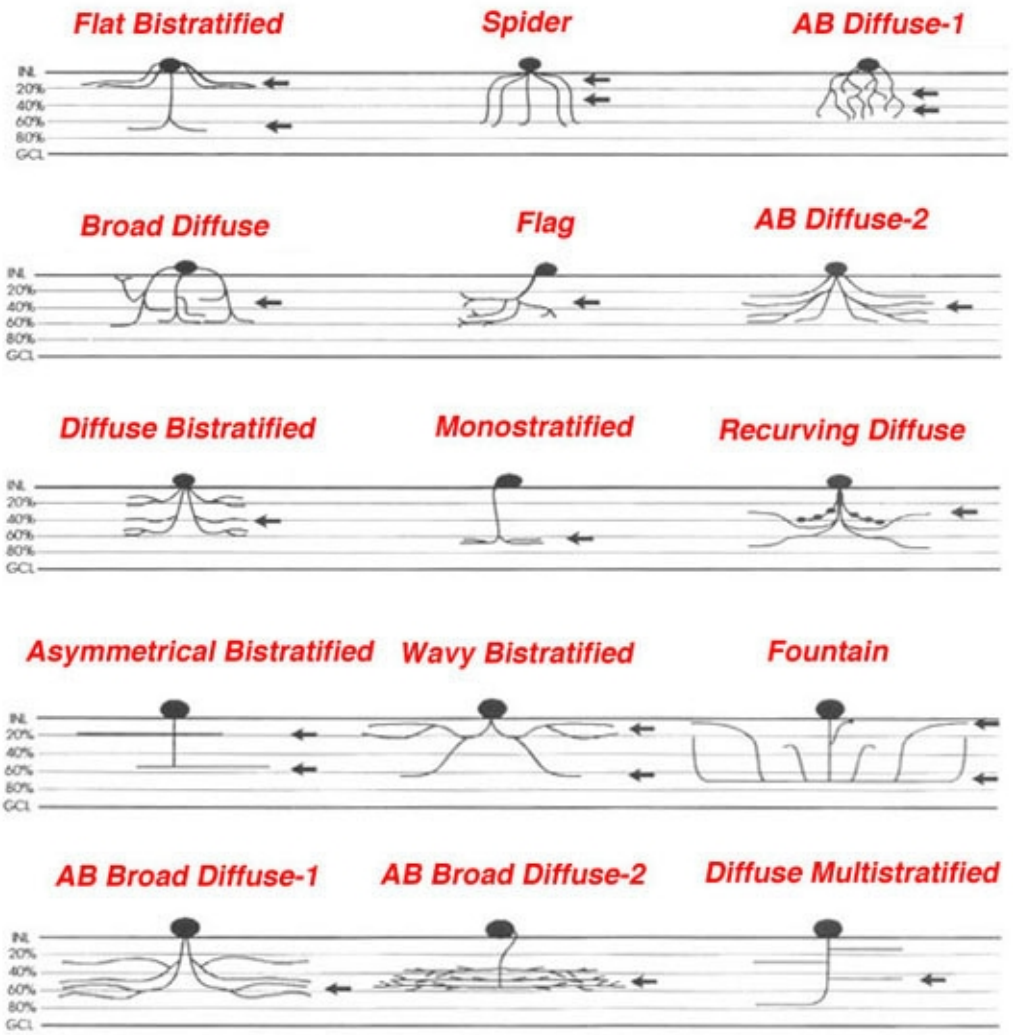

Figure 4b. Small-field and medium-field amacrine cells of the rabbit retina. AII cells, DAPI-3 cells, starburst type a cells, and indoleamine-containing cells are shown.

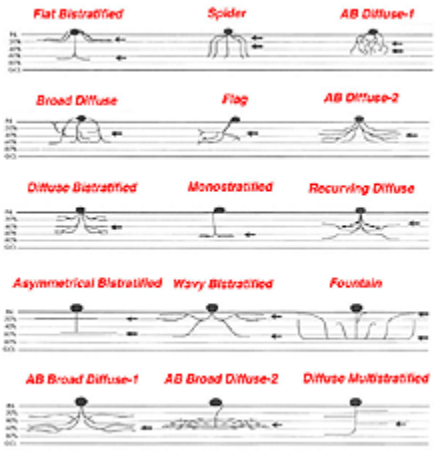

Figure 4c. Narrow- and medium-field cells of the rabbit retina.

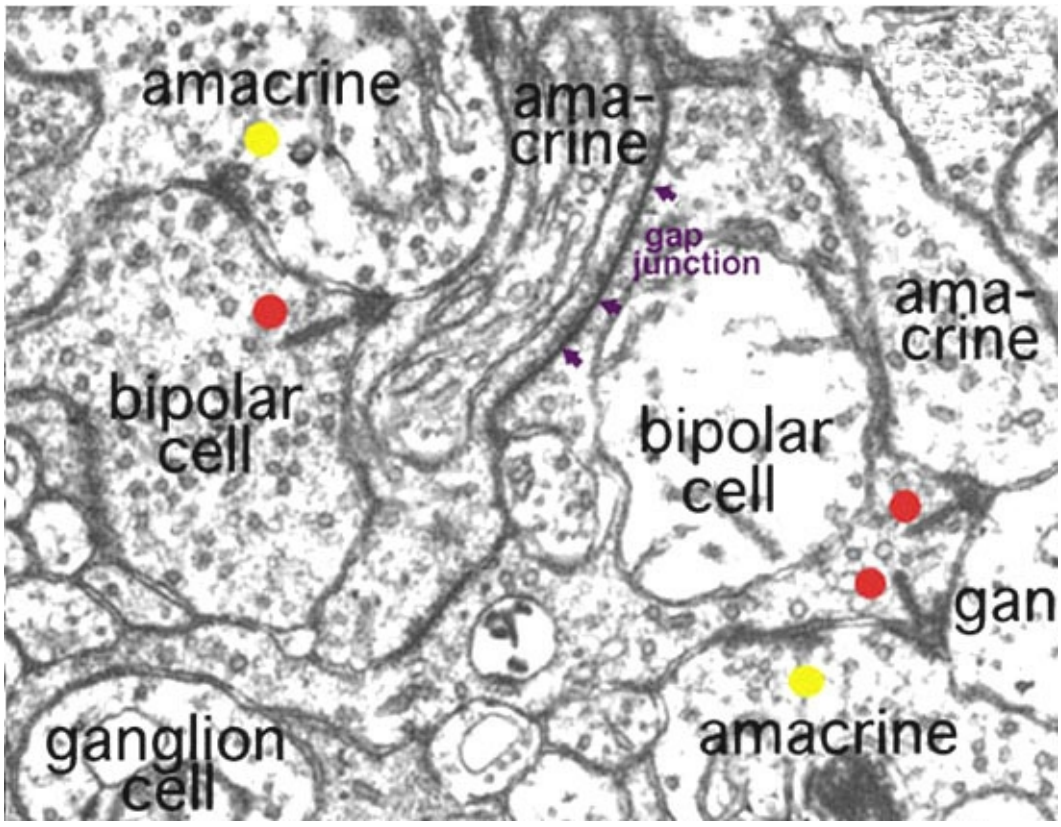

Figure 5. Electron micrograph of the various synapses in the IPL. Red dots indicate bipolar ribbon synapses; yellow dots are reciprocal amarcine synapses. Small arrows point to a gap junction between a bipolar cell and an All amacrine cell profile.

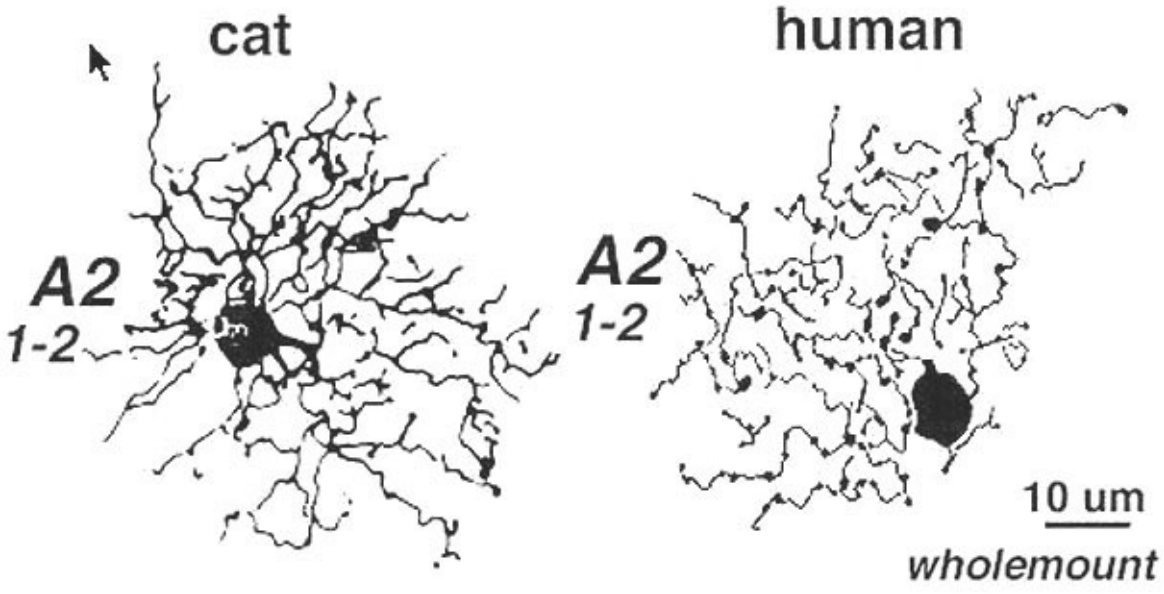

Figure 6. Golgi drawings of A2 amacrine cells.

dendritic tree in strata 3-4 (23). AII amacrine cells are glycine immunoreactive (28, 29) and contain the calcium-binding proteins parvalbumin, calbindin, and calretinin (Fig. 13) (30).

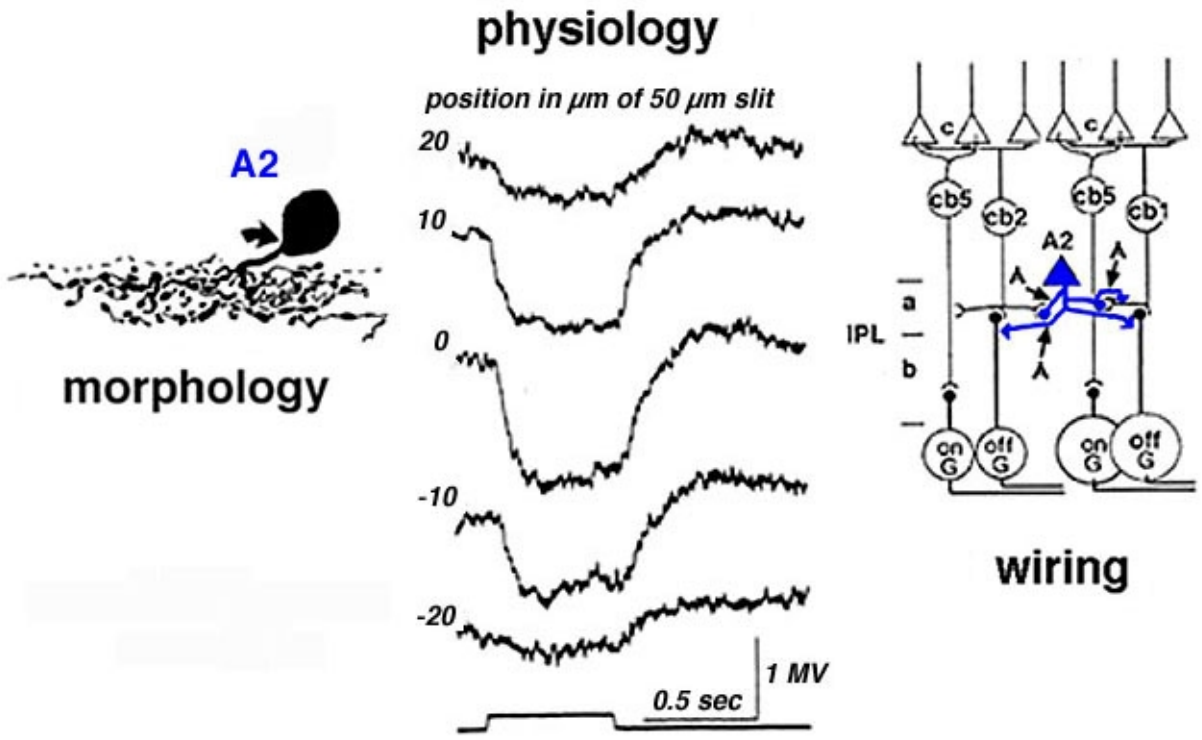

Figure 7. Summary diagram of A2 amacrine cells.

The AII amacrine cells are the major carriers of rod signals to the ganglion cells in the retina. As such, they play a role in speeding up the slow potential rod messages for presentation to ganglion cells (18, 31). Their distribution in the retina suggests that they tile the complete retina (32). AII amacrine cells peak in density at 1.5 mm from the foveal center in monkey and at the area centralis in cat (33). In addition, because of their high density across all parts of the retina and their synaptic involvement with millions of rod bipolar cells, they may contribute in a major way to the pattern ERG (34).

A8: A Bistratified Cone Amacrine Cell

A8 is a bistratified, narrow-field amacrine cell that is easy to confuse with AII in whole-mount, stained retina. It actually looks like an upside-down AII cell. A8 has short, wispy processes coming from the apical dendrite to ramify in sublamina **a** of the IPL, whereas heavy-beaded dendrites penetrate down to sublamina **b** to run in strata 4 and 5. This cell type may correspond to the DAPI-3 of the rabbit retina, described by Vaney (32) and Bloomfield (21) (Fig. 14).

The A8 cell has been intracellularly recorded and studied by electron microscopy after iontophoresis of horseradish peroxidase. In Fig. 15, we shown two of the most important synapses of this cell type.

The A8 amacrine cell is involved in the cone pathways of the cat retina, rather than the rod pathways that the AII is committed to. Thus, in sublamina **a**, excitatory cone-driven signals come from cone bipolar cells such as cb2, which we know are OFF-center in physiology (Fig. 16, yellow cb profile), and in sublamina **b** from cb6, another OFF-center bipolar cell (Fig. 16, cb, pink profile) (35). Altogether cone bipolar synapses account for 42% of the input to A8 cells. Lesser rod bipolar input (20%) also occurs to the lower dendrites in sublamina **b** of the IPL. Like AII amacrine cells, A8 cells also engage in gap junctions with a cone bipolar type of sublamina **b**, but the bipolar is a different type and, in addition to the gap junction, makes the common ribbon synapse to A8

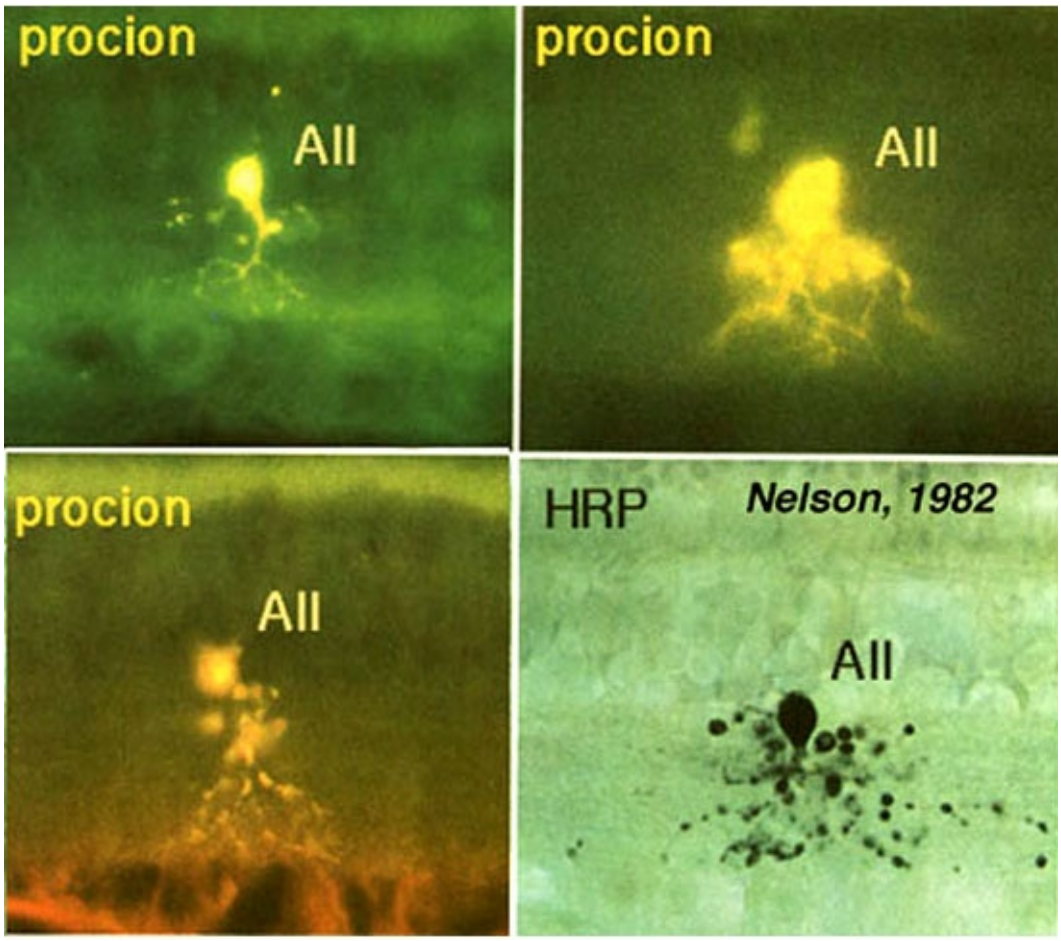

Figure 8. AII amacrine cells stained with different methods.

dendrites (Fig. 16; see an animation of the wiring pattern). A8's major output is to beta ganglion cell dendrites in sublamina **a** of the IPL (above GC). We have not seen A8 synapses to alpha cells in the cat retina (36).

The intracellular response of A8 indicates a hyperpolarization to light at the receptive field center with a rather transient OFF-response to light. The transientness could reflect the amacrine synapses (38% of input) occurring over all parts of its dendritic tree (Fig. 16, red arrowheads) (0, response is at largest magnitude).

Both rod-driven and cone-driven signals contribute to the response. Its receptive field extent can be mapped with a slit of light. As the slit is stepped some distance to either side of the center of the receptive field, the response of the cell inverts and a depolarizing or ON-surround appears by 700 μm from the central position (Fig. 17, top and bottom trace) (36).

Some part of the amacrine input to A8, particularly that upon its cell body and proximal dendrites in stratum 1 of the IPL, may be from dopaminergic amacrine cells (A18) (25). So it is probable that this cell type is also under the control of the dopaminergic amacrine cells, similar to the AII amacrine cell (see above). Thus, the dopamine cell may control A8's spatial characteristics through gating its gap junctions in light and dark. A8 is intensely glycine immunoreactive (28, 29). We have suggested that A8 cells also function in the disinhibition of ganglion cell receptive field centers (36).

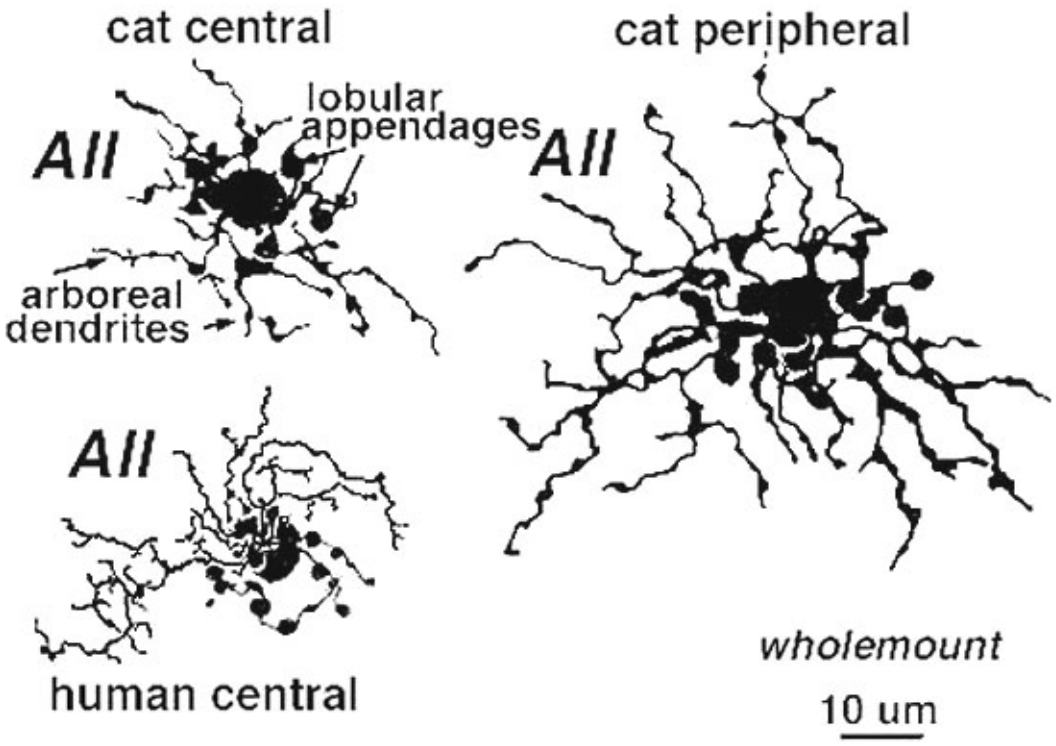

Figure 9. AII amacrine cells.

A13: A Small-field Diffuse Amacrine Cell of the Cone System

Cell A13 is a diffusely branched cell with a large cell body (12 μm diameter) and fine dendrites bearing distinct beads at regular intervals that run through mostly strata 3-5 of sublamina **b** of the IPL to end up along the top of ganglion cell bodies. The complete tree covers a 100-μm area (Fig. 18).

Electron microscopy shows that A13 cells, similar to A8 cells, get only a minor rod bipolar cell (12%) input, whereas three different types of cone bipolar cell have major synaptic input (28%). The cone bipolar inputs are from axons in sublamina **a**, stratum 3-4 of sublamina **b**, and stratum 5 of sublamina **b**. A13 cells appear to make reciprocal synapses upon cone bipolar cells and possibly also upon rod bipolar cells. Amacrine cells provide much more synaptic input than bipolar cells (60%). A13 makes synaptic output to OFF-center ganglion cells, of both alpha and beta types, in sublamina **a**. Gap junctions link A13 cells at their beaded dendrites (36) (Fig. 19; see an animation of the wiring pattern).

The intracellular response of A13 is a slow potential, hyperpolarizing response, looking much like a horizontal cell response in the cat retina. Mixtures of rod and cone signals contributed to the intracellular response of A13 cells. Its receptive field is large and does not appear to exhibit a surround. The spatial extent of the receptive field is very suggestive of a coupled electrical syncytium of cells at least seven cells wide (Fig. 20) (36).

A17: The Wide-field Reciprocal Rod Amacrine Cell

A17 is a wide-field *diffuse* amacrine. Its dendritic tree can span close to a millimeter of retinal surface. Its very fine dendrites bear pronounced beads at regular intervals along their lengths. The majority of the dendritic tree runs in sublamina **b** of the IPL, along the top of the ganglion cell layer in stratum 5 as a dense network of fine

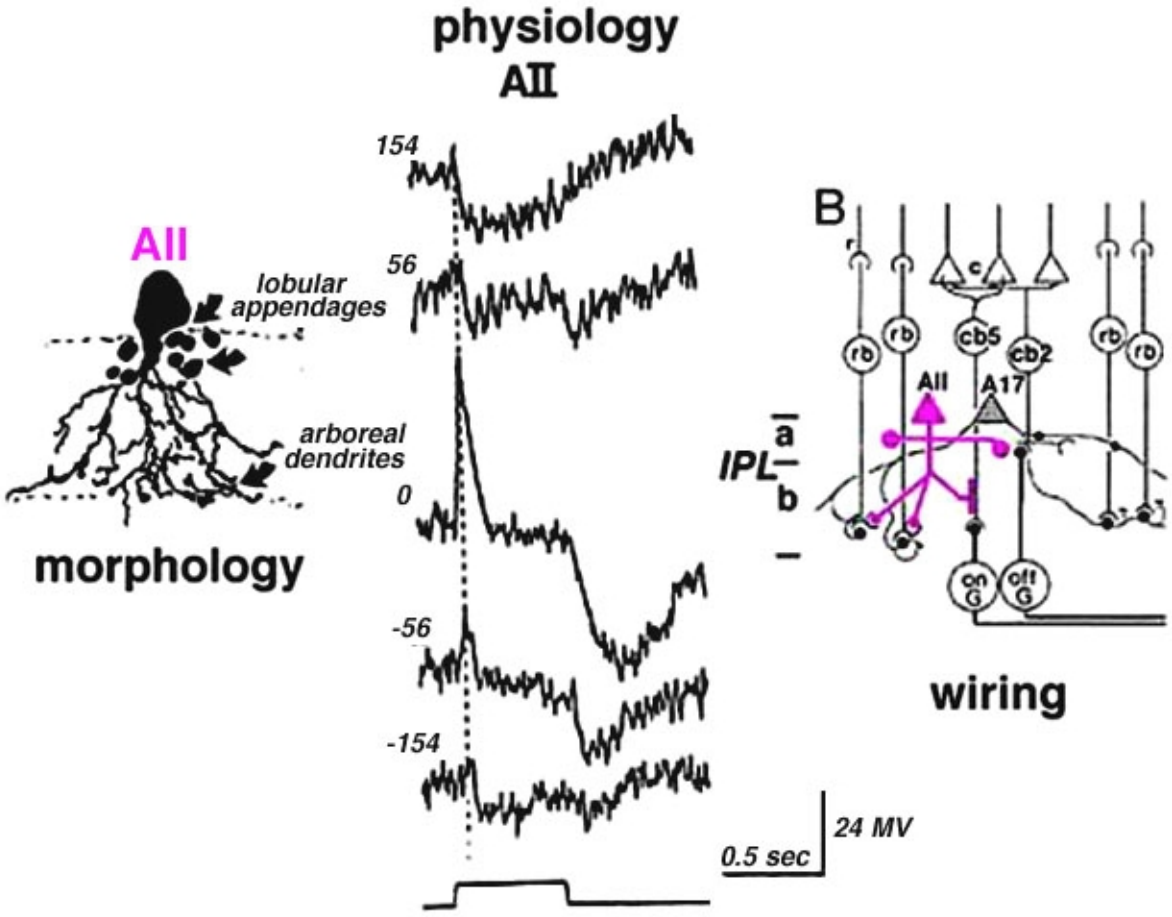

Figure 10. Schematic diagram of the morphology, physiology, and wiring pattern of the AII amacrine cell.

fibers. Over 1000 beads have been counted on such A17 amacrine cells in the cat retina (37), and as we shall see later, the beads are the synaptic points where reciprocal synapses with rod bipolar cells occur (38) (Fig. 21).

Electron microscopy shows that A17 cells are the predominant reciprocal amacrine cell at the rod bipolar cell axon terminals in sublamina **b** of the IPL. In addition, their fine dendrites in sublamina **a** receive some synapses from the dopaminergic amacrine cell A18 (Fig. 22). However, there has not yet been discovered any synaptic output of the A17 except the reciprocal synapses with the rod bipolar axon.

A17 cells are driven almost exclusively by rod-matched stimulating conditions. In the intensity series is shown using wavelengths of light matched for rods at rod- and cone-stimulating wave lengths. The responses at each light intensity superimpose, indicating that only a single receptor mechanism is present, that due to the rods. At all intensities, the response is a depolarization and, up until the highest intensities (Fig. 23, bottom trace), essentially a slow potential response. At the highest light intensity, the response becomes slightly transient, although there is a depolarizing plateau phase. The response now resembles that of its input neuron, the rod bipolar cell (22). A17 cells do not appear to have inhibitory surrounds, although they exhibit spatially dependent characteristics to their response amplitudes with far surround stimulation (37).

The A17 cell wiring diagram is shown in Fig. 23. Its huge coverage of the IPL neuropil by its up-to-a-millimeter dendritic spread allows it to collect scotopic rod signals from several thousand rod bipolar axons. Its high sensitivity to scotopic conditions (rod-driven light intensities) suggests hat this amacrine plays a role in converging rod signals from huge areas of retina and in amplifying them at very low light intensities. A17 is

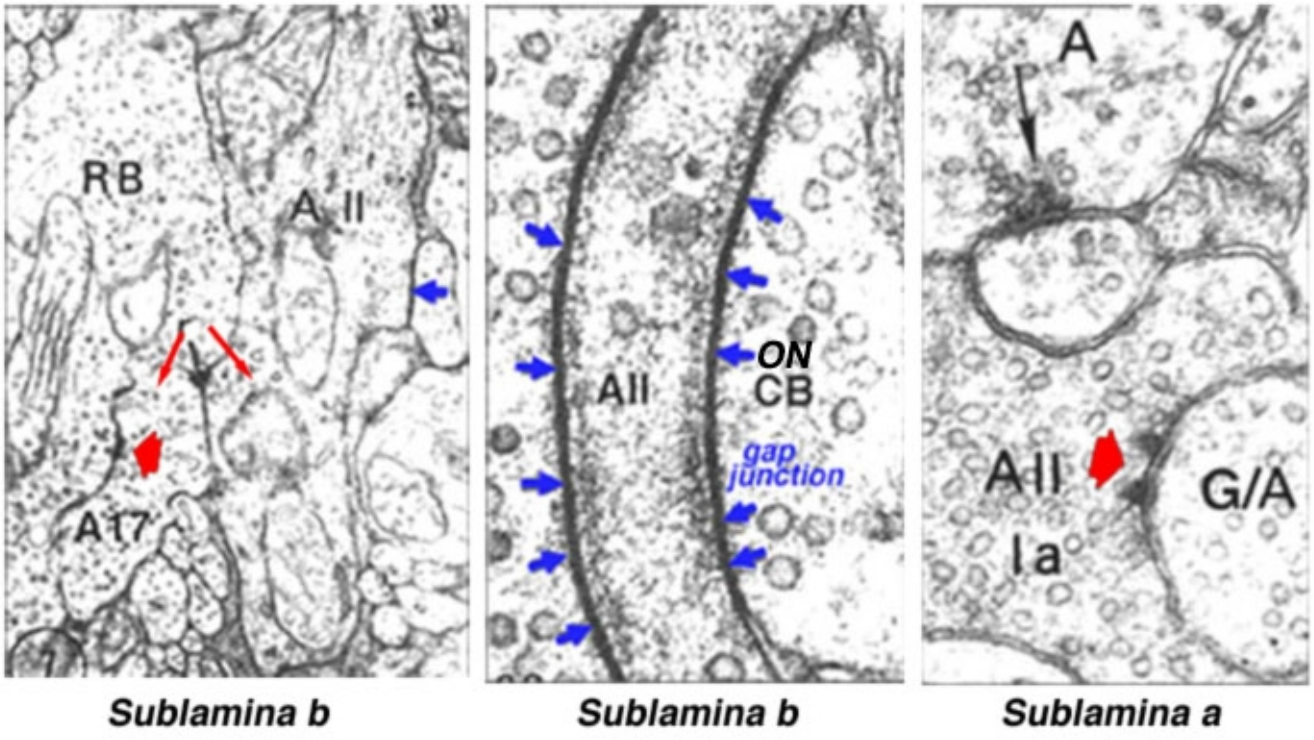

Figure 11. Electron micrographs of AII amacrine synapses.

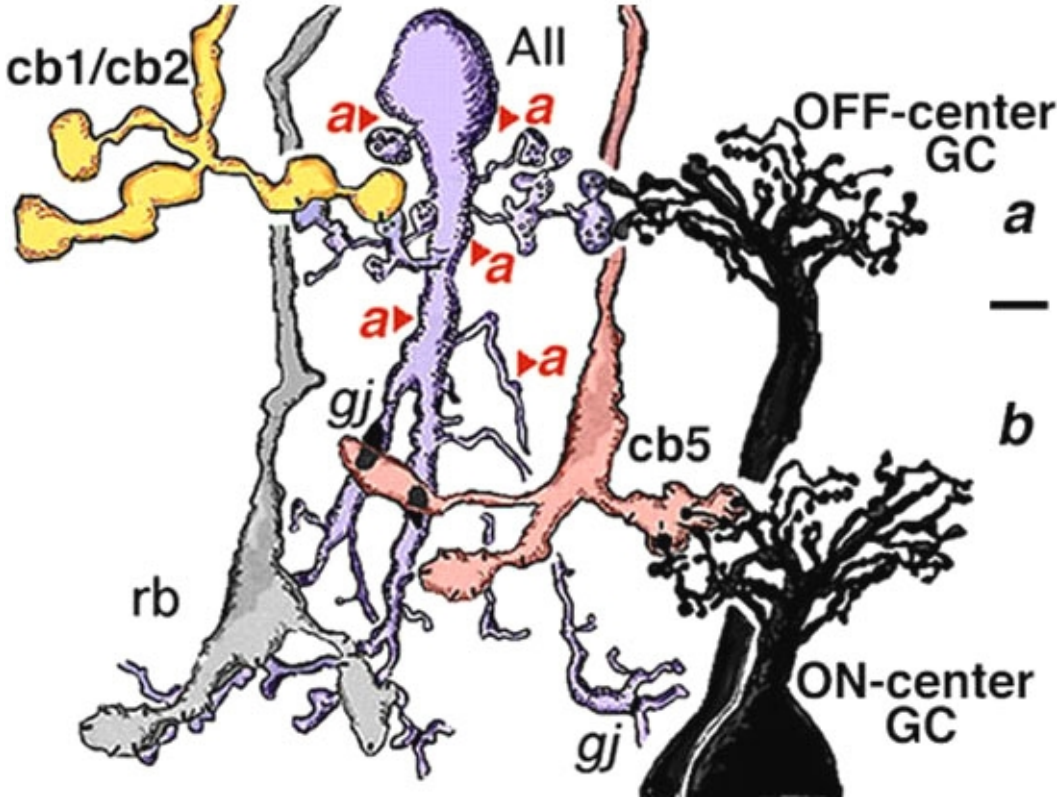

Figure 12. Schematic drawing of the wiring pattern of the AII amacrine cell.

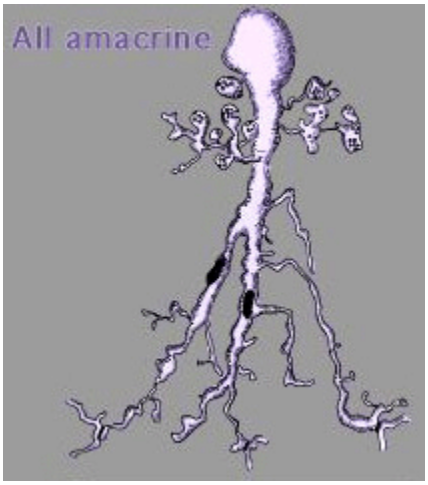

Movie 1. Animation of the wiring pattern of the AII amacrine cells.
Download video

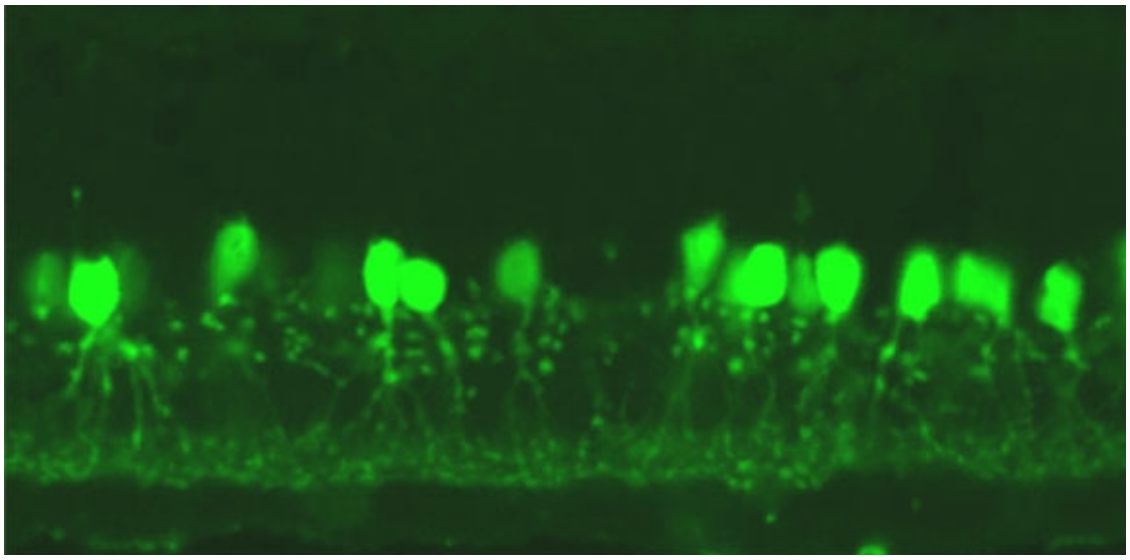

Figure 13. Parvalbumin staining of AII amacrine cells in hamster retina.

known to accumulate serotonin in rabbit retina (39) but is thought to be a GABAergic neuron in terms of neurotransmission in all mammalian retinas (16).

A19 and A20: ON-OFF Wide-field Amacrine Cells

A19 and A20 are similar appearing, wide-field radiate amacrine cells with 300-500-µm-diameter fields. However, their fields are further expanded to several mm by the presence of fine axon-like processes coming either from the ends of tapering dendrites (A19, A20) or from primary dendrites or even from the cell body (Fig. 24).

They differ in stratification levels levels in the IPL, although A19 stratifies on the sublamina **a**/**b** border and A20 in stratum 2 of sublamina **a.** A19 has distinctly spiny dendrites, whereas A20 has long, smooth, spineless but beaded dendrites.

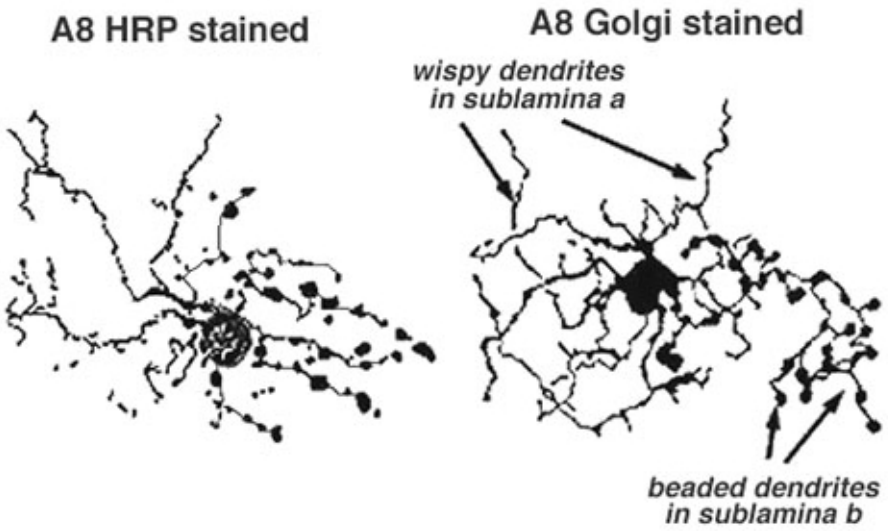

Figure 14. Golgi and HRP appearance of A8 amacrine cells.

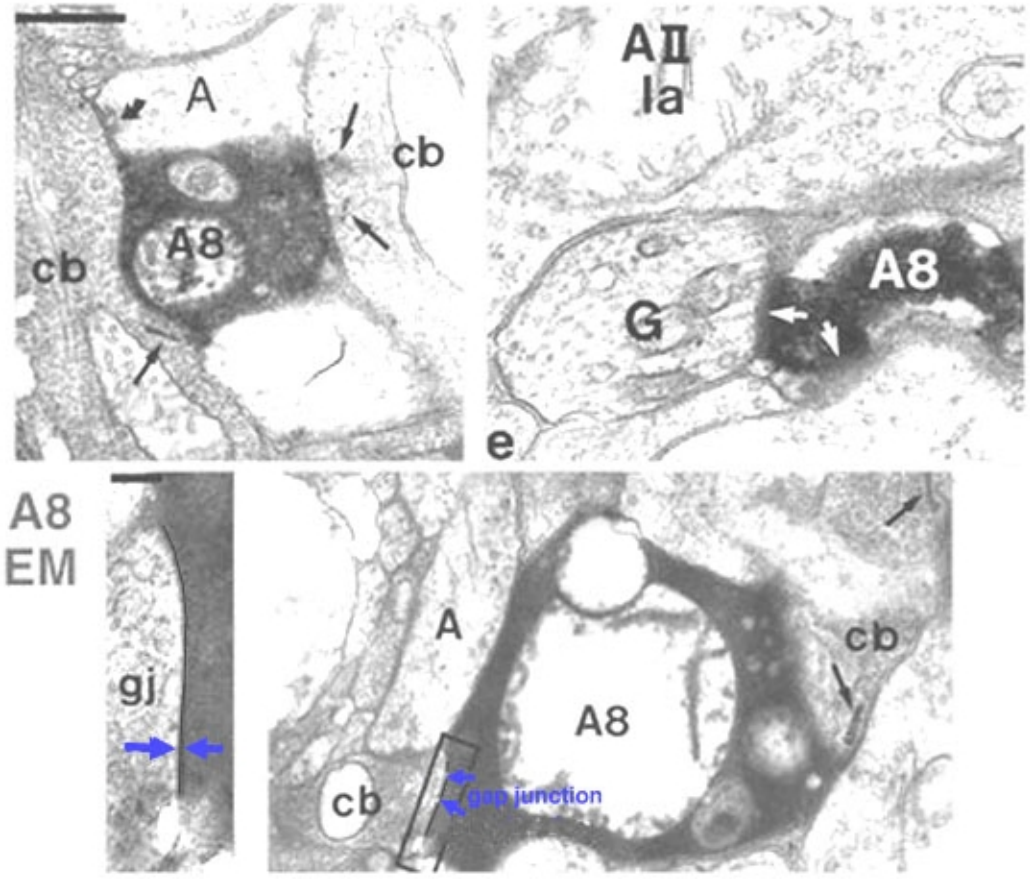

Figure 15. Electron micrograph of A8 synapses in the IPL.

A19 and A20 are both transient depolarizing ON-OFF cells, otherwise known as ON-OFF amacrine cells in response type. Such cells have been difficult to record long-term responses from in a mammalian retina (40), and the example illustrated in Fig. 25 of an A19 is one of the longest held, and thus a receptive field was mapped.

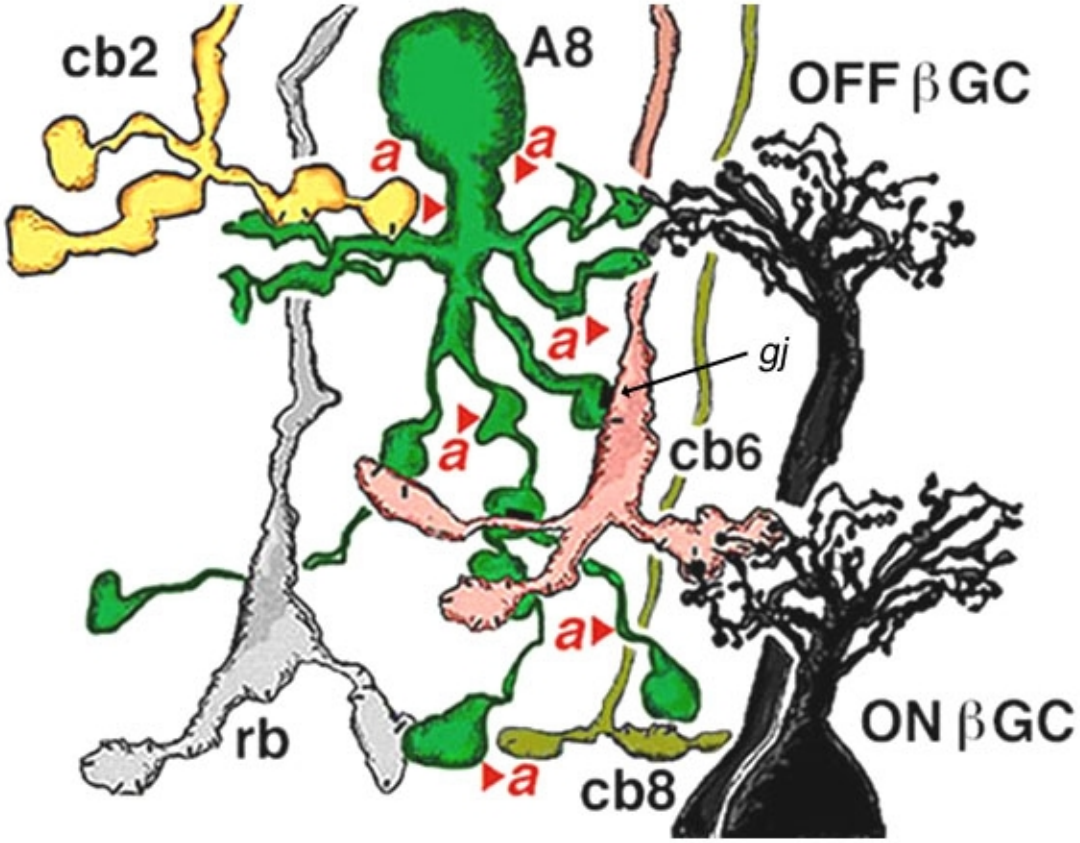

Figure 16. Summary diagram of the wiring pattern of the A8 amacrine cell.

Movie 2. Animation of the wiring pattern of the A8 amacrine cells.
Download video

The receptive fields are large, i.e., >550 μm radius, rather larger than their immediate dendritic tree sizes, and undoubtedly due to their axon-like extensions (40). Neither A19 nor A20 exhibited antagonistic surrounds.

Electron microscopy for circuitry of A19 and 22 has been performed. A19 receives two types of cone bipolar input (24%): the first is from OFF-center cb2 cone bipolar cells of sublamina **a**, while the other is ON-center input from cb5 at the sublamina **a/b** border, where cb5 passes in to sublamina **b**. OFF- and ON-center bipolar input could account for this cell's ON-OFF physiology. The predominant input is from amacrine cells of sublamina **a**, though (76%). Some of the amacrine inputs could be from rod amacrine AII cells, others from A2 cells, while some looked like they could be from other A19 cells. A19's output is reciprocal synapses to both

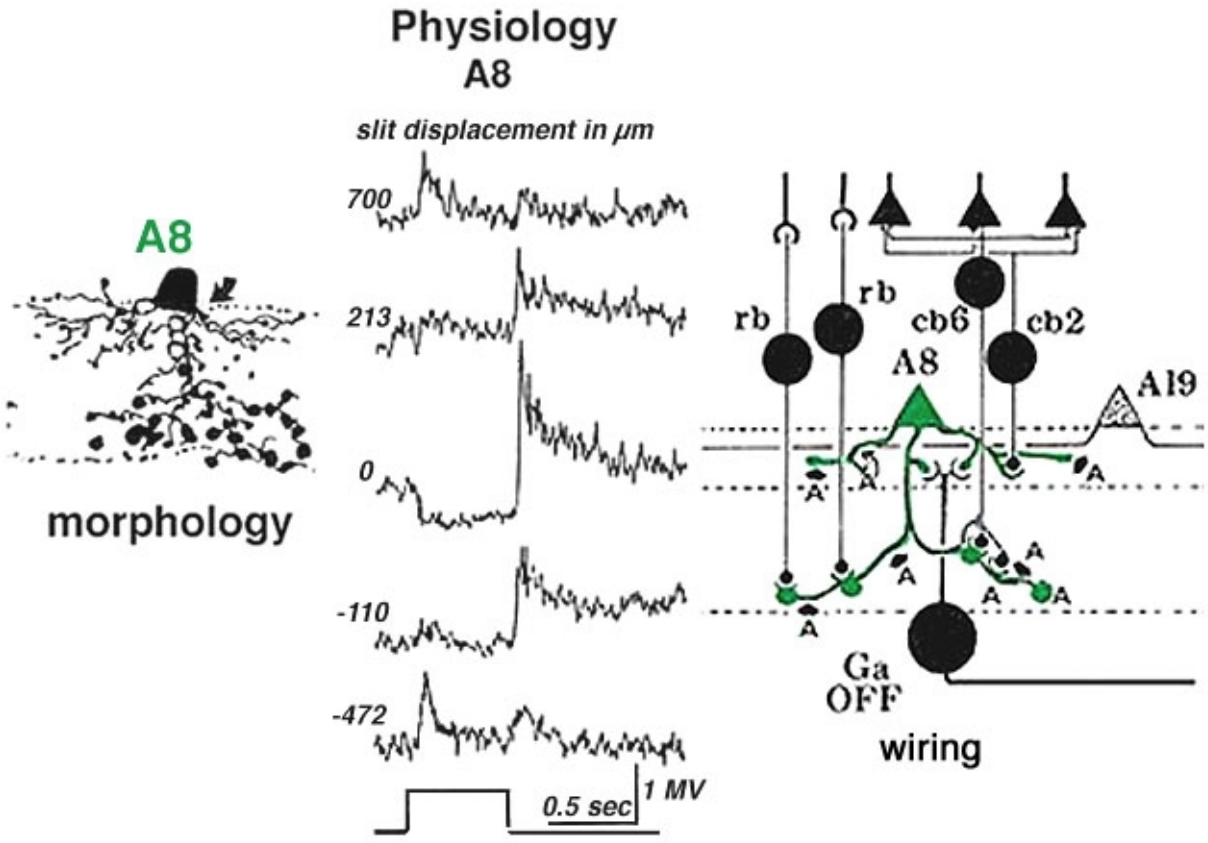

Figure 17. Summary diagram of the A8 amacrine cell.

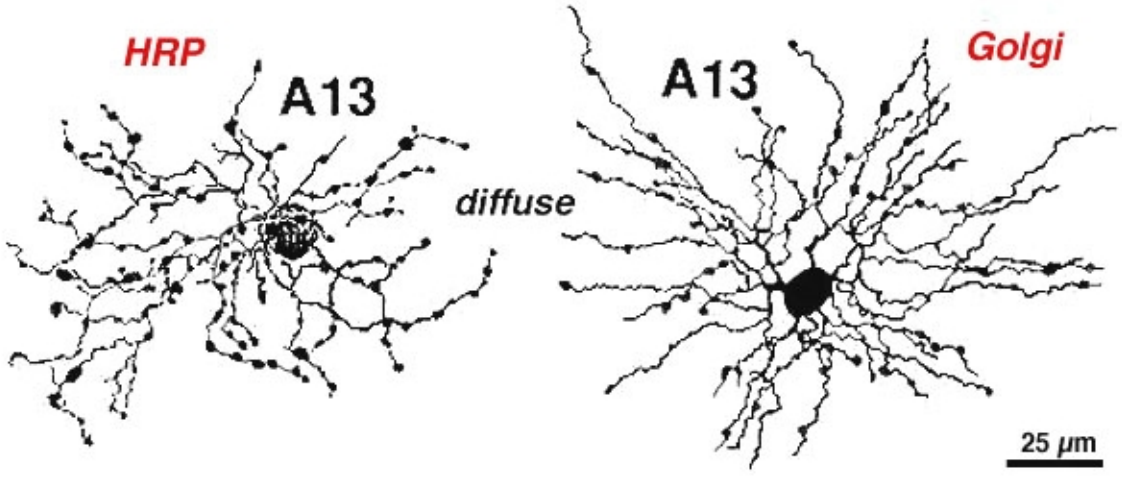

Figure 18. HRP and Golgi appearance of A13 amacrine cells.

types of bipolar (40%), to unknown dark amacrines (40%) and possibly some fine-diameter ganglion cell dendrites (20%) (40) (Fig. 26).

Gap junctions may connect A19 dendrites one to another (Fig. 11, A19, gj). A19 is GABAergic (16).

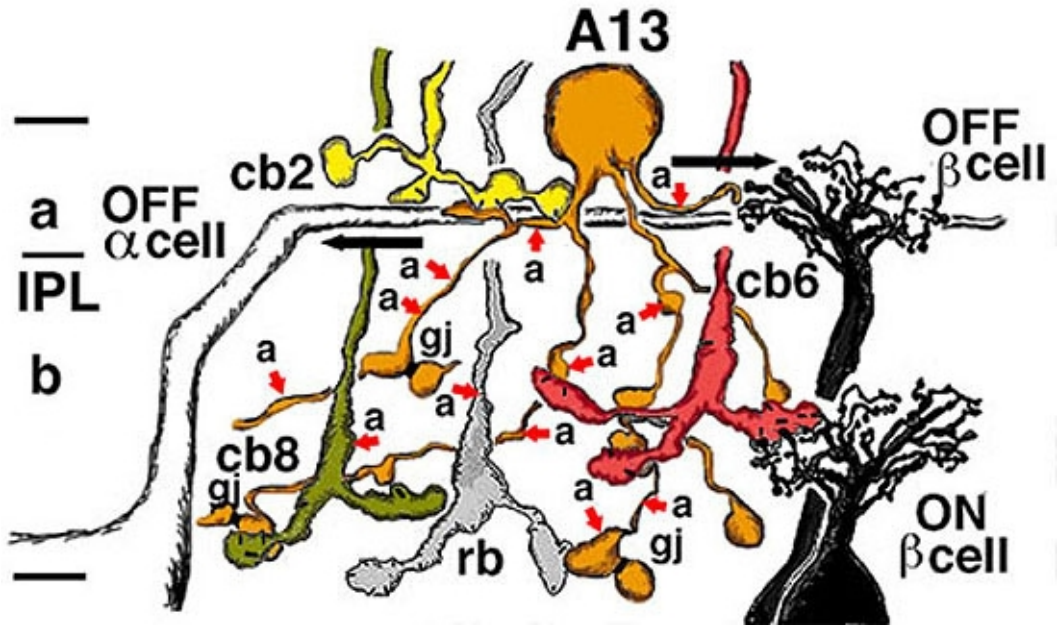

Figure 19. Wiring pattern of the A13 amacrine cell.

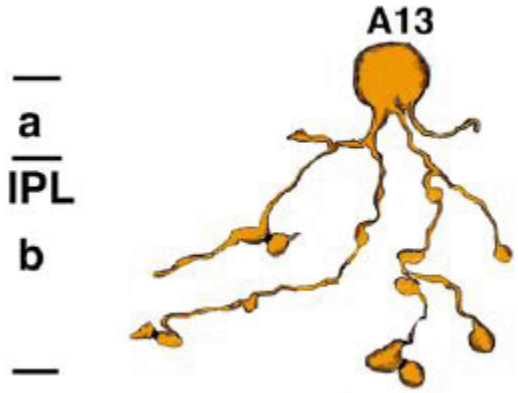

Movie 3. Animation of the wiring pattern of the A13 amacrine cell.
Download video

A20 cells, running in upper stratum 2 of sublamina **a**, have slightly different synaptic relationships with other nerve cells in the neuropil from A19, which will be remembered, sits on the sublamina **a/b** border (Fig. 27). Thus, A20 receives some cone bipolar inputs in stratum 1/2 and 2 (7%), but they are dominated by amacrine cell inputs (93%). Much of this input is recognizable as being from lobular appendages of rod AII cells. A20's output is about equally as reciprocal synapses to bipolar cells (5%) and synapses to amacrine cells (5%), but the cells have major output to alpha ganglion cells of sublamina **a** (90%). The latter ganglion cells would be OFF-center types, of course.

Both A19 and A20 cells are probably involved in the transfer of fast messages from one area of retina to another. They may be the basis of the proximal negative response recordable in the intraretinal ERG and in the shift effect in Y-type ganglion cells.

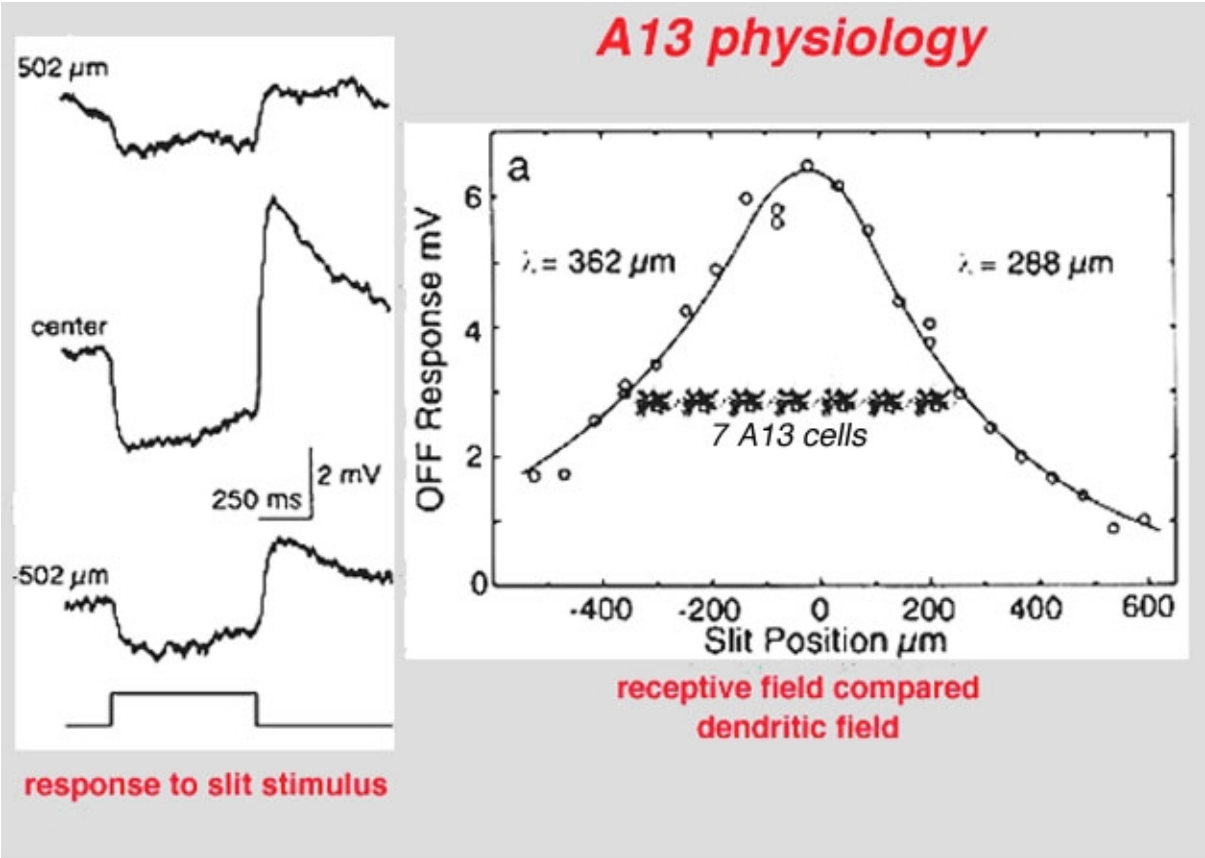

Figure 20. Physiology of the A13 amacrine cell.

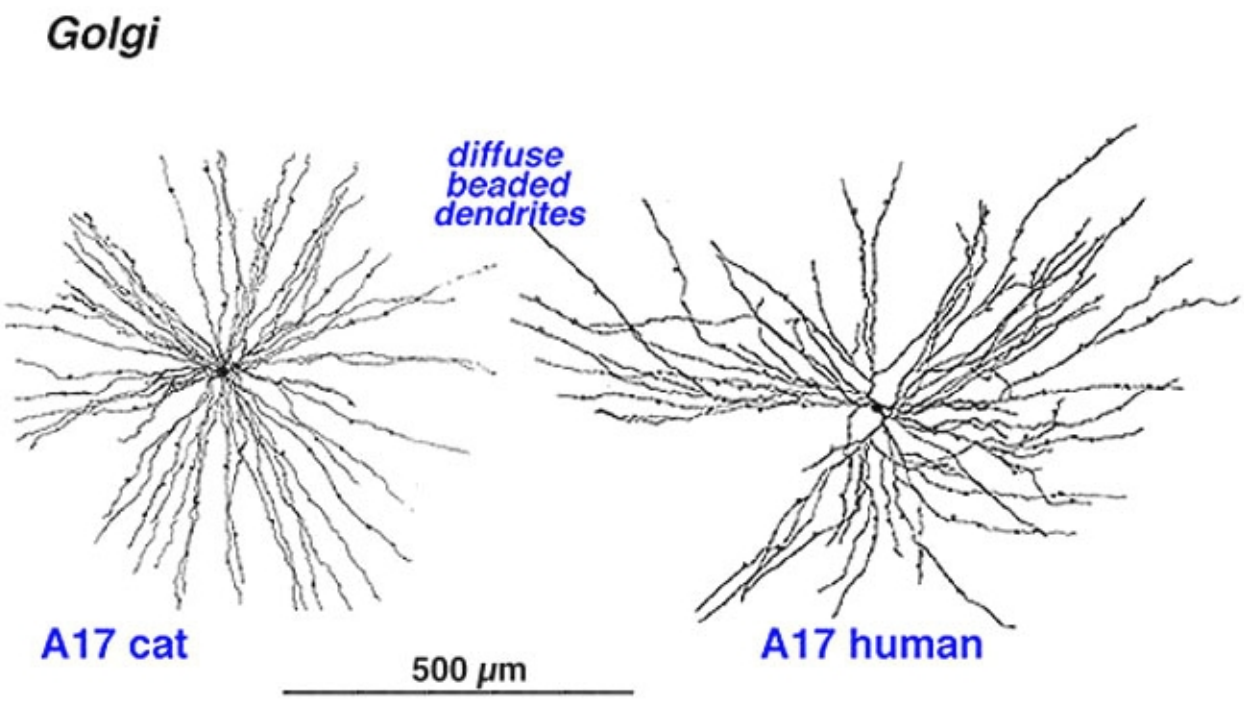

Figure 21. Golgi staining of A17 amacrine cells.

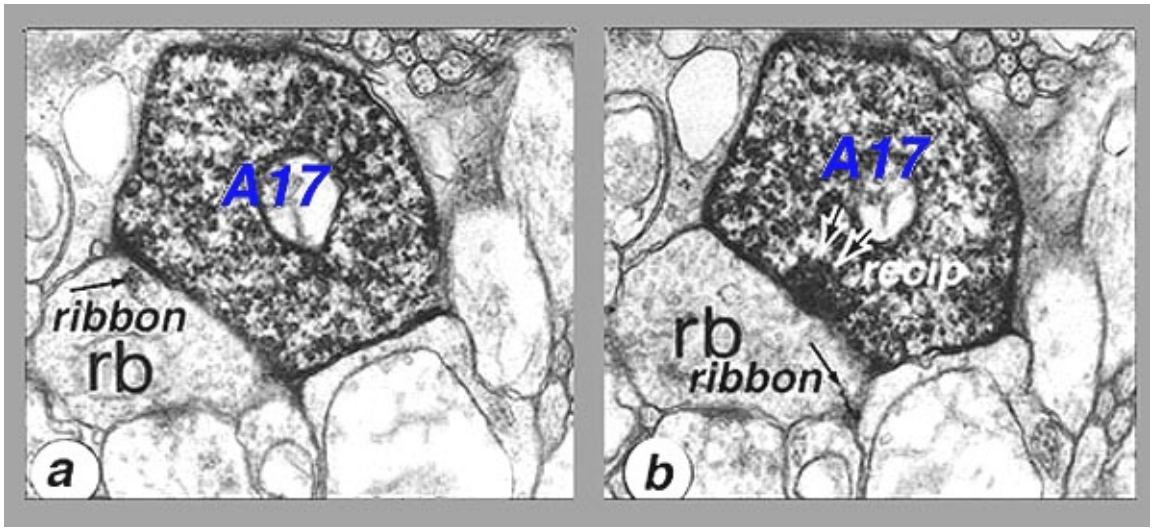

Figure 22. Electron micrograph of reciprocal synapse.

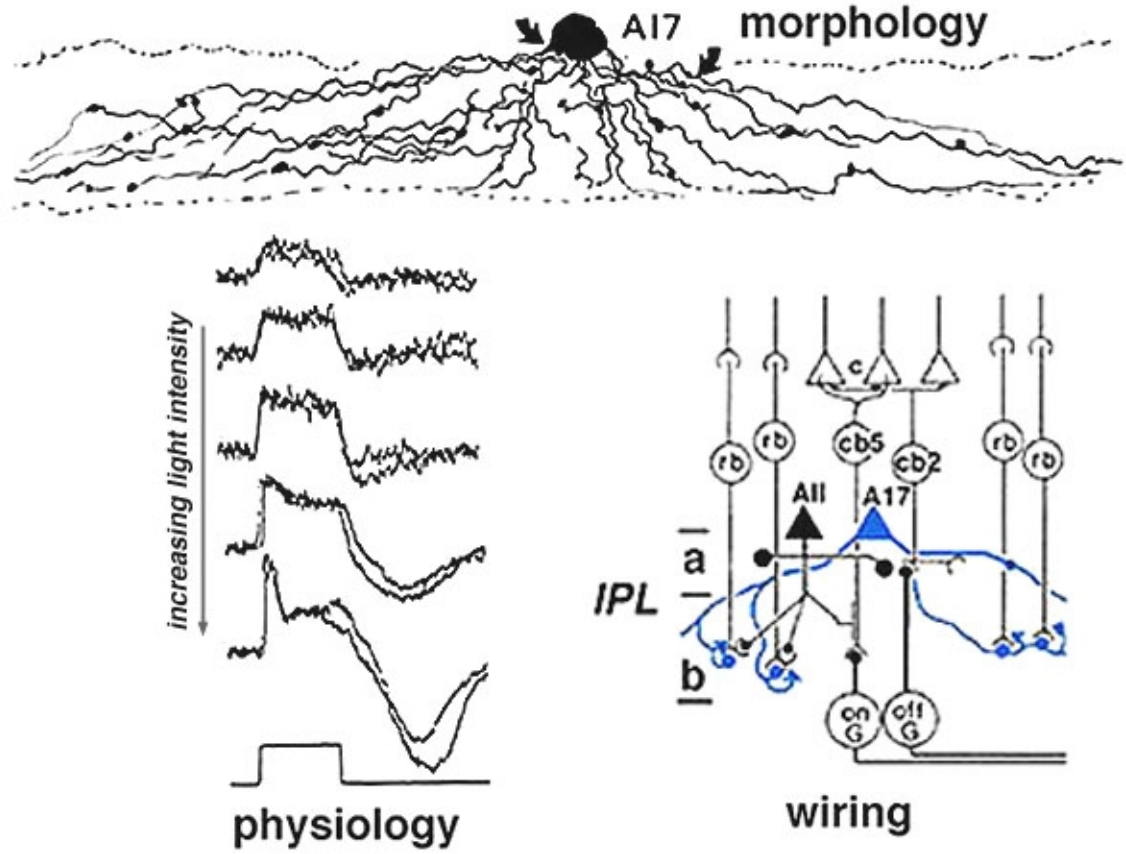

Figure 23. Summary diagram of the morphology, physiology, and wiring pattern of the A17 amacrine cell.

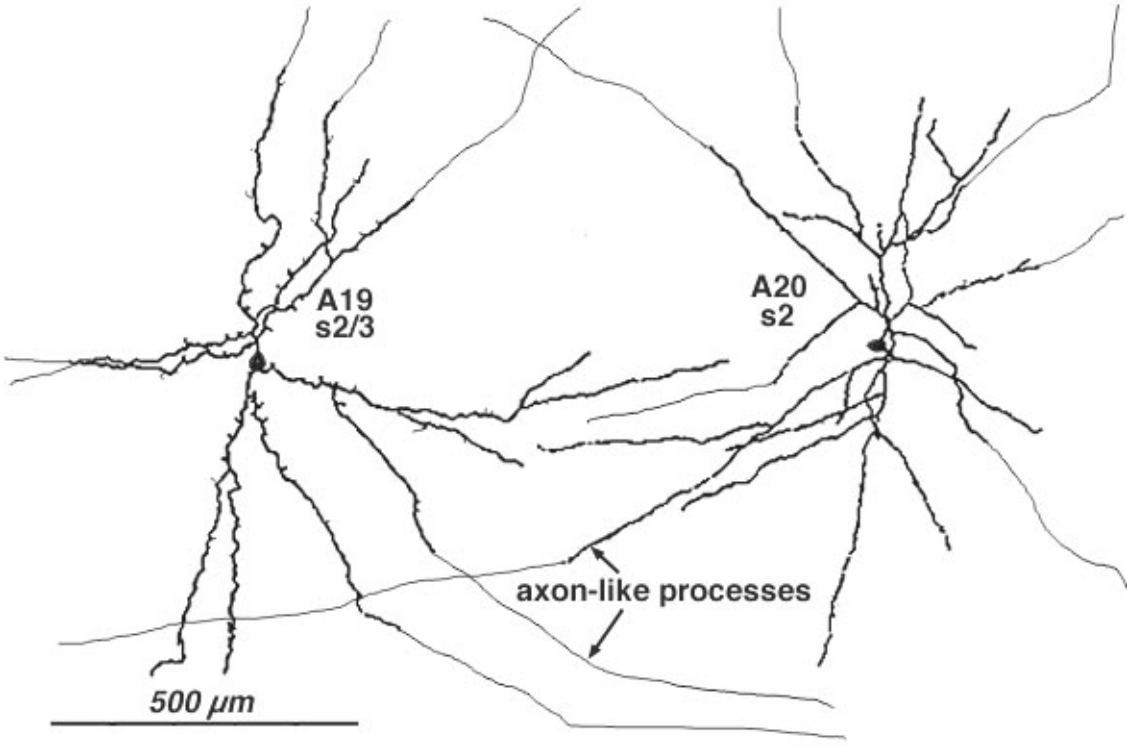

Figure 24. A19 and A20 amacrine cell subtypes.

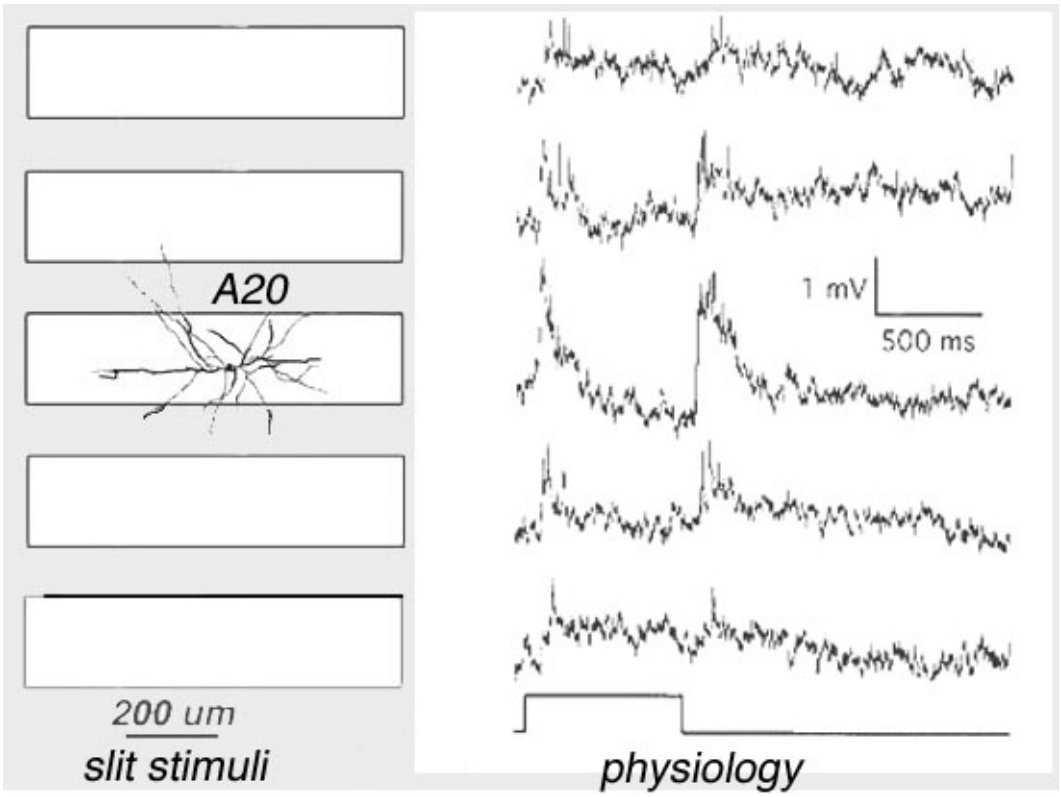

Figure 25. Physiological responses of the A20 amacrine cell.

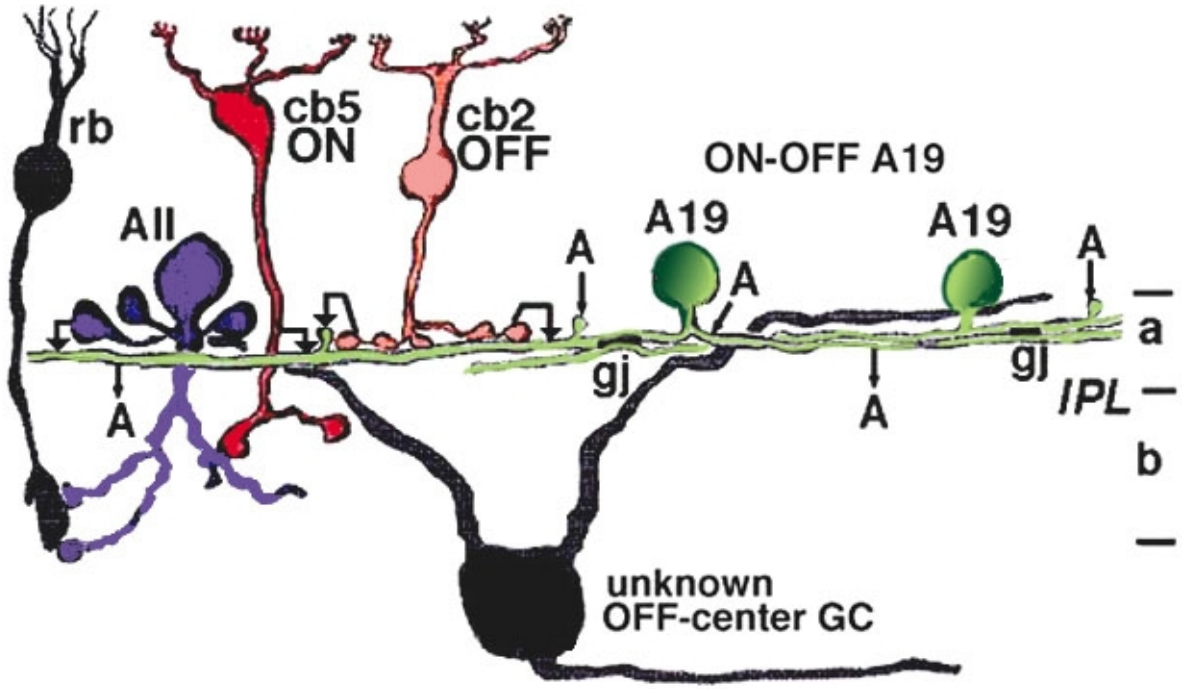

Figure 26. Wiring diagram of the ON-OFF A19 amacrine cell.

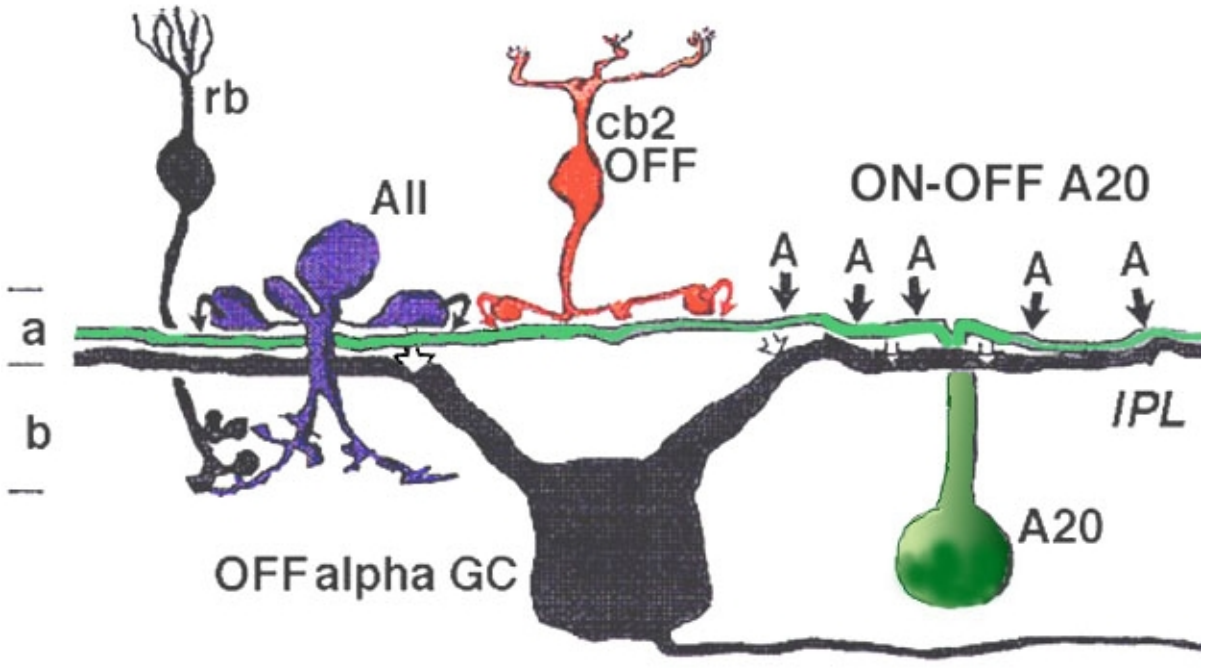

Figure 27. Wiring diagram of the ON-OFF A20 amacrine cell.

A22: A Putative Substance P-containing, ON-OFF Neuron of the Cone System

Immunocytochemical staining with antibodies against the neuropeptide substance P (SP) reveals a large-field amacrine cell in human retina (41). The SP-containing amacrine is possibly equivalent to the wide-field A22 cell of cat that has been intracellularly recorded as an ON-OFF cell (Fig. 27) (40).

SP-containing and A22 cells are wide-field amacrine cells (dendritic trees of 500-µm span), often having large cell bodies (14-16 µm) displaced to the ganglion cell layer, with their major dendritic stratification in strata 3 and 4 of sublamina **b** of the IPL. Both cells have long axon-like processes that pass up into sublamina **a** to run for up to 1 mm and also down into stratum to run over ganglion cell bodies. Their major dendrites are covered with spines (Fig. 28).

Electron microscopy shows that the spines are postsynaptic with reciprocal synapses to cone bipolar cells. They also receive synapses from unidentified amacrine cells and other SP-IR cell dendrites. They are presynaptic to ganglion cell dendrites and directly to ganglion cell bodies (possibly some of the latter are of SP-IR ganglion cells). Their axonal processes are presynaptic to amacrine and ganglion cells in stratum 5 and in stratum 1 of the IPL. Probably the latter ganglion cells are OFF-center (see above). They receive cone bipolar input from a cone bipolar type in stratum 1 of the IPL. Almost certainly A22 cells, SP-IR amacrine cells of cat and human, are GABAergic (42). This ON-OFF cell probably plays a similar role as the A19 and A20 cells above in being recordable in the proximal negative response (PNR) (43) and being involved in fast-moving aspects of visual coding (Fig. 29).

A18: The Dopaminergic Amacrine Cell

The dopaminergic amacrine cell types have been revealed by immunostaining with an antibody directed against tyrosine hydroxylase (TOH) (the rate-limiting enzyme for dopamine) and are wide-field cells that stratify almost exclusively in stratum 1 of the IPL (under the amacrine cell bodies). It has been identified with A18 cells or type 1CA (CA = catecholamine) of the Golgi studies (2, 10). Their dendrites form a densely packed network of processes leaving only few "rings" for other amacrine cell bodies and major dendrites to pass through. The rings are are beaded dendrites that appear to be synaptic points on amacrine cells, particularly the AII amacrine cell of the rod system (Fig. 30). Another feature of dopamine cells is only seen after dye injection (44) or immunostaining (45) (Fig. 31), and this that their dendrites emit long, axon-like processes running in different strata of the IPL, in the ganglion cell layer and sometimes into the outer plexiform layer (OPL).

A second type of dopaminergic cell has been described in the monkey and human retinas (28, 46). This type 2 CA cell is described as a "wispy" cell in Golgi studies (10) (Fig. 32).

There is still not a convincing electrophysiological study of the dopamine cell in the mammalian retina. However, in turtle and fish retinas, the equivalent to type 1 CA cells is an ON-center cell. In turtle, the cell gives as light ON transient, which continues as a sustained depolarization during the light ON. At light OFF, it has a very distinct, slow, sustained hyperpolarization that lasts for several seconds. The increasing spot sizes bring out the depolarizing ON-plateau, whereas with an annulus, a sustained OFF-surround is evident (see Fig. 33a) (47).

Synaptic relations of Type 1 CA cells have been studied by electron microscopy. This amacrine makes most of its synaptic arrangements in stratum 1 of the IPL as would be predicted from its branching pattern. Sparse cone bipolar input occurs to the cell's primary dendrites in stratum 1. The cone bipolar input is either from a diffuse cone bipolar that has axons in startum 1 or else from giant bistratified cone bipolar cells known to be present in cat and monkey retinas. Both bipolar types are probably hyperpolarizing (OFF-center) in response. Thus, the fact that the dopamine amacrine cell is a depolarizing ON-center cell makes the OFF-center bipolar input difficult to understand. Both the cell body and primary dendrites in stratum 1 of the IPL also receive GABAergic

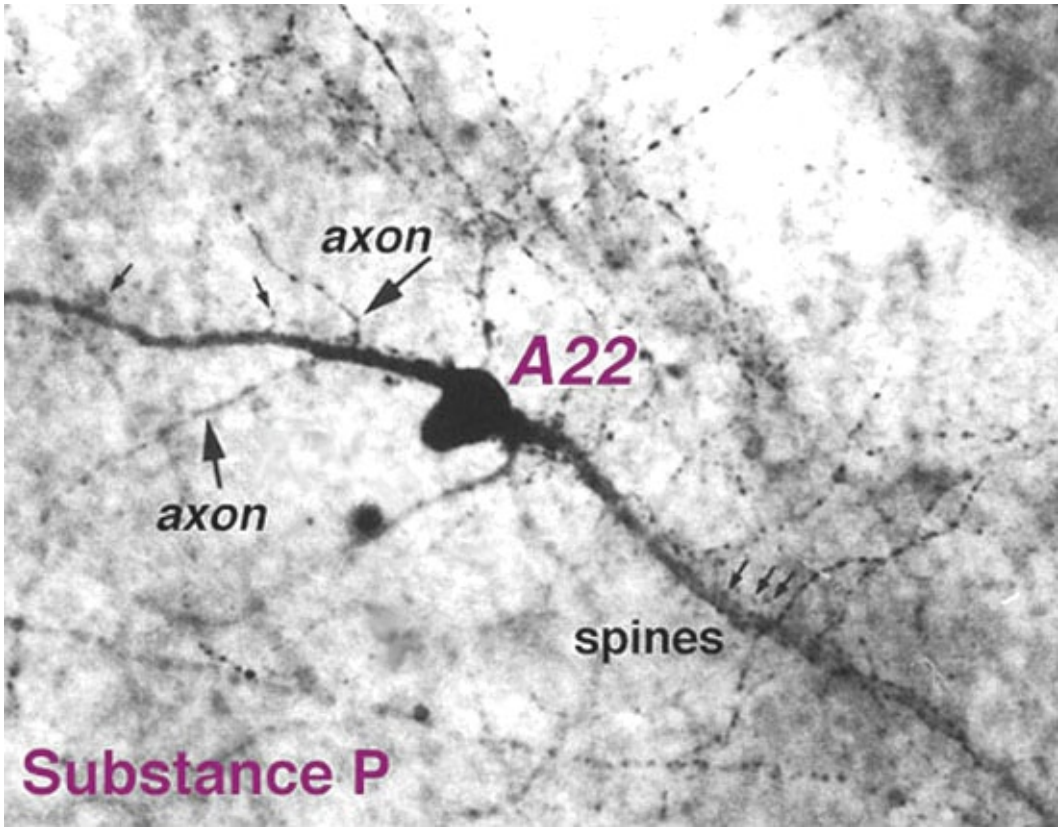

Figure 28. Substance P-containing amacrine cell in human retina.

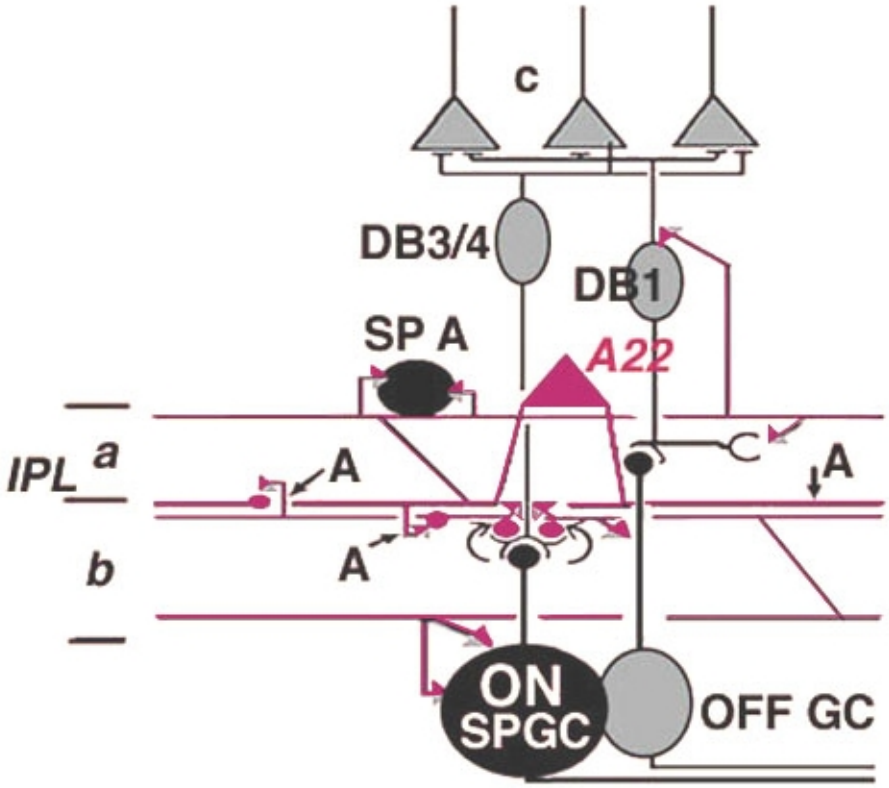

Figure 29. Diagram of the organization of the A22 amacrine cell.

and glycinergic amacrine cell inputs. Therefore, it has been suggested (48) that the GABAergic amacrine input comes from a GABAergic amacrine intermediary between the OFF-center bipolar and the dopamine cell, thereby giving the dopamine cell its ON-center response (Fig. 33b). The major output of the A18 cell is in the fine network of dendrites and axon terminals surrounding the cell bodies and apical dendrites of AII and A8 cells (25). The rings of dopamine processes surround many unfilled, stained cell bodies (Fig. 31). So we also think it probable that the dopamine cell in the mammal makes ring contacts upon both A17 and A13 cell bodies and main dendrites in stratum 1 of the IPL (Fig. 33b). Dopamine cell axons also contact AII dendrites in sublamina **b** of the IPL, and the few processes that run into the OPL make synapses upon the GABAergic interplexiform cell (25).

Dopamine cells in the fish retina are true interplexiform cells (IPC) and have profuse arborations in the inner nuclear layer and very extensive synapses upon the three types of horizontal cells. In the inner plexiform layer, the dopamine IPC makes some synaptic connections with the Mb (rod-dominated) bipolar axon terminals (49) (Fig. 34a).

Dopamine IPCs are thought to be influential upon the horizontal cells by decreasing their light responsiveness (50) and modulating their spatial extent by uncoupling their gap junctions (51). Horizontal cells in all retinas are joined by gap junctions in a strong syncytium (52) (reviewed by Negishi et al. (53)). Dopamine uncouples horizontal cells from the syncytium by interacting with D1 receptors, on the horizontal cell bodies and dendrites, linked to the second messenger cyclic AMP (see Dowling (54) and Witkovsky and Dearry (55) for reviews on dopamine effects in the retina). In the mammalian retina, a similar but lesser amount of uncoupling of horizontal cells due to dopamine has been reported (56, 57) (Fig. 34b).

The dopamine cell is, however, primarily an amacrine cell and not an interplexiform cell in the mammalian retina; thus, their effect on inner retina circuitry would be expected to be more pronounced than on the outer retina. We know that ganglion cells have their spiking properties variously altered by dopamine and by agonists and antagonists of dopamine and D1 receptors (58-61). These neuromodulatory effects are thought to occur via amacrine intermediaries, particularly the AII cell, or by diffusion of dopamine transmitter from a distance to ganglion cell bodies and dendrites, because there are no direct contacts of dopamine amacrine cells and ganglion cell dendrites. Both D1 and D2 receptors have been seen upon some ganglion cell bodies (62-64). The second effect of dopamine in the inner retina is thought to be upon amacrine cell coupling via gap junctions, somewhat analogous to the effect upon gap junction between horizontal cells in the outer plexiform layer. Dopamine uncouples AII amacrine cells in the mammalian retina, mediated through a D1 receptor (see above) (65, 66).

ACh Amacrines: Mirror Symmetric Starburst Cells

Golgi studies and intracellular Lucifer yellow staining has revealed amacrine cells that are known to use acetylcholine as a neurotransmitter (67). These cells have also been called "starburst" amacrine cells and are particularly striking in appearance in turtle, rabbit, and ground squirrel retinas (32, 68-71) (Fig. 35 and Fig. 36).

ACh amacrines occur as two mirror symmetric pairs of cells. One type, ACh-a type, has its cell body in the amacrine cell layer, and its dendrites stratify in stratum 2 of sublamina **a.** The other type, ACh-b type, has a cell body displaced to the ganglion cell layer, and its dendrites stratify in stratum 4 of sublamina **b.** ACh-b cells are medium-field in size but have a tremendous overlap of their dendritic trees such that as many as 70 cells overlap a single central cell in peripheral retina (33, 71). ACh-a type cells have slightly larger dendritic tree sizes (13% larger), and their overlap values can reach 90 or more (24). The ACh cells in the human retina are similar to those in rabbit but less dramatic in shape and branching pattern (see below). ACh starburst cells are particularly striking in the turtle retina, where the mirror symmetric amacrines are arranged in an essentially one-to-one relationship (Fig. 37a and Fig. 37b) (see a rotation of the mirror symmetric starburst cells).

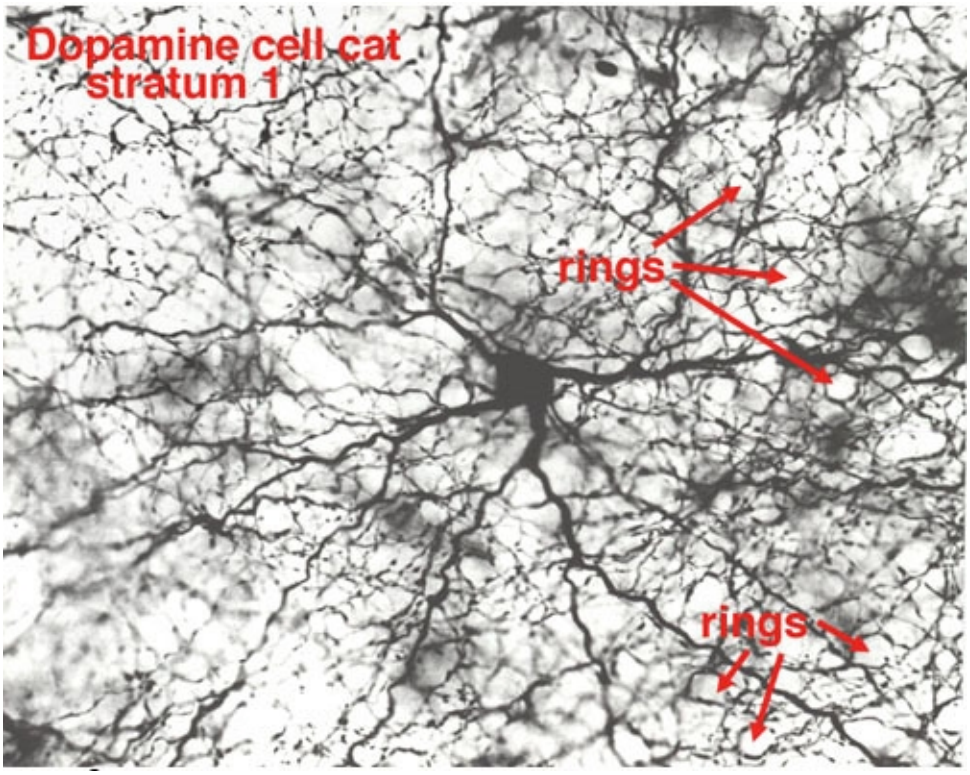

Figure 30. Immunostaining with antibodies to TOH. A18 amacrine cells stain and have overlapping dendrites that form into rings.

Golgi ACh-containing starburst amacrine cells of the rabbit retina have been extensively studied by electron microscopy (72). Cone bipolar and amacrine cell inputs are distributed irregularly over the entire dendritic tree, but the proximal dendrites to the cell body, containing small spines, are particularly choice for bipolar input. A small amount of AII amacrine input may occur to the proximal dendrites of the ACh-a type cell. The varicosities on the distal dendrites (see above) are the only sites of synaptic output to ganglion cells. The postsynaptic ganglion cells for both ACh-a and ACh-b type cells, are thought to be ON-OFF directional selective bistratified ganglion cells (32, 66, 71-75). Additionally, the monostratified ON-directionally selective ganglion cell may be postsynaptic to the ACh-b type cell (72) (Fig. 38).

Both mirror symmetric pairs of starburst cells of the rabbit retina have been intracellularly recorded from and dye marked by Bloomfield (21). The a-type of the pair is an OFF-center cell, giving a transient burst of small spikes at light off, whereas the ACh-b type is an ON-center cell (Fig. 38, top traces, above). Both types have antagonistic surrounds (Fig. 38, bottom trace).

ACh amacrine cells are thus thought to be involved in the generation of directional selectivity (DS) in certain retinal ganglion cells, particularly in rabbits and turtles with visual streak topography. They may not be as well developed in form and function in foveal-based retinas, such as cat and human (Fig. 39).

DAPI-3 Cells in the Rabbit Retina

In 1997, another bistratified, medium-field amacrine cell that is nucleus stained with DAPI was revealed by intracellular dye injection of Lucifer yellow. It was given the name DAPI-3 (76). Since then, the DAPI-3 cell has also been revealed by the fluoresecent rhodamine probe used by MacNeil and Masland (8) (see Fig. 4a, Roles of amacrine cells) and glycine immunoreactivity in the rabbit and ground squirrel retinas (77, 78). DAPI-3 cells are medium-field in size, i.e.. have a 100-μm field diameter and a profusion of overlapping dendrites, as seen in whole-mount views (Fig. 40b) that prove to be the two tiers of branches of a bistratified cell (Fig. 40d). One of

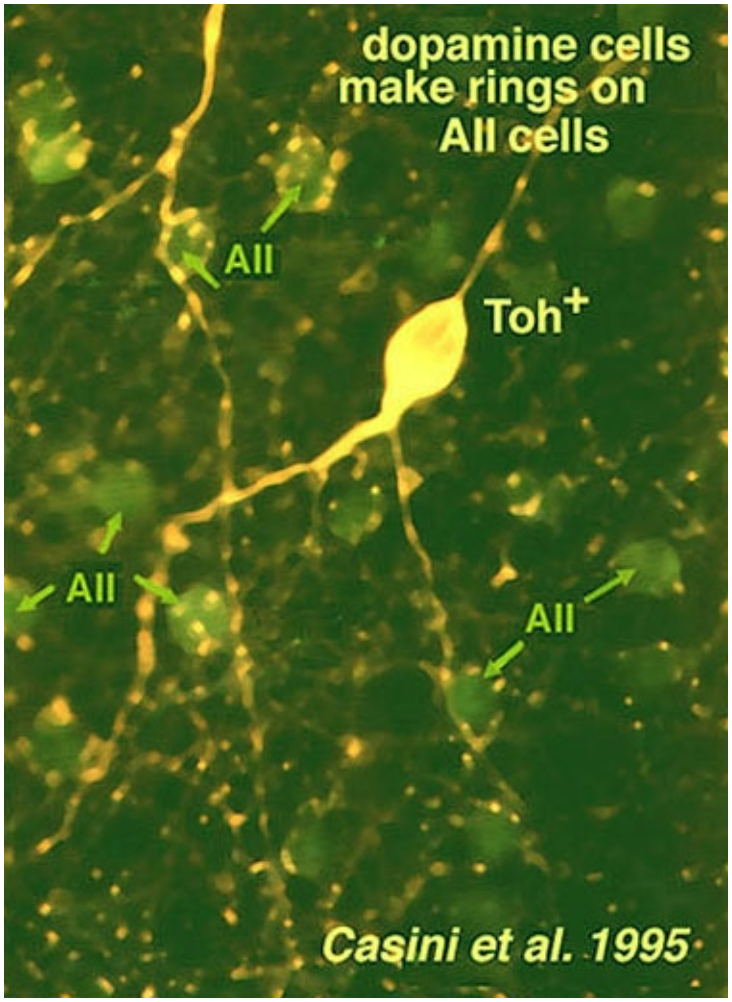

Figure 31. Dopaminergic and AII cells. From Casini et al. (82).

the tiers of dendrites in sublamina **a** run just below the ACh-a type (starburst a type), and the other tier run in sublamina **b**, just above the ACh b type (starburst b type) cells (Fig. 40d).

The DAPI-3 cell proves to be glycinergic and can be stained with the glycine transporter (Fig. 40c, green). It is also immunopositive for $GABA_A$ receptors (Fig. 40c, red). Thus, the cell appears to be orange in the figure (Fig. 40c, red and green combine to make orange-stained cells with a blue DAPI nucleus, arrows). The starburst ACh cells stains with CHAT in Fig. 40d, and the overlapping dendrites of the DAPI-3 cell stained for $GABA_A$ receptors are juxtaposed to the cholinergic cell's dendrites.

Zucker and Ehinger's (79) nice study on the DAPI-3 cells and immunostaining with the glycine and $GABA_A$ transporter/receptors allowed them to draw a summary diagram of the probable manner on which the DAPI-3 amacrine cells interact with the starburst ACh cells (Fig. 41). The DAPI-3 cell is acetylcholine receptive at nicotinic and muscarinic synapses and feeds back upon the starburst cell via a glycinergic synapse (glycine receptors have been identified on starburst cells). The DAPI-3 cell also contacts the cone bipolar cell that has input to the starburst cell. We know the starburst cell contains GABA in addition to acetylcholine, and the starburst cell can presumably feed forward to the DAPI-3 cell at a GABAergic synapse with $GABA_A$ receptors on the DAPI-3 cells. The starburst cell is known to synapse upon a directionally selective ganglion cell type in rabbit retina (Fig. 41). It is not clear yet whether the DAPI-3 cell exists in other mammals that do not have a pronounced visual streak as does the rabbit.

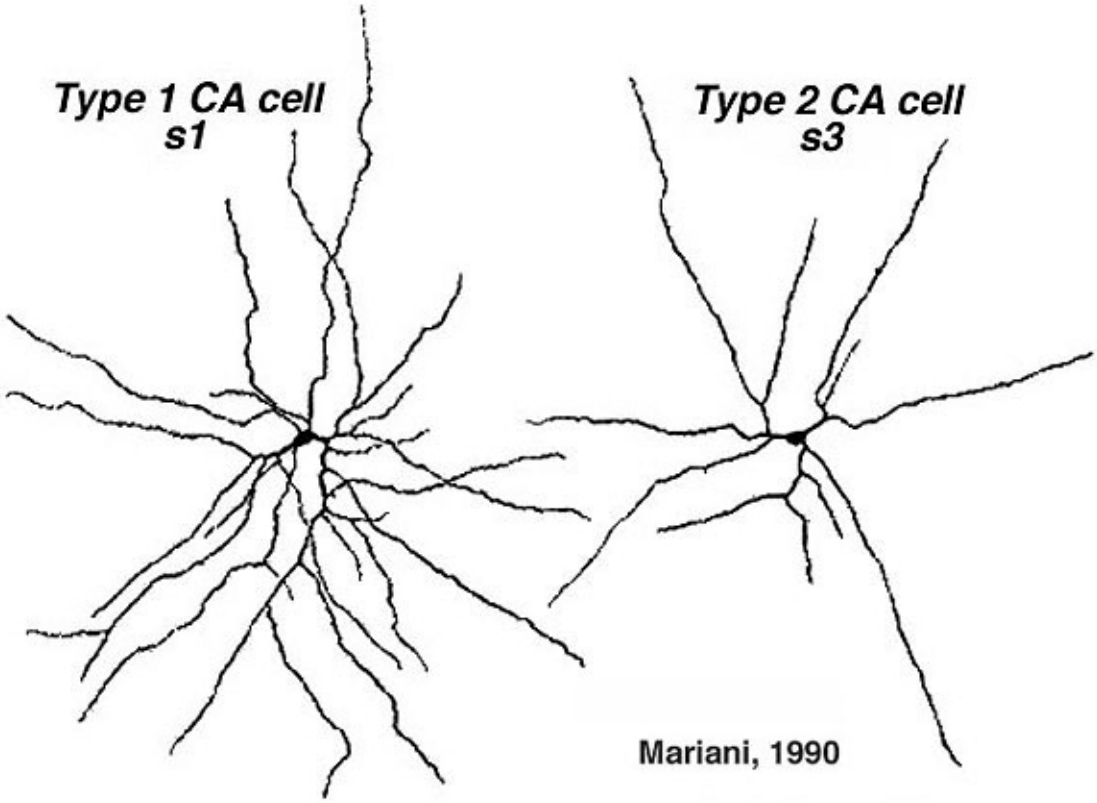

Figure 32. Types of dopaminergic cells.

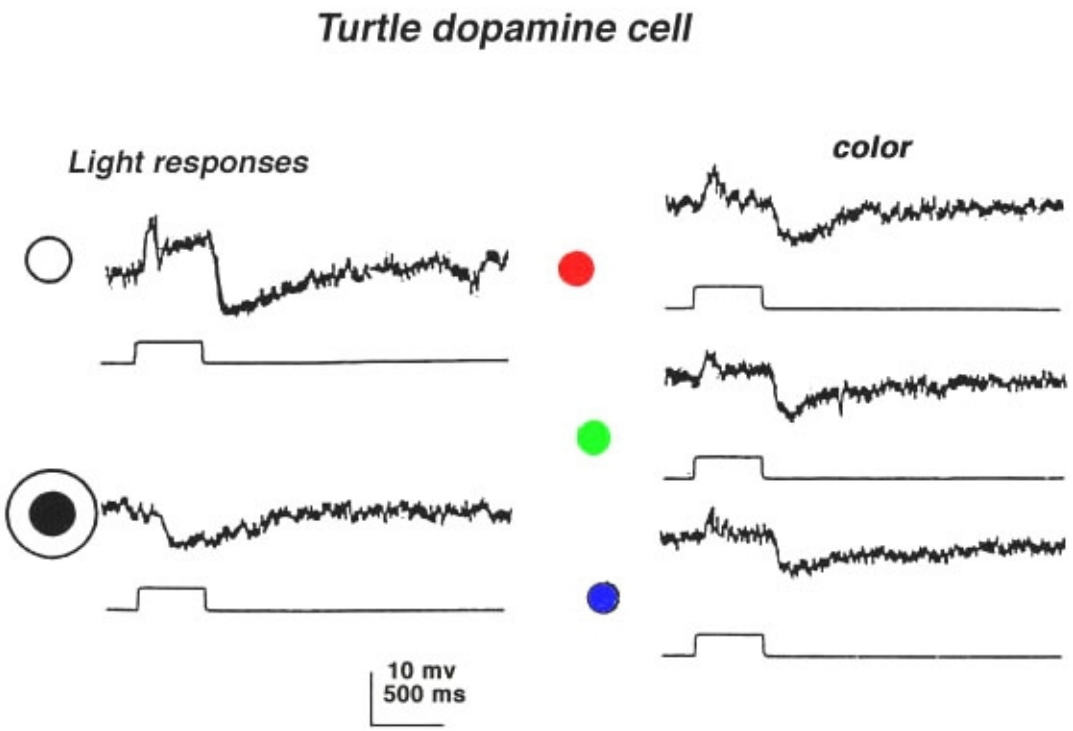

Figure 33a. Light responses of the dopaminergic amacrine cell in the turtle retina (47).

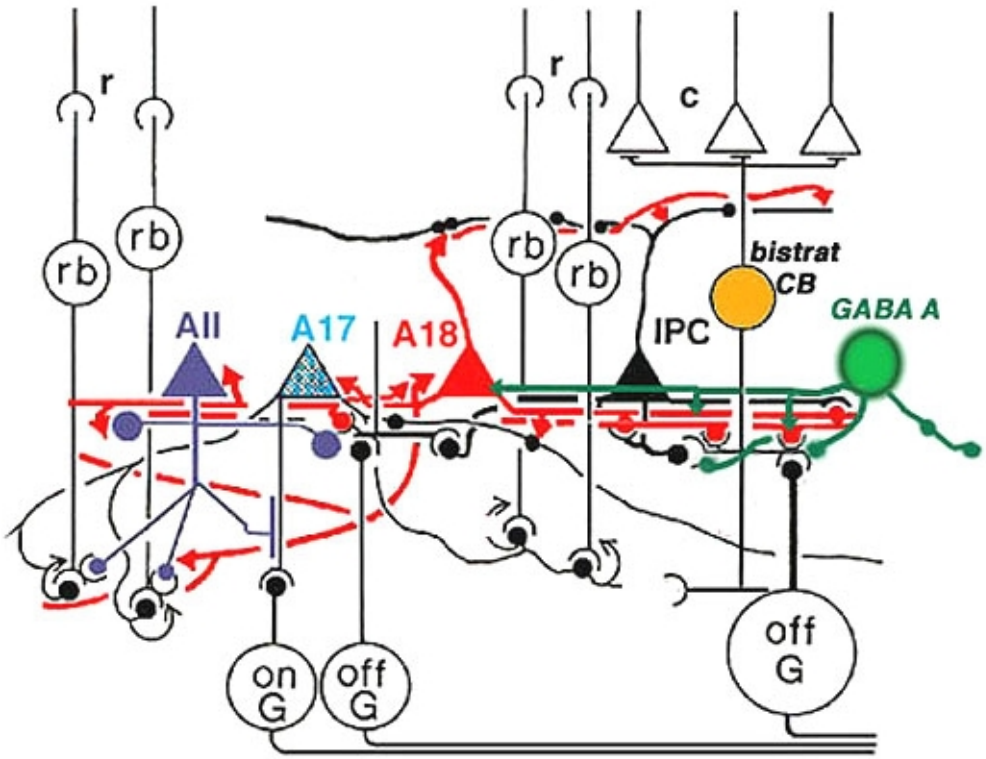

Figure 33b. Wiring diagram of the A18 amacrine cell.

Midget System Amacrine Cell

The calcium binding protein calretinin is found in three types of amacrine cell in the monkey and human retinas (80). The most numerous population are the AII amacrine cells, but a small- to medium-field diffuse amacrine cell and a large-field, stratified A19 type are also calretinin immunoreactive (IR). Of these non-AII cell types, the small diffuse (or tristratified cell type, difficult to know which) is of particular interest.

Its appearance is shown in Fig. 42 (A, arrow) in immunostained slice preparations. The cell has a large cell body, but unlike the AII cells (Fig. 42, AII), many fine dendrites are given off the cell body instead of the typical AII thick primary dendrite. The dendrites pass down to all levels of the IPL as thin, beaded, and branched processes (Fig. 42, fine arrows). This small-field diffuse calretinin-IR cell is found in high numbers in the foveal, rod-free area of the retina and in lesser numbers in the peripheral retina. Electron microscopic examination of foveal diffuse calretinin-IR cells has shown that they get synaptic input from ON- and OFF-midget bipolar terminals, reciprocate synapses to these bipolars, and have synaptic output to ON-center midget ganglion cells (Fig. 43, wiring diagram). In more central to peripheral retina where rods are present, the diffuse calretinin-IR amacrines are probably also in synaptic interplay with both diffuse bipolar cells and larger parasol ganglion cells (Fig. 43). Because these calretinin-IR amacrines are found in the fovea and have particular relationships with the midget bipolar and ganglion cell systems, we have suggested that they may have a role in the antagonistic surround generation for midget ganglion cells. Moreover, they could also contribute to color opponency in these ganglion cells (80).

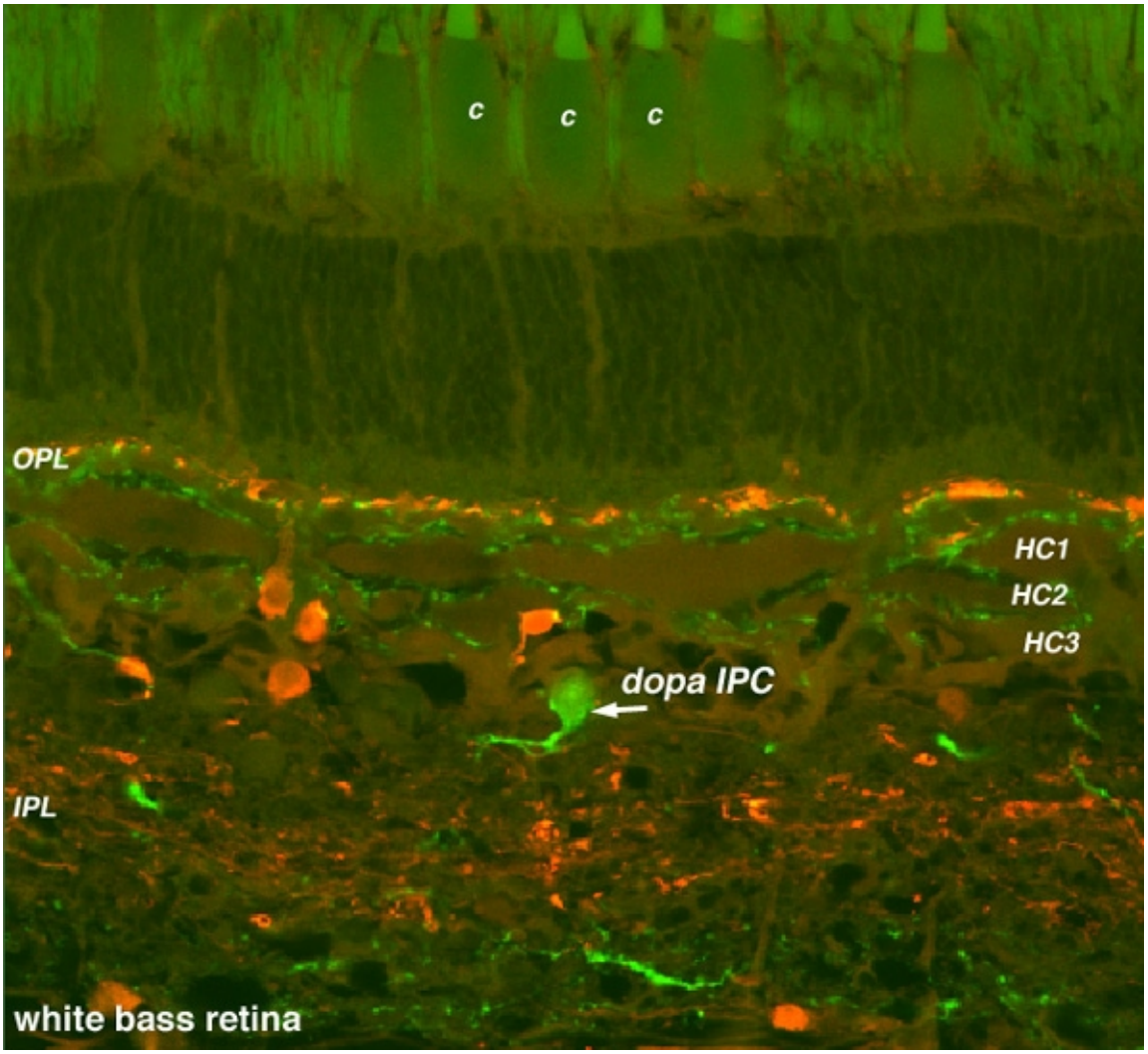

Figure 34a. The dopaminergic interplexiform cell of the fish retina.

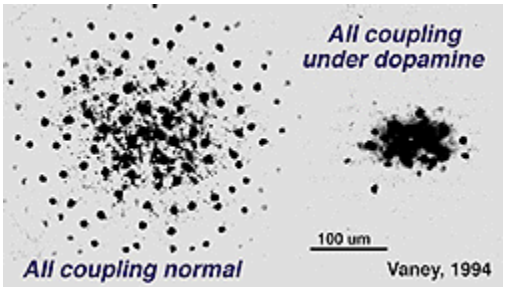

Figure 34b. Effects of dopamine on AII amacrine cell coupling.

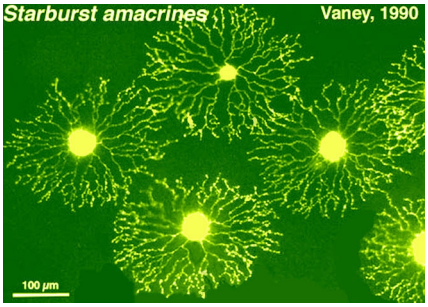

Figure 35. Starbust amacrine cells as stained with Lucifer yellow in whole-mount rabbit retina. From Vaney (32).

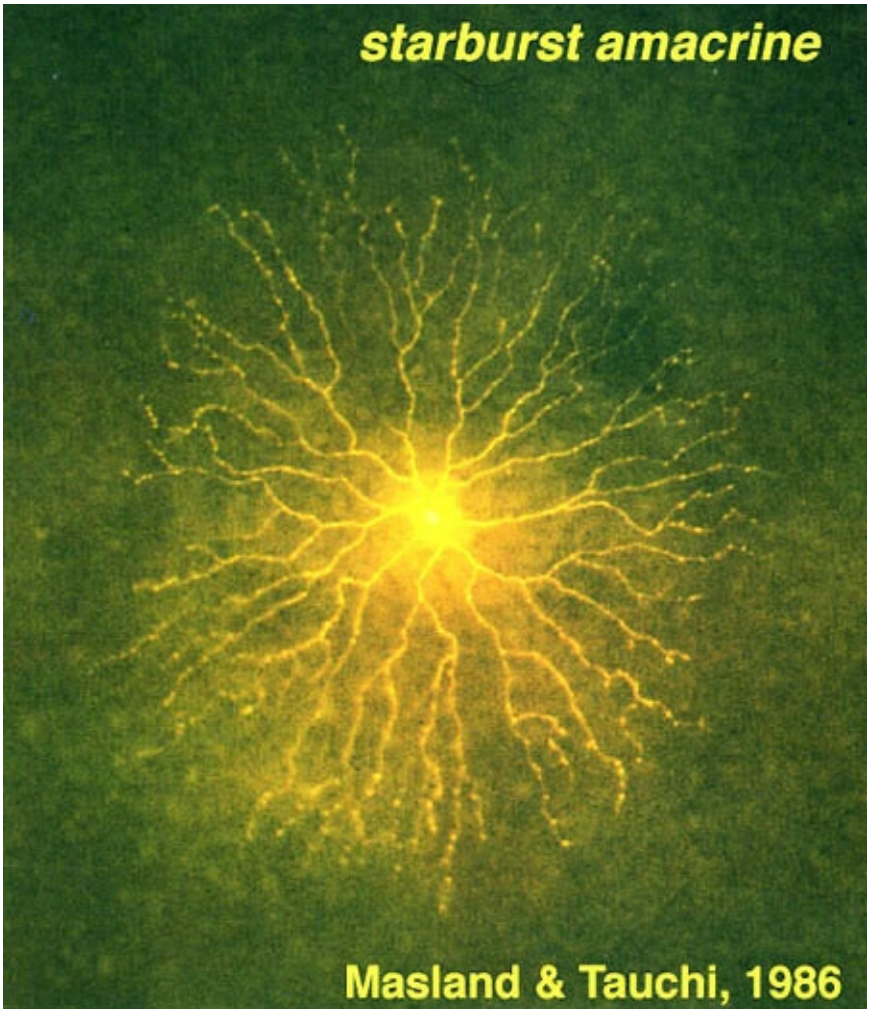

Figure 36. Lucifer yellow labeling of a starburst amacrine cell. From Masland and Tauchi (67).

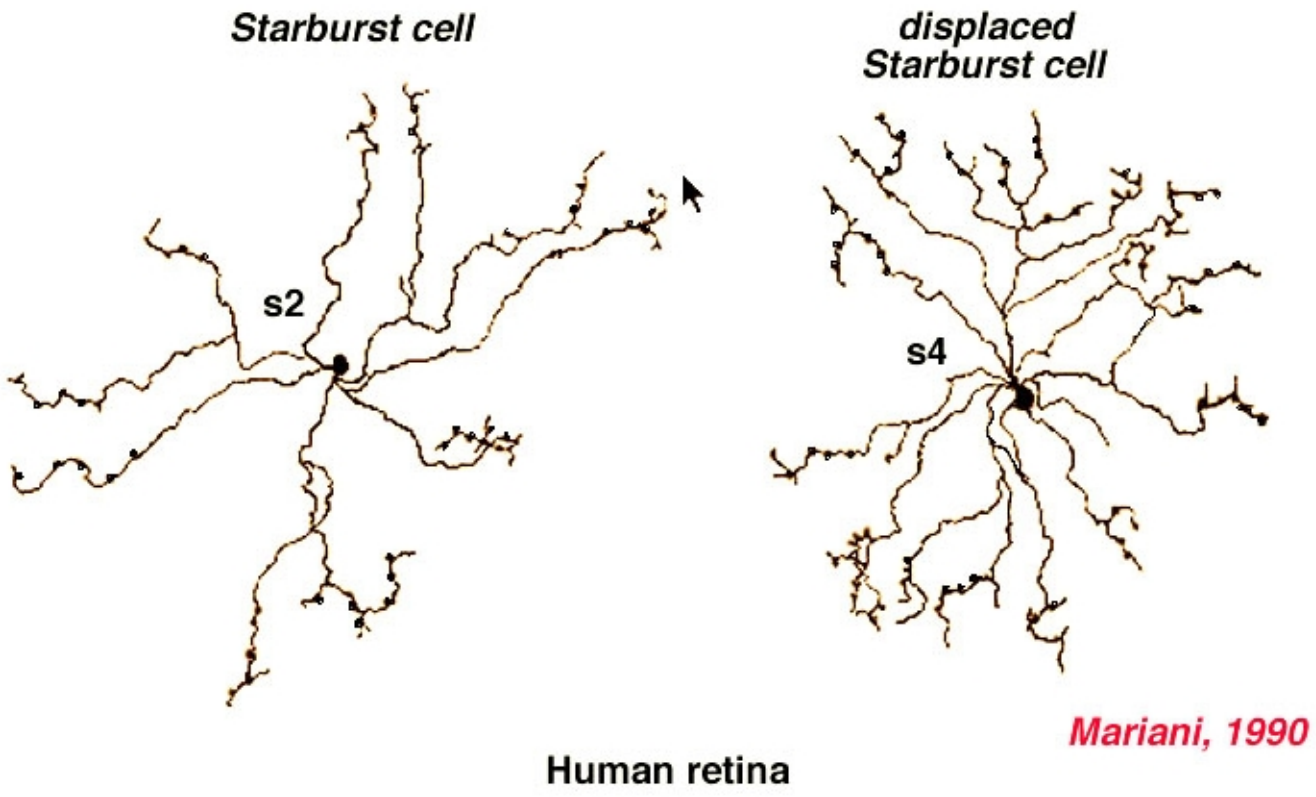

Figure 37a. Golgi staining of ACh-containing amacrine cells in human retina. From Mariani (10).

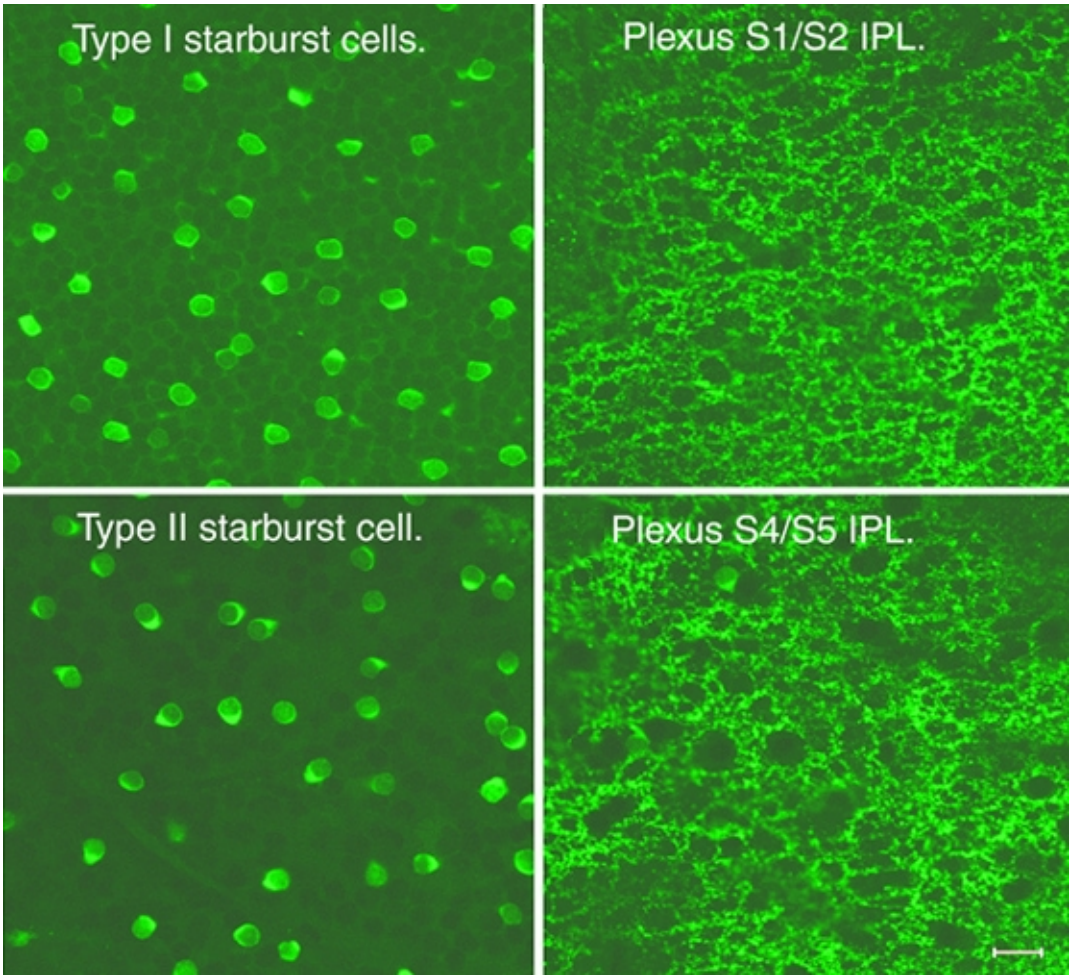

Figure 37b. Immunioabeling of a starburst amacrine cell with ChAT in turtle whole-mount retina.

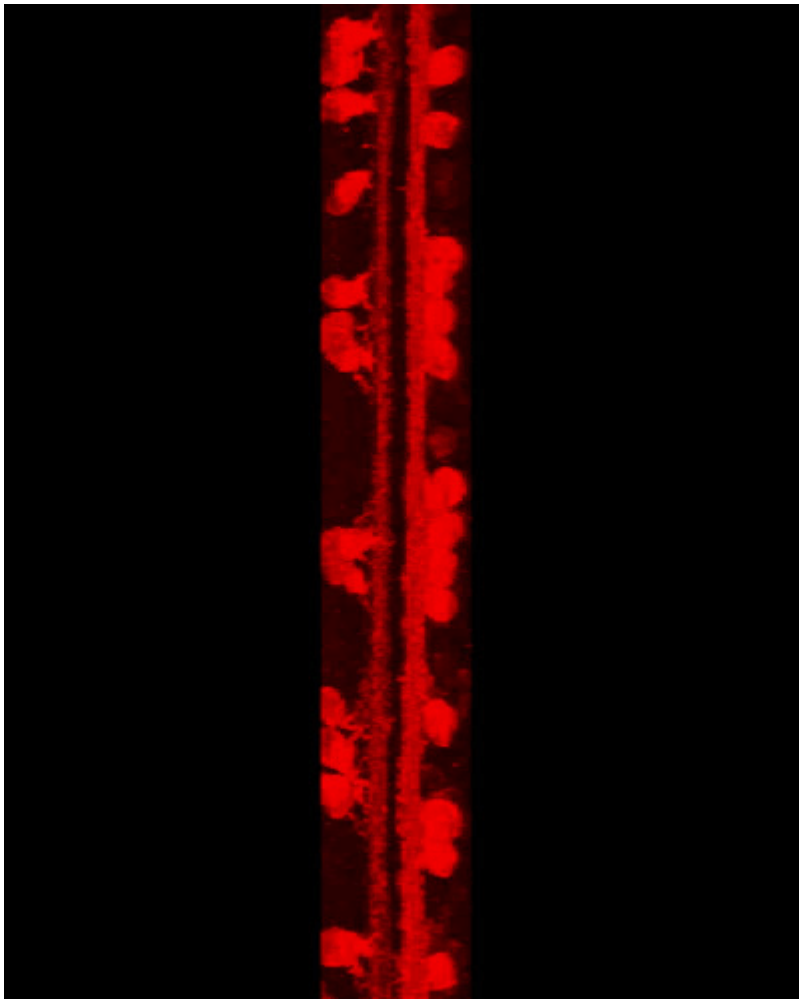

Movie 4. A rotation of the mirror symmetric starburst cells of the turtle retina. Immunostaining to ChAT. Courtesy Nicolas Cuenca.
Download video

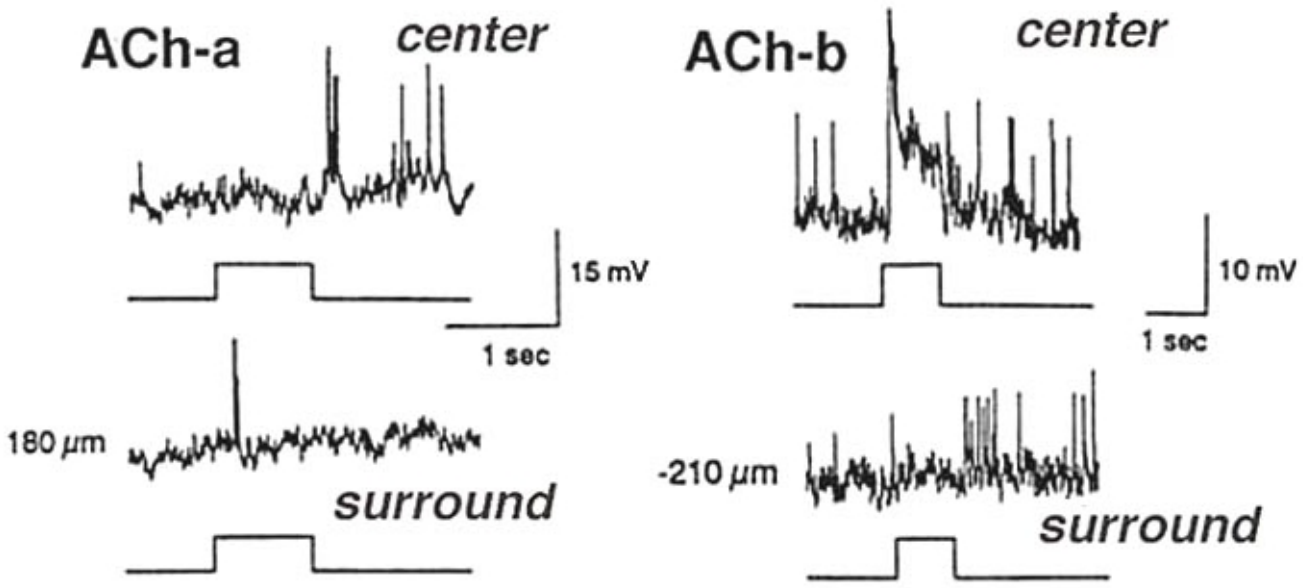

Figure 38. Intracellular recordings of ACh-containing amacrine cells. From Bloomfield (21).

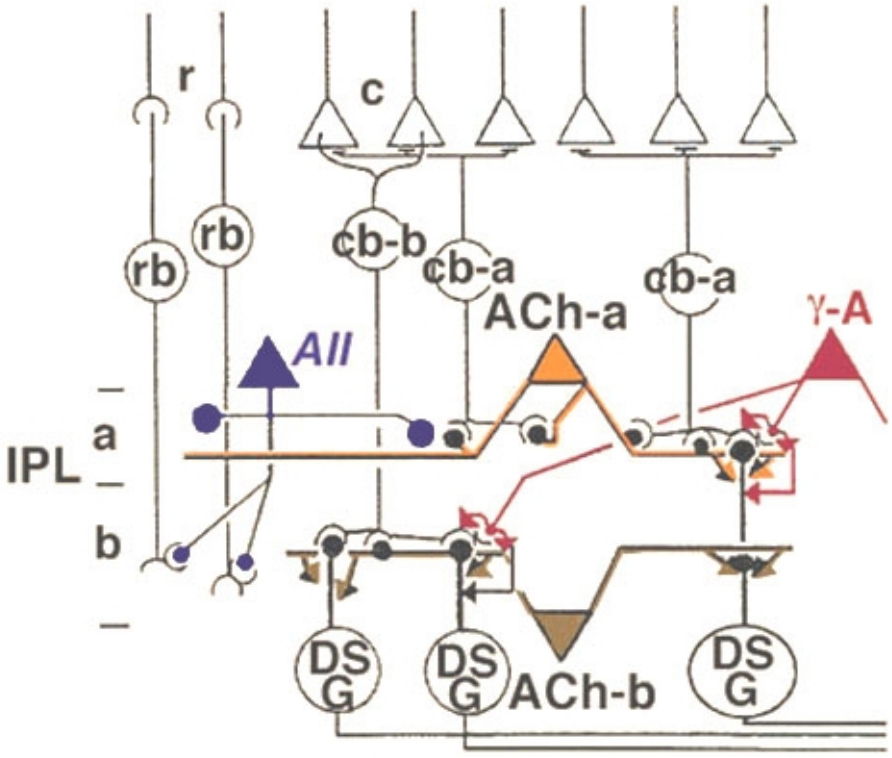

Figure 39. Wiring diagram of the two types of ACh-containing amacrine cells.

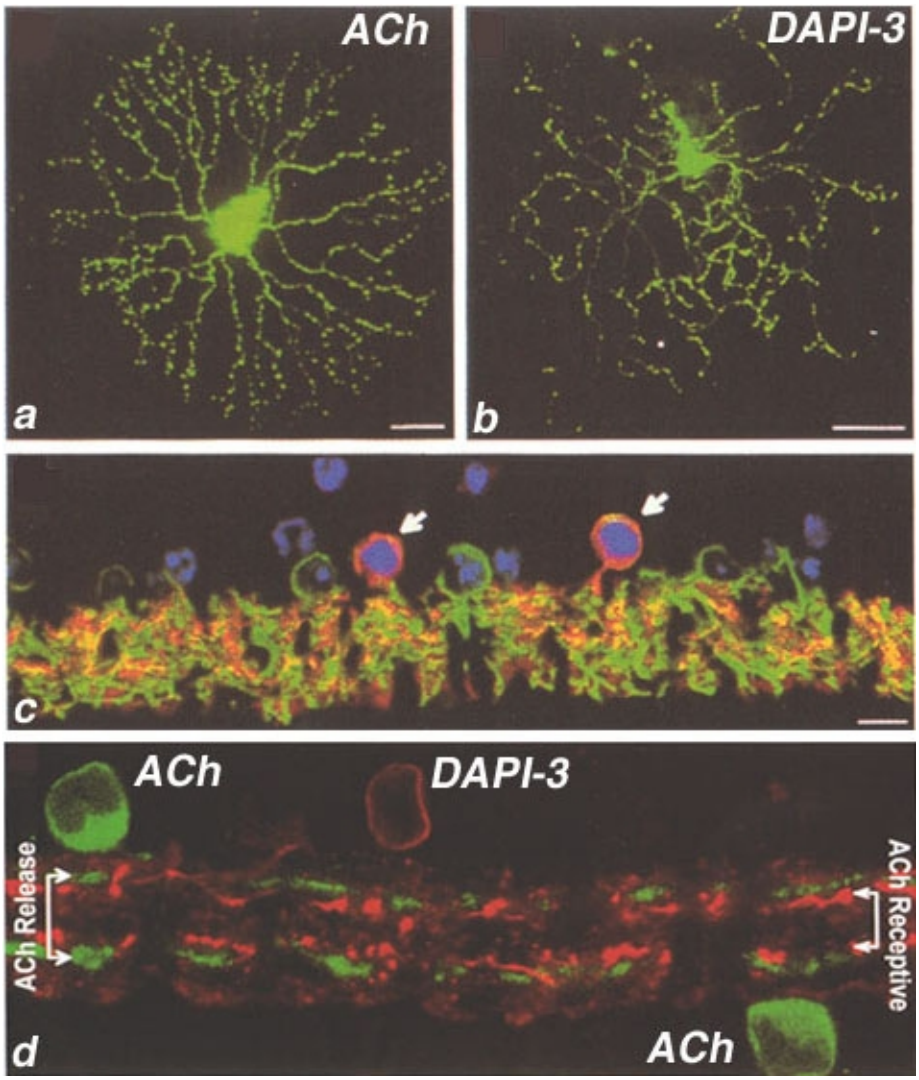

Figure 40. A comparison between DAPI-3 cells and cholinergic ACh cells. Adapted from Zucker and Ehinger (79).

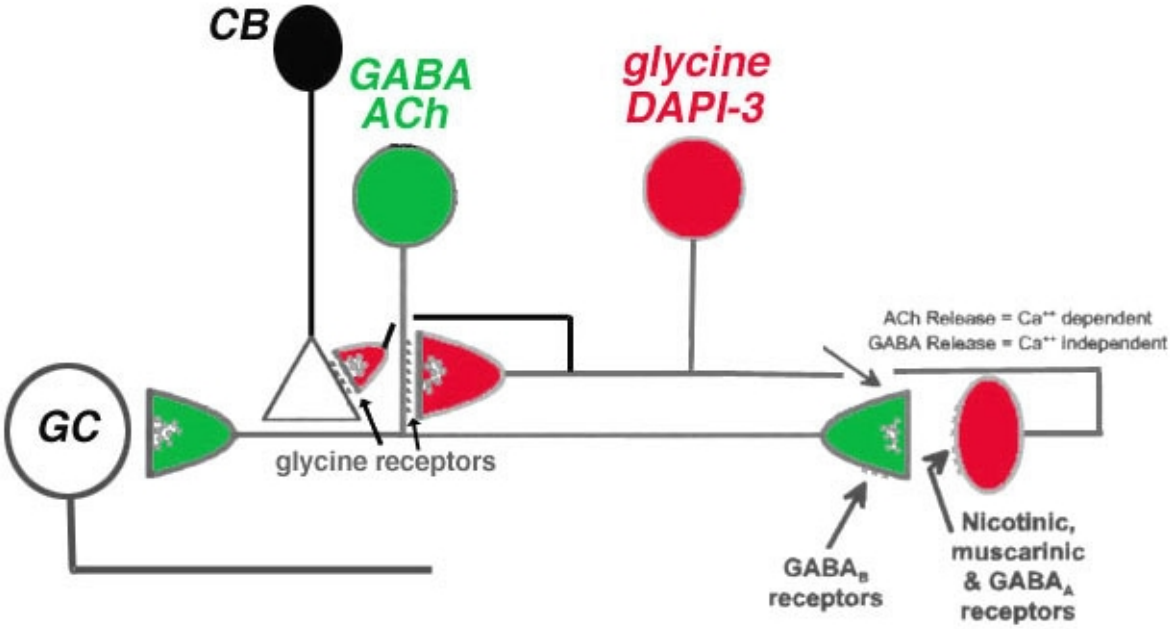

Figure 41. Wiring diagram of the DAPI-3 cell and its relationship to the ACh amacrine cell.

Figure 42. Cryostat sections of calretinin-IR monkey retina to show the different amacrine cell types that are immunoreactive. Three calretinin-IR cells are shown, of which only one has all the features of an AII amacrine cell (AII). The middle cell (A, curved arrow) has very fine, beaded dendrites running in S1, S3, and S5 (fine arrows). The third cell is difficult to identify (A).

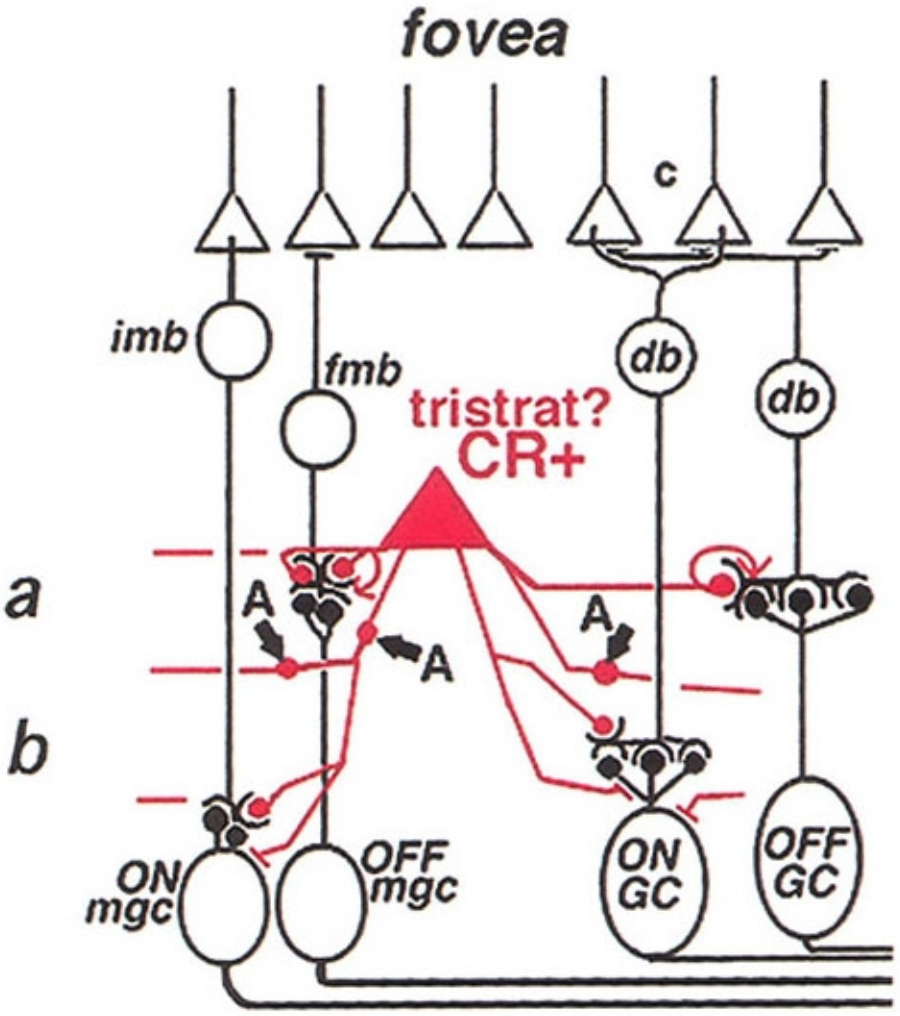

Figure 43. The calretinin-IR amacrine of the rod-free fovea (red cell) receives inputs from diffuse cone bipolar cells (db) and both invaginating and flat midget bipolar cells (imb and fmb) and many amacrine cells types (A arrows). It makes synapses upon ON-center midget (ON mgc) and other ON-center ganglion cells (ON GCs) in sublamina b of the IPL. OFF-center ganglion cells (OFF GC) in sublamina a could be indirectly affected by the tristratified calretinin-IR amacrines through their reciprocal synapses to dbs or fmb bipolar cells (return arrows).

References

1. Cajal SR. In: Thorpe SA, Glickstein M., translators. 1892. The structure of the retina. Springfield (IL): Thomas; 1972.
2. Kolb H, Nelson R, Mariani A. Amacrine cells, bipolar cells and ganglion cells of the cat retina: a Golgi study. Vision Res. 1981;21:1081–1114. PubMed PMID: 7314489.
3. Famiglietti EV, Kolb H. Structural basis for ON- and OFF-center responses in retinal ganglion cells. Science. 1976;194:193–195. PubMed PMID: 959847.
4. Nelson R, Famiglietti EV, Kolb H. Intracellular staining reveals different levels of stratification for on- and off-center ganglion cells in cat retina. J Neurophysiol. 1978;41:472–483. PubMed PMID: 650277.
5. Boycott BB, Kolb H. The horizontal cells of the rhesus monkey retina. J Comp Neurol. 1973;148:115–140. PubMed PMID: 4121525.
6. Stell WK, Witkovsky P. Retinal structure in the smooth dogfish, Mustelus canis: light microscopy of photoreceptor and horizontal cells. J Comp Neurol. 1973;148:33–46. PubMed PMID: 4349223.

7. Karten HJ, Brecha N. Localization of substance P immunoreactivity in amacrine cells of the retina. Nature. 1980;283:87–88. PubMed PMID: 6985713.
8. MacNeil MA, Masland RH. Extreme diversity among amacrine cells: implications for function. Neuron. 1998;20:971–982. PubMed PMID: 9620701.
9. Kolb H, Linberg KA, Fisher SK. The neurons of the human retina: a Golgi study. J Comp Neurol. 1992;318:147–187. PubMed PMID: 1374766.
10. Mariani AP. Amacrine cells of the rhesus monkey retina. J Comp Neurol. 1990;301:382–400. PubMed PMID: 2262597.
11. Kidd M. Electron microscopy of the inner plexiform layer of the retina in the cat and the pigeon. J Anat. 1962;96:179–187. PubMed PMID: 14455782.
12. Dowling JE, Boycott BB. Organization of the primate retina: electron microscopy. Proc R Soc Lond B Biol Sci. 1966;166:80–111. PubMed PMID: 4382694.
13. Famiglietti EV, Kolb H. A bistratified amacrine cell and synaptic circuitry in the inner plexiform layer of the retina. Brain Res. 1975;84:293–300. PubMed PMID: 1111833.
14. Kolb H. The inner plexiform layer in the retina of the cat: electron microscopic observations. J Neurocytol. 1979;8:295–329. PubMed PMID: 490185.
15. Kolb H, Nelson R. Neural architecture of the cat retina. Prog Ret Res. 1984;3:21–60.
16. Pourcho RG, Goebel DJ. Neuronal subpopulations in cat retina which accumulate the GABA agonist (3H) muscimol: a combined Golgi and autoradiographic study. J Comp Neurol. 1983;219:25–35. PubMed PMID: 6619330.
17. Kolb H, Nelson R. Off-alpha and off-beta ganglion cells in the cat retina. II. Neural circuitry as revealed by electron microscopy of HRP stains. J Comp Neurol. 1993;329:85–110. PubMed PMID: 8454727.
18. Nelson R. AII amacrine cells quicken the time course of rod signals in the cat retina. J Neurophysiol. 1982;47:928–947. PubMed PMID: 6177841.
19. Kolb H., Famiglietti E. V. Rod and cone pathways in the inner plexiform layer of the cat retina. Science. 1974;186:47–49. PubMed PMID: 4417736.
20. Vaney DI, Gynther IC, Young HM. Rod-signal interneurons in the rabbit retina: 2. AII amacrine cells. J Comp Neurol. 1991;310:154–169. PubMed PMID: 1955580.
21. Bloomfield SA. Relationship between receptive and dendritic field size of amacrine cells in the rabbit retina. J Neurophysiol. 1992;68:711–725. PubMed PMID: 1432044.
22. Dacheux RF, Raviola E. The rod pathway in the rabbit: a depolarizing bipolar and amacrine cell. J Neurosci. 1986;6:331–345. PubMed PMID: 3950701.
23. Strettoi E, Raviola E, Dacheux RF. Synaptic connections of the narrow-field, bistratified rod amacrine cell (AII) in the rabbit retina. J Comp Neurol. 1992;325:152–168. PubMed PMID: 1460111.
24. Vaney DI. Patterns of neuronal coupling in the retina. Prog Ret Res. 1994;13:301–389.
25. Kolb H, Cuenca N, DeKorver L. Post embedding immunocytochemistry for GABA and glycine reveals the synaptic relationships of the dopaminergic amacrine cell of the cat retina. J Comp Neurol. 1991;310:267–284. PubMed PMID: 1720142.
26. Voigt T, Wässle H. Dopaminergic innervation of AII amacrine cells in mammalian retina. J Neurosci. 1987;7:4115–4128. PubMed PMID: 2891802.
27. Daw NW, Jensen RJ, Brunken WJ. Rod pathways in mammalian retinae. Trends Neurosci. 1990;13:110–115. PubMed PMID: 1691871.
28. Crooks J, Kolb H. Localization of GABA, glycine, glutamate and tyrosine hydroxylase in the human retina. J Comp Neurol. 1992;315:287–302. PubMed PMID: 1346792.
29. Pourcho RG, Goebel DJ. A combined Golgi and autoradiographic study of 3(H) glycine-accumulating amacrine cells in the cat retina. J Comp Neurol. 1985;233:473–480. PubMed PMID: 2984258.
30. Wässle H, Grünert U, Chun M-H, Boycott BB. The rod pathways of the macaque monkey retina: identification of AII-amacrine cells with antibodies against calretinin. J Comp Neurol. 1995;361:537–551. PubMed PMID: 8550898.

31. Smith RG, Vardi N. Simulation of the AII amacrine cell of mammalian retina: functional consequences of electrical coupling and regenerative membrane potentials. Vis Neurosci. 1995;12:851–860. PubMed PMID: 8924409.
32. Vaney DI. The mosaic of amacrine cells in the mammalian retina. Prog Ret Res. 1990;9:49–100.
33. Vaney DI. The morphology and topographic distribution of AII amacrine cells in the cat retina. Proc R Soc Lond B Biol Sci. 1985;224:475–488. PubMed PMID: 2862635.
34. Zrenner E. The physiological basis of the pattern electroretinogram. Prog Ret Res. 1990;9:427–464.
35. Nelson R, Kolb H. Synaptic patterns and response properties of bipolar and ganglion cells in the cat retina. Vision Res. 1983;23:1183–1195. PubMed PMID: 6649437.
36. Kolb H, Nelson R. Hyperpolarizing, small-field amacrine cells in cone pathways of cat retina. J Comp Neurol. 1996;371:415–436. PubMed PMID: 8842896.
37. Nelson R, Kolb H. A17: a broad-field amacrine cell of the rod system in the retina of the cat. J Neurophysiol. 1985;54:592–614. PubMed PMID: 4045539.
38. Sandell JH, Masland RH, Raviola E, Dacheux RF. Connections of indole amine-accumulating cells in the rabbit retina. J Comp Neurol. 1989;283:303–313. PubMed PMID: 2738200.
39. Vaney DI. Morphological identification of serotonin-accumulating neurons in the living retina. Science. 1986;233:444–446. PubMed PMID: 3726538.
40. Freed MA, Pflug R, Kolb H, Nelson R. ON-OFF amacrine cells in cat retina. J Comp Neurol. 1996;364:556–566. PubMed PMID: 8820883.
41. Cuenca N, De Juan J, Kolb H. Substance P-immunoreactive neurons in the human retina. J Comp Neurol. 1995;356:491–504. PubMed PMID: 7560262.
42. Pourcho RG, Goebel DJ. Co-localization of substance P and GABA in amacrine cells of the cat retina. Brain Res. 1988;447:164–168. PubMed PMID: 2454701.
43. Burkhardt DA. Proximal negative response of frog retina. J Neurophysiol. 1970;33:405–420. PubMed PMID: 5439344.
44. Dacey DM. The dopaminergic amacrine cell. J Comp Neurol. 1990;301:461–489. PubMed PMID: 1979792.
45. Kolb H, Cuenca N, Wang HH, Dekorver L. The synaptic organization of the dopaminergic amacrine cell in the cat retina. J Neurocytol. 1990;19:343–366. PubMed PMID: 2391538.
46. Hokoc JN, Mariani AP. Tyrosine hydroxylase immunoreactivity in the rhesus monkey retina reveals synapses from bipolar cells to dopaminergic amacrine cells. J Neurosci. 1987;7:2785–2793. PubMed PMID: 2887643.
47. Ammermüller J, Kolb H. The organization of the turtle inner retina. I. The organization of on- and off-center pathways. J Comp Neurol. 1995;358:1–34. PubMed PMID: 7560272.
48. Critz SD, Marc RE. Glutamate antagonists that block hyperpolarizing bipolar cells increase the release of dopamine from turtle retina. Vis Neurosci. 1992;9:271–278. PubMed PMID: 1327088.
49. Yazulla S, Studholme KM, Fan S-F, Mora-Ferrer C. Neuromodulation of voltage-dependent K+ channels in bipolar cells: immunocytochemical and electrophysiological studies. In: Kolb H, Ripps H, Wu S, editors. Concepts and challenges in retinal biology: a tribute to John E. Dowling. 2001. p. 201-213.
50. Hedden WL, Dowling JE. The interplexiform cell system. II. Effects of dopamine on goldfish retinal neurones. Proc R Soc Lond B Biol Sci. 1978;201:27–55. PubMed PMID: 27790.
51. Teranishi T, Negishi K, Kato S. Dopamine modulates S-potential amplitude and dye-coupling between external horizontal cells in carp retina. Nature. 1983;301:243–246. PubMed PMID: 6401844.
52. Kaneko A. Elecrical connections between horizontal cells in the dog fish retina. J Physiol. 1971;213:95–105. PubMed PMID: 5575346.
53. Negishi K, Teransihi T, Kato S. The dopamine system of the teleost fish retina. Prog Ret Res. 1990;9:1–48.
54. Dowling JE. The retina: an approachable part of the brain. Cambridge (MA): The Belknap Press, Harvard University Press; 1987.
55. Witkovsky P, Dearry A. Functional roles of dopamine in the vertebrate retina. Prog Ret Res. 1991;11:247–292.

56. Bloomfield SA, Xin D, Persky SE. A comparison of receptive field and tracer coupling size of horizontal cells in the rabbit retina. Vis Sci. 1995;12:985–999. PubMed PMID: 8924420.
57. Pflug R, Nelson R. Dopaminergic effects on response kinetics of rabbit and cat horizontal cells. Invest Ophthalmol Vis Sci. 1989;30Suppl.18.
58. Ikeda H, Priest TD, Robbins J, Wakakuwa K. Silent dopaminergic synapses at feline retinal ganglion cells? Clin. Vis Res. 1986;1:25–38.
59. Jensen RJ, Daw NW. Effects of dopamine antagonists on receptive fields of brisk cells and directionally selective cells in the rabbit retina. J Neurosci. 1984;4:2972–2985. PubMed PMID: 6502216.
60. Jensen RJ, Daw NW. Effects of dopamine and its agonists and antagonists on the receptive field properties of ganglion cells in the rabbit retina. Neuroscience. 1986;17:837–855. PubMed PMID: 3703255.
61. Thier P, Alder V. Action of iontophoretically applied dopamine on cat rerinal ganglion cells. Brain Res. 1984;292:109–121. PubMed PMID: 6697199.
62. Dearry A, Falardeau P, Shores C, Caron MG. D2 dopamine receptors in the human retina: cloning of cDNA and localization of mRNA. Cell Mol Neurobiol. 1991;11:437–453. PubMed PMID: 1835903.
63. Veruki ML, Wässle H. Localization and function of dopamine D1 receptors in rat retina. Soc Neurosci Abstr. 1995;21:900.
64. Wagner H-J, Luo B-G, Ariano MA, Sibley DR, Stell WK. Localization of D2 dopamine receptors in vertebrate retinae with anti-peptide antibodies. J Comp Neurol. 1993;331:469–481. PubMed PMID: 8509505.
65. Hampson ECGM, Vaney DI, Weiler R. Dopaminergic modulation of gap junction permeability between amacrine cells in mammalian retina. J Neurosci. 1992;12:4911–4922. PubMed PMID: 1281499.
66. Vaney DI. Territorial organization of direction-selective ganglion cells in rabbit retina. J Neurosci. 1994;14:6301–6316. PubMed PMID: 7965037.
67. Masland RH, Tauchi M. The cholinergic amacrine cells. Trends Neurosci. 1988;9:218–223.
68. Cuenca N, Deng P, Linberg K, Fisher SK, Kolb H. Acetylcholine is found in a second type of amacrine cell in the ground squirrel retina. Brain Res. 2003;964:21–30. PubMed PMID: 12573509.
69. Famiglietti EV. Starburst" amacrine cells and cholinergic neurons: mirror-symmetric ON and OFF amacrine cells of rabbit retina. Brain Res. 1983;261:138–144. PubMed PMID: 6301622.
70. Linberg KA, Suemune S, Fisher SK. Retinal neurons of the Californian ground squirrel, *Spermophilus beecheyi*: a Golgi study. J Comp Neurol. 1996;365:173–216. PubMed PMID: 8822165.
71. Tauchi M, Masland RH. The shape and arrangement of the cholinergic neurons in the rabbit retina. Proc R Soc Lond B Biol Sci. 1984;223:101–119. PubMed PMID: 6151180.
72. Famiglietti EV. Synaptic organization of starburst amacrine cells in rabbit retina: analysis of serial thin sections by electron microscopy and graphic reconstruction. J Comp Neurol. 1991;309:40–70. PubMed PMID: 1894768.
73. Amthor FR, Oyster CW, Takahashi ES. Morphology of on-off direction-selective ganglion cells in the rabbit retina. Brain Res. 1984;298:187–190. PubMed PMID: 6722555.
74. Amthor FR, Takahashi ES, Oyster CW. Morphologies of rabbit retinal ganglion cells with complex receptive fields. J Comp Neurol. 1989;280:97–121. PubMed PMID: 2918098.
75. Famiglietti EV. Starburst amacrine cells in cat retina are associated with bistratified, presumed directionally selective, ganglion cells. Brain Res. 1987;413:404–408. PubMed PMID: 3607491.
76. Wright LL, Macqueen CL, Elston GN, Young HM, Pow DV, Vaney DI. The DAPI-3 amacrine cells of the rabbit retina. Vis Neurosci. 1997;14:473–492. PubMed PMID: 9194315.
77. Cuenca N, Deng P, Linberg K, Lewis GP, Fisher SK, Kolb H. The neurons of the ground squirrel retina as revealed by immunostaining for calcium binding proteins and neuro transmitters. J Neurocytol. 2002;31:649–666. PubMed PMID: 14501205.
78. Zucker CL, Ehinger BE. Distribution of GABAA receptors on a bistratified amacrine cell type in the rabbit retina. J Comp Neurol. 1998;393:309–319. PubMed PMID: 9548552.

79. Zucker CL, Ehinger BE. Complexities of retina circuitry revealed by neurotransmitter receptor localization. In: Kolb H, Ripps H, Wu S, editors. Concepts and challenges in retinal biology: a tribute to John E. Dowling. Progress in Brain Research, Vol. 131. 2001. p. 71-81.
80. Kolb H., Zhang L., DeKorver L, Cuenca N. A new look at calretinin-immunoreactive amacrine cell types in the monkey retina. J Comp Neurol. 2002;453:168–184. PubMed PMID: 12373782.
81. Polyak SL. The retina. Chicago: University of Chicago; 1941.
82. Casini G, Rickman DW, Brecha NC. AII amacrine cell population in the rabbit retina identified by parvalbum in immunoreactivity. J Comp Neurol. 1995;356:132–142. PubMed PMID: 7629307.

AII Amacrine Cells

Mahnoosh Farsaii and Victoria P. Connaughton

Created: June 1, 2005; Updated: April 26, 2007.

Introduction

The AII amacrine cell is characterized by a multifaceted connectivity and physiology. It is unique among amacrine cells in that it participates predominantly in the vertical flow of information though the inner retina, contributing to center mechanisms, rather than in lateral inhibitory pathways. As its multilayer stratification, and synaptic partners, suggest, the AII transmits both rod and cone-driven signals within the ON- and OFF-retinal pathways to the inner retina. This chapter summarizes the morphological and physiological characteristics of AII cells focusing on data obtained from four mammalian species: rat, cat, rabbit, and monkey.

Morphology and Distribution

The AII amacrine cell, originally described by Kolb and Famiglietti (1, 2) is the most studied amacrine cell of the vertebrate retina. It has been identified in a variety of mammalian retinas. The AII is a narrow-field, bistratified amacrine cell that is involved in synaptic contacts throughout the IPL. Its morphology has been identified using a variety of staining methods, such as Golgi techniques (Fig. 1a) (1-3), Lucifer and HRP labeling of recorded neurons (4), and fluorescent dyes such as 4,6-diamidino-2-phenylindole (DAPI) followed by Lucifer Yellow injection (5-7), or by small-spot photo-oxidation of dihydrorhodamine 123 (8, 9).

More recently, immunocytochemical methods targeting various calcium-binding proteins (parvalbumin and calretinin) have been used to selectively label AII cells in rabbit (10, 11) and rodent (Fig. 1b) (12). Primate AII cells are also labeled with calretinin (11, 13), although not selectively (14). Regardless of technique used, the AII cell has a consistent morphology (Fig. 1a) with a round or oval-shaped cell body 8-10 µm in diameter located in the proximal inner nuclear layer. In peripheral retina, the cell body often extends into the IPL. The distribution of AII cell bodies is non-random, forming a regular mosaic (5, 6, 15). Calculated regularity indices range from 4.0 (inferior retina) to 5.4 (temporal midperipheral retina) in rabbit (16), cat (6), and rat (12); a lower value was calculated in monkey (13). AII dendritic trees are reported to be more regularly distributed than their cell bodies, with their processes filling in gaps between adjacent cell bodies to get full coverage of the IPL (13, 16).

The bistratified nature of AII cells arises from two distinct dendritic trees (Fig. 1a and Fig. 1b). The dendritic tree in sublamina **a** (s1 and s2) is composed of short, thin processes ending in lobular appendages that radiate in all directions from typically a single primary dendrite (1, 17-19). Quantitative analysis of serial sections of one particular rabbit AII cell (18) identified 21 lobular appendages ranging in diameter from 1.6 to 5.5 µm. In contrast, the processes that form the dendritic tree in sublamina **b** are called the distal (or arboreal) dendrites and terminate predominantly in stratum 5. The distal dendrites are thin processes that possess spines along their length and branch more widely than the lobular appendages (Fig. 1a). The above characteristics are conserved in rabbit, rat, cat, and macaque monkey retinas (6, 12, 13, 20-22).

AII distribution and morphology is different in central *versus* peripheral retina. AII density is greatest in extrafoveal central retina and decreases with increasing eccentricity. Simultaneously, both dendritic fields enlarge with eccentricity (Fig. 2a) (5, 12, 16, 19, 23), with a more pronounced change reported for the distal dendrites. For example, AII cell density in central cat retina is maximal at 5,300 cells/mm^2 and decreases to 500-800 cells/mm^2 in the peripheral retina. The diameter of the lobular appendage field increases from 16 µm (central retina) to 30 µm (8mm eccentricity), whereas the diameter of the distal arbor expands from 18 µm to 58 µm (6) (Fig. 2b). This morphological trend has also been identified in other mammalian retinas.

The distal dendrites in sublamina **b** of adjacent AII cells overlap. The amount of overlap has been quantified by calculating the coverage (dendritic field area × cell density) of each cell (10). In rabbit, a coverage value of 1.8

was calculated for distal dendrites in the central retina (visual streak) and 2.4 in the inferior retina. The greatest overlap is seen in the superior peripheral retina, where a coverage value of ~10 was calculated (16). In contrast, there is little or no overlap between the lobular dendrites in sublamina **a** of adjacent rabbit AII cells, as coverage varied from ~1.0 in the inferior retina and ~0.8 in the superior retina (16) were calculated. These values show that the lobular appendages maintain a constant coverage over the entirety of the retinal area, whereas the distal processes vary in overlap along both central-to-peripheral and superior-to-inferior axes. Similar differences in AII dendritic processes have been reported in cat, monkey, and rat, suggesting differences in function between AII processes in the distal and proximal IPL (6, 12, 13).

Synaptic Connectivity

Chemical Inputs to Distal Dendrites in Sublamina b

The AII receives direct glutamatergic inputs in sublamina **b** (s5) from rod bipolar cells (RBC) (Fig. 3). At this synapse, the AII forms one member of the postsynaptic dyad (1, 2, 18, 24-27); the other member (discussed below) is a GABA-containing amacrine cell known as A17 in cat and S1/S2 in rabbit (28). The latter cell types make reciprocal synapses back onto the RBC terminal at $GABA_C$ receptors on the RBC (24, 26, 27, 29-33). Each AII receives input from several RBCs.

In all mammals, physiological studies show that glutamate-elicited currents in AII amacrine cells are mediated by AMPA-preferring receptors (34-36) sensitive to the nonselective antagonist CNQX and the AMPA receptor-specific compounds GYKI-52466 and cyclothiazide (36-38). The receptors are formed from GluR3 (39-42) and/or GluR4 (43, 44) subunits (Fig. 4), which confer high calcium permeability to the channel.

NMDA responses have also been identified on rat (45) and rabbit (46) AII cells. These findings contradict immunocytochemical studies that note the absence of NMDA receptor subunits on AII dendritic processes (47-50). Recent findings indicate that NMDA responses do not mediate transmission at the RBC-to-AII synapse (37), suggesting that these receptors, when present, may be located extrasynaptically. The NMDA response in AII cells may also depend on an intracellular signaling pathway, because the response runs down quickly in patch-clamp studies (45).

Although one AII amacrine cell is associated with almost all RBC dyads, rod bipolar connections make up only ~30% of the inputs to AII cells (18). These cells also receive chemical inputs from other amacrine cells within s1 and s5 in rabbit and s1, s3-s5 in rat and cat and in monkey. The amacrine cell(s) presynaptic to AII distal dendrites have not generally been identified, except for dopaminergic amacrine cells in cat (51). Amacrine contacts make up ~40% of the synaptic inputs in sublamina **b** according to Strettoi et al. (18).

Electrical Connections of Distal Dendrites in Sublamina b

AIIs are electrically coupled to ON cone bipolar cells (CBC) throughout sublamina **b** (Fig. 3) (1, 2, 18, 52, 53) and to other AII cells in s5 (18, 27, 54). AII/AII junctions are structurally formed from connexin 36 (55, 56). Signal propagation is bidirectional, promoting synchronized responses (i.e., action potentials) among connected cells (57).

Dopamine application reduces AII/AII coupling (58) through the activation of D1-type dopamine receptors (59) and the formation of cAMP (Fig. 5a) (59, 60). In contrast, gap junctions formed between AII and ON-CBC are heterologous, formed by connexin 36 on AII processes and either connexin 36 or another (possibly 45) connexin on CBC (55, 56, 61). These junctions are also bidirectional (35, 46, 62), although signals are more effectively propagated in the direction of AII to ON-CBC (53). The permeability of AII/ON-CBC channels appears to be regulated by nitric oxide and cGMP (58). Nitric oxide activates guanylate cyclase (increasing intracellular cGMP) and decreases coupling between these cell types.

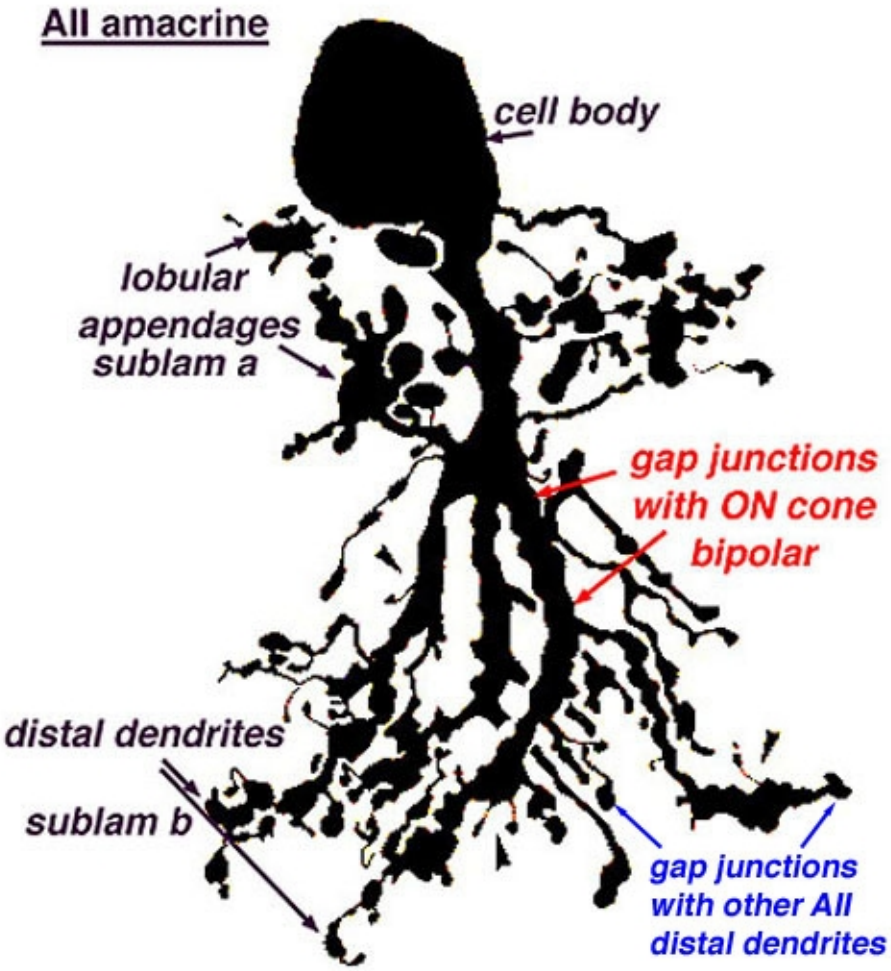

Figure 1a. A Golgi-stained example of an AII amacrine cell in cat retina.

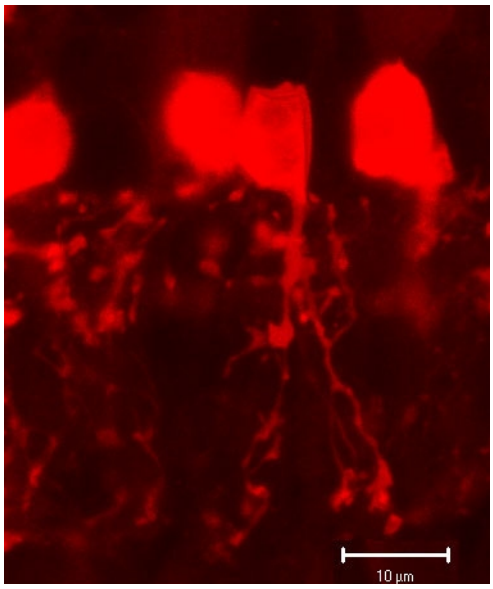

Figure 1b. AII amacrine cells immunocytochemically stained with anti-parvalbumen in rodent retina. Courtesy of Nicolas Cuenca.

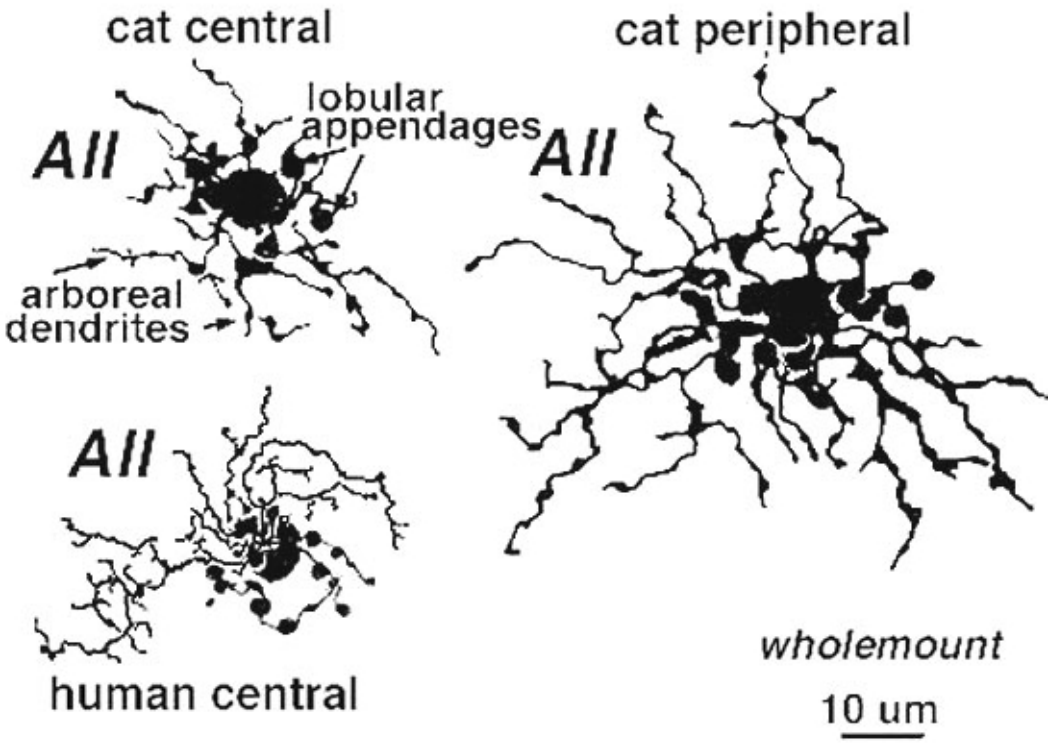

Figure 2a. Golgi-stained whole-mount views of AII amacrine cells.

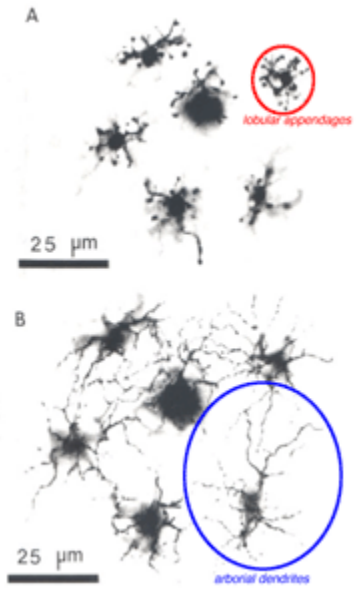

Figure 2b. AII amacrine cells stained with Lucifer Yellow and viewed in whole-mounts reveal two distinct types of processes. In sublamina a, the shorter lobular dendrites (A) encircle the cell body, whereas in sublamina b, thin distal dendrites (B), end in stratum 5. From Mills & Massey (5).

The reported extent of coupling among AII cells varies greatly, from modeling estimates that each AII is coupled to three other AII cells (63) to dye-coupling studies showing that the network can range from ~20 to >300 coupled cells (7, 64). This difference in coupling extent is dependent upon adaptational state (Fig. 5b). Changes

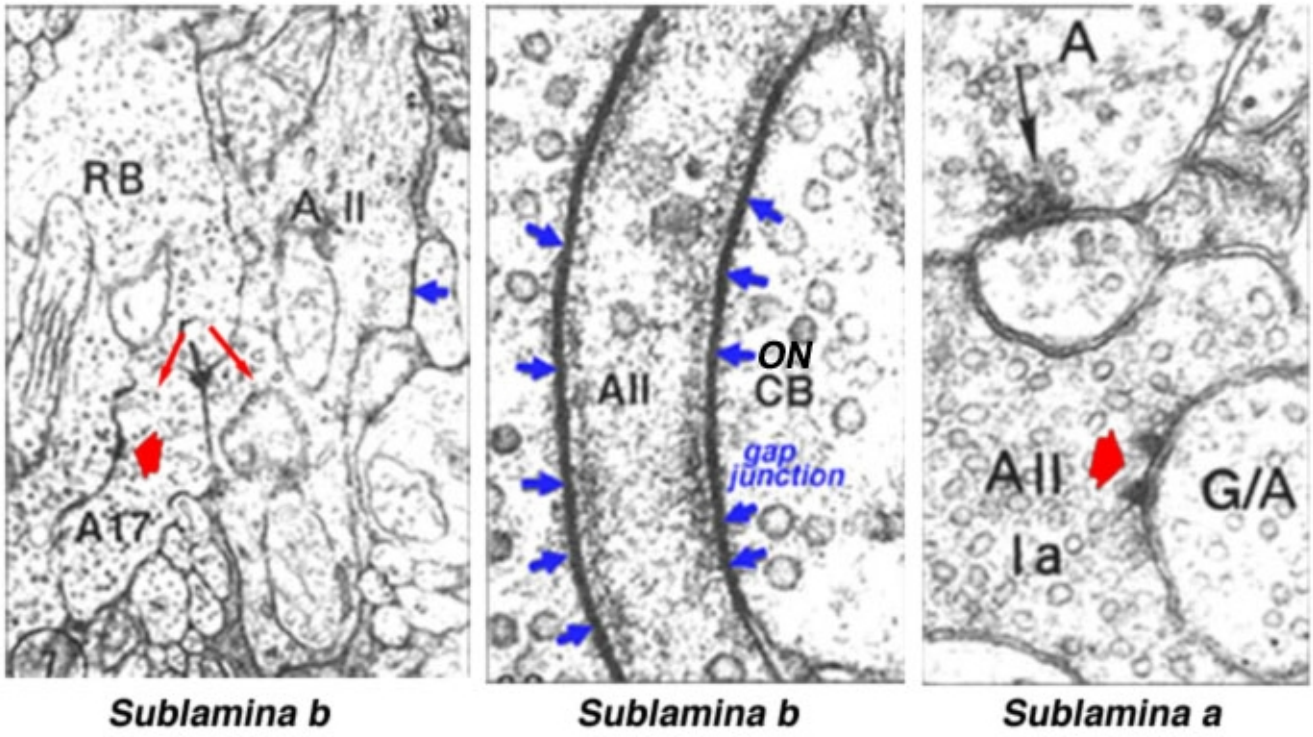

Figure 3. Electron micrographs of AII amacrine synapses. In sublamina a, AII cells synapse on cone bipolar, ganglion cells, and amacrine cells. In sublamina b, AII cells receive ribbon synapses from rod bipolar cells and make gap junctions with ON-center cone bipolar cells.

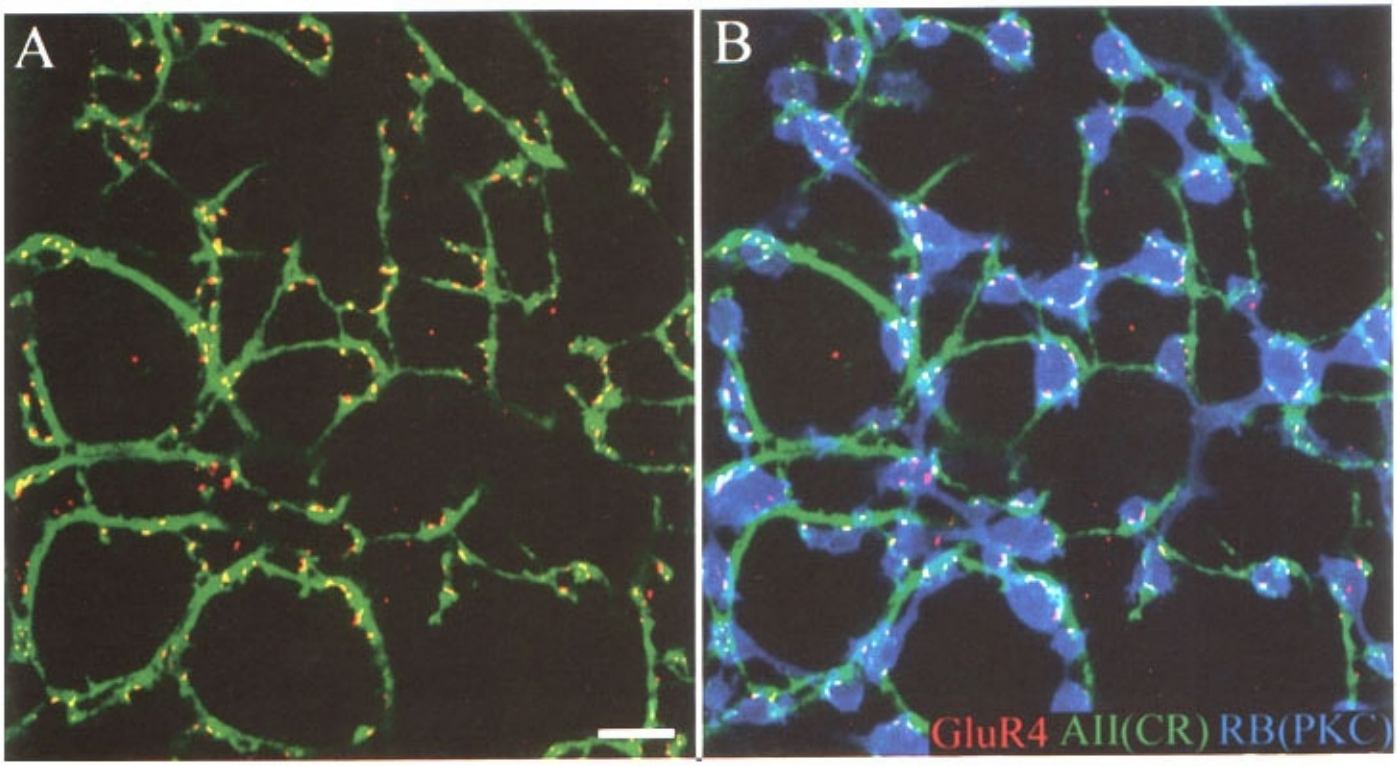

Figure 4. Immunostaining of AII distal dendrites (calretinin, green) and rod bipolar cell terminal (protein kinase C, blue). The yellow/white dots indicate immunostaining for GluR4 receptors at the rod bipolar-AII amacrine synapses. From Li et al. (44).

in AII/AII coupling have been shown to reflect changes in the diameter of the receptive field center (Fig. 5b). For example, in dark-adapted tissue, one AII cell is coupled to a network of ~20 other cells, and the corresponding diameter of the receptive field center averages ~74 μm (64). When the intensity of light is increased but still within the operating range of the cell (~2.25 log intensity unit), both the extent of coupling and the diameter of the receptive field center increase (Fig. 5b). Further increases in light intensity actually results in a decrease in coupling to levels comparable with those seen in dark-adapted conditions (Fig. 5b). Thus, the cells are extensively coupled over their operating range but uncouple at the edges of this range.

What is the benefit of varying the extent of coupling? AII/AII coupling is integral in optimizing the signal-to-noise ratio of the AII network (64, 65) because it allows the smaller correlated rod signals to be increased while uncorrelated noise is decreased (63, 66). This would be important when the retina is operating at dim light intensities (mesopic conditions) because increased coupling maximizes the area from which each AII can merge spatially correlated signals, thereby increasing signal-to-noise ratio. In dark-adapted conditions, however, a miniscule number of photons are intermittently absorbed by the rods, and the correlated signals are few (65). Because coupled AII cells all receive common inputs, AII coupling would strengthen the response by summing correlated signals and reducing noise (63, 66). However, given that the number of correlated signals reaching the AII network is few, extensive coupling at these low light levels is of no advantage because it would increase background noise, causing the faint signals to spread laterally and decrease the overall amplitude of the response. Coupling is also reduced in light-adapted conditions, reducing the transmission, and loss, of cone signals through the AII network, facilitating the high spatial acuity in photopic conditions (65). Furthermore, the high signal-to-noise levels in the cone system reduce the need for spatial averaging.

Gap junctions between AII/ON-CBC provide the mechanism through which rod signals reach ON-ganglion cells (52) via the circuit: rod-to-rod bipolar to AII to ON-cone bipolar cell to ON-ganglion cell (Fig. 6, red circle, blue square). Because these gap junctions are also bidirectional, they provide an alternate pathway through which AIIs receive cone-driven inputs (35, 67, 68). The alternative route would be through rod/cone gap junctions, thus getting rod signals into cone photoreceptors themselves (69). Rod signals would be transmitted to cone bipolar cells and then pass to AIIs in the circuit rod-cone-ON-cone bipolar-AII (67). Signals originating in cone photoreceptors would be relayed via this path as well, and cone-driven responses have been recorded in AII cells (4, 68). Photopic inputs from ON-CBC depolarize AII cells which, in turn, hyperpolarize OFF-CBC (Fig. 6), suppressing light-adapted OFF-center responses (68). As noted above, AII/ON-CBC junctions appear to be modulated by NO, but not by light as physiological studies report changes in background light levels do not alter the observed overall extent of AII/ON-CBC coupling (64), and cone-driven responses can be recorded from AII cells in photopic conditions (4, 68).

Given the morphological diversity of CBC types, it is useful to identify which specific cell(s) is coupled to AIIs to better understand the underlying circuitry. Mills and Massey (70) identified electrical coupling between AIIs and the calbindin-positive bipolar cell in rabbit. However, because only one-quarter of the bipolar cells (23%) tracer-coupled to AIIs are calbindin positive, more than one type of ON-CBC probably makes gap junctions with AIIs (70, 71). In agreement with this, a recent study by Veruki & Harveit (53) examining the electrical properties of AII/ON-CBC gap junctions in rat identified four types of bipolar cells, namely CB5 through CB8, electrically coupled to AIIs in rat (72). Furthermore, the latest evidence from Masland's group suggest that some of the ON cone bipolars coupled to AII cells express connexin 45 but not connexin 36 (61). In cat, the cb5 bipolar cell was found to be coupled to AII processes (73). The cb5 bipolar cell probably corresponds to the calbindin bipolar cell in rabbit, because the latter makes the greatest number of gap junctions with AII cells (54).

Thus, electrical coupling within the AII network functions to maximize signal transmission to postsynaptic ganglion cells. As AIIs receive both rod- and cone-driven inputs, the caliber of the signal varies, depending on stimulus intensity. Consequently, the dynamics of the AII network must also vary continuously. In contrast, synaptic transmission through AII/ON-CBC gap junctions is not affected by adaptational state (64), suggesting

this pathway may function on a sustained level, continually relaying signals independent of light level to ganglion cells.

Synapses of the Lobular Appendages in Sublamina a

The lobular appendages are the major chemical synaptic output sites of AII amacrine cells (Fig. 3) (1, 18). These appendages form reciprocal, inhibitory synapses in s1-s2 (18) with OFF-CBC terminals (18, 24, 74, 75). These synapses account for 90% of the output from AII cells in rabbit (18). AII amacrine cells in rabbit rarely synapse directly onto OFF-ganglion cells, whereas in cat and monkey synapses to OFF ganglion cells are common (52, 76). Inhibitory signals from AIIs are passed to OFF-CBC, decreasing glutamate release onto OFF-type ganglion cells during light stimulation (Fig. 6, blue circle).

Merighi et al. (75) have shown in rabbit that at least two different OFF-CBC types (DAPI-Ba1 and DAPI-Ba2) are postsynaptic to AII cell lobular appendages in different regions of the inner plexiform layer (IPL). The axon terminal of DAPI-Ba1 cells ramifies in s2, whereas DAPI-Ba2 cells are multistratified with boutons located within s1-s3. In cat, cb1 and cb2 bipolar cells (23), which correspond to DAPI-Ba2 and DAPI-Ba1 cells, respectively, contact AII cells in sublamina **a**. In primates, AII lobular appendages participate in reciprocal synapses with calbindin-positive DB3 axon terminals in s2 (77). Another bipolar cell in macaque, DB2, is similar in stratification pattern to the rabbit DAPI-Ba2.

Both AII dendrites and the cell body are postsynaptic to other amacrine cells in S1. Double labeling studies have shown that the dendrites of dopaminergic amacrine cells encircle AII somata, forming characteristic rings as shown in Fig. 7 (78-80). These dopaminergic inputs are believed to mediate changes in AII/AII coupling that occur with adaptational state. However, recent findings show that direct contacts between the dopaminergic processes and AII somata are GABAergic rather than dopaminergic (because dopaminergic amacrines are said to be also GABA positive (81)). Thus, AII cells may receive direct GABAergic inputs at the cell body, which could also regulate AII cell light responses. These GABA-elicited responses, from $GABA_A$ receptor activation, would result in a faster modification of AII responses compared with dopamine actions, which are mediated through slower second messenger cascades and may be considered paracrine in nature. It has to be mentioned here that the dopaminergic amacrine cell is now considered to contain glutamate (82), and if this is the case, a faster transmitter action would also be expected.

Physiological Responses

AII cells themselves are inhibitory glycinergic neurons (83, 84). Their strongest response, and unique role, is during scotopic levels of illumination. In this case, the AII assists in increasing both the speed of transmission and the amplitude of the rod signals seen by the ganglion cells (4).

AII amacrine cells are also called the "rod amacrine cell" because they have response characteristics, such as threshold, saturation level, and spectral sensitivities, similar to rods (4, 65). These cells display complex physiological responses that serve both rod and cone retinal pathways and are sensitive to adaptational state (Fig. 8a). In general, AIIs generate TTX-sensitive action potentials and respond to the exogenous application of GABA, glycine, and glutamate (34). AIIs are classified as ON-center amacrine cells that display center-surround antagonism (4, 39, 68, 85) when dark-adapted; surround antagonism is abolished in light-adapted cells (68).

Generation of the ON-Center Response

On the basis of the synaptic connections of AII cells, ON-center responses could be generated via two pathways: 1) direct rod-driven inputs from (ON-type) RBC at chemical synapses or 2) direct cone-driven inputs from (ON-type) CBC via electrical synapses. Physiological recordings showing rod- and cone-driven responses in AII

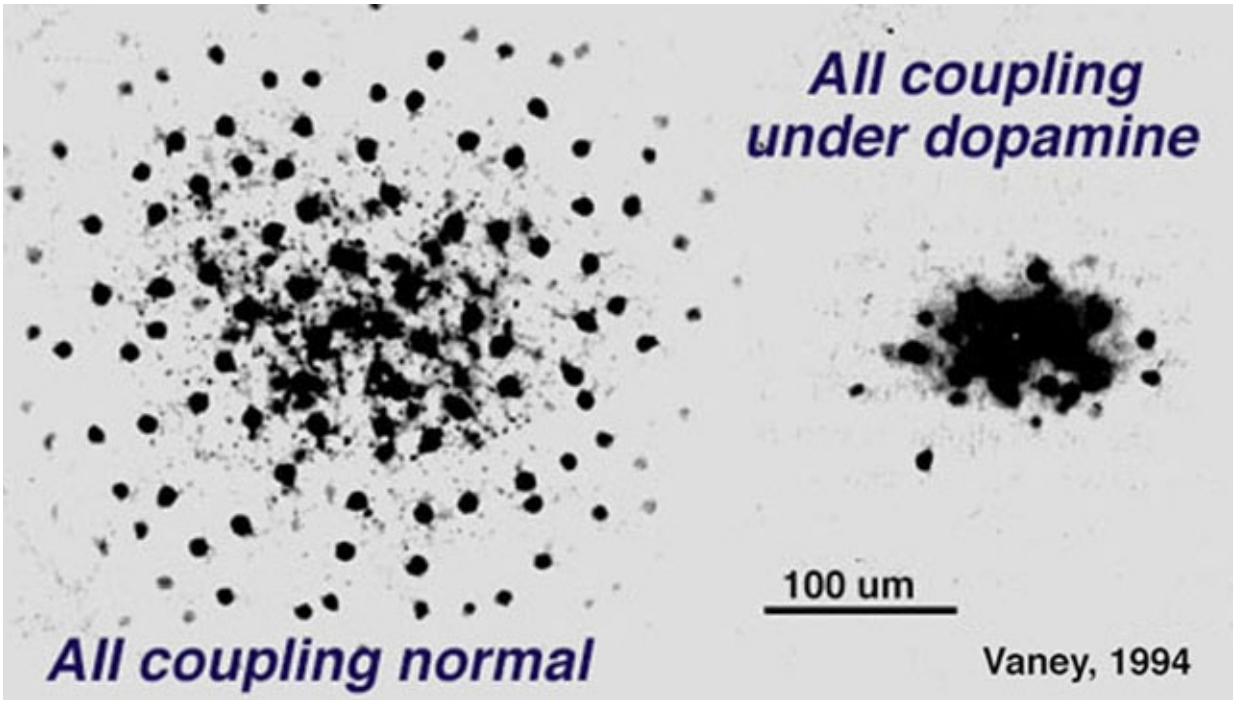

Figure 5a. Dopamine application to retina when the AII cells are injected with biocytin cause a reduction in the numbers of cells that are coupled via gap junctions as compared with normal conditions. Rabbit retina. From Hampson et al. (59).

cells (68, 85) and pharmacological studies (68) indicate that ON-center responses are blocked by the application of 2-amino-4-phosphonobutyric acid (APB), indicating they are generated by ON-type bipolar cells (86, 87).

How is the ON-center response generated? Interestingly, signals transmitted within both of the above pathways can generate the center response, with the contributions of each pathway varying, depending on the intensity of the stimulus (Fig. 8b). In dark-adapted conditions, center responses are derived from rod-driven or cone-driven inputs transmitted directly to AIIs from rod BCs or from cone BCs through gap junctions. Exogenous application of either 8-bromo-cGMP or SNAP, which uncouple AII/ON-CBC gap junctions, does not block scotopic ON-center responses but does block the cone signal component. Bright stimuli saturate the rods, reducing rod-driven inputs to AIIs. In these conditions, ON-center responses are blocked when AII/ON-CBC junctions are pharmacologically uncoupled (68). Thus, the ON-center responses in AII cells comes from either rods or cones. Rod signals depolarize AIIs in dark-adapted (scotopic) conditions; cone-driven signals are relayed in light (photopic) conditions (Fig. 8a and Fig. 8b). Interestingly, a temporary OFF-center response has also been identified in light-adapted AII cells. This response is blocked by CNQX and is believed to be generated via direct glutamatergic inputs from OFF-cone bipolar cells onto AII lobular appendages in sublamina **a** (68).

The AII light response is biphasic, with an initial transient depolarization followed by a more sustained component (Fig. 9). This allows the AII to respond faster to a light stimulus than the presynaptic rod bipolar cell and to reach its maximum amplitude more rapidly. In fact, at the peak of the AII response, the rod bipolar response is one-third of its maximum amplitude (see Fig. 9). The AII cell also repolarizes at a faster rate (4). The transient nature of the AII light response is unexpected because both presynaptic RBC (39) and rod photoreceptors generate slow sustained responses. This leads to the conclusion that the change from a sustained to a transient signal originates in the AII and serves to quicken rod signals relayed to the inner retina (4). What underlying mechanism accounts for the change in response kinetics? This question was answered in a recent paper by Singer and Diamond (37). They examined the RBC/AII synapse using dual patch clamp techniques in rat retinal slices. The transient component of the AII response was not attributable to feedback inhibition onto RBC or to postsynaptic AMPA receptor desensitization, because it was present when either picrotoxin or

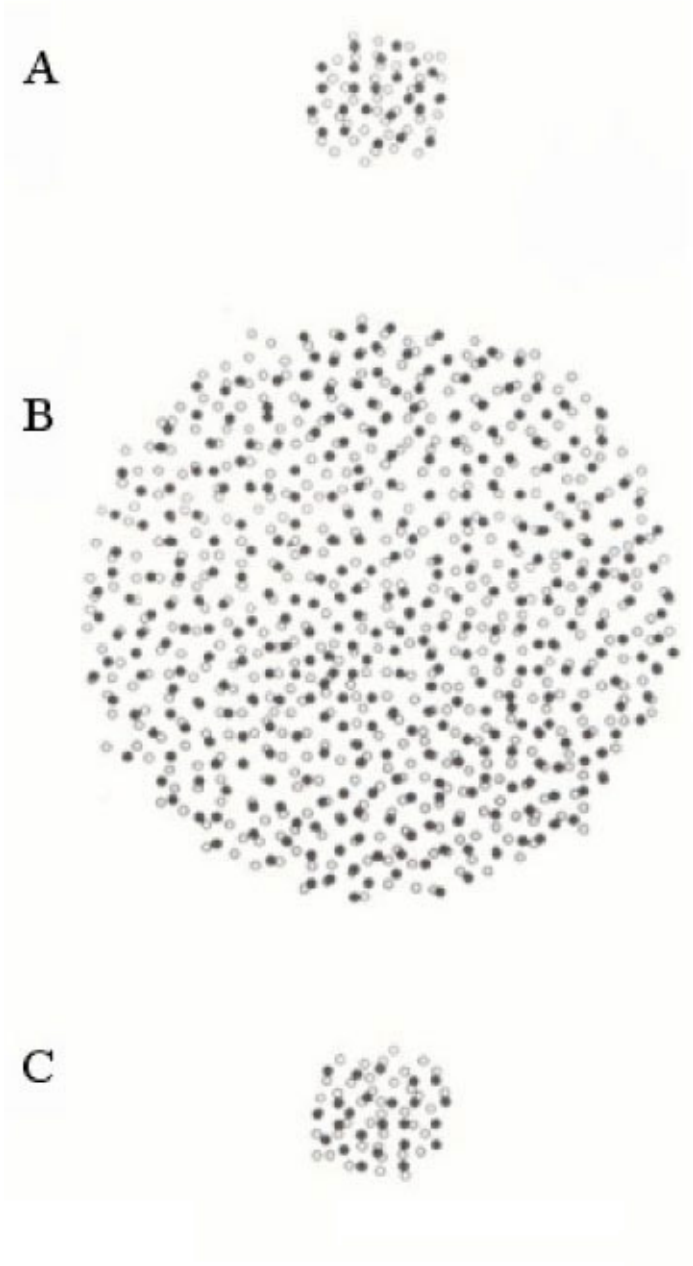

Figure 5b. Coupling between AII cells changes with the level of illumination. In dark-adapted (starlight/scotopic) rabbit retinas (A), only a small number of AII amacrine cells are coupled. Retinas that are light adapted at low/mesopic/twilight intensities (B) display the greatest degree of AII coupling. When light-adapted at the cone threshold/daylight (C), the extent of AII/AII coupling decreases to a value similar to (A). These observed changes in AII/AII coupling reflect changes in the diameter of the receptive field center. Overall coupling between AII/ON-cone bipolar cells did not vary with light level (65).

cyclothiazide was applied. However, the EPSC waveform did vary with calcium influx into the presynaptic terminal, suggesting that activation of calcium channels limits the rate of exocytosis. The authors conclude that the initial transient component of the AII light response is due to the rapid rate of neurotransmitter release from RBC terminals coupled to the fast kinetics of postsynaptic AMPA receptors (37).

Generation of the OFF-Surround Response

In the initial physiological characterization of AIIs, surround responses were only identified in some cells (4). Subsequently, it was shown that the antagonistic surround is present only when cells are dark adapted (46, 68). A

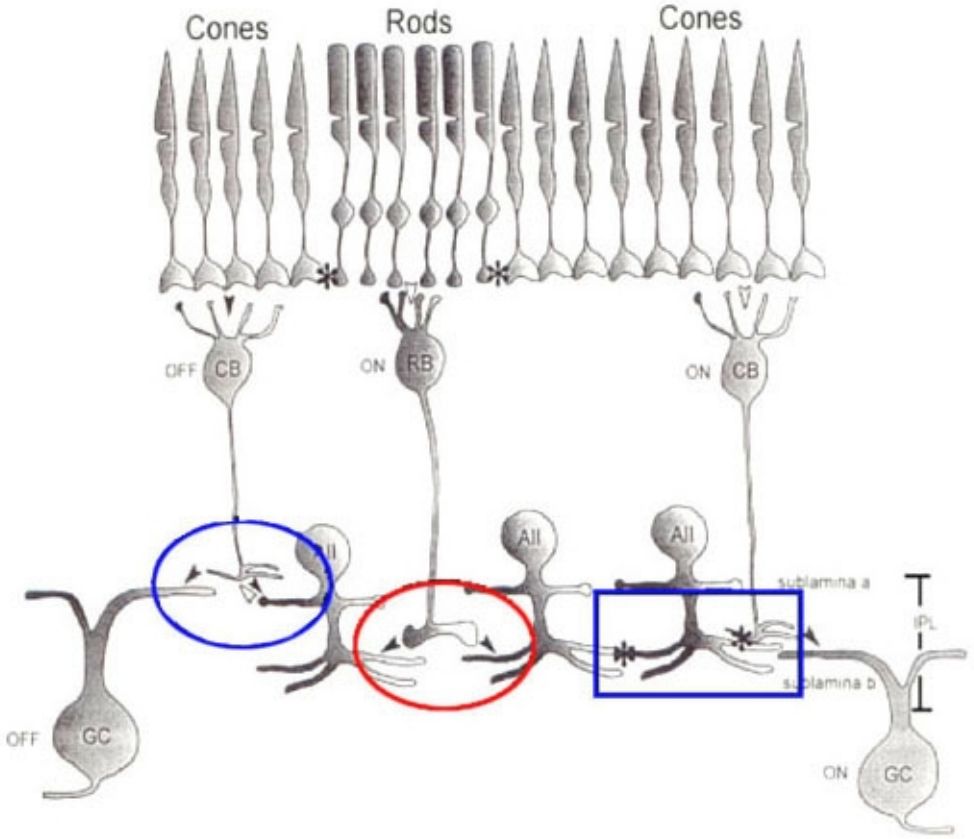

Figure 6. The AII has synaptic contacts throughout the inner plexiform layer (IPL), including synapses with both rod (RB) and cone bipolar (CB) cell types. AII cell processes are postsynaptic to rod bipolar terminals in sublamina b (red circle). In this region, the terminal dendrites also participate in gap junctions (*, blue rectangle) with other AII cells and with ON-CB. In sublamina a, AII cells form synapses (often reciprocal) with OFF-CBC processes (blue circle). GC, ganglion cell; ON, ON-center; OFF, OFF-center. Open arrowheads indicate sign-inverting synapses; filled arrowheads indicate sign-conserving synapses. From Xin and Bloomfield (68).

reasonable hypothesis, given AII morphology, would be that the surround is generated through connections between AII cells and OFF-CBC, because this synapse would be functioning in dark-adapted conditions. However, the surround response is blocked by CNQX (consistent with a role for OFF-CBC) and is also blocked by APB, suggesting that the surround originates at rod bipolar synapse(s) in the IPL (sublamina **b**), although RBC themselves do not display center/surround organization (46, 68).

Two pathways have been proposed to account for the circuitry underlying the OFF-surround response (Fig. 10). First, another amacrine cell may synapse directly with and provide inhibitory inputs to AII distal dendrites, as suggested by anatomical studies. Second, inhibitory feedback synapses onto RBC terminals from A17 amacrine cells may generate surround responses (46, 88). Recent evidence favors this latter pathway, which is summarized below (Fig. 10).

The A17 amacrine cell in cat, rat, and monkey is equivalent to the S1/S2 indolamine-accumulating amacrine cell in rabbit (32). This cell, like the AII, is rod driven (89) and transmission from RBC to A17 cells in rat is blocked by CNQX (90). In other species, however, immunocytochemical studies have identified metabotropic glutamate receptors (91) and GluR1/2 receptor subunits (43, 44) on A17 dendrites. These findings suggest that information flow across the RBC dyad may be mediated by several different glutamatergic mechanisms (43, 44). Cat A17 cells display a sustained light response and lack an antagonistic surround (89), whereas center-surround antagonism has been reported for rat A17 cells (92).

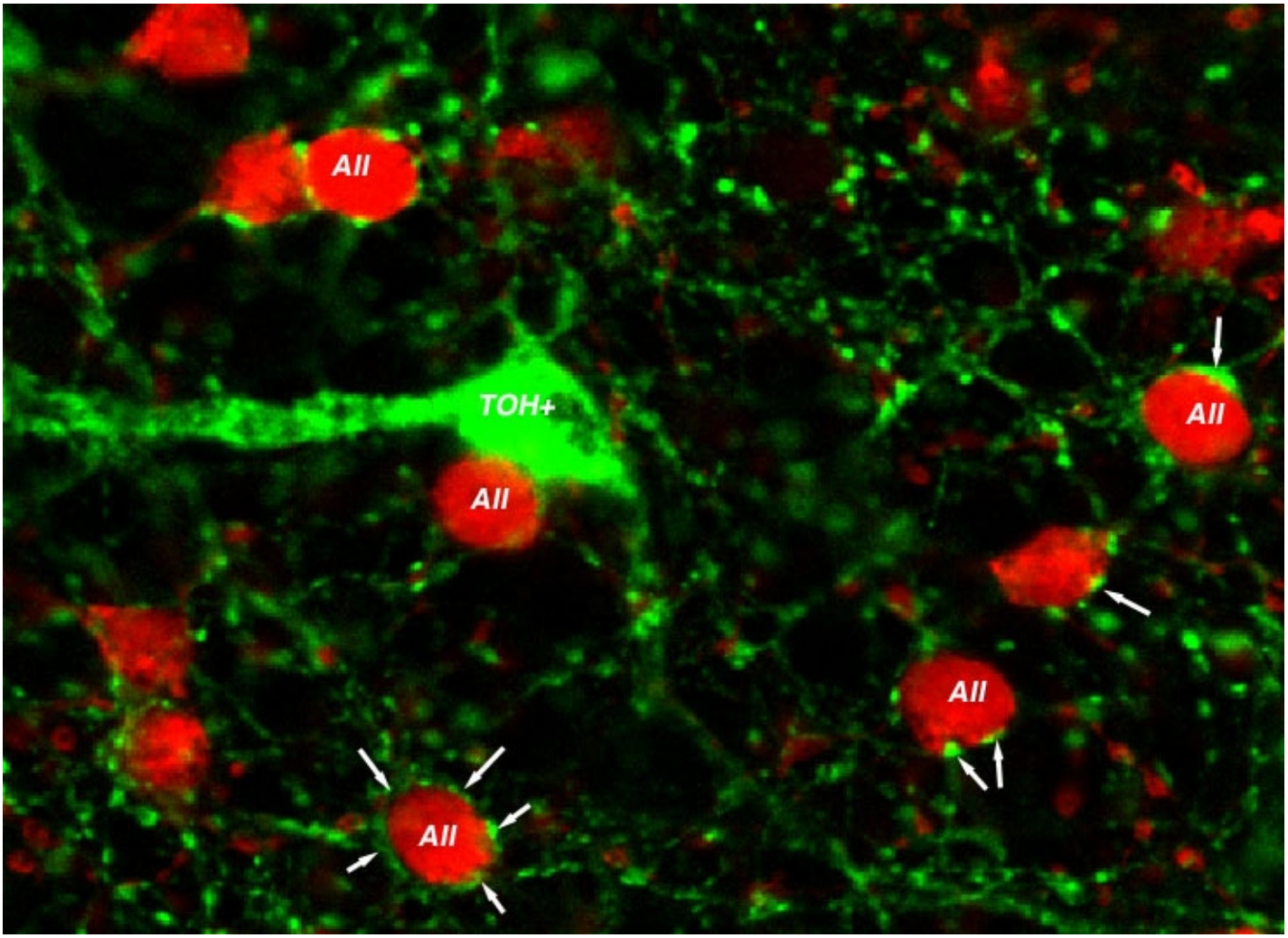

Figure 7. A dopaminergic amacrine cell immunolabeled for tyrosine hydroxylase TOH+ (TOH+green) has fine terminal dendrite "rings" that surround AII amacrine cell bodies (red, AII) in S1 of the IPL. Courtesy of Nicolas Cuenca.

A17 and S1/S2 amacrine cells make reciprocal contacts onto RBC terminals. A17 cells contain GABA (26, 28, 31, 93) and inhibit RBC through the activation of $GABA_C$ receptors (33, 94). This GABAergic feedback is modulated by light intensity; the activation of $GABA_A$ receptors (94) also present on rod bipolar terminals (29, 30, 88, 95, 96), and the activation of presynaptic mGluR1/5 receptors (95). Physiologically, this feedback changes rod bipolar responses, making the scotopic b-wave more transient (94), and may be involved in altering calcium currents in RBC terminals (97), ultimately modifying glutamate release contributing to the surround mechanism in both ganglion cells (98) and AII amacrine cells (88).

In cat, the A17 cell is always the other member of the postsynaptic dyad with AII amacrine distal processes, although other amacrine cell types also receive inputs from rod bipolar cells (74). In contrast, in rabbit, either the S1 or the S2 indolamine-accumulating amacrine cell could partner with the AII at the dyad. Why is this synapse more complex in rabbit? The answer can be found in the differences in morphology and coupling extent between these two cell types. S1 cells are wide-field amacrine cells that display extensive coupling with other S1 cells (i.e., up to ~130 cells coupled), whereas S2 cells are smaller and not as extensively coupled (maximum of 35 cells coupled) (44). These differences suggest that S1 cells provide a wide-field component to the AII surround response, whereas S2 cells provide inputs from a more local circuit (33, 44).

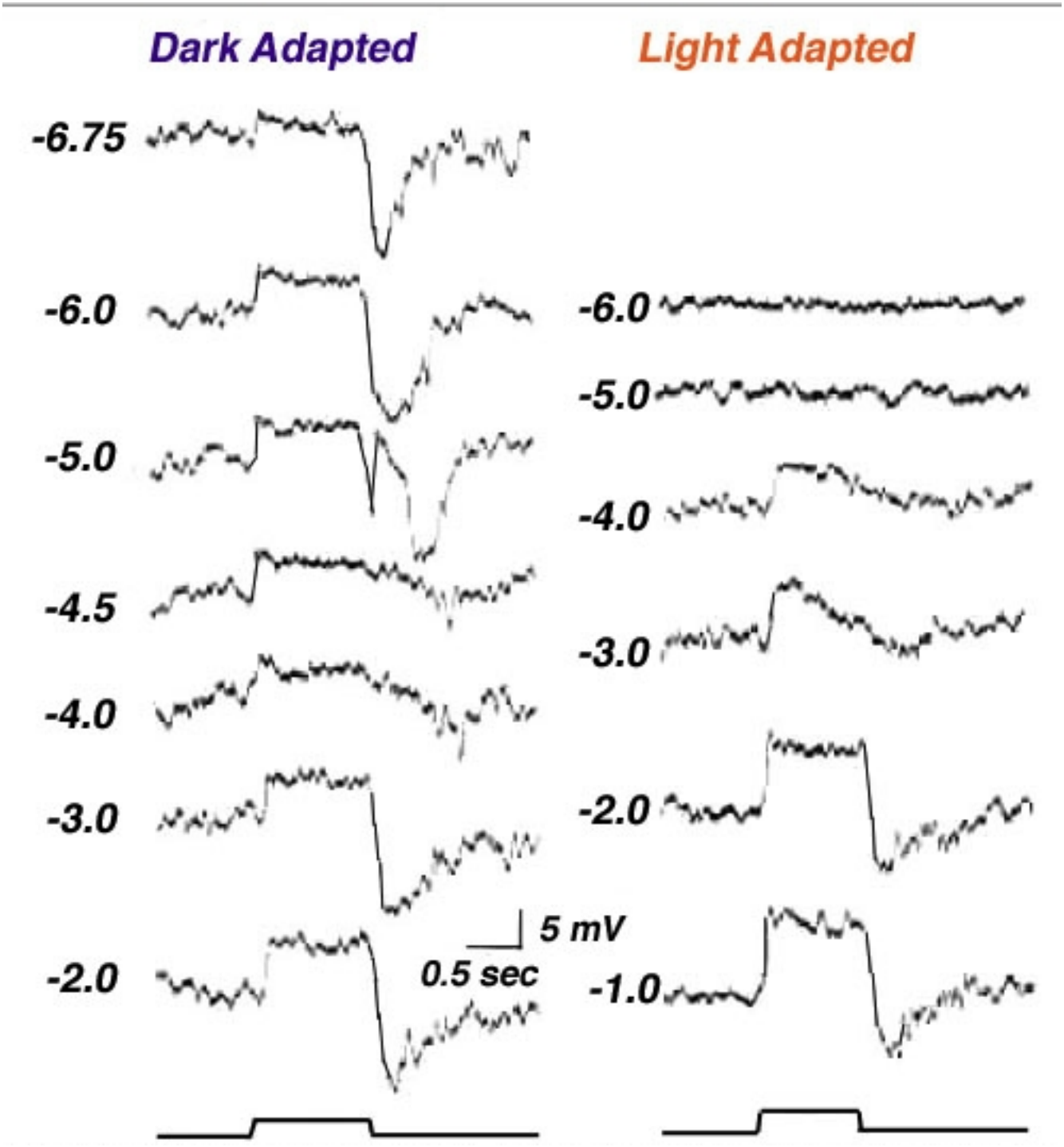

Figure 8a. In dark-adapted conditions (A, left), an ON-center response was recorded at all light intensities tested (threshold = log -6.75). The amplitude of the ON-center response increased with increasing light intensity until saturation at ~ log -4.5 to log -4.0. An ON-center response was also recorded from light-adapted cells (A, right), although the threshold under these conditions was higher (~ log -4.0). The light-adapted ON-center response also increased with increasing light intensity but reached saturation (log -1.0 to 0.0) at a higher light intensity than dark-adapted AIIs. From Xin and Bloomfield (68).

Role in Duplex Vision

The AII amacrine is the place where rod and cone pathways, as well as ON- and OFF-pathways, cross. It is central to scotopic (night) vision. The complex physiology of AII cells is paralleled by their diffuse morphology:

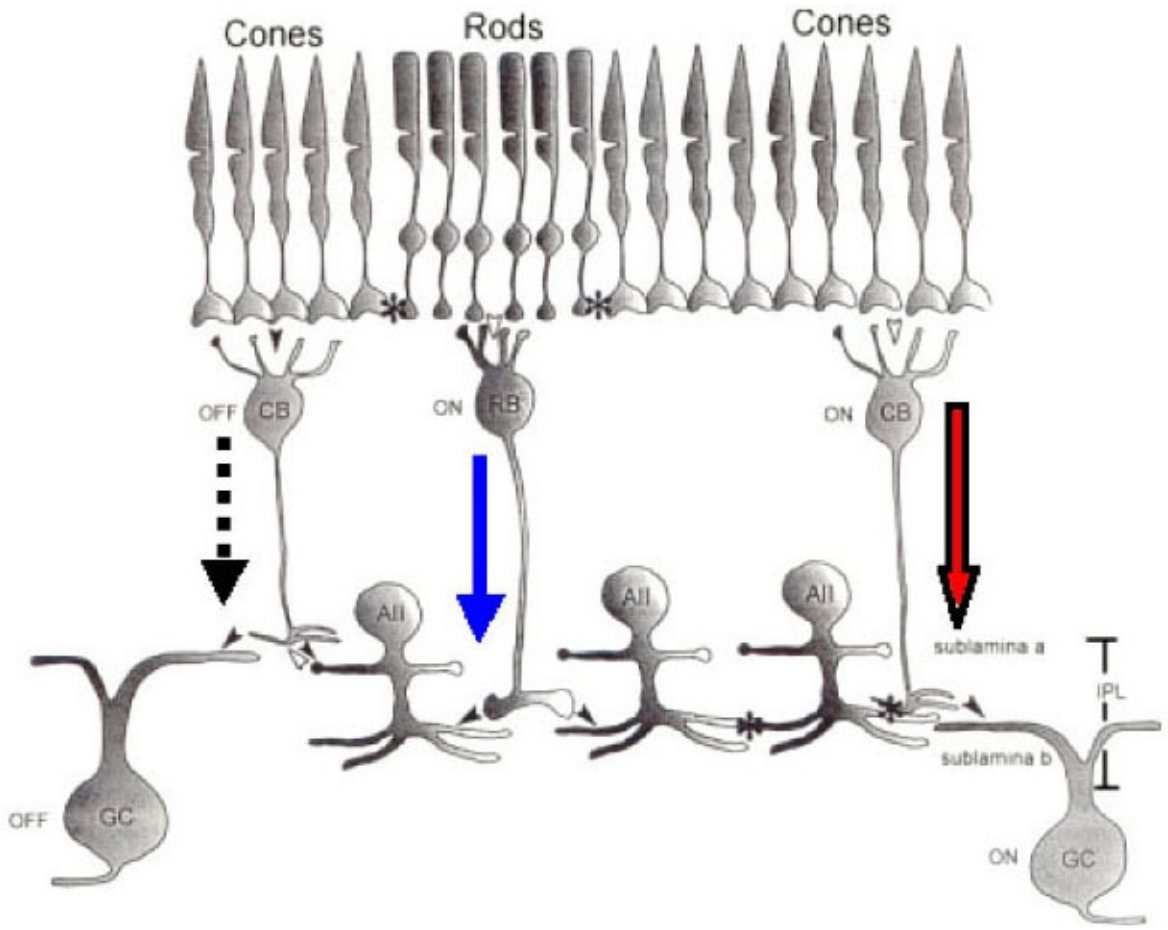

Figure 8b. Schematic diagram showing the circuitry underlying AII ON-center responses. In dark-adapted conditions, the scotopic ON-center response results from direct glutamatergic inputs from rod bipolar cells (RB) (blue arrow). In contrast, cone-driven ON-center responses occur as AIIs are depolarized by signals relayed through AII/ON-CB gap junctions (red arrow). Both of these inputs occur onto the distal dendrites in sublamina b. Light-adapted AIIs also display a small, transient OFF-center responses due to direct inputs from OFF-CB onto lobular appendages in sublamina a (dashed arrow). The ON- and OFF-center responses of light-adapted AII cells are generated simultaneously. From Xin and Bloomfield (68).

their processes are located throughout the IPL, and synapses have been observed within all strata (i.e., chemical synapses in s1, s2, and s5; electrical synapses in s3, s4, and s5). Because of these connections and the parallel retinal pathways, AII amacrine cells always receive inputs, providing the inner retina with a sustained inhibitory pathway (35).

Within the rod pathway (or scotopic levels of light), the light-stimulated decrease in rod photoreceptor glutamate release depolarizes rod bipolar cells, in turn causing the release of glutamate from rod bipolar terminals onto the postsynaptic dyad elements—the indolamine-accumulating or the A17 amacrine cell and the AII amacrine cell. Glutamate excites the AII, resulting in three simultaneous synaptic events: 1) the release of glycine onto OFF-CBC, ultimately inhibiting OFF-ganglion cells; 2) the depolarization of ON-CBC (via AII/ON-CBC gap junctions) and the subsequent depolarization of ON-ganglion cells; and 3) and increase in signal-to-noise ratio due to the spread of the signal among the coupled AII network. In addition, cat, monkey, and rat AII cells synapse directly onto OFF-ganglion cells, resulting in direct glycinergic inhibition of these cells (76, 99). AII responses are modified by inhibitory inputs from depolarized A17 (S1/S2) cells, which feed back onto rod bipolar terminals. The overall effect is inhibition of the OFF-pathway and excitation in the ON-pathway, both by rod-driven signals.

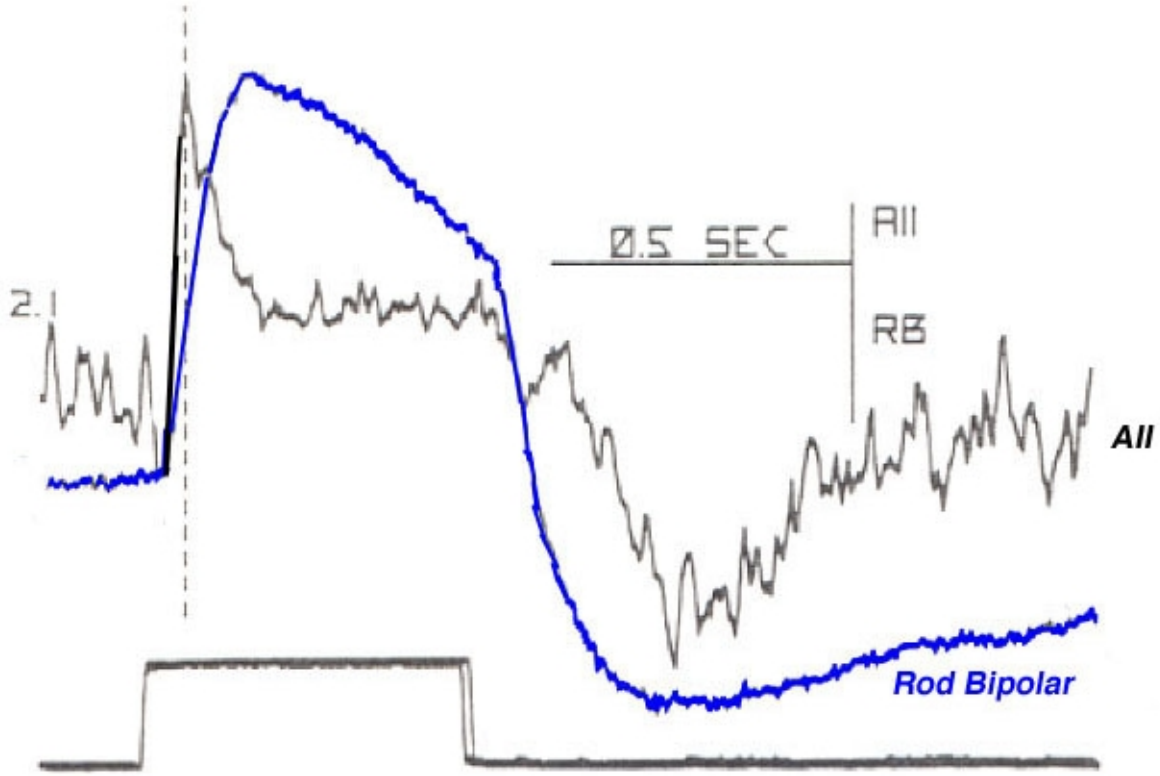

Figure 9. The waveform of the AII amacrine cell reaches its maximum amplitude more rapidly than the presynaptic rod bipolar cell. At the peak of the AII cell's response, the response of the rod bipolar is only one-third of its maximum amplitude. Trace at bottom indicates the duration of the light stimulus. From Nelson (4).

In bright light (photopic) conditions, ON- and OFF-center responses have been recorded from AII cells (68). Both responses are generated via inputs from CBC, with the transient OFF-center response arising from glutamatergic inputs from OFF-CBC and the ON-response arising from transmission through ON-CBC/AII gap junctions. Although both ON- and OFF-responses may be found in the same AII cell, the ON-center response predominates. These inputs from ON-CBC depolarize the AII cells, causing glycinergic inhibition of OFF-CBC and OFF-ganglion cells (99). In addition, under bright light conditions, coupling within the AII network is reduced, preventing the dissipation of cone signals before reaching the ganglion cells. The overall result, again, is that the OFF-pathway is inhibited by the ON-pathway, while high-acuity cone signals are maintained. In this way, the AII mixes not only rod and cone signals but ON- and OFF-pathways as well.

Thus, the inclusion of the AII in the rod circuit (scotopic conditions) is required for the vertical flow of information within the IPL, because it functions to amplify the signal, increase transience, and reduce noise before reaching the ganglion cells. In cone-driven circuits, inputs from ON-CBCs directly stimulate AIIs and ON-ganglion cells. The AII response is a depolarization, with robust ON-center response, resulting in glycine release and the inhibition of OFF-type responses. These glycinergic inputs to postsynaptic CBC and/or ganglion cells allow ON-signals to predominate in the inner retina under these conditions. Thus, AII is always receiving inputs, although the type of input varies (depending on stimulus intensity), causing the AII cell to "shift its focus" from one input pathway to another and from one function to another.

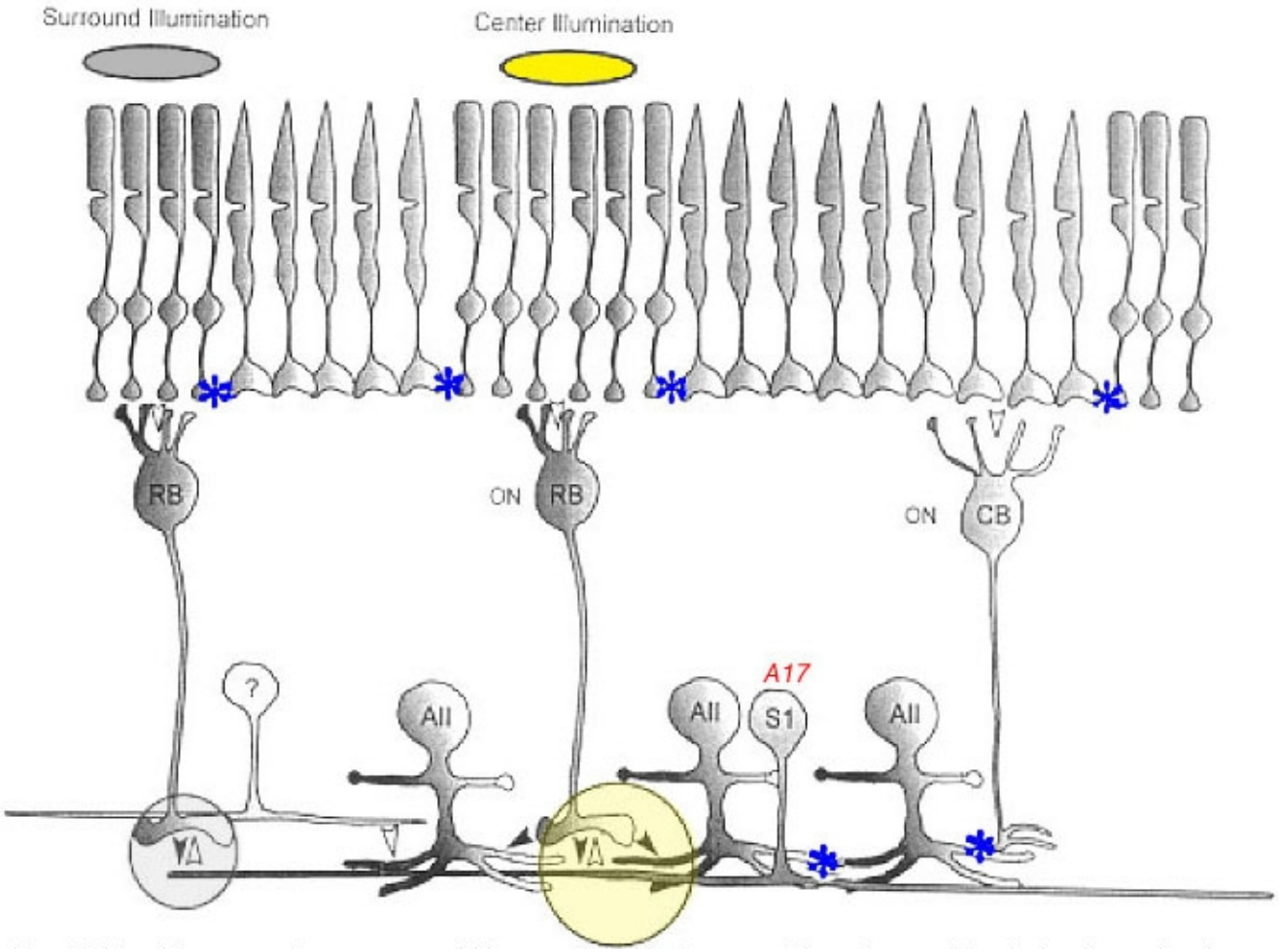

Figure 10. The AII surround response could be generated by two possible pathways. The first pathway involves direct inputs from a GABAergic amacrine cell (labeled with a "?") presynaptic to the distal dendrites in sublamina b. These synapses have been described in many species, although the specific presynaptic cell has not been identified. The second pathway involves an indolamine-accumulating amacrine cell (S1, A17 in cat), which releases GABA at reciprocal synapses onto rod bipolar (RB) terminals. In this diagram, presentation of a light stimulus in the surround region of the AII cell's receptive field (gray circle, left) depolarizes the rod bipolar cell, leading to a release of glutamate onto the process of an S1 amacrine cell (gray circle to the left). The depolarizing signal is transmitted centrally, where the S1 process (yellow circle) releases GABA onto the rod bipolar terminal. GABA inhibition of the rod bipolar cell reduces subsequent release of glutamate onto the AII cell. Experiments suggest that it is the pathway involving the S1 cell that generates the AII surround response. From Bloomfield and Xin (46).

References

1. Famiglietti EV, Kolb H. A bistratified amacrine cell and synaptic circuitry in the inner plexiform layer of the retina. Brain Res. 1975;84:293–300. PubMed PMID: 1111833.
2. Kolb H, Famiglietti EV. Rod and cone pathways in the inner plexiform layer of the cat retina. Science. 1974;186:47–49. PubMed PMID: 4417736.
3. Mariani AP. Amacrine cells of the rhesus monkey retina. J Comp Neurol. 1990;301:382–400. PubMed PMID: 2262597.
4. Nelson R. AII amacrine cells quicken the time course of rod signals in the cat retina. J Neurophysiol. 1982;47:928–947. PubMed PMID: 6177841.
5. Mills SL, Massey SC. Labeling and distribution of AII amacrine cells in the rabbit retina. J Comp Neurol. 1991;304:491–501. PubMed PMID: 1850763.

6. Vaney DI. The morphology and topographic distribution of AII amacrine cells in the cat retina. Proc R Soc Lond B Biol Sci. 1985;224:475–488. PubMed PMID: 2862635.
7. Vaney DI. Many diverse types of retinal neurons show tracer coupling when injected with biocytin or neurobiotin. Neurosci Lett. 1991;125:187–190. PubMed PMID: 1715532.
8. MacNeil MA, Heussy JK, Dacheux RF, Raviola E, Masland RH. The shapes and numbers of amacrine cells: matching photofilled with Golgi-stained cells in the rabbit retina and comparison with other mammalian species. J Comp Neurol. 1999;413:305–326. PubMed PMID: 10524341.
9. MacNeil MA, Masland RH. Extreme diversity among amacrine cells: implications for function. Neuron. 1998;20:971–982. PubMed PMID: 9620701.
10. Casini G, Rickman DW, Brecha NC. AII amacrine cell population in the rabbit retina: identification by parvalbumin immunoreactivity. J Comp Neurol. 1995;356:132–142. PubMed PMID: 7629307.
11. Massey SC, Mills SL. Antibody to calretinin stains AII amacrine cells in the rabbit retina: double-label and confocal analyses. J Comp Neurol. 1999;411:3–18. PubMed PMID: 10404104.
12. Wassle H, Grunert U, Rohrenbeck J. Immunocytochemical staining of AII-amacrine cells in the rat retina with antibodies to parvalbumin. J Comp Neurol. 1993;332:407–420. PubMed PMID: 8349840.
13. Wassle H, Grunert U, Chun M-H, Boycott BB. The rod pathway of the macaque monkey retina: identification of AII-amacrine cells with antibodies against calretinin. J Comp Neurol. 1995;361:537–551. PubMed PMID: 8550898.
14. Kolb H, Zhang L, Dekorver L, Cuenca N. A new look at calretinin-immunoreactive amacrine cell types in the monkey retina. J Comp Neurol. 2002;453:168–184. PubMed PMID: 12373782.
15. H. Kolb, E. Fernandez, R. Nelson, R. (2000). Webvision: the organization of the vertebrate retina [online]. Available from: http://webvision.med.utah.edu/.
16. Vaney DI, Gynther IC, Young HM. Rod-signal interneurons in the rabbit retina: 2. AII amacrine cells. J Comp Neurol. 1991;310:154–169. PubMed PMID: 1955580.
17. Kolb H, Famiglietti EV. Rod and cone pathways in the retina of the cat. Invest Ophthalmol. 1976;15:935–945.
18. Strettoi E, Raviola E, Dacheux RF. Synaptic connections of the narrow-field, bistratified rod amacrine cell (AII) in the rabbit retina. J Comp Neurol. 1992;325:152–168. PubMed PMID: 1460111.
19. Vaney DI, Young HM, Gynther IC. The rod circuit in the rabbit retina. Vis Neurosci. 1991;7:141–154. PubMed PMID: 1931798.
20. Kolb H, Famiglietti EV Jr, Nelson R. Neural connections in the inner plexiform layer of the cat's retina. In: The structure of the eye. Vol. III. 1976.
21. Kolb H, Linberg KA, Fisher SK. Neurons of the human retina: a Golgi study. J Comp Neurol. 1992;318:147–187. PubMed PMID: 1374766.
22. Mills SL, Massey SC. AII amacrine cells limit scotopic acuity in central macaque retina: a confocal analysis of calretinin labeling. J Comp Neurol. 1999;411:19–34. PubMed PMID: 10404105.
23. Kolb H, Nelson R, Mariani A. Amacrine cells, bipolar cells, and ganglion cells of the cat retina: a Golgi study. Vision Res. 1981;21:1081–1114. PubMed PMID: 7314489.
24. Chun MH, Han S-H, Chung J-W, Wassle H. Electron microscopic analysis of the rod pathway of the rat retina. J Comp Neurol. 1993;332:421–432. PubMed PMID: 8349841.
25. Grunert U, Martin PR. Rod bipolar cells in the macaque monkey retina: immunoreactivity and connectivity. J Neurosci. 1991;11:2742–2758. PubMed PMID: 1715391.
26. Kim I-B, Lee M-Y, Oh S-J, Kim K-Y, Chun M-H. Double-labeling techniques demonstrate that rod bipolar cells are under GABAergic control in the inner plexiform layer of the rat retina. Cell Tissue Res. 1998;292:17–25. PubMed PMID: 9506908.
27. Strettoi E, Dacheux RF, Raviola E. Synaptic connections of rod bipolar cells in the inner plexiform layer of the rabbit retina. J Comp Neurol. 1990;295:449–466. PubMed PMID: 2351763.
28. Massey SC, Mills SL, Marc RE. All indolamine-accumulating cells in the rabbit retina contain GABA. J Comp Neurol. 1992;322:275–291. PubMed PMID: 1522254.

29. Fletcher EL, Koulen P, Wassle H. $GABA_A$ and $GABA_C$ receptors on mammalian rod bipolar cells. J Comp Neurol. 1998;396:351–365. PubMed PMID: 9624589.
30. Fletcher EL, Wassle H. Indoleamine-accumulating amacrine cells are presynaptic to rod bipolar cells through $GABA_C$ receptors. J Comp Neurol. 1999;413:155–167. PubMed PMID: 10464377.
31. Grunert U, Wassle H. GABA-like immunoreactivity in the Macaque monkey retina: a light and electron microscopic study. J Comp Neurol. 1990;297:509–524. PubMed PMID: 2384611.
32. Sandell JH, Masland RH, Raviola E, Dacheux RF. Connections of the indoleamine-accumulating cells in the rabbit retina. J Comp Neurol. 1989;283:303–313. PubMed PMID: 2738200.
33. Zhang J, Li W, Trexler EB, Massey SC. Confocal analysis of reciprocal feedback at rod bipolar terminals in the rabbit retina. J Neurosci. 2002;22:10871–10882. PubMed PMID: 12486181.
34. Boos R, Schneider H, Wassle H. Voltage- and transmitter-gated currents of AII-amacrine cells in a slice preparation of the rat retina. J Neurosci. 1993;13:2874–2888. PubMed PMID: 7687279.
35. Cohen ED, Miller RF. The network-selective actions of quinoxalines on the neurocircuitry operations of the rabbit retina. Brain Res. 1999;831:206–228. PubMed PMID: 10412000.
36. Morkve SH, Veruki ML, Hartveit E. Functional characteristics of non-NMDA-type ionotropic glutamate receptor channels in AII amacrine cells in rat retina. J Physiol. 2002;542:147–165. PubMed PMID: 12096058.
37. Singer JH, Diamond JS. Sustained Ca^{2+} entry elicits transient postsynaptic currents at a retinal ribbon synapse. J Neurosci. 2003;23:10923–10933. PubMed PMID: 14645488.
38. Veruki ML, Morkve SH, Hartveit E. Functional properties of spontaneous EPSCs and non-NMDA receptors in rod amacrine (AII) cells in the rat retina. J Physiol. 2003;549:759–774. PubMed PMID: 12702738.
39. Dacheux RF, Raviola E. The rod pathway in the rabbit retina: a depolarizing bipolar and amacrine cell. J Neurosci. 1986;6:331–345. PubMed PMID: 3950701.
40. Gabriel R, De Souza S, Ziff EB, Witkovsky P. Association of the AMPA receptor-related postsynaptic density proteins GRIP and ABP with subsets of glutamate-sensitive neurons in the rat retina. J Comp Neurol. 2002;449:129–140. PubMed PMID: 12115684.
41. Qin P, Pourcho RG. Localization of AMPA-selective glutamate receptor subunits in the cat retina: a light- and electron-microscopic study. Vis Neurosci. 1999;16:169–177. PubMed PMID: 10022488.
42. Qin P, Pourcho RG. AMPA-selective glutamate receptor subunits GluR2 and GluR4 in the cat retina: an immunocytochemical study. Vis Neurosci. 1999;16:1105–1114. PubMed PMID: 10614590.
43. Ghosh KK, Haverkamp S, Wassle H. Glutamate receptors in the rod pathway of the mammalian retina. J Neurosci. 2001;21:8636–8647. PubMed PMID: 11606651.
44. Li W, Trexler EB, Massey SM. Glutamate receptors at rod bipolar ribbon synapses in the rabbit retina. J Comp Neurol. 2002;448:230–248. PubMed PMID: 12115706.
45. Hartveit E, Veruki ML. AII amacrine cells express functional NMDA receptors. Neuroreport. 1997;8:1219–1223. PubMed PMID: 9175117.
46. Bloomfield SA, Xin D. Surround inhibition of mammalian AII amacrine cells is generated in the proximal retina. J Physiol. 2000;523:771–783. PubMed PMID: 10718754.
47. Fletcher EL, Hack I, Brandstatter JH, Wassle H. Synaptic localization of NMDA receptor subunits in the rat retina. J Comp Neurol. 2000;420:98–112. PubMed PMID: 10745222.
48. Goebel DJ, Aurelia JL, Tai Q, Jojich L, Poosch MS. Immunocytochemical localization of the NMDA-R2A receptor subunit in the cat retina. Brain Res. 1998;808:141–154. PubMed PMID: 9767152.
49. Grunert U, Haverkamp S, Fletcher EL, Wassle H. Synaptic distribution of ionotropic glutamate receptors in the inner plexiform layer of the primate retina. J Comp Neurol. 2002;447:138–151. PubMed PMID: 11977117.
50. Hartveit E, Brandstatter JH, Sassoe-Pognetto M, Laurie DJ, Seeburg PH, Wassle H. Localization and developmental expression of the NMDA receptor subunit NR2A in the mammalian retina. J Comp Neurol. 1994;348:570–582. PubMed PMID: 7836563.
51. Kolb H, Cuenca N, Wang H-H, Dekorver L. The synaptic organization of the dopaminergic amacrine cell in the cat retina. J Neurocytol. 1990;19:343–366. PubMed PMID: 2391538.

52. Kolb H. The inner plexiform layer in the retina of the cat: electron microscope observation. J Neurocytol. 1979;8:295–329. PubMed PMID: 490185.
53. Veruki ML, Hartveit E. Electrical synapses mediate signal transmission in the rod pathway of the mammalian retina. J Neurosci. 2002;22:10558–10566. PubMed PMID: 12486148.
54. Strettoi E, Dacheux RF, Raviola E. Cone bipolar cells as interneurons in the rod pathway of the rabbit retina. J Comp Neurol. 1994;347:139–149. PubMed PMID: 7798378.
55. Feigenspan A, Teubner B, Willecke K, Weiler R. Expression of neuronal connexin 36 in AII amacrine cells of the mammalian retina. J Neurosci. 2001;21:230–239. PubMed PMID: 11150340.
56. Mills SL, O'Brien JJ, Li W, O'Brien J, Massey SC. Rod pathways in the mammalian retina use connexin 36. J Comp Neurol. 2001;436:336–350. PubMed PMID: 11438934.
57. Veruki ML, Hartveit E. AII (rod) amacrine cells for a network of electrically coupled interneurons in the mammalian retina. Neuron. 2002;33:935–946. PubMed PMID: 11906699.
58. Mills SL, Massey SC. Differential properties of two gap junctional pathways made by AII amacrine cells. Nature. 1995;377:734–737. PubMed PMID: 7477263.
59. Hampson EC, Vaney DI, Weiler R. Dopaminergic modulation of gap junction permeability between amacrine cells in mammalian retina. J Neurosci. 1992;12:4911–4922. PubMed PMID: 1281499.
60. Cooper JR, Bloom FE, Roth RH. The biochemical basis of neuropharmacology. New York: Oxford University Press; 1996.
61. Lin B, Jakobs TC, Masland RH. Different functional types of bipolar cells use different gap-junctional proteins. J Neurosci. 2005;25:6696–6701. PubMed PMID: 16014731.
62. Trexler EB, Li W, Mills SL, Massey SC. Coupling from AII amacrine cells to ON cone bipolar cells is bidirectional. J Comp Neurol. 2001;437:408–422. PubMed PMID: 11503143.
63. Vardi N, Smith RG. The AII amacrine network: coupling can increase correlated activity. Vision Res. 1996;36:3743–3757. PubMed PMID: 8994576.
64. Bloomfield SA, Xin D, Osborne T. Light-induced modulation of coupling between AII amacrine cells in the rabbit retina. Vis Neurosci. 1997;14:565–576. PubMed PMID: 9194323.
65. Bloomfield SA, Dacheux RF. Rod vision: pathways and processing in the mammalian retina. Prog Retin Eye Res. 2001;20:351–384. PubMed PMID: 11286897.
66. Smith RG, Vardi N. Simulation of the AII amacrine cell of mammalian retina: functional consequences of electrical coupling and regenerative membrane properties. Vis Neurosci. 1995;12:851–860. PubMed PMID: 8924409.
67. DeVries SH, Baylor DA. An alternative pathway for signal flow from rod photoreceptors to ganglion cells in mammalian retina. Proc Natl Acad Sci U S A. 1995;92:10658–10662. PubMed PMID: 7479860.
68. Xin D, Bloomfield SA. Comparison of the responses of AII amacrine cells in the dark- and light-adapted rabbit retina. Vis Neurosci. 1999;16:653–665. PubMed PMID: 10431914.
69. Nelson R. Cat cones have rod input: a comparison of the response properties of cones and horizontal cell bodies in the retina of the cat. J Comp Neurol. 1977;172:109–136. PubMed PMID: 838876.
70. Massey SC, Mills SL. A calbindin-immunoreactive cone bipolar cell type in the rabbit retina. J Comp Neurol. 1996;366:15–33. PubMed PMID: 8866843.
71. Kim I.-B., Park M.T.-H.K., Lee E.-J., Kang M.-S., Chun M.-H. Synaptic circuitries of two types of ON-cone bipolar cells in the rabbit retina. Investigative Ophthalmology and Visual Science. 2004;45:E-abstract 5357.
72. Euler T, Schneider H, Wassle H. Glutamate responses of bipolar cells in a slice preparation of the rat retina. J Neurosci. 1996;16:2934–2944. PubMed PMID: 8622124.
73. Nelson R, Kolb H. Synaptic patterns and response properties of bipolar and ganglion cells in the cat retina. Vision Res. 1983;23:1183–1195. PubMed PMID: 6649437.
74. Kolb H, Nelson R. Rod pathways in the retina of the cat. Vision Res. 1983;23:301–312. PubMed PMID: 6880030.
75. Merighi A, Raviola E, Dacheux R. Connections of two types of flat cone bipolars in the rabbit retina. J Comp Neurol. 1996;371:164–178. PubMed PMID: 8835725.

76. Grunert U, Wassle H. Glycine receptors in the rod pathway of the macaque monkey retina. Vis Neurosci. 1996;13:101–115. PubMed PMID: 8730993.
77. Jacoby RA, Marshak DW. Synaptic connections of DB3 diffuse bipolar cell axons in macaque retina. J Comp Neurol. 2000;416:19–29. PubMed PMID: 10578100.
78. Kolb H, Cuenca N, Dekorver L. Postembedding immunocytochemistry for GABA and glycine reveals the synaptic relationships fo the dopaminergic amacrine cell of the cat retina. J Comp Neurol. 1991;310:267–284. PubMed PMID: 1720142.
79. Pourcho RG. Dopaminergic amacrine cells in the cat retina. Brain Res. 1982;252:101–109. PubMed PMID: 7172014.
80. Voigt T, Wassle H. Dopaminergic innervation of A II amacrine cells in the mammalia retina. J Neurosci. 1987;7:4115–4128. PubMed PMID: 2891802.
81. Contini M, Raviola E. GABAergic synapses made by a retinal dopaminergic neuron. Proc Natl Acad Sci U S A. 2003;100:1358–1363. PubMed PMID: 12547914.
82. Jones BW, Watt CB, Marc RE. Dopamine amacrine and interplexiform cells exhibit glutamatergic signatures. Rockville (MD): Association for Research in Vision and Ophthalmology; 2004.
83. Menger N, Pow DV, Wassle H. Glycinergic amacrine cells of the rat retina. J Comp Neurol. 1998;401:34–46. PubMed PMID: 9802699.
84. Pourcho RG. Neurotransmitters in the retina. Curr Eye Res. 1996;15:797–803. PubMed PMID: 8670790.
85. Dacey DM. Primate retina: cell types, circuits, and color opponency. Prog Retin Eye Res. 1999;18:737–763. PubMed PMID: 10530750.
86. Slaughter MM, Miller RF. 2-Amino-4-phosphonobutyric acid: a new pharmacological tool for retina research. Science. 1981;211:182–185. PubMed PMID: 6255566.
87. Slaughter MM, Miller RF. Characterization of an extended glutamate receptor on the ON bipolar neuron in the vertebrate retina. J Neurosci. 1985;5:224–233. PubMed PMID: 2981298.
88. Volgyi B, Xin D, Bloomfield SA. Feedback inhibition in the inner plexiform layer underlies the surround-mediated responses of AII amacrine cells in the mammalian retina. J Physiol. 2002;539:603–614. PubMed PMID: 11882691.
89. Nelson R, Kolb H. A17: a broad-field amacrine cell in the rod system of the cat retina. J Neurophysiol. 1985;54:592–614. PubMed PMID: 4045539.
90. Hartveit E. Reciprocal synaptic interactions between rod bipolar cells and amacrine cells in the rat retina. J Neurophysiol. 1999;81:2923–2936. PubMed PMID: 10368409.
91. Cai W, Pourcho RG. Localization of metabotropic glutamate receptors mGluR1alpha and mGluR2/3 in the cat retina. J Comp Neurol. 1999;407:427–437. PubMed PMID: 10320222.
92. Menger N, Wassle H. Morphological and physiological properties of the A17 amacrine cell of the rat retina. Vis Neurosci. 2000;17:769–780. PubMed PMID: 11153656.
93. Pourcho RG, Goebel DJ. Neuronal subpopulations in cat retina which accumulate the GABA agonist (3H)muscimol: a combined Golgi and autoradiographic study. J Comp Neurol. 1983;219:25–35. PubMed PMID: 6619330.
94. Dong C-J, Hare WA. Temporal modulation of scotopic visual signals by A17 amacrne cells in mammalian retina in vivo. J Neurophysiol. 2003;89:2159–2166. PubMed PMID: 12686583.
95. Euler T, Wassle H. Different contributions of $GABA_A$ and $GABA_C$ receptors to rod and cone bipolar cells in a rat retinal slice preparation. J Neurophysiol. 1998;79:1384–1395. PubMed PMID: 9497419.
96. McGillem GS, Rotolo TC, Dacheux RF. GABA responses of rod bipolar cells in rabbit retinal slices. Vis Neurosci. 2000;17:381–389. PubMed PMID: 10910106.
97. Pan Z-H. Voltage-activated Ca^{2+} channels and ionotropic GABA receptors localized at axon terminals of mammalian retinal bipolar cells. Vis Neurosci. 2001;18:279–288. PubMed PMID: 11417802.
98. Shields CR, Lukasiewicz PD. Spike-dependent GABA inputs to bipolar cell axon terminals contribute to lateral inhibition of retinal ganglion cells. J Neurophysiol. 2003;89:2449–2458. PubMed PMID: 12611993.
99. Muller F, Wassle H, Voight T. Pharmacological modulation of rod pathway in the cat retina. J Neurophysiol. 1988;59:1657–1672. PubMed PMID: 3404200.

Midget pathways of the primate retina underlie resolution and red green color opponency

Helga Kolb, PhD[1]

Created: May 24, 2007; Updated: April 4, 2012.

1 General characteristics

The specialized cone pathways of the central fovea of human and monkey retinas have the least convergence and the greatest resolution capabilities of the visual system. This is accomplished by making the connections as "private" as possible and narrowing them to a one to one relationship in the so-called midget pathways. Figure 1 shows an older drawing from Polyak's book (1) that shows the very narrowest field bipolars and ganglion cells of the fovea.

The midget pathways consist of midget bipolar cells and midget ganglion cells, the latter of which project to individual parvocellular layer cells of the lateral geniculate nucleus in the brain. Because of the need for the high acuity midget pathways also to be organized into ON- and OFF-center channels like the diffuse cone pathways for maximization of contrast, it means that every cone of the fovea will have dual midget pathways. The two midget bipolars will be an ON-center type and an OFF-center type and will connect with ON-center and OFF-center midget ganglion cells respectively. Because midget bipolar/ganglion cell circuits are devoted to a single cone, and the individual cones are of different spectral type maximally excited by short (S-cone/blue), medium (M-cone/green) or long (L-cone/red) wavelengths, they must carry sensitivity information about one wavelength. Thus the midget system concerned with the M- and L-cones in particular are considered also to carry L- or M-signals to the brain where further processing takes place to allow us the red and green discriminations of color vision.

The S-cone system is rather different from the M- and L-cone systems from the initial level of the cone itself to its circuitry though the retina and into the brain. We do not consider the S-cone pathway as a midget pathway (see later chapter on S-cone pathways). So this chapter is devoted to the M- and L-midget pathways and as we shall see, they carry both a resolution and a chromatic message through the retina to the brain.

2 Visual acuity starts with cone spacing and midget circuitry

Visual acuity is a measure of our ability to discriminate the finest detail: either by discriminating two parallel lines apart (Vernier acuity) or two tiny spots or stars apart (point discrimination). The primate and human visual system is capable of acuity of 1 min of arc or 60 cycles/degree of visual angle. One degree of visual angle is thought to cover approximately 280-300 um of retinal distance (2). The area of the retina where the cone photoreceptors are most closely packed in a more or less hexagonal array, is, of course, the center of the fovea and is about one degree across (Fig. 2). So visual discrimination of 1 min of arc is about the center to center spacing (3 μm) of the cones of the central mosaic in the foveola (Fig. 3).

If the minimum center to center spacing (a) is 3 μm for the cones of the fovea, then the grating resolution limit, known as the Nyquist limit, is $a\sqrt{3}$, about 1 min of arc. One may ask why the grating resolution is not better than 1 min of arc and the size of, or even less than the diameter of each cone, i.e. a or $< a$. For these narrower gratings, the spatial interference of the packed cones would apparently cause Moire effects, or aliasing, if line separations of less than $a\sqrt{3}$ are used, as shown below (3) (Fig. 4). These interference patterns, with a repeat length that

Author Affiliation: 1 Professor Emeritus of Ophthalmolgy & Visual Sciences, The University of Utah School of Medicine.; Email: helga.kolb@hsc.utah.edu.

Corresponding author.

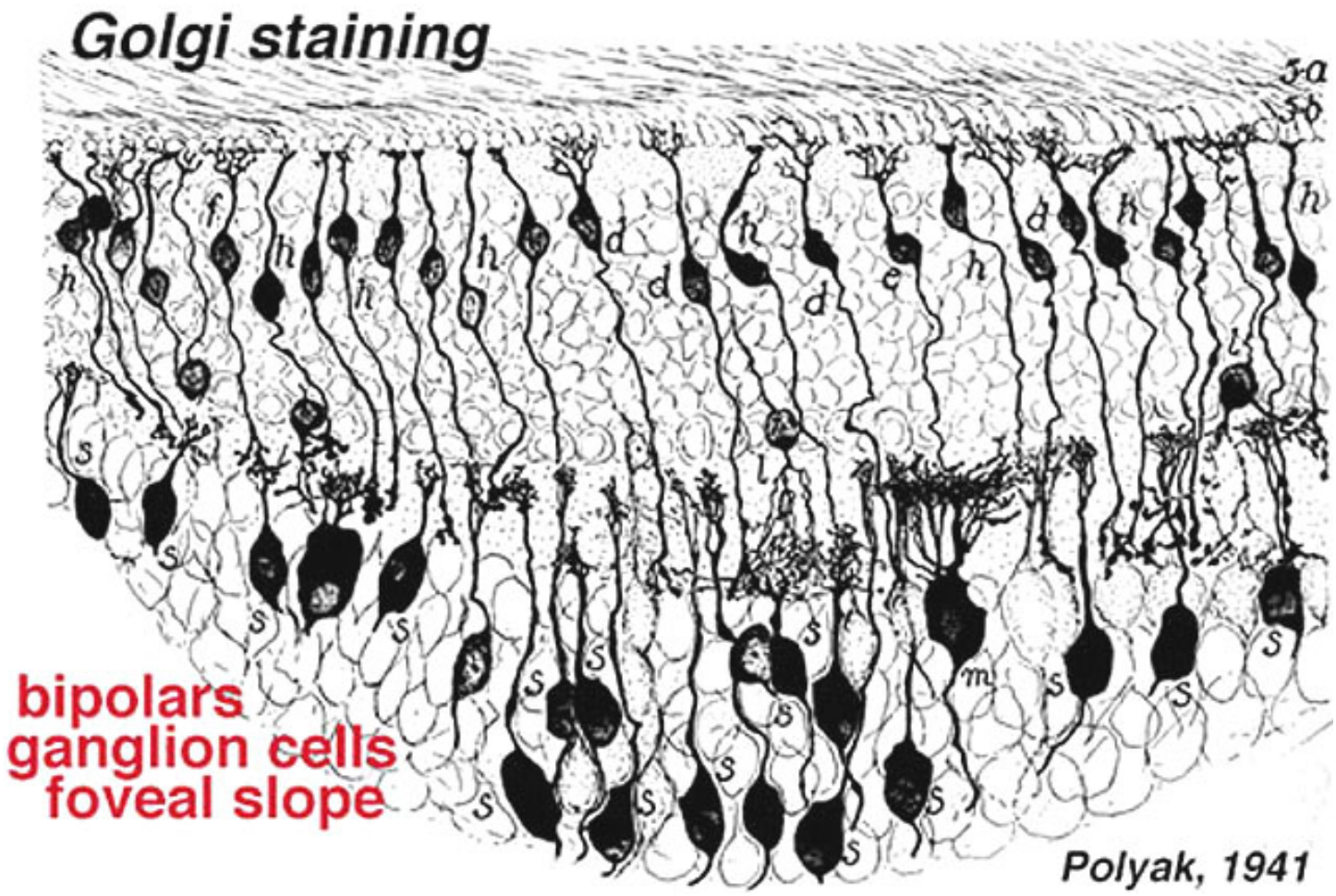

Figure 1. Polyak's drawing of bipolar and ganglion cells in the foveal slope of the monkey retina. The illustration is taken from Polyak, 1941 (1).

depends on the angle that the grating makes with the cone mosaic, make it impossible to determine the wavelength of the grating. It turns out that under normal conditions, the optics of the eye do not sharply image gratings of greater than 60 cycles/degree (4). The optical blur of the eye minimizes Moire effects in spatial sampling (Fig. 4).

The image is also blurred by the optics of the eye to project onto about 10 cones (Fig. 4). Lateral shifts of this image can then be compared over these 10 cones and their midget chains of neurons for later computation in the brain. This allows better discrimination (resolution) because of the possibility of imposing antagonism from neighboring cone systems, i.e. surrounds on the pathways and increasing contrast and discrimination between the several midget-single-cone originating pathways (5).

We know that three classes of cone comprise the cone foveal mosaic, but we have long been curious as to how the three different spectral types of cone are arranged in the hexagonal mosaic. The S-cones (blue cones) are fairly easily picked out from the L-cones (red cones) and M-cone (green cones) on some distinguishing morphological features (see chapter on S-cone pathways). In fact the S-cones are seen as the larger profiles disrupting the hexagonal mosaic in the wholemount view of the foveal mosaic of Figure 2 (arrows point to S-cones). In the foveal region of the cone mosaic S-cones form from 8-12% of the cones (6). The very center of the foveal pit is almost devoid of S-cones. So the remainder of the cones are somehow divided into the L- and M-cone populations. In the human fovea, psychophysical measurements have suggested that red cones outnumber green by 2:1 (7). However, direct measurements by microspectrophotometry of all cones in small patches of

cones in the fovea of monkeys, has revealed that red and green cones occur in about equal proportion (Fig. 5) (8). Roorda and Williams (9) made direct measurements of spectral sensitivity of foveal cones in the living human eye by a sophisticated technique of adaptive optics to increase spatial resolution. They found that humans varied greatly in their proportions of red cones to green cones: some individuals have almost equal proportions while others have a higher proportion of red cones, to the extreme of 2 red cones to every green cone. The red and green cones lie randomly in the mosaic meaning that clusters of cones of the same spectral type will occur together as illustrated in figure 5 from Mollon and Bowmaker's paper. An interesting point can be deduced from these findings. It does appear possible then, that a multiheaded midget or diffuse cone bipolar with a small dendritic tree, could contact all the same spectral type of cones in the primate fovea.

3. Cone to midget bipolar cell connections

Polyak (Fig. 6) had already described two types of midget ganglion cell in the primate retina in 1941 (1). He had studied and drawn ganglion cells from vertical sections of Golgi-stained monkey retina and noticed that the midget ganglion cells in particular (although it is also true of the small and large parasol ganglion cells) had dendrites branching at one of two levels in the IPL: close to the ganglion cell bodies (the area we now know as sublamina b) or in neuropil close to the amacrine cell bodies (the area we now know as sublamina a). He had also drawn and remarked on the fact that midget bipolar cells came in long and short axon varieties to fit the two midget ganglion cell varieties (Fig. 7) (1)).

The important distinction between two types of midget bipolar cell was not made until an electron microscope study was able to show differences in their synaptic contacts with the cone pedicle (10). Thus, invaginating midget bipolar cells (imb) were found to connect with cone pedicles at central elements, invaginating synapses at the cone pedicle ribbons (Fig. 8 and Fig. 9). Flat midget bipolar cells connect to cone pedicles at wide-cleft, basal junctions (fmb), most often on either side of the invaginating dendrite of the imb (Fig. 8 and Fig. 10).

4. Midget ganglion cells

Viewing Golgi stained whole-mount primate retinas has been particularly helpful in revealing the differences between the three ganglion cell types that are involved with spatial and color vision: namely the midget ganglion cells, the blue/yellow ganglion cells and the parasol ganglion cells (1, 11, 12). The midget ganglion cells are thought to be high acuity cells that also carry a red or green color specific signal. They project to the parvocellular layers of the lateral geniculate nucleus and are thus called P cells (Fig. 11) (13). Midget ganglion cells come in high branching varieties that are probably OFF-center physiologically and low branching types that are ON-center physiologically. Movie 1 is a through focus series of an ON and OFF midget pair in human retina.

Figure 11 shows two midget ganglion cells in comparison with a parasol ganglion cell (M cell) of peripheral human retina. The one midget ganglion cell has an 18 μm diameter dendritic tree and the other has a larger dendritic field at 35 μm in diameter. The movie above shows that the midget ganglion cell with the smaller dendritic field comes into focus at a different level from the larger field cell. The former midget ganglion cell branches high in the IPL and so is probably an OFF center type physiologically. The lower branching midget ganglion cell with the larger dendritic tree is probably an ON center type. Why the OFF center type has a smaller dendritic tree compared with ON center type remains a mystery at present but one implication may be that the midget OFF system acuity is higher in acuity than the ON system (14).

The connections between the midget bipolar and the midget ganglion cells have always been thought to be "private", i.e. one to one. Because of the similar size and branching level of the axon terminal of the bipolar cell and the dendritic arbor of the midget ganglion cell in the foveal area particularly, it has been assumed that axon terminal and dendritic field overlap and synapse, with no room for convergence from more than one bipolar axon per ganglion cell. However, the story may be different in the peripheral retina where the midget ganglion

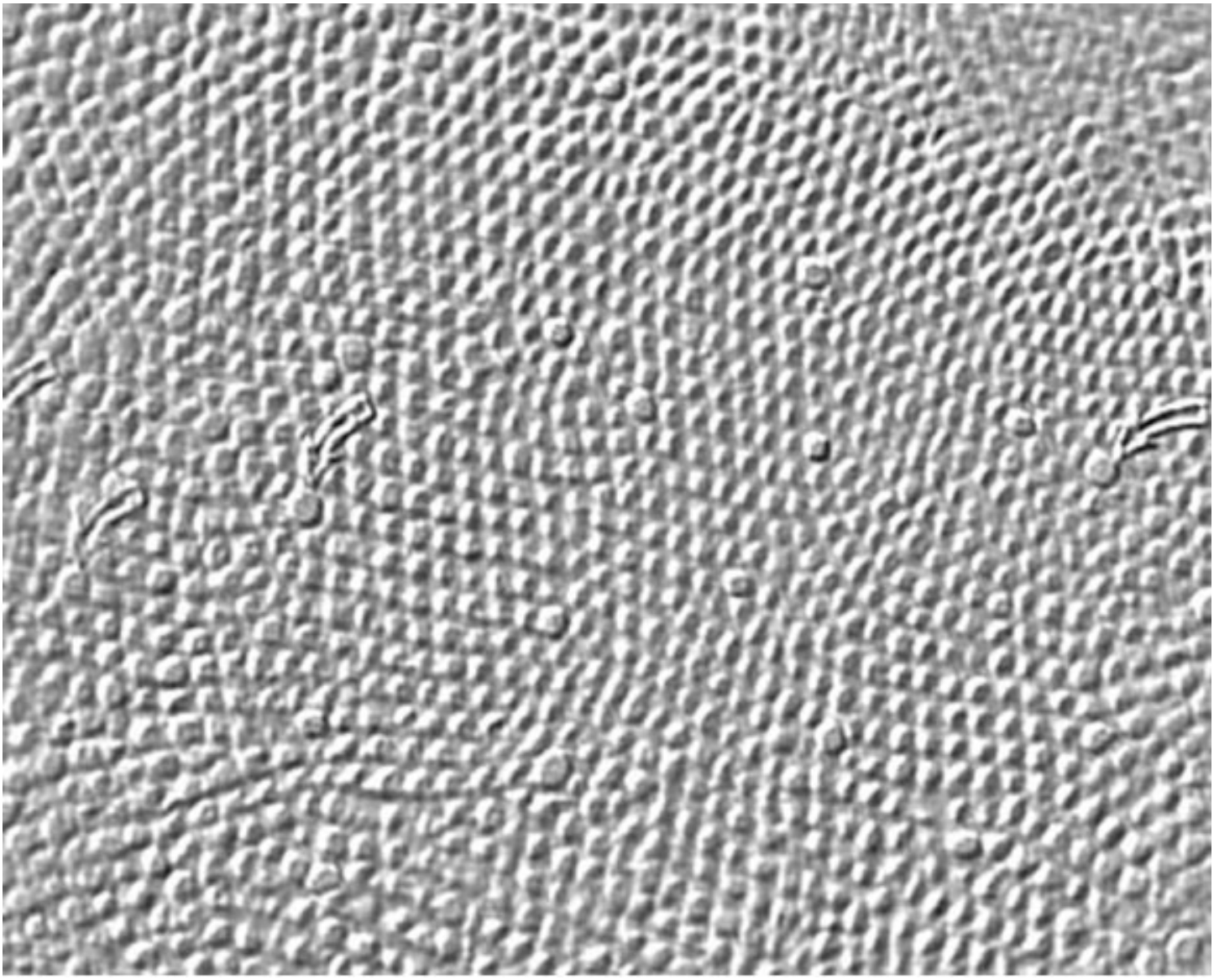

Figure 2. Tangential section through the human fovea. The larger cones (arrows) are blue cones. The illustration is taken from Ahnelt et al., 1987 (6).

cells have larger dendritic fields. Obviously more than one midget bipolar axon could fit the dendritic tree of the receiving peripheral midget ganglion cell as seen in Figure 12.

The one to one relationship was positively proven to be the case in the parafoveal area by an electron microscope study and reconstruction of serially sectioned midget ganglion cells and their input midget bipolar cell axons in parafovea, about 2 mm from the foveal pit (Fig 14) (15). More recently we have also performed a serial section electron microscope study of foveal midget bipolar axons and their connections with the dendrites of foveal midget ganglion cells (Fig. 13) (14).

The respective midget bipolar cells are almost solely synaptic upon single midget ganglion cells (Fig. 14), except in the very central fovea where a few midget bipolar synapses are shared with neighboring midget ganglion cells because of the crowding of neurons and neuropil (Fig. 13). Since we know (16) that ganglion cells branching in sublamina **a** will be OFF center and those branching in sublamina **b** will be ON center we can be sure that midget ganglion cells branching close to the amacrine cell layer will be OFF center and those branching close to the ganglion cell layer will be ON center. This ON and OFF midget ganglion cell organization in primate has

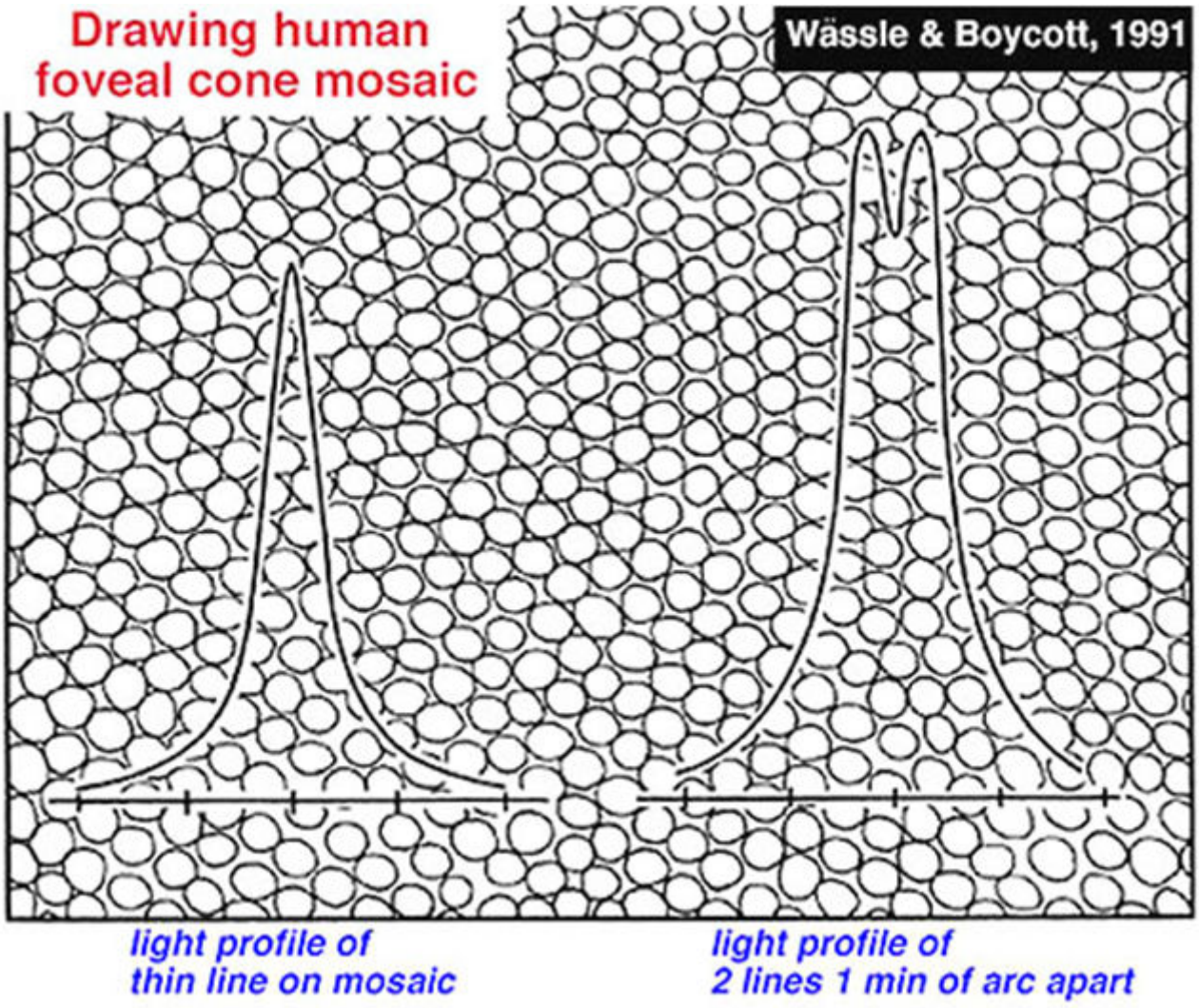

Figure 3. Human foveal cone mosaic. Visual discrimination of 1 min of arc is about the center to center spacing (3 μm) of the cones of the central mosaic in the foveola. The illustration is from Wässle and Boycott, 1991 (3).

now been shown conclusively by Chichilnisky's group (17). So it appears that in the foveal region and out to the borders of the central retina (about 4 mm from the fovea center) the midget pathways of the human fovea are organized in the following manner: 1 cone to 2 midget bipolar cells (ON- and OFF-center bipolar types) to 2 midget ganglion cells (ON- and OFF-center ganglion cell types).

What we find more difficult to say is what spectral type of cone is connected in the midget bipolar to midget ganglion cell chain. M- and L-cones are indistinguishable anatomically. Where we can recognize S-cone (blue) pedicles on unusual morphological features (6, 18, 19) (see chapter on S-cone pathways), the M- and L-cones look the same. There is some evidence that M- and L-connected midget bipolar cells have different numbers of synaptic ribbons associated with their axons and therefore different quantities of output sites to their midget ganglion cell in the fovea (20): but which axon terminal/ganglion cell pair is associated with M- or L-cone pathways is still a moot question.

Four to five millimetres beyond the fovea, in near periphery, the midget bipolar cells become 2- and 3-headed, connecting to 2 and 3 cones respectively (1, 12, 21). Midget ganglion cells are found throughout the near and mid peripheral retina (1, 12, 22, 23) and their dendritic trees increase in size but are often composed of several domains of dendrites. The further peripheral it gets, the more domains of dendrites compose the dendritic tree

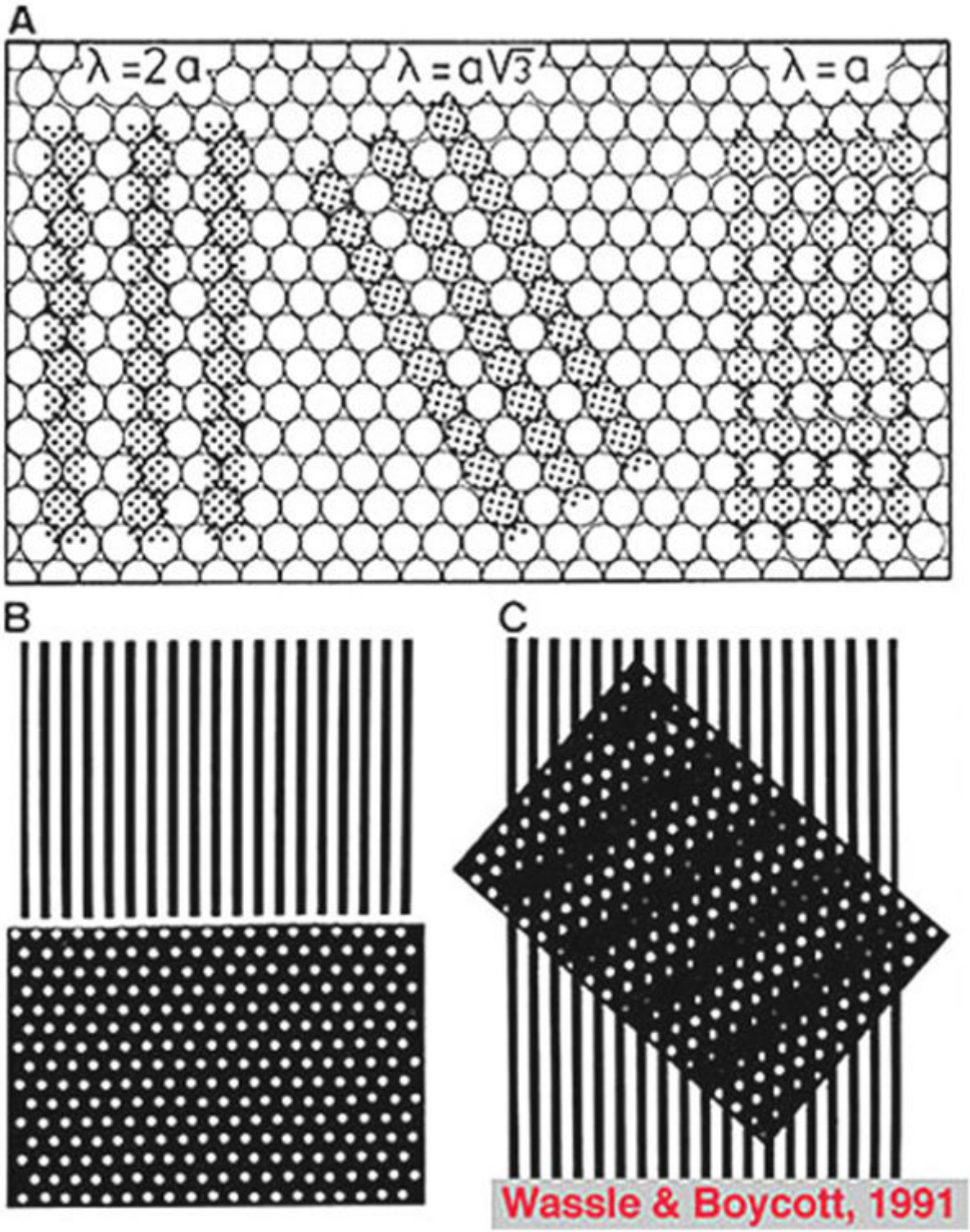

Figure 4. The minimum center to center spacing (*a*) is 3 μm for the cones of the fovea. This determines the Nyquist spatial resolution limit, a√3, approximately 1 min of arc. If the grating wavelength (λ) is less than this, Moire patterns (*B* and *C*) result which vary depending of the angle of the mosaic to the grating. Thus the grating can't be uniquely resolved. The illustration is from Wässle and Boycott, 1991 (3).

of midget ganglion cells. So it seems likely, that more than one midget bipolar cell will synapse upon each midget ganglion cell, probably each bipolar occupying one of the domains of the dendritic tree.

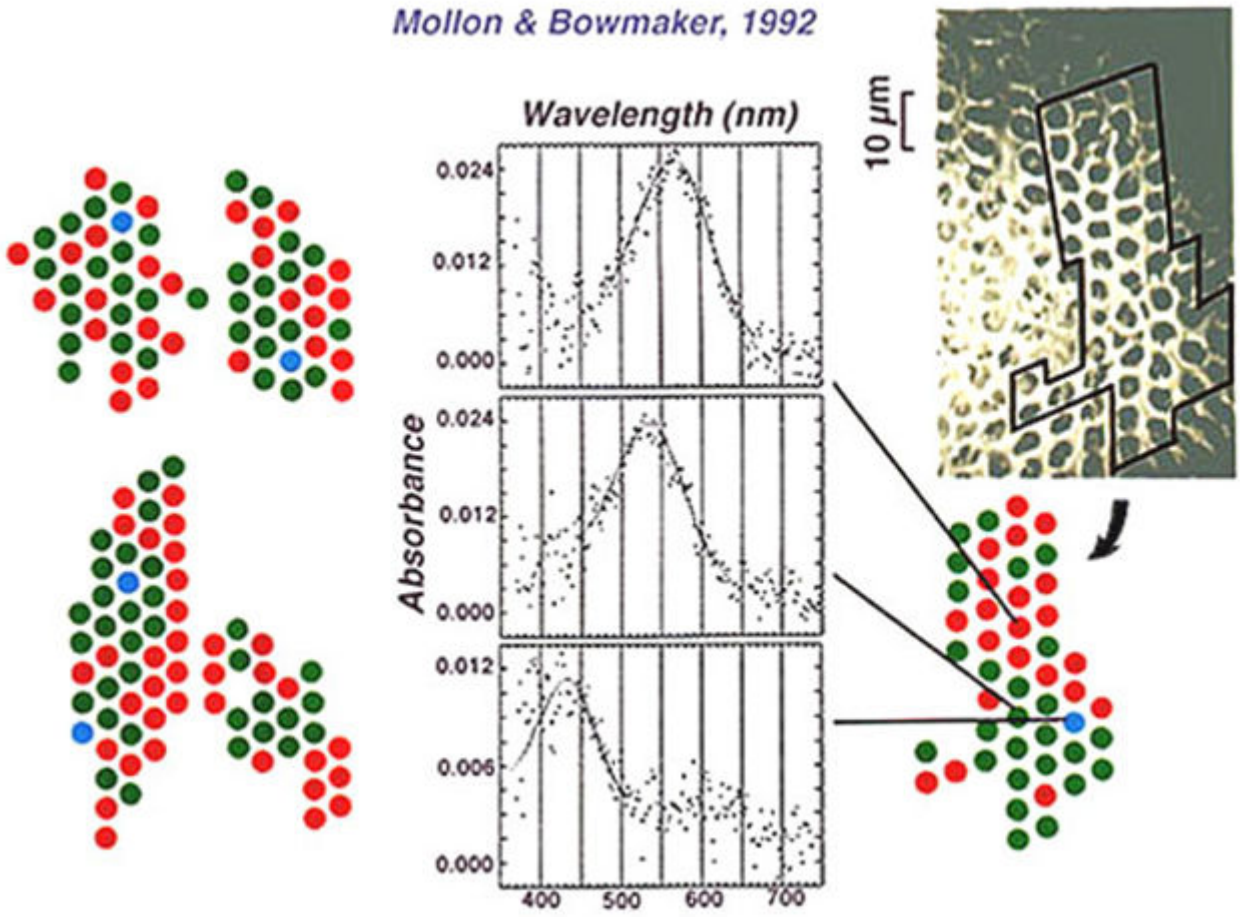

Figure 5. Absorbance spectra of three cone types as measured in foveal patches of cones in rhesus monkey. The spectral composition of these cone patches are shown. The illustration is from Mollon and Bowmaker, 1992 (8).

Serial section electron microscopy and reconstruction of axons and dendrites of midget ganglion cells at the edge of the central area (i.e. 4 mm from the foveal center) and from peripheral retina (12 mm from the foveal center) indicate that the prediction of multiple input from cones to midget bipolar cells, and multiple inputs from midget bipolar cells to midget ganglion cells is correct in peripheral retina (Fig. 15 and Fig. 16). Our estimation (14) is that 3 midget bipolar cells synapse on a single ganglion cell 4 mm from the fovea (Fig. 15) (14). Even more convergence of midget bipolar cells to midget ganglion cells occurs in far peripheral retina where we estimated at least 3 multi-headed midget bipolar cells synapse on a single midget ganglion (Fig. 16).

In the fovea where a single cone connects with its midget bipolar and midget ganglion cell system, the pathway will of necessity be carrying a single color receptive field center. Beyond the fovea where the midget pathway is 2 and 3 channeled and/or many midget bipolars have input, the midget ganglion cell's center may be a mixture of cone color types. Despite the patchy and random nature of the red and green cone mosaic and multiple midget bipolar inputs, does the midget ganglion cell retain a dominant commitment to one spectral class of cone and a color opponent center surround organization? This is in fact is what is concluded in both physiological (24-26) and the most recent functional connectivity report from Chichilnisky's group (Fig. 17) (17). Figure 17 shows the results of midget ganglion cell measurements with multielectrode recordings and high resolution stimulation of single cone types included in these ganglion cells' receptive fields. Although both red and green cones input the cell, single spectral type of cone i.e. either red types or green types, dominate the receptive field centers (Fig. 17, white outlined, and white lines).

Figure 6. Stephen L. Polyak (1889-1955) is a major authority on the anatomy and neural organization of the primate eye.

5. Circuits underlying red and green color opponency in the human retina

Midget ganglion cells of the monkey retina (presumably also of human retina) are known to respond to light with an opponent chromatic organization in their surround (5, 27, 28) (Fig. 18). That is, midget ganglion cells of central retina, when recorded from electrophysiologically, have the smallest receptive fields, and are organized as

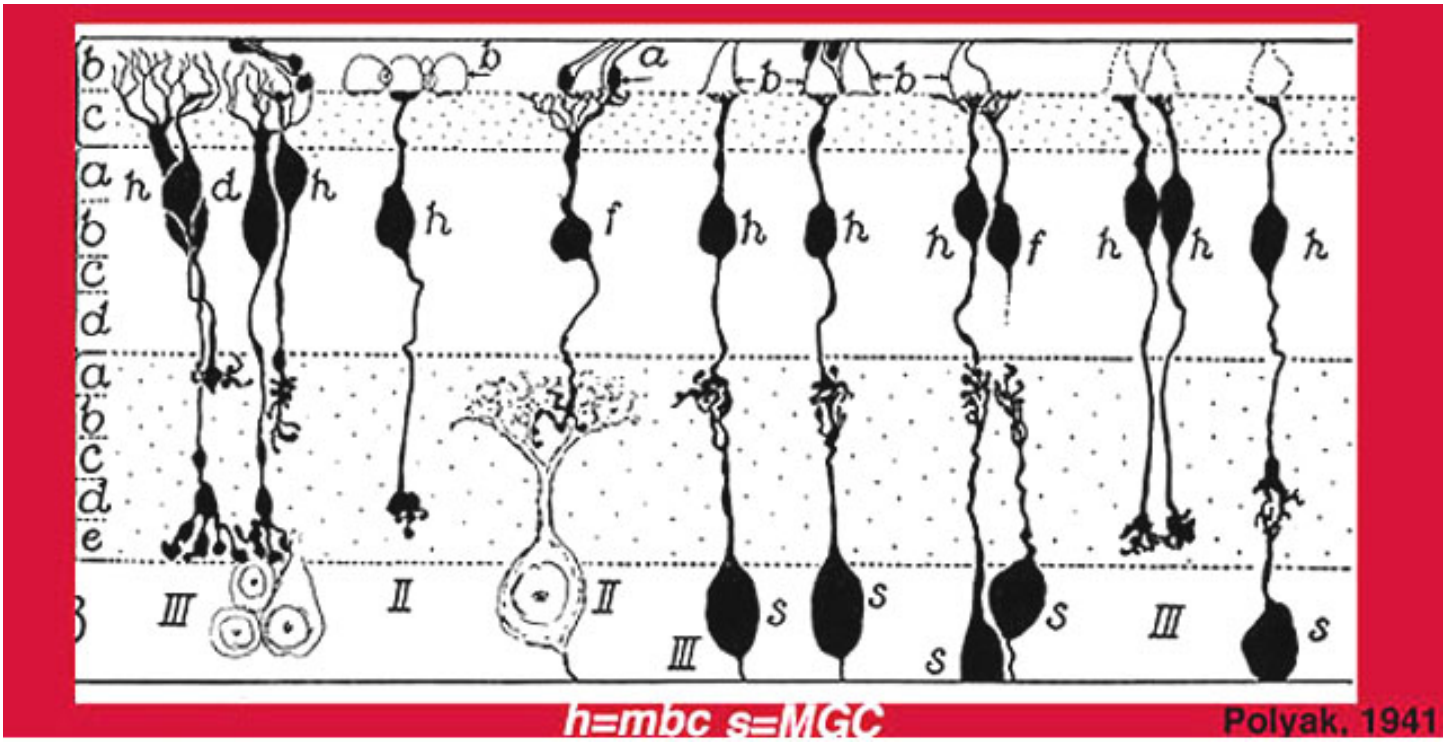

Figure 7. Drawing of Golgi-stained midget bipolar cells (h) in the monkey retina by Polyak, 1941 (1).

L-cone ON or OFF center, and M-cone ON or OFF center. Each midget ganglion cell type has a larger surround of the opposite polarity and the opponent color. The surrounds of the midget ganglion cells, as Chichilnisky's group have elegantly shown (17), That the surround is comprised of many red and green cone inputs, suggesting non-specific, but mixed spectral input to surrounds (Fig. 17e-g, black lines and circles).

The parasol varieties of ganglion cells are the non-color opponent, phasic varieties of ganglion cell recorded in the retina (28) and are also called M cells projecting to the lateral geniculate nucleus (13, 28, 29). A smaller field, tonic and not clearly color opponent ganglion cell type is also recorded in the retina and parvocellular layers of the geniculate nucleus (Fig. 18) (5). Whether these are the minority extrafoveal midget ganglion cells that are no longer color specific like some of the cells in the Field et al., study (17) remains to be seen.

The opponent color surrounds recorded in midget ganglion cells (28) provide color and spatial opponency. It appears clear now that all primate cone bipolar types have a center/surround organization (Fig. 19) (17, 30). This includes the midget bipolar cells (Fig. 19) (30). Where does this antagonistic surround organization come from?

The horizontal cells are thought to contribute to the surround response of bipolar cells in submammalian species and particularly in creatures with good color vision. Horizontal cells have been shown to be color opponent in response in fish and turtles for example (31-34). The situation is different in primate retina where color opponency has been difficult to detect in intracellular recordings of monkey horizontal cells (35) despite the anatomical findings on spectrally selective connectivity (35, 36).

However, it has recently been shown by elegant experiments in macaque monkey that red and green cones receive an antagonistic surround response from horizontal cells, presumably HI cells (37). Similarly, primate (blue) S-cones clearly have an opponent yellow surround that appears to come from horizontal cells driven by L- and M-cones according to Packer and co-authors (38). Very recent evidence from the same group (39) indicates quite definitively that horizontal cell feedback can account for surround opponency to red and green midget ganglion cells in primate retina, showing that the midget bipolar cells are already color opponent in nature. There does not appear to be any inner retina (amacrine cell) input to organize surrounds in midget bipolar cells

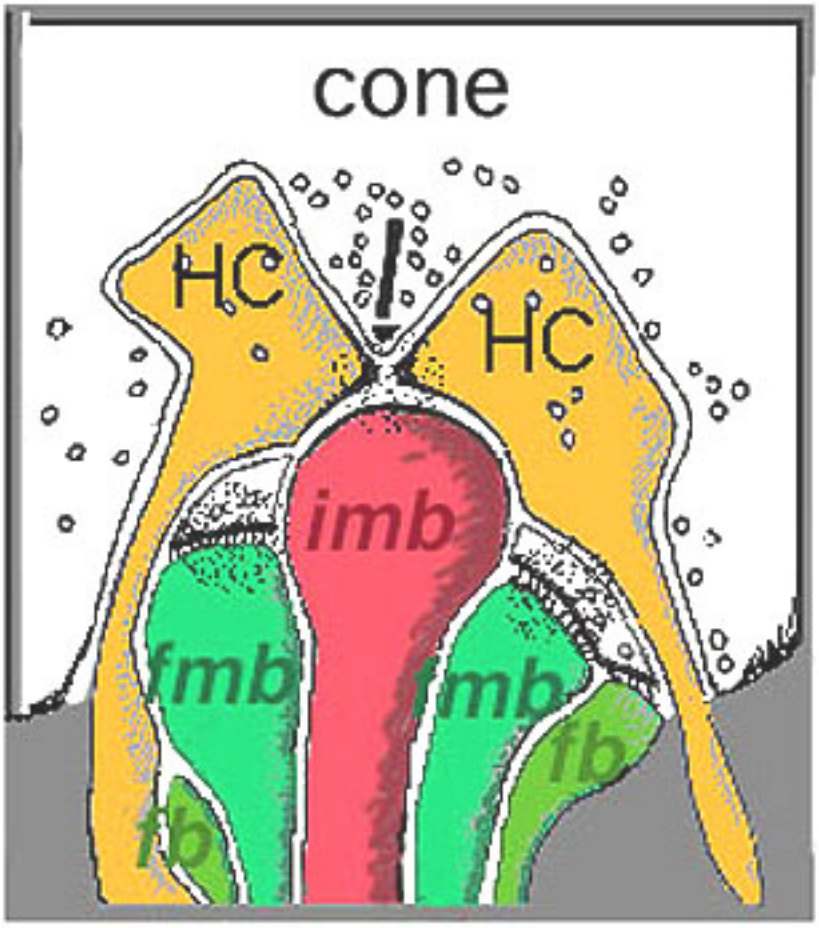

Figure 8. Schematic drawing of a cone pedicle ribbon triad to show the differences in synaptic contacts of invaginating midget and flat midget bipolar cell dendrites.

and midget ganglion cells. The possibility exists that some large field diffuse cone bipolar types that are not spectrally opponent, and have surrounds consistently larger than midget bipolar cells, could involve an amacrine cell content (30, 40).

We believe that L- and M-midget ganglion cell responses are organized in the manner shown in Figure 20. An L-cone would contact two L-cone midget bipolars and through them, two L-cone midget ganglion cells. For example, an L-cone ON-center midget bipolar would contact a single L-cone at invaginating synapses in the OPL, and a single L-cone ON-center midget ganglion cell in sublamina **b** of the IPL. The same L-cone would also be contacted by a single OFF-center midget bipolar at basal junctions, and the bipolar would, in turn, contact a single OFF-center midget ganglion cell in sublamina **a** of the the IPL (Fig. 20, left). Thus L-cone ON- and L-cone OFF-center receptive field ganglion cell types are generated (red + center and orange - center, Fig. 20, left). M-cones would be connected in a similar manner to two midget bipolars (ON and OFF types) and two midget ganglion cells which would also be ON and OFF-center receptive field types (dark green + center and light green - center, Fig. 20, right).

All of the three types of horizontal cell, HI, HII and HIII could make M-cone surrounds to L-cone center bipolars, and L-cone surrounds to M-cone center bipolar cells. However the HII cell may be more involved with spectrally antagonistic fields in the blue/yellow bipolar cell pathways (see Webvision: S-Potentials and Horizontal Cells).

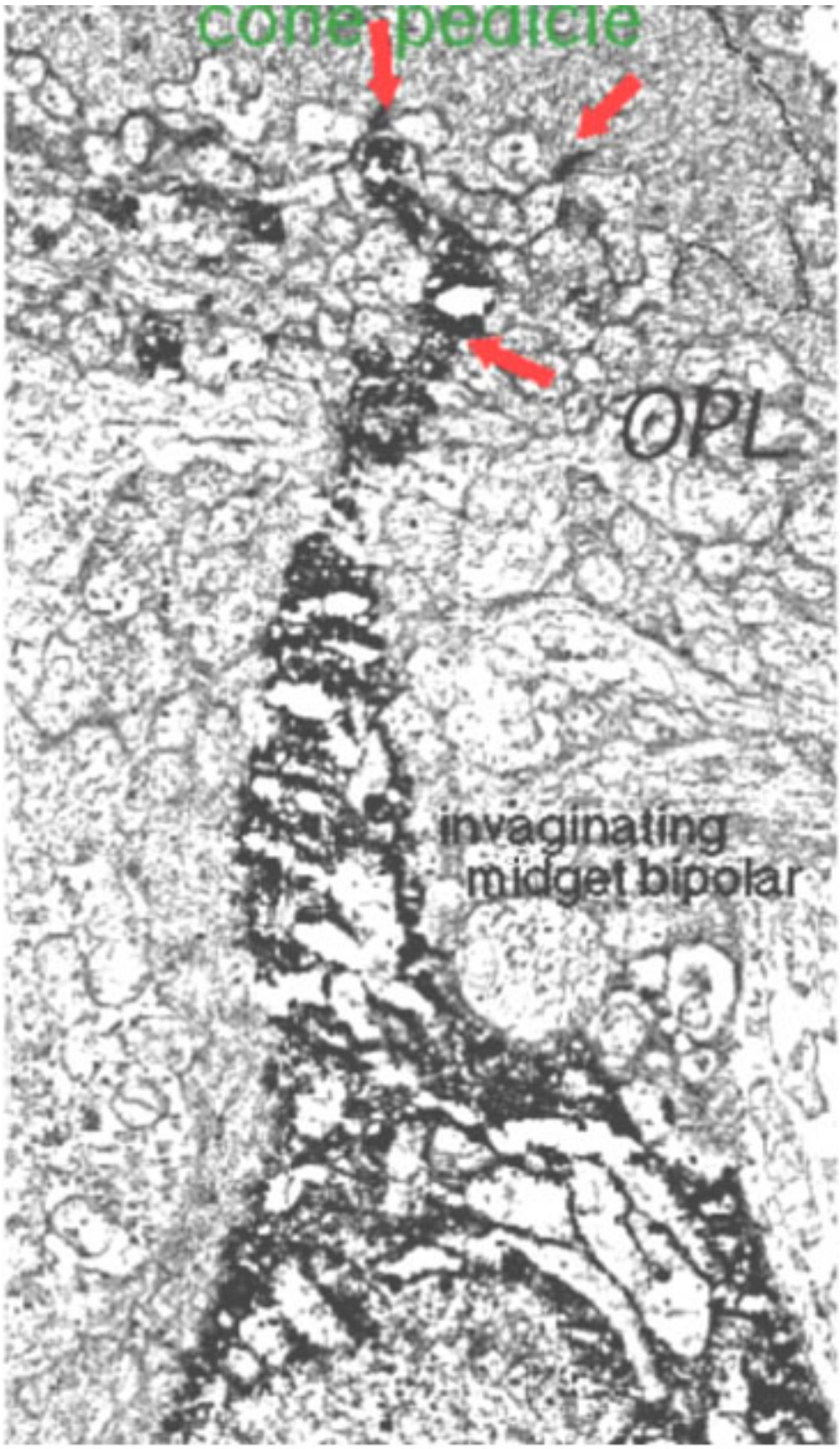

Figure 9. EM of a Golgi stained invaginating midget bipolar cell in the monkey retina. OPL, outer plexiform layer.

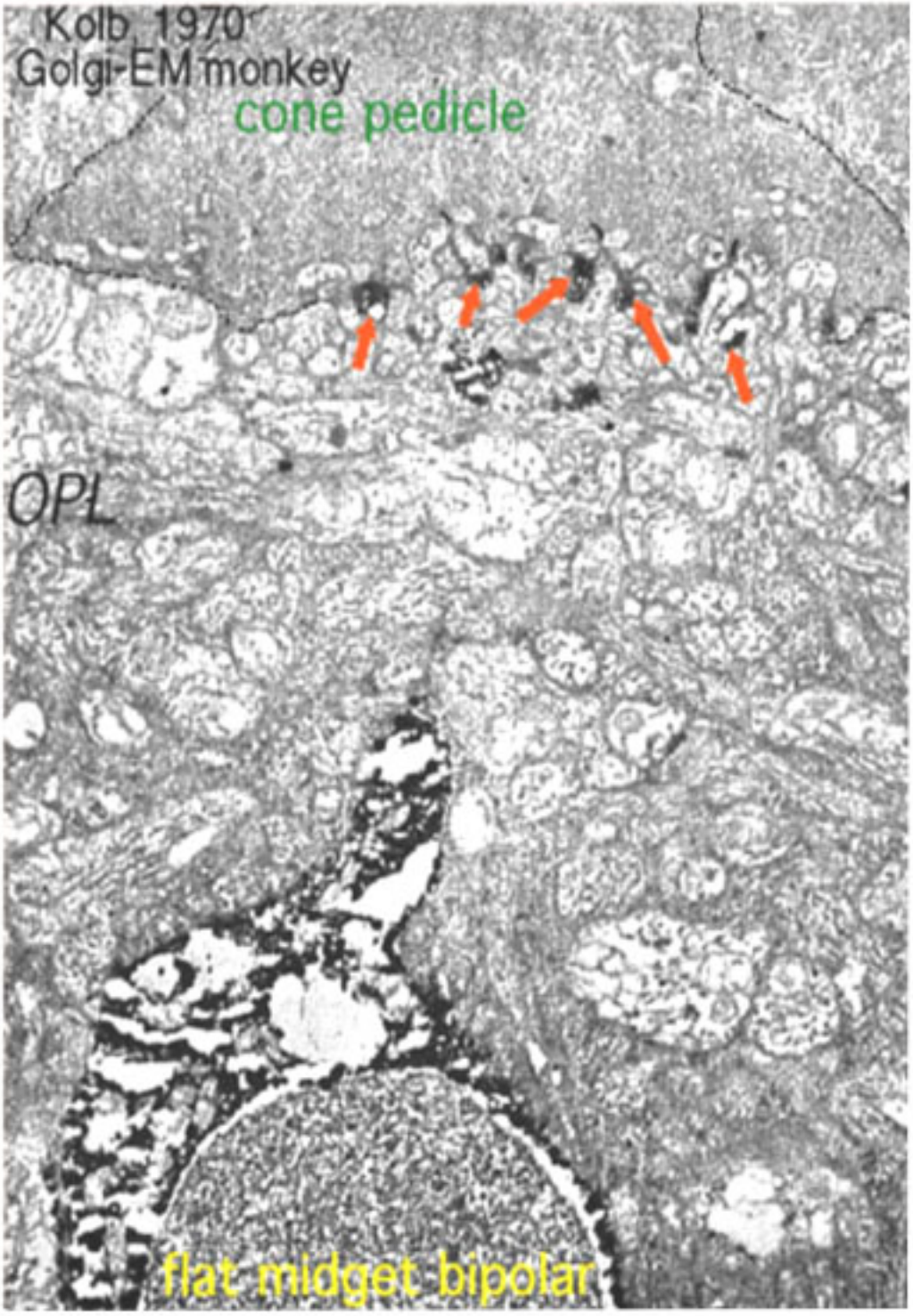

Figure 10. EM of a Golgi-stained flat midget bipolar cell in the monkey retina. OPL, outer plexiform layer. The illustration is from Kolb, 1970 (10).

6. Magnocellular and blue/yellow ganglion cells

The large field parasol cells of the primate retina are thought to convey achromatic information concerning low spatial acuity, movement and luminance messages (41, 42). Parasol cells come in ON- and OFF-center varieties like the midget ganglion cells and project to the magnocellular layers of the lateral geniculate nucleus (Fig. 21):

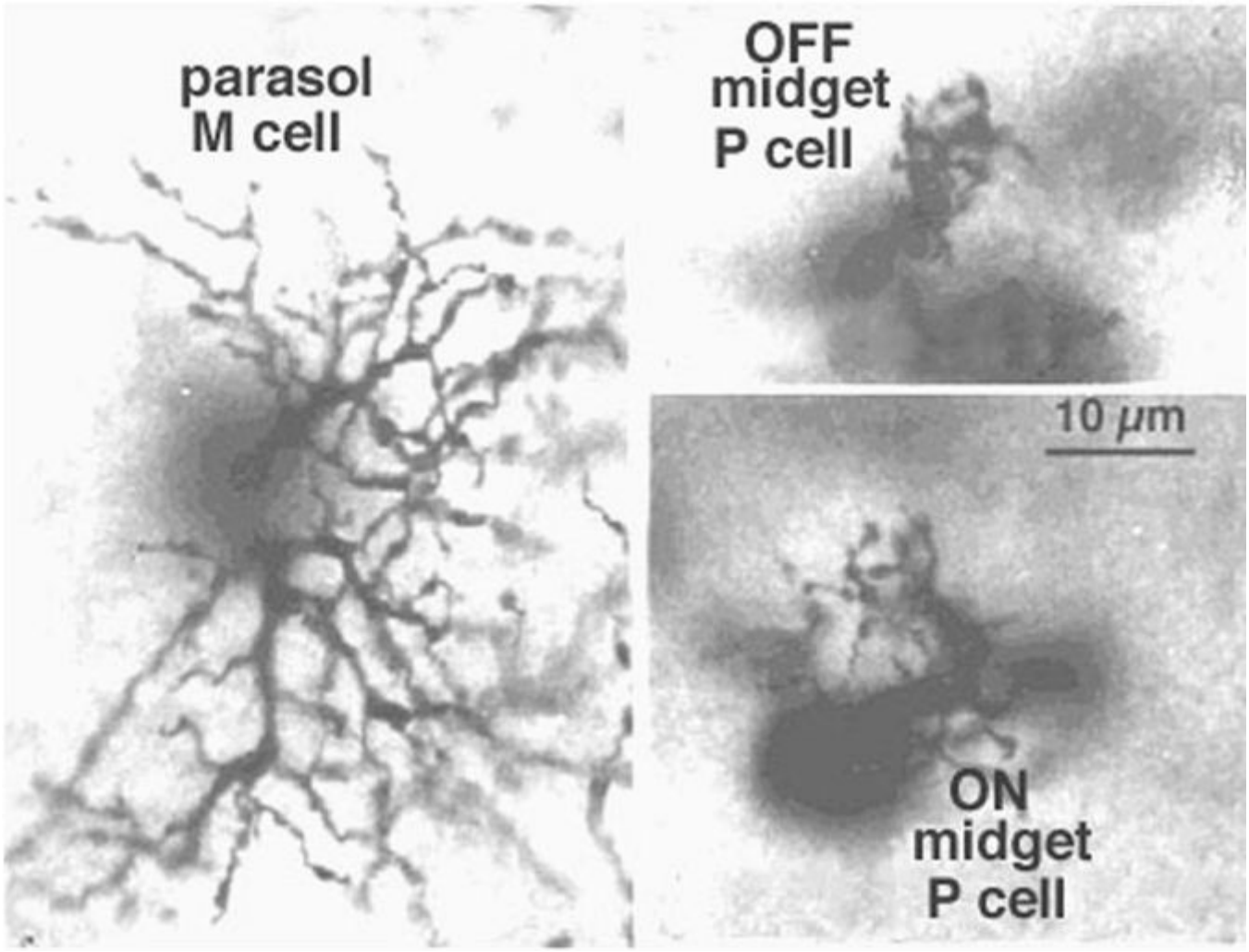

Figure 11.Golgi staining of parasol (M) and midget (P) ganglion cells in the human retina. Scale bar 10 μm for all images. The illustration is from Kolb, Lindberg and Fisher, 1992 (12)

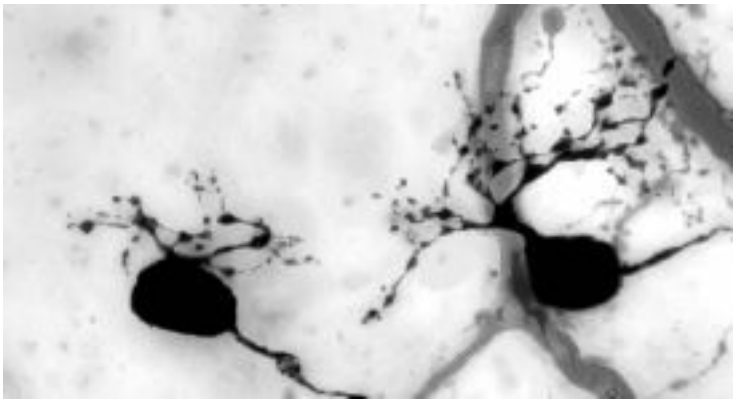

Movie 1. A focus series of two Golgi-stained P or midget ganglion cells in the human retina.

Download video

hence they are also called M cells (13, 43). Parasol ganglion cells also have a surround mechanism to their receptive field physiology, that, like the midget ganglion cells, is thought to originate mainly in the outer

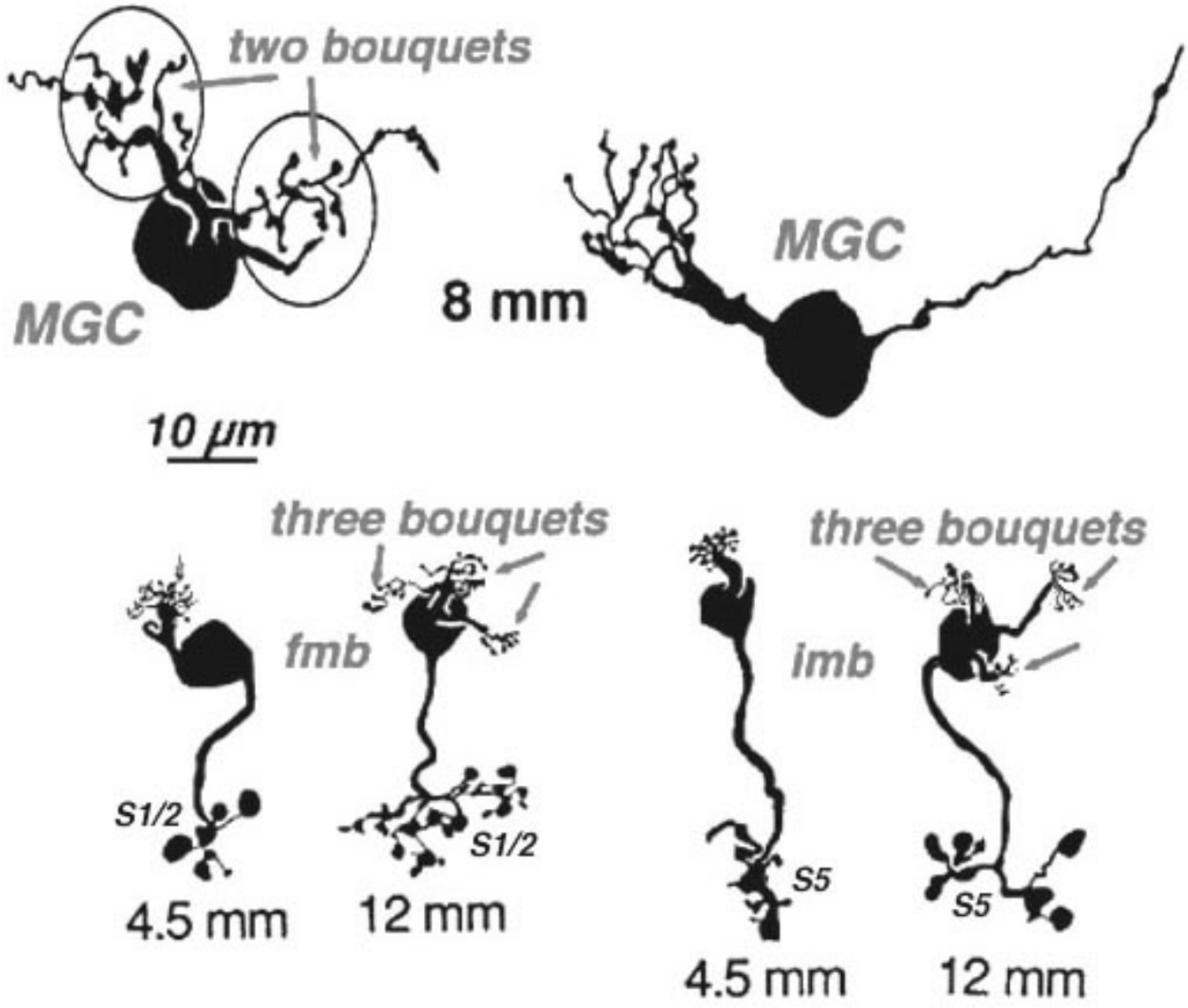

Figure 12. Midget bipolar cells (imb, fmb) have larger axon terminals at greater distances from the fovea (retinal eccentricity of 4.5mm as compared to 12 mm). Midget ganglion cells (MGC) have larger dendritic fields (here seen at 8 mm) as they increase in eccentricity..

plexiform layer from a horizontal cell feedback mechanism (44). The blue yellow ganglion cells (Fig. 21) are a bistratified type and thought to be driven by blue-specific bipolar cells, and other midget or diffuse types to give them their yellow response (11). They project to a special layer of the geniculate nucleus called the koniocellular layer or K layer (45, 46) (Fig. 20). We shall deal with the short wavelength sensitive system in another chapter (Webvision: S-cone pathways) and so will say little more about these ganglion cells here.

About the Authors

The biosketch for Helga Kolb can be found in the About the Editors section of Webvision.

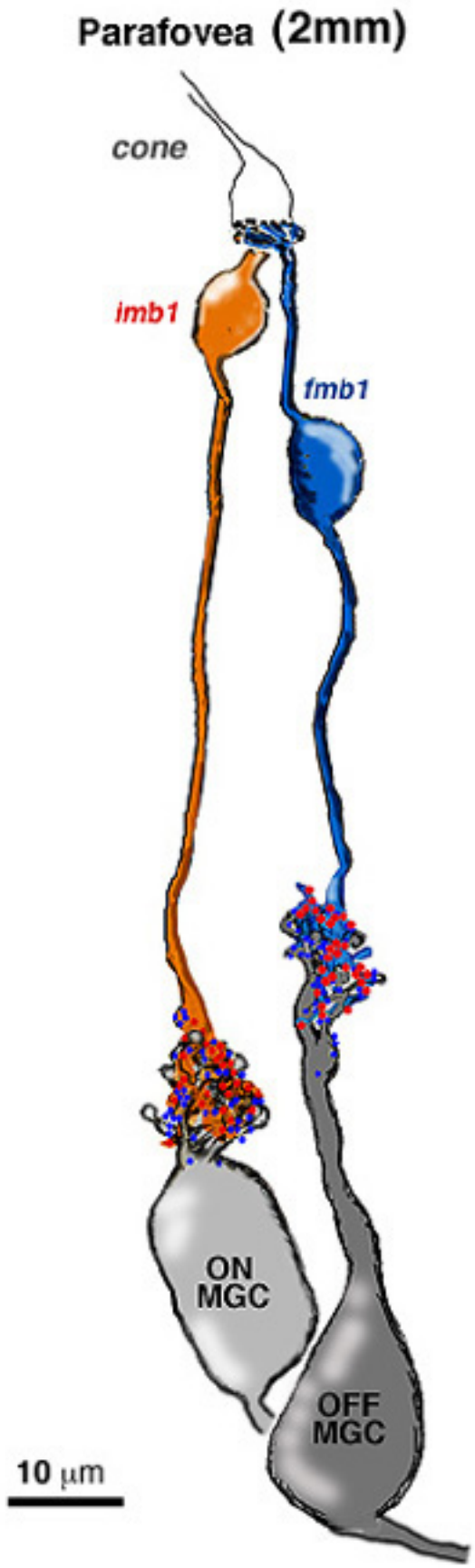

Figure 14. 3-D reconstruction taken from serial electron micrographs of a flat and an invaginating midget bipolar cell and their respective midget ganglion cells at 2mm from the foveal center in human retina..

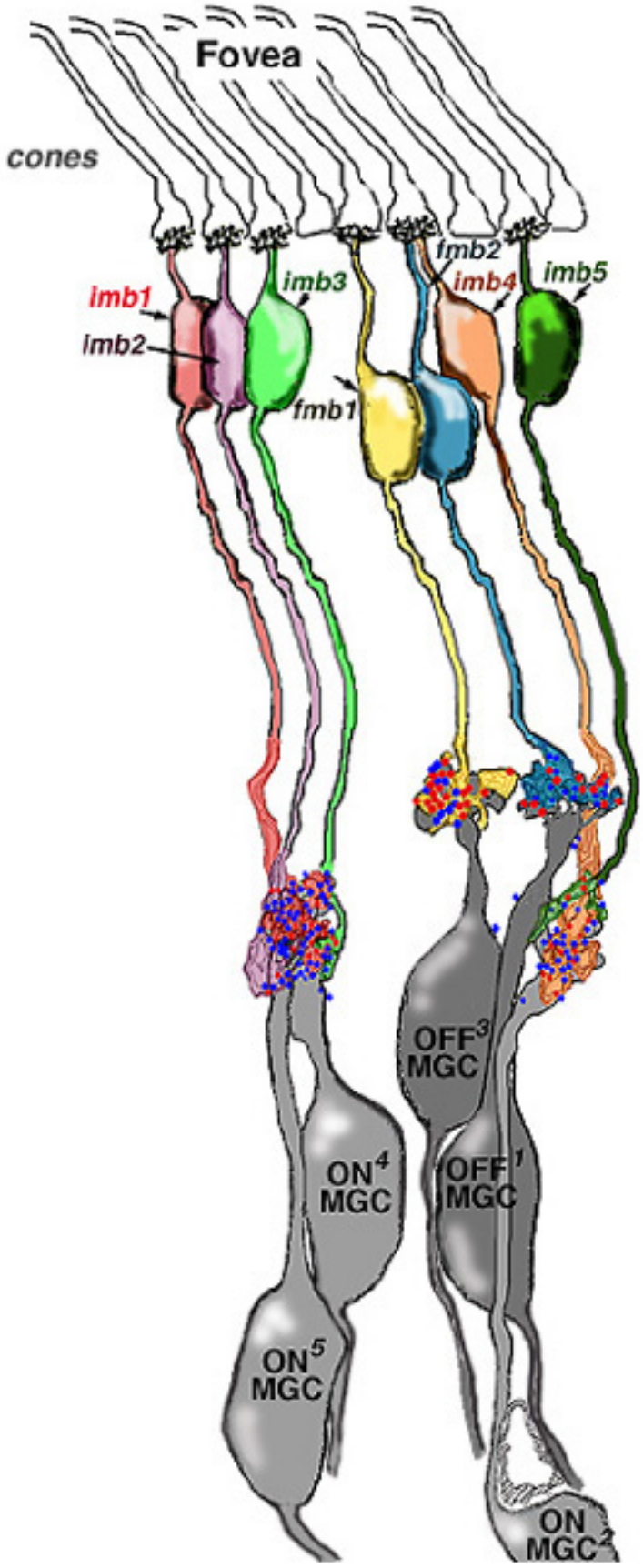

Figure 13. 3-D reconstruction in human fovea taken from serial electron micrographs of a group of neighboring midget bipolar cells and their post-synaptic midget ganglion cells..

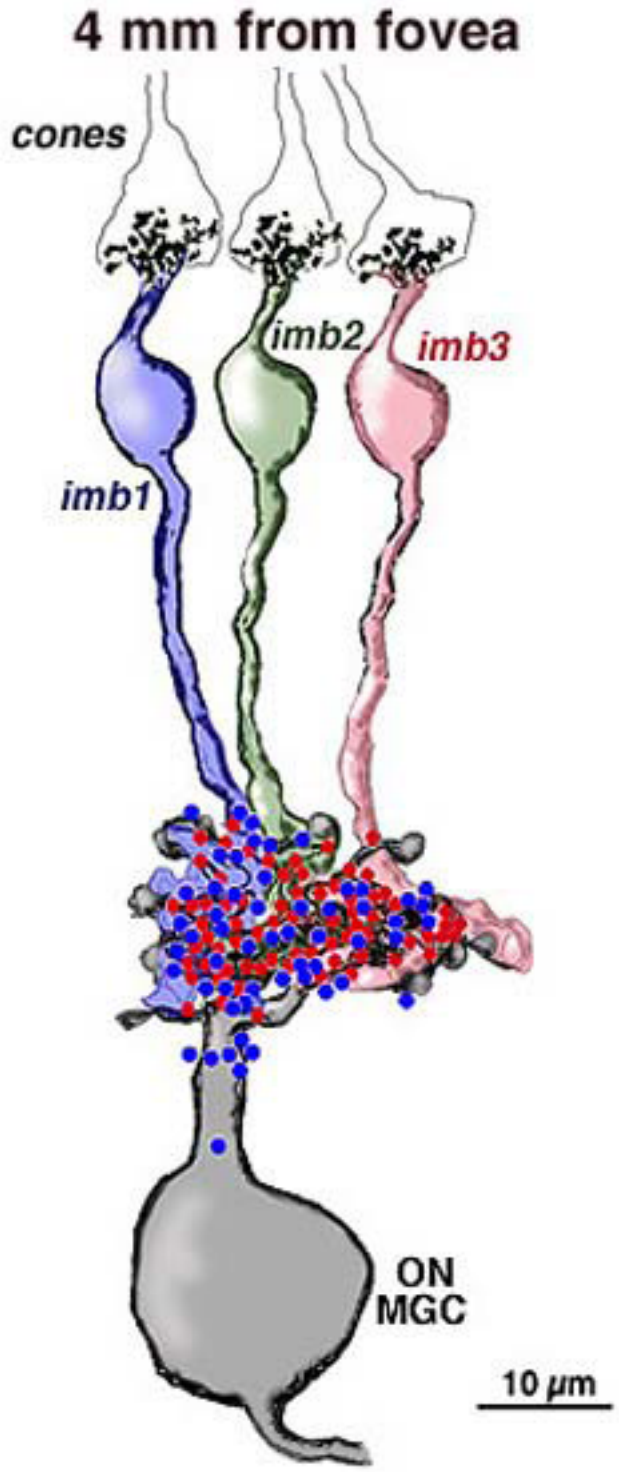

Figure 15. 3-D reconstruction taken from serial electron micrographs of a single midget ganglion cell (ON MGC) at 4 mm eccentricity from the foveal center in macaque retina. Three midget bipolar cells (imb1, imb2, imb3) synapse upon the midget ganglion cell, each in contact with a single cone. Thus 3 cones input to this midget ganglion cell.

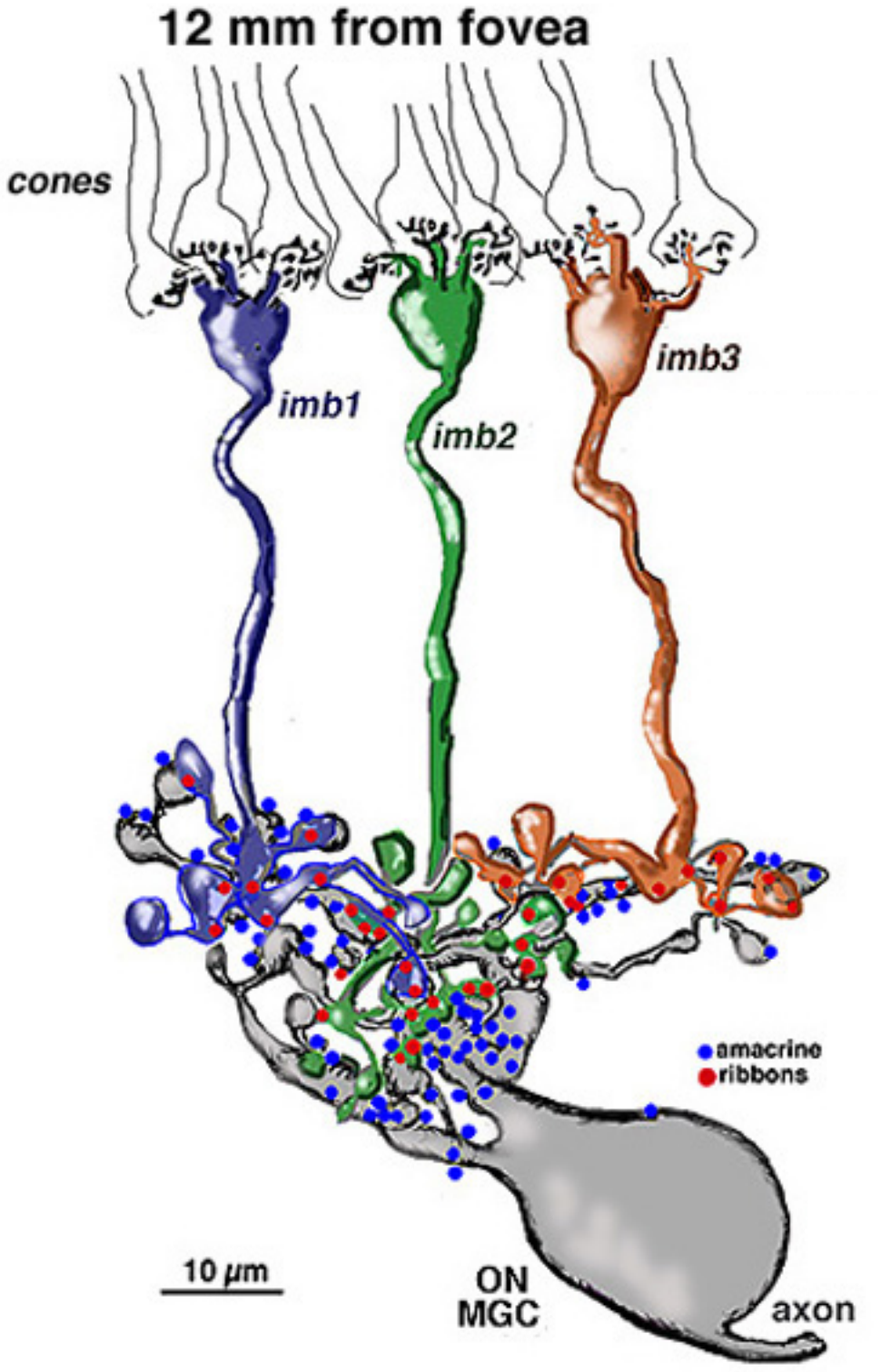

Figure 16. 3-D reconstruction taken from serial electron micrographs of a peripheral midget ganglion cell (ON MGC). Three domains of its dendrites receive from three midget bipolar cells (imb1, imb2, imb3). As each midget bipolar cell is likely to be three-headed at this eccentricity, it is likely that 9 cones are connected to this ganglion cell.

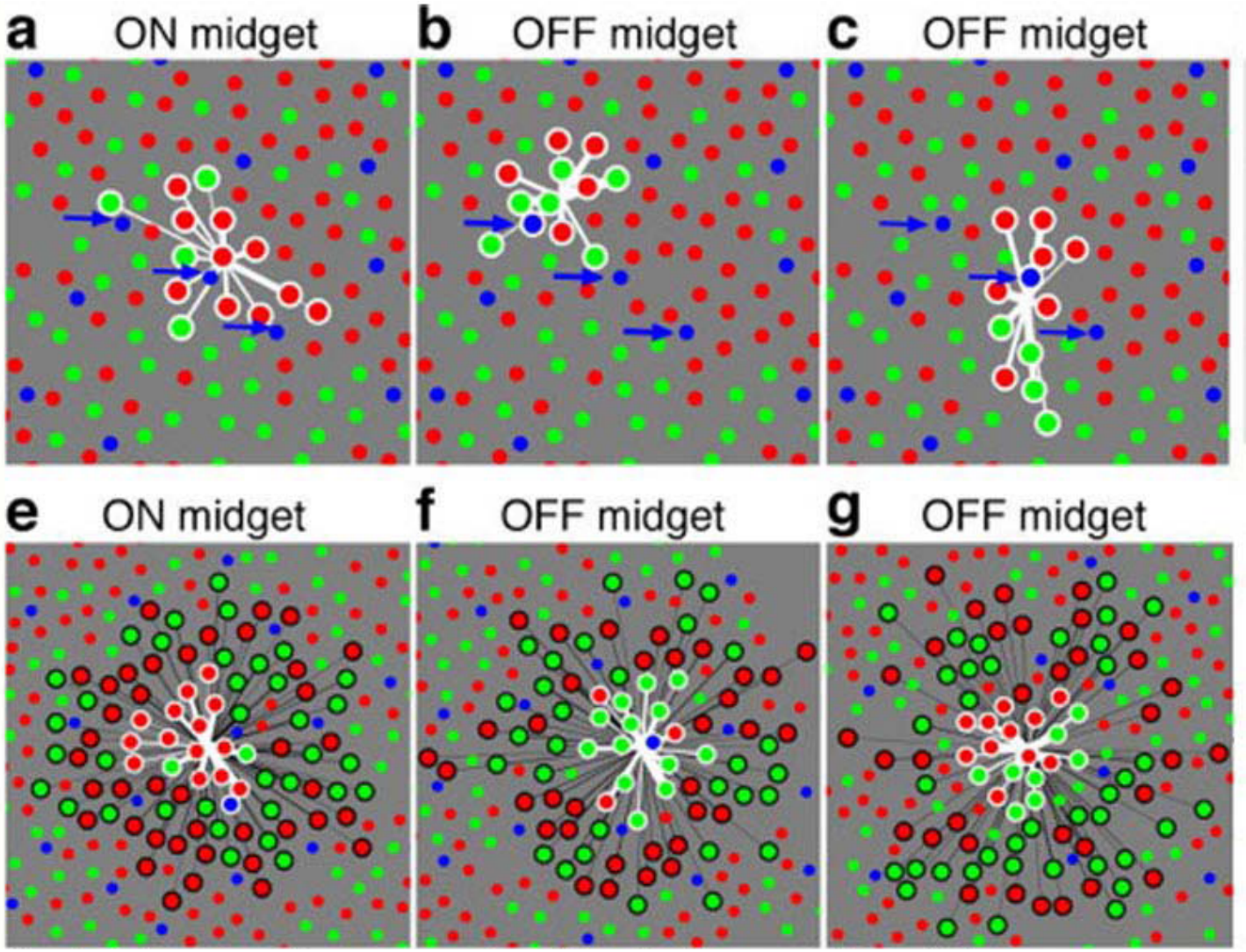

Figure 17. The cone wiring pattern of peripheral midget ganglion cells in macaque monkey retina. a) to c) Functional mapping of cones by ON and OFF midget ganglion cell centers. Spectral composition is mainly a mixture of red and green cones. The white circles indicate central cone input. Note in b) and c) a blue cone provides input. In the surrounds of such midget ganglion cell, e) to g) (black circles), many red and green cones have input, suggesting non-specific, but mixed spectral input to surrounds. The illustration is from Field et al, 2010, including many contributors from the Chichilnisky group (17).

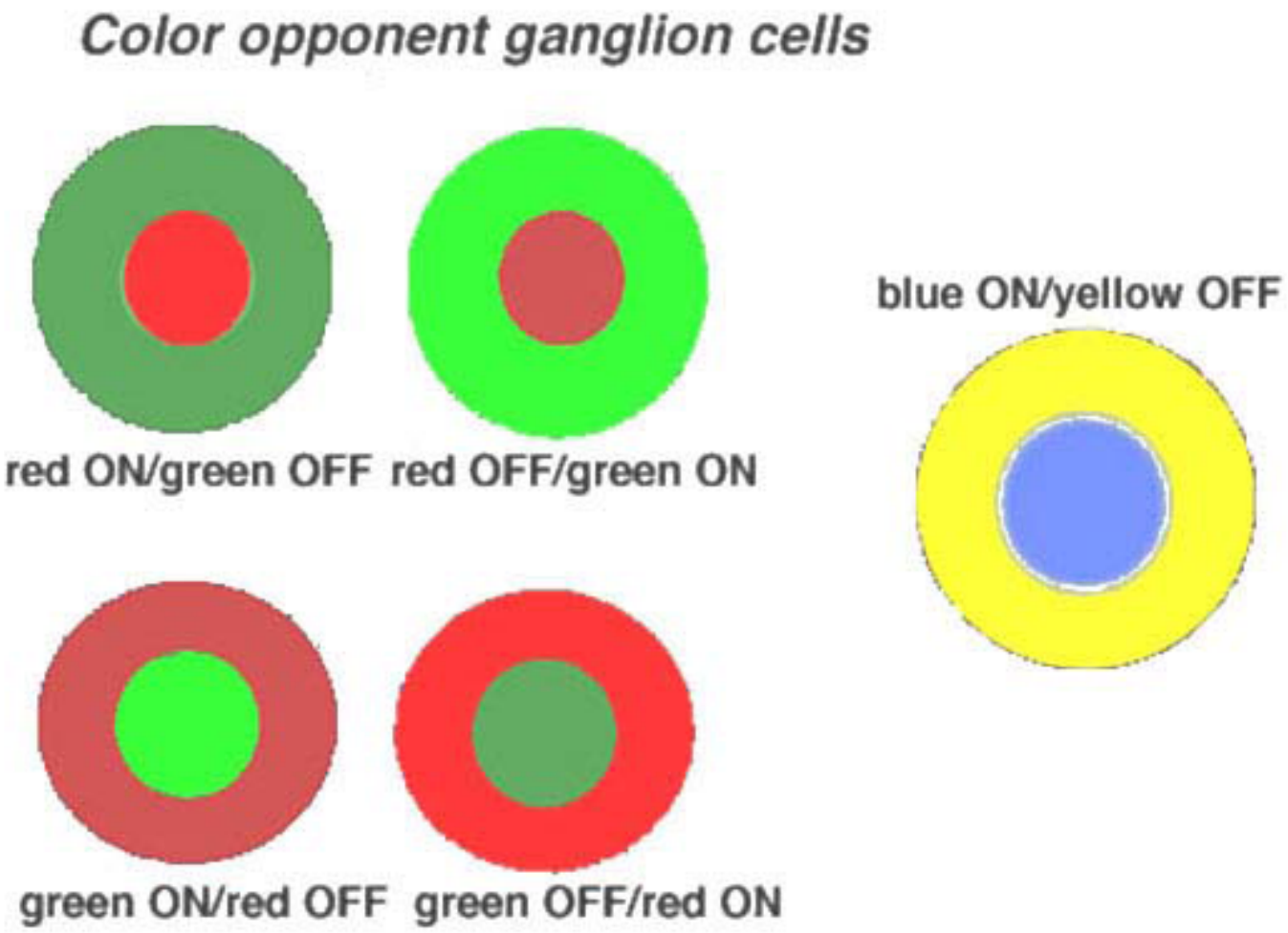

Figure 18. Color-opponent units as recorded in monkey retina. The illustration is from Gouras, 1968 (28).

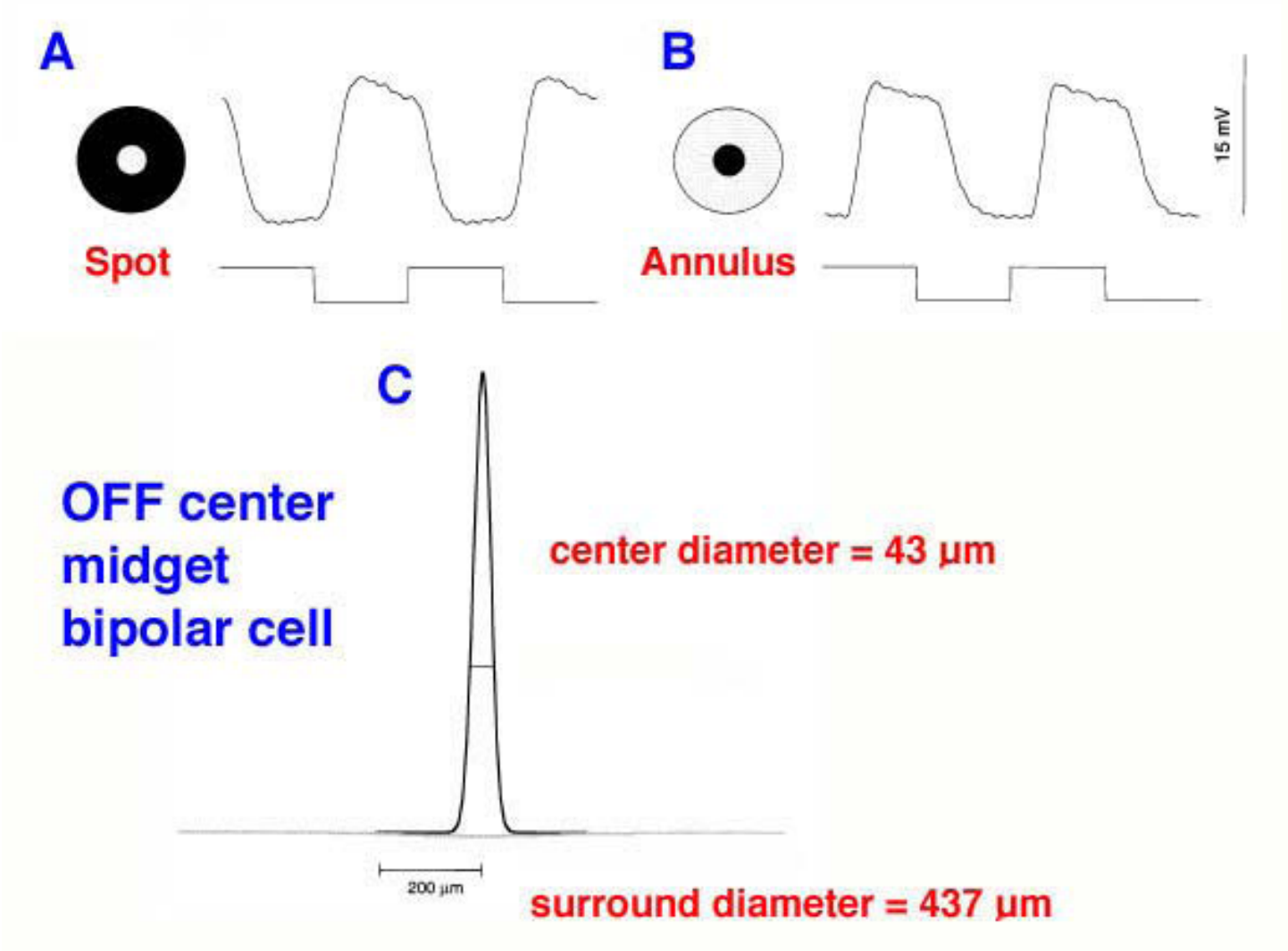

Figure 19. Center-surround receptive field structure of monkey bipolar cells. (A) Bipolar cell hyperpolarized to a small 150 µm diameter spot centered on the receptive field. (B) Cell depolarized to an annulus (inner diameter 150 µm; outer diameter 1200 µm), Stimulus wave-form is shown below the traces in A and B. (C) Plot of the center and surround Gaussians, giving the center (43 µm) and surround (437 µm) mean receptive field diameters. The illustration is from Dacey et al., 2000 (30).

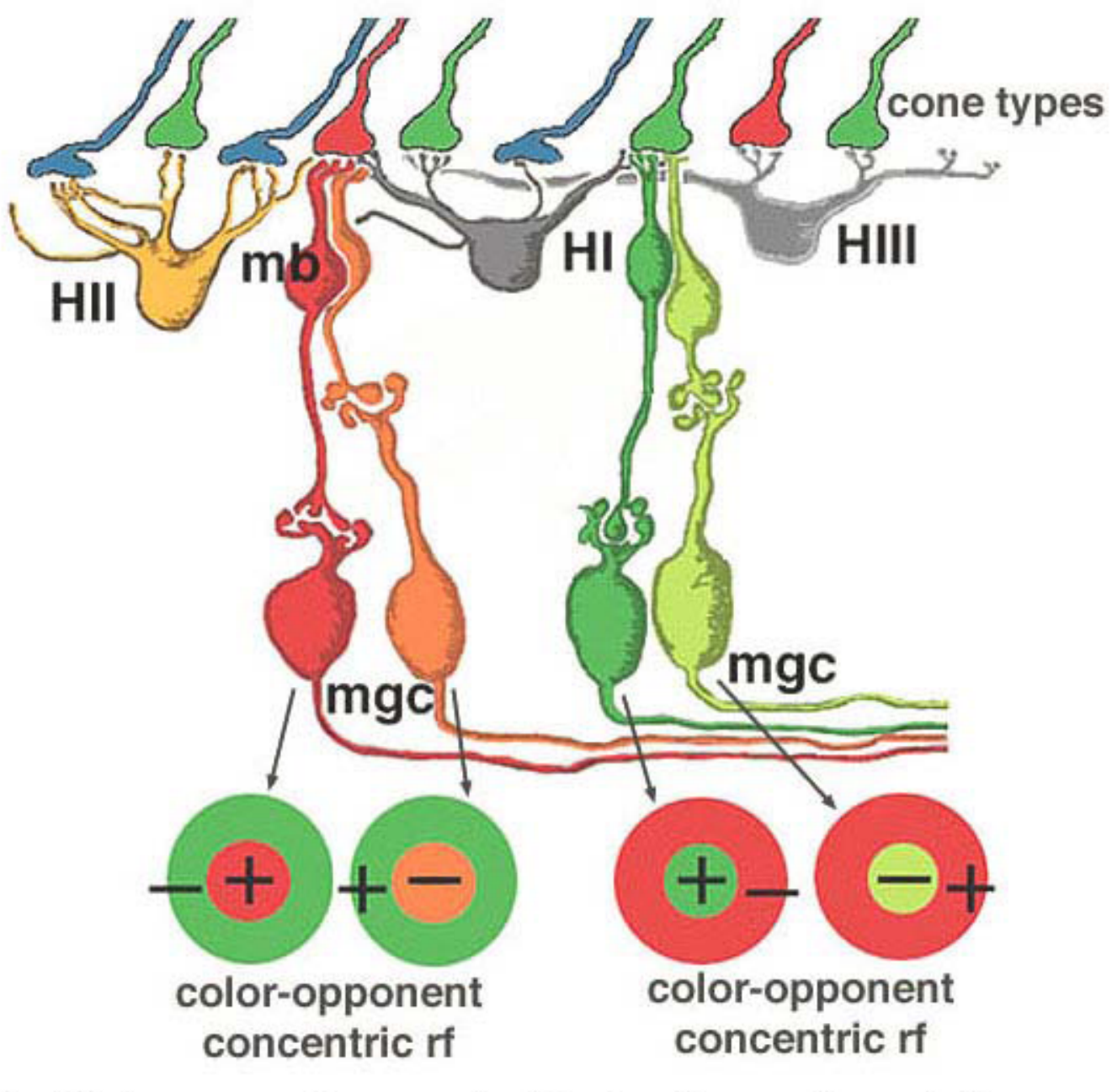

Figure 20. Summary diagram of midget pathways through the primate retina with color opponent centers and surrounds (red/green) and ON (+) or OFF(-) centers and surrounds.

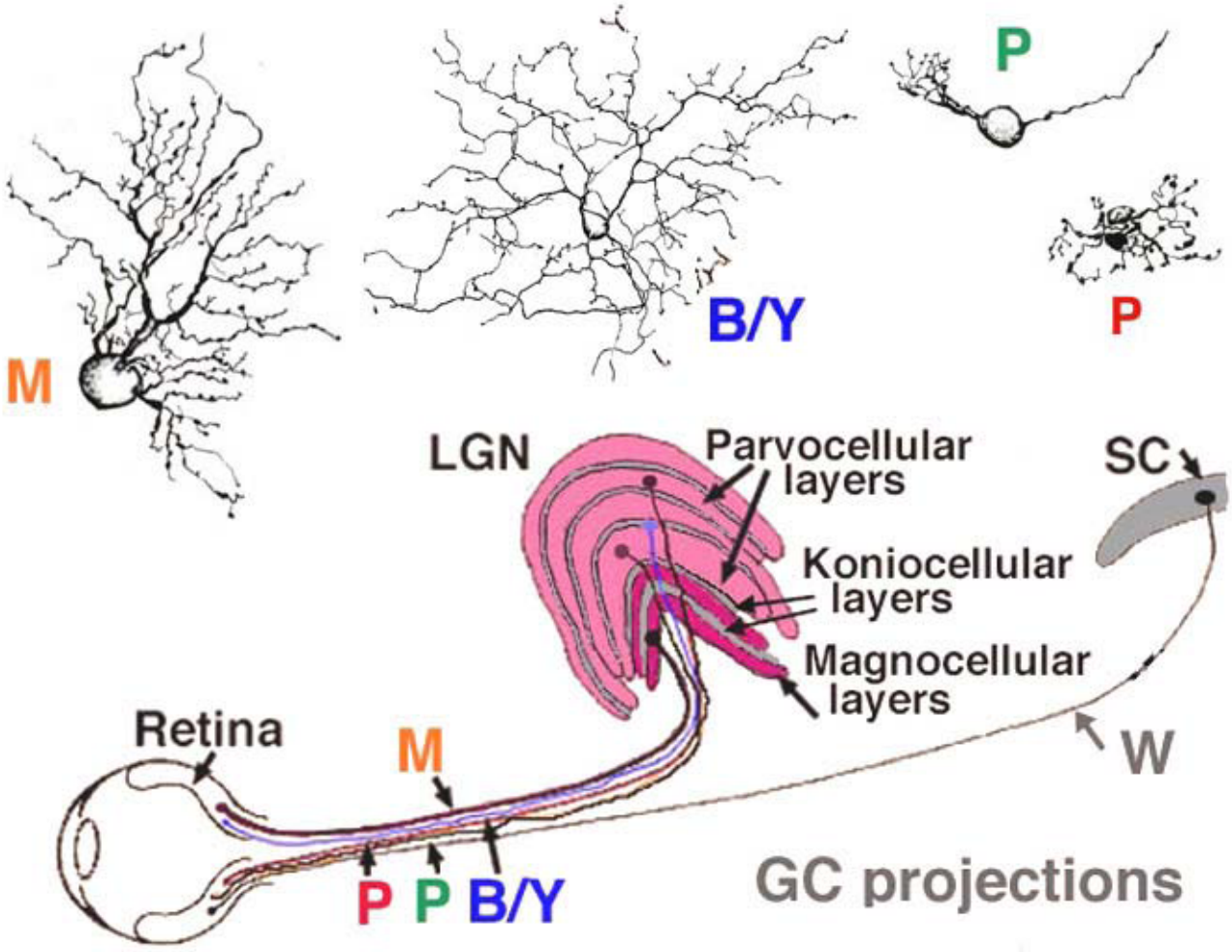

Figure 21. Diagram of the projections of primate ganglion cells to the lateral geniculate nucleus an the superior colliculus. The illustration B/Y above is from Dacey and Lee, 1994 (11). The LGN illustration is from Shapley and Perry, 1986 (13).

References

1. Polyak, S.L., *The Retina*1941, Chicago: University of Chicago.
2. Drasdo N., Fowler C.W. *Non-linear projection of the retinal image in a wide-angle schematic eye.* .Br J Ophthalmol. 1974;58(8):709–14. PubMed PMID: 4433482.
3. Wässle H., Boycott B.B. *Functional architecture of the mammalian retina.* .Physiol Rev. 1991;71(2):447–80. PubMed PMID: 2006220.
4. Campbell F.W., Gubisch R.W. *Optical quality of the human eye.* .J Physiol. 1966;186(3):558–78. PubMed PMID: 5972153.
5. Gouras P. *Retinal circuitry and its relevance to diagnostic psychophysics and electrophysiology.* .Current Opinion in Ophthalmology. 1992;3(6):803–812.
6. Ahnelt P.K., Kolb H., Pflug R. *Identification of a subtype of cone photoreceptor, likely to be blue sensitive, in the human retina.* .J Comp Neurol. 1987;255(1):18–34. PubMed PMID: 2434534.
7. Cicerone C.M., Nerger J.L. *The relative numbers of long-wavelength-sensitive to middle-wavelength-sensitive cones in the human fovea centralis.* .Vision Res. 1989;29(1):115–28. PubMed PMID: 2773329.
8. Mollon J.D., Bowmaker J.K. *The spatial arrangement of cones in the primate fovea.* .Nature. 1992;360(6405):677–9. PubMed PMID: 1465131.

9. Roorda A., Williams D.R. *The arrangement of the three cone classes in the living human eye.* .Nature. 1999;397(6719):520–2. PubMed PMID: 10028967.
10. Kolb H. *Organization of the outer plexiform layer of the primate retina: electron microscopy of Golgi-impregnated cells.* .Philosophical Transactions of the Royal Society, London, B. 1970;258(823):261–283. PubMed PMID: 22408829.
11. Dacey D.M., Lee B.B. *The 'blue-on' opponent pathway in primate retina originates from a distinct bistratified ganglion cell type.* .Nature. 1994;367(6465):731–5. PubMed PMID: 8107868.
12. Kolb H., Linberg K.A., Fisher S.K. *Neurons of the human retina: a Golgi study.* .J Comp Neurol. 1992;318(2):147–87. PubMed PMID: 1374766.
13. Shapley R., Perry V.H. *Cat and monkey retinal ganglion cells and their visual functional roles.* .Trends Neurosci. 1986;9:229–235.
14. Kolb H., Marshak D. *The midget pathways of the primate retina.* .Doc Ophthalmol. 2003;106(1):67–81. PubMed PMID: 12675488.
15. Kolb H., Dekorver L. *Midget ganglion cells of the parafovea of the human retina: a study by electron microscopy and serial section reconstructions.* .J Comp Neurol. 1991;303(4):617–36. PubMed PMID: 1707423.
16. Nelson R., Famiglietti E.V. Jr, Kolb H. *Intracellular staining reveals different levels of stratification for on- and off-center ganglion cells in the cat retina.* .J. Neurophysiol. 1978;41(2):472–483. PubMed PMID: 650277.
17. Field G.D.et al. *Functional connectivity in the retina at the resolution of photoreceptors.* .Nature. 2010;467(7316):673–7. PubMed PMID: 20930838.
18. Ahnelt P., Keri C., Kolb H. *Identification of pedicles of putative blue-sensitive cones in the human retina.* .J Comp Neurol. 1990;293(1):39–53. PubMed PMID: 2312791.
19. Kolb H.et al. *Uniqueness of the S-cone pedicle in the human retina and consequences for color processing.* .J Comp Neurol. 1997;386(3):443–60. PubMed PMID: 9303428.
20. Calkins D.J.et al. *M and L cones in macaque fovea connect to midget ganglion cells by different numbers of excitatory synapses.* .Nature. 1994;371(6492):70–2. PubMed PMID: 8072528.
21. Boycott B.B., Hopkins J.M. *Cone bipolar cells and cone synapses in the primate retina.* .Vis Neurosci. 1991;7(1-2):49–60. PubMed PMID: 1931800.
22. Dacey D.M., Petersen M.R. *Dendritic field size and morphology of midget and parasol ganglion cells of the human retina.* .Proc Natl Acad Sci U S A. 1992;89(20):9666–70. PubMed PMID: 1409680.
23. Rodieck R.W., Binmoeller K.F., Dineen J. *Parasol and midget ganglion cells of the human retina.* .J Comp Neurol. 1985;233(1):115–32. PubMed PMID: 3980768.
24. Martin P.R.et al. *Transmission of colour and acuity signals by parvocellular cells in marmoset monkeys.* .J Physiol. 2011;589(Pt 11):2795–812. PubMed PMID: 21486786.
25. Martin P.R.et al. *Chromatic sensitivity of ganglion cells in the peripheral primate retina.* .Nature. 2001;410(6831):933–6. PubMed PMID: 11309618.
26. Reid R.C., Shapley R.M. *Space and time maps of cone photoreceptor signals in macaque lateral geniculate nucleus.* .J Neurosci. 2002;22(14):6158–75. PubMed PMID: 12122075.
27. Dacey D.M., Packer O.S. *Colour coding in the primate retina: diverse cell types and cone-specific circuitry.* .Curr Opin Neurobiol. 2003;13(4):421–7. PubMed PMID: 12965288.
28. Gouras P. *Identification of cone mechanisms in monkey ganglion cells.* .J Physiol. 1968;199(3):533–47. PubMed PMID: 4974745.
29. Wiesel T.N., Hubel D.H. *Spatial and chromatic interactions in the lateral geniculate body of the rhesus monkey.* .J Neurophysiol. 1966;29(6):1115–56. PubMed PMID: 4961644.
30. Dacey D.et al. *Center surround receptive field structure of cone bipolar cells in primate retina.* .Vision Res. 2000;40(14):1801–11. PubMed PMID: 10837827.
31. Connaughton V.P., Nelson R. *Spectral Responses in Zebrafish Horizontal Cells Include a Tetraphasic Response and a Novel UV-Dominated Triphasic Response.* .J Neurophysiol. 2010;104(5):2407–22. PubMed PMID: 20610786.

32. Kamermans, M. and H. Spekreijse, *Spectral behavior of cone-driven horizontal cells in teleost retina*, Volume 14, in *Progress in Retinal and Eye Research*, N. Osborne and G. Chader, Editors. 1995, Elsevier Science Ltd. p. 313-360.
33. Kolb, H. and L.E. Lipetz, *The anatomical basis for colour vision in the vertebrate retina* in *Vision and Visual Dysfunction*, Volume 6, J. Cronly-Dillon, Series Editor. in *The Perception of Colour*, P. Gouras, Editor. 1991, Macmillan Press Ltd.: London. p. 128-145.
34. Stell W.K., Lightfoot D.O. *Color-specific interconnections of cones and horizontal cells in the retina of the goldfish.* .J Comp Neurol. 1975;159(4):473–502. PubMed PMID: 1092733.
35. Dacey D.M.et al. *Horizontal cells of the primate retina: cone specificity without spectral opponency.* .Science. 1996;271(5249):656–9. PubMed PMID: 8571130.
36. Ahnelt P., Kolb H. *Horizontal cells and cone photoreceptors in primate retina: a Golgi-light microscopic study of spectral connectivity.* .J Comp Neurol. 1994;343(3):387–405. PubMed PMID: 8027449.
37. Verweij J., Hornstein E.P., Schnapf J.L. *Surround antagonism in macaque cone photoreceptors.* .J Neurosci. 2003;23(32):10249–57. PubMed PMID: 14614083.
38. Packer O.S.et al. *Blue-yellow opponency in primate S cone photoreceptors.* .J Neurosci. 2010;30(2):568–72. PubMed PMID: 20071519.
39. Crook J.D.et al. *Horizontal cell feedback without cone type-selective inhibition mediates "red-green" color opponency in midget ganglion cells of the primate retina.* .J Neurosci. 2011;31(5):1762–72. PubMed PMID: 21289186.
40. Taylor W.R. *TTX attenuates surround inhibition in rabbit retinal ganglion cells.* .Vis Neurosci. 1999;16(2):285–90. PubMed PMID: 10367963.
41. Merigan W.H. *Chromatic and achromatic vision of macaques: role of the P pathway.* .J Neurosci. 1989;9(3):776–83. PubMed PMID: 2926482.
42. Merigan W.H., Maunsell J.H. *Macaque vision after magnocellular lateral geniculate lesions.* .Vis Neurosci. 1990;5(4):347–52. PubMed PMID: 2265149.
43. Kaplan E., Shapley R.M. *The primate retina contains two types of ganglion cells, with high and low contrast sensitivity.* .Proc Natl Acad Sci U S A. 1986;83(8):2755–7. PubMed PMID: 3458235.
44. McMahon M.J., Packer O.S., Dacey D.M. *The classical receptive field surround of primate parasol ganglion cells is mediated primarily by a non-GABAergic pathway.* .J Neurosci. 2004;24(15):3736–45. PubMed PMID: 15084653.
45. Martin P.R.et al. *Evidence that blue-on cells are part of the third geniculocortical pathway in primates.* .Eur J Neurosci. 1997;9(7):1536–41. PubMed PMID: 9240412.
46. Roy S.et al. *Segregation of short-wavelength-sensitive (S) cone signals in the macaque dorsal lateral geniculate nucleus.* .Eur J Neurosci. 2009;30(8):1517–26. PubMed PMID: 19821840.

S-Cone Pathways

Helga Kolb

Created: May 1, 2005; Updated: May 4, 2007.

General Characteristics

Over the last few years, psychophysicists, electrophysiologists, geneticists, and anatomists have concluded that there is something unique about the short wavelength system compared with the two longer wavelength systems in the visual system.

There are differences in the genetic structure and locus of the S-cone visual pigment compared with the L- and M-cone pigments (1), yet the S-cones are common to all vertebrate retinas and always form a consistent 8-10% of the cone photoreceptor population (2, 3) (Fig. 1). The S-cones are, however, very few in the fovea center, thus causing a so-called S-cone blind spot (4), but they peak in number on the foveal slope at about 12% of the population (Fig. 2).

The short wavelength system has a lower spatial and temporal resolution than the other two cone systems (5, 6) but is probably the only system to truly carry color information through the retina (7, 8).

The pathways for transmitting information from the short-wavelength cones to ganglion cells appear to be different from the midget pathways for the medium- and long-wavelength cones. As we have discussed in a previous chapter, the latter two chromatic pathways are via midget bipolar and midget ganglion cell connections related to a single spectral type of cone, either L-cone or M-cone.

Blue Cones

Of the three spectral types of cone found in the normal human retina, only the S-cone or blue cone can be distinguished from the others in the mosaic. Using special antibodies generated against cone opsins, which are the visual pigments contained within the cone, it is possible to selectively stain the short-wavelength-sensitive pigment (or blue pigment)-bearing cones (Fig. 3) (9, 10).

Before the development of the antibody though, the S-cones were recognizable by staining with fluorescent dyes like Lucifer yellow (11) or from careful quantitative light microscopy of monkey and human retinas (12).

They are distinguished from other cones in the fovea by their larger inner segment diameter and their occurrence in a different mosaic than the the more numerous, hexagonally packed L- and M-cones. Thus, the S-cones seem to break up the regular hexagonal array into small distorted patches of the other cones (Fig. 1).

In vertical sections of human retina, the S-cone is recognized by having a longer inner segment that sticks further into subretinal space than neighboring cones (Fig. 4). It also has a narrower "waist" at the outer limiting membrane than neighboring cones and often sits adjacent to another cone cell body without intervening rods. Pedicles belonging to S-cones project deeper into the outer plexiform layer (OPL) and have a smaller or unusually shaped pedicle compared with other cone pedicles (Fig. 4 and Fig. 5) (13, 14).

In peripheral retina, S-cone pedicles are bilobed in shape, with synaptic invaginations and ribbons separated to the two lobes (Fig. 6). They do not exhibit the long telodendria typical of other cone pedicles, so they remain rather isolated from gap junction contacts, with L- or M-cones at the level of the OPL (14).

S-Cone Bipolar Cell

The S-cone pedicle is only contacted by a special S-cone bipolar cell, which was originally described by Mariani (15) and shown later to be selectively stainable with antibodies to the peptide cholecystokinin (16). This bipolar

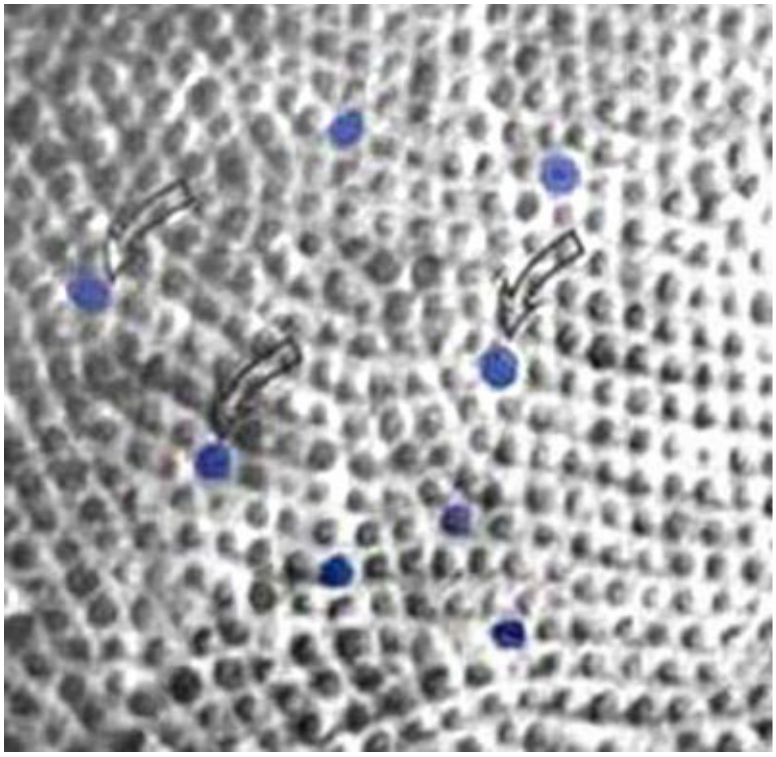

Figure 1. Cone mosaic in the fovea where the S-wave or blue cones are evident by size and density differences.

is not like other midget bipolar cells, although in the central retina, it is related mostly to a single S-cone (16). It differs primarily in its axonal ending in the inner plexiform layer (IPL), from the regular midget bipolar cells that contact M- and L-cones. The S-cone bipolar axon ends deep in the IPL with a long-ranging terminal that runs among the rod bipolar axon terminals in stratum 5 (Fig. 7).

The S-cone bipolar cell makes an invaginating ribbon junction with the cone pedicle as well as a basal junction type of contact (Fig. 6, violet profile, sb). A small number of additional fine bipolar dendrites make basal junction contacts only (Fig. 6, green profile, fb) and so belong to some other kind of diffuse bipolar type, possibly one called GBB, a giant bistratified type (Fig. 7) (17). The HII horizontal cells make many of the lateral element contacts with the S-cone in both lobes (Fig. 6, orange profiles, HII). A small number of contacts come from HI cells (Fig. 6, red profiles, HI) (13).

S-Cone Horizontal Cell

Originally, there was thought to be only one type of horizontal cell in the primate retina—a long-axoned cell type that connected with cones at its dendrites and rods at its axonal endings (18-20). However, in 1980 a second type of horizontal cell was described (21) and proposed to be more concerned with S-cones than the original long-axoned HI type. The HII cell was distinguished on its bushy dendritic tree with fine irregular dendrites and without clear clusters destined for cones (Fig. 8a, compare H1 and H2 cells morphology). Electron microscopy finally showed that the HII type of horizontal cell indeed sent many dendritic processes to the few S-cones in its dendritic field and lesser concentrations of processes to overlying M- and L-cones. The short axons of these HII cells contact S-cones exclusively (Fig. 8b) (13). Intracellular recordings from H2 horizontal cells in monkey retina have proved conclusively that this horizontal cell is blue sensitive and an important element of the S-cone pathway in the primate retina (22).

It has been demonstrated that horizontal cells produce negative feedback to cones (23-25) and are engaged in center-surround generation in bipolar cells and color opponent responses in horizontal cells of animals with

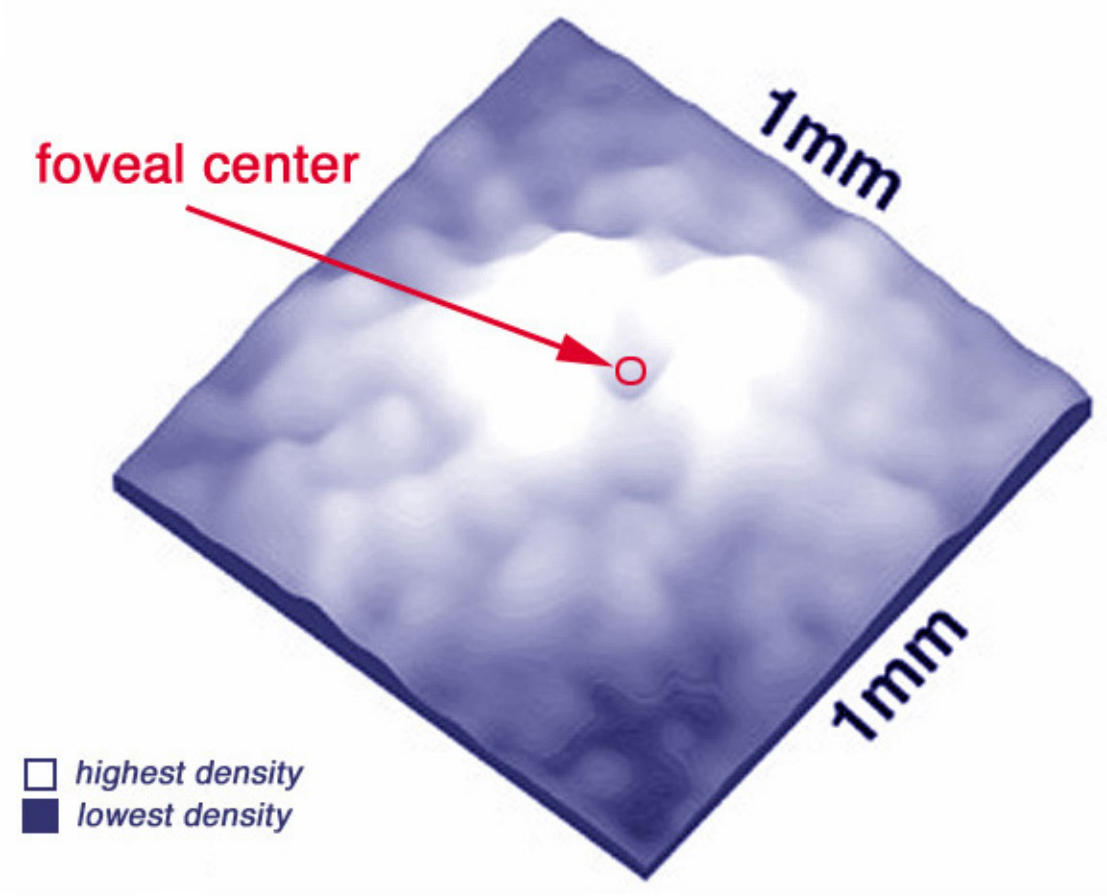

Figure 2. 3D map of the blue or S-cone density around the foveal center. The peak density occurs on the foveal slope. From Ahnelt and Kolb (9).

good color vision (24). In the case of the HI and HII horizontal cells of the primate retina, it has been difficult to demonstrate color opponency in intracellular recording and dye-markings (22), although anatomically, we know there is color selectivity of their contacts (13). Dacey and coauthors (22) concluded that HII cells, which of course make contact with L- and M-cones as well but are primarily concerned with S-cones, do not engage in feedback signals with the longer wavelength cones. However, it is possible that HII cells feed back only to their S-cones, thereby forming opponency in the S-cones themselves and their S-cone bipolar cells. This should result in an opponent S-cone bipolar S-ON, L-/M-OFF (blue ON/yellow OFF) channel that could be carried straight to the ganglion cells (Fig. 9).

S-Cone Ganglion Cell

Early electrophysiological investigation of monkey retinal ganglion cells indicated that blue/yellow opponency was carried primarily by an S-cone ON-center ganglion cell type with a much larger receptive field center than is typical of the L- or M-cone color and spatially opponent midget ganglion cells (26). The S-cone ganglion cell did not appear to have a spatially antagonistic receptive field structure. Instead, the yellow opponency was coextensive with the center of the receptive field. Interestingly, there are very few recordings of the opposite type of ganglion cell, i.e., yellow-ON and blue-OFF.

The morphology of the blue-ON/yellow-OFF ganglion cell has been known since Dacey and Lee (27) made intracellular recordings and staining of these ganglion cells in monkey retina. It turns out to be a relatively small-

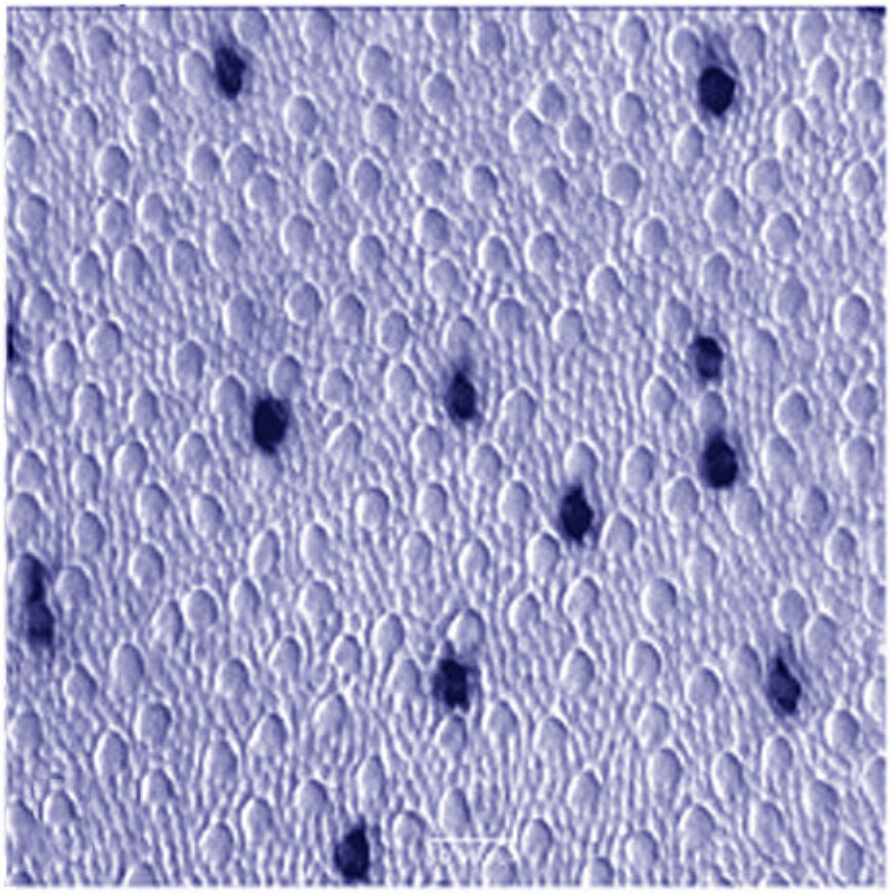

Figure 3. Blue or S-cones can be marked with anti-S-cone pigment antibodies. From Ahnelt and Kolb (9).

field bistratified ganglion cell (28) with its major dendritic branching in stratum 5 of the IPL and a small tier of dendrites in stratum 1 of the IPL (Fig. 10).

Circuits for the S-Cone Pathways in the Primate Retina

Hypothetical wiring diagrams of the S-cone pathway through the primate retina in comparison with the L- and M-cone midget pathways are shown in Fig. 11. The S-cone bipolar would carry ON signals to the lower dendrites of the bistratified ganglion cell, which may be the dominant input. It is possible, though, that the bipolar is already S-ON and yellow-OFF, in response to the HII cell influence, as mentioned above. Then both ON and OFF spectrally antagonistic components would drive the ganglion cell. However, the yellow-OFF response could also be complemented by an OFF bipolar that contacts L- and M-cones as well, making synapses upon the upper dendrites of the bistratified ganglion cell (Fig. 11).

The equivocal existence of the OFF S-cone channels (29, 30) in the retina could be because only a small number of S-cone OFF ganglion cells are present, and they are difficult to record. Very recent preliminary recordings and markings of an OFF-blue cone ganglion cell indicate that it is a small-bodied, wide-field cell type with thin dendrites in S5 of the IPL (31). Wiring of such a cell type must involve amacrine circuitry to get blue-OFF and yellow-ON signals to the ganglion cell (Fig. 11).

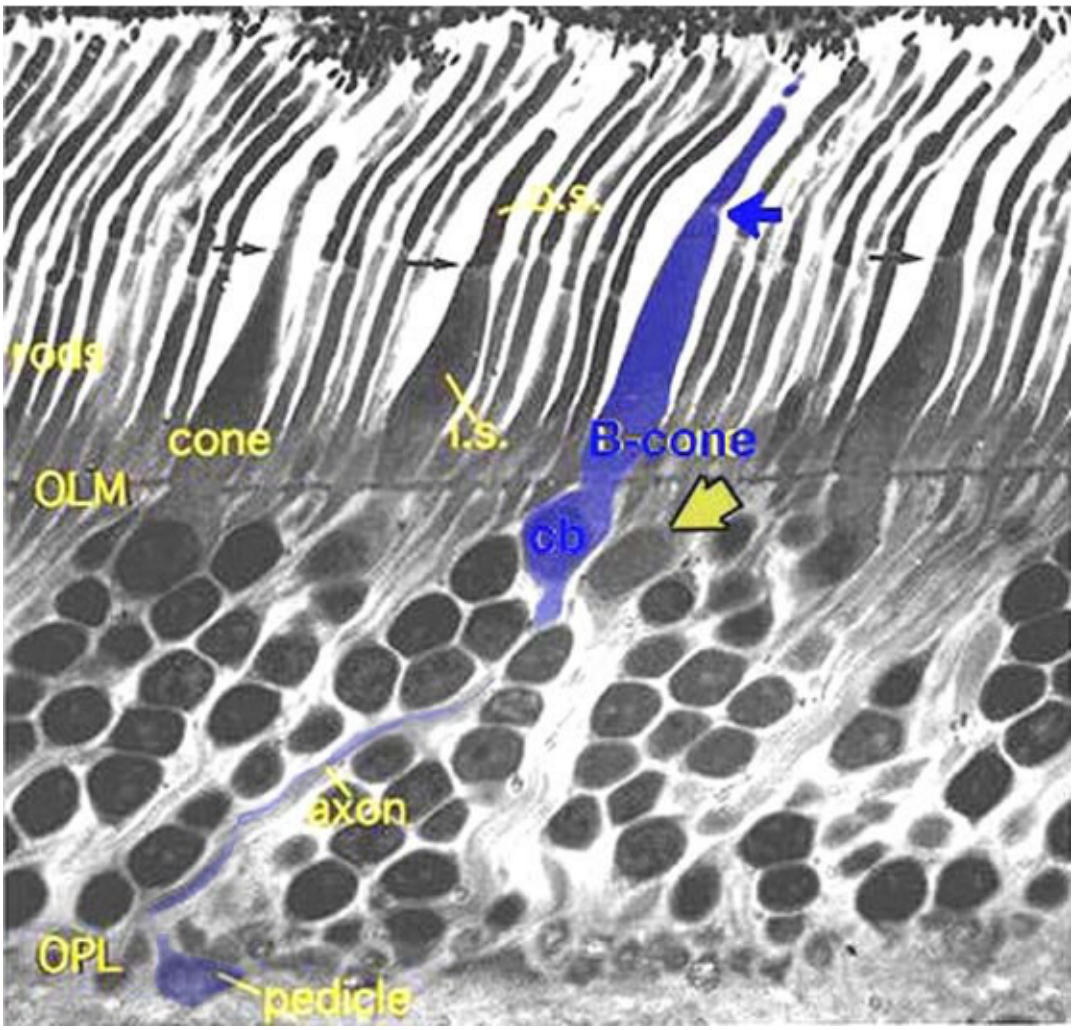

Figure 4. Blue cone in a vertical section through human retina.

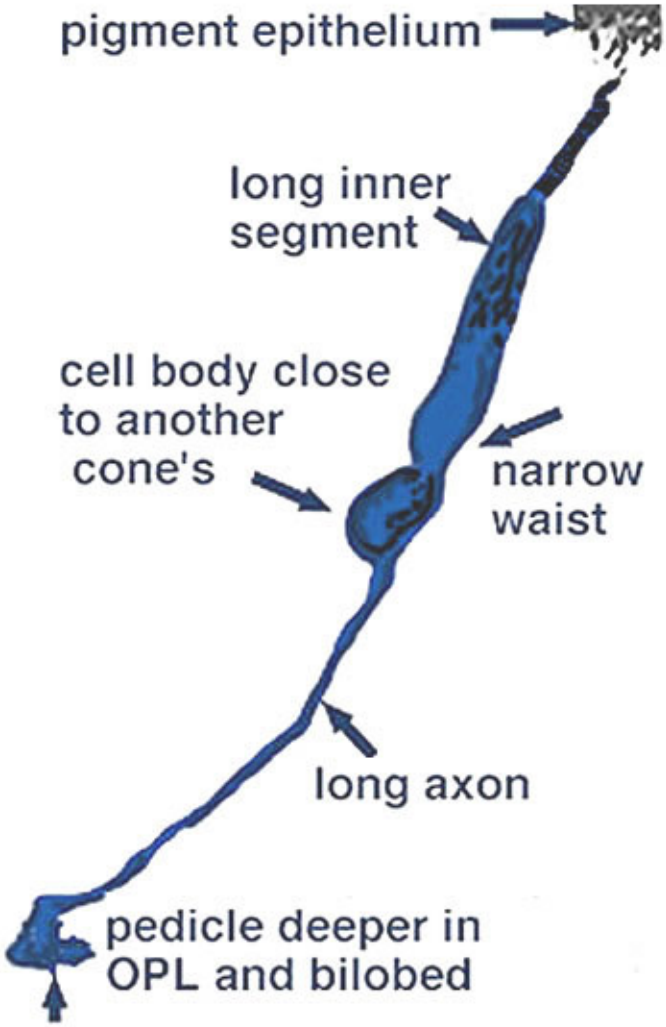

Figure 5. Schematic drawing of a blue cone.

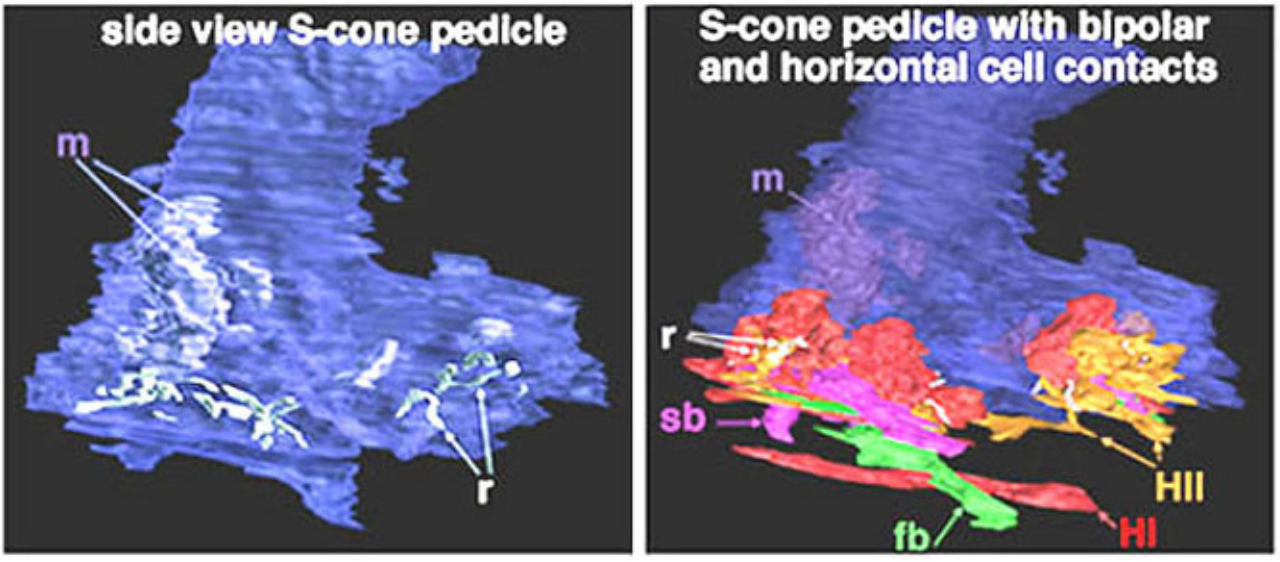

Figure 6. 3D computer reconstructions of an S-cone pedicle.

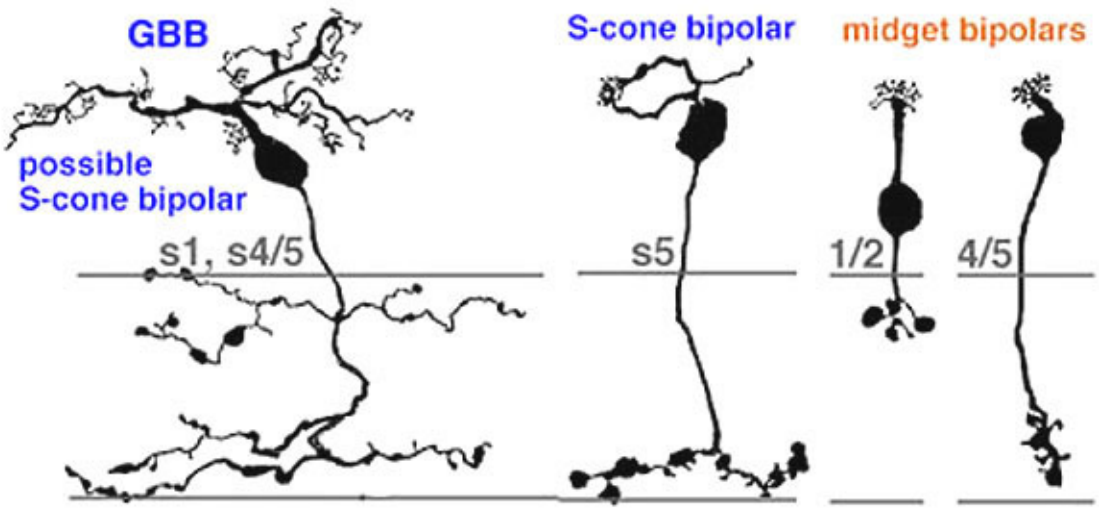

Figure 7. S-cone bipolar cell types of primate retina. The giant bistratified bipolar (GBB) has not yet been proved to be blue exclusive. Midget bipolars are for M- and L-cones.

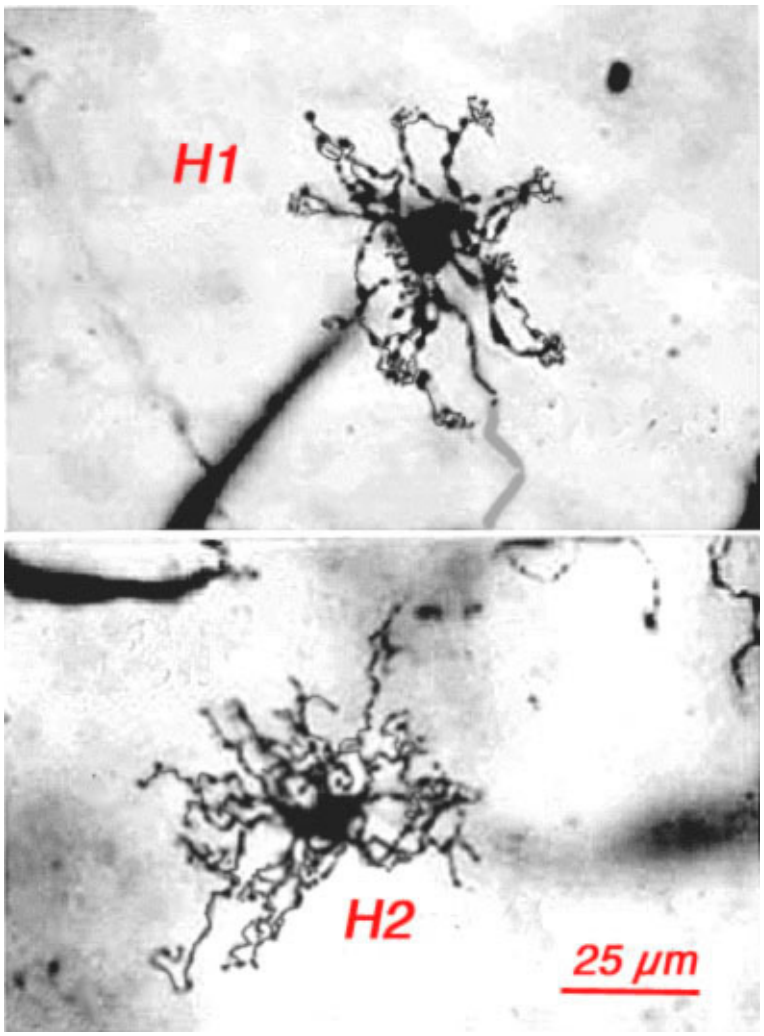

Figure 8a. Comparisons of HI and HII cells in primate retina. Golgi staining.

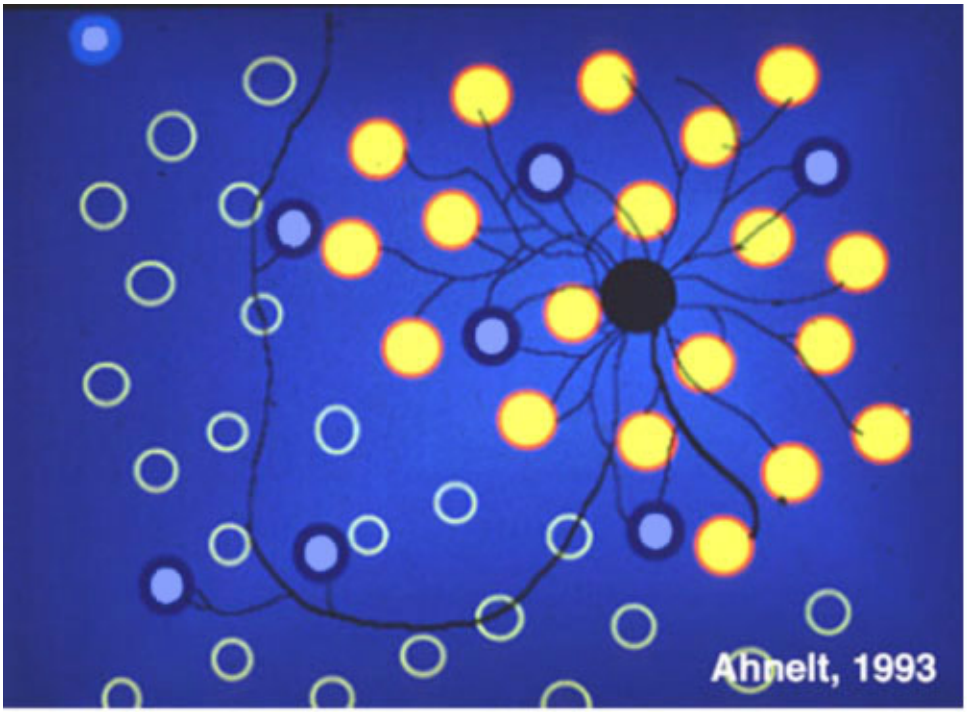

Figure 8b. Schematic of the S-cone-specific HII horizontal cell in primate retina.

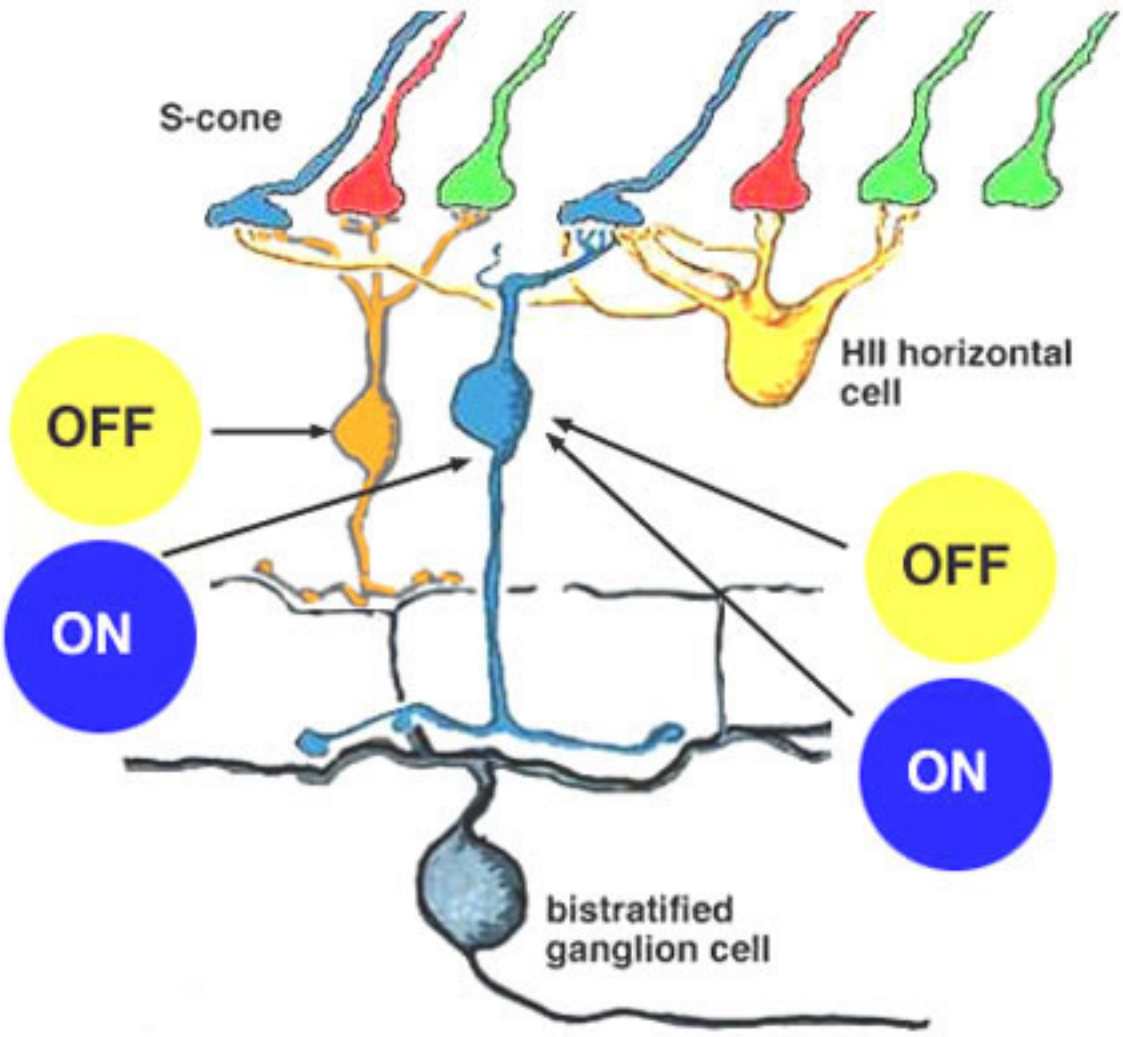

Figure 9. Neurons of the S-cone pathways.

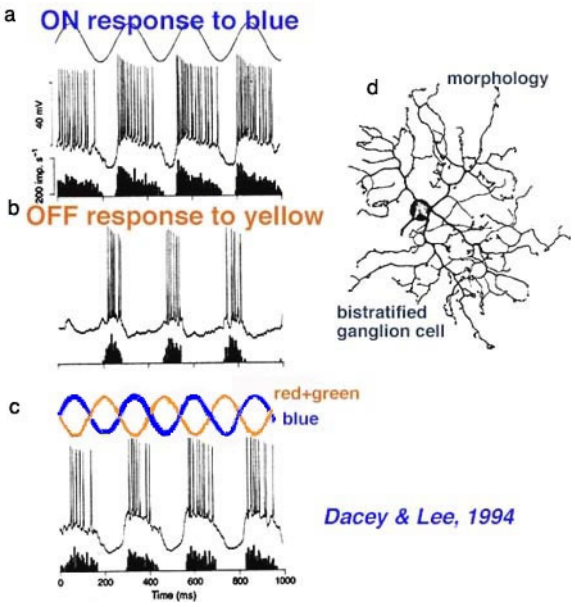

Figure 10. Blue-ON, yellow-OFF chromatic ganglion cell in monkey retina. a, alternating blue and dark stimuli evoke ON responses. b, alternating yellow and dark stimuli evoke OFF responses. c, alternating blue and yellow colors matched in brightness evoke blue-ON, yellow-OFF responses. d–f, Morphological appearance of the small bistratified ganglion cell from which blue-sensitive responses were recorded. From Dacey and Lee (27).

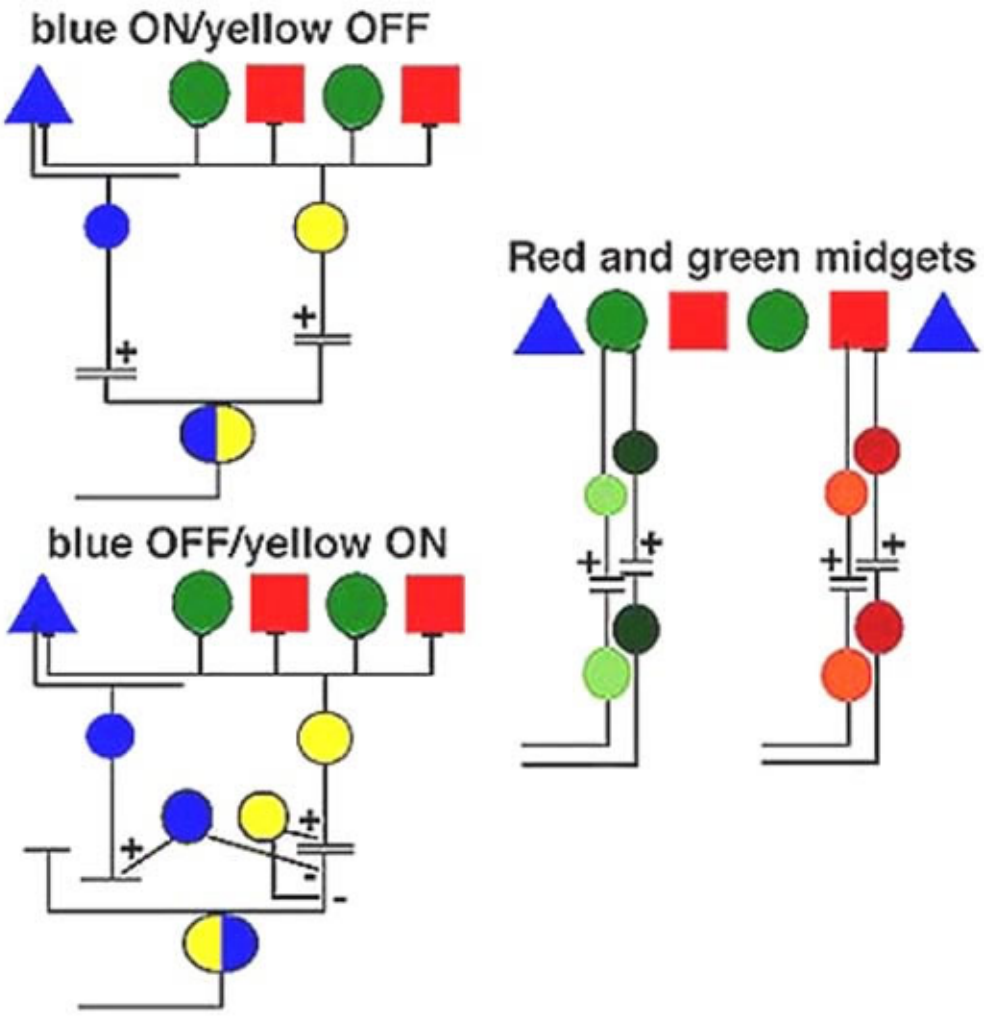

Figure 11. Hypothetical wiring diagrams of the S-cone pathways.

References

1. Nathans J, Thomas D, Hogness DS. Molecular genetics of human color vision: the genes encoding the blue, green and red pigments. Science. 1986;232:193–202. PubMed PMID: 2937147.
2. Kolb H, Lipetz LE. The anatomical basis for colour vision in the vertebrate retina. In: Gouras P, editor. Vision and visual dysfunction. Vol. 6. The perception of colour. London: Macmillan Press Ltd.; 1991. p. 128-145.
3. Marc RE. Chromatic organization of the retina. In: LaVail M, Hollyfield J, editors. Cell biology of the eye. New York: Academic Press; 1982. p.435-473.
4. Williams DR, MacLeod DIA, Hayhoe M. Punctate sensitivity of the blue-sensitive mechanisms. Vision Res. 1981;21:1357–1375. PubMed PMID: 7314519.
5. Humanski RA, Wilson HR. Spatial frequency mechanisms withshort-wavelength-sensitive cone inputs. Vision Res. 1992;32:549–560. PubMed PMID: 1604842.
6. Stockman A, MacLeod DIA, DePriest DD. The temporal properties of the human short-wave photoreceptors and their associated pathways. Vision Res. 1991;31:189–208. PubMed PMID: 2017881.
7. Gouras P. Retinal circuitry and its relevance to diagnostic psychophysics and electrophysiology. Curr Opin Ophthalmol. 1992;3:803–812.
8. Rodieck RW. In: Valberg A, Lee BB, editors. From pigments to perception. New York: Plenum Publishing Corp.; 1991. p. 83-94.

9. Ahnelt P, Kolb H. The mammalian photoreceptor mosaic-adaptive design. Prog Ret Eye Res. 2000;19:711–777.
10. Szel A, Diamanstein T, Röhlich P. Identification of blue-sensitive cones in the mammalian retina by antivisual pigment antibody. J Comp Neurol. 1988;273:593–602. PubMed PMID: 3209737.
11. DeMonasterio FM, Schein SJ, McCrane EP. Staining of blue-sensitive cones of the macaque retina by fluorescent dye. Science. 1981;213:1278–1281. PubMed PMID: 7268439.
12. Ahnelt PK, Kolb H, Pflug R. Identification of a subtype of cone photoreceptor, likely to be blue sensitive, in the human retina. J Comp Neurol. 1987;255:18–34. PubMed PMID: 2434534.
13. Ahnelt P, Kolb H. Horizontal cells and cone photoreceptors in human retina: a Golgi-electron microscopic study of spectral connectivity. J Comp Neurol. 1994;343:406–427. PubMed PMID: 8027450.
14. Kolb H, Goede P, Roberts S, McDermott R, Gouras P. Uniqueness of the S-cone pedicle in the human retina and consequences for color processing. J Comp Neurol. 1997;386:443–460. PubMed PMID: 9303428.
15. Mariani AP. Bipolar cells in monkey retina selective for cones likely to be blue-sensitive. Nature. 1984;308:184–186. PubMed PMID: 6199677.
16. Kouyama N, Marshak DW. Bipolar cells specific for blue cones in the macaque retina. J Neurosci. 1992;12:1233–1252. PubMed PMID: 1556594.
17. Mariani AP. Giant bistratified bipolar cells in the monkey retina. Anat Rec. 1983;206:215–220.
18. Boycott BB, Dowling JE. Organization of the primate retina: light microscopy. Philos Trans R Soc B. 1969;255:109–184.
19. Kolb H. Organization of the outer plexiform layer of the primate retina: electron microscopy of Golgi-impregnated cells. Philos Trans R Soc Lond B Biol Sci. 1970;258:261–283.
20. Polyak SL. The retina. Chicago: University of Chicago Press; 1941.
21. Kolb H, Mariani A, Gallego A. A second type of horizontal cell in the monkey retina. J Comp Neurol. 1980;189:31–44. PubMed PMID: 6766145.
22. Dacey DM, Lee BB, Stafford DK, Pokorny J, Smith VC. Horizontal cells of the primate retina: cone specificity without spectral opponency. Science. 1996;271:656–659. PubMed PMID: 8571130.
23. Baylor DA, Fuortes MGF, O'Bryan PM. Receptive fields of the cones in the retina of the turtle. J Physiol. 1971;214:265–294. PubMed PMID: 5579638.
24. Fuortes MGF, Simon EJ. Interactions leading to horizontal cellresponses in the turtle retina. J Physiol. 1974;240:177–199. PubMed PMID: 4852507.
25. Burkhardt DA. Synaptic feedback, depolarization, and color opponency in cone photoreceptors. Vis Neurosci. 1993;10:981–989. PubMed PMID: 8257672.
26. Gouras P. Progress in human visual evoked responses. J Clin Neurophysiol. 1984;1:77–82. PubMed PMID: 6400021.
27. Dacey DM, Lee BB. The "blue-on" opponent pathways in primate retina originates from a distinct bistratified ganglion cell. Nature. 1994;367:731–735. PubMed PMID: 8107868.
28. Dacey DM. Morphology of a small-field bistratified ganglion cell type in the macaque and human retina. Vis Neurosci. 1993;10:1081–1089. PubMed PMID: 8257665.
29. Gouras P, Zrenner E. Color vision: a review from a neurophysiological perspective. In: Autrum H, Ottoson D, Perl ER, Schmidt RF, editors. Progress in sensory physiology. Vol. 1. Berlin: Springer-Verlag; 1981. p.139-179.
30. Lennie P. Recent developments in the physiology of color vision. Trends Neurosci. 1984;5:243–248.
31. Dacey D.M., Peterson B.B., Gamlin P.D., Robinson F.R. Retrograde photofilling reveals the complete morphology of diverse new ganglion cell types that project to the lateral geniculate nucleus in macaque monkey. Invest Ophthal Vis Sci. 2001.

Feedback Loops in the Retina

Helga Kolb

Created: May 1, 2005; Updated: May 4, 2007.

General Characteristics

At every level of the retina, there are reciprocal or feedback loops in the circuitry so that certain neurons can interact laterally within the same layer, vertically from one layer to the other, and indeed from the brain to the retina. The intra-layer feedback loops are typically provided by neurons that use inhibitory neurotransmitters, such as GABA, and have a function in sharpening the image by adding lateral inhibition or antagonism to receptive fields of the neurons, whereas the feedback loops between the layers or from the brain are less clear in function. The latter loops tend to use neuromodulators as their transmitters and thereby have a more generalized effect on groups of neurons, or on the state of excitability of the neuron chains (adaptation, for example).

Feedback in the Outer Retina

As mentioned in previous chapters, it has been well demonstrated in turtle and fish retinas that cones receive an antagonistic reciprocal feedback message from horizontal cells (1), which serves to provide a restricted concentric receptive field for the individual cones (Fig. 1 and Fig. 2). Evidence for feedback synapses have been difficult to demonstrate, either electrophysiologically or morphologically, in the cones of the mammalian retinas. However, the rod axon terminals of HI horizontal cells ending in the rod spherules are seen to make small punctate chemical synapses, consisting a small cluster of vesicles at a single dense projection in the membrane, upon both the rod spherule (Fig. 2) and upon the rod bipolar cell dendrite (not illustrated) in human retina (2). A similar-appearing small cluster of vesicles is occasionally seen in horizontal cell dendrites in the cone pedicle triads in human retina as well (Fig. 3).

In the inner plexiform layer, many amacrine cell types probably provide feedback information to bipolar axon terminals. One we know something about is the reciprocal synapses from the wide-field rod amacrine A17 upon the rod bipolar axon terminal. It is intriguing that this IPL input/output synaptology between the rod bipolar and A17 amacrine parallels the input/output of the photoreceptor and horizontal cell at the outer plexiform layer (OPL) and suggests some necessity of the rod system, in the mammalian retina at least, to be in repetitive feedback loops all through the retina (Fig. 4).

Where A17 is a **rod** system bipolar cell feedback amacrine cell, A4, A13, and wide-field amacrines like A19 are **cone** system feedback amacrine cells. Similar to A17 cells of the rod system, these amacrine cells are probably also GABAergic. The amacrine cell feedback loop seen below occurs commonly at the midget bipolar axon terminal in the human retina in close proximity to the ribbon synapse of the related midget ganglion cell (Fig. 5).

It is possible that feedback (reciprocal) synapses, in these cases, are involved with phasic or transient components of these cell response characteristics. They may sharpen and speed up otherwise slow potential responses of the bipolar cell by feedback to the bipolar before output to the ganglion cell (see an animation of the feedback synapses).

Interplexiform Cells

A neuron in the retina of just about every species studied, including humans, links the two plexiform layers by receiving synaptic input in the IPL and having synaptic output upon neurons of the OPL. It is known as the interplexiform cell, an **IPC**. The interplexiform cell, first described by Gallego (3) in the cat retina, has been studied extensively in the goldfish retina by Dowling and coauthors (4) and now also in the cat and the human

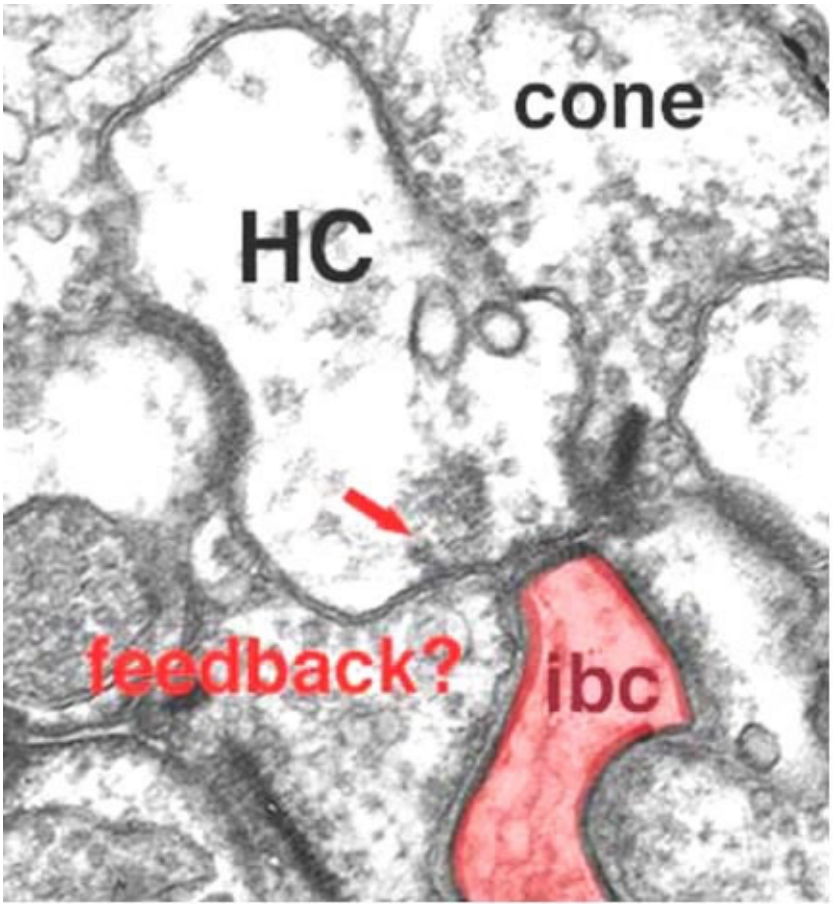

Figure 1. Electron micrograph of a cone pedicle.

retinas (2, 5, 6). In cat and human retinas, such interplexiform cells are medium field and tristratified in branching pattern in the inner plexiform layer. Either from the cell body or from one of the dendrites in stratum 1 of the IPL, processes ascend through the inner nuclear layer to the outer plexiform layer. There they run for a short distance (Fig. 6 and Fig. 7).

Electron microscopy has been performed on examples of this type of IPC in cat and human retinas. They get input from amacrine cells of unknown type and make some synapses upon rod and cone bipolar axons (5, 7) with their inner plexiform layer branches. Through the inner nuclear layer and into the outer plexiform layer, processes of IPCs cell make numerous conventional synapses upon rod and cone bipolar cell bodies and dendrites (Fig. 8).

In both cat and human, the interplexiform cell has processes that touch cone pedicles but make rather unspecialized junctions at this site, so we have been reluctant to call these synapses. The interplexiform cell, just described in the human and cat, is known to be GABAergic. This differs considerably from the interplexiform cell of the fish retina, where it is known to be dopaminergic (8). In the fish retina, the dopaminergic interplexiform cell is known to have synapses in the OPL, primarily upon horizontal cells. Thus, it seems that the fish interplexiform cell has a rather different role to play in the retina compared with the GABAergic interplexiform cell of the human (Fig. 9).

Dopaminergic Cells in Mammals

In both human and cat retinas, there exists a dopaminergic amacrine cell, called A18, which we think is involved in the rod system pathways of the IPL and particularly with the rod amacrine AII cells (see previous chapters).

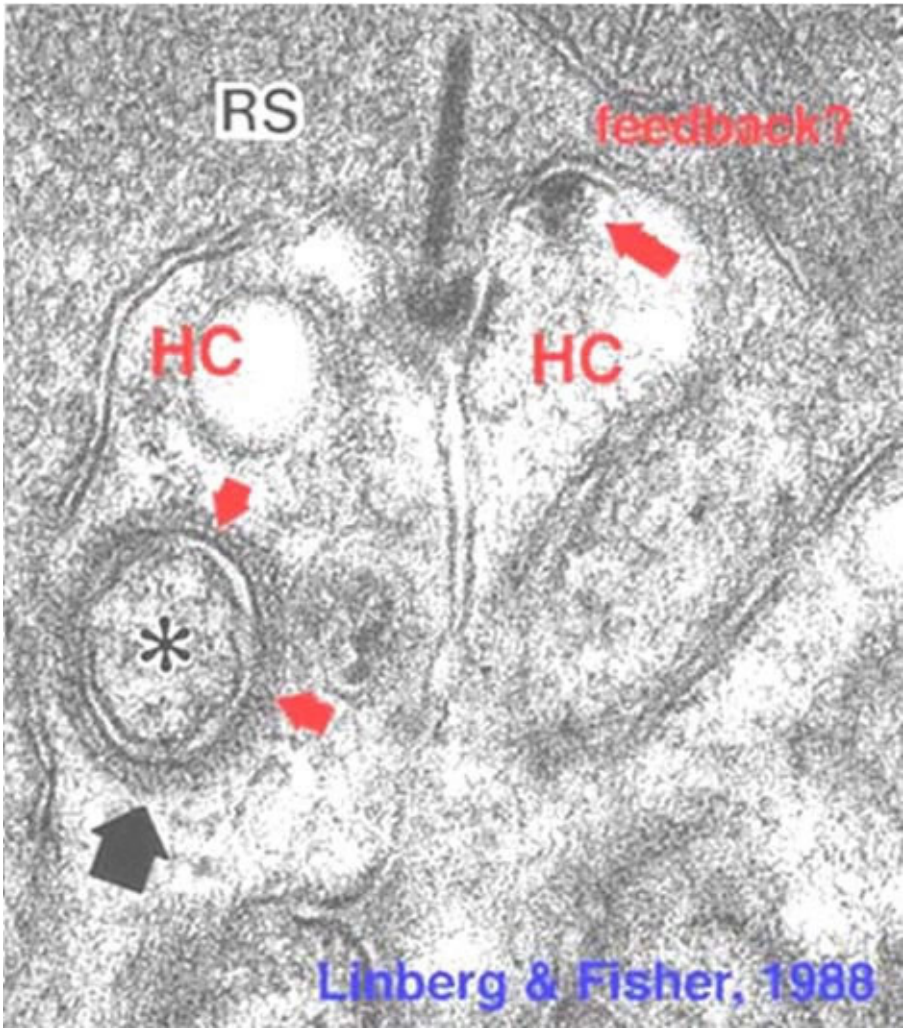

Figure 2. Electron micrograph of a rod spherule.

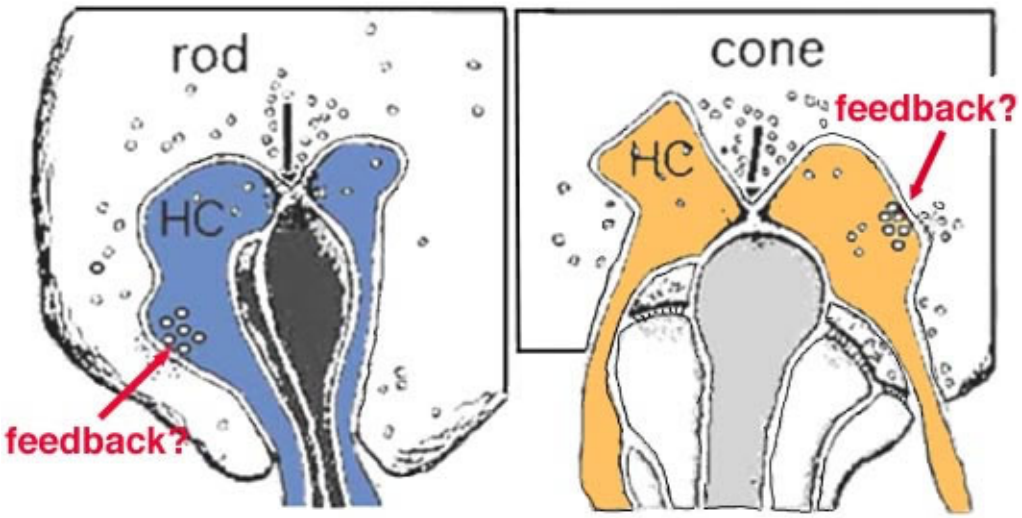

Figure 3. Diagram of the organization of a cone pedicle and a rod spherule.

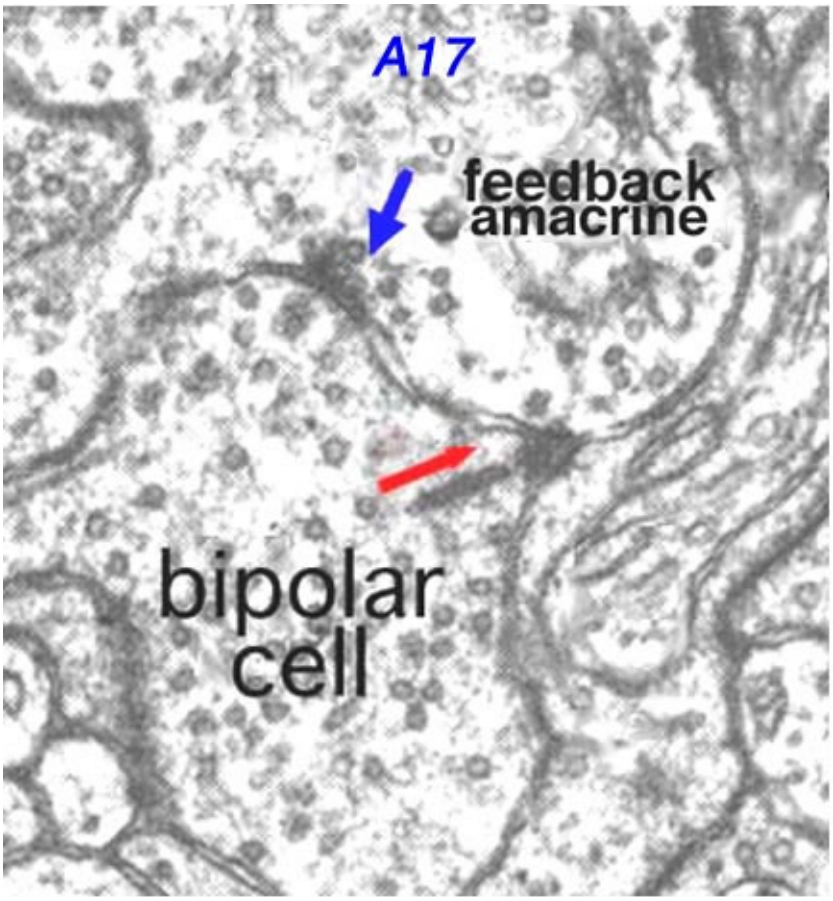

Figure 4. Electron micrograph of a reciprocal synapse of a rod amacrine cell (A17) upon a rod bipolar axon terminal.

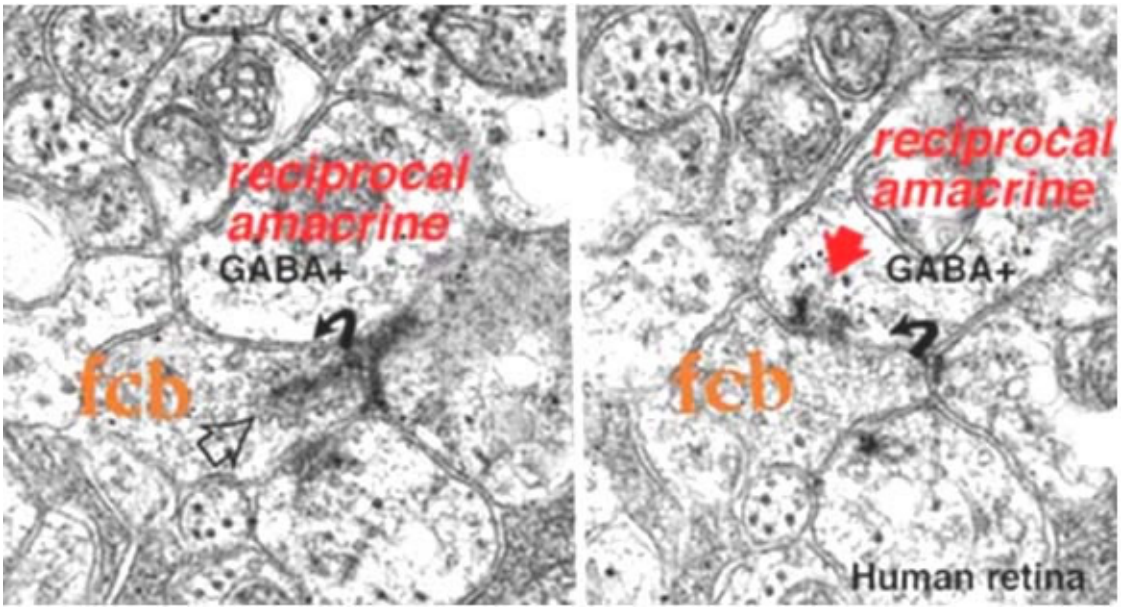

Figure 5. Electron micrograph of a reciprocal GABAergic synapse.

However, sometimes these A18 cells can be seen to have processes ascending from their cell bodies or from their plexus of dendrites in stratum 1 of the innerplexiform layer, to pass up to the outer plexiform layer. In these layers, dopaminergic processes may be presynaptic to horizontal cells in the human retina (9). In the cat retina,

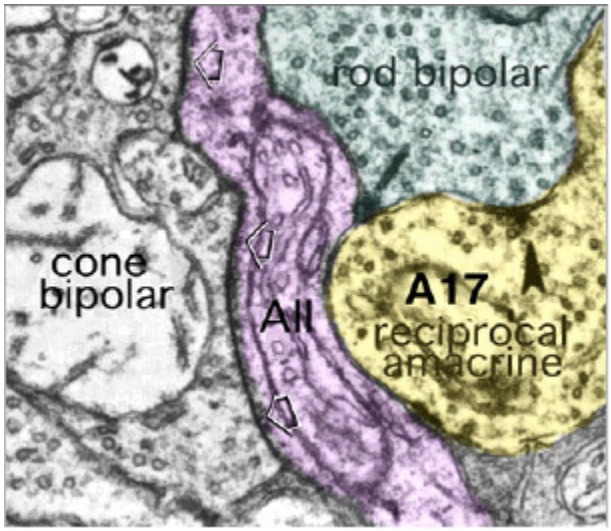

Movie 1. An animation of the feedback synapses.
Download video

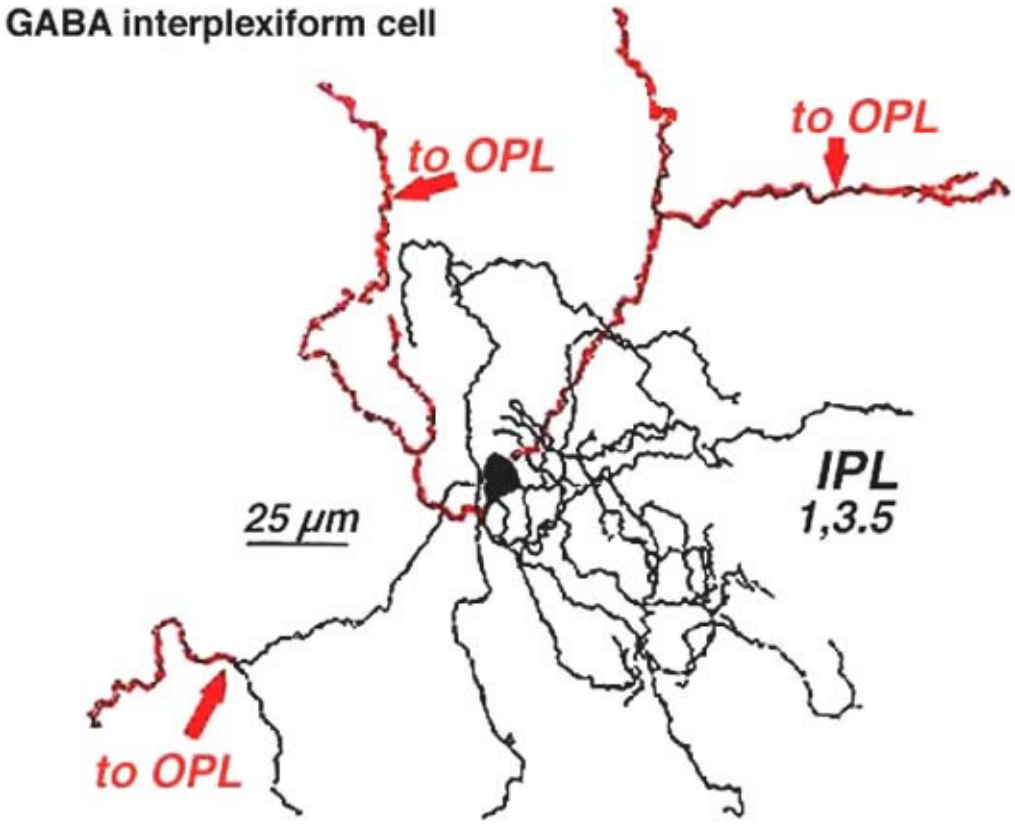

Figure 6. Whole-mount view of an interplexiform cell in human retina.

however, we have seen these ascending dopaminergic processes (marked by their content of Toh immunoreactivity) to be presynaptic to the conventional IPC of the cat, i.e., the cell described above (10, 11) (Fig. 10 and Fig. 11).

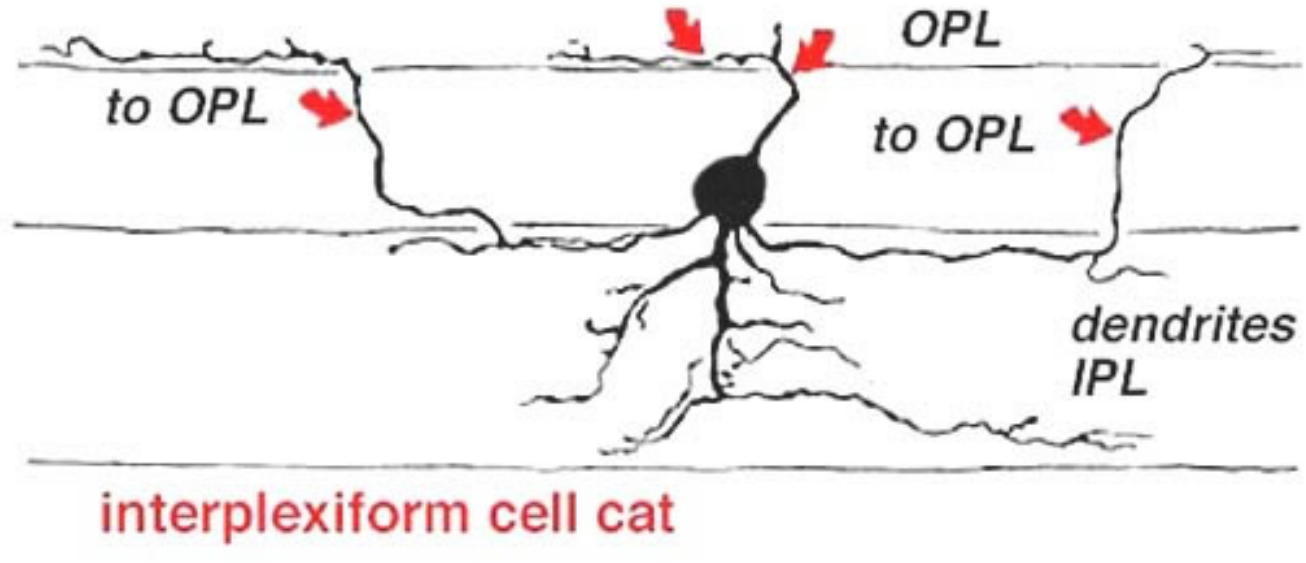

Figure 7. Vertical view of a Golgi-stained interplexiform cell in human retina.

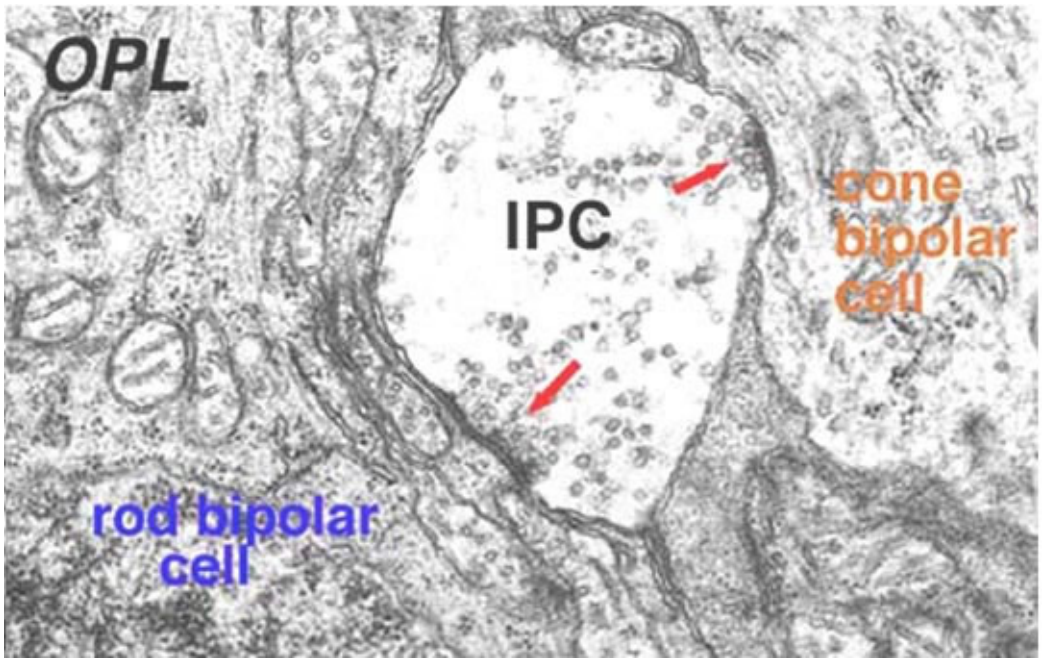

Figure 8. Electron micrograph of output synapses of an interplexiform cell.

Centrifugal Fibers in Mammalian Retinas

Centrifugal fibers arising in brain nuclei and passing back to the retina have been noted sporadically in mammals but with few details and no ideas about which brain centers they might derive from. Centrifugal fibers are particularly well developed in the avian retina (12-14). A few centrifugal fibers were described in the monkey retina by Polyak (15) and later by Honrubia and Elliot (16). According to Polyak (15), the centrifugal fibers in monkey have varicose, bulbous terminals that end in the inner plexiform layer close to amacrine cell bodies. In the human retina, they have been followed across the nerve fiber layer into the inner nuclear layer before disappearing (17) (Fig. 12).

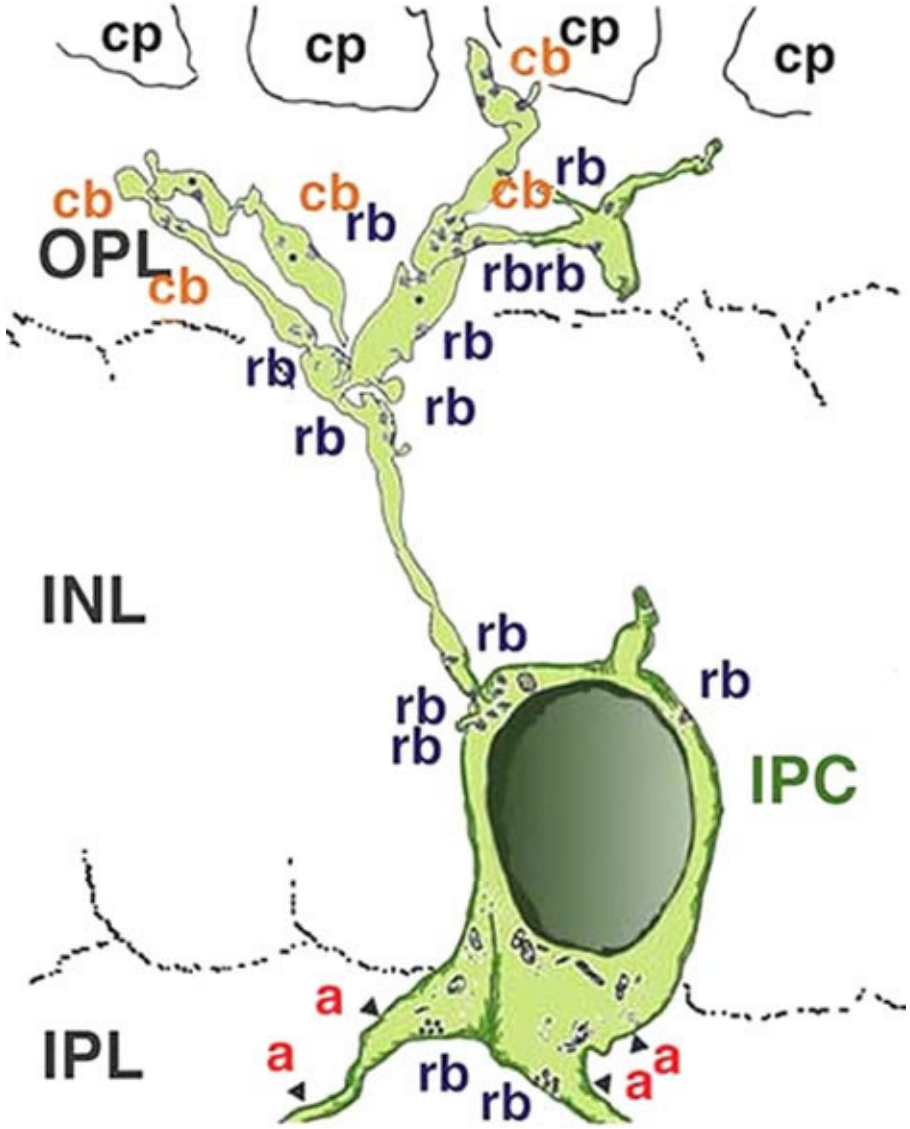

Figure 9. Summary diagram of the organization of the interplexiform cell in human retina.

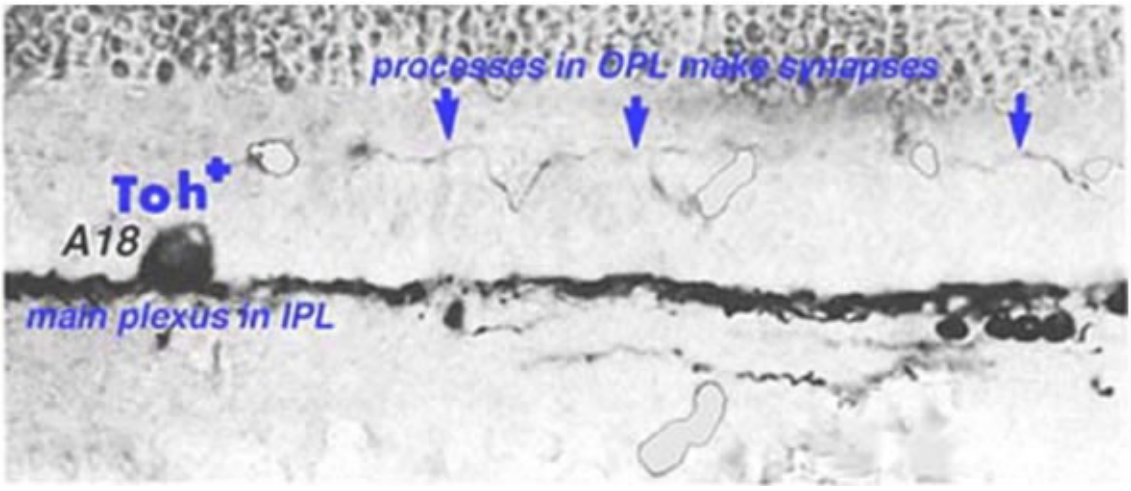

Figure 10. Light micrograph of a dopaminergic cell.

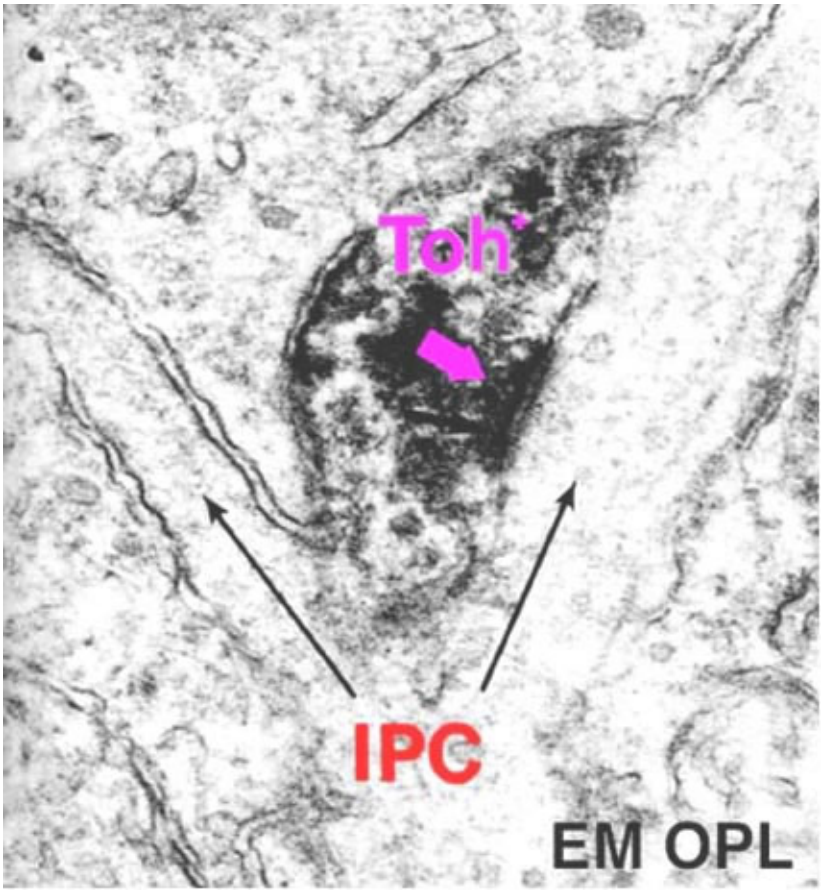

Figure 11. Electron micrograph of a dopaminergic cell.

Recently, it has been discovered that centrifugal axons arising in the hypothalamus project to various parts of the brain, including the retina in the macaque monkey. Interestingly, these axons contain histamine (18). The histamine-immunoreactive axons run from the optic nerve head in a broad circular band around the far side of the fovea in temporal retina and appear to return to the optic disc (see Fig. 13). Many of these axons branch extensively and emerge out of the nerve fiber layer into the inner plexiform layer. Sometimes the histaminergic axons are associated with retinal blood vessels. It will be extremely interesting to discover whether these histamine-containing centrifugal fibers have interactions with amacrine or other cells of the retina, similar to what is proposed for centrifugal fibers in other species.

In the fish retina, we know that centrifugal fibers use the hormones FMRF amide and luteinizing hormone-releasing hormone as neurotransmitters (19). They synapse in the fish directly upon cell bodies of the dopamine interplexiform cell (20). In turtle retina, only three to six efferent fibers that are immunoreactive to the peptide MET-enkephalin are known to enter the retina and pass up to the amacrine cell area. These fibers originate in the caudal mesencephalon, but their function and action in the retina are still unknown (21).

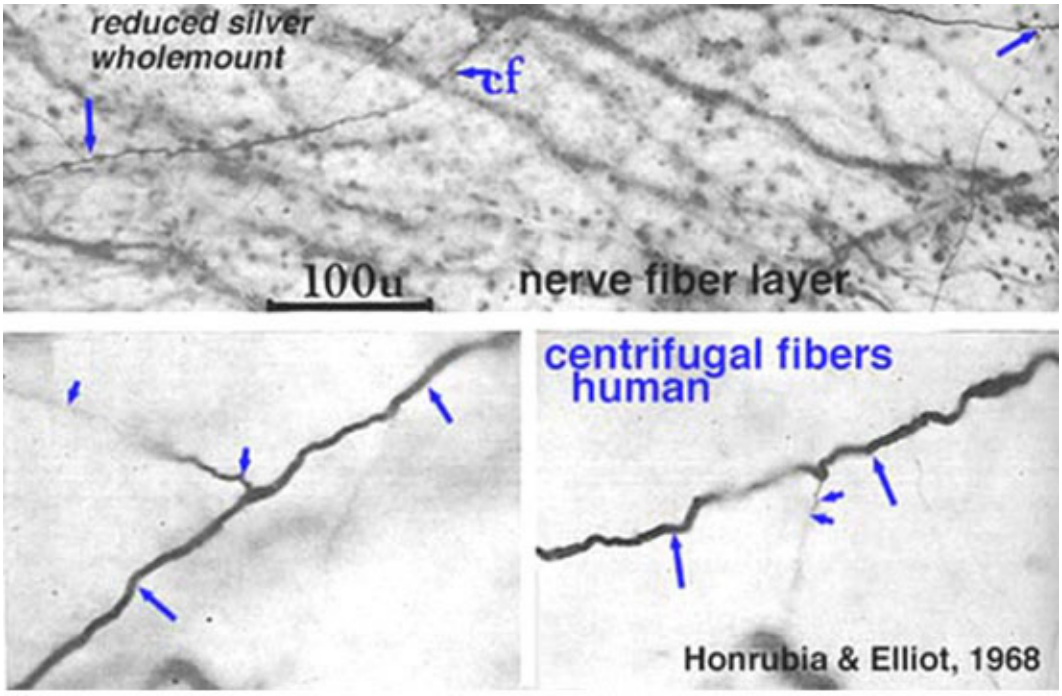

Figure 12. Centrifugal fibers in human retina.

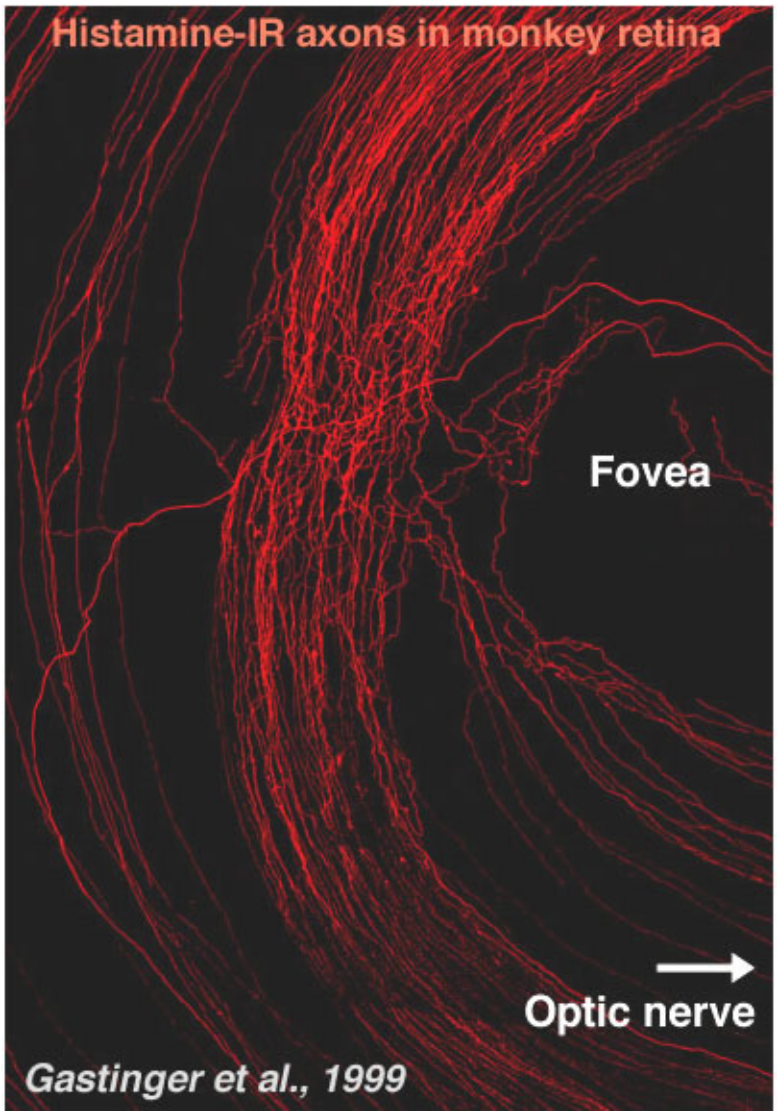

Figure 13. Photomontage of histamine-immunoreactive axons from the area temporal to the fovea. In this region, most histamine-IR axons made collateral branches in the optic fiber layer that continued around the fovea and returned to the optic disc. One large axon passed through this dense network of collaterals and ultimately made an orthogonally projecting branch to the inner plexiform layer. In the parafovea, a few of the smaller collaterals terminated in the inner plexiform layer, and the remainder ended in small swellings in the optic fiber layer.

References

1. Baylor DA, Fuortes MGF, O'Bryan PM. Receptive fields of the cones in the retina of the turtle. J Physiol. 1971;214:265–294. PubMed PMID: 5579638.
2. Linberg KA, Fisher SK. Ultrastructural evidence that horizontal cell axon terminals are presynaptic in the human retina. J Comp Neurol. 1988;268:281–297. PubMed PMID: 3360989.
3. Gallego A. Celules interplexiformes en la retine del gato. Arch Soc Esp Oftal. 1971;31:299–304.
4. Dowling JE, Ehinger B. Synaptic organization of the amine-containing interplexiform cells of the goldfish and Cebus monkey retinas. Science. 1975;188:270–273. PubMed PMID: 804181.
5. Kolb H, West RW. Synaptic connections of the interplexiform cell in the retina of the cat. J Neurocytol. 1977;6:155–170. PubMed PMID: 853310.
6. Kolb H, Linberg KA, Fisher SK. The neurons of the human retina: a Golgi study. J Comp Neurol. 1992;318:147–187. PubMed PMID: 1374766.

7. Nakamura Y, McGuire BA, Sterling P. Interplexiform cell in cat retina: identification by uptake of [gamma]-[^{3}H] aminobutyric acid and serial reconstruction. Proc Natl Acad Sci U S A. 1980;77:658–661. PubMed PMID: 6928650.
8. Ehinger B, Falck B, Laties AM. Adrenergic neurons in teleostretina. Z Zellforsch Mikrosk Anat. 1969;97:285–297. PubMed PMID: 4907380.
9. Frederick JM, Rayborn ME, Laties AM, Lam DM-K, Hollyfield JG. Dopaminergic neurons in the human retina. J Comp Neurol. 1982;210:65–79. PubMed PMID: 6127354.
10. Kolb H, Cuenca N, DeKorver L. Postembedding immunocytochemistry for GABA and glycine reveals the synaptic relationships of the dopaminergic amacrine cell of the cat retina. J Comp Neurol. 1991;310:267–284. PubMed PMID: 1720142.
11. Kolb H, Cuenca N, Wang H-H, DeKorver L. The synaptic organization of the dopaminergic amacrine cell in the cat retina. J Neurocytol. 1990;19:343–366. PubMed PMID: 2391538.
12. Cajal SR. (1892). In: Thorpe SA, Glickstein M, translators. The structure of the retina. Springfield (IL): Thomas, 1972.
13. Maturana HR, Frenk S. Synaptic connections of the centrifugal fibres in the pigeon retina. Science. 1965;150:359–361. PubMed PMID: 5833792.
14. Ogden TE. On the function of efferent retinal fibres. In: Structure and function of inhibitory neuronal mechanisms. New York: Pergamon Press; 1968. p. 89-109.
15. Polyak SL. The retina. Chicago: University of Chicago Press; 1941.
16. Honrubia FM, Elliott JH. Efferent innervation of the retina. II. Morphologic study of the monkey retina. Invest. Ophthal. 1970;9:971–976. PubMed PMID: 4098604.
17. Honrubia FM, Elliott JH. Efferent innervation of the retina. I. Morphologic study of the human retina. Arch Ophthal. 1968;80:98–103. PubMed PMID: 4873166.
18. Gastinger MJ, O'Brian JJ, Larsen JNJ, Marshak DW. Histamine immunoreactive axons in the macaque retina. Invest Ophthal Vis Sci. 1999;40:487–495. PubMed PMID: 9950609.
19. 19. Stell WK. Putative peptide transmitters, amacrine cell diversity and function in the inner plexiform layer. In: Gallego A, Gouras G, editors. Neurocircuitry of the retina: a Cajal memorial. New York: Elsevier; 1985. p. 171-187
20. Zucker CL, Dowling JE. Centrifugal fibres synapse on dopaminergic interplexiform cells in the teleost retina. Nature. 1987;330:166–168. PubMed PMID: 2890106.
21. Weiler R. Afferent and efferent peptidergic pathways in the turtle retina. In: Gallego A, Gouras P, editors. Neurocircuitry of the retina: a Cajal memorial. New York: Elsevier; 1985. p. 245-256.

Myriad roles for gap junctions in retinal circuits

Stuart Trenholm, Ph.D.[1,*] and Gautam B. Awatramani, Ph. D[2,†]

Created: September 20, 2019.

Abstract

Gap junctions are recognized in the electron microscope as dense starchy areas of opposed membrane between two cells. Small tracer molecules such as Neurobiotin pass through the gap junction pore, marking interconnected cells. Electrical signals pass through these junctions, extending the region of neuronal data collection, modifying the dynamic properties of the signal, and synchronizing impulse generation. In the retina, circuits comprised of many neuronal types transform information within the visual environment into a series of highly processed, simplified spike trains that are relayed to higher visual areas. Retinal signal processing relies on intricate interactions between specific cell types, which are mediated by both chemical and electrical synapses. In the field, great strides have been made in understanding the diversity of retinal cell types, of which there are likely at least 100 unique types, and how they connect to form cell-type-specific circuits. Here, we provide an overview of electrical coupling in the retina and outline the varied roles that gap junctions play in processing information in healthy and diseased states.

Introduction

The retina is built from approximately 100 distinct neuronal cell types, which reside in specific retinal layers and connect with one another to form intricate microcircuits (1-5). These circuits serve to extract principle features of the visual world, which get parsed into distinct visual channels via different retinal ganglion cell types. These differentially processed visual signals are then relayed out of the retina to a large number of higher visual areas (6, 7). Interestingly, microcircuits in the retina are connected through both chemical synapses and bi-directional electrical synapses formed by gap junctions. The rich interactions between electrical and chemical synapses enable circuits to operate in highly flexible and dynamic ways. Moreover, as the strength of gap junctions can be modified over a variety of timescales, they can reconfigure retinal microcircuits on both a millisecond time-scale as well as over the course of the day/night cycle. In addition, gap junctions exert their effects over a range of spatial scales, synchronizing activity at the sub-cellular level as well as across wide swaths of the retina. Given these diverse roles for gap junctions in retinal signal processing, it is not surprising that electrical synapses also play many roles in disease states. Finally, despite the advances outlined here regarding our understanding of the various roles for gap junctions in retinal signaling, it is likely that we are still only scratching the surface in identifying the full repertoire of their functional roles.

Gap junctions in the retina and how they affect receptive field size

The vertebrate retina contains five principal neuron classes: photoreceptors (rods and cones), horizontal cells, bipolar cells, amacrine cells and ganglion cells. For each class of neuron, we describe electrical and chemical synaptic connectivity patterns (**Figure 1**). For electrical synapses, when known, we outline the connexin

Author Affiliations: 1 Montreal Neurological Institute, McGill University, Montreal, Canada; Email: stuart.trenholm@mcgill.ca. 2 Department of Biology, University of Victoria, Victoria, Canada; Email: gautam@uvic.ca.

Corresponding author.

* About the authors

† About the authors

subtypes involved in forming gap junctions and describe their biophysical properties. Also, whenever possible, we describe the strength of gap junctions between pairs of neurons, represented as either the junctional conductance or the coupling coefficient (i.e. the change in membrane potential of a post-junctional cell divided by the change in the membrane potential in a pre-junctional cell when then membrane potential of the pre-junctional cell is altered).

Despite the characterizations of coupling strength that we will outline below, it is important to keep in mind that the conductance through a gap junction is not static, and changes to the conductance can have significant effects on the roles that electrical synapses play in neuronal circuits. For instance, modifying the strength of gap junction coupling can significantly alter the receptive field size of retinal neurons by modifying the strength and extent of their excitatory receptive field surround. For many neurons in the retina, light adaptation or circadian rhythm can modulate the strength of electrical coupling and thus alter receptive field sizes. Changes to coupling strength could also modify other roles for gap junctions in retinal circuits. While molecular mechanisms underlying changes in coupling strength have been studied in detail (8), in the following section we focus on the functional outcomes of modifications in coupling strength on receptive field size.

Photoreceptors

Vision starts in rod and cone photoreceptors, as photons are converted into an electro-chemical signal (See Webvision chapter Phototransduction in Rods and Cones). Photoreceptors make glutamatergic synapses with horizontal and bipolar cells (ionotropic sign conserving synapses with horizontal cells and OFF bipolar cells; metabotropic sing-inverting synapses with ON bipolar cells). Photoreceptors also form both homologous (i.e. cone-cone and rod-rod) and heterologous (rod-cone) electrical synapses (**Figure 2**) (9-17).

Cone gap junctions contain connexin 36 (Cx36) in mammals (**Figure 3**) (18-21) and Cx35 in zebrafish (22), while the connexin involved in rod electrical synapses has not been definitively identified (22-24), and coupling between rods and cones appears to rely on Cx36 (25). Photoreceptor gap junctions are localized around the axon terminal of cones (11, 16, 26-28).

Based on physiological recordings, it appears that homologous photoreceptor coupling is stronger than heterologous coupling. The junctional conductance of cone-cone and rod-rod gap junctions appears to be bidirectionally symmetrical and in the range of 200-800 pS (**Figure 4**) (12, 14, 15, 27, 29), with a coupling coefficient of around 0.15 (14, 30). The junctional conductance of rod-cone gap junctions has been reported to be bidirectionally symmetrical and in the range of 40-200 pS (31), with a coupling coefficient of around 0.04 (32). From tracer dye experiments where the dye is injected into cones, it appears that being coupled to rods is more common than being coupled to only cones or to both rods and cones, and some cones may be uncoupled (13). In contrast, from tracer dye experiments where the dye is injected into rods, rod-rod coupling seems to be more common than rod-cone coupling and some rods may be uncoupled (15).

Circadian rhythm, and not light adaptation, appears to be the main controller for altering the strength of electrical coupling in photoreceptors in fish and mouse retinae (33). Psychophysical experiments in humans have indicated that cone coupling appears to be unaffected by light adaptation, but effects of circadian rhythm have not been tested (12). In contrast, light adaptation, not circadian rhythm, appears to modulate electrical coupling strength between salamander photoreceptors (31). Altering the strength of gap junctions can modify the receptive field size of photoreceptors. For instance, cones have larger receptive fields during states in which rods and cones are more strongly electrically coupled (33). Similarly, rod receptive fields are also expected to be larger when they are more strongly coupled, and coupling decreases trial-to-trial variability in their responses to dim flashes (15). Finally, heterotypic gap junctions allow cone responses to pass into rods (34), and rod responses to pass into cones (**Figure 5**) (13, 35-37), meaning that increases in electrical coupling should extend the range of light intensities over which a given rod or cone can respond, and at least for cones such coupling could result in increased reliability of threshold responses.

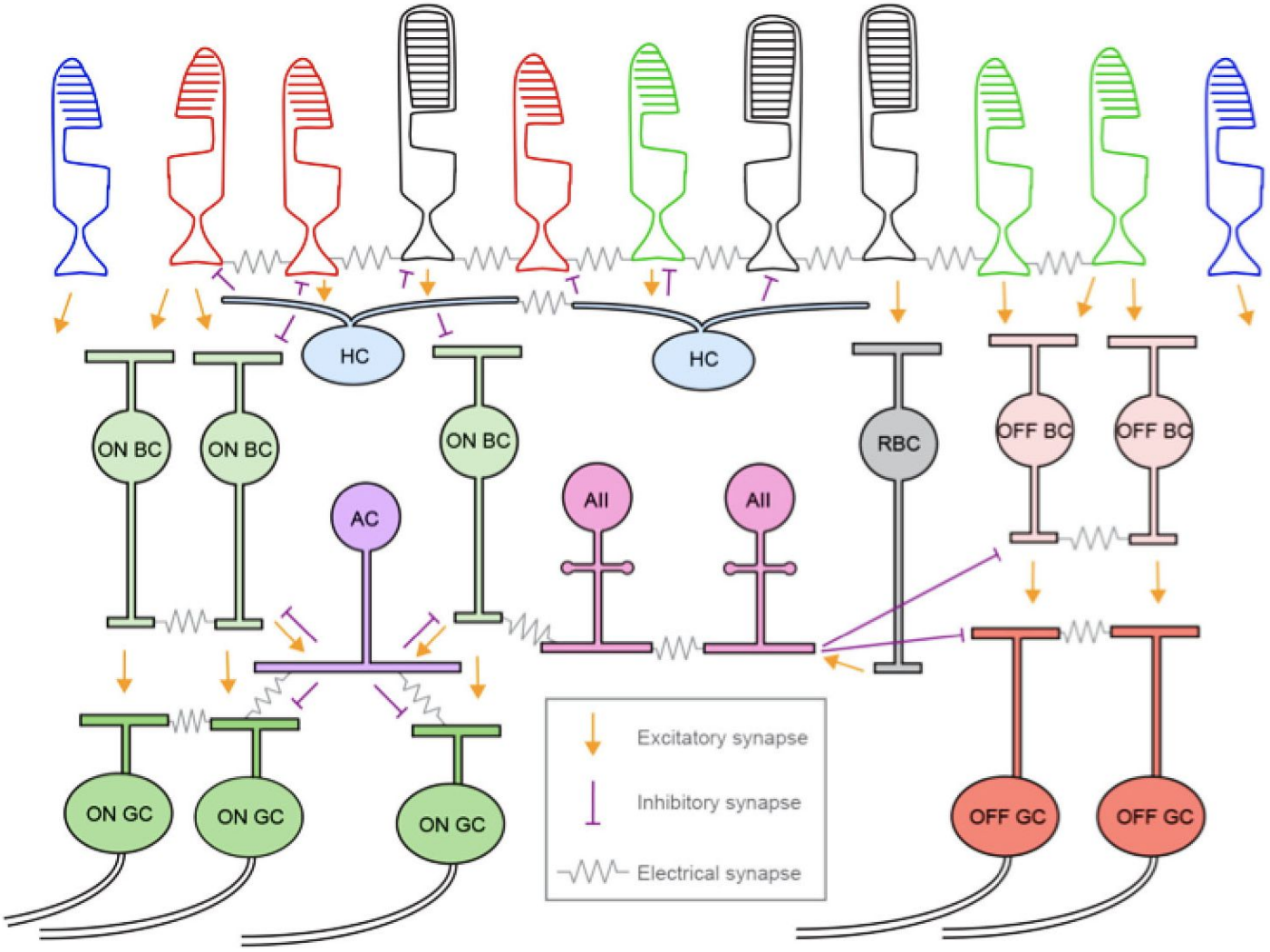

Figure 1. *Retinal anatomy and synaptic connectivity.* A schematic of the vertebrate retina. Photoreceptors (top), showing rods (black), and cones, colored according to wavelength. Note that blue cones may be uncoupled (14, 27). Horizontal cells (HC, blue), ON bipolar cells (ON BC, green), OFF bipolar cells (OFF BC, light red), and rod bipolar cells (RBC, gray) are shown in the middle, as are AII amacrine cells (pink), as well as a generic amacrine cell (AC, purple). ON and OFF ganglion cells (ON GC, green; OFF GC red) are on the bottom. Taken from Trenholm and Awatramani (2017) (197).

Horizontal cells

Horizontals receive glutamatergic inputs from photoreceptors, and in turn provide negative feedback to photoreceptors and possibly feedforward inhibition to bipolar cells (See Webvision chapter S-potentials and Horizontal cells). The mechanisms of feedback interactions are still actively being studied (38). Additionally, horizontal cells are densely interconnected with gap junctions (**Figure 6**) (26, 39).

Horizontal cell gap junctions can be either axoaxonic or dendrodendritic. In mouse, Cx57 is present in both types of gap junctions (**Figure 7**) (40, 41), while Cx50 is localized in axonal gap junctions (42). In rabbit A-type horizontal cells, Cx50 localizes in dendritic gap junctions (43), and Cx57 is found in axonal gap junctions in B-type horizontal cells (44). In zebrafish, horizontal cell gap junctions appear to be comprised of Cx52.6, 52.9 and 55.5 (45, 46).

Coupling between horizontal cells appears to be very strong, with a bidirectional and symmetrical junctional conductance of > 1ns and with a coupling coefficient of 0.5 or greater in cultured horizontal cells (47-50). From

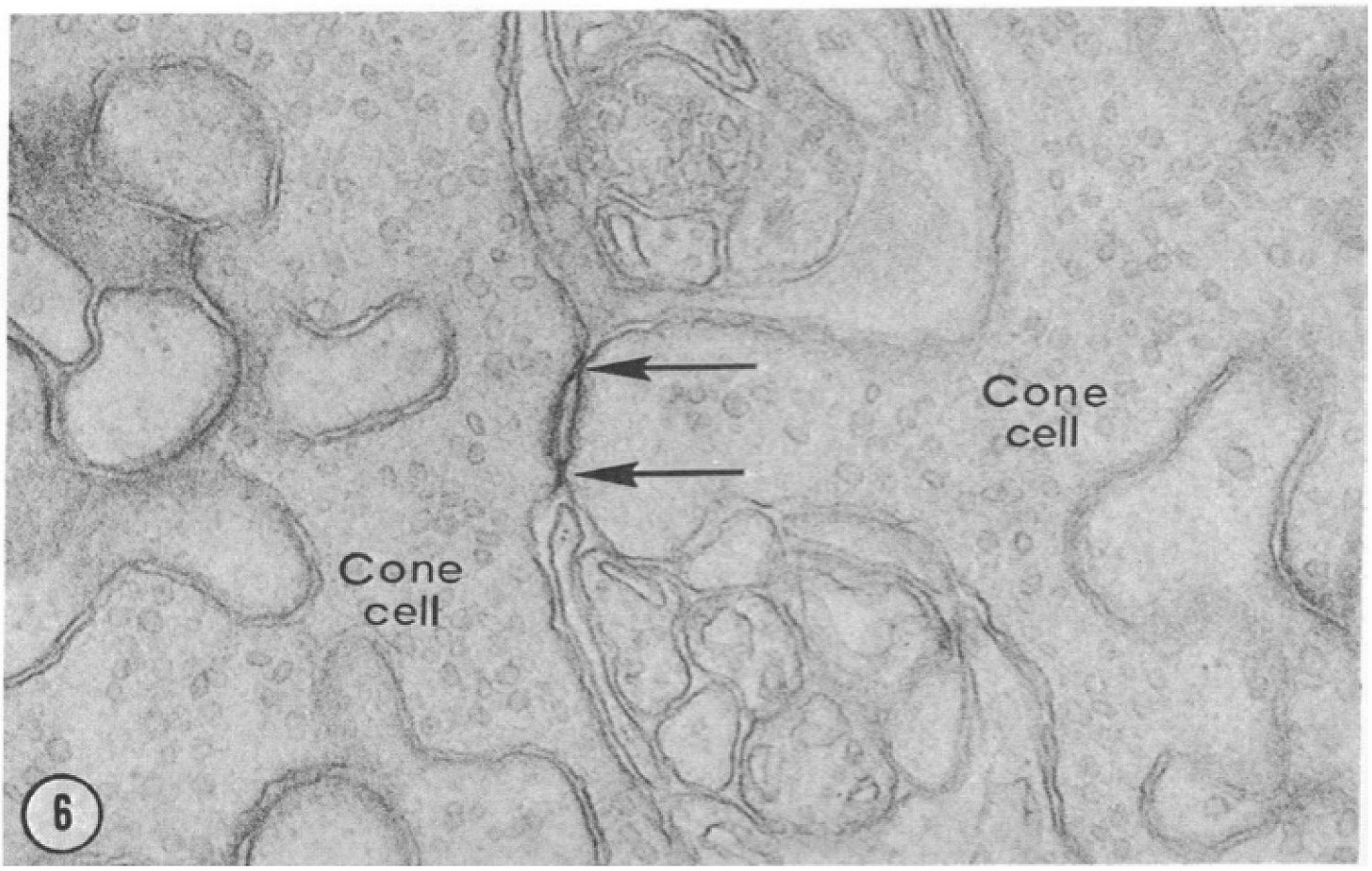

Figure 2. *Gap junctions between cone photoreceptors*. Electron micrograph of a tangential retinal section showing two gap junctions (black arrows) between cone photoreceptors in macaque retina. Magnification: x 55000. Taken from Raviola and Gilula (1973) (16).

remarkable tracer dye experiments, where dye is injected into a single horizontal cell, it has been found that dye can spread into more than 1000 surrounding horizontal cells extending across a distance of over 1 mm (**Figure 8**) (51).

In horizontal cells, light adaptation appears to be the main factor controlling the strength of gap junction coupling (52, 53). Horizontal cell coupling has been shown to exhibit a tri-phasic relationship depending on luminance levels: tracer coupling experiments show minimal coupling in the dark adapted or "dark-suppressed" state; tracer coupling is greatly increased in medium light levels, during the so-called "light-sensitized" state; tracer coupling is very weak during the light adapted state (**Figure 9**) (51).

Horizontal cell coupling seems to strongly affect receptive field size (54), with receptive fields being approximately three times larger in the light-sensitized state (51). Consistent with this finding, knocking out Cx57 in mice decreases the size of horizontal cell receptive fields (**Figure 10**) (55).

As horizontal cells provide negative feedback to photoreceptors, it has been posited that they might be responsible for generating inhibitory surround receptive fields in downstream ganglion cells (56, 57) in which case modifying horizontal cell coupling strength would modify ganglion cell receptive field size. However, the effect of horizontal cell feedback on ganglion cell surround responses remains uncertain, and at least in some cases horizontal cells do not drive significant surround responses in ganglion cells (58-60). Additionally, despite reducing horizontal cell receptive field size, knocking out Cx57 has little effect on ganglion cell spatial tuning and on visual acuity in mice (61). In contrast, horizontal cells might play a role in temporal tuning of ganglion cells. For instance, it has been suggested that strong electrical coupling might functionally remove horizontal

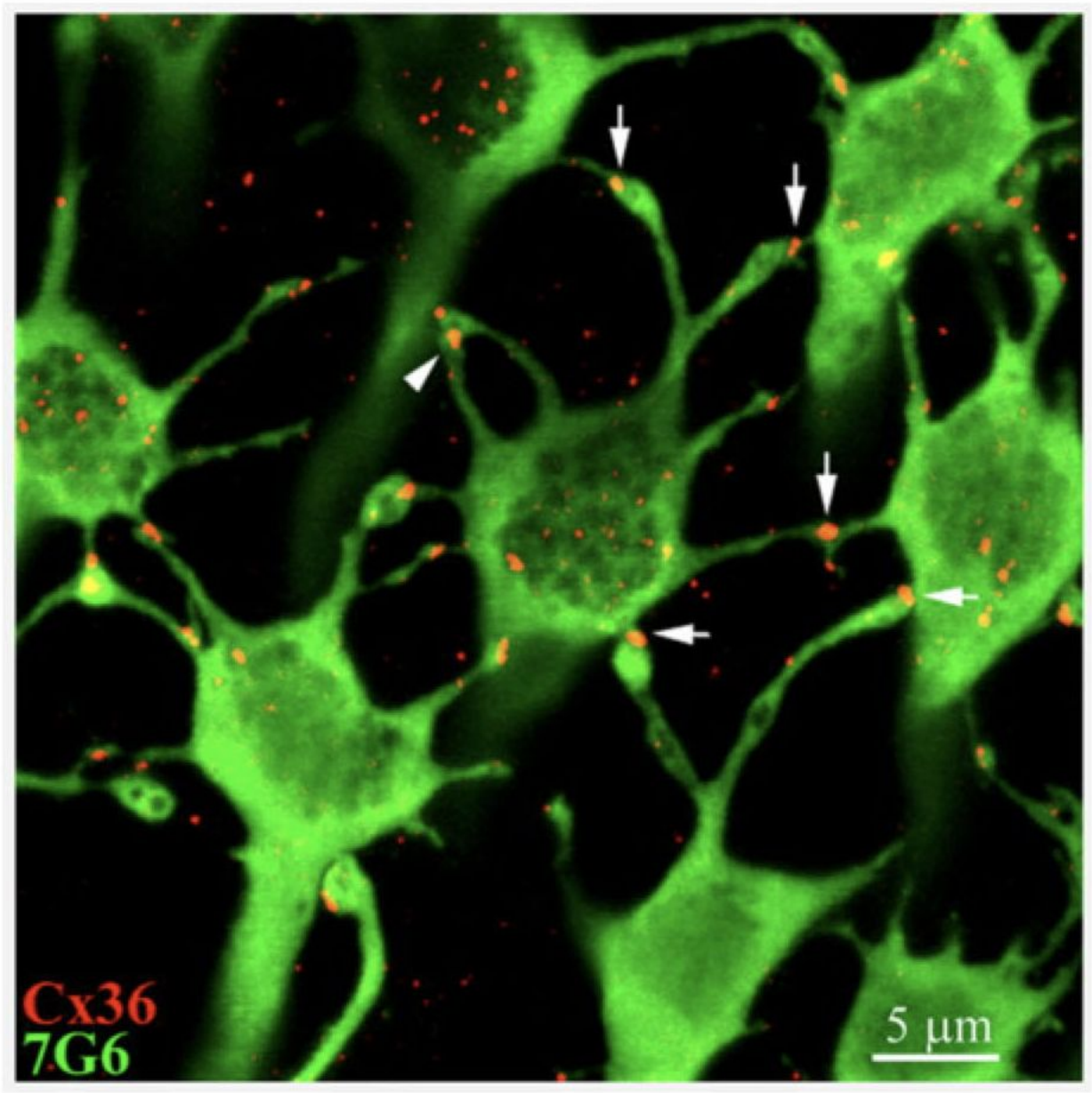

Figure 3. *Connexin 36 is present in telodendria contacts between pedicles of adjacent cones.* Connexin 36 (Cx36, red) is localized at contact points (white arrows) between neighbouring cone terminals (7G6, green, cone arrestin antibody) in macaque retina. Taken from O'Brien et al. (2012) (21).

cells from the retinal circuit, by effectively shunting their input current from photoreceptors. In such a situation, modifying coupling strength could switch the retina from a mode of short integration time in daylight conditions to a mode of long integration time in nightlight conditions (62). In another study, horizontal cell feedback to photoreceptors was shown to differentially affect transient and/or sustained portions of ganglion cell responses (58), and this could provide another mechanism whereby changes in horizontal cell coupling could affect temporal tuning in ganglion cells.

Bipolar cells

Bipolar cells, of which there are at least 10 types (63), pass photoreceptor signals onto amacrine and ganglion cells at glutamatergic synapses (See Webvision chapter Bipolar Cell Pathways in the Vertebrate Retina).

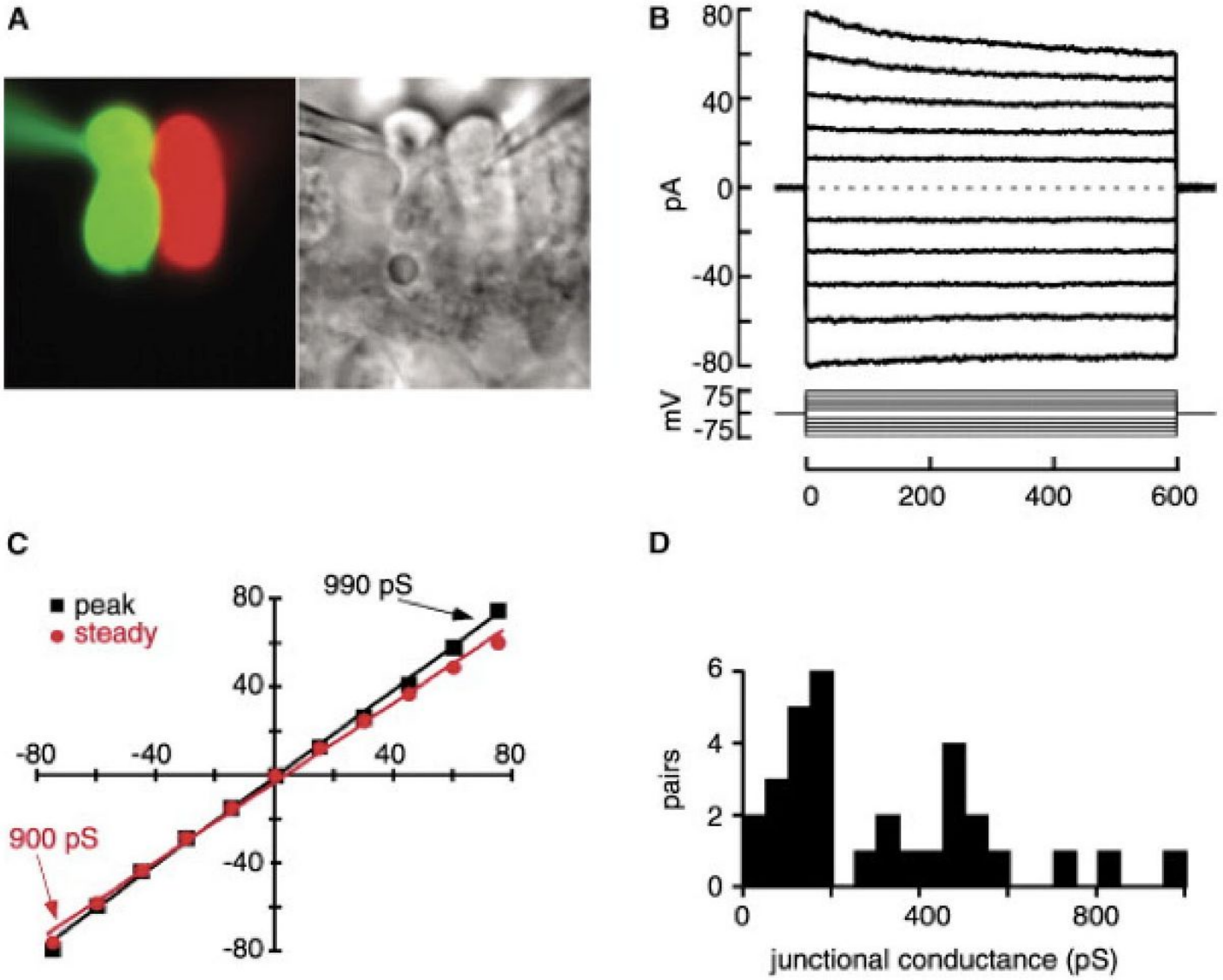

Figure 4. *Paired whole-cell voltage clamp recordings from ground squirrel retina*. **A**, Patch pipette recording from a pair of cones, labelled in green and red, in a retinal slice preparation (shown in grey on the right). **B**, Changing the resting voltage in one cell (*bottom*) results in transjunctional currents in the neighbor (*top*). **C**, Conductance is plotted for both peak and steady state transjunctional currents to a variety of membrane changes in the pre-junctional cell (x-axis represents mV; y-axis represents pA). **D**, Distribution of measured junctional conductances for different pairs of cells. Taken from Devries et al. (2002) (12).

Additionally, bipolar cells can be electrically coupled to other bipolar cells and amacrine cells. Most commonly, bipolar cells are coupled to AII amacrine cells (**Figure 11**) (64), though recent work shows that certain ON cone bipolar cells form gap junctions with non-AII amacrine cells (59, 65). See Webvision chapter on AII amacrine cells.

Gap junctions between bipolar cells can be localized in dendrites (66) or axon terminals (67, 68), though gap junctions between ON cone bipolar cells and AII amacrine cells are localized in the bipolar cell axon terminal (69). In mouse retina, bipolar cell gap junctions contain either Cx36 or Cx45 (**Figure 12**) (18, 70-73).

Bipolar cell to bipolar cell gap junctions are bidirectional and symmetrical, with a junctional conductance of around 1 nS and a coupling coefficient of around 0.3 (**Figure 13**) (66, 74-77).

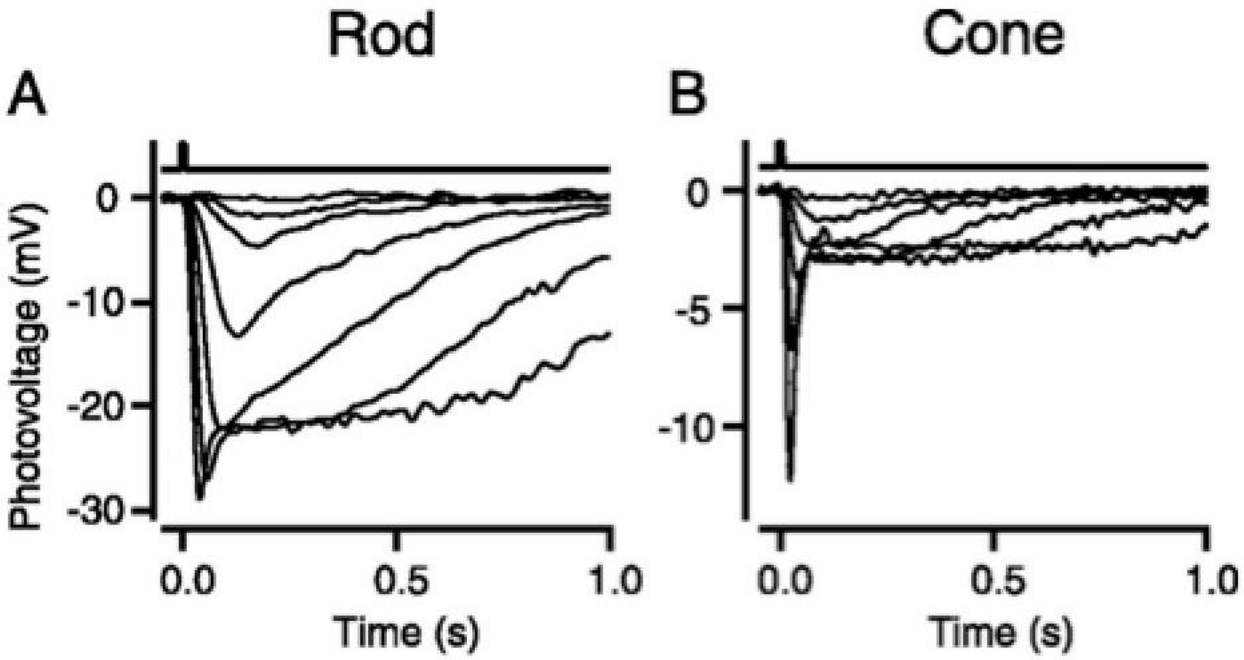

Figure 5. *Rod-generated signals measured in rods and cones of macaque*. **A**, Photovoltage responses from a rod for flashes of increasing brightness (from 0.3 to 803 photons um^{-2}). **B**, Photovoltage responses from a cone for flashes of increasing brightness (from 2.0 to 3874 photons um^{-2}). Slow, rod-like responses are present in cones at dim light levels. The stimulating wavelength is 500 nm. Taken from Hornstein et al. (2005) (13).

ON cone bipolar cells form gap junctions with AII amacrine cells that are bidirectional but asymmetric, though this measured asymmetry is likely an artifact of differences in input resistance. Between ON cone bipolar cells and AII amacrine cells the junctional conductance is approximately 1 nS, with a coupling coefficient between 0.3-0.6 (**Figure 14**) (64, 70, 78-80).

The gap junction conductance between electrically connected bipolar cells increases in the light adapted state, at least as shown in goldfish for Mb-1 bipolar cells (66). While it has been suggested that bipolar cell coupling can result in increased receptive field sizes, which some studies have found to be significantly larger than dendritic field sizes (74, 75, 81), but also see (82), to our knowledge the effect of changing light adaptation state on bipolar cell coupling and receptive field size has never been directly tested. Furthermore, since previous work has shown that light adaptation can produce antagonistic surround receptive fields in bipolar cells (83), such surround inhibition would be expected to counteract excitatory surround responses provided via gap junction inputs from neighbouring cells, thus limiting the ability of gap junction coupling to expand receptive field size. As such, while bipolar cell gap junctions appear to enhance their ability to integrate spatially separated stimuli and preferentially enhance their signaling of low contrast stimuli (84), further study is required to define the effect of light adaptation on the strength of gap junction coupling for bipolar cells, and for examining whether such changes effectively modify receptive field size.

Amacrine cells

Amacrine cells, of which there are more than 45 types (5, 85), provide inhibition, via GABA or glycine release, to bipolar cells, other amacrine cells and ganglion cells. Some amacrine cells can also co-release acetylcholine (86-88), dopamine (89), or glutamate (90). Many amacrine cells form homologous gap junctions (78, 79, 91-93), and heterologous gap junctions with bipolar cells – as described above – and ganglion cells (94, 95). AII amacrine cells form gap junctions with one another in their dendritic arbors (**Figure 15**) (69). It seems likely

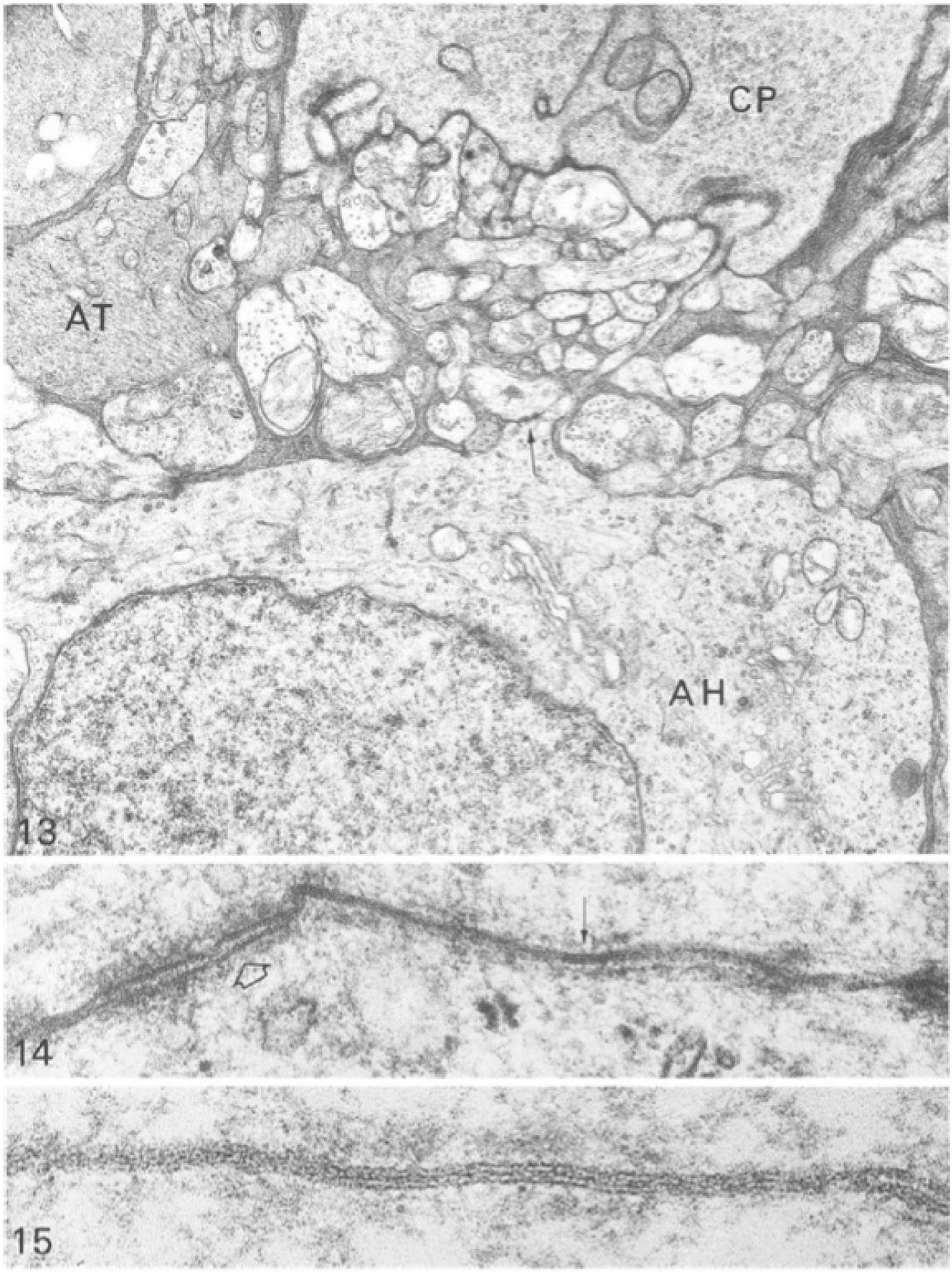

Figure 6. *Gap junctions between horizontal cells*. **13**, An electron micrograph of an A-type horizontal cell (AH), an axon terminal tract (AT) and a cone pedicle (CP) from cat retina, revealing a small gap junction (black arrow) on the horizontal cell dendrite. Magnification: x 18000. **14**, A gap junction (small arrow) between two A-type horizontal cell processes, as well as a macula adherens (large arrow). Magnification: x 90000. **15**, A higher resolution view of gap junctions between two A-type horizontal cell dendrites. Magnification x 180000. Taken from Kolb (1977) (26).

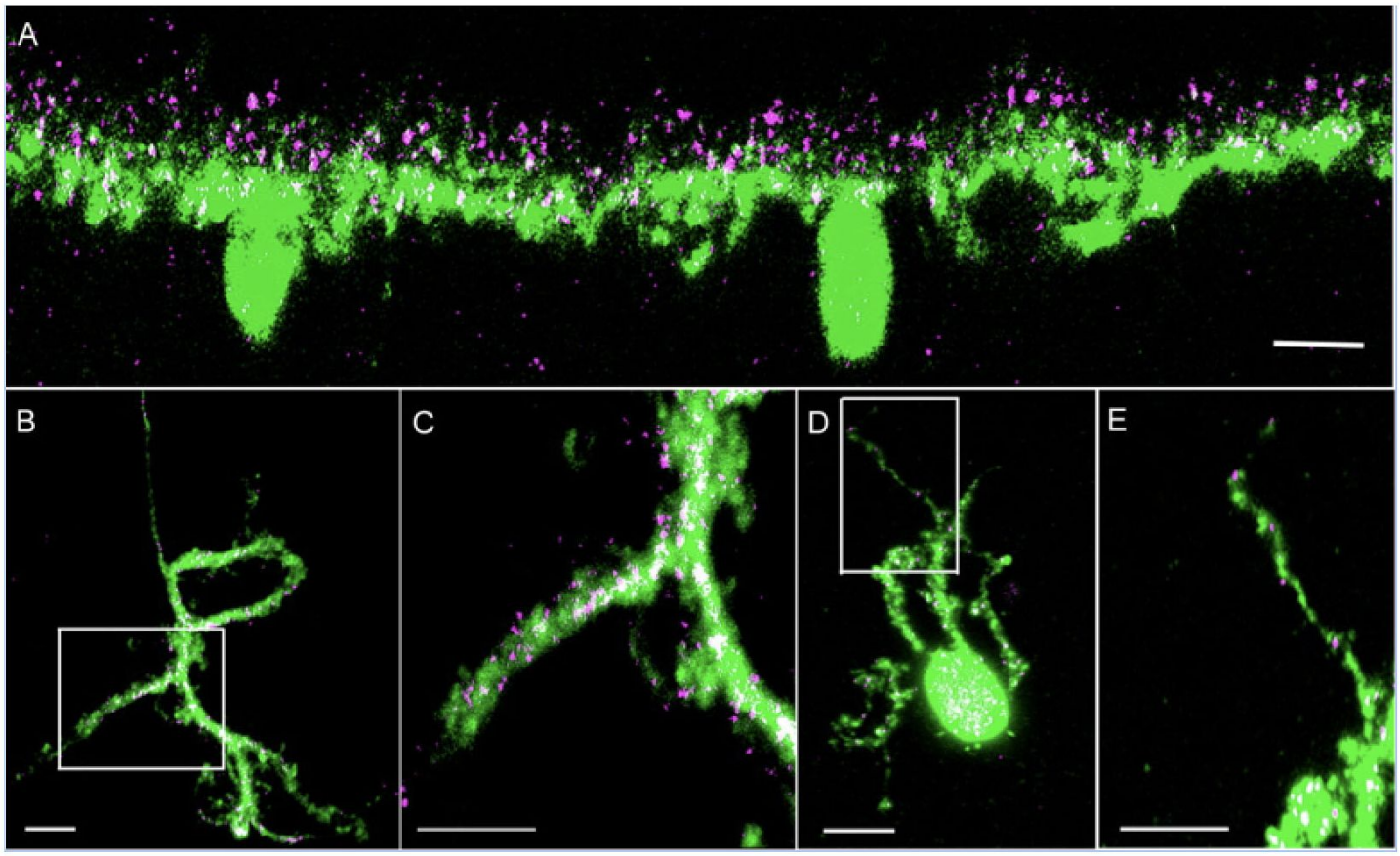

Figure 7. *Cx57 is localized in the processes of mouse horizontal cells*. **A**, Calbindin (green) stained horizontal cells in a retina slice, co-labelled for Cx57 (purple) revealing dense Cx57 expression in horizontal cell processes. **B**, An isolated horizontal axon terminal. **C**, A higher magnification view of the area outlined in (B). **D**, An isolated horizontal cell body and processes. **E**, A higher magnification view of the area indicated in (D). Scale bars: 20 μm in A, B, D; 10 μm in C, E. Taken from Janssen-Bienhold et al. (2009) (41).

that other amacrine cell types also make dendrodendritic gap junctions with amacrine and ganglion cells, as this is often the only location where their processes overlap.

AII amacrine cells appear to form gap junctions with ON cone bipolar cells with Cx36. Coupling between AII amacrine cells is bidirectional and symmetric, with a junctional conductance of ~700 pS and a coupling coefficient of ~ 0.3 (**Figure 16**) (78).

Other amacrine cell types form gap junctions with amacrine or ganglion cells with electrical synapses comprising either Cx36 or Cx45 (96, 97). nNOS-2 amacrine cells, which are the main source of nitric oxide in the mouse retina, have been shown be extensively interconnected with what appear to be Cx45 containing gap junctions, and exhibit a bidirectional and symmetrical conductance, with a junctional conductance that was modeled to be very large (4.4 nS, **Figure 17**) (98). The measured coupling coefficient for nNOS-2 amacrine cell gap junctions was ~0.08 (98).

Light adaptation state appears to strongly control coupling strength in amacrine cells (94). Similar to horizontal cells, tracer coupling experiments indicate that AII amacrine cells exhibit minimal coupling during both very dim and bright conditions, and strong coupling during mid light conditions (**Figure 18**) (94).

Such changes in coupling strength appear to strongly influence receptive field size, as AII amacrine cell receptive fields can be 2-3 times larger than their dendritic fields in the light-sensitized state (94). However, a direct relationship between coupling strength and receptive field size does not appear to hold across all amacrine cell

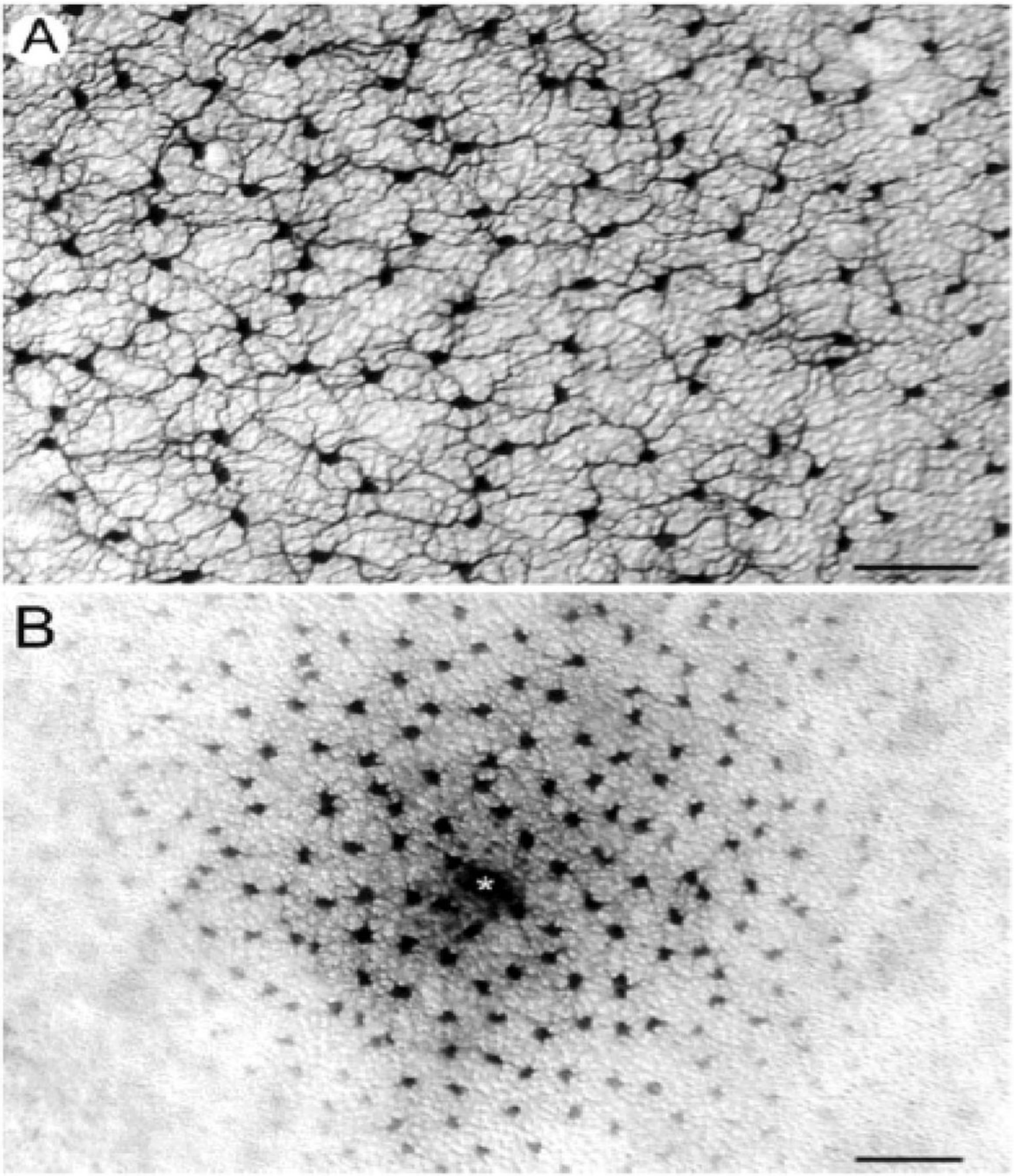

Figure 8. *Extensive tracer coupling in horizontal cells in the dark-adapted rabbit retina.* **A**, Neurobiotin injected into A-type horizontal cell spread into over 1000 neighboring cells, spanning across a distance of over 2 mm (a more restricted view is shown here). **B**, Neurobiotin injected into a B-type horizontal cell spread into over 200 neighboring cells. Scale bar, 50 μm. Taken from Xin and Bloomfield (1999) (51).

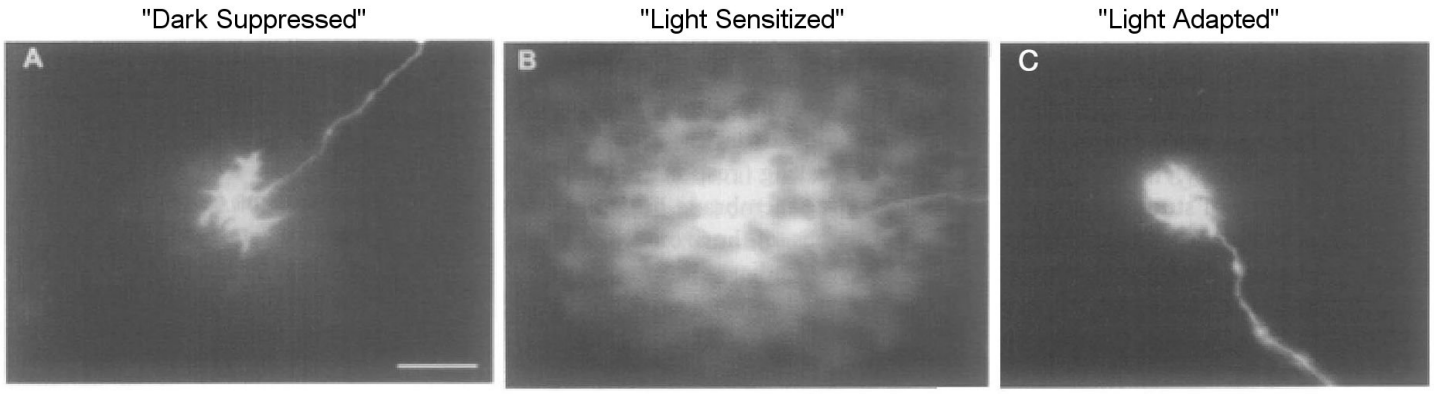

Figure 9. *Triphasic adaptation of horizontal cell tracer coupling.* Injecting Lucifer yellow dye into a single H1 horizontal cell in goldfish retina results in little tracer coupling in dark adapted ("Dark Suppressed") retina (**A**), extensive tracer coupling in the "Light Sensitized" state (**B**), and little if any tracer coupling in the "Light Adapted" state (**C**). Taken from Baldridge (2001) (198).

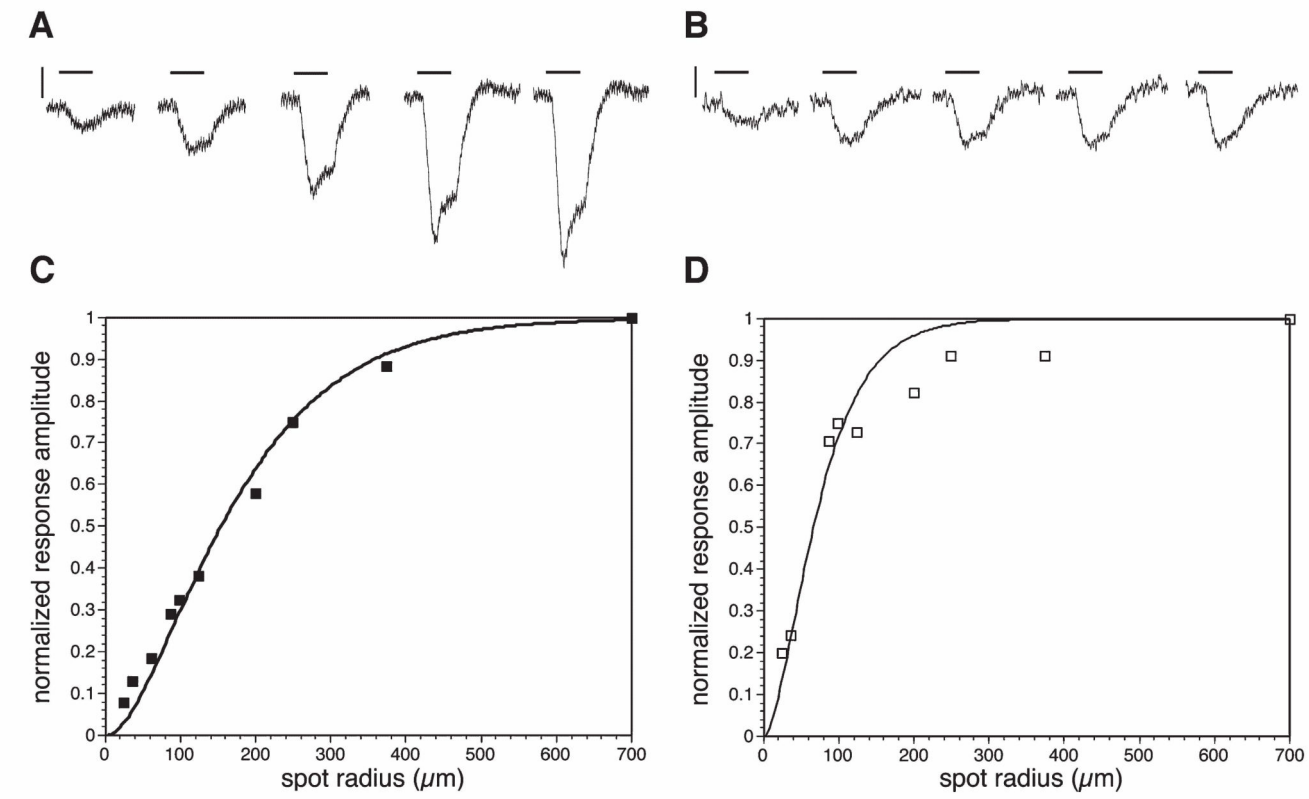

Figure 10. *Spatial integration is impaired in horizontal cells in Cx57 KO mouse retina.* **A**, Spots of light of increasing radii (40, 90, 200, 375, and 700 μm) were presented to a horizontal cell and membrane voltage responses are shown (scale bar, 2 mV). **B**, The same experiment as in (A), but in Cx57 KO retina. **C**,**D**, Response amplitude vs. spot size is plotted for wild type (C) and Cx57 KO (D) horizontal cells. In Cx57 retina, horizontal cells reach their peak response amplitude at small spot sizes. Note that response amplitude is also significantly decreased in Cx57 knockout, as seen in panels A and B. Taken from Shelley et al. (2006) (55).

types. For instance, unlike AII amacrine cells, work with some other types of amacrine cells did not indicate a strong effect of light adaptation on receptive field size, despite the fact that tracer coupling experiments showed light-adaptation dependent changes in tracer coupling patterns (**Figure 19**) (94). Why the effect of gap junction coupling on receptive field size does not appear consistent across all amacrine cell types remains unclear, though it could have to do with the fact that the dendrites of some amacrine cell types appear to perform local

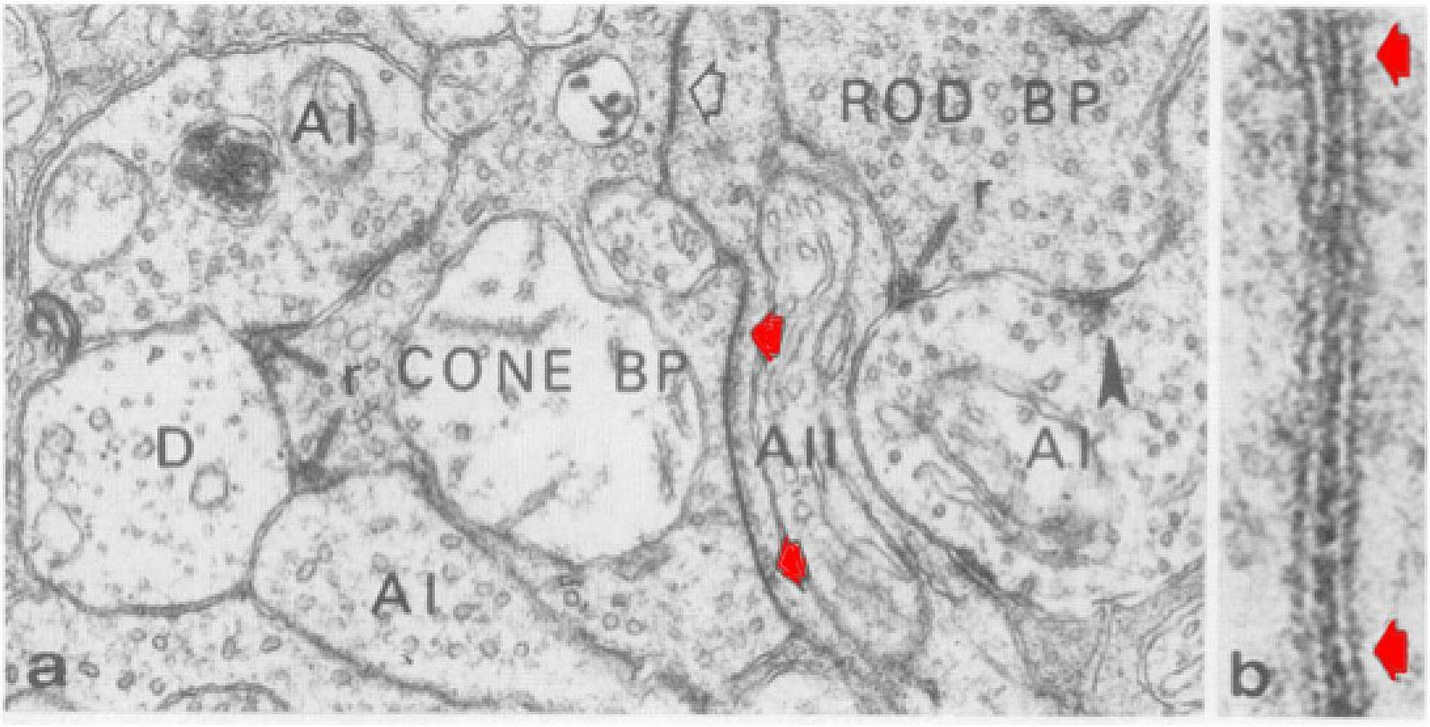

Figure 11. Gap junctions between a cone bipolar cell and an AII amacrine cell. **a** An electron micrograph from a section of cat retina showing a cone bipolar cell (CONE BP), that makes extensive gap junctions connections (red arrows) with an AII amacrine cell. Also seen are bipolar cell ribbon synapses (r) onto a ganglion cell dendrite (D) as well as a synapse of an AI amacrine cell making a synapse (arrowhead) on a rod bipolar cell (ROD BP). AI is also known as A17. Magnification: x 33000. **b** A higher resolution view of a gap junction between a bipolar cell and an AII amacrine cell. Magnification: x 250000. Taken from Kolb and Famiglietti (1974) (64).

computations (99), which might therefore not require global changes in receptive field size for changes in junctional conductance to have an effect on circuit function. Another possibility for the difference of light adaptation on amacrine cell coupling could be differential regulation by dopamine. Indeed, gap junction coupling of A8 amacrine cells, which are coupled to both ON and OFF bipolar cells with Cx36 gap junctions, does not appear to be modulated by dopamine receptor D_1 activation, in contrast to AII amacrine cells (100). Finally, in mouse nNOS-2 amacrine cells, there appears to be a remarkable self-regulation between light activation and coupling state. nNOS-2 cells are extensively electrically coupled in the dark-adapted retina, whereas upon light activation they produce nitric oxide which in turn decouples the network (98). Whether this light-activated decoupling affects receptive field size remained to be tested.

Ganglion cells

Ganglion cells, of which there are upwards of 30 types (101-103), receive excitatory glutamatergic input from bipolar cells and inhibitory GABAergic and glycinergic input from amacrine cells, and send their signals, via the optic nerve, to multiple higher visual areas (6, 7) (See Webvision chapter Visual Responses of Ganglion Cells). Ganglion cells also form dendrodendritic gap junctions with amacrine cells and other ganglion cells (**Figure 20**) (91, 95, 104-108).

Ganglion cell gap junctions are frequently comprised of connexin 36 (**Figure 21**) (96, 109-111), though some contain connexin 45 (109) and possibly also connexin 30.2 (109).

Ganglion cell to ganglion cell coupling appears to be exclusively homologous, with no coupling between different ganglion cell types (95, 105, 112, 113), though possibly there are exceptions (114). Furthermore, distinct ganglion cell subtypes have unique coupling patterns (Figure 22) (95). Less is known about ganglion cell-

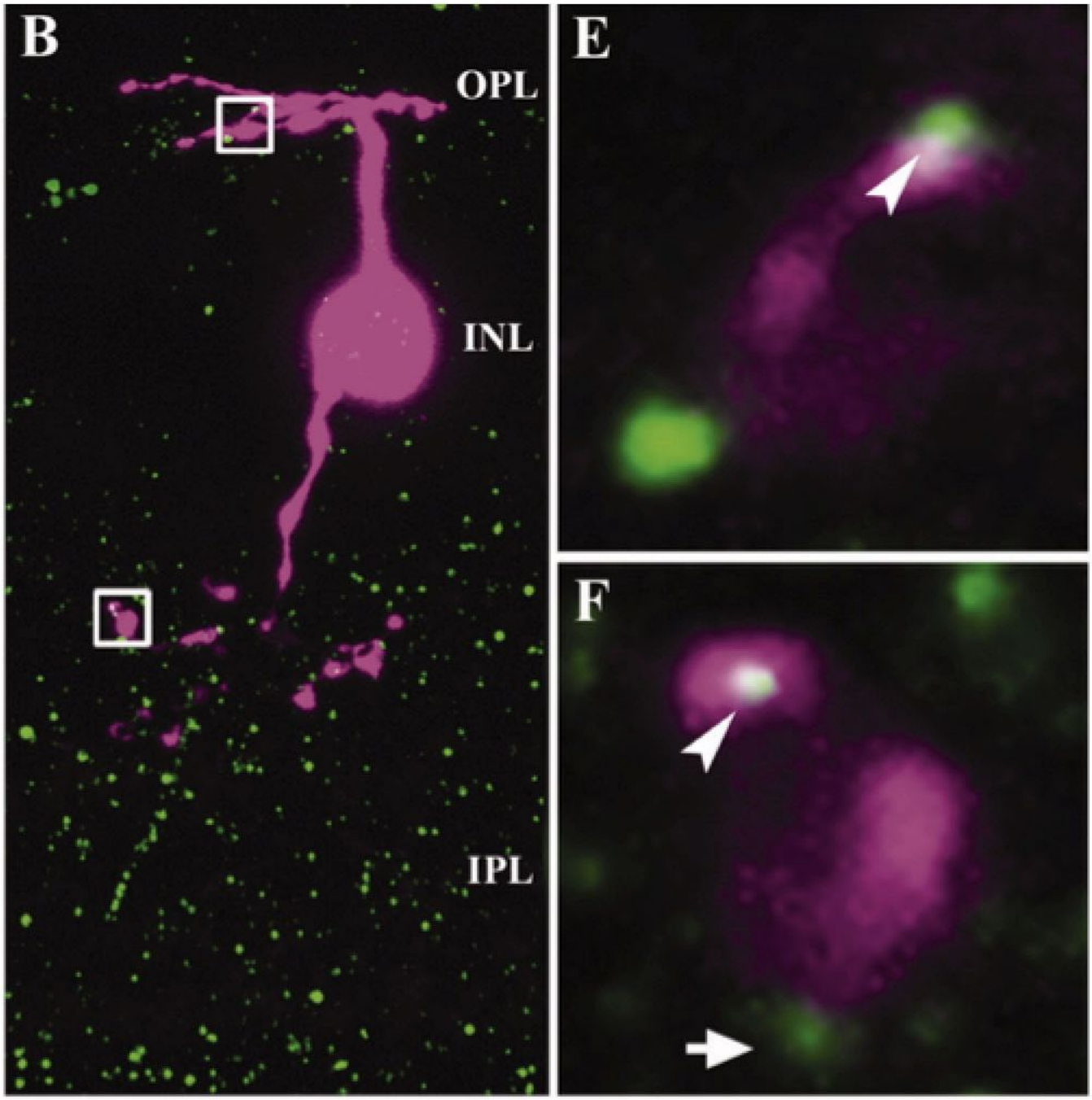

Figure 12. *Connexin 45 is present on certain bipolar cells*. **B**, An Alexa-594 filled type 1 cone bipolar cell in mouse retina (magenta) stained for Cx45 (green). Overlap between a bipolar cell dendrite and Cx45 (**E**), and a bipolar cell axonal bouton and Cx45 (**F**) are show for regions outlined in (B). Taken from Hilgen et al. (2011) (72).

amacrine cell coupling, though tracer coupling work suggests that specific ganglion cells form gap junctions with specific types of amacrine cells (**Figure 22**) (95).

Gap junctions between ganglion cells are bidirectional and have a symmetrical junctional conductance of around 1 nS and a coupling coefficient of around 0.15 (**Figure 23**) (106, 113).

In ganglion cells, light adaptation appears to control coupling strength, with coupling being reduced in the dark adapted state and increased in the light adapted state (at least as has been shown for OFF α cells in the rabbit retina (115); though this may not be the case for all ganglion cell types (111)). Interestingly, while increased

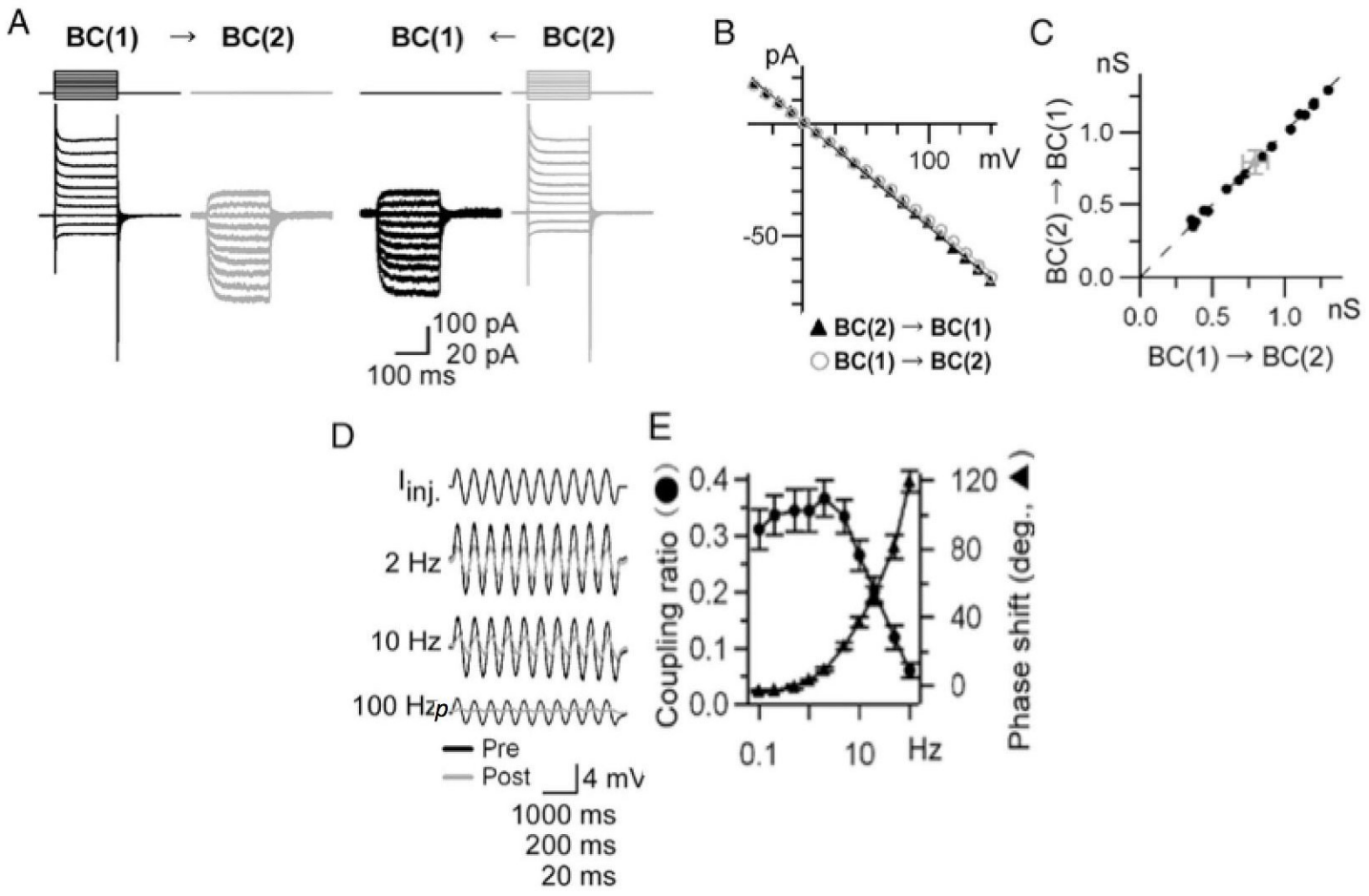

Figure 13. *Biophysical properties of gap junctions between bipolar cells*. **A**, A pair of Mb1 bipolar cells in goldfish retina were voltage clamped at -60 mV, and voltage steps (-100 to +90 mV) were applied to one cell in the pair while currents were measured in the other cell. **B**, The junctional I-V curves from the experiment shown in (A). **C**, Bidirectional junctional conductance plotted for 16 pairs of cells. **D**, Example voltage responses (both pre and postjunctional) to sinusoidal current injections into a prejunctional cell (20 pA peak to peak current injection) at various frequencies. **E**, Coupling ratio (i.e. coupling coefficient) and phase shift plotted against frequency. Taken from Arai et al. (2010) (66).

coupling strength does not seem to alter the size of the classical (spiking) receptive field (115, 116), gap junction inputs from neighboring cells endow electrically coupled ganglion cells with extensive subthreshold excitatory surround receptive fields (113). Furthermore, for many ganglion cells, receptive field size actually decreases in light adapted conditions (117-119), likely due to a strengthening of inhibitory surround responses arising from either horizontal and/or amacrine cells. For instance, it was found that for mouse ON and OFF α-like ganglion cells (59) and directionally selective ganglion cells (60), surround inhibition in ganglion cells is provided by wide-field amacrine cells, and this surround inhibition appears to be activated only at light intensities that activate cones. In this bright light, amacrine-cell-mediated surround inhibition is thought to rely on electrical coupling between a wide-field amacrine and ON cone bipolar cells. Knocking out Cx36 eliminates the bright light induced reduction in receptive field size of α-like ganglion cells (59). As such, classical receptive field size in ganglion cells appears to be most strongly controlled by amacrine cell mediated surround inhibition: one recent study suggests that horizontal cells may only contribute as little as ~15% to the surround inhibition of ganglion cells (58).

Much less is known about the properties of ganglion cell-amacrine cell coupling. Nonetheless, the gap junction strength appears to be strong enough such that current injected into one ganglion cell can pass via gap junctions

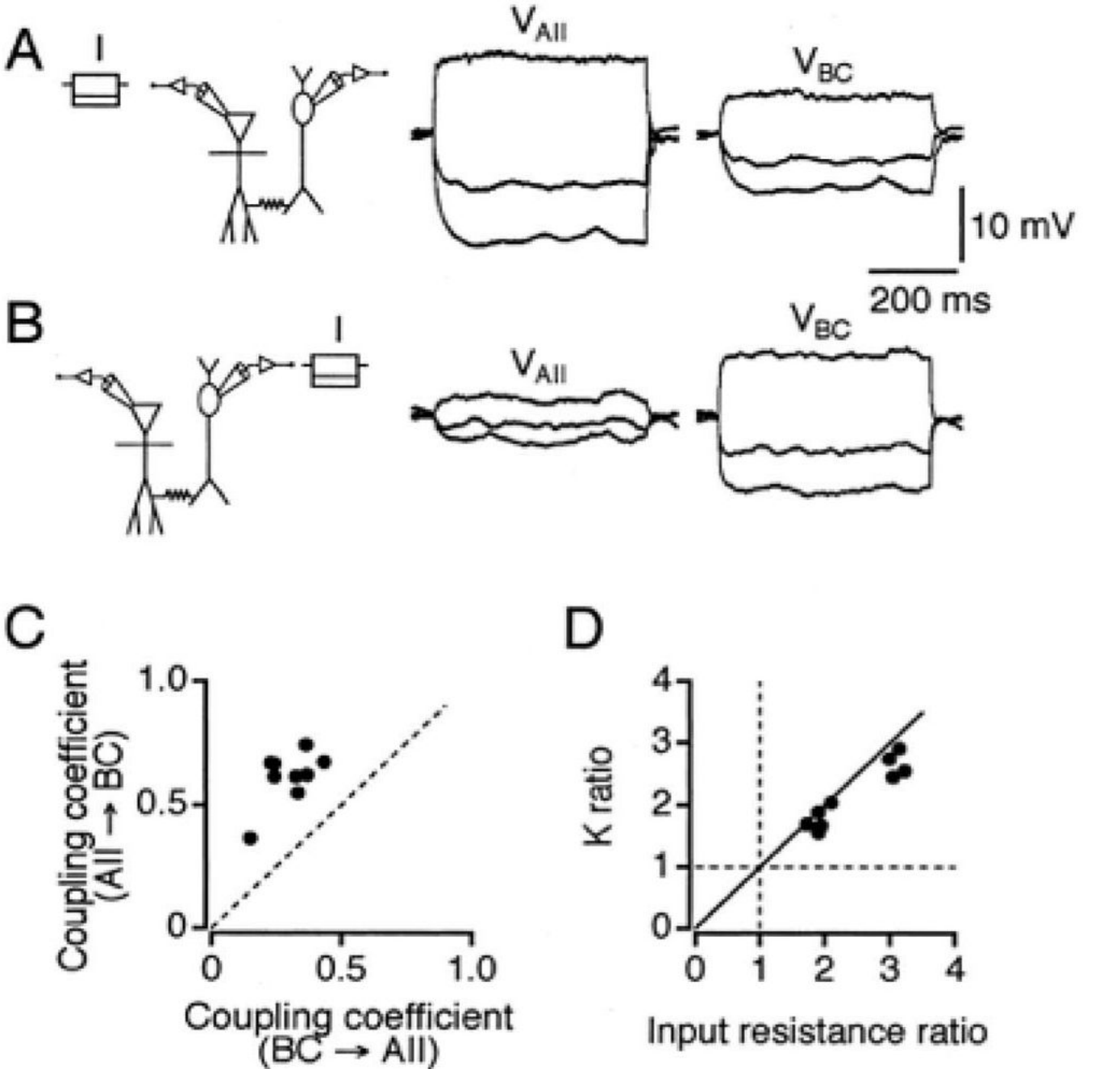

Figure 14. *Coupling coefficient of gap junctions between ON bipolar cells and AII amacrine cells.* **A**, Paired current clamp recording from an ON bipolar cell and an AII amacrine cell in rat retina, with current pulses (-50, -25 and +50 pA) applied to the AII amacrine cell. **B**, The same experiment but with current pulses (-20, -10 and +20 pA) applied to the bipolar cell. **C**, Plotting the reciprocal coupling coefficient suggests asymmetric coupling. **D**, Compensating for differences in input resistance between ON bipolar cells and AII amacrine cells results in a more symmetrical coupling coefficient between pairs of cells. Taken from Veruki and Hartveit (2002a) (199).

into an amacrine cell, and then via additional gap junctions into a nearby ganglion cell, driving measurable responses in the indirectly coupled ganglion cell (**Figure 24**) (120).

Gap junctions and scotopic vision

In dark (scotopic) light conditions, when rods are the active photoreceptor, gap junctions are critical for passing rod-mediated signals throughout the retina. In the classical rod pathway, rods form glutamatergic synapses with

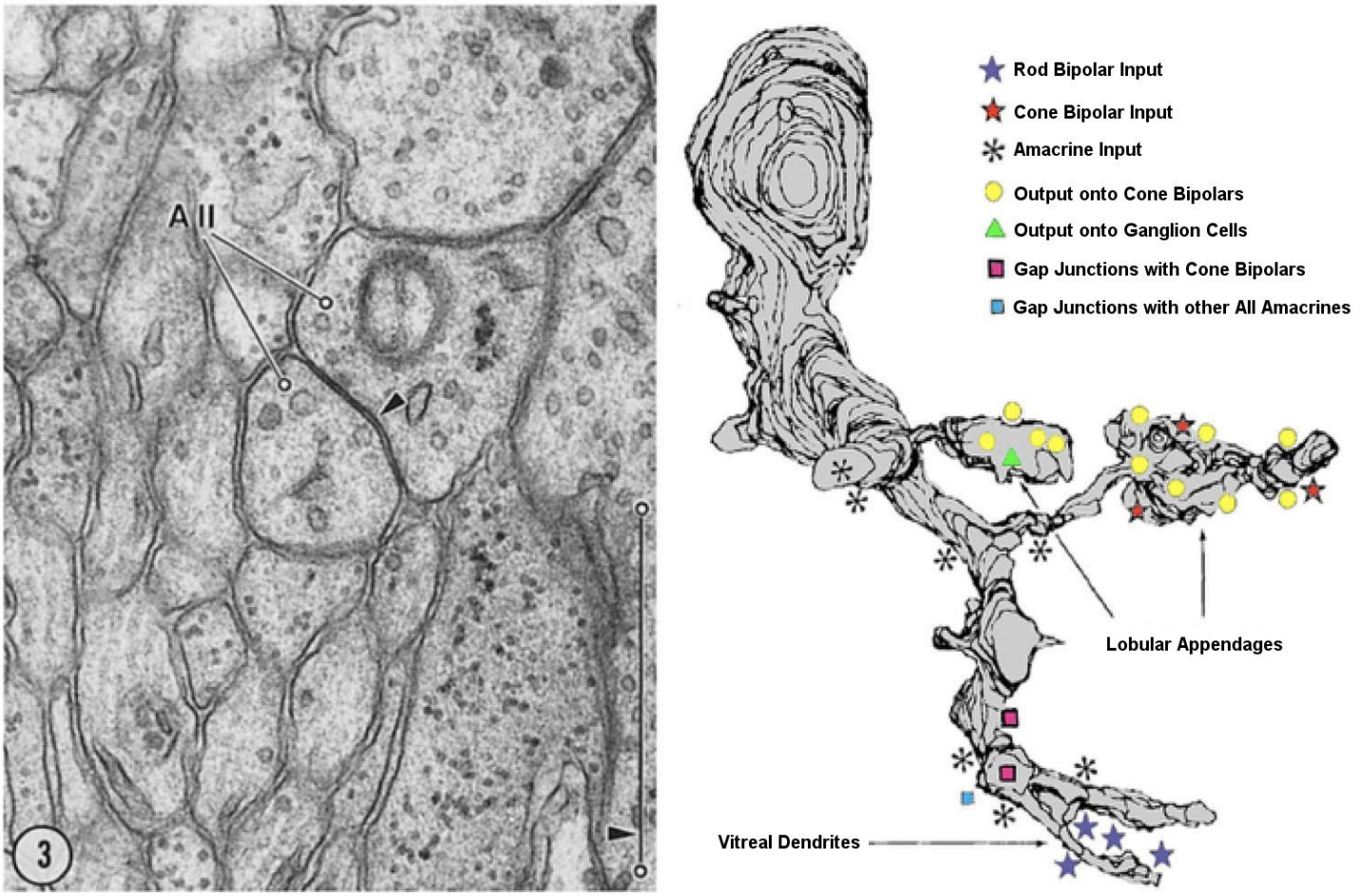

Figure 15. *Electrical synapses between AII amacrine cells. Left*, an electron micrograph showing a gap junction (arrow) between a pair of AII amacrine cells in rabbit retina. Magnification: x27000. *Right*, reconstruction of a portion of an AII amacrine cell indicating the location of different types of synaptic inputs and outputs. Adapted from Strettoi et al. (1992) (69).

rod bipolar cells, which in turn form glutamatergic synapses with AII amacrine. These AII amacrine cells then transfer rod-generated signals to the ON cone bipolar cells, via gap junctions with ON cone bipolar cells. In addition, AII amacrine cells also make glycinergic synapses with OFF bipolar cells (**Figure 25 A**) (64, 79, 80, 121-124). In the second route, rod signals pass directly into cones, via rod-cone electrical synapses, and are thus passed onto the inner retina (**Figure 25 B**) (36, 122, 125, 126). In the third route, some rods appear to form glutamatergic synapses with OFF bipolar cells, and pooling of signals between electrically coupled rods has been hypothesized to increase sensitivity of this pathway (**Figure 25 C**) (17, 127, 128).

Consistent with an important role for gap junction signaling during rod-mediated scotopic vision, knocking out Cx36 greatly impairs rod-mediated responses in the inner retina (**Figure 26**) (70, 122, 126). Additionally, gap junctions between certain types of amacrine and ganglion cells could also aid in high-sensitivity detection of dim light (129).

Gap junctions are thought to play another important role in rod signaling by allowing rods to increase their signal-to-noise ratio. Intrinsic noise in photoreceptors is unique to individual cells, whereas gap junctional coupling allows light-evoked signals to be shared, resulting in more effective detection of relatively weak signals and a decrease in response variability. Note however that these gains may result in a loss of absolute sensitivity and resolution in dim conditions (12, 13, 15, 32, 130-132). A final possible role for gap junctions in rod signaling relates to the nature of synaptic transmission between rods and rod bipolar cells. There appears to be significant

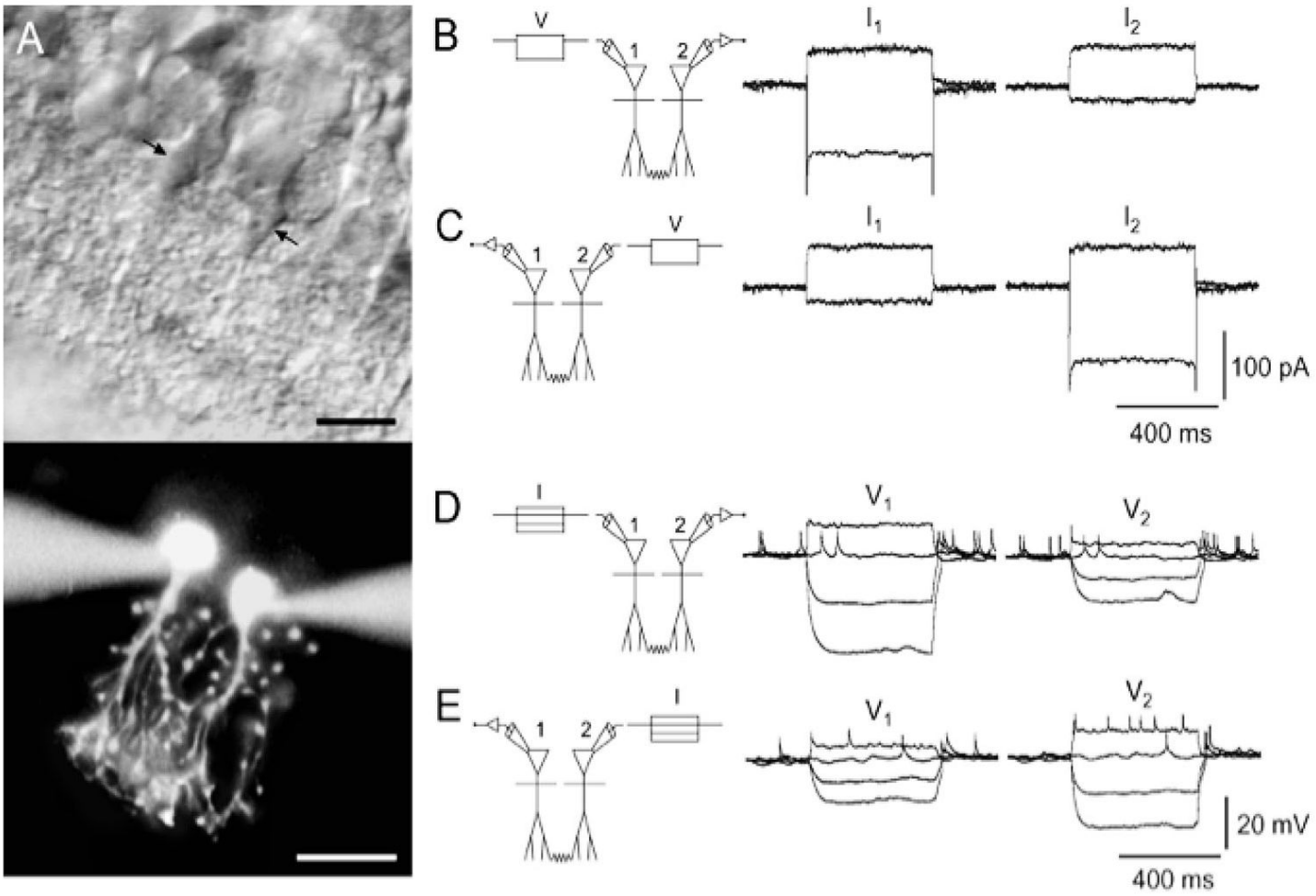

Figure 16. *Properties of electrical synapses between AII amacrine cells*. **A**, A paired recording from AII amacrine cells in a slice from rat retina (top view, DIC; bottom view, fluorescence from Lucifer yellow delivered via the patch pipettes). **B**,**C**, Paired voltage clamp recordings, with cells held at -60 mV, and voltage steps (-30 mV and +10 mV) injected into one of the cells while current is monitored in the other cell. **D**,**E**, Paired current clamp recordings when current steps (-50, -25, 0 and +25 pA) are injected into one of the cells while voltage is monitored in the other cell. Taken from Veruki and Hartveit (2002b) (78).

signal clipping (i.e. saturation of synaptic transmission) between rods and rod bipolar cells, and it has been posited that electrical coupling between rods could allow spatially-restricted visual stimuli to activate several rods, via junctional spread, and that this activated group of rods would then more effectively activate bipolar cells (133).

Gap junctions and synchrony

One of the best described roles for gap junctions in the CNS is that they can synchronize activity between coupled cells (134, 135). Classical work in the retina revealed that neighboring retinal ganglion cells exhibit significant spike synchrony (136-139). Subsequent studies verified that electrical synapses are responsible for driving diverse types of fine-scale synchrony between ganglion cells, in many species (112, 116, 140-143).

Correlations between neighbouring pairs of ganglion cells are generally classified, based on temporal characteristics, as either narrow, medium or broad (**Figure 27**) (140, 142, 144). Narrow synchrony occurs within ± 2 ms, with a trough in the cross-correlogram at 0 ms delay. Medium correlations have a cross-correlogram peak at 0 ms delay, and occur somewhere between 2-10 ms (144), ~ 25-50 ms (140), and less than 100 ms (142). Broad correlations generally exhibit a 0 ms delay peak in the cross-correlogram, and occur on a timescale of

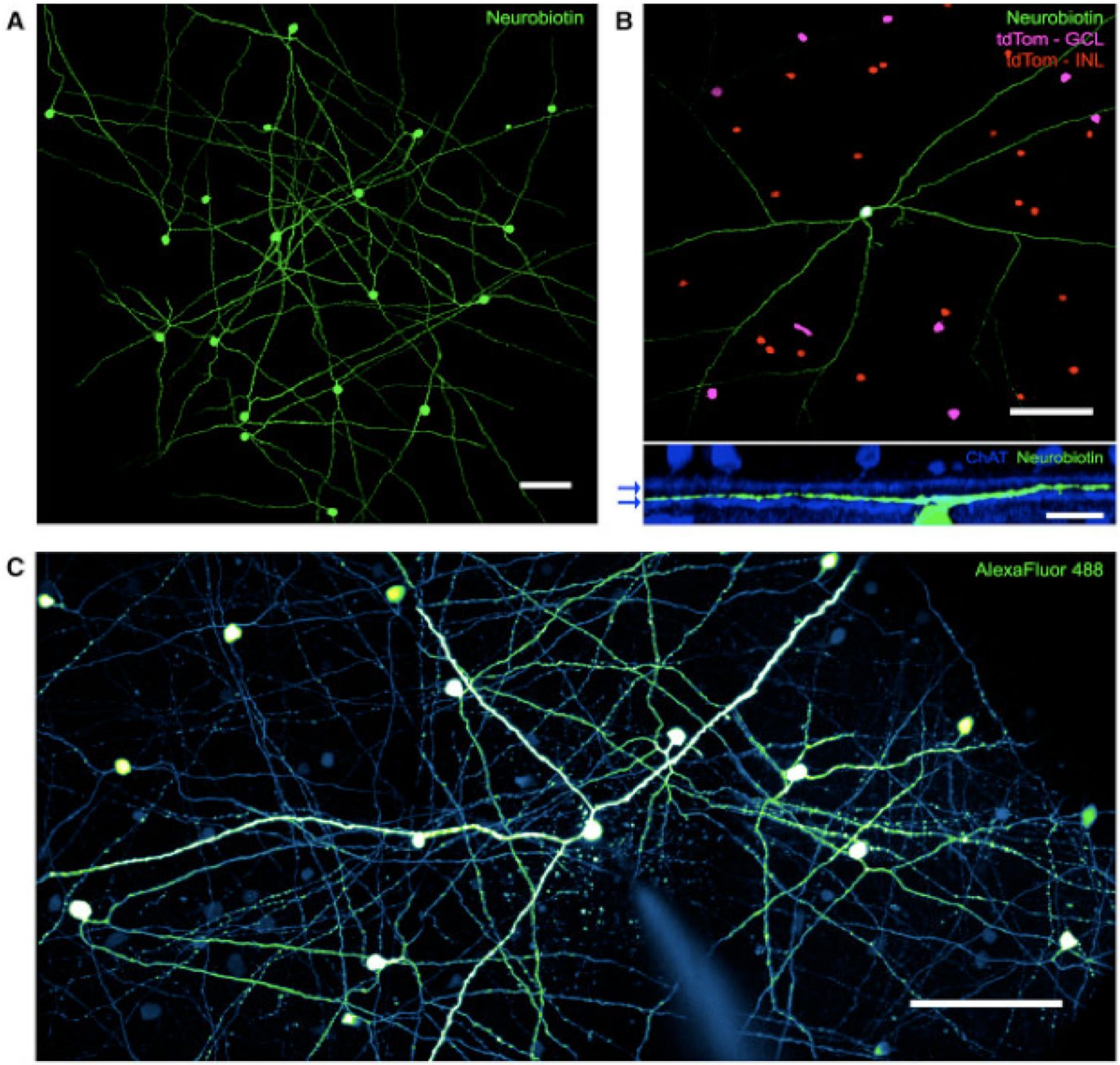

Figure 17. *Tracer coupling between nNOS-2 amacrine cells in mouse retina*. **A**, Tracer coupling when a single amacrine cell in the center of the field of view was injected with Neurobiotin (green). **B** (*top*), Injecting an nNOS-2 amacrine cell with Neurobiotin in the presence of the gap junction blocker meclofenamic acid results in no neighbouring cells being tracer coupled. Red and pink cells indicate the positions of nearby nNOS-2 amacrine cells in both the ganglion cell layer (GCL, pink) and the inner nuclear layer (INL, red). **B** (*bottom*), Side projection of a Neurobiotin (green) filled nNOS-2 amacrine cell co-stained with choline acetyltransferace (ChAT) which labels starburst amacrine and helps to delineate the inner plexiform layer. **C**, A 2-photon image from an acute retinal preparation showing that Alexa Fluor 488 (green), delivered to a single nNOS-2 amacrine via a patch pipette, can spread throughout the coupled network. Blue represents tdTomato transgenically labelled nNOS-2 amacrine cells. Taken from Jacoby et al. (2018) (98).

around 50 ms (144), greater than 50 ms (140) and greater than 100 ms (142), though between pairs of ON and OFF ganglion cells, broad correlations can exhibit a trough at 0 ms, indicative of a slow anti-correlation (137, 138, 144).

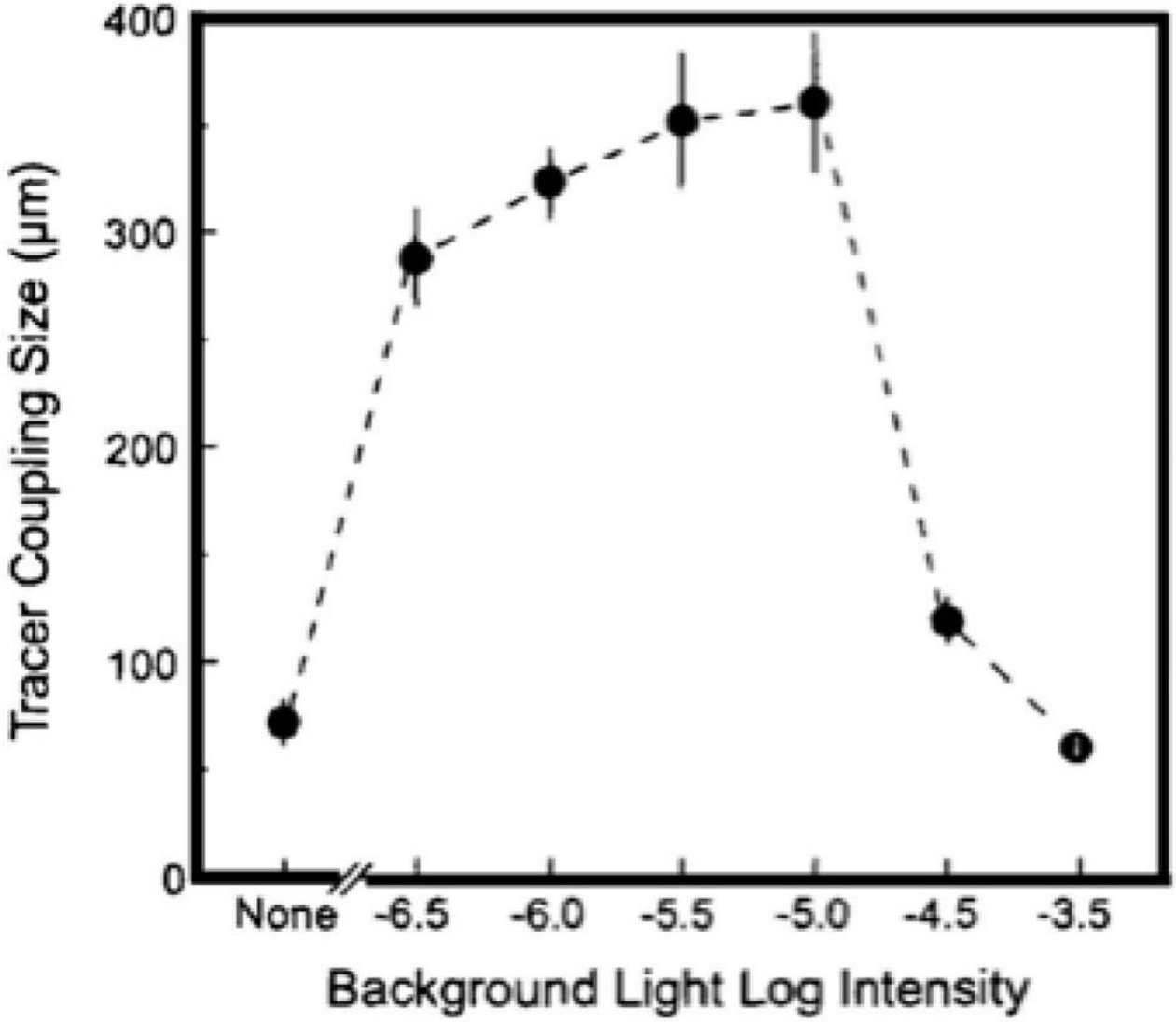

Figure 18. *Coupling between AII amacrine cells in rabbit retina is controlled by illumination conditions*. The average extent of tracer coupling in AII amacrine cells when Neurobiotin was injected into a single AII amacrine cell at different background intensities of light. Taken from Bloomfield et al. (1997) (200).

Pharmacological and genetic knockout experiments have been performed to tease apart the role of electrical and chemical synaptic transmission in these different types of ganglion cell correlations. Pharmacological studies indicate that narrow and medium correlations are unaffected by a cocktail of chemical synaptic blockers, but are inhibited by application of gap junction blockers (140). Cx36 knockout experiments have indicated that broad correlations may also rely upon gap junction signaling (142). Based on these studies, it is thought that broad correlations arise initially in photoreceptors. In contrast, medium correlations are thought to be generated when pairs of ganglion cells are indirectly coupled via an amacrine cell (116, 140, 142, 144, 145), and narrow correlations form between reciprocally coupled ganglion cells (106, 111, 112, 116, 139, 140, 142, 143). In the rest of this section, we mostly focus on homologous coupling between ganglion cells and narrow correlations.

It is thought that narrow spike synchrony arises when one neuron fires an action potential and thus biases spike firing in its neighbor within a short time window. However, as gap junctions act as low-pass filters which significantly reduce the amplitude of action potential mediated signals as they pass across the junction **(Figure**

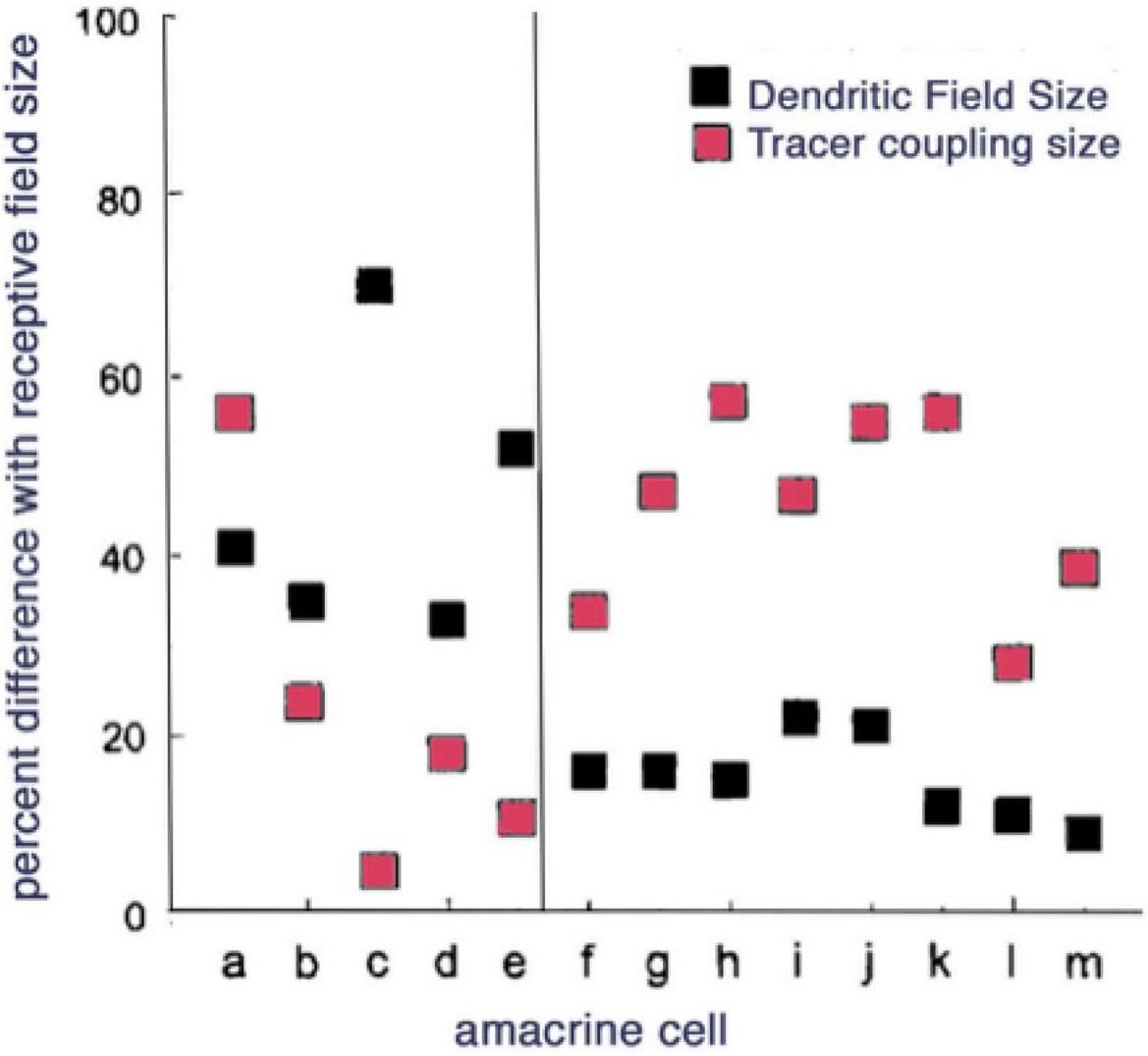

Figure 19. *Relationship between tracer coupling and receptive field size in rabbit amacrine cells.* A scatterplot comparing how different the receptive field size is from the dendritic field size (black squares) and the extent of tracer coupling (pink squares). Cells to the left of the dotted vertical line are AII amacrine cells and have receptive fields closer in size to their tracer coupled networks than their dendritic fields, whereas the non- AII amacrine cells to the right of the vertical line have receptive fields that more closely align with their dendritic fields. Taken from Bloomfield and Xin (1997) (200).

28) (134, 135, 146), it was not immediately evident how such small signals can generate such robust synchrony (120).

While it has been suggested that an action potential in one ganglion cell can directly drive a spike in a coupled neighbour (112), more direct experimental evidence indicates that action potentials in one ganglion cell practically never drive suprathreshold responses in coupled ganglion cells (143). Consistent with this finding, early work in the field suggested that a spike in one ganglion cell will directly drive a spike in a coupled neighbor with a success rate of less than 5% (139). Furthermore, the classical receptive field of ganglion cells is not significantly increased by the presence of gap junctions (but see also112, 113, 116). Why is a spike in one ganglion cell ineffective in directly driving spikes in a neighour? It turns out that in ganglion cells, coupled spikelets – at least when measured with a patch-pipette at the post-junctional soma – are small in amplitude (**Figure 23**; ~ 1 mV), though they do arrive with little delay (< 1 ms) (113). As such, coupling between ganglion cells is similar to coupling between most other neurons in the CNS, in which spiking in a pre-junctional neuron

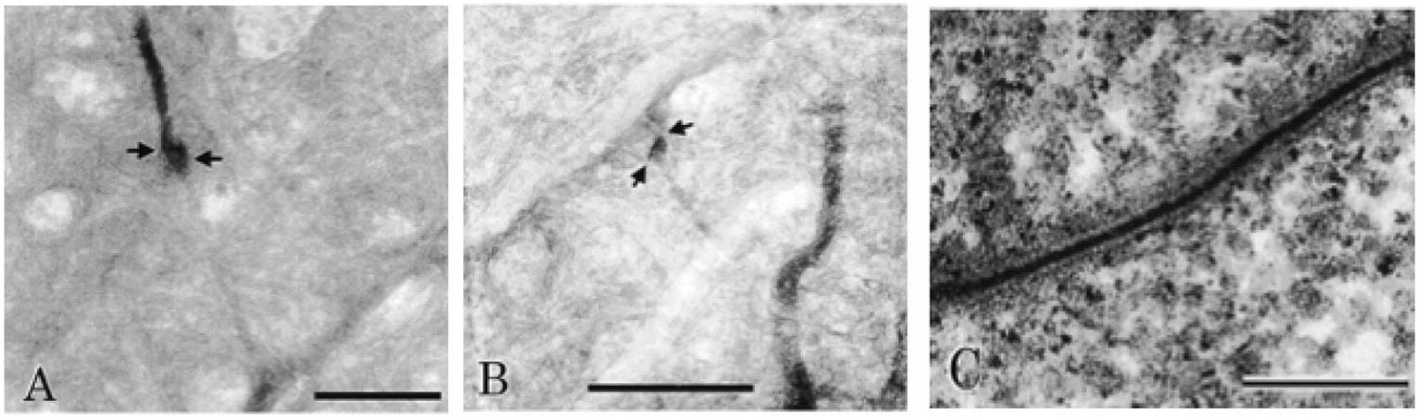

Figure 20. *Dendrodendritic gap junctions between ganglion cells*. **A**,**B**, Electron micrographs showing dendrodendritic gap junctions between Neurobiotin coupled alpha ganglion cells in rat retina. **C**, High resolution view of a gap junction between dendrites of coupled ganglion cells. Scale bars: A,B, 10 μm; C, 200 nm. Taken from Hidaka et al. (2004) (106).

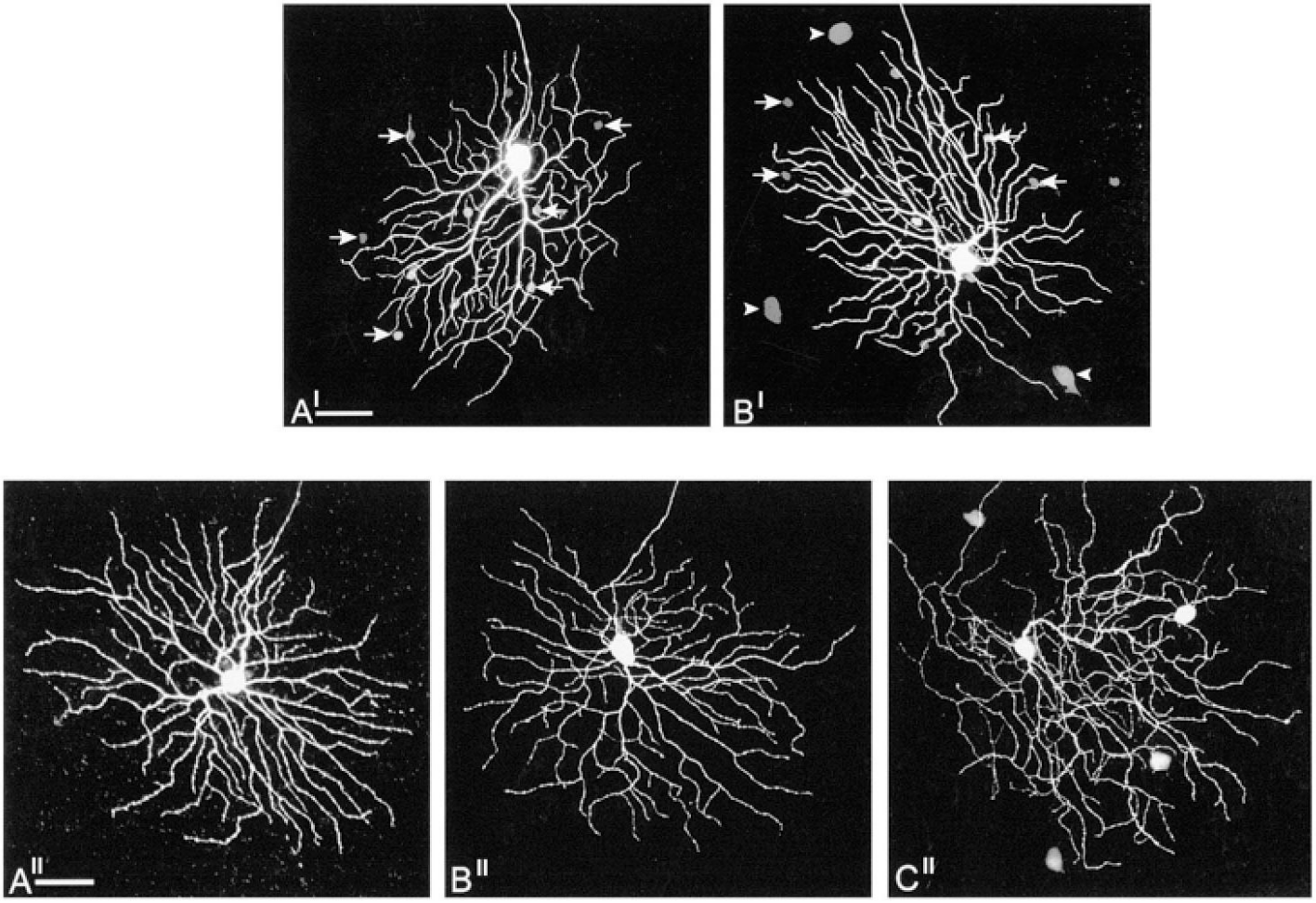

Figure 21. *Tracer coupling from certain ganglion cell types is dependent on Cx36*. $\mathbf{A^{I}}$, Neurobiotin injected into an ON alpha ganglion in wild type mouse retina cell results in tracer dye labelling the somata of neighbouring amacrine cells (white arrows). $\mathbf{B^{I}}$, Neurobiotin injected into an OFF alpha ganglion cell in wild type mouse retina results in tracer dye labelling the soma of neighbouring amacrine cells (white arrows) and ganglion cells (arrowheads). $\mathbf{A^{II}}$, $\mathbf{B^{II}}$, Neurobiotin injected into a pair of OFF alpha ganglion cells in Cx36 KO retina shows no tracer coupling. $\mathbf{C^{II}}$, Neurobiotin injected into a bistratified ganglion cell shows tracer coupling to neighbouring ganglion cells in the Cx36 KO retina. Adapted from Schubert et al. (2005a) (201).

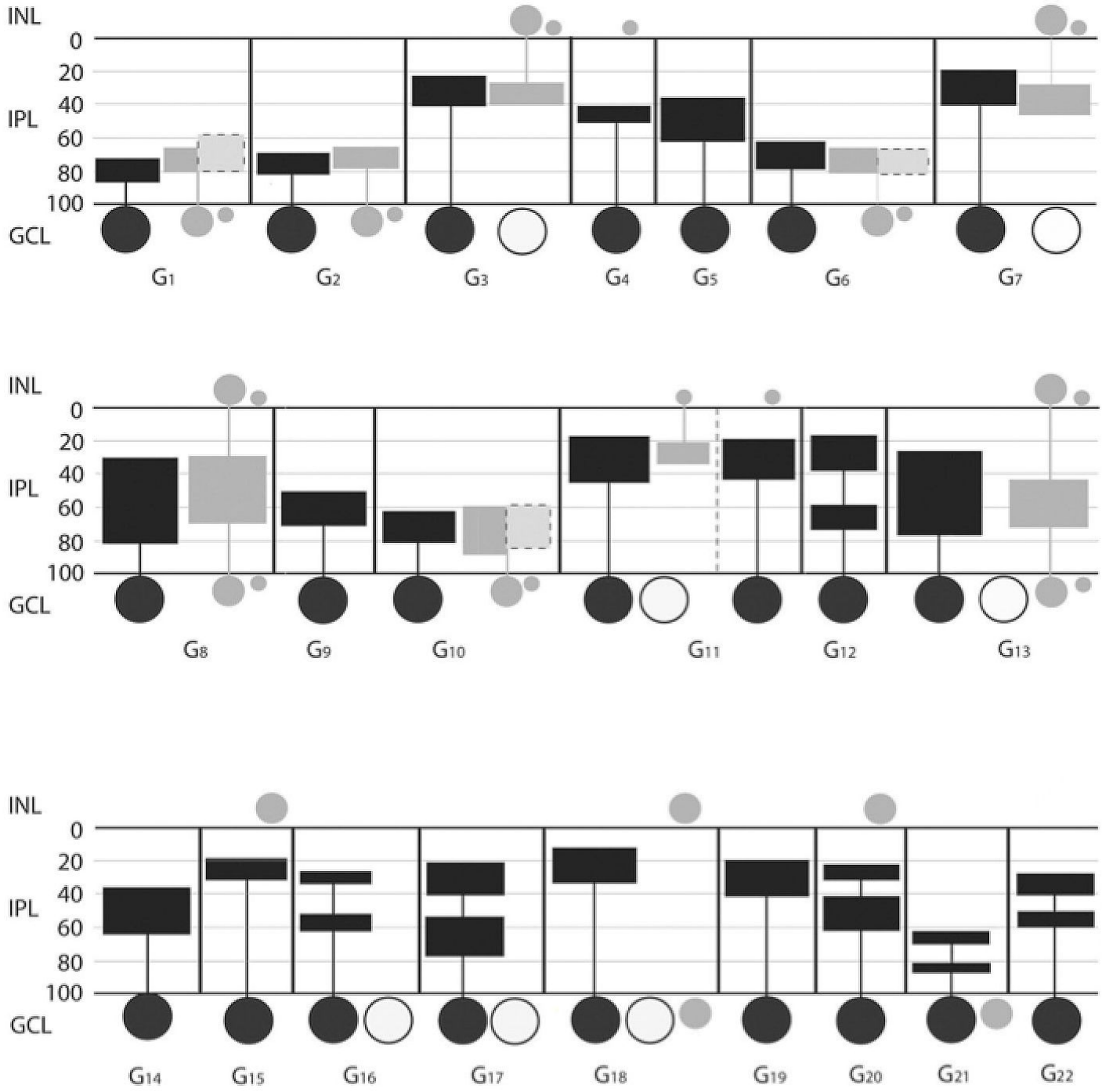

Figure 22. *Diverse coupling patterns of different retinal ganglion cell types.* Schematic outlining differential coupling patterns (as determined via tracer coupling experiments) of 22 types of ganglion cells in the mouse retina. Dendritic stratification patterns in the inner plexiform layer (IPL) for each ganglion cell (black) and its coupled amacrine cells (grey) are shown. Large unfilled circles in the ganglion cell layer indicate tracer coupled ganglion cells. Filled grey circles represent coupled amacrine cells (the size of the circle varies depending the soma size, and if also labelled, amacrine cell dendrites/axons are shown). Taken from Völgyi et al. (2009) (95).

only drives subthreshold activity in post-junctional neighbors (134). How then do subthreshold coupled spikelets drive synchronous activity in coupled ganglion cells?

ON-OFF directionally selective (DS) ganglion cells have been an ideal model for studying how coupled spikelets can drive synchrony via non-linear dendritic signaling. DS ganglion cells generate Na^+-channel dependent, TTX-sensitive dendritic spikes that trigger action potentials with high reliability (147, 148). There are at least

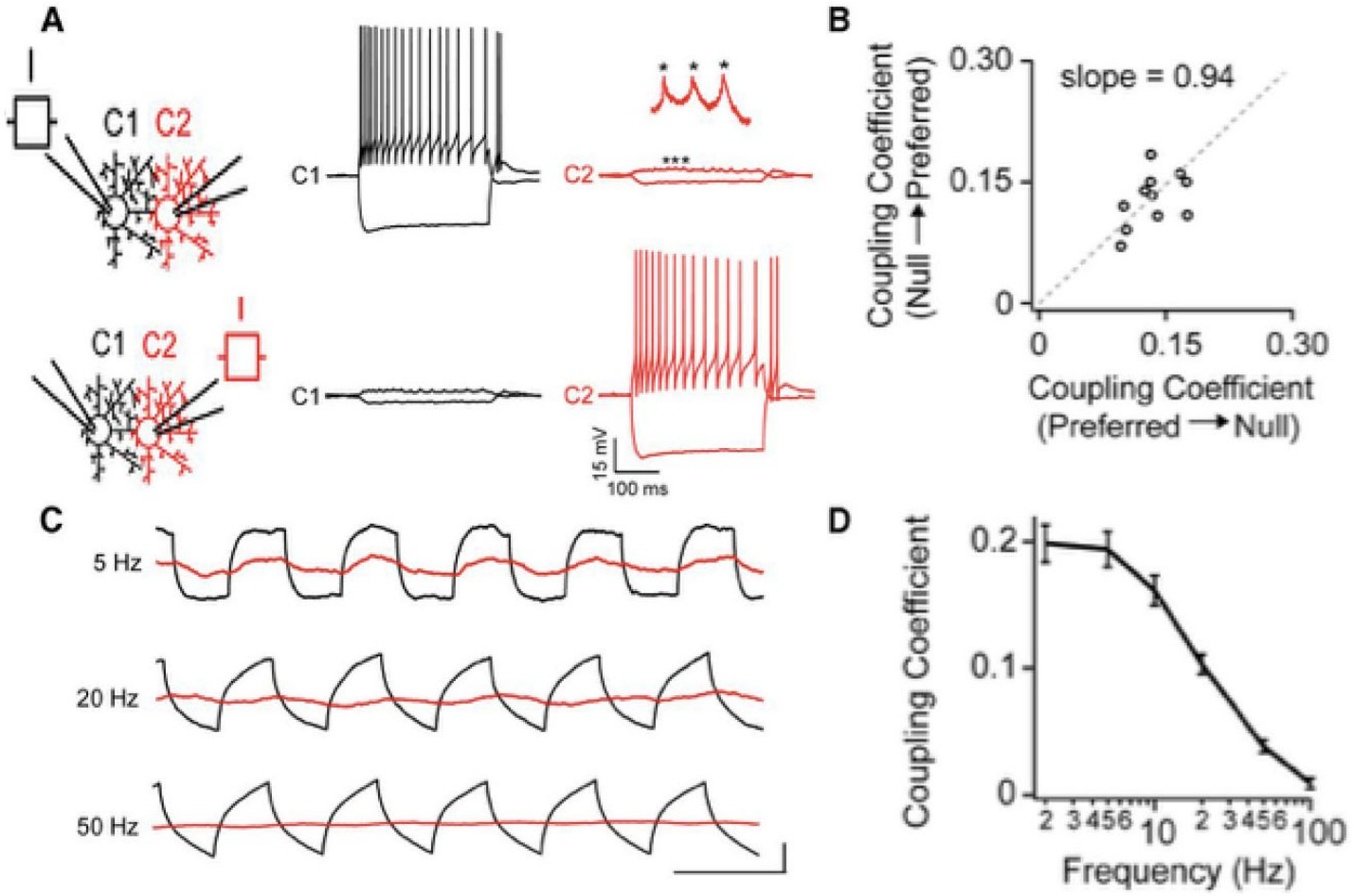

Figure 23. *Properties of gap junctions between ganglion cells in mouse retina*. **A**, Paired current clamp recordings, in which current steps (-200 and +120 pA) were injected into one cell while, membrane responses were monitored in the other cell. The 'I' and current steps in the diagram indicates which cell of the pair is having current injected into it. **B**, Bidirectional coupling coefficient is plotted for 11 pairs of cells. **C**, The membrane responses of both cells when current pulses of different frequencies where injected into one cell (black) and the voltage responses in the postjunctional cell (red) were monitored. **D**, The coupling coefficient is plotted for different frequencies of current injections. Taken from Trenholm et al. (2013a) (113).

four types of ON-OFF DS ganglion cells, coding the cardinal directions (149). For reasons that are not entirely clear, only ON-OFF DS cells that prefer superior motion in the visual field (ventral motion on the retina) exhibit homologous electrical coupling in the adult mammalian retina, at least in rabbit and mouse retinas (**Figure 29**) (105, 113, 150).

Interestingly, when coupled spikelets were simulated via current injection at the soma (with a patch pipette) in coupled DS ganglion cells, they did not significantly modulate action potential timing, raising the possibility that their site of action was in the dendrites (143). Furthermore, coupled spikelets do not appear large enough to directly initiate dendritic spikes themselves. It turns out that to drive spike synchrony in neighbouring cells, coupled spikelets must interact non-linearly with chemical synaptic inputs in the overlapping dendrites of neighbouring ganglion cells (143). Flashing light at a shared location of receptive overlap between a pair of neighboring coupled ganglion cells drives significant spike correlations, whereas flashing two spots of light at two different spatial locations to activate the same pair of ganglions at the same time but with non-overlapping chemical synaptic inputs, does not drive significant correlations (**Figure 30**) (143).

Despite its prevalence, it remains unclear what role correlated ganglion cell activity plays in higher visual processing. One hypothesized role is that it could enhance synaptic transmission in retinorecipient cells. In the

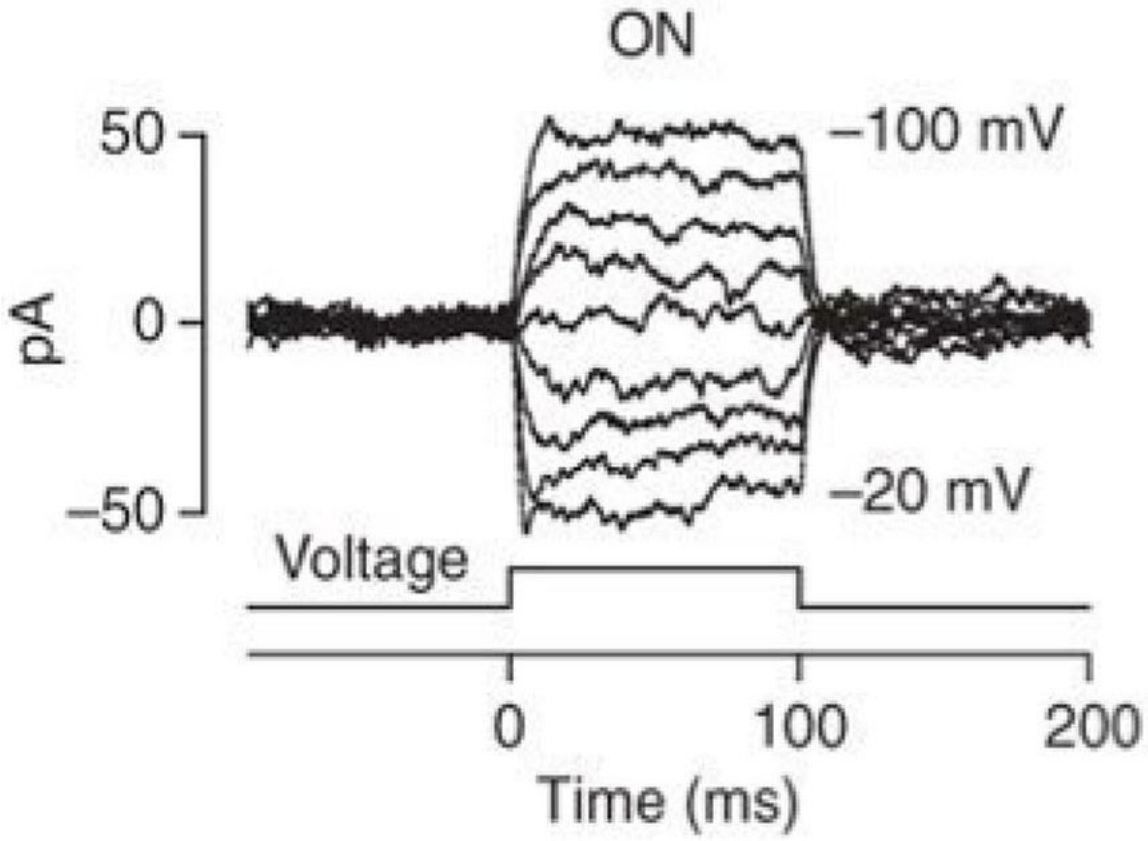

Figure 24. *Properties of gap junctions between ganglion cells and amacrine cells in primate retina.* **A**, Coupling mediated currents in an ON parasol cell when the membrane potential of a neighbouring ON parasol cell was changed from -100 to -20 mV in 10 mV steps (from a holding potential of -60 mV). This coupling current was present despite minimal dendritic overlap between neighbouring ON parasol ganglion cells, and no tracer coupling between ganglion cells, thus suggesting that the coupling was indirect via an amacrine cell. Taken from Trong and Rieke (2008) (120).

lateral geniculate nucleus (LGN), retinal inputs with short inter-spike intervals greatly increase synaptic efficacy (151, 152). Considering that multiple neighbouring ganglion cells converge onto individual LGN relay neurons (153-156), ganglion cell synchrony appears to be a highly plausible strategy for effectively driving LGN neurons. Another hypothesized role for ganglion cell synchrony is that it enhances bandwidth of the optic nerve (145, 157). Since correlated ganglion cell spikes tend to occur when light activates overlapping areas between neighbouring ganglion cell receptive fields (**Figure 31**) (145, 157), correlated activity contains unique spatial information which could subsequently be decoded separately from uncorrelated activity.

Furthermore, since the strength of narrow gap junction mediated ganglion cell correlations appears to decrease with increasing spike rates (143, 158), though an inhibitory mechanism may sometimes concomitantly lower spike rates and reduce medium-scale gap-junction mediated synchrony (159), correlated ganglion cell activity could relay information to downstream targets independent from spike rate (**Figure 32**). Whether these types of parallel decoding strategies are actually implemented in higher visual areas remains to be examined.

Aside from the above described forms of synchrony, which tend to be restricted to neighbouring retinal neurons, gap junctions also appear to play an important role in synchronizing activity across wide regions of the retina. Classic work with paired recordings revealed the presence of long-range correlated activity in the retina across distances larger than 20 degrees of visual space (160). Such synchrony appeared to arise when pairs of distally located ganglion cells were responding to a visual image that fell upon their receptive fields as well as the space in between them (160). More recent work has shown that this long-range synchrony arises from gap junction

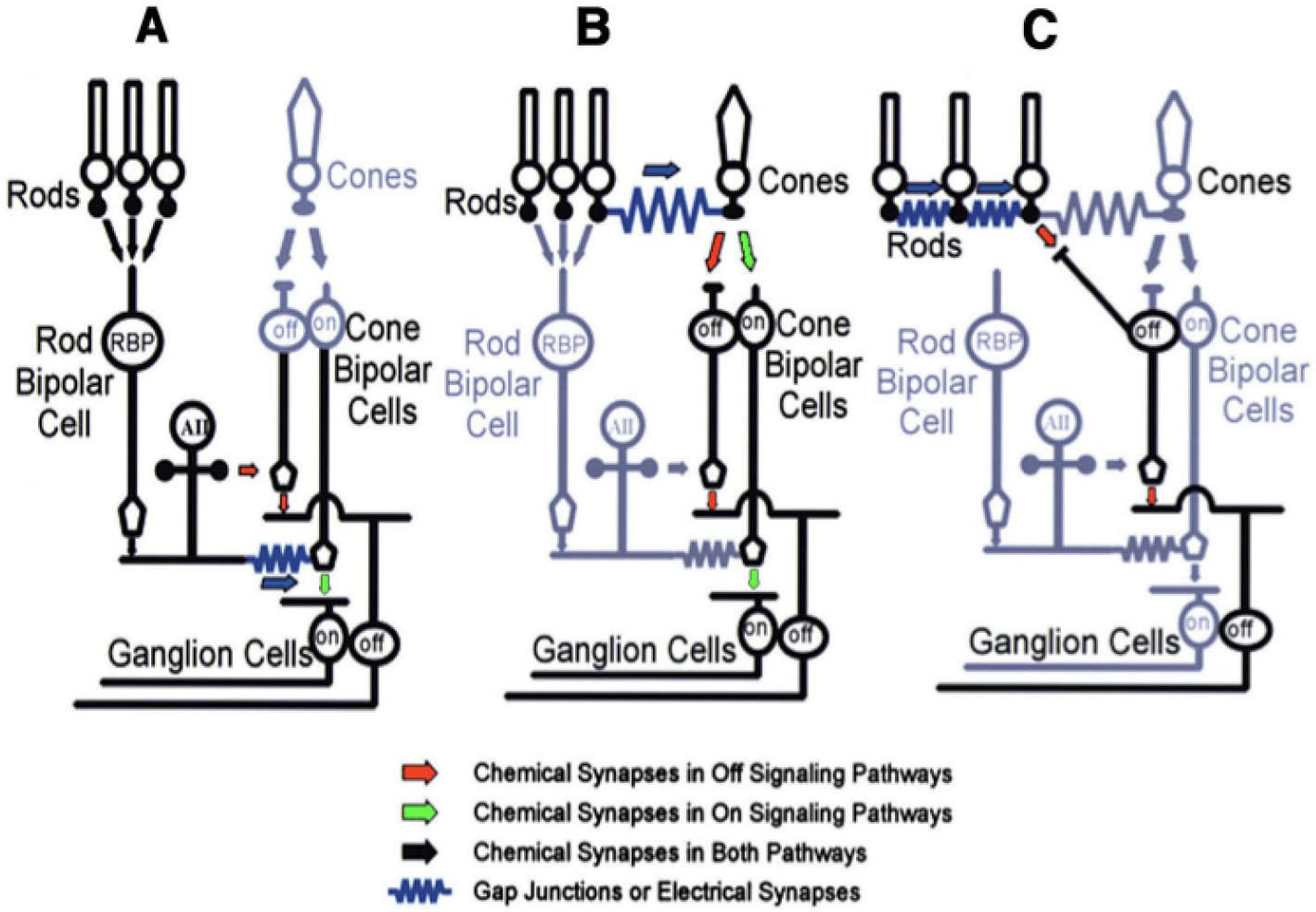

Figure 25. *Three rod vision circuits in the mammalian retina.* **A**, Rod signals pass to rod bipolar cells, then onto AII amacrine cells, and then onto bipolar and ganglion cells. **B**, Rod signals pass into cones via gap junctions. **C**, Rods directly synapse onto OFF bipolar cells. Taken from Deans et al. (2002) (70).

connectivity between ganglion cells, likely via an intermediary widefield amacrine cell (161). Remarkably, as was originally hypothesized (160), this long-range synchrony appears to play an important behavioral role in an animal's ability to bind together distal portions of the same visual image (161).

Gap junctions and moving visual stimuli

The classical view of the excitatory retinal signaling pathway is of a vertical circuit from photoreceptors to bipolar cells to ganglion cells. Placing gap junctions between neighbouring cells adds a lateral excitatory connection to this vertical pathway. Unsurprisingly, adding such a lateral excitatory pathway endows retinal circuits with distinct advantages when it comes to processing moving visual stimuli.

Motion sensitivity

Lateral gap junction connectivity, in both bipolar cells and ganglion cells, has been shown to selectively modify and enhance responses to moving stimuli. In mouse retina, it has been shown that gap junction inputs to bipolar cells (which can represent > 30% of their excitatory synaptic input), can endow bipolar cells with supralinear spatial summation, which selectively enhances processing of spatio-temporally correlated inputs (i.e. stimuli moving in a coherent direction). This results in enhanced responses to motion in retinal ganglion cells **(Figure**

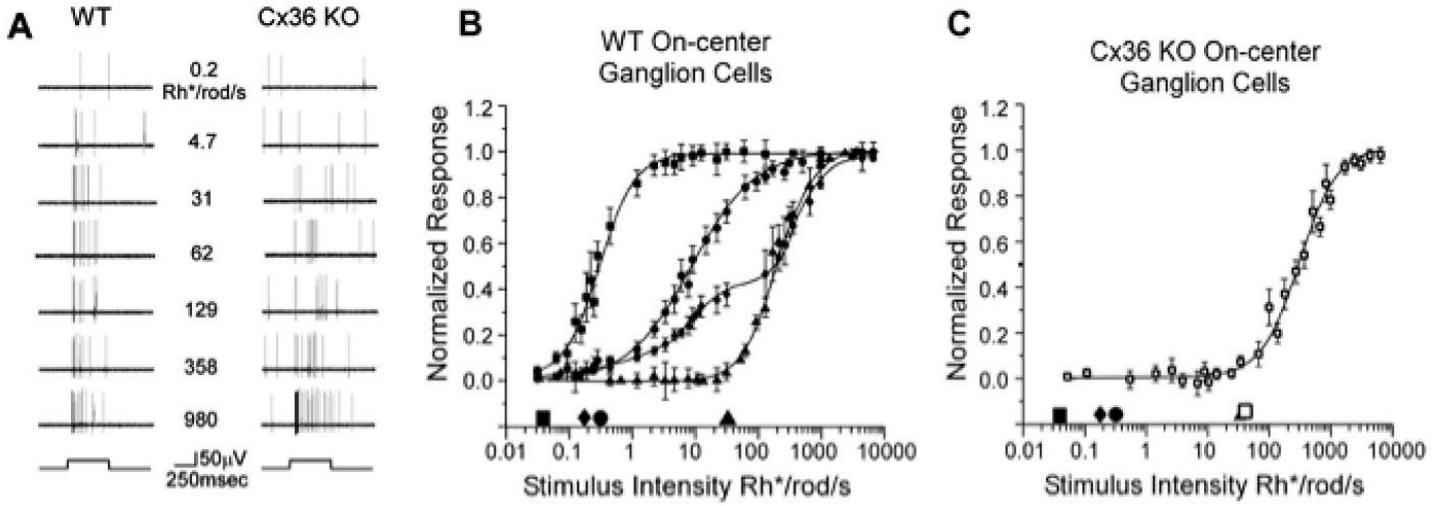

Figure 26. *Cx36 containing gap junctions are required for rod-mediated signals to pass to ganglion cells*. **A**, Example of spiking responses from ON ganglion cells in wild type (WT, left) and Cx36 KO mouse retina (right) to a series of flashes of different intensities. **B**, Ganglion cells in wild-type retina were grouped into 4 different categories based on their stimulus response profiles, with many cells being activated by dim flashes. **C**, In Cx36 retina, all ganglion cells resembled the least sensitive group identified in wild type retina. Taken from Deans et al. (2002) (70).

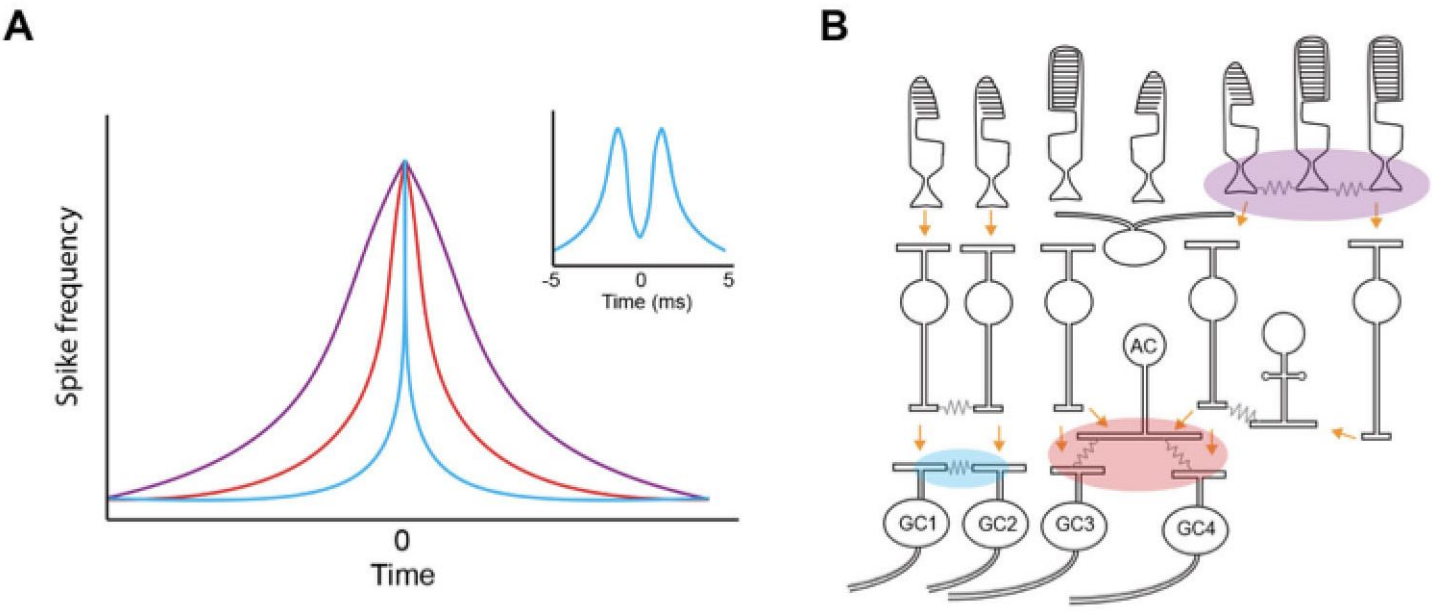

Figure 27. *Correlated spike activity in pairs of retinal ganglion cells*. **A**, Schematic cross-correlogram outlining broad (purple), medium (red) and narrow (blue) spike correlations between pairs of retinal ganglion cells. The inset shows a zoomed in view of the narrow correlations, with a trough in the cross-correlogram at 0 ms delay. **B**, Schematic of the retinal synaptic locations where broad (purple), medium (blue) and narrow (red) correlations are thought to arise. Taken from Trenholm and Awatramani (2017) (197).

33) (84). Related work has been done in primate retina, in which bipolar cell gap junction coupling appears to contribute to motion sensitivity of parasol ganglion cells (162). The general principles underlying motion facilitation in gap junction networks in bipolar cells appears to be similar to that described in more detail in a later section on ganglion cells (163).

Finally, in mouse retina, at low light levels, homologously coupled direction selective ganglion cells have broader tuning curves than their uncoupled counterparts. As such, gap junction connectivity appears to allow these cells

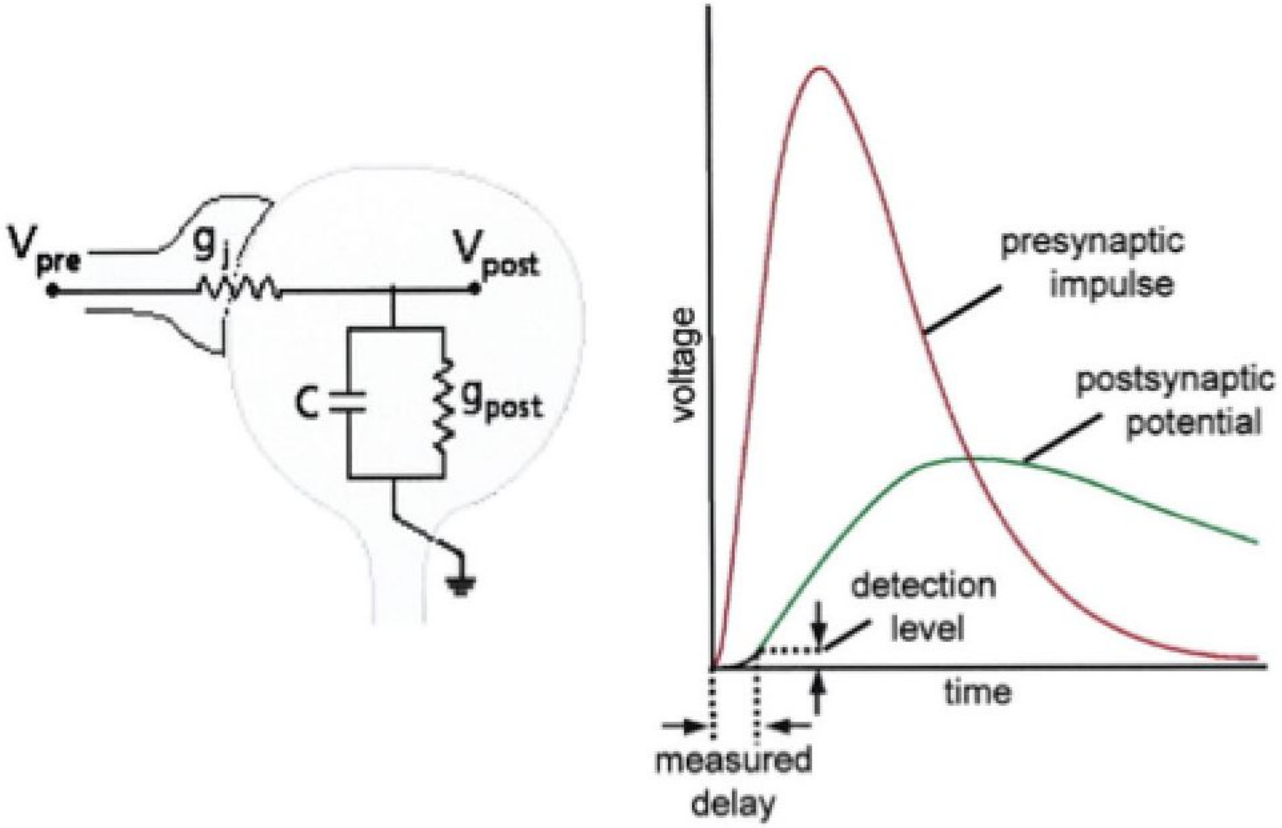

Figure 28. *Gap junctions act as low-pass filters. Left*, An equivalent circuit of a gap junction. *Right*, Electrical signals pass through gap junctions with a short delay, and high frequency presynaptic signal components are more highly attenuated upon passing to the postsynaptic cell. Taken from Bennett and Zukin (2004) (146).

to strike a balance, in low light levels, between detecting dim moving stimuli and accurately reporting the direction of movement **(Figure 34)** (111).

Motion anticipation

When light is flashed on the retina, it takes roughly 50 ms or more for a ganglion cell to fire a light-evoked action potential. Most of this delay is due to phototransduction in rods and cones, the relatively slow process whereby incoming photons are converted into an electro-chemical signal. This delay poses a problem, given that the same retinal circuity can process both static and moving stimuli. For static images, this delay does not pose a significant problem, as when a ganglion cell spikes the stimulus it is encoding is still in the appropriate position. In contrast, when a moving image activates photoreceptors in one location, the image will have moved to a different spatial location by the time the ganglion cells vertically connected to the photoreceptors at the earlier position begin to respond. The lag between where a ganglion cell reports an image is, compared to where the image actually is in space, increases as movement gets faster. One method that has been hypothesized for the retina to address this problem is for ganglion cells to dynamically shift the peak of their receptive field toward the leading edge of a moving stimulus (164, 165), which could theoretically be read out by downstream targets as anticipation if they decode position based on peak spike rate. Another method that has been proposed to compensate for the lag that arises when coding moving stimuli involves using gap junctions to allow upstream retinal ganglion cells to alert their downstream neighbors to the presence of an incoming image. This phenomenon, termed lag normalization, arises in homologously coupled retinal ganglion cells which exhibit a coupling-mediated subthreshold excitatory receptive field that surrounds their receptive field center **(Figure 35)** (113).

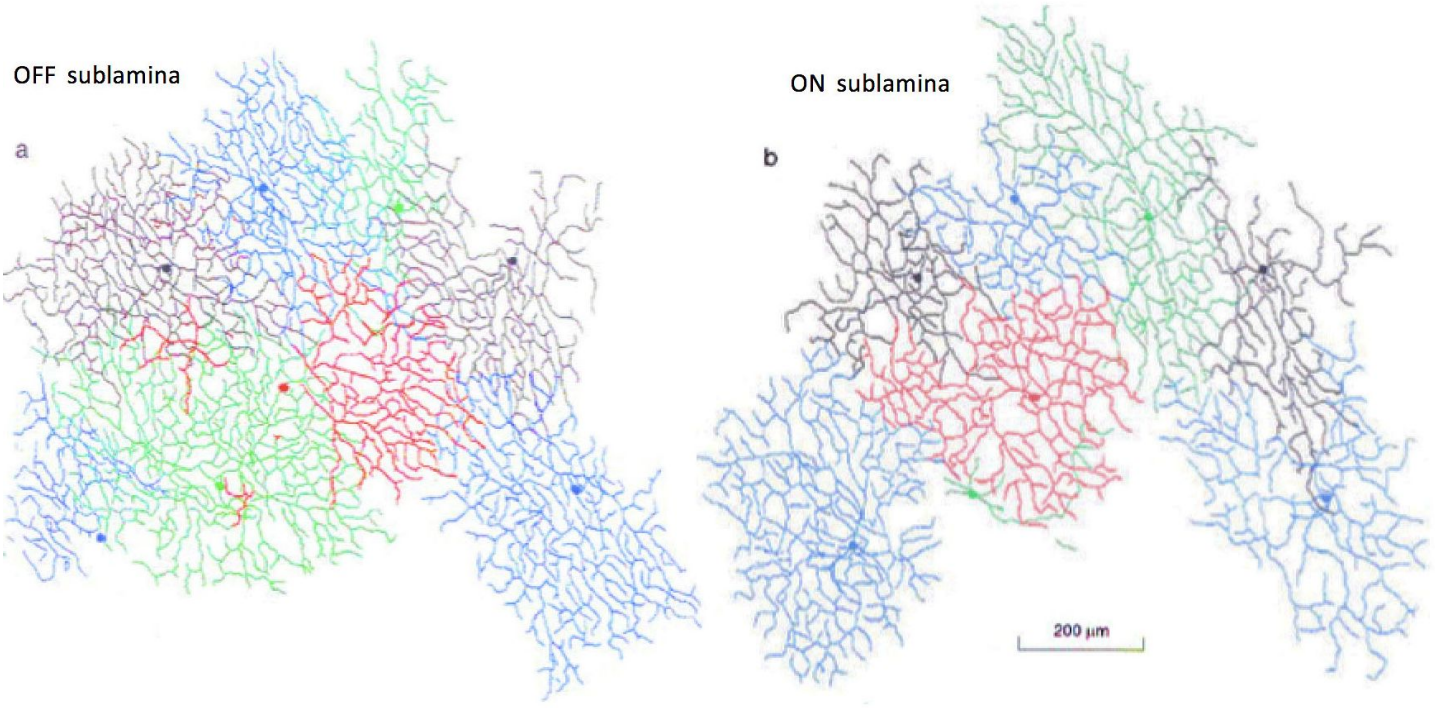

Figure 29. *Homologous coupling between directionally selective ganglion cells*. Neurobiotin injected into a single bistratified directionally selective ganglion in rabbit retina results in dye passing into neighbouring bistratified ganglion cells, with largely non-overlapping dendritic trees. **a**, OFF sublamina. **b**, ON sublamina. Taken from Vaney (1994) (105).

For moving images, the gap junction inputs spread laterally from one ganglion cell to another, and are able to combine with weak bipolar cell mediated chemical synaptic inputs to allow the ganglion cell to begin responding outside of the receptive area that drove spiking activity to static stimuli (166). Moreover, when these coupled ganglion cells are stimulated with images moving at various speeds, they can initiate their responses at nearly the same spatial location (i.e. they 'lag normalize'), in contrast to uncoupled ganglion cells which initiate their responses at positions further and further in space when presented with faster and faster speeds of moving images **(Figure 36)** (166).

Looming

Effective detection of looming visual stimuli, like an approaching predator, can be a matter of life or death. Accordingly, looming (or approaching) visual stimuli drive behavioral reflexes that are found across many species, including humans (167-171). In the retina, it appears that lateral gap junction connectivity – between AII amacrine cells and ON cone bipolar cells – plays a role in allowing a specific retinal ganglion cell to preferentially detect looming visual images. In mouse retina, the looming sensitive cell is an OFF ganglion cell, termed the PV-5 cell (124). When static decrements of light are presented over the receptive field of this cell, they evoke transient OFF excitation, followed by transient ON inhibition when the light level returns to baseline (124). As a large dark stimulus gets smaller over the receptive field of this cell, it exclusively drives ON inhibition and no excitatory OFF response, and thus does not result in spiking. On the other hand, if the same stimulus is now played backwards and the black area expands over the receptive field of the cell, it exclusively drives OFF excitation that drives robust spiking responses. Based on the described response properties, this cell should also respond reasonably well to moving stimuli that pass across the receptive field, which would drive a mix of OFF excitation and ON inhibition. However, the ON inhibitory input to the PV-5 cell is very fast and appears to arise via gap junction signals passed from ON cone bipolar cells to AII amacrine cells, which weaken the effect of concomitant excitatory OFF inputs. Indeed, when Cx36 was knocked out, PV-5 cells no longer responded

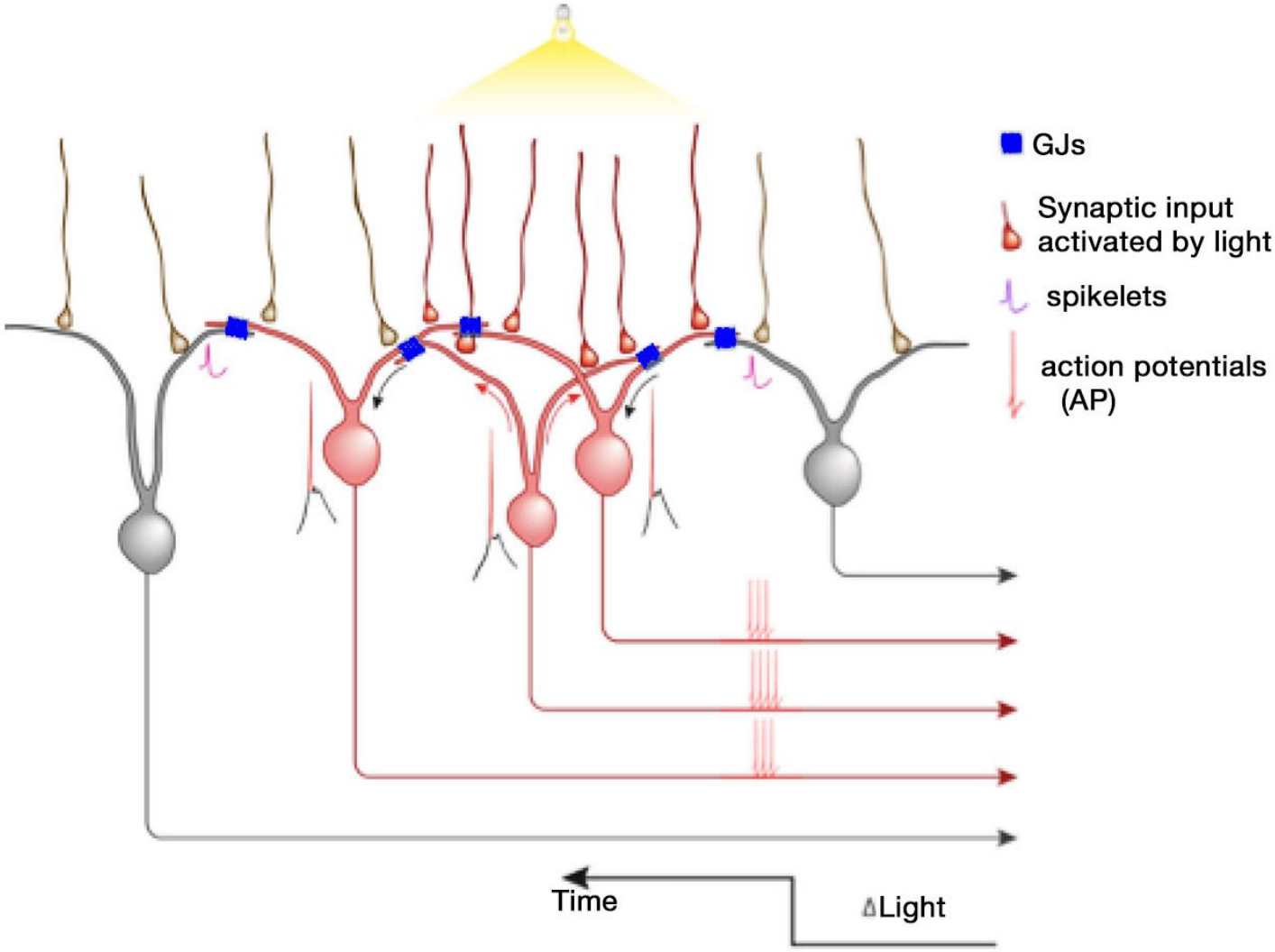

Figure 30. *Non-linear interactions between coupled spikelets and chemical synaptic inputs drive correlated spiking.* A flash of light drives an action potential (AP) in the central ganglion cell. The action potential back-propagates into the dendritic tree (red arrows), crosses gap junctions (GJs), which become coupled spikelets in the dendrites of coupled neighbors. Coupled spikelets integrate with light-evoked chemical synaptic inputs from bipolar cells to trigger dendritic spikes that in turn propagate to the soma (black arrows), where they generate a synchronized action potential. Taken from Lanore and Silver (2014) (202).

preferentially to looming stimuli over stimuli that simply moved across the receptive field (124). In mice, this retinal cell type is thought to underlie innate freezing/fleeing behavioral responses when dark looming stimuli are presented above the head of a mouse (172). Whether similar retinal circuitry underlies behavioral responses to looming visual stimuli in primates remains to be tested.

Gap junctions, retinal degeneration and spontaneous activity

While, as outlined above, gap junctions serve many functions in the healthy retina, they also promote aberrant neuronal activity following retinal degeneration (rd). In rodent rd models, following photoreceptor degeneration, instead of becoming silent many ganglion cells exhibit spontaneous oscillations with a frequency of around 10 Hz (**Figure 37**) (173-179). Understanding the source of this aberrant activity is important since it could underlie phosphenes experienced by patients suffering from vision loss (180, 181), and could impact the success of therapeutic strategies including electrical implants (182) and optogenetic vision therapy (183).

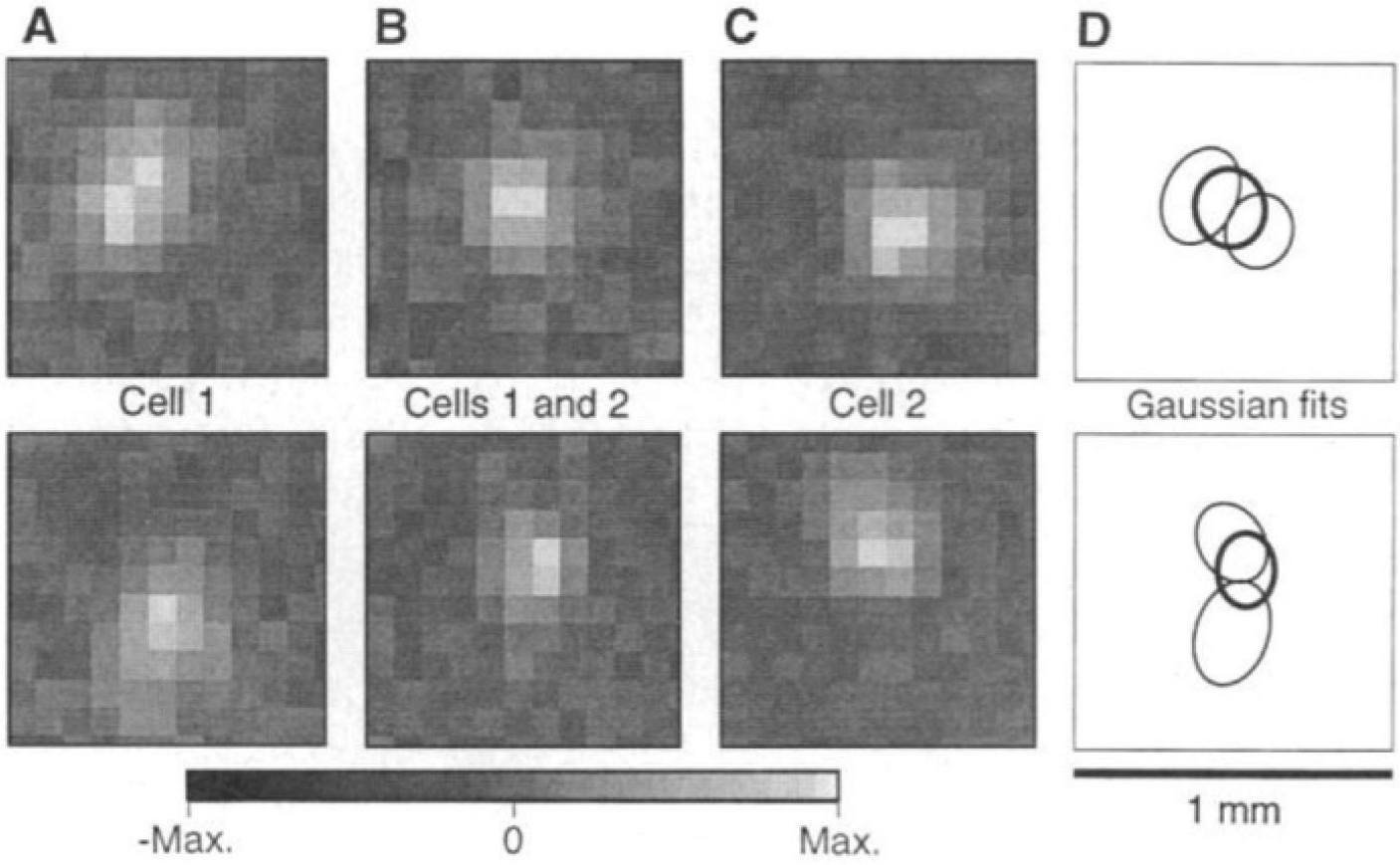

Figure 31. *Correlated spikes carry unique spatial information*. Receptive fields, generated with a flickering checkerboard stimulus, are plotted for two cells (**A**) and (**C**), and the 'receptive field' in which they exhibited correlated spiking is shown in the middle (**B**). **D**, Gaussian fit contours of the receptive fields from (A-C). Top and bottom rows are from different cell pairs. Taken from Meister et al (1995) (157).

In rd retina, ganglion cells oscillate as the result of receiving excitatory and inhibitory oscillatory inputs (174, 175, 179, 184). Application of chemical synaptic blockers inhibits ganglion cell oscillations, indicating that spontaneous oscillations do not arise in ganglion cells themselves (174, 176), but see also (185). In contrast, membrane oscillations in ON cone bipolar cells and AII amacrine cells, which also occur with a frequency of around 10 Hz, persist upon application of chemical synaptic blockers, indicating that spontaneous oscillations arise intrinsically within the coupled network of ON cone bipolar cells and AII amacrine cells (174). As evidence that gap junctions between bipolar cells and AII amacrine cells are important in this pathophysiology, pharmacologically blocking gap junctions inhibits oscillations in ganglion cells (176, 186), AII amacrine cells and ON cone bipolar cells **(Figure 38)** (186). Furthermore, spontaneous ganglion cell oscillations were greatly reduced in rd mice in which connexin 36 was knocked out (187).

Considering that there is extensive coupling between ON cone bipolar cells and AII amacrine cells in wild type retina, what occurs during retinal degeneration that promotes aberrant network activity? Experiments in wild type retina suggest that the main trigger for spontaneous activity relates to altered glutamate release from photoreceptors, as either pharmacologically blocking photoreceptor output in wild type retina or photobleaching the wild type retina with bright light (both of which would hyperpolarize the AII amacrine/ON cone bipolar cell network) can drive spontaneous activity similar to that found in the rd retina (186), though recent work also implicates retinoic acid in this hyperactivity (188). Consistent with the former idea, the resting membrane potential of AII amacrine cells in the degenerating retina appears to be hyperpolarized compared to those in the wild type retina (189). Such hyperpolarization could activate rhythmogenic conductances, such as

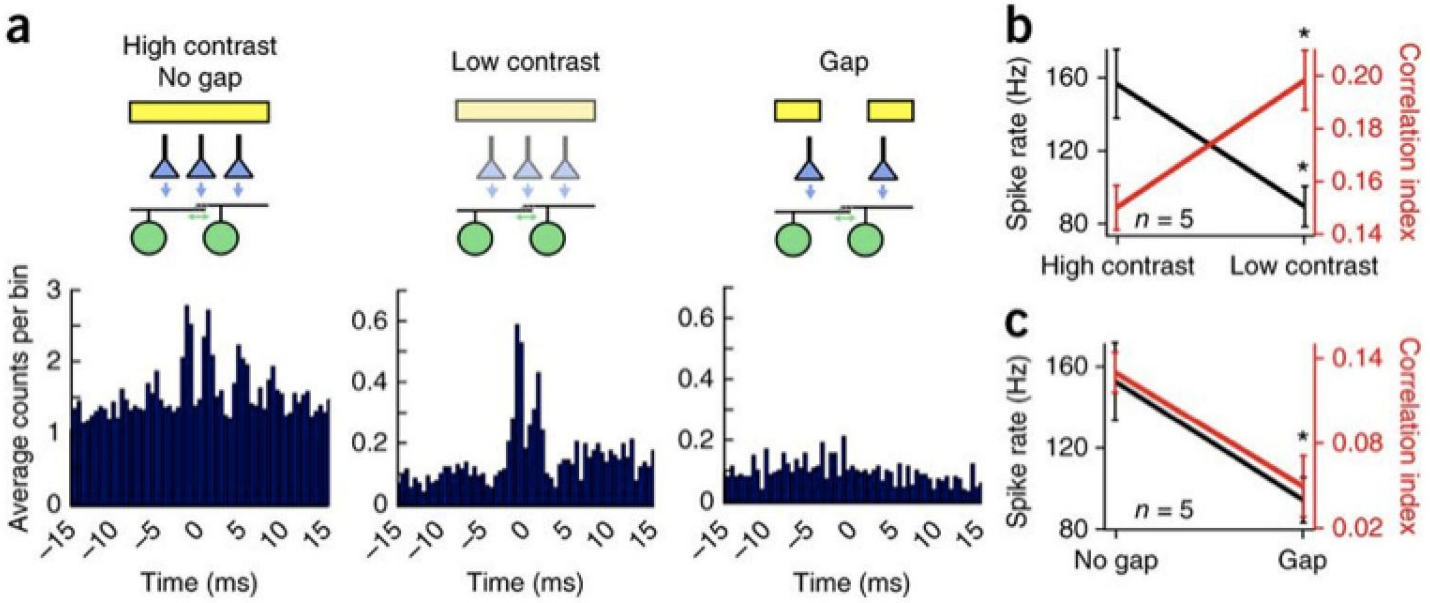

Figure 32. *Correlated spikes contain information that is independent from the spike rate*. **a** (*top*), Spikes are recorded from a pair of coupled ganglion cells when (*left*) a bright bar of light is flashed that covers both cells' receptive fields, (*middle*) the same bar of light is shown, but at low contrast, or (right) the same contrast of stimuli is shown as on the left, but is only presented to each cell in a portion of their receptive fields that is not shared between to the two cells, but that drives a similar amount of spiking as the middle stimulus. **a** (*bottom*), Cross-correlograms for the stimuli described above. **b**, Decreasing the contrast results in lower spike rates but higher spike correlations. **c**, Not stimulating the region of receptive field overlap between the pair of cells reduces spike rate but decreases correlation strength. Taken from Trenholm et al. (2014) (143).

I_h, which is present in some ON cone bipolar cells and has been shown to modulate oscillations in the rd retina (186). These oscillations have also been shown to be reliant on TTX-sensitive Na^+ channels in AII amacrine cells (186). Finally, it has been shown that gap junctional coupling of AII amacrine cells in the rd retina appears to be increased (as measured via an increase in phosphorylated Cx36), which could exacerbate aberrant activity following photoreceptor degeneration (190). As such, membrane conductances and gap junctions in the AII amacrine and ON bipolar cell network act in tandem following photoreceptor degeneration to elicit spontaneous membrane oscillations (**Figure 39**).

Conclusions

It is well established that the retina is extensively gap junction coupled, and that these connections endow retinal circuits with a plethora of functional properties. In the retina, gap junctions are associated with night vision, controlling receptive field size, signal correlation, spatial integration, and motion detection. Despite these findings, many unknowns remain. First, many critical experiments into the roles of gap junctions in the retina have employed either pharmacological agents or Cx36 KO to examine the roles of gap junctions in retinal circuits. However, simultaneously blocking gap junctions at all levels of the retina makes it difficult to assign roles for specific electrical synapses between given cell types. As such, future research will need to endeavor to modify gap junctions in specific cell types (111). Second, related to the first point, while it is clear that the retina splits incoming visual signals into over 30 distinct retinal channels (made up of distinct cell types, connected in distinct ways), unique roles for gap junctions in each of these channels is only beginning to be studied. Third, given that gap junctions are known to play important roles in retinal development (191), and may affect susceptibility to disease pathologies (192-195), it will be important to examine whether gap junctions play precise cell-type-specific roles in development (196) and disease. Finally, in addition to increasing our knowledge into the fine details of roles for gap junctions in microcircuits, it will be important to characterize

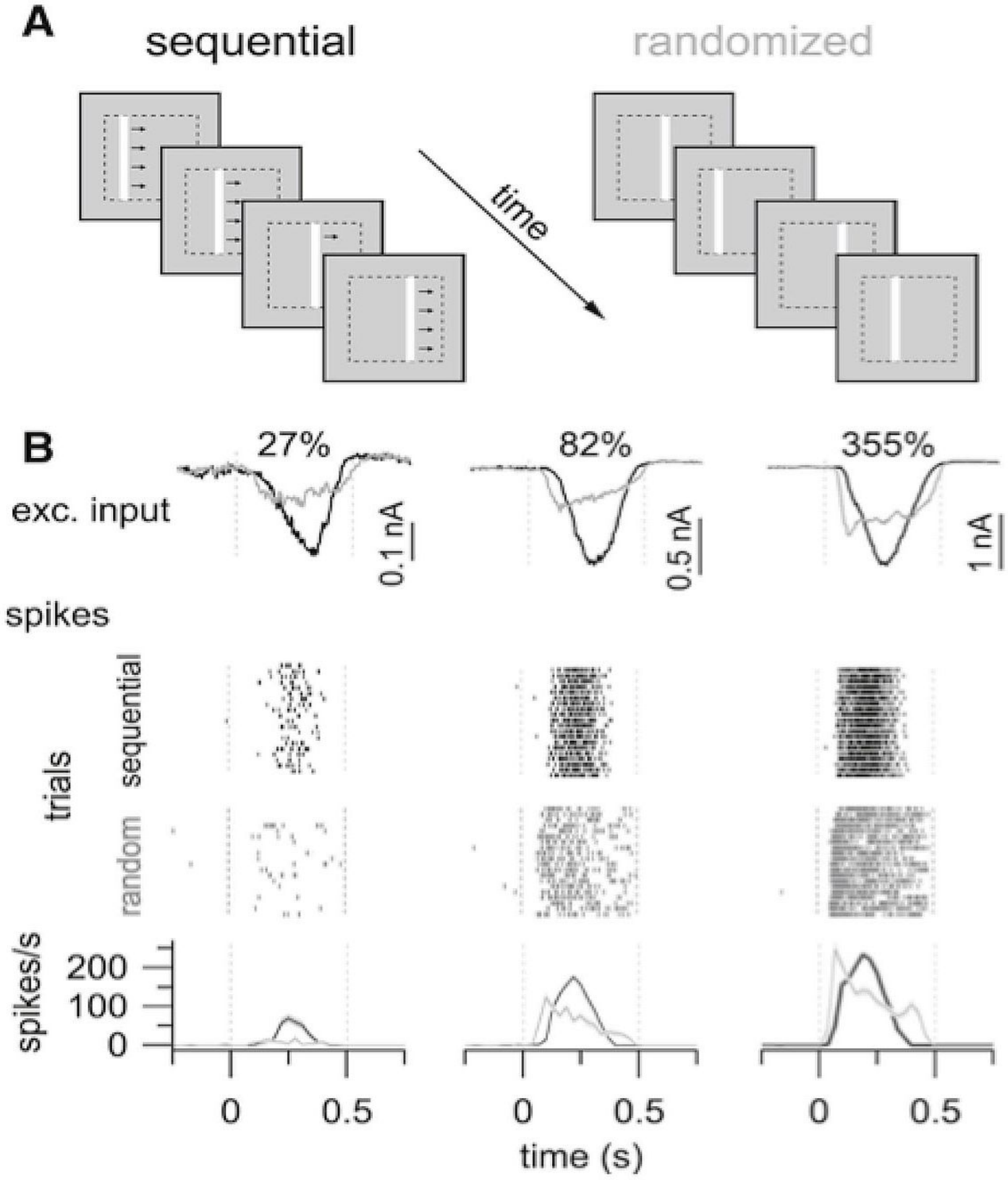

Figure 33. *Enhanced motion responses in retinal ganglion cells*. **A**, Two stimulus patterns, in which a bar of light is either flashed sequentially in space (left), mimicking coherent motion, or the same number of bars are presented in the same locations but in a random spatial order (right). **B**, The excitatory input and spiking responses of an ON sustained alpha ganglion cell in mouse retina is shown for the two stimulus paradigms described in (A). Spatio-temporally correlated stimuli drive stronger responses, and this is thought to arise from gap junction dependent spatial integration in presynaptic bipolar cells. Taken from Kuo et al. (2016) (84).

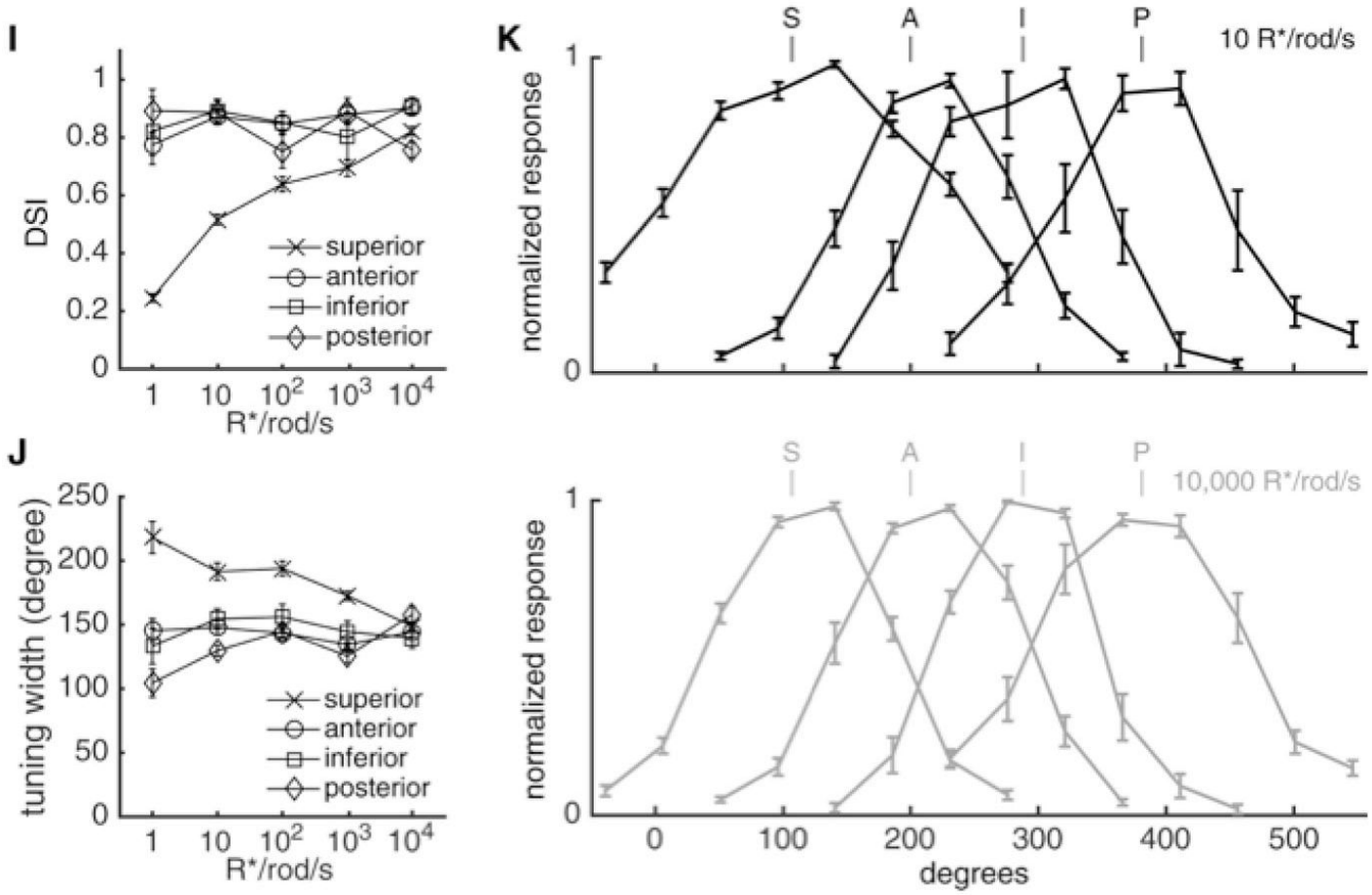

Figure 34. *The direction tuning of electrically coupled directionally selective ganglion cells changes at different light levels*. **I**, **J**, The direction selective index (DSI) and tuning width (high tuning width values mean a cell responds strongly to a wider angle of directions of motion) are plotted for direction selective ganglion cells coding the four cardinal directions (note that only superior coding direction selective cells are electrically coupled). **K**, Normalized tuning curves, to 8 directions of moving stimuli, are plotted for the four directions of ganglion cells, at dim (*top*) and bright (*bottom*) light levels. Taken from Yao et al. (2018) (111).

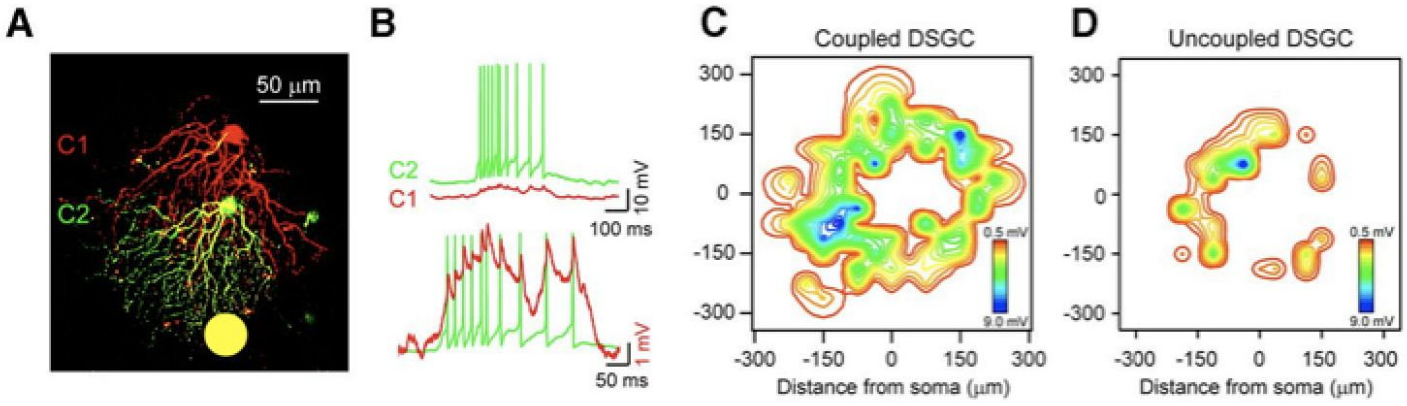

Figure 35. *Electrically coupled ganglion cells exhibit gap junction mediated excitatory subthreshold surround receptive fields*. **A**, An image of a pair of coupled ganglion cells in mouse retina, whose membrane responses to a flash of light (yellow spot) are shown in panel (B). **B**, A flash of light over the receptive field of cell 2 drives a strong spiking response in cell 2, which propagates via gap junctions into cell 1 as a subthreshold response including many coupled spikelets. **C**, **D**, The area surrounding coupled directionally selective ganglion cells (DSGC, (C)), and an uncoupled DSGC (D), where a small flash of light drives subthreshold depolarizations. Taken from Trenholm et al. (2013a) (113).

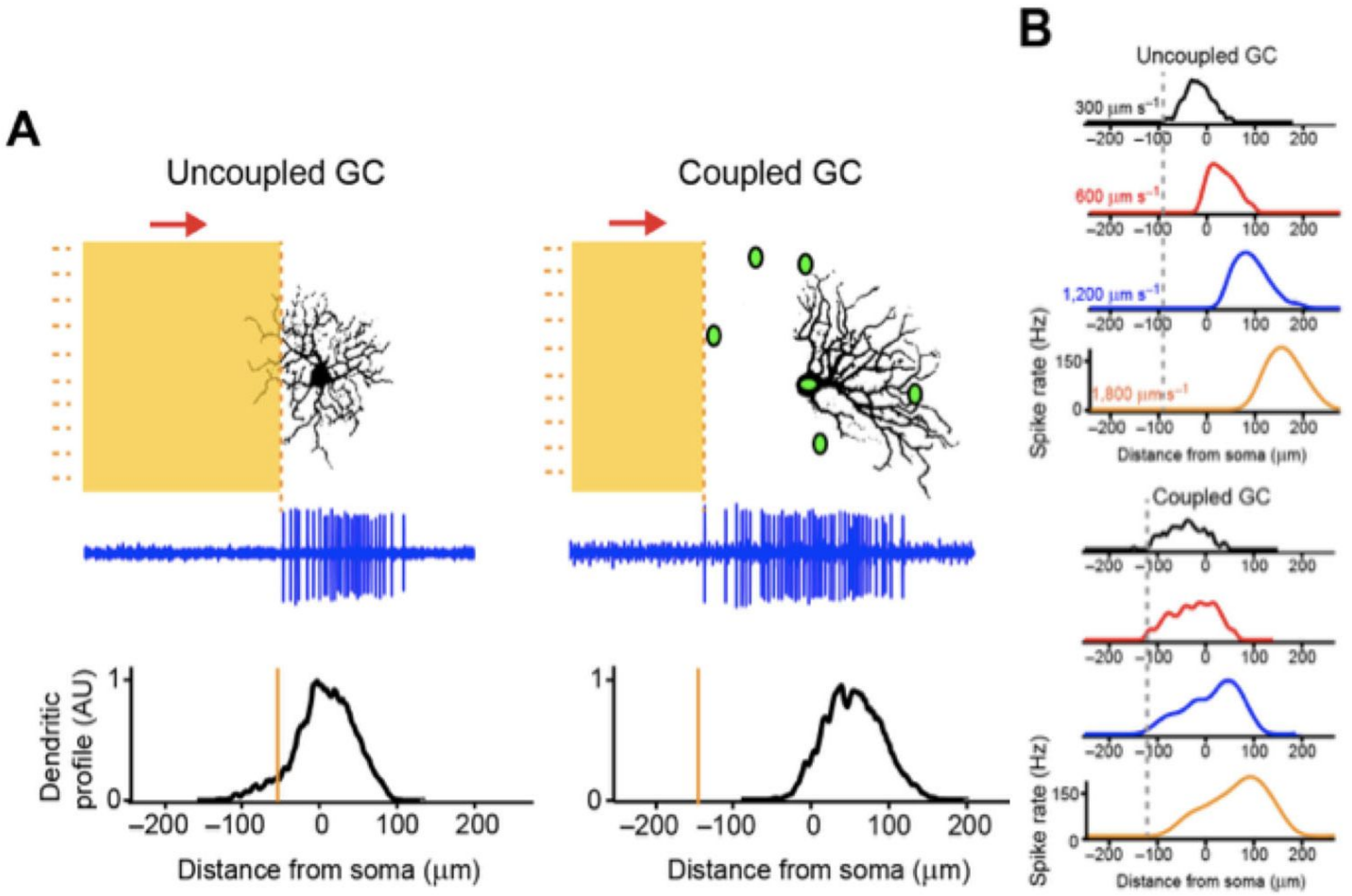

Figure 36. *Lag normalization in coupled ganglion cells*. **A**, A moving bar of light drives spiking responses in an uncoupled (left) and a coupled (right) ganglion cell (GC) in mouse retina. For the coupled cell, the locations of nearby coupled ganglion cells are plotted in green. The spike train elicited by the moving bar is shown in blue. The moving bar (yellow) is shown at the spatial location where it initiated responses. Below are average positions where spiking initiated (orange vertical line) compared to the average dendritic tree location (black lines) of uncoupled (left) and coupled (right) ganglion cells (n = 9 for each group). **B**, PSTHs of the spike rate of uncoupled (top) and coupled (bottom) ganglion cells to bars moving at 4 different speeds. On the X-axis, the spike rate is plotted with respect to where in space the leading edge of the moving stimulus was with respect to the soma (soma position is at 0 μm). Taken from Trenholm et al. (2013b) (166).

different manners in which gap junction connections are plastic, and thus allow circadian rhythm, light adaptation, or neuronal activity to gate their activity and modify circuit function.

Acknowledgements

This work was supported by Canada Research Chairs to ST and GBA.

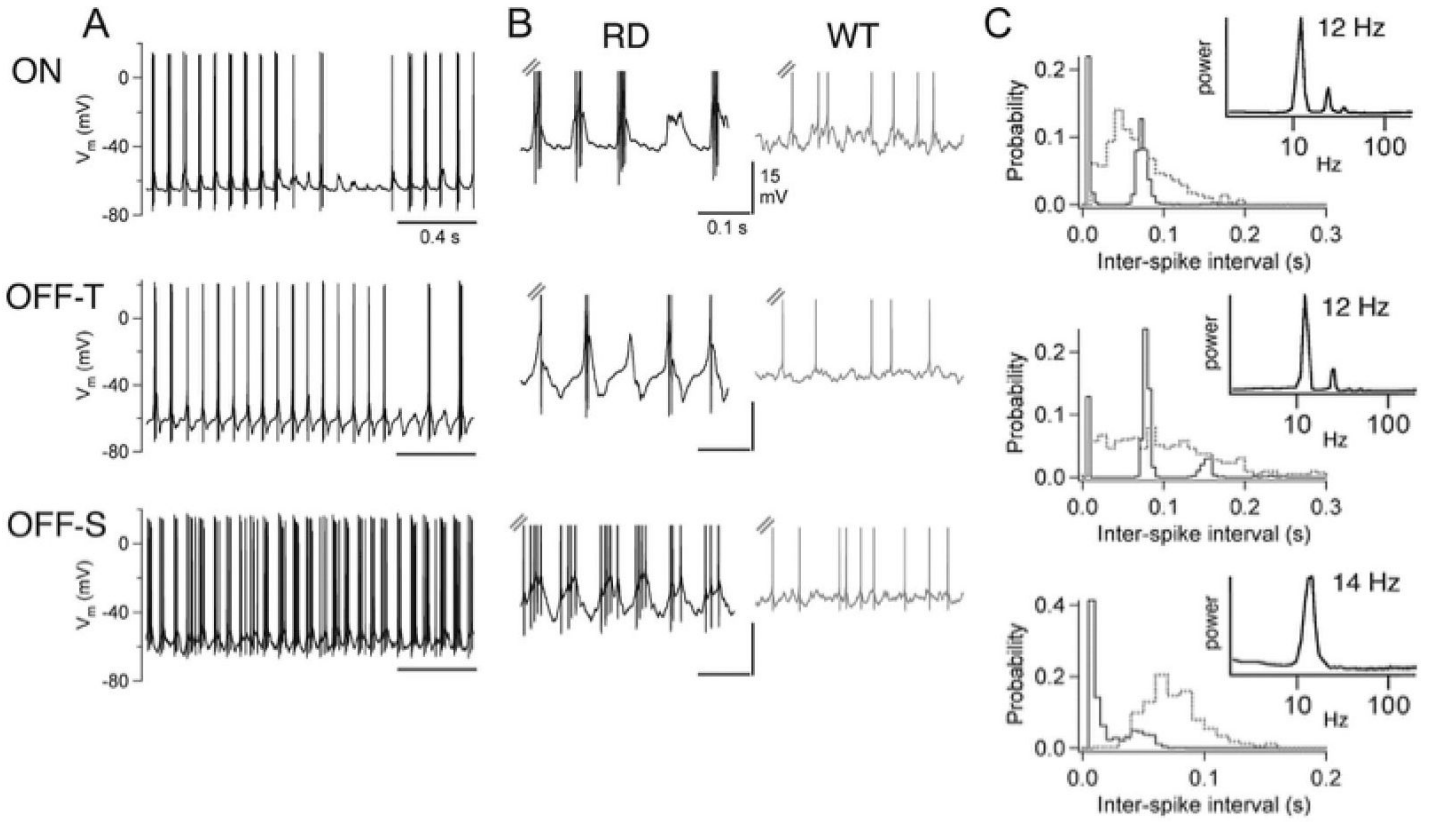

Figure 37. *Spontaneous ganglion cell oscillations in the rd retina*. **A**, Current clamp recordings from an ON, an OFF transient, and an OFF sustained ganglion cell in the rd1 mouse retina. **B**, Responses are shown at an expanded time scale, action potentials are clipped to focus on membrane oscillations, and wild type spontaneous activity is plotted to show that it is not oscillatory. **C**, Inter-spike intervals are plotted for rd (solid line) and wild type (dotted lines) ganglion cells. Power spectra are shown for rd1 oscillations. Taken from Margolis et al. (2008) (175).

About the authors

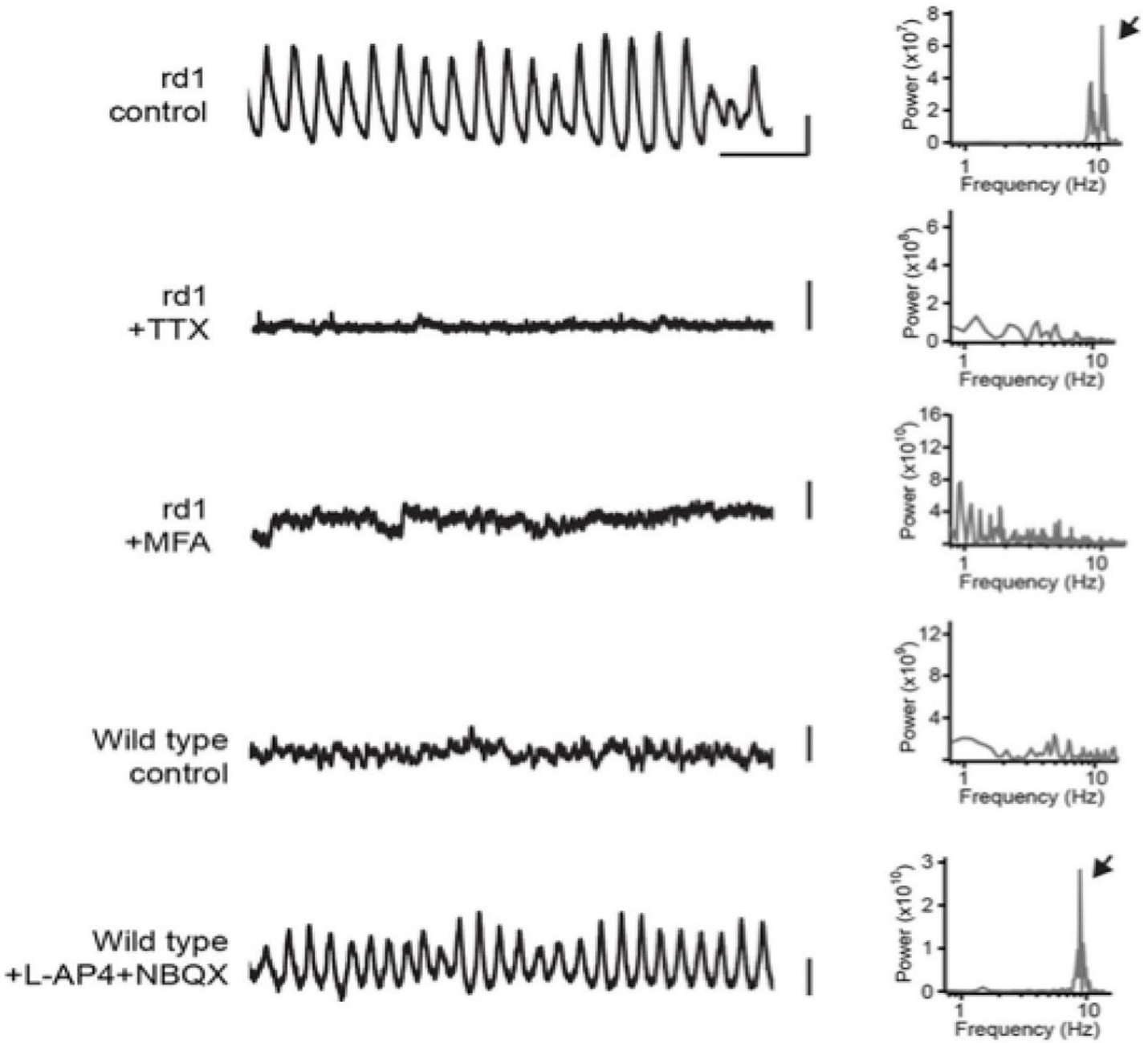

Figure 38. rd1 membrane oscillations are inhibited by TTX and gap junction blockers, and similar oscillations can be elicited in wild type retina. Left (top three traces), Current clamp recordings reveal membrane oscillations in an rd1 ON cone bipolar cell that are blocked by the voltage-gated Na^+-channel blocker tetrodotoxin (TTX) and the gap junction blocker meclofenamic acid (MFA). Left (bottom two traces), Current clamp recordings from a wild type ON cone bipolar cell in control (second trace from the bottom) and when glutamatergic input from photoreceptors was pharmacologically blocked (bottom trace). Right, Power spectra are shown for the traces on the left. Adapted from Trenholm and Awatramani (2015) (203).

Dr. Stuart Trenholm received his PhD in neuroscience from Dalhousie University, in Halifax Canada, in the lab of Dr. Gautam Awatramani. Subsequently he was a postdoctoral fellow in neuroscience in the lab of Dr. Botond Roska, at the Friedrich Miescher Institute for Biomedical Research in Basel, Switzerland. He is now an Assistant Professor at the Montreal Neurological Institute at McGill University, in Montreal, Canada. His lab examines the neuronal circuitry underlying visual perception and studies vision rehabilitation strategies.

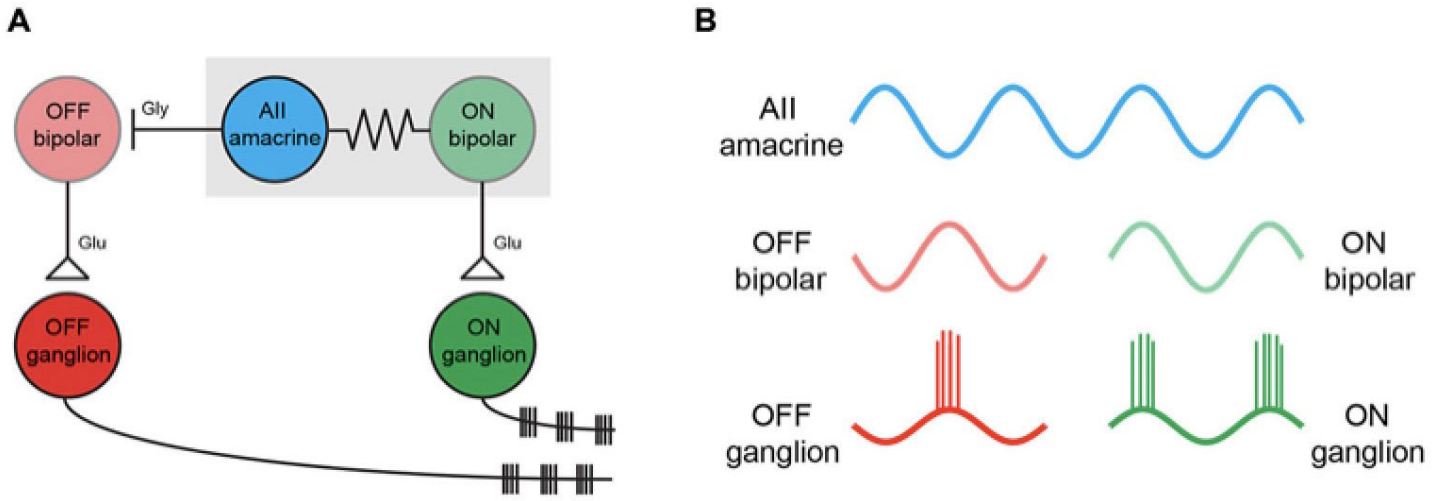

Figure 39. Model for spontaneous oscillations in rd retina. **A**, Upon losing normal glutamatergic input from photoreceptors following retinal degeneration, aberrant activity arises in the coupled AII amacrine cell-ON cone bipolar cell network, that then propagates through the rest of the retina (**B**). Taken from Trenholm and Awatramani (2015) (203).

Dr. Gautam Awatramani received his B.S. from the University of Rochester (1995) and then did his Ph.D. in Physiology and Biophysics under the supervision of Dr. Malcolm Slaughter at SUNY Buffalo. He was a postdoctoral fellow at the Vollum Institute (Portland, OR, 2000-2004) with Dr. Laurence Trussell, at the University of British Columbia (Vancouver, B.C, 2005-2007) with Dr. Tim Murphy and at the Friedrich Miescher Institute (Basel, CH, 2008) with Dr. Botond Roska. He then started his own lab at Dalhousie University (Halifax 2008-2011) and subsequently moved to the University of Victoria (Victoria, B.C.) where he is currently an Associate Professor/CRC chair in Physiology. His work currently focusses on understanding the synaptic mechanisms underlying the generation of direction selectivity in the retina.

References

1. Masland R.H. The fundamental plan of the retina. Nature Neuroscience. 2001;4(9):877–886. PubMed PMID: 11528418.
2. Gollisch T., Meister M. Eye smarter than scientists believed: neural computations in circuits of the retina. Neuron. 2010;65(2):150–164. PubMed PMID: 20152123.
3. Azeredo da Silveira R., Roska B. Cell types, circuits, computation. Current Opinion in Neurobiology. 2011;21(5):664–671. PubMed PMID: 21641794.
4. Masland R.H. The neuronal organization of the retina. Neuron. 2012;76(2):266–280. PubMed PMID: 23083731.

5. Diamond J.S. Inhibitory Interneurons in the Retina: Types, Circuitry, and Function. Annual Review of Vision Science. 2017;3:1–24. PubMed PMID: 28617659.
6. Martersteck E.M., Hirokawa K.E., Evarts M., Bernard A., Duan X., Li Y., Ng L., Oh S.W., Ouellette B., Royall J.J., Stoecklin M., Wang Q., Zeng H., Sanes J.R., Harris J.A. Diverse Central Projection Patterns of Retinal Ganglion Cells. Cell Reports. 2017;18(8):2058–2072. PubMed PMID: 28228269.
7. Robles E., Laurell E., Baier H. The retinal projectome reveals brain-area-specific visual representations generated by ganglion cell diversity. Current biology: CB. 2014;24(18):2085–2096. PubMed PMID: 25155513.
8. Ribelayga, C.P. and J. O'Brien, *Chapter 10 - Circadian and Light-Adaptive Control of Electrical Synaptic Plasticity in the Vertebrate Retina*, in *Network Functions and Plasticity*, J. Jing, Editor. 2017, Academic Press. p. 209-241.
9. Baylor D.A., Fuortes M.G., O'Bryan P.M. Receptive fields of cones in the retina of the turtle. The Journal of Physiology. 1971;214(2):265–294. PubMed PMID: 5579638.
10. Copenhagen D.R., Owen W.G. Coupling between rod photoreceptors in a vertebrate retina. Nature. 1976;260(5546):57–59. PubMed PMID: 1264196.
11. Custer N.V. Structurally specialized contacts between the photoreceptors of the retina of the axolotl. The Journal of Comparative Neurology. 1973;151(1):35–56. PubMed PMID: 4731301.
12. DeVries S.H., Qi X., Smith R., Makous W., Sterling P. Electrical coupling between mammalian cones. Current biology: CB. 2002;12(22):1900–1907. PubMed PMID: 12445382.
13. Hornstein E.P., Verweij J., Li P.H., Schnapf J.L. Gap-junctional coupling and absolute sensitivity of photoreceptors in macaque retina. The Journal of Neuroscience: The Official Journal of the Society for Neuroscience. 2005;25(48):11201–11209. PubMed PMID: 16319320.
14. Hornstein E.P., Verweij J., Schnapf J.L. Electrical coupling between red and green cones in primate retina. Nature Neuroscience. 2004;7(7):745–750. PubMed PMID: 15208634.
15. Li P.H., Verweij J., Long J.H., Schnapf J.L. Gap-junctional coupling of mammalian rod photoreceptors and its effect on visual detection. The Journal of Neuroscience: The Official Journal of the Society for Neuroscience. 2012;32(10):3552–3562. PubMed PMID: 22399777.
16. Raviola E., Gilula N.B. Gap junctions between photoreceptor cells in the vertebrate retina. Proceedings of the National Academy of Sciences of the United States of America. 1973;70(6):1677–1681. PubMed PMID: 4198274.
17. Tsukamoto Y., Morigiwa K., Ueda M., Sterling P. Microcircuits for night vision in mouse retina. The Journal of Neuroscience: The Official Journal of the Society for Neuroscience. 2001;21(21):8616–8623. PubMed PMID: 11606649.
18. Feigenspan A., Janssen-Bienhold U., Hormuzdi S., Monyer H., Degen J., Söhl G., Willecke K., Ammermüller J., Weiler R. Expression of connexin36 in cone pedicles and OFF-cone bipolar cells of the mouse retina. The Journal of Neuroscience: The Official Journal of the Society for Neuroscience. 2004;24(13):3325–3334. PubMed PMID: 15056712.
19. Kántor O., Benkő Z., Énzsöly A., Dávid C., Naumann A., Nitschke R., Szabó A., Pálfi E., Orbán J., Nyitrai M., Németh J., Szél Á., Lukáts Á., Völgyi B. Characterization of connexin36 gap junctions in the human outer retina. Brain Structure & Function. 2016;221(6):2963–2984. PubMed PMID: 26173976.
20. Lee E.-J., Han J.-W., Kim H.-J., Kim I.-B., Lee M.-Y., Oh S.-J., Chung J.-W., Chun M.-H. The immunocytochemical localization of connexin 36 at rod and cone gap junctions in the guinea pig retina. The European Journal of Neuroscience. 2003;18(11):2925–2934. PubMed PMID: 14656288.
21. O'Brien J.J., Chen X., Macleish P.R., O'Brien J., Massey S.C. Photoreceptor coupling mediated by connexin36 in the primate retina. The Journal of Neuroscience: The Official Journal of the Society for Neuroscience. 2012;32(13):4675–4687. PubMed PMID: 22457514.
22. Li H., Chuang A.Z., O'Brien J. Photoreceptor coupling is controlled by connexin 35 phosphorylation in zebrafish retina. The Journal of Neuroscience: The Official Journal of the Society for Neuroscience. 2009;29(48):15178–15186. PubMed PMID: 19955370.

23. Li H., Zhang Z., Blackburn M.R., Wang S.W., Ribelayga C.P., O'Brien J. Adenosine and dopamine receptors coregulate photoreceptor coupling via gap junction phosphorylation in mouse retina. The Journal of Neuroscience: The Official Journal of the Society for Neuroscience. 2013;33(7):3135–3150. PubMed PMID: 23407968.
24. Zhang J., Wu S.M. Connexin35/36 gap junction proteins are expressed in photoreceptors of the tiger salamander retina. The Journal of Comparative Neurology. 2004;470(1):1–12. PubMed PMID: 14755521.
25. Asteriti S., Gargini C., Cangiano L. Connexin 36 expression is required for electrical coupling between mouse rods and cones. Visual Neuroscience. 2017;34:E006. PubMed PMID: 28965521.
26. Kolb H. The organization of the outer plexiform layer in the retina of the cat: electron microscopic observations. Journal of Neurocytology. 1977;6(2):131–153. PubMed PMID: 856949.
27. Li W., DeVries S.H. Separate blue and green cone networks in the mammalian retina. Nature Neuroscience. 2004;7(7):751–756. PubMed PMID: 15208635.
28. Tsukamoto Y., Masarachia P., Schein S.J., Sterling P. Gap junctions between the pedicles of macaque foveal cones. Vision Research. 1992;32(10):1809–1815. PubMed PMID: 1337638.
29. Zhang J., Wu S.M. Physiological properties of rod photoreceptor electrical coupling in the tiger salamander retina. The Journal of Physiology. 2005;564(Pt 3):849–862. PubMed PMID: 15746168.
30. Werblin F.S. Transmission along and between rods in the tiger salamander retina. The Journal of Physiology. 1978;280:449–470. PubMed PMID: 211229.
31. Gao F., Pang J.-J., Wu S.M. Sign-preserving and sign-inverting synaptic interactions between rod and cone photoreceptors in the dark-adapted retina. The Journal of Physiology. 2013;591(22):5711–5726. PubMed PMID: 24000179.
32. Attwell D., Wilson M., Wu S.M. A quantitative analysis of interactions between photoreceptors in the salamander (Ambystoma) retina. The Journal of Physiology. 1984;352:703–737. PubMed PMID: 6747904.
33. Ribelayga C., Cao Y., Mangel S.C. The circadian clock in the retina controls rod-cone coupling. Neuron. 2008;59(5):790–801. PubMed PMID: 18786362.
34. Wu S.M., Yang X.L. Electrical coupling between rods and cones in the tiger salamander retina. Proceedings of the National Academy of Sciences of the United States of America. 1988;85(1):275–278. PubMed PMID: 3422423.
35. Asteriti S., Gargini C., Cangiano L. Mouse rods signal through gap junctions with cones. eLife. 2014;3:e01386. PubMed PMID: 24399457.
36. Nelson R. Cat cones have rod input: a comparison of the response properties of cones and horizontal cell bodies in the retina of the cat. The Journal of Comparative Neurology. 1977;172(1):109–135. PubMed PMID: 838876.
37. Schneeweis D.M., Schnapf J.L. Photovoltage of rods and cones in the macaque retina. Science (New York, N.Y.). 1995;268(5213):1053–1056. PubMed PMID: 7754386.
38. Thoreson W.B., Mangel S.C. Lateral interactions in the outer retina. Progress in Retinal and Eye Research. 2012;31(5):407–441. PubMed PMID: 22580106.
39. Raviola E., Gilula N.B. Intramembrane organization of specialized contacts in the outer plexiform layer of the retina. A freeze-fracture study in monkeys and rabbits. The Journal of Cell Biology. 1975;65(1):192–222. PubMed PMID: 1127010.
40. Hombach S., Janssen-Bienhold U., Söhl G., Schubert T., Büssow H., Ott T., Weiler R., Willecke K. Functional expression of connexin57 in horizontal cells of the mouse retina. The European Journal of Neuroscience. 2004;19(10):2633–2640. PubMed PMID: 15147297.
41. Janssen-Bienhold U., Trümpler J., Hilgen G., Schultz K., Müller L.P.D.S., Sonntag S., Dedek K., Dirks P., Willecke K., Weiler R. Connexin57 is expressed in dendro-dendritic and axo-axonal gap junctions of mouse horizontal cells and its distribution is modulated by light. The Journal of Comparative Neurology. 2009;513(4):363–374. PubMed PMID: 19177557.
42. Dorgau B., Herrling R., Schultz K., Greb H., Segelken J., Ströh S., Bolte P., Weiler R., Dedek K., Janssen-Bienhold U. Connexin50 couples axon terminals of mouse horizontal cells by homotypic gap junctions. The Journal of Comparative Neurology. 2015;523(14):2062–2081. PubMed PMID: 25823610.

43. O'Brien J.J., Li W., Pan F., Keung J., O'Brien J., Massey S.C. Coupling between A-type horizontal cells is mediated by connexin 50 gap junctions in the rabbit retina. The Journal of Neuroscience: The Official Journal of the Society for Neuroscience. 2006;26(45):11624–11636. PubMed PMID: 17093084.
44. Pan F., Keung J., Kim I.-B., Snuggs M.B., Mills S.L., O'Brien J., Massey S.C. Connexin 57 is expressed by the axon terminal network of B-type horizontal cells in the rabbit retina. The Journal of Comparative Neurology. 2012;520(10):2256–2274. PubMed PMID: 22495514.
45. Klaassen L.J., Sun Z., Steijaert M.N., Bolte P., Fahrenfort I., Sjoerdsma T., Klooster J., Claassen Y., Shields C.R., Ten Eikelder H.M.M., Janssen-Bienhold U., Zoidl G., McMahon D.G., Kamermans M. Synaptic transmission from horizontal cells to cones is impaired by loss of connexin hemichannels. PLoS biology. 2011;9(7):e1001107. PubMed PMID: 21811399.
46. Shields C.R., Klooster J., Claassen Y., Ul-Hussain M., Zoidl G., Dermietzel R., Kamermans M. Retinal horizontal cell-specific promoter activity and protein expression of zebrafish connexin 52.6 and connexin 55.5. The Journal of Comparative Neurology. 2007;501(5):765–779. PubMed PMID: 17299759.
47. DeVries S.H., Schwartz E.A. Modulation of an electrical synapse between solitary pairs of catfish horizontal cells by dopamine and second messengers. The Journal of Physiology. 1989;414:351–375. PubMed PMID: 2558170.
48. Lasater E.M., Dowling J.E. Dopamine decreases conductance of the electrical junctions between cultured retinal horizontal cells. Proceedings of the National Academy of Sciences of the United States of America. 1985;82(9):3025–3029. PubMed PMID: 3857632.
49. McMahon D.G. Modulation of electrical synaptic transmission in zebrafish retinal horizontal cells. The Journal of Neuroscience: The Official Journal of the Society for Neuroscience. 1994;14(3 Pt 2):1722–1734. PubMed PMID: 8126566.
50. McMahon D.G., Mattson M.P. Horizontal cell electrical coupling in the giant danio: synaptic modulation by dopamine and synaptic maintenance by calcium. Brain Research. 1996;718(1-2):89–96. PubMed PMID: 8773769.
51. Xin D., Bloomfield S.A. Dark- and light-induced changes in coupling between horizontal cells in mammalian retina. The Journal of Comparative Neurology. 1999;405(1):75–87. PubMed PMID: 10022197.
52. Ribelayga C., Mangel S.C. Absence of circadian clock regulation of horizontal cell gap junctional coupling reveals two dopamine systems in the goldfish retina. The Journal of Comparative Neurology. 2003;467(2):243–253. PubMed PMID: 14595771.
53. Ribelayga C., Mangel S.C. Tracer coupling between fish rod horizontal cells: modulation by light and dopamine but not the retinal circadian clock. Visual Neuroscience. 2007;24(3):333–344. PubMed PMID: 17640444.
54. Mangel S.C., Dowling J.E. Responsiveness and receptive field size of carp horizontal cells are reduced by prolonged darkness and dopamine. Science (New York, N.Y.). 1985;229(4718):1107–1109. PubMed PMID: 4035351.
55. Shelley J., Dedek K., Schubert T., Feigenspan A., Schultz K., Hombach S., Willecke K., Weiler R. Horizontal cell receptive fields are reduced in connexin57-deficient mice. The European Journal of Neuroscience. 2006;23(12):3176–3186. PubMed PMID: 16820008.
56. Mangel S.C. Analysis of the horizontal cell contribution to the receptive field surround of ganglion cells in the rabbit retina. The Journal of physiology. 1991;442(1):211–234. PubMed PMID: 1665857.
57. Werblin F.S., Dowling J.E. Organization of the retina of the mudpuppy, Necturus maculosus. II. Intracellular recording. Journal of Neurophysiology. 1969;32(3):339–355. PubMed PMID: 4306897.
58. Drinnenberg A., Franke F., Morikawa R.K., Jüttner J., Hillier D., Hantz P., Hierlemann A., Azeredo da Silveira R., Roska B. How Diverse Retinal Functions Arise from Feedback at the First Visual Synapse. Neuron. 2018;99(1):117–134.e11. PubMed PMID: 29937281.
59. Farrow K., Teixeira M., Szikra T., Viney T.J., Balint K., Yonehara K., Roska B. Ambient illumination toggles a neuronal circuit switch in the retina and visual perception at cone threshold. Neuron. 2013;78(2):325–338. PubMed PMID: 23541902.

60. Hoggarth A., McLaughlin A.J., Ronellenfitch K., Trenholm S., Vasandani R., Sethuramanujam S., Schwab D., Briggman K.L., Awatramani G.B. Specific wiring of distinct amacrine cells in the directionally selective retinal circuit permits independent coding of direction and size. Neuron. 2015;86(1):276–291. PubMed PMID: 25801705.
61. Dedek K., Pandarinath C., Alam N.M., Wellershaus K., Schubert T., Willecke K., Prusky G.T., Weiler R., Nirenberg S. Ganglion cell adaptability: does the coupling of horizontal cells play a role? PloS One. 2008;3(3):e1714. PubMed PMID: 18320035.
62. Pandarinath C., Bomash I., Victor J.D., Prusky G.T., Tschetter W.W., Nirenberg S. A novel mechanism for switching a neural system from one state to another. Frontiers in Computational Neuroscience. 2010;4:2. PubMed PMID: 20407612.
63. Wässle H., Puller C., Müller F., Haverkamp S. Cone contacts, mosaics, and territories of bipolar cells in the mouse retina. The Journal of Neuroscience: The Official Journal of the Society for Neuroscience. 2009;29(1):106–117. PubMed PMID: 19129389.
64. Kolb H., Famiglietti E.V. Rod and cone pathways in the inner plexiform layer of cat retina. Science (New York, N.Y.). 1974;186(4158):47–49. PubMed PMID: 4417736.
65. Lee S.C.S., Meyer A., Schubert T., Hüser L., Dedek K., Haverkamp S. Morphology and connectivity of the small bistratified A8 amacrine cell in the mouse retina. The Journal of Comparative Neurology. 2015;523(10):1529–1547. PubMed PMID: 25630271.
66. Arai I., Tanaka M., Tachibana M. Active roles of electrically coupled bipolar cell network in the adult retina. The Journal of Neuroscience: The Official Journal of the Society for Neuroscience. 2010;30(27):9260–9270. PubMed PMID: 20610761.
67. Jacoby R.A., Marshak D.W. Synaptic connections of DB3 diffuse bipolar cell axons in macaque retina. The Journal of Comparative Neurology. 2000;416(1):19–29. PubMed PMID: 10578100.
68. Marc R.E., Liu W.L., Muller J.F. Gap junctions in the inner plexiform layer of the goldfish retina. Vision Research. 1988;28(1):9–24. PubMed PMID: 3414003.
69. Strettoi E., Raviola E., Dacheux R.F. Synaptic connections of the narrow-field, bistratified rod amacrine cell (AII) in the rabbit retina. The Journal of Comparative Neurology. 1992;325(2):152–168. PubMed PMID: 1460111.
70. Deans M.R., Volgyi B., Goodenough D.A., Bloomfield S.A., Paul D.L. Connexin36 is essential for transmission of rod-mediated visual signals in the mammalian retina. Neuron. 2002;36(4):703–712. PubMed PMID: 12441058.
71. Han Y., Massey S.C. Electrical synapses in retinal ON cone bipolar cells: subtype-specific expression of connexins. Proceedings of the National Academy of Sciences of the United States of America. 2005;102(37):13313–13318. PubMed PMID: 16150718.
72. Hilgen G., von Maltzahn J., Willecke K., Weiler R., Dedek K. Subcellular distribution of connexin45 in OFF bipolar cells of the mouse retina. The Journal of Comparative Neurology. 2011;519(3):433–450. PubMed PMID: 21192077.
73. Maxeiner S., Dedek K., Janssen-Bienhold U., Ammermüller J., Brune H., Kirsch T., Pieper M., Degen J., Krüger O., Willecke K., Weiler R. Deletion of connexin45 in mouse retinal neurons disrupts the rod/cone signaling pathway between AII amacrine and ON cone bipolar cells and leads to impaired visual transmission. The Journal of Neuroscience: The Official Journal of the Society for Neuroscience. 2005;25(3):566–576. PubMed PMID: 15659592.
74. Dacey D., Packer O.S., Diller L., Brainard D., Peterson B., Lee B. Center surround receptive field structure of cone bipolar cells in primate retina. Vision Research. 2000;40(14):1801–1811. PubMed PMID: 10837827.
75. Kujiraoka T., Saito T. Electrical coupling between bipolar cells in carp retina. Proceedings of the National Academy of Sciences of the United States of America. 1986;83(11):4063–4066. PubMed PMID: 16593707.
76. Mills S.L. Unusual coupling patterns of a cone bipolar cell in the rabbit retina. Visual Neuroscience. 1999;16(6):1029–1035. PubMed PMID: 10614585.
77. Umino O., Maehara M., Hidaka S., Kita S., Hashimoto Y. The network properties of bipolar-bipolar cell coupling in the retina of teleost fishes. Visual Neuroscience. 1994;11(3):533–548. PubMed PMID: 8038127.

78. Veruki M.L., Hartveit E. AII (Rod) amacrine cells form a network of electrically coupled interneurons in the mammalian retina. Neuron. 2002;33(6):935–946. PubMed PMID: 11906699.
79. Marc R.E., Anderson J.R., Jones B.W., Sigulinsky C.L., Lauritzen J.S. The AII amacrine cell connectome: a dense network hub. Frontiers in Neural Circuits. 2014;8:104. PubMed PMID: 25237297.
80. Graydon C.W., Lieberman E.E., Rho N., Briggman K.L., Singer J.H., Diamond J.S. Synaptic Transfer between Rod and Cone Pathways Mediated by AII Amacrine Cells in the Mouse Retina. Current biology: CB. 2018;28(17):2739–2751.e3. PubMed PMID: 30122532.
81. Saito T., Kujiraoka T. Characteristics of bipolar-bipolar coupling in the carp retina. The Journal of General Physiology. 1988;91(2):275–287. PubMed PMID: 3373179.
82. Berntson A., Taylor W.R. Response characteristics and receptive field widths of on-bipolar cells in the mouse retina. The Journal of Physiology. 2000;524(Pt 3):879–889. PubMed PMID: 10790165.
83. Werblin F.S. Response of retinal cells to moving spots: intracellular recording in Necturus maculosus. Journal of Neurophysiology. 1970;33(3):342–350. PubMed PMID: 5439341.
84. Kuo S.P., Schwartz G.W., Rieke F. Nonlinear Spatiotemporal Integration by Electrical and Chemical Synapses in the Retina. Neuron. 2016;90(2):320–332. PubMed PMID: 27068789.
85. Masland R.H. The tasks of amacrine cells. Visual Neuroscience. 2012;29(1):3–9. PubMed PMID: 22416289.
86. Masland R.H., Mills J.W. Autoradiographic identification of acetylcholine in the rabbit retina. The Journal of Cell Biology. 1979;83(1):159–178. PubMed PMID: 92476.
87. Lee S., Kim K., Zhou Z.J. Role of ACh-GABA cotransmission in detecting image motion and motion direction. Neuron. 2010;68(6):1159–1172. PubMed PMID: 21172616.
88. Sethuramanujam S., McLaughlin A.J., deRosenroll G., Hoggarth A., Schwab D.J., Awatramani G.B. A Central Role for Mixed Acetylcholine/GABA Transmission in Direction Coding in the Retina. Neuron. 2016;90(6):1243–1256. PubMed PMID: 27238865.
89. Zhang D.-Q., Zhou T.-R., McMahon D.G. Functional heterogeneity of retinal dopaminergic neurons underlying their multiple roles in vision. The Journal of Neuroscience: The Official Journal of the Society for Neuroscience. 2007;27(3):692–699. PubMed PMID: 17234601.
90. Baden T., Euler T. Retinal Physiology: Non-Bipolar-Cell Excitatory Drive in the Inner Retina. Current biology: CB. 2016;26(15):R706–R708. PubMed PMID: 27505240.
91. Xin D., Bloomfield S.A. Tracer coupling pattern of amacrine and ganglion cells in the rabbit retina. The Journal of Comparative Neurology. 1997;383(4):512–528. PubMed PMID: 9208996.
92. Li W., Zhang J., Massey S.C. Coupling pattern of S1 and S2 amacrine cells in the rabbit retina. Visual Neuroscience. 2002;19(2):119–131. PubMed PMID: 12385625.
93. Abdel-Majid R.M., Archibald M.L., Tremblay F., Baldridge W.H. Tracer coupling of neurons in the rat retina inner nuclear layer labeled by Fluorogold. Brain Research. 2005;1063(2):114–120. PubMed PMID: 16263096.
94. Bloomfield S.A., Xin D. A comparison of receptive-field and tracer-coupling size of amacrine and ganglion cells in the rabbit retina. Visual Neuroscience. 1997;14(6):1153–1165. PubMed PMID: 9447695.
95. Völgyi B., Chheda S., Bloomfield S.A. Tracer coupling patterns of the ganglion cell subtypes in the mouse retina. The Journal of Comparative Neurology. 2009;512(5):664–687. PubMed PMID: 19051243.
96. Pan F., Paul D.L., Bloomfield S.A., Völgyi B. Connexin36 is required for gap junctional coupling of most ganglion cell subtypes in the mouse retina. The Journal of Comparative Neurology. 2010;518(6):911–927. PubMed PMID: 20058323.
97. Pang J.-J., Paul D.L., Wu S.M. Survey on amacrine cells coupling to retrograde-identified ganglion cells in the mouse retina. Investigative Ophthalmology & Visual Science. 2013;54(8):5151–5162. PubMed PMID: 23821205.
98. Jacoby J., Nath A., Jessen Z.F., Schwartz G.W. A Self-Regulating Gap Junction Network of Amacrine Cells Controls Nitric Oxide Release in the Retina. Neuron. 2018;100(5):1149–1162.e5. PubMed PMID: 30482690.

99. Grimes W.N., Zhang J., Graydon C.W., Kachar B., Diamond J.S. Retinal parallel processors: more than 100 independent microcircuits operate within a single interneuron. Neuron. 2010;65(6):873–885. PubMed PMID: 20346762.
100. Yadav S.C., Tetenborg S., Dedek K. Gap Junctions in A8 Amacrine Cells Are Made of Connexin36 but Are Differently Regulated Than Gap Junctions in AII Amacrine Cells. Frontiers in Molecular Neuroscience. 2019;12:99. PubMed PMID: 31065239.
101. Dacey, D., *Origins of perception: retinal ganglion cell diversity and the creation of parallel visual pathways*, in *The Cognitive Neurosciences*. 2004, MIT Press.
102. Sanes J.R., Masland R.H. The types of retinal ganglion cells: current status and implications for neuronal classification. Annual Review of Neuroscience. 2015;38:221–246. PubMed PMID: 25897874.
103. Baden T., Berens P., Franke K., Román Rosón M., Bethge M., Euler T. The functional diversity of retinal ganglion cells in the mouse. Nature. 2016;529(7586):345–350. PubMed PMID: 26735013.
104. Vaney D.I. Many diverse types of retinal neurons show tracer coupling when injected with biocytin or Neurobiotin. Neuroscience Letters. 1991;125(2):187–190. PubMed PMID: 1715532.
105. Vaney D.I. Territorial organization of direction-selective ganglion cells in rabbit retina. The Journal of Neuroscience: The Official Journal of the Society for Neuroscience. 1994;14(11 Pt 1):6301–6316. PubMed PMID: 7965037.
106. Hidaka S., Akahori Y., Kurosawa Y. Dendrodendritic electrical synapses between mammalian retinal ganglion cells. The Journal of Neuroscience: The Official Journal of the Society for Neuroscience. 2004;24(46):10553–10567. PubMed PMID: 15548670.
107. Müller L.P.d.S., Do M.T.H., Yau K.-W., He S., Baldridge W.H. Tracer coupling of intrinsically photosensitive retinal ganglion cells to amacrine cells in the mouse retina. The Journal of Comparative Neurology. 2010;518(23):4813–4824. PubMed PMID: 20963830.
108. Reifler A.N., Chervenak A.P., Dolikian M.E., Benenati B.A., Li B.Y., Wachter R.D., Lynch A.M., Demertzis Z.D., Meyers B.S., Abufarha F.S., Jaeckel E.R., Flannery M.P., Wong K.Y. All Spiking, Sustained ON Displaced Amacrine Cells Receive Gap-Junction Input from Melanopsin Ganglion Cells. Current biology: CB. 2015;25(21):2878. PubMed PMID: 28843289.
109. Schubert T., Maxeiner S., Krüger O., Willecke K., Weiler R. Connexin45 mediates gap junctional coupling of bistratified ganglion cells in the mouse retina. The Journal of Comparative Neurology. 2005;490(1):29–39. PubMed PMID: 16041717.
110. Kántor O., Szarka G., Benkő Z., Somogyvári Z., Pálfi E., Baksa G., Rácz G., Nitschke R., Debertin G., Völgyi B. Strategic Positioning of Connexin36 Gap Junctions Across Human Retinal Ganglion Cell Dendritic Arbors. Frontiers in Cellular Neuroscience. 2018;12:409. PubMed PMID: 30524239.
111. Yao X., Cafaro J., McLaughlin A.J., Postma F.R., Paul D.L., Awatramani G., Field G.D. Gap Junctions Contribute to Differential Light Adaptation across Direction-Selective Retinal Ganglion Cells. Neuron. 2018;100(1):216–228.e6. PubMed PMID: 30220512.
112. Hu E.H., Bloomfield S.A. Gap junctional coupling underlies the short-latency spike synchrony of retinal alpha ganglion cells. The Journal of Neuroscience: The Official Journal of the Society for Neuroscience. 2003;23(17):6768–6777. PubMed PMID: 12890770.
113. Trenholm S., McLaughlin A.J., Schwab D.J., Awatramani G.B. Dynamic tuning of electrical and chemical synaptic transmission in a network of motion coding retinal neurons. The Journal of Neuroscience: The Official Journal of the Society for Neuroscience. 2013;33(37):14927–14938. PubMed PMID: 24027292.
114. Cooler, S. and G.W. Schwartz, *An on-primary retinal ganglion cell receives off input via a heterotypic RGC gap junction*, in *Annual Meeting of the Society for Neuroscience*. 2019, Society for Neuroscience: Chicago. p. 225.08.
115. Hu E.H., Pan F., Völgyi B., Bloomfield S.A. Light increases the gap junctional coupling of retinal ganglion cells. The Journal of Physiology. 2010;588(Pt 21):4145–4163. PubMed PMID: 20819943.
116. DeVries S.H. Correlated firing in rabbit retinal ganglion cells. Journal of Neurophysiology. 1999;81(2):908–920. PubMed PMID: 10036288.

117. Barlow H.B., Fitzhugh R., Kuffler S.W. Change of organization in the receptive fields of the cat's retina during dark adaptation. The Journal of Physiology. 1957;137(3):338–354. PubMed PMID: 13463771.
118. Peichl L., Wässle H. The structural correlate of the receptive field centre of alpha ganglion cells in the cat retina. The Journal of Physiology. 1983;341:309–324. PubMed PMID: 6620182.
119. Muller J.F., Dacheux R.F. Alpha ganglion cells of the rabbit retina lose antagonistic surround responses under dark adaptation. Visual Neuroscience. 1997;14(2):395–401. PubMed PMID: 9147490.
120. Trong P.K., Rieke F. Origin of correlated activity between parasol retinal ganglion cells. Nature Neuroscience. 2008;11(11):1343–1351. PubMed PMID: 18820692.
121. Nelson R. AII amacrine cells quicken time course of rod signals in the cat retina. Journal of Neurophysiology. 1982;47(5):928–947. PubMed PMID: 6177841.
122. Völgyi B., Deans M.R., Paul D.L., Bloomfield S.A. Convergence and segregation of the multiple rod pathways in mammalian retina. The Journal of Neuroscience: The Official Journal of the Society for Neuroscience. 2004;24(49):11182–11192. PubMed PMID: 15590935.
123. Ivanova E., Müller U., Wässle H. Characterization of the glycinergic input to bipolar cells of the mouse retina. The European Journal of Neuroscience. 2006;23(2):350–364. PubMed PMID: 16420443.
124. Münch T.A., da Silveira R.A., Siegert S., Viney T.J., Awatramani G.B., Roska B. Approach sensitivity in the retina processed by a multifunctional neural circuit. Nature Neuroscience. 2009;12(10):1308–1316. PubMed PMID: 19734895.
125. Trexler E.B., Li W., Massey S.C. Simultaneous contribution of two rod pathways to AII amacrine and cone bipolar cell light responses. Journal of Neurophysiology. 2005;93(3):1476–1485. PubMed PMID: 15525810.
126. Abd-El-Barr M.M., Pennesi M.E., Saszik S.M., Barrow A.J., Lem J., Bramblett D.E., Paul D.L., Frishman L.J., Wu S.M. Genetic dissection of rod and cone pathways in the dark-adapted mouse retina. Journal of Neurophysiology. 2009;102(3):1945–1955. PubMed PMID: 19587322.
127. Soucy E., Wang Y., Nirenberg S., Nathans J., Meister M. A novel signaling pathway from rod photoreceptors to ganglion cells in mammalian retina. Neuron. 1998;21(3):481–493. PubMed PMID: 9768836.
128. Li W., Keung J.W., Massey S.C. Direct synaptic connections between rods and OFF cone bipolar cells in the rabbit retina. The Journal of Comparative Neurology. 2004;474(1):1–12. PubMed PMID: 15156575.
129. Murphy G.J., Rieke F. Electrical synaptic input to ganglion cells underlies differences in the output and absolute sensitivity of parallel retinal circuits. The Journal of Neuroscience: The Official Journal of the Society for Neuroscience. 2011;31(34):12218–12228. PubMed PMID: 21865465.
130. Fain G.L. Quantum sensitivity of rods in the toad retina. Science (New York, N.Y.). 1975;187(4179):838–841. PubMed PMID: 1114328.
131. Lamb T.D., Simon E.J. The relation between intercellular coupling and electrical noise in turtle photoreceptors. The Journal of Physiology. 1976;263(2):257–286. PubMed PMID: 1018249.
132. Tessier-Lavigne M., Attwell D. The effect of photoreceptor coupling and synapse nonlinearity on signal:noise ratio in early visual processing. Proceedings of the Royal Society of London. Series B, Biological Sciences. 1988;234(1275):171–197. PubMed PMID: 2905460.
133. Attwell D., Borges S., Wu S.M., Wilson M. Signal clipping by the rod output synapse. Nature. 1987;328(6130):522–524. PubMed PMID: 3039370.
134. Connors B.W., Long M.A. Electrical synapses in the mammalian brain. Annual Review of Neuroscience. 2004;27:393–418. PubMed PMID: 15217338.
135. Pereda A.E., Curti S., Hoge G., Cachope R., Flores C.E., Rash J.E. Gap junction-mediated electrical transmission: regulatory mechanisms and plasticity. Biochimica Et Biophysica Acta. 2013;1828(1):134–146. PubMed PMID: 22659675.
136. Arnett D., Spraker T.E. Cross-correlation analysis of the maintained discharge of rabbit retinal ganglion cells. The Journal of Physiology. 1981;317:29–47. PubMed PMID: 7310736.
137. Mastronarde D.N. Correlated firing of cat retinal ganglion cells. I. Spontaneously active inputs to X- and Y-cells. Journal of Neurophysiology. 1983;49(2):303–324. PubMed PMID: 6300340.

138. Mastronarde D.N. Correlated firing of cat retinal ganglion cells. II. Responses of X- and Y-cells to single quantal events. Journal of Neurophysiology. 1983;49(2):325–349. PubMed PMID: 6300341.
139. Mastronarde D.N. Interactions between ganglion cells in cat retina. Journal of Neurophysiology. 1983;49(2):350–365. PubMed PMID: 6300342.
140. Brivanlou I.H., Warland D.K., Meister M. Mechanisms of concerted firing among retinal ganglion cells. Neuron. 1998;20(3):527–539. PubMed PMID: 9539126.
141. Greschner M., Shlens J., Bakolitsa C., Field G.D., Gauthier J.L., Jepson L.H., Sher A., Litke A.M., Chichilnisky E.J. Correlated firing among major ganglion cell types in primate retina. The Journal of Physiology. 2011;589(Pt 1):75–86. PubMed PMID: 20921200.
142. Völgyi B., Pan F., Paul D.L., Wang J.T., Huberman A.D., Bloomfield S.A. Gap junctions are essential for generating the correlated spike activity of neighboring retinal ganglion cells. PloS One. 2013;8(7):e69426. PubMed PMID: 23936012.
143. Trenholm S., McLaughlin A.J., Schwab D.J., Turner M.H., Smith R.G., Rieke F., Awatramani G.B. Nonlinear dendritic integration of electrical and chemical synaptic inputs drives fine-scale correlations. Nature Neuroscience. 2014;17(12):1759–1766. PubMed PMID: 25344631.
144. Mastronarde D.N. Correlated firing of retinal ganglion cells. Trends in Neurosciences. 1989;12(2):75–80. PubMed PMID: 2469215.
145. Schnitzer M.J., Meister M. Multineuronal firing patterns in the signal from eye to brain. Neuron. 2003;37(3):499–511. PubMed PMID: 12575956.
146. Bennett M.V.L., Zukin R.S. Electrical Coupling and Neuronal Synchronization in the Mammalian Brain. Neuron. 2004;41(4):495–511. PubMed PMID: 14980200.
147. Oesch N., Euler T., Taylor W.R. Direction-selective dendritic action potentials in rabbit retina. Neuron. 2005;47(5):739–750. PubMed PMID: 16129402.
148. Sivyer B., Williams S.R. Direction selectivity is computed by active dendritic integration in retinal ganglion cells. Nature Neuroscience. 2013;16(12):1848–1856. PubMed PMID: 24162650.
149. Oyster C.W., Barlow H.B. Direction-selective units in rabbit retina: distribution of preferred directions. Science (New York, N.Y.). 1967;155(3764):841–842. PubMed PMID: 6019094.
150. Xu Z., Zeng Q., Shi X., He S. Changing coupling pattern of The ON-OFF direction-selective ganglion cells in early postnatal mouse retina. Neuroscience. 2013;250:798–808. PubMed PMID: 23791968.
151. Usrey W.M., Reppas J.B., Reid R.C. Paired-spike interactions and synaptic efficacy of retinal inputs to the thalamus. Nature. 1998;395(6700):384–387. PubMed PMID: 9759728.
152. Carandini, M., J.C. Horton, and L.C. Sincich, *Thalamic filtering of retinal spike trains by postsynaptic summation.* Journal of Vision. 2007; 7(14):20.1-11.
153. Cleland B.G., Dubin M.W., Levick W.R. Simultaneous recording of input and output of lateral geniculate neurones. Nature: New Biology. 1971;231(23):191–192. PubMed PMID: 4325715.
154. Chen C., Regehr W.G. Developmental remodeling of the retinogeniculate synapse. Neuron. 2000;28(3):955–966. PubMed PMID: 11163279.
155. Morgan J.L., Berger D.R., Wetzel A.W., Lichtman J.W. The Fuzzy Logic of Network Connectivity in Mouse Visual Thalamus. Cell. 2016;165(1):192–206. PubMed PMID: 27015312.
156. Rompani S.B., Müllner F.E., Wanner A., Zhang C., Roth C.N., Yonehara K., Roska B. Different Modes of Visual Integration in the Lateral Geniculate Nucleus Revealed by Single-Cell-Initiated Transsynaptic Tracing. Neuron. 2017;93(4):767–776.e6. PubMed PMID: 28231464.
157. Meister M., Lagnado L., Baylor D.A. Concerted signaling by retinal ganglion cells. Science (New York, N.Y.). 1995;270(5239):1207–1210. PubMed PMID: 7502047.
158. Xiao L., Zhang M., Xing D., Liang P.-J., Wu S. Shifted encoding strategy in retinal luminance adaptation: from firing rate to neural correlation. Journal of Neurophysiology. 2013;110(8):1793–1803. PubMed PMID: 23864383.
159. Ackert J.M., Wu S.H., Lee J.C., Abrams J., Hu E.H., Perlman I., Bloomfield S.A. Light-induced changes in spike synchronization between coupled ON direction selective ganglion cells in the mammalian retina. The

Journal of Neuroscience: The Official Journal of the Society for Neuroscience. 2006;26(16):4206–4215. PubMed PMID: 16624941.
160. Neuenschwander S., Singer W. Long-range synchronization of oscillatory light responses in the cat retina and lateral geniculate nucleus. Nature. 1996;379(6567):728–732. PubMed PMID: 8602219.
161. Roy K., Kumar S., Bloomfield S.A. Gap junctional coupling between retinal amacrine and ganglion cells underlies coherent activity integral to global object perception. Proceedings of the National Academy of Sciences of the United States of America. 2017;114(48):E10484–E10493. PubMed PMID: 29133423.
162. Manookin M.B., Patterson S.S., Linehan C.M. Neural Mechanisms Mediating Motion Sensitivity in Parasol Ganglion Cells of the Primate Retina. Neuron. 2018;97(6):1327–1340.e4. PubMed PMID: 29503188.
163. Murphy-Baum B.L., Awatramani G.B. An Old Neuron Learns New Tricks: Redefining Motion Processing in the Primate Retina. Neuron. 2018;97(6):1205–1207. PubMed PMID: 29566789.
164. Berry M.J., Brivanlou I.H., Jordan T.A., Meister M. Anticipation of moving stimuli by the retina. Nature. 1999;398(6725):334–338. PubMed PMID: 10192333.
165. Johnston J., Lagnado L. General features of the retinal connectome determine the computation of motion anticipation. eLife. 2015.:4. PubMed PMID: 25786068.
166. Trenholm S., Schwab D.J., Balasubramanian V., Awatramani G.B. Lag normalization in an electrically coupled neural network. Nature Neuroscience. 2013;16(2):154–156. PubMed PMID: 23313908.
167. Ball W., Tronick E. Infant responses to impending collision: optical and real. Science (New York, N.Y.). 1971;171(3973):818–820. PubMed PMID: 5541165.
168. Ishikane H., Gangi M., Honda S., Tachibana M. Synchronized retinal oscillations encode essential information for escape behavior in frogs. Nature Neuroscience. 2005;8(8):1087–1095. PubMed PMID: 15995702.
169. King S.M., Dykeman C., Redgrave P., Dean P. Use of a distracting task to obtain defensive head movements to looming visual stimuli by human adults in a laboratory setting. Perception. 1992;21(2):245–259. PubMed PMID: 1513673.
170. Schiff W., Caviness J.A., Gibson J.J. Persistent fear responses in rhesus monkeys to the optical stimulus of "looming". Science (New York, N.Y.). 1962;136(3520):982–983. PubMed PMID: 14498362.
171. Temizer I., Donovan J.C., Baier H., Semmelhack J.L. A Visual Pathway for Looming-Evoked Escape in Larval Zebrafish. Current biology: CB. 2015;25(14):1823–1834. PubMed PMID: 26119746.
172. Yilmaz M., Meister M. Rapid innate defensive responses of mice to looming visual stimuli. Current biology: CB. 2013;23(20):2011–2015. PubMed PMID: 24120636.
173. Biswas S., Haselier C., Mataruga A., Thumann G., Walter P., Müller F. Pharmacological analysis of intrinsic neuronal oscillations in rd10 retina. PloS One. 2014;9(6):e99075. PubMed PMID: 24918437.
174. Borowska J., Trenholm S., Awatramani G.B. An intrinsic neural oscillator in the degenerating mouse retina. The Journal of Neuroscience: The Official Journal of the Society for Neuroscience. 2011;31(13):5000–5012. PubMed PMID: 21451038.
175. Margolis D.J., Newkirk G., Euler T., Detwiler P.B. Functional stability of retinal ganglion cells after degeneration-induced changes in synaptic input. The Journal of Neuroscience: The Official Journal of the Society for Neuroscience. 2008;28(25):6526–6536. PubMed PMID: 18562624.
176. Menzler J., Zeck G. Network oscillations in rod-degenerated mouse retinas. The Journal of Neuroscience: The Official Journal of the Society for Neuroscience. 2011;31(6):2280–2291. PubMed PMID: 21307264.
177. Stasheff S.F. Emergence of sustained spontaneous hyperactivity and temporary preservation of OFF responses in ganglion cells of the retinal degeneration (rd1) mouse. Journal of Neurophysiology. 2008;99(3):1408–1421. PubMed PMID: 18216234.
178. Stasheff S.F., Shankar M., Andrews M.P. Developmental time course distinguishes changes in spontaneous and light-evoked retinal ganglion cell activity in rd1 and rd10 mice. Journal of Neurophysiology. 2011;105(6):3002–3009. PubMed PMID: 21389300.
179. Yee C.W., Toychiev A.H., Sagdullaev B.T. Network deficiency exacerbates impairment in a mouse model of retinal degeneration. Frontiers in Systems Neuroscience. 2012;6:8. PubMed PMID: 22383900.

180. Lepore F.E. Spontaneous visual phenomena with visual loss: 104 patients with lesions of retinal and neural afferent pathways. Neurology. 1990;40(3 Pt 1):444–447. PubMed PMID: 2314586.
181. Murtha T., Stasheff S.F. Visual dysfunction in retinal and optic nerve disease. Neurologic Clinics. 2003;21(2):445–481. PubMed PMID: 12916487.
182. Weiland J.D., Humayun M.S. Retinal prosthesis. IEEE transactions on bio-medical engineering. 2014;61(5):1412–1424. PubMed PMID: 24710817.
183. Busskamp V., Picaud S., Sahel J.A., Roska B. Optogenetic therapy for retinitis pigmentosa. Gene Therapy. 2012;19(2):169–175. PubMed PMID: 21993174.
184. Yee C.W., Toychiev A.H., Ivanova E., Sagdullaev B.T. Aberrant synaptic input to retinal ganglion cells varies with morphology in a mouse model of retinal degeneration. The Journal of Comparative Neurology. 2014;522(18):4085–4099. PubMed PMID: 25099614.
185. Sekirnjak C., Jepson L.H., Hottowy P., Sher A., Dabrowski W., Litke A.M., Chichilnisky E.J. Changes in physiological properties of rat ganglion cells during retinal degeneration. Journal of Neurophysiology. 2011;105(5):2560–2571. PubMed PMID: 21389304.
186. Trenholm S., Borowska J., Zhang J., Hoggarth A., Johnson K., Barnes S., Lewis T.J., Awatramani G.B. Intrinsic oscillatory activity arising within the electrically coupled AII amacrine-ON cone bipolar cell network is driven by voltage-gated Na+ channels. The Journal of Physiology. 2012;590(10):2501–2517. PubMed PMID: 22393249.
187. Ivanova E., Yee C.W., Baldoni R., Sagdullaev B.T. Aberrant activity in retinal degeneration impairs central visual processing and relies on Cx36-containing gap junctions. Experimental Eye Research. 2016;150:81–89. PubMed PMID: 26005040.
188. Telias, M., B. Denlinger, Z. Helft, C. Thornton, B. Beckwith-Cohen, and R.H. Kramer, *Retinoic Acid Induces Hyperactivity, and Blocking Its Receptor Unmasks Light Responses and Augments Vision in Retinal Degeneration.* Neuron. 2019; 102(3):574-586. e5.
189. Choi H., Zhang L., Cembrowski M.S., Sabottke C.F., Markowitz A.L., Butts D.A., Kath W.L., Singer J.H., Riecke H. Intrinsic bursting of AII amacrine cells underlies oscillations in the rd1 mouse retina. Journal of Neurophysiology. 2014;112(6):1491–1504. PubMed PMID: 25008417.
190. Ivanova E., Yee C.W., Sagdullaev B.T. Increased phosphorylation of Cx36 gap junctions in the AII amacrine cells of RD retina. Frontiers in Cellular Neuroscience. 2015;9:390. PubMed PMID: 26483638.
191. Cook J.E., Becker D.L. Gap-junction proteins in retinal development: new roles for the "nexus". Physiology (Bethesda, Md.). 2009;24:219–230. PubMed PMID: 19675353.
192. Akopian A., Atlasz T., Pan F., Wong S., Zhang Y., Völgyi B., Paul D.L., Bloomfield S.A. Gap junction-mediated death of retinal neurons is connexin and insult specific: a potential target for neuroprotection. The Journal of Neuroscience: The Official Journal of the Society for Neuroscience. 2014;34(32):10582–10591. PubMed PMID: 25100592.
193. Kranz K., Paquet-Durand F., Weiler R., Janssen-Bienhold U., Dedek K. Testing for a gap junction-mediated bystander effect in retinitis pigmentosa: secondary cone death is not altered by deletion of connexin36 from cones. PloS One. 2013;8(2):e57163. PubMed PMID: 23468924.
194. Paschon V., Higa G.S.V., Resende R.R., Britto L.R.G., Kihara A.H. Blocking of connexin-mediated communication promotes neuroprotection during acute degeneration induced by mechanical trauma. PloS One. 2012;7(9):e45449. PubMed PMID: 23029016.
195. Striedinger K., Petrasch-Parwez E., Zoidl G., Napirei M., Meier C., Eysel U.T., Dermietzel R. Loss of connexin36 increases retinal cell vulnerability to secondary cell loss. The European Journal of Neuroscience. 2005;22(3):605–616. PubMed PMID: 16101742.
196. Arroyo D.A., Kirkby L.A., Feller M.B. Retinal Waves Modulate an Intraretinal Circuit of Intrinsically Photosensitive Retinal Ganglion Cells. The Journal of Neuroscience: The Official Journal of the Society for Neuroscience. 2016;36(26):6892–6905. PubMed PMID: 27358448.
197. Trenholm, S. and G.B. Awatramani, *Chapter 9 - Dynamic Properties of Electrically Coupled Retinal Networks*, in *Network Functions and Plasticity*, J. Jing, Editor. 2017, Academic Press. p. 183-208.

198. Baldridge W.H. Triphasic adaptation of teleost horizontal cells. Progress in Brain Research. 2001;131:437–449. PubMed PMID: 11420961.
199. Veruki M.L., Hartveit E. Electrical synapses mediate signal transmission in the rod pathway of the mammalian retina. The Journal of Neuroscience: The Official Journal of the Society for Neuroscience. 2002;22(24):10558–10566. PubMed PMID: 12486148.
200. Bloomfield S.A., Xin D., Osborne T. Light-induced modulation of coupling between AII amacrine cells in the rabbit retina. Visual Neuroscience. 1997;14(3):565–576. PubMed PMID: 9194323.
201. Schubert T., Degen J., Willecke K., Hormuzdi S.G., Monyer H., Weiler R. Connexin36 mediates gap junctional coupling of alpha-ganglion cells in mouse retina. The Journal of Comparative Neurology. 2005;485(3):191–201. PubMed PMID: 15791644.
202. Lanore F., Silver R.A. Reading dendritic activity with gap junctions. Nature Neuroscience. 2014;17(12):1625–1627. PubMed PMID: 25413085.
203. Trenholm S., Awatramani G.B. Origins of spontaneous activity in the degenerating retina. Frontiers in Cellular Neuroscience. 2015;9:277. PubMed PMID: 26283914.

Neuroactive Substances in the Retina

Neurotransmitters in the Retina

Helga Kolb

Created: May 1, 2005; Updated: June 1, 2009.

General Characteristics

Today's research on the retina focuses a great deal of attention on neurotransmission between the neurons of the retina. Various techniques using autoradiography, immunocytochemistry and molecular biology are being used to mark neurons for neurochemicals, their synthesizing enzymes, calcium binding proteins and receptors and transporters of these neurochemicals. Cells immunostained with antibodies to the various neurotransmitter candidates give particularly spectacular images by confocal microscopy because they become stained to their finest dendrites and so can be readily classified against their Golgi-stained equivalents. Furthermore, the whole population of neurotransmitter specific neurons are stained so one can understand their topographical organization into mosaics across the entire retina. Some immunocytochemistry for the common neurotransmitter candidates has been performed on the human retina (1, 2) but most have been done in the cat, rabbit and mouse retinas and so far the findings are the same in general. The consistency of cell types staining across species boundaries, in mammals at least, suggest that most, with a few exceptions, of the neurotransmitters, neuromodulators and neuropeptides discovered in nonhuman retinas are present in human retina too.

The Neurotransmitter of Neurons of the Vertical Pathways through the Retina is Glutamate

Glutamate is the neurotransmitter of the neurons of the vertical pathways through the retina. All photoreceptor types, rods and cones, use the excitatory amino acid glutamate to transmit signals to the next order neuron in the chain (see chapter on glutamate and Massey (3) for review). There was originally some evidence for the closely related amino acid, aspartate, being present in rods but the later sophisticated techniques of demonstrating amino acid signatures in retinal neurons cannot confirm aspartate as a retinal neurotransmitter at all (4). Uptake, release and action of glutamate and agonists upon second-order neurons in slice preparations or isolated cells in tissue culture have also all confirmed glutamate to be the neurotransmitter acting at the first synapse in the retina (see Lasater and Lam (5) for review). The action of the photoreceptor neurotransmitter upon the second-order neurons is through two different types of sensory channels though. The one type of postsynaptic receptor type is the metabotropic glutamate channel (mGluR6) that involves a second messenger cascade and cyclic GMP for activation of the channel (in the ON-center bipolar cell) whereas the other is an ionotropic channel via at least two types of AMPA receptors and Na ions (OFF-center bipolar and horizontal cells) (6-9). Photoreceptors in most vertebrates including human, havea content of D2 dopamine receptors somewhere upon there surface (10).

Glutamate is also considered to be the neurotransmitter of all bipolar cells and most ganglion cells in the vertebrate retina including the monkey retina (Kalloniatis and Marc, personal communication and Marc et. al. (4)). In an immunocytochemical study of the human retina a similar conclusion was drawn by us. All the ganglion cells appeared to label strongly with antibodies to glutamate (2) (see Fig. 1).

Bipolar cells have receptor channels that are either of the metabotropic type, mGluR6,(APB sensitive) or ionotropic type (AMPA) at their dendrites in the OPL, while their axonal ending in the IPL have channels and receptors for GABA (A, B and C types), D1 dopamine and glycine because, of course, all kinds of amacrine cells are presynaptic at these sites in the IPL neuropil. Ganglion cells are as diverse in receptor sensors as the bipolar cells with the addition of receptors to acetylcholine (11), and the first appearance in the retina of NMDA glutamate receptors that are typical in the brain (12, 13).

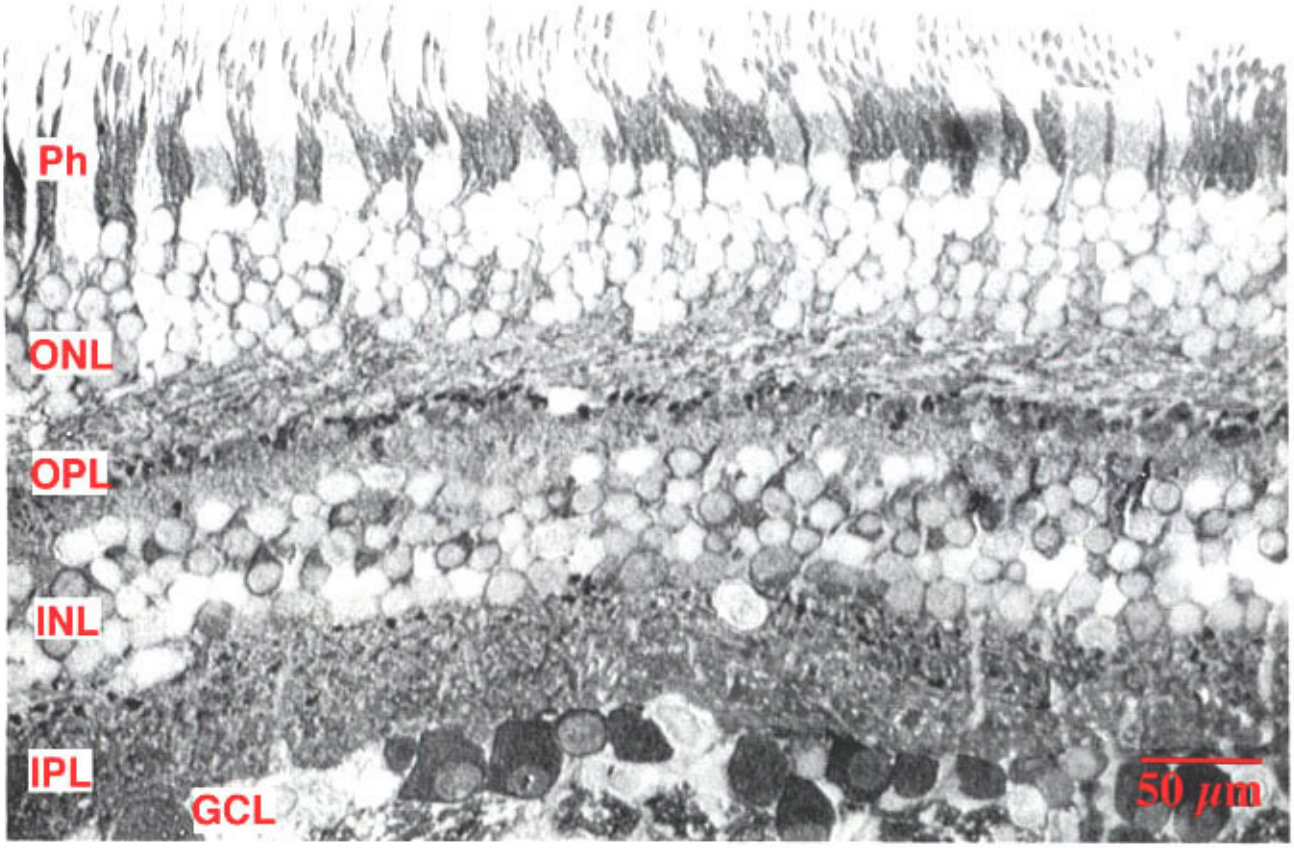

Figure 1. Distribution of Glutamate immunoreactivity in human retina.

Amacrine cells

Recently an amacrine cell type has also been shown to contain the glutamate transporter, vesicular glutamate transporter 3, shortened to VGLUT3 (14, 15). VGLUTs are used to concentrate cystolic glutamate into the synaptic vesicles. Typically in the retina the VGLUT1 isoform is expressed in photoreceptors and bipolar cells and the VGLUT2 in ganglion cells. The amacrine cell type that can be immunostained to the antibody to VGLUT3 is found to be a small-field amacrine cell with varicose processes that are restricted in branching to the OFF laminae (S1 and S2) of the IPL (Fig. 2A). It is also immunoreactive to the transmitter glycine as seen in Fig. 2, B and C, but not reactive for GABA, dopamine (Fig. 3, A-C) or acetylcholine. Fig. 3, A-C, shows that the dopamine cell and its dendrites run above the branches of the VGLUT3 cell and indeed appear to be able to make synaptic contact with the cell bodies of the latter cell type, in the way we know dopamine cell processes do (see below and amacrine cell chapter). The VGLUT3 amacrines appear to be in a good position to interact with OFF center ganglion cell, stained for MAP-1, dendrites as shown in Fig. 3, D-F.

Electron microscopy of VGLUT3 dendrites in the IPL, indicate that they are postsynaptic to OFF cone bipolar cell axons (Fig. 4B) and presynaptic to OFF ganglion cell dendrites (Fig. 4A).

Recent evidence from the metabolic mapping technique of Marc and Jones (16) indicates that a dopaminergic amacrine cell type also has a content of glutamate. However, from the above evidence on VGLUT3 immunostaining it is clear that the dopaminergic type 1 cell does not use that particular vesicular glutamate transporter.

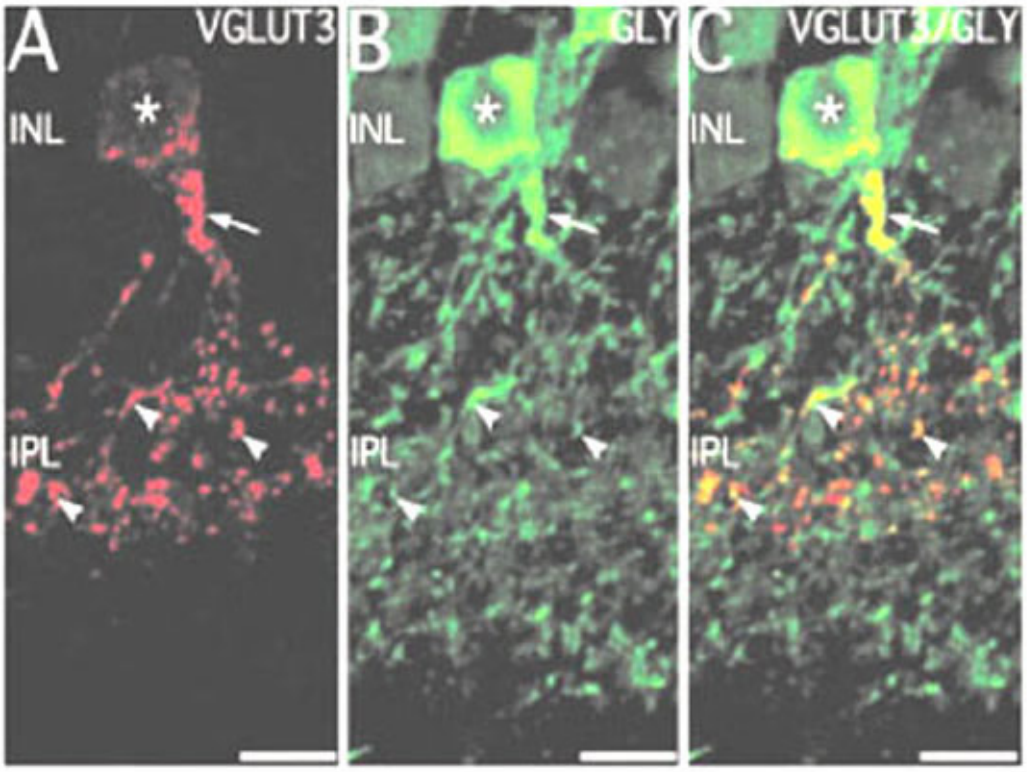

Figure 2. VGLUT3 immunostaining (A, red) shows a small-field amacrine cell. It also Immunostains for glycine (B,C).

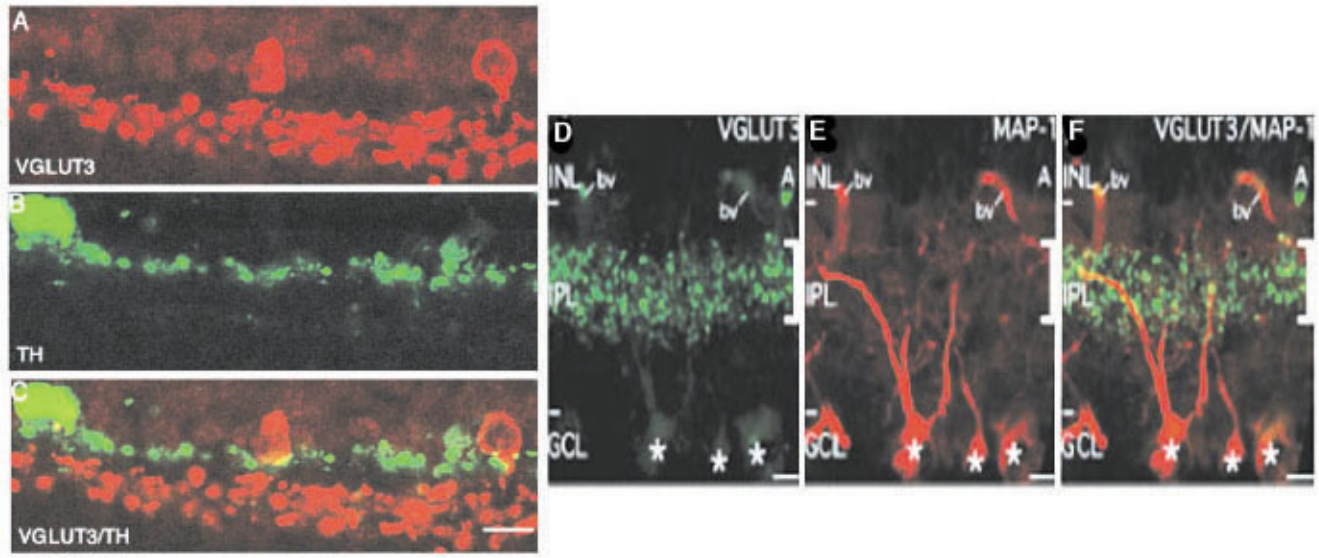

Figure 3. A-C, VGLUT3 cell has dendritic branching in S1 and S2. Dopamine cells branch above the main plexus of the VGLUT3 cell. D-F, The MAP-1 ganglion cells (red) branch in the same layers as the dendrites of the VGLUT3 cell.

Gamma Aminobutyric Acid

The classical inhibitory neurotransmitter gamma aminobutyric acid (GABA) occurs in many different varieties of amacrine cells, and in one or more classes of horizontal cell in most vertebrate retinas (4). There is still some controversy over whether GABA is contained within horizontal cells in monkey and human retina.

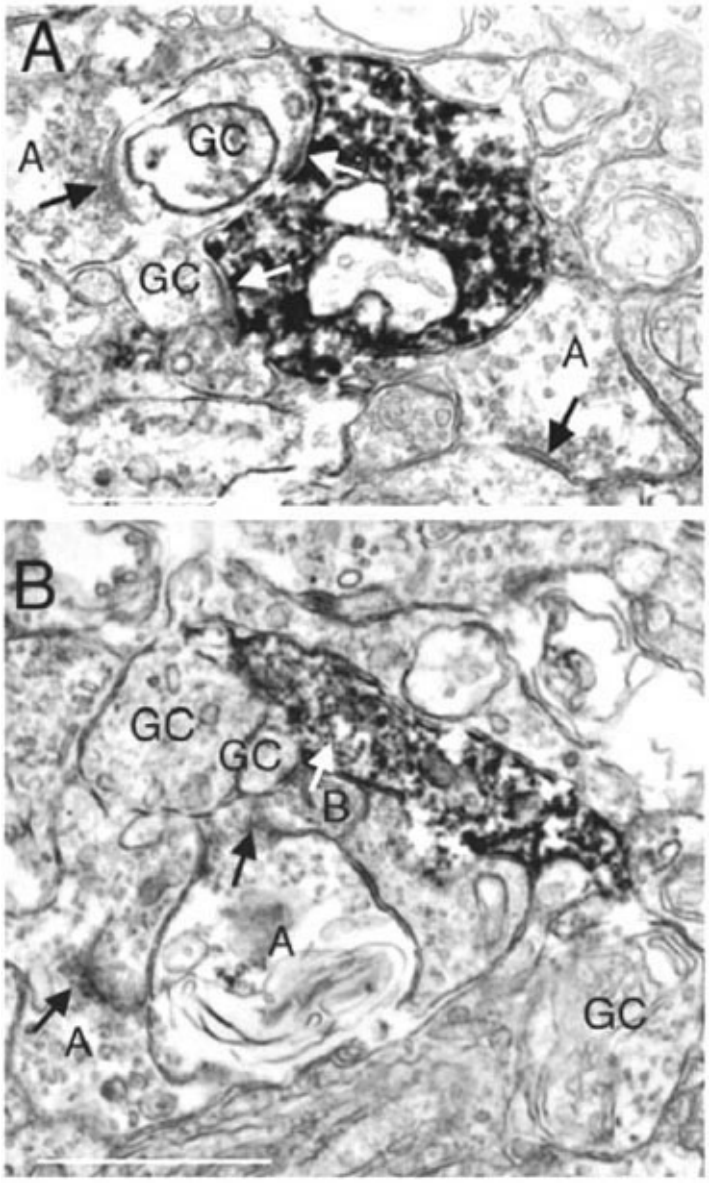

Figure 4. Electron microscopy of VGLUT3 immunostained processes in the IPL of the rat retina.

In this figure (Fig. 5a) taken from human peripheral retina, it can be seen that there is heavy staining with antibodies to GABA in the inner plexiform layer (three heavier bands can be discerned) and in about half of the amacrine cell bodies in the lower row of amacrine cells in the inner nuclear layer. Some displaced amacrines and interplexiform cells are also revealed with GABA immunocytochemistry (2). However, the horizontal cells are not stained at all in peripheral retina although they are in foveal retina apparently (Cuenca, personal communication).

A valuable identification of individual cell types that contain GABA has come from double staining techniques upon Golgi stained cell types (17). The amacrine cell that are contain GABA are all of the large-field types. Thus we know now that A10, A13, A17, A19, and the interplexiform cell accumulate GABA and probably use it as their primary neurotransmitter (Fig. 5b). Many large field amacrine cells also colocalize GABA with another neurotransmitter. Thus the GABAergic A17 colocalizes serotonin, the acetylcholine (starburst amacrine) colocalizes GABA and so does the dopamine A18 cell (18). Neuropetides (see later) are also commonly colocalized with GABA i.e. substance P in A22 is almost certainly the secondary transmitter to GABA as the primary. GABAergic amacrine cells and IPCs act upon bipolar, amacrine and ganglion cell processes or cell

bodies in the neuropils of the retina via all the three varieties of GABA receptors (a, b and c types). It appears clear that A17 type or the type that makes reciprocal synapse with the rod bipolar axon terminal uses a GABAc receptor (see chapter by Haohua Qian) (19). However, for most amacrine cells, what GABA receptors are associated with which morphological or physiological subtype of amacrine cell, still need more elucidation.

Glycine

The other classic inhibitory neurotransmitter glycine, accounts for most of the small-field types of amarine cell. All amacrine cells in the vertebrate retina can be accounted for by the two inhibitory neurotransmitters GABA and glycine (4). In addition one or more types of bipolar cell are also thought to contain glycine in mammalian retinas including monkey and human.

In Fig. 6 it can be seen that the immunostaining for glycine is just as strong in the inner plexiform layer as GABA staining. About the same number of amacrine cells are revealed. However there is an addition of some small bipolar cell bodies in the inner nuclear layer and the occasional large cell body of a ganglion cell type in the ganglion cell layer (2).

Pourcho and Goebel (20) showed quite clearly that tritiated glycine accumulated in Golgi stained AII, A4, and A8 cells in cat retina. More recently as many as 10 different morphological types of small field amacrine cells have been demonstrated by immunocytochemistry and GFP (green fluorescent protein) staining in mouse retina (21, 22). The A8 cell was the most strongly glycinergic of the small field amacrine cells according to Pourcho and Goebel, with the rod amacrine AII cell being also very clearly glycinergic. Fig. 7 shows the commonest glycinergic amacrine cells present in the mouse retina (22). These cells are presumably also so in the cat and primate retinas.

Glycine receptors are found on all the neurons that are postsynaptic to these glycinergic (all small-field) amacrine cells. Thus receptors are found on certain bipolar cell axons, and on many amacrine and ganglion cell dendrites. Again like for the GABA receptors, linking receptor type to morphological type of postsynaptic cell is still a hot topic for research in the retina (22, 23).

Dopamine Is Present in Amacrine Cells in the Mammalian Retina

The neuromodulator dopamine is found in one or more types of amacrine cell in the mammalian retina. The most robustly stained dopaminergic cell after immunocytochemistry to the rate limiting enzyme of dopamine synthesis, tyrosine hydroxylase (Toh), is recognized as an A18 cell of the Golgi descriptions (24, 25) (Fig. 8).

It is very characteristic in wholemount appearance, with a large cell body and a dense plexus of dendrites in stratum 1 of the inner plexiform layer. Holes or "rings" in the plexus of criss-crossing stained dendrites are sites of amacrine cell bodies or large amacrine dendrites (see chapter on amacrine cells) on which the processes of the Toh stained plexus synapse. The Type 1 dopamine cell (A18) is known to synapse upon the AII rod amacrine cell and possibly also upon A8 and A17 cells (26-29).

A second type of dopamine amacrine cell has also been described in the monkey and human retinas (2, 30). The Type 2 CA cell has dendrites stratifying in stratum 3 of the IPL and in vertical views of Toh processed human retinas these dendrites can be seen quite clearly below those of the Type 1 (A18) dendritic plexus in stratum 1 (orange arrows, Fig. 9).

Type 1 dopamine cells provide ascending processes to the outer plexiform layer (see above) which are known to synapse on the GABAergic interplexiform cell (see previous chapter on feed-back loops).GABA and dopamine colocalize to the A18 cell type (Type 1 CA cell) and serotonin has also been found to co-exist in in the same amacrine cells in cat retina (31).

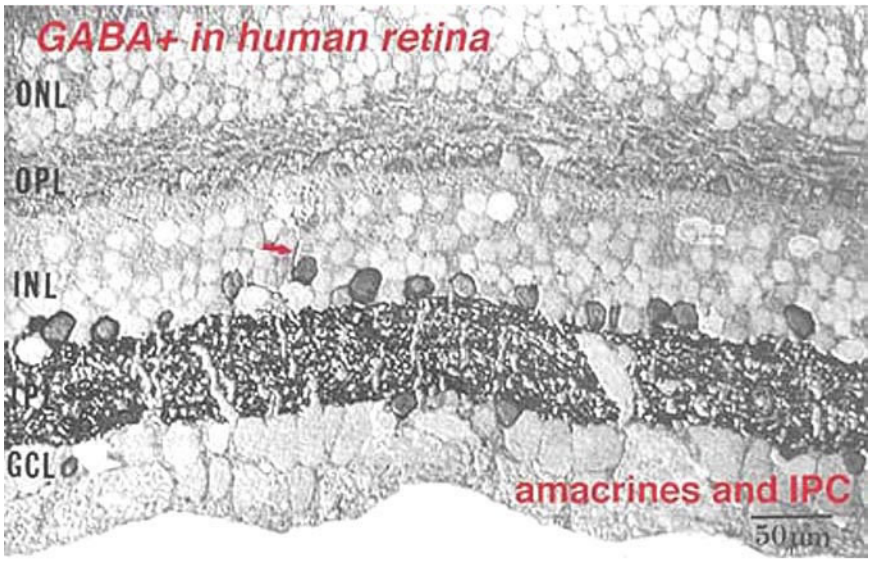

Figure 5a. Expression pattern of GABA immunoreactivity in human retina.

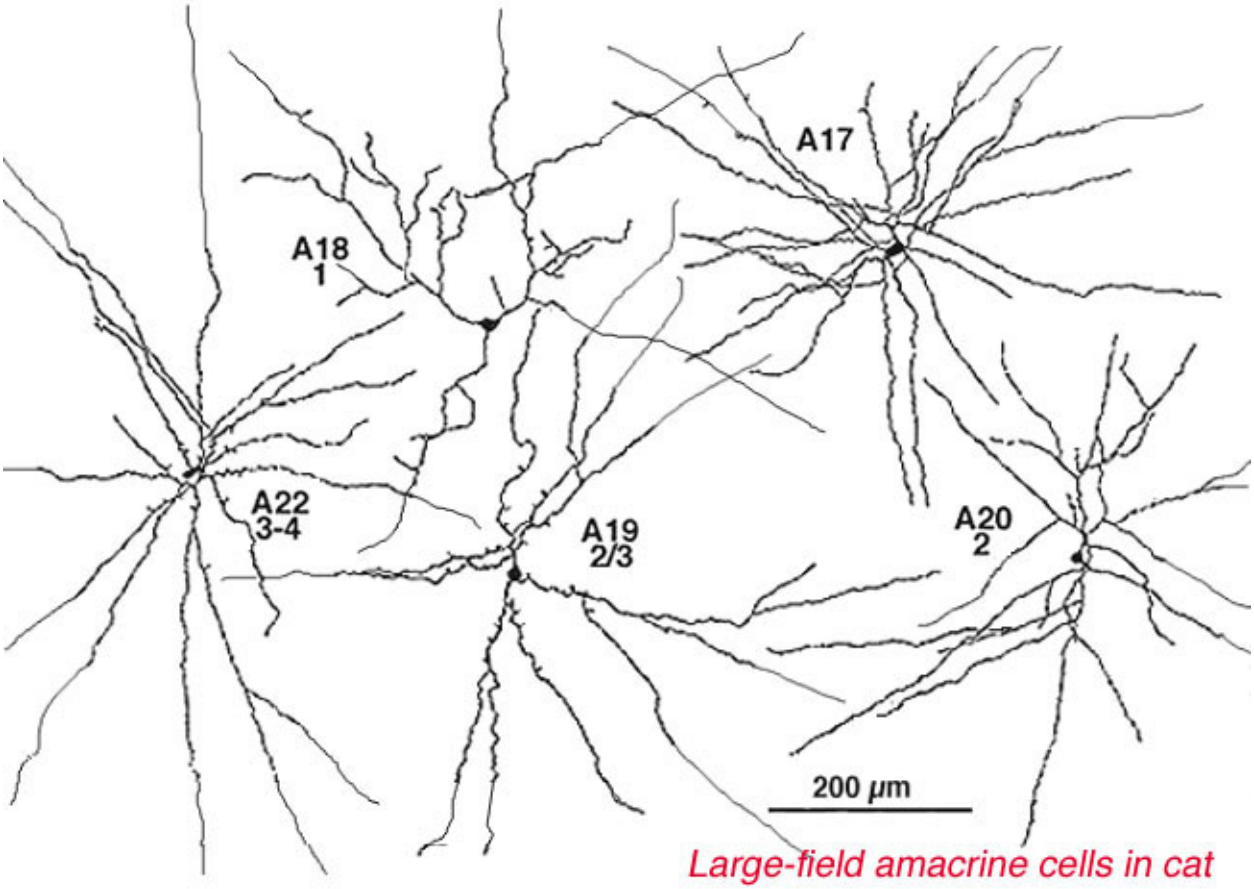

Figure 5b. Large-field amacrine cells in all retinas use gabaergic transmission. Illustration of large-field cell types in cat retina.

Both D1 and D2 receptor types have been found on neurons of the inner and outer retina in many vertebrates. It is thought that the D1 receptor is particularly associated with cells that are coupled by gap junctions, because of dopamine's known action in cyclic AMP regulation of gap junction channels (32). Thus D1 receptors have been

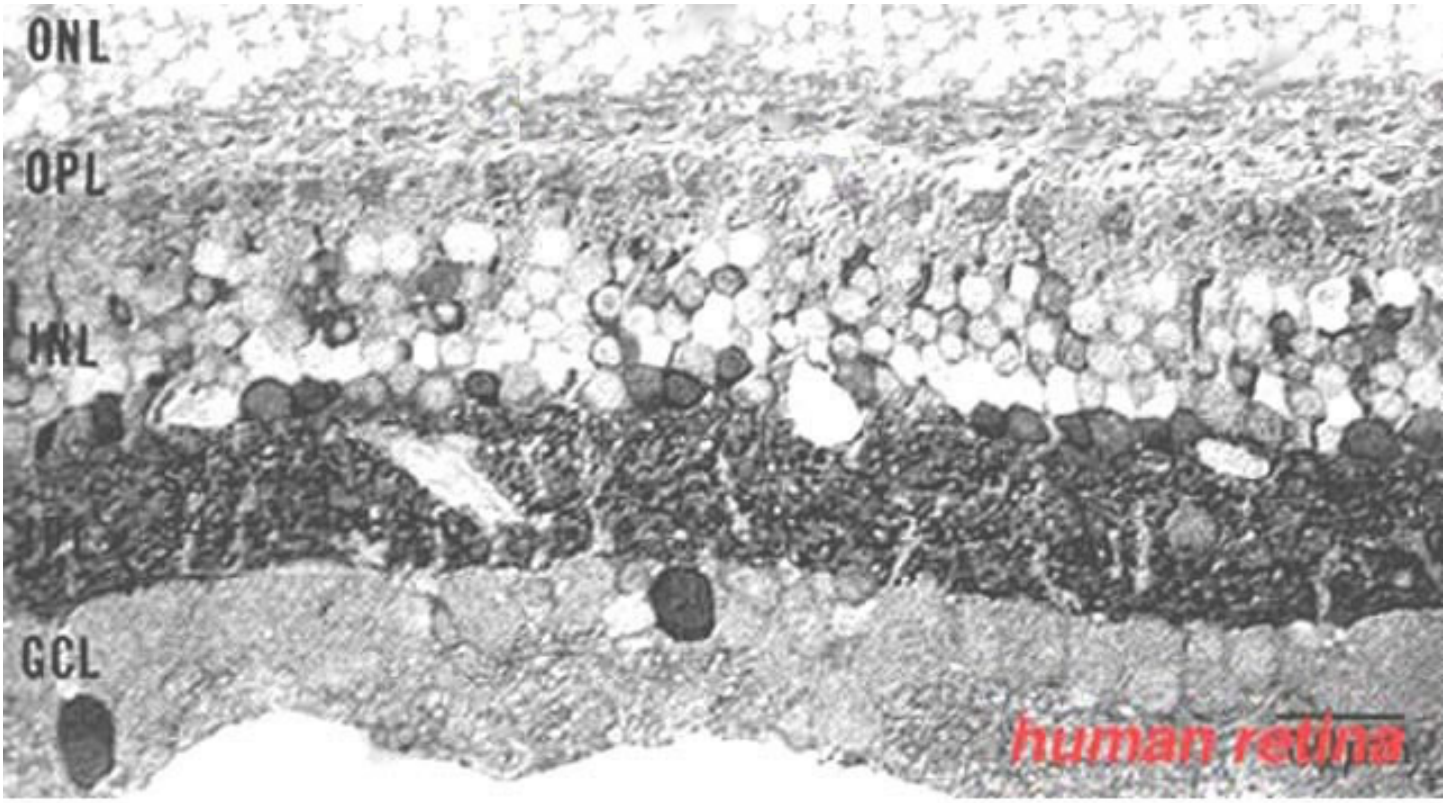

Figure 6. Expression pattern of glycine immunoreactivity in human retina.

demonstrated in association with horizontal cells of the OPL and some amacrine cells of the IPL. D1 receptors are robust on ganglion cell bodies as well (personal observations), despite the fact that the dopamine amacrine cell is not known to make direct synapses upon ganglion cells. D2 receptors are also found in the retina associated with photoreceptors in the outer nuclear layer, outer limiting membrane and retinal pigment epithelium even. Also they are present in the IPL but the target cells in this neuropil are not well understood yet.

Acetylcholine

The classic fast excitatory neurotransmitter of the peripheral nervous system, acetylcholine (ACh), is found in a mirror symmetric pair of amacrine cells in the vertebrate retina. In the rabbit such cells have been named starburst cell (33, 34). One of the mirror pair occurs in the amacrine cell layer with dendrites in sublamina **a** (OFF sublamina of the IPL). The other of the pair has its cell body displaced to the ganglion cell layer and its dendrites stratify in sublamina **b** (ON sublamina of the IPL).

These ACh containing amacrine cells are common to almost all vertebrate retinas and have been described morphologically in human retina too (25, 35) (see previous chapter on amacrine cells). Both muscarinic and nicotinic receptors have been demonstrated in the mammalian retina, particularly associated with transient phasic ganglion cells (Y cells) (36, 37) and effects of ACh and antagonists on ganglion cell responses are documented but not well understood (Fig. 10).

Serotonin

There are two types of serotonin-accumulating amacrine cell in the rabbit retina (38). One of these is almost certainly the A17 cell or the reciprocal amacrine cell of the rod system in the rabbit (see previous chapters) (Fig. 11). However, in cat retina, a completely different amacrine cell type stains with antibodies against serotonin.

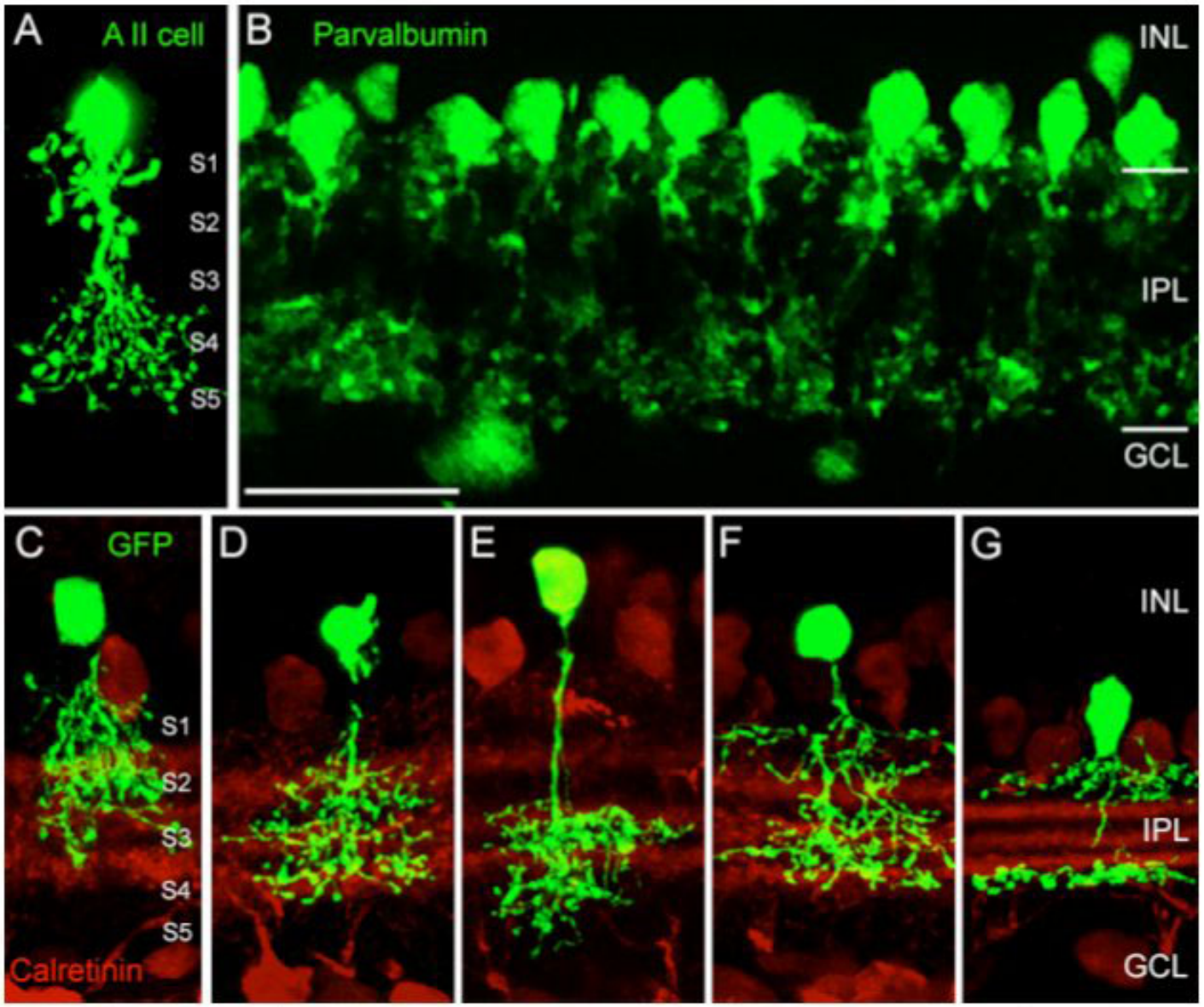

Figure 7. Expression of glycine immunoreactivity in small-field amacrine cells of mouse retina. A-B, aII amacrine cells; C, Type 2 cell (A2 cell); D, Type 3 cells (A4 cell); E, Type 4 cell (A6 cell); F, Type 7 cell (A9? cell): G, A8 cell (Kolb et al. (24)). (Adapted from Waessle et al. (22)).

One cell type in cat is similar to the wide-field cell A20, while the other may be the A18 or dopamine cell (31). Even where serotonin is strongly demonstrated in these amacrine cells in rabbit retina, it is not thought to be the neurotransmitter.

Serotonin co-exists with GABA, in the A17 cell and the latter is thought to be the releasable transmitter (18, 39). A few cold-blooded vertebrates have a bistratified amacrine cell and a bipolar cell type that immunostain for serotonin (40, 41).

Adenosine May Be a Retinal Neurotransmitter

The purine nucleotide, adenosine may be a neurotransmitter or neuromodulator in the mammalian retina. Autoradiography and immunocytochemistry for adenosine has revealed cell bodies in the amacrine and

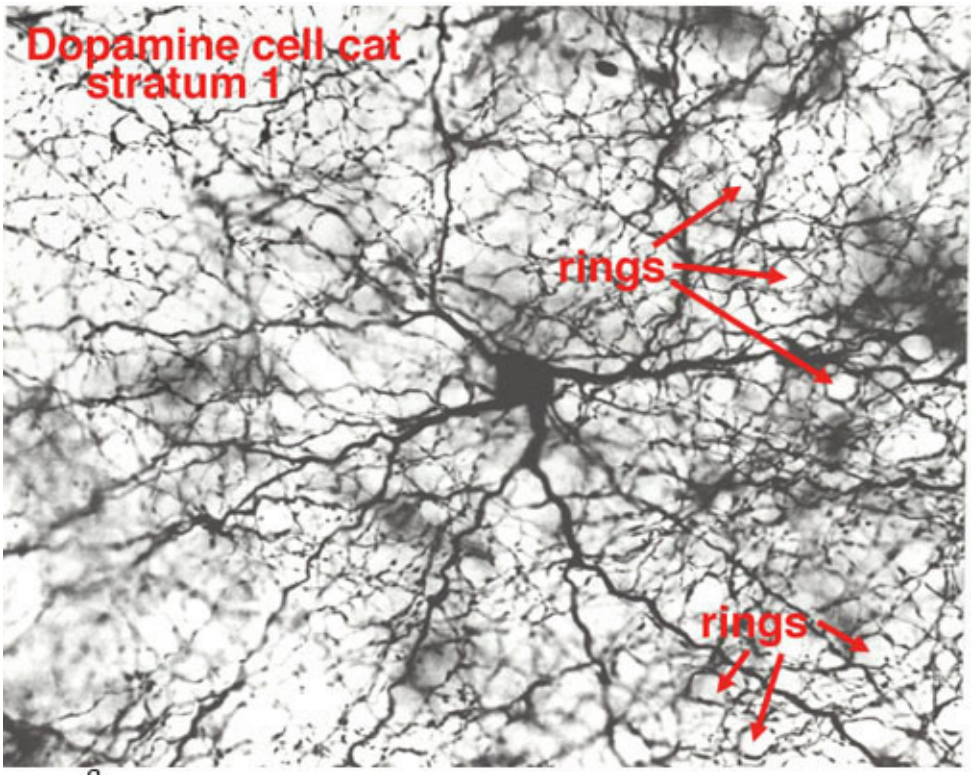

Figure 8. Immunostaining with antibodies to TOH. A18 amacrine cells stain and have overlapping dendrites that form into rings.

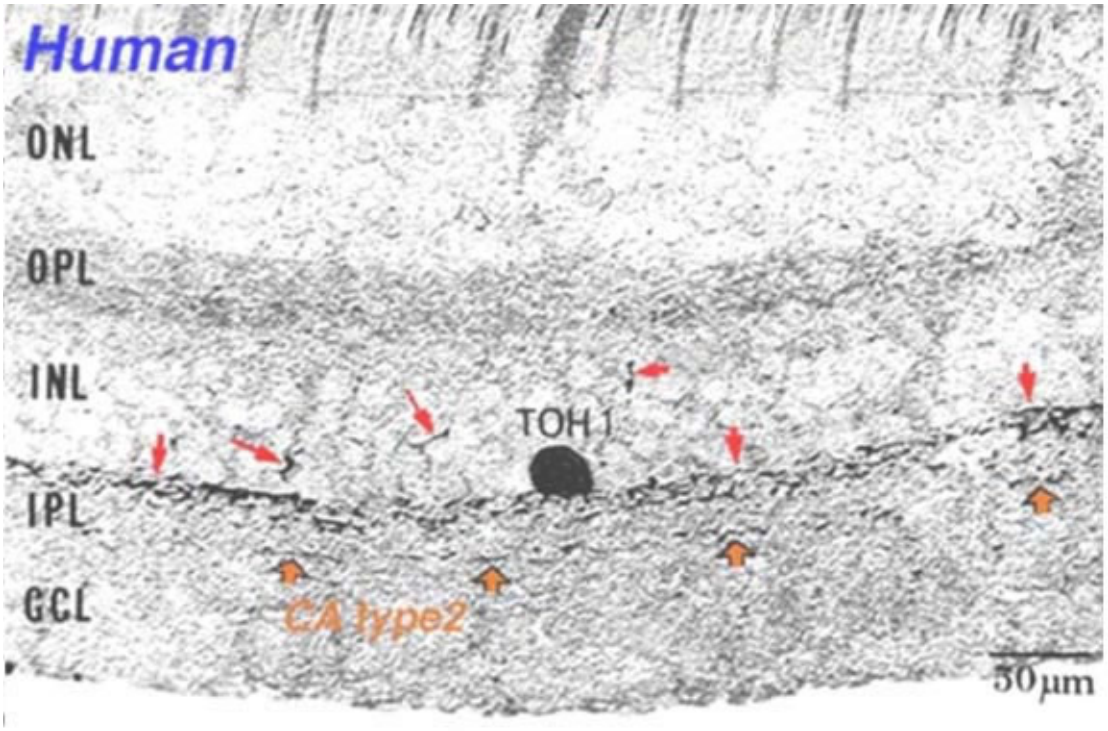

Figure 9. Vertical section of a type 1 TOH+ amacrine cell.

ganglion cell layers (42). Probably most of these cells are amacrine cells but some in the ganglion cell layer may be true ganglion cells. In human retina additional cells that could be bipolar or horizontal cell label too. K+ and light evoked release of adenosine can be measured in rabbit and chick retinas. And the vertical pathway

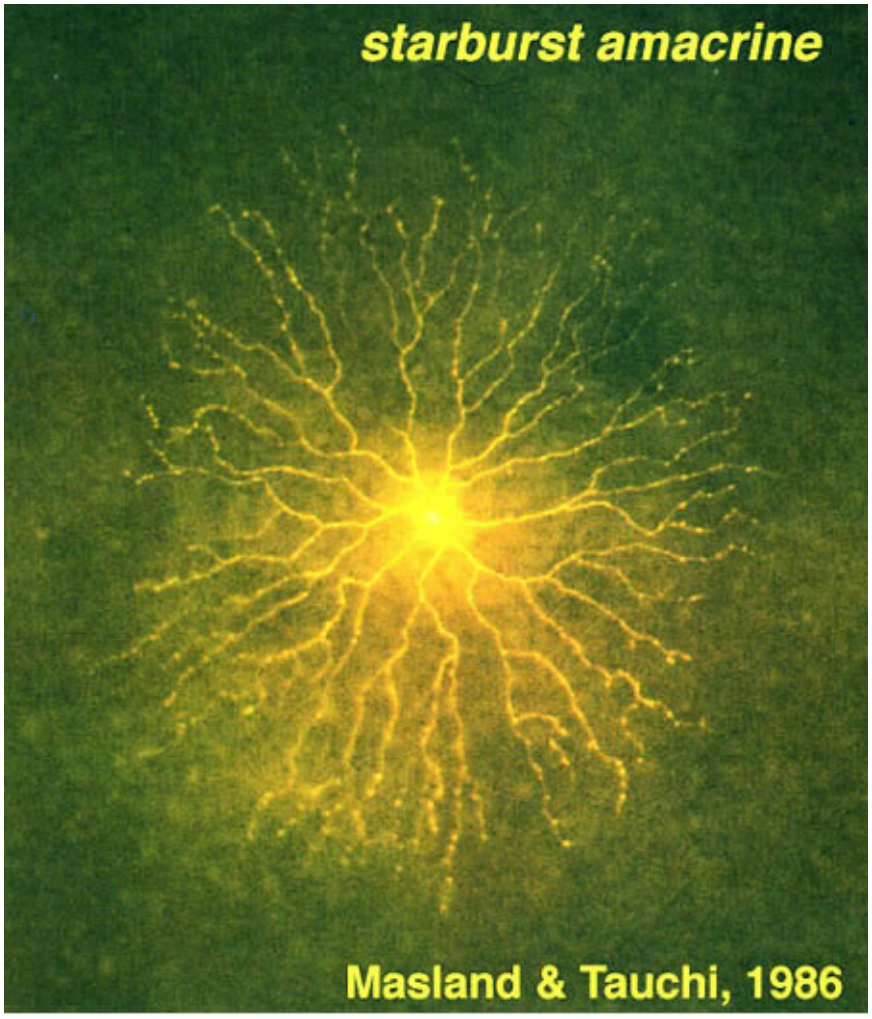

Figure 10. ACh containing amacrine cell stained with Lucifer yellow.

neurotransmitter glutamate can induce adenosine release from [^{3}H]-adenosine preloaded rabbit retina. Additionally some effects of adenosine on the ERG generated in the retina and on the activity of ganglion cell terminals in the superior colliculus have been recorded and the information points to the strong likelihood that adenosine does play a neurotransmitter role in the vertebrate retina (See review by Blazynski and Perez (42)). Adenosine colocalizes with GABA, acetylcholine and serotonin in various retinas. Much more research is needed in this area.

Substance P Occurs in an Amacrine Type and a Ganglion Cell Type

Substance P (SP) is a neuropeptide belonging to the tachykinin family that include neurokinin A, neuropeptide K and neurokinin B, as well. Substance P is thought to be a neurotransmitter or neuromodulator in the vertebrate retina (See Kolb et al. (43) for a review).

SP-IR amacrine cells appear to be of a single type in the human retina (Fig. 12). They are large-field cells with large cell bodies (16 um diameter) lying in normal or displaced positions on either side of the inner plexiform layer (IPL).

Their sturdy, spiny and appendage-bearing dendrites stratify in stratum 3 (S3) of the IPL, where many overlapping fine dendrites intermingle to form a plexus of stained processes. Either cell bodies or primary

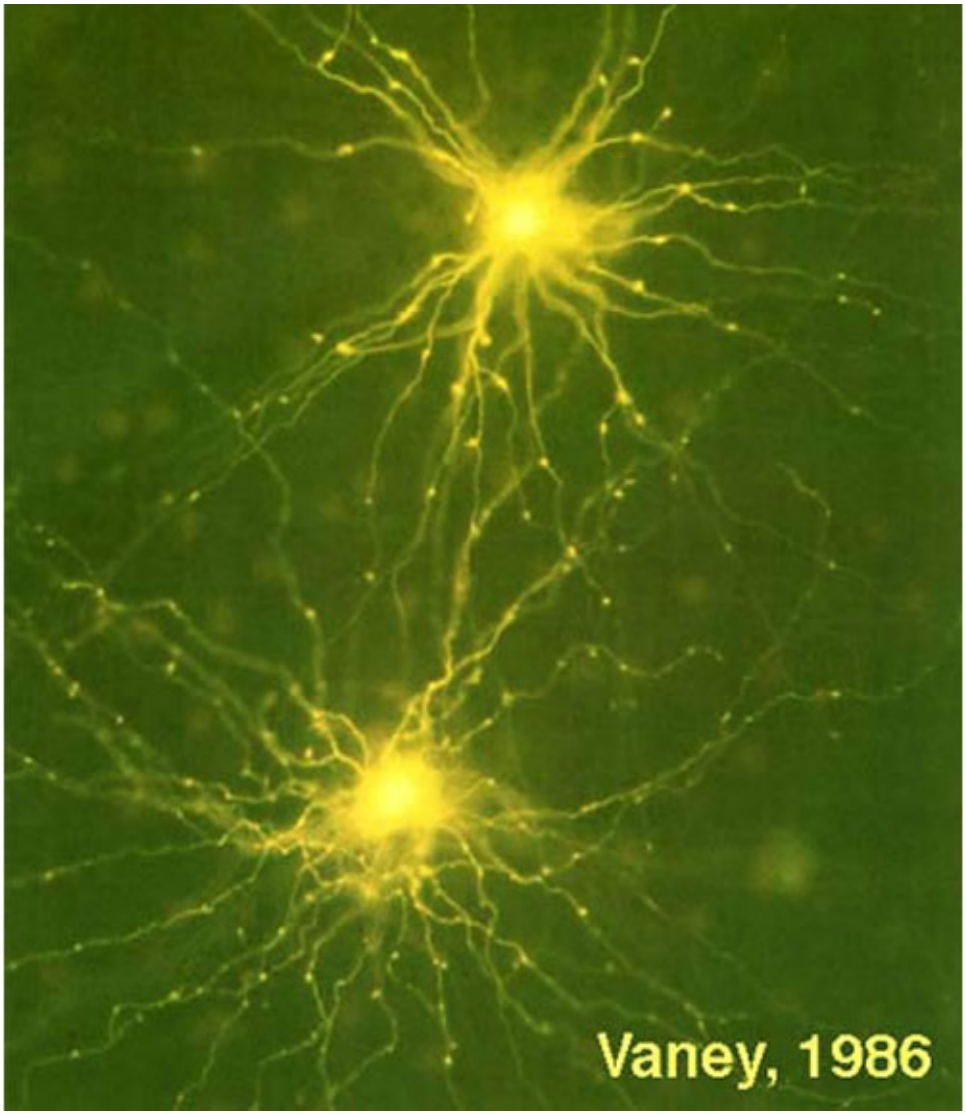

Figure 11. Serotonin accumulating amacrine cells in rabbit retina known as A17 GABAergic cells in cat and primate retinas.

dendrites emit "axon-like" process which divides typically into two long, fine processes that run in opposite directions for hundreds of microns in S5 and S3 before disappearing as distinct entities in the stained plexus in S3. Long fine dendrites also pass from the dendritic plexus to run in S5 and down to the nerve fibre layer to end as large varicosities at blood vessel walls. In addition fine processes are emitted from the dendritic plexus that run in S1, and some pass up to the outer plexiform layer (OPL) to run therein for short distances. The SP-IR amacrine cell has many similarities to thorny type 2 amacrine cells described in Golgi studies. SP amacrine cells co-localize GABA as a neurotransmitter (44).

In addition to the SP-IR amacrine cells, a ganglion cell type is immunostained with SP (Fig. 13). Its 20- 22 um cell body gives rise to a radiate, sparsely-branched, wide-spreading dendritic tree running in S3. Its dendrites and cell body become enveloped by the more intensely SP-IR processes and boutons from the SP-IR amacrine cell type (Fig. 13, fine arrows). The SP-IR ganglion cell type most resembles G21 of a Golgi study. A ganglion cell type in rabbit retina has definitely been proved to contain substance P. Such ganglion cells almost certainly colocalize a more standard neurotransmitter like glutamate too (45).

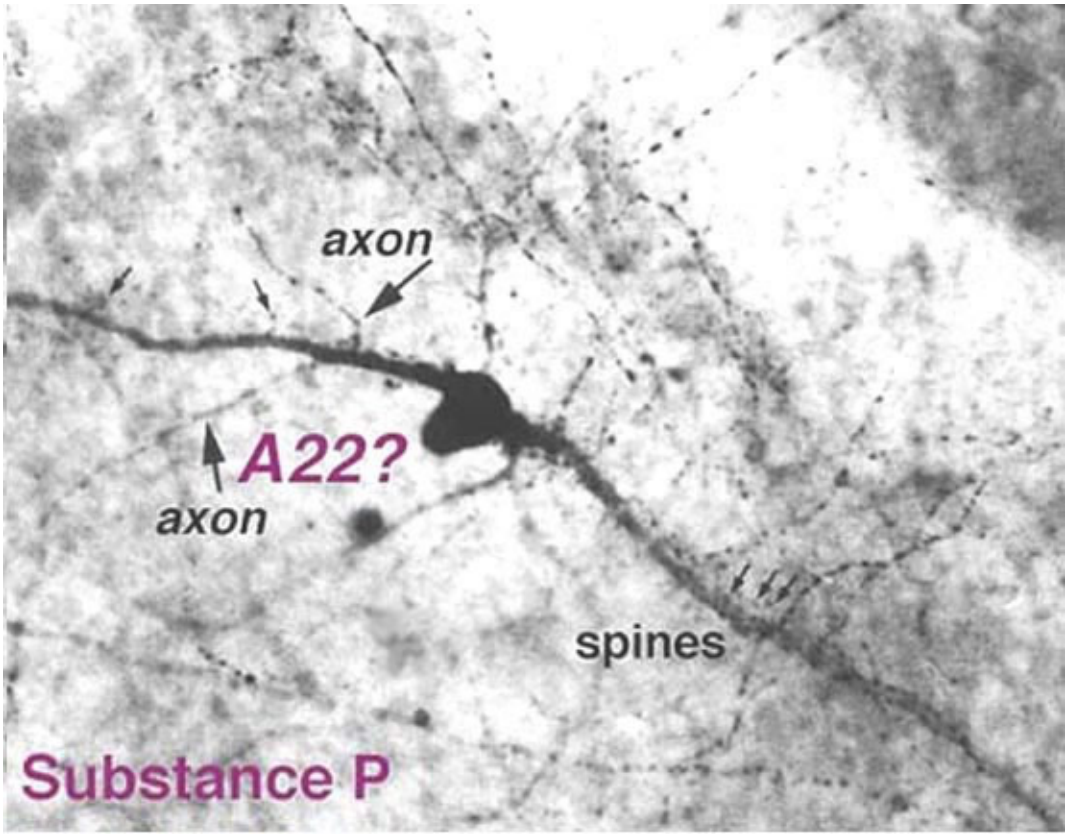

Figure 12. Substance P containing amacrine cell in human retina.

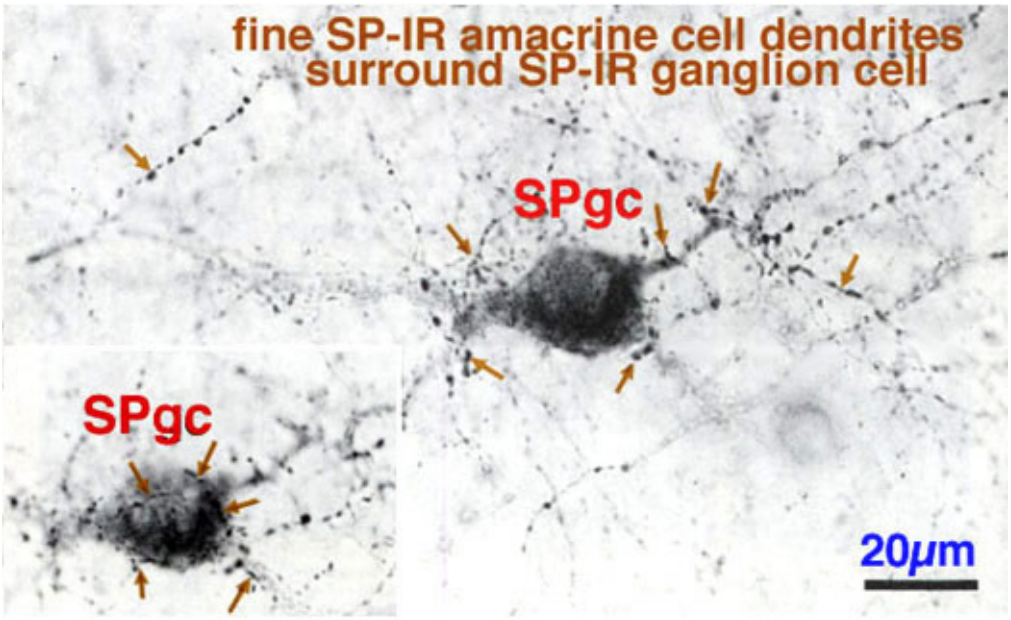

Figure 13. Substance P containing ganglion cell in human retina.

Other Neuropeptides

Immunostaining with antibodies against somatostatin has revealed a small population of neurons in the ganglion cell layer in the rabbit retina (46). They are distributed only in the inferior retina and in the far

peripheral circumference of the retina. However, in the monkey and human retinas these amacrines are more uniformly distributed. The somatostatin-IR amacrines have long fibers that distribute across the entire retina running in three plexuses in the middle and outer and inner strata of the inner plexiform layer (Fig. 14, from Marshak (47)). In the human and monkey most of the somatostatin-IR cells have their cell bodies in the ganglion cell layer (Fig. 14) and they emit fibers or axon-like processes that can be measured running 20 mm across the entire retina (48). Because these axon like processes stay within the retina, not passing to the optic nerve, the somatostatin-immunoreactive cells are likened to the associational neurons of Cajal (49).

Corticotropin releasing factor (CRF) is contained within a population of wide-field tristratified amacrines with long axon like processes, very similar in morphology to those containing somatostatin (Fig. 15) (47). Colocalization of the two peptides has not been attempted yet but it seems probably that they are one and the same cell type.

Vasoactive Intestinal peptide (VIP) immunostains a population of amacrine cells that can be normally place in the INL or displaced to the ganglion cell layer (Fig. 16). They appear to have a medium size dendritic field and dendrites that branch diffusely through the middle strata of the IPL. They may be equivalent to the A12 type of Mariani (50).

Amacrine cells that immunostain for neuropeptide Y are quite regularly stained in the primate and rodent retina. These amacrine cells have a characteristic sparsely branched wide-field dendritic tree with dendrites running in stratum 1 of the IPL (Fig. 17) (47). Recent research wherby NPY amacrine cells can be selectively ablated indicates that these cells have a role in low spatial frequency tuning of certain large ganglion cell types (51). Both ON and OFF center ganglion cell types are said to be equally affected by loss of NPY amacrine cells, which is a strange finding considering the OFF stratum branching of these particuar amacrine cells. Presumably another chain of amacrine cells is involved in spatial tuning of ganglion in addition to the NPY type.

Using antibodies to the glycine extended form of cholecystokinin, Marshak and colleagues were able to demonstrate the presence of two different morphological types of amacrine cell and a single morphological type of bipolar cell in the monkey retina (47, 52). The amacrines come as pairs that are either bistratified in the strata 2 and 4 and a larger bodied monstratified pair, again branching in either stratum 2 or 4 (Fig. 18). The blue cone specific bipolar cell is well characterized by CCK immunostaining and its distribution, contact with blue cones specfically and its probably ON center physiology is now well known (52, 53) (see chapter on S-cone pathways).

NADPH-Diaphorase Staining and the Possibility That There are Nitric Oxide Containing Neurons in the Retina

Nitric oxide is formed in many nerve cells of the peripheral and central nervous system. It is known to play a role in second messenger cascades by activating guanylyl cyclase and elevating cyclic GMP levels. Since many neurotransmitters and transduction events utilize cyclic GMP in the retina (notable phototransduction in the photoreceptors and activation of metabotropic glutamate receptors) the idea that nitric oxide might play a key role in retinal neurotransmission has been forwarded. Nitric oxide synthase the enzyme required for synthesis of nitric oxide requires NADPH as a cofactor in the cell. Thus the simple histochemical technique to reveal NADPH in a cell by the reduction of tetrazolium salts has proved to be a good marker of neurons that contain NADPH-diaphorase and hence possibly also nitric oxide synthase. An antibody has been made against the synthase but staining and identification of morphological cell types that contain this enzyme have been unsatisfactory to date for the retina. Thus the NADPH-diaphorase histochemical technique is still more reliable.

In monkey retina, three types of amacrine cell and one type of ganglion cell appear clearly stained with NADPH-diaphorase. The commonest type is the one shown above (Fig. 19 and Fig. 20) and occurs at a maximum density of 280 cell/mm2 at 1 mm from the fovea (Cuenca, personal communication). It has a large cell body that lies either in the amacrine cell layer or can be displaced to the ganglion cell layer. The dendrites radiate out from the

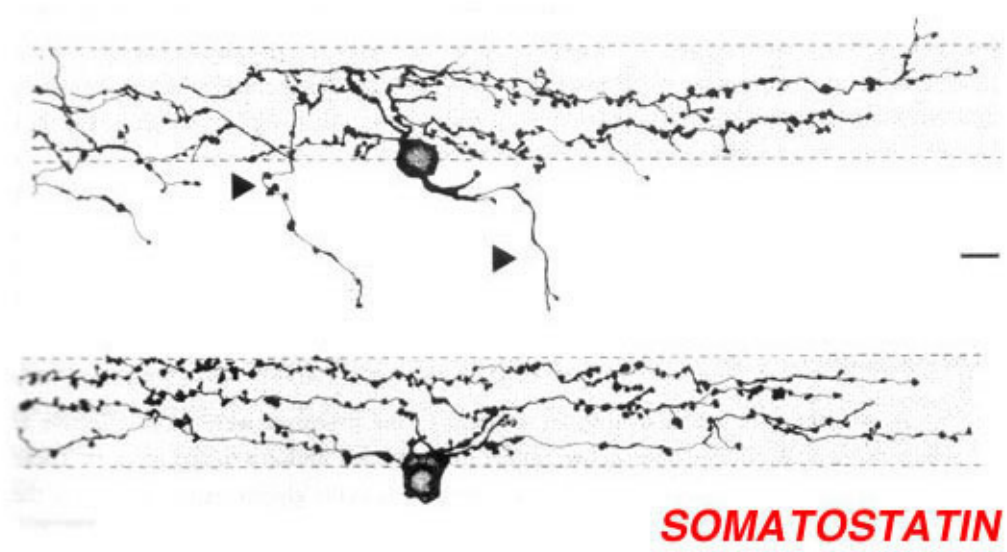

Figure 14. Somatostatin-IR amacrine cells of the monkey retina (47).

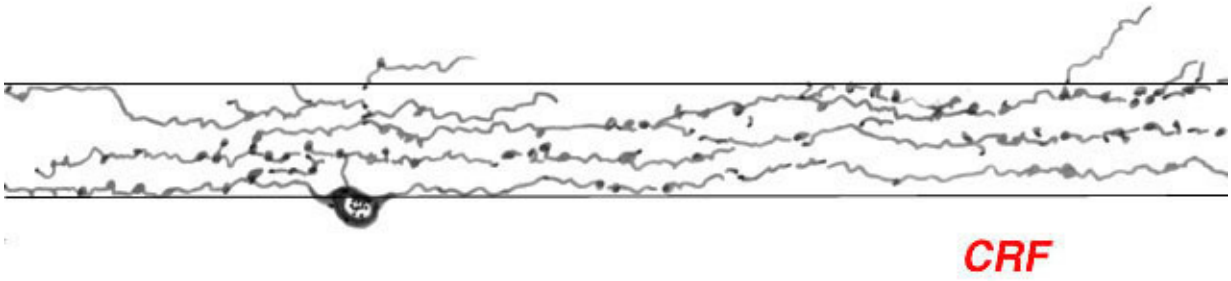

Figure 15. Vertical section of CRF-IR amacrine cells are probably the same type as those labelling with somatostatin (47).

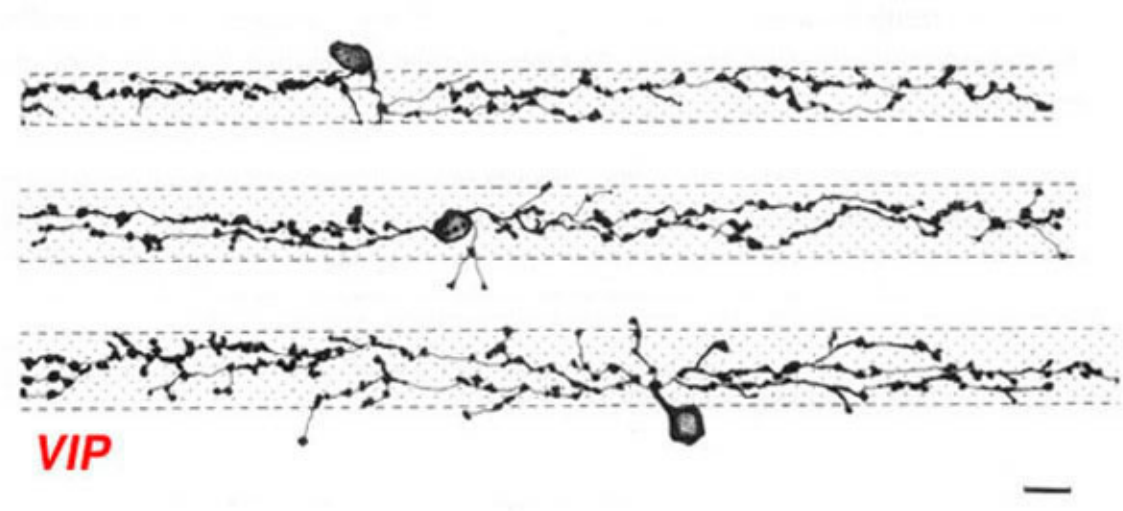

Figure 16. Vasoactive Intestinal peptide-IR amacrine cells of the monkey retina (47).

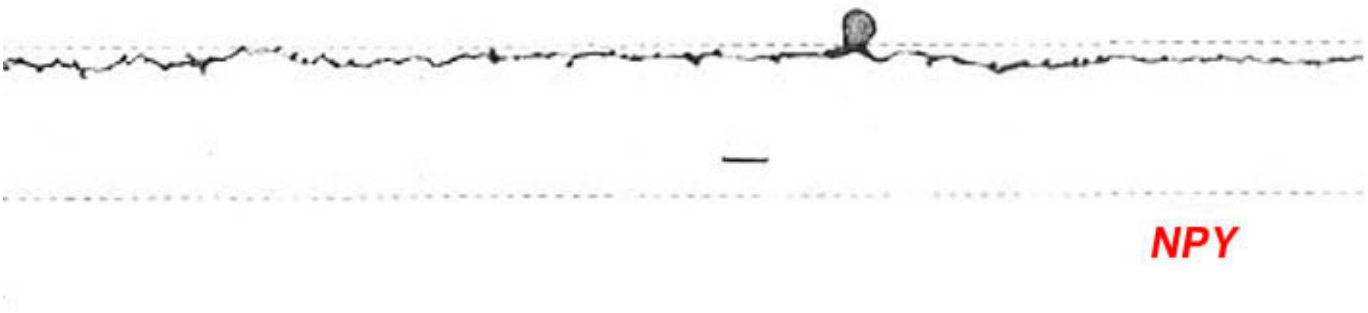

Figure 17. Vertical section of neuropeptide Y-IR amacrine cells are wide-field and unistratified in stratum 1 of the IPL (47).

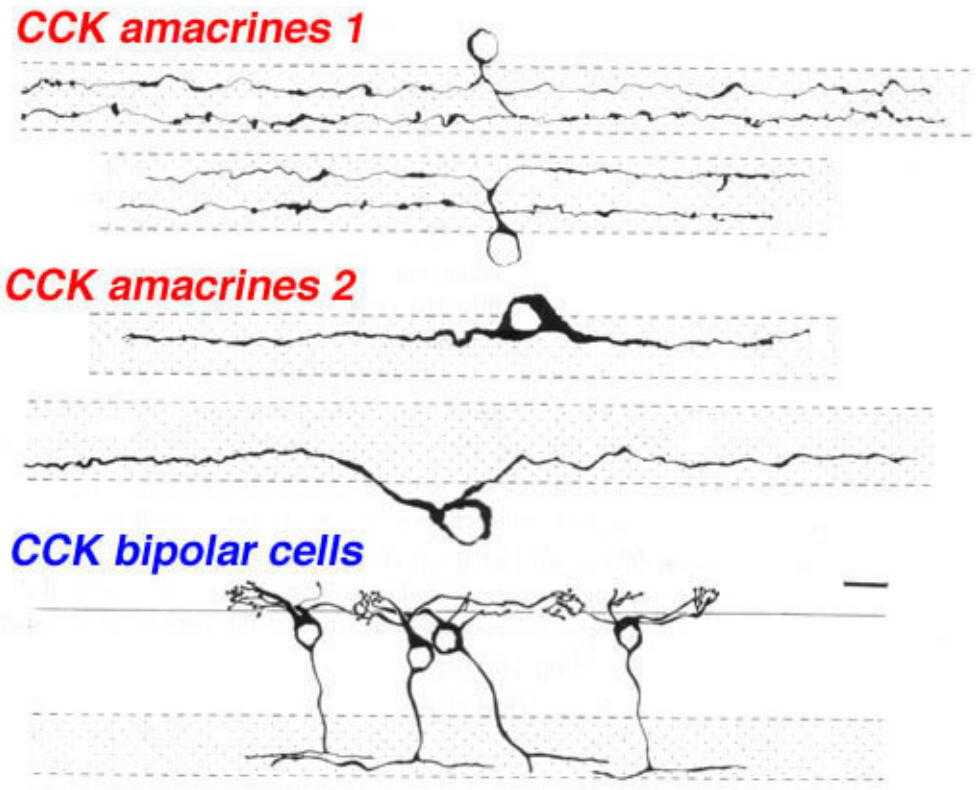

Figure 18. Two type of amacrine (1 and 2,) and a type of bipolar cell known to contact blue cones is immunostained with the peptide cholecystokinin (47).

cell body like the spokes of a wheel, contain, many fine spines, and lie on one plane in stratum 3 of the IPL. Fine axon like processes arise from the main dendritic tree that is about 300 um in diameter to run for mm in all directions. The cell is probably the equivalent of a spiny amacrine described by Mariani (50) and a cell type stained by Dacey as axon bearing (54).

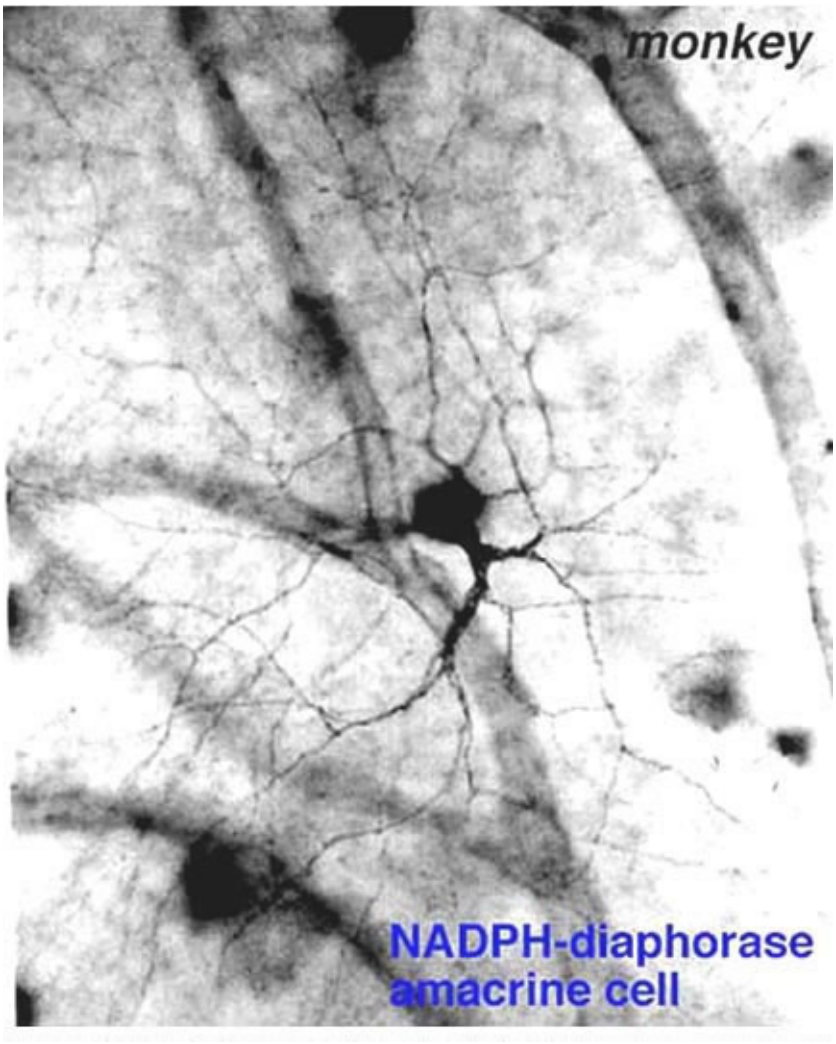

Figure 19. NADPH-diaphorase histochemical staining of an amacrine cell in monkey retina.

Amacrine Cell Populations and Mosaics Arrangements Are Revealed by Neurotransmitter Immunocytochemistry

Table 1 lists the amacrine cell types that have now become associated with particular neurotransmitter substances in the mammalian retina. The list is compiled primarily from data of cat and rabbit retinas. However, some clearly recognizable amacrine cell types of the monkey and human retina have been included. The list is as yet incomplete concerning an exact classification of each cell type by neurotransmitter signature because of the difficulty of agreeing on correspondence between different authors classification schemes and making cross species comparisons. The review article by Vaney (18) is the most comprehensive treatment on the subject of the differences between cat and rabbit retina in this regard.

Immunocytochemical staining of amacrine cells, when done on wholemounts of retina, can reveal every cell of the population that are immunoreactive to the antibody used. Thus we are increasingly acquiring population maps and distribution maps of all the different types of amacrine cells according to neurotransmitter content. Most amacrine types are arranged in regular mosaics and the individual cells have certain overlap characteristics that can be calculated from nearest neighbor statistics. The cat and monkey amacrine mosaics peak in cell density with closest packing of their smallest dendritic trees in the fovea or area centralis. Then from center to periphery the neurons distribute evenly in concentric rings of decreasing density and increasing dendritic field

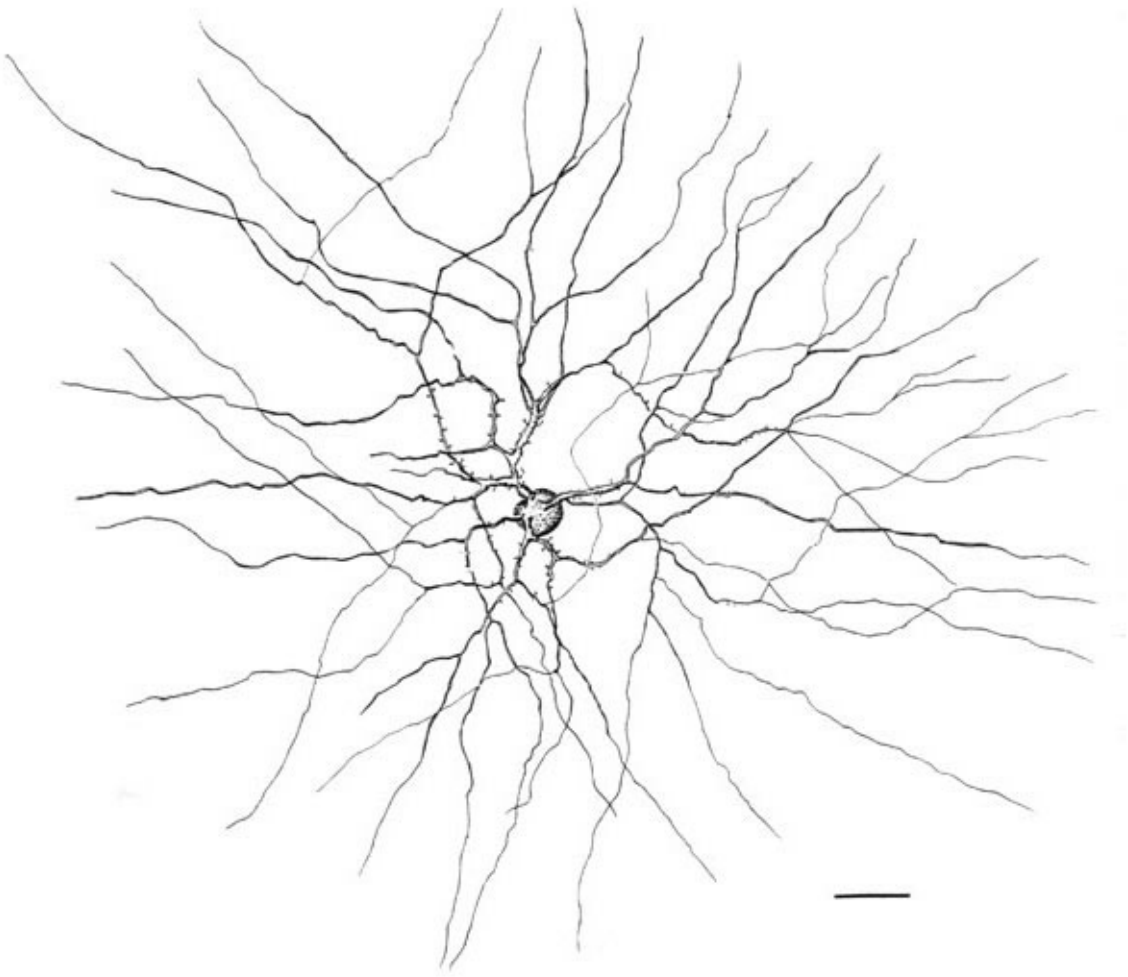

Figure 20. Drawing from wholemount retina stained with NADPH-diaphorase of the commonly stained amacrine cell.

sizes. The rabbit amacrine mosaics peak along the horizontally-organized visual streak and fall off therefrom linearly into superior and inferior retina (18). Some of the more sparsely distributed neurotransmitter types, have unique distributions. For example, the somatostatin-immunoreactive associational neurons in rabbit retina are located almost exclusively in inferior retina.

The commonest amacrine cell type of the cat and rabbit retina is the glycinergic AII amacrine (estimated 512,000 total in cat retina) followed by the serotonin-accumulating amacrines (between 170,000 and 230,000 cells in rabbit), cholinergic cells (approximately 130,000 in rabbit retina) and substance P-containing cell types (39,000 cells in cat retina). Dopaminergic amacrine cells are some of the lowest density populations of cells (3-5,000 in cat; 6-8,000 in rabbit). Somatostatin occurs in a small population of only 1000 cells in rabbit retina (Fig. 21).

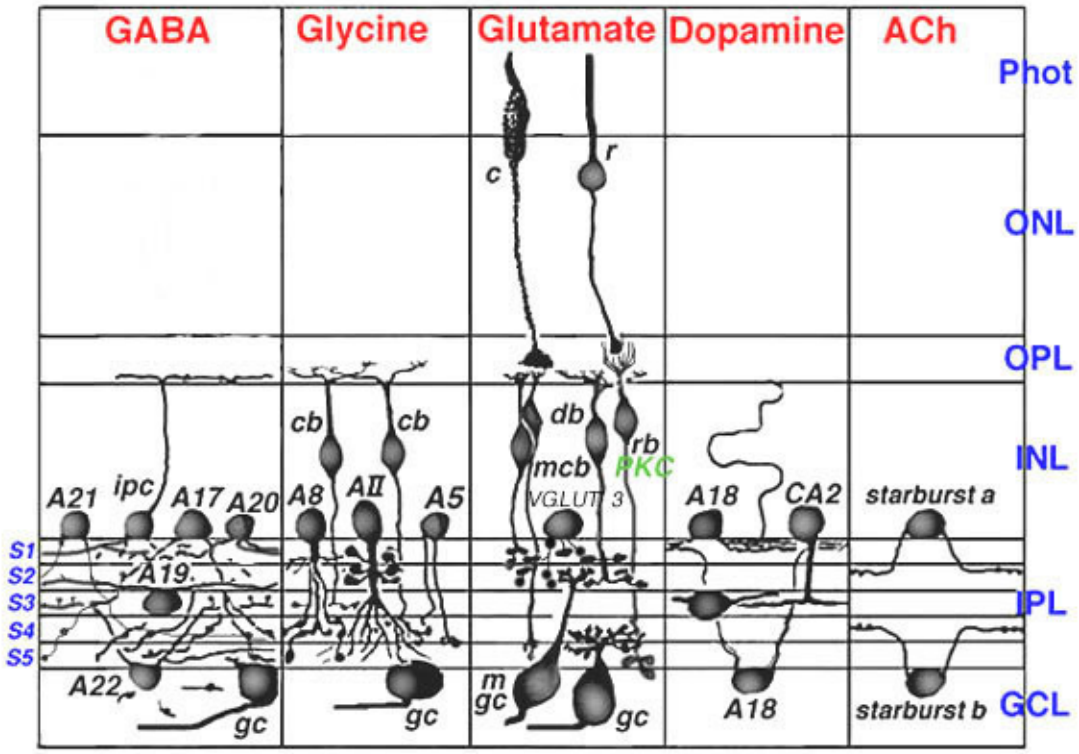

Figure 21. Summary diagram of the organization of neurotransmitters in the retina.

Table 1. Common neurotransmitter substances found in mammalian amacrine cells

Neurotransmitter		Amacrine cell type	
	rabbit	cat	primate
GABA		A2, A10, A13, A17, A19, A22, A20	same as cat
glycine	All DAPI-3	A3, A4 All A8	same as cat
acetylcholine	"starburst" Ca, Cb	"starburst" a-type, b-type	"starburst" a-type, b-type
dopamine	Toh-IR CA1, CA2, CA3	A18	CA-type1 CA-type2
serotonin	S1, S2	A20 and A22	A17
substance P	tri-stratified	A22	thomy 2
VIP	Tri-stratified		
somatostatin	association neuron long axon-like processes		
nitric oxide	NADPH-diaphorase cell		multiaxonal spiny

Compiled from Vaney (18)

References

1. Davanger S, Ottersen OP, Storm-Mathisen J. Glutamate, GABA and glycine in the human retina: An immunocytochemical investigation. J Comp Neurol. 1991;311:483–494. PubMed PMID: 1684589.

2. Crooks J, Kolb H. Localization of GABA, glycine, glutamate and tyrosine hydroxylase in the human retina. J Comp Neurol. 1992;315:287–302. PubMed PMID: 1346792.
3. Massey SC. Cell types using glutamate as a neurotransmitter in the vertebrate retina. Prog Ret Res. 1990;9:399–425.
4. Marc RE, Murry RF, Basinger SF. Pattern recognition of amino acid signatures in retinal neurons. J Neurosci. 1995;15(7 Pt 2):5106–29. PubMed PMID: 7623139.
5. Lasater EM, Lam DMK. Membrane properties of distal retinal neurons. Prog Ret Res. 1992;11:215–246.
6. Slaughter MM, Miller RF. 2-amino-4-phosphonobutyric acid: A new pharma-cological tool for retina research. Science. 1981;211:182–184. PubMed PMID: 6255566.
7. Slaughter MM, Miller RF. An excitatory amino acid antagonist blocks cone input to sign-conserving second-order retinal neurons. Science. 1983a;219:1230–1232. PubMed PMID: 6131536.
8. Slaughter MM, Miller RF. Bipolar cells in the mudpuppy retina use an excitatory amino acid neurotransmitter. Nature. 1983b;303:537–538. PubMed PMID: 6134238.
9. Nawy S, Jahr CE. Supression by glutamate of cGMP activated conductance in retinal bipolar cells. Nature. 1990;346:269–271. PubMed PMID: 1695713.
10. Witkovsky P, Dearry A. Functional roles of dopamine in the vertebrate retina. Prog Ret Res. 1991;11:247–292.
11. Keyser KT, Britto LRG, Schoepfer R, Whiting P, Cooper J, Conroy W, Brozozowska-Prechtl A, Karten HJ, Linstrom J. Three subtypes of alpha-bungarotoxin-sensitive nicotinic acetylcholine receptors are expressed in chick retina. J Neurosci. 1993;13:442–454. PubMed PMID: 8426223.
12. Massey SC, Miller RF. Glutamate receptors of ganglion cells in the rabbit retina: Evidence for glutamate as a bipolar cell transmitter. J Physiol (Lond). 1988;405:635–655. PubMed PMID: 2908248.
13. Yazejian B, Fain GL. Excitatory amino acid receptors on isolated retinal ganglion cells from the goldfish. J Neurophysiol. 1992;67:94–106. PubMed PMID: 1372651.
14. Johnson J, Sherry DM, Liu X, Fremeau RT, Seal RP, Edwards RH, Copenhagen DR. Vesicular glutamate transporter 3 expression identifies glutamatergic amacine cells in the rodent retina. J Comp Neurol. 2004;477:386–398. PubMed PMID: 15329888.
15. Haverkamp S, Wassle H. Characterization of an amacrine cell type of the mammalian retina immunoreactive for vesicular glutamate transporter 3. J Comp Neurol. 2004;468:251–263. PubMed PMID: 14648683.
16. Marc RE, Jones BW. Molecular phenotyping of retinal ganglion cells. J Neurosci. 2002;22(2):413–27. PubMed PMID: 11784786.
17. Pourcho RG, Goebel DJ. Neuronal subpopulations in cat retina which accumulate the GABA agonist (3H)muscimol: a combined Golgi and autoradiographic study. J Comp Neurol. 1983;219:25–35. PubMed PMID: 6619330.
18. Vaney DI. The mosaic of amacrine cells in the mammalian retina. Prog Ret Res. 1990;9:49–100.
19. Lukasiewicz PD, Wong ROL. GABAC receptors on ferret retinal bipolar cells: a diversity of subtypes in mammals? Vis Neurosci. 1997;14:989–994. PubMed PMID: 9364734.
20. Pourcho RG, Goebel DJ. A combined Golgi and autoradiographic study of 3(H)glycine-accumulating amacrine cells in the cat retina. J Comp Neurol. 1985;233:473–480. PubMed PMID: 2984258.
21. Menger N, Pow DV. Glycinergic amacrine cells of the rat retina. J Comp Neurol. 1998;401:34–46. PubMed PMID: 9802699.
22. Waessle H, Heinze L, Ivanova E, Majumdar S, Weiss J, Harvey RJ, Haverkamp S. (2009). Glycinergic transmission in the mammalian retina . Frontiers in Molecular Neuroscience, www.frontiersin.org
23. Grünert U, Wässle H. Immunocytochemical localization of glycine receptors in the mammalian retina. J Comp Neurol. 1993;335:523–537. PubMed PMID: 8227534.
24. Kolb H, Nelson R, Mariani A. Amacrine cells, bipolar cells and ganglion cells of the cat retina: A Golgi study. Vision Res. 1981;21:1081–1114. PubMed PMID: 7314489.
25. Kolb H, Linberg KA, Fisher SK. The neurons of the human retina: a Golgi study. J Comp Neurol. 1992;318:147–187. PubMed PMID: 1374766.

26. Pourcho RG. Dopaminergic amacrine cells in the cat retina. Brain Res. 1982;252:101–109. PubMed PMID: 7172014.
27. Kolb H, Cuenca N, DeKorver L. Postembedding immunocytochemistry for GABA and glycine reveals the synaptic relationships of the dopaminergic amacrine cell of the cat retina. J Comp Neurol. 1991;310:267–284. PubMed PMID: 1720142.
28. Wässle H, Voight T, Patel B. Morphological and immunocytochemical identification of indoleamine-accumulating neurons in the cat retina. J Neurosci. 1987;7:1574–1585. PubMed PMID: 3553450.
29. Casini G, Rickman DW, Brecha NC. AII amacrine cell population in the rabbit retina: Identification by parvalbumin immunoreactivity. J Comp Neurol. 1995;356:132142.
30. Mariani AP, Hokoc JM. Two types of tyrosine hydroxylase-immunoreactive amacrine cells in the rhesus monkey. J Comp Neurol. 1988;276:81–91. PubMed PMID: 2903868.
31. Wässle H, Chun MH. Dopaminergic and indoleamine-accumulating amacrine cells express GABA-like immunoreactivity in cat retina. J Neurosci. 1988;8:3383–3394. PubMed PMID: 2902202.
32. Lasater EM, Dowling JE. Dopamine decreases conductance of the electrical junctions between cultured retinal horizontal cells. Proc Natl Acad Sci USA. 1985;82:3025–3029. PubMed PMID: 3857632.
33. Famiglietti EV. 'Starburst' amacrine cells and cholinergic neurons: mirror-symmetric ON and OFF amacrine cells of rabbit retina. Brain Res. 1983;261:138–144. PubMed PMID: 6301622.
34. Masland RH, Tauchi M. The cholinergic amacrine cell. TINS. 1986;9:218–223.
35. Hutchins JB, Hollyfield JG. Cholinergic neurons in the human retina. Exp Eye Res. 1987;44:363–376. PubMed PMID: 3297747.
36. Hughes TE, Grunert U, Karten HJ. GABAA receptors in the retina of the cat: an immunohistochemical study of wholemounts, sections, and dissociated cells. Vis Neurosci. 1991;6:229–238. PubMed PMID: 1647196.
37. Keyser KT, Hughes TE, Whiting PJ, Lindstrom JM, Karten HJ. Cholinoceptive neurons in the retina of the chick: an immunohistochemical study of the nicotinic acetylcholine receptors. Vis Neurosci. 1988;1:349–366. PubMed PMID: 3154804.
38. Vaney DI. Morphological identification of serotonin-accumulating neurons in the living retina. Science. 1986;233:444–446. PubMed PMID: 3726538.
39. Ehinger B, Dowling JE. Retinal neurocircuitry and transmission. In "Handbook of chemical neuroanatomy, vol. 5 Integrated systems of the CNS, part 1 (A Bjorklund, T Hokfelt and LW Swanson, eds) Elsevier Science Publishers BV; 1987, pp. 389-446.
40. Schütte M, Weiler R. Morphometric analysis of serotonergic bipolar cells in the retina and its implication for retinal image processing. J Comp Neurol. 1987;260:619–626. PubMed PMID: 3301919.
41. Hurd LB, Eldred WD. Synaptic microcircuitry of bipolar and amacrine cells with serotonin-like immunoreactivity in the retina of the turtle Pseudemys scripta elegans. Vis Neurosci. 1993;10:455–472. PubMed PMID: 8494799.
42. Blazynski C, Perez, MTR. Neuroregulatory functions of adenosine in the retina. Prog ret Res. 1991; 11: 293-332.
43. Kolb H, Fernandez E, Ammermüller J, Cuenca N. Substance P: A neurotransmitter of amacrine and ganglion cells in the vertebrate retina. Histol Histopathol. 1995;10:947–968. PubMed PMID: 8574015.
44. Pourcho RG, Goebel DJ. Colocalization of substance P and GABA in amacrine cells of the cat retina. Brain Res. 1988;447:164–168. PubMed PMID: 2454701.
45. Brecha NC, Johnson D, Bolz J, Sharma S, Parnavelas JG, Lieberman AR. Substance P immunoreactive retinal ganglion cells and their central axon terminals in the rabbit. Nature. 1987;327:155–158. PubMed PMID: 2437459.
46. Sagar SM. Somatostatin-like immunoreactive material in the rabbi retina: immunohistochemical staining using monoclonal antibodies. J Comp Neurol. 1987;266:291–299. PubMed PMID: 2893815.
47. Marshak DW. Peptidergic neurons of the Macaque monkey retina. Neurosci Res. (Suppl., 10) 1989; S117-130.

48. Sagar SM, Marshall PE. Somatostatin-like immunoreactive material in associational ganglion cells of human retina. Neurosci. 1988;27:507–516.
49. Cajal RS. The structure of the retina. (Thorpe SA, Glickstein M, Trans) Springfield, IL: Thomas; 1892, 1972.
50. Mariani AP. Amacrine cells of the rhesus monkey retina. J Comp Neurol. 1990;301:382–400. PubMed PMID: 2262597.
51. Sinclair JR, Jacobs AL, Nirenberg S. Selective ablation of a class of amacrine cells alters spatial processing in the retina. J Neurosci. 2004;24:1459–1467. PubMed PMID: 14960619.
52. Kouyama N, Marshak DW. Bipolar cells specific for blue cones in the macaque retina. J Neurosci. 1992;12:1233–1252. PubMed PMID: 1556594.
53. Kolb H, Goede P, Roberts S, McDermott R, Gouras P. The uniqueness of the S-cone pedicle in the human retina and consequences for color processing. J Comp Neurol. 1997;386:443–460. PubMed PMID: 9303428.
54. Dacey DM. Axon-bearing amacrine cells of the Macaque monkey retina. J Comp Neurol. 1989;284:275–293. PubMed PMID: 2754037.

$GABA_C$ Receptors in the Vertebrate Retina

Haohua Qian

Created: May 1, 2005; Updated: June 1, 2007.

Properties of GABA Receptors

γ-Aminobutyric acid (GABA) is the main inhibitory neurotransmitter in the central nervous system. The inhibitory action of GABA is mediated by the receptors present on the cell membrane and results in a reduction of neuronal excitability. At least three types of GABA receptors have been characterized. Table 1 summarizes some of the general properties of these three types of GABA receptors. $GABA_A$ receptors are ligand-gated chloride channels. They mediate fast inhibition and have a wide distribution throughout the central nervous system. $GABA_A$ receptors have a diverse molecular composition. At least 16 subunits in six groups have been identified. Pharmacologically, these receptors are antagonized by bicuculline. $GABA_A$ receptors are also the targets of many therapeutic compounds (such as general anaesthetics, sedative drugs, and alcohols). These compounds allosterically modulate $GABA_A$ receptor channel activities. $GABA_B$ receptors belong to the G-protein-coupled receptor superfamily. The inhibition of $GABA_B$ receptors is mediated by indirect gating of either potassium or calcium channels. $GABA_B$ receptors are activated by baclofen and antagonized by phaclofen and saclofen. The subunits of $GABA_B$ receptors have recently been cloned. $GABA_C$ receptors are the newly identified member of the GABA receptor family. They are also linked to chloride channels, with distinct physiological and pharmacological properties. In contrast to the fast and transient responses elicited from $GABA_A$ receptors, $GABA_C$ receptors mediate slow and sustained responses. Pharmacologically, $GABA_C$ receptors are bicuculline- and baclofen-insensitive and are not modulated by many $GABA_A$ receptor modulators (such as benzodiazepines and barbiturates). GABA ρ subunits are thought to participate in forming $GABA_C$ receptors on the neuronal membrane, but the exact molecular composition of these receptors is yet to be determined. $GABA_C$ receptors are expressed in many brain regions, with prominent distributions on retinal neurons, suggesting that these receptors play important roles in retinal signal processing.

Table 1. Characteristics of GABA receptors.

	$GABA_A$ receptor	$GABA_B$ receptor	$GABA_C$ receptor
Category	Ligand-gated channel	G-protein-coupled receptor	Ligand-gated channel
Subunits	α, β, γ, δ, ε, π	GBR1, GBR2	ρ
Agonists	Muscimol, THIP	Baclofen	
Antagonists	Bicuculline, picrotoxin	Phaclofen	TPMPA, picrotoxin
Desensitization	Yes	No	No
Modulator	Benzodiazepine barbiturates		Zinc

$GABA_C$ Responses on Retinal Neurons

The term "$GABA_C$ receptor" was first used by Johnston to describe a novel GABA binding site on neuronal membranes (1, 2). Although recent studies indicate a wide distribution of $GABA_C$ receptors in many parts of the central nervous system (3-7), these receptors are most prominently expressed in the vertebrate retina. In the fish white perch retina, rod-driven (H4) horizontal cells were the first retinal neurons where $GABA_C$ receptors were characterized (8). Subsquently, $GABA_C$ receptor-mediated responses have been detected in many types of retinal neurons, including bipolar cells (9-15), cone-driven horizontal cells in catfish (16, 17), cone photoreceptors (18), and ganglion cells (19). Among all these retinal neurons, the rod-driven horizontal cells of white perch are the only cells where GABA responses are mediated solely by $GABA_C$ receptors. The GABA responses elicited from

other cells are usually a mixture of GABA receptors and/or GABA transporters. The unique properties of the white perch rod-driven horizontal cell provided an excellent model to characterize the physiological and pharmacological properties of $GABA_C$ receptors on retinal neurons (8, 20).

An example of a solitary rod-driven horizontal cell isolated from white perch retina is shown in Fig. 1, together with a typical GABA-elicited response from such a cell. These horizontal cells receive input from rod photoreceptors in the retina; and when isolated, they keep their typical morphology in culture. Rod-driven horizontal cells have a flat cell body with diameter of 50-100 μm. There are several thick primary dendrites from which many fine processes extend. As shown in Fig. 1, GABA elicits a slow and sustained response from these cells. The GABA-induced membrane currents are mediated by chloride ions and, therefore, exhibit inhibitory actions on these neurons. The responses showed no sign of desensitization, i.e., the responses are maintained at a steady level as long as GABA is present. Furthermore, the GABA responses elicited from these horizontal cells exhibit slow kinetics, which could best be observed in the offset response. After the termination of GABA application, the membrane current returns to the baseline very slowly, with a time constant of ~15 seconds. Such slow and sustained response properties are typical of $GABA_C$ receptors.

It is interesting to note that the neurons in distal retina (i.e., photoreceptors, horizontal cells, and bipolar cells) do not produce action potentials at all. They only generate slow graded responses to light stimuli. It has always been thought that retinal neurons must have special ways to process and analyze such slow signals compared with fast transient neurons of the brain. The kinetics of $GABA_C$ receptor-mediated responses are thus particularly suited for the generatation of signals in distal retinal neurons.

Pharmacology of $GABA_C$ Receptors

$GABA_C$ receptors exhibit a distinct pharmacology that differs from classical $GABA_A$ or $GABA_B$ receptors. $GABA_C$ receptors were first described by Johnston for bicuculline- and baclofen-insensitive GABA binding sites on neuronal membranes (1, 2). More detailed studies indicated that $GABA_C$ receptors on retinal neurons are not sensitive to the competitive antagonists of either $GABA_A$ receptors (such as SR95531 and hydrastine) or $GABA_B$ receptors (such as phaclofen and saclofen). Because the competitive antagonists are thought to interact with the GABA binding sites on the receptors, these results indicate that a different conformation of GABA molecule is preferred for binding to the $GABA_C$ receptor. In agreement with such a notion, the specific agonists of $GABA_A$ and $GABA_B$ receptors exhibit quite different activity on $GABA_C$ receptors. They either have no effect (isonipecotic acid, baclofen), act as partial agonists (isoguvacine, muscimol), or as antagonists (THIP, P4S, 3-APA, and 3-APMPA) (20, 21). I4AA, a partial agonist of $GABA_A$ receptors, behaves as a potent antagonist on $GABA_C$ responses of retinal neurons and as a partial agonist on expressed $GABA_C$ receptors in *Xenopus* oocytes (20, 22).

$GABA_C$ receptors also differ from classical $GABA_A$ receptors in terms of their responses to various modulators. Two groups of compounds, benzodiazepine and barbiturates, are well-known to modulate $GABA_A$ activity. On the other hand, none of these compounds have any significant influence on responses mediated by $GABA_C$ receptors (23). For example, the GABA-elicited response on white perch rod-driven horizontal cells are virtually identical in the presence or absence of either diazepam or pentobarbital (8). Another class of $GABA_A$ receptor modulators, known as neuroactive steroids, has different effects on the expressed $GABA_C$ receptor in *Xenopus* oocytes. Whereas some of them modulate GABA responses on these receptors, others do not (24, 25). The effect of these neuroactive steroids on $GABA_C$ receptors on neurons has yet to be determined.

Although both $GABA_A$ and $GABA_C$ receptors are linked to chloride channels, the channel properties of these two receptors are quite different. Unlike $GABA_A$ receptors, picrotoxin inhibition on $GABA_C$ receptors in white perch horizontal cells exhibits both competitive and non-competitive mechanisms (20). In mammalian retina (rat), on the other hand, $GABA_C$ receptors are insensitive to picrotoxin blockage (9, 13). The unusual features of $GABA_C$ receptors in rat retina are attributed to a single amino acid substitution in the receptor subunit (26).

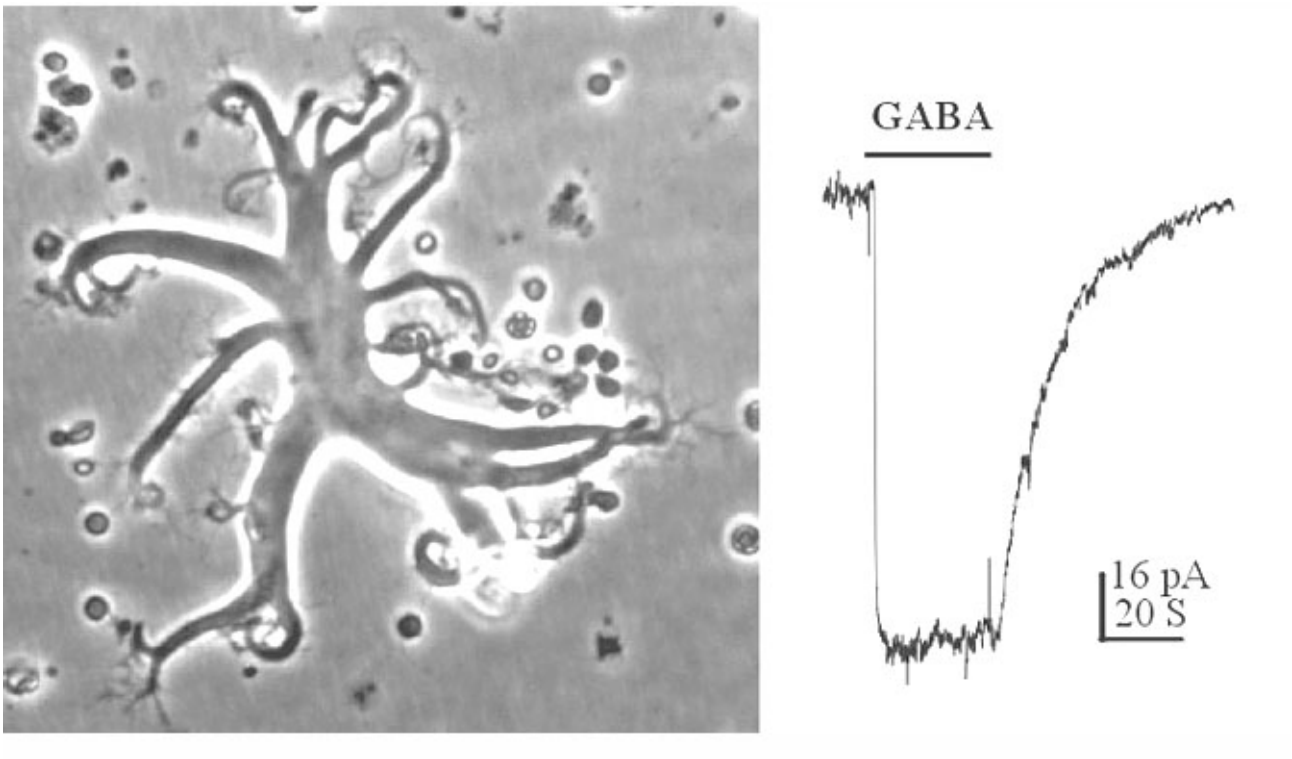

Figure 1. An example of a rod-driven (H4) horizontal cell (left) isolated from white perch retina. GABA elicits a sustained and slow response (right) from these cells mediated by GABA$_C$ receptors. Thus far, this is the only preparation in which the GABA response is mediated solely by GABA$_C$ receptors.

Furthermore, TBPS (like picrotoxin, another chloride channel blocker on GABA$_A$ receptors) does not block the responses mediated by GABA$_C$ receptors (20, 27). In addition, GABA$_C$ receptor-gated chloride channels exhibit a very small single channel conductance (14, 28).

GABA$_C$ receptor activities are modulated by divalent cations (17, 29-31). In particular, GABA$_C$ receptor-mediated responses are inhibited by low concentrations of zinc ions. The high sensitivity of GABA$_C$ receptors to zinc inhibition is attributed to a histidine residue on the extracellular domain of the subunits (32).

Recently, a new GABA$_C$ receptor antagonist, TPMPA, has become available commercially. This compound is thought to be a specific inhibitor of the GABA$_C$ receptor (33). The availability of such a drug will greatly facilitate further studies of this receptor.

Molecular Biology of GABA$_C$ Receptors

The GABA$_C$ receptor is a member of the ligand-gated channel superfamily. By analogy to the well-studied nicotinic acytocholine receptors, GABA$_C$ receptors are thought to exhibit the structure shown schematically in Fig. 2. These receptors are pentamers, i.e., five subunits constitute the functional channel (34). The receptors have a long extracellular domain containing ligand binding sites and several modulatory sites. In the middle of the receptor, GABA gates an ionic channel. Binding of GABA to the receptor induces a conformational change in receptor structure, which leads to the opening of the channel.

For each subunit forming the receptor, the structure is thought to be that shown in Fig. 3. The subunit contains a long extracellular N-terminal domain that has ligand binding sites, four transmembrane domains, and a large intracellular loop that connects the third and the fourth transmembrane domains. The ionic channel is formed by the second transmembrane domain of each subunit. For the large intracellular loop, there are several putative

phosphorylation sites, indicated as colored circles with letter "P" in the figure. Phosphorylation of these residues is implicated for modulation of receptor activities. For example, it has been reported that dopamine modulates $GABA_C$ receptor activity in both catfish cone-driven horizontal cells and tiger salamander bipolar cell terminals (35, 36). On rat bipolar cells, the $GABA_C$ receptor activities are modulated by protein kinase C (37). The modulation of receptor activities by intracellular second messenger systems is also observed at $GABA_C$ receptors expressed on *Xenopus* oocytes (38). However, the mechanisms for modulation by intracellular second messager systems are yet to be determined. Recently, Filippova and coauthors (39) provided evidence for $GABA_C$ receptor internalization upon phosphorylation of the subunits. In addition, there is evidence that the large intracellular loop of $GABA_C$ receptor subunits is involved in the interaction of receptor protein with other intracellular proteins, which may play an important role in the clustering of the receptors on neuronal membranes (40).

There is much evidence to indicate that $GABA_C$ receptors are composed of GABA ρ subunits. These were first cloned from a human retinal cDNA library (41, 42). When expressed in *Xenopus* oocytes, GABA ρ subunits formed functional homo-oligomeric receptors with properties similar to those of $GABA_C$ receptors in retinal neurons (43). Furthermore, the expression of GABA ρ subunits has been detected on retinal neurons where $GABA_C$ receptor-mediated responses have been recorded (44-46). In white perch retina, we have now cloned five forms of GABA ρ subunits (22, 46). Fig. 4 shows a comparison of white perch GABA ρ subunits and those cloned from mammalian retinas. The distances between the various connecting elements represent the degree of divergence among subunits. Unlike the mammalian retina, where only one form of ρ1 and ρ2 subunits has been identified, in white perch there are two forms of the subunit for each ρ1 and ρ2 family. In accordance with their deduced amino acid sequences and the properties of the receptors they formed on *Xenopus* oocytes, each ρ1 and ρ2 family was subdivided into A and B forms. All white perch GABA ρ1 and ρ2 subunits are able to form functional homo-oligomeric receptors when expressed in *Xenopus* oocytes. GABA-elicited responses in these expressed receptors are sustained, bicuculline insensitive, and are not modulated by either benzodiazepines or barbiturates, features typical of $GABA_C$ receptors. Similar to $GABA_C$ receptors on retinal neurons, GABA ρ receptors also gate chloride channels. However, the receptors expressed by each of the GABA ρ subunits display unique response properties that distinguish one from the other. For example, the sensitivity of GABA activation and picrotoxin inhibition varies among subunits. In addition, I4AA acts as an antagonist on A-type ρ receptors, whereas it is a partial agonist on B-type ρ receptors (22).

The waveform of receptor-mediated responses plays an important role in shaping the neuronal signal. Interestingly, the kinetics of the GABA response are also different for the receptors formed by each individual subunits. Current-trace responses to application of 10 μM GABA are illustrated in Fig. 5. These recordings indicate that there are significant differences in the kinetics of the GABA responses from *Xenopus* oocytes, depending on which white perch GABA ρ subunitis are expressed. To quantitate the kinetics of the GABA response, the offset GABA responses (current traces after GABA application is terminated) were replotted on a semi-logarithmic scale, with the amplitudes normalized to their initial values (Fig. 6). In each case, the data were fit by a straight line, indicating that offset responses can be described by a single exponential function. The slope of the line represents the time constant of the decay and shows that the receptors formed by the various ρ subunits exhibit significant differences in their response kinetics. The average time constants of offset responses elicited from receptors formed by various white perch GABA ρ subunits are shown in the bar graph in Fig. 6C. There are consistent differences between the response kinetics of the two receptor families and between their subgroups. For example, the responses from ρ1 receptors were significantly slower than those of ρ2 receptors. Such difference in the response kinetics among ρ1 and ρ2 receptors are determined, in large part, by a single residue at the second transmembrane domain of the subunits (47). This dichotomy among ρ1 and ρ2 subunits is well conserved in all species where GABA ρ subunits have been cloned. ρ1 subunits, which have a proline at the residue site, combine to make a receptor with slower kinetics, whereas ρ2 subunits, which contain a serine at the residue site, form receptors with faster response rate. Thus, receptors made of human ρ1 subunits exhibit slower response kinetics than receptors made of ρ2 subunits (5). The kinetic differences among the receptors formed by

various GABA ρ subunits could provide building blocks for the nevous system to construct different types of signal filters and different types of neuronal signaling in the nervous system.

Function of GABA$_C$ Receptors in the Retina

Although rod-driven horizontal cells provide an excellent model in which to characterize GABA$_C$ receptors in the retina, recent studies indicate that GABA$_C$ receptors are present on various other types of retinal neurons. GABA$_C$ receptor-mediated responses have been recorded from cone-driven horizontal cells in catfish (16, 17), cone photoreceptors (18), and some types of ganglion cells (19). GABA$_C$ responses are particularly prominent in bipolar cells of every species examined thus far (9-12, 14, 15), and both immunocytochemistry and *in situ* hybridization studies indicate that GABA$_C$ receptors are present on bipolar cells (15, 44, 45, 48). It appears that these receptors play an important role in shaping signal transmission from bipolar cells to third-order neurons in the retina.

Fig. 7 illustrates some examples of bipolar cells isolated from white perch retina. These bipolar cells keep their morphology when isolated in culture. They usually have a pear-shaped cell body from which several dendrites and one axon extend. The GABA responses of bipolar cells in white perch retina have both transient and sustained components, indicating both GABA$_A$ and GABA$_C$ receptors are present, as shown in Fig. 8. The transient component can be selectively blocked by the co-application of bicuculline, leaving a more sustained response. Thus, the electrophysiological and pharmacological properties of GABA$_C$ receptors on bipolar cells are very similar to those of GABA$_C$ receptors on rod-driven horizontal cells (11, 14, 37, 49).

Different kinetic properties of GABA$_A$ and GABAc receptors suggest that they play different roles in mediating inhibition on bipolar cell terminals (15, 46, 50). Furthermore, various subtypes of bipolar cells exhibit different proportions of GABA$_A$ and GABA$_C$ receptors. For example, in the rat retina, there is a clear difference in the contribution of GABA$_A$ and GABA$_C$ receptors to rod and cone bipolar cells (51). In white perch, too, different morphological types of bipolar cells exhibit different proportions of GABA$_C$ receptor-mediated components (14). These results strongly suggest that different subtypes of bipolar cell use various mixtures of GABA$_A$ and GABA$_C$ receptors to perform different activities and help create the variety of functional pathways through the retina.

Because of the presence of multiple GABA receptors on retinal neurons, it is sometimes difficult to isolate the contributions of each receptor. Recent studies on ganglion cell responses reveal some interesting features of GABA$_C$ receptors in retinal information processing. For example, activation of GABA$_C$ receptors leads to more transient light responses in ganglion cells (52) and the delayed inhibition mediated by GABA$_C$ receptors is thought to play a major role in shaping edge-enhancement of ganglion cell receptive fields (53). The bipolar cell to ganglion cell synapse is probably heavily influenced by inhibitory amacrine feed-forward or feedback synapses, and these appear to be via primarily GABA$_C$ receptors.

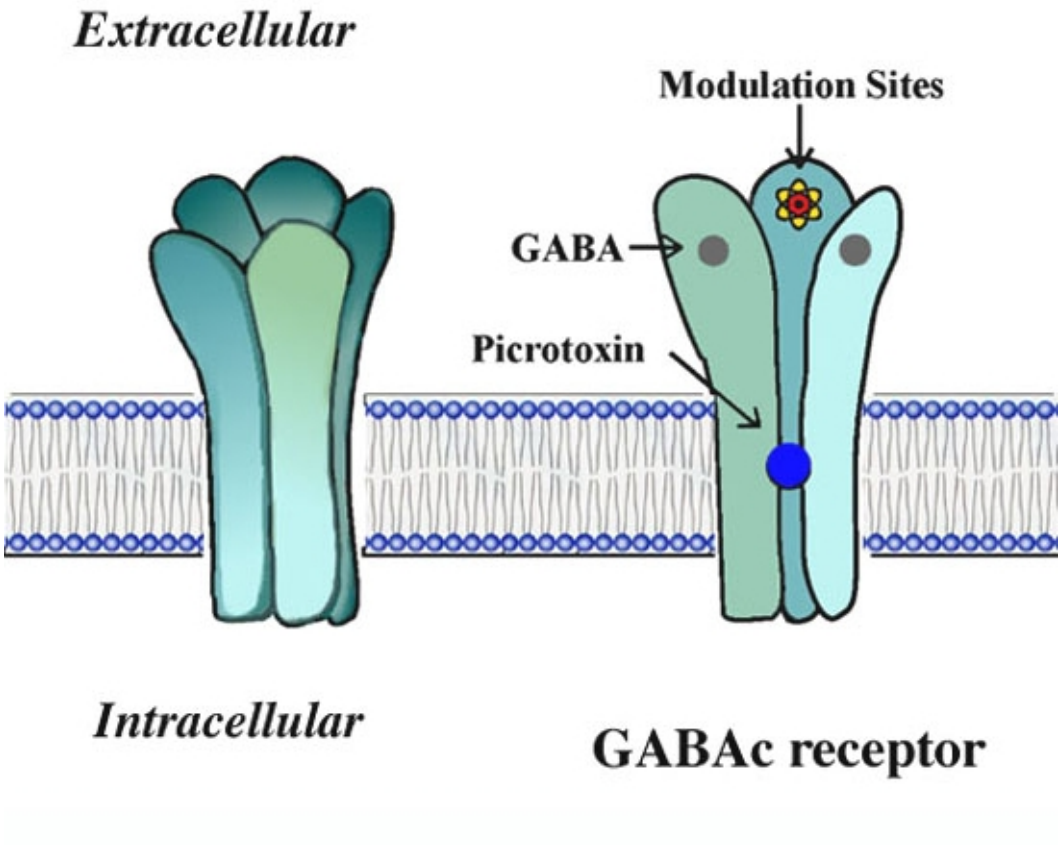

Figure 2. Schematic diagram of $GABA_C$ receptors. These receptors are formed by five subunits with an ionic channel in the middle of the receptor. On the extracellular side, the receptor contains the binding site for GABA and several modulatory sites.

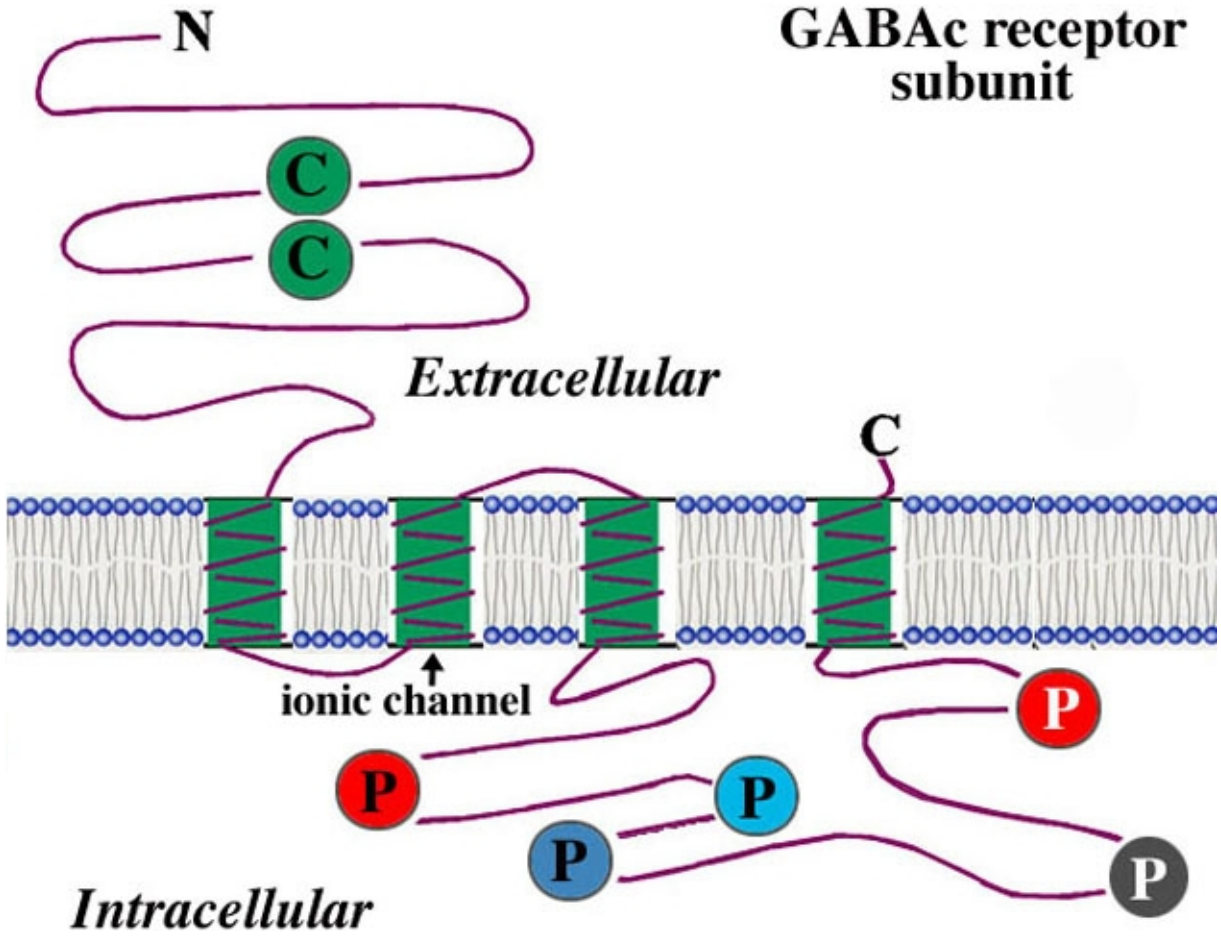

Figure 3. Schematic digram of the GABA$_C$ receptor subunits. Each subunit contains a long extracellular N-terminal region that contains two cystine residues thought to form disulfide bonds. The extracellular domain forms the GABA binding sites and other modulatory sites. The subunit crosses the cell membrane four times with a short C-terminal region on the outside of the cell. The second transmembrane domain forms the ionic channel of the receptor. There are several putative phosphorylation sites on the large intracellular loop between the third and the fourth transmembrane domains (colored circles with letter "P").

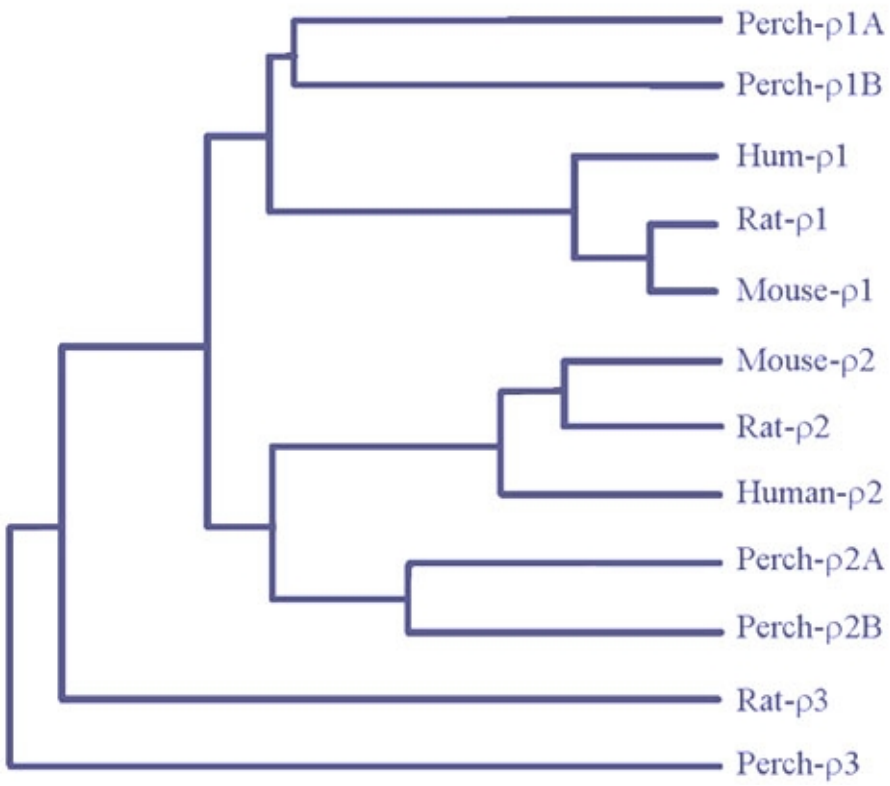

Figure 4. Dendrogram showing the relation of the GABA ρ subunits cloned from white perch retina to those cloned from mammalian retinas. Analysis was performed on the deduced amino acid sequence of each subunit.

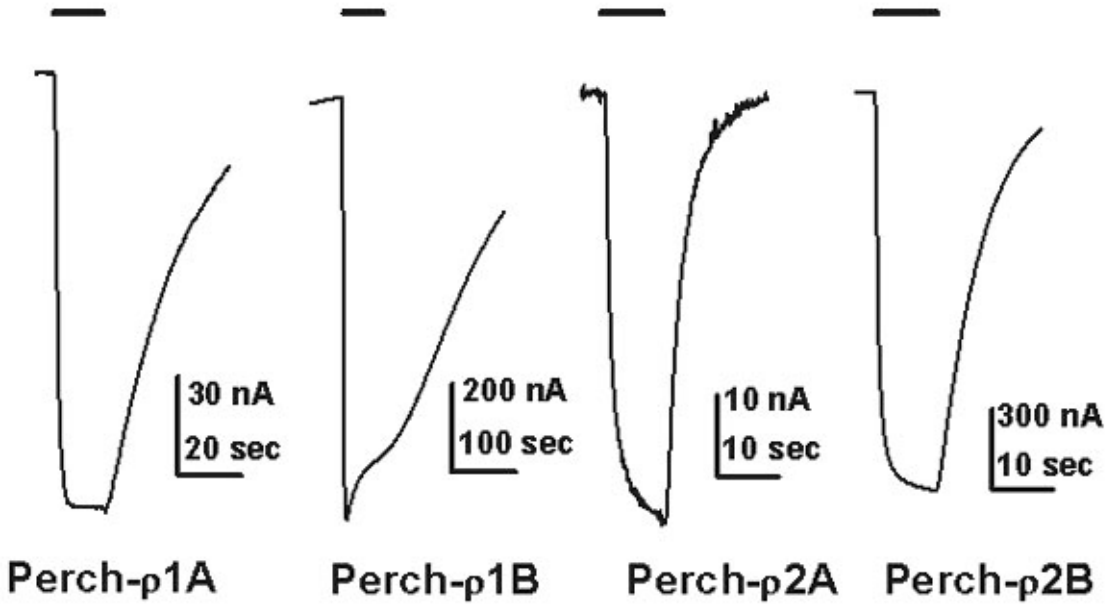

Figure 5. GABA (10 μM) induced responses from white perch GABA ρ subunits expressed in *Xenopus* oocytes. The duration of GABA application is shown by the bar above each trace. Variations in response amplitude often result from the different level of receptor expression in individual oocytes; response kinetics are a relatively stable feature, independent of amplitude.

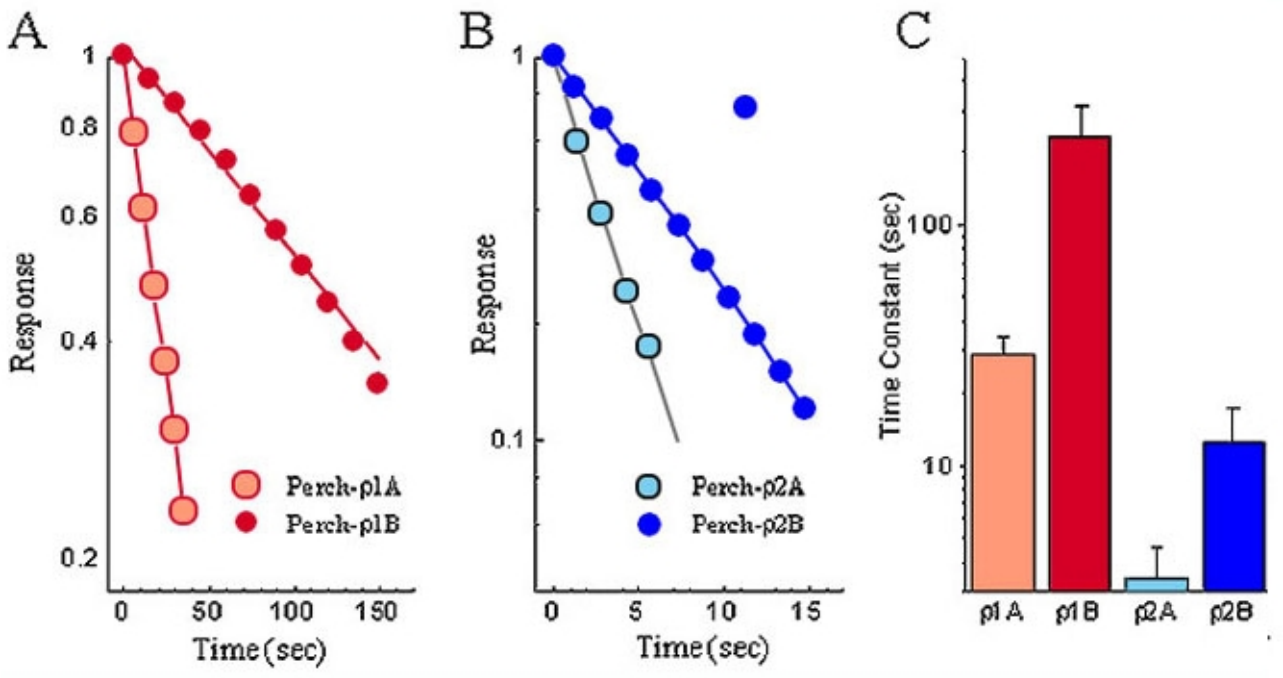

Figure 6. Kinetics of the GABA responses obtained from the white perch GABA ρ receptors expressed in *Xenopus* oocytes. A. Semi-logarithmic plot of GABA responses measured at various times following the offset of drug application (10 μM GABA); the responses were normalized to their initial amplitude at the time of offset. The responses are well fit by straight lines, indicating that the relationship can be described by a single exponential function. B. A similar analysis applied to the offset GABA responses obtained from perch ρ2 receptors. Note different time scales in A and B. C. Comparison of the time constants calculated from GABA offset responses elicited from various GABA ρ receptors.

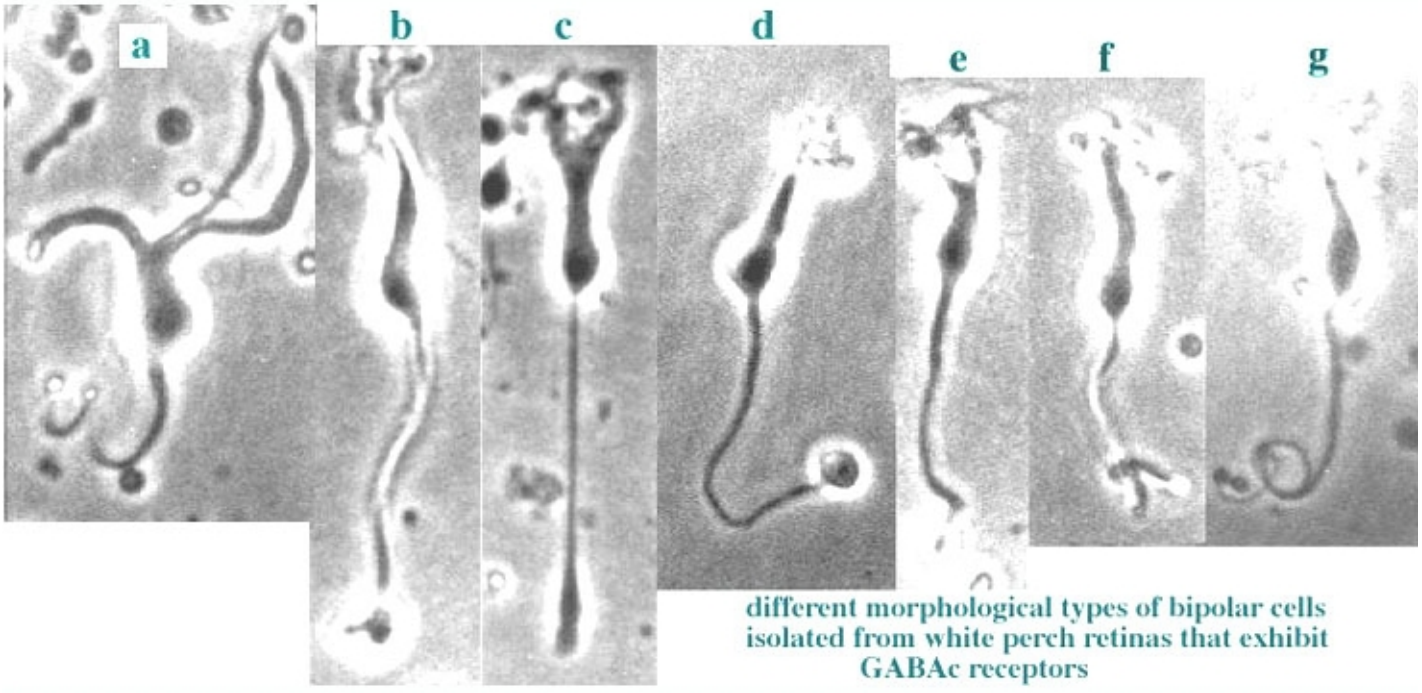

Figure 7. Examples of solitary white perch bipolar cells in culture.

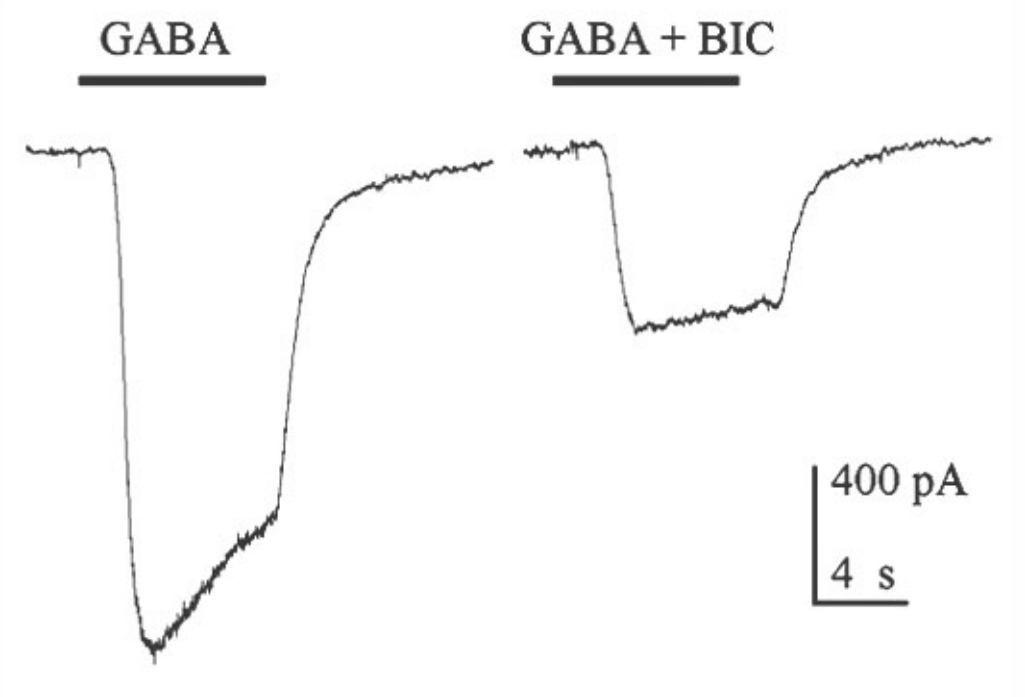

Figure 8. GABA-elicited responses from isolated white perch bipolar cells. The membrane currents elicited by GABA application (left) contain both transient and sustained components, indicating both $GABA_A$ and $GABA_C$ receptors are present. In the pesence of bicuculline, $GABA_A$ receptor activity is inhibited, revealing sustained GABA responses mediated by $GABA_C$ receptors (right).

About the Author

Dr. Haohua Qian was born in Jiangsu, China. He received his B.A. in Biology from Nanjing University (1982), M.S. in Neurobiology from Shanghai Institute of Physiology (1985), and Ph.D. in Anatomy and Cell Biology from University of Illinois at Chicago (1991). He is currently an Assistant Professor of Neurosciences in the Department of Ophthalmology and Visual Sciences at the University of Illinois at Chicago. During his postdoctoral studies with Dr. John E. Dowling at Harvard University, he characterized a new type of GABA receptor, the $GABA_C$ ρ receptor, on retinal neurons. He is currently continuing these studies on the molecular structure and physiological functions of $GABA_C$ receptors in the vertebrate retina.

References

1. Johnston GAR. Multiplicity of GABA receptors. In: Olsen RW, Venter JC, editors. Receptor biochemistry and methodology. Vol. 5. Alan R. Liss, Inc.; 1986. p. 57-71.
2. Johnston GAR. GABAc receptors: relatively simple transmitter-gated ion channels? Trends Pharmacol Sci. 1996;17:319–323. PubMed PMID: 8885697.
3. Albrecht BE, Breitenbach U, Stuhmer T, Harvey RJ, Darlison MG. In situ hybridization and reverse transcription-polymerase chain reaction studies on the expression of the GABA(C) receptor rho1- and rho2-subunit genes in avian and rat brain. Eur J Neurosci. 1997;9:2414–2422. PubMed PMID: 9464935.
4. Boue-Grabot E, Roudbaraki M, Bascles L, Tramu G, Bloch B, Garret M. Expression of GABA receptor rho subunits in rat brain. J Neurochem. 1998;70:899–907. PubMed PMID: 9489708.
5. Enz R, Cutting GR. GABAC receptor rho subunits are heterogeneously expressed in the human CNS and form homo- and heterooligomers with distinct physical properties. Eur J Neurosci. 1999;11:41–50. PubMed PMID: 9987010.
6. Sivilotti L, Nistri A. GABA receptor mechanisms in the central nervous system. Prog Neurobiol. 1991;36:35–92. PubMed PMID: 1847747.
7. Wegelius K, Pasternack M, Hiltunen JO, Rivera C, Kaila K, Saarma M, Reeben M. Distribution of GABA receptor rho subunit transcripts in the rat brain. Eur J Neurosci. 1998;10:350–357. PubMed PMID: 9753143.
8. Qian H, Dowling JE. Novel GABA responses from rod-driven retinal horizontal cells. Nature. 1993;361:162–164. PubMed PMID: 8421521.
9. Feigenspan A, Wässle H, Bormann J. Pharmacology of GABA receptor Cl^- channels in rat retinal bipolar cells. Nature. 1993;361:159–163. PubMed PMID: 7678450.
10. Lukasiewicz PD, Wong ROL. GABAC receptors on ferret retinal bipolar cells: a diversity of subtypes in mammals? Vis Neurosci. 1997;14:989–994. PubMed PMID: 9364734.
11. Lukasiewicz PD, Maple BR, Werblin FS. A novel GABA receptor on bipolar cell terminals in the tiger salamander retina. J Neurosci. 1994;14:1202–1212. PubMed PMID: 8120620.
12. Nelson R, Schaffner AE, Li Y-X, Walton MC. Distribution of GABA(C)-like responses among acutely dissociated rat retinal neurons. Vis Neurosci. 1999;16:179–190. PubMed PMID: 10022489.
13. Pan Z-H, Lipton SA. Multiple GABA receptor subtypes mediate inhibition of calcium influx at rat retinal bipolar cell terminals. J Neurosci. 1995;15:2668–2679. PubMed PMID: 7722621.
14. Qian H, Dowling JE. GABAA and GABAC receptors on hybrid bass retinal bipolar cells. J Neurophysiol. 1995;74:1920–1928. PubMed PMID: 8592185.
15. Qian H, Li L, Chappell RL, Ripps H. GABA receptors of bipolar cells from the skate retina: actions of zinc on GABA-mediated membrane currents. J Neurophysiol. 1997b;78:2402–2412. PubMed PMID: 9356392.
16. Dong CJ, Picaud SA, Werblin FS. GABA transporters and GABAC-like receptors on catfish cone- but not rod-driven horizontal cells. J Neurosci. 1994;14:2648–2658. PubMed PMID: 8182433.
17. Kaneda M, Mochizuki M, Kaneko A. Modulation of GABAC response by Ca2+ and other divalent cations in horizontal cells of the catfish retina. J Gen Physiol. 1997;110:741–747. PubMed PMID: 9382900.
18. Picaud S, Pattnaik B, Hicks D, Forster V, Fontaine V, Sahel J, Dreyfus H. GABAA and GABAC receptors in adult porcine cones: evidence from a photoreceptor-glia co-culture model. J Physiol. 1998;513:33–42. PubMed PMID: 9782157.
19. Zhang J, Slaughter MM. Perferential suppression of the ON pathway by GABAC receptors in the amphibian retina. J Neurophysiol. 1995;74:1583–1592. PubMed PMID: 8989395.
20. Qian H, Dowling JE. Pharmacology of novel GABA receptors found on rod horizontal cells of the white perch retina. J Neurosci. 1994;14:4299–4307. PubMed PMID: 8027780.
21. Woodward RM, Polenzani L, Miledi R. Characterization of bicuculline/baclofen-insensitive (r-like) g-aminobutyric acid receptors expressed in Xenopus oocytes. II. pharmacology of g-aminobutyric acid A and g-aminobutyric acid B receptor agonists and antagonists. Mol Pharmacol. 1993;43:609–625. PubMed PMID: 8386310.

22. Qian H, Dowling JE, Ripps H. Molecular and pharmacological properties of GABA-rho subunits from white perch retina. J Neurobiol. 1998;37:305–320. PubMed PMID: 9805275.
23. Polenzani L, Woodward RM, Miledi R. Expression of mammalian g-aminobutyric acid receptors with distinct pharmacology in Xenopus oocytes. Proc Natl Acad Sci U S A. 1991;88:4318–4322. PubMed PMID: 1709741.
24. Morris KD, Moorefield CN, Amin J. Differential modulation of the gamma-aminobutyric acid type C receptor by neuro active steroids. Mol Pharmacol. 1999;56:752–759. PubMed PMID: 10496958.
25. Woodward RM, Polenzani L, Miledi R. Effects of steroids on g-aminobutyric acid receptors expressed in Xenopusoocytes by poly(A)+ RNA from mammalian brain and retina. Mol Pharmacol. 1992a;41:89–103. PubMed PMID: 1370710.
26. Zhang D, Pan ZH, Zhang X, Brideau AD, Lipton SA. Cloning of a gamma-aminobutyric acid type C receptor subunit in rat retina with a methionine residue critical for picrotoxin in channel block. Proc Natl Acad Sci U S A. 1995;92:11756–11760. PubMed PMID: 8524843.
27. Woodward RM, Polenzani L, Miledi R. Characterization of bicuculline/baclofen-insensitive g-aminobutyric acid receptors expressed in Xenopus oocytes I. effects of Cl- channel inhibitors. Mol Pharmacol. 1992b;42:165–173. PubMed PMID: 1378924.
28. Chang Y, Weiss DS. Channel opening locks agonist on to the GABAC receptor. Nat Neurosci. 1999;2:219–225. PubMed PMID: 10195213.
29. Calvo DJ, Vazquez AE, Miledi R. Cationic modulation of r1-type g-aminobutyrate receptors expressed in Xenopus oocytes. Proc Natl Acad Sci U S A. 1994;91:12725–12729. PubMed PMID: 7809110.
30. Chang Y, Amin J, Weiss DS. Zinc is a mixed antagonist of homomeric r1 g-aminobutyric acid-activated channels. Mol Pharmacol. 1995;47:595–602. PubMed PMID: 7535381.
31. Dong CJ, Werblin FS. Zinc down modulates the GABAc receptor current in cone horizontal cells acutely isolated from the catfish retina. J Neurophysiol. 1995;73:916–919. PubMed PMID: 7760150.
32. Wang TL, Hackam A, Guggino WB, Cutting GR. A single histidine residue is essential for zinc inhibition of GABA rho 1 receptors. J Neurosci. 1995;15:7684–7691. PubMed PMID: 7472519.
33. Ragozzino D, Woodward RM, Murata Y, Eusebi F, Overman LE, Miledi R. Design and in vitro pharmacology of a selective gamma-aminobutyric acid C receptor antagonist. Mol Pharmacol. 1996;50:1024–1030. PubMed PMID: 8863850.
34. Amin J, Weiss DS. Insights into the activation mechanism of rho1 GABA receptors obtained by coexpression of wild type and activation-impaired subunits. Proc Biol Sci. 1996;263:273–282. PubMed PMID: 8920250.
35. Dong CJ, Werblin FS. Dopamine modulation of GABAC receptor function in an isolated retinal neuron. J Neurophysiol. 1994;71:1258–1260. PubMed PMID: 8201417.
36. Wellis DP, Werblin FS. Dopamine modulates GABAc receptors mediating inhibition of calcium entry into and transmitter release from bipolar cell terminals in tiger salamander retina. J Neurosci. 1995;15:4748–4761. PubMed PMID: 7623108.
37. Feigenspan A, Bormann J. Modulation of GABAC receptors in rat retinal bipolar cells by protein kinase C. J Physiol. 1994a;481:325–330. PubMed PMID: 7738828.
38. Kusama T, Sakurai M, Kizawa Y, Uhl GR, Murakami H. GABA rho1 receptor: inhibition by protein kinase C activators. Eur J Pharmacol. 1995;291:431–434. PubMed PMID: 8719430.
39. Filippova N, Dudley R, Weiss DS. Evidence for phosphorylation-dependent internalization of recombinant human r1 GABAC receptors. J Physiol. 1999;518:385–399. PubMed PMID: 10381587.
40. Hanley JG, Koulen P, Bedford F, Gordon-Weeks PR, Moss SJ. The protein MAP-1B links GABA(C) receptors to the cytoskeleton at retinal synapses. Nature. 1999;397:66–69. PubMed PMID: 9892354.
41. Cutting GR, Lu L, Zoghbi H, O'Hara BF, Kasch LM, Montrose-Rafizader C, Donovan DM, Shimada S, Antonarakis SE, Guggino W, Uhl GR, Kazazian HH. Cloning of the g-aminobutyric acid (GABA) rho1 cDNA: a GABA receptor subunit highly expressed in the retina. Proc Natl Acad Sci U S A. 1991;88:2673–2677. PubMed PMID: 1849271.

42. Cutting GR, Curristin S, Zoghbi H, O'Hara B, Selden MF, Uhl GR. Identification of a putative gamma-aminobutyric acid (GABA) receptor subunit rho2 cDNA and colocalization of the genes encoding rho2 (GABRR2) and rho1 (GABRR1) to human chromosome 6q14-q21 and mouse chromosome 4. Genomics. 1992;12:801–806. PubMed PMID: 1315307.
43. Shimada S, Cutting G, Uhl GR. g-Aminobutyric acid A or C receptor? g-Aminobutyric acid r1 receptor RNA induces bicuculline-, barbiturate-, and benzodiazepine-insensitive g-aminobutyric acid responses in Xenopus oocytes. Mol Pharmacol. 1992;41:683–687. PubMed PMID: 1314944.
44. Enz R, Brandstätter JH, Hartveit E, Wässle H, Bormann J. Expression of GABA receptor rho 1 and rho2 subunits in the retina and brain of the rat. Eur J Neurosci. 1995;7:1495–1501. PubMed PMID: 7551175.
45. Enz R, Brandstätter JH, Wässle H, Bormann J. Immunocytochemical localization of the GABAC receptor rho subunits in the mammalian retina. J Neurosci. 1996;16:4479–4490. PubMed PMID: 8699258.
46. Qian H, Hyatt G, Schanzer A, Hazra R, Hackam A, Cutting GR, Dowling JE. A comparison of GABAC and rho subunit receptors from the white perch retina. Vis Neurosci. 1997a;14:843–851. PubMed PMID: 9364723.
47. Qian H, Dowling JE, Ripps H. A single amino acid in the second transmembrane domain of GABA r subunits is a determinant of the response kinetics of GABAC receptors. J Neurobiol. 1999;40:67–76. PubMed PMID: 10398072.
48. Koulen P, Brandstätter JH, Kröger S, Enz R, Bormann J, Wässle H. Immunocytochemical localization of the GABA(C) receptor rho subunits in the cat, goldfish, and chicken retina. J Comp Neurol. 1997;380:520–532. PubMed PMID: 9087530.
49. Feigenspan A, Bormann J. Differential pharmacology of GABAA and GABAC receptors on rat retinal bipolar cells. Eur J Pharmacol. 1994b;288:97–104. PubMed PMID: 7535710.
50. Lukasiewicz PD, Shields CR. Different combinations of GABAA and GABAC receptors confer distinct temporal properties to retinal synaptic responses. J Neurophysiol. 1998;79:3157–3167. PubMed PMID: 9636116.
51. Euler T, Wassle H. Different contributions of GABAA and GABAC receptors to rod and cone bipolar cells in a rat retinal slice preparation. J Neurophysiol. 1998;79:1384–1395. PubMed PMID: 9497419.
52. Dong CJ, Werblin FS. Temporal contrast enhancement via GABAC feedback at bipolar terminals in the tiger salamander retina. J Neurophysiol. 1998;79:2171–2180. PubMed PMID: 9535976.
53. Jacobs AL, Werblin FS. Spatio temporal pattern sat the retinal output. J Neurophysiol. 1998;80:447–451. PubMed PMID: 9658062.

Glycine Receptor Diversity in the Mammalian Retina

Silke Haverkamp, PhD[1]

Created: March 27, 2012.

1 Introduction

Glycine is a major inhibitory neurotransmitter in the mammalian central nervous system (CNS). Its receptors, the inhibitory glycine receptors (GlyRs), are ligand-gated chloride channels composed of ligand-binding α and β subunits (1, 2). In mature neurons, the activation of GlyRs allows for an influx of chloride ions into the cytoplasm, which hyperpolarizes the postsynaptic membrane and, thereby, reduces neuronal firing. Inversely, the blockade of GlyRs by the competitive antagonist strychnine causes overexcitation resulting in pain, muscle cramps and exaggerated startle responses (3). Apart from its major transmitter function in spinal cord and brainstem, glycine also mediates substantial inhibitory neurotransmission via glycinergic amacrine cells in the mammalian retina. Thus, the abundant and highly complex expression patterns of different GlyR subtypes in the inner plexiform layer create an appealing field of retinal research.

2 Structure of glycine receptors

The GlyR was the first neurotransmitter receptor protein to be isolated from the mammalian CNS. Purification of the GlyR from rat spinal cord by strychnine affinity chromatography revealed three distinct polypeptides of molecular mass 48, 58 and 98 kDa (4). The 48 and 58 kDa peptides were shown to correspond to the α1 and β subunits, respectively. The 98 kDa peptide was later identified as the cytoplasmic protein, gephyrin, which is essential for clustering GlyRs at postsynaptic densities via direct interactions between the GlyR β subunit and intracellular microtubules (5).

GlyRs are pentameric ligand-gated ion channel receptors of the Cys-loop family, which also include $GABA_{A/C}$ receptors, muscle and neuronal nicotinic acetylcholine receptors, and serotonin type 3 receptors. Members of this superfamily share a common proposed structure (Fig. 1). Each subunit consists of a large N-terminal extracellular domain, four transmembrane segments (TM1–TM4), a long intracellular loop connecting TM3 and TM4, and a short extracellular C-terminus. The second transmembrane segment, TM2, lines the inner ion pore which, in GlyRs and $GABA_{A/C}$ receptors, displays strict anion selectivity.

Molecular cloning has revealed four genes encoding the α subunits (α1, α2, α3, α4) and only one gene encoding the β subunit (6, 7). In the adult organism, two copies of the α subunit and three copies of the β subunit form the pentameric receptor protein (8).

3. Developmental expression

Glycine is excitatory during embryonic development and around birth. The neonatal form of the GlyR is thought to be a homopentamer of α2 subunits that are mainly found extrasynaptically in vivo, whereas adult synaptic GlyRs are heteromeric αβ receptors. It seems that homomeric α2 GlyRs mediate a depolarizing glycine-gated chloride flux that in turn stimulates the calcium influx necessary for the development of numerous neuronal specializations, including glycinergic synapses (2, 9). Surprisingly, however, knockout of the α2 subunit has no obvious effect on neuronal development (10), whereas an α1 knockout (*Glra1*$^{spd\text{-}ot}$*"oscillator")* has severe

Author Affiliation: 1 Neuroanatomy, Max-Planck-Institute for Brain Research, Frankfurt/Main, Germany.; Email: silke.haverkamp@brain.mpg.de.

Corresponding author.

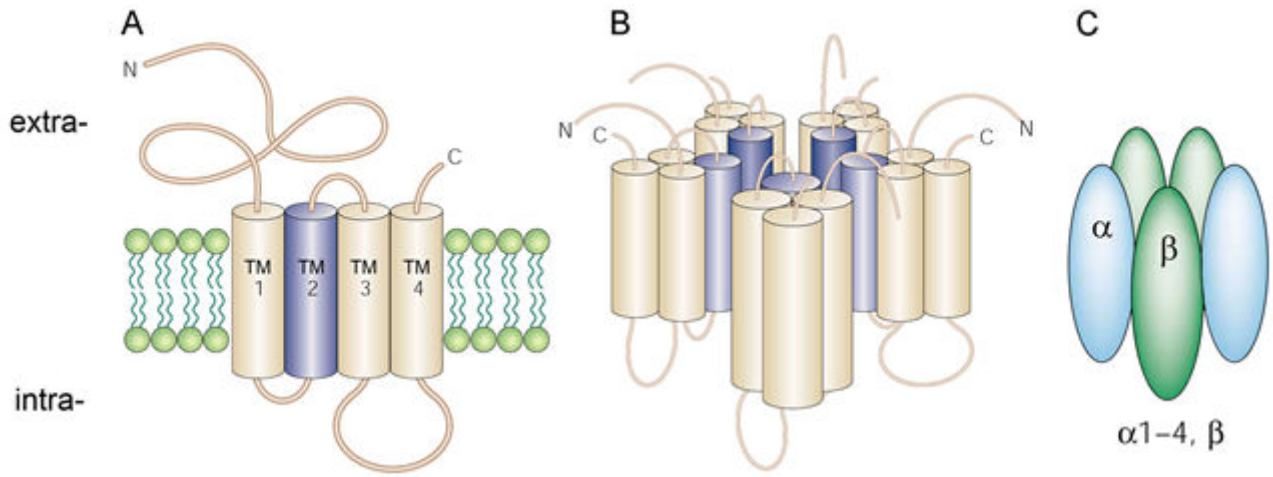

Figure 1. Structure of ligand-gated ion channels. A. Each GlyR subunit consists of a large N-terminal extracellular domain, four transmembrane segments (TM1–TM4), a long intracellular loop connecting TM3 and TM4, and a short extracellular C-terminus. B. Proposed structure of a ligand-gated ion channel. TM2 forms the lining of the ion pore. C. Glycine receptors are pentamers constructed from α and β subunits in a ratio of 2α:3β. From Moss and Smart, 2001 (54).

consequences: mice appear normal until the 2nd postnatal week whereupon they show prolonged periods of rapid tremor, producing extreme rigor and stiffness, and die within 10 days (11, 12).

4. Glycinergic amacrine cells

In the retina, approximately half of the amacrine cells release glycine at their synapses with bipolar, other amacrine, and ganglion cells. Glycinergic amacrine cells can be immunolabeled with antibodies against glycine or against the glycine transporter GlyT1 (13-15). Figure 2 shows a vertical section through a mouse retina that was double immunolabeled for glycine and for GlyT1 (16). Strong glycine immunoreactivity can be observed in amacrine cell bodies and their dendrites descending into the inner plexiform layer (IPL) or in dendrites from interplexiform amacrine cells ascending into the outer plexiform layer (OPL). Weak glycine expression is also found in putative ON-cone bipolar cells in the outer half of the inner nuclear layer (INL). The section was also immunolabeled for GlyT1 which labels all glycinergic amacrine cells but not bipolar cells. Bipolar cells do not express GlyT1 but they receive glycine by diffusion through electrical synapses (gap junctions) from glycinergic amacrine cells (17). In other parts of the CNS, GlyT1 has been localized to glial cells, while GlyT2 is now known to represent the presynaptic neuronal glycine transporter. Surprisingly, GlyT2 does not appear to be expressed in the mammalian retina (18).

5. Morphological types of glycinergic amacrine cells

Glycinergic amacrine cells are small-field amacrine cells with principally vertically oriented dendrites, and they comprise more than 10 different morphological types (13, 19). Most of them have small, diffuse dendritic trees and perform local circuit operations between the different sublayers of the IPL.

The most prominent and also most numerous glycinergic amacrine cell is the AII amacrine cell which transfers the light signal from rod bipolar cells into the cone pathway (20). In the inner IPL, AII cells receive direct glutamatergic input from rod bipolar cells, but they are also engaged with ON-cone bipolar cell axon terminals via electrical synapses (gap junctions). In the outer IPL. AII cell lobular dendrites provide glycinergic, chemical output synapses onto OFF-cone bipolar cell axon terminals and dendrites of OFF ganglion cells. Further glycinergic, small-field amacrine cells were identified in the cat retina by combined Golgi-staining and glycine

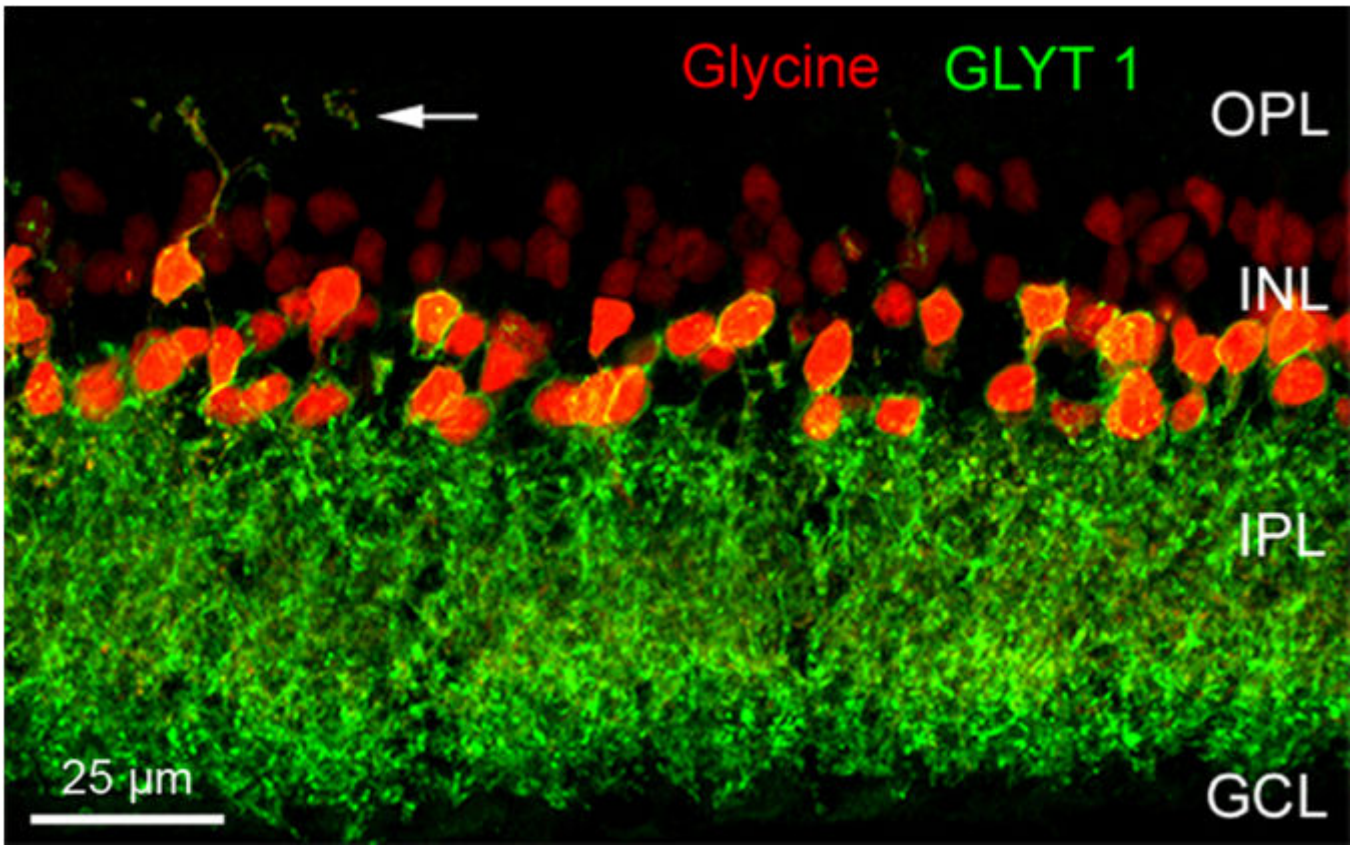

Figure 2. Glycinergic amacrine cells of the mouse retina. A vertical section was double immunolabeled for glycine (red) and the glycine transporter GlyT1 (green). The arrows indicate an interplexiform process ascending to the OPL (OPL: outer plexiform layer; INL: inner nuclear layer; IPL: inner plexiform layer; GCL; ganglion cell layer). From Haverkamp and Wässle, 2000 (16).

uptake (21), and Menger et al. (13) identified at least 8 different glycinergic amacrine cells in the rat retina (Fig. 3).

Recently it became possible to study glycinergic amacrine cells in the retina of transgenic mice which express green fluorescent protein (GFP) under the control of the Thy1 promotor (Thy1-GFP-O) (22, 23). Three such cells are illustrated in figure 4, with double labeling for calcium binding protein 5 (CaBP5) in order to reveal the different sublaminas of the IPL and possible bipolar cell candidates as synaptic partners. The cells in figures 4A and B have small, diffuse dendritic trees; the cell in figure 4C has a bistratified appearance and has been identified as A8 cell in cats and human retinas (24-26) (see also chapter on 'Roles of Amacrine Cells', Webvision).

6. GlyR diversity in the mouse retina

The diversity of types of glycinergic amacrine cells is paralleled by the striking heterogeneity of glycine receptors. All four α subunits of the GlyR have been localized to specific synapses within the mammalian retina (23, 27-30). When subunit selective antibodies were applied to lightly fixed tissue, they each produced a distinct punctate immunofluorescence pattern (Figure 5).

The GlyRα1 subunit is expressed in a sparse population of puncta in the OPL, which represent synapses between glycinergic interplexiform cells and bipolar cell dendrites (Fig. 5A). In the outer IPL (stratum S1 and S2) GlyR α1 immunoreactivity is found in large puncta, which occur at high density. They represent synapses between AII amacrine cells and OFF-cone bipolar cells (30). In the inner IPL (stratum S3-S5) smaller GlyRα1 immunoreactive puncta can be observed representing synapses onto ganglion cell dendrites and rod bipolar cell axons (31, 32). The GlyRα2 subunit is more uniformly distributed across all strata (Fig. 5B), and GlyRα2

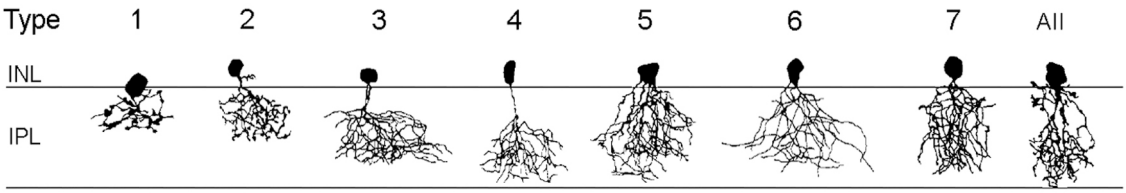

Figure 3. Glycinergic amacrine cells of the rat retina. From Menger, Pow and Wässle, 1998 (13).

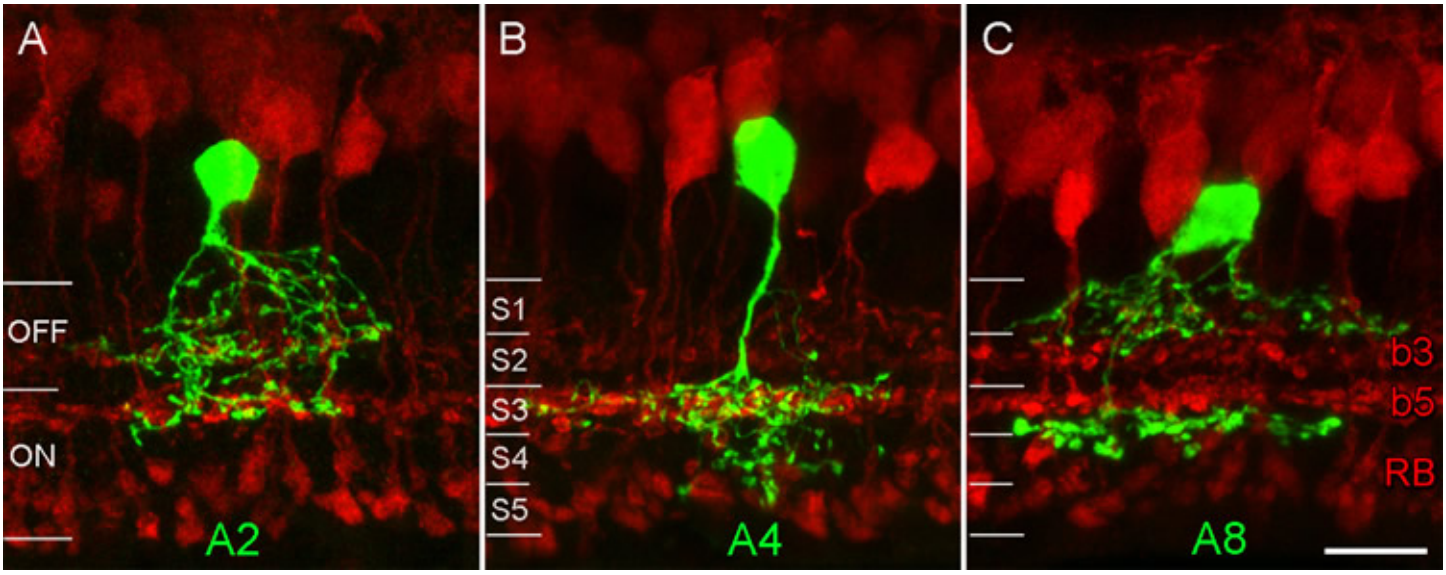

Figure 4. Glycinergic amacrine cells expressing GFP in the Thy1-GFP-O mouse. Sections are double labeled for bipolar cell marker CaBP5 (red). CaBP5 is expressed in rod bipolar cells (RB), in type 5 ON-cone bipolar cells (b5), and in type 3 OFF-cone bipolar cells (b3) (55). A2 and A4 amacrine cells are classified according to the scheme of Menger et al., 1998 (13); A8 according to Kolb et al., 1981 (26). Scale bar: 25 µm. Unpublished data.

immunoreactive puncta occur at the highest density amongst the four α subunits (28). The GlyRα3 subunit (Fig. 5C) shows four bands whose density of puncta successively declines towards the ON sublamina (27). Lastly, the GlyRα4 subunit (Fig. 5D) shows a band of high density of puncta at the border between stratum 3 and 4 and further small and sparsely distributed puncta throughout the remaining strata (23). Taken together, the characteristic distribution of subunits across the IPL suggests that the GlyR subtypes are expressed at different synapses and are involved with different neuronal circuits.

Electron microscopy confirms the notion that the immunofluorescent puncta represent clusters of GlyRs at postsynaptic sites. Antibodies against the α1 subunit recognize extracellular epitopes of the receptor. Thus, staining from preembedding immunoelectron-microscopic experiments appears in the synaptic cleft of the synapse (Fig. 6A). Accordingly, postembedding immunoelectron microscopy showed that the α3 subunit was localized at the postsynaptic membrane (Fig. 6B).

7. Co-localization of GlyR subunits at postsynaptic sites

Since synaptic GlyRs are composed of 2α and 3β subunits (8) there is the possibility that two different α subunits co-exist in a single heteromeric GlyR. In addition, it is possible that two different GlyR subtypes, such as α2β and α3β GlyRs co-distribute at the same postsynaptic sites. In both cases, the immunoreactive hot spots should coincide. However, when retinal sections were double labeled for the GlyRα1 subunit and the other three GlyRα subunits, no statistically significant coincidence rate of immunoreactive puncta was observed. When retinal

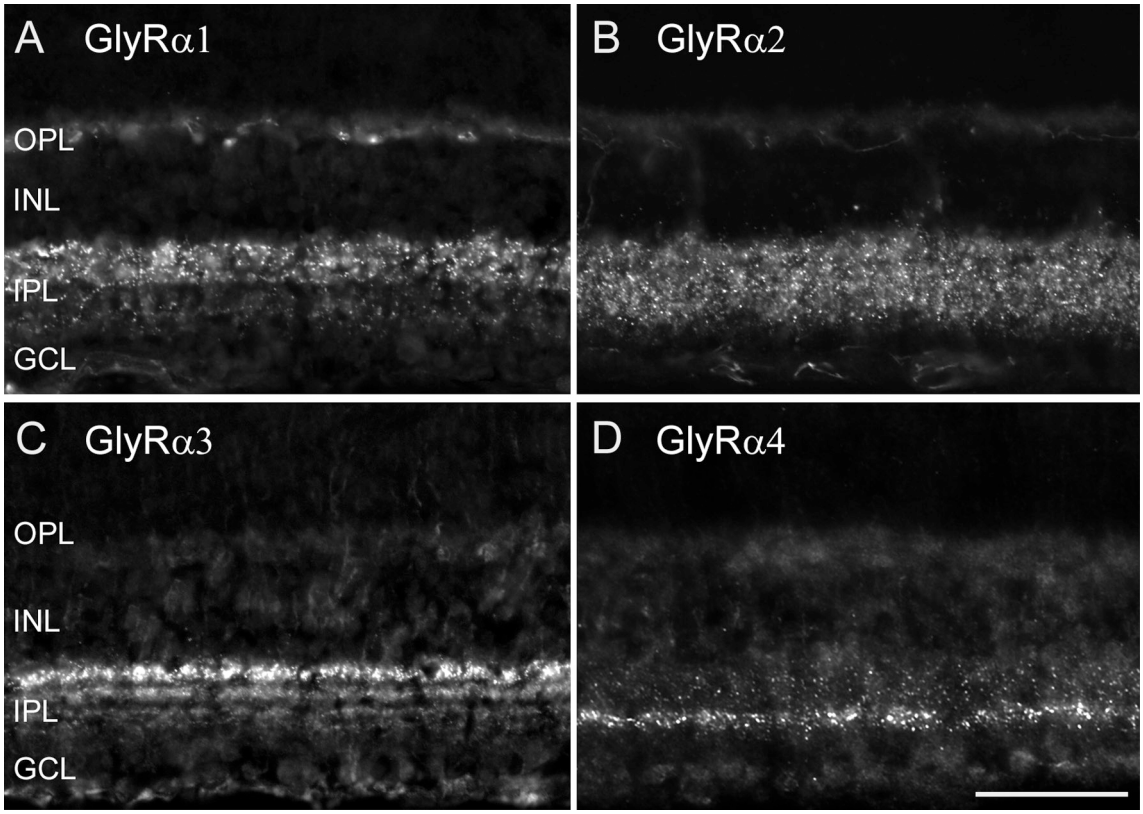

Figure 5. Diversity of GlyR subtypes in the mouse retina. A. GlyRα1 immunoreactive puncta are most prominent in the outer IPL (OFF sublamina). B. GlyRα2 immunofluorescence is more evenly distributed across the IPL. C. GlyRα3 expression is found in four bands. D. GlyRα4 is most prominent in a small band at sublamina 3/4 border. Scale bar: 50 μm. From Heinze et al., 2007 (23).

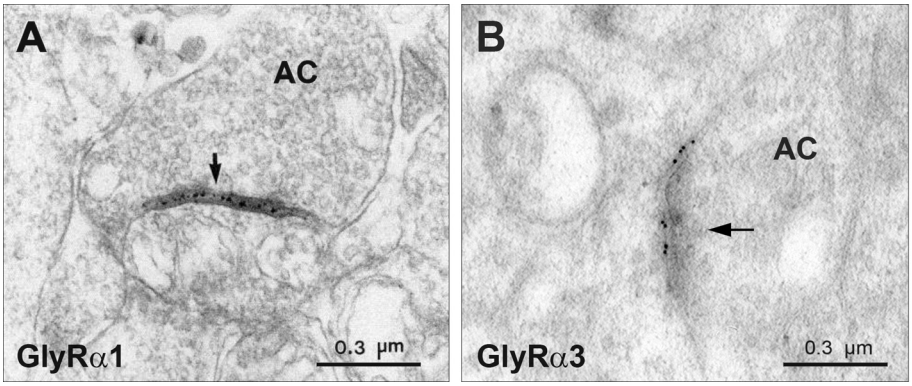

Figure 6. Synaptic localization of two GlyR subunits at conventional synapses in the IPL. A. Preembedding electron microscopy on vibratome sections of rat retina. The figure shows an amacrine cell synapse (AC, arrow) with GlyRα1 immunoreactivity. From Sassoè-Pognetto et al., 1994 (30). B. Postembedding electron microscopy of GlyRα3 on ultrathin sections of mouse retina. The GlyR subunit is localized at the postsynaptic membrane of an amacrine cell synapse (provided by Christian Puller, unpublished data).

sections were double labeled for the GlyRα2 and α3 subunits a coincidence rate of 26.7% was found (28). In retinal sections double labeled for the GlyRα3 and α4 subunits no significant coincidence rate was found (23). In sections double labeled for the GlyRα4 and α2 subunits, 31.5% of the α4 immunoreactive clusters also contained the α2 subunit (Fig. 7). The results indicate that postsynaptic GlyR clusters usually contain only one type of α subunit. The exception is approximately one third of synapses immunoreactive for GlyR α2 which can also contain the α3 or the α4 subunits.

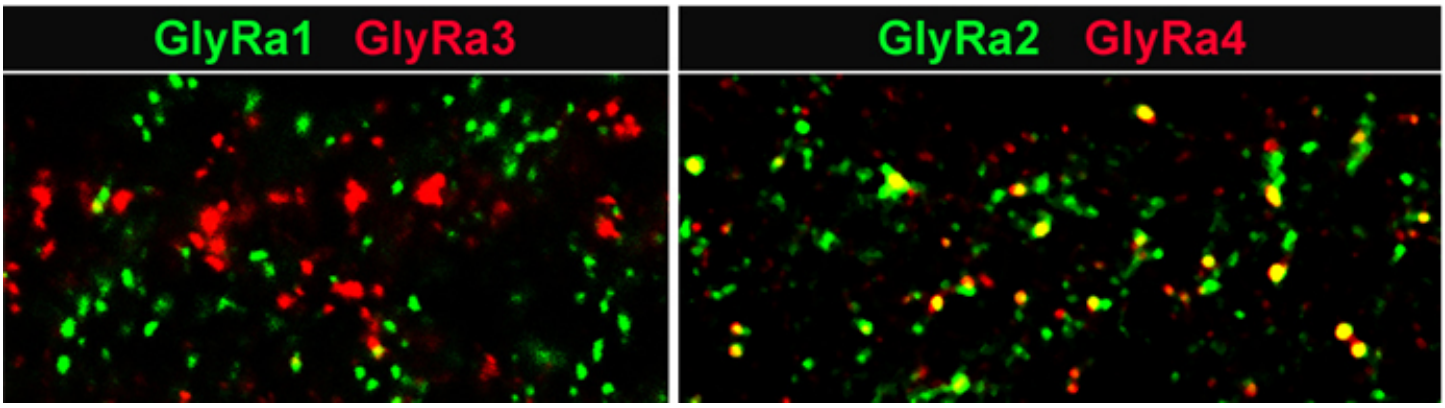

Figure 7. Colocalization of GlyR subunits at postsynaptic sites. GlyRα3 and GlyRα1 immunoreactive puncta are not colocalized whereas GlyRα2 and GlyRα4 immunoreactive puncta sometimes colocalize. From Haverkamp et al., 2003 (27); Heinze et al., 2007 (23).

8. Expression of GlyRs by identified neurons

In order to reveal the involvement of selected GlyR subtypes with different retinal circuits, identified neurons were immunostained for the different GlyR α subunits. Figure 8 shows a GFP labeled A-type ganglion cell in a whole mount of Thy1-GFP-O mouse retina (32). The retina was immunolabeled for the GlyRα1 subunit demonstrating that many GlyRα1 immunoreactive puncta decorate the dendrites of this A-type ON ganglion cell. A coincidence of puncta and dendrites was also obvious for A-type OFF ganglion cells, which suggests that both ON and OFF A-type ganglion cells receive glycinergic input through α1 subunit expressing synapses. A-type ganglion cells were also double labeled for the other α subunits but quantification showed that the predominant input is through GlyRα1 containing synapses (32).

Figure 9 shows a vertical view of a Type 3 glycinergic amacrine cell in the Thy1-GFP-O mouse retina (33). Many GlyRα2 immunoreactive puncta (red) coincide with dendritic varicosities of the Type 3 cell (green) (Fig. 9D-F). Since this cell is a glycinergic amacrine cell, the puncta may represent input synapses the cell receives from other glycinergic amacrine cells or output synapses the cell makes onto other, non-labeled neurons. The fact that the red GlyRα2 immunoreactive puncta are always slightly displaced from the green varicosities (Fig. 9F) indicates that these synaptic GlyRα2 clusters are expressed by unknown neurons that are postsynaptic to this Type 3 cell.

The two examples of cells presented in figure 8 and figure 9 suggest a correlation between the morphological type of a given neuron and the molecular signature of the glycinergic synapse it receives or forms onto postsynaptic neurons. In this context one interesting question is whether the presynaptic neuron instructs the postsynaptic cell to express certain GlyR subunits or whether a given postsynaptic neuron expresses an exclusive GlyR subtype. To address this question a detailed physiological characterization of selected synaptic GlyRs on individual cells is essential.

To date, selective agonists or antagonists that distinguish different isoforms of synaptic GlyRs have not been identified (1, 34). However, mutant mice are available that have dysfunction of specific GlyR subunits and thus it became possible to study details of the glycinergic synaptic transmission in the mammalian retina (31, 32, 35, 36). The kinetic properties of GlyRs were measured by recording spontaneous inhibitory postsynaptic currents (sIPSCs) from identified retinal neurons in wild-type mice and mice lacking GlyR α subunit (*Glra1*$^{spd\text{-}ot}$, *Glra2* and *Glra3*. From the observed differences of sIPSCs in wild-type and mutant mice, the cell-type specific subunit composition of GlyRs can be defined.

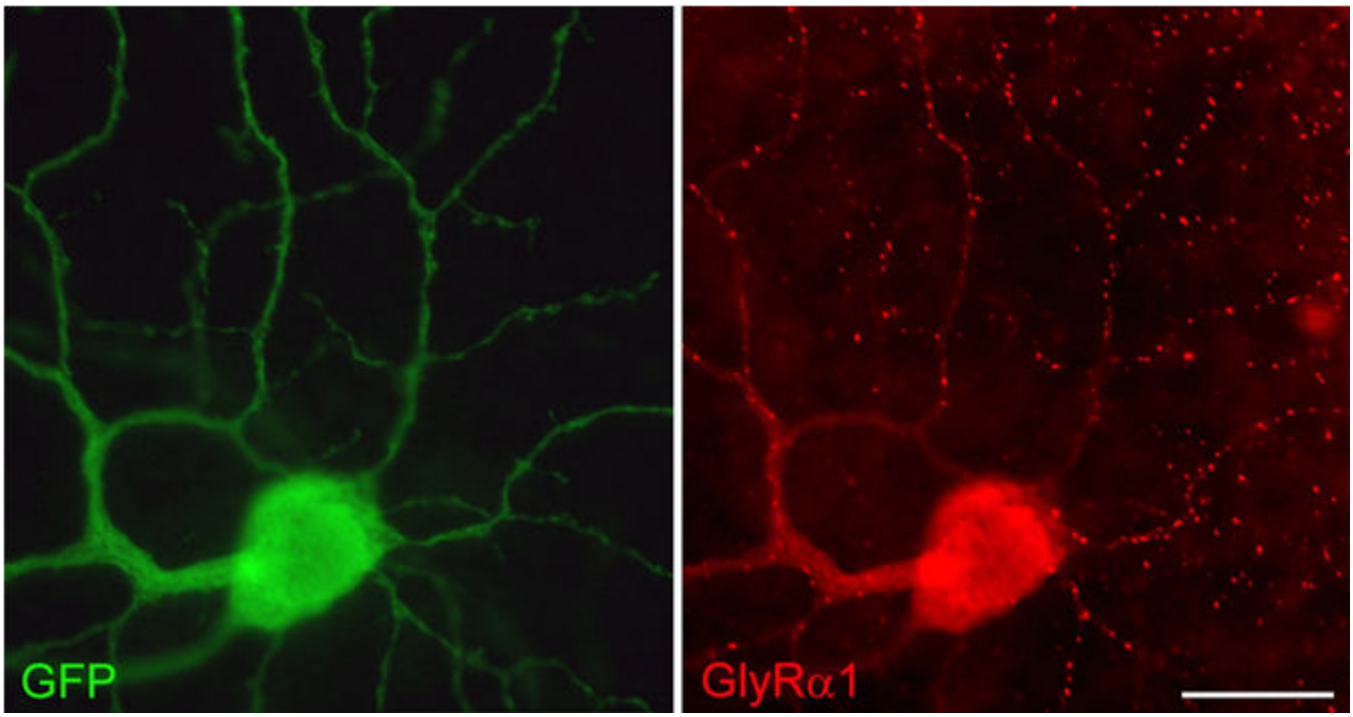

Figure 8. Colocalization of GlyRα1 with the dendrites of an A-type ganglion cell. The image on the left shows an A2-ON ganglion cell in the Thy1-GFP-O mouse (22). The whole mount was also immunostained for GlyRα1 and many immunoreactive puncta decorate the dendrites of this ganglion cell. Scale bar: 20 μm. From Majumdar et al., 2007 (32).

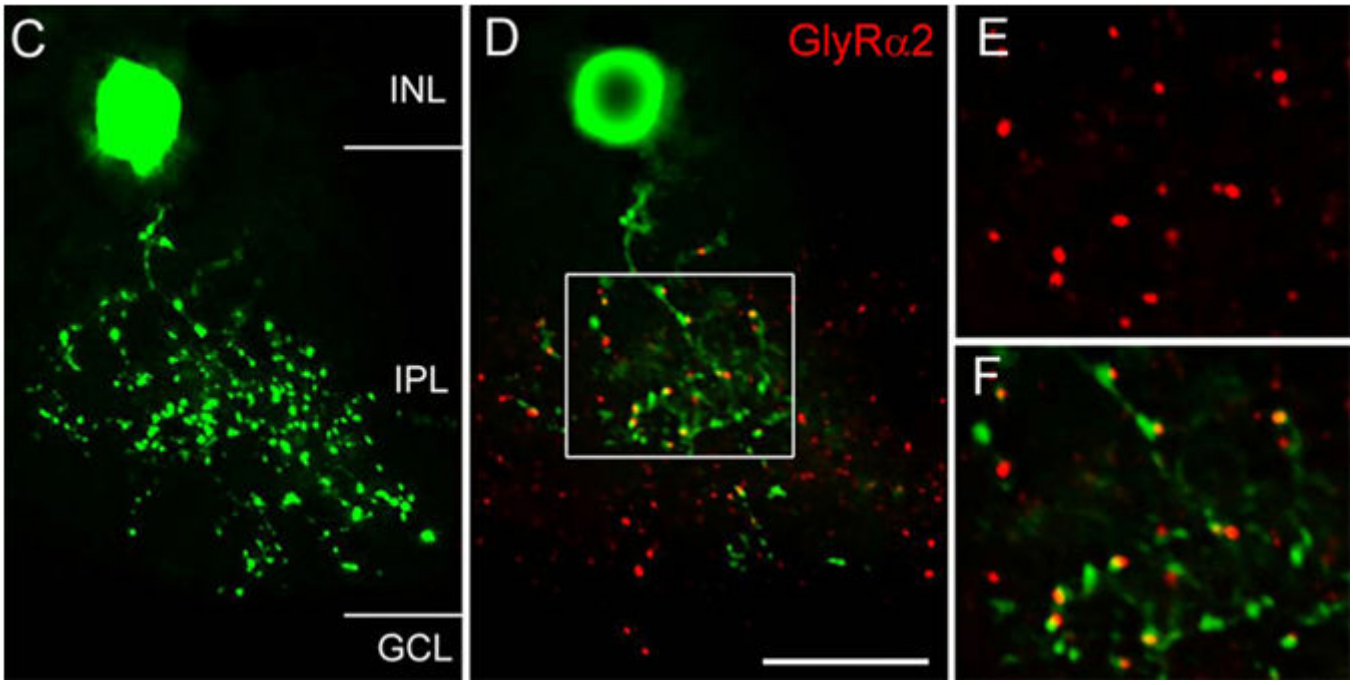

Figure 9. Association of GlyRα2 with a glycinergic amacrine cell. C. Type 3 amacrine cell from the Thy1-GFP-O mouse retina. D. Single confocal section of the cell in C also immunostained for GlyRα2. The boxed area is shown at higher magnification in E and F. Scale bar: 17 μm in C & D, 10 μm in E & F. From Wässle et al., 2009 (33).

Glycine receptors expressed by bipolar cells

Patch-clamp recordings performed from identified bipolar cells in slices of the mouse retina (31) enabled the study of GlyRs by the application of exogenous glycine and by recording glycinergic spontaneous inhibitory postsynaptic currents (sIPSCs). Glycine application elicited large-amplitude currents in all OFF-cone and rod bipolar cells while ON-cone bipolar cells exhibited only very small, if any, glycinergic currents (Fig. 10 (31, 37),). By comparing sIPSCs of bipolar cells in wild-type and *Glra3*$^{-/-}$ mice, no statistically significant differences were found; whereas glycine-induced currents and sIPSCs were absent from all bipolar cells of *Glra1*$^{spd\text{-}ot}$ mice. Thus, OFF-cone and rod bipolar cells receive kinetically fast glycinergic inputs, preferentially mediated by GlyRs composed of α1 and β subunits (decay time constant τ ~ 5 ms). Slow sIPSCs, the characteristic of GlyRs containing the α2 subunit, were not observed in bipolar cells.

Glycine receptors on AII and narrow-field amacrine cells

Amacrine cells are known to express strychnine-sensitive glycine receptors. The GlyRs expressed by AII amacrine cells and by the narrow-field (NF) amacrine cells (Fig. 11A) were studied by patch-clamp recordings in mouse retinal slices (36). Glycinergic sIPSCs of AII cells displayed medium fast kinetics (τ ~ 11 ms, Fig. 11B), which were completely absent in the *Glra3*$^{-/-}$ mouse, indicating that synaptic GlyRs of AII cells mainly contain the α3 subunit. Glycinergic sIPSCs of NF cells had slow kinetics (τ ~ 27 ms, Figs. 11B and 12C) that were significantly prolonged in *Glra2*$^{-/-}$ mice (τ ~ 69 ms, Fig. 12F). These data show that morphologically distinct amacrine cells express different sets of glycine receptors.

Glycine receptors expressed by wide-field amacrine cells

Glycine induced currents and sIPSCs were also recorded from displaced wide-field, putative GABAergic amacrine cells. These GlyRs had slow kinetics (τ ~ 25 ms) (35, 38) comparable to NF amacrine cells. ON-starburst (cholinergic amacrine cells) had sIPSCs with extremely long decay time constants (τ ~ 50 - 70 ms), which did not differ between wild-type and the three mutant mice (35). Since GlyR α4 immunoreactive puncta (Fig. 5D) occur at higher density along the dendrites of ON-starburst amacrine cells, it is possible that GlyRs of ON-starburst cells are dominated by the α4 subunit. This would in turn suggest that GlyRs containing the α4 subunit have slow kinetics.

Glycine receptors expressed by ganglion cells

There are more than ten different types of ganglion cells in any mammalian retina. The GlyRs expressed by A-type ganglion cells (alpha-cell homologues) of the mouse retina were also investigated both in wild-type and mutant mice (32). In the wild-type retina, glycinergic sIPSCs of A-type ganglion cells have fast kinetics (mean τ = 3.9 ± 2.5 ms). Glycinergic sIPSCs recorded from *Glra2*$^{-/-}$ and *Glra3*$^{-/-}$ mice did not differ from those of wild-type mice. However, the number of glycinergic sIPSCs was significantly reduced in *Glra1*$^{spd\text{-}ot}$ mice and the remaining sIPSCs had slower kinetics. These results show that A-type ganglion cells receive preferentially kinetically fast glycinergic inputs, mediated by GlyRs containing the α1 subunit.

B-type cells (beta-cell homologues) are probably involved with sustained neurotransmission. They are also believed to perform complex tasks like local edge detection. However, the specific roles of different B-type cells in the mouse retina are not yet clearly understood. There are four classes of small-field B-type ganglion cells (39), and there seems to be a substantial heterogeneity with respect to GlyR expression in these cell types. GlyRs of B1 cells are dominated by the α1 subunit, while in B4 cells the α3 subunit plays an important role. B2 and B3 cells express a more balanced mixture of fast (α1) and slow (α2, α3, α4) GlyR subunits (40).

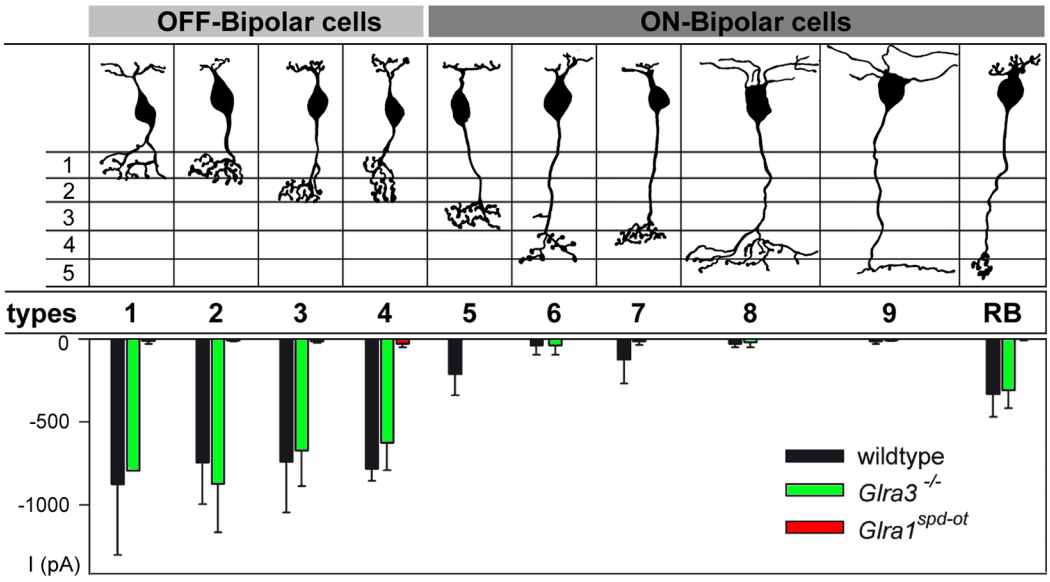

Figure 10. Glycine-induced currents from mouse bipolar cells. OFF- and ON-bipolar cells of the mouse retina as described by Ghosh et al., 2004 (55) and summary diagram of the peak amplitudes of inward currents elicited by the application of glycine (1–2 mM) in the nine cone bipolar cell types and rod bipolar (RB) cells of wild-type, Glra3$^{-/-}$ and Glra1$^{spd\text{-}ot}$ mice. From Ivanova et al., 2006 (31).

9. Summary and conclusion

All four GlyR α subunits are clustered in synaptic hot spots (Fig. 5) that show characteristic distributions across the IPL of the mouse retina (23). Gephyrin is responsible for clustering GlyRs to postsynaptic sites by linking the GlyR β subunit to the cytoskeleton (5, 41). No GlyR clusters could be detected in gephyrin deficient mouse retinas (42), which suggests that synaptic GlyRs in the retina are always heteromeric. In the adult, two copies of the α subunit and three copies of the β subunit form the pentameric receptor protein (8).

Bipolar cells and A-type ganglion cells represent the fast transfer channel of the mammalian retina and, therefore, express α1β GlyRs with fast kinetics. AII amacrine cells relay rod light signals with lower temporal resolution and express α3β GlyRs with medium-fast kinetics. NF amacrine cells are modulatory interneurons, where temporal precision seems less important and they express the α2β and α4β GlyRs with slow kinetics.

Both GABA and glycine inhibition are used to modulate different aspects of ganglion cell responses and receptive field (RF) organization (43-45). GABAergic amacrine cells often provide feedforward inhibition and target both $GABA_A$Rs and $GABA_C$Rs in reciprocal inhibitory circuits to modulate the RF center excitation (46), and they target $GABA_A$Rs to amplify and refine the RF surround (47). Glycinergic inhibition on the other hand modulates less spatial than temporal properties and may increase the gain of the ganglion cell response. Glycinergic amacrine cells often use (crossover) inhibition to modulate ganglion cell excitatory inputs within their RF center (48-52).

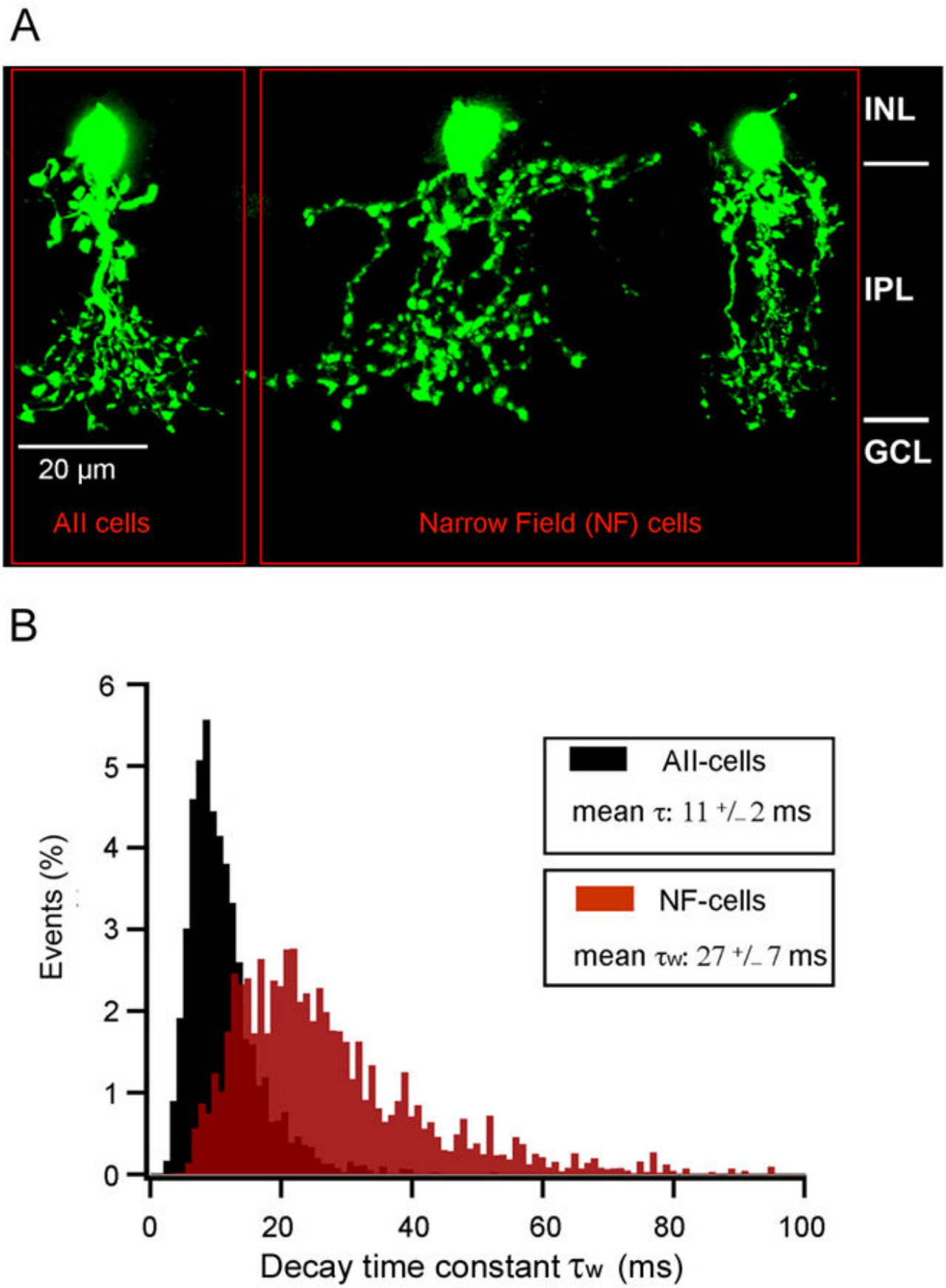

Figure 11. Glycinergic sIPSCs of mouse narrow-field amacrine cells. A. Examples of recorded AII, and narrow field (NF) glycinergic amacrine cells. B. Frequency histogram of decay time constants of glycinergic sIPSCs recorded from AII cells and from NF cells in wild-type mice. From Weiss et al., 2008 (36).

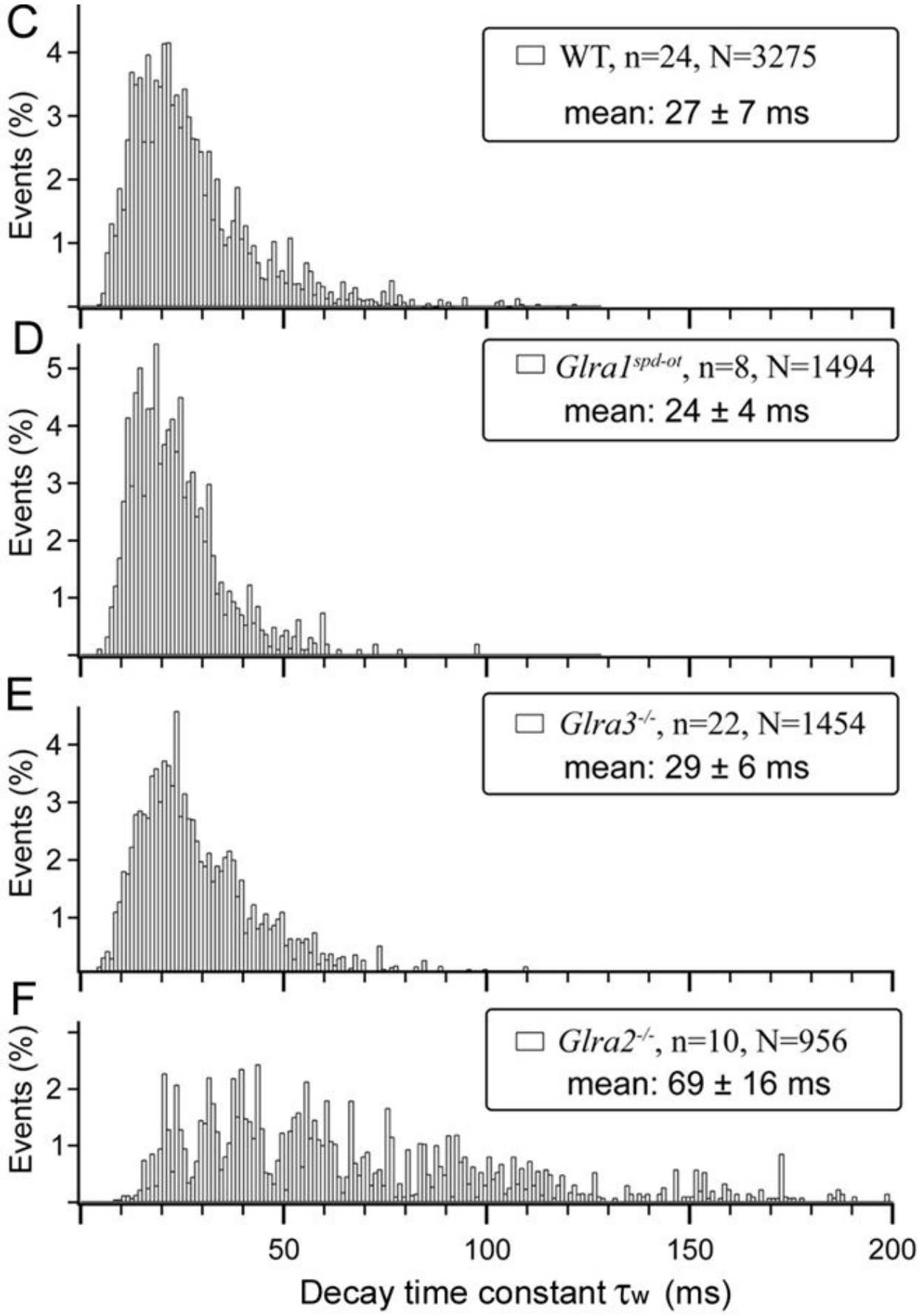

Figure 12. Mutations of glycine receptor α subunits change sIPSC decay times. C-F. Decay time constants of glycinergic sIPSCs recorded from narrow field (NF) cells of wild-type, *Glra*$^{spd\text{-}ot}$, *Glra3*$^{-/-}$ and *Glra2*$^{-/-}$ mice. From Weiss et al., 2008 (36).

About the Authors

Silke Haverkamp received her PhD from the Carl von Ossietzky Universität Oldenburg, Germany, in Visual Neuroscience under the mentorship of Josef Ammermüller. She was a postdoctoral researcher at the Boston University with Bill Eldred and then at the Moran Eye Center in Salt Lake City with Helga Kolb. Afterwards, Silke moved back to Germany to join the Department of Neuroanatomy headed by Heinz Wässle at the Max Planck Institute of Brain Research in Frankfurt. She has now her own research group at the Institute and focuses on the structure and function of neurons and synaptic circuits within the mammalian retina, using neuroanatomical and electrophysiological methods.

References

1. Betz H., Laube B. *Glycine receptors: recent insights into their structural organization and functional diversity.* .J Neurochem. 2006;97(6):1600–10. PubMed PMID: 16805771.
2. Lynch J.W. *Native glycine receptor subtypes and their physiological roles.* .Neuropharmacology. 2009;56(1):303–9. PubMed PMID: 18721822.
3. Harvey R.J.et al. *The genetics of hyperekplexia: more than startle!* .Trends Genet. 2008;24(9):439–47. PubMed PMID: 18707791.
4. Pfeiffer F., Graham D., Betz H. *Purification by affinity chromatography of the glycine receptor of rat spinal cord.* .J Biol Chem. 1982;257(16):9389–93. PubMed PMID: 6286620.
5. Meyer G.et al. *Identification of a gephyrin binding motif on the glycine receptor beta subunit.* .Neuron. 1995;15(3):563–72. PubMed PMID: 7546736.
6. Harvey R.J.et al. *Glycine receptors containing the alpha4 subunit in the embryonic sympathetic nervous system, spinal cord and male genital ridge.* .Eur J Neurosci. 2000;12(3):994–1001. PubMed PMID: 10762330.
7. Matzenbach B.et al. *Structural analysis of mouse glycine receptor alpha subunit genes. Identification and chromosomal localization of a novel variant.* .J Biol Chem. 1994;269(4):2607–12. PubMed PMID: 7507926.
8. Grudzinska J.et al. *The beta subunit determines the ligand binding properties of synaptic glycine receptors.* .Neuron. 2005;45(5):727–39. PubMed PMID: 15748848.
9. Kirsch J., Betz H. *Glycine-receptor activation is required for receptor clustering in spinal neurons.* .Nature. 1998;392(6677):717–20. PubMed PMID: 9565032.

10. Young-Pearse T.L.et al. *Characterization of mice with targeted deletion of glycine receptor alpha 2.* .Mol Cell Biol. 2006;26(15):5728–34. PubMed PMID: 16847326.
11. Buckwalter M.S.et al. *A frameshift mutation in the mouse alpha 1 glycine receptor gene (Glra1) results in progressive neurological symptoms and juvenile death.* .Hum Mol Genet. 1994;3(11):2025–30. PubMed PMID: 7874121.
12. Kling C.et al. *The frameshift mutation oscillator (Glra1(spd-ot)) produces a complete loss of glycine receptor alpha1-polypeptide in mouse central nervous system.* .Neuroscience. 1997;78(2):411–7. PubMed PMID: 9145798.
13. Menger N., Pow D.V., Wässle H. *Glycinergic amacrine cells of the rat retina.* .J Comp Neurol. 1998;401(1):34–46. PubMed PMID: 9802699.
14. Pow D.V. *Transport is the primary determinant of glycine content in retinal neurons.* .J Neurochem. 1998;70(6):2628–36. PubMed PMID: 9603230.
15. Pow D.V., Hendrickson A.E. *Distribution of the glycine transporter glyt-1 in mammalian and nonmammalian retinae.* .Vis Neurosci. 1999;16(2):231–9. PubMed PMID: 10367958.
16. Haverkamp S., Wässle H. *Immunocytochemical analysis of the mouse retina.* .J Comp Neurol. 2000;424(1):1–23. PubMed PMID: 10888735.
17. Vaney D.I., Nelson J.C., Pow D.V. *Neurotransmitter coupling through gap junctions in the retina.* .J Neurosci. 1998;18(24):10594–602. PubMed PMID: 9852595.
18. Zafra F.et al. *Glycine transporters are differentially expressed among CNS cells.* .J Neurosci. 1995;15(5 Pt 2):3952–69. PubMed PMID: 7751957.
19. MacNeil M.A., Masland R.H. *Extreme diversity among amacrine cells: implications for function.* .Neuron. 1998;20(5):971–82. PubMed PMID: 9620701.
20. Kolb H., Famiglietti E.V. *Rod and cone pathways in the inner plexiform layer of cat retina.* .Science. 1974;186(4158):47–9. PubMed PMID: 4417736.
21. Pourcho R.G., Goebel D.J. *A combined Golgi and autoradiographic study of (^{3} H)glycine-accumulating amacrine cells in the cat retina.* .J Comp Neurol. 1985;233(4):473–80. PubMed PMID: 2984258.
22. Feng G.et al. *Imaging neuronal subsets in transgenic mice expressing multiple spectral variants of GFP.* .Neuron. 2000;28(1):41–51. PubMed PMID: 11086982.
23. Heinze L.et al. *Diversity of glycine receptors in the mouse retina: localization of the alpha4 subunit.* .J Comp Neurol. 2007;500(4):693–707. PubMed PMID: 17154252.
24. Kolb H., Linberg K.A., Fisher S.K. *Neurons of the human retina: a Golgi study.* .J Comp Neurol. 1992;318(2):147–87. PubMed PMID: 1374766.
25. Kolb H., Nelson R. *Hyperpolarizing, small-field, amacrine cells in cone pathways of cat retina.* .J Comp Neurol. 1996;371(3):415–36. PubMed PMID: 8842896.
26. Kolb H., Nelson R., Mariani A. *Amacrine cells, bipolar cells and ganglion cells of the cat retina: a Golgi study.* .Vision Res. 1981;21(7):1081–1114. PubMed PMID: 7314489.
27. Haverkamp S.et al. *Diversity of glycine receptors in the mouse retina: localization of the alpha3 subunit.* .J Comp Neurol. 2003;465(4):524–39. PubMed PMID: 12975813.
28. Haverkamp S.et al. *Diversity of glycine receptors in the mouse retina: localization of the alpha2 subunit.* .J Comp Neurol. 2004;477(4):399–411. PubMed PMID: 15329889.
29. Jusuf P.R., Haverkamp S., Grunert U. *Localization of glycine receptor alpha subunits on bipolar and amacrine cells in primate retina.* .J Comp Neurol. 2005;488(2):113–28. PubMed PMID: 15924342.
30. Sassoe-Pognetto M., Wässle H., Grunert U. *Glycinergic synapses in the rod pathway of the rat retina: cone bipolar cells express the alpha 1 subunit of the glycine receptor.* .J Neurosci. 1994;14(8):5131–46. PubMed PMID: 8046473.
31. Ivanova E., Műller F. *Retinal bipolar cell types differ in their inventory of ion channels.* .Vis Neurosci. 2006;23(2):143–54. PubMed PMID: 16638168.
32. Majumdar S.et al. *Glycine receptors of A-type ganglion cells of the mouse retina.* .Vis Neurosci. 2007;24(4):471–87. PubMed PMID: 17550639.

33. Wässle H.et al. *Glycinergic transmission in the Mammalian retina.* .Front Mol Neurosci. 2009;2:6. PubMed PMID: 19924257.
34. Webb T.I., Lynch J.W. *Molecular pharmacology of the glycine receptor chloride channel.* .Curr Pharm Des. 2007;13(23):2350–67. PubMed PMID: 17692006.
35. Majumdar S., Weiss J., Wässle H. *Glycinergic input of widefield, displaced amacrine cells of the mouse retina.* .J Physiol. 2009;587(Pt 15):3831–49. PubMed PMID: 19528249.
36. Weiss J.et al. *Glycinergic input of small-field amacrine cells in the retinas of wildtype and glycine receptor deficient mice.* .Mol Cell Neurosci. 2008;37(1):40–55. PubMed PMID: 17920294.
37. Eggers E.D., Lukasiewicz P.D. *GABA $_A$, GABA $_C$ and glycine receptor-mediated inhibition differentially affects light-evoked signalling from mouse retinal rod bipolar cells.* .J Physiol. 2006;572(Pt 1):215–25. PubMed PMID: 16439422.
38. Veruki M.L., Gill S.B., Hartveit E. *Spontaneous IPSCs and glycine receptors with slow kinetics in wide-field amacrine cells in the mature rat retina.* .J Physiol. 2007;581(Pt 1):203–19. PubMed PMID: 17331993.
39. Sun W., Li N., He S. *Large-scale morphological survey of mouse retinal ganglion cells.* .J Comp Neurol. 2002;451(2):115–26. PubMed PMID: 12209831.
40. Majumdar, S., L. Heinze, and H. Wässle, *Glycinergic Synaptic Inputs of B-type Ganglion Cells of the Mouse Retina.* ARVO Meeting Abstracts, 2007**48**(5): p. 4597.
41. Kirsch J., Betz H. *Widespread expression of gephyrin, a putative glycine receptor-tubulin linker protein, in rat brain.* .Brain Res. 1993;621(2):301–10. PubMed PMID: 8242343.
42. Fischer F.et al. *Reduced synaptic clustering of GABA and glycine receptors in the retina of the gephyrin null mutant mouse.* .J Comp Neurol. 2000;427(4):634–48. PubMed PMID: 11056469.
43. Caldwell J.H., Daw N.W. *Effects of picrotoxin and strychnine on rabbit retinal ganglion cells: changes in centre surround receptive fields.* .J Physiol. 1978;276:299–310. PubMed PMID: 650452.
44. Chen X.et al. *Three forms of spatial temporal feedforward inhibition are common to different ganglion cell types in rabbit retina.* .J Neurophysiol. 2010;103(5):2618–32. PubMed PMID: 20220071.
45. O'Brien B.J., Richardson R.C., Berson D.M. *Inhibitory network properties shaping the light evoked responses of cat alpha retinal ganglion cells.* .Vis Neurosci. 2003;20(4):351–61. PubMed PMID: 14658764.
46. Eggers E.D., Lukasiewicz P.D. *Multiple pathways of inhibition shape bipolar cell responses in the retina.* .Vis Neurosci. 2011;28(1):95–108. PubMed PMID: 20932357.
47. Flores-Herr N., Protti D.A., Wässle H. *Synaptic currents generating the inhibitory surround of ganglion cells in the mammalian retina.* .J Neurosci. 2001;21(13):4852–63. PubMed PMID: 11425912.
48. Hsueh H.A., Molnar A., Werblin F.S. *Amacrine-to-amacrine cell inhibition in the rabbit retina.* .J Neurophysiol. 2008;100(4):2077–88. PubMed PMID: 18667544.
49. Manookin M.B.et al. *Disinhibition combines with excitation to extend the operating range of the OFF visual pathway in daylight.* .J Neurosci. 2008;28(16):4136–50. PubMed PMID: 18417693.
50. van Wyk M., Wässle H., Taylor W.R. *Receptive field properties of ON- and OFF-ganglion cells in the mouse retina.* .Vis Neurosci. 2009;26(3):297–308. PubMed PMID: 19602302.
51. Wässle H., Schafer-Trenkler I., Voigt T. *Analysis of a glycinergic inhibitory pathway in the cat retina.* .J Neurosci. 1986;6(2):594–604. PubMed PMID: 3950712.
52. Werblin F.S. *Six different roles for crossover inhibition in the retina: correcting the nonlinearities of synaptic transmission.* .Vis Neurosci. 2010;27(1-2):1–8. PubMed PMID: 20392301.
53. Stafford B.K.et al. *Spatial-Temporal Patterns of Retinal Waves Underlying Activity-Dependent Refinement of Retinofugal Projections.* .Neuron. 2009;64(2):200–212. PubMed PMID: 19874788.
54. Moss S.J., Smart T.G. *Constructing inhibitory synapses.* .Nat Rev Neurosci. 2001;2(4):240–250. PubMed PMID: 11283747.
55. Ghosh K.K.et al. *Types of bipolar cells in the mouse retina.* .J Comp Neurol. 2004;469(1):70–82. PubMed PMID: 14689473.

Role of Dopamine in Retinal Function

Elka Popova, Ph.D.[1,*]

Created: May 28, 2020.

Abstract

Dopamine (DA) is the major catecholamine in all vertebrate retinas including man. All vertebrates have dopaminergic neurons identified as amacrine cells (ACs) and interplexiform cells (IPCs), with great variations among different species. DA neurons are comparatively rare with density about 10-100 per mm^2, which means that they are less than 1% of all amacrine cells. In retinal circuitry DA serves principally as a neuromodulator, which reaches distant target cells by diffusion, and thus exerts a "volume transmission" mode of communication. Dopamine release appears to be circadian, with high release levels during the day in many species, and is a counterpart to the circadian rhythm in melatonin, which is released at night. Dopamine regulates voltage-gated ion channels and alters chemical and electrical synaptic transmission through five D_1-like and D_2-like G-protein-coupled receptors. DA is particularly associated with retinal circuitry reconfigurations with nighttime and daytime vision. DA actions are highly cell type, species and context dependent. DA acts through multiple intracellular pathways, in particular G-protein activated Adenylate Cyclase (AC) and Phospholipase C (PLC) pathways.

Introduction

In 1970 Julius Axelrod received the Nobel prize for Neuropharmacological studies of brain neurotransmitter pathways, among them biogenic amines such as dopamine (DA). His work was key in developing a treatment for Parkinsonism, a DA deficiency disorder (1). The discovery of enzymatic pathways of DA synthesis, an early histochemical DA marker involving formaldehyde-induced fluorescence for biogenic amines (2), and association with a prominent neurological disease gave incentive to study actions of DA circuitry in retina. DA is the major catecholamine in all vertebrate retinas including man. All vertebrates have dopaminergic neurons identified as amacrine cells (ACs) and interplexiform cells (IPCs) with great variations in neural types represented among different species. DA neurons are comparatively rare with density about 10-100 per mm^2, which means that they are less than 1% of cells in the amacrine cell layer of the retinal inner nuclear layer. In retinal circuitry dopamine serves principally as a neuromodulator, which reaches distant target cells by diffusion and thus exerts a "volume" transmission mode of communication. DA regulates voltage-gated ion channels and alters chemical and electrical synaptic transmission through five D_1-like and D_2-like G-protein-coupled receptors. It is particularly associated with retinal circuitry reconfigurations undergone with nighttime and daytime vision. DA acts through multiple intracellular pathways, in particular, G-protein activated Adenylate Cyclase (AC) and Phospholipase C (PLC) pathways. Dopamine receptors also directly modulate voltage-gated membrane channels through protein-protein interactions as well as G-proteins. DA actions are highly cell type, species and context dependent. This article reviews five decades of DA research of actions on and within neurons of the retina.

Morphology and circuitry of Dopaminergic neurons in the retina

The distribution of DA among retinal cell types varies with species. Some species (*amphibians*) have both dopamine cell types (ACs and IPCs), while others (*elasmobranch fishes, reptiles, birds ,cats, rabbits, monkeys,*

Author Affiliation: 1 Department of Physiology, Medical University of Sofia, Bulgaria; Email: epopova@abv.bg.

Corresponding author.

* About the authors

human) have only DA **amacrine** cells that spread over a wide field in stratum 1 of the inner plexiform layer (IPL) (**Figure 1 a, b**). *Teleost fish* have only DA IPCs (**Figure 1 c, d**) (3, 4). IPCs are wide field amacrine-like cells that have dendrites running through both the IPL and outer plexiform layer (OPL). *Turtles* appear to have DA cells with tristratified IPL dendritic trees but no dendrites to the OPL (5). In *human, cat,* and *ground squirrel* retinas dopaminergic ACs have some rare processes projecting towards and into the OPL (6-8) but their major dendritic plexus is in stratum 1 of the IPL (**Figure 1 a, b; Figure 2 a, b**). In *cat* the OPL-running DA dendrites make synaptic contacts upon a different IPC, which is GABAergic, and possibly upon B-type horizontal cells (7) (**Figure 2 a**, **b**). In primates, mouse, and rabbit retinas a second type of catecholamine amacrine (CA) is seen, called Type 2 CA (9-12) (see also Webvision chapter on Neurotransmitters in the Retina).

The primary Type 1 DA cell in mammals is very characteristic with a large cell body and a dense plexus of dendrites in stratum S1 of the inner plexiform layer (**Figure 2 a**, **c**). Holes or "rings" in the plexus of criss-crossing stained dendrites are sites of amacrine cell bodies or large amacrine dendrites (**Figure 2 b**), on which the processes of the DA cell plexus synapse. In this respect the processes of DA cells appear to be axon-like (**Figure 2 a**, **b**, **c**).

Electron microscopy of a cat Type 1 DA cell, in tyrosine hydroxylase (Toh) immunostained retinas (7), shows that Toh amacrine dendritic rings synapse upon the glycinergic AII rod amacrine cells (**Figure 3 b**), A8 glycinergic amacrine cells (**Figure 3 a**), and upon GABAergic A17 amacrine cells (not shown) (7, 13, 14). The type 1 DA cell is postsynaptic to OFF-bipolar cells in stratum 1 (**Figure 4 a**) and to occasional ectopic synapses from an ON-bipolar axon passing through the OFF layer (not shown) (15). The main DA plexus in S1 sends a few processes to the S3 level of the IPL (7, 11, 16) (**Figure 2 d**) where they are postsynaptic to ON-bipolar cells (**Figure 4 b**) (16). Glycinergic and GABAergic amacrine cells (**Figure 4 c-f**), melanopsin M1 ganglion cells (17-19) and histaminergic centrifugal fibers (20) make synapses upon the Type 1 DA cell as well (see chapters on Roles of Amacrine Cells and Melanopsin-expressing, Intrinsically Photosensitive Retinal Ganglion Cells (ipRGCs) in Webvision).

In cat the OPL-running DA dendrites make synaptic contacts upon a non-dopaminergic IPC, which is GABAergic, and possibly upon B-type horizontal cells (7) (**Figure 3 c and d**). These contacts are, however, probably not signs of synaptic vesicle release of transmitter because no synaptic vesicle proteins have been found at these attachment points. They are possibly sites of dopamine release and action through "volume transmission".

The DA Type 1 cell exhibits glutamate, GABA and histamine H1 receptors (7, 19, 20). Glutamate (21), GABA and dopamine colocalize to the Type 1 DA cell (22, 23), and serotonin has also been found to co-exist in these same amacrine cells in cat retina (23). Thus, the dopamine amacrine cells of the vertebrate retina are a complex cell type, differing in branching patterns in different species, making different synaptic connections dependent on species, and synthesizing multiple neurotransmitters. A general summary diagram of the DA cell in *mammalian* retinas with the synaptic inputs and outputs is shown in **Figure 5** (explanations are in the figure legend).

Physiology of Dopaminergic amacrine cells

DA amacrine cells fire spontaneously at a modest rate (< 10 spikes/s) and the action potentials trigger dopamine release by exocytosis (22, 24). In the dark, the spontaneous spike activity differs markedly among DA cells. The characteristics of their spike activity falls into four categories in intact *mouse* retina: quiet cells that generated spikes infrequently at random intervals (**Figure 6**, **A1**), rhythmic cells that fire spikes at a maintained rate, and cells that generate bursts that are either mixed with single spikes (**Figure 6 B1**) or occur in discrete bursts at regular intervals (**Figure 6**, **C1**, **D**) (25). The bursting, but not the overall firing rate, increases during blockade of the GABAergic and glycinergic retinal synapses, indicating that an inhibitory synaptic input from amacrine cells in the dark modulates the bursting aspect of DA cell spontaneous activity (12). On the other hand, blockade of

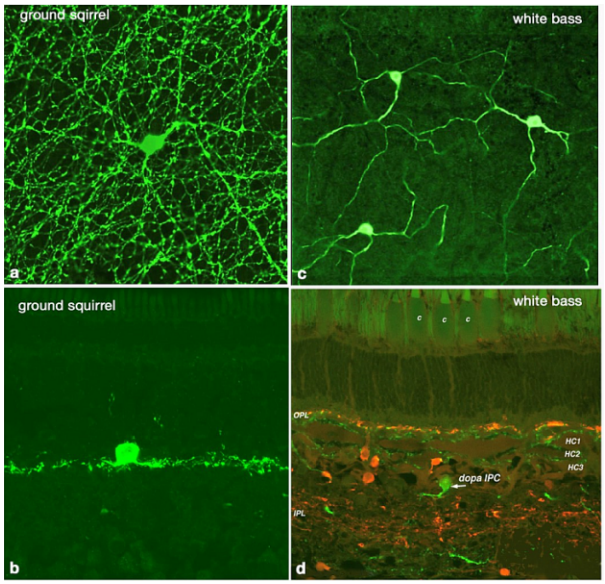

Figure 1. Confocal images of Tyrosine hydroxylase (Toh) immunostained dopaminergic amacrine cells in *ground squirrel* (typical of mammalian retinas) and in *white bass* retina (typical of teleost fish). (a, c) are whole mount retinas, while (b, d) are vertically sectioned retinas. In (d) dopaminergic interplexiform cell (***dopa IPC***), type 1, 2, and 3 horizontal cells (***HC1***, ***HC2***, ***HC3***). Courtesy of Nicolas Cuenca.

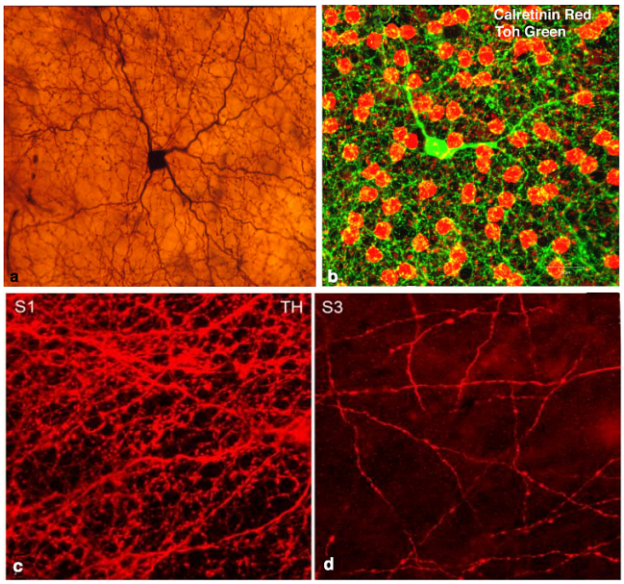

Figure 2. (a) Immunostained Toh dopamine amacrine cell in wholemount the *cat* retina. Many fine processes make rings around spaces occupied by amacrine cell bodies. (b) Double immunostaining for Toh-labeled DACs (green) and Calretinin-labeled AII amacrine cells (red) in wholemount *monkey* retina. Many of the Toh-labeled dendritic rings are occupied by AII amacrine cell bodies. (a, b) courtesy of Nicolas Cuenca. (c) Toh-immunostained DA cell processes in stratum 1 (S1) of the mouse IPL form a dense monolayered plexus. (d) A few processes descend from the S1 plexus to ramify loosely in S3 of the IPL. (c, d) from Contini et al. (16).

AMPA/kainate-type or NMDA-type glutamate receptors affects neither the firing rate nor the firing pattern of DA cells, indicating a lack of direct excitatory glutamate synaptic input from bipolar cells in the dark.

In contrast to spontaneous firing, the light-evoked activity of DA cells in *mammalian retina* is modulated by the excitatory glutamatergic input from the ON cone bipolar cells (CBCs) (16) and melanopsin-expressing intrinsically photosensitive retinal ganglion cells (ipRGCs) (19) (**Figure 7**) (for relationship between DA and

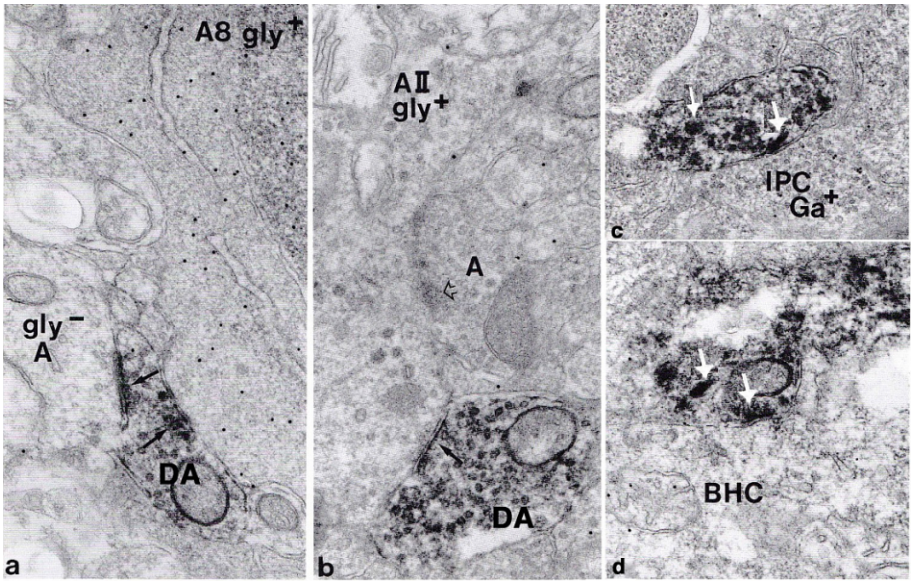

Figure 3. EM of dopamine amacrine processes (**DA**) immunostained with Toh in *cat* retina. These processes are synaptic upon (a) **A8** amacrine cell bodies and (b) **AII** amacrine cell bodies. The A8 amacrine cell is heavily counterstained by colloidal gold techniques for glycine (small black spots), whereas the AII cell is only lightly stained. The AII amacrine cell body receives a glycine-negative synapse on its cell body (open arrow, b). The DA process in (a) synapse nearby to a glycine negative cell body. (c) Toh-stained processes in the OPL are closely opposed to an interplexiform cell (**IPC**) that is GABAergic (black spots of **Ga$^+$** immunogold). (d) In the OPL, the same Toh-stained profile as (c) is attached to a B-type horizontal cell (**BHC**). The attachment points (c, d) are characterized by dense-cored vesicles in the Toh-stained profiles (white arrows). From Kolb et al. (7).

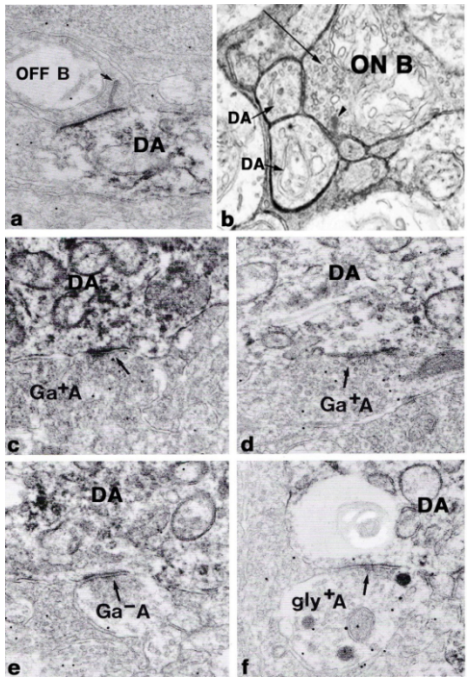

Figure 4. EM of synaptic input to **DA** cells in *cat* retina. (a) An OFF cone bipolar cell in stratum 1 of the IPL (**OFF B**) makes a ribbon synapses (arrow) upon a DA process immunostained for Toh. (b) An ON cone bipolar in stratum 3 of the IPL (**ON B**) makes a ribbon synapse (arrowhead) upon two postsynaptic dopaminergic amacrine cell processes (short arrows, DA) in a transgenic mouse immunolabeled with human placental alkaline phosphatase (PLAP). A precipitate of lead phosphate labels DA processes on the external plasma membrane as a black precipitate. From Contini et al., 2010 (16). (c-f) Toh-immunolabelled DA amacrine cell body receives synapses from immune gold labeled GABA positive amacrine cell processes (small black spots, **Ga$^+$ A,** d) and GABA negative amacrine cell processes (**Ga$^-$ A**, e). (f) Glycine positive amacine processes (**gly$^+$ A**) also synapse upon the Toh-stained cell body (small black spots). From Kolb et al., (7).

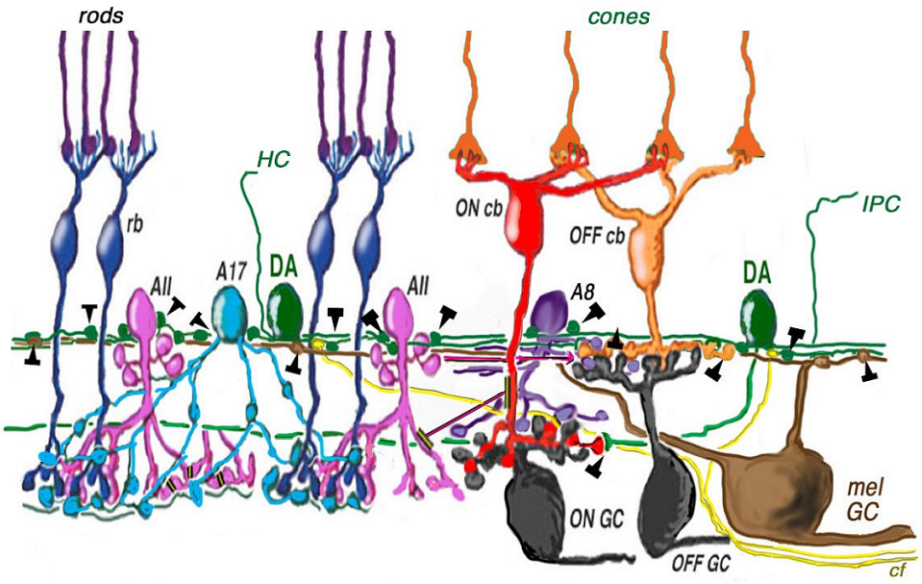

Figure 5. Summary diagram of the synaptic relationships of the dopaminergic amacrine cell (**DA**, green) in the *mammalian* retina. The **DA** cells are characterized by a dense plexus of processes in stratum 1, under the amacrine cell bodies, in the inner plexiform layer (IPL). In this plexus DA cells are postsynaptic to OFF cone bipolar cells (***OFF cb***, orange) and occasional ectopic synapses from ON cone bipolar cells (***ON cb***, red). Several glycinergic and GABAergic amacrine cells, the melanopsin Type 1 intrinsically photosensitive ganglion cell (***mel GC***, brown) and histaminergic centrifugal fibres that run in stratum 1 (***cf***, yellow) are synaptic upon the **DA** cell in that stratum of the IPL (black arrowheads). **DA** cells form presynaptic in rings upon amacrine cell bodies of ***AII*** cells (pink) *A8* cells (purple) and ***A17*** cells (light blue) (black arrowheads). A few DA processes run in stratum 3 of the IPL where they are postsynaptic to ribbon synapses of ON cone bipolar cells (***ON cb***, red bipolar, arrowhead). In addition, a few, scarcely observed, ascending processes go to the outer plexiform layer and seem closely applied to the non-dopaminergic mammalian interplexiform cell (***IPC***) and B-type horizontal cell bodies (***HC***). These attachments associate with clusters of dense cored vesicles. From Kolb et al (7).

ipRGCs see Melanopsin-expressing, Intrinsically Photosensitive Retinal Ganglion Cells (ipRGCs) in Webvision). All mammalian DA amacrine cells are ON-type, while amphibian DA amacrine cells showed excitatory ON and OFF responses (26). Inputs from ON-BCs probably account for the light-evoked ON-transient responses of mammalian DA cells, while inputs from ipRGCs likely account for ON-sustained DA cells.

Zhang et al. (12, 19, 27) found that all ON-transient, but not ON-sustained light responses of DA neurons were entirely eliminated in photoreceptor degenerate mouse retinas and under the influence of L-AP4, which blocked the transmission from rod/cones to ON bipolar cells. On the other hand, the ON-transient light responses persisted in melanopsin knockout mice, where all ON-sustained light responses were eliminated, supporting the dependence of the latter on the inputs only from ipRGCs. Other authors argued, however, that the nature of generated spike response (sustained or transient) of DA neurons depended only on stimulus intensity (25). Newkirk et al. (25) showed that the sustained spike trains were evoked by weak stimuli, whereas the transient trains were evoked by bright light, because the latter caused a depolarization block that limited the ON response to an initial transient burst of spikes. This was also the case in DA cells that generated exceptionally prolonged large depolarizing responses to strong stimuli, which they considered to be the result of direct excitatory input from ipRGCs. Newkirk et al. (25) suggested that a reduced light sensitivity of the retina in experiments of Zhang et al. (12, 19), due to differences in methodology, may account for the discrepancies between the results of the two groups. The reduced sensitivity may serve to reduce the amplitude of the depolarizing response evoked by excitatory input to a level that was not sufficient to cause a depolarizing spike block. This could explain the presence of sustained spike train in response to saturating light in experiments of Zhang et al. (12, 19). This suggestion could not explain, however, why all DA cells had transient responses in melanopsin knockout mice under the same conditions of stimulation and adaptation (27).

The relative contribution of different photoreceptor inputs to the light-evoked ON responses of DA cells was recently investigated in *mouse* retina (28). It was found that rods excited the dark-adapted DA amacrine cells across a wide range of stimulation intensities (6 log units) primarily (but not solely) through connexin-36-dependent rod pathways. This result is at odds with previous findings that DA cell threshold response to scotopic stimuli was generated only by inhibitory input at light onset from glycinergic ACs (25). The discrepancy between cited results is probably due to the different adaptation state of the retina. Zhao et al. (28) performed their recordings in dark-adapted retina, while Newkirk et al. (25) conducted their experiments under weak background illumination that could eliminate the ON-EPSPs evoked by dimmer light. Zhao et al. (28) found that the ON-responses of DA cells to prolonged adapting light were mediated by rods under dim lighting conditions, rods/M-cones/melanopsin under intermediate lighting conditions, and cones and melanopsin under bright lighting conditions (**Figure 7**). Thus, it appears that mammalian DA cells receive excitatory ON inputs from all photoreceptor types and can influence their target cells under different conditions of light stimulation and adaptation. It should be mentioned that not all DA cells have light-modulated responses. Some authors reported that 40% of mouse DA cells are unresponsive to light (12), while other authors (25) reported much smaller portion (1 out of 300 cells).

The light-evoked activity of DA cells is modulated also by inhibitory glycinergic and GABAergic AC synaptic inputs (25, 29). This inhibitory input can occur during light onset and/or at light offset. It appears that the ON inhibition is mediated by glycinergic ACs (25, 29), while the OFF inhibition is mediated by GABAergic ACs solely (25) or by GABAergic and glycinergic ACs (29). In addition to their intraretinal inputs, DA cells receive centrifugal influences from different brain structures. In *fishes* the activity of DA-IPCs cells was modulated by centrifugal fibers originating in the olfactory bulb and containing FMRFamide-like and luteinizing hormone releasing hormone (30, 31). In other species (*guinea pig, mouse, rat, monkey*) histaminergic centrifugal fibers originating in the tuberomamillary nucleus of hypothalamus innervated retina and they may also modulate the activity of DA cells (20).

The output synapses of DA amacrine cells are in the IPL, while DA interplexiform cells transmit signals from inner to outer retina. The main output synapses of mammalian DA amacrine cells in the IPL are onto two types of amacrine cells - AII (glycinergic) and A17 (GABAergic), which belong to the rod pathway (see Webvision: AII Amacrine Cells and Roles of amacrine cells). In addition, DA cells make reciprocal, conventional GABAergic synapses onto the presynaptic ON CBCs (16). These synapses probably function to exert an inhibitory feedback onto the presynaptic bipolar cell. DA amacrine cells synapse also onto ipRGS and thus can modulate their activity (17, 18) (see Webvison: Melanopsin-expressing, Intrinsically Photosensitive Retinal Ganglion Cells (ipRGCs). In cold blooded animals, DA amacrine cells make output synapses onto other amacrine cells, ganglion cells and axon terminals of bipolar cells (32, 33). The well-known synaptic outputs of DA IPCs in the OPL are on the GABAergic IPC as seen in *cat* (7, 8), horizontal cells of *cat* (7, 8), *Cebus monkey* and *goldfish* (34), *human* (6), and on bipolar cells of *Cebus monkey* and *goldfish* (34). In rodent retina, DA IPC distal processes have multiple varicosities that terminate throughout the INL, the OPL, and, rarely, in the layer of photoreceptor cells without making morphologically defined synapses (35). Dopamine is packed into membrane-bound compartments that are not conventional synaptic vesicles. These reside in the dendritic varicosities and can be released from them at multiple horizontal levels of the outer retina. Dopamine reaches its target cells by diffusion over distances of up to tens of microns giving rise to the concept of "volume transmission" (36, 37).

It is known that DA amacrine cells co-localize GABA, in *cat* (23, 38), *turtle, chick, mouse* (39) and *rat* (38, 40, 41). It was shown that a proportion of the secretory organelles in the cytoplasm of mouse DA cell bodies contained both GABA and dopamine and that both transmitters were released simultaneously by exocytosis upon depolarization of the cell membrane (22). The synapses made by rodent DA cells onto AII amacrine cells appeared to be GABAergic, since $GABA_A$ but not DA receptors were clustered in the postsynaptic active zone (42). A hypothesis exists that GABA, released by the DA cell, acts on the ionotropic GABA receptors clustered at the postsynaptic active zone of AII amacrine cell, whereas dopamine diffuses to more distant, slower-acting

metabotropic receptors (22, 42). This hypothesis is probably not true for rabbit retina, where synapses made by DA amacrine cells on AII cells were not GABAergic (43). Lee et al. (43) suggested that AII synaptic input from DACs in the rabbit retina may be mediated only by dopamine. This is consistent with earlier results showing that a very few rabbit DACs contained very low levels of GABA (38). GABA co-localization was not observed in DA cells of some lower vertebrates including amphibians and fishes (39).

Photic and circadian regulation of dopamine release

Much data indicates that endogenous dopamine release is low in darkness but increases during retinal exposure to constant or flickering light, as seen in *frog* (37, 44, 45), *turtle* (46), *pigeon* (47), *chick* (48, 49), *duck* (50), *rodents* (29, 51, 52), *rabbit* (53-56), *cat* (57), and *monkey* (58). These results led to the suggestion that dopamine functions as a chemical signal for light (59-62). However, there are some opposite results, indicating that the dopamine release was high in darkness and decreased during retinal illumination as seen in *cat* (63, 64). According to some authors the latter effect was seen only when the experiments were performed at night, not at day (65). There is some suggestion that in *mammalian retina* there is a U-shaped relationship between dopamine release and light intensity (66, 67). In total darkness, when DA cells receive no input, they fire spontaneously and release dopamine. The release of dopamine diminishes at the low scotopic range, because the DA cells are inhibited by GABAergic amacrine cells driven through the OFF system (67) or through rod BCs via AII amacrine cells (66). There is no consensus among the authors cited, however, at what intensity range the DA release increases again. According to Marshak (66) it occurs in the higher scotopic range, when the DA cells receive direct excitatory input from ON cone bipolar cells driven from the less sensitive rod pathway via rod-cone junctions (**Figure 8**). According to Pérez-Fernández et al. (67) it occurs at light intensities when transition from mesopic to photopic vision takes place (> 6 log units above ERG threshold). The latter authors suggest that under scotopic and mesopic light stimuli, although the glutamate release increases and stimulates synaptic AMPA/kainite receptors, it does not outweigh the inhibition caused by the GABAergic system and DA release is low (**Figure 9**). Under bright light conditions both inhibition and excitation are increased, but due to glutamate spill over to extra-synaptic NMDA receptors the level of excitation tips the balance and allows a large release of dopamine.

Pérez-Fernández et al. (67) presented evidence that DA release in mouse retina depended neither on cone photoreceptors nor on ipRGC function and they insist that it entirely depended on the rod pathway function. This suggestion is not supported by results of Cameron et al. (51), who reported that light-induced dopamine release was retained in mice lacking rod phototransduction, although the magnitude of this response was substantially reduced compared with wild-types. By contrast, light-induced dopamine release was not evident in mice lacking both rods and cones, indicating that light regulation of retinal dopamine release relies upon both rod and cone function.

Another hypothesis is proposed by Dowling (68), who suggested that different types of dopaminergic cells in mammalian retina, as described by Zhang (12), can account for the dopamine release under different conditions of light stimulation. The spontaneously active dopaminergic cells, which are not light-driven, would release dopamine in the dark. The ON-transient cells would release dopamine best when exposed to flickering light and the ON-sustained dopaminergic cells would release dopamine best in steady light. The amount of dopamine released, however, may be determined not only by spike frequency, but also by the pattern of spike activity (single spike, random, or bursting). It was shown that bursting stimulations were twice as potent as regularly spaced ones having the same average frequency in evoking dopamine release from brain dopaminergic neurons (69). In this regard, Cameron et al. (51) suggested that the slow sustained activation, typically associated with ipRGCs, could account for their inability to release measurable amounts of DA from the dopaminergic cells upon light stimulation, although ipRGCs send excitatory outputs onto the dopaminergic cells.

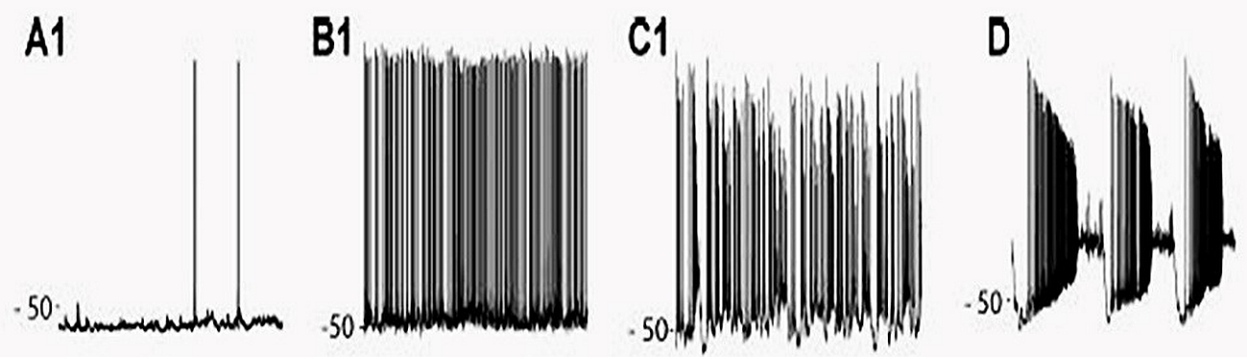

Figure 6. Cellular properties of dopaminergic cells in *mouse* retina. Resting spontaneous spike activities in 4 different cells provide examples of cells that are nearly silent (**A1**), continuously active (**B1**), or exhibit steady discharge with intermixed bursts of spikes (**C1**) or periodic bursts (**D**). Resting membrane potentials (in mV) are indicated at left of each trace. From Newkirk et al. (25).

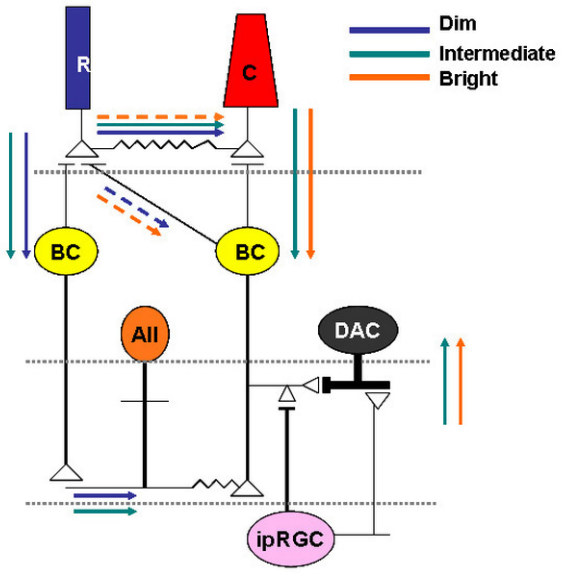

Figure 7. Proposed inputs from three distinct photoreceptor classes to dopaminergic amacrine cells (**DAC**) under different lighting conditions. Under dim lighting conditions, DACs receive equal input from rods (**R**) through the primary (rod — > rod BC — > AII amacrine — > cone BC) and secondary (rod — > cone) rod pathways (blue arrows) and possibly from the tertiary rod pathway (rod — > cone BC) (dashed blue line/arrow). Under intermediate lighting conditions, DACs receive input from rods (green arrows), cones (**C**) and melanopsin intrinsically photosensitive retinal ganglion cells (**ipRGC**) (green arrows). Under bright lighting conditions, DACs receive cone input (orange arrows) and melanopsin input (orange arrow); melanopsin may contribute to DAC signaling in the ventral retina as well (dashed orange line/ arrow). Under bright lighting conditions, rods may also excite DACs through the secondary and tertiary rod pathways (dashed orange line/arrow). Form Zhao et al. (28).

In some *non-mammalian species* (fishes, reptiles, birds), dopamine synthesis and release are controlled by a circadian clock so that dopamine release is highest during the daytime in light and lowest at night in darkness, as seen in *fish* (70-72), *iguana* (73, 74), *pigeon* (47), *turkey* (75), *quail* (76), *chick* (48, 49), and *duck* (50). In *fish retina*, the circadian rhythm of dopamine release was eliminated during the continuous presence of melatonin and melatonin receptor antagonists, indicating that the circadian rhythm of dopamine release was primarily driven by the circadian rhythm of melatonin (71). Similar results were obtained in *reptiles*, where the circadian rhythm of retinal dopamine content and metabolism was abolished in melatonin depleted eyes (73). Whether dopamine release is predominantly light-driven or controlled by a circadian rhythm in *birds* is a subject of dispute. It was shown that retinal DA content oscillated rhythmically in pigeons kept for 4 days under continuous dim light illumination, indicating the dominant role of circadian oscillator for retinal dopamine

release (47). In these cases, the dopamine rhythms were not just driven by melatonin rhythms, because inhibition of melatonin release by quinpirole did not always change dopamine level (77). However, in retinas of *chick* (49, 61), *quail* (76) and *turkey* (75), a progressive decline of rhythmic oscillations of DA, its synthesis and degradation products was observed in constant darkness, emphasizing the important role of light as a stimulatory signal for the retinal dopaminergic system, in addition to the circadian pacemaker. The authors cited proposed that the small circadian increase in dopamine synthesis, release, and metabolism resulted from disinhibition of dopaminergic neurons from the suppressive action of melatonin during the light phase of the cycle.

A consensus is lacking regarding the circadian regulation of dopamine metabolism in *mammalian retina*. Although the concentration and release of dopamine was higher during the day and lower at night in *mouse* (78, 79), *rat* (80-84), *rabbit* (55), *human* (85), some authors reported no circadian rhythm in dopamine synthesis and utilization in *rats* (81), *rabbits* (55), *mice* (79) kept in constant darkness. The latter authors suggested that the diurnal changes of dopamine synthesis and utilization are entirely dependent on the presence or absence of light and not driven by a circadian clock. Other authors, however, demonstrated circadian rhythm of dopamine content and turnover that persisted in constant darkness (78, 80, 84). The circadian rhythm of dopamine content and metabolism was evident in mice that synthesize melatonin, but not in mice that were genetically incapable of synthesizing melatonin. Daily injections of melatonin induced circadian rhythms of dopamine in retinas of mice that were unable to synthesize melatonin (78). These observations suggest that the circadian rhythm of dopamine synthesis in the mouse retina, like fishes and reptiles, is controlled by rhythmic release of melatonin from the photoreceptors. It is tempting to speculate that melatonin released from photoreceptor cells is required to entrain the circadian oscillators in dopamine ACs to the daily light-dark cycle. However, when photoreceptors degenerate (as in Royal College of Surgeons rats), the retinal dopamine content, its metabolites and melatonin synthesis still displayed circadian rhythms (80, 86), thus suggesting the presence of a circadian clock outside the photoreceptors. It was shown that the mouse dopaminergic neurons expressed core circadian clock genes (87-90), which supports the hypothesis that dopaminergic amacrine cells may contain an autonomous circadian clock.

It appears that at least two different circadian pacemakers are present in the mammalian retina. The first pacemaker drives the circadian rhythm of melatonin synthesis and is likely to be located in the photoreceptor cells, while the second pacemaker drives the circadian rhythm of dopamine and is located in neurons of the inner retina (91). It was postulated that the melatonin secreting photoreceptors and dopaminergic amacrine/interplexiform cells are components of a mutually interplaying system (in a negative manner) and act as chemical analogs of light and darkness, respectively (62, 92). Melatonin appears to contribute to the nocturnal suppression of DA release and to its circadian rhythm. Dopamine, on the other hand, feeds back to the photoreceptor cells to inhibit melatonin synthesis, contributing to the suppression of melatonin synthesis in the daytime. Dopamine also serves as a zeitgeber that together with light entrains the photoreceptor clock (**Figure 10**).

Some data suggest that the circadian regulation of dopamine synthesis in mouse retina depended also on melanopsin ipRGCs. It was shown that lack of melanopsin (in melanopsin$^{-/-}$knockout mouse retinas) prevented the light-dependent increase of tyrosine hydroxylase mRNA and of dopamine and, in constant darkness, led to comparatively high levels of both components (93).

Dopamine receptors in the retina

Dopamine actions are mediated by five G-protein-coupled receptors named D_1 to D_5. These receptors are allocated to two groups: **1.** The D_1-like (including D_1 and D_5 subtypes), which are generally coupled to $G\alpha_{s/olf}$ and stimulate the production of cyclic Adenosine Monophosphate (cAMP) and the activity of Protein Kinase A (PKA). **2.** The D_2-like (including D_2, D_3 and D_4 subtypes), which are coupled to $G\alpha_{i/o}$ and negatively regulate

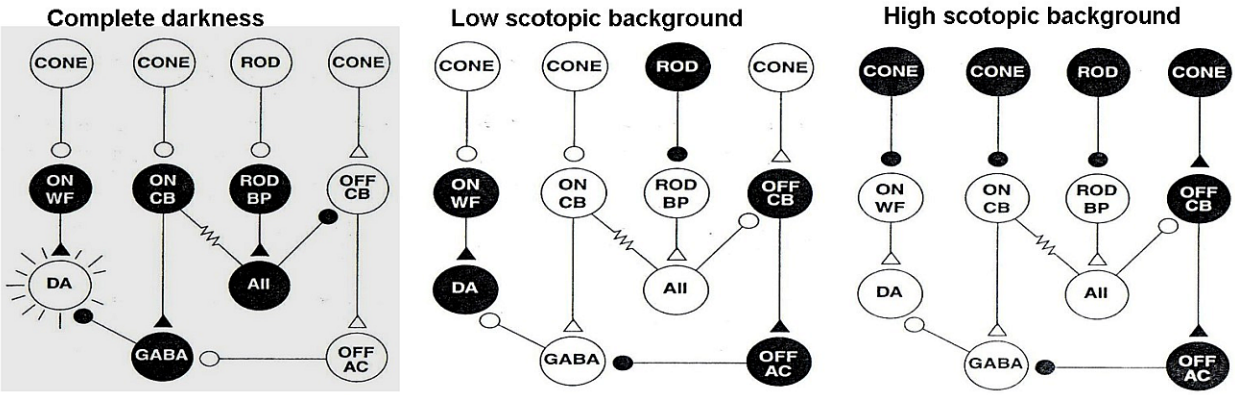

Figure 8. Marshak model for dopamine release. In the dark dopaminergic cells (**DA**) are spontaneously active and release high levels of dopamine. Rods, cones, cone OFF bipolar cells (**OFF CB**) and OFF ACs (**OFF AC**) are depolarized (white), while rod bipolar cells (**RB**), ON-cone BCs (**ON CB**), ON cone wild field BCs (**ON WF**), AII amacrine cells (**AII**) and GABAergic ACs (**GABA**) are hyperpolarized (black). In low scotopic backgrounds, rods are hyperpolarized and cones are depolarized. Rod BCs are depolarized, which leads to depolarization of **AII**, ON-cone BCs and GABAergic ACs. The latter inhibit DA cells and dopamine release decreases. In high scotopic backgrounds, rods and cones are hyperpolarized, which leads to depolarization of RBs, ON-WF, ON-CBs and GABAergic ACs, while OFF-CBs and OFF-ACs remained hyperpolarized. The activity of DA cells reflects a balance between excitatory input from ON-WF BCs and inhibitory input from GABAergic cells so that the release is greater than under low scotopic backgrounds. From Marshak (66).

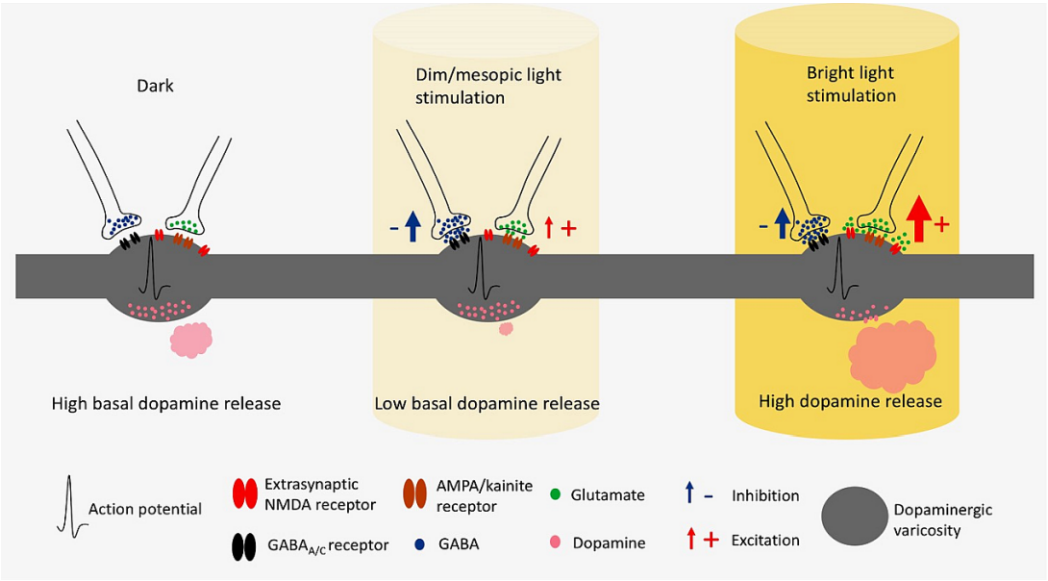

Figure 9. Model of Pérez-Fernández et al. for dopamine release. In the dark, the dopamine release is not inhibited, resulting in a high basal release. Under scotopic/mesopic light stimulation, rod activation drives GABAergic inhibition, and a small excitatory glutamatergic input only to synaptic AMPA/kainite receptors, causing reduced basal dopamine release. Under bright light stimulation, the rod activation also drives GABAergic inhibition, but activates extra-synaptic NMDA receptors via glutamate spillover resulting in more excitation than inhibition causing a large release of dopamine. From Pérez-Fernández et al. (67).

the production of cAMP, resulting in a decrease in PKA activity. This is reviewed in Beaulieu and Gainetdinov (94). Activation of PKA by D_1-like receptors also results in the phosphorylation of the cyclic AMP-regulated phosphoprotein, 32 kDa (DARPP-32), which is an inhibitor of protein phosphatase 1 and thus prevents dephosphorylation of activated proteins (**Figure 11**). In addition to this main pathway for intracellular signaling, dopamine receptors can also utilize other pathways. Some data indicate that the D_5 dopamine receptor can be coupled to Gαq to regulate PLC activity and intracellular calcium signaling, as reviewed in articles by Beaulieu

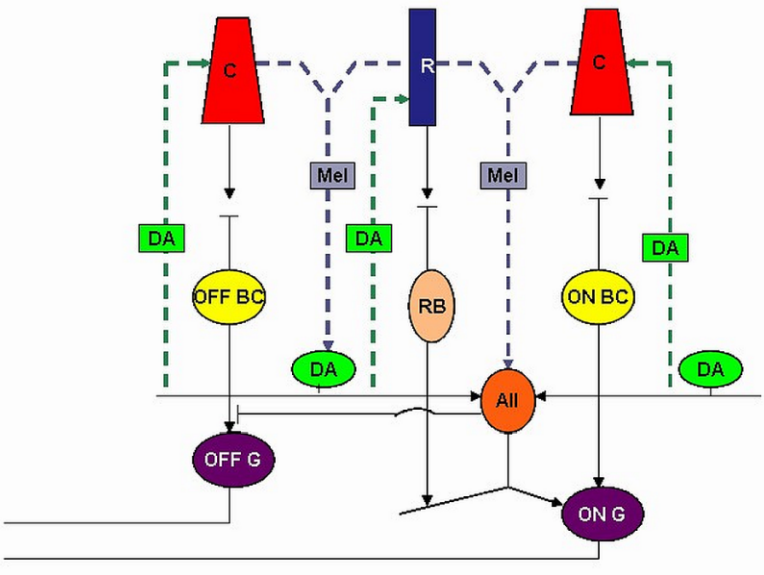

Figure 10. Melatonin–dopamine circadian clock network. Melatonin (**Mel**) is released from rods (**R**) and cones (**C**) at night and inhibits dopamine (**DA**) release both directly, and indirectly though GABA amacrine cells (not shown), thus contributing to the nocturnal suppression of DA release and to DA circadian rhythm. Dopamine, on the other hand, feeds back to the photoreceptor cells to inhibit melatonin synthesis, contributing to the suppression of melatonin synthesis in the daytime. This reciprocal paracrine feedback loop may function to stabilize circadian output in the inner and outer plexiform layer. Melatonin and dopamine probably have opposing effects on AII amacrine cell physiology. Modified from Iuvone et al. (92).

(94, 95) (**Figure 11**). The participation of the D_1 receptor in the same signaling pathway is uncertain. The D_2-like receptors acting through $G_{\beta\gamma}$ subunits of heterotrimeric G- proteins can increase the activity of inwardly rectifying potassium channels (94, 96) and reduce the activity of L-type and N-type calcium channels (97) (**Figure 11**). Similar to D_1-like receptors, D_2-like receptors can also modulate intracellular calcium levels (98, 99). Some of these actions may be mediated by $G_{\beta\gamma}$ subunits of heterotrimeric G-proteins that could activate PLC and thus lead to release of Ca^{2+} from intracellular stores (94, 100). Other data suggest, however, that the calcium signal from D_2-like receptor activation may originate from activation of D_1-D_2 or D_5-D_2 receptor hetero-oligomeric complexes, reviewed in Hasbi et al (101, 102).

It was shown that D_1–D_2 receptor heteromer activation (by SKF 83959) led to a rapid, transient, intracellular calcium mobilization (via Gq, PLC, PKC, IP_3), independent of extracellular calcium influx (**Figure 12**), that was not observed with either D_1R or D_2R activation alone. The activation of the D_5 receptor had similar effects, with the exception that the calcium signal depended on calcium influx. The formation of the D_2–D_5 receptor heteromers resulted in an attenuation of the D_5 receptor induced calcium signal, which could be restored only when both receptors are concomitantly activated (**Figure 13**).

Some authors question these results because SKF 83959 may not exhibit selective activation of D_1-D_2 heteromers, and also may show cross-reactivity to other receptors, as reviewed in Lee et al (103). One might conclude that current evidence does not allow us to determine the detailed mechanism by which D_1, D_5 or D_1–D_2 dopamine receptors participate in calcium signaling in target cells. In addition to their G-protein dependent action, the D_1 and D_2 receptors could directly alter the activity of the ion channels in the cell membrane. It was shown that both D_1 and D_2 receptors inhibited the activity of N-type calcium channels through a direct protein-protein interaction (104). Direct interaction of D_1 and D_2 receptors and Na^+-K^+-ATPase was also demonstrated (105, 106). Finally, there is strong evidence that dopamine receptors can signal *in vivo* by activating cAMP-independent mechanisms involving the multifunctional adaptor protein β-arrestin 2 and transactivation of receptor tyrosine kinases in different experimental systems, as reviewed by Beaulieu et al (95).

The D_1-like receptors are found exclusively postsynaptically on dopamine target cells, whereas D_2-like receptors are expressed both postsynaptically and presynaptically on dopaminergic neurons (107, 108). The presynaptic autoreceptors generally provide an important negative feedback mechanism, which regulates the synthesis and release of the neurotransmitter in response to changes in its extracellular concentration (109, 110). The D_2-like receptors, including those in the retina, are 2-3 times more sensitive to dopamine than D_1-like receptors (62, 98, 111-113).

All dopamine receptors undergo desensitization as a result of prolonged exposure to DA or its agonists (114-117). This is a characteristic feature of G-protein-coupled receptors. On the other hand, the receptors can undergo sensitization when an agonist does not activate them for an extended period. Some data indicated that retinal dopamine receptors in rat developed a state of hypersensitivity during period of prolonged light deprivation (118). The hypersensitivity of D_1-like receptors developed earlier (within 6 hours) in comparison with that of the D_2-like receptors (after 2 or, even better, 4 days). Hypersensitivity of D_2-like receptors regulating serotonin N-acetyltransferase activity was found in kainic acid treated chick retinas, where retinal levels of dopamine were markedly reduced (119).

The activity of all neurons in the retina might be modulated by dopamine because all express D_1- or D_2-like receptors. Rod and cone photoreceptors have D_2-like receptors in all species studied. This includes *frog* (120, 121), *salamander* (120), *turtle* (121), *fish* (121), *chick* (121, 122), *rat* (36, 121, 123-126), *bovine* (121, 127), *rabbit* (121, 123), and *human* (128). Some D_1R-immunoreactivity was observed on the axons of cones (129) and in the outer segments of the photoreceptor layer (36). It was shown that dopamine receptors on photoreceptors were of the D_4 type in the retinas of *rodents*, *birds* and *fishes* (120, 130-134). Horizontal cells (HC), bipolar cells (BC), amacrine and ganglion cells (GC) are thought to express mainly D_1-like receptors. The species studied were *frog* (135), *turtle* (135), *fish* (129, 136), *chick* (137), *rat* (124, 138, 139), and *mouse* (140-142). D_1-like receptors were expressed in a type-dependent manner on the ON-CBCs and OFF-CBCs, but not rod BCs (RBC) in mouse retina (140). In ON CBCs, they were expressed in transient, but not sustained cells, while in OFF CBCs they were expressed in sustained, but not transient cells. In addition to the photoreceptors, D_2-like receptors were localized on horizontal cells in *fish* (136), amacrine cells in *frog* (120), *salamander* (120), or *rat* (131), and in cells resembling amacrines and bipolars in the *chick* (121, 122), *rat* (36, 121, 125), *bovine* (121), *rabbit* (121), and *human* (128), and in the ganglion cell layer of *chick* (121, 122), *rat* (36, 121, 125), *bovine* (121), and *rabbit* (121) retinas. The dopaminergic neurons themselves express D_2-like autoreceptors, which function to inhibit dopamine release (125, 131, 143). The Műller glial cells also express dopamine receptors in *frog* (120, 135), *salamander* (120), *turtle* (135), *chick* (144), *mouse* (144), *rat* (129, 145) and *guinea pig* (145).

Effects of dopamine on photoreceptors

Dopamine has numerous effects on photoreceptors. It inhibits the synthesis of melatonin (119, 146), influences retinomotor movements, as reviewed by Popova (147), inhibits hyperpolarization-activated currents as seen in *frog* (148, 149) and *human* (149), modulates light-evoked responses, changes the coupling between photoreceptors, etc. Most of these effects are mediated through D_2-like receptors expressed on the photoreceptors. It was shown that activation of dopamine D_4 receptors in photoreceptors suppressed the light-sensitive pool of cAMP (130, 150-152), reduced the PKA activity and down-regulated the type1 Adenylyl cyclase (AC1) expression (153). In addition, the regulation of cAMP level in photoreceptors by dopamine may occur indirectly, via regulation of the intracellular calcium concentration (154). It was shown that dopamine, quinpirole and the selective D_4 receptor agonist PD 168,077 significantly suppressed K^+-stimulated uptake of Ca^{2+} and decreased $[Ca^{2+}]_i$ in *chicken* cones. The effects of the agonists were blocked by dopamine D_2/D_4 receptor antagonists or by pertussis toxin. Because quinpirole inhibited the increase in cAMP level elicited by K^+, which requires Ca^{2+} influx through voltage-gated Ca^{2+} channels, but not that induced by the calcium ionophore A23187, the authors concluded that the decrease of cAMP elicited by dopamine D_4 receptor

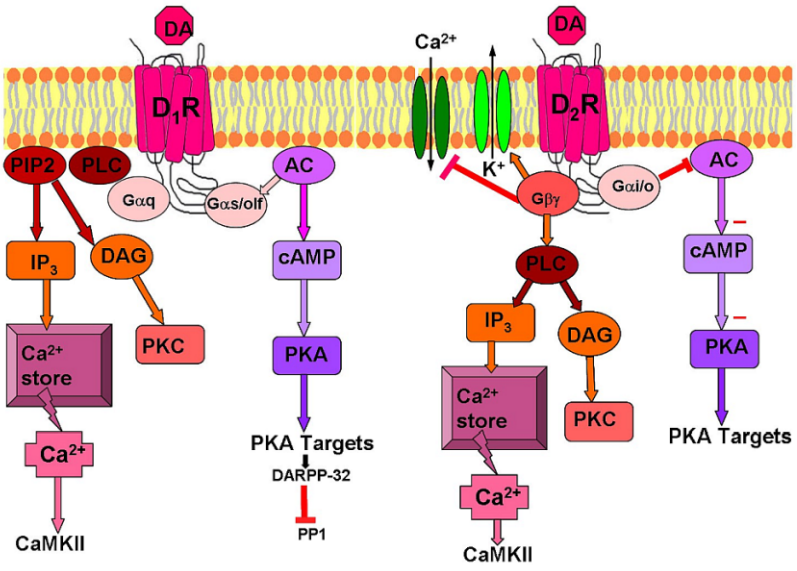

Figure 11. Signaling pathways regulated by dopamine through D_1-like (**D_1R**) and D_2-like (**D_2R**) receptors. Arrows indicate activation, red T-symbols indicate inhibition. Phosphatidylinositol 4,5-bisphosphate (PIP2), Inositol trisphosphate (IP3), Phospholipase C (PLC), Diacyl Glycerol (DAG), Protein kinase C (PKC), Gq, protein alpha subunit (Gαq), Guanine nucleotide-binding protein (Golf) subunit alpha (Gαs/olf), Adenylate cyclase (AC), cyclic Adenosine monophosphate (cAMP), Protein kinase A (PKA), dopamine and cyclic AMP-regulated phosphoprotein (DARPP-32), Protein phosphatase 1 (PP1), G beta-gamma (Gβγ), Gi protein alpha subunit (Gαi/o), Ca2+/calmodulin-dependent protein kinase II (CaMKII).

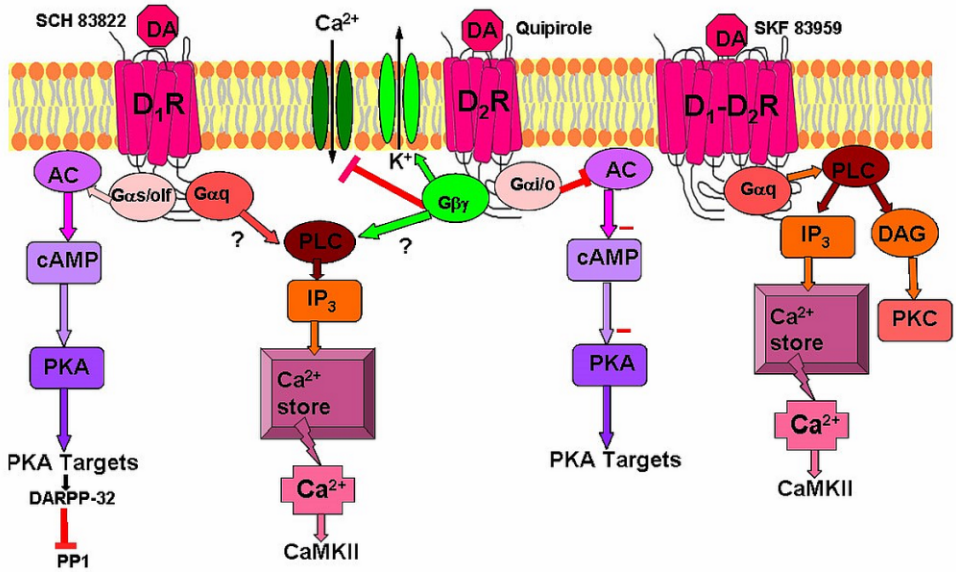

Figure 12. Signaling pathways through dopamine homomeric D_1 and D_2 receptors and heteromeric D_1–D_2 receptors. The respective agonists of the different receptor types are shown above the receptors. The abbreviations are as in Figure 11 legend. Modified from Hasbi et al. (102).

stimulation may be secondary to decreased $[Ca^{2+}]_i$. The latter was probably evoked by a direct action of dopamine on photoreceptor calcium permeability.

Other authors showed, however, that the suppressive action of dopamine and quinpirole on the influx of Ca^{2+} through L-type channels in *salamander* large cones depended on the activation of D_2-like receptors acting through $G_{i/o}$, AC1, cAMP and PKA pathway (155). A suggestion was proposed that dopamine via D_2-like

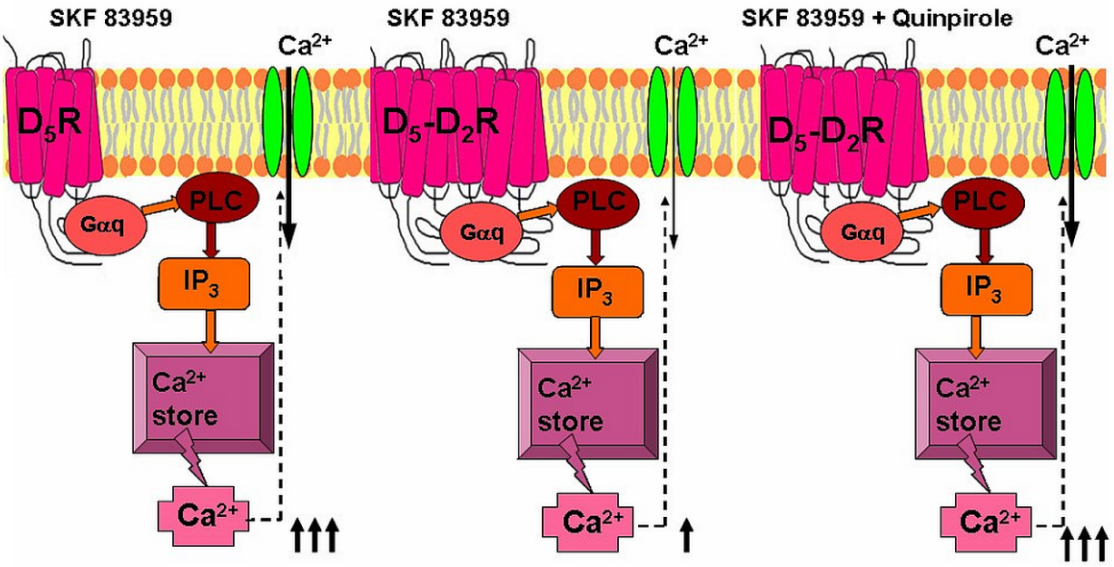

Figure 13. The activation of D_5 receptor homo-oligomers results in a robust rise in intracellular calcium due to PLC activation and extracellular calcium influx (left panel). The formation of the D_2–D_5 receptor heteromers results in an attenuation of the D_5 receptor induced calcium signal (middle panel), which could be restored only when both receptors are concomitantly activated (right panel). The abbreviations are the same as in Figure 11. Modified from Hasbi et al. (102).

receptors triggered two parallel intracellular calcium signaling pathways in photoreceptors (156). One pathway involved inhibition of AC1 (via Gi/o), leading to a decrease in $[cAMP]_i$, a decrease in PKA activity and to a reduction in the calcium permeability of photoreceptor plasma membrane channels. The other pathway included a direct action of dopamine on photoreceptor calcium permeability, leading to a decreased Ca^{2+} influx, a decrease in $[Ca^{2+}]_i$, a decrease in calcium-dependent AC1 activity, and a decrease in $[cAMP]_i$ (**Figure 14**). It was shown, however, that the dopamine effect on calcium influx current was not one and the same in all photoreceptors, but it strongly depended on the photoreceptor type (155). Dopamine reduced I_{Ca} in salamander large single cones, but enhanced I_{Ca} in rods and in all spectral subtypes of small single cones. Surprisingly, Stella and Thoreson (155) found that the intracellular mechanism of those opposite dopamine effects on I_{Ca} was one and the same - via Gi/o, AC1, cAMP and PKA. They proposed that differences among calcium channel subtypes may account for differences among photoreceptors in their responses to activation of the D_2-like receptors. Because of dopamine-induced changes in I_{Ca}, rods would have an augmented release of neurotransmitter, while the large cones would have a diminished release of neurotransmitter. Thoreson et al. (157) showed, however, that although the rod calcium currents were elevated, rod input to second order retinal neurons was diminished. They provided evidence that dopamine and D_2R agonists activated calcium-dependent chloride channels, leading to efflux of Cl^- from rods, resulting in subsequent fall of $[Ca^{2+}]_i$. Thus, the transmitter released by rods diminished without changing the membrane potential. In *mammalian (rat) retina*, however, it appeared that dopamine had no modulatory effect on the photoreceptor Ca^{2+} signals (evoked by high K^+ stimulus), because neither D_2R antagonist spiperone nor D_1R agonist SKF38393 had effect on them (158).

The effect of dopamine on the photoreceptor light responses is not well established. In *goldfish* dopamine did not affect the amplitude of light-evoked responses in green- and red-sensitive cones (159). The only effect of dopamine on the cone responses was to abolish the initial transient phase of membrane relaxation that occurred after the hyperpolarization peak (**Figure 15**). Similar results were obtained in *turtles*, where neither the rods, long-wavelength-sensitive, or medium-wavelength-sensitive cones exhibited any apparent change in responsiveness to light under the influence of dopamine (160). No dopamine-induced changes of rod light-evoked responses were seen in *Xenopus* retina (161) (**Figure 16 A**). In contrast to the above cited results, Hare and Owen (162) demonstrated that dopamine decreased the light-evoked responses of rods over the whole

intensity range tested in *tiger salamander* retina (**Figure 16 B**). In *mammalian retina*, the effects of dopamine on the rod light responses depended critically on the time of the day (163). Jin et al. (163) demonstrated that application of spiperone during the subjective day in *mice* decreased the amplitude and slowed the kinetics of rod responses, so that they resembled the responses typically observed at night. Application of the D_2R agonist quinpirole during the subjective night had opposite effects – enhancing the amplitude and speeding up the kinetics of rod responses. The same pharmacologic agents had no significant effect on the rod light responses, when they were applied during the opposite phase of the diurnal cycle. Jin et al. (163) concluded that a circadian clock in mouse retina controlled the light-evoked responses of rod photoreceptors and that the pathway of this control included dopamine and D_2-like receptors.

Much data indicates that dopamine influences the electrical coupling between rods and cones, but the effects described are contradictory. Some authors presented evidence that dopamine, acting through D_2-like receptors, increased the electrical coupling between rods and cones in *amphibian* retina (164-166). Krizaj (164) suggests that the effect is most important in the mesopic state, when both rods and cones are light responsive, and the electrotonic rod-cone bridges would permit one photoreceptor class to serve as a conduit for signals arising in the other class. At night or following prolonged dark adaptation, when dopamine levels are low, the rod-cone coupling is minimal, and this would prevent the shunting of the rod signal into the cones. Thus, the greater sensitivity to light of the rods would be preserved in postsynaptic cells. Neither light nor dopamine modulated rod-rod coupling in amphibian retina (165, 167), indicating that the modulation of electrical synapses between photoreceptors is specifically related to light adaptation. Other authors suggest, however, that the electrical communication between rods and cones in *fish* and *mammalian* retinas (*rabbit, mouse*) is weak during the day, when dopamine levels are high and robust at night, when dopamine levels are low (168-171). It was found that cones and cone-connected second order neurons could respond to very dim light stimuli in the scotopic range at night, but not during the day, indicating that rods could shunt currents to cones only during the night (170, 171). The authors suggest that the retinal circadian clock decreases both rod-cone tracer coupling and rod input to second order retinal neurons in the day by increasing dopamine D_2R, but not D_1R activation in the outer retina. The changes in photoreceptor coupling were driven by PKA-dependent phosphorylation of gap junctions (168, 169). There was a direct correlation between connexin 36/35 phosphorylation and rod-cone coupling such that both were high in darkness at night, and low under daytime illumination (168, 169, 172, 173). Pharmacological blockade of D_4 receptors under photopic light exposure in daytime resulted in significantly increased rod-cone coupling (169). This effect was also observed by the Li et al. (169) during adenosine A_{2a} receptor activation under the same conditions of light stimulation. Conversely, inhibiting A_{2a} or activating D_4 receptors in daytime dark-adapted retina decreased Cx36 phosphorylation with similar PKA dependence. Li et al. (169) concluded that adenosine and dopamine co-regulated photoreceptor coupling through opposite action on the PKA pathway and Cx36 phosphorylation (**Figure 17**).

This allows the photoreceptors to respond to extracellular cues that have opposite phases (dopamine: high in the day, low at night; adenosine: high at night, low in the day). Dopamine acting through D_2-like receptors during daytime not only suppressed rod-cone coupling in *mouse* retina, but it reduced the rod-rod coupling as well (163). The authors presented evidence that rod-rod coupling was weak during daytime (or subjective day) and stronger during nighttime (or subjective night). Application of quinpirole during the subjective night mimicked the daytime state, while application of spiperone during the subjective day mimicked the night-time state. It appears that a circadian clock in mammalian retina uses dopamine to control both rod-rod and rod-cone electrical coupling. It remains to be determined why dopamine, acting on D_2-like receptors, has no effect on rod-rod coupling in *amphibian* retina, but strongly modulates rod-rod coupling in *mouse* retina and why it has opposite effects on rod-cone coupling in *amphibian* vs *fish*, *mouse* and *rabbit* retinas. A possible explanation for the latter observation is that the decreased cAMP levels and suppressed PKA activity, due to D_2R activation, may have different effect on gap junction conductance in different species. It should be noted that electrophysiological studies on monkey photoreceptors failed to find any modulation of rod-cone coupling by dim backgrounds, dopamine or flupenthixol, a D_1/D_2 dopamine receptor blocker (174).

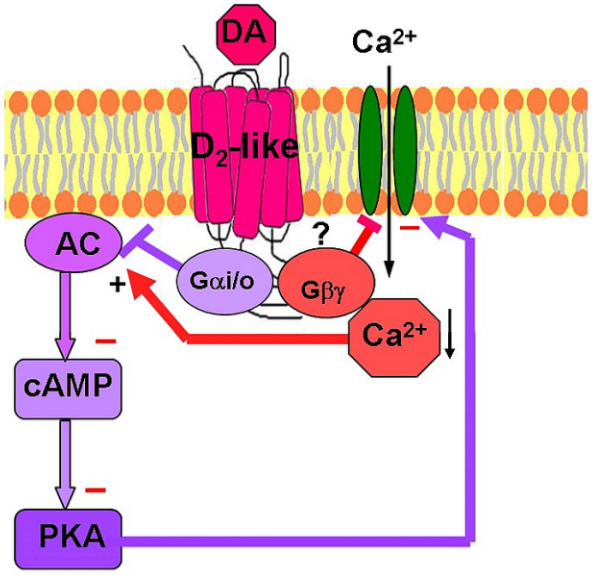

Figure 14. Action of dopamine on photoreceptor Ca^{2+} concentration. Dopamine via D_2-like receptors triggers two parallel intracellular calcium signaling pathways. One pathway involves reduction in the calcium permeability of photoreceptor membrane through $G_{i/o}$, AC1, cAMP and PKA. The other pathway includes a direct inhibitory action of dopamine on photoreceptor calcium permeability (via unknown mechanism, it may be Gβγ), that leads to a decreased $[Ca^{2+}]_i$, a decrease in calcium-dependent AC1 activity, and a decrease in $[cAMP]_i$. Type1 adenylyl cyclase (AC1). Model proposed by Firsov and Astakhova (156).

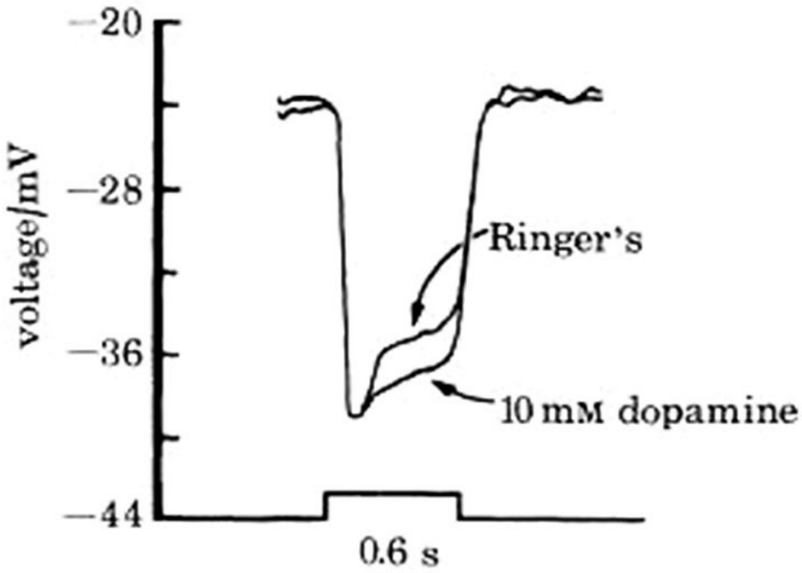

Figure 15. Red cone response to dopamine in *goldfish* retina. A response evoked in the presence of Ringer's solution is compared with one elicited after treatment with 10 mM dopamine. The flash duration is indicated by the raised bar. Both stimuli delivered 9 x 10^{10} photon·cm^{-2}·s^{-1}. Although the resting potential and response amplitude were unaffected by dopamine, the initial transient was abolished by the drug. From Hedden and Dowling (159).

Effects of dopamine on horizontal cells

Horizontals cells are one of major targets of dopamine actions in the distal retina. Dopamine reduced HC calcium currents through L-type channels via D_1R activation (175), affected spinule formation in HC dendrites, as reviewed in (147), strongly influenced the electrical coupling between adjacent HCs, changed HC responsiveness to light, and modulated the balance between HC rod and cone inputs, etc.

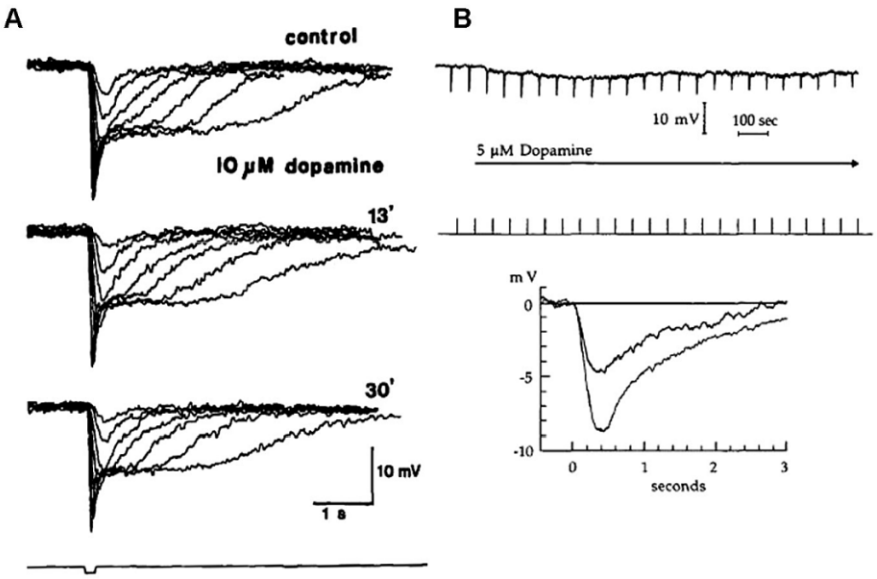

Figure 16. (**A**) Effect of dopamine on rod light-evoked responses in *Xenopus* retina. Voltage-intensity series from a rod recorded before (control) and during exposure (13 min, middle traces; 30 min lower traces) to 10 μM dopamine. The retina was stimulated with a 200 ms flash of 527 nm light (photocell trace is indicated at bottom). Stimulus intensities ranged from 9.68-12.27 log quanta·cm^{-2} ·s^{-1}. It is apparent that dopamine has no effect on light-evoked responses of Xenopus rods. From Witkovsky et al. (161). **(B)** Effects of dopamine on the dark potential and response amplitude of rods in *tiger salamander* retina. Stimuli were circular spots of 492 nm light, 600 μm in diameter, 20 ms in duration. Stimulus irradiance was fixed at 3.9 hv·μm^{-2} ·flash^{-1}. Typical responses of the same rod to the same stimulus recorded in control Ringer's solution (lighter trace) and 20 min after switching to a solution containing 5 μM dopamine (heavier trace) are presented on the lower row. It is apparent that dopamine caused a small hyperpolarization of the dark potential and attenuated the light-evoked responses of *salamander* rods. From Hare and Owen (162).

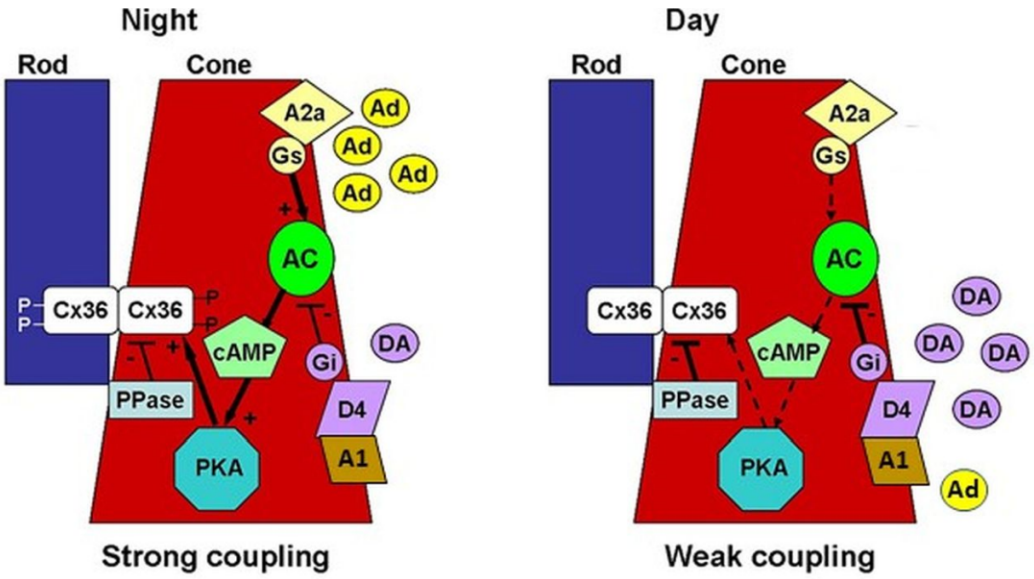

Figure 17. Molecular mechanisms that control photoreceptor coupling. At night, extracellular adenosine (**Ad**) is relatively high and dopamine (**DA**) relatively low, favoring activation of adenosine **A2a** receptors and stimulation of adenylyl cyclase (**AC**) and **PKA** through **Gs** signaling. **PKA** phosphorylates **Cx36** and thus increases coupling between rods and cones. In the day, extracellular dopamine is relatively high and adenosine relatively low, favoring activation of dopamine D4 receptors and adenosine A1 receptors. These both inhibit **AC** and **PKA** through **Gi** signaling and thus decrease the phosphorylation of **Cx36**. The phosphatase (**PPase**) is critical for regulation of coupling, but it is not known if its activity is constitutive or regulated. Modified from O'Brien (336).

The dopamine action on the electrical coupling between adjacent horizontal cells was studied in a number of species. Exogenous dopamine uncoupled horizontal cells in non-mammalian species: *amphibia* (162, 176), *reptiles* (177, 178), *fishes* (143, 179-187) and mammalian species: *rodents* (188-190), *rabbit* (191, 192). As a result, the response amplitude to a centered light spot increased, while that to an eccentric light spot or annulus decreased (64, 143, 177, 178, 180, 186-188, 193-197). According to Tornqvist et al. (64) this effect was seen in the first 5-7 minutes of dopamine application, while application of dopamine for longer periods of time (17–20 minutes) reduced the responses to both small and large spot stimuli. They suggested that the earlier effect was due to the uncoupling of HCs and the latter effect was due to suppressed responsiveness of HCs caused by dopamine (see below). Dopamine-induced uncoupling caused a marked reduction of the HC receptive field size (160, 177, 180, 186, 194, 195, 198, 199). Destruction of retinal dopaminergic neurons with 6-hydroxydopamine, on the other hand, broadened the receptive field profile of HCs (180, 186, 187, 199, 200). According to some authors this effect in fishes was seen only in cone-, but not rod-driven HCs (201, 202), while other authors observed it in rod-driven HCs as well (185, 203). The uncoupling effect of dopamine was mediated by D_1-like receptors, because D_1-, but not D_2-R agonists mimicked the uncoupling effect of exogenous dopamine and the effect was antagonized by D_1R, but not D_2R antagonists (162, 176, 178, 184, 188, 191, 192, 204) (**Figure 18**).

Whether the release of endogenous dopamine uncouples HCs via action on D_1R is a matter of debate. Some authors reported that application of D_1R antagonists alone had no effect on the coupling between HCs (184, 185, 192, 205), while other authors reported an increase of coupling between HCs and therefore insisted that HC coupling was tonically modulated by the endogenous dopamine (176, 188-191, 204). Activation of D_1R in HCs led to cAMP production, the latter likely modified the gap junction conduction between HCs by alteration in protein phosphorylation (**Figure 19**).

It was reported that elevated levels of cAMP in HCs decreased the electrical coupling between horizontal cells (178, 179, 181, 186, 189-192, 206). The effect in *fishes* and *mice* was independent of changes in $[Ca^{2+}]_i$ or pH (179, 190), while in *rabbit* retina, it was pH-gated and thus, may be mediated by a different mechanism (192). Dopamine reduced the open probability of gap-junction channels by reducing both the duration and frequency of channel opening (182, 183). The electrical coupling of HCs may be modulated also by dopamine acting on D_2-like receptors. Some authors found that D_2R agonists increased the HC coupling and D_2R antagonists decreased it (143, 176, 199, 207). The coupling effect of D_2R agonists was blocked completely by prior application of D_1R agonists or treatment with 6-OHDA. These results supported the suggestion that activation of D_2 autoreceptors on dopaminmergic IPCs inhibited dopamine release onto HCs so that the electrical coupling between *fish* horizontal cells increased (143, 199). In *turtle* retina, however, the effect of D_2 agonists was preserved in the presence of a D_1R antagonist, indicating that D_2R played a direct role in electrical coupling between HCs (207).

There is no consensus among authors how the electrical coupling and receptive field size of horizontal cells change with retinal adaptation. Some authors insisted that background illumination had no effect on the HC coupling and receptive field size (177, 208), while other authors stated that background light significantly decreased electrical coupling among HCs (176, 184, 204, 209-212). Still other authors reported that electrical coupling between horizontal cells increased during light adaptation (213) and had minimal values during prolong periods in darkness (64, 194, 195, 214). An interesting relationship between retinal adaptation state and HC coupling was suggested for *fish* and *rabbit* retina. Baldridge (209) proposed a triphasic model for adaptation changes of teleost H_1 cells. He suggested that the HC responsiveness and receptive field sizes were minimal during prolonged darkness but increased considerably when moderate illumination was applied after darkness. Coupling decreased again following exposure to bright illumination. Similar triphasic adaptation was suggested to exist in rabbit HCs (215). It was shown that the coupling between HCs was relatively weak in darkness as well as under background illumination with intensity higher than 3 log units above the rod threshold (**Figure 20**). The coupling between cells increased only under dim background illumination with intensity from one-quarter to 1.5 log units above the rod threshold (215).

Most authors related the changes of electrical coupling between HCs during dark or light adaptation to changes of endogenous dopamine release. According to some, dopamine mimicked the effect of a prolonged period of darkness, but not continuous light background (64, 195, 214), while others suggested that dopamine was responsible for the uncoupling effect of the adapting light (176, 212). The latter suggestion was supported by the fact that the uncoupling effect of both flickering and steady adapting light was blocked by nonselective DR antagonist fluphenazine (212) and selective D_1R antagonist SCH 23390 (176). Some authors argued that dopamine is not the signal of HC adaptation to steady illumination in *teleosts*, because DA depletion or application of DR antagonists did not alter the effect of background illumination upon fish horizontal cell coupling and receptive field size (209, 211). In the case of flickering light adaptation, however, dopamine did seem to be involved, because haloperidol blocked the reduction of HC receptive field size induced by a flickering light (211). In *primate* retina, SCH 23390 only partially blocked the effect of background light on the HC receptive field size, suggesting that other mechanisms, in addition to the dopaminergic system, may be involved in background-induced reduction of HC receptive field size (204).

Dopamine has an additional effect on the horizontal cells that is independent of its action on the electrical coupling between adjacent horizontal cells. It decreased the response of *fish* cone-HCs to full-field stimuli and enhanced glutamate- and kainate-induced currents (64, 143, 159, 194, 195, 199, 216). Thus, dopamine, by enhancing the potency of the photoreceptor transmitter, rendered the light-induced reduction of transmitter release from the photoreceptors less effective, leading to decreased amplitude of the HC response to light. Some authors suggested that dopamine was responsible for the strongly suppressed light responsiveness of cone HCs in prolonged darkness (64, 194, 195, 202).

Yang et al. (202) demonstrated that HCs became highly responsive to illumination in dopamine depleted retinas maintained in prolonged darkness (**Figure 21**). Furthermore, application of DA to dopamine-depleted or light-sensitized retinas strongly suppressed the responsiveness of cone HCs, mimicking the effects of prolonged darkness. The effect was probably mediated by D_1-like receptors, because SCH 23390 (a specific D_1R antagonist), enhanced the responsiveness of cone HCs in prolonged darkness, mimicking the effect of background illumination. It was suggested that DA was released in the dark by the IPCs and enhanced the potency of the photoreceptor transmitter (202, 217). Dowling (217) proposed a hypothesis that dopamine increased cAMP which activated kinases that phosphorylated both glutamate-gated channels and gap-junction channels (**Figure 19**). Destruction of dopaminergic neurons significantly decreased, but not fully eliminated the suppressive effect of prolonged darkness on responsiveness of fish cone HCs in vivo (218). The latter result suggests that a substance or substances other than dopamine may contribute to the dark suppression effect. In *turtle* retina, dopamine reduced the responsiveness of all except L_1-type horizontal cells (160). A reduction of the response amplitude to full field stimuli caused by dopamine was observed in *mammalian* rod-driven HCs (188, 219). The effect was mediated by D_1-like receptors, because it was reversed effectively by the co-application of the D_1R antagonist SCH 23390, but not by the D_2R antagonist L-sulpiride (219) (**Figure 22**). SCH 23390 alone, but not sulpiride, enhanced the responses to full-field light stimuli, revealing an active endogenous DA input to HCs. Because the DA effect on HCs was not seen in preparations with blocked synaptic transmission, Hankins and Ikeda (188) suggested that dopamine action resulted from modulation of the L-glutamate activated currents of these cells. The described two effects of dopamine on horizontal cells – decreasing light responsiveness and shrinking receptive field size – are effective ways to lessen HC influence upon the other retinal neurons. It was suggested (159, 194, 195) that these effects of dopamine may account for the reduced or fully eliminated antagonistic surrounds of ganglion cells with prolonged time in the dark (**Figure 23**). Baldridge (209) proposed that the reduction of HC receptive field size following light adaptation would narrow the receptive filed surround of GCs and therefore permit spatial contrast analysis to be done more locally.

Much data indicate that dopamine effects on the HC light responses depend on the photoreceptor input. Separate horizontal cells in *fishes* receive inputs from cones or rods. It was shown that dopamine had apparent effects on light responses of cone-driven HCs, while contradictory results exist concerning its effects on the light

responses of rod-driven HCs. Some authors found that dopamine effects on the rod-driven HCs were similar to those on cone-driven HCs (196), other authors obtained much smaller effects on rod- than cone-driven HCs, as in *perch* (64, 195, 202) and still other authors found no dopamine effects on the rod-driven HCs in *skate* (208), *dogfish* (220) or *goldfish* (159). In *amphibian* retina, where horizontal cells receive converging synaptic inputs from both rods and cones, dopamine enhanced the amplitude of the cone-mediated component of the HC response, but diminished the amplitude of the rod-mediated one (161, 162, 164, 221). The authors cited suggested that dopamine decreased the gain of the rod-HC synapse and increased the gain of the cone-HC synapse. Dopamine action was probably mediated by postsynaptic D_1-like receptors, because D_1 activation eliminated the rod component of the flash response and caused the HCs to display all the signs characteristic of the photopic state (164). The effect of injecting cAMP was identical to that obtained by the application of the D_1R agonist or by adapting the retina with strong background light. Krizaj (164) concluded that dopamine via D_1R acted as a postsynaptic switch modulating the balance between the rod and cone pathways, and that intracellular cAMP could play an important role in regulating the relative weight of rod and cone information in retinal cells. Other authors argued, however, that the dopamine effect on the rod-cone balance in amphibian HCs was mediated synergistically by both D_1- and D_2-like receptors (162, 221). How dopamine influences the balance between rod and cone inputs to *mammalian* HCs is not well evaluated. Ribelayga and Mangel (170) reported that the blockade of D_2R, but not D_1R during the day increased the absolute and relative light sensitivity of *rabbit* A-type HCs, so that their responses resembled those typically recorded at night. The authors proposed that the retinal circadian clock increased the dopamine levels and D_2R activation in the outer retina during the day, so that rod input (via rod-cone coupling) to A-type HCs was greatly reduced. On the other hand, Pflug et al. (222) found that D_1R agonists depolarized somata of both A- and B-type HCs in rabbit retina and enhanced the overall and flicker amplitudes of their scotopic responses, but almost completely suppressed the cone flicker amplitudes of the photopic responses, without changing the overall response amplitude (222). The authors proposed that the dopamine-induced HC depolarization caused a shift of the cone I_{Ca} activation curve to more positive values and thus reduced the transmission of the most hyperpolarizing cone signal component, i.e. the cone flickering part of the light response. Pflug et al. (222) imply that shifting the operating range of cone synapses to more depolarized levels increases the gain for low amplitude rod signals which enter cones through rod-cone gap junctions but did not elaborate on the mechanism, whether at the rod-cone gap junctions, or at the tuning of the cone synapse itself. More studies are needed to fully understand how the dopamine action upon mammalian HCs depends on the photoreceptor input.

Dopamine may participate in the control of spectral responses of cone luminosity (H_1) and chromaticity (C-type) horizontal cells in *fish* and *turtle* retina. Mangel and Dowling (195) reported that dopamine reduced the responses to long wavelength full-field light stimuli more than the responses to short wavelength stimuli in one third of carp H_1 cells. Contrary to this observation, other authors found that dopamine increased the responses of carp H_1 cells to long wavelengths (223, 224), but had no effect (224) or decreased (223) responses to short wavelengths. In the latter case, dopamine decreased the blue/red response amplitude ratio in a way similar to that induced by red-background adaptation (223). The effect of light adaptation, however, was also recorded in dopamine depleted retinas and in the presence of haloperidol, indicating that dopamine was not responsible for the effect of light adaptation on the spectral response characteristics of H_1 cells. Djamgoz et al. (223) suggested that spectral responses of H_1 cells were controlled independently by light-adaptation (primarily by long wavelengths) and dopamine. The effects of dopamine on C-type HCs are not well understood. No differential spectral response effects of dopamine on C-type HCs were observed in turtle (160) or carp retina (195). In goldfish retina, dopamine increased the hyperpolarizing component evoked with white light, but decreased the depolarizing component evoked with red light in half of C-type HCs, while in the other half it had no effect irrespective of the cell subtype (159). In roach retina, haloperidol increased the hyperpolarizing component (to blue-green light), but decreased the depolarizing component (to red light) of biphasic (green/red) H_2 horizontal cells (225). In addition, haloperidol prevented the enhancement of the depolarizing component induced by light adaptation. Destruction of the DA cells with 6-OHDA also prevented the enhancing effect of red flickering light

on the depolarizing response of R/G HCs in carp retina (226). The effect was probably mediated by D_2R, because application of D_2R, but not D_1R antagonists was similar to that of 6-OHDA. Liu et al. (226) suggested that the activation of D_2R in the OPL might be related to the synaptic plasticity of the GABAergic pathway between HCs and cones, which is responsible for the change in red flickering induced responsiveness in the R/G HCs.

Effects of dopamine on bipolar cells

There are not many studies undertaken to evaluate dopamine action on retinal bipolar cells; however, the effects of DA on the ionic currents (Ca^{2+}, Na^+, K^+), membrane potential, light-evoked responses and responses to other neurotransmitter of retinal BCs have been reported. It was shown that dopamine and D_1R agonist ADTN potentiated the voltage dependent Ca^{2+} currents in presynaptic terminals of all bipolar cells in *fish* retina (227, 228). The effects of dopamine antagonists on the same currents, however, depended on the BC type (ON or OFF) (227). The D_1R antagonist SCH 23390 strongly suppressed Ca^{2+} currents at all stimulus intensities in OFF BCs but in ON BCs, SCH 23390 augmented Ca^{2+} currents at lower stimulus intensities but did not change them at higher intensities. The D_2R antagonist sulpiride had similar effect as SCH 23390 upon the ON BCs, while it enhanced the Ca^{2+} currents at lower stimulus intensities and diminished them at higher intensities in the OFF BCs. The mechanism for the differential effects of dopamine antagonists on the ON and OFF pathways is still not clear. In *amphibian* retina, dopamine had no apparent effect on Ca^{2+} entry into the bipolar terminals, but it blocked the GABAergic inhibition on this entry and thus increased the transmitter release (229). The effect was similar for the ON and OFF BCs. In addition to Ca^{2+} currents, dopamine, via D_1R, modulated the voltage-gated Na^+ currents in amphibian transient ON BCs (230). The dopamine receptor agonist ADTN markedly reduced the Na^+ currents in dim light conditions, while SCH 23390 prevented the depressing effect of light adaptation on these currents. Dopamine modulated also the K^+ currents in retinal BCs. Dopamine acting via D_1R-coupled G-protein pathways decreased the voltage-dependent K^+ currents in ON BCs in *zebrafish* retina (231). In *goldfish* retina, dopamine depressed K^+ currents but only in high concentrations, while in low concentrations it enhanced these currents in mixed rod-cone ON bipolar cells (Mb) (232, 233). Both the enhancement and suppressive effects were blocked by SCH23390, indicating involvement of D_1-like receptors. Fan and Yazulla (233) proposed that D_1R activation should make the ON response of Mb BCs more phasic by enhancing K^+ currents. Depletion of retinal dopamine reduced by about half the amplitude of voltage-dependent K^+ currents in Mb BCs (234).

The actions of dopamine on membrane potential and light-evoked responses of retinal BCs were investigated mainly in fish and amphibian retina. In *fish* retina dopamine produced a hyperpolarization of the membrane potential of cone BCs and rod BCs (159, 220, 235). Dopamine enhanced the center light responses, but it reduced the antagonistic surround responses of both ON and OFF BCs under conditions in which the responses were mediated by cones (159, 235) (**Figure 24**). This effect is consistent with the suppressive action of dopamine on HC responsiveness, because the latter cells are thought to mediate the antagonistic surround of BC receptive field (68). In the all-rod retina of dogfish, dopamine reduced the responses to light flashes of ON RBCs (220) (**Figure 25**). The suppressive effect of dopamine on RBCs was not due to its effect on HCs, because neither the membrane potential nor the light responses of rod HCs were influenced by dopamine. Thus, it appears that dopamine enhanced the responses of fish cone BCs but suppressed the responses of rod BCs.

In *amphibian* retina, where bipolar cells receive mixed rod and cone inputs, dopamine produced variable effects upon the dark membrane potential of OFF BCs, but upmodulated their glutamate-gated currents through D_1R and cAMP-PKA pathway (236). Dopamine caused a significant reduction in the amplitudes of rod-driven responses, while it enhanced the cone-driven responses elicited from the receptive field center (162). It did not change the balance between center and surround of the BC receptive field, when the responses were rod-driven, but it favored the center over surround, when the responses were cone-driven. Opposite results were reported for the action of dopamine on the light responses of cone-driven transient ON BCs in the same species (230). It was

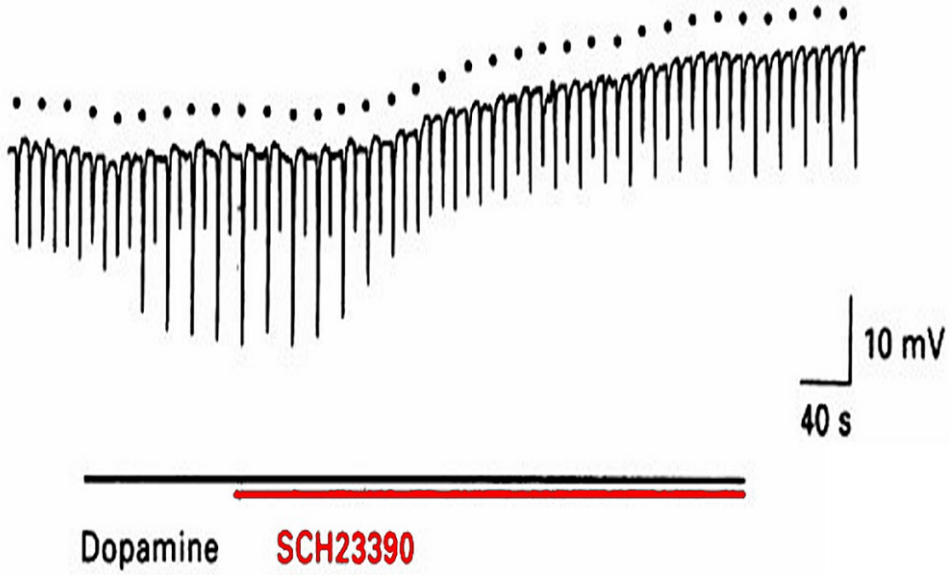

Figure 18. Effect of exogenous dopamine and SCH23390 on horizontal cell responses to center and surround illumination in dark adapted *mudpuppy* retina. Responses to alternating spot (indicated by dots) and annulus stimuli are presented. Dopamine decreases the responses to annular stimuli and increases the responses to spot stimuli. SCH23390 blocks the effect of exogenous dopamine. From Dong and McReynolds (176).

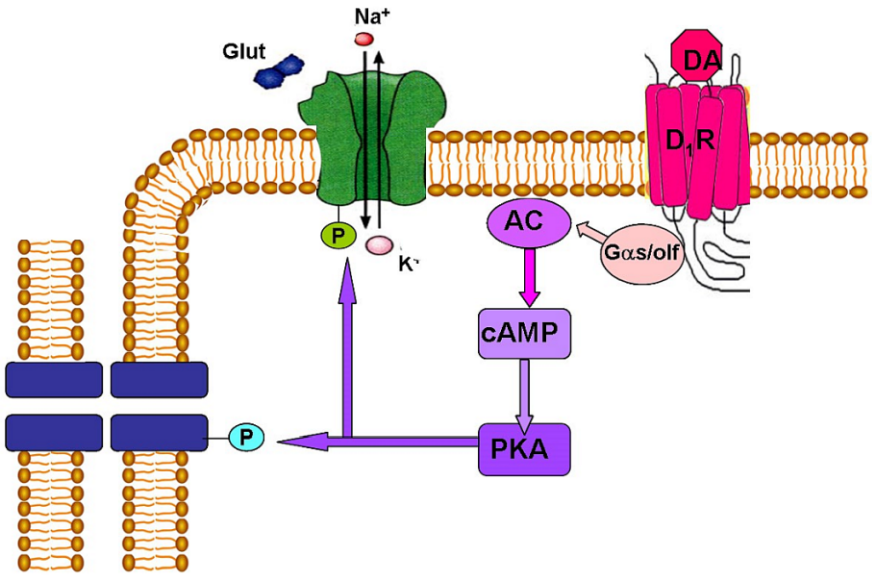

Figure 19. Scheme showing the effects of dopamine (**DA**), acting via D_1-like receptors (**D_1R**), on the fish horizontal cells. Dopamine via **cAMP**-**PKA** pathway causes phosphorylation (**P**) of the gap-junction channels and glutamate (**Glut**) channels and thus reduces the electrical coupling between horizontal cells but increases their responsiveness to L-glutamate (the photoreceptor transmitter). Modified from Dowling (217).

shown that D_1 agonist SKF38393 reduced the L-EPSPs in dim light conditions and thus mimicked the effect of bright light. On the other hand, D_1 antagonist SCH23390 blocked the suppressive effect of bright light on L-EPSPs. The effect was seen in transient, but not sustained ON BCs. The authors concluded that dopamine released in bright light, attenuated the sodium channel-dependent amplification of L-EPSPs in transient cone-driven ON BCs and thus prevented response saturation. It remains to be determined if the opposite, depressing effects of D_1R activation on the cone-mediated responses of ON BCs (230) and enhancing effects on OFF BCs (162) are species specific or they represent general ON/OFF asymmetry in dopamine action on BCs. The effects

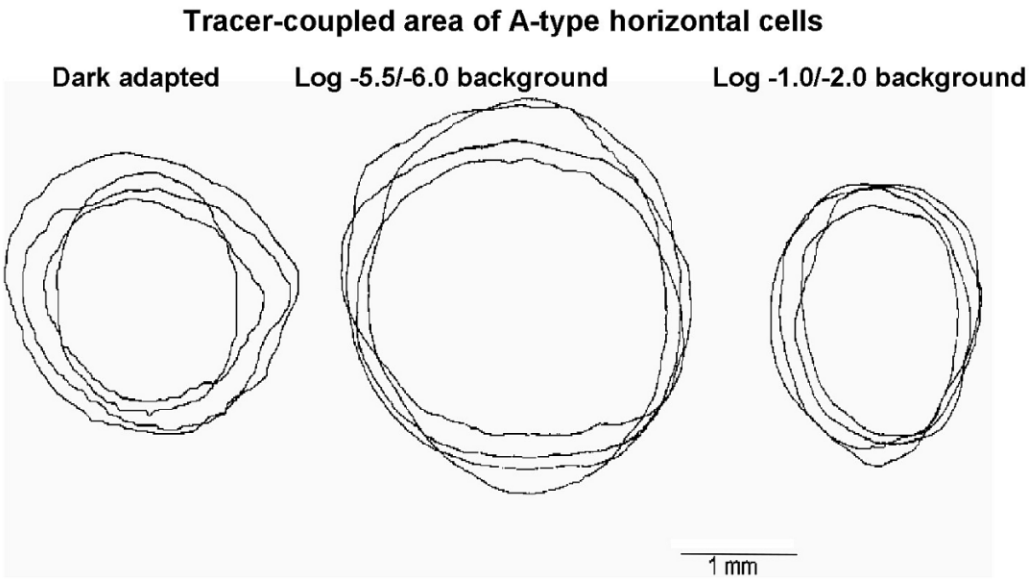

Figure 20. Tracer-coupling area of A-type horizontal cells in different conditions of light adaptation in *rabbit* retina. Each drawing outlines the area occupied by a group of tracer-coupled A-type cells. Four outlines, representing four different Neurobiotin injections, are shown for each level of adaptation. For dark-adapted cells, each outline represents the largest tracer-coupled group in each quartile of 12 total cells. From Xin and Bloomfield (215).

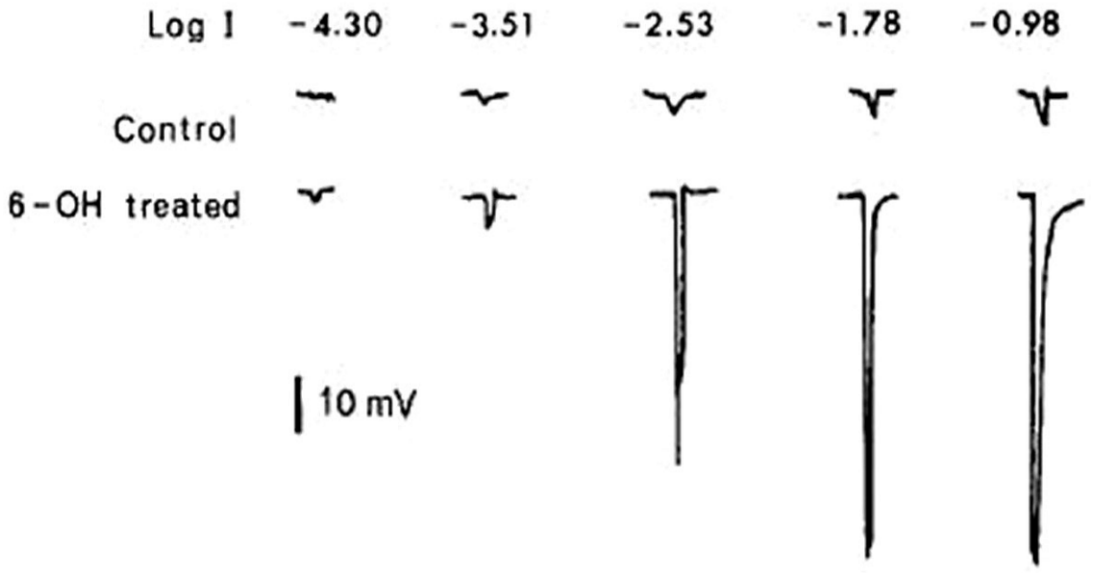

Figure 21. Responses of L-type cone horizontal cells to full-field white flashes recorded in an untreated *white perch* retina (upper row) and in a 6-OHDA-treated retina (lower row) maintained in prolonged (> 2 hr) darkness. The responses recorded from the 6-OHDA-treated retina were much larger in size and had faster-rising phases and on-transients. Intensities of the light flashes, indicated above the response traces, are in relative log units. Form Yang et al. (202).

of dopamine on the *mammalian* bipolar cells are largely unknown. It was shown that dopamine induced changes of receptive field organization of *rabbit* ON-CBCs in the dark similar to those observed during light adaptation (237). During dopamine treatment, the ON-CBCs exhibited center and surround responses similar to those of bright-light-adapted ON-CBCs in intact retinal preparations. The dopamine effect was probably mediated by D_1-like receptors, because the surround responses were not observed during D_1R blockade but were preserved during D_2R blockade.

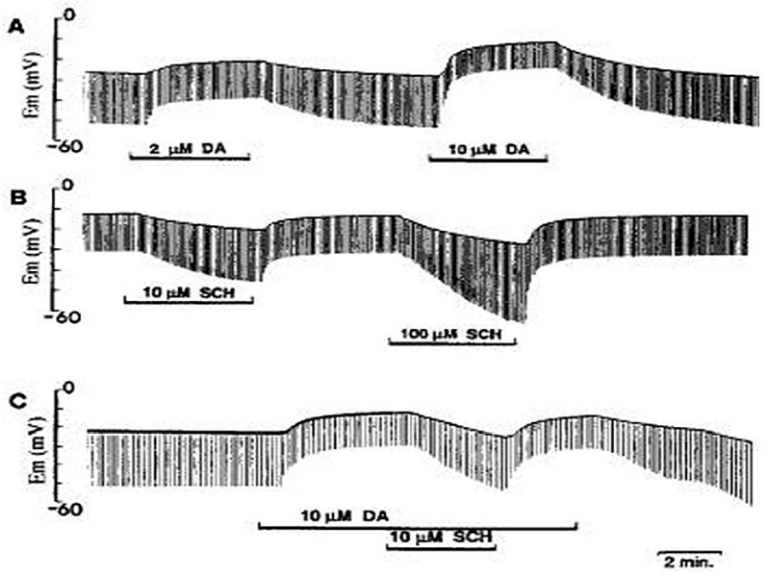

Figure 22. Effects of dopamine and SCH23390 on the membrane potential and the light-evoked S-potentials of rod-driven (A-type) horizontal cells in *rat* retina. **(A)** Dopamine (2 and 10 µM) evokes a dose-related depolarization associated with a significant reduction in the full-field light response. **(B)** SCH23390 (SCH; 10 and 100 µM) evokes a dose-dependent hyperpolarization accompanied by a significant enhancement of the full-field light response. **(C)** The effects of exogenous dopamine (10 µM) on the membrane potential and light responses of HCs are effectively reversed by the co-application of 10 µM SCH 23390. From Djamgoz et al. (219).

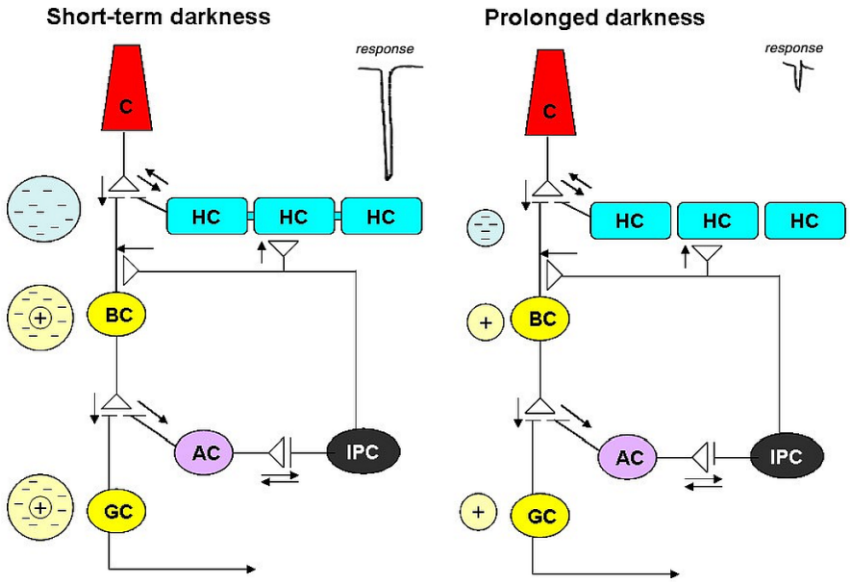

Figure 23. Changes of coupling between cone horizontal cells (**HC**) and receptive field profiles of HCs, bipolar cells (**BC**) and ganglion cells (**GC**) in short-term darkness and prolonged darkness in fish retina. Dopamine, released by interplexiform cells (**IPC**) in prolonged darkness, decreases the responsiveness of HCs to light and uncouples HCs (depicted here as disconnected cells) thus leading to reduction of the size of HC receptive fields. These effects of dopamine lead to reduction of antagonistic receptive field surrounds of BCs and GCs in prolonged darkness. Plus symbols (+) refer to receptive field centers of BCs and GCs, while dashes (-) refer to the receptive field of HCs and to the receptive field surrounds of BCs and GCs. Modified from Mangel and Dowling (195).

Dopamine may modulate the responses of bipolar cells to other neurotransmitters such as glutamate and GABA. Dopamine enhanced the response to glutamate in *amphibian* OFF BCs (236). The effect was mediated by D_1-like receptors, because it was blocked by D_1R antagonist SCH 23390, but not the D_2R antagonist spiperone. Activation of D_1 receptors in the dendrites of bipolar cells led to stimulation of Adenyl cyclase, which through

cAMP and PKA enhanced a glutamate-gated current in BC dendrites. Dopamine plays a very important role in modulating the GABAergic inhibition onto BCs as a part of the light adaptation process. It was shown that activation of D_1R significantly decreased the frequency and amplitude of spontaneous inhibitory postsynaptic currents (S-IPSCs) and the amplitudes of light-evoked inhibitory postsynaptic currents (L-IPSCs) evoked by full-field stimuli in dark adapted *mouse* rod BCs, the effect being similar to light adaptation (238, 239). Flood et al. (238) showed also that D_1R activation directly diminished the inhibitory output of non-reciprocal ACs onto rod BCs, in the absence of serial inhibition. They proposed the following model for the inhibition of rod BCs under dark adapted conditions and D_1R activation. In dim light, rod BCs receive reciprocal inhibition from A17 amacrine cells and lateral inhibition from wide-field GABAergic ACs, as well as narrow-field glycinergic ACs. When light stimuli of sufficient size are used, the strength of lateral inhibition to rod BCs is diminished by serial inhibition. When D_1Rs are activated, the inhibition to rod BCs is greatly decreased, because the strength of serial inhibition is increased and the GABA release by ACs that mediate lateral inhibition is decreased (**Figure 26**).

However, unlike light adaptation, D_1R activation did not shorten L-IPSC decays in rod BCs and its effect on the amplitude of L-IPSCs was smaller than that of light adaptation, indicating that some D_1R independent component also played a role in the modulation of rod BC inhibition with light adaptation (238). Dopamine modulated also the GABAergic inhibition on the cone BCs. It was recently shown that bright-light-induced activation of D_1Rs located on the ON CBC dendrites in *rabbit* retina increased the expression and activity of $GABA_A$ receptors on the dendrites of the cell (237). Endogenous activation of these receptors participated in the generation of the surround light responses of CBCs, which were diminished in maintained darkness and during D_1R blockade (with SCH 23390). Dopamine via D_1R modulated also the local glycinergic, but not GABAergic inhibition to *mouse* OFF cone bipolar cells (239). D_1R activation significantly decreased the frequency and amplitude of S-IPSCs and L-IPSCs in OFF CBCs, evoked by local light stimuli in the dark (238, 239). The effect of D_1R activation on the glycinergic L-IPSCs was similar, but not identical to the effect of light adaptation. D_1R activation had no significant effect on the time course of the glycinergic L-IPSCs, while those currents become more transient with light adaptation. Mazade et al. (239) concluded that D_1 receptors were not the only neuromodulator influencing light adapted changes in local inhibition of OFF BCs.

The overall activity of BCs in living animals could be monitored by recording the electroretinogram (ERG), because the b-wave (in response to stimulus onset) and the d-wave (in response to stimulus offset) are thought to depend mainly on the activity of ON and OFF bipolar cells, respectively, as reviewed by Frishman (240), see also Webvision: The Electroretinogram. Thus, the significance of dopaminergic neurotransmission for bipolar cell function could be investigated by exploring the effects of dopamine and DR agonists and antagonists on the ERG b- and d-waves.

Effects of dopamine on the diffuse electroretinogram

The ERG b-wave amplitude displayed a *circadian rhythm* in constant conditions in *fishes* (241), *birds* (76, 242-244), *reptiles* (245, 246), and *mammals*: *rabbit* (247, 248), *mouse* (249-252). Generally, the b-wave amplitude was highest during the subjective day and lowest during the subjective night. In dopamine depleted nonmammalian animals, no circadian rhythm of the b-wave amplitude was seen (**Figure 27**), indicating that retinal endogenous dopaminergic system is essential for the circadian rhythm of the b-wave amplitude as seen in *zebrafish* (241), *iguana* (74) and *quail* (76). The circadian rhythm was markedly changed during D_2R, but not D_1R manipulation in *quail*, indicating involvement of D_2R mechanisms in its generation. Li and Dowling (241) found, however, that not all circadian effects were absent in dopamine-depleted *fishes*. In the latter animals, an ERG OFF-response was observed at subjective dusk, but not at subjective dawn, as also found in the control fishes (**Figure 27**). In *mice*, the cone-, but not rod-mediated ERG was under circadian control (249-251, 253). The role played by endogenous dopamine in this control is an object of debate. Sengupta et al. (251) observed that the circadian regulation in the photopic ERG was absent in *mice* lacking melatonin receptor type 1,

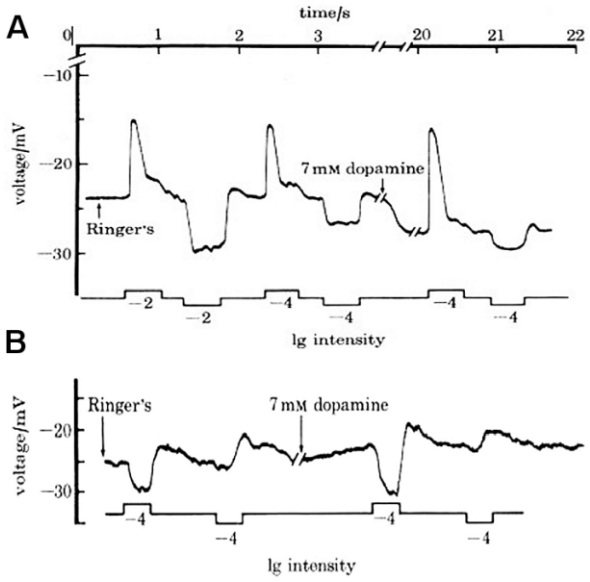

Figure 24. Responses of *goldfish* cone-driven bipolar cells to dopamine. Responses of an ON bipolar cell **(A)** and an OFF BC **(B)** obtained with alternately flashed spots (raised bars) and annuli (lowered bars) are presented during the control period (Ringer) and during treatment with dopamine. The intensities are given on the figure. Dopamine evoked an enhanced central response and a depressed surround response in both cells. From Hedden and Dowling (159).

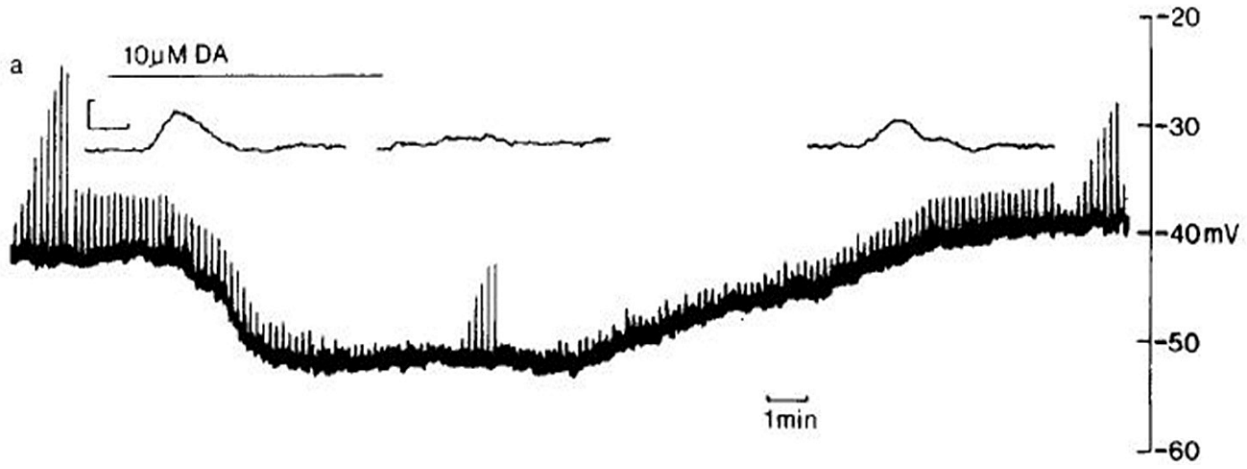

Figure 25. Effect of dopamine (**DA**) on the membrane potential and response to light of a rod ON bipolar cell in *dogfish* retina. Test flashes of constant low intensity and of 15-ms duration were applied every l0 s. At intervals, the cell's light intensity-response relation (which appears as a decreasing, then increasing staircase of responses) was determined by changing the light intensity by factors of approximately 2. 10 μM **DA** was applied for the duration indicated by the bar. Above the continuous trace are shown single responses on an expanded timescale, corresponding to the test responses following the intensity-response determinations. Bars = 5 mV, 200 ms. From Shiells and Falk (220).

although the circadian regulation of dopamine turnover was preserved. These results led to the suggestion that the circadian regulation of dopamine turnover did not drive the mouse cone-mediated ERG rhythm. Jackson et al. (253) reported, however, that the circadian rhythm of the light-adapted b-wave amplitude was lost in mice lacking retinal dopamine (with disrupted tyrosine hydroxylase), indicating that endogenous dopamine was essential for the circadian rhythm of the mouse ERG. This action of dopamine was probably mediated by D_4 receptors, because the circadian rhythm was abolished in D_4R-KO mice, but not in D_1R-KO mice. However, D_4Rs did not maintain circadian rhythm at DD1 (18–30 h in dark), since a substantial b-wave decrease was observed at midnight relative to midday in D_4R-KO mice. Smith et al. (254) presented evidence that the robust

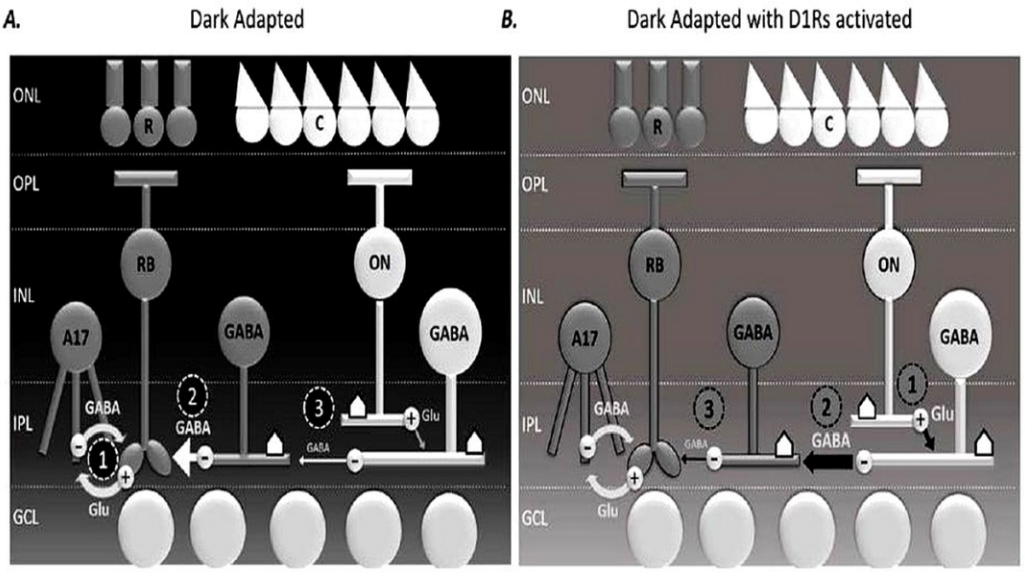

Figure 26. Sources of inhibition to rod bipolar cells under dark-adapted conditions and upon D_1 receptor activation in *mouse* retina. **(*A*)**. In darkness, rod BCs (**RB**) receive reciprocal inhibition from A17 amacrine cells, '**1**' and lateral inhibition from wide-field GABAergic amacrine cells '**2**'. When light stimuli of sufficient size are used, the strength of lateral inhibition to rod BCs is diminished by serial inhibition '**3**'. **(*B*).** When D_1Rs are activated, the strength of serial inhibition is increased '**2**' and the GABA release by amacrine cells that mediate lateral inhibition is decreased and becomes independent of serial inhibitory influences '**3**'. These effects lead to diminished inhibition upon rod BCs. From Flood et al. (238).

circadian rhythm seen after 6–18 h in dark (DD1) was controlled predominantly by D_1R and Na_V channels. They proposed that circadian modulation of cone pathway function in mice involved an early mechanism based on D_1Rs and Nav channels on ON-CBCs that acted in the short-term time scale (DD1, 6–18 h) and a longer-term modulation taken over by a mechanism based on D_4Rs affecting persistent circadian rhythms after 42 h (DD2). Melanopsin-containing retinal ganglion cells probably are also involved in the circadian regulation of mouse cone-mediated b-wave, because genetic ablation of melanopsin blunted the circadian rhythm of b-wave amplitude and speed (249). Barnard et al. (249) suggested that melanopsin-containing retinal ganglion cells could influence dopaminergic amacrine cells via gap junctions and thus entrain a local retinal clock in inner retina.

There is no consensus among the authors about the role played by the dopaminergic system for the *non-circadian* regulation of ERG b-wave amplitude in *nonmammalian* retinas. In *fish* retina, some authors observed no apparent changes of the b-wave amplitude during blockade of retinal dopaminergic transmission in either dark or light adapted eyes (241, 255, 256), while other authors reported that the D_1R agonist SKF 38393 as well as exogenous dopamine increased, while D_1R antagonist SCH 23390 either decreased the cone-mediated b-wave amplitude (257), or led to a separation of the signal into transient peaks, emphasizing those components, and sharpening the peaks (258). Manipulation of D_2R had opposite effects to those described for the manipulation of D_1R (257, 258) (**Figure 28**). The conflicting results obtained in fish retina may be due in part to differences in light stimulation used by the authors. While Kim and Jung (257) used a small spot light, other authors (241, 255, 256) used full field light stimuli. This suggestion is supported by the fact that meclofenamic acid (a non-specific gap junction blocker), which had similar action to that of dopamine on the fish ERG, had 5 times greater effect on the b-wave obtained with small spot than large spot (257).

In *amphibian* retina, a reduction of the suprathreshold b- and d-wave amplitudes was reported during blockade of the dopaminergic transmission (259-261). The isolated blockade of D_1R with SCH 23390 and D_2R with sulpiride had differential effects on the ERG waves depending on photoreceptor input (262-264). Both blockers enhanced the rod-mediated suprathreshold b- and d-waves, while the action on the cone-mediated responses

was in an opposite direction. The D_1R blocker enhanced the amplitude of the cone-dominated b- and d-waves, while D_2R blocker diminished them (**Figure 29**). These results suggested that activation of D_1R by endogenous dopamine inhibited frog ERG ON and OFF responses, which was opposite to its action on fish photopic ON response (257). The inhibitory effect of endogenous dopamine on the frog b- and d-wave amplitudes may be due to D_1R-induced GABA release, because this effect was prevented during ionotropic GABA receptor blockade (265).

In *chicken* retina, exogenous dopamine had no effect (266) or it had diverse effects on the b- and d-wave amplitudes depending on light stimulation conditions (267). The blockade of dopaminergic transmission (with haloperidol) caused a reduction of the b-wave amplitude at all stimulus intensities, indicating that endogenous dopamine had an enhancing effect on the chicken ERG ON response recorded under conditions of dim ambient illumination (268). In *quail*, the b-wave amplitude was reduced by the D_2R agonist quinpirole injected during the subjective night and increased by D_2R antagonist eticlopride injected during the subjective day, while manipulation of D_1R had no effect (76). These results suggest that endogenous dopamine via D_2R decreased the b-wave amplitude during the day in quail. In *iguana*, the manipulation of D_1R had no effect on the dark-adapted b-wave, while D_2R manipulation had opposite effects to those observed in quail (74). Quinpirole increased the amplitude of the b-wave, when it was injected during the subjective night and eticlopride reduced the b-wave amplitude, when it is injected during the subjective day. Miranda-Anaya et al. (74) suggested that endogenous dopamine increased the b-wave amplitude during the subjective day directly via D_2R and indirectly by inhibiting melatonin synthesis. Because the phases of the rhythm of dopamine synthesis were similar in quail and iguana (74, 76), whereas the phase of the rhythm of b-wave amplitude and the effect of quinpirole and eticlopride were opposite, it seemed likely that dopamine exerted its effects on the ERGs of the two species by different mechanisms.

The dopaminergic modulation of *mammalian ERG* was investigated in many studies. Most of the authors reported that application of exogenous dopamine, its nonselective agonist apomorphine and the dopamine uptake blocker nomifensine decreased the amplitude of the b-wave as seen in *rabbit* (269-274) and *cat* (275, 276).The blockade of dopaminergic transmission, on the other hand, caused an increase of the suprathreshold b-wave amplitude as seen in *cat* (275, 277, 278), *rabbit* (272, 279) and *monkey* (280) without altering the dark adapted threshold ERG (275). The b-wave *V - log I* curve was shifted to the left along the intensity axis, indicating an increased relative sensitivity of the response during dopaminergic blockade (277). The effects of dopaminergic manipulation were maximal under scotopic conditions but were also seen in mesopic and photopic conditions (270, 278) (**Figure 30 A**).

All these results suggested that endogenous dopamine had a general suppressive influence on retinal ON channel activity in rabbits, cats and monkeys and that this influence did not depend critically on conditions of light adaptation. The DA receptors involved in this suppressive action appear to differ among species. In *cats*, the inhibitory effect of endogenous dopamine on the ERG b-wave was probably mediated through D_2-like receptors, because sulpiride, similar to 6-OHDA, caused an increase of the scotopic b-wave amplitude (277, 278) (**Figure 30 B**). In contrast to cats, in *rabbits* the inhibitory action of exogenous dopamine and apomorphine upon the b-wave amplitude was probably mediated by D_1-like receptors, because D_1R agonists (SKF38393, A77636), but not a D_2R agonist (NPA) decreased the b-wave amplitude in all conditions of illumination (281) (**Figure 30 C**). Contrary to these species, in *patients with Parkinson's disease*, who had lower than normal retinal dopamine concentration, a reduction of both the scotopic and photopic b-wave amplitude was reported (282-284). Treatment with L-DOPA in these patients increased the amplitude of the scotopic and photopic b-wave (285), while treatment with L-DOPA in healthy humans increased the scotopic, but not the photopic b-wave amplitude (286-288). It appears that endogenous dopamine has an overall stimulating action on the ON-BC activity (reflected in ERG b-wave) in human retina opposite to its suppressive action in monkey, rabbit and cat retina. What types of dopamine receptors mediate this stimulating action in human retina is not determined yet.

Similar to humans, a decrease of the b-wave amplitude was reported in *mouse* retina when dopaminergic transmission was compromised (253, 289, 290). This effect probably involved D_1R, because SCH 23390 also diminished the b-wave amplitude (291). The action of SCH 23390 on the rod-mediated b-wave amplitude resembled the ERG phenotype of the D_1R knockout mouse. In both cases a substantial reduction in dark sensitivity and compression of the operational range of the b-wave was observed. The authors reported that similar changes were seen when retinal $GABA_CR$, but not $GABA_AR$ signaling was prevented. In addition, Herrmann et al. (291) demonstrated that the lack of D_1R-mediated signaling could be completely masked by exogenous GABA, consistent with a role for D_1R in modulating a $GABA_CR$ input onto rod-driven ON BC (**Figure 31**).They proposed that dopamine via D_1R caused a release of GABA (possibly by HCs), which acted on $GABA_CR$ on rod BCs and thus increased their sensitivity and operational range. Travis et al. (141) eliminated the horizontal cells as a potential source of GABA release in this mechanism, because rod BC sensitivity was unaffected by horizontal cell-specific knockouts of either D_1R or VGAT. The wide-field amacrine cells, whose activity is regulated by $GABA_AR$-dependent serial inhibition, probably had an important role in GABA-induced rod BC sensitization (141, 292). Smith et al. (292) demonstrated that blocking of D_1R did not suppress rod-driven ON-BC sensitivity when $GABA_A$-mediated serial inhibition was blocked by gabazine, suggesting that the reduction in rod-driven BC sensitivity in the absence of D_1R receptors was due to disinhibition of serial inhibitory GABAergic circuitry rather than a direct facilitatory effect on GABA release, as proposed by Herrmann et al. (291). Smith et al. (292) suggested that D_1Rs may be expressed in all wide-field amacrine cells in this circuit, while Travis et al. (141) concluded that D_1R-mediated regulation took place at the secondary GABAergic cell, responsible for the serial inhibition of the primary cell (**Figure 32**). This suggestion is supported by the fact that neither D_1R full agonist SKF81297 not D_1R antagonist SKF83566 changed the rod bipolar cell sensitivity when serial inhibition was blocked. Regardless of the exact mechanism of D_1R-mediated action, it is clear that endogenous dopamine acting via D_1-like receptors caused a sensitization of mouse rod BCs. Confirming this, a reduction of the b-wave amplitude was obtained by other authors working with D_1R knockout mice (253, 293, 294). Lavoie et al. (294) reported that the b-wave amplitude decreased over the entire intensity range in scotopic and photopic conditions, while He et al. (293) observed reduced b-wave amplitude only for some stimulus intensities mostly towards the higher light intensities. All cited results obtained in mouse retina indicate that activation of D_1R by endogenous dopamine has an enhancing effect on the ERG b-wave amplitude in both scotopic and photopic conditions.

Smith et al. (254) reported, however, that the D_1R agonist SKF38393 reduced the mouse photopic b-wave amplitude at all stimulus intensities during daytime (**Figure 33 A**). They presented evidence that this suppressive effect was due to a direct inhibition of Na_v channels in ON-cone BCs. The D_1R antagonist SKF83566 increased the light-adapted b-wave amplitude during circadian midnight, but surprisingly it reduced the light-adapted b-wave amplitude during circadian midday (**Figure 33 B**). The authors proposed that at night, dopamine released during light adaptation was able to strongly suppress Nav channels via D_1R, while at midday the light adaptation was unable to cause enough dopamine release to strongly suppress Na_v channels on the ON-cone BCs. The D_2-like receptors appeared to have a smaller role in dopamine actions on *mouse* ERG than D_1-like receptors. In D_2R knockout mice no significant changes of the b-wave amplitude were observed in either scotopic or photopic conditions (291, 294). The b-wave amplitude was decreased, however, in D_4R-KO mice in the first 10 minutes of dark adaptation after turning off a rod desensitizing ganzfeld background (151). Nir et al. (151) suggested that both rod and cone photoreceptors of the D_4R-KO mouse had limited capacity to adapt to prolonged bright light exposure, although dopamine did not appreciably impact the phototransduction response to a flash stimulus. A decrease of the b-wave amplitude was obtained under photopic conditions of illumination, but not in the dark in D_4R knockout mice (151, 253). Because the effect was similar to that obtained in D_1R-KO *mice*, Jackson et al. (253) concluded that "both D_1 and D_4 receptors act to increase the amplitude of the light adapted ERG b-wave, with D_4 receptors acting through circadian regulation of the ERG and D_1 receptors acting on baseline amplitude in a non-circadian manner". Thus, it appears that dopamine receptors belonging to the two main classes (D_1 and

D_2) may have similar action on *mouse* cone-mediated b-wave amplitude (253), but opposite action on cone-mediated b-wave amplitude in *fishes* (257, 258) and *frogs* (262, 264).

Effect of dopamine on amacrine cells

One of the most studied effects of dopamine on the amacrine cell network was the effect it had on the electrical coupling of AII ACs, which are critical elements in the primary rod pathway of the *mammalian* retina (see Webvision chapter on AII Amacrine Cells, see also Webvision chapter Myriad roles for gap junctions in retinal circuits). It is well known that these cells receive excitatory input from ON-rod BCs (RBC) and they in turn form sign-conserving electrical synapses with the axon terminals of ON-cone BCs (CBC), and sign-inverting glycinergic chemical synapses with the axon terminals of OFF-CBCs (see chapter on AII ACs in Webvision). AII amacrine cells form homotypic gap junctions with neighboring AII amacrine cells, involving connexin 36 (Cx36) as seen in *rat* (295), *rabbit* (296) and *mouse* (297-299). Exogenous dopamine reduced the tracer coupling between adjacent AII amacrine cells in *rabbit* (300-302) (see Webvision chapter on AII ACs). The effect was mediated through activation of D_1R, because it was mimicked by the specific D_1R agonist SKF38393 and blocked by selective D_1R antagonist SCH23390, an action seen in both *rabbit* (300, 303) and *mouse* (142). The dopamine antagonist SCH 23390, on its own, in low concentration (10 μM) did not increase significantly the extent of tracer coupling (142, 299, 300), while in higher concentration (100 μM) it increased the coupling (303). The exact mechanism underlying the D_1R mediated uncoupling of AII ACs is a matter of debate. Some authors (299-302) suggested that uncoupling of gap junctions involved phosphorylation via protein kinase A of Cx36. Other authors, however, presented evidence that D_1R-driven uncoupling of the AII network resulted from protein kinase A activation of protein phosphatase 2A and subsequent dephosphorylation of Cx36 (303). The AII amacrine cells undergo well-known and prominent changes in electrical coupling driven by light adaptation that contribute to rewiring retinal circuitry from rod-pathway-dominated during dim light conditions to cone-pathway-dominated during bright light conditions. In *rabbit* retina, changes in light adaptation affected the coupling between AII amacrine cells in a triphasic manner (215, 304). Dark-adapted AII cells were coupled in relatively small groups and showed relatively small receptive fields. Exposure to dim background light increased both parameters approximately sevenfold allowing for summation of coincident signals and improved signal to noise ratio. Further light adaptation brought about a decrease in coupling to levels similar to those seen in dark-adapted retinas, which may act to prevent contamination of cone photoreceptor signals in cone bipolar cells by saturated rod signals in AII amacrine cells (See Webvision chapter on AII ACs). It is apparent that modulation of gap junctions between AII ACs is of physiological importance since it regulates the balance between sensitivity and spatial resolution in adjustment to the ambient light. Dopamine signaling alone cannot account, however, for the described 'inverted U' shaped AII coupling-background light relationship, because dopamine release increased steadily with increasing background illumination (54). It was shown that activation of extrasynaptic NMDA receptors on AII ACs led to increased phosphorylation of Cx36 and increased coupling between ACs (305). Kothmann et al. (305) proposed that the glutamate released from some rod BCs under scotopic conditions would depolarize AII ACs via postsynaptic AMPA receptors and would drive opening of nonsynaptic NMDA receptors on depolarized AII dendrites, thus leading to increased local coupling between ACs. The coupling between ACs would increase with increased background illumination in the scotopic range, because the latter would stimulate more strongly a larger pool of rod BCs. This glutamate-driven increase in Cx36 phosphorylation and AII coupling is opposed by dopamine-driven decrease in Cx36 phosphorylation via D_1R (305). Retinal dopamine secretion would be increased by bright light adaptation and it would be sufficient to overwhelm the pathway favoring increased Cx36 phosphorylation (**Figure 34**). This push-pull organization would result in the 'U-shaped' relationship between AII coupling and background illumination.

Modulation of the heterocellular gap junctions between AII amacrine cells and ON-cone bipolar cells by dopamine and cAMP is a matter of debate. In older studies it was reported that AII/CBC coupling, in contrast to AII/AII coupling, was modulated by NO through increases in cGMP concentration, but not by dopamine and

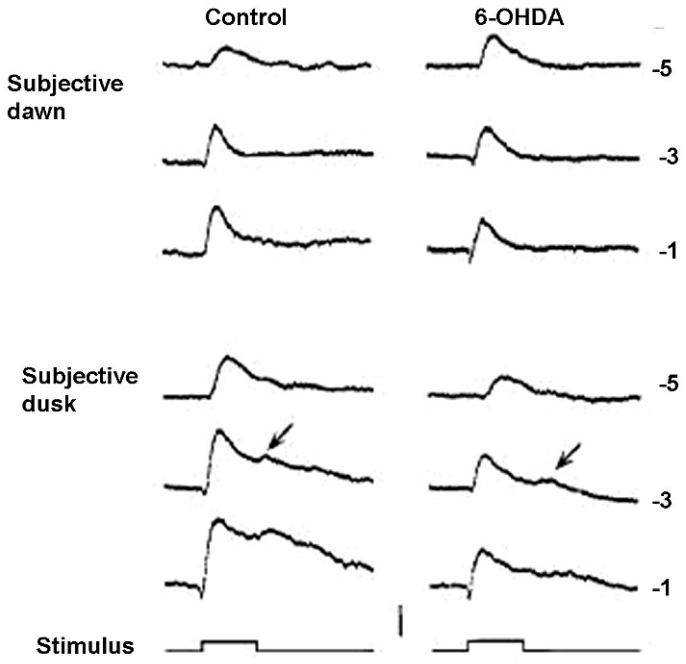

Figure 27. Electroretinograms recorded from a control and a DA depleted (6-OHDA) *zebrafish* at subjective dawn and dusk in animals kept in constant darkness. It is seen that the ERG b-wave amplitudes generated at all light intensities were reduced at subjective dawn as compared with those generated at subjective dusk in the control animal, while the b-wave amplitudes were similar when determined at subjective dusk and dawn in a DA depleted animal. Note at subjective dusk, both ON and OFF responses were recorded in both the control and DA-depleted fish, while no OFF responses were evident at subjective dawn in either fish. OFF responses are indicated by *arrows*. Stimuli, 500 msec. Calibration, 100 mV. From Li and Dowling (241).

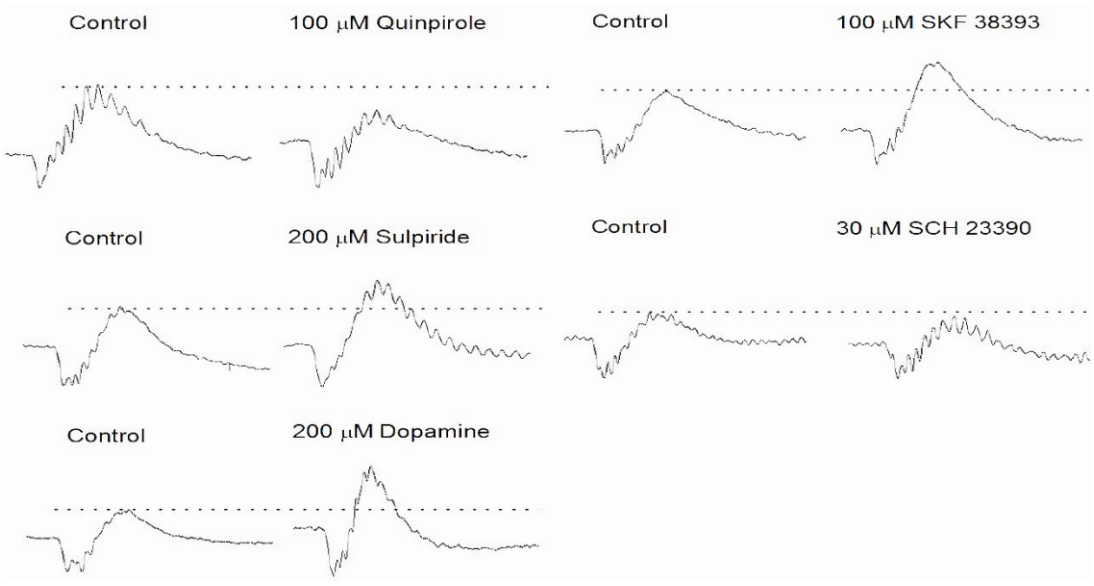

Figure 28. Effects of dopamine, D_1R agonist (SKF38393), D_1R antagonist (SCH23390), D_2R agonist (quinpirole) and D_2R antagonist (sulpiride) on the ERG b-waves in light adapted *goldfish*. Dopamine and the D_1R agonist increased, while The D_2R agonist decreased the b-wave amplitude. Antagonists had opposite effects of those seen during agonist treatment. Dotted lines indicate the peak amplitudes of control b-waves. From Kim and Jung (257).

cAMP (300, 301). In more recent studies evidence was presented that the AII/ON-CBC coupling was reduced by dopamine, D_1R agonists and intracellular cAMP, and enhanced by D_1R antagonist SCH23390 and thus resembled modulation of AII/AII coupling, as seen in both *mouse* (142, 299) and *rabbit* (302). Xia and Mills

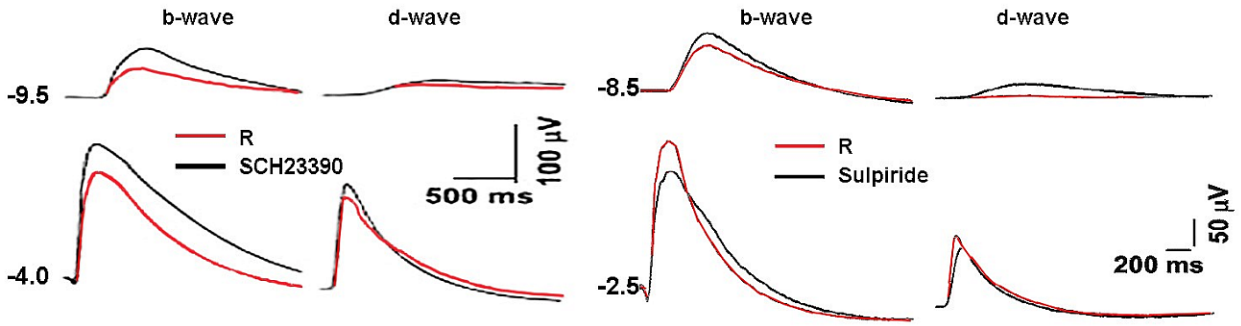

Figure 29. Effects of D_1R antagonist SCH23390 and D_2R antagonist sulpiride on the ERG b- and d-waves in dark adapted *frog* eyecups. ERGs were recorded with two different stimulus intensities (indicated on the left) during the control period (R – red lines) and during antagonist treatment (black lines). Both antagonists increased the b- and d-wave amplitude at lower stimulus intensity, while SCH23390 increased, but sulpiride decreased the b- and d-wave amplitude at higher intensity. Adapted from Popova and Kupenova (264).

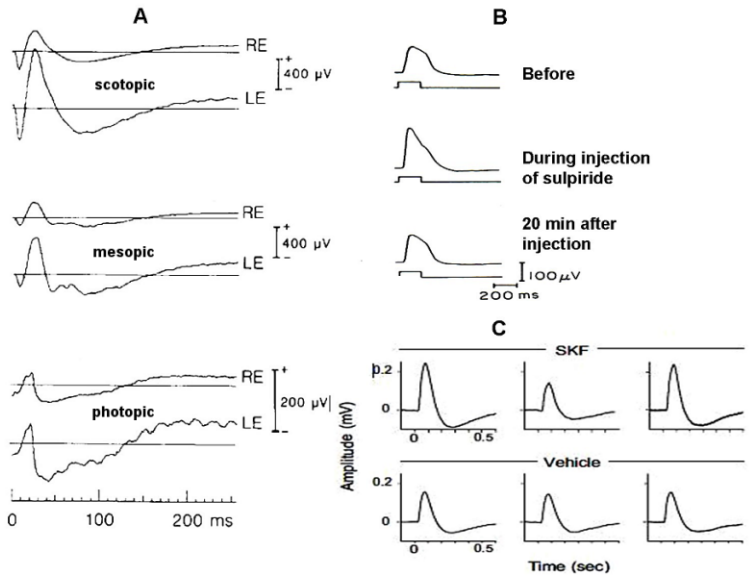

Figure 30. **(A)** Original ERGs recorded simultaneously from the right (RE) and left eye (LE) of *cats* were elicited by 20 flashes of intensity $9.3x10^4$ cd/m^2. The left eye was injected with 20 µg 6-OHDA 23 hours previously while the right eye was injected with saline. The larger ERG amplitudes were recorded from the 6-OHDA-injected left eye. The effect was most pronounced in the scotopic conditions. From Skrandies and Wässle (278). **(B)** Effect of D_2R antagonist sulpiride of the b-wave in dark adapted *cat*. Sulpiride caused a reversible b-wave amplitude increase. From Schneider and Zrenner (277). **(C)** Effect of D_1R agonist SKF38393 on the *rabbit* scotopic b-wave. SKF38393 caused a reversible reduction of about 30% of the b-wave amplitude. Injection of sterile water (vehicle) in the contralateral eye failed to modify the ERG waveform (bottom traces). From Huppé-Gourgues et al. (281).

(302) showed, however, that dopamine reduced the AII/AII coupling more than AII/ON-CBC coupling, while cAMP affected them equally. The authors proposed that cAMP modulated gating in both hemichannels, while dopamine modulated gating on only the AII side of the channel, because dopamine-induced cAMP elevations normally occurred on only the AII side (**Figure 35**).

Nitric oxide, on the other hand, modulated the AII/ON-CBC hemichannel, but not AII/AII hemichannel and it acted independently of dopamine. Xia and Mills (302) suggested that the functional role of dopamine is to reduce both the scotopic flow via the AII pathway into cone pathway as well as the photopic flow from ON-CBCs into AII ACs, when light level (and dopamine) increases. Further reduction might occur with independent rises in cGMP in ON cone BCs possibly arising from nearby nitric oxide generators. There is no evidence,

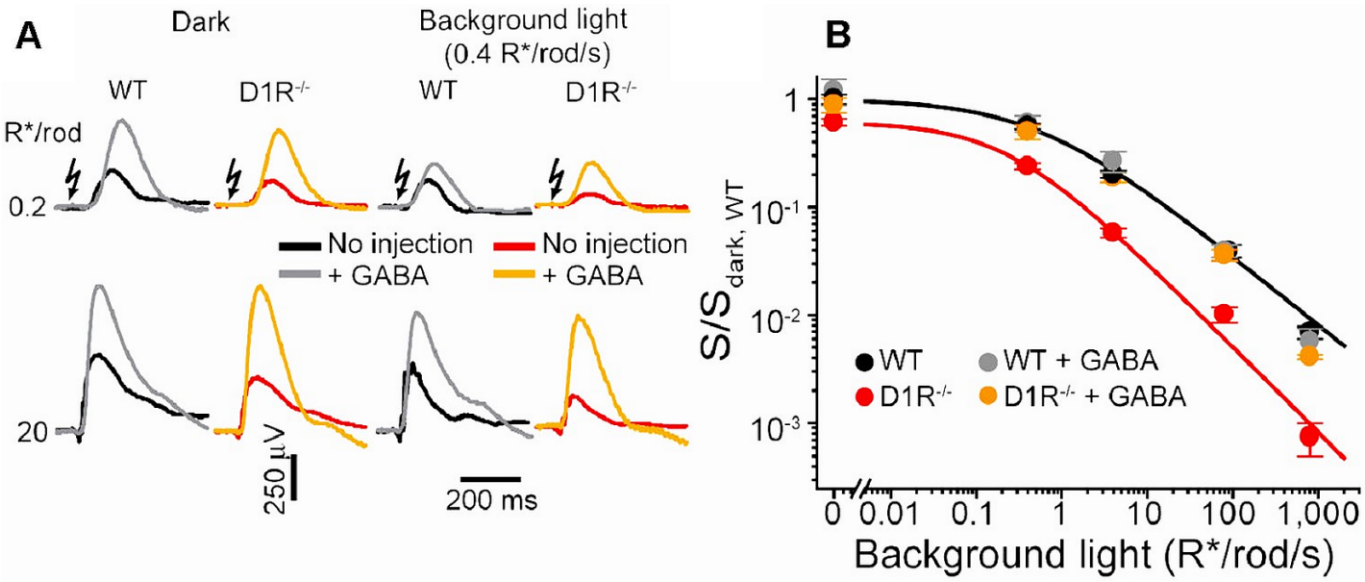

Figure 31. GABA increases b-wave sensitivity, but GABA release is inhibited by D_1R. **(A)** ERG recordings from dark- or light-adapted wild type (WT) and D_1R knockout ($D_1R^{-/-}$) *mice* with and without GABA injections. **(B)** WT and $D_1R^{-/-}$ ERG b-wave sensitivity plots in the absence or presence of injected GABA. Stimuli given in photoexcited rhodopsin molecules per rod per second (R^*/rod/s). Sensitivity (S/S_{dark}) is normalized. From Herrmann et al. (291).

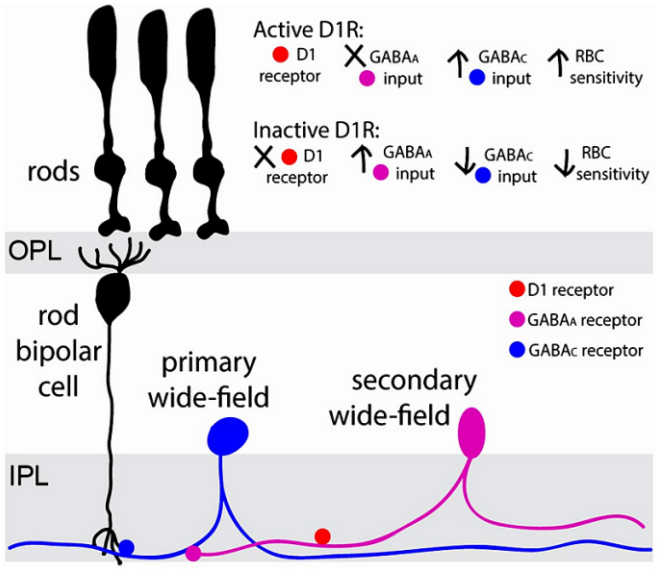

Figure 32. The circuit responsible for rod bipolar cell sensitization by the dopamine and GABA dependent mechanism. A subset of wide field amacrine cells (primary wide-field cell in blue) provides sustained GABA release onto $GABA_CRs$ located in the rod bipolar cell axon. This GABA release can be suppressed by upstream amacrine cells (secondary wide-field cell in magenta), which release GABA onto $GABA_ARs$ located at the primary wide-field amacrine cell. This serial inhibition is suppressed by dopamine acting through the D_1 receptors located on the secondary cells. When these D_1Rs are blocked, secondary cells inhibit primary cells through the $GABA_AR$-dependent mechanism, which ultimately causes reduction in rod bipolar cell sensitivity. From Travis et al. (141).

however, that the AII/ON-CBC coupling is modulated by background light as it was shown for the AII/AII coupling. Bloomfield et al. (306) could not find any light-induced modulation of AII/ON-CBC gap junctions under the 1000-fold range of background light intensities studied. No effect on Cx36 phosphorylation of AII/AII and AII/ON-BC gap junctions was found, when dark adapted retina cultures were submitted to day lighting conditions (299). Urschel et al. (299) proposed that the dopamine released upon light stimulation was diluted

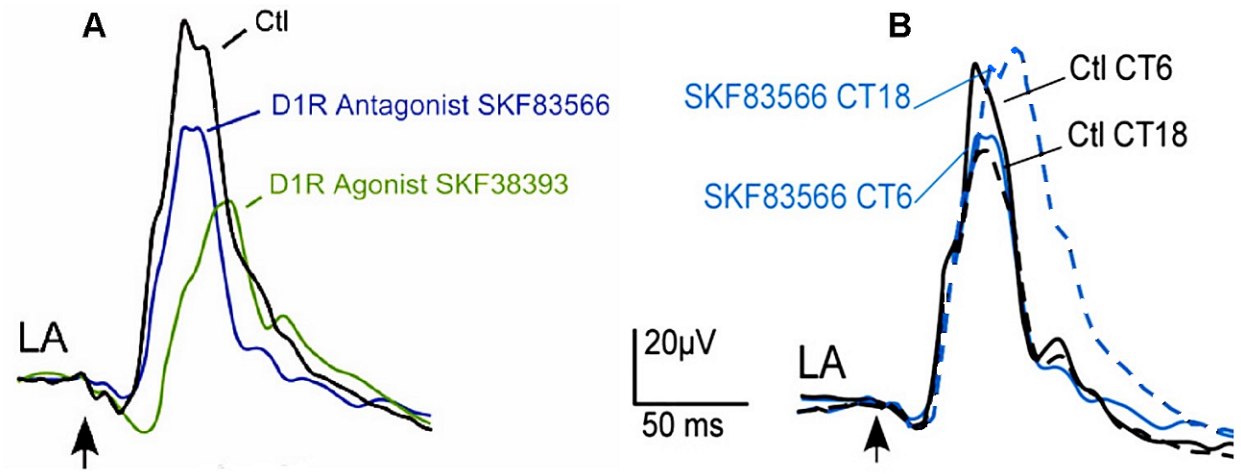

Figure 33. **(A)** ERG recordings in daytime from light-adapted *mice* (LA) during control conditions (black) and after injecting D_1R antagonist SKF83566 (blue) or D_1R agonist SKF38393 (light green). Stimulus intensity: 1.0 log cd s m^{-2}. Both agonist and antagonist caused a decrease of the b-wave amplitude. **(B)** ERG recordings from light-adapted (LA) *mice* obtained during the circadian midday (CT6, solid lines) and circadian midnight (CT18, dotted lines) in control conditions (black) and after injection of D_1R antagonist SKF83566 (blue). The D_1R antagonist decreased the b-wave amplitude during the circadian midday but increased the b-wave amplitude during the circadian midnight. In other experiments the sodium channel blocker TTX blocks actions of D_1R ligands. From Smith et al. (254).

too fast into the surround culture medium and therefore it could not reach threshold concentration to affect Cx36 phosphorylation.

Dopamine modulates the gap junctions formed by other types of ACs and between ACs and GCs. It was shown that dopamine decreased homotypic coupling between AC1 (GABAergic) cells via D_1R and PKA-induced phosphorylation, while DA acting via D_2R inhibited PKA and decreased phosphorylation of homotypic gap junctions between OFF α GCs in *rabbit* retina (54). A surprising inference is that, in contrast to AC1cells, ganglion cell hemichannels were closed by a decrease in phosphorylation. The heterotypic gap junctional channels between AC1 and OFF *α* GCs likely involved differential modulation of the two different types of hemichannels. One hemichannel was closed by phosphorylation on the side of AC1 cells, while the other hemichannel was opened by phosphorylation on the GC side. This differential modulation of the two hemichannels was accomplished by employing different dopamine receptors and opposite responses of two different hemichannels to PKA phosphorylation. Mills et al. (54) proposed that in the dark, where dopamine levels are minimal, both types of hemichannels may be relatively open and neighboring GCs will fire synchronously. As dopamine increases with background light, D_2R will be activated first and will cause decrease in phosphorylation and closure of the GC channels. Ganglion-amacrine gap junctions would also be closed, although to a lesser extent, because there is only a single D_2-sensitive hemichannel on the GC side. As dopamine levels increase with higher background intensities, activation of D_1R accelerates the closure of the ganglion-amacrine cell channels and begins uncoupling the amacrine cells as well (**Figure 36**).

Thus, dopamine might regulate both the strength and spatial extent of inhibition mediated by the coupled AC1 GABAaergic amacrine cells as well as the degree of synchronous firing of the ganglion cells. It was shown, however, that light adaptation resulted in a dramatic increase instead of decrease in the coupling of *α*-GCs to both neighboring ganglion cells and amacrine cells in *mouse* and *rabbit* retina (307), which did not support the model of Mills et al. (54).

In contrast to the AII cells, dopamine, the D_1R agonist SKF38393 and D_1R antagonist SCH23390 did not modulate the homotypic and heterotypic gap junctions made by *mouse* A8 ACs (glycinergic), although the latter cells expressed D_1 receptors and formed Cx36-containing junctions just like AII cells (142). A8 cells formed gap

junctions with OFF bipolar cells, whereas AII cells only contacted ON CBCs via electrical synapses. It appears that dopaminergic regulation of amacrine cell gap junctions depends both on type and functional role. Exogenous dopamine did not influence the electrical coupling between ACs in *carp* retina, although it decreased coupling between horizontal cells (308).

How dopamine modulates the light-evoked responses of ACs is largely unknown. In *goldfish* it was shown that exogenous dopamine had no effect on the sustained ACs, while it depolarized the transient ACs and reduced their responsiveness to light stimuli (159).

Effect of dopamine on ganglion cells

Dopamine can modulate homotypic coupling among retinal GCs of the same subtype, which underlies the coherent firing of neighboring cells. This concerted firing is thought to form a separate stream of information to the brain, in addition to the asynchronous signals from individual ganglion cells (309, 310) (see also Webvision chapter Myriad roles for gap junctions in retinal circuits). Hu et al. (307) found that the D_1R agonist SKF38393 and the D_1R antagonist SCH23390 produced no significant change in the coupling of dark-adapted OFF α-GCs, while D_2R antagonists (eticlopride and spiperone) produced a dramatic increase of homotypic (GC/GC) and heterotypic (GC/AC) coupling in OFF α-GCs and increased the concerted activity of α-GC neighbors in *rabbit* and *mouse* retina. These effects were like the effects obtained by the authors during light adaptation. Application of D_2R agonists on light adapted retinas had no effect on coupling, while the D_1R antagonist SCH23390 reduced both the coupling and the number of cells showing correlated light-evoked spike activity. Inhibition of adenylate cyclase and PKA in light adapted retinas had similar effect to those obtained with SCH23390. The authors proposed that the basal levels of dopamine in dark-adapted retinas activated high-affinity D_2R resulting in an inhibition of adenylate cyclase, a dephosphorylation of connexins and a reduction in the permeability of α-GC gap junctions. Under mesopic/photopic conditions, dopamine levels increased and activated low-affinity D_1R which, via a cAMP-mediated activation of PKA, increased connexin phosphorylation, and as a consequence, increased the coupling of the α-GC network (**Figure 37**). Thus, light-induced enhancement of GC coupling was due to activation of D_1R, while uncoupling of dark-adapted GCs was due to activation of D_2R. It is evident that the model of Hu et al. (307) differs markedly from the model of Mills et al (54), although they concern one and the same type of GC in rabbit retina.

Dopamine can modulate coupling among GCs in *amphibian* retina as well. Dopamine enhanced the synchronization of dimming detector (sustained OFF GCs) firing in bullfrog retina (311, 312). In addition, dopamine prevented the changes in synchronization and receptive field size induced by contrast adaptation. Li et al. (312) showed that single neuronal receptive field size was reduced during contrast adaptation, which was accompanied by weakening in synchronization strength between adjacent neurons' activities. Dopamine increased the synchronization strength index and the mean receptive field size, indicating that dopamine caused a significant strengthening of the gap junctional connections among dimming detectors. Dopamine eliminated both the adaptation-related receptive field area shrinkage and the synchronization weakening. Application of the D_2R antagonist sulpiride, but not D_1R antagonist SCH23390, had effects similar to that obtained with dopamine. Li et al. (312) proposed that in early-adaptation, light-induced increase in dopamine release activated D_1R and desensitized D_2R. Thus, the gap junction conductance between ganglion cells was enhanced to a relatively high level, resulting in stronger synchronization. In late adaptation, as dopamine release declined, both the decrease in D1R activation and probable recovery of D_2R from desensitized status in low dopamine concentration induced the decrease of gap junctional conductance. Bu et al. (311) found that the spatial correlation of dimming detector activity was enhanced, while temporal correlation in a single spike train was greatly decreased during dopamine treatment. The D_2R antagonist sulpiride, but not D_1R antagonist SCH23390 had similar effects to those of exogenous dopamine and Bu et al. (311) suggested that "endogenous dopamine influence on spatial and temporal correlation of firing activities of dimming detectors might be due to the activation of D_1R". Li and Liang (313) reported, however, that the exogenous dopamine did not alter the

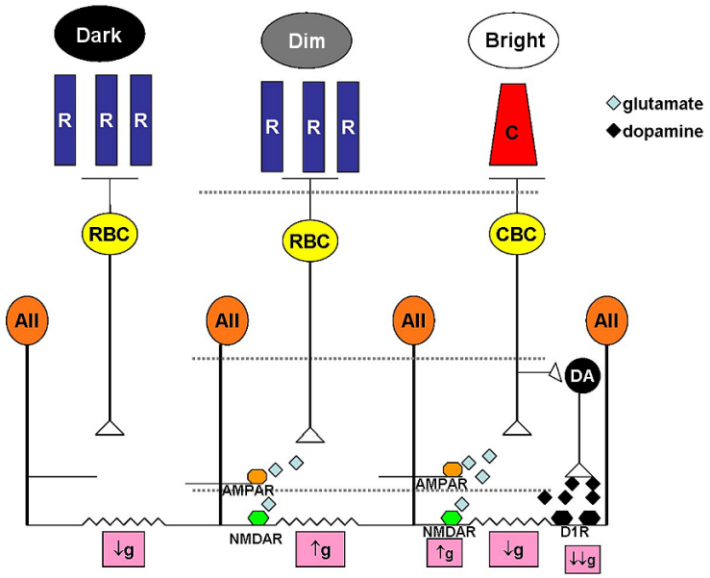

Figure 34 Mechanisms that control AII amacrine cell coupling under different conditions of light adaptation. In the dark (left panel), rod BCs (RBC) are hyperpolarized and release no glutamate. The AII amacrine cells (AII) are uncoupled (↓g). In dim light (middle panel), non-synaptic NMDA receptors associated with the Cx36 gap junctions are activated by spillover glutamate derived from RBCs in response to light. NMDA receptor activation in turn activates CaMKII and phosphorylates Cx36 to enhance coupling (↑g). In the presence of bright light (right panel), dopaminergic amacrine cells (DA) secrete dopamine, which activates D_1 receptors on AII amacrine cells, leading to activation of AC-PKA-PP2A and dephosphorylation of Cx36 to reduce coupling (↓↓g). This action of dopamine is enough to overwhelm the pathway favoring increased Cx36 phosphorylation. Modified from O'Brien (336).

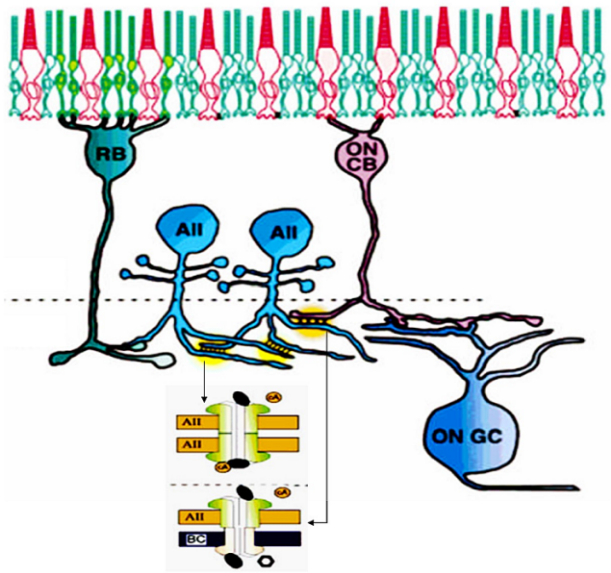

Figure 35. AII amacrine cells (**AII**) relay input from rod bipolar cells (**RB**) to ON cone bipolar cells (**ON CB**), which contact ON ganglion cells (**ON GC**). Each AII amacrine cell makes gap junctions both with neighboring AII amacrine cells and with ON CBs. The model predicts two cAMP-sensitive gap-junction hemi-channels gate signals between AII pairs, and between AII and ON CB pairs, but cAMP is elevated on only the AII side, leading to lesser modulation of the AII to ON CB junction. From Xia and Mills (302).

temporal structure of the firing sequences in single bullfrog neurons, although it decreased firing rates in response to three different stimulus patterns. Dopamine enhanced the synchronization of the GC population activity but decreased the rate of correct stimulus pattern discrimination and eliminated the linear correlation between correct rate and group size. Exogenous dopamine attenuated also the encoding of information about

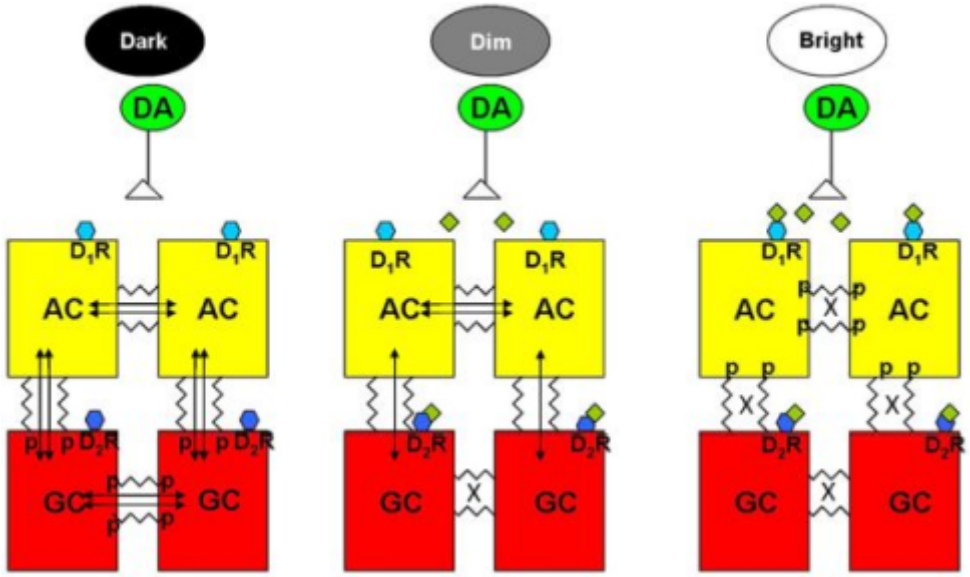

Figure 36. Effects of dopamine on the gap junctions between AC1 amacrine cells and OFF α GCs in rabbit retina. In the dark (left panel), no dopamine is released, and the gap junctions are open. The gap junctions between neighboring ACs are dephosphorylated, while these between neighboring GCs are phosphorylated (p). The gap junctions between AC and GCs are phosphorylated on the GC site and dephosphorylated on the AC site. In dim light (middle panel), small amounts of dopamine are released and act on the more-sensitive D_2Rs on GCs, leading to dephosphorylation of the gap junctions and their closure. In the presence of bright light (right panel), dopamine levels increase and activate both D_1R on ACs and D_2R on GCs leading to closure of their gap junctions. Model proposed by Mills et al. (54).

the stimulus duration carried by the response latency and not by the firing rate, although it increased the firing rate and shortened the latency of both the ON and OFF responses of bullfrog ON-OFF GCs (314).

Dopamine changes the sustained lateral inhibition of *amphibian* GCs during light adaptation (315). It was shown that both light adaptation and dopamine caused a decrease in the sustained lateral inhibition produced by distant windmill stimuli and an increase in the sustained lateral inhibition produced by nearby windmill stimuli. The authors suggested that the observed effects were due to a dopamine induced decrease of electrical coupling in the OPL and IPL and this might serve to increase contrast detection at higher spatial frequencies. Dopamine had no effect on the transient lateral inhibition of GCs, which was evident in light, but not in dark adapted amphibian retina. This type of inhibition was mediated by transient ACs and spread laterally via action potentials.

In cell culture dopamine may act directly on retinal ganglion cells to regulate excitability by affecting voltage-gated currents. It was shown that dopamine did not change the membrane potential or membrane resistance but reduced the excitability of dissociated GCs through activation of D_1R in nonmammalian retina as seen in both *turtle* (316) and *goldfish* (317, 318). In *turtles*, the dopamine effect was attributed to changes in conductance of voltage-gated Ca^{2+} channels (316), while in *goldfish* the effect did not depend on voltage-gated Ca^{2+} currents (318) and it was probably due to a reduction of the voltage-gated Na^{+} current amplitude (317). Reduced excitability of dissociated GCs by the action of dopamine was obtained also in *rat* retina, but the underlying mechanism is a matter of debate (319-321). Chen and Yang (319) showed that exogenous dopamine, acting via D_1R, induced a small depolarization of GC membrane potential, associated with decreased membrane resistance and diminished number of current-evoked action potentials (**Figure 38**).

The membrane potential effects of dopamine were prevented by the blockade of hyperpolarization-activated cation currents (I_h) with ZD7288, while dopamine alone increased the amplitude of I_h. Therefore Chen and Yang (319) suggested that the depressing effects of dopamine on rat GCs may be, at least in part, mediated by increasing the I_h amplitude through the cAMP- and PKA-dependent pathway. Hayashida et al. (320) suggested

that dopamine and D_1R agonists inhibited GC spiking primarily by reducing Na^+ currents, because dopamine reduced the amplitude of both voltage-gated Na^+ currents and current-evoked action potentials and it also slowed the rising and repolarizing sides of each spike. The reported effects were not affected by the blockade of I_h. Involvement of intracellular Ca^{2+} in the depressant effect of dopamine on current-evoked GC spiking was proposed by Ogata et al. (321). The authors demonstrated that dopamine and SKF 83959 (an agonist that activates heteromeric, but not homomeric DR) induced a Ca^{2+} influx in GCs, which was prevented by lowering of extracellular Ca^{2+}, by SCH23390 and by eticlopride. The blockade of IP_3-mediated Ca^{2+} release also prevented the dopamine-induced rise in intracellular Ca^{2+}. All these data indicated that rat GCs possessed heterodimeric D_2-D_5 receptors that mediated the dopamine-induced Ca^{2+} influx. Ogata et al. (321) showed that D_1R and D_2R antagonists blocked also light-induced rises in cAMP and activation of Ca^{2+}/calmodulin-dependent protein kinase II, suggesting that dopamine may activate two pairs of signaling pathways in rat GCs: cAMP and PKA, and Ca^{2+} and CaMKII. Dopamine may modulate K^+ currents of dissociated rat GCs as well. Li et al. (322) demonstrated that D_1R agonist SKF81297 suppressed the GC outward K^+ currents, mainly mediated by Gb-sensitive and 4-AP-sensitive components, through the intracellular PKA and CaMKII signaling pathways. Cui et al. (323) reported that D_1R activation suppressed K_{ir} currents through cAMP/ PKA signaling pathway and thus leading to enhancement of the temporal summation of EPSPs in GC dendrites. They showed that D_1R activation increased the spontaneous firing of GCs and induced cell depolarization (**Figure 39**), strongly suggesting that D_1R activation increased the excitability of rat GCs, instead of decreasing it (319, 320). The cause for these opposite results obtained in rat retina, is unclear.

Dopamine acting via the D_1R signaling pathway (cAMP/PKA) directly affected the intrinsically photosensitive retinal ganglion cells (ipRGCs) in *rat* retina (324). Dopamine and D_1R agonist SKF38393 attenuated the ipRGC photocurrent and dramatically reduced the light-evoked cell spiking. D_1R activation caused a modest depolarization and input resistance decrease of ipRGCs without significantly altering the number of spikes evoked by injection of depolarizing current. The authors suggested that the effects of D_1R activation on membrane properties of ipRGCs were due to modulation of the I_h and not of voltage-gated Na^+ channels, while the exact mechanism of the effects on melanopsin phototransduction cascade was unclear. Van Hook et al. (324) proposed that dopamine acting via D_1R activation contributed to light-driven desensitization in ipRGCs and thus supported a form of light adaptation. On the other hand, Sakamoto et al. (83) found that dopamine via D_2R modulated the photic and circadian regulation of melanopsin mRNA in rat ipRGCs. Thus, it appears that the two classes of dopamine receptors have distinct roles in regulating activity of rat ipRGCs.

Much data suggests that dopamine depresses retinal ganglion cell activity in *intact mammalian retina*. In *cat* retina dopamine reduced the spontaneous and light-evoked firing of GCs irrespectively of their type (ON or OFF, transient or sustained) and these effects were essentially the same under scotopic, mesopic and photopic conditions (325-327) (**Figure 40**). Dopamine antagonists haloperidol (mixed D_1/D_2R antagonist), flupenthixol (selective D_1R antagonist) or sulpiride (selective D_2R antagonist) had no effect on spontaneous or light-induced activity of GCs, suggesting there was no endogenous dopamine present on the dopamine receptors of retinal GCs (325). Ikeda et al. (325) suggested that the retinal GCs may initially be innervated by dopaminergic cells, but the connection is eliminated during formation of GABA and glycine synapses. Other authors showed, however, that the impairment of dopaminergic transmission (with 6-OHDA or haloperidol) in adult cat retina led to a marked ON/OFF asymmetry in transient GC activity under photopic conditions of illumination (328, 329). The maintained activity of OFF-Y GCs was decreased, while that of ON-Y GCs was increased during either treatment (6-OHDA or haloperidol). Maguire and Smith (329) found that the proportion of OFF, but not ON GCs, which displayed nonlinear spatial summation was larger in the 6-OHDA treated than in the control eyes. The modulation of shift response (elicited with a peripheral square-wave grating) became larger in OFF-Y, but smaller in ON-Y GCs and the light-evoked responses of OFF-Y cells became even more transient in 6-OHDA treated eyes. The effect of haloperidol on the shift response of ON-Y GCs was like that of 6-OHDA, while its effect on the shift response of OFF-Y GCs showed great dynamics with time. The response disappeared at 25 min postinjection, but reappeared and increased to supranormal levels reaching a 50% increase in response

modulation over control at 4 h 30 min (328). The peak firing rate of the center responses to flashing spots was greatly decreased at all stimulus intensities during haloperidol and SCH23390 treatment in the OFF Y GCs, while in the ON Y GCs the response diminution was much smaller (328). Whether the impairment of dopaminergic transmission caused a similar ON/OFF asymmetry in sustained (X) GC activity in cats is a matter of debate.

Maguire and Smith (329) found that the intensity-response function of center responses was unaffected for both ON and OFF X cells during 6-OHDA treatment, while Maguire and Hamasaki (328) found that the same function was shifted to the right for the OFF-X cells and not changed for the ON-X cells during haloperidol application. It was also shown that the blockade of D_1R with SCH23390 altered the dark-adaptation function of OFF-Y and OFF-X GCs so that no rod-cone break was observed; rather the threshold of the cell fell quickly in a single exponential function to rod levels (328) (**Figure 41**). Therefore, the authors proposed that one of the operations of retinal dopamine may be to eliminate rod input to GCs during brief periods of decreased retinal illumination. Maguire and Hamasaki (328) suggested that without dopamine acting on D_1-like receptors, "rapid changes from light to dark would allow the rod photoreceptors to activate GCs and lead to a noisy system with poor spatial and temporal resolution".

An ON/OFF imbalance of ganglion cell activity, caused by dopamine, was described also in *rabbit* retina (330-333). It was shown that exogenous dopamine increased the spontaneous activity of OFF GCs, but reduced the spontaneous activity of ON GCs (330, 331). In accordance with these findings, dopamine nonselective antagonists (haloperidol, fluphenazine, cis-flupenthixol) caused a decrease in the spontaneous activity of OFF GCs and an increase of the spontaneous activity of ON GCs, indicating that there was a continuous dopamine release in light adapted rabbit retinas (331-333). These results are similar to those obtained in cat retina (328, 329). The involvement of the two DR types in the observed effects was studied with selective D_1R and D_2R agonists and antagonists. It was demonstrated that D_2R agonist LY 141865 and D_1R antagonist SCH 23390 decreased the spontaneous activity of OFF GCs and increased of the spontaneous activity of ON GCs, while D_2R antagonist sulpiride decreased the spontaneous activity of both OFF GCs and ON transient GCs (331). The authors proposed that D_1R mediated the effects of dopamine on spontaneous firing of GCs, while D_2R may function at presynaptic autoreceptors that reduced the release of dopamine. It remained unclear why both activation and blockade of D_2R decreased the spontaneous activity of OFF GCs. How exogenous dopamine affected the light-evoked responses of rabbit GCs is a matter of debate. Ames and Pollen (330) reported that the light-evoked responses of OFF GCs were usually unaffected by dopamine, while Jensen and Daw (331) demonstrated that dopamine reduced the light-evoked responses of these cells and shifted the intensity-response function of cell center and surround response to the right by an equal amount. Thus, exogenous dopamine reduced OFF GC sensitivity to light without altering the center-surround balance. Exogenous dopamine exerted a suppressive action also on the light-evoked responses of two thirds of ON and ON-OFF GCs (330). Dopamine suppressed the light responses of all ON-transient GCs and ON-OFF GCs, while it had no effect on the responses of the ON-sustained GCs (331). The blockade of dopamine receptors revealed effects on the GC light responses that were not seen during the action of exogenous dopamine. Application of haloperidol reduced and delayed the antagonistic surround responses in both OFF and ON brisk GCs and shifted their center-surround balance in favor of the center (333). Similar effects were found with D_1R antagonist SCH23390, but not D_2R antagonist sulpiride (**Figure 42**) with the exception of OFF large field units (331).

In the latter, sulpiride also caused a shift in center-surround balance in favor of the center. Thus, it appears that D_1R mediated the effects of endogenous dopamine on the center-surround balance of ON-brisk GCs, while both D_1R and D_2R mediated those effects on the OFF large field units. An interesting observation was reported for ON brisk-sustained GCs, in which haloperidol and SCH23390, but not sulpiride, caused a reduction of sustained ON activity to spots of light and in some of the cells, in others the sustained excitation to spots of light actually turned into sustained inhibition (331, 333). The latter effect was not seen during application of dopamine. Endogenous dopamine, acting via D_1R was probably involved also in the directional selectivity of rabbit GCs. It

was shown that haloperidol and SCH23390, but not sulpiride, reduced the leading edge response, while either not affecting or increasing slightly the trailing edge response to a moving light stimulus of the ON-OFF directionally selective cells (331, 333). Exogenous dopamine had similar action in 3 out of 5 directionally selective cells.

The effects of dopamine on the activity of other mammalian GCs (except cat and rabbit) are not thoroughly investigated. It was shown that in light-adapted *mouse* retina, D_1R antagonist (SCH23390) decreased, while D_2R antagonist (spiperone) increased the light-evoked OFF responses of GCs, indicating that D_1 and D_2 receptors played opposite roles in OFF response generation (334). Simultaneous inhibition of both receptor types (D_1 and D_2) increased the OFF responses, showing that the D_2R-mediated effect was stronger and it dominated over that mediated by D_1R. The authors gave no proposal for the mechanism underlying the OFF-response enhancement caused by D_2R blockade. In *rat* retina, the D_2/D_3 receptor antagonists (sulpiride and eticlopride) had no significant effect on the spontaneous activity of either ON or OFF GCs in a dimly lighted environment (335). On the other hand, the specific D_4R antagonist L-745,870 reduced the spontaneous activity of OFF GCs but had no significant effect on the spontaneous firing of ON GCs. In addition, L-745,870 decreased both the light sensitivity (by 0.32 log unit) and the maximum peak response of the ON and OFF GCs, while sulpiride and eticlopride reduced only light sensitivity (0.23 log unit) without changing the maximum peak response. Jensen (335) proposed that D_4R, like D_2R, functions to regulate dopamine release, but did not provide any suggestion why the effect of D_4R blockade inhibited the GC spontaneous and light-evoked activity more strongly than D_2R blockade. More studies are needed to fully understand the role of dopamine in ganglion cell function in both mammalian and nonmammalian retina.

Summary

Dopamine is synthesized and released by a group of cells in the retinal amacrine cell layer. This group represents less than 1% of cells in this layer. Dopaminergic cells are morphologically either interplexiform cells, with dendritic arbors in both inner and outer plexiform layers, or large-bodied amacrine cells. The latter typically have dense, wide-field dendritic arbors in stratum S1 of the inner plexiform layer, adjacent to the amacrine cell layer, but sparse branching in more proximal inner plexiform layer strata. Dopaminergic amacrine or interplexiform cells synapse directly on other retinal neurons, but much of the dopaminergic action is thought to be 'paracrine', exerted by diffusion of dopamine to different target cells. Dopaminergic cells release other neurotransmitters such as GABA. Dopamine release appears to be circadian, with high release levels during the day in many species, and is a counterpart to circadian rhythms in melatonin, which is released at night. Consistent with a role as a humoral neuromodulator, dopaminergic actions are found in every retinal cell type, mediated through both D_1-like and D_2 like G-protein coupled receptors. One particularly prominent action is diurnal modulation of gap-junction coupling between horizontal, amacrine, ganglion cells, clearly observed in the regulation of tracer molecule spread among like cell types. In mammals gap-junction modulation corresponds to a retinal circuitry reconfiguration in rod and cone pathways so as to optimize nocturnal and diurnal vision. Further actions are found in the modulation of voltage-gated channels and chemical neurotransmission. Nonetheless, there are no general rules concerning dopaminergic action, which vary considerably depending on species, neural cell type, and the experimental context.

Acknowledgements

The author thanks Helga Kolb (University of Utah) for giving the idea for writing this chapter and her valuable support during the whole process of chapter construction. She especially helped for writing the section concerning the morphology and circuity of retinal dopaminergic cells. The author thanks also Dr. Ralph Nelson (NIH) for chapter editing and helpful comments.

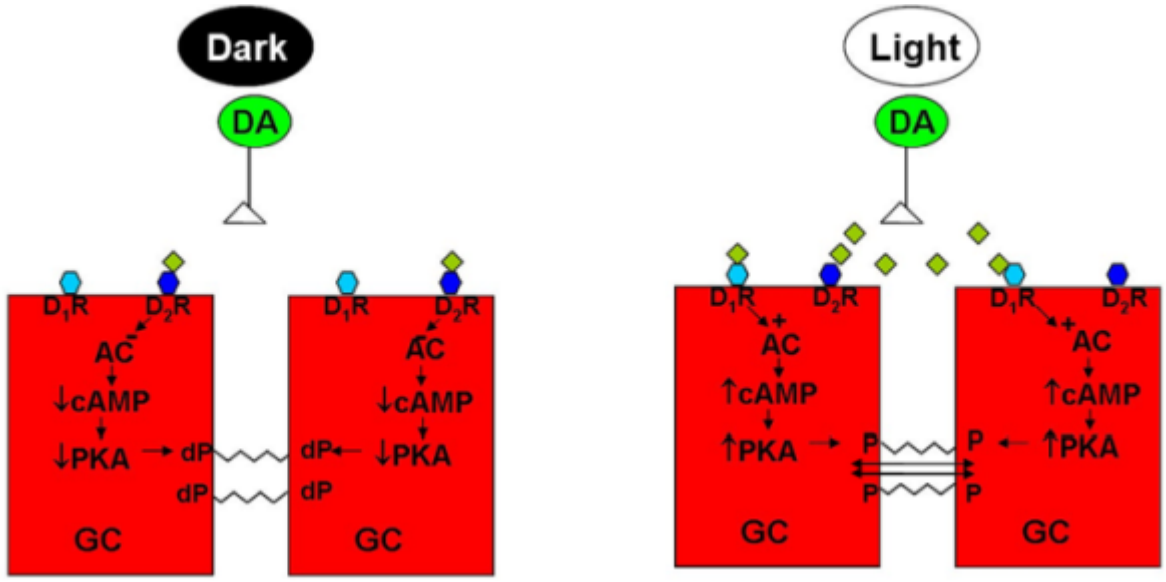

Figure 37. Schematic diagram of the intracellular pathway proposed to control the conductance of α-GC gap junctions under dark- and light-adapted conditions. In the dark (left panel) dopamine levels are low and dopamine activates the more sensitive D_2 receptors, which, through reduction of cAMP and PKA activity, cause dephosphorylation (dP) of connexin protein and a reduction of gap junction permeability. During light adaptation (right panel) dopamine levels increase and dopamine activates D_1 receptors, which, through an increase of cAMP and PKA activity, cause phosphorylation (P) of connexins and an increase in gap junctional conductance. Modified from Hu et al. (307).

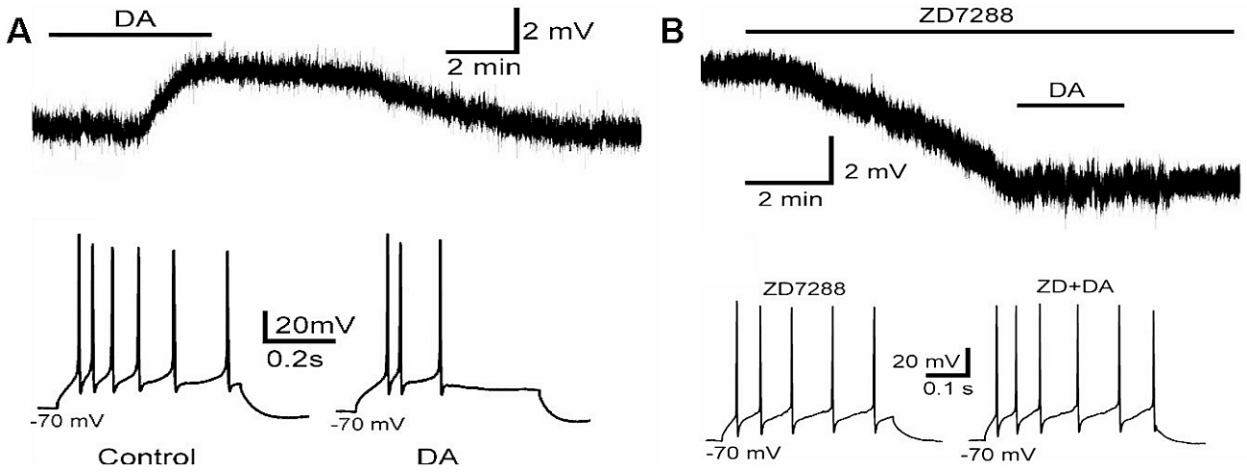

Figure 38. Modulation of membrane properties and excitability of *rat* ganglion cells by dopamine (DA) in a retinal slice preparation. **(A)** Bath application of 10 μM DA produced a small and reversible depolarization of the membrane potential (upper row). Action potentials evoked by depolarizing current injection (80 pA, 400 ms) at a holding potential of -70 mV in the lower row. **(B)** Application of 30 μM ZD7288, an HCN channel blocker, produced a hyperpolarization of the membrane potential, and addition of DA (10 μM) failed to further change the membrane potential (upper row). Effects of DA on the number of evoked action potentials are prevented when the cell was incubated with ZD7288 (lower row). From Chen and Yang (319).

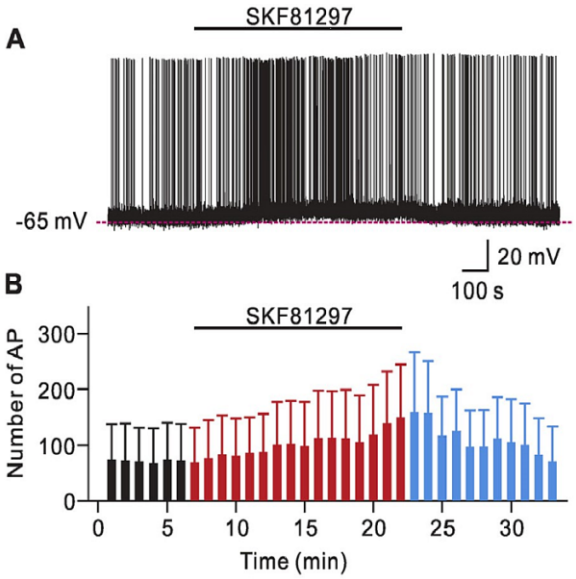

Figure 39. Effects of D1 receptor activation by the agonist SKF81297 on the membrane potential and spontaneous firing of *rat* retinal ganglion cells. **(A)** Representative trace recorded from an RGC, showing that the perfusion of SKF81297 significantly increased the spontaneous firing and induced a small depolarization of Em. (**B)** Bar chart showing SKF81297-induced increase in the number of spontaneous action potentials (AP) as a function of time. Bin size: 1 min. From Cui et al. (323).

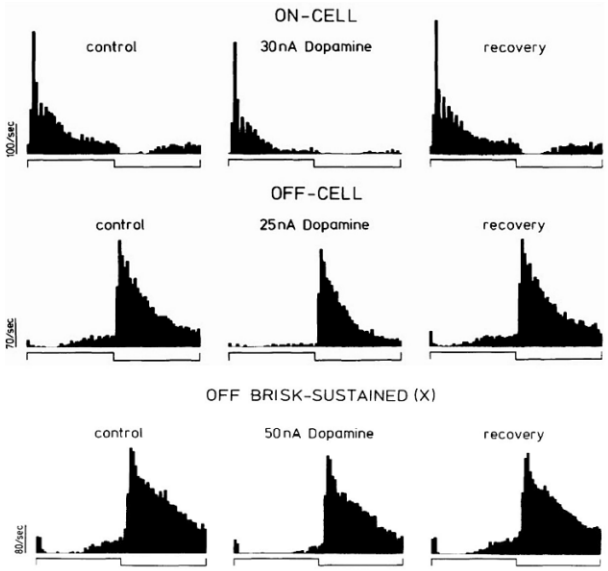

Figure 40. Effects of dopamine on the optimal spot response histograms of 3 different ganglion cells in *cat* retina. Responses of ON brisk-transient (Y) cell (top row), OFF brisk-transient (Y) cell (middle row) and OFF brisk-sustained (X) cell (bottom row) are presented prior to, during and after the administration of dopamine. The stimulus was on when the trace beneath the histograms was shifted upwards. All histograms summed 32 stimulus representations. Stimulus period 1024 ms with light on for 512 ms. Note that dopamine reduces the firing rate in both ON and OFF phases of the response. Dopamine applied to individual cells by iontophoresis from a 7 barrel pipette with iontophoresis current given in nanoAmperes (nA). Adapted from Thier and Alder (327).

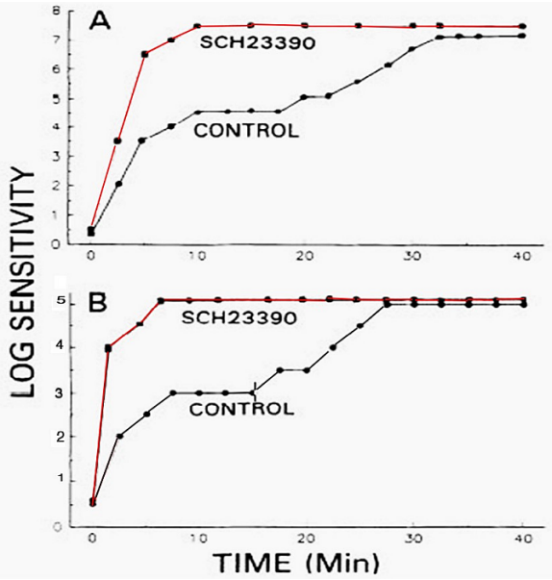

Figure 41. Effects of the D_1R antagonist SCH23390 on the dark-adaptation curves of OFF GCs in *cat* retina. Changes of light sensitivity were measured in a 40 min period immediately after extinguishing white background light with luminance of 61 cd/m^2. **(A)** Dark-adaptation curve for an OFF Y-GC. It is evident that in control conditions the dark adaptation curve has two branches (first: cone-mediated, second: rod-mediated), while after administration of SCH23390 (50 pg) the curve quickly sensitizes to that branch representing the rod system. **(B)** Dark-adaptation curve for an OFF X-GC as described above for the OFF Y-GC. From Maguire and Hamasaki (328).

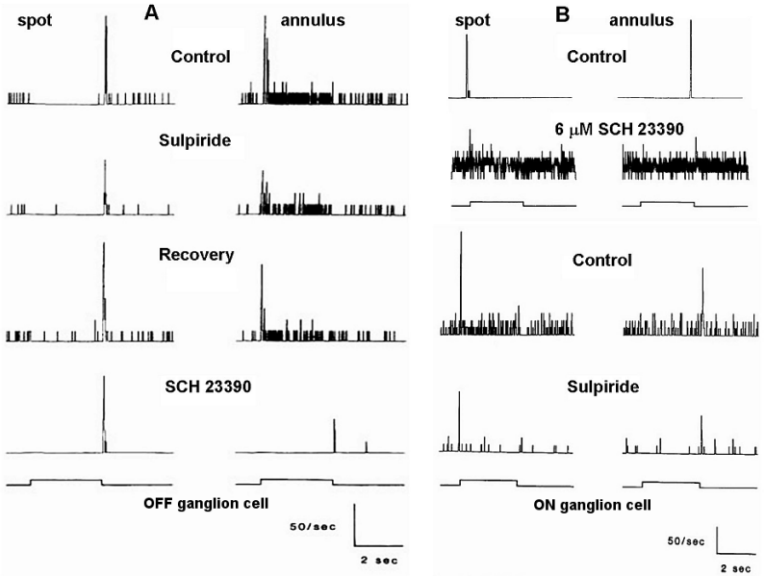

Figure 42. Effects of the D_2R antagonist sulpiride and the D_1R antagonist SCH-23390 on the light-evoked responses of *rabbit* retinal ganglion cells. **(A)** Effects of sulpiride (143 μM) and SCH 23390 (25 μM) on the responses of an OFF ganglion-cell. Responses to a spot (0.5 mm square) and an annulus (0.7 mm inner diameter and 3.0 mm outer diameter) of light are presented. Recovery records were taken about 7 min after application of sulpiride. Stimulus intensity, 1.7 log lux. **(B)** Effects of SCH 23390 (6 μM) and sulpiride (78 μM) on the responses of an ON transient ganglion cell to a spot and annulus of light. Stimulus intensity, 1.1 log lux in SCH23390 and 0.5 log lux in sulpiride experiment. From Jensen and Daw (331).

About the author

Dr. Elka Popova, MD, PhD, was born in Sofia, Bulgaria. She received a Medical Degree from Medical University of Sofia in 1979 and started her work as assistant professor in the Department of Physiology at the same university. Dr. Popova worked in the visual electrophysiological laboratory of the department and received her Ph.D. in 2001 and her associated professor position in 2003. Her work is in the field of retinal physiology and includes investigation of various excitatory and inhibitory neurotransmitters (GABA, glycine, dopamine, histamine, serotonin, purines, enkephalins) and ion channel (Na_V, HCN) modulation on the electroretinogram and ganglion cell activity in cold blooded species. She has a special interest in revealing the differences between retinal ON and OFF channels and the interaction between the two channels at different retinal levels. Dr. Popova investigates how some of these differences and interactions depend on different neurotransmitter systems and ion channels.

References

1. Goldstein D.S., Eisenhofer G., Kopin I.J. Clinical catecholamine neurochemistry: a legacy of Julius Axelrod. Cellular and molecular neurobiology. 2006;26(4-6):693–700. PubMed PMID: 16871444.
2. Falck B., Hillarp N.-Å., Thieme G., Torp A.a. Fluorescence of catechol amines and related compounds condensed with formaldehyde. Journal of Histochemistry & Cytochemistry. 1962;10(3):348–354.
3. Djamgoz M., Wagner H.-J. Localization and function of dopamine in the adult vertebrate retina. Neurochemistry international. 1992;20(2):139–191. PubMed PMID: 1304857.
4. Massey S.C., Redburn D.A. Transmitter circuits in the vertebrate retina. Progress in neurobiology. 1987;28(1):55–96. PubMed PMID: 2881324.
5. Kolb H., Cline C., Wang H.H., Brecha N. Distribution and morphology of dopaminergic amacrine cells in the retina of the turtle (Pseudemys scripta elegans). Journal of neurocytology. 1987;16(5):577–588. PubMed PMID: 2891796.
6. Frederick J.M., Rayborn M.E., Laties A.M., Lam D.M., Hollyfield J.G. Dopaminergic neurons in the human retina. Journal of Comparative Neurology. 1982;210(1):65–79. PubMed PMID: 6127354.
7. Kolb H., Cuenca N., Dekorver L. Postembedding immunocytochemistry for GABA and glycine reveals the synaptic relationships of the dopaminergic amacrine cell of the cat retina. Journal of Comparative Neurology. 1991;310(2):267–284. PubMed PMID: 1720142.
8. Kolb H., Cuenca N., Wang H.-H., Dekorver L. The synaptic organization of the dopaminergic amacrine cell in the cat retina. Journal of neurocytology. 1990;19(3):343–366. PubMed PMID: 2391538.
9. Crooks J., Kolb H. Localization of GABA, glycine, glutamate and tyrosine hydroxylase in the human retina. Journal of Comparative Neurology. 1992;315(3):287–302. PubMed PMID: 1346792.

10. Mariani A.P., Hokoc J.N. Two types of tyrosine hydroxylase-immunoreactive amacrine cell in the rhesus monkey retina. Journal of Comparative Neurology. 1988;276(1):81–91. PubMed PMID: 2903868.
11. Tauchi M., Madigan N.K., Masland R.H. Shapes and distributions of the catecholamine-accumulating neurons in the rabbit retina. Journal of Comparative Neurology. 1990;293(2):178–189. PubMed PMID: 19189710.
12. Zhang D.-Q., Zhou T.-R., McMahon D.G. Functional heterogeneity of retinal dopaminergic neurons underlying their multiple roles in vision. Journal of Neuroscience. 2007;27(3):692–699. PubMed PMID: 17234601.
13. Casini G., Rickman D.W., Brecha N.C. AII amacrine cell population in the rabbit retina: identification by parvalbumin immunoreactivity. Journal of Comparative Neurology. 1995;356(1):132–142. PubMed PMID: 7629307.
14. Voigt T., Wassle H. Dopaminergic innervation of A II amacrine cells in mammalian retina. Journal of Neuroscience. 1987;7(12):4115–4128. PubMed PMID: 2891802.
15. Dumitrescu O.N., Pucci F.G., Wong K.Y., Berson D.M. Ectopic retinal ON bipolar cell synapses in the OFF inner plexiform layer: contacts with dopaminergic amacrine cells and melanopsin ganglion cells. Journal of Comparative Neurology. 2009;517(2):226–244. PubMed PMID: 19731338.
16. Contini M., Lin B., Kobayashi K., Okano H., Masland R.H., Raviola E. Synaptic input of ON-bipolar cells onto the dopaminergic neurons of the mouse retina. Journal of Comparative Neurology. 2010;518(11):2035–2050. PubMed PMID: 20394057.
17. Viney T.J., Balint K., Hillier D., Siegert S., Boldogkoi Z., Enquist L.W., Meister M., Cepko C.L., Roska B. Local retinal circuits of melanopsin-containing ganglion cells identified by transsynaptic viral tracing. Current Biology. 2007;17(11):981–988. PubMed PMID: 17524644.
18. Vugler A.A., Redgrave P., Lawrence J., Greenwood J., Coffey P.J. Dopamine neurones form a discrete plexus with melanopsin cells in normal and degenerating retina. Experimental neurology. 2007;205(1):26–35. PubMed PMID: 17362933.
19. Zhang D.-Q., Wong K.Y., Sollars P.J., Berson D.M., Pickard G.E., McMahon D.G. Intraretinal signaling by ganglion cell photoreceptors to dopaminergic amacrine neurons. Proceedings of the National Academy of Sciences. 2008;105(37):14181–14186. PubMed PMID: 18779590.
20. Frazao R., McMahon D.G., Schunack W., Datta P., Heidelberger R., Marshak D.W. Histamine elevates free intracellular calcium in mouse retinal dopaminergic cells via H1-receptors. Investigative ophthalmology & visual science. 2011;52(6):3083–3088. PubMed PMID: 21310914.
21. Marc R.E., Jones B.W., Watt C.B., Anderson J.R., Sigulinsky C., Lauritzen S. Retinal connectomics: towards complete, accurate networks. Progress in retinal and eye research. 2013;37:141–162. PubMed PMID: 24016532.
22. Hirasawa, H., M. Contini, and E. Raviola, *Extrasynaptic release of GABA and dopamine by retinal dopaminergic neurons.* Philosophical Transactions of the Royal Society B: Biological Sciences. 2015; 370(1672):20140186.
23. Wassle H., Chun M. Dopaminergic and indoleamine-accumulating amacrine cells express GABA-like immunoreactivity in the cat retina. Journal of Neuroscience. 1988;8(9):3383–3394. PubMed PMID: 2902202.
24. Puopolo M., Hochstetler S.E., Gustincich S., Wightman R.M., Raviola E. Extrasynaptic release of dopamine in a retinal neuron: activity dependence and transmitter modulation. Neuron. 2001;30(1):211–225. PubMed PMID: 11343656.
25. Newkirk G.S., Hoon M., Wong R., Detwiler P.B. Inhibitory inputs tune the light response properties of dopaminergic amacrine cells in mouse retina. Journal of neurophysiology. 2013;110(2):536–552. PubMed PMID: 23636722.
26. Yang C.Y., Lukasiewicz P., Maguire G., Werblin F.S., Yazulla S. Amacrine cells in the tiger salamander retina: morphology, physiology, and neurotransmitter identification. Journal of Comparative Neurology. 1991;312(1):19–32. PubMed PMID: 1683878.

27. Zhang D.-Q., Belenky M.A., Sollars P.J., Pickard G.E., McMahon D.G. Melanopsin mediates retrograde visual signaling in the retina. PloS one. 2012;7(8) PubMed PMID: 22880066.
28. Zhao X., Wong K.Y., Zhang D.-Q. Mapping physiological inputs from multiple photoreceptor systems to dopaminergic amacrine cells in the mouse retina. Scientific reports. 2017;7(1):1–14. PubMed PMID: 28801634.
29. Qiao S.-N., Zhang Z., Ribelayga C.P., Zhong Y.-M., Zhang D.-Q. Multiple cone pathways are involved in photic regulation of retinal dopamine. Scientific reports. 2016;6:28916. PubMed PMID: 27356880.
30. Li L., Dowling J.E. Disruption of the olfactoretinal centrifugal pathway may relate to the visual system defect in night blindness bmutant zebrafish. Journal of Neuroscience. 2000;20(5):1883–1892. PubMed PMID: 10684889.
31. Zucker C.L., Dowling J.E. Centrifugal fibres synapse on dopaminergic interplexiform cells in the teleost retina. Nature. 1987;330(6144):166–168. PubMed PMID: 2890106.
32. Kolb H., Netzer E., Ammermüller J. Neural circuitry and light responses of the dopamine amacrine cell of the turtle retina. Molecular vision. 1997;3(6) PubMed PMID: 9238095.
33. Yazulla S., Zucker C.L. Synaptic organization of dopaminergic interplexiform cells in the goldfish retina. Visual neuroscience. 1988;1(1):13–29. PubMed PMID: 2908724.
34. Dowling J.E., Ehinger B. Synaptic organization of the amine-containing interplexiform cells of the goldfish and Cebus monkey retinas. Science. 1975;188(4185):270–273. PubMed PMID: 804181.
35. Witkovsky P., Gábriel R., Križaj D. Anatomical and neurochemical characterization of dopaminergic interplexiform processes in mouse and rat retinas. Journal of Comparative Neurology. 2008;510(2):158–174. PubMed PMID: 18615559.
36. Bjelke B., Goldstein M., Tinner B., Andersson C., Sesack S.R., Steinbusch H.W., Lew J.Y., He X., Watson S., Tengroth B. Dopaminergic transmission in the rat retina: evidence for volume transmission. Journal of chemical neuroanatomy. 1996;12(1):37–50. PubMed PMID: 9001947.
37. Witkovsky P., Nicholson C., Rice M.E., Bohmaker K., Meller E. Extracellular dopamine concentration in the retina of the clawed frog, Xenopus laevis. Proceedings of the National Academy of Sciences. 1993;90(12):5667–5671. PubMed PMID: 8516316.
38. Young H. Co-localization of GABA-and tyrosine hydroxylase-like immunoreactivities in amacrine cells of the rabbit retina. Vision research. 1994;34(8):995–999. PubMed PMID: 7909184.
39. Wulle I., Wagner H.J. GABA and tyrosine hydroxylase immunocytochemistry reveal different patterns of colocalization in retinal neurons of various vertebrates. Journal of Comparative Neurology. 1990;296(1):173–178. PubMed PMID: 1972711.
40. Kosaka T., Kosaka K., Hataguchi Y., Nagatsu I., Wu J.-Y., Ottersen O., Storm-Mathisen J.a., Hama K. Catecholaminergic neurons containing GABA-like and/or glutamic acid decarboxylase-like immunoreactivities in various brain regions of the rat. Experimental brain research. 1987;66(1):191–210. PubMed PMID: 2884126.
41. Nguyen-Legros J., Versaux-Botteri C., Savy C. Dopaminergic and GABAergic retinal cell populations in mammals. Microscopy research and technique. 1997;36(1):26–42. PubMed PMID: 9031259.
42. Contini M., Raviola E. GABAergic synapses made by a retinal dopaminergic neuron. Proceedings of the National Academy of Sciences. 2003;100(3):1358–1363. PubMed PMID: 12547914.
43. Lee J.W., Lim M.Y., Park Y.S., Park S.J., Kim I.-B. Reexamination of Dopaminergic Amacrine Cells in the Rabbit Retina: Confocal Analysis with Double-and Triple-labeling Immunohistochemistry. Experimental neurobiology. 2017;26(6):329–338. PubMed PMID: 29302200.
44. Boatright J.H., Hoel M.J., Iuvone P.M. Stimulation of endogenous dopamine release and metabolism in amphibian retina by light-and K+-evoked depolarization. Brain research. 1989;482(1):164–168. PubMed PMID: 2706474.
45. Boatright J.H., Rubim N.M., Iuvone P.M. Regulation of endogenous dopamine release in amphibian retina by melatonin: the role of GABA. Visual neuroscience. 1994;11(5):1013–1018. PubMed PMID: 7947394.
46. Kolbinger W., Weiler R. Modulation of endogenous dopamine release in the turtle retina: effects of light, calcium, and neurotransmitters. Visual neuroscience. 1993;10(6):1035–1041. PubMed PMID: 7903046.

47. Adachi A., Nogi T., Ebihara S. Phase-relationship and mutual effects between circadian rhythms of ocular melatonin and dopamine in the pigeon. Brain research. 1998;792(2):361–369. PubMed PMID: 9593995.
48. Megaw P., Morgan I., Boelen M. Vitreal dihydroxyphenylacetic acid (DOPAC) as an index of retinal dopamine release. Journal of neurochemistry. 2001;76(6):1636–1644. PubMed PMID: 11259481.
49. Zawilska J.B., Bednarek A., Berezińska M., Nowak J.Z. Rhythmic changes in metabolism of dopamine in the chick retina: the importance of light versus biological clock. Journal of neurochemistry. 2003;84(4):717–724. PubMed PMID: 12562516.
50. Zawilska J.B., Berezińska M., Rosiak J., Vivien-Roels B., Nowak J.Z. The relationship between melatonin and dopamine rhythms in the duck retina. Neuroscience letters. 2003;347(1):37–40. PubMed PMID: 12865136.
51. Cameron M.A., Pozdeyev N., Vugler A., Cooper H., Iuvone P.M., Lucas R.J. Light regulation of retinal dopamine that is independent of melanopsin phototransduction. European Journal of Neuroscience. 2009;29(4):761–767. PubMed PMID: 19200071.
52. Gibson C.J. A simple perfusion system for measuring endogenous retinal dopamine release. Journal of neuroscience methods. 1990;32(1):75–79. PubMed PMID: 2335969.
53. Godley B.F., Wurtman R.J. Release of endogenous dopamine from the superfused rabbit retina in vitro: effect of light stimulation. Brain research. 1988;452(1-2):393–395. PubMed PMID: 3401747.
54. Mills S.L., Xia X.-B., Hoshi H., Firth S.I., Rice M.E., Frishman L.J., Marshak D.W. Dopaminergic modulation of tracer coupling in a ganglion-amacrine cell network. Visual neuroscience. 2007;24(4):593–608. PubMed PMID: 17711603.
55. Nowak J., Zurawska E. Dopamine in the rabbit retina and striatum: diurnal rhythm and effect of light stimulation. Journal of neural transmission. 1989;75(3):201–212. PubMed PMID: 2926383.
56. Parkinson D., Rando R. Effect of light on dopamine turnover and metabolism in rabbit retina. Investigative ophthalmology & visual science. 1983;24(3):384–388. PubMed PMID: 6131875.
57. Kramer S.G. Dopamine: A retinal neurotransmitter: I. Retinal uptake, storage, and light-stimulated release of H3-dopamine in vivo. Investigative ophthalmology & visual science. 1971;10(6):438–452. PubMed PMID: 4325307.
58. Boelen M.K., Boelen M.G., Marshak D.W. Light-stimulated release of dopamine from the primate retina is blocked by l-2-amino-4-phosphonobutyric acid (APB). Visual neuroscience. 1998;15(1):97–103. PubMed PMID: 9456509.
59. Besharse J.C., Iuvone P.M. Is dopamine a light-adaptive or a dark-adaptive modulator in retina? Neurochemistry international. 1992;20(2):193–199. PubMed PMID: 1304858.
60. Luft W., Iuvone P., Stell W. Spatial, temporal, and intensive determinants of dopamine release in the chick retina. Visual neuroscience. 2004;21(4):627–635. PubMed PMID: 15579225.
61. Megaw P.L., Boelen M.G., Morgan I.G., Boelen M.K. Diurnal patterns of dopamine release in chicken retina. Neurochemistry international. 2006;48(1):17–23. PubMed PMID: 16188347.
62. Witkovsky, P., *Dopamine and retinal function.* Documenta ophthalmologica. 2004; 108(1):17-39.
63. Hamasaki D., Trattler W.B., Hajek A.S. Light on depresses and light off enhances the release of dopamine from the cat's retina. Neuroscience letters. 1986;68(1):112–116. PubMed PMID: 3725212.
64. Tornqvist K., Yang X., Dowling J. Modulation of cone horizontal cell activity in the teleost fish retina. III. Effects of prolonged darkness and dopamine on electrical coupling between horizontal cells. Journal of Neuroscience. 1988;8(7):2279–2288. PubMed PMID: 3249225.
65. Weiler R., Baldridge W.H., Mangel S.C., Dowling J.E. Modulation of endogenous dopamine release in the fish retina by light and prolonged darkness. Visual neuroscience. 1997;14(2):351–356. PubMed PMID: 9147486.
66. Marshak, D., *Synaptic input to dopaminergic neurons in mammalian retina*, in *Concepts and Challenges in retinal Physiology*, H. Kolb, R. H, and W. S, Editors. 2001, Elsevier Sci B.V. : Netherlands.
67. Pérez-Fernández, V., N. Milosavljevic, A.E. Allen, K.A. Vessey, A.I. Jobling, E.L. Fletcher, P.P. Breen, J.W. Morley, and M.A. Cameron, *Rod photoreceptor activation alone defines the release of dopamine in the retina.* Current Biology. 2019; 29(5):763-774. e5.

68. Dowling, J., *The retina: an approachable part of the brain, Revised edn*. 2012, World: Belknap Press. 384.
69. Gonon F. Nonlinear relationship between impulse flow and dopamine released by rat midbrain dopaminergic neurons as studied by in vivo electrochemistry. Neuroscience. 1988;24(1):19–28. PubMed PMID: 3368048.
70. McCormack C.A., Burnside B. Light and circadian modulation of teleost retinal tyrosine hydroxylase activity. Investigative ophthalmology & visual science. 1993;34(5):1853–1860. PubMed PMID: 8097190.
71. Ribelayga C., Wang Y., Mangel S.C. A circadian clock in the fish retina regulates dopamine release via activation of melatonin receptors. The Journal of physiology. 2004;554(2):467–482. PubMed PMID: 14565990.
72. Wulle I., Kirsch M., Wagner H.-J. Cyclic changes in dopamine and DOPAC content, and tyrosine hydroxylase activity in the retina of a cichlid fish. Brain research. 1990;515(1-2):163–167. PubMed PMID: 1972642.
73. Bartell P.A., Miranda-Anaya M., McIvor W., Menaker M. Interactions between dopamine and melatonin organize circadian rhythmicity in the retina of the green iguana. Journal of biological rhythms. 2007;22(6):515–523. PubMed PMID: 18057326.
74. Miranda-Anaya M., Bartell P.A., Menaker M. Circadian rhythm of iguana electroretinogram: the role of dopamine and melatonin. Journal of biological rhythms. 2002;17(6):526–538. PubMed PMID: 12465886.
75. Lorenc-Duda A., Berezińska M., Urbańska A., Gołembiowska K., Zawilska J.B. Dopamine in the turkey retina—an impact of environmental light, circadian clock, and melatonin. Journal of molecular neuroscience. 2009;38(1):12–18. PubMed PMID: 18953673.
76. Manglapus M.K., Iuvone P.M., Underwood H., Pierce M.E., Barlow R.B. Dopamine mediates circadian rhythms of rod–cone dominance in the Japanese quail retina. Journal of Neuroscience. 1999;19(10):4132–4141. PubMed PMID: 10234041.
77. Adachi A., Suzuki Y., Nogi T., Ebihara S. The relationship between ocular melatonin and dopamine rhythms in the pigeon: effects of melatonin inhibition on dopamine release. Brain research. 1999;815(2):435–440. PubMed PMID: 9878866.
78. Doyle S.E., Grace M.S., McIvor W., Menaker M. Circadian rhythms of dopamine in mouse retina: the role of melatonin. Visual neuroscience. 2002;19(5):593–601. PubMed PMID: 12507326.
79. Nir I., Haque R., Iuvone P.M. Diurnal metabolism of dopamine in the mouse retina. Brain research. 2000;870(1-2):118–125. PubMed PMID: 10869508.
80. Doyle S.E., McIvor W.E., Menaker M. Circadian rhythmicity in dopamine content of mammalian retina: role of the photoreceptors. Journal of neurochemistry. 2002;83(1):211–219. PubMed PMID: 12358745.
81. Melamed E., Frucht Y., Lemor M., Uzzan A., Rosenthal Y. Dopamine turnover in rat retina: a 24-hour light-dependent rhythm. Brain research. 1984;305(1):148–151. PubMed PMID: 6744054.
82. Pozdeyev N., Lavrikova E. Diurnal changes of tyrosine, dopamine, and dopamine metabolites content in the retina of rats maintained at different lighting conditions. Journal of Molecular Neuroscience. 2000;15(1):1–9. PubMed PMID: 11211232.
83. Sakamoto K., Liu C., Kasamatsu M., Pozdeyev N.V., Iuvone P.M., Tosini G. Dopamine regulates melanopsin mRNA expression in intrinsically photosensitive retinal ganglion cells. European Journal of Neuroscience. 2005;22(12):3129–3136. PubMed PMID: 16367779.
84. Wirz-Justice A., Da Prada M., Remé C. Circadian rhythm in rat retinal dopamine. Neuroscience letters. 1984;45(1):21–25. PubMed PMID: 6728302.
85. Di Paolo T., Harnois C., Daigle M. Assay of dopamine and its metabolites in human and rat retina. Neuroscience letters. 1987;74(2):250–254. PubMed PMID: 3574761.
86. Sakamoto K., Liu C., Tosini G. Classical photoreceptors regulate melanopsin mRNA levels in the rat retina. Journal of Neuroscience. 2004;24(43):9693–9697. PubMed PMID: 15509757.
87. Dorenbos R., Contini M., Hirasawa H., Gustincich S., Raviola E. Expression of circadian clock genes in retinal dopaminergic cells. Visual neuroscience. 2007;24(4):573–580. PubMed PMID: 17705893.

88. Gustincich S., Contini M., Gariboldi M., Puopolo M., Kadota K., Bono H., LeMieux J., Walsh P., Carninci P., Hayashizaki Y. Gene discovery in genetically labeled single dopaminergic neurons of the retina. Proceedings of the National Academy of Sciences. 2004;101(14):5069–5074. PubMed PMID: 15047890.
89. Ruan G.-X., Zhang D.-Q., Zhou T., Yamazaki S., McMahon D.G. Circadian organization of the mammalian retina. Proceedings of the National Academy of Sciences. 2006;103(25):9703–9708. PubMed PMID: 16766660.
90. Witkovsky P., Veisenberger E., LeSauter J., Yan L., Johnson M., Zhang D.-Q., McMahon D., Silver R. Cellular location and circadian rhythm of expression of the biological clock gene Period 1 in the mouse retina. Journal of Neuroscience. 2003;23(20):7670–7676. PubMed PMID: 12930806.
91. Sakamoto K., Liu C., Kasamatsu M., Iuvone P.M., Tosini G. Intraocular injection of kainic acid does not abolish the circadian rhythm of arylalkylamine N-acetyltransferase mRNA in rat photoreceptors. Mol Vis. 2006;12:117–24. PubMed PMID: 16518309.
92. Iuvone P.M., Tosini G., Pozdeyev N., Haque R., Klein D.C., Chaurasia S.S. Circadian clocks, clock networks, arylalkylamine N-acetyltransferase, and melatonin in the retina. Progress in retinal and eye research. 2005;24(4):433–456. PubMed PMID: 15845344.
93. Dkhissi-Benyahya O., Coutanson C., Knoblauch K., Lahouaoui H., Leviel V., Rey C., Bennis M., Cooper H.M. The absence of melanopsin alters retinal clock function and dopamine regulation by light. Cellular and molecular life sciences. 2013;70(18):3435–3447. PubMed PMID: 23604021.
94. Beaulieu J.-M., Gainetdinov R.R. The physiology, signaling, and pharmacology of dopamine receptors. Pharmacological reviews. 2011;63(1):182–217. PubMed PMID: 21303898.
95. Beaulieu J.M., Espinoza S., Gainetdinov R.R. Dopamine receptors–IUPHAR review 13. British journal of pharmacology. 2015;172(1):1–23. PubMed PMID: 25671228.
96. Kuzhikandathil E.V., Yu W., Oxford G.S. Human dopamine D3 and D2L receptors couple to inward rectifier potassium channels in mammalian cell lines. Molecular and Cellular Neuroscience. 1998;12(6):390–402. PubMed PMID: 9888991.
97. Yan Z., Song W.-J., Surmeier D.J. D2 dopamine receptors reduce N-type Ca2+ currents in rat neostriatal cholinergic interneurons through a membrane-delimited, protein-kinase-C-insensitive pathway. Journal of neurophysiology. 1997;77(2):1003–1015. PubMed PMID: 9065864.
98. Missale C., Nash S.R., Robinson S.W., Jaber M., Caron M.G. Dopamine receptors: from structure to function. Physiological reviews. 1998;78(1):189–225. PubMed PMID: 9457173.
99. Nishi A., Snyder G.L., Greengard P. Bidirectional regulation of DARPP-32 phosphorylation by dopamine. Journal of Neuroscience. 1997;17(21):8147–8155. PubMed PMID: 9334390.
100. Hernandez-Lopez S., Tkatch T., Perez-Garci E., Galarraga E., Bargas J., Hamm H., Surmeier D.J. D2 dopamine receptors in striatal medium spiny neurons reduce L-type Ca2+ currents and excitability via a novel PLC [beta] 1-IP3-calcineurin-signaling cascade. The Journal of Neuroscience: the Official Journal of the Society for Neuroscience. 2000;20(24):8987–8995. PubMed PMID: 11124974.
101. Hasbi A., O'Dowd B.F., George S.R. Dopamine D1-D2 receptor heteromer signaling pathway in the brain: emerging physiological relevance. Molecular brain. 2011;4(1):26. PubMed PMID: 21663703.
102. Hasbi A., O'Dowd B.F., George S.R. Heteromerization of dopamine D2 receptors with dopamine D1 or D5 receptors generates intracellular calcium signaling by different mechanisms. Current opinion in pharmacology. 2010;10(1):93–99. PubMed PMID: 19897420.
103. Lee S.-M., Yang Y., Mailman R.B. Dopamine D1 Receptor Signaling: Does GαQ–Phospholipase C Actually Play a Role? Journal of Pharmacology and Experimental Therapeutics. 2014;351(1):9–17. PubMed PMID: 25052835.
104. Kisilevsky A.E., Zamponi G.W. D2 dopamine receptors interact directly with N-type calcium channels and regulate channel surface expression levels. Channels. 2008;2(4):269–277. PubMed PMID: 18719394.
105. Blom H. D. RöNnlund, L. Scott, Z. Spicarova, V. Rantanen, J. Widengren, A. Aperia, and H. Brismar, *Nearest neighbor analysis of dopamine D1 receptors and Na+-K+-ATPases in dendritic spines dissected by STED microscopy.* Microscopy research and technique. 2012;75(2):220–228. PubMed PMID: 21809413.

106. Hazelwood L.A., Free R.B., Cabrera D.M., Skinbjerg M., Sibley D.R. Reciprocal modulation of function between the D1 and D2 dopamine receptors and the Na+, K+-ATPase. Journal of Biological Chemistry. 2008;283(52):36441–36453. PubMed PMID: 18984584.
107. Rankin, M.L., L.A. Hazelwood, R.B. Free, E. Rex, R. Roof, and D. Sibley, *Molecular Pharmacology of the Dopamine Receptors*, in *Dopamine handbook*, L. Iversen, et al., Editors. 2010, Oxford University Press: New York. p. 63–87.
108. Rondou P., Haegeman G., Van Craenenbroeck K. The dopamine D4 receptor: biochemical and signalling properties. Cellular and molecular life sciences. 2010;67(12):1971–1986. PubMed PMID: 20165900.
109. Sibley D.R. New insights into dopaminergic receptor function using antisense and genetically altered animals. Annual review of pharmacology and toxicology. 1999;39(1):313–341. PubMed PMID: 10331087.
110. Wolf M.E., Roth R.H. Autoreceptor regulation of dopamine synthesis. Annals of the New York Academy of Sciences. 1990;604(1):323–343. PubMed PMID: 2171398.
111. Civelli O., Bunzow J.R., Grandy D.K. Molecular diversity of the dopamine receptors. Annual review of pharmacology and toxicology. 1993;33(1):281–307. PubMed PMID: 8494342.
112. Ribelayga C., Wang Y., Mangel S.C. Dopamine mediates circadian clock regulation of rod and cone input to fish retinal horizontal cells. The Journal of physiology. 2002;544(3):801–816. PubMed PMID: 12411525.
113. Seeman P., Van Tol H.H. Dopamine receptor pharmacology. Trends in pharmacological sciences. 1994;15(7):264–270. PubMed PMID: 7940991.
114. Barton A.C., Black L.E., Sibley D.R. Agonist-induced desensitization of D2 dopamine receptors in human Y-79 retinoblastoma cells. Molecular pharmacology. 1991;39(5):650–658. PubMed PMID: 1674585.
115. Gardner B., Liu Z.F., Jiang D., Sibley D.R. The role of phosphorylation/dephosphorylation in agonist-induced desensitization of D1 dopamine receptor function: evidence for a novel pathway for receptor dephosphorylation. Molecular pharmacology. 2001;59(2):310–321. PubMed PMID: 11160868.
116. Ito K., Haga T., Lameh J., Sadée W. Sequestration of dopamine D2 receptors depends on coexpression of G-protein-coupled receptor kinases 2 or 5. European journal of biochemistry. 1999;260(1):112–119. PubMed PMID: 10091590.
117. Ko F., Seeman P., Sun W., Kapur S. Dopamine D2 receptors internalize in their low-affinity state. Neuroreport. 2002;13(8):1017–1020. PubMed PMID: 12060799.
118. Nowak J.Z., Sek B., Schorderet M. Dark-induced supersensitivity of dopamine D-1 and D-2 receptors in rat retina. NeuroReport. 1991;2(8):429–432. PubMed PMID: 1717048.
119. Zawilska J.B., Iuvone P.M. Melatonin synthesis in chicken retina: effect of kainic acid-induced lesions on the diurnal rhythm and D2-dopamine receptor-mediated regulation of serotonin N-acetyltransferase activity. Neuroscience letters. 1992;135(1):71–74. PubMed PMID: 1347416.
120. Muresan Z., Besharse J.C. D2-like dopamine receptors in amphibian retina: Localization with fluorescent ligands. Journal of Comparative Neurology. 1993;331(2):149–160. PubMed PMID: 8509497.
121. Wagner H.J., Luo B.G., Ariano M.A., Sibley D.R., Stell W.K. Localization of D2 dopamine receptors in vertebrate retinae with anti-peptide antibodies. Journal of Comparative Neurology. 1993;331(4):469–481. PubMed PMID: 8509505.
122. Rohrer B., Stell W.K. Localization of putative dopamine D2-like receptors in the chick retina, using in situ hybridization and immunocytochemistry. Brain research. 1995;695(2):110–116. PubMed PMID: 8556320.
123. Elena P., Denis P., Kosina-Boix M., Lapalus P. Dopamine receptors in rabbit and rat eye: characterization and localization of DA1 and DA2 binding sites. Current eye research. 1989;8(1):75–83. PubMed PMID: 2707038.
124. Tran V.T., Dickman M. Differential localization of dopamine D1 and D2 receptors in rat retina. Investigative ophthalmology & visual science. 1992;33(5):1620–1626. PubMed PMID: 1532792.
125. Veruki M.L. Dopaminergic neurons in the rat retina express dopamine D2/3 receptors. European Journal of Neuroscience. 1997;9(5):1096–1100. PubMed PMID: 9182963.
126. Vuvan T., Geffard M., Denis P., Simon A., Nguyen-Legros J. Radioimmunoligand characterization and immunohistochemical localization of dopamine D2 receptors on rods in the rat retina. Brain research. 1993;614(1-2):57–64. PubMed PMID: 8348331.

127. Brann M.R., Young W.S. III. Dopamine receptors are located on rods in bovine retina. Neuroscience letters. 1986;69(3):221–226. PubMed PMID: 3763052.
128. Dearry A., Falardeau P., Shores C., Caron M.G. D 2 dopamine receptors in the human retina: Cloning of cDNA and localization of mRNA. Cellular and molecular neurobiology. 1991;11(5):437–453. PubMed PMID: 1835903.
129. Mora-Ferrer C., Yazulla S., Studholme K.M., Haak-Frendscho M. Dopamine D1-receptor immunolocalization in goldfish retina. Journal of Comparative Neurology. 1999;411(4):705–714. PubMed PMID: 10421879.
130. Cohen A.I., Todd R.D., Harmon S., O'Malley K.L. Photoreceptors of mouse retinas possess D4 receptors coupled to adenylate cyclase. Proceedings of the National Academy of Sciences. 1992;89(24):12093–12097. PubMed PMID: 1334557.
131. Derouiche A., Asan E. The dopamine D2 receptor subfamily in rat retina: ultrastructural immunogold and in situhybridization studies. European Journal of Neuroscience. 1999;11(4):1391–1402. PubMed PMID: 10103134.
132. Hillman D.W., Lin D., Burnside B. Evidence for D4 receptor regulation of retinomotor movement in isolated teleost cone inner-outer segments. Journal of neurochemistry. 1995;64(3):1326–1335. PubMed PMID: 7861165.
133. Klitten L.L., Rath M.F., Coon S.L., Kim J.-S., Klein D.C., Møller M. Localization and regulation of dopamine receptor D4 expression in the adult and developing rat retina. Experimental eye research. 2008;87(5):471–477. PubMed PMID: 18778704.
134. Zawilska J., Nowak J. Dopamine D4-like receptors in vertebrate retina: does the retina offer a model for the D4-receptor analysis? Polish journal of pharmacology. 1997;49(4):201–211. PubMed PMID: 9437763.
135. Zhekova D., Vitanova L. Tyrosine hydroxylase activity and dopamine receptors D1 and D5 in frog and turtle retina: An immunofluorescence study. Comptes rendus de l'Académie bulgare des Sciences. 2016;69(2):191–196.
136. Yazulla S., Lin Z.-S. Differential effects of dopamine depletion on the distribution of [3H] SCH 23390 and [3H] spiperone binding sites in the goldfish retina. Vision Research. 1995;35(17):2409–2414. PubMed PMID: 8594810.
137. Firth S., Morgan I., Boelen M. Localization of D, dopamine receptors in the chicken retina. Australian and New Zealand journal of ophthalmology. 1997;25(4):64–66. PubMed PMID: 9267629.
138. Koulen P. Postnatal development of dopamine D1 receptor immunoreactivity in the rat retina. Journal of neuroscience research. 1999;56(4):397–404. PubMed PMID: 10340747.
139. Veruki M.L., Wässle H. Immunohistochemical Localization of Dopamine D Receptors in Rat Retina. European Journal of Neuroscience. 1996;8(11):2286–2297. PubMed PMID: 8950093.
140. Farshi P., Fyk-Kolodziej B., Krolewski D.M., Walker P.D., Ichinose T. Dopamine D1 receptor expression is bipolar cell type-specific in the mouse retina. Journal of Comparative Neurology. 2016;524(10):2059–2079. PubMed PMID: 26587737.
141. Travis A.M., Heflin S.J., Hirano A.A., Brecha N.C., Arshavsky V.Y. Dopamine-dependent sensitization of rod bipolar cells by GABA is conveyed through wide-field amacrine cells. Journal of Neuroscience. 2018;38(3):723–732. PubMed PMID: 29217689.
142. Yadav S.C., Tetenborg S., Dedek K. Gap junctions in A8 amacrine cells are made of connexin36 but are differently regulated than gap junctions in AII amacrine cells. Frontiers in molecular neuroscience. 2019;12:99. PubMed PMID: 31065239.
143. Wang Y., Harsanyi K., Mangel S.C. Endogenous activation of dopamine D2 receptors regulates dopamine release in the fish retina. Journal of Neurophysiology. 1997;78(1):439–449. PubMed PMID: 9242292.
144. Kubrusly R.C., Panizzutti R., Gardino P.F., Stutz B., Reis R.A., Ventura A.L.M., de Mello M.C.F., de Mello F.G. Expression of functional dopaminergic phenotype in purified cultured Müller cells from vertebrate retina. Neurochemistry international. 2008;53(3-4):63–70. PubMed PMID: 18582514.
145. Biedermann B., Fröhlich E., Grosche J., Wagner H.-J., Reichenbach A. Mammalian Müller (glial) cells express functional D2 dopamine receptors. Neuroreport. 1995;6(4):609–612. PubMed PMID: 7605910.

146. Nguyen-Legros J., Chanut E., Versaux-Botteri C., Simon A., Trouvin J.H. Dopamine inhibits melatonin synthesis in photoreceptor cells through a D2-like receptor subtype in the rat retina: biochemical and histochemical evidence. Journal of neurochemistry. 1996;67(6):2514–2520. PubMed PMID: 8931485.
147. Popova E. Role of dopamine in distal retina. Journal of Comparative Physiology A. 2014;200(5):333–358. PubMed PMID: 24728309.
148. Akopian A., Witkovsky P. D2 dopamine receptor-mediated inhibition of a hyperpolarization-activated current in rod photoreceptors. Journal of Neurophysiology. 1996;76(3):1828–1835. PubMed PMID: 8890295.
149. Kawai F., Horiguchi M., Miyachi E.-i. Dopamine modulates the voltage response of human rod photoreceptors by inhibiting the h current. Investigative ophthalmology & visual science. 2011;52(7):4113–4117. PubMed PMID: 21421871.
150. Cohen A.I., Blazynski C. Dopamine and its agonists reduce a light-sensitive poor of cyclic AMP in mouse photoreceptors. Visual Neuroscience. 1990;4(1):43–52. PubMed PMID: 1702315.
151. Nir I., Harrison J.M., Haque R., Low M.J., Grandy D.K., Rubinstein M., Iuvone P.M. Dysfunctional light-evoked regulation of cAMP in photoreceptors and abnormal retinal adaptation in mice lacking dopamine D4 receptors. Journal of Neuroscience. 2002;22(6):2063–2073. PubMed PMID: 11896146.
152. Patel S., Chapman K.L., Marston D., Hutson P.H., Ragan C.I. Pharmacological and functional characterisation of dopamine D4 receptors in the rat retina. Neuropharmacology. 2003;44(8):1038–1046. PubMed PMID: 12763097.
153. Jackson C.R., Chaurasia S.S., Zhou H., Haque R., Storm D.R., Iuvone P.M. Essential roles of dopamine D4 receptors and the type 1 adenylyl cyclase in photic control of cyclic AMP in photoreceptor cells. Journal of neurochemistry. 2009;109(1):148–157. PubMed PMID: 19166506.
154. Ivanova T.N., Alonso-Gomez A.L., Iuvone P.M. Dopamine D4 receptors regulate intracellular calcium concentration in cultured chicken cone photoreceptor cells: relationship to dopamine receptor-mediated inhibition of cAMP formation. Brain research. 2008;1207:111–119. PubMed PMID: 18371938.
155. Stella S.L. Jr, Thoreson W.B. Differential modulation of rod and cone calcium currents in tiger salamander retina by D2 dopamine receptors and cAMP. European Journal of Neuroscience. 2000;12(10):3537–3548. PubMed PMID: 11029623.
156. Firsov M., Astakhova L. The role of dopamine in controlling retinal photoreceptor function in vertebrates. Neuroscience and Behavioral Physiology. 2016;46(2):138–145.
157. Thoreson W.B., Stella S.L., Bryson E.J., Clements J., Witkovsky P. D 2-like dopamine receptors promote interactions between calcium and chloride channels that diminish rod synaptic transfer in the salamander retina. Visual neuroscience. 2002;19(3):235–247. PubMed PMID: 12392173.
158. Liu X., Hirano A.A., Sun X., Brecha N.C., Barnes S. Calcium channels in rat horizontal cells regulate feedback inhibition of photoreceptors through an unconventional GABA-and pH-sensitive mechanism. The Journal of physiology. 2013;591(13):3309–3324. PubMed PMID: 23613534.
159. Hedden W. Jr, Dowling J. The interplexiform cell system II. Effects of dopamine on goldfish retinal neurones. Proceedings of the Royal Society of London. Series B. Biological Sciences. 1978;201(1142):27–55. PubMed PMID: 27790.
160. Ammermüller J., Weiler R., Perlman I. Short-term effects of dopamine on photoreceptors, luminosity-and chromaticity-horizontal cells in the turtle retina. Visual neuroscience. 1995;12(3):403–412. PubMed PMID: 7654600.
161. Witkovsky P., Stone S., Besharse J.C. Dopamine modifies the balance of rod and cone inputs to horizontal cells of the Xenopus retina. Brain research. 1988;449(1-2):332–336. PubMed PMID: 3293703.
162. Hare W.A., Owen W.G. Similar effects of carbachol and dopamine on neurons in the distal retina of the tiger salamander. Visual neuroscience. 1995;12(3):443–455. PubMed PMID: 7654602.
163. Jin N.G., Chuang A.Z., Masson P.J., Ribelayga C.P. Rod electrical coupling is controlled by a circadian clock and dopamine in mouse retina. The Journal of physiology. 2015;593(7):1597–1631. PubMed PMID: 25616058.

164. Krizaj D. Mesopic state: Cellular mechanisms involved in pre-and post-synaptic mixing of rod and cone signals. Microscopy research and technique. 2000;50(5):347–359. PubMed PMID: 10941171.
165. Krizaj D., Gábriel R., Owen W.G., Witkovsky P. Dopamine D2 receptor-mediated modulation of rod-cone coupling in the Xenopus retina. Journal of Comparative Neurology. 1998;398(4):529–538. PubMed PMID: 9717707.
166. Krizaj, D., T. Vu, and D.R. Copenhagen, *On the shaping, modulation and synaptic transmission of rod and cone signals*, in *The retinal basis of vision*, J. Toyoda, et al., Editors. 1999, Elsevier Press. p. 7-83.
167. Yang X.-L., Wu S.M. Modulation of rod-cone coupling by light. Science. 1989;244(4902):352–354. PubMed PMID: 2711185.
168. Li H., Chuang A.Z., O'Brien J. Photoreceptor coupling is controlled by connexin 35 phosphorylation in zebrafish retina. Journal of Neuroscience. 2009;29(48):15178–15186. PubMed PMID: 19955370.
169. Li H., Zhang Z., Blackburn M.R., Wang S.W., Ribelayga C.P., O'Brien J. Adenosine and dopamine receptors coregulate photoreceptor coupling via gap junction phosphorylation in mouse retina. Journal of Neuroscience. 2013;33(7):3135–3150. PubMed PMID: 23407968.
170. Ribelayga C., Mangel S.C. Identification of a circadian clock-controlled neural pathway in the rabbit retina. PloS one. 2010;5(6) PubMed PMID: 20548772.
171. Ribelayga C., Cao Y., Mangel S.C. The circadian clock in the retina controls rod-cone coupling. Neuron. 2008;59(5):790–801. PubMed PMID: 18786362.
172. Li, H. and J. O'Brien, *Regulation of gap junctional coupling in photoreceptors*, in *Photoreceptors: Physiology, Types and Abnormalities*, E. Akutagawa and K. Ozaki, Editors. 2012, Nova Science: Hauppauge, NY. p. 97-112.
173. Zhang Z., Li H., Liu X. J. O'BRIEN, and C.P. Ribelayga, *Circadian clock control of connexin36 phosphorylation in retinal photoreceptors of the CBA/CaJ mouse strain.* Visual neuroscience. 2015.:32.
174. Schneeweis D.M., Schnapf J.L. The photovoltage of macaque cone photoreceptors: adaptation, noise, and kinetics. Journal of Neuroscience. 1999;19(4):1203–1216. PubMed PMID: 9952398.
175. Liu X., Grove J.C., Hirano A.A., Brecha N.C., Barnes S. Dopamine D1 receptor modulation of calcium channel currents in horizontal cells of mouse retina. Journal of neurophysiology. 2016;116(2):686–697. PubMed PMID: 27193322.
176. Dong C., McReynolds J.S. The relationship between light, dopamine release and horizontal cell coupling in the mudpuppy retina. The Journal of Physiology. 1991;440(1):291–309. PubMed PMID: 1687151.
177. Perlman I., Ammermuller J. Receptive-field size of L1 horizontal cells in the turtle retina: effects of dopamine and background light. Journal of Neurophysiology. 1994;72(6):2786–2795. PubMed PMID: 7897489.
178. Piccolino M., Neyton J., Gerschenfeld H. Decrease of gap junction permeability induced by dopamine and cyclic adenosine 3': 5'-monophosphate in horizontal cells of turtle retina. Journal of Neuroscience. 1984;4(10):2477–2488. PubMed PMID: 6092564.
179. DeVries S., Schwartz E. Modulation of an electrical synapse between solitary pairs of catfish horizontal cells by dopamine and second messengers. The Journal of physiology. 1989;414(1):351–375. PubMed PMID: 2558170.
180. Hida E., Negishi K., Naka K.I. Effects of dopamine on photopic L-type s-potentials in the catfish retina. Journal of neuroscience research. 1984;11(4):373–382. PubMed PMID: 6748110.
181. Lasater E.M., Dowling J.E. Dopamine decreases conductance of the electrical junctions between cultured retinal horizontal cells. Proceedings of the National Academy of Sciences. 1985;82(9):3025–3029. PubMed PMID: 3857632.
182. McMahon D.G., Brown D.R. Modulation of gap-junction channel gating at zebrafish retinal electrical synapses. Journal of neurophysiology. 1994;72(5):2257–2268. PubMed PMID: 7533830.
183. McMahon D.G., Mattson M.P. Horizontal cell electrical coupling in the giant danio: synaptic modulation by dopamine and synaptic maintenance by calcium. Brain research. 1996;718(1-2):89–96. PubMed PMID: 8773769.

184. Ribelayga C., Mangel S.C. Absence of circadian clock regulation of horizontal cell gap junctional coupling reveals two dopamine systems in the goldfish retina. Journal of Comparative Neurology. 2003;467(2):243–253. PubMed PMID: 14595771.
185. Ribelayga C., Mangel S.C. Tracer coupling between fish rod horizontal cells: modulation by light and dopamine but not the retinal circadian clock. Visual neuroscience. 2007;24(3):333–344. PubMed PMID: 17640444.
186. Teranishi T., Negishi K., Kato S. Dopamine modulates S-potential amplitude and dye-coupling between external horizontal cells in carp retina. Nature. 1983;301(5897):243–246. PubMed PMID: 6401844.
187. Teranishi T., Negishi K., Kato S. Regulatory effect of dopamine on spatial properties of horizontal cells in carp retina. Journal of Neuroscience. 1984;4(5):1271–1280. PubMed PMID: 6726332.
188. Hankins M., Ikeda H. Non-NMDA type excitatory amino acid receptors mediate rod input to horizontal cells in the isolated rat retina. Vision research. 1991;31(4):609–617. PubMed PMID: 1688218.
189. He S., Weiler R., Vaney D.I. Endogenous dopaminergic regulation of horizontal cell coupling in the mammalian retina. Journal of Comparative Neurology. 2000;418(1):33–40. PubMed PMID: 10701754.
190. Weiler R., Pottek M., He S., Vaney D.I. Modulation of coupling between retinal horizontal cells by retinoic acid and endogenous dopamine. Brain research reviews. 2000;32(1):121–129. PubMed PMID: 10751661.
191. Reitsamer H.A., Pflug R., Franz M., Huber S. Dopaminergic modulation of horizontal-cell-axon-terminal receptive field size in the mammalian retina. Vision research. 2006;46(4):467–474. PubMed PMID: 16023694.
192. Hampson E.C., Weiler R., Vaney D.I. pH-gated dopaminergic modulation of horizontal cell gap junctions in mammalian retina. Proceedings of the Royal Society of London. Series B: Biological Sciences. 1994;255(1342):67–72. PubMed PMID: 8153138.
193. Drujan, B., K. Negishi, and M. Laufer, *Studies on putative neurotransmitters in the distal retina*, in *Neurochemistry of the Retina*. 1980, Elsevier. p. 143-150.
194. Mangel S.C., Dowling J. Responsiveness and receptive field size of carp horizontal cells are reduced by prolonged darkness and dopamine. Science. 1985;229(4718):1107–1109. PubMed PMID: 4035351.
195. Mangel S.C., Dowling J. The interplexiform–horizontal cell system of the fish retina: effects of dopamine, light stimulation and time in the dark. Proceedings of the Royal society of London. Series B. Biological sciences. 1987;231(1262):91–121. PubMed PMID: 2888119.
196. Negishi K., Drujan B. Effects of catecholamines on the horizontal cell membrane potential in the fish retina. Sensory Processes. 1978;2(4):388–395. PubMed PMID: 755294.
197. Negishi K., Drujan B. Effects of catecholamines and related compounds on horizontal cells in the fish retina. Journal of Neuroscience Research. 1979;4(5-6):311–334. PubMed PMID: 522194.
198. Bornstein O., Twig G., Benda J., Weiler R., Perlman I. Dynamic changes in the receptive fields of L1-type horizontal cells in the retina of the turtle Mauremys caspica. Visual neuroscience. 2002;19(5):621–632. PubMed PMID: 12507328.
199. Harsanyi K., Mangel S.C. Activation of a D2 receptor increases electrical coupling between retinal horizontal cells by inhibiting dopamine release. Proceedings of the National Academy of Sciences. 1992;89(19):9220–9224. PubMed PMID: 1357661.
200. Cohen J.L., Dowling J.E. The role of the retinal interplexiform cell: effects of 6-hydroxydopamine on the spatial properties of carp horizontal cells. Brain research. 1983;264(2):307–310. PubMed PMID: 6405977.
201. Qian H., Malchow R.P., Ripps H. Gap-junctional properties of electrically coupled skate horizontal cells in culture. Visual neuroscience. 1993;10(2):287–295. PubMed PMID: 8485091.
202. Yang X., Tornqvist K., Dowling J. Modulation of cone horizontal cell activity in the teleost fish retina. II. Role of interplexiform cells and dopamine in regulating light responsiveness. Journal of Neuroscience. 1988;8(7):2269–2278. PubMed PMID: 2470870.
203. Yamada M., Shigematsu Y., Umetani Y., Saito T. Dopamine decreases receptive field size of rod-driven horizontal cells in carp retina. Vision research. 1992;32(10):1801–1807. PubMed PMID: 1337637.
204. Zhang A.J., Jacoby R., Wu S.M. Light-and dopamine-regulated receptive field plasticity in primate horizontal cells. Journal of Comparative Neurology. 2011;519(11):2125–2134. PubMed PMID: 21452210.

205. Piccolino M., Witkovsky P., Trimarchi C. Dopaminergic mechanisms underlying the reduction of electrical coupling between horizontal cells of the turtle retina induced by d-amphetamine, bicuculline, and veratridine. Journal of Neuroscience. 1987;7(8):2273–2284. PubMed PMID: 3112324.
206. Miyachi E., Murakami M. Decoupling of horizontal cells in carp and turtle retinae by intracellular injection of cyclic AMP. The Journal of physiology. 1989;419(1):213–224. PubMed PMID: 2559975.
207. Piccolino M., Demontis G., Witkovsky P., Strettoi E., Cappagli G., Porceddu M., De Montis M., Pepitoni S., Biggio G., Meller E. Involvement of D1 and D2 dopamine receptors in the control of horizontal cell electrical coupling in the turtle retina. European Journal of Neuroscience. 1989;1(3):247–257. PubMed PMID: 12106155.
208. Qian H., Ripps H. Receptive field properties of rod-driven horizontal cells in the skate retina. The Journal of general physiology. 1992;100(3):457–478. PubMed PMID: 1359000.
209. Baldridge, W.H., *Triphasic adaptation of teleost horizontal cells*, Volume 131, in *Progress in brain research*. 2001, Elsevier. p. 437-449.
210. Shigematsu Y., Yamada M. Effects of dopamine on spatial properties of horizontal cell responses in the carp retina. Biomedical Research-Tokyo. 1988;9:125–130. PubMed PMID: 3231368.
211. Umino O., Lee Y., Dowling J.E. Effects of light stimuli on the release of dopamine from interplexiform cells in the white perch retina. Visual neuroscience. 1991;7(5):451–458. PubMed PMID: 1764415.
212. Weiler R., Akopian A. Effects of background illuminations on the receptive field size of horizontal cells in the turtle retina are mediated by dopamine. Neuroscience letters. 1992;140(1):121–124. PubMed PMID: 1407690.
213. Villa P., Bedmar M., Barón M. Studies on rod horizontal cell s-potential in dependence of the dark/light adapted state: a comparative study in Cyprinus carpio and Scyliorhinus canicula retinas. Vision research. 1991;31(3):425–435. PubMed PMID: 1843752.
214. Yang, X.-L., *Modulation of synaptic transmission in the retina*. Documenta ophthalmologica. 1991; 76(4):377-387.
215. Xin D., Bloomfield S.A. Dark-and light-induced changes in coupling between horizontal cells in mammalian retina. Journal of Comparative Neurology. 1999;405(1):75–87. PubMed PMID: 10022197.
216. Knapp A.G., Dowling J.E. Dopamine enhances excitatory amino acid-gated conductances in cultured retinal horizontal cells. Nature. 1987;325(6103):437–439. PubMed PMID: 2880299.
217. Dowling J.E. Retinal neuromodulation: the role of dopamine. Visual neuroscience. 1991;7(1-2):87–97. PubMed PMID: 1718402.
218. Yang X.-L., Fan T.-X., Shen W. Effects of prolonged darkness on light responsiveness and spectral sensitivity of cone horizontal cells in carp retina in vivo. Journal of Neuroscience. 1994;14(1):326–334. PubMed PMID: 8283240.
219. Djamgoz M., Hankins M., Hirano J., Archer S. Neurobiology of retinal dopamine in relation to degenerative states of the tissue. Vision research. 1997;37(24):3509–3529. PubMed PMID: 9425527.
220. Shiells R., Falk G. Dopamine hyperpolarizes and reduces the light responses of rod ON-centre bipolar cells in the retina of the dogfish, Scyliorhinus canicula. Neuroscience letters. 1985;55(3):331–336. PubMed PMID: 4011036.
221. Witkovsky P., Stone S., Tranchina D. Photoreceptor to horizontal cell synaptic transfer in the Xenopus retina: modulation by dopamine ligands and a circuit model for interactions of rod and cone inputs. Journal of Neurophysiology. 1989;62(4):864–881. PubMed PMID: 2530319.
222. Pflug R., Nelson R., Huber S., Reitsamer H. Modulation of horizontal cell function by dopaminergic ligands in mammalian retina. Vision research. 2008;48(12):1383–1390. PubMed PMID: 18440579.
223. Djamgoz M.B., Fitzgerald E.M., Yamada M. Spectral Plasticity of H1 Horizontal Cells in Carp Retina: Independent Modulation by Dopamine and Light-adaptation. European Journal of Neuroscience. 1996;8(8):1571–1579. PubMed PMID: 8921249.
224. Yasui S., Yamada M., Djamgoz M. Dopamine and 2-amino-4-phosphonobutyrate differentially modify spectral responses of H1 horizontal cells in carp retina. Experimental brain research. 1990;83(1):79–84. PubMed PMID: 2073952.

225. Djamgoz M., Kirsch M., Wagner H.-J. Haloperidol suppresses light-induced spinule formation and biphasic responses of horizontal cells in fish (roach) retina. Neuroscience letters. 1989;107(1-3):200–204. PubMed PMID: 2616031.
226. Liu Y., Luo F.-J., Liang P.-J. Dopamine effect on the stimulus pattern related changes in response characteristics of R/G horizontal cells in carp retina. Brain research. 2003;973(2):190–195. PubMed PMID: 12738062.
227. Esposti F., Johnston J., Rosa J.M., Leung K.-M., Lagnado L. Olfactory stimulation selectively modulates the OFF pathway in the retina of zebrafish. Neuron. 2013;79(1):97–110. PubMed PMID: 23849198.
228. Heidelberger R., Matthews G. Dopamine enhances Ca2+ responses in synaptic terminals of retinal bipolar neurons. Neuroreport. 1994;5(6):729–732. PubMed PMID: 8199349.
229. Wellis D.P., Werblin F.S. Dopamine modulates GABAc receptors mediating inhibition of calcium entry into and transmitter release from bipolar cell terminals in tiger salamander retina. Journal of Neuroscience. 1995;15(7):4748–4761. PubMed PMID: 7623108.
230. Ichinose T., Lukasiewicz P.D. Ambient light regulates sodium channel activity to dynamically control retinal signaling. Journal of Neuroscience. 2007;27(17):4756–4764. PubMed PMID: 17460088.
231. Yu C.J., Li L. Dopamine modulates voltage-activated potassium currents in zebrafish retinal on bipolar cells. Journal of neuroscience research. 2005;82(3):368–376. PubMed PMID: 16206280.
232. Fan S.-F., Yazullla S. Modulation of voltage-dependent K+ currents (I K (V)) in retinal bipolar cells by ascorbate is mediated by dopamine D1 receptors. Visual neuroscience. 1999;16(5):923–931. PubMed PMID: 10580728.
233. Fan S.-F., Yazulla S. Reciprocal inhibition of voltage-gated potassium currents (I K (V)) by activation of cannabinoid CB 1 and dopamine D 1 receptors in ON bipolar cells of goldfish retina. Visual neuroscience. 2005;22(1):55–63. PubMed PMID: 15842741.
234. Fan S.-F., Yazulla S. Dopamine depletion with 6-OHDA enhances dopamine D1-receptor modulation of potassium currents in retinal bipolar cells. Visual neuroscience. 2001;18(2):327–337. PubMed PMID: 11417806.
235. Yamada M., Saito T. Effects of dopamine on bipolar cells in the carp retina. BIOMEDICAL RESEARCH-TOKYO. 1988;9:125–130.
236. Maguire G., Werblin F. Dopamine enhances a glutamate-gated ionic current in OFF bipolar cells of the tiger salamander retina. Journal of Neuroscience. 1994;14(10):6094–6101. PubMed PMID: 7931565.
237. Chaffiol, A., M. Ishii, Y. Cao, and S.C. Mangel, *Dopamine regulation of GABAA receptors contributes to light/dark modulation of the ON-cone bipolar cell receptive field surround in the retina.* Current Biology. 2017; 27(17):2600-2609. e4.
238. Flood M.D., Moore-Dotson J.M., Eggers E.D. Dopamine D1 receptor activation contributes to light-adapted changes in retinal inhibition to rod bipolar cells. Journal of neurophysiology. 2018;120(2):867–879. PubMed PMID: 29847232.
239. Mazade R.E., Flood M.D., Eggers E.D. Dopamine D1 receptor activation reduces local inner retinal inhibition to light-adapted levels. Journal of neurophysiology. 2019;121(4):1232–1243. PubMed PMID: 30726156.
240. Frishman, L.J., *Origins of the electroretinogram*, Volume 2, in *Principles and practice of clinical electrophysiology of vision*, J. Heckenlively and A. GB, Editors. 2006, MIT Press: London. p. 139-183.
241. Li L., Dowling J.E. Effects of dopamine depletion on visual sensitivity of zebrafish. Journal of Neuroscience. 2000;20(5):1893–1903. PubMed PMID: 10684890.
242. Lu J., Zoran M., Cassone V. Daily and circadian variation in the electroretinogram of the domestic fowl: effects of melatonin. Journal of Comparative Physiology A. 1995;177(3):299–306. PubMed PMID: 7643319.
243. McGoogan J.M., Cassone V.M. Circadian regulation of chick electroretinogram: effects of pinealectomy and exogenous melatonin. American Journal of Physiology-Regulatory, Integrative and Comparative Physiology. 1999;277(5):R1418–R1427. PubMed PMID: 10564215.
244. Wu W.Q., McGoogan J.M., Cassone V.M. Circadian regulation of visually evoked potentials in the domestic pigeon, Columba livia. Journal of Biological Rhythms. 2000;15(4):317–328. PubMed PMID: 10942263.

245. Miranda-Anaya M., Bartell P.A., Yamazaki S., Menaker M. Circadian rhythm of ERG in Iguana iguana: role of the pineal. Journal of biological rhythms. 2000;15(2):163–171. PubMed PMID: 10762034.
246. Shaw A.P., Collazo C.R., Easterling K., Young C.D., Karwoski C.J. Circadian rhythm in the visual system of the lizard Anolis carolinensis. Journal of biological rhythms. 1993;8(2):107–124. PubMed PMID: 8369548.
247. Brandenburg J., Bobbert A., Eggelmeyer F. Circadian changes in the response of the rabbit's retina to flashes. Behavioural brain research. 1983;7(1):113–123. PubMed PMID: 6824525.
248. White M.P., Hock P.A. Effects of continuous darkness on ERG correlates of disc shedding in rabbit retina. Experimental eye research. 1992;54(2):173–180. PubMed PMID: 1559546.
249. Barnard A.R., Hattar S., Hankins M.W., Lucas R.J. Melanopsin regulates visual processing in the mouse retina. Current biology. 2006;16(4):389–395. PubMed PMID: 16488873.
250. Cameron M.A., Barnard A.R., Hut R.A., Bonnefont X., van der Horst G.T., Hankins M.W., Lucas R.J. Electroretinography of wild-type and Cry mutant mice reveals circadian tuning of photopic and mesopic retinal responses. Journal of biological rhythms. 2008;23(6):489–501. PubMed PMID: 19060258.
251. Sengupta A., Baba K., Mazzoni F., Pozdeyev N.V., Strettoi E., Iuvone P.M., Tosini G. Localization of melatonin receptor 1 in mouse retina and its role in the circadian regulation of the electroretinogram and dopamine levels. PloS one. 2011;6(9) PubMed PMID: 21915336.
252. Storch K.-F., Paz C., Signorovitch J., Raviola E., Pawlyk B., Li T., Weitz C.J. Intrinsic circadian clock of the mammalian retina: importance for retinal processing of visual information. Cell. 2007;130(4):730–741. PubMed PMID: 17719549.
253. Jackson C.R., Ruan G.-X., Aseem F., Abey J., Gamble K., Stanwood G., Palmiter R.D., Iuvone P.M., McMahon D.G. Retinal dopamine mediates multiple dimensions of light-adapted vision. Journal of Neuroscience. 2012;32(27):9359–9368. PubMed PMID: 22764243.
254. Smith B.J., Côté P.D., Tremblay F. D1 dopamine receptors modulate cone ON bipolar cell Nav channels to control daily rhythms in photopic vision. Chronobiology international. 2015;32(1):48–58. PubMed PMID: 25157610.
255. Lin Z.-S., Yazulla S. Depletion of retinal dopamine does not affect the ERG b-wave increment threshold function in goldfish in vivo. Visual neuroscience. 1994;11(4):695–702. PubMed PMID: 7918220.
256. Yazulla S., Lin Z.-S., Studholme K.M. Doparninergic control of light-adaptive synaptic plasticity and role in goldfish visual behavior. Vision research. 1996;36(24):4045–4057. PubMed PMID: 9068857.
257. Kim D.-Y., Jung C.-S. Gap junction contributions to the goldfish electroretinogram at the photopic illumination level. The Korean Journal of Physiology & Pharmacology. 2012;16(3):219–224. PubMed PMID: 22802705.
258. Mora-Ferrer C., Behrend K. Dopaminergic modulation of photopic temporal transfer properties in goldfish retina investigated with the ERG. Vision research. 2004;44(17):2067–2081. PubMed PMID: 15149838.
259. Citron M.C., Erinoff L., Rickman D.W., Brecha N.C. Modification of electroretinograms in dopamine-depleted retinas. Brain research. 1985;345(1):186–191. PubMed PMID: 3933762.
260. Kupenova P., Belcheva S. Effects of haloperidol, methylergometrine and phentolamine on the frog ERG. Experientia. 1981;37(8):852–854. PubMed PMID: 7286136.
261. Wachtmeister L. Further studies of the chemical sensitivity of the oscillatory potentials of the electroretinogram (ERG) II. Glutamate-aspartate-and dopamine antagonists. Acta ophthalmologica. 1981;59(2):247–258. PubMed PMID: 7257744.
262. Popova E. Effects of dopamine receptor blockade on the intensity-response function of electroretinographic b-and d-waves in light-adapted eyes. Journal of Neural Transmission. 2014;121(3):233–244. PubMed PMID: 24150276.
263. Popova E., Kupenova P. Effects of dopamine D1 receptor blockade on the intensity-response function of ERG b-and d-waves under different conditions of light adaptation. Vision research. 2011;51(14):1627–1636. PubMed PMID: 21605587.
264. Popova E., Kupenova P. Effects of dopamine receptor blockade on the intensity-response function of ERG b-and d-waves in dark adapted eyes. Vision research. 2013;88:22–29. PubMed PMID: 23810982.

265. Popova E., Kostov M., Kupenova P. Effects of dopamine D 1 receptor blockade on the ERG b-and d-waves during blockade of ionotropic GABA receptors. Eye and Vision. 2016;3(1):32. PubMed PMID: 27981058.
266. Sato, T., T. Yoneyama, H. Kim, and T. Suzuki, *Effect of dopamine and haloperidol on the c-wave and light peak of light-induced retinal responses in chick eye.* Documenta ophthalmologica. 1987; 65(1):87-95.
267. Fujikado T. The effect of dopamine on the response to pattern stimulation--study of the chick ERG. Japanese journal of ophthalmology. 1994;38(4):368–374. PubMed PMID: 7723204.
268. Wioland, N., G. Rudolf, and N. Bonaventure, *Electrooculographic and electroretinographic study in the chicken after dopamine and haloperidol.* Documenta ophthalmologica. 1990; 75(2):175-180.
269. Gottvall, E. and O. Textorius, *Concentration-dependent effects of dopamine on the direct current electroretinogram of pigmented rabbits during prolonged intermittent recording.* Documenta ophthalmologica. 2003; 106(2):161-169.
270. Jagadeesh J., Sanchez R. Effects of apomorphine on the rabbit electroretinogram. Investigative ophthalmology & visual science. 1981;21(4):620–624. PubMed PMID: 7287352.
271. Kobayashi A., Shirao Y., Tagawa S., Katoh K., Tamura T. Effects of retinal intrinsic dopamine on the in in vivo electroretinogram of rabbits. Nippon Ganka Gakkai zasshi. 1996;100(2):111–117. PubMed PMID: 8851149.
272. Nakagawa T., Kurasaki S., Masuda T., Ukai K., Kubo S., Kadono H. Effects of some psychotropic drugs on the b-wave of the electroretinogram in isolated rabbit retina. Jpn J Pharmacol. 1988;46:97–100. PubMed PMID: 3367551.
273. Starr M.S. The effects of various amino acids, dopamine and some convulsants on the electroretinogram of the rabbit. Experimental eye research. 1975;21(1):79–87. PubMed PMID: 1140222.
274. Textorius, O., S.E.G. Nilsson, and B.-E. Andersson, *Effects of intravitreal perfusion with dopamine in different concentrations on the DC electroretinogram and the standing potential of the albino rabbit eye.* Documenta ophthalmologica. 1989; 73(2):149-162.
275. Naarendorp F., Hitchock P., Sieving P.A. Dopaminergic modulation of rod pathway signals does not affect the scotopic ERG of cat at dark-adapted threshold. Journal of neurophysiology. 1993;70(4):1681–1691. PubMed PMID: 8283223.
276. Naarendorp, F. and P.A. Sieving, *The scotopic threshold response of the cat ERG is suppressed selectively by GABA and glycine.* Vision research. 1991; 31:1:15.
277. Schneider T., Zrenner E. Effects of D-1 and D-2 dopamine antagonists on ERG and optic nerve response of the cat. Experimental eye research. 1991;52(4):425–430. PubMed PMID: 2037020.
278. Skrandies W., Wässle H. Dopamine and serotonin in cat retina: electroretinography and histology. Experimental brain research. 1988;71(2):231–240. PubMed PMID: 2901977.
279. Olivier, P., F. Jolicoeur, G. Lafond, A. Drumheller, and J. Brunette, *Effects of retinal dopamine depletion on the rabbit electroretinogram.* Documenta ophthalmologica. 1987; 66(4):359-371.
280. Bodis-Wollner I., Marx M., Ghilardi M. Systemic haloperidol administration increases the amplitude of the light-and dark-adapted flash ERG in the monkey. Clinical vision sciences. 1989;4(1):19–26.
281. Huppé-Gourgues F., Coudé G., Lachapelle P., Casanova C. Effects of the intravitreal administration of dopaminergic ligands on the b-wave amplitude of the rabbit electroretinogram. Vision research. 2005;45(2):137–145. PubMed PMID: 15581915.
282. Burguera J., Vilela C., Traba A., Ameave Y., Vallet M. The electroretinogram and visual evoked potentials in patients with Parkinson's disease. Archivos de neurobiologia. 1990;53(1):1–7. PubMed PMID: 2393335.
283. Gottlob I., Schneider E., Heider W., Skrandies W. Alteration of visual evoked potentials and electroretinograms in Parkinson's disease. Electroencephalography and clinical neurophysiology. 1987;66(4):349–357. PubMed PMID: 2435514.
284. Nightingale S., Mitchell K., Howe J. Visual evoked cortical potentials and pattern electroretinograms in Parkinson's disease and control subjects. Journal of Neurology, Neurosurgery & Psychiatry. 1986;49(11):1280–1287. PubMed PMID: 3794734.

285. Jaffe M., Bruno G., Campbell G., Lavine R., Karson C., Weinberger D. Ganzfeld electroretinographic findings in parkinsonism: untreated patients and the effect of levodopa intravenous infusion. Journal of Neurology, Neurosurgery & Psychiatry. 1987;50(7):847–852. PubMed PMID: 3625207.
286. Filipova M., Balik J., Filip V., Rodný J., Krejcova H. Electroretinographic changes in patients with parkinsonism treated with various classes of antiparkinsonian drugs. Activitas nervosa superior. 1979;21(3):136–138. PubMed PMID: 517077.
287. Fornaro P., Castrogiovanni P., Perossini M., Placidi G., Cavallacci G. Electroretinography (ERG) as a tool of investigation in human psychopharmacology. Electroretinographic changes induced by a combination of carbi-dopa and levo-dopa. Acta neurologica. 1980;2(4):293–299. PubMed PMID: 7211516.
288. Gottlob I., Weghaupt H., Vass C. Effect of levodopa on the human luminance electroretinogram. Investigative ophthalmology & visual science. 1990;31(7):1252–1258. PubMed PMID: 2365557.
289. Adachi-Usami E., Ikeda H., Satoh H. Haloperidol delays visually evoked cortical potentials but not electroretinograms in mice. Journal of Ocular Pharmacology and Therapeutics. 1990;6(3):203–210. PubMed PMID: 2290068.
290. Mizota, A. and E. Adachi-Usami, *Electroretinographic effects of haloperidol on the mouse retina.* Documenta ophthalmologica. 1993; 85(2):151-160.
291. Herrmann R., Heflin S.J., Hammond T., Lee B., Wang J., Gainetdinov R.R., Caron M.G., Eggers E.D., Frishman L.J., McCall M.A. Rod vision is controlled by dopamine-dependent sensitization of rod bipolar cells by GABA. Neuron. 2011;72(1):101–110. PubMed PMID: 21982372.
292. Smith B.J., Côté P.D., Tremblay F. Dopamine modulation of rod pathway signaling by suppression of GABAC feedback to rod-driven depolarizing bipolar cells. European Journal of Neuroscience. 2015;42(6):2258–2270. PubMed PMID: 26080286.
293. He Q., Xu H.-p., Wang P., Tian N. Dopamine D1 receptors regulate the light dependent development of retinal synaptic responses. PloS one. 2013;8(11) PubMed PMID: 24260267.
294. Lavoie J., Illiano P., Sotnikova T.D., Gainetdinov R.R., Beaulieu J.-M., Hébert M. The electroretinogram as a biomarker of central dopamine and serotonin: potential relevance to psychiatric disorders. Biological psychiatry. 2014;75(6):479–486. PubMed PMID: 23305992.
295. Feigenspan A., Teubner B., Willecke K., Weiler R. Expression of neuronal connexin36 in AII amacrine cells of the mammalian retina. Journal of Neuroscience. 2001;21(1):230–239. PubMed PMID: 11150340.
296. Mills S.L., O'Brien J.J., Li W., O'Brien J., Massey S.C. Rod pathways in the mammalian retina use connexin 36. Journal of Comparative Neurology. 2001;436(3):336–350. PubMed PMID: 11438934.
297. Deans M.R., Volgyi B., Goodenough D.A., Bloomfield S.A., Paul D.L. Connexin36 is essential for transmission of rod-mediated visual signals in the mammalian retina. Neuron. 2002;36(4):703–712. PubMed PMID: 12441058.
298. Meyer A., Hilgen G., Dorgau B., Sammler E.M., Weiler R., Monyer H., Dedek K., Hormuzdi S.G. AII amacrine cells discriminate between heterocellular and homocellular locations when assembling connexin36-containing gap junctions. Journal of cell science. 2014;127(6):1190–1202. PubMed PMID: 24463820.
299. Urschel S., Höher T., Schubert T., Alev C., Söhl G., Wörsdörfer P., Asahara T., Dermietzel R., Weiler R., Willecke K. Protein kinase A-mediated phosphorylation of connexin36 in mouse retina results in decreased gap junctional communication between AII amacrine cells. Journal of biological chemistry. 2006;281(44):33163–33171. PubMed PMID: 16956882.
300. Hampson E.C., Vaney D.D.I., Weiler R. Dopaminergic modulation of gap junction permeability between amacrine cells in mammalian retina. Journal of Neuroscience. 1992;12(12):4911–4922. PubMed PMID: 1281499.
301. Mills S.L., Massey S.C. Differential properties of two gap junctional pathways made by AII amacrine cells. Nature. 1995;377(6551):734–737. PubMed PMID: 7477263.
302. Xia X.-B., Mills S.L. Gap junctional regulatory mechanisms in the AII amacrine cell of the rabbit retina. Visual neuroscience. 2004;21(5):791–805. PubMed PMID: 15683564.

303. Kothmann W.W., Massey S.C., O'Brien J. Dopamine-stimulated dephosphorylation of connexin 36 mediates AII amacrine cell uncoupling. Journal of Neuroscience. 2009;29(47):14903–14911. PubMed PMID: 19940186.
304. Bloomfield S.A., Völgyi B. Function and plasticity of homologous coupling between AII amacrine cells. Vision research. 2004;44(28):3297–3306. PubMed PMID: 15535997.
305. Kothmann W.W., Trexler E.B., Whitaker C.M., Li W., Massey S.C., O'Brien J. Nonsynaptic NMDA receptors mediate activity-dependent plasticity of gap junctional coupling in the AII amacrine cell network. Journal of Neuroscience. 2012;32(20):6747–6759. PubMed PMID: 22593045.
306. Bloomfield S.A., Xin D., Osborne T. Light-induced modulation of coupling between AII amacrine cells in the rabbit retina. Visual neuroscience. 1997;14(3):565–576. PubMed PMID: 9194323.
307. Hu E.H., Pan F., Völgyi B., Bloomfield S.A. Light increases the gap junctional coupling of retinal ganglion cells. The Journal of physiology. 2010;588(21):4145–4163. PubMed PMID: 20819943.
308. Teranishi T., Negishi K. Double-staining of horizontal and amacrine cells by intracellular injection with lucifer yellow and biocytin in carp retina. Neuroscience. 1994;59(1):217–226. PubMed PMID: 7514770.
309. Bloomfield S.A., Völgyi B. The diverse functional roles and regulation of neuronal gap junctions in the retina. Nature Reviews Neuroscience. 2009;10(7):495–506. PubMed PMID: 19491906.
310. Mastronarde D.N. Correlated firing of cat retinal ganglion cells. I. Spontaneously active inputs to X-and Y-cells. Journal of Neurophysiology. 1983;49(2):303–324. PubMed PMID: 6300340.
311. Bu J.-Y., Li H., Gong H.-Q., Liang P.-J., Zhang P.-M. Gap junction permeability modulated by dopamine exerts effects on spatial and temporal correlation of retinal ganglion cells' firing activities. Journal of computational neuroscience. 2014;36(1):67–79. PubMed PMID: 23748559.
312. Li H., Liu W.-Z., Liang P.-J. Adaptation-dependent synchronous activity contributes to receptive field size change of bullfrog retinal ganglion cell. PLoS One. 2012;7(3) PubMed PMID: 22479604.
313. Li H., Liang P.-J. Stimulus discrimination via responses of retinal ganglion cells and dopamine-dependent modulation. Neuroscience bulletin. 2013;29(5):621–632. PubMed PMID: 23990220.
314. Xiao L., Zhang P.-M., Gong H.-Q., Liang P.-J. Effects of dopamine on response properties of ON-OFF RGCs in encoding stimulus durations. Frontiers in neural circuits. 2014;8:72. PubMed PMID: 25071453.
315. Cook P.B., McReynolds J.S. Modulation of sustained and transient lateral inhibitory mechanisms in the mudpuppy retina during light adaptation. Journal of neurophysiology. 1998;79(1):197–204. PubMed PMID: 9425191.
316. Liu Y., Lasater E.M. Calcium currents in turtle retinal ganglion cells. II. Dopamine modulation via a cyclic AMP-dependent mechanism. Journal of Neurophysiology. 1994;71(2):743–752. PubMed PMID: 8176436.
317. Hayashida Y., Ishida A.T. Dopamine receptor activation can reduce voltage-gated Na+ current by modulating both entry into and recovery from inactivation. Journal of neurophysiology. 2004;92(5):3134–3141. PubMed PMID: 15486428.
318. Vaquero C.F., Pignatelli A., Partida G.J., Ishida A.T. A dopamine-and protein kinase A-dependent mechanism for network adaptation in retinal ganglion cells. Journal of Neuroscience. 2001;21(21):8624–8635. PubMed PMID: 11606650.
319. Chen L., Yang X.-L. Hyperpolarization-activated cation current is involved in modulation of the excitability of rat retinal ganglion cells by dopamine. Neuroscience. 2007;150(2):299–308. PubMed PMID: 17942239.
320. Hayashida Y., Rodríguez C.V., Ogata G., Partida G.J., Oi H., Stradleigh T.W., Lee S.C., Colado A.F., Ishida A.T. Inhibition of adult rat retinal ganglion cells by D1-type dopamine receptor activation. Journal of Neuroscience. 2009;29(47):15001–15016. PubMed PMID: 19940196.
321. Ogata G., Stradleigh T.W., Partida G.J., Ishida A.T. Dopamine and full-field illumination activate D1 and D2-D5-type receptors in adult rat retinal ganglion cells. Journal of Comparative Neurology. 2012;520(17):4032–4049. PubMed PMID: 22678972.
322. Li Q., Wu N., Cui P., Gao F., Qian W.-J., Miao Y., Sun X.-H., Wang Z. Suppression of outward K+ currents by activating dopamine D1 receptors in rat retinal ganglion cells through PKA and CaMKII signaling pathways. Brain research. 2016;1635:95–104. PubMed PMID: 26826585.

323. Cui P., Li X.-Y., Zhao Y., Li Q., Gao F., Li L.-Z., Yin N., Sun X.-H., Wang Z. Activation of dopamine D1 receptors enhances the temporal summation and excitability of rat retinal ganglion cells. Neuroscience. 2017;355:71–83. PubMed PMID: 28499973.
324. Van Hook M.J., Wong K.Y., Berson D.M. Dopaminergic modulation of ganglion-cell photoreceptors in rat. European Journal of Neuroscience. 2012;35(4):507–518. PubMed PMID: 22304466.
325. Ikeda H., Priest T., Robbins J., Wakakuwa K. Silent dopaminergic synapse at feline retinal ganglion -cells. Clinical Vision Sciences. 1986;1(1):25–38.
326. Straschill M., Perwein J. The inhibition of retinal ganglion cells by catecholeamines and γ-aminobutyric acid. Pflügers Archiv. 1969;312(3):45–54. PubMed PMID: 5388469.
327. Thier P., Alder V. Action of iontophoretically applied dopamine on cat retinal ganglion cells. Brain research. 1984;292(1):109–121. PubMed PMID: 6697199.
328. Maguire G., Hamasaki D. The retinal dopamine network alters the adaptational properties of retinal ganglion cells in the cat. Journal of Neurophysiology. 1994;72(2):730–741. PubMed PMID: 7983531.
329. Maguire G.W., Smith E. 3rd. Cat retinal ganglion cell receptive-field alterations after 6-hydroxydopamine induced dopaminergic amacrine cell lesions. Journal of neurophysiology. 1985;53(6):1431–1443. PubMed PMID: 2861256.
330. Ames A. 3rd, Pollen D. Neurotransmission in central nervous tissue: a study of isolated rabbit retina. Journal of Neurophysiology. 1969;32(3):424–442. PubMed PMID: 4308417.
331. Jensen R., Daw N. Effects of dopamine and its agonists and antagonists on the receptive field properties of ganglion cells in the rabbit retina. Neuroscience. 1986;17(3):837–855. PubMed PMID: 3703255.
332. Jensen R.J., Daw N.W. Towards an understanding of the role of dopamine in the mammalian retina. Vision research. 1983;23(11):1293–1298. PubMed PMID: 6659376.
333. Jensen R.J., Daw N.W. Effects of dopamine antagonists on receptive fields of brisk cells and directionally selective cells in the rabbit retina. Journal of Neuroscience. 1984;4(12):2972–2985. PubMed PMID: 6502216.
334. Yang J., Pahng J., Wang G.Y. Dopamine modulates the off pathway in light-adapted mouse retina. Journal of neuroscience research. 2013;91(1):138–150. PubMed PMID: 23023788.
335. Jensen R. Effects of dopamine D2-like receptor antagonists on light responses of ganglion cells in wild-type and P23H rat retinas. PloS one. 2015;10(12) PubMed PMID: 26717015.
336. O'Brien J. The ever-changing electrical synapse. Current opinion in neurobiology. 2014;29:64–72. PubMed PMID: 24955544.

Phototransduction and Photoreceptor Synaptic Pathways

Phototransduction in Rods and Cones

Yingbin Fu, PhD[1]

Created: April 1, 2010.

1. Introduction

Vertebrates rely on retinal rods and cones for the conventional, image-forming vision while non-image-forming vision is mediated by intrinsically photosensitive retinal ganglion cells (ipRGCs) (see chapter on Melanopsin Ganglion Cells). Rods are specialized for low-light vision. They are extremely sensitive and can signal the absorption of single photons. Cones mediate daylight vision (Figure 1). They are much less sensitive to light than rods, but have higher temporal resolution. They also mediate color vision by several cone types with different pigment spectra sensitivity.

Great progress has been made in understanding rod phototransduction since the introduction of the suction-electrode recording technique in the late 1970s (1). Individual amphibian and mammalian (including primate) photoreceptors can be recorded with this method. Bovine retina, on the other hand, has been a favorite preparation for studying phototransduction by biochemists because of the abundance of tissue available. The mouse, however, has become an increasingly popular animal model for study in the past decade through the advent of gene-targeting techniques. When combined with electrophysiology, mouse genetics provides unmatched power in elucidating the in vivo functions of key phototransduction proteins, most of which have been knocked out, overexpressed or mutated in rods, yielding a rich body of information on the mechanisms underlying the amplification, recovery and adaptation of rod/cone photoresponses (Table 1, Figure 2, Figure 3).

I shall first give a brief description of the structure and the development of mouse photoreceptors, followed by a summary of recent studies on rod phototransduction with emphasis on information gleaned from mouse models. Finally, a recent advance in studying mouse cones will be mentioned.

Author Affiliation: 1 University of Utah.

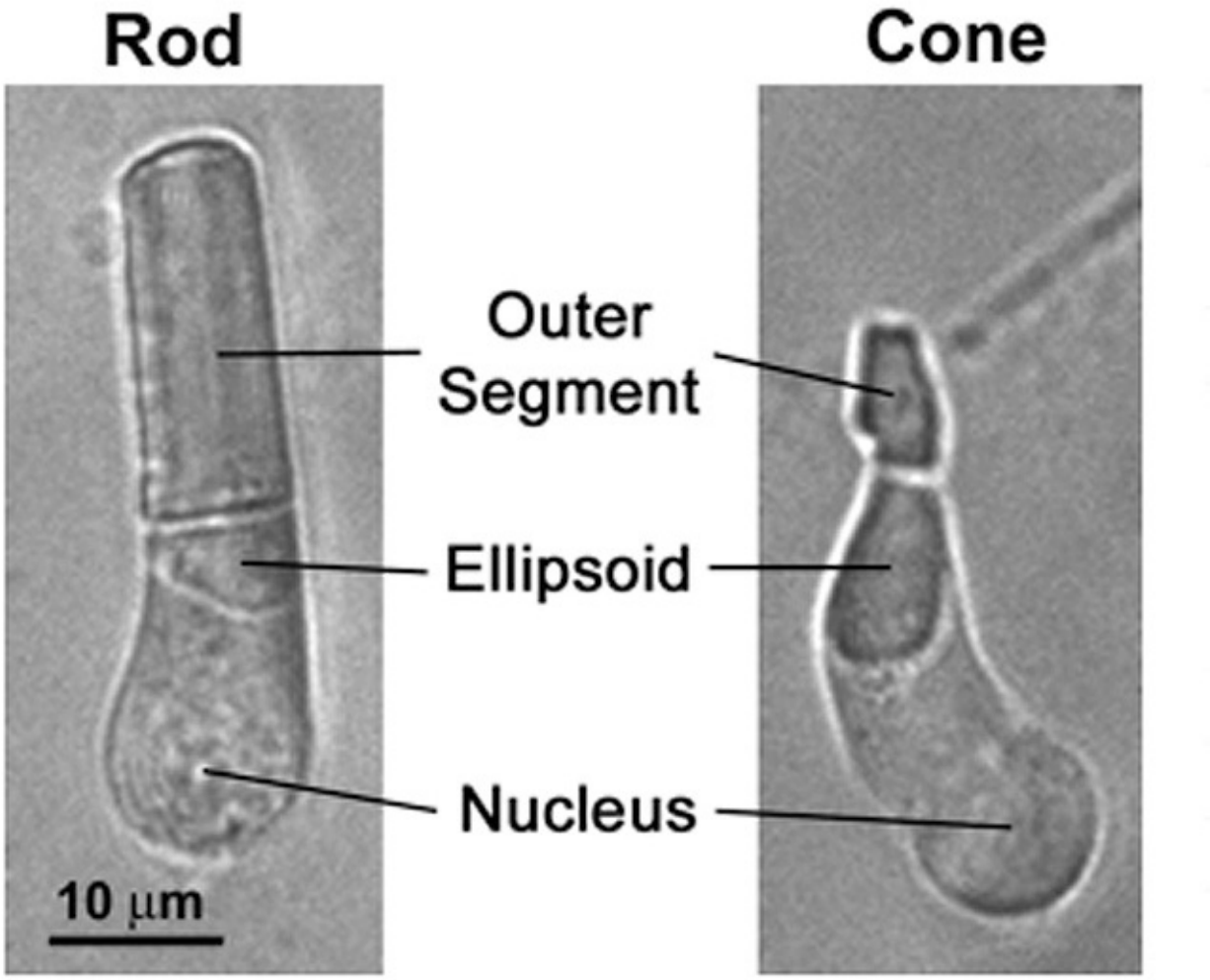

Figure 1. Brightfield images of living rod and cone photoreceptors isolated from a salamander retina. Phototransduction takes place in the outer segment, while the ellipsoid is densely packed with mitochondria. Rods are responsible for dim light vision, cones for bright light vision. Courtesy of Yiannis Koutalos.

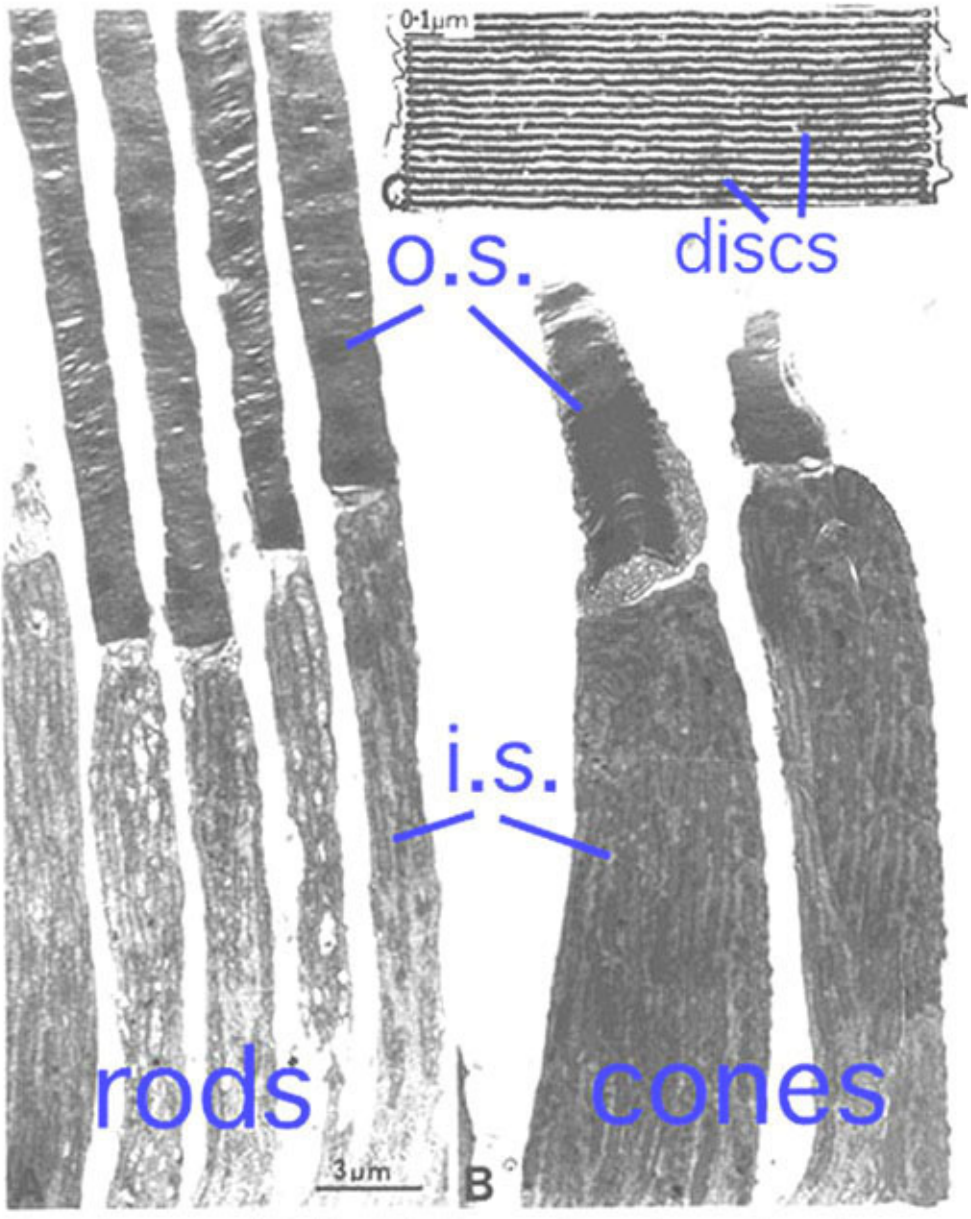

Figure 2. Low magnification EM image of monkey rods and cones with an enlargement of the outer segment discs.

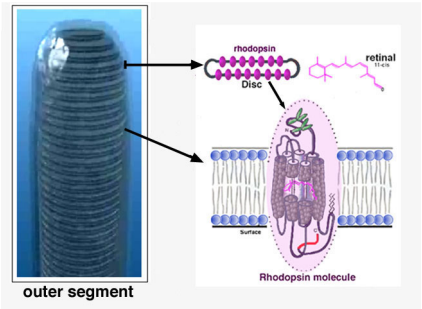

Figure 3. Schematic diagram of rhodopsin in the outer segment discs. When the outer segments are magnified further, stacked membrane disks are visible inside. The disks are studded with thousands of rhodopsin complexes. Each rhodopsin consists of a membrane-traversing protein with a retinal molecule embedded in its core.

Table 1. List of major proteins involved in mouse rod and cone phototransductions that have been knocked out, overexpressed or mutated.

Proteins	Manipulation	Phenotype	References
Rhodopsin	knockout	no ROS formation, no rod photoresponse	Humphries et al., 1997; Lem et al., 1999 (3, 4)
Transducin $G\alpha_{t1}$	knockout	no rod photoresponse	Calvert et al., 2000 (85)
Transducin $G\alpha_{\gamma 1}$	knockout	down regulation of $G\alpha_{t1}$ & $G_{\beta 1}$, reduced rod sensitivity, retinal degeneration	Lobanova et al., 2008 (210)
Transducin $G\alpha_{\gamma 1}$	S70L mutation	deficit in light adaptation in rods	Kassai et al., 2005 (90)
phosducin	knockout	reduced rod sensitivity	Krispel et al., 2007 (211)
PDE_{β}	mutation	rd mouse, retinal degeneration	Bowes et al., 1990; Pittler and Baehr, 1991(105, 106)
PDE_{γ}	knockout	reduced PDE activity, retinal degeneration	Tsang et al., 1996 (102)
PDE_{γ}	overexpression	reduced gain, accelerated shutoff in rods	Tsang et al., 2006 (212)
PDE_{γ}	W70A	reduced sensitivity, slow shutoff in rods	Tsang et al., 1998 (109)
CNGB1	knockout	no rod photoresponse, retinal degeneration	Huttl et al., 2005; Zhang et al., 2009 (127, 213)
CNGA3	knockout	no cone photoresponse, slow cone degeneration	Biel et al., 1999a (121)
GRK1	knockout	slow shutoff in rods & cones	Chen et al., 1999; Nikonov et al., 2005 (139, 146)
GRK1	overexpression	normal rod photoresponse	Krispel et al., 2006 (77)
Arrestin1	knockout	slow shutoff in rods	Xu et al., 1997 (155)
Arrestin1& 42	Double knockout	slow shutoff in rods and cones	Nikonov et al., 2008 (168)
Recoverin	knockout	reduced rod sensitivity, decreased signal transfer between rods and rod bipolar cells	Makino et al., 2004; Sampath et al., 2005 (154, 214)
RGS9-13	overexpression	accelerated shutoff in rods	Krispel et al., 2006 (77)
RGS9-1	knockout	slow shutoff in rods and cones	Chen et al., 2000; Lyubarsky et al., 2001 (172, 215)
Gβ5-L	knockout	same as RGS9-1 knockout	Krispel et al., 2003b (180)
R9AP	knockout	same as RGS9-1 knockout	Keresztes et al., 2004 (174)
GC1	knockout	normal rod response, no cone response, cone dystrophy	Baehr et al., 2007; Yang et al., 1999 (187, 188)
GC2	knockout	Normal rod & cone responses	Baehr et al., 2007 (187)
GC1 & 2	Double knockout	No light response in rods & cones, cone degeneration	Baehr et al., 2007 (187)
GCAP2	knockout	Rods recover more slowly, more sensitive to flashes, saturate at lower intensities	Makino et al., 2008 (200)

Table 1. continued from previous page.

GCAP1 & 2	Double knockout	larger amplitude, delayed recovery in rods and cones	Mendez et al., 2001; Pennesi et al., 2003 (193, 199)

1 Due to space limitation, not all the genetically engineered mouse lines are listed. For those included, only the most salient phenotypes are listed, please refer to the text for more complete description.
2 Arrestin4 is also called cone arrestin or X-arrestin (168, 216).
3 RGS9-1 overexpression was achieved by overexpressing R9AP, which resulted in overexpression of all three components of the GAP complex, RGS9-1, Gβ5-L and R9AP.

2. Structure of rods and cones.

Rods constitute ~97% of mouse retinal photoreceptors, with cones accounting for the remainder (2). The mouse photoreceptors are broadly similar to primate photoreceptors in physical dimensions (Table 2, Figure 2). The outer segment is about 1.4 μm in diameter and 24 μm in length for rods, and, correspondingly, about 1.2 μm and 13 μm for cones. These dimensions are significantly smaller than those of amphibian photoreceptors (Figure 1), which explain physiologists' longtime favor for the latter.

Rods and cones have four primary structural/functional regions: outer segment, inner segment, cell body and synaptic terminal. The outer segment is connected to the inner segment through a thin connecting cilium. The outer segment is filled with a dense stack of membrane discs (Figure 2 and Figure 3), spaced at intervals of about 28 nm. The discs carry the visual pigment (rhodopsin in rods and cone pigment in cones) and other transduction components either as transmembrane or peripheral membrane proteins (Figure 3). Visual pigment is the most abundant protein in the outer segment. The importance of visual pigment as a major structural component is demonstrated by the rhodopsin-knockout mouse, the rod outer segments of which fail to form (3, 4). The rod photoreceptors of this mouse degenerate, followed suit by cones. The packing density of pigment molecules on the discs is remarkably uniform across different vertebrate species, being ~25000 mm^2, corresponding to a concentration of ~ 3mM (5). The total number of pigment molecules in the outer segment can thus be calculated roughly from its envelope volume. The dense stack of discs greatly increases the probability of photon capture. An interesting difference between rods and cones is that the rod discs (except for the nascent discs at the base of the outer segment) are completely internalized and therefore physically separate from the plasma membrane, whereas the cone discs remain as foldings of the plasma membrane. The open cone discs offer a much larger surface area for rapid fluxes of substances between the cell exterior and interior, such as chromophore transfer for pigment regeneration and fast calcium dynamics during light adaptation.

The inner segment contains the endoplasmic reticulum and the Golgi apparatus. It is also packed with mitochondria immediately adjacent to the outer segment (Figure 2, Figure 3) in order to meet the high demand for metabolic energy associated with phototransduction. All proteins destined for the outer segment must pass through a narrow connecting cilium between the outer and the inner segments.

The synaptic terminal transmits the light signal to the second-order neurons in the retina: the bipolar and horizontal cells. In darkness, there is a steady inward current (the "dark current") through a cation conductance on the outer-segment membrane (6), depolarizing the rod or cone and maintaining a steady synaptic release of glutamate. Light closes this cation conductance (the "light-sensitive" conductance, consisting of cGMP-gated channels) to stop the dark current and produce a membrane hyperpolarization as the response. This hyperpolarization decreases or terminates the dark glutamate release. The signal is further processed by other neurons in the retina before being transmitted to higher centers in the brain.

Table 2. Physical dimensions of the outer segment of mouse rods and cones. Salamander and primate photoreceptors are included for comparison purpose.

		Rods			Cones	

Table 2. continued from previous page.

	Mouse	Primate	Salamander	Mouse	Primate	Salamander
Length (μm)	23.6	25	22	13.4	13	8
Diameter[a] (μm)	1.4	2	11	1.2	3_{base}, 1_{tip}	4_{base}, 2.5_{tip}
Volume (μm^3)	36	40	2000	14	30	70
References	Carter-Dawson and LaVail, 1979 (2)	Baylor et al., 1984 (217)	Baylor and Nunn, 1986 (218)	Carter-Dawson and LaVail, 1979 (2)	Pugh and Lamb, 2000 (101)	Pugh and Lamb, 2000 (101)

3. Can we see a single photon?

The minimum number of photons required to produce a visual effect was first successfully determined by Hecht, Schlaer and Pirenne in a landmark experiment (7). Human subjects were allowed to stay in the dark for 30 minutes to have optimal visual sensitivity. The stimulus was presented 20 degrees to the left of the point of focus so that the light would fall on the region of the retina with the highest concentration of rods. The stimulus was a circle of red light with a diameter of 10 minutes (1 minute=1/60th of a degree). The subjects were asked whether they had seen a flash. The light was gradually reduced in intensity until the subjects could only guess the answer. It was found that between 54 and 148 photons were required in order to elicit visual experience. After corrections for corneal reflection (4%), ocular media absorption (50%) and photons passed through retina (80%), only 5 to 14 photons were actually absorbed by the retinal rods. The small number of photons in comparison with the large number of rods (500) involved makes it very unlikely that any rod will take up more than one photon. Therefore, one photon must be absorbed by each of 5 to 14 rods in the retina to produce a visual effect.

In the same publication (7), Hecht and co-workers determined the visual threshold of human vision by the famous "frequency-of-seeing-curves" experiment. The theory is that photon absorptions vary according to a Poisson probability distribution. If *a* is the average number of photons absorbed per flash, the probability Pn that any number *n* will be absorbed is: $Pn = a^n/(e^a n!)$. Some of these Possson integral curves (n from 1 to 9) are shown in Figure 4. By measuring the frequency of seeing against the logarithm of the brightness experimentally, one can fit the experimental curve with one of the probability distribution in Figure 4b to reveal the value *n*, which lies between 5 and 8 (Figure 4b). This agrees well with the value 5 to 14 photons absorbed by rods!

4. Development of mouse photoreceptors

Rods and cones renew their outer segments continually (8, 9). Newly formed disks at the base of the outer segment progressively displace previously synthesized disks toward the apical end. The disks reaching the apex of the outer segment are shed and phagocytosed on a daily basis by the adjacent retinal pigment epithelium (RPE) (10). The rate of formation and disposal of the disks are roughly equal so that a constant outer-segment length is maintained in the adult retina.

The mouse rod outer segment (ROS) changes little in diameter during development, but it elongates at a rapid and almost linear rate from postnatal day (P) 11 to 17, reaching adult length by P19-25 (11). The increase in ROS length parallels the almost linear rise in rhodopsin content from P8 to P23 (12). At the peak rate of growth during P13-P17, ~120 disks are synthesized per day compared with 75 disks in adult retina (8, 11).

The dark current recorded in developing mouse rods increases roughly in direct proportion to the length of the mouse ROS between P12 (around the time of eye-opening in neonate) and P45 (adult) (13). The kinetics of the dim-flash response changes rather little during development and the flash sensitivity of rods increases by approximately 1.5-fold, reflecting the presence in neonatal rods of a small percentage (~1%) of free opsin (i.e.

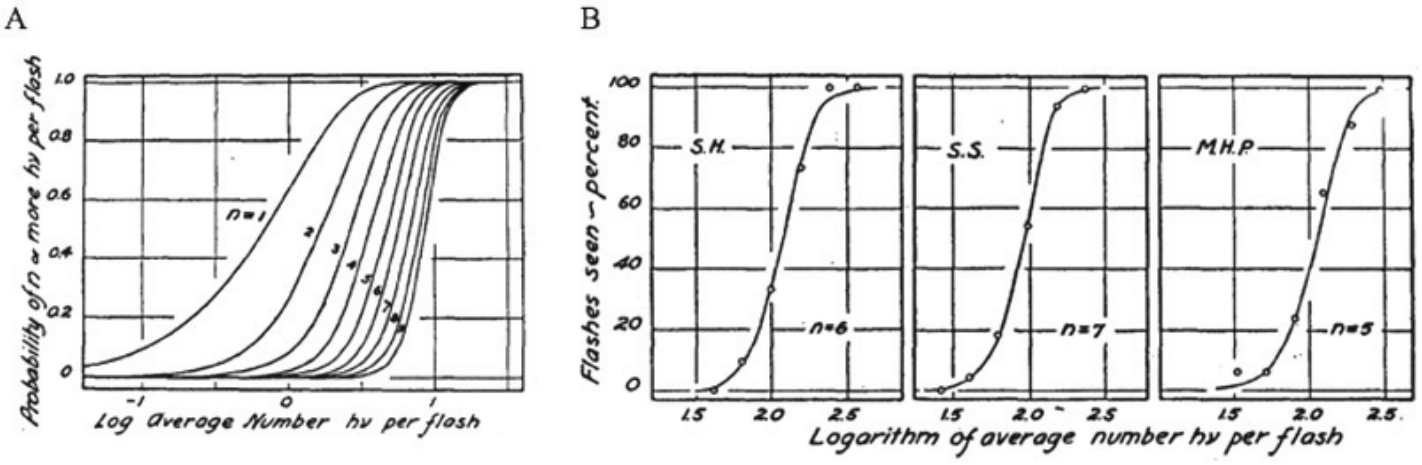

Figure 4. Frequency of seeing curve experiment. (A) Poisson probability distribution. For any average number of quanta (hv) per flash, the ordinates give the probabilities that the flash will deliver to the retina *n* or more photons, depending on the value assumed for *n*. (B) Relation between the average energy content of a flash of light (in number of (hv)) and the frequency with which it is seen by three observers. From Figs. 6 & 7 of Hecht et al (7).

devoid of chromophore) even after overnight dark-adaptation. The constitutive activity of this small amount of opsin mildly triggers adaptation mechanisms and therefore causes a small reduction in the sensitivity of the cell (see later). A similar small, age-dependent increase in rod sensitivity was found for rat. Previously, a 50-fold increase in rod sensitivity was reported for rat from neonate to adulthood (14), but now this appears to be incorrect.

5. Vertebrate rods are highly efficient photon detectors

Psychophysical experiments performed by Hecht, Schlaer and Pirenne in 1942 suggested that human retinal rods can detect single photons (7) (Figure 4). Thirty seven years later, suction pipette recordings from isolated toad rods by Baylor, Lamb and Yau confirmed this remarkable ability of vertebrate rods (Figure 5) (15). The amazing ability of vertebrate rods to detect single photons can be attributed to at least three factors: high quantum efficiency of photoactivation, low intrinsic noise, and a powerful signal amplification cascade. Two other factors greatly increase the photon capture ability of vertebrate rods, numerical dominance of rods over cones and a highly specialized outer segment structure. The dense stack of discs of the rod outer segment ensures that virtually every photon traveling axially will be captured. In a sense, vertebrate rods can be viewed as sophisticated three-dimensional photon capture devices.

6. Phototransduction in rods: a G-protein-signaling pathway

Rod phototransduction is one of the best-characterized G-protein-signaling pathways (Figure 6, Figure 7, Figure 8). The receptor is rhodopsin (R), the G protein is transducin (G), and the effector is cGMP phosphodiesterase (PDE or PDE6). Upon photon absorption, the rhodopsin molecule becomes enzymatically active (R*) and catalyzes the activation of the G protein transducin to G*. Transducin, in turn, activates the effector phosphodiesterase (PDE) to PDE*. PDE* hydrolyzes the diffusible messenger cGMP. The resulting decrease in the cytoplasmic free cGMP concentration leads to the closure of the cGMP-gated channels on the plasma membrane. Channel closure leads to localized reduction on the influx of cations into the outer segment, which results in membrane hyperpolarization, i.e. the intracellular voltage becoming more negative (Figures 6).) This hyperpolarization decreases or terminates the dark glutamate release at the synaptic terminal. The signal is further processed by other neurons in the retina before being transmitted to higher centers in the brain.

This phototransduction cascade is shown in Figures 6 and 7.

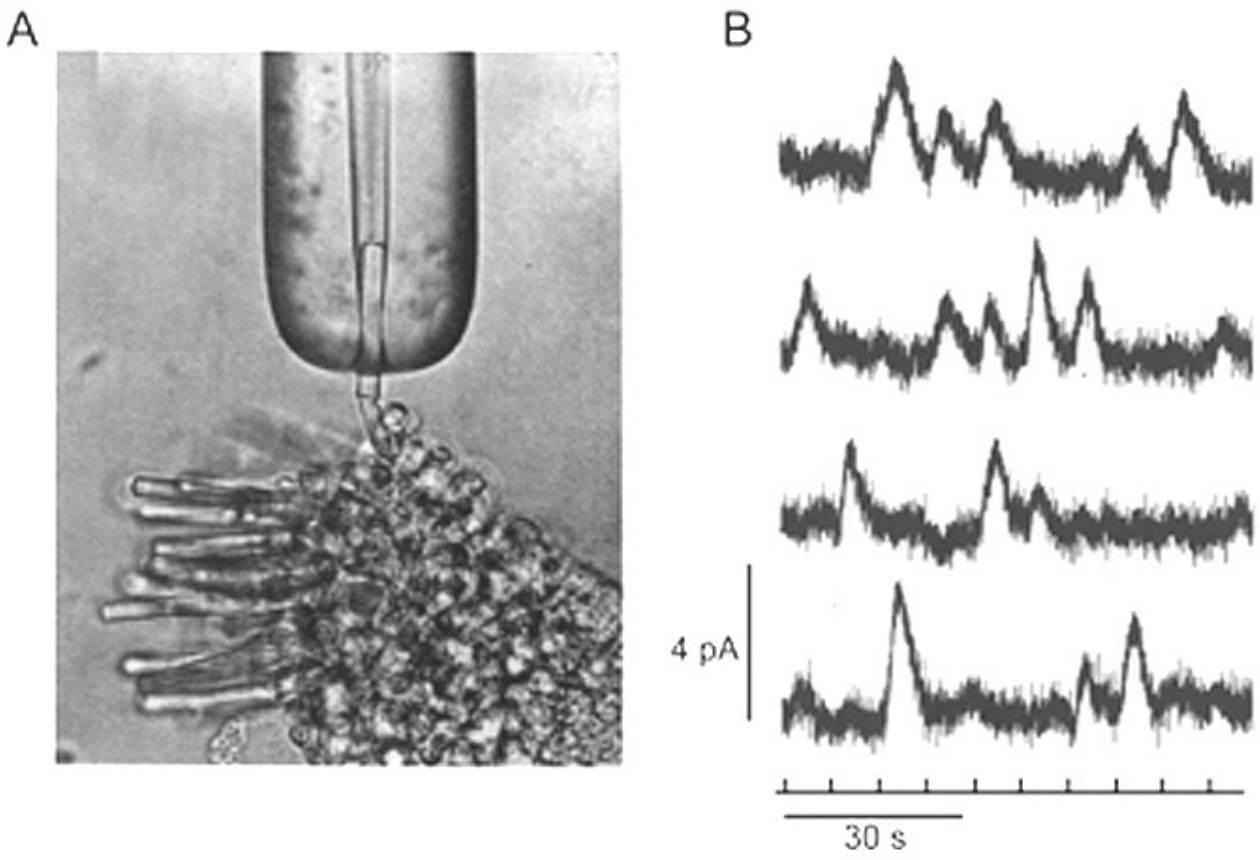

Figure 5. Suction-electrode recording on the membrane current of a single toad rod. (A) The outer segment of a rod projecting from a piece of retina was sucked in position in a suction electrode. Proximal end of cell remains attached to retina. Boundary between inner and outer segments is visible. (B) Response of rod outer segment to a series of 40 consecutive dim flashes. 20 msec flash delivering 0.029 photons μm^{-2} at 500 nm, flash timing monitored below. The rod showed no response to some flashes, or a small response of ~ 1 pA to others, and occasionally a larger response. This suggests that the flash response is quantized, as might be expected when on average very few photons are absorbed. With further analysis, the authors demonstrated that each quantal electrical event resulted from a single photo-isomerization with mean amplitude of ~ 1 pA - the single-photon response. Modified from Baylor et al. (15)

Following light activation, a timely recovery of the photoreceptor is essential so that it can respond to subsequently absorbed photons, and signal rapid changes in illumination (Figure 8). This recovery from light requires the efficient inactivation of each of the activated components: R*, G*, and PDE*, as well as the efficient regeneration of rhodopsin (R) and the rapid restoration of the cGMP concentration. The termination rates of the activation steps set the time course of the photoresponse.

Although rod phototransduction is the best characterized sensory transduction pathway, rods differ from other sensory cells in that light leads to hyperpolarization rather than depolarization. Rods respond to light with graded hyperpolarization whose amplitude increases monotonically as a function of flash intensity until saturation. One hallmark of rod phototransduction is the reproducibility of its single-photon response in both amplitude and kinetics. This is quite remarkable considering the fact that events generated by single molecules are stochastic in nature. The study on the underlying mechanisms has long been a hot topic in the vision field. Recent research pointed to two possible mechanisms: 1. Rhodopsin inactivation is averaged over multiple shutoff steps so that the integrated R* activity varies less than otherwise controlled by a single step. 2. Averaging over the deactivation of multiple G protein molecules is important for the constancy in response decay.

The details of the activation phase of rod phototransduction are now well established. A quantitative description is achieved that reproduces the activation kinetics of the rod response under physiological conditions (16-19).

We shall discuss below the major proteins mediating the activation phase in mouse rods - visual pigment, transducin, the effector PDE, and the cGMP-gated channel. The focus will be on studies with combined approaches from mouse genetics and physiology.

7. Visual Pigments of Mouse Rods and Cones

Mouse has a single rod pigment, rhodopsin, and two cone pigments: S- and M- cone pigments, with maximal spectral sensitivity at 360 nm and 508 nm, respectively. Mouse is unusual in that individual cones express both S- and M-cone pigments, with the M-pigment level decreasing in a gradient from dorsal to ventral retina (20).

Mouse rhodopsin and cone pigments belong to the super family of G-protein coupled receptors (GPCRs). A high-resolution (2.8 Å), three-dimensional structure of the ground state of bovine rhodopsin was determined in 2000 by Palczewski et al. (Figure 9a) (21, 22). The future challenge is to solve the structure of cone pigments, which is much more unstable than rhodopsin.

Visual pigments from most vertebrate species, including mammals, use 11-cis-retinal (denoted A1), while those from many water-based animals use 11-cis-3,4-dehydroretinal (denoted A2), as their natural ligand (23-25). George Wald first identified vitamin A in the retina (26) and later showed how it functions with light, which forms the molecular basis of vision (Nobel Prize 1967). The chromophore is covalently bound via a Schiff-base linkage to a conserved lysine residue (K296 in mammalian rhodopsin) in the seventh transmembrane helix (Figure 9a and 9b). In darkness, the 11-cis-retinal acts as an inverse agonist to lock rhodopsin in an inactive state by preventing free opsin from activating the transduction cascade. The "locking" role of 11-cis-retinal as was clearly demonstrated in RPE65-null mice. RPE65 functions as an isomerase in the RPE visual cycle, which is important for regenerating rod and cone pigments. $Rpe65^{-/-}$ retina has virtually no 11-cis-retinal (27). Rod photoreceptors degenerate slowly due to the constant activation of phototransduction by the large amount of free rod opsin. This degeneration can be prevented by deleting the transducin α-subunit, which blocks the activation of the downstream cascade (28). In a separate experiment, K296 is mutated to glutamic acid, producing an opsin with no chromophore-binding site (29). Although the K296E opsin constitutively activates transducin in vitro, the constitutive activity of the mutant opsin in vivo was turned off due to phosphorylation by rhodopsin kinase followed by arrestin binding (see R* termination).

Even with 11-cis-retinal attached, rhodopsin occasionally undergoes spontaneous (thermal) activation in the dark, producing responses identical to those triggered by photons (30). Spontaneous activation of visual pigment molecules sets an ultimate limit on visual sensitivity (31-34). In a toad rod, the rate of thermal activation of rhodopsin was measured to be 0.031 $s^{-1}rod^{-1}$ at 22 (C, corresponding to an average wait of 2000 years for the spontaneous activation of a given rhodopsin molecule to occur, based on a total of $2x10^9$ rhodopsin molecules per cell (35). This great stability makes it possible for rods to pack many rhodopsin molecules to the rod discs to increase their photon-capture ability while keeping the dark noise low. In wild-type mouse rods, it is rather difficult to measure the discrete noise arising from the thermal activation of rhodopsin because of the relatively small amplitude of the single-photon response. However, the measurement has been achieved with $GCAPs^{-/-}$ rods (36), the single-photon response of which is nearly five times that of wild type as a result of the elimination of the Ca^{2+}-mediated negative feedback on guanylate cyclase (see later). The rate is ~0.012 $s^{-1}rod^{-1}$ at 36°C.

It should be mentioned that the question of dark noise in vision has had a long intellectual history from the point of view of psychophysics and system neuroscience. As early as 1940s and 1950s, Hecht and Barlow have estimated the amount of "dark light" in human rods based on psychophysical experiments (7, 37). More than 30 years later, Baylor and colleagues used suction-pipette recording technique on primate rods to demonstrate that the very low quantal noise from rhodopsin, corresponding to ~ 0.01 event s^{-1} rod^{-1} in darkness), indeed matches the human psychophysical scotopic threshold. The quantitative agreement between the quantal noise measured from single rods and that measured in human psychophysics was considered a breakthrough in the

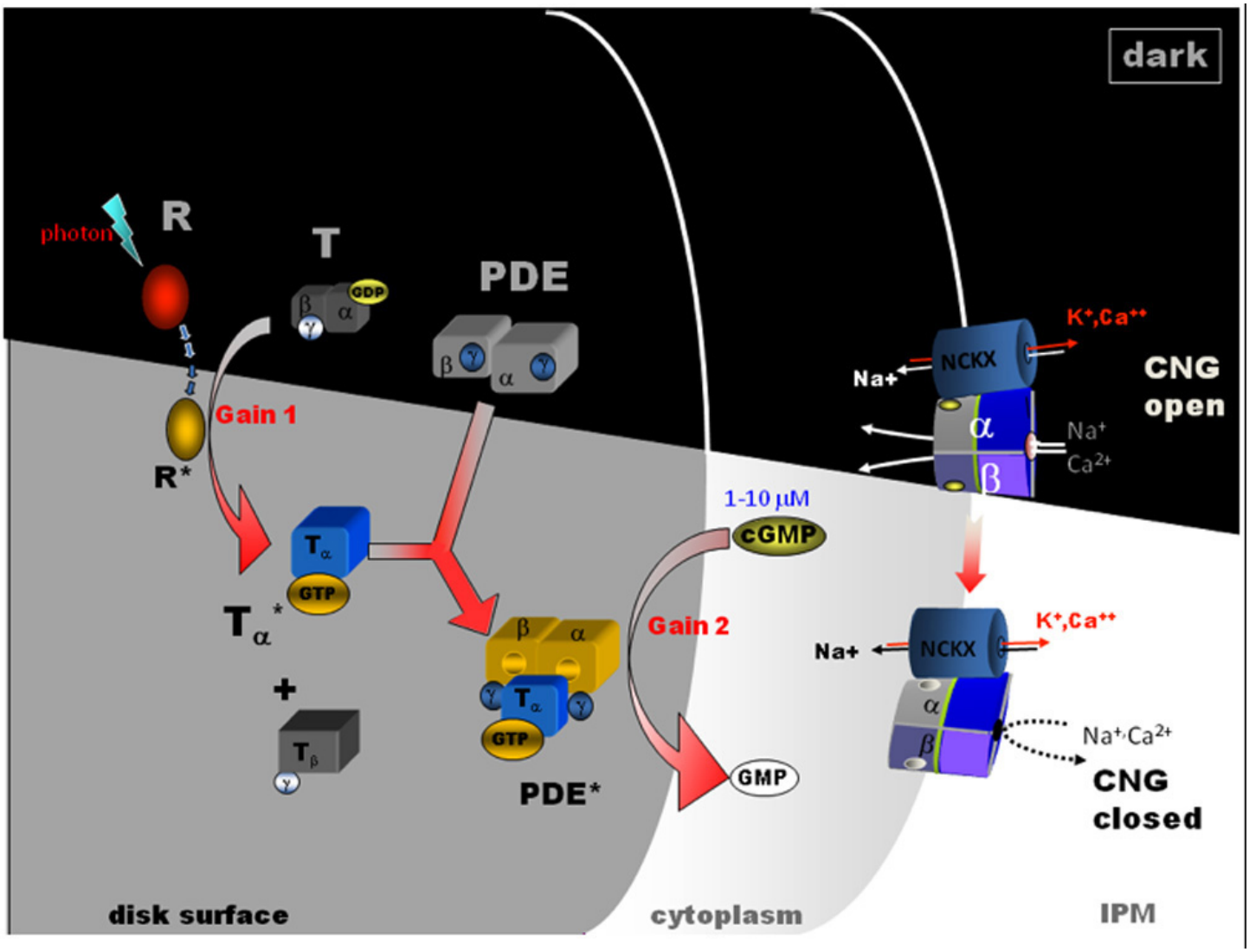

Figure 6. Activation of rod phototransduction cascade that results in the closure of cGMP-gated channels on the plasma membrane (from dark to light state). R, rhodopsin (inactive); R*, rhodopsin (active); T, transducin; PDE, phosphodiesterase (inactive); PDE*, phosphodiesterase (active); NCKX, Na/Ca,K exchanger. IPM, interphotoreceptor matrix. Courtesy of Wolfgang Baehr.

vision field and a wonderful convergence between cell physiology and human psychophysics/systems neuroscience - the goal of modern neuroscience after all!

Red cone pigment is much more prone to spontaneous isomerization than rhodopsin (38, 39), but it is difficult to measure the rate from native cones (38). By expressing human red cone pigment transgenically in GCAPs$^{-/-}$ rods, the rate of human red cone pigment was found to be surprisingly low at ~10 $s^{-1}cone^{-1}$ (molecular rate constant ~1.35 x 10^{-7} sec^{-1}) (40), almost 1000-fold lower than the overall dark transduction noise previously reported in primate cones (41, 42). Thus, the overwhelming amount of dark noise in the primate red cone originates not from spontaneous isomerization of the pigment, but most probably from constitutive activity in the downstream phototransduction steps, such as the phosphodiesterase (43).

The molecular rate constant for thermal isomerization of A2 human red cone pigment was determined to be ~5.6 x 10^{-6} sec^{-1} by expressing human red cone pigment in Xenopus rods (38). Since mammals use A1 chromophore, A1 red cone pigment is perhaps 40-fold less prone to spontaneous isomerization than the A2 form (40). This is likely due to the fact that the A2 chromophore has an additional double bond in the β-ionone ring, which has been suggested to lower the energy barrier for isomerization (44). Consequently, this introduces

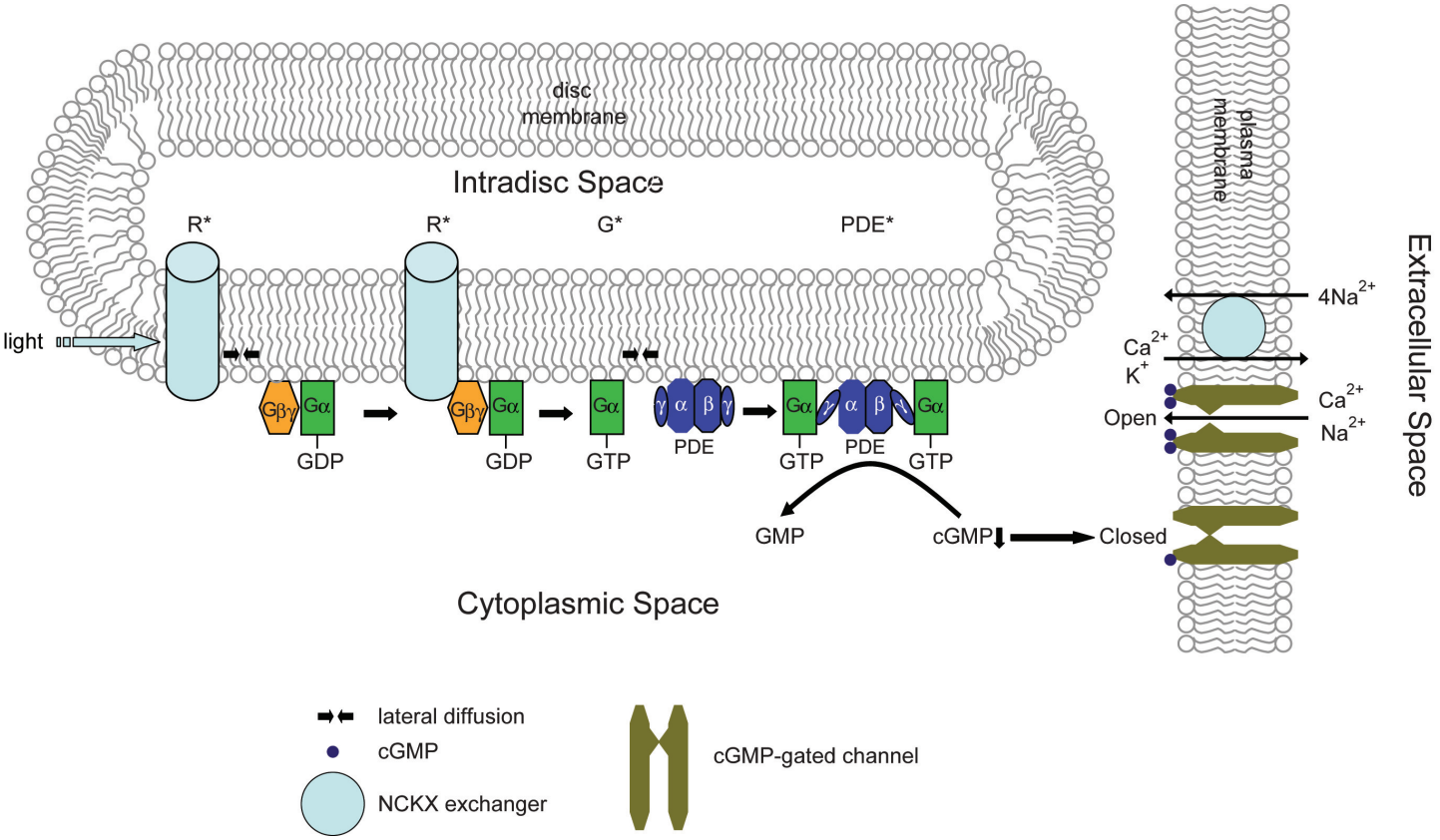

Figure 7. Schematic representation on the activation of vertebrate rod phototransduction. Following photon absorption, the activated rhodopsin (R*) activates the heterotrimeric G protein, catalyzing the exchange of GDP for GTP, producing the active Gα*-GTP. Two Gα*-GTP bind to the two inhibitory (subunits of PDE, thereby releasing the inhibition on the catalytic α and β subunits, forming PDE*, which in turn catalyzes the hydrolysis of cGMP. The consequent decrease in the cytoplasmic free cGMP concentration leads to the closure of the cGMP-gated channels on the plasma membrane and blockage of the influx of cations into the outer segment, which results in the reduction of the circulating dark current.

a red shift in absorption (45) and decreases the thermal stability of the A2 pigment. Incidentally, A1 rhodopsin was found to be 30 times more stable than A2 rhodopsin, rather similar to the finding for red cone pigment (46). More importantly, unlike in lower vertebrates such as salamander where A2 red cone pigment is sufficiently noisy as to impose a potential adaptational influence on cones even in darkness (38, 39, 47), A1 red cone pigment (and likewise for green and blue cone pigments) in primates and presumably other mammals should be quiet enough to have hardly any adaptational influence on cone sensitivity. In other words, the much lower absolute sensitivity of mammalian cones compared to mammalian rods appears to arise not from quantal noise in the pigments themselves, but from other phototransduction steps (48-50). This may explain why primate red, green and blue cones, unlike their amphibian counterparts (51, 52), all have similar sensitivities irrespective of their difference in visual pigments (41).

Photon absorption by 11-cis-retinal triggers the cis-to-trans isomerization of the retinoid chromophore (53, 54). As early as in the 1930s-1950s, vision scientists knew that rhodopsin bleaches in stages over intermediates that were short-lived at room temperature, yet stable at low temperatures (55-57), (Figure 10). Hubbard and Kropf measured the "bleaching intermediates (a mixture of lumirhodopsin and metarhodopsin) " by spectrophotometry at -17 °C (58). Photo-isomerization rapidly converts the ligand from a powerful inverse agonist to a powerful agonist, leading to the formation of a series of spectrally distinct intermediates of rhodopsin in the order of bathorhodopsin, lumirhodopsin, metarhodopsin I (Meta I), and metarhodopsin II (Meta II) within a few millisecond (Figure 10) (reviewed in Okada and Palczewski, 2001 (59)). Meta II is the active form of rhodopsin (R*), which in turn decays to the inactive Meta III. The Meta-II state of cone pigment

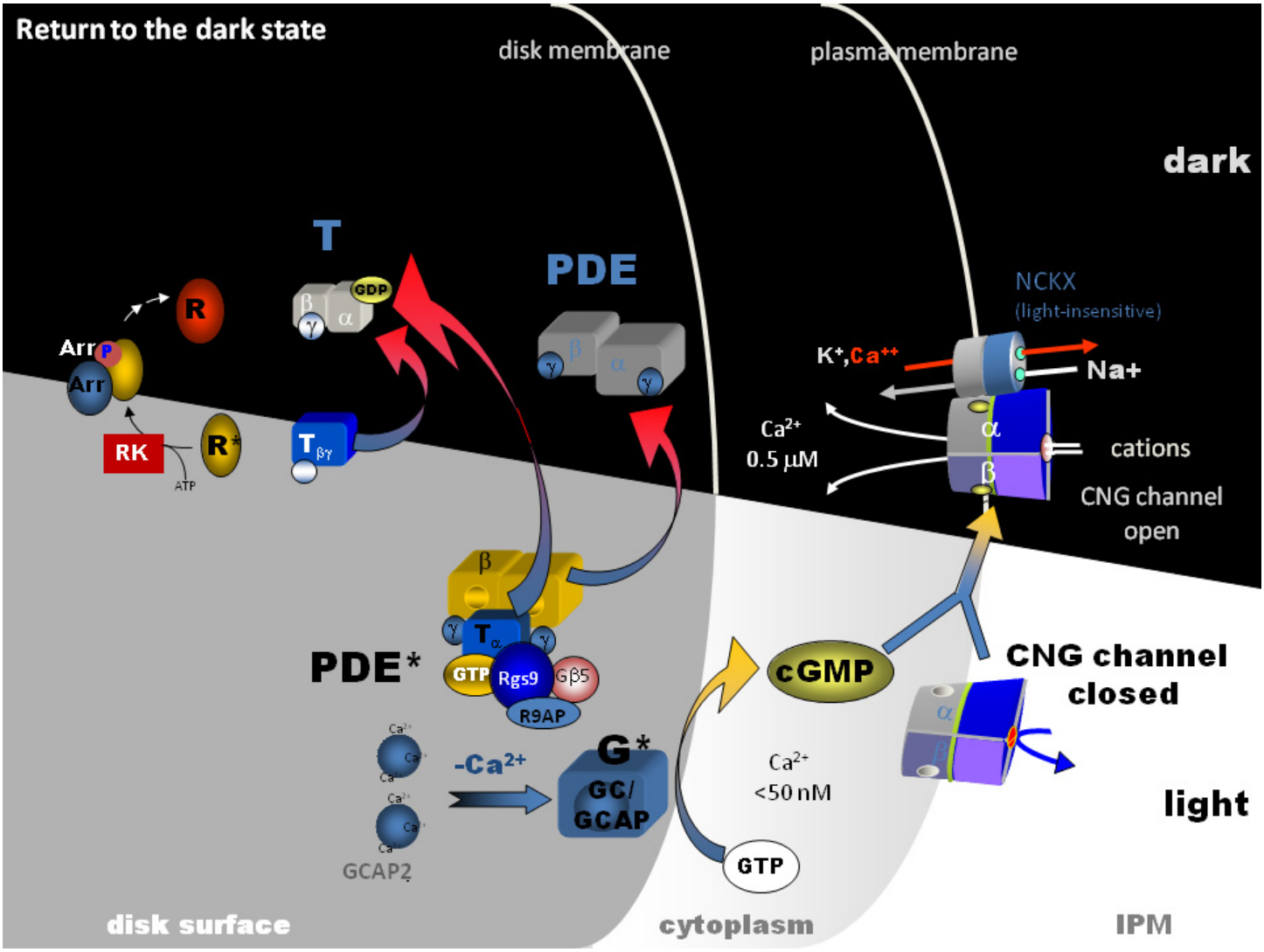

Figure 8. Recovery of rod phototransduction cascade that results in the re-openning of cGMP-gated channels on the plasma membrane (from light to dark state). IPM, interphotoreceptor matrix; R, rhodopsin (inactive); R*, rhodopsin (active); T, transducin; PDE, phosphodiesterase (inactive); PDE*, phosphodiesterase (active); Rgs9, regulator-of-G-protein-signaling protein 9; R9AP, RGS9 anchor protein; GC, guanylate-cyclase; NCKX, Na/Ca,K exchanger; Arr, arrestin; GCAP, guanylate-cyclase-activating protein. Courtesy of Wolfgang Baehr.

decays 50 times more rapidly than that of rhodopsin (60-62). Despite this difference, rhodopsin and transgenic red cone cone pigment, and vice versa, signal identically downstream when compared side-by-side in the same Xenopus rod or cone (38). The same was found for rhodopsin and transgenic red cone pigment in mouse rod (40). Thus, not only do rod and cone pigments interact with a given transducin, pigment kinase and arrestin in quantitatively identical ways, but the shutoff mediated by pigment kinase and arrestin also precedes the Meta-II decay of rod and cone pigments, rendering the decay of Meta II non-rate-limiting under normal conditions (see R* termination).

Retinal absorbs maximally in the UV-range (max ~380 nm) when in solution or bound to opsin in the unprotonated form. The absorption shifts into the visible region when the Schiff-base (SB) is protonated. Like other vertebrate pigments, mouse rhodopsin and M-cone pigment are protonated. On the other hand, mouse S-cone pigment is unprotonated, explaining its absorption in the UV-region (63). The positively charged Schiff-base is stabilized by the counterion E113 (residue number according to mouse rhodopsin) in rhodopsin and M-cone pigment (21, 64-66). Rhodopsin activation involves a "counterion switch" mechanism in which E181

located in the extracellular loop II transfers a proton via a hydrogen-bonded network to the primary counterion, E113, during the formation of Meta I. Therefore, E181 replaces E113 as the counterion to stabilize the protonated Schiff-base in the transition stage before its eventual deprotonation ((67), Figure 11).

Because the mouse S-cone pigment is not protonated and the nearby E113 is neutral, the interesting questions are: does a protonation event occur during light activation, and does it involve a "counterion switch" mechanism? Remarkably, after the 11-cis isomerization, the Schiff-base picked up a proton in the Lumi state from E108 to become transiently protonated (68) and a counterion switch occurs from E108 (E113 in rhodopsin) to E176 (E181 in rhodopsin) during the Lumi to Meta I transition, in close analogy to rhodopsin ((69), Figure 12). The photoactivation mechanism of S-cone pigment, SB → PSB (protonated Schiff-base) (+):E108(-) → PSB(+):E176(-) → SB, makes vision possible in the UV region. Thus, the counterion switch appears to be a general mechanism for the activation of all visual pigments.

The decay of R* eventually leads to the departure of all-trans-retinal from the protein. The all-trans chromophore is converted back to 11-cis-retinal through a cascade of enzymatic reactions called the visual cycle in the adjacent RPE, before being used again for the regeneration of visual pigments (for example, see review McBee et al., 2001 (70)).

Visual pigment is a major structural component of rods and cones. It is not surprising that genetic deletion of mouse rhodopsin results in rods without proper outer-segment formation (3, 4). Is half the amount of normal rhodopsin enough for maintaining a healthy ROS? In rho$^{+/-}$ mouse, rods are properly formed despite only half of the normal level of rhodopsin being present. However, a progressive mild degeneration of the rods does occur. Interestingly, the activation rate of the photoresponse of rho$^{+/-}$ rods is twice that of normal (71). The explanation for this observation was originally proposed that a lower rhodopsin concentration reduces protein crowding on the disc membrane, thereby increasing rhodopsin's diffusion coefficient and its rate of encounter with transducin. This finding thus would point to the diffusional encounter of transducin by photoexcited rhodopsin as the rate-limiting step in the activation of the rod photoresponse. However, Liang et al. subsequently reported that rods in rho$^{+/-}$ mouse are not completely normal in that rhodopsin exists in small raft-like structures as well as in large and organized para-crystals (72). In addition, there is an approximate 40% reduction in the ROS volume, in the rhodopsin content and in the 11-cis-retinal level in these cells. These authors suggested that the observed acceleration of phototransduction in rho$^{+/-}$ rods was not due to a lower density of rhodopsin on the disc surface but to the structural changes in the whole ROS.

8. High quantum efficiency of photoactivation

The quantum efficiency of photoactivation measures the probability that the adsorption of a photon initiates photoactivation. This probability is defined as the ratio between the number of photoactivated molecules and the number of molecules that absorbed a photon. Quantum efficiency of visual pigments is wavelength-independent at ~ 0.7 in the spectrum of visible light whereas it falls to about 0.25 for wavelengths shorter than 300 nm (73). This suggests that every absorbed photon in the visible range can activate rhodopsin equally well. The quantum efficiency of 0.7 is very similar across all visual pigments. This high efficiency seems to be a common feature of most vertebrate visual pigments.

9. The activation of transducin constitutes the first amplification step

Photoactivated pigment binds the transducin heterotrimer and catalyzes the exchange of GTP for GDP on the α-subunit. Gα-GTP (G*) dissociates from R* as well as its native partners, Gβν and interacts with the cGMP phosphodiesterase (PDE) to carry the signal forward. Released R* is free to activate additional transducin molecules. Transducin activation by R* represents the first amplification step in the phototransduction cascade.

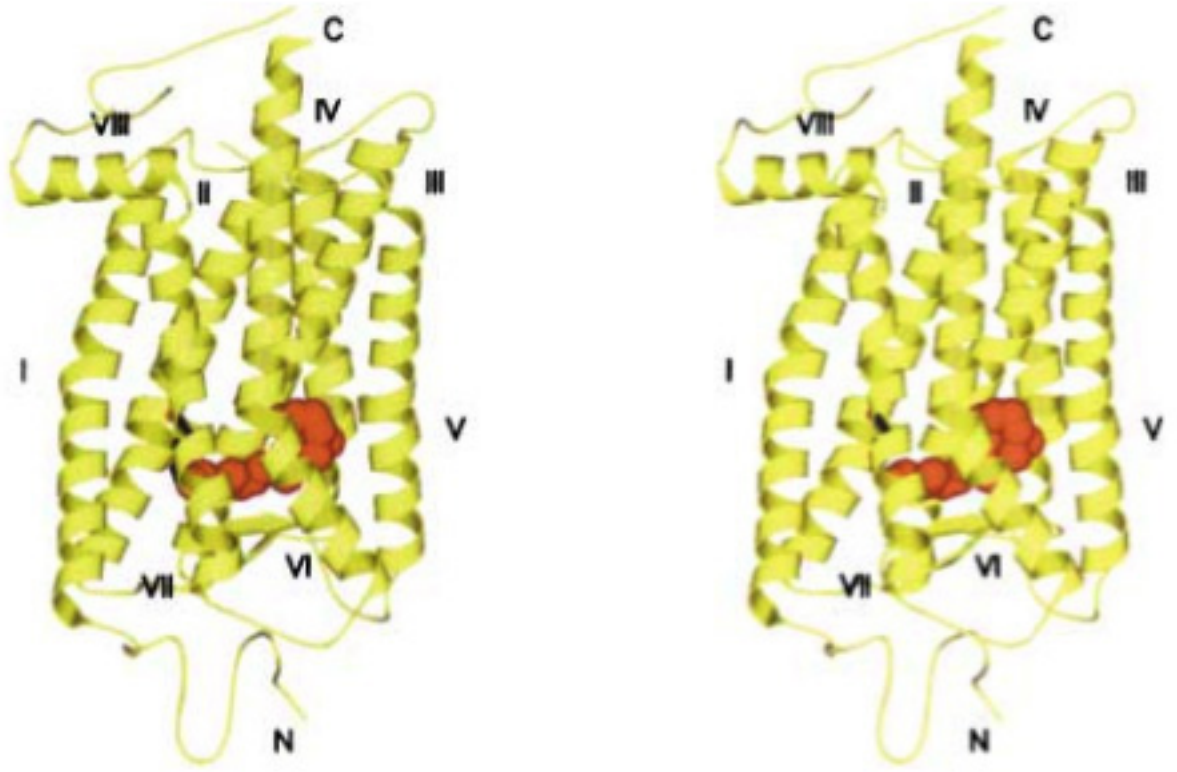

Figure 9a Stereo pair of the crystal structure of rhodopsin. From Stenkamp et al. 2002 (209).

The estimated rate of transducin activation by a single R* has ranged from 10 to over 3000 s^{-1} at room temperature (for review see Pugh and Lamb, 1993). More recently, a rate of ~ 120 s^{-1} was reported to be more consistent with biochemical, light-scattering, and electrophysiological measurements ((74), but see (75)). The rate is roughly doubled in mammalian rods due to a difference in body temperature. Until recently, it was believed that over a hundred transducins are activated during the lifetime of a single R* in mammalian rods (76). This number is now revised to be ~ 20 in mouse rods, based on the shorter life time of R* (80 msec) and 240 s^{-1} activation rate of transducin by R* (77).

Transducin is present at 10% the amount of pigment. Rods and cones have different isoforms of transducin, being $G\alpha t_1 G\beta_1\gamma_1$ in rods and $G\alpha t_2 G\beta_3\gamma_8$ in cones (78-81). The C-terminal of the γ subunit is farnesylated and the N-terminal of the α subunit is acylated (82-84). These lipid modifications help anchor the holo-transducin to the disc membrane. The importance of transducin for conveying the signal from R* to PDE was confirmed by gene-targeting experiments, in which rods of Gαt1-null mice (gnat1$-/-$) were found to lose all light sensitivity (85). The gnat1$^{-/-}$ mouse line has proven to be a valuable tool for blocking rod phototransduction in many studies (86-88). It was also used successfully to delineate two apoptotic pathways in light-induced retinal degeneration (89). Bright light triggers apoptosis of photoreceptors through a mechanism requiring the activation of rhodopsin but not transducin signaling. In contrast, low-intensity light induces apoptosis that is predominantly dependent on transducin signaling.

Almost two decades ago, rod transducin was found to undergo light-dependent redistribution (164, 219). Great progress has been made in the past few years by using mouse (or rat) models for study. Both Gαt2 and $G\beta_1\gamma_1$ subunits are present predominantly in the ROS in darkness, but translocate in bright light, with slightly different time courses, to the inner segment and the inner nuclear layer (90). This phenomenon has been suggested to contribute to light adaptation of rods (91), but others argue that the main function of transducin translocation is to provide protection for rods in bright light when rods contribute little to vision (92). In contrast, Gαt2 has been

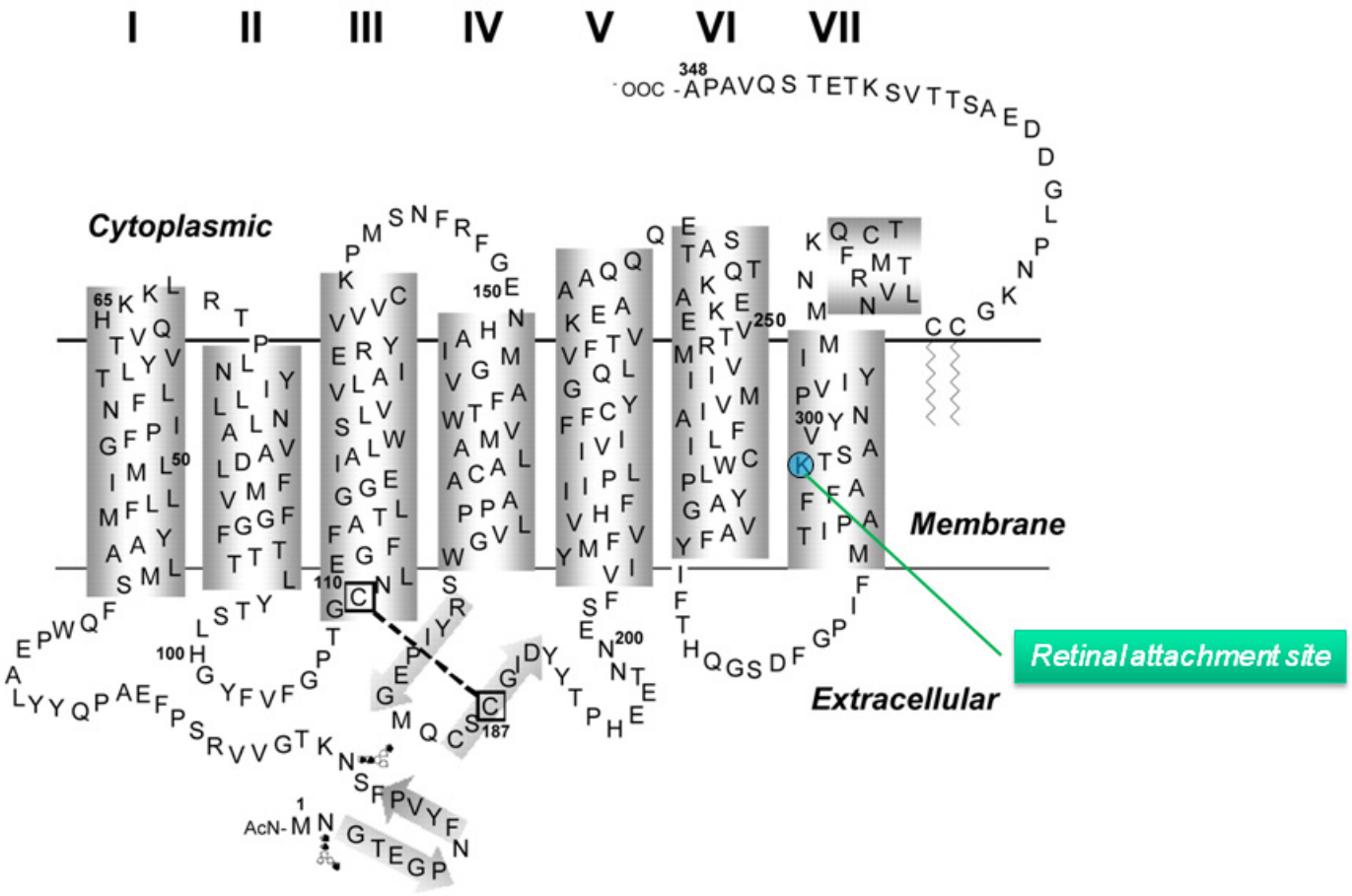

Figure 9b. Structural model of bovine rhodopsin showing seven transmembrane components and the attachment site for retinal. The seven-TM helices are shown by numbered gray boxes, and β-strands are shown by arrows. The respective residue ranges of these TM helices are as follows: I, 35-60; II, 71-100; III, 107-137; IV, 151-173; V, 200-225; VI, 247-277; VII, 286-306; VIII, 310-324. The dashed line indicates the C110-C187 disulfide bond located at the interface between the TM and EC domains. Reprinted from (208)

found not to translocate from the cone outer segment (COS) in light under physiological conditions (92-94) and only translocates away from the cone outer segment under very high-intensity light (95). This might be consistent with the need for cones to function in bright light (92).

$G_{\gamma 1}$ in rods and $G_{\gamma 8}$ in cones are farnesylated with a 15-carbon chain, but all other G_{γ} subunits are geranylgeranylated with a 20-carbon chain. What is the significance of this difference? Knock-in mice expressing geranylgeranylated instead of farnesylated $G_{\gamma 1}$ exhibited impaired properties in light adaptation because the stronger attachment by geranylgeranylation attenuated the light-dependent translocation of $G_{\gamma 1}$ from ROS to the inner region (90). It thus appears that the selective farnesylation is important for the regulation of visual sensitivity by providing sufficient but not excessive anchoring of $G\beta_{1\gamma 1}$ to the membrane.

10. The high catalytic power of PDE accounts for the second amplification step

PDE is the third component of vertebrate phototransduction. It is a tetrameric protein consisting of two equally active catalytic subunits, α and β, and two identical ν subunits (96-98). PDE is anchored to the disc membrane by isoprenylation of the C-termini of the two catalytic subunits (99, 100). The density of PDE is ~1-2% of rhodopsin. Thus, the first three components of phototransduction are present in the ratio of 100R:10G:1PDE.

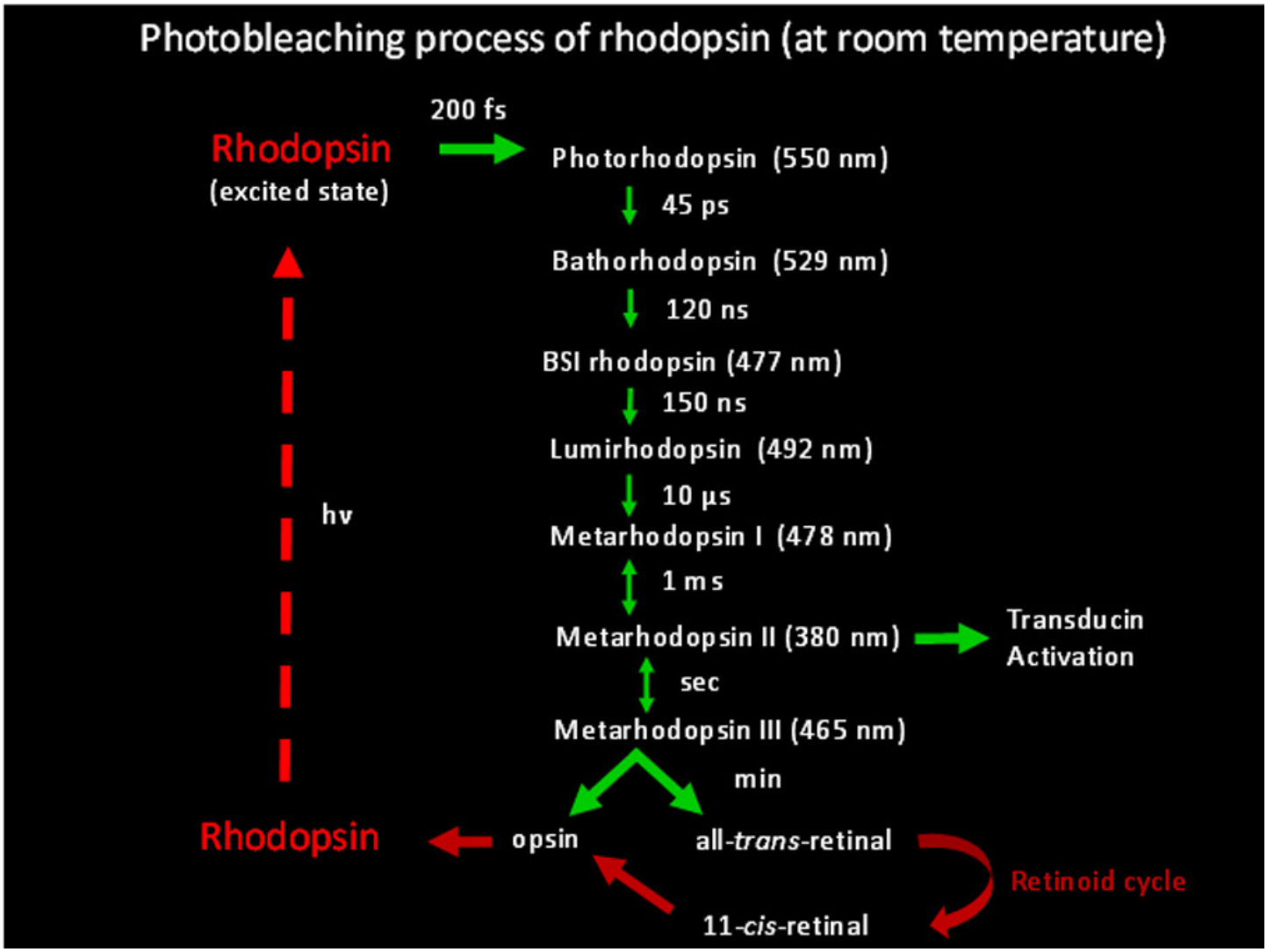

Figure 10. Photobleaching process of bovine rhodopsin. After photon absorption and electronic excitation, fast isomerization of the chromophore leads to the formation of a series of intermediate states of rhodopsin. This is called the "bleaching process" because rhodopsin loses its color. The intermediate states were identified by both low-temperature and time-resolved spectroscopy. The peak spectral sensitivity of each state was indicated. BSI, blue-shifted intermediate. Modified from Wolfgang Baehr.

In the dark, the two γ subunits act as inhibitory subunits by binding to the two catalytic subunits. In the light, Gα-GTP encounters PDEγ and sterically displaces the latter (still associated with PDEαβ, therefore relieving its inhibitory effect on the catalytic subunits and permitting the hydrolysis of cGMP to proceed.

In contrast to the amplification achieved during transducin activation by R*, the activation of PDE by G* constitutes no gain, i.e. with an efficiency approaching at most unity. It is the catalytic power of PDE* that provides the second amplification step. It was reported that PDE* hydrolyzes cGMP at a rate close to the limit set by aqueous diffusion, with a Km of ~ 10 µM and a Kcat of 2200 s^{-1} (74, 96). The combined amplification provided by rhodopsin and PDE are very high (~ 10^5-10^6), ensuring the high sensitivity of rods, including the ability of rods to detect single photons (for review see (19, 101)).

One might have expected that the deletion of PDEγ from mouse rods would unleash the full catalytic power of PDEαβ. However, Tsang et al. found that, in the absence of PDEγ, the PDEαβ dimer actually lacked hydrolytic activity, and the photoreceptors of the mutant mouse rapidly degenerated (102). Thus, the inhibitory PDEγ subunit appears to be necessary for the integrity of the catalytic PDEαβ subunits. The degeneration might be caused by an abnormally high cGMP concentration due to the lack of hydrolysis. A related example is the rd

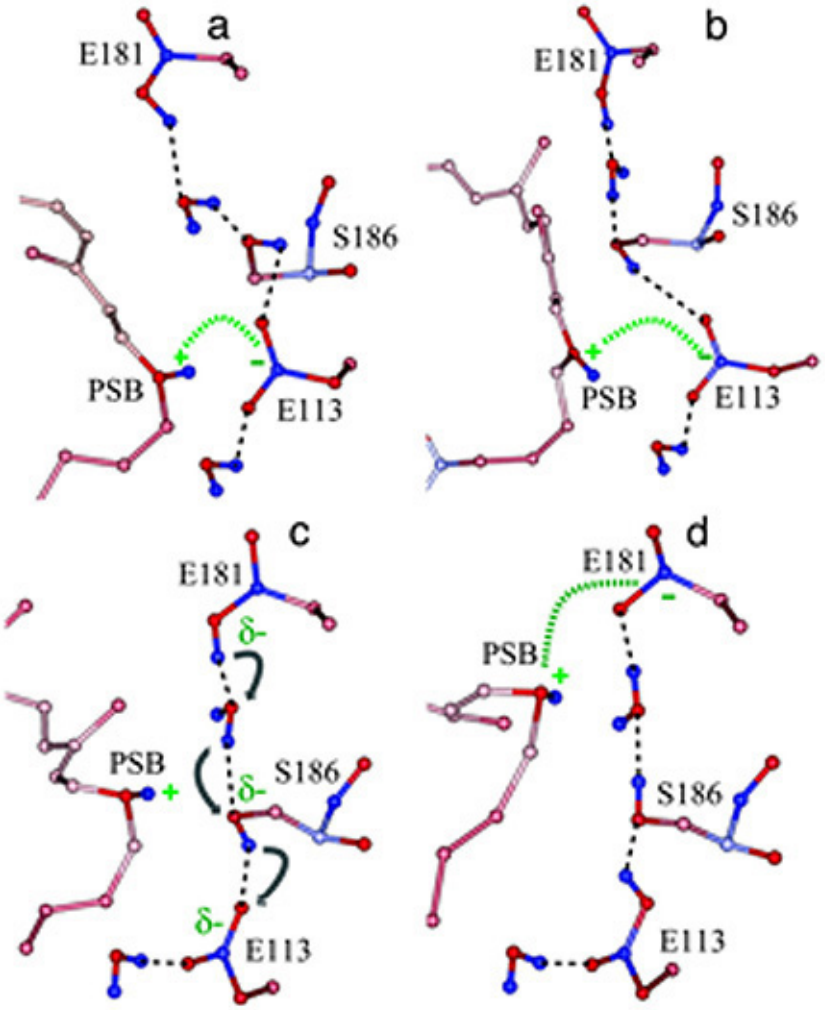

Figure 11. Schematic of the proposed proton transfer mechanism for switching the protonated Schiff-base (PSB) counterion in rhodopsin. (a) Rhodopsin: two water molecules and Ser-186 form a H-bond chain between Glu-113 and Glu-181. Electrostatic interaction between the PSB and Glu-113 is indicated by the green dashed line. (b) Blue-shifted intermediate: after photoisomerization, the H-bond chain evolves so that the two water molecules and Ser-186 are lined up to prepare for the proton transfer and the PSB has shifted relative to Glu-113. (c) Lumirhodopsin: the PSB shifts further away from Glu-113 toward Glu-181. The gray arrows indicate a possible proton transfer pathway. (d) Metarhodopsin I: proton transfer is completed. The PSB group is now close to Glu-181 to establish the electrostatic interaction (green dashed line) with the new counterion. Reprinted from Yan et al., 2003 (67).

mouse, which is one of the best-known models for retinal degeneration. The rod cells in the rd mouse begin to degenerate at about P8, followed by cones; by 4 weeks, virtually no photoreceptors are left (103, 104). Degeneration in this mouse model is preceded by the accumulation of cGMP in the retina, correlated with deficient activity of the rod PDE due to a mutation in the β subunit (105, 106). It is worth noting that the rd mouse was instrumental in suggesting that inner retinal neurons could mediate non-image-forming vision (107, 108).

In addition to its inhibitory function, PDEγ accelerates the GAP (GTPase Activating Protein) activity of G* for self-shutoff (see G*-PDE* termination). Mouse rods carrying the W70A point mutation of PDEγ which impairs the $G\alpha t_1$-PDEγ interaction, showed a greatly reduced sensitivity to light and a slower recovery from the flash response than wild type (109).

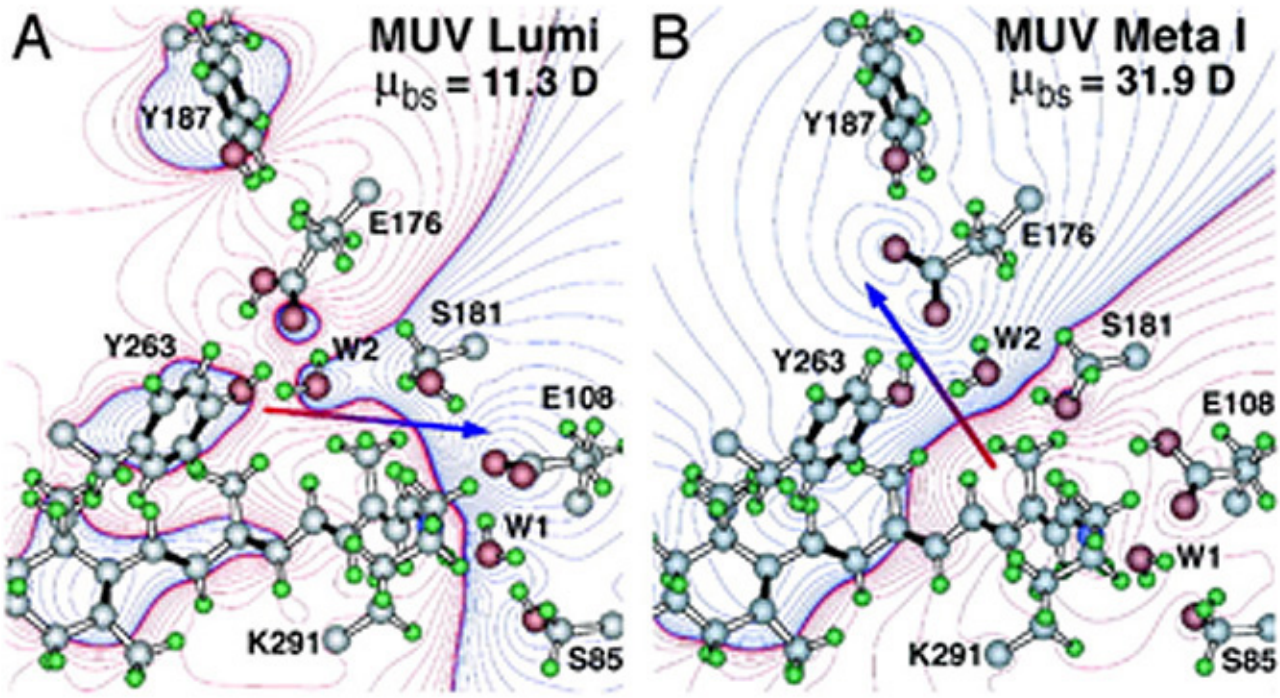

Figure 12. Molecular models of the lumi (A) and meta I (B) intermediates of mouse S-cone (UV) pigment based on the assumption that a counterion switch occurs during the lumi (E108 counterion) to meta I (E176 counterion) transformation. The dipole moments of the binding site residues, μ_{bs}, are given in the upper right of A and B and the dipole moment vector is shown by using red-to-blue arrows. Reprinted from Kusnetzow et al., 2004 (69).

11. cGMP is the second messenger mediating rod phototransduction

By 1970, scientists generally believed that a second messenger was required to mediate the rod photoresponse based on several lines of evidence. First, light absorption occurs on the rod disc membrane, whereas the light sensitive conductance is in the plasma membrane. Since rod discs are separate from the plasma membrane, a second messenger is required to connect the two. Second, the dim-flash response of rods lasts a few seconds, which is too long to be accounted by the open time of known membrane conductance. However, it took more than a decade before the identity of the second messenger was finally determined to be cGMP (reviewed in (110). The "fierce battle was fought" on the validity between two competing candidates, Ca^{2+} and cGMP. According to the Ca^{2+} hypothesis, which was first proposed by Hagins (6), the concentration of intracellular free Ca^{2+} is low in the dark and rises in the light to block light-sensitive current. The main supporting evidence was that reducing the concentration of external Ca^{2+} dramatically increases the dark current, suggesting internal Ca^{2+} inhibits the dark current. On the other hand, the cGMP hypothesis proposed that the concentration of cGMP was high in the dark to maintain a cGMP-dependent conductance. Light led to the hydrolysis of cGMP and the subsequent closing of the conductance. The supporting evidence is that intracellular injection of cGMP increases the amplitude and latency of the photoresponse. Adding to the complexity is the finding that the free cGMP concentration varies inversely with the free Ca^{2+} concentration in rods, making it difficult to separate the effect of the two.

This debate was finally settled with the discovery of cGMP-gated channels in rods by Fesenko and colleagues in 1985 (111). By using the patch-clamp technique, they showed that cGMP increased a cation conductance of

inside-out patches of outer-segment plasma membrane without the need of ATP. The direct channel gating by cGMP is surprising because cyclic nucleotides were generally believed to act through cyclic-nucleotide dependent kinases and protein phosphorylation on target proteins at that time. This dogma partially explained scientists' reluctance to embrace the cGMP hypothesis because protein phosphorylation was too slow. Another monumental work by Yau and Nakatani was published at the same year that helped the anointment of cGMP as the right candidate (112). An identical cGMP-gated cation conductance was found on a truncated rod outer segment with an intact plasma membrane. Most importantly, this conductance could be suppressed by light, suggesting that the long-sought light-sensitive conductance is the cGMP-gated conductance. The publications by Fesenko and Yau marked the end of the Ca^{2+} hypothesis.

12. The cGMP-gated channel provides the final step of photo-activation

The cGMP-gated channel belongs to the family of cyclic-nucleotide-gated (CNG) channels, which are non-selective cation channels (reviewed in (113, 114)). The channel is located on the plasma membrane and is the last component in the activation phase of phototransduction. In the dark, a basal concentration of one to several μM cGMP keeps a small percentage of the CNG channels open (115). The decline in cGMP concentration upon illumination leads to rapid closure of the channels with a sub-millisecond delay (116). The gating of the rod channel by cGMP is cooperative with a Hill coefficient of ~ 3; therefore, the light-triggered suppression of the dark current is 3 times larger than the decrease in the intracellular cGMP concentration.

For a long time, the rod channel was believed to be a hetero-tetramer consisting of 2 CNGA1 and 2 CNGB1 subunits. In 2002, a number of laboratories made the surprising discovery that the rod channel actually has a 3CNGA1:1CNGB1 subunit composition (117-119), whereas the cone channel supposedly exhibits a 2CNGA3: 2CNGB3 stoichiometry (120). CNGA1 and CNGA3 subunits form functional homomeric channels by themselves when heterologously expressed. Although CNGB1 and CNGB3 do not form functional channels by themselves, they confer several properties typical of native channels when co-expressed with A subunits: flickery opening behavior, increased sensitivity to L-cis-diltiazem (a CNG channel-specific inhibitor), and weaker block by extracellular calcium (113, 121-123).

In humans, mutations in CNGA1 causes retinitis pigmentosa (124), while mutations in both CNGA3 (125) and CNGB3 (126) cause achromatopsia. Mouse models carrying null mutations of CNGB1 (127) and CNGA3 (121) are available. CNGB1 was found to be crucial for the targeting of the native CNG channel in rods. Thus, only trace amounts of the CNGA1 subunit were found on the ROS in CNGB1-null mice and the majority of rod photoreceptors failed to respond to light (127). CNGA3-deficient mice selectively lost their cone photoresponse with the rod pathway intact. Analogous to the case of rod transducin, CNGA3-null mice were used to block cone phototransduction in studying the intrinsically photosensitive retinal ganglion cells (86, 87).

In the dark, the concentration of free cGMP in the rod outer segment was estimated to be several μM, which is lower than the K1/2 (~ 10-40 μM depending on Ca^{2+} concentration), the concentration of cGMP necessary to half-maximally activate the channel. As a result, only ~ 1% of the CNG channels are open! In other words, 99% of the channels are already closed in the dark and light can only suppress the remaining 1% channels. This explains why current induced by cGMP injection is more than 10 times larger than the dark current.

The inward current through the cGMP-gated channel is composed of ~85% Na^+ because Na^+ is the predominant external cation and the channel is non-selective to monovalent cations. The remaining current is mainly carried by Ca^{2+} with a minor contribution from Mg^{2+} (115, 128). Extracellular Ca^{2+} actually partially blocks the channel to reduce its conductance under physiological conditions. The inward current is balanced by an outward current flowing across the inner-segment membrane, which is mainly carried by potassium ions. This "circulating current" is also called "dark current" in both rods and cones (6). Unlike other ligand-gated

channels, the CNG channel does not desensitize to cGMP, which is important for rods to maintain a steady dark current ranging between 20 and 70 pA in vertebrate rods. The rod photoresponse is essentially a transient suppression of the circulating current. It was estimated that the dark current was carried by ~ 10, 000 channels. The participation of large numbers of "micro" channels averages out the channels noise, i.e. reduce an otherwise substantial stochastic channel noise if the dark current were carried out by a few "macro" channels. This feature improves the sensitivity of rods.

Two extrusion mechanisms are critical to maintain ionic balance in rods. An energy-dependent Na-K ATPase at the inner segment pumped Na^+ out and K^+ into the cells. A Na/Ca,K exchanger (NCKX) in the outer-segment plasma membrane extrudes one Ca^{2+} and one K^+ outward in exchange for four Na^+ inward producing the net entry of one positive charge. The exchanger and the CNG channel were found to form a stable complex on the plasma membrane, likely as a way to control the stoichiometry between the two, which is critical for regulating Ca^{2+} concentration in the rod outer segment. During the light response, the influx of Ca^{2+} is reduced due to the closure of some CNG channels while the efflux of Ca^{2+} through the exchanger is maintained. The resulting Ca^{2+} decline triggers negative feedback to produce light adaptation.

13. Phototransduction termination

Following light activation, a timely recovery of the photoreceptor is essential so that it can respond to subsequently absorbed photons, and signal rapid changes in illumination. This recovery from light requires the efficient inactivation of each of the activated components: R*, G*, and PDE*, as well as a rapid restoration of the cGMP concentration. The termination rates of the activation steps set the time course of the photoresponse.

In the past decade, knowledge gained from genetically engineered mouse lines has provided major advances in understanding the termination of the rod photoresponse. In the following sections, we shall discuss separately the events responsible for the inactivations of R*, G* and PDE*, followed by the restoration of cGMP.

14. R* termination

Activated rhodopsin (R*) is inactivated by a two-step process. First, R* is phosphorylated by rhodopsin kinase (GRK1), which lowers the activity of R*. Second, the protein arrestin (Arr1) binds to phosphorylated R*, capping its residual activity (129, 130).

Multiple serine/threonine residues at the C-terminal of rhodopsin (six in mice and seven in humans) provide the phosphorylation sites for GRK1. Cone pigments have more potential phosphorylation sites at the C-terminal than rhodopsin. For example, human red cone pigment has 10 such sites. Even though biochemical experiments originally suggested that rhodopsin is predominantly phosphorylated at only one serine residue following light exposure (131), subsequent recordings from transgenic mouse rods carrying phosphorylation-site mutations suggested that the reproducible deactivation of R* requires at least three phosphorylation events (132). In addition, all six sites need to be phosphorylated in order for the normal decline of the response to proceed.

Multiple phosphorylation events are also proposed to underlie the reproducibility of rod responses to single-photons (132-134). Despite the fact that events generated by single molecules are stochastic in nature, the single-photon response of rods shows remarkable reproducibility in amplitude and shape (15, 135, 136). By averaging over multiple shutoff steps, the integrated R* activity varies less than otherwise controlled by a single step. This hypothesis is supported by experiments using transgenic mouse rods carrying phosphorylation-site mutations (137). The authors showed that the reproducibility of the single-photon response varies in a graded and systematic manner with the number, but not the identity, of the phosphorylation sites. Each phosphorylation site provides an independent step in rhodopsin deactivation and that, collectively, these steps tightly control the lifetime of R*.

Much less is known about the role of the phosphorylation sites in cone pigments. The only in vivo experiment was done by Kefalov et al. (38), showing that transgenic frog rods expressing a human red cone pigment with all 10 putative phosphorylation sites mutated gave a prolonged response. It suggests that activated cone pigment is quenched by a similar two-step shutoff mechanism even though its active lifetime is much shorter than that of rhodopsin.

In addition to mutations of all of the C-terminal serine and threonine residues to alanine (132), rhodopsin phosphorylation can also be prevented by deleting the C-terminal region of the pigment (138) or ablating GRK1 (139). As expected, rods from all three transgenic mouse lines showed similar properties of the single-photon response, with an amplitude reaching a plateau about twice that of wild-type and decaying stochastically to baseline after a long interval of 3 to 5 seconds. GRK1-mediated phosphorylation begins to reduce the activity of R* at ~100 msec after the flash, because this is the time point at which the transgenic response starts to deviate from the WT response (Figure 13). As mentioned earlier, it was estimated in a recent study that the lifetime of R* is ~80 msec (77), suggesting that arrestin binding occurs rapidly after phosphorylation of the pigment. Therefore, GRK1/arrestin mediated shutoff occurs in rods even earlier than the fast Meta-II decay of cone pigment (38), which is of the order of 1 s after flash (60, 62, 140). The GRK1-mediated shutoff likely happens even faster in cones (see below).

Mouse and rat are unusual in that the same GRK1 is present in both rods and cones. In all other species studied, another pigment kinase (the so called "cone pigment kinase"), GRK7, is present in cone photoreceptors (141-144). Indeed, many animal species, including human, have both GRK1 and GRK7 in cones. This explains why Oguchi patients with a defective GRK1 gene have normal daytime vision whereas GRK1-null mice have prolonged cone photoresponses (145, 146). Interestingly, GRK7 was shown to have considerably higher specific activity than GRK1 and, in fish, is present at a much higher concentration in cones than GRK1 is in rods (142, 147). This difference has been proposed as a potential mechanism underlying the faster shutoff and lower sensitivity of cones than rods (reviewed in (148)).

Biochemical experiments suggest that GRK1-mediated phosphorylation of R* is regulated by recoverin (Rec) (149-152), which belongs to a family of calcium-binding proteins. The hypothesis is that, when intracellular free Ca^{2+} concentration is high in the dark, Rec-Ca^{2+} binds to GRK1 and inhibits R* phosphorylation. When Ca^{2+} concentration decreases in the light, Ca^{2+} dissociates from recoverin; consequently, the resulting affinity between recoverin and GRK1 is reduced, and its inhibition on R* phosphorylation is released. However, this hypothesis was challenged by in vitro measurements suggesting that the extent of R* phosphorylation was unaffected by light adaptation and by changes in intracellular Ca^{2+} (153). This controversy was finally settled by recordings from Rec$^{-/-}$ mouse rods (154), which showed that Rec-Ca^{2+} prolongs the dark-adapted flash response and increases the rod's sensitivity to dim steady light, probably by inhibiting the phosphorylation of R* by GRK1. Furthermore, Rec$^{-/-}$ rods had faster Ca^{2+} dynamics, indicating that recoverin is a significant Ca^{2+} buffer in the ROS.

In the second step for the deactivation of R*, arrestin binds to phosphorylated R* (R*-P) to cap its catalytic activity. In mouse, the dim-flash responses from rods of arrestin-knockout (Arr$^{-/-}$) mice do not differ greatly from the wild-type response until in its falling phase, when recovery reaches approximately halfway back to baseline (155). Therefore, phosphorylation alone can reduce R*'s activity significantly. The response of Arr$^{-/-}$ rods on average recovers ~10 times more slowly than the response of rods lacking rhodopsin phosphorylation (Figure 13), presumably reflecting the continuous activity of the phosphorylated meta-II state of R* until it decays to inactive meta III. In rods lacking both GRK1 and arrestin (GRK1$^{-/-}$Arr$^{-/-}$), the activation phase and peak amplitude of the dim-flash response resemble those of GRK1$^{-/-}$ rods but then decay slowly with a time constant similar to that of the Arr$^{-/-}$ response (156), reflecting the decay of non-phosphorylated R. It thus appears that phosphorylation does not influence the decay of R*.

At least two splice variants exist for rod arrestin: a full-length (p48) and a C-terminal truncated form (p44) (157). P44 has a faster on-rate than p48 for binding R* and R*-P (158, 159). In addition, p44 is more efficient than p48 in turning off R* in vitro (158, 160). Although p48 is ~10 times more abundant than p44, it translocates from ROS to the rest of the cell in the dark, therefore largely absent in dark-adapted ROS (161-164). This raises an interesting question about the roles of individual isoforms of arrestin in the intact rods. By selectively expressing the two isoforms in mouse rods lacking endogenous arrestin, it was found that both isoforms could quench the activity of phosphorylated R* rapidly. However, only p48 was able to quench the activity of non-phosphorylated R* (156).

Cones express their own arrestin called cone arrestin or X-arrestin (Arr4) (165, 166). Surprisingly, both the rod and cone forms of arrestin exist in mouse cones (167). Arr1 in cones is ~50-fold higher than that of Arr4 (168). Single cell recordings from cones of mice with one or both arrestins knocked out shows that arrestin is required for normal cone inactivation although removal of one arrestin has negligible effect (168).

15. G*-PDE* termination

Earlier, genetically engineered mouse lines were designed to disrupt R* termination. More recent studies have centered on G*-PDE* termination. G* is inactivated when its bound GTP is hydrolyzed to GDP. Although transducin has a slow intrinsic GTPase activity, the hydrolysis is greatly accelerated by the GAP complex. The complex is composed of a member of the family of regulator-of-G-protein-signaling proteins (RGS9-1 (169),), the long form of Gβ5 subunit (Gβ5-L (170),), and a membrane-anchor protein (R9AP (171),). RGS9-1 has a G protein γ-like (GGL) domain that binds to Gβ5-L, and has an N-terminal DEP (Dishevell/Eg110/Pleckstrin) domain that interacts with R9AP. After hydrolysis, Gα-GDP dissociates from PDEγ which allows the latter to re-exert its inhibition on the catalytic PDEαβ subunits (reviewed in (76)). The molecular reactions underlying this step are shown schematically in Figure 14.

Even though only RGS9-1 has GAP activity, all three components of the GAP complex are obligatory partners because genetic ablation of any one of them in mouse resulted in an increased instability of the other two through a posttranscriptional mechanism (172-174). This is why transgenic mouse rods lacking RGS9-1, Gβ5-L, or R9AP display a similar delay in the recovery phase of the flash response without much noticeable differences in the activation phase (172, 174, 175). In addition, the GAP activity on transducin is enhanced by PDEγ (109, 169, 176, 177) see PDE section). This provides an elegant mechanism for ensuring that excitation does not normally decay until G* has bound to the effector, PDE. The same GAP complex is present in both rods and cones; however, its concentration is much higher in cones than in rods (178, 179). This has been suggested to contribute to the faster response kinetics of cones than rods.

Overexpression of PDEγ in mouse rods can accelerate the shutoff of light response independent of the GAP complex, suggesting that the inhibitory sites on PDE α and β are accessible to excess PDEγ after endogenous PDEγ has been displaced by G* upon illumination (109). Overexpression also reduces the gain of transduction apparently through the "dominant negative effect" of interfering with the binding of G* to endogenous PDEγ.

Termination of phototransduction requires the shutoff of both R* and G*-PDE*, with the slower step determining the overall rate of response recovery. The identity of the rate-limiting step for rod recovery has been a long-standing question until recently (135, 180-183). By overexpressing the GAP complex in mouse rods, Krispel et al showed that the recovery of rod response was dramatically accelerated whereas overexpression of GRK1 had no effect (77). This experiment unequivocally demonstrated that the termination of G*-PDE* is the rate-limiting step. It is worthwhile to note that the same step is not necessarily the rate-limiting step in cone recovery because there is a much higher concentration of the GAP complex in cones. The same "overexpression" technique can be used in cones to answer this question.

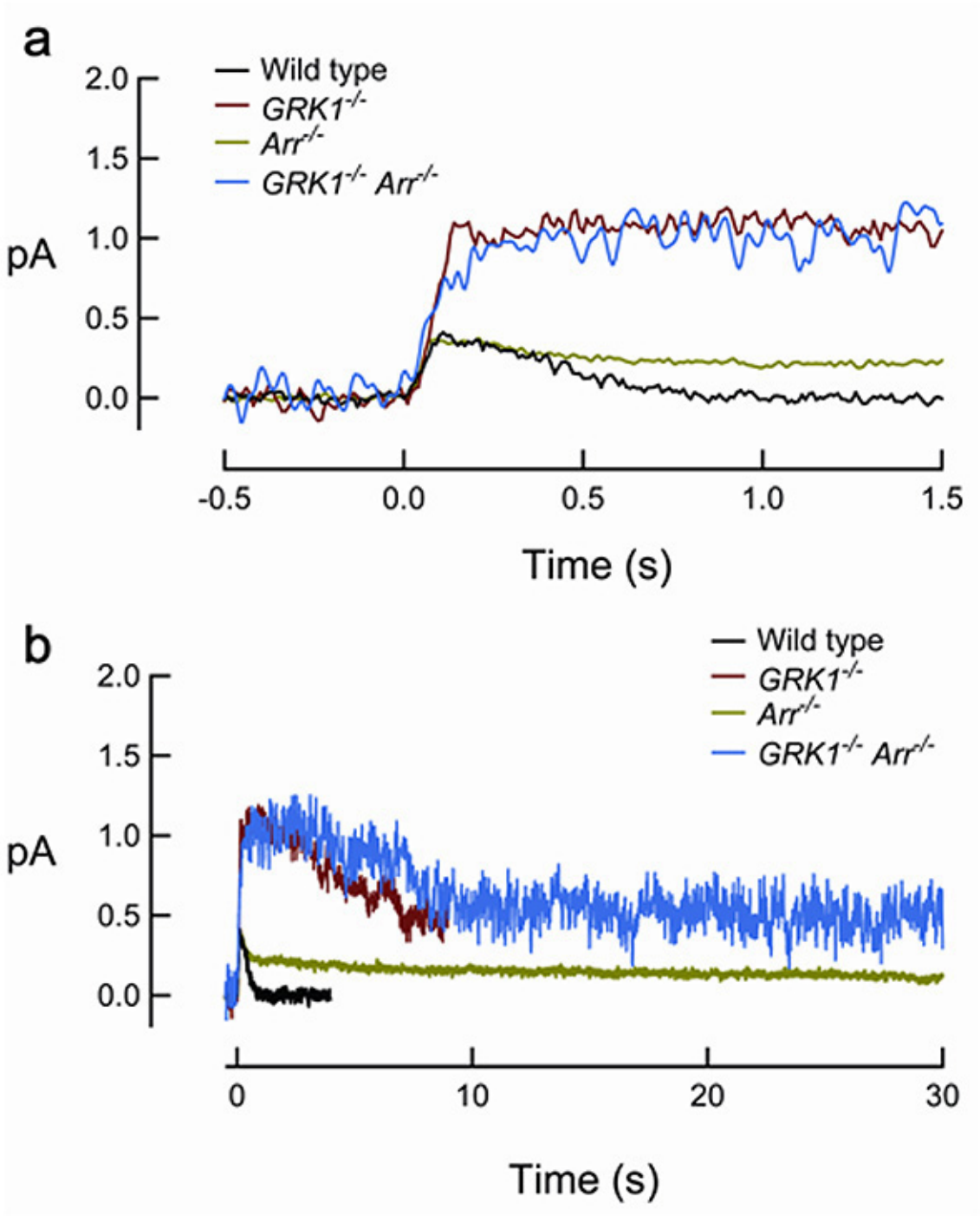

Figure 13. Form of the single-photon response from knockout mouse rods with deficient R* termination on fast (a) and slow (b) time scales. Flashes were delivered at t = 0. Courtesy of Marie E. Burns.

Another implication of the above finding has to do with the question of the reproducibility of the single-photon response (see R* Termination). Because G* deactivation is 2.5 times slower than R* deactivation (77), the slower G* termination dictates the recovery kinetics of the single-photon response of rods. In addition to the multi-step involved in the shutoff of R*, the activation of ~20 transducin by one R* can provide the necessary averaging for an otherwise stochastic process.

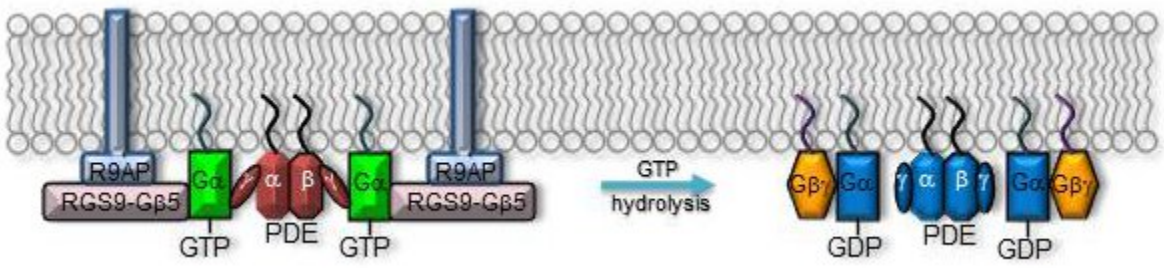

Figure 14. Schematic on the termination G*-PDE*. Gα*-GTP binds to PDEγ and activates PDE. The deactivation of Gα*-GTP is accelerated by the GAP complex, R9AP-RGS9-1-Gβ5L, in which RGS9-1 facilitates the hydrolysis of the bound GTP to GDP, leading to the re-formation of the inactive heterotrimeric Gα-GDP-Gβγ and inactive PDE. This step was found to be the rate-limiting step of rod recovery (77).

16. Restoration of cGMP

The free concentration of cGMP is determined by the PDE-mediated hydrolysis and guanylate-cyclase (GC)-mediated synthesis. For the photoreceptor to recover, not only is the light-stimulated cGMP hydrolysis by PDE required to terminate as discussed in the previous sections, but the dark level of cGMP also has to be restored. There are two GCs in mouse photoreceptors: GC1 (GC-E) and GC2 (GC-F). GC1 is present in both rods and cones (184, 185), and GC2 is present only in rods (186). It seems that the basal activity of either GC1 or GC2 is sufficient to maintain dark current in rods (187, 188). Deletion of either GC has no significant impact on rod sensitivity. GC1 is important for cone function because cones degenerate in its absence. Deletion of both GC1 and GC2 rendered rod and cone photoreceptors nonfunctional and unstable (187).

GC activity is regulated by Ca^{2+}, mediated by the guanylate-cyclase-activating proteins (GCAPs). This regulation is the most important negative-feedback mechanism triggered by Ca^{2+} in the light. For topics on other Ca^{2+}-feedback effects and light adaptation, readers can refer to the following publications (101, 115, 189, 190).

GCAPs belong to a large family of calmodulin-like Ca^{2+}-binding proteins. Two GCAPs are present in mouse retinas, GCAP1 and GCAP2. Both GCAPs are expressed in mouse rods, but GCAP1 is primarily expressed in cones (191, 192). In darkness, the relatively high Ca2+ concentration promotes the formation of the Ca^{2+}-bound form of GCAPs, which inhibits GCs. When the Ca^{2+} concentration declines during the light response, the dissociation of Ca^{2+} allows GCAP to activate GC, thereby quickly restoring the basal cGMP concentration (Figure 15).

The two GCAP genes were knocked out in mouse simultaneously by taking advantage of their tail-to-tail arrangement on chromosome 17 (193). The flash response of GCAPs$^{-/-}$ rods showed a larger amplitude and delayed decline compared to wild type, consistent with a delay in cGMP synthesis during recovery when the associated Ca^{2+}-feedback was removed. The power of Ca^{2+}-mediated regulation through GCAP can be appreciated from the fact that the single-photon response of GCAPs$^{-/-}$ rods is nearly 5 times that of wild type, versus the 2-fold increase when pigment phosphorylation is prevented. By comparing the light response of GCAPs$^{-/-}$ rods with that of wild-type rods, Burns et al. found that the activation of GC resulting from a change in Ca^{2+}-dependent GCAP activity occurs within ~40 ms after the flash and in a highly cooperative manner, with a Hill coefficient of 4 (189). Therefore, the effect occurs much earlier than pigment phosphorylation, which is 80-100 msec after the flash (see R* termination). The rapid feedback to GC has dual effects on photoreceptors, decreasing the dark-adapted flash sensitivity (132) and speeding the restoration of the dark current (36).

What are the functional differences between the two GCAPs? In vitro, GCAP1 activates GC1 more efficiently than GC2 (194, 195), whereas GCAP2 activates both GC1 and GC2 with similar efficiency (186, 196, 197). In vivo, transgenic GCAP1 can rescue the GCAPs$^{-/-}$ phenotype in rods and cones, as tested by single rod cell recordings and electroretinography, even in the absence of GCAP2 (198, 199). Expression of bovine GCAP2 in GCAPs$^{-/-}$ rods restored the recovery of rods to saturating flashes but failed to restore the recovery kinetics of responses initiated by sub-saturating flashes and, in particular, failed to rescue the fast initial phase of recovery (193), suggesting that GCAP1 is responsible for the initial rapid phase of response recovery. GCAP2 speeds up the recovery of flash responses and adjusts the operating range of rods to higher intensities of ambient illumination (200).

17. Mouse model of cone phototransduction

Recently, there have been substantial advances in the understanding of cone transduction with fish as the model (142, 143, 147, 201, 202). On the other hand, despite the enormous success in studying rod phototransduction by a combination of mouse genetics and suction-electrode recording in recent years, the usage of mouse as a model system for studying cone phototransduction has until recently been limited to ERG studies. This is mainly due to the rarity of cones (~3%) and the fragility of the cone outer segment (COS).

This hurdle was finally overcome by Pugh and colleagues (146, 203). The conventional suction-pipette recording, which involves drawing the ROS into the suction pipette ("OS in"), is not tolerated well by the more fragile COS. Instead, Pugh and colleagues drew a portion of the inner segment ("OS out") of a cone photoreceptor in a retinal slice into the suction pipette, allowing long, stable recordings. Previously, it was shown that the same information could be obtained by recording from either outer or inner segment of amphibian rods and cones (204) as expected from the nature of the circulating current.

To overcome the difficulty of identifying the ~3% cones in mouse retina, Pugh and colleagues used three different mouse lines. The first lacks the neural leucine zipper transcription factor (Nrl) (205), which drastically alters the cell fate of rod photoreceptors by turning them into cone-like photoreceptors (146, 206). The second expresses EGFP in mouse cones, which facilitates/verifies their identification (207). The third lacks the rod transducin α-subunit (gnat1$^{-/-}$), which blocks rod phototransduction (85).

In the case of the EGFP mouse line, background light is required in order to suppress the rod response so that the cone response can be isolated. As a result, the cone response is slightly light-adapted, therefore slightly faster and smaller for a given test-flash intensity than that from gnat1$^{-/-}$ or Nrl$^{-/-}$ cones. When this factor is taken into consideration, the light response properties of mouse cones recorded from the three mouse lines are very similar and are as expected from mammalian cones (Figure 16, Table 3) (203). Prominent among these features is that mouse cones are far more tolerant than mouse rods to bleached pigment. The dark current recovers substantially in both S- and M-type cones following strong flashes that bleach a substantial fraction of the pigment. One surprising finding, however, is that the inactivation of M pigment is more retarded than that of S pigment in the absence of GRK1, suggesting the existence of a GRK1-independent inactivation mechanism for the S pigment. Nrl$^{-/-}$ cones differ from wild type in certain respects. Their outer segments are shorter, more disordered and undergo a slow degeneration (206). In addition, in contrast to wild type, Nrl$^{-/-}$ cones express a much higher percentage of S-opsin. Thus, transgenic mice expressing EGFP in their cones and gnat1$^{-/-}$ mice are better than Nrl$^{-/-}$ mice for studying cone physiology.

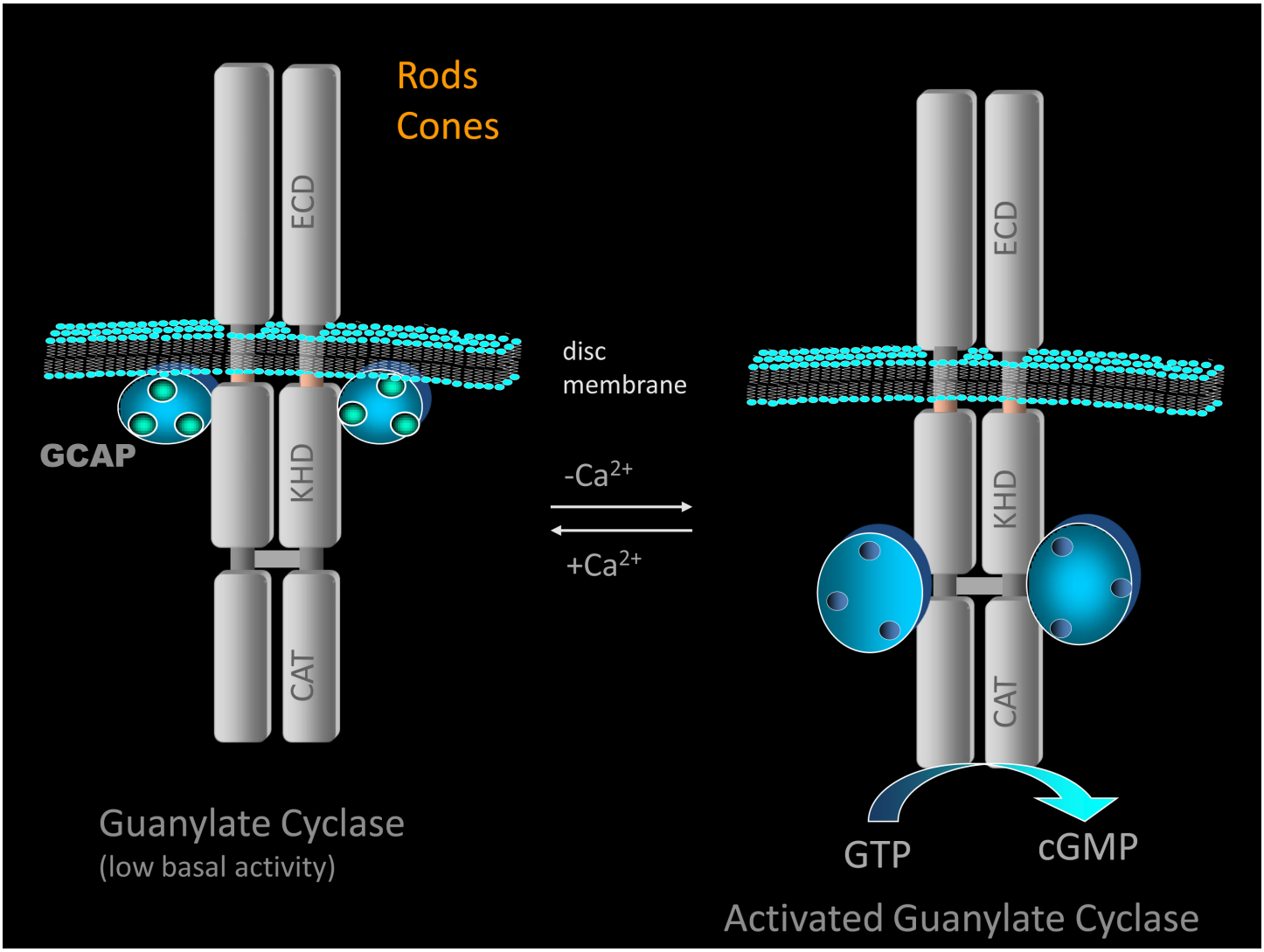

Figure 15. GCs and GCAPs in rods and cones. ECD, extracellular domain, KHD, kinase homology domain, CAT, catalytic domain. Courtesy of Wolfgang Baehr.

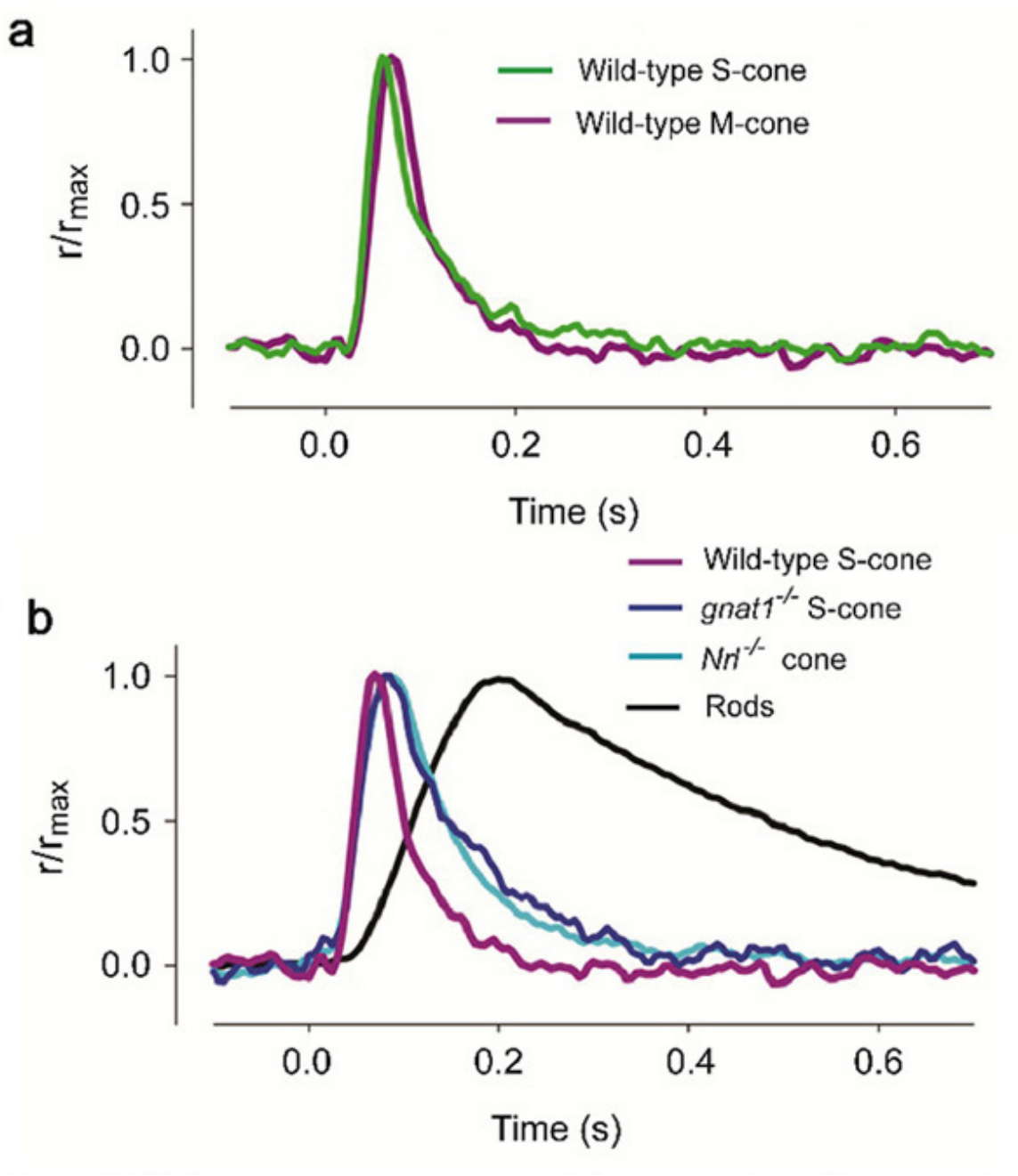

Figure 16. Flash responses of mouse cone photoreceptors from different genotypes. a. Comparison of the average response of S-cones to 361-nm flashes and M-cones to 510-nm flashes. b. Comparison of the average flash responses to 361-nm flashes of wild-type S-cones, gnat1$^{-/-}$ S-cones, Nrl$^{-/-}$ cones, and rods recorded under the same "OS out" conditions. Each trace is scaled to unity at its peak. Data from Fig. 4E & F of Nikonov et al., 2006 (203) with permission from the Rockefeller University Press.

Table 3. Kinetic and Sensitivity Parameters of mouse rods and cones. I_d, dark current. t_p, the time to peak of the dim-flash response. τ_D, the dominant recovery time constant. $I_{1/2}$, Flash strength that elicited a half-maximal response, uncorrected for pigment bleaching for cones. Data from Table 1 of Nikanov, 2006 (203)

	I_d (pA)	t_p (ms)	τ_D (ms)	$I_{1/2}$ (photons μm^{-2} s^{-1})
S-cone (n = 21)	6 ± 1	73 ± 5	73 ± 10	$(1.8 \pm 0.6) \times 10^5$
M-cone (n = 8)	8 ± 2	63 ± 5	68 ± 18	$(2.5 \pm 0.9) \times 10^5$
Rods (n = 26)	20 ±6	205 ± 10	235 ± 20	350

18. Concluding remarks

In the past decade, great progress has been made in using mouse models to elucidate the mechanisms of activation and termination of the rod phototransduction pathway. Although there are still questions to be answered about the rod pathway such as the reproducibility of the single-photon response, the current frontier of phototransduction research lies in cones, which, for human vision, are far more important than rods. The recent success in recording from single mouse cones ushers in a new era in research on vertebrate cone phototransduction. Many long standing questions, e.g., the mechanisms for the enormous ability of cones to adapt to light, and the differences between rods and cones in sensitivity and kinetics, can now be addressed with a combination of mouse genetics and electrophysiology.

About the Author

Dr. Yingbin Fu is presently an Assistant Professor in the Department of Ophthalmology and Visual Science, John Moran Eye Center, University of Utah. He received his B.S in Biochemistry at Peking University, Beijing, China. After receiving his Ph.D. in Biochemistry at Michigan State University, East Lansing, Michigan, Dr. Fu's interests turned into retina and he joined Dr. King-Wai Yau's lab as a postdoc fellow at the Johns Hopkins University School of Medicine in Baltimore, Maryland. His postdoc experience turned out to be quite fruitful after he successfully brought his expertise in Xenopus and mouse genetics to the Yau lab, a world-class electrophysiology lab. Dr. Fu made significant discoveries on the role of visual pigments in rod and cone phototransduction, and the role of melanopsin in intrinsically photosensitive retinal ganglion cells. After moving to Utah to establish his own lab, Dr. Fu's research primarily focuses on two objectives: 1. To understand the mechanisms governing the assembly/trafficking of key photoreceptor proteins and its role in photoreceptor survival; 2. To perform functional characterization on genetic variants that are associated with age-related macular degeneration (AMD) with animal models. Email: yingbin.fu@hsc.utah.edu

References

1. Baylor D.A., Lamb T.D., Yau K.W. *The membrane current of single rod outer segments.* .J Physiol. 1979;288:589–611. PubMed PMID: 112242.
2. Carter-Dawson L.D., LaVail M.M. *Rods and cones in the mouse retina. I. Structural analysis using light and electron microscopy.* .J Comp Neurol. 1979;188(2):245–62. PubMed PMID: 500858.
3. Humphries M.M.et al. *Retinopathy induced in mice by targeted disruption of the rhodopsin gene.* .Nat Genet. 1997;15(2):216–9. PubMed PMID: 9020854.
4. Lem J.et al. *Morphological, physiological, and biochemical changes in rhodopsin knockout mice.* .Proc Natl Acad Sci U S A. 1999;96(2):736–41. PubMed PMID: 9892703.
5. Harosi F.I. *Absorption spectra and linear dichroism of some amphibian photoreceptors.* .J Gen Physiol. 1975;66(3):357–82. PubMed PMID: 808586.
6. Hagins W.A., Penn R.D., Yoshikami S. *Dark current and photocurrent in retinal rods.* .Biophys J. 1970;10(5):380–412. PubMed PMID: 5439318.
7. Hecht S., Shlaer S., Pirenne M.H. *Energy, Quanta, and Vision.* .J Gen Physiol. 1942;25(6):819–840. PubMed PMID: 19873316.
8. Young R.W. *The renewal of photoreceptor cell outer segments.* .J Cell Biol. 1967;33(1):61–72. PubMed PMID: 6033942.
9. Young R.W., Droz B. *The renewal of protein in retinal rods and cones.* .J Cell Biol. 1968;39(1):169–84. PubMed PMID: 5692679.
10. Young R.W., Bok D. *Participation of the retinal pigment epithelium in the rod outer segment renewal process.* .J Cell Biol. 1969;42(2):392–403. PubMed PMID: 5792328.
11. LaVail M.M. *Kinetics of rod outer segment renewal in the developing mouse retina.* .J Cell Biol. 1973;58(3):650–61. PubMed PMID: 4747920.
12. Caravaggio L.L., Bonting S.L. *The rhodopsin cycle in the developing vertebrate retina. II. Correlative study in normal mice and in mice with hereditary retinal degeneration.* .Exp Eye Res. 1963;2:12–9. PubMed PMID: 14018516.
13. Luo D.G., Yau K.W. *Rod sensitivity of neonatal mouse and rat.* .J Gen Physiol. 2005;126(3):263–9. PubMed PMID: 16129773.
14. Ratto G.M.et al. *Development of the light response in neonatal mammalian rods.* .Nature. 1991;351(6328):654–7. PubMed PMID: 2052091.
15. Baylor D.A., Lamb T.D., Yau K.W. *Responses of retinal rods to single photons.* .J Physiol. 1979;288:613–34. PubMed PMID: 112243.
16. Arshavsky V.Y., Lamb T.D., Pugh E.N. Jr. *G proteins and phototransduction.* .Annu Rev Physiol. 2002;64:153–87. PubMed PMID: 11826267.
17. Lamb T.D. *Gain and kinetics of activation in the G-protein cascade of phototransduction.* .Proc Natl Acad Sci U S A. 1996;93(2):566–70. PubMed PMID: 8570596.
18. Lamb T.D., Pugh E.N. Jr. *A quantitative account of the activation steps involved in phototransduction in amphibian photoreceptors.* .J Physiol. 1992;449:719–58. PubMed PMID: 1326052.
19. Pugh E.N. Jr, Lamb T.D. *Amplification and kinetics of the activation steps in phototransduction.* .Biochim Biophys Acta. 1993;1141(2-3):111–49. PubMed PMID: 8382952.
20. Applebury M.L.et al. *The murine cone photoreceptor: a single cone type expresses both S and M opsins with retinal spatial patterning.* .Neuron. 2000;27(3):513–23. PubMed PMID: 11055434.
21. Palczewski K.et al. *Crystal structure of rhodopsin: A G protein-coupled receptor.* .Science. 2000;289(5480):739–45. PubMed PMID: 10926528.
22. Stenkamp R.E., Teller D.C., Palczewski K. *Crystal structure of rhodopsin: a G-protein-coupled receptor.* .Chembiochem. 2002;3(10):963–7. PubMed PMID: 12362360.

23. Bridges, C.D.B., *The rhodopsin-porphyropsin visual system.* Handbook of Sensory Physiology, VII/1. Photochemistry of Vision, ed. H.J.A. Dartnall. Vol. VII/1. 1972, Berlin-Heidelberg-NewYork: Springer. 417-480.
24. Dartnall H.J., Lythgoe J.N. *The spectral clustering of visual pigments.* .Vision Res. 1965;5(3):81–100. PubMed PMID: 5862952.
25. Wald G. *On the Distribution of Vitamins a(1) and a(2).* .J Gen Physiol. 1939;22(3):391–415. PubMed PMID: 19873110.
26. Wald G. *Vitamin a in Eye Tissues.* .J Gen Physiol. 1935;18(6):905–915. PubMed PMID: 19872899.
27. Redmond T.M.et al. *Rpe65 is necessary for production of 11-cis-vitamin A in the retinal visual cycle.* .Nat Genet. 1998;20(4):344–51. PubMed PMID: 9843205.
28. Woodruff M.L.et al. *Spontaneous activity of opsin apoprotein is a cause of Leber congenital amaurosis.* .Nat Genet. 2003;35(2):158–64. PubMed PMID: 14517541.
29. Li T.et al. *Constitutive activation of phototransduction by K296E opsin is not a cause of photoreceptor degeneration.* .Proc Natl Acad Sci U S A. 1995;92(8):3551–5. PubMed PMID: 7724596.
30. Baylor D.A., Matthews G., Yau K.W. *Two components of electrical dark noise in toad retinal rod outer segments.* .J Physiol. 1980;309:591–621. PubMed PMID: 6788941.
31. Aho A.C.et al. *Low retinal noise in animals with low body temperature allows high visual sensitivity.* .Nature. 1988;334(6180):348–50. PubMed PMID: 3134619.
32. Autrum H. *Über kleinste Reize bei Sinnesorganen.* .Biologisches Zentralblatt. 1943;63:209–236.
33. Barlow H.B. *Retinal noise and absolute threshold.* .J Opt Soc Am. 1956;46(8):634–9. PubMed PMID: 13346424.
34. Donner K. *Noise and the absolute thresholds of cone and rod vision.* .Vision Res. 1992;32(5):853–66. PubMed PMID: 1604854.
35. Yau K.W., Matthews G., Baylor D.A. *Thermal activation of the visual transduction mechanism in retinal rods.* .Nature. 1979;279(5716):806–7. PubMed PMID: 109776.
36. Burns M.E.et al. *Dynamics of cyclic GMP synthesis in retinal rods.* .Neuron. 2002;36(1):81–91. PubMed PMID: 12367508.
37. Barlow H.B. *Increment thresholds at low intensities considered as signal/noise discriminations.* .J Physiol. 1957;136(3):469–88. PubMed PMID: 13429514.
38. Kefalov V.et al. *Role of visual pigment properties in rod and cone phototransduction.* .Nature. 2003;425(6957):526–31. PubMed PMID: 14523449.
39. Rieke F., Baylor D.A. *Origin and functional impact of dark noise in retinal cones.* .Neuron. 2000;26(1):181–6. PubMed PMID: 10798402.
40. Fu Y.et al. *Quantal noise from human red cone pigment.* .Nat Neurosci. 2008;11(5):565–71. PubMed PMID: 18425122.
41. Schnapf J.L.et al. *Visual transduction in cones of the monkey Macaca fascicularis.* .J Physiol. 1990;427:681–713. PubMed PMID: 2100987.
42. Schneeweis D.M., Schnapf J.L. *The photovoltage of macaque cone photoreceptors: adaptation, noise, and kinetics.* .J Neurosci. 1999;19(4):1203–16. PubMed PMID: 9952398.
43. Holcman D., Korenbrot J.I. *The limit of photoreceptor sensitivity: molecular mechanisms of dark noise in retinal cones.* .J Gen Physiol. 2005;125(6):641–60. PubMed PMID: 15928405.
44. Bridges C.D. *Spectroscopic properties of porphyropsins.* .Vision Res. 1967;7(5):349–69. PubMed PMID: 5613301.
45. Donner K., Firsov M.L., Govardovskii V.I. *The frequency of isomerization-like 'dark' events in rhodopsin and porphyropsin rods of the bull-frog retina.* .J Physiol. 1990;428:673–92. PubMed PMID: 2231428.
46. Ala-Laurila P.et al. *Chromophore switch from 11-cis-dehydroretinal (A2) to 11-cis-retinal (A1) decreases dark noise in salamander red rods.* .J Physiol. 2007;585(Pt 1):57–74. PubMed PMID: 17884920.
47. Kefalov V.J.et al. *Breaking the Covalent Bond- A Pigment Property that Contributes to Desensitization in Cones.* .Neuron. 2005;46(6):879–90. PubMed PMID: 15953417.

48. Miller J.L., Picones A., Korenbrot J.I. *Differences in transduction between rod and cone photoreceptors: an exploration of the role of calcium homeostasis.* .Curr Opin Neurobiol. 1994;4(4):488–95. PubMed PMID: 7812136.
49. Nakatani K., Yau K.W. *Sodium-dependent calcium extrusion and sensitivity regulation in retinal cones of the salamander.* .J Physiol. 1989;409:525–48. PubMed PMID: 2479741.
50. Tachibanaki S.et al. *Molecular mechanisms characterizing cone photoresponses.* .Photochem Photobiol. 2007;83(1):19–26. PubMed PMID: 16706600.
51. Ma J.et al. *A visual pigment expressed in both rod and cone photoreceptors.* .Neuron. 2001;32(3):451–61. PubMed PMID: 11709156.
52. Perry R.J., McNaughton P.A. *Response properties of cones from the retina of the tiger salamander.* .J Physiol. 1991;433:561–87. PubMed PMID: 1841958.
53. Hubbard R., Wald G. *Cis-trans isomers of vitamin A and retinene in the rhodopsin system.* .J Gen Physiol. 1952;36(2):269–315. PubMed PMID: 13011282.
54. Wald G. *The chemistry of rod vision.* .Science. 1951;113(2933):287–91. PubMed PMID: 14817272.
55. Lythgoe R.J., Quilliam J.P. *The relation of transient orange to visual purple and indicator yellow.* .J Physiol. 1938;94(3):399–410. PubMed PMID: 16995053.
56. Wald G. *On Rhodopsin in Solution.* .J Gen Physiol. 1938;21(6):795–832. PubMed PMID: 19873085.
57. Wald G., Durell J., St George C.C. *The light reaction in the bleaching of rhodopsin.* .Science. 1950;111(2877):179–81. PubMed PMID: 15403120.
58. Hubbard R., Kropf A. *The Action of Light on Rhodopsin.* .Proc Natl Acad Sci U S A. 1958;44(2):130–9. PubMed PMID: 16590155.
59. Okada T., Palczewski K. *Crystal structure of rhodopsin: implications for vision and beyond.* .Curr Opin Struct Biol. 2001;11(4):420–6. PubMed PMID: 11495733.
60. Imai H.et al. *Photochemical and biochemical properties of chicken blue-sensitive cone visual pigment.* .Biochemistry. 1997;36(42):12773–9. PubMed PMID: 9335534.
61. Kuwayama S.et al. *Amino acid residues responsible for the meta-III decay rates in rod and cone visual pigments.* .Biochemistry. 2005;44(6):2208–15. PubMed PMID: 15697246.
62. Shichida Y.et al. *Is chicken green-sensitive cone visual pigment a rhodopsin-like pigment? A comparative study of the molecular properties between chicken green and rhodopsin.* .Biochemistry. 1994;33(31):9040–4. PubMed PMID: 8049204.
63. Vought B.W.et al. *Photochemistry of the primary event in short-wavelength visual opsins at low temperature.* .Biochemistry. 1999;38(35):11287–97. PubMed PMID: 10471278.
64. Nathans J. *Determinants of visual pigment absorbance: identification of the retinylidene Schiff's base counterion in bovine rhodopsin.* .Biochemistry. 1990;29(41):9746–52. PubMed PMID: 1980212.
65. Sakmar T.P., Franke R.R., Khorana H.G. *Glutamic acid-113 serves as the retinylidene Schiff base counterion in bovine rhodopsin.* .Proc Natl Acad Sci U S A. 1989;86(21):8309–13. PubMed PMID: 2573063.
66. Zhukovsky E.A., Oprian D.D. *Effect of carboxylic acid side chains on the absorption maximum of visual pigments.* .Science. 1989;246(4932):928–30. PubMed PMID: 2573154.
67. Yan E.C.et al. *Retinal counterion switch in the photoactivation of the G protein-coupled receptor rhodopsin.* .Proc Natl Acad Sci U S A. 2003;100(16):9262–7. PubMed PMID: 12835420.
68. Dukkipati A.et al. *Phototransduction by vertebrate ultraviolet visual pigments: protonation of the retinylidene Schiff base following photobleaching.* .Biochemistry. 2002;41(31):9842–51. PubMed PMID: 12146950.
69. Kusnetzow A.K.et al. *Vertebrate ultraviolet visual pigments: protonation of the retinylidene Schiff base and a counterion switch during photoactivation.* .Proc Natl Acad Sci U S A. 2004;101(4):941–6. PubMed PMID: 14732701.
70. McBee J.K.et al. *Confronting complexity: the interlink of phototransduction and retinoid metabolism in the vertebrate retina.* .Prog Retin Eye Res. 2001;20(4):469–529. PubMed PMID: 11390257.
71. Calvert P.D.et al. *Membrane protein diffusion sets the speed of rod phototransduction.* .Nature. 2001;411(6833):90–4. PubMed PMID: 11333983.

72. Liang, Y., et al., *Rhodopsin signaling and organization in heterozygote rhodopsin knockout mice.* J Biol Chem, 2004
73. Kropf A. *Photosensitivity and quantum efficiency of photoisomerization in rhodopsin and retinal.* .Methods Enzymol. 1982;81:384–92. PubMed PMID: 7098885.
74. Leskov I.B.et al. *The gain of rod phototransduction: reconciliation of biochemical and electrophysiological measurements.* .Neuron. 2000;27(3):525–37. PubMed PMID: 11055435.
75. Heck M., Hofmann K.P. *Maximal rate and nucleotide dependence of rhodopsin-catalyzed transducin activation: initial rate analysis based on a double displacement mechanism.* .J Biol Chem. 2001;276(13):10000–9. PubMed PMID: 11116153.
76. Makino C.L., Wen X.H., Lem J. *Piecing together the timetable for visual transduction with transgenic animals.* .Curr Opin Neurobiol. 2003;13(4):404–12. PubMed PMID: 12965286.
77. Krispel C.M.et al. *RGS expression rate-limits recovery of rod photoresponses.* .Neuron. 2006;51(4):409–16. PubMed PMID: 16908407.
78. Fung B.K., Lieberman B.S., Lee R.H. *A third form of the G protein beta subunit. 2. Purification and biochemical properties.* .J Biol Chem. 1992;267(34):24782–8. PubMed PMID: 1332966.
79. Lee R.H.et al. *A third form of the G protein beta subunit. 1. Immunochemical identification and localization to cone photoreceptors.* .J Biol Chem. 1992;267(34):24776–81. PubMed PMID: 1447215.
80. Lerea C.L.et al. *Identification of specific transducin alpha subunits in retinal rod and cone photoreceptors.* .Science. 1986;234(4772):77–80. PubMed PMID: 3529395.
81. Peng Y.W.et al. *Retinal rods and cones have distinct G protein beta and gamma subunits.* .Proc Natl Acad Sci U S A. 1992;89(22):10882–6. PubMed PMID: 1438293.
82. Fukada Y.et al. *Phosphorylation of iodopsin, chicken red-sensitive cone visual pigment.* .Biochemistry. 1990;29(43):10102–6. PubMed PMID: 2271641.
83. Kokame K.et al. *Lipid modification at the N terminus of photoreceptor G-protein alpha-subunit.* .Nature. 1992;359(6397):749–52. PubMed PMID: 1436039.
84. Neubert T.A.et al. *The rod transducin alpha subunit amino terminus is heterogeneously fatty acylated.* .J Biol Chem. 1992;267(26):18274–7. PubMed PMID: 1326520.
85. Calvert P.D.et al. *Phototransduction in transgenic mice after targeted deletion of the rod transducin alpha -subunit.* .Proc Natl Acad Sci U S A. 2000;97(25):13913–8. PubMed PMID: 11095744.
86. Fu Y.et al. *Intrinsically photosensitive retinal ganglion cells detect light with a vitamin A-based photopigment, melanopsin.* .Proc Natl Acad Sci U S A. 2005;102(29):10339–44. PubMed PMID: 16014418.
87. Hattar S.et al. *Melanopsin and rod-cone photoreceptive systems account for all major accessory visual functions in mice.* .Nature. 2003;424(6944):76–81. PubMed PMID: 12808468.
88. Lyubarsky A.L.et al. *Functionally rodless mice: transgenic models for the investigation of cone function in retinal disease and therapy.* .Vision Res. 2002;42(4):401–15. PubMed PMID: 11853756.
89. Hao W.et al. *Evidence for two apoptotic pathways in light-induced retinal degeneration.* .Nat Genet. 2002;32(2):254–60. PubMed PMID: 12219089.
90. Kassai H.et al. *Farnesylation of retinal transducin underlies its translocation during light adaptation.* .Neuron. 2005;47(4):529–39. PubMed PMID: 16102536.
91. Sokolov M.et al. *Massive light-driven translocation of transducin between the two major compartments of rod cells: a novel mechanism of light adaptation.* .Neuron. 2002;34(1):95–106. PubMed PMID: 11931744.
92. Elias R.V.et al. *Temporal kinetics of the light/dark translocation and compartmentation of arrestin and alpha-transducin in mouse photoreceptor cells.* .Mol Vis. 2004;10:672–81. PubMed PMID: 15467522.
93. Coleman J.E., Semple-Rowland S.L. *GC1 deletion prevents light-dependent arrestin translocation in mouse cone photoreceptor cells.* .Invest Ophthalmol Vis Sci. 2005;46(1):12–6. PubMed PMID: 15623748.
94. Kennedy M.J., Dunn F.A., Hurley J.B. *Visual pigment phosphorylation but not transducin translocation can contribute to light adaptation in zebrafish cones.* .Neuron. 2004;41(6):915–28. PubMed PMID: 15046724.
95. Chen J.et al. *Light Threshold-Controlled Cone {alpha}-Transducin Translocation.* .Invest Ophthalmol Vis Sci. 2007;48(7):3350–5. PubMed PMID: 17591908.

96. Baehr W., Devlin M.J., Applebury M.L. *Isolation and characterization of cGMP phosphodiesterase from bovine rod outer segments.* .J Biol Chem. 1979;254(22):11669–77. PubMed PMID: 227876.
97. Deterre P.et al. *cGMP phosphodiesterase of retinal rods is regulated by two inhibitory subunits.* .Proc Natl Acad Sci U S A. 1988;85(8):2424–8. PubMed PMID: 2833739.
98. Hurley J.B., Stryer L. *Purification and characterization of the gamma regulatory subunit of the cyclic GMP phosphodiesterase from retinal rod outer segments.* .J Biol Chem. 1982;257(18):11094–9. PubMed PMID: 6286681.
99. Anant J.S.et al. *In vivo differential prenylation of retinal cyclic GMP phosphodiesterase catalytic subunits.* .J Biol Chem. 1992;267(2):687–90. PubMed PMID: 1309771.
100. Qin N., Baehr W. *Expression and mutagenesis of mouse rod photoreceptor cGMP phosphodiesterase.* .J Biol Chem. 1994;269(5):3265–71. PubMed PMID: 8106363.
101. Pugh, E.N., Jr. and T.D. Lamb, *Phototransduction in Vertebrate Rods and Cones: Molecular Mechanisms of Amplification, Recovery and Light Adaptation.*, in *Handbook of Biological Physics*, D.G. Stavenga, W.J. de Grip, and E.N. Pugh, Jr., Editors. 2000, Elsevier Science B.V.: Amsterdam. p. 183-255.
102. Tsang S.H.et al. *Retinal degeneration in mice lacking the gamma subunit of the rod cGMP phosphodiesterase.* .Science. 1996;272(5264):1026–9. PubMed PMID: 8638127.
103. Carter-Dawson L.D., LaVail M.M., Sidman R.L. *Differential effect of the rd mutation on rods and cones in the mouse retina.* .Invest Ophthalmol Vis Sci. 1978;17(6):489–98. PubMed PMID: 659071.
104. LaVail M.M., Sidman R.L. *C57BL-6J mice with inherited retinal degeneration.* .Arch Ophthalmol. 1974;91(5):394–400. PubMed PMID: 4595403.
105. Bowes C.et al. *Retinal degeneration in the rd mouse is caused by a defect in the beta subunit of rod cGMP-phosphodiesterase.* .Nature. 1990;347(6294):677–80. PubMed PMID: 1977087.
106. Pittler S.J., Baehr W. *Identification of a nonsense mutation in the rod photoreceptor cGMP phosphodiesterase beta-subunit gene of the rd mouse.* .Proc Natl Acad Sci U S A. 1991;88(19):8322–6. PubMed PMID: 1656438.
107. Freedman M.S.et al. *Regulation of mammalian circadian behavior by non-rod, non-cone, ocular photoreceptors.* .Science. 1999;284(5413):502–4. PubMed PMID: 10205061.
108. Lucas R.J.et al. *Regulation of the mammalian pineal by non-rod, non-cone, ocular photoreceptors.* .Science. 1999;284(5413):505–7. PubMed PMID: 10205062.
109. Tsang S.H.et al. *Role for the target enzyme in deactivation of photoreceptor G protein in vivo.* .Science. 1998;282(5386):117–21. PubMed PMID: 9756475.
110. Luo D.G., Xue T., Yau K.W. *How vision begins: an odyssey.* .Proc Natl Acad Sci U S A. 2008;105(29):9855–62. PubMed PMID: 18632568.
111. Fesenko E.E., Kolesnikov S.S., Lyubarsky A.L. *Induction by cyclic GMP of cationic conductance in plasma membrane of retinal rod outer segment.* .Nature. 1985;313(6000):310–3. PubMed PMID: 2578616.
112. Yau K.W., Nakatani K. *Light-suppressible, cyclic GMP-sensitive conductance in the plasma membrane of a truncated rod outer segment.* .Nature. 1985;317(6034):252–5. PubMed PMID: 2995816.
113. Kaupp U.B., Seifert R. *Cyclic nucleotide-gated ion channels.* .Physiol Rev. 2002;82(3):769–824. PubMed PMID: 12087135.
114. Molday, R.S. and U.B. Kaupp, *Ion channels of vertebrate photoreceptors*, in *Handbook of Biological Physics*, D.G. Stavenga, W.J. de Grip, and E.N. Pugh, Jr., Editors. 2000, Elsevier Science B.V.: Amsterdam.
115. Yau K.W. *Phototransduction mechanism in retinal rods and cones. The Friedenwald Lecture.* .Invest Ophthalmol Vis Sci. 1994;35(1):9–32. PubMed PMID: 7507907.
116. Karpen J.W.et al. *Gating kinetics of the cyclic-GMP-activated channel of retinal rods: flash photolysis and voltage-jump studies.* .Proc Natl Acad Sci U S A. 1988;85(4):1287–91. PubMed PMID: 2448798.
117. Weitz D.et al. *Subunit stoichiometry of the CNG channel of rod photoreceptors.* .Neuron. 2002;36(5):881–9. PubMed PMID: 12467591.
118. Zheng J., Trudeau M.C., Zagotta W.N. *Rod cyclic nucleotide-gated channels have a stoichiometry of three CNGA1 subunits and one CNGB1 subunit.* .Neuron. 2002;36(5):891–6. PubMed PMID: 12467592.

119. Zhong H.et al. *The heteromeric cyclic nucleotide-gated channel adopts a 3A:1B stoichiometry.* .Nature. 2002;420(6912):193–8. PubMed PMID: 12432397.
120. Peng C., Rich E.D., Varnum M.D. *Subunit configuration of heteromeric cone cyclic nucleotide-gated channels.* .Neuron. 2004;42(3):401–10. PubMed PMID: 15134637.
121. Biel M.et al. *Selective loss of cone function in mice lacking the cyclic nucleotide-gated channel CNG3.* .Proc Natl Acad Sci U S A. 1999;96(13):7553–7. PubMed PMID: 10377453.
122. Finn J.T., Grunwald M.E., Yau K.W. *Cyclic nucleotide-gated ion channels: an extended family with diverse functions.* .Annu Rev Physiol. 1996;58:395–426. PubMed PMID: 8815801.
123. Matulef K., Zagotta W.N. *Cyclic nucleotide-gated ion channels.* .Annu Rev Cell Dev Biol. 2003;19:23–44. PubMed PMID: 14570562.
124. Dryja T.P.et al. *Mutations in the gene encoding the alpha subunit of the rod cGMP-gated channel in autosomal recessive retinitis pigmentosa.* .Proc Natl Acad Sci U S A. 1995;92(22):10177–81. PubMed PMID: 7479749.
125. Kohl S.et al. *Total colourblindness is caused by mutations in the gene encoding the alpha-subunit of the cone photoreceptor cGMP-gated cation channel.* .Nat Genet. 1998;19(3):257–9. PubMed PMID: 9662398.
126. Kohl S.et al. *Mutations in the CNGB3 gene encoding the beta-subunit of the cone photoreceptor cGMP-gated channel are responsible for achromatopsia (ACHM3) linked to chromosome 8q21.* .Hum Mol Genet. 2000;9(14):2107–16. PubMed PMID: 10958649.
127. Huttl S.et al. *Impaired channel targeting and retinal degeneration in mice lacking the cyclic nucleotide-gated channel subunit CNGB1.* .J Neurosci. 2005;25(1):130–8. PubMed PMID: 15634774.
128. Chen C., Nakatani K., Koutalos Y. *Free magnesium concentration in salamander photoreceptor outer segments.* .J Physiol. 2003;553(Pt 1):125–35. PubMed PMID: 14500766.
129. Kuhn H., Wilden U. *Deactivation of photoactivated rhodopsin by rhodopsin-kinase and arrestin.* .J Recept Res. 1987;7(1-4):283–98. PubMed PMID: 3040978.
130. Wilden U., Hall S.W., Kuhn H. *Phosphodiesterase activation by photoexcited rhodopsin is quenched when rhodopsin is phosphorylated and binds the intrinsic 48-kDa protein of rod outer segments.* .Proc Natl Acad Sci U S A. 1986;83(5):1174–8. PubMed PMID: 3006038.
131. Ohguro H.et al. *Rhodopsin phosphorylation and dephosphorylation in vivo.* .J Biol Chem. 1995;270(24):14259–62. PubMed PMID: 7782279.
132. Mendez A.et al. *Rapid and reproducible deactivation of rhodopsin requires multiple phosphorylation sites.* .Neuron. 2000;28(1):153–64. PubMed PMID: 11086991.
133. Gibson S.K., Parkes J.H., Liebman P.A. *Phosphorylation modulates the affinity of light-activated rhodopsin for G protein and arrestin.* .Biochemistry. 2000;39(19):5738–49. PubMed PMID: 10801324.
134. Hamer R.D.et al. *Multiple steps of phosphorylation of activated rhodopsin can account for the reproducibility of vertebrate rod single-photon responses.* .J Gen Physiol. 2003;122(4):419–44. PubMed PMID: 12975449.
135. Rieke F., Baylor D.A. *Origin of reproducibility in the responses of retinal rods to single photons.* .Biophys J. 1998;75(4):1836–57. PubMed PMID: 9746525.
136. Whitlock G.G., Lamb T.D. *Variability in the time course of single photon responses from toad rods: termination of rhodopsin's activity.* .Neuron. 1999;23(2):337–51. PubMed PMID: 10399939.
137. Doan T.et al. *Multiple phosphorylation sites confer reproducibility of the rod's single-photon responses.* .Science. 2006;313(5786):530–3. PubMed PMID: 16873665.
138. Chen J.et al. *Mechanisms of rhodopsin inactivation in vivo as revealed by a COOH-terminal truncation mutant.* .Science. 1995;267(5196):374–7. PubMed PMID: 7824934.
139. Chen C.K.et al. *Abnormal photoresponses and light-induced apoptosis in rods lacking rhodopsin kinase.* .Proc Natl Acad Sci U S A. 1999;96(7):3718–22. PubMed PMID: 10097103.
140. Kuwayama S.et al. *Conserved proline residue at position 189 in cone visual pigments as a determinant of molecular properties different from rhodopsins.* .Biochemistry. 2002;41(51):15245–52. PubMed PMID: 12484762.
141. Rinner O.et al. *Knockdown of cone-specific kinase GRK7 in larval zebrafish leads to impaired cone response recovery and delayed dark adaptation.* .Neuron. 2005;47(2):231–42. PubMed PMID: 16039565.

142. Tachibanaki S.et al. *Highly effective phosphorylation by G protein-coupled receptor kinase 7 of light-activated visual pigment in cones.* .Proc Natl Acad Sci U S A. 2005;102(26):9329–34. PubMed PMID: 15958532.
143. Tachibanaki S., Tsushima S., Kawamura S. *Low amplification and fast visual pigment phosphorylation as mechanisms characterizing cone photoresponses.* .Proc Natl Acad Sci U S A. 2001;98(24):14044–9. PubMed PMID: 11707584.
144. Weiss E.R.et al. *Species-specific differences in expression of G-protein-coupled receptor kinase (GRK) 7 and GRK1 in mammalian cone photoreceptor cells: implications for cone cell phototransduction.* .J Neurosci. 2001;21(23):9175–84. PubMed PMID: 11717351.
145. Lyubarsky A.L.et al. *Mice lacking G-protein receptor kinase 1 have profoundly slowed recovery of cone-driven retinal responses.* .J Neurosci. 2000;20(6):2209–17. PubMed PMID: 10704496.
146. Nikonov S.S.et al. *Photoreceptors of Nrl -/- mice coexpress functional S- and M-cone opsins having distinct inactivation mechanisms.* .J Gen Physiol. 2005;125(3):287–304. PubMed PMID: 15738050.
147. Wada Y.et al. *GRK1 and GRK7: unique cellular distribution and widely different activities of opsin phosphorylation in the zebrafish rods and cones.* .J Neurochem. 2006;98(3):824–37. PubMed PMID: 16787417.
148. Tachibanaki, S., et al., *Molecular Mechanisms Characterizing Cone Photoresponses.* Photochem Photobiol, 2006
149. Chen C.K.et al. *Ca(2+)-dependent interaction of recoverin with rhodopsin kinase.* .J Biol Chem. 1995;270(30):18060–6. PubMed PMID: 7629115.
150. Kawamura S. *Light-sensitivity modulating protein in frog rods.* .Photochem Photobiol. 1992;56(6):1173–80. PubMed PMID: 1337215.
151. Kawamura S. *Rhodopsin phosphorylation as a mechanism of cyclic GMP phosphodiesterase regulation by S-modulin.* .Nature. 1993;362(6423):855–7. PubMed PMID: 8386803.
152. Klenchin V.A., Calvert P.D., Bownds M.D. *Inhibition of rhodopsin kinase by recoverin. Further evidence for a negative feedback system in phototransduction.* .J Biol Chem. 1995;270(27):16147–52. PubMed PMID: 7608179.
153. Otto-Bruc A.E.et al. *Phosphorylation of photolyzed rhodopsin is calcium-insensitive in retina permeabilized by alpha-toxin.* .Proc Natl Acad Sci U S A. 1998;95(25):15014–9. PubMed PMID: 9844007.
154. Makino C.L.et al. *Recoverin regulates light-dependent phosphodiesterase activity in retinal rods.* .J Gen Physiol. 2004;123(6):729–41. PubMed PMID: 15173221.
155. Xu J.et al. *Prolonged photoresponses in transgenic mouse rods lacking arrestin.* .Nature. 1997;389(6650):505–9. PubMed PMID: 9333241.
156. Burns M.E.et al. *Deactivation of phosphorylated and nonphosphorylated rhodopsin by arrestin splice variants.* .J Neurosci. 2006;26(3):1036–44. PubMed PMID: 16421323.
157. Smith W.C.et al. *A splice variant of arrestin. Molecular cloning and localization in bovine retina.* .J Biol Chem. 1994;269(22):15407–10. PubMed PMID: 7515057.
158. Palczewski K.et al. *Characterization of a truncated form of arrestin isolated from bovine rod outer segments.* .Protein Sci. 1994;3(2):314–24. PubMed PMID: 8003967.
159. Pulvermuller A.et al. *Functional differences in the interaction of arrestin and its splice variant, p44, with rhodopsin.* .Biochemistry. 1997;36(30):9253–60. PubMed PMID: 9230059.
160. Langlois G.et al. *Responses of the phototransduction cascade to dim light.* .Proc Natl Acad Sci U S A. 1996;93(10):4677–82. PubMed PMID: 8643463.
161. Broekhuyse R.M.et al. *Light induced shift and binding of S-antigen in retinal rods.* .Curr Eye Res. 1985;4(5):613–8. PubMed PMID: 2410196.
162. Mangini N.J., Pepperberg D.R. *Immunolocalization of 48K in rod photoreceptors. Light and ATP increase OS labeling.* .Invest Ophthalmol Vis Sci. 1988;29(8):1221–34. PubMed PMID: 3138199.
163. Philp N.J., Chang W., Long K. *Light-stimulated protein movement in rod photoreceptor cells of the rat retina.* .FEBS Lett. 1987;225(1-2):127–32. PubMed PMID: 2826235.
164. Whelan J.P., McGinnis J.F. *Light-dependent subcellular movement of photoreceptor proteins.* .J Neurosci Res. 1988;20(2):263–70. PubMed PMID: 3172281.

165. Craft C.M., Whitmore D.H. *The arrestin superfamily: cone arrestins are a fourth family.* .FEBS Lett. 1995;362(2):247–55. PubMed PMID: 7720881.
166. Murakami A.et al. *X-arrestin: a new retinal arrestin mapping to the X chromosome.* .FEBS Lett. 1993;334(2):203–9. PubMed PMID: 8224247.
167. Zhu, X., et al., *Rod arrestin expression and function in cone photoreceptors.* Invest. Ophthalmol. Vis. Sci., 2005. 46: p. E-Abstract 1179.
168. Nikonov S.S.et al. *Mouse cones require an arrestin for normal inactivation of phototransduction.* .Neuron. 2008;59(3):462–74. PubMed PMID: 18701071.
169. He W., Cowan C.W., Wensel T.G. *RGS9, a GTPase accelerator for phototransduction.* .Neuron. 1998;20(1):95–102. PubMed PMID: 9459445.
170. Makino E.R.et al. *The GTPase activating factor for transducin in rod photoreceptors is the complex between RGS9 and type 5 G protein beta subunit.* .Proc Natl Acad Sci U S A. 1999;96(5):1947–52. PubMed PMID: 10051575.
171. Hu G., Wensel T.G. *R9AP, a membrane anchor for the photoreceptor GTPase accelerating protein, RGS9-1.* .Proc Natl Acad Sci U S A. 2002;99(15):9755–60. PubMed PMID: 12119397.
172. Chen C.K.et al. *Slowed recovery of rod photoresponse in mice lacking the GTPase accelerating protein RGS9-1.* .Nature. 2000;403(6769):557–60. PubMed PMID: 10676965.
173. Chen C.K.et al. *Instability of GGL domain-containing RGS proteins in mice lacking the G protein beta-subunit Gbeta5.* .Proc Natl Acad Sci U S A. 2003;100(11):6604–9. PubMed PMID: 12738888.
174. Keresztes G.et al. *Absence of the RGS9.Gbeta5 GTPase-activating complex in photoreceptors of the R9AP knockout mouse.* .J Biol Chem. 2004;279(3):1581–4. PubMed PMID: 14625292.
175. Krispel C.M.et al. *Novel form of adaptation in mouse retinal rods speeds recovery of phototransduction.* .J Gen Physiol. 2003;122(6):703–12. PubMed PMID: 14610022.
176. Angleson J.K., Wensel T.G. *Enhancement of rod outer segment GTPase accelerating protein activity by the inhibitory subunit of cGMP phosphodiesterase.* .J Biol Chem. 1994;269(23):16290–6. PubMed PMID: 8206935.
177. Skiba N.P., Hopp J.A., Arshavsky V.Y. *The effector enzyme regulates the duration of G protein signaling in vertebrate photoreceptors by increasing the affinity between transducin and RGS protein.* .J Biol Chem. 2000;275(42):32716–20. PubMed PMID: 10973941.
178. Cowan C.W.et al. *High expression levels in cones of RGS9, the predominant GTPase accelerating protein of rods.* .Proc Natl Acad Sci U S A. 1998;95(9):5351–6. PubMed PMID: 9560279.
179. Zhang X., Wensel T.G., Kraft T.W. *GTPase regulators and photoresponses in cones of the eastern chipmunk.* .J Neurosci. 2003;23(4):1287–97. PubMed PMID: 12598617.
180. Krispel C.M.et al. *Prolonged photoresponses and defective adaptation in rods of Gbeta5-/- mice.* .J Neurosci. 2003;23(18):6965–71. PubMed PMID: 12904457.
181. Nikonov S., Engheta N., Pugh E.N. Jr. *Kinetics of recovery of the dark-adapted salamander rod photoresponse.* .J Gen Physiol. 1998;111(1):7–37. PubMed PMID: 9417132.
182. Pepperberg D.R.et al. *Light-dependent delay in the falling phase of the retinal rod photoresponse.* .Vis Neurosci. 1992;8(1):9–18. PubMed PMID: 1739680.
183. Sagoo M.S., Lagnado L. *G-protein deactivation is rate-limiting for shut-off of the phototransduction cascade.* .Nature. 1997;389(6649):392–5. PubMed PMID: 9311782.
184. Cooper N.et al. *The bovine rod outer segment guanylate cyclase, ROS-GC, is present in both outer segment and synaptic layers of the retina.* .J Mol Neurosci. 1995;6(3):211–22. PubMed PMID: 8672403.
185. Liu X.et al. *Ultrastructural localization of retinal guanylate cyclase in human and monkey retinas.* .Exp Eye Res. 1994;59(6):761–8. PubMed PMID: 7698269.
186. Lowe D.G.et al. *Cloning and expression of a second photoreceptor-specific membrane retina guanylyl cyclase (RetGC), RetGC-2.* .Proc Natl Acad Sci U S A. 1995;92(12):5535–9. PubMed PMID: 7777544.
187. Baehr W.et al. *The function of guanylate cyclase 1 and guanylate cyclase 2 in rod and cone photoreceptors.* .J Biol Chem. 2007;282(12):8837–47. PubMed PMID: 17255100.

188. Yang R.B.et al. *Disruption of a retinal guanylyl cyclase gene leads to cone-specific dystrophy and paradoxical rod behavior.* .J Neurosci. 1999;19(14):5889–97. PubMed PMID: 10407028.
189. Burns M.E., Baylor D.A. *Activation, deactivation, and adaptation in vertebrate photoreceptor cells.* .Annu Rev Neurosci. 2001;24:779–805. PubMed PMID: 11520918.
190. Fain G.L.et al. *Adaptation in vertebrate photoreceptors.* .Physiol Rev. 2001;81(1):117–151. PubMed PMID: 11152756.
191. Cuenca N.et al. *The localization of guanylyl cyclase-activating proteins in the mammalian retina.* .Invest Ophthalmol Vis Sci. 1998;39(7):1243–50. PubMed PMID: 9620085.
192. Howes K.et al. *Gene array and expression of mouse retina guanylate cyclase activating proteins 1 and 2.* .Invest Ophthalmol Vis Sci. 1998;39(6):867–75. PubMed PMID: 9579466.
193. Mendez A.et al. *Role of guanylate cyclase-activating proteins (GCAPs) in setting the flash sensitivity of rod photoreceptors.* .Proc Natl Acad Sci U S A. 2001;98(17):9948–53. PubMed PMID: 11493703.
194. Haeseleer F.et al. *Molecular characterization of a third member of the guanylyl cyclase-activating protein subfamily.* .J Biol Chem. 1999;274(10):6526–35. PubMed PMID: 10037746.
195. Krylov D.M.et al. *Mapping sites in guanylyl cyclase activating protein-1 required for regulation of photoreceptor membrane guanylyl cyclases.* .J Biol Chem. 1999;274(16):10833–9. PubMed PMID: 10196159.
196. Dizhoor A.M.et al. *The human photoreceptor membrane guanylyl cyclase, RetGC, is present in outer segments and is regulated by calcium and a soluble activator.* .Neuron. 1994;12(6):1345–52. PubMed PMID: 7912093.
197. Laura R.P., Hurley J.B. *The kinase homology domain of retinal guanylyl cyclases 1 and 2 specifies the affinity and cooperativity of interaction with guanylyl cyclase activating protein-2.* .Biochemistry. 1998;37(32):11264–71. PubMed PMID: 9698373.
198. Howes K.A.et al. *GCAP1 rescues rod photoreceptor response in GCAP1/GCAP2 knockout mice.* .Embo J. 2002;21(7):1545–54. PubMed PMID: 11927539.
199. Pennesi M.E.et al. *Guanylate cyclase-activating protein (GCAP) 1 rescues cone recovery kinetics in GCAP1/GCAP2 knockout mice.* .Proc Natl Acad Sci U S A. 2003;100(11):6783–8. PubMed PMID: 12732716.
200. Makino C.L.et al. *A role for GCAP2 in regulating the photoresponse. Guanylyl cyclase activation and rod electrophysiology in GUCA1B knock-out mice.* .J Biol Chem. 2008;283(43):29135–43. PubMed PMID: 18723510.
201. Kawamura, S., et al., *Mechanism of rapid visual pigment phosphorylation in carp cones.* Invest. Ophthalmol. Vis. Sci., 2004. 45: p. E-Abstract 2207.
202. Shimauchi-Matsukawa Y.et al. *Isolation and characterization of visual pigment kinase-related genes in carp retina: polyphyly in GRK1 subtypes, GRK1A and 1B.* .Mol Vis. 2005;11:1220–8. PubMed PMID: 16402022.
203. Nikonov S.S.et al. *Physiological features of the S- and M-cone photoreceptors of wild-type mice from single-cell recordings.* .J Gen Physiol. 2006;127(4):359–74. PubMed PMID: 16567464.
204. Yau K.W., McNaughton P.A., Hodgkin A.L. *Effect of ions on the light-sensitive current in retinal rods.* .Nature. 1981;292(5823):502–5. PubMed PMID: 6265800.
205. Mears A.J.et al. *Nrl is required for rod photoreceptor development.* .Nat Genet. 2001;29(4):447–52. PubMed PMID: 11694879.
206. Daniele L.L.et al. *Cone-like morphological, molecular, and electrophysiological features of the photoreceptors of the Nrl knockout mouse.* .Invest Ophthalmol Vis Sci. 2005;46(6):2156–67. PubMed PMID: 15914637.
207. Fei Y., Hughes T.E. *Transgenic expression of the jellyfish green fluorescent protein in the cone photoreceptors of the mouse.* .Vis Neurosci. 2001;18(4):615–23. PubMed PMID: 11829307.
208. Rader A.J.et al. *Identification of core amino acids stabilizing rhodopsin.* .Proc Natl Acad Sci U S A. 2004;101(19):7246–51. PubMed PMID: 15123809.
209. Stenkamp D.L., Cameron D.A. *Cellular pattern formation in the retina: retinal regeneration as a model system.* .Mol Vis. 2002;8:280–93. PubMed PMID: 12181523.
210. Lobanova E.S.et al. *Transducin gamma-subunit sets expression levels of alpha- and beta-subunits and is crucial for rod viability.* .J Neurosci. 2008;28(13):3510–20. PubMed PMID: 18367617.

211. Krispel C.M.et al. *Phosducin regulates the expression of transducin betagamma subunits in rod photoreceptors and does not contribute to phototransduction adaptation.* .J Gen Physiol. 2007;130(3):303–12. PubMed PMID: 17724163.
212. Tsang S.H.et al. *GAP-independent termination of photoreceptor light response by excess gamma subunit of the cGMP-phosphodiesterase.* .J Neurosci. 2006;26(17):4472–80. PubMed PMID: 16641226.
213. Zhang Y.et al. *Knockout of GARPs and the beta-subunit of the rod cGMP-gated channel disrupts disk morphogenesis and rod outer segment structural integrity.* .J Cell Sci. 2009;122(Pt 8):1192–200. PubMed PMID: 19339551.
214. Sampath A.P.et al. *Recoverin improves rod-mediated vision by enhancing signal transmission in the mouse retina.* .Neuron. 2005;46(3):413–20. PubMed PMID: 15882641.
215. Lyubarsky A.L.et al. *RGS9-1 is required for normal inactivation of mouse cone phototransduction.* .Mol Vis. 2001;7:71–8. PubMed PMID: 11262419.
216. Gurevich E.V., Gurevich V.V. *Arrestins: ubiquitous regulators of cellular signaling pathways.* .Genome Biol. 2006;7(9):236. PubMed PMID: 17020596.
217. Baylor D.A., Nunn B.J., Schnapf J.L. *The photocurrent, noise and spectral sensitivity of rods of the monkey Macaca fascicularis.* .J Physiol. 1984;357:575–607. PubMed PMID: 6512705.
218. Baylor D.A., Nunn B.J. *Electrical properties of the light-sensitive conductance of rods of the salamander Ambystoma tigrinum.* .J Physiol. 1986;371:115–45. PubMed PMID: 2422346.
219. Brann M.R., Cohen L.V. *Diurnal expression of transducin mRNA and translocation of transducin in rods of rat retina.* .Science. 1987;235(4788):585–7. PubMed PMID: 3101175.

S-Potentials and Horizontal Cells

Ido Perlman, PhD,[1] Helga Kolb, PhD,[2] and Ralph Nelson, PhD[3]

Created: May 1, 2007; Updated: December 30, 2011.

1. Introduction

Horizontal cells are the interneurons of distal vertebrate retina. They provide the pathways for both local and long range interactions between photoreceptors. These interactions are called feedback signals. Feedback signals adjust the gain of photoreceptor synaptic output, both as seen in the horizontal cells themselves and in the adjacent, proximally projecting bipolar cells. In forming a distal, lateral synaptic network, horizontal cells enrich not only their own physiology but that of presynaptic and postsynaptic partners. They generate spatial opponency in both cones and bipolar cells. They also generate color opponency in cones, bipolar cells, and chromatic horizontal-cell subtypes. The actions of horizontal cells propagate forward in the retina, can be identified in the physiology of retinal ganglion cells, and in visual perception. Horizontal cell actions are in turn tuned by neuromodulators released by other retinal neurons.

2. History

The first intracellular, light-evoked responses recorded in the vertebrate retina were slow, negative going changes in membrane potential that lasted for as long as the light stimulus was present (Fig. 1). Before the morphological source of these responses became clear, they were called simply S-potentials (1). As shown in figure 1, S-potentials are membrane hyperpolarizations that last for as long as the light stimulus is present. The graded character of the S-potential is evident in figure 1A. The brighter the stimulus, the larger the amplitude of the S-potential until a saturation level is reached. In figure 1B, the duration of a light stimulus of fixed intensity is altered in order to examine the temporal properties of S-potentials. For long stimuli, the S-potential only changes in duration but the amplitude remains constant (2 leftmost responses in Fig. 1B). Further reduction in the stimulus duration causes a decrease in amplitude (Fig. 1B). This illustrates the temporal summation of the S-potential, following Bloch's law. Up to certain stimulus durations, in this case about 10 msec, the amplitude is directly related to the quantal content of the stimulus (quantal flux multiplied by duration), while for stimuli of longer duration, the amplitude is related to the quantal flux, that is, the rate of quantal absorption by photoreceptors (1). In S-potentials this 'critical duration' varies considerably with stimulus conditions (2). It is likely that S-potentials were named in honor of their discoverer, Gunnar Svaetichin, although 'slow potential' is another common interpretation.

S-potentials puzzled neurophysiologists of the 1950s when they were first described. At that time, neurons were thought only to be depolarized by synaptic inputs (inside becoming more positive relative to outside), thus having their inside-negative resting membrane potentials become reduced. This depolarization was thought of as excitation, and if the excitation was large enough, action potentials, or nerve spikes, were generated to transfer signals down the length of the nerve-cell axon. S-potentials, however, were not depolarized by light, but rather hyperpolarized, and did not fire action potentials, even with the brightest light stimuli.

At first, the cell type of origin for S-potentials was not really known other than that microelectrode tips were somewhere in the outer retina. In fact, initially Svaetichin thought S-potentials arose from cones (1). However, later intracellular marking techniques, in which dyes were injected from the electrode tips into the cytoplasm of

Author Affiliations: 1 Technion - Israel Institute of Technology, Haifa; Email: iperlman@tx.technion.ac.il. 2 Moran Eye Institute, University of Utah School of Medicine, Salt Lake City; Email: Helga.kolb@hsc.utah.edu. 3 National Institute of Neurological Disorders and Stroke, NIH, Bethesda MD; Email: nelsonr@ninds.nih.gov.

Corresponding author.

the recorded neuron, revealed that horizontal cells, second order neurons postsynaptic to cones, were the source of the S-potentials (3, 4). Since being first described in fish retinas, S-potentials have been recorded from retinal horizontal cells in all vertebrate classes. These include both cold-blooded vertebrates (4-13), household mammals (14-20) and primates (21-26). Horizontal cells have now been studied by numerous investigators using anatomical, biochemical, pharmacological and electrophysiological techniques. In this chapter, we shall try to summarize our current knowledge of horizontal cells in the vertebrate retina.

3. Morphology and Circuitry

Horizontal cells are second order neurons contacting photoreceptors directly all across the plane of the retina's outer plexiform layer. These cell types were first described as huge brick-like structures occupying much of the inner nuclear layer in the fish retina (27, 28). Early interpretations assumed these cells to be glial cells, mainly because they gave rise to hyperpolarizing slow responses to light (S-potentials) rather than true depolarizing spikes like 'real neurons'. Now we know horizontal cells to be true neurons that make true, if unique, synapses and exhibit most of the structural and ultrastructural characteristics of neurons. Through Golgi staining, intracellular marking and immunostaining techniques we have learned that horizontal cells can adapt various morphologies in the retinas of different vertebrate species (6, 29-44).

Selective rod and cone contacts of horizontal cells

There are two morphological types of horizontal cell in the majority of terrestrial vertebrate retinas, B-type cells with axons and A-type cells that are axonless (Fig. 2a). In mammals the dendrites of both B- and A-types contact cones, while the axon terminals of B-type cells contact rods (gray area, Fig. 1A). In birds and reptiles, horizontal cells come in further axonless subtypes with color specific cone connections (Fig. 2a, axonless). Figure 2a shows the morphologies of these different types of horizontal cells in different species as indicated. Also shown are the spectral types of cone (red, blue and green dots) that connect with each type.

In fish retinas, short-axon or axonless horizontal cells (type H4) contact only rods (45, 46), while the dendrites of all axon bearing cells contact only cones (Fig. 2b). The axons of fish horizontal cells do not contact photoreceptors. There are multiple types of axon bearing, cone-contacting, horizontal cells in fish (H1, H2, H3), each with different patterns of cone selectivity. In the zebrafish example (Fig. 2b), most are excited by 2 of the 4 cone types and avoid excitatory input from other types. The exception is the H3 UV triphasic type that appears to be selectively excited by either UV or blue cones. H2 and H3 types are color opponent in wavelength physiology, but H1 is not.

Mammalian and reptilian B-type horizontal cells code changes in brightness but do not discriminate color. They regulate adaptational and spatial responses of cones and bipolar cells. These are luminosity type horizontal cells whose physiology will be discussed later. These B-Type cells can often be identified with antibodies against calcium binding proteins (47-49) and some contain the neurotransmitter GABA (47, 50, 51). In turtle retina, acetylcholine has been located in H1 type horizontal cell dendrites where they invaginate the cone pedicles (47). H1 type cells of turtles are morphologically analogous to mammalian B-type cells. The dendrites of B-type horizontal cells in mammalian retinas are bushy and contact all cones within the dendritic field. The axon emerges from one of these dendrites. At its distal end, an axon terminal sprouts to collect signals from large numbers of rods at some distance from the cone-contacting dendritic field. The length and thinness of the axon is believed to electrically isolate one portion of the cell from the other, thereby, separating a cone-photoreceptor-involved compartment of the cell from a rod-photoreceptor-involved compartment (17). In species where there are few rods (Fig. 2a, turtle) the B-type axon terminal makes sparse contacts with both red cones and the few rods present in this retina (36, 52). Nonetheless soma-dendritic and axon terminal compartments maintain physiological separation, as evidenced by different summation areas (53). The type I horizontal cell of pigeon

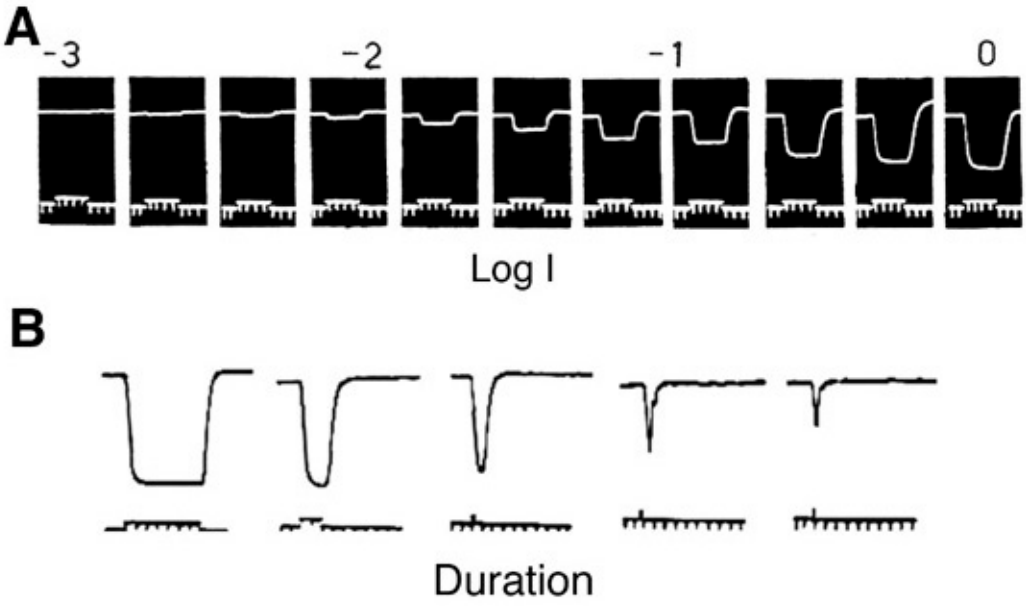

Figure 1. The S-potential of the fish retina. Light stimuli of fixed duration and different irradiances (A) and light stimuli of fixed irradiance but different durations (B) were used to elicit these potentials. Lower traces in A and B record light-stimulus duration and provide 100 msec 'tick-marks'. The illustrations are from Svaetichin,1953 (1).

retina is axon bearing and also appears analogous to mammalian B-type cells. Similar to turtle, the axon terminal contacts a mixture of rods and cones, while the dendrites contact cones (35).

A-type horizontal cells in mammals are purely cone connecting (most species have only green and blue cones). They have no connections with rod photoreceptors at all. The H2 cell of the trichromatic primate retina (humans and old world monkeys) is a kind of A-type cell. Even the H2 cell, where one or more dendrites are elongated and axon-like, contacts only cones. Interestingly enough, these longer dendrites contact principally blue cones. This may be a general theme for mammalian axonless horizontal cells that is only now being realized. In certain big cats (not yet confirmed in domestic cat), the elongated dendritic tips of A-type cells contact blue cones, while the dendrites closer to the cell body are in contact with both red cones and blue cones (54). In horses the A-type cell is apparently only connected to blue cones (Fig. 2a) (38, 40).

In reptiles, and birds with well developed color vision, typically there are two axonless horizontal cell types. Each of these connects selectively with a cone type. In turtles, birds, and fish, species with excellent color vision, type H2 and type H3 horizontal cells are large, stellate cells. In birds and turtles these cells lack axons, but in fish H2 and H3 are axon-bearing. These cells contact cones selectively and sense color (Fig. 2a, axonless, color-opponent types of birds and reptiles; Fig. 2b, H2 and H3 axon bearing types of fish). H2 and H3 respond to some wavelengths with hyperpolarization, and to other wavelengths with depolarization. Thus, in turtle (pentachromats) and fish (trichromats or tetrachromats), H2 horizontal cells connect to green and blue cones and H3 to blue cones (Fig. 2a, Fig. 2b), or to blue cones and ultraviolet cones (6, 7, 36, 37, 41, 43, 52, 55, 56). In the turtle and zebrafish, ultraviolet-sensitive cones appear to connect only with H3 type horizontal cells, sharing this type with blue cones. Some chromatic horizontal cells can be recognized in immunohistochemistry. The C-type horizontal cells of the turtle can be labeled with antibodies to nitric oxide synthase and calcium binding proteins (47); the former suggests a role for NO in their functioning (see section on Neuromodulation).

Gunnar Svaetichin (1915-1981) mastered high impedance microelectrode techniques while studying neurophysiology in the Karolinska Institute with Ragnar Granit (nobel prize, 1967). These enabled intracellular recording of light responses from retinal interneurons, a field that he founded. It was an imaginative area to pursue in the 1940's. He is the discoverer of S-potentials, now known to be retinal horizontal cell responses, and discovered both color opponent and non opponent types. The discovery of neural color opponency ranks with the most significant findings in color vision in the 20th century (292). The later decades of his career were spent at the Venezuelan Institute for Scientific Research.

Lateral elements and spinules

Horizontal cells always interact with photoreceptor terminals at what are known as 'lateral elements' post-synaptic to photoreceptor ribbons (Fig. 3a, le, arrow). In fish retinas, the horizontal cell connections with cones at the lateral elements are characterized by minute projections called spinules (Fig. 3b). Spinules are dynamic and change shape with the level of illumination. Spinule formation is stimulated by background illumination, while darkness causes retraction (57, 58). These plastic spinules are known to contain the calcium binding proteins caldendrin and CaMKII (59). Spinules are under an endogenous circadian control but need centrifugal control from the brain via FMR-amide-like and GnRH-like hormone releasing hormones (60, 61) acting upon the dopaminergic interplexiform cell system in the retina (62, 63). These spinules appear also to be under the local control of the visual-cycle byproduct retinoic acid (64, 65).

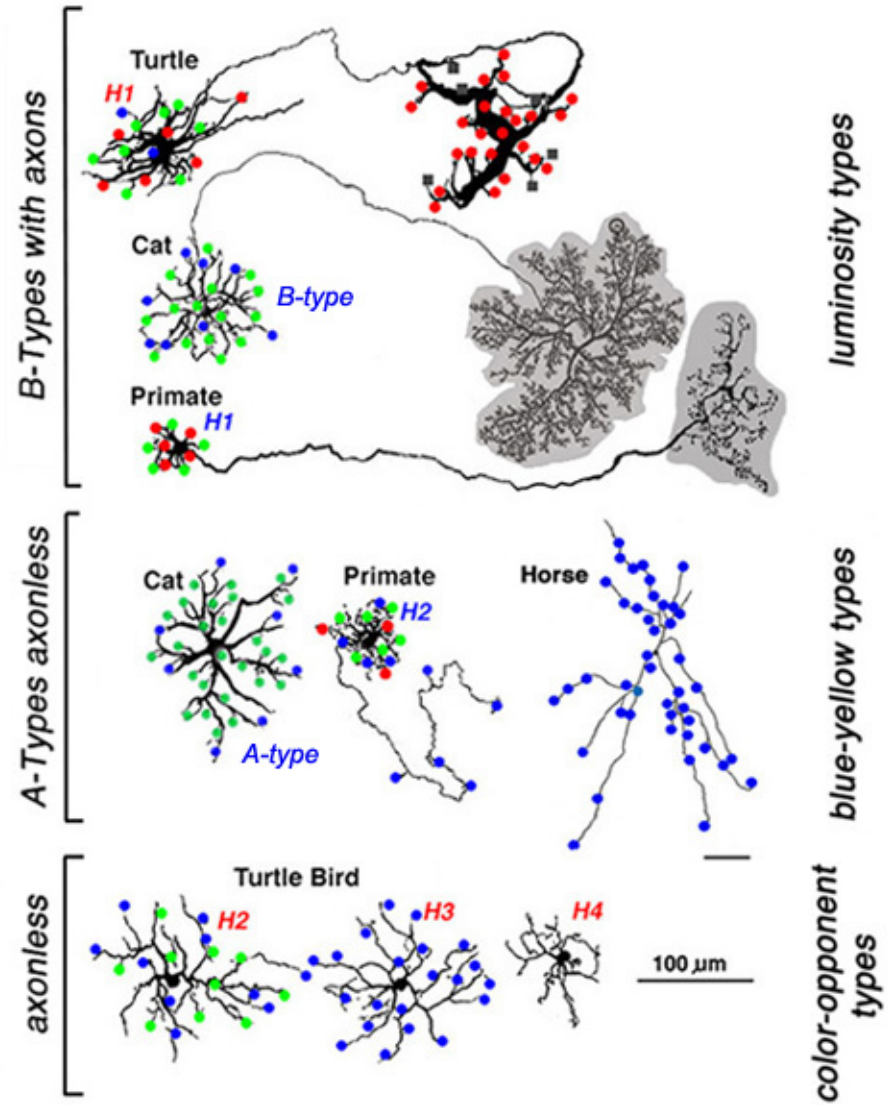

Figure 2a. The morphologies of different types of horizontal cell and their known connectivities with rod and cone photoreceptors. The cells are drawn from Golgi stained or Neurobiotin filled retinal cells and viewed in flat whole-mounted preparations. B-type cells with axons, and A-type axonless cells exist in most vertebrate retinas. The physiological type that is associated with each morphological type is indicated to the right of the figure, i.e luminosity, blue-yellow and color-opponent types. Red-, green- and blue-dots represent inputs from red-, green-, and blue cones respectively. Black squares or shaded gray areas represent rod inputs. The turtle H1 cell is from Ammermüller and Kolb, 1995 (84); H2-H4 are from Kolb et al., 1988 (293). The cat B-type is from Nelson et al., 1975 (17); the A-type is from Kolb, 1974 (294). Primate H1 and H2 types are from Helga Kolb not elsewhere published. The horse axonless horizontal cell is from Sandmann et al., 1996 (40).

Gap-junction contacts and connexins

Retinal horizontal cells in all species are interconnected to homologous neighbors, by areas of gap junctions. These occur between dendrites, between axon terminals, and occasionally between dendrites and cell bodies. Gap junctions are very selective, occurring only between cells of the same type (that is H1 to H1 etc). This exclusivity even extends to axon terminal regions and dendritic regions of B-type horizontal cells, that is, gap junctions connect dendrite to dendrite, and axon terminal to axon terminal, but not axon terminal to dendrite (66, 67). The gap junctions can be extremely large, appearing as plaques (Fig. 3c). First described in fish retinas by Yamada and Ishikawa (28), gap junctions were considered “fused membrane structures” specialized for electrical transmission. Procion Yellow dye diffusion between morphologically similar horizontal cells was noted

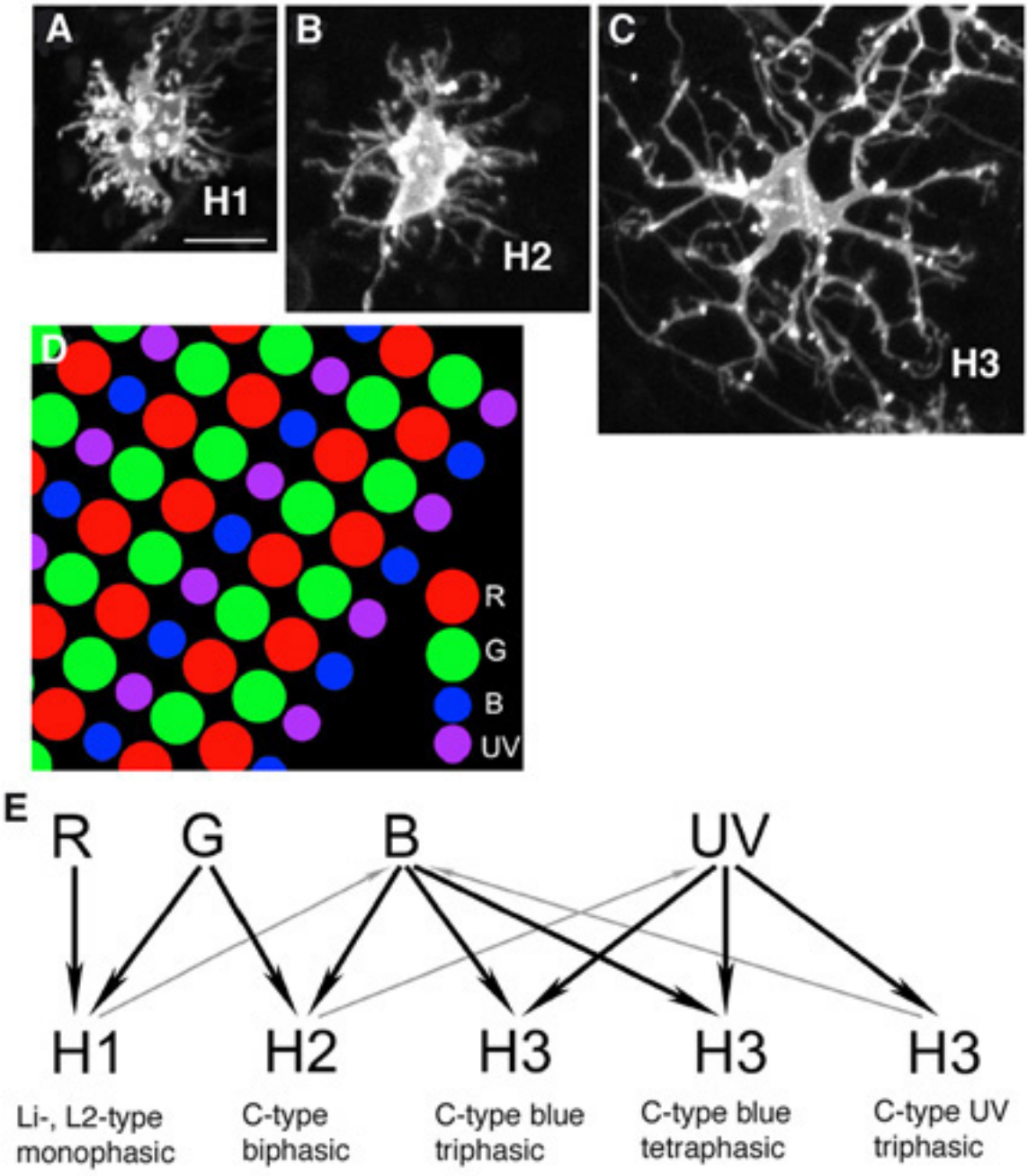

Figure 2b. Cone contacts of H1, H2 and H3 horizontal cell types in zebrafish retina (*A*, *B*, *C* respectively). These neurons were back-labeled with DiI through crystals placed on their axons. Dendritic tips and spines contact cones, sometimes in clusters called 'rosettes'. *D*. Zebrafish cones form a regular mosaic of red (R), green (G), blue (B) and ultraviolet (UV) types. The position of horizontal-cell contacts within the mosaic identifies the cone color type that is contacted. *E*. Summary of cone contacts for H1, H2 and H3 types. Black arrows are contacts proposed for feed-forward excitation, while gray arrows are contacts proposed for feedback inhibition. Except for the UV triphasic H3 cell, all horizontal cells are excited by 2 cone types. The figure is from Li, et al, 2009 (37), with physiological identifications based on Connaughton and Nelson, 2010 (6).

by Kaneko (66) and indicated that the electrical junctions could pass small molecules freely through the so-called S-space of horizontal cells (10).

Gap junctions are formed at closely opposed plasma membranes (2-4 nm gap) from two horizontal cell processes (Fig. 3c). Each of the interacting cells supplies connexons or hemichannels to complete the gap

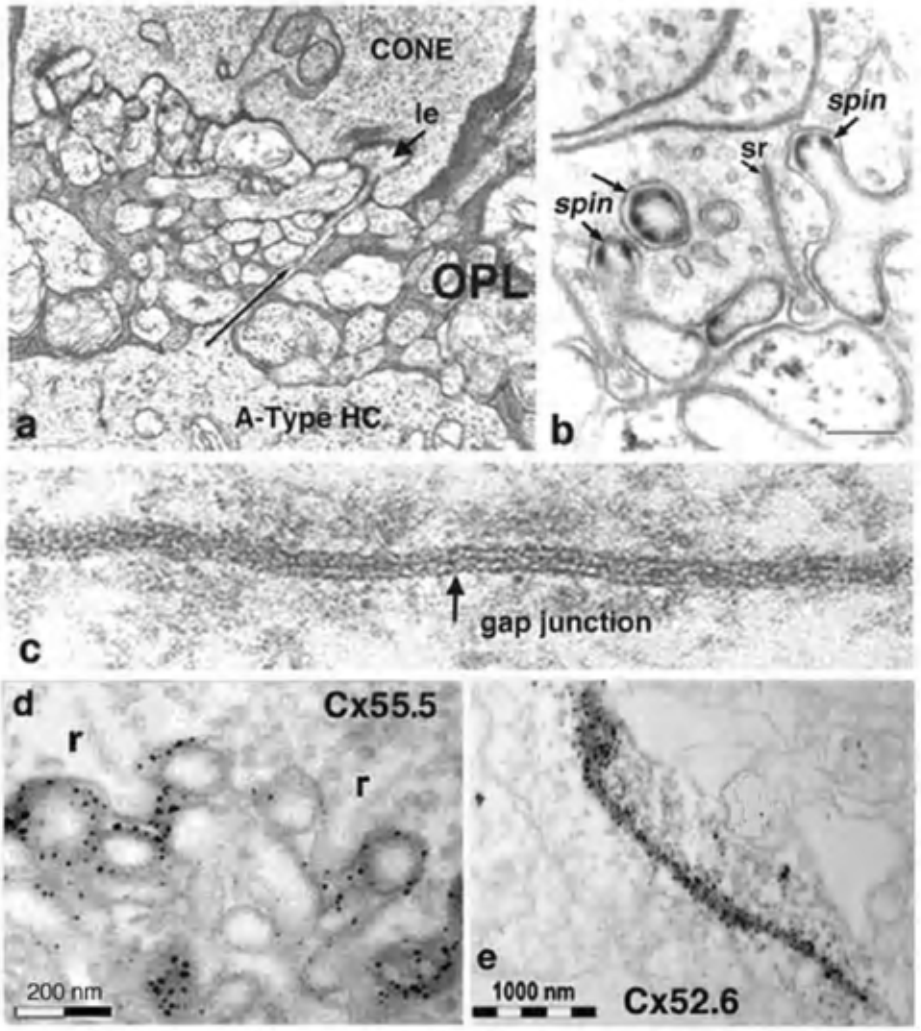

Figure 3. *a*) Electron micrograph of cat outer plexiform layer (OPL) shows an A-type horizontal cell dendritic terminal entering an overlying cone pedicle to form a lateral element (le) at a ribbon triad. *b*) Light adapted fish retina exhibits spinules (spin) on horizontal cell lateral elements in cone pedicles at synaptic ribbon (31) synapses. *c*) High magnification electron micrograph of a gap junction between two A-type horizontal cell dendrites in the cat retina. The latest information concerning gap junction connexins in zebrafish retina shows that *d*) Cx 55.5 forms a hemi- gap junction between HC dendrites and cone pedicles at the ribbon synapse (arrow), while *e*) complete gap junctions between HC dendrites are made by Cx 52.6. The illustrations in *a* and *c* are from Kolb (1977) (103). The illustration in *b* is from From DeJuan and Garcia, (2001) (62). Both *d* and *e* are taken from Shields et al., (2007) (72).

junction contact. These channels can consist of homomeric or heteromeric connexin subunits, thus, potentially allowing a huge variety of gap junctions with slightly different properties to exist between various neurons. Each connexon channel contains six connexins (Cx) surrounding the channel pore. In fish and turtle retinas Cx43 and Cx26 were originally thought to comprise the horizontal cell gap junction connexins (68, 69). However more recently connexin 57 has been demonstrated to be expressed at the protein level and to mediate dendritic gap junctions between mouse B-type horizontal cells. The number of junctions appears to increase with light adaptation (70). In a study on rabbit retina where, unlike mouse, both A- and B-type horizontal cells occur, O'Brien and colleagues have found that Cx50 is the connexin between A-type horizontal-cell dendrites (71). In zebrafish multiple connexins are expressed, in particular Cx52.6 that participates in dendro-dendritic junctions (Fig. 3e) and Cx55.5 that forms hemi-gap-junction channels with cones at lateral elements (Fig. 3d) (72). In zebrafish with Cx55.5 knockout, horizontal-cell color opponency is reduced (73). This connexin is important for feedback modulation of cone synapses. In addition to Cx55.5, another connexin (52.9) is also expressed in zebrafish horizontal cells. It is found both in lateral elements where it may participate in feedback, and in gap

junctions between horizontal cell dendrites within the outer plexiform layer (73). Horizontal cell gap junctions pass not only ions but small cytoplasmic molecules and tracer dyes of less than 500 Dalton size (74). Gap junctions enlarge horizontal cell receptive fields (see section on gap junction physiology), and are modulated by retinal neurotransmitters or humoral factors (see section on neuromodulation).

4. Physiological Types

The vertebrate retina contains a mosaic of rod- and cone-photoreceptors that serve for dark- and light-adapted vision respectively. Multiple cone types, each selectively expressing a visual pigment tuned to a specific region of the visible spectrum, provide vertebrates with the opportunity to discriminate colors. Cone types are defined by the spectral preference of their visual pigment; e.g. short-wavelength (SW) cones, medium-wavelength (MW) cones and long-wavelength (LW) cones, also referred to as blue/UV cones, green cones and red cones respectively. Most mammals are dichromats (2 cone types); however, old world monkeys and humans are trichromats (3 different cone types), and many non-mammalian species are also trichromats or even tetrachromats (4 different cone types). In the retinas of birds, fish and reptiles, a class of SW cones that are sensitive to ultraviolet light (UV cones) can be found (27, 75-79), in addition to the LW, MW, and typical SW cones (red, green and blue cones respectively). Since rods and cones of different spectral types are directly connected to horizontal cells, it is of interest to explore how horizontal cells integrate and process this richness of spectral information.

Physiologists recognize two major types of horizontal cell, luminosity and chromaticity. These can be distinguished by photoresponses to lights of different wavelength. The luminosity (L-type) horizontal cells always respond with hyperpolarization to light stimuli of any wavelength within the visible range of the spectrum, while the chromaticity (C-type) horizontal cells respond with different polarity to light stimuli of different wavelengths (80).

L-type horizontal cells

Luminosity (L-type) horizontal cells are found in every retina that has been studied, non-mammalian vertebrates, mammals and primates. Figure 4 shows the photoresponses of luminosity-type horizontal cells from toad (A), rabbit (B) and monkey (C) retinas. Regardless of the wavelength, these cells respond with membrane hyperpolarization that depends only on the brightness and duration of the stimulus. In some species, two classes of L-type horizontal cells can be distinguished both by anatomical structure and physiological properties. In the turtle retina, the L1 and L2 types are similar in spectral sensitivity but differ in receptive field size and in photoresponse kinetics to red and green light (53, 81). Anatomically, these two L-type horizontal cell physiologies are respectively the axon terminal and the soma of the turtle H1 horizontal cell (Fig. 2a).

In cat and rabbit retinas, A-type and B-type cells (Fig. 2a) are both luminosity types. They differ in morphology and in connectivity with rods and cones but respond only with hyperpolarizations to light stimuli (14, 15, 17). Differences in A- and B-type spectral properties have not yet been reported. Like turtle retinas, the retinas of cyprinids and old world monkeys have both red and green cones. In these species some L-type horizontal cells favor green cone signals, while others favor red cone signals. In cyprinids, the former is called an L1 type, and the latter an L2 type (82). In old world primates both red and green favoring L-type signals arise from the H1 morphological type. Rather than two discrete types, there is a distribution in the balance of red cone and green cone signals for H1 cells (21, 24). In zebrafish also, there is a distribution in red-green balance on the H1 cell, yielding at the extremes L1 green-peaking types, and L2 red-peaking types (6).

C-type horizontal cells

In 1959, Svaetichin and MacNichol (80) first reported on extreme wavelength-dependency of some S-potentials (Fig. 5). As shown in the figure, the photoresponses of this S-unit reversed in polarity at a wavelength of about

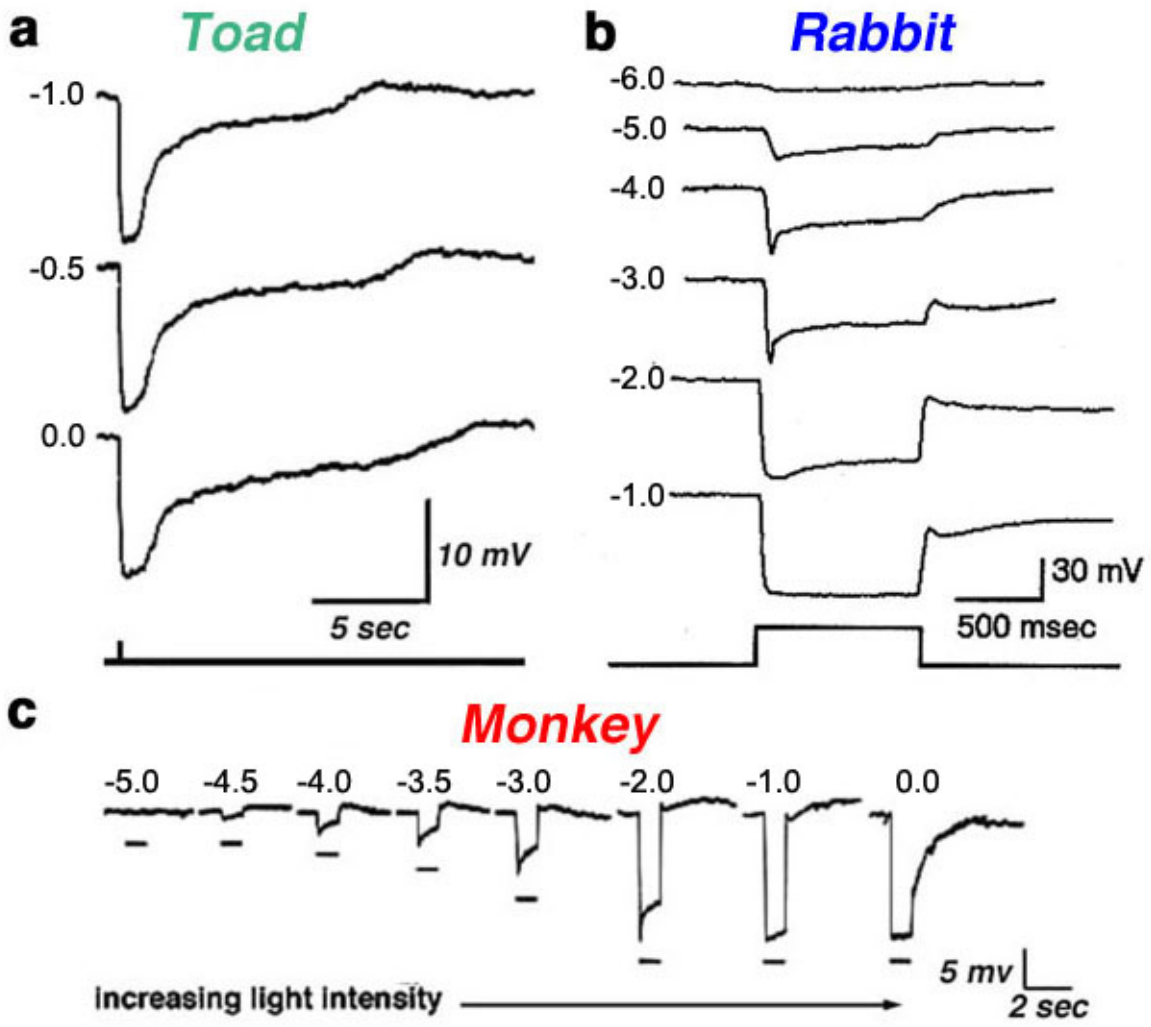

Figure 4. Photoresponses recorded from luminosity-type horizontal cells of toad, rabbit and monkey retinas. In each case, photoresponses were elicited by light stimuli of different intensities. Stimulus intensity is given in log units relative to the most intense stimulus available for the particular recording system. The illustration in *a* is from Normann and Pochobradsky, 1976 (295); in *b* from Bloomfield, 1992 (296), and in *c* from Dacheux and Raviola, 1990 (23).

560 nm. Photoresponses to light stimuli of longer wavelength depolarized the cell membrane, while stimuli of shorter wavelengths hyperpolarized the cell membrane. Svaetichin and MacNichol called these 'color opponent' S-units chromaticity or C-type horizontal cells. C-type horizontal cells have been extensively studied in turtle, amphibian and fish retinas (7, 9, 55, 83-94). Horizontal cells are named by the number of wavelengths at which response polarity reverses; no reversal – monophasic (or L-type) cells, one reversal – biphasic C-type cells, two reversals – triphasic C-type cells, three reversals – tetraphasic C-type cells. Wavelengths at which response polarity reverses are called 'null wavelengths'. In fish retinas, three types of chromaticity horizontal cells have been described; biphasic, triphasic and tetraphasic (6, 86, 95, 96). In the bowfin retina, the null wavelength for the biphasic cells is around 640 nm, while null wavelengths of the triphasic cells are; in the regions of 500-530 nm and 650-670 nm respectively (95). The biphasic and triphasic C-type horizontal cells of the fish retina are identified morphologically as H2 and H3 types respectively (Fig. 2b). In zebrafish the H3 morphological type has taken on as many as 3 physiological identities: the blue triphasic, analogous to previous findings in fish, a UV triphasic type, and a tetraphasic type (6).

In the turtle retina, two classes of biphasic C-type horizontal cells have been identified (7, 85, 91). Typical photoresponses of L-type and C-type horizontal cells in the turtle Mauremys caspica to light stimuli of different wavelength and intensity are shown in figure 6. For each wavelength, a series of photoresponses to different intensities is shown. The L-type horizontal cell (1st row in Fig. 6) responds to all stimuli with graded hyperpolarizations regardless of wavelength. The red/green biphasic C-type horizontal cell (2nd row, Fig 6) responds with graded depolarizations to red light stimuli and with graded hyperpolarizations to yellow, green and blue stimuli. The yellow/blue biphasic horizontal cell (3rd row, Fig. 6), responds with depolarizations to red and yellow light stimuli and with hyperpolarizations to blue light stimuli.

In order to define the spectral properties of the horizontal cells, monochromatic light stimuli of dim intensities are used to elicit small amplitude (<1mV) photoresponses. These photoresponses are within the linear range of the cells and can be used to calculate light sensitivities. Sensitivity is defined as the volts of evoked response per quantum of light and is calculated by dividing the voltage response by the number of quanta in the stimulus. The relationship between light sensitivity and wavelength is the action spectrum of the cell and describes the threshold spectral properties. Figure 7 shows the mean action spectra of 8 L-types, 7 red/green types and 6 yellow/blue types of horizontal cell (*A*, *B* and *C* respectively) from the turtle Mauremys caspica. These spectra clearly demonstrate that the L-type horizontal cells are most sensitive to long-wavelength stimuli, with the major excitatory input coming from red cones (7, 85). These cells receive additional excitatory input from green cones and to a lesser extent from blue cones (85). The red/green C-type horizontal cells are characterized by reversal of response polarity around 600 nm (Fig. 7*B*). These cells are excited by green and blue cones and inhibited by red cones (7, 85). The yellow/blue C-type horizontal cells are inhibited by green and red cones and excited by blue cones (7, 85) and interestingly, also by UV cones (27, 97). Their photoresponses reverse in polarity around 540 nm (Fig. 7C).

Triphasic color responses are only rarely reported in turtle horizontal cells (94), but they are common to some cyprinid retinas, where even tetraphasic responses occur (6, 86, 95, 96). The processing of spectral information at just this first post-photoreceptor synapse in these species is quite amazing. Six spectral configurations occur in zebrafish retina (6). The most elaborate of these is the tetraphasic response, with three null points across the spectrum. It is depolarized by UV light, hyperpolarized by blue, depolarized by blue-green, and hyperpolarized by yellow and red (Fig. 8A). Spectral analysis shows that tetraphasic types are depolarized by both green and UV cones, and hyperpolarized by red and blue cones (6). Like other fish (95), zebrafish has triphasic responses, but there are two types, one hyperpolarized primarily by UV cones (Fig. 8B) and the other hyperpolarized primarily by blue cones (Fig. 8C). Both these triphasic cells depolarize with middle-wavelength (green cone) stimulation, and hyperpolarize with long-wavelength (red cone) stimulation. The biphasic cells of zebrafish (Fig. 8D) are depolarized by long wavelengths (red cones) and hyperpolarized by short and medium wavelengths (both blue and green cones) (6). The zebrafish L-type horizontal cells (Fig. 8E, 8F) are hyperpolarized by input from both red and green cones, but are little influenced by blue cone and UV cone signals. When response amplitudes at different wavelengths are fit by a spectral model that takes into account the shapes of zebrafish cone pigments (6, 98), L-type responses to blue and UV stimuli (Figs. 8E, 8F) are shown to result from stimulation of the short-wavelength absorbance limbs of red and green cones. L1 types show a balance of red and green cone signals and L2 cells hyperpolarize predominantly in response to red cone stimulation (6).

Mammals lack C-type horizontal cells

Given the diversity of horizontal-cell physiology in lower vertebrates, where dendritic contacts with cones containing different visual pigments frequently produce chromatically opponent responses, it is surprising that in mammalian retinas, whose horizontal-cell dendrites also contact cones with different visual pigments, only luminosity-type horizontal cell responses can be recorded (18, 19, 22, 99, 100). For example, both cat A- and B-horizontal cells are luminosity types (Fig. 9), that are dominated by red-cone input, although low-level

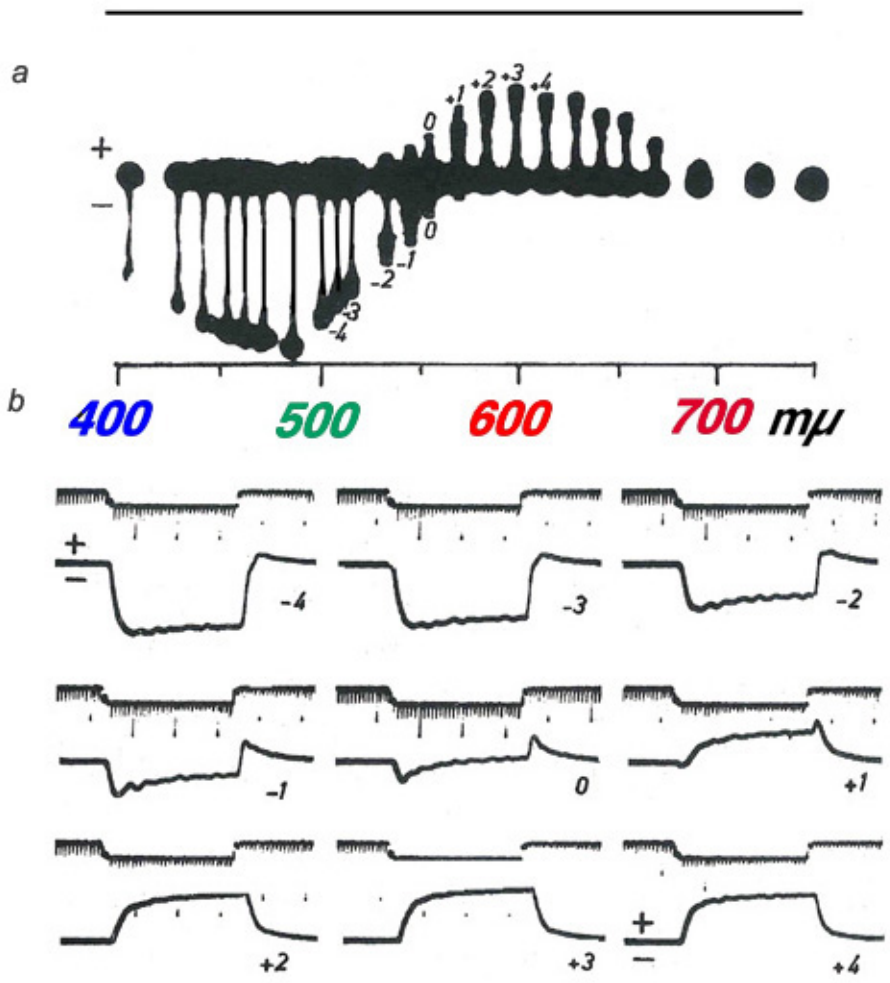

Figure 5. Color opponency of S-potentials in the fish retina. *a*. Responses were recorded as a function of wavelength covering the entire visible spectrum using light stimuli of different wavelength but similar quantal content. *b*. The responses that were elicited by selected light stimuli, numbered in *a* from -4 to +4, are shown at greater time resolution. The longer time marks on the rectangular stimulus traces (upper traces in *b*) are 100 msec, the shorter, 10 msec. The illustration is from Svaetichin and MacNichol, 1959 (80).

synergistic input from blue cones can be detected using specific spectral stimulating and adapting conditions (100). In both A- and B- type cells, rod signals (Fig. 9) are intermixed with cone signals (16, 17).

The failure of mammalian horizontal cells to be color opponent may correlate with the absence of a horizontal cell that avoids contact with long-wavelength cones. The biphasic responses in zebrafish retinas are thought to arise from an H2 type horizontal cell that avoids contact with red cones, while selectively contacting green, blue, and UV cones. Excitatory input arises from the blue and green cone contacts, and the red inhibitory input arises from feedback contacts from red-cone dominated H1, L-type horizontal cells, onto blue cones (Fig.2b, panel E). In the H2 cell there is no red hyperpolarizing signal to mask the H1 red-inhibitory feedback onto the blue cones. This allows the H2 cell to show the color opponent feedback signal (37).

In primate retina, despite a full complement of red, green and blue cone types, horizontal cells also only occur as luminosity types (22, 23). H1 cells receive synergistic signals from long- and medium-wavelength cones (red and green cones), while H2 cells receive synergistic input from all three spectral types of cones; long- medium- and short-wavelength (red, green and blue cones) as shown in figure 10. Anatomically H1 type horizontal cells tend to avoid the pedicles of blue cones (Fig. 10, Neurobiotin-injected H1 cell) (22, 101) and are therefore not responsive to blue-cone isolating stimuli (Fig. 10E). On the other hand, large numbers of H2 dendrites contact

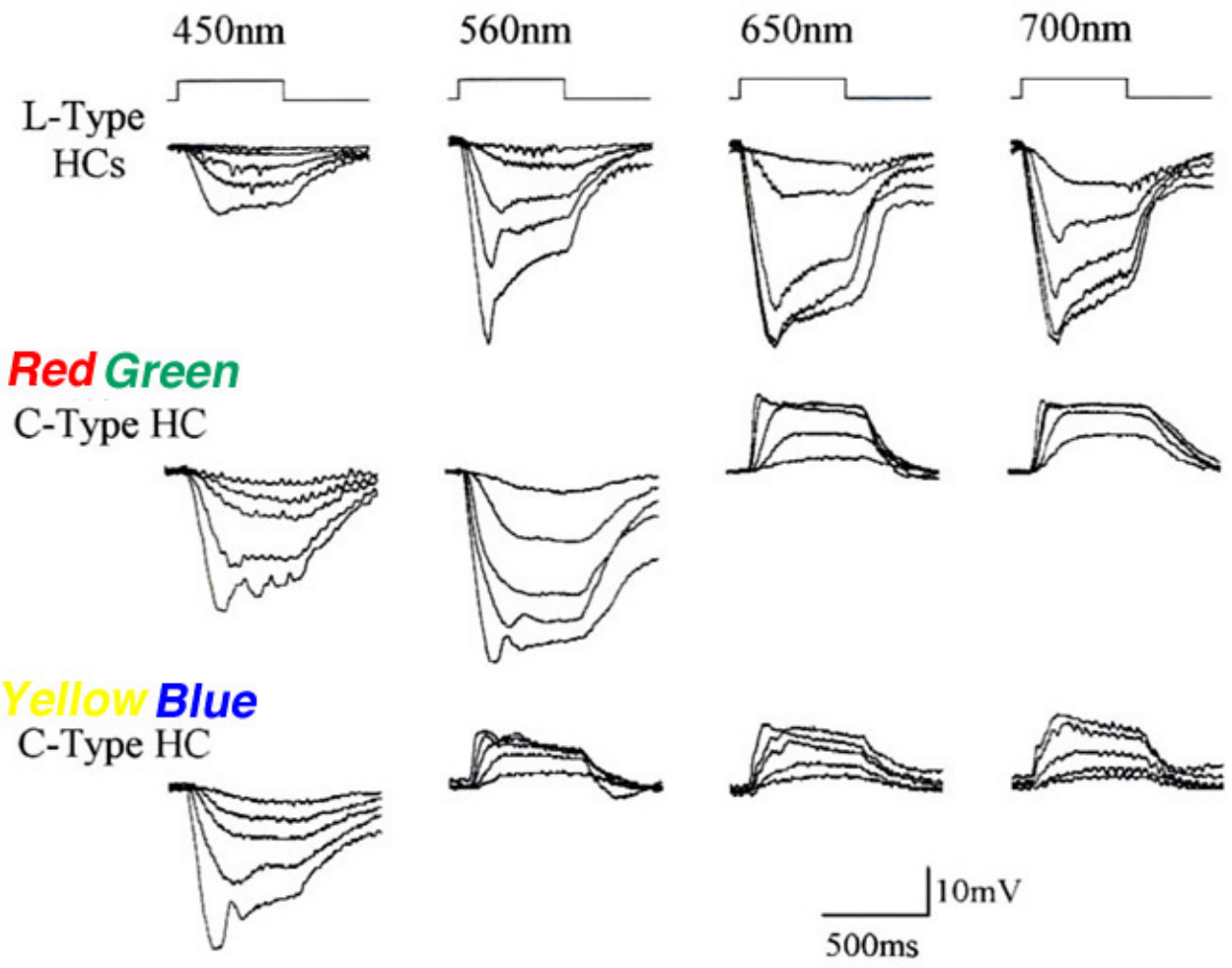

Figure 6. Wavelength dependency of the photoresponses from an L-type horizontal cell, a red/green C-type horizontal cell, and a yellow/blue C-type horizontal cell in the retina of the turtle Mauremys caspica. For each wavelength, several intensities are nested. The illustration is from Twig et al., 2003 (92).

blue cone pedicles (Fig. 10, Neurobiotin-injected H2 cells, outlined clusters) (22, 101, 102). The H2 cell is indeed very sensitive to the blue end of the spectrum (Fig. 10J). Yet, the responses of both horizontal cell types are only of hyperpolarizing polarity to all wavelengths (22). Thus, it appears that subsets of mammalian and primate L-type horizontal cells are devoted primarily to processing of either red green and blue signals or red and green signals, but spectral opponency is not part of the processing regime.

5. Rod and cone contributions and passive electrical models

Mixing of rod and cone signals

Steinberg (19, 99) was the first to distinguish separate rod and cone signals in S-potentials from a mammalian retina. He made intracellular recordings from horizontal cells in the cat retina and saw the typical graded hyperpolarizing responses that depended upon the intensity of the light stimulus. However, unlike the responses seen in non-mammalian retinas, Steinberg's S-potential recordings revealed much more distinct rod and cone contributions to the response. A very slow phase of membrane repolarization seen after termination of the light stimulus was identified as the rod contribution. Steinberg called this the 'rod after effect' (Fig. 9). The difference

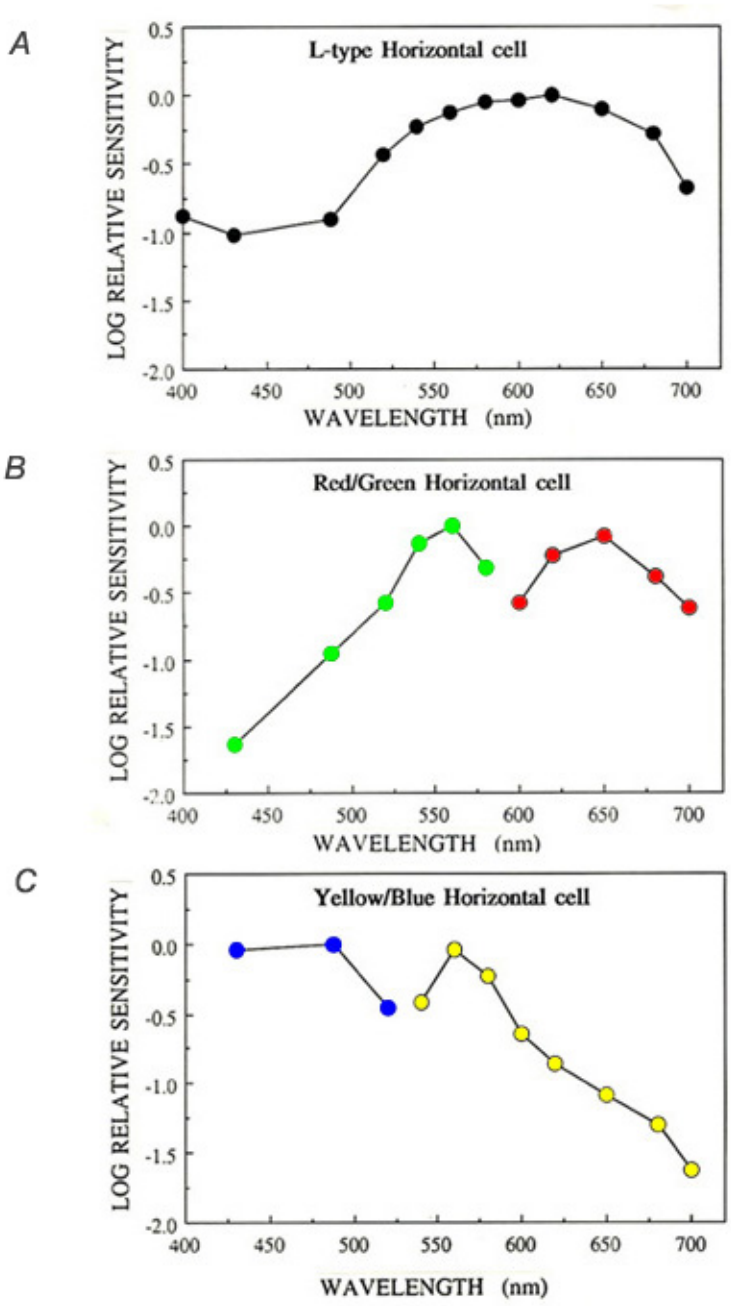

Figure 7. Action spectra of 8 L-type (*A*), 7 red/green C-type (*B*) and 6 yellow/blue C-type (*C*) horizontal cells in the turtle retina (Mauremys caspica). Sensitivity data were calculated from photoresponses of small amplitude (<1 mV) that were elicited by dim light stimuli illuminating the entire receptive field of the studied cells. In order to compare the different action spectra, the spectrum of each cell was normalized to the peak sensitivity. In (*A*), all responses were of hyperpolarizing polarity. In (*B*) and (*C*), depolarizing responses are marked respectively by red and yellow circles, and hyperpolarizing responses by green and blue circles. Reproduced from Asi and Perlman, 1998 (85).

in offset kinetics for rod and cone signal components provides a convenient assay for separating rod and cone inputs to S-potentials in rod-dominated mammalian retinas (16). In Figure 9, typical mixed rod and cone signals of all three horizontal cell structures in cats are shown (17). In A- and B-type horizontal cell bodies, rod and cone signals are about equal in amplitude, whereas in the axon terminal of the B-type cell, the slowly recovering response characteristic of rod signals occurs. This is interpreted to indicate that rod and cone signals are almost

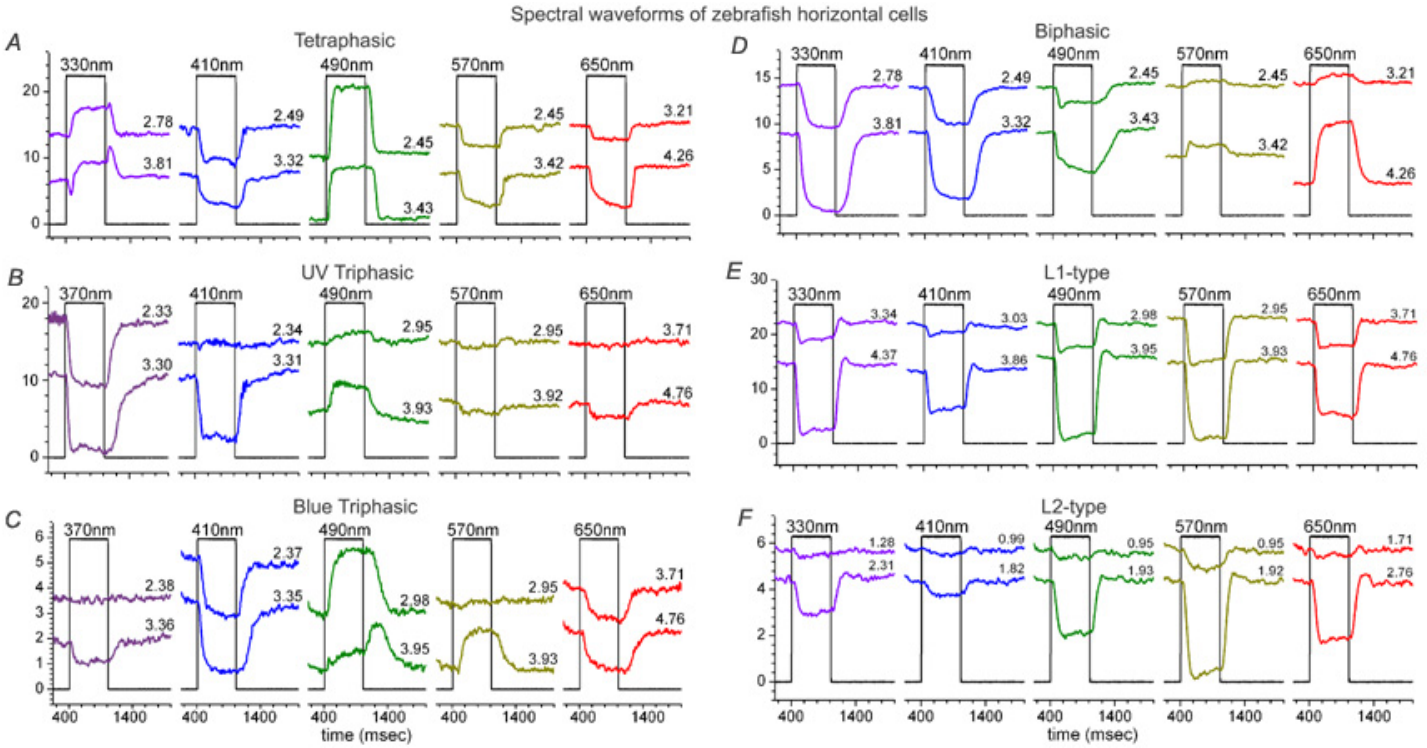

Figure 8. Color physiology of zebrafish horizontal cells. *A*. Tetraphasic type is depolarized by ultraviolet (UV-330nm) hyperpolarized by blue (410nm) depolarized by blue-green (490nm) and hyperpolarized both by yellow (570nm) and red (650nm) wavelengths. *B*. UV triphasic cell hyperpolarizes at full amplitude for both irradiances of the UV 330nm stimuli but is depolarized by the dimmer of the blue 410nm stimuli and hyperpolarized by the brighter 410nm stimulus. For 490nm the cell depolarizes, but at longer wavelengths the cell hyperpolarizes. The blue triphasic cell (*C*) hyperpolarizes fully for both 410nm blue stimuli, but responds only weakly to 330nm UV stimuli. Depolarization occurs in the blue-green (490nm) and yellow (570nm) but the cell hyperpolarizes for red stimuli (650nm). The biphasic cell (*D*) is hyperpolarized for short-wavelengths (330nm, 410nm, and 490nm) but is depolarized by long wavelengths (570nm, 650nm). Two L-type cells, L1 (*E*) and L2 (*F*) hyperpolarize at all wavelengths, but the amplitude ratio at 490nm and 570nm favors 570nm for the L2-type, and is more evenly balanced for the L1-type. All amplitudes are given in mV. Numbers to the right of each trace are stimulus irradiance, given in $\log(h\nu \cdot \mu m^{-2} \cdot s^{-1})$. Illustrations are from Connaughton and Nelson, 2010 (6).

equally mixed in cat horizontal cell bodies, but only rod signals are seen in the axon terminals. The 'rod after effect' grows increasingly prolonged with bright light stimuli (Fig. 9, bottom).

Further evidence for the mixing of rod and cone inputs to cat horizontal cells is seen during light adaptation. When retinas are light adapted by steady background lights, rod signals saturate and rod contributions to the horizontal cell photoresponses, including rod after-effects, vanish. In contrast, the cones adapt to the brighter conditions and their input remains robust. These properties of rod and cone inputs are easily seen in the photoresponses of mammalian horizontal cells such as cats and rabbits (15, 17, 19). The photoresponses of the rod-dominated B-type horizontal cell axon terminals are virtually abolished by light adaptation. In the horizontal cell bodies (A and B types), which receive mixed rod and cone inputs, light adaptation selectively reduces the rod contribution but large cone signals remain and therefore, these horizontal cell elements continue to respond well in the presence of background lights (16).

Axon terminals of the axon-bearing B-type horizontal cells in the cat receive an excitatory feed-forward input only from rods, but the cell bodies of A-type and B-type cells contact only cones. So where does the large rod component of the S-potential in the cell bodies of cat horizontal cell bodies come from? Electron microscope observations show gap junctions linking rod and cone photoreceptors in the mammalian outer plexiform layer (103, 104). These electrical synapses introduce rod signals into cones and thence into horizontal cells. This rod/

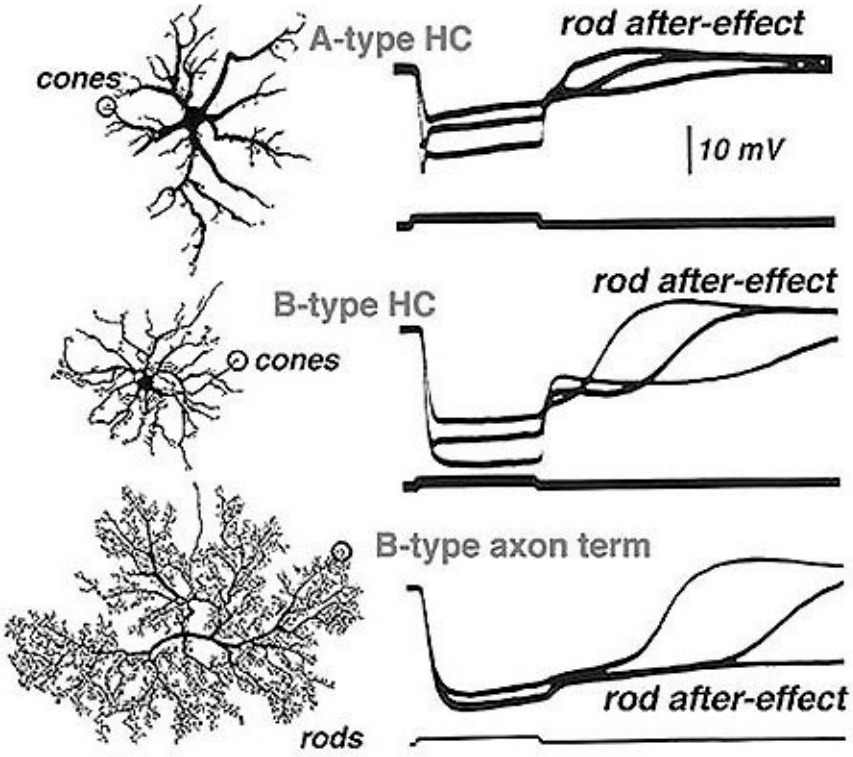

Figure. 9. Rod-cone mixing in horizontal cells of the cat retina. Responses to light stimuli of different intensities were recorded from the cell bodies of A-type and B-type horizontal cells and from the axon terminal of the B-type horizontal cell. Brighter stimuli produce greater amplitudes from the cones, and longer 'rod after-effects' from the saturated rod signals. The illustration is adapted from Nelson et al., 1975 (17).

cone mixing in the photoreceptors is now considered one of the pathways whereby rod driven inputs pass to horizontal cells and to all subsequent second and third order cells in the retina (105-108).

In other species, similar characteristics of rod-cone mixing can be found in horizontal cells. In the rabbit retina, as in the cat retina, rod-dominated input to the axon terminal is identified by waveform, sensitivity and the presence of after-potentials (15, 109). Also in primate retina, the axon terminals of the axon-bearing H1-type horizontal cells produce rod signals while the cell bodies produce cone or mixed rod-cone signals (22, 23, 26). Similar to other mammalian retinas, the somata of primate H1-type horizontal cells receive rod input indirectly via gap junctions between rods and cones (26).

Horizontal cells of reptiles and amphibians, like mammals, mix rod and cone signals. In the retina of the turtle Chelydra serpentina, the photoresponses of H1 axon terminals contain slow, low-amplitude components that are contributed by rod photoreceptors, despite the major excitatory input being from long-wavelength sensitive cones. The cell bodies of the same H1 horizontal cells receive input only from long- and medium-wavelength sensitive cones (110). In Xenopus, horizontal cell dendrites contact both rods and cones (111). Similar to mammals, waveforms characteristic of rods and cones, including rod after-effects are recorded in these cells with light stimulation (112). The amphibian circuitry, with direct rod contacts onto horizontal cell dendrites, differs from mammals, where only cones are contacted, and rod signals enter cones directly through gap junctions. No rod signals have been reported in the purely cone-contacting horizontal cells of fish (Fig. 2b, Fig. 8). In fish rod signals are restricted to H4, a special rod-connected horizontal cell type (45, 46).

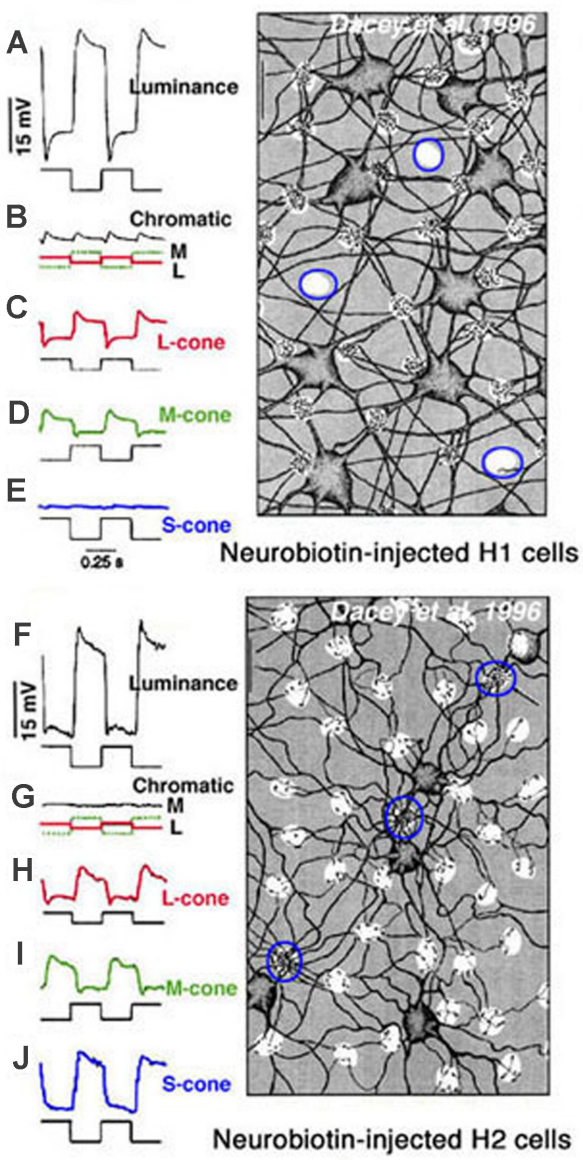

Figure 10. Connectivity and physiology of horizontal cells in the monkey retina. Above: Intracellular staining and chromatic responses of H1 cells. These cells avoid dendritic contact with S-cones (blue outlined white circles). There is no response to S-cone (blue-cone) isolating stimuli (trace *E*). Below: Intracellular staining and chromatic responses of H2 cells. These cells send many dendrites to S-cones (blue outlined cones) as well as to red and green cones. The response to S-cone isolating stimuli is large (*J*). The illustration is from Dacey, 1996 (22).

Passive electrical models

All vertebrate retinas contain at least one horizontal cell type that is an axon-bearing cell (Fig. 2a, *B-types*). The axon terminals and somata of these horizontal cell types are connected by a long thin axon, but in many cases each end behaves as an isolated physiological unit. In the turtle Pseudemys scripta elegans, both axon terminals and somata receive excitatory input mainly from red cones but differ in spatial properties and response kinetics for red and green stimuli (53, 81). In another turtle species, Chelydra serpentina, the axon terminal receives excitatory input from red cones and rods while the cell body dendrites contact red and green cones (110). In domestic mammals (cat, rabbit) and in primates (monkey), the dendrites of the cell body receive input from cones while the terminals of the axon contact thousands of rods. No evidence has been found to indicate any synaptic or electrical interaction between the axon terminal and the soma of the same cell in any of these cases.

Where horizontal cell types have the dendritic portion of the cell much distant from the axonal ending (Fig. 2a, *B-types*), calculations based on the anatomical dimensions and geometry of the neuron, and ohmic linear properties of cell membrane and cytoplasm, indicate that the axons are too long and thin to allow significant passive electrotonic spread of signals from one end of the cell to the other (17, 26, 36, 110). Such models tell us that signals in cell bodies and axon terminals of horizontal cells reflect only the local synaptic inputs. Indeed, the two portions of the same cell act as independent units (17), in clear violation of neuron theory.

The exception to this rule of physiological separation between cell body and axon terminal appears to be the cone-connected horizontal cells in fish. The cone responses of axon terminals in these cells are similar to the cell bodies (3). As there are no cone contacts from/to the axon terminals in fish, it appears likely that signals are passively conducted from the cell body. The high impedance of the simple unbranched axon terminal may be permissive to the passive propagation of signals through the axon.

6. Ionic conductances

Ionotropic glutamate-gated channels

Photoreceptors excite horizontal cells through sign-conserving synapses. In darkness, photoreceptors continuously release an excitatory neurotransmitter that opens horizontal-cell cationic channels with a depolarized reversal potential. Therefore, the horizontal cells are maintained at a relatively depolarized potential in darkness. When the photoreceptors are hyperpolarized by a light stimulus, neurotransmitter release is reduced, the post-synaptic ligand-gated channels close and the horizontal cells hyperpolarize. Neurotransmitter release from photoreceptor terminals is calcium dependent. Exposing the retina to ions that interfere with calcium influx through voltage-dependent calcium channels blocks neurotransmitter release from the photoreceptors, and consequently horizontal cells hyperpolarize (113-115).

Early experiments in intact retinas pointed to the excitatory amino acids L-glutamate and L-aspartate as putative candidates for the photoreceptor neurotransmitter (116-120). Exposing the retina to either L-glutamate or L-aspartate caused depolarization of horizontal cells and loss of photoresponses as shown in figure 11A for horizontal cells in the intact rabbit retina (116). These observations are consistent with the notions that an excitatory amino acid is continuously released by the photoreceptors in the dark, and that light-induced hyperpolarization of horizontal cells reflects the reuptake of the amino acid from the synaptic cleft. Accordingly, exogenously applied neurotransmitter saturates the receptor sites in the horizontal cells causing further depolarization. Since the horizontal cells are saturated with the *ex*ogenously applied neurotransmitter, modulation of *end*ogenous transmitter release by light stimuli has little effect on membrane potential and the photoresponses are eliminated. In the experiment described in figure 11A, solutions containing 15 mM L-aspartate or L-glutamate were needed to induce depolarization of rabbit horizontal cells and loss of photoresponses. These and other studies raised two major questions (1). Why were relatively high concentrations (in the millimolar range) of excitatory amino acids needed to exert the effects shown in figure 11A (78)? Which of the two excitatory amino acids was the photoreceptor neurotransmitter?

The first question was answered by the identification of efficient uptake systems for glutamate and aspartate by excitatory amino acid transporters (EAATs) (121, 122). EAATs efficiently remove excitatory amino acids from extracellular space, thereby greatly reducing the concentration of the exogenously applied aspartate or glutamate reaching the cone-to-horizontal-cell synapses. Retinal glutamate transporters are reviewed elsewhere in Webvision. When non-transportable analogues of excitatory amino acids are applied, considerably lower concentrations are needed to exert effects on horizontal cells (109, 123). This is illustrated in figure 12 where the effect of 10 mM L-glutamate (A) is compared to that of 0.1 mM kainic acid (B). Kainic acid, an agonist for AMPA-kainate-type glutamate receptors in vertebrate horizontal cells, but not a substrate for EAATs, exerts effects similar to L-glutamate at a concentration lower by 100 fold. In both cases horizontal cells are depolarized

and photoresponses lost. In further support of the excitatory amino acid receptor hypothesis, kynurenic acid, a non-selective antagonist of excitatory amino acid receptors (124) hyperpolarizes horizontal cells, also with loss of photoresponse (Fig, 12 C).

The exact identity of the excitatory amino acid was debated for more than a decade. A variety of experiments in intact retinas were designed to decide between L-glutamate and L-aspartate as candidates for photoreceptor neurotransmitter, but with conflicting conclusions. It was not until the development of the isolated cell preparation that a clear answer to this question was obtained. Lasater and Dowling (125), in their pioneering work, isolated horizontal cells from the carp retina and recorded the membrane potentials with sharp microelectrodes. Since these horizontal cells in culture were separated from all other influences of retinal circuitry, including photoreceptor stimulation, they were characterized by hyperpolarized resting potentials (close to the potassium equilibrium potential). Application of low doses of L-glutamate, but not of L-aspartate or D-glutamate, induced depolarization, indicating that selective receptors for L-glutamate existed in the horizontal cell membrane (Fig. 11B). With this experimental approach, a low concentration of L-glutamate was sufficient to induce effects, because in this preparation, removal of extracellular L-glutamate by uptake systems is negligible.

Voltage- and current-clamp techniques have been applied to isolated horizontal cells from a variety of species in order to reveal the properties of the glutamate-gated channels. These channels have a reversal potential around 0 mV, depending upon the composition of the intra-pipette and extracellular solutions (123, 126-128). Pharmacological analysis of the properties of the glutamate-gated channels in horizontal cells, using specific agonists and antagonists, revealed them to be of the AMPA/KA type. They are specifically activated by α-amino-3-hydroxy-5-methyl-4-isoxazole propionic acid (AMPA) or kainic acid (KA) and are antagonized by 6-cyano-7-nitroquinoxaline (CNQX) or cis-2, 3-piperidine-dicarboxylic acid (PDA) (129, 130). When AMPA/KA ion channels are activated by the agonist kainic acid, the induced currents are considerably larger than those elicited by L-glutamate, even at higher concentrations (127, 131). This effect has been attributed to fast desensitization of the AMPA/KA type channels by L-glutamate but not by kainic acid (132, 133). Selective blockers of the glutamate-induced desensitization (e.g. cyclothiazide) cause glutamate-induced currents to reach levels similar to those elicited by kainic acid, buttressing the conclusion that horizontal cells express largely AMPA-type glutamate receptors (134-136). Catfish horizontal cells, which express NMDA receptors in addition to AMPA/KA receptors, appear to be an exception to the above general conclusion (131). Further, there is physiological evidence for kainate receptors in addition to AMPA receptors in horizontal cells cultured from human retina (137).

Metabotropic glutamate actions

Glutamate also influences horizontal cells through metabotropic pathways. Unlike ionotropic AMPA-glutamate responses, metabotropic actions do not spread globally through membrane voltage changes within the horizontal cell network, but remain local, influencing only nearby cytoplasmic chemistry. DL-AP4, a glutamate analogue selective for type III metabotropic glutamate receptors, suppresses nearby voltage sensitive potassium channels (138). Similarly, group I and group III metabotropic glutamate receptors increase the amplitudes of nearby voltage-gated calcium currents in horizontal cells (139). Glutamate provides further metabotropic regulation of calcium and potassium channels through modulation of cytoplasmic pH (140). NMDA receptors on catfish horizontal cells have been observed to down-regulate voltage dependent sodium and calcium channel activity through a calmodulin-dependent mechanism, also a type of metabotropic effect (141). Furthermore sodium entry through stimulated AMPA-glutamate channels stimulates local activity of Na^+K^+ ATPase. This in turn appears important in setting membrane potential (142). Thus, in addition to causing the light response itself, photoreceptor glutamate regulates a variety of cellular and membrane functions.

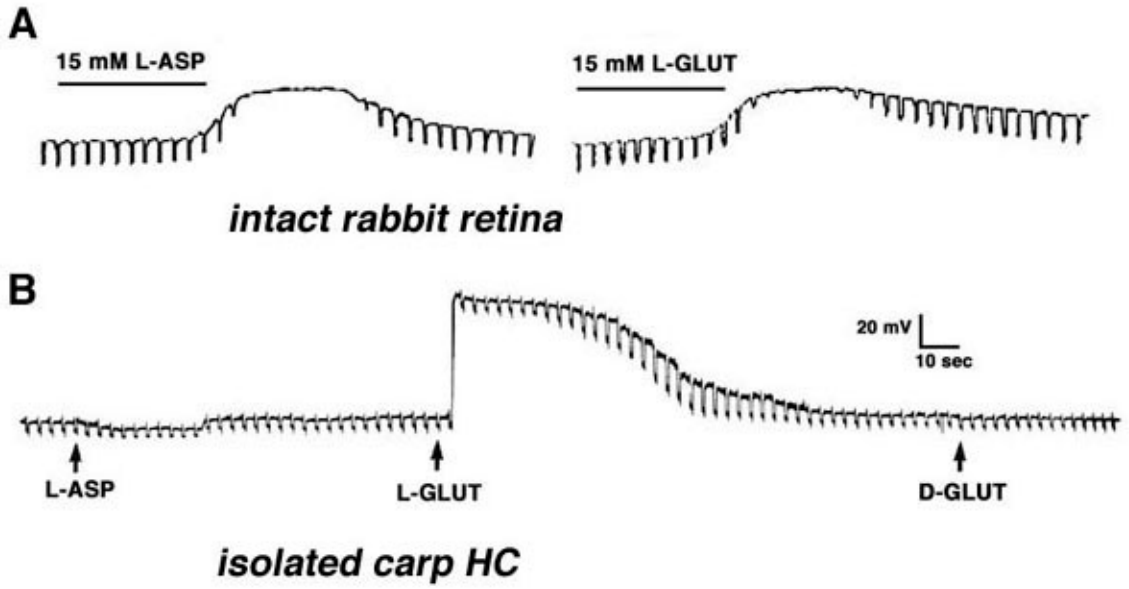

Figure 11. *A*. L-aspartate and L-glutamate depolarize horizontal cell membrane potential and abolish horizontal cell photoresponses in intact rabbit retina. These photoresponses were elicited by diffuse light stimuli. The illustration is from Bloomfield and Dowling, 1985 (116). *B*. L-glutamate depolarizes the membrane potential of a horizontal cell isolated from the carp retina, while L-aspartate and D-glutamate exert no effect. Each application pipette was filled with 500 μM of drug. Current pulses measure changes in membrane resistance. The illustration is from Lasater and Dowling, 1982 (125)

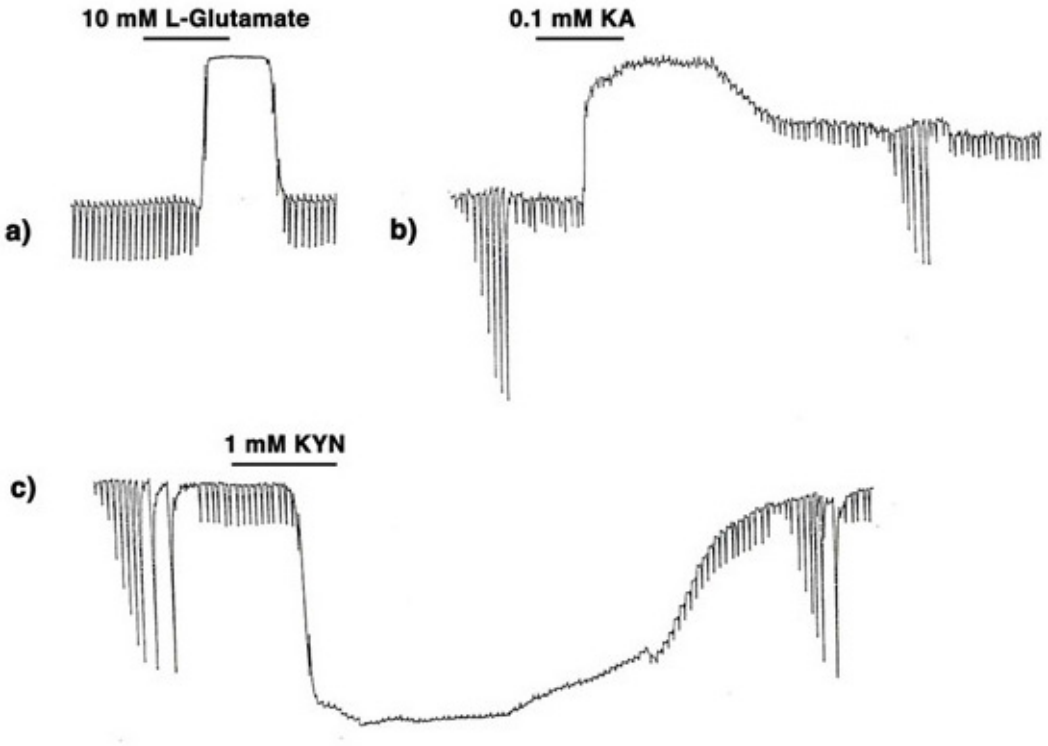

Figure 12. The effects of L-glutamate (*a*), kainic acid (*b*) and kynurenic acid (*c*) upon the membrane potential and photoresponses of L-type horizontal cells in the retina of the turtle Mauremys caspica. The illustrations are from Perlman.

Voltage- and time-dependent membrane channels

The photoresponses of horizontal cells from cold-blooded, as well as warm-blooded mammalian retinas, are shaped by voltage- and time-dependent ionic channels located within the plasma membrane (143-146). Five types of ionic currents; a sodium current, a calcium current and three types of potassium current have been identified in isolated horizontal cells of goldfish (147), catfish (148), white perch (143), skate (149), turtle (150), rabbit (145) and cat (146).

Voltage steps evoke membrane current responses for two types of horizontal cells isolated from the cat retina (Fig. 13A) and four types of horizontal cells isolated from the retina of the white perch (Fig. 13B). In cat horizontal cells, the inward sodium current is clearly evident during the first 10 ms of the current responses while at the steady state, a sustained outward potassium current is seen (Fig. 13A). Fish horizontal cells exhibit a more complex array of currents as evident from the current waveforms and the I-V curves for transient and sustained portions of the response to electrical stimulation (Fig. 13B). Basically all four types of fish horizontal cells exhibit similar ionic currents but they differ in relative magnitude. The sodium current is inward going and is seen during the initial 10ms of the current pulses that are recorded when the horizontal cells are depolarized from a negative holding potential (about -70mV) to around 0mV. It is very similar to the regenerative sodium current typical of spiking neurons. The physiological role of this current in horizontal cells is not known since these cells do not exhibit action potentials. Three types of potassium channel have been identified by their voltage- and time-dependency and by their sensitivity to specific blockers. The inwardly rectifying channels conduct an inward current when the cells are hyperpolarized below potassium equilibrium potential. In some species, extracellular sodium ions influence the reversal potential of these channels making the currents functional at physiological potentials (151). The sustained outward potassium current (delayed rectifier) is activated at potentials more depolarized than the resting, dark potential of the horizontal cells. The outward transient potassium current (I_A), is activated upon fast depolarization from negative potentials. In the intact turtle retina, the outward transient potassium current is activated upon termination of a bright light stimulus, speeding the recovery of the L-type horizontal cell from the depolarizing overshoot at light offset back to the dark level. This effect allows the L-type horizontal cells to follow fast flickering stimuli and thus, improves the frequency response curve of the cells (152).

L-type calcium responses are a prominent feature of isolated horizontal cells. These channels inactivate only slowly resulting in long duration spikes and persistent depolarized states (142, 146, 148, 153). Outward potassium currents appear in themselves too weak to inactivate calcium currents in these cells (154), however glutamate activation of the electrogenic Na/K ATPase appears sufficient to restore hyperpolarized membrane potentials (142). Calcium currents may sometimes contribute to oscillations in the light responses of horizontal cells (155).

GABA receptors and transporters

Some, but not all, horizontal-cell types accumulate GABA (51). A likely target of horizontal-cell GABA is other horizontal cells. Kamermans suggested GABA as mediator of positive feedback between these neurons (156). In many species $GABA_A$ and/or $GABA_C$ receptors are located on horizontal cells. Qian and Dowling discovered retinal $GABA_C$ receptors. They were localized on the membranes of isolated rod horizontal cells of white perch (157). Retinal $GABA_C$ receptors are reviewed elsewhere in Webvision. Currents from $GABA_A$ receptors are found in dissociated rabbit horizontal cells (158). Both $GABA_A$ and $GABA_C$ receptor currents as well as GABA transporter currents occur in isolated catfish horizontal cells (159, 160). Isolated horizontal cells from skate (161) or zebrafish (162) show no evidence of GABA receptor physiology, but do possess GABA transporter physiology. Horizontal-cell GABA circuits are species specific, nonetheless GABA would appear to be an important signaling molecule within the vertebrate outer plexiform layer, and GABA roles include signaling between horizontal cells.

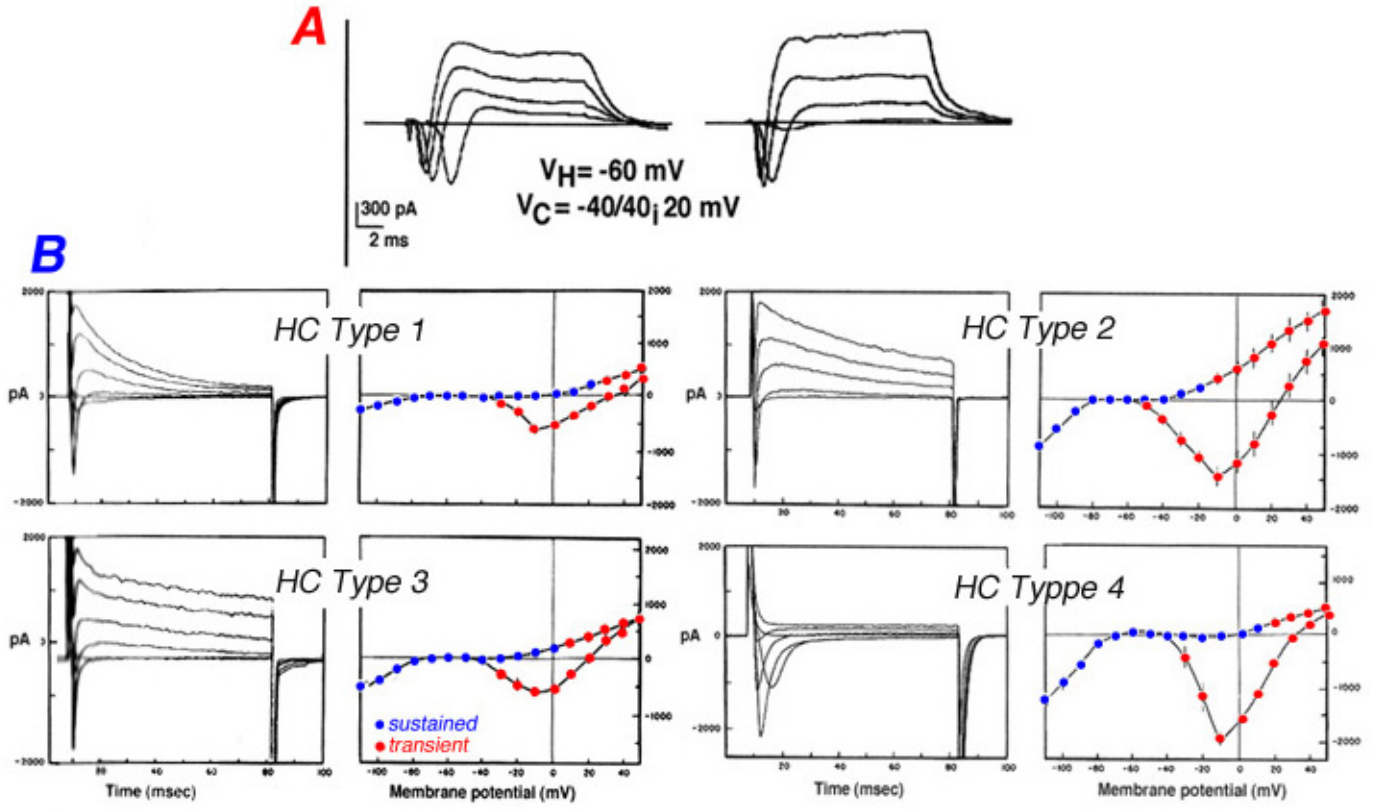

Figure 13. Voltage- and time-dependent ionic conductances in isolated horizontal cells. *A*. Current responses to different voltage steps from a holding potential at -60mV in horizontal cells from the cat retina, from Ueda et al., 1992 (146). *B*. Current responses and I-V curves from 4 types of horizontal cells that were isolated from the retina of the white perch, from Lasater, 1986 (143).

7. Gap junctions and spatial characteristics

Gap junctions

In all vertebrate retinas including mammals, horizontal cells are characterized by large-surface-area gap junctions (Fig. 3c) between each others' dendrites (163, 164). These junctions allow lateral flow of small molecules and ions within the horizontal cell network. Gap-junction-permeant tracers such as Lucifer yellow or Neurobiotin that are injected into one horizontal cell in the layer spread to hundreds of neighboring cells, forming striking images of the interconnected horizontal cell network (Figs. 14, 15A) (14, 66, 67, 84, 165, 166). Gap junctions are formed only between neighboring horizontal cells of the same physiological type as shown in figures 14 and 15A. Networks of turtle H2 cells (Fig. 15A, left panel) and of rabbit A-type cells (Fig. 15A, right panel) are revealed by neurobiotin injection into one cell of the network. Gap-junction connexons between rabbit A-type horizontal cells accommodate molecules as large as 500 Daltons (74). The permeance of the gap junctions between horizontal cells and therefore, dye coupling, is influenced by the intracellular and extracellular milieu and by chemicals such as dopamine, retinoic acid, nitric oxide or hydrogen ions that are released by other retinal cells (see section on neuromodulators).

Receptive field properties

The gap junctions between horizontal cells are highly permeable to small ions and therefore, serve as low-resistance pathways for electrical signals to spread laterally within the horizontal cell layer. Thus, horizontal cells receive excitatory input directly from photoreceptors via chemical synapses and also indirectly via gap junctions

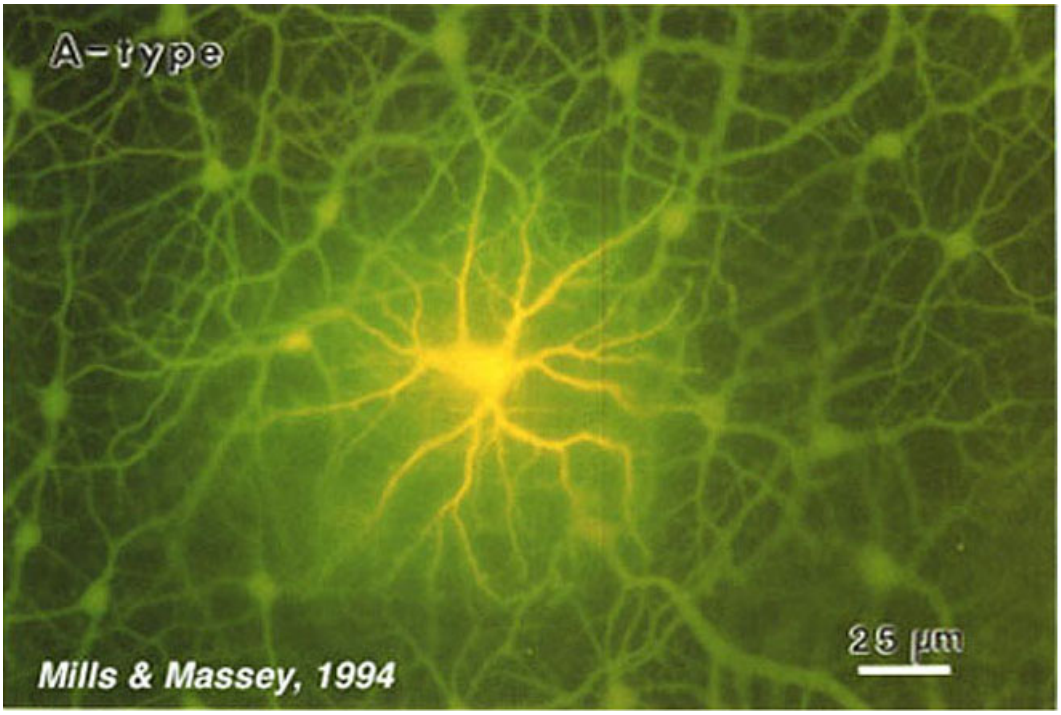

Figure 14. Rabbit horizontal cell network revealed by dye injection. Lucifer dye, injected into one cell, spreads via the gap junctions linking A-Type horizontal cells to reveal the centrally injected cell and hundreds of neighboring cells. The illustration is from Mills and Massey, 1994 (67).

with neighboring horizontal cells. The physiological consequence of the gap junctions between horizontal cells is to create a very large receptive field that spreads out to distant retinal regions, regions beyond the extent of direct dendritic contact with photoreceptors (10, 66).

The receptive fields of horizontal cells are measured by several spatial protocols. The most common are (1) examining responses to a series of concentric spots of increasing diameter but fixed irradiance, or (78) examining responses to long narrow slits of light presented at different positions across the retina. In either case response amplitudes can be modeled, at least to first order, by differential equations describing current flow in a resistive plane (16, 167, 168), or equivalently by discrete passive networks of interconnected resistors (53). An experiment in which an L-type horizontal cell in the retina of the turtle Pseudemys scripta elegans was stimulated with a series of concentric spots of fixed intensity is shown in figure 15B. The first photoresponse to the left was elicited with a stimulus of super-saturating intensity that illuminated the entire receptive field of the cell. This is the maximal photoresponse. A series of 6 photoresponses were then elicited by sub-saturating light stimuli with different stimulus diameters, as illustrated diagrammatically above each response. The photoresponse amplitude gradually decreases as the size of the illuminated retinal area is reduced (Fig. 15B; graph). This reduction of amplitude is not due to diminution of photoreceptor synaptic input to the recorded cell, as even the small spot stimuli are larger than the dendritic extent of the cell. Thus, it is suggested that the low amplitude of the responses to small spot light stimuli are due to shunting of the local photoreceptor input into neighboring horizontal cells through gap junctions. With full-field illumination, all the horizontal cells are evenly illuminated, equipotential, and therefore, no current flows between them. With small spot illumination, the membrane potential of non-illuminated horizontal cells is different from that of illuminated cells causing electrical currents to flow between them and thus, to shunt the responses of the illuminated cells.

The receptive field of a cat A-type horizontal cell, mapped with a narrow slit of light, is shown in figure 16. Exponential decay of response amplitude flanks both sides of the maximal response, which is elicited when the narrow slit is centered on the studied cell. Note that this maximal slit response is always smaller than the one

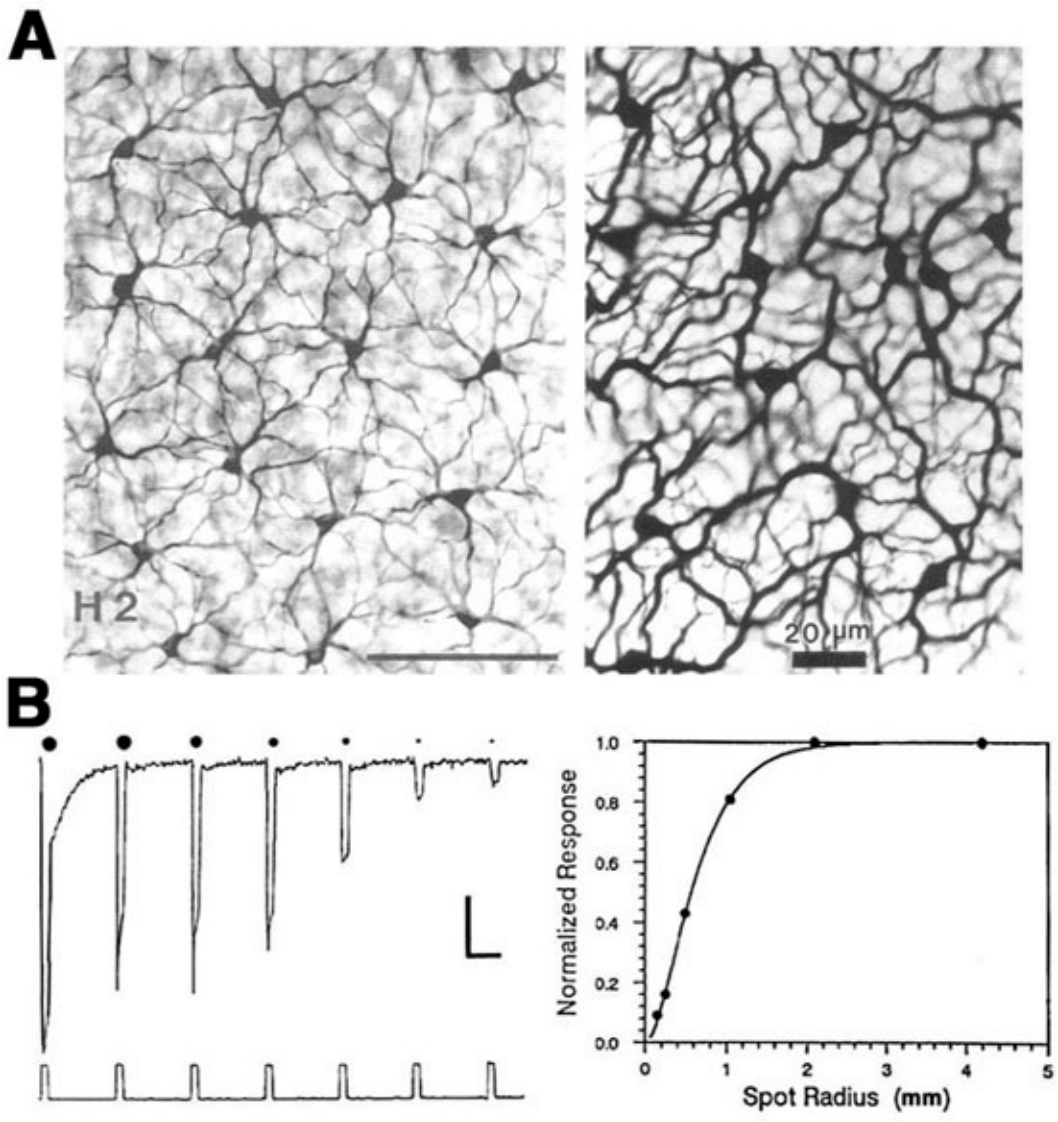

Figure 15. *A*. The syncytia of H2 cells in turtle retina (left) and A-type horizontal cells in the rabbit (right) as revealed by Neurobiotin injection into one cell in each syncytium. The illustration in turtle retina is from Ammermüller et al, 1996 (84); the rabbit retina illustration is from Mills and Massey, 1994 (67). *B*. The size of the receptive field of a turtle L-type horizontal cell as determined from the photoresponses that were elicited by concentric light stimuli of different diameters (left). The peak amplitude, normalized to the response to full field illumination (2^{nd} response from the left), is plotted as a function of spot radius in order to derive the length constant (right). The illustration is from Perlman and Ammermüller, 1994 (176).

elicited by a large light stimulus of the same intensity that covers the entire receptive field of the studied cell (V_{max}). The red receptive field (Fig. 16A) measures the spatial extent of cat red cone signals, while the blue receptive field (Fig. 16B) measures the spatial extent of rod signals, both signal components occur in the same horizontal cell. These signals share a common center, but differ in space constant.

The dimension of the horizontal cell receptive field can be quantified. Using variable diameter spots, one common procedure is to find the minimum spot diameter that elicits a maximal response. Another measure is the receptive-field length constant lambda (λ). For models based on electrical current flow in the horizontal cell layer, lambda is defined as the slit displacement required to reduce response amplitude by 1/e (16, 167, 169, 170). Some other definitions of lambda based on empirical curve fitting of data have also been suggested (10, 171). For models based on electrical current flow in the horizontal-cell syncytium, receptive field size is directly related to lambda, and lambda is directly related to the membrane resistance of the horizontal cell, and inversely related to

the coupling resistance between the horizontal cells. The space constant of the cone signal components in a cat A-type horizontal cell (Fig. 16A) is 250 μm. The space constant for the rod signal component in the same cell is 200 μm (Fig. 16B). This illustrates the point that even in the same cell, depending on what is being measured; somewhat different receptive fields can be inferred. The concept of field size is not monolithic.

The exceptional width of horizontal-cell receptive fields finds several uses. First, horizontal-cell actions on photoreceptors and bipolar cells, both of which are much narrower in receptive field centers than horizontal cells, can be seen in the distal limbs of area functions in these narrower-field neurons. Second, horizontal cell types can be distinguished by the size and properties of receptive fields. In the turtle retina, two types of luminosity horizontal cells were early recognized; L1 and L2 (53) or respectively, large receptive field (LRF) and small receptive field (SRF) horizontal cells (81). The L1 (LRF) cells are characterized by receptive fields of large diameter (>3 mm) while the L2 (SRF) cells have a receptive field diameter of about 2 mm. These two L-type horizontal cells also differ with regards to spectral properties (172) and responsiveness to surround illumination (173). The anatomical stains of LRF and SRF cells actually reveals that they are two, electrically isolated, parts of the same cell. LRF is the axon terminal of H1, and SRF is the cell body (Fig. 2a) (53). Thus receptive field measurements add further evidence that a single horizontal cell may have 2 independent area summation regions.

The horizontal cell syncytium cannot be fully described by static passive electrical models. The resistances within the horizontal cell layer change with illumination and time and therefore, the size of the receptive field (magnitude of lambda, or the length constant) changes also (169, 174, 175). In general, the size of the receptive-field length constant is related to the intensity of the light stimulus used to measure it (16, 167, 172, 176, 177). When the irradiance of the ambient illumination is increased, the length constant first increases to a peak value and then decreases (16, 169, 175). The spatial properties of C-type horizontal cells in the turtle retina depend upon the color of the light stimuli (91, 178). The waveform of the photoresponses of C-type horizontal cells may change dramatically when the spatial pattern of the light stimulus is changed, especially when the wavelength of the light is close to the zone where response polarity reverses (91). This is because depolarizing and hyperpolarizing mechanisms may differ in size. In isolated pairs of horizontal cells, coupling current decreases somewhat over time (179), potentially introducing another time-dependence in receptive fields. A further receptive field size dependency is introduced by neuromodulators such as dopamine (see below).

8. Feedback

Effects on cone receptive fields

Horizontal cells are post-synaptic to photoreceptors, but are also pre-synaptic, forming a *feedback* loop. Horizontal cells send wide-field visual signals back to the narrow center mechanism of cones through these feedback pathways (180-186). The effects of these pathways is revealed by adjusting the size, shape and color of the light stimuli used to evoke responses from cones. The effects of area and brightness on cone photoresponses from the retina of the tiger salamander are shown in figure 17 (183). Each pair of responses was elicited by light stimuli of the same intensity but different size. The early ON-phase of each pair of photoresponses (initial hyperpolarization) is identical regardless of the size of the stimulus, but the later phases are considerably affected by the stimulus size. With a small spot stimulus, following the initial hyperpolarization, the cell slightly recovers towards the dark potential but the membrane potential is maintained at a hyperpolarized level for the entire duration of the stimulus. When a large spot stimulus is used, a significant depolarization is seen after the initial hyperpolarizing phase (arrows in Fig. 17). This result appears independent of stimulus intensity. The late depolarizing potential reflects the activation of the negative feedback pathway from the horizontal cells to cones. Feedback effects are particularly large when cone intracellular chloride concentrations are artificially elevated (183, 185).

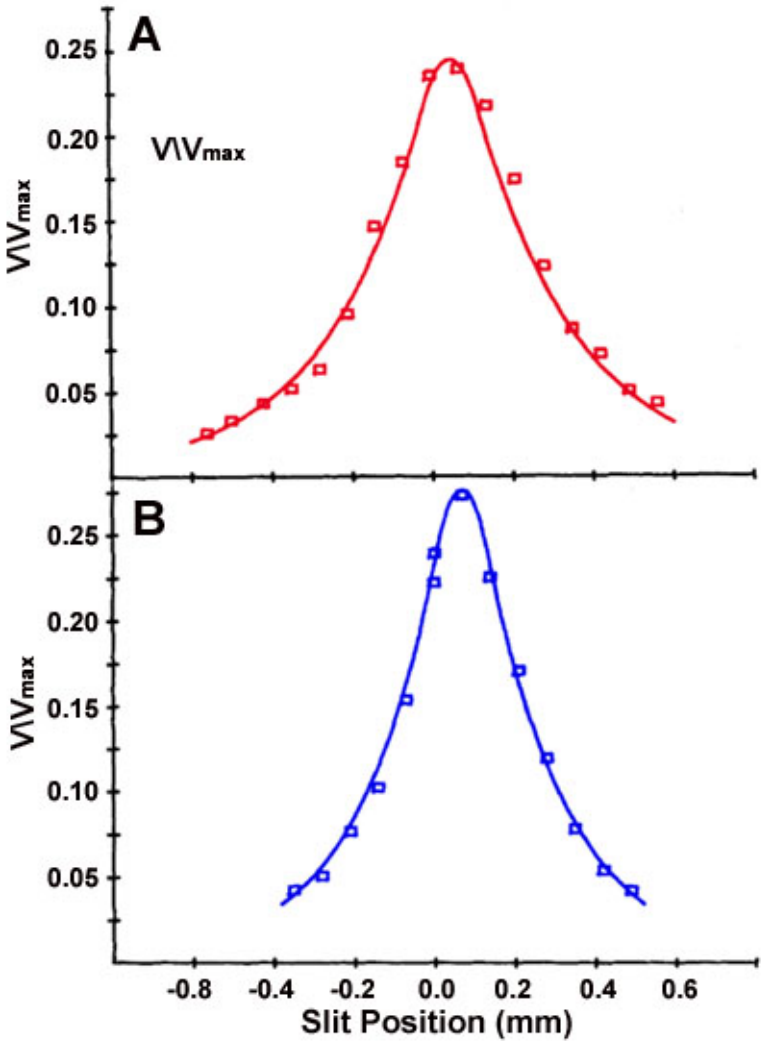

Figure 16. A-type horizontal-cell receptive field in cat retina is mapped with a long narrow slit (100 x 5000 μm). *A*. The wavelength is 647nm (242) that stimulates a mixture of cat red cone and rod responses. *B*. The wavelength is 441nm (blue) and dim enough to stimulate only rods. Rod and cone receptive fields share a common center, but differ in size. The continuous curves are generated by the conductive sheet model, with a space constant of 250 μm in *A*. and 200 μm in *B*. The figure is from Nelson, 1977 (16).

In turtle retina, the feedback pathway from horizontal cells to cones can be revealed by experiments examining the effects of size and color on cone responses (Fig. 18). With small spots, red and green light stimuli can be adjusted in brightness until equal amplitude hyperpolarizations are elicited from red and green cones. With these small-spot stimuli, the photoresponses of the red cone are very similar in shape, regardless of wavelength (upper pairs of responses). However, when the same two wavelengths of light stimuli were increased in diameter, the excitatory input from the green cones to the L1-type horizontal cells activated the feedback pathway, and caused the response of the red cone to the green light stimulus to become transient and biphasic (Fig. 18, lower left pair). In the green cone, the contribution of the feedback pathway from the red-cone input to L1-type horizontal cells is even more pronounced, and a depolarizing photoresponse is elicited in the green cone with a large diameter red-light stimulus (Fig. 18, bottom right pair). Blue cones also receive feedback signals from L-type horizontal cells (187) as shown in figure 18 (right hand traces). A large diameter red light stimulus was used to selectively isolate possible inputs that were mediated by these feedback pathways. In the dark-adapted state, a small depolarizing after potential is seen following the initial hyperpolarizing phase (trace 1). During a red background light, that selectively desensitized the red cones (L-cones), a pure hyperpolarizing photoresponse was elicited by the red light stimulus (trace 2), while a blue background augmented the relative contribution of

the feedback pathway and therefore a depolarizing photoresponse was obtained (trace 3). These and other anatomical and physiological studies provide the basis for proposing that a feedback model between cones and horizontal cells could underlie color opponency (37, 42, 86, 188).

While mammals lack color opponent horizontal cells, color opponent responses are seen in primate short-wavelength cones (blue cones) (185). With short-wavelength stimulation, primate blue cones produce outward currents in response to the closing of outer-segment cation channels by phototransduction. But long-wavelength stimuli evoke inward currents (Fig. 19A). The primate blue cone, then, is similar to the turtle blue cone in exhibiting negative feedback from long-wavelength-selective L-type horizontal cells. The long-wavelength inward currents, the feedback responses, are abolished by CNQX, an antagonist of horizontal-cell AMPA/kainate membrane channels (Fig. 19B), supporting the notion that horizontal cells are the source of the negative feedback input in cone photoreceptors. Further, the characteristics of blue-cone feedback currents resemble those of calcium currents (185), supporting the long-held idea that horizontal-cell feedback to cones operates through a modulation of calcium channels (183, 189).

Thus, in primate retina there are color opponent blue cones, but not color opponent horizontal cells. The difference with other vertebrates would appear to reside with horizontal cell circuitry. While the H2 cell of primate retina is somewhat blue cone selective (Fig. 10), it apparently is not selective enough to reveal the blue-cone depolarizing feedback signals to red stimuli. The direct hyperpolarizing long-wavelength cone input to H2 cells may mask the blue-cone feedback response.

The feedback synapse

The negative feedback circuit from horizontal cells to cones is thought to occur at the horizontal-cell lateral elements that invaginate photoreceptor terminals at the triad ribbon synapses (Fig. 3a). The problem has been that no images of a synapse with presynaptic vesicle clusters has ever been seen within the lateral elements, except for human retina (190), and there it was only noticed for axon terminal invaginations within rod spherules. However syntaxin-4, a SNARE protein involved in fusion of synaptic vesicles to the plasma membrane, has been localized to the lateral elements of mouse horizontal cells in both cones and rods (Fig 20) (191), as has VGAT, the vesicular GABA transporter (Fig. 21) (192). These molecules both suggest presynaptic activity in horizontal cells. Further, fish retinas have distinctive spinules on the dendritic endings of the horizontal-cell lateral elements in cone pedicles (Fig. 3b). Spinules may be the sites of feedback from horizontal cells to cones because they change shape and enlarge during background illumination when the effects of negative feedback are most apparent (57, 58, 193-196).

There are several candidates for the feedback neurotransmitter. In cyprinid retinas H1 horizontal cells transport GABA, which accumulates in the cytoplasm (47, 51, 162, 197, 198). GABA-induced currents can be recorded from the terminals of red-sensitive and green-sensitive cones isolated from the turtle retina (199, 200). Color opponency in fish C-type horizontal cells is eliminated upon exposure to GABA or its antagonists (201, 202). However, studies in other species have failed to show GABA effects that are supportive of a role for GABA as the inhibitory feedback neurotransmitter of the horizontal cell. GABA did not eliminate C-type responses in turtle (203) or Xenopus (89), and did not affect cone surround responses in monkey (204). In L-type horizontal cells of turtle, catfish, skate and goldfish retinas, GABA and related drugs induce depolarizations that are consistent with the activation of electrogenic GABA transporters in the horizontal cell membrane (149, 159, 160, 203, 205). Although these cells clearly have GABA uptake systems and accumulate GABA, the idea that GABA mediates the negative feedback of horizontal cells to cone photoreceptors has not received universal experimental validation. Horizontal-cell GABA could still have a feed-forward action directly upon bipolar cell dendrites or other horizontal-cell processes (156, 205). Alternatively GABA receptors on horizontal cells might simply serve the purpose of limiting transporter-generated membrane depolarizations in the presence of extracellular GABA.

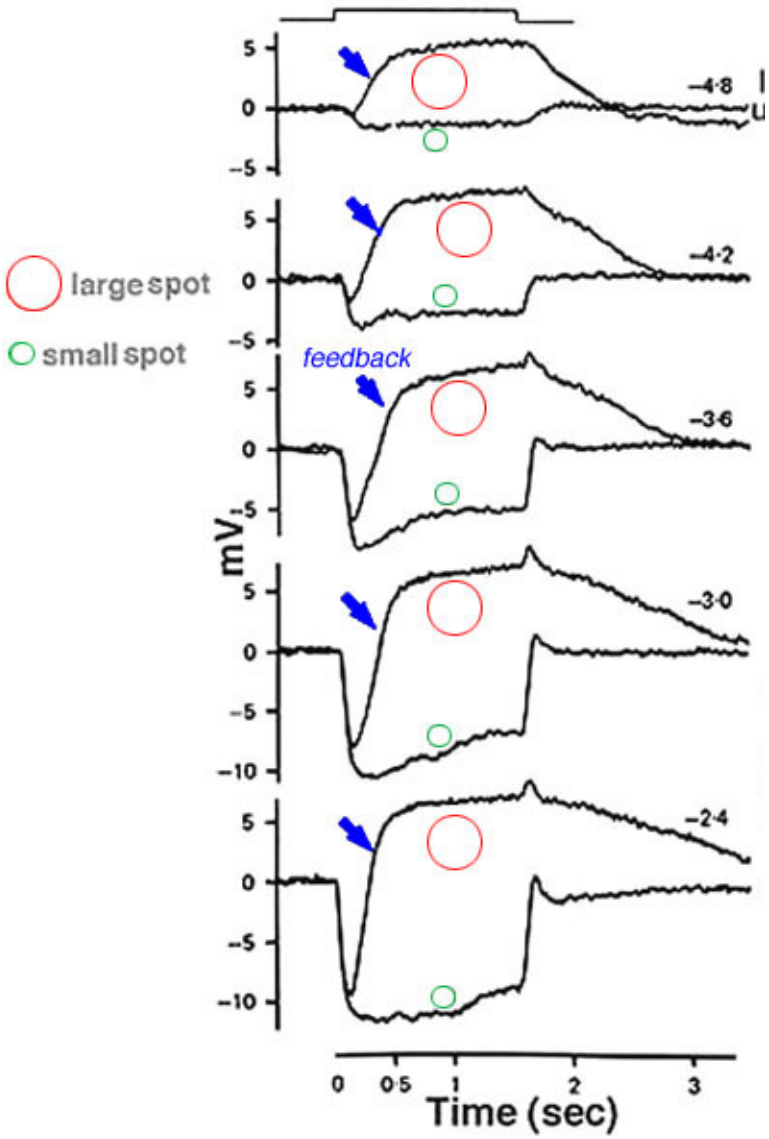

Figure 17. The contribution of the feedback pathway from L-type horizontal cells to cone responses in the retina of the tiger salamander. Cone photoresponses were elicited by light stimuli of different intensities covering a small or a large spot as indicated. The illustration is from Lasansky, 1981 (183).

A further feedback model proposes that elevated proton concentration in the synaptic cleft mediates feedback by inhibiting photoreceptor calcium channels (206). Proton buffers, particularly amino sulfonates like HEPES, block feedback (207-212). While there is general agreement that some pH buffers block feedback, there is currently disagreement whether alteration of pH in the synaptic cleft is the mechanism (213, 214).

Most feedback models propose that modulation of presynaptic calcium channels in the photoreceptor terminals is the key. Using voltage-clamp recordings from cones during illumination with spots or annuli of light, Verweij et al (1996) (215) suggest that feedback modulates the voltage-dependency of the calcium channels in the cone pedicles (Fig. 22A). The explanation takes off from an old electrical model (5) and proposes that horizontal cells can initiate large extracellular current flow through hemi-gap-junction channels into the restricted extracellular space within the triad synapse of the cone (Fig. 22B) (68, 70, 72, 189, 216). During light stimulation, the L-type horizontal cells hyperpolarize, increasing the magnitude of the inward flow of cations from extracellular space, through hemi-gap-junction channels, into horizontal cell lateral elements. This causes hyperpolarization of the extracellular space. Such hemi-gap-junctions, consisting of connexin Cx55.5, have been demonstrated

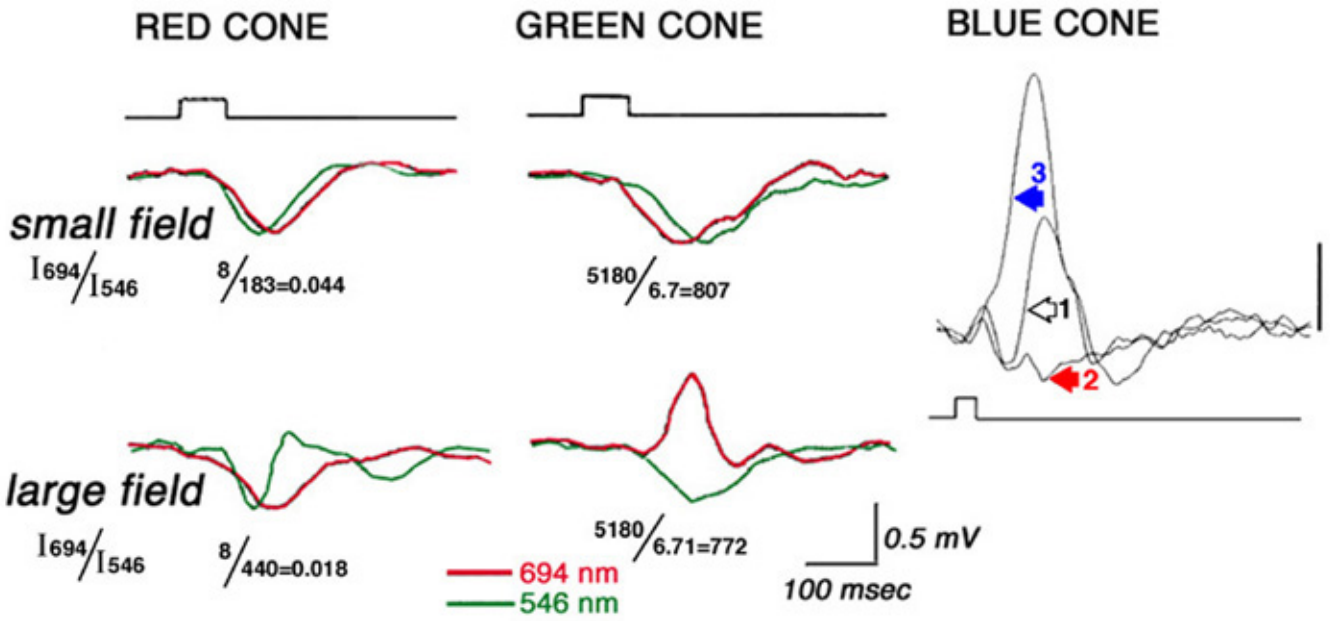

Figure 18. The contribution of negative feedback from L-type horizontal cells to the photoresponses of cones in the turtle retina. Red and green cones were stimulated with either small field or large field stimuli of either red or green light. The contribution of the negative feedback from the L-type horizontal cells was most apparent in the recording from the green cone stimulated with a large field red light stimulus. The illustration is from Perlman et al., 1985 (172). The blue cone from the retina of the turtle (*Mauremys caspica*) was stimulated with a red (700nm) light stimulus covering a large retinal area in the dark-adapted state (trace 1) and during red (trace 2) or blue (trace 3) background lights. Depolarizing feedback signals from red cone stimulation are most apparent on the blue background (trace 3). The illustration is from Itzhaki et al., 1992 (187)

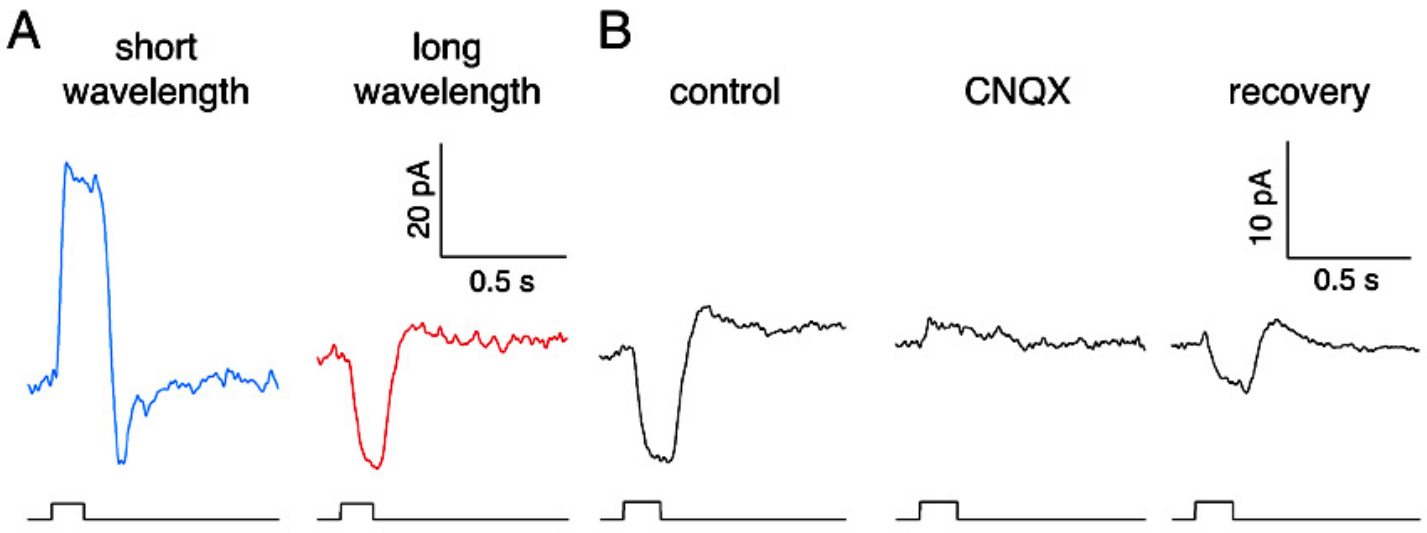

Figure 19. In monkey retina, inhibition of blue cones by long wavelength light is mediated by horizontal cell feedback. *A*. Short-wavelength blue light evokes outward photocurrents in the blue cone, but long-wavelength yellow light evokes inward feedback currents. *B*. Inward feedback currents elicited by long-wavelength stimuli are blocked by 20μM CNQX, a blocker of horizontal-cell light responses. Blue cones are voltage clamped at -40mV. The figure is adapted from Packer et al., 2010 (185).

anatomically in horizontal cell lateral elements in zebrafish retinas (Fig. 3d).The extracellular hyperpolarization activates voltage dependent calcium channels which sense the change in the same way as intracellular depolarization, leading to calcium entry, and an increase in glutamate release. The idea finds some support because when the hemi-channels are blocked with carbenoxolone (a specific gap junction blocker), the feedback signal in the cone is eliminated (189, 204).

Further evidence for the importance of connexin 55.5 and hemi gap-junctions for feedback comes from a genetic knockout in zebrafish. Feedback to cones, behavioral contrast sensitivity, and horizontal-cell color opponency were all weakened in this knockout. As this connexin is only expressed in horizontal cells, a perturbation of horizontal-cell circuitry is a likely cause. Curiously the knockout effects were strongest when horizontal cells were in a hyperpolarized state, but were less evident when they were in a depolarized state (73).

9. Modulation of physiology

The properties of horizontal cells are altered by a variety of humoral factors released by retinal cells during changing conditions of illumination. These chemicals, generally referred to as neuromodulators, are believed to adjust the modes of information processing in the retina in order to match retinal function to ambient condtions. Neuromodulators reach horizontal cells either via direct synaptic interactions or by volume transmission. In the latter mode, inter-cellular communication is mediated by passive diffusion of the chemical following its release from the source cells into extracellular space. Dopamine is the most extensively studied retinal neuromodulator, but in recent years nitric oxide and retinoic acid have been added to the list. In this section the actions of these neuromodulators on vertebrate horizontal cells is discussed.

Dopamine

Dopamine-containing neurons reside in the amacrine cell layer of the retina. In fish, where they were first discovered, dopaminergic cells are interplexiform cells (IPCs), having cell bodies in the amacrine cell layer and sending long processes to the outer plexiform layer where they arborize and synapse on horizontal cells. In other species (e.g. turtle, most mammals), the dopaminergic cells are amacrine cells with few, if any, processes extending to the outer plexiform layer (217), and therefore dopamine has to reach the horizontal cells by volume diffusion through the inner nuclear layer. The action of dopamine upon vertebrate horizontal cells has been extensively studied and reviewed (218) and involves at least 4 distinct actions.

1. Dopamine reduces the extent of gap-junction coupling, as shown by dye coupling experiments, by electrophysiological determination of receptive field size (119, 166, 176, 219-222), and by patch recordings from isolated cell pairs (69). Dopamine shrinks the receptive field, and reduces photoresponse amplitude in horizontal cells from intact fish retina (Fig. 23A). Photoresponses that were recorded during superfusion with dopamine solutions were larger in amplitude with small spot stimuli than those recorded with the same stimuli under control conditions (Fig 23A). The increase in the response to spot stimuli indicates less shunting by neighboring non-illuminated horizontal cells and is consistent with the notion that dopamine uncouples the horizontal cell network (220). Gap junction conductance is reduced through activation of adenylate cyclase by dopamine D1-type receptors (223).

By reducing gap-junction coupling, dopamine limits the spread of Neurobiotin, a low-molecular weight (323 Dalton) tracer molecule, after injection of this molecule into a cell within the horizontal cell layer. In H1 cells of monkey retina the Neurobiotin tracer field is maximal during dark adaptation (Fig. 24A). The dopamine D1 agonist SKF38393 reduces the size of the tracer field (Fig. 24D), as does light adaptation (Fig. 24B) and the gap junction blocking agent meclofenamic acid (Fig. 24C). Dark adapted space constants in monkey H1 cells are very large, in excess of 1000 μm (222). Similar results are seen in mouse retina where additionally, blockade of the dopamine D1 receptor with a D1 antagonist (SCH23390) widens the area of tracer spread, and the cAMP

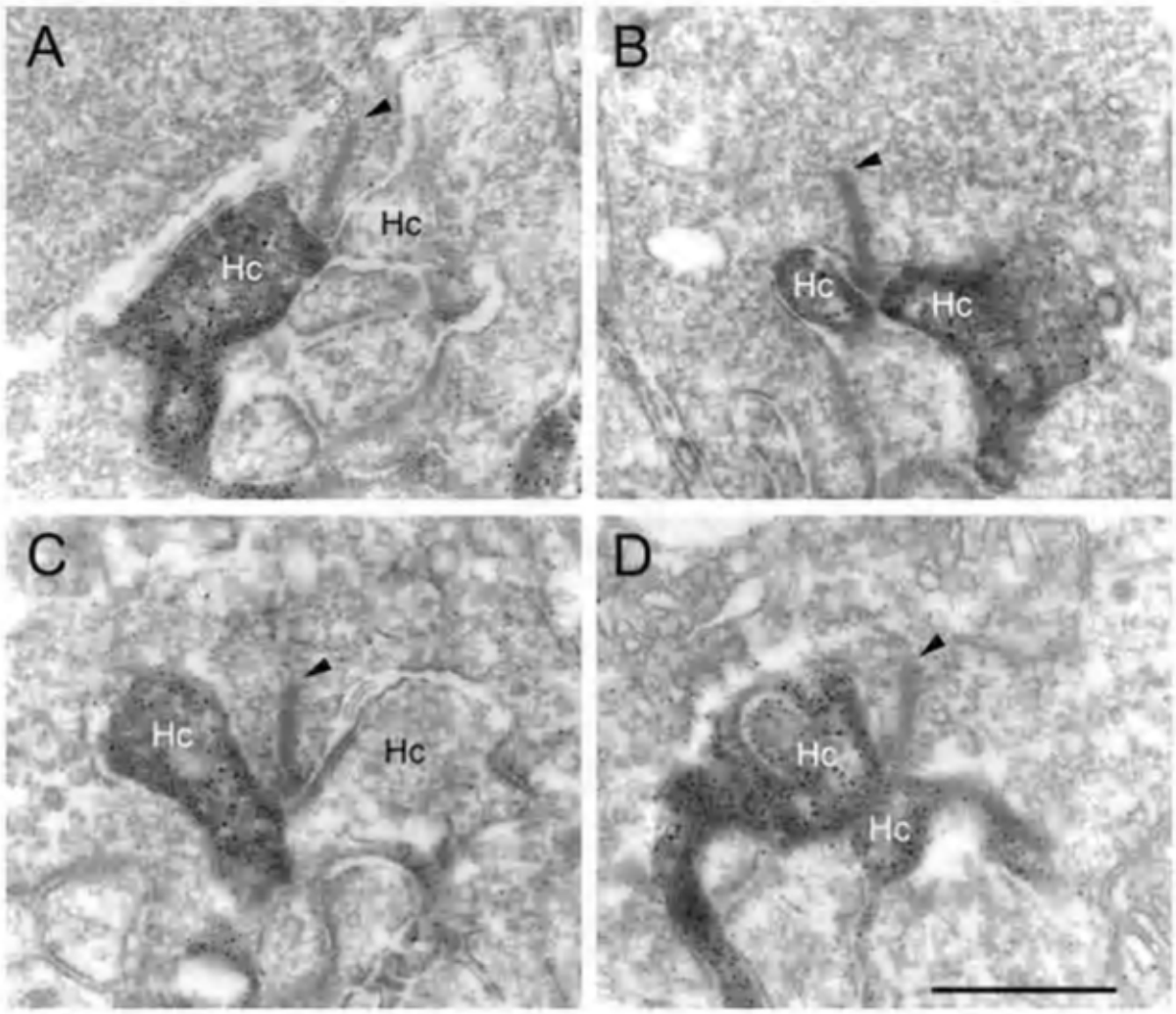

Figure 20. Electron microscopy of immunolabeled mouse retina demonstrates localization of syntaxin-4 (black granular staining) to the lateral elements of horizontal cells (Hc) in rod (*A* and *B*) and cone (*C* and *D*) ribbon synapses (arrow heads). Syntaxin-4 occurs in one or both lateral elements. The immunolabel is seen also in horizontal-cell axons and dendrites. The scale bar is 0.5 μm for *A-D*. The figure is from Hirano et al., 2007 (191).

analogue 8-bromo cyclic GMP reduces the spread of the tracer. All observations are consistent with a D1 receptor, cAMP-mediated mechanism (224).

Receptive field modulation by dopamine varies somewhat with species. Neurobiotin spread between rabbit A-type cell bodies is highly pH sensitive (165), in fact only observable at pH 7.2 +/- 0.05. Nonetheless, a particularly striking modulation of receptive field size occurs in the axon terminal systems of rabbit B-type horizontal cells (225). Modulation of tracer coupling by dopamine is robust in mouse retina (224) and in monkey retina (Fig. 24) (222). Tracer coupling between the rod-driven horizontal cells of skate retina was dopamine insensitive (226).

In isolated horizontal cell pairs dopamine uncouples gap junctions (69). In this preparation the biophysics of gap junction coupling and its modulation by dopamine can be examined in detail. In zebrafish the unitary conductance of a gap-junction channel is 50-60 pS and the open time is ~10 msec. Dopamine reduces the open time and the frequency of opening of these channels for a net reduction of 2-3 fold (227). The action is mediated through a D1 agonist and is mimicked by the cAMP analogue 8-Bromo-cAMP, suggesting an intracellular mechanism that involves increases in cAMP, a common action of D1 receptors (179). A parallel study in isolated

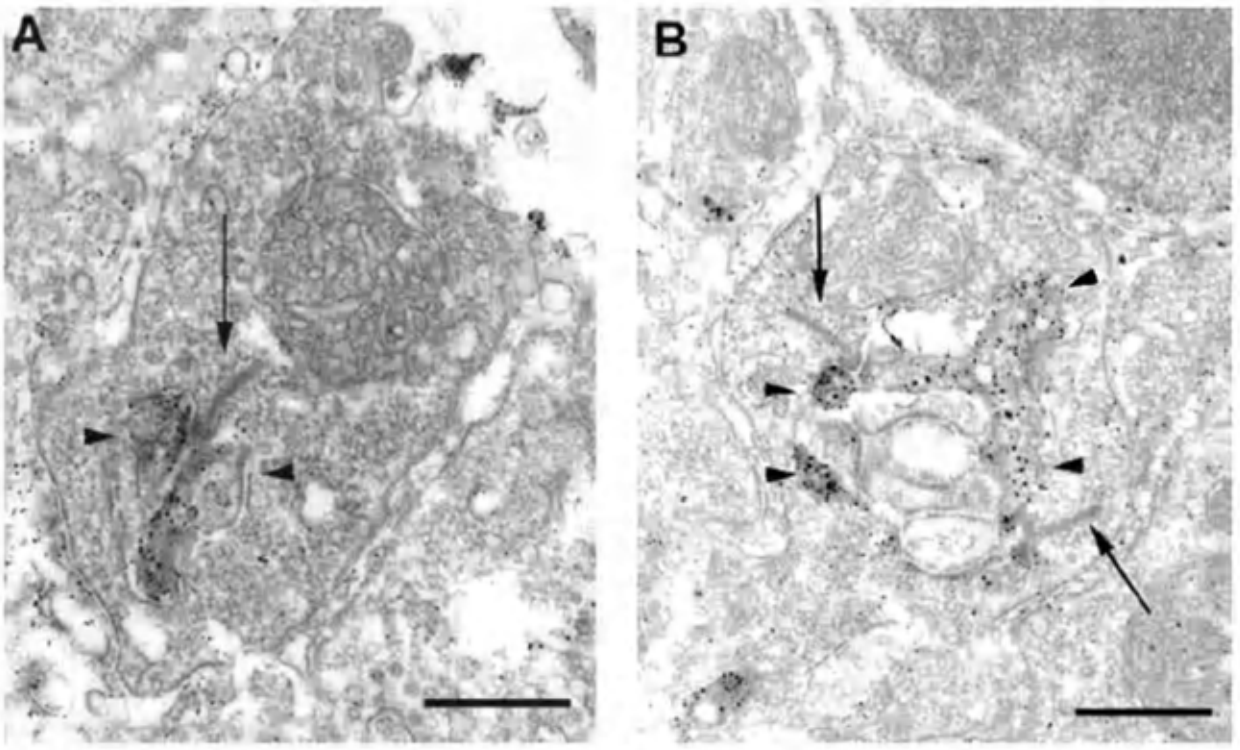

Figure 21. Electron microscopy shows immunolabeling (dark granules) for vesicular γ-aminobutryric acid transporter (VGAT) in mouse (*A*) and rat (*B*) horizontal cell lateral elements (arrow heads) in rod spherules. Rod synaptic ribbons are indicated by long arrows. The scale bars are 0.5 μm. The illustration is from Cueva et al., 2002 (192).

catfish horizontal-cell pairs yielded similar results. Dopamine D1 receptors raised intracellular cAMP, closing gap junctions. Further, intracellular pH and Ca^{2+} ions were ruled out as mediators (228).

2. Dopamine induces the formation of spinules in fish horizontal cells in a manner similar to that seen with bright-light background illumination (193, 229).

3. In fish retina, dopamine reduces the amplitude of horizontal-cell photoresponses (220, 230), as shown in figure 23A. This phenomenon is attributed to dopamine modulation of the interaction between L-glutamate and AMPA/KA receptors on the horizontal cell membrane. Dopamine increases the binding of L-glutamate to horizontal-cell-membrane receptors (231), as illustrated in figure 23B. Dopamine by itself evoked no current in the isolated horizontal cell (Fig. 23B, upper trace), but it significantly augmented the kainate-induced glutamate-receptor current (Fig. 23B, lower traces). Further studies show that this dopamine action is dependent on extracellular magnesium ions (232). In the intact retina, the photoresponses of horizontal cells reflect the unbinding of glutamate from its receptors. If dopamine increases the affinity of glutamate for its receptors on the horizontal cell membrane, then unbinding at light onset will be at a slower rate. The flicker photoresponses of cat and rabbit horizontal cells were in fact phase-delayed by both D1 and D2 selective dopamine agonists, in agreement with the idea of slower unbinding of glutamate. In these species flicker photoresponses increased in amplitude with dim lights, but decreased with bright lights (233). Pflug et al (233) suggest that the dopamine-induced increase in glutamate binding by horizontal cells may induce a maintained depolarized bias that shifts cone calcium activation through feedback interaction towards more depolarized levels, tending to facilitate dim-stimulus synaptic transmission, while truncating bright-stimulus transmission (233), an elaboration of the ideas put forward by Mangel and Dowling (234).

In other species this appears not to be the case. Such modulations are not clear in the turtle retina (176, 221).

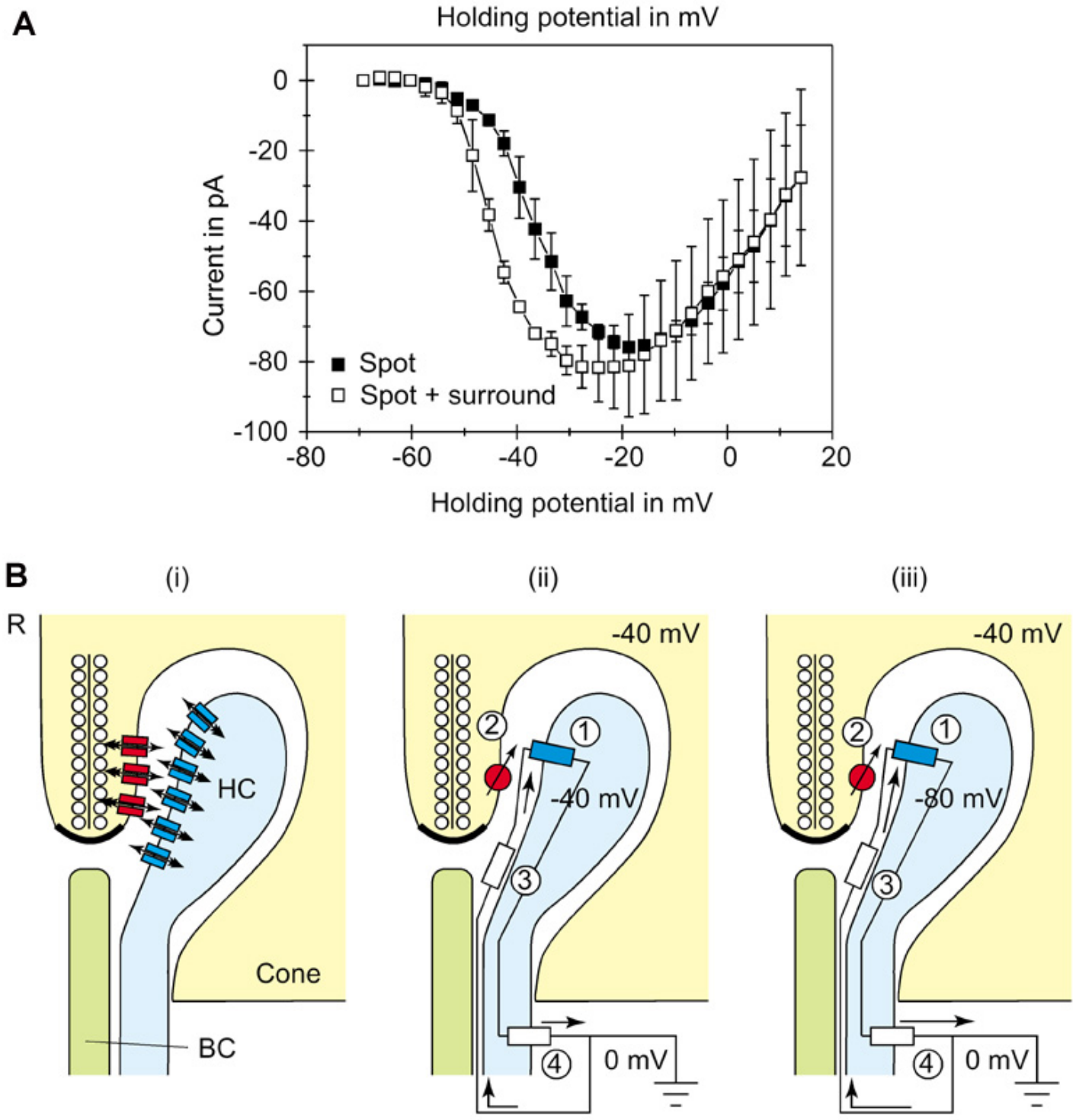

Figure 22. Electrical feedback model. *A*. The activation range of calcium currents in cone synaptic terminals shifts towards more hyperpolarized values during surround stimuli that hyperpolarize horizontal cells. *B.* The electrical or 'ephaptic' feedback model argues that the voltage within the enclosed extracellular space surrounding horizontal-cell invaginated dendritic tips is influenced by horizontal-cell membrane polarization. With surround stimulation, these dendrites hyperpolarize, causing extracellular space to hyperpolarize also. This affects synaptic calcium channels in the same way as would intracellular depolarization of the cone terminal. The more hyperpolarized the horizontal cell dendrite, the more calcium enters the cone terminal, and the more neurotransmitter is released. The effect is opposite to the light-induced closing of cone outer segment cation channels that suppress neurotransmitter release. (i) Calcium channels (242) are located on the cone presynaptic membrane, adjacent to the ribbon. Gap junction hemichannels (blue), polarize adjacent extracellular space. Extracellular current flow hyperpolarizes extracellular space to a greater extent in the light (ii) than in the dark (i) The illustration is from Kamermans and Fahrenfort, 2004 (216).

4. Dopamine changes the balance between rod and cone inputs to horizontal cells in Xenopus retina, in order to augment the rod contribution in the dark-adapted state and the cone contribution in the light-adapted state. This action is thought to depend on different dopamine sensitivities of AMPA/KA receptors postsynaptic to rods and cones (235, 236).

Nitric oxide

Involvement of nitric oxide (NO) in physiolological regulation of retina is indicated by the presence of cells containing the enzyme nitric oxide synthase (NOS) that synthesizes NO from L-arginine (237). Immunoreactivity to NOS isoforms or demonstration of NADPH-diaphorase activity has been seen in every vertebrate retina studied (238). In all species NOS occurs in some types of amacrine cells, but reports of NOS in photoreceptors, horizontal cells, bipolar cells and Müller cells have also been published. In fish retinas, evidence for NOS in horizontal cells has been demonstrated by immunostaining and NADPH diaphorase histochemistry (239-241). In the turtle retina, n-NOS has been reported in horizontal cell processes at photoreceptor ribbon synapses and in the inner segments of the photoreceptors, and e-NOS has been seen in the H1 cell axon terminals and in Müller cells (47, 242-244). In the rabbit retina, NADPH diaphorase activity, an indicator for NOS presence in horizontal cells, has been shown to depend upon the state of adaptation and the activity of glutamatergic pathways. It is increased in the dark-adapted state (245) or by the activation of AMPA/KA type receptors (246). Indeed nitric oxide has been suggested as a player in horizontal-cell feedback mechanisms (247).

Regardless of the exact cellular source of NO, this molecule exerts profound effects on the physiology of horizontal cells. Raising NO level by either exogenous application (NO donors) or by adding L-arginine, the substrate for its synthesis, reduces the size of the horizontal cell receptive field (177, 248, 249). This effect reflects direct action of NO on the gap junctions between adjacent horizontal cells. It is thought to be mediated through cGMP-dependent protein kinase pathways (249, 250), in a pathway parallel to cAMP, dopaminergic modulation.

NO modifies the photoresponses of both A-type and B-type horizontal cells in the rabbit retina (Fig. 25). These responses were elicited by a series of disks of fixed intensity and different radii, both in control conditions and during exposure to SNAP (an NO donor). For every light stimulus, the photoresponse is larger during SNAP application as compared to control conditions (gray vs black responses, Fig.25). This is illustrated graphically in figure 25B and 25D where the peak responses of photoresponses shown in parts A and C respectively are plotted as a function of stimulus diameter. SNAP clearly causes augmentation of the photoresponses to large diameter stimuli. NO acts in the distal rabbit retina to augment the photoresponses of the horizontal cells and to reduce the receptive field size (249).

A similar augmentation of horizontal-cell responses by NO has been seen in L-type horizontal cells of carp (177) and turtle retinas (251). The NO effect in horizontal cells can reflect either NO action upon the phototransduction process in the photoreceptor outer segments (251, 252) or upon the neurotransmitter release from the photoreceptors (253). Furthermore, NO can modulate the interaction between L-glutamate and its receptors on the horizontal cell membrane (254), and thus can alter the responsivity of horizontal cells independently of effects upon phototransduction. In order to distinguish the above possibilities, the influence of NO-related drugs on the transfer function between cone photoreceptors and L1-type horizontal cells (L1-HC) were studied in the turtle eyecup preparation as shown in figure 26 (251). In the dark-adapted state (Fig. 26A), the cone to L1-HC synapse is non-linear and is characterized by high amplification for dim light stimuli that elicit low amplitude cone photoresponses. Reducing the retinal level of NO by adding L-NAME, increased this non-linearity, while raising retinal NO level by adding either L-arginine or SNP, reduced the non-linearity and linearized the cone-to-horizontal cell transfer function. In the light-adapted state (Fig. 26B), the cone to L1-HC transfer function was linear under control conditions consistent with high NO level. Further increase of retinal NO (adding L-arginine or SNP) did not change the transfer function or synaptic amplification, while lowering retinal level of NO (adding L-NAME) changed the transfer function into a non-linear one with high amplification for small amplitude cone photoresponses. What is clear in figure 26 is a direct effect on synaptic

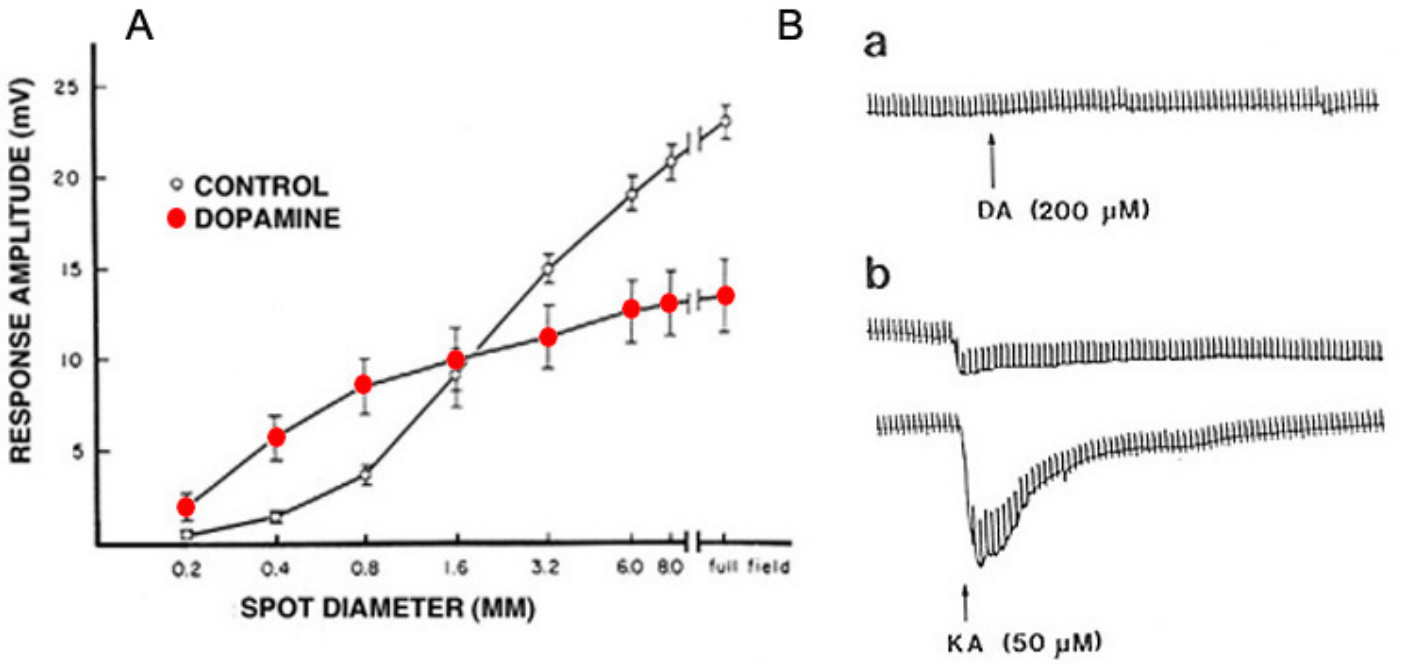

Figure 23. Dopamine affects synaptic gain and receptive fields in fish horizontal cells. *A*. Photoresponses were recorded from a horizontal cell in the intact carp retina using light stimuli of fixed intensity but different diameter, under control conditions and after exposure to dopamine. The illustration is from Mangel and Dowling, 1985 (220). *B*. Dopamine by itself did not elicit any current response in a horizontal cell isolated from white perch retina (upper trace). However in the presence of dopamine the inward current elicited by the AMPA/kainate agonist kainic acid (middle trace) was significantly augmented (bottom trace). The illustration is from Knapp and Dowling, 1987 (231).

transfer from cones to horizontal cells. This may include neurotransmitter release and/or neurotransmitter interactions with its post-synaptic receptors.

In contrast to dopamine, NO does not influence the process of spinule formation in fish horizontal cells during exposure to background lights (177).

Retinoic acid

Retinoids are of great importance in the eye having roles in both the photopigment cycle and in the embryonic development of the eye. The retinoid 11-cis retinaldehyde serves as the chromophore of the rhodopsin molecule, the visual pigment of the vertebrate photoreceptors (255, 256). The retinoid retinoic acid activates transcription factors which are important during eye development (257-260). Most recently a further role for retinoic acid has been proposed; that of a neuromodulator linked to background adaptation, affecting horizontal cells in particular (64, 65, 261). Retinoic acid is produced in the pigment epithelium as a side effect of the rhodopsin transduction process in bright illumination.

Retinoic acid induces synaptic plasticity at the terminal dendrites of horizontal cells and promotes the growth of spinules in fish horizontal cells, in a pattern similar to that induced by background lights (64, 65). It exerts a pronounced effect on the electrical coupling between horizontal cells in mammalian and non-mammalian retinas and reduces the receptive fields of the horizontal cells (261, 262) as shown in figure 27. Adding retinoic acid to retinal preparations of carp, rabbit and mouse, reduces the conductance of the gap junctions between neighboring horizontal cells thus reducing the degree of dye coupling (Fig. 27a), in a manner similar to that seen during background illumination. Intracellular recordings in horizontal cells also show that retinoic acid produces effects similar to those of light adaptation. The amplitudes of the horizontal cell photoresponses to full

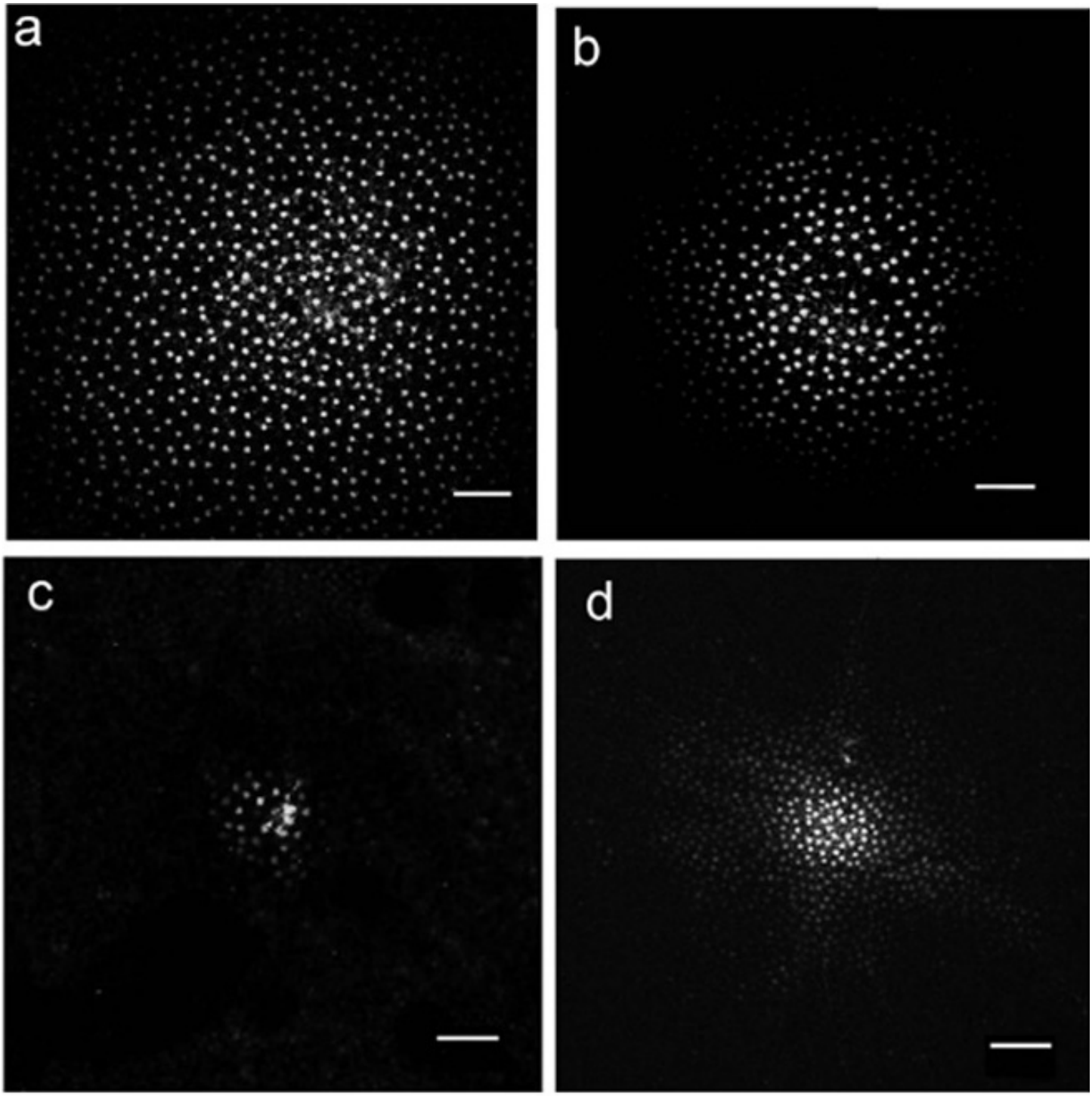

Figure 24. Modulation of horizontal-cell coupling in monkey retina. *a*. Neurobiotin tracer reveals maximal coupling-field occurs in H1 horizontal cells under dark adaptation. *b*. Mesopic (500 nm) background illumination shrinks the coupling field. *c*. Meclofenamic acid, a gap junction blocking agent, prevents tracer spread. *d*. The dopamine D1 receptor agonist SKF38393 greatly reduces the spread of tracer. The scale bars are 100 μm. The illustration is from Zhang, Jacoby and Wu, 2011 (222).

field stimuli are increased by retinoic acid (Fig. 27b). The responses to stimulation with bright light annuli are reduced by retinoic acid, and those to spot illumination are increased (Fig. 27c). Thus, retinoic acid, like dopamine and nitric oxide, seems to modulate the physiological properties of vertebrate horizontal cells in order to adjust their function during changing conditions of ambient illumination.

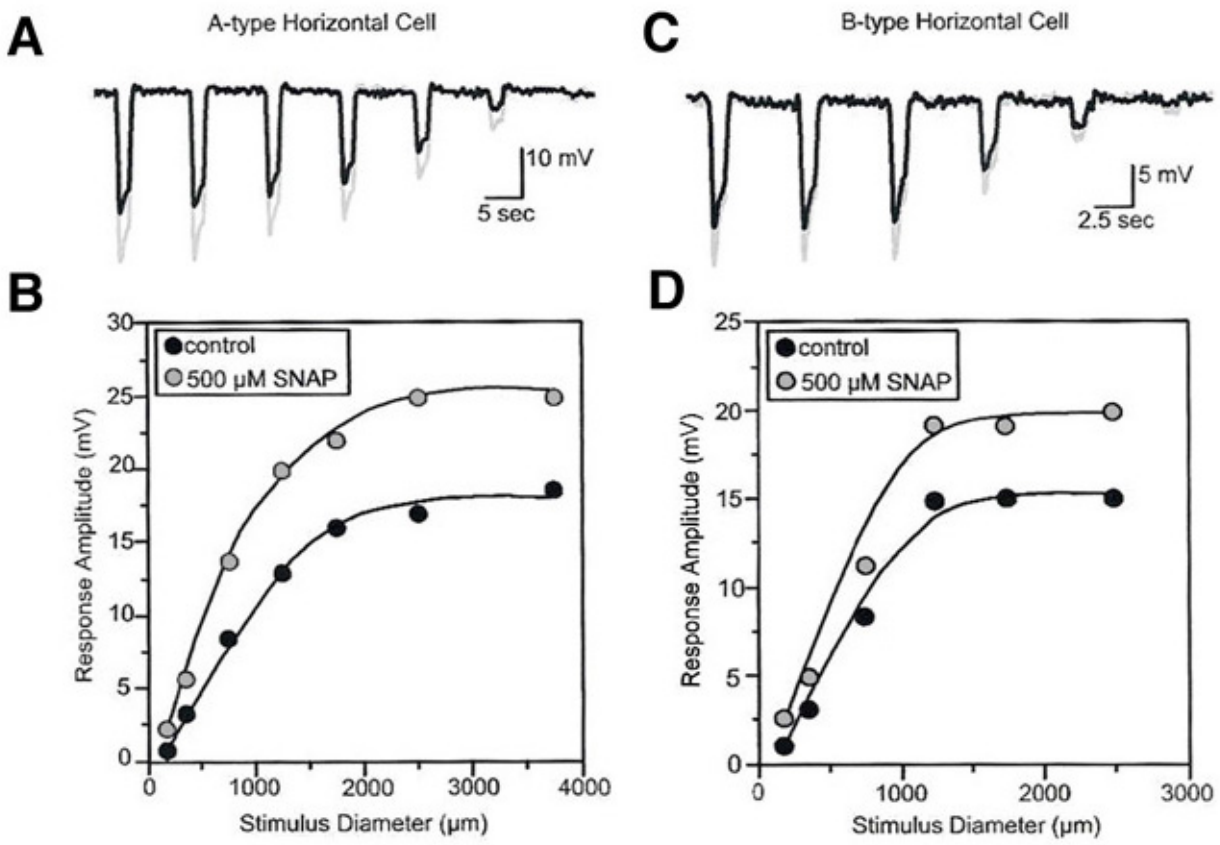

Figure 25. The actions of nitric oxide (NO) upon the physiology of horizontal cells in the rabbit retina. *A.* & *C.* The effects of NO were tested by adding SNAP, an NO donor, and observing the effects upon photoresponses that were elicited by disks of fixed intensity but different diameters. *B.* & *D.* The relationship between response amplitudes and stimulus diameters indicates that NO augments the photoresponses of both A-type and B-type horizontal cells and reduces their receptive field sizes (black traces, control; gray traces, SNAP). The illustration is from Xin and Bloomfield, 2000 (249).

10. Functional Roles

The major functional roles of horizontal cells in the vertebrate retina are 1) initiating the organization of spatially opponent receptive fields for second and third order neurons in the retina, 2) modulation of the photoreceptor signal with different lighting conditions and 3) adjustment of synaptic gain. These roles represent both neuronal signal processing and neuronal adaptation at the first synaptic level in the retina.

In the half century since Svaetichin (80, 263) first described S-potentials in the vertebrate retina, we have made progress in our understanding of the many ways that horizontal cells can influence the kinetics and spatial organization of the photoreceptor response, and as a consequence, the physiology of all downstream retinal neurons. These include rod-cone balance changes, distal color opponency, center surround opponency, and gain regulation at the photoreceptor synapse. Further, the horizontal cell itself is under neuromodulatory control, and reorganizes its synaptic connections, glutamate sensitivity, and receptive field under the influence of dopamine, retinoic acid and nitric oxide. The horizontal cell forms an important link between inner and outer retina because this cell type controls distal retinal signal processing, while being itself under the influence of centrifugal neuromodulatory control from both within the retina and even from the brain itself.

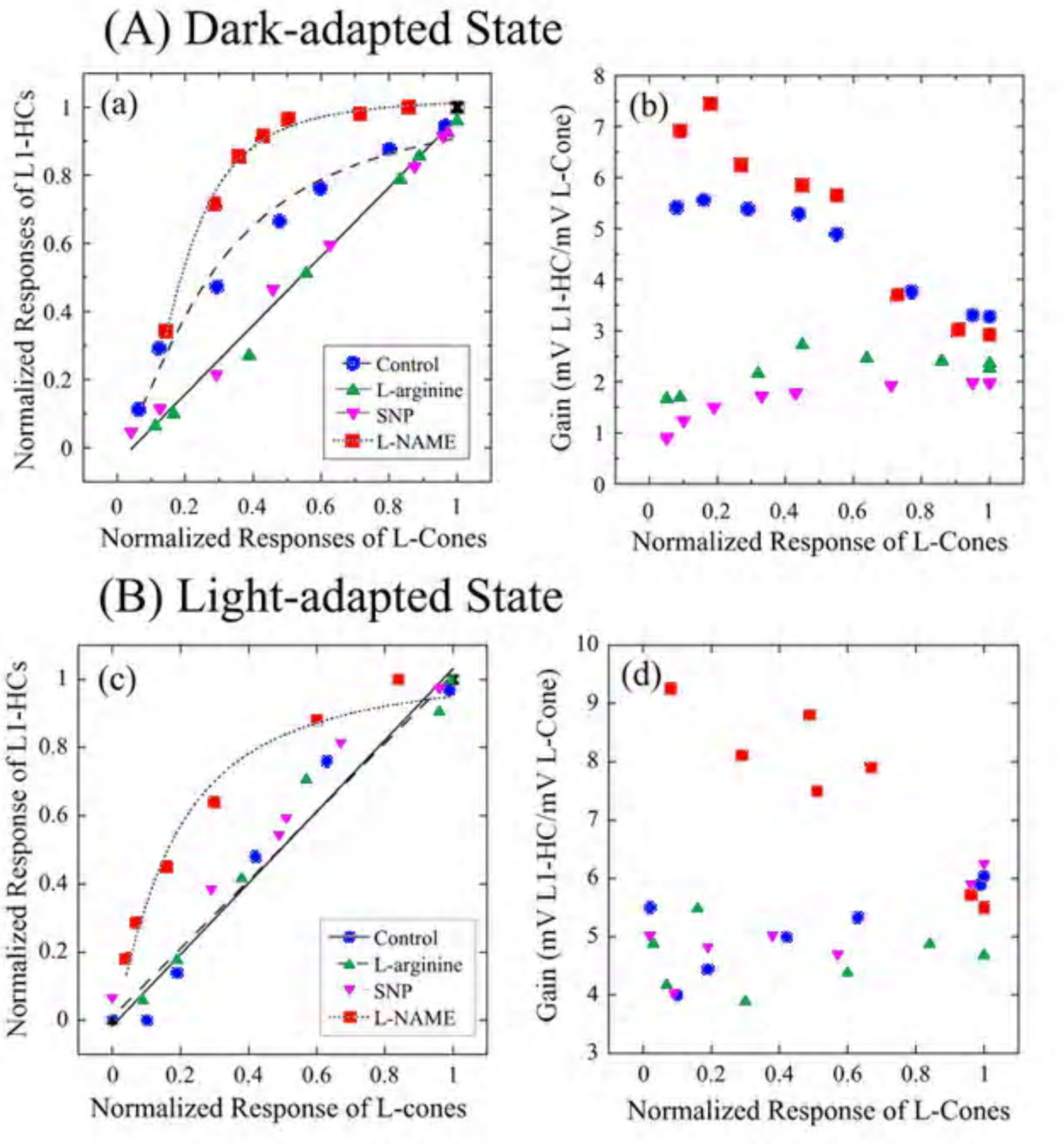

Figure 26. The effects of nitric oxide (NO) upon transfer function and synaptic amplification between cone photoreceptors and L1-type horizontal cells in the turtle eyecup preparation. The transfer function and synaptic amplification were calculated by comparing the mean photoresponses of L1-horizontal cells to those of cones for each recording condition. *A*. In the dark-adapted state, the transfer function under control conditions is non-linear (open circles) having highest synaptic amplification for small amplitude cone photoresponses, elicited by dim light stimuli. Lowering retinal NO level by adding L-NAME, increased non-linearity (open squares), while raising retinal NO level, by adding L-arginine or sodium nitroprusside (SNP), linearized the transfer function and made synaptic amplification independent of cone response amplitude (triangles and inverted triangles respectively). *B*. The control light-adapted transfer function is linear having constant synaptic amplification for the entire range of cone photoresponses (open circles). Raising retinal NO level (L-arginine – triangles; SNP – inverted triangles) had no effect, while lowering retinal NO level (adding L-NAME) transformed the transfer function into a non-linear function having highest synaptic amplification for small amplitude cone photoresponses (open squares). The figure is adopted from Levy et al., 2004 (251).

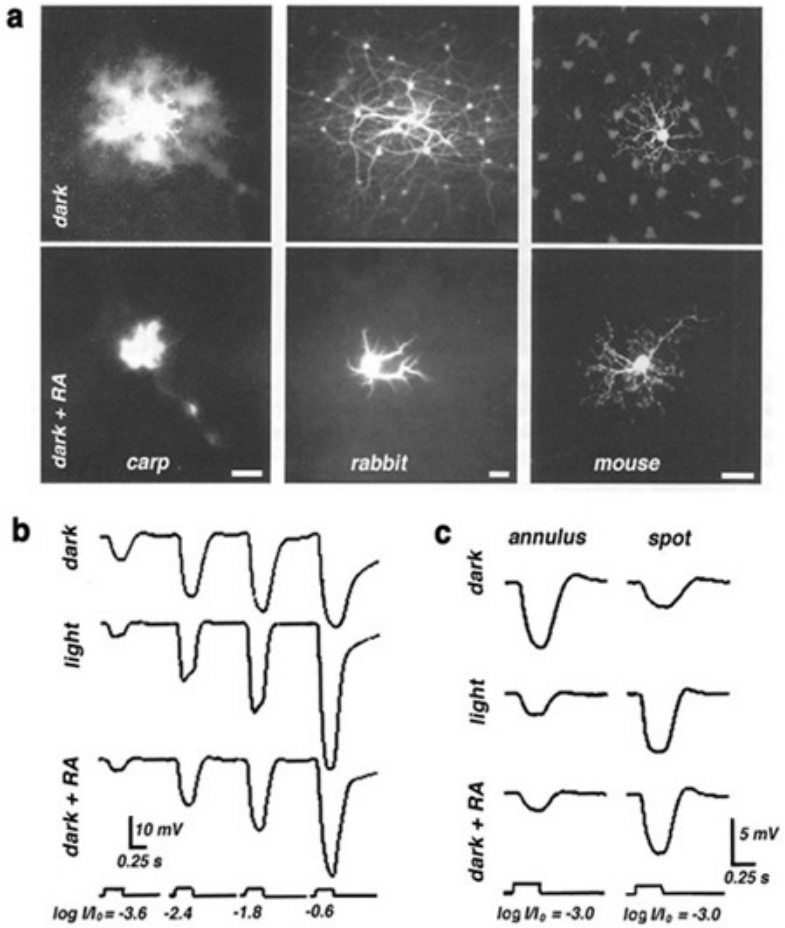

Figure 27. The effects of retinoic acid upon the physiology of horizontal cells in different species. *a*. In carp, rabbit and mouse retinas, retinoic acid added in the dark-adapted state reduced the extent of dye coupling. *b*. Retinoic acid added in the dark-adapted state exerts effects similar to those of light adaptation by augmenting the photoresponses of fish horizontal cells. *c*. Retinoic acid, like background illumination, reduces the response to an annulus stimulus and augments that to a spot stimulus in fish horizontal cells. The illustration is from Weiler et al., 2001 (261).

Photoreceptor synaptic modulation

Calcium entry into synaptic structures induces the release of neurotransmitter by promoting fusion of neurotransmitter-laden synaptic vesicles with the presynaptic membrane. Calcium enters through specialized membrane channels regulated by voltage, by second messengers, and by neurotransmitters. In the ephaptic model for horizontal cell modulation of gain at cone synapses (189, 215, 216), depolarized, dark-adapted horizontal cells produce an electrical gradient in the extracellular space that reduces the rate of calcium entry into cone terminals. This in turn, reduces the rate of neurotransmitter release (Fig. 22B). Background illumination hyperpolarizes horizontal cells, increases the extracellular currents, shifts the voltage dependency of the calcium channels in the cone terminals to more hyperpolarized levels (Fig. 22A), and increases the rate of transmitter release for a given potential of the cone as compared to the rate of release in the absence of horizontal cell feedback. Light-evoked hyperpolarization of horizontal cells increases neurotransmitter release from cones, while light evoked hyperpolarization of cones depresses the same release.

Horizontal-cell feedback modulation of horizontal cells

Horizontal-cell modulation of transmitter release from cones serves to complete a negative feedback loop between horizontal cells and cones. This in turn regulates the horizontal cell membrane potential. When

horizontal cells become depolarized, calcium influx into the cone synapse is reduced, as is transmitter efflux from the synapse. The effect sends horizontal cell membrane potential in a hyperpolarized direction. Thus horizontal cell membrane potential becomes controlled by the network, rather than strictly by factors intrinsic to the cell itself.

Horizontal cells do not express overt center-surround organization of their receptive fields; however, they do express color opponency, a very likely result of their own feedback. This is discussed in the section Physiological types above. Horizontal-cell receptive fields also show evidence of spatial effects from their own feedback circuitry. Small spot responses from horizontal cells are increased in amplitude and quickened in time course when a feedback-stimulating annular background is added (Fig. 28). In the illustration (264) small-spot, white-noise stimuli are used to calculate impulse functions under conditions where the spot is presented either with, or without an annulus. The white noise impulse function provides a very accurate depiction of changes in response dynamics. It is clear that the gain of the small spot response is increased, and the temporal tuning of the response is changed to higher frequencies and shorter latencies in the presence of the feedback-stimulating annulus. The increased gain agrees with the idea that an inhibitory feedback influence on photoreceptor synaptic transmission has been removed by the annulus causing greater transmitter release, and consequently greater modulation of that release by light. The change in dynamics is not yet modeled, but it would appear that clearance of glutamate from the photoreceptor synaptic cleft has been accelerated through feedback also.

The illustrated effect (Fig. 28) is shown for turtle and catfish horizontal cells (264), but has also been reported in Xenopus, mudpuppy and cat horizontal cells (168, 265, 266). In these latter species horizontal cell responses contain mixed rod and cone signals. In these species it is particularly rod-selective wide-field stimuli that are effective in increasing the amplitudes of cone-driven spot responses and shortening their latencies (168, 265, 266). The effect is thought to be analogous to 'suppressive rod cone interaction' (SRCI), a behavioral paradigm where dim rod backgrounds make flickering, cone-selective, small spots more visible (267). These observations suggest that feedback provides more than just wide field inhibition of cones, it also regulates synaptic gain and response dynamics.

Bipolar cell receptive fields

Bipolar cells respond with opposite voltage polarity to light stimuli illuminating either the center or the surround (4, 268). Bipolar cells perceive horizontal-cell negative feedback and synaptic gain modulation as spatial opponency. This is true for both ON- and OFF-center bipolar cells. The increase in photoreceptor transmitter release caused by horizontal cell hyperpolarization due to annular light stimuli is just the reverse of the decrease in transmitter release that occurs as cones are hyperpolarized by small spots of light. Thus through horizontal cell feedback onto cones, for bipolar cells, wide field annular stimuli have just the opposite effect as small spot stimuli. Feedback also provides synaptic gain in bipolar cells. Small-spot center responses of bipolar cells, as well as small-spot responses of horizontal cells, are amplified by feedback (265, 269).

Horizontal cell feedback is not necessarily the only way of influencing bipolar cell receptive field architecture. Horizontal cells can impinge directly on bipolar cells, feeding visual information forward to these second-order retinal neurons. Typical chemical synapses from horizontal to bipolar cells have been described in non-mammalian retinas (270, 271). In one study, in the presence of APB to block synaptic transmission from photoreceptors to ON-center bipolar cells, the light stimulus induced a hyperpolarizing response in the bipolar cell thus supporting the idea of a direct input, possibly from horizontal cells (123).

The best candidate for the feed-forward neurotransmitter is GABA, as seen in experiments on salamander retina (272). Horizontal cells make the GABA synthetic enzyme GAD in one of two isoforms, GAD 65 or GAD 67 (273); and further, in some species, they express uptake systems for GABA (51, 161). $GABA_A$ receptors are found postsynaptic to horizontal cells on the dendritic tips of both flat and invaginating bipolar cells in cat, macaque, and human retinas (274, 275). While GABA inhibition from horizontal cells might serve for the

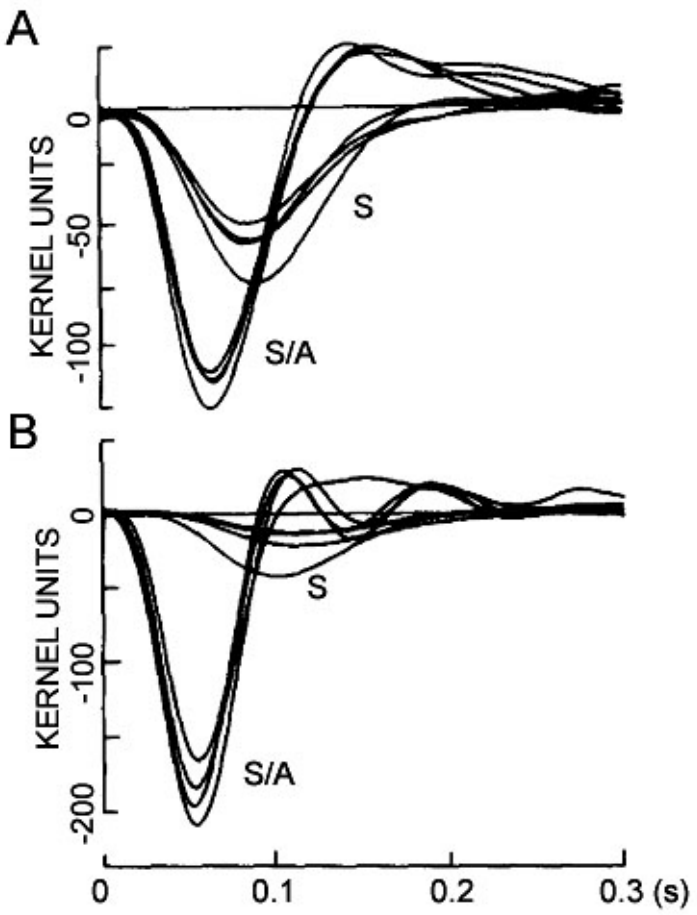

Figure 28. The effects of feedback on horizontal-cell gain and speed. Using small-spot, white-noise stimuli, impulse functions were calculated for horizontal-cell light responses. S is the impulse function for the spot stimulus alone. S/A is the impulse function for the spot stimulus with additional maintained annular stimulation in the surround to stimulate feedback. In the presence of an annulus the peak time of the spot impulse function shortens, the amplitude increases, and the shape becomes biphasic or differentiating. *A*. Turtle horizontal cells. *B*. Catfish horizontal cells. In each case results are superimposed for 4 different horizontal cells. The illustration is from Chappell, et al., 1985 (264)

antagonistic surround of OFF bipolar cells, GABA excitation would be required for ON-bipolar cells. GABA responses are mediated by the chloride gradient in post-synaptic bipolar cells. This gradient is governed in part by the actions of chloride transporters. The transporter KCC2 localized on the dendritic tips of OFF-center bipolar cells, probably maintains a chloride gradient suitable for GABA inhibition (276). ON bipolar cell dendrites express the chloride transporter NKCC, as do horizontal cells, setting up a chloride gradient suitable for GABAergic excitation. A further potential excitatory pathway for GABA in the distal retina might be provided by GABA transporters. These induce sodium entry, depolarizing, at least, horizontal cells (161, 162), but possibly some bipolar cells as well.

Not all bipolar cells exhibit spatial antagonism. The ON-bipolar for the rod system and some OFF-center cone bipolar cells in cat retina appear to lack surrounds (277, 278). Regardless of the exact neuronal pathway, whether feedforward or feedback, it is generally accepted that horizontal cells play an important role in spatial information processing in retinal neurons in the distal retina (3, 4, 171, 279-287).

Horizontal cell feedback also serves to generate color opponency in bipolar cells and therefore contributes to the physiology of color-opponent ganglion cells. Figure 29B summarizes, the manner in which single and double opponent bipolar-cell receptive fields can be formed in the fish retina according to the cascade model of color

opponency (43, 86, 288). The opponent surround of the single opponent cell is easy to model (Fig. 29B, top). This bipolar cell receives an excitatory input from red cones only and therefore, is defined as a red OFF-center cell. Negative feedback from monophasic and biphasic horizontal cells oppose each other in the red range of the spectrum and strengthen each other in the green and blue range. If the degree of feedback from both horizontal cells is the same, then the bipolar surround will be of an ON pattern with spectral sensitivity highest in the green part of the spectrum. If the feedback from the monophasic horizontal cell is weaker compared to that of the biphasic horizontal cell, then the spectral response of the bipolar cell to surround illumination will be hyperpolarizing for red light and depolarizing for green light (R-G+) (86).

In the double opponent bipolar cell (Fig. 29B, bottom), the bipolar cell responds in its center with hyperpolarizations to red light stimuli and with depolarizations to green and blue light stimuli. This central color opponency is generated by different types of inputs from different types of cones; excitatory input from the red cones and inhibitory input from the green cones. Indeed in the retina of giant danio a color opponent cone bipolar cell with bistratified axonal morphology has been found to respond to both AMPA/kainate agonists (OFF type receptors) and to EAAT agonists (ON type receptors) suggesting both ON and OFF dendritic input from spectrally distinct cones (289). If the monophasic and the biphasic horizontal cells feed back onto both spectral types of cone (86), then the feedback through the green cones would work against the feedback through the red cones because of the different synaptic interactions. When the feedback pathways from each horizontal cell onto the red and green cones differ, then color opponency can be generated by the feedback pathways. However, when the strength of the feedback from each horizontal cell to both types of cones is equal, the surround response could be achromatic. Under these conditions, color opponency in the surround of the bipolar cell can occur only through direct input from one or both horizontal cells to the bipolar cell itself.

Horizontal cells influence ganglion-cell discharge

In experiments where horizontal-cell membrane potentials are directly polarized by injections of current through intracellular microelectrodes (Fig. 30), ganglion cell discharges characteristic of 'surround responses' or 'large-spot responses' are evoked (284, 290). A hyperpolarizing current step injected into a rabbit horizontal cell depresses the firing rate in an ON-center ganglion cell, but increases the firing rate in an OFF-center ganglion cell (Fig. 30). Both actions resemble surround responses. This current-evoked response reflects the negative feedback pathway from horizontal cells to cones and/or direct input from the horizontal cells to bipolar cells. Evidence for both possibilities has been reported. The glutamate agonist 2-amino-4 phosphonobutyrate (APB), a selective blocker for transmission between cones and ON-center bipolar cells, blocks the light responses of ON-center ganglion cells, and also the 'surround-like' responses evoked by injection of current into horizontal cells (290). Moreover, sub-millimolar concentrations of cobalt ions selectively block the feedback pathway from horizontal cells to cone photoreceptors. In turtles this results in the absence of surround components in ganglion cells in proximal retina (291). Similarly the feedback blocker HEPES, a cationic buffer which selectively attenuates horizontal-cell area effects in cone responses, blocks the surround responses of parasol ganglion cells in monkey (209). This evidence suggests that a major influence of horizontal cells at the ganglion cell level is through interactions with photoreceptors, that this interaction influences the discharge patterns of ganglion cells, and by extension, plays a very important role in vision and visual perception.

About the Authors

The biosketches for Ido Perlman, Helga Kolb and Ralph Nelson appear elsewhere in Webvision.

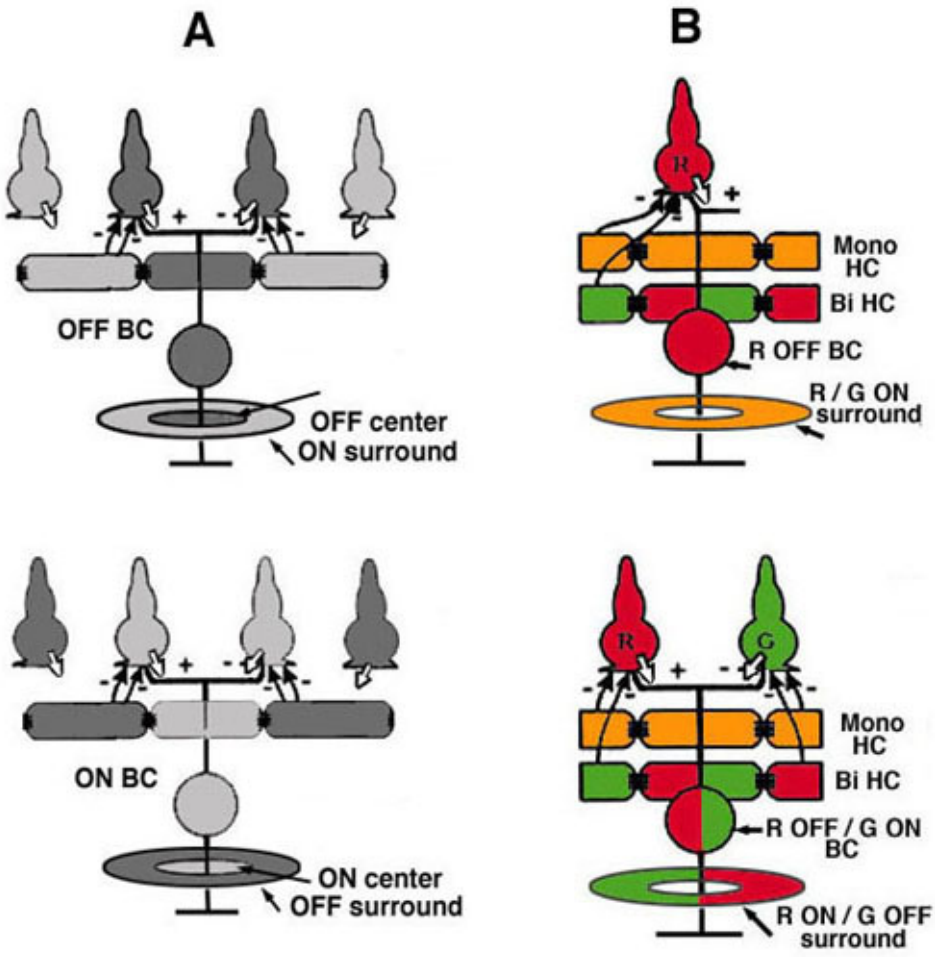

Figure 29. Schematic drawing of the horizontal-cell lateral inhibition onto cones that forms the concentrically organized receptive fields of bipolar cells. In (*A*), a simple feedback from monophasic (L-type) horizontal cells onto cones can affect the hyperpolarizing OFF-center or depolarizing ON-center bipolar cells to provide the opponent ON- or OFF- surround respectively. In (*B*), the same mechanism can be used to model the generation of color opponent responses in bipolar cells. The drawing illustrates the manner in which biphasic (Bi) chromaticity horizontal cells and monophasic (Mono) luminosity horizontal cells can feed back through a single cone type to give the opponent color surround to a red OFF bipolar cell. In the lower cartoon, red cones provide excitatory input and green cone inhibitory input to produce a red OFF, green ON center double opponent bipolar cell. The red ON and green OFF surround is added by the chromatic (Bi) and luminosity (mono) horizontal cells. The model is adapted from Kamermans and Spekreijse, 1995 (86).

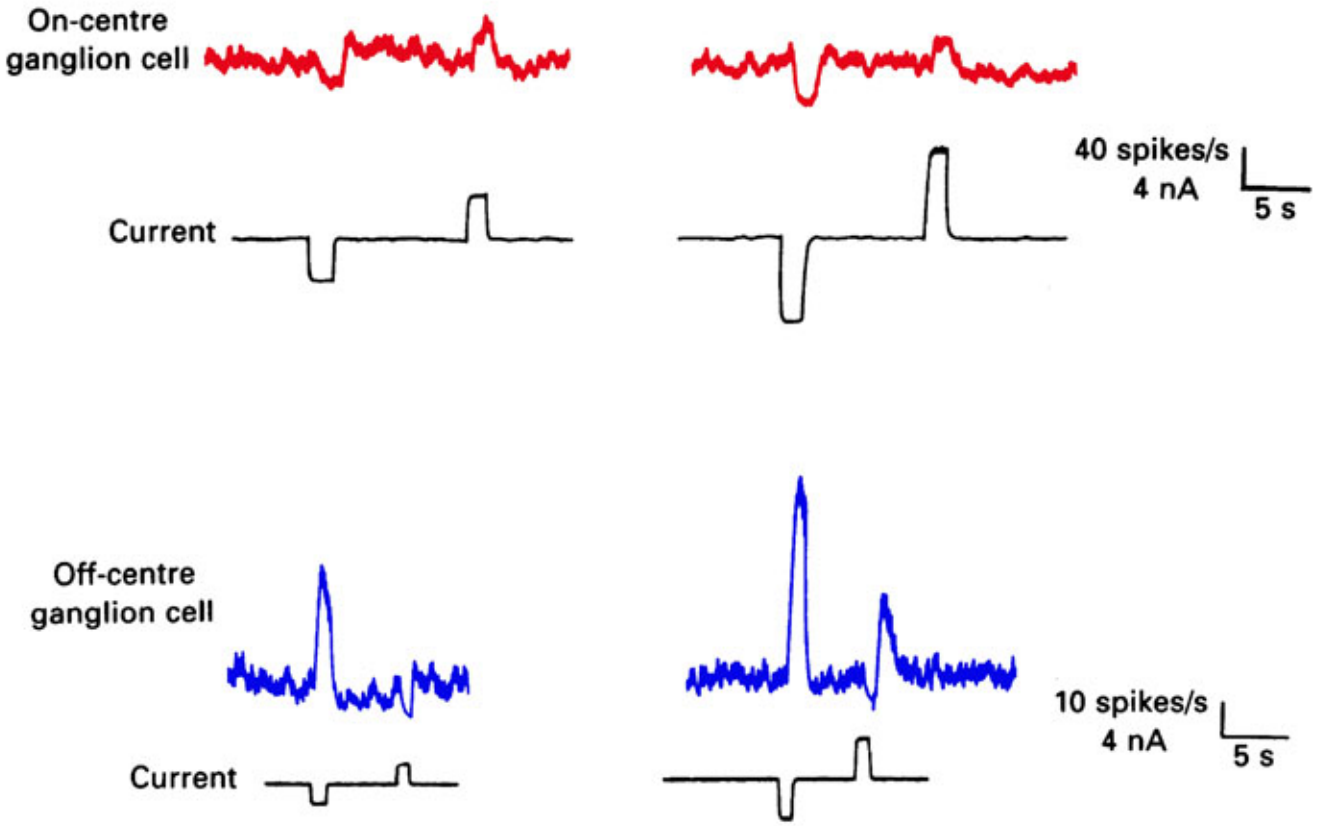

Figure 30. Retinal ganglion cells are influenced by current injection into horizontal cells. Horizontal cells were penetrated with intracellular electrodes while extracellular spikes were recorded from ganglion cells close to the horizontal cell recording site. The firing rate of an ON-center ganglion cell was reduced by hyperpolarizing current injection, and increased by depolarizing currents (red, above). The firing rate of an OFF-center ganglion cell was increased by hyperpolarizing currents, and slightly decreased by depolarizing currents (blue, below). The actions mimicked ganglion-cell surround responses. The illustration is taken from Mangel, 1991 (290).

References

1. Svaetichin G. *The cone action potential.* .Acta Physiol. Scand. 1953;29 Suppl. 106:565–600.
2. Daly S.J., Normann R.A. *Temporal information processing in cones: effects of light adaptation on temporal summation and modulation.* .Vision Res. 1985;25(9):1197–206. PubMed PMID: 4071999.
3. Kaneko A. *Physiological and morphological identification of horizontal, bipolar and amacrine cells in goldfish retina.* .J Physiol. 1970;207(3):623–33. PubMed PMID: 5499739.
4. Werblin F.S., Dowling J.E. *Organization of the retina of the mudpuppy, Necturus maculosus. II. Intracellular recording.* .J Neurophysiol. 1969;32(3):339–55. PubMed PMID: 4306897.
5. Byzov A.L., Trifonov J.A. *The response to electric stimulation of horizontal cells in the carp retina.* .Vision Res. 1968;8(7):817–22. PubMed PMID: 5664016.
6. Connaughton V.P., Nelson R. *Spectral Responses in Zebrafish Horizontal Cells Include a Tetraphasic Response and a Novel UV-Dominated Triphasic Response.* .J Neurophysiol. 2010;104(5):2407–22. PubMed PMID: 20610786.
7. Fuortes M.G., Simon E.J. *Interactions leading to horizontal cell responses in the turtle retina.* .J Physiol. 1974;240(1):177–98. PubMed PMID: 4852507.
8. Itzhaki A., Perlman I. *Light adaptation in luminosity horizontal cells in the turtle retina. Role of cellular coupling.* .Vision Res. 1984;24(10):1119–26. PubMed PMID: 6523733.

9. Naka K.I., Rushton W.A. *S-potentials from colour units in the retina of fish (Cyprinidae).* .J Physiol. 1966;185(3):536–55. PubMed PMID: 5918058.
10. Naka K.I., Rushton W.A. *The generation and spread of S-potentials in fish (Cyprinidae).* .J Physiol. 1967;192(2):437–61. PubMed PMID: 6050157.
11. Normann R.A., Perlman I. *Signal transmission from red cones to horizontal cells in the turtle retina.* .J Physiol. 1979;286:509–24. PubMed PMID: 220415.
12. Norton A.L.et al. *Receptive field organization of the S-potential.* .Science. 1968;160(831):1021–2. PubMed PMID: 5647849.
13. Sakai H., Naka K. *Neuron network in catfish retina.* .Neurosci Res Suppl. 1985;2:S227–38. PubMed PMID: 3866154.
14. Bloomfield S.A., Miller R.F. *A physiological and morphological study of the horizontal cell types of the rabbit retina.* .J Comp Neurol. 1982;208(3):288–303. PubMed PMID: 6288777.
15. Dacheux R.F., Raviola E. *Horizontal cells in the retina of the rabbit.* .J Neurosci. 1982;2(10):1486–93. PubMed PMID: 6181232.
16. Nelson R. *Cat cones have rod input: a comparison of the response properties of cones and horizontal cell bodies in the retina of the cat.* .J Comp Neurol. 1977;172(1):109–35. PubMed PMID: 838876.
17. Nelson R.et al. *Horizontal cells in cat retina with independent dendritic systems.* .Science. 1975;189(4197):137–9. PubMed PMID: 1138370.
18. Niemeyer G., Gouras P. *Rod and cone signals in S-potentials of the isolated perfused cat eye.* .Vision Res. 1973;13(8):1603–12. PubMed PMID: 4719089.
19. Steinberg R.H. *Rod and cone contributions to S-potentials from the cat retina.* .Vision Res. 1969;9(11):1319–29. PubMed PMID: 5358837.
20. Suzuki H., Pinto L.H. *Response properties of horizontal cells in the isolated retina of wild-type and pearl mutant mice.* .J Neurosci. 1986;6(4):1122–8. PubMed PMID: 3009732.
21. Dacey D.M.et al. *Physiology of L- and M-cone inputs to H1 horizontal cells in the primate retina.* .J Opt Soc Am A Opt Image Sci Vis. 2000;17(3):589–96. PubMed PMID: 10708040.
22. Dacey D.M.et al. *Horizontal cells of the primate retina: cone specificity without spectral opponency.* .Science. 1996;271(5249):656–9. PubMed PMID: 8571130.
23. Dacheux R.F., Raviola E. *Physiology of HI horizontal cells in the primate retina.* .Proc R Soc Lond B Biol Sci. 1990;239(1295):213–30. PubMed PMID: 1970436.
24. Deeb S.S.et al. *Interindividual and topographical variation of L:M cone ratios in monkey retinas.* .J Opt Soc Am A Opt Image Sci Vis. 2000;17(3):538–44. PubMed PMID: 10708035.
25. Lee B.B.et al. *Horizontal cells reveal cone type-specific adaptation in primate retina.* .Proc Natl Acad Sci U S A. 1999;96(25):14611–6. PubMed PMID: 10588753.
26. Verweij J.et al. *Sensitivity and dynamics of rod signals in H1 horizontal cells of the macaque monkey retina.* .Vision Res. 1999;39(22):3662–72. PubMed PMID: 10746136.
27. Ammermüller J.et al. *UV-sensitive input to horizontal cells in the turtle retina.* .Eur J Neurosci. 1998;10(5):1544–52. PubMed PMID: 9751127.
28. Yamada E., Ishikawa T. *The fine structure of the horizontal cells in some vertebrate retinae.* .Cold Spring Harb Symp Quant Biol. 1965;30:383–92. PubMed PMID: 5219489.
29. Boycott, B.B. and J.E. Dowling, *Organization of the primate retina: light microscopy.* Phil. Trans. R. Soc., B 1969**255**: p. 109-184.
30. Boycott B.B., Peichl L., Wässle H. *Morphological types of horizontal cell in the retina of the domestic cat.* .Proc R Soc Lond B Biol Sci. 1978;203(1152):229–45. PubMed PMID: 84387.
31. Cajal, S., *The Structure of the retina. In: Thorpe SA, Glickstein M, translators (1972).* 1892, Springfield: Thomas.
32. Gallego A. *Comparative studies on horizontal cells and a note on microglial cells* .Progress in Retinal Research. 1986;5:165–206.
33. Kolb H. *Organization of the outer plexiform layer of the primate retina: electron microscopy of Golgi-impregnated cells.* .Philosophical Transactions of the Royal Society, London, B. 1970;258:261–283.

34. Kolb H., Mariani A., Gallego A. *A second type of horizontal cell in the monkey retina.* .J Comp Neurol. 1980;189(1):31–44. PubMed PMID: 6766145.
35. Mariani A.P., Leure-DuPree A.E. *Horizontal cells of the pigeon retina.* .J Comp Neurol. 1977;175(1):13–26. PubMed PMID: 886024.
36. Leeper H.F. *Horizontal cells of the turtle retina. I. Light microscopy of Golgi preparations.* .J Comp Neurol. 1978;182(4 Pt 2):777–93. PubMed PMID: 730847.
37. Li Y.N., Matsui J.I., Dowling J.E. *Specificity of the horizontal cell-photoreceptor connections in the zebrafish (Danio rerio) retina.* .J Comp Neurol. 2009;516(5):442–53. PubMed PMID: 19655401.
38. Peichl, L., D. Sandmann, and B.B. Boycott, eds. *Comparative anatomy and function of mammalian horizontal cells*. Development and Organization of the Retina, ed. L.M. Chalupa and B.L. Finaly. 1998, Plenum Press: New York.
39. Polyak, S.L., *The Retina*1941, Chicago: University of Chicago.
40. Sandmann D., Boycott B.B., Peichl L. *Blue-cone horizontal cells in the retinae of horses and other equidae.* .J Neurosci. 1996;16(10):3381–96. PubMed PMID: 8627374.
41. Song P.I., Matsui J.I., Dowling J.E. *Morphological types and connectivity of horizontal cells found in the adult zebrafish (Danio rerio) retina.* .J Comp Neurol. 2008;506(2):328–38. PubMed PMID: 18022944.
42. Stell W.K.et al. *Goldfish retina: functional polarization of cone horizontal cell dendrites and synapses.* .Science. 1975;190(4218):989–90. PubMed PMID: 1188380.
43. Stell W.K., Lightfoot D.O. *Color-specific interconnections of cones and horizontal cells in the retina of the goldfish.* .J Comp Neurol. 1975;159(4):473–502. PubMed PMID: 1092733.
44. Wässle H., Riemann H.J. *The mosaic of nerve cells in the mammalian retina.* .Proc R Soc Lond B Biol Sci. 1978;200(1141):441–61. PubMed PMID: 26058.
45. Kaneko A., Yamada M. *S-potentials in the dark-adapted retina of the carp.* .J Physiol. 1972;227(1):261–73. PubMed PMID: 4646582.
46. Tsukamoto Y., Yamada M., Kaneko A. *Morphological and physiological studies of rod-driven horizontal cells with special reference to the question of whether they have axons and axon terminals.* .J Comp Neurol. 1987;255(2):305–16. PubMed PMID: 3819018.
47. Cuenca N., Haverkamp S., Kolb H. *Choline acetyltransferase is found in terminals of horizontal cells that label with GABA, nitric oxide synthase and calcium binding proteins in the turtle retina.* .Brain Res. 2000;878(1-2):228–39. PubMed PMID: 10996158.
48. Wässle H., Boycott B.B. *Functional architecture of the mammalian retina.* .Physiol Rev. 1991;71(2):447–80. PubMed PMID: 2006220.
49. Wässle H., Boycott B.B., Rohrenbeck J. *Horizontal Cells in the Monkey Retina: Cone connections and dendritic network.* .Eur J Neurosci. 1989;1(5):421–435. PubMed PMID: 12106129.
50. Marc R.E. *Mapping glutamatergic drive in the vertebrate retina with a channel-permeant organic cation.* .J Comp Neurol. 1999;407(1):47–64. PubMed PMID: 10213187.
51. Marc R.E.et al. *GABA-ergic pathways in the goldfish retina.* .J Comp Neurol. 1978;182(2):221–44. PubMed PMID: 212456.
52. Leeper H.F. *Horizontal cells of the turtle retina. II. Analysis of interconnections between photoreceptor cells and horizontal cells by light microscopy.* .J Comp Neurol. 1978;182(4 Pt 2):795–809. PubMed PMID: 730848.
53. Simon E.J. *Two types of luminosity horizontal cells in the retina of the turtle.* .J Physiol. 1973;230(1):199–211. PubMed PMID: 4702422.
54. Ahnelt P.K.et al. *Irregular S-cone mosaics in felid retinas. Spatial interaction with axonless horizontal cells, revealed by cross correlation.* .J Opt Soc Am A Opt Image Sci Vis. 2000;17(3):580–8. PubMed PMID: 10708039.
55. Miller W.H.et al. *Physiological and morphological identification of L- and C-type S-potentials in the turtle retina.* .Vision Res. 1973;13(2):443–7. PubMed PMID: 4120837.
56. Lipetz, L.E., ed. *A model of function at the outer plexiform layer of cyprinid retina.* Frontiers of Visual Science. 1978, Springer-Verlag: Berlin-Heidelberg. pp 471-482.

57. Raynauld J.P., Laviolette J.R., Wagner H.J. *Goldfish retina: a correlate between cone activity and morphology of the horizontal cell in clone pedicules.* .Science. 1979;204(4400):1436–8. PubMed PMID: 451577.
58. Weiler R., Wagner H.J. *Light-dependent change of cone-horizontal cell interactions in carp retina.* .Brain Res. 1984;298(1):1–9. PubMed PMID: 6326947.
59. Schultz K.et al. *Calcium-binding protein Caldendrin and CaMKII are localized in spinules of the carp retina.* .J Comp Neurol. 2004;479(1):84–93. PubMed PMID: 15389610.
60. Münz H.et al. *Centrifugal innervation of the retina by luteinizing hormone releasing hormone (LHRH)-immunoreactive telencephalic neurons in teleostean fishes.* .Cell Tissue Res. 1982;222(2):313–23. PubMed PMID: 7044556.
61. Stell W.K.et al. *The goldfish nervus terminalis: a luteinizing hormone-releasing hormone and molluscan cardioexcitatory peptide immunoreactive olfactoretinal pathway.* .Proc Natl Acad Sci U S A. 1984;81(3):940–4. PubMed PMID: 6199789.
62. De Juan J., Garcia M. *Spinules and nematosomes in retinal horizontal cells: a "thorny" issue.* .Prog Brain Res. 2001;131:519–37. PubMed PMID: 11420967.
63. Zucker C.L., Dowling J.E. *Centrifugal fibres synapse on dopaminergic interplexiform cells in the teleost retina.* .Nature. 1987;330(6144):166–8. PubMed PMID: 2890106.
64. Pottek M., Weiler R. *Light-adaptive effects of retinoic acid on receptive field properties of retinal horizontal cells.* .Eur J Neurosci. 2000;12(2):437–45. PubMed PMID: 10712624.
65. Weiler R.et al. *Retinoic acid has light-adaptive effects on horizontal cells in the retina.* .Proc Natl Acad Sci U S A. 1998;95(12):7139–44. PubMed PMID: 9618552.
66. Kaneko A. *Electrical connexions between horizontal cells in the dogfish retina.* .J Physiol. 1971;213(1):95–105. PubMed PMID: 5575346.
67. Mills S.L., Massey S.C. *Distribution and coverage of A- and B-type horizontal cells stained with Neurobiotin in the rabbit retina.* .Vis Neurosci. 1994;11(3):549–60. PubMed PMID: 7518689.
68. Janssen-Bienhold U.et al. *Molecular diversity of gap junctions between horizontal cells.* .Prog Brain Res. 2001;131:93–107. PubMed PMID: 11420985.
69. McMahon D.G., Knapp A.G., Dowling J.E. *Horizontal cell gap junctions: single-channel conductance and modulation by dopamine.* .Proc Natl Acad Sci U S A. 1989;86(19):7639–43. PubMed PMID: 2477845.
70. Janssen-Bienhold U.et al. *Connexin57 is expressed in dendro-dendritic and axo-axonal gap junctions of mouse horizontal cells and its distribution is modulated by light.* .J Comp Neurol. 2009;513(4):363–74. PubMed PMID: 19177557.
71. O'Brien J.J.et al. *Coupling between A-type horizontal cells is mediated by connexin 50 gap junctions in the rabbit retina.* .J Neurosci. 2006;26(45):11624–36. PubMed PMID: 17093084.
72. Shields C.R.et al. *Retinal horizontal cell-specific promoter activity and protein expression of zebrafish connexin 52.6 and connexin 55.5.* .J Comp Neurol. 2007;501(5):765–79. PubMed PMID: 17299759.
73. Klaassen L.J.et al. *Synaptic transmission from horizontal cells to cones is impaired by loss of connexin hemichannels.* .PLoS Biol. 2011;9(7):e1001107. PubMed PMID: 21811399.
74. Mills S.L., Massey S.C. *A series of biotinylated tracers distinguishes three types of gap junction in retina.* .J Neurosci. 2000;20(22):8629–36. PubMed PMID: 11069972.
75. Goldsmith T.H. *Hummingbirds see near ultraviolet light.* .Science. 1980;207(4432):786–8. PubMed PMID: 7352290.
76. Goldsmith T.H. *What birds See.* .Scientific American. 2006;295(1):69–75.
77. Harosi F.I., Hashimoto Y. *Ultraviolet visual pigment in a vertebrate: a tetrachromatic cone system in the dace.* .Science. 1983;222(4627):1021–3. PubMed PMID: 6648514.
78. Hughes A.et al. *Cone contributions to the photopic spectral sensitivity of the zebrafish ERG.* .Vis Neurosci. 1998;15(6):1029–37. PubMed PMID: 9839967.
79. Robinson J.et al. *Zebrafish ultraviolet visual pigment: absorption spectrum, sequence, and localization.* .Proc Natl Acad Sci U S A. 1993;90(13):6009–12. PubMed PMID: 8327475.
80. Svaetichin G., MacNichol E.F. Jr. *Retinal mechanisms for chromatic and achromatic vision.* .Ann N Y Acad Sci. 1959;74(2):385–404. PubMed PMID: 13627867.

81. Perlman I., Normann R.A. *Short-wavelength input to luminosity-type horizontal cells in the turtle retina.* .Vision Res. 1979;19(8):903–6. PubMed PMID: 516459.
82. Ruddock K.H., Svaetichin G. *The effects of maintained light stimulation on S-potentials recorded from the retina of a teleost fish.* .J Physiol. 1975;244(3):569–88. PubMed PMID: 1133771.
83. Ammermüller J., Kolb H. *The organization of the turtle inner retina. I. ON- and OFF-center pathways.* .J Comp Neurol. 1995;358(1):1–34. PubMed PMID: 7560272.
84. Ammermüller J., Kolb H. *Functional architecture of the turtle retina.* .Progress in Retinal and Eye Research. 1996;15(2):393–433.
85. Asi H., Perlman I. *Neural interactions between cone photoreceptors and horizontal cells in the turtle (Mauremys caspica) retina.* .Vis Neurosci. 1998;15(1):1–13. PubMed PMID: 9456500.
86. Kamermans, M. and H. Spekreijse, *Spectral behavior of cone-driven horizontal cells in teleost retina*, in *Progress in Retinal and Eye Research*, N. Osborne and G. Chader, Editors. 1995, Elsevier Science Ltd. p. 313-360.
87. Kolb, H. and L.E. Lipitz, eds. *The anatomical basis for colour vision in the vertebrate retina.* Vision and Visual Dysfunction ed. P. Gouras. Vol. 6. 1991, Macmillan Press Ltd.: London. 128-145.
88. Spekreijse H., Norton A.L. *The dynamic characteristics of color-coded S-potentials.* .J Gen Physiol. 1970;56(1):1–15. PubMed PMID: 5514159.
89. Stone S., Witkovsky P., Schutte M. *A chromatic horizontal cell in the Xenopus retina: intracellular staining and synaptic pharmacology.* .J Neurophysiol. 1990;64(6):1683–94. PubMed PMID: 1705962.
90. Twig G., Levy H., Perlman I. *Turtle C-type horizontal cells act as push-pull devices.* .Vis Neurosci. 2001;18(6):893–900. PubMed PMID: 12020079.
91. Twig G., Levy H., Perlman I. *Spatial-chromatic interactions in C-type horizontal cells of the turtle (Mauremys caspica) retina.* .Vis Neurosci. 2002;19(1):71–84. PubMed PMID: 12180861.
92. Twig G., Levy H., Perlman I. *Color opponency in horizontal cells of the vertebrate retina.* .Prog Retin Eye Res. 2003;22(1):31–68. PubMed PMID: 12597923.
93. Twig G., Perlman I. *Homogeneity and diversity of color-opponent horizontal cells in the turtle retina: Consequences for potential wavelength discrimination.* .J Vis. 2004;4(5):403–14. PubMed PMID: 15330723.
94. Yazulla S. *Cone input to horizontal cells in the turtle retina.* .Vision Res. 1976;16(7):727–35. PubMed PMID: 960597.
95. Gottesman J., Burkhardt D.A. *Response properties of C-type horizontal cells in the retina of the bowfin.* .Vision Res. 1987;27(2):179–89. PubMed PMID: 3576978.
96. Hashimoto Y.et al. *Ultra-violet-sensitive cones in the color-coding systems of cyprinid retinas.* .Neurosci Res Suppl. 1988;8:S81–95. PubMed PMID: 3231369.
97. Zana Y.et al. *Tetrachromatic input to turtle horizontal cells.* .Vis Neurosci. 2001;18(5):759–65. PubMed PMID: 11925011.
98. Nelson R.F., Singla N. *A spectral model for signal elements isolated from zebrafish photopic electroretinogram.* .Vis Neurosci. 2009;26(4):349–63. PubMed PMID: 19723365.
99. Steinberg R.H. *Rod-cone interaction in S-potentials from the cat retina.* .Vision Res. 1969;9(11):1331–44. PubMed PMID: 5358838.
100. Nelson R. *Spectral properties of cat horizontal cells.* .Neurosci Res Suppl. 1985;2(83):S167–83. PubMed PMID: 3935989.
101. Ahnelt P., Kolb H. *Horizontal cells and cone photoreceptors in primate retina: a Golgi-light microscopic study of spectral connectivity.* .J Comp Neurol. 1994;343(3):387–405. PubMed PMID: 8027449.
102. Ahnelt P., Kolb H. *Horizontal cells and cone photoreceptors in human retina: a Golgi-electron microscopic study of spectral connectivity.* .J Comp Neurol. 1994;343(3):406–27. PubMed PMID: 8027450.
103. Kolb H. *The organization of the outer plexiform layer in the retina of the cat: electron microscopic observations.* .J Neurocytol. 1977;6(2):131–53. PubMed PMID: 856949.
104. Raviola E., Gilula N.B. *Intramembrane organization of specialized contacts in the outer plexiform layer of the retina. A freeze-fracture study in monkeys and rabbits.* .J Cell Biol. 1975;65(1):192–222. PubMed PMID: 1127010.

105. Sharpe L.T., Stockman A. *Rod pathways: the importance of seeing nothing.* .Trends Neurosci. 1999;22(11):497–504. PubMed PMID: 10529817.
106. Smith R.G., Freed M.A., Sterling P. *Microcircuitry of the dark-adapted cat retina: functional architecture of the rod-cone network.* .J Neurosci. 1986;6(12):3505–17. PubMed PMID: 3794785.
107. Sterling, P., *Retina*, in *The Synaptic Organization of the Brain*, G.M. Shepard, Editor. 1990, Oxford University Press: New York. p. 170-213.
108. Stockman A.et al. *Slow and fast pathways in the human rod visual system: electrophysiology and psychophysics.* .J Opt Soc Am A. 1991;8(10):1657–65. PubMed PMID: 1941296.
109. Massey S.C., Miller R.F. *Excitatory amino acid receptors of rod- and cone-driven horizontal cells in the rabbit retina.* .J Neurophysiol. 1987;57(3):645–59. PubMed PMID: 3031231.
110. Leeper H.F., Copenhagen D.R. *Mixed rod-cone responses in horizontal cells of snapping turtle retina.* .Vision Res. 1979;19(4):407–12. PubMed PMID: 473609.
111. Witkovsky P., Stone S., MacDonald E.D. *Morphology and synaptic connections of HRP-filled, axon-bearing horizontal cells in the Xenopus retina.* .J Comp Neurol. 1988;275(1):29–38. PubMed PMID: 3170790.
112. Witkovsky P., Stone S. *Rod and cone inputs to bipolar and horizontal cells of the Xenopus retina.* .Vision Res. 1983;23(11):1251–8. PubMed PMID: 6659374.
113. Cervetto L., Piccolino M. *Synaptic transmission between photoreceptors and horizontal cells in the turtle retina.* .Science. 1974;183(123):417–9. PubMed PMID: 4358073.
114. Dowling J.E., Ripps H. *Effect of magnesium on horizontal cell activity in the skate retina.* .Nature. 1973;242(5393):101–3. PubMed PMID: 4348460.
115. Kaneko A., Shimazaki H. *Effects of external ions on the synaptic transmission from photorecptors to horizontal cells in the carp retina.* .J Physiol. 1975;252(2):509–22. PubMed PMID: 173833.
116. Bloomfield S.A., Dowling J.E. *Roles of aspartate and glutamate in synaptic transmission in rabbit retina. I. Outer plexiform layer.* .J Neurophysiol. 1985;53(3):699–713. PubMed PMID: 2858516.
117. Cervetto L., MacNichol E.F. Jr. *Inactivation of horizontal cells in turtle retina by glutamate and aspartate.* .Science. 1972;178(62):767–8. PubMed PMID: 5082843.
118. Marshall L.M., Werblin F.S. *Synaptic transmission to the horizontal cells in the retina of the larval tiger salamander.* .J Physiol. 1978;279:321–46. PubMed PMID: 209177.
119. Negishi K., Drujan B.D. *Effects of some amino acids on horizontal cells in the fish retina.* .J Neurosci Res. 1979;4(5-6):351–63. PubMed PMID: 118265.
120. Normann R.A., Perlman I., Daly S.J. *The effects of continuous superfusion of L-aspartate and L-glutamate on horizontal cells of the turtle retina.* .Vision Res. 1986;26(2):259–68. PubMed PMID: 2872748.
121. Eliasof S.et al. *Localization and function of five glutamate transporters cloned from the salamander retina.* .Vision Res. 1998;38(10):1443–54. PubMed PMID: 9667010.
122. Rauen T.et al. *High-affinity glutamate transporters in the rat retina: a major role of the glial glutamate transporter GLAST-1 in transmitter clearance.* .Cell Tissue Res. 1998;291(1):19–31. PubMed PMID: 9394040.
123. Yang X.L., Wu S.M. *Feedforward lateral inhibition in retinal bipolar cells: input-output relation of the horizontal cell-depolarizing bipolar cell synapse.* .Proc Natl Acad Sci U S A. 1991;88(8):3310–3. PubMed PMID: 1849650.
124. Mayer M.L., Westbrook G.L. *The physiology of excitatory amino acids in the vertebrate central nervous system.* .Prog Neurobiol. 1987;28(3):197–276. PubMed PMID: 2883706.
125. Lasater E.M., Dowling J.E. *Carp horizontal cells in culture respond selectively to L-glutamate and its agonists.* .Proc Natl Acad Sci U S A. 1982;79(3):936–40. PubMed PMID: 6278502.
126. Hals G.et al. *Voltage-clamp analysis of currents produced by glutamate and some glutamate analogues on horizontal cells isolated from the catfish retina.* .J Neurophysiol. 1986;56(1):19–31. PubMed PMID: 3746395.
127. Perlman I., Knapp A.G., Dowling J.E. *Responses of isolated white perch horizontal cells to changes in the concentration of photoreceptor transmitter agonists.* .Brain Res. 1989;487(1):16–25. PubMed PMID: 2568870.

128. Tachibana M. *Permeability changes induced by L-glutamate in solitary retinal horizontal cells isolated from Carassius auratus.* .J Physiol. 1985;358:153–67. PubMed PMID: 2580079.
129. Peng Y.W.et al. *Distribution of glutamate receptor subtypes in the vertebrate retina.* .Neuroscience. 1995;66(2):483–97. PubMed PMID: 7477889.
130. Wu S.M. *Synaptic transmission in the outer retina.* .Annu Rev Physiol. 1994;56:141–68. PubMed PMID: 8010738.
131. O'Dell T.J., Christensen B.N. *Horizontal cells isolated from catfish retina contain two types of excitatory amino acid receptors.* .J Neurophysiol. 1989;61(6):1097–109. PubMed PMID: 2473174.
132. Eliasof S., Jahr C.E. *Rapid AMPA receptor desensitization in catfish cone horizontal cells.* .Vis Neurosci. 1997;14(1):13–8. PubMed PMID: 9057264.
133. Schmidt K.F., Kruse M., Hatt H. *Dopamine alters glutamate receptor desensitization in retinal horizontal cells of the perch (Perca fluviatilis).* .Proc Natl Acad Sci U S A. 1994;91(17):8288–91. PubMed PMID: 7520178.
134. Blanco R., de la Villa P. *Ionotropic glutamate receptors in isolated horizontal cells of the rabbit retina.* .Eur J Neurosci. 1999;11(3):867–73. PubMed PMID: 10103080.
135. Shen Y., Lu T., Yang X.L. *Modulation of desensitization at glutamate receptors in isolated crucian carp horizontal cells by concanavalin A, cyclothiazide, aniracetam and PEPA.* .Neuroscience. 1999;89(3):979–90. PubMed PMID: 10199629.
136. Yang J.H.et al. *Postsynaptic responses of horizontal cells in the tiger salamander retina are mediated by AMPA-preferring receptors.* .Brain Res. 1998;797(1):125–34. PubMed PMID: 9630565.
137. Shen W., Finnegan S.G., Slaughter M.M. *Glutamate receptor subtypes in human retinal horizontal cells.* .Vis Neurosci. 2004;21(1):89–95. PubMed PMID: 15137585.
138. Dixon D.B., Copenhagen D.R. *Metabotropic glutamate receptor-mediated suppression of an inward rectifier current is linked via a cGMP cascade.* .J Neurosci. 1997;17(23):8945–54. PubMed PMID: 9364042.
139. Linn C.L., Gafka A.C. *Activation of metabotropic glutamate receptors modulates the voltage-gated sustained calcium current in a teleost horizontal cell.* .J Neurophysiol. 1999;81(2):425–34. PubMed PMID: 10036249.
140. Takahashi K.I., Copenhagen D.R. *Modulation of neuronal function by intracellular pH.* .Neurosci Res. 1996;24(2):109–16. PubMed PMID: 8929916.
141. Davis S.F., Linn C.L. *Mechanism linking NMDA receptor activation to modulation of voltage-gated sodium current in distal retina.* .Am J Physiol Cell Physiol. 2003;284(5):C1193–204. PubMed PMID: 12676655.
142. Nelson R., Bender A.M., Connaughton V.P. *Stimulation of sodium pump restores membrane potential to neurons excited by glutamate in zebrafish distal retina.* .J Physiol. 2003;549(3):787–800. PubMed PMID: 12730339.
143. Lasater E.M. *Ionic currents of cultured horizontal cells isolated from white perch retina.* .J Neurophysiol. 1986;55(3):499–513. PubMed PMID: 2420944.
144. Lasater E.M. *Characteristics of single-channels activated by quisqualate and kainate in teleost retinal horizontal cells.* .Vision Res. 1991;31(3):413–24. PubMed PMID: 1726896.
145. Lohrke S., Hofmann H.D. *Voltage-gated currents of rabbit A- and B-type horizontal cells in retinal monolayer cultures.* .Vis Neurosci. 1994;11(2):369–78. PubMed PMID: 7516179.
146. Ueda Y., Kaneko A., Kaneda M. *Voltage-dependent ionic currents in solitary horizontal cells isolated from cat retina.* .J Neurophysiol. 1992;68(4):1143–50. PubMed PMID: 1279133.
147. Tachibana M. *Ionic currents of solitary horizontal cells isolated from goldfish retina.* .J Physiol. 1983;345:329–51. PubMed PMID: 6420548.
148. Shingai R., Christensen B.N. *Excitable properties and voltage-sensitive ion conductances of horizontal cells isolated from catfish (Ictalurus punctatus) retina.* .J Neurophysiol. 1986;56(1):32–49. PubMed PMID: 2427666.
149. Malchow R.P.et al. *Structural and functional properties of two types of horizontal cell in the skate retina.* .J Gen Physiol. 1990;95(1):177–98. PubMed PMID: 2299330.
150. Golard A., Witkovsky P., Tranchina D. *Membrane currents of horizontal cells isolated from turtle retina.* .J Neurophysiol. 1992;68(2):351–61. PubMed PMID: 1382117.

151. Pfeiffer-Linn C.L., Perlman I., Lasater E.M. *Sodium dependency of the inward potassium rectifier in horizontal cells isolated from the white bass retina.* .Brain Res. 1995;701(1-2):81–8. PubMed PMID: 8925302.
152. Perlman I., Sullivan J.M., Normann R.A. *Voltage- and time-dependent potassium conductances enhance the frequency response of horizontal cells in the turtle retina.* .Brain Res. 1993;619(1-2):89–97. PubMed PMID: 8374796.
153. Tachibana M. *Membrane properties of solitary horizontal cells isolated from goldfish retina.* .J Physiol (Lond). 1981;321:141–61. PubMed PMID: 7338808.
154. Sullivan J.M., Lasater E.M. *An unusually small potassium current that is well-suited to a retinal neuron which is chronically depolarized.* .Brain Res. 1990;528(1):130–2. PubMed PMID: 2245330.
155. Akopian A., Krizaj D., Witkovsky P. *Both high- and low voltage-activated calcium currents contribute to the light-evoked responses of luminosity horizontal cells in the Xenopus retina.* .Brain Res. 1997;762(1-2):121–30. PubMed PMID: 9262166.
156. Kamermans M., Werblin F. *GABA-mediated positive autofeedback loop controls horizontal cell kinetics in tiger salamander retina.* .J Neurosci. 1992;12(7):2451–63. PubMed PMID: 1351934.
157. Qian H., Dowling J.E. *Novel GABA responses from rod-driven retinal horizontal cells.* .Nature. 1993;361(6408):162–4. PubMed PMID: 8421521.
158. Blanco R., Vaquero C.F., de la Villa P. *The effects of GABA and glycine on horizontal cells of the rabbit retina.* .Vision Res. 1996;36(24):3987–95. PubMed PMID: 9068851.
159. Cammack J.N., Schwartz E.A. *Ions required for the electrogenic transport of GABA by horizontal cells of the catfish retina.* .J Physiol. 1993;472:81–102. PubMed PMID: 8145174.
160. Dong C.J., Picaud S.A., Werblin F.S. *GABA transporters and GABA $_C$ -like receptors on catfish cone- but not rod-driven horizontal cells.* .J Neurosci. 1994;14(5 Pt 1):2648–58. PubMed PMID: 8182433.
161. Malchow R.P., Ripps H. *Effects of gamma-aminobutyric acid on skate retinal horizontal cells: evidence for an electrogenic uptake mechanism.* .Proc Natl Acad Sci U S A. 1990;87(22):8945–9. PubMed PMID: 2247470.
162. Nelson R., Bender A.M., Connaughton V.P. *Transporter-mediated GABA responses in horizontal and bipolar cells of zebrafish retina.* .Vis Neurosci. 2008;25(2):155–65. PubMed PMID: 18442438.
163. Kolb H., West R.W. *Synaptic connections of the interplexiform cell in the retina of the cat.* .J Neurocytol. 1977;6(2):155–70. PubMed PMID: 853310.
164. Witkovsky P., Dowling J.E. *Synaptic relationships in the plexiform layers of carp retina.* .Z Zellforsch Mikrosk Anat. 1969;100(1):60–82. PubMed PMID: 5354186.
165. Hampson E.C., Weiler R., Vaney D.I. *pH-gated dopaminergic modulation of horizontal cell gap junctions in mammalian retina.* .Proc Biol Sci. 1994;255(1342):67–72. PubMed PMID: 8153138.
166. Teranishi T., Negishi K., Kato S. *Dopamine modulates S-potential amplitude and dye-coupling between external horizontal cells in carp retina.* .Nature. 1983;301(5897):243–6. PubMed PMID: 6401844.
167. Lamb T.D. *Spatial properties of horizontal cell responses in the turtle retina.* .J Physiol. 1976;263(2):239–55. PubMed PMID: 1018237.
168. Nelson R., Pflug R., Baer S.M. *Background-induced flicker enhancement in cat retinal horizontal cells. II. Spatial properties.* .J Neurophysiol. 1990;64(2):326–40. PubMed PMID: 2213121.
169. Kamermans M.et al. *The size of the horizontal cell receptive fields adapts to the stimulus in the light adapted goldfish retina.* .Vision Res. 1996;36(24):4105–19. PubMed PMID: 9068862.
170. Lankheet M.J., Frens M.A., van de Grind W.A. *Spatial properties of horizontal cell responses in the cat retina.* .Vision Res. 1990;30(9):1257–75. PubMed PMID: 2219744.
171. Hare W.A., Owen W.G. *Spatial organization of the bipolar cell's receptive field in the retina of the tiger salamander.* .J Physiol. 1990;421:223–45. PubMed PMID: 2348392.
172. Perlman I.et al. *Chromatic and spatial information processing by red cones and L-type horizontal cells in the turtle retina.* .Vision Res. 1985;25(4):543–9. PubMed PMID: 4060606.
173. Piccolino M., Neyton J., Gerschenfeld H. *Center-surround antagonistic organization in small-field luminosity horizontal cells of turtle retina.* .J Neurophysiol. 1981;45(3):363–75. PubMed PMID: 7218006.
174. Byzov A.L., Shura-Bura T.M. *Spread of potentials along the network of horizontal cells in the retina of the turtle.* .Vision Res. 1983;23(4):389–97. PubMed PMID: 6880037.

175. Borenstein, O., *Lateral spread of electrical signals in the horizontal cells layer of the turtle retina* 1999, Technion-Israel Institute of Technology: Haifa.
176. Perlman I., Ammermüller J. *Receptive-field size of L1 horizontal cells in the turtle retina: effects of dopamine and background light.* .J Neurophysiol. 1994;72(6):2786–95. PubMed PMID: 7897489.
177. Pottek M., Schultz K., Weiler R. *Effects of nitric oxide on the horizontal cell network and dopamine release in the carp retina.* .Vision Res. 1997;37(9):1091–102. PubMed PMID: 9196728.
178. Kato S. *C-type horizontal cell responses to annular stimuli.* .Exp Eye Res. 1979;28(6):627–39. PubMed PMID: 467520.
179. McMahon D.G. *Modulation of electrical synaptic transmission in zebrafish retinal horizontal cells.* .J Neurosci. 1994;14(3 Pt 2):1722–34. PubMed PMID: 8126566.
180. Baylor D.A., Fuortes M.G., O'Bryan P.M. *Receptive fields of cones in the retina of the turtle.* .J Physiol. 1971;214(2):265–94. PubMed PMID: 5579638.
181. Burkhardt D.A. *Responses and receptive-field organization of cones in perch retinas.* .J Neurophysiol. 1977;40(1):53–62. PubMed PMID: 833628.
182. Fuortes M.G., Schwartz E.A., Simon E.J. *Colour-dependence of cone responses in the turtle retina.* .J Physiol. 1973;234(1):199–216. PubMed PMID: 4766220.
183. Lasansky A. *Synaptic action mediating cone responses to annular illumination in the retina of the larval tiger salamander.* .J Physiol. 1981;310:205–14. PubMed PMID: 7230033.
184. O'Bryan P.M. *Properties of the depolarizing synaptic potential evoked by peripheral illumination in cones of the turtle retina.* .J Physiol. 1973;235(1):207–23. PubMed PMID: 4778138.
185. Packer O.S.et al. *Blue-yellow opponency in primate S cone photoreceptors.* .J Neurosci. 2010;30(2):568–72. PubMed PMID: 20071519.
186. Wu S.M. *Input-output relations of the feedback synapse between horizontal cells and cones in the tiger salamander retina.* .J Neurophysiol. 1991;65(5):1197–206. PubMed PMID: 1651374.
187. Itzhaki A., Malik S., Perlman I. *Spectral properties of short-wavelength (blue) cones in the turtle retina.* .Vis Neurosci. 1992;9(3-4):235–41. PubMed PMID: 1390383.
188. Witkovsky P.et al. *Feedback from luminosity horizontal cells mediates depolarizing responses of chromaticity horizontal cells in the Xenopus retina.* .Proc Natl Acad Sci U S A. 1995;92(8):3556–60. PubMed PMID: 7724597.
189. Kamermans M.et al. *Hemichannel-mediated inhibition in the outer retina.* .Science. 2001;292(5519):1178–80. PubMed PMID: 11349152.
190. Linberg K.A., Fisher S.K. *Ultrastructural evidence that horizontal cell axon terminals are presynaptic in the human retina.* .J Comp Neurol. 1988;268(2):281–97. PubMed PMID: 3360989.
191. Hirano A.A.et al. *Robust syntaxin-4 immunoreactivity in mammalian horizontal cell processes.* .Vis Neurosci. 2007;24(4):489–502. PubMed PMID: 17640443.
192. Cueva J.G.et al. *Vesicular gamma-aminobutyric acid transporter expression in amacrine and horizontal cells.* .J Comp Neurol. 2002;445(3):227–37. PubMed PMID: 11920703.
193. Djamgoz M.B., Kirsch M., Wagner H.J. *Haloperidol suppresses light-induced spinule formation and biphasic responses of horizontal cells in fish (roach) retina.* .Neurosci Lett. 1989;107(1-3):200–4. PubMed PMID: 2616031.
194. Downing J.E., Djamgoz M.B. *Quantitative analysis of cone photoreceptor-horizontal cell connectivity patterns in the retina of a cyprinid fish: electron microscopy of functionally identified and HRP-labelled horizontal cells.* .J Comp Neurol. 1989;289(4):537–53. PubMed PMID: 2592596.
195. Wagner H.J. *Light-dependent plasticity of the morphology of horizontal cell terminals in cone pedicles of fish retinas.* .J Neurocytol. 1980;9(5):573–90. PubMed PMID: 7441304.
196. Kirsch M., Djamgoz M.B., Wagner H.G. *Correlation of spinule dynamics and plasticity of the horizontal cell spectral response in cyprinid fish retina: quantitative analysis.* .Cell & Tissue Research. 1990;260(1):123–130.
197. Connaughton V.P.et al. *Immunocytochemical localization of excitatory and inhibitory neurotransmitters in the zebrafish retina.* .Vis Neurosci. 1999;16(3):483–90. PubMed PMID: 10349969.

198. Yazulla S., Kleinschmidt J. *Carrier-mediated release of GABA from retinal horizontal cells.* .Brain Res. 1983;263(1):63–75. PubMed PMID: 6132667.
199. Tachibana M., Kaneko A. *gamma-Aminobutyric acid acts at axon terminals of turtle photoreceptors: difference in sensitivity among cell types.* .Proc Natl Acad Sci U S A. 1984;81(24):7961–4. PubMed PMID: 6595670.
200. Tatsukawa T.et al. *GABA-mediated component in the feedback response of turtle retinal cones.* .Vis Neurosci. 2005;22(3):317–24. PubMed PMID: 16079007.
201. Murakami M.et al. *GABA-mediated negative feedback and color opponency in carp retina.* .Jpn J Physiol. 1982;32(6):927–35. PubMed PMID: 7169700.
202. Murakami M.et al. *GABA-mediated negative feedback from horizontal cells to cones in carp retina.* .Jpn J Physiol. 1982;32(6):911–26. PubMed PMID: 7169699.
203. Perlman I., Normann R.A. *The effects of GABA and related drugs on horizontal cells in the isolated turtle retina.* .Vis Neurosci. 1990;5(5):469–77. PubMed PMID: 1963078.
204. Verweij J., Hornstein E.P., Schnapf J.L. *Surround antagonism in macaque cone photoreceptors.* .J Neurosci. 2003;23(32):10249–57. PubMed PMID: 14614083.
205. Verweij J.et al. *GABA sensitivity of spectrally classified horizontal cells in goldfish retina.* .Vis Neurosci. 1998;15(1):77–86. PubMed PMID: 9456507.
206. Hirasawa H., Kaneko A. *pH changes in the invaginating synaptic cleft mediate feedback from horizontal cells to cone photoreceptors by modulating* Ca^{2+} *channels.* .J Gen Physiol. 2003;122(6):657–71. PubMed PMID: 14610018.
207. Babai N., Thoreson W.B. *Horizontal cell feedback regulates calcium currents and intracellular calcium levels in rod photoreceptors of salamander and mouse retina.* .J Physiol. 2009;587(Pt 10):2353–64. PubMed PMID: 19332495.
208. Cadetti L., Thoreson W.B. *Feedback effects of horizontal cell membrane potential on cone calcium currents studied with simultaneous recordings.* .J Neurophysiol. 2006;95(3):1992–5. PubMed PMID: 16371457.
209. Davenport C.M., Detwiler P.B., Dacey D.M. *Effects of pH buffering on horizontal and ganglion cell light responses in primate retina: evidence for the proton hypothesis of surround formation.* .J Neurosci. 2008;28(2):456–64. PubMed PMID: 18184788.
210. Thoreson W.B., Babai N., Bartoletti T.M. *Feedback from horizontal cells to rod photoreceptors in vertebrate retina.* .J Neurosci. 2008;28(22):5691–5. PubMed PMID: 18509030.
211. Trenholm S., Baldridge W.H. *The effect of aminosulfonate buffers on the light responses and intracellular pH of goldfish retinal horizontal cells.* .J Neurochem. 2009;115(1):102–11.
212. Vessey J.P.et al. *Proton-mediated feedback inhibition of presynaptic calcium channels at the cone photoreceptor synapse.* .J Neurosci. 2005;25(16):4108–17. PubMed PMID: 15843613.
213. Fahrenfort I.et al. *Hemichannel-mediated and pH-based feedback from horizontal cells to cones in the vertebrate retina.* .PLoS One. 2009;4(6):e6090. PubMed PMID: 19564917.
214. Kreitzer M.A.et al. *Modulation of extracellular proton fluxes from retinal horizontal cells of the catfish by depolarization and glutamate.* .J Gen Physiol. 2007;130(2):169–82. PubMed PMID: 17664345.
215. Verweij J., Kamermans M., Spekreijse H. *Horizontal cells feed back to cones by shifting the cone calcium-current activation range.* .Vision Res. 1996;36(24):3943–53. PubMed PMID: 9068848.
216. Kamermans M., Fahrenfort I. *Ephaptic interactions within a chemical synapse: hemichannel-mediated ephaptic inhibition in the retina.* .Curr Opin Neurobiol. 2004;14(5):531–41. PubMed PMID: 15464885.
217. Witkovsky P., Gabriel R., Krizaj D. *Anatomical and neurochemical characterization of dopaminergic interplexiform processes in mouse and rat retinas.* .J Comp Neurol. 2008;510(2):158–74. PubMed PMID: 18615559.
218. Witkovsky P. *Dopamine and retinal function.* .Doc Ophthalmol. 2004;108(1):17–40. PubMed PMID: 15104164.
219. Dong C.J., McReynolds J.S. *The relationship between light, dopamine release and horizontal cell coupling in the mudpuppy retina.* .J Physiol. 1991;440:291–309. PubMed PMID: 1687151.

220. Mangel S.C., Dowling J.E. *Responsiveness and receptive field size of carp horizontal cells are reduced by prolonged darkness and dopamine.* .Science. 1985;229(4718):1107–9. PubMed PMID: 4035351.
221. Piccolino M., Neyton J., Gerschenfeld H.M. *Decrease of gap junction permeability induced by dopamine and cyclic adenosine 3′:5′-monophosphate in horizontal cells of turtle retina.* .J Neurosci. 1984;4(10):2477–88. PubMed PMID: 6092564.
222. Zhang A.J., Jacoby R., Wu S.M. *Light- and dopamine-regulated receptive field plasticity in primate horizontal cells.* .J Comp Neurol. 2011;519(11):2125–34. PubMed PMID: 21452210.
223. Dowling J.E. *Retinal neuromodulation: the role of dopamine.* .Vis Neurosci. 1991;7(1-2):87–97. PubMed PMID: 1718402.
224. He S., Weiler R., Vaney D.I. *Endogenous dopaminergic regulation of horizontal cell coupling in the mammalian retina.* .J Comp Neurol. 2000;418(1):33–40. PubMed PMID: 10701754.
225. Reitsamer H.A.et al. *Dopaminergic modulation of horizontal-cell-axon-terminal receptive field size in the mammalian retina.* .Vision Res. 2006;46(4):467–74. PubMed PMID: 16023694.
226. Qian H., Ripps H. *Receptive field properties of rod-driven horizontal cells in the skate retina.* .J Gen Physiol. 1992;100(3):457–78. PubMed PMID: 1359000.
227. McMahon D.G., Brown D.R. *Modulation of gap-junction channel gating at zebrafish retinal electrical synapses.* .J Neurophysiol. 1994;72(5):2257–68. PubMed PMID: 7533830.
228. DeVries S.H., Schwartz E.A. *Modulation of an electrical synapse between solitary pairs of catfish horizontal cells by dopamine and second messengers.* .J Physiol. 1989;414:351–75. PubMed PMID: 2558170.
229. Weiler R.et al. *Glutamate and dopamine modulate synaptic plasticity in horizontal cell dendrites of fish retina.* .Neurosci Lett. 1988;87(3):205–9. PubMed PMID: 2898116.
230. Yang X.L., Tornqvist K., Dowling J.E. *Modulation of cone horizontal cell activity in the teleost fish retina. II. Role of interplexiform cells and dopamine in regulating light responsiveness.* .J Neurosci. 1988;8(7):2269–78. PubMed PMID: 2470870.
231. Knapp A.G., Dowling J.E. *Dopamine enhances excitatory amino acid-gated conductances in cultured retinal horizontal cells.* .Nature. 1987;325(6103):437–9. PubMed PMID: 2880299.
232. Schmidt K.F. *Divalent cations modulate glutamate receptors in retinal horizontal cells of the perch (Perca fluviatilis).* .Neurosci Lett. 1999;262(2):109–12. PubMed PMID: 10203243.
233. Pflug R.et al. *Modulation of horizontal cell function by dopaminergic ligands in mammalian retina.* .Vision Res. 2008;48(12):1383–90. PubMed PMID: 18440579.
234. Mangel S.C., Dowling J.E. *The interplexiform-horizontal cell system of the fish retina: effects of dopamine, light stimulation and time in the dark.* .Proc R Soc Lond B Biol Sci. 1987;231(1262):91–121. PubMed PMID: 2888119.
235. Witkovsky P., Stone S., Besharse J.C. *Dopamine modifies the balance of rod and cone inputs to horizontal cells of the Xenopus retina.* .Brain Res. 1988;449(1-2):332–6. PubMed PMID: 3293703.
236. Witkovsky P., Stone S., Tranchina D. *Photoreceptor to horizontal cell synaptic transfer in the Xenopus retina: modulation by dopamine ligands and a circuit model for interactions of rod and cone inputs.* .J Neurophysiol. 1989;62(4):864–81. PubMed PMID: 2530319.
237. Nathan C. *Nitric oxide as a secretory product of mammalian cells.* .FASEB J. 1992;6(12):3051–64. PubMed PMID: 1381691.
238. Koistinaho J., Sagar S.M. *Light-induced c-fos expression in amacrine cells in the rabbit retina.* .Brain Res Mol Brain Res. 1995;29(1):53–63. PubMed PMID: 7770001.
239. Liepe B.A.et al. *Nitric oxide synthase in Muller cells and neurons of salamander and fish retina.* .J Neurosci. 1994;14(12):7641–54. PubMed PMID: 7527846.
240. Ostholm T.et al. *Nitric oxide synthase in the CNS of the Atlantic salmon.* .Neurosci Lett. 1994;168(1-2):233–7. PubMed PMID: 7518064.
241. Weiler R., Kewitz B. *The marker for nitric oxide synthase, NADPH-diaphorase, co-localizes with GABA in horizontal cells and cells of the inner retina in the carp retina.* .Neurosci Lett. 1993;158(2):151–4. PubMed PMID: 7694204.

242. Haverkamp S., Eldred W.D. *Localization of nNOS in photoreceptor, bipolar and horizontal cells in turtle and rat retinas.* .Neuroreport. 1998;9(10):2231–5. PubMed PMID: 9694205.
243. Haverkamp S., Kolb H., Cuenca N. *Endothelial nitric oxide synthase (eNOS) is localized to Muller cells in all vertebrate retinas.* .Vision Res. 1999;39(14):2299–303. PubMed PMID: 10367050.
244. Haverkamp S., Kolb H., Cuenca N. *Morphological and neurochemical diversity of neuronal nitric oxide synthase-positive amacrine cells in the turtle retina.* .Cell Tissue Res. 2000;302(1):11–9. PubMed PMID: 11079711.
245. Zemel E.et al. *NADPH diaphorase activity in mammalian retinas is modulated by the state of visual adaptation.* .Vis Neurosci. 1996;13(5):863–71. PubMed PMID: 8903029.
246. Zemel E., Lei B., Perlman I. *NADPH diaphorase activity in the rabbit retina is modulated by glutamatergic pathways.* .J Comp Neurol. 2001;431(1):28–38. PubMed PMID: 11169988.
247. Savchenko A., Barnes S., Kramer R.H. *Cyclic-nucleotide-gated channels mediate synaptic feedback by nitric oxide.* .Nature. 1997;390(6661):694–8. PubMed PMID: 9414163.
248. Miyachi E., Murakami M., Nakaki T. *Arginine blocks gap junctions between retinal horizontal cells.* .Neuroreport. 1990;1(2):107–10. PubMed PMID: 2129864.
249. Xin D., Bloomfield S.A. *Effects of nitric oxide on horizontal cells in the rabbit retina.* .Vis Neurosci. 2000;17(5):799–811. PubMed PMID: 11153659.
250. Lu C., McMahon D.G. *Modulation of hybrid bass retinal gap junctional channel gating by nitric oxide.* .J Physiol. 1997;499(Pt 3):689–99. PubMed PMID: 9130165.
251. Levy H., Twig G., Perlman I. *Nitric oxide modulates the transfer function between cones and horizontal cells during changing conditions of ambient illumination.* .Eur J Neurosci. 2004;20(11):2963–74. PubMed PMID: 15579150.
252. Tsuyama Y., Noll G.N., Schmidt K.F. *L-arginine and nicotinamide adenine dinucleotide phosphate alter dark voltage and accelerate light response recovery in isolated retinal rods of the frog (Rana temporaria).* .Neurosci Lett. 1993;149(1):95–8. PubMed PMID: 8469390.
253. Kurenny D.E.et al. *Modulation of ion channels in rod photoreceptors by nitric oxide.* .Neuron. 1994;13(2):315–24. PubMed PMID: 7520253.
254. McMahon D.G., Ponomareva L.V. *Nitric oxide and cGMP modulate retinal glutamate receptors.* .J Neurophysiol. 1996;76(4):2307–15. PubMed PMID: 8899605.
255. Dowling J.E., Wald G. *The Biological Function of Vitamin a Acid.* .Proc Natl Acad Sci U S A. 1960;46(5):587–608. PubMed PMID: 16590647.
256. Wald G. *Carotenoids and the Visual Cycle.* .J Gen Physiol. 1935;19(2):351–71. PubMed PMID: 19872932.
257. Hyatt G.A.et al. *Retinoic acid-induced duplication of the zebrafish retina.* .Proc Natl Acad Sci U S A. 1992;89(17):8293–7. PubMed PMID: 1518861.
258. Marsh-Armstrong N.et al. *Retinoic acid is necessary for development of the ventral retina in zebrafish.* .Proc Natl Acad Sci U S A. 1994;91(15):7286–90. PubMed PMID: 8041782.
259. Wagner M., Han B., Jessell T.M. *Regional differences in retinoid release from embryonic neural tissue detected by an in vitro reporter assay.* .Development. 1992;116(1):55–66. PubMed PMID: 1483395.
260. Dräger U.C., McCaffery P. *Retinoic acid and development of the retina.* .Progress in Retinal and Eye Research. 1997;16(3):323–351.
261. Weiler R.et al. *Retinoic acid, a neuromodulator in the retina.* .Prog Brain Res. 2001;131:309–18. PubMed PMID: 11420951.
262. Weiler R., He S., Vaney D.I. *Retinoic acid modulates gap junctional permeability between horizontal cells of the mammalian retina.* .Eur J Neurosci. 1999;11(9):3346–50. PubMed PMID: 10510200.
263. MacNichol E.J., Svaetichin G. *Electric responses from the isolated retinas of fishes.* .Am J Ophthalmol. 1958;46(3 Part 2):26–40. PubMed PMID: 13571357.
264. Chappell R.L., Naka K., Sakuranaga M. *Dynamics of turtle horizontal cell response.* .J Gen Physiol. 1985;86(3):423–53. PubMed PMID: 4056733.
265. Frumkes T.E., Eysteinsson T. *Suppressive rod-cone interaction in distal vertebrate retina: intracellular records from Xenopus and Necturus.* .J Neurophysiol. 1987;57(5):1361–82. PubMed PMID: 3585472.

266. Pflug R., Nelson R., Ahnelt P.K. *Background-induced flicker enhancement in cat retinal horizontal cells. I. Temporal and spectral properties.* .J Neurophysiol. 1990;64(2):313–25. PubMed PMID: 2213120.
267. Goldberg S.H., Frumkes T.E., Nygaard R.W. *Inhibitory influence of unstimulated rods in the human retina: evidence provided by examining cone flicker.* .Science. 1983;221(4606):180–2. PubMed PMID: 6857279.
268. Dowling J.E., Werblin F.S. *Organization of retina of the mudpuppy, Necturus maculosus. I. Synaptic structure.* .J Neurophysiol. 1969;32(3):315–38. PubMed PMID: 5787842.
269. Frumkes T.E., Eysteinsson T. *The cellular basis for suppressive rod-cone interaction.* .Vis Neurosci. 1988;1(3):263–73. PubMed PMID: 3154799.
270. Dowling J.E. *Organization of vertebrate retinas.* .Invest Ophthalmol. 1970;9(9):655–80. PubMed PMID: 4915972.
271. Kolb H., Jones J. *Synaptic organization of the outer plexiform layer of the turtle retina: an electron microscope study of serial sections.* .J Neurocytol. 1984;13(4):567–91. PubMed PMID: 6481412.
272. Wu S.M. *Effects of gamma-aminobutyric acid on cones and bipolar cells of the tiger salamander retina.* .Brain Res. 1986;365(1):70–7. PubMed PMID: 3947987.
273. Vardi N., Auerbach P. *Specific cell types in cat retina express different forms of glutamic acid decarboxylase.* .J Comp Neurol. 1995;351(3):374–84. PubMed PMID: 7706548.
274. Vardi N., Masarachia P., Sterling P. *Immunoreactivity to GABA $_A$ receptor in the outer plexiform layer of the cat retina.* .J Comp Neurol. 1992;320(3):394–7. PubMed PMID: 1377202.
275. Vardi N., Sterling P. *Subcellular localization of GABA $_A$ receptor on bipolar cells in macaque and human retina.* .Vision Res. 1994;34(10):1235–46. PubMed PMID: 8023433.
276. Vardi N.et al. *Evidence that different cation chloride cotransporters in retinal neurons allow opposite responses to GABA.* .J Neurosci. 2000;20(20):7657–63. PubMed PMID: 11027226.
277. Bloomfield S.A., Xin D. *Surround inhibition of mammalian AII amacrine cells is generated in the proximal retina.* .J Physiol. 2000;523(Pt 3):771–83. PubMed PMID: 10718754.
278. Nelson R., Kolb H. *Synaptic patterns and response properties of bipolar and ganglion cells in the cat retina.* .Vision Res. 1983;23(10):1183–95. PubMed PMID: 6649437.
279. Ammermüller J.et al. *Effects of horizontal cell network architecture on signal spread in the turtle outer retina. Experiments and simulations.* .Vision Res. 1996;36(24):4089–103. PubMed PMID: 9068861.
280. Ammermüller J., Muller J.F., Kolb H. *The organization of the turtle inner retina. II. Analysis of color- coded and directionally selective cells.* .J Comp Neurol. 1995;358(1):35–62. PubMed PMID: 7560276.
281. Lasansky A. *Contacts between receptors and electrophysiologically identified neurones in the retina of the larval tiger salamander.* .J Physiol. 1978;285:531–42. PubMed PMID: 217992.
282. Marchiafava P.L., Weiler R. *Intracellular analysis and structural correlates of the organization of inputs to ganglion cells in the retina of the turtle.* .Proc R Soc Lond B Biol Sci. 1980;208(1170):103–13. PubMed PMID: 6105651.
283. Naka K. *Neuronal circuitry in the catfish retina.* .Invest Ophthalmol. 1976;15(11):926–935.
284. Naka K.I. *Receptive field mechanism in the vertebrate retina.* .Science. 1971;171(972):691–3. PubMed PMID: 5540311.
285. Saito T., Kondo H., Toyoda J. *Ionic mechanisms of two types of on-center bipolar cells in the carp retina. II. The responses to annular illumination.* .J Gen Physiol. 1981;78(5):569–89. PubMed PMID: 7310376.
286. Saito T., Kondo H., Toyoda J.I. *Ionic mechanisms of two types of on-center bipolar cells in the carp retina. I. The responses to central illumination.* .J Gen Physiol. 1979;73(1):73–90. PubMed PMID: 438766.
287. McReynolds, J.S. and P.D. Lukasiewicz, eds. *Integration of synaptic input from on and off pathways in mudpuppy retinal ganglion cells.* Neurobiology of the Inner Retina, ed. R. Weiler and N.N. Osborne. Vol. H31. 1989, Springer-Verlag: Berlin, Heidelberg. 209-220.
288. Stell W.K. *Functional polarization of horizontal cell dendrites in goldfish retina.* . .Invest Ophthalmol. 1976;15(11):895–908.
289. Wong K.Y., Dowling J.E. *Retinal Bipolar Cell Input Mechanisms in Giant Danio: III. ON-OFF Bipolar Cells and Their Color-Opponent Mechanisms.* .J Neurophysiol. 2005;94(1):265–272. PubMed PMID: 15758056.

290. Mangel S.C. *Analysis of the horizontal cell contribution to the receptive field surround of ganglion cells in the rabbit retina.* .J Physiol. 1991;442:211–34. PubMed PMID: 1665857.
291. Vigh J., Witkovsky P. *Sub-millimolar cobalt selectively inhibits the receptive field surround of retinal neurons.* .Vis Neurosci. 1999;16(1):159–68. PubMed PMID: 10022487.
292. Gouras P. *Gunnar Svaetichin. 1915-1981.* .Vision Res. 1982;22(3):339–40. PubMed PMID: 7046222.
293. Kolb H., Perlman I., Normann R.A. *Neural organization of the retina of the turtle Mauremys caspica: a light microscope and Golgi study.* .Vis Neurosci. 1988;1(1):47–72. PubMed PMID: 3154788.
294. Kolb H. *The connections between horizontal cells and photoreceptors in the retina of the cat: electron microscopy of Golgi preparations.* .J Comp Neurol. 1974;155(1):1–14. PubMed PMID: 4836060.
295. Normann R.A., Pochobradsky J. *Oscillations in rod and horizontal cell membrane potential: evidence for feed-back to rods in the vertebrate retina.* .J Physiol. 1976;261(1):15–29. PubMed PMID: 825636.
296. Bloomfield S.A. *A unique morphological subtype of horizontal cell in the rabbit retina with orientation-sensitive response properties.* .J Comp Neurol. 1992;320(1):69–85. PubMed PMID: 1401243.

Glutamate and Glutamate Receptors in the Vertebrate Retina

Victoria Connaughton

Created: May 1, 2005; Updated: May 7, 2007.

General Overview of Synaptic Transmission

Cells communicate with each other electrically, through gap junctions, and chemically, using neurotransmitters. Chemical synaptic transmission allows nerve signals to be exchanged between cells that are electrically isolated from each other. The chemical messenger, or neurotransmitter, provides a way to send the signal across the extracellular space, from the presynaptic neuron to the postsynaptic cell. The space is called a **cleft** and is typically more than 10 nanometers across. Neurotransmitters are synthesized in the presynaptic cell and stored in vesicles in presynaptic processes, such as the axon terminal. When the presynaptic neuron is stimulated, calcium channels open, and the influx of calcium ions into the axon terminal triggers a cascade of events leading to the release of neurotransmitter. Once released, the neurotransmitter diffuses across the cleft and binds to receptors on the postsynaptic cell, allowing the signal to propagate. Neurotransmitter molecules can also bind onto presynaptic autoreceptors and transporters, regulating subsequent release and clearing excess neurotransmitter from the cleft. Compounds classified as neurotransmitters have several characteristics in common (reviewed in Massey (1) and Erulkar (2)).

Briefly: 1) the neurotransmitter is synthesized, stored, and released from the presynaptic terminal; 2) specific neurotransmitter receptors are localized on the postsynaptic cells; and 3) there exists a mechanism to stop neurotransmitter release and clear molecules from the cleft. Common neurotransmitters in the retina are glutamate, GABA, glycine, dopamine, and acetylcholine. Neurotransmitter compounds can be small molecules, such as glutamate and glycine, or large peptides, such as vasoactive intestinal peptide (VIP). Some neuroactive compounds are amino acids, which also have metabolic functions in the presynaptic cell.

Glutamate (Fig. 1) is believed to be the major excitatory neurotransmitter in the retina. In general, glutamate is synthesized from ammonium and α-ketoglutarate (a component of the Krebs cycle) and is used in the synthesis of proteins, other amino acids, and even other neurotransmitters (such as GABA) (3). Although glutamate is present in all neurons, only a few are glutamatergic, releasing glutamate as their neurotransmitter. Neuroactive glutamate is stored in synaptic vesicles in presynaptic axon terminals (4). Glutamate is incorporated into the vesicles by a glutamate transporter located in the vesicular membrane. This transporter selectively accumulates glutamate through a sodium-independent, ATP-dependent process (4-6), resulting in a high concentration of glutamate in each vesicle. Neuroactive glutamate is classified as an excitatory amino acid (EAA), because glutamate binding onto postsynaptic receptors typically stimulates, or depolarizes, the postsynaptic cells.

Histological Techniques Identify Glutamatergic Neurons

Using immunocytochemical techniques, neurons containing glutamate are identified and labeled with a glutamate antibody. In the retina, photoreceptors, bipolar cells, and ganglion cells are glutamate immunoreactive (7-12) (Fig. 2). Some horizontal and/or amacrine cells can also display weak labeling with glutamate antibodies (7, 8, 10, 13). These neurons are believed to release GABA, not glutamate, as their neurotransmitter (14), suggesting that the weak glutamate labeling reflects the pool of metabolic glutamate used in the synthesis of GABA. This has been supported by the results from double-labeling studies using antibodies to both GABA and glutamate; glutamate-positive amacrine cells also label with the GABA antibodies (8, 13).

Photoreceptors, which contain glutamate, actively take up radiolabeled glutamate from the extracellular space, as do Muller cells (Fig. 3) (15, 16). Glutamate is incorporated into these cell types through a high-affinity glutamate transporter located in the plasma membrane. Glutamate transporters maintain the concentration of glutamate within the synaptic cleft at low levels, preventing glutamate-induced cell death (17). Although Muller cells take

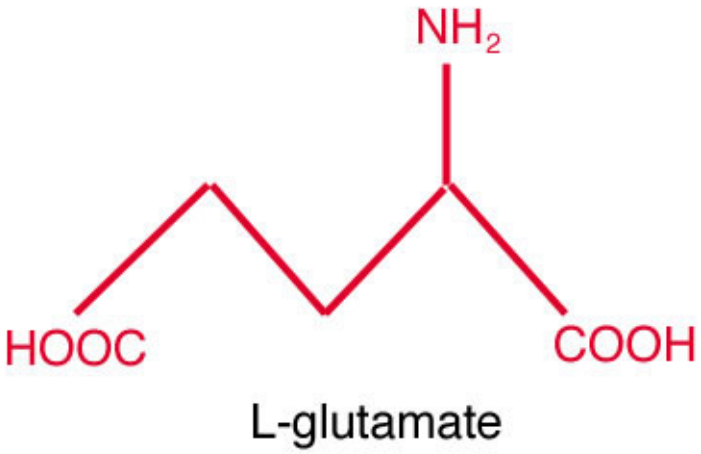

Figure 1. Structure of the glutamate molecule.

up glutamate, they do not label with glutamate antibodies (8). Glutamate incorporated into Muller cells is rapidly broken down into glutamine, which is then exported from glial cells and incorporated into surrounding neurons (18). Neurons can then synthesize glutamate from glutamine (18, 19).

Thus, histological techniques are used to identify potential glutamatergic neurons by labeling neurons containing glutamate (through immunocytochemistry) and neurons that take up glutamate (through autoradiography). To determine whether these cell types actually release glutamate as their neurotransmitter, however, the receptors on postsynaptic cells have to be examined.

Glutamate Receptors

Once released from the presynaptic terminal, glutamate diffuses across the cleft and binds onto receptors located on the dendrites of the postsynaptic cell(s). Multiple glutamate receptor types have been identified. Although glutamate will bind onto all glutamate receptors, each receptor is characterized by its sensitivity to specific glutamate analogs and by the features of the glutamate-elicited current. Glutamate receptor agonists and antagonists are structurally similar to glutamate (Fig. 4), which allows them to bind onto glutamate receptors. These compounds are highly specific and, even in intact tissue, can be used in very low concentrations because they are poor substrates for glutamate uptake systems (20, 21).

Two classes of glutamate receptors (Fig. 5) have been identified: 1) ionotropic glutamate receptors, which directly gate ion channels; and 2) metabotropic glutamate receptors, which may be coupled to an ion channel or other cellular functions via an intracellular second messenger cascade. These receptor types are similar in that they both bind glutamate, and glutamate binding can influence the permeability of ion channels. However, there are several differences between the two classes.

Ionotropic Glutamate Receptors

Glutamate binding onto an ionotropic receptor directly influences ion channel activity because the receptor and the ion channel form one complex (Fig. 5a). These receptors mediate fast synaptic transmission between neurons. Each ionotropic glutamate receptor, or iGluR, is formed from the co-assembly of individual subunits. The assembled subunits may or may not be homologous, with the different combinations of subunits resulting in channels with different characteristics (22-26).

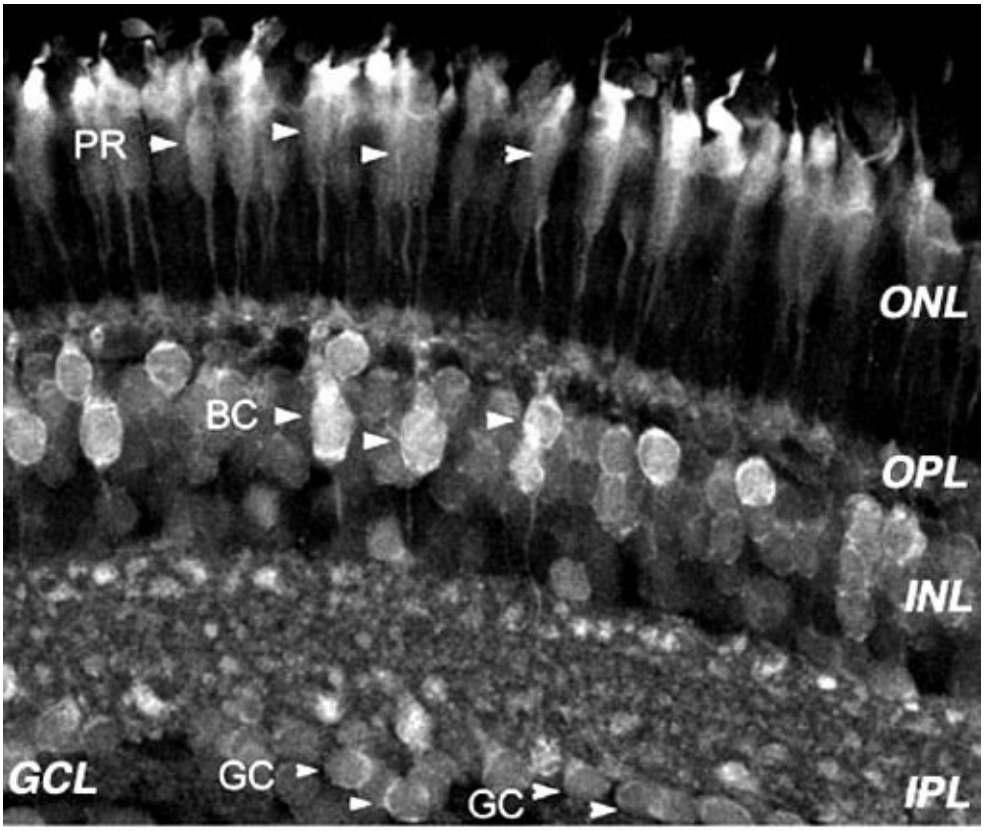

Figure 2. Glutamate immunoreactivity.

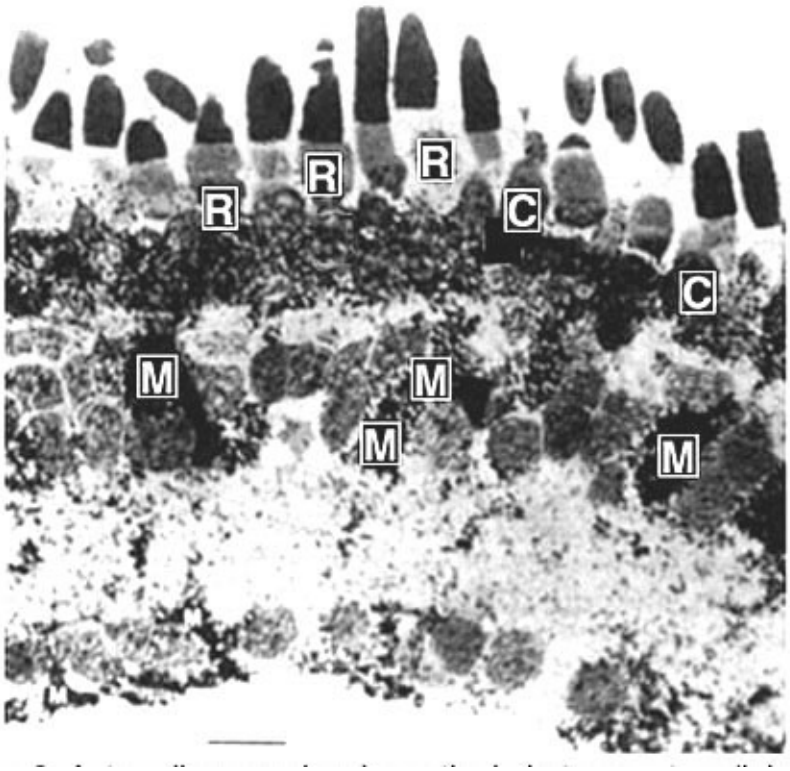

Figure 3. Autoradiogram of glutamate uptake through glutamate transporters.

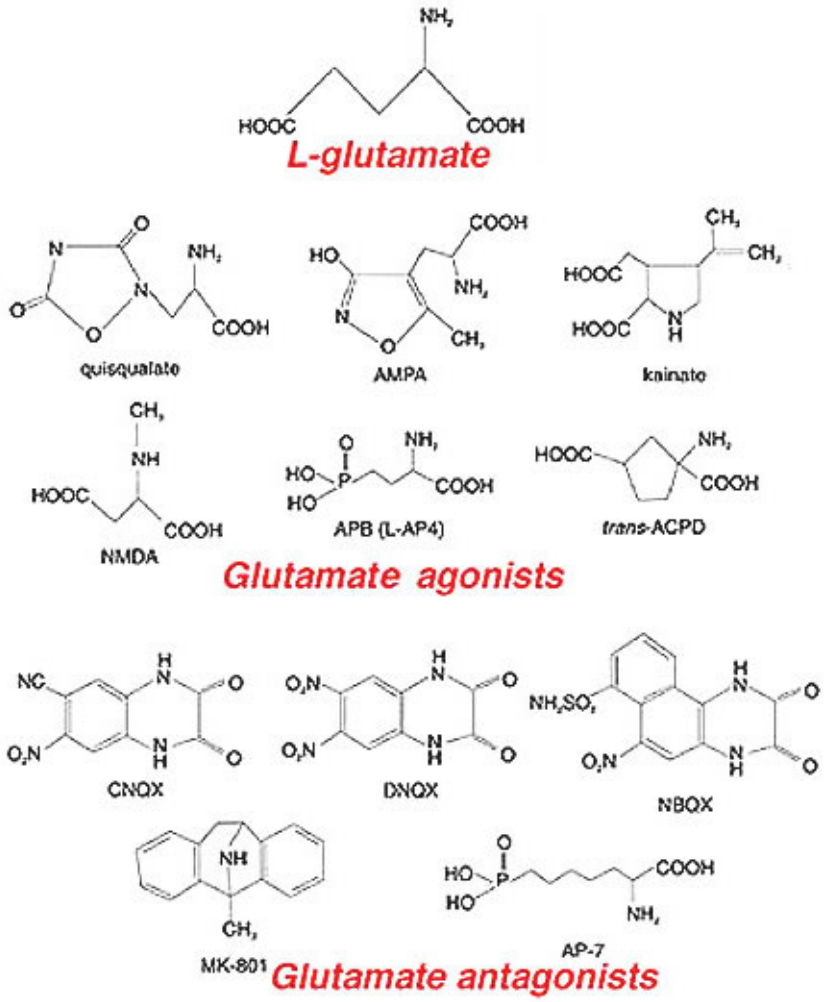

Figure 4. Glutamate receptor agonists and antagonists.

Two iGluR types (Fig. 6) have been identified: 1) NMDA receptors, which bind glutamate and the glutamate analog *N*-methyl-D-aspartate (NMDA) and 2) non-NMDA receptors, which are selectively agonized by kainate, AMPA, and quisqualate, but not NMDA.

Non-NMDA Receptors

Glutamate binding onto a non-NMDA receptor opens non-selective cation channels more permeable to sodium (Na^+) and potassium (K^+) ions than calcium (Ca^{2+}) (27). Glutamate binding elicits a rapidly activating inward current at membrane potentials negative to 0 mV and an outward current at potentials positive to 0 mV. Kainate, quisqualate, and AMPA (α-amino-3-hydroxy-5-methyl-4-isoxazolepropionic acid) are the specific agonists at these receptors; CNQX (6-cyano-7-nitroquinoxaline-2,3-dione), NBQX (1,2,3,4-tetrahydro-6-nitro-2,3-dione-benzo[*f*]quinoxaline-7-sulfonamide), and DNQX (6,7-dinitroquinoxaline-2,3-dione) are the antagonists.

In retina, non-NMDA receptors have been identified on horizontal cells, OFF-bipolar cells, amacrine cells, and ganglion cells (see below). Patch clamp recordings (28-32) indicate that AMPA, quisqualate, and/or kainate application can evoke currents in these cells. However, the kinetics of the ligand-gated currents differ. AMPA- and quisqualate-elicited currents rapidly desensitize, whereas kainate-gated currents do not (Fig. 7a). The desensitization at AMPA/quisqualate receptors can be reduced (Fig. 7b) by adding cyclothiazide (33), which stabilizes the receptor in an active (or non-desensitized) state (33, 34).

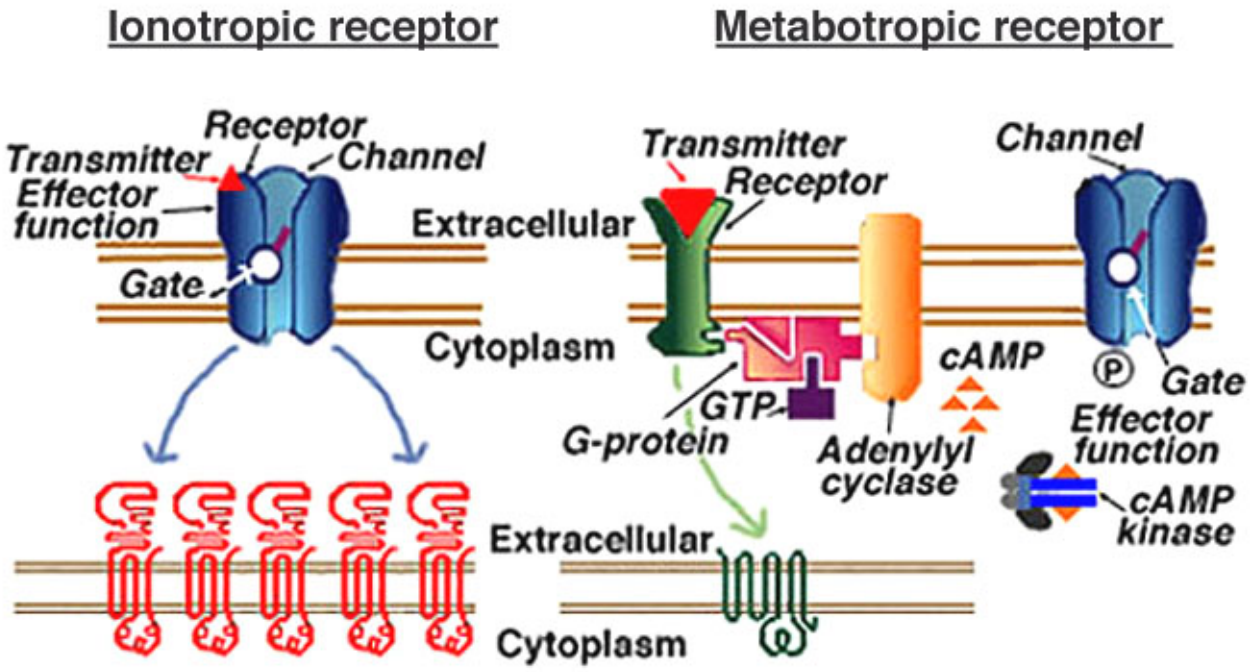

Fig. 5a. Ionotropic receptors and their associated ion channels form one complex (top). Each iGluR is formed from the co-assembly of multiple (4-5) subunits (From Kandel et al., 1991).

Fig. 5b. Metabotropic receptors are coupled to their associated ion channels by a second messenger cascade (top). Each mGluR is composed of one polypeptide, which is coupled to a G-protein (from Kandel et al., 1991).

Figure 5. Ionotropic and metabotropic glutamate receptors and channels. From Kandel et al. (127).

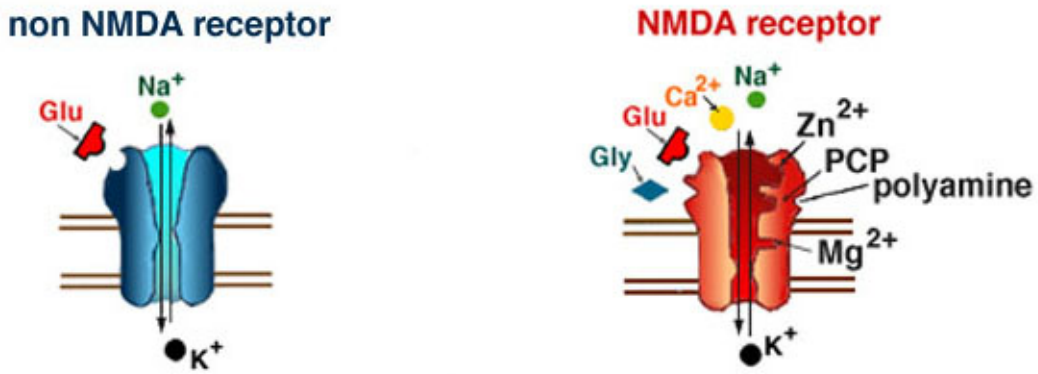

Fig. 6a. Non-NMDA receptors are selectively agonized by kainate, AMPA and quisqualate. The associated ion channels are more perm eable to Na+ and K+ ions tha Ca+2 (from Kandel et al,.1991).

Fig. 6b. NMDA receptors are structurally complex, with separate binding sites for glutamate, glycine MG+2, Zn+2 and polyamines. NMDA-gated channels are more permeable to Ca+2 than Na+ ions (from Kandel et al., 1991).

Figure 6. Comparison between NMDA and non-NMDA receptors. From Kandel et al. (127).

Each non-NMDA receptor is formed from the co-assembly of several subunits (25, 35, 36). To date, seven subunits (named GluR1 through GluR7) have been cloned (22, 35-40). Expression of subunit clones in *Xenopus* oocytes revealed that GluR5, GluR6, and GluR7 (along with subunits KA1 and KA2) co-assemble to form kainate(-preferring) receptors, whereas GluR1, GluR2, GluR3, and GluR4 are assembled into AMPA(-preferring) receptors (25).

NMDA Receptors

Glutamate binding onto an NMDA receptor also opens non-selective cation channels, resulting in a conductance increase. However, the high conductance channel associated with these receptors is more permeable to Ca^{2+} than Na^{+} ions (27), and NMDA-gated currents typically have slower kinetics than kainate- and AMPA-gated channels. As the name suggests, NMDA is the selective agonist at these receptors. The compounds MK-801, AP-5 (2-amino-5-phosphonopentanoic acid), and AP-7 (2-amino-7-phosphoheptanoic acid) are NMDA receptor antagonists.

NMDA receptors are structurally complex, with separate binding sites for glutamate, glycine, magnesium ions (Mg^{2+}), zinc ions (Zn^{2+}), and a polyamine recognition site (Fig. 6b). There is also an antagonist binding site for PCP and MK-801 (41). The glutamate, glycine, and magnesium binding sites are important for receptor activation and gating of the ion channel. In contrast, the zinc and polyamine sites are not needed for receptor activation but affect the efficacy of the channel. Zinc blocks the channel in a voltage-independent manner (42). The polyamine site (43, 44) binds compounds such as spermine or spermidine, either potentiating (43, 44) or inhibiting (44) the activity of the receptor, depending on the combination of subunits forming each NMDA receptor (44).

To date, five subunits (NR1, NR2a, N2b, N2c, and N2d) of NMDA receptors have been cloned (45-49). As with non-NMDA receptors, NMDA receptor subunits can co-assemble as homomers (i.e., five NR1 subunits) (23, 49) or heteromers (one NR1 + four NR2 subunits) (23, 46-48). However, all functional NMDA receptors express the NR1 subunit (23, 25, 46).

The glutamate, glycine, and Mg^{2+} binding sites confer both ligand-gated and voltage-gated properties onto NMDA receptors. NMDA receptors are ligand gated because the binding of glutamate (ligand) is required to activate the channel. In addition, micromolar concentrations of glycine must also be present (Fig. 8) (50, 51). The requirement for both glutamate and glycine makes them co-agonists (51) at NMDA receptors.

Mg^{2+} ions provide a voltage-dependent block of NMDA-gated channels (52). This can be seen in the current-voltage (I-V) relationship presented in Fig. 9 (from Nowak et al. (52)). I-V curves plotted from currents recorded in the presence of Mg^{2+} have a characteristic J-shape (Fig. 9, dotted line), whereas a linear relationship is calculated in Mg^{2+}-free solutions (Fig. 9, solid line). At negative membrane potentials, Mg^{2+} ions occupy the binding site, causing less current to flow through the channel. As the membrane depolarizes, the Mg^{2+} block is removed (52).

Retinal ganglion cells and some amacrine cell types express functional NMDA receptors in addition to non-NMDA receptors (i.e., 29, 53-57). The currents elicited through these different iGluR types can be distinguished pharmacologically. Non-NMDA receptor antagonists block a transient component of the ganglion cell light response, whereas NMDA receptor antagonists block a more sustained component (29, 53, 57, 58). These findings suggest that the currents elicited through colocalized NMDA and non-NMDA receptors mediate differential contributions to the ON- and OFF-light responses observed in ganglion cells (53).

Metabotropic Glutamate Receptors

Unlike ionotropic receptors, which are directly linked to an ion channel, metabotropic receptors are coupled to their associated ion channel through a second messenger pathway. Ligand (glutamate) binding activates a G-

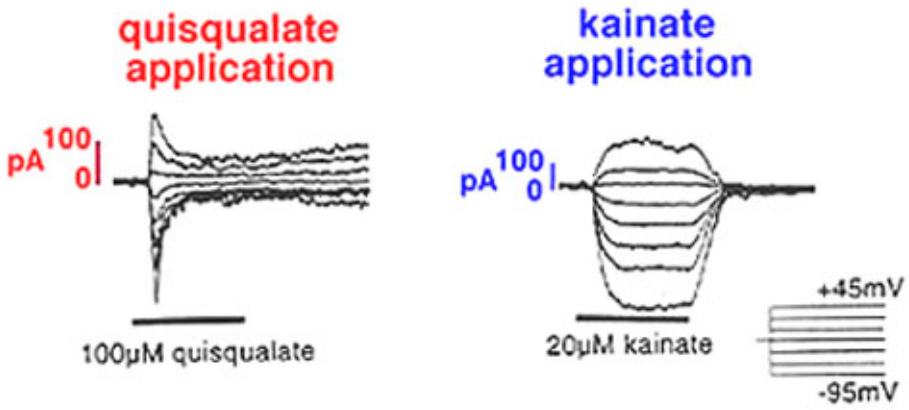

Fig. 7a. Families of whole-cell current traces show the rapid kinetics and desensitization of quisqualate- (and AMPA-) gated currents (left traces). Kainate-gated currents (right), in contrast, do not desensitize (from Gilbertson et al., 1991, Fig. 1).

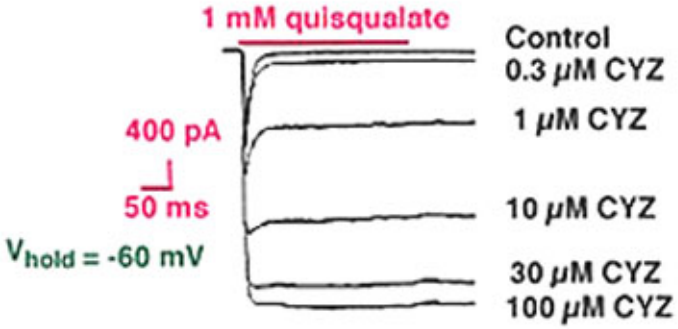

Fig. 7b. Cyclothiazide (CYZ) reduces desensitization at quisqualate receptors in a concentration-dependent manner (from Yamada and Tang, 1993, Fig. 2).

Figure 7. Whole-cell patch clamp to show quisqualate- and kainate-gated currents.

Figure 8. NMDA receptor activation.

protein and initiates an intracellular cascade (59). Metabotropic glutamate receptors (mGluRs) are not co-assembled from multiple subunits but are one polypeptide (Fig. 5b). To date, eight mGluRs (mGluR1 through mGluR8) have been cloned (60-66). These receptors are classified into three groups (I, II, and III) based on

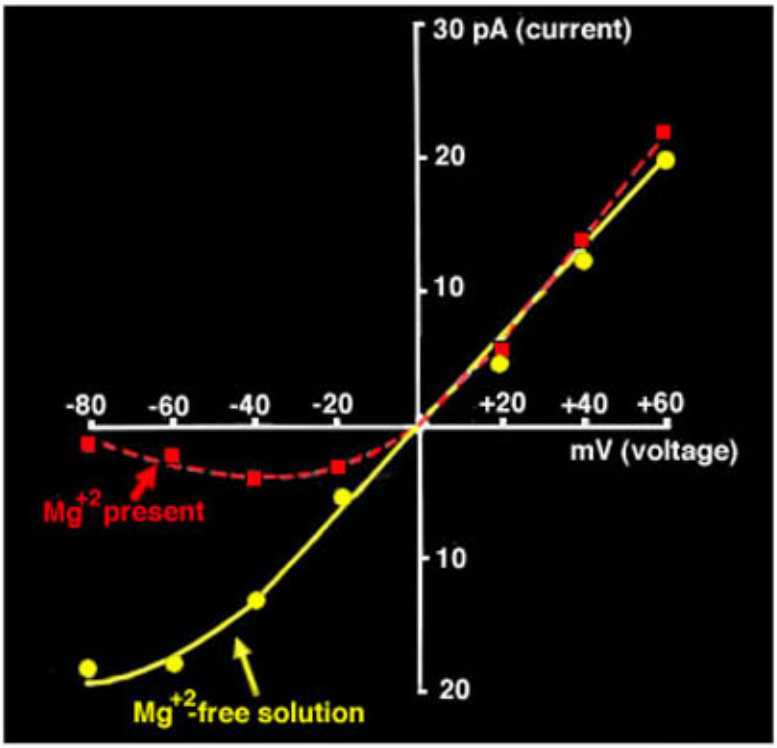

Figure 9. Mg^{2+} ions block NMDA receptor channels.

structural homology, agonist selectivity, and their associated second messenger cascade (Table 1) (reviewed in Nakanishi (67), Knopel et al. (68), Pin and Bockaert (69), and Pin and Duvoisin (70)).

In brief, Group I mGluRs (mGluR1 and mGluR5) are coupled to the hydrolysis of fatty acids and the release of calcium from internal stores. Quisqualate and *trans*-ACPD are Group I agonists. Group II (mGluR2 and mGluR3) and Group III (mGluR4, mGluR6, mGluR7, and mGluR8) receptors are considered inhibitory because they are coupled to the downregulation of cyclic nucleotide synthesis (70). L-CCG-1 and *trans*-ACPD agonize Group II receptors; L-AP4 (also called APB) selectively agonizes Group III receptors. *In situ* hybridization studies have revealed that the mRNAs encoding Groups I, II, and III mGluRs are present in retina (see below); however, with the exception of the APB receptor, the function of all of these receptor types in retina has not been characterized.

Table 1. Metabotropic glutamate receptor groups (from Pin and Duvoisin (70)).

Group	mGluR	Agonist(s)	Intracellular pathway
I	mGluR1, mGluR5	quisqualate, ACPD	Increase phospholipase C activity, increase cAMP levels, increase protein kinase A activity
II	mGluR2, mGluR3	L-CCG-1, ACPD	Decrease cAMP levels
III	mGluR4, mGluR6. mGluR7, mGluR8	L-AP4 (APB)	Decrease cAMP or cGMP levels

APB Receptor

In contrast to non-NMDA and NMDA receptors, glutamate binding onto an APB receptor elicits a conductance decrease (71-73) because of the closure of cGMP-gated, non-selective cation channels (74) (Fig. 10).

APB application selectively blocks the ON-pathway in the retina (Fig. 11) (73), i.e., ON-bipolar cell responses and the ON-responses in amacrine cells (75) and ganglion cells (29, 76, 77) are eliminated by APB. Experimental evidence (73, 78) suggests that the APB receptor is localized to ON-bipolar cell dendrites. Inhibition of amacrine and ganglion cell light responses, therefore, is due to a decrease in the input from ON-bipolar cells, not a direct effect on postsynaptic receptors.

APB (2-amino-4-phosphobutyric acid, also called L-AP4) is the selective agonist for all Group III mGluRs (mGluR4, mGluR6, mGluR7, and mGluR8). So, which is the APB receptor located on ON-bipolar cell dendrites? MGluR4, mGluR7, and mGluR8 expression has been observed in both the inner nuclear layer and the ganglion cell layer (61, 79), suggesting that these mGluRs are associated with more than one cell type. In contrast, mGluR6 expression has been localized to the inner nuclearmlayer (INL) (64, 79) and the outer plexiform layer (OPL) (80), where bipolar cell somata and dendrites are located. Furthermore, ON-responses are abolished in mice lacking mGluR6 expression (81). These mutants also display abnormal ERG b-waves, suggesting an inhibition of the ON-retinal pathway at the level of bipolar cells (81). Taken together, these findings suggest that the APB receptor on ON-bipolar cells is mGluR6.

Glutamate Transporters and Transporter-like Receptors

Glutamate transporters have been identified on photoreceptors (15, 21, 82) and Muller cells (15, 16). From glutamate labeling studies, the average concentration of glutamate in photoreceptors, bipolar cells, and ganglion cells is 5 mM (10). Physiological studies using isolated cells indicate that only μM levels of glutamate are required to activate glutamate receptors (32, 83, 84). Thus, the amount of glutamate released into the synaptic cleft is several orders of magnitude higher than the concentration required to activate most postsynaptic receptors. High-affinity glutamate transporters located on adjacent neurons and surrounding glial cells rapidly remove glutamate from the synaptic cleft to prevent cell death (17). Five glutamate transporters, EAAT-1 (or GLAST), EAAT-2 (or GLT-1), EAAT-3 (or EAAC-1), EAAT-4, and EAAT-5, have been cloned (85-90).

Glutamate transporters are pharmacologically distinct from both iGluRs and mGluRs. L-Glutamate, L-aspartate, and D-aspartate are substrates for the transporters (21, 82, 91); glutamate receptor agonists (20, 21, 82, 91) and antagonists (82, 92) are not. Glutamate uptake can be blocked by the transporter blockers dihydrokainate (DHKA) and DL-*threo*-β-hydroxyaspartate (HA) (82, 92).

Glutamate transporters incorporate glutamate into Muller cells along with the co-transport of three Na^+ ions (91, 93) and the antiport of one K^+ ion (93, 94) and either one OH– or one HCO^{3-} ion (94) (Fig. 12). The excess sodium ions generate a net positive inward current, which drives the transporter (91, 93). More recent findings indicate that a glutamate-elicited chloride current is also associated with some transporters (85, 95).

It should be noted that the glutamate transporters located in the plasma membrane of neuronal and glial cells (discussed in this section) are different from the glutamate transporters located on synaptic vesicles within presynaptic terminals (see General Overview of Synaptic Transmission). The transporters in the plasma membrane transport glutamate in a Na^+- and voltage-dependent manner independent of chloride (17, 91, 93). L-Glutamate, L-aspartate, and D-aspartate are substrates for these transporters (91). In contrast, the vesicular transporter selectively concentrates glutamate into synaptic vesicles in a Na+-independent, ATP-dependent manner (4-6) that requires chloride (4, 6).

Glutamate receptors with transporter-like pharmacology have been described in photoreceptors (96-98) and ON-bipolar cells (99, 100). These receptors are coupled to a chloride current. The pharmacology of these receptors is similar to that described for glutamate transporters, because the glutamate-elicited current is: 1) dependent upon external Na^+; 2) reduced by transporter blockers; and 3) insensitive to glutamate agonists and antagonists. However, altering internal Na^+ concentration does not change the reversal potential (100) or the amplitude (96, 99) of the glutamate-elicited current, suggesting that the receptor is distinct from glutamate

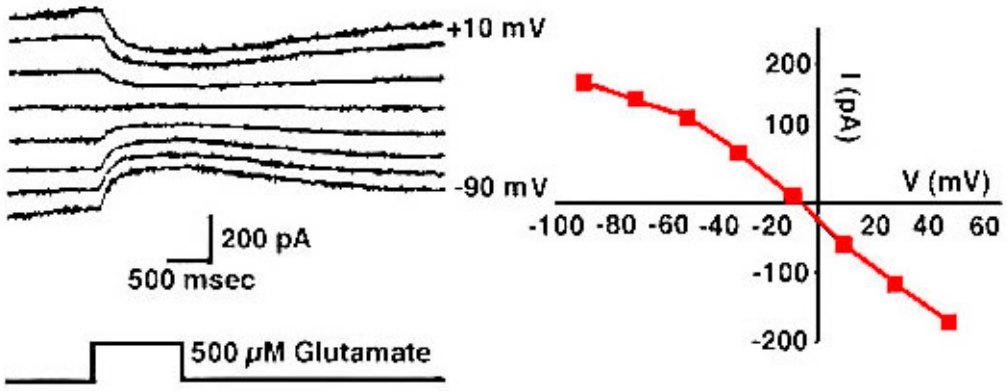

Figure 10. Whole-cell current traces to show kinetics of APB receptor-gated currents.

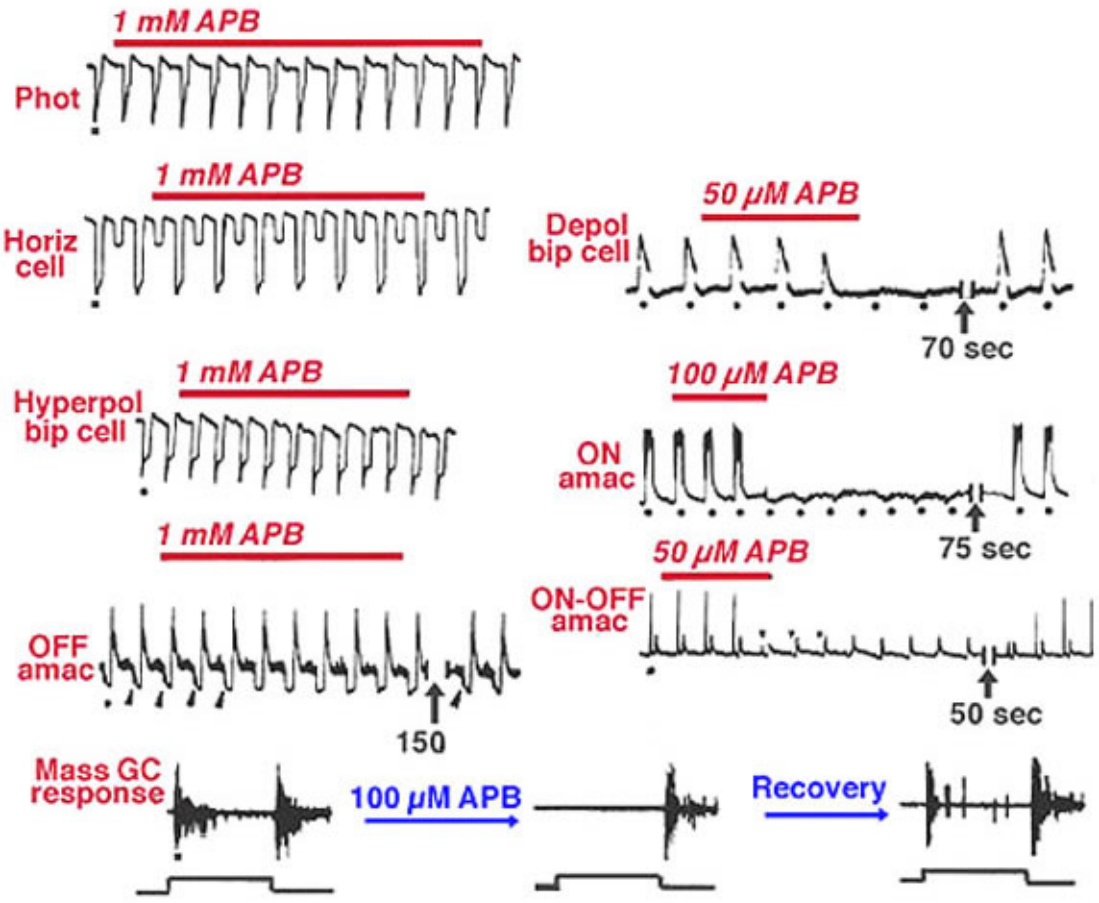

Figure 11. Intracellular recordings to show that APB selectively antagonizes the ON-pathways.

transporters. At the photoreceptor terminals, the glutamate-elicited chloride current may regulate membrane potential and subsequent voltage-gated channel activity (99). Postsynaptically, this receptor is believed to mediate conductance changes underlying photoreceptor input to ON-cone bipolar cells (99).

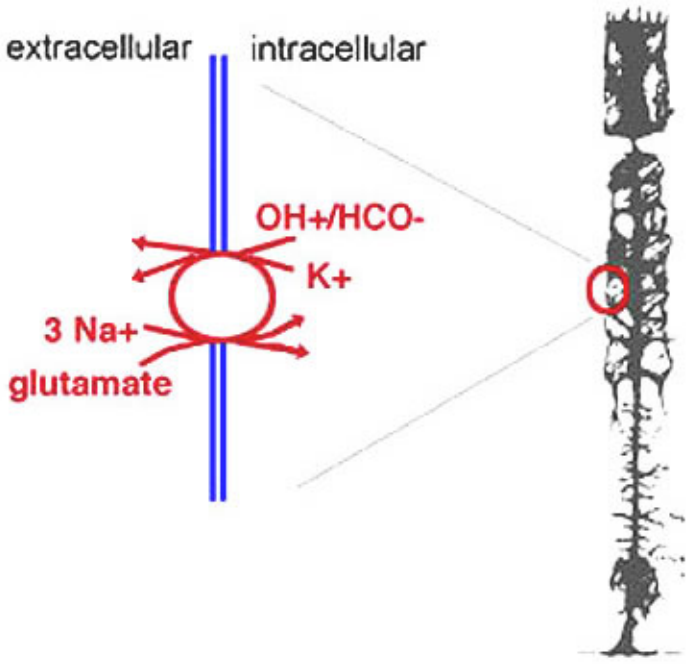

Figure 12. Glutamate transporters in Muller cells are electrogenic.

Localization of Glutamate Receptor Types in the Retina

Photoreceptor, bipolar, and ganglion cells compose the vertical transduction pathway in the retina. This pathway is modulated by lateral inputs from horizontal cells in the distal retina and amacrine cells in the proximal retina (Fig. 13). As described in the previous sections, photoreceptor, bipolar, and ganglion cells show glutamate immunoreactivity. Glutamate responses have been electrically characterized in horizontal and bipolar cells, which are postsynaptic to photoreceptors, and in amacrine and ganglion cells, which are postsynaptic to bipolar cells. Taken together, these results suggest that glutamate is the neurotransmitter released by neurons in the vertical pathway. Recent *in situ* hybridization and immunocytochemical studies have localized the expression of iGluR subunits, mGluRs, and glutamate transporter proteins in the retina. These findings are summarized below.

Retinal Neurons Expressing Ionotropic Glutamate Receptors

In both higher and lower vertebrates, electrophysiological recording techniques have identified ionotropic glutamate receptors on the neurons composing the OFF-pathway (Table 2). In the distal retina, OFF-bipolar cells (Fig. 14) (84, 101, 102) and horizontal cells (Fig. 15) (32, 103, 104) respond to kainate, AMPA, and quisqualate application, but not NMDA nor APB. (However, NMDA receptors have been identified on catfish horizontal cells (105, 106), and APB-induced hyperpolarizations have been reported in some fish horizontal cells (107-109)).

Non-NMDA agonists also stimulate both amacrine cells (Fig. 16a) (28, 54, 55) and ganglion cells (Fig. 16b) (29, 31, 53, 57, 58). Ganglion cells responses to NMDA have been observed (29, 53, 55-57), whereas NMDA responses have been recorded in only some types of amacrine cells (28, 54, 55) but see Hartveit and Veruki (110).

Consistent with this physiological data, antibodies to the different non-NMDA receptor subunits differentially label all retinal layers (Table 3) (111-114), and mRNAs encoding the different non-NMDA iGluR subunits are similarly expressed (115-117). In contrast, mRNAs encoding NMDA subunits are expressed predominantly in

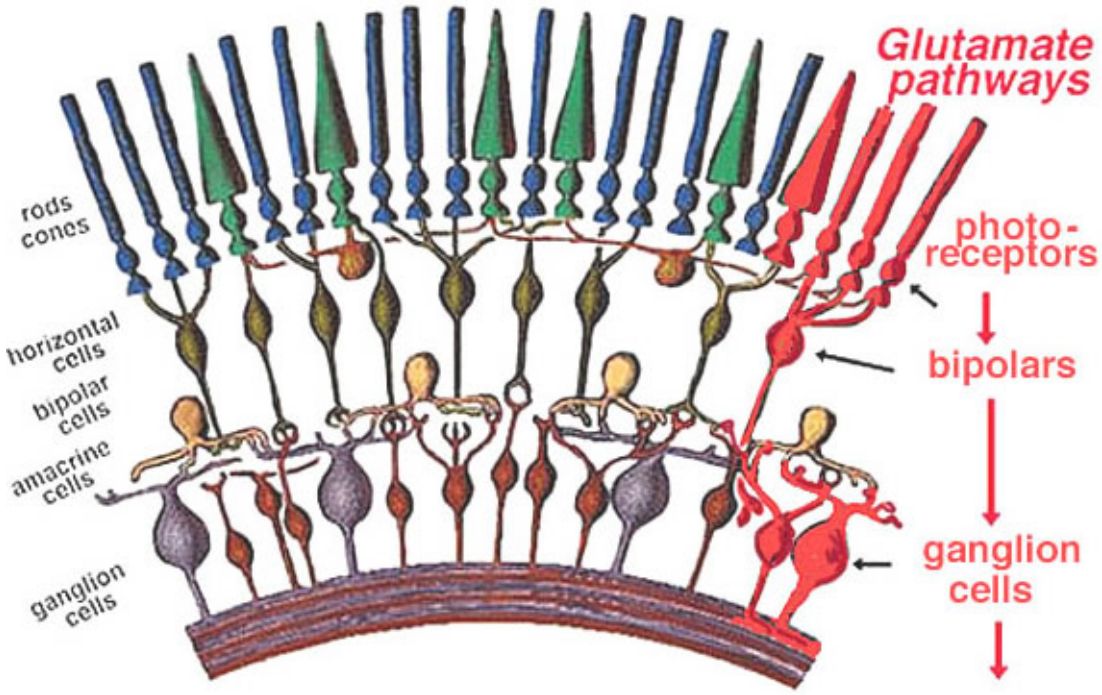

Figure 13. The types of neurons in the vertebrate retina.

the proximal retina, where amacrine and ganglion cells are located (INL, IPL, GCL) (Table 3) (111, 115), although mRNA encoding the NR2a subunit (111) has been observed in the OPL and antibodies to the NR2d (118) and the NR1 subunits (112) label rod bipolar cells.

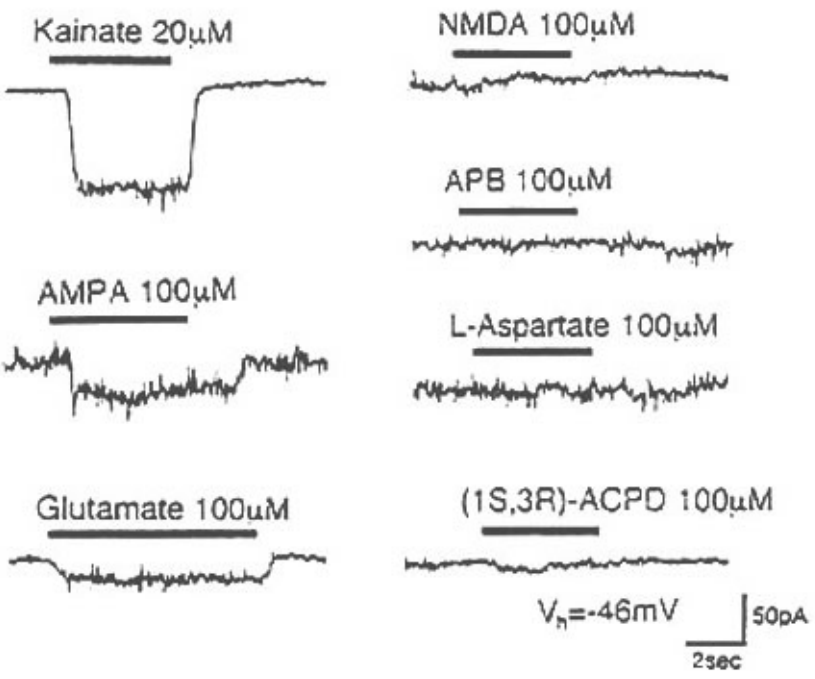

Figure 14. Whole-cell currents in OFF bipolar cells.

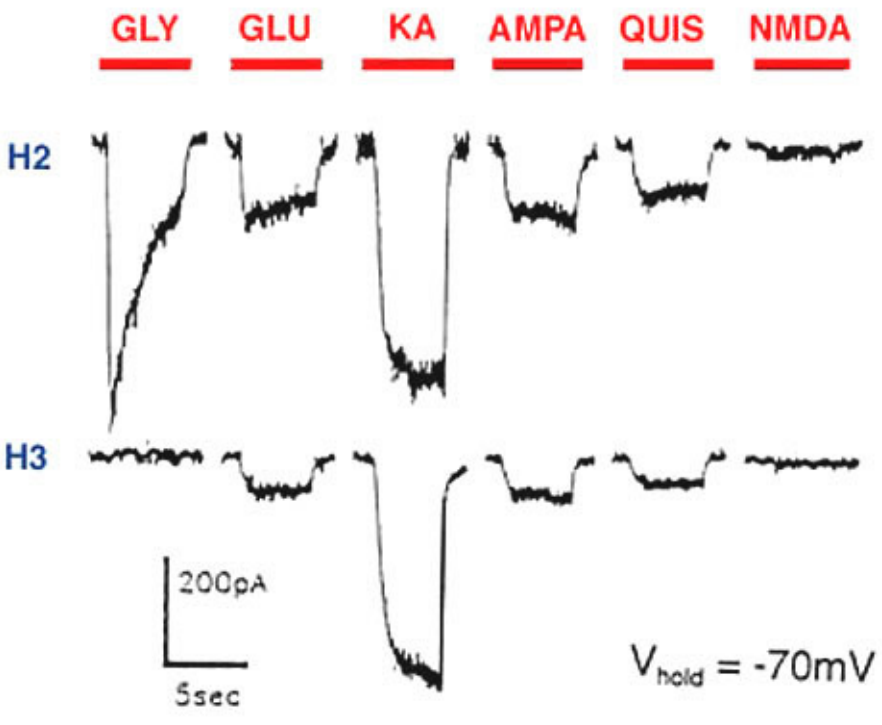

Figure 15. Whole-cell currents in horizontal cells.

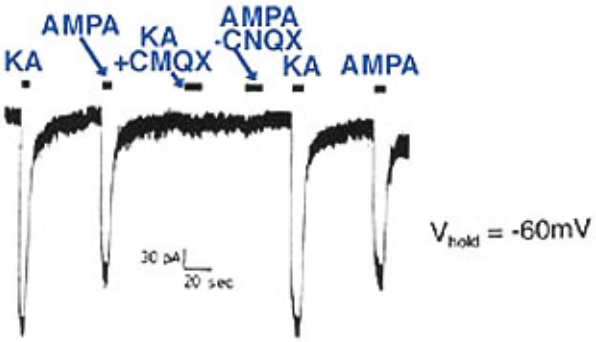

Fig. 16a. Representative whole cell current trace showing the glutamate receptors on amacrine cells are depolarized by the iGluR agonists kainate and AMPA. These responses are blocked by the antagonist CNQX (from Boos et al., 1993, Fig. 13.).

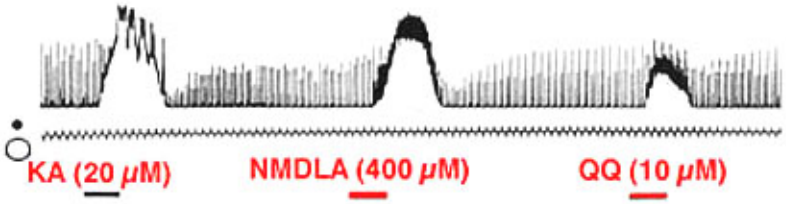

Fig. 16b. Representative ratemeter recording showing an increase in firing rate in ganglion cells in response to NMDA, kainate and quisqualate application (from Massey and Miller, 1988, Fig. 10)

Figure 16. Glutamate receptors on amacrine and ganglion cells.

Table 2. Glutamate receptor types on retinal neurons, electrophysiological measurements.

Retinal cell type	Non-NMDA receptor	NMDA receptor	mGluR	Glutamate receptor with transporter-like pharmacology	Species	Reference
Photoreceptors				++ (cones)	Salamander	Eliasof & Werblin (82); Picaud et al (98).
				++ (rods)	Salamander	Grant & Werblin (96)
OFF-bipolar cells	++				Mudpuppy	Slaughter & Miller (73, 128)
	++				Cat	Sasaki & Kaneko (84)
	++				Salamander	Hensley et al. (58)
	++				Rat	Euler et al. (102)
	++				Mudpuppy	Slaughter & Miller (128)
ON-bipolar cells	++		++ (APB)		Mudpuppy	Slaughter & Miller (73, 128)
			++ (APB)	++	White perch	Grant & Dowling (99, 100)

Table 2 continued from previous page.

Retinal cell type	Non-NMDA receptor	NMDA receptor	mGluR	Glutamate receptor with transporter-like pharmacology	Species	Reference
			++ (APB)		Salamander	Hirano & MacLeish (129)
			++ (L-AP4)		Salamander	Hensley et al. (58)
			++ (AP-4)		Rat	Euler et al. (101)
			++ (APB and cGMP)		Salamander	Nawy & Jahr (74)
			++ (APB and cGMP)		Cat	de la Villa et al. (130)
Horizontal cells	++				White perch	Zhou et al. (32)
	++				Mudpuppy	Slaughter & Miller (128)
	++				Salamander	Yang & Wu (104)
	++	++			Catfish	O'Dell & Christensen (106); Eliasof & Jahr (105)
Amacrine cells	++ (AII)				Rat	Boos et al. (28)
	++	++			Mudpuppy	Slaughter & Miller (128)
	++	++			Rabbit	Massey & Miller (55)
	++	++			Rat	Harveit & Veruki (110)
	++ (transient & sustained AC)	++ (transient AC)			Salamander	Dixon & Copenhagen (54)
Ganglion cells	++	++			Salamander	Diamond & Copenhagen (53); Mittman et al (57); Hensley et al (58).
	++	++			Primates	Cohen & Miller (29)
	++	++			Rat	Aizenman et al. (83)
	++	++			Mudpuppy	Slaughter & Miller (128)
	++	++			Cat	Cohen & Miller (29)
	++	++			Rabbit	Massey & Miller (55, 56)

Table 3. Ionotropic glutamate receptor expression in retinal neurons and retinal layers, immunocytochemistry, and *in situ* hybridization.

Retinal cell type or layer	Non-NMDA receptor subunits	NMDA receptor subunits	Species	Reference
Photoreceptors	GluR6/7 (single cone outer segments)		Goldfish	Peng et al. (113)
	GluR1 (cone pedicles)		Cat	Pourcho et al. (114)
OPL	GluR2, GluR2/3, GluR6/7		Rat	Peng et al. (113)
		NR2A (punctate)	Cat	Harveit et al. (111)

Table 3 continued from previous page.

Retinal cell type or layer	Non-NMDA receptor subunits	NMDA receptor subunits	Species	Reference
	GluR2, GluR2/3 (photoreceptors)		Goldfish	Peng et al. (113)
Bipolar cells	GluR2 (Mb cells)		Goldfish	Peng et al. (113)
	GluR2, GluR2/3		Rat	Peng et al. (113)
		NR2D (RBC)	Rat	Wenzel et al. (118)
	GluR2 and/or GluR4	NR1 (RBC)	Rat	Hughes (112)
	GluR2 (RBC)		Rat	Hughes et al. (117)
Horizontal cells	GluR6/7		Goldfish	Peng et al. (113)
	GluR2/3		Cat	Pourcho et al. (114)
INL	GluR2/3, GluR6/7		Rat	Peng et al. (113)
		NR2A (inner)	Rat	Hartveit et al. (111)
	GluR1, 2, 5 > GluR4 (outer third), GluR1, 2, 5 (middle third), GluR1-5 (inner third)		Rat	Hughes et al. (117)
	GluR1-7		Rat, cat	Hamassaki-Britto et al. (116)
	KA2 (homogeneous), GluR6 (inner), GluR7 (inner two-thirds)	NR1 (homogeneous), NR2A-B (inner third, patchy), NR2C (inner two-thirds)	Rat	Brandstatter et al. (115)
IPL	GluR1, GluR2/3, GluR6/7		Rat	Peng et al. (113)
		NR2A	Rat, cat, rabbit, monkey	Harveit et al. (111)
Amacrine cells	GluR6	NR2A-C	Rat	Brandstatter et al. (115)
	GluR2/3		Cat	Pourcho et al. (114)
	GluR1, GluR2/3		Rat	Peng et al. (113)
Ganglion cells	GluR1		Rat	Peng et al. (113)
GCL	GluR2/3, GluR6/7		Rat	Peng et al. (113)
	GluR1-5		Rat	Hughes et al. (117)
	GluR1-7		Rat, cat	Hamassaki-Britto et al. (115)
	GluR6/7, KA2	NR1, NR2A-C	Rat	Brandstatter et al. (115)
Muller cells	GluR4		Rat	Peng et al. (113)

Retinal Neurons Expressing Metabotropic Glutamate Receptors

All metabotropic glutamate receptors, except mGluR3, have been identified in retina either through antibody staining (113, 114, 119, 120) or *in situ* hybridization (61, 64, 79). MGluRs are differentially expressed throughout the retina, specifically in the outer plexiform layer, inner nuclear layer, inner plexiform layer, and the ganglion cell layer (Table 4). Although different patterns of mGluR expression have been observed in the retina, only the APB receptor on ON-bipolar cells has been physiologically examined.

Table 4. Metabotropic glutamate receptor expression in retinal neurons and retinal layers, immunocytochemistry, and in situ hybridization.

Retinal cell type or layer	Group I	Group II	Group III	Species	Reference
OPL	mGluR1alpha, mGluR5a (RBC dendrites)			Rat	Koulen et al. (120)
			mGluR6 (RBC dendrites)	Rat	Nomura et al. (80)
INL	mGluR8			Mouse	Duvoisin et al. (61)
			mGluR6	Rat	Nakajima et al. (64)
	mGluR5 (BC, HC), mGluR1 (AC)	mGluR2 (AC)	mGluR6 (RBC), mGluR7 (BC), mGluR4, 7 (AC)	Rat	Hartveit et al. (79)
IPL	mGluR1alpha			Rat	Peng et al. (113)
			mGluR7 (CBC terminals; AC dendrites; few GC dendrites)	Rat	Brandstatter et al. (115)
	mGluR1alpha, mGluR5a (AC dendrites)			Rat	Koulen et al. (120)
Amacrine cells	mGluR1alpha			Rat	Peng et al. (113)
	mGluR1alpha			Cat	Pourcho et al. (114)
Ganglion cells	mGluR1alpha			Rat	Peng et al. (113)
GCL			mGluR8	Mouse	Duvoisin et al. (61)
	mGluR1alpha	mGluR2/3		Cat	Pourcho et al. (114)
	mGluR1	mGluR2	mGluR4, 7	Rat	Hartveit et al. (79)

Retinal Neurons Expressing Glutamate Transporters

The glutamate transporters GLAST, EAAC1, and GLT-1have been identified in retina (Table 5). GLAST (L-**gl**utamate/L-**as**partate **t**ransporter) immunoreactivity is found in all retinal layers (121) but not in neuronal tissue. GLAST is localized to Muller cell membranes (121-124). In contrast, EAAC-1 (**e**xcitatory **a**mino **a**cid **c**arrier-1) antibodies do not label Muller cells or photoreceptors. EAAC-1 immunoreactivity is observed in ganglion and amacrine cells in chicken, rat, goldfish, and turtle retinas. In addition, bipolar cells positively labeled with EAAC-1 antibody in lower vertebrates, and immunopositive horizontal cells were observed in rat (90). GLT-1 (**gl**utamate **t**ransporter-1) proteins have been identified in monkey (125), rat (124), and rabbit (126) bipolar cells. In addition, a few amacrine cells were weakly labeled with the GLT-1 antibody in rat (124), as were photoreceptor terminals in rabbit (126).

Table 5. Glutamate transporters in retinal neurons and retinal layers, immunocytochemical localizations.

Retinal cell type	EAAC-1	GLAST	GLT-1	Species	Reference
Photoreceptors			+ (cone soma to pedicles)	Rabbit	Massey et al. (126)
OPL	++			Rat	Rauen et al. (124)
			++ (rod spherules > cone pedicles)	Rabbit	Massey et al. (126)
Horizontal cells	++			Rat	Schultz & Stell (90); Rauen et al (124).

Table 5 continued from previous page.

Retinal cell type	EAAC-1	GLAST	GLT-1	Species	Reference
Bipolar cells			++ (2 types of CBCs)	Rabbit	Massey et al. (126)
	++ (faint)		++	Rat	Rauen et al. (124)
	++			Turtle, salamander	Schultz & Stell (90)
			++ (DB2, flat midget bipolar cells)	Monkey	Grunert et al. (125)
IPL			++ (diffuse)	Rabbit	Massey et al. (126)
	++		++	Rat	Rauen et al. (124)
	++			Goldfish, salamander, turtle, chicken, rat	Schultz & Stell (90)
Amacrine cells	++		++	Rat	Rauen et al. (124)
	++				Schultz & Stell (90)
Ganglion cells	++			Chicken, rat, goldfish, turtle	Schultz & Stell (90)
	++			Rat	Rauen et al. (124)
Muller cells		++		Rat	Rauen et al. (124); Lehre et al (123); Deroiche & Rauen (122)

Summary and Conclusions

Histological analyses of presynaptic neurons and physiological recordings from postsynaptic cells suggest that photoreceptor, bipolar, and ganglion cells release glutamate as their neurotransmitter. Multiple glutamate receptor types are present in the retina. These receptors are pharmacologically distinct and differentially distributed. IGluRs directly gate ion channels and mediate rapid synaptic transmission through either kainate/AMPA or NMDA receptors. Glutamate binding onto iGluRs opens cation channels, depolarizing the postsynaptic cell membrane. Neurons within the OFF-pathway (horizontal cells, OFF-bipolar cells, amacrine cells, and ganglion cells) express functional iGluRs. mGluRs are coupled to G-proteins. Glutamate binding onto mGluRs can have a variety of effects, depending on the second messenger cascade to which the receptor is coupled. The APB receptor, found on ON-bipolar cell dendrites, is coupled to the synthesis of cGMP. At these receptors, glutamate decreases cGMP formation, leading to the closure of ion channels. Glutamate transporters, found on glial and photoreceptor cells, are also present at glutamatergic synapses (Fig. 17). Transporters remove excess glutamate from the synaptic cleft to prevent neurotoxicity. Thus, postsynaptic responses to glutamate are determined by the distribution of receptors and transporters at glutamatergic synapses which, in retina, determine the conductance mechanisms underlying visual information processing within the ON- and OFF-pathways.

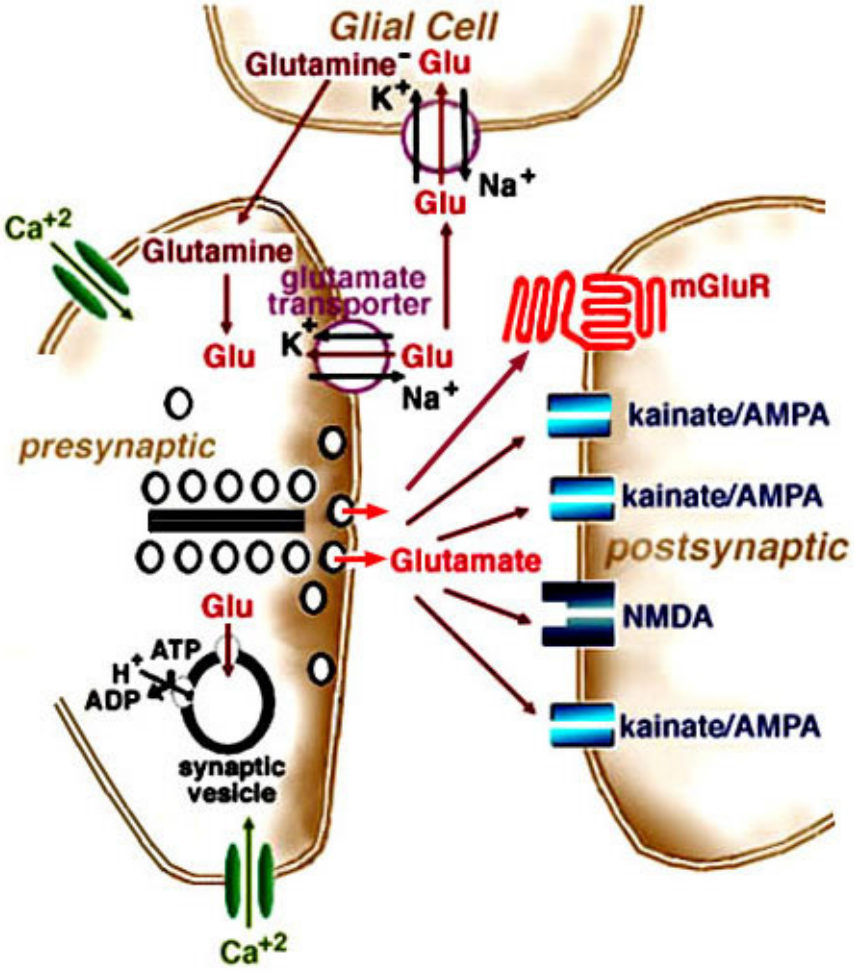

Figure 17. The ribbon glutamatergic synapse in the retina.

About the Author

Dr. Victoria Connaughton was born in Sellersville, Pennsylvania. She received her B.A. from Bucknell University in Biology in 1989 and her Ph.D. in Marine Studies from The University of Delaware in 1994. She is currently an Assistant Professor in the Biology Department at American University, Washington, DC. In her thesis work under Dr. Charles Epifano, she studied the visually guided feeding behavior of larval fish. Dr. Connaughton pursued postdoctoral studies with Dr. Greg Maguire at the University of Houston and Dr. Ralph Nelson at the National Institutes of Health. Dr. Connaughton's current research interests include electrophysiological examination of zebrafish mutants with visual system defects and the characterization of light responses in zebrafish retinal bipolar cells.

References

1. Massey SC. Cell types using glutamate as a neurotransmitter in the vertebrate retina. Prog Retinal Res. 1990;9:399–425.
2. Erulkar SD. Chemically mediated synaptic transmission: an overview. In: Siegel GJ, Agranoff BJ, Albers RW, Molinoff PB, editors. Basic neurochemistry, 5th ed. New York: Raven Press; 1994. p. 181-208.
3. Stryer L. Biochemistry. 3rd ed. New York: W.H. Freeman; 1988.
4. Fykse EM, Fonnum F. Amino acid neurotransmission: dynamics of vesicular uptake. Neurochem Res. 1996;21:1053–1060. PubMed PMID: 8897468.
5. Naito S, Ueda T. Adenosine triphosphate-dependent uptake of glutamate into protein I-associated synaptic vesicles. J Biol Chem. 1983;258:696–699. PubMed PMID: 6130088.
6. Tabb JS, Ueda T. Phylogenetic studies on the synaptic vesicle glutamate transporter. J Neurosci. 1991;11:1822–1828. PubMed PMID: 2045887.
7. Ehinger B, Ottersen OP, Storm-Mathisen J, Dowling JE. Bipolar cells in the turtle retina are strongly immunoreactive for glutamate. Proc Natl Acad Sci U S A. 1988;85:8321–8325. PubMed PMID: 2903503.

8. Jojich L, Pourcho RG. Glutamate immunoreactivity in the cat retina: a quantitative study. Vis Neurosci. 1996;13:117–133. PubMed PMID: 8730994.
9. Kalloniatis M, Fletcher EL. Immunocytochemical localization of the amino acid neurotransmitters in the chicken retina. J Comp Neurol. 1993;336:174–193. PubMed PMID: 7902364.
10. Marc RE, Liu W-LS, Kalloniatis M, Raiguel SF, Van Haesendonck E. Patterns of glutamate immunoreactivity in the goldfish retina. J Neurosci. 1990;10:4006–4034. PubMed PMID: 1980136.
11. Van Haesendonck E, Missotten L. Glutamate-like immunoreactivity in the retina of a marine teleost, the dragonet. Neurosci Lett. 1990;111:281–286. PubMed PMID: 2336203.
12. Yang C-Y, Yazulla S. Glutamate-, GABA-, and GAD-immunoreactivities co-localize in bipolar cells of tiger salamander retina. Vis Neurosci. 1994;11:1193–1203. PubMed PMID: 7841126.
13. Yang C-Y. Glutamate immunoreactivity in the tiger salamander retina differentiates between GABA-immunoreactive and glycine-immunoreactive amacrine cells. J Neurocytol. 1996;25:391–403. PubMed PMID: 8866240.
14. Yazulla S. GABAergic neurons in the retina. Prog Retinal Res. 1986;5:1–52.
15. Marc RE, Lam DMK. Uptake of aspartic and glutamic acid by photoreceptors in goldfish retina. Proc Natl Acad Sci U S A. 1981;78:7185–7189. PubMed PMID: 6118867.
16. Yang JH, Wu SM. Characterization of glutamate transporter function in the tiger salamander retina. Vision Res. 1997;37:827–838. PubMed PMID: 9156180.
17. Kanai Y, Smith CP, Hediger MA. A new family of neurotransmitter transporters: the high-affinity glutamate transporters. FASEB J. 1993;7:1450–1459. PubMed PMID: 7903261.
18. Pow DV, Crook DR. Direct immunocytochemical evidence for the transfer of glutamine from glial cells to neurons: use of specific antibodies directed against the D-stereoisomers of glutamate and glutamine. Neuroscience. 1996;70:295–302. PubMed PMID: 8848133.
19. Hertz L. Functional interactions between neurons and astrocytes. I. Turnover and metabolism of putative amino acid transmitters. Prog Neurobiol. 1979;13:277–323. PubMed PMID: 42117.
20. Schwartz EA, Tachibana M. Electrophysiology of glutamate and sodium co-transport in a glial cell of the salamander retina. J Physiol. 1990;426:43–80. PubMed PMID: 2231407.
21. Tachibana M, Kaneko A. L-Glutamate-induced depolarization in solitary photoreceptors: a process that may contribute to the interaction between photoreceptors in situ. Proc Natl Acad Sci U S A. 1988;85:5315–5319. PubMed PMID: 2899327.
22. Keinanen K, Wisden W, Sommer B, Werner P, Herb A, Versoorn TA, Sakmann B, Seeburg PH. A family of AMPA-selective glutamate receptors. Science. 1990;249:556–560. PubMed PMID: 2166337.
23. Monyer H, Sprengel R, Schoepfer R, Herb A, Higuchi M, Lomeli H, Burnashev N, Sakmann B, Seeburg PH. Heteromeric NMDA receptors: molecular and functional distinction of subtypes. Science. 1992;256:1217–1221. PubMed PMID: 1350383.
24. Verdoorn TA, Burnashev N, Monyer H, Seeburg PH, Sakmann B. Structural determinants of ion flow through recombinant glutamate receptor channels. Science. 1991;252:1715–1718. PubMed PMID: 1710829.
25. Nakanishi S. Molecular diversity of glutamate receptors and implications for brain function. Science. 1992;258:597–603. PubMed PMID: 1329206.
26. Ozawa S, Rossier J. Molecular basis for functional differences of AMPA-subtype glutamate receptors. News Physiol Soc. 1996;11:77–82.
27. Mayer ML, Westbrook GL. Permeation and block of N-methyl-D-aspartic acid receptor channels by divalent cations in mouse cultured central neurones. J Physiol. 1987;394:501–527. PubMed PMID: 2451020.
28. Boos R, Schneider H, Wassle H. Voltage- and transmitter-gated currents of AII amacrine cells in a slice preparation of the rat retina. J Neurosci. 1993;13:2874–2888. PubMed PMID: 7687279.
29. Cohen ED, Miller RF. The role of NMDA and non-NMDA excitatory amino acid receptors in the functional organization of primate retinal ganglion cells. Vis Neurosci. 1994;11:317–332. PubMed PMID: 8003456.

30. Gilbertson TA, Scobey R, Wilson M. Permeation of calcium ions through non-NMDA glutamate channels in retinal bipolar cells. Science. 1991;251:1613–1615. PubMed PMID: 1849316.
31. Yu W, Miller RF. NBQX, an improved non-NMDA antagonist studied in retinal ganglion cells. Brain Res. 1995;692:190–194. PubMed PMID: 8548303.
32. Zhou ZJ, Fain GL, Dowling JE. The excitatory and inhibitory amino acid receptors on horizontal cells isolated from the white perch retina. J Neurophysiol. 1993;70:8–19. PubMed PMID: 8103091.
33. Yamada KA, Tang C-M. Benzothiadiazides inhibit rapid glutamate receptor desensitization and enhance glutamatergic synaptic currents. J Neurosci. 1993;13:3904–3915. PubMed PMID: 8103555.
34. Kessler M, Arai A, Quan A, Lynch G. Effect of cyclothiazide on binding properties of AMPA-type glutamate receptors: lack of competition between cyclothiazide and GYKI 52466. Mol Pharmacol. 1996;49:123–131. PubMed PMID: 8569697.
35. Boulter J, Hollmann M, O'Shea-Greenfield A, Hartley M, Deneris E, Maron C, Heinemann S. Molecular cloning and functional expression of glutamate receptor subunit genes. Science. 1990;249:1033–1037. PubMed PMID: 2168579.
36. Nakanishi N, Schneider NA, Axel R. A family of glutamate receptor genes: evidence for the formation of heteromultimeric receptors with distinct channel properties. Neuron. 1990;5:569–581. PubMed PMID: 1699567.
37. Bettler B, Boulter J, Hermans-Borgmeyer I, O'Shea-Greenfield A, Deneris ES, Moll C, Borgmeyer U, Hollmann M, Heinemann S. Cloning of a novel glutamate receptor subunit, GluR5: expression in the nervous system during development. Neuron. 1990;5:583–595. PubMed PMID: 1977421.
38. Bettler B, Egebjerg J, Sharma G, Pecht G, Hermans-Borgmeyer I, Moll C, Stevens CF, Heinemann S. Cloning of a putative glutamate receptor: a low affinity kainate-binding subunit. Neuron. 1992;8:257–265. PubMed PMID: 1371217.
39. Egebjerg J, Bettler B, Hermans-Borgmeyer I, Heinemann S. Cloning of a cDNA for a glutamate receptor subunit activated by kainate but not AMPA. Nature. 1991;351:745–748. PubMed PMID: 1648177.
40. Hollmann M, O'Shea-Greenfield A, Rogers SW, Heinemann S. Cloning by functional expression of a member of the glutamate receptor family. Nature. 1989;342:643–648. PubMed PMID: 2480522.
41. Lodge D. Subtypes of glutamate receptors. Historical perspectives on their pharmacological differentiation. In: Monaghan DT, Weinhold RJ, editors. The ionotropic glutamate receptors. Totowa (NJ): Humana Press; 1997. p. 1-38.
42. Westbrook GL, Mayer ML. Micromolar concentrations of Zn^{2+} antagonize NMDA and GABA responses of hippocampal neurons. Nature. 1987;328:640–643. PubMed PMID: 3039375.
43. Ransom RW, Stec NL. Cooperative modulation of [3H}MK-801 binding to the N-methyl-D-aspartate receptor-ion channel complex by L-glutamate, glycine, and polyamines. J Neurochem. 1988;51:830–836. PubMed PMID: 2457653.
44. Williams K, Zappia AM, Pritchett DB, Shen YM, Molinoff PB. Sensitivity of the N-methyl-D-aspartate receptor to polyamines is controlled by NR2 subunits. Mol Pharmacol. 1994;45:803–809. PubMed PMID: 8190097.
45. Ikeda K, Nagasawa M, Mori H, Araki K, Sakimura K, Watanabe M, Inoue Y, Mishina M. Cloning and expression of the 4 subunit of the NMDA receptor channel. FEBS Lett. 1992;313:34–38. PubMed PMID: 1385220.
46. Ishii T, Moriyoshi K, Sugihara H, Sakurada K, Kadotani H, Yokoi M, Akazawa C, Shigemoto R, Mizuno N, Masu M, Nakanishi S. Molecular characterization of the family of N-methyl-D-aspartate receptor subunits. J Biol Chem. 1993;268:2836–2843. PubMed PMID: 8428958.
47. Kutsuwada T, Kashiwabuchi N, Mori H, Sakimura K, Kushiya E, Araki K, Meguro H, Masaki H, Kumanishi T, Arakawa M, Mishina M. Molecular diversity of the NMDA receptor channel. Nature. 1992;358:36–41. PubMed PMID: 1377365.
48. Meguro H, Mori H, Araki K, Kushiya E, Kutsuwada T, Yamazaki M, Kumanishi T, Arakawa M, Sakimura K, Mishina M. Functional characterization of a heteromeric NMDA receptor channel expressed from cloned cDNAs. Nature. 1992;357:70–74. PubMed PMID: 1374164.

49. Moriyoshi K, Masu M, Ishii T, Shigemoto R, Mizuno N, Nakanishi S. Molecular cloning and characterization of the rat NMDA receptor. Nature. 1991;354:31–37. PubMed PMID: 1834949.
50. Johnson JW, Ascher P. Glycine potentiates the NMDA response in cultured mouse brain neurons. Nature. 1987;325:529–531. PubMed PMID: 2433595.
51. Kleckner NW, Dingledine R. Requirement for glycine activation of NMDA-receptors expressed in Xenopus oocytes. Science. 1988;241:835–837. PubMed PMID: 2841759.
52. Nowak L, Bregestovski P, Ascher P, Herbet A, Prochiantz A. Magnesium gates glutamate-activated channels in mouse central neurones. Nature. 1984;307:462–465. PubMed PMID: 6320006.
53. Diamond JS, Copenhagen DR. The contribution of NMDA and non-NMDA receptors to the light-evoked input-output characteristics of retinal ganglion cells. Neuron. 1993;11:725–738. PubMed PMID: 8104431.
54. Dixon DB, Copenhagen DR. Two types of glutamate receptors differentially excite amacrine cells in the tiger salamander retina. J Physiol. 1992;449:589–606. PubMed PMID: 1355793.
55. Massey SC, Miller RF. Glutamate receptors of ganglion cells in the rabbit retina: evidence for glutamate as a bipolar cell transmitter. J Physiol. 1988;405:635–655. PubMed PMID: 2908248.
56. Massey SC, Miller RF. N-Methyl-D-aspartate receptors of ganglion cells in rabbit retina. J Neurophysiol. 1990;63:16–30. PubMed PMID: 2153770.
57. Mittman S, Taylor WR, Copenhagen DR. Concomitant activation of two types of glutamate receptor mediates excitation of salamander retinal ganglion cells. J Physiol. 1990;428:175–197. PubMed PMID: 2172521.
58. Hensley SH, Yang X-L, Wu SM. Identification of glutamate receptor subtypes mediating inputs to bipolar cells and ganglion cells in the tiger salamander retina. J Neurophysiol. 1993;69:2099–2107. PubMed PMID: 7688801.
59. Nestler EJ, Duman ES. G proteins and cyclic nucleotides in the nervous system. In: Siegel GJ, Agranoff BW, Albers RW, Molinoff PB, editors. Basic Neurochemistry. 5th ed. New York: Raven Press; 1994. p. 429-448.
60. Abe T, Sugihara H, Nawa H, Shigemoto R, Mizuno N, Nakanishi S. Molecular characterization of a novel metabotropic glutamate receptor mGluR5 coupled to inositol phosphate/Ca^{2+} signal transduction. J Biol Chem. 1992;267:13361–13368. PubMed PMID: 1320017.
61. Duvoisin RM, Zhang C, Ramonell K. A novel metabotropic glutamate receptor expressed in the retina and olfactory bulb. J Neurosci. 1995;15:3075–3083. PubMed PMID: 7722646.
62. Houamed KM, Kuijper JL, Gilbert TL, Haldeman BA, O'Hara PJ, Mulvihill ER, Almers W, Hagen FS. Cloning, expression, and gene structure of a G protein-coupled glutamate receptor from rat brain. Science. 1991;252:1318–1321. PubMed PMID: 1656524.
63. Masu M, Tanabe Y, Tsuchida K, Shigemoto R, Nakanishi S. Sequence and expression of a metabotropic glutamate receptor. Nature. 1991;349:760–765. PubMed PMID: 1847995.
64. Nakajima Y, Iwakabe H, Akazawa C, Nawa H, Shigemoto R, Mizuno N, Nakanishi S. Molecular characterization of a novel retinal metabotropic glutamate receptor mGluR6 with a high agonist selectively for L-2-amino-4-phosphobutyrate. J Biol Chem. 1993;268:11868–11873. PubMed PMID: 8389366.
65. Tanabe Y, Masu M, Ishii T, Shigemoto R, Nakanishi S. A family of metabotropic glutamate receptors. Neuron. 1992;8:169–179. PubMed PMID: 1309649.
66. Saugstad JA, Kinzie JM, Mulvihill ER, Segerson TP, Westbrook GL. Cloning and expression of a new member of the L-2-amino-4-phosphobutyric acid-sensitive class of metabotropic glutamate receptors. Mol Pharmacol. 1994;45:367–372. PubMed PMID: 8145723.
67. Nakanishi S. Metabotropic glutamate receptors: synaptic transmission, modulation, and plasticity. Neuron. 1994;13:1031–1037. PubMed PMID: 7946343.
68. Knopfel T, Kuhn R, Allgeier H. Metabotropic glutamate receptors: novel targets for drug development. J Med Chem. 1995;38:1417–1426. PubMed PMID: 7738999.
69. Pin JP, Bockaert J. Get receptive to metabotropic glutamate receptors. Curr Opin Neurobiol. 1995;5:342–349. PubMed PMID: 7580157.
70. Pin JP, Duvoisin R. Review: Neurotransmitter receptors. I. The metabotropic glutamate receptors: structure and functions. Neuropharmacology. 1995;34:1–26. PubMed PMID: 7623957.

71. Nawy S, Copenhagen DR. Multiple classes of glutamate receptor on depolarizing bipolar cells in retina. Nature. 1987;325:56–58. PubMed PMID: 3025746.
72. Nawy S, Copenhagen DR. Intracellular cesium separates two glutamate conductances in retinal bipolar cells of goldfish. Vision Res. 1990;30:967–972. PubMed PMID: 1975465.
73. Slaughter MM, Miller RF. 2-Amino-4-phosphobutyric acid: a new pharmacological tool for retina research. Science. 1981;211:182–184. PubMed PMID: 6255566.
74. Nawy S, Jahr CE. Suppression by glutamate of cGMP-activated conductance in retinal bipolar cells. Nature. 1990;346:269–271. PubMed PMID: 1695713.
75. Taylor WR, Wassle H. Receptive field properties of starburst cholinergic amacrine cells in the rabbit retina. Eur J Neurosci. 1995;7:2308–2321. PubMed PMID: 8563980.
76. Jin XT, Brunken WJ. A differential effect of APB on ON- and OFF-center ganglion cells in the dark adapted rabbit retina. Brain Res. 1996;708:191–196. PubMed PMID: 8720878.
77. Kittila CA, Massey SC. Effect of ON pathway blockade on directional selectively in the rabbit retina. J Neurophysiol. 1995;73:703–712. PubMed PMID: 7760129.
78. Massey SC, Redburn DA, Crawford MLJ. The effects of 2-amino-4-phosphobutyric acid (APB) on the ERG and ganglion cell discharge of rabbit retina. Vision Res. 1983;23:1607–1613. PubMed PMID: 6666062.
79. Hartveit E, Brandsttter JH, Enz R, Wassle H. Expression of the mRNA of seven metabotropic glutamate receptors (mGluR1 to 7) in the rat retina. An in situ hybridization study on tissue section and isolated cells. Eur J Neurosci. 1995;7:1472–1483. PubMed PMID: 7551173.
80. Nomura A, Shigemoto R, Nakamura Y, Okamoto N, Mizuno N, Nakanishi S. Developmentally regulated postsynaptic localization of a metabotropic glutamate receptor in rat bipolar cells. Cell. 1994;77:361–369. PubMed PMID: 8181056.
81. Masu M, Iwakabe H, Tagawa Y, Miyoshi T, Yamashita M, Fukuda Y, Sasaki H, Hiroi K, Nakamura Y, Shigemoto R, Takada M, Nakamura K, Makao K, Katsuki M, Nakanishi S. Specific deficit of the ON response in visual transmission by targeted disruption of the mGluR6 gene. Cell. 1995;80:757–765. PubMed PMID: 7889569.
82. Eliasof S, Werblin F. Characterization of the glutamate transporter in retinal cones of the tiger salamander. J Neurosci. 1993;13:402–411. PubMed PMID: 8093715.
83. Aizenman E, Frosch MP, Lipton SA. Responses mediated by excitatory amino acid receptors in solitary retinal ganglion cells from rat. J Physiol. 1988;396:75–91. PubMed PMID: 2842491.
84. Sasaki T, Kaneko A. L-Glutamate-induced responses in OFF-type bipolar cells of the cat retina. Vision Res. 1996;36:787–795. PubMed PMID: 8736215.
85. Arriza JL, Eliasof S, Kavanaugh MP, Amara SG. Excitatory amino acid transporter 5, a retinal glutamate transporter coupled to a chloride conductance. Proc Natl Acad Sci U S A. 1997;94:4155–4160. PubMed PMID: 9108121.
86. Fairman WA, Vandengerg RJ, Arriza JL, Kavanaugh MP, Amara SG. An excitatory amino-acid transporter with properties of a ligand-gated chloride channel. Nature. 1995;375:599–603. PubMed PMID: 7791878.
87. Kanai Y, Hediger MA. Primary structure and functional characterization of a high-affinity glutamate transporter. Nature. 1992;360:467–471. PubMed PMID: 1280334.
88. Kanai Y, Trotti D, Nussberger S, Hediger MA. 1997. The high-affinity glutamate transporter family, structure, function, and physiological relevance. In: Reith MEA, editor. Neurotransmitter transporters: structure, function, and regulation. Totowa (NJ): Humana Press; 1997. p. 171-213.
89. Pines G, Danbolt NC, Bjoras M, Zhang Y, Bendahan A, Eide L, Koepsell H, Storm-Mathisen J, Seeberg E, Kanner BI. Cloning and expression of a rat brain L-glutamate transporter. Nature. 1992;360:464–467. PubMed PMID: 1448170.
90. Schultz K, Stell WK. Immunocytochemical localization of the high-affinity glutamate transporter, EAAC1, in the retina of representative vertebrate species. Neurosci Lett. 1996;211:191–194. PubMed PMID: 8817573.
91. Brew H, Attwell D. Electrogenic glutamate uptake is a major current carrier in the membrane of axolotl retinal glial cells. Nature. 1987;327:707–709. PubMed PMID: 2885752.

92. Barbour B, Brew H, Attwell D. Electrogenic uptake of glutamate and aspartate into glial cells isolated from the salamander (Ambystoma) retina. J Physiol. 1991;436:169–193. PubMed PMID: 1676418.
93. Barbour B, Brew H, Attwell D. Electrogenic glutamate uptake in glial cells is activated by intracellular potassium. Nature. 1988;335:433–435. PubMed PMID: 2901670.
94. Bouvier M, Szatkowski M, Amato A, Attwell D. The glial cell glutamate uptake carrier countertransports pH-changing ions. Nature. 1992;360:471–474. PubMed PMID: 1448171.
95. Eliasof S, Jahr CE. Retinal glial cell glutamate transporter is coupled to an anionic conductance. Proc Natl Acad Sci U S A. 1996;93:4153–4158. PubMed PMID: 8633032.
96. Grant GB, Werblin FS. A glutamate-elicited chloride current with transporter-like properties in rod photoreceptors of the tiger salamander. Vis Neurosci. 1996;13:135–144. PubMed PMID: 8730995.
97. Picaud S, Larsson HP, Wellis DP, Lecar H, Werblin F. Cone photoreceptors respond to their own glutamate release in the tiger salamander. Proc Natl Acad Sci U S A. 1995a;92:9417–9421. PubMed PMID: 7568144.
98. Picaud SA, Larsson HP, Grant GB, Lecar H, Werblin FS. Glutamate-gated chloride channel with glutamate-transporter-like properties in cone photoreceptors of the tiger salamander. J Neurophysiol. 1995b;74:1760–1771. PubMed PMID: 8989410.
99. Grant GB, Dowling JE. A glutamate-activated chloride current in cone-driven ON bipolar cells of the white perch retina. J Neurosci. 1995;15:3852–3862. PubMed PMID: 7538566.
100. Grant GB, Dowling JE. ON bipolar cell responses in the teleost retina are generated by two distinct mechanisms. J Neurophysiol. 1996;76:3842–3849. PubMed PMID: 8985882.
101. Euler T, Schneider H, Wassle H. Glutamate responses of bipolar cells in a slice preparation of the rat retina. J Neurosci. 1996;16:2934–2944. PubMed PMID: 8622124.
102. Hartveit E. Functional organization of cone bipolar cells in the rat retina. J Neurophysiol. 1997;77:1716–1730. PubMed PMID: 9114231.
103. Krizaj D, Akopian A, Witkovsky P. The effects of L-glutamate, AMPA, quisqualate, and kainate on retinal horizontal cells depend on adaptational state: implications for rod-cone interactions. J Neurosci. 1994;14:5661–5671. PubMed PMID: 7521912.
104. Yang X-L, Wu SM. Coexistence and function of glutamate receptor subtypes in the horizontal cells of the tiger salamander retina. Vis Neurosci. 1991;7:377–382. PubMed PMID: 1661137.
105. Eliasof S, Jahr CE. Rapid AMPA receptor desensitization in catfish cone horizontal cells. Vis Neurosci. 1997;14:13–18. PubMed PMID: 9057264.
106. O'Dell TJ, Christensen BN. Horizontal cells isolated from catfish retina contain two types of excitatory amino acid receptors. J Neurophysiol. 1989;61:1097–1109. PubMed PMID: 2473174.
107. Furukawa T, Yamada KM, Petruv R, Djamgoz MBA, Yasui S. Nitric oxide, 2-amino-4-phosphobutyric acid and light/dark adaptation modulate short-wavelength-sensitive synaptic transmission to retinal horizontal cells. Neurosci Res. 1997;27:65–74. PubMed PMID: 9089700.
108. Nawy SE, Sie A, Copenhagen DR. The glutamate analog 2-amino-4-phosphonobutyrate antagonizes synaptic transmission from cones to horizontal cells in the goldfish retina. Proc Natl Acad Sci U S A. 1989;86:1726–1730. PubMed PMID: 2537984.
109. Takahashi K, Copenhagen DR. APB suppresses synaptic input to retinal horizontal cells in fish: a direct action on horizontal cells modulated by intracellular pH. J Neurophysiol. 1992;67:1633–1642. PubMed PMID: 1352805.
110. Hartveit E, Veruki ML. AII amacrine cells express functional NMDA receptors. Neuroreport. 1997;8:1219–1223. PubMed PMID: 9175117.
111. Hartveit E, Brandstatter JH, Sasso-Pognetto M, Laurie DJ, Seeburgh PH, Wassle H. Localization and developmental expression of the NMDA receptor subunit NR2A in the mammalian retina. J Comp Neurol. 1994;348:570–582. PubMed PMID: 7836563.
112. Hughes TE. Are there ionotropic glutamate receptors on the rod bipolar cell of the mouse retina? Vis Neurosci. 1997;14:103–109. PubMed PMID: 9057273.
113. Peng YW, Blackstone CD, Huganir RL, Yau KW. Distribution of glutamate receptor subtypes in the vertebrate retina. Neuroscience. 1995;66:483–497. PubMed PMID: 7477889.

114. Pourcho RG, Cai W, Qin P. Glutamate receptor subunits in cat retina: light and electron microscopic observations. Invest Ophthal Vis Sci. 1997;38:S46.
115. Brandstatter JH, Hartveit E, Sasso-Pognetto M, Wassle H. Expression of NMDA and high-affinity kainate receptor subunit mRNAs in the adult rat retina. Eur J Neurosci. 1994;6:1100–1112. PubMed PMID: 7952290.
116. Hamassaki-Britto DE, Hermans-Borgmeyer I, Heinemann S, Hughes TE. Expression of glutamate receptor genes in the mammalian retina: the localization of GluR1 through GluR7 mRNAs. J Neurosci. 1993;13:1888–1898. PubMed PMID: 8478682.
117. Hughes TE, Hermans-Borgmeyer I, Heinemann S. Differential expression of glutamate receptor genes (GluR1-5) in the rat retina. Vis Neurosci. 1992;8:49–55. PubMed PMID: 1310870.
118. Wenzel A, Benke D, Mohler H, Fritschy J-M. N-Methyl-D-aspartate receptors containing the NR2D subunit in the retina are selectively expressed in rod bipolar cells. Neuroscience. 1997;78:1105–1112. PubMed PMID: 9174077.
119. Brandstatter JH, Koulen P, Kuhn R, van der Putten H, Wassle H. Compartmental localization of a metabotropic glutamate receptor (mGluR7): two different active sites at a retinal synapse. J Neurosci. 1996;16:4749–4756. PubMed PMID: 8764662.
120. Koulen P, Kuhn R, Wassle H, Brandstatter JH. Group I metabotropic glutamate receptors mGluR1 and mGluR5a: localization in both synaptic layers of the rat retina. J Neurosci. 1997;17:2200–2211. PubMed PMID: 9045744.
121. Otori Y, Shimada S, Tanaka T, Ishimoto I, Tana Y, Tohyama M. Marked increase in glutamate-aspartate transporter (GLAST/GluT-1) mRNA following transient retinal ischemia. Brain Res Mol Brain Res. 1994;27:310–314. PubMed PMID: 7898315.
122. Derouiche A, Rauen T. Coincidence of L-glutamate/L-aspartate transporter (GLAST) and glutamine synthetase (GS) immunoreactions in retinal glia: evidence for coupling of GLAST and GS in transmitter clearance. J Neurosci Res. 1995;42:131–143. PubMed PMID: 8531222.
123. Lehre KP, Davanger S, Danbolt NC. Localization of the glutamate transporter protein GLAST in rat retina. Brain Res. 1997;744:129–137. PubMed PMID: 9030421.
124. Rauen T, Rothstein JF, Wassle H. Differential expression of three glutamate transporter subtypes in the rat retina. Cell Tissue Res. 1996;286:325–336. PubMed PMID: 8929335.
125. Grunert U, Martin PR, Wassle H. Immunocytochemical analysis of bipolar cells in the macaque monkey retina. J Comp Neurol. 1994;348:607–627. PubMed PMID: 7530731.
126. Massey SC, Koomen JM, Liu S, Lehre KP, Danbolt NC. Distribution of the glutamate transporter GLT-1 in the rabbit retina. Invest Ophthal Vis Sci. 1997;38:S689.
127. Kandel ER, Schwartz JH, Jessell TM. Principles of neuroscience. 3rd ed. New York: Elsevier Publishing Co; 1991.
128. Slaughter MM, Miller RF. The role of excitatory amino acid transmitters in the mudpuppy retina: an analysis with kainic acid and N-methyl aspartate. J Neurosci. 1983;3:1701–1711. PubMed PMID: 6135763.
129. Hirano AA, MacLeish PR. Glutamate and 2-amino-4-phosphobutyric acid evoke an increase in potassium conductance in retinal bipolar cells. Proc Natl Acad Sci U S A. 1991;88:805–809. PubMed PMID: 1671534.
130. de la Villa P, Kurahashi T, Kaneko A. L-Glutamate-induced responses and cGMP-activated channels in three subtypes of retinal bipolar cells dissociated from the cat. J Neurosci. 1995;15:3571–3582. PubMed PMID: 7538564.

Bipolar Cell Pathways in the Vertebrate Retina

Ralph Nelson, PhD[1] and Victoria Connaughton, PhD[2]

Created: May 24, 2007; Updated: January 20, 2012.

1. Introduction

Retinal ganglion cells are typically only two synapses distant from retinal photoreceptors, yet ganglion cell responses are far more diverse than those of photoreceptors. The most direct pathway from photoreceptors to ganglion cells is through retinal bipolar cells. Thus, it is of great interest to understand how bipolar cells transform visual signals.

Light response physiology

Werblin and Dowling (1) were among the first to investigate light-evoked responses of retinal bipolar cells. Based on these studies using penetrating microelectrodes, they proposed that retinal bipolar cells lacked impulse activity, and that they processed visual signals through integration of analogue signals, that is synaptic currents and non-spike-generating voltage-gated membrane currents. They also proposed that retinal bipolar cells come in two fundamental varieties: ON-center and OFF-center (Fig. 1). Both types displayed a surround region in their receptive field that opposed the center, similar to the classic, antagonistic center-surround organization earlier described for ganglion-cell receptive fields (2). Ganglion cell receptive field organization is further reviewed in the Webvision chapter on ganglion cells. ON-center bipolar cells are depolarized by small spot stimuli positioned in the receptive field center. OFF-center bipolar cells are hyperpolarized by the same stimuli. Both types are repolarized by light stimulation of the peripheral receptive field outside the center (Fig. 1). Bipolar cells with ON-OFF responses were not encountered (1). ON-OFF responses, excitation at both stimulus onset and offset, first occur among amacrine cells, neurons postsynaptic to bipolar cells.

The Werblin and Dowling characterization of bipolar-cell physiology has proved quite durable over many decades. The notion that bipolar cells do not spike has found exception for some bipolar types. Dark-adapted Mb1 (rod bipolar cells) of goldfish generate light-evoked calcium spikes. These spikes originate in bipolar-cell axon terminals (3, 4). Through genetic imaging techniques this finding has been extended to the axon terminals of many zebrafish bipolar-cell types. In these studies bipolar terminals were labeled transgenically with the Ca^{2+} reporter protein SyGCaMP2 and light-induced fluctuations in Ca^{2+} were followed by 2-photon photometry. Fully 65% of the terminals delivered a spiking Ca^{2+} signal (4). In the cb5b bipolar-cell type of ground squirrel retina Na^{+} action potentials are driven by light. Other bipolar types in this retina do not exhibit spiking (5). These results suggest that bipolar cells are responsible for significantly more of the encoding of visual signals than had been previously supposed, and that axon-terminal spiking is actively involved. Impulse generation in bipolar cells is further discussed in the section on *Voltage-gated currents*.

Morphology and connectivity

Anatomical investigations of bipolar cells reveal a multiplicity (4-22 depending on species) of different morphological types (6-12), significantly more than the just two types that early physiology implied. The diversity of human retinal bipolar types is illustrated in Fig. 2. Nonetheless all of these are either ON- or OFF-types and their diversity results from other factors, such as differing connectivity with photoreceptors and differing postsynaptic targets, as evidenced in the diversity of dendritic and axon-terminal ramification patterns. Some bipolar cells are postsynaptic only to rods, others only to cones (Fig. 2), and still others receive mixed rod-

Author Affiliations: 1 National Institute of Neurological Disorders and Stroke, NIH, Rockville, MD; Email: nelsonr@ninds.nih.gov. 2 Department of Biology, American University, Washington, DC; Email: vconn@american.edu.

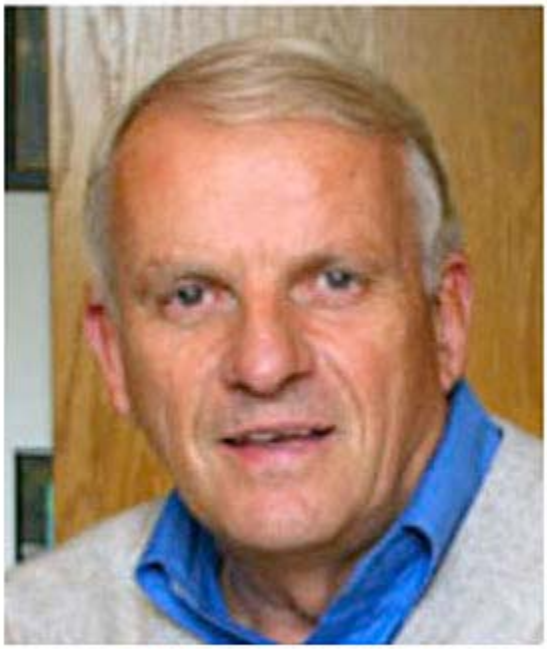

John E. Dowling

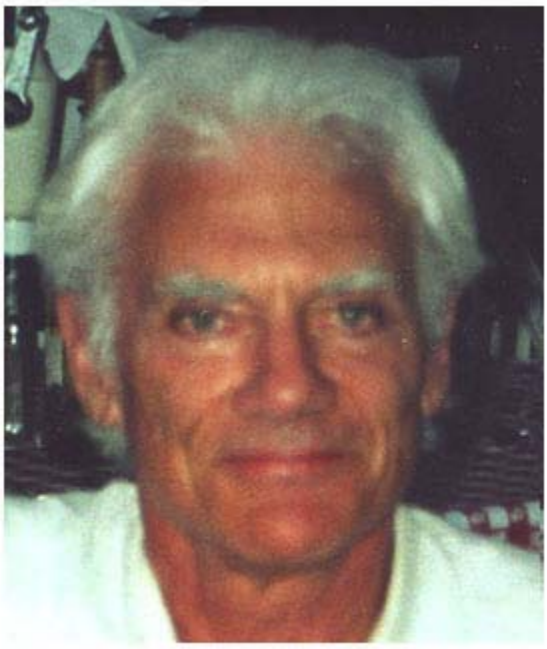

Frank Werblin

Frank Werblin and John Dowling discovered the 'ON or OFF' light-evoked physiology of retinal bipolar cells (1). They characterized these neurons as processors of analogue visual signals that did not use impulse generation. The work was done at Johns Hopkins University as a part of Frank Werblin's doctoral dissertation under the John Dowling's mentorship.

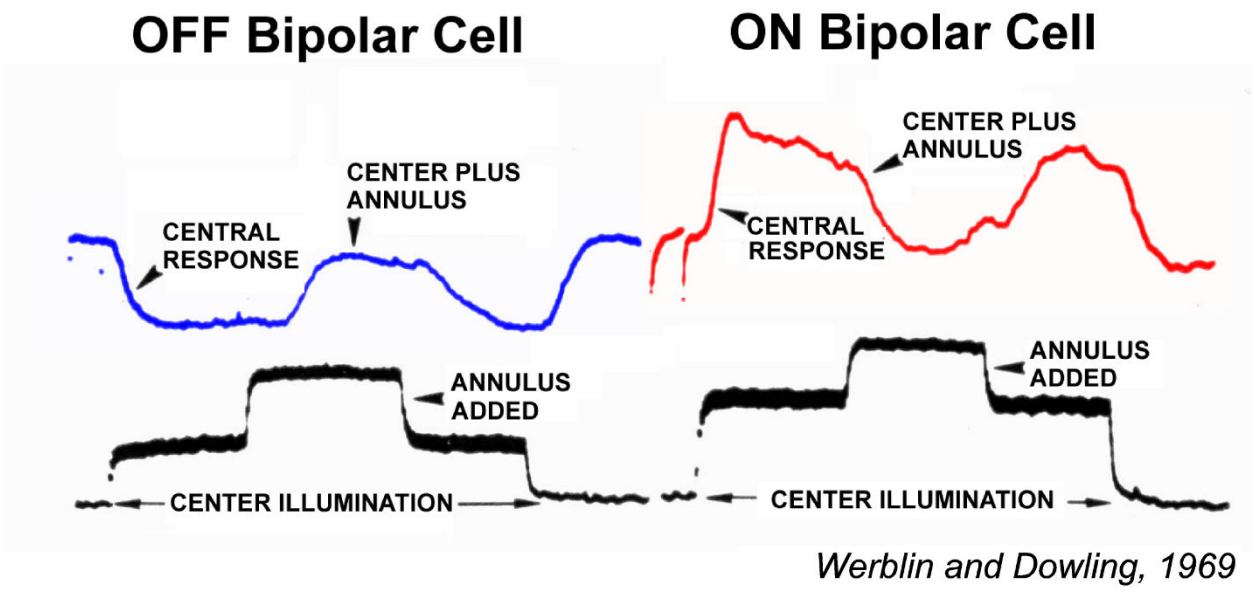

Figure 1. Retinal bipolar cells initiate ON and OFF pathways. Microelectrode recordings of voltage responses from mudpuppy retinal neurons reveal two sorts of retinal bipolar cells: those hyperpolarized by central illumination (OFF Bipolar Cell) and those depolarized by central illumination (ON Bipolar Cell). In each case membrane potential is restored by concomitant illumination of annular rings surrounding the center. Such responses are typically 10 mV in amplitude and lack impulse activity. The absolute response latency to the light step above is about 100 msec for these suprathreshold stimuli. The illustration is taken from Werblin and Dowling, 1969 (1).

cone input. Among cone-selective bipolar cells, some innervate only red, green, or blue cones, while others are 'diffuse', that is, not selective (13-19). Different bipolar types express different glutamate receptors at subsynaptic contacts with cones.

Bipolar cell axon terminals are either mono- or multistratified, depending on the location of axonal boutons and branches in the inner plexiform layer (IPL). Differing terminal position and branching morphology within the IPL suggests that different morphological types selectively innervate different types of amacrine and ganglion cell (Fig 2). In primate retinas, bipolar cells are described as diffuse or midget types, based on the extent of the dendritic arbor. Midgets contact only a single cone, while diffuse types contact multiple cones. Bipolar cells are also termed 'flat' or 'invaginating' (20) depending on the placement of dendritic tips, either on the surface of (flat), or penetrating within photoreceptor synaptic terminals to approach presynaptic ribbons (invaginating). Fig. 2 illustrates 11 morphological types of bipolar cell seen in Golgi-stained human retinas.

2. Different glutamate receptor types for ON and OFF bipolar cells

Light responses in bipolar cells are initiated by synapses with photoreceptors. Photoreceptors release only one neurotransmitter, glutamate (21); yet bipolar cells react to this stimulus with two different responses, ON-center (glutamate hyperpolarization) and OFF-center (glutamate depolarization). Different postsynaptic glutamate receptor proteins mediate these different membrane polarizing mechanisms. The different glutamate-gated responses are associated with the differential expression of either ionotropic (iGluR) glutamate receptors (OFF bipolar cells), metabotropic (mGluR) glutamate receptor types (ON bipolar cells) or glutamate transporters (ON bipolar cells). As a result, signal transduction at the photoreceptor-to-bipolar synapse has a range of properties. The process of splitting images into multiple components tuned to selective visual features begins with differentiation of different photoreceptor types but is then greatly elaborated at the synapses between photoreceptors and bipolar cells.

Metabotropic responses of ON bipolar cells: mGluR6, G_o, TRPM1, Nyctalopin

The conductance of ON bipolar cells increases in the light, whereas OFF bipolar cell conductance decreases (22, 23). The decrease in OFF bipolar cell conductance is easily explained as a loss of excitation by glutamate, as light inhibits glutamate release from photoreceptors (24). The positive reversal potential of the ON bipolar cell light response, coupled with a conductance increase (22, 25), implies that glutamate blocks a cation-permeable channel. Originally a puzzle, this was the first evidence of what we now understand as the action of metabotropic glutamate receptors (mGluRs). These receptors do not form ion channels themselves, but act as isolated antennae on the cell surface sensing glutamate and activating intracellular pathways, ultimately affecting membrane potential through mechanisms several steps removed from the binding site for glutamate. Metabotropic receptors have been identified on the axon terminals of both photoreceptors (26) and bipolar cells (27) where they serve as autoreceptors regulating glutamate release. However, the expression of one specific mGluR in the subsynaptic membrane of ON bipolar cell dendrites, the APB receptor, is unique to retina, where it is used in the direct signal transmission pathway from photoreceptors to ON bipolar cells.

The mGluR6 receptor

Slaughter and Miller (28) were the first to observe that the metabotropic glutamate agonist 2-amino-4-phosphonobutric acid (APB or DL-AP4, with the L enantiomer being effective) completely blocks the light responses of ON bipolar cells. In these neurons, APB acts as a substitute for photoreceptor-released glutamate (Fig. 3AB). Thus, ON bipolar cells utilize a metabotropic pathway to sense light-induced variations in release of photoreceptor glutamate. The metabotropic receptor has been identified as mGluR6 (29, 30). Transgenic

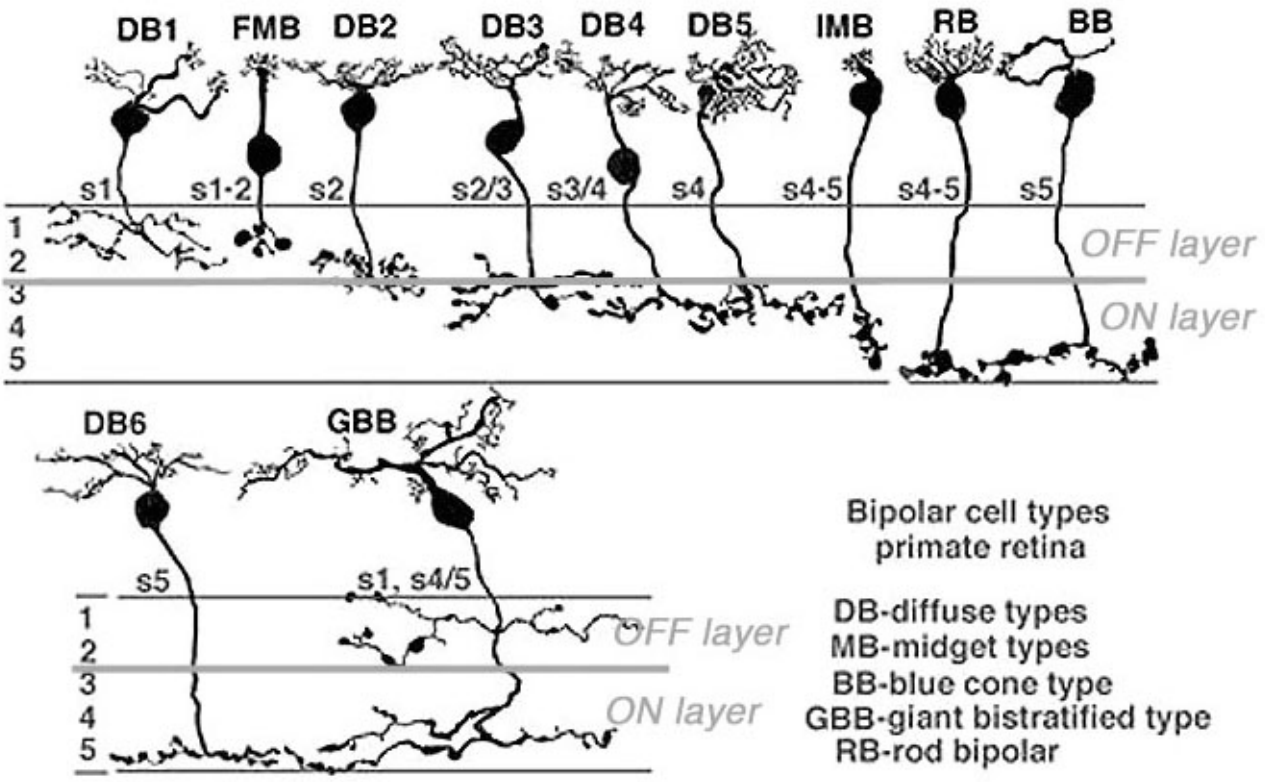

Figure 2. Dendritic and axonal stratification patterns of bipolar cell types in human retina. The illustration is courtesy of Helga Kolb.

knockout mice lacking the mGluR6 gene lack the electroretinographic b-wave (Fig. 4AB), an evoked-potential component associated with ON bipolar activity (31). The relation of electroretinogram components to cellular electrophysiology is further discussed in the Webvision chapter '*The Electroretinogram: ERG*'. Immunocytochemical localization for mGluR6 shows staining in the invaginating dendritic tips of monkey bipolar cells (Fig. 5) (32). Invaginating bipolar cells are thought to be mainly ON types in primate retina. Some foveal flat contacts also stained for mGluR6 (32).

The G-protein G_o

In addition to mGluR6, the G-protein G_o is cytoplasmically localized in the dendritic tips of ON bipolar cells (Fig. 6) (33). Removal of the alpha subunit ($G\alpha_o$) by knockout results in b-wave loss (34), similar to the mGluR6 knockout. G_o was originally localized in rod bipolar cells, known to be ON-type, in a screen of potential G-protein second messengers for the metabotropic light response (35). This suggests that G_o is directly involved in the intracellular pathway following mGluR6 activation.

The ion channel coupled to the APB receptor was originally thought to be cGMP-modulated (36).The closure of ion channels following APB binding onto mGluR6 seemed to require GTP and phosphodiesterase similar to phototransduction (36). However, the exact cascade by which this happened was less clear, as blocking phosphodiesterase (PDE) activity, or adding non-hydrolyzable cGMP analogs, did not inhibit the glutamate responses generated through APB-receptors (37). Further, it was G_o that suppressed glutamate-gated current in ON bipolar cells, not transducin, the G-protein of the phototransduction cascade (37). Thus, removal of cGMP appears not to be required for channel closure (37).

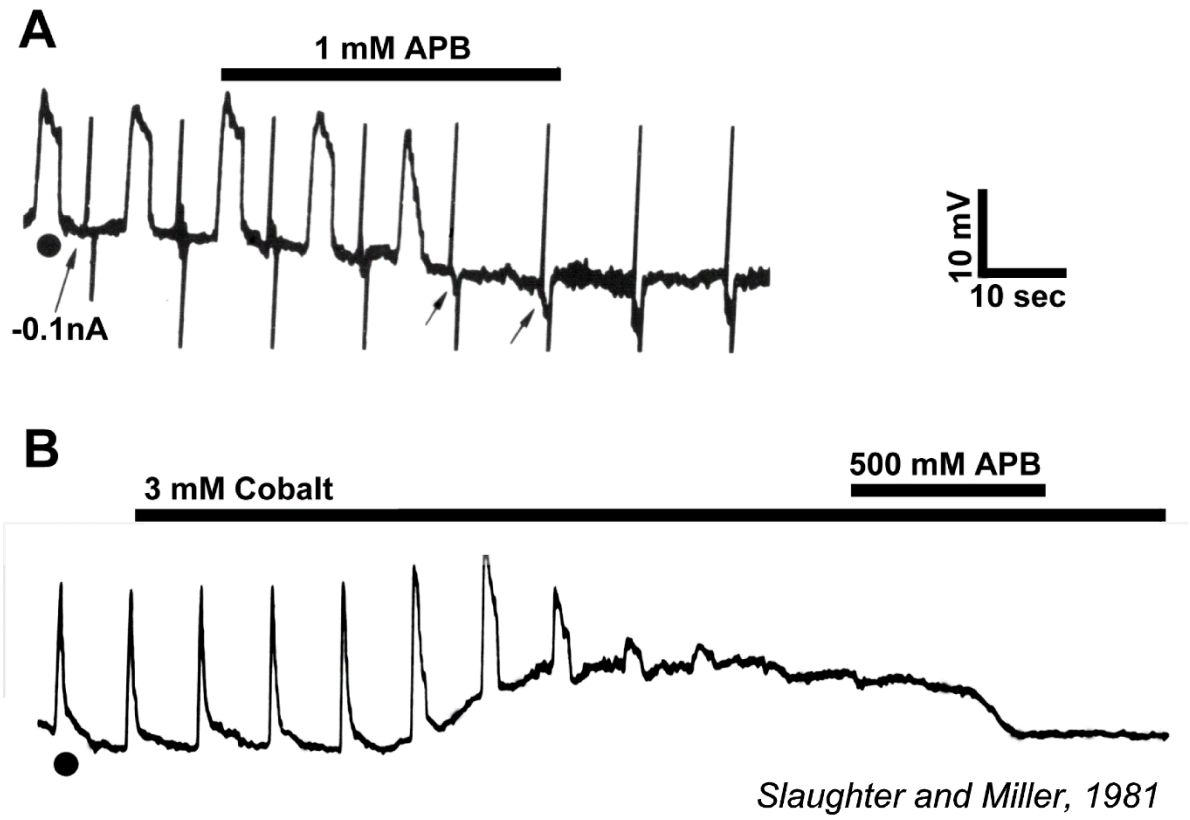

Figure 3. Metabotropic glutamate receptors in the ON pathway. The glutamate agonist 2-Amino-4-Phosphonobutric acid (APB, later termed DL-AP4) interferes with light responses and membrane physiology of ON-center bipolar cells in mudpuppy. *A*. APB abolishes light responses (the rectangular depolarizing events), hyperpolarizes the membrane potential, and increases the membrane resistance. The latter is measured by the amplitude of voltage responses to injected current pulses (arrow). *B*. 3 mM cobalt, a blocker for synaptic release of glutamate from photoreceptors, abolishes light responses in an ON bipolar cell and depolarizes the membrane potential. The membrane potential can be later restored by application of APB, which acts as a substitute for the missing photoreceptor glutamate. As APB is selective for a subset of metabotropic glutamate receptors, synaptic transmission of light responses to ON bipolar cells must rely on a metabotropic mechanism. The illustration is adapted from Slaughter and Miller, 1981 (28).

The TRPM1 channel

In agreement with these findings, recent work suggests the ON-bipolar-cell ion channel downstream of the mGluR6 receptor is not cGMP-gated (38). Rather, this non-selective cation channel – identified as a TRPM1-L channel – appears to be regulated by $G\alpha_o$ (38-40) in conjunction with $G\beta\gamma$ (41). The activity of the TRPM1 channel requires the presence of mGluR6, as the channel, though present, can not be activated in mGluR6 knockout mice (42).

TRP channels, or transient receptor potential channels, first identified in *Drosophila* photoreceptors (43), are present in all animal groups, including vertebrates (44), and as many as 28 channel subtypes have been identified. The TRP superfamily includes 7 subfamilies separated into two groups: TRPC, TRPV, TRPM, TRPN, and TRPA channels form Group 1; TRPP and TRPML channels form Group 2. TRPM1-L or melastatin, a melanoma related TRP channel, belongs to Group 1, and is found in ON bipolar cells. All channels share structural similarities and are permeable to cations; however, there is great functional diversity among the different channel subtypes. TRP channels are involved in many sensory systems including vision, hearing, taste, temperature-sensitivity, and osmoregulation, and are also involved in human disease (44-48).

In retina, TRP channels have been identified on photoreceptors (49), amacrine cells (50, 51), and ON-type bipolar cells. ON-bipolars (Fig. 7A), specifically, are antigenic for TRPM1 channels (52, 53) or TRPM1-L (38, 39,

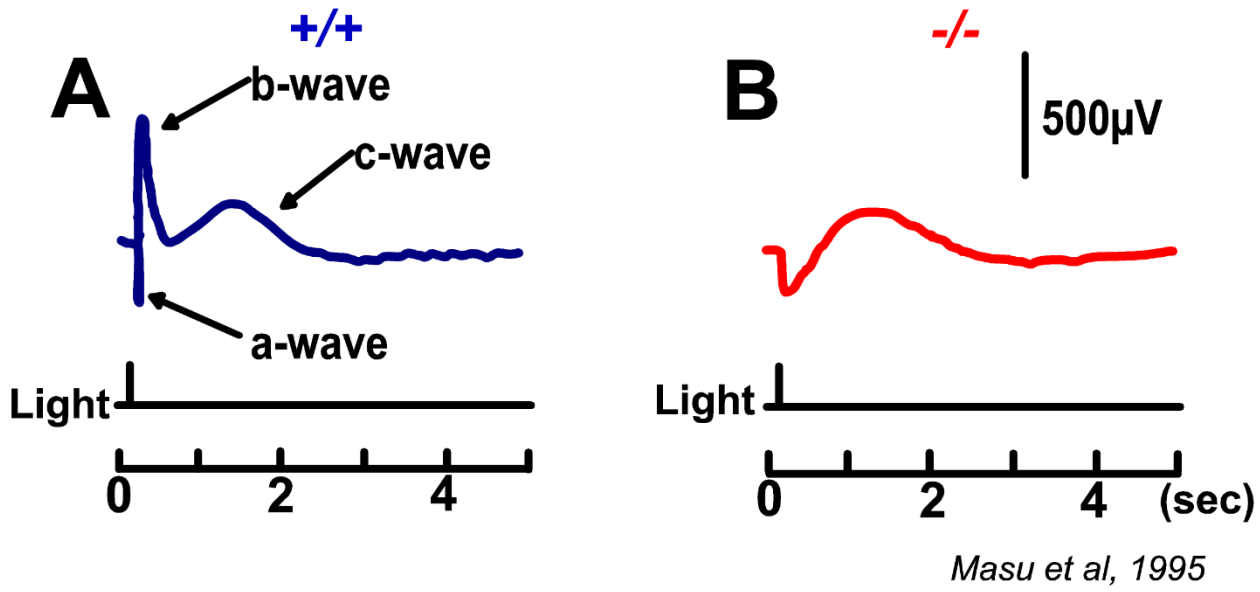

Figure 4. MGluR6 is the metabotropic glutamate receptor expressed by ON bipolar cells. Light evoked ERG responses from the eye of a wild type (*A*, +/+) and a mutant (*B*, -/-) mouse deficient in the gene encoding mGluR6. The b-wave, which originates from the light responses of ON bipolar cells is absent in the mutant mouse. The illustration is adapted from Masu et al, 1995 (31)..

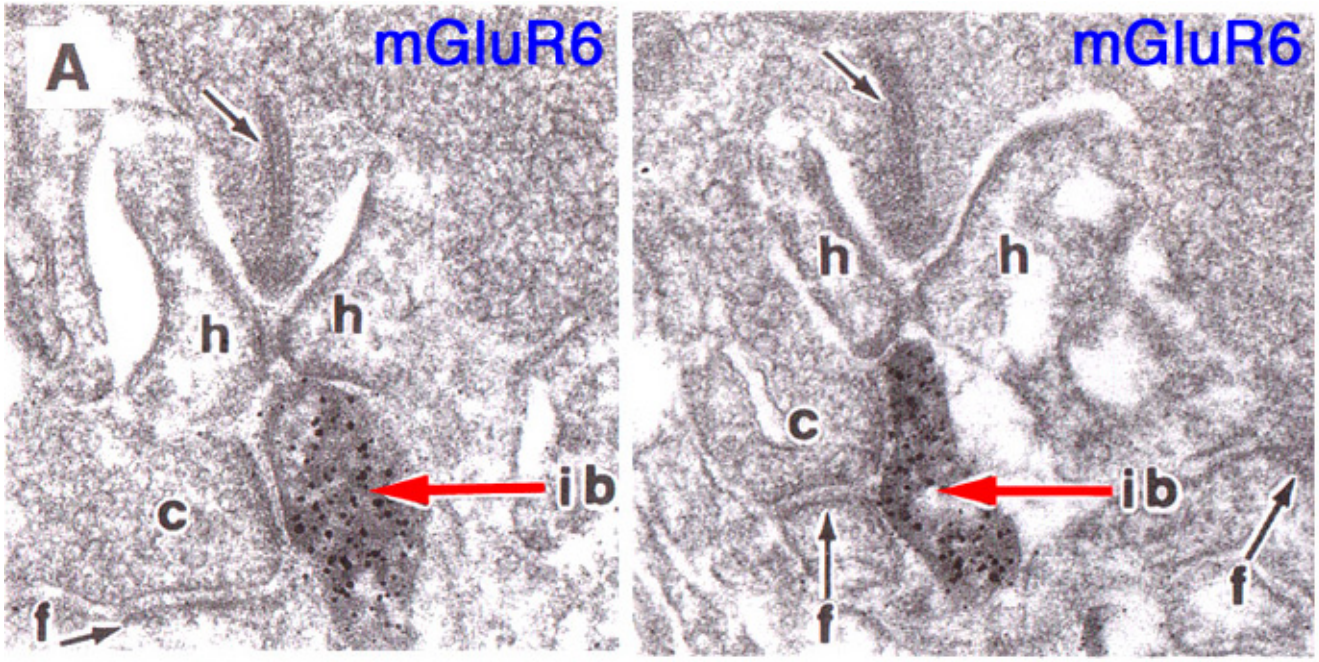

Figure 5. Immunostaining for the metabotropic glutamate receptor mGluR6 selectively labels dendritic tips of invaginating bipolar cells (ib) in monkey retina. The adjacent dendritic contacts from horizontal cells (h) and the flat contact (f) from a flat cone bipolar cell are not labeled, nor is the presynaptic cone pedicle (c).The illustration is from Vardi et al., 1998 (33).

54). Immunocytochemical and/or *in situ* hybridization studies have localized TRPM1 expression to the dendritic tips of ON-bipolar cells (38, 39, 52), though labeling is seen in cell bodies and axons as well (Fig. 7A). TRP channels are absent in OFF-type bipolar cells. TRPM1-L channel currents have a reversal potential ~0mV (38) similar to the reversal potential of glutamate-gated currents in these cells. TRPM1-L has been shown to co-localize with and/or be functionally coupled to mGluR6 (38, 40, 42, 52). In transfected CHO cells that express

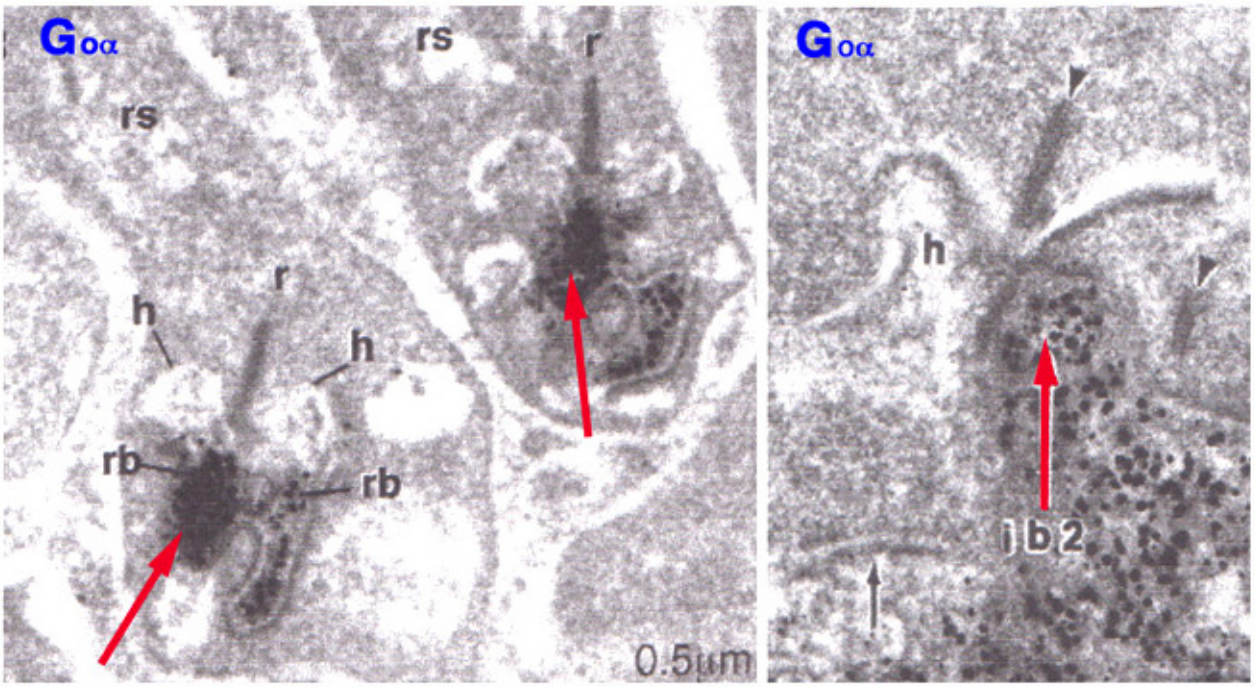

Figure 6. Immunostaining for $G\alpha_o$, the the alpha subunit of the G-protein G_o, localizes to the invaginating dendritic tips of a rod bipolar cell (left) and a cone bipolar cell (right) in cat retina. $G\alpha_o$ is required for light activation of ON bipolar cells. The illustration is from Vardi, 1998 (33).

mGluR6, $G\alpha_o$, and TRPM1-L, Koike and colleagues (38) showed that all three of these components must be present for glutamate-evoked whole-cell currents to be recorded. Cells expressing only mGluR6 and $G\alpha_o$, or only $G\alpha_o$ and TRPM1-L, did not respond to glutamate application (38, 39). These findings suggest TRPM1 channels are downstream of the mGluR6 receptor and are necessary for glutamate-elicited responses in these cells. Further, TRPM1 -/- knockout mice (Fig. 7B) do not have light-evoked ON-bipolar-cell responses and there is no ERG b-wave (38, 39, 55). The loss of response is similar to that reported for mGluR6 -/- mice (Fig. 4) (31, 56), again suggesting that both mGluR6 and TRPM1 channels are required for ON-bipolar-cell photic responses. While all cone bipolar cells in mouse appear to use an mGluR6 synapse with cones, there is evidence that some of these cells may modulate a cation channel in addition to TRPM1-L. In the TRPM1 -/- mouse, the mGluR6 antagonist CPPG still blocks a minor APB-induced membrane current (52).

The proteoglycan nyctalopin

Nyctalopin is another protein expressed on the dendritic tips of ON-bipolar cells (Fig. 8a). It is encoded by the *NYX* gene. *NYX* is required for light- and glutamate-elicited responses in ON bipolar cells (57). Mutant *nob* mice (58) lack an ERG b-wave and are not responsive to focal applications of glutamate onto the bipolar cell dendritic arbor (57). In wild type mice ON bipolar cells respond with outward currents to this treatment, but in *nob* mice they do not (Fig. 9). The *nob* strain is an *NYX* -/- mutant (59). Generation of transgenic *nob* mice selectively expressing EYFP-nyctalopin fusion protein in bipolar cells completely rescued the mutant phenotype. Cellular expression was restricted to bipolar cells using a regulatory sequence for GABAcρ1, a GABA receptor subunit selectively produced by bipolar cells. In the EYFP-*NYX* line, the fusion protein expression was localized to the tips of ON-bipolar cells (Fig. 8a), the b-wave was restored, and inner retinal function was similar to controls (57).

In zebrafish a membrane-targeted yellow fluorescent protein (MYFP) reporter strain has been generated using the upstream regulatory sequences for the *NYX* gene to express MYFP. This reporter marks a subset of ON-type bipolar cells with characteristic long axons and terminal boutons restricted to the inner half of the inner

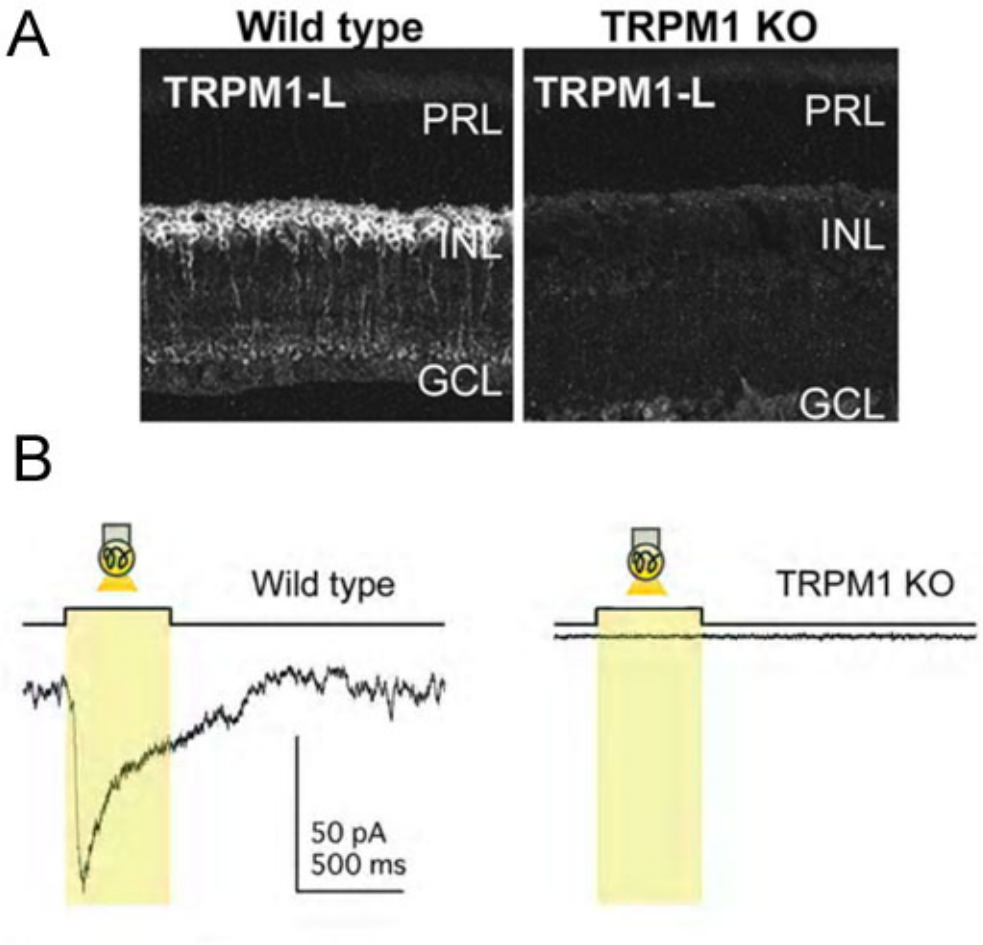

Figure 7. TRPM1 channel knockouts lack photoresponses in ON-bipolar cells. *A*. In a wild type mouse, antibody staining for TRPM1 reveals localization in bipolar cells. No antibody staining is evident in the knockout. *B*. ON-bipolar-cell patch recordings in wild type mice reveal inward currents in response to light stimulation. This is the normal response of an ON-type bipolar cell as these cells are excited by light. No inward currents occur in ON-bipolar-cell recordings from the knockout. The illustrations are from Koike et al, 2010 (38).

plexiform layer. Many of these also express the ON-bipolar marker protein kinase C (PKC) (60). This genetic reporter shows the complete morphology of the cells expressing the nyctalopin gene. This transgenic tool was used to follow embryonic refinement and development of axonal projection patterns for nyctalopin-expressing ON bipolars (60) (Fig. 8b).

Subsequent studies have reported that nyctalopin complexes with both mGluR6 and TRPM1 channels in ON-bipolar cells, serving a structural role that allows proper assembly and organization of the receptor and the channel (61). In addition, nyctalopin is able to modulate TRPM1 channels, as is mGluR6 (42, 62). Thus, glutamate binding onto mGluR6 activates a G-protein ($G\alpha_o$ and/or $G\beta\gamma$) leading to the closure of TRPM1 channels. The receptor and the channel are held in close proximity by nyctalopin. Alteration or mutation of any of these components - mGluR6, nyctalopin, TRPM1, and/or G_o – can lead to a loss of response by ON-bipolar cells. In agreement with this, individuals with congenital stationary night blindness (CSNB – discussed below) display a loss of ON-bipolar cell responses as evidenced in an absent ERG b-wave, and mutations in the genes encoding mGluR6, nyctalpin, and TRPM1 are associated with at least 75% of CSNB cases (62).

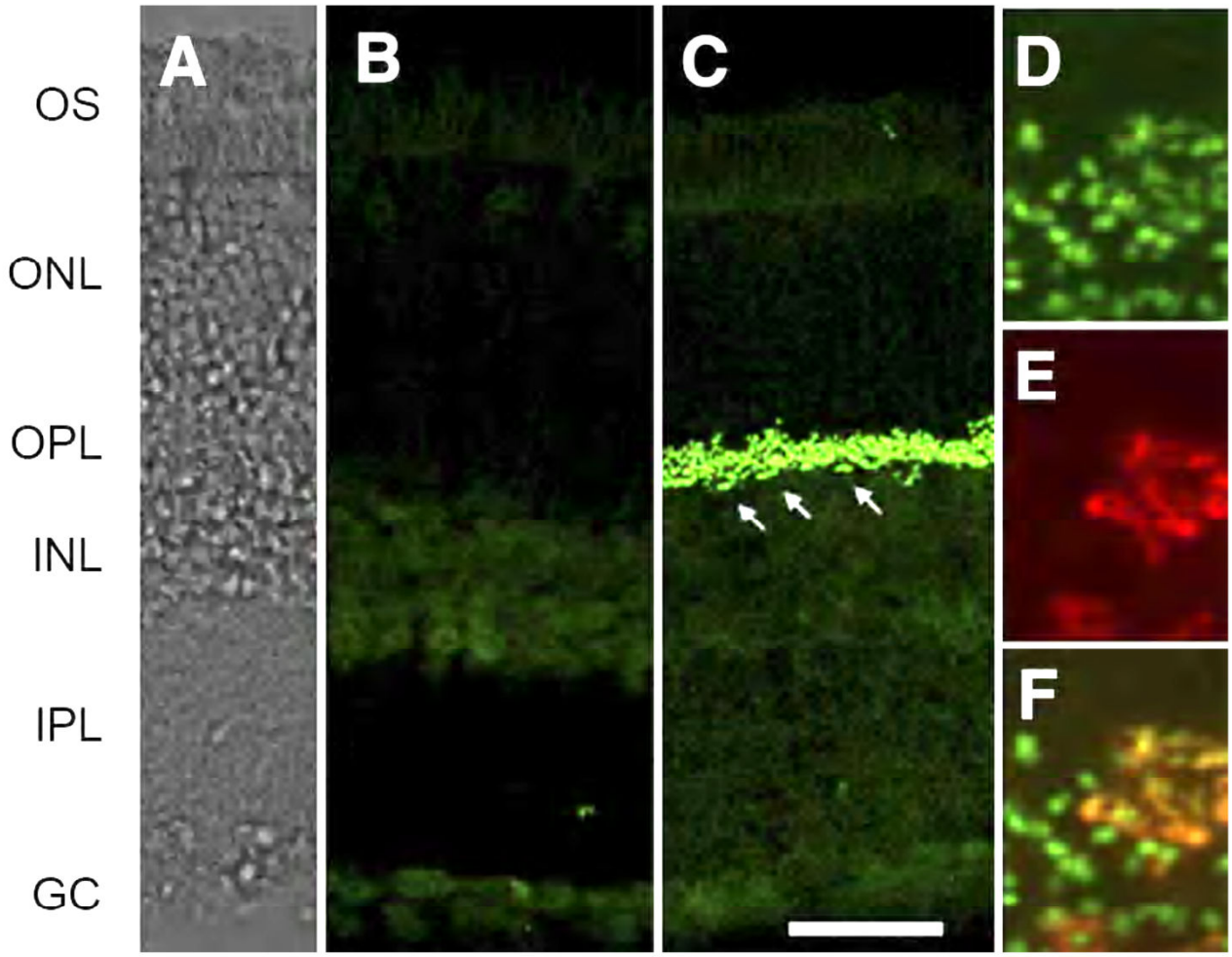

Figure 8a. The insertion of the fusion protein EYFP-nyctalopin into *nob NYX* -/- mice re-establishes nyctalpin expression. Expression can be localized with EYFP antibodies. *A*. DIC image of mouse retinal slice. OS, outer segments; ONL, outer nuclear layer; OPL, outer plexiform layer; INL, inner nuclear layer; IPL, inner plexiform layer; GC, ganglion cell layer. *B*. Wild type mouse is not labeled by anti-GFP. *C*. *EYFP-NYX* rescue mouse shows fusion protein localization in bipolar-cell dendritic tips within the OPL. *D*. High magnification of C. *E*. peanut agglutinin reaction labels cone terminals. *F*. Overlay of D and E shows *NYX* expression (nyctalpin) is localized in cone terminals (yellow). Green localization is presumed in rod terminals. Scale bar in *A*, *B* and *C* is 50 μm. The illustration is from Gregg et al, 2007 (57).

Modulators and subtypes

Calcium ions are a modulator of the ON bipolar metabotropic ion channel. Calcium ions, entering through the TRPM1 ion channel (63, 64) affect channel function, either by directly down regulating the channel (63) or by activating calcium-dependent enzymes, such as CaMKII (65-67), which modulate ion channel conductance. cGMP has been shown to selectively enhance ON bipolar cell responses to dim light, and may play a modulatory role for the TRPM1 channel (68).

Metabotropic receptors for ON-center bipolar cells have sustained and transient subtypes (69). The molecular basis is not yet known. However, it appears that the sustained and transient responses of ON-center ganglion cells, such as the classic X- and Y-types (70), may have their origin, at least in part, in the type of glutamate receptor expressed on the bipolar cells which innervate them (71).

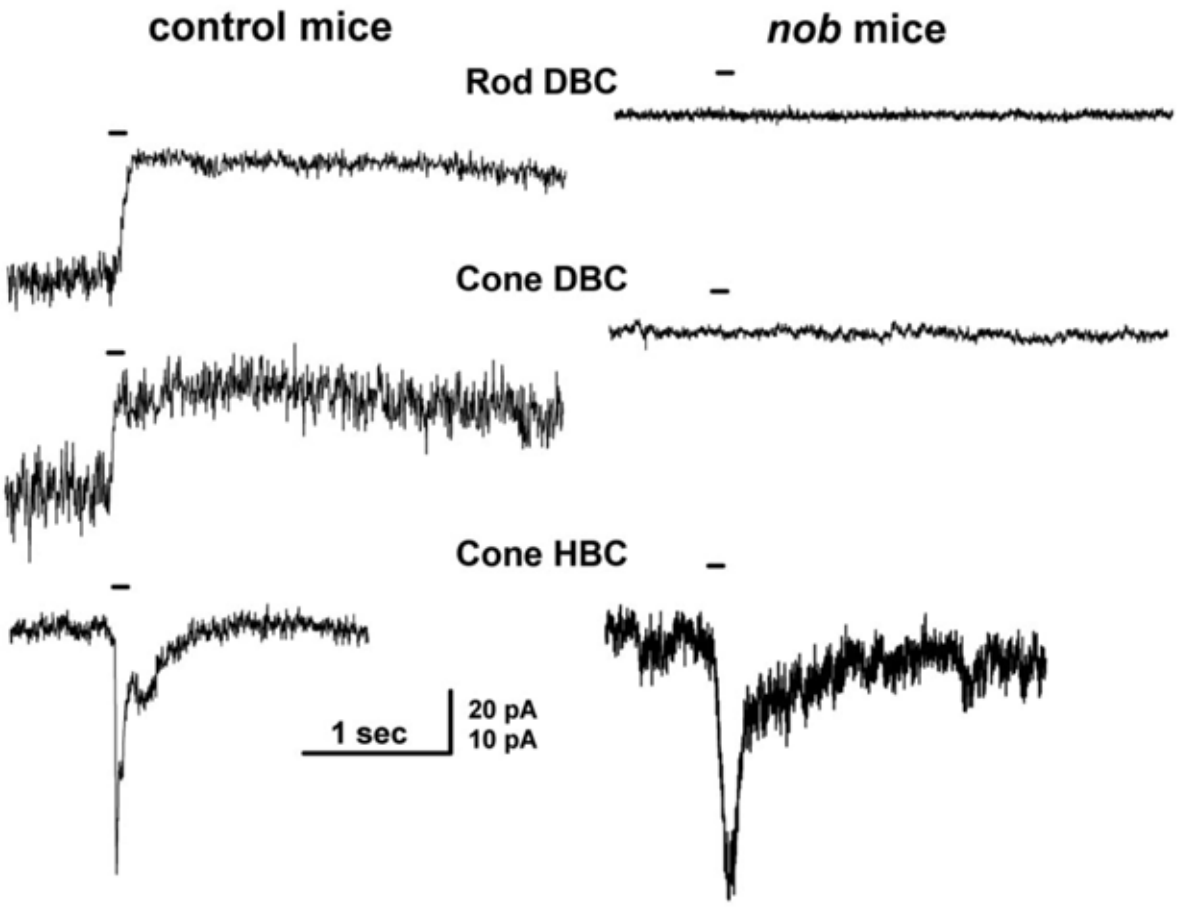

Figure 9. Bipolar-cell glutamate responses in the *nob* (nyctalopin) knockout mouse. Patch recordings of glutamate-responses reveal outward, metobotropic glutamate, currents in both rod bipolar cells and ON-type cone bipolar cells (DBC) in control mice. No glutamate currents are recorded for these cell types in *nob* mice. OFF cone bipolar cells (HBC) respond with inward AMPA/kainate currents in both control and *nob* mice. The holding potential was -60 mV. Glutamate puffs are 100 msec from pipettes filled with 1-5mM glutamate. The illustration is from Gregg et al, 2007 (57).

Glutamate transporter mediated responses of ON bipolar cells

Ionotropic glutamate receptors with transporter-like properties are also present on some ON-center bipolar-cell dendrites. When photoreceptor glutamate binds to these transporters, a Cl^- conductance forms and hyperpolarizes the cells in the dark (Fig. 10). Release from this Cl^- inhibition occurs in the light with the decrease in glutamate released from photoreceptors. This allows the bipolar cells to depolarize (Fig. 10). Like transporters, this glutamate-gated Cl^- mechanism requires $[Na^+]_o$ in order to function. Thus far this mechanism has been found as a dendritic glutamate 'receptor' only in cyprinid ON bipolar cells (72-74), though it is reported in turtle, salamander and mouse photoreceptors (75-78) and is also present in mammalian central nervous system (79). Interestingly it occurs on the axon terminals of mouse rod and cone bipolar cells, where it acts to regulate glutamate release through inhibitory feedback (78).

Some non-mammalian bipolar cells contain both the APB and the ionotropic (transporter-like) receptor on their dendrites, while other ON-cells express either the metabotropic or the ionotropic receptor but not both (72, 73). EAAT5 has been identified as the chloride-channel-forming glutamate transporter (80). The ionotropic mechanism is used for sustained transmission between cones and bipolar cells (81, 82), and is likely to be a fast

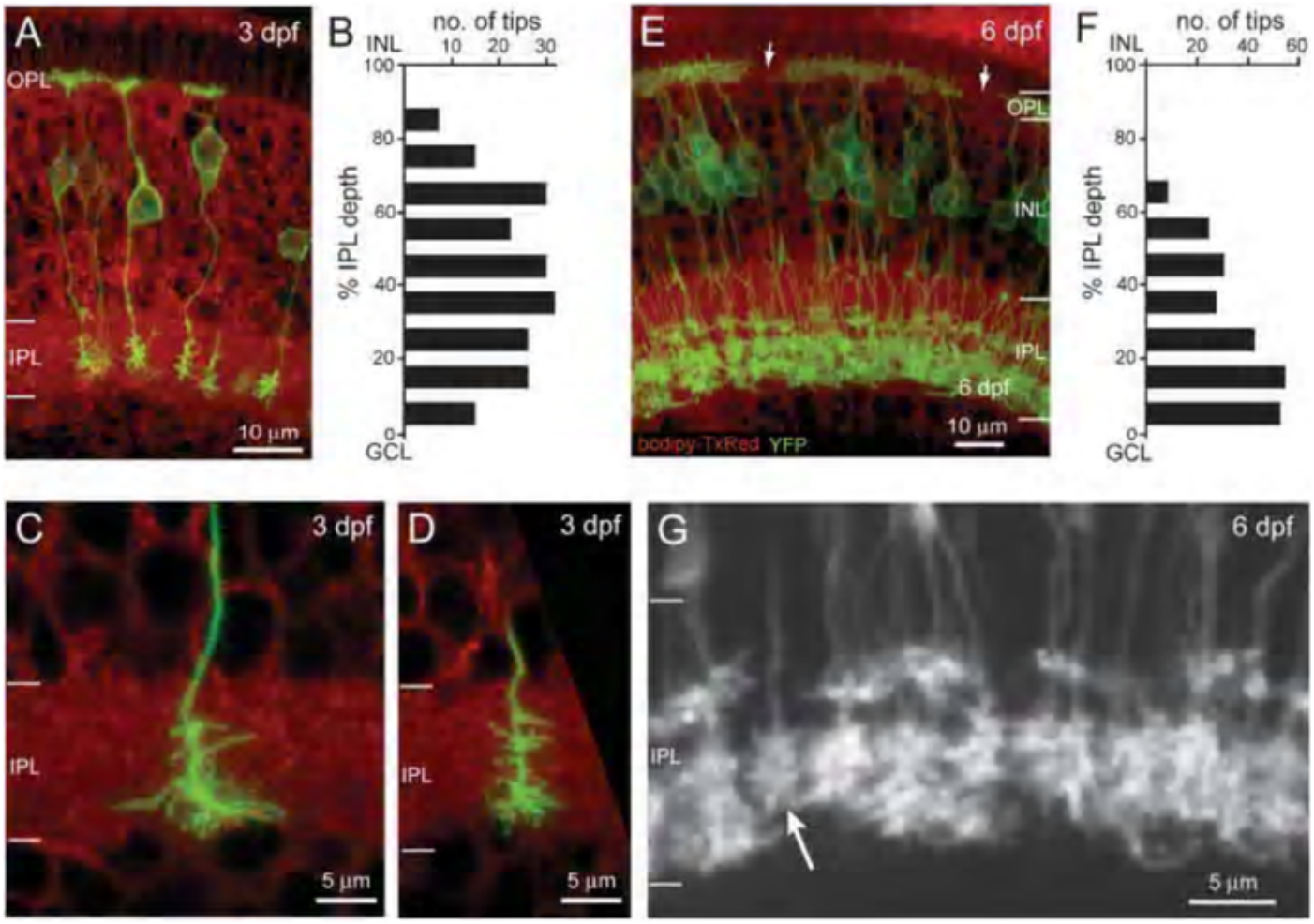

Figure 8b. Morphology of zebrafish retinal neurons expressing nyctalopin. The transgenic strain contains an MYFP gene driven by the regulatory sequence for *NYX* (nyctalopin). *A-D* retinas from 3-day post fertilization (3 dpf) larvae show only bipolar cells, with a broad distribution of axonal filopodia within the inner plexiform layer (IPL). *E-G*. By 6 dpf the filopdial pattern of bipolar cell axons is restricted to the inner half of the IPL, a characteristic of ON bipolar morphology. The illustration is from Schroeter, Wong and Gregg, 2006 (60).

mechanism as compared to metabotropic pathways, which involve multi-step intracellular pathways and are often relatively slow (22).

The classic Mb rod bipolar cell of fish makes synapses with both rods and cones. The rod synapse mediates a conductance increase with reversal potential positive to resting potential. The cone synapse mediates a conductance decrease with reversal potential negative to the resting potential (82). Both mechanisms provide ON-type photic responses. In retrospect it would appear that the rod synapse is metabotropic, while the cone synapse is transporter-like, two different, selectively directed post-synaptic glutamate mechanisms on the same neuron.

AMPA kainate receptor expression in ON bipolar cells

ON-center bipolar cells of mammals are immunoreactive for ionotropic AMPA receptors as well as metabotropic mGluR6 receptors (83-85). In figure 11 (left panel) and figure 12 (right panel) immunoreactivity for GluR1 and GluR2/3, ionotropic AMPA subunits, appeas at invaginating, ON-type ribbon contacts in cat. Similarly in teleost retinas, ON-center bipolar cells are immunoreactive for ionotropic kainate receptors (86, 87). Particularly in mammals, no physiological role has been suggested for these conventional ionotropic receptors, usually

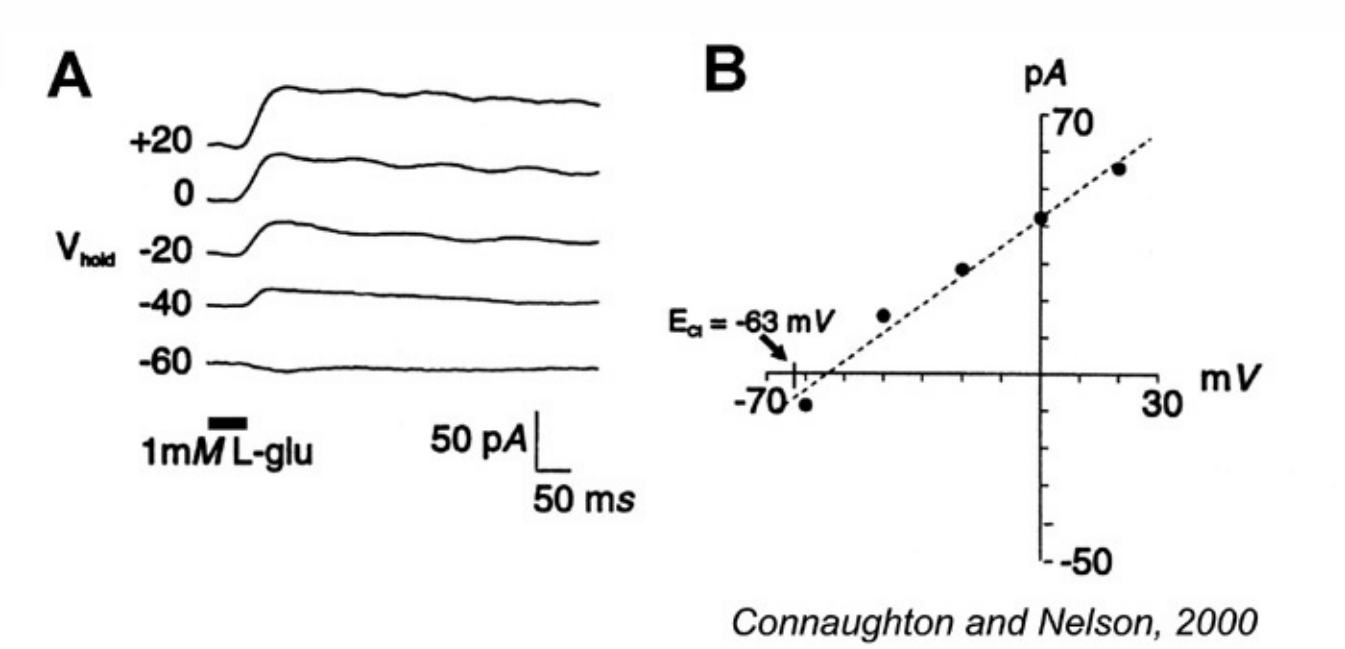

Figure 10. An alternate ON-bipolar synaptic mechanism is a glutamate-activated-chloride channel. Puffs of glutamate mimic photoreceptor dark release in patch recordings from bipolar cells in a zebrafish retinal slice. *A*. Glutamate-evoked currents are outwards for physiological ranges of membrane potential, which are positive to ECl (Cl^- reversal potential). They are inwards at more negative potentials. The results are consistent with an ON-center mechanism driven by changes in Cl^- conductance. *B*. The –63 mV reversal potential is consistent with a model where photoreceptor glutamate opens Cl^- channels. Glutamate gated Cl^- currents are called I_{glu} (73) and result from the binding of glutamate to excitatory amino acid (EAAT) transporters. The illustration is from Connaughton and Nelson, 2000 (72).

associated with OFF bipolar cells, but also seen in ON-center bipolar cells. In giant danio Wong and Dowling find that bistratified cone bipolar cells mix ON-type and OFF-type glutamate receptor mechanisms, and utilize both transporter-like receptors and AMPA/kainate receptors in generating ON and OFF color responses respectively to different spectral stimuli (88).

Ionotropic glutamate responses of OFF bipolar cells

Like ON bipolar cells, OFF bipolar cells express more than one type of glutamate receptor, though all are ionotropic. There are three principal types of ionotropic glutamate receptors (AMPA, kainate, and NMDA) as originally defined by agonist selectivity. Though immunocytochemical studies (84, 89, 90) and in situ hybridization (91) have identified specific NMDA receptor subunits in the outer retina, OFF bipolar cells have never been observed to utilize NMDA receptors in the generation of light responses. OFF bipolar cells selectively express either AMPA or kainate receptors (92, 93). AMPA receptor subunit GluR1 immunoreactivity is found at the 'flat' contacts between OFF- bipolar-cell dendrites and cones (Fig. 11, left and right). Kainate receptor subunit GluR6/7 immunoreactivity is also found at these flat contacts (Fig. 12, left). AMPA and kainate receptors resensitize at different rates after exposure to glutamate (Fig. 13), and as a result, emphasize different temporal characteristics of the light signal. Kainate-type glutamate receptors transfer the sustained characteristics of the visual stimulus. AMPA receptors are more selective for the transient components of the signal (92). In ground squirrel retina bipolar cells are selective for one or the other (93). The situation is interesting in so far as neurons using kainate receptors exclusively are rare in the central nervous system. Nonetheless, AMPA and kainate receptors on retinal bipolar cells are pharmacologically well-behaved. Bipolar-cell AMPA-type responses can be selectively suppressed by the lipophilic AMPA receptor antagonist GYKI 52466 (94). Conversely, bipolar-cell kainate-type responses are blocked by the desensitizing kainate receptor agonist SYM 2081 (95).

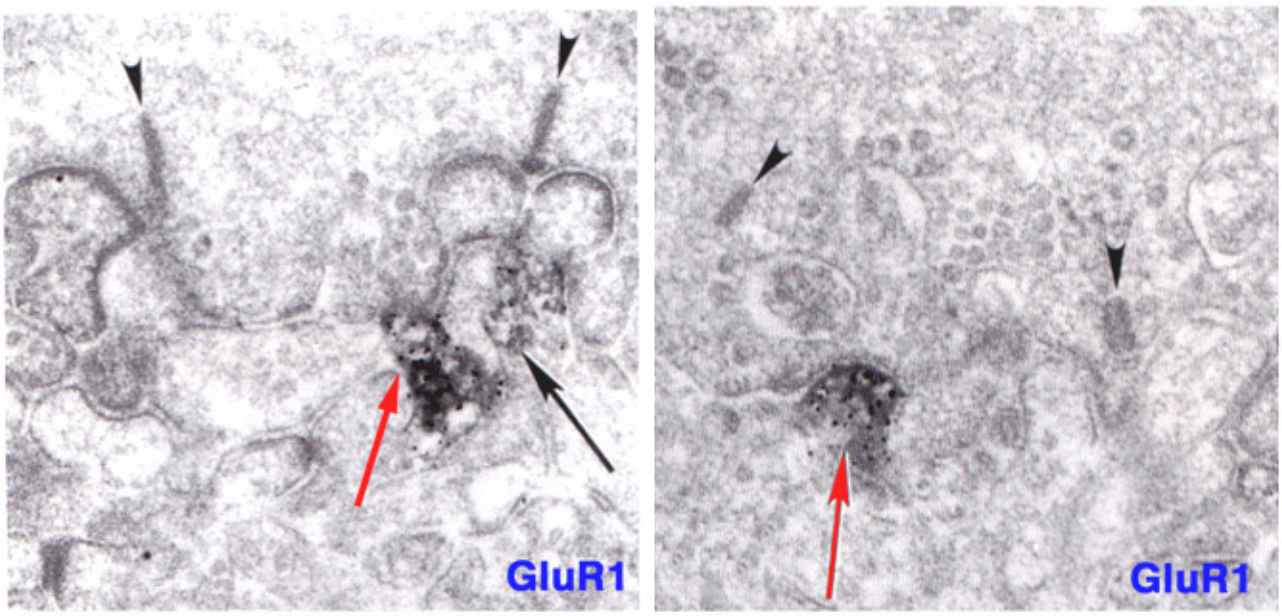

Figure 11. Immunostaining for the ionotropic glutamate receptor GluR1 in bipolar cell dendrites contacting cone pedicles in cat retina. Red arrows point to flat contacts, the black arrow points to an invaginating contact, and the arrowheads point to synaptic ribbons in the cone pedicle. The illustration is from Qin and Pourcho, 1999 (261).

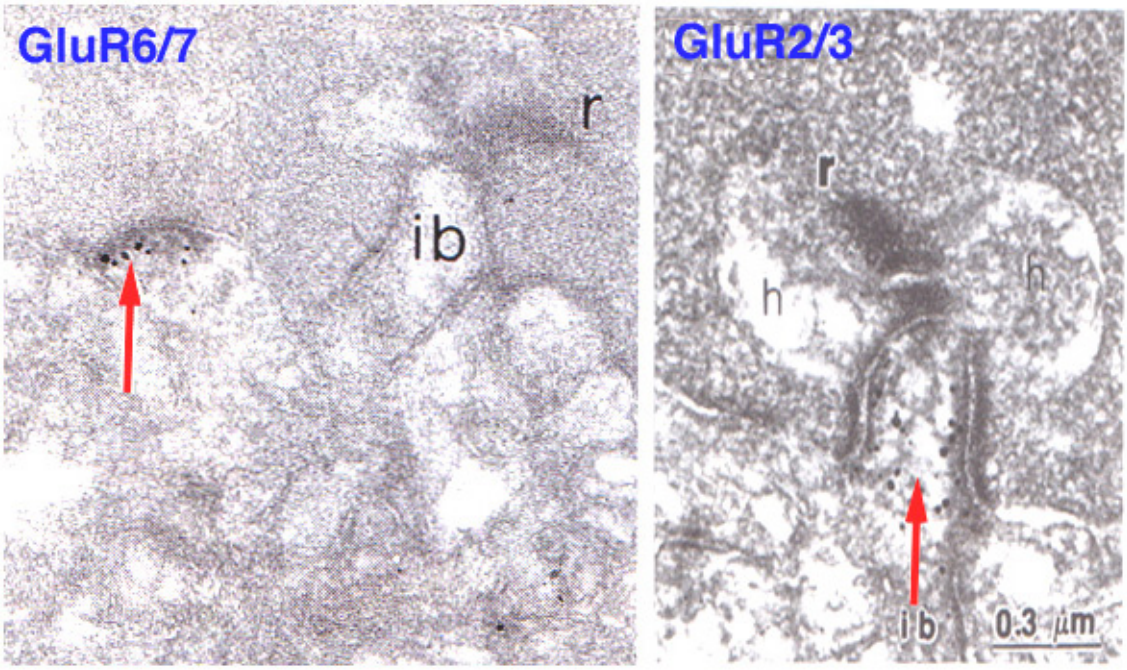

Figure 12. Immunostaining for ionotropic glutamate receptors in the dendritic tips of cat bipolar cells. GluR6/7 subunits are found in kainate receptors. GluR2/3 subunits are found in AMPA receptors. The red arrow (left, GluR6/7) points to a immuno-stained flat contact. The red arrow (right, GluR2/3) points to an immuno-stained invaginating contact. Letter labels are invaginating bipolar (ib), horizontal cell lateral element (h), and rod (r). The illustration is from Vardi et al., 1998 (83). .

While all retinas contain ON and OFF bipolar cell pathways, it is easy to imagine that among these pathways natural selection might cause a divergence in the expression of dendritic glutamate receptor types depending on the visual requirements of the species. In agreement with this hypothesis, species-specific differences between ON and OFF bipolar cell dendritic glutamate responses have been found. For example, ionotropic glutamate

channels with transporter-like pharmacology occur exclusively in ON type bipolar cells in fish retinas. Conversely in salamander, OFF bipolar cells utilize only AMPA receptors (96). This may also be the case in zebrafish retina where dissociated cells fail to respond to the kainate agonist SYM 2081 (86) and electroretinographic OFF responses (d-waves) are blocked by the AMPA antagonist GYKI 52466 (97). One might expect also that even within the broad classes of AMPA and kainate receptors, subforms may have evolved to fit particular visual niches. In salamander retina indeed, there are separate classes of AMPA receptors postsynaptic to rods and to cones (96, 98).

3. Bipolar-cell axons: ON and OFF lamination in the inner plexiform layer

In work performed at the National Institutes of Health in the mid 1970s (99, 100), it was noted that the ON or OFF property of cat retinal ganglion cells was related to the level of stratification of dendrites within the retinal inner plexiform layer. This led to a general scheme for ON and OFF layering illustrated in figure 14. The dendrites of OFF-center ganglion cells always arborize distal to the dendrites of ON-center ganglion cells. The zone of OFF-center dendritic arborization is called sublamina *a*, while the zone of ON-center dendritic arborization is called sublamina *b* (Fig. 14). Within each sublamina ganglion cells make selective contacts with ON- or OFF-type bipolar cells. The pattern of ON and OFF layering of bipolar cell synaptic terminals and ganglion cell dendrites has proved to be a consistent pattern among all vertebrate retinas examined (101, 102). ON and OFF layering is particularly pronounced in retinas where ganglion cell types are predominantly monostratified. However, in more anatomically complex retinas, (i.e., turtle) with multistratified and/or diffusely stratified ganglion cell types, the ON vs. OFF layering pattern applies to monostratified cells only. The physiology of cells with processes ramifying throughout the IPL is more difficult to predict based on morphology alone (103).

Stratification of cone bipolar cell axon terminals

The axon terminals of ON and OFF bipolar cells ramify in distinct IPL layers, where they are presynaptic to ON- and OFF-type ganglion cells, respectively. The axon terminal arborizations of OFF-type cone-contacting bipolar cells lie in sublamina a, where they synapse with the dendrites of OFF-type ganglion cells, while the axon terminal arborizations of ON-type cone contacting bipolar cells lie in sublamina b, where they contact the dendrites of ON-center ganglion cells. Synapses between OFF-type bipolar terminals and ganglion cell dendrites in sublamina a, and ON-type cells in sublamina b, have been observed electron-microscopically (104-109). Synapses between pairs of bipolar and ganglion cells with mismatched response polarity were never observed, even where processes come in close proximity (105). Melanopsin ganglion cells may provide an exception to this rule. The outer stratifying melanopsin ganglion cells of mouse and primate receive synapses from ON-cone bipolar cell axons en passant (110, 111).

Awatramani and Slaughter (69) proposed a further refinement of the bipolar-cell stratification scheme: cells with a glutamate receptor physiology emphasizing transients in the visual pattern are layered more toward the center of the IPL, while those with glutamate receptor patterns emphasizing sustained contrast are layered more towards IPL inner and outer edges. Although based in salamander retina, such a pattern would be appropriate to the layering of the sustained X (IPL inner and outer edge) and transient Y type ganglion cells of the cat retina (central IPL), as well as P and M cells of the primate retina. Wu et al (11) find a similar pattern in salamander, but attribute it to an elaboration of other circuitry elements, as bipolar cells with arbors in the mid-IPL tend to be cone dominated, emphasizing speed and transient response, whereas bipolar cells with axon terminals stratified at the inner and outer edges of the IPL process rod signals, which are relatively more lethargic in wave form (11).

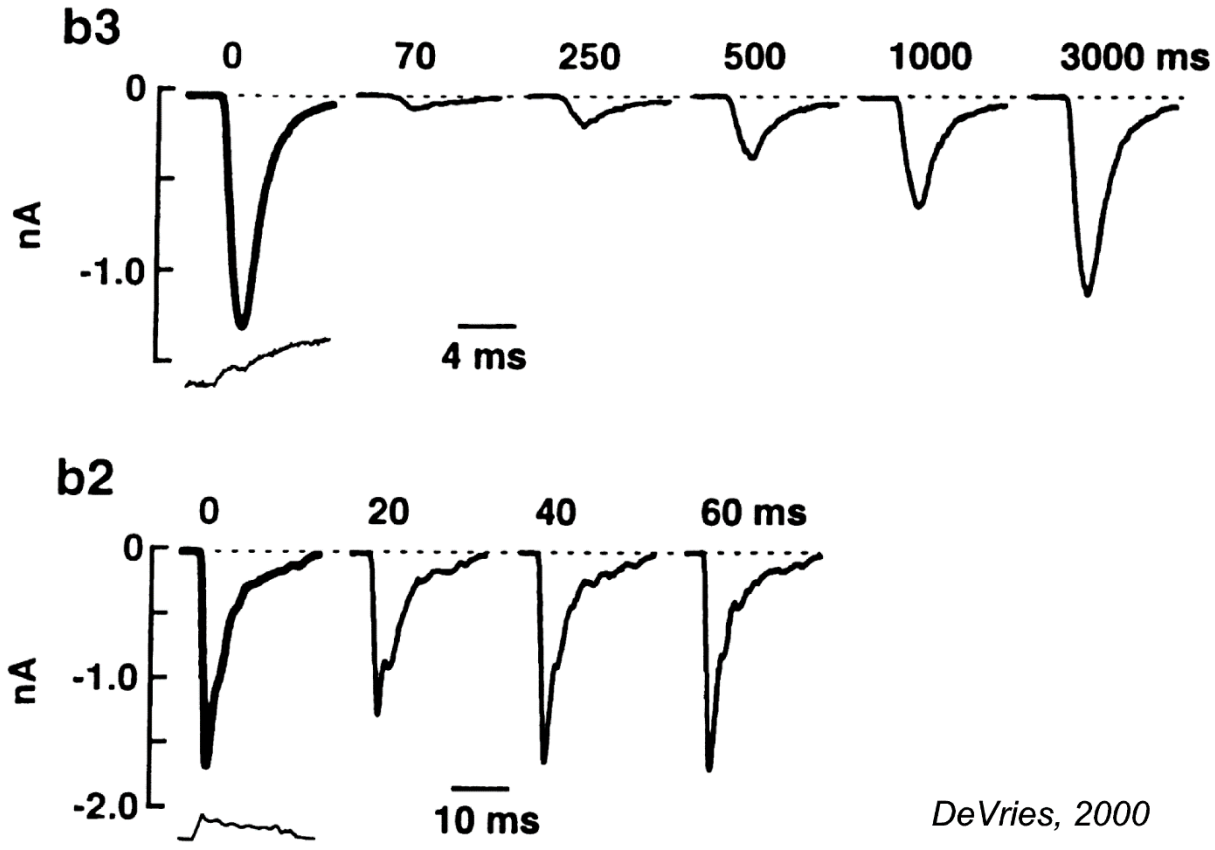

Figure 13. Different OFF bipolar cells re-sensitize at different rates after glutamate treatment. In whole cell patch recordings from ground squirrel retina, bipolar cells b3 and b2 are desensitized by an initial glutamate pulse ('0'). The time course of recovery is measured by responses to a second pulse after different delays. Type b3 (Fig. 16) bipolar cells utilize kainate-type glutamate receptors and require several seconds for complete recovery. Type b2 bipolar cells (Fig. 16) utilize AMPA-type glutamate receptors and recover 100 times faster. The illustration is from DeVries, 2000 (92, 93)..

Exhaustive correlations of ON or OFF bipolar cell physiology with axonal stratification patterns are now available for several species. Light responses or, as a surrogate for light responses, either dendritic glutamate responses, or responses to electrical stimulation of individual cones, can be measured in patch microelectrode recordings in retinal slice. Electrophysiological findings are correlated with axonal and dendritic morphology through microelectrode staining.

Salamander

In salamander retina Pang, Gao and Wu (2004) (112) separated bipolar-cell light-evoked responses into cationic currents originating from glutamatergic synapses with photoreceptors, and chloride currents originating with GABAergic or glycinergic synapses with amacrine cells. The polarity of light-evoked cationic currents (ΔI_C) correlated perfectly with axonal branching levels in the inner plexiform layer. Salamander bipolar cell types 1-5, with axonal stratification in the outer half of the inner plexiform layer (sublamina *a*), were OFF types, giving outward ΔI_C. Types 6-10, with axonal stratification in the inner half of the inner plexiform layer (sublamina *b*), were ON-types, giving inward ΔI_C (Fig. 15). The cationic synaptic currents were isolated from inhibitory chloride currents by clamping the cells at chloride reversal potential (V_m = −60 mV). Light evoked inhibitory chloride currents (ΔI_{Cl}) were examined by clamping the cells at cationic reversal potential (V_m = 0 mV). Both ON and OFF bipolar cells were inhibited by chloride currents, most likely generated by glycinergic and GABAergic synapses from amacrine cells onto bipolar cell axon terminals (Fig. 21, Fig. 22). One inhibitory

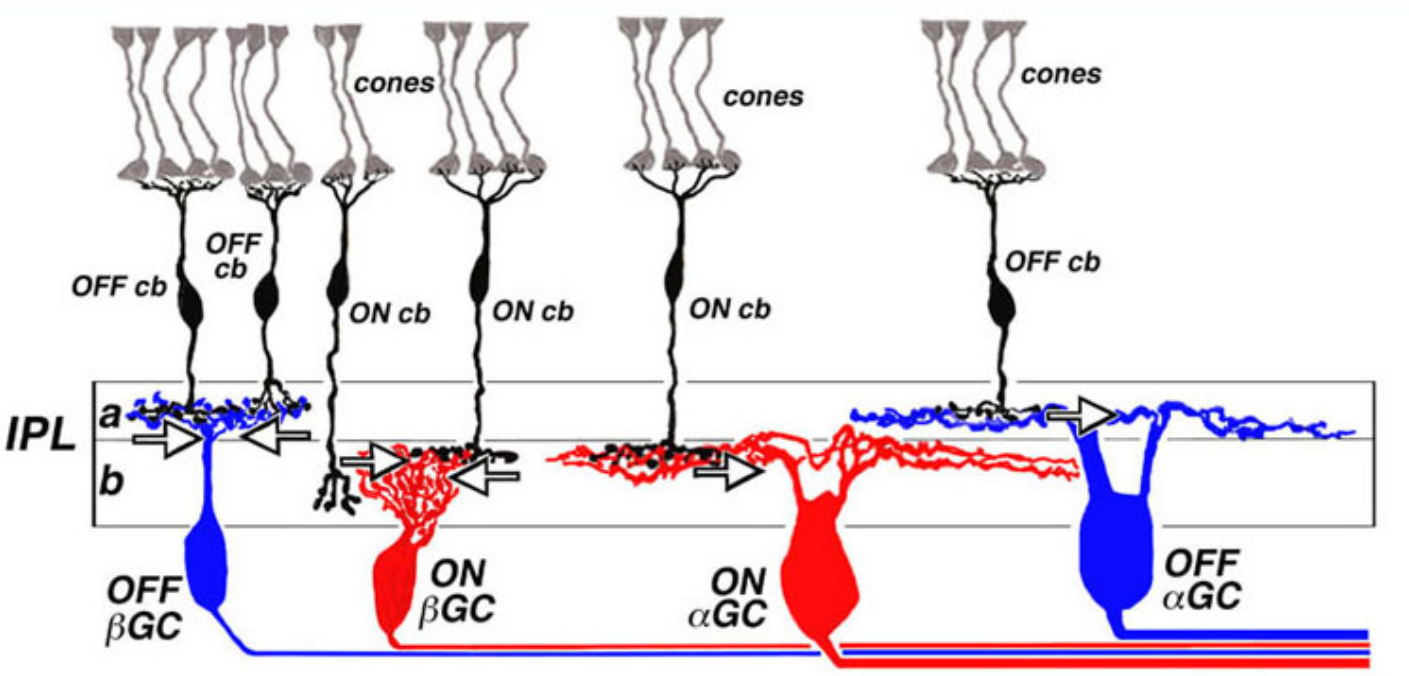

Figure 14. Layering of ON and OFF bipolar cell axons in the cat inner plexiform layer (IPL). OFF ganglion cell (*αGC* and *βGC*) dendrites and OFF cone bipolar cell axons (*OFF cb*) co-stratify in sublamina *a* of the IPL. ON bipolar axons (O*N cb*) and ON ganglion cell dendrites co-stratify in sublamina *b* of the IPL. These are the parallel ON and OFF cone pathways that originate with bipolar-cell dendritic contacts with cones. The illustration is modified from Nelson et al, 1978 (100)..

pattern was ON-sustained, while the other was ON/OFF. In addition to bipolar cells with highly stratified axon terminals (Fig. 15) others with broader stratification or even bistratification were encountered, giving a total of 22 morphological types (12). These latter types also followed the ON-OFF stratification rule, except for the types that were bistratified in both sublaminae, the a/b types. These could be either ON or OFF, but often a dual ON and OFF dendritic input could be dissected with pharmacological treatments (112).

Rod-dominated mammals

In rat retina, bipolar cell axon terminal arborization appears to obey perfectly the rule of ON and OFF layering (7). As judged by the level of axonal stratification, there are 9 bipolar types. The axons of cone bipolar cells 1-5 branch in the outer half of rat IPL (sublamina *a*). These cells responded with inward currents when stimulated with kainate, an agonist for AMPA/kainate receptors on the dendrites of OFF bipolar cells. Of a combined 15 recordings from types 1-5, only one cell responded to APB (DL AP-4), a glutamate agonist selective for ON center bipolar cells. Four cone bipolar cell types (types 6-9) with axons branching in the inner half of rat IPL (sublamina *b*) were identified. In net 12 of 14 of cells of these types responded with outward currents to APB, whereas only one responded to kainate (7). This is a better than 90% compliance with the ON and OFF stratification pattern for cone bipolar cell axon terminals in rat retina. Bipolar cell branching patterns in mouse retina appear similar to rat (113). A more limited set of recordings in cat and monkey retinas suggest also that there may be good adherence to ON and OFF stratification of bipolar terminals (109, 114).

Ground squirrel

Li and DeVries (15) have provided a significant technical advance in the mapping of form onto function for biplolar cells of the all-cone retina of ground squirrel. In these studies one patch electrode was used to electrically stimulate an individual cone within the dendritic arbor of a bipolar cell simultaneously patched and

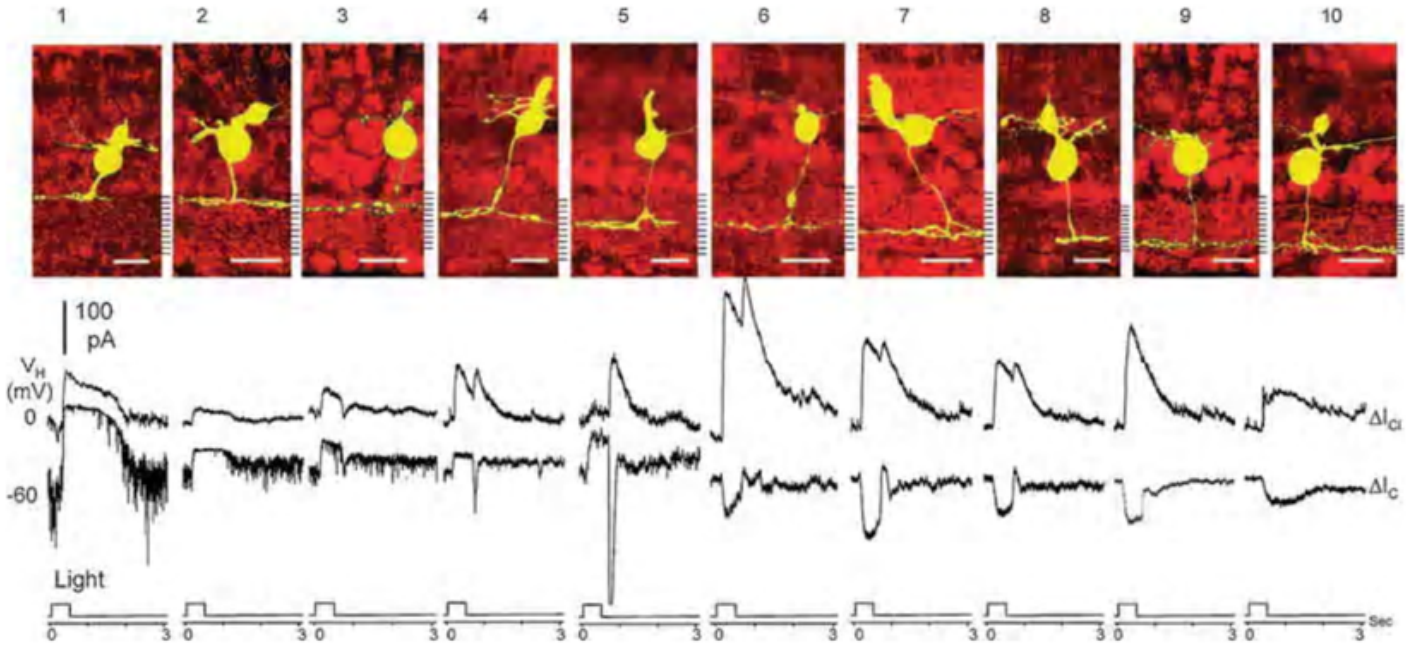

Figure 15. Functional stratification of bipolar-cell axon terminals in salamander retina. Types 1-5 are OFF bipolar cells with axonal branching in the outer half of the inner plexiform layer (IPL sublamina *a*). The light-evoked cationic currents (ΔI_C), obtained at a holding voltage (V_H) of -60 mV, are all outward, characteristic of dendritic AMPA receptors. Types 6-10 are all ON bipolar cells with axonal branching in the inner half of the inner plexiform layer (IPL sublamina *b*). The light-evoked cationic currents are all inward, characterisitic of dendritic mGluR6 receptors. Inhibitory chloride currents (ΔI_{Cl}) are seen at the cationic reversal potential ($V_H = 0$). These are either sustained ON, or transient ON/OFF. Inhibitory currents arise mainly from amacrine cells. The illustration is from Pang et al, 2004 (112).

stained by a second microelectrode. In this way both the cone contacts and the nature of these contacts onto bipolar cells are directly verified. Six cone bipolar types have been mapped by this technique, one ON type contacting only blue cones, an ON and an OFF type contacting both blue and green cones, and remaining types contacting only green cones (Fig. 16). No color opponent cone synaptic inputs using different glutamate receptors were detected in ground squirrel bipolar cells. The lamination patterns for ON and OFF types follows that proposed for rod-dominated mammalian retinas (100, 115).

Cyprinids

In anatomical studies using a technique called 'diolistic labeling', Connaughton et al (2004) (6) distinguished 17 bipolar-cell types in zebrafish based on axonal stratification patterns. In work still in progress in the Dowling laboratory, cone contact patterns have been added to axonal stratification patterns (116, 117), resulting in perhaps 20 or more bipolar types that can be anatomically distinguished. However, in the latter studies 90% of the examples are accounted for by as few as 9 of these types. There are 5 exclusively cone-contacting groups that are distinguished by the pattern of cones contacted and by axonal stratification. There are 4 types that contact rods in addition to various cone groupings (Mb types). The most selective cone-contacting type contacts only green-cones. It is very wide in dendritic and axonal field and is OFF-stratified. The most diffuse pattern of photoreceptor contacts is an OFF stratified type that contacts all photoreceptors, rods, red, blue, green, and UV cones. In mammals it appears that all the dendritic contacts emanating from a single bipolar cell express the same glutamate receptor (15). This appears not to be the case in fish or amphibian bipolar cells, where the same cell may express different glutamate receptors at different dendritic tips (72, 82, 88, 112), with each receptor type segregating according to the photoreceptor type contacted (82, 88).

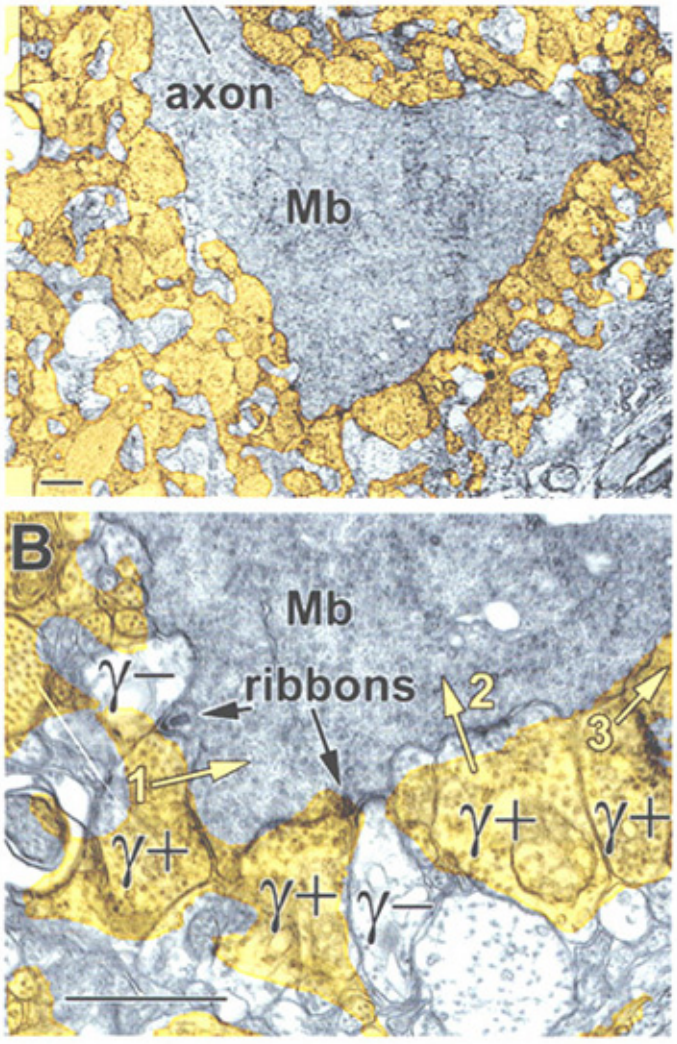

Figure 21. Immunostaining for the inhibitory neurotransmitter GABA (γ^+) in goldfish retina shows dense innervation of type Mb bipolar axon terminals. The yellow image for light-microsocpic immunostaining (yellow) is superimposed upon the electron micrograph image of an Mb (ON-type mixed rod/cone bipolar) axon terminal. The illustration is from Marc and Liu, 2000 (168).

Glutamate responses of zebrafish bipolar cells with axonal boutons in sublamina a (Group a) and sublamina b (Group b) are summarized in Fig. 17. Bipolar cells with 1 or 2 terminal boutons restricted either to sublamina a or to sublamina b obey the ON and OFF stratification rule. OFF cells branching in sublamina a express AMPA/KA type receptors. ON cells branching in sublamina b express either or both of two inhibitory glutamate mechanisms, ionotropic (I_{glu}, transporter-like chloride current) or metabotropic (APB receptor).

Carp retina (115, 118) also exhibits a bisublaminar organization of bipolar-cell terminals.

Bistratified axon terminals

Bisublaminar orderliness breaks down to some extent in species where multistratified bipolar cell axons are common. While multistratified cells exist in mammals like monkeys, cats, and squirrels (10, 15, 119, 120) (Fig. 2-GBB; Fig. 16 b3), these types are much more common in birds, reptiles, amphibians and fishes. Multistratified types selectively contact cones (19, 120) and so may be characteristic of cone-dominated species. If broad or multistratified bipolar terminals are restricted to either the ON or the OFF sublaminae (i.e. all branches and boutons within the same sublamina), the ON and OFF stratification rules apply. This is seen for type b3 bipolar cells in ground squirrel (Fig. 16). However, if the axonal stratification pattern crosses the ON-OFF boundary, the

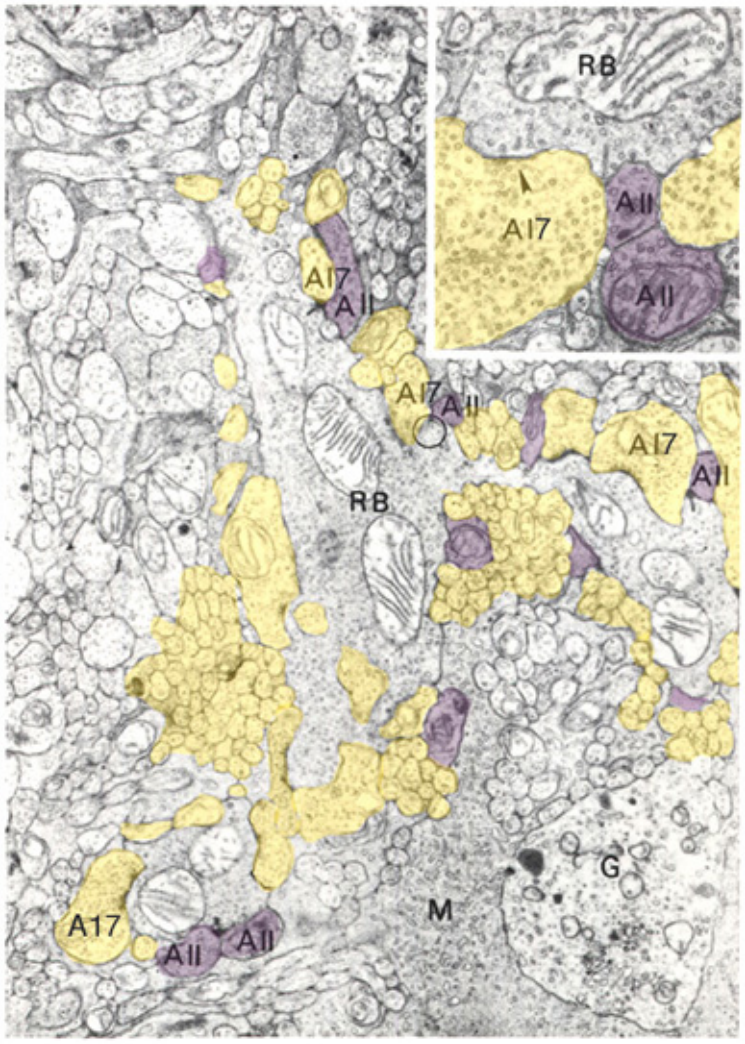

Figure 22. GABAergic and glycinergic inhibitory terminals surround a rod bipolar axon terminal (RB) in cat retina. The A17 amacrine cell (yellow) is GABAergic and transmits at $GABA_A$ receptors on the rod bipolar axon terminal. The AII amacrine cell is known to be glycinergic (purple). The electron micrograph is adapted from Kolb, 1979 (105).

cells may be either ON-type or OFF-type (11, 72, 103). In some cases such multistratified bipolar cells may even express both ON and OFF physiologies (11, 88, 112), with the OFF physiology mediated by AMPA receptors, and the ON physiology mediated by either mGluR6, or EAAT. In giant danio such cells are color opponent (88). In zebrafish multistratified bipolar cells with boutons in both sublaminae were found to be either ON or OFF types Fig. 17. Connaughton and Nelson concluded that multistratified ON types use only I_{glu}, the transporter-like chloride current (72), however in the related giant danio, Wong et al find a bistratified type that is both ON and OFF, expressing both I_{glu} and AMPA/kainate receptors (88). The pattern for other giant danio ON bipolar cells is similar to zebrafish where the I_{glu}, or excitatory amino acid transporter (EAAT), mechanism is found particularly in ON-type cone contacting bipolar cells, while the mixed Mb rod and cone contacting types utilize both EAAT and MGluR6 mechanisms (121). The glutamate transporter blockers TBOA was found effective in blocking EAAT transmission (121).

Stratification of rod bipolar cell axon terminals and rod pathways

Rod bipolar cells are unique. These cells are easily identified in both mammals and fish (122). In most mammals, judged by axonal stratification pattern and contacts with photoreceptors, there is only a single class of rod bipolar cell (20, 122). The axon descends deep into ON sublamina *b* of the IPL, where it arborizes in a bulbous

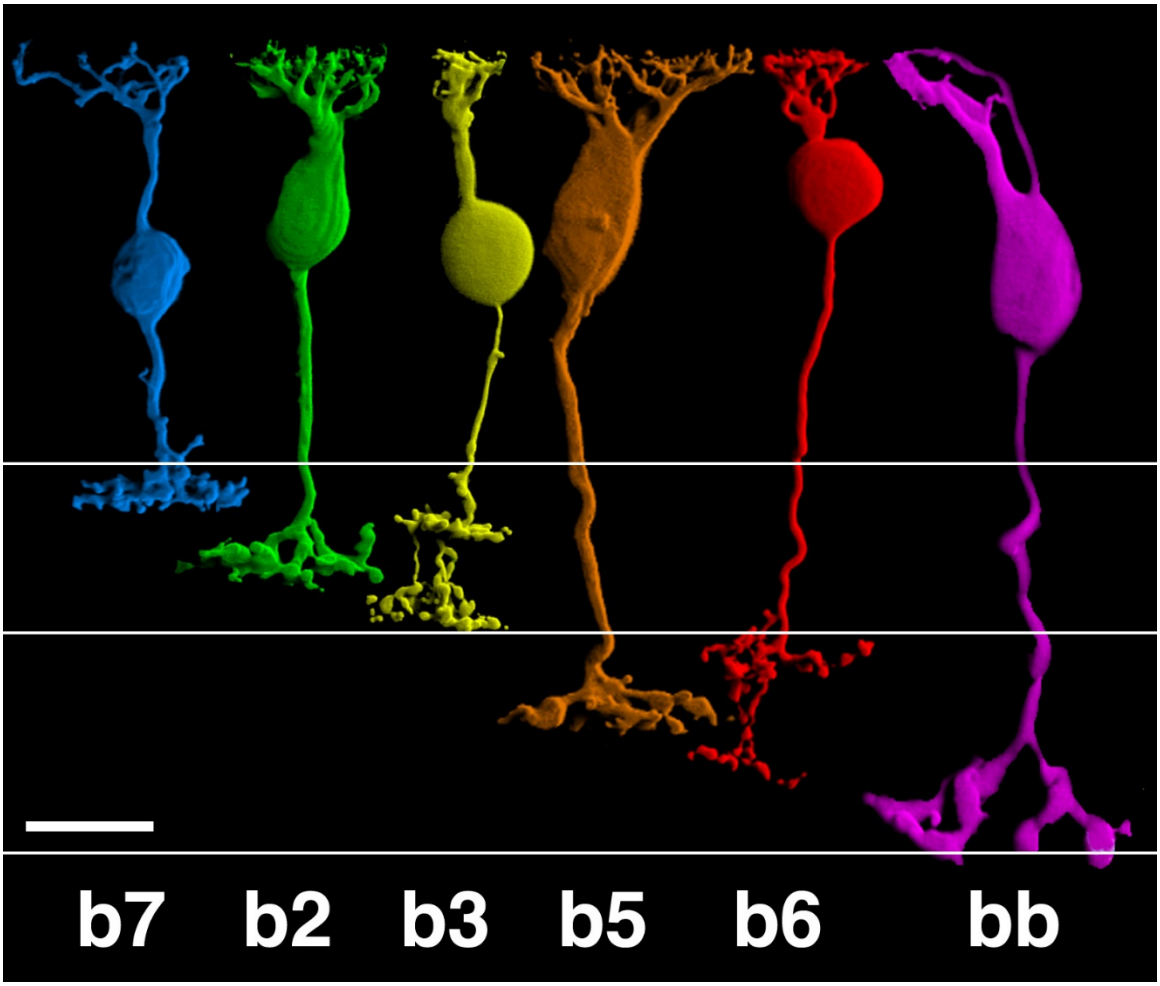

Figure 16. Axonal stratification of bipolar cells in ground squirrel retina. Bipolar cells are stained by dye-filled patch electrodes while recording responses to microelectrode stimulation of individual cones contacting the dendritic tips. 'bb' is an ON-type blue cone bipolar cell; 'b2' is and OFF-type bipolar cell (Fig.13) that contacts both blue and green cones. 'b5' is an ON bipolar cell contacting both blue and green cones. Both 'b3' (Fig.13) and 'b7' are OFF-type bipolar cells that contact only green cones. 'b6' is a heterogeneous grouping of ON cells contacting almost exclusively green cones. While the cone contacts vary, the ON and OFF stratification of axon terminals follow the typical vertebrate pattern. The scale bar is 10μm. The illustration is from Li and DeVries, 2006 (15).

terminal just adjacent to ganglion cells (Fig. 18, rb). The mammalian rod bipolar cell is an ON-type cell (123) utilizing metabotropic APB-sensitive, glutamate receptors (31, 32, 64, 124). In fish, the comparable cell type is the Mb bipolar cell (125). In fish retinas, rod-contacting bipolar cells also contact cones. Five such types are found in goldfish retina, including multiple ON types with axon terminals branching in sublamina *b*, and likely OFF types with axon terminals branching in sublamina *a* (14). Interestingly in mouse retina there also appear to be multiple ON type rod bipolar cells. While axon-terminal morphology differs only subtly, light-evoked signals in DBC_{R1} are completely rod dominated, whereas DBC_{R2}, similar to fish, receives substantial cone signal input in addition to rod input. The cone signals in DBC_{R2} types disappear in connexin 36 knockout mice (126, 127). Regardless of species, classic ON-center rod bipolar cells are all universally recognized by high immunoreactivity for protein kinase C (PKC) (64, 113, 126, 128-130).

Although the axon terminals of rod bipolar cells are directly adjacent to ganglion cells, they do not contact them directly. In the mammalian retina, the AII amacrine cell (105, 131, 132) is the first intermediary in transferring rod bipolar signals to ganglion cells. The AII cell achieves this through direct innervations of cone bipolar processes within the IPL, either by means of chemical synapses with OFF bipolar cells (large arrow in sublamina *a*, Fig. 18) or through gap junctions between AII dendrites and ON cone bipolar axons (large arrow with red

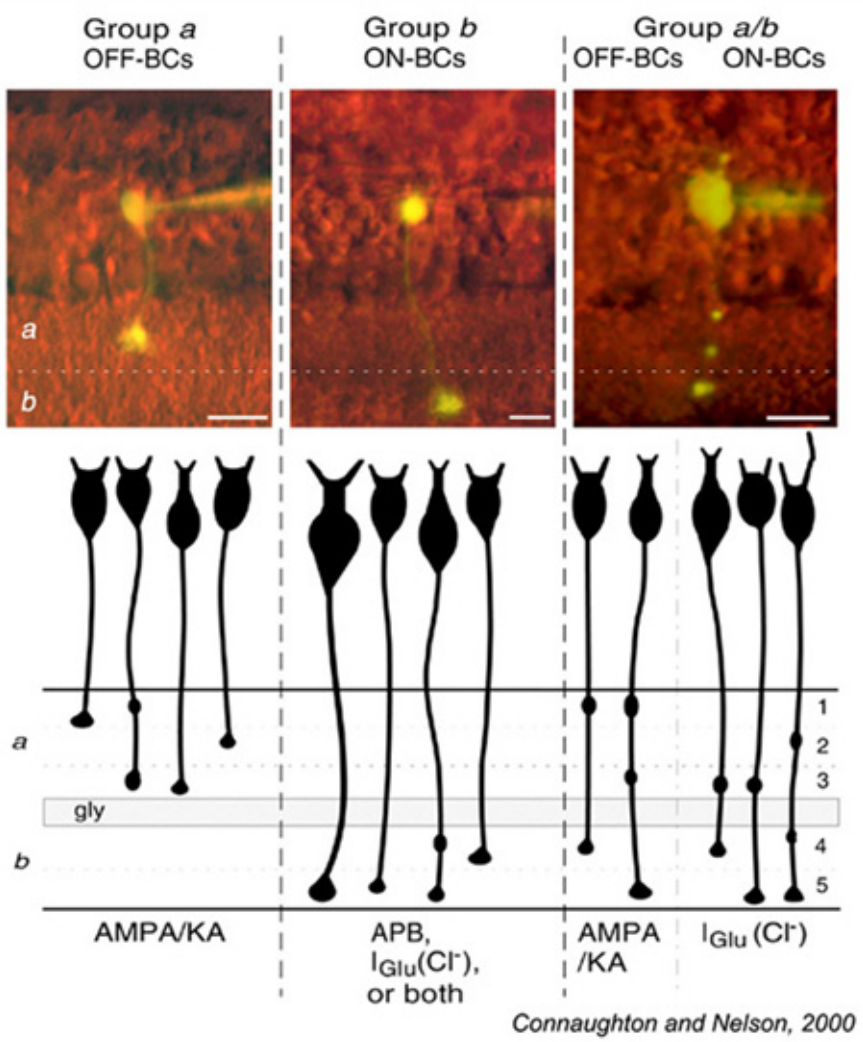

Figure 17. ON and OFF stratification of bipolar-cell axon terminals in zebrafish retina. There are three groupings: axonal boutons only in IPL sublamina *a* (Group *a*), axonal boutons only in sublamina *b* (Group *b*), axonal boutons in both sublaminae (Group *a/b*). ON and OFF properties and glutamate receptor types were determined from whole-cell currents evoked by puffs of glutamate, kainate, APB or NMDA directed at dendritic arbors. AMPA/KA shows cells responding to glutamate or kainate with inward currents. APB shows cells responding to glutamate, APB, or both with outward currents and reversal potentials at or beyond 0 mV. $I_{Glu}(Cl^{-})$ shows cells responding to glutamate with outward currents reversing at -60 mV, the I_{Glu} or EAAT mechanism. NMDA evoked no responses. There is an immunoreactive band for glycine (gly) that appears to separate IPL sublamina *a* from *b*. The scale bar is 10 μm. The illustration is from Connaughton and Nelson, 2000 (72)..

asterisk, Fig. 18). The cone bipolar axon terminals are the second intermediary in transferring rod bipolar signals to ganglion cells. The AII-amacrine-to-cone-bipolar gap junction is down-regulated by the humeral factor nitric oxide acting through an intracellular cGMP pathway (133) and also is susceptible to pharmacological blockade by meclofenamic acid (134).

Cone bipolar cells participate in transferring ON and OFF rod signals from distal retina to ganglion cells even without AII amacrine intermediation. This occurs through two pathways. In the first, signals flow through gap junctions between rods and cones (135-139), and by this pathway into cone bipolar cells. In the second, cone-contacting bipolar cells make direct dendritic contact with rods, as commonly occurs in non-mammals (14, 117, 140, 141). In mammals this type of cone bipolar pathway is usually restricted to OFF cone bipolar cell dendritic contacts with rods (139, 142, 143). This pathway bypasses the slower, albeit higher gain and more sensitive, metabotropic pathway of rod bipolar cells using the faster ionotropic pathways in the OFF cone bipolar cells

(143). In contrast to the typical mammalian pattern, mouse retina shows an analogy to fish retina in having ON cone bipolar cells that directly contact rods (144). Separate rod signaling pathways can be distinguished in humans, both behaviorally, and in evoked potential recordings (145). A sensitive scotopic pathway may represent the rod-bipolar-to-AII pathway, whereas a less sensitive and faster mesopic pathway may represent a rod-to-cone gap-junction pathway, or perhaps additionally, an OFF cone bipolar pathway with direct rod input.

4. Electrical properties, lateral inhibition, and synaptic release

Voltage-gated currents

Voltage-gated channels permeate the membranes of retinal bipolar cells and contribute to voltage responses. In general, these channels carry calcium (Ca^{2+}) and/or potassium (K^+) ionic currents. Intracellular recordings show bipolar cells produce graded potentials in response to a light stimulus, but not action potentials (1). This finding is supported by several studies in which voltage-gated Na^+ currents were not identified in bipolar neurons (146-148). However, some other studies do report voltage-gated Na^+ currents in some cone bipolar cells in rat (149-151) and in goldfish (152). In general such Na^+ currents may not produce action potentials, except sometimes under special conditions where K^+ channels are blocked. It seems rather that these currents may typically serve to amplify synaptic events and shape photoresponse waveforms.

The cb5b bipolar cell of ground squirrel retina is an exception. Spontaneous and light-evoked Na^+ spikes can be recorded from these bipolar cells using perforated patch recordings (Fig. 19) (5). The light-evoked bipolar spikes appear to trigger impulse generation in post-synaptic ganglion cells.

Na^+ spikes have not been seen in rod bipolar cells. However in fish retinas, Ca^{2+} spikes have been identified in the rod bipolar axon terminals (3, 153, 154). In zebrafish with bipolar cells transgenically labeled with the Ca^{2+} fluorescent indicator SyGCaMP2, 65% of bipolar terminals produced at least 1 Ca^{2+} spike every second (4). This suggests that Ca^+ spikes occur in the axon terminals of both rod and cone bipolar cells. As yet light-evoked Ca^{2+} spiking is only reported in cyprinid retinas.

All bipolar cells examined to date express inward Ca^{2+} currents in response to membrane depolarizations. The Ca^{2+} currents are either transient (T-type/low voltage activated) and/or sustained (L-type/high voltage activated). The expression of these different Ca^{2+} current types varies among vertebrate species. For example, in goldfish, L-type Ca^{2+} currents are present (155, 156); whereas, mouse bipolar cells express only a transient T-type current (156, 157). In salamander (158) and zebrafish (146), however, both T- and L-type Ca^{2+} channels are present, with the L-type localized to the axon terminal. Recordings of a zebrafish bipolar cell expressing both L-type and T-type Ca^{2+} currents appear in figure 20, I_{Ca}.

A number of potassium (K^+) currents have been identified in bipolar cells. Membrane depolarization typically elicits a combination of outward K^+ currents. In goldfish (159) and tiger salamander retina (25), a slowly activating, delayed rectifying (I_K) potassium current, modulated by dopamine (160), is activated. In contrast, axolotl bipolar neurons (161) express a rapidly activating, slowly inactivating I_A current in response to depolarizing membrane potentials. Bipolar cells in fish, such as white bass and zebrafish, express one or the other of these two types of K^+ currents, suggesting that these neurons can be differentiated into distinct populations based on the voltage-gated currents they express (146, 148). Membrane depolarizations also elicit a calcium-dependent K^+ current ($I_{K(Ca)}$) that contributes to the overall outward current amplitude observed (146, 148, 159). These outward currents tend to hyperpolarize the cell, restoring membrane potential after depolarization. On the other hand membrane hyperpolarizations elicit the slowly activating, inward rectifying (I_h) current (146-148, 159). This also tends to restore membrane potential. Examples of K^+ currents evoked by membrane depolarization (I_K, I_A, $I_{K(Ca)}$), or hyperpolarization (I_{sust}, I_h) appear in figure 20. These were recorded in zebrafish retinal bipolar cells.

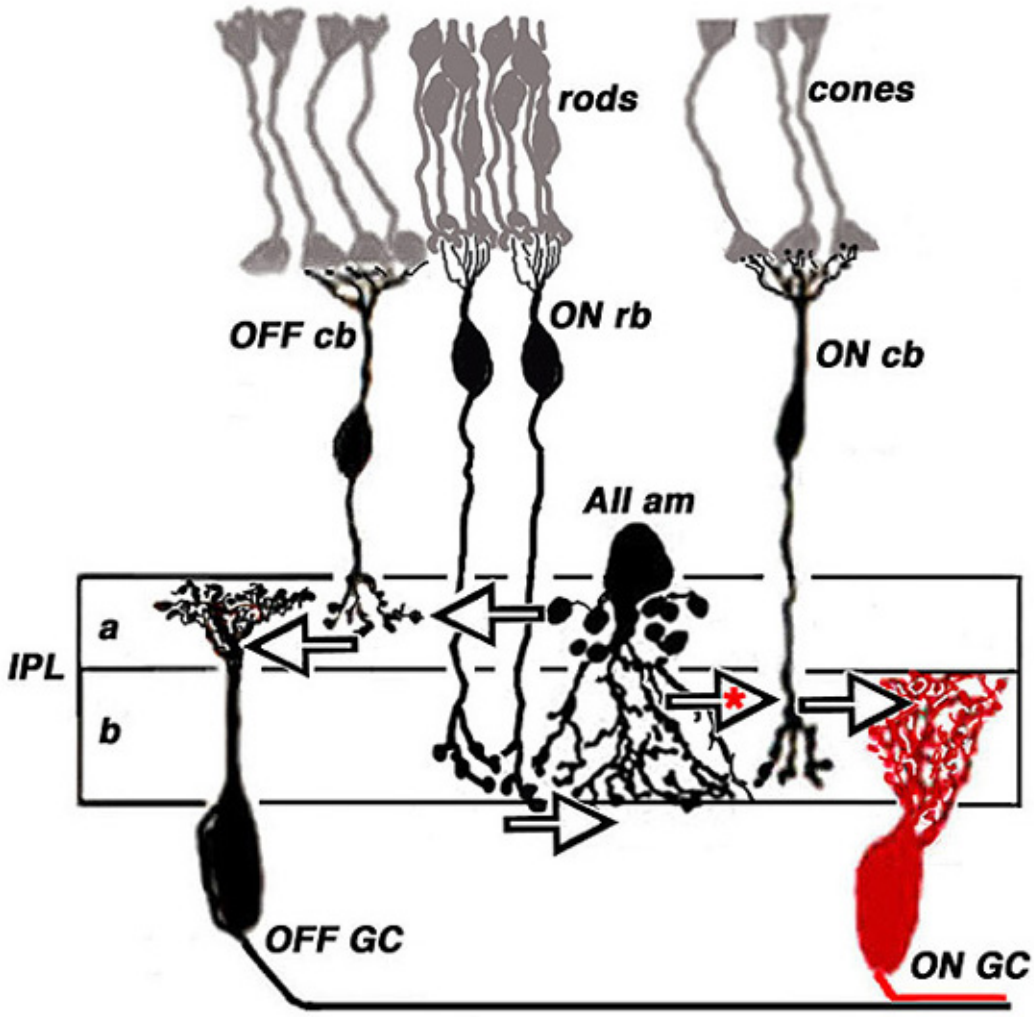

Figure 18. Rod bipolar cells in the mammalian retina are ON type (*ON rb*). Rod bipolar cell signals are split into ON and OFF components by the glycinergic AII amacrine cell (*AII am*, center arrows). Rod ON signals flow from rod bipolar cell to AII amacrine cell to ON cone bipolar cells at gap junctions (asterisk) in IPL sublamina *b*. Rod OFF signals are generated at inhibitory glycinergic synapses between AII amacrine cells and OFF cone bipolar cells within IPL sublamina *a*. The illustration is modified from Kolb and Famiglietti, 1974 (131)..

Inhibitory GABA-gated currents

As described above, light stimulation of the bipolar cell receptive field reveals characteristic center-surround antagonism (Fig. 1), where the response of the center is of opposite polarity to the response of the surround. It is believed that the center component of the bipolar cell light response arises from direct glutamatergic inputs from photoreceptors, while the surround response is generated indirectly by horizontal-cell suppression of glutamate release from cones (162). Horizontal-cell feedback to cones is further discussed in the Webvision chapter *S-potentials and horizontal cells*.

A further potential surround mechanism is through direct inhibitory GABAergic and/or glycinergic inputs from horizontal cells or amacrine cells. These neurotransmitters open chloride channels and generate signals of either hyperpolarizing or depolarizing polarity, depending on the sign of the chloride (Cl^-) gradient across the synaptic membranes (163). Chloride-mediated responses at light onset and offset have been observed in ON bipolar cells of tiger salamander (12, 25, 112). These components appear to originate with AMPA excitation of GABAergic and glycinergic inhibitory interneurons, rather than with photoreceptors directly (25, 164). The

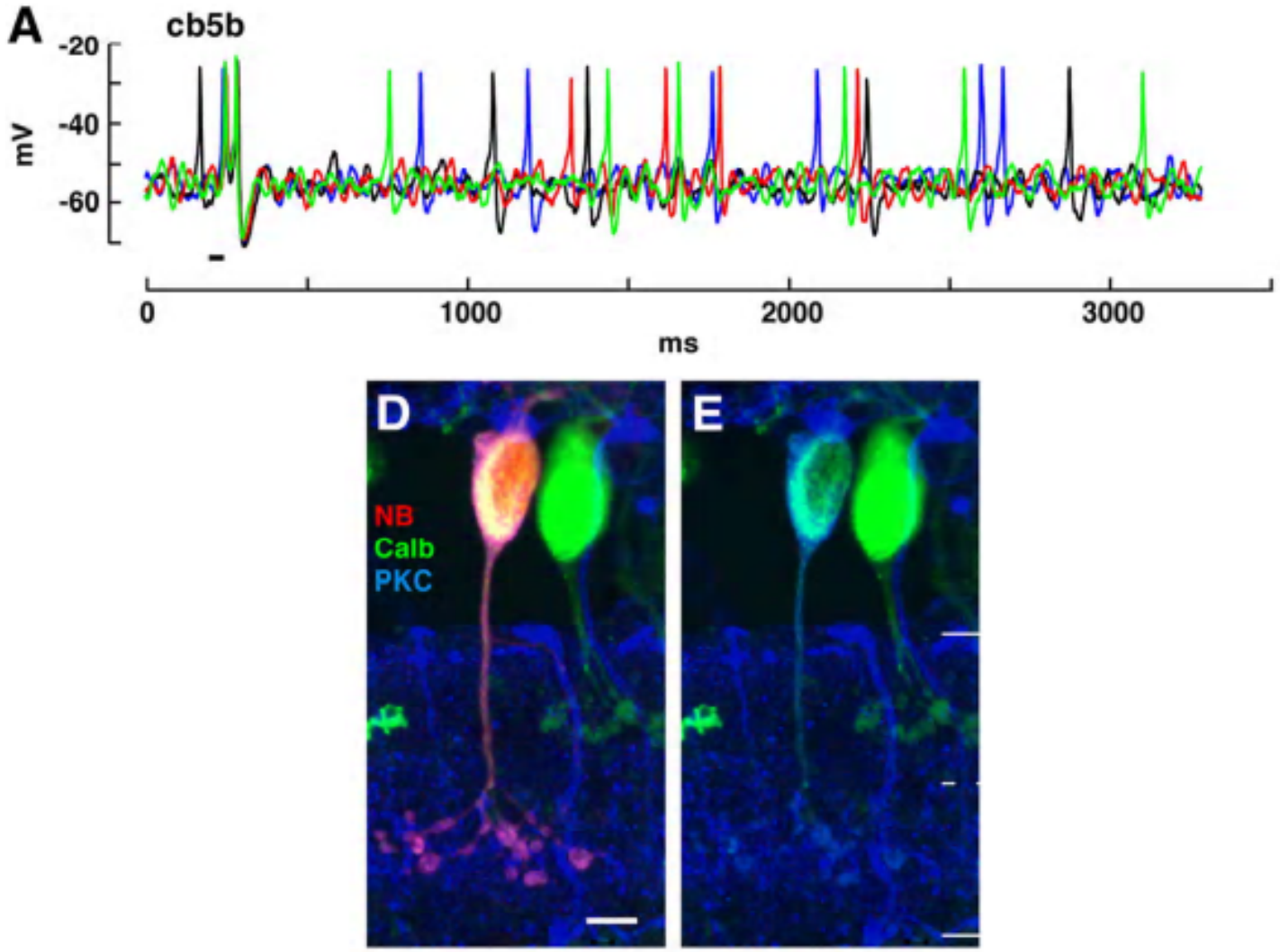

Figure 19. Spontaneous and light-evoked actions potentials in a ground squirrel bipolar cell. Four traces are superimposed in *A*. The short horizontal bar represents a 40 msec light flash that evokes a spike doublet at the beginning of each trace. The remaining spikes are spontaneous activity. In *D* the red label is the neurobiotin (NB) injected cb5b bipolar cell. In *E* this cell labels for protein kinase C (PKC), characteristic of ON bipolar cells, and calbindin (Calb). The green label in *D* and *E* is a calbindin reactive cb2 OFF bipolar cell, not recorded in this session. The scale bar is 5 µm. The illustration is modified from Saszik and DeVries, 2012 (5)...

waveforms of these ON or OFF inhibitions depend on whether the excitatory ON responses are rod or cone dominated. Rod dominated cells tend to have sustained ON inhibition without offset inhibitory transient, whereas cone dominated cells are transiently inhibited at both onset and offset of the stimulus (112). Immunocytochemical studies show that bipolar-cell dendrites and terminals are surrounded by GABAergic processes. In the OPL, these processes belong to horizontal cells; whereas, in the IPL, GABAergic amacrine cell processes surround bipolar terminals (165-170). Illustrations of the GABAergic inhibitory synaptic arrangements surrounding bipolar cell axon terminals appear in figure 21 for a cyprinid Mb (rod bipolar) terminal and in figure 22 for a cat rod bipolar cell axon terminal.

Bipolar cell processes are selectively sensitive to external GABA application (Fig. 23). GABA-evoked currents are typically greatest at the axon terminals (171-174), though smaller amplitude currents can be elicited from the soma and/or dendrites (Fig. 23). This suggests a major inhibitory feedback circuit from neighboring amacrine cells (171-175) occurs through direct GABAergic input onto bipolar-cell terminals. GABAergic inputs to bipolar dendrites may also occur indirectly, through a feedback synapse involving photoreceptors (176-179).

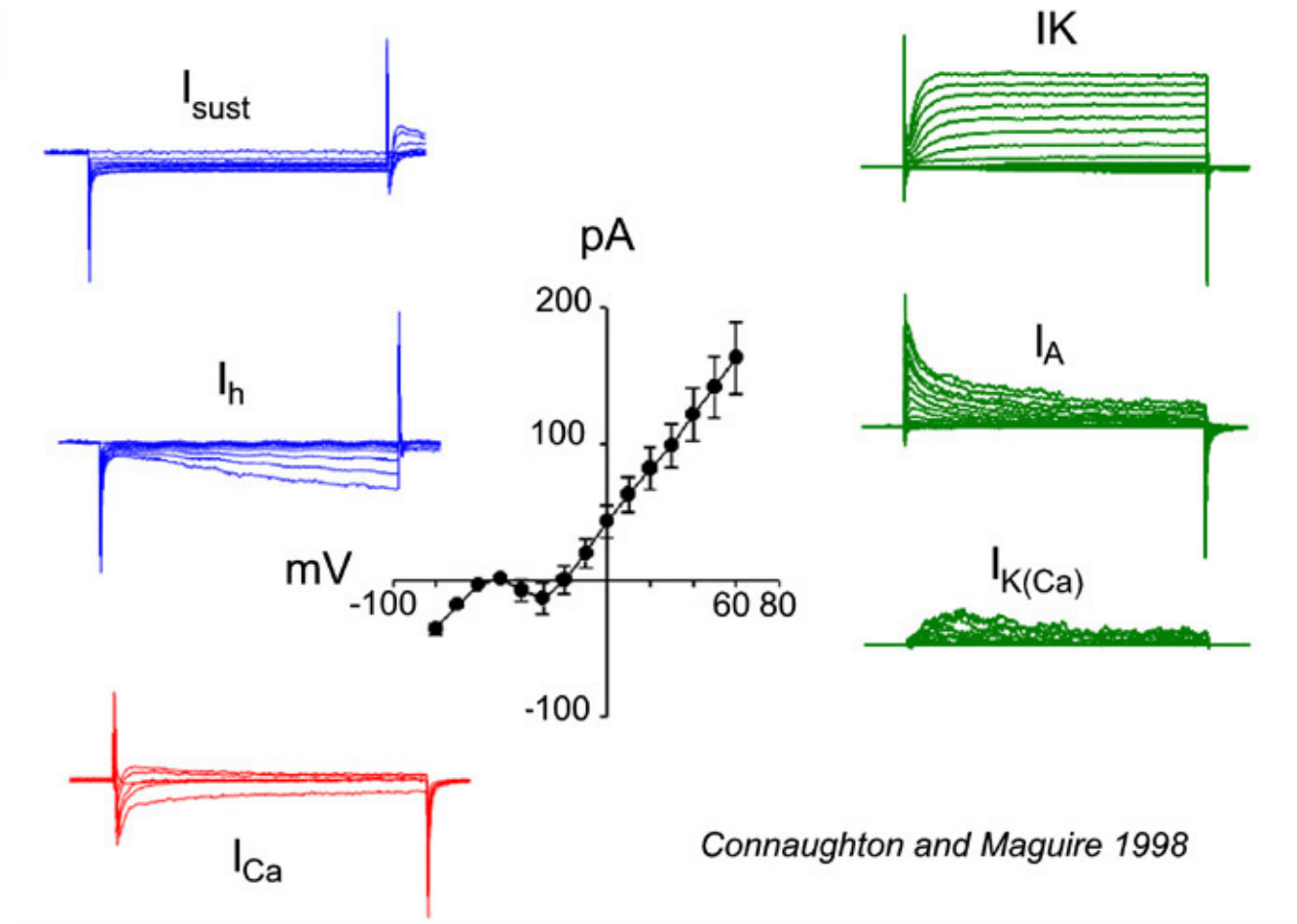

Figure 20. Voltage gated currents found in zebrafish bipolar cells. Inward currents (I_{sust} or I_h) are evoked by hyperpolarizing voltage (blue traces, left). Outward currents (IK, I_A and $I_{K(Ca)}$) are evoked by stepping membrane potential from -90 mV to a maximum of +60 mV (green traces, right). IK is the delayed rectifying K^+ current, I_A is the transient K^+ 'A' current, and $I_{K(Ca)}$ is the Ca^{2+} activated potassium current. I_A and I_{sust} tend to be found in the same cells, as do IK and I_h. I_{Ca} (below, red trace) is the depolarization-activated Ca^{2+} current. Both T (transient) and L (sustained) type Ca^{2+} currents are seen. In the center is the mean bipolar cell I-V plot, the prominent dip at -30 mV is caused by Ca^{2+} currents. The illustration is modified from Connaughton and Maguire, 1998 (146).

GABA application elicits a chloride (Cl^-) current. Depending on the Cl^- gradient either depolarization or hyperpolarization may result, though the most common result is hyperpolarization. GABA-elicited currents have both transient and sustained components. The transient response is mediated by $GABA_A$ receptors; while the sustained component results from the activation of $GABA_C$ receptors (173, 180-187). The sustained components of $GABA_C$ responses last many minutes and the hyperpolarizing action is readily seen in voltage probe studies of dissociated bipolar cells using oxonol, a slow distributive probe, as voltage reporter (171, 188). The different time courses of $GABA_A$ and $GABA_C$ currents and the different sensitivity to selective antagonists are illustrated for ferret bipolar cells in figure 24. The molecular properties of retinal $GABA_C$ receptors are explained in the Webvision chapter *GABAc Receptors in the Vertebrate Retina*. Interestingly, though most bipolar cells appear to express both $GABA_A$ and $GABA_C$ receptors, it is the $GABA_C$ receptor that underlies 70-80% of GABA-elicited responses. With light stimuli these receptors transfer more net charge to bipolar cell terminals than either $GABA_A$ or glycine receptors (189). Expression of both $GABA_A$ and $GABA_C$ receptors allows bipolar axon terminals to respond to a range of GABA concentrations and time courses within the synaptic cleft, as these different receptor types display collectively high sensitivity to long duration applications of low GABA doses ($GABA_C$), and short duration applications of high GABA doses ($GABA_A$) (181, 183).

$GABA_B$ is the 'metabotopic' GABA receptor. These receptors have been identified on the axon terminals of salamander and goldfish bipolar cells, where they reduce calcium influx (158, 190), modulating synaptic release of bipolar-cell glutamate.

Functional consequences of GABA inhibitory circuitry

GABA receptors affect the dynamics of retinal light responses (191-194). $GABA_A$ antagonists cause ganglion cell ON discharges to become more transient (193, 195), an effect seen in ON bipolar cells (195). Zhang et al suggest a serial synaptic pathway to explain this counterintuitive result. On this model, the native action of GABA, not GABA antagonists, is to make light responses more transient, through delayed inhibition. Amacrine cells synapsing on bipolar cells with $GABA_C$ synapses, however, are themselves inhibited by other amacrine cells utilizing $GABA_A$ synapses. Blockade of the $GABA_A$ input causes more robust inhibition of bipolar terminals by $GABA_C$ and further transience of light responses. In this model a counterintuitive action is explained by a polysnaptic pathway. $GABA_C$ currents measured in bipolar cells actually do increase in the presence of the $GABA_A$ antagonist bicuculline (189). GABA release from amacrine cells activates receptors on bipolar cell terminals, causing the suppression of a depolarization-elicited calcium current (158, 196) and associated synaptic release (197) presumably modulating or reducing neurotransmitter release from these cells (198). Measurement of the light evoked excitatory currents in amacrine cells postsynaptic to bipolar cells suggests that the kinetically slower $GABA_C$ inhibition limits the duration of excitatory post-synaptic events, whereas the faster glycine and $GABA_A$ inhibition limits the peak amplitude of postsynaptic excitatory events (191).

GABAergic synapses between A17 amacrine cells and rod bipolar cells (Fig. 22) activate $GABA_A$ receptors (199). While being wide in dendritic field, the action of A17 amacrine cells on rod-bipolar axon terminals is local (200, 201) and depends on calcium entry through local A17 AMPA channels excited by the rod-bipolar-cell ribbon synapse (201), not impulses propagating in the A17 dendrites (200). $GABA_C$ inhibition of rod bipolar terminals is long range and depends on impulse activity (200). These two inhibitory systems have been dissected in the Diamond laboratory. The short range reciprocal $GABA_A$ feedback is eliminated by ablating A17 amacrine cells with 5,7 dihydroxytryptamine (DHT), a toxic serotonin analogue that is selectively taken up by A17. The long range $GABA_C$ feedback is abolished by tetrodotoxin (TTX). This abolishes nerve spikes that allow signal propagation along amacrine cell dendrites other than A17. Interestingly, though wide in dendritic field, the regulatory actions of A17 appear to be independent local-circuit reciprocal interactions with rod bipolar cells (Fig. 25).

Inhibitory glycine-gated currents

Glycine applied to bipolar cells elicits a strychnine-sensitive, hyperpolarizing chloride current. As with GABA, different bipolar-cell regions are differentially sensitive to glycine. In mouse (156, 202) and carp (177) the axon terminal shows the greatest sensitivity; while in rat (147) and salamander (203) the dendrites are more sensitive. There is a tendency for glycinergic inhibitory circuitry to impinge selectively on OFF cone bipolar cells (177, 204); the outstanding example is AII amacrine innervation of the mammalian OFF cone bipolar cells (105, 205-207). In this case glycine acts as a neurotransmitter intermediary in the pathway to dark adapted ganglion-cell center responses (Fig. 18). In general the inhibitory pathway onto cone-bipolar-cell axon terminals uses glycine, whereas the rod bipolar axon terminal receives GABAergic inhibition (208). Glycine, however, is a component of inhibition on rod bipolar terminals. This pathway is innervated by both ON and OFF bipolar cells through a preferentially NMDA glutamate receptor mechanism impinging on amacrine cells (209). Dendritic impulse propagation plays a role in the transmission of glycinergic inhibition at this synapse. Noise analysis performed on glycine-elicited currents from dendrites and axon terminal suggests that each region may express a different subtype of glycine receptor (210). In fish retinas glycinergic inputs to bipolar-cell dendrites and axon terminals are believed to arise directly from populations of amacrine and glycinergic interplexiform cells (203).

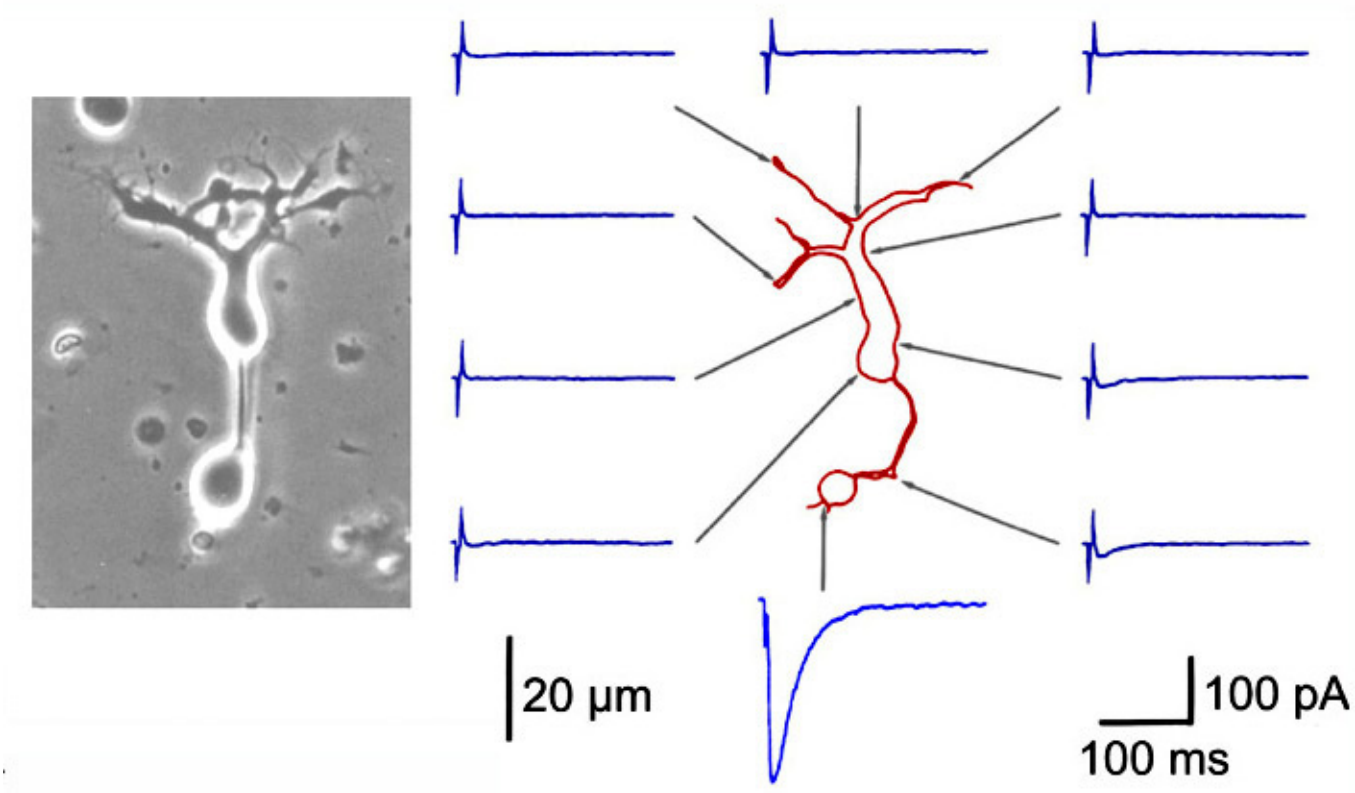

Figure 23. A rod bipolar cell is dissociated from goldfish retina (left). When the selected cellular regions are stimulated with micro puffs of GABA, the most sensitive region is the axon terminal (right). The figure is modified from Tachibana and Kaneko, 1987 (173).

Glycine-containing interplexiform cells have only been seen so far in fish retinas; glycine receptors can be found on processes postsynaptic to photoreceptors, including bipolar cell dendritic processes (211).

Glycine is believed to modulate the surround light responses of bipolar cells, though the reported effects of glycine are not consistent. Stone and Schutte (1991) (212), working in Xenopus, report that glycine application eliminated surround responses in both ON- and OFF-type bipolar cells. In contrast, surround responses in salamander are not blocked by glycine (213). While GABA application elicits responses in all bipolar cells examined, glycine elicits responses from only a subset of bipolar cells, such as OFF bipolar cells in carp (177) and the small-field bipolar cells in skate (214), suggesting glycine may have a selective role in retina. Glycinergic feedback connections between amacrine and bipolar cells decrease light-evoked glutamate release onto ganglion cell dendrites (198). Glycinergic feed-forward synapses transfer rod bipolar signals from AII amacrine cells to OFF cone bipolar terminals in mammalian retinas (105, 215). Thus, glycinergic synapses onto bipolar cells may be important in mediating the transfer of information among neurons in both the proximal and distal retina.

Glutamate release from vesicles in goldfish bipolar cell axon terminals

Due to their large size, the axon terminals of goldfish Mb1-type ON-bipolar cells are used as a model system in which to examine neurotransmitter release. The axon terminal can be directly recorded in patch clamp studies (216). Changes in internal calcium (217) and both exocytosis and endocytosis activity (217, 218) can be detected using fluorescent calcium probes and observing capacitance changes as vesicle membrane is added or removed from this presynaptic terminal. Images of releasing vesicles at Mb1 terminals are seen by evanescent fluorescence microscopy in figure 26.

Neurotransmitter release from bipolar terminals occurs at ribbon synapses (219, 220); conventional synapses are rare in bipolar axon terminals although they have been seen in some species (221, 222). Each ribbon is an

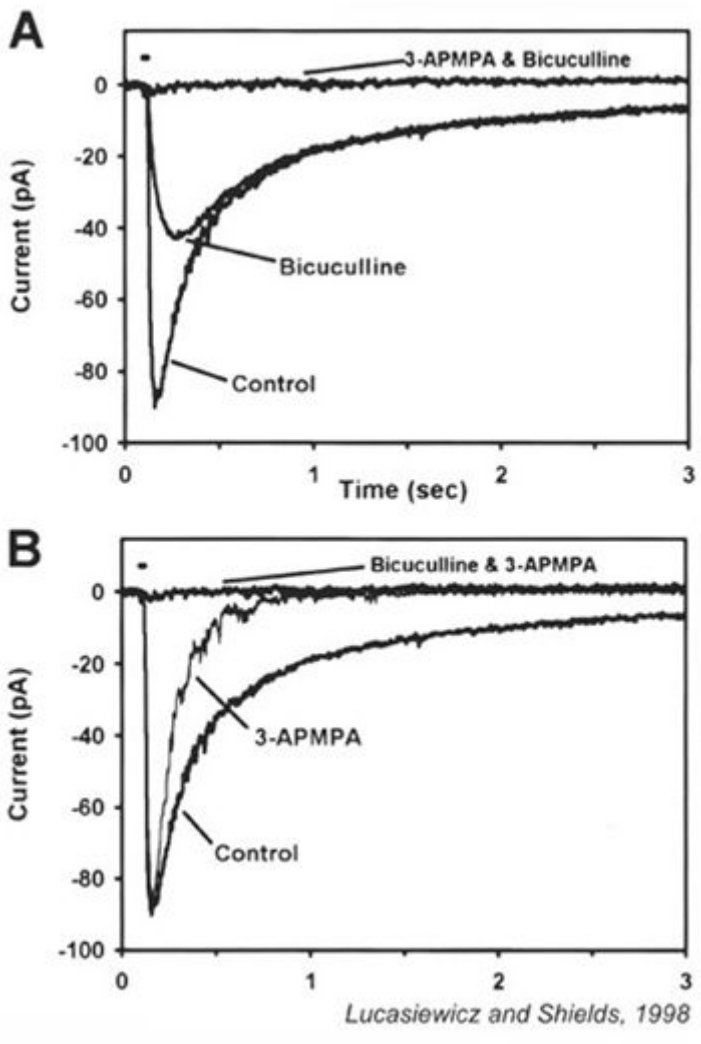

Figure 24. Mixtures of $GABA_A$ and $GABA_C$ receptors in ferret OFF bipolar cells are separately blocked by selective antagonists. *A*. The transient $GABA_A$ response component is blocked by bicuculline (200 μM), leaving a slowly desensitizing $GABA_C$ waveform. *B*. The $GABA_C$ response component is blocked by 3-APMPA (300 μM), leaving the rapidly desensitizing $GABA_A$ waveform. When both antagonists are mixed together, the GABA response is fully blocked. The illustration is from Lukasiewicz and Shields, 1998 (182).

electron dense structure oriented perpendicular to the plasma membrane. One ribbon may contain as many as ~110 tethered vesicles along the sides. Vesicles along the base of the ribbon, or "docked vesicles", are in contact with the presynaptic membrane (216). The arrangement of the ribbon synapse at the bipolar cell axon terminal and associated post-synaptic events are shown in figure 27. All vesicles associated with the ribbon constitute the readily releasable pool of vesicles. Since one axon terminal averages 55 active zones in the goldfish, each with an associated ribbon (218), there are ~6000 tethered or rapidly releasable vesicles per terminal (von Gersdorff et al., 1996). Combining these values with capacitance measurements indicates that maximal release per active zone occurs at a rate of ~500 vesicles/sec (216). Species with smaller rod or cone bipolar axon terminals (amphibians, reptiles and mammals) have smaller numbers of ribbons and smaller volumes to contain synaptic vesicles so the release rates may be different compared with the model goldfish system.

The ribbon synapse, in the absence of light, releases vesicles spontaneously. The single spontaneous excitatory postsynaptic synaptic currents (sEPSCs) can be studied by voltage clamp techniques in ganglion cells (221). It is thought that normal spontaneous release activates AMPA receptors located immediately below the active release zone (Fig. 27). Light stimulation of ON bipolar cells induces release of many vesicles along a single ribbon site and glutamate spillover activates both AMPA and NMDA receptors (Fig. 27). The patch recordings of sEPSCs,

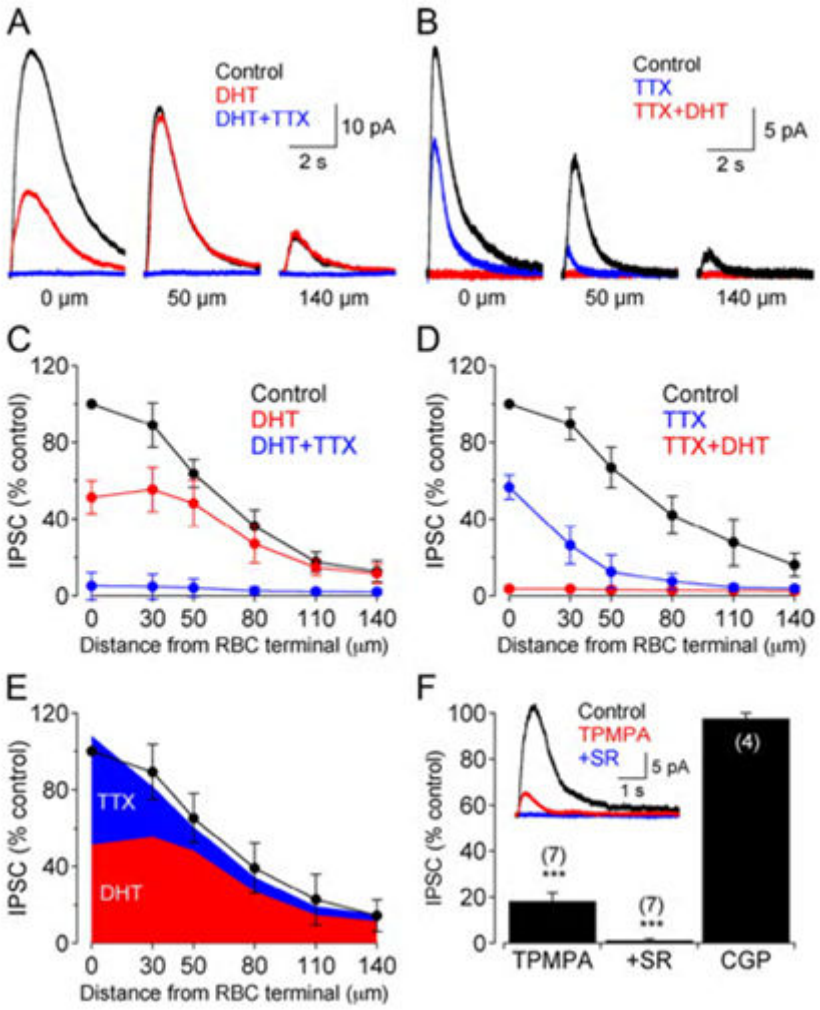

Figure 25. Long-range and short-range inhibitory circuits for rod-bipolar-cell axon terminals. Ablation of A17 amacrine cells in rat retina with 5,7 dihydroxytramine (DHT) eliminates local GABAergic inhibitory post synaptic currents (IPSC) in rod bipolar terminals. Tetrodotoxin (TTX), which blocks nerve spikes, eliminates long range IPSC's. *A-D*. The spatial profiles of GABA inhibitory responses are evaluated by puffing glutamate at different distances. This excites all GABAergic amacrine cells. DHT-ablated retinas lack local feedback from A17 amacrine cells. TTX treated retinas lack long range feedback. *E*. TTX and DHT sensitive inhibition add to produce total observed inhibition. This suggests a lack of interaction between the two systems. *F*. TPMPA, a $GABA_C$ antagonist blocks virtually all inhibition in DHT treated retinas, suggesting long range inhibition acts through $GABA_C$ receptors. The illustration is from Chavez, Grimes and Diamond, 2010 (200).

under conditions of hyperosmotic Ringer to enhance rates of spontaneous events, reveal large and small as well as fast and slow events (Fig. 27, control). The sEPSCs are mostly eliminated by NBQX, a highly selective antagonist for AMPA and kainate receptors (Fig. 27, NBQX). But small amplitude events still are seen (Fig. 27, NBQX) until the NMDA antagonist D-AP7 is added (Fig. 27, NBQX+DAP7). This indicates that both AMPA and NMDA receptors are active in post-synaptic ganglion cells (223). Further, a maintained inward current is also blocked by both these antagonists, suggesting bipolar-cell ribbon synapses transfer information across a broad temporal spectrum.

Vesicular release at the bipolar ribbon synapse occurs in a calcium-dependent manner (224-226), though there does not appear to be a selective requirement for calcium, as other divalent ions, such as strontium and barium, can stimulate exocytosis, though to a lesser degree (227). Calcium entry occurs through L-type channels in goldfish (155) and/or T-type channels in mouse (228). These channels are located on the axon terminal

membrane. Internal calcium concentrations of 10-20 μM stimulate exocytosis (155) of the readily releasable pool (216, 218, 229). Exocytosis occurs in two phases. Initially, membrane depolarization elicits an increase in capacitance (time constant ~1.5 ms) corresponding to the rapid release of docked vesicles. This is followed by a second capacitance increase with a slower time constant (~250-300ms), believed to represent the movement of tethered vesicles to the active zone and their subsequent release (218, 230). Estimates indicate that 20% or ~1100 vesicles (of the 6000 in the readily releasable pool) are released during rapid exocytosis (229, 230), with the remainder released during the slow component. The depleted pool is restocked with a time constant of about 8s (231). Both the fast and slow phases are calcium-dependent, though they display differential sensitivities to calcium buffers (230).

Following neurotransmitter release, the vesicular membrane is recovered rapidly (226) and continuously (217, 232). The continual cycling of vesicles through the processes of exocytosis and endocytosis, is compatible with tonic release of neurotransmitter (217). This is suspected as bipolar cells generate sustained responses to light, and at least in some cases, transmit sustained signals to postsynaptic neurons (1). Though neurotransmitter is released following continuous or paired-pulse stimulation of the terminals, release decreases with time (229, 230). This synaptic depression is believed to be due to depletion of the readily releasable pool and a decrease in exocytosis of this pool (229).

Vesicle release at the mammalian rod-bipolar-to-AII-amacrine synapse

The pharmacology and kinetics of the mammalian ribbon synapse between rod bipolar cells and AII amacrine cells has been studied by simultaneous patch recording of presynaptic and postsynaptic cells (199). This glutamatergic synapse uses exclusively AMPA receptors (233). Within the retinal inner plexiform layer there is a transformation from the largely sustained light response of bipolar cells to the largely transient responses of amacrine cells (1). The mechanism of this transformation is a major topic for retinal neural circuitry. Rod bipolar cells respond to maintained light stimuli with maintained depolarizations (123), whereas the AII amacrine response to light is a transient depolarization (123, 132). Singer and Diamond (2003) (199) argue that vesicle depletion, at least a higher stimulus levels, is a major contributor to the sustained-transient transformation (123, 132). The rod-bipolar-to-AII synapse is fast, rising to peak in about 1 ms following depolarization of the rod bipolar. It is also transient, responding to a depolarizing rectangular voltage step in the presynaptic rod bipolar with a saw-toothed waveform decaying to a lesser steady-state release level within 20 msec. Presynaptic calcium currents that lead to vesicle release are L-type and sustained and do not explain the decay (199). The sustained-to-transient transformation occurs even in the presence of inhibitory synaptic blockers that block reciprocal $GABA_A$ feedback. GABA feedback could be observed as a delayed transient outward current in the rod bipolar recording, but did not measurably alter synaptic release.

After the decaying phase of the response completes, a residual train of small synaptic events persists. The transient waveform slows, but is evident, even at stimulation threshold (199). Singer and Diamond (2003) conclude that presynaptic vesicle depletion within a 'releasable pool' accounts for the transient waveform of the synapse. Decline in the number of available vesicles reduces the number of vesicles released over time, even though for an individual vesicle this probability may remain constant. This is typical of synaptic transmission. One unique feature of this synapse however is synchronous release of vesicle pairs (234). Singer and Diamond (2006) (235) estimate the readily releasable pool in the rat rod-bipolar-cell terminal is in net about 70 vesicles, which amounts to about 7 vesicles per ribbon. The synapse appears able to replace vesicles at about 0.5 vesicles/ms, giving each ribbon a steady-state release rate of about 50/s. Release is easily depressed in paired pulse experiments and recovers with a time constant only of about 4 s, but sustained exocytosis appears to accelerate vesicle recovery. These properties may confer the ability for synaptically-based neural adaptation (235).

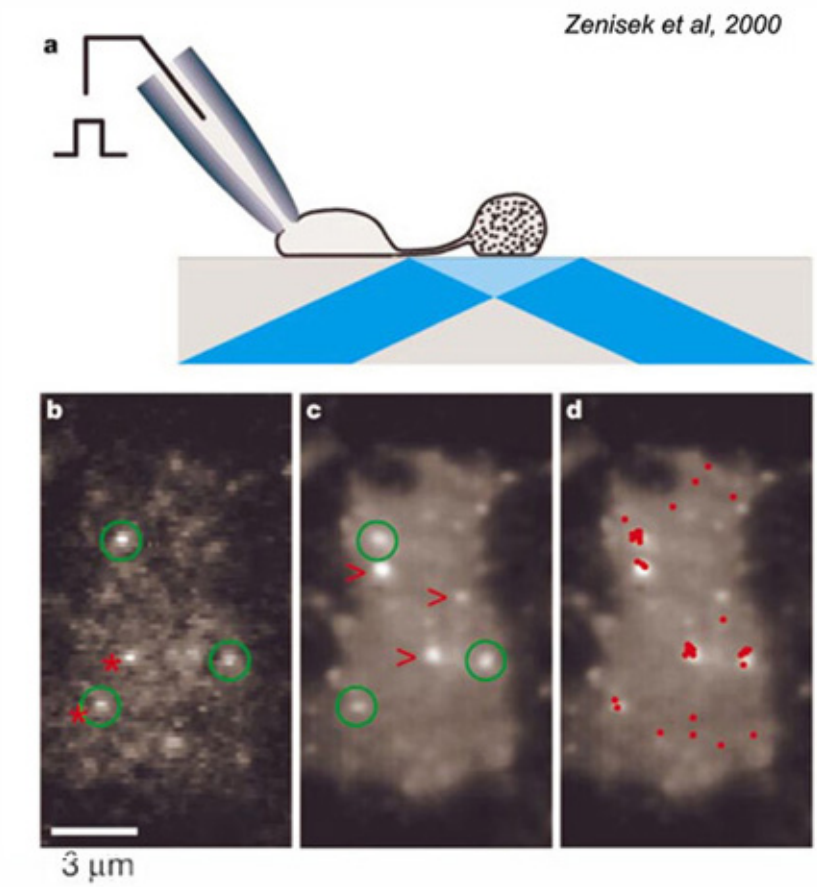

Figure 26. Vesicle release at Mb-1 bipolar terminals can be observed by evanescent fluorescence microscopy. *a*. Schematic showing simultaneous stimulation of release by patch recording, and dark-field evanescent fluorescence imaging of FM1-43 loaded fluorescent vesicles. *b*. Single frame showing vesicles near the membrane. The asterisked vesicles were released and disappeared in subsequent frames *c* and *d*. Averages of multiple images show preferred sites of vesicle docking and or release (circles and arrowheads in *c*, *d*. The actual sites of release during the averaged image are indicated as red dots. The illustration is from Zenesek et al, 2000 (218).

5. Behavioral and clinical implications of bipolar-cell abnormalities

ON bipolar cells appear uniquely vulnerable to insult. The mGluR6 receptor, for example, can be selectively removed (i.e., knocked out) without major effect on other neural pathways. This can be accomplished through a variety of techniques, such as use of selective pharmacological blocking agents (i.e., APB) or site directed mutagenisis techniques designed to eliminate the mGluR6 receptors themselves (Fig. 4). Further, naturally occurring mutations and disease processes related to mGluR6 selectively target ON bipolar cells. These include compromise of the TRPM1 channel (Fig. 7), and the associated glycoprotein nyctalopin (Fig. 9). Other disease processes also single out ON bipolar cells. Surprisingly humans or animal models with ON-bipolar deficit(s) perform visual tasks relatively normally. The major problem is loss of nocturnal vision, which appears dependent on the physiological integrity of a single ON bipolar-cell type, the mammalian rod bipolar cell.

Mice with ON bipolar knockout perform visual tasks

The electrophysiological consequences of site-directed mutagenisis directed at the ON pathway are seen in figure 4 for mGluR6 deficient mice. The electroretinographic b-wave component, which arises from the activity of ON bipolar cells, is abolished (31). These authors further demonstrate that light-evoked field potentials from the

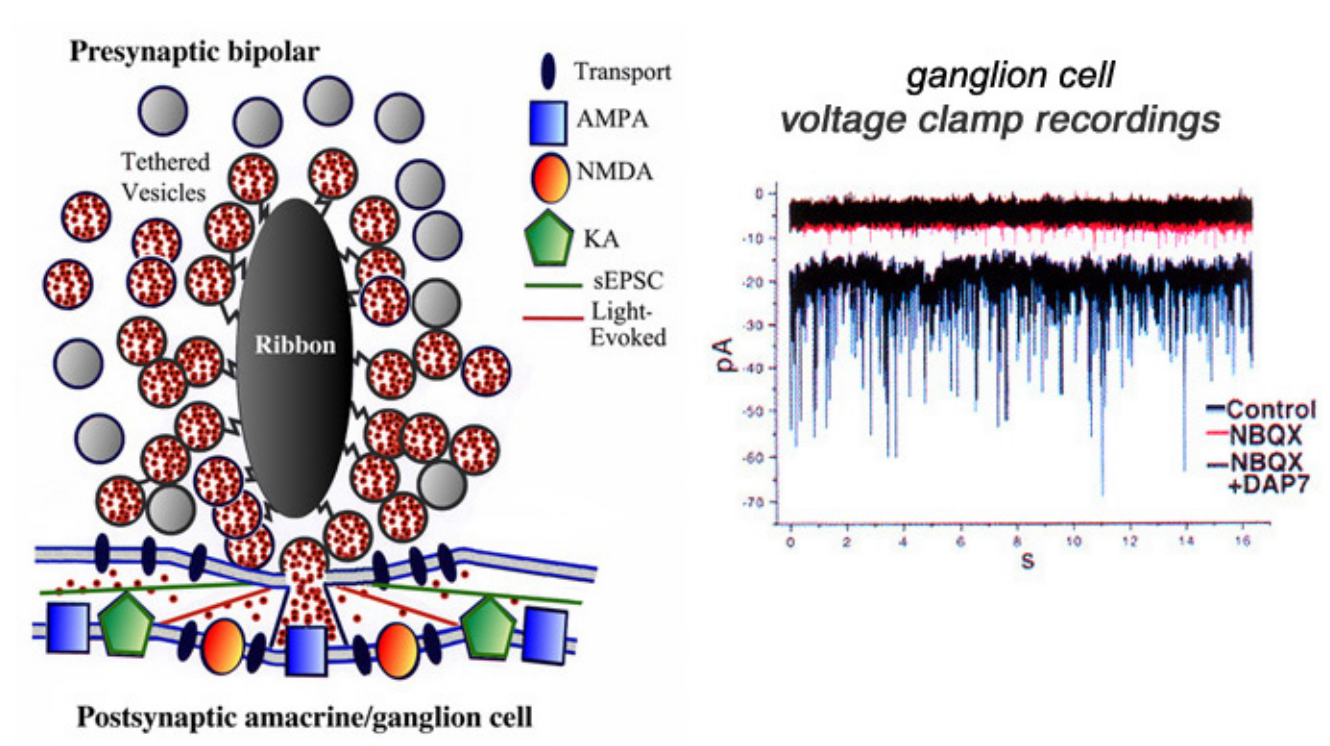

Figure 27. *Left*, cartoon of a ribbon synapse at a salamander ON bipolar synapse. Docked vesicles, release sites, transporters and postsynaptic receptors are indicated. *Right*, voltage clamp recordings (V_H= −70 mV) from a salamander ganglion cell postsynaptic to an ON bipolar cell show rapid inward events (EPSCs) as large as 50 pA, as well as baseline fluctuations, suggesting that both fast and slow events contribute to the responses. NBQX, a selective antagonist for AMPA and KA receptors, eliminates most large spontaneous events but the addition of D-AP7 (NMDA specific antagonist) is needed to eliminate the small amplitude events. The illustration is from Miller et al., 2001 (221).

superior colliculus, which in mouse is the main termination site for ganglion cell axons, lack ON responses, though OFF-type waves appear. In wild type mice, transient collicular waves are seen at both onset and cessation of light stimuli. The altered mGluR6 physiology would seem to imply a behavioral deficit.

Interestingly some tests do suggest deficits in behavior while others do not. In a shuttle box avoidance learning analysis, both mutant and wild type mice performed equally well (31). Since the original site-directed mutant line was created, a forward-genetic mGluR6-mutant line, nob4, has been found (236). Circadian clocks, characterized by wheel running activity in the dark phase, are normal in both mutants. In each mutant light stops this activity (237, 238). In the site-directed mutant this action is phase delayed (237); in nob4 this action is sensitized, a seemingly paradoxical result (238). In both mutants pupillary responses were observed only at high light levels (238, 239). In the site-directed mutant optokinetic responses were seen only at high contrasts (239), suggesting a general loss of sensitivity. These studies indicate that the OFF bipolar cells alone can mediate vision, even if somewhat impaired. Interestingly the ON and OFF layering of the inner plexiform layer persists in the site-directed mutant (240).

Melanoma-associated retinopathy (MAR)

Some patients with malignant melanomas lose night vision. They may further report hallucinations consisting of shimmering blobs of white light (241, 242). Visual processing in daylight appears otherwise normal. Color vision is not affected, nor is visual acuity dramatically worsened. Electroretinography reveals ON bipolar cell deficits for these patients. As with mGluR6 deficient mice, the b-wave is selectively absent in both rod and cone driven

responses (243) and the patients may have reduced contrast sensitivity (244). Although originally thought to be a side effect of chemotherapy (242), it became clear that the syndrome might arise in cancer patients prior to chemotherapy (241, 243). The IgG serum fraction of MAR patients induces reversible electroretinographic disturbances similar to MAR when injected into the eyes of monkeys (245). Electroretinographic a-waves and d-waves remain; the b-wave is lost from both rod and cone responses (Fig. 28). MAR appears to be caused by an autoimmune attack against retinal ON bipolar cells for both rod and cone vision. Antibodies induced by the melanoma cause the visual deficit. One of the epitopes appears to be the ON-bipolar-cell TRPM1 channel (246, 247), perhaps not surprisingly as the channel name derives from 'melanoma related'. MAR is one of several paraneoplastic retinopathies (PR) or cancer-associated retinopathies (CAR).

Congenital stationary night blindness (CSNB)

This visual dysfunction is an inherited retinal disease very similar in symptoms to MAR. In the Schubert-Bornschein, or complete, type (248), there is loss of nocturnal or rod vision (Fig. 29), but in daylight, cone-mediated color vision and visual acuity are relatively normal (249, 250), though the sensitivity of cone vision is somewhat reduced (250, 251). The disease is X-linked, affecting primarily males (250, 251).

Electroretinograms (Fig. 29) reveal a loss of b-waves for both the rod and cone systems. ON bipolar cell signals appear greatly depressed or absent, OFF cone bipolar signals, as represented by the electroretinographic d-wave, are spared (243), as is the rod a-wave (249). The presence of a rod a-wave but not b-wave provided the first suggestion that the retina could have genetic diseases of the post receptor, neural processing machinery (249).

Early on it became apparent that CSNB was a heterogeneous disease. Miyake et al (250) classified CSNB as 'complete' and 'incomplete'. 'Complete' or 'Shubert-Bornshein' type lacked all rod function and had no b-wave. 'Incomplete' or 'Riggs' type had reduced b-wave and rod function. Both 'complete' and 'incomplete' forms occurred nearly exclusively in males (50 of 55 examples) (250), and so both were X-linked, but multiple examples within a family tree were only of one type. Genetic analysis reveals that the complete form of CSNB involves defects in the glycoprotein nyctalopin (252). Animal models of this gene defect appear in the section *Metabotropic responses of ON bipolar cells*. Mutant proteins disrupt neurotransmission in ON bipolar cells. The genetic defect in incomplete CSNB has been localized to a gene uniquely expressed in retina and similar to the L-type calcium channel alpha subunit (253). Defects in this gene, CACNA1F, provide an example of a human retinal channelopathy.

There are also examples of human mutations in the *GRM6* gene, the gene that encodes mGluR6. This defect also results in CSNB, a type called 'arCSNB', 'ar' for 'autosomal recessive'. In this type an abnormal 15Hz flicker response near rod threshold distinguishes the electrical phenotype (254). The authors interpret this phase-reversed scotopic threshold response as the survival of an alternative rod pathway, perhaps an element of the 2 rod pathway model (145). More recently another autosomal recessive form of 'Complete CSNB' has been identified. This is a particularly common in females. The ON-bipolar-cell TRPM1 cation channel is the genetic defect (62). In this case the 15Hz rod flicker is similar to X-linked (*NYX* -/-) CSNB. Animal models of these defects are discussed above (see *Metabotropic responses of ON bipolar cells*).

6. Visual processing under mGluR6 blockade of the ON bipolar cells

Lateral geniculate and cortical neurons.

The responses of visual neurons in the central nervous system of primates have been investigated under conditions of ON-bipolar blockade using the metabotropic glutamate receptor agonist APB (DL AP-4). Recordings from the dorsal lateral geniculate nucleus (LGNd) indicate that light responses of ON-center geniculate neurons are completely blocked by APB (255, 256). ON-center geniculate cells are also blocked

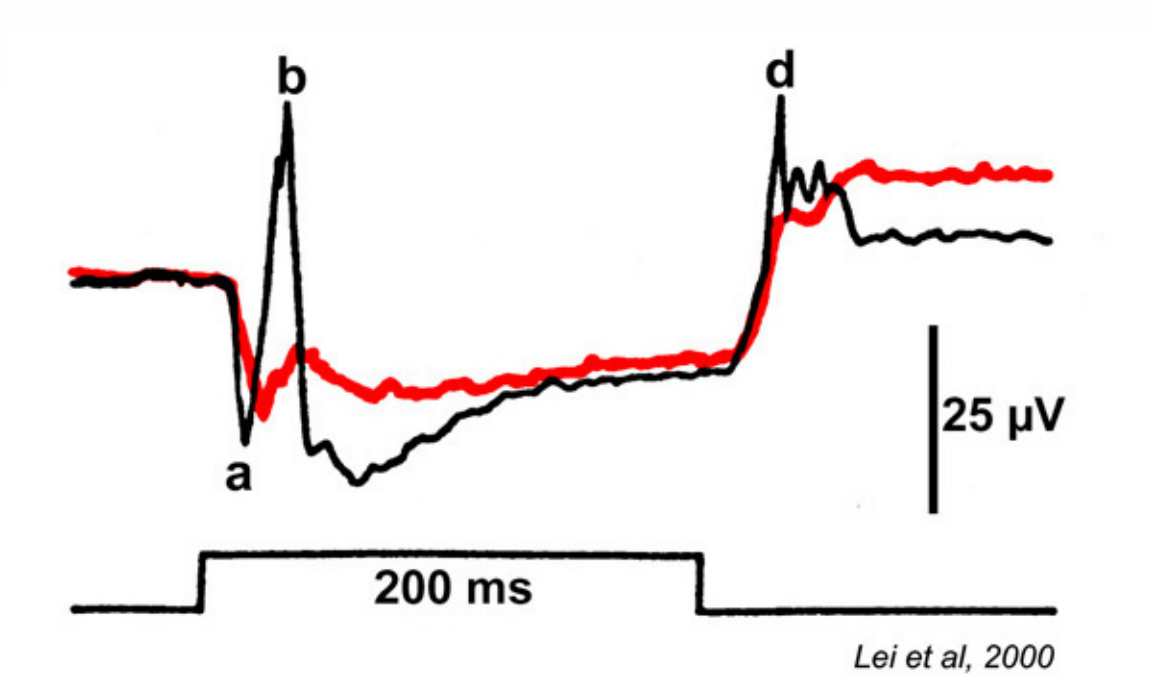

Figure 28. The ERG recordings are from a non-human primate model of melanoma-associated retinopathy (MAR), a disease sometimes associated with a primary cancer. The thin black trace represents a normal ERG with a, b and d waves. The red trace was recorded from an eye treated with an intravitrial injection of IgG from a patient experiencing MAR. There is a marked reduction in the b-wave. The illustration is from Lei et al, 2000 (245).

selectively in rabbit (257). Projection of retinal ganglion cells onto geniculate relay cells is selective for physiological types (258) so that ON and OFF pathways are preserved and can be selectively affected by retinal blockers.

Recordings of light responses of individual neurons in visual cortex suggest this is the site of final integration for ON and OFF bipolar-cell signals and their associated retinal neurons. Complex cortical cells continue to respond under APB blockade of ON bipolar cells, but leading edge responses to bright squares drifting through the receptive field are lost (255). The directional selectivity and orientation selectivity of these cortical cells appears unperturbed by the blockade (255). In a parallel study, monkeys under APB blockade were found to have much poorer perception of light increments than light decrements, but relatively unimpaired perception of simultaneous spatial contrast (259). Elimination of synaptic function for all ON bipolar types in mammals leaves a surprisingly functional visual system.

Dim light responses require ON bipolar cells

One common feature of rod-dominated mammalian retinas is the emergence of a single, ON-type bipolar cell for rods (64, 123, 124) dominated by the metabotropic, mGluR6, glutamate receptor and associated molecules. Pharmacological blockade of this pathway leads to physiological deficits in night vision. This is true behaviorally for both light increments and decrements (260), as well as for dim light responses in ON or OFF ganglion cells (205). Knockout of ON bipolar cell signals in mGluR6-deficient mice leads to loss of light sensitivity evident in the electroretinogram (31). As noted above ON bipolar cell diseases in humans are always accompanied by a loss of nocturnal vision. The secondary rod pathways that utilize either cone-system OFF bipolar cells or gap-junction pathways between rods and cones appear not to be involved in rod-mediated nocturnal vision, but rather it is rod-bipolar-cell metabotropic receptors that mediate dim light responses.

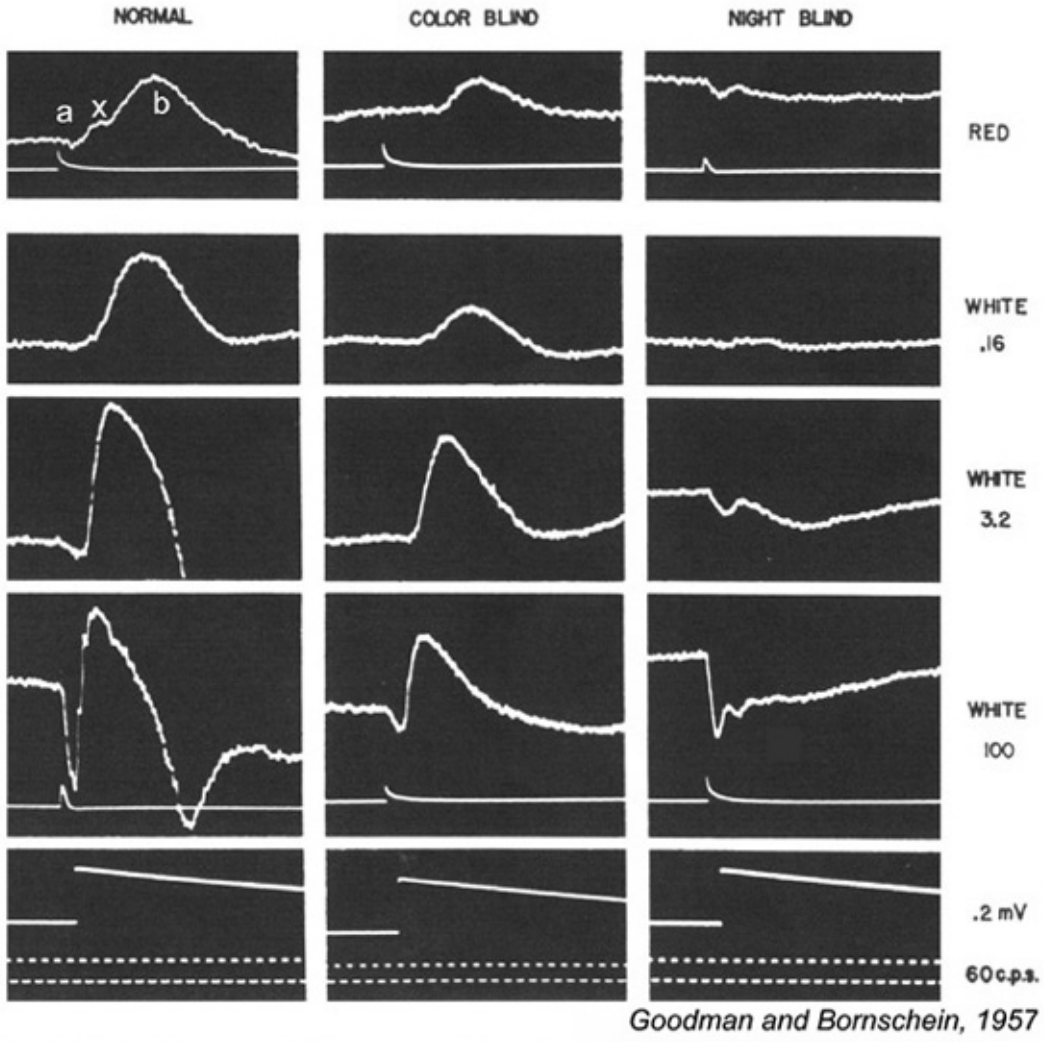

Figure 29. ERG responses from humans with a genetic retinal defect are compared to a normal subject. The color blind subject (middle column) lacks the x-wave, but has a normal b-wave and ON bipolar function. The night-blind subject (right) responds with an x-wave to red stimulation, but lacks a b-wave for any stimulation. An isolated a-wave appears with bright stimulation. The night blind subject is an early example of congenital stationary night blindness (CSNB).The illustration is from Goodman and Bornschien, 1957 (249).

7. Summary and conclusions

Bipolar cells are functionally crucial neurons that comprise the middle component of the vertical transduction pathway through the retina. ON- and OFF-type bipolar cells are presynaptic to similarly polarized ganglion cells in the retinal inner plexiform layer and can be distinguished by morphology, by light response, and by different types of dendritic glutamate receptor expression. These cells serve as models in which to examine different aspects of neurobiology, including embryological development, postsynaptic receptor systems, neurotransmitter release mechanisms, neural circuitry interactions, and visual system defects. ON and OFF bipolar cells initiate two functionally independent pathways, the ON and the OFF, each with center-surround organization, and each with a splitting into both transient and sustained signal types postsynaptic to bipolar cells. Each bipolar pathway is capable of independent image processing. The signals of ON and OFF bipolar cells are relayed separately to higher brain centers. ON bipolar cells appear selectively vulnerable to diseases, genetic defects, or pharmacological assault. Loss of ON bipolar cells results in a loss of nocturnal vision.

About the Authors

The biosketch for Ralph Nelson can be found in the About the Editors section of Webvision.

Victoria Connaughton, Ph.D. is an Associate Professor of Biology at American University in Washington DC. Born in Sellersville, Pennsylvania, Vikki earned a B. S. degree from Bucknell University and Ph. D in Marine Science from the University of Delaware, Lewes. She has been a postdoctoral fellow at the University of Texas, Houston in the Department of Neurobiology and Anatomy, and also at the National Institutes of Health where she continued studies of zebrafish retinal neuroanatomy and neurophysiology with co-author Ralph Nelson. Dr. Connaughton's current research interests encompass the disciplines of developmental biology (nervous system development) and neurobiology. Specifically, she is interested in examining the relation between visually-guided behaviors in larval teleosts and maturation of retinal neurons, circuits, and receptor mechanisms. She is also interested in examining how the development of neural connections can be altered due to mutations or drugs. She has performed experiments that address behavioral/ecological questions, as well as those that employ cell biology techniques to examine retinal circuitry in both developing and adult retinal tissue.

References

1. Werblin F.S., Dowling J.E. Organization of the retina of the mudpuppy, Necturus maculosus. II. Intracellular recording. J Neurophysiol. 1969;32(3):339–55. PubMed PMID: 4306897.
2. Kuffler S.W. Discharge patterns and functional organization of mammalian retina. J Neurophysiol. 1953;16(1):37–68. PubMed PMID: 13035466.
3. Protti D.A., Flores-Herr N., von Gersdorff H. Light evokes Ca^{2+} spikes in the axon terminal of a retinal bipolar cell. Neuron. 2000;25(1):215–27. PubMed PMID: 10707985.
4. Dreosti E., et al. In vivo evidence that retinal bipolar cells generate spikes modulated by light. Nat Neurosci. 2011;14(8):951–2. PubMed PMID: 21706020.

5. Saszik S., DeVries S.H. A Mammalian Retinal Bipolar Cell Uses Both Graded Changes in Membrane Voltage and All-or-Nothing Na^+ Spikes to Encode Light. J Neurosci. 2012;32(1):297–307. PubMed PMID: 22219291.
6. Connaughton V.P., Graham D., Nelson R. Identification and morphological classification of horizontal, bipolar, and amacrine cells within the zebrafish retina. Journal of Comparative Neurology. 2004;477:371–385. PubMed PMID: 15329887.
7. Euler T., Schneider H., Wässle H. Glutamate responses of bipolar cells in a slice preparation of the rat retina. J Neurosci. 1996;16(9):2934–44. PubMed PMID: 8622124.
8. Kolb H., Nelson R., Mariani A. Amacrine cells, bipolar cells and ganglion cells of the cat retina: a Golgi study. Vision Res. 1981;21(7):1081–1114. PubMed PMID: 7314489.
9. Wässle H., Boycott B.B. Functional architecture of the mammalian retina. Physiol Rev. 1991;71(2):447–80. PubMed PMID: 2006220.
10. West R.W. Light and electron microscopy of the ground squirrel retina: functional considerations. J Comp Neurol. 1976;168(3):355–77. PubMed PMID: 950385.
11. Wu S.M., Gao F., Maple B.R. Functional architecture of synapses in the inner retina: segregation of visual signals by stratification of bipolar cell axon terminals. J Neurosci. 2000;20(12):4462–70. PubMed PMID: 10844015.
12. Wu S.M. Synaptic organization of the vertebrate retina: general principles and species-specific variations: the Friedenwald lecture. Invest Ophthalmol Vis Sci. 2010;51(3):1263–74. PubMed PMID: 20185835.
13. Boycott B.B., Wässle H. Morphological Classification of Bipolar Cells of the Primate Retina. Eur J Neurosci. 1991;3(11):1069–1088. PubMed PMID: 12106238.
14. Ishida A.T., Stell W.K., Lightfoot D.O. Rod and cone inputs to bipolar cells in goldfish retina. J Comp Neurol. 1980;191(3):315–35. PubMed PMID: 7410596.
15. Li W., DeVries S.H. Bipolar cell pathways for color and luminance vision in a dichromatic mammalian retina. Nat Neurosci. 2006;9(5):669–75. PubMed PMID: 16617341.
16. MacNeil M.A., Gaul P.A. Biocytin wide-field bipolar cells in rabbit retina selectively contact blue cones. J Comp Neurol. 2008;506(1):6–15. PubMed PMID: 17990268.
17. Mariani A.P. The neuronal organization of the outer plexiform layer of the primate retina. Int Rev Cytol. 1984;86:285–320. PubMed PMID: 6368448.
18. Marshak D.W., et al. Localization of immunoreactive cholecystokinin precursor to amacrine cells and bipolar cells of the macaque monkey retina. J Neurosci. 1990;10(9):3045–55. PubMed PMID: 2398370.
19. Scholes J.H. Colour receptors, and their synaptic connexions, in the retina of a cyprinid fish. Philos Trans R Soc Lond B Biol Sci. 1975;270(902):61–118. PubMed PMID: 234623.
20. Kolb H. Organization of the outer plexiform layer of the primate retina: electron microscopy of Golgi-impregnated cells. Philos Trans R Soc London. 1970;258:261–283. [Biol]. PubMed PMID: 22408829.
21. Ayoub G.S., Copenhagen D.R. Application of a fluorometric method to measure glutamate release from single retinal photoreceptors. J Neurosci Methods. 1991;37(1):7–14. PubMed PMID: 1677056.
22. Nelson R. A comparison of electrical properties of neurons in Necturus retina. J Neurophysiol. 1973;36(3):519–535. PubMed PMID: 4349059.
23. Toyoda J. Membrane resistance changes underlying the bipolar cell response in the carp retina. Vision Res. 1973;13(2):283–94. PubMed PMID: 4348152.
24. Dacheux R.F., Miller R.F. Photoreceptor-bipolar cell transmission in the perfused retina eyecup of the mudpuppy. Science. 1976;191(4230):963–4. PubMed PMID: 175443.
25. Lasansky A. Properties of depolarizing bipolar cell responses to central illumination in salamander retinal slices. Brain Res. 1992;576(2):181–96. PubMed PMID: 1515915.
26. Hirasawa H., Shiells R., Yamada M. A metabotropic glutamate receptor regulates transmitter release from cone presynaptic terminals in carp retinal slices. J Gen Physiol. 2002;119(1):55–68. PubMed PMID: 11773238.
27. Awatramani G.B., Slaughter M.M. Intensity-dependent, rapid activation of presynaptic metabotropic glutamate receptors at a central synapse. J Neurosci. 2001;21(2):741–9. PubMed PMID: 11160453.

28. Slaughter M.M., Miller R.F. 2-amino-4-phosphonobutyric acid: a new pharmacological tool for retina research. Science. 1981;211(4478):182–5. PubMed PMID: 6255566.
29. Nakajima Y., et al. Molecular characterization of a novel retinal metabotropic glutamate receptor mGluR6 with a high agonist selectivity for L-2-amino-4-phosphonobutyrate. J Biol Chem. 1993;268(16):11868–73. PubMed PMID: 8389366.
30. Nomura A., et al. Developmentally regulated postsynaptic localization of a metabotropic glutamate receptor in rat rod bipolar cells. Cell. 1994;77(3):361–9. PubMed PMID: 8181056.
31. Masu M., et al. Specific deficit of the ON response in visual transmission by targeted disruption of the mGluR6 gene. Cell. 1994;80(5):757–65. PubMed PMID: 7889569.
32. Vardi N., et al. Localization of mGluR6 to dendrites of ON bipolar cells in primate retina. J Comp Neurol. 2000;423(3):402–412. PubMed PMID: 10870081.
33. Vardi N. Alpha subunit of G_o localizes in the dendritic tips of ON bipolar cells. J Comp Neurol. 1998;395(1):43–52. PubMed PMID: 9590545.
34. Dhingra A., et al. The light response of ON bipolar neurons requires G[alpha]o. J Neurosci. 2000;20(24):9053–8. PubMed PMID: 11124982.
35. Vardi N., et al. Identification of a G-protein in depolarizing rod bipolar cells. Vis Neurosci. 1993;10(3):473–8. PubMed PMID: 8388245.
36. Nawy S., Jahr C.E. Suppression by glutamate of cGMP-activated conductance in retinal bipolar cells. Nature. 1990;346(6281):269–71. PubMed PMID: 1695713.
37. Nawy S. The metabotropic receptor mGluR6 may signal through G(o), but not phosphodiesterase, in retinal bipolar cells. J Neurosci. 1999;19(8):2938–44. PubMed PMID: 10191311.
38. Koike C., et al. TRPM1 is a component of the retinal ON bipolar cell transduction channel in the mGluR6 cascade. Proc Natl Acad Sci U S A. 2010;107(1):332–7. PubMed PMID: 19966281.
39. Koike C., et al. TRPM1: a vertebrate TRP channel responsible for retinal ON bipolar function. Cell Calcium. 2010;48(2-3):95–101. PubMed PMID: 20846719.
40. Nakamura M., et al. TRPM1 mutations are associated with the complete form of congenital stationary night blindness. Mol Vis. 2010;16:425–37. PubMed PMID: 20300565.
41. Xu, Y. and N. Vardi, *Modulation of the Light-Activated Cation Channel in Retinal ON Bipolar Cells by G-Protein Subunits.* ARVO Meeting Abstracts, 2010. 51(5): p. 4797.
42. Xu Y., et al. mGluR6 Deletion Renders the TRPM1 Channel in Retina Inactive. J Neurophysiol. 2011. PubMed PMID: 22131384.
43. Montell C., Rubin G.M. Molecular characterization of the Drosophila trp locus: a putative integral membrane protein required for phototransduction. Neuron. 1989;2(4):1313–23. PubMed PMID: 2516726.
44. Myers B.R., et al. Multiple unbiased prospective screens identify TRP channels and their conserved gating elements. J Gen Physiol. 2008;132(5):481–6. PubMed PMID: 18955590.
45. Abramowitz J., Birnbaumer L. Physiology and pathophysiology of canonical transient receptor potential channels. FASEB J. 2009;23(2):297–328. PubMed PMID: 18940894.
46. Montell C. The TRP superfamily of cation channels. Sci STKE. 2005;2005(272):re3. PubMed PMID: 15728426.
47. Montell C., Birnbaumer L., Flockerzi V. The TRP channels, a remarkably functional family. Cell. 2002;108(5):595–8. PubMed PMID: 11893331.
48. Nishida M., Kurose H. Roles of TRP channels in the development of cardiac hypertrophy. Naunyn Schmiedebergs Arch Pharmacol. 2008;378(4):395–406. PubMed PMID: 18600314.
49. Krizaj D. Compartmentalization of calcium entry pathways in mouse rods. Eur J Neurosci. 2005;22(12):3292–6. PubMed PMID: 16367794.
50. Ke J.B., et al. Characterization of spontaneous inhibitory postsynaptic currents in cultured rat retinal amacrine cells. Neuroscience. 2010;165(2):395–407. PubMed PMID: 19819309.
51. Sosa R., et al. Metabotropic glutamate receptor 5 and calcium signaling in retinal amacrine cells. J Neurochem. 2002;81(5):973–83. PubMed PMID: 12065609.

52. Morgans C.W., et al. TRPM1 is required for the depolarizing light response in retinal ON-bipolar cells. Proc Natl Acad Sci U S A. 2009;106(45):19174–8. PubMed PMID: 19861548.
53. Shen Y., et al. A transient receptor potential-like channel mediates synaptic transmission in rod bipolar cells. J Neurosci. 2009;29(19):6088–93. PubMed PMID: 19439586.
54. Koike C., et al. The functional analysis of TRPM1 in retinal bipolar cells. Neurosci Res. 2007;58S:S41.
55. Morgans C.W., Brown R.L., Duvoisin R.M. TRPM!: the endpoint of the mGluR6 signal transduction cascade in retinal ON-bipolar cells. Bioessays. 2010;32:609–614. PubMed PMID: 20544736.
56. Koyasu T., et al. Photopic electroretinograms of mGluR6-deficient mice. Curr Eye Res. 2008;33(1):91–9. PubMed PMID: 18214746.
57. Gregg R.G., et al. Nyctalopin expression in retinal bipolar cells restores visual function in a mouse model of complete X-linked congenital stationary night blindness. J Neurophysiol. 2007;98(5):3023–33. PubMed PMID: 17881478.
58. Pardue M.T., et al. A naturally occurring mouse model of X-linked congenital stationary night blindness. Invest Ophthalmol Vis Sci. 1998;39(12):2443–9. PubMed PMID: 9804152.
59. Gregg R.G., et al. Identification of the gene and the mutation responsible for the mouse nob phenotype. Invest Ophthalmol Vis Sci. 2003;44(1):378–84. PubMed PMID: 12506099.
60. Schroeter E.H., Wong R.O., Gregg R.G. In vivo development of retinal ON-bipolar cell axonal terminals visualized in nyx::MYFP transgenic zebrafish. Vis Neurosci. 2006;23(5):833–43. PubMed PMID: 17020638.
61. Cao Y., Posokhova E., Martemyanov K.A. TRPM1 forms complexes with nyctalopin in vivo and accumulates in postsynaptic compartment of ON-bipolar neurons in mGluR6-dependent manner. J Neurosci. 2011;31(32):11521–6. PubMed PMID: 21832182.
62. van Genderen M.M., et al. Mutations in TRPM1 are a common cause of complete congenital stationary night blindness. Am J Hum Genet. 2009;85(5):730–6. PubMed PMID: 19896109.
63. Nawy S. Regulation of the on bipolar cell mGluR6 pathway by Ca^{2+}. J Neurosci. 2000;20(12):4471–9. PubMed PMID: 10844016.
64. Yamashita M., Wässle H. Responses of rod bipolar cells isolated from the rat retina to the glutamate agonist 2-amino-4-phosphonobutyric acid (APB). J Neurosci. 1991;11(8):2372–82. PubMed PMID: 1714492.
65. Shiells R.A., Falk G. A rise in intracellular Ca^{2+} underlies light adaptation in dogfish retinal 'on' bipolar cells. J Physiol (Lond). 1999;514(Pt 2):343–50. PubMed PMID: 9852318.
66. Shiells R.A., Falk G. Activation of Ca^{2+}--calmodulin kinase II induces desensitization by background light in dogfish retinal 'on' bipolar cells. J Physiol. 2000;528(Pt 2):327–38. PubMed PMID: 11034622.
67. Walters R.J., Kramer R.H., Nawy S. Regulation of cGMP-dependent current in On bipolar cells by calcium/calmodulin-dependent kinase. Vis Neurosci. 1998;15(2):257–61. PubMed PMID: 9605527.
68. Snellman J., Nawy S. cGMP-dependent kinase regulates response sensitivity of the mouse on bipolar cell. J Neurosci. 2004;24(29):6621–8. PubMed PMID: 15269274.
69. Awatramani G.B., Slaughter M.M. Origin of transient and sustained responses in ganglion cells of the retina. J Neurosci. 2000;20(18):7087–95. PubMed PMID: 10995856.
70. Enroth-Cugell C., Robson J.G. The contrast sensitivity of retinal ganglion cells of the cat. J Physiol. 1966;187(3):517–52. PubMed PMID: 16783910.
71. Demb J.B., et al. Bipolar cells contribute to nonlinear spatial summation in the brisk-transient (Y) ganglion cell in mammalian retina. J Neurosci. 2001;21(19):7447–54. PubMed PMID: 11567034.
72. Connaughton V.P., Nelson R. Axonal stratification patterns and glutamate-gated conductance mechanisms in zebrafish retinal bipolar cells. J Physiol. 2000;524(Pt 1):135–146. PubMed PMID: 10747188.
73. Grant G.B., Dowling J.E. A glutamate-activated chloride current in cone-driven ON bipolar cells of the white perch retina. J Neurosci. 1995;15(5):3852–62. PubMed PMID: 7538566.
74. Grant G.B., Dowling J.E. On bipolar cell responses in the teleost retina are generated by two distinct mechanisms. J Neurophysiol. 1996;76(6):3842–9. PubMed PMID: 8985882.
75. Grant G.B., Werblin F.S. A glutamate-elicited chloride current with transporter-like properties in rod photoreceptors of the tiger salamander. Vis Neurosci. 1996;13(1):135–44. PubMed PMID: 8730995.

76. Picaud S.A., et al. Glutamate-gated chloride channel with glutamate-transporter-like properties in cone photoreceptors of the tiger salamander. J Neurophysiol. 1995;74(4):1760–71. PubMed PMID: 8989410.
77. Tachibana M., Kaneko A. L-glutamate-induced depolarization in solitary photoreceptors: a process that may contribute to the interaction between photoreceptors in situ. Proc Natl Acad Sci U S A. 1988;85(14):5315–9. PubMed PMID: 2899327.
78. Wersinger E., et al. The glutamate transporter EAAT5 works as a presynaptic receptor in mouse rod bipolar cells. J Physiol. 2006;577(Pt 1):221–34. PubMed PMID: 16973698.
79. Otis T.S., Jahr C.E. Anion currents and predicted glutamate flux through a neuronal glutamate transporter. J Neurosci. 1998;18(18):7099–110. PubMed PMID: 9736633.
80. Arriza J.L., et al. Excitatory amino acid transporter 5, a retinal glutamate transporter coupled to a chloride conductance. Proc Natl Acad Sci U S A. 1997;94(8):4155–60. PubMed PMID: 9108121.
81. Saito T., Kondo H., Toyoda J. Ionic mechanisms of two types of on-center bipolar cells in the carp retina. II. The responses to annular illumination. J Gen Physiol. 1981;78(5):569–89. PubMed PMID: 7310376.
82. Saito T., Kondo H., Toyoda J.I. Ionic mechanisms of two types of on-center bipolar cells in the carp retina. I. The responses to central illumination. J Gen Physiol. 1979;73(1):73–90. PubMed PMID: 438766.
83. Vardi N., et al. Neurochemistry of the mammalian cone 'synaptic complex'. Vision Res. 1998;38(10):1359–69. PubMed PMID: 9667004.
84. Hughes T.E. Are there ionotropic glutamate receptors on the rod bipolar cell of the mouse retina? Vis Neurosci. 1997;14(1):103–9. PubMed PMID: 9057273.
85. Hughes T.E., Hermans-Borgmeyer I., Heinemann S. Differential expression of glutamate receptor genes (GluR1-5) in the rat retina. Vis Neurosci. 1992;8(1):49–55. PubMed PMID: 1310870.
86. Nelson R., et al. Physiological responses associated with kainate receptor immunoreactivity in dissociated zebrafish retinal neurons: a voltage probe study. Prog Brain Res. 2001;131:255–65. PubMed PMID: 11420945.
87. Peng Y.W., et al. Distribution of glutamate receptor subtypes in the vertebrate retina. Neuroscience. 1995;66(2):483–97. PubMed PMID: 7477889.
88. Wong K.Y., Dowling J.E. Retinal Bipolar Cell Input Mechanisms in Giant Danio: III. ON-OFF Bipolar Cells and Their Color-Opponent Mechanisms. J Neurophysiol. 2005. PubMed PMID: 15758056.
89. Pourcho R.G., Qin P., Goebel D.J. Cellular and subcellular distribution of NMDA receptor subunit NR2B in the retina. J Comp Neurol. 2001;433(1):75–85. PubMed PMID: 11283950.
90. Wenzel A., et al. N-methyl-D-aspartate receptors containing the NR2D subunit in the retina are selectively expressed in rod bipolar cells. Neuroscience. 1997;78(4):1105–12. PubMed PMID: 9174077.
91. Brandstatter J.H., et al. Expression of NMDA and high-affinity kainate receptor subunit mRNAs in the adult rat retina. Eur J Neurosci. 1994;6(7):1100–12. PubMed PMID: 7952290.
92. DeVries S.H. Bipolar cells use kainate and AMPA receptors to filter visual information into separate channels. Neuron. 2000;28(3):847–56. PubMed PMID: 11163271.
93. DeVries S.H., Schwartz E.A. Kainate receptors mediate synaptic transmission between cones and 'Off' bipolar cells in a mammalian retina. Nature. 1999;397(6715):157–60. PubMed PMID: 9923677.
94. Paternain A.V., Morales M., Lerma J. Selective antagonism of AMPA receptors unmasks kainate receptor-mediated responses in hippocampal neurons. Neuron. 1995;14(1):185–9. PubMed PMID: 7826635.
95. Jones K.A., et al. Desensitization of kainate receptors by kainate, glutamate and diastereomers of 4-methylglutamate. Neuropharmacology. 1997;36(6):853–63. PubMed PMID: 9225313.
96. Maple B.R., Gao F., Wu S.M. Glutamate receptors differ in rod- and cone-dominated off-center bipolar cells. Neuroreport. 1999;10(17):3605–10. PubMed PMID: 10619652.
97. Wesolowska, A., R. Nelson, and V. Connaughton, *Glutamate Mechanisms Involved in the OFF Pathway of Zebrafish Retina.* Invest. Ophthalmol. Vis. Sci., 2002. 43(12): p. E-abstract 1826.
98. Kim H.G., Miller R.F. Properties of synaptic transmission from photoreceptors to bipolar cells in the mudpuppy retina. J Neurophysiol. 1993;69(2):352–60. PubMed PMID: 8384660.
99. Famiglietti E.V. Jr, Kolb H. Structural basis for ON-and OFF-center responses in retinal ganglion cells. Science. 1976;194(4261):193–5. PubMed PMID: 959847.

100. Nelson R., Famiglietti E.V. Jr, Kolb H. Intracellular staining reveals different levels of stratification for on- and off-center ganglion cells in the cat retina. J. Neurophysiol. 1978;41(2):472–483. PubMed PMID: 650277.
101. Amthor F.R., Takahashi E.S., Oyster C.W. Morphologies of rabbit retinal ganglion cells with concentric receptive fields. J Comp Neurol. 1989;280(1):72–96. PubMed PMID: 2918097.
102. Bloomfield S.A., Miller R.F. A functional organization of ON and OFF pathways in the rabbit retina. J Neurosci. 1986;6(1):1–13. PubMed PMID: 3944611.
103. Ammermüller J., Kolb H. The organization of the turtle inner retina. I. ON- and OFF-center pathways. J Comp Neurol. 1995;358(1):1–34. PubMed PMID: 7560272.
104. Cohen E., Sterling P. Microcircuitry related to the receptive field center of the on-beta ganglion cell. J Neurophysiol. 1991;65(2):352–9. PubMed PMID: 2016645.
105. Kolb H. The inner plexiform layer in the retina of the cat: electron microscopic observations. J Neurocytol. 1979;8(3):295–329. PubMed PMID: 490185.
106. Kolb H., Dekorver L. Midget ganglion cells of the parafovea of the human retina: a study by electron microscopy and serial section reconstructions. J Comp Neurol. 1991;303(4):617–36. PubMed PMID: 1707423.
107. Kolb H., Nelson R. OFF-alpha and OFF-beta ganglion cells in cat retina: II. Neural circuitry as revealed by electron microscopy of HRP stains. J Comp Neurol. 1993;329(1):85–110. PubMed PMID: 8454727.
108. McGuire B.A., Stevens J.K., Sterling P. Microcircuitry of bipolar cells in cat retina. J Neurosci. 1984;4(12):2920–38. PubMed PMID: 6502212.
109. Nelson R., Kolb H. Synaptic patterns and response properties of bipolar and ganglion cells in the cat retina. Vision Res. 1983;23(10):1183–95. PubMed PMID: 6649437.
110. Dumitrescu O.N., et al. Ectopic retinal ON bipolar cell synapses in the OFF inner plexiform layer: contacts with dopaminergic amacrine cells and melanopsin ganglion cells. J Comp Neurol. 2009;517(2):226–44. PubMed PMID: 19731338.
111. Grunert U., et al. Bipolar input to melanopsin containing ganglion cells in primate retina. Vis Neurosci. 2011;28(1):39–50. PubMed PMID: 20950505.
112. Pang J.J., Gao F., Wu S.M. Stratum-by-stratum projection of light response attributes by retinal bipolar cells of Ambystoma. J Physiol. 2004;558(Pt 1):249–62. PubMed PMID: 15146053.
113. Ghosh K.K., et al. Types of bipolar cells in the mouse retina. J Comp Neurol. 2004;469(1):70–82. PubMed PMID: 14689473.
114. Dacey D.M., Lee B.B. The 'blue-on' opponent pathway in primate retina originates from a distinct bistratified ganglion cell type. Nature. 1994;367(6465):731–5. PubMed PMID: 8107868.
115. Famiglietti E.V. Jr, Kaneko A., Tachibana M. Neuronal architecture of on and off pathways to ganglion cells in carp retina. Science. 1977;198(4323):1267–9. PubMed PMID: 73223.
116. Li, Y.N. and J.E. Dowling, *Specificity in the Bipolar Cell-Photoreceptor Connections in the Zebrafish Retina.* ARVO Meeting Abstracts, 2010. 51(5): p. 4125.
117. Li, Y.N., et al., *Bipolar Cell-Photoreceptor Connections in the Zebrafish Retina.* ARVO Meeting Abstracts, 2011. 52(6): p. 2573.
118. Saito T., et al. Reexamination of photoreceptor-bipolar connectivity patterns in carp retina: HRP-EM and Golgi-EM studies. J Comp Neurol. 1985;236(2):141–60. PubMed PMID: 4056093.
119. Kolb H., Nelson R. Amacrine cells of the cat retina. Vision Res. 1981;21(11):1625–33. PubMed PMID: 7336596.
120. Mariani A. Giant Bistratified Bipolar Cells in Monkey Retina. Anatomical Record. 1983;206(2):215–220. PubMed PMID: 6846872.
121. Wong K.Y., Cohen E.D., Dowling J.E. Retinal bipolar cell input mechanisms in giant danio. II. Patch-clamp analysis of on bipolar cells. J Neurophysiol. 2005;93(1):94–107. PubMed PMID: 15229214.
122. Cajal, S., *The Structure of the retina. In: Thorpe SA, Glickstein M, translators (*1972*).* 1892, Springfield: Thomas.

123. Dacheux R.F., Raviola E. The rod pathway in the rabbit retina: a depolarizing bipolar and amacrine cell. J Neurosci. 1986;6(2):331–45. PubMed PMID: 3950701.
124. de la Villa P., Kurahashi T., Kaneko A. L-glutamate-induced responses and cGMP-activated channels in three subtypes of retinal bipolar cells dissociated from the cat. J Neurosci. 1995;15(5 Pt 1):3571–82. PubMed PMID: 7538564.
125. Sherry D.M., Yazulla S. Goldfish bipolar cells and axon terminal patterns: a Golgi study. J Comp Neurol. 1993;329(2):188–200. PubMed PMID: 8454729.
126. Pang J.J., et al. Direct rod input to cone BCs and direct cone input to rod BCs challenge the traditional view of mammalian BC circuitry. Proc Natl Acad Sci U S A. 2010;107(1):395–400. PubMed PMID: 20018684.
127. Pang J.J., Gao F., Wu S.M. Light-evoked current responses in rod bipolar cells, cone depolarizing bipolar cells and AII amacrine cells in dark-adapted mouse retina. J Physiol. 2004;558(Pt 3):897–912. PubMed PMID: 15181169.
128. Greferath U., Grunert U., Wässle H. Rod bipolar cells in the mammalian retina show protein kinase C-like immunoreactivity. J Comp Neurol. 1990;301(3):433–42. PubMed PMID: 2262600.
129. Kolb H., Zhang L., Dekorver L. Differential staining of neurons in the human retina with antibodies to protein kinase C isozymes. Vis Neurosci. 1993;10(2):341–51. PubMed PMID: 8485096.
130. Negishi K., Kato S., Teranishi T. Dopamine cells and rod bipolar cells contain protein kinase C-like immunoreactivity in some vertebrate retinas. Neurosci Lett. 1988;94(3):247–52. PubMed PMID: 3205402.
131. Kolb H., Famiglietti E.V. Rod and cone pathways in the inner plexiform layer of cat retina. Science. 1974;186(4158):47–9. PubMed PMID: 4417736.
132. Nelson R. AII amacrine cells quicken time course of rod signals in the cat retina. J Neurophysiol. 1982;47(5):928–47. PubMed PMID: 6177841.
133. Mills S.L., Massey S.C. Differential properties of two gap junctional pathways made by AII amacrine cells.Nature. 1995;377(6551):734–7. *[see comments]* . PubMed PMID: 7477263.
134. Veruki M.L., Hartveit E. Meclofenamic acid blocks electrical synapses of retinal AII amacrine and on-cone bipolar cells. J Neurophysiol. 2009;101(5):2339–47. PubMed PMID: 19279153.
135. Kolb H. The organization of the outer plexiform layer in the retina of the cat: electron microscopic observations. J Neurocytol. 1977;6(2):131–53. PubMed PMID: 856949.
136. Nelson R. Cat cones have rod input: a comparison of the response properties of cones and horizontal cell bodies in the retina of the cat. J Comp Neurol. 1977;172(1):109–35. PubMed PMID: 838876.
137. Raviola E., Gilula N.B. Gap junctions between photoreceptor cells in the vertebrate retina. Proc Natl Acad Sci U S A. 1973;70(6):1677–81. PubMed PMID: 4198274.
138. Smith R.G., Freed M.A., Sterling P. Microcircuitry of the dark-adapted cat retina: functional architecture of the rod-cone network. J Neurosci. 1986;6(12):3505–17. PubMed PMID: 3794785.
139. Tsukamoto Y., et al. Microcircuits for night vision in mouse retina. J Neurosci. 2001;21(21):8616–23. PubMed PMID: 11606649.
140. Lasansky A. Organization of the outer synaptic layer in the retina of the larval tiger salamander. Philos Trans R Soc Lond B Biol Sci. 1973;265(872):471–89. PubMed PMID: 4147132.
141. Stell W.K., Ishida A.T., Lightfoot D.O. Structural basis for on-and off-center responses in retinal bipolar cells. Science. 1977;198(4323):1269–71. PubMed PMID: 201028.
142. Hack I., Peichl L. Horizontal cells of the rabbit retina are non-selectively connected to the cones. Eur J Neurosci. 1999;11(7):2261–74. PubMed PMID: 10383615.
143. Li W., Chen S., DeVries S.H. A fast rod photoreceptor signaling pathway in the mammalian retina. Nat Neurosci. 2010;13(4):414–6. PubMed PMID: 20190742.
144. Tsukamoto Y., et al. A novel connection between rods and ON cone bipolar cells revealed by ectopic metabotropic glutamate receptor 7 (mGluR7) in mGluR6-deficient mouse retinas. J Neurosci. 2007;27(23):6261–7. PubMed PMID: 17553999.
145. Sharpe L.T., Stockman A. Rod pathways: the importance of seeing nothing. Trends Neurosci. 1999;22(11):497–504. PubMed PMID: 10529817.

146. Connaughton V.P., Maguire G. Differential expression of voltage-gated K^+ and Ca^{2+} currents in bipolar cells in the zebrafish retinal slice. Eur J Neurosci. 1998;10(4):1350–62. PubMed PMID: 9749789.
147. Karschin A., Wässle H. Voltage- and transmitter-gated currents in isolated rod bipolar cells of rat retina. J Neurophysiol. 1990;63(4):860–76. PubMed PMID: 2341882.
148. Lasater E.M. Membrane currents of retinal bipolar cells in culture. J Neurophysiol. 1988;60(4):1460–80. PubMed PMID: 3193166.
149. Pan Z.H., Hu H.J. Voltage-dependent Na(+) currents in mammalian retinal cone bipolar cells. J Neurophysiol. 2000;84(5):2564–71. PubMed PMID: 11067998.
150. Ma Y.P., Cui J., Pan Z.H. Heterogeneous expression of voltage-dependent Na^+ and K^+ channels in mammalian retinal bipolar cells. Vis Neurosci. 2005;22(2):119–33. PubMed PMID: 15935105.
151. Cui J., Pan Z.H. Two types of cone bipolar cells express voltage-gated Na+ channels in the rat retina. Vis Neurosci. 2008;25(5-6):635–45. PubMed PMID: 19094370.
152. Zenisek D., et al. Voltage-dependent sodium channels are expressed in nonspiking retinal bipolar neurons. J Neurosci. 2001;21(13):4543–50. PubMed PMID: 11425883.
153. Protti D.A., Llano I. Calcium currents and calcium signaling in rod bipolar cells of rat retinal slices. J Neurosci. 1998;18(10):3715–24. PubMed PMID: 9570802.
154. Zenisek D., Matthews G. Calcium action potentials in retinal bipolar neurons. Vis Neurosci. 1998;15(1):69–75. PubMed PMID: 9456506.
155. Heidelberger R., Matthews G. Calcium influx and calcium current in single synaptic terminals of goldfish retinal bipolar neurons. J Physiol. 1992;447:235–56. PubMed PMID: 1317429.
156. Kaneko A., et al. Membrane currents and pharmacology of retinal bipolar cells: a comparative study on goldfish and mouse. Comp Biochem Physiol C. 1991;98(1):115–27. PubMed PMID: 1673905.
157. Kaneko A., Pinto L.H., Tachibana M. Transient calcium current of retinal bipolar cells of the mouse. J Physiol. 1989;410:613–29. PubMed PMID: 2552084.
158. Maguire G., et al. Gamma-aminobutyrate type B receptor modulation of L-type calcium channel current at bipolar cell terminals in the retina of the tiger salamander. Proc Natl Acad Sci U S A. 1989;86(24):10144–7. PubMed PMID: 2557620.
159. Kaneko A., Tachibana M. A voltage-clamp analysis of membrane currents in solitary bipolar cells dissociated from Carassius auratus. J Physiol. 1985;358:131–52. PubMed PMID: 2580078.
160. Fan S.F., Yazulla S. Dopamine depletion with 6-OHDA enhances dopamine D1-receptor modulation of potassium currents in retinal bipolar cells. Vis Neurosci. 2001;18(2):327–37. PubMed PMID: 11417806.
161. Tessier-Lavigne M., et al. Membrane currents in retinal bipolar cells of the axolotl. J Gen Physiol. 1988;91(1):49–72. PubMed PMID: 3125305.
162. Kamermans M., et al. Hemichannel-mediated inhibition in the outer retina. Science. 2001;292(5519):1178–80. PubMed PMID: 11349152.
163. Vardi N., et al. Evidence that different cation chloride cotransporters in retinal neurons allow opposite responses to GABA. J Neurosci. 2000;20(20):7657–63. PubMed PMID: 11027226.
164. Thoreson W.B., Miller R.F. Membrane currents evoked by excitatory amino acid agonists in ON bipolar cells of the mudpuppy retina. J Neurophysiol. 1993;70(4):1326–38. PubMed PMID: 7506752.
165. Connaughton V.P., et al. Immunocytochemical localization of excitatory and inhibitory neurotransmitters in the zebrafish retina. Vis Neurosci. 1999;16(3):483–90. PubMed PMID: 10349969.
166. Freed M.A., Nakamura Y., Sterling P. Four types of amacrine in the cat retina that accumulate GABA. J Comp Neurol. 1983;219(3):295–304. PubMed PMID: 6619340.
167. Freed M.A., Smith R.G., Sterling P. Rod bipolar array in the cat retina: pattern of input from rods and GABA-accumulating amacrine cells. J Comp Neurol. 1987;266(3):445–55. PubMed PMID: 3693619.
168. Marc R.E., Liu W. Fundamental GABAergic amacrine cell circuitries in the retina: nested feedback, concatenated inhibition, and axosomatic synapses. J Comp Neurol. 2000;425(4):560–82. PubMed PMID: 10975880.
169. Marc R.E., et al. GABA-ergic pathways in the goldfish retina. J Comp Neurol. 1978;182(2):221–44. PubMed PMID: 212456.

170. Pourcho R.G., Goebel D.J. Neuronal subpopulations in cat retina which accumulate the GABA agonist, (^{3}H)muscimol: a combined Golgi and autoradiographic study. J Comp Neurol. 1983;219(1):25–35. PubMed PMID: 6619330.
171. Connaughton V.P., Nelson R., Bender A.M. Electrophysiological evidence of $GABA_A$ and $GABA_C$ receptors on zebrafish retinal bipolar cells. Vis Neurosci. 2008;25(2):139–53. PubMed PMID: 18442437.
172. Lukasiewicz P.D., Maple B.R., Werblin F.S. A novel GABA receptor on bipolar cell terminals in the tiger salamander retina. J Neurosci. 1994;14(3 Pt 1):1202–12. PubMed PMID: 8120620.
173. Tachibana M., Kaneko A. gamma-Aminobutyric acid exerts a local inhibitory action on the axon terminal of bipolar cells: evidence for negative feedback from amacrine cells. Proc Natl Acad Sci U S A. 1987;84(10):3501–5. PubMed PMID: 3472220.
174. Tachibana M., Kaneko A. Retinal bipolar cells receive negative feedback input from GABAergic amacrine cells. Vis Neurosci. 1988;1(3):297–305. PubMed PMID: 2856476.
175. Lukasiewicz P.D., Werblin F.S. A novel GABA receptor modulates synaptic transmission from bipolar to ganglion and amacrine cells in the tiger salamander retina. J Neurosci. 1994;14(3 Pt 1):1213–23. PubMed PMID: 7907138.
176. Burkhardt D.A. Responses and receptive-field organization of cones in perch retinas. J Neurophysiol. 1977;40(1):53–62. PubMed PMID: 833628.
177. Kondo H., Toyoda J. GABA and glycine effects on the bipolar cells of the carp retina. Vision Res. 1983;23(11):1259–64. PubMed PMID: 6659375.
178. Wu S.M. Effects of gamma-aminobutyric acid on cones and bipolar cells of the tiger salamander retina. Brain Res. 1986;365(1):70–7. PubMed PMID: 3947987.
179. Wu S.M., Maple B.R. Amino acid neurotransmitters in the retina: a functional overview. Vision Res. 1998;38(10):1371–84. PubMed PMID: 9667005.
180. Feigenspan A., Wässle H., Bormann J. Pharmacology of GABA receptor Cl^- channels in rat retinal bipolar cells. Nature. 1993;361(6408):159–62. PubMed PMID: 7678450.
181. Lukasiewicz P.D., Shields C.R. Different combinations of $GABA_A$ and $GABA_C$ receptors confer distinct temporal properties to retinal synaptic responses. J Neurophysiol. 1998;79(6):3157–67. PubMed PMID: 9636116.
182. Lukasiewicz P.D., Shields C.R. A diversity of GABA receptors in the retina. Semin Cell Dev Biol. 1998;9(3):293–9. PubMed PMID: 9665865.
183. Lukasiewicz P.D., Wong R.O. $GABA_C$ receptors on ferret retinal bipolar cells: a diversity of subtypes in mammals? Vis Neurosci. 1997;14(5):989–94. PubMed PMID: 9364734.
184. McGillem G.S., Rotolo T.C., Dacheux R.F. GABA responses of rod bipolar cells in rabbit retinal slices. Vis Neurosci. 2000;17(3):381–9. PubMed PMID: 10910106.
185. Qian H., Dowling J.E. Novel GABA responses from rod-driven retinal horizontal cells. Nature. 1993;361(6408):162–4. PubMed PMID: 8421521.
186. Qian H., Dowling J.E. $GABA_A$ and $GABA_C$ receptors on hybrid bass retinal bipolar cells. J Neurophysiol. 1995;74(5):1920–8. PubMed PMID: 8592185.
187. Vaquero C.F., de la Villa P. Localisation of the $GABA_C$ receptors at the axon terminal of the rod bipolar cells of the mouse retina. Neurosci Res. 1999;35(1):1–7. PubMed PMID: 10555158.
188. Nelson R., Connaughton V.P., Schaffner A.E. Voltage probe measurements of glutamate responses form acutely dissociated zebrafish retinal neurons. Invest Ophthalmol Vis Sci. 1999;40:S242.
189. Eggers E.D., Lukasiewicz P.D. $GABA_A$, $GABA_C$ and glycine receptor-mediated inhibition differentially affects light-evoked signalling from mouse retinal rod bipolar cells. J Physiol. 2006;572(Pt 1):215–25. PubMed PMID: 16439422.
190. Heidelberger R., Matthews G. Inhibition of calcium influx and calcium current by gamma-aminobutyric acid in single synaptic terminals. Proc Natl Acad Sci U S A. 1991;88(16):7135–9. PubMed PMID: 1651495.
191. Eggers E.D., Lukasiewicz P.D. Receptor and transmitter release properties set the time course of retinal inhibition. J Neurosci. 2006;26(37):9413–25. PubMed PMID: 16971525.

192. Frumkes T.E., Nelson R. Functional role of GABA in cat retina: I. Effects of $GABA_A$ agonists. Vis Neurosci. 1995;12(4):641–50. PubMed PMID: 8527366.
193. Frumkes T.E., Nelson R., Pflug R. Functional role of GABA in cat retina: II. Effects of $GABA_A$ antagonists. Vis Neurosci. 1995;12(4):651–61. PubMed PMID: 8527367.
194. Freed, M.A., *GABAergic circuits in the mammalian retina*, in *GABA in the retina and central visual system*. 1992, Elsevier: Amsterdam.
195. Zhang D.Q., Yang X.L. OFF pathway is preferentially suppressed by the activation of GABA(A) receptors in carp retina. Brain Res. 1997;759(1):160–2. PubMed PMID: 9219876.
196. Matthews G., Ayoub G.S., Heidelberger R. Presynaptic inhibition by GABA is mediated via two distinct GABA receptors with novel pharmacology. J Neurosci. 1994;14(3 Pt 1):1079–90. PubMed PMID: 7509862.
197. Mack A.F., Behrens U.D., Wagner H.J. Inhibitory control of synaptic activity in goldfish Mb bipolar cell terminals visualized by FM1-43. Vis Neurosci. 2000;17(6):823–9. PubMed PMID: 11193098.
198. Pang J.J., Gao F., Wu S.M. Relative contributions of bipolar cell and amacrine cell inputs to light responses of ON, OFF and ON-OFF retinal ganglion cells. Vision Res. 2002;42(1):19–27. PubMed PMID: 11804628.
199. Singer J.H., Diamond J.S. Sustained Ca^{2+} entry elicits transient postsynaptic currents at a retinal ribbon synapse. J Neurosci. 2003;23(34):10923–33. PubMed PMID: 14645488.
200. Chavez A.E., Grimes W.N., Diamond J.S. Mechanisms underlying lateral GABAergic feedback onto rod bipolar cells in rat retina. J Neurosci. 2010;30(6):2330–9. PubMed PMID: 20147559.
201. Chavez A.E., Singer J.H., Diamond J.S. Fast neurotransmitter release triggered by Ca influx through AMPA-type glutamate receptors. Nature. 2006;443(7112):705–8. PubMed PMID: 17036006.
202. Suzuki S., Tachibana M., Kaneko A. Effects of glycine and GABA on isolated bipolar cells of the mouse retina. J Physiol. 1990;421:645–62. PubMed PMID: 1693403.
203. Maple B.R., Wu S.M. Glycinergic synaptic inputs to bipolar cells in the salamander retina. J Physiol. 1998;506(Pt 3):731–44. PubMed PMID: 9503334.
204. Cunningham R., Miller R.F. Electrophysiological analysis of taurine and glycine action on neurons of the midpuppy retina. I. Intracellular recording. Brain Res. 1980;197(1):123–38. PubMed PMID: 6249454.
205. Műller F., Wässle H., Voigt T. Pharmacological modulation of the rod pathway in the cat retina. J Neurophysiol. 1988;59(6):1657–72. PubMed PMID: 3404200.
206. Pourcho R.G., Goebel D.J. A combined Golgi and autoradiographic study of (^{3}H)glycine-accumulating amacrine cells in the cat retina. J Comp Neurol. 1985;233(4):473–80. PubMed PMID: 2984258.
207. Wässle H., Schafer-Trenkler I., Voigt T. Analysis of a glycinergic inhibitory pathway in the cat retina. J Neurosci. 1986;6(2):594–604. PubMed PMID: 3950712.
208. Eggers E.D., Lukasiewicz P.D. Multiple pathways of inhibition shape bipolar cell responses in the retina. Vis Neurosci. 2011;28(1):95–108. PubMed PMID: 20932357.
209. Chavez A.E., Diamond J.S. Diverse mechanisms underlie glycinergic feedback transmission onto rod bipolar cells in rat retina. J Neurosci. 2008;28(31):7919–28. PubMed PMID: 18667624.
210. Du J.L., Yang X.L. Glycinergic synaptic transmission to bullfrog retinal bipolar cells is input-specific. Neuroscience. 2002;113(4):779–84. PubMed PMID: 12182885.
211. Smiley J.F., Yazulla S. Glycinergic contacts in the outer plexiform layer of the Xenopus laevis retina characterized by antibodies to glycine, GABA and glycine receptors. J Comp Neurol. 1990;299(3):375–88. PubMed PMID: 2172330.
212. Stone S., Schutte M. Physiological and morphological properties of off- and on-center bipolar cells in the Xenopus retina: effects of glycine and GABA. Vis Neurosci. 1991;7(4):363–76. PubMed PMID: 1751422.
213. Hare W.A., Owen W.G. Receptive field of the retinal bipolar cell: a pharmacological study in the tiger salamander. J Neurophysiol. 1996;76(3):2005–19. PubMed PMID: 8890310.
214. Qian H., et al. Responses of small- and large-field bipolar cells to GABA and glycine. Brain Res. 2001;893(1-2):273–7. PubMed PMID: 11223017.
215. Merighi A., Raviola E., Dacheux R.F. Connections of two types of flat cone bipolars in the rabbit retina. J Comp Neurol. 1996;371(1):164–78. PubMed PMID: 8835725.

216. von Gersdorff H., et al. Evidence that vesicles on the synaptic ribbon of retinal bipolar neurons can be rapidly released. Neuron. 1996;16(6):1221–7. PubMed PMID: 8663998.
217. Lagnado L., Gomis A., Job C. Continuous vesicle cycling in the synaptic terminal of retinal bipolar cells. Neuron. 1996;17(5):957–67. PubMed PMID: 8938127.
218. Zenisek D., Steyer J.A., Almers W. Transport, capture and exocytosis of single synaptic vesicles at active zones. Nature. 2000;406(6798):849–54. PubMed PMID: 10972279.
219. Dowling, J.E., *The retina: an approachable part of the brain.* 1987, Cambridge (MA): Belknap Press of Harvard University Press.
220. Dowling J.E., Boycott B.B. Organization of the primate retina: electron microscopy. Proc R Soc Lond B Biol Sci. 1966;166(2):80–111. PubMed PMID: 4382694.
221. Miller R.F., et al. Pre- and postsynaptic mechanisms of spontaneous, excitatory postsynaptic currents in the salamander retina. Prog Brain Res. 2001;131:241–53. PubMed PMID: 11420944.
222. Wong-Riley M.T. Synaptic orgnization of the inner plexiform layer in the retina of the tiger salamander. J Neurocytol. 1974;3(1):1–33. PubMed PMID: 4132946.
223. Gottesman J., Miller R.F. Pharmacological properties of N-methyl-D-aspartate receptors on ganglion cells of an amphibian retina. J Neurophysiol. 1992;68(2):596–604. PubMed PMID: 1382121.
224. Heidelberger R., Matthews G. Dopamine enhances Ca^{2+} responses in synaptic terminals of retinal bipolar neurons. Neuroreport. 1994;5(6):729–32. PubMed PMID: 8199349.
225. Morgans C.W. Neurotransmitter release at ribbon synapses in the retina. Immunol Cell Biol. 2000;78(4):442–6. PubMed PMID: 10947871.
226. von Gersdorff H., Matthews G. Inhibition of endocytosis by elevated internal calcium in a synaptic terminal. Nature. 1994;370(6491):652–5. PubMed PMID: 8065451.
227. Neves G., Neef A., Lagnado L. The actions of barium and strontium on exocytosis and endocytosis in the synaptic terminal of goldfish bipolar cells. J Physiol. 2001;535(Pt 3):809–24. PubMed PMID: 11559777.
228. Pan Z.H. Voltage-activated Ca^{2+} channels and ionotropic GABA receptors localized at axon terminals of mammalian retinal bipolar cells. Vis Neurosci. 2001;18(2):279–88. PubMed PMID: 11417802.
229. Burrone J., Lagnado L. Synaptic depression and the kinetics of exocytosis in retinal bipolar cells. J Neurosci. 2000;20(2):568–78. PubMed PMID: 10632586.
230. Mennerick S., Matthews G. Ultrafast exocytosis elicited by calcium current in synaptic terminals of retinal bipolar neurons. Neuron. 1996;17(6):1241–9. PubMed PMID: 8982170.
231. von Gersdorff H., Matthews G. Depletion and replenishment of vesicle pools at a ribbon-type synaptic terminal. J Neurosci. 1997;17(6):1919–27. PubMed PMID: 9045721.
232. Rouze N.C., Schwartz E.A. Continuous and transient vesicle cycling at a ribbon synapse. J Neurosci. 1998;18(21):8614–24. PubMed PMID: 9786969.
233. Veruki M.L., Morkve S.H., Hartveit E. Functional properties of spontaneous EPSCs and non-NMDA receptors in rod amacrine (AII) cells in the rat retina. J Physiol. 2003;549(Pt 3):759–74. PubMed PMID: 12702738.
234. Singer J.H., et al. Coordinated multivesicular release at a mammalian ribbon synapse. Nat Neurosci. 2004;7(8):826–33. PubMed PMID: 15235608.
235. Singer J.H., Diamond J.S. Vesicle depletion and synaptic depression at a mammalian ribbon synapse. J Neurophysiol. 2006;95(5):3191–8. PubMed PMID: 16452253.
236. Pinto L.H., et al. Generation, identification and functional characterization of the nob4 mutation of Grm6 in the mouse. Vis Neurosci. 2007;24(1):111–23. PubMed PMID: 17430614.
237. Takao M., et al. Impaired behavioral suppression by light in metabotropic glutamate receptor subtype 6-deficient mice. Neuroscience. 2000;97(4):779–87. PubMed PMID: 10842024.
238. Thompson S., et al. Different inner retinal pathways mediate rod-cone input in irradiance detection for the pupillary light reflex and regulation of behavioral state in mice. Invest Ophthalmol Vis Sci. 2011;52(1):618–23. PubMed PMID: 20847113.
239. Iwakabe H., et al. Impairment of pupillary responses and optokinetic nystagmus in the mGluR6-deficient mouse. Neuropharmacology. 1997;36(2):135–43. PubMed PMID: 9144650.

240. Tagawa Y., et al. Immunohistological studies of metabotropic glutamate receptor subtype 6-deficient mice show no abnormality of retinal cell organization and ganglion cell maturation. J Neurosci. 1999;19(7):2568–79. PubMed PMID: 10087070.
241. Berson E.L., Lessell S. Paraneoplastic night blindness with malignant melanoma. Am J Ophthalmol. 1988;106(3):307–11. PubMed PMID: 2971322.
242. Ripps H. Night blindness revisited: from man to molecules. Proctor lecture. Invest Ophthalmol Vis Sci. 1982;23(5):588–609. PubMed PMID: 6127328.
243. Alexander K.R., et al. 'On' response defect in paraneoplastic night blindness with cutaneous malignant melanoma. Invest Ophthalmol Vis Sci. 1992;33(3):477–83. PubMed PMID: 1544774.
244. Alexander K.R., et al. Contrast-processing deficits in melanoma-associated retinopathy. Invest Ophthalmol Vis Sci. 2004;45(1):305–10. PubMed PMID: 14691188.
245. Lei B., et al. Human melanoma-associated retinopathy (MAR) antibodies alter the retinal ON-response of the monkey ERG in vivo. Invest Ophthalmol Vis Sci. 2000;41(1):262–6. PubMed PMID: 10634629.
246. Dhingra A., et al. Autoantibodies in melanoma-associated retinopathy target TRPM1 cation channels of retinal ON bipolar cells. J Neurosci. 2011;31(11):3962–7. PubMed PMID: 21411639.
247. Kondo M., et al. Identification of autoantibodies against TRPM1 in patients with paraneoplastic retinopathy associated with ON bipolar cell dysfunction. PLoS One. 2011;6(5):e19911. PubMed PMID: 21611200.
248. Schubert G., Bornschein H.Ophthalmologica. 1952;123(6):396–413. *[Analysis of the human electroretinogram]* . PubMed PMID: 14957416.
249. Goodman G., Bornschein H. Comparative electroretinographic studies in congenital night blindness and total color blindness. AMA Arch Ophthalmol. 1957;58(2):174–82. PubMed PMID: 13443574.
250. Miyake Y., et al. Congenital stationary night blindness with negative electroretinogram. A new classification. Arch Ophthalmol. 1986;104(7):1013–20. PubMed PMID: 3488053.
251. Miyake, Y., *[Establishment of the concept of new clinical entities--complete and incomplete form of congenital stationary night blindness].* Nihon Ganka Gakkai Zasshi, 2002. 106(12): p. 737-55; discussion 756.
252. Bech-Hansen N.T., et al. Mutations in NYX, encoding the leucine-rich proteoglycan nyctalopin, cause X-linked complete congenital stationary night blindness. Nat Genet. 2000;26(3):319–23. PubMed PMID: 11062471.
253. Bech-Hansen N.T., et al. Loss-of-function mutations in a calcium-channel alpha1-subunit gene in Xp11.23 cause incomplete X-linked congenital stationary night blindness. Nat Genet. 1998;19(3):264–7. PubMed PMID: 9662400.
254. Zeitz C., et al. Mutations in GRM6 cause autosomal recessive congenital stationary night blindness with a distinctive scotopic 15-Hz flicker electroretinogram. Invest Ophthalmol Vis Sci. 2005;46(11):4328–35. PubMed PMID: 16249515.
255. Schiller P.H. Central connections of the retinal ON and OFF pathways. Nature. 1982;297(5867):580–3. PubMed PMID: 7088141.
256. Schiller P.H. The connections of the retinal on and off pathways to the lateral geniculate nucleus of the monkey. Vision Res. 1984;24(9):923–32. PubMed PMID: 6506480.
257. Knapp A.G., Mistler L.A. Response properties of cells in rabbit's lateral geniculate nucleus during reversible blockade of retinal on-center channel. J Neurophysiol. 1983;50(5):1236–45. PubMed PMID: 6644369.
258. Cleland B.G., Dubin M.W., Levick W.R. Sustained and transient neurones in the cat's retina and lateral geniculate nucleus. J Physiol. 1971;217(2):473–96. PubMed PMID: 5097609.
259. Dolan R.P., Schiller P.H. Effects of ON channel blockade with 2-amino-4-phosphonobutyrate (APB) on brightness and contrast perception in monkeys. Vis Neurosci. 1994;11(1):23–32. PubMed PMID: 8011580.
260. Dolan R.P., Schiller P.H. Evidence for only depolarizing rod bipolar cells in the primate retina. Vis Neurosci. 1989;2(5):421–4. PubMed PMID: 2487079.
261. Qin P., Pourcho R.G. Localization of AMPA-selective glutamate receptor subunits in the cat retina: a light- and electron-microscopic study. Vis Neurosci. 1999;16(1):169–77. PubMed PMID: 10022488.

Retinal Neurogenesis

Early stages in the Development of Neurons and Pathways

Development of Cell Types and Synaptic Connections in the Retina

Josh Morgan and Rachel Wong

Created: May 1, 2005; Updated: May 29, 2007.

Introduction

Synaptic connections of the vertebrate retina are organized into distinct laminae (Fig. 1). In the outer retina, photoreceptors contact horizontal cells and bipolar cells within a single lamina, the outer plexiform layer (OPL). Within the inner retina, synapses between retinal ganglion cells and their presynaptic partners, the amacrine and bipolar interneurons, are localized to the inner plexiform layer (IPL). Connections between cells that are depolarized upon an increase in illumination (ON) occupy approximately the inner half of the IPL, whereas connectivity of cells hyperpolarized (OFF) by light is confined to the outer half of the IPL. What factors control the precision by which each cell type forms synaptic connections within the IPL and OPL are not completely understood. However, structural and functional studies have significantly improved our understanding of the mechanisms underlying retinal circuit development, aided in part by new technological advances.

Sequence of Circuit Assembly in the Vertebrate Retina

Ultrastructural studies (1-3) suggest that synaptogenesis between the major neuronal classes of the vertebrate retina occurs in three major phases (Fig. 2, illustrated for the mouse retina). Retinal ganglion cells and amacrine cells are the first cell classes to differentiate and form the earliest functional circuits in the IPL of the developing retina. Shortly after, horizontal cells and photoreceptors differentiate and contact each other in the outer retina, forming the OPL. The vertical networks in the inner and outer retina are later interconnected when bipolar cells are born and connections with ganglion cells are established. This sequential pattern of retinal circuit development is common across species, although the separation in time between inner and outer retinal circuit development varies, ranging from a few hours in animals such as the zebrafish to many days and weeks in mammals. The emergence of the IPL and OPL plexuses can be observed in the zebrafish embryo by *in vivo* time-lapse confocal imaging as visualized in Movie 1.

Structural Assembly

New Approaches

The morphology of the pre- and postsynaptic arbors of retinal neurons have been documented from Golgi staining many decades ago (4). These studies provided a wealth of information, not only aiding classification of distinct morphological cell types in the mature retina but also enabling visualization of the structure of their immature counterparts. More recently, fluorescent markers have been used to specifically label retinal cell classes and their subtypes. Cells can be targeted by intracellular dye filling methods using glass micropipettes (5, 6). This method leads to rapid labeling of the cell and its processes, within seconds to minutes. Intracellular dye filling has been used to visualize developing retinal neurons and remains a popular technique to determine their morphology at different ages.

Since its discovery, green fluorescent protein (GFP) has been used extensively as a live-cell marker. Its resistance to bleaching, compared with most fluorescent dyes, together with its lack of toxicity, make GFP ideal for studying how retinal neurons alter their structure in tissue explants or *in vivo*. GFP and its spectral variants can be expressed in retinal neurons either by transient transfection or in stable transgenic lines. To randomly label retinal neurons in explant cultures, a gene-gun can be used to deliver plasmids encoding GFP (7) (Fig. 3). Other color fluorescent proteins (FPs: yellow, cyan, red) can also be expressed this way. Electroporation can be used to

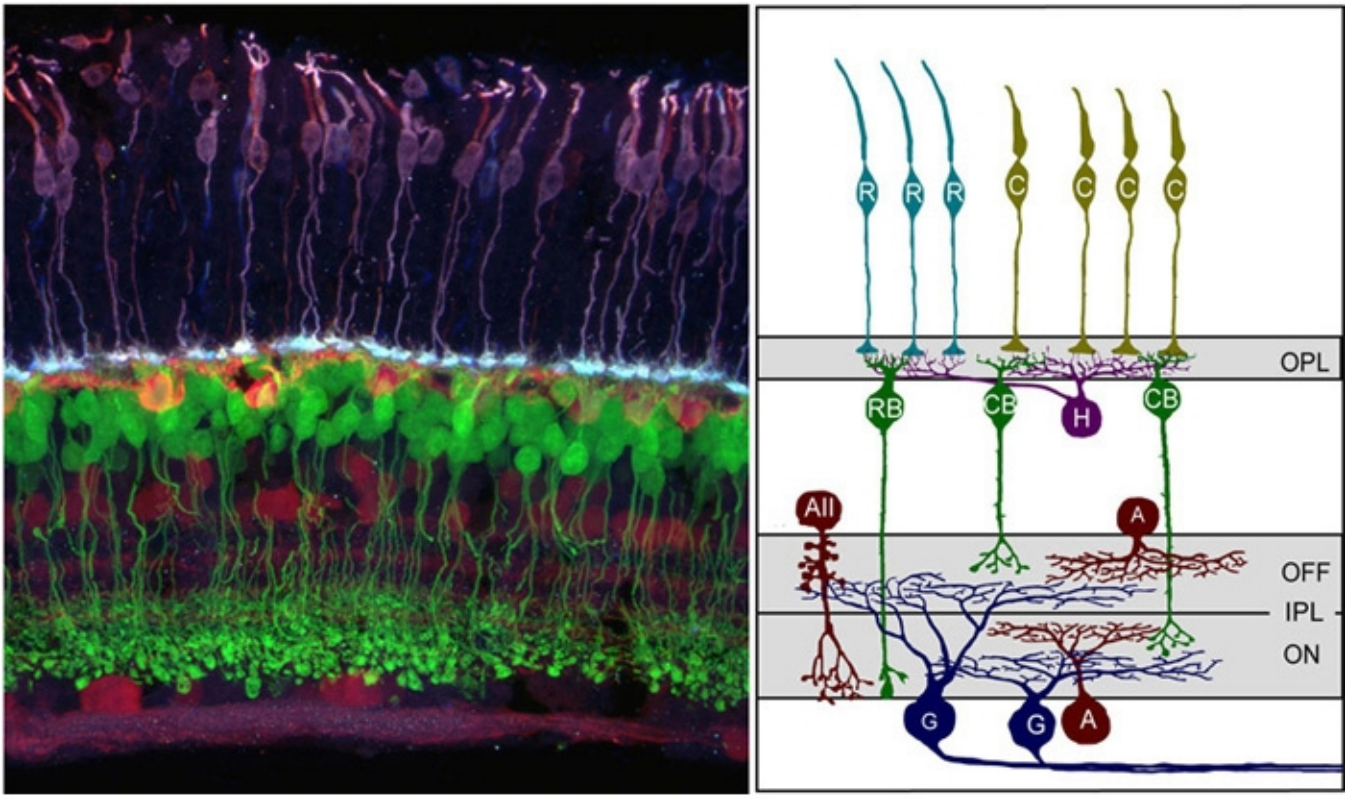

Figure 1. (left) Cross-section of an immunostained mature mouse retina showing lamination of cell bodies and synaptic terminals. Photoreceptors (bluish-purple) immunolabeled with anti-cone arrestin (gift of Cheryl Craft); amacrine and ganglion cells immunstained for calbindin (red), and bipolar cells immunoreacted for GFP (section from a transgenic animal in which ON bipolar cells express GFP under the mGluR6 promoter; generated by Anuradha Dhingra and Noga Vardi). (right) Schematic diagram illustrating the major cell components and their projection patterns in the mature vertebrate retina.

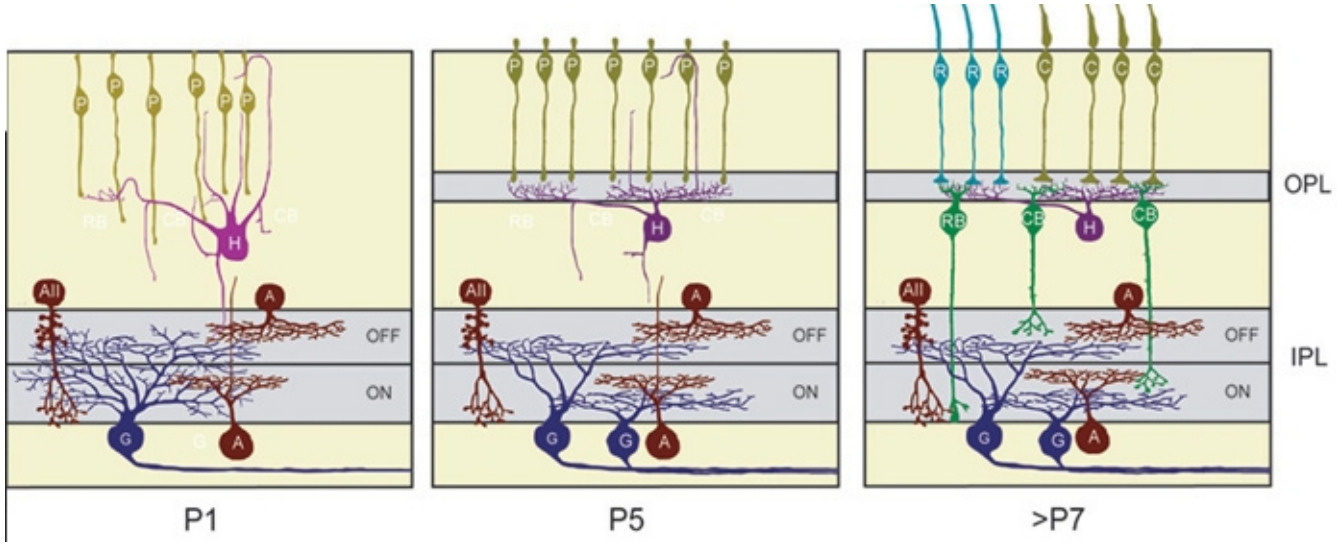

Figure 2. Schematic showing the sequence of circuit assembly in the vertebrate retina, illustrated for the mouse. P = postnatal day. IPL= inner plexiform layer; OPL= outer plexiform layer.

specifically target and label individual cells *in vitro* and *in vivo* (8). This technique involves intraocular DNA injection before high-voltage pulses are applied across the eye (9) (Fig. 4).

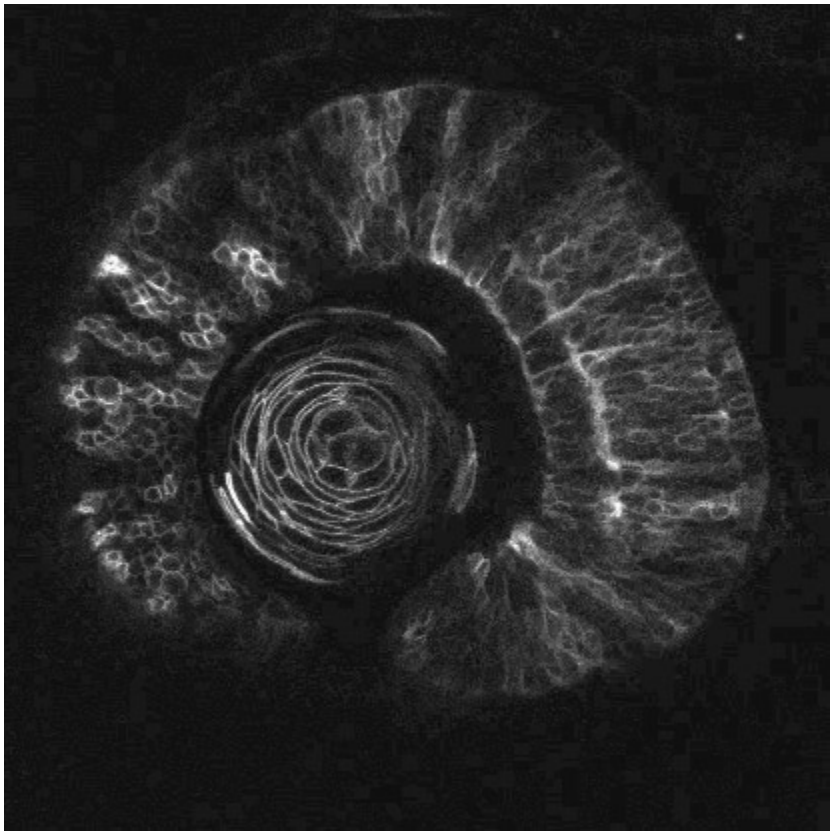

Movie 1. A movie of the emergence of the IPL and OPL plexuses in the zebrafish embryo by *in vivo* time-lapse confocal imaging.
Download video

Alternatively, as cell type-specific promoters become increasingly available, labeling of retinal neurons in the developing and adult retina can be achieved by generating transgenic animals. For example, GFP expression is driven in cone photoreceptors in mice shortly after birth using the human L- and M-cone promoter (10) (Fig. 5). Also, a subset of bipolar cells expresses GFP in the gustducin-GFP mouse (11) (Fig. 5), and retinal ganglion cells are found to express fluorescent proteins under the Thy-1 promoter (12) (Fig. 5).

Zebrafish in which retinal neurons express fluorescent proteins have also been generated (Fig. 6). The major advantage for generating fluorescent proteins expressing transgenic lines is that structural development of the various retinal neuronal cell types can be followed in live tissue, or in the intact animal using time-lapse microscopy. The zebrafish, in particular, is highly suited for *in vivo* imaging because of its relatively rapid development and transparency during embryonic development. Details of how to image fluorescently labeled retinal neurons in zebrafish embryos is provided by Lohmann et al. (13).

Development of Pre- and Postsynaptic Processes

There are at least two features of the structure of retinal neurons that impact their connectivity and therefore the circuits that they form. The first relates to the lateral branching patterns of their axons and dendrites. The lateral organization of the pre- and postsynaptic arbors of retinal neurons determines the spatial coverage of the cell, and possibly the density of input and output that they form. The second, as mentioned earlier, is that the pre- and postsynaptic arbors of retinal neurons are highly restricted to laminae in the inner and outer retina. This laminar organization in structure reflects the connectivity between specific subsets of cells. Thus, one way to gain a better understanding of how retinal circuits form appropriately is to determine the mechanisms that regulate the lateral and vertical organization of the axonal and dendritic arbors of retinal neurons.

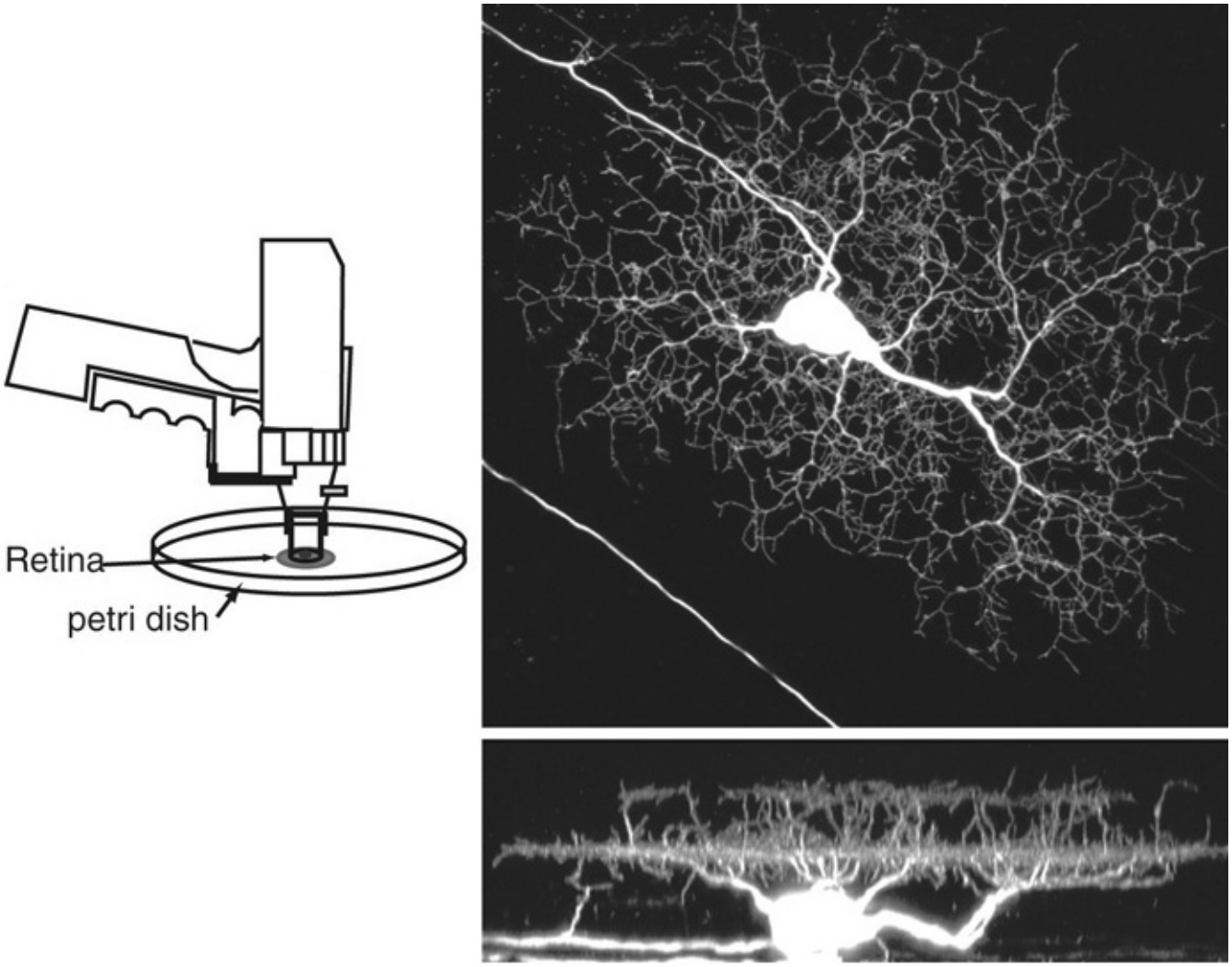

Figure 3. Biolistic delivery of plasmid encoding fluorescent protein by a gene-gun (diagram to the left) results in exquisite labeling of retinal ganglion cells in live, developing retina. Shown here is a YFP-expressing embryonic chick retinal ganglion cell.

Retinal Ganglion Cells

There are many types of retinal ganglion cells, each with characteristic branching patterns, arbor size, and amount of overlap with neighbors of the same subtype. Both intrinsic and environmental cues appear to shape the branching patterns of retinal neurons, at least for ganglion cells (reviewed in Sernagor et al. (14)). When retinal ganglion cells are isolated in culture without contact with other cells, they elaborate a dendritic arbor that is complex in branching and resembles cells *in vivo*. Stereotypic organization of the branching patterns of the various cell types (for example, alpha cells and beta cells in the cat retina) also argue that cell intrinsic mechanisms help define their branching patterns.

However, the shape and size of the ganglion cell dendritic arbor changes when the density of neighboring ganglion cells is altered during development (Fig. 7). Laser ablation or axon section results in a local lesion depleted of retinal ganglion cells (15). This manipulation results in cells at the edge of the lesion projecting their dendrites into the ganglion cell-free region. Experimental manipulation of eye size that causes an increase in the spacing between cells is paralleled by an increase in their arbor size (16). However, for certain subtypes of ganglion cells in the mouse retina, a reduction in ganglion cell density does not affect the size and patterning of their dendritic arbors (17). These differences raise the possibility that the balance between cell-intrinsic and cell-

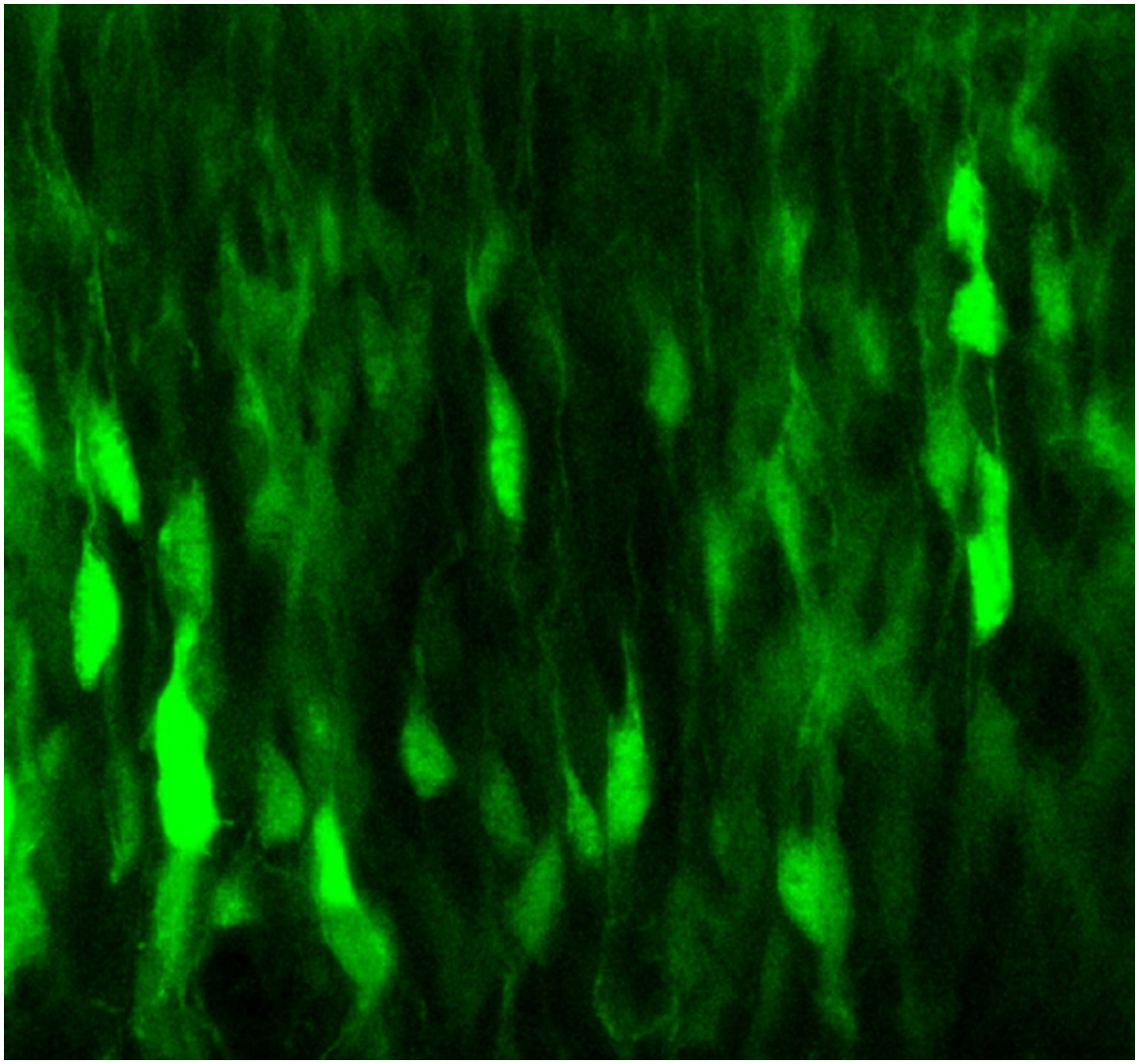

Figure 4. Retinal cells are labeled by GFP expression *in vivo* using electroporation methods. Shown here is a cross-section of a neonatal mouse retina (provided by Mike Dyer).

extrinsic cues in shaping the lateral organization of ganglion cell dendritic arbors may vary from one cellular subtype to another, or perhaps even across species.

If cell–cell interactions influence the branching and territorial size of ganglion cell dendritic arbors, what might be the signals? One way to address this is to better understand the dynamic behavior of ganglion cell dendrites during the period when their branching patterns and territories are established. Time-lapse imaging experiments of developing chick and mouse retinal ganglion cells reveal that dendritic branches are both added and eliminated over time, before the adult branching patterns are attained. Dynamic alterations to the dendritic territory upon branch addition and loss can be appreciated in Movie 2.

What cellular mechanisms might neurotransmission evoke to regulate dendritic branching in retinal ganglion cells? Live-imaging studies of embryonic chick retinas reveal that ganglion cell dendritic stability is calcium dependent. In low extracellular calcium, the dendrites of retinal ganglion cells retract (Fig. 8). Dendritic retraction can be locally controlled by calcium-induced calcium release (CICR) from intracellular stores (18). Spontaneous CICR is observed in small dendritic segments during calcium imaging of immature retinal ganglion cells. The pathways that CICR activates to stabilize the dendritic cytoskeleton remains to be determined. One possibility is that transmission from presynaptic terminals causes local CICR that then stabilize

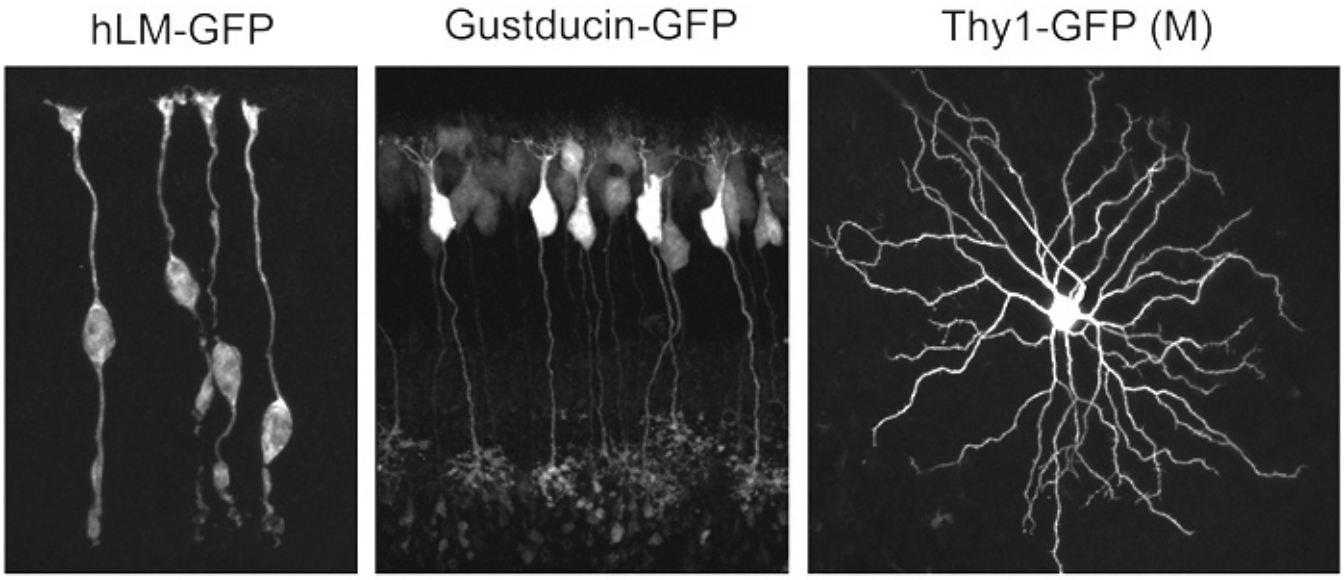

Figure 5. Examples of GFP-expressing retinal neurons in stable transgenic lines. Cone expression is driven by the human L- and M-opsin promoter (image provided by Rachel Huckfeldt); a subset of bipolar cells express GFP under the gustducin promoter, and a ganglion cell in the Thy-1-GFP M-line.

the contacted dendritic segments (18). Future time-lapse imaging experiments are needed to directly address whether nascent synapses stabilize dendrites of retinal ganglion cells upon contact, as has been demonstrated in zebrafish tectal neurons (19).

What factors shape dendritic stratification of retinal ganglion cells during development? In mammals, retinal ganglion cells initially project dendrites throughout the depth of the IPL (Fig. 9). Stratification occurs progressively and becomes precise by maturity (Fig. 9). Some insight into what mechanisms underlie ganglion cell dendritic stratification was gained by early studies where intraocular injections of 2-amino-4-phosphonobutyrate (APB, a mGluR6 receptor agonist) prevented the emergence of stratified alpha and beta ganglion cell dendritic arbors in cat (20, 21) and ferret (22) retina. Thus, neurotransmission may be involved in sculpting the final arrangement of ganglion cell dendrites. This is supported by pharmacological studies in turtles and chick, whereby blockade of cholinergic or glutamatergic transmission, respectively, resulted in ganglion cells with relatively smaller and less branched arbors (7, 23).

Amacrine Cells

How immature amacrine cells elaborate their processes after neuronal differentiation has been described by Golgi (24) and electron microscope (25, 26) studies a few decades ago. From observations of retinas fixed at different ages, it is thought that cells in the differentiating inner nuclear layer that are multipolar in shape are immature amacrine cells. Such cells extend neurites in many different directions before reaching the border of the INL and IPL. Thereafter, amacrine cells elaborate processes within the IPL to form their arbors (Fig. 10).

Time-lapse studies of amacrine cells labeled by expression of fluorescent protein in stable transgenic zebrafish lines have provided some insight into the lamination of amacrine cell neurites (27). In a transgenic line in which subpopulations of ON and OFF amacrine cells express GFP, it is possible to visualize the emergence of a plexus of processes from these amacrine cells (see Movie 1). Initially, it appears that GFP-positive amacrine cell processes contributing to the nascent IPL are diffusely arranged, because no sublamination is observed. However, over time, two distinct bands of bright fluorescence resolve, corresponding in depth to sublamina **a** (OFF) and sublamina **b** (ON) of the IPL. To determine how individual amacrine cells target their appropriate sublamina during development, it will be necessary to visualize and follow the development of individual

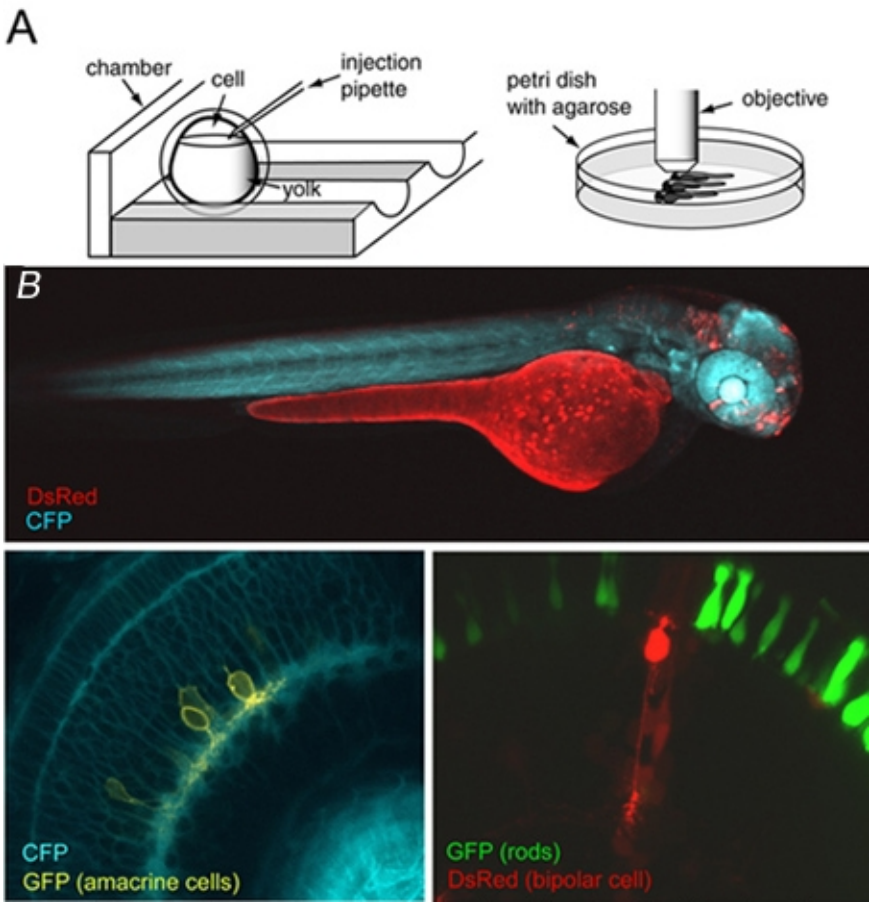

Figure 6. (A) Transient expression of fluorescent proteins is attained in zebrafish embryos by injection of plasmid into the fertilized egg at the one-cell stage. Imaging of this expression is possible in anesthetized embryos embedded in low-melting point agarose using a water objective. Reproduced in part from Lohmann et al. (13). (B) Examples of zebrafish neurons expressing fluorescent proteins by transient transfection or in stable transgenic lines. Transient DsRed expression driven by the alpha-tubulin promoter. GFP-expressing amacrine cells in the Pax6-DF4:mGFP transgenic line (27) crossed to a Pax6-DF4:mCFP line (58); rod photoreceptors (green) in the XOPs-GFP line (59). Reproduced in part from Mumm et al. (58).

amacrine cells over time *in vivo*. This is because it is impossible to differentiate between closely apposed, but segregated, arbors in the IPL from arbors that are intermingled in depth.

It is evident that even after amacrine cell neurites have attained their correct sublamination, their arbors still undergo significant reoroganization in the lateral dimension before achieving their mature form. Starburst amacrine cells in the mammalian retina show a distinctive radial morphology early in development, but their detailed branching pattern alters with maturation. Similar to retinal ganglion cells, the morphological changes primarily involve the loss of small protrusions and the emergence of bouton-like structures at the distal branches (28) that, in the mature cell, are sites of presynaptic transmitter release (see chapters on amacrines and neuroactive substances).

What factors influence the development of amacrine cell neurites? First, it is evident that retinal ganglion cells, although a major postsynaptic target of amacrine cells, are not required for lamination of amacrine cell arbors. Optic nerve section in rodents that leads to ganglion cell death does not alter the stratification of starburst amacrine cells (reviewed in Chalupa and Gunhan (29). In mutant animals in which ganglion cells do not differentiate (Math5 knockout mice (30, 31) and the zebrafish lakritz mutant), amacrine cell lamination also occurs (Fig. 11). Because bipolar cells differentiate only after amacrine cell lamination has taken place, it is unlikely that these neurons influence the initial stratification of amacrine cells. It is possible that interactions

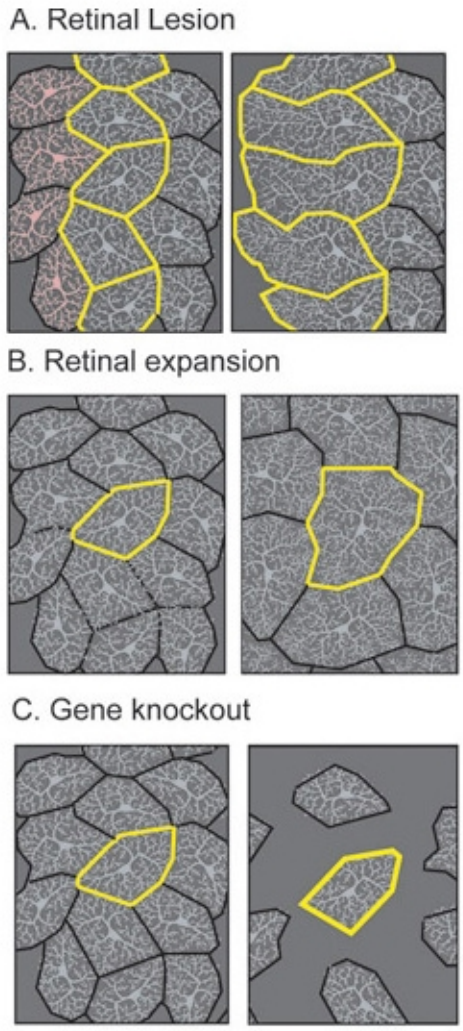

Figure 7. Schematized organization of dendritic territories of retinal ganglion cells under various conditions of manipulation. (A) Pink cells are lesioned by a laser (15). (B) Expansion of the retinal area induced by form deprivation (16). (C) Territories of SMI-32 immunopositive ganglion cells in the Brn3b knockout mouse retina (17).

between amacrine cells that are specific to each subtype result in the formation of their separate laminae. Alternatively, lamination cues may arise from Muller glial cells or their precursors. Such cues may be diffusible, creating a gradient of permissive or repulsive factors with retinal depth, or are contact mediated. Because amacrine cells express neurotransmitters even before their cell bodies reach the INL/IPL border, it also remains plausible that communication between these cells via secretion of transmitters influences their arborization. Mutant animals in which specific forms of neurotransmission are absent would help address this possibility.

Bipolar Cells

Axo- and dendrogenesis of bipolar cells are not well understood because of the lack of markers for these cells early in development. However, Golgi studies of the chick retina suggest that the axonal and dendritic arbors of developing bipolar cells elaborate from vertical processes terminating in the inner and outer limiting membranes (32) (Fig. 12). The use of cell-specific markers to identify bipolar cells would further test this model of bipolar cell development.

Stratification of the axonal arbors of bipolar cells may be influenced by interactions with amacrine cells. AII amacrine cells, which are the postsynaptic targets of rod bipolar cells, have a bistratified arbor, each with

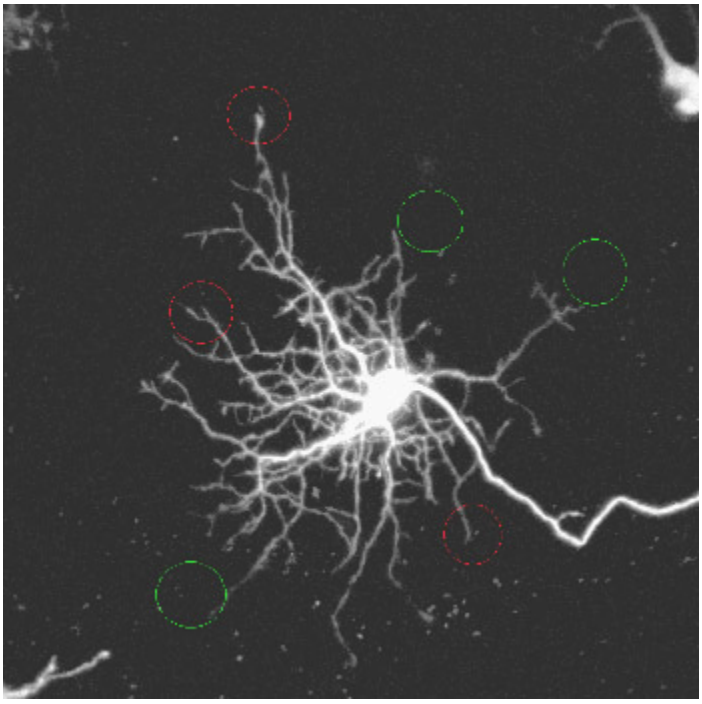

Movie 2. A movie of the emergence of dendrites (to green circles) and elimination of others (in red circles) in developing ganglion cells in the zebrafish retina.

Download video

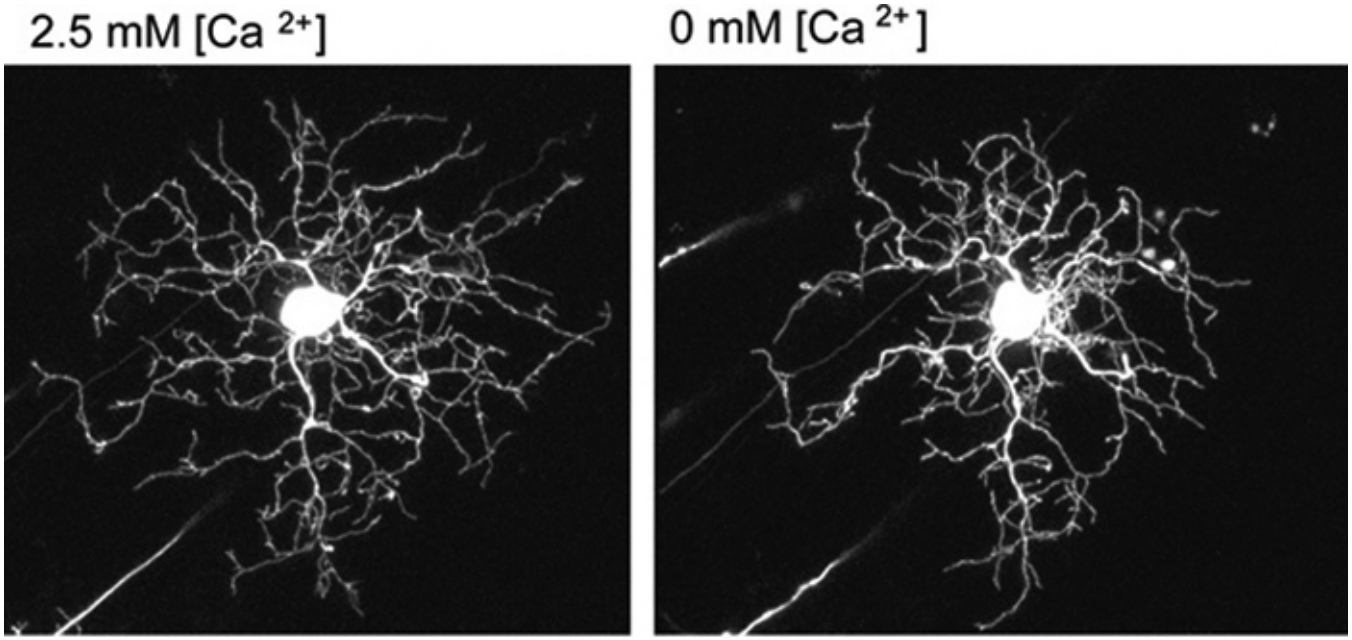

Figure 8. Live confocal imaging of a GFP-expressing chick retinal ganglion cell during embryonic development. Removing extracellular calcium causes shrinkage of the dendritic arbor.

stereotypic morphology. The outer arbor (OFF sublamina) comprises lobular appendages, whereas the inner arbor (ON) is finely branched (see chapter on AII amacrine cells). AII amacrine cells express Disabled1, an adaptor protein involved in the reelin pathway (33). In the reeler mouse in which reelin is absent, the distribution of lobular and non-lobular appendages of the AII amacrine cells is imprecise. Likewise, some rod

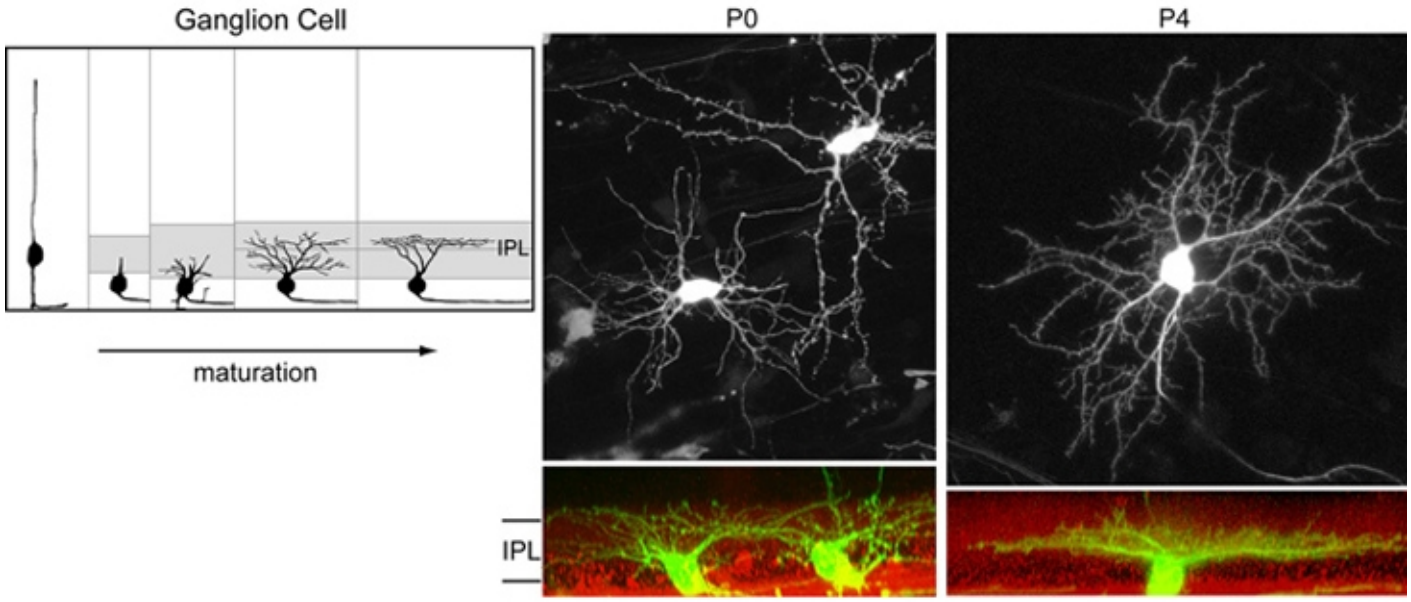

Figure 9. (left) Proposed sequence of dendritic development of mammalian retinal ganglion cells. (right) Labeling of mouse retinal ganglion cells at birth (P0) and at P4 demonstrates that initially, the arbors of these ganglion cells are unstratified. The depth of the IPL is judged by reflected light microscopy (red regions). The distribution of dendrites (green) with depth is best observed in the orthogonal rotations of confocal optical stacks encompassing the arbors, shown below the whole-mount images of the cells.

bipolar cells are found to have axonal stratification defects (Fig. 13). Also in the lakritz mutant, bipolar axonal terminals are similarly perturbed in their organization in local regions of disrupted amacrine cell lamination (Fig. 13). ON and OFF bipolar cell lamination persists in the absence of ganglion cells (30, 31, 34). Together, these observations raise the possibility that amacrine cells, rather than ganglion cells, provide lamination cues for bipolar axon terminals.

Horizontal Cells

Early Golgi studies and immunolabeling for GAD67 (35), one of the two synthetic enzymes for GABA, suggest that horizontal cell processes undergo dramatic progression from a radial to lateral organization during development (Fig. 14). Horizontal cells achieve this lateral organization in the absence of cone photoreceptors (36). However, abnormal lamination patterns in horizontal cells are observed in the Rb mouse during development in regions where rods are absent (37).

In the mature retina, horizontal cells do not contact cones uniformly within their dendritic fields. The number of dendritic terminals (Fig. 15A, examples of terminals) that contact cones decreases as a function of distance from the cell body (Fig. 15B). Interestingly, in developing horizontal cells, the number of terminals does not vary greatly with distance from the cell body. Because the overlap of dendritic fields of neighboring horizontal cells is relatively unchanged after birth in the mouse, horizontal cells appear to lose peripheral terminals but gain central terminals with maturation (Fig. 15B). The terminal branching pattern of horizontal cell dendrites is altered in the coneless mouse (36) (Fig. 15C). This suggests that contact with cones is either important in the initial organization, or in the maintenance, of these structures.

Photoreceptors

Structural changes in the morphology and axonal targeting of photoreceptors have been assessed using immunolabeling methods (schematized in Fig. 16A). In a variety of species, these studies reveal that the terminals of a large number of rods (80% of the population) and some cones project beyond the forming OPL,

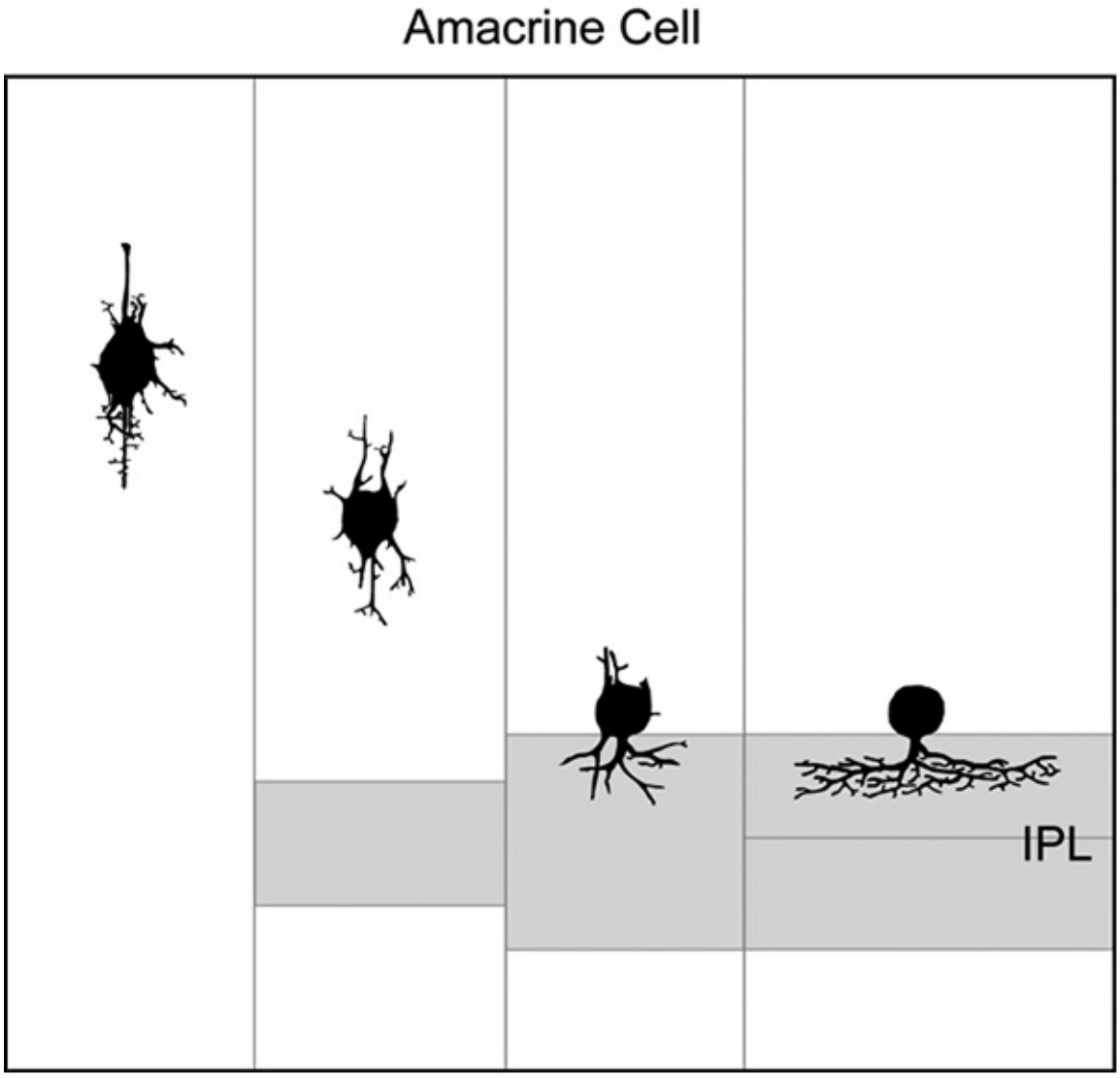

Figure 10. Proposed sequence of amacrine cell neurite development from serial EM studies (25).

reaching the IPL (38) (reviewed by Reese (39)) (Fig. 16). With maturation, all photoreceptor terminals become restricted to the OPL. The transient projection of photoreceptor terminals to the IPL is not perturbed when retinal ganglion cells are ablated. However, pharmacological deletion of amacrine cells, for example with VAChT-saporin, results in these photoreceptor terminals ending at various depths of the IPL, and even extending into the GCL. This implicates the amacrine cells as targets of the immature photoreceptor terminals (40) (Fig. 16).

Functional Assembly

New Approaches

Physiological properties of developing retinal neurons have often been assessed at the single-cell level using patch clamp, intracellular and extracellular recording methods. Simultaneous recording from large populations of developing retinal neurons became possible upon the development of multielectrode arrays (41) and advances in optical imaging methods (reviewed in Morgan et al. (42)). Both approaches have been used to assess activity patterns of retinal networks during development.

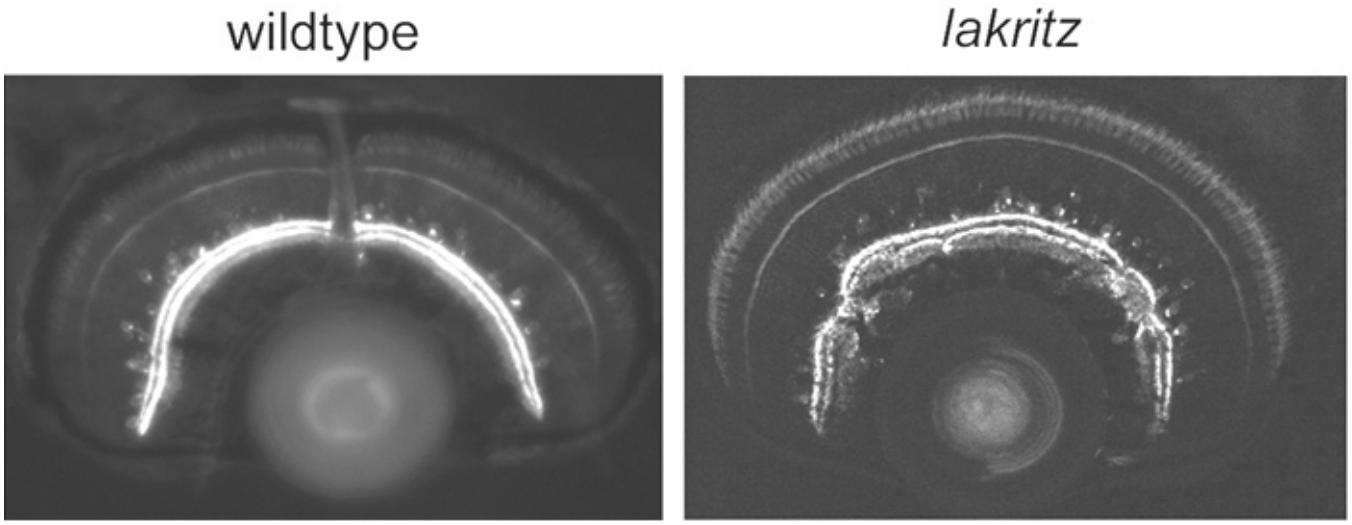

Figure 11. Sublamination of amacrine cell neurites is still apparent in the absence of retinal ganglion cells, as evident in the lakritz zebrafish retina (reprinted from Kay et al. (27).

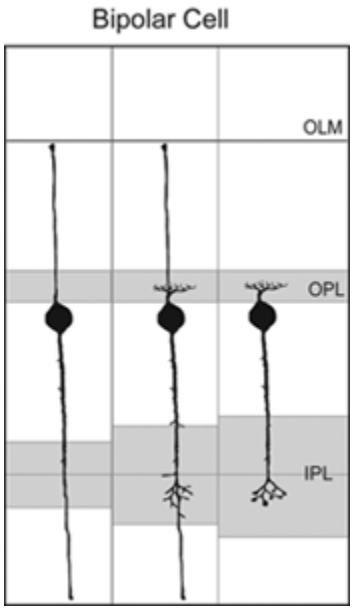

Figure 12. Proposed sequence of development of bipolar cell axons and dendrites from Golgi studies.

Multielectrode recording planar electrode arrays with 60 or more extracellular electrodes permit simultaneous recordings from tens of ganglion cells (Fig. 17) (see Movie 3). However, because they are extracellular recordings, it is not straightforward to determine which cells within the sampled area are associated with spike trains detected at each electrode site. These arrays are commercially available from several sources. Shown is an example of an array from multichannel systems used for recording spikes from the developing retina (43, 44).

Calcium Imaging

Calcium imaging approaches have been used to assess retinal neuronal activity at the single-cell level and to simultaneously monitor intracellular calcium levels in populations of cells (see chapter on retinal development by Marla Feller). The use of calcium indicator dyes is widely documented (see Lohmann et al. (45) for a detailed description of the methodology). Both membrane-permeant forms of indicators as well as genetically encoded

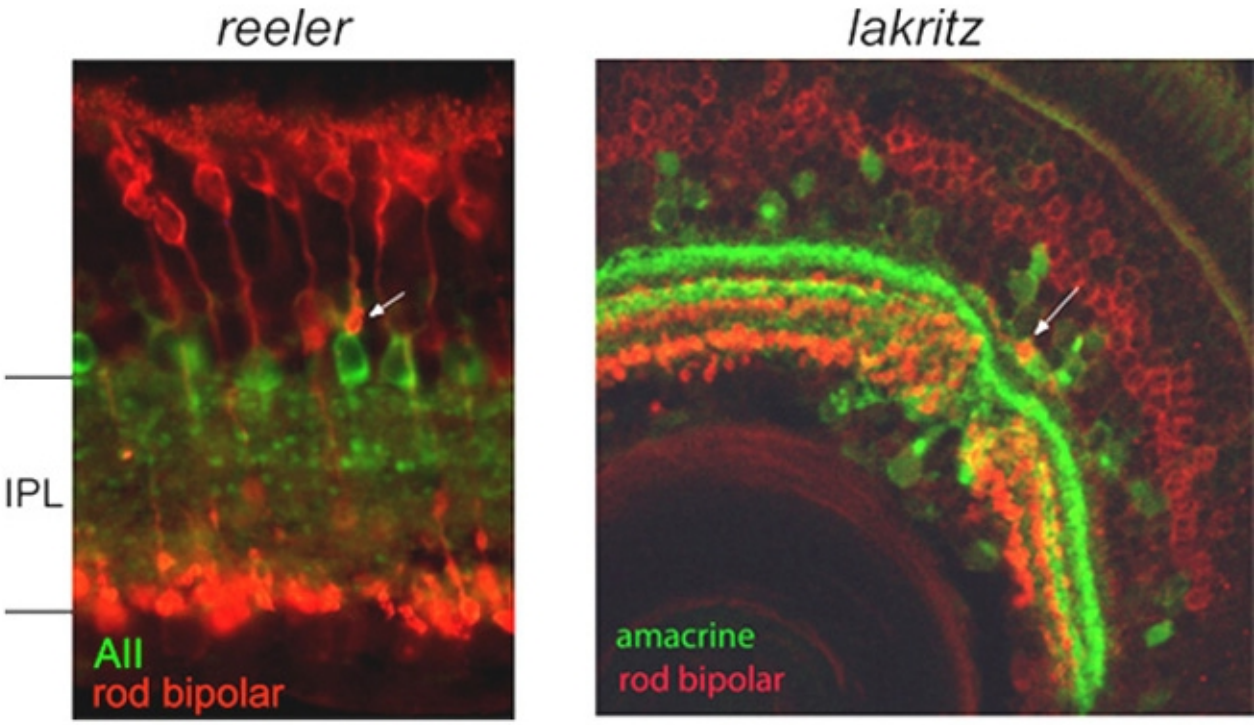

Figure 13. Bipolar cell axonal stratification is affected in the reeler mouse (left) and lakritz (right) zebrafish mutant at regions where amacrine stratification is disrupted (e.g., arrow). Image of cross-section of reeler retina provided by Dennis Rice, and lakritz retinal section reprinted from Kay et al. (27).

indicators are available and have been used successfully. Shown in Movie 4 is an example of spontaneous activity in an embryonic chick retina, showing elevations in intracellular calcium levels as there is increase in fluorescence intensity. The calcium levels elevate across the array in a wave formation. Ballistic delivery of calcium indicators can be used to actually visualize the processes of individual cells (18).

Development of Synaptic Connectivity

Functional drive onto retinal ganglion cells is first observed shortly after conventional synapses are present in the IPL, as assessed by electron microscopy. During this period of development, spontaneous excitatory postsynaptic currents (EPSCs) are detected in retinal ganglion cells and amacrine cells. These excitatory currents are mediated by acetylcholine, GABA, or glycine (14), transmitters used by amacrine cells. As in other parts of the CNS, GABA is depolarizing to retinal ganglion cells before the appearance of glutamatergic drive. Spontaneous glutamatergic drive is first observed in the mouse retina around P7, when bipolar terminals are clearly present in the IPL (46). Whether photoreceptors transiently projecting to the IPL provide glutamatergic drive to inner retinal neurons is not known, although it is suggested by the presence of synaptophysin-positive terminals (39).

Fig. 18 summarizes the time-line of key events associated with circuit development in the developing mouse retina.

Spontaneous Activity

Prior to vision, the inner retina generates a pattern of activity that is unique to the developing retina. Neighboring retinal ganglion cells exhibit rhythmic bursting activity that is correlated by propagating waves (reviewed in Wong (47)) (see Marla Feller's chapter). These waves are visualized by calcium imaging and are also

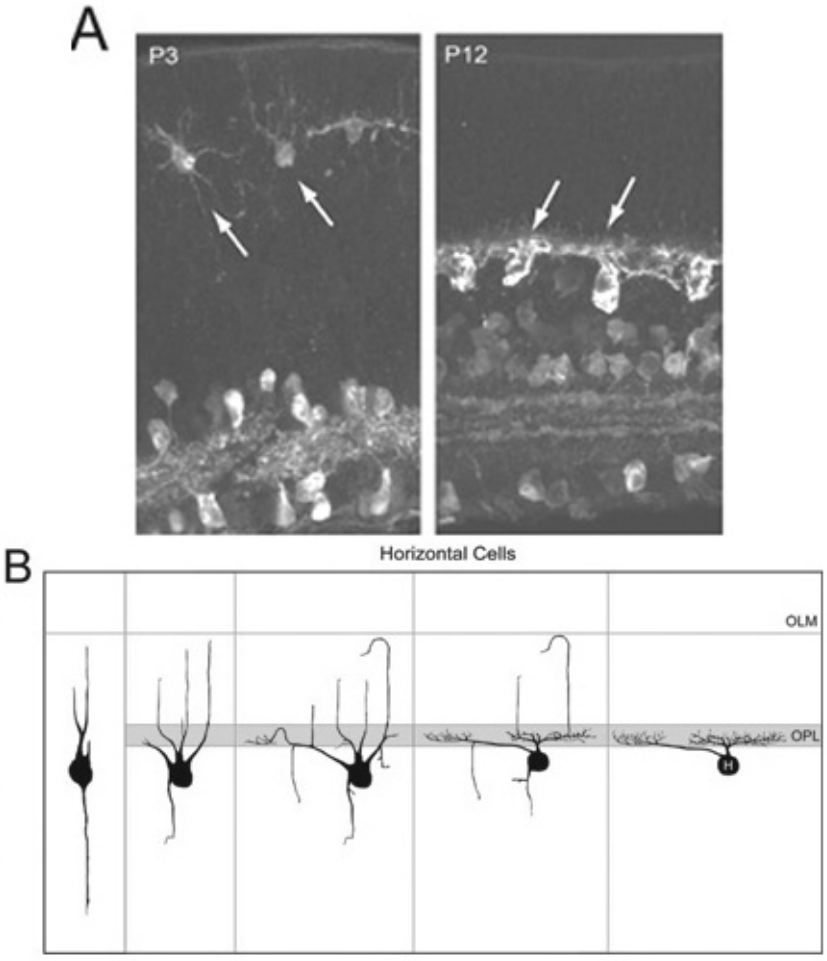

Figure 14. Horizontal cells (arrows) undergo dramatic remodeling of their processes during development, as visualized by immunolabeling for calbindin in the neonatal mouse (A) retina, and illustrated in the schematic diagram (B). OLM = outer limiting membrane; OPL = outer plexiform layer.

detected using multielectrode arrays (see Movie 3). Retinal waves disappear shortly after eye-opening (Fig. 19). The properties and significance of these retinal waves are discussed in the chapter by Marla Feller. Although there is increasing evidence for a role of waves in the refinement of connectivity between the retina (48) and its central targets, their role in shaping intra-retinal circuits, although possible, remains to be determined.

Light Responses

Emergence of ON *versus* OFF Responses

Immunolabeling studies show that VGlut1, a vesicular glutamate transporter, first appears in the axonal terminals of OFF bipolar cells, before being present in ON bipolar cells (49). This would suggest that the OFF pathway may become functional somewhat earlier than the ON pathway. However, immature amacrine cells in the developing rabbit retina show a predominantly ON response to light (50). Thus, to further ascertain whether ON and OFF transmission matures at different rates, it is necessary to record spontaneous glutamatergic currents and visual responses from identified ON and OFF retinal ganglion cells during development.

At the stage when ferret retinal ganglion cells are still diffusely unstratified, they are found to respond to both increments and decrements in light intensity (51). In mouse, multielectrode recordings show that a higher proportion of units sampled have ON-OFF responses during development, compared with the adult (52). Thus,

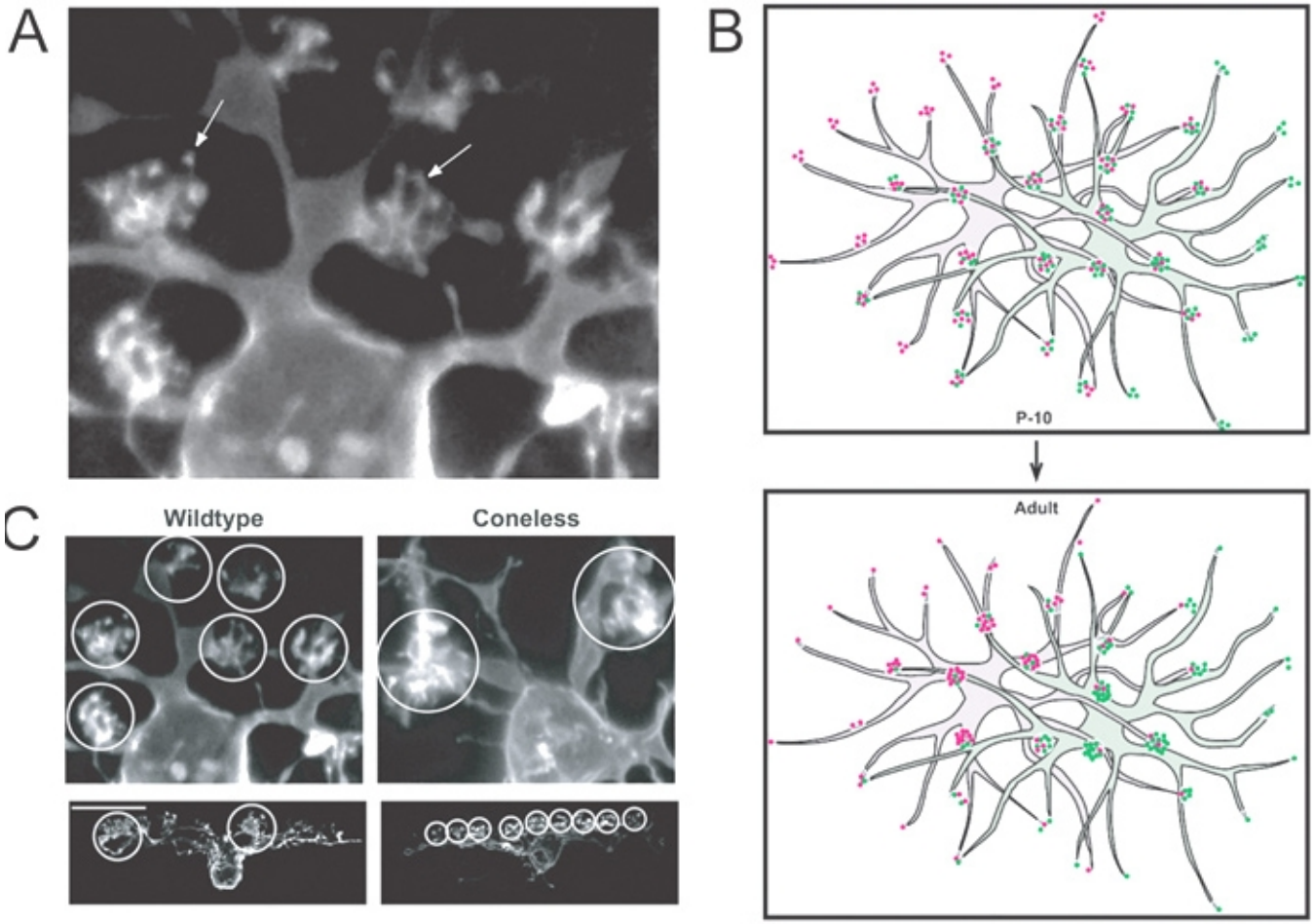

Figure 15. Development of horizontal cell terminals. (A) DiI labeling of a mouse horizontal cell, showing terminals that contact cone photoreceptors. (B) Developmental rearrangements in the organization of terminals across the arbor. (C) Dendritic terminals of horizontal cells are abnormal in the coneless mouse. Images provided by Ben Reese.

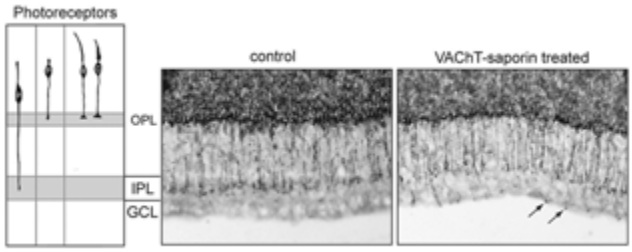

Figure 16. Structural development of photoreceptor axonal terminals. In ferret, the axonal terminals of recoverin-positive photoreceptors reach the IPL. Treatment with VAChT-saporin that kills cholinergic amacrine cells results in overprojection of these terminals into the GCL. OPL = outer plexiform layer. Images provided by Ben Reese (unpublished data).

it appears that significant refinement of ON and OFF bipolar axonal projections to the retinal ganglion cells occurs during maturation of the mammalian retina. One set of projections becomes dominant, and the other is eliminated. In addition to preventing dendritic stratification of retinal ganglion cells, intraocular injections of APB also results in a higher incidence of ON-OFF cells in the cat retina (20). Because APB suppresses spontaneous activity of both ON and OFF ganglion cell subtypes during development, how chronic treatment with this glutamate analog might affect the maturation of ON and OFF connectivity is not yet known.

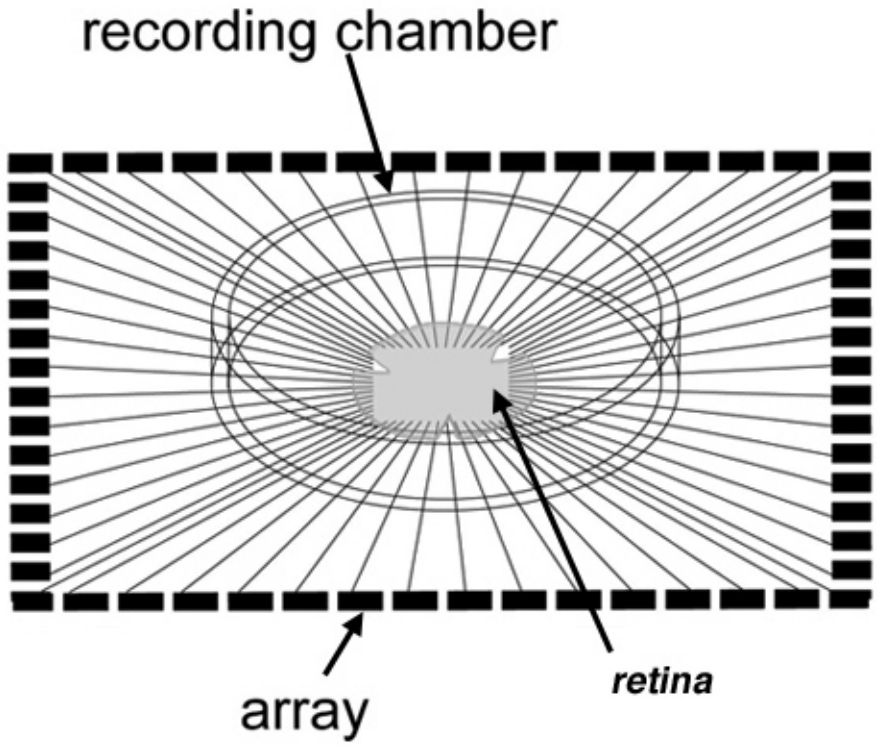

Figure 17. Schematic of multielectrode array produced by Multichannel Systems showing a central recording chamber surrounding a planar electrode array (60 electrodes).

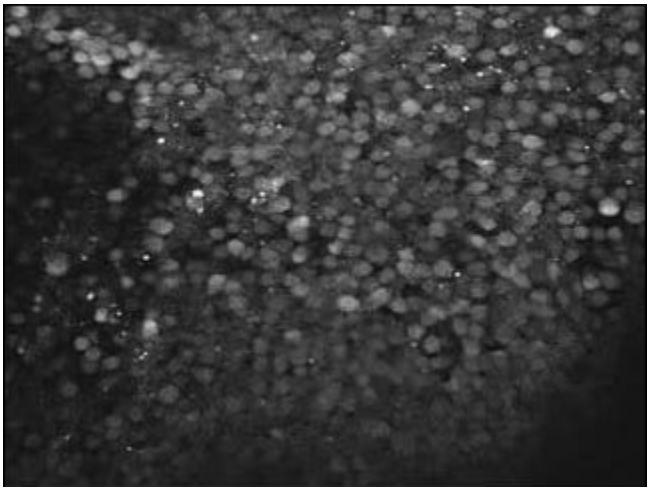

Movie 4. A movie of calcium indicator fluorescence in embryonic chick retina. At-rest background fluorescence of individual ganglion cells can be seen. Passage of the wave produces an intense flash as calcium levels synchronously increase.

Download video

Emergence of Receptive Fields

In vivo recordings from cat retina show that center-surround organization of receptive fields is apparent as soon as light responses are detected (53). Unlike the mature retina, however, receptive field center sizes appear larger than dendritic field size during development (53). In contrast to ganglion cells, the surrounds of rabbit bipolar cells appear after receptive field centers are clearly present (54).

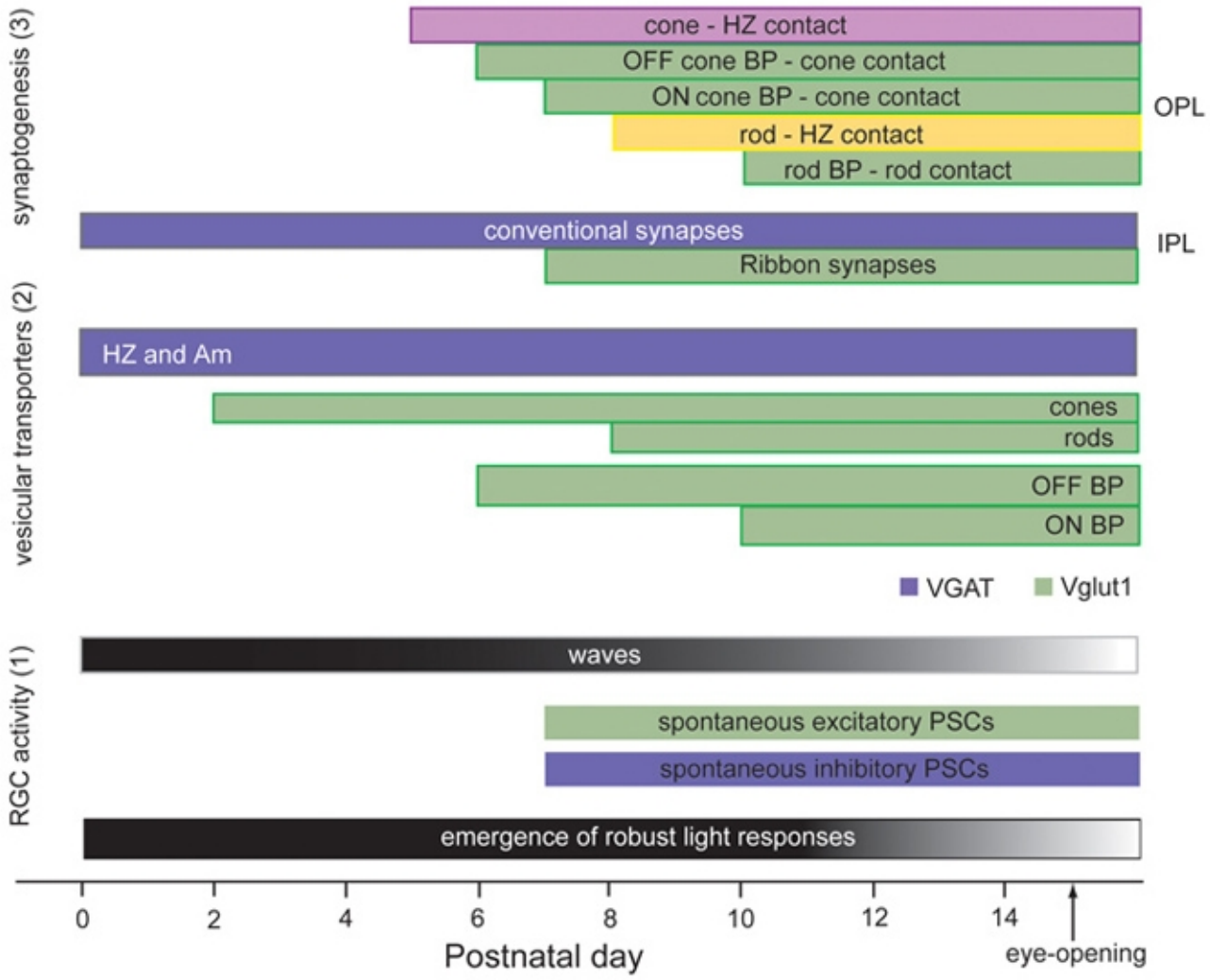

Figure 18. Summary of key physiological events during circuit assembly and maturation in the mouse retina. References for: ROC activity (46, 47);vesicular transporters (46, 49); synaptogenesis (1-3).

Specialized receptive field properties, such as direction-selectivity, can be detected before eye-opening in the rabbit retina (55). Recordings from the developing turtle retina, however, suggest that ganglion cells initially have "anisotropic" receptive fields, with more "isotropic" fields emerging only with maturation (56) (Fig. 20).

Influence of Light in Shaping Receptive Field Properties

Multielectrode recordings in the mouse retina suggest that light stimulation is necessary to facilitate the age-related loss of ON-OFF ganglion cells with maturation (52). Dark-reared mice, until about 3 weeks after birth, have an increase in the fraction of bistratified, ON-OFF ganglion cells in the retina (Fig. 21). This observation would suggest that interactions between bipolar cells and the retinal ganglion cells, or amacrine cells, act to fine-tune the extent of convergence of the vertical pathways onto an individual ganglion cell. This study also underscores the ability of retinal circuits to undergo reorganization, physiologically and structurally, after eye-opening.

Experiments in the turtle retina also implicate light stimulation in prolonging the period of spontaneous wave activity. This in turn affects receptive field maturation (57). Dark-rearing causes an expansion of receptive field size; however, this expansion is prevented when cholinergic-driven spontaneous activity is blocked.

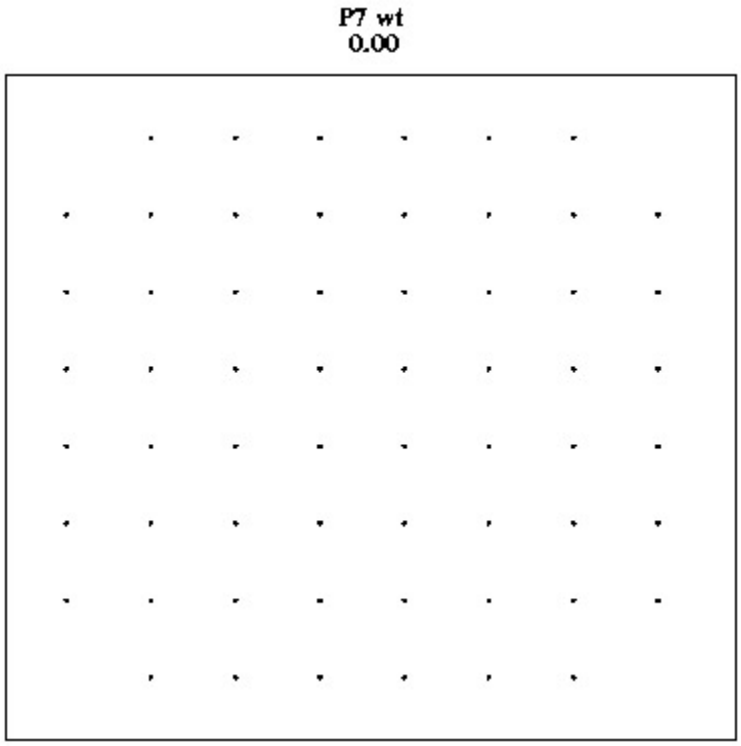

Movie 3. A movie of multielectrode array recording from a week-old mouse retina. Each dot represents the location of an electrode site. The size of the dot is proportional to the firing rate. A wave of activity can be seen to propagate cross the array. Time in seconds.

Download video

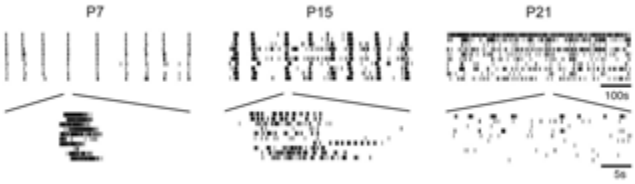

Figure 19. Examples of spontaneous activity patterns in the neonatal mouse retina recorded in the dark using a multielectrode array (Fig. 17). At each age, spike rates are shown for 10 representative cells at two different time scales. Correlated bursting activity is evident at postnatal day (P7) and gradually disappears with maturation. For details, see Demas et al. (43).

Summary

Much remains to be determined as to how retinal circuits are assembled precisely. Because the retina comprises a large diversity of cell components and numerous circuits, determining the cellular and molecular mechanisms regulating its wiring is a challenging task. Nevertheless, as retinal subcircuits with defined visual properties become identified (such as the direction-selective circuit), elucidating the developmental mechanisms regulating their assembly should become more tractable. Combined electrophysiological and anatomical techniques are necessary, and with rapid advancement in both approaches, it is likely that significant progress will be made in the near future.

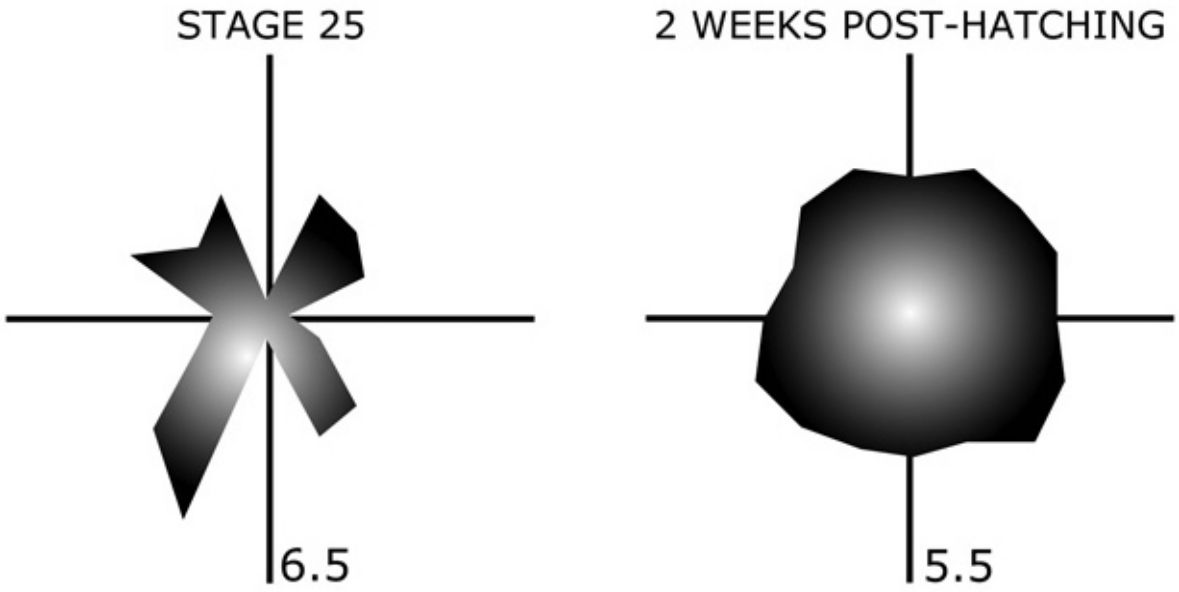

Figure 20. Example of receptive fields in the developing turtle retina. Note the initial anisotropic nature of the receptive field, suggesting sensitivity in different directions early on. Numbers indicate spikes/second rate.

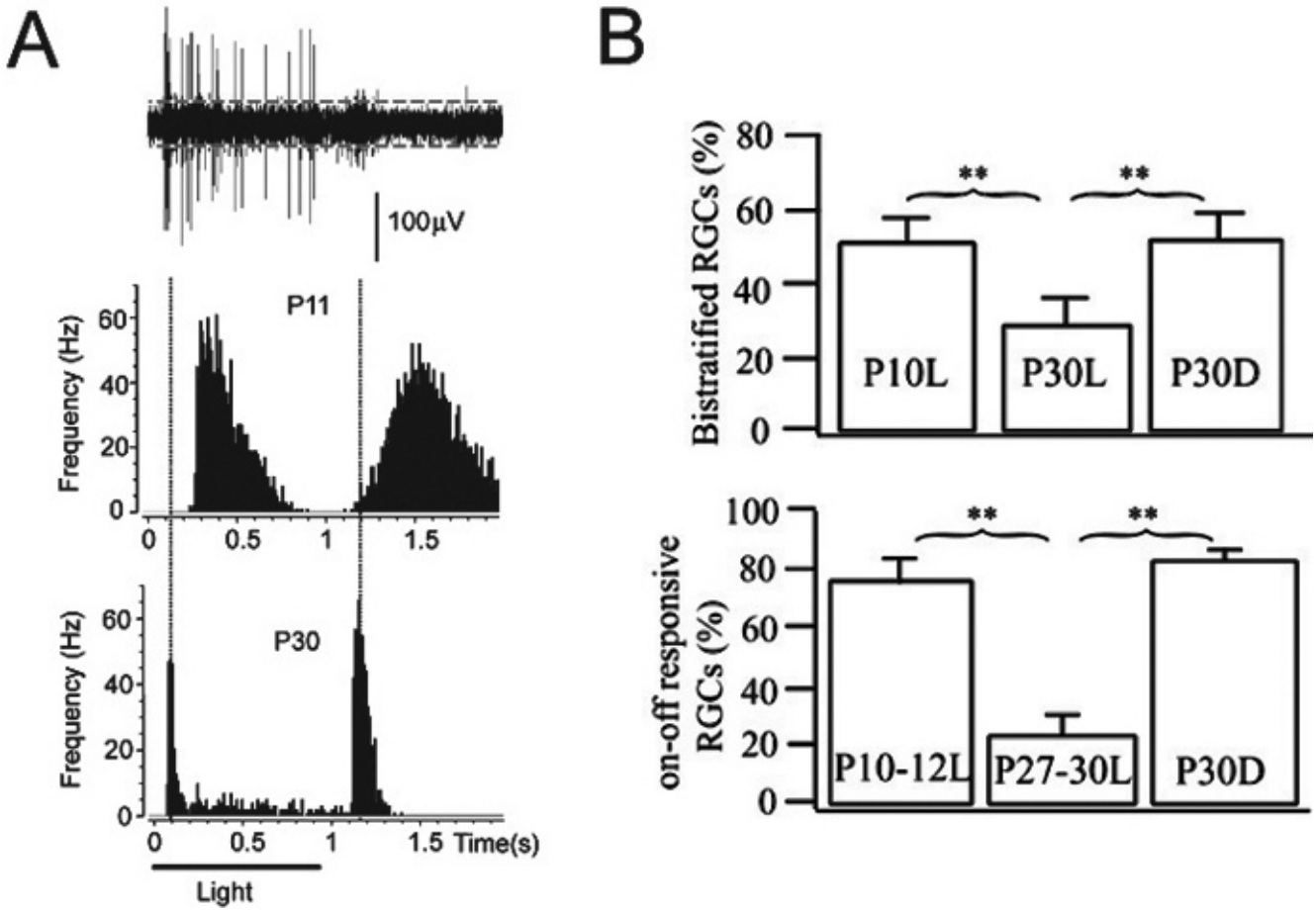

Figure 21. (A) Examples of ON and OFF light responses from neonatal mouse retinal ganglion cells to adult age. Recorded with a multielectrode array. (B) Effects of dark-rearing (P30D) compared with normal (P10L and P30L) on the fraction of bistratified cells and ON-OFF retinal ganglion cells during postnatal development. Figures provided by Ning Tian.

About the Authors

Josh Morgan received his B.A at New College of the University of South Florida with an area of concentration in neurobiology. He is currently a graduate student in Rachel Wong's lab in the Anatomy and Neurobiology Department of Washington University in St. Louis. He expects to spend his life imaging neural circuit development and has focused his graduate work on studying the development of bipolar cells, retinal ganglion cells, and the connections between the two.

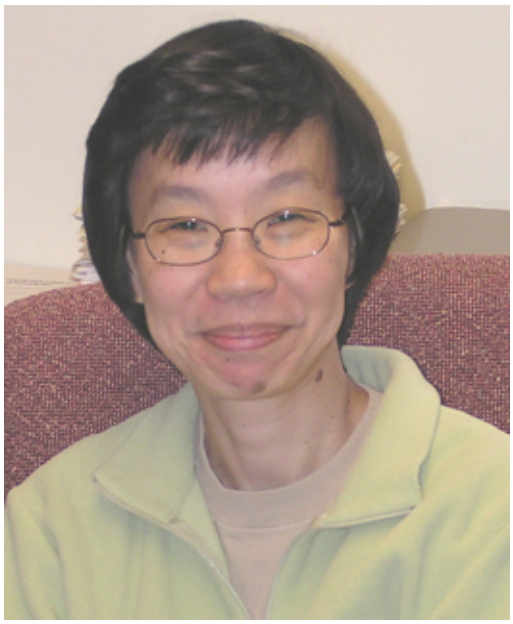

Rachel Wong obtained her PhD from the Australian National University, Canberra, Australia, in Visual Neuroscience under the mentorship of Abbie Hughes. She then worked in the laboratory of Carla Shatz at Stanford University, focusing on early activity patterns of the retina together with Markus Meister and Denis Baylor. Subsequently, Rachel moved back to Australia to join the Vision group in the Vision, Touch and Hearing Research Centre, University of Queensland. From 1994-2010, she joined the Department of Anatomy and Neurobiology at Washington University School of Medicine, St. Louis. Now she is Professor of Neurobiology in the Department of Biological Structure, University of Washington, Seattle. Research interests concern how

neural circuits are developed in the vertebrate visual system using mice and chick retinas and now examining by in vivo analyses, the development of synaptic layers in the zebrafish retina.

References

1. Blanks JC, Adinolfi AM, Lolley RN. Synaptogenesis in the photoreceptor terminal of the mouse retina. J Comp Neurol. 1974;156:81–93. PubMed PMID: 4836656.
2. Fisher LJ. Development of synaptic arrays in the inner plexiform layer of neonatal mouse retina. J Comp Neurol. 1979;187:359–372. PubMed PMID: 489784.
3. Olney JW. An electron microscopic study of synapse formation, receptor outer segment development, and other aspects of developing mouse retina. Invest Ophthalmol. 1968;7:250–268. PubMed PMID: 5655873.
4. Cajal RY. Studies on vertebrate neurogenesis .Springfield (IL): Thomas; 1960.
5. Sakaguchi DS. The development of retinal ganglion cells deprived of their targets. Dev Biol. 1989;134:103–111. PubMed PMID: 2731644.
6. Vaney DI. 'Coronate' amacrine cells in the rabbit retina have the 'starburst' dendritic morphology. Proc R Soc Lond B Biol Sci. 1984;220:501–508. PubMed PMID: 6142459.
7. Wong WT, Faulkner-Jones B, Sanes JR, Wong ROL. Rapid dendritic remodeling in the developing retina: dependence on neurotransmission and reciprocal regulation by Rac and Rho. J Neurosci. 2000;20:5024–5036. PubMed PMID: 10864960.
8. Haas K, Jensen K, Sin WC, Foa L, Cline HT. Targeted electroporation in Xenopus tadpoles in vivo--from single cells to the entire brain. Differentiation. 2002;70:148–154. PubMed PMID: 12147134.
9. Matsuda T, Cepko CL. Electroporation and RNA interference in the rodent retina in vivo and in vitro. Proc Natl Acad Sci U S A. 2004;101:16–22. PubMed PMID: 14603031.
10. Fei Y, Hughes TE. Transgenic expression of the jellyfish green fluorescent protein in the cone photoreceptors of the mouse. Vis Neurosci. 2001;18:615–623. PubMed PMID: 11829307.
11. Huang L, Max M, Margolskee RF, Su H, Masland RH, Euler T. G protein subunit G gamma 13 is coexpressed with G-alphao, G-beta3, and G-beta4 in retinal ON bipolar cells. J Comp Neurol. 2003;455:1–10. PubMed PMID: 12454992.
12. Feng G, Mellor RH, Bernstein M, Keller-Peck C, Nguyen QT, Wallace M, Nerbonne JM, Lichtman JW, Sanes JR. Imaging neuronal subsets in transgenic mice expressing multiple spectral variants of GFP. Neuron. 2000;28:41–51. PubMed PMID: 11086982.
13. Lohmann C, Mumm JS, Morgan J, Godinho L, Schroeter E, Stacy R, Wong WT, Oakley D, Wong ROL. Imaging the developing retina. In: Rafael Y, Konnerth A, editors. Imaging in neuroscience and development. Cold Spring Harbor (NY): Cold Spring Harbor Laboratory Press; 2005. p. 159-170.
14. Sernagor E, Eglen SJ, Wong RO. Development of retinal ganglion cell structure and function. Prog Retin Eye Res. 2001;20:139–174. PubMed PMID: 11173250.
15. Eysel UT, Peichl L, Wassle H. Dendritic plasticity in the early postnatal feline retina: quantitative characteristics and sensitive period. J Comp Neurol. 1985;242:134–145. PubMed PMID: 2416785.
16. Troilo D, Xiong M, Crowley JC, Finlay BL. Factors controlling the dendritic arborization of retinal ganglion cells. Vis Neurosci. 1996;13:721–733. PubMed PMID: 8870228.
17. Lin B, Wang SW, Masland RH. Retinal ganglion cell type, size, and spacing can be specified independent of homotypic dendritic contacts. Neuron. 2004;43:475–485. PubMed PMID: 15312647.
18. Lohmann C, Myhr KL, Wong RO. Transmitter-evoked local calcium release stabilizes developing dendrites. Nature. 2002;418:177–181. PubMed PMID: 12110889.
19. Niell CM, Meyer MP, Smith SJ. In vivo imaging of synapse formation on a growing dendritic arbor. Nat Neurosci. 2004;7:254–260. PubMed PMID: 14758365.
20. Bodnarenko SR, Chalupa LM. Stratification of ON and OFF ganglion cell dendrites depends on glutamate-mediated afferent activity in the developing retina. Nature. 1993;364:144–146. PubMed PMID: 8100613.

21. Bodnarenko SR, Jeyarasasingam G, Chalupa LM. Development and regulation of dendritic stratification in retinal ganglion cells by glutamate-mediated afferent activity. J Neurosci. 1995;15:7037–7045. PubMed PMID: 7472459.
22. Bodnarenko SR, Yeung G, Thomas L, McCarthy M. The development of retinal ganglion cell dendritic stratification in ferrets. Neuroreport. 1999;10:2955–2959. PubMed PMID: 10549804.
23. Sernagor E, Mehta V. The role of early neural activity in the maturation of turtle retinal function. J Anat. 2001;199:375–383. PubMed PMID: 11693298.
24. Prada C, Puelles L, Genis-Galvez JM, Ramirez G. Two modes of free migration of amacrine cell neuroblasts in the chick retina. Anat Embryol (Berl). 1987;175:281–287. PubMed PMID: 3826654.
25. Hinds JW, Hinds PL. Early development of amacrine cells in the mouse retina: an electron microscopic, serial section analysis. J Comp Neurol. 1978;179:277–300. PubMed PMID: 641219.
26. Hinds JW, Hinds PL. Development of retinal amacrine cells in the mouse embryo: evidence for two modes of formation. J Comp Neurol. 1983;213:1–23. PubMed PMID: 6826785.
27. Kay JN, Roeser T, Mumm JS, Godinho L, Mrejeru A, Wong RO, Baier H. Transient requirement for ganglion cells during assembly of retinal synaptic layers. Development. 2004;131:1331–1342. PubMed PMID: 14973290.
28. Wong ROL, Collin SP. Dendritic maturation of displaced putative cholinergic amacrine cells in the rabbit retina. J Comp Neurol. 1989;287:164–178. PubMed PMID: 2477402.
29. Chalupa LM, Gunhan E. Development of On and Off retinal pathways and retinogeniculate projections. Prog Retin Eye Res. 2004;23:31–51. PubMed PMID: 14766316.
30. Brown NL, Patel S, Brzezinski J, Glaser T. Math5 is required for retinal ganglion cell and optic nerve formation. Development. 2001;128:2497–2508. PubMed PMID: 11493566.
31. Wang SW, Kim BS, Ding K, Wang H, Sun D, Johnson RL, Klein WH, Gan L. Requirement for math5 in the development of retinal ganglion cells. Genes Dev. 2001;15:24–29. PubMed PMID: 11156601.
32. Quesada A, Prada F, Armengol JA, Genis-Galvez JM. Early morphological differentiation of the bipolar neurons in the chick retina. A Golgi analysis. Anat Histol Embryol. 1981;10:328–341. PubMed PMID: 6462068.
33. Rice DS, Nusinowitz S, Azimi AM, Martinez A, Soriano E, Curran T. The reelin pathway modulates the structure and function of retinal synaptic circuitry. Neuron. 2001;31:929–941. PubMed PMID: 11580894.
34. Gunhan-Agar E, Kahn D, Chalupa LM. Segregation of on and off bipolar cell axonal arbors in the absence of retinal ganglion cells. J Neurosci. 2000;20:306–314. PubMed PMID: 10627608.
35. Schnitzer J, Rusoff AC. Horizontal cells of the mouse retina contain glutamic acid decarboxylase-like immunoreactivity during early developmental stages. J Neurosci. 1984;4:2948–2955. PubMed PMID: 6502214.
36. Reese BE, Raven MA, Stagg SB. Afferents and homotypic neighbors regulate horizontal cell morphology, connectivity, and retinal coverage. J Neurosci. 2005;25:2167–2175. PubMed PMID: 15745942.
37. Donovan SL, Dyer MA. Developmental defects in Rb-deficient retinae. Vision Res. 2004;44:3323–3333. PubMed PMID: 15536000.
38. Johnson PT, Williams RR, Cusato K, Reese BE. Rods and cones project to the inner plexiform layer during development. J Comp Neurol. 1999;414:1–12. PubMed PMID: 10494074.
39. Reese BE. Developmental plasticity of photoreceptors. Prog Brain Res. 2004;144:3–19. PubMed PMID: 14650837.
40. Johnson PT, Raven MA, Reese BE. Disruption of transient photoreceptor targeting within the inner plexiform layer following early ablation of cholinergic amacrine cells in the ferret. Vis Neurosci. 2001;18:741–751. PubMed PMID: 11925009.
41. Meister M, Wong RO, Baylor DA, Shatz CJ. Synchronous bursts of action potentials in ganglion cells of the developing mammalian retina. Science. 1991;252:939–943. PubMed PMID: 2035024.
42. Morgan J, Huckfeldt R, Wong RO. Imaging techniques in retinal research. Exp Eye Res. 2005;80:297–306. PubMed PMID: 15721612.

43. Demas J, Eglen SJ, Wong RO. Developmental loss of synchronous spontaneous activity in the mouse retina is independent of visual experience. J Neurosci. 2003;23:2851–2860. PubMed PMID: 12684472.
44. Tian N, Copenhagen DR. Visual deprivation alters development of synaptic function in inner retina after eye opening. Neuron. 2001;32:439–449. PubMed PMID: 11709155.
45. Lohmann C, Demas J, Morgan JL, Wong ROL. A practical guide: calcium imaging of the retina. In: Rafael Y, Konnerth A. Imaging in neuroscience and development. Cold Spring Harbor (NY): Cold Spring Harbor Laboratory Press; 2005. p. 283-288.
46. Johnson J, Tian N, Caywood MS, Reimer RJ, Edwards RH, Copenhagen DR. Vesicular neurotransmitter transporter expression in developing postnatal rodent retina: GABA and glycine precede glutamate. J Neurosci. 2003;23:518–529. PubMed PMID: 12533612.
47. Wong ROL. Retinal waves and visual system development. Annu Rev Neurosci. 1999;22:29–47. PubMed PMID: 10202531.
48. McLaughlin T, Torborg CL, Feller MB, O'Leary DD. Retinotopic map refinement requires spontaneous retinal waves during a brief critical period of development. Neuron. 2003;40:1147–1160. PubMed PMID: 14687549.
49. Sherry DM, Wang MM, Bates J, Frishman LJ. Expression of vesicular glutamate transporter 1 in the mouse retina reveals temporal ordering in development of rod vs. cone and ON vs. OFF circuits. J Comp Neurol. 2003;465:480–498. PubMed PMID: 12975811.
50. Dacheux RF, Miller RF. An intracellular electrophysiological study of the ontogeny of functional synapses in the rabbit retina. II. Amacrine cells. J Comp Neurol. 1981;198:327–334. PubMed PMID: 7240449.
51. Wang GY, Liets LC, Chalupa LM. Unique functional properties of on and off pathways in the developing mammalian retina. J Neurosci. 2001;21:4310–4317. PubMed PMID: 11404416.
52. Tian N, Copenhagen DR. Visual stimulation is required for refinement of ON and OFF pathways in postnatal retina. Neuron. 2003;39:85–96. PubMed PMID: 12848934.
53. Tootle JS. Early postnatal development of visual function in ganglion cells of the cat retina. J Neurophysiol. 1993;69:1645–1660. PubMed PMID: 8509831.
54. Dacheux RF, Miller RF. An intracellular electrophysiological study of the ontogeny of functional synapses in the rabbit retina. I. Receptors, horizontal, and bipolar cells. J Comp Neurol. 1981;198:307–326. PubMed PMID: 7240448.
55. Masland RH. Maturation of function in the developing rabbit retina. J Comp Neurol. 1977;175:275–286. PubMed PMID: 903424.
56. Sernagor E, Grzywacz NM. Emergence of complex receptive field properties of ganglion cells in the developing turtle retina. J Neurophysiol. 1995;73:1355–1364. PubMed PMID: 7643153.
57. Sernagor E, Grzywacz NM. Influence of spontaneous activity and visual experience on developing retinal receptive fields. Curr Biol. 1996;6:1503–1508. PubMed PMID: 8939611.
58. Mumm JS, Godinho L, Morgan JL, Oakley DM, Schroeter EH, Wong RO. Laminar circuit formation in the vertebrate retina. Prog Brain Res. 2005;147:155–169. PubMed PMID: 15581704.
59. Fadool JM. Development of a rod photoreceptor mosaic revealed in transgenic zebrafish. Dev Biol. 2003;258:277–290. PubMed PMID: 12798288.

Formation of Early Retinal Circuits in the Inner-Plexiform Layer

Kevin Ford, PhD[1] and Marla Feller, PhD[1]

Created: May 1, 2005; Updated: January 16, 2012.

1. Introduction

The mammalian retina has long been a model system for study of development of neural circuits in the CNS because the adult network is well organized into cell-type specific layers, and the anatomy, physiology and function of many of the retinal cell types is well characterized. A major focus of research in the retina is directed toward understanding how functional circuits arise during development.

The development of the retina requires several steps. The first step is to create the right proportion of the 7 cell types that comprise the retina. This process occurs primarily through genesis of the correct number of each cell type. Only ganglion cells have their final number regulated by cell death, which reduces the number of ganglion cells by as much as 50% in some species. The second step is for cells to migrate into the correct location. The third step is for neurons to form synaptic connections with other retinal neurons. Finally, for some of these groups of synaptically coupled cells, synaptic refinement is necessary to generate the circuits that comprise the adult retina.

The process of neuronal migration in the retina has been the focus of developmental biologists since the time of Cajal, who used Golgi staining techniques (Fig. 1). Progenitor cells in the neurepithelium lining the surface of the neural tube later become the ventricular zone of the optic vesicles, optic cup and early retina. Postmitotic cells leave the ventricular zone to migrate to one of three cell layers in the retina remaining attached radially from one side of the retina to the other. The neural cells lie at different levels in the retina and, when in correct position, lose their anchoring radial connections. Then polarity of the differentiating cells occurs and dendrites and axons grow out appropriately. The ganglion cells are the first to emerge as recognizable neurons with axons passing to the optic nerve and central brain structures (Fig. 1a and b). Then amacrine cells (Fig. 1c), Müller cells, bipolar cells (Fig. 1d), and horizontal cells form in the correct layer and finally photoreceptors remain to line the top layers (Fig. 1e and f).

Before the neural circuits that underlie visual processing emerge, the retina assembles and disassembles a series of intermediate circuits. These transient connections between cells produce the propagating spontaneous activity that is termed retinal waves (1-3). As the retina develops, so do the circuits that underlie retinal waves. The earliest spontaneous retinal waves are propagated via electrical coupling between cells. Then, around birth in mice, waves are produced by a transient network consisting of cholinergic connections between amacrine cells. Finally, just before visual processing begins, they are driven by early glutamatergic signaling.

In this chapter we will discuss how these transient circuits of the inner plexiform layer (IPL) assemble to produce specific patterns of neural activity, and how they transition from one circuit into the next. Finally, we will discuss the role of spontaneous activity in shaping the development of the visual system within both the retina and the brain.

Author Affiliation: 1 Department of Molecular & Cell Biology, University of California, Berkeley, Berkeley, CA; Email: kford@berkeley.edu; Email: mfeller@berkeley.edu.

Corresponding author.

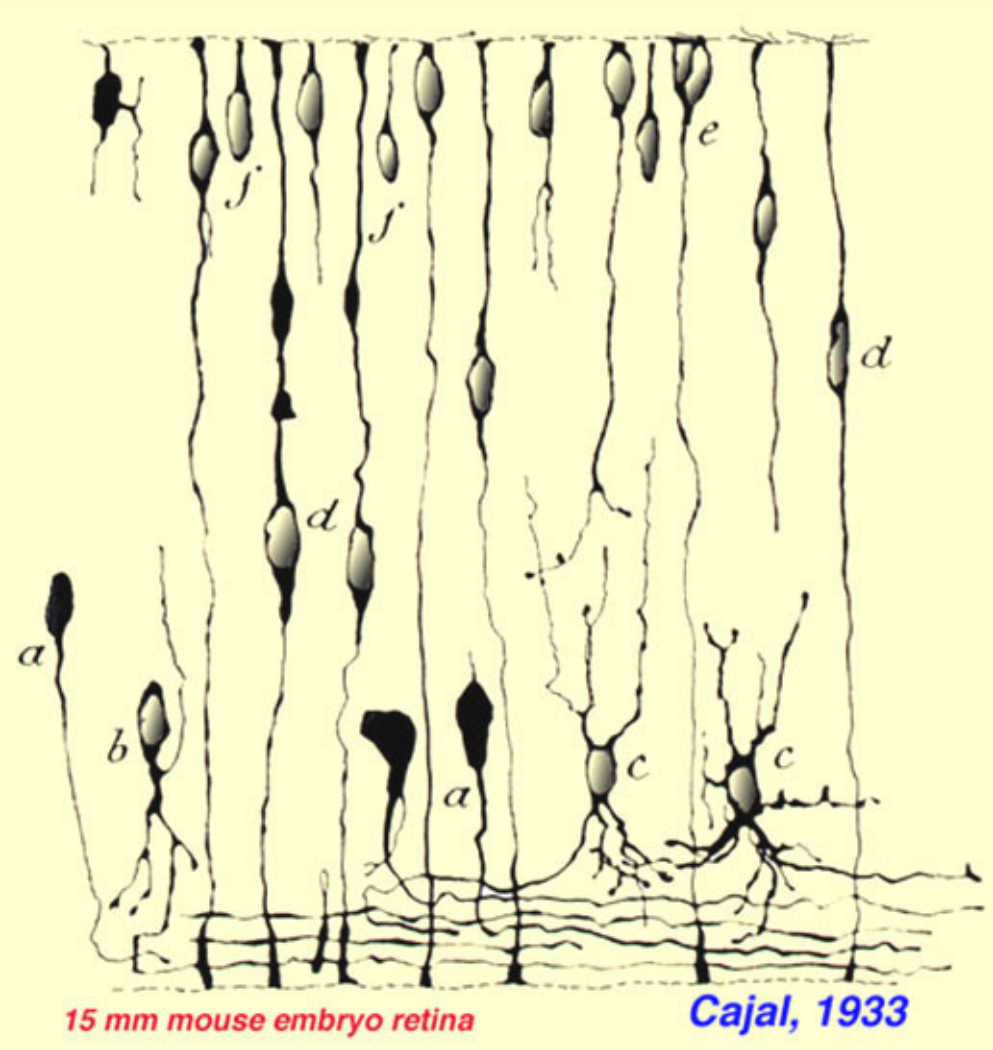

Fig. 1. Golgi stained embryonic mouse retina to show the differentiating cells migrating to the correct layer of the retina. From Cajal, 1933.

Figure 1. Golgi stained embryonic mouse retina shows the differentiating cells migrating to the correct layer of the retina. From Cajal, 1894, Translation, 1972 (70).

2. Neurotransmitters and Early Retinal Development

Early in development, neurotransmitters can function in the absence of traditional synapses (4). Ultrastructurally identified conventional synapses within the IPL are first formed a few days after birth in mice (5). However, even before that there is evidence of neurotransmitters. Below we discuss the role of early neurotransmitters and their receptors prior to the formation of circuits that mediate vision.

Acetylcholine

Acetylcholine (ACh) signaling plays a key role in the development of the retina. Prior to synapse formation, paracrine action of ACh is essential for regulating early developmental events, such as the regulation of the cell cycle (6) and the growth of neurites (7). In addition, cholinergic synapses are among the earliest to mature and thereby constitute the earliest functional circuits in the retina.

ACh in the retina is produced solely by one cell type, the starburst amacrine cell (SAC), a type of amacrine cell named for its radially symmetric processes (8). In the mature retina, released ACh acts on both muscarinic and nicotinic receptors to modulate the response properties of many different types of ganglion cells (9-13), but it does not affect the SACs themselves (14). However, during development, cholinergic signaling does occur between SACs (14). During the first week after birth in mice, ACh released from SACs activates nicotinic acetylcholine receptors (nAChRs) on neighboring SACs and thus gives rise to a cholinergic network. A key developmental function of this cholinergic network is the generation of retinal waves. This network appears at birth in mice and mediates the initiation and propagation of waves.

Aside from the effect ACh has on ganglion and amacrine cells via nicotinic acetylcholine receptors, it also acts on the muscarinic acetylcholine receptors (mAChRs) of many cells in the neuroblastic layer (15, 16) (Fig. 2). Figure 2 shows the effect of acetylcholine on progenitor cells in rabbit retina. A one-day old rabbit retina is loaded with Fura-2. Images show responses to bath application of 200μM nicotine (Nic, left), which activates nicotinic acetylcholine receptors, or 100μM carbachol (CCh, right), which activates muscarinic acetylcholine receptors. Red indicates cells that had increases in intracellular calcium whereas blue indicates cells without increases in intracellular calcium.

The mAChRs are G-protein coupled receptors that lead to an increase in intracellular calcium via release of calcium from internal stores, as opposed to influx through ligand- or voltage-activated channels. Interestingly, the ACh released during retinal waves drives correlated mAChR-dependent calcium transients in undifferentiated cells of the ventricular zone (Fig. 2) (15). Hence, it is possible that ACh released by retinal waves induces signaling that is important for early phases of neurogenesis and for cell migration (17).

GABA

GABA is expressed in more cells during development than during adulthood, thus suggesting that it plays a transient role in circuit formation (18). During the first few postnatal days in rabbit, GABA displays a high transient expression in the ganglion cell layer. Moreover, the IPL of P0 ferret exhibits markers for enzymes involved in the synthesis of GABA (19).

During development, GABA initially serves to depolarize neurons. When activated, ionotropic GABA receptors, $GABA_A$ and $GABA_C$, flux chloride (Fig. 3A). Since the chloride concentration within developing retinal neurons is high due to low expression of the potassium-chloride co-transporter, KCC2, receptor activation leads to an efflux of negatively charged chloride ions through the open channels and thus causes depolarization of the cell (Fig. 3A, B left). KCC2 expression gradually increases during the first two weeks after birth in mice (20). Thus there is a 'switch' from excitation to inhibition as the reversal potential for chloride drops below the threshold for firing action potentials (Fig. 3 A, B right).

In turtle retina, the timing of the GABA switch correlates with a decrease in propagating spontaneous activity (21), suggesting that GABA depolarization plays a role in this propagation. In mammalian retina, GABA plays a minor role in correlated spontaneous activity during its excitatory period (1, 22, 23). However, after the GABA switch, GABA's inhibitory action takes on a prominent role in shaping spontaneous activity. Blocking $GABA_A$ receptors greatly increases the frequency of spontaneous retinal waves (22, 24).

What underlies the switch of GABA's action from depolarizing to hyperpolarizing? Several environmental factors, including neural activity (25), have been implicated in the timing of this switch in the retina. A recent study used acutely isolated retinas from knockout mice and pharmacological manipulations in retinal explants demonstrates that the timing of the GABA switch in retinal ganglion cells is unaffected by blocking specific neurotransmitter receptors or global activity (26) (Fig. 4). Purified retinal ganglion cells remain depolarized by muscimol for at least two weeks in culture (Fig 4, right), indicating that the GABA switch is not cell-autonomous. Purified ganglion cells co-cultured with other retinal neurons also remain depolarized by

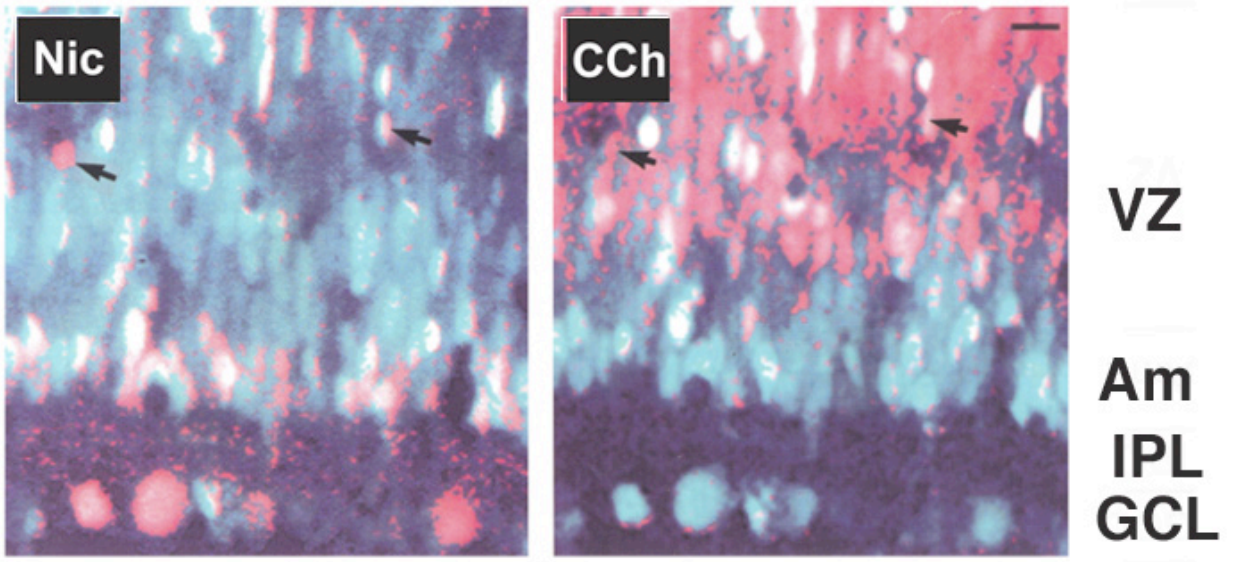

Figure 2. Acetylcholine acts on nicotinic receptors in ganglion and amacrine cells and on muscarinic receptors on progenitor cells. Adapted from Wong, 1995. VZ ventricular zone; Am, amacrine cell layer, IPL, inner plexiform layer; GCL, ganglion cell layer.

Figure 2. Acetylcholine acts on muscarinic receptors in progenitor cells and nicotinic receptors in ganglion and amacrine cells. Adapted from Wong et al, 1995 (16).

muscimol (Fig. 4, middle). However, culturing purified ganglion cells with dissociated cells from the superior colliculus (Fig. 4, right), or treating purified ganglion cells with media conditioned by superior colliculus cultures (Fig. 4C, red), results in a switch to inhibition by muscimol after two weeks in culture, indicating that a diffusible signal independent of local circuit activity regulates the maturation of GABAergic transmission.

Glutamate

Glutamatergic signaling is the last to develop within the IPL. Glutamate is released primarily from bipolar cells and a small subset of amacrine cells (27, 28). In mice, the axons of bipolar cells first express VGLUT1, the enzyme responsible for packaging glutamate into vesicles, around one week after birth (29). Although, ribbon synapses between bipolar cells axons and the dendrites of amacrine and ganglion cells do not form until 11 days after birth (5), glutamatergic currents can be measured before this (24, 29).

State-of-the-art transgenic and imaging techniques have characterized the distribution of glutamatergic synapses onto ganglion cells and between particular subtypes of bipolar and ganglion cells (30, 31). Before the functional maturation of bipolar cell ribbon synapses and long before the structural maturation of the ganglion cell dendritic arbor, adult-like patterns of glutamatergic synapses can be seen. However, between some subtypes of bipolar and ganglion cells, there appears to be an activity dependent remodeling of these synapses (30).

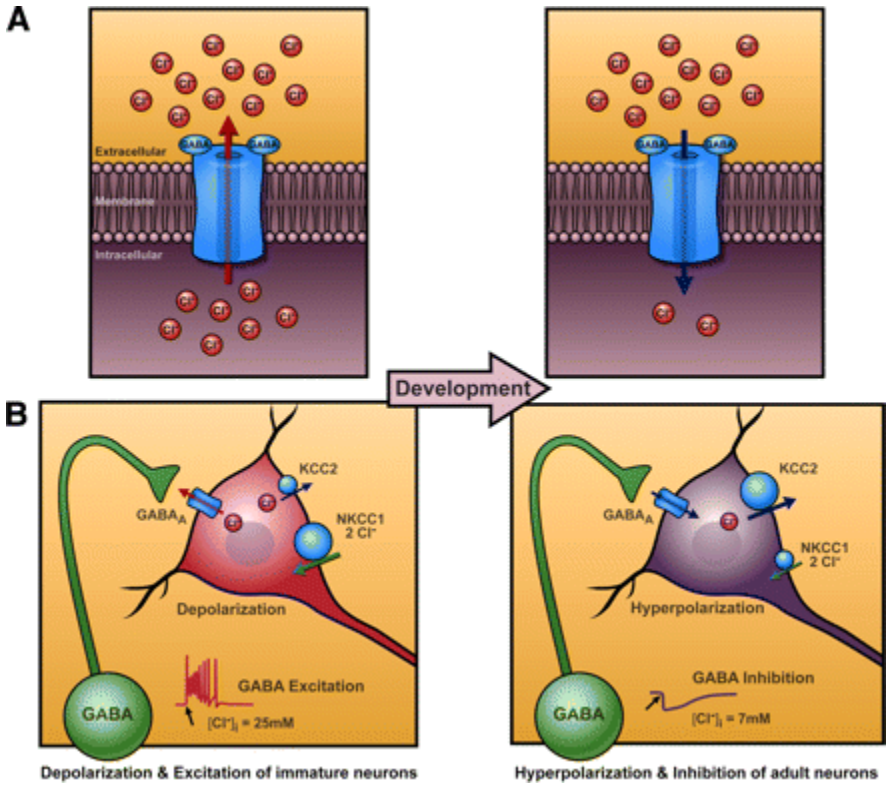

Figure 3. GABA switches from depolarizing to hyperpolarizing during development. From Ben-Ari et al. 2007 (71).

3. Spontaneously active synaptic circuits in the inner plexiform layer

Retinal Waves

Prior to photoreceptor maturation and eye opening, retinal ganglion cells periodically fire bursts of action potentials on the order of once per minute. This spontaneous rhythmic activity was first measured in fetal rat pups and was found to be highly correlated among neighboring ganglion cells (32).

Extracellular recordings using a multielectrode array (2) (Movie 1) and imaging of calcium transients (Movie 2) associated with bursts of action potentials (1, 33) have revealed that these spontaneous bursts propagate from one cell to the next in a wavelike manner. These retinal waves are an extremely robust phenomenon, observed in a large variety of vertebrate species, including chick, turtle, mouse, rabbit, rat, ferret and cat (34).

Retinal waves persist for an extended period throughout development as shown in Figure 5. However, as the retina matures, the circuitry underlying these retinal waves changes. Thus the wave generating circuits progress through three distinct stages, reflecting the nature of the connections and the cells that are involved (Fig. 5).

Embryonic waves

The earliest waves recorded in mammals are thought to be propagated via gap junctions. Retinal waves before embryonic day 23 in rabbit persist in the presence of antagonists to ionotropic GABA, glycine, ACh, and glutamate receptors, but are completely blocked by 18β-GA, a blocker of gap junction coupling (22). Similarly, mice prior to birth exhibit waves that are insensitive to chemical transmission antagonists (35). How waves are initiated and propagated during this early stage of development is still not clear. During the first week after birth in ferret and mouse, neurobiotin coupling between ganglion cells of the same subtype and amacrine cells has

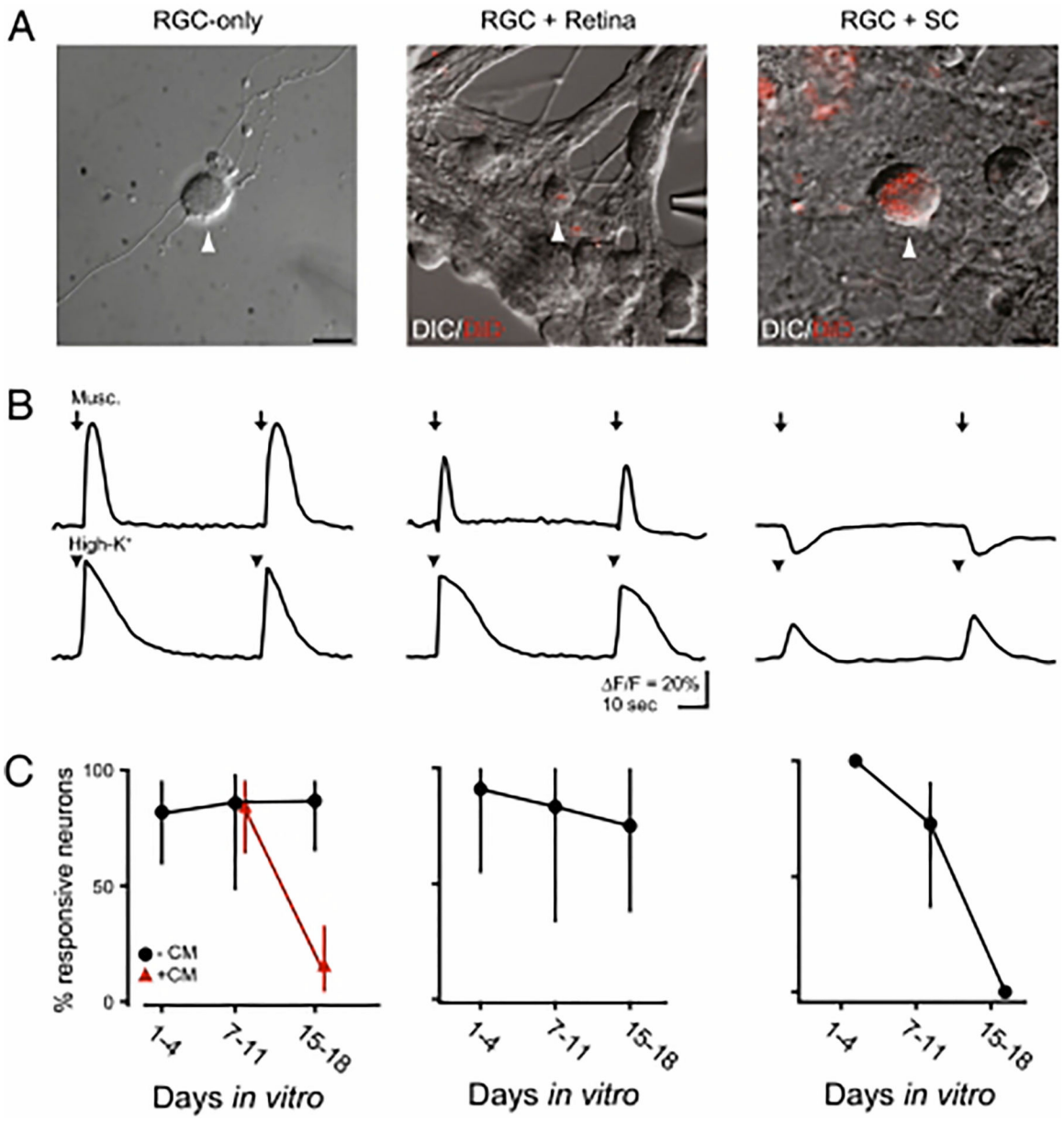

Figure 4. The GABA switch in retinal ganglion cells is due to a diffusible factor. From Barkis et al., 2010 (26).

been seen (3, 36). However, ganglion cell coupling is initially weak and becomes stronger with age, while the correlations generated by waves become weaker with age (37). In addition, tracer coupling is found primarily between retinal ganglion cells of the same subtype and many other ganglion cells are not gap junction coupled. Thus, the issue of wave propagation in this early network still remains to be explored.

Neurotransmitters play a modulatory role during early stage waves. At the earliest ages studied in chick retina (E8-E11), wave frequency decreases in the presence of an ACh antagonist and increases with an ACh agonist but waves are not blocked. These waves are unaffected by $GABA_A$ and glutamate receptor antagonists (38). Similarly, embryonic waves in mouse are reduced in ACh receptor antagonists (35). In addition, in rabbit, early waves are blocked by the activation of $GABA_B$ receptors and are increased in frequency by the inhibition of these receptors (22).

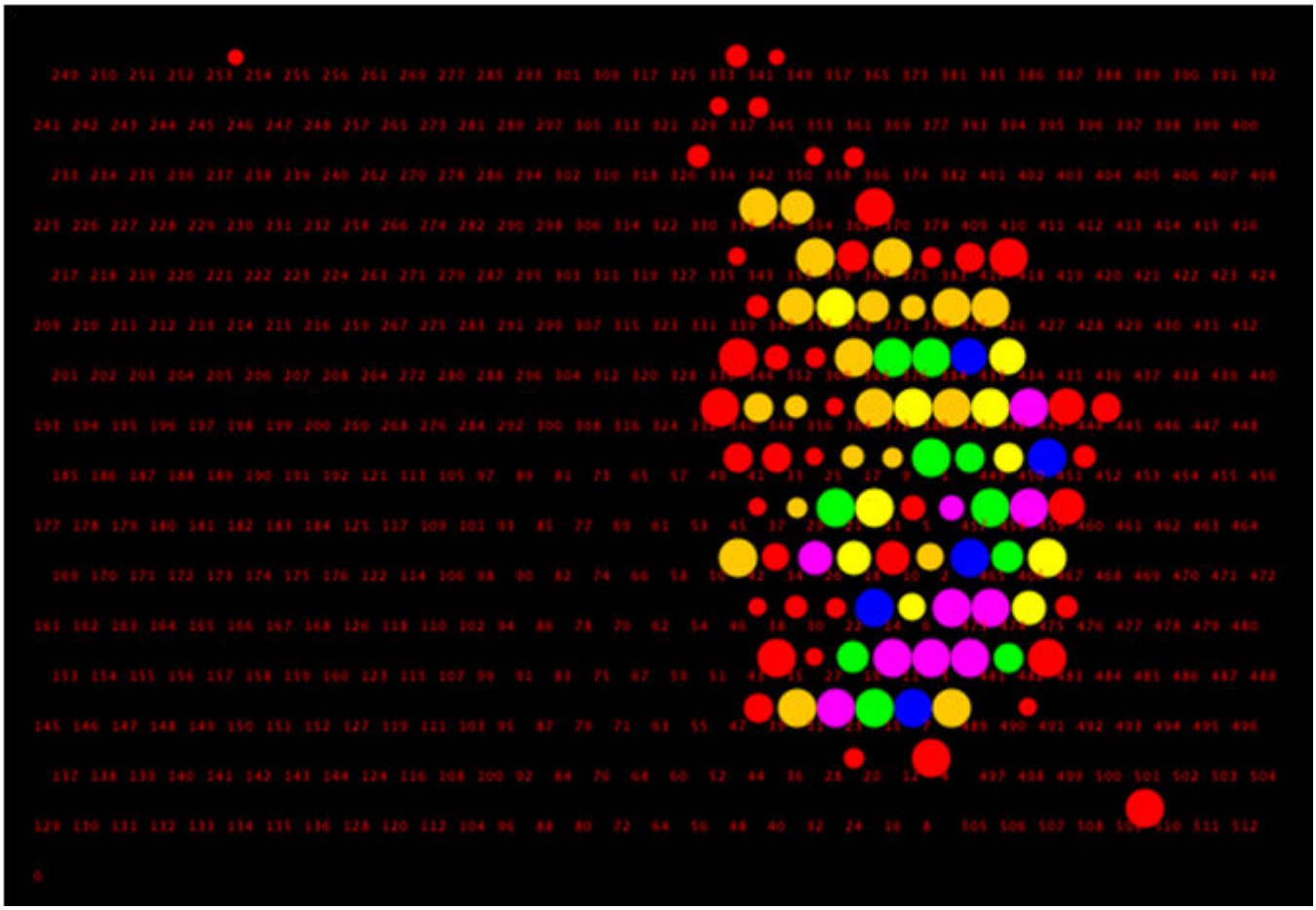

Movie 1. Multi-electrode array recording of cholinergic waves. 512 electrode array recording from the mouse at 37°. Each dot represents multiunit activity recorded on an electrode at that site. The size of the dot is proportional to the amplitude of the signal, and the color is proportional to the frequency of the signal. Movie is at 5× normal speed. From Stafford et al, 2009 (43).

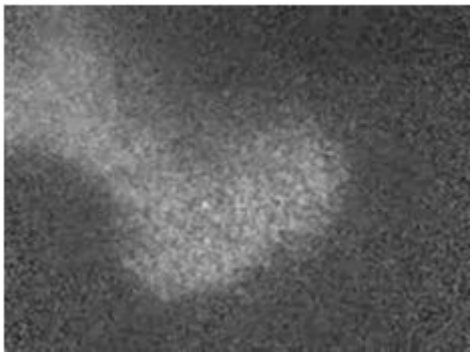

Movie 2. Calcium imaging of cholinergic waves. P3 mouse retina loaded with Oregon Green-Bapta-1AM. Playback 10x, size 800x600 μm (unpublished).

Cholinergic waves

Several experimental results show that chemical synaptic transmission is a prerequisite for cholinergic wave propagation. First, simultaneous whole cell voltage clamp recordings from ganglion cells demonstrate that increases in $[Ca^{2+}]_i$ correlated across cells are driven by compound synaptic inputs (1). Second, the compound postsynaptic currents measured from ganglion cells are blocked by bath application of Cd^{2+}, a blocker of

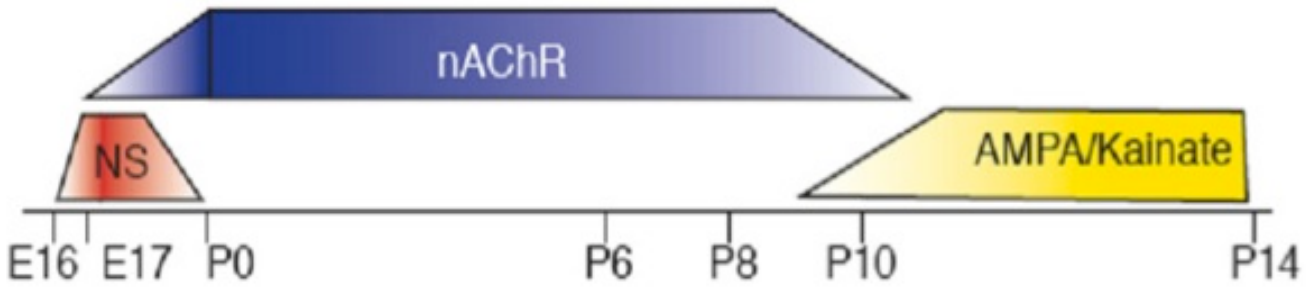

Figure 5. Retinal waves occur in three stages. Before birth in mice, waves are mediated by non-synaptic (NS) circuits. From around birth until 10 days after birth, waves are mediated by acetylcholine acting on nicotinic acetylcholine receptors (nAChRs). From 10 days after birth until the end of the second week, waves are mediated by ionotropic glutamate receptors. Modified from Bansal et al. 2000 (35).

calcium channels that are associated with transmitter release (1). Third, the periodic Ca^{2+} increases, action potentials, and compound postsynaptic currents associated with waves can all be blocked by a variety of nAChRs antagonists (1, 39). Finally, genetic deletion of the beta2 subunit of the nAChR receptor (35) or deletion of the enzyme responsible for synthesis of ACh (40) results in the disruption of normal waves during the first week after birth.

The spatiotemporal properties of cholinergic retinal waves have been well-characterized by fluorescence imaging of calcium indicators, which are reliable markers of cell depolarizations. Figure 6 schematizes these waves (41). Waves initiate in small clusters of coactive neurons and then propagate over spatially restricted areas of the retina. Initiation sites and wave boundaries are distributed randomly across a given retina, indicating that the global patterns of waves are not determined by fixed structures such as pacemaker cells or by repeated activation of the same clusters of neurons. Instead, the propagation boundaries of waves are determined in part by wave-induced refractory regions that last for 40-50 seconds. These observations have led to the hypothesis that every region of the retina is equally likely to initiate or propagate a wave, and therefore the global spatial patterns of waves are determined by the local history of retinal activity (Feller et al., 1997).

Recent studies in rabbit (Zheng et al., 2004; Zheng et al., 2006) and mouse (Ford et al. 2012) retina have revealed the cellular properties of starburst amacrine cells (SACs), the cell type that gives rise to cholinergic waves (Fig. 7) (42). Identifying SACs in mouse retinas was facilitated by the use of a line of mice in which GFP is expressed in SACs (mGluR2-GFP, Fig 7A). Using calcium imaging, spontaneous depolarizations of individual SACs were observed in the absence of synaptic excitation (Fig 7A), indicating that SACs themselves may be the source of initiation for waves. Paired recording between SACs revealed reciprocal cholinergic transmission (Fig 7C), indicating that waves are propagated via these slow, excitatory connections between neighboring SACs. Finally, wave boundaries are thought to arise from a slow after-hyperpolarization in the SACs that recovers over the course of tens of seconds following the depolarization during waves (Fig 7B).

Cholinergic waves may play a role in terminating early stage gap-junction mediated waves. Knock-out animals that lack nAChR receptor subunits still exhibit wave like activity under certain recording conditions, such as elevated temperature [alpha3(-/-) (35), beta2(-/-)(43, 44)]. This activity is likely mediated by gap junctions (44). Moreover, a study using a genetic model that eliminates ChAT in a large portion of the retina found normal cholinergic waves in the spared region, but compensatory waves in the region lacking ChAT (40). These studies suggest a sequential maturation of the retinal circuitry that relies on checkpoints to make transitions from one stage (gap-junction mediated waves) to the next (cholinergic transmission mediated waves). This sort of

checkpoint model of neuronal development (45) is further supported by the disassembly of the cholinergic network to make way for glutamatergic signaling (46).

Glutamatergic waves

The synaptic circuitry that drives retinal waves changes postnatally. Though retinal waves early in development require cholinergic neurotransmission, studies in older ferret, rabbit, and mouse indicate that waves become insensitive to cholinergic antagonists and can be blocked by glutamate receptor antagonists (35, 47, 48). This switch in the requisite transmitter occurs at the age that bipolar cells make their initial synaptic connections with ganglion cells and conventional synapses between amacrine and ganglion cells become morphologically mature and numerous. This timing suggests that perhaps waves are mediated by neurotransmitters only when the synapses are first forming.

Glutamatergic waves have distinct spatial and temporal features. Unlike cholinergic waves that drive correlations in all neighboring ganglion cells regardless of subtype, glutamatergic waves occur more frequently in OFF cells than in ON cells (49) (Fig. 8). Waves occur in rapid clusters separated by periods of silence lasting about one minute (24). Within clusters, there is a distinct pattern of firing where ON and OFF cells alternate in firing bursts of action potentials (50) (Fig. 8). These spatial and temporal features are significantly shaped by inhibitory circuits. Blocking ionotropic GABA receptors increases wave frequency (51). Blocking glycine receptors does the same but also eliminates the asynchronous firing between ON and OFF cells.

Similar to the transition from gap-junction to cholinergic waves, the onset of glutamatergic waves may play an active role in the disassembly of the cholinergic circuits (46). Mice lacking the vesicular glutamate transporter VGLUT1 lack glutamate release from bipolar cells. However, these mice still have retinal waves during the time that littermate control animals have glutamatergic waves. Interestingly, these waves in the VGLUT1 knockout mice are unaffected by glutamate receptor antagonists but are blocked by nAChR antagonists (24). Thus, glutamate signaling from bipolar cells seems necessary for dismantling the cholinergic network.

There is some evidence that the transitions between the different circuits that mediate waves are linked. Prior to birth waves are thought to propagate via gap-junctions between ganglion cells (Fig. 9A, left). From postnatal day 1-10 waves are propagated via SAC release of acetylcholine onto other SACs (Fig 9A, Middle, black box). Acetylcholine also depolarizes ganglion cells. During this period of development, the gap-junction signaling between ganglion cells is reduced (Fig 9A, Middle, red box). From P10-P15 bipolar cells release glutamate to propagate waves in a mechanism that is thought to involve spillover of glutamate to excite neighboring bipolar cells (Fig. 9A right, black box). Cholinergic signaling between SACs is reduced (Fig. 9A right, red box).

Genetic disruption of cholinergic or glutamatergic waves result in an extended action of the previous wave generating circuit (Fig. 9B). In wild type mice gap-junction mediated waves (gray) are followed by cholinergic waves (blue) starting at P0, then glutamatergic waves (green) at P10. In mice lacking the Beta2 subunit of the nicotinic acetylcholine receptor, gap-junction mediated waves persist until ~P8. In mice lacking vesicular glutamate transporter VGLUT1, cholinergic waves persist through the second postnatal week.

Gap junctions and waves

Gap junctions are thought to play a role in the generation of embryonic waves, as described above. At later ages in mammals, however, gap junctions also play a minor role in the propagation of retinal waves. Gap junction antagonists reduce or partially block retinal waves after birth in mice (36) and at later stages in rabbit (22) when waves depend critically on chemical transmission. However, these antagonists also have several non-specific effects so these results are inconclusive. A different approach is to study mice in which specific connexins are genetically deleted (Fig. 10). Knockouts of connexins 36 and 45, the two major gap junction forming connexins in the IPL, have normal wave propagation (Fig. 10 A) but the firing between waves at later stages is increased (Fig 10B). Glutamatergic waves and the firing between waves is eliminated by the application of bipolar cell

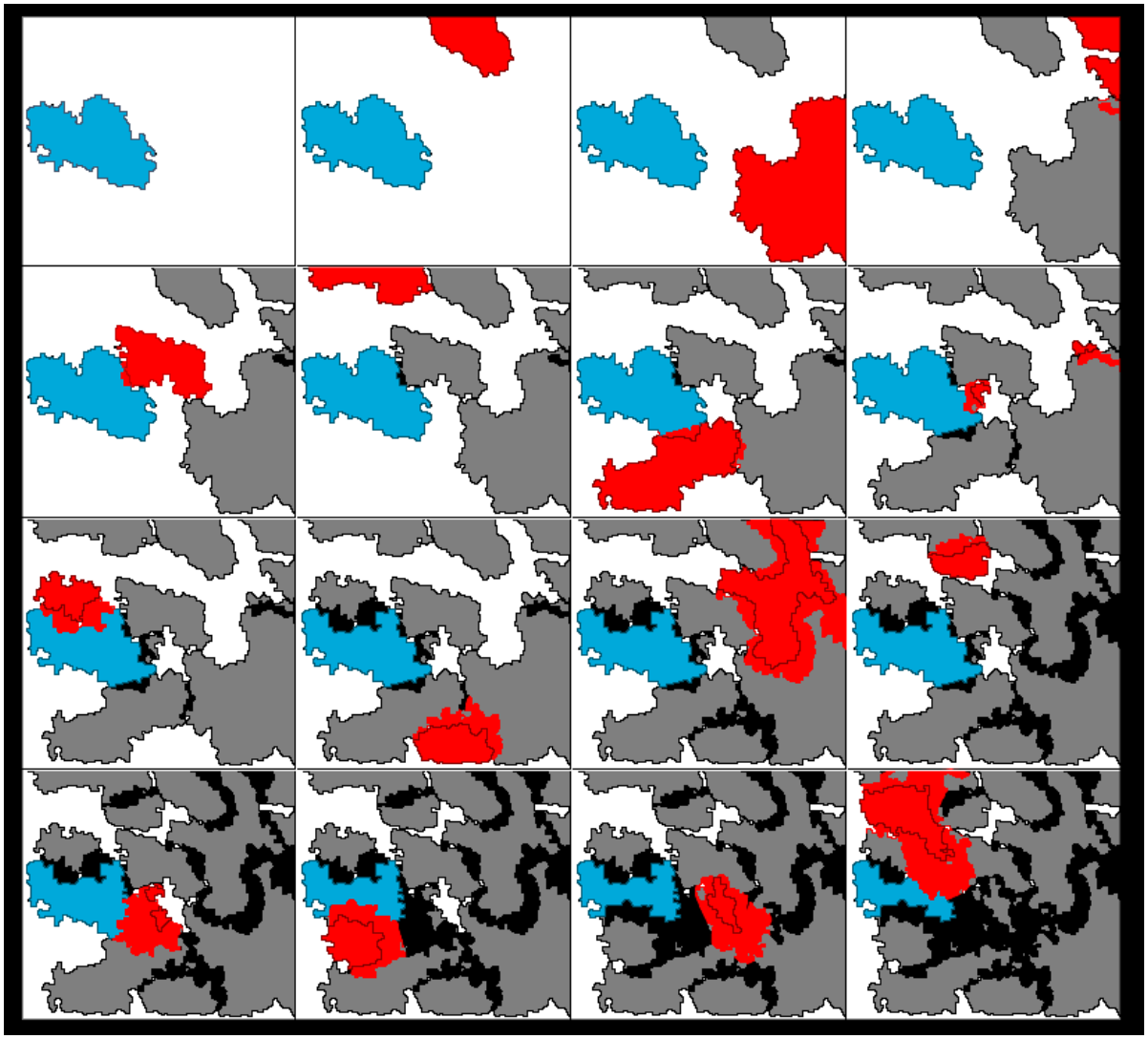

Figure 6. Cholinergic retinal waves tile the retina. Pictured is a sequence of retinal waves that were measured using calcium imaging in a P2 ferret retina loaded with the calcium dye fura-2AM (read from left to right, top row first). This analysis is used to show that a mosaic of waves is created by sequential waves to tile the entire retina. The blue figure in the first frame represents the total spatial extent of a single wave, which is termed a domain. The red domain in each frame corresponds to a new wave arising in the same region of retina monitored with fura-2 imaging. Gray shapes represent the regions of retina that previously supported a wave. Black corresponds to overlapping regions in which more than one wave occurs. This first domain remains blue through all of the subsequent frames to demonstrate that subsequent waves initiated within 10s of seconds of that first wave do not significantly invade its territory. The fact that almost the entire region is gray after 90 seconds indicates that the entire retina is tiled but that domain boundaries change constantly over time. The entire sequence corresponds to 90 seconds of recording. The total field of view is 1.2 x 1.4 mm. From Feller et al, 1997 (41).

synapse antagonists DNQX and AP5, indicating that bipolar input is important for the generation of waves as in wild type retinas (52).

In contrast, in the chick retina, gap junctions were found to be involved in wave generation at all ages. Octanol, a significant inhibitor of waves in E8 chick retina, restricts tracer coupling between ganglion cells and other cell types but not between ganglion cells themselves, indicating that the circuitry mediating these waves involves cells other than ganglion cells (38).

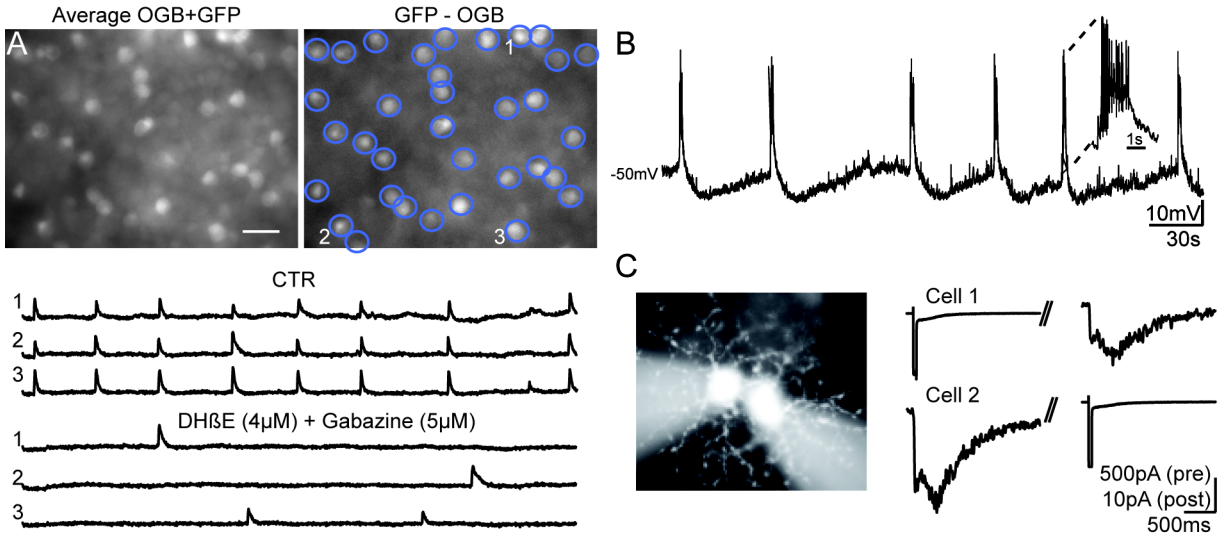

Figure 7. Cellular features of starburst amacrine cells underlie the spatiotemporal properties of retinal waves. (A) Fluorescence image of an mGluR2-GFP retina loaded with OGB. Right, Fluorescence image of GFP cells. Regions of interest are shown around each SAC. Scale bar, 20 µm. B, Time course of DF/F averaged over the somas of three cells (labeled in A) in the absence (CTR, top) and in the presence of nAChR antagonist DHβE (4µM) and GABA-A receptor antagonist gabazine (5µM) (bottom). (B) Current-clamp recording from a SAC showing wave evoked depolarizations followed by sAHPs. (C) Voltage-clamp recordings from pairs of neighboring SACs show both fast slow cholinergic postsynaptic currents. From Ford, Felix and Feller, 2012 (42)

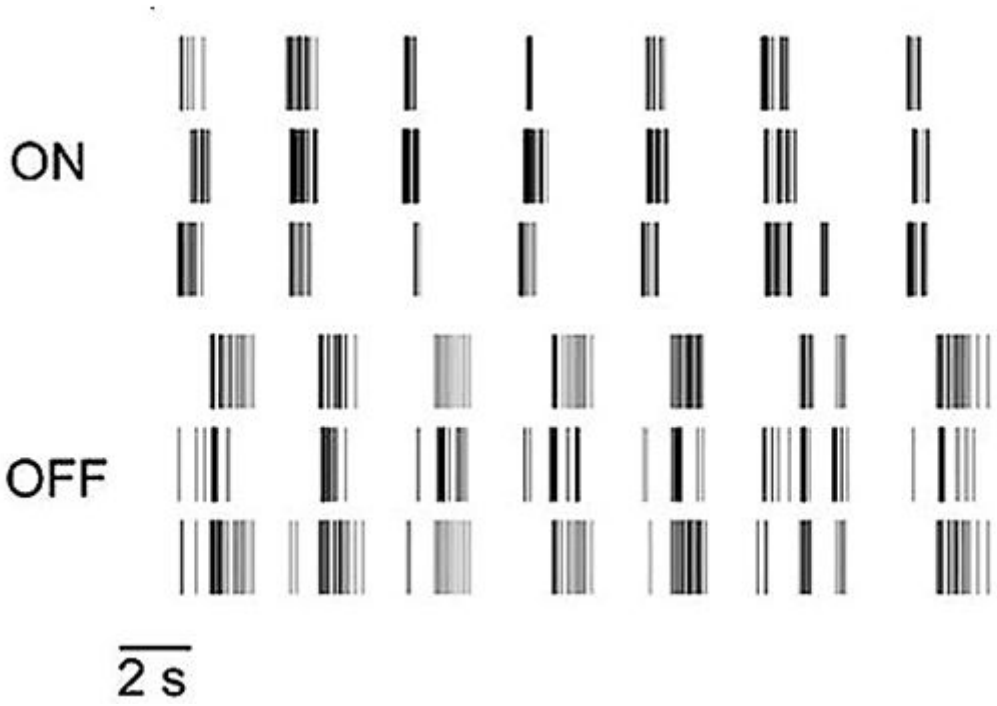

Figure 8. Glutamatergic waves occur in clusters of asynchronous ON/OFF bursts. Multi-electrode array recording of glutamatergic waves from a 12 day old mouse. ON ganglion cells precede OFF ganglion cells during burst clusters. Adapted from Kerchensteiner and Wong, 2008 (50).

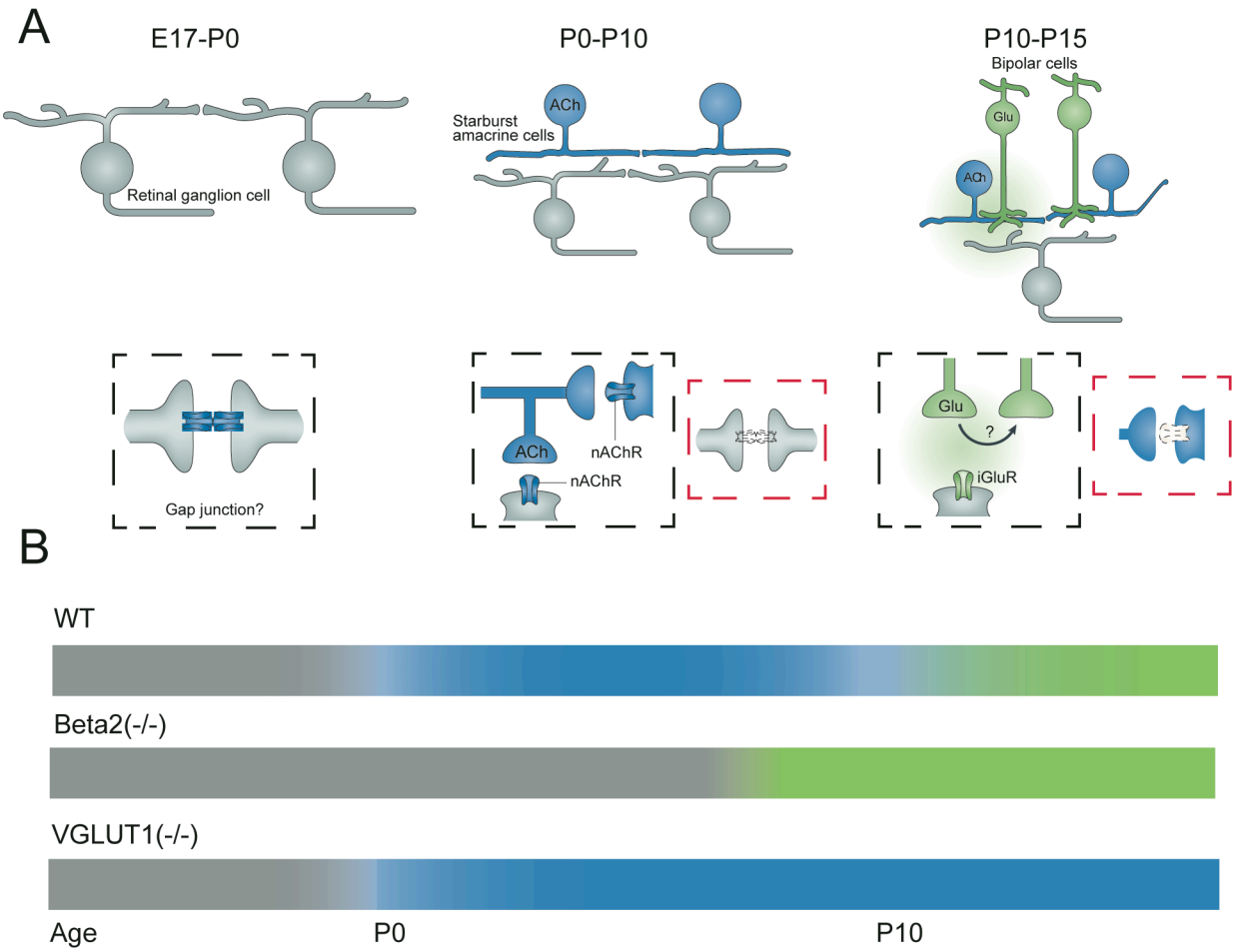

Figure 9. *A*. Transitions between waves stages are homeostatically regulated. Different circuits mediated waves at different ages. *B.* In wild type mice gap-junction mediated waves (gray) are followed by cholinergic waves (blue) starting at P0, then glutamatergic waves (green) at P10. In mice lacking the Beta2 subunit of the nicotinic acetylcholine receptor, gap-junction mediated waves persist until ~P8. In mice lacking vesicular glutamate transporter VGLUT1, cholinergic waves persist through the second postnatal week. From Ford and Feller, 2011 (72).

4. Role of activity in formation of visual circuitry

Spontaneous activity in the developing retina occurs while functional circuits are forming within the retina and projections from the retina are undergoing refinement at their target regions in the brain. What role do retinal waves play in sculpting the circuits that mediate vision?

ON/OFF circuitry within the retina

Two sub-circuits that have been well characterized in the adult retina are the ON and OFF pathways. The classes of bipolar cells that transmit responses to the onset of light (ON responses) are distinct from those that transmit responses to the cessation of light (OFF responses). These ON and OFF circuits have ganglion cell dendrites, amacrine cell processes and bipolar cell inputs that are physically segregated from each other into what are called the ON and OFF layers of the IPL. The formation of these ON or OFF circuits involves the dendritic maturation of ganglion cell types.

The dendrites of most retinal ganglion cells arborize diffusely within the IPL before restricting their dendrites to distinct lamina (35, 53-57) (Fig. 11). Some studies have suggested that this segregation of ganglion cell dendrites into ON and OFF layers involves bipolar cell activity. First, this segregation is prevented by applying APB to

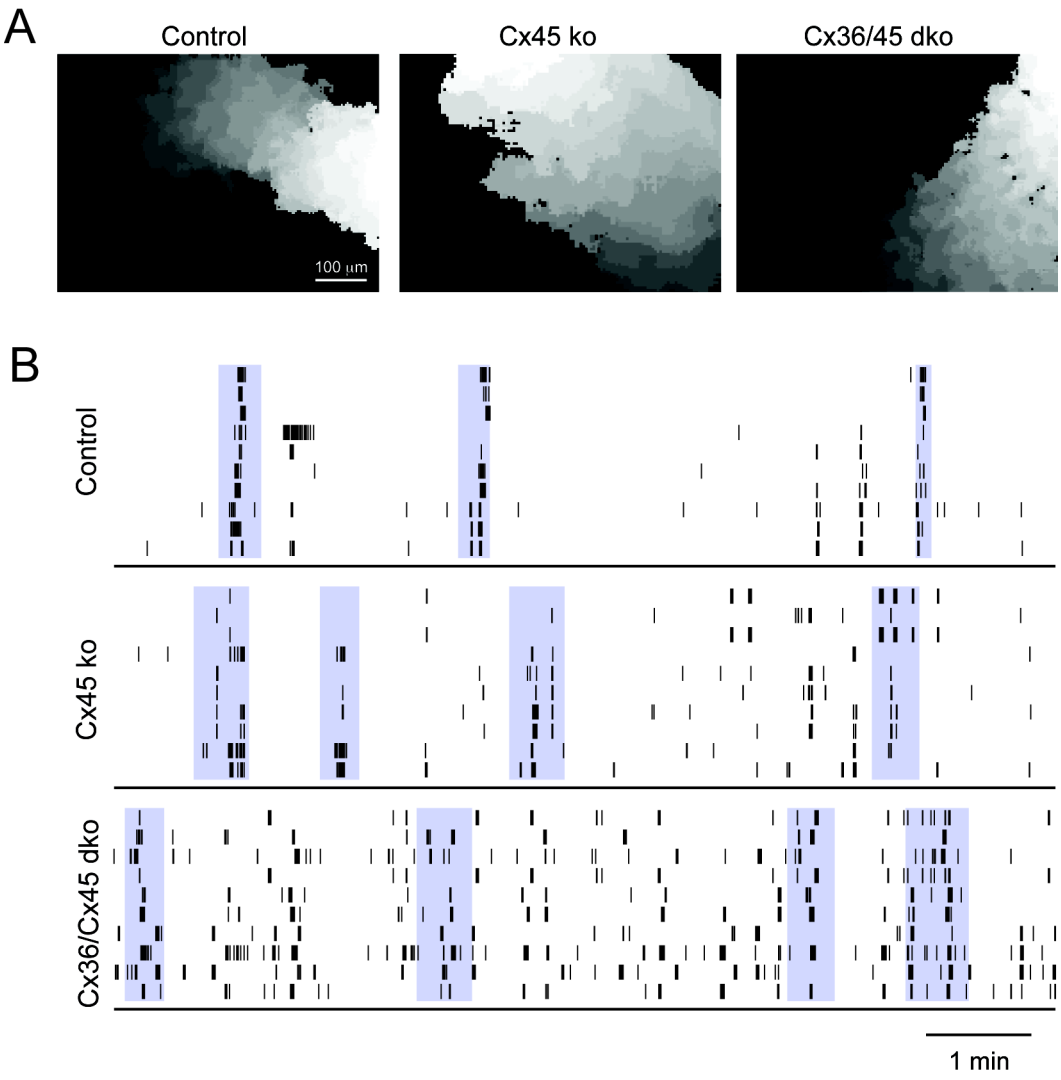

Figure 10. Spatiotemporal properties of retinal waves are similar in control, Cx45, and Cx36/45 double knockout mice. A, Examples of waves recorded in different genotypes. Each grayscale value represents an active area in one frame, with darker shades corresponding to later points in time during the wave. B, Raster plot of ganglion cell action potentials taken from multi-electrode array recordings from different genotypes. Correlated firing during wave events are shown in blue. From Blankenship et al. 2011 (52).

hyperpolarize ON bipolar cells during the period of glutamatergic retinal waves (Fig. 12) (58, 59). Second, mice that lack the MHCI receptor CD3zeta, and thus display altered glutamatergic retinal waves, have ganglion cells with reduced dendritic motility and more diffuse dendrites within the IPL (60) (Fig. 11). However, not all manipulations of spontaneous retinal activity during development alter dendritic stratification. Preventing synaptic release of glutamate from ON bipolar cells by expressing tetanus toxin does not prevent the stratification of ganglion cell dendrites, but it does reduce synapse formation onto the ON bipolar cells (30).

Is there a role for cholinergic waves in this ganglion cell stratification process? Several studies suggest that there is. First, blocking nAChRs during the period of cholinergic waves reduces the motility of filipodia on the dendrites of ganglion cells (61), demonstrating that cholinergic waves can drive structural changes in dendrites. Second, studies in turtle demonstrate that blocking cholinergic waves with nAChR antagonists reduces receptive field sizes (62). Finally, mice lacking the beta2 subunit of the nAChR exhibit a delay in, but not an absence of, the fine stratification of ganglion cell dendrites (35). These findings indicate that cholinergic waves do influence the outgrowth of ganglion cell dendrites but they are not the primary factor that dictates their final organization.

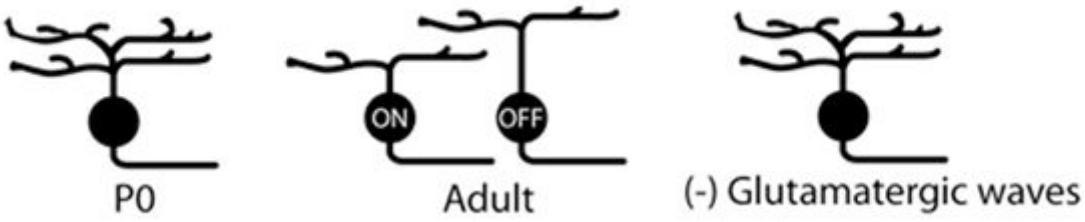

Figure 11. Retinal waves drive refinement of some retinal ganglion cell dendrites.

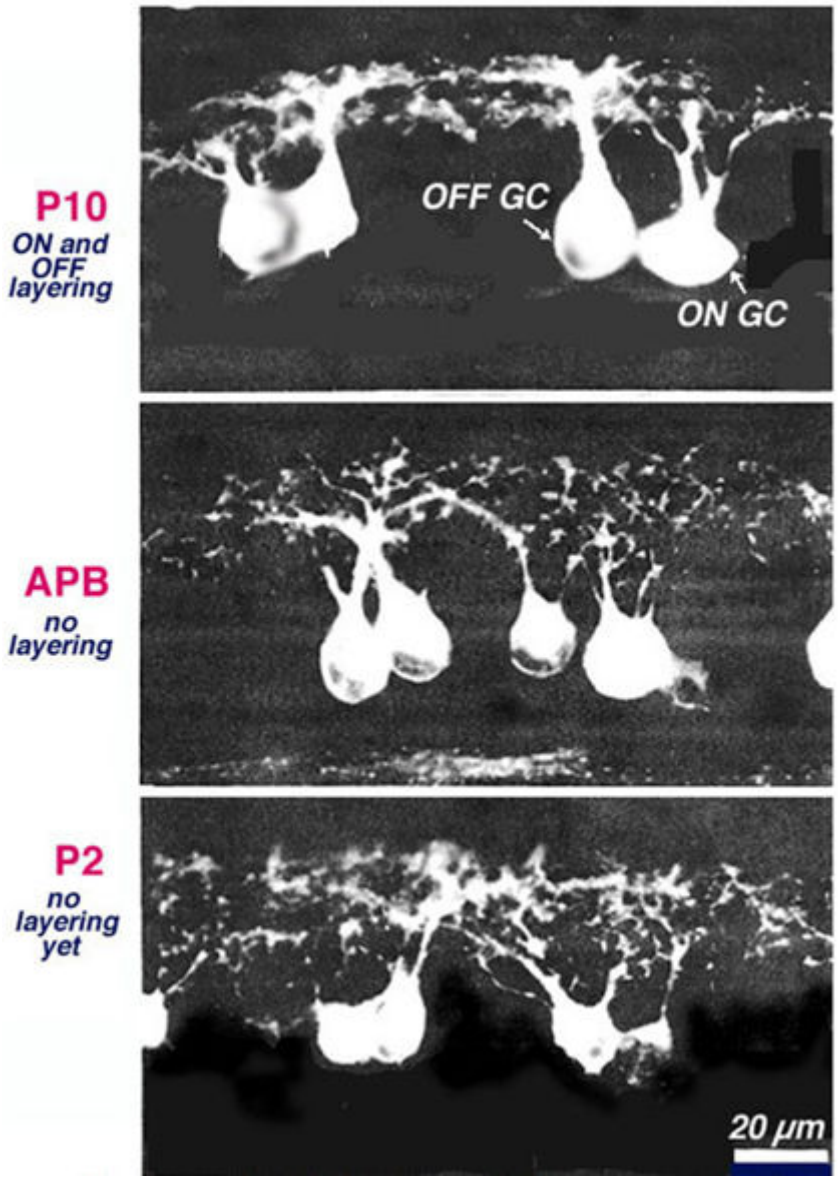

Figure 12. Activity dependent maintenance of ganglion cell dendritic stratification in the developing cat retina. From Bodnarenko and Chalupa, 1993 (58) .

Refinement of retinal projections

Retinal axons undergo a period of refinement before vision begins. At birth in mice, axons from both eyes reside in overlapping regions of the dorsal lateral geniculate nucleus of the thalamus. By about two weeks after birth, the axon terminals from the ganglion cells of each eye separate into non-overlapping regions. Similarly, within the superior colliculus, retinal axons at birth extend over the entire area of the colliculus. However, over the course of about one week, these axons retract to their appropriate retinotopic regions and extensively arborize within a small target zone. These processes of eye-specific segregation and retinotopic map refinement occur during the period of retinal waves. Thus, the hypothesis has emerged that waves might provide cues within their activity pattern to instruct these developmental processes.

The refinement of retinal projections to the brain is thought to be driven by the precise initiation, propagation and termination properties of cholinergic waves (63). The periodic initiation of waves induces depolarizations and calcium transients that may be tuned to drive axon guidance (64, 65) and plasticity mechanisms (66, 67). Propagation speed sets the time scale over which neighboring cells are correlated, and thus may be critical for retinotopic map refinement (68). The spatial extent of wave propagation has been shown to be important for establishing eye-specific segregation of retinal inputs within the thalamus (69).

Retinal waves determine the final size of termination zones of retinal projections to the superior colliculus (SC, Figure 13A). Focal labeling of retinal ganglion cells using DiI labels in retina (Retina) gives small target zones in superior colliculus (WT, Fig. 13A, left). In knockout mice lacking normal cholinergic waves (β2-nAChR KO, Fig. 13A middle), termination zones are less compact. Rescue of the β2-nAChR gene in a subset of retinal cells (Fig. 13 β2 tg) produce small waves, which are sufficient to rescue normal retinotopic map refinement.

Retinal waves also play a role in eye-specific segregation of retinal ganglion cell projections to the lateral geniculate nucleus of the thalamus (Fig. 13b). In wild type mice, there is little overlap between ipsi- and contra-lateral projections. Mice lacking cholinergic waves (β2 KO) and mice with small waves (β2 tg) have significantly overlapping projections from either eye.

Retinal waves also play a role in eye-specific segregation of retinal ganglion cell projections to the lateral geniculate nucleus of the thalamus (Fig. 13b). In wild type mice, there is little overlap between ipsi- and contra-lateral projections. Mice lacking cholinergic waves (β2 KO) and mice with small waves (β2 tg) have significantly overlapping projections from either eye.

5. Conclusion

The neural circuits within the inner plexiform layer are highly organized, making them an ideal system for the study of circuit formation. Understanding how this organized structure and intricate connectivity arise during development is an important endeavor. It is clear that on the path to forming the circuits that mediate vision, the retina creates a series of intermediate circuits that generate spontaneous activity. These transitory circuits are then dismantled as the retina matures. During their brief existence, these transient networks play an important role in shaping the circuits both within the retina and from the retina to the brain.

A wealth of new tools will lead the way to a greater understanding of how these neural circuits develop. Several recent studies have identified lines of mice with GFP or Cre recombinase expression that is restricted to specific classes and even to subsets of retinal neurons. The ability to identify and alter the activity of specific components of a neural circuit will allow future experimentalists to observe how these circuits form and to ask what role spontaneous activity plays in their formation.

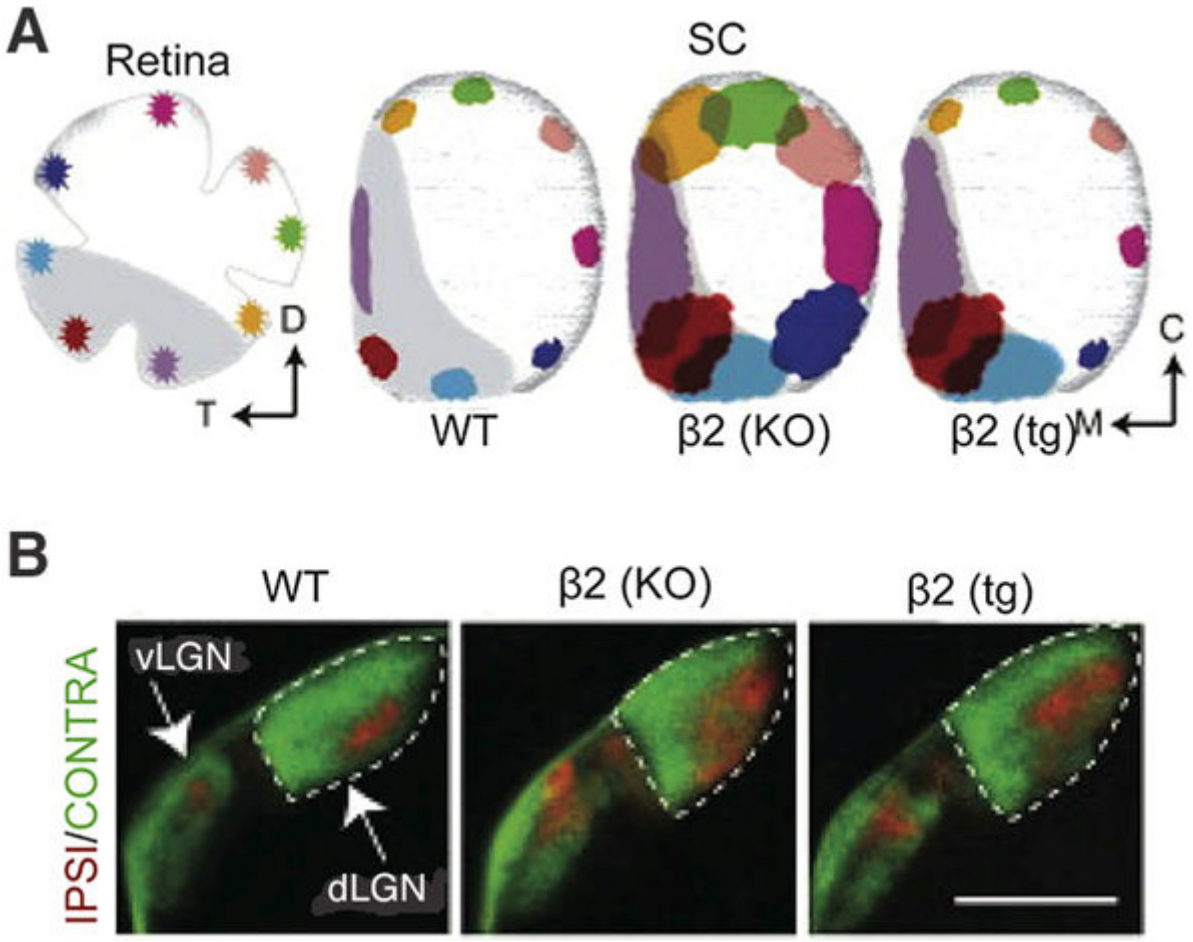

Figure 13. Retinal waves drive refinement of central projections. *A*. Schematic showing results of several experiments based on DiI anterograde labeling to determine the retinotopic projection of retinal ganglion cells to the superior colliculus. Results for WT mice, knockout mice lacking the beta2-subunit of nAChR, and tg mice in which b2 has is rescued in a subset of RGCs in the beta2-nAChR KO mice. *B*. Fluorescent images of retinal ganglion cell axon terminals from ipsilateral (red) and contralateral (green) projections. Axons labeled by fluorescently tagged cholera toxin. From Xu et al., 2011 (69).

About the Authors

Dr. Kevin Ford received his B.S. in Biology from UC San Diego in 2005. He did his graduate work with Marla Feller first at UC San Diego and then UC Berkeley, receiving his Ph.D. in Molecular and Cell Biology from UC Berkeley in 2011. During his graduate career, he researched the cellular mechanisms underlying retinal waves in the developing mouse retina. He is still in Marla's laboratory at Berkeley.

Dr. Marla Feller received her B.A. and Ph.D. in Physics from University of California at Berkeley in 1985 and 1992 respectively. She was a postdoctoral researcher with at Bell Laboratories with Dr. David Tank (1992-1994) and then at UC Berkeley with Dr. Carla Shatz (1994-1998). She headed a laboratory at the National Institutes of Neurological Disorders (1998-2000), was at UC San Diego (2000-2007) and is now at UC Berkley Neuroscience as an Associate Professor of Neurobiology. She has done research in the elucidating the circuits that mediate retinal waves and also in what role retinal waves play in the establishment of retinal projections to the brain. Currently Marla is investigating the mechanisms underlying the generation of this highly patterned activity and exploring the role it plays in the development and shaping of ganglion cell responses, particularly those generated by a cholinergic amacrine cell network.

References

1. Feller M.B., et al. Requirement for cholinergic synaptic transmission in the propagation of spontaneous retinal waves. Science. 1996;272(5265):1182. PubMed PMID: 8638165.
2. Meister M., et al. Synchronous bursts of action potentials in ganglion cells of the developing mammalian retina. Science. 1991;252(5008):939–43. PubMed PMID: 2035024.
3. Penn A.A., Wong R.O., Shatz C.J. Neuronal coupling in the developing mammalian retina. J Neurosci. 1994;14(6):3805–15. PubMed PMID: 8207489.

4. Redburn D.A., Rowe-Rendleman C. Developmental neurotransmitters. Signals for shaping neuronal circuitry. Invest Ophthalmol Vis Sci. 1996;37(8):1479–82. PubMed PMID: 8675389.
5. Fisher L.J. Development of synaptic arrays in the inner plexiform layer of neonatal mouse retina. J Comp Neurol. 1979;187(2):359–72. PubMed PMID: 489784.
6. Pearson R., et al. Purinergic and muscarinic modulation of the cell cycle and calcium signaling in the chick retinal ventricular zone. The Journal of Neuroscience: The Official Journal of the Society for Neuroscience. 2002;22(17):7569–7579. PubMed PMID: 12196580.
7. Lohmann C., Myhr K.L., Wong R.O. Transmitter-evoked local calcium release stabilizes developing dendrites. Nature. 2002;418(6894):177–81. PubMed PMID: 12110889.
8. Hayden S.A., Mills J.W., Masland R.M. Acetylcholine synthesis by displaced amacrine cells. Science (New York, N.Y.). 1980;210(4468):435–437. PubMed PMID: 7433984.
9. Baldridge W.H. Optical recordings of the effects of cholinergic ligands on neurons in the ganglion cell layer of mammalian retina. The Journal of Neuroscience: The Official Journal of the Society for Neuroscience. 1996;16(16):5060–5072. PubMed PMID: 8756436.
10. Masland R.H., Ames A. 3rd. Responses to acetylcholine of ganglion cells in an isolated mammalian retina. J Neurophysiol. 1976;39(6):1220–35. PubMed PMID: 993829.
11. Masland RH, Mills JW, Cassidy C. The functions of acetylcholine in the rabbit retina. Proc R Soc Lond B Biol Sci. 1984;223:121–39. PubMed PMID: 6151181.
12. Schmidt M., Humphrey M.F., Wässle H. Action and localization of acetylcholine in the cat retina. Journal of Neurophysiology. 1987;58(5):997–1015. PubMed PMID: 3694255.
13. Strang CE, Andison ME, Amthor FR, Keyser KT. Rabbit retinal ganglion cells express functional alpha7 nicotinic acetylcholine receptors. Am J Physiol Cell Physiol. 2005;289:C644–55. PubMed PMID: 15872006.
14. Zheng J.J., Lee S., Zhou Z.J. A developmental switch in the excitability and function of the starburst network in the mammalian retina. Neuron. 2004;44(5):851–64. PubMed PMID: 15572115.
15. Syed M.M., et al. Spontaneous waves in the ventricular zone of developing mammalian retina. J Neurophysiol. 2004;91(5):1999–2009. PubMed PMID: 14681336.
16. Wong R.O., et al. Early functional neural networks in the developing retina. Nature. 1995;374(6524):716–8. PubMed PMID: 7715725.
17. Martins R.A.P., Pearson R.A. Control of cell proliferation by neurotransmitters in the developing vertebrate retina. Brain Research. 2008;1192:37–60. PubMed PMID: 17597590.
18. Sandell J.H. GABA as a developmental signal in the inner retina and optic nerve. Perspect Dev Neurobiol. 1998;5(2-3):269–78. PubMed PMID: 9777642.
19. Karne A., et al. Immunocytochemical localization of GABA, GABAA receptors, and synapse-associated proteins in the developing and adult ferret retina. Vis Neurosci. 1997;14(6):1097–108. PubMed PMID: 9447691.
20. Zhang L.L., et al. Shift of intracellular chloride concentration in ganglion and amacrine cells of developing mouse retina. J Neurophysiol. 2006;95(4):2404–16. PubMed PMID: 16371454.
21. Sernagor E., Young C., Eglen S.J. Developmental modulation of retinal wave dynamics: shedding light on the GABA saga. The Journal of Neuroscience: The Official Journal of the Society for Neuroscience. 2003;23(20):7621–7629. PubMed PMID: 12930801.
22. Syed M.M., et al. Stage-dependent dynamics and modulation of spontaneous waves in the developing rabbit retina. J Physiol. 2004;560(Pt 2):533–49. PubMed PMID: 15308679.
23. Wang C.-T., et al. GABAA Receptor-Mediated Signaling Alters the Structure of Spontaneous Activity in the Developing Retina. J. Neurosci. 2007;27(34):9130. PubMed PMID: 17715349.
24. Blankenship A.G., et al. Synaptic and extrasynaptic factors governing glutamatergic retinal waves. Neuron. 2009;62(2):230–241. PubMed PMID: 19409268.
25. Leitch E., et al. GABA type-A activity controls its own developmental polarity switch in the maturing retina. J Neurosci. 2005;25(19):4801–5. PubMed PMID: 15888655.

26. Barkis W.B., Ford K.J., Feller M.B. Non-cell-autonomous factor induces the transition from excitatory to inhibitory GABA signaling in retina independent of activity. Proc Natl Acad Sci U S A. 2010;107(51):22302–7. PubMed PMID: 21135238.
27. Haverkamp S., Wassle H. Characterization of an amacrine cell type of the mammalian retina immunoreactive for vesicular glutamate transporter 3. J Comp Neurol. 2004;468(2):251–63. PubMed PMID: 14648683.
28. Johnson J., et al. Vesicular glutamate transporter 3 expression identifies glutamatergic amacrine cells in the rodent retina. J Comp Neurol. 2004;477(4):386–98. PubMed PMID: 15329888.
29. Johnson J., et al. Vesicular Neurotransmitter Transporter Expression in Developing Postnatal Rodent Retina: GABA and Glycine Precede Glutamate. The Journal of Neuroscience. 2003;23(2):518–529. PubMed PMID: 12533612.
30. Kerschensteiner D., et al. Neurotransmission selectively regulates synapse formation in parallel circuits in vivo. Nature. 2009;460(7258):1016–20. PubMed PMID: 19693082.
31. Morgan J.L., Schubert T., Wong R.O. Developmental patterning of glutamatergic synapses onto retinal ganglion cells. Neural Dev. 2008;3:8. PubMed PMID: 18366789.
32. Galli L., Maffei L. Spontaneous impulse activity of rat retinal ganglion cells in prenatal life. Science. 1988;242(4875):90–1. PubMed PMID: 3175637.
33. Wong R.O. Cholinergic regulation of [Ca2+]i during cell division and differentiation in the mammalian retina. The Journal of Neuroscience: The Official Journal of the Society for Neuroscience. 1995;15(4):2696–2706. PubMed PMID: 7722623.
34. Wong R.O. Retinal waves and visual system development. Annu Rev Neurosci. 1999;22:29–47. PubMed PMID: 10202531.
35. Bansal A., et al. Mice lacking specific nicotinic acetylcholine receptor subunits exhibit dramatically altered spontaneous activity patterns and reveal a limited role for retinal waves in forming ON and OFF circuits in the inner retina. J Neurosci. 2000;20(20):7672. PubMed PMID: 11027228.
36. Singer J.H., Mirotznik R.R., Feller M.B. Potentiation of L-type calcium channels reveals nonsynaptic mechanisms that correlate spontaneous activity in the developing mammalian retina. J Neurosci. 2001;21(21):8514–22. PubMed PMID: 11606640.
37. Wong R.O., Meister M., Shatz C.J. Transient period of correlated bursting activity during development of the mammalian retina. Neuron. 1993;11(5):923–38. PubMed PMID: 8240814.
38. Catsicas M., et al. Spontaneous Ca2+ transients and their transmission in the developing chick retina. Curr Biol. 1998;8(5):283–6. PubMed PMID: 9501073.
39. Penn A.A., et al. Competition in retinogeniculate patterning driven by spontaneous activity. Science (New York, N.Y.). 1998;279(5359):2108–2112. PubMed PMID: 9516112.
40. Stacy R.C., et al. Disruption and Recovery of Patterned Retinal Activity in the Absence of Acetylcholine. J. Neurosci. 2005;25(41):9347–9357. PubMed PMID: 16221843.
41. Feller M.B., et al. Dynamic Processes Shape Spatiotemporal Properties of Retinal Waves. Neuron. 1997;19(2):293. PubMed PMID: 9292720.
42. Ford K.J., Felix A.L., Feller M.B. Cellular mechanisms underlying spatiotemporal features of cholinergic retinal waves. J Neurosci. 2012;32(3):850–63. PubMed PMID: 22262883.
43. Stafford B.K., et al. Spatial-Temporal Patterns of Retinal Waves Underlying Activity-Dependent Refinement of Retinofugal Projections. Neuron. 2009;64(2):200–212. PubMed PMID: 19874788.
44. Sun C., et al. Retinal waves in mice lacking the β2 subunit of the nicotinic acetylcholine receptor. Proceedings of the National Academy of Sciences. 2008;105(36):13638–13643. PubMed PMID: 18757739.
45. Ben-Ari Y., Spitzer N.C. Phenotypic checkpoints regulate neuronal development. Trends in Neurosciences. 2010;33(11):485–492. PubMed PMID: 20864191.
46. Blankenship A.G., Feller M.B. Mechanisms underlying spontaneous patterned activity in developing neural circuits. Nat Rev Neurosci. 2010;11(1):18–29. PubMed PMID: 19953103.

47. Wong W.T., et al. Developmental changes in the neurotransmitter regulation of correlated spontaneous retinal activity. The Journal of Neuroscience: The Official Journal of the Society for Neuroscience. 2000;20(1):351–360. PubMed PMID: 10627612.
48. Zhou Z.J., Zhao D. Coordinated transitions in neurotransmitter systems for the initiation and propagation of spontaneous retinal waves. The Journal of Neuroscience: The Official Journal of the Society for Neuroscience. 2000;20(17):6570–6577. PubMed PMID: 10964962.
49. Wong R.O., Oakley D.M. Changing patterns of spontaneous bursting activity of on and off retinal ganglion cells during development. Neuron. 1996;16(6):1087–1095. PubMed PMID: 8663985.
50. Kerschensteiner, D. and R.O.L. Wong, A Precisely Timed Asynchronous Pattern of ON and OFF Retinal Ganglion Cell Activity during Propagation of Retinal Waves. 2008. **58**(6): p. 851.
51. Fischer K.F., Lukasiewicz P.D., Wong R.O. Age-dependent and cell class-specific modulation of retinal ganglion cell bursting activity by GABA. J Neurosci. 1998;18(10):3767–78. PubMed PMID: 9570807.
52. Blankenship A.G., et al. The role of neuronal connexins 36 and 45 in shaping spontaneous firing patterns in the developing retina. J Neurosci. 2011;31(27):9998–10008. PubMed PMID: 21734291.
53. Bodnarenko S.R., et al. The development of retinal ganglion cell dendritic stratification in ferrets. Neuroreport. 1999;10(14):2955–2959. PubMed PMID: 10549804.
54. Coombs J.L., Van Der List D., Chalupa L.M. Morphological properties of mouse retinal ganglion cells during postnatal development. The Journal of Comparative Neurology. 2007;503(6):803–814. PubMed PMID: 17570502.
55. Kim I.-J., et al. Laminar restriction of retinal ganglion cell dendrites and axons: subtype-specific developmental patterns revealed with transgenic markers. The Journal of Neuroscience: The Official Journal of the Society for Neuroscience. 2010;30(4):1452–1462. PubMed PMID: 20107072.
56. Sernagor E., Eglen S.J., Wong R.O. Development of retinal ganglion cell structure and function. Progress in Retinal and Eye Research. 2001;20(2):139–174. PubMed PMID: 11173250.
57. Xu H., Tian N. Pathway-specific maturation, visual deprivation, and development of retinal pathway. The Neuroscientist: A Review Journal Bringing Neurobiology, Neurology and Psychiatry. 2004;10(4):337–346. PubMed PMID: 15271261.
58. Bodnarenko S.R., Chalupa L.M. Stratification of ON and OFF ganglion cell dendrites depends on glutamate-mediated afferent activity in the developing retina. Nature. 1993;364(6433):144–6. PubMed PMID: 8100613.
59. Bodnarenko S.R., Jeyarasasingam G., Chalupa L.M. Development and regulation of dendritic stratification in retinal ganglion cells by glutamate-mediated afferent activity. J Neurosci. 1995;15(11):7037–45. PubMed PMID: 7472459.
60. Xu H.P., et al. The immune protein CD3zeta is required for normal development of neural circuits in the retina. Neuron. 2010;65(4):503–15. PubMed PMID: 20188655.
61. Wong W.T., Wong R.O. Changing specificity of neurotransmitter regulation of rapid dendritic remodeling during synaptogenesis. Nature Neuroscience. 2001;4(4):351–352. PubMed PMID: 11276221.
62. Sernagor E., Grzywacz N.M. Influence of spontaneous activity and visual experience on developing retinal receptive fields. Current Biology: CB. 1996;6(11):1503–1508. PubMed PMID: 8939611.
63. Huberman A.D., Feller M.B., Chapman B. Mechanisms Underlying Development of Visual Maps and Receptive Fields. Annual Review of Neuroscience. 2008;31(1):479–509. PubMed PMID: 18558864.
64. Nicol X., et al. cAMP oscillations and retinal activity are permissive for ephrin signaling during the establishment of the retinotopic map. Nat Neurosci. 2007;10(3):340–7. PubMed PMID: 17259982.
65. Pfeiffenberger C., Yamada J., Feldheim D.A. Ephrin-As and Patterned Retinal Activity Act Together in the Development of Topographic Maps in the Primary Visual System. J. Neurosci. 2006;26(50):12873–12884. PubMed PMID: 17167078.
66. Butts D.A., Kanold P.O., Shatz C.J., Burst-Based A. "Hebbian" Learning Rule at Retinogeniculate Synapses Links Retinal Waves to Activity-Dependent Refinement. PLoS Biol. 2007;5(3):e61. PubMed PMID: 17341130.

67. Shah R.D., Crair M.C. Retinocollicular Synapse Maturation and Plasticity Are Regulated by Correlated Retinal Waves. J. Neurosci. 2008;28(1):292–303. PubMed PMID: 18171946.
68. Chandrasekaran A.R., Shah R.D., Crair M.C. Developmental Homeostasis of Mouse Retinocollicular Synapses. J. Neurosci. 2007;27(7):1746–1755. PubMed PMID: 17301182.
69. Xu H.P., et al. An instructive role for patterned spontaneous retinal activity in mouse visual map development. Neuron. 2011;70(6):1115–27. PubMed PMID: 21689598.
70. Ramón y Cajal, S., The structure of the retina. 1894, Translated by S.A. Thorpe and M. Glickstein 1972, Springfield, Ill.,: C. C. Thomas. xxxix, 196 p.
71. Ben-Ari Y., et al. GABA: a pioneer transmitter that excites immature neurons and generates primitive oscillations. Physiol Rev. 2007;87(4):1215–84. PubMed PMID: 17928584.
72. Ford K.J., Feller M.B. Assembly and disassembly of a retinal cholinergic network. Vis Neurosci. 2011.:1–11. PubMed PMID: 21787461.

Development of Retinal Ganglion Cell Dendritic Structure and Synaptic Connections

Ning Tian, MD-PhD[1]

Created: June 13, 2012.

1 Introduction

The neuronal information of the visual scene that is processed by the retina is conducted to the brain by a set of separate spatio-temporal synaptic pathways. The morphological basis for the formation of these parallel synaptic pathways is the laminar-specific structure of the retina, in which specific subtypes of retinal neurons form synapses only with highly selective presynaptic and postsynaptic cells (1-3).

Retinal ganglion cells (RGCs) are the output neurons of the retina. In the retina, RGCs synapse with bipolar and amacrine cells in the inner plexiform layer (IPL) to receive excitatory and inhibitory synaptic inputs respectively. The axons of RGCs travel through the optic nerve to retinorecipient structures in the brain, where they transfer their specific aspects of visual information to the higher centers (3). Because different subtypes of bipolar cells (Fig 1) (4) and amacrine cells (Fig. 2) (5) have their axonal/dendritic terminals in the specific sublaminae of the IPL, it is crucial that dendrites of individual RGCs are also confined to specific strata in order to synapses with them.

Thus, the synaptic circuitries processing distinct visual features, the so called "parallel pathways" (1, 2, 6-10), start in the retina. In most mammals, RGCs can be divided into about 20 morphological subtypes based on their distinctive dendritic structure and synaptic connections (11-19). The wholemount drawings of mouse RGCs (Fig. 3) illustrate the diversity of morphologies present in mammalian RGCs ((19). See also RGCs of human, cat and rabbit retinas in the ganglion cell chapter in Webvision).

Most of these RGCs have specific dendritic distribution in the IPL in adult retina as exemplified by the schematic (Fig. 4) showing the branching patterns of mouse RGCs. In most mammals, these lamina-restricted distributions of RGC dendrites and synaptic connections are formed during pre- and post-natal development. The question is how this lamination arises.

2 Neurogenesis and synaptogenesis of retina

The neurogenesis and synaptogenesis of mammalian retina is an orderly process. Figure 5 shows an overview drawing of the development of mouse retinal neurons. RGCs differentiate first followed by amacrine cells, cones and horizontal cells. Rod photoreceptors differentiate shortly afterward. Bipolar cells are the last neurons to differentiate. In mammals most retinal neurons differentiate before birth (20-22).

The order of synaptogenesis of retinal neurons is somewhat different from the order of neurogenesis. The synapses of amacrine cells in the IPL appear first. These are followed by the synaptic formation between photoreceptors and horizontal cells in the OPL. The last synaptic element to link photoreceptors in the outer retina and RGCs in the inner retina is the synaptic connection between bipolar cells and RGCs (Fig. 5A) (23, 24). In mouse, the density of both ribbons and conventional synapses in the IPL continuously increases after eye opening and reaches the peak level by the age of P21 (Fig. 5B). Functionally, the strength of RGC synaptic inputs measured by the frequency of spontaneous synaptic activity is low before eye opening in mice. After eye

Author Affiliation: 1 Associate Professor of Ophthalmology and Neurobiology, Moran Eye Center, University of Utah School of Medicine.; Email: Ning.Tian@hsc.utah.edu.

Corresponding author.

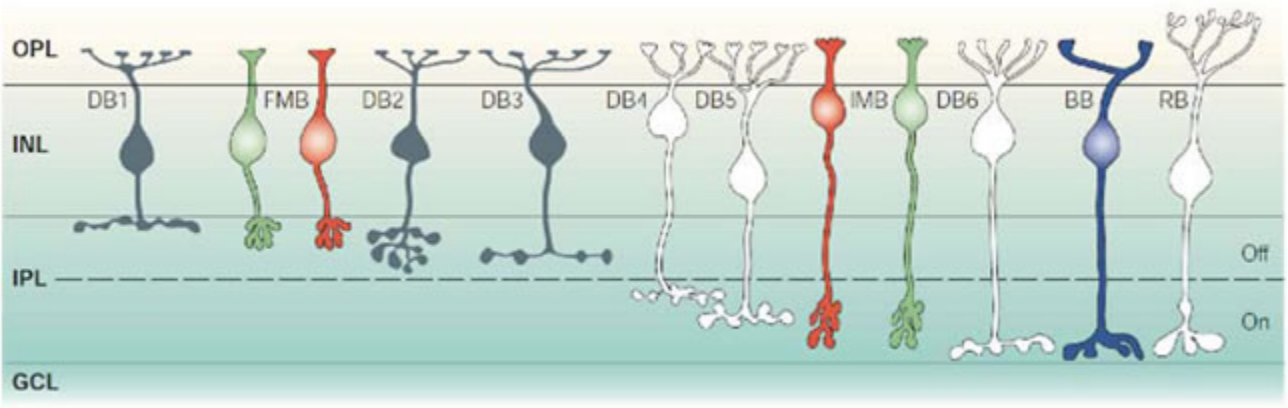

Figure 1: The major subtypes of bipolar cells of primate retina (Adapted from Wässle, 2004 (10)). Similar types have been observed in the rats (4), rabbit, cat (15, 74), monkey (75) and human (76).

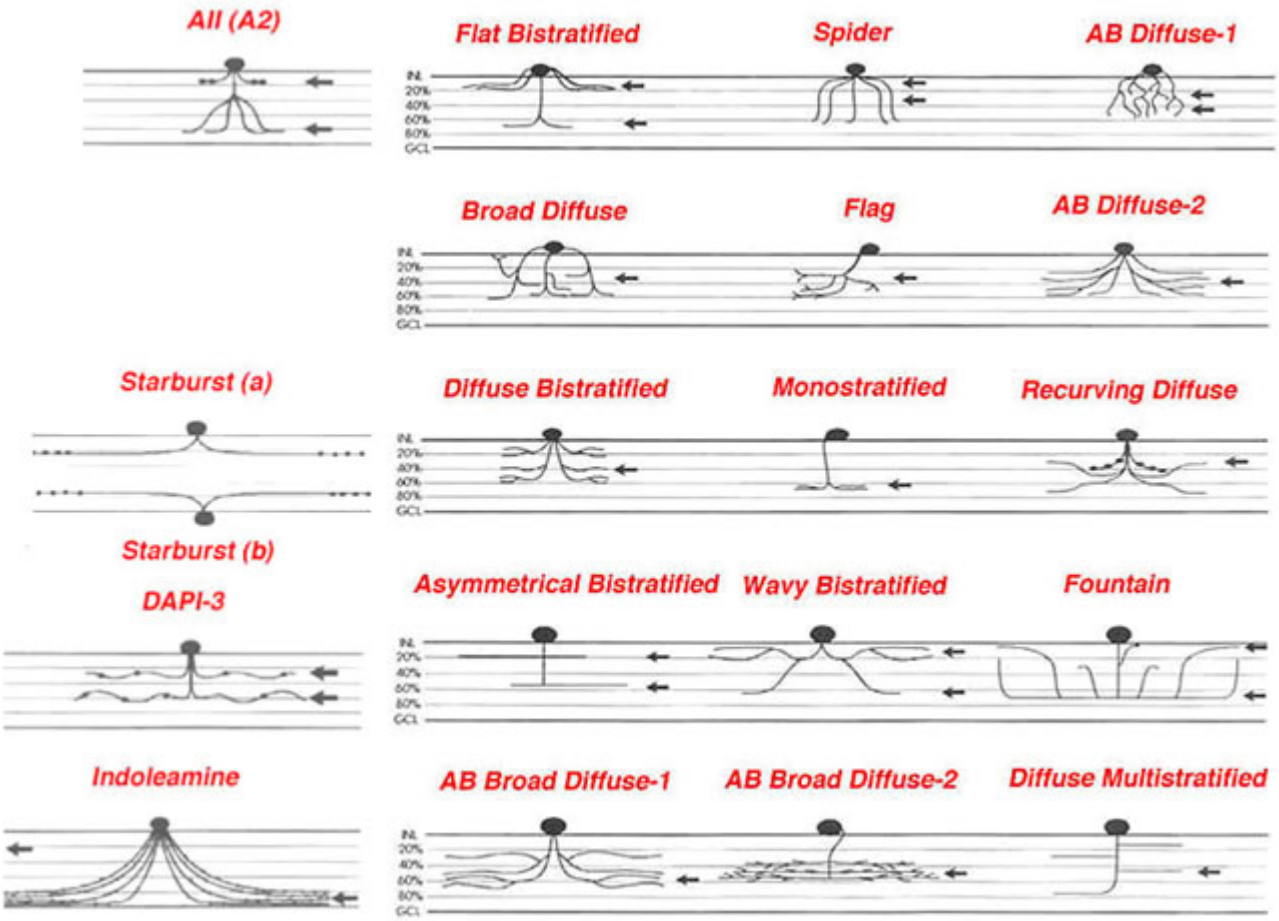

Figure 2. Schematic drawings of some of the amacrine cells of rabbit retina show each type has a characteristic morphology and stratification of the dendrites to specific strata (1-5) of the inner plexiform layer. All other mammals have similar cells. Adapted from MacNeil and Masland, 1998 (5).

opening, a surge of glutamate receptor-mediated spontaneous excitatory postsynaptic currents (sEPSCs) and GABA/glycine receptor-mediated spontaneous inhibitory postsynaptic currents emerges around P25 (Fig. 5B). Amplitudes of RGC light responses in cat and ferret retina are also found to increase after eye opening (25, 26).

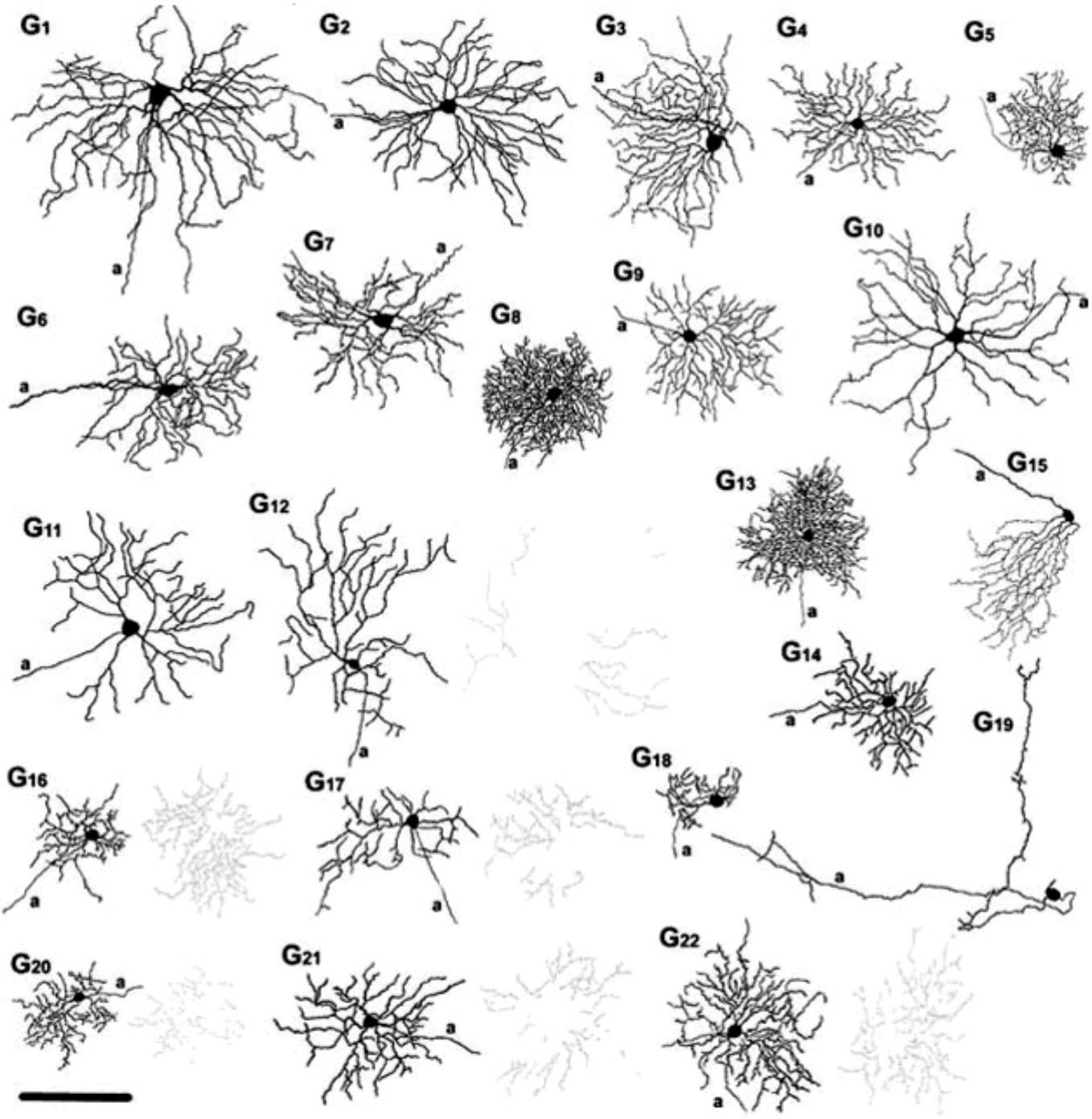

Figure 3. About 22 subtypes of retinal ganglion cells (RGCs) are present in the mammalian retina (See chapter on ganglion cells, Webvision). Camera lucida drawings show the RGCs of mouse retina. Adapted from Volgyi et al., 2009 (19).

In rabbit and rat, the amplitudes of retinal light responses measured by electroretinography continuously increases in the first month after birth and reaches the adult level by the ages of P30 to P40 (27, 28).

During synaptogenesis, the dendrites of mouse RGCs undergo very active remodeling. More than 30% of dendritic filopodial branches in the mouse are replaced every hour by continuous dendritic growth and elimination (pruning) between P10-13 (see Fig 6 and movie 1). This developmental remodeling of RGC dendrites is thought to play an important role in synaptogenesis and the formation of lamina-restricted dendritic distributions of RGCs.

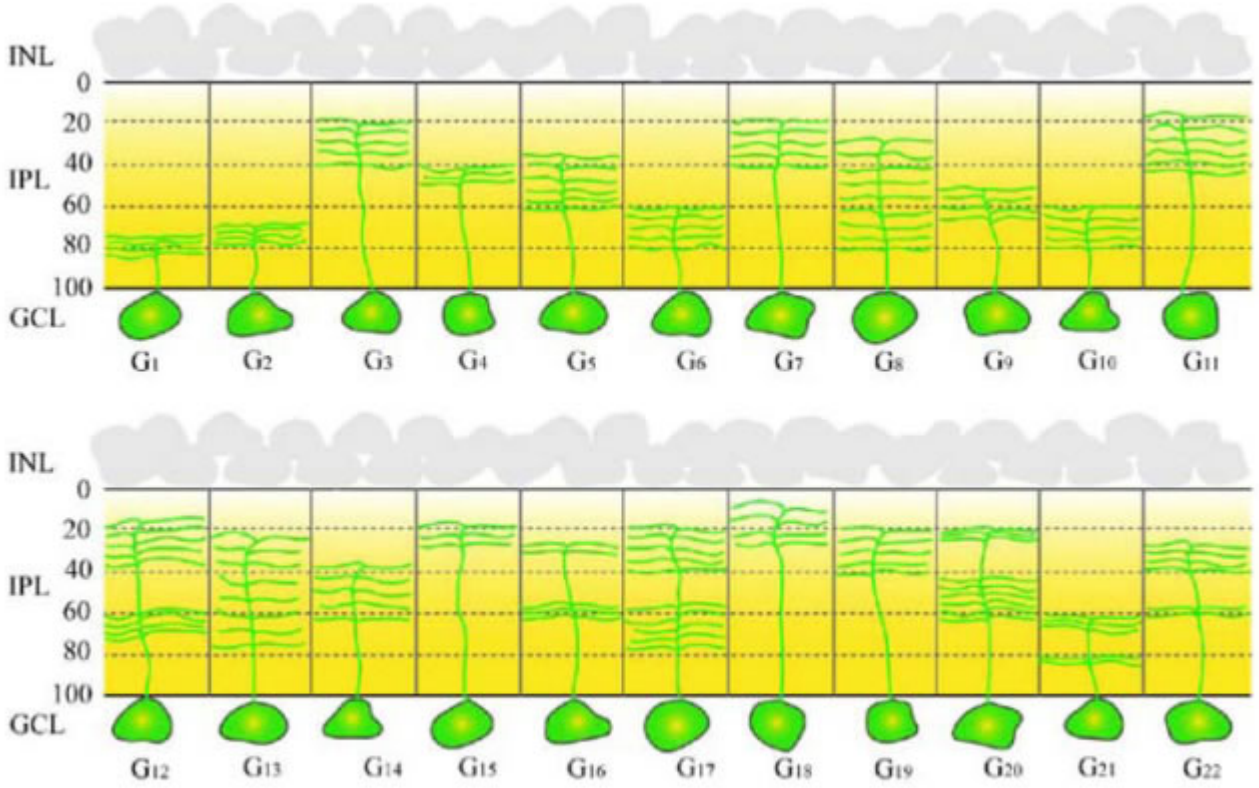

Figure 4. Dendritic ramification depth of the 22 mouse RGC subtypes (From Volgi et al., 2009 (19)). Solid horizontal lines represent the inner and outer borders of the IPL, whereas dashed lines separate the 5 IPL strata. Numbers on the left represent percent depth level in the IPL. Summary diagrams of RGCs are separated by vertical lines into the subtypes but do not represent the diameter of the dendritic trees.

3. Formation of lamina-restricted dendritic distributions of RGCs

Many studies have shown that the dendritic morphology and synaptic connections of RGCs undergo profound refinement during postnatal development. Early in postnatal development, the dendrites of many RGCs ramify diffusely throughout the IPL of the retina in cats, rats and mice (Fig. 7, A1, A2). With subsequent maturation, RGC dendrites become much more narrowly stratified in the IPL (Fig. 7, A2, B2 and B3) (26, 29-34) at least partially due to a developmental restriction of RGC dendrites (31). Recent studies suggest that different subtypes of RGCs acquire their lamina-restricted dendritic ramification patterns in different ways.

Some RGCs seem to achieve their restricted lamina patterns by direct targeting without significant pruning. In Figure 8 A1-A3, a bistratified RGC has a bistratified dendritic distribution pattern early at P5 (A1) and retains this bistratified pattern into adulthood (A2 and A3) without an initial diffuse distribution pattern. Similarly in Zebrafish some RGCs directly elaborate their dendrites to the middle of the IPL and later became strictly monostratified, occupying a single stratum in the middle of the IPL (Fig. 8 B1, B2 and B3) (35).

It is also clear that some RGCs form their lamina-restricted dendritic patterns through both direct targeting and selective dendritic pruning (Fig. 9). In Figure 9, A1-A3, the dendritic trees of a subtype of RGCs are diffusely ramified with many side branches originally and become bistratified to two strata above and below the

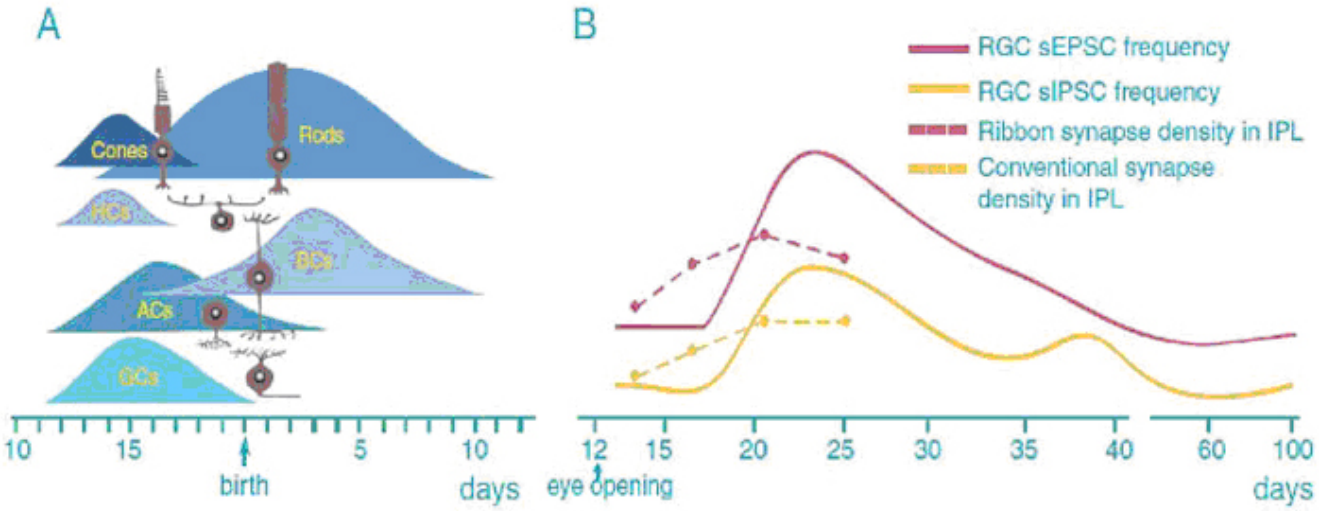

Figure 5. In mouse retina, neurogenesis begins before birth and is largely completed shortly after birth (A.). However neurogenesis of rods and bipolar cells starts before birth and continues for 1-2 weeks after birth (77). B: Synaptogenesis of mouse retina begins before eye opening and continues for several weeks after eye opening. The density of both ribbon and conventional synapses in the IPL reaches peak at P21 (78). The synaptic strength measured as the frequency of RGC spontaneous activity increases with age and peaks around 2 weeks after eye opening (55). The curves show the relative cell populations, synaptic densities and frequencies of spontaneous synaptic inputs as a function of time. Adapted from Xu and Tian, 2004 (79).

cholinergic starburst type a cell with significant pruning of their dendritic branches (33). Similarly in Figure 9 B1-B3, a zebrafish RGC starts its dendrites in the inner strata of the IPL and then selectively prunes the dendrites in the inner strata and grows the dendrites in the outer strata of the IPL over time (35).

4. Regulation of the formation of lamina-restricted dendritic patterns of RGCs

The regulatory mechanisms for the formation of the lamina-restricted dendritic patterns of RGCs are not completely understood. It has been reported that many molecular cues play crucial roles in the formation of laminar-restricted dendritic pattern of some subtypes of RGCs. The immunoglobulin superfamily adhesion molecules, DSCAMs and sidekicks, have been reported to direct laminar-specific axonal and dendritic ramification of bipolar cells and RGCs in chick retina (36) and RGC neurite arborization and mosaic formation in mouse retina (37). The transmembrane semaphorin Sema6A and its receptor PlexinA4 (PlexA4) have also been reported to control the stratification of the dendrites of dopaminergic amacrine cells, melanopsin containing RGCs and calbindin-positive cells into ON and OFF sublaminae of the IPL in mouse retina (38). Fig 10A shows that transmembrane semaphorin Sema5A and Sema5B normally constrain dendritic targeting of melanopsin-expressing RGCs to the IPL. In Sema5A-/- and Sema5B-/- mice the RGCs exhibit aberrant dendritic branching in INL, OPL and ONL (Fig. 10B, 10C and 10G).

Several reports have also shown that both spontaneous synaptic activity mediated by glutamate receptor (GluR) before eye opening and light evoked retinal activity after eye opening regulate the normal development of the lamina-restricted dendritic patterns of RGCs. In an early developing vertebrate retina like mouse, RGCs fire periodic bursts of action potentials that are highly correlated and propagate across the RGC layer in a wave-like fashion (39). These spontaneous retinal waves are mainly mediated by cholinergic and glutamatergic synaptic transmission (40-45) (see chapter by Ford and Feller, Webvision). The retinal wave mediated by AChR seems to

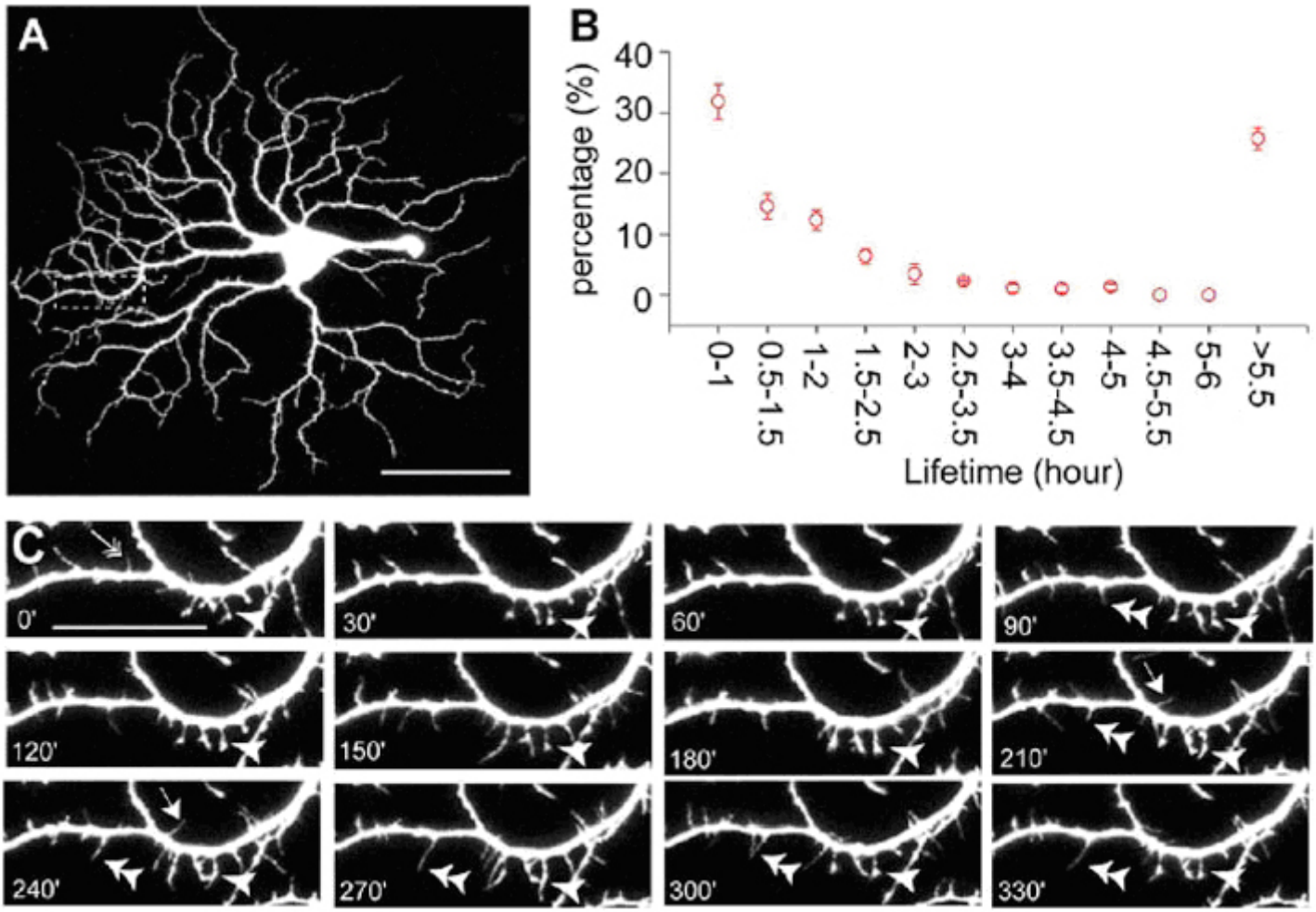

Figure 6: Dendrites of mouse RGCs undergo very active remodeling during synaptogenesis in postnatal development. RGC dendritic motility was examined using time-lapse confocal imaging on retinas of YFP+ mice at P13-14. A: Representative image of an A1 YFP+ RGC of a Thy1-YFP mouse. Scale bar, 60 µm. B: Average lifetime of RGC filopodia of P13-14 mice. Note that more than 30% of the filopodia are replaced every hour. Filopodia that existed at the beginning and disappeared before the end of the recording period and filopodia that emerged during the recording period and persisted until the end of the recording were discarded since the lifetime of these filopodia could not be determined. C: Representative time-lapse images of a segment of the dendrite from the RGC shown in (A) (indicated by the dash-line box) taken at 30 min intervals. Arrow, transient filopodia; arrowhead, static filopodia: double arrowhead, new filopodia; double-headed arrow, filopodia lost over the recording period. Scale bar, 20 µm. See also Movie . Adapted from Xu et al., 2010 (44).

have little effect on the formation of laminar-restricted dendritic pattern of RGCs. In mice, genetic deletion of β2 subunits of nAChR or the sole synthetic enzyme for acetylcholine, choline acetyltransferase, eliminates the retinal waves mediated by nAChRs and causes an insignificant or non detectable change of the development of the lamina-restricted dendritic ramification of RGCs (40, 46).

On the other hand, intraocular injection of APB, an agonist for class III metabotropic GluRs (mGluR6), results in a blockade of glutamate release from ON and rod bipolar cells and causes an arrest of the developmental stratification and segregation of RGC dendrites into ON and OFF synaptic pathways in cats, ferrets and rats (29, 30, 47, 48) (Fig 11).

Also, intraocular injection of antagonists for NMDA and AMPA receptors, AP5 and NBQX, increases the density of filopodia by more than 100% after 5 days of treatment in mice (see Fig 12, compare A and B). Xu et al. (44) showed that pharmacological blockade of GluR-mediated activity slows the kinetics of RGC dendritic

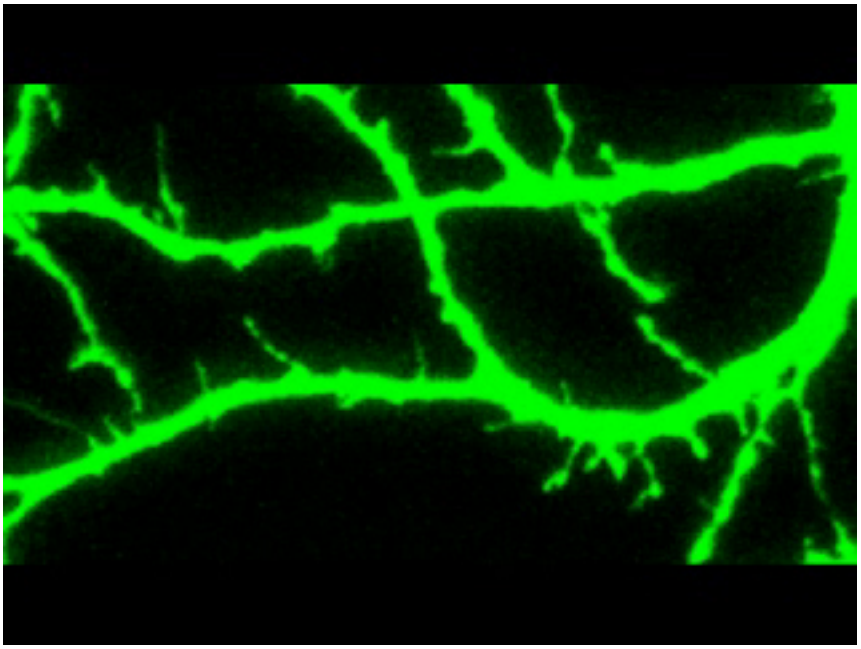

Movie 1. Changes in filopodial growth and shape in the course of one hour.
Download video

growth and elimination by approximately 50% (Fig. 12D). The disrupted GluR-mediated activity in retina during early postnatal development is associated with profound and permanent defects of RGC dendritic morphology and synaptic function in adults (44). Similarly, Lau et al. (49) showed that blockade of NMDA receptors before eye opening increases the spine density of RGCs in hamsters.

However, genetic blockade of glutamate release from ON bipolar cells eliminates spontaneous and light evoked synaptic inputs to ON RGCs without effect on the spontaneous and light evoked synaptic activity of OFF RGCs and causes no detectable effect on the lamina-restricted dendritic ramification of either ON or OFF RGCs (50). In addition, genetic deletion of the mGluR6 receptor, which blocks ON bipolar cell light evoked synaptic activity, failed to impair dendritic stratification of mouse RGCs (51). Therefore, the effect of GluR-mediated synaptic activity on the development of the lamina-restricted dendritic ramification and synaptic connections of RGCs is somewhat controversial and needs to be further investigated. The effect of light evoked synaptic activity on the development of RGC dendritic restriction and synaptic connection seems to vary among subtypes of RGCs and selective to some synaptic features. Morphologically, dark rearing blocks an age-dependent remodeling of dendritic complexity of a class of "aberrant" RGCs in hamster retina (52). In mice, light deprivation increases the density of conventional synapses in the IPL (53). The developmental ramification of RGC dendrites into OFF lamina of the IPL is selectively impaired by light deprivation in RGCs of mouse retina (54). Functionally, light deprivation blocks the surge of spontaneous synaptic inputs to RGCs, the age-dependent increase of inner retinal light responses measured by ERG oscillatory potentials (55, 56), the segregation of RGC synaptic inputs from ON and OFF synaptic pathways (54), and the maturation of the size of inhibitory receptive field of RGCs (57).

However, light deprivation seems preferentially to affect the maturation of dendrites of OFF RGCs, but not ON RGCs. Xu and Tian (54) quantitatively analyzed the developmental refinement of the dendrites of a random group of RGCs in mouse retina and determined the ramification depth and width of RGC dendrites in the IPL at different postnatal ages (Fig. 13). They showed that a large proportion of RGCs have a single layer of narrowly stratified dendritic plexus ramifying near the centre of the IPL before eye opening (P12), where they could synapse with both ON and OFF bipolar cells. After eye opening, a significant portion of RGCs redistribute their

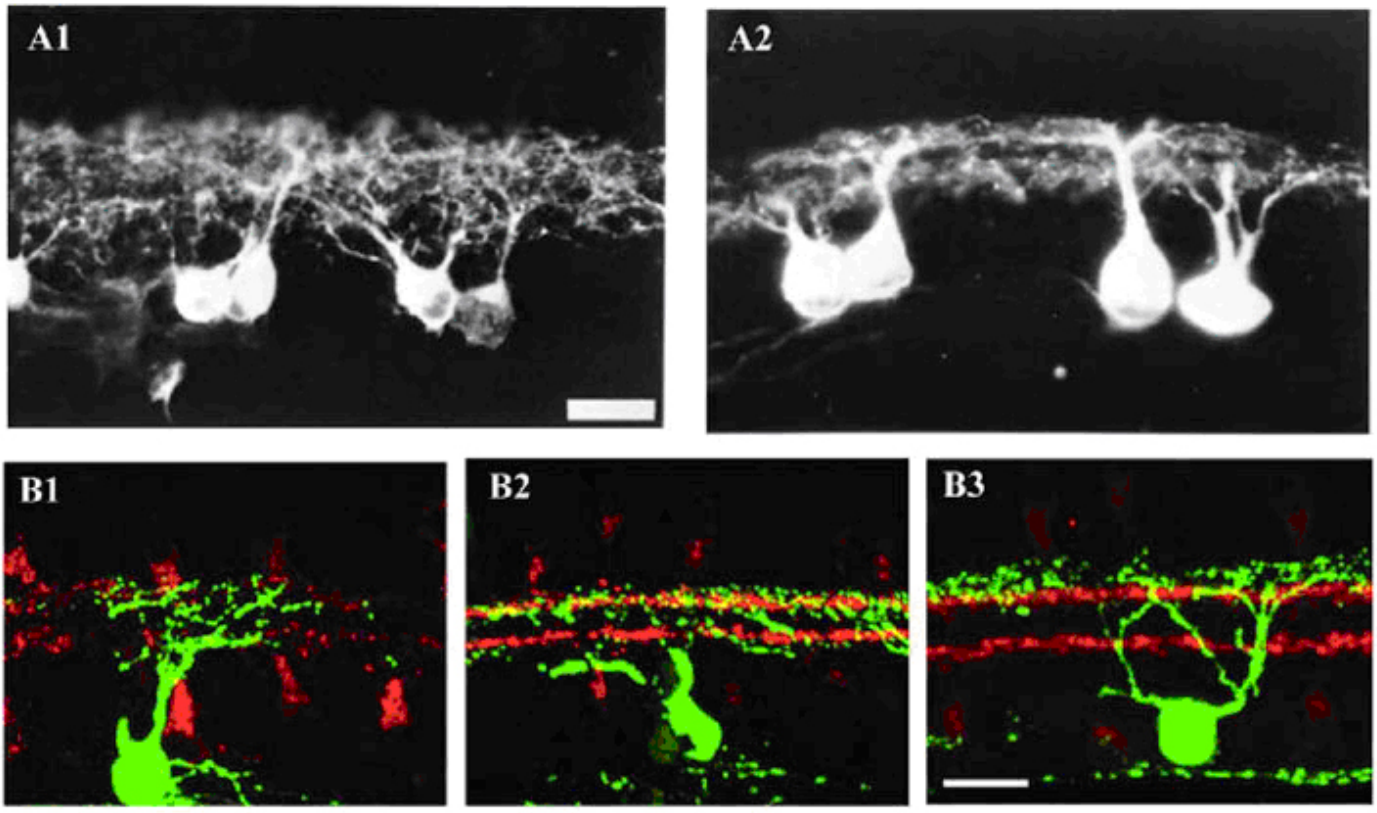

Figure 7: Dendrites of RGCs can reach mature stratified pattern through selective pruning. A1 and A2: Light micrographs of DiI (1,10-dioctadecyl-3,3,30,30-tetramethyl indocarbocyanine perchlorate) labeled RGCs from transverse sections of the central region of a P2 and a P10 cat, respectively. In A1, the RGC dendrites are distributed throughout the total IPL at P2 while, in A2, the dendrites have the distinct appearance of two tiers of dendrites within the IPL and the stratification pattern of ON and OFF layers. Scale bar in A1, 20 um. Reproduced from Bodnarenko and Chalupa, 1993 (29). B1, B2 and B3: Retinal sections from P5, P8, and P12-P13 JAM-B mice, respectively. RGCs were labeled with anti-GFP (green) and starburst amacrines with anti-ChAT (red). In B1, the dendrites of JAM-B RGC are distributed throughout the total IPL at P5. At P8 (B2), the JAM-B RGC selectively loses dendrites in the inner IPL. At P12-13 (B3), the dendrites of JAM-B RGC exhibit a lamina-restricted distribution in the outer IPL. Scale bar in B3, 20 um. Adapted from Kim et al., 2010 (33).

dendrites from the centre of the IPL toward the inner and outer borders of the IPL (Fig. 14A). This laminar-specific redistribution of RGC dendrites is associated with an age-dependent decrease of the number of RGCs receiving synaptic inputs from both ON and OFF bipolar cells (Fig. 14C). In dark reared mice, the RGC dendritic redistribution from the centre of the IPL to sublamina a of the IPL is blocked, which results in a significant increase of the number of RGCs ramifying at the center of the IPL, and a decrease of the number of RGCs ramifying only in sublamina a, in comparison with age-matched controls (Fig. 14A). Physiologically, the number of RGCs responding to both the onset and the offset of light stimulation of mice raised in constant darkness from birth to the ages of P27-30 was 4-fold higher than that of age-matched controls raised in cyclic light, but comparable to the percentage of ON-OFF responsive RGCs of P10-12 mice (58) (Fig. 14C). Similarly, long-term treatment of cat eyes with intraocular injection of APB significantly reduced the number of αRGCs ramifying in the sublamina a and increased the number of multistratified α cells (48).

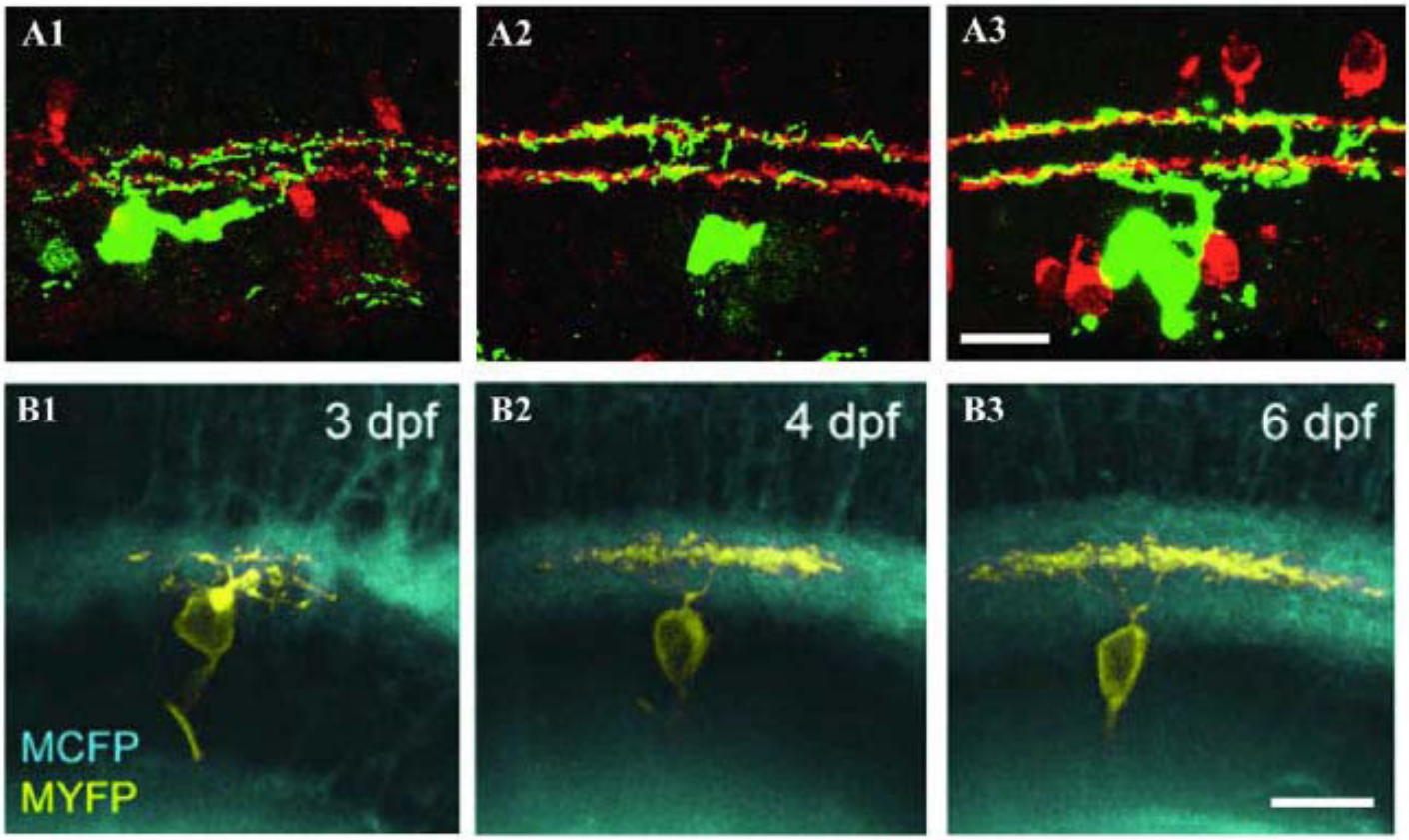

Figure 8. Dendrites of RGCs can reach mature stratified pattern by direct targeting. A1, A2 and A3: Retinal sections from P5, P8, and P12-P13 BD mice, respectively. RGCs were labeled with anti-GFP (green) and starburst amacrines with anti-ChAT (red). The BD RGC forms the distinct bistratified dendritic distribution pattern early during postnatal development at P5 (A1) without an initial diffuse distribution pattern. The bistratified distribution pattern remains throughout the postnatal development to adulthood (A2 and A3). Scale bar in A3, 20 um. Adapted from Kim et al., 2010 (33). B1, B2 and B3: In vivo time-lapse image of an isolated immature RGC (MYFP) in the Q01 background (MCFP) transgenic zebrafish retina. Time-lapse images taken at 3, 4 and 6 dpf, respectively, show orthogonally oriented image stacks of the entire arbor of the RGC. This RGC directly elaborates its dendrites targeting the inner half of the IPL that later became monostratified, occupying a single stratum in the middle of the IPL. Scale bar in B3, 10 um. Adapted from Mumm et al., 2006 (35).

5. The possible mechanisms of developmental regulation of RGC dendrites

During developmental refinement, the dendritic arborizations of RGCs undergo dynamic elaboration, maintenance or elimination to attain their lamina-restricted ramification pattern. Although neuronal activity influences this remodeling in many subtypes, the underlying molecular mechanisms have not yet been identified. Several studies suggest that calcium is important to link the neuronal activity with dendritic growth and patterning (59). Thus, it has been reported that synaptic stimulation induces calcium influx through voltage-dependent calcium channels and is sufficient to activate a transcriptional program that regulates dendritic growth (60).

BDNF/TrkB has also been shown to play an essential role in the activity-dependent development of RGC dendrites (61). Activation of BDNF promotes the anatomical segregation of the dendrites of ON- and OFF-center RGCs in different sublaminae of the IPL (61, 62), while deletion of TrkB strongly inhibits visual experience-dependent refinement of RGC dendrites (62). In addition, the expression of BDNF in the retina is up-regulated by visual stimulation (61, 63-65). This suggests that light deprivation retards RGC dendritic

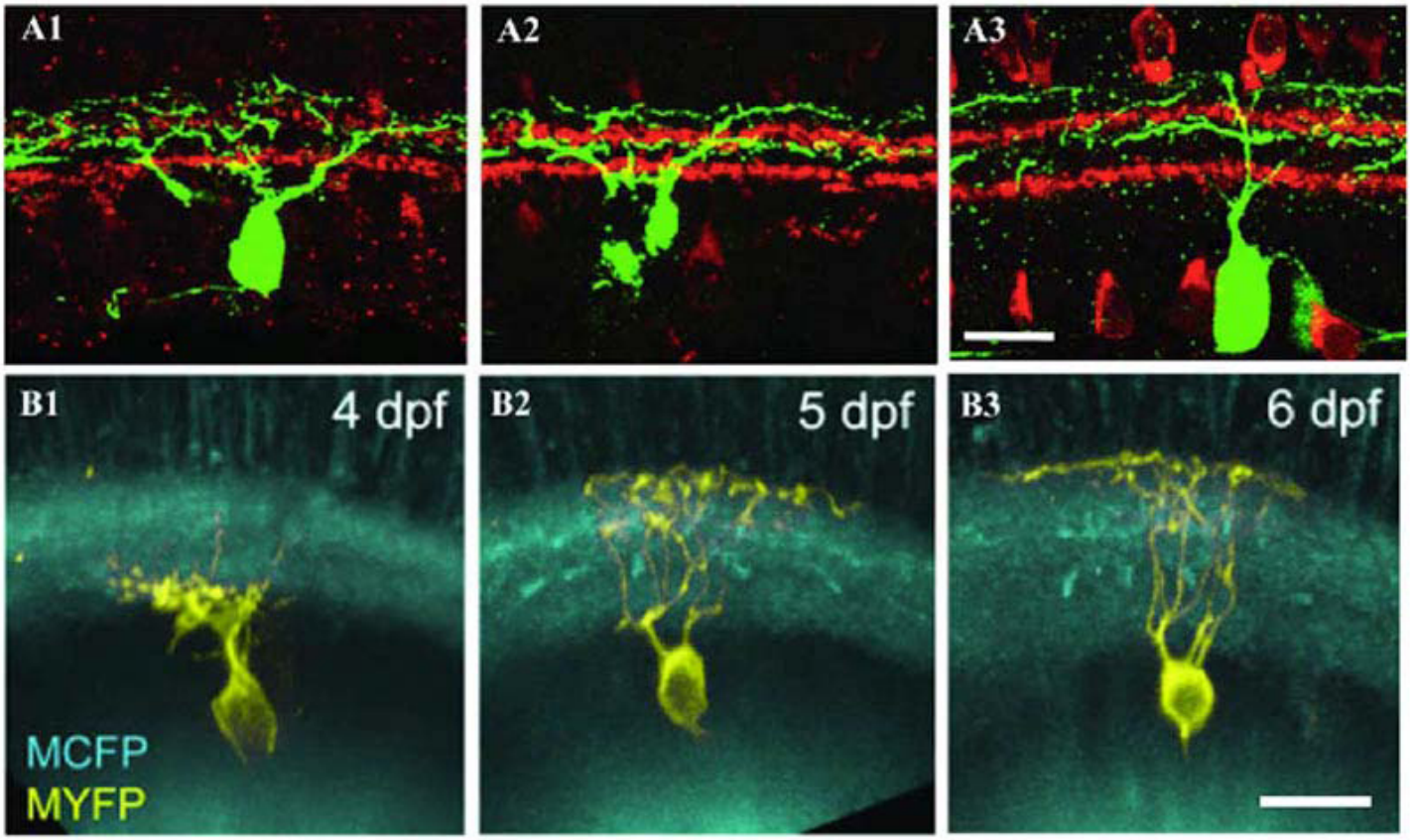

Figure 9. Dendrites of RGCs can reach mature stratified pattern by targeted growth and selective pruning. A1, A2 and A3: Retinal sections from P5, P8, and P12-P13 W7 mice, respectively. RGCs were labeled with anti-GFP (green) and starburst amacrines with anti-ChAT (red). The W7 RGCs selectively distributed their dendrites in the outer IPL at P5 (A1). With development, the dendritic complex is further pruned to form two narrowly restricted strata in the outer IPL at P12-13 (A3). Scale bar in A3, 20 μm. Adapted from Kim et al., 2010 (33). B1, B2 and B3: In vivo time-lapse image of an isolated immature RGC (MYFP) in the Q01 background (MCFP) transgenic zebrafish retina. Time-lapse images taken at 4, 5 and 6 dpf, respectively, show orthogonally oriented image stacks of the entire arbor of the RGC. This RGC initially ramifies its dendrites in the inner IPL at 4 dpf (B1). With development, the inner arbor of this RGC was pruned, the cell selectively grew dendrites toward the outer IPL and developed a narrowly restricted lamina of dendrites in the outer IPL at 6 dpf. Scale bar in B3, 10 μm. Adapted from Mumm et al., 2006 (35).

maturation by reduction of the expression of BDNF. Conversely, over-expression of BDNF precludes the retardation of laminar refinement in dark reared mice (62).

Recent studies demonstrated that genes typically associated with the immune system, such as those in the major histocompatibility complex (MHC), are expressed by neurons in various regions of the CNS, including retina, and play important roles in synapse formation and activity-dependent synaptic plasticity (66-72). Genetic deletion or mutation of a number of MHC class I genes result in the failure of eye-specific segregation of RGC axon projections to the dosal lateral geniculat nucleus (dLGN) (68, 72). Also, long-term potentiation, long-term depression, learning, memory, and neurogenesis in hippocampus are impaired (68, 73).

Xu et al. (44) reported that the key component of MHCI receptor, CD3ζ is specifically expressed by RGCs in mouse retina. Similar to the pharmacological blockade of GluR-mediated activity, genetic mutation of CD3ζ profoundly reduces the kinetics of RGC dendritic growth and pruning, and impairs the lamina-specific segregation of RGC dendrites in the IPL. In addition, CD3ζ-/- mice show a selective reduction of GluR-mediated synaptic transmission in RGCs suggesting that CD3ζ-mediated signaling participates in activity-dependent synaptic maturation of RGCs. However, some of the important questions, such as what are the exact molecule mechanisms with which activation of MHC/CD3ζ on neurons affects the maturation of RGC dendrites, and how

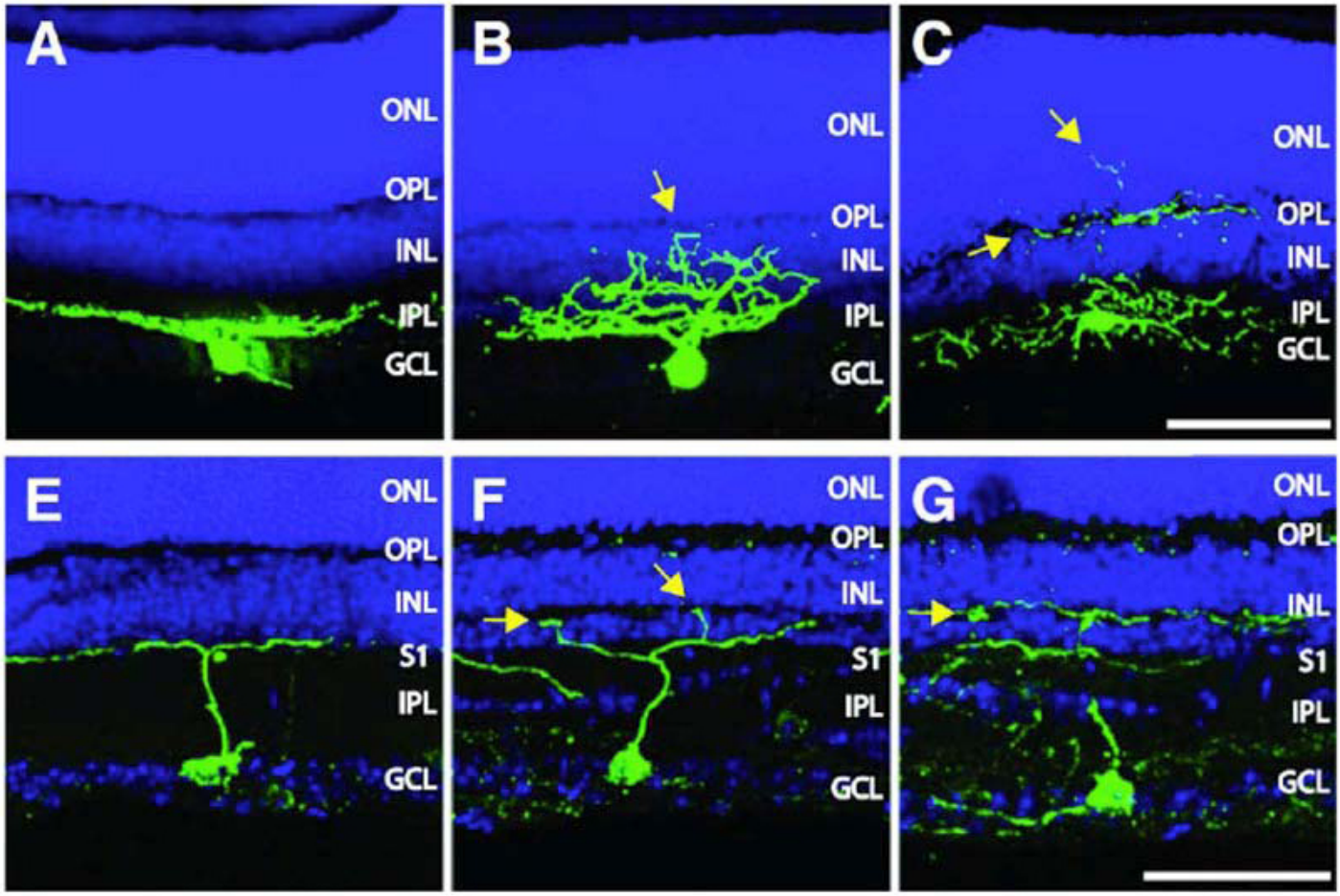

Figure 10. Sema5A and Sema5B constrain dendritic targeting of RGCs to the IPL. WT; Thy-1:GFP-M (A) and Sema5A-/-; Sema5B-/-; Thy-1:GFP-M (B and C) adult retina sections were immunostained with anti-GFP or WT (E) and Sema5A-/-; Sema5B-/- (F and G) adult retina sections were immunostained with an antibody against melanopsin. A: A representative RGC in WT; Thy-1:GFP-M retina exhibits narrowly stratified dendritic plexus. B: A GFP-expressing RGC in a Sema5A-/-; Sema5B-/-; Thy-1:GFP-M retina shows dendritic arbors that aberrantly extend into the INL. C: Another GFP-expressing RGC in a Sema5A-/-; Sema5B-/-; Thy-1:GFP-M retina shows dendritic arbors that aberrantly extend into the INL, OPL and ONL. E: A representative M1-type ipRGCs in a WT adult retina, which normally exhibits dendritic stratification within the S1 sublamina of the IPL. F: A M1-type ipRGCs in a Sema5A-/-; Sema5B-/- retina shows dendritic arbors that aberrantly extend into the INL. G: Another M1-type ipRGCs in a Sema5A-/-; Sema5B-/- retina shows dendritic arbors that aberrantly extend into the INL as well as other sublaminae of the IPL. Scale bars, 50 um. Adapted from Matsuoka et al., 2011b (80).

MHC/CD3ζ-mediated signaling interacts with neurotransmitter-mediated synaptic activity in dendritic maturation, need to be further addressed.

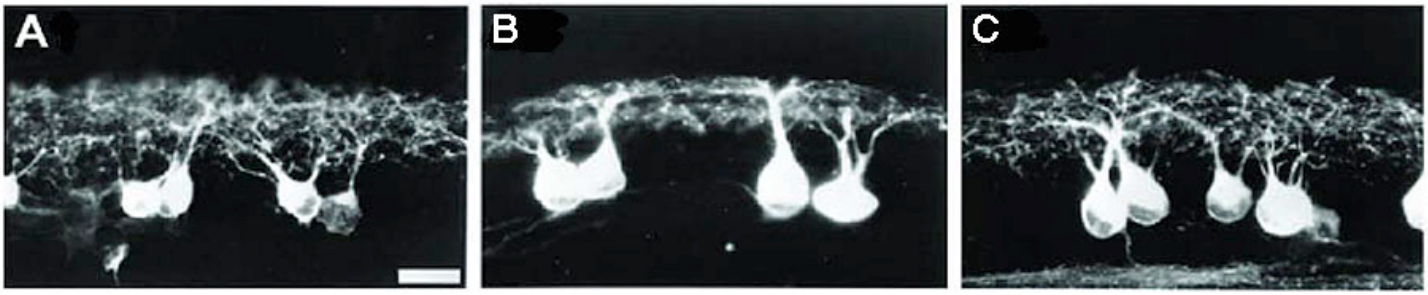

Figure 11. Glutamate released from bipolar cells regulates the dendritic development of RGCs. A, B and C: Light micrographs of DiI labeled RGCs from sections of a P2, a P10 and an APB-treated P10 cat retina, respectively. At P2 the RGC dendrites are distributed throughout the total IPL (A), at P10 the dendrites have the distinct appearance of two tiers of dendrites within the IPL (B). APB treatment prevented the formation of the lamina-restricted distribution of RGC dendrites (C). Scale bar in A, 20 um. Reproduced from Bodnarenko and Chalupa, 1993 (29).

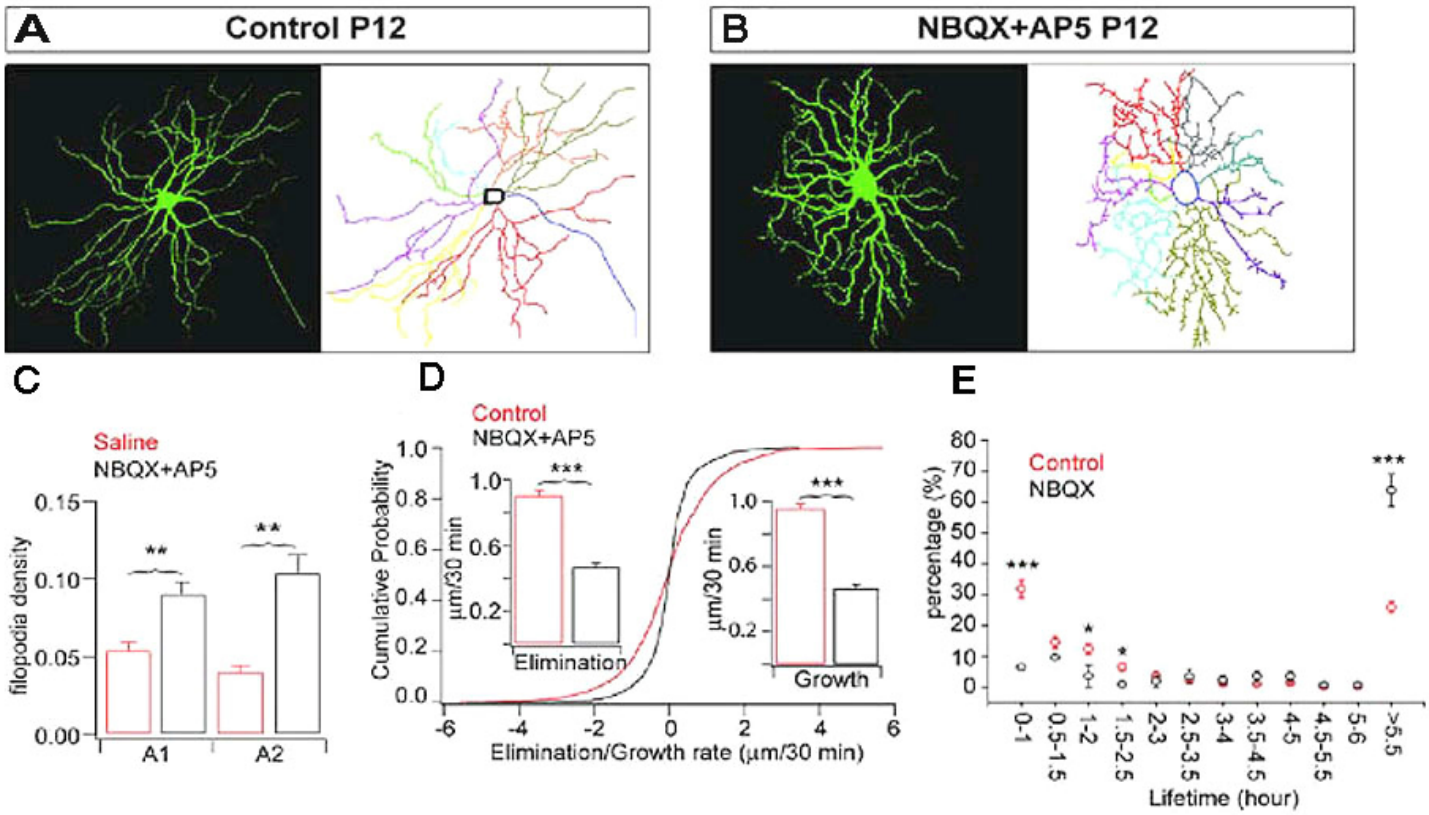

Figure 12. GluR-mediated activity regulates the dendritic development of RGCs. A and B: Representative images and dendritic reconstructions of YFP-expressing RGCs of P12 retinas in control and with intraocular treatment of NBQX+AP5. Note that NBQX +AP5 treatment significantly increase the number of filopodia. C: The average densities of filopodia of A1 and A2 RGCs of NBQX +AP5 treated retinas are 80-100% higher than that untreated retinas. D: The speeds of filopodia growth and elimination are reduced by NBQX+AP5 treatement. Filopodia growth and elimination were determined by the difference of the length of the filopodia recorded at two succeeding time points (recording time interval, 30 minutes). E: Average lifetime of RGC filopodia was significantly prolonged in NBQX+AP5 treated retinas. Adapted from Xu et al., 2010 (44).

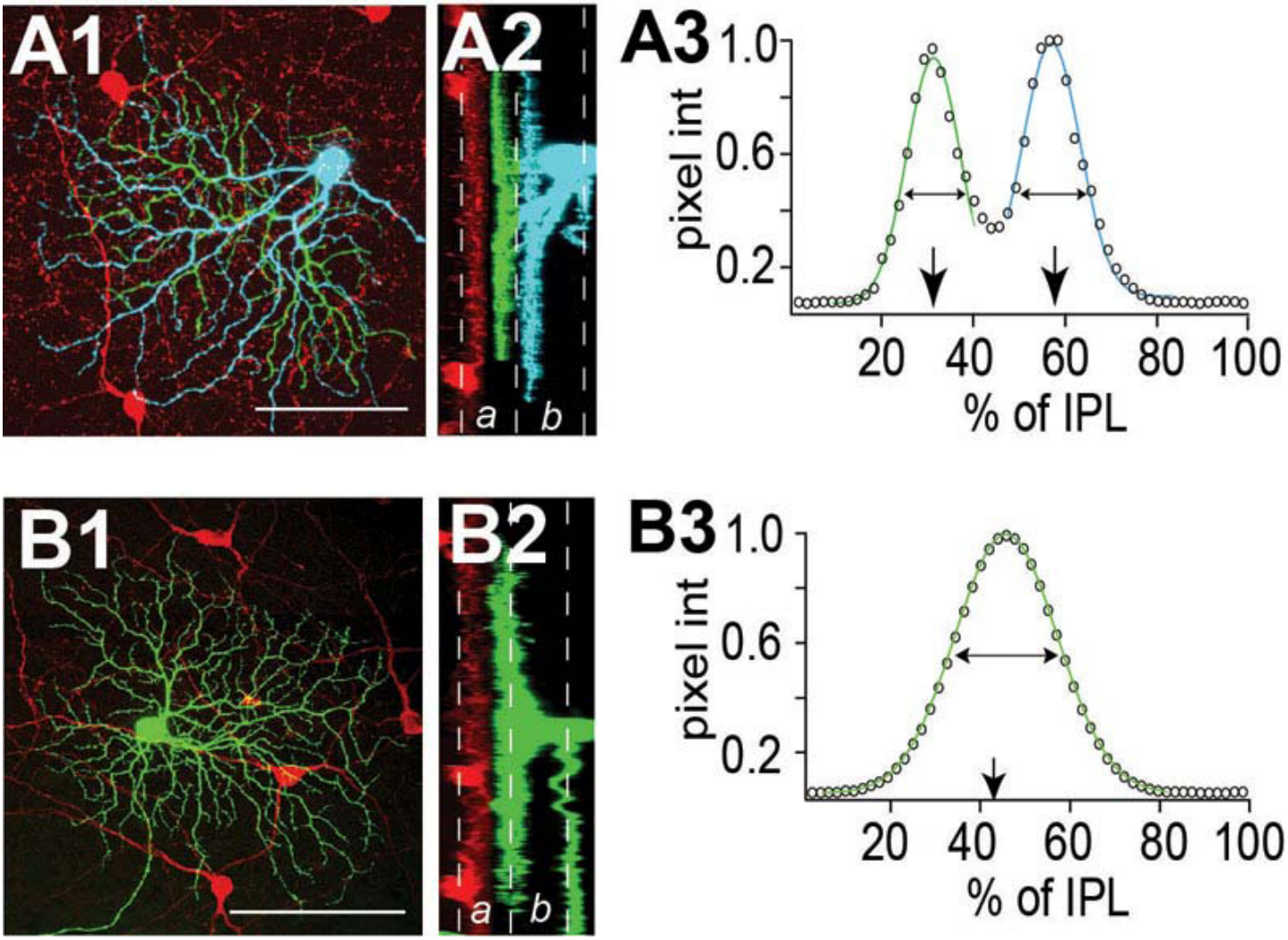

Figure 13. RGC dendritic distribution in the IPL can be quantified. The dendritic distribution of YFP-expressing RGCs in the IPL was quantified from confocal images Thy1-YFP mice. A: A stacked image (A1), the 90° rotation view (A2) and the quantitative dendritic distribution (A3) of a bistratified RGC. The dendrites ramified in the sublamina b are colored in blue and the dendrites ramified in the sublamina a are colored in green. Dopaminergic amacrine cells are colored in red. In A2, the three dashed lines indicate the inner and outer borders of the IPL, and the boundary of the sublaminae a and b, respectively. In A3, double-arrow lines indicate dendritic widths. Single arrows indicate the locations of the two peaks of dendritic density. B: A stacked image (B1), the 90° rotation view (B2) and the quantitative dendritic distribution (B3) of a mono-stratified RGC. Adapted from Xu and Tian, 2007 (54)..

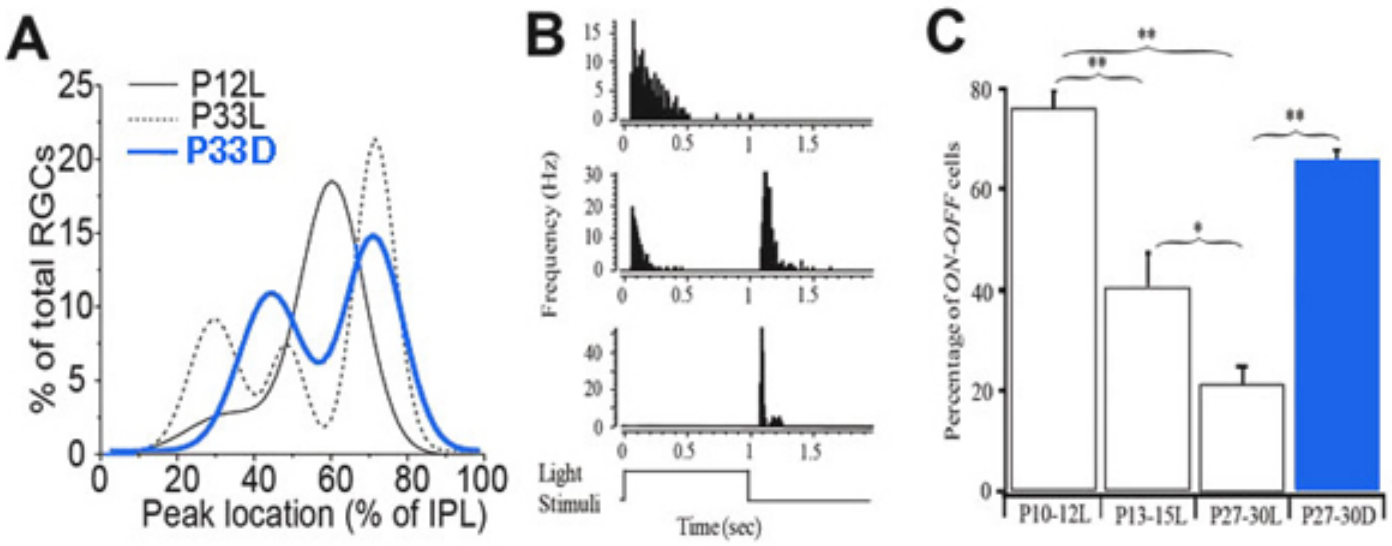

Figure 14. Light deprivation alters the dendritic ramification and synaptic inputs of mouse RGCs. A: Peak dendritic location of all mono-stratified RGCs of P12, P33 and P33 dark-reared mice. Note that the number of RGC with peak located near 30% of the IPL is significantly reduced in dark-reared mice (P33D). B: Representative frequency histograms of RGC light responses of an ON cell (top), an ON-OFF cell (middle), and an OFF cell (bottom), recorded using a multielectrode array system. C: Percentage of RGCs that are ON-OFF to light decrease with age. Note that light deprivation from birth (blue) prevents the age-dependent decrease of ON-OFF responding cells. Reproduced from Xu and Tian, 2007 (54); Tian and Copenhagen, 2003 (58).

About the Author

Dr. Ning Tian was initially trained as a physician in China (Yichang Medical School) and then received his Master Degree in clinical visual physiology from Zhong-sen Ophthalmic Center, Sun Yat-sen University of Medical Sciences, China. He practiced clinical ophthalmology for a while before doing a PhD in Biophysics and Physiology at the State University of New York at Buffalo with Dr. Malcolm Slaughter. Ning then did a postdoc with Dr. David Copenhagen at University of California, San Francisco. After being an Assistant Research Ophthalmologist at the University of California, San Francisco from 1998-2000, he headed a laboratory at Yale

University (2000-2009). Ning is presently an Associate Professor of Ophthalmology and Neurobiology in the Moran Eye Center, University of Utah. His research is focused on understanding the cellular and molecular mechanisms that regulate the maturation of retinal ganglion cell synaptic function and dendritic structure.

References

1. Famiglietti E.V. Jr, Kolb H. *Structural basis for ON-and OFF-center responses in retinal ganglion cells.* .Science. 1976;194(4261):193–5. PubMed PMID: 959847.
2. Nelson R., Famiglietti E.V. Jr, Kolb H. *Intracellular staining reveals different levels of stratification for on- and off-center ganglion cells in the cat retina.* .J. Neurophysiol. 1978;41(2):472–483. PubMed PMID: 650277.
3. Schiller P.H. *Parallel information processing channels created in the retina.* .Proc Natl Acad Sci U S A. 2010;107(40):17087–94. PubMed PMID: 20876118.
4. Euler T., Wassle H. *Immunocytochemical identification of cone bipolar cells in the rat retina.* .J Comp Neurol. 1995;361(3):461–78. PubMed PMID: 8550893.
5. MacNeil M.A., Masland R.H. *Extreme diversity among amacrine cells: implications for function.* .Neuron. 1998;20(5):971–82. PubMed PMID: 9620701.
6. Ghosh K.K.et al. *Types of bipolar cells in the mouse retina.* .J Comp Neurol. 2004;469(1):70–82. PubMed PMID: 14689473.
7. . J., C. and L.M. Chalupa, *Morphological, functional, and developmental properties of mouse retinal ganglion cells.*, in *Eye, retina, and visual system of the mouse*, L.M. Chalupa and R.W. Williams, Editors. 2008, MIT Press: Cambridge, Mass. p. 189-199.
8. Kuffler S.W. *Discharge patterns and functional organization of mammalian retina.* .J Neurophysiol. 1953;16(1):37–68. PubMed PMID: 13035466.
9. Masland R.H. *The fundamental plan of the retina.* .Nat Neurosci. 2001;4(9):877–86. PubMed PMID: 11528418.
10. Wässle H. *Parallel processing in the mammalian retina.* .Nat Rev Neurosci. 2004;5(10):747–57. PubMed PMID: 15378035.
11. Badea T.C., Nathans J. *Quantitative analysis of neuronal morphologies in the mouse retina visualized by using a genetically directed reporter.* .J Comp Neurol. 2004;480(4):331–51. PubMed PMID: 15558785.
12. Berson, D.M., *Retinal ganglion cell types and their central projections.*, Volume 1, in *The senses : a comprehensive reference*, A.I. Basbaum, et al., Editors. 2008, Elsevier: Amsterdam; Boston. p. 491–520.
13. Coombs J.et al. *Morphological properties of mouse retinal ganglion cells.* .Neuroscience. 2006;140(1):123–36. PubMed PMID: 16626866.
14. Dacey D.M., Packer O.S. *Colour coding in the primate retina: diverse cell types and cone-specific circuitry.* .Curr Opin Neurobiol. 2003;13(4):421–7. PubMed PMID: 12965288.
15. Kolb H., Nelson R., Mariani A. *Amacrine cells, bipolar cells and ganglion cells of the cat retina: a Golgi study.* .Vision Res. 1981;21(7):1081–1114. PubMed PMID: 7314489.
16. Kong J.H.et al. *Diversity of ganglion cells in the mouse retina: unsupervised morphological classification and its limits.* .J Comp Neurol. 2005;489(3):293–310. PubMed PMID: 16025455.
17. Rockhill R.L.et al. *The diversity of ganglion cells in a mammalian retina.* .J Neurosci. 2002;22(9):3831–43. PubMed PMID: 11978858.
18. Sun W., Li N., He S. *Large-scale morphological survey of mouse retinal ganglion cells.* .J Comp Neurol. 2002;451(2):115–26. PubMed PMID: 12209831.
19. Volgyi B., Chheda S., Bloomfield S.A. *Tracer coupling patterns of the ganglion cell subtypes in the mouse retina.* .J Comp Neurol. 2009;512(5):664–87. PubMed PMID: 19051243.
20. Cepko C.L.et al. *Cell fate determination in the vertebrate retina.* .Proc Natl Acad Sci U S A. 1996;93(2):589–95. PubMed PMID: 8570600.
21. . D, A., T. D, and C.L. Cepko, *Specification of cell types in the vertebrate retina.* in *Proceedings of the Retina Research Foundation symposia*, Volume 3, in *Development of the Visual System*, D.M.-K. Lam and C.J. Shatz, Editors. 1991, MIT Press: Cambridge, Mass. p. 37-58.

22. Marquardt T., Gruss P. *Generating neuronal diversity in the retina: one for nearly all.* .Trends Neurosci. 2002;25(1):32–8. PubMed PMID: 11801336.
23. Nishimura Y., Rakic P. *Development of the rhesus monkey retina: II. A three-dimensional analysis of the sequences of synaptic combinations in the inner plexiform layer.* .J Comp Neurol. 1987;262(2):290–313. PubMed PMID: 3624556.
24. Stone, J. and D.H. Rapaport, *The development of the topographical organization of the cat's retina.*, in *Development of visual pathways in mammals : proceedings of a satellite symposium of the XXIX International Congress of the Union of Physiological Sciences, held in Sydney, Australia, August 24-27, 1983*, J. Stone, B. Dreher, and D.H. Rapaport, Editors. 1984, A.R. Liss: New York. p. 1-21.
25. Tootle J.S. *Early postnatal development of visual function in ganglion cells of the cat retina.* .J Neurophysiol. 1993;69(5):1645–60. PubMed PMID: 8509831.
26. Wang G.Y., Liets L.C., Chalupa L.M. *Unique functional properties of on and off pathways in the developing mammalian retina.* .J Neurosci. 2001;21(12):4310–7. PubMed PMID: 11404416.
27. Gorfinkel J., Lachapelle P., Molotchnikoff S. *Maturation of the electroretinogram of the neonatal rabbit.* .Doc Ophthalmol. 1988;69(3):237–45. PubMed PMID: 3168725.
28. Wachtmeister L. *Oscillatory potentials in the retina: what do they reveal.* .Prog Retin Eye Res. 1998;17(4):485–521. PubMed PMID: 9777648.
29. Bodnarenko S.R., Chalupa L.M. *Stratification of ON and OFF ganglion cell dendrites depends on glutamate-mediated afferent activity in the developing retina.* .Nature. 1993;364(6433):144–6. PubMed PMID: 8100613.
30. Bodnarenko S.R., Jeyarasasingam G., Chalupa L.M. *Development and regulation of dendritic stratification in retinal ganglion cells by glutamate-mediated afferent activity.* .J Neurosci. 1995;15(11):7037–45. PubMed PMID: 7472459.
31. Coombs J.L., Van Der List D., Chalupa L.M. *Morphological properties of mouse retinal ganglion cells during postnatal development.* .J Comp Neurol. 2007;503(6):803–14. PubMed PMID: 17570502.
32. Diao L.et al. *Development of the mouse retina: emerging morphological diversity of the ganglion cells.* .J Neurobiol. 2004;61(2):236–49. PubMed PMID: 15389605.
33. Kim I.J.et al. *Laminar restriction of retinal ganglion cell dendrites and axons: subtype-specific developmental patterns revealed with transgenic markers.* .J Neurosci. 2010;30(4):1452–62. PubMed PMID: 20107072.
34. Maslim J., Stone J. *Time course of stratification of the dendritic fields of ganglion cells in the retina of the cat.* .Brain Res Dev Brain Res. 1988;44(1):87–93. PubMed PMID: 3233733.
35. Mumm J.S.et al. *In Vivo Imaging Reveals Dendritic Targeting of Laminated Afferents by Zebrafish Retinal Ganglion Cells.* .Neuron. 2006;52(4):609–621. PubMed PMID: 17114046.
36. Yamagata M., Sanes J.R. *Dscam and Sidekick proteins direct lamina-specific synaptic connections in vertebrate retina.* .Nature. 2008;451(7177):465–9. PubMed PMID: 18216854.
37. Fuerst P.G.et al. *Neurite arborization and mosaic spacing in the mouse retina require DSCAM.* .Nature. 2008;451(7177):470–4. PubMed PMID: 18216855.
38. Matsuoka R.L.et al. *Transmembrane semaphorin signalling controls laminar stratification in the mammalian retina.* .Nature. 2011;470(7333):259–63. PubMed PMID: 21270798.
39. Wong R.O. *Retinal waves and visual system development.* .Annu Rev Neurosci. 1999;22:29–47. PubMed PMID: 10202531.
40. Bansal A.et al. *Mice lacking specific nicotinic acetylcholine receptor subunits exhibit dramatically altered spontaneous activity patterns and reveal a limited role for retinal waves in forming ON and OFF circuits in the inner retina.* .J Neurosci. 2000;20(20):7672–81. PubMed PMID: 11027228.
41. Demas J., Eglen S.J., Wong R.O. *Developmental loss of synchronous spontaneous activity in the mouse retina is independent of visual experience.* .J Neurosci. 2003;23(7):2851–60. PubMed PMID: 12684472.
42. Feller, M. and A. Blankenship, *The function of the retina prior to vision: The phenomenon of retinal waves and retinotopic refinement.*, in *Eye, retina, and visual system of the mouse*, L.M. Chalupa and R.W. Williams, Editors. 2008, MIT Press: Cambridge, Mass. p. 343-351.
43. Feller M.B.et al. *Requirement for cholinergic synaptic transmission in the propagation of spontaneous retinal waves.* .Science. 1996;272(5265):1182–7. PubMed PMID: 8638165.

44. Xu H.P.et al. *The immune protein CD3ζ is required for normal development of neural circuits in the retina.* .Neuron. 2010;65(4):503–15. PubMed PMID: 20188655.
45. Zhou Z.J. *The function of the cholinergic system in the developing mammalian retina.* .Prog Brain Res. 2001;131:599–613. PubMed PMID: 11420974.
46. Stacy R.C.et al. *Disruption and recovery of patterned retinal activity in the absence of acetylcholine.* .J Neurosci. 2005;25(41):9347–57. PubMed PMID: 16221843.
47. Bodnarenko S.R.et al. *The development of retinal ganglion cell dendritic stratification in ferrets.* .Neuroreport. 1999;10(14):2955–9. PubMed PMID: 10549804.
48. Deplano S.et al. *Long-term treatment of the developing retina with the metabotropic glutamate agonist APB induces long-term changes in the stratification of retinal ganglion cell dendrites.* .Dev Neurosci. 2004;26(5-6):396–405. PubMed PMID: 15855769.
49. Lau K.C., So K.F., Tay D. *Postnatal development of type I retinal ganglion cells in hamsters: a lucifer yellow study.* .J Comp Neurol. 1992;315(4):375–81. PubMed PMID: 1560113.
50. Kerschensteiner D.et al. *Neurotransmission selectively regulates synapse formation in parallel circuits in vivo.* .Nature. 2009;460(7258):1016–20. PubMed PMID: 19693082.
51. Tagawa Y.et al. *Immunohistological studies of metabotropic glutamate receptor subtype 6-deficient mice show no abnormality of retinal cell organization and ganglion cell maturation.* .J Neurosci. 1999;19(7):2568–79. PubMed PMID: 10087070.
52. Wingate R.J., Thompson I.D. *Targeting and activity-related dendritic modification in mammalian retinal ganglion cells.* .J Neurosci. 1994;14(11 Pt 1):6621–37. PubMed PMID: 7965065.
53. Fisher L.J. *Development of retinal synaptic arrays in the inner plexiform layer of dark-reared mice.* .J Embryol Exp Morphol. 1979;54:219–27. PubMed PMID: 528867.
54. Xu H.P., Tian N. *Retinal ganglion cell dendrites undergo a visual activity-dependent redistribution after eye opening.* .J Comp Neurol. 2007;503(2):244–59. PubMed PMID: 17492624.
55. Tian N., Copenhagen D.R. *Visual deprivation alters development of synaptic function in inner retina after eye opening.* .Neuron. 2001;32(3):439–49. PubMed PMID: 11709155.
56. Vistamehr S., Tian N. *Light deprivation suppresses the light response of inner retina in both young and adult mouse.* .Vis Neurosci. 2004;21(1):23–37. PubMed PMID: 15137579.
57. Di Marco S.et al. *Permanent functional reorganization of retinal circuits induced by early long-term visual deprivation.* .J Neurosci. 2009;29(43):13691–701. PubMed PMID: 19864581.
58. Tian N., Copenhagen D.R. *Visual stimulation is required for refinement of ON and OFF pathways in postnatal retina.* .Neuron. 2003;39(1):85–96. PubMed PMID: 12848934.
59. Wong R.O., Ghosh A. *Activity-dependent regulation of dendritic growth and patterning.* .Nat Rev Neurosci. 2002;3(10):803–12. PubMed PMID: 12360324.
60. Redmond L., Kashani A.H., Ghosh A. *Calcium regulation of dendritic growth via CaM kinase IV and CREB-mediated transcription.* .Neuron. 2002;34(6):999–1010. PubMed PMID: 12086646.
61. Landi S.et al. *Environmental enrichment effects on development of retinal ganglion cell dendritic stratification require retinal BDNF.* .PLoS One. 2007;2(4):e346. PubMed PMID: 17406670.
62. Liu X.et al. *Brain-derived neurotrophic factor and TrkB modulate visual experience-dependent refinement of neuronal pathways in retina.* .J Neurosci. 2007;27(27):7256–67. PubMed PMID: 17611278.
63. Mandolesi G.et al. *A role for retinal brain-derived neurotrophic factor in ocular dominance plasticity.* .Curr Biol. 2005;15(23):2119–24. PubMed PMID: 16332537.
64. Pollock G.S.et al. *Effects of early visual experience and diurnal rhythms on BDNF mRNA and protein levels in the visual system, hippocampus, and cerebellum.* .J Neurosci. 2001;21(11):3923–31. PubMed PMID: 11356880.
65. Seki M.et al. *BDNF is upregulated by postnatal development and visual experience: quantitative and immunohistochemical analyses of BDNF in the rat retina.* .Invest Ophthalmol Vis Sci. 2003;44(7):3211–8. PubMed PMID: 12824273.
66. Baudouin S.J.et al. *The signaling adaptor protein CD3zeta is a negative regulator of dendrite development in young neurons.* .Mol Biol Cell. 2008;19(6):2444–56. PubMed PMID: 18367546.

67. Corriveau R.A., Huh G.S., Shatz C.J. *Regulation of class I MHC gene expression in the developing and mature CNS by neural activity.* .Neuron. 1998;21(3):505–20. PubMed PMID: 9768838.
68. Huh G.S.et al. *Functional requirement for class I MHC in CNS development and plasticity.* .Science. 2000;290(5499):2155–9. PubMed PMID: 11118151.
69. Ishii T., Hirota J., Mombaerts P. *Combinatorial coexpression of neural and immune multigene families in mouse vomeronasal sensory neurons.* .Curr Biol. 2003;13(5):394–400. PubMed PMID: 12620187.
70. Syken J.et al. *PirB restricts ocular-dominance plasticity in visual cortex.* .Science. 2006;313(5794):1795–800. PubMed PMID: 16917027.
71. Syken J., Shatz C.J. *Expression of T cell receptor beta locus in central nervous system neurons.* .Proc Natl Acad Sci U S A. 2003;100(22):13048–53. PubMed PMID: 14569018.
72. Xu, Y. and N. Vardi, *Modulation of the Light-Activated Cation Channel in Retinal ON Bipolar Cells by G-Protein Subunits.* ARVO Meeting Abstracts, 2010**51**(5): p. 4797.
73. Ziv Y.et al. *Immune cells contribute to the maintenance of neurogenesis and spatial learning abilities in adulthood.* .Nat Neurosci. 2006;9(2):268–75. PubMed PMID: 16415867.
74. Sterling, P., *Retina*, in *The Synaptic Organization of the Brain*, G.M. Shepard, Editor. 1990, Oxford University Press: New York. p. 170-213.
75. Boycott B.B., Wässle H. *Morphological Classification of Bipolar Cells of the Primate Retina.* .Eur J Neurosci. 1991;3(11):1069–1088. PubMed PMID: 12106238.
76. Kolb H., Linberg K.A., Fisher S.K. *Neurons of the human retina: a Golgi study.* .J Comp Neurol. 1992;318(2):147–87. PubMed PMID: 1374766.
77. Young R.W. *Cell differentiation in the retina of the mouse.* .Anat Rec. 1985;212(2):199–205. PubMed PMID: 3842042.
78. Fisher L.J. *Development of synaptic arrays in the inner plexiform layer of neonatal mouse retina.* .J Comp Neurol. 1979;187(2):359–72. PubMed PMID: 489784.
79. Xu H., Tian N. *Pathway-specific maturation, visual deprivation, and development of retinal pathway.* .Neuroscientist. 2004;10(4):337–46. PubMed PMID: 15271261.
80. Matsuoka R.L.et al. *Class 5 transmembrane semaphorins control selective Mammalian retinal lamination and function.* .Neuron. 2011;71(3):460–73. PubMed PMID: 21835343.

Evolution of the Vertebrate Eye

Evolution of Phototransduction, Vertebrate Photoreceptors and Retina

Trevor D Lamb, PhD[1]

Created: May 14, 2013; Updated: July 10, 2013.

1. Introduction

"Nothing in biology makes sense except in the light of evolution" (1).

Theodosius Dobzhansky's insight is especially apposite in trying to comprehend the nature of our rod and cone photoreceptors, and the organization of our retina. Unless we understand how these cells and structures arose, through hundreds of millions of years of evolution, we have little prospect of making sense of their morphological and molecular structure, or being able to answer the recurring conundrum 'Why does the retina do it this way?'. In addition to providing a rationale for the arrangement of our retina, a study of the evolution of our eye and its cones and rods is immensely satisfying, in offering potential answers to questions such as 'How and when did our eyes originate?' and 'Why should we and all other vertebrates possess eyes so different from those of (for example) insects?'.

The apparent lack of transitional forms that have been preserved during the course of vertebrate eye evolution has provided perennial fodder for 'creationists'. But, as Charles Darwin (2) explained,

"if numerous gradations from a perfect and complex eye to one very imperfect and simple, each grade being useful to its possessor, can be shown to exist ... and if any variation or modification in the organ be ever useful to an animal under changing conditions of life, then the difficulty of believing that a perfect and complex eye could be formed by natural selection, though insuperable by our imagination, can hardly be considered real".

One of the goals of this article is to document evidence for such gradations in the photoreceptors, in the phototransduction cascade, and in the retina, during the course of chordate and vertebrate evolution. A second major aim is to construct a set of 'scenarios' for the long sequence of events that contributed; in this regard the term 'scenario' is used in its dictionary sense of 'a postulated sequence or development of events'.

Historically, three main avenues for studying eye evolution have been utilized: examination of eyes in the fossil record, examination of the structure of eyes in extant species, and examination of embryological development. Recently, a number of powerful new avenues have been developed, utilizing molecular evidence; for example, comparative molecular genetics across extant species, as well as the combination of evolutionary and developmental analysis (evo-devo approaches). This article concentrates on the eyes of extant chordates, and examines clues to eye evolution that can be obtained from morphological, embryological and molecular features. In doing so, it builds on the scenarios put forward by Lamb et al (3, 4).

For other recent reviews of various aspects of the evolution of phototransduction and photoreception, see Arendt et al (5), Vopalensky & Kosmik (6), Larhammar et al (7), Shichida & Matsuyama (8), Kusakabe et al (9), Collin et al (10), Fain et al (11), Porter et al (12) and Nilsson (13). For descriptions of the types of eyes that have evolved across the entire animal kingdom (rather than primarily in chordates, as treated here), see the lavishly illustrated book by Schwab (14). For the evolution of vertebrate sensory systems and brains, see Butler (15) and Butler & Hodos (16).

Author Affiliation: 1 Australian National University, Canberra.; Email: Trevor.Lamb@anu.edu.au.

Corresponding author.

One question that has often been asked is *'How many times have eyes and photoreceptors evolved independently?'* Answers to this question can vary greatly, depending on one's concept of 'independence'. As we shall see below, the common ancestor of cnidaria, protostomes and deuterostomes already possessed the great majority of the components needed for constructing an ocellus and/or a retina; e.g. it already possessed transcription factors, growth factors, opsins, photoreceptor cells (of the ciliary and microvillar forms), pigment cells, and neurons, etc. Using this common set of tools, different events occurred in different lineages, leading to very different eyes. In certain protostomes, a simple ocellus replicated many times to form a compound eye; in our own lineage, an extensive light-sensitive retina formed and a single optical element developed in front of it.

Although the eyes that have resulted are radically different from each other, it turns out that the photoreceptors upon which they are based are remarkably similar to each other, and indeed are derived from a common ancestral type, so that one can now conclusively reject the claim of Salvini-Plawen & Mayr (17) that "Photoreceptors have originated independently in at least 40, but possibly up to 65 or more different phyletic lines".

As was so aptly pointed out by Jacob (18), it is important to realize that evolution works by 'tinkering' with what is already available, and without any overall 'purpose' (such as to give rise to vision). In the case of the evolution of phototransduction, photoreceptors, and retina, numerous examples of such tinkering will become apparent in the Sections ahead; see also Goldsmith (19).

2. Origins

By way of background, the following sub-sections briefly summarize in turn: the origin of vertebrates, the origin of the vertebrate-style eye, the origin of opsins, and the origin of photoreceptor cells.

Origin of vertebrates

A summary view of the origin of vertebrates is presented in Figure 1, on a timescale extending from 700 to 400 Mya (millions of years ago); this diagram primarily illustrates extant taxa that are relevant to vertebrate evolution, though three extinct taxa of interest are also shown (using dashed lines). Although there is widespread agreement about the sequence of the branchings that occurred, there is less certainty about the timings of the various divergences. Molecular evidence suggests that many of the branchings occurred considerably earlier than is recorded in the fossil record, and the timings shown in Figure 1 are based on a recent reconciliation of molecular and fossil evidence, as reported by Erwin et al (20). In the following discussion, the branchings will be described from the perspective of our own direct ancestors, shown by the red curve, with various important branchings numbered as #1 to #5.

Around 700 Mya (#1), the early Eumetazoa that were our distant ancestors separated into Cnidaria (e.g. jellyfish, corals, etc.) and our own line of bilaterally symmetric animals (Bilateria). Then, around 665 Mya (#2), the ancestors of the great majority of extant invertebrate species (Protostomes) diverged from our Deuterostome line. A few million years later, the common ancestor of Hemichordates and Echinoderms (e.g. sea urchins) diverged from our ancestors. Shortly afterwards, around 655 Mya (#3), Cephalochordates (e.g. amphioxus) diverged Â– and from the time of that split (at the latest) our ancestors have been chordates. After perhaps another 50 million years, at ~600 Mya (#4), Tunicates (e.g. sea squirts) diverged, and then a further 100 million years elapsed before the occurrence of the next split from which descendants have survived, when ancestors of the extant jawless vertebrates (Agnathans) diverged from our own lineage of jawed vertebrates (Gnathostomes), around 500 Mya (#5). From the time of that divergence (and possibly from some time before it) our ancestors have been vertebrates.

The preceding interval of ~100 million years, between #4 and #5 (from ~600–500 Mya), was important not only for the evolution of the vertebrate eye, but also more generally as a period of exceptional innovation in the

evolution of body plans. Frustratingly, though, two factors complicate analysis of the transitions that occurred through that period. First, none of the numerous intermediate forms that diverged from our own lineage during that 100 million year time-span have survived to the present day. A few important examples of extinct species are indicated in Figure 1, but there is a huge gap between extant species. Secondly, soft tissues are poorly preserved in the fossil record, so that few clues to transitional forms of chordate eyes can be obtained from the extinct species that are known.

Despite these difficulties, there is a remarkable amount that we can surmise about vertebrate eye evolution, (*i*) from comparative analysis of the eyes of extant animals, (*ii*) from analysis of embryonic eye development, and (*iii*) from molecular genetic analysis of photoreceptors and retinas. But before we look in detail at the eyes of living vertebrates, it will help to set the scene if we briefly consider the origin of the vertebrate-style eye, the origin of opsin photopigments, and the origin of photoreceptor cells.

Origin of the vertebrate-style eye

To help answer the question *"When did the vertebrate-style eye arise?"* one can usefully examine the eyes of extant chordates - jawed vertebrates, cyclostomes, tunicates, and cephalochordates.

Jawed vertebrates. The eyes of all extant jawed vertebrates (e.g. fish, tetrapods, birds) are remarkably similar and appear to be built to a common plan. As a result, we can be certain that the last common ancestor of all extant jawed vertebrates, that lived ~420 Mya, possessed a 'vertebrate-style eye'. But can we delve even further back into the past?

Lampreys. The ancestors of lampreys diverged from our own ancestors around 500 Mya (Figure 1), yet the lamprey's camera-style eyes are extremely similar to the eyes of jawed fish and other jawed vertebrates. Thus, the lamprey's eye has a lens, an iris, and a set of six extraocular muscles that are broadly homologous to those of jawed vertebrates (Section 3). Furthermore, the lamprey retina has a structure closely comparable to that of vertebrates, with the five classes of homologous neurons (photoreceptors, horizontal, bipolar, amacrine and ganglion cells) distributed into three main nuclear layers and two plexiform layers. The southern hemisphere lamprey Geotria australis possesses five morphological classes of retinal photoreceptor cell together with five classes of opsin, each of which is closely related to the retinal opsins of jawed vertebrates (see Section 6 for details); northern hemisphere lamprey species, however, have lost several opsin classes.

In view of the overwhelming parallels between the eyes of lampreys and jawed vertebrates, it seems a near certainty that the last common ancestor of these taxa possessed a camera-type eye, broadly comparable to that of extant lampreys and gnathostomes, and hence that the vertebrate-style eye already existed ~500 Mya. However, one cannot totally reject the possibility that, even though the last common ancestor of lampreys and jawed vertebrates possessed the requisite genes, its eyes might have exhibited a form more rudimentary than a fully-developed camera-style eye, and that both lampreys and gnathostomes perfected the physical manifestation of the eye by some degree of convergent evolution.

Hagfish. The 'eyes' of hagfish represent a special case that will be considered in detail in Section 3. Although hagfish are descended from a lamprey-like ancestor, their 'eyes' exhibit a much more rudimentary form than the eyes of lampreys, and it will be argued that there are strong grounds for thinking that those features are retained from an earlier stage of eye evolution.

Tunicates and cephalochordates. Of the chordate taxa that diverged prior to the agnathans (lampreys and hagfish), none of those that survive to the present day possess an organ that can properly be described as an eye. The cephalochordate amphioxus possesses several groupings of photoreceptors, and larval tunicates possess a simple ocellus. In both cases ciliary photoreceptors with C-opsins are present, and appear homologous to our own cones and rods. Although their photoreceptors and opsins hold important clues to the evolution of

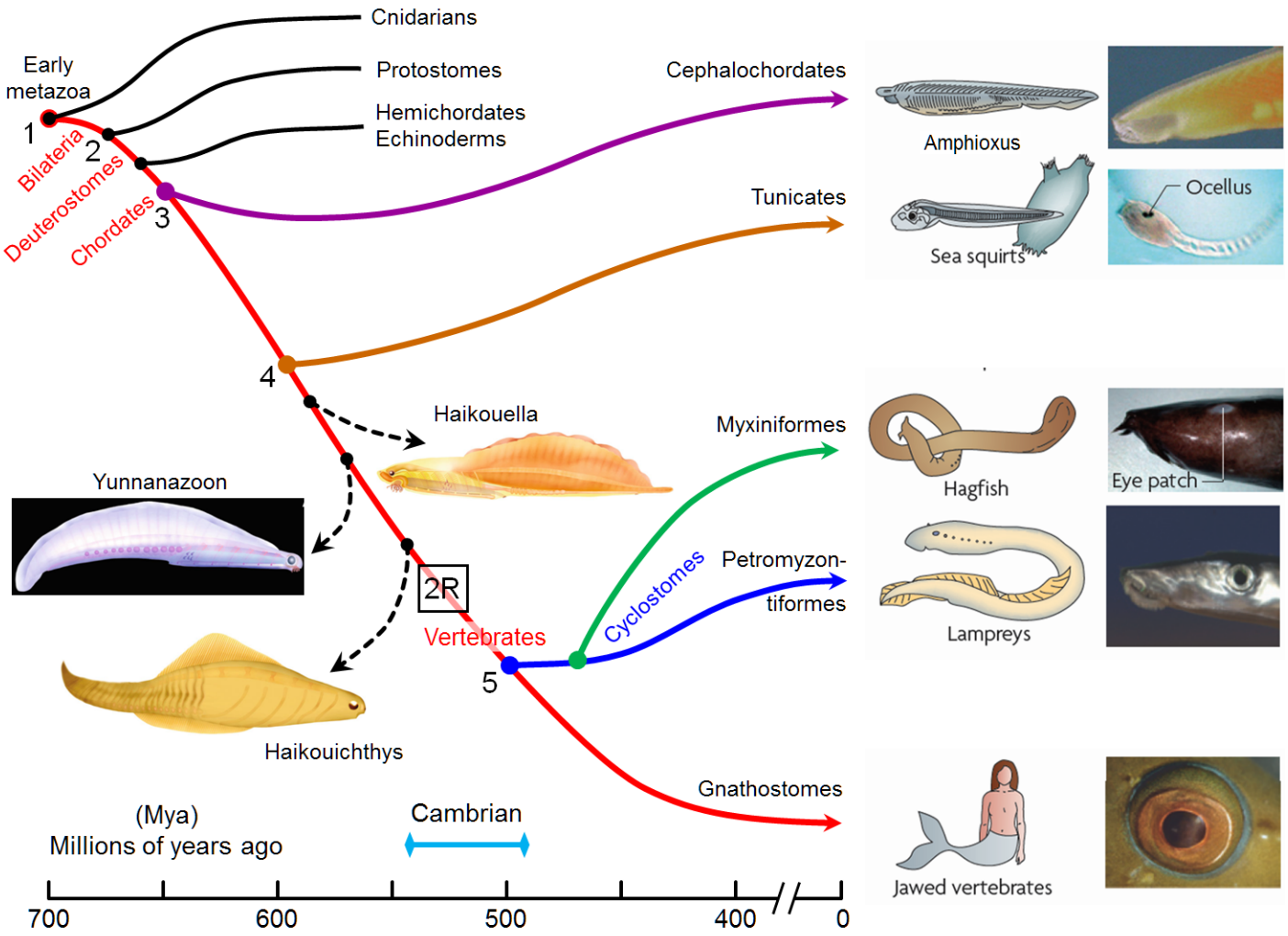

Figure 1. The origin of vertebrates, over a time-scale from roughly 700 to 400 million years ago (Mya), with timings of the branchings taken from a reconciliation of fossil and molecular data by Erwin et al (2011). The red curve indicates our direct ancestors, beginning with early metazoans, and the numbers along the curve denote major branchings that are significant to the evolution of the vertebrate eye. #1, Cnidarians branched off around 700 Mya, and since then our ancestors have been bilaterally symmetric (bilaterians). #2, Protostomes branched off around 665 Mya, and since then our ancestors have been termed deuterostomes. #3, #4, By the time that cephalochordates and then tunicates diverged (around 650 and 600 Mya), our ancestors possessed a notochord, and are referred to as chordates. #5, By the time that the ancestors of lampreys diverged around 500 Mya, they and our own ancestors were vertebrates. It has recently been confirmed that the '2R' two rounds of whole-genome duplication occurred prior to that divergence of ancestral lampreys. Subsequently (by around 420 Mya) our own ancestors evolved jaws and hence became jawed vertebrates (gnathostomes). Black curves indicate taxa that are not considered in any detail in this article; dashed black curves indicate extinct taxa of potential interest. See text for details. Source of illustrations: *Haikouella*, *Yunnanazoon* and *Haikouichthys* from Chen (21); remainder from Lamb et al (3), where original sources are given.

vertebrate photoreceptors, these primitive organisms clearly diverged prior to the evolution of the vertebrate-style camera eye.

Some extinct chordates of interest. Three extinct species of early chordates are indicated schematically in Figure 1 (diagrams from Chen (21)). These are the earliest known chordates to have possessed structures that in extant vertebrates arise from migratory neural crest tissue, and accordingly they have been named 'crest animals', or Cristozoa, by Chen and colleagues. These pre-craniate crest fossils have been found only in the Lower Cambrian strata of Yunnan in south-western China; they are around 3 cm in length. Of the three species, *Haikouella lanceolata* has the most basal form, and *Yunnanazoon lividum* appears somewhat more developed, while

Haikouichthys ercaicunensis is the most developed and appears to be a transitional form to craniates. Each of these fossil species is reported to exhibit paired eyes, with diameters of around 0.3, 0.6 and 0.4 mm respectively, but unfortunately so little detail of these soft tissues is preserved that it is not possible to describe the internal features of the eyes - even, for example, whether they possessed a lens.

Comparison of chordate eye features. Item A compares a number of features of the eyes (or eyespots) of the extant chordate species referred to above. There seems little doubt that the last common ancestor we shared with lampreys (~500 Mya, Figure 1, #5) possessed a fully-fledged 'vertebrate-style camera eye' while, further back, it seems inconceivable that our last common ancestor with sea squirts (~600 Mya, Figure 1, #4) could have had anything more complicated than a simple eyespot.

A crucial period for eye evolution in chordates and other phyla. Clearly then, the interval #4 to #5, from 600-500 Mya, was crucial to the evolution of the vertebrate-style eye. Furthermore, it seems plausible that the most profound changes in physical appearance occurred towards the end of that period, during the time of the Cambrian 'explosion' in body forms. At roughly the same time, eyes were evolving in a number of other phyla as well, often with radically different physical form (14, 22).

Recent discoveries of exceptionally well preserved fossil eyes from the Early Cambrian (~515 Mya) have shown that some of the earliest arthropods already possessed compound eyes containing many thousands of ommatidia. Paterson et al (23) have reported that *Anomalocaris* had eyes at least 12 mm in diameter, containing well over 16,000 ommatidia. These animals, which had bodies up to 90 cm long, are acknowledged as free-swimming apex predators, and have now been confirmed to have possessed compound eyes with the potential for high spatial resolution (~1°). Our own ancestors were tardy in developing eyes, and they may have been preyed upon by visually-guided protostomes for tens of millions of years.

Driving force for the evolution of eyes? In analyzing the emergence of sensory systems in the Cambrian, Plotnick et al (24) have proposed that two factors that rendered the acquisition of spatial vision highly valuable were, firstly, the enormous increase in spatial complexity in the landscape that occurred during the Cambrian and, secondly, the need of free-swimming organisms to navigate. Optic-flow information from spatial vision provided at least a partial solution to the latter requirement. On top of these pressures there was of course the need to detect prey and to avoid predators.

Origin of opsins

Opsins, and their major divisions (25) arose very early in metazoan evolution. In this article the term 'opsin' will refer only to 'Type 2 animal opsins', and not to the 'Type 1 microbial opsins' of bacteria or the 'channelrhodopsins' of algae, both of which are unrelated and appear to have arisen by convergent evolution. The phylogeny of ciliary opsins will be considered in Sections 5 and 6 for chordates generally, and for the vertebrate retina, but for now the questions are: *How did the ancestral opsin originate?* and *What were the initial stages in its diversification?*. In addressing these questions, important clues have been obtained through analysis of a number of cnidarian opsin sequences that have become available since 2007 (12, 26-31).

Animal opsins evolved from within the eponymous 'Rhodopsin family' of the 'GRAFS' superfamily of G-protein coupled receptors (GPCRs), and it is known that this superfamily originated in an ancient eukaryote that existed prior to the divergence of fungi (32)). Recently, Feuda et al (30)) analyzed the phylogeny of opsins and proposed a scheme for the early origin of opsins. They showed that the closest relatives of the opsins are found in the lineage that includes the vertebrate receptors for melatonin. However, for the corresponding GPCRs in invertebrates the ligand has not yet been identified, and so it is not clear what the ancestral ligand might have been at the time that the opsin lineage diverged.

One potential problem with the analysis of Feuda et al (30) is its reliance on the (unproven) existence of R-opsins in cnidaria, but that issue appears to have been resolved by an independent and nearly simultaneous study of

Table 1. Comparisons between eyes and eyespots of extant chordate groups

	Amphioxus	Sea squirt	Hagfish	Lamprey	Jawed vertebrate
Camera-type eye	x	x	x	✓	✓
Lens	x	x	x	✓	✓
Transparent cornea	x	x	x	✓	✓
Extraocular muscles	x	x	x	6	6
Retinal cell layers	–	–	2	3	3
Photoreceptor class	Both	Ciliary	Ciliary	Ciliary	Ciliary
Cones / Rods	?	1 ?	1 ?	5 Cones ?	4 Cones + Rod
Ribbon synapse	?	?	x	✓	✓
RPE65	x	x	?	✓	✓
Central projection	?	?	Hypothalamus	Tectum	Tectum / thalamus

Presence or absence of features is indicated by: ✓, present; x, absent; ?, unknown/uncertain.

Item A: Comparisons between eyes and eyespots of extant chordate groups

opsins from a coral (31), that clearly identified the existence of an R-opsin. The following scenario for the early origin of animal opsins, illustrated in Figure 2B builds on the report of Feuda et al (30), and is presented here as the first in a series of scenarios/hypotheses for the events that gave rise to photoreceptors:

A-1) The forerunner of the first opsin arose through duplication of a GPCR in an ancient metazoan, at a time prior to the divergence of the amoeba-like placozoans.

A-2) That forerunner protein did not possess the retinal-binding lysine ('K296') in the seventh transmembrane helix (30); this suggests that retinaldehyde ligand occupied the internal cavity by means of non-covalent binding, as for ligands in conventional GPCRs, and in Figure 2B this pre-opsin is termed a 'retinaldehyde receptor'. The placozoan Trichoplax has a homolog of opsin (dubbed placopsin by Feuda et al, 2012), that likewise is devoid of the retinal-binding lysine residue.

A-3) Acquisition of an appropriately situated lysine residue within the seventh transmembrane segment of that receptor allowed the retinaldehyde ligand to bind covalently. Initially, the Schiff base bond is likely to have been unprotonated, so that the molecule would have absorbed in the UV. Acquisition of an appropriately located negatively charged residue (e.g. E181) permitted the bond to be protonated, thereby creating the ancestral opsin, and enabling the absorption peak to be shifted into the 'visible' spectrum.

A-4) As for most opsins (though not for vertebrate visual opsins), the activated metarhodopsin state of this opsin was thermally stable and could undergo photoreversal to the rhodopsin state. Hence this protein probably did not require a source of 11-*cis* retinal and could instead utilize all-*trans* retinal perfectly well.

A-5) Subsequently, two duplications of that earliest opsin occurred, during the relatively short interval between the divergence of placozoa and the divergence of cnidarians from bilaterians. Thus, all of the duplications

indicated in Figure 2B took place shortly prior to the first of the numbered branchings shown in Figure 1 (i.e. prior to #1).

Hypothesized association between opsin type and membrane type . A contributory factor in the co-evolution of opsin classes and photoreceptor classes may have been a preferential association of the different opsins with different regions of membrane, as indicated in Figure 2B. Accordingly, the hypothetical scenario for the early evolution of opsins is extended as follows:

A-6) The two variants of opsin that emerged after the first duplication event may have trafficked preferentially to the membrane of sub-cellular organelles and to surface membrane. Those variants would have given rise to the RGR- division and the C-/R- division, respectively, of modern opsins.

A-7) Following the duplication event that created the distinction between C- and R-opsins, these two variants trafficked to ciliary and microvillar membrane, respectively. In Figure 2B this duplication is shown as having occurred subsequent to the duplication mentioned in the previous point, but at present one cannot reliably distinguish the order in which this pair of duplication events occurred.

A-8) Subsequently, cells expressing the C- and R-opsin classes became distinct from each other, through a process termed 'division of labor' (5, 33), leading to (a) ciliary photoreceptors that possessed C-opsins and (b) microvillar photoreceptors that possessed R-opsins; see next Section. The third variant of opsin, RGR-opsin, tended to be expressed in the membranes of intracellular organelles, possibly as an additional opsin in the first two classes of photoreceptors.

A-9) Later in evolution, further division of labor occurred, so that (for example) RGR-opsin could be expressed in separate cells. This would explain how it is possible, on the one hand, for squid photoreceptors to contain an R-opsin in their microvillar membranes as well as retinochrome (an RGR-opsin) in their intracellular organelles, and, on the other hand, for vertebrate cones and rods to contain only a C-opsin in their outer segments whereas RPE cells contain only RGR-opsin in their endoplasmic reticulum.

Classification and diversity of photoreceptor cell types

A view that pervades quite widely is that photoreceptor cells fall into two varieties: rhabdomeric photoreceptors in the eyes of invertebrates (protostomes) and ciliary photoreceptors in the eyes of chordates. However, neither the rigid association of photoreceptor type with phylum, nor the rigid classification of photoreceptors into two categories, can be supported.

Ciliary and rhabdomeric classification. Based on the manner in which the opsin-containing region is elaborated into an extensive surface area, Eakin and his collaborators discerned two classes of photoreceptor: the **ciliary** form, exemplified by vertebrate rod and cone photoreceptors, where the membrane expansion forms a modified cilium, radiating from a classic 9+0 non-motile axonemal structure, and the **rhabdomeric** form, exemplified by insect photoreceptors, where the membrane expansion occurs as microvilli arranged in a highly-ordered manner (33); see for example Figure 3 and Figure 4 below.

Based to a substantial extent on Eakin's classification, three theories were proposed to account for the evolution of photoreceptor types. Eakin himself proposed what became known as a diphyletic model of photoreceptor evolution, wherein the rhabdomeric line of photoreceptors arose in protostomes, as a variant of the ancestral line of ciliary photoreceptors (34). Eakin acknowledged a number of exceptions to his model (such as deuterostomes with microvillar photoreceptors), but he proposed that those exceptions arose via independent evolution.

In a variant of Eakin's model, Vanfleteren & Coomans (35) interpreted rhabdomeric photoreceptors to represent a modified form of the ancestral ciliary photoreceptors, in which the elaboration of the microvillar membranes is induced to occur by a ciliary structure that often degenerates subsequently; other authors termed this a monophyletic model of photoreceptor evolution. In contra-distinction to both these models, Salvini-Plawen &

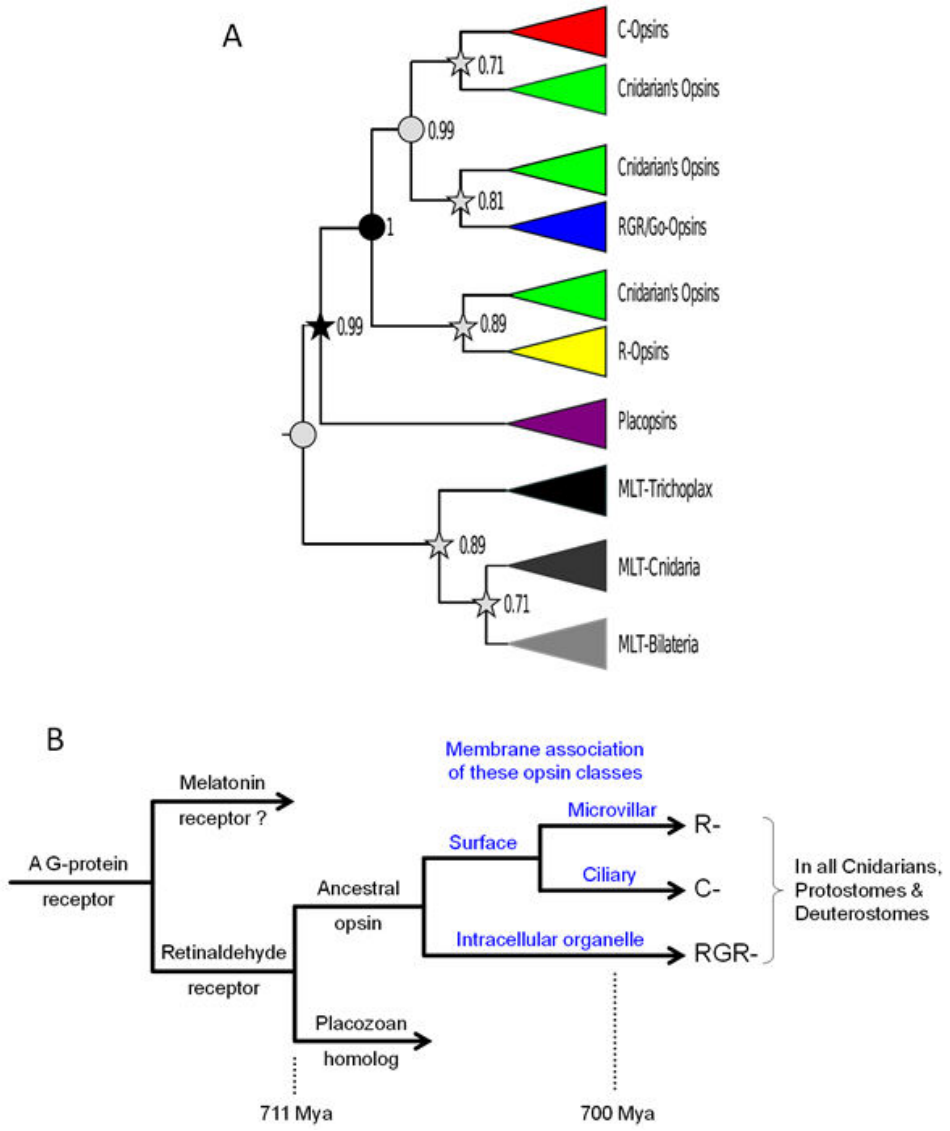

Figure 2. Origin of opsins, and their possible association with membrane type. A, Opsin phylogeny. Cnidarians have orthologs of each bilaterian opsin subfamily; i.e. the C-, R-, and RGR/Go-opsin subfamilies. Numbers indicate support values (Bayesian PPs) for key nodes. From Feuda et al (30). B, Hypothesized duplications of ancestral opsin and its precursors, and suggested association with membrane type. An ancient GPCR (related to extant vertebrate melatonin receptors) duplicated, and its ligand became retinaldehyde, which bound non-covalently; this is denoted as 'Retinaldehyde receptor'. After the divergence of the amoeba-like placozoans (~711 Mya), this GPCR evolved a lysine residue in its seventh transmembrane segment and a negatively charged residue (counterion) so that retinaldehyde bound covalently via a protonated Schiff base linkage; this form is denoted 'Ancestral opsin'. Within a relatively short interval (prior to the divergence of cnidarians, ~700 Mya), this opsin duplicated twice, giving rise to three major families of opsins: C-opsins, R-opsins, and RGR/Go-opsins. It is proposed that these three opsins preferentially associated with ciliary membrane, microvillar membrane, and the membranes of intracellular organelles, respectively. Note that all these events occurred just prior to the starting point of Figure 1.

Mayr (17) proposed that photoreceptors had evolved independently on at least 40 occasions, in what they termed a polyphyletic origin of photoreceptors. With the benefit of hindsight, one can see that there are aspects of both Eakin's and Vanfleteren & Coomans' models that had merit.

Diversity of photoreceptor types. The diversity of photoreceptor types across the animal kingdom is truly remarkable, to the extent that in perhaps the majority of organisms photoreceptor morphology fails to fall neatly into the two categories of ciliary and rhabdomeric. For an overview of the range of light-sensitive structures that occur in different organisms, the interested reader is referred to the comprehensive summary of photoreceptor

morphology provided by Vanfleteren (36). Numerous kinds of membrane elaboration occur, quite apart from the conventional 'ciliary' and 'rhabdomeric' structures.

Furthermore both ciliary and microvillar forms of membrane frequently co-occur within a single type of photoreceptor, as sketched in Figure 3 (36). For example, microvillar photoreceptors often exhibit ciliary structures such as centrioles during development (Figure 3A), though in most cases in protostomes these cilia are transient.

Importantly, such co-occurrence is also seen in deuterostome (and even vertebrate) photoreceptors. In the microvillar photoreceptors of amphioxus, the cilia persist; thus, Hesse cells bear a single 9+0 cilium, while Joseph cells bear two (37). And vertebrate ciliary photoreceptors typically possess microvilli that emanate from the distal region of the inner segment and that appear closely associated with the ciliary outer segment (Figure 3B3); however, these microvilli do not exhibit the organization typical of rhabdomeric photoreceptors, at right angles to the incident light, and instead they are arranged longitudinally. A third example amongst deuterostomes is found in hemichordates, where the cerebral eyes in the larvae of an acorn worm contain photoreceptor cells that possess both a well-developed cilium and numerous microvilli closely packed and at right-angles to the axis (38).

A final illuminating example comes from a marine gastropod, *Aporrhais pespelecani*. In the larval eye, the photoreceptors are ciliary, but at metamorphosis the ciliary photoreceptors additionally develop microvilli, thereby undergoing conversion into mixed ciliary-plus-microvillar photoreceptors in the adult (39); unfortunately, the nature of the opsin and transduction cascade in these photoreceptors is not known.

Even the extreme cases are homologous. In light of the sheer diversity in photoreceptor morphologies, one can view the classical cases of the fly photoreceptor and the vertebrate rod cell as representing extrema in a vast gradation of photoreceptor structural types. But even though the morphological disparity between these two cell types is large, the homology between them (Figure 4) is quite remarkable, as noted by Ready & Tepass (40). Both cells develop from a simple columnar epithelium. Both retain a zonula adherens (ZA) region that delineates basal from apical membrane, and that links neighboring cells; in the vertebrate retina, these intercellular contacts form the outer limiting membrane. In developing photoreceptors of both types, two sub-domains develop in the membrane apical to the ZA. The first is a Crumbs-rich supporting domain that in *Drosophila* forms the fly stalk, and that in vertebrate photoreceptors forms the inner segment. The second more apical sub-domain expands massively to form the light-sensitive membrane, in *Drosophila* as microvilli, and in vertebrate photoreceptors as the ciliary sacs or discs.

Scenario for the origin of photoreceptor cells

By drawing together threads from the concepts above, the following scenario is proposed for the origin of the main two morphological variants of photoreceptor, namely **ciliary** and **microvillar**:

B-1) The ciliary variant represents the ancestral class of photoreceptor. That ancestral photoreceptor expressed the ancestral opsin in its ciliary membrane and it also exhibited microvilli extending from its soma in the vicinity of the cilium.

B-2) In deuterostomes and cnidarians, mechanisms evolved for the massive elaboration of the ciliary region of cell membrane.

B-3) After R-opsins diverged from C-opsins (see above), they tended to traffic to microvillar membranes.

B-4) In bilaterians, mechanisms evolved for the elaboration of those microvillar membranes, leading to the principal distinction between 'ciliary' and 'microvillar' photoreceptors.

B-5) In certain arthropods and mollusks the elaboration of microvilli culminated in the formation of highly-organized rhabdomeres, and hence the evolution of a number of cases of truly 'rhabdomeric' photoreceptors.

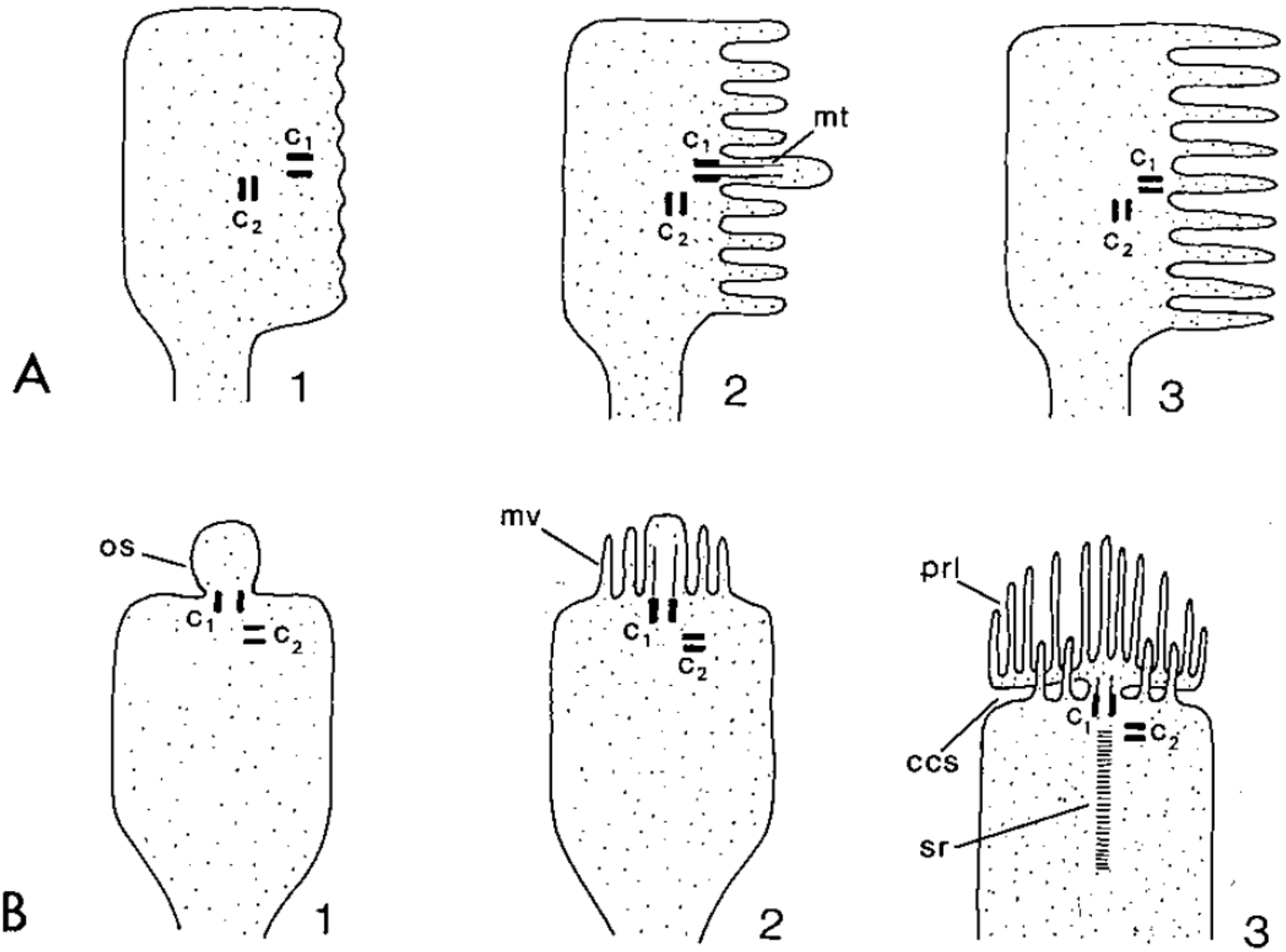

Figure 3. Co-occurrence of ciliary and microvillar structures within photoreceptors. Sketches of three steps in the development of a rhabdomeric photoreceptor (A) and a ciliary photoreceptor (B). A, Arthropod rhabdomeric photoreceptor. B, Tunicate ciliary photoreceptor. In both cases paired centrioles (c_1, c_2 are seen. In rhabdomeric photoreceptors, the ciliary apparatus may disappear during subsequent development. In the chordate photoreceptor, an outer segment bud appears first, then microvilli develop, and subsequently the ciliary membrane (of the outer segment) expands. Note that this diagram was designed to illustrate Vanfleteren & Coomans model of ciliary induction of photoreceptor membrane (35), but is here presented simply to sketch the concept of co-occurrence of structures. c_1, c_2, distal and proximal centrioles; ccs, circumciliary space; mt, microtubules; mv, microvilli; os, outer segment; prl, photoreceptive lamellae; sr, striated rootlet. From Vanfleteren (36).

B-6) Many different mechanisms for elaboration of the opsin-containing membrane have arisen, that have led to the evolution of many different varieties of membrane specialization, and hence to the formation of a vast number of photoreceptor morphologies in different organisms.

Association between opsin class and transduction cascade. There is a strong association between the class of opsin and the nature of the G-protein transduction cascade in the photoreceptor. In vertebrates, C-opsins typically activate a member of the Gi family (which includes Gt and Ggust), leading to modulation of cyclic nucleotide levels and to altered opening of CNGCs (cyclic nucleotide gated channels) and thereby to generation of the electrical response. R-opsins instead activate a Gq, which uses a PLC (phospholipase C) as the effector protein, with TRP/C channels usually generating the electrical activity. Plachetzki et al (27) provide evidence that the ancestral opsin is likely to have employed CNGCs to mediate its electrical response, and that the linkage of R-

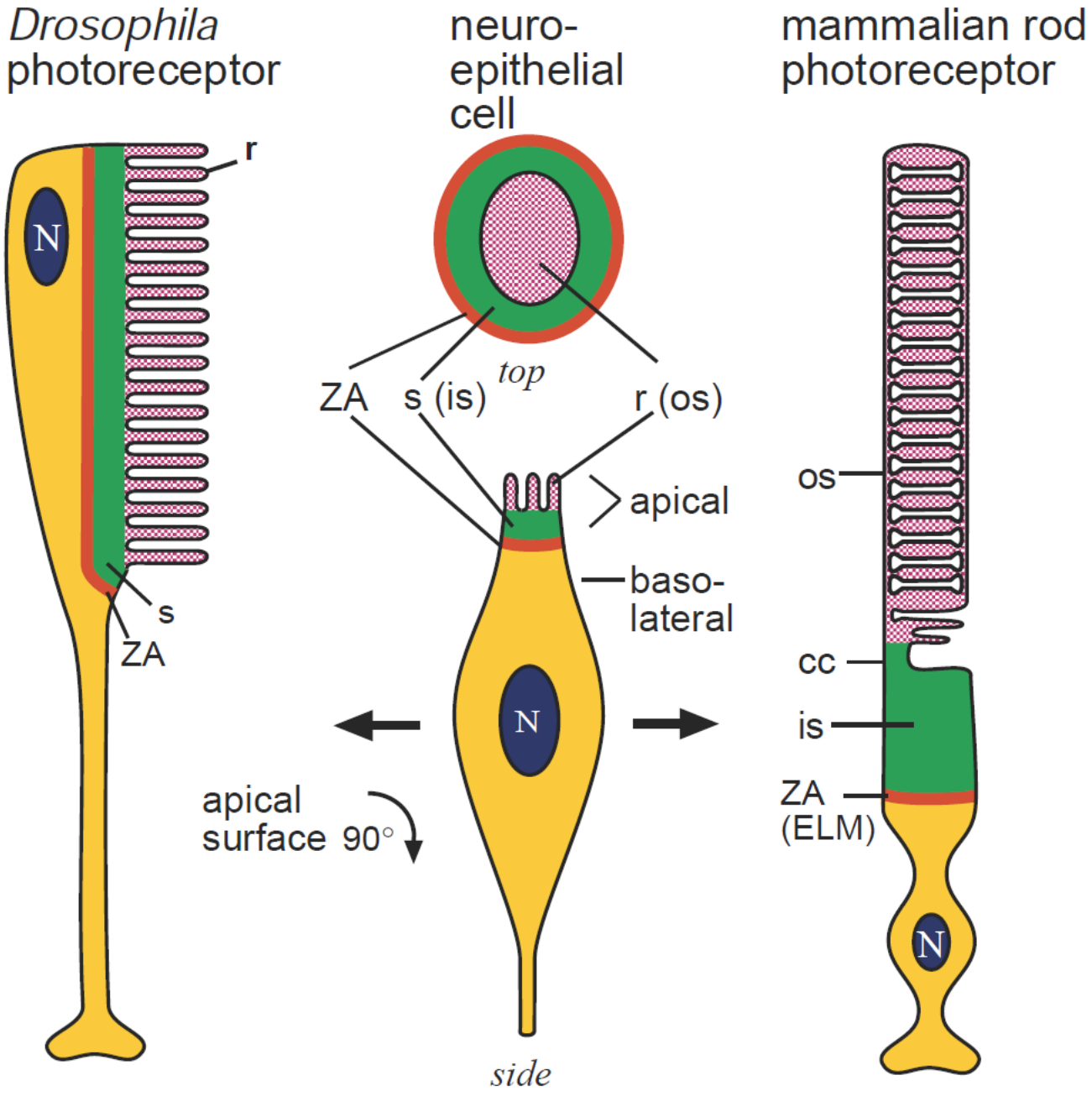

Figure 4. Rhabdomeric and ciliary photoreceptors and their homologies. Conservation of cell polarity and topology between *Drosophila* rhabdomeric photoreceptor (left) and vertebrate rod photoreceptor (right). The center image pair, in top and side view, depicts an ancestral (or an immature) photoreceptor, which can evolve (or develop) into either of the two illustrated final forms simply by different modes of expansion of the apical membrane (pink); that apical membrane is separated from the baso-lateral membrane (yellow) by a zonula adherens (ZA, brown). r, rhabdomere; s, fly stalk; os, outer segment; cc, connecting cilium; is, inner segment; ELM, external limiting membrane; N, nucleus. From Ready & Tepass (40).

opsins to TRP/C channels is likely to have arisen subsequently. The molecular genetic evidence for the co-evolution of opsins and their transduction cascades will be expanded upon in Section 8.

3. Ciliary photoreceptors in the eyes of extant chordates

In order to understand vertebrate eye evolution, one of the primary challenges is to explain the sequence of events by which a handful of photoreceptors and a pigment cell in an ancient chordate ancestor could have evolved into an exquisite retina, by the time that vertebrates appeared. (Closely related issues, that will not be treated here, concern the co-evolution of the requisite optical and motor apparatus, and of appropriate brain areas.) In considering the evolution of the vertebrate retina, we will now survey the light-sensitive organs of living chordate species, beginning with the simplest ocelli and progressing to the vertebrate retina. For each example of chordate light-sensitive organ, we will briefly examine the general features of the organ, and then concentrate on its ciliary photoreceptors.

In Section 7 we will consider why it was ciliary photoreceptors rather than microvillar photoreceptors that triumphed in chordate and vertebrate eyes. Then in later sections we will examine the embryological development of the mammalian retina, as well as molecular clues to eye evolution.

Cephalochordate light-sensitive organs (amphioxus)

Lacalli (41, 42) has described four distinct light-sensing regions in the cephalochordate, amphioxus (Figure 5). Each of these regions lies along the neural tube, in a fairly dorsal position, on the midline (i.e. unpaired), and none has any kind of lens or other imaging apparatus. Two of these organs contain ciliary cells (usually presumed to be photoreceptors) whereas the other two contain microvillar photoreceptors. Although these latter cells have in the past often been referred to as 'rhabdomeric' cells, they do not actually display the highly-organized structure of genuine rhabdomeres and it is preferable to refer to them as 'microvillar', as used by Gomez et al (43) and co-workers.

Ciliary photoreceptors. The 'frontal eye' is a tiny rostral region containing a few ciliary cells that has been proposed to be the homolog of the vertebrate lateral eyes. The 'lamellar body', not far behind the frontal eye, also contains ciliary cells, which in this case exhibit very extensive lamellar membranes; this organ has been proposed as the homolog of the vertebrate pineal. Although the lamellar body is present as a distinct organ in larvae, the cells appear to disperse in the adult. To date, neither of these types of ciliary cell (frontal eye or lamellar body) has actually been shown to be light-responsive.

Microvillar photoreceptors. A little more caudally, a set of 'Joseph cells' is found, each being a microvillar photoreceptor, and further caudally a chain of 'dorsal ocelli' or 'organs of Hesse' are found, that each contain a microvillar photoreceptor partly enveloped by a pigment cell. Recently, it has been established that phototransduction in these cells is closely homologous to that in rhabdomeric photoreceptors of protostomes, utilizing the R-opsin melanopsin (44) to trigger a classical 'rhabdomeric' transduction cascade that involves Gq and PLC (45, 46), and that presumably is closely similar to the cascade in the intrinsically photosensitive retinal ganglion cells (ipRGCs) of the vertebrate retina.

Molecular markers. Very recently, Vopalensky et al (47) identified a number of molecular markers expressed in cells of the frontal eye of amphioxus (Figure 5C), and they concluded that this organ indeed appears homologous to the lateral eyes of vertebrates. In particular, the simple ciliary cells in the first row of the frontal eye appear homologous to cone and rod photoreceptors, in co-expressing C-opsins along with the transcription factors Pax4/6, Otx and Six3/6; furthermore, the presence of the inhibitory Gi-type G-protein alpha subunit is suggestive of the vertebrate-style OFF response to light. Cells in the second row might conceivably be homologous to retinal ganglion cells; they project axons to the neuropil, and they contain serotonin, though so far there is insufficient information to decide on their possible homology to ganglion cells. Finally, the pigmented cells appear homologous to vertebrate RPE cells, in terms of melanin content, location adjacent to the photoreceptors, and regulatory signature (of Mitf, Otx, and Pax2/5/8).

The previously proposed homology of the lamellar body to the vertebrate pineal organ is not supported, because of the demonstrated absence of both Otx and Rx - as well as by the inability to detect an opsin. Thus, although the cells of the lamellar body clearly exhibit a ciliary lamellate ultrastructure, there is as yet no evidence that they are photoreceptors, and the organ appears not to be homologous to the vertebrate eyes or pineal.

Electrophysiology. The Joseph cells and dorsal ocellar cells of amphioxus have recently been studied using electrophysiological techniques, and unequivocally identified as microvillar photoreceptors (43), but the ciliary cells of the frontal eye and lamellar body have not yet been studied in this way.

Tunicate ocellus (larval *Ciona* and *Aplidium*)

Ocellus. The closest extant sister group to vertebrates comprises the tunicates, including sea squirts such as *Ciona intestinalis* and *Aplidium constellatum*. The sessile adult form of the sea squirt has not been reported to possess any kind of discrete eyespot, though scattered opsin-expressing cells apparently occur. However, the tadpole-like larval stage (Figure 6A) has a simple photosensory organ, termed an ocellus (Figure 6D), that contains a handful of ciliary photoreceptors surrounded by a single large pigment-containing cell. It has been suggested that this ocellus is the remnant of paired ocelli in an ancestor (48). The larva does little, beyond swimming to the bottom, embedding its head on a rock, dissolving its nervous system, and transforming itself into a squirt.

Photoreceptor cells. The ciliary photoreceptors of two species of sea squirt are illustrated in Figures 6B-E (from (49, 50)). A total of a dozen or so photoreceptor cells (about seven are sectioned in Figure 6B) protrude through the single pigment cell, with their outer segments lying beneath the lens formed by the three lens vesicle (LV) cells. A schematized *Ciona* photoreceptor is shown in Figure 6C. A large somatic region gives rise at its base to an axonal process (AX), while from its upper end a process penetrates the pigmented cell and gives rise to the axoneme (A), from which expands the outer segment (OS) with its lamellae (L). The electron micrographs from the closely-related ascidian, *Aplidium*, were obtained transversely (Figure 6D) and longitudinally (Figure 6E) with respect to the axis of the outer segment, and show the rather 'petal-like' concentric arrangement of lamellae. Both the studies above reported microvilli interdigitating with the lamellae, though Eakin & Kuda (50) suggested that these originated from the pigment cell (Figure 6C) whereas Barnes (49) reported that they originated from the inner segment of the photoreceptor (see Figure 6E).

Electrophysiology. Electrical responses have been recorded from ascidian ciliary photoreceptors in only one study, on *Aplidium constellatum* (51), where it was reported that it "proved exceedingly difficult to record electrical activity from these preparations, possibly because the retinal cells, which lie close to the surface of the small animal, are often damaged by the removal of the thick tunic". The rare penetrations gave resting potentials of -5 to -20 mV, with hyperpolarizing light responses of small amplitude (2 to 7 mV) that were accompanied by a decrease in membrane conductance. These responses are qualitatively similar to those of vertebrate retinal photoreceptors (with the small amplitude probably explained by damage), though there is insufficient data to allow a proper comparison to be made.

Hagfish eye (*Eptatretus* species)

There is now strong evidence that hagfish are descendants of a lamprey-like ancestor and that many of their morphological features have 'degenerated' from a more complex form. That interpretation is certainly accepted here but, notwithstanding this, the viewpoint that will be advanced below is that the hagfish eye provides a window into an early transitional form in the evolution of the vertebrate-style eye, as suggested previously by Lamb et al (3).

Although controversy has long surrounded the phylogenic position of hagfish, there is now powerful evidence that hagfish form a clade with lampreys (52), as indicated in Figure 1. Hagfish have the simplest body plan of all vertebrates (Figure 7A, B). They inhabit the oceans around most continents, often at great depths (in many cases 200 m or more) where they scavenge fallen carcasses; recently they have been found also to be predatory (53).

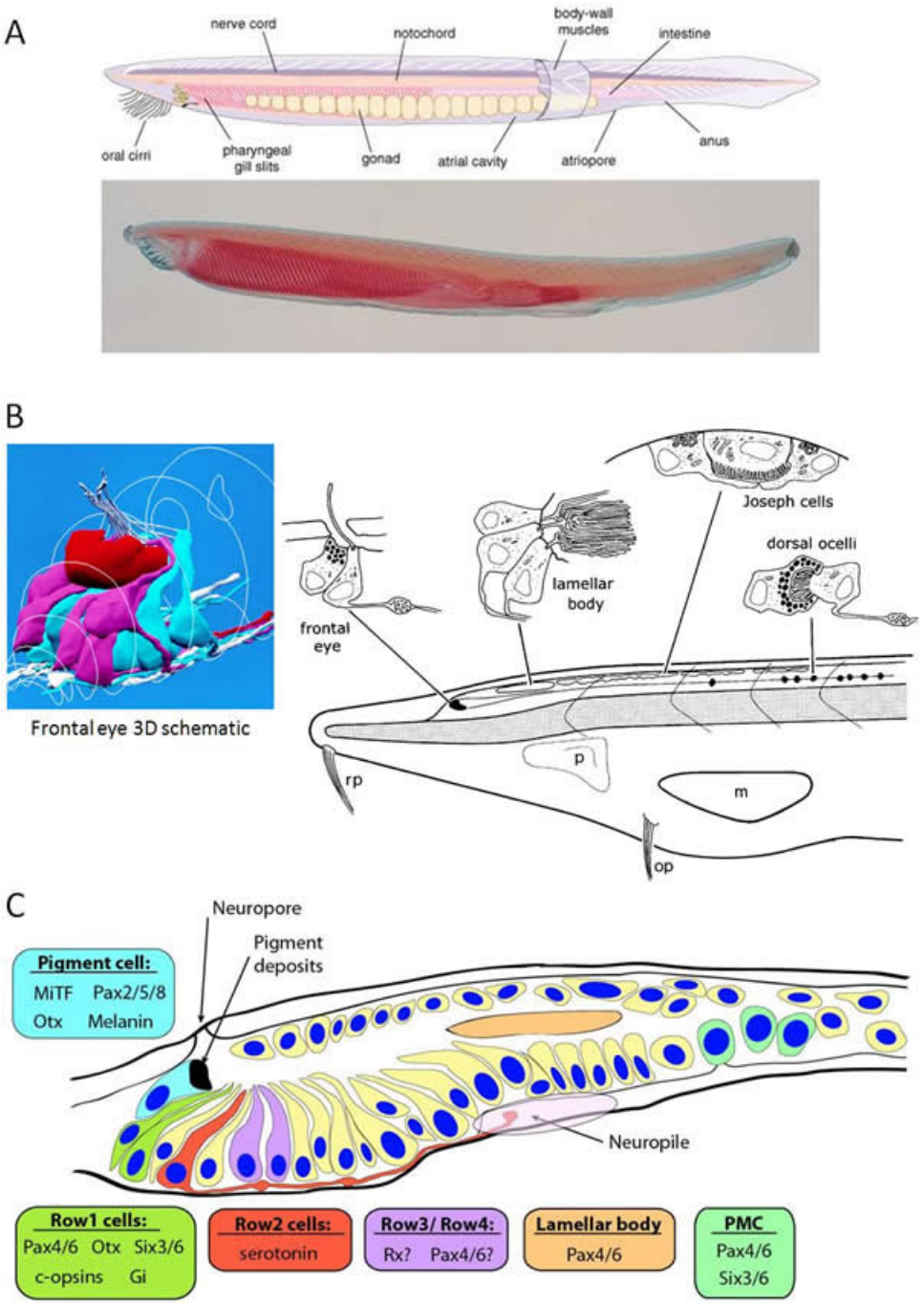

Figure 5. Amphioxus photoreceptors. A, Amphioxus adult, schematic and image. Typical length 2-3 cm. B, Light-sensitive organs in the head region of the larval amphioxus. The frontal eye and lamellar body contain ciliary cells; the Joseph cells and pigmented dorsal ocelli are rhabdomeric. The notochord is shaded; m, mouth. From Lacalli (42). C, Molecular fingerprint of the frontal eye of larval amphioxus. The expression profile of vertebrate eye-specific regulatory genes (Rx, Otx, Pax4/6, Mitf) and eye-associated proteins (C-opsins, Gi, melanin) supports the homology of Row 1 cells with vertebrate photoreceptors, and of pigment cells with vertebrate RPE cells. From Vopalensky et al (47).

Behaviorally, hagfish appear blind. However, in captivity, exposure to the onset of bright light leads, after a long delay (of the order of 10 s or more), to the onset of swimming and sometimes attempted burrowing. Upon removal of the animal's eyes, Newth & Ross (54) reported that the delay was unchanged, though Kobayashi (55) instead reported that it nearly doubled from around 10 s to 20 s. In either case, the eyes of the hagfish appear to mediate little in the way of rapid photosensitive behavior.

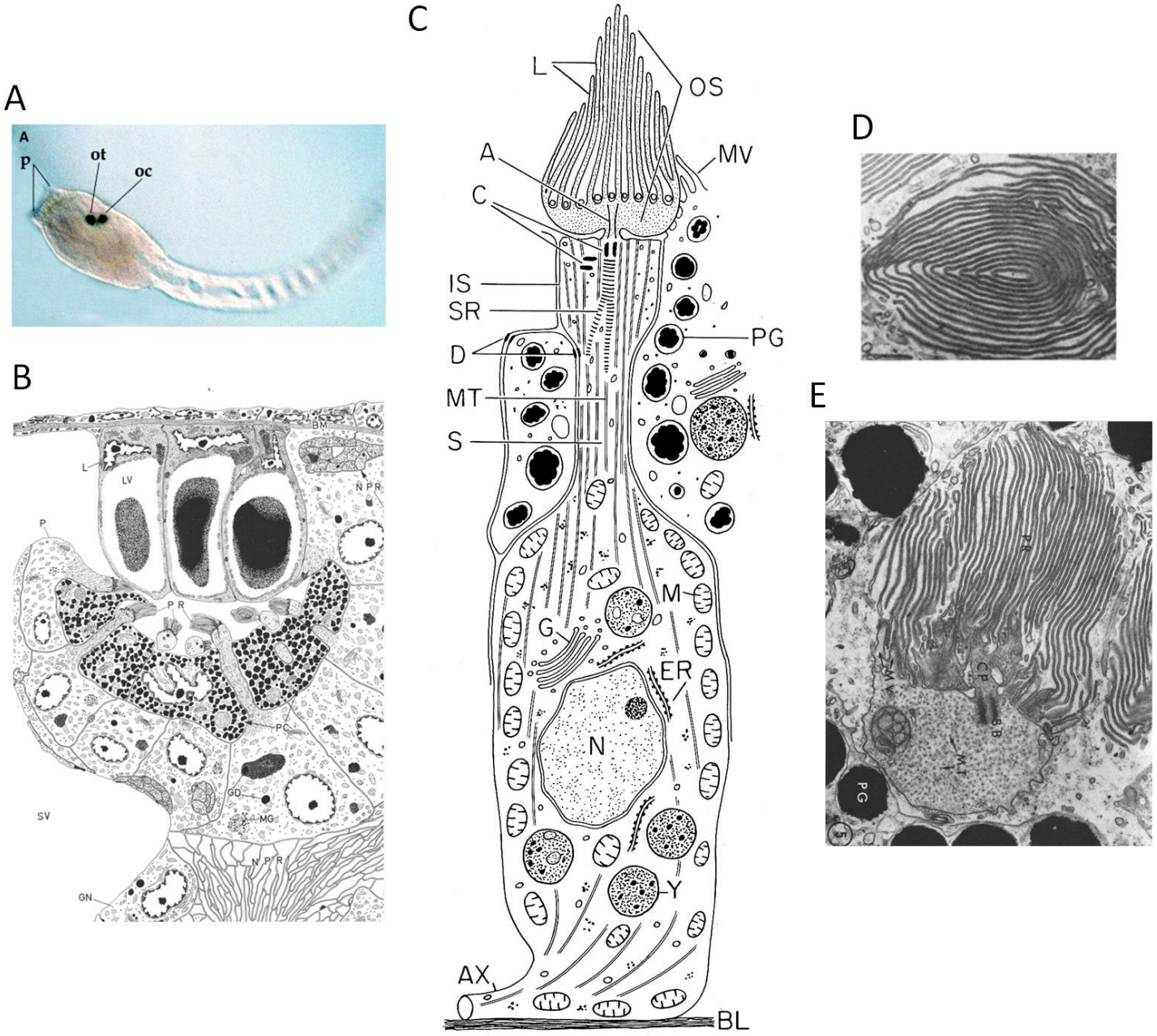

Figure 6. Photoreceptors of ascidian larvae, *Ciona* and *Aplidium*. A, *Ciona intestinalis* larva. Diameter of head is ~80-100 µm. ot, otolith; oc, ocellus. From D'Aniello et al (266). B, Schematic of eyespot of *Aplidium constellatum* larva at low magnification. LV, lens vesicle (3 cells); PR, photoreceptor cells (~7 are shown); NPR, neuronal processes extending from basal region of the photoreceptor cells; PC, pigment cell (a single cell). From Barnes (49). C, Schematic of a photoreceptor protruding through part of the pigment cell, in *Ciona intestinalis* larva. Abbreviations for photoreceptor: OS, outer segment; L, lamellae; A, axoneme (9+0 double filaments); MT, microtubules; N, nucleus; AX, axon. For pigment cell: MV, microvilli; PG, pigment granules. From Eakin & Kuda (50). D, E, Outer segment of a photoreceptor of *Aplidium constellatum* larva. D, Transverse section, showing concentric arrangement of lamellae. E, Longitudinal section. BB, basal body; CP, connecting piece; MV, microvilli. From Barnes (49).

Hagfish are able to secrete a potent slime from a series of lateral pores (Figure 7B), and this slime functions as a highly-effective defense mechanism. The spectacular movies (Supplementary Video S1, Supplementary Video S2) obtained by Zintzen et al (53) show the rapid release of slime into the mouth of a predator at the moment that it bites a hagfish, accompanied by an almost instantaneous gagging reaction and retreat by the predator. Of 14 attacks that were filmed, none was successful, and in each case the hagfish continued swimming as if nothing

had happened. The evolution of such a successful defense mechanism may have enabled hagfish to have survived in their niche virtually unaltered for hundreds of millions of years.

Hagfish eyes. Locket & Jorgensen (56) provided a comprehensive review of hagfish eyes, which had first been studied in the late nineteenth century, and then using electron microscopy in the late twentieth century. The following description for *Eptatretus* species is based largely on the reports of Holmberg (57, 58), Fernholm & Holmberg (59) and Locket & Jorgensen (56).

General features of the hagfish eye. At the location on the head where one would expect to find an eye, the hagfish simply has a patch of translucent (almost transparent) skin (Figure 7D). Beneath this translucent patch of skin is what in the hagfish passes for an eye (Figure 8A, Figure 8B). This organ has no extraocular muscles, no lens, and no iris, and is embedded in fat, through which a very slender optic nerve passes. The size of the eye varies considerably between individuals, but is typically around 1 - 1.5 mm in diameter, though rarely spherical in shape. The sclera/cornea is not divided into separate opaque and transparent regions, and is instead fairly uniformly translucent. No pigmentation is found in the eye, either in the sclera, choroid, or retinal epithelium, even though the skin of the animal may be darkly pigmented. Lining the sclera is a tenuous layer of capillaries, presumably comparable to the choroidal vasculature of jawed vertebrates. In the absence of a lens, much of the chamber is filled with the vitreous body. The optic nerve is thin, containing only a couple of thousand unmyelinated axons. Neither hagfish nor lampreys exhibit myelin (60, 61), and these axons project predominantly to the hypothalamus (62, 63), just as their likely homologs, the melanopsin-expressing ipRGCs, do in mammals (64).

The hagfish retina is roughly cup-shaped and lines half to two-thirds of the globe, though the choroid fissure often remains open (65). As for jawed vertebrates, the retina comprises two apposed layers, the neural retina and the retinal epithelium, though in hagfish the epithelial layer is unpigmented. Several authors have remarked that the neural retina and retinal epithelium often seem to be separated by a gap, but it is possible that this is a fixation artifact (perhaps arising from dilution of the high tonicity extracellular medium, which resembles sea-water). At the peripheral margin of the retina, the inner layer reduces to a single layer of cells and is continuous with the outer layer, though there is no extension to a ciliary body or iris.

Neural retina. The neural retina (Figure 8B) of hagfish is simpler than that of lampreys or jawed vertebrates, with only two layers of somata, comprising photoreceptor cells and projection neurons. No author has reported identifiable horizontal cells or bipolar cells, though Locket & Jorgensen (56) reported some instances of a ciliated structure resembling a Landolt club. The neural arrangement of the hagfish retina is strongly reminiscent of the pineal organ in non-mammalian vertebrates (see Section 3) and, interestingly, the hagfish lacks a pineal. It is presumed that hagfish photoreceptors make direct synaptic contact onto the projection neurons (ganglion cells), though as yet the identity of the cells that are post-synaptic at the photoreceptor synapse has not been determined. There are distinct outer and inner limiting membranes bounding the retina.

Photoreceptor morphology. The morphology of photoreceptors from the hagfish *Eptatretus stoutii* is illustrated in Figure 9 (57). The schematic in Figure 9A shows the general arrangement, of roughly cylindrical receptor cells (R) surrounded by glial cells (G). The region corresponding to the inner segment lies vitreal to the outer limiting membrane, in contrast to the situation in jawed vertebrates and lampreys. It contains a region corresponding to the ellipsoid, packed with mitochondria (Figure 9C), from which the cilium arises, but there is no sign of a paraboloid or myoid. The outer segment protrudes through the outer limiting membrane into the ventricular/extracellular space (ES), where it comes into contact with a non-pigmented epithelial cell (E) and the fine processes that descend from that cell. Compared with other vertebrate retinas, the outer segments are packed very sparsely in the ventricular space (Figure 8B and Figure 9A).

The electron micrographs in Figure 9B and Figure 9C show the lamellar arrangement of the outer segment membranes. According to Holmberg (57) and Locket & Jorgensen (56) the lamellae are enclosed by the plasma

membrane, though this is not clear-cut from the micrographs. Some authors report the lamellae to be quite regular (Figure 9B (57)), while others do not; e.g. "These discs in *Eptatretus*, however, are not stacked closely, but in a loose and often disordered way" (56). The cilium has the classical 9+0 double filament structure, but unusually is located centrally, on the axis of the inner and outer segments, so that the outer segment lamellae extend roughly symmetrically on either side of the cilium (Figure 9C); this contrasts with the situation in vertebrate cones and rods where the cilium is located at the edge of the outer segment.

At its base, the receptor cell is invaginated by a synaptic contact (Figure 9A), and the synaptic zone (Figure 9D) is characterized by synaptic vesicles surrounding a 'synaptic body' (SB), rather than a conventional synaptic ribbon. The contact is of the dyad type, rather than the triad found in the photoreceptors of lampreys and most jawed vertebrates, though (as mentioned above) the identity of the post-synaptic elements has not been reported. Nevertheless, it is presumed that there must be direct synaptic contact from photoreceptors onto projection neurons, as no other cell types have been reported.

Electrophysiology. Single cell recordings have not been made from hagfish photoreceptors, though ERG recordings were reported by Kobayashi (55), for a species named as *Myxine garmani* but subsequently reported by Fernholm & Holmberg (59) to have been *Eptatretus burgeri*. The excised eye was used, and recordings were made between a wick electrode on the surface of the eye and a moistened cloth on which the eye sat. Dim flashes elicited a slow response of characteristic positive-then-negative shape, and the amplitude of this complex response saturated at a relatively low intensity of ~10 lux. For bright flashes a small slow negative-going wave preceded this complex response. The spectral sensitivity of the response was maximal at around 500 nm, suggestive of rhodopsin.

Although Kobayashi interpreted the complex positive-then-negative wave as analogous to the b-wave of the ERG from the vertebrate eye, there were some remarkable properties that suggest a different interpretation. First, this response exhibited a relatively long latency of ~350 ms prior to a fairly rapid climb to its positive peak in a further ~200 ms. Secondly, the form of this complex response was completely unchanged, either when the flash intensity was further increased or when the flash duration was varied from 3 ms up to 1 s. Thirdly, the response exhibited a lengthy refractory period, so that an interval of ~4 s was required after a flash of 10 lux, before any response could be elicited from a second identical flash. Fourthly, dim adapting light could completely eliminate this response, and then during subsequent dark adaptation the response reappeared fairly abruptly.

From the combination of these features I suggest the alternative interpretation that the positive-then-negative response actually reflected the synchronous firing of very slow regenerative potentials ('action potentials') in the projection neurons (ganglion cells). For the future, it should be possible to test this assertion by making more comprehensive electrophysiological recordings from hagfish retinal cells, including intracellular recordings from ganglion cells, suction pipette recordings from photoreceptors, and further ERG recordings.

Hagfish photoreceptors exhibit some rod-like properties. In summary, the photoreceptors of *Eptatretus* species exhibit a number of rod-like properties: e.g. the outer segment lamellae are reported to be disc-like, the inner segment lacks a paraboloid or myoid, and the electrical response shows peak sensitivity at around 500 nm. However, there is still no evidence as to whether these cells can respond reliably to individual photons.

Lamprey pineal (*Petromyzon marinus* ammocoete)

Like the retina of the lateral eyes, the pineal is an evagination of the diencephalon, though it emerges upwards on the dorsal midline (see Section 13). In non-mammalian vertebrates, the pineal contains light-sensitive ciliary photoreceptors, and all ultrastructural work has shown the existence of only three main cell types: photoreceptors, projection neurons (ganglion cells), and glial cells. The photoreceptors make ribbon synapses onto ganglion cells, which send axons to the hypothalamus.

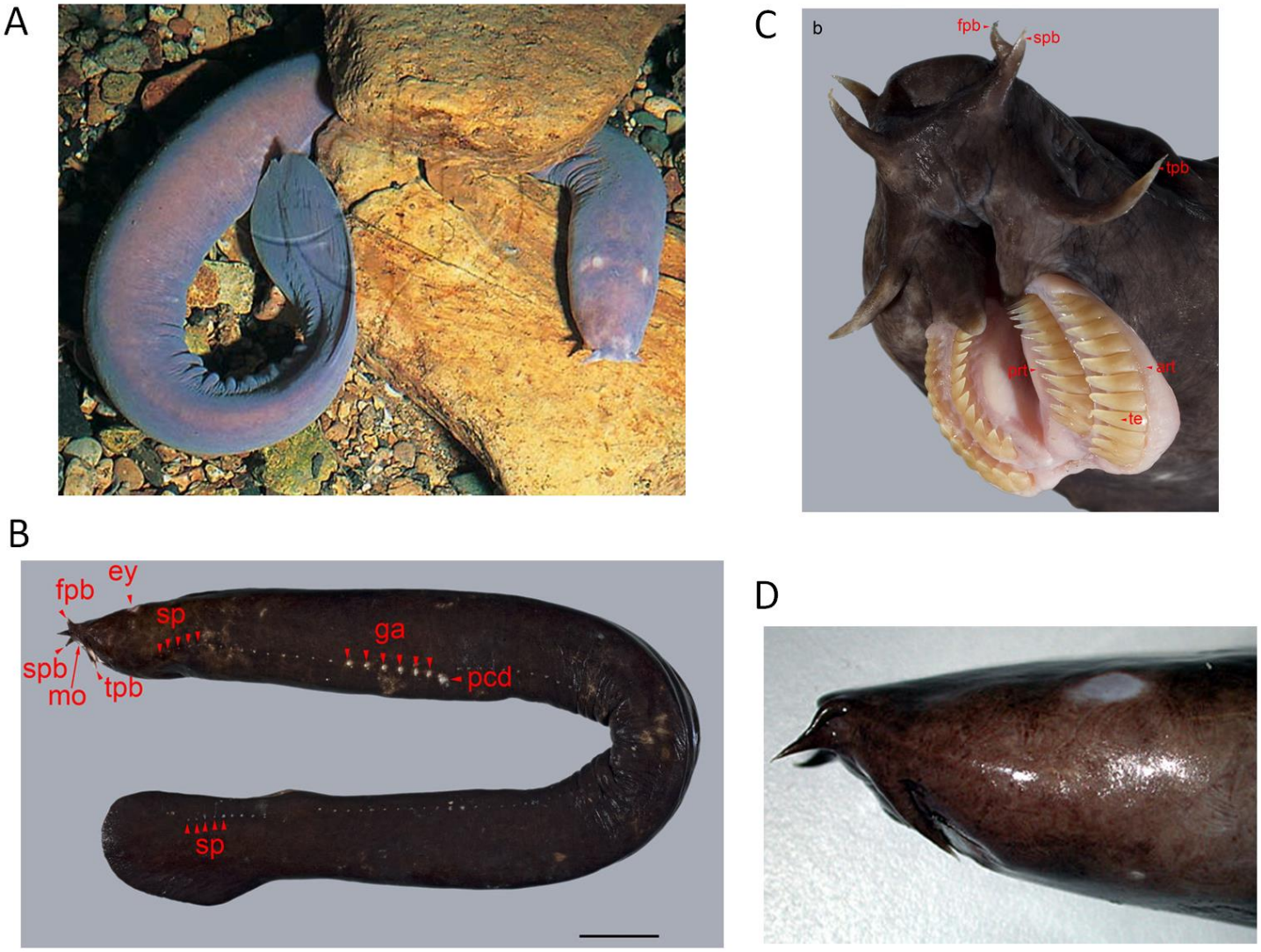

Figure 7. New Zealand Hagfish (*Eptatretus cirrhatus*) A, Living hagfish. Photograph Peter Batson, Imagequestmarine.com. B, Slime pores (sp) and gill apertures (ga) of hagfish. From Zintzen et al (53). C, Tentacles and mouth of hagfish. From Zintzen et al (53). B and C courtesy of Te Papa (collections.tepapa.govt.nz). D, Side view of hagfish head, showing pale eyespot. Photograph David Greenhalgh, copyright Australian Museum.

The photoreceptors in the pineal of the larval sea lamprey, *Petromyzon marinus*, have been investigated by Pu & Dowling (66), using light and electron microscopy as well as intracellular electrophysiological recording, and the following is based on their report. Figure 10 illustrates pineal photoreceptors and their organization within the pineal. The diagram in Figure 10A sketches the overall arrangement of the organ, while the schematic in Figure 10B illustrates the detailed features of the photoreceptor cell and its synaptic contacts.

Photoreceptor morphology. As sketched in Figure 10B (67), the photoreceptor cell is approximately cylindrical for most of its length, with a diameter approaching 10 µm, but the outer segments are often broader, with widths of 10 - 25 µm. The outer segment contains numerous lamellae, that can number more than 100 (Figure10C), which contrasts with the view of Nilsson (13) that there is "very limited membrane stacking" of pineal membranes. The lamellae are rarely flat, but usually somewhat curved, and they are reported to be somewhat less regularly stacked than for cone and rod outer segments in gnathostome retinas. The outer segment membrane is like that of cones, in being continuous with the plasma membrane (Figure 10C).

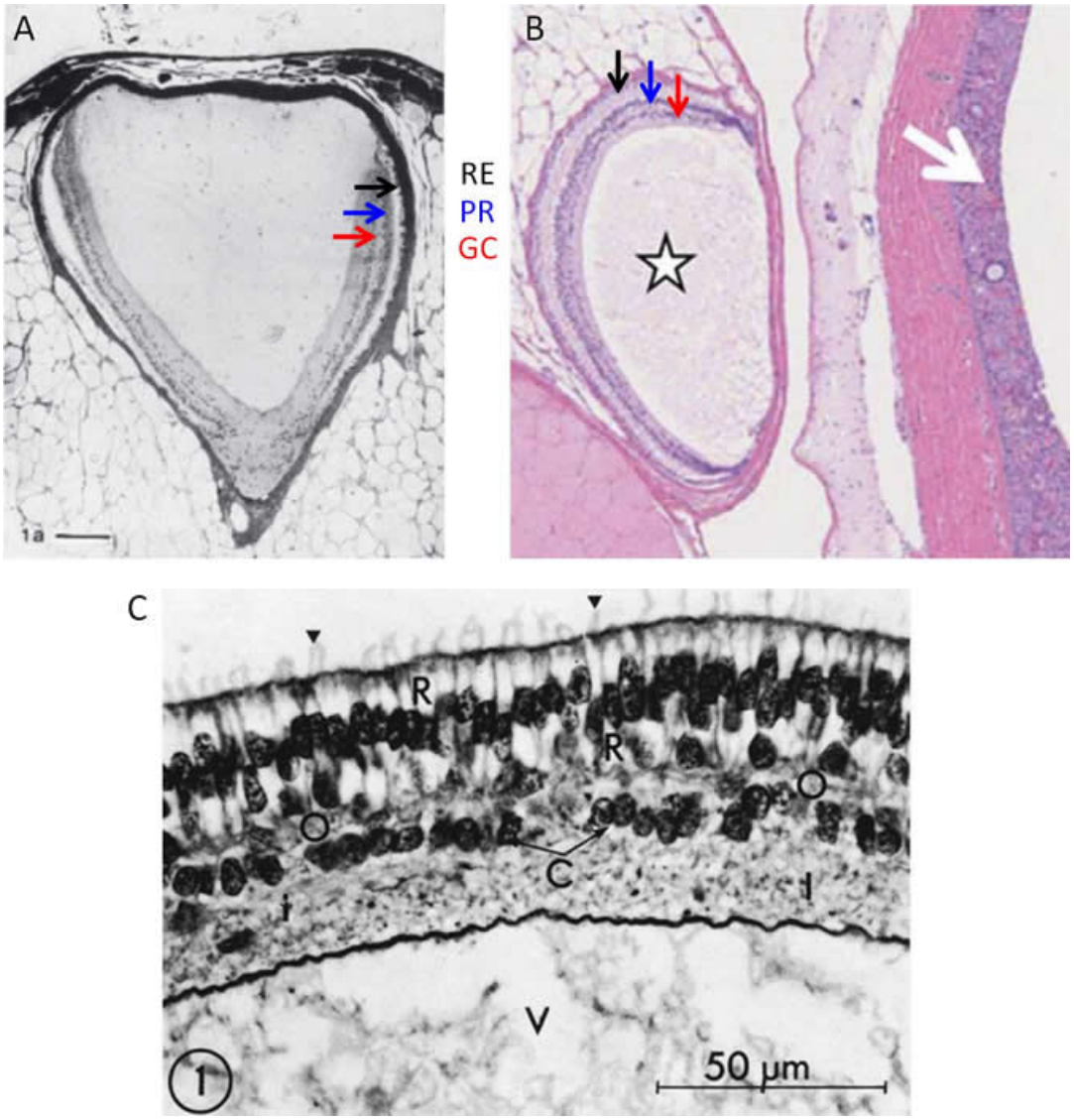

Figure 8. A,B, Light micrographs of sections through hagfish eyes. A, *Eptatretus burgeri*. Scale bar 0.15 mm. From Locket & Jorgensen (56). B, *Eptatretus stoutii*. Eye (starred) and eye-patch (arrowed). Stain: Hematoxylin and Eosin. From Zeiss et al (267). Arrows indicate nuclear layers as follows: red (GC) ganglion cells; blue (PR) photoreceptors; and black (RE) retinal epithelial cells. C, Electron micrograph of retinal section, *Eptatretus stoutii*. The two triangles mark two outer segments. R, receptor cells; O, outer synaptic layer; C, cell bodies of projection neurons; I, inner fiber layer; V, vitreous body. Distinct outer and inner limiting membranes are visible. Stain: Heidenhain's Azan. From Holmberg (57).

As well as the outer segment, a prominent inner segment protrudes into the lumen. At the base of the cell, synaptic contact is made with ganglion cells, predominantly at flat ribbon synapses (Figure 10B, Figure 10D), arranged either as dyads (Figure 10D) or 'monads'; triads were never seen, and nor were feedback synapses (66).

Electrical response to light. Pu & Dowling (66) made intracellular voltage recordings from these pineal photoreceptors, and response to flashes and steps of light are shown in Figure 11. The response was always a slow graded hyperpolarization, broadly similar to that recorded from vertebrate cones or rods, though without the characteristic rapid relaxation from an initial peak back to a plateau for bright stimuli. The flash responses were more than a log unit less sensitive than for cones (of the mudpuppy) and the spectral sensitivity peaked at around 545 nm. The time-to-peak for dim flashes was around 1 s (Figure 11A), much slower than for cones at room temperature, though similar to rods. The response-versus-intensity relation for flashes followed a hyperbolic saturation, $I / (I+\sigma)$. In response to prolonged illumination, the response slowly sagged, except at the

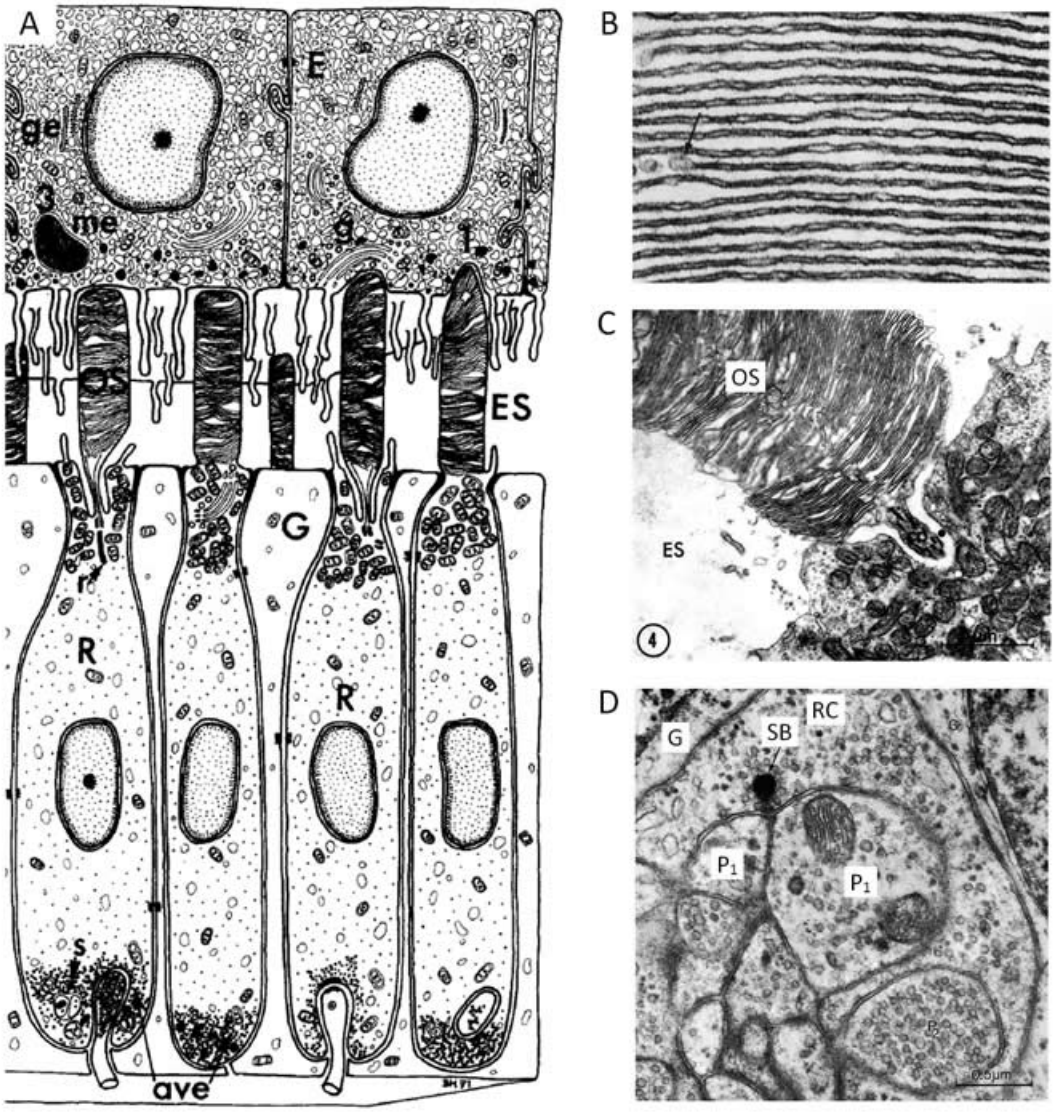

Figure 9. Photoreceptors of Pacific hagfish, *Eptatretus stoutii*. A, Schematic, showing four receptor cells (R) with outer segments (OS) protruding into the extracellular space (ES), and making contact with epithelial cells (E). Invaginating synapses are seen at the base: s, synaptic body; ave, agranular vesicles. G, glial cell. B, Outer segment lamellae are often stacked in an orderly manner. Interruptions of the kind marked by the arrow were presumed to be fixation artifacts, as they were seen only with osmium tetroxide and not with formaldehyde-glutaraldehyde. C, Lower power image, showing outer segment (OS) and connecting cilium. It is not clear whether the outer segment lamellae are enclosed by a plasma membrane or not. ES, extracellular space. The inner segment region contains an accumulation of mitochondria, analogous to the ellipsoid. D, Synaptic terminal. Within the terminal of the receptor cell (RC), a synaptic body (SB) is surrounded by vesicles, and makes contact with two post-synaptic processes (P_1, P_1). From Holmberg (57, 58).

highest intensities, for which it remained saturated (Figure 11B). Responses to incremental flashes were desensitized, roughly according to Weber's law, though much of the desensitization was the result of response compression, and only about 1.5 log units was due to a scaling of σ. At the cessation of steady light, the response began recovering immediately, as occurs in cones. Following intense 'bleaching' exposures, the sensitivity was fully recovered within 4 min, again similar to cones rather than rods.

Kusmic et al (68) obtained broadly comparable results in trout pineal photoreceptors, and additionally showed that the molecular mechanism appeared similar to that in retinal photoreceptors. Voltage clamp experiments showed that the light response was accompanied by a reduction in membrane conductance (as in retinal photoreceptors); however, bright flashes reduced the total conductance only by ~10%, which may explain a contrary report of a light-induced conductance increase by Morita et al (69). In addition, application of the

phosphodiesterase inhibitor IBMX led to an increase in the size of the light responses, as in retinal photoreceptors, and consistent with a light-induced decrease in cGMP concentration. Furthermore, the response-versus-intensity relation measured at a fixed time (prior to the peak) exhibited an exponential saturation, as expected for the classic vertebrate phototransduction cascade (70).

The light adaptation behavior reported by Kusmic et al (68) differed somewhat from that reported by Pu & Dowling (66), in that the responses to steady illumination did not sag at all. Further, for superimposed test flashes the time-to-peak did not shorten in the presence of background illumination. For dim test flashes, the time-to-peak was around 1.5 s in dark-adapted conditions and it remained the same in the presence of backgrounds; likewise, responses to brighter test flashes (which had shorter times-to-peak in darkness) did not accelerate.

From the spectral sensitivity reported by Pu & Dowling (66), and from the in situ hybridization results of Koyanagi et al (71), it seems likely that the opsin in the pineal photoreceptors recorded above was rhodopsin (though with a vitamin A_2-based chromophore in the larval lamprey), and the cells were probably from the ventral region of the organ. Photoreceptors in the dorsal region express parapinopsin (71) and exhibit UV-sensitive hyperpolarizations (71, 72).

Despite the fact that the pineal photoreceptors described above probably use rhodopsin as the visual pigment, their electrical responses can generally be described as resembling 'slow and insensitive cone-like responses', except for two properties. Firstly, light adaptation occurs without response acceleration. Secondly (and probably related), the response saturates in bright steady lights. In contrast, no matter how bright the steady light, the cones of jawed vertebrates always manage to return their circulating current and intracellular voltage to an operating point that permits them to continue responding to incremental stimuli (73).

Pineal ganglion cell responses. A typical response for a standard 'luminosity OFF' ganglion cell to moderately bright illumination is shown in Figure 12 (69), and compared schematically with a photoreceptor response. For sub-saturating intensities the form of the graded response in the ganglion cell closely resembles that in the photoreceptor. In other experiments it has been shown that maintained exposures reduce the firing rate in proportion to the logarithm of the intensity, over a range as great as 8 log units (74).

Lamprey lateral eye

Eye. The lateral eye of adult lampreys (Figure 13B, Figure 13C) bears a striking similarity to that of jawed fish. It is a camera-style eye, with a lens, an iris, and a set of six extraocular muscles. These extraocular muscles are in part homologous to those of jawed vertebrates (75) and interestingly an intermediate arrangement of muscles has been documented (76, 77) in a fossil placoderm, an agnathan armored fish that diverged from our lineage after the ancestors of lampreys had diverged.

Retina. As shown schematically in Figure 14, the retina of the silver lamprey (a northern hemisphere species) appears very similar to that of gnathostomes, and contains the conventional five classes of neuron (photoreceptors, horizontal, bipolar, amacrine and ganglion cells) as well as Müller glial cells. The nuclei are distributed into three main nuclear layers, and there are two plexiform layers, though one difference between lamprey and gnathostome retinas is an apparent 'flipping' of the ganglion cell layer and inner plexiform layer - thus, the bulk of the retinal ganglion cells and their fibers are positioned scleral to the inner plexiform layer in the lamprey (compare Figure 14A and Figure 14B) (75). Fritzsch has proposed that this arrangement in the lamprey retina (and likewise in some brain areas) is basal, and that the flipping of retinal layers in gnathostomes is derived (78, 79).

Also shown for comparison in Figure 14C, Figure 14D is a schematic of the retina of the southern hemisphere lamprey, *Geotria australis*, in its 'downstream' and 'upstream' migratory phases; the downstream phase is just post-metamorphic, when the juveniles migrate down to the sea, while in the upstream phase the fully-grown

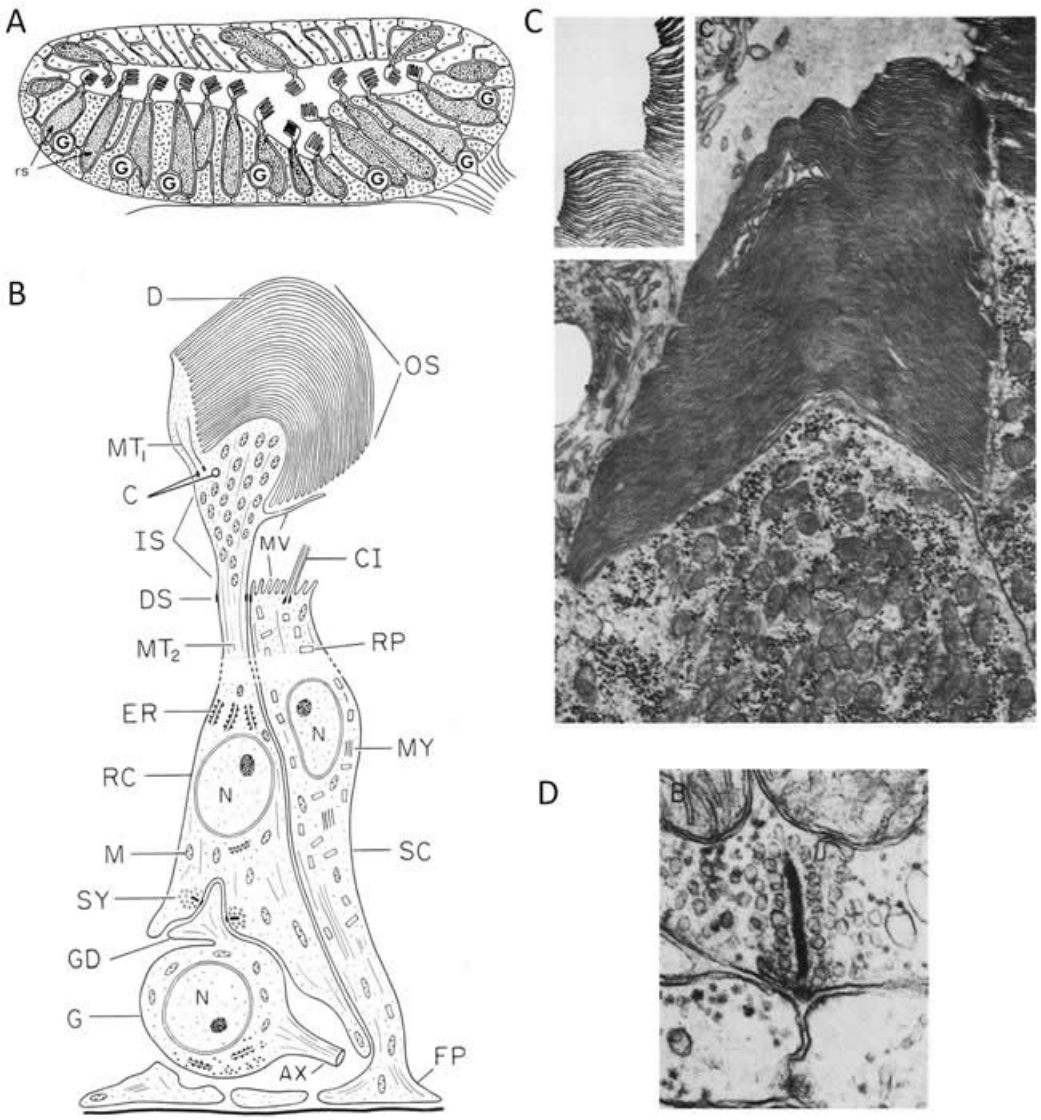

Figure 10. Lamprey pineal photoreceptors. A, Schematic of the pineal. Photoreceptors are darkly stippled, and are shown with their outer segments protruding into the lumen; glial cells are lightly stippled. Ganglion cells (G) lie near the basal end of the photoreceptors. B, Schematic of cellular organization in the pineal of the larval lamprey. A photoreceptor cell (RC) is shown making synaptic contacts with a ganglion cell (G). The outer segment (OS) is short but broad, and there is a distinct inner segment (IS) distal to the tips of the glial (supportive) cell (SC). No other identifiable classes of neuron are present. Sections deleted from cells are indicated by dashed lines. Selected abbreviations: C, centrioles; CI, cilium of supporting cell; D, discs (though these are actually cone-like sacs); MV, microvilli. From Eakin (67). C, Outer segment showing sacs, with membranes that are continuous with the plasma membrane (inset). The stacking of membranes may be less orderly than in vertebrate retinal photoreceptors. D, Synaptic terminal, showing a distinct ribbon contact onto a dyad; triads are not observed. A, C, D, From Pu & Dowling (66).

adults migrate back upstream to spawn near where they hatched. The retina of *G. australis* is broadly similar to those of other lampreys. Figure 14C, Figure 14D indicates the substantial increase in the size of the photoreceptors that occurs during the intervening marine phase.

The distribution of immunoreactivity for amino acid neurotransmitters and calcium-binding proteins in the retina of *G. australis* has recently been examined by Nivison-Smith et al (80), and shown to be generally similar to that found in jawed vertebrates. Experiments with the small organic cation agmatine were consistent with cation entry into photoreceptors and horizontal cells, again broadly similar to that seen in the jawed vertebrate retina.

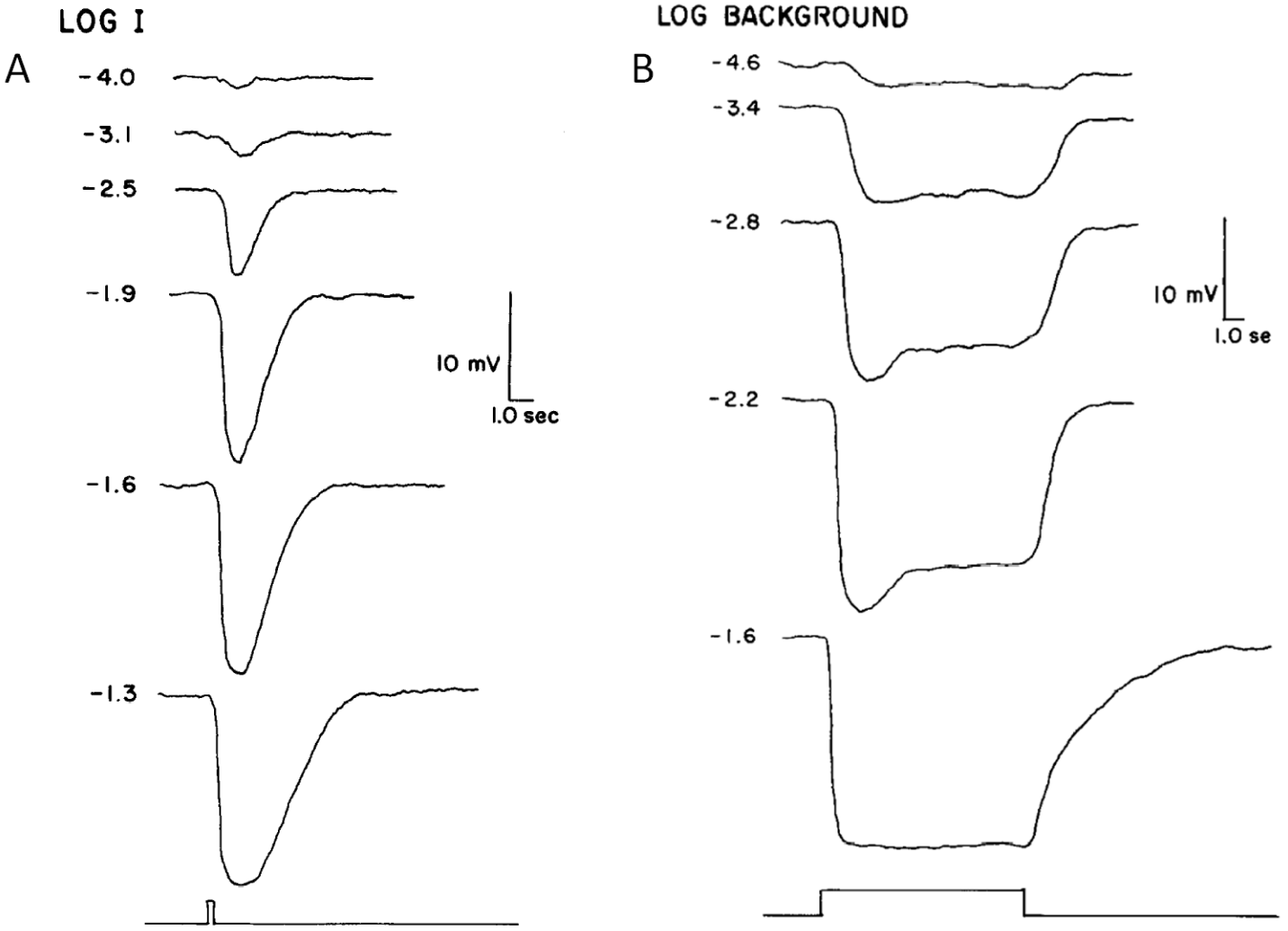

Figure 11. Intracellular light responses of pineal photoreceptors. Intracellular voltage responses of a dark-adapted pineal photoreceptor from a *Petromyzon marinus* ammocoete. Exposures of progressively higher intensity were presented as 200 ms flashes (A) or as steps of 9 s duration (B); white light. Numbers to the left of the traces give the log10 intensity, relative to the unattenuated intensity, which corresponded to ~10^{13} photons cm^{-2} s^{-1} measured at 540 nm. From Pu & Dowling (66).

Classes of opsin and photoreceptor. Lamprey opsins fall into five classes, that appear to be homologous (or nearly so) to those of jawed vertebrates; thus, the southern hemisphere lamprey *Geotria australis* clearly possesses LWS, SWS1 and SWS2 opsins, and its remaining two opsins, RhA and RhB, may well be members of the Rh1 and Rh2 families, respectively (81, 82). Furthermore, this species possesses five distinct classes of photoreceptor (83). Although the distribution of expression of opsin classes amongst photoreceptor classes has not yet been determined definitively, circumstantial evidence suggests the distribution indicated in Figure 15B (Shaun P Collin, personal communication). In contrast to the case in *G. australis,* other species of lamprey have lost varying numbers of classes of opsin and photoreceptor; thus, another southern hemisphere species *Mordacia mordax* has only a single class of opsin and a single class of photoreceptor, while northern hemisphere species generally have two classes of opsin (Rh1 and LWS) and two classes of photoreceptor.

Photoreceptor morphology. In northern hemisphere lampreys, these two types of photoreceptor have been termed 'long' and 'short', based on the length of their inner segments; somewhat confusingly, their outer segments are the reverse of this. Thus the 'long' cells have short (~7 μm long) conical outer segments arranged in a distal layer in close contact with the retinal pigment epithelium, whereas the 'short' cells (which outnumber the long cells

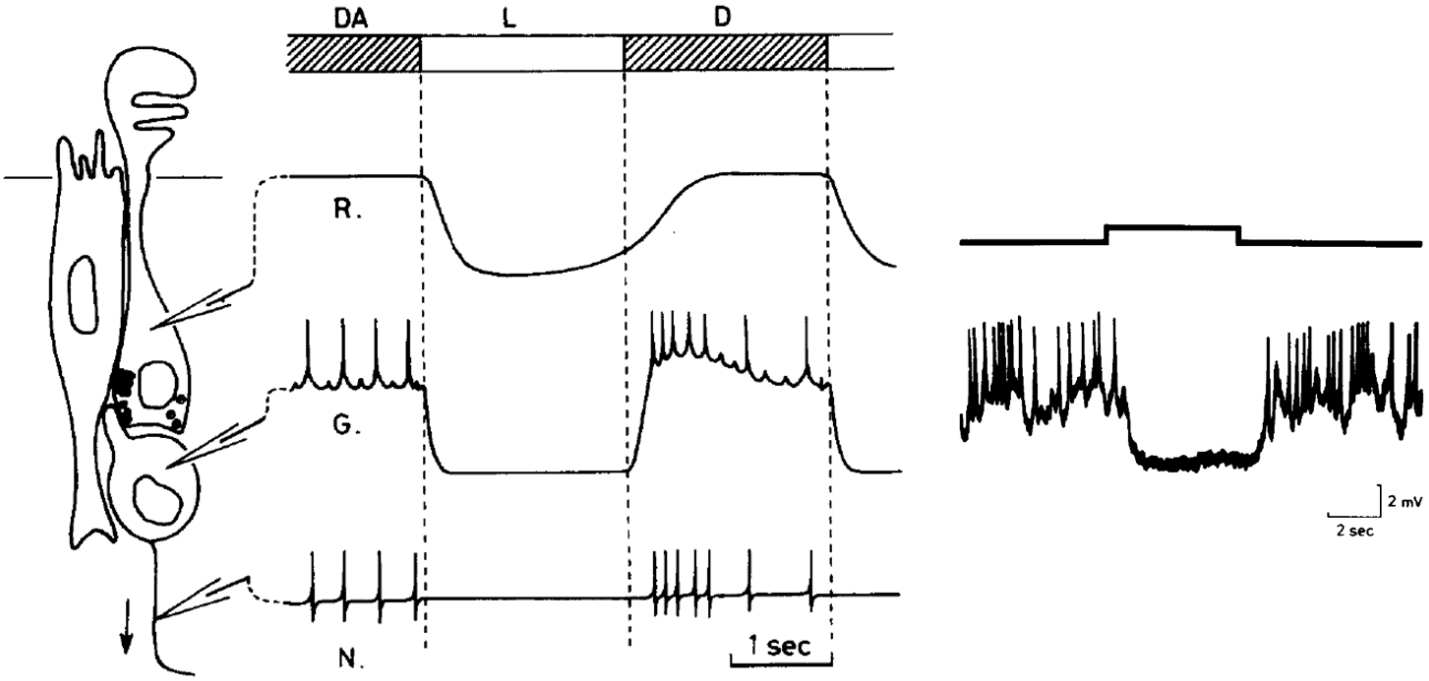

Figure 12. Light response of a pineal luminosity ganglion cell. Left, Schematic of pineal cells and recording electrodes. Middle, schematic of light responses in: R, photoreceptor (intracellular); G, ganglion cell (intracellular); N, nerve fiber (extracellular). Light monitor indicates: DA, dark-adapted; L, light; D, dark. Right, Intracellular recordings from a luminosity ganglion cell. Typical intracellular responses from photoreceptors were shown in Figure 11. From Morita et al (69).

3:1) have longer (~25 μm) cylindrical outer segments arranged in a proximal layer, and only their tips reach the RPE.

The ultrastructure of retinal photoreceptors in the lamprey *Petromyzon marinus* was examined by Dickson & Graves (84), who reported that both classes of cell (short and long) exhibited cone-like rather than rod-like morphology. Thus, in both cell types the outer segment membrane appeared to be continuous with the plasma membrane. Although small groups of sacs/discs were found to be surrounded by plasma membrane, there were frequent openings to the exterior, as illustrated in Figure 15C, Figure 15D. Autoradiography with labeled amino acids showed that newly-synthesized protein was distributed uniformly throughout the outer segment, as found in cones. In addition, the outer segments never exhibited incisures (the deep longitudinal infoldings of the surface membrane that divide the discs of the rods of jawed vertebrates into lobules). Finally, the synaptic terminals (Figure 15E) were reported to resemble cone pedicles rather than rod spherules. Thus, on all the conventional criteria that are used to distinguish cones from rods in jawed vertebrates, the short and long receptors of *P. marinus* would both be classified as cones.

Broadly comparable results were obtained in the southern hemisphere lamprey, *G. australis*, where ultrastructural examination led to the proposal that all five classes of photoreceptor are cone-like (83, 85). In each of the five classes of photoreceptor, the outer segment membrane is continuous with the extracellular matrix (Figure 15A), and the synaptic terminals contain between one and five synaptic ribbons. Furthermore, at least three of the cell classes contain a filtering pigment in the inner segment (Figure 15B).

Proteins of phototransduction. As will be described in Section 8, the distribution of isoforms of opsin, of transducin alpha, and of PDE catalytic and regulatory subunits, has been determined for *P. marinus* by Muradov et al (86, 87). The long receptors express an LWS opsin, a transducin alpha subunit GαL that may be ancestral, a common PDE6 that appears ancestral, and a PDE gamma subunit that clades with the gnathostome cone isoform. The short receptors express an Rh1 rhodopsin, a rod-like transducin alpha subunit GαS that

nevertheless retains cone-like features, the common PDE6 that appears ancestral, and a PDE gamma subunit that clades with the gnathostome rod isoform.

Lamprey genome. The first whole genome sequence and assembly for a lamprey has very recently been reported by Smith et al (88), for *P. marinus*. Analysis indicates that the '2R' two rounds of whole genome duplication that occurred near the base of the vertebrate lineage had already taken place prior to the divergence of the ancestral lamprey and gnathostome lineages (i.e. prior to 5 in Figure 1).

Electrophysiology. Govardovskii & Lychakov (89) examined the ERG response properties of the long and short photoreceptors of *Lampetra fluviatilis.* At scotopic intensities, they observed a b-wave driven by the 517 nm pigment (known to be present in the short cells), though this ERG response was not as sensitive as seen in the frog retina. At photopic intensities the a-wave was a combination of signals from the two spectral classes, and both sets of spectral response exhibited light-adaptation and could not be saturated. Thus, while both long and short cells had cone-like morphology, the short cells behaved electrophysiologically somewhat like rods, but both classes exhibited cone-like adaptation.

Did 'rods' exist in the ancestral vertebrate? As discussed above, lamprey 'rhodopsin' RhA/Rh1 is closely homologous to jawed vertebrate rhodopsin Rh1 (82, 83, 90). Pisani et al (82) have interpreted the sequence analyses to indicate that the common ancestor of lampreys and jawed vertebrates possessed an Rh1 gene. They went on to say: "The function of Rh1 in agnathans is not yet known, but assuming its function in the vertebrate cenancestor was not dramatically different from its scotopic function in most vertebrates, this implies that both photopic and scotopic vision evolved in the stem vertebrate lineage and must have been in place in the Cambrian by about 522-518 Ma". However, there is not yet sufficient evidence to go this far, because it is by no means certain that this Rh1 opsin was expressed in a 'true rod' or that the Rh1 actually mediated 'scotopic vision'. On current evidence, it is entirely possible that the ancestral Rh1-containing photoreceptor functioned simply as a 'slow sensitive cone', rather than as a true rod capable of reliably detecting individual photons, as is required in order for the visual system to attain the ultimate in scotopic performance, of the kind that is attained in jawed vertebrates. All that can be said for certain from this evidence is that the common ancestor of jawed and jawless vertebrates is highly likely to have had a rod-like opsin; but this is not at all sufficient to deduce that it had scotopic vision.

Summary of lamprey photoreceptor features. In northern hemisphere lamprey species that have long and short photoreceptors, the long cells have all the features of cones in jawed vertebrates. The short cells have most of the features of cones, though they express rhodopsin as well as a somewhat rod-like transducin alpha subunit and a rod-like PDE regulatory subunit; other components of phototransduction are yet to be classified. The short cells have high sensitivity, though as yet there is no evidence that they can reliably signal individual photon hits. In southern hemisphere lampreys, there are five classes of photoreceptor that all appear to have most of the features of cones. One of these expresses rhodopsin, but as yet there is insufficient evidence to say whether it has rod-like functional properties.

Jawed vertebrate lateral eye

The eyes of all jawed vertebrates are remarkably similar, in terms of overall layout and features. The retina has the same set of cell classes, and is organized in fundamentally the same way. Furthermore, the cone photoreceptors of all gnathostomes (and likewise the rods) are closely similar in structure, apart from size differences, and their electrical responses to light are also closely comparable. In view of the period of over 400 million years that has elapsed since the emergence of the first jawed vertebrates, it is impressive how little change has occurred in the basic plan of the eye and in the structure and response properties of the photoreceptors.

The structure and responses of cone and rod photoreceptors, as well as the process of phototransduction, in jawed vertebrates are dealt with comprehensively elsewhere (see other sections of Webvision; Ebrey and Koutalos

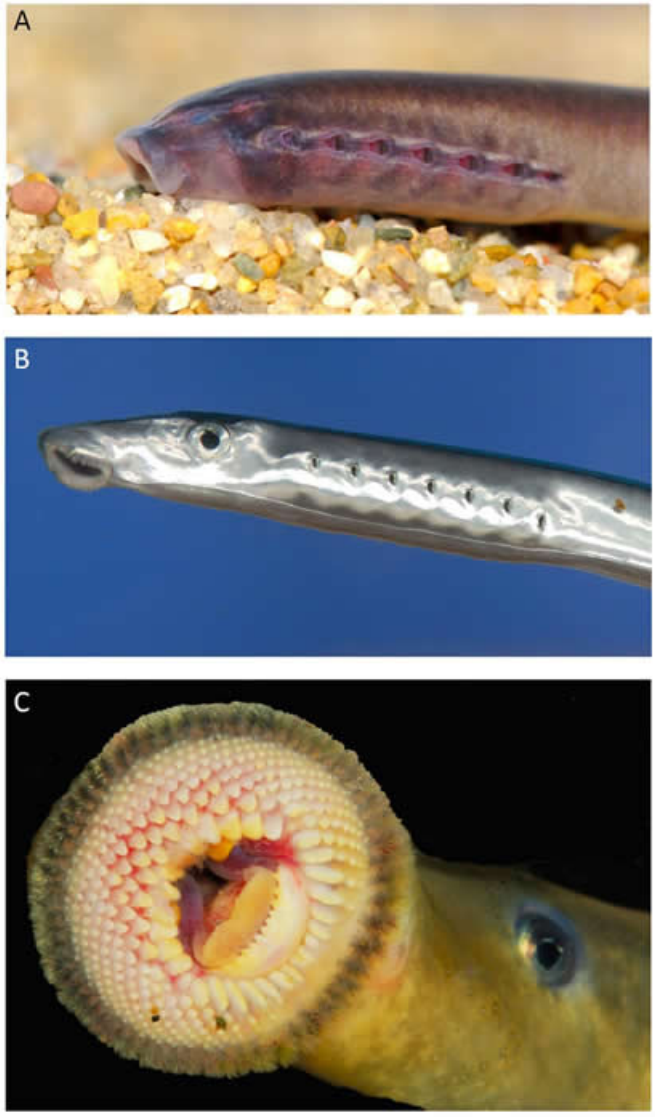

Figure 13. Lamprey (*Geotria australis*) and its lateral eyes. A, Ammocoete. The ammocoete's rudimentary 'eyes' cannot be seen as they are embedded beneath the skin. B, Downstream migrant. C, Upstream migrant. All images courtesy of Shaun P Collin.

(91); etc.), and will not be repeated here. For completeness, though, Figure 16 illustrates the main ultrastructural features of mammalian photoreceptors, for comparison with those of other chordates. The functional properties of cones and rods will be contrasted in Section 7 and the molecular components of the transduction cascade will be reviewed in Section 8.

4. Gradations in chordate eyes: retina and photoreceptors

From the descriptions in Section 3, one can discern gradations in types of retina and types of ciliary photoreceptor, that will now be described. Likewise, one finds gradations in the properties of the opsins (C-opsins), and these will be covered in Section 6.

Categories of chordate retina

The light-sensitive neural tissue in extant chordates can be classified into three groups:

a. *No 'retina'*. The 'primitive' chordates (cephalochordates and tunicates) do not have a retina, in the sense that the term is generally used, but rather a handful of ciliary photoreceptors associated with a pigment

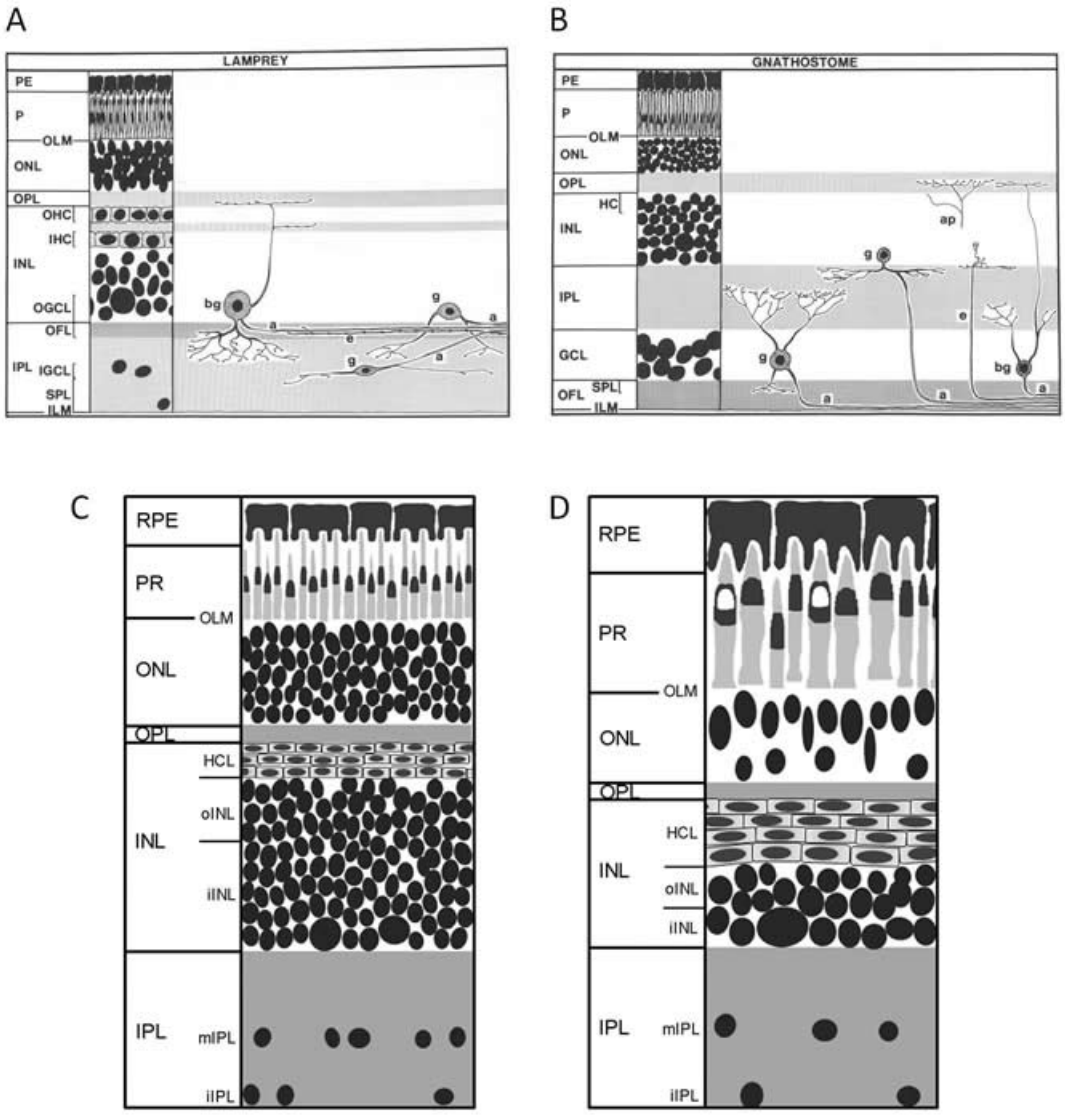

Figure 14. Comparison of lamprey and gnathostome retinas. Schematics of the organization of the retina of the lamprey lateral eye. A, Silver lamprey *(Ichthyomyzon unicuspis*, post-metamorphic juveniles). B, Gnathostome. The main difference is that in the lamprey the inner plexiform layer is vitreal to the majority of ganglion cells, so that most of the ganglion cells are located in the inner nuclear layer. C, D, Southern hemisphere lamprey, *Geotria australis*: in two of the animal's adult forms: (C) downstream migrant phase (post-metamorphic juvenile), and (D) upstream migrant phase (ready to spawn). The retina of the downstream migrant is densely packed with cells, lying ~10 layers deep in the INL (including at least two layers of horizontal cells); the retina of the upstream migrant is much larger, and is dominated by large photoreceptors and reduced layering of cells in the INL. Abbreviations in upper case are standard, with the addition of: IGCL, OGCL, inner and outer ganglion cell layers; IHC, OHC, inner and outer horizontal cells; OFL, optic fiber layer; SPL, superficial plexiform layer. a, axon; ap, ascending process of unknown origin; bg, biplexiform ganglion cell; e, efferent fiber; g, ganglion cell. A, B, from Fritzsch & Collin (75). C, D from Nivison-Smith et al (80).

cell, in the frontal eye and in the ocellus, respectively. In the tunicate ocellus, the ciliary photoreceptors each give rise to an axon, but its synaptic contacts have not been determined. In the cephalochordate frontal eye, it appears that the output axons arise from a second row of cells rather than from the ciliary photoreceptors themselves.

b. *Two-layered retina.* The hagfish lateral 'eye' and the dorsal light-sensitive organs of non-mammalian jawed vertebrates (pineal / parapineal / parietal) exhibit a two-layered retina, with ciliary photoreceptors making ribbon synapse contacts onto projection neurons (ganglion cells). The photoreceptors and projection neurons are embedded amongst glial cells, but no other classes of neuron have been identified (though their existence cannot be ruled out).

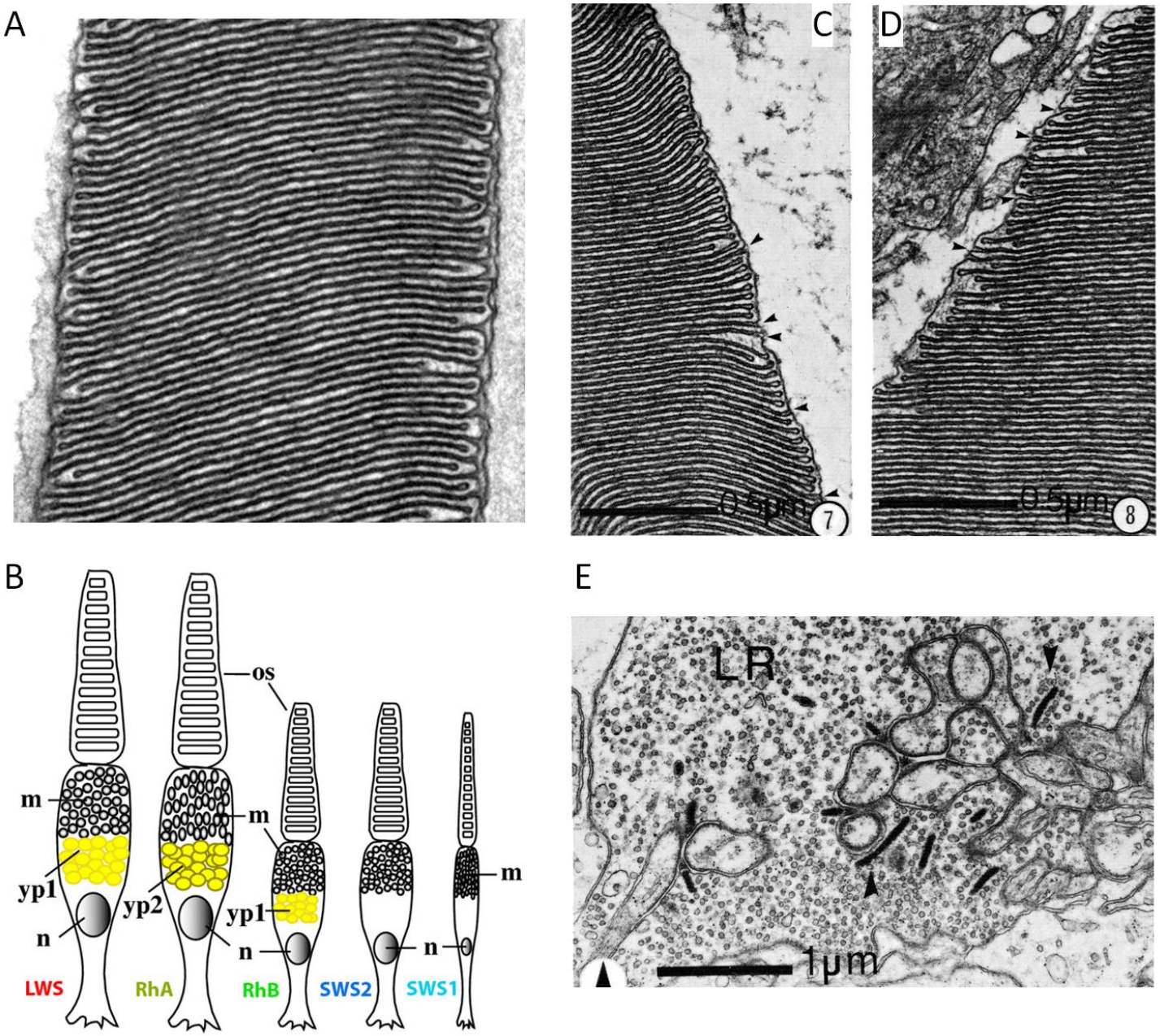

Figure 15. Lamprey retinal photoreceptors. Photoreceptors of *Geotria australis*, a southern hemisphere species (A, B), and of *Petromyzon marinus*, a northern hemisphere species (C, D, E). A, Outer segment, showing ordered stacking of sac-like membranes. From Collin & Trezise (85). B, Schematic of *G. australis* photoreceptors, showing the five distinct morphologies, and making a tentative assignment of the five classes of opsins (based on personal communication from Shaun P Collin). Abbreviations: m, mitochondria; n, nucleus; os, outer segment; yp1, yp2, yellow pigments 1 and 2. Modified from Collin (10). C, D: Outer segment ultrastructure, for long (C) and short (D) photoreceptors of *P. marinus*. E, Synaptic ribbons in the synaptic terminal of long photoreceptor (LR). C, D and E from Dickson & Collard (84).

c. *Three-layered retina.* The lateral eyes of lampreys and jawed vertebrates exhibit a three-layered retina, with bipolar cells interposed between ciliary photoreceptors and retinal ganglion cells, and with two additional classes of neuron in the form of horizontal cells and amacrine cells.

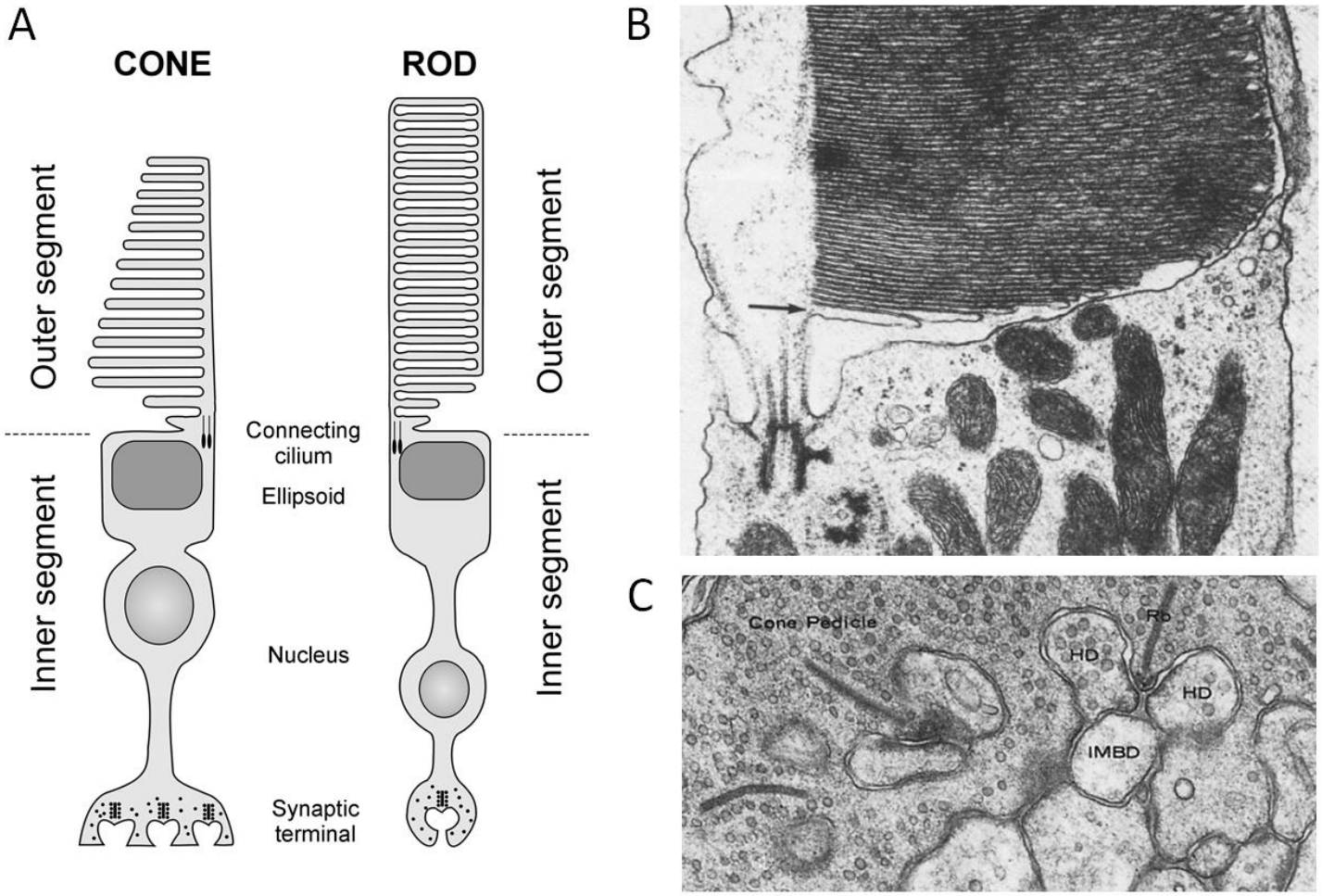

Figure 16. Jawed vertebrate retinal photoreceptors. A, Schematic of jawed vertebrate cone and rod photoreceptors. From Burns & Lamb (268). B, Outer segment, connecting cilium, and distal inner segment of a rhesus monkey cone. From Steinberg et al (129). C, Synaptic ribbons in the synaptic pedicle of a macaque cone. From Raviola & Gilula (269).

Gradations in morphological types of chordate ciliary photoreceptor

On morphological grounds, the ciliary photoreceptor cells of the chordate retinas described in Section 3 can be described as indicated schematically in Figure 17. In all cases, the light-sensitive outer segment is formed by a massive expansion of membrane surface, in the form of lamellae arising from a cilium that is characterized by 9+0 double filaments. This outer segment membrane is packed with a high concentration of visual pigment, together with lower levels of other proteins of phototransduction. The cell body is in most cases roughly cylindrical in shape, both above and below the nucleus. Synaptic output occurs at the end of the cell opposite the outer segment (i.e. at the 'base'), which is sometimes separated from the soma by an intervening 'axonal' segment. These features permit classification into at least five groups, as follows:

i. *Ascidian-style.* The outer segment lamellae are arranged rather like petals, lying roughly longitudinally around the centrally positioned connecting cilium. An axon leaves the base of the cell, but its synaptic contacts are not known.
ii. *Hagfish-style.* The outer segment lamellae are splayed out to either side of the connecting cilium, which lies centrally. Synaptic output occurs at a basal invagination, where synaptic vesicles are arranged around a 'spherical body' rather than a ribbon.

iii. *Pineal-style.* The outer segment lamellae are very broad, and often lie in a curve. It is generally reported that the lamellae constitute cone-like sacs rather than rod-like discs. The basal invaginating synapse exhibits synaptic ribbons, and makes a dyad (or sometimes monad) contact with ganglion cells.
iv. *Cones.* The outer segment lamellae (sacs) are arranged highly regularly, and their membranes form a continuum with the plasma membrane of the inner segment. In mammals the outer segment is roughly cylindrical in shape, though in non-mammalian vertebrates it tends to be conical. The inner segment can contain a variety of specializations, including the ellipsoid (with mitochondria, and sometimes spectrally-filtering oil droplet or vesicles), the contractile myoid, and the paraboloid.
v. *Rods.* Morphologically, rods are very similar to cones, though a significant exception relates to the topology of the outer segment membrane. During outer segment synthesis, cone-like sacs are generated, but these proceed to form a seal around the rim with neighboring sacs, to form discs separated from the plasma membrane, with the result that the narrow intradiscal space is isolated from the extracellular space.

Gradations provide evidence for gradual transitions during eye evolution. The gradations in type of retina and type of photoreceptor listed above provide powerful evidence that the vertebrate eye did not 'suddenly appear', and instead support the view that the evolution of our eye proceeded via myriad tiny changes. This conclusion, based (up until here) primarily on the morphology of ciliary photoreceptors, is greatly strengthened by evidence from analysis of gradations in opsins (Section 5 and Section 6), from analysis of the molecular genetics of the transduction cascade (Section 8), and from studies of embryonic eye development (Section 13 and Section 14).

5. Pre-vertebrate chordate C-opsins

As a result of recent work, it has become possible to track the changes that enabled an ancestral chordate C-opsin (that exhibited many properties in common with R-opsins) to evolve into the immediate pre-cursor of modern cone and rod opsins.

Thermal stability and photoreversal

Two ways in which cone and rod C-opsins differ substantially from their R-opsin cousins (including melanopsin) relate to the thermal stability of the photo-activated all-*trans* 'metarhodopsin' state and its ability to undergo photoreversal (Figure 18).

In R-opsins, the photo-activated metarhodopsin is thermally stable (Figure 18 right), with a half-life usually of hours or even days. This active form is rapidly inactivated by the binding of an arrestin molecule, but it remains stably in its all-*trans* configuration. In most cases this metarhodopsin has its peak absorption in the visible region of the spectrum, indicating that, in its enzymatically active configuration, the Schiff base bond of the all-*trans* retinaldehyde remains protonated. Furthermore, upon absorption of a further photon, this stable all-*trans* metarhodopsin (even when arrestin-bound) can undergo photoreversal back to its 11-*cis* rhodopsin form. Indeed, for most practical purposes this photoreversal is the only short-term mechanism available for the regeneration of visual pigment in many microvillar (rhabdomeric) photoreceptors.

In contrast, the photo-activated metarhodopsin II state of cone and rod opsins is thermally unstable (Figure 18, left), decaying with a half-life that is short (seconds) in cone opsins and somewhat longer (minutes) in rhodopsin (for values, see Table 2 of Imai et al (92)). Fast inactivation occurs as a result of arrestin binding, enabled by rapid phosphorylation. The active meta II absorbs in the UV (~380 nm), because the Schiff base is now un-protonated. Although the protonated meta I intermediate can undergo photoreversal to the 11-cis configuration, the active meta II state is incapable of undergoing such photoreversal, even if it absorbs a blue/UV photon (see Figure 7 of Ritter et al (93)), and this inability is apparently a consequence of an internal molecular rearrangement that accompanies activation.

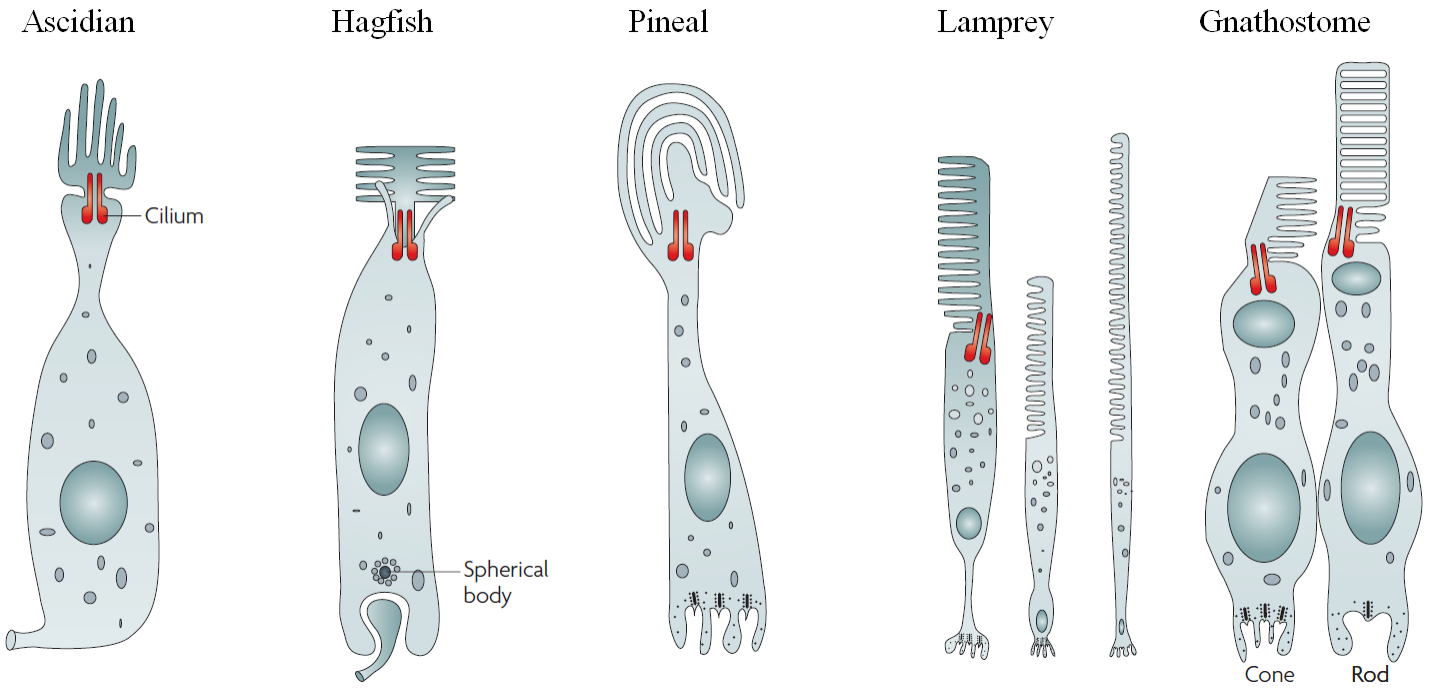

Figure 17. Schematic of transitions in ciliary photoreceptor morphology across chordates Schematic morphology of the ciliary photoreceptors of extant chordate species provides suggestive evidence of the remnants of a gradual transition in the morphology of ciliary photoreceptors during chordate evolution. Note the transitions, from left to right, towards (1) a highly organized laminar structure in the outer segment, and (2) the appearance of ribbons in the synaptic terminal. From Lamb et al (3).

Phylogeny, and gradation in properties, of chordate C-opsins

The C-opsins comprise a large family, with representatives in cnidaria and protostomes, as well as in deuterostomes (including chordates and vertebrates). Apart from the well-known retinal cone and rod opsins, vertebrates also express several additional categories of C-opsin, including: Opn3 (encephalopsin / TMT opsin), parietopsin, parapinopsin, VA (vertebrate ancient), and pinopsin. From their molecular phylogeny, as well as from the gradation (now to be described) in functional properties of the five groups that have been investigated, these C-opsins reflect an evolutionary sequence preceding the advent of the cone and rod opsins.

Figure 19 presents a shortened molecular phylogeny of opsins, together with a tabulation of the amino acid residues at a number of important locations (94). In the cladogram on the left, note that the lengths of the lines do not indicate evolutionary distance, and so the horizontal positions of the branch points do not represent timings of divergences. And in the tabulation on the right (as well as throughout this article), note that residues are numbered in accordance with the bovine rhodopsin sequence.

As indicated by the phylogeny in Figure 19, vertebrate C-opsins fall into the sequence (from most ancient to most recent) of: Opn3 (encephalopsin), parietopsin, parapinopsin, VA opsin, pinopsin, cone opsins, rhodopsin. For each of these C-opsins, the functional molecular properties are briefly described below and summarized in Item B; much of this information has come from recent studies of recombinant proteins.

In evaluating the relative properties of these C-opsins, comparison will be made with a 'typical' R-opsin, exhibiting photoreversible transitions between two stable states. As indicated above, vertebrate cone and rod opsins do not exhibit photoreversal, and instead release their all-*trans* retinoid. On the other hand they exhibit stronger activation of the G-protein. We will now see that the other vertebrate C-opsins exhibit properties intermediate between these.

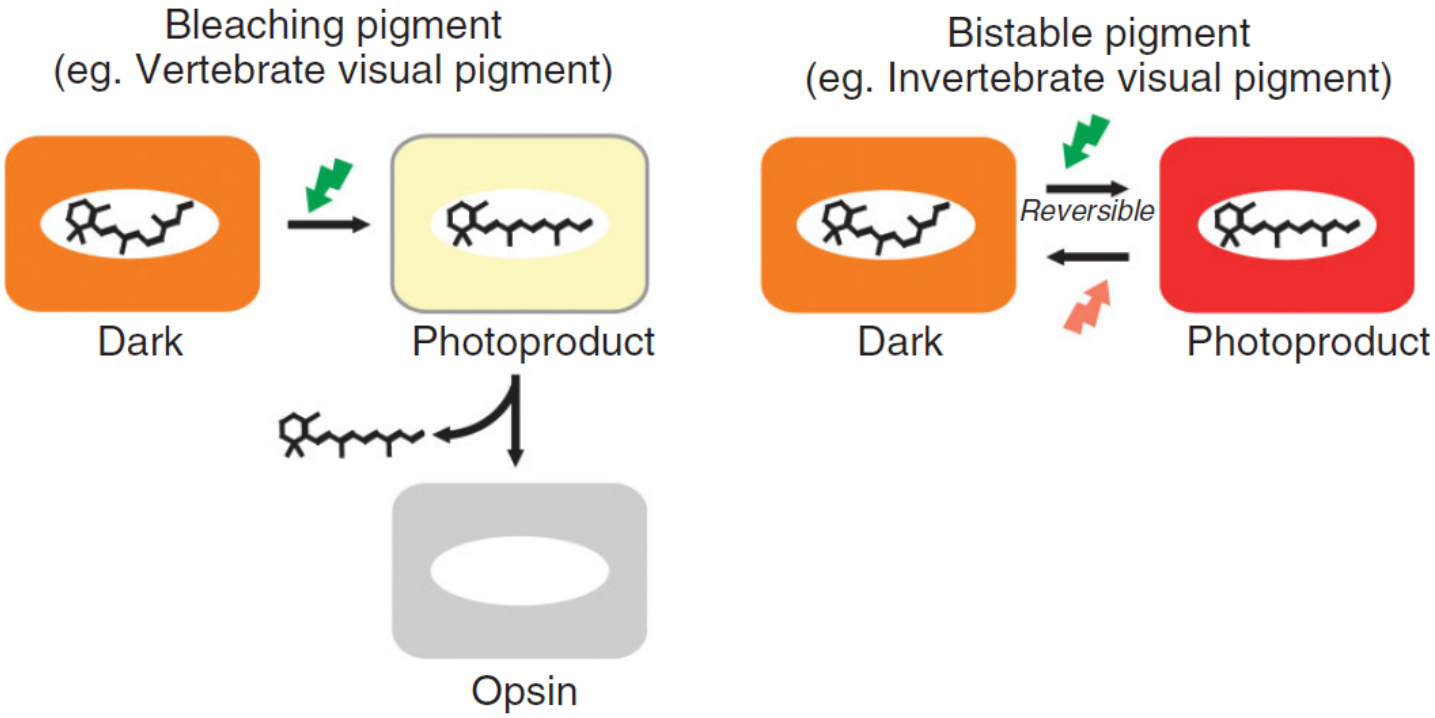

Figure 18. Thermally unstable pigment contrasted with bistable/photoreversible pigment Left: Cone pigments and rhodopsin are thermally unstable upon activation. The metarhodopsin photoproduct absorbs in the UV, so that it is colorless to human vision and hence the pigment is said to 'bleach' in the light. This metarhodopsin decays fairly rapidly, releasing all-trans retinal; cone metarhodopsin II decays in a matter of seconds, and rod metarhodopsin decays in minutes. Right: R-opsins and many C-opsins (other than vertebrate visual opsins) are bistable. The activated all-*trans* metarhodopsin is photoreversible; it absorbs in the visible part of the spectrum, and upon absorption of a photon is isomerized back to the 11-*cis* isomer. From Terakita et al (103).

Opn3. The Opn3 group of opsins includes mammalian Opn3 (formerly called encephalopsin or panopsin), TMT (teleost multiple tissue) opsin, insect pteropsin, and annelid C-opsin. This group clades near the base of C-opsins, and the sequences quite closely resemble those of R-opsins. For most members of the group, the two potential sites (113 and 181) for the counterion to the protonated Schiff base have the R-opsin form, Y113 and E181, indicating that E181 serves as the counterion; however, in mammals Opn3 has D113. Mammalian Opn3 is expressed in scattered cells in deep brain areas.

The molecular properties of Opn3 opsins have only very recently been studied (95), by expression in cultured cells. Pufferfish TMT opsin was shown to bind 11-cis retinal, to form a visual pigment absorbing in the blue (~460 nm); this pigment was bistable, being isomerized to a slightly red-shifted all-*trans* form by short-wavelength light, and isomerized back to the 11-*cis* form by long-wavelength light. The light- activated form could activate Gi and Go, though with only ~10% of the efficacy of activated rhodopsin, but it did not activate Gq, Gs or Gt (transducin). Similar results were found for a mosquito Opn3 homolog, though its activity was higher. Although mammalian Opn3 itself has not yet been successfully expressed in cultured cells, Koyanagi et al (95) suggest that it is likely to exhibit similar properties.

Parietopsin. Parietopsin was first identified in photoreceptors in the parietal eye of the lizard. Its functional properties have recently been explored by Sakai et al (96), who showed that the Schiff base counterion is located in the 'invertebrate' position of 181, consistent with the residues Q113 and E181. The expressed pigment had its absorption peak at 520 nm, and its photosensitivity and molar extinction coefficients were marginally lower than those of cone and rod opsins, as is often characteristic of invertebrate visual opsins. On the other hand, its photochemical properties resembled those of cone and rod pigments, with the formation of decaying metarhodopsin intermediates (I, II and III), rather than the typical invertebrate photoreversible metarhodopsin.

Parapinopsin. Parapinopsin was first identified in the catfish parapineal organ. It was subsequently identified in the lamprey pineal, where it was shown to be a UV-sensitive bistable opsin (97). Koyanagi et al (71) found parapinopsin to be expressed in the ciliary photoreceptors only on the distal side of the lamprey pineal and parapineal organs, and they examined its functional properties. They discovered that illumination of parapinopsin caused the conventional 11-*cis* to all-*trans* isomerization of the chromophore, to yield a product with a spectral peak at 515 nm. However, in contrast to the case for UV-sensitive (SWS1) cone opsins, this metarhodopsin was found to be stable, and to exhibit photoreversal upon absorption of a subsequent photon; indeed it was possible to repeatedly interconvert between parapinopsin and its meta state by illumination successively with UV and then orange light. Intracellular electrical recordings from pineal photoreceptors expressing parapinopsin showed that flashes of UV light elicited slow hyperpolarizing responses, consistent with a phototransduction cascade of the vertebrate style. The efficacy of activation of G-protein by activated parapinopsin was shown to be around 20-fold lower than that by activated rhodopsin (97).

VA/VAL opsin. VA opsin was first identified in salmon retina, and then soon after in other teleost retinas, where a longer splice variant (VAL) was also found, and then in other vertebrates. The functional properties of VAL opsin have recently been investigated by Sato et al (98). Like vertebrate visual opsins, VA/VAL has E113 at the usual site for the counterion to the resting state but, uniquely, the site of the ancestral counterion location is S181. Sato et al (98) found that light activation caused *cis* to *trans* isomerization, but that the activated intermediate absorbed in the visible region, at 455 nm, indicating that the Schiff base remained protonated. Although this intermediate absorbed visible light, it did not exhibit photoreversal (as for vertebrate visual opsins). This intermediate could activate the Gi G-protein, though with an efficacy around 5-fold lower than that of activated rhodopsin. Hence, they showed that several of the properties of VA/VAL opsin are intermediate between those of parapinopsin and pinopsin (see below).

Pinopsin. Pinopsin was first cloned from the chicken pineal, and was found to clade with the LWS cone opsin near the base of the phylogenetic tree of vertebrate visual opsins (99). However, there is no clear evidence as to exactly where or how it diverged from visual opsins, and there is a distinct possibility that it could be ancestral. Its functional properties were examined by Nakamura et al (100), and found to be closely similar to those of vertebrate visual opsins. The resting dark form absorbed at 465 nm, in the blue region of the spectrum, similar to the absorption of the SWS cone opsins (e.g. SWS2, Rh2). Light absorption triggered its progression through a sequence of photoproducts (batho, lumi, meta I, meta II, meta III) analogous to those triggered by activation of rhodopsin. The lifetimes of these intermediates were comparable to those of cone opsins, except for the meta II state, which exhibited a longer lifetime more typical of rhodopsin.

Improvements in the performance of C-opsins during chordate evolution

By comparing the sequences, structures, and functional properties of chordate C-opsins, Akihisa Terakita and Yoshinori Shichida and their colleagues have elucidated a set of transitions that occurred during evolution, that endowed chordate C-opsins with improved performance (reviewed by Tsutsui & Shichida (101); Tsukamoto & Terakita (102); Terakita et al (103)). These changes included the translocation of the counterion site (for the protonated Schiff base) from residue 181 to residue 113, as well as molecular rearrangements of the protein that provided enhanced tilt of helix 6 during activation, and hence led to much stronger activation of the G- protein.

Counterion relocation. To provide stability for the positive charge on the protonated Schiff base in the resting opsin, there is a requirement for a nearby negatively charged counterion. In most opsins (including R- opsins, Go-opsins, RGR-opsins, and photoisomerases) this counterion is located at position 181 (in bovine rhodopsin numbering) which is occupied by glutamate, E181, whereas in cone and rod opsins the counterion is located at position 113, occupied by glutamate E113. Terakita et al (97) found clear evidence that the E181 location represented the ancestral position, and showed that during the evolution of chordate C-opsins the counterion site had migrated to position 113 (Figure 20).

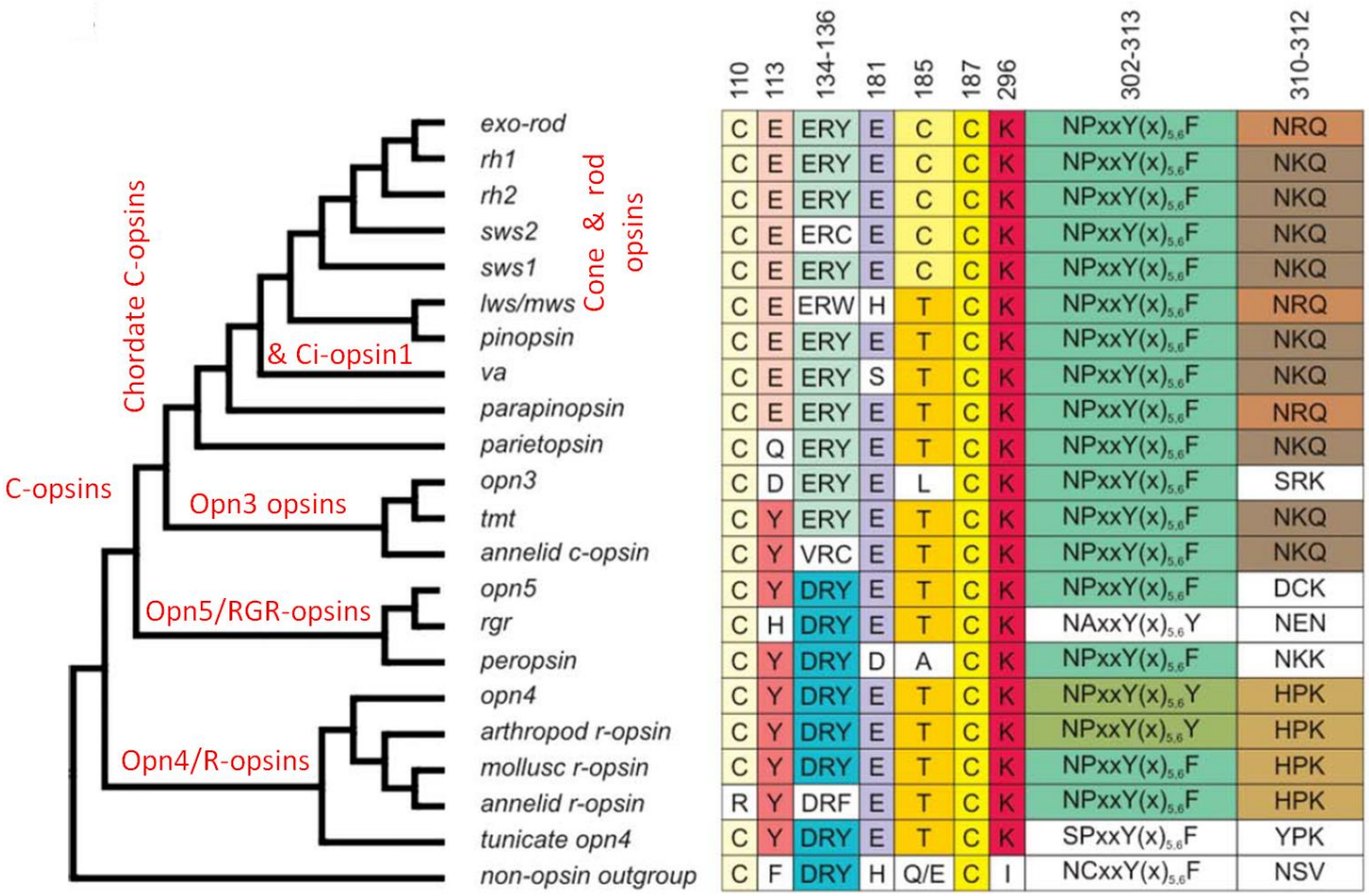

Figure 19. Abbreviated phylogeny of opsins, together with residues of interest Left: Phylogeny of a subset of opsins, comprising vertebrate C-opsins together with a selection of other opsins of interest. Note that the lengths of the lines do not indicate evolutionary distance, and so the horizontal positions of the branch points do not represent the timings of divergences. The C-opsin from *Ciona intestinalis* (Ci-Opsin1) is not included in this diagram, but its position in the tree is close to that of VA/VAL. Right: Residues at several locations that are known to be important for a variety of functions. Here and throughout the article, residue numbering is in accordance with bovine rhodopsin. From Davies et al (94).

Counterion functions. In addition to its role in stabilizing the protonated Schiff base in the resting state, the E113 counterion in cone and rod opsins has a number of other important functions (reviewed by Tsutsui & Shichida, (101)). Perhaps most importantly, it acts as an acceptor for the proton from the Schiff base during activation (see description of molecular mechanism below). Very recently it has been shown that it has two additional crucial functions, in enabling the rapid hydrolysis of the Schiff base bond after light absorption (which is important in cones) and likewise in enabling the rapid binding of 11-*cis* retinal (104)); these roles will be described below, and a comparison between cone and rod opsins will be made in Section 6. The counterion also exerts a powerful effect on the spectral tuning of the resting opsin state. Finally, it is also important in reducing the constitutive activity of the resting opsin; mutants that lack the E113 counterion typically exhibit substantial rates of G-protein activation in darkness. Thus, the acquisition of this alternative location for the counterion has proved enormously important in the evolution of vertebrate retinal opsins.

Increased efficacy of G-protein activation. It has been found (Item B) that the light-activated forms of cone and rod opsins exhibit much greater efficacy of activation of the G-protein than do the active forms of R-opsins, and furthermore that there is a gradation in this property amongst chordate C-opsins. Tsukamoto et al (105) used site-directed fluorescence labeling to examine the changes in the protein that occurred during light activation,

Table 2. Properties of chordate C-opsins

	113	181	λ_{max} (nm) Dark	λ_{max} (nm) Meta	Rev.	ε	G	Effic.	Reference
Cone/rod	E	E	vis.	~380	N	40.6	Gt	[1]	
Pinopsin	E	E	465	385	N		Gt		Nakamura et al (1999)
VA opsin	E	S	501	455	N		Gt	0.2	Sato et al (2011)
Parapinopsin	E	E	370	515	Y		Gt	0.05	Terakita et al (2004) Koyanagi et al (2004)
Parietopsin	Q	E	520	~380	N	31.7	Gt		Sakai et al (2012)
Opn3 opsins	D/Y	E	~460	~470	Y		Gi/Go	~0.1	Koyanagi et al (2013)
Box jellyfish C-opsin	A	E	500	455	N		Gs		Koyanagi et al (2008)
R-opsins	Y/F	E	vis.	vis.	Y	27-35	Gq	0.02	

Item B: For each of the chordate C-opsins, the columns give the following information, where known: 113, 181: Identity of amino acid residue at the two potential counterion sites. λ_{max} Dark: Wavelength of peak absorbance of the 11-*cis* configuration, 'rhodopsin'. λ_{max} Meta: Wavelength of peak absorbance of the all-*trans* configuration, 'metarhodopsin'. Rev: Photoreversal (Y or N). ε: Absorption coefficient of 'rhodopsin' at its peak wavelength (in units of 103 M^{-1} cm^{-1}). G: The class of G-protein that is preferentially activated. Effic.: Efficacy of G-protein activation, relative to efficacy of activated bovine rhodopsin.

and they found a strong correlation between the degree of movement of helix 6 relative to helix 5 during activation and the strength of the opsin's ability to activate the G-protein.

Pre-vertebrate duplication of the ancestral cone opsin. The 'improved' C-opsin that had emerged during chordate evolution, with a high efficacy of G-protein activation and with rapid release of all-*trans* retinal, became the ancestral cone opsin. Furthermore, there is strong evidence that, prior to the '2R' whole genome duplications at the base of the vertebrate lineage, this ancestral cone opsin had already duplicated into the ancestral pair of SWS and LWS cone opsins. However, it is more convenient to consider that evidence later, in Section 6 on vertebrate visual opsins.

Molecular mechanism of activation in vertebrate rhodopsin

The mechanism underlying activation of the metarhodopsin state in bovine rhodopsin is now understood at a molecular level, based to a large extent on examination of the crystal structure of the activated form (106, 107). It seems very likely that fundamentally the same mechanism applies for cone opsins, and therefore that it had arisen prior to the '2R' whole genome duplications. Figure 21 provides a schematic illustration of the events involved in activation (108). Within a few microseconds of photon absorption, a state (meta I) is reached, in which the excitation remains in the twist of the retinoid, and where there has been little movement in the protein. Within a few milliseconds, though, meta I relaxes thermally to the form known as meta II, which

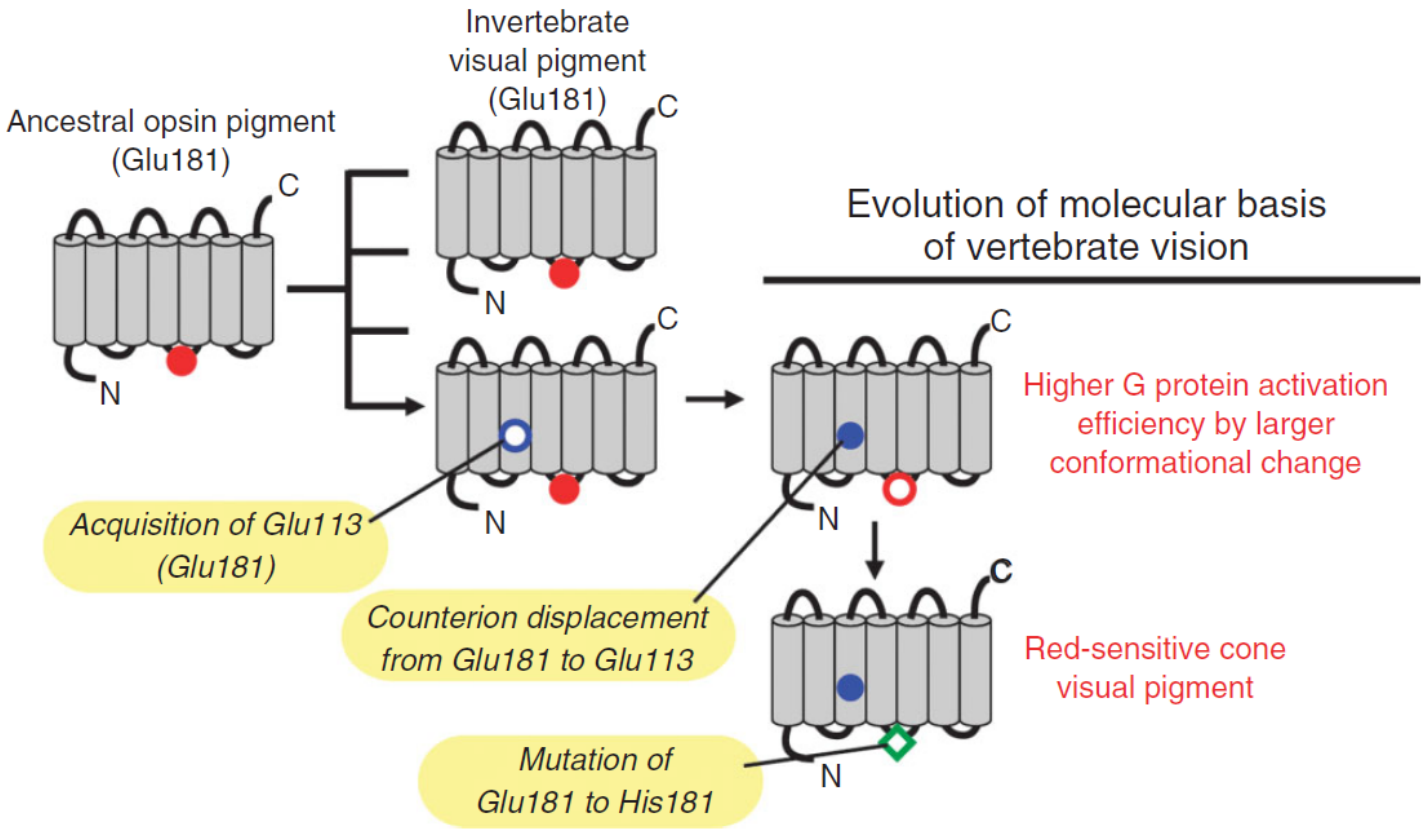

Figure 20. Counterion relocation and molecular rearrangements in chordate C-opsins. The ancestral opsin employed site 181 for the counterion (Glu181 = E181) that stabilizes the protonated Schiff base bond to 11-cis retinal. During the evolution of chordate opsins the site of the counterion relocated to position 113 following acquisition of a glutamate residue (Glu113 = E113) at that site. Both the new (Glu113) and former (Glu181) counterion residues could in principle facilitate the acquisition of new molecular properties for opsin photopigments. In vertebrate visual opsins the Glu113/Glu181 combination appears to have permitted a molecular rearrangement that led to a larger conformational change upon light activation. In one opsin lineage (LWS), mutation of site 181 from glutamate to histidine caused a significant red-shift in sensitivity through the formation a chloride binding site. From Terakita et al (103).

actually comprises an equilibrium between three different (though spectroscopically equivalent) forms. In the first step, a proton translocation occurs, deprotonating the Schiff base of meta I and protonating the E113 residue (109), creating meta IIa. In the second step, meta IIa undergoes an outward tilt of helix 6, opening up a crevice for interaction with the G-protein, creating meta IIb. In the third step, a proton is taken up onto E134 of the 'ERY' motif, which locks helix 6 in relation to helix 3. This form has been termed 'meta IIb H+' and is the enzymatically active form R* that activates the G- protein very efficiently. However, it is unable to undergo photoreversal back to the resting 11-*cis* configuration.

A schematic model for the configuration changes in the opsin/rhodopsin molecule during activation has very recently been proposed by Piechnick et al (110); see their Figure 4. On their model the protein can exist on the one hand in a 'compact inactive' configuration, either when it is ligand-free (as free opsin) or after binding 11–*cis* retinal (as rhodopsin), or alternatively it can exist in an 'opened-up active' configuration, either upon isomerization of rhodopsin to meta II (as R*) or when ligand-free (as Opsin*). Exit or entry of all–*trans* or 11–*cis* retinal is possible only from/to the opened-up active configuration, and such access appears to occur via a retinoid channel that opens between the retinoid binding pocket and the lipid membrane. A separate hydrophilic channel, that permits entry/exit of water during Schiff base hydrolysis/formation, is also proposed to open and close at the same times. This model appears capable of explaining many of the known features of retinoid entry/exit, Schiff base formation/hydrolysis, and switching of the protein's ability to activate the G-

protein. In Section 6 it will be suggested that one difference between rhodopsin and the cone opsins is that access by water is greater, and that it remains possible in the cone pigment's 'compact inactive' configuration.

Rapid hydrolysis of the Schiff base bond after light activation. Recently, Chen et al (104) have shown that the presence of the relocated counterion (the equivalent of E113 in bovine rhodopsin) is crucial in enabling rapid hydrolysis of the Schiff base bond in the light-activated metarhodopsin II state (which occurs ~200× more rapidly for the cone form than for rod metarhodopsin II). As described above, in meta II the Schiff base bond is deprotonated while the counterion site is protonated. However, hydrolysis of the Schiff base bond requires its transient protonation, and Chen et al (104) showed that the proton donor is the protonated counterion residue; water is then able to attack the protonated Schiff base, breaking the covalent bond and thereby leaving all-*trans* retinal non-covalently attached in the retinoid-binding pocket. Hence, we can conclude that the relocation of the counterion site was instrumental in generating a visual pigment that could rapidly release its all-*trans* retinal, thereby contributing to the rapid shut-off of activation needed for a rapid response in cones, and also rapidly readying the opsin for binding 11-*cis* retinal. As will be discussed in Section 6, at a subsequent stage in evolution the Rh1 opsin (rhodopsin) found a way to prevent this rapid decay of meta II, thereby enabling activated rhodopsin to integrate the photon-triggered signal for longer times than could be achieved with the rapidly decaying meta II.

Scenario for the pre-vertebrate evolution of C-opsins

In view of the information above, the following scenario can be hypothesized for the developments that occurred during the evolution of C-opsins in the chordate lineage (modified slightly from the interpretations of Terakita, Shichida, and colleagues):

C-1) An ancestral chordate possessed a C-opsin photopigment that exhibited close homology to extant Opn3 (encephalopsin and TMT-opsin), as well as to cnidarian and protostome C-opsins and even to R-opsins. E181 served as the Schiff base counterion, and site 113 was not negatively charged, and was instead probably either Y or F. This photopigment was bistable and could undergo photoreversal from its active state. It activated a Gi protein, though at a much lower rate than modern cone or rod opsins activate Gt.

C-2) This C-opsin gained a glutamate at position 113. Subsequently this E113 adopted the role of counterion to the Schiff base in the dark resting state, while the ancient E181 may have played a role in stabilizing the protonated Schiff base in the first metarhodopsin intermediate, metarhodopsin I.

C-3) Further mutations occurred, that permitted a larger tilt of helix 6 in the active state thereby improving interaction with the G-protein. This new configuration was stabilized by protonation of the ERY motif, creating the highly-active form metarhodopsin II that is unique to vertebrate 'visual' opsins. This metarhodopsin state exhibits very efficient activation of the G-protein in comparison with its predecessors, but is no longer capable of undergoing photoreversal upon absorption of another quantum (and it also has its absorption maximum in the UV).

C-4) Relocation of the counterion site also expedited hydrolysis of the Schiff-base bond in the activated state, providing a short lifetime of meta II and hence a more rapid photoresponse in those early cones.

C-5) The vertebrate C-opsins Opn3, parietopsin, parapinopsin, VA opsin, and probably pinopsin, represent modern versions of intermediate forms that occurred in this evolutionary progression, and show various degrees of modification of their functional properties from those of the ancestral chordate C-opsin, that remain useful for applications in different types of light-sensitive cell.

C-6) Hence, the ancestral opsin of the first cone photoreceptor in the lateral light-sensitive organs of the proto-vertebrate exhibited highly-efficient activation of the G-protein, along with rapid shut-off; it is also likely that by this stage the G-protein of the cone had evolved to become Gt (transducin).

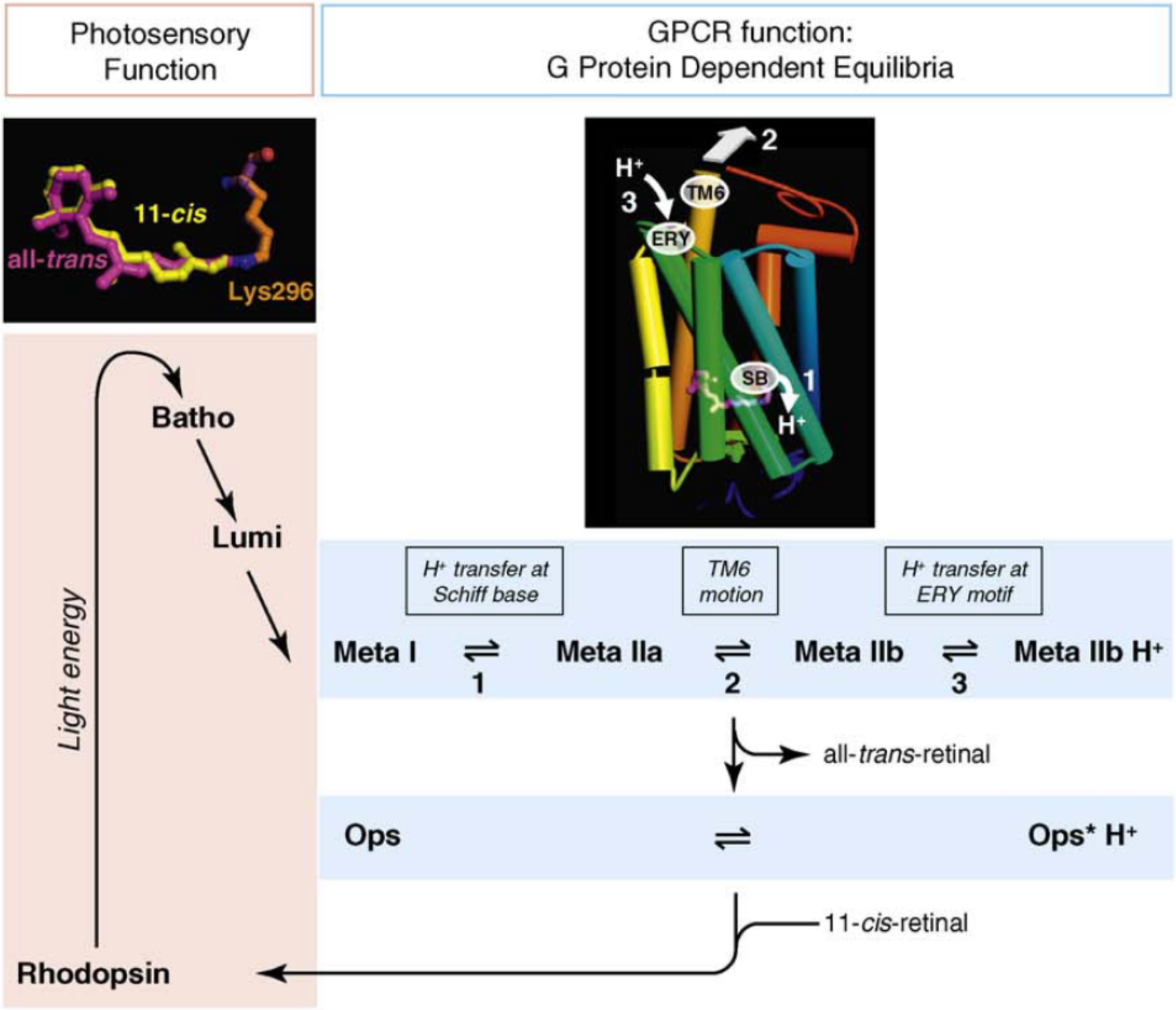

Figure 21. Molecular mechanism of activation of metarhodopsin II in vertebrate rhodopsin. Metarhodopsin II comprises three configurations that are indistinguishable spectroscopically, Meta IIa, IIb, and IIb H+. These are formed sequentially, from meta I: (1) by proton translocation from the Schiff base to E113; (2) by an outward tilt of helix 6; and (3) by protonation of E134 in the 'ERY' motif, that locks the molecule in its active form. From Hofmann et al (108).

C-7) As will be discussed in the next Section, this first cone opsin duplicated, giving rise to what became the SWS and LWS (short- and long-wave sensitive) divisions of cone opsins.

C-8) These events all occurred prior to the '2R' whole-genome duplications that occurred around the base of the vertebrate radiation.

6. Vertebrate 'visual' opsins

A characteristic feature of the retina of jawed vertebrates is its use of cone opsins and a cone-based pathway for intensities from twilight upwards (photopic vision) but rhodopsin and a rod-based pathway for the very lowest intensities (scotopic vision), in what has historically been termed a 'duplex' organization of the retina. It is of

considerable interest to understand how, when, and why this division arose. Along with many of the other advents that occurred in the stem vertebrate lineage, it seems that a major factor contributing to the duality of cones and rods was the occurrence of two rounds of whole genome duplication ('2R'), as proposed originally by Ohno (111) and subsequently confirmed in numerous studies.

By way of background, we will begin by reviewing the phylogeny of cone and rod opsins. Recently, substantial progress has been made in understanding the contribution of the '2R' duplications through studies of gene arrangements on chromosomes, and here we will examine results relevant to opsins. Then we will examine the differences in functional properties between cone opsins and rhodopsin.

In addition to the opsins expressed in cones and rods, the vertebrate retina also expresses a number of other opsins, including melanopsin and VA opsin. Furthermore, it has been shown that the intrinsically-photosensitive retinal ganglion cells (ipRGCs) that express melanopsin comprise a number of subtypes with diverse functions (112, 113). Different subtypes receive synaptic input from different sub-laminae of the inner plexiform layer, and project to different brain areas. Some subtypes are able to contribute to form vision in mouse. However, the following discussion of vertebrate 'visual' opsins will be restricted to the opsins of cones and rods.

Phylogeny of vertebrate 'visual' opsins

Phylogeny. The phylogeny of opsins, including vertebrate 'visual' opsins, has been reviewed in a number of publications, including Terakita (25), Bowmaker (114), Shichida & Matsuyama (8), Davies et al (94), and Porter et al (12), amongst others.

Cone opsins are ancestral to rhodopsin. One of the most important discoveries about the origin of vertebrate retinal opsins was made by Okano et al (115), who showed conclusively that the rod photopigment rhodopsin had evolved from one of the pre-existing cone photopigments. Furthermore, they showed that the first split in the ancestral vertebrate visual opsins had given rise to the SWS and LWS distinction; i.e. to the long-wave-sensitive (LWS) cone opsin on the one hand, and on the other hand to all the other cone opsins plus rhodopsin (the 'SWS' division, that now comprises SWS1, SWS2, Rh2 and Rh1). These fundamental results, which are illustrated by the more recent phylogeny in Figure 22, have been confirmed by all subsequent studies.

Timing of the SWS/LWS split. The evidence to be presented in the next Section (on paralogon arrangement of chromosomes) indicates that ancestral SWS and LWS opsins already existed prior to the '2R' whole genome duplications that occurred at the base of the vertebrate lineage. These two cone opsins already exhibited highly effective activation of transducin, as a result of the molecular rearrangements that had followed relocation of the site for the Schiff base counterion from position 181 to 113. The advent of LWS red-shifted-sensitivity appears to have occurred as follows.

LWS opsins: Red-shift through acquisition of a chloride binding site. As residue E181 was no longer required as the counterion to the resting state, mutations were not as constrained as previously. A mutation of E181 to H181 created a chloride ion binding site that permitted a substantial red-shift in the opsin's peak absorption, giving rise to the ancestral LWS cone opsin. (Note that this numbering is relative to bovine rhodopsin; in the frame of human OPN1LW the residues are H197/K200.) A history of investigations into the nature of this chloride-binding site is given in the recent study of Yamashita et al (116). Wang et al (117) showed that the two residues H181 and K184 contributed to the effect, with H181 being the primary residue contributing the red-shift; the K184 may contribute to enhancing the stabilization of chloride binding. Davies et al (118)and Yamashita et al (116) have recently shown that two other residues, 289 and 292, are also involved in the chloride effect.

As an aside, it is interesting that a handful of mammalian LWS cone opsins have subsequently reverted to a blue-shifted 'MWS' sensitivity through loss of the chloride binding site. One example is mouse 'MWS' opsin, which has the 181 position mutated to tyrosine (Y181); it shows no chloride effect because positions 289 and 292 have

both also mutated to serine (Yamashita et al, 2013). On the other hand, guinea-pig 'MWS' opsin (also with Y181) retains a partial chloride effect, as positions 289 and 292 both remain occupied by alanine.

SWS opsin duplications. The ancestral SWS pigment duplicated twice, to produce four opsins with peak sensitivities in the blue/green region of the spectrum; the next Section will present evidence suggesting that this quadruplication occurred as part of the vertebrate '2R' whole-genome duplications.

Vertebrate cone opsins. As a result of these duplications, the first vertebrates (jawless at that stage) possessed a complement of five distinct cone opsins, that are conventionally classified using the rather confusing terminology of SWS1, SWS2, Rh2, Rh1, and LWS (Figure 22). Those five classes have been inherited by all the descendants of the ancestral vertebrate, though some classes of opsin have been lost in different lineages. For example, monotremes lost the SWS1 opsin (119), while placental mammals lost the SWS2 and Rh2 opsins; for more complete information, see Davies et al (120).

Where they are retained in extant vertebrate species, the four opsin classes SWS1, SWS2, Rh2, and LWS, continue to be expressed in cones. At some subsequent stage (Section 11), the cone photoreceptor that expressed the Rh1 opsin evolved to become a rod. A second type of rod exists in amphibia, utilizing the SWS2 opsin, but the timing of its origin is unclear.

Paralogon arrangement of opsin genes

In order to help determine the role of whole-genome and other large-scale duplications in the evolution of the genes encoding the opsins and associated proteins of phototransduction, Larhammar and colleagues have studied the paralogon arrangement of the genes (7, 121). The term 'paralogon' applies to the (usually) quartet arrangement of related chromosome regions within the genome, that still persist (though often greatly modified) some 500 million years after the two rounds of genome duplication.

Chromosomal arrangement of opsins. The results of Nordström et al (121) and Larhammar et al (7) for the paralogon arrangement of the human opsin genes (as well as the genes for transducin alpha subunits) are shown schematically in Figure 23. The genes for rhodopsin (=RHO), SWS1 (=OPN1SW), and LWS (=OPN1LW) lie in corresponding positions on chromosomes 3, 7, and X. In view of the fact that phylogenetic trees for vertebrate visual opsins always have the SWS and LWS opsins as the most basal divergence (Section 6), they proposed that the locations of the ancestral genes (prior to quadruplication) had been as indicated in the top row. Following the two genome duplications, the ancestral SWS was proposed to have evolved into the SWS1, SWS2, Rh2, and Rh1 opsins of basal vertebrates, of which Rh2 and SWS2 have been lost in mammals (crosses in first column). In addition, it appeared that the LWS opsin had been preserved in only one member of the quartet (now on the X chromosome in humans).

The chromosomal arrangement of the genes for all the other proteins involved in the phototransduction cascade will be deferred to Section 8.

Discrepancy between observed phylogenetic tree and that predicted by '2R' duplications. It is important to recognize a discrepancy between the observed phylogenetic tree for vertebrate cone/rod opsins and the tree expected for whole-genome duplications. From first principles, one would expect that the pair of '2R' whole-genome duplications would have produced a 'forked' phylogenetic tree with a double bifurcation, of the form ((SWS1,SWS2), (Rh2,Rh1)), in contrast to the 'nested' tree (SWS1,(SWS2,(Rh2,Rh1))) that is always observed. In fact, a doubly bifurcating tree might be expected for all gene families that survived the quadruplication event, and the general absence of such forms was originally taken by some as evidence against the occurrence of '2R' duplications.

However, if (as is generally thought) the two duplication events occurred close together in time, relative to the time that has elapsed since, then a variety of influences could alter the form of the phylogenetic tree that is

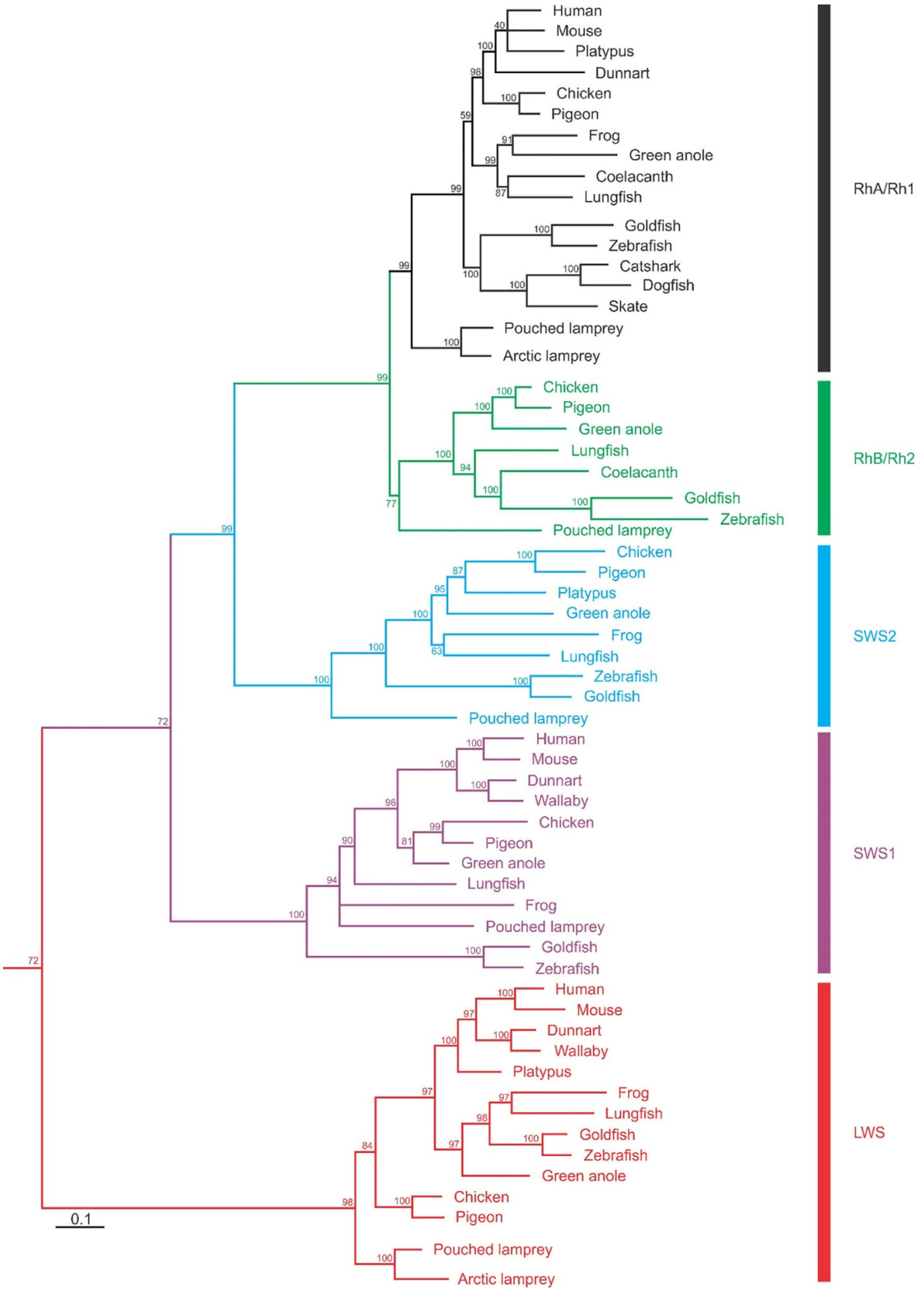

Figure 22. Phylogeny of vertebrate cone and rod opsins. Phylogeny of the gene families of vertebrate visual pigments (i.e. cone opsins and rhodopsin): LWS, SWS1, SWS2, RHB/RH2 and RHA/RH1. Posterior probability values (as percentages) are indicated at the base of each node. The scale bar indicates the number of nucleotide substitutions per site. Branch lengths reflect evolutionary distances. From Collin et al (10).

obtained. In general, any tendency towards different rates of incorporation of substitutions in the different branches could lead to a distortion of the extracted tree topology. For the visual opsins, which have adopted different spectral positions and different kinetic properties, it is plausible that there could have been competition between these (or other) properties, in the different branches, that in practice led to different rates of substitutions at residues in different branches.

As one example, consider what might have happened if the ancestral SWS opsin exhibited its peak absorption close to the UV, and underwent two successive duplications. After the first duplication, it seems likely that selective pressures would have caused a separation of peak wavelengths of the two opsins. However, this pressure is likely to have been asymmetric, because a shift of peak sensitivity further into the UV is unlikely to have been advantageous to the organism, whereas a shift of one of the opsins to longer wavelengths (to occupy the gap between SWS and LWS) is likely to have been advantageous. Comparable arguments would apply after a second duplication. Hence it is possible to envisage that selective pressures would initially have favored a general shifting *apart* of the spectral absorption peaks of the different opsins, though with a 'barrier' at the UV end. On this basis, whichever opsin was nearest to the UV end of the spectrum would have been under selective pressure not to alter its absorption peak, as a shift in either direction would have proved disadvantageous. As a result, it might be expected that the opsin that we now call SWS1 will have experienced a lower rate of substitutions at residues that affect its spectral tuning than have the other opsins. This could have the effect of distorting the extracted phylogenetic tree in a manner that would tend to make the SWS1 opsin appear more ancient than it really is.

It therefore seems that the observed nested phylogeny that is recovered for the visual opsins cannot necessarily be taken as a basis for rejection of the hypothesis that the four SWS opsins (SWS1, SWS2, Rh2, and Rh1) arose from the '2R' pair of whole genome duplications that occurred near the base of the vertebrate lineage. But on the other hand, neither has it been proven that '2R' does indeed account for the existence of the five classes of vertebrate cone and rod opsin.

Differences in functional properties between cone and rod opsins

Differences in functional properties between cone opsins and rhodopsin, and the dependence of these differences on amino acid sequence, have been reviewed by Imai et al (92). Three substantial differences involve: (*i*) the short lifetime of cone metarhodopsins, (*ii*) the rapid regeneration of cone pigments, and (*iii*) the high susceptibility of cone opsins to hydroxylamine attack.

Short lifetime of cone meta II. Many studies have shown that the lifetime of the meta II state is orders of magnitude shorter in cone opsins than in rhodopsin. Shichida's group (reviewed in Imai et al (92)) examined the properties of purified extracted opsins from native membranes or from cultured opsins with point mutations, using spectrophotometry, at a range of temperatures and other conditions. For WT chicken opsins, the meta II decay times were short for cone opsins (~2, ~1, 7 and 16 s for SWS1, SWS2, Rh2 and LWS) but far longer for rhodopsin (210 s), in each case at room temperature and with extraction in CHAPS. More recently, Chen et al (104) reported a similar difference in *Xenopus*, where the meta II for blue/violet-sensitive (SWS1) cone opsin decayed with a time constant of ~3 s compared with ~800 s for bovine rhodopsin (Rh1), both at 20 °C and pH 6 with extraction in 0.1% dodecyl maltoside. Their method involved fluorescence microscopy measurements to monitor the release of all-*trans* retinal, presumed to reflect the decay of meta II.

The large observed difference in speed of meta II decay (or retinal release) is not due to extraction/purification, because Golobokova & Govardovskii (122) found a similar effect in intact individual cones and rods of the goldfish using a fast-scanning dichroic microspectrophotometer. For both the red-sensitive (LWS) and green-sensitive (Rh2) cone opsins they found a meta II lifetime of ~5 s, compared with ~330 s for rhodopsin (Rh1). Hence each of these approaches shows that the decay of meta II occurs 100× (or more) faster for cone opsins than for rhodopsin.

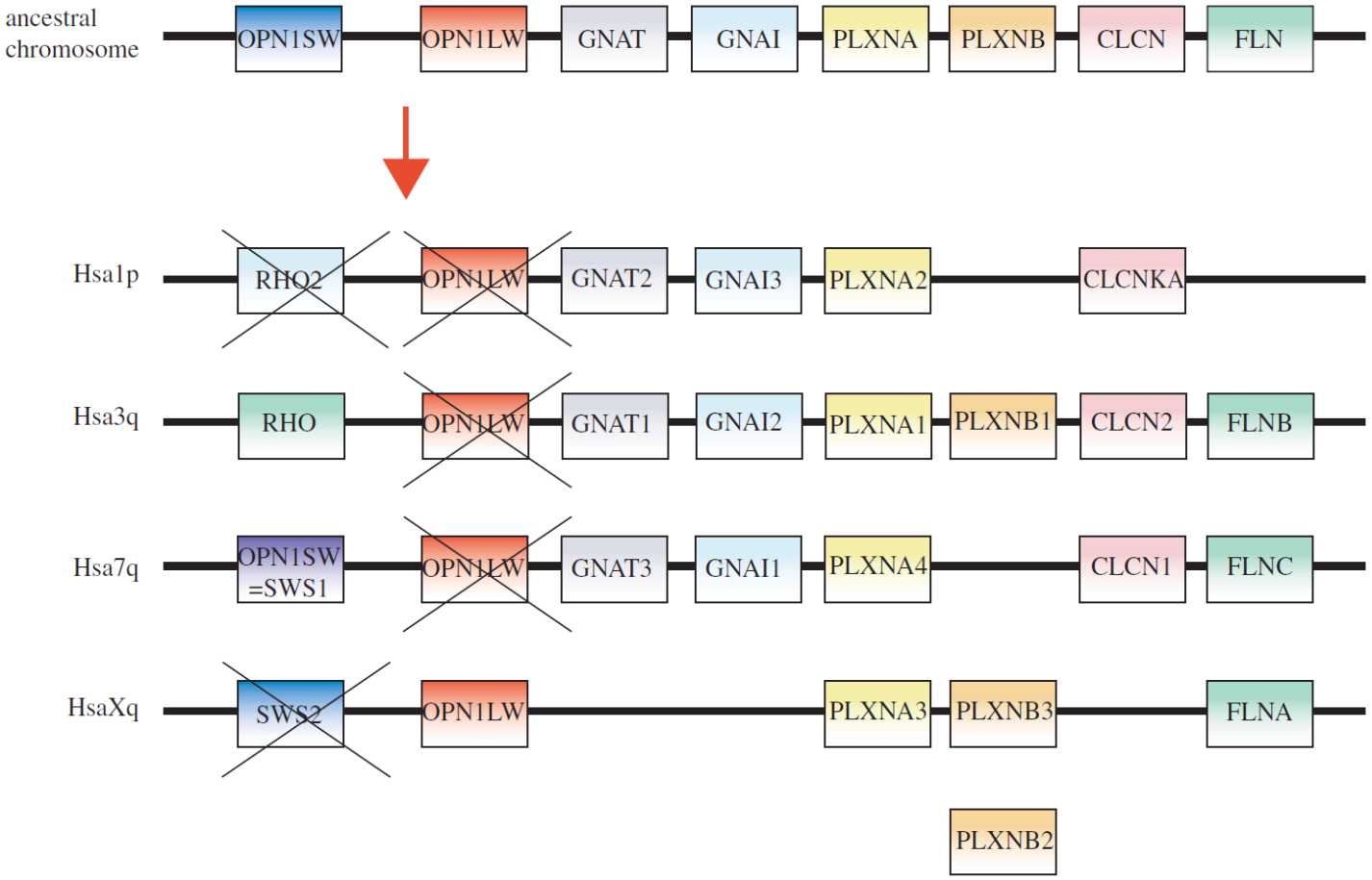

Figure 23. Paralogon arrangement of genes for opsins and transducin alpha subunits Chromosomal locations of vertebrate visual opsin gene family members in the human genome (Hsa for *Homo sapiens*) are shown in the lower four rows. The top row gives the arrangement postulated by Larhammar et al (7) for the ancestral genes, prior to quadruplication, and below, the crosses indicate the positions of the ancient blue- (SWS2) and green-sensitive (RHO2) opsins that have been lost in mammals. The proposed position for the ancient green-sensitive opsin (RHO2) is confirmed by the present location of its ortholog in the chicken genome, in a region with conserved synteny with Hsa1. The ancestral chromosome (top) was postulated to have possessed the SWS and LWS gene pair (OPN1SW and OPN1LW) before the chromosome quadruplication, because phylogenetic trees for vertebrate visual opsins always have SWS and LWS as the most basal divergence (e.g. see Bowmaker, 2008, and Figs. 19, 22). The transducin α subunit is located in the same paralogon, with GNAT1 expressed in rods and GNAT2 in cones (see Figure 26). From Larhammar et al (7).

Role of sites 122 and 189. Yoshinori Shichida's group has employed site-directed mutagenesis to determine the importance of the residues at sites 122 and 189 (in bovine rhodopsin numbering) for these differences in meta II lifetime, as well as for differences in pigment regeneration time (reviewed in Imai et al (92)). Residue 122 is conserved as E122 in all rhodopsins apart from those of deep-sea fish (see below), but in cone opsins it may be I, L, M or Q. Residue 189 is conserved as P in all cone opsins, but it is I in most rhodopsins. Mutations in these two residues act synergistically in determining both the lifetime of meta II and the rate of pigment regeneration. Thus, the presence of the rod forms (E122 and I189) both contributed to slow decay of meta II and to slow regeneration of visual pigment, whereas the presence of the cone forms (I/L/M/Q122 and P189) both contributed to faster kinetics. Together, the effects of these two residues accounted for all of the observed cone/rod difference in meta II kinetics. Although synergistic, the effects at the two locations were not equally strong, with the residue at position 122 being more effective in rods and the residue at position 189 being more effective in cones.

Role of the counterion site 113. The recent study of Chen et al (104) investigated the role of the counterion site in the speed of meta II decay. As mentioned in Section 5, they showed that all-trans retinal was released around 200× faster from the SWS1 cone opsin than from rhodopsin. In the *Xenopus* SWS1 opsin the counterion residue is aspartate (D108), and its removal (by mutation to alanine) led to extremely slow release of all-trans retinal; note that this visual pigment had an unprotonated Schiff base and hence was UV-sensitive so that it needed to be activated by UV rather than blue light. The re-introduction of aspartate at an alternative location (residue 85), also close to the Schiff base, restored absorption in the violet and in addition restored release of all-*trans* retinal. They also compared release of retinal from cone opsin and rhodopsin, when the counterion was removed from each (in bovine rhodopsin by mutation to glutamine); the measurements required higher temperature and longer monitoring times, but remarkably the release rate was equally slow in the two mutant opsins.

From these and further experiments Chen et al (104) concluded that the rate of hydrolysis of the Schiff base bond was similar in cone opsins and rhodopsin, and that what differed was the rate of release of retinal from the opsin after the covalent bond had been broken. This could result from either a difference in the chromophore's interaction with the retinal binding pocket or a difference in its ability to traverse the opsin protein (i.e. its accessibility). As mentioned in Section 5, they proposed a molecular model for hydrolysis of the Schiff base, in which the protonated residue at the counterion site acted as a proton donor to transiently protonate the bond and thereby render it susceptible to attack by water.

Susceptibility to hydroxylamine attack. Cone opsins are subject to degradation by hydroxylamine, whereas most rhodopsins are not. (This applies to rhodopsins of placental mammals, though some non-mammalian and monotreme rhodopsins have been shown to be slowly degraded; (123, 124).) Hydroxylamine attacks the Schiff base bond, and is able to do so in the resting cone opsin as well as in the metarhodopsin state of activated rhodopsin. Hydroxylamine is thought to attack the Schiff base in much the same way as occurs in the normal decay of meta II, by transient protonation of the bond, so that the cone/rod opsin difference in susceptibility to attack by hydroxylamine simply reflects the accessibility of the binding site to hydroxylamine.

Molecular mechanism limiting the speed of metarhodopsin II decay and formation of rhodopsin. Decay from the metarhodopsin II state involves hydrolysis of the Schiff base bond followed by release of all–*trans* retinal from the chromophore pocket, and there has been controversy as to which of these represents the rate-limiting step. By combining the recent work of Chen et al (104) and Piechnick et al (110), the following is proposed. The meta II state has to be transiently protonated, and the proton donor for this is the protonated counterion residue. Water access is required, and is relatively unhindered in cone opsins, but in rhodopsin can only occur via the hydrophilic channel that opens up in the meta II state. Likewise, when 11–*cis* retinal binds to form rhodopsin, a water molecule must be able to exit the binding site via this same route. In the molecular model of Piechnick et al (110), the hydrophilic channel in rhodopsin permits slow access/removal of water in the 'opened-up active' configuration, but very effectively protects the binding site in the 'compact inactive' state. For cone opsins it is simply necessary to postulate that access for water is much less restricted in both the active and inactive configurations.

Rhodopsin inaccessibility. Hence, the three major differences between cone opsins and rhodopsin (meta II lifetime, regeneration time, and hydroxylamine susceptibility) may all simply be manifestations of the fact that the rhodopsin molecule is much more effective at 'shielding' the retinal covalent binding site from small molecules, including water and hydroxylamine. Furthermore, it appears that this major cone/rod difference is contributed by the residues at sites 122 and 189. In other words, the acquisition of these residues may have permitted the rhodopsin molecule to adopt the more compact 'shielded' configuration that excludes water access in the resting state while permitting slow access in the meta II state (see Piechnick et al (110)). Thus, it seems entirely possible that essentially all of the important molecular differences between cone and rod opsins stem from this difference in accessibility, determined mainly by the residues at these two sites.

Evolution of this difference between cone opsins and rhodopsin. In terms of evolution, we can rationalize the above findings with the view (as explained in Section 5) that the ancestral C-opsin of cones had already evolved the relocation of its counterion site, which enabled both the increase in efficacy of G-protein activation and the release of all-trans retinal, with that latter contributing in part to a fast response. But subsequently (after the '2R' duplication) the pressure for increased sensitivity provided an advantage in attaining a longer lifetime of activated meta II for one of the opsins, and this was accomplished in the Rh1 opsin when site 122 mutated to glutamate and site 189 mutated to isoleucine, their present forms in rhodopsin.

The slow decay of metarhodopsin II may additionally have provided an advantage in reducing the toxicity that could have been elicited by a massive rapid release of all-*trans* retinaldehyde in intense light (e.g. sunlight); if so, this would have provided pressure for the retention of E122 and I189 in rhodopsins.

Residue 122 in deep-sea fish. Interestingly, in the rhodopsins of deep-sea fish, residue 122 is often occupied by glutamine (Q122), and this provides a significant blue-shift in the absorption spectrum (125). It is conceivable that the extremely low light intensities that are experienced at great depths lead to so little retinal being released that there is never a toxicity problem with E122Q in these species, whereas there is an advantage in the shift to a shorter wavelength of peak absorption.

Similarity. One interesting similarity, rather than difference, between cone and rod photopigments is that they are all remarkably stable against spontaneous thermal isomerization to the active state. The comparative details of this stability will be treated in Section 10.

Scenario for the evolution of vertebrate 'visual' opsins

From the information presented up to here, the following scenario is proposed for the sequence of evolutionary events that led to the emergence of four cone opsins plus rhodopsin in the vertebrate retina:

D-1) Prior to the large-scale duplication events that occurred at the base of the vertebrate lineage, the rostral region of the central nervous system (that would expand as the diencephalon) contained neurons (some of them ciliary photoreceptors) that expressed a range of C-opsins, including members of the classes parietopsin, parapinopsin, VA opsin, pinopsin, and an ancestral cone opsin.

D-2) In the ancestral cone opsin (and some of the earlier C-opsins), the counterion site had migrated to position 113. Subsequently, changes occurred that permitted greater movement of helix 6. The new meta II form exhibited a high efficacy of activation of the G-protein, and it decayed rapidly to release all-trans retinal.

D-3) This ancestral cone opsin duplicated to form two divisions, SWS and LWS opsins, that were expressed in two separate classes of cone photoreceptor in the part of the diencephalon that was expanding laterally.

D-4) In the LWS opsin, the ancestral counterion site E181 (in bovine rhodopsin numbering) had undergone mutation to H181, to create a chloride ion binding site, thereby giving a substantial red-shift in the pigment's peak absorption.

D-5) The genes for the SWS and LWS opsins were adjacent on a chromosome. Not far downstream were the genes for the alpha subunits of Gt (transducin) and Gi.

D-6) Two rounds of whole-genome duplication gave rise to four copies of the SWS gene, which underwent mutations to become the founding SWS1, SWS2, Rh2 and Rh1 opsins. When bound to 11-*cis* retinal, these visual pigments had peak spectral sensitivities ranging from the UV to the green region of the spectrum. Of the quartet of LWS genes that resulted from the duplications, only one copy survived, corresponding to the LWS (also sometimes called MWS) gene of all extant vertebrates.

D-7) Upon activation by a photon, all of these cone opsins exhibited a high efficacy of activation of the G-protein transducin; none exhibited photoreversal once they relaxed from the meta I state to meta II; and all underwent relatively rapid thermal decay from the active meta II state, releasing all-*trans* retinal.

D-8) In the Rh1 opsin, two mutations occurred (at residues 122 and 189) that led to slower decay of the meta II intermediate. This enabled the photoreceptor expressing the Rh1 opsin to integrate the photon signal for longer, thereby endowing it with higher sensitivity; but a trade-off was the slower re-binding of 11-*cis* retinal and hence slower regeneration of visual pigment. There was little else that distinguished this Rh1 'rhodopsin' from the other 'cone opsins'.

D-9) The thermal stability of these opsins against isomerization (i.e. their ability to avoid spontaneously entering the active all-trans state) was a function of the wavelength of absorption to which they were tuned (see subsequent Section 10), but all of these opsins were highly stable.

7. Vertebrate retinal cones and rods

The triumph of ciliary cells as the primary photoreceptors in vertebrates

In view of the fact that the image-forming eyes of most protostomes employ microvillar photoreceptors, it is natural to ask why vertebrate eyes instead opted for ciliary photoreceptors. Furthermore, given that a single type of fly rhabdomeric photoreceptor can reliably detect individual photons, and also respond very rapidly over an enormous range of intensities (reviewed in Yau & Hardie (126)), it is also appropriate to ask why vertebrates instead use a duplex retina with separate cone and rod divisions.

In considering the relative merits of ciliary and microvillar photoreceptors, and the likely reasons why one or other of these classes triumphed in different organisms, it is important to avoid the error of simply comparing properties between the photoreceptors of living organisms. For example, it is not appropriate to argue on the basis of a comparison between the properties of modern rhabdomeric photoreceptors in flies and modern cone and rod photoreceptors. Instead, one needs to take into consideration the properties of the photoreceptors, and the circumstances of the organisms, at the relevant stage in evolution when the cell type gained its dominance; i.e. at the time when the 'choice' of photoreceptor class was made. At the stage when ciliary photoreceptors first became dominant in the retinas of chordates, more than 500 Mya, the evidence suggests that rods had not yet evolved. Likewise, at the stage when microvillar photoreceptors gained their dominance in protostome compound eyes, possibly more than 550 Mya, it is unlikely that they had yet become true rhabdomeric photoreceptors or that they had yet evolved the highly specialized (and possibly unique) kind of phototransduction cascade of *Drosophila* eyes (127). Accordingly, one needs to investigate the relative merits of the rather simpler ciliary and microvillar photoreceptors that were likely to have existed in those ancient times.

With those points in mind, we can list a number of advantages that ciliary photoreceptors might have had over microvillar ones, at the time that the 'choice' between them was made:

E-1) Firstly, the polarity of response (hyperpolarizing to light and depolarizing to darkness) meant that ciliary photoreceptors would have been ideally suited for shadow detection in ancient organisms. The depolarization induced by a shadow could have triggered either an action potential or an increase in release of synaptic transmitter without additional logic, and this might have been advantageous for an animal with a simple nervous system.

E-2) Secondly, there may have been little difference in gain between the two classes of photoreceptor. Very recently, Ferrer et al (46) have shown that the gain of transduction in amphioxus microvillar photoreceptors is much lower than the gain in modern rhabdomeric photoreceptors. However, the extremely short duration of the quantal response in chordate microvillar photoreceptors (a few ms; (43)) may have been disadvantageous in comparison with the slower responses of ciliary photoreceptors.

E-3) Thirdly, it has been calculated that in a bright environment the energy consumption is lower for a hyperpolarizing ciliary photoreceptor, in which the ionic currents decrease in the light, than for a depolarizing microvillar photoreceptor, in which the ionic currents increase in the light; on the other hand the energy consumption of the two classes of photoreceptor is comparable in darkness (128). A duplex retina has a further advantage in a bright environment because the rods saturate, thereby reducing their energy consumption to a low level, and it is only the cones that continue to generate a circulating current with its consequent energy demand (11).

E-4) Fourthly, chordate ciliary opsins (but not other ciliary opsins) underwent intra-molecular changes that substantially increased the efficacy of their activation of the G-protein. As a consequence, though, they lost the ability to undergo photoreversal.

E-5) Fifthly, these new ciliary opsins exhibited quite rapid decay of the active metarhodopsin II state, releasing bound all-*trans* retinal, and thereby enabling the binding of 11-*cis* retinal. Such release would have been made essential by the inability of the pigment to undergo photoreversal; however it is also possible that this change preceded the increase in activation efficacy. In the case of bistable opsins (R-opsins and the early C-opsins), the activated pigment remains in the metarhodopsin state for an extended period after exposure to light, so that the pool of rhodopsin available to detect incident photons is depleted. In this respect, a bistable photopigment may have been severely disadvantageous when an organism moved from a bright environment to a dim environment and needed to dark-adapt rapidly. Chordate ciliary photoreceptors may thus have provided a distinct advantage under such conditions.

E-6) Finally, an additional benefit to the organism may have arisen not directly from the properties of the phototransduction process, but from the fact that the ciliary cells evolved synaptic transmission onto their microvillar counterparts (see Section 15), thereby constituting a dual photoreceptive system via a single afferent pathway.

In any case, as the discussion above shows, it is possible to point to several important ways in which ciliary photoreceptors may have proved superior to microvillar photoreceptors in ancient chordates. For one reason or another, ciliary photoreceptors did indeed triumph in the light-sensitive organs of proto-vertebrates.

Multiple classes of vertebrate retinal photoreceptor

For a review of the distribution of opsins and the variations in morphology and in transduction pathways across classes of vertebrate photoreceptors, see Ebrey & Koutalos (91).

As described in Section 6, the ancestral vertebrate possessed five classes of cone/rod opsin photopigment. In addition it possessed five morphological classes of cone/rod photoreceptor. On the basis of the norm in photoreceptors of jawed vertebrates, as well as circumstantial evidence from extant lampreys (Figure 15), it seems likely that each class of photoreceptor expressed a single class of opsin.

In jawed vertebrates, these photoreceptors comprise four classes of cone, expressing their individual cone opsins (SWS1, SWS2, Rh2, LWS), plus a single class of rod photoreceptor expressing the rod photopigment, rhodopsin (Rh1). However, at least in amphibia, the SWS2 'cone' opsin can additionally be expressed in another class of rods (called 'green rods' because of their greenish tint). In living lampreys, all five classes of photoreceptor appear cone-like, though the class that expresses 'rhodopsin' has some rod-like properties (Section 3). As a result, it is plausible that 'true' rods had not evolved prior to point #5 in Figure 1. The timing of the emergence of rods will be discussed in Section 11.

Currently it is not clear whether the initial driving force for the multiplicity of spectral classes of cone photoreceptor was simply in order to cover more of the 'visible' spectrum, given that each opsin absorbs over a relatively narrow region of the spectrum, or whether it was to provide 'color vision'. But it seems reasonable to

think that, almost as soon new spectral information became available to an organism, it would have been utilized by the nervous system to provide color information.

Morphological differences between cones and rods

Details of the morphology of cone and rod photoreceptors are given in Webvision Part I, Chapter 2 'Photoreceptors'; here we will simply concentrate on *differences* between the two classes of cell.

Sac versus disc structure. The most marked morphological difference between mammalian cones and rods relates to the topology of the outer segment membrane. In cones, the entire membrane is continuous with the plasma membrane of the inner segment, whereas in rods the bulk of the outer segment membrane is sealed off from the plasma membrane in the form of discs that resemble deflated balloons. These discs are not actually 'free floating', but appear to be tethered to the plasma membrane by proteins including peripherin/RDS, Rom1, and the GARP domain of the cyclic nucleotide-gated channel.

In both cell types, new outer segment membrane is continually being formed in the vicinity of the ciliary neck, and bulges outwards, so that new sacs are repeatedly formed beneath recently formed ones, in a mechanism that was documented experimentally by Steinberg, Fisher & Anderson (129); see Figure 16B above. They showed that a process of rim formation occurs between the membranes of adjacent sacs, though in cones it proceeds only part way around the circumference, so that the sacs are always open to the exterior (patent). In rods, however, this process of rim formation proceeds all the way around the circumference (bi-directionally), zippering together the apposed surfaces, and thereby forming a disc pinched-off from the plasma membrane.

As a result of this 'sealing over' of discs in rods, newly synthesized protein is trapped in the newly formed discs. As additional discs are created, those formed earlier slowly migrate outward along the length of the outer segment, over a period of weeks, before being phagocytosed by the RPE. This localization and migration of proteins can be demonstrated experimentally by autoradiographic examination at successive times after application of labeled amino acids (130). In contrast, what is seen in cones is a uniform distribution of label over the entire outer segment, as expected if protein is able to diffuse (even very slowly) throughout the continuous plasma membrane of the outer segment.

Other morphological differences. A further morphological difference between their outer segments is the existence of one or more incisure(s) in rods; these deep longitudinal indentations into the outer segments provide an increased cross-section of cytoplasmic space that increases the effective longitudinal diffusion coefficient for intracellular messengers (see also Section 11). At the level of the inner segment, cones exhibit specializations that do not occur in rods, including the paraboloid and sometimes spectral filters (an oil droplet or vesicles, in the ellipsoid). Probably because of its high refractive index, the inner segment of cones is very effective in funneling incident light into the outer segment, and this gives rise to a marked Stiles-Crawford directional effect in cones, and a weak one in rods. At their synaptic terminals, cones and rods differ substantially, with the cones exhibiting large pedicles and the rods exhibiting smaller spherules. In addition, there are other subtle morphological differences between cones and rods.

Overview of functional differences between cones and rods

The light response properties of cone and rod photoreceptors are remarkably similar to each other (see below), and the cells exhibit just a few major differences:

a. *Rods*. The defining feature in the response of the rod photoreceptor is its ability, under dark-adapted conditions, to respond reliably (i.e. with good signal-to-noise ratio) to the absorption of individual photons of light (131, 132). This single-photon detection performance is possible because the noise, expressed as 'dark light', is very low in rods; this dark light is many orders of magnitude lower in rods than in LWS cones, though the difference may be smaller in the case of SWS cones.

b. *Cones*. The defining features in the responses of the cone photoreceptor are its ability: (*i*) to respond rapidly, (*ii*) to function over an enormous range of intensities, so that (*iii*) it never saturates in steady light, no matter how bright the intensity, and (*iv*) its ability to recover much of its responsiveness almost instantaneously when an intense light is extinguished (reviewed in Lamb (133)).

Cone/rod similarities. In most other respects, the responses of cone and rod photoreceptors are remarkably similar to each other, as shown in Item C for human LWS cones compared with rods. For example, the amplification of the phototransduction cascade appears to be reasonably similar in mammalian cones and rods. The observed difference in sensitivity between them (of around 20-fold) results in large part from the more rapid shut-off of the cone response, which is typically around 5-times faster than in rods under dark-adapted conditions. As illustrated in Figure 24, cone and rod responses begin rising with broadly similar gain, but the cone responses recover much sooner. It has also been shown that the shapes of the light responses (i.e. their kinetics) are closely similar, apart from an overall scaling of the time axis.

However, the gain of transduction and the rate of activation of G-protein by activated opsin are probably not exactly equal in cones and rods, and indeed there are several reports of a lower gain in cones. Kawamura & Tachibanaki (134) reviewed measurements from isolated cones and rods of fish and salamander, and concluded that the gain in the cones was considerably lower. More recently, Tachibanaki et al (135) conducted careful experiments on the rate of G-protein activation by light-activated visual pigment, and found this rate to be ~5× lower in cones than in rods. Nevertheless, a recurring difficulty in measurements of cone biochemistry is that the shut-off reactions are so fast that this creates problems in determining activation rates. Overall, it seems likely that the gain of transduction in cones lies somewhere in the range 0.2-1× that in rods.

The responses in Figure 24 also illustrate the general observation that cone photoreceptors expressing blue/green-sensitive opsins (i.e. those with the SWS1, SWS2, or Rh2 opsin) typically tend to display response properties intermediate between those of LWS cones and rods; thus, blue/green-sensitive cones are slower and more sensitive than red-sensitive cones.

Major cone/rod differences in performance. In Item C the parameters exhibiting major differences between cones and rods are indicated in red. Firstly, although cones and rods both exhibit classical Weber-law light adaptation, for rods this occurs only over a restricted range of intensities before they saturate, whereas for cones the adaptation continues up to indefinitely high intensities so that they never saturate in steady light. Secondly, rods typically display a very low rate of photon-like events in darkness, of the order of one event per tens or hundreds of seconds, whereas in LWS cones the 'dark light' may typically be of the order of hundreds of photon events per second. Although much of this difference in dark light stems from the difference in wavelength of peak absorbance (Section 10), a small part appears to be due to intrinsic differences between rhodopsin and cone opsins. Finally, following extinction of a steady light that bleaches more than 90% of the photopigment, human cones recover their circulating current within ~20 ms (136), whereas for human rods comparable recovery of circulating current may take 20 mins, which is slower by a factor of ~60,000×.

These differences will be treated according to the photoreceptor class that exhibits the superior performance. Thus, the avoidance of saturation and the speed of response will be dealt with in Section 9 on cone photoreceptors, while transduction noise and the ability to resolve individual photons will be treated in Section 10 and Section 11.

8. Evolution of the vertebrate retinal phototransduction cascade

In this Section we will investigate the evolution of the 'vertebrate-style' phototransduction cascade that is employed in chordate ciliary photoreceptors, with emphasis on those of the vertebrate retina. The similar cascades utilized in protostome and cnidarian ciliary photoreceptors will be mentioned only in passing. The aims will be (1) to determine the nature of the phototransduction cascade that existed in a chordate ancestor of

	Parameter	Cone	Rod	Units	Qualitative effect	Ratio
Adaptational range and dark noise	Saturating intensity	–	100	Td	**Low in rods, but unlimited in cones**	**>10,000×**
	Weber fraction	0.5	10	%	Better in cones	~20×
	'Dark light'	>100	0.01	R*/s	**Enormously lower in rods**	**~10,000×**
Response kinetics and sensitivity (dark-adapted)	Response time-to-pk	25	125	ms	Faster in cones	~5×
	Sensitivity	0.1	2	pA/R*	Higher in rods	~20×
	Gain of transduction	5	10	s^{-2}/R*	Slightly lower in cones	~0.5×
Speed of reactions (dark-adapted)	R* lifetime	3	40	ms	Faster in cones	~10×
	G*/PDE* lifetime	10	200	ms	Faster in cones	~20×
	cGMP turnover time	350	250	ms	Similar	~1×
	Ca^{2+} turnover time	3	50	ms	Faster in cones	~20×
Dark adaptation after very large bleach	Time for recovery of circulating current	0.02	1200	s	**Enormously faster in cones**	**~60,000×**
	Time for regeneration of visual pigment	3	15	min	Faster in cones	~5×
	Time for full recovery of visual sensitivity	5	50	min	Faster in cones	~10×

Item C: Comparison of light response properties of human LWS cones and rods. Parameter values are representative, and have been taken from numerous different sources. The parameters with very large cone versus rod differences are shown in bold red. Note that the turnover time for cGMP in cones is effectively much shorter than shown, even for the dim-flash response, because of the combination of the flash-induced activation of PDE within each sac and the calcium feedback loop.

ours, just prior to the '2R' rounds of whole-genome duplication, and (2) to determine the manner in which that cascade became specialized in cones and rods. Thus, we will be examining the co-evolution of components of the cascade, initially in pre-vertebrate chordates, and thereafter in the earliest vertebrates.

Evolution of bilaterian phototransduction cascades

In Figure 25A, the major components of several phototransduction cascades are contrasted, for vertebrate photoreceptors (top), for other ciliary photoreceptors, and for microvillar photoreceptors (103). Each of these cascades appears to have evolved from a common ancestral form.

Co-evolution of cascade components. The co-evolution of molecular components across phototransduction cascades was investigated by Arendt & Wittbrodt (137), who compared the phylogenies of the genes for opsin,

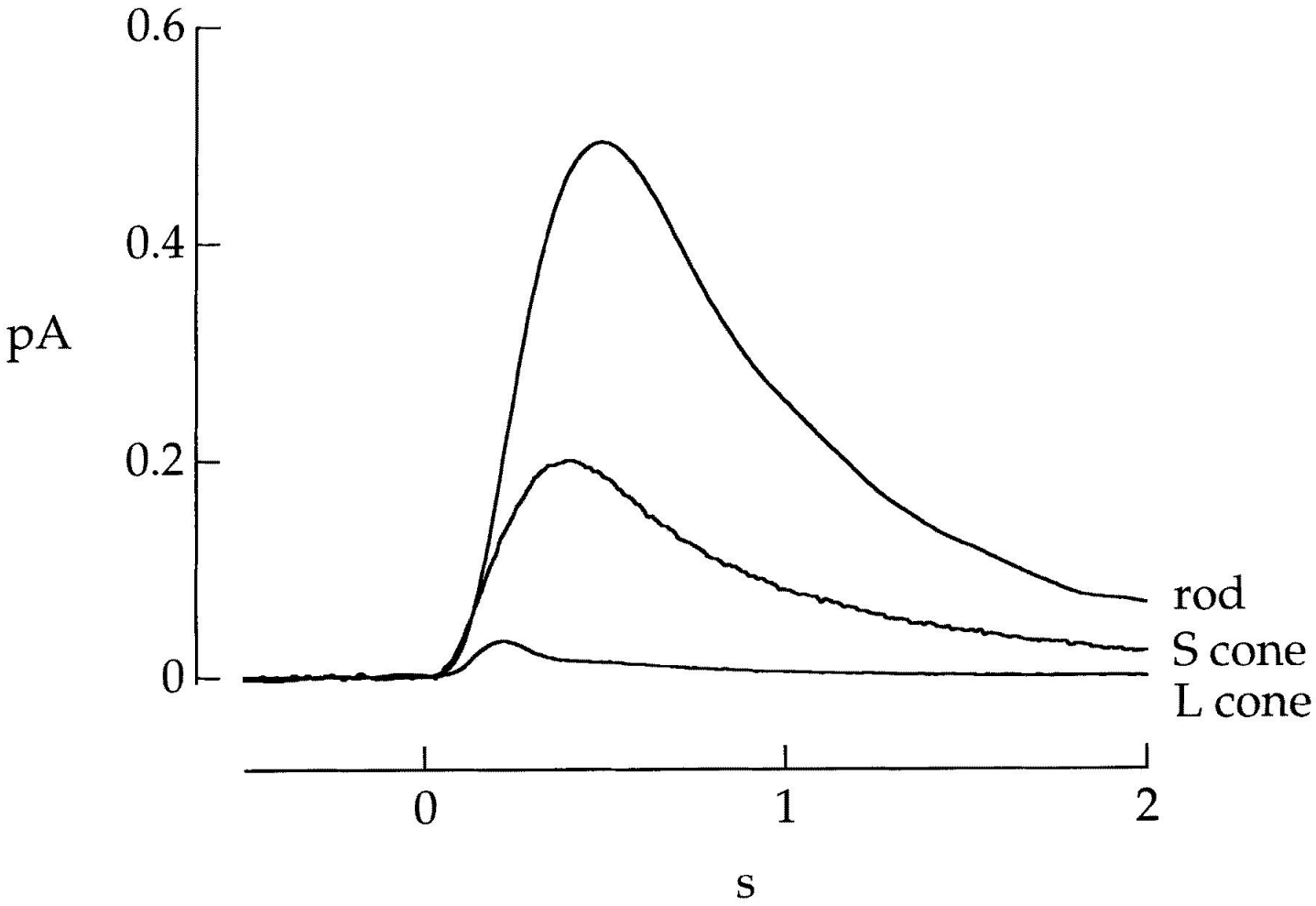

Figure 24. Comparison of single-photon responses in LWS and SWS cones and a rod. Averaged responses to a single photoisomerization in representative dark-adapted photoreceptors of the salamander. The photopigments in these cells are: L cone, LWS; S cone, SWS2; rod, Rh1. The responses reach peak in approx. 200, 400 and 600 ms, and their amplitudes are roughly in the ratio 1 : 6 : 12. From Rieke & Baylor (270).

plus its G-protein, kinase, and arrestin, across protostomes and deuterostomes. They found clear evidence that all four of these components must have been present in the common bilaterian ancestor.

Coupling to G-proteins. The coupling of opsin type with G-protein type was examined by Koyanagi et al (138) and has recently been reviewed by Terakita et al (103). They categorized opsins into four groups according to the G-proteins to which they coupled. Chordate C-opsins couple to Gi/Gt; at least one cnidarian C-opsin couples to Gs; invertebrate 'Go-opsins' couple to Go; while all R-opsins couple to Gq.

Origin of cascades using CNGCs. The evolution of the coupling of opsin via its G-protein to an ion channel was investigated by Plachetzki et al (26, 27). For the downstream effector mechanism, at the level of the cell's electrical response, Plachetzki et al (27) provided evidence that the ancestral cascade had employed CNGCs (cyclic nucleotide-gated channels), as illustrated in Figure 25B. Furthermore, the alternative TRP/TRPL (transient receptor potential-like) channel mechanism appeared to have arisen at a later stage, probably in bilaterians, and was employed in microvillar photoreceptors, where the R-opsin couples via Gq.

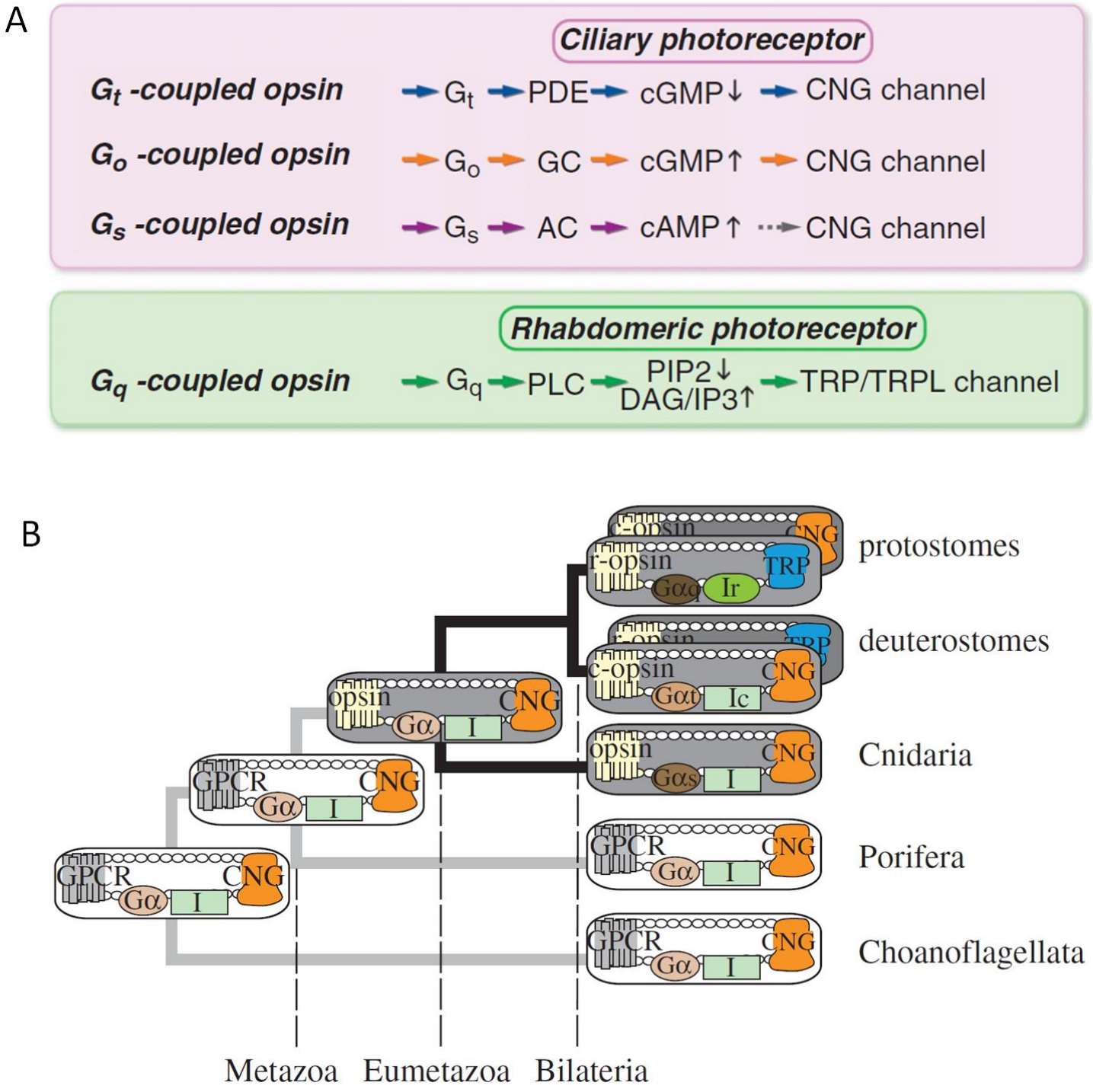

Figure 25. Co-evolution of components of phototransduction cascades. A, Components of the phototransduction cascades in ciliary and microvillar (rhabdomeric) photoreceptors. From Terakita et al (103). B, Sequence of evolution for the components of phototransduction cascades proposed by Plachetzki et al (27). Bottom left: The ancestral (non-photosensitive) G-protein cascade utilized a GPCR that coupled ultimately to a CNG (cyclic nucleotide-gated) channel. Third from left: The mechanism in the ancestral light-sensitive cell was similar. Top right: Early in the bilaterian lineage two variants of this scheme arose, both of which have been preserved in protostomes and deuterostomes. (Note that the obscured rear diagram for protostomes is the same as the front diagram for deuterostomes, and vice versa.) The ancestral mechanism was retained only slightly modified in the ciliary variety of photoreceptors, that expressed C-opsins. But the microvillar variety of photoreceptors, that expressed R-opsins, instead coupled via a Gq G-protein (and unknown intermediaries) to a TRP (transient receptor potential) channel. Additional abbreviations: I, intermediary molecules; Ic, ciliary intermediaries such as phosphodiesterase (PDE) and guanylyl cyclase (GC); Ir, rhabdomeric intermediaries such as phospholipase C (PLC), DAG (diacylglycerol) and PIP2 (phosphatidylinositol-4,5-biphosphate). From Plachetzki et al (27).

Molecular components of the vertebrate phototransduction cascade

The molecular and cellular mechanisms underlying activation and recovery of the (modern) vertebrate phototransduction cascade are dealt with in detail in Webvision 'Phototransduction in Rods and Cones', as well as in numerous reviews, including Lamb & Pugh (139), Wensel (140), Yau & Hardie (126), etc. The principal proteins involved, both in cones and rods, are shown schematically in Figure 26. For an overview of these proteins and their functions, see Wensel (140); for a review of the proteins mediating shut-off of R*, see Gurevich et al (141).

Summary of molecular mechanisms. The molecular mechanisms of phototransduction are almost identical in cones and rods. Photoisomerization of a molecule of visual pigment to its active form R* triggers the catalytic activation of the G-protein (Gt, transducin) to G*, which in turn activates the cGMP phosphodiesterase (PDE6) to E*. The increased hydrolysis of cGMP lowers its cytoplasmic concentration, causing closure of cyclic nucleotide-gated channels (CNGCs). This suppresses the circulating electrical current that had been flowing in darkness, hyperpolarizing the cell; in addition, it leads to lowered cytoplasmic Ca^{2+} concentration through the continued activity of a $Na^{+}/Ca^{2+},K^{+}$ exchanger, and this drop in Ca^{2+} level is important for response recovery. Response shut-off requires inactivation of each of the activated forms, as well as restoration of cGMP levels. R* is rapidly inactivated by the binding of arrestin, but this step first requires the R* to have been phosphorylated by a G-protein receptor kinase (GRK). The G*/E* complex is rapidly inactivated by hydrolysis of the terminal phosphate of the GTP bound to G*, through the action of the GTPase accelerating (GAP) activity of the RGS9-Gβ5-R9AP complex. The drop in Ca^{2+} concentration permits Mg^{2+} to bind to guanylyl cyclase activating proteins (GCAPs), thereby activating guanylyl cyclase (GC), restoring cGMP levels, and hence causing the re-opening of ion channels. This action of Ca^{2+} endows the photoreceptor with a powerful negative feedback loop that helps stabilize the electrical current.

Differences in isoforms and activities between cone and rod proteins

The proteins mediating the light response in cones and rods are closely similar; indeed a few of the proteins are identical in the two classes of photoreceptor, though in most cases distinct but closely related isoforms are expressed, as indicated by the gene names shown in Figure 26 and listed in Item D. A number of online resources exist for examining the genes involved in the eye, and two useful resources are RetinaCentral.org (with the 'retinome', or transcriptome of the retina/RPE; (142)) and RetNet, sph.uth.edu/retnet (with retinal disease genes).

When we come to compare the functional properties of cones and rods in Sections 9 to 11, we will see that it is possible to view the rod transduction cascade as a variant of the cone transduction cascade, in which the main difference is that each of the shut-off steps in the dim flash response has been slowed down. For several of the phototransduction proteins, the expression levels in cones are much higher than in rods, and this probably accounts for several instances of more rapid shut-off of the light-activated molecules. A notable example is the 10-fold higher expression level in cones of the molecular complex RGS9/Gβ5/R9AP that shuts off the activated G-protein, transducin, when it is bound to the PDE. For shutting off activated rhodopsin, cones and rods in many species employ different isoforms of the GRK (G-protein receptor kinase): in cones it is typically GRK7 whereas in rods it is GRK1; in this case, the difference in isoform probably contributes substantially to slowing the shut-off of activated rhodopsin and therefore in increasing the sensitivity of the response (134, 143, 144). For dim flashes the recovery kinetics are also determined by the turnover time in darkness for cGMP, and in rods this turnover time is slowed as a result of a lower basal activity of the rod PDE6 (145).

The overall effects of the differences in activities and expression levels of the different isoforms of phototransduction proteins have been analyzed and modeled by Kawamura & Tachibanaki (134) and Korenbrot (144), who have been able to account well for the observed differences in kinetics and sensitivity between cones and rods.

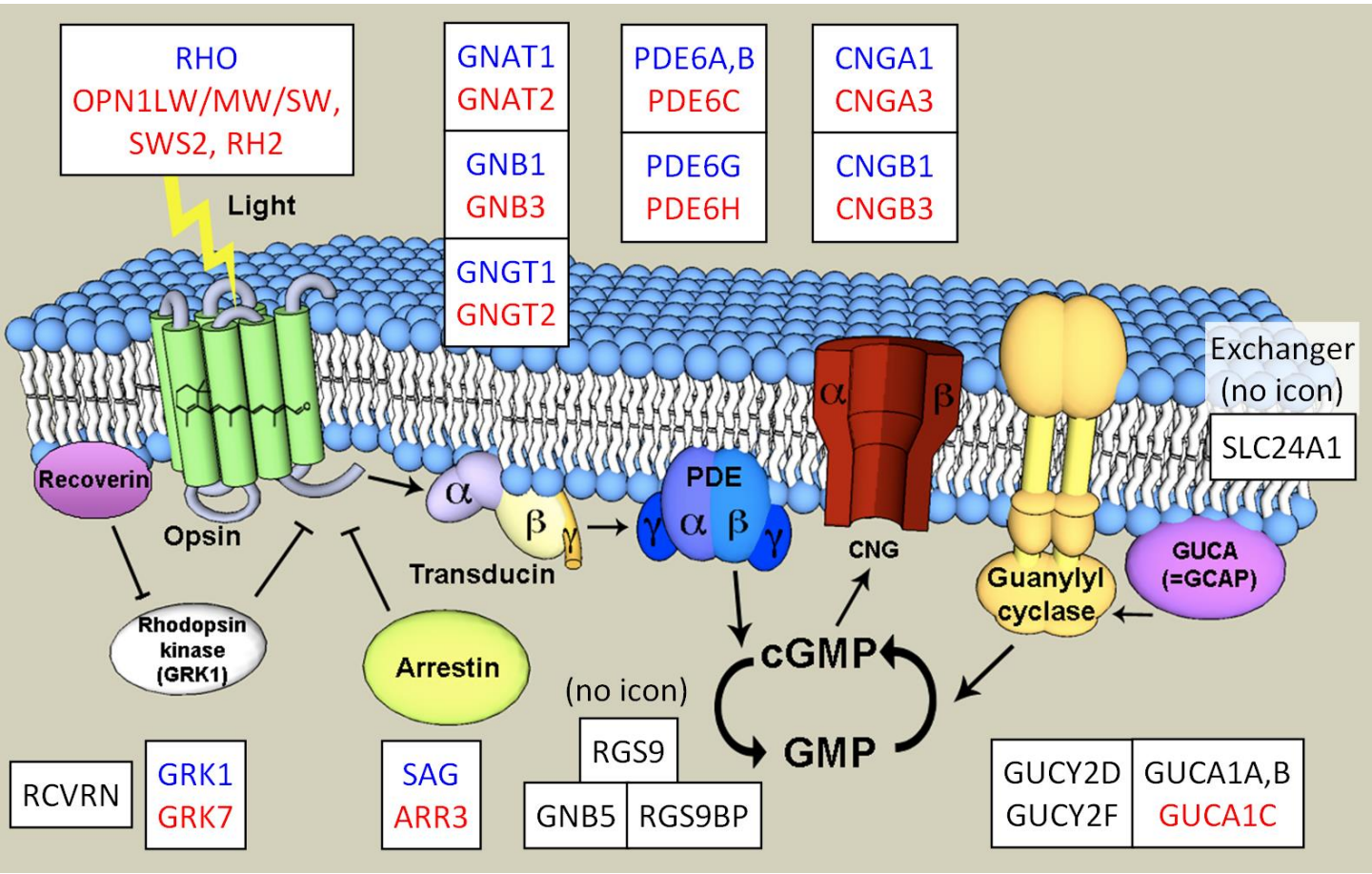

Figure 26. Molecular components of the vertebrate phototransduction cascade. The proteins underlying the activation phase of the phototransduction cascade in a cone are illustrated schematically; because the membrane configuration of a cone rather than a rod is illustrated, the ion channel and ion exchanger are in the same membrane as the other proteins. From Larhammar et al (7). The names of the corresponding genes are listed nearby, with those for activation above and those for recovery and regulation below or to the right. Note, though, that icons for the RGS9/Gβ5/R9AP complex and the Na+/Ca2+,K+ exchanger (SLC24A1) are not included in this diagram. Where there is a clear distinction between expression in cones and rods, the genes are colored red for cones and blue for rods, while black indicates expression in both cones and rods; see Nordström et al (121) for references. A more complete list of the proteins/genes involved in phototransduction, as well as those involved in the recycling of retinoid, is given in Item D. Note that the arrestin gene SAG (retinal S-antigen) is sometimes known as ARR1, and that ARR3 is sometimes known as ARRX. The ion channel is a tetramer, composed of both α and β subunits, and is permeable to monovalent and divalent cations. In cones, it comprises two CNGA3 and two CNGB3 subunits; in rods, it comprises three CNGA1 subunits and a single CNGB1.

Evolution of components of the vertebrate phototransduction cascade

For vertebrate phototransduction, Hisatomi & Tokunaga (146) compared the phylogenies of the genes for eight families of the proteins involved (transducin, PDE, CNGC, GRK, arrestin, recoverin, GC, GCAP). They noted close similarity in the branching patterns of the gene dendrograms, and concluded that each of these families appeared to have evolved 'cone' and 'rod' branches, though in two cases (PDE and GCAP) there had been a further duplication in the rod branch. More recent results, examining the evolution of individual components of the phototransduction cascade, will now be presented.

Transducin. The origin of transducin alpha subunits was investigated by Muradov et al (87), who identified two isoforms in lamprey, that they named GαL and GαS, for their expression in the long (cone-like) and short (rod-like) photoreceptors, respectively. GαL is roughly equally distantly related to cone and rod transducin alpha subunits of jawed vertebrates, and might represent the ancestral form, whereas GαS clades with the rod version, though it retains certain cone-like characteristics such as the presence of the 'hallmark' four-residue sequence

Protein name	Gene name in human	Has role in:	Cell	Protein description
Rh (Rh1)	RHO	Activation	Rod	Rhodopsin
LWS	OPN1LW OPN1MW	Activation	L-cone M-cone	Long-wave-sensitive opsin
SWS1	OPN1SW	Activation	S-cone	Short-wave-sensitive opsin
SWS2	–	Activation	Cone (or rod)	Blue/green-sensitive opsin
Rh2	–	Activation	Cone	Blue/green-sensitive opsin
Gα	GNAT1 GNAT2	Activation	Rod Cone	Transducin α subunit
Gβ	GNB1 GNB3	Activation	Rod Cone	G-protein β subunit
Gγ	GNGT1 GNGT2	Activation	Rod Cone	Transducin γ subunit
PDEα PDEβ PDEα'	PDE6A PDE6B PDE6C	Activation	Rod Rod Cone	PDE6 hydrolytic subunits
PDEγ PDEγ'	PDE6G PDE6H	Activation	Rod Cone	PDE6 inhibitory subunits
CNGCα	CNGA1 CNGA3	Activation	Rod Cone	Cyclic nucleotide-gated channel α
CNGCβ	CNGB1 CNGB3	Activation	Rod Cone	Cyclic nucleotide-gated channel β
GRK	GRK1 GRK7	Recovery	Rod Cone	G-protein receptor kinase
Arr	ARR1/SAG ARR4	Recovery	Rod Cone	Arrestin
Rec	RCVRN	Recovery	Both	Recoverin
RGS9	RGS9	Recovery	Both	Regulator of G-protein signaling 9
Gβ5	GNB5	Recovery	Both	G-protein β subunit 5
R9AP	R9AP	Recovery	Both	RGS9 anchor protein
GC	GUCY2D GUCY2F	Recovery	Both	Guanylyl cyclase
GCAP	GUCA1A,B GUCA1C	Recovery	Rod Cone	GC activating protein
Exchanger	SLC24A1	Recovery	Both	$Na^+/Ca^{2+},K^+$ ion exchanger
at-RDH	RDH8, 12	Retinoid	Both	all-*trans* Retinol dehydrogenase
ABCR	ABCA4	Retinoid	Both	ATP-binding cassette transporter
IRBP	RBP3	Retinoid	RPE	Interphotoreceptor retinoid-binding protein
CRBP	RBP1	Retinoid	RPE	Cellular retinol-binding protein
LRAT	LRAT	Retinoid	RPE	lecithin:retinol acyltransferase
RPE65	RPE65	Retinoid	RPE	Isomerohydrolase, RPE65
11c-RDH	RDH5	Retinoid	RPE	11-*cis* Retinol dehydrogenase
CRALBP	RLBP1	Retinoid	RPE	Cellular retinal-binding protein

Item D: Genes for proteins with known function in phototransduction or retinoid cycling. List of proteins with known functions in activation and recovery of the phototransduction cascade, and in the RPE retinoid cycle. Names of the human genes are given in column 2. Where there is a clear distinction between expression in cones and rods, the genes are colored red for cones and blue for rods, while black (and 'Both') indicates expression in both cones and rods, as in Figure 26 and Figure 27. Not enough is known about the intra-retina retinoid cycle in order to list its components. Many additional proteins have important functions in cones, rods, and RPE cells, apart from involvement in phototransduction and retinoid cycling, but are not listed here. Likewise, numerous other proteins are involved in signal transmission and neural processing within the retina

near the N-terminus. In order to determine the timing of the duplication that gave rise to these two transducin alpha subunits, there is additional information that can be obtained from analysis of the location of genes on chromosomes (see Section 8 below).

Phosphodiesterase. The phosphodiesterase (PDE6) used in vertebrate phototransduction is unique in its ability to be regulated by the gamma subunit (Pγ), and the co-evolution of these two components has been investigated by Muradov et al (86) and Zhang & Artemyev (147). Muradov et al (86) cloned both components from lamprey. For the PDE6 catalytic unit, they found that lamprey has a single isoform (as in cones), with high homology to jawed vertebrate PDE6 catalytic units, though equally distantly related to those of cones and rods, and their results were consistent with the notion that PDE6 arose from a common PDE5/6/11 ancestor in the chordate lineage. They identified a tunicate PDE that grouped with vertebrate PDE6, but they could find no other non-vertebrate sequences grouping with PDE6.

For the regulatory Pγ subunits, they found two isoforms, one cone-like and the other intermediate between cone and rod sequences; no sign of similar sequences was found in tunicate databases. Their evidence suggested that these regulatory subunits arose in the stem vertebrate lineage, and that the common ancestor of lampreys and jawed vertebrates was likely to have already possessed two isoforms. This analysis was extended by Zhang & Artemyev (147) who provided evidence that, although Pγ is a strictly vertebrate invention, the capacity of the PDE catalytic units to bind Pγ predated the emergence of the inhibitory subunit; indeed their analysis predicted that the PDE5/6-like enzymes of cnidaria should interact with vertebrate Pγ.

CNGCs. In cones the cyclic nucleotide-gated channel comprises two α subunits (CNGA3) and two β subunits (CNGB3), configured as A3-A3-B3-B3 (148), whereas in rods the channel comprises three α subunits (CNGA1) and a single β subunit (CNGB1). Nordström et al (121) found strong evidence that the duplication that gave rise to the α and β subunits of the cyclic nucleotide-gated channel took place prior to the divergence of protostomes and deuterostomes, and they also found suggestive evidence that the multiple versions of α and β subunits may have arisen in the '2R' duplications.

GRKs. Mushegian et al (149) have recently investigated the origin and evolution of G-protein receptor kinases (GRKs). They found evidence that GRKs originated prior to metazoa, through the insertion of a kinase (similar to a ribosomal protein S6 kinase) into a loop in a domain with homology to RGS (regulator of G-protein signaling). During chordate evolution an ancestral GRKa split into the GRK1/7 and GRK4/5/6 lineages. Mushegian et al (149) suggest that this coincided with the first round of '2R' whole-genome duplication, though it is possible that the split may have occurred earlier, as an apparently ancestral GRK1/7 is present in the tunicate *Ciona intestinalis.* The results of Larhammar et al (7) (see next Section) suggest that the distinction between GRK1 and GRK7 arose during the '2R' duplications. However, further work is needed to resolve the origin of these isoforms.

Arrestin. The phylogeny of arrestins (including 'visual' arrestin) has been studied by Gurevich & Gurevich (150) and Alvarez (151), and the function of these proteins has been comprehensively reviewed by Gurevich et al (141). Arrestins arose very early in metazoan evolution, with the family comprising both the β-arrestins (named after their interaction with the β-adrenergic receptor) and the 'visual' arrestins, having diverged from a much larger family in pre-bilaterian times (151). A clue to the nature of the much more recent split between vertebrate visual arrestins and β-arrestins has been provided by Kawano-Yamashita et al (152) who reported that the pineal non-bleaching opsin, parapinopsin, appeared to be inactivated by a β-arrestin through a process of internalization (as in other β-arrestins). They noted that *Ciona intestinalis* photoreceptors apparently use a β-arrestin, and they proposed that the vertebrate-style visual arrestin had evolved specifically for use in shutting-off opsins that release their retinoid; i.e. specifically in the case of vertebrate visual opsins.

Chromosomal arrangement of phototransduction genes

The paralogon arrangement of the opsin genes was presented in Section 6. Here we consider the results of Larhammar et al (7) relating to the paralogon arrangement of other components of phototransduction.

Transducin alpha subunits. Interestingly, Larhammar et al (7) showed that the gene for the transducin alpha subunits was in the same paralogon as the opsins, and close by (see Figure 23). Recently, Lagman et al (153) have combined an analysis of the gene arrangements for each of the three subunits of the trimeric transducins with sequence-based analyses, and they have provided evidence that all three families of transducin subunit expanded during the early vertebrate tetraploidizations. They concluded that the early vertebrate tetraploidizations provided the basis for the subsequent specialization of transducin subunits leading to differential expression between cones and rods.

The original GNAT gene may have arisen by duplication within the deuterostome lineage of the ancestral GNAI/GNAT gene present in bilaterians, as some protostomes have homologs of GNAI, but none have homologs of GNAT; alternatively, the duplication could have occurred earlier, but with GNAT being lost in protostomes.

Other components of the phototransduction cascade. Larhammar et al (7) also found apparent remnants of a paralogon arrangement in a local grouping of the genes for the transducin beta subunits, for the GRKs, and for the arrestins (their Fig. 5). In addition they found evidence for '2R' expansion of the genes for PDE6, and for both the alpha and beta subunits of the CNGC channel, as well as for arrestin and the GRKs.

Interpretation. For many of the proteins involved in the phototransduction cascade, there is a difference (either partial or complete) in the distribution of isoforms between cones and rods, and for at least 10 of the 13 protein components studied by Larhammar et al (7) the differentially-distributed isoforms arose as a result of the '2R' duplications at the base of the vertebrate lineage. Accordingly, there seems little doubt that much of the distinction between the cone and rod transduction cascades can be traced to the reduction in constraints on gene mutation that resulted from the two whole-genome duplications.

Hypothesized nature of pre-vertebrate ciliary photoreceptor and transduction cascade

From the available evidence, it does not yet seem feasible to paint a scenario for the detailed sequence of events that transformed an ancestral bilaterian photoreceptor into a vertebrate photoreceptor. However, it is possible to propose the following for the state that had been reached, in the evolution of the 'proto-cone' photoreceptor and its phototransduction cascade, just prior to the '2R' whole-genome duplications that occurred near the base of the vertebrate lineage:

F-1) The ancestral cone opsin of the 'proto-cone' photoreceptor was broadly similar to modern pinopsin and SWS and LWS cone opsins, and in particular it had evolved a high efficacy of activation of the G-protein.

F-2) Duplication of that ancestral cone opsin created a pair of retinal cone opsins: an SWS opsin with the standard E181 residue, and an LWS opsin with the H181/K184 combination that provided a chloride-binding site giving a substantially red-shifted absorption. The SWS and LWS opsins were expressed in separate, but closely similar, cones. The output signals from those cones could potentially have been utilized to provide dichromatic color vision.

F-3) The primary additional proteins involved in activation of the cascade had evolved to become: (*i*) the ancestral transducin Gt, with unique alpha, beta and gamma subunits; (*ii*) the ancestral PDE6 cyclic GMP phosphodiesterase, comprising a pair of identical catalytic subunits and a pair of identical regulatory (gamma) subunits; and (*iii*) a tetrameric cyclic nucleotide-gated channel composed of two classes of subunit, alpha and beta.

F-4) The Gαt had probably arisen from a common ancestral Gαi / Gαt during chordate evolution. The PDE6 had arisen from a common ancestral PDE5/6/11 during chordate evolution. The PDE regulatory subunit had arisen late in chordate evolution, after the divergence of tunicates (i.e. after #4 in Figure 1).

F-5) The primary proteins involved in response recovery and regulation had evolved to become the ancestral 'cone' components, specified by the genes GRK7, ARR3, RGS9, GUCY2D/F, GUCA1C, SLC24A1 and RCV1, in addition to the cone opsins themselves.

F-6) The presence of all these components suggests that response shut-off occurred in a manner fundamentally similar to that in modern vertebrate photoreceptors.

F-7) In particular, the co-existence of the components required for the Ca^{2+} feedback loop (GUCA1C, GUCY2D/F, CNGA3/B3) provides strong circumstantial evidence that the negative-feedback loop that stabilizes the circulating current, and assists in light adaptation, was already present.

F-8) All the components of the transduction cascade were expressed in the membranes of the lamellar sacs that radiated laterally from the cilium of the proto-cone.

F-9) Because of the release of all-*trans* retinoid from activated opsin, the photoreceptor's outer segment required a source of 11-*cis* retinoid, and this may have been provided by the glial (Müller) cells.

F-10) The cell had evolved a simple glutamatergic synapse, permitting synaptic transmission.

9. Cones: Photoreceptors with exceptional performance

Cones exhibit high sensitivity, high speed, and high contrast sensitivity

High sensitivity. Despite frequent claims to the contrary, cone photoreceptors are highly sensitive, and the amplification of transduction appears to be quite similar to that of rods. Indeed, when one views a dim star at night, it is the cones (and the photopic system) that detect the star. For example, in viewing the Pleiades (Seven Sisters), although one will be aware of the cluster as a blur in the parafoveal field by means of scotopic vision, when one fixates the individual stars then it is the cones that are detecting them. The rod system is much better for the diffuse cluster, because of its wide spatial summation, but the cone system is better at detecting individual stars, because of its higher spatial resolution. The sensitivity of individual cones is sufficient to detect quite dim stars, though for very dim stars one may be better off using parafoveal rod vision.

High-speed response. The speed of response in cone photoreceptors is far higher than in rods, and this speed increases with increasing background intensity. In bright illumination, the human photopic visual system is able to resolve sinusoidal or square-wave flicker at frequencies of around 100 Hz (154), for which the brighter/dimmer periods are ~5 ms each. Thus, it seems that light-adapted cones are able to generate a resolvable signal when the illumination is extinguished for as short a duration as about 5 ms.

High contrast sensitivity. The human photopic (cone) system is able to detect very small fractional changes in intensity. Thus, under light-adapted conditions, an observer can detect a contrast of 0.5%; for comparison the contrast sensitivity of the scotopic (rod) system is at least an order of magnitude poorer, at >5%.

Hence, the cone system is extremely sensitive, extremely fast, and it has excellent contrast sensitivity.

Avoidance of saturation by cones: Unlimited upper operating intensity

In contrast to rod photoreceptors, which saturate at quite low intensities, cone photoreceptors are remarkable for their ability to function well during steady illumination - no matter how intense that steady background is made (155, 156). Although cones may saturate transiently at the onset of intense illumination, they rapidly recover and are able to signal increments and decrements, even when the illumination is so bright that it bleaches a large

proportion of the photopigment. To account for this, Lamb & Pugh (139) compared the shut-off reactions in human cones and rods; they showed that the ability of the cones to avoid saturation can be explained in terms of the combination of the ~20-fold faster shut-off of the activated cone photopigment, and the ~20-fold faster shut-off of the activated cone Gt/PDE complex.

In human rod photoreceptors *in vivo,* the circulating current is halved at a steady intensity of ~70 scotopic trolands (600 $R^* s^{-1}$), with complete saturation occurring at ~1000 scotopic trolands (~10^4 $R^* s^{-1}$). If the activation gain of transduction is comparable in human cones and rods, then the two very short cone time constants would elevate the intensities required for half and full saturation by some ~400×, to levels of ~240,000 and ~4×10^6 $R^* s^{-1}$ in cones. Two additional factors are that the gain of transduction may be slightly lower in cones, and that the cGMP-gated channels of mammalian cones (in contrast to those of rods) show increased affinity for cGMP when Ca^{2+} falls (157); these factors would further increase the R* rate required to saturate the cone. Now, the highest *steady* rate of photoisomerization that can ever be reached in a human cone, *by exposure to steady light,* corresponds to the maximal rate of pigment regeneration, which has been shown by Mahroo & Lamb (158) to be 0.75%/s, which in a cone containing 40 million molecules of cone opsin corresponding to ~300,000 $R^* s^{-1}$. Hence, this maximum possible rate of steady photoisomerizations is lower than the isomerization rate calculated above to be needed to saturate the cone, meaning that the cone can never be saturated by steady light.

A more intuitive way of understanding this is to say that very high steady intensities cause the cone opsin to bleach to a level low enough to prevent saturation of the response by the steady light. As a result, the photopic visual system is able to function over (i.e. to adapt to) an enormous range of intensities, from moon-lit conditions to the brightest sun-lit scenes.

Extremely rapid recovery of cone circulating current

When the human eye is exposed to steady light sufficiently intense to bleach 90% of the photopigment in the rods, full recovery of the rod circulating current takes around 20 mins after extinction of the light (159). In contrast, a steady light that bleaches 90% of the LWS/MWS cone photopigment does not saturate the cone response (see above), and around half the circulating current remains. Upon extinction of that light, the cone circulating current recovers fully within ~20 ms, around 60,000-fold faster than for the rod (136).

As in the case of the cone's avoidance of saturation, the molecular mechanisms that enable this extremely rapid recovery of circulating current lie in the rapidity of the inactivation steps. Kenkre et al (136) estimated that in the presence of bright light the time constants for the shut-off reactions were as follows: for R*, ~5 ms; for G*/E*, ~13 ms; and for cGMP turnover, ~4 ms. Using these parameters in a simple model of cGMP kinetics and channel activation, they were able to accurately fit their experimental measurements of the time-course of recovery of cone current. In rods, the extremely slow recovery of current is caused not by the slowness of inactivation/shut-off steps in the G-protein cascade, but instead by the slowness of the regeneration of visual pigment, combined with the fact that unregenerated opsin activates the cascade; for a full account of this slow recovery, see Lamb & Pugh (160).

Morphological features required by a cone

The operational requirements of cone photoreceptors place certain constraints on the morphological features of the cells.

High surface to volume ratio of outer segment. In order to achieve rapid response kinetics, all the recovery reactions must be fast, including the Ca^{2+}-mediated acceleration of guanylyl cyclase activity that permits rapid re-opening of the cyclic nucleotide-gated ion channels. This means that the time constant for equilibration of cytoplasmic Ca^{2+} concentration (τ_{Ca}) must be short. In mammalian (including human) cones, τ_{Ca} has been estimated as ~3 ms (161, 162), in contrast to its value in amphibian rods of the order of 400 ms or more.

Simulations showed that if τ_{Ca} was not kept as short as the longest of the other shut-off time constants, then the responses became strongly biphasic or even oscillatory.

Straightforward analysis shows that τ_{Ca} should be inversely proportional to the activity of the $Na^+/Ca^{2+},K^+$ exchanger, but directly proportional to cytoplasmic volume (see eqn 15 of Lagnado et al (163)). Accordingly, a high surface-to-volume ratio for the outer segment, that allows a large number of molecules of exchanger per unit volume of cytoplasm, will provide a short time constant τ_{Ca} for Ca^{2+} and will therefore be advantageous for cones. In addition, the calcium buffering power of the outer segment will need to be kept low for cones.

Function of open sacs. The above requirement for a high surface-to-volume ratio no doubt provided a powerful driving force for the opsin-containing membrane of cones to remain in contact with the extracellular medium, and hence for the outer segment membrane not to seal over in the way it does in rods. In LWS cones, an additional driving force for the retention of open sacs may relate to the chloride-binding site, H197 (=H181 in the bovine rhodopsin frame), that confers a substantial red-shift in spectral sensitivity. This site is in the second extracellular loop, and in order to provide a high (and stable) chloride ion concentration on this side of the membrane, it is probably necessary for this region to remain extracellular, instead of transforming to become intradiscal as occurs in the discs of rods.

The existence of the sac structure in cone photoreceptors would appear likely to restrict both the membrane-based reactions and the cytoplasmic reactions resulting from a single photoisomerization to the domain of just a single sac; this could conceivably be either advantageous or disadvantageous, depending on the response property under consideration.

Synaptic release constraints. In order for cone photoreceptors to be able to transmit their graded (i.e. analog) signals rapidly, it is essential that the rate of release of synaptic vesicles be extremely high. This is necessary because the post-synaptic signal needs to be detected above the noise that is intrinsic to the quantal release of neurotransmitter vesicles. In order to be able to detect a change of (say) 1% in the release of vesicles, it is necessary that the mean number of vesicles released should be of the order of $1/(0.01)^2$, or 10,000. And in order for this to be achievable in (say) 100 ms, the rate of vesicle release would need to be around 100,000 vesicle s^{-1} which is enormously high. Accordingly, the cone's synaptic terminal requires a very large area for the active release zone, in order to achieve this kind of rate of vesicle release. For comparison, in a rod the response to a single photoisomerization is considerably larger than the cell's baseline noise, so that it may be adequate to be able to detect a change of the order of (say) 10%; in addition the rod's response is a much slower than the cone's. Hence, a far lower rate of vesicle release (and hence a smaller synapse) would suffice to provide a sufficiently reliable post-synaptic signal from a rod.

Scenario for the refinement of vertebrate phototransduction in cones

The following scenario is proposed for the refinement of the phototransduction cascade in chordate ciliary photoreceptors, that occurred during the early evolution of the vertebrate retina:

G-1) By the time that the chordate lateral retinas began signaling spatial (i.e. visual) information (see Section 17) there was great evolutionary pressure for rapid responses, for high sensitivity, for the ability to adapt to different intensities, and for high contrast sensitivity.

G-2) Those pressures led to acceleration of each of the recovery steps in the cascade; i.e.: shut-off of activated opsin, shut-off of G-protein/PDE, turnover time for Ca^{2+} concentration, and Ca^{2+} feedback to the re-opening of ion channels.

G-3) To compensate for the reduced sensitivity that would inevitably have accompanied the faster responses, there would have been a continuation of the pressure for increased efficacy of activation of the G-protein by the activated opsin.

G-4) Given the existence of multiple classes of cone, not all of these needed to be equally fast or equally sensitive. The systems with shorter wavelength (and hence more thermally stable) opsins could afford to become slower, in order to achieve higher sensitivity. The LWS system, with its high intrinsic noise, was better suited to achieving the fastest performance.

G-5) In response to the intense pressure to be able to transmit responses rapidly, and also to be able to signal small changes in light level (low contrasts), changes took place in the synaptic terminal that led to very high rates of release of synaptic transmitter. In this way, even brief and small changes in cone intracellular voltage led to changes in post-synaptic transmitter concentration that could be detected above the noise inherent in the vesicular nature of release.

G-6) By the time that the first (jawless) vertebrates evolved, their lateral retinas possessed five spectral classes of cone photoreceptor that exhibited exceptional responses properties, broadly similar to those of modern vertebrate cones.

10. Noise: Thermal isomerization and other sources of noise

This Section examines sources of noise (fluctuations) in the responses of photoreceptors, beginning with intrinsic properties of the opsins and then within the transduction cascade.

Thermal isomerization of cone opsins and rhodopsin

In considering the differences between cones and rods, one major disparity relates to the level of noise: LWS cones are many orders of magnitude noisier than rods (Item C). Here we will examine the extent to which this difference in noise is a function of the stability of opsin molecules with different peak wavelengths.

More than 60 years ago, Stiles (164) developed a model describing the long-wavelength decline in spectral sensitivity of visual pigments, later expanded by Lewis (165), invoking the concept that the thermal energy of vibration in the molecule could add to the energy of a photon in order to trigger activation. Barlow (166) extended this concept, with the proposal that spontaneous thermal activation could occur, at a very low rate, even in the absence of light, and he predicted reduced stability (greater noise) for pigments of longer wavelength. Barlow's prediction has been borne out in numerous experimental studies (167, 168), and theoretical models of varying complexity have been proposed to account for the exact relationship between peak wavelength and rate of thermal activation (165, 168-170).

One important observation is that 'cone' opsins can be incredibly stable, and this is most obvious when that particular opsin is expressed in a rod. In amphibia, the so-called 'green rods' (that absorb in the blue, and hence appear green) express a blue-sensitive pigment, which has been shown to be the SWS2 opsin that is also expressed in blue-sensitive cones in the same retina (171). Early electrophysiological experiments showed that green rods of the toad exhibit a very low rate of spontaneous thermal isomerizations (172), and more recent experiments have shown this rate to be amazingly low, at $<10^{-14}$ s^{-1} at 23 °C (168). This means that the SWS2 (cone) pigment, when expressed naturally in a toad rod, only activates spontaneously on average once every ~10^{14} s, or ~4000 years. Thus, this 'cone' pigment is the most stable of all known opsins, including conventional rhodopsins!

Cones: Dark noise

Intracellular voltage recordings from LWS cones in turtle have shown very high levels of noise (173). Usually, this noise is reduced in amplitude by the 'averaging out' that results from the extensive lateral spread of signals across the electrically coupled network that is created by the gap junctions that link neighboring cones (174). But in a cone that is not coupled to its neighbors (an 'electrically isolated' cone), the observed amplitude of dark noise, of around 3000 μV peak-to-peak, is truly enormous when compared with the mean single-photon

response amplitude of only 25 μV, and utterly precludes the resolution of individual photon events. Calculations indicate that this dark noise is equivalent to the quantal fluctuations that would be produced by a real light of a little over 2000 photoisomerizations s^{-1}; this parameter is termed the 'dark light' experienced by the cone. Experiments with backgrounds showed that application of a real light of this intensity roughly halved the flash sensitivity of the cone. Subsequently, in intracellular measurements from macaque LWS/MWS cones, Schneeweis & Schnapf (175) found dark noise that they calculated to be equivalent to >3000 R^* s^{-1}per cone.

The source of these dark fluctuations in the intracellular voltage of LWS cones has not been established. In turtle cones, a significant contribution would be expected to come from thermal activation of the opsin (see above), because the wavelength of peak absorption is exceptionally long, at around 620 nm; indeed this appears to be the longest known wavelength of peak sensitivity of any opsin. If all the dark noise originated from thermal isomerizations, then the cone's opsin content of ~10^8 molecules divided by the event rate of 2000 s^{-1} would yield a mean thermal lifetime of 0.5 × 10^5 s, which is not far from the prediction of Luo et al (168); their Fig. 4C) for a cone opsin of this wavelength. In addition to photopigment noise, the transduction process is also expected to contribute noise (see below). And finally, the chattering activity of ion channels in the synaptic terminal should contribute additional noise. To date, the relative contribution of these potential sources has not been evaluated. One way to investigate the contributions would be to use suction pipette experiments, though a potential drawback is that separation of the cone outer segment from its normal enmeshment amongst the processes of the RPE cells might conceivably alter the cone's performance compared with that in the intact retina.

Rods: Transduction noise and variability of the single-photon response

Transduction noise in rods. In rods, it is possible to separate noise in the transduction process (and subsequently) from the noise caused by thermal isomerization of rhodopsin, because of the fact that the spontaneous photon-like events are individually resolvable (at least, under dark-adapted conditions). In dark-adapted toad rods, Baylor et al (176) reported that the residual 'continuous' noise corresponded to shot events with an amplitude around 1/400 of the single-photon event and occurring randomly at a mean rate of around 6000 events s^{-1}. In functional terms, this source of noise can be considered low, simply on the basis that the great majority of single-photon responses are resolvable despite its presence. It seems likely that the proteins of the rod transduction cascade have evolved greater stability against spontaneous activation than have those of the cone cascade, as exemplified by the results of Muradov et al (145) for PDE6, which showed that the rod form has a lower basal hydrolytic activity in conjunction with a weaker affinity for transducin (see also Section 8).

Variability of the rod single-photon response. Despite the contrary view that is painted in most publications on the subject, the single-photon response of rods is quite variable, especially in terms of its time-course, yet most authors describe the kinetics as 'reproducible'. For toad rods, Whitlock & Lamb (177) illustrated the wide variability in time-course of the single-photon response visually, by matching individual responses that began rising with a similar slope, and showing how different the peaks and falling phases could be. When they estimated the variation in a single shut-off step that was needed to account for the experimental measurements, they found a coefficient of variation (standard deviation divided by mean) of ~0.4. This is sufficiently high that it is not reasonable to describe the quantal responses as exhibiting 'reproducible' kinetics. The substantial variability in time-course, and also in amplitude, is a perfectly normal (and expected) feature of the known shut-off steps in the rod photoresponse, and has been accurately modeled by Hamer et al (178, 179) and Gross et al (180).

Magnitude of the rod single-photon response. It has recently been shown that mouse rods in the retinal slice preparation exhibit considerably larger single-photon responses than reported previously using the suction pipette approach, with mean amplitudes of 2-3 mV in cells with ~20 mV maximal responses (181). With a single-photon response as large as this, reliable synaptic transmission of that response to rod bipolar cells is far less problematic than has frequently been suggested in the literature.

11. Rod specializations and the origin of rods

As discussed in Section 7, the defining feature that distinguishes a rod photoreceptor from a cone photoreceptors is its ability, under dark-adapted conditions, to respond reliably (i.e. with good signal-to-noise ratio) to the absorption of individual photons of light (131, 132). Although numerous differences between cones and rods have been catalogued, in terms of morphology, molecular components, and response properties, there has never been a compelling account of what it is that enables vertebrate rods to achieve their photon-resolving performance.

This Section first analyzes structural features that contribute to the ability of rods to reliably signal individual photoisomerizations. It then examines two unusual types of 'rod': those of the nocturnal gecko, where the photoreceptors exhibit rod-like properties, yet are relatively recently descended from cones; and those in the all-rod retina of the skate, where the rods exhibit certain cone-like properties. Thereafter the emergence of rods in early vertebrates is considered, and finally a scenario is painted for the evolution of rod photoreceptors.

Structure as a factor in the rod's ability to signal individual photoisomerizations

In order to achieve a single-photon response amplitude of reasonable amplitude (say 5% of the circulating dark current), ion channels must be affected over a moderate length of the outer segment, and this necessitates longitudinal spread of the cytoplasmic messenger cGMP along the outer segment. The situation in a typical cone, where the cytoplasmic message is restricted primarily to the interior of a single sac during the short duration of the cone response, cannot provide a single-photon signal of more than 1/N of the circulating current, where N is the number of sacs in the outer segment (typically >500).

More effective longitudinal spread (a higher longitudinal diffusion coefficient) can be achieved by increasing the cross-sectional area available for longitudinal diffusion, as was originally modeled by Lamb et al (182). In a cone outer segment, only a tiny proportion of the circumference of the sac is available as an intracellular route for longitudinal communication, and hence the effective longitudinal diffusion coefficient is low. But, by enclosing the sac membranes within the plasma membrane, through the formation of pinched-off discs, then essentially the entire circumference is available as a longitudinal conduit. The longitudinal diffusion coefficient can be further increased by the use of one or more incisures (longitudinal infoldings of the outer segment membrane), as this will increase the total length of the gap that encircles the discs, and hence will increase the cross-sectional area of the cytoplasmic path along the outer segment.

In the large rods of toads, Lamb et al (182) measured the longitudinal spread of activation to have a length constant of the order of 3 μm at the time of the peak of the single-photon response, and they measured the steady-state spread of desensitization during light adaptation to have a length constant of around 6 μm. Subsequent studies have confirmed and extended these observations to mammalian rods.

With this extent of longitudinal spread of cytoplasmic messenger in the outer segment, the rod is readily able to achieve an amplitude for the single-photon response of 5% of the circulating dark current (provided that its shut-off reactions have been made sufficiently slow). The effect of such longitudinal diffusion on the time-course of the single-photon response was modeled by Lamb & Pugh (70); their Appendix B).

Nocturnal gecko: Cones exhibiting rod-like properties

The photoreceptors of nocturnal species of gecko provide an important test of what is needed to make a 'rod', because in essence they are cones with a few rod-like features, yet they exhibit rod-like response properties. Walls (183, 184) proposed that the photoreceptors of nocturnal geckos had been 'transmuted' from cones into rods. He suggested that extant geckos were derived from a diurnal ancestor that had possessed an all-cone retina

(i.e. one from which the rods had been completely lost). He suggested that nocturnal species of gecko had adapted by evolving rod-like outer segments, while retaining other morphological features of cones together with the organization of an all-cone retina. In more recent literature, most authors have referred to the retina of the nocturnal gecko (e.g. *Gekko gekko*) as being 'all-rod', and the photoreceptors as being 'rods', but this is *not* the case (see below).

Light responses. Intracellular recordings of light responses were made from photoreceptors of *Gekko gekko* by Kleinschmidt & Dowling (185), who reported response properties broadly similar to those found in the rods of other species. The responses to dim flashes had a slow time-to-peak, of around 700 ms at 25 °C. Although those responses appeared very sensitive (and hence rod-like), I have not been able to extract a quantitative value for their sensitivity. The family of responses to flashes of increasing intensity is reminiscent of rod families. The response to a bright flash had an amplitude of ~20 mV, and exhibited a rapid sag from a peak to a plateau; this sag was eliminated by treatment with 100 mM aspartate, suggesting that it arose through feedback from horizontal cells; if so this aspect would be cone-like rather than rod-like, because rods typically display a rapid sag originating in the inner segment. In the presence of steady backgrounds, the photoreceptor's response light-adapted, over a range of ~4 $\log_{10}$ units, before saturating; such saturation is rod-like.

Rispoli et al (186) reported voltage-clamp electrical recordings from isolated outer segments of *Gekko gekko* photoreceptors, that had been detached at the connecting cilium and then dialyzed with an energy-rich intracellular solution. The mean dark current was ~67 pA, and the family of responses to flashes of increasing intensity was remarkably similar to that seen in rods of other species. Responses to dim flashes had a time-to-peak of ~1.1 s at 17 °C, with kinetics of the form reported for rods. The dark-adapted flash sensitivity was calculated (from intensity measurements) to correspond to a single-photon response amplitude of ~0.8 pA, while fluctuation analysis (ensemble variance divided by mean) gave a marginally smaller value of ~0.6 pA. This indicates that the single-photon response corresponded to ~1% of the dark current, far larger than in conventional cones though somewhat smaller than in most rods.

Taken together, the results of these two studies indicate that the electrical responses of *Gekko gekko* photoreceptors to illumination exhibit predominantly rod-like properties, though the amplitude of the single-photon response may not be as large as in true rods of other species.

Photoreceptor morphology. In an ultrastructural study, Röll (187) showed conclusively that almost every morphological feature of the photoreceptors of nocturnal geckos is actually cone-like, confirming the original view of Walls (183, 184), and contradicting more recent assertions that they are rods. The only features that are rod-like relate to the outer segment, and are: (1) the large size of the outer segment, (2) the existence of outer segment 'discs' that for the most part are enclosed by the plasma membrane, and (3) the existence of an incisure. The cone-like features that she demonstrated in the photoreceptors from all species of gecko studied (both nocturnal and diurnal) were as follows: the connecting cilium was short; the inner segment contained a glycogen-rich paraboloid, and an ellipsoid (with oil droplets in diurnal species); the nuclei contained dispersed chromatin; and the synaptic terminals closely resembled cone pedicles. She concluded that "the retinae of nocturnal geckos have definitely to be classified as cone retinae".

The disc-like structure of the photoreceptor outer segment in the nocturnal gecko had previously been reported by Yoshida (188), and the study of Röll (187) was in close agreement. Yoshida (188) stated that "as in other vertebrate rods, the stack of double membrane discs of the outer segment of the photoreceptor cells in the retina of adult [nocturnal] geckos is enclosed by the plasma membrane, except for the proximal zone of the outer segment". Both studies found the great majority of discs to be enclosed by plasma membrane, but both also reported frequent cone-like openings to the exterior, scattered along the length of the outer segment. Both also reported the existence of one (or rarely two) rod-like incisures.

Gekko opsins. The differences between cone and rod opsins were presented in Section 6. The two primary opsins of *Gekko gekko* have been shown to clade with the LWS and Rh2 cone opsins of other vertebrates, and to exhibit cone-like biochemical properties (189). In particular, the gecko Rh2 opsin has the Q122 and P189 that have been reported to underlie the cone visual pigment properties of fast meta II decay and fast pigment regeneration (92), Section 6).

Gecko phototransduction cascade. The proteins of the transduction cascade in *Gekko gekko* were investigated by Zhang et al (190) and, in all the proteins that they were able to identify, the sequences were cone-like rather than rod-like; those identified proteins comprised the α subunit of Gt (GNAT2), the catalytic and inhibitory subunits of the PDE6 (PDE6C and PDE6H), the α subunit of the cyclic nucleotide-gated channel (CNGA3), and arrestin (ARR3). Although these proteins were predominantly cone-like, a few residues were identified as being rod-like. On the other hand, in measuring expression levels and activities, they found that RGS9 was expressed at the low level expected for rods rather than the high level characteristic of cones, and the resulting GAP activity was correspondingly low; likewise, the low dark basal activity of the PDE was typical of rods rather than of cones.

Taken together, these results on the opsin and the cascade appear to indicate that the proteins of *Gekko gekko* photoreceptors are overwhelmingly cone-like, but that the expression levels and/or activities of at least two of the proteins that are important in generating slow responses (GAP activity and basal PDE activity) are instead rod-like.

Skate: Rods that can exhibit cone-like properties

Some deep-water species of skate have been shown to possess pure rod retinas, but their rods are able to function in a cone-like manner at intensities that would normally saturate rods (191). The outer segments of the rods in these species have all the morphological and other features of classical rods, in terms of large cylindrical outer segment, sealed-off discs, microspectrophotometric peak at 500 nm, and band-like incorporation of labeled amino acid. On the other hand, the ultrastructure of the synaptic terminal is intermediate between that of conventional rods and cones, with multiple synaptic ribbons and contacts at both invaginating and flat contacts (192).

The electrical responses of these cells were recorded by Dowling & Ripps (193) using the aspartate-isolated trans-retinal potential from the isolated retina, which reflects photoreceptor activity. Under dark-adapted conditions the electrical responses closely resembled those of conventional rods. Furthermore, application of steady background illumination led to saturation at relatively low intensities, as in other rods. However, when these backgrounds were left on for extended periods the rods slowly recovered and were able to respond to incremental stimuli. For backgrounds of moderate intensity, a steady state of adaptation was reached within 5-10 min, but for more intense backgrounds the rods took 20 min or more to recover from saturation and to reach a steady adaptational state. Those findings from trans-retinal recordings were subsequently confirmed by suction pipette recordings from skate rods, under dark-adapted conditions and at a single moderately bright background intensity (194). The suction pipette measurements showed that the acceleration of the flash response that occurs when the cell recovers from the initial saturation involves speeding-up of each of the shut-off reactions, in much the same way as occurs in a conventional rod exposed to steady backgrounds or to temperature changes.

These results are consistent with the notion that rods in the skate all-rod retina function as conventional rods under fully dark-adapted conditions and in dim illumination. However, upon exposure to brighter steady backgrounds, the skate rods initially saturate but then recover after tens of minutes and display adaptational properties that are reminiscent of those of cones. Hence it would appear that, in this retina that lacks cones, the rods have become modified in a way that permits them to slowly change their response properties from rod-like to somewhat more cone-like. At present, the cellular and molecular mechanisms that enable this transition are not known.

In a conventional 'duplex' retina, containing both rods and cones, there is no need for the rods to function at moderate to high background intensities. Indeed, there is a distinct advantage in the rods becoming saturated at the intensities at which cones operate, because this reduces the metabolic load on the outer retina and permits the oxygen tension to be maintained at a reasonable level for the cones. But in the all-rod skate retina, it seems that the rods have had to forgo this energy-saving trick in order to enable the animal to continue to see at intensities that would otherwise be blinding.

What is needed to make a 'true rod'?

In light of the results presented in Section 10 and up to here in Section 11, the following interpretations are drawn regarding the crucial features that are needed to make a 'true rod', defined as one that reliably signals the occurrence of individual photoisomerizations, as distinct from a photoreceptor with cone-like properties:

H-1) First, the photoreceptor needs to express an opsin with a peak spectral sensitivity shorter than about 520 nm, in order to achieve a sufficiently low rate of thermal isomerizations; hence, LWS opsins are effectively ruled out.

H-2) The amplification of the phototransduction cascade does not need to differ significantly from that in a conventional cone.

H-3) One essential change is that all of the shut-off reactions underlying recovery of the dim-flash response need to be slow enough that the response to a single photoisomerization can build up sufficiently to suppress at least 1% (and preferably more) of the circulating dark current.

H-4) In comparison with typical cone shut-off, the required slowing necessitates concerted changes that: (1) slow the shut-off of R*; (2) slow the shut-off of G*/E*; (3) slow the cGMP turnover time in darkness; and (4) slow the Ca^{2+}-mediated negative feedback loop so that the recovery of cGMP levels and the re-opening of ion channels are slowed. It is not crucial whether these changes are achieved by alteration in the activities of the proteins, or by altered expression levels.

H-5) The way that this slowing was actually achieved appears to have included: slowing the rate at which the GRK and arrestin could phosphorylate and bind to R*; slowing the GAP activity by lowering the concentration of the RGS9 complex; and slowing the cGMP turnover time in darkness by lowering the basal activity of the PDE6.

H-6) Secondly, the cytoplasmic messengers (cGMP and Ca^{2+}) need to be able to diffuse substantial distances axially along the outer segment, and this requires a significant change in outer segment morphology: the sac membranes need to be enclosed by the plasma membrane (in effect forming discs) in a manner that provides an enlarged conduit for axial movement. In addition, one or more longitudinal incisures in the outer segment can further assist in axial diffusion.

H-7) An additional change that will assist in rendering the (now) large single-photon response detectable above the background noise is a lowering of the intrinsic fluctuations in the phototransduction process through increased stability of the proteins of the cascade.

H-8) Through the combination of all the above changes, it should be possible to convert a cone photoreceptor that is specialized for high-performance rapid photopic vision into a rod photoreceptor that can reliably signal individual photoisomerizations under dark-adapted conditions. An inevitable consequence of the slowing of shut-off reactions, though, will be that this cell saturates at low to moderate background intensities.

Timing of the emergence of rods

In Section 10 it was shown that modern SWS2 'cone' opsins have an exceedingly low rate of thermal isomerization, making them exceptionally well adapted to act as the photopigment in the green rods of amphibia. We cannot be certain that the ancestral SWS2 opsin was equally as stable as this. But, even if its thermal stability had been several orders of magnitude poorer, then that would have been entirely adequate to support reliable single-photon detection if that opsin had been expressed in a 'rod'. We can conclude that cone opsins (at least of the SWS2 variety) already exhibited thermal stability sufficient to enable single-photon detection before rhodopsin evolved, and therefore presumably before rods evolved. Hence, it would appear that thermal stability of the opsin molecule was not the limiting factor in the evolution of rods (at least, when 'rods' are characterized by their ability to detect single photons).

It seems clear that photoreceptors with certain rod-like features had evolved prior to the divergence of cyclostomes from the lineage leading to jawed vertebrates. Thus, hagfish photoreceptors have been reported to have discs enclosed by plasma membrane, and their peak spectral sensitivity is at 500 nm (Section 3). Likewise, one class of lamprey photoreceptor has a number of rod-like features, including the expression of an opsin that appears homologous with Rh1, though the cell also retains other cone-like features, both anatomically and electrophysiologically (Section 3). Unfortunately, though, it has not yet been discovered whether these hagfish and lamprey photoreceptors are able to respond reliably to the absorption of individual photons of light - in other words whether they achieve the ultimate sensitivity that is the defining feature of the 'true rods' of jawed vertebrates. If future experiments were to show that both hagfish and lamprey photoreceptors indeed meet this criterion, then this would be evidence in support of the notion that their common ancestor likewise possessed true rods.

Until this issue can be resolved, it is not possible to confidently go further than to say, firstly, that it seems highly probable that the last common ancestor of hagfish and lampreys possessed a class of photoreceptor with a number of rod-like features and, secondly, that 'true rods' had definitely evolved by the time that the first jawed vertebrates appeared.

Scenario for the emergence of 'true rod photoreceptors'

The following steps are proposed as the likely means by which rod photoreceptors emerged from their cone photoreceptor forerunners:

I-1) Following the '2R' rounds of whole-genome duplication, the lateral retina of an early vertebrate possessed five classes of cone-like photoreceptor cell, each expressing one of the five opsin classes (LWS, SWS1, SWS2, Rh2, Rh1).

I-2) In the photoreceptor expressing the Rh1 opsin, a number of changes gradually occurred, that led to a slowing of the response and concomitantly to an increase in its sensitivity.

I-3) These changes in the photoreceptor expressing Rh1 included slowing of the three shut-off reactions and slowing of the negative feedback loop. Some of these changes involved specialization of the shut-off proteins expressed in that cell, some involved altered expression levels, and some involved changes in morphology.

I-4) R* shut-off became slower, in part because of the slower decay of metarhodopsin II due to the mutations at residues 122 and 189, and in part through changes in the kinase and arrestin (GRK1 and SAG).

I-5) G*/E* shut-off became slower primarily as a result of lowered levels of the RGS complex (RGS9-Gβ5-R9AP).

I-6) The turnover time for cGMP in darkness lengthened as a result of lowered resting phosphodiesterase activity (PDE6A, B).

I-7) The time constant for equilibration of cytoplasmic Ca^{2+} concentration increased in parallel, through a reduction in the number of $Na^+/Ca^{2+},K^+$ exchangers per unit volume of outer segment, in part as a result of lowered surface-to-volume ratio, and in part through an increase in cytoplasmic Ca^{2+}-buffering power.

I-8) Changes at the rim of the outer segment lamellae led to the plasma membrane enclosing groups of lamellae (which thereby became groups of discs), providing an enhanced cross-sectional area for axial diffusion in the cytoplasm.

I-9) With these changes occurring gradually, but in concert, the photoreceptor expressing the Rh1 opsin would, over time, have become steadily slower and more sensitive.

I-10) Eventually almost the entire outer segment became sealed over, providing extensive longitudinal spread, and the shut-off reactions became sufficiently slow that the response to a single photoisomerization became large enough to exceed the level of noise in the cell.

I-11) Any further slowing of the shut-off reactions would then have been disadvantageous.

I-12) The synapse of this cell had a less demanding role, because the signal-to-noise ratio was higher and the kinetics were slower, and hence the synapse was able to function satisfactorily with less expenditure on synaptic machinery (i.e. with less extensive ribbon and fewer vesicles).

I-13) The eventual outcome of these combined gradual changes was the emergence of a 'true rod' photoreceptor, that reliably signaled individual photoisomerizations.

12. Retinoid re-isomerization in darkness

As discussed in Section 5, a major difference between vertebrate retinal photopigments and those of invertebrates is that the vertebrate visual opsins release their all-*trans* retinoid following light activation. The vertebrate retina therefore requires a continual supply of 11-*cis* retinal, in order to silence the residual activity of the free opsin and at the same time regenerate native rhodopsin for further signaling by light. This is accomplished by two biochemical pathways that operate in darkness (Figure 27; reviewed in Lamb & Pugh, (160); Wang & Kefalov, (195); Saari, (196)). One is the classical 'retinoid cycle of vision' (Figure 27B), in which all-*trans* retinoid is transported to the RPE, isomerized to the 11-*cis* isomer, and then transported back to the retina. The second is a less well understood pathway, internal to the retina, involving Müller cells and cone inner segments, that is thought to contribute to the regeneration of cone visual pigment.

Intra-retina retinoid cycle

Although most work on retinoid recycling over the past four decades has concentrated on the RPE cycle, the fact that cone photoreceptors pre-date rod photoreceptors raises the distinct possibility that the ancestral retinoid cycle of the vertebrate eye may have been the intra-retina cycle involving the cones and Müller cells, with the RPE cycle having evolved subsequently. The intra-retina cycle appears simpler, in that it involves isomerization of all-*trans* retinol (vitamin A) directly to 11-*cis* retinol (bottom of Figure 27A), via what has been termed ‘isomerase 2’ in Müller cells, without requiring initial esterification followed by an isomerohydrolase reaction as in the RPE (see below). A very recent report has indicated that this second isomerase might be the desaturase, DEGS1 (197), but the identity of the other enzymes that contribute to this intra-retina cycle are only just beginning to emerge. Unfortunately, as this cycle has been less intensively studied, it has not yet proven possible to investigate its evolutionary roots.

RPE retinoid cycle

Two recent papers have made important advances in determining the origin of the classical RPE retinoid cycle. Albalat (198) and Poliakov et al (199) have shown that this cycle is present only in vertebrates, as

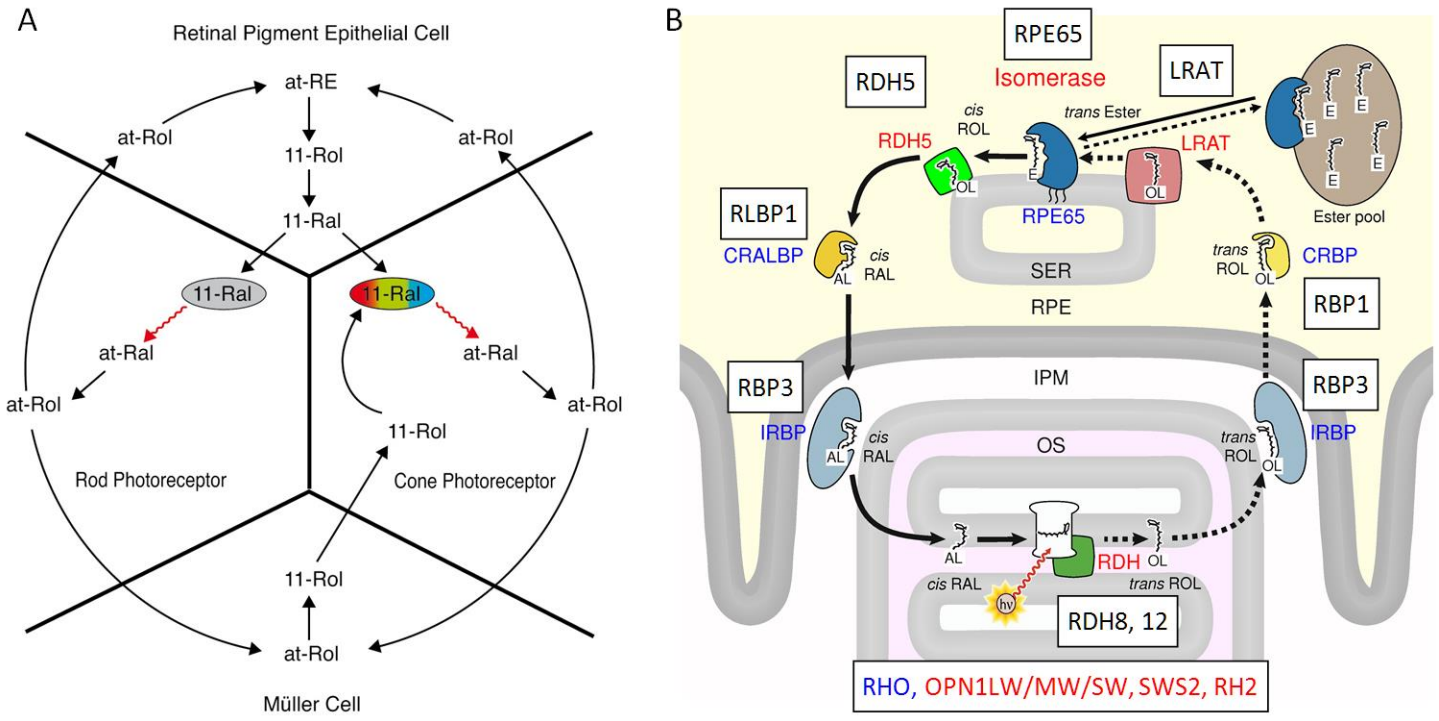

Figure 27. Retinoid cycles: Overview of the two cycles, and flow in the RPE cycle. A, Overview of the flow of retinoid in the two cycles. The areas separated by solid lines represent cellular compartments of a retinal pigment epithelial cell (top), a rod and a cone photoreceptor cell (middle), and a Müller cell (bottom). The ovals surrounding 11-Ral represent rhodopsin (gray) and cone opsins (tricolor). Photoisomerization reactions are shown in red. All other chemical reactions are catalyzed by enzymes. Retinoids are chaperoned by retinoid-binding proteins (not shown) during intercellular and intracellular movement. Abbreviations: at-RE, all-*trans* retinyl esters; at-Ral, all-*trans* retinal; at-Rol, all-*trans* retinol (= vitamin A); 11-Ral, 11-*cis* retinal; 11-Rol, 11-*cis* retinol. From Saari (196). B, Flow of retinoid in the RPE cycle. Delivery of 11-*cis* retinoid is shown by solid arrows, while removal of all-*trans* retinoid is shown by dashed arrows. Abbreviations: OS, outer segment; IPM, inter-photoreceptor matrix; RPE, retinal pigment epithelium; SER, smooth endoplasmic reticulum. RAL, retinaldehyde; ROL, retinol. For the chemical icons: AL, OL and E denote the aldehyde, alcohol, and ester groups attached to the retinoid hydrocarbon chain. Enzymes (in red): RDH, all-*trans* retinol dehydrogenase; LRAT; lecithin:retinol acyltransferase; RDH5, 11-*cis* retinol dehydrogenase. Chaperone proteins (in blue): IRBP, inter-photoreceptor retinol binding protein; CRBP, cellular retinol binding protein; RPE65, retinal pigment epithelium 65 kDa protein, now known to be the isomerohydrolase; CRALBP, cellular retinal binding protein. The ABCA4 transporter is not shown; this rescues the very small proportion of all-trans retinoid that inadvertently reaches the luminal leaflet of the disc membrane, and it has only a minor role in total retinoid cycling. From Lamb & Pugh (139). Gene names are given in boxes; see also Item D.

cephalochordates and tunicates do not possess the required enzymes, implying that the cycle evolved during the 100 million year interval from #4 to #5 in Figure 1.

Two crucial enzymes in the retinoid cycle are LRAT (lecithin:retinol acyltransferase) and RPE65. LRAT esterifies vitamin A (all-*trans* retinol) to all-*trans* retinyl ester, which is the substrate for RPE65, which actually performs the isomerization while at the same time cleaving the ester bond, in a so-called 'isomerohydrolase' reaction. This step generates 11-*cis* retinol which is subsequently oxidized to the aldehyde, 11-*cis* retinal, and then transported to the retina.

Albalat (198) undertook an *in silico* search for the genetic machinery of retinoid processing amongst invertebrates, and he analyzed the likely function of the components that he found. He concluded that "genome surveys, phylogenetic reconstructions and structural analyses of invertebrate components similar to those of the vertebrate retinoid cycle - that is, Rdh8, Rdh12, Lrat, Rpe65, Rdh5, Rlbp1, and Rbp3 - did not provide any evolutionary or functional support for the existence of the genetic machinery of the retinoid cycle outside vertebrates".

Poliakov et al (199) extended that approach, by experimentally determining the functional activity of the key enzymes LRAT and RPE65 (and similar molecules) in lamprey and in tunicate. In lamprey (*Petromyzon marinus*), they showed that LRAT and RPE65 are both present and functional, and further that the key sites for RPE65's ability to act an isomerohydrolase are remarkably similar to those of jawed vertebrates. On the other hand, their phylogenetic analyses confirmed that neither RPE65 nor LRAT have orthologs in the cephalochordate (amphioxus) or the tunicate (*Ciona intestinalis*). They showed that an enzyme previously proposed (and named) as a *Ciona* ortholog of RPE65 by Takimoto et al (200) has no isomerohydrolase activity, confirming the report of Kusakabe et al (9), and they showed that it functions instead as a BCMO (β-carotene mono-oxygenase).

Taken together, these results show that both the crucial transition from a BCMO to a true RPE65 isomerohydrolase, and also the origin of LRAT, occurred only in the lineage leading to vertebrates (jawless and jawed), after the divergence of tunicates. Hence, the RPE retinoid cycle evolved only in vertebrates.

In a number of invertebrate species, it has been known for many years that rhodopsin can be regenerated in darkness (201), but there is scant evidence as to how this occurs. In *Drosophila*, evidence has recently been obtained for the likely existence of a retinoid cycle, though rather different from that in the RPE (202).

Scenario of the origin of retinoid recycling in the vertebrate retina/RPE

From our current knowledge of the intra-retinal and RPE retinoid cycles, it is possible to hypothesize the following scenario for the evolution of retinoid processing in the vertebrate eye:

J-1) At around the time that chordate ciliary opsins lost their bistable (photoreversible) properties and instead released their all-*trans* retinoid, an intra-retinal retinoid processing cycle arose, that utilized an isomerase (currently termed isomerase 2) in the Müller cells to isomerize retinol from its all-*trans* to its 11-*cis* form.

J-2) Subsequently, around the time that the RPE became specialized as a monolayer apposed to the retina, the two crucial enzymes LRAT and RPE65 evolved, and the RPE was able to adopt an additional role in retinoid re-isomerization.

13. Development of the retina at a macroscopic level

Clues to the evolution of the vertebrate eye can be obtained by studying its embryonic development, though caution is required. Nearly 200 years ago, Karl Ernst von Baer (203) observed that organisms with widely different adult forms have embryos that resemble each other closely, and he suggested that the developmental stages through which the embryo passes might to some extent reflect the evolutionary history of the organism; for a recent evaluation of von Baer's ideas, see Brauckmann (204).

This concept was extended by Ernst Haeckel (205) to the extreme view that 'ontogeny recapitulates phylogeny'; i.e. that each step in development reflects a corresponding step in the evolutionary sequence. The problem with this strict relationship is that it implies that evolution can work only by altering or adding to the final stage of embryogenesis, and this is clearly not correct. Nevertheless, despite the fact that all stages of development are subject to evolution, there is a marked tendency for more ancient steps to be preserved, so that the fundamental body plan that was established early in evolution appears seldom to be altered in a major way during embryogenesis, and instead there appears to be a tendency for newly-evolved features to be 'tacked-on' to later stages of embryogenesis.

Because of the likelihood that events that occurred in the distant past during eye *evolution* have left remnant traces in the process of eye *development,* we shall now examine several aspects of eye embryology: firstly, the overall sequence of eye development across jawed vertebrates, lampreys and hagfish; secondly, the sequential differentiation of cell classes in the vertebrate retina; and thirdly, the maturation of photoreceptors and the

formation of their neural connections. Inevitably, this leads on to the nature and origin of retinal bipolar cells. Analysis of each of these topics provides important clues to the evolution of the retina.

Development of diencephalic light-sensitive organs in jawed vertebrates

During vertebrate embryonic development, a small region of the anterior neural plate (the eye fields) contains cells that will give rise to several distinct light-sensitive organs: the paired lateral eyes, the pineal organ, and the parapineal organ or the parietal eye, though not all are present in all vertebrate species (Figure 28; (206, 207)). Each of these organs arises as an evagination from the developing diencephalon; the dorsal evagination begins as a single bulge, but then becomes constricted, dividing into paired evaginations that take up rostral and caudal positions, with the caudal vesicle becoming the pineal organ and the rostral vesicle becoming either the parapineal organ or parietal eye (206). These organs share close homologies with each other, and the evolutionary significance of these parallels have been highlighted in a number of studies, including Reichenbach and Robinson (208), Vigh et al (207, 209), Ekström & Meissl (210), Klein (211), Mano & Fukada (212).

Polarity of the developing diencephalic vesicles. The developing light-sensitive outgrowths from the diencephalon (retina, pineal, parapineal, parietal) become rather flattened – compare Figure 10A for the lamprey pineal with Figure 29F for the lateral retina and RPE. One significant difference between the organs concerns the side of the vesicle that develops as the retina (or its homolog). In the pineal and parapineal organs, and in the parietal eye, it is primarily the proximal side of the vesicle (nearest the brain) that develops as a 2-layered retina, so that the photoreceptor outer segments (which project into the lumen) point out towards the external world. As the projection neurons are on the outer surface, their axons have no need to penetrate the organ, and are able to run directly to the CNS. The distal side of the organ (facing the external world) develops differently, in some cases as non-photoreceptive tissue; e.g. in the parietal eye as a so-called 'lens', and in the pineal as a thinner layer either containing either occasional photoreceptors or sometimes UV-sensitive photoreceptors (71). In comparison with these dorsal organs, the polarity is reversed in the lateral eyes, with the proximal side developing as a monolayer of RPE cells, and with the distal side differentiating as the multi-layered retina. It will be suggested below that the signal for this inverted polarity came from an ancestral placode in the stem vertebrate, that subsequently evolved to become the lens placode.

In the parietal eye, and also in the pineal organ of non-mammalian vertebrates, the glial cells (amongst which the photoreceptors are embedded) are pigmented; in the parietal eye, these glia contain black pigment granules (213), whereas in the pineal organ they contain reflective organelles that give a slate gray appearance.

Lateral eye development at a macroscopic level. The paired lateral evaginations of the developing diencephalon give rise to the eyes, in a sequence (Figure 29 and the animation below) that was described nicely by Walls (184) and that has been reviewed recently in Martinez-Morales & Wittbrodt (214). On each side of the rostral neural plate a depression forms, termed the optic groove (Figure. 29B). As the neural plate folds upwards and inwards (Figure 29B, Figure 29C), meeting and closing over to form the neural tube, these growing regions bulge outwards (Figure 29D) and are now termed optic vesicles. However, it appears that the luminal space is minimal, so that the interior surfaces of the vesicle remain effectively in contact with each other, somewhat like a deflated balloon. Contact between the expanding optic vesicle and the surface ectoderm (Figure 29E), at a region termed the lens placode, induces changes in both, with the ectoderm thickening progressively and eventually forming the lens (Figure 29G). Although it has sometimes been suggested that invagination of the optic cup is a physical result of growth of the lens, this cannot be the case, because a normal eye-cup and retina can develop in the absence of a lens, as in human congenital primary aphakia (215). Remarkably, such development can also occur in cell culture, in the absence of ectoderm or lens tissue (216), see below).

Click below for an animation of vertebrate eyecup development:
Lamb et al (3) Supplementary Animation S1

Specification of retina and RPE. The initial polarization of the lateral eye vesicles into RPE and retina is under the control of a number of extracellular signaling molecules, including FGFs released from the surface ectoderm, but also involving Bmp, Activin and Wnt. Very recently, evidence has been found for a positive feedback circuit involving Pax6 whereby, once the initial specification of RPE and retina has begun, the signals within the retina/RPE become self-reinforcing (217). These authors propose that, when expressed in conjunction with Mitf or Tfec, Pax6 acts as a pro-RPE (i.e. anti-retina) factor, whereas in conjunction with other retinogenic genes it acts as a pro-retina factor. Thus, once there is a bias towards an initial retina/RPE polarity, this bias becomes self-reinforcing by signaling events that are internal to the developing retina/RPE.

A further exciting and intriguing recent finding is that when aggregates of mouse embryonic stem cells are grown entirely in vitro, as vesicles in 3D culture, they are capable of autonomously organizing themselves into eye-cups with appropriately oriented retina and RPE (216), as illustrated in the movie linked below. This observation is again consistent with the notion of a signaling system internal to the retina/RPE that can regulate its development in the absence of external signals.

Click below for movies of spontaneous formation of eye-cup in vitro:
Eiraku et al (2011) Supplementary information , especially Movie 2

Coordinated migration of cells. The early steps in formation of the zebrafish eye vesicle have been monitored in several studies that have used time-lapse video imaging (218-220), so that individual cells could be visualized and their migration tracked. The movies (linked below) from each of these studies provide impressive visualizations of the coordinated cell migrations that occur in zebrafish. Thus, the macroscopic development (indicated, for example, in Figure 29) can be visualized as the coordinated migration of individual cells, firstly as primarily outward migrations, and then through a combination of inward migration of those cells near the locus of contact with the placode, together with continued outward migration of new cells into the eye vesicle (see movies).

Click below for movies of cell migrations in formation of zebrafish eye vesicle and eye cup:
England et al (218) Supplementary material, especially Movie S1
Rembold et al (219) Supporting online material, especially Movie S1
Kwan et al (220) Supplementary material, especially Movie S1

Scenario for the evolution of chordate diencephalic light-sensitive structures

It seems reasonable to think that the events in vertebrate embryonic development described above may represent a shadow of the sequence of steps that occurred during chordate evolution, in the interval between the divergence of tunicates and the emergence of vertebrates (i.e. between #4 and #5 in Figure 1). Accordingly, the following steps (also explained in the schematic in Figure 30) are suggested to have occurred:

K-1) The anterior neural tube of an early chordate contained a light-sensitive region that sent axons to relevant parts of the nervous system (e.g. to the forerunner of the hypothalamus).

K-2) The inner surface (in contact with the CSF) contained ciliary photoreceptors, while microvillar photoreceptors (that later simply became projection neurons) were located on the outer side (Figure 30A). Pigment-containing cells were also present.

K-3) This light-sensitive region expanded, possibly initially simply as a means of increasing the number of photoreceptors and thereby increasing the organism's ability to catch light. In doing so, it bulged outwards in different directions, dorsally and laterally (Figure 30B).

K-4) As these regions expanded, the somata of the ciliary photoreceptors and the microvillar photoreceptors (i.e. projection neurons) remained in close proximity to each other, while the axons of the projection neurons

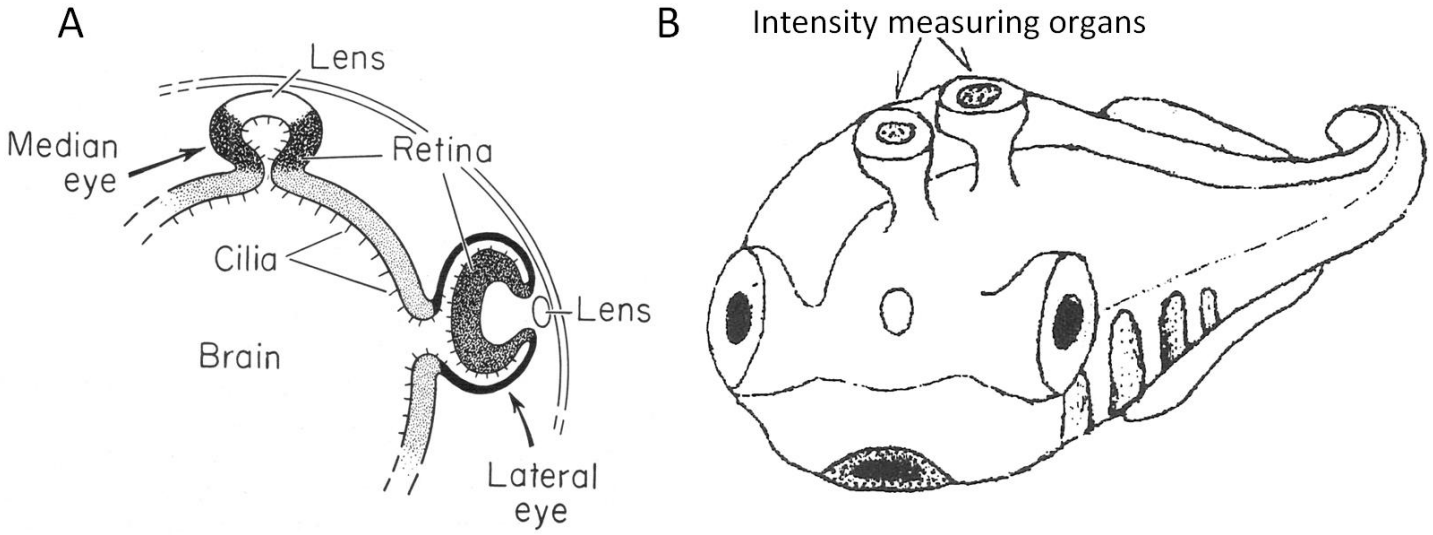

Figure 28. Light-sensitive organs that evaginate from the diencephalon. A, Schematic of the light-sensitive organs that evaginate from the developing diencephalon. The median (or parietal) eye is often found in reptiles and amphibia. During development an initially single dorsal evagination then divides into two roughly bilaterally symmetric organs that rotate their location to become a caudal pineal organ and a rostral median eye or parapineal organ. The developing vesicles of the paired visual eyes evaginate laterally to form eye-cups; they retain very little luminal space and thereby appear invaginated. From Eakin (206). B, Schematic of the possible arrangement of light-sensitive organs in a proto-vertebrate. In addition to the paired lateral eyes, there were two dorsal organs that measured light intensity. From Vigh et al (207).

lengthened so that they continued to reach their targets in the CNS; thus the cell bodies remained close together but the axons of the projection neurons 'stretched'.

K-5) The interior of each bulge (the luminal space, containing CSF) remained relatively small, so that the inner surface of the epithelium (with ciliary photoreceptors and pigment cells) became folded in upon itself, resembling a deflated balloon rather than an inflated one.

K-6) Initially, this double layer of epithelial tissue was probably spatially uniform, with ciliary photoreceptors, pigment cells and projection neurons distributed across the entire surface of the organ (not shown in Figure 30).

K-7) In due course each of the organs (dorsal and lateral) tended to develop a polarity, with one side remaining predominantly light-sensitive and with the other side adopting a different role (e.g. as a lens in the parietal eye).

K-8) In the lateral bulges, but not in the dorsal bulges, the orientation of this polarization was such that only the distal (outer) side remained light sensitive, and only the proximal side (closer to the brain) made pigment cells (see Figure 30B). In this way, ciliary photoreceptors occupied the entire cross-sectional area struck by incident light, and the pigmented cells were behind the photoreceptors yet still in close contact with them.

K-9) In these lateral organs, the axons continued to run across the outer surface, which now comprised the vitreal surface of the retina. As they headed centrally they converged as a bundle running along a groove under the optic stalk (Figure 30C). With continued lateral and downward expansion of the retina/RPE, the narrowing gap around the optic stalk became the optic fissure. At some (possibly later) stage in evolution this fissure sealed over, so that the optic nerve penetrated the lateral eyecup.

Eye development in lampreys and hagfish

Lamprey eye development. Lampreys have a larval form (the ammocoete, Figure 13A) that develops slowly over a period of 5 years or more, before metamorphosing into the adult (see for example Dickson & Collard (84)). The ammocoete is effectively blind, and its eyes resemble those of the hagfish, in being small and buried beneath

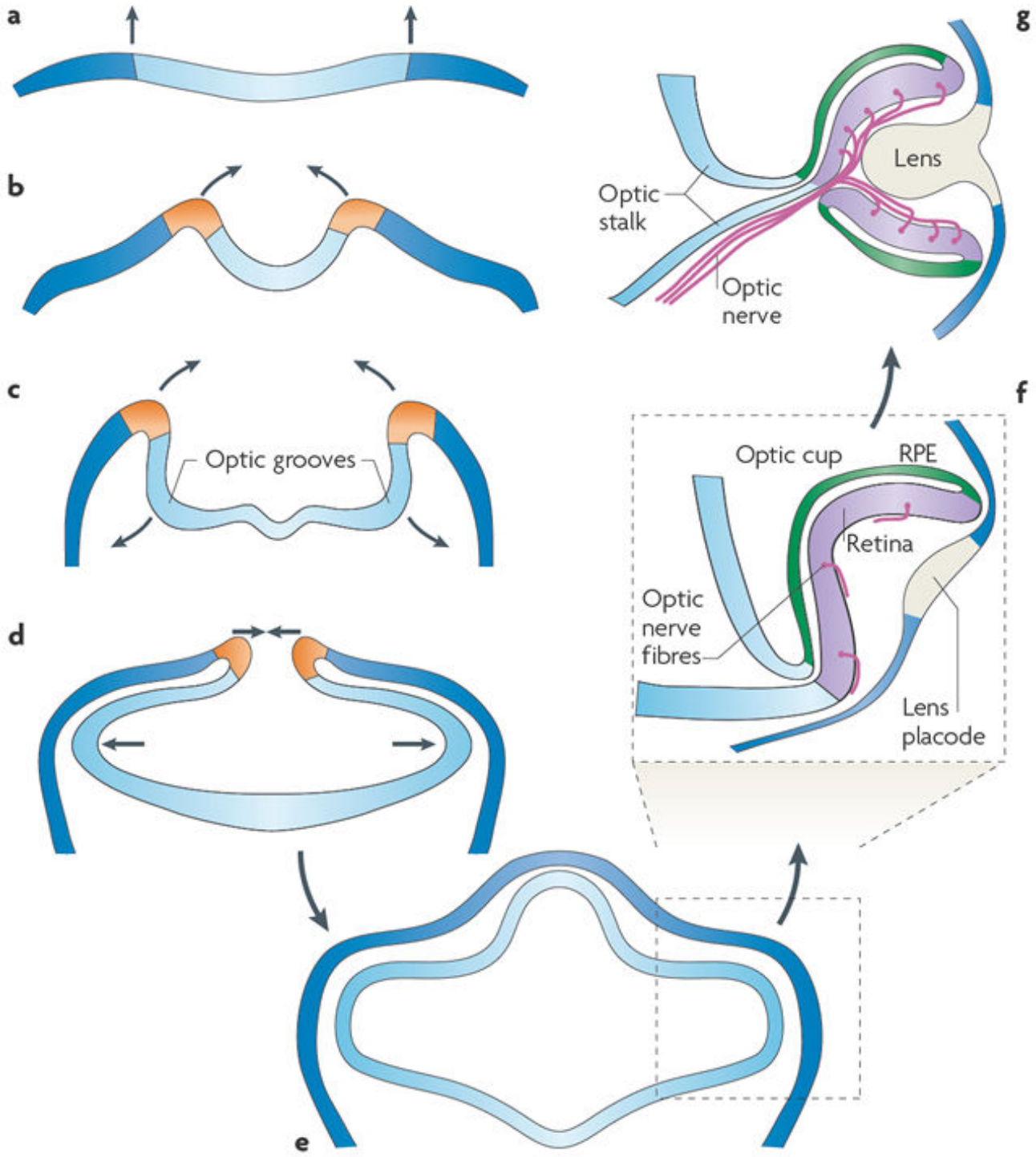

Figure 29. Development of the vertebrate eye cup. (a) The neural plate is the starting point for development of the neural tube. (b) The neural plate folds upwards and inwards. (c) The optic grooves form, and begin to evaginate. (d) The lips of the neural folds approach each other, and the optic vesicles bulge outwards. (e) After the lips have sealed, the neural tube is pinched off. At this stage the forebrain grows upwards and the optic vesicles continue to grow outwards. One aspect of this diagram that is not accurate is that the expanding optic vesicles actually have very little luminal/ventricular space; i.e. the wall thickness is much greater than shown here. (f) The expanding optic vesicles contact the surface ectoderm at the lens placode, inducing changes in both tissues. The optic vesicle now appears invaginated, and with the future retina closely apposed to the future RPE; what little ventricular space had been present between them disappears. Developing retinal ganglion cells send axons out across the retinal surface. The surface ectoderm at the lens placode thickens, forming the lens pit. The section in (f) is midline in the right eye, through the choroid fissure, so that only the upper region of retina/RPE is visible. (g) The eyecup continues to grow, through a combination of new material expanding outwards and continued warping of the eye cup. This expansion eventually causes the choroid fissure to seal over, thereby enclosing the axons of the optic nerve (as well as the hyaloid/retinal vessels; not shown). The ectodermal tissue continues to differentiate, eventually forming the lens. From Lamb et al (3). The text provides a link to an animation of this developmental progression.

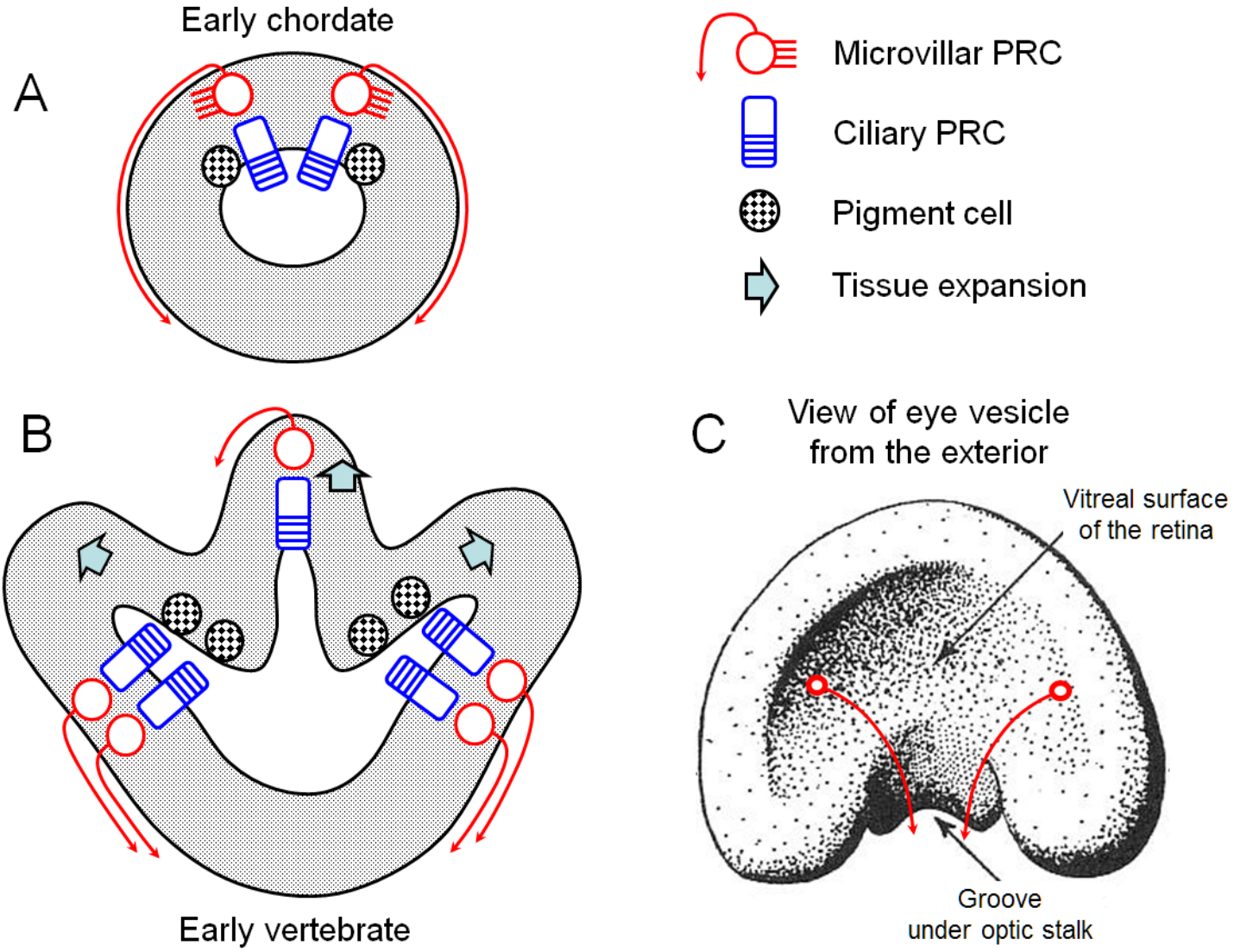

Figure 30. Schematic for evolution of chordate diencephalic light-sensitive structures A, B, Schematic sections through rostral neural tube, at stages corresponding to an early chordate and an early vertebrate. The key at the upper right identifies the icons; PRC, photoreceptor cell. A, In the early chordate (i.e. around the time that tunicates diverged), a region of the rostral neural tube was light-sensitive. On its inner surface, in contact with the CSF, there were ciliary photoreceptors (blue), and on its outer surface there were microvillar photoreceptors (red) that sent axons out to other regions of the nervous system (e.g. to the forerunner of the hypothalamus). Pigment cells (stippled black) were also present. It seems likely that each of these cell types (as well as glial cells) was descended from a single multifunctional type of ancestral cell. B, Later in chordate evolution, around the time that the earliest vertebrates appeared, the light-sensitive region of the rostral neural tube had expanded, bulging outwards (gray arrows), both dorsally and laterally. In each of these regions the ciliary photoreceptors retained their positions at the inner surface, while the microvillar photoreceptors remained near the external surface; by this stage most of the microvillar cells had lost their microvilli and their R-opsin, and had become projection neurons. In the lateral bulges (the eye vesicles), signals from the surface ectoderm (not shown) initiated polarization of the vesicles, so that only the outward-facing surface made photoreceptors and projection neurons, and only the rear surface made pigment cells. C, A view of (either) lateral eye vesicle from the exterior. Projection neurons from all across the retinal surface sent their axons across the surface and out along a groove, under what by that stage had become the optic stalk, eventually to reach their targets, probably in the hypothalamus. Diagram in C modified from Walls (184).

skin. The initial stages of eye development occur at an early age in the ammocoete, and appear comparable to the initial stages of eye development in jawed vertebrates. However, eye development then becomes arrested; for the remainder of the ammocoete phase (i.e. perhaps 5 years) the main change to the eye is that it (and its lens) slowly grows in size as the animal grows.

The bulk of the ammocoete retina is undifferentiated, with a thick neuroblastic layer, though a narrow central region (~50 μm wide, adjacent to the optic nerve) is differentiated (84, 221-223). Although it has been reported that all the conventional layers of the vertebrate retina are present, re-examination of those micrographs suggests that bipolar cells may not in fact be present in the ammocoete retina. A slow process of neural differentiation occurs, over a period of years, and this accelerates as metamorphosis approaches. The area of differentiated cells spreads outward, and the cells differentiate in the following sequence: ganglion cells, amacrine and horizontal cells, photoreceptors, and finally bipolar cells (221, 222); i.e. in broadly the same order as occurs much more rapidly during embryogenesis in jawed vertebrates (see Section 14).

Then, at metamorphosis, development of the lamprey's eye resumes, apace. The eye and lens grow rapidly in size, differentiation of the retina reaches completion, the cornea splits into scleral and dermal layers (allowing the eye to move with respect to the epidermis, as in jawed fish; (224)), extraocular muscles develop, and the eye erupts at the surface, as a vertebrate-style visual organ (Figure 13B).

Hagfish eye development. The development of hagfish embryos was first studied by Price (225), and comprehensive accounts were given by Dean (226, 227) and von Kupffer (228), though there was only limited data on the eye in any of these. The embryonic development of hagfish eyes was investigated by Allen (65) and Stockard (229), with particular reference to the origin (or the absence) of a lens. The combined results of those early studies are consistent with the following description.

The developing eye is always very small in comparison with the size of the embryo. At a very early stage the optic vesicle contacts the surface ectoderm and a definite 'lens placode' is seen, though even at its thickest (in a 15 mm embryo) this placode is only a few cells deep (229); thereafter the lens placode thins and disappears. Allen (65) concluded by suggesting that, if the thickening of the lens placode represented a rudimentary lens, then "we should have a clear case of arrested development resulting in the continuance of an embryonic condition into adult life. This view is strongly supported by the condition of the retina with its space of separation between the inner and outer layers of the optic-cup, by the rudimentary iris, and by the often persistent choroid fissure".

Following those studies, it did not prove possible to obtain viable fertilized hagfish eggs for about 100 years; it would be exciting to continue those earlier studies using the procedures recently developed in Shigeru Kuratani's laboratory (230).

Implications of cyclostome eye development for vertebrate eye evolution

In view of the comparative aspects of cyclostome and jawed vertebrate eye development described above, the following implications for evolution of the vertebrate eye are hypothesized (3):

L-1) The 'arrested development' of the hagfish eye (65) may reflect a failure of hagfish eye development to proceed beyond a point corresponding to an earlier stage in vertebrate eye evolution. Hagfish do not undergo metamorphosis, and in the absence of the developmental changes that occur at metamorphosis, perhaps the hagfish eye has been 'frozen' in its earlier evolutionary state. In other words, eye development (and perhaps all development) in hagfish might correspond to a kind of neoteny.

L-2) If this is correct, then the hagfish eye and retina provide an invaluable window into an important stage of vertebrate eye evolution, with the following additional implications.

L-3) The retina of the stem vertebrate would, at some stage of evolution, have resembled that of the hagfish, with photoreceptors directly contacting projection neurons (ganglion cells). Further evidence relating to this notion will be presented in Section 14 on maturation of retinal connectivity.

L-4) The failure of the hagfish 'lens' placode to develop into a lens would suggest that the ancestral function of this placode may have been to influence the orientation of polarization of the retina/RPE (see above), rather

than to form a lens. On this basis, the evolution of the lens would have occurred subsequent to the evolution of the paired lateral 'eye-cups' that comprised infolded, two-layered retinas.

L-5) Likewise, the extraocular muscles would not have evolved until after the lateral eye-cups were already present.

L-6) Taken together, these interpretations further suggest that the ancestral function of the paired lateral retinas was not for image-forming vision, because the evidence suggests that these retinas were present before the evolution of a lens, of extraocular muscles, or of anything more than the most basic computational power in the retina. Instead, these lateral counterparts of the pineal organ may have subserved a function in circadian and/or seasonal timekeeping, or perhaps in shadow detection, or even in control of axial orientation (i.e. roll).

L-7) Hence, it is suggested that at an early stage in vertebrate evolution, *after* the '2R' genome duplications but before the divergence of cyclostomes from the jawed lineage, a pair of primitive lateral retinas with RPE had evolved in the stem vertebrate. These retinas possessed early forms of the five 'visual' ciliary opsins, expressed in cones and in a rod-like photoreceptor. Bipolar cells had not evolved, nor had a lens or extraocular muscles. It is suggested that the ancestral function of the 'lens placode' was to specify the polarity of the lateral eyecup, possibly by releasing molecules like fibroblast growth factors (FGFs).

L-8) It is suggested that a state resembling this is retained in the eyes of living hagfish, possibly as a result of neoteny. In lampreys (and in their ancestors) the subsequent stages of eye development occur (and may have occurred) slowly, predominantly during metamorphosis. But in living jawed vertebrates those subsequent stages of eye development occur rapidly, and inseparably from the earlier stages.

14. Molecular signatures and cell differentiation in the vertebrate retina

Molecular signatures of neurons in the developing vertebrate retina

In the developing nervous systems of both protostomes and deuterostomes the specification of neuronal cell fate appears to be determined by the combinatorial code of transcription factors (mainly of the bHLH and homeodomain superfamilies) that are expressed. In the differentiating cell, the particular combination of transcription factors regulates the programs controlling cellular morphology, outgrowth of axons, and the expression of effector molecules (such as members of transduction cascades, neurotransmitter-synthesizing enzymes, ion channels, etc.). For a review of the deployment of transcription factors in eye development across phyla, see Vopalensky & Kozmik (6).

A comparison of the molecular factors that underlie the differentiation of cell types has been applied to the retina, both within an organism and between organisms, by Detlev Arendt and his colleagues, in order to gain insight into the evolutionary history of the component cells (231). Arendt refers to the approach as 'comparative molecular cell biology'.

Sister and homologous cell types. Arendt (231) defined 'sister' and 'homologous' cell types as follows. Within an organism, 'sister cell types' are those that have evolved from one common precursor, by diversification of cell type. And across the evolutionary tree, 'homologous cell types' are those that have evolved from the same type of precursor cell in the last common ancestor of the groups being compared. Using these definitions he argued that, within any vertebrate species, the horizontal cells, amacrine cells, and ganglion cells are 'sister' cell types, having descended from a single ancestral cell type. And across phyla, he argued that rhabdomeric photoreceptors and vertebrate retinal ganglion cells are 'homologous' cell types, having descended from a microvillar photoreceptor in the last common (bilaterian) ancestor.

The evidence supporting the former assertion is illustrated in Figure 31 which compares the transcription factors and effector genes expressed in the different cell types of the vertebrate retina. Cone and rod photoreceptors are clearly sister cell types, having descended from a common ancestral ciliary photoreceptor (see Section 11). Although Arendt was equivocal about the origin of retinal bipolar cells, it will be argued subsequently (Section 16) that the bipolar cells are also sister cells of ciliary photoreceptors.

The lower part of Figure 31 shows that the transcription factors and effector genes expressed in horizontal, amacrine, and ganglion cells are closely similar (for detailed comparisons, see Arendt (231)). Furthermore, most notably in the case of ganglion cells, these factors are fundamentally the same as the factors that underlie differentiation and that specify phototransduction in the rhabdomeric photoreceptors of *Drosophila*. By Arendt's analysis, horizontal, amacrine, and ganglion cells appear to have descended from an ancestral microvillar photoreceptor, so not only are they 'sister' cell types (to each other) but they are also each 'homologous' cell types to protostome rhabdomeric photoreceptors.

Complications. Two observations that complicate this relatively simple account have been pointed out by Davies et al (94). Firstly, despite their postulated common origin as microvillar photoreceptors, some horizontal cells and some ganglion cells express a C-opsin (VA/VAL). Secondly, it appears that this C-opsin VA/VAL is frequently co-expressed with the R-opsin melanopsin. What might lead to expression or co-expression of a C-opsin in a cell that has descended from an ancestral microvillar photoreceptor? In addition to this complication with the opsins, it is now known that the set of transcription factors is more extensive than shown in Figure 31, and as a result the grouping of cell types is less distinct.

Solution? One possible solution to this conundrum (as well as to other issues) would be to take the view that all vertebrate retinal and RPE cells are descended from a single pre-bilaterian cell type that combined the features of a photoreceptor cell, a pigment cell, and a glial cell; i.e. from an ancestral cell of the kind envisaged in the 'division of labor' model proposed by Arendt et al (5). Such a view seems consistent with knowledge of cell differentiation in the vertebrate retina (see next sub-Section), where it has been shown that progenitor cells are initially unrestricted in their cell fate, and are potentially able to form any type of retinal cell. By taking this viewpoint, one would not need to apply the restriction that all vertebrate retinal/RPE cell types had proceeded through antecedents that were either strictly 'ciliary photoreceptor type' or strictly 'microvillar photoreceptor type' before reaching their current forms. Instead, some cell types (such as horizontal cells) might be descended from intermediate cell type(s) that had not committed to either a ciliary or a microvillar form of photoreceptor. If this were the case, then modern cells in the retina and RPE might share certain features with one more of the ancestral ciliary, microvillar, pigment, or glial categories, in what might resemble a mix-and-match fashion.

This concept will be followed up after a brief description of cell differentiation in the vertebrate retina.

Cell differentiation in the vertebrate retina

For reviews of cell differentiation and neuronal development in the retina, the reader is referred to Webvison "Retinal neurogenesis" as well as to the chapters in Sernagor et al (232), and to Agathocleous & Harris (233), Swaroop et al (234), Reese (235) and Chen et al (21). Here the briefest of summaries is given.

Cells in the neuroepithelium of the optic vesicle, that will generate the retina, proceed through the standard cycle of cell replication in much the same way as in other regions of the brain. The soma of a progenitor cell migrates vertically within the neuroepithelium, between the outer (ventricular) and inner (vitread) surfaces, in a characteristic pattern, and when a daughter cell exits the cell cycle its soma then migrates towards its final position within the retinal layer. Differentiation begins in the central retina and proceeds outwards to the periphery.

Fate, competence, and birth order. Initially, progenitor cells are unrestricted in fate, with the capacity to form any class of retinal cell. Nevertheless, the order in which different classes of retinal cell are 'born' (i.e. exit the cell

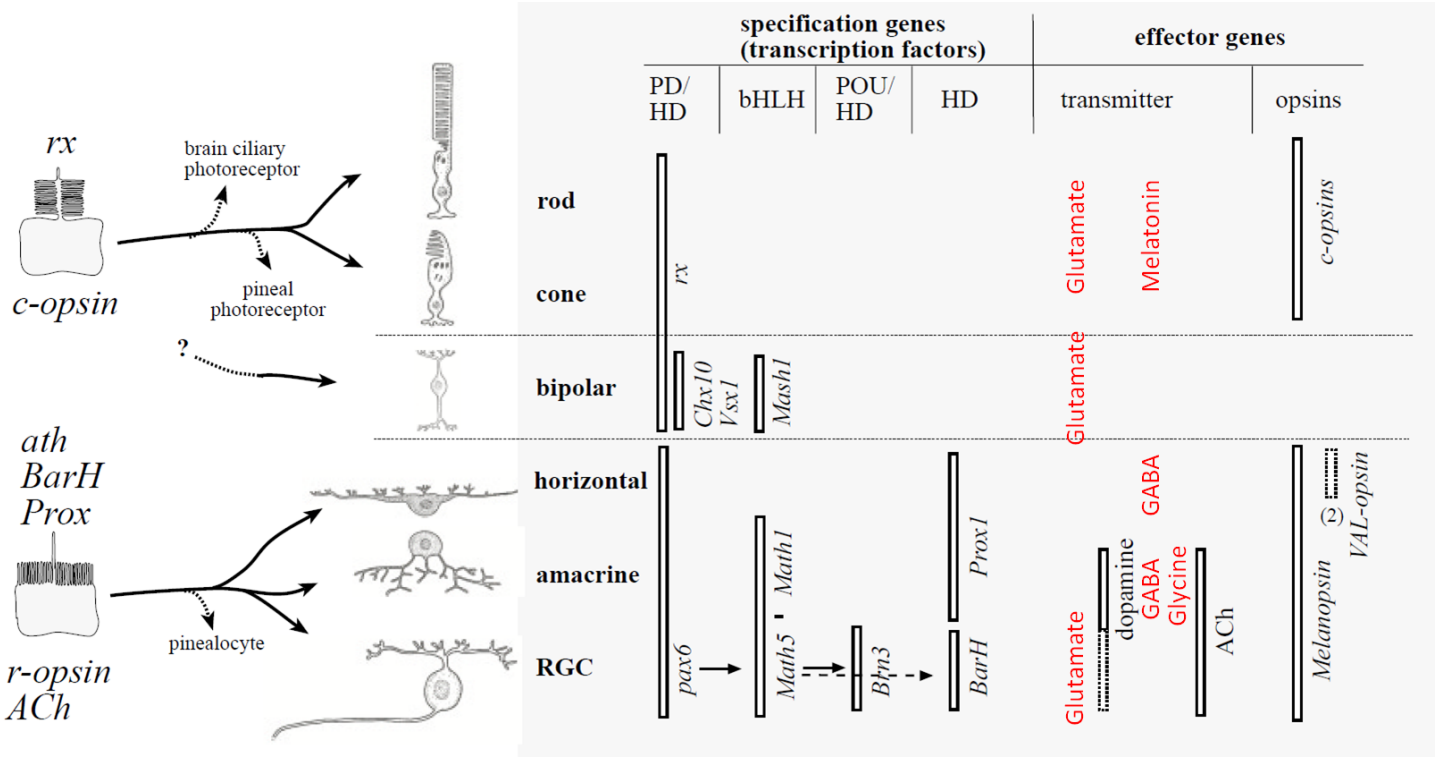

Figure 31. Molecular signatures and possible origins of vertebrate retinal neurons. Diversification of cell types in the vertebrate retina, as proposed by Arendt (231). Comparative molecular cell biological analysis indicates (Top) that cones and rods have evolved from a common ciliary photoreceptor precursor, and also suggests (Bottom) that retinal ganglion, amacrine and horizontals may have evolved from a common ancestral microvillar photoreceptor precursor. Black arrows represent cell type evolution. The evolutionary origin of bipolar cells was unclear from this kind of analysis. The right-hand side of the diagram shows the transcription factors and also the genes for neurotransmitters and opsins that have been identified in these cell classes. Additional neurotransmitters not indicated in the original diagram are shown in red. From Arendt (231).

cycle) is well defined within a species, as illustrated in Figure 32 and well conserved across vertebrate species. In particular, most cone photoreceptors are born before most rod photoreceptors, and most bipolar cells are born very late, though there is temporal overlap in the generation of different classes (236, 237).

A number of models have been put forward to explain the experimental results that have been amassed on the determination of retinal cell fate, and three are illustrated schematically in Figure 33. One model, termed serial competence (Figure 33A(a)), proposes that at any time a given progenitor has competence to produce cells of only one or a few types, and that the progenitors proceed through multiple states of this kind. Another model, progressive restriction (Figure 33A(b)), proposes that early progenitors have competence to produce all cell fates and that this competence is steadily lost (restricted) over time.

An explicit scheme under the latter model is shown in Figure 33B, from Reese (235). This scheme is based on the results of Wong & Rapaport (238), which suggested that restriction of competence represents a unidirectional sequence through which progenitors progress. The diagram illustrates the (unusual) case in which a single progenitor cell generates the entire set of retinal cell classes. As we shall see below, though, not every division produces one post-mitotic daughter cell plus one continuing progenitor cell; some divisions can produce a pair of post-mitotic daughter cells (e.g. a ganglion cell and a cone, or a pair of horizontal cells), while some can produce a Müller cell and a progenitor, or a pair of progenitors. Importantly, though, in the scheme of Wong & Rapaport (238), at every division the competence of the progenitor is progressively restricted, so that cells corresponding to an 'earlier' stage can no longer be created. In Figure 33B, the presumed influence of signaling

molecules is indicated by the broader shaded arrows: diagonal colored arrows indicate signals from the different classes of newly-born cells, while vertical gray arrows indicate Notch-Delta mediated lateral inhibition.

Alternative stochastic scheme. Recently, Gomes et al (239)proposed an alternative stochastic model (Figure 33C) in which the sequential order of cell birth in the overall population results from random choices of cell fate at each cell division, and both they and He et al (240) have obtained evidence in support of this stochastic model. Intuitively, it may be difficult to envisage how it could be possible for random divisions to lead to a deterministic make-up of cell classes, but He et al (240) provide numerical simulations that support their contention.

Three modes of cell division are possible (Figure 33C). In the first mode, termed 'PP', the progenitor cell gives rise to a pair of progenitors, resulting in an expansion of the progenitor population. In the second mode, 'PD', it gives rise to one continuing progenitor and one daughter cell that exits the cell cycle. In the third mode, it gives rise to two daughter cells, 'DD', thereby terminating the lineage. The analysis of He et al (240) showed that as the progenitors proceeded through multiple mitoses, they exhibited a shift from the initially preferred PP mode to the PD mode and finally to the DD mode. Furthermore, the types of daughter cell appeared to be correlated with the PD and DD division modes. In particular, most RGCs arose from PD mode divisions; amacrine cells arose from either PD or DD modes; but horizontal cells, photoreceptors, and bipolar cells mostly arose from DD divisions. They also showed that Ath5 was required both for the specification of RGCs and also for the PD mode of division, explaining why RGC differentiation is always earlier than that of other cell types.

Through the combination of these (and probably additional) factors influencing the probabilities of individual stochastic divisions, the overall effect at a macroscopic level is that the cells of the retina are born (on average) in a well-defined sequence, and also that the final composition of retinal cell types is determined appropriately.

Horizontal cells. In spite of the general understanding that retinal precursors undergo mitosis at the outer (ventricular) surface, and that the daughter cells migrate vertically to their final position in the retina, an exception applies to horizontal cells (at least in the zebrafish retina). In the case of zebrafish horizontal cells, the great majority of precursor cells (90% of the final population) undergo a symmetrical 'DD' mode of mitosis at the laminar position of the mature horizontal cells, giving rise to a pair of horizontal cell daughters (241). This mode of division at the final laminar position may assist in the formation of the layer of horizontal cells, and in achieving lateral connectivity between these cells.

Photoreceptors. The birth and differentiation of photoreceptors is influenced by a plethora of transcription factors and other messengers, as reviewed in Swaroop et al (234). Interestingly, the default situation for a newly-born mammalian photoreceptor cell is that, in the absence of other influences, it will become an S-cone (expressing the SWS1 opsin). In the absence of exposure to the factors NRL/NR2E3 the generic photoreceptor will become a cone, and in the absence of the factor TRβ2 it will become an S-cone. Exposure of the cone to TRβ2 will cause it to express an LWS opsin, with the choice (in human) between L- and M- (via the tandem OPN1LW and OPN1MW genes) being under control of an upstream locus control region. Exposure of the generic photoreceptor to NRL/NR2E3 will commit the cell to becoming a rod.

The default condition, of producing an S-cone, makes sense if one assumes that the ancestral cone type was the SWS variety. At the stage in chordate evolution, prior to '2R', when this ancestral cone and its opsin duplicated, an additional signal would have been needed to specify the alternative LWS fate. Likewise, at the later stage of vertebrate evolution when rods emerged, an appropriate signal would have been needed to specify that fate.

Hypotheses for the evolutionary origin of cells in the vertebrate retina/RPE

On the basis of the observations in the preceding sections, the following hypotheses are advanced for the evolutionary origin of cells in the vertebrate retina/RPE:

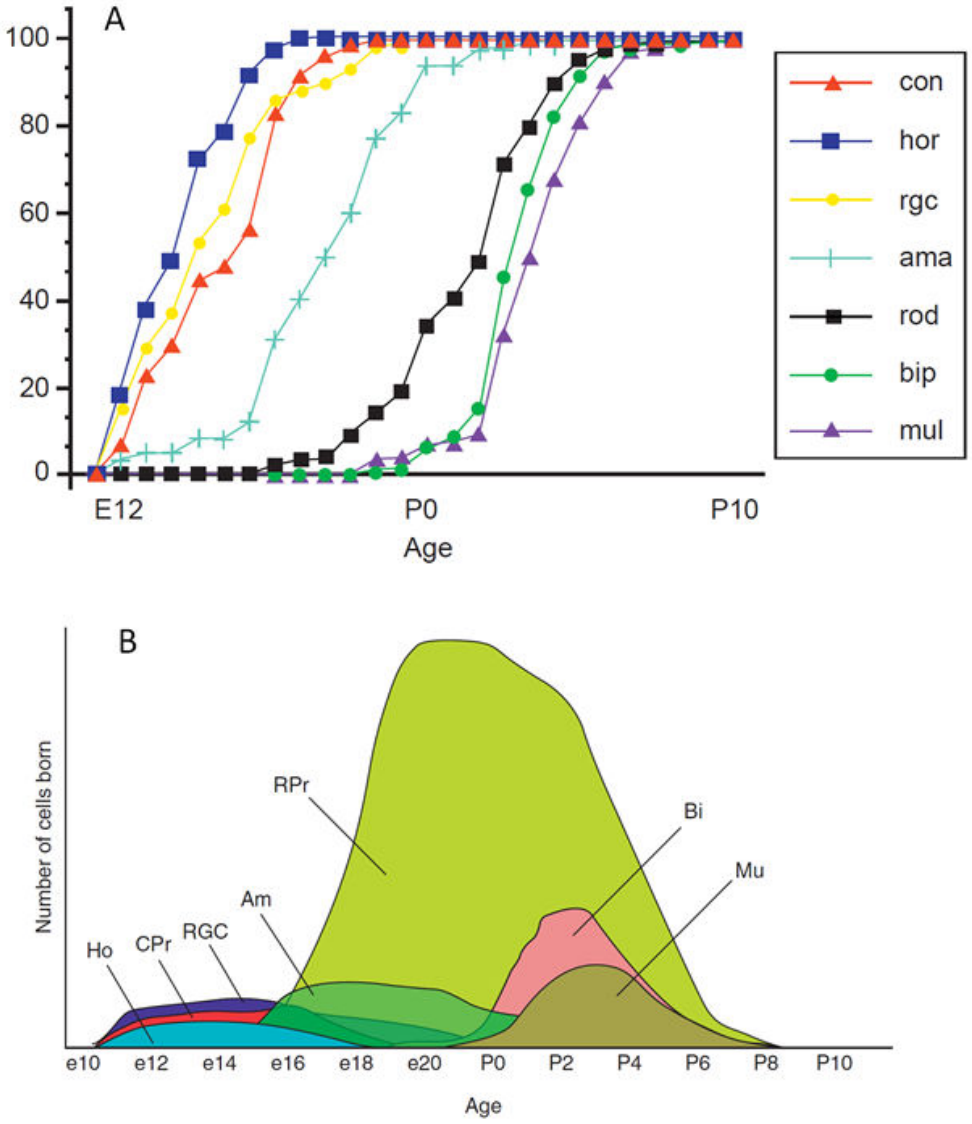

Figure 32. Sequential generation of classes of retinal neuron in the mammalian retina. Two representations of data obtained by Rapaport et al (237) for the rat retina. A, Cumulative percentage of cells in each class, as a function of age. From Brzezinski & Reh (271). B, Rate at which cells in each class were born, in absolute numbers, as a function of age. From (272). Abbreviations in the two panels are as follows. Horizontal cells: hor, Ho. Retinal ganglion cells: rgc, RGC. Cone photoreceptors: con, CPr. Amacrine cells: ama, Am. Rod photoreceptors: rod, RPr. Bipolar cells: bip, Bi. Müller cells: mul, Mu.

M-1) All the cell types in the vertebrate retina/RPE are descended from a single ancestral type of multifunctional cell, that existed in a pre-bilaterian organism, and that functioned as a photoreceptor and that also contained shielding pigment.

M-2) That cell expressed the ancestral opsin and activated a G-protein cascade, and it probably employed cyclic nucleotide-gated channels to generate its electrical response; it might also have had additional (e.g. motile) functions.

M-3) During evolution, subsequent duplications and division of labor gave rise to separate ciliary and microvillar photoreceptors, as well as (in some cases) to separate pigment cells and separate glial cells, in bilaterian organisms.

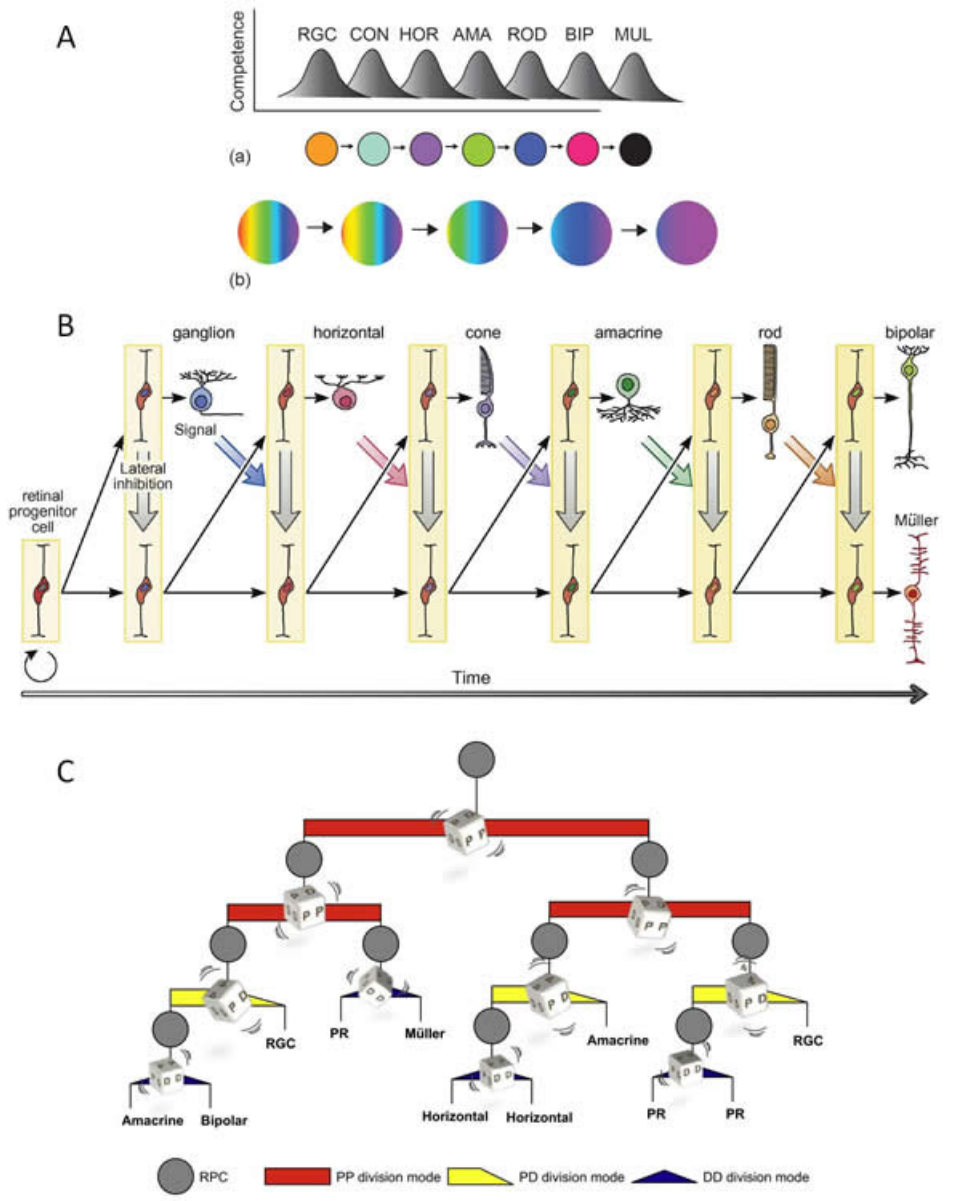

Figure 33. Models for the generation of retinal cell classes. A, Models of serial competence (a) and progressive fate restriction (b). From Brzezinski & Reh (271). B, Sequence of retinal cell classes that would be produced in the special case of a progenitor cell that gave rise to all the possible classes. From Reese (235). C, Stochastic model proposed by Gomes et al (239) and He et al (240). From Chen et al (273). See text for further details.

M-4) Since ancient times, development of the light-sensitive region has involved divisions of a multipotent progenitor cell. In early bilaterians, that progenitor might have given rise only to ciliary photoreceptors, microvillar photoreceptors, pigment cells, and glial cells.

M-5) In the vertebrate lineage, probably after the time of the '2R' duplications but before the divergence of the jawed and jawless lineages, other cell types emerged, as variants of the pre-existing cells (including the microvillar and ciliary photoreceptors). In due course these new cells became horizontal cells, amacrine cells, rod photoreceptors, and bipolar cells.

M-6) In the expanding vertebrate lateral vesicles, a polarity arose, possibly triggered by a signal from the ancestral 'lens placode', causing the outer layer to generate only epithelial cells (RPE), and causing the inner layer to generate all the other classes of cells (the retina). In the dorsal vesicles (pineal, parapineal and parietal) that

lacked the placode signal, the same polarization did not occur, leading to a somewhat different distribution of cell classes.

In considering the data on the order of cell birth in the retina, Dowling (242) has suggested that the early birth of ganglion cells, cones, and horizontal cells may indicate that these were the original classes of cells in the ancestral retina. He notes that horizontal cells share many properties with glial cells, and suggests that the original glia took on neuronal properties and thereby became horizontal cells, with a new class of glia (the Müller cells) emerging; thereafter amacrine cells, rods, and bipolar cells were added. Dowling's scheme represents an explicit proposal for the origin of horizontal cells in step M-5) above.

Uncoupling of differentiation and lateral expansion. As a final point, it is interesting to note that the differentiation of retinal neurons is not obligatorily coupled to the lateral expansion of the eye vesicles. Thus, Manns & Fritzsch (243)showed that application of retinoic acid to *Xenopus* embryos could prevent the formation of eye vesicles, yet in this case an apparently normal set of retinal and RPE cells could differentiate in the dorsal region of the forebrain, with the photoreceptors protruding into the third ventricle.

15. Synaptic transmission from photoreceptors to ganglion cells

Development of photoreceptor connectivity in the mammalian retina

The process of development of photoreceptor neural connectivity is intriguing, and may represent an informative relic of retinal evolution. The process is probably common across mammalian species, though it has been studied most comprehensively (244, 245) in the ferret, which has proved convenient as the young are born at a relatively immature stage of retinal development, and eye-opening does not occur for a further 2 weeks. The process is illustrated by the micrographs and the schematized sequence in Figure 34.

Initially (during the first post-natal week in the ferret) the photoreceptors have a simple bipolar form, making it almost impossible to identify them on purely morphological grounds. But even these very young cells express markers specific for photoreceptors (e.g. recoverin, vGluT1, rhodopsin), and they do so long before they exhibit the characteristic morphology of mature photoreceptors. In the immunofluorescence image of Figure 34A, the young rods are labeled green as a result of reactivity for rhodopsin, which is found to be distributed throughout the entire cytoplasm of the rods before the outer segments have differentiated.

Transient contacts at the inner plexiform layer. At very early times each immature cone or rod photoreceptor sends a process directly to the inner plexiform layer (schematic in Figure 34C). Over the course of the first two post-natal weeks, more and more photoreceptors form, and their processes continue to penetrate the location of the nascent outer plexiform layer, even though the horizontal cells with which they will eventually connect are already in their final positions and have begun to extend their processes laterally (schematic in Figure 34D). Within the IPL, the processes of the young photoreceptors terminate in two discrete sub-layers, coincident with the stratifying processes of cholinergic amacrine cells (micrographs of Figure 34A,Figure 34B and schematic in Figure 34E). The photoreceptor terminals express the synaptic proteins synaptophysin and synaptotagmin, and have the morphological appearance of functional synapses (245). However, it has not been established whether the post-synaptic processes that they contact are amacrine or ganglion cells.

Mature contacts at the outer plexiform layer. Subsequently (around post-natal day 14 in the ferret), these transient processes retract from the IPL, and the photoreceptors instead make synaptic contacts within the developing OPL (schematic in Figure 34F). This phase of retraction coincides in time with maturation of the bipolar cells and with continued maturation of horizontal cells and the OPL. At the developing OPL, each photoreceptor terminal develops a ribbon synapse which first forms a dyad contact with a pair of horizontal cell processes, and is thereafter contacted by a bipolar cell process, giving rise to the adult triad arrangement of the ON pathway. At

around the same time, the distal process of each photoreceptor penetrates the outer limiting membrane, and begins to form an inner segment and an outer segment.

The above developmental sequence, whereby the route for signal transmission from the photoreceptor initially occurs via direct synaptic contact onto the output layer, but is subsequently transformed by the insertion of a bipolar cell into the afferent pathway, is consistent with the notion that a comparable transformation occurred during the evolution of the retina.

Photoreceptor connectivity in organs other than gnathostome retina

Pineal organ: Photoreceptor connectivity to ganglion cells. In non-mammalian vertebrates, pineal photoreceptor cells make direct synaptic contact via ribbon synapses onto projection neurons ('ganglion cells'), as indicated previously in Figure 10A,Figure 10D and reviewed in Dodt (246) and Ekström & Meissl (247). It is generally thought that the pineal organ contains only photoreceptors, ganglion cells, and glial cells, and that it completely lacks the other classes of neuron that characterize the lateral retinas; however, Ekström & Meissl (247) reported the occurrence of a single case of a presumed interneuron that exhibited electrical response properties closely similar to those of the photoreceptors.

Pineal ganglion cell responses are predominantly 'luminosity OFF' units, showing sustained firing in darkness and a graded inhibition of firing during illumination at any wavelength (69, 74, 246, 248). Typical responses for a pineal photoreceptor and a standard 'luminosity OFF' pineal ganglion cell to moderately bright illumination were indicated schematically in Figure 12. For sub-saturating intensities the form of the graded response in the ganglion cell closely resembles that in the photoreceptor. For maintained exposures, the firing rate is reduced in proportion to the logarithm of the intensity, over a range as great as 8 log units (74).

In addition, some luminosity cells are transient, showing little spike activity in darkness but giving a burst of firing at the cessation of a light stimulus. Occasionally, chromatic responses are seen, that involve antagonism between UV-sensitive photoreceptors on the distal side of the organ and the main rhodopsin-containing photoreceptors.

The interpretation of these results is as follows. In the light-sensitive pineal organ of non-mammalian vertebrates, the photoreceptor cells make direct synaptic contact onto ganglion cells via ribbon synapse junctions. The high rate of release of glutamate in darkness leads to a sustained depolarization and steady firing in the ganglion cells. In response to light, the photoreceptors hyperpolarize, reducing their release of glutamate, and eliciting graded responses of similar form in the ganglion cells. The resulting sign-preserving responses in the ganglion cells are accordingly of 'OFF' polarity; they are maintained during steady illumination and show a logarithmic relation to intensity. There is no 'ON' pathway, and no evidence for the involvement of cells other than the photoreceptors and ganglion cells. Given that the pineal organ may well have antedated the lateral retinas of vertebrates, these results suggest that the ancestral pathway for signal flow in the vertebrate retina could conceivably have been directly from cones to OFF retinal ganglion cells.

Hagfish 'eye': Photoreceptor connectivity to ganglion cells. In the hagfish eye, the only known classes of neuron are ciliary photoreceptors and projection neurons. The synaptic terminals of the photoreceptor cells have been shown to form dyad contacts with post-synaptic elements, though to date the identity of those post-synaptic processes has not been determined; nevertheless, it is presumed that they are the projection neurons. Hence the presumption is that the ciliary photoreceptors make direct synaptic contact onto the projection neurons in hagfish.

Contact between ciliary and microvillar cells in amphioxus? The kind of molecular homologies discovered by Arendt and his colleagues, between the vertebrate and *Drosophila* retinas, have recently been extended to the frontal eye of amphioxus. As presented in Section 3, Vopalensky et al (47) have shown a close homology between ciliary photoreceptors in Row 1 of the amphioxus frontal eye and the cone and rod photoreceptors of the

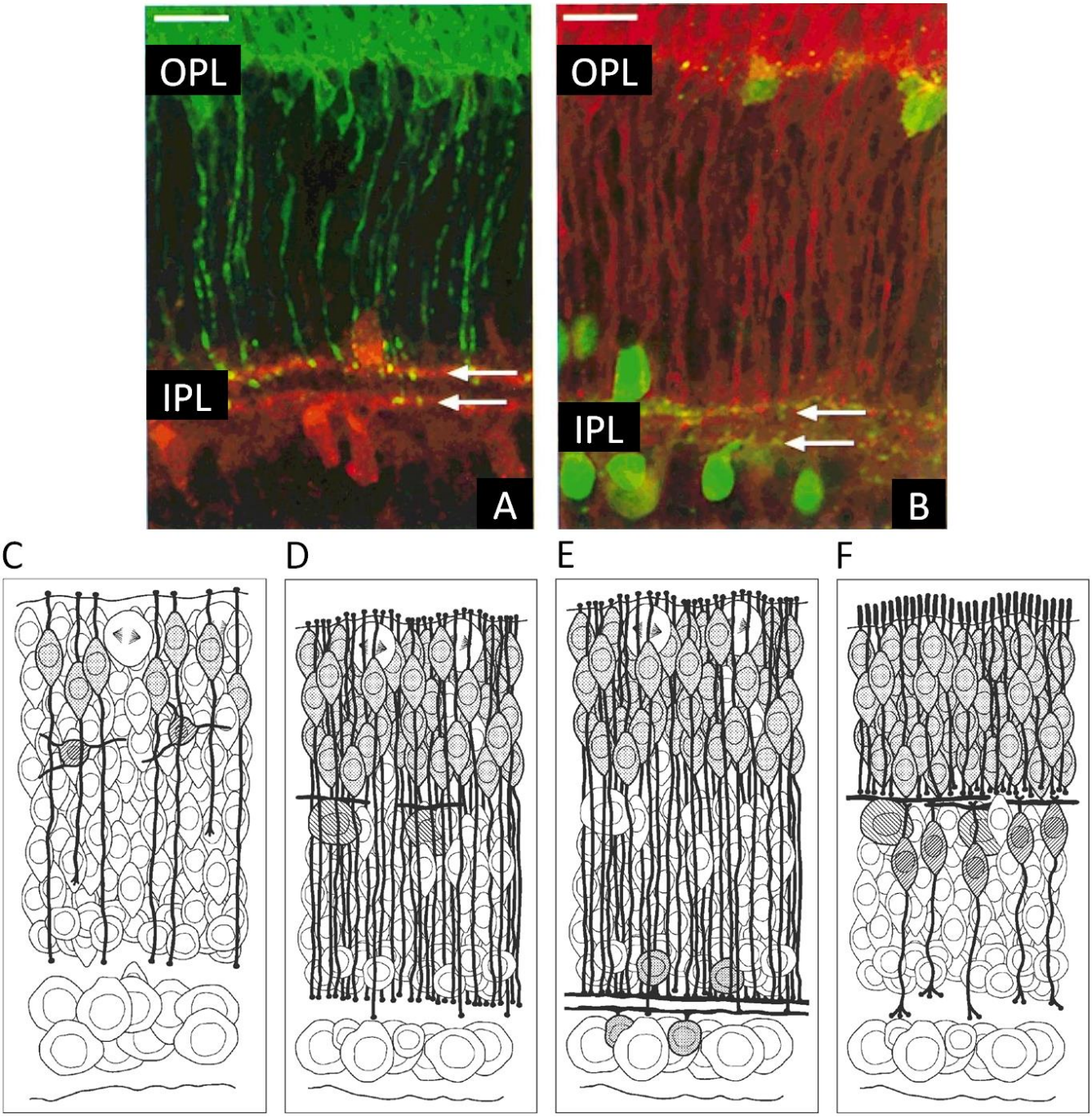

Figure 34. Photoreceptor transient contacts at IPL and final contacts at OPL. Top row: Immunolabeling of ferret retina at P15 (post-natal day 15), the day on which the density of rods projecting to the IPL is highest. Scale bars 10 μm. Modified from Johnson et al (245). A, Rod photoreceptors (green, rhodopsin labeled) send processes to the IPL, where their terminals overlap with the two strata (arrowed) of dendrites from cholinergic and displaced amacrine cells (red, ChAT labeled). B, Cone photoreceptors (red, recoverin labeled) send processes to the IPL, where their terminals overlap with the two strata (arrowed) of dendrites from amacrine and ganglion cells (green, parvalbumin labeled). Bottom row: Schematic representation of the development of photoreceptor and bipolar cell connectivity, in the course of the first (C), second (D, E) and third (F) post-natal weeks. From Reese (274). C, First week. Photoreceptors (pale stippling) extend processes through the neuroblast and amacrine cell layers to the IPL. Horizontal cells (diagonal shading) have migrated into the neuroblast layer, to the site of the future OPL, yet despite their presence the photoreceptors extend beyond them. D, Second week, showing horizontal cells. Horizontal cells (diagonal shading) begin elaborating their horizontally oriented dendrites, giving rise to the OPL. E, Second week, showing cholinergic amacrine cells. Photoreceptor cell processes terminate at two levels within the IPL, coincident with the stratifying processes of the cholinergic amacrine cells (dark stippled cells at the bottom). F, Third week. Horizontal cells, and then bipolar cells (diagonal shading), continue to mature, giving rise to a continuous plexus of processes within the OPL. The photoreceptors retract their terminals from the IPL and form synapses within the OPL. Outer segments begin forming.

vertebrate retina; in addition, it is possible that the Row 2 cells might be homologous to retinal ganglion cells. Elsewhere in the brain of amphioxus, microvillar photoreceptors (Joseph cells) are immediately adjacent to the cells of the lamellar organ, with the Joseph cells 'capping' the lamellate cells (37, 249, 250). Although there is no evidence that the lamellate cells are actually photoreceptors, these reports at least show that during evolution microvillar photoreceptors have come into very close apposition with lamellate ciliary cells.

Scenario for origin of synaptic transmission from photoreceptors to ganglion cells

In light of these observations, the following scenario is proposed for the origin of synaptic transmission from ciliary photoreceptors onto projection neurons in a proto-vertebrate retina (see Figure 35):

N-1) At an early stage in chordate evolution, ciliary photoreceptors and microvillar photoreceptors (that had descended from a common ancestral cell) lay adjacent to each other. They responded to light with hyperpolarizing and depolarizing responses, respectively. These photoreceptor cells were embedded amongst pigmented cells, and possibly separate glial cells, that had likewise descended from the common ancestral cell.

N-2) At this stage, the ciliary photoreceptors conveyed their output via a 'local circuit' or paracrine mechanism, probably releasing melatonin, and possibly also glutamate. This paracrine release may well have had a circadian or seasonal time-keeping function.

N-3) The microvillar photoreceptors signaled their output to other regions of the CNS via axon terminals that released glutamate as synaptic transmitter.

N-4) Over time, the microvillar photoreceptors additionally came to express glutamate receptors and thus were able to respond to signals from the ciliary photoreceptor, and in due course full-blown synaptic contacts evolved. At this stage, the microvillar photoreceptors acted as projection neurons and could transmit the responses of the ciliary photoreceptors rapidly, via their axons and synaptic outputs.

N-5) At some stage (probably coinciding with the improvements in C-opsin performance and the invention of retinoid re-isomerization in darkness), the signals from the ciliary photoreceptors provided virtually all the information that was needed by the organism, and the phototransduction machinery in most of the projection neurons became redundant and withered away.

N-6) The region in which these cells were located was the forerunner of the 'eye fields' that in the future would give rise to the several diencephalic light-sensitive organs. Its expansion occurred as described above in Section 13.

16. Retinal processing: Bipolar cells and the photopic and scotopic pathways

The nature and origin of retinal bipolar cells

Retinal bipolar cells share a large repertoire of features with cone and rod photoreceptors. Structurally, retinal bipolar cells have the same 'bipolar' shape as is initially exhibited by developing photoreceptors, prior to the differentiation of their inner and outer segments.

Landolt's club. Some bipolar cells possess an appendage, the Landolt's club (Figure 36) that bears a striking similarity to the inner segment of the photoreceptor (251-253). This organelle has microtubules organized in the 9+0 pattern characteristic of non-motile cilia, and is located at the outer limiting membrane, though it differs from the inner segment in not giving rise to an outer segment. In the chick retina, Quesada & Genis-Galvez

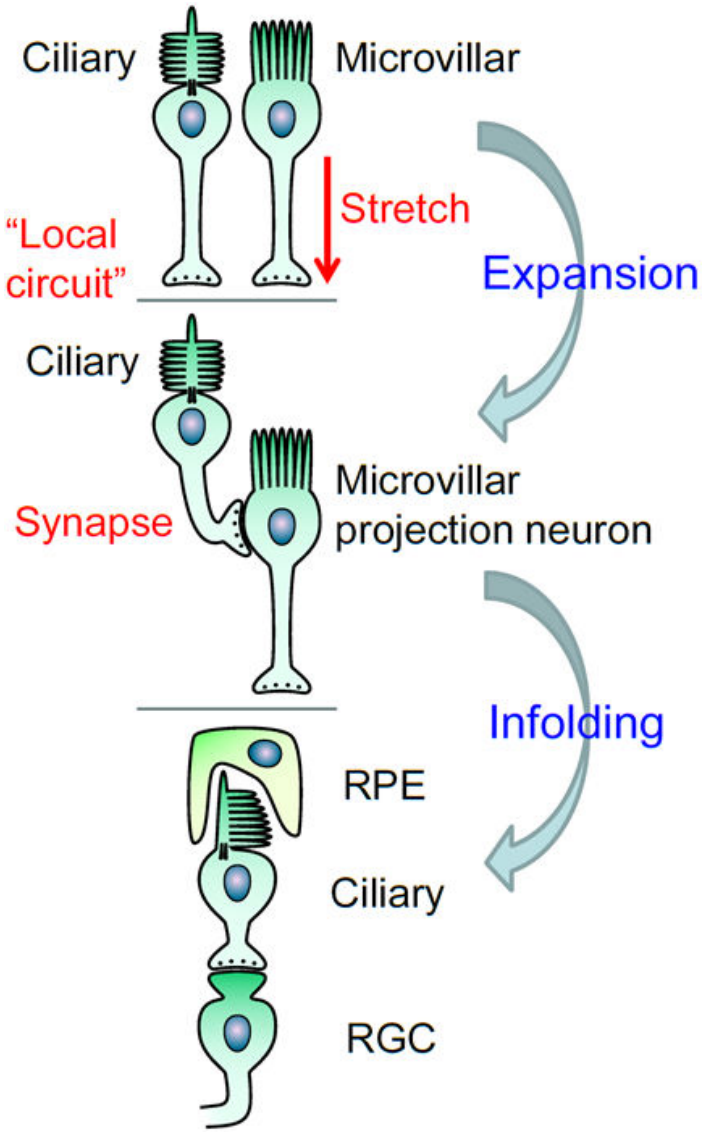

Figure 35. Ciliary photoreceptors make synaptic contact onto ganglion cells. Hypothesized sequence of steps for the formation of the photoreceptor to retinal ganglion cell pathway from ciliary and microvillar photoreceptors. Top: At some stage, ciliary and microvillar photoreceptors co-existed in close proximity to each other; pigmented glial cells were also present but are not shown. The ciliary photoreceptor is envisaged to have had a 'local circuit' or paracrine role, in releasing one or more chemical messengers (perhaps melatonin and glutamate), whereas the microvillar photoreceptor made synaptic contacts onto target cells (not shown). Middle: As this light-sensitive region of the diencephalon expanded, the ciliary and microvillar photoreceptors maintained their respective 'local circuit' and synaptic transmission modes, with the axons of the microvillar cells elongating to reach their targets, and with the paracrine release from the ciliary cells developing into synaptic transmission with the expression of glutamate receptors on the microvillar cells. At this stage it is envisaged that both sets of cells would have responded to light, though with opposite polarity, and the axons of the microvillar cells provided the neural output for both sets of photoreceptors. Bottom: With the in-folding of the eye-cup, the outer segments of the ciliary photoreceptors came into close apposition with the monolayer of retinal pigment epithelial cells, and at this stage the pigment cells that had previously been present in the retina were able to be dispensed with. At some stage, most of the formerly microvillar cells lost their microvillar membrane and their phototransduction cascade, though a subset retained vestiges, as intrinsically photosensitive retinal ganglion cells. Modified from Lamb, Pugh & Collin (275).

(254) have reported that in early embryonic stages all of the bipolar cells are connected to the outer limiting membrane by a Landolt's club, and that during development many of these processes retract.

Transduction. In terms of transduction mechanisms, the G-protein cascade of the ON bipolar cells bears a remarkable similarity to the phototransduction cascade in vertebrate photoreceptors. In addition, the output

synapse of the bipolar cell is very similar to that of the photoreceptor, employing synaptic ribbon structures that are not found in any other types of retinal neuron. Finally, many proteins expressed in retinal bipolar cells are either identical to, or else represent isoforms of, proteins found in cone and rod photoreceptors; for example, recoverin, potassium channels, and the molecular machinery of ribbon synapses.

In view of these close similarities, as well as the order of differentiation of retinal cells (Figure 33) it is possible to view retinal bipolar cells as probable 'descendants' of retinal ciliary photoreceptors, in the sense that they appear to have evolved as a kind of variant of the established ciliary photoreceptor theme and have thereby inherited a great many of the properties of those photoreceptors. If this is indeed the case then one might anticipate that cone ON bipolar cells would have descended from cones, and that rod bipolar cells might have descended from rods rather than from cone bipolar cells.

An alternative (though perhaps less likely) possibility that might account for these observations is that photoreceptors and bipolar cells are independent descendants of the 'proto-neuron' that has been hypothesized to have been the most ancient type of vertebrate nerve cell (208, 209, 255). However, this hypothesis would not seem to sit well with the evidence that cone and rod photoreceptors are descended from an ancestral ciliary photoreceptor. An extant representative of the presumed ancestral proto-neuron has been suggested to be the sensory 'cerebrospinal fluid (CSF)-contacting neuron' present in the CNS of amphioxus, hagfish (256) and lampreys (257), as well as jawed vertebrates.

Scenario for evolution of the photopic signaling pathway via bipolar cells

From the observations in Section 14 on the development of photoreceptor contacts in the embryonic retina, and the observations above on the nature of bipolar cells, as well as the findings in Section 14 on the timing of retinal development, the following is proposed as the likely sequence of events that occurred during evolution of the afferent pathway in the vertebrate retina:

O-1) At the stage of eye evolution where the eye vesicles had bulged laterally to form the ancestral retina/RPE, the photoreceptors already made synaptic contacts directly onto ganglion cells, which projected axons to the CNS.

O-2) Horizontal cells evolved, and made synaptic contacts with photoreceptors at ribbon synapses in a dyad structure; they provided spatial integration of light signals, and fed this spatially-averaged signal back (inverted) onto the photoreceptor terminals thereby generating an element of spatial contrast.

O-3) Subsequently, a modified class of 'pseudo photoreceptor' cell evolved, that had lost the capability of expressing visual pigment and an outer segment, but that expressed metabotropic glutamate receptors.

O-4) During retinal development, this new class of cell, the retinal ON bipolar cell, inserted its dendritic terminals into photoreceptor dyads, to form triads, while its afferent process made the same journey to the IPL that its predecessor (the photoreceptor) had made.

O-5) A variant of this cell expressed ionotropic glutamate receptors and became the OFF bipolar cell.

O-6) Overall, a new twin-set of neural elements had been incorporated into the ancestral two-layered retina, greatly expanding the retina's capacity to perform spatiotemporal processing computations.

Dedicated scotopic pathway for rod signals

The existence of unexpected retinal circuitry in the rod pathway of mammals was first described by Kolb & Famiglietti (258), Nelson (259) and Kolb and Nelson (260); see chapters in webvision on "Circuitry for rod signals", "AII amacrine cells" and "Bipolar cell pathways". The details of this circuitry were expanded upon by Strettoi et al (261) and Vaney et al (262), and shortly afterwards Strettoi et al (263) set out the concept that the

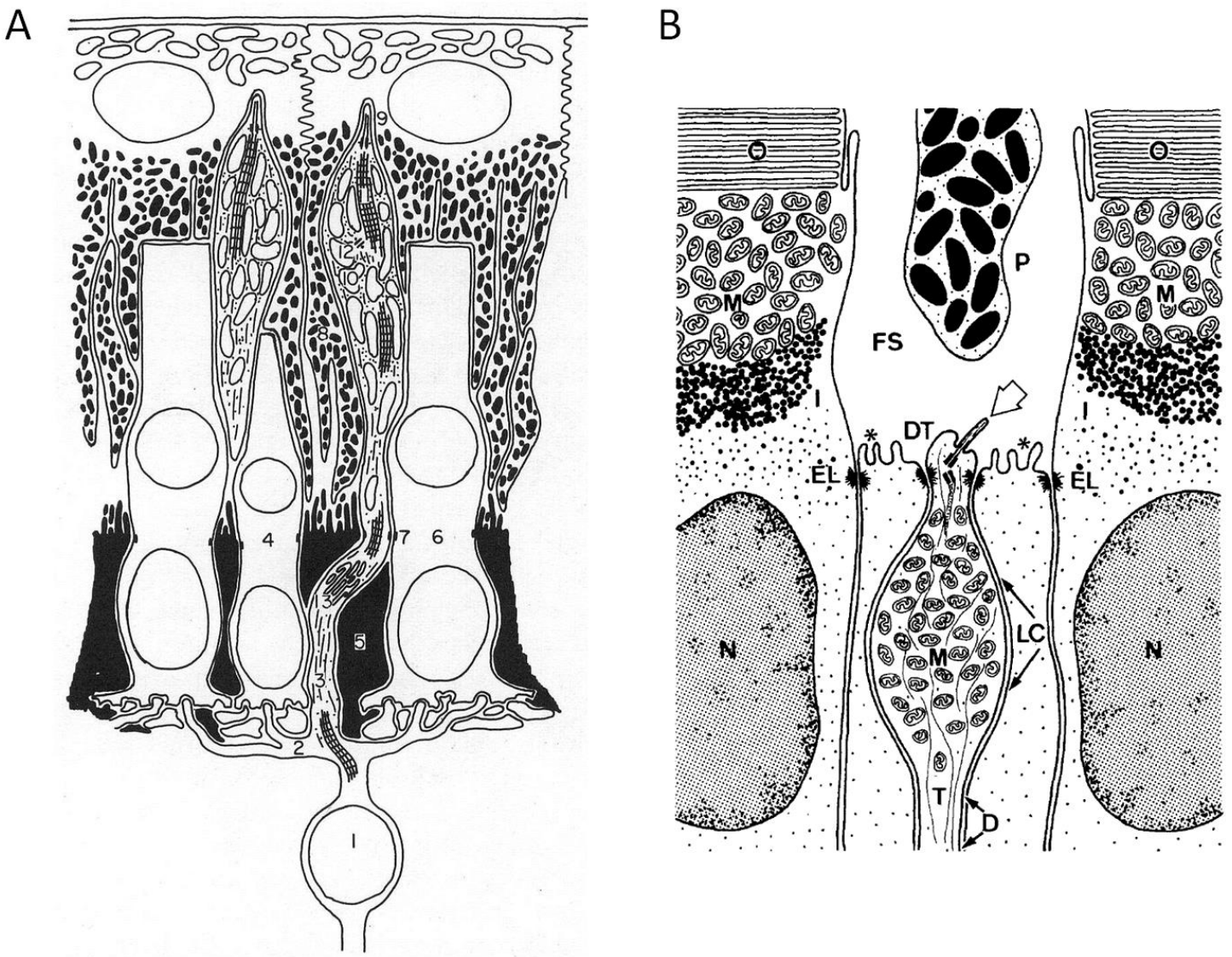

Figure 36. Landolt's club. Two schematic representations of Landolt's clubs in the retinas of different species, showing several points of resemblance to photoreceptor inner and outer segments. A, Schematic of bipolar cell and Landolt's club in lungfish retina. The bipolar cell of origin (1) gives rise to a tuft of dendrites (2) from which the stalk (3) of Landolt's club arises. Beyond the outer limiting membrane (7), the club expands and is closely apposed to the cone and rod inner and outer segments and to the processes (8) of RPE cells. The club terminates in a 9+0 cilium (9) that inserts into the RPE cell. The expanded region of the club is packed with mitochondria (10) and contains the ciliary rootlets (11). Cone (4); rod (6). From Locket (252). B, Schematic of Landolt's club for a generalized vertebrate retina. The club (LC) expands from a bipolar cell dendrite (D) and is packed with mitochondria (M); it is shown enwrapped by a Müller cell. Its dendritic terminal (DT) and 9+0 cilium (broad arrow) penetrate the outer limiting membrane (EL), and enter the sub-retinal space (FS). I, O, inner and outer segments of photoreceptors. From Vigh et al (253).

mammalian scotopic (rod-driven) retinal pathway 'piggybacks' on a pre-existing photopic (cone-driven) pathway. Coincidentally, this was the same year that Okano et al (115) discovered that rod opsins had evolved from cone opsins.

In functional terms, the main advantage of this piggyback arrangement is that the duplex cone-plus-rod system does not require duplicate pathways for neural processing in the retina, and nor does it require a duplicate set of nerve fibers to the brain. Instead, the rod signals enter the pre-existing sophisticated cone neural processing circuitry, where they can be seamlessly integrated. For visual perception, this means that it is almost impossible for one to distinguish whether it is one's scotopic or photopic system that is being utilized.

The manner in which the rod signals are injected into the mammalian cone system looks complicated (Figure 37), but it cleverly avoids introducing major compromises, especially by avoiding the generation of additional noise. From mesopic (twilight) light levels down to high scotopic (moonlight) levels, the rod signals pass via gap junctions onto cones (denoted ON2 and OFF2 in Figure 37) thereby employing the photopic pathway in its entirety. But at very low scotopic (starlight) levels, a separate dedicated system comes into operation, utilizing the rod bipolar cell and the AII amacrine cell.

For the ON system, illustrated on the left side of Figure 37, the photopic pathway uses a sign-inverting synapse (red arrow) from cone photoreceptor to cone ON bipolar cell (via a metabotropic glutamate receptor mechanism), followed by a sign-preserving synapse (green) from cone ON bipolar cell to ON ganglion cell. Thus, at low light levels, when the cones are contributing little in the way of signals, the ON bipolar cell is hyperpolarized and the synapse from ON bipolar cell to ganglion cell is quiescent. At low scotopic levels (indicated ON1), rod activity is signaled via a sign-inverting synapse onto the rod bipolar cell, and thence via a sign-preserving synapse to the AII amacrine cell, so that dim scotopic illumination causes depolarization of the AII amacrine cells (i.e. the same polarity as any light-stimulated activity in the cone ON bipolar cells). The scotopic signals are then coupled into the cone pathway, with no additional noise contribution, via gap junction electrical connections from the AII amacrine cells onto the cone ON bipolar cells (indicated in orange). In bright light, when the rods are saturated, and the rod bipolar cells and AII amacrine cells are strongly depolarized, it is possible that the gap junctions close, to prevent the intrusion of unwanted signals. If instead the rod bipolar cells had connected directly onto the ON ganglion cells synaptically (as for cone bipolar cells), a major disadvantage would have been the injection of large levels of synaptic noise into the photopic system when the rods were saturated.

For the OFF system, illustrated on the right of Figure 37, the photopic pathway uses a sign-preserving synapse (green arrow) from cone to OFF bipolar cell (via an ionotropic glutamate receptor mechanism), followed by a second sign-preserving synapse (green) from cone OFF bipolar cell to OFF ganglion cell. As a result, in the quiescent dark state, the cone OFF bipolar cell is depolarized and is continually releasing synaptic transmitter (glutamate) onto the OFF ganglion cell at a high rate. How, then, could activity from the scotopic system be injected into the cone OFF pathway, in the presence of this continual synaptic input? The answer that has been adopted is to employ a sign-inverting synaptic input from the AII amacrine cell onto the pre-synaptic terminal of the cone OFF bipolar cell (indicated OFF1). In this way, dim scotopic light leads to hyperpolarization of the cone OFF bipolar cell's synaptic terminal, thereby suppressing its on-going high rate of release of synaptic transmitter, just as occurs for signals that come from the cones.

This analysis shows that, by the time that mammals appeared, evolution had found a means by which to superimpose the single-photon detection capabilities of the more recently evolved rods onto a pre-existing cone neural processing pathway, in a seamless manner, with minimal additional wiring, and in a way that introduced minimal additional noise and that minimally perturbed the sophisticated signal processing functions of the cone circuitry. However, it is not yet clear whether this was the first solution that had been adopted in the early vertebrate retina.

Thus, it will be important to discover whether similar AII amacrine cell circuitry is employed in the retinas of vertebrates other than mammals, but so far a definitive answer to this question does not appear to have been established. In non-mammalian vertebrate retinas, it is clear that scotopic signals are processed via bipolar cells that are highly sensitive and that display response properties very similar to those of mammalian rod bipolar cells; e.g. Ashmore & Falk (264) in dogfish. Likewise, ERG recordings in lamprey retina have show a sensitive *b*-wave signal at very low light intensities However, the circuitry by which rod and cone signals are combined is not entirely clear. One possibility is that in non-mammalian retinas rod and cone signals are merged solely at the level of the outer plexiform layer, via gap junctions between rods and cones, and possibly via synaptic input from both rods and cones onto a single class of bipolar cell. In this case the bipolar cells would be of the mixed rod-

cone type, and thereafter the signals would be processed by the conventional cone pathway, comprising bipolar cell to ganglion cell. Alternatively, it is possible that circuitry analogous to that of the AII amacrine cell exists in the inner retina. Until the details of the scotopic circuitry of non-mammalian vertebrate species have been elucidated, it may not be possible to ascertain the extent to which the ancestral vertebrate retina employed the outer versus the inner plexiform layer to inject its rod-derived signals into the cone pathway. But in either case it is clear that, as a minimum, the output (ganglion cell) stage of the pre-existing cone system was utilized.

At this stage, there is insufficient information available to justify the proposal of explicit steps in the evolution of the dedicated scotopic pathway.

17. When did spatial (imaging) vision arise in the chordate lineage?

It was argued above, in Section 13, that the retina of the vertebrate lateral eyes evolved first as a non-imaging light-sensitive organ, with many similarities to the two-layered retina in the dorsal organs (pineal, parapineal, and parietal eye) of extant non-mammalian vertebrates. But when did that two-layered retina first emerge? And when, and by what means, did that pair of 'lateral pineal-like organs' evolve to become imaging organs for a visual system?

There is no evidence to suggest that the last common ancestor that we share with tunicates (at point #4 in Figure 1) could have possessed anything resembling a retina. On the other hand, our last common ancestor with lampreys (at point #5 in Figure 1) seems almost certain to have possessed a fully-fledged vertebrate-style eye, with three-layered retina, lens, extraocular muscles, and so on. Unfortunately, none of the numerous organisms that diverged from our own lineage (represented by the red curve in Figure 1) between those times has survived to the present day. Several extinct species that diverged during that interval are known from the fossil record. Although these fossil species have been reported to have possessed 'eyes', the preservation of their soft tissues is so imperfect that it is not even known whether those organs contained a lens. It seems that the fossilized lateral impressions described as 'eyes' tend to be black, or at least dark, which might be consistent with their having contained pigment.

Accordingly, it does not currently seem possible to be more specific than to say that the lateral two-layered retina arose some time after point #4 in Figure 1 and that the full-blown lateral eyes arose subsequently, at some time prior to point #5 in Figure 1. On the basis of the dates put forward by Erwin et al (20), these divergences occurred 600 Mya and 500 Mya, respectively. So, unfortunately, we do not appear to be in a position to tie down the relevant times of evolution of these important features any more precisely than within that interval of 100 million years.

If it were possible to date with any precision the timing of the occurrences of the '2R' pair of whole genome duplications, then it might be possible to narrow down the timing of the events of interest in eye evolution. Thus, the ciliary opsin quadruplication did not appear until after '2R', and hence the present five classes of ciliary opsin could not have appeared before that time, so that (for example) rods could not have appeared before that time.

A calculation has been made by Nilsson & Pelger (265) of the time required for a lens to evolve. This calculation assumed that a fully functional retina was already present, and that it was already connected appropriately to the brain, but the calculation did not take account of other changes that might be required, such as the emergence of a system of muscles to orient the eye. Hence, the time that they calculated, of approaching 1 million years, would appear to enormously underestimate the time required to transform a handful of photoreceptors into a functional eye.

Instead, we can expect that the transitions described above might have taken far longer, because each must have involved a long sequence of changes. To transform a handful of ciliary and microvillar photoreceptors into a

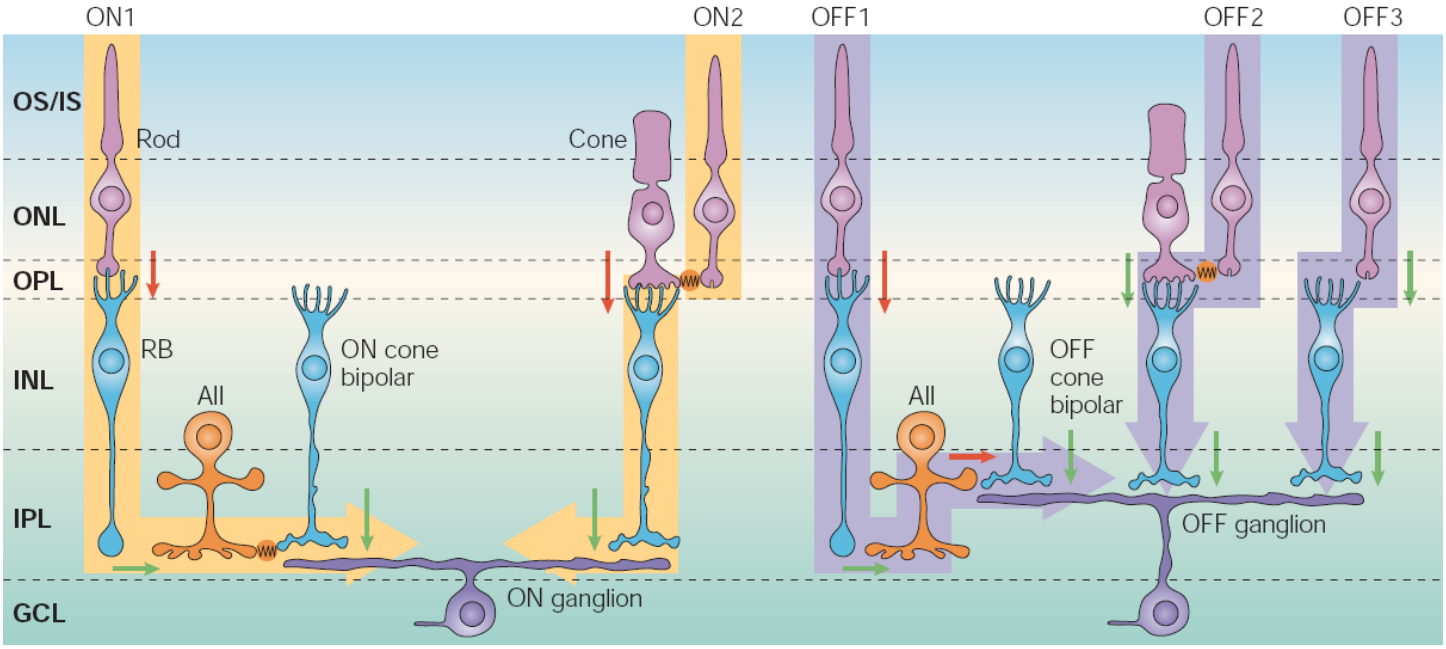

Figure 37. Cone and rod afferent pathways through the mammalian retina. Schematic wiring diagram of the mammalian retina, emphasizing the rod (scotopic) pathways. Left, ON pathways. Right, OFF pathways. Cone circuitry is indicated using just two cone photoreceptors; that in the left half is shown connecting via an ON cone bipolar cell to an ON ganglion cell; that in the right half is shown connecting via an OFF cone bipolar cell to an OFF ganglion cell. The rod pathways are described in the text. From Wässle (276).

pineal-like retina would have required numerous steps. Thereafter, to add bipolar cells, to add a lens and cornea, to add extraocular muscles, and (possibly most demandingly) to create a processing center in the brain that could deal with this spatial information, would have required enormous numbers of parallel steps. It does not seem unreasonable to contemplate that the time taken to implement the combination of these major transformations (first to non-imaging retinas, and then to imaging eyes) might have occupied a very substantial proportion of the 100 million year interval that is currently thought to have been available.

18. Conclusions: Scenario for the evolution of photoreceptors and the vertebrate retina

The following sub-sections set out a proposed scenario for the sequence of the more important of the numerous steps that were involved in the evolution of photoreceptors cells and of the vertebrate retina, using the epoch numbering scheme from Figure 1.

Early metazoans: Prior to point #1 (>700 Mya)

Sensory cell. The sensory cell from which all animal photoreceptors evolved employed a G-protein coupled receptor (GPCR), which triggered a G-protein cascade that is likely to have employed cyclic nucleotide gated channels (CNGCs).

Opsins. The original opsin arose during the relatively short interval (of ~10 million years), just prior to 700 Mya (see Figure 2), between the divergence first of placozoans and then of cnidarians from our own lineage. Prior to this, mutations in a GPCR had changed its binding specificity so that the ligand that activated it became retinaldehyde, and this modified GPCR thereby became a retinaldehyde receptor; as in other GPCRs the ligand bound non-covalently. (One of the close relatives of this GPCR appears to have given rise to the melatonin receptors of vertebrates.) After placozoans had diverged, mutation of this retinaldehyde receptor gave it a lysine

residue in its seventh transmembrane helix (corresponding to K296), so that the retinaldehyde ligand could now bind covalently via a Schiff base bond. A further mutation added a negatively charged residue nearby (corresponding to E181) that acted as a counterion, enabling the Schiff base to be protonated. This molecule thus became the ancestral opsin. It would have absorbed at the short-wavelength end of the spectrum, though we cannot be sure whether its peak would have been in what we call the 'visible' part of the spectrum or in the UV. Subsequently, this ancestral opsin duplicated twice, prior to the divergence of cnidaria, giving rise to three major branches of opsins, namely C-, R-, and RGR/Go-opsins.

Photoreceptor cells and phototransduction cascades. Once that ancestral opsin appeared, the ancestral photoreceptor had been born. It seems likely that this original photoreceptor cell resembled the ciliary category, with the opsin expressed in the membrane of the cilium and coupling via a Gi and/or Gs cascade to modulate cyclic nucleotide levels and CNGC activity. It is possible that this ancestral photoreceptor cell possessed the components of more than one G-protein signaling cascade, but at present there is too little information available to be sure about its transduction cascade(s). In the short time before cnidaria diverged, it is possible that two classes of opsin-containing cell had come into existence, with one expressing the ancestral C-opsin in its ciliary surface membrane and the other expressing the RGR/Go-opsin in the membrane of intracellular organelles. One likely function of the ancestral RGR/Go-opsin was as a retinoid photoisomerase that used light to convert the all-*trans* isomer to the 11-*cis* isomer. While it is possible that separate microvillar photoreceptors using the R-opsin had also emerged, and that they later disappeared in cnidaria, it is suggested that the microvillar class of photoreceptor arose only in bilaterians.

Other components of the ancestral light-sensitive cells. It is likely that the ancestral light-sensitive cells in those early metazoa were multifunctional, additionally expressing pigment that could act as a light shield, and it is also possible that these cells had motile functions (79). The animals possessing these cells would have been very small and would not have had a recognizable nervous system. Their cells would have been able to signal to each other by means of diffusible chemical messengers; i.e. by paracrine release. A chemical messaging system to control the basic features of differentiation in these cells would need to have been laid down by this time. Thus, the ancestral system of transcription factors specific to light-sensitive tissue was probably already in place.

Division of labor. As proposed by Arendt et al (5), it seems likely that processes of gene duplication and evolution led to the emergence of more specialized daughter cells, that shared out between them roles that had originally been performed by a single cell. If, as is suggested above, an ancient multifunctional photoreceptor cell had expressed more than one class of opsin and transduction cascade, and also functioned as a pigment cell and had a motile role, then over time these functions may have been delegated to separate specialized cells that inherited only the components relevant to a subset of the original functions. Thus, motile cells and pigment cells became separate from those that performed phototransduction; likewise, the 'photoisomerase' opsins could have been relegated to separate cells (for example, to the pigment cells). Similarly, the different opsins and their transduction cascades became separated into distinct cell types.

Bilaterians, protostomes, and early deuterostomes

Early bilaterians. In the bilaterian lineage (i.e. after the divergence of cnidaria), at least two variants of photoreceptor cell were present: a ciliary photoreceptor class expressing a C-opsin, and a microvillar photoreceptor class expressing an R-opsin. It seems likely that these two classes of cell came to be utilized for different functions. One possibility is that the ciliary photoreceptors adopted a role in diurnal and seasonal time-keeping functions, whereas microvillar photoreceptors adopted a role in phototactic behavior, providing the signal for the organism to move either towards or away from light (e.g. up or down in the water column).

Protostomes. Following the split between protostomes and deuterostomes (at point #2, Figure 1), it would appear that some protostomes evolved a lens in front of a handful of microvillar photoreceptors, in what would have become an ocellus or a single ommatidium. Perhaps signals evolved that led to the duplication/multiplication of

a number of such adjacent ommatidia, leading to the formation of compound eyes. At some later stage, the microvillar photoreceptors in some protostome lineages developed a highly organized sub-cellular structure (the rhabdomere) and a highly-specialized version of the transduction cascade, and gave rise to rhabdomeric photoreceptors. Until the advent of full-blown rhabdomeric photoreceptors in those particular lineages, it is entirely plausible that microvillar photoreceptors may not have been very sensitive. In the chordate lineage, for example, microvillar photoreceptors in amphioxus have much lower sensitivity than their protostome counterparts that evolved rhabdomeric structure (46).

Early deuterostomes. No such developments (in the form of either a lens or a rhabdomere structure) appear to have occurred in the deuterostome lineage. Thus, although microvillar photoreceptors persisted in deuterostomes, they remained as relatively simple cells, sparsely distributed, sometimes in association with pigmented cells. Likewise, relatively little seems to have occurred in the way of changes to the ciliary photoreceptors in the early deuterostome lineage.

Chordates - Early events: From point #3 onwards (Since ~650 Mya)

Refinement of C-opsins. The transformation of an ancestral C-opsin into vertebrate visual opsins appears to have involved a prolonged sequence. One of the most important changes was the re-location of the counterion site (from 181 to 113), as this allowed the meta II state to be modified in a way that achieved a higher rate of activation of the G-protein and it also allowed the meta II state to decay fairly rapidly, releasing all-*trans* retinal.

In the phylogenetic tree of C-opsins (Figure 19), there are several extant opsins that clade between the most basal C-opsin and the cone opsins, and these include Opn3, parietopsin, parapinopsin, VA/VAL-opsin, and possibly pinopsin. The functional properties of these opsins also tend to follow a sequence (Section 5), and it seems clear that the performance of C-opsins was steadily enhanced during chordate evolution, reaching a high level by the time that the first cone opsin emerged (Section 5) Thereafter this ancestral cone opsin duplicated to form both an SWS and an LWS opsin. The tunicate *Ciona intestinalis*, which diverged at point #4 (Figure 1), possesses a single C-opsin, Ci-Opsin1, that clades close to VA/VAL (though this is not shown explicitly in Figure 19. Accordingly it seems plausible that the refinement of chordate C-opsins that ultimately gave rise to cone opsins was only partway through by the time that tunicates diverged, and perhaps that the entire process of refinement may have stretched out over much of the 150 million year period from #3 to #5 in Figure 1.

Refinement of the phototransduction cascade. Over the course of chordate evolution, it appears that refinements also occurred in the phototransduction cascade. These changes include: the emergence of a Gt variant of the G-protein alpha subunit (i.e. transducin), apparently through duplication of a common Gαi / Gαt ancestor; the emergence of PDE6 specific for cGMP; the emergence of its regulatory PDEγ subunits; and so on. While the exact sequence of these developments remains obscure, and the chain of events was no doubt prolonged, it seems clear that, prior to the '2R' whole-genome duplications, the phototransduction cascade in the ancestral cone photoreceptor had already reached a state that would have been fundamentally similar to that in modern vertebrate cones.

Synaptic contact from ciliary photoreceptors onto microvillar photoreceptors. There are few landmarks to indicate when it was that synaptic contact became established between ciliary photoreceptors and their microvillar counterparts (most of which subsequently lost their light sensitivity). Amphioxus possesses microvillar photoreceptors (Joseph cells) that are immediately adjacent to cells of the lamellar organ, with the microvillar cells 'capping' the lamellate cells (Section 15) although these lamellate cells have generally been presumed to be ciliary photoreceptors, this has not been confirmed through electrophysiological recording and nor has an opsin yet been identified in them. In the 'frontal eye' of amphioxus, it has recently been shown that ciliary photoreceptors (Row 1 cells) are positioned immediately adjacent to projection neurons (Row 2 cells) that may conceivably be homologous to retinal ganglion cells (6). Hence it is possible that the last common ancestor we

share with amphioxus already had ciliary photoreceptors making synaptic contact onto microvillar photoreceptors.

Chordate to vertebrate transition: Interval #4 - #5 (~600 - 500 Mya)

In the chordate lineage, it would seem that most of the transformations that distinguish an 'eyespot' from an 'eye' are likely to have occurred during the 100 million year interval from #4 to #5 (Figure 1), around 600-500 Mya. In the light-sensitive tissue itself, these transformations included: massive enlargement of the tissue to form a retina; the invention of a means of re-isomerization of retinoid in darkness; the elaboration of retinal processing power, including the invention of bipolar cells; and the transformation of one class of cone into more rod-like cells. Outside the retina, the transformations included: the formation of accessory structures, including the lens, the cornea, the iris, and intra- and extra-ocular muscles, as well as the formation of brain regions to process the visual information and to control the motor system.

Expansion of diencephalic light-sensitive region. The region comprising the light-sensitive tissue expanded, both dorsally and laterally, at some stage during chordate evolution; most of this expansion appears to have occurred after the divergence of tunicates. The initial driving force for expansion may simply have been the need to achieve greater sensitivity, and that may have led to the deployment of a larger area for absorption of incident light. One factor favoring expansion in the lateral direction may have been the shielding of down-welling light that accompanied the expansion of the primitive brain and the formation of a cartilaginous cranium. The advantages to the organism would have been not only increased light sensitivity, but the potential for shadow detection and a crude comparison of the direction of incident illumination.

In the tissue expansion that occurred, it seems that only the microvillar photoreceptor cells extended axons to their pre-existing targets in more central brain regions, and that the ciliary photoreceptor cells continued to signal in a purely local manner. At some stage, their signaling mechanism became synaptic, rather than paracrine, though the ciliary photoreceptors have retained to this day the capacity to release melatonin.

The region that bulged appears to have had minimal luminal space, so that its apposing luminal (interior) surfaces were in contact with each other; the innermost surface of each side contained ciliary photoreceptors embedded amongst pigment cells and glial cells. This expanding vesicle developed a 'polarity', that rendered the two sides different, and that in due course gave rise to a complete distinction between 'retina' on one side and 'RPE' on the other; the signal for this development of polarity may have been generated by the ancestral placode that subsequently evolved into the lens placode. As a result of the polarization, pigment cells no longer formed on the side facing the external world, while neural elements formed only on that side. This afforded a major advantage to the organism, in terms of increased light sensitivity, because the entire cross-sectional area of the organ was now tiled with photoreceptors, whereas previously a substantial proportion of that area had been occupied by pigment cells; instead, the pigment cells were now effectively placed behind the photoreceptors (in terms of the incident light path) but nevertheless still in physical contact with them.

This expansion and bulging, combined with the retention of minimal luminal volume and the development of a polarity to the organ, is what gave rise to the 'inside-out' vertebrate retina.

At this stage of chordate evolution, it is suggested that the rudimentary 'eye' had not yet evolved optical components (lens, etc.), or sophisticated neural processing power (bipolar cells, etc.), or a motor system for orienting it, and that instead it probably bore a close resemblance to the 'eye' of extant hagfish.

Dark re-isomerization of retinoid. Concomitant with the improvement in efficacy of G-protein activation that evolved in chordate C-opsins was the loss of ability of the active metarhodopsin to undergo photoreversal to the 11-*cis* isomeric form (Section 5). This necessitated release of the all-*trans* retinoid and its re-isomerization via some other route. Potentially, that could have utilized a separate photoisomerase, along the lines of the retinochrome that is used in the squid eye - and possibly such an isomerase was at some stage used, given the

presence in the RPE of RGR-opsin that is capable of such *trans*-to-*cis* photoisomerization. However, it appears that what was of greater importance in the chordate lineage was a chemical route for isomerization in darkness (Section 12). In living vertebrate species there is clear evidence for the existence of an intra-retina retinoid cycle, available to cones, though the details are obscure and the origins unknown - but it is entirely possible that this intra-retina cycle might represent the ancestral pathway for isomerization of the all-*trans* form to the 11-*cis* isomer in darkness. The better known pathway, involving retinoid transport to the RPE and back, evolved after the divergence of tunicates, judging from the absence of a true RPE65 or LRAT in *Ciona*.

Triumph of ciliary photoreceptors. The advent of a chemical route for re-isomerization in darkness is likely to have invested chordate ciliary photoreceptors with a major advantage over microvillar photoreceptors that utilized bistable photopigments. Whenever the animal moved from a brightly-lit environment to a dimly-lit one, the microvillar photoreceptors would have been burdened by a large complement of stable metarhodopsin, with no way to rapidly convert it back to rhodopsin; hence the content of useful rhodopsin would have remained low, and these photoreceptors would have exhibited a prolonged reduction in sensitivity. In contrast, the ciliary photoreceptors would have been able to 'dark adapt' through release of all-*trans* retinoid and re-binding of 11-*cis* retinal to form rhodopsin; to maintain this ability in the long-term, the released all-*trans* retinoid needed to be chemically isomerized back to the 11-*cis* form in darkness. As a result, pre-vertebrate chordates are likely to have had a distinct advantage over organisms with stable photopigments, when they entered dim environments during the daytime, as well as at the fading of sunlight. Likewise, the ciliary photoreceptors may have enjoyed a sufficiently large advantage over their microvillar companions within the same retina, in terms of higher sensitivity and the ability to dark adapt, that there was little to be gained in retaining both sets of photoreceptor. Instead, the microvillar cells for the most part lost their photoreceptive properties and instead became specialized as projection neurons, though some retained a role in signaling light for circadian entrainment and other 'non-visual' purposes.

Multiple classes of retinal opsin and photoreceptors. Prior to the '2R' rounds of whole-genome duplication, there appear to have been just two types of cone opsin (SWS and LWS) that were expressed in two classes of cone. Then, as a result of the '2R' duplications, the SWS opsin quadruplicated into SWS1, SWS2, Rh2 and Rh1 opsins, expressed in what originally would have been four classes of short-to-mid-wave-sensitive cone photoreceptors. However, the pressure for high sensitivity at low light levels would have made it advantageous for the meta II lifetime to have lengthened in (at least) one of these opsins, so that the light response could be integrated for longer. This appears to have led to mutations at sites 122 and 189 in the Rh1 opsin, that lengthened the meta II lifetime by partly shielding the retinoid binding site from access by water. The same pressure additionally led to the slowing of other recovery steps in the cells expressing the Rh1 opsin, so that modified versions of the GRK, arrestin and PDE6 arose. Although the LWS opsin is likewise assumed to have quadruplicated, only a single copy has survived.

Even by the stage at which lampreys diverged from our own lineage (i.e. #5 in Figure 1), it seems unlikely that 'true rods' had evolved; thus, although the short photoreceptors of northern hemisphere lampreys express an Rh1 opsin and are quite sensitive, they exhibit a number of cone-like properties and it remains to be determined whether they are capable of reliably signaling individual photon hits. True rods, of the kind we recognize in jawed vertebrates, may not have been perfected until after that divergence.

Evolution of retinal bipolar cells. In vertebrate light-sensitive regions other than the lateral retinas (i.e. in the pineal organ, the parapineal organ, and the parietal eye), and also in the retina of the hagfish eye, the ciliary photoreceptors make synaptic contact directly onto projection neurons which, as argued above, are likely to represent descendants of microvillar photoreceptors. In contrast, the cone and rod photoreceptors of the vertebrate retina communicate with their projection neurons via an intervening bipolar cell. Examination of retinal development shows that these bipolar cells differentiate later than all other retinal neurons, and

furthermore that the developing bipolar cells become interposed into a circuit that initially comprises direct contact from photoreceptors onto ganglion cells.

These findings are consistent with the notion that retinal bipolar cells evolved late, after a two-layered retina had already been established (comprising ciliary photoreceptors connected to projection neurons) and that these newer cells became inserted into the pre-existing neural pathway. That new arrangement provided an enormous increase in computational power in the retina, allowing the pooling of photoreceptor signals, as well as comparisons of different signals, as in center-surround processing and spectral (color) comparisons.

Accessory structures (lens, cornea, muscle). The accessory structures that enable a retina to function as the 'sensor' in a camera-style eye include the lens, the cornea and sclera, the iris, and the intra- and extra-ocular muscles. In addition, and arguably most importantly, there needs to be a neural processing center in the brain to interpret the information and act on it, as well as to control the movement of the eyes. Although it is clear that these structures must have evolved in parallel with the evolution of the retina, unfortunately any account of their evolution is beyond the scope of this article.

Jawed vertebrates: After point #5 (Since 500 Mya)

After the divergence of cyclostomes, the fundamental bauplan of the eyes of jawed vertebrates did not change substantially. Nevertheless, numerous refinements occurred, many of which relate to the optics of the eye, and especially to the optics required with an air interface once tetrapods emerged. Those changes will not be discussed here.

One major change that evolved within the jawed vertebrate retina involved scotopic pathways. As far as we know, neither lampreys nor hagfish possess a 'duplex' retina of the kind that evolved in jawed vertebrates, with true rods capable of reliably detecting single photon hits and with a dedicated scotopic visual system. Instead, lamprey photoreceptors that express the rod-like Rh1/RhA opsin retain a variety of cone-like features. On current evidence I suggest that the ultimate scotopic sensitivity exhibited by modern vertebrates, that is made possible by the retina's ability to 'count' individual photons hitting 'true rods', did not evolve until after our ancestors had diverged from the ancestors of lampreys and hagfish. It will be important to test this assertion through future research.

19. Summary

The following is an abbreviated summary of the main events hypothesized to have contributed to the evolution of vertebrate cone and rod photoreceptors and their transduction cascades, and to the evolution of the vertebrate retina:

1. An ancestral cyclic nucleotide version of a G-protein cascade arose very early in metazoan evolution. In that cascade a (non-light-sensitive) GPCR activated a G-protein that coupled to an effector enzyme that modulated cyclic nucleotide levels, thereby modulating the opening of CNGCs.
2. One type of GPCR evolved the ability to bind retinaldehyde non-covalently, as its ligand, and hence effectively became a retinaldehyde receptor. This occurred prior to the divergence of placozoans. Subsequently, the lysine 296 residue evolved, so that the binding of retinoid became covalent, via a Schiff base bond. A counterion site (e.g. E181) also evolved, enabling the Schiff base bond to be protonated, and generating the ancestral opsin that would have had its peak absorption near the shortwave end of the spectrum.
3. The cell that expressed this first opsin thereby became the ancestral metazoan photoreceptor cell. It employed a G-protein cascade broadly comparable to that of modern ciliary photoreceptors, and in particular it used a cyclic nucleotide as cytoplasmic messenger to modulate the opening of cyclic nucleotide-gated ion channels.

4. The organism in which this photoreceptor cell evolved was very small, and did not yet possess what could be described as a nervous system. The cell signaled its response to other cells by the local release of one of more chemical messengers, probably melatonin and glutamate.
5. This cell probably did not require a source of 11-*cis* retinal, because the opsin apoprotein could bind all-*trans* retinal, and because the resulting visual pigment could undergo photoreversal from the active metarhodopsin state to the ground state rhodopsin (as can most opsins, with the exception of vertebrate cone and rod opsins).
6. Variants of this cell arose, through a number of duplications, leading to different cell types that expressed a C-opsin, an R-opsin, or an RGR-opsin.
7. In the cell expressing the ancestral C-opsin, the opsin trafficked to the plasma membrane of the cilium. In time, mechanisms evolved for the massive expansion of this ciliary membrane. At first, these expansions were poorly organized; often they tended to align parallel to the axis of the cilium (longitudinally).
8. In the deuterostome/chordate lineage, these expansions of the ciliary membrane progressively evolved greater degrees of organization, becoming flattened (lamellar) by the time that cephalochordates diverged, and as rather bud-like lamellar petals by the time that ascidia diverged, and then subsequently being splayed-out at right angles to the ciliary axis by the time that vertebrates appeared.
9. During early chordate evolution there was probably just a single type of C-opsin, probably of the Opn3 family, that in many respects did not differ greatly from R-opsins. But during early vertebrate evolution a number of variants of this C-opsin arose, of which residual members in living vertebrates include parietopsin, parapinopsin, VA opsin, and pinopsin.
10. During this progression, the counterion for the Schiff base migrated from site 181 to site 113, and this re-location turns out to have been important in at least three ways. First, it permitted release of all-*trans* retinal and hence the rapid regeneration of visual pigment in darkness (from a store of 11-*cis* retinal); secondly, it improved the time resolution of the cone by shortening the lifetime of active meta II; and thirdly, it paved the way for the achievement of a higher efficacy of G-protein activation by enabling further intra-molecular rearrangements that led to a large tilt in helix 6 in the meta II state. That last improvement prevented photoreversal of meta II, and made the release of all-*trans* retinal essential.
11. Hence the ancestral cone photoreceptor utilized an opsin (the ancestral cone opsin) that was expressed in lamellar sac membranes that radiated laterally from the cilium. It required a source of 11-*cis* retinoid, which (by analogy with modern cones) was probably provided by the Müller cells.
12. The primary proteins involved in activation of the cascade had evolved to become: (*i*) the ancestral transducin, with its Gt alpha subunit duplicated and modified from an earlier Gi, and with a ubiquitous beta and unique gamma subunit; (*ii*) the ancestral PDE6 cyclic GMP phosphodiesterase, comprising a pair of identical catalytic subunits and a pair of regulatory (gamma) subunits; and (*iii*) a tetrameric cyclic nucleotide-gated channel composed of two classes of subunit, alpha and beta.
13. The primary proteins involved in response recovery and regulation had evolved to become the ancestral 'cone' components: GRK7, ARR3, RGS9, GUCY2D, GUCA1C, SLC24A1, RCVRN.
14. Duplication of the first cone opsin gave rise to a pair of retinal cone opsins: an SWS opsin with the standard E181 residue, and an LWS opsin with the H181/K184 combination that provided a chloride-binding site and a substantially red-shifted absorption. These two opsins were expressed in separate, but closely similar, cone photoreceptors. Their outputs provided signals that could have been utilized to provide dichromatic processing.
15. Also present nearby were microvillar photoreceptors that had descended from a common ancestral photoreceptor. The paracrine release mechanism of the ciliary photoreceptors evolved into synaptic contacts onto the neighboring microvillar photoreceptors. At some stage, the performance of the ciliary photoreceptors (as transmitted to the cells of microvillar origin) became sufficient to signal all the features of illumination that were important to the organism, and thereafter the majority of the

microvillar photoreceptors dispensed with their opsin and phototransduction cascade, and specialized as projection neurons.

16. All the above events took place prior to the '2R' two rounds of whole-genome duplication that occurred at the base of the vertebrate lineage.
17. As a result of the two genome duplications, the quadruplication of the SWS opsin gave rise to the vertebrate SWS1, SWS2, Rh2, and Rh1 opsin classes. Only a single copy of the LWS quadruplication survived. These five opsins were expressed in five classes of cones.
18. The genome duplications additionally gave rise to the cone versus rod differences in isoforms of many of the components of the phototransduction cascade.
19. In the cone photoreceptor that expressed the Rh1 opsin, the confluence of a number of changes led to a slowing of response shut-off, which elicited a larger response per photoisomerization. One of these changes was an increase in lifetime of meta II that occurred as a result of mutations at sites 122 and 189. This also reduced the rate at which rhodopsin could be regenerated, and probably explains the resistance of rhodopsin to hydroxylamine.
20. Ultrastructural changes in the outer segment of this cell, including the enclosure of lamellae within the plasma membrane, permitted more extensive longitudinal spread of messengers.
21. In due course, the combination of these changes gave rise to a photoreceptor that was capable of reliably signaling individual photoisomerizations, and that thereby deserved the title of 'first true rod'. Whether this stage was reached before or after the divergence of cyclostomes is not yet certain, but it seems likely to have been after.
22. At around the time that chordate C-opsins lost their ability to undergo photoreversal, one or more mechanisms arose for the re-isomerization of retinoid in darkness. It is possible that the first of these mechanisms was the intra-retina cycle that modern cones have access to. The other cycle, involving transport of retinoid to and from the RPE, had not arisen by the time that tunicates diverged, and hence (among extant species) is a purely vertebrate phenomenon.
23. The light-sensitive region in the anterior neural tube of an ancestral chordate expanded dorsally and laterally. The ciliary photoreceptors and the projection neurons remained in close proximity to each other, and what 'stretched' was the axon of the projection neuron that conveyed information to other areas of the brain.
24. The lateral vesicles developed a sidedness, such that the side facing outwards made only the cells of the neural retina whereas the proximal side made only the epithelial cells that provided supportive, nutritional, and retinoid processing functions, as well as pigment to absorb unwanted light. At that stage of evolution the lateral retinas broadly resembled the retinas of modern hagfish.
25. As a consequence of the genome duplications, two new classes of retinal cells appeared. These horizontal cells and amacrine cells made synaptic connections with ciliary photoreceptors and ganglion cells, respectively, in a manner that mediated lateral interactions between cells and possibly mediated extraction of simple spatial contrast.
26. Also as a consequence of the genome duplications, another new class of cell, the retinal bipolar cell, evolved. It closely resembled the ciliary photoreceptor cells in many ways, though instead of making an outer segment it expressed glutamate receptors. This new cell became incorporated into the neural pathway from ciliary photoreceptors to ganglion cells, and thereby permitted a great increase in the computational ability of the retina.
27. Relics of the evolution of retinal cells and the evolution of retinal wiring are retained in various features of retinal cell differentiation and the early connectivity of retinal cells.
28. Spatial vision in chordates arose gradually, through parallel changes not just in the photoreceptors and the retina, but also through the formation of an imaging element (the lens) and other ancillary structures such as the cornea/sclera, the iris, and intra- and extra-ocular muscles, as well as through elaboration of brain structures that could make use of spatial information.

29. The advent of spatial vision provided immense survival value to the organism, but the process occurred slowly, over countless steps, with the transition from a simple eye spot in an early chordate to the vertebrate-style camera eye possibly taking as long as 100 million years.

I should emphasize that the brief summary painted above represents my best guess at the events underlying the evolution of vertebrate photoreceptors and retina, distilled from a large body of experimental data in the literature. The purpose of presenting an explicit proposal for events that occurred over 500 million years ago is to stimulate further experiment, in order to test and thereby refine or reject specific proposals. I look forward to updating the ideas that I have presented above, in the light of the results of future experiments.

Acknowledgements

I am extremely grateful to Helga Kolb for stimulating me to undertake this project, to Nansi Colley, Tom Cronin, John Dowling, Martin Heck, Dan Larhammar, Robert Marc, Ralph Nelson and Yoshinori Shichida for helpful comments on a draft of this article, and to Shaun Collin for the use of images. Supported by grants CE0561903 and DP110103294 from the Australian Research Council.

About the Author

Trevor D. Lamb received a degree in Electronic Engineering from Melbourne University in 1971 and then moved to Cambridge, UK, to do his graduate studies under the guidance of Sir Alan Hodgkin, working with Denis Baylor on retinal horizontal cells and photoreceptors. He received his PhD in 1975. Then as a post-doc at Stanford, USA, Denis Baylor, King-Wai Yau and Trevor developed the suction pipette technique for recording from photoreceptors. For the following 25 years he again worked in Cambridge, UK, on phototransduction and light- and dark-adaptation. He was elected a Fellow of the Royal Society in 1993. With Ed Pugh in the USA he developed a mathematical description of the molecular reactions underlying the photoreceptor light response, as well as a model of dark adaptation and the retinoid cycle. In 2003, Trevor returned to Australia, as a Federation Fellow at the Australian National University (ANU), in Canberra. Since 2011 he has been an Emeritus Professor at ANU, where he pursues his current interest in the evolutionary origin of photoreceptors and the retina. e-mail Trevor at *Trevor.Lamb@anu.edu.au*

References

1. Dobzhansky T. Nothing in biology makes sense except in light of evolution. American Biology Teacher. 1973;35:125–129.
2. Darwin, C., *On the origin of species by means of natural selection*. 1859, London,: J. Murray. 502 p.
3. Lamb T.D., Collin S.P., Pugh E.N. Jr. Evolution of the vertebrate eye: opsins, photoreceptors, retina and eye cup. Nat Rev Neurosci. 2007;8(12):960–76. PubMed PMID: 18026166.
4. Lamb T.D. Evolution of vertebrate retinal photoreception. Philos Trans R Soc Lond B Biol Sci. 2009;364:2911–24. PubMed PMID: 19720653.
5. Arendt D., Hausen H., Purschke G. The 'division of labour' model of eye evolution. Philos Trans R Soc Lond B Biol Sci. 2009;364:2809–17. PubMed PMID: 19720646.
6. Vopalensky P., Kozmik Z. Eye evolution: common use and independent recruitment of genetic components. Philos Trans R Soc Lond B Biol Sci. 2009;364:2819–32. PubMed PMID: 19720647.
7. Larhammar D., Nordstrom K., Larsson T.A. Evolution of vertebrate rod and cone phototransduction genes. Philos Trans R Soc Lond B Biol Sci. 2009;364:2867–80. PubMed PMID: 19720650.
8. Shichida Y., Matsuyama T. Evolution of opsins and phototransduction. Philos Trans R Soc Lond B Biol Sci. 2009;364:2881–95. PubMed PMID: 19720651.
9. Kusakabe T.G., et al. Evolution and the origin of the visual retinoid cycle in vertebrates. Philos Trans R Soc Lond B Biol Sci. 2009;364:2897–910. PubMed PMID: 19720652.
10. Collin S.P., et al. The evolution of early vertebrate photoreceptors. Philos Trans R Soc Lond B Biol Sci. 2009;364:2925–40. PubMed PMID: 19720654.
11. Fain G.L., Hardie R., Laughlin S.B. Phototransduction and the evolution of photoreceptors. Curr Biol. 2010;20(3):114–24. PubMed PMID: 20144772.
12. Porter M.L., et al. Shedding new light on opsin evolution. Proc R Soc Lond. 2012;279:3–14. [Biol]. p. PubMed PMID: 22012981.
13. Nilsson D.E. Eye evolution and its functional basis. Vis Neurosci. 2013;30(1-2):5–20. PubMed PMID: 23578808.
14. Schwab, I.R., R.R. Dubielzig, and C. Schobert, *Evolution's witness : how eyes evolved*. 2012, New York: Oxford University Press. 306 p.
15. Butler A.B. Chordate evolution and the origin of craniates: an old brain in a new head. Anat Rec. 2000;261(3):111–25. PubMed PMID: 10867629.
16. Butler, A.B. and W. Hodos, *Comparative vertebrate neuroanatomy : evolution and adaptation*. 2nd ed. 2005, Hoboken, N.J.: Wiley-Interscience. 715 p.
17. Salvini-Plawen L., Mayer E. On the evolution of photoreceptors and eyes. Evol Biol. 1977;10:207–263.
18. Jacob F. Evolution and tinkering. Science. 1977;196:1161–6. PubMed PMID: 860134.
19. Goldsmith T.H. Evolutionary tinkering with visual photoreception. Vis Neurosci. 2013;30(1-2):21–37. PubMed PMID: 22391141.
20. Erwin D.H., et al. The Cambrian conundrum: early divergence and later ecological success in the early history of animals. Science. 2011;334:1091–7. PubMed PMID: 22116879.
21. Chen, J.-Y., *Evolutionary scenario of the early history of the animal kingdom: Evidence from Precambrian (Ediacaran) Weng'an and Early Cambrian Maotianshan biotas, China.*, in *Earth and Life, Springer*, J.A. Talent, Editor. 2012, Springer.
22. Land, M.F. and D.-E. Nilsson, *Animal eyes*. Oxford animal biology series. 2002, New York: Oxford University Press. 221 p.
23. Paterson J.R., et al. Acute vision in the giant Cambrian predator Anomalocaris and the origin of compound eyes. Nature. 2011;480:237–40. PubMed PMID: 22158247.
24. Plotnick R.E., Dornbos S.Q., Chen J. Information landscapes and sensory ecology of the Cambrian Radiation. Paleobiology. 2010;36:303–317.
25. Terakita A. The opsins. Genome Biol. 2005;6(3):213. PubMed PMID: 15774036.

26. Plachetzki D.C., Degnan B.M., Oakley T.H. The origins of novel protein interactions during animal opsin evolution. PLoS One. 2007;2(10):e1054. PubMed PMID: 17940617.
27. Plachetzki D.C., Fong C.R., Oakley T.H. The evolution of phototransduction from an ancestral cyclic nucleotide gated pathway. Proc R Soc Lond. 2010;277:1963–9. [Biol]. p. PubMed PMID: 20219739.
28. Kozmik Z., et al. Assembly of the cnidarian camera-type eye from vertebrate-like components. Proc Natl Acad Sci U S A. 2008;105(26):8989–93. PubMed PMID: 18577593.
29. Suga H., Schmid V., Gehring W.J. Evolution and functional diversity of jellyfish opsins. Curr Biol. 2008;18(1):51–5. PubMed PMID: 18160295.
30. Feuda R., et al. Metazoan opsin evolution reveals a simple route to animal vision. Proc Natl Acad Sci U S A. 2012;109(46):18868–72. PubMed PMID: 23112152.
31. Mason B., et al. Evidence for multiple phototransduction pathways in a reef-building coral. PLoS One. 2012;7(12):e50371. PubMed PMID: 23227169.
32. Krishnan A., et al. The origin of GPCRs: identification of mammalian like Rhodopsin, Adhesion, Glutamate and Frizzled GPCRs in fungi. PLoS One. 2012;7(1):e29817. PubMed PMID: 22238661.
33. Eakin R.M. Evolution of photoreceptors. Cold Spring Harb Symp Quant Biol. 1965;30:363–70. PubMed PMID: 5219487.
34. Eakin R.M. Morphology of invertebrate photoreceptors. Methods Enzymol. 1982;81:17–25. PubMed PMID: 7098862.
35. Vanfleteren J.R., Coomans A. Photoreceptor evolution and phylogeny. J Zool Syst Evol Res. 1976;14:157–168.
36. Vanfleteren, J.R., *A monophyletic line of evolution? Ciliary induced photoreceptor membranes.*, in *Visual cells in evolution*, J.A. Westfall, Editor. 1982, Raven Press: New York. p. 107-136.
37. Ruiz M.S., Anadon R. Some considerations on the fine structure of rhabdomeric photoreceptors in the amphioxus, Branchiostoma lanceolatum (Cephalochordata). J Hirnforsch. 1991;32(2):159–64. PubMed PMID: 1791297.
38. Brandenburger J.L., Woollacott R.M., Eakin R.M. Fine structure of eyespots in tornarian larvae (phylum: Hemichordata). Z Zellforsch Mikrosk Anat. 1973;142(1):89–102. PubMed PMID: 4356037.
39. Blumer M. Alterations of the eyes during ontogenesis in Aporrhais pespelecani (Mollusca, Caenogastropoda). Zoomorphology. 1996;116:123–131.
40. Ready, D.F. and U. Tepass, *Crumbs-dependent epithelial organization in retinal morphogenesis and disease*, Volume 10, in *Recent Advances in Human Biology* D.S. Williams, Editor. 2004, World Scientific Publishing: River Edge, NJ. p. 7-27.
41. Lacalli T.C. Frontal eye circuitry, rostral sensory pathways and brain organization in amphioxus larvae: Evidence from 3D reconstructions. Philos Trans R Soc London. 1996;351:243–263. [Biol]. p.
42. Lacalli T.C. Sensory systems in amphioxus: a window on the ancestral chordate condition. Brain Behav Evol. 2004;64(3):148–62. PubMed PMID: 15353907.
43. Gomez M.P., Angueyra J.M., Nasi E. Light-transduction in melanopsin-expressing photoreceptors of Amphioxus. Proc Natl Acad Sci U S A. 2009;106(22):9081–6. PubMed PMID: 19451628.
44. Koyanagi M., et al. Cephalochordate melanopsin: evolutionary linkage between invertebrate visual cells and vertebrate photosensitive retinal ganglion cells. Curr Biol. 2005;15(11):1065–9. PubMed PMID: 15936279.
45. Angueyra J.M., et al. Melanopsin-expressing amphioxus photoreceptors transduce light via a phospholipase C signaling cascade. PLoS One. 2012;7(1):e29813. PubMed PMID: 22235344.
46. Ferrer C., et al. Dissecting the determinants of light sensitivity in amphioxus microvillar photoreceptors: possible evolutionary implications for melanopsin signaling. J Neurosci. 2012;32(50):17977–87. PubMed PMID: 23238714.
47. Vopalensky P., et al. Molecular analysis of the amphioxus frontal eye unravels the evolutionary origin of the retina and pigment cells of the vertebrate eye. Proc Natl Acad Sci U S A. 2012;109(38):15383–8. PubMed PMID: 22949670.

48. Sorrentino M. Evolution of cerebral vesicles and their sensory organs in an ascidian larva. Acta Zool-Stockholm. 2000;81(3):243.
49. Barnes S.N. Fine structure of the photoreceptor and cerebral ganglion of the tadpole larva of Amaroucium constellatum (Verril) (subphylum: Urochordata; class: Ascidiacea). Z Zellforsch Mikrosk Anat. 1971;117(1):1–16. PubMed PMID: 5559422.
50. Eakin R.M., Kuda A. Ultrastructure of sensory receptors in Ascidian tadpoles. Z Zellforsch Mikrosk Anat. 1971;112(3):287–312. PubMed PMID: 5542324.
51. Gorman A.L., McReynolds J.S., Barnes S.N. Photoreceptors in primitive chordates: fine structure, hyperpolarizing receptor potentials, and evolution. Science. 1971;172:1052–4. PubMed PMID: 5573956.
52. Heimberg A.M., et al. microRNAs reveal the interrelationships of hagfish, lampreys, and gnathostomes and the nature of the ancestral vertebrate. Proc Natl Acad Sci U S A. 2010;107(45):19379–83. PubMed PMID: 20959416.
53. Zintzen V., et al. Hagfish predatory behaviour and slime defence mechanism. Sci Rep. 2011;1:131. PubMed PMID: 22355648.
54. Newth D.R. On the reaction to light of Myxine glutinosa L. J Exp Biol. 1955;32(1):4.
55. Kobayashi H. On the photo-perceptive function in the eye of the hagfish, Myxine garmani Jordan et Snyder. Journal of National Fisheries University. 1964;13:67–83. (formely Journal of Shimonoseki Fisheries University). p.
56. Locket, N.A. and J.M. Jorgensen, *The biology of hagfishes*, in *The biology of hagfishes*, J.M. Jørgensen, et al., Editors. 1998, Chapman & Hall: London; New York. p. 541-546.
57. Holmberg K. The hagfish retina: electron microscopic study comparing receptor and epithelial cells in the Pacific hagfish, Polistotrema stouti, with those in the Atlantic hagfish, Myxine glutinosa. Z Zellforsch Mikrosk Anat. 1971;121(2):249–69. PubMed PMID: 4330182.
58. Holmberg, K., *The cyclostome retina.* Handbook of Sensory Physiology, 1977. **7**(5): p. 47-66.
59. Fernholm B., Holmberg K. The eyes in three genera of hagfish (Eptatretus, Paramyxine and Myxine)--a case of degenerative evolution. Vision Res. 1975;15(2):253–9. PubMed PMID: 1129982.
60. Bullock T.H., Moore J.K., Fields R.D. Evolution of myelin sheaths: both lamprey and hagfish lack myelin. Neurosci Lett. 1984;48(2):145–8. PubMed PMID: 6483278.
61. Schultz R., Berkowitz E.C., Pease D.C. The electron microscopy of the lamprey spinal cord. J Morphol. 1956;98(2):251–273.
62. Kusunoki T., Amemiya F. Retinal projections in the hagfish, Eptatretus burgeri. Brain Res. 1983;262(2):295–8. PubMed PMID: 6839158.
63. Wicht H., Northcutt R.G. Retinofugal and retinopetal projections in the Pacific hagfish, Eptatretus stouti (Myxinoidea). Brain Behav Evol. 1990;36(5):315–28. PubMed PMID: 2285858.
64. Hattar S., et al. Central projections of melanopsin-expressing retinal ganglion cells in the mouse. J Comp Neurol. 2006;497(3):326–49. PubMed PMID: 16736474.
65. Allen B.M. The eye of Bdellostoma stouti. Anat. Anz. 1905;26:208–211.
66. Pu G.A., Dowling J.E. Anatomical and physiological characteristics of pineal photoreceptor cell in the larval lamprey, Petromyzon marinus. J Neurophysiol. 1981;46(5):1018–38. PubMed PMID: 7299444.
67. Eakin, R.M., *The third eye*. 1973, Berkeley,: University of California Press. 157 p.
68. Kusmic C., Marchiafava P., Strettoi E. Photoresponses and light adaptation of pineal photoreceptors in the trout. Proc R Soc Lond. 1992;248:149–157. [Biol]. p.
69. Morita Y., Tabata M., Tamotsu S. Intracellular response and input resistance change of pineal photoreceptors and ganglion cells. Neurosci Res Suppl. 1985;2:S79–88. PubMed PMID: 3866157.
70. Lamb T.D., Pugh E.N. Jr. A quantitative account of the activation steps involved in phototransduction in amphibian photoreceptors. J Physiol. 1992;449:719–58. PubMed PMID: 1326052.
71. Koyanagi M., et al. Bistable UV pigment in the lamprey pineal. Proc Natl Acad Sci U S A. 2004;101(17):6687–91. PubMed PMID: 15096614.
72. Uchida K., Morita Y. Intracellular responses from UV-sensitive cells in the photosensory pineal organ. Brain Res. 1990;534(1-2):237–42. PubMed PMID: 2073583.

73. Burkhardt D.A. Synaptic feedback, depolarization, and color opponency in cone photoreceptors. Vis Neurosci. 1993;10(6):981–9. PubMed PMID: 8257672.
74. Meissl, H., T. Nakamura, and G. Thiele, *Neural response mechanisms in the photoreceptive pineal organ of goldfish.* Comp Biochem Physiol A Comp Physiol, 1986. **84**(3): p. 467-73.
75. Fritzsch B., Collin S.P. Dendritic distribution of two populations of ganglion cells and the retinopetal fibers in the retina of the silver lamprey (Ichthyomyzon unicuspis). Vis Neurosci. 1990;4(6):533–45. PubMed PMID: 2278933.
76. Young G.C. Number and arrangement of extraocular muscles in primitive gnathostomes: evidence from extinct placoderm fishes. Biology Letters. 2007;4:110–114. PubMed PMID: 18077236.
77. Young G.C. Number and arrangement of extraocular muscles in primitive gnathostomes: evidence from extinct placoderm fishes. Biol Lett. 2008;4(1):110–4. PubMed PMID: 18077236.
78. Fritzsch, B., *Ontogenetic clues to the phylogeny of the visual system*, in *The changing visual system : maturation and aging in the central nervous system*, P. Bagnoli and W. Hodos, Editors. 1991, Plenum Press: New York. p. 33-49.
79. Fritzsch, B. and J.C. Glover, *Evolution of the deuterostome central nervous system: an intercalation of developmental patterning processes with cellular specification processes*, Volume 2, in *Evolution of nervous systems : a comprehensive reference*, J.H. Kaas, Editor. 2007, Elsevier Academic Press: Amsterdam; Boston.
80. Nivison-Smith L., et al. Retinal amino acid neurochemistry of the southern hemisphere lamprey, Geotria australis. PLoS One. 2013;8(3):e58406. PubMed PMID: 23516473.
81. Collin S.P., et al. Ancient colour vision: multiple opsin genes in the ancestral vertebrates. Curr Biol. 2003;13(22):R864–5. PubMed PMID: 14614838.
82. Pisani, D., et al., *Molecular evidence for dim-light vision in the last common ancestor of the vertebrates.* Curr Biol, 2006. **16**(9): p. R318-9; author reply R320.
83. Collin S.P., et al. Morphology and spectral absorption characteristics of retinal photoreceptors in the southern hemisphere lamprey (Geotria australis). Vis Neurosci. 2003;20(2):119–30. PubMed PMID: 12916734.
84. Dickson D.H., Collard T.R. Retinal development in the lamprey (Petromyzon marinus L.): premetamorphic ammocoete eye. Am J Anat. 1979;154(3):321–36. PubMed PMID: 433786.
85. Collin, S.P. and A.E.O. Tresize, *Evolution of colour discrimination in vertebrates and its implications for visual communication*, in *Communication in fishes*, F. Ladich, Editor. 2006, Science Publishers: Enfield, NH. p. 303-335.
86. Muradov H., et al. PDE6 in lamprey Petromyzon marinus: implications for the evolution of the visual effector in vertebrates. Biochemistry. 2007;46(35):9992–10000. PubMed PMID: 17685558.
87. Muradov H., et al. Unique transducins expressed in long and short photoreceptors of lamprey Petromyzon marinus. Vision Res. 2008;48(21):2302–8. PubMed PMID: 18687354.
88. Smith, J.J., et al., *Sequencing of the sea lamprey (Petromyzon marinus) genome provides insights into vertebrate evolution.* Nat Genet, 2013. **45**(4): p. 415-21, 421e1-2.
89. Govardovskii V., Lychakov D. Visual cells and visual pigments of the lamprey, Lampetra fluviatilis. J Comp Physiol [A]. 1984;154(2):279–286.
90. Davies W.L., et al. Functional characterization, tuning, and regulation of visual pigment gene expression in an anadromous lamprey. FASEB J. 2007;21(11):2713–24. PubMed PMID: 17463225.
91. Ebrey T., Koutalos Y. Vertebrate photoreceptors. Prog Retin Eye Res. 2001;20(1):49–94. PubMed PMID: 11070368.
92. Imai H., et al. Molecular properties of rod and cone visual pigments from purified chicken cone pigments to mouse rhodopsin in situ. Photochem Photobiol Sci. 2005;4(9):667–74. PubMed PMID: 16121275.
93. Ritter E., et al. Transition of rhodopsin into the active metarhodopsin II state opens a new light-induced pathway linked to Schiff base isomerization. J Biol Chem. 2004;279(46):48102–11. PubMed PMID: 15322129.
94. Davies W.L., Hankins M.W., Foster R.G. Vertebrate ancient opsin and melanopsin: divergent irradiance detectors. Photochem Photobiol Sci. 2010;9(11):1444–57. PubMed PMID: 20922256.

95. Koyanagi M., et al. Homologs of vertebrate Opn3 potentially serve as a light sensor in nonphotoreceptive tissue. Proc Natl Acad Sci U S A. 2013;110(13):4998–5003. PubMed PMID: 23479626.
96. Sakai K., et al. Photochemical nature of parietopsin. Biochemistry. 2012;51(9):1933–41. PubMed PMID: 22303823.
97. Terakita A., et al. Counterion displacement in the molecular evolution of the rhodopsin family. Nat Struct Mol Biol. 2004;11(3):284–289. PubMed PMID: 14981504.
98. Sato K., et al. Vertebrate ancient-long opsin has molecular properties intermediate between those of vertebrate and invertebrate visual pigments. Biochemistry. 2011;50(48):10484–90. PubMed PMID: 22066464.
99. Okano T., Yoshizawa T., Fukada Y. Pinopsin is a chicken pineal photoreceptive molecule. Nature. 1994;372:94–7. PubMed PMID: 7969427.
100. Nakamura A., et al. Chimeric nature of pinopsin between rod and cone visual pigments. Biochemistry. 1999;38(45):14738–45. PubMed PMID: 10555955.
101. Tsutsui K., Shichida Y. Multiple functions of Schiff base counterion in rhodopsins. Photochem Photobiol Sci. 2010;9(11):1426–34. PubMed PMID: 20842311.
102. Tsukamoto H., Terakita A. Diversity and functional properties of bistable pigments. Photochem Photobiol Sci. 2010;9(11):1435–43. PubMed PMID: 20852774.
103. Terakita A., Kawano-Yamashita E., Koyanagi M. Evolution and diversity of opsins. Wiley Interdisciplinary Reviews: Membrane Transport and Signaling. 2012;1(1):104–111.
104. Chen M.H., et al. Rapid release of retinal from a cone visual pigment following photoactivation. Biochemistry. 2012;51(20):4117–25. PubMed PMID: 22217337.
105. Tsukamoto H., et al. The magnitude of the light-induced conformational change in different rhodopsins correlates with their ability to activate G proteins. J Biol Chem. 2009;284(31):20676–83. PubMed PMID: 19497849.
106. Choe H.W., et al. Crystal structure of metarhodopsin II. Nature. 2011;471(7340):651–5. PubMed PMID: 21389988.
107. Scheerer P., et al. Crystal structure of opsin in its G-protein-interacting conformation. Nature. 2008;455:497–502. PubMed PMID: 18818650.
108. Hofmann K.P., et al. A G protein-coupled receptor at work: the rhodopsin model. Trends Biochem Sci. 2009;34(11):540–52. PubMed PMID: 19836958.
109. Yan E.C., et al. Retinal counterion switch in the photoactivation of the G protein-coupled receptor rhodopsin. Proc Natl Acad Sci U S A. 2003;100(16):9262–7. PubMed PMID: 12835420.
110. Piechnick R., et al. Effect of channel mutations on the uptake and release of the retinal ligand in opsin. Proc Natl Acad Sci U S A. 2012;109(14):5247–52. PubMed PMID: 22431612.
111. Ohno, S., *Evolution by gene duplication*. 1970, Berlin, New York,: Springer-Verlag. xv, 160 p.
112. Ecker J.L., et al. Melanopsin-expressing retinal ganglion-cell photoreceptors: cellular diversity and role in pattern vision. Neuron. 2010;67(1):49–60. PubMed PMID: 20624591.
113. Schmidt T.M., Chen S.K., Hattar S. Intrinsically photosensitive retinal ganglion cells: many subtypes, diverse functions. Trends Neurosci. 2011;34(11):572–80. PubMed PMID: 21816493.
114. Bowmaker J.K. Evolution of vertebrate visual pigments. Vision Res. 2008;48(20):2022–41. PubMed PMID: 18590925.
115. Okano T., et al. Primary structures of chicken cone visual pigments: vertebrate rhodopsins have evolved out of cone visual pigments. Proc Natl Acad Sci U S A. 1992;89(13):5932–6. PubMed PMID: 1385866.
116. Yamashita T., et al. Chloride-dependent spectral tuning mechanism of L-group cone visual pigments. Biochemistry. 2013;52(7):1192–7. PubMed PMID: 23350963.
117. Wang Z., Asenjo A.B., Oprian D.D. Identification of the Cl(-)-binding site in the human red and green color vision pigments. Biochemistry. 1993;32(9):2125–30. PubMed PMID: 8443153.
118. Davies W.I., et al. Anion sensitivity and spectral tuning of middle- and long-wavelength-sensitive (MWS/LWS) visual pigments. Cell Mol Life Sci. 2012;69(14):2455–64. PubMed PMID: 22349213.

119. Davies W.L., et al. Visual pigments of the platypus: a novel route to mammalian colour vision. Curr Biol. 2007;17(5):R161–3. PubMed PMID: 17339011.
120. Davies W.I., Collin S.P., Hunt D.M. Molecular ecology and adaptation of visual photopigments in craniates. Mol Ecol. 2012;21(13):3121–58. PubMed PMID: 22650357.
121. Nordstrom K., Larsson T.A., Larhammar D. Extensive duplications of phototransduction genes in early vertebrate evolution correlate with block (chromosome) duplications. Genomics. 2004;83(5):852–72. PubMed PMID: 15081115.
122. Golobokova E.Y., Govardovskii V.I. Late stages of visual pigment photolysis in situ: cones vs. rods. Vision Res. 2006;46(14):2287–97. PubMed PMID: 16473387.
123. Kawamura S., Yokoyama S. Functional characterization of visual and nonvisual pigments of American chameleon (Anolis carolinensis). Vision Res. 1998;38(1):37–44. PubMed PMID: 9474373.
124. Bickelmann C., et al. Functional characterization of the rod visual pigment of the echidna (Tachyglossus aculeatus), a basal mammal. Vis Neurosci. 2012;29(4-5):211–7. PubMed PMID: 22874131.
125. Hunt D.M., et al. The molecular basis for spectral tuning of rod visual pigments in deep-sea fish. J Exp Biol. 2001;204(Pt 19):3333–44. PubMed PMID: 11606607.
126. Yau K.W., Hardie R.C. Phototransduction motifs and variations. Cell. 2009;139(2):246–64. PubMed PMID: 19837030.
127. Hardie R.C., Franze K. Photomechanical responses in Drosophila photoreceptors. Science. 2012;338:260–3. PubMed PMID: 23066080.
128. Okawa H., et al. ATP consumption by mammalian rod photoreceptors in darkness and in light. Curr Biol. 2008;18(24):1917–21. PubMed PMID: 19084410.
129. Steinberg R.H., Fisher S.K., Anderson D.H. Disc morphogenesis in vertebrate photoreceptors. J Comp Neurol. 1980;190(3):501–8. PubMed PMID: 6771304.
130. Young R.W. Visual cells and the concept of renewal. Invest Ophthalmol Vis Sci. 1976;15(9):700–25. PubMed PMID: 986765.
131. Hecht S., Shlaer S., Pirenne M.H. Energy, Quanta, and Vision. J Gen Physiol. 1942;25(6):819–40. PubMed PMID: 19873316.
132. Baylor D.A., Lamb T.D., Yau K.W. Responses of retinal rods to single photons. J Physiol. 1979;288:613–34. PubMed PMID: 112243.
133. Lamb, T.D., *Phototransduction: Adaptation in cones.*, Volume 3, in *Encyclopedia of the eye*, D.A. Dartt, J.C. Besharse, and R. Dana, Editors. 2010, Academic Press: Oxford. p. 354-360.
134. Kawamura S., Tachibanaki S. Rod and cone photoreceptors: molecular basis of the difference in their physiology. Comp Biochem Physiol A Mol Integr Physiol. 2008;150(4):369–77. PubMed PMID: 18514002.
135. Tachibanaki S., et al. Low activation and fast inactivation of transducin in carp cones. J Biol Chem. 2012;287(49):41186–94. PubMed PMID: 23045532.
136. Kenkre J.S., et al. Extremely rapid recovery of human cone circulating current at the extinction of bleaching exposures. J Physiol. 2005;567(Pt 1):95–112. PubMed PMID: 15932890.
137. Arendt D., Wittbrodt J. Reconstructing the eyes of Urbilateria. Philos Trans R Soc London. 2001;356:1545–1563. [Biol]. p. PubMed PMID: 11604122.
138. Koyanagi M., et al. Jellyfish vision starts with cAMP signaling mediated by opsin-Gs cascade. Proc Natl Acad Sci U S A. 2008;105(40):15576–15580. PubMed PMID: 18832159.
139. Lamb T.D., Pugh E.N. Jr. Phototransduction, dark adaptation, and rhodopsin regeneration the proctor lecture. Invest Ophthalmol Vis Sci. 2006;47(12):5137–52. PubMed PMID: 17122096.
140. Wensel T.G. Signal transducing membrane complexes of photoreceptor outer segments. Vision research. 2008;48(20):2052–2061. PubMed PMID: 18456304.
141. Gurevich V.V., et al. The functional cycle of visual arrestins in photoreceptor cells. Prog Retin Eye Res. 2011;30(6):405–430. PubMed PMID: 21824527.
142. Schulz H.L., et al. The Retinome–Defining a reference transcriptome of the adult mammalian retina/retinal pigment epithelium. BMC genomics. 2004;5(1):50. PubMed PMID: 15283859.

143. Vogalis F., et al. Ectopic expression of cone-specific G-protein-coupled receptor kinase GRK7 in zebrafish rods leads to lower photosensitivity and altered responses. J Physiol. 2011;589(9):2321–2348. PubMed PMID: 21486791.
144. Korenbrot J.I. Speed, sensitivity, and stability of the light response in rod and cone photoreceptors: Facts and models. Prog Retin Eye Res. 2012;31(5):442–466. PubMed PMID: 22658984.
145. Muradov H., Boyd K.K., Artemyev N.O. Rod phosphodiesterase-6 PDE6A and PDE6B subunits are enzymatically equivalent. J Biol Chem. 2010;285(51):39828–34. PubMed PMID: 20940301.
146. Hisatomi O., Tokunaga F. Molecular evolution of proteins involved in vertebrate phototransduction. Comparative Biochemistry and Physiology Part B: Biochemistry and Molecular Biology. 2002;133(4):509–522. PubMed PMID: 12470815.
147. Zhang Z., Artemyev N.O. Determinants for Phosphodiesterase 6 Inhibition by Its γ-Subunit. Biochemistry. 2010;49(18):3862–3867. PubMed PMID: 20397626.
148. Peng C., Rich E.D., Varnum M.D. Subunit configuration of heteromeric cone cyclic nucleotide-gated channels. Neuron. 2004;42(3):401–410. PubMed PMID: 15134637.
149. Mushegian A., Gurevich V.V., Gurevich E.V. The origin and evolution of G protein-coupled receptor kinases. PloS one. 2012;7(3):e33806. PubMed PMID: 22442725.
150. Gurevich E.V., Gurevich V.V. Arrestins: ubiquitous regulators of cellular signaling pathways. Genome biology. 2006;7(9):236. PubMed PMID: 17020596.
151. Alvarez C.E. On the origins of arrestin and rhodopsin. BMC evolutionary biology. 2008;8(1):222. PubMed PMID: 18664266.
152. Kawano-Yamashita E., et al. Beta-Arrestin Functionally Regulates the Non-Bleaching Pigment Parapinopsin in Lamprey Pineal. PloS one. 2011;6(1):e16402. PubMed PMID: 21305016.
153. Lagman D., et al. Expansion of transducin subunit gene families in early vertebrate tetraploidizations. Genomics. 2012. PubMed PMID: 22814267.
154. Tyler C.W., Hamer R.D. Analysis of visual modulation sensitivity. IV. Validity of the Ferry-Porter law. JOSA A. 1990;7(4):743–758. PubMed PMID: 2338596.
155. Normann R.A., Werblin F.S. Control of retinal sensitivity I. Light and dark adaptation of vertebrate rods and cones. J Gen Physiol. 1974;63(1):37–61. PubMed PMID: 4359063.
156. Burkhardt D.A. Light adaptation and photopigment bleaching in cone photoreceptors in situ in the retina of the turtle. J Neurosci. 1994;14(3 Pt 1):1091–105. PubMed PMID: 8120614.
157. Rebrik T.I., et al. CNG-modulin: a novel Ca-dependent modulator of ligand sensitivity in cone photoreceptor cGMP-gated ion channels. J Neurosci. 2012;32(9):3142–53. PubMed PMID: 22378887.
158. Mahroo O., Lamb T. Recovery of the human photopic electroretinogram after bleaching exposures: estimation of pigment regeneration kinetics. J Physiol. 2004;554(2):417–437. PubMed PMID: 14594984.
159. Thomas M., Lamb T. Light adaptation and dark adaptation of human rod photoreceptors measured from the a-wave of the electroretinogram. J Physiol. 1999;518(2):479–496. PubMed PMID: 10381594.
160. Lamb T., Pugh E. Dark adaptation and the retinoid cycle of vision. Prog Retin Eye Res. 2004;23(3):307–380. PubMed PMID: 15177205.
161. van Hateren H. A cellular and molecular model of response kinetics and adaptation in primate cones and horizontal cells. J Vis. 2005;5(4) PubMed PMID: 15929656.
162. Van Hateren J., Lamb T. The photocurrent response of human cones is fast and monophasic. BMC neuroscience. 2006;7(1):34. PubMed PMID: 16626487.
163. Lagnado L., Cervetto L., McNaughton P. Calcium homeostasis in the outer segments of retinal rods from the tiger salamander. J Physiol. 1992;455(1):111–142. PubMed PMID: 1282928.
164. Stiles, W., *The physical interpretation of the spectral sensitivity curve of the eye*, in *Transactions of the Optical Convention of the Worshipful Company of Spectacle Makers*. 1948, Spectacle Makers' Company: London. p. 97-107.
165. Lewis P. A theoretical interpretation of spectral sensitivity curves at long wavelengths. J Physiol. 1955;130(1):45. PubMed PMID: 13278884.
166. Barlow H. Purkinje shift and retinal noise. Nature. 1957;179:255–256. PubMed PMID: 13407693.

167. Ala-Laurila P., et al. On the relation between the photoactivation energy and the absorbance spectrum of visual pigments. Vision Res. 2004;44(18):2153–2158. PubMed PMID: 15183682.
168. Luo D.-G., et al. Activation of visual pigments by light and heat. Science. 2011;332:1307–3012. PubMed PMID: 21659602.
169. Ala-Laurila P., Donner K., Koskelainen A. Thermal activation and photoactivation of visual pigments. Biophys J. 2004;86(6):3653–3662. PubMed PMID: 15189862.
170. Gozem S., et al. The Molecular Mechanism of Thermal Noise in Rod Photoreceptors. Science. 2012;337:1225–1228. PubMed PMID: 22955833.
171. Ma J., et al. A visual pigment expressed in both rod and cone photoreceptors. Neuron. 2001;32(3):451–61. PubMed PMID: 11709156.
172. Matthews G. Photocurrents of single retinal rods from Rana pipiens tadpoles. Vision Res. 1984;24(8):821–5. PubMed PMID: 6332411.
173. Lamb T.D., Simon E.J. Analysis of electrical noise in turtle cones. J Physiol. 1977;272(2):435–68. PubMed PMID: 592199.
174. Lamb T.D., Simon E.J. The relation between intercellular coupling and electrical noise in turtle photoreceptors. J Physiol. 1976;263(2):257–86. PubMed PMID: 1018249.
175. Schneeweis D.M., Schnapf J.L. The photovoltage of macaque cone photoreceptors: adaptation, noise, and kinetics. J Neurosci. 1999;19(4):1203–16. PubMed PMID: 9952398.
176. Baylor D.A., Matthews G., Yau K.W. Two components of electrical dark noise in toad retinal rod outer segments. J Physiol. 1980;309:591–621. PubMed PMID: 6788941.
177. Whitlock G.G., Lamb T.D. Variability in the time course of single photon responses from toad rods: termination of rhodopsin's activity. Neuron. 1999;23(2):337–51. PubMed PMID: 10399939.
178. Hamer R.D., et al. Toward a unified model of vertebrate rod phototransduction. Vis Neurosci. 2005;22(4):417–36. PubMed PMID: 16212700.
179. Hamer R.D., et al. Multiple steps of phosphorylation of activated rhodopsin can account for the reproducibility of vertebrate rod single-photon responses. J Gen Physiol. 2003;122(4):419–44. PubMed PMID: 12975449.
180. Gross O.P., Pugh E.N. Jr, Burns M.E. Calcium feedback to cGMP synthesis strongly attenuates single-photon responses driven by long rhodopsin lifetimes. Neuron. 2012;76(2):370–82. PubMed PMID: 23083739.
181. Cangiano L., et al. The photovoltage of rods and cones in the dark-adapted mouse retina. J Physiol. 2012;590(Pt 16):3841–55. PubMed PMID: 22641773.
182. Lamb T.D., McNaughton P.A., Yau K.W. Spatial spread of activation and background desensitization in toad rod outer segments. J Physiol. 1981;319:463–96. PubMed PMID: 6798202.
183. Walls G.L. The reptilian retina. Am. J. Ophthalmol. 1934;17:892–915.
184. Walls, G.L., *The vertebrate eye and its adaptive radiation*. Cranbrook Institute of Science. 1942, Bloomfield Hills, Michigan: Cranbrook Institute of Science. 785 p.
185. Kleinschmidt J., Dowling J.E. Intracellular recordings from gecko photoreceptors during light and dark adaptation. J Gen Physiol. 1975;66(5):617–48. PubMed PMID: 1194887.
186. Rispoli G., Sather W.A., Detwiler P.B. Visual transduction in dialysed detached rod outer segments from lizard retina. J Physiol. 1993;465:513–37. PubMed PMID: 8229848.
187. Roll B. Gecko vision-visual cells, evolution, and ecological constraints. J Neurocytol. 2000;29(7):471–84. PubMed PMID: 11279363.
188. Yoshida M. Some observations on the patency in the outer segments of photoreceptors of the nocturnal gecko. Vision Res. 1978;18(2):137–43. PubMed PMID: 664283.
189. Kojima D., et al. Cone visual pigments are present in gecko rod cells. Proc Natl Acad Sci U S A. 1992;89(15):6841–5. PubMed PMID: 1379723.
190. Zhang X., Wensel T.G., Yuan C. Tokay gecko photoreceptors achieve rod-like physiology with cone-like proteins. Photochem Photobiol. 2006;82(6):1452–60. PubMed PMID: 16553462.

191. Ripps H., Dowling J.E. Structural features and adaptive properties of photoreceptors in the skate retina. J Exp Zool Suppl. 1990;5:46–54. PubMed PMID: 1982495.
192. Dowling J.E., Ripps H. On the duplex nature of the skate retina. J Exp Zool Suppl. 1990;5:55–65. PubMed PMID: 1982496.
193. Dowling J.E., Ripps H. Adaptation in skate photoreceptors. J Gen Physiol. 1972;60(6):698–719. PubMed PMID: 4645677.
194. Cornwall M.C., et al. Membrane current responses of skate photoreceptors. J Gen Physiol. 1989;94(4):633–47. PubMed PMID: 2614369.
195. Wang J.-S., Kefalov V.J. The cone-specific visual cycle. Prog Retin Eye Res. 2011;30(2):115–128. PubMed PMID: 21111842.
196. Saari J.C. Vitamin A metabolism in rod and cone visual cycles. Annu Rev Nutr. 2012;32:125–45. PubMed PMID: 22809103.
197. Kaylor J.J., et al. Identification of DES1 as a vitamin A isomerase in Muller glial cells of the retina. Nat Chem Biol. 2013;9(1):30–6. PubMed PMID: 23143414.
198. Albalat R. Evolution of the genetic machinery of the visual cycle: a novelty of the vertebrate eye? Mol Biol Evol. 2012;29(5):1461–9. PubMed PMID: 22319134.
199. Poliakov E., et al. Origin and evolution of retinoid isomerization machinery in vertebrate visual cycle: hint from jawless vertebrates. PLoS One. 2012;7(11):e49975. PubMed PMID: 23209628.
200. Takimoto N., et al. Origin of the vertebrate visual cycle: III. Distinct distribution of RPE65 and beta-carotene 15,15'-monooxygenase homologues in Ciona intestinalis. Photochem Photobiol. 2006;82(6):1468–74. PubMed PMID: 16544957.
201. Stavenga, D.G., *Dark regeneration of invertebrate visual pigments*, in *Photoreceptor Optics*, A.W. Synder and R. Menzel, Editors. 1975, Springer. p. 290-295.
202. Wang X., et al. Requirement for an enzymatic visual cycle in Drosophila. Curr Biol. 2010;20(2):93–102. PubMed PMID: 20045325.
203. Baer, K.v., *Entwicklungsgeschichte der thiere: Beobachtung und reflexion.* Bornträger, Königsberg, 1828. 1837.
204. Brauckmann S. Karl Ernst von Baer (1792-1876) and evolution. Int J Dev Biol. 2012;56(9):653–60. PubMed PMID: 23319342.
205. Haeckel, E., *Natürliche schöpfungsgeschichte. Gemeinverständliche wissenschaftliche vorträge über die entwickelungslehre im allgemeinen und diejenige von Darwin, Goethe und Lamarck im besonderen*. 5. verb. aufl. Mit dem porträt des verfassers (nach einer photographie) und mit 16 tafeln, 19 holzschnitten, 18 stammbäumen und 19 systematischen tabellen. ed. 1874, Berlin,: G. Reimer. xlvi, 2, 688 p.
206. Eakin R.M. A Third Eye: A century-old zoological enigma yields its secrets to electron-microscopist and neurophysiologist. American Scientist. 1970;58(1):73–79.
207. Vigh B., et al. The pineal organ as a folded retina: immunocytochemical localization of opsins. Biol Cell. 1998;90(9):653–9. PubMed PMID: 10085541.
208. Reichenbach A., Robinson S.R. Phylogenetic constraints on retinal organisation and development. Prog Retin Eye Res. 1995;15:139–171.
209. Vigh B., et al. Nonvisual photoreceptors of the deep brain, pineal organs and retina. Histol Histopathol. 2002;17(2):555–90. PubMed PMID: 11962759.
210. Ekstrom P., Meissl H. Evolution of photosensory pineal organs in new light: the fate of neuroendocrine photoreceptors. Philos Trans R Soc Lond B Biol Sci. 2003;358(1438):1679–700. PubMed PMID: 14561326.
211. Klein D.C. Evolution of the vertebrate pineal gland: the AANAT hypothesis. Chronobiol Int. 2006;23(1-2):5–20. PubMed PMID: 16687276.
212. Mano H., Fukada Y. A median third eye: pineal gland retraces evolution of vertebrate photoreceptive organs. Photochem Photobiol. 2007;83(1):11–8. PubMed PMID: 16771606.
213. Eakin R.M., Westfall J.A. Further observations on the fine structure of the parietal eye of lizards. J Biophys Biochem Cytol. 1960;8:483–99. PubMed PMID: 13725484.
214. Martinez-Morales J.R., Wittbrodt J. Shaping the vertebrate eye. Curr Opin Genet Dev. 2009;19(5):511–7. PubMed PMID: 19819125.

215. Valleix S., et al. Homozygous nonsense mutation in the FOXE3 gene as a cause of congenital primary aphakia in humans. Am J Hum Genet. 2006;79(2):358–64. PubMed PMID: 16826526.
216. Eiraku M., et al. Self-organizing optic-cup morphogenesis in three-dimensional culture. Nature. 2011;472(7341):51–6. PubMed PMID: 21475194.
217. Bharti K., et al. A regulatory loop involving PAX6, MITF, and WNT signaling controls retinal pigment epithelium development. PLoS Genet. 2012;8(7):e1002757. PubMed PMID: 22792072.
218. England S.J., et al. A dynamic fate map of the forebrain shows how vertebrate eyes form and explains two causes of cyclopia. Development. 2006;133(23):4613–7. PubMed PMID: 17079266.
219. Rembold M., et al. Individual cell migration serves as the driving force for optic vesicle evagination. Science. 2006;313:1130–4. PubMed PMID: 16931763.
220. Kwan K.M., et al. A complex choreography of cell movements shapes the vertebrate eye. Development. 2012;139(2):359–72. PubMed PMID: 22186726.
221. Rubinson K., Cain H. Neural differentiation in the retina of the larval sea lamprey (Petromyzon marinus). Vis Neurosci. 1989;3(3):241–8. PubMed PMID: 2487105.
222. Rubinson K. The developing visual system and metamorphosis in the lamprey. J Neurobiol. 1990;21(7):1123–35. PubMed PMID: 2258725.
223. Meyer-Rochow V.B., Stewart D. Review of larval and postlarval eye ultrastructure in the lamprey (Cyclostomata) with special emphasis on Geotria australis (Gray). Microsc Res Tech. 1996;35(6):431–44. PubMed PMID: 9016447.
224. Dickson D.H., Graves D.A., Moyles M.R. Corneal splitting in the developing lamprey Petromyzon marinus L. eye. Am J Anat. 1982;165(1):83–98. PubMed PMID: 7137060.
225. Price G.C. *Some points in the development of a myxinoid (Bdellostoma stouti Lockington).* Verhandlungen der Anatomischen Gesellschaft. Anatomischer Anzeiger. 1896;6:81–86.
226. Dean B. On the development of the Californian hag-fish, Bdellostoma stouti, Lockington. Q J Microsc Sci. 1897;40:269–280.
227. Dean, B., *On the embryology of Bdellostoma stouti: A general account of myxinoid development from the egg and segmentation to hatching*, in *Festschrift zum siebensigsten Geburtstag von Carl von Kupffer*. 1899, Gustav Fisher: Jena.
228. von Kupffer, C., *Zur Kopfentwicklung von Bdellostoma. Studien zur vergleichenden Entwicklungsgeschichte des Kopfes der Kranioten, Heft 4.* 1900, München: Lehman.
229. Stockard C.R. The embryonic history of the lens in Bdellostoma stouti in relation to recent experiments. Am J Anat. 1906;6(1):511–515.
230. Ota K.G., Kuraku S., Kuratani S. Hagfish embryology with reference to the evolution of the neural crest. Nature. 2007;446(7136):672–5. PubMed PMID: 17377535.
231. Arendt D. Evolution of eyes and photoreceptor cell types. Int J Dev Biol. 2003;47(7-8):563–71. PubMed PMID: 14756332.
232. Sernagor, E., et al., *Retinal development*. 2006, Cambridge: Cambridge University Press. 383 p.
233. Agathocleous M., Harris W.A. From progenitors to differentiated cells in the vertebrate retina. Annu Rev Cell Dev Biol. 2009;25:45–69. PubMed PMID: 19575661.
234. Swaroop A., Kim D., Forrest D. Transcriptional regulation of photoreceptor development and homeostasis in the mammalian retina. Nat Rev Neurosci. 2010;11(8):563–76. PubMed PMID: 20648062.
235. Reese B.E. Development of the retina and optic pathway. Vision Res. 2011;51(7):613–32. PubMed PMID: 20647017.
236. Rapaport, D.H., *Retinal neurogenesis*, in *Retinal development*, E. Sernagor, et al., Editors. 2006, Cambridge University Press: Cambridge. p. 30-58.
237. Rapaport D.H., et al. Timing and topography of cell genesis in the rat retina. J Comp Neurol. 2004;474(2):304–24. PubMed PMID: 15164429.
238. Wong L.L., Rapaport D.H. Defining retinal progenitor cell competence in Xenopus laevis by clonal analysis. Development. 2009;136(10):1707–15. PubMed PMID: 19395642.

239. Gomes F.L., et al. Reconstruction of rat retinal progenitor cell lineages in vitro reveals a surprising degree of stochasticity in cell fate decisions. Development. 2011;138(2):227–35. PubMed PMID: 21148186.
240. He J., et al. How variable clones build an invariant retina. Neuron. 2012;75(5):786–98. PubMed PMID: 22958820.
241. Godinho L., et al. Nonapical symmetric divisions underlie horizontal cell layer formation in the developing retina in vivo. Neuron. 2007;56(4):597–603. PubMed PMID: 18031679.
242. Dowling, J.E., *The retina : an approachable part of the brain*. Rev. ed. 2012, Cambridge, Massachusetts: Belknap Press of Harvard University Press. xvi, 355 p.
243. Manns M., Fritzsch B. The eye in the brain: retinoic acid effects morphogenesis of the eye and pathway selection of axons but not the differentiation of the retina in Xenopus laevis. Neurosci Lett. 1991;127(2):150–4. PubMed PMID: 1881624.
244. Johnson P.T., Raven M.A., Reese B.E. Disruption of transient photoreceptor targeting within the inner plexiform layer following early ablation of cholinergic amacrine cells in the ferret. Vis Neurosci. 2001;18(5):741–51. PubMed PMID: 11925009.
245. Johnson P.T., et al. Rods and cones project to the inner plexiform layer during development. J Comp Neurol. 1999;414(1):1–12. PubMed PMID: 10494074.
246. Dodt, E., *The parietal eye (pineal and parietal organs) of lower vertebrates*, in *Visual Centers in the Brain (Handbook of Sensory Physiology)*, R. Jung, Editor. 1973, Springer. p. 113-140.
247. Ekstrom P., Meissl H. Intracellular staining of physiologically identified photoreceptor cells and hyperpolarizing interneurons in the teleost pineal organ. Neuroscience. 1988;25(3):1061–70. PubMed PMID: 3405424.
248. Uchida K., Nakamura T., Morita Y. Signal transmission from pineal photoreceptors to luminosity-type ganglion cells in the lamprey, Lampetra japonica. Neuroscience. 1992;47(1):241–7. PubMed PMID: 1315936.
249. Meves A.Z Zellforsch Mikrosk Anat. 1973;139(4):511–32. *[Electron microscopical investigation on the cytoarchitecture of the brain of Branchiostoma lanceolatum]* . p. PubMed PMID: 4724529.
250. Ruiz S., Anadon R. The fine structure of lamellate cells in the brain of amphioxus (Branchiostoma lanceolatum, Cephalochordata). Cell Tissue Res. 1991;263(3):597–600. PubMed PMID: 1878939.
251. Hendrickson A. Landolt's club in the amphibian retina: a Golgi and electron microscope study. Invest Ophthalmol. 1966;5(5):484–96. PubMed PMID: 4162899.
252. Locket N.A. Landolt's club in the retina of the African lungfish, Protopterus aethiopicus, Heckel. Vision Res. 1970;10(4):299–306. PubMed PMID: 5483268.
253. Vigh B., et al. Cerebrospinal fluid-contacting neurons, sensory pinealocytes and Landolt's clubs of the retina as revealed by means of an electron-microscopic immunoreaction against opsin. Cell Tissue Res. 1983;233(3):539–48. PubMed PMID: 6226359.
254. Quesada A., Genis-Galvez J.M. Morphological and structural study of Landolt's club in the chick retina. J Morphol. 1985;184(2):205–14. PubMed PMID: 3989868.
255. Vigh B., Vigh-Teichmann I. Cytochemistry of CSF-contacting neurons and pinealocytes. Prog Brain Res. 1992;91:299–306. PubMed PMID: 1410413.
256. David C., et al. Cerebrospinal fluid contacting neurons in the reduced brain ventricular system of the atlantic hagfish, Myxine glutinosa. Acta Biol Hung. 2003;54(1):35–44. PubMed PMID: 12705320.
257. García-Fernández J.M., Foster R.G. Immunocytochemical identification of photoreceptor proteins in hypothalamic cerebrospinal fluid-contacting neurons of the larval lamprey (Petromyzon marinus). Cell Tissue Res. 1994;275(2):319–326.
258. Kolb H., Famiglietti E.V. Rod and cone pathways in the inner plexiform layer of cat retina. Science. 1974;186:47–9. PubMed PMID: 4417736.
259. Nelson R. AII amacrine cells quicken time course of rod signals in the cat retina. J Neurophysiol. 1982;47(5):928–47. PubMed PMID: 6177841.
260. Kolb H., Nelson R. Neural architecture of the cat retina. Prog Retin Eye Res. 1984;3:21–60.

261. Strettoi E., Dacheux R.F., Raviola E. Synaptic connections of rod bipolar cells in the inner plexiform layer of the rabbit retina. J Comp Neurol. 1990;295(3):449–66. PubMed PMID: 2351763.
262. Vaney D.I., Young H.M., Gynther I.C. The rod circuit in the rabbit retina. Vis Neurosci. 1991;7(1-2):141–54. PubMed PMID: 1931798.
263. Strettoi E., Raviola E., Dacheux R.F. Synaptic connections of the narrow-field, bistratified rod amacrine cell (AII) in the rabbit retina. J Comp Neurol. 1992;325(2):152–68. PubMed PMID: 1460111.
264. Ashmore J.F., Falk G. Responses of rod bipolar cells in the dark-adapted retina of the dogfish, Scyliorhinus canicula. J Physiol. 1980;300:115–50. PubMed PMID: 7381782.
265. Nilsson D.E., Pelger S. A pessimistic estimate of the time required for an eye to evolve. Proc Roy Soc B. 1994;256:53–8. PubMed PMID: 8008757.
266. D'Aniello S., et al. The ascidian homolog of the vertebrate homeobox gene Rx is essential for ocellus development and function. Differentiation. 2006;74(5):222–34. PubMed PMID: 16759288.
267. Zeiss C.J., et al. Comparative retinal morphology of the platypus. J Morphol. 2011;272(8):949–57. PubMed PMID: 21567446.
268. Burns, M.E. and T.D. Lamb, *Visual transduction by rod and cone photoreceptors*, in *The visual neurosciences*, J.S. Werner and L.M. Chalupa, Editors. 2004, MIT Press: Cambridge, Mass. p. 215-233.
269. Raviola E., Gilula N.B. Intramembrane organization of specialized contacts in the outer plexiform layer of the retina. A freeze-fracture study in monkeys and rabbits. J Cell Biol. 1975;65(1):192–222. PubMed PMID: 1127010.
270. Rieke F., Baylor D.A. Origin and functional impact of dark noise in retinal cones. Neuron. 2000;26(1):181–6. PubMed PMID: 10798402.
271. Brzezinski, J. and T. Reh, *Retinal Histogenesis*, in *Encyclopedia of the Eye. Elsevier Ltd*. 2010. p. 73-80.
272. Gomes, F.L. and M. Cayouette, *Retinal development: Cell type specification*, in *Encyclopedia of neuroscience*, L.R. Squire, Editor. 2009, Elsevier/Academic Press: Amsterdam; Boston. p. 203-209.
273. Chen Z., Li X., Desplan C. Deterministic or stochastic choices in retinal neuron specification. Neuron. 2012;75(5):739–42. PubMed PMID: 22958814.
274. Reese B.E. Developmental plasticity of photoreceptors. Prog Brain Res. 2004;144:1–19. PubMed PMID: 14650837.
275. Lamb T.D., Pugh E.N. Jr, Collin S.P. *The origin of the vertebrate eye.* Evolution. Education and Outreach. 2008;1(4):415–426.
276. Wässle H. Parallel processing in the mammalian retina. Nat Rev Neurosci. 2004;5(10):747–57. PubMed PMID: 15378035.

Neural Basis of Color Perception

Color Vision

Peter Gouras

Created: May 1, 2005; Updated: July 1, 2009.

Introduction

Color vision is an illusion created by the interactions of billions of neurons in our brain. There is no color in the external world; it is created by neural programs and projected onto the outer world we see. It is intimately linked to the perception of form where color facilitates detecting borders of objects (Fig. 1).

Color is created by utilizing two properties of light, energy and frequency of vibration or wavelength. How our brain separates these two properties of light, energy and wavelength, and then recombines them into color perception is a mystery that has intrigued scientists through the ages. We know much about the nature of light and the subjective impressions of color, definable by physical standards (1) but ultimately color should be explained at the level of single cells in our brain. Examination of the responses of single neurons or arrays of such neurons provides the best insights into the physiology of color vision. Ultimately our understanding of this process will allow us to model the neural circuits that underlie the perception of color and form. Although still beyond reach, progress is being made in deciphering these clever circuits that create our perception of the external world.

We start by describing the nature of the photoreceptors that convert light energy into neural signals. Then we consider the parallel channels leading from the retina to the thalamus carrying information into visual cortex, where color is ultimately determined. Lastly we use our current understanding to speculate on how visual cortex uses neural circuits to create the perception of color and form.

The Photoreceptors

Photoreceptors are neurons specialized to detect light. The detection occurs in an organelle called the outer segment, a membranous structure where light absorbing proteins, opsins, are embedded. There are two major types of photoreceptors in most vertebrate eyes, rods and cones. Rods are very sensitive but slow and their response saturates at light levels where cones function optimally. Rods are not used much in modern society where artificial illumination adequate for cone vision is ubiquitous. Cones are less sensitive but are fast and can adapt to the brightest lights, being almost impossible to saturate. Cones evolved before rods undoubtedly in areas of strong sunlight where vision was a great advantage. In broad sunlight, shadows are strong and more important to detect than increments of light in the struggle for survival. Shadows depolarize cones leading to a release of a transmitter that influences second order retinal neurons. The appearance of light hyperpolarizes cones leading to a curtailing of this transmitter.

A cone responds only to the energy it absorbs (2). All wavelength of light can produce identical responses from a cone if the energy absorbed by the cone is the same for these wavelengths (Fig. 2). Cones are therefore color blind producing a univariant response reflecting only the amount of energy they absorb. Detecting objects by the energy reflected from their surfaces, however, can fail when objects reflect a similar amount of energy as their background. Here is where color vision becomes important. Wavelength contrast can detect objects when energy contrast is absent or minimal. An object can reflect the same energy but seldom reflects the same wavelength composition as its background. Color vision combines both energy and wavelength contrasts to detect objects and this advantage must have evolved early in the evolution of vision.

In order to detect objects by differences in spectral reflectance, two or more different types of cones are needed. This is an important concept for understanding color vision. For divariant color vision, two cone types must exist and be sensitive to different parts of the visible spectrum, preferably as different as possible. The range of the visible spectrum depends on the ability of light to penetrate the eye and be absorbed by the photoreceptors.

Figure 1. A floral scene with and without color.

Ultra-violet light is absorbed by the anterior segment of our eyes and seldom reaches the photoreceptors. Infra-red light penetrates our eye readily but its quantal energy may be too small to activate opsins. Therefore early in the evolution of color vision, opsins sensitive to the middle of our visible spectrum evolved, near spectral yellow, and a short wavelength opsin evolved in a second type of cone, near spectral blue (Fig. 3). These have been called L (long wavelength sensitive) and S (short wavelength sensitive) cones, respectively, and this was a first step in the evolution of color vision.

In animals with large eyes, an interesting strategy evolved. L-cones were used to detect both energy and wavelength contrast but S-cones were used only for wavelength contrast. This was due to chromatic aberration. Short wavelength images are out of focus when longer wavelength images are in focus on the photoreceptor mosaic. Chromatic aberration increases greatly at short wavelengths, which led to the L cone system dominating energy contrast. As a result there are many more L than S cones in many mammals in order to gain spatial resolution by achromatic contrast detectable by L cones.

In animals with small eyes, like mice and rats, ultra-violet light can reach the photoreceptor mosaic and in this case ultra-violet sensitive cone opsins have evolved to widen the spectral range of vision and if combined with L cones could allow color vision (3-5). Chromatic aberration is reduced in these small, highly spherical eyes which have outer segments as long as animals with large eyes. This increases their depth of focus minimizing chromatic aberration, an advantage of being small. Their retinal images are less magnified, however, than those in large eyes.

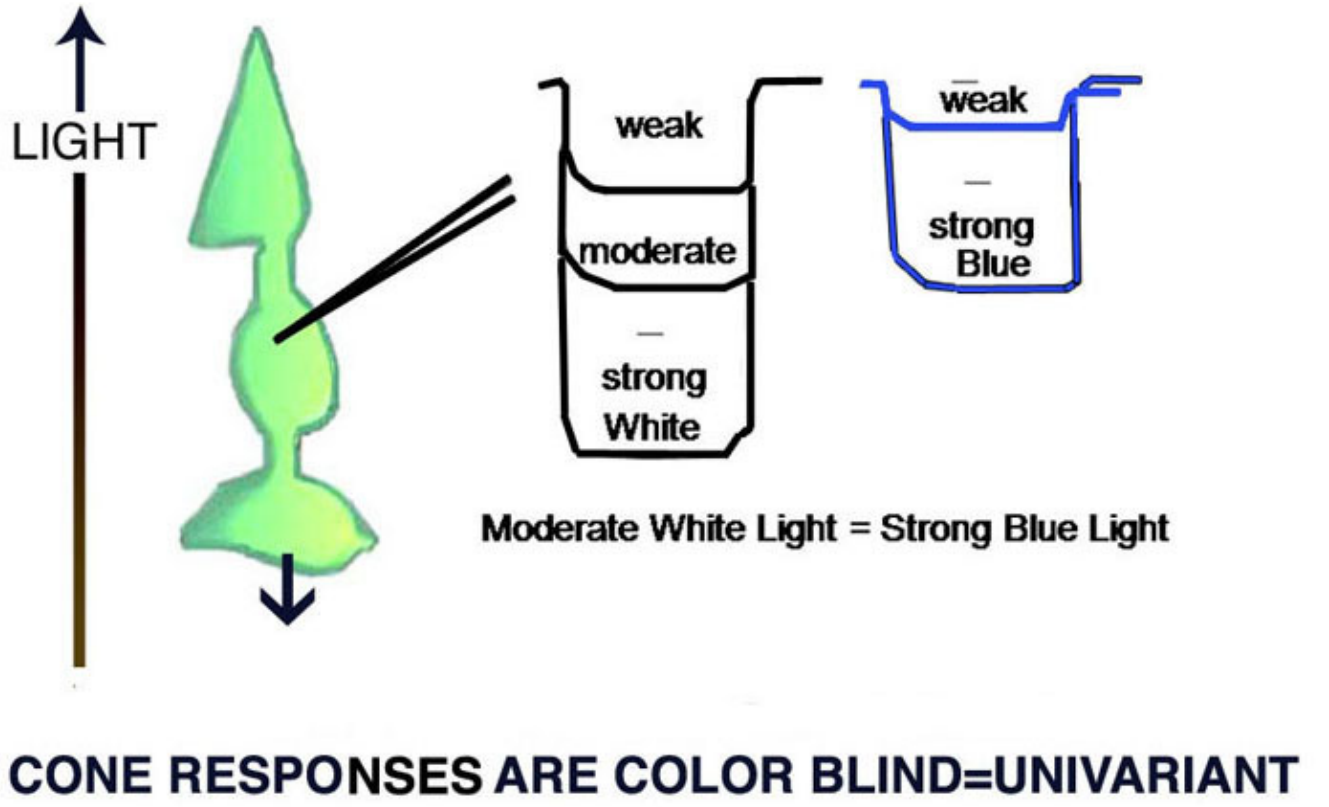

Figure 2. Different wavelengths (colors) producing identical responses from cones.

Chromatic and Achromatic Contrast

In order to establish chromatic contrast it is necessary to compare the responses of a group of cones of one type with the responses of a group of cones of another type within the same area of visual space. One cannot compare only two neighboring cones such as the S and the L cone in Fig. 4A.

If an image of gray and yellow were to cover these two cones in an inappropriate way as done in Fig. 4A the brain would reach an erroneous conclusion about this border because the S cone would not be affected by the yellow side and the L cone would be strongly affected by the gray side. The brain might consider this to be a black/yellow border rather than a yellow/gray border. Even if a slit of light imaged on only the more numerous L cones (Fig. 4B), there would be ambiguity about the colors of adjacent images. If only L cones are affected by both yellow and gray light, the brain would not see any border here. Only when a larger image covers a number of S and L cones (Fig. 4C) can an unequivocal decision be made about the color of these bordering images. In this case the left side, which is yellow, would strongly affect L but not S cones and therefore be judged to be yellow. The right side of this border, which is gray, would strongly affect both L and S cones and therefore would appear white or gray. For achromatic contrast, smaller images can be analyzed for border contrasts and in most cases only two neighboring cones would be sufficient to distinguish a light/dark border. This is why a unit area of achromatic space is smaller than a unit area of chromatic space.

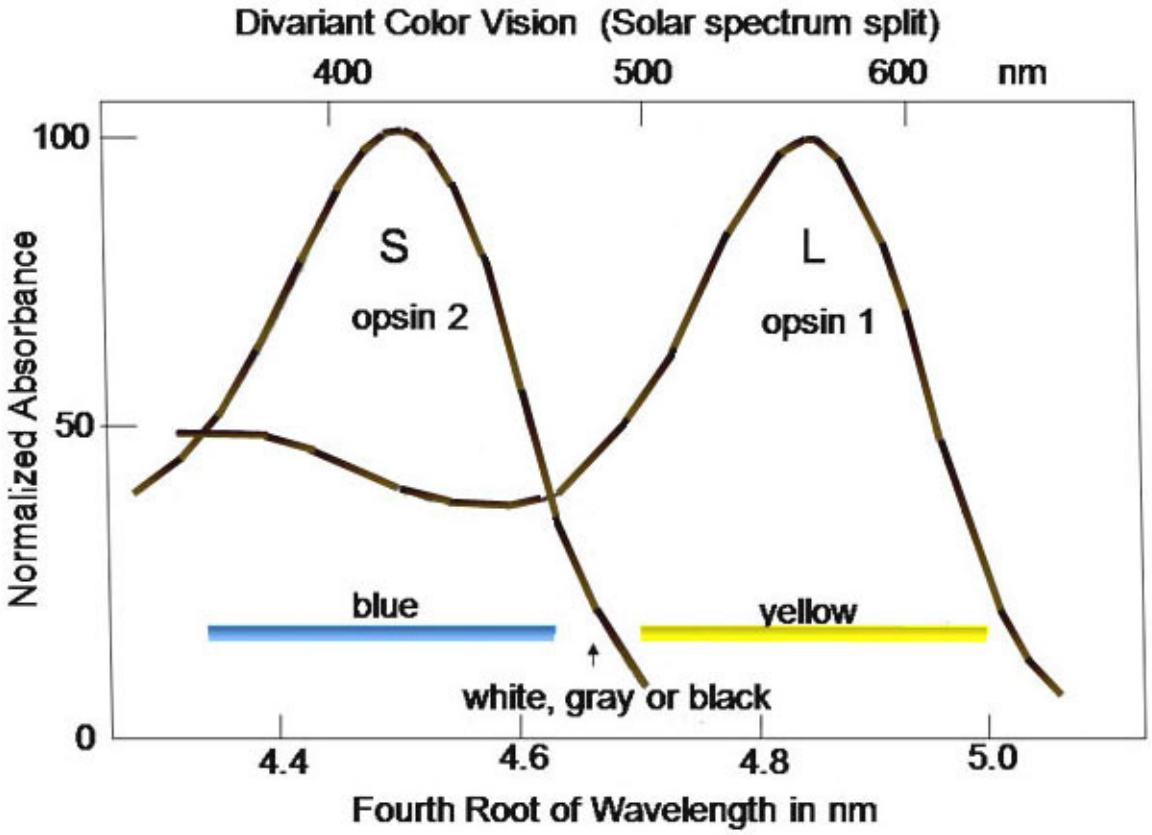

Figure 3. The normalized absorption spectra of the S and L cone opsins mediating divariant color vision. Strong absorption by the S cone opsin alone induces "blue"; strong absorption by L cone opsin induces "yellow" and absorption by both induces "white or gray" depending on achromatic contrast of light and dark. The 4th root makes the curves identical in shape.

Horizontal Cells

Cones receive an antagonistic input from horizontal cells, whose cell bodies reside in the outer nuclear layer and whose processes contact the spherules of rods and the pedicles of cones (6). There are at least two varieties of cone horizontal cells (Fig. 5).

One variety (H1) only contacts L cones; the other variety contacts both S and L cones (H2). Cone horizontal cells receive an excitatory input from cones and send back an inhibitory input to cones. This is a type of negative feedback. When a cone is hyperpolarized by an increment or depolarized by a decrement of light, it receives an opposing input from horizontal cells after a brief synaptic delay. This dampens the response and can also reduce the effects of scattered light by minimizing cone responses outside of the focal image on the retina. In color vision the horizontal feedback also acts to narrow the action spectrum of cone bipolar cells. In divariant color vision this can narrow the action spectrum of S cone bipolar cells. This occurs because the processes of the H2 horizontal cell that reach L cones are only post-synaptic to S cones. Therefore L cones can send an antagonistic signal to S cones which can reduce the effectiveness of wavelengths, absorbed by both L and S cones and this narrows the action spectrum of the S cone channels (7).

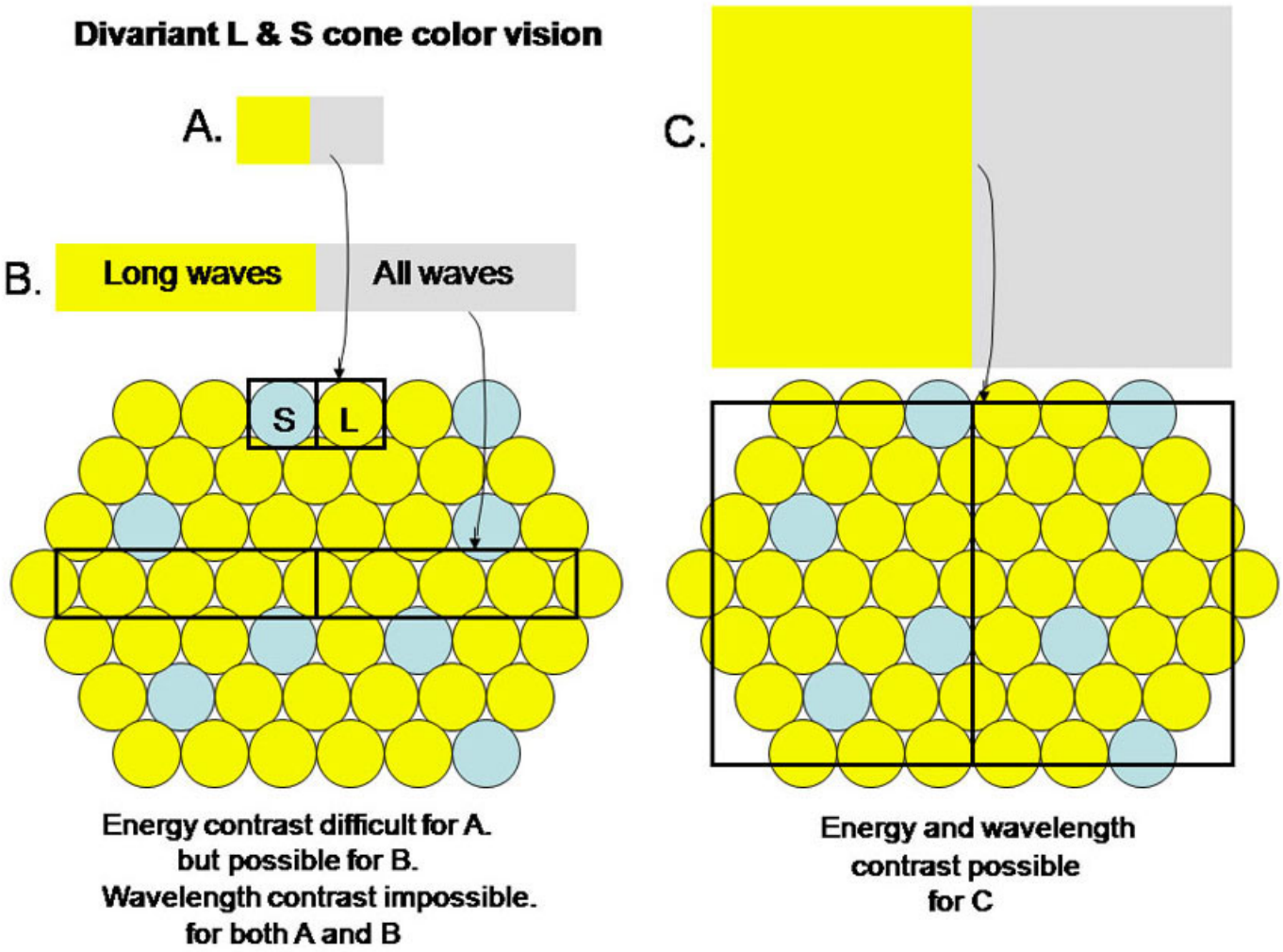

Figure 4. The difficulty determining the color of small objects.

Bipolar and Ganglion Cells

The retina is composed of three layers of neurons, the outermost being the photoreceptors, rods and cones, which for divariant color vision are L and S cones. A second layer of bipolar cells transmits the signals of the photoreceptors to a third layer of neurons, the ganglion cells whose axons form the optic nerve. The ganglion cells serving the two photoreceptor systems are quite different. The L cones synapse with unique bipolar cells, called "midget" bipolar. These single cone detectors were discovered by Stephan Polyak (8) in monkey retina using the Golgi method of silver impregnation. Because of their small size they were called "midget" bipolar cells. This provides the brain with the ultimate in spatial resolution, a single cone, and in addition isolates the signals of L cones which can be used for color vision. A feature of this L cone bipolar system is the presence of two types of cells (Fig. 6). One type of L cone bipolars depolarizes whenever the cone or cones they synapse with hyperpolarize; this set is called on-bipolars because they are excited (turned on) by light. The other set is depolarized whenever the cones they synapse with detect decrements of light; this set is called off-bipolars because they are excited by darkness and inhibited (turned off) by light. These two sets of cone bipolar cells synapse with separate sets of on and off ganglion cells at two levels in the inner plexiform layer of the retina, a more external off-lamina and a more internal on-lamina (9).

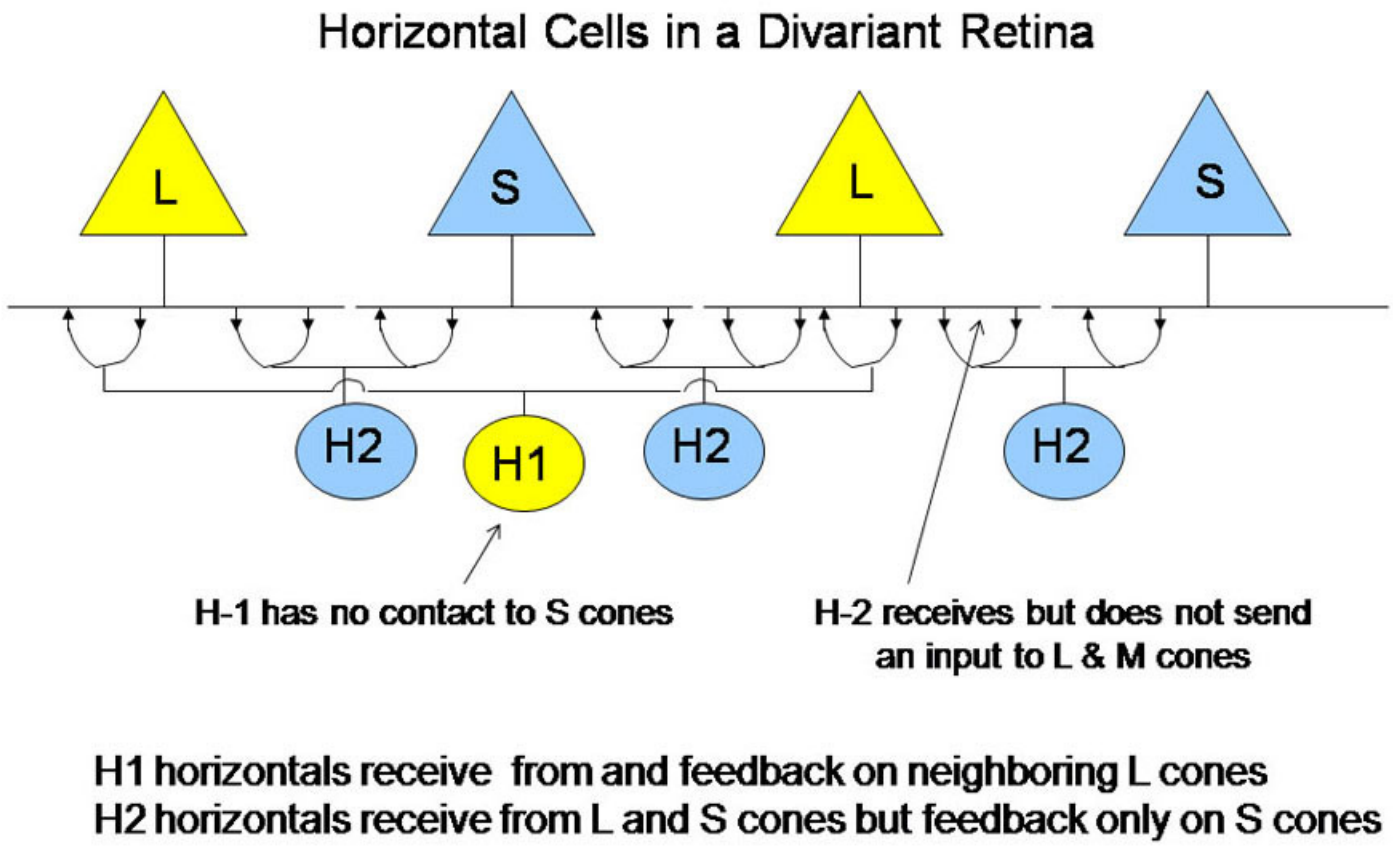

Figure 5. Two varieties of horizontal cells and their relation to L and S cones in a divariant retina.

These parallel channels, transmitting lightness and darkness from local retinal areas, are maintained throughout the visual pathway to visual cortex. This "push-pull" system of neurons is thought to increase the dynamic range for detecting decrements and increments of light in local areas of the retinal image. Only L cones seem to be connected to both on and off bipolar cells while S cones are connected to only on-bipolar cells. The reason for this may be that the latter are only involved in chromatic vision while the former are involved in both chromatic and achromatic vision. Achromatic vision involves the detection of lightness and darkness while chromatic vision involves the detection of color. Not only do S cones lack an off-bipolar system but they have a much different route to the ganglion cell output layer. The S cone on bipolar excite the internal arbor of a bistratified ganglion cell while a wide-field L cone off bipolar excites the external arbor of this same ganglion cell (10). This S cone system is absent in the very center of the fovea where achromatic contrast is mediated by the L cone midget system. Away from the fovea the L cone midget system begins to contact more than one cone and therefore loses spatial resolution.

There is a second ganglion cell system that plays no role in color vision but is also connected to only L cones. These are parasol ganglion cells. They are larger cells with faster conduction velocities and they target the magno-cellular layers of the lateral geniculate nucleus (LGN). They appear to play a role in the detection of movement and possibly slow tracking movements. There is some evidence that they might receive an input from S cones but I have never been able to detect such an input. Barry Lee's group considers these cells play a role in the detection of luminance (11).

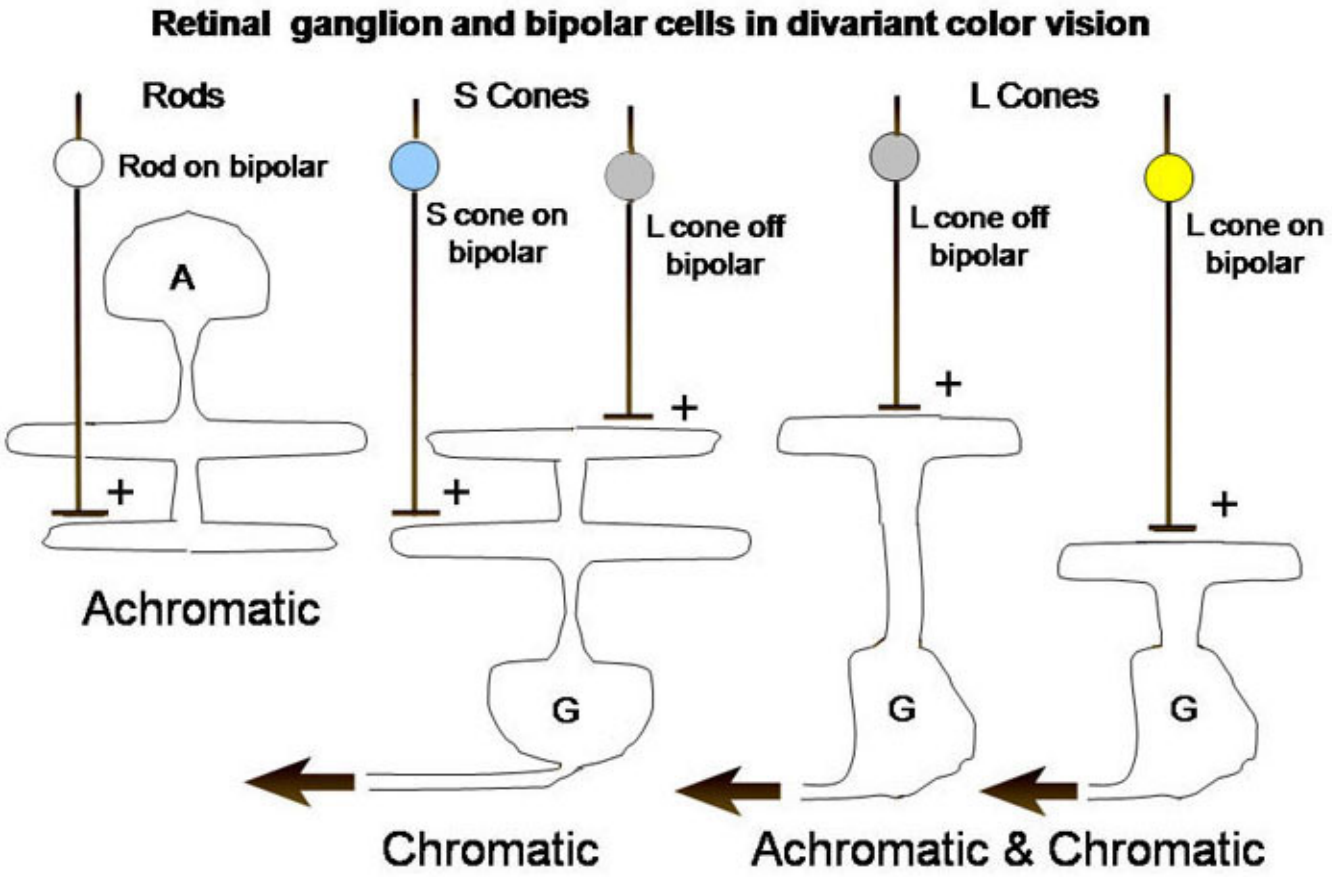

Figure 6. The currently understood retinal ganglion cells responsible for rod (achromatic) and cone achromatic and chromatic signals being sent to the lateral geniculate nucleus. We assume that the L cone off bipolar signals darkness but it could also be blue.

Divariant Blue/Yellow Color Vision

The ganglion cells in Fig. 6 are thought by most to be the essential channels for divariant color vision. The bistratifid S cone on-cells and the L cone midget cells monitor the light absorption of S and L cones respectively. The signals from these two channels must be compared in the same areas of visual space for color vision. The cone bipolar cells driving the bistratified S cone on-ganglion cells have co-extensive fields (Fig. 7), which is ideal for comparing differences between two cone mechanisms in the same area of visual space.

These two different bipolar inputs to the bistratified ganglion cell do not appear to oppose each other because these cells are excited by white light. Another more indirect input to these cells comes from the H2 horizontal cell which transmits antagonistic signals from L to S cones. This input provides spectral antagonism to the bistratified ganglion cell because light activation of L cones will produce a depolarizing signal in S cones that counteracts the hyperpolarization produced by short wavelength light. The strong response to white light, however, implies that this H2 mediated antagonism is relatively weak.

The channel transmitting L cone signals for spectral contrast in visual cortex has been considered to be the midget system, at least in primates. These midget ganglion cells are considered to receive no input from S cones, either synergistic or antagonistic, although there are connections to S cones through H2 horizontal cells. In trivariant monkey retina there is no evidence of S cone input to either the midget or the parasol ganglion cell

systems which implies that H2 horizontal cells are only post- and not pre- synaptic to L cones. The H1 horizontal cell only contacts L cones and therefore provides only spatial antagonism to neighboring L cones and does not produce spectral antagonism.

This previous picture is not accepted by everyone. There is evidence that a L cone on/S cone off ganglion cell exists to provide an opponent L cone on input to visual cortex (12-15). It has been difficult to find such a ganglion cell in primate retina but they they have been reported in the koniocellular layers of the primate lateral geniculate nucleus. These geniculate cells have been traced back to their retinal ganglion cell inputs, which have their dendritic arbors in the on-lamina of the inner plexiform layer, quite different than the bistratified arbors of S on/ L off ganglion cells. This produces a curious difference in the blue/yellow channels of color vision in primates. In small animals, ground squirrels, guinea pigs and mice, there appears to be a more symmetrical system of S cone on/Lcone off and M cone on/S cone off opponent ganglion cells, both of which send their dendrites to the on-lamina of the inner plexiform layer. This implies that the horizontal cells and/or intervening amacrine cells are involved in their unique opponent organization, perhaps more similar to the rod system. The existence of this retinal L cone on/S cone off channel would preclude the midget cells depicted in Fig. 7 from contributing to color vision in animals with divariant color vision.

A more iconoclastic hypothesis recently proposed by the Neitz group (13) considers the bistratified S cone on/L cone off retinal ganglion cell to play no role in color vision proposing that its signals go to the brain stem where they mediate unconscious visual functions together with light sensitive retinal melanopsin ganglion cells. They propose that surround antagonism from the H2 horizontal cell turns L cone off-center midget bipolar cells into S cone-on/L cone-off cells and L cone-on/S cone-off cells. This hypothesis brings S cone signals into the midget ganglion cell system designed for high spatial resolution. Evidence that the bistratified S cone on-cell does affect conscious vision comes from an observation of W.S. Stiles (16) that his S cone mechanism, isolated psychophysically, affects conscious experience because it exhibits a curious behavior; its sensitivity declines when a long wavelength adapting light, which has no effect on S cones, is turned off. The bistratified S-cone ganglion cell exhibits this same behavior implying that its signals do reach visual cortex and consciousness. It is also possible, however, that the unusual midget cells proposed by the Neitz team (13) also exhibit this phenomenon, which has been labeled "transient tritanopia".

Regardless of which of these three hypotheses is correct, there must be a way for the visual cortex to compare L with S cone activity in the same area of visual space in order to produce color vision. In Fig. 8 we use two of the ideas that are demonstrated in Fig. 7 to illustrate how striate cortex uses these retino-geniculate inputs to construct cells that are more responsive to color.

Fig. 9 shows a logical way to extract the signals from the cone mosaic into parallel channels mediating achromatic contrast with high spatial resolution and chromatic contrast with lower spatial resolution from the same mosaic.

The perception of color mixes both achromatic with chromatic signals to create the combined experience of color. In this arrangement the S cone system only plays a role in chromatic vision while the L cone system contributes to both chromatic and achromatic vision. The repertoire of colors that are produced and their relationship to the activity of the two cone mechanisms involved are shown in Fig. 10; these colors are shown at borders of minimum achromatic contrast where chromatic contrast becomes most important.

Color Constancy and Double Opponency

The schemes of the previous figures neglect a problem called "ch22color constancy". We see colors as unchanged even when there are large changes in the spectral properties of an illuminant. The colors in a scene illuminated by fluorescent lights, which generate much short wavelength energy or by tungsten filament lights, which generate much long wavelength energy are not significantly altered by such changes. In other words we should

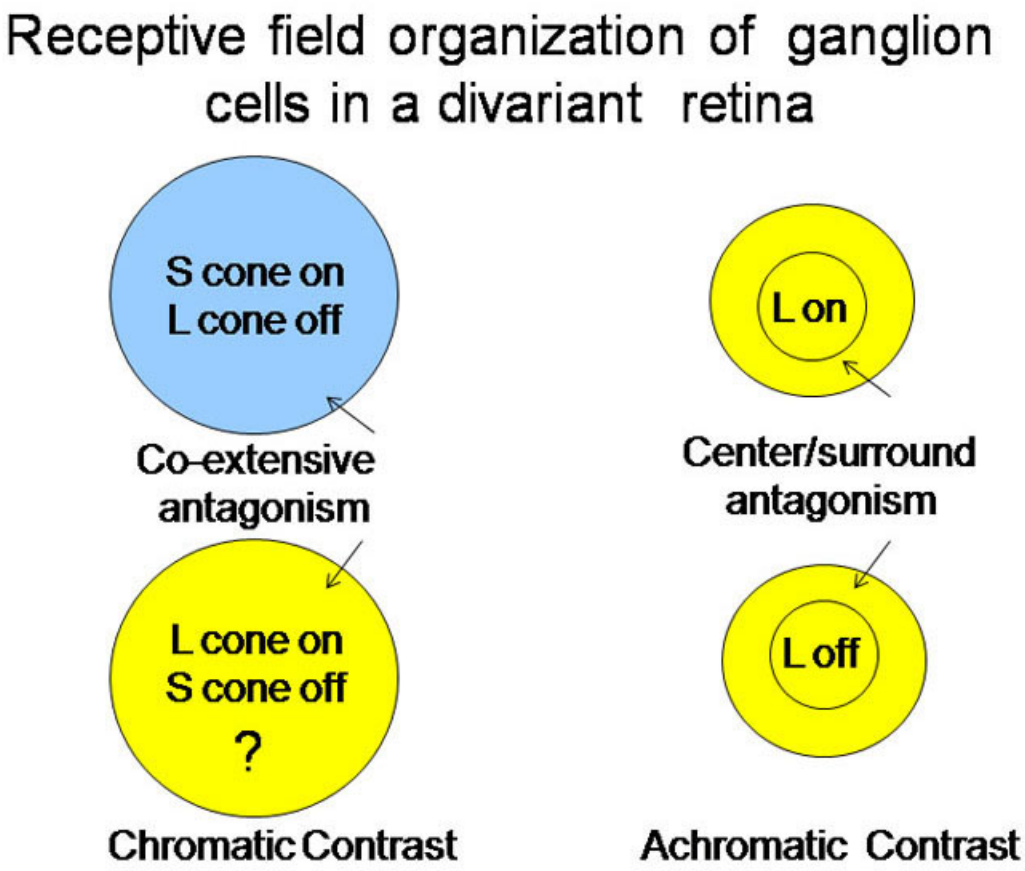

Figure 7. Two options being considered for the ganglion cell system providing chromatic and achromatic information to the lateral geniculate nucleus for divariant color vision.

see things "bluer" in fluorescent light and redder in tungsten light but we don't. This constancy of colors despite changes in illumination intrigued Edwin Land, the founder of the Polaroid Corporation, who spent years investigating this phenomenon and demonstrating significant global aspects of color vision (17). Local objects can reflect identical spectral components from their surfaces but will appear of different color because of the influence of the entire scene. He proposed a model in which the signals from each cone mechanism are normalized over the entire visual scene before being compared with each other locally to generate the perception of the color of an object scene. Fig. 11 illustrates why this idea is reasonable. Here two lights beams, one white, the other yellow illuminate a screen.

An arrow blocks a portion of the yellow beam and this produces a shadow that appears "blue". If one determines the light energy being absorbed by the L and S cones from the screen, it is apparent that there is more light affecting the L than the S cones coming from the shadow, which would suggest that the shadow should look yellow and not blue. But if one normalizes the light coming from the entire screen to 100%, then the relative effect on the S cones becomes greater than that on the L cones and the shadow appears "blue". This supports the idea that responses from each cone mechanism across the entire visual scene are first normalized before being compared with each other locally to produce the perception of color from specific objects in the scene. Such normalization could occur if S cone and L cone transmitting neurons were to inhibit each other following the rules outlined in Fig. 12. This could reduce the responses to global illumination that affected one cone mechanism more strongly than the other and support color constancy. If, in addition, the excitation of these cone specific channels were organized so that each local area of color space would be enhanced by neighboring spectral contrast between cone mechanisms it would lead to simultaneous color contrast.

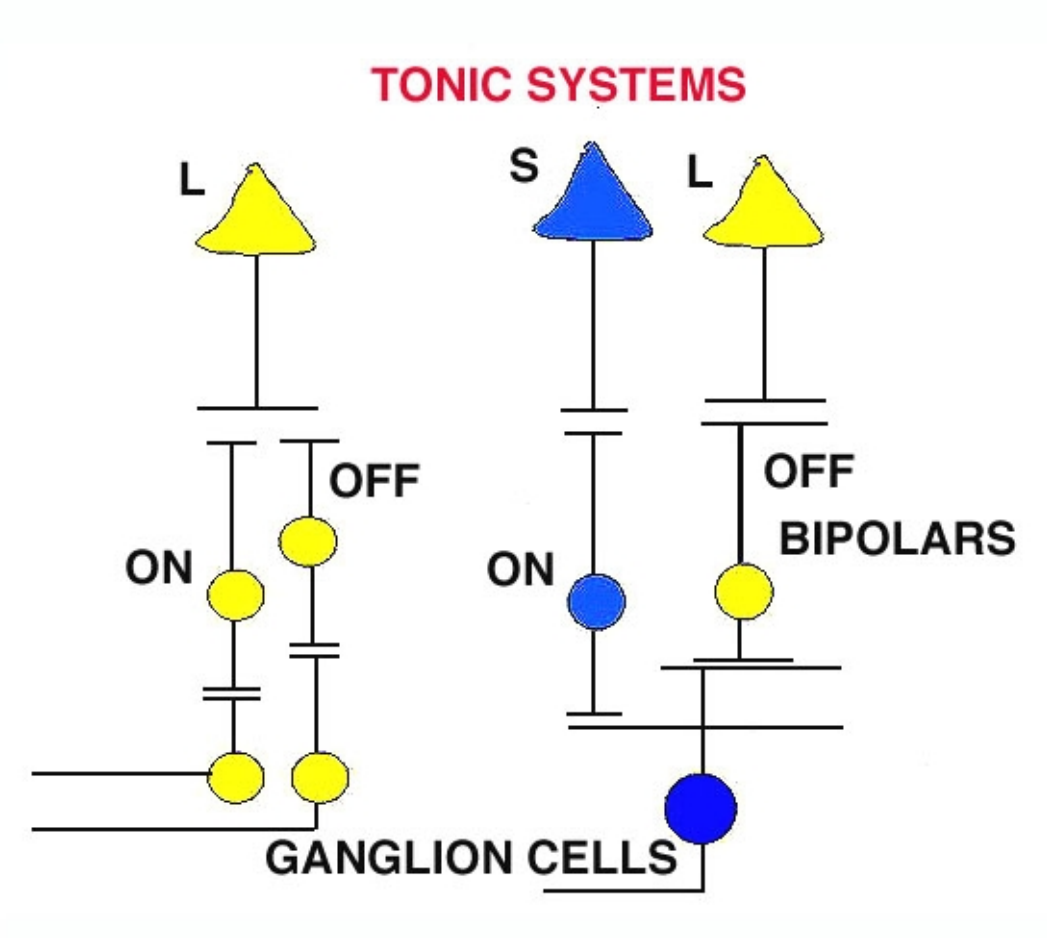

Figure 8. How retino-geniculate inputs are used to build cells with spectral antagonism, i.e., selectivity for certain wave-bands and ultimately color. This figure illustrates interaction between the achromatic system that determines the lightness or darkness of an object and the chromatic system that detects "hue". Together they create color.

By the rules of Fig. 12, a unit area of color space A would appear "blue" if there were short wavelengths and no long wavelengths in area A; the converse would lead to "yellow". This blueness or yellowness would be enhanced if the surrounding areas of color space were activated by the opposite color, i.e. simultaneous color contrast. Such cells have been called "double opponent" cells because they have one form of antagonism between cone mechanisms mediating a local area of color space and an opposite arrangement in neighboring areas of color space. Charles Michaels (18) found such cells in striate cortex of non-human primates following up on observations of Nigel Daw (19) in goldfish retina. Double opponency tends to separate spectral from energy contrast.

Trivariant Color Vision

In primates, high resolution vision and trivariant color vision evolved to enhance survival. A fovea formed to facilitate high resolution achromatic vision and a third opsin evolved from the original mammalian L cone opsin to create a new dimension of color in higher primates (20). The gene for the L cone opsin duplicated itself and one of the paired genes developed polymorphisms to absorb further into the long wavelength region of the spectrum. The original long wave sensitive L cone now became an M cone being the partner of an even longer wavelength sensitive L cone. Fig. 13 shows that a trivariant system can detect a larger variety of spectral reflectances (21). In Fig. 13 above right, one sees that a divariant color vision system can detect spectral contrasts

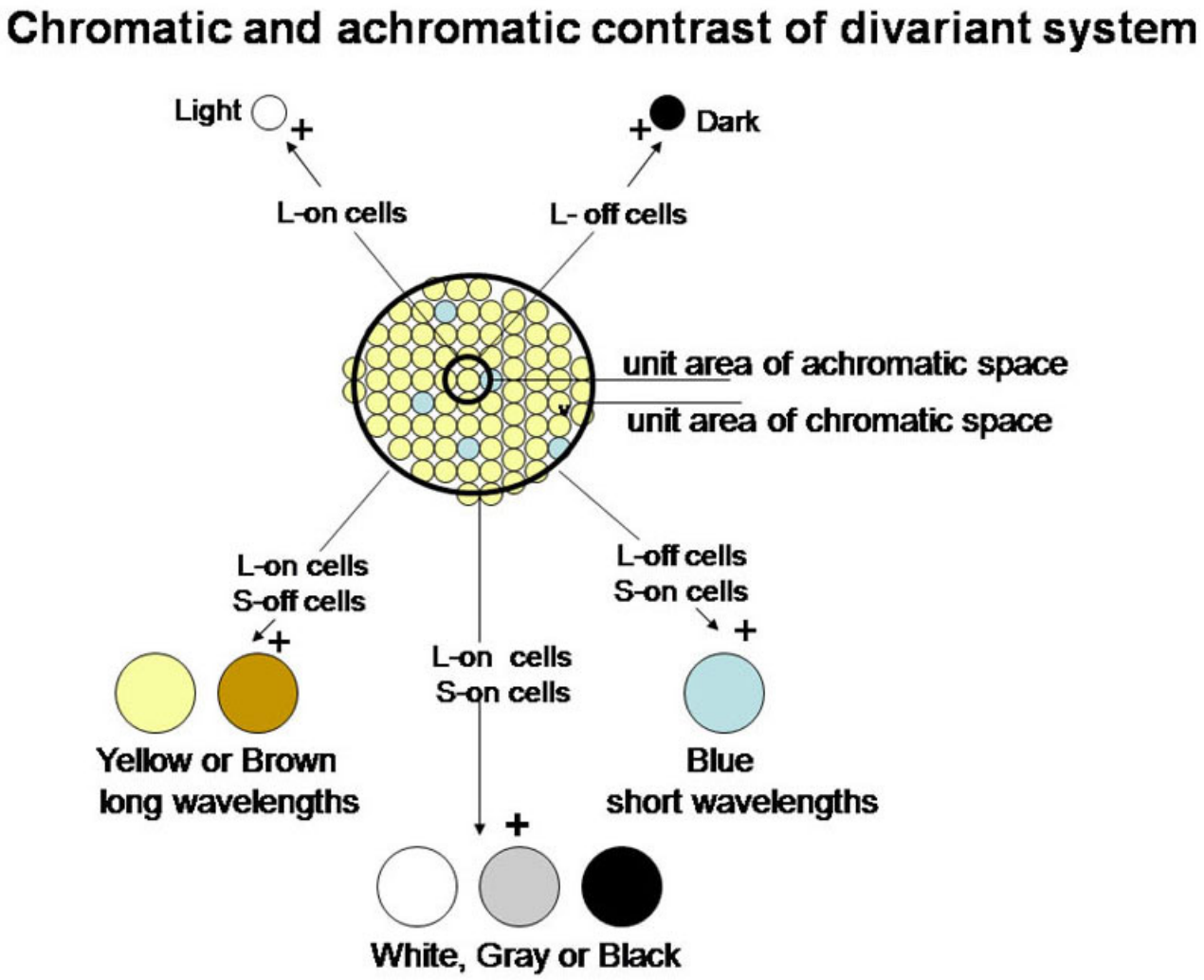

Figure 9. Parallel pathways extract chromatic and achromatic contrast from the same cone mosaic. The unit area of achromatic space is smaller than that of chromatic space.

that reflect more at one end than at the other end of the spectrum; these reflectances tend to tilt the solar spectrum.

If, however, a surface reflects less from both sides of the visible spectrum, i.e. bending the solar spectrum, it might be invisible to a divariant system because both cone types could be absorbing the same amount of light from the object and its background (Fig. 13 lower left). A trivariant system detects this object because it is impossible for all three cones to be absorbing the same amount of light from the object and its background (Fig. 13 lower right). More complex reflecting surfaces might confuse even a trivariant system but they are probably very rare in the natural world. This change split the yellow region of the original spectrum and created two new chromatic percepts, red and green (Fig.14). It is noteworthy that a rise in the beta-band absorption of this new L cone pigment also provided a long wave influence at the short wavelength region of the spectrum.

Fig. 15 shows how a trivariant system facilitates the distinguishing of red and green objects which would remain indistinguishable for a divariant observer.

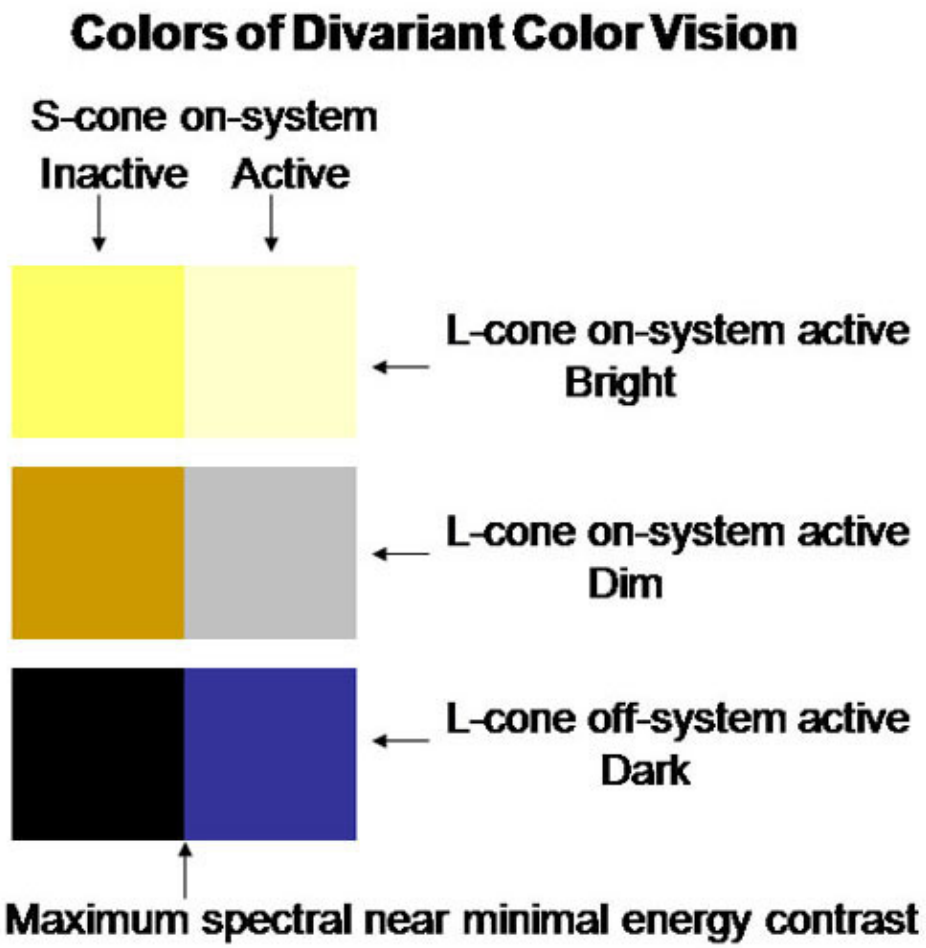

Figure 10. The variety of colors seen by a divariant color vision system using only L and S cones. Each of these colors is related to a certain combination of on and off cell systems.

In the fovea, the same midget cells which had been contacting only single L cones for divariant color vision now contacted either an L or an M cone (Fig. 16), providing the brain with separate channels for these two different cones and another opportunity for chromatic contrast.

In Fig. 16 it is assumed that the bistratified S cone on cell conveys S cone signals from the retina and the midget cell system conveys the signals of L or M cones for color vision (6). The midget cell system is currently assumed to play a role as a "double duty" detector contributing to both high spatial resolution achromatic vision and lower spatial resolution chromatic vision.

Fig. 17 (upper) shows the responses of a midget ganglion cell receiving an excitatory L cone input. This cell is continuously excited by the red adapting field; under these conditions the cell does not respond to the small red spot. A blue adapting field stops this continuous discharge and under these circumstances the cell responds to the small red spot. Fig. 17 (lower) shows the responses of an L cone on midget ganglion cell (large amplitude) and a M cone on midget-like ganglion cell (small amplitude) responding to a small red spot in the presence of the same adapting fields. The red adapting field continuously excites the L cone cell and inhibits the M cone cell; under these conditions the small red spot inhibits the L cone cell, an inhibition mediated by M cones.

Fig. 18 shows an S cone on-cell responding to spectrally narrow stimuli.

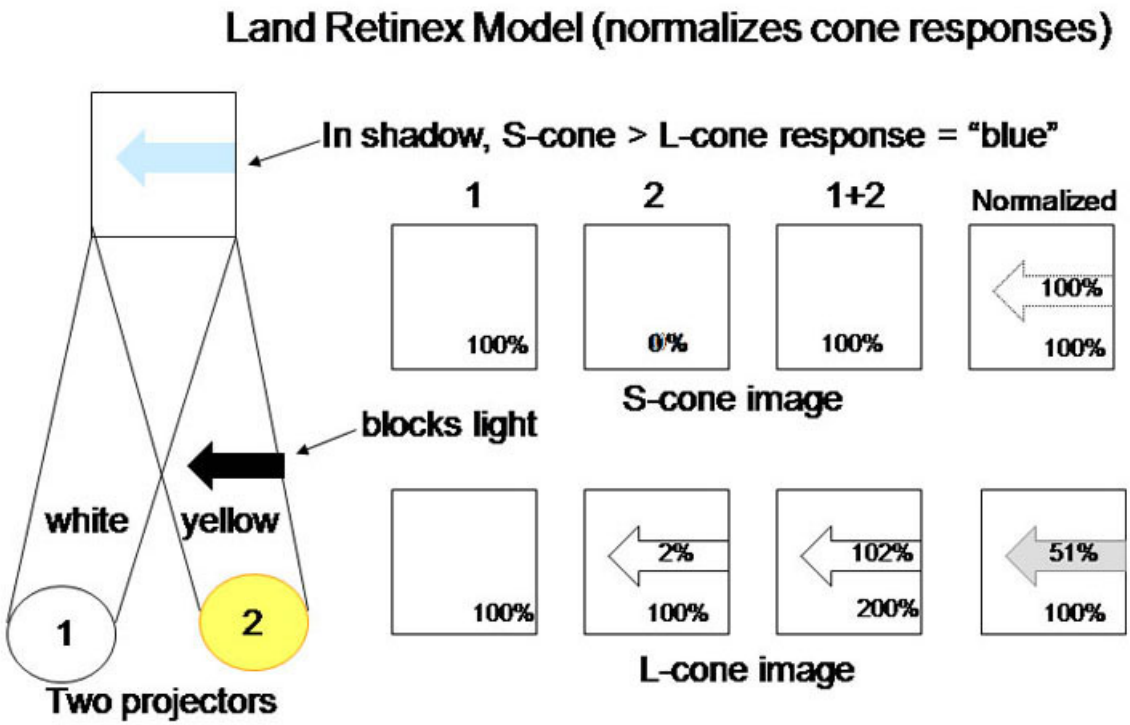

Figure 11. An experiment of Edwin Land. Two projectors cast a mixture of white and yellow light on a screen and an object (arrow) is placed in the yellow beam which leads to the appearance of a "blue" shadow of the arrow on the screen. This somewhat paradoxical appearance of the shadow can be explained if one assumes that the effects of the separate cone mechanisms viewing this screen have their responses normalized across the screen before being compared with each other to produce color.

The cell is excited by the blue spot on the yellow background and is profoundly excited by the turning off of the yellow adapting light. The cell is not responsive to the red spot in the presence of the yellow adapting light but is inhibited by the red spot in the absence of the adapting light.

Fig. 19 illustrates how these midget cells could participate in both chromatic and achromatic vision. The same concentrically organized retinal and geniculate cells feed two different circuits in striate cortex. One achromatic with a large number of orientation selective neurons capable of high spatial resolution and the other chromatic built up from the same center/surround organized midget-like cells. How center/surround cells can build up a circuit which is more co-extensively organized more suitable for chromatic processing remains enigmatic.

David Hubel (22) and the late Bob Rodieck (23) have suggested that the midget system may not be involved in mediating chromatic vision but another much less common ganglion cell type with a receptive field in which L and M cones driving these cells are co-extensively rather than concentrically organized in the receptive field of these cells. It has been difficult to obtain any evidence for such a cell.

The evolution of trivariant color vision in higher primates increased the repertoire of colors we perceive and the power of spectral contrast to detect objects. The original blue/yellow form of color vision was now accompanied by a parallel system of red/green colors occurring in the yellow region of the spectrum where brightness is maximal (24). Where the dynamic range of achromatic contrasts are maximal is where chromatic contrast can contribute most to detecting borders when achromatic contrast is minimal. Fig. 20 shows how the activity of this trivariant cone system contributes to the variety of major colors we see. The borders of effective energy contrast for each of these colors are minimal, which is where color contrast is especially important.

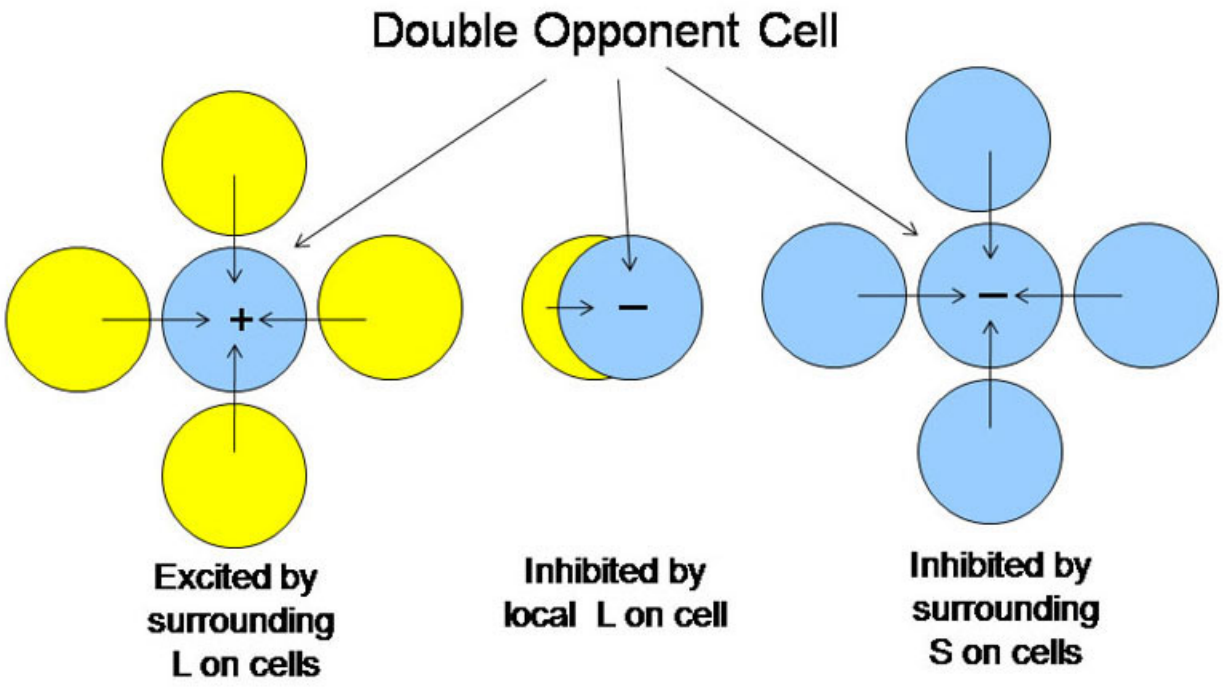

Figure 12. How double opponent cells can be constructed. The central two on cells, one S on and the other L on, inhibit each other. The surround L on cells excite the central S on cell and inhibit the central L on cell. the surround S on cells excite the central L on cell and inhibit the central S cone on cell (not shown).

The Cone Mosaic of Trivariant Color Vision

The division of a single L cone type into two spectrally different L and M cones produced a mosaic of L, M and S cones from which each ganglion cell picks out the input of one or the other of these cone mechanisms to transmit to the brain. Adaptive optics has revealed significant differences in the number of L versus M cones in normal subjects (25) (Fig. 21).

Some subjects have 15 times as many L than M cones and others have twice as many M than L cones but all have normal color vision. This reinforces the idea that a unit area of color space involves comparisons of large groups of cones. What remains problematic is how midget-like ganglion cells in the parafovea select only L or only M cones to form synaptic contact within this variegated cone field.

A Parallel System of Achromatic Ganglion Cells

In addition to midget and midget-like ganglion cells described there is another parallel system of larger ganglion cells with less representation in the fovea than the midget cell system (26). These ganglion cells also have: on- and off-varieties mediated by a separate set of cone bipolar cells and are known to be the "parasol" ganglion cells found by the Golgi method of silver impregnation. They seem to receive their inputs from only L and M cones through a different set of bipolar cells than those serving the midget cell system. Fig. 22 shows two retinal ganglion cells in rhesus monkey retina.

The cell with smaller amplitude is a phasic on-cell that responds at on to all three wavelengths with a shorter latency than the tonic S cone on cell which is excited only by the deep blue light (419 nm) and inhibited by the longer wavelengths (610 and 509 nm). It is thought that a separate relatively wide field bipolar cell feeds these

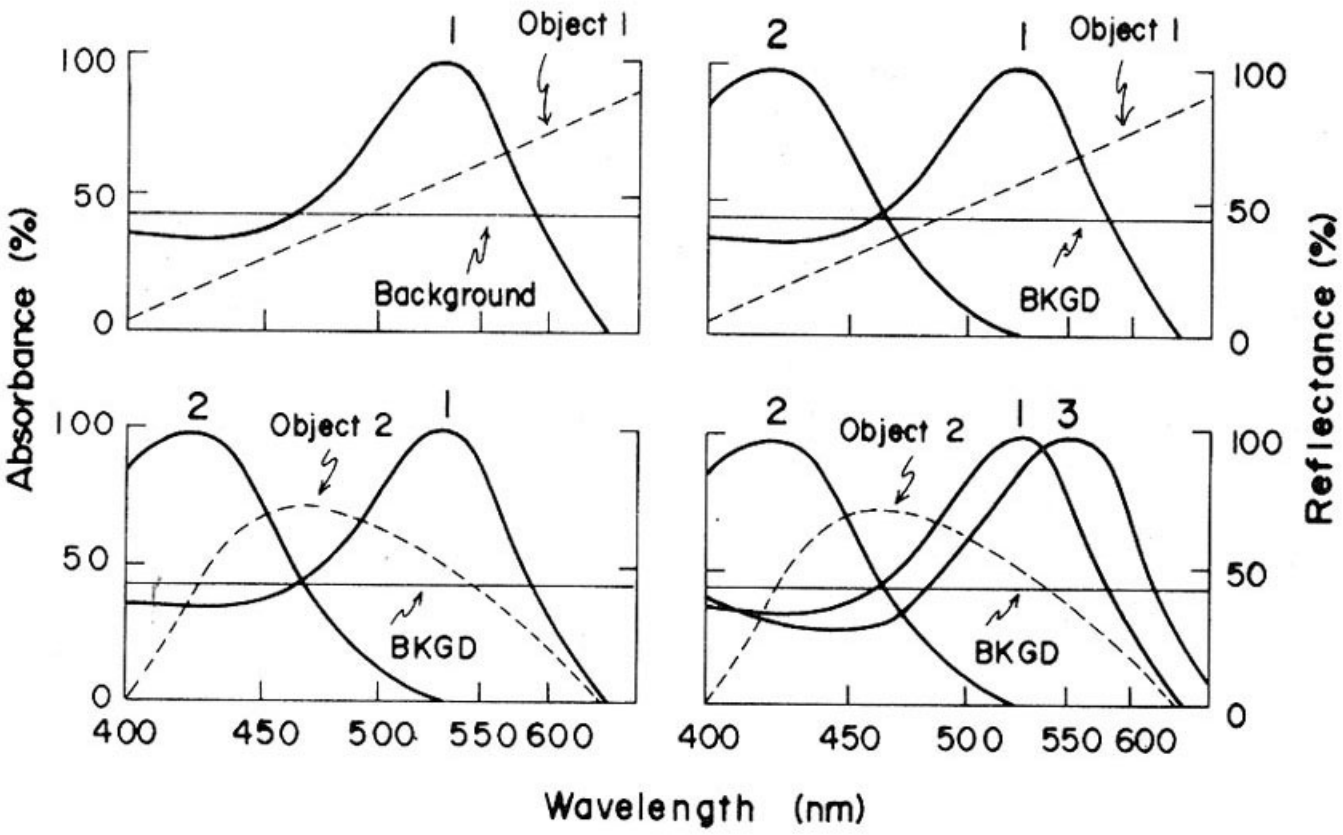

Figure 13. An Object 1 that just "tilts" the solar spectrum but causes as much light absorption as the background will not be detectable by a retina with only 1 photopigment (opsin) in one class of cones (1). In order to detect this Object 1 by its spectral contrast it is essential to have a second type of cone (2) which will always recognize this Object 1 by its spectral reflectance relative to its background. If an object arises such as Object 2 that "bends" the solar reflectance by having a reflectance maxima in the middle of the spectrum it could become invisible relative to its Background for both cones 1 and 2. For such reflectances three types of cones are needed to detect this object under all conditions.

phasic cells. These cells receive similar inputs from both L and M cones and therefore cannot play a role in "red/green" color vision and probably no role in blue/yellow color vision. Fig. 23 is evidence that they receive no input from S cones. The threshold spectral function obtained on a strong yellow adapting field shows no evidence of an S cone input. The S cone on-cell has a threshold spectral function that shows it lowest threshold to blue light. The phasic cells have their lowest threshold resembling that of the photopic luminosity function.

The retinal latencies at of these two types of cells show a significant difference between the tonic and phasic cells indicating a faster transmission of the latter through the inner nuclear layer by the phasic system. In addition the larger size of the axons of the phasic system allows this system to transmit its signals to visual cortex much quicker than the tonic system. The role of the phasic "parasol" ganglion cell system in vision is not entirely clear. It seems to play a role in the detection of motion and to target different areas of visual cortex. Whether it plays any role in color vision is moot.

The Lateral Geniculate Nucleus (LGN)

The LGN reorganizes the parallel ganglion cell systems serving local retinal areas into separate layers from where their axons project to specific layers in striate cortex (12, 15, 27). Signals from nasal retina of the contralateral

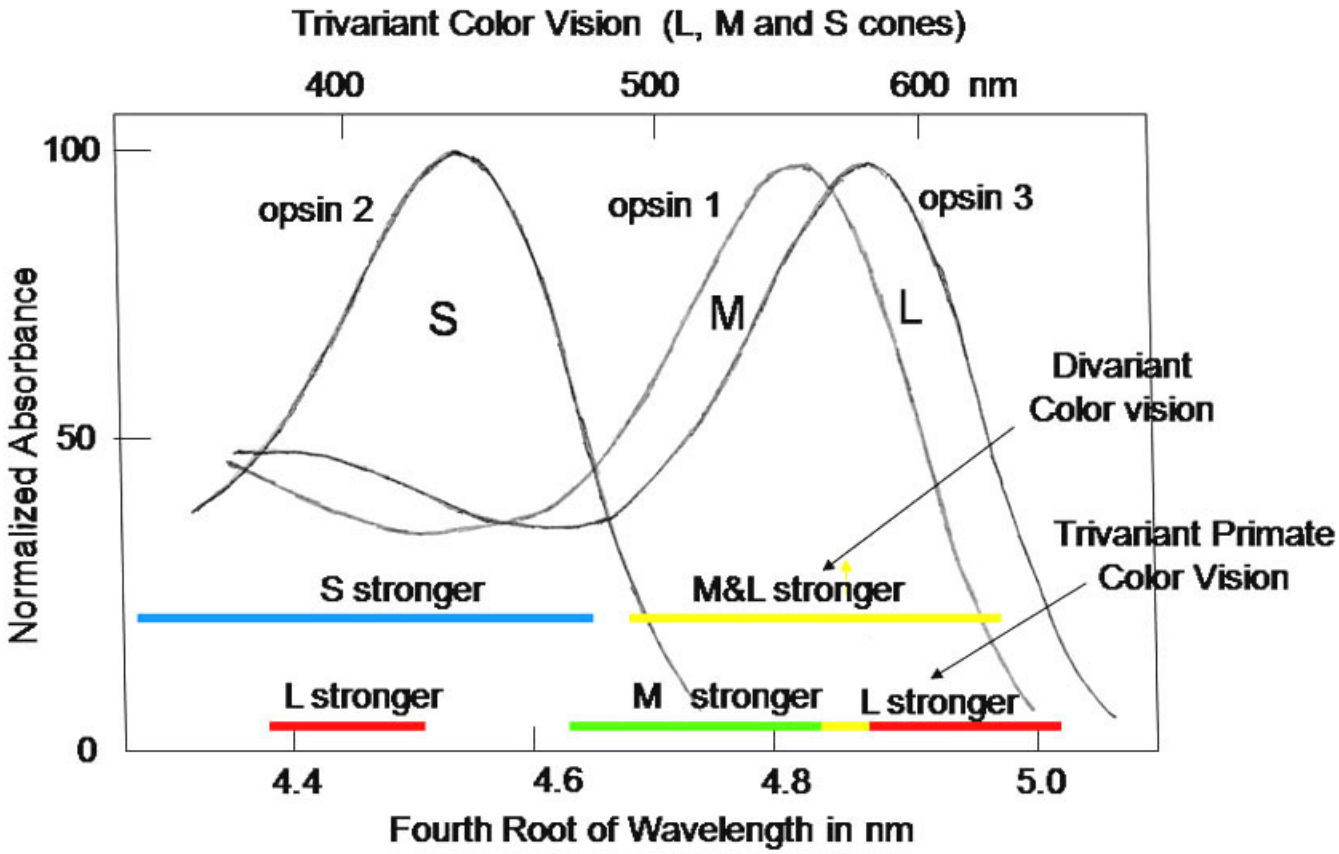

Figure 14. The normalized absorption spectra of the three cone mechanisms that mediate primate trivariant color vision. The original L cone system of divariant color vision split into two slightly different long wavelength sensitive cones straddling the yellow region of the visible spectrum.

eye are separated into different layers from those coming from the temporal area of the ipsilateral eye. This is needed for stereopsis where changes in eye position require comparing signals from different corresponding retinal regions and accordingly different ganglion cells. Binocular interactions begin for the first time in visual cortex. The parallel channels coming from the same retina are also separated into different layers. The phasic achromatic ganglion cell system goes to the magno-cellular layers, one layer for each eye. The midget and midget-like retinal ganglion cells transmitting signals for high resolution achromatic vision and "red-green" color vision are placed in four parvo-cellular layers, two for each eye. The S-cone mediating retinal ganglion cells which are involved in "blue-yellow" color vision go to the konio-cellular layers. These parallel systems of ganglion cells project to specific layers of striate cortex where form, color, movement, direction and stereopsis are processed.

An interesting but unknown role must be played by the numerous centrifugal axons that arise from striate cortical layers and impinge upon the cells in the LGN. Whether this shapes or influences chromatic and achromatic contrasts that are involved in form vision is unknown.

Striate Cortex

The LGN transmits its signals to striate cortex, the first visual area (V1) to process visual signals in cerebral cortex. There is a retinotopic order to the projection of these producing a map of the visual field. The map is distorted because the fovea occupies a relatively large area compared to the more peripheral retina. There are columns of cells extending from the upper to the lower layers, one column receiving signals from one eye and a

Figure 15. Trivariant color vision distinguishes red from green, expanding the repertoire of colors.

neighboring column receiving signals from the other eye (Fig. 24). Within each of these "ocularity" columns there are micro-columns of cells favoring a particular orientation of an extended light stimulus. Together these sets of columns have been called a "hyper-column". Within each hyper-column there is a local area that receives inputs from chromatic selective cells, i.e. the S cone on and off cells and the L and M cone midget and midget-like cells; these areas have been called "blobs", and are thought to be where color is processed.

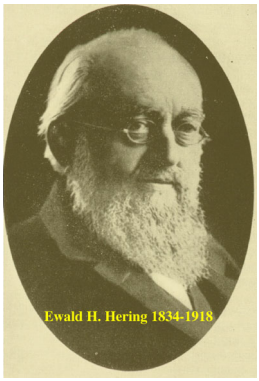

Figure 16. Four varieties of ganglion cells considered to mediate trivariant color vision in primates. The L cone on/ S cone off cells reported to be in the koniocellular layers of the lateral geniculate nucleus are not included here.

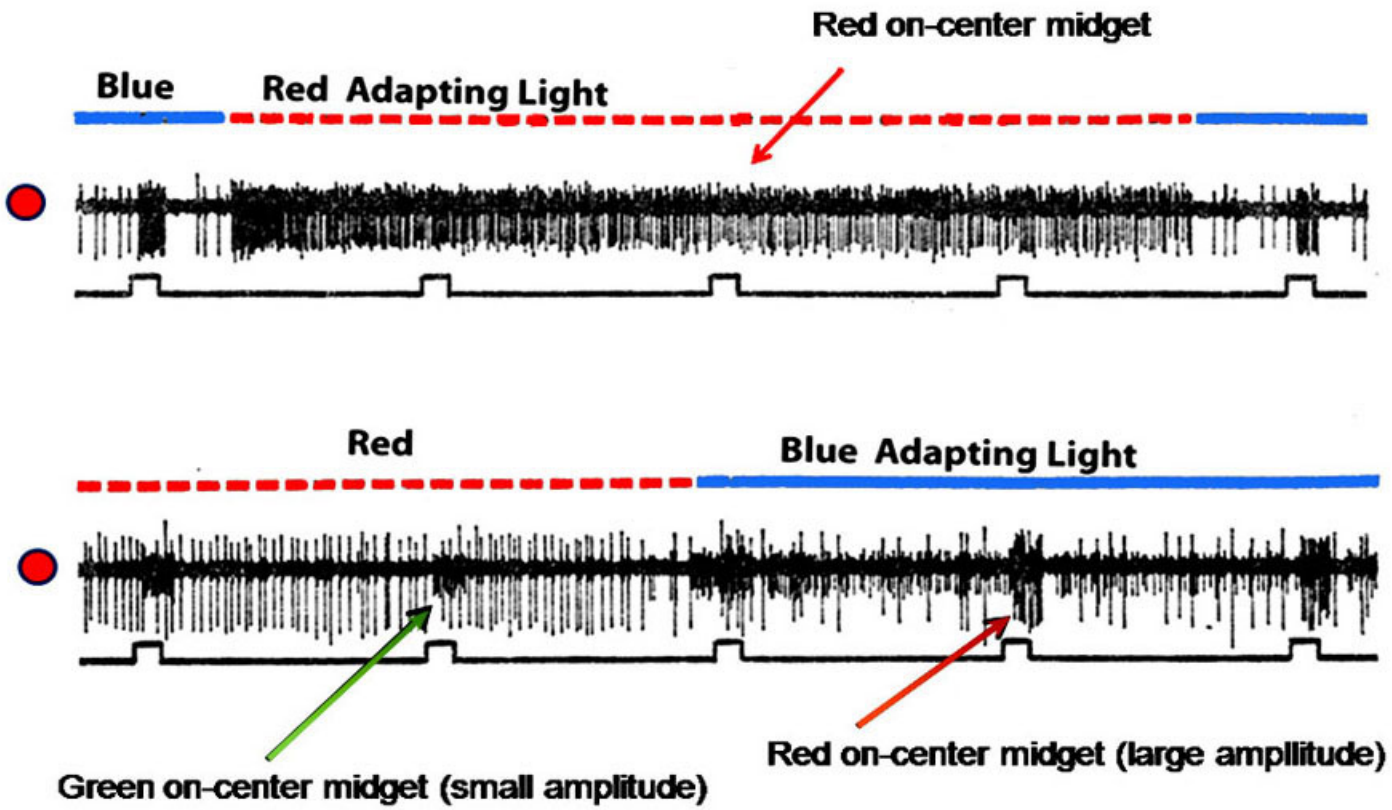

Figure 17. Midget-like ganglion cell responses. Figure 17(upper) shows an L cone on midget-like ganglion cell being stimulated by a red and blue adapting light while the center of its receptive field is being stimulated with a small red spot. The blue light suppresses the discharge but the cell responds to the red spot. The red adapting light excites the cell tonically but the cell no longer responds to the red spot. Figure 17 (lower) shows the responses of two midget-like ganglion cells. The one of small amplitude responds to the red spot on the red background and is excited tonically by the blue background. The one of large amplitude is excited tonically by the red background light and is inhibited by the red spot. It is suppressed by the blue adapting light but is then excited by the red spot. The latter is a L cone on cell with an antagonistic M cone surround; the former cell is the converse.

There are six distinct layers extending from an upper layer 1 down to a lowermost layer, 6. The projections from the functionally different layers of the LGN target different layers to synapse on cortical cells (Fig. 24).

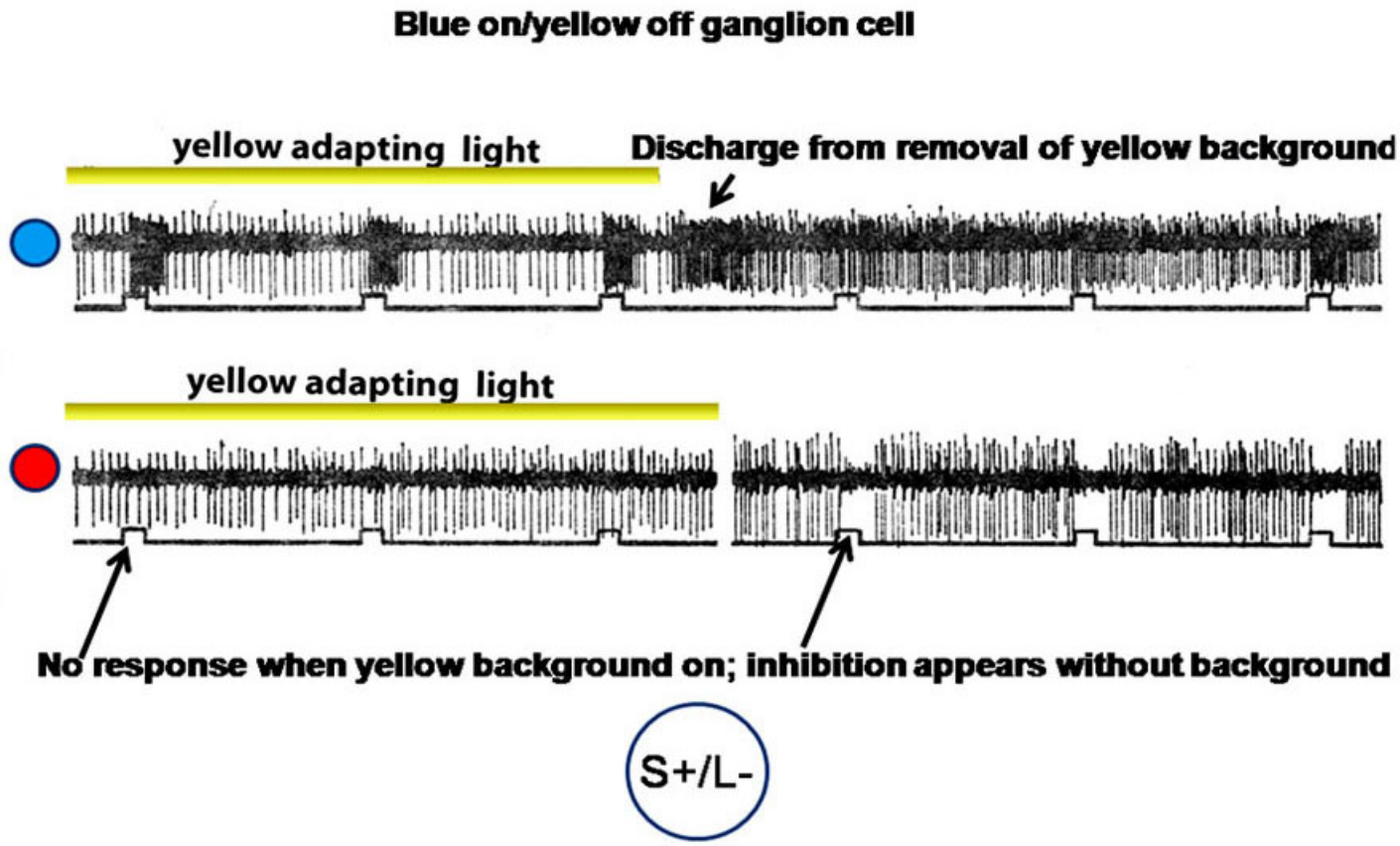

Figure 18. An S cone on/L+M off cell responding to a blue spot (above) and a red spot (below) in the presence and absence of a yellow adapting light.

The L and M midget and midget-like cells, projecting from the parvo-cellular layers, synapse in layer 4Cbeta from which their post-synaptic target cells appear to send axons to layer 3 within "blobs". The S cone system, projecting from the konio-cellular layers, appears to send axons directly to layer 3 within blobs. The fact that the parvo-cellular input, incorporating the L and M cone midget and midget-like cells, makes an intermediary synapse may be due to the double duty role these cells play in handling both achromatic and chromatic vision. The area surrounding blobs process achromatic contrast, undoubtedly receiving their input from the parvo-cellular layers. The magno-cellular layers of the LGN target cells in layer 4Calpha from which postsynaptic cells send axons to layer 4B. Therefore there is segregation of cell systems, some playing a role in chromatic contrast and others playing a role in achromatic contrast and movement. The existence of "double opponent" cells in blobs supports the idea that this zone within each hyper-column is devoted to detecting chromatic contrast for color vision. There are many unknowns in this structure that can only be solved by more single cell physiology combined with anatomical insights into the circuitry. What seems clear is that each unit area of visual space is processed in parallel by achromatic and chromatic mechanisms (28).

Pure Spectral Contrast

Double opponent cells tend to eliminate the influence of energy contrast establishing pure spectral contrast as an indicator of the borders of objects. With trivariant color vision this can be formed by comparing L with M cone responses and/or by S cone versus L&M cone responses. Fig. 25 illustrates the organization of a "red/green" double opponent cell. The system uses spectral contrast.

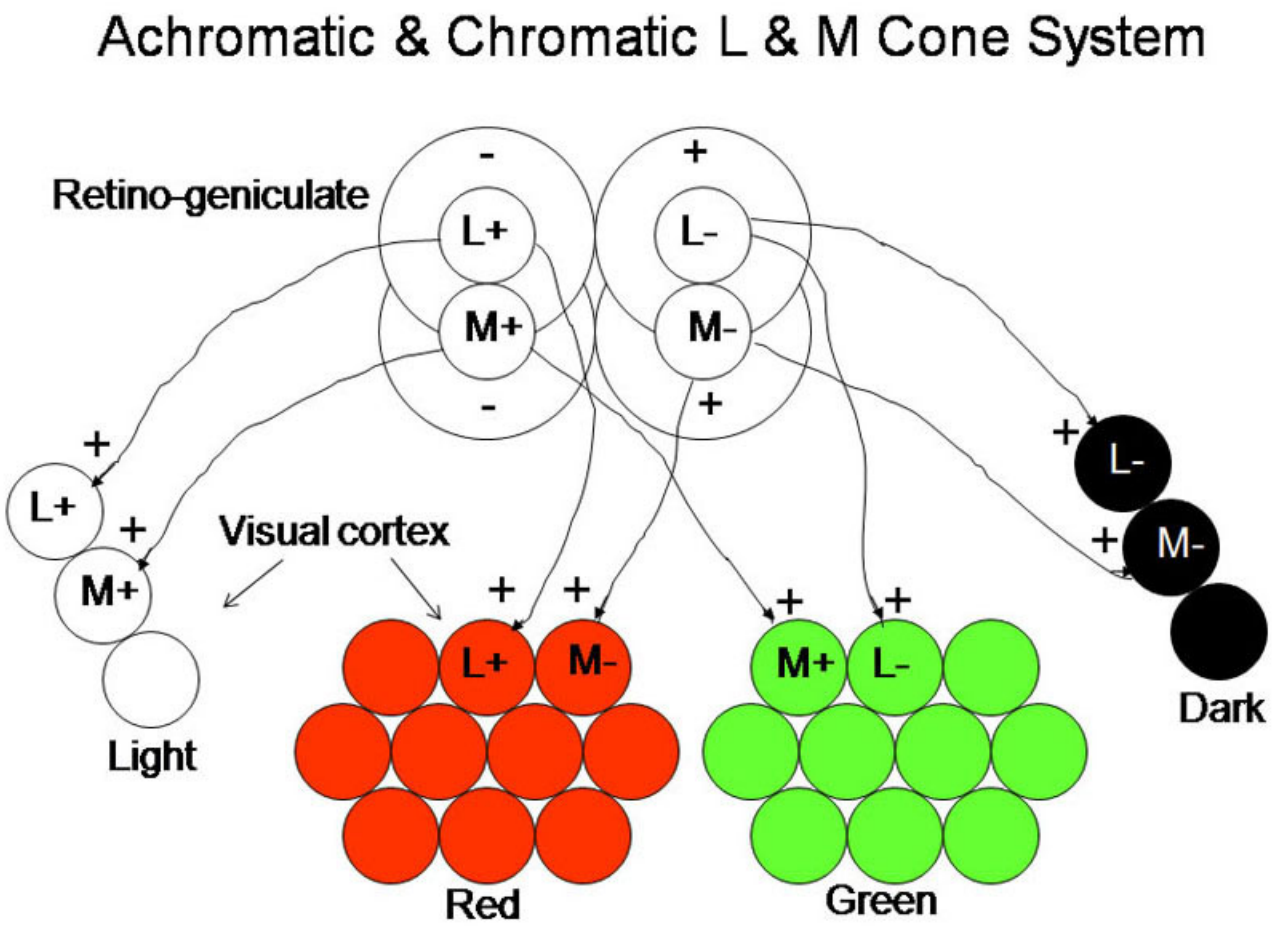

Figure 19. L and M cone midget-like cells can be used to extract achromatic high spatial resolving vision and chromatic "red/green" chromatic vision of lower spatial resolution.

Fig. 25 shows how concentrically organized double opponent cells can be constructed by having identical (red) neighboring cells inhibit a central cell (red) and have opposite neighboring cells (green) excite the central cell (red) making it most sensitive to a red central object in a green background and unresponsive to the converse. Such a cell responds to spectral rather than energy contrast as an indicator of a border. This behavior is illustrated by a cell detected in visual cortex that responds exclusively to spectral and not to energy contrast (Fig. 26). The stimuli with maximum energy contrasts such as a red or green bar on a black background or a black bar on a green or red background produce no response from the cell. But a green bar on a red background where energy contrast is minimal generates a large response. The brain has now separated the two major forms of contrast, spectral versus energy contrast to use them as independent variables to create color.

Simple, Complex and Hypercomplex Double Opponent Cells

One of the remarkable discoveries in visual cortex has been that of a unique body of cells that exhibit definable patterns of responses all based on orientation selectivity. One group called "simple" cells show orientation selectivity which can be predicted by the organization of responses produced within their receptive field. Another group called "complex" cells also show orientation selectivity but are less obviously related to the distribution of responses within their receptive field. A third group of "hypercomplex" cells are orientation-selective but are "end-stopped" being inhibited if the oriented stimulus is too long. These three types of cells are thought to contribute to form vision based on energy contrast. Charles Michael (18) has shown that a similar

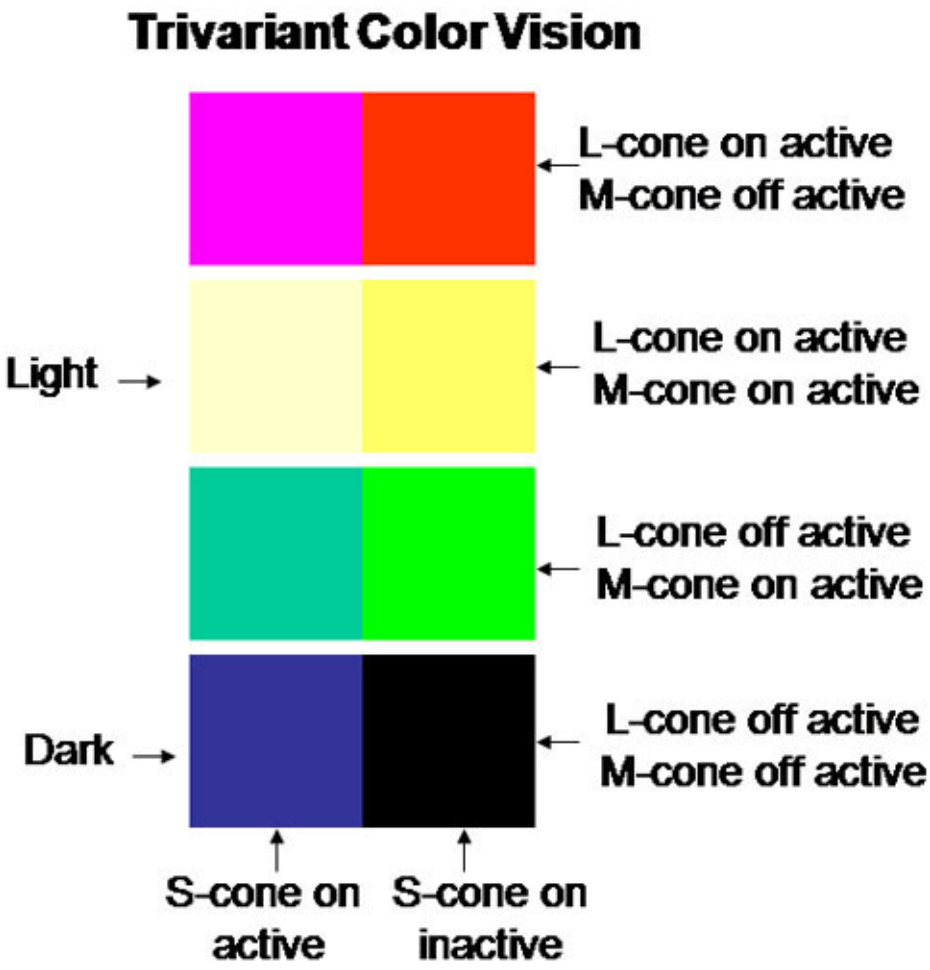

Figure 20. The major colors produced by trivariant color vision in primates. The figure indicates the synaptic pattern in which the three cone inputs of on and off cells make to produce particular colors.

group of double opponent cells exist in striate cortex of monkeys. Fig. 27 shows such a simple cell responding best to strong spectral contrast.

Fig. 27 shows that this cell is excited when an oriented red bar moving upward crosses the red selective area of its receptive field and inhibited when it crosses the green selective area; it produces an off-response when it leaves this green selective area. A green bar produces excitation when it crosses the green selective area only. A green-red and a red-green bar produce strong responses but the responses occur at different points in the receptive field and are therefore totally out of phase with each other. This cell responds poorly to white bars being spectrally selective. Fig. 28 shows a complex cell that responds to spectral and not energy contrasts. It is both orientation and directionally selective and refuses to respond to energy but responds strongly to spectral "red/green" contrast.

Hypercomplex double opponent cells (Fig. 29) are also detectable in striate cortex completing the variety based on energy contrasts. Therefore the same repertoire of orientation selective cells responsive to energy contrasts in striate cortex can also be found for spectral contrast. It is thought that both groups of cells play a role in form vision. Parallel systems of cells are detecting the forms of objects, one based on energy and the others based on spectral contrast. Because energy contrasts allow a higher spatial resolution, more of visual cortex is dedicated to achromatic than chromatic contrast detection.

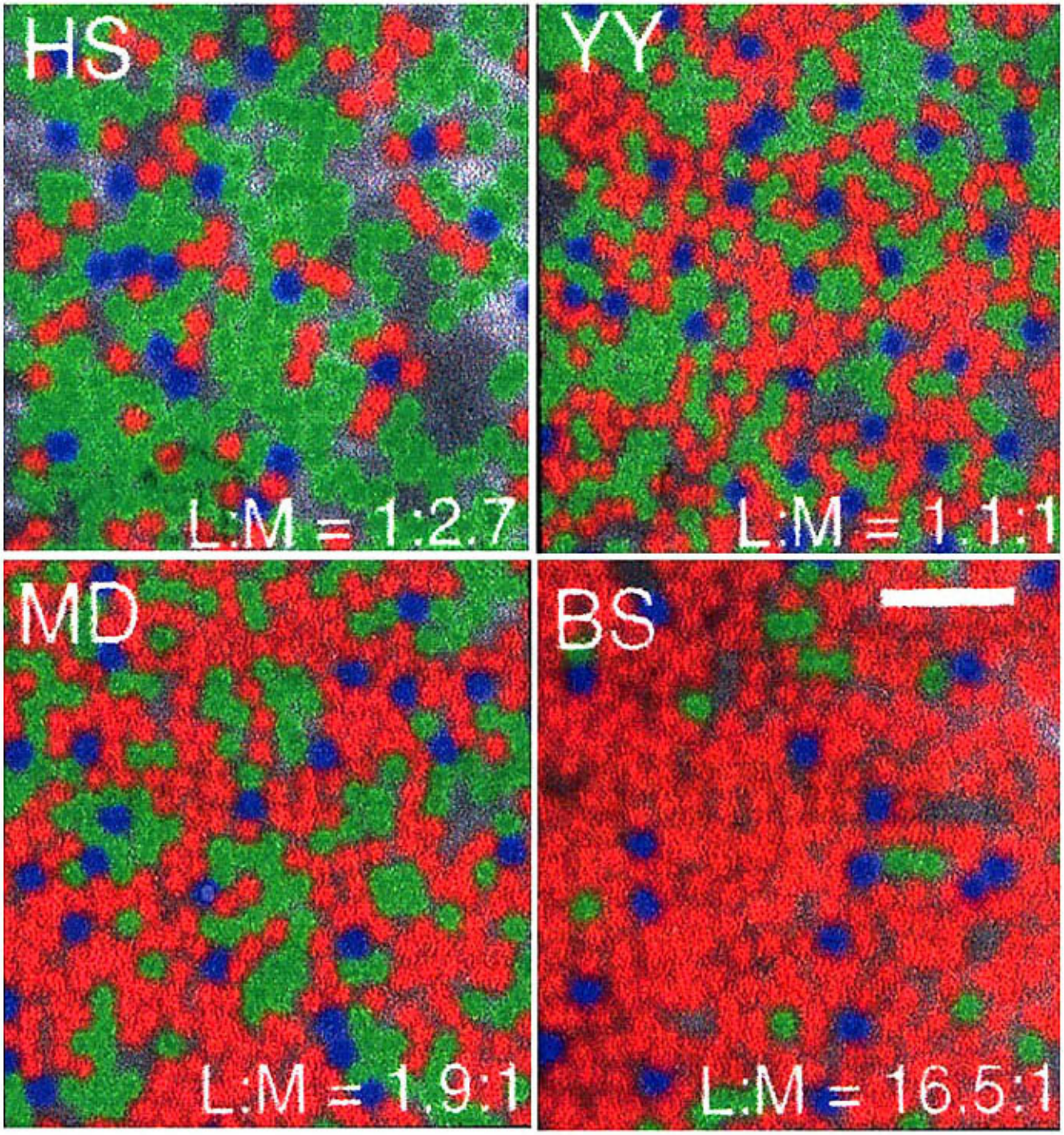

Figure 21. An adaptive optics view of the mosaic of L (red), M (green) and S (blue) cones in four human subjects with normal color vision. The ratio of S to L and M cones is constant but thaf of L to M cones varies from 1:2.7 (M:L) to 16.5:1 (L:M). (Adapted from Williams).

Fig. 30 shows how these two parallel contrast detecting systems could work in detecting a red object. Both simple cells of different orientation selectivity can detect the border of this cross, one set based on energy contrast and with a higher spatial resolution and the other set based on spectral contrast and with a lower spatial resolution. Sharp corners in the object would be detected by end-stopped hypercomplex cells. This creates two different views of the object which may be fused into one colored object just as two similar stereoscopic views are fused into an object in depth. Together they create shapes in full color (Fig. 30).

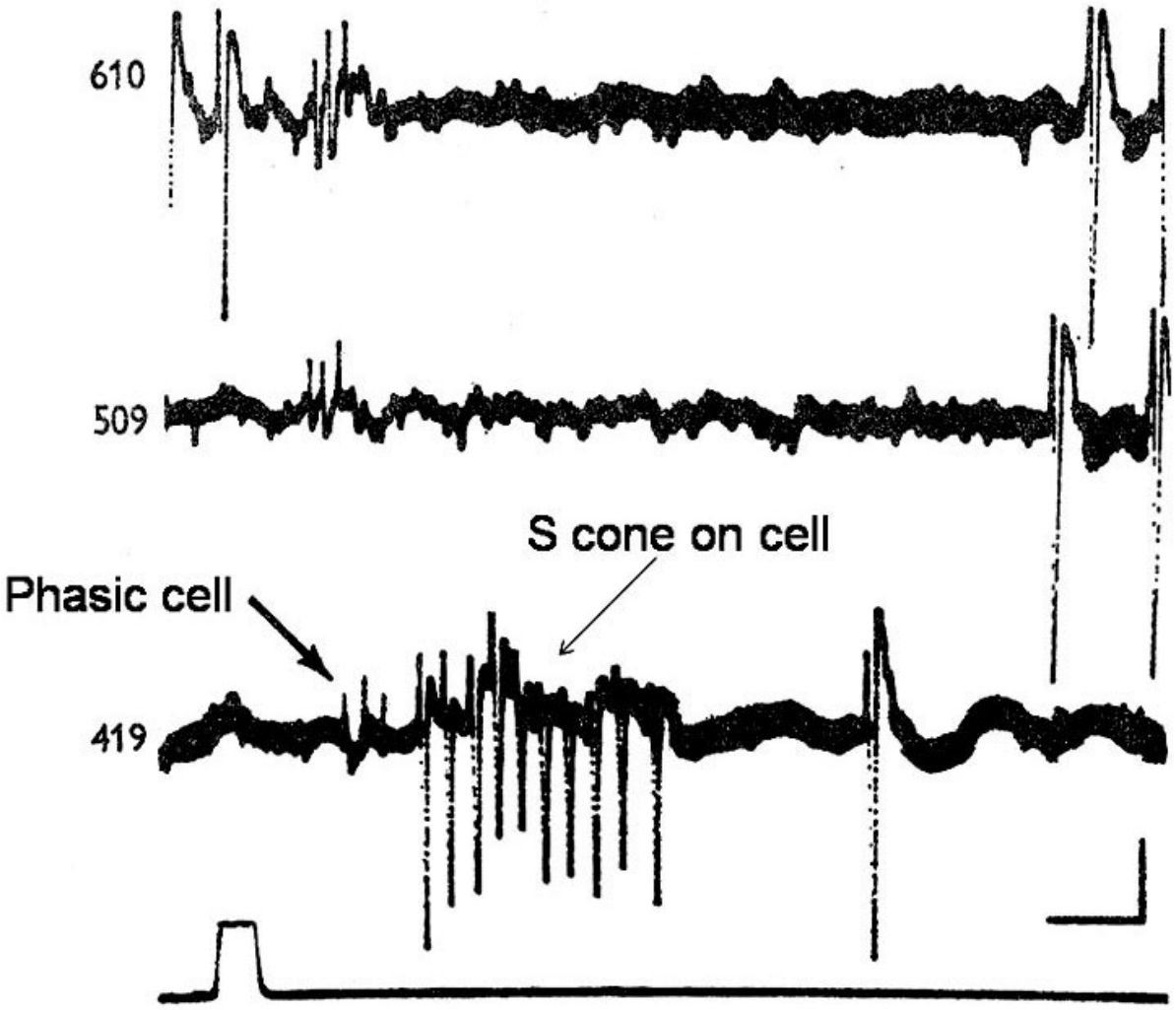

Figure 22. A magno-cellular on cell (small amplitude) and an S cone on cell (large amplitude) responding to three different parts of the spectrum (419, 509 and 610 nm). The calibration, lower right , indicates 200 microvolts vertically and 20 msec horizontally. The lower trace shows the duration of the light stimulus. Positivity is upwards.

A similar system for using spectral contrast created by double opponent S cone versus L cones or L+M cones must create another spectral view of objects by border contrasts (Fig. 31 and Fig. 32). In Fig. 31 groups of double opponent simple cells detect a circular blue form on a yellow background. In Fig. 32, similar simple cells detect a border of contrast between yellow and white, allowing the detection of an object of minimum energy contrast.

This highlights an important role of the S cone mechanism in vision to detect border contrasts of white versus yellow which are difficult for the achromatic system which is mediated only by L and M cones. This scheme implies that for color vision three different views of the same object are formed and then fused to provide colors that represent mixtures of the red/green and the blue/yellow spectral contrasts systems. If there is no activity in the spectral contrast detectors then only the energy (achromatic) system is active and the object is pure white, gray or black. There are some different views on these ideas. Single opponent cells are thought to detect surface color while double opponent cells detect borders (29). Others have suggested that neurons involved in the analysis of color should retain their chromatic properties in the face of changes in other components of stimulation, orientation, size and contrast and this may not be the case for color selective neurons found in striate cortex (30).

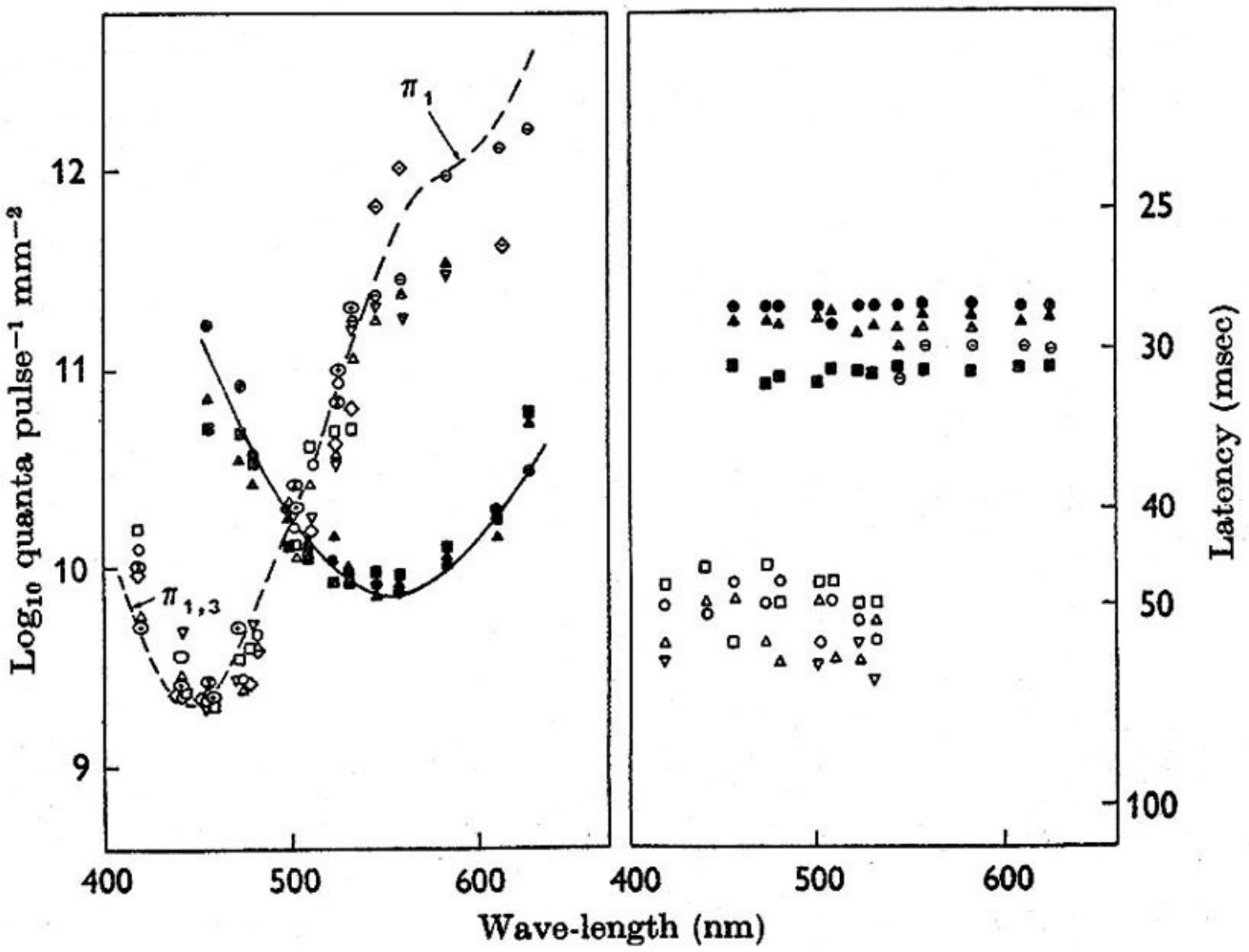

Figure 23. The threshold (left) in log relative quanta of 3 on-center phasic cells (filled symbols) and 7 S cone on/L cone off cells (open symbols) and their latencies at threshold (right) on a reciprocal scale of milliseconds. The dashed line indicates the Stiles' [1] 1 and 4 mechanisms. The continuous line is the CIE (Commission Internationale de l' Eclairage) luminosity function.

The Stabilized Retinal Image

If an image is made stationary on the retina it will disappear in seconds. Fig. 33 illustrates what is perceived by a subject presented with a stabilize image of a red/green boundary based on the research of the Russian physiologist Yarbus (31) and others (32). Initially the subject sees the red/green scene but in several seconds it fades into a featureless field. If a pale blue light is added to both sides only a blue field is seen without the red/green scene. This also fades within seconds. If the pale blue field is removed the subject sees a faint red/green scene but this fades again. This indicates that we only see in transients determined by change in the retinal image.

If the retinal image does not change in space and/or time, it will disappear. Constant small micro-movements of the eye continue to produce transient changes at the borders of objects that are able to maintain an undiminished view of the external world. This supports the idea that objects are seen because of their borders, as depicted by the orientation selective border contrast cells illustrated previously, which must be continuously moved across the retina to maintain their visibility. Fig. 34 illustrates how the responses of on and off cells contribute to maintaining strong responses to movements of borders of contrast. When a long wavelength (red) surface enters the receptive fields of on and off cells, the on-cell (L off) responds more strongly than the off-cell if

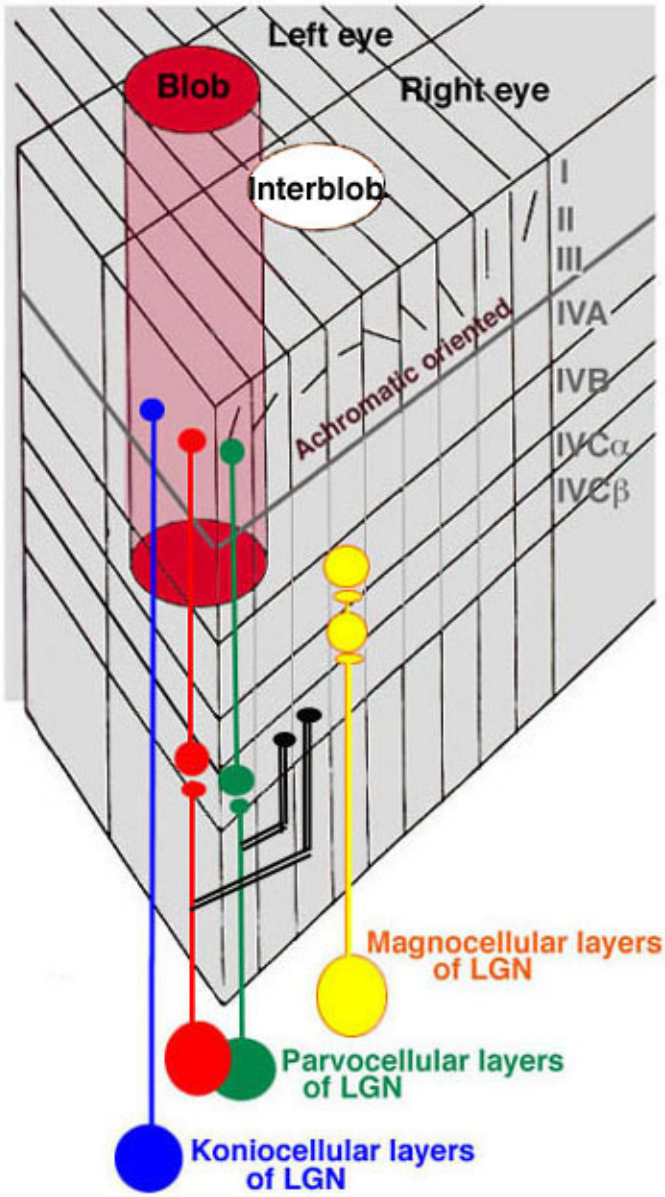

Figure 24. S cone on and off cells of the koniocellular layers and the four varieties of L and M midget-like cells of the parvo-cellular layers of the LGN target different layers of striate cortex. The midget system must project to both the achromatic areas as well as the "blobs" involved in chromatic vision. The parasol cells from the magno-cellular layers of the LGN target a different layer than the previous cells.

there is an increment in energy contrast. But the off-cell (M off) will respond more strongly if there is a decrement in energy contrast. These two systems are showing their ability to respond to increments and decrements of energy contrast but also manage to favor long over other shorter wavelengths, which is a key for their role in color vision. M on and L off -cells would respond weakly to such a moving border.

Color Vision Beyond Striate Cortex

An intriguing but poorly understood aspect of visual cortex is the remapping of visual space into multiple adjacent visual areas where a retinotopic order is maintained. Fig. 33 shows how V1 projects to V2, a second visual area juxtaposed to V1 where there continues to be a segregation of functionally different cells. The "blob" areas of V1 appear to project to "slabs" of cells in V2, which project to "globs" of cells in V4 (Fig. 35).

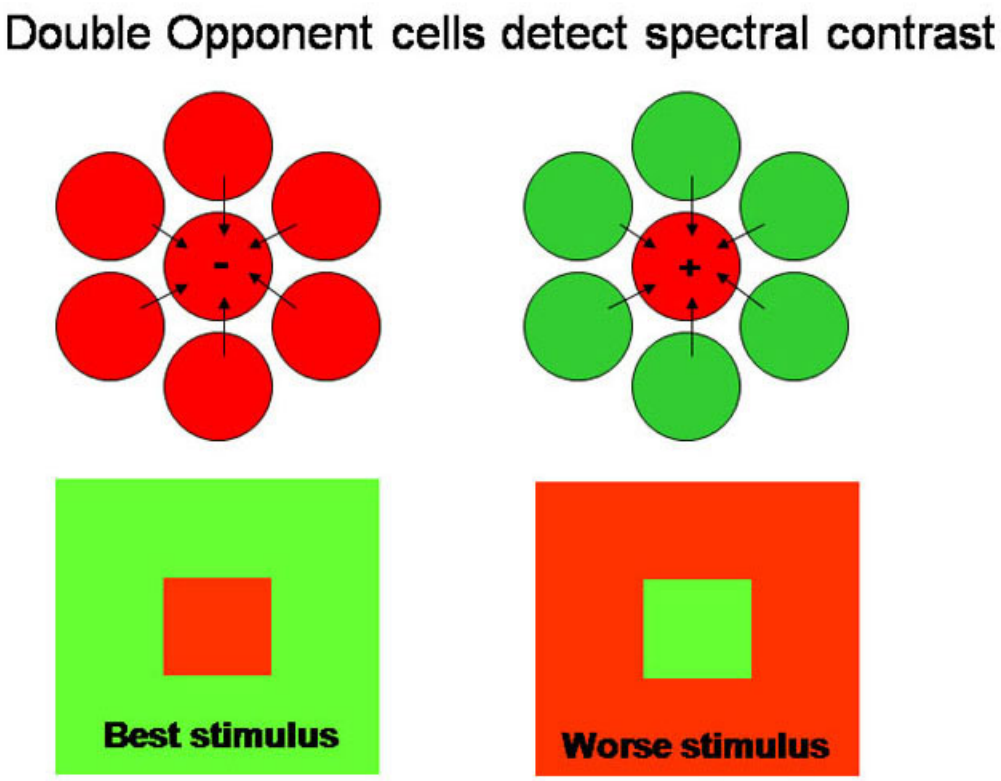

Figure 25. Concentrically organized double opponent cells can be constructed by having identical (red) neighboring cells inhibit a central cell (red) and have opposite neighboring cells (green) excite the central (red) making it more sensitive to a red central object in a green background and unresponsive to the converse.

Within these three interconnected areas spectral contrast is processed, presumably to determine its contribution to color, i.e., hue. Adjacent areas processing energy (achromatic) contrasts contribute to determining the saturation and brightness in colors. The achromatic areas are larger because of the higher spatial resolution of energy contrasts. The receptive field sizes of cells in these higher visual areas tend to be larger than they are in V1 suggesting that, several blobs in V1 project to a single slab in V2 and several slabs in V2 project to a single glob in V4 (33-35). The functional roles of these higher areas could be to recognize objects better as they come closer to the observer when they cast a larger retinal image. It is known that the perception of color increases with the size of an object over sizes as large as 20 degrees of visual angle. Under ideal conditions i.e. a well lit surface, we can perceive at least a million different colors. Fig. 36 shows how more basic hues determined by single cells in blobs could be used to build higher order colors that combine the inputs of the more basic hue determining cells. As one develops more experience with colors even higher order cells could be formed allowing the distinguishing of many different shades of color.

There is a question as to whether a single cell is committed to detecting a particular color or whether a group of cells are involved. This might depend on the practice one has in working with colors such as artists who may form single cells that are sensitive to a particular color and capable of contributing to even higher order colors while those who are less involved have fewer such cells and depend on less fastidious interactions.

There has been a controversy about whether color processing is exclusively segregated to V4 while achromatic processing occurs in another complete area of visual space. Evidence implying this type of organization involves rare individuals who have lost all color vision but can see objects with high spatial resolution in black and white.

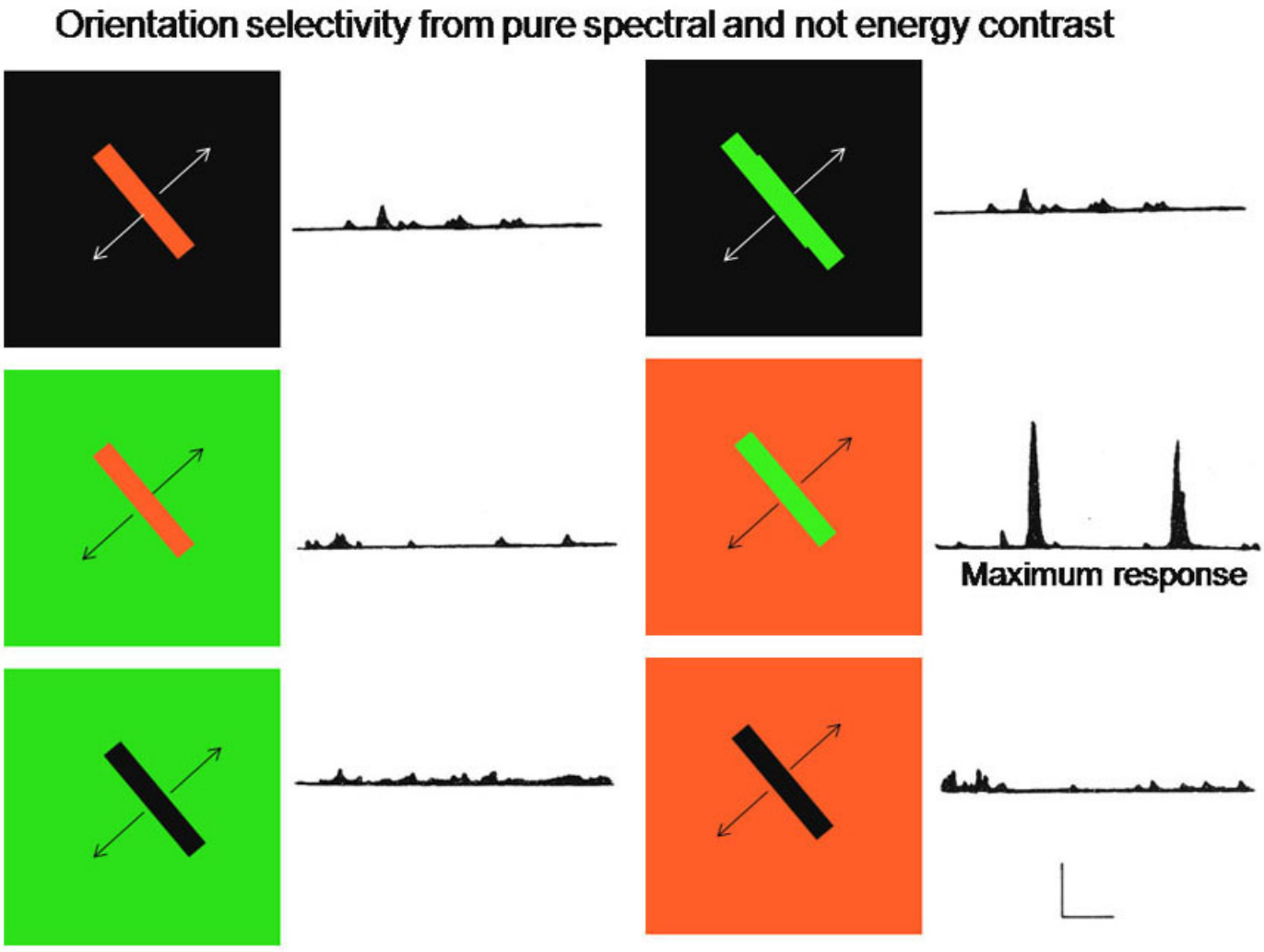

Figure 26. A cell selective for orientation based on pure spectral contrast. It fails to respond to strong energy contrast such as occurs with the movement of the colored bar on a dark background (above) and a dark bar on a color background (below).

This hypothesis was championed by Semir Zeki (36) but the existence of "globs" related to spectral contrast in V4 surrounded by larger areas of achromatic contrast detecting cells tends to weaken this idea. Because "globs" are relatively large it was perhaps possible for an investigator making a limited number of penetrations to conclude that all of V4 is devoted to chromatic vision. Nevertheless there must be an explanation of why in these very rare patients color can be lost without a loss in spatial resolution which depends entirely on achromatic contrast. The enigma may be explicable by damage to higher areas of the brain where interpretation and language are involved linking vision to external communication.

Redness at short wavelengths

It is well known that short wavelengths can produce a reddish sensation that makes blue appear violet. This affect appears to arise from the beta-band of L cone opsin which makes this opsin more sensitive to light than M cone opsin at this region of the spectrum (see Fig. 14). This effect is best observed in midget-like cone opponent retinal ganglion cells which are excited by long wavelengths and inhibited at wavelengths at the middle of the spectrum. In many of these cells excitation appears with short wavelength stimulation implying that the L cone response is overpowering the M cone antagonism. This is supported by the fact the L cone response is

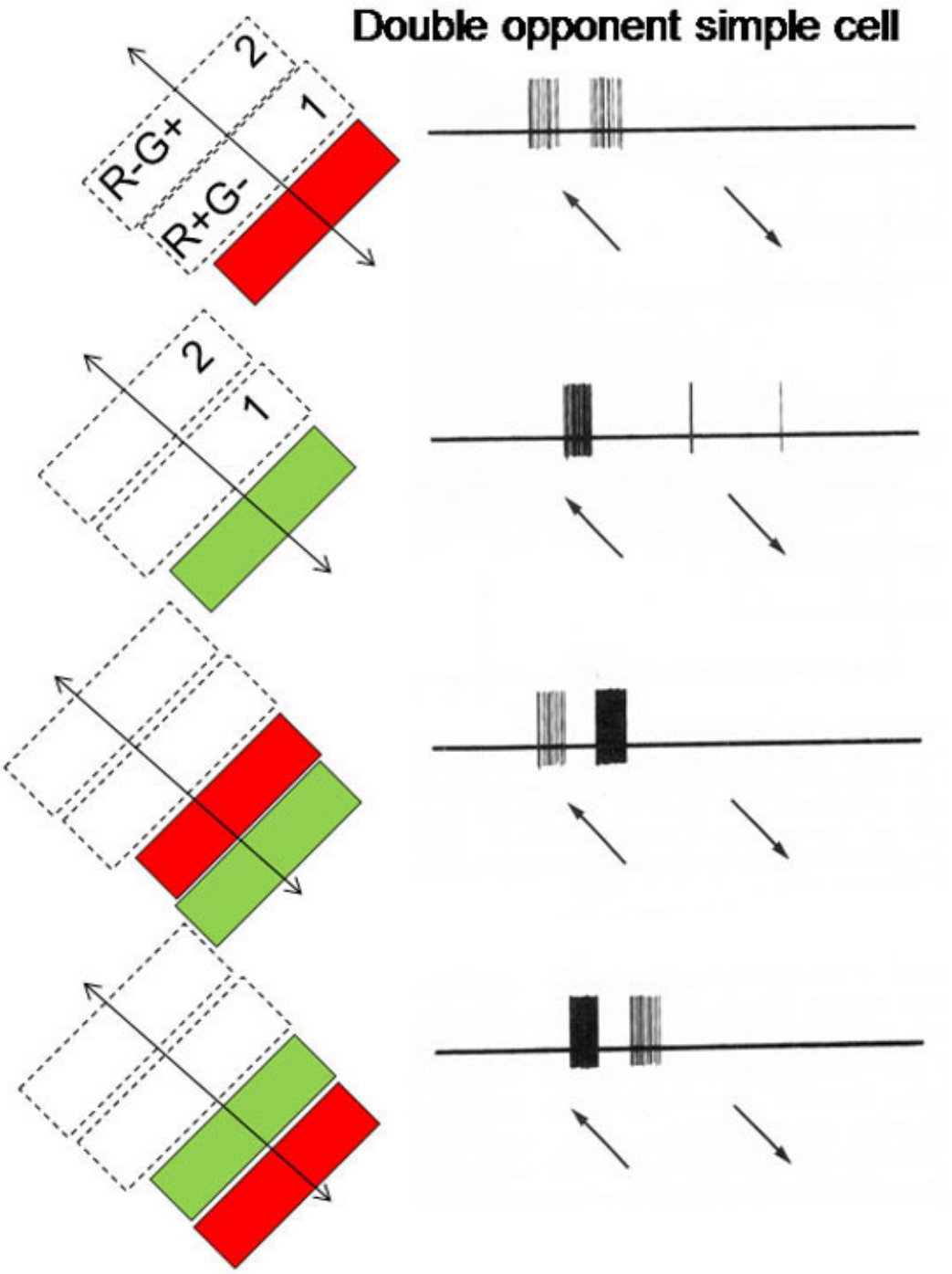

Figure 27. A simple cell responding best to strong spectral contrast.

strengthened by a blue adapting light, which selectively depresses the responses of M cones. Had this short wavelength excitatory input been due to S cones, it would have been weakened by the blue adapting light.

Hering's Theory of Color Vision

An insightful theory was proposed by Ewald Hering (37) in Prague in 1874 which was resisted by many leading scientists in the field, such as Herman von Helmholtz (38). Hering noted that the sensations of blue and yellow

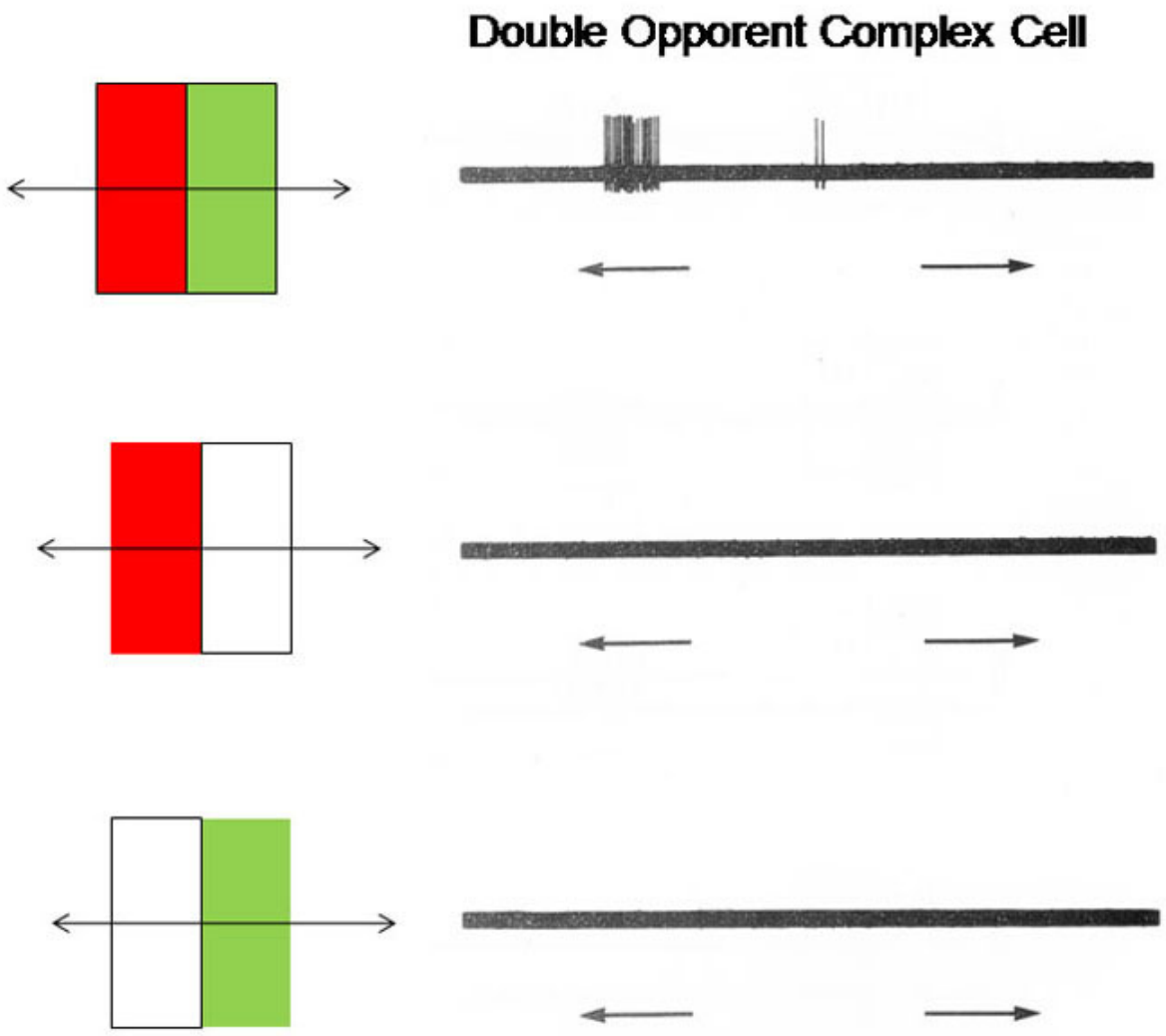

Figure 28. A complex cell responding to spectral contrast but not to energy contrasts.

opposed each other so that when seen simultaneously, the original colors were lost and a new sensation of a totally different color "white" was seen. Similarly the colors red and green exhibited a similar opposing relationship. When mixed they lose all traces of the original colors to create a new sensation "yellow". Hering suggested that there were two pairs of opponent processes underlying human color vision. This contrasted with the fact that there are only three variables underlying human color vision. This three dimensional system was suggested by Thomas Young in 1802 (39) and proven by James Clerk Maxwell in 1872 (2) and strongly promulgated by Helmholtz in 1852 (38). The Hering theory suggested that there are two pairs of basic colors that have a unique opponent relationship for each pair. He was correct in this analysis although his idea that the opponency between colors was occurring in the photoreceptors was incorrect.

At Hering's time the understanding of neuro-physiology was poor and the concepts of excitation and inhibition of neurons in unique and complex ways was unknown. The first suggestion that antagonism between colors could be due to excitation and inhibition between nerve cells, that I have found, was in a paper by the Swedish physiologist Gustaf F. Gothlin in 1944 (40). He had followed Sherington's work on the spinal cord where the idea of excitation and inhibition between nerve cells first evolved. Fig. 37 shows how prophetic Gothlin's ideas were. Here he creates an antagonistic balance between blue and yellow processes as a first stage and then hangs a scale

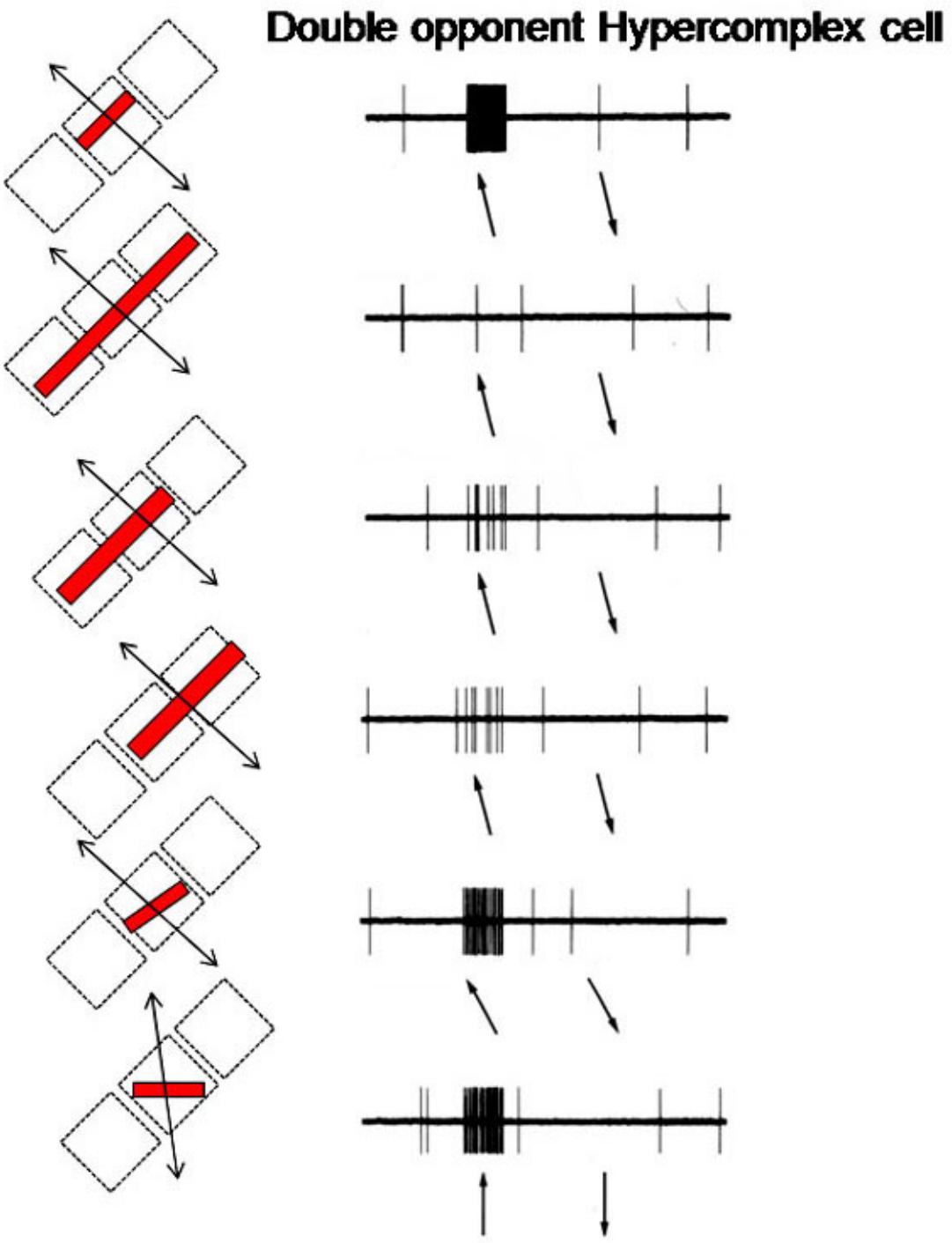

Figure 29. A double opponent orientation and directionally selective hypercomplex cell, characteristically failing to respond if the red bar is elongated.

on the yellow side of the blue/yellow balance to show an antagonistic relationship between red and green. He predicts that these antagonistic interactions were due to excitation and inhibition between neurons. It is interesting that the pioneer of exploring nerve cell responses to spectral stimuli in the retina, the Nobel Prize winner, Ragnar Granit, also a Swedish physiologist, made no reference of Gothlin's concept in any of his writings on retinal responses to color.

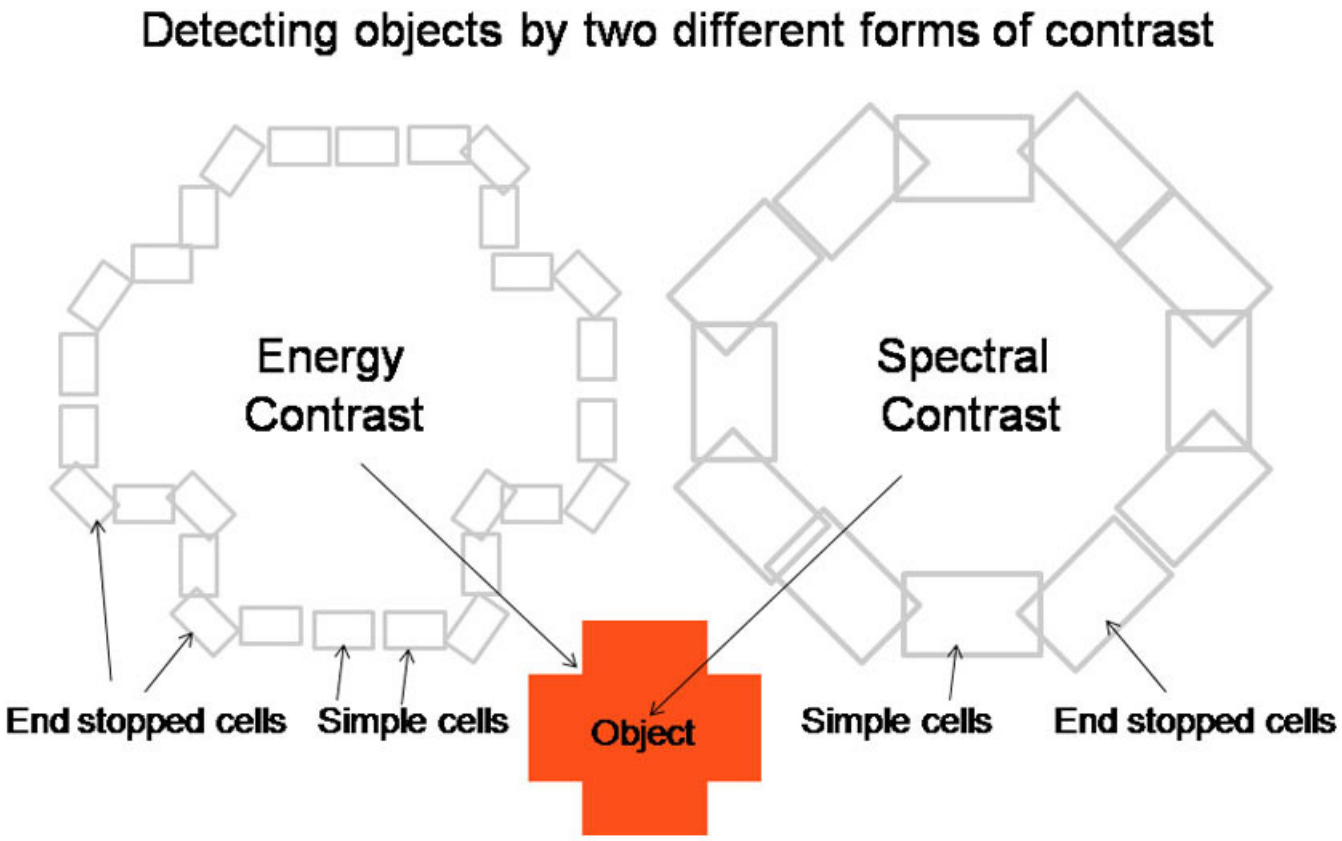

Figure 30. Two systems, one based on achromatic contrast with finer spatial resolution and a second based on spectral contrast, detect the borders of an object using simple cells and end-stopped cells with orientation selectivity (30).

Granit (41) proposed in 1947 a dominator/modular theory of color vision in which there were some retinal neurons which responded to only a narrow part of the visible spectrum, "modulators", and another group that responded to a broad band of the spectrum, "dominators". He thought the modulators were more involved in color vision but never mentioned the concept of excitation and inhibition between colors or cone mechanisms as Gothlin did. The first American studies of single visual neuron responses to monochromatic stimuli were obtained in the monkey's lateral geniculate nucleus by Russel DeValois and associates in 1958 (42). They emphasized the presence of narrow-band responding cells resembling the modulators of Granit but they also noted some cells that gave on responses to red and off responses to green light but again Hering's concept of opponent colors was not mentioned. The experiments that brought Hering's opponent color theory to the forefront were done in fish retina by another Swede, Gunter Svaetichin (1956) using glass instead of metal electrodes, enabling him to record intra-cellularly from horizontal cells. This allowed him to see both depolarizing and hyperpolarizing responses, the latter not obvious with extra-cellular recordings, where one sees only a silence or perhaps an off response from inhibition (hyperpolarizing) which could easily be overlooked. Svaetichin's results gave rise to a resurgence in Hering's opponent color theory (43, 44). This quickly led to the idea that there were three retinal channels representing Hering's color opponent channels, red opposing green, yellow opposing blue and white opposing black. This idea, however, was short lived. First of all it became apparent that the red/green opponent cells had concentrically organized receptive fields with the color opponent inputs coming from adjacent retinal regions. One would expect the color opponent signal should involve the same area of visual space and not neighboring areas. In addition the red-green opponent ganglion cells seemed to be the midget cell system which was the logical mediator of high spatial resolution. This created a dilemma in having a red/green color opponent channel carrying achromatic information for high spatial resolution. In

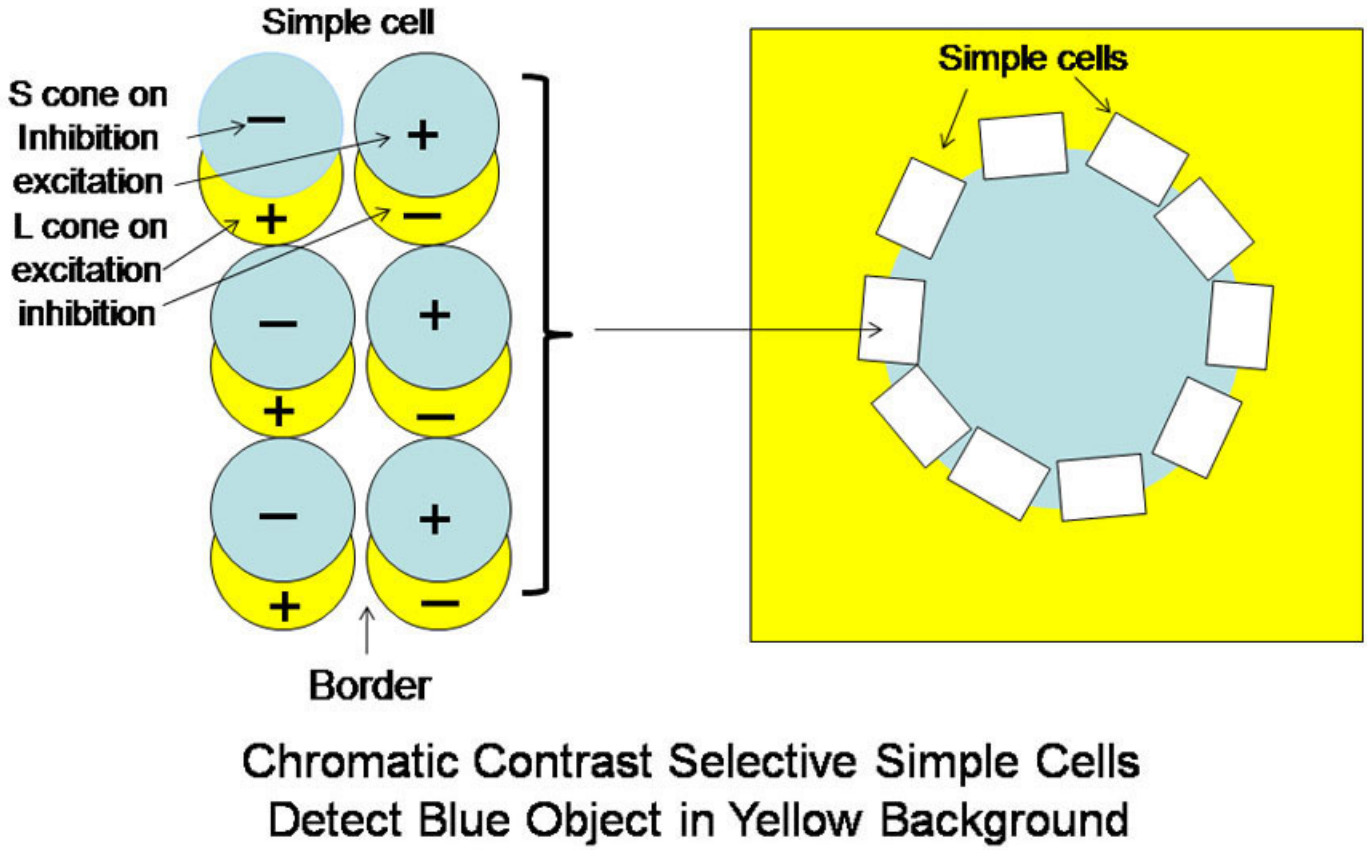

Figure 31. Double opponent simple cells with orientation selectivity detect a blue object in a yellow background. A population of such cells with slightly different orientation preferences detects a circular object.

addition the S cone channel was opposed by yellow light but not strongly enough to stop responses to white. The S cone on ganglion cells appeared to be transmitting a signal that said that the S cones were absorbing light but not that this light was "blue"; it could be white, grey as well. The so called white/black channel was receiving no input from S cones which is not what is expected for a channel signaling white. The contribution of activation of the S cone retinal ganglion cells is illustrate by the after images produced in Fig. 38.

Therefore the link between Hering's opponent color theory and retinal ganglion cell signals was scrapped. Because the neurons in the lateral geniculate nucleus responded similarly to what was found in the retina, attention went to striate cortex to explain opponent color theory by physiology. The initial ideas of channels signaling color at the retinal level were wrong; the opponent signals detectable in the retina were cone opponent and not color opponent. Color vision turned out to be more sophisticated, more arcane but more realistic.

The Future

Certainly the future will involve anatomical definition of how the projections from the lateral geniculate synapse in striate cortex and begin to define the neurocircuitry of this hexalaminar cortical structure. The dendritic input and axonal output of each functionally unique cell must be defined as has been done to a large degree in the retina. This strategy must be repeated in higher areas of visual cortex, perhaps the most intriguing phase of this crusade. New optical techniques that combine both anatomical identification and physiological responses of the same cells could expedite this enormous task. But this is the only way to understand how the most complex

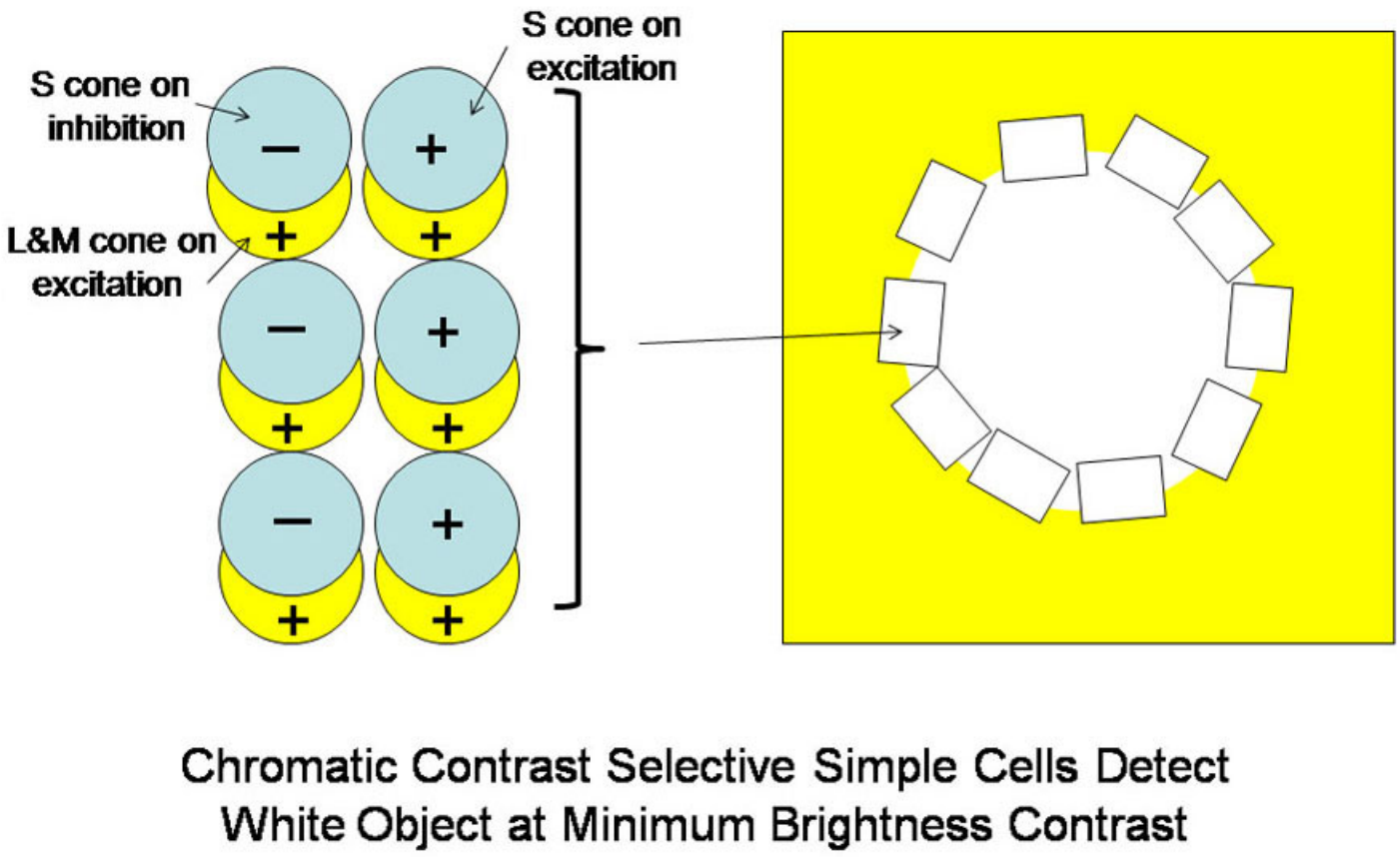

Figure 32. Spectral contrast based simple cells with orientation selectivity detect a white object in a yellow background. A population of cells with slightly different orientation preferences detects a circular object. Note the synergism of L & S cones at one edge of the simple cell.

machine in our universe, the cerebral cortex works. For this color vision is an ideal starting point because it has carried us further into this organ than any other neural process.

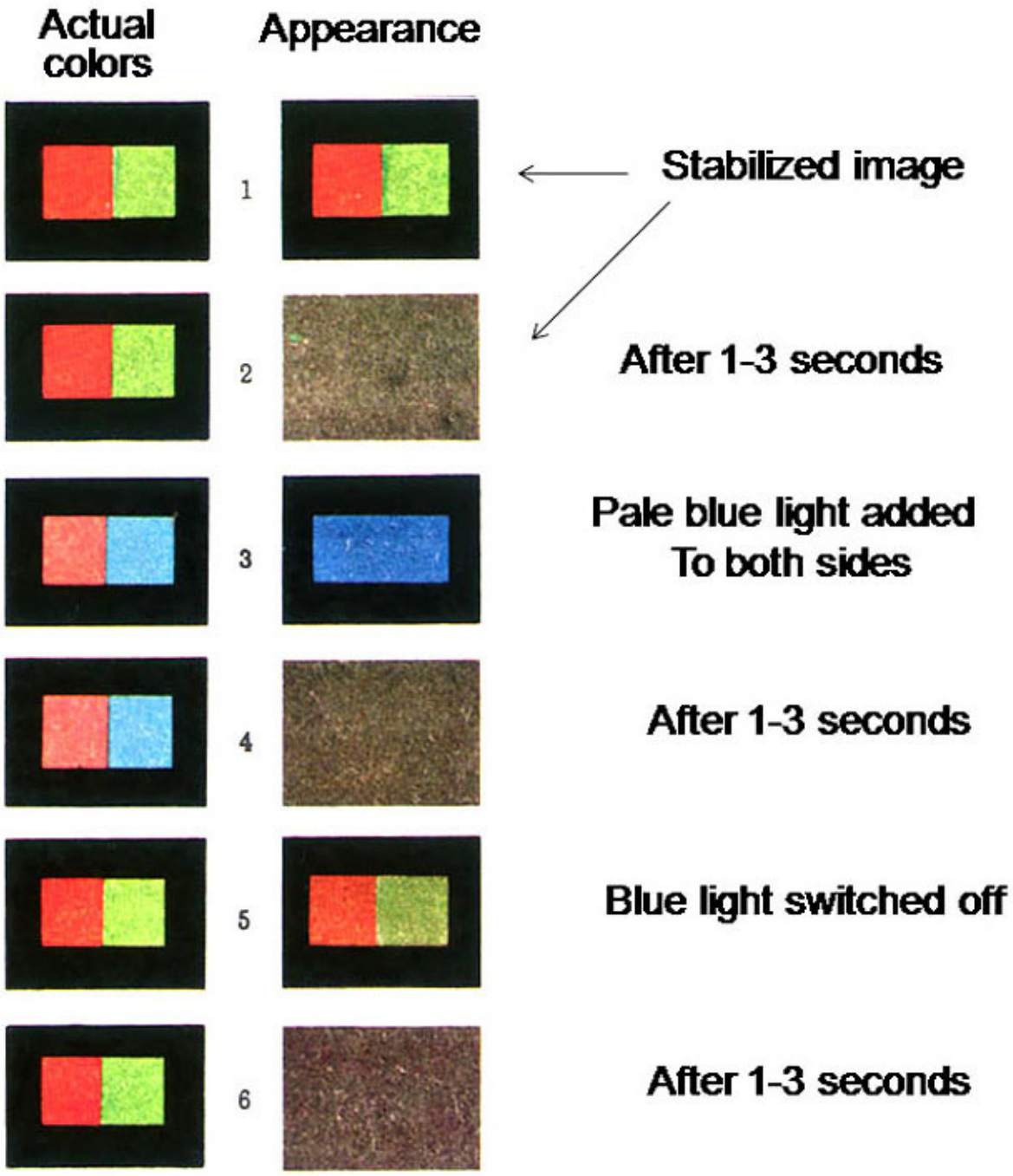

Figure 33. A stabilized retinal image of a red/green scene changes with time and its modification by additional stimulation (from Iarbus, 1967).

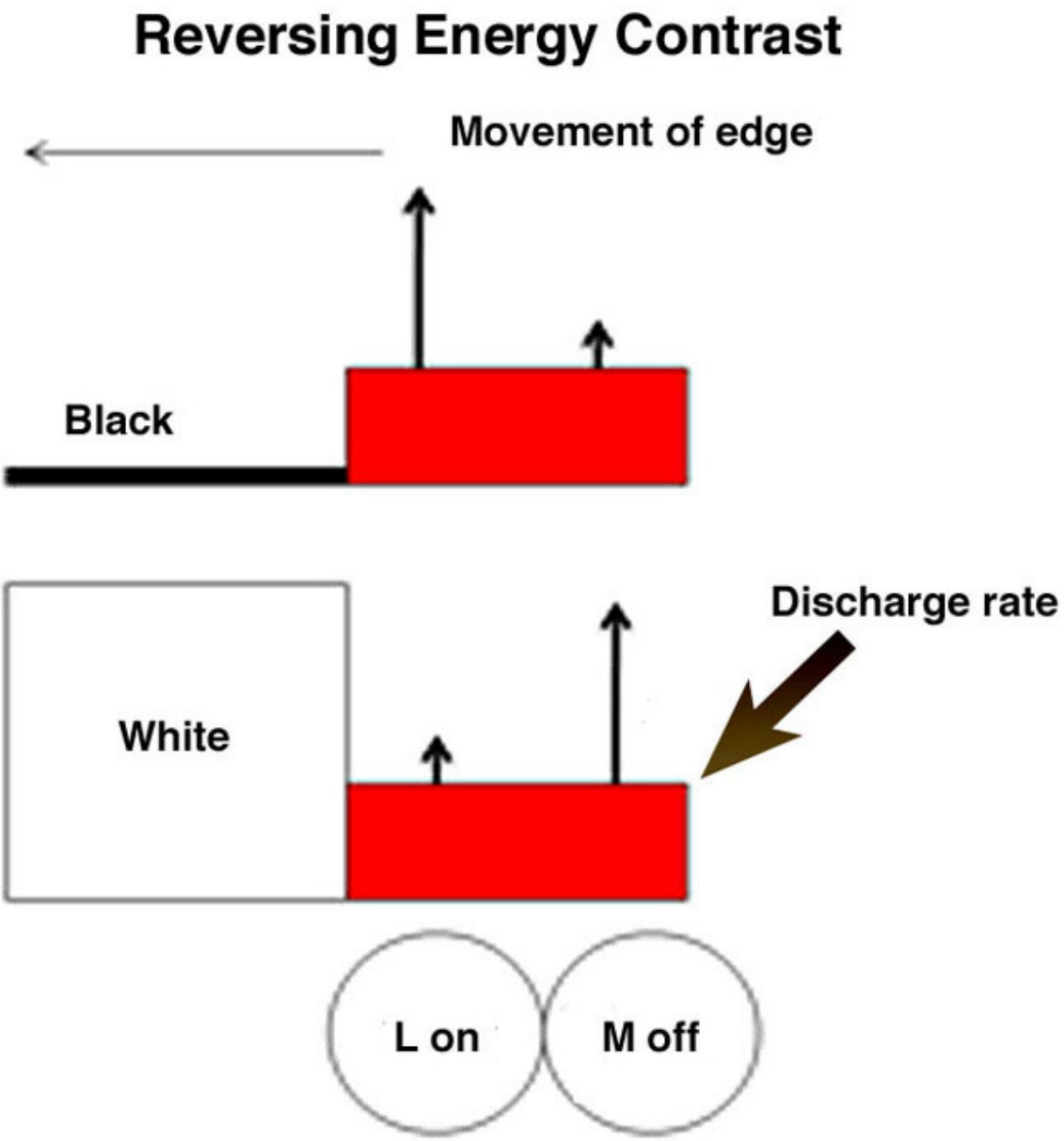

Figure 34. A moving border affects neighboring midget-like ganglion cells when there is a change in wavelength as well as a large change in energy contrast. When there is an increment in energy contrast the L on cell responds more strongly; when there is a decrement of energy contrast the M off cell responds more strongly. Both contribute to the sensation or red.

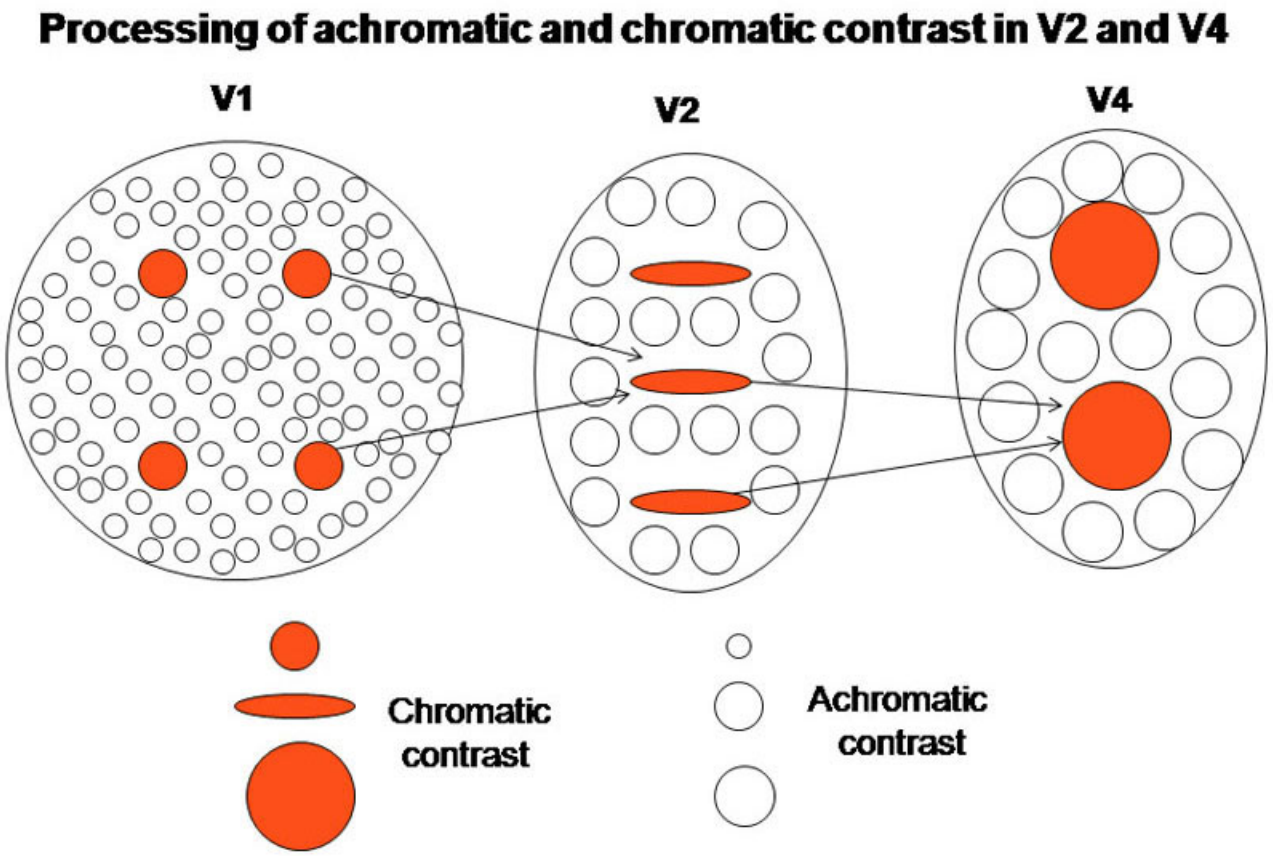

Figure 35. "Blobs" of V1 target slabs of cells in V2 which target "globs" of cells in V4 producing a hierarchy of chromatic processing embedded in areas involved in achromatic vision (33-35).

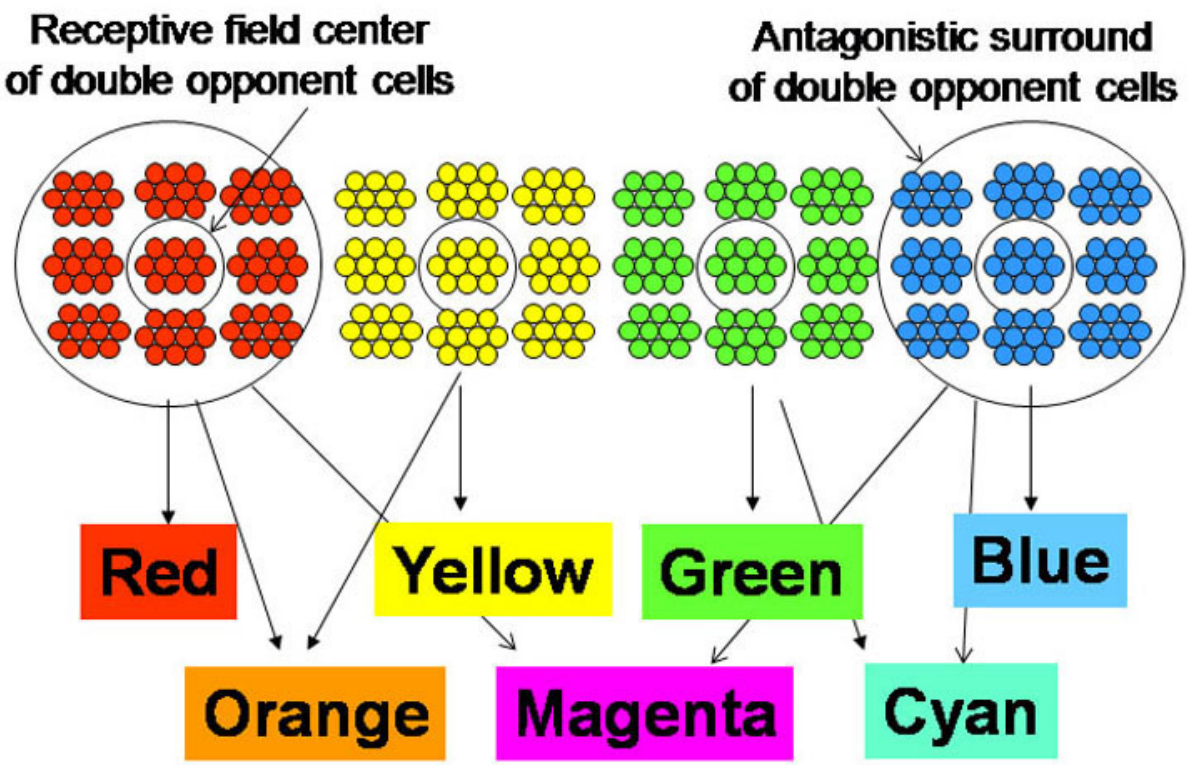

Figure 36. More basic hue responsive cells could be used to create higher order hue responsive cells.

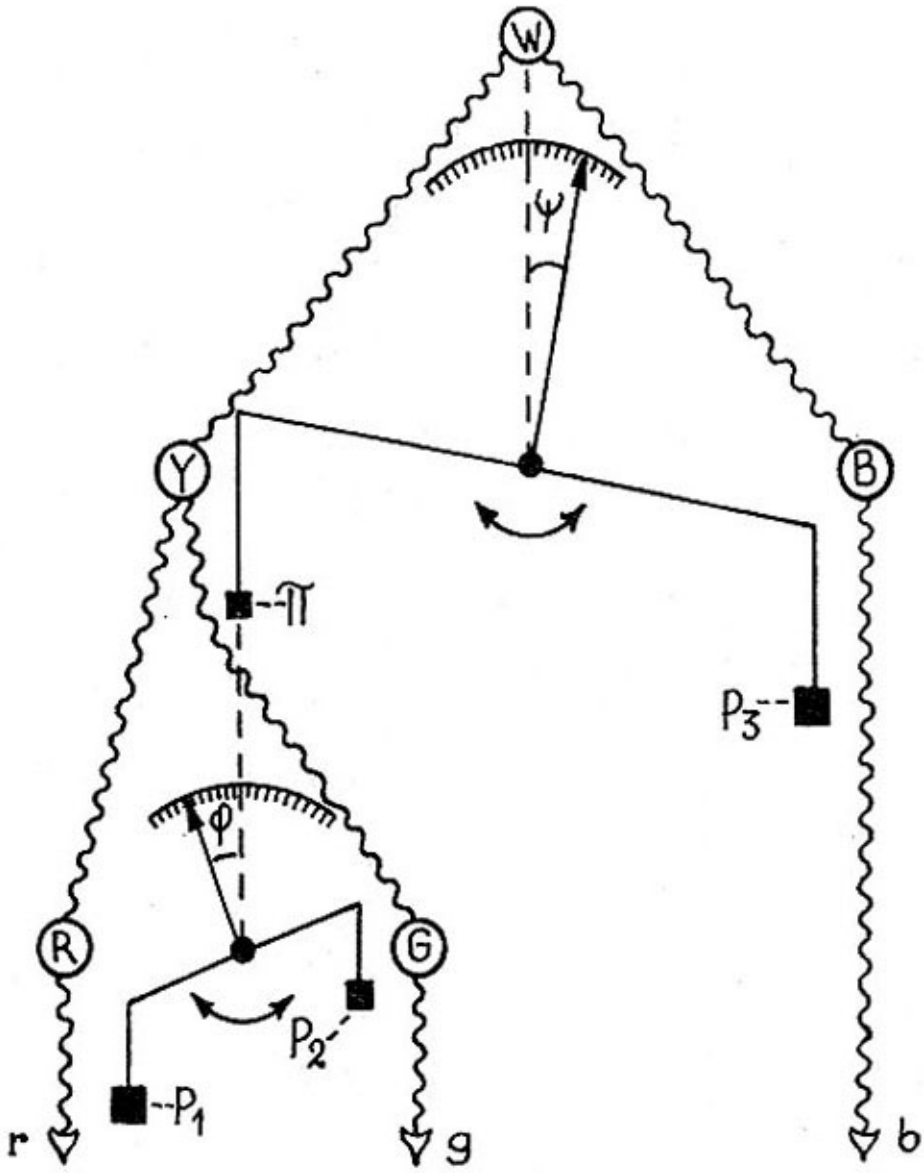

Figure 37. Gothlin's concept of a two stage representation of the three component theory of man's color vision on the assumption that the fundamental colors are red, green and blue but are organized into two antagonistic pairs. The color depicted here is an unsaturated purple.

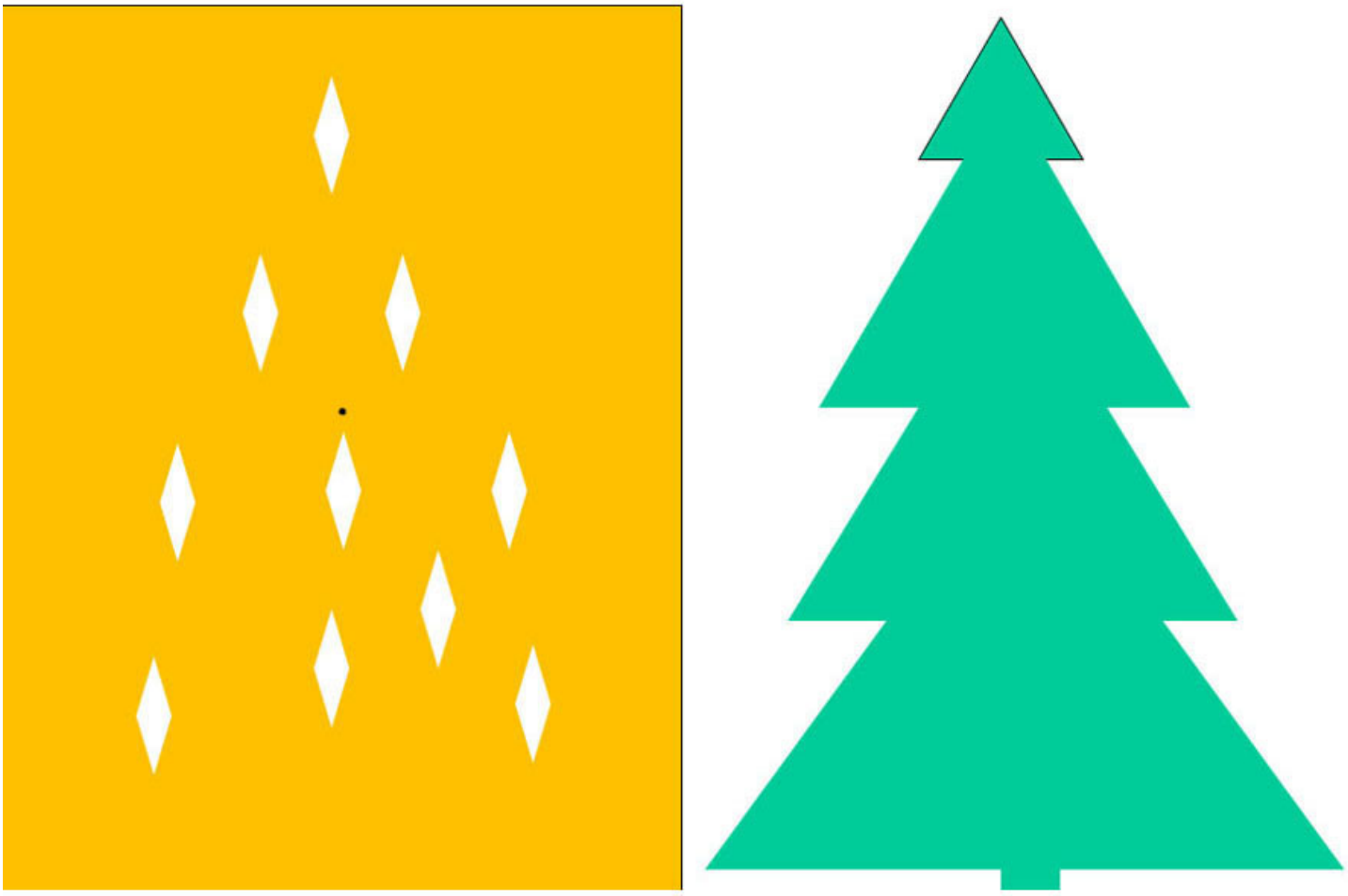

Figure 38. The after image of a white object is the opposing color to blue which is yellow. By fixating on the black spot on the left for a minute and then glancing over to the right, one sees yellow, not black, candles on the tree.

About the Author

Peter Gouras was born in Brooklyn, New York. He received an MD degree from Johns Hopkins University School of Medicine and proceeded directly into a career in eye research at the National Institutes of Health, as part of the Public Health Service, at first in the Neurological Institute and the Division of Blindness and later in the National Eye Institute. Dr. Gouras is renowned in three areas of vision research, all of which he has been a pioneer and leader. For most of his career, he has been active in the fields of basic and clinical research on the ERG. In the late 1960s, he pioneered recordings of primate ganglion cells in the fovea and did pivotal work on the analysis of color pathways from the retina through LGN to the visual cortex. On his moving to the faculty of Harkness Eye Institute at Columbia Medical School, New York City in the mid-1970s, Dr. Gouras made daring strides into the area of pigment epithelium transplantation for the treatment of retinal and macular disease. He is the author of several hundred papers and many chapters and books, particularly concerning color vision and retinal information processing.

References

1. Wright WD. Researches on Normal and Defective Colour Vision. London: Henry Kimpton; 1946.
2. Maxwell JC. On colour vision. Proc R Inst. Great Britain. 1872; 6:260-271.
3. Haverkamp S, Wassle H, Duebel J, Kuner T, Augustine GJ, Feng G, Euler T. The primordial, blue-cone color system of the mouse retina. J Neurosci. 2005; 25:5438 -5445.22:3831-3843.
4. Ekesten B, Gouras P. Cone and rod inputs to murine retinal ganglion cells: Evidence of cone opsin specific channels. Vis Neurosci. 2005;22:893–903. PubMed PMID: 16469196.

5. Yin L, Smith RG, Sterling P, Brainard DH. Physiology and morphology of Color-Opponent ganglion cells in a retina expressing a dual gradient of S and M opsins. J Neurosci. 2009;29:2706–2724. PubMed PMID: 19261865.
6. Kolb H. Anatomical pathways for color vision in the human retina. Visual Neurosci. 1991;7:61–74.
7. Packer O, Verweij J, Schnapf JL, Dacey DM. Primate S cones have blue-yellow opponent receptive fields. Invest Ophthalmol Vis Sci. 2007;48:2849.
8. Polyak, SL. The Retina. Chicago: Univ. Chicago Press; 1941.
9. Nelson R, Famiglietti EV, Kolb H. Intracellular staining reveals different levels of stratification for on-center and off-center ganglion cells in the cat retina. J Neurophyiol. 1978;41:427–483.
10. Dacey DM, Lee BB. The "blue-on" opponent pathway in primate retina originates from a distinct bistratified cell type. Nature. 1994;367:731–735. PubMed PMID: 8107868.
11. Lee BB. Neural models and physiological reality. Vis Neurosci. 2008;25:231–41. PubMed PMID: 18321399.
12. Tailby C, Szmajda BA, Buzas P, Lee BB, Martin PR. Transmission of blue (S) cone signals through the primate lateral geniculate nucleus. J Physiol. 2008;586:5947–67. PubMed PMID: 18955378.
13. Neitz J, Neitz M. Colour vision: the wonder of hue. Curr Biol. 2008;26(18):R700–702.
14. Martin PR., White AJR, Goodchild AK, Wilder H D, Sefton A E. Evidence that blue-on cells are partof the third geniculocortical pathway in primates. Eur. J. Neurosci. 1997;9:1536–1541. PubMed PMID: 9240412.
15. Chatterjee S, Callaway EM. Parallel colour opponent pathways to primary visual cortex. Nature. 2003;426:668–671. PubMed PMID: 14668866.
16. Stiles WS. Increment thresholds and the mechanisms of colour vision. Dcoumenta Ophth. 1949;3:138–165.
17. Land EH. An alternative technique for the computation of the designators in the Retinex theory of color vision. Proc Natl Acad Sci USA. 1986;83:3078–3085. PubMed PMID: 3458165.
18. Michael CR. Columnar organization of color cells in monkey's striate cortex. J Neurophysiol. 1981;46:587–604. PubMed PMID: 7299435.
19. Daw NW. The psychology and physiology of colour vision. Trends in Neurosci. 1984;7:330–335.
20. Jacobs GH. Primate color vision: a comparative perspective. Vis Neurosci. 2008;25(5-6):619–33. PubMed PMID: 18983718.
21. Mollon JD. "Tho' she kneel'd in that place where they grew. . ." The uses and origins of primate colorvision. J Exp Biol. 1989;146:21–38. PubMed PMID: 2689563.
22. Hubel DH. Eye, Brain and Vision. NY: Scientific American Library; 1988.
23. Rodieck RW. The primate retina. In: Comparative Primate Biology Series, Volume 4: Neurosciences (eds. Steklis H and Erwin J). New York: Alan R. Liss. 1988; pp. 203-278.
24. Mullen KT, Kingdom FA. Differential distributions of red-green and blue-yellow cone opponency across the visual field. Vis Neurosci. 2002;19:109–118. PubMed PMID: 12180855.
25. Hofer H, Carroll J, Neitz J, Neitz M, Williams DR. Organization of the human trichromatic cone mosaic. J Neurosci. 2005;25:9669–9679. PubMed PMID: 16237171.
26. Gouras P. Antidromic stimulataion of orthodromically identified ganglion cells in monkey retina. J Physiol. 1969;204:407–419. PubMed PMID: 4980966.
27. Martin PR, White AJR, Goodchild AK, Wilder HD, Sefton AE. Evidence that blue-on cells are partof the third geniculocortical pathway in primates. Eur J Neurosci. 1997;9:1536–1541. PubMed PMID: 9240412.
28. Livingstone MS, Hubel DH. Psychophysical evidence for separate channels for the perception of form, color, movement and depth. J Neurosci. 1987;11:3416–68.
29. Johnson EN, Hawken MJ, Shapley R. The orientation selectivity of color-responsive neurons in macaque V1. J Neurosci. 2008;28:8096–8106. PubMed PMID: 18685034.
30. Solomon SG, Lennie P. The Machinery of Colour Vision. Nature Reviews Neurosci. 2007;8:275–286.
31. Yarbus AL. Eye Movements and Vision. New York: Plenum Press; 1967.
32. Ditchburn R. Eye Movements and Visual Perception. Claredon Press; 1973.
33. Conway BR, Hubel DH, Livingstone MS. Color contrast in macaque V1. Cereb Cortex. 2002;12:915–925. PubMed PMID: 12183391.

34. Conway BR, Livingstone MS. Spatial and temporal properties of cone signals in alert macaque primaryvisual cortex. J Neurosci. 2006;26:10826–10846. PubMed PMID: 17050721.
35. Conway BR, Moeller S, Tsao DV. Specialized color modules in Macaque extrastriate cortex. Neuron. 2007;56:560–573. PubMed PMID: 17988638.
36. Zeki S. A vision of the brain. Oxford: Blackwell Scientific Publications; 1993.
37. Hering E. Outlines of a theory of the light sense (translated by Leo M Hurvich and Dorothea Jameson). Cambridge (MA): Harvard University Press; 1964.
38. Helmholtz HLF von. Handbuch der Physiologischen Optik, 2nd edition. Hamburg: Voss. (3rd edition, Hamburg:Voss, 1909); 1852.
39. Young T. On theory of light and colours. Phil Trans R Soc. 1802;92:12–48.
40. Gothlin GF. Interaction of excitatory and inhibitory processes in the synthesis of the sensation of colour and of white. Upsala Lek refurenings Furhandlingar. 1944; 49: 433-446.
41. Granit R. Sensory Mechanisms of the Retina. London: Oxford University Press; 1947.
42. De Valois RL, Smith CJ, Kitai ST, Karoly AJ. Responses of single cells in monkey lateral geniculate nucleus to monochromatic light. Science. 1958;127:238–239. PubMed PMID: 13495504.
43. Hurvich L. Color Vision. Sunderland (MA): Sinauer Associates; 1981.
44. Hurvich LM, Jameson D. An opponent-process theory of color vision. Psychol Rev. 1957;64:384–404. PubMed PMID: 13505974.

Visual Behavior

Principles of Vision

Michael Kalloniatis and Charles Luu.[1]

Created: May 1, 2005; Updated: June 4, 2007.

Introduction

From the earliest dawn of history, man must have wondered how the outside world became apparent to him through his eyes. He must have pondered what forces cause an observing eye to see an object. Why did the world look light or dark or nature have such bright colors? Although early man could not understand the concept of the physics of light or that perception occurred in the brain, he must have understood that the eye was the organ of vision, and without eyes we were blind. Thus, the earliest concerns of the ancient civilizations of India, Babylon, China, and Egypt were certainly to attempt to restore or improve eye sight when it was failing, even without understanding much else. It was the Greek philosophers (Hippocrates, Aristotle, Plato) who provided the first known theories concerning the eye, its function, anatomy, and treatment. Originally, the Aristotelian idea was that rays of light emanated from the eyes to illuminate the world around. When it was dark, the air became murky so the rays could not penetrate, but a candle could burn off the opacity in the air, allowing sight to penetrate. Also strangely enough, the Homeric Greeks lacked a word for blue. Homer described the sea as "wine colored".

Eventually, Aristotle proposed that visual sensation passed from the eye to the **heart**, which was at that time considered the center of sensation and psychic function. The brain was thought to be a cooling device (3). This **cardiocentric** nature of sensation continued into the Middle Ages (as depicted by the sixteenth century illustration in Fig. 1), despite the direct experimental evidence of Galen (A.D. 129–200). Galen, a Greek scientist working within the Roman empire, showed that pressing on the heart in human subjects did not lead to loss of consciousness or loss of sensation, but severing the spinal cord in animals abolished sensory responses after brain stimulation.

The ideas of the Greeks from centuries B.C. were perpetuated and preserved by the writings and drawings of the Arab world until well into the Middle Ages A.D. Thus, one of the earliest diagrams of the eye was from an ancient Arab manuscript (circa A.D. 860), and this was probably a copy of an older Greek illustration now lost (Fig. 2) (4).

According to early ideas, the eye had a central crystalline lens that had a photoreceptor role. Furthermore, the belief was that the optic nerve was hollow and that a mysterious **visual spirit** existed in front of the lens (Fig. 2). Interestingly, the general theory advanced by the majority of Greek anatomists was that the retina, because of its abundant blood vessels, was an organ of nutrition rather than of sight, although one Greek, Galen, hypothesized correctly, as we now know, that the retina was a displaced part of the brain. It was not until the 12th century A.D that a Moor scientist, Averroes, living in Spain, proposed that the retina and not the lens was the visual receptor (3). And it was not until 500 years after Galen that Kepler and others expanded on this principle (4).

Our knowledge of the eye continued to show the Arab influence up until the 16th century (Fig. 3, left). Even the great anatomist and artist Leonardo da Vinci (1452–1519) based his anatomical sketches of the eye on the older incorrect Arab drawings. Leonardo was convinced that the image was formed in the eye but did not know how, and for the good reason that there was still not yet an understanding of physiological optics. In fact, it was not until the early 17th century that more correct drawings of the eye were made independently by the little known anatomists and scientists, Girolamo Fabrizzi d'Aquapendente and Christopher Scheiner (Fig. 3, right) (4). By

Author Affiliation: 1 Department of Optometry and Vision Sciences University of Melbourne, Australia.

this time, the Swiss anatomist, Platter in 1583, had proposed that the role of the lens was to collect light rays, and the retina was the photoreceptor.

Again it was the early Greek physicists (Euclid, Archimedes, and Ptolemy) that hypothesized concerning the fundamental properties of light: that light traveled in straight lines and could be reflected from polished planes and curved mirrors. It seems likely that the Greeks and then the Romans used polished glass as early magnifiers. These items were preserved in the lava covering the destroyed city of Pompeii (destroyed A.D. 79). There is little evidence for any real design of spectacles though, until about the 13th century A.D. One of the earliest depictions of spectacles to correct eyesight (Fig. 4) is shown in a man's portrait found in a church at Rothenburgh, Germany, dating from the year 1466 (4).

Johannes Kepler (1571–1630) in his "Dioptrice" established the principle of dioptrics, which is fundamental to an understanding of how the image is formed in the eye. He understood that the cornea and lens collected and refracted the light rays, and that the image was "painted" on the retina as an aggregation of many image points. Kepler was also able to explain presbyopia and myopia. Kepler was indeed the father of the science of optics (4). Subsequently, many great scientists, including Rene des Cartes (1596–1650) (Fig. 5) and Sir Isaac Newton (1642–1727) with their work put the study of optics and ocular dioptrics on a solid scientific foundation, from which stems all our modern knowledge of how the eye functions and the visual image is formed.

Perceptual studies of how we see became possible as a result of the development of mathematical formulae and other measuring techniques proposed in the early 17th century. They include Newton's great discovery of the spectrum, which is the foundation for the study of color vision (3). The discipline, known as psychophysics—psycho = perception and physics = physical nature of the stimulus—is an essential discipline for probing perception. In the chapter that follows, we outline common psychophysical procedures and methods in use today, likely to be encountered in vision science, optometry, and ophthalmology.

Measurement of Light

Light can be measured and specified in two units: radiometric units and photometric units. We consider "light" to be a form of visible electromagnetic radiation. It is part of the electromagnetic spectrum between the wavelengths of 380 nm (blue light) and 750 nm (red light) (Fig. 6). Electromagnetic radiation is emitted from a source in small packets of energy called quanta or photons.

In a vacuum, a photon travels at a velocity of 3×10^8m/second. The velocity, frequency (cycles/vibrations per second of the photon), and the wavelength is related by Eq. 1:

$$\text{Equation 1: } c = \nu\lambda$$

where c is the velocity of light in a vacuum (e.g., m/s), ν is the frequency in Hertz (e.g., cycles per second), and λ is the wavelength (e.g., in meters) (see Fig. 7 for this relationship). It is important to note that the frequency is inversely proportional to the wavelength as the velocity of light is fixed.

The velocity of light in a vacuum (c) is higher than in any other medium (V_m). Therefore, the refractive index in any given medium (n_m), is defined as the ratio of the two velocities. Furthermore, for any given frequency, the wavelength in a vacuum, (λ_c) and the wavelength in a medium (λ_m), gives the refractive index (Eq. 2):

$$\text{Equation 2: } n_m = c/V_m = \lambda_c/\lambda_m$$

Energy and frequency of the photon can be related using Einstein's equation (Eq. 3):

$$\text{Equation 3: } E = h\nu$$

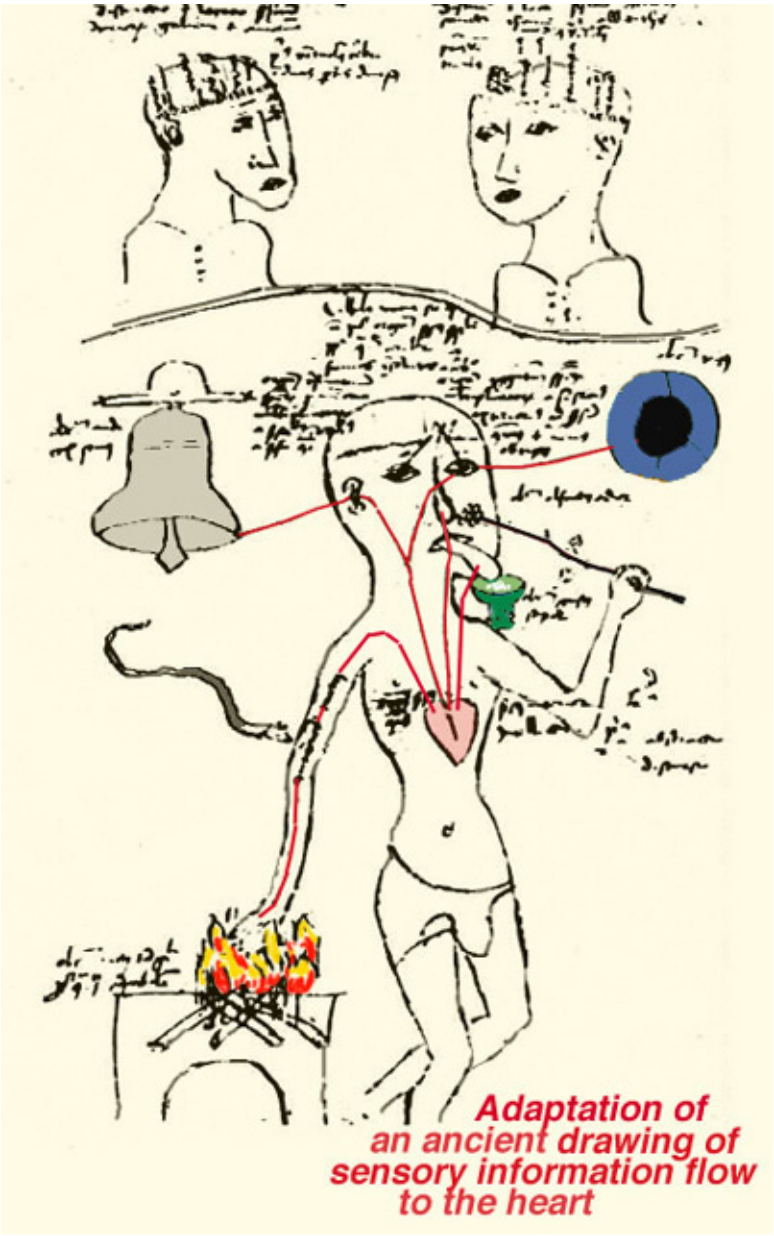

Figure 1. Aristotelian concept of five senses projecting to the heart, either directly or via the "sensus communis" in the anterior part of the head (lower panel). The upper panel shows the four (Galen's and Avicennas's) or five (Albertus Magnus's) brain compartments. From Jung (3).

where E is the energy in Joules, h is Planck's constant ($6.624 \times 10{-}^{34}$ joule · sec) and ν is the frequency in Hertz (cycles per second of the photon). The unit for energy is joules (J).

As frequency is inversely proportional to its wavelength (Eq. 4):

$$\text{Equation 4: } \nu = c/\lambda$$

where λ is the wavelength in meters and ν is the frequency in Hertz (cycles per second of the photon).

The above two equations can be combined to give (Eq. 5):

$$\text{Equation 5: } E = hc/\lambda$$

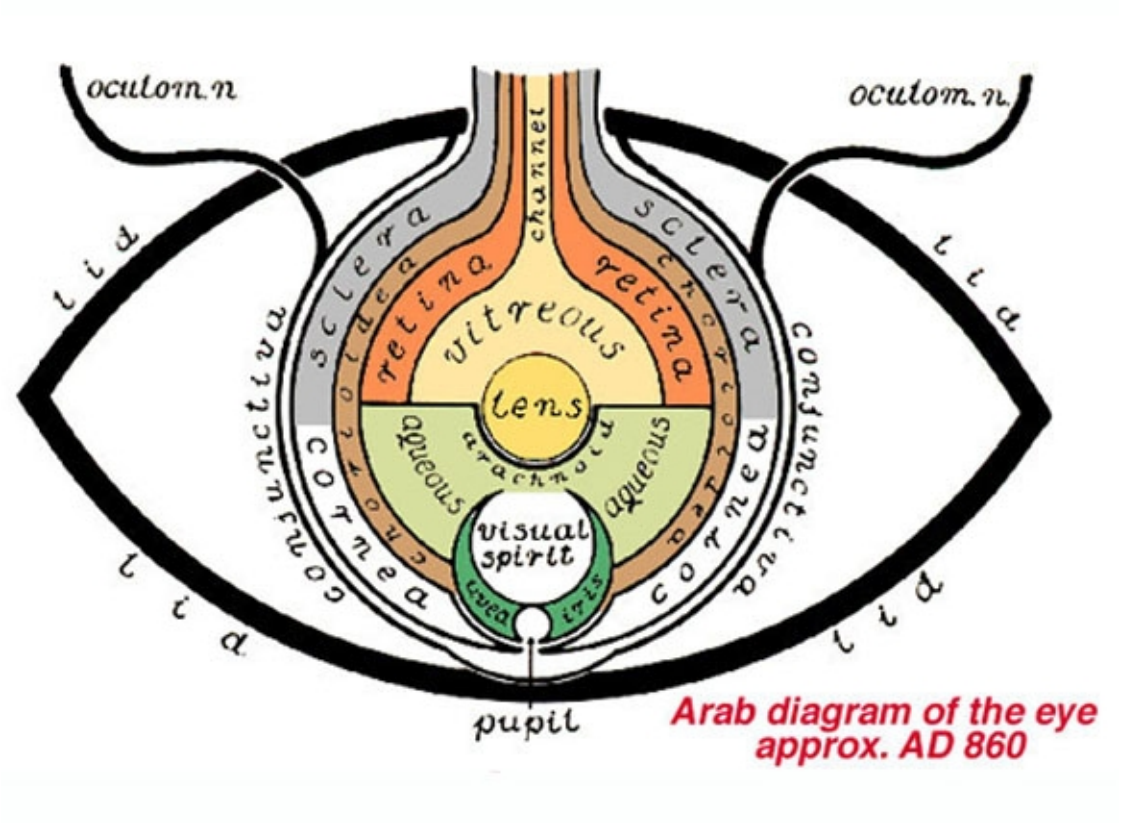

Figure 2. The earliest Arabic drawing of the structure of the eye. From Polyak (4).

Or (Eq. 6):

Equation 6: $E = hV_m/\lambda_m$

This fundamental equation is important in relating energy and wavelength of light. Because energy and wavelength are inversely proportional, this implies that short wavelength photons have higher energy. Furthermore, it is important to bear in mind that it is only photon energy and frequency that are conserved when light passes from one medium to another.

Another important term is power. Power is defined as the rate of work done, that is, the amount of work or energy output over a given time. The watt (W) is the SI unit for power. One watt is equivalent to one joule per second.

Radiometry

There are two parallel sets of units for measuring light. One is based on the psychophysical impact of the light on a human observer, the other on detection by physical radiometric devices. The two units are interconvertible, but sometimes only with difficulty. Measurement of light energy from a source can be specified in radiometric units. Radiometric units specify the amount of radiant energy present in light (see Table 1 for radiometric concepts and SI units).

All light measurement is derived from radiant flux. Subsequently, radiometric units are defined with respect to direction and surface, and all photometric units are derived from radiometric units using the photopic luminous efficiency functions or the scotopic luminous efficiency function.

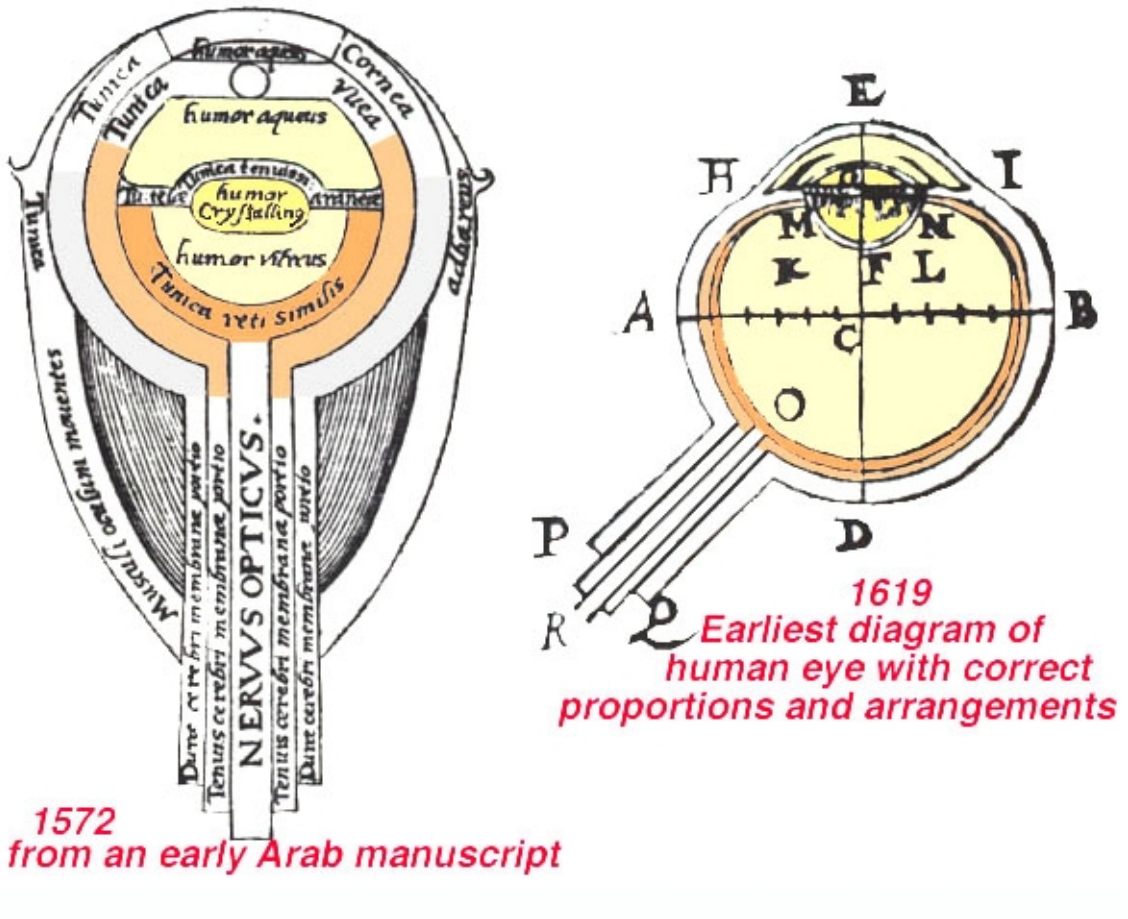

Figure 3. Drawings of the structure of the eye from the 16th and 17th centuries. From Polyak (4).

There are two main ways in which energy produces photons: incandescence and luminescence. These correspond to thermal and non-thermal mechanisms, respectively. With incandescence, photons are released from thermally agitated electrons. The frequency of photons from this type of radiation is relatively wide and continuous, regardless of the substance, with a spectrum dependent only on temperature. Luminescence involves electron excitation in an atom, molecule, or crystal. Emission of photons results from the energy given up by the electron as it moves from one excitation shell to another. The frequency of the photon emission has a pattern characteristic of the substance.

Luminescent production of photons can be achieved in a gas discharge tube. These tubes contain gas vapor such as sodium, mercury, or neon. Electrons are accelerated from one electrode to the other in these tubes. These high-velocity electrons bombard the gas atoms and cause a displacement of electrons. When the electrons return to the normal state, this excitation energy is emitted as photons. Neon and mercury sources are often used in optics.

Fluorescence is another example of luminescence. In fluorescent tubes, electrons collide with atoms of mercury, resulting in a quanta of ultraviolet light being emitted. Part of the energy of the ultraviolet quanta is absorbed by the phosphor coating of the tube and subsequently releases a quanta of light in the visible spectrum.

A tungsten filament lamp is an example of incandescence. Tungsten spectral emission resembles that of a black body. A black body is a theoretically perfect radiator. As the energy is increased, the spectral emission changes. Color temperature is a term used when the color of the radiator is the same color as the black body at a certain

Figure 4. An early painting of a man wearing spectacles. Portrait dated 1466. From Polyak (4).

temperature (measured in Kelvin). For example, a black body with a temperature of 2700 K would have a similar color to tungsten; therefore, tungsten is said to have a color temperature of 2700 K.

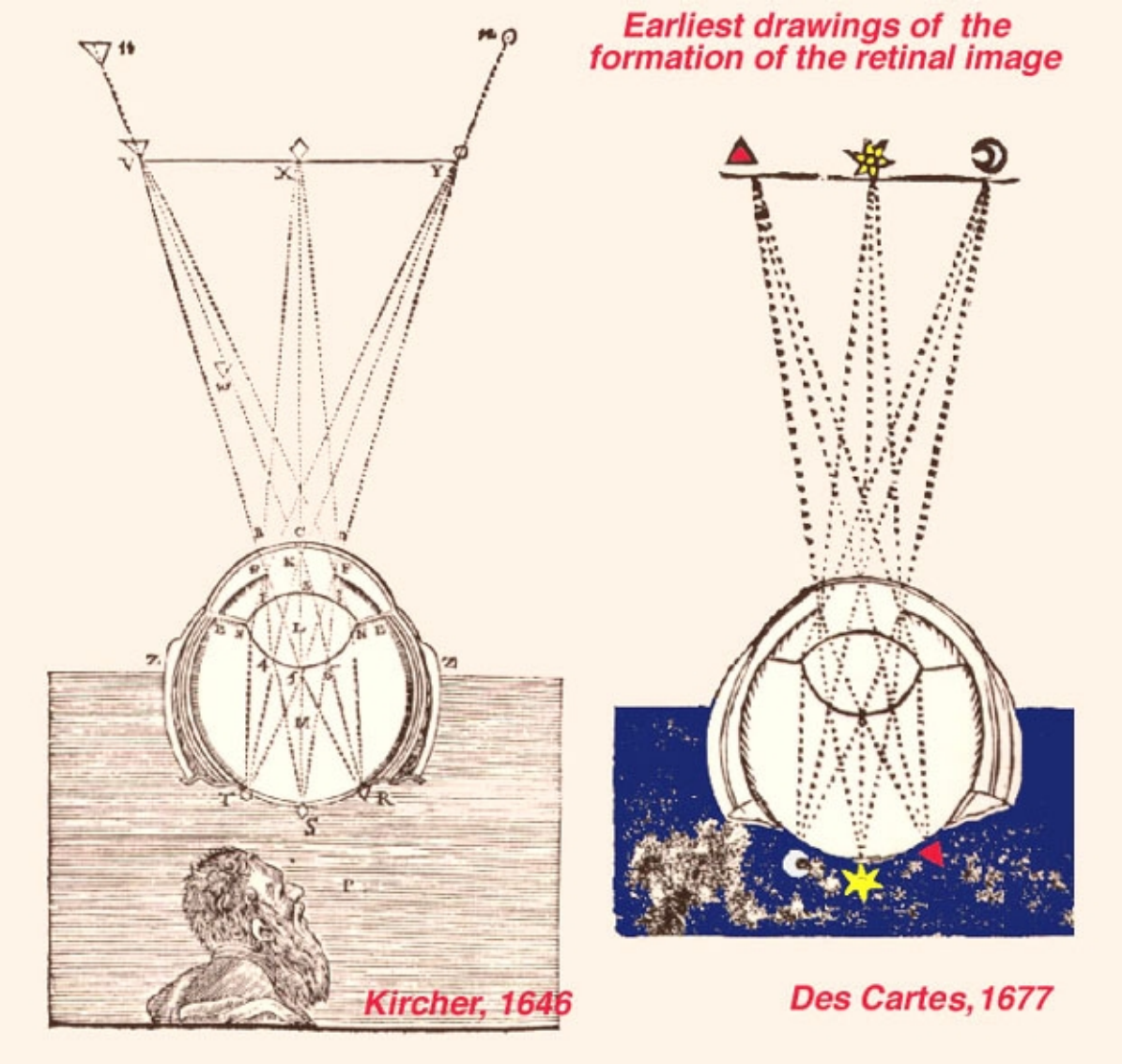

Figure 5. Diagrams showing the formation of the retinal image from Kirscher (1646) (left) and Des Cartes (1677) (right). From Polyak (4).

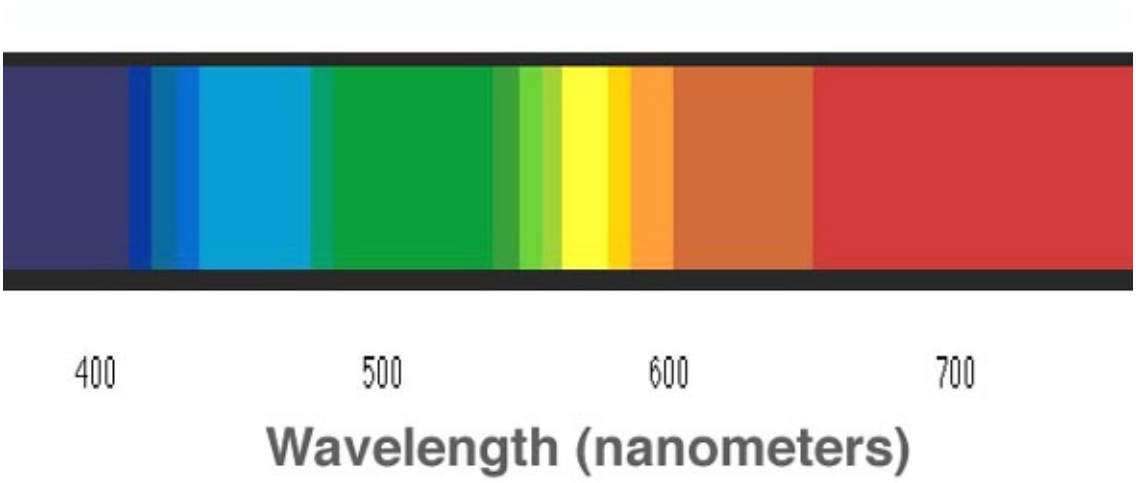

Figure 6. Visible spectrum of electromagnetic radiation.

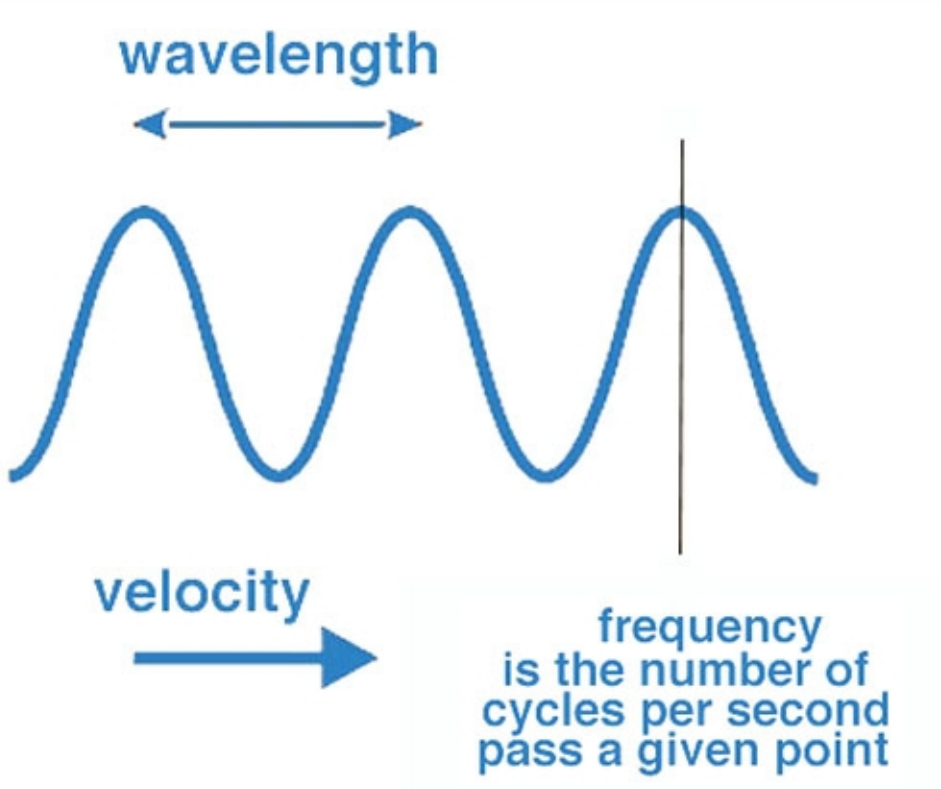

Figure 7. Velocity, frequency, and wavelength characteristics of light.

Table 1. **Radiometric concepts and units.**

Term	Symbol	Defining Equation	Applications	SI Unit
Radiant Flux	F_e	$F_e = \frac{\delta Q}{\delta t}$	Specification of the total quantity of light emitted from a source.	watt = joule/sec (W)
Radiant Intensity	I_e	$I_e = \frac{\delta F_e}{\delta \omega}$	Specification of the total quantity of light emitted by a point source, in a given solid angle.	watt/ω
Irradiance e	E_e	$E_e = \frac{\delta F_e}{\delta A_r}$	Specification of density of light incident on a surface or in a given plane.	watt/m^2
Radiance e	L_e	$L_e = \frac{\delta I_e}{\delta A_s \cos\theta}$	Specification of the amount of light emitted or reflected from an extended source in a given direction.	watt/ω/m^2

δQ is the total energy emitted by a source (in watts)
δt is the time (in sec)
$\delta \omega$ is the solid angle (in steradian) of the source
A_r is the surface area of the receiving element
A_s is the surface area of the source (in m^2)
θ is the angle between the given direction and normal to the emitting surface

Photometry

Photometry is the measurement and specification of light relating to its effect on vision. The eye can be regarded as a radiant energy detector with a selective spectral response. In a well-lit environment, it is maximally sensitive to light of about 555 nm (yellow-green light) and relatively insensitive to far-red and -blue light. The function describing the response of the human eye to different wavelengths is known as the relative luminous efficiency function.

Measurement of light from a source can be specified in photometric units. Photometric units take into account both the quantity of radiant energy and sensitivity of the eye to the wavelength(s) of the radiation. In other words, the photometric quantities specify the capacity of radiant energy to evoke a visual response (see Table 2 for photometric concept and SI units).

All light measurement is derived from radiant flux, converted to luminous flux. As with radiometric units, subsequent photometric units are also defined with respect to direction and surface (Fig. 8).

A patient's visual fields are commonly examined in clinical practice. The luminance of the background (bowl) of the visual field analyser are as follows: 1) Humphrey automated visual field analyser, 10 cd/m^2; 2) Goldmann visual field analyser, 4 cd/m^2; and 3) the Medmont automated visual field analyser, 4 cd/m^2. From these values, retinal illuminance can be calculated. Also, from Table 3, we can see that the luminance of the visual field analysis places the patient just above mesopic light levels.

V(λ) *versus* V'(λ) is the relative luminous efficiency function used to describe the response of the human eye to different wavelengths. The values used are those defined by the International Commission of Illumination (CIE) for a standard observer, as adopted in 1924 (for photopic vision) and 1951 (for scotopic vision). Thus, the photometric quantity of luminous flux is given by the equations below (Eq. 7 for photopic conditions and Eq. 8 for scotopic conditions, respectively):

$$\text{Equation 7: } F = K_m \int F_e(\lambda) V(\lambda)\, d\lambda$$

and

$$\text{Equation 8: } F_s = K'_m \int F_e(\lambda) V'(\lambda)\, d\lambda$$

where $F_e(\lambda)$ is the corresponding radiometric quantity (in this case, radiant flux) and $V(\lambda)$ is a luminous efficiency constant (which equals 683 lm/W for photopic conditions and 1700 lm/W for scotopic conditions), and K_m is a luminous efficiency constant. Eq. 8 outlines scotopic flux (F_s) in scotopic lumens from which other scotopic units, such as scotopic troland, can be obtained. Convention dictates that unless otherwise stated, all units are photopic quantities.

A candela is the unit for luminous intensity. In a given direction, it is defined as a source that emits monochromatic radiant energy of frequency 540×10^{12} Hertz and whose radiant intensity is 1/683 watts per steradian in that direction.

A lumen (unit of luminous flux) is the luminous flux emitted within a unit solid angle (one steradian), by a point source having a uniform luminous intensity of 1 candela. Therefore, a lumen can be defined as the luminous flux of monochromatic radiant energy whose radiant flux is 1/683 watt and whose frequency is 540×10^{12} Hertz (converts to 555 nm in air). The definition for a candle at 555 nm is identical for scotopic and photopic system. Consequently, the peak of the two functions will be different, as shown in Fig. 9. The amount of light required to stimulate the eye under scotopic conditions is much less than under potpie condition (Fig. 9). The difference in absolute sensitivity is reflected by the different constants, K_m and K'_m values for the photopic and scotopic luminous efficacy, respectively.

Fig. 10 shows normalised data, where the maximum value is set at 1 for comparison. Therefore, the curves peak at the same level. To set the maximum at unity, the constants K_m and K'_m, which correspond to the peaks of the photopic and scotopic luminous efficacy curve, respectively, are used. These constants are used to relate back to the actual photopic luminous efficacy, $K(\lambda)$, and actual scotopic luminous efficacy, $K'(\lambda)$. The relationship between $K(\lambda)$, $V(\lambda)$, and K_m are given as this equation (unnumbered):

$$K(\lambda) = K_m V(\lambda) \text{ and } K'(\lambda) = K'_m V'(\lambda)$$

The visual system is sensitive over a wide range of luminance. Table 3 illustrates this range. The top row shows luminances that extend from the minimum required for detection to levels at which damage to the visual system is possible. The second row relates the luminance to familiar viewing conditions by indicating the luminance of

white paper under illumination from starlight to sunlight. Finally, the bottom row links the physical stimulus to a variety of visual functions. When patients are asked to read the chart to measure their visual acuity as in Fig. 3, their visual system is functioning in the low photopic range.

SI (International Standard) units should always be used when reporting photometric quantities (Table 4). See the Units and Conversion Tables (Table 4) for conversion factors for some common (and not so common) non-SI units. To convert to SI units, multiply the non-SI unit by the conversion factor. The best source of light measurement units is from the Light Measurements Handbook.

A convenient measure of retinal illuminance is based on the unit of the troland. One troland (Td) of retinal illuminance is produced by an extended source of 1 cd/m^2 seen through a pupil of 1 mm^2. Thus, retinal illuminance *E* in trolands is given by Eq. 9:

$$\text{Equation 9: } E = LA$$

where *L* is the luminance in $cd/m^2$and *A* is pupil area in mm^2. Thus, the unit for troland is $cd/m^2.mm^2$. If scotopic units are used, luminance is defined as scotopic cd/m^2, and the troland is called a scotopic troland.

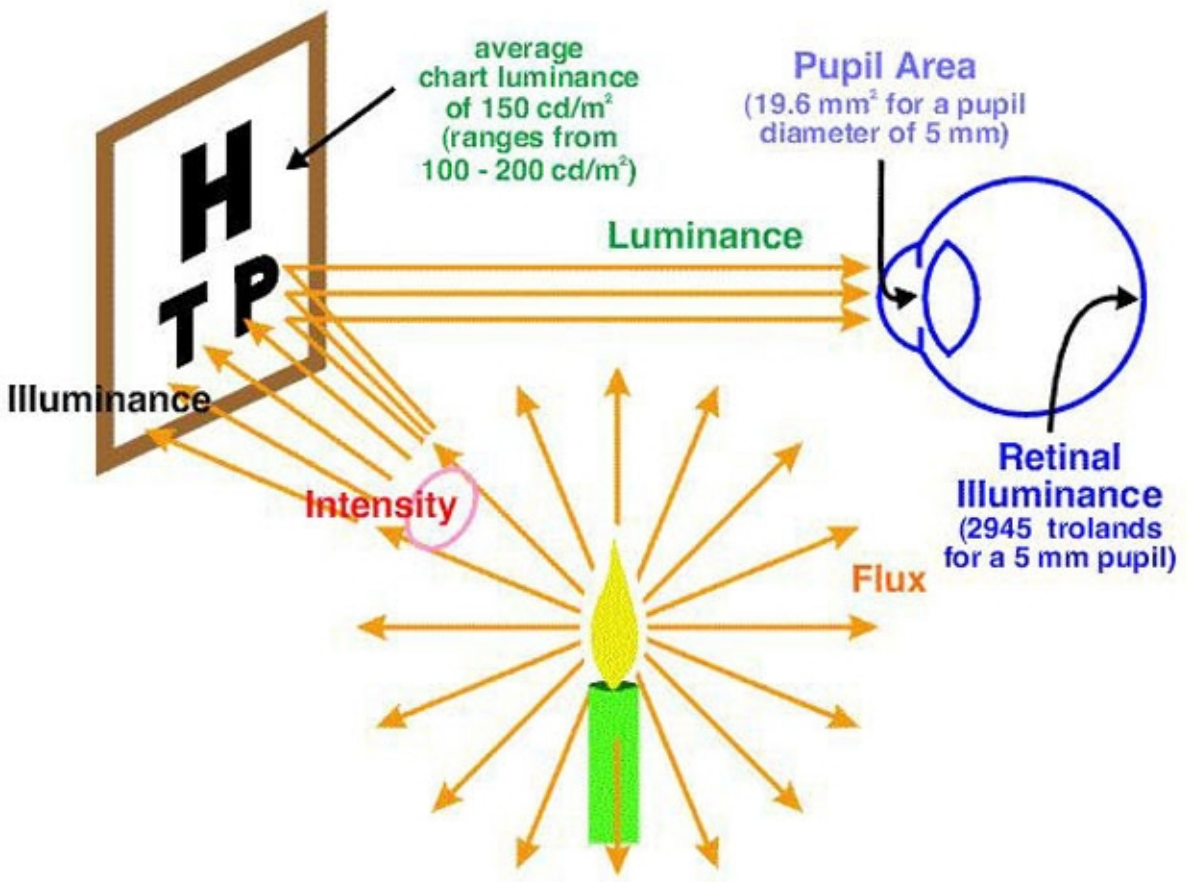

Figure 8. Photometric quantities illustrating flux, intensity, illuminance, and luminance. Retinal illuminance of 2945 trolands is achieved through a pupil diameter of 5 mm and a chart luminance of 150 cd/m^2.

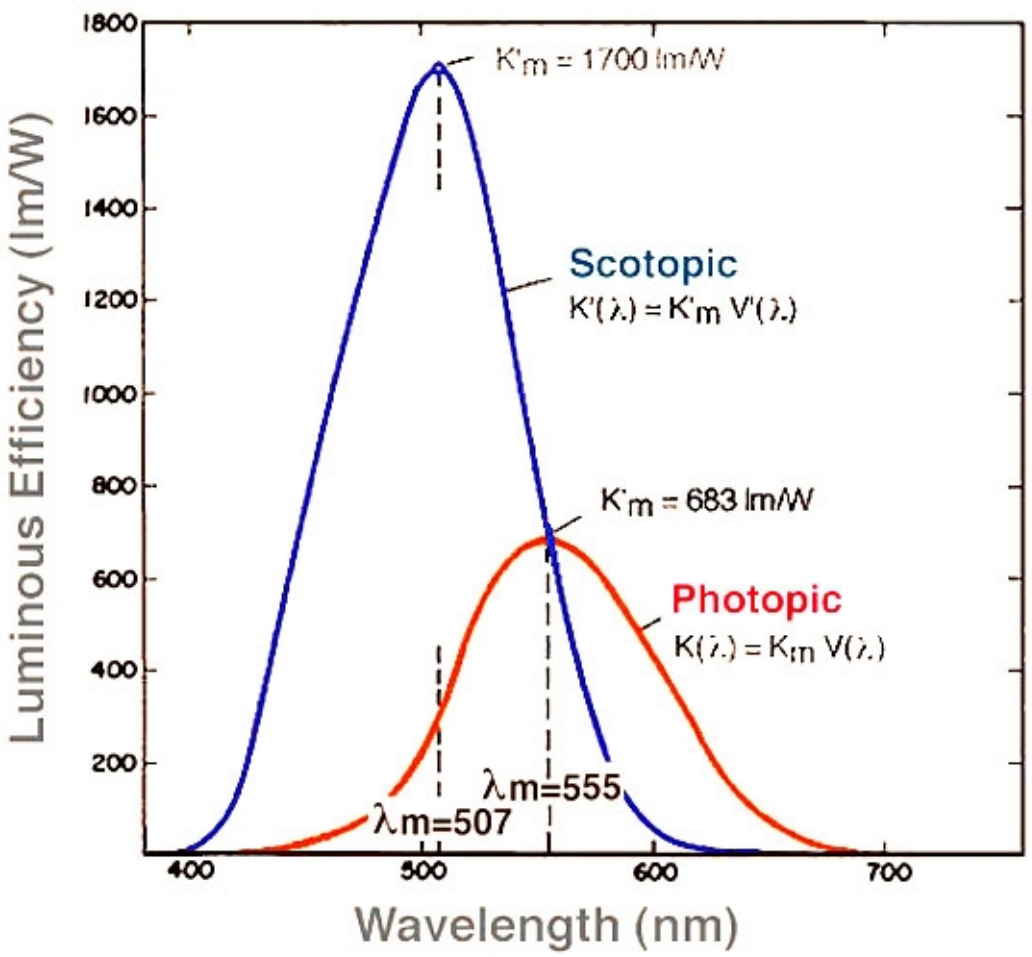

Figure 9. The scotopic and the photopic curves of spectral luminous efficacy (non-normalized values).

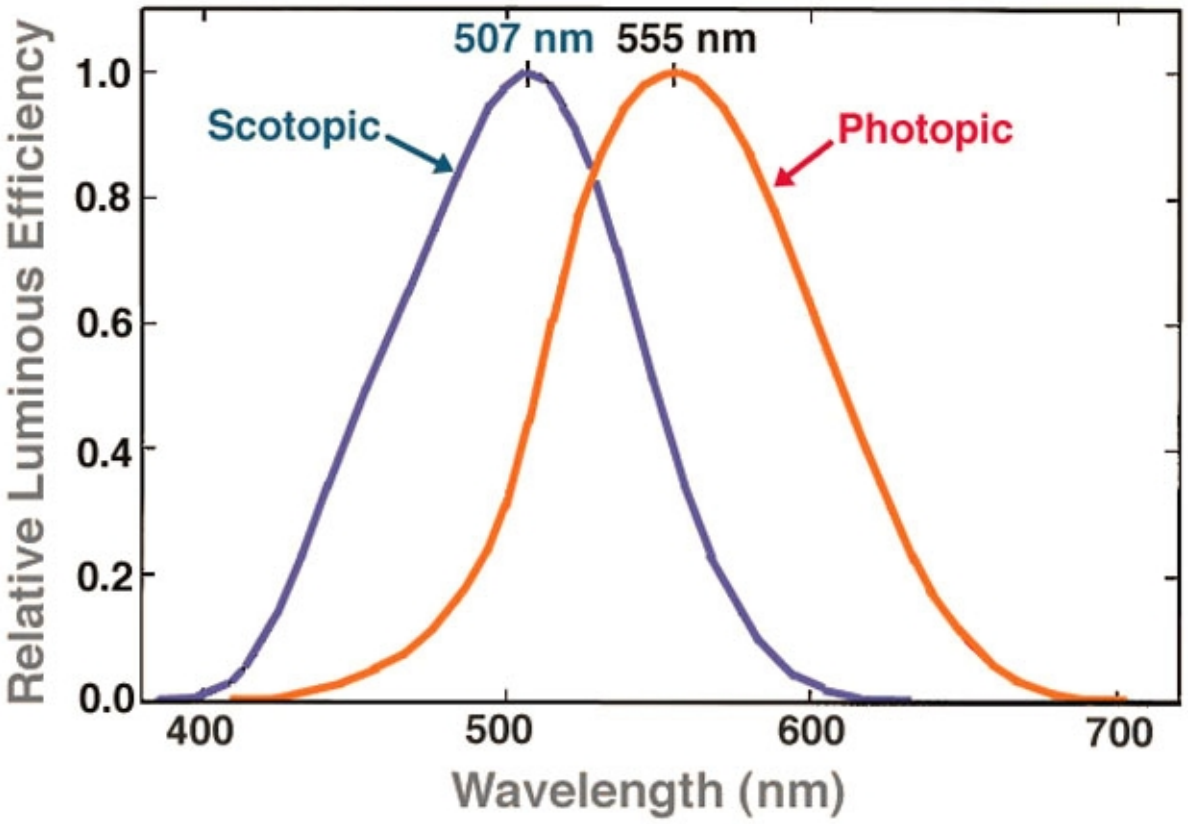

Figure 10. The scotopic and the photopic curves of relative spectral luminous efficiency as specified by the CIE (normalized values).

Table 2. **Photometric concepts and units.**

Term	Symbol	Defining Equation	Applications	SI Unit
Luminous Flux	F	$F = K_m \int F_e(\lambda) V(\lambda) d\lambda$	Specification of the total quantity of light emitted from a source.	lumen (lm)
Luminous Intensity	I	$I = \frac{\delta F}{\delta \Omega}$	Specification of the total quantity of light emitted by a point source, in a given solid angle.	candela (cd) (lumens/ω)
Illuminance	E	$E = \frac{\delta F}{\delta A_r}$	Specification of density of light incident on a surface or in a given plane.	lumens/m^2 (lux)
Luminance	L	$L = \frac{\delta I}{\delta A_s \cos\theta}$	Specification of the amount of light emitted or reflected from an extended source in a given direction.	cd/m^2 nit (nt)

K_m is the maximum spectral luminous efficacy
$F_e(\lambda)$ is the radial flux at specific wavelength
$\delta\Omega$ is the solid angle (in steradian) of the source
A_r is the surface area of the receiving element
A_s is the surface area of the source (in m^2)
θ is the angle between the given direction and the normal to the emitting surface

Table 3. **The dynamic range of the visual system.**

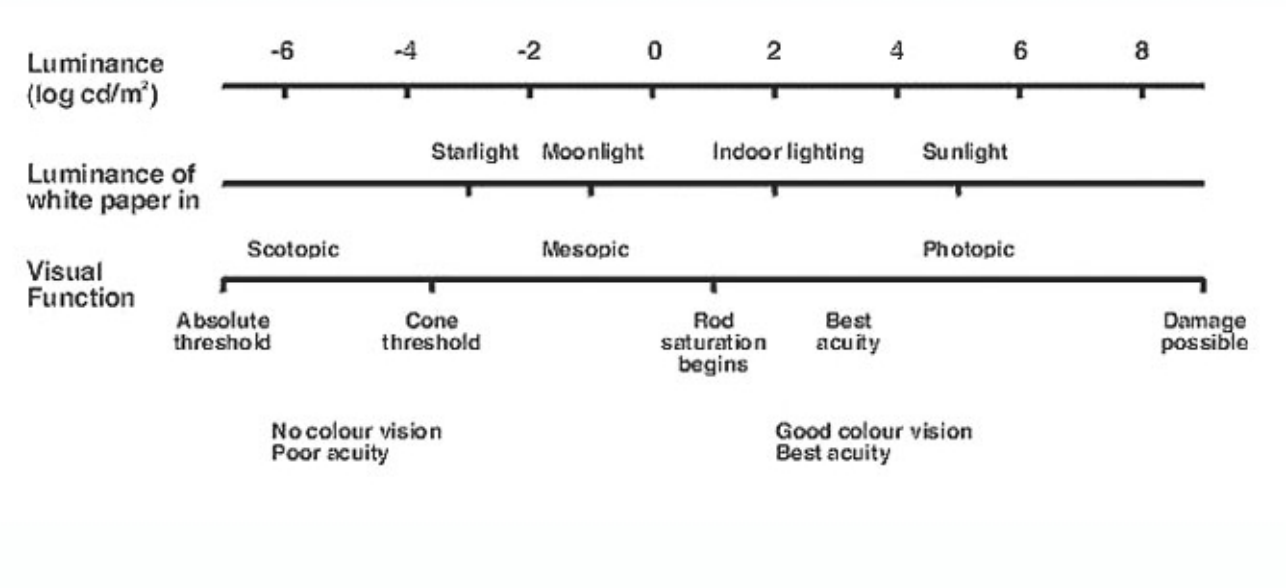

Table 4. **SI units and non-SI units and conversion factors.**

Term	SI unit	Non-SI unit	Conversion factor
Illuminance	Lux (lx)	Phot	10000
		Footcandle	10.76
Luminance	cd/m^2	Stilb	10000
		Apostilb	0.3183
		Lambert	3183
		Millilambert	3.183
		Footlambert	3.426
		cd/ft^2	10.76
		cd/in^2	1550

Inverse Square Law

The illuminance (E) of a surface due to a point source of light is proportional to the luminous intensity (I) of the source in the direction of that surface and inversely proportional to the square of the distance (d) between the surface and the source. The angle θ is the angle of incidence (Eq. 10):

$$\text{Equation 10: } E = I/d^2 . \cos\theta$$

Remember, the rule of thumb for all laws dealing with light measurement is that radiation is derived from a point source. For practical purposes, a source is considered to be a point source when the distance from the source is greater that five times its diameter.

Luminance and Illuminance Calculations

When light falls on a surface, the luminance from this surface is proportional to its reflectance and the angle of incidence (Eq. 11):

$$\text{Equation 11: } L = Er/\pi \cdot \cos\theta$$

where L is luminance of the surface (cd/m^2), E is the illuminance (lux), r is the reflectance, and θ is the angle of incidence of the luminous flux.

Filters

Neutral density filters are used to decrease the transmittance. Transmittance is calculated using the following formula (Eq. 12):

$$\text{Equation 12: } T = L/L_o$$

where L is luminance of the source with no filter in place and L_o is the luminance of the source with the filter. The optical density of the filters is given by Eq. 13:

$$\text{Equation 13: } D = -\log_{10} T$$

where T is the transmittance.

According to Beer's law, the optical density of a solution is given by Eq. 14:

$$\text{Equation 14: } D = a\ e\ l$$

where a is the concentration of the solution in gram-molecules per liter, e is the molar extinction coefficient, and l is the path length in cm. Eq. 13 and Eq. 14 can be equated to relate Beer's law to transmittance.

In visual field measures, the attenuation of light from the maximum available is expressed in decibel (dB) values. For example, in the Humphrey Visual Field analyser, the luminance of the light can be modulated over a 5.1 log unit range (i.e., 51dB, where 0.1 log unit of attenuation = 1 dB). The maximum brightness spot is 3,183 cd/m^2, and when it is attenuated with a 51dB filter, it has a luminance of 0.025 cd/m^2.

Psychophysical Measurements

Psychophysical methods and procedures are useful in determining threshold, including visual field analysis. For a perfect observer, threshold is the point where the stimulus can just be detected or where you just cannot detect the stimulus. Humans are not perfect observers, and often thresholds are defined in probabilistic terms: for example, half the points presented would be detected and half would not. So under certain psychophysical techniques, threshold can be considered the point where 50% of the stimuli are detected. Threshold variability most likely depends on neural noise. One aspect of visual psychophysics deals with noise and is termed Signal Detection Theory, but this will not be covered here.

Measurement of visual response can be achieved through several methods. These methods include: 1) Method of Adjustment; 2) Method of Limits; 3) Staircase Method (modified Method of Limits); and 4) Method of Constant Stimuli.

The **Method of Adjustment** involves asking the subject to either increase the stimulus intensity from non-seeing until the stimulus can just be seen or to decrease the stimulus intensity until the stimulus has just disappeared. This method also suffers from both errors of habituation and anticipation (these two errors are discussed below) but is useful to obtain an estimate of threshold that can be investigated with more complex techniques (see Fig. 11).

The **Method of Limits** involves presenting a stimulus well above threshold and decreasing the stimulus intensity in small steps until the subject cannot detect the stimulus (threshold). This is called descending limits. Ascending limits is when a stimulus is first presented well below threshold, then the stimulus intensity is increased to reach threshold. Ascending limits and descending limits are used to estimate the threshold. Threshold is considered the average of the threshold points estimated by several ascending and descending limits (Fig. 11).

Ascending and descending limits is a quick method of determining threshold; however, like the Method of Adjustment, two errors can occur; the errors of habituation and the errors of anticipation. The error of habituation occurs when subjects develop a habit of responding to a stimulus. For example, in ascending limits, the subject may respond to seeing the stimulus three steps past the threshold every time, thus giving a false threshold point. The error of anticipation occurs when subjects prematurely report seeing the stimulus before the threshold has been reached. Clear instructions, demonstrations, and practice runs can reduce the errors of habituation. Errors of anticipation can be minimized by changing the starting intensity for each trial.

A variation of the method of limits is the **Staircase Method**, which involves both the ascending and descending limits in a trial. Stimulus intensity is progressively increased (ascending limits) until the subject reports seeing the stimulus. At this point, the intensity value is recorded, and the stimulus intensity is then progressively reduced (descending limits) until the subject reports not seeing the stimulus. Threshold is considered the average of several of these reversal points (see Fig. 12). Threshold estimates using this method are also prone to the errors noted above, and consequently, multiple simultaneous staircases are used to minimize such errors.

The **Method of Constant Stimuli** involves the repeated presentation of a number of stimuli. The threshold value of 50% lies somewhere within this range. Other psychophysical techniques are used to estimate threshold and determine stimuli intensities to be used for presentation. These stimuli are randomly presented. The percentage of detection is determined as a function of stimulus intensity. Some high-intensity points will always be detected, whereas other low-intensity points will never to detected. The percentage of detection *versus* the stimulus intensity is graphed in Fig. 13. This graph is called the psychometric function and looks like an S-shaped curve, sometimes referred to as an ogive. The threshold value is defined as the value where 50% of the stimuli are detected. Thus, the threshold for the data below is 23.5.

Psychophysical procedures are used to minimize the variability in obtaining threshold by requiring subjects to commit to an answer.

The **YES-NO PROCEDURE** involves the subject judging the presence or absence of the signal. A stimulus is presented, during which the subject has to make a yes or no response. A correct response can range from 0% to 100%, as shown in Fig. 13.

The **FORCED CHOICE PROCEDURE** involves forcing the subject to choose from alternative choices, one of which contains the stimulus. A two-alternative forced choice (2AFC) describes a subject choosing between two alternatives. Choosing from four alternatives and six alternatives are called 4AFC and 6AFC, respectively. The percentage correct for the various stimuli intensities can be used to construct a psychometric function to determine threshold. Because there is already a 50% chance of a correct response with 2AFC, threshold is commonly considered as 75% (see Fig. 14).

For a 4AFC, threshold is considered to be at the 62.5% seen level, because this is halfway between 25% and 100%. The ogive starts at 25% because there is already a 25% chance of a correct response with 4AFC, as shown in Fig. 15.

Stimulus Intensity	A	D	A	D	A	D	A	D
9		Y						
8		Y				Y		Y
7		Y		Y		Y		Y
6		Y		Y		Y		Y
5		Y		Y		Y		Y
4	Y	Y		Y		Y		Y
3	N	Y	Y	Y	Y	Y		Y
2	N	N	N	Y	N	N	Y	Y
1	N	N	N	N	N		N	N
0	N		N		N		N	
-1	N		N		N		N	
-2	N		N		N		N	
-3	N		N		N		N	
-4	N		N		N		N	
-5	N		N				N	
-6	N						N	
Transition Points	3.5	2.5	2.5	1.5	2.5	2.5	1.5	1.5

Mean Threshold = 2.25

Figure 11. Threshold determination using the method of limits. A = ascending limits; D = descending limits; Y = Yes, the stimulus is seen; and N = No, the stimulus cannot be seen.

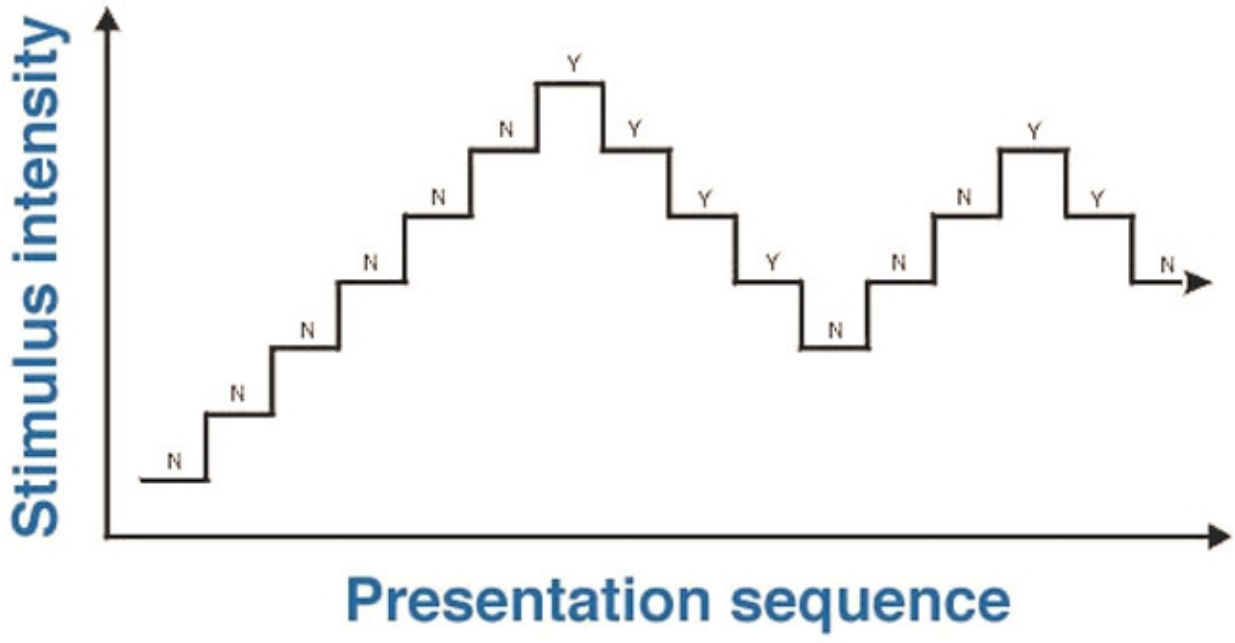

Figure 12. Staircase method. Y = Yes, the stimulus can be seen; and N = No, the stimulus cannot be seen.

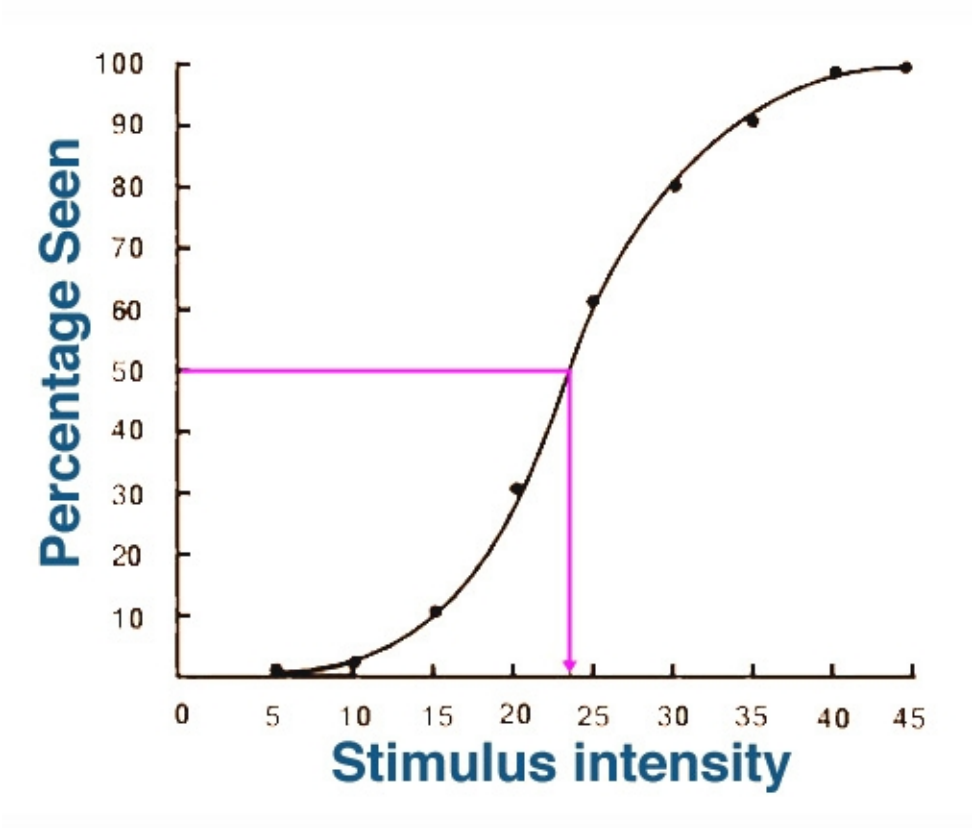

Figure 13. Psychometric function for a YES-NO paradigm.

Adaptive Psychophysical Methods

ADAPTATIVE METHODS involve presenting signals based on the performance of the subject's previous response while in **FORCED CHOICE TRACKING** a forced choice procedure is used. When subjects correctly respond three times, stimulus intensity is decreased by one step. An incorrect response will result in a one step increase in stimulus intensity. The size of the ascending and descending steps remain the same throughout the session. The session ends when a narrow range of stimuli level is reached. Threshold is considered the average of the intensity level within the period of stable tracking.

The size of the steps is an important factor. If the steps are too small, the subject may not be able to discern differences in intensity. Reaching the threshold range with small steps will also be time consuming. Large steps may miss the threshold range altogether, with swings from well above threshold to well below threshold.

PARAMETER ESTIMATION BY SEQUENTIAL TESTING (PEST) was designed to address the problem of step size and starting intensity. PEST techniques begin the session with large steps (large changes in intensity), with the intensity progressively halved until the smallest specified step to determine threshold (Fig. 16). PEST is actually a little more complicated than explained here.

MAXIMUM LIKELIHOOD METHODS. With both forced choice tracking and PEST, subsequent changes in stimulus intensity relies on the subjects previous two or three responses. In maximum likelihood methods, the stimulus intensity presented at each trial is determined by statistical estimation of the subjects threshold based on all responses from the beginning of the session. After each trial, a new estimation of threshold is determined, and the stimulus intensity is adjusted accordingly. Threshold is taken at the point where there is little change in stimulus intensity.

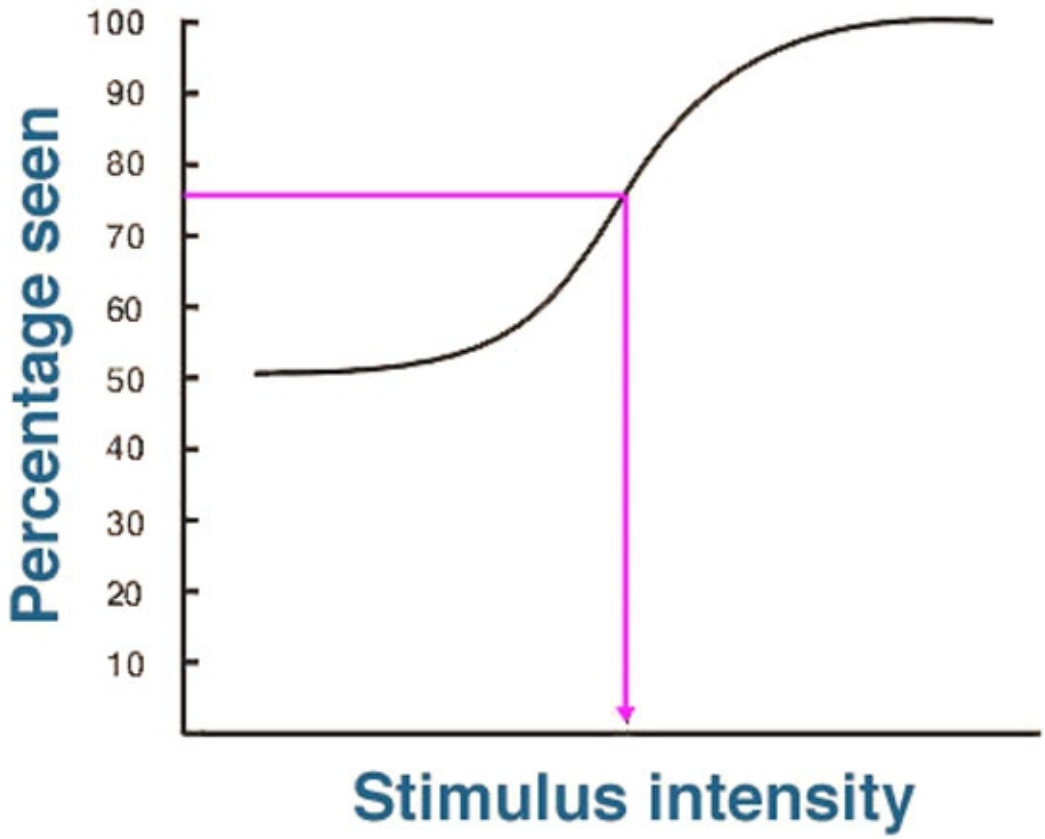

Figure 14. Psychometric function for 2AFC. Threshold is taken at the 75%-seen level.

Several examples of maximum likelihood methods are QUEST (quick estimate by sequential testing), ZEST (zippy estimate of sequential testing), and SITA (Swedish interactive threshold algorithm, which is a modified ZEST). These methods require prior information about the population's distribution of threshold and is used to construct a probability distribution function (PDF). Prior PDF is based on previously published data, pilot studies, or the expectations of the experimenter. On the basis on the PDF, the mode (QUEST) or the mean (ZEST) stimulus intensity that is most likely to be the subject's threshold is presented. The subject's response is then used to construct a new PDF using Bayes' rule of combining probability. The next stimulus intensity is presented at the new level that is most likely threshold. At the end of the procedure, the mode (QUEST) or the mean (ZEST) of the final PDF is considered the best estimate of the subject's threshold.

For additional readings, see Geischeider (1), Graham (2), Schwartz (5), and Wyszecki and Stiles (6).

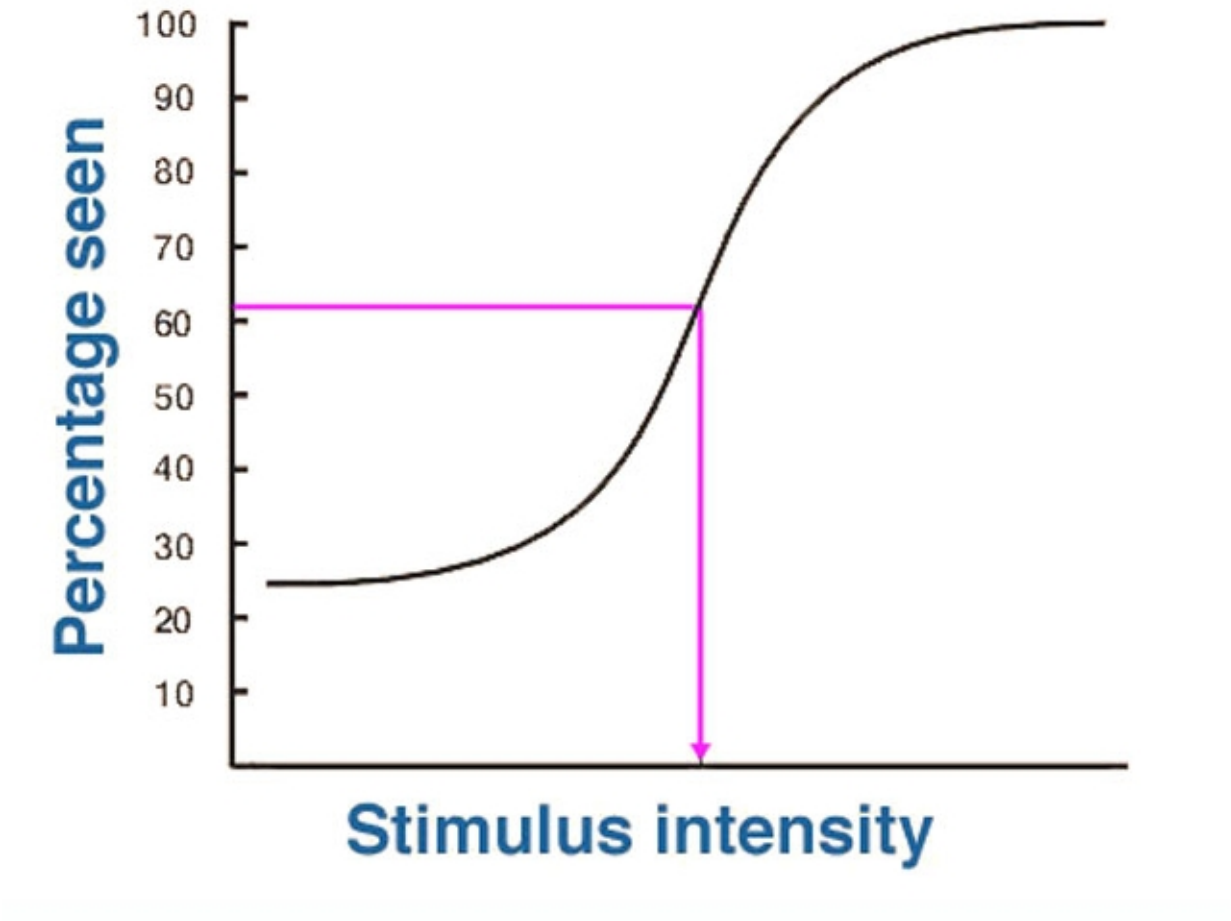

Figure 15. Psychometric function for 4AFC. Threshold is taken at the 62.5%-seen level.

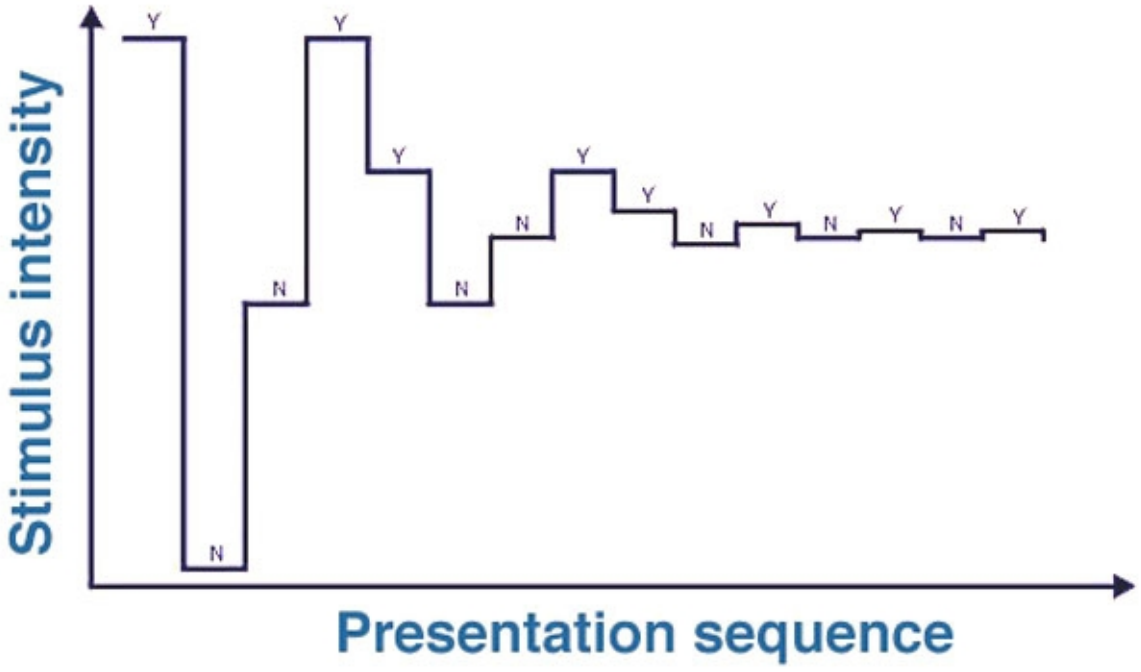

Figure 16. Tracking record using PEST. Y = Yes, there is a stimulus; and N = No, there is not a stimulus.

About the Authors

Michael Kalloniatis was born in Athens Greece in 1958. He received his optometry degree and Master's degree from the University of Melbourne. His PhD was awarded from the University of Houston, College of Optometry, for studies investigating colour vision processing in the monkey visual system. Post-doctoral training continued at the University of Texas in Houston with Dr Robert Marc. It was during this period that he developed a keen interest in retinal neurochemistry, but he also maintains an active research laboratory in visual psychophysics focussing on colour vision and visual adaptation. He was a faculty member of the Department of Optometry and Vision Sciences at the University of Melbourne until his recent move to New Zealand. Dr. Kalloniatis is now the

Robert G. Leitl Professor of Optometry, Department of Optometry and Vision Science, University of Auckland.
e-mail: m.kalloniatis@unsw.edu.au

Charles Luu was born in Can Tho, Vietnam in 1974. He was educated in Melbourne and received his optometry degree from the University of Melbourne in 1996 and proceeded to undertake a clinical residency within the Victorian College of Optometry. During this period, he completed post-graduate training and was awarded the post-graduate diploma in clinical optometry. His areas of expertise include low vision and contact lenses. During his tenure as a staff optometrist, he undertook teaching of optometry students as well as putting together the "Cyclopean Eye", in collaboration with Dr Michael Kalloniatis. The Cyclopean Eye is a Web based interactive unit used in undergraduate teaching of vision science to optometry students. He is currently in private optometric practice as well as a visiting clinician within the Department of Optometry and Vision Science, University of Melbourne.

References

1. Geischeider GA. Psychophysics: the fundamentals. 3rd ed. (NJ): Lawrence Erlbaum Associates, Inc; 1997.
2. Graham CH. Vision and visual perception. New York: John Wiley and Sons, Inc; 1965.
3. Jung R. Sensory research in historical perspective: some philosophical foundations of perception. In: Darian-Smith I, editor. Handbook of physiology. Bethesda (MD): American Physiological Society; 1984. p. 1-74.
4. Polyak S. The vertebrate visual system. Chicago: University of Chicago Press; 1957.
5. Schwartz SH. Visual perception: a clinical orientation. 2nd ed. (CT): Appleton and Lange; 1999.
6. Wyszecki G, Stiles WS. Color science: concepts and methods. Quantitative data and formulae. 2nd ed. New York: John Wiley and Sons, Inc; 1982.

Visual Acuity

Michael Kalloniatis and Charles Luu.[1]

Created: May 1, 2005; Updated: June 5, 2007.

Introduction

Visual acuity is the spatial resolving capacity of the visual system. This may be thought of as the ability of the eye to see fine detail. There are various ways to measure and specify visual acuity, depending on the type of acuity task used. Visual acuity is limited by diffraction, aberrations, and photoreceptor density in the eye (1). Apart from these limitations, a number of factors also affect visual acuity, such as refractive error, illumination, contrast, and the location of the retina being stimulated.

Types of Acuity Tasks

Target **detection** requires only the perception of the presence or absence of an aspect of the stimuli, not the discrimination of target detail (Fig. 1). The Landolt C and the Illiterate E are other forms of detection used in visual acuity measurement in the clinic. The task required here is to detect the location of the gap (Fig. 2).

Target **recognition** tasks, which are most commonly used in clinical visual acuity measurements, require the recognition or naming of a target, such as with Snellen letters. Test objects used here are large enough that detection is not a limiting factor (Fig. 3), but careful letter choice and chart design are required to ensure that letter recognition tasks are uniform for different letter sizes and chart working distances (2).

Snellen letters are constructed so that the size of the critical detail (stroke width and gap width) subtends 1/5th of the overall height. To specify a person's visual acuity in terms of Snellen notation, a determination is made of the smallest line of letters of the chart that he/she can correctly identify. Visual acuity (VA) in Snellen notation is given by the relation:

$$VA = D'/D$$

where D' is the standard viewing distance (usually 6 meters) and D is the distance at which each letter of this line subtends 5 minutes of arc (each stroke of the letter subtending 1 minute) (Fig. 4).

The reciprocal of the Snellen Notation equals the angle (in minutes of arc) that the strokes of the letter subtend at the person's eye. This angle is also used to specify visual acuity (Fig. 5). It is called the minimum angle of resolution (MAR) and can also be given in log10 form (logMAR).

Some European countries specify their visual acuities in decimal form, which is simply the decimal of the Snellen fraction (Table 1).

Target resolution thresholds are usually expressed as the smallest angular size at which subjects can discriminate the separation between critical elements of a stimulus pattern such as a pair of dots, a grating, or a checkerboard (Fig. 6).

Target **localization** involves discriminating differences in the spatial position of segments of a test object, such as a break or discontinuity in contour. Visual acuity measured in this way is called Vernier acuity (a type of hyperacuity), and the discontinuity is specified in terms of its angular size (Fig. 7).

Author Affiliation: 1 Department of Optometry and Vision Sciences University of Melbourne, Australia.

Resolution, localization, or detection tasks produce hyperacuity or levels of performance over and above the recognition (normal visual acuity) limit and indicate that the mechanisms involved in making such judgements are not restricted to the retinal level (3, 4).

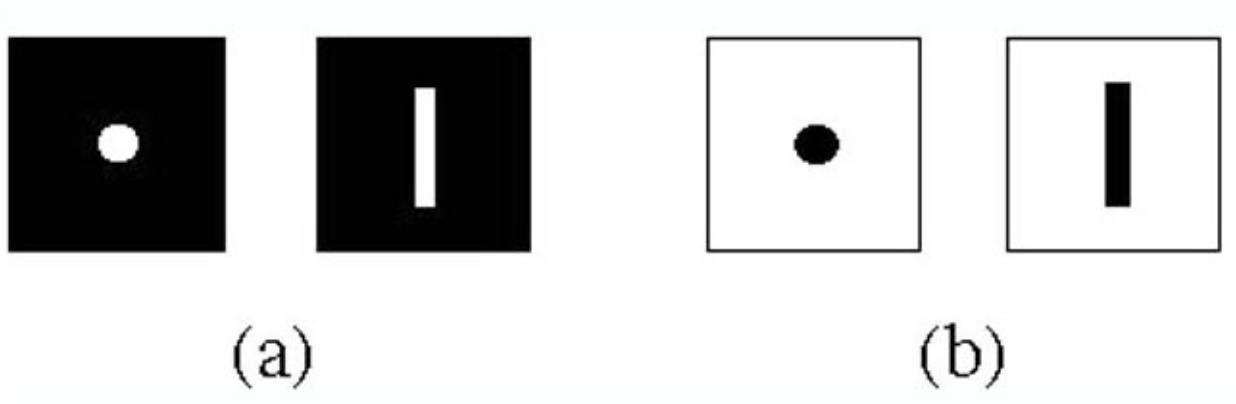

Figure 1. The task of detection involves stating whether the spot or line is present. (a) Bright test object on a dark background. (b) Dark test object on a bright background.

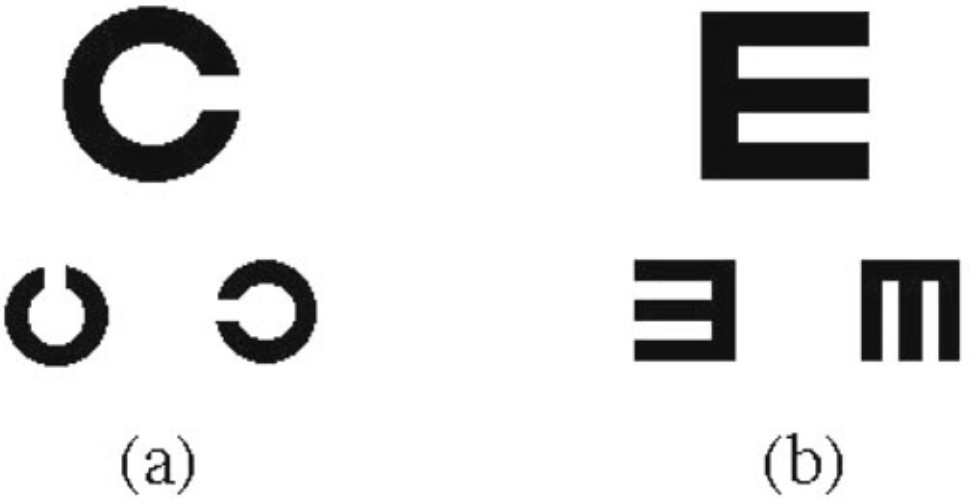

Figure 2. (a) Landolt C. (b) Illiterate E.

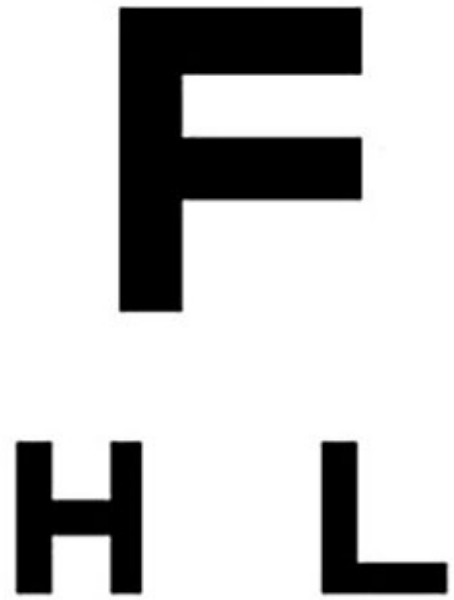

Figure 3. The task of recognition. Naming the test objects, in this case, letters of the alphabet (Snellen).

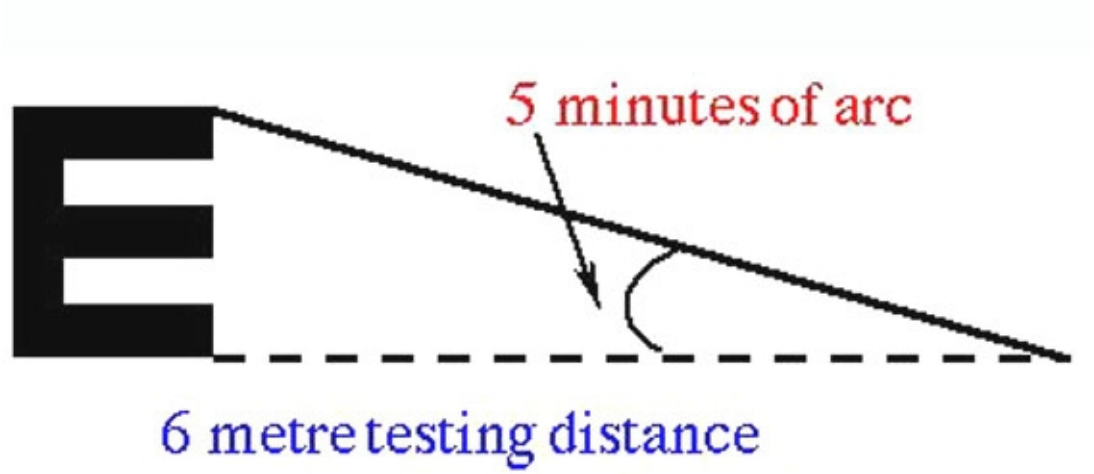

Figure 4. For a visual acuity of 6/6, the whole letter subtends an angle of 5 minutes of arc at the eye and is viewed at 6 meters (20 feet).

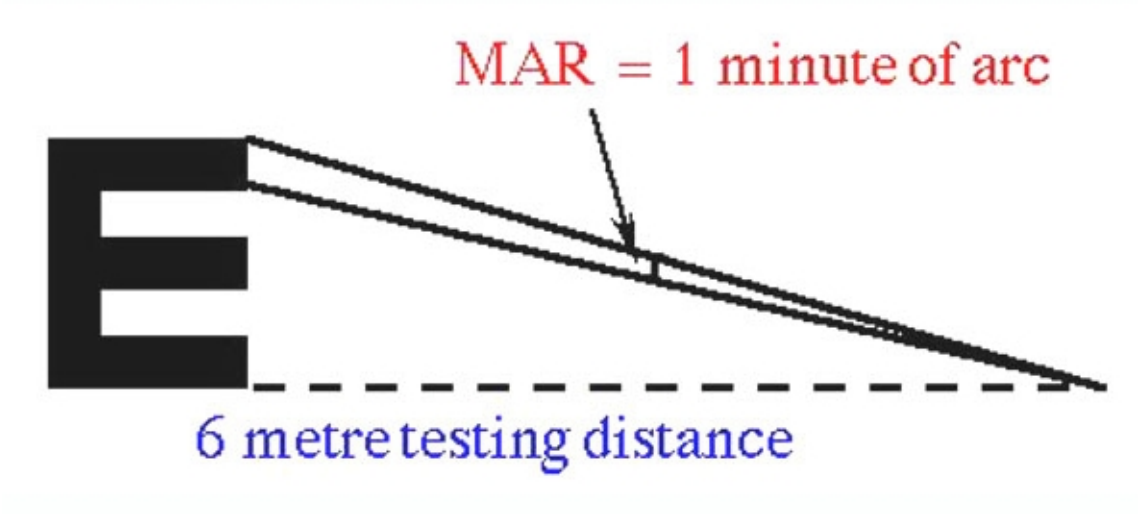

Figure 5. For a visual acuity of 6/6 (20/20), one of the strokes of the letter subtends one minute of arc at the eye. Therefore, theminimum angle of resolution (MAR) is one minute of arc and the logMAR is 0.

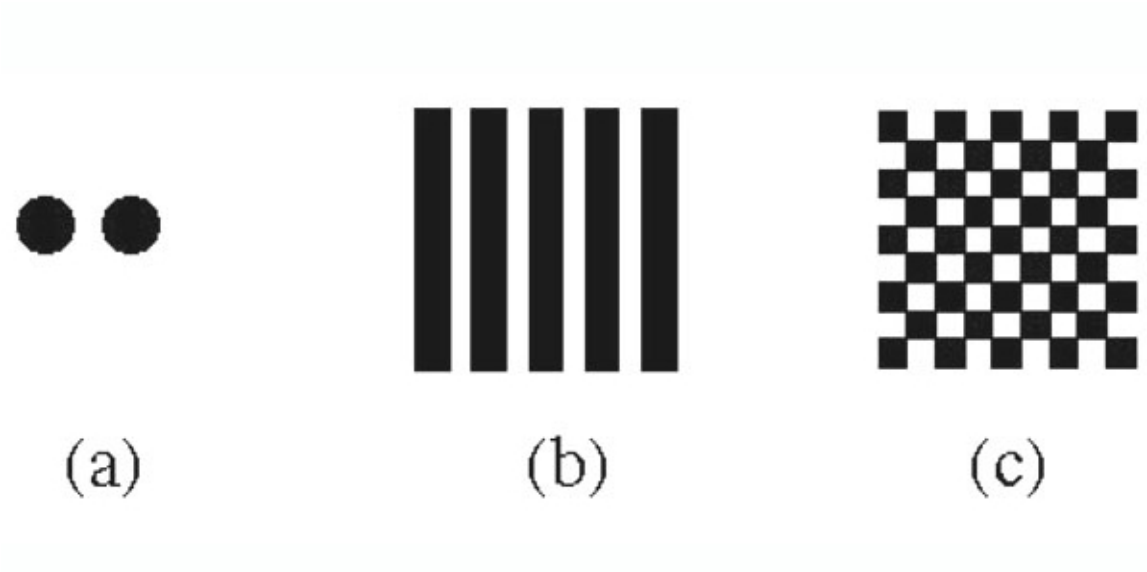

Figure 6. The task of resolution. (a) Double dot target. (b) Acuity grating. (c) Checkerboard.

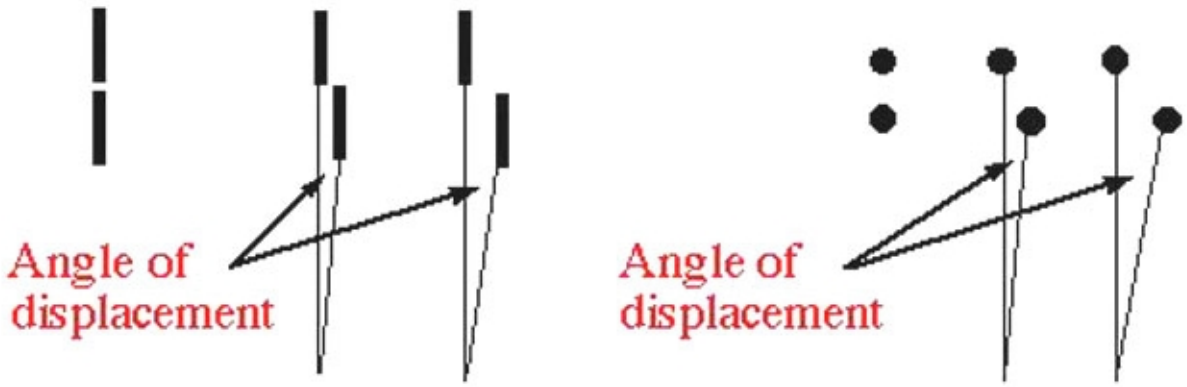

Figure 7. The task of localization. The above is an example of Vernier acuity.

Table 1. Relationship between Snellen notation, minimum angle of resolution (MAR), and the logarithmic minimum angle of resolution (logMAR).

Snellen notation		MAR	logMAR	Decimal
Metric imperial				
6/60	20/200	10	1.0	0.10
6/48	20/160	8.0	0.9	0.13
6/38	20/125	6.3	0.8	0.16
6/30	20/100	5.0	0.7	0.20
6/24	20/80	4.0	0.6	0.25
6/19	20/60	3.2	0.5	0.32
6/15	20/50	2.5	0.4	0.40
6/12	20/40	2.0	0.3	0.50
6/9.5	20/30	1.6	0.2	0.63
6/7.5	20/25	1.25	0.1	0.80
6/6	20/20	1.00	0.0	1.00
6/4.8	20/16	0.80	−0.1	1.25
6/3.8	20/12.5	0.63	−0.2	1.58
6/3.0	20/10	0.50	−0.3	2.00

Visual Acuity Limitations

For the smallest point to be detected or the finest detail to be resolved requires a good optical system and appropriately spaced detectors. Visual acuity will be limited by one of these. Objects we look at will be imaged at the back of the eye. If we take a point source, the image will be distributed on the retina as a point spread function due to distortions created by the optics of the eye (Fig. 8).

A point spread function describes the light distribution on the retina of a point source in visual space. An Airy disk pattern would be formed from a point source due to the diffraction of light (Fig. 9). A line spread function describes the light distribution of an extended source and is often used to simplify calculations.

The angular radius, *a*, of the first ring is given by:

$$a = 1.22\ l/d$$

where *l* is the wavelength of light and *d* is the diameter of the pupil. The angular radius is in radians. To convert from radians to degrees, multiply by 180/*p*. Two point sources produce two-point spread functions at the back of the eye (Fig. 10). These two points are said to be just resolved if they meet Rayleigh's criterion (see below). Clearly, if the retinal image of the two point sources was not degraded, it would be possible to have higher resolution limits (with the appropriate detector array).

Raleigh's Criterion

Raleigh's criterion is used to calculate the resolution of the eye for stimuli that are degraded by the optics of the eye. The criterion states that two points or lines are just resolved if the peak of the point spread function lies on the first trough of the other point spread function (Fig. 11).

Two points are resolved if their angular separation, α_S, is:

$$\alpha_S = 1.22\ l/d$$

In effect, this equation mathematically states that resolution is possible if two objects are separated by the width of their point spread function. If two objects are within this distance (Fig. 12), our perception of them is that of one uniform distribution (part b); and hence, we will not be able to discern the two objects.

Dimension of the Retinal Mosaic

Other than diffraction limiting visual acuity according the Raleigh's criterion, retinal cone spacing is another limiting factor, at least with in the central two degrees (5). Helmholtz (6) proposed that a grating would be resolved if there is a row of unstimulated cone between rows of stimulated cones. This is considered the Yes-No-Yes response of the cone receptors. For example, if two lines are to be resolved, a detector array needs to be fine enough to detect a gap between the two lines (Fig. 13). From Fig. 13, it can be seen that detectors A and B will not be able to resolve the two lines. However, with a fine detector array of detectors C, D, E, and F, the two lines would be resolved.

The same principle applies to sinusoidal gratings where a detector array must be fine enough to detect the gap between the lines or gratings. The bars of a sinusoidal grating do not change abruptly as with square wave gratings (Fig. 14).

Gratings can be used as another method of measuring visual acuity. Visual acuity in Snellen notation can be expressed in spatial frequency and *vice versa* (Fig. 15).

Sinusoidal gratings were used by Campbell and Green (7) to determine the maximum resolution of the eye. They used interference patterns generated by a laser to bypass the optics of the eye to create a sinusoidal grating at the back of the eye. They found that the maximum resolution was about 60 cycles per degree, whereas a free viewing screen resulted in reduced resolution capabilities. More recent work on photoreceptor density and spatial resolution has shown that the receptor array in the human visual system can resolve in the order of 6/1 (20/3) or ~150 cycles/degree (8, 9). Cone spacing at the fovea is approximately 2.5 μm (8) or approximately 28 seconds of arc. On the basis of cone spacing, a maximum of about 60 cycles per degree is possible, which is well above

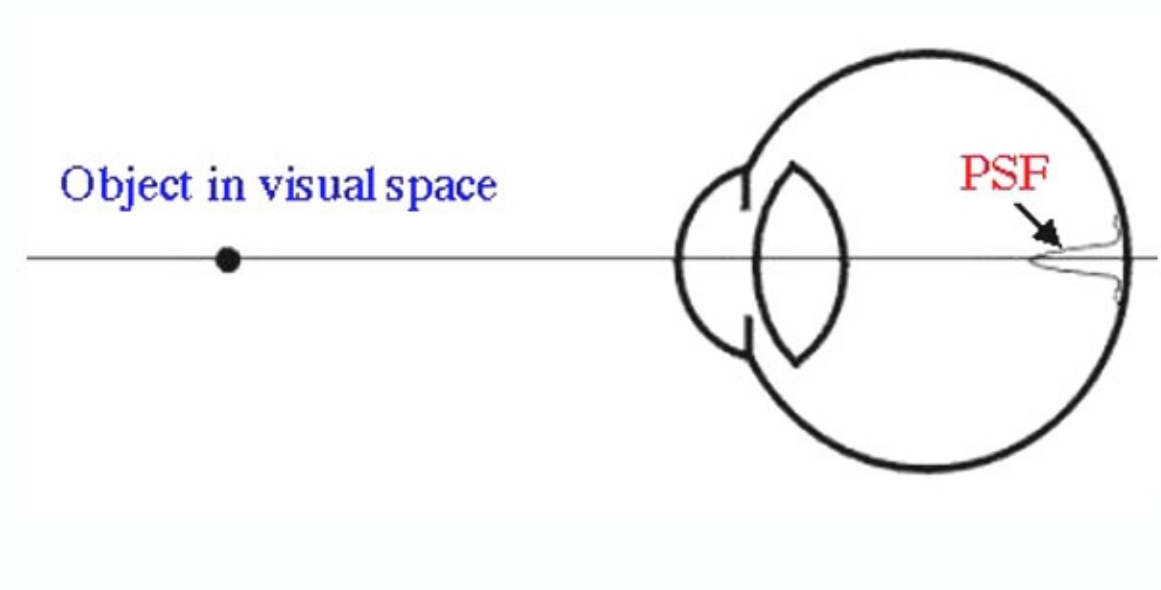

Figure 8. Image of a point at the back of the eye.

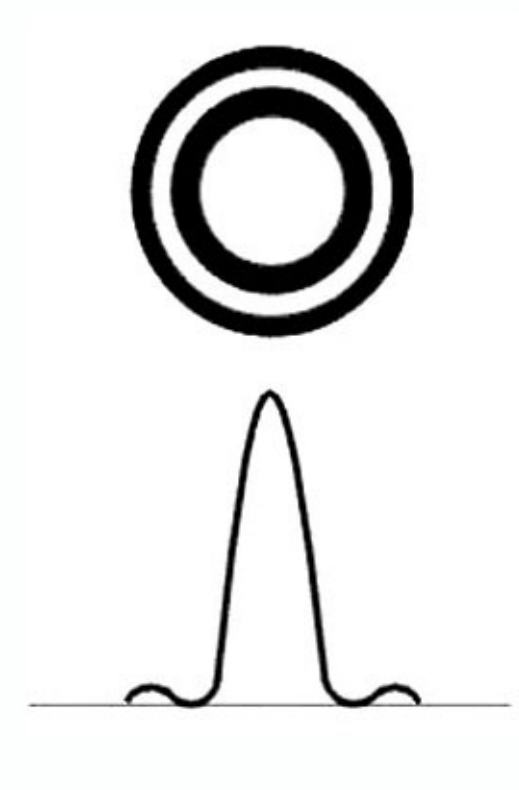

Figure 9. Point spread function (Airy disk pattern) of a point source. The upper component represents the perception of the light distribution when viewing an Airy disc.

conventional clinical measures because this does not compensate for the optics of the eye and post-receptoral neural processing.

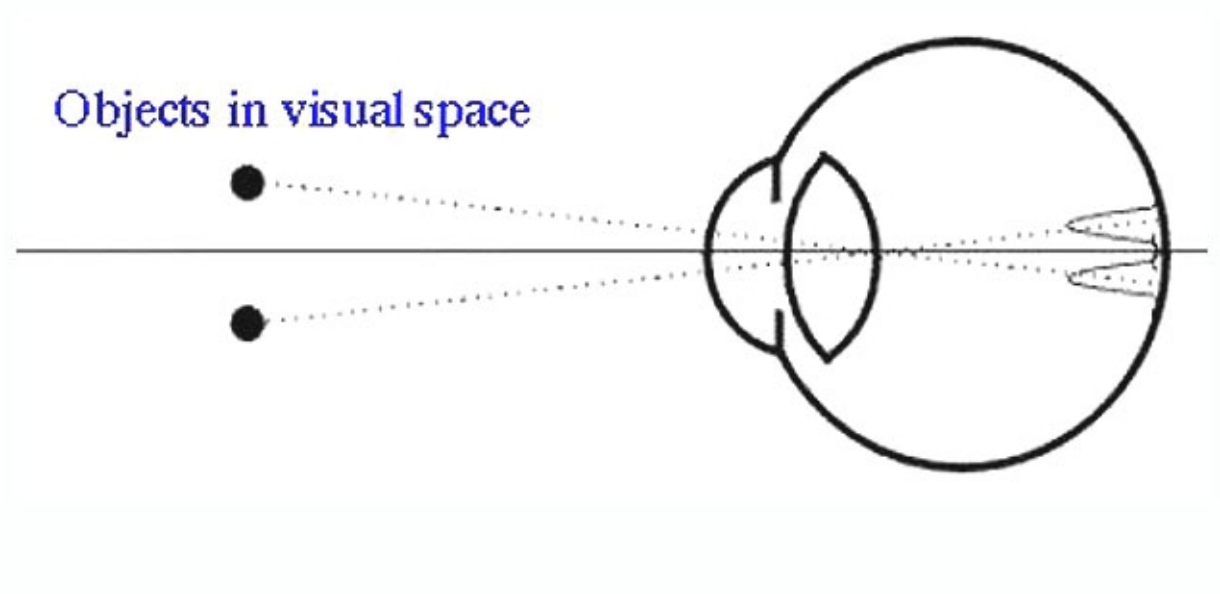

Figure 10. Two point sources and their point spread function at the back of the eye.

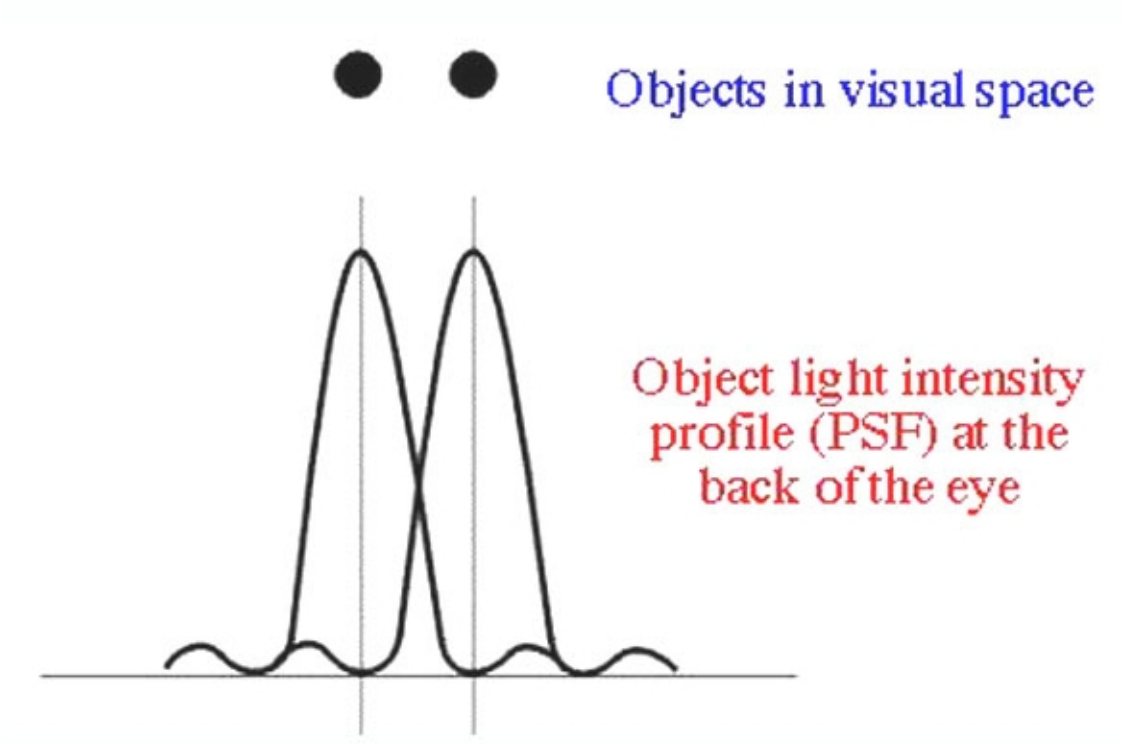

Figure 11. Raleigh's criterion.

Factors Affecting Visual Acuities

Apart from the two main limiting factors above, visual acuity also depends on a number of factors including:

- refractive error
- size of the pupil
- illumination

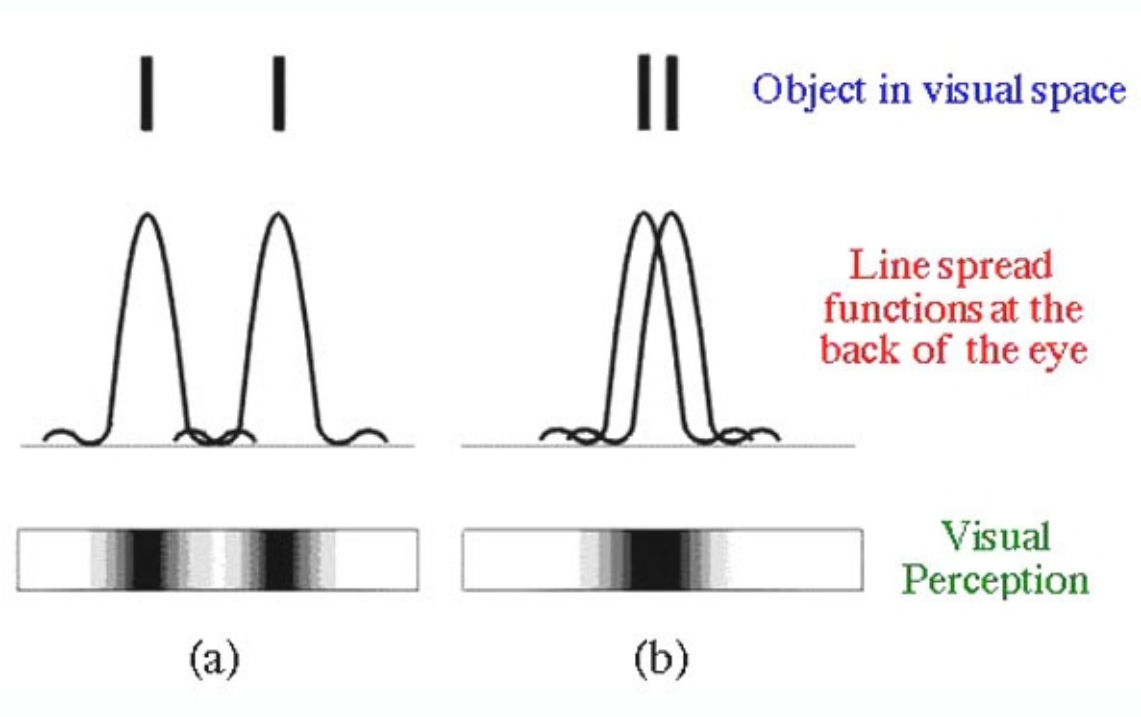

Figure 12. The representation between two lines, their line spread function, and a person's perception of the two lines. (a) Two lines are resolved. (b) Two lines that cannot be resolved and are perceived as one thick line.

- time of exposure of the target
- area of the retina stimulated
- state of adaptation of the eye
- eye movement

Refractive Error

Refractive errors will affect visual acuity by causing defocus at the retina. Defocus will blur out fine detail, sharp edges, and contrast sensitivity by affecting its point spread function (Fig. 16). Refractive errors such as myopia (short-sightedness) and hyperopia (long-sightedness) causes the point spread function to spread more laterally, affecting resolution (Fig. 17). The image at the back of the eye of an object is focused sharply on the retina in an emmetropic eye. In a myopic eye, the optical system can be considered to be too strong, thus the image is focused in front of the retina. The reverse occurs with a hyperopic eye where the optical system is too weak so the image is focused behind the retina.

Pupil Size

The size of the pupil is an important factor affecting visual acuity. Large pupils allow more light to stimulate the retina and reduces diffraction, but resolution will be affected by aberrations of the eye. On the other hand, a small pupil will reduce optical aberrations, but resolution will be diffraction limited. Therefore, a mid-size pupil of about 3 to 5 mm would be optimal, because this is a compromise between the diffraction and aberration limits (1, 10). As noted earlier, pupil area affects the size of the point spread function, and hence resolution.

Illumination

For recognition tasks, visual acuity is greatly affected by the level of background luminance (Fig. 18). Two branches are evident: the lower branch belongs to the rod (scotopic) function, and the upper branch belongs to

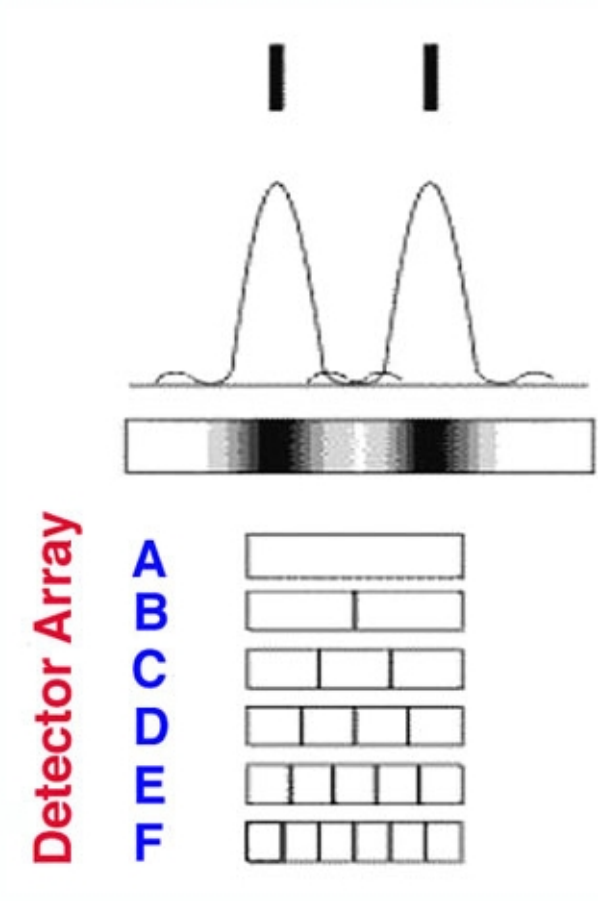

Figure 13. Two lines with their line spread function, person's perception of the two lines, and various detector arrays. Only detector arrays C (3 detectors) through F (6 detectors) have a fine enough detector density to resolve the two lines, i.e., detect the gap. Detector array A or B, which have one and two detectors, respectively, cannot signal a yes-no-yes response.

the cone (photopic) function. Note the asymptote for both, indicating the maximum visual acuity (arrows). The cone branch has a long "linear" range of about 3 log units, with the asymptote at the photopic level of about 300 cd/m^2.

One theory put forward by Hecht (11) is that within the rod population and within the cone population, there are differing sensitivities that are distributed randomly. Therefore, at high luminance, all cells are active for a high level of visual acuity. At low luminances, only cells sensitive to that level of luminances are active, and because they are distributed randomly, the retinal mosaic is coarser; thus, a lower level of visual acuity is achieved (12).

Another possible explanation is that under limited quantal availability, quantal capture is more probable in the para-central and peripheral retinal because of greater spatial summation. Because photoreceptor density in this area is low, resolution is poorer. As light levels increase, quantal capture occurs more successfully at the central retinal (macula and fovea). A higher level of visual acuity is achieved because of the high photoreceptor density.

Time of Exposure of the Target

To detect a small bright spot, detection is greatly dependent on the quantity of light rather than the exposure time. However, to detect a line, the acuity (reciprocal width of the line) is proportional to the exposure time. There is no simple acuity–exposure time relationship for the resolution of the target.

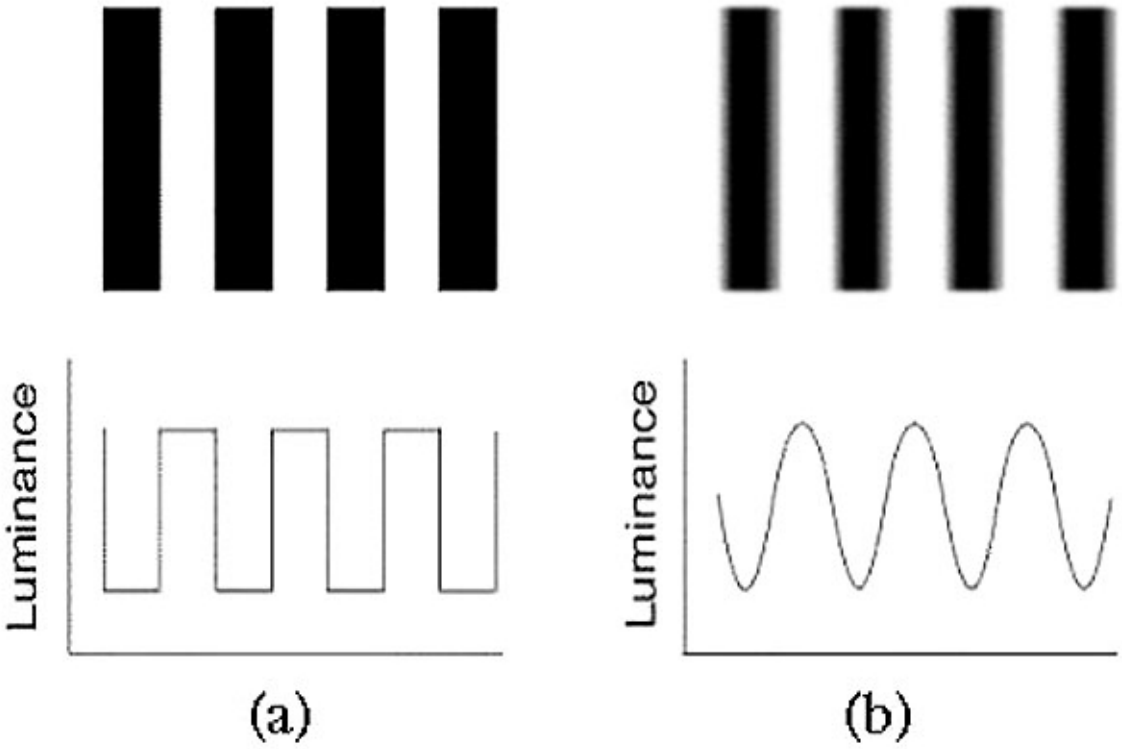

Figure 14. Square wave grating (a) and sinusoidal wave grating (b) with their luminance profile.

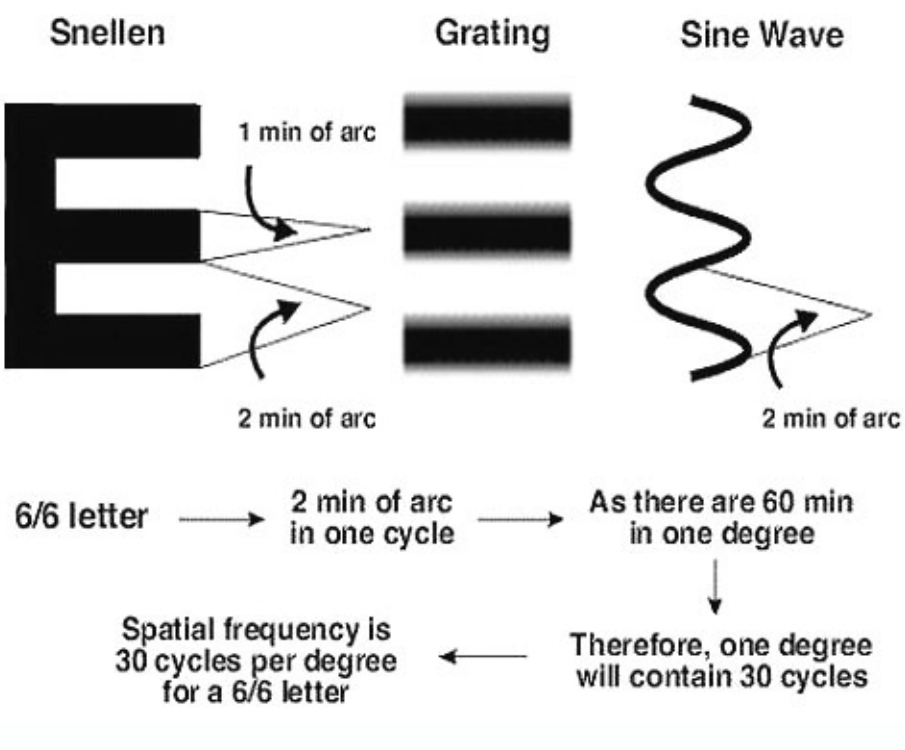

Figure 15. Visual acuity in Snellen notation and its conversion to spatial frequency.

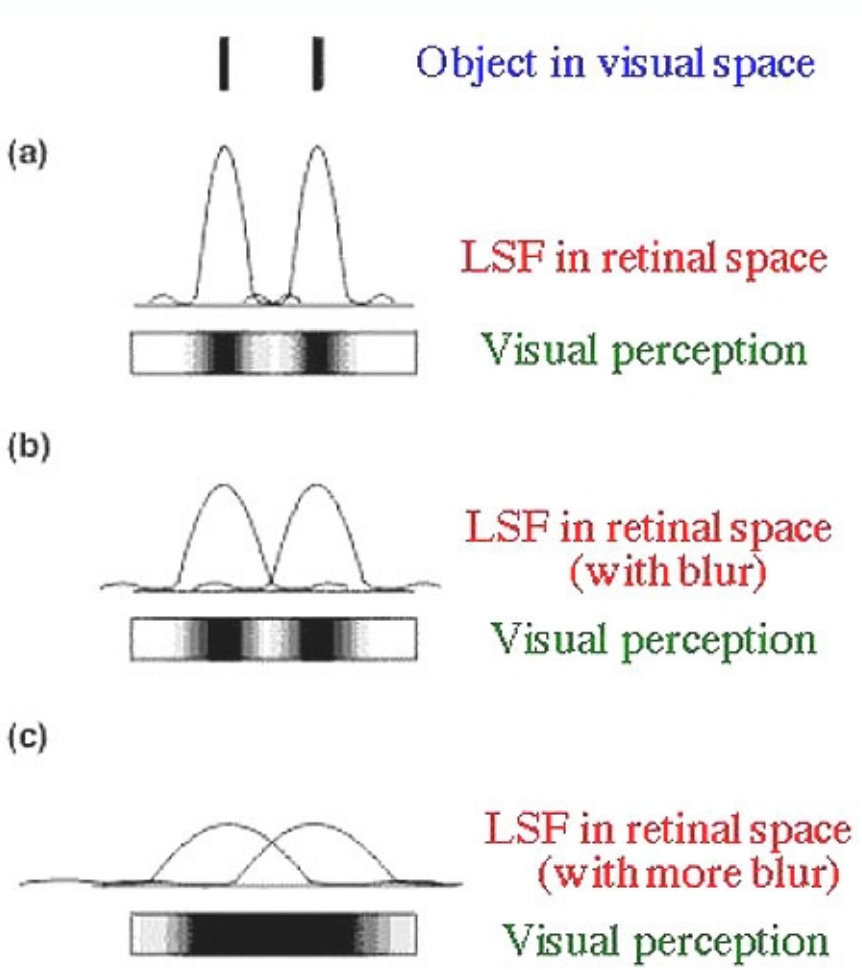

Figure 16. Line spread function (LSF) of two lines with various amounts of blur. With increasing blur, the discrimination of the two lines is lost.

Area of the Retina Stimulated

Because of the densely packed cones at the fovea, visual acuity is the greatest at the center of fixation. At a distance of 5 minutes of arc from the center of fixation, there is a measurable loss in visual acuity. At 10 minutes of arc (1/6 of a degree) from fixation, there is a 25% loss of visual acuity (Fig. 19). When comparisons were made of cone packing density and photopic resolution, close correlation was evident up to approximately 2 degrees eccentricity (5). At larger eccentricities, visual acuity is worse than that predicted by cone spacing, which may indicate that another post-receptoral retinal element is the limiting factor (see the discussion below for scotopic visual acuity).

State of Adaptation of the Eye

The highest level of visual acuity is achieved if the eye is adapted to the same level as the test luminance for test luminances of 34 cd/m^2 to 34,000 cd/m^2. For test luminances less than 34cd/m^2, adapting to a lower luminance will achieve a slightly better acuity.

The high density of cones at the fovea is responsible for the high levels of visual acuity under photopic conditions. Under scotopic conditions, the AII amacrine cell, which is an interneuron identified in the primate retina (13, 14), appears to limit resolution. Maximum scotopic acuity occurs at ~5-15° eccentricity, which corresponds to the AII amacrine cell density, whereas peak rod density occurs at about 15-20°. The arrow in Fig.

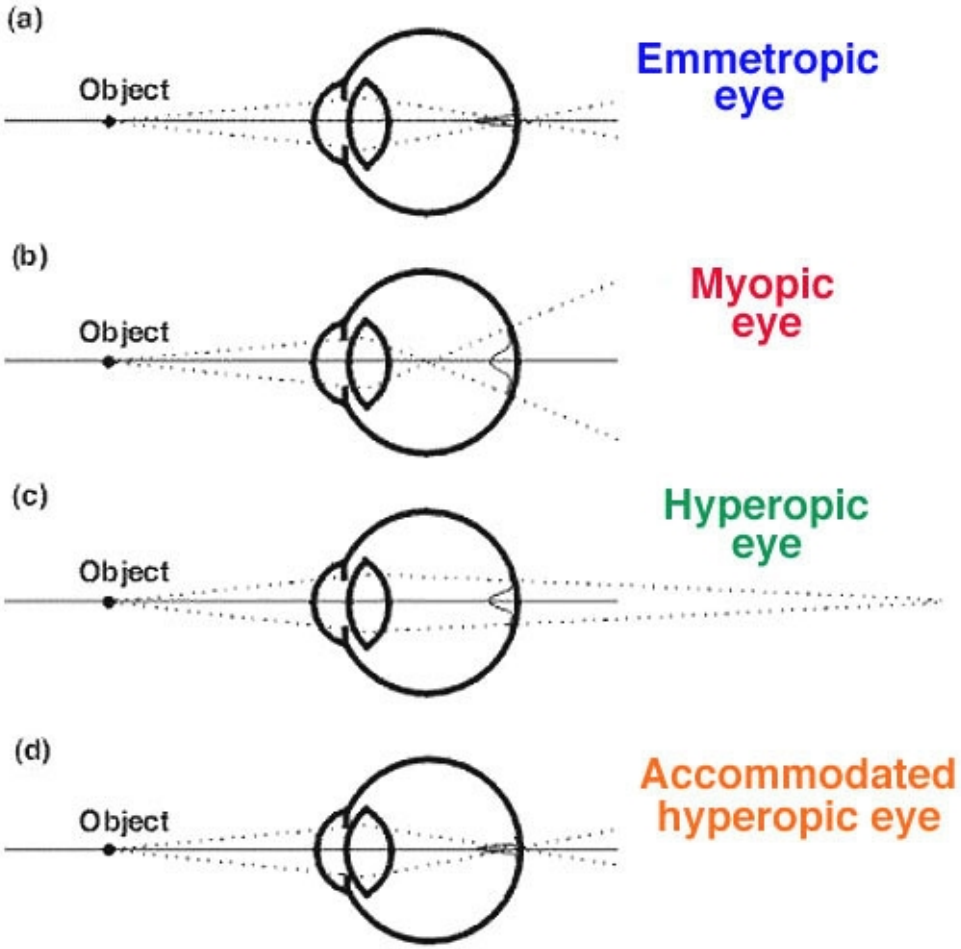

Figure 17. Point spread function at the back of the eye with different refractive errors.

20 shows that at eccentricities less than 15°, scotopic acuity is limited by the AII amacrine cell. Beyond 15°, scotopic acuity is limited by the midget ganglion cell (P cell) (15).

As noted above, a similar process may occur in the photopic system (5), where photopic resolution beyond an eccentricity of 2° falls below that predicted by cone density. The works by both Green (5) and Mills and Massey (15) provide evidence that post-receptoral processing is another factor that may limit visual acuity.

Eye Movement

During steady fixation, the eyes are in constant motion. Under these conditions, retinal images traverse a distance of about 3 minutes of arc in one second.

Contrast Sensitivity

Contrast is an important parameter in assessing vision. Visual acuity measurement in the clinic uses high contrast, that is, black letters on a white background. In reality, objects and their surroundings are of varying contrast. Therefore, the relationship between visual acuity and contrast allows a more detailed understanding of our visual perception.

Grating patterns are used as a means of measuring the resolving power of the eye because the gratings can be adjusted to any size. The contrast of the grating is the differential intensity threshold of a grating, which is defined as the ratio:

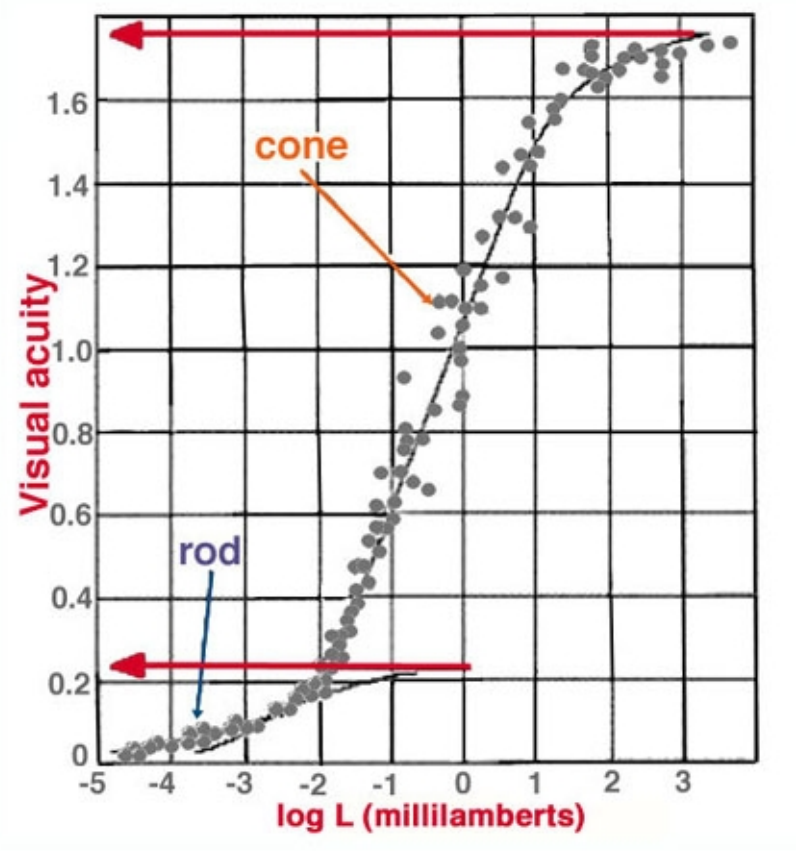

Figure 18. Relationship between visual acuity (decimal notation) and background luminance. The shallow curve at low luminances is attributable to the rod response, and the large sigmoidal curve is attributable to the cone response. The horizontal arrow identifies the maximum resolution of rod and cone systems. Konig's data from Riggs (21).

$$C = (L_{max} - L_{min})/(L_{max} + L_{min})$$

where C can have a value between 0.0 and 1.0; sometimes C is called the modulation, Raleigh or Michelson contrast (Fig. 21). The luminance of contrast gratings vary in a sinusoidal manner (Fig. 21). This allows the contrast of the grating to be altered without changing the average luminance of the screen displaying the gratings.

The size of the bars of the grating can be expressed in terms of the number of cycles (one cycle consists of one light bar plus one dark bar of the grating) per degree subtended at the eye. This is called the spatial frequency of the grating and can be thought of as a measure of the fineness or coarseness of the grating. The units can be cycles per degree (Fig. 22).

We can determine the sensitivity of the visual system as a function of grating size (spatial frequency). The contrast of the grating patterns is adjusted to determine the threshold for a given spatial frequency. That is, with a given spatial frequency, the contrast can be lowered until detection of the grating becomes impossible (contrast threshold). The reciprocal of this contrast threshold is called contrast sensitivity.

The contrast required for the visual system to reach a certain threshold can be expressed as a sensitivity on a *decibel* (dB) scale (contrast sensitivity in dB = $-20 \log_{10} C$). A plot of (contrast) sensitivity *versus* spatial frequency is called the **spatial contrast sensitivity function** (SCSF, or usually abbreviated to CSF).

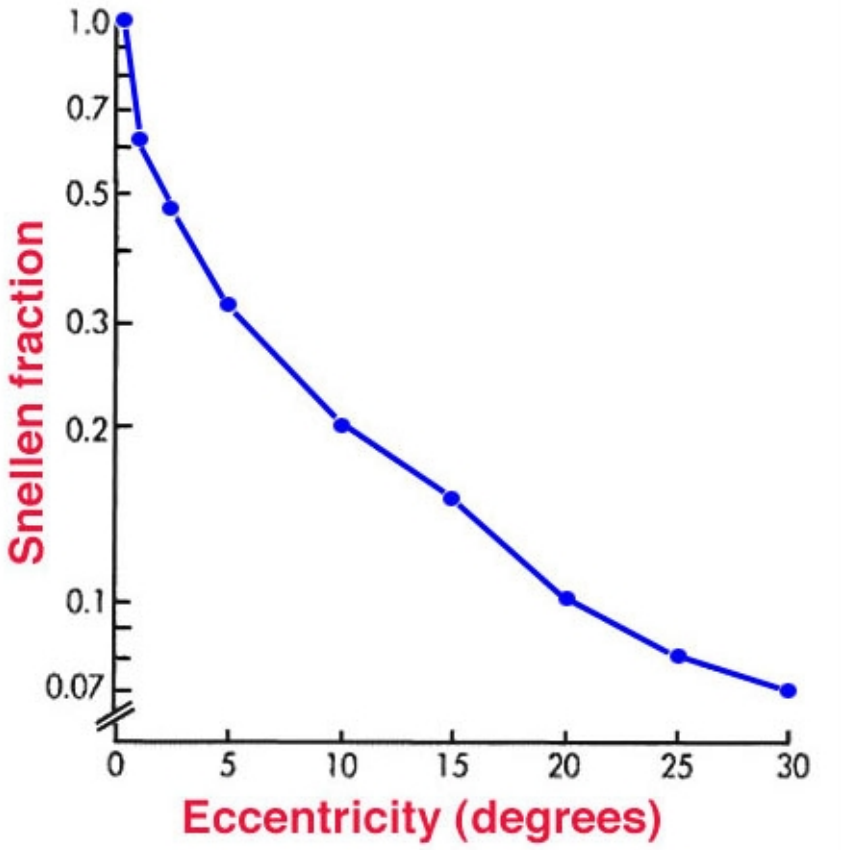

Figure 19. The effects of eccentricity on visual acuity (expressed in decimal notation). From Westheimer (22).

Contrast Sensitivity Function

Under photopic conditions, contrast sensitivity measurements reveal a band-pass function when using sinusoidal gratings (Fig. 23). The peak of the CSF function is in the mid-spatial range, and only under high contrast conditions is resolution at its maximal level.

The shape and critical parameters of the CSF depends on a number of factors including: the mean luminance of the grating, whether the luminance profiles of the gratings are sinusoidal or square waveforms; the level of defocus; and the clarity of the optics of the eye. At low light levels, maximum contrast sensitivity is approximately 8% and maximum resolution is approximately 6 cycles per degree. As mean light levels increase, the peak of the contrast sensitivity function is now close to 0.5% contrast, and the high spatial frequency cut off is at about 50 to 60 cycles per degree (~6/3 or 20/10). Also shown in Fig. 24, at photopic light levels, the peak contrast sensitivity is at approximately 5 to 10 cycles per degree (16).

The contrast sensitivity function provides a more thorough representation of the visual system. For example, the pivotal visual developmental study of Harwerth et al. (17) characterized the changes in the contrast sensitivity function after different periods of monocular deprivation in monkeys. The loss of sensitivity in the mid to high spatial frequencies was profound during abnormal visual development, with increased deprivation leading to further contrast losses. Not only will certain disease/disorders of the eye reduce visual acuity, contrast sensitivity will also be affected (18). For example, patients with multiple sclerosis will have mid to low contrast sensitivity losses (Fig. 25B), whereas patients with cataracts will have an overall reduction in contrast sensitivity (Fig. 25C). Mild refractive error or mild amblyopia will lead to a CSF similar to D in Fig. 25, with more severe refractive errors or severe amblyopia, resulting in a CSF similar to curve C.

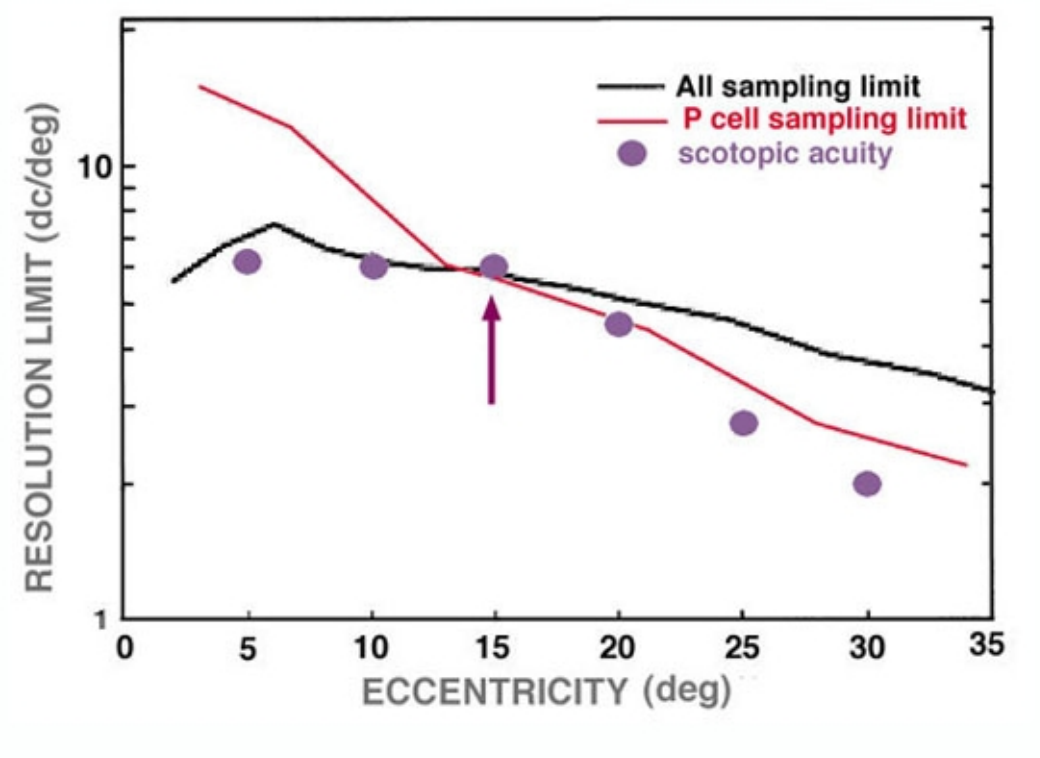

Figure 20. Scotopic acuity is limited by the AII amacrine cells at eccentricities less that 15° (open circles following the black line). After 15°, scotopic acuity is limited by P cells (open circles following the gray line). The arrow indicates the approximate location of maximum rod density. From Mills and Massey (15).

Spatial Summation

Spatial summation describes the eye's ability to summate or add up quanta over a certain area. This area over which spatial summation operates is called the critical diameter. According to Ricco's law, within this critical diameter, the threshold is reached when the total luminous energy reachs a constant value (k). Threshold is reached when the product of luminance (L) and stimulus area (A) equals or exceeds this constant value. In other words, when luminance is halved, a doubling in stimulus area is required to reach threshold. When luminance is doubled, the stimulus area can be halved and still reach threshold. Ricco's law is expressed as:

$$L \cdot A^{n} = k$$

where L is the luminance of the stimulus, A is the area of the stimulus, k is a constant value, and n describes whether spatial summation is complete ($n = 1$) or partial ($0 < n < 1$). No spatial summation occurs when $n = 0$. Critical area varies with eccentricity. Ricco's law holds for an area of 30 minutes of arc in the parafoveal area (4 to 7° eccentricity) and increasing to an area of about 2° at an eccentricity of 35° (19).

Spatial summation occurs because of the convergence of photoreceptors onto ganglion cells. This convergence of photoreceptors form a receptive field; thus, stimulating different photoreceptors within this receptive field would result in one signal. Receptive field sizes vary with eccentricity (Fig. 26) and helps explain the reason why critical area varies with eccentricity (20). Clearly, the size of spatial summation (functional receptive field) will limit resolution capabilities as outlined earlier.

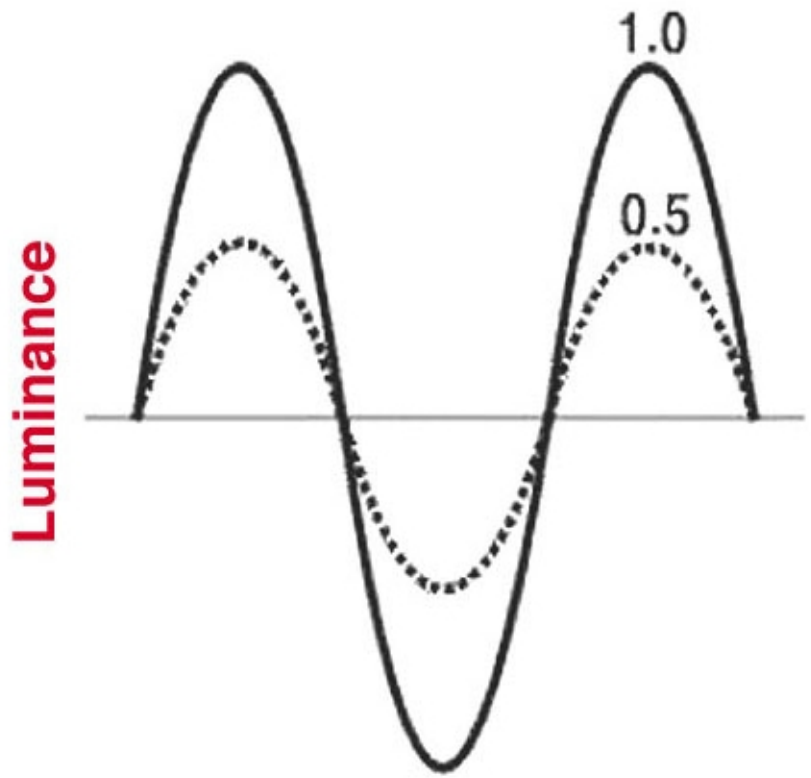

Figure 21. Luminance profile of sinusoidal gratings of contrast ratio of 1.0 and 0.5. For the contrast value of 1, the grating would have the maximum and minimum available luminances.

A schematic spatial summation graph is shown in Fig. 27. A simple logarithmic transform of $L \cdot A = k$ results in the log$L$ *versus* log$A$ plot having a straight line with a slope of −1 (complete spatial summation within Ricco's law). Outside the critical area, such a plot has a slope of 0, indicating that the size of the target does not affect the threshold.

Fig. 28 shows data on spatial summation where spots of light with different background luminances are presented 6.5° nasally from the fovea. Ricco's law of complete spatial summation holds when the gradient is −1 (solid line). Note that the critical area is larger for low luminance and smaller for high luminance. Such a change reflects the functional alteration of receptive field size with changes in adaptation level (20).

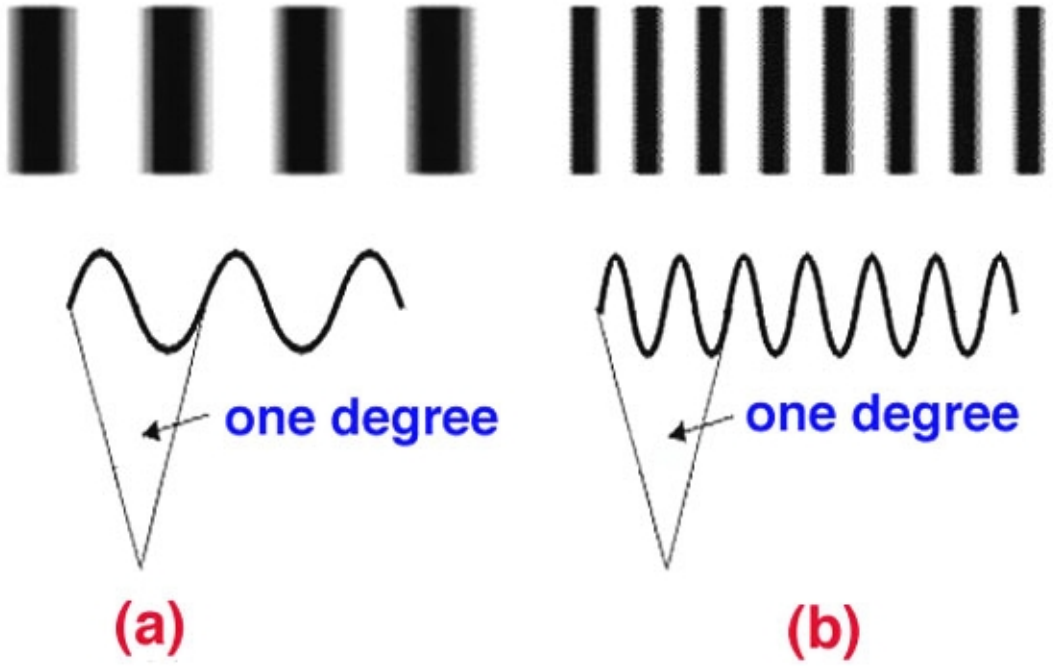

Figure 22. Spatial frequency is a measure of the number of cycles subtended at the eye per degree. (a) One cycle per degree. (b)Two cycles per degree.

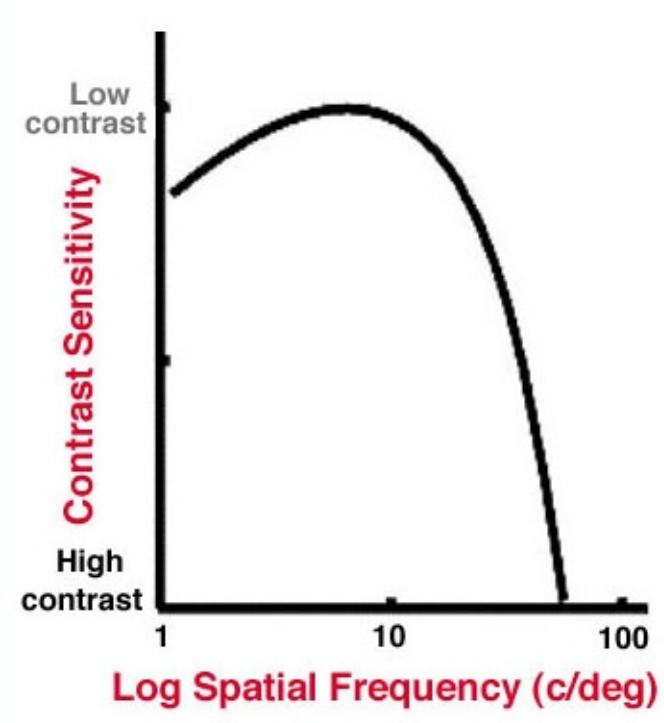

Figure 23. Photopic contrast sensitivity function.

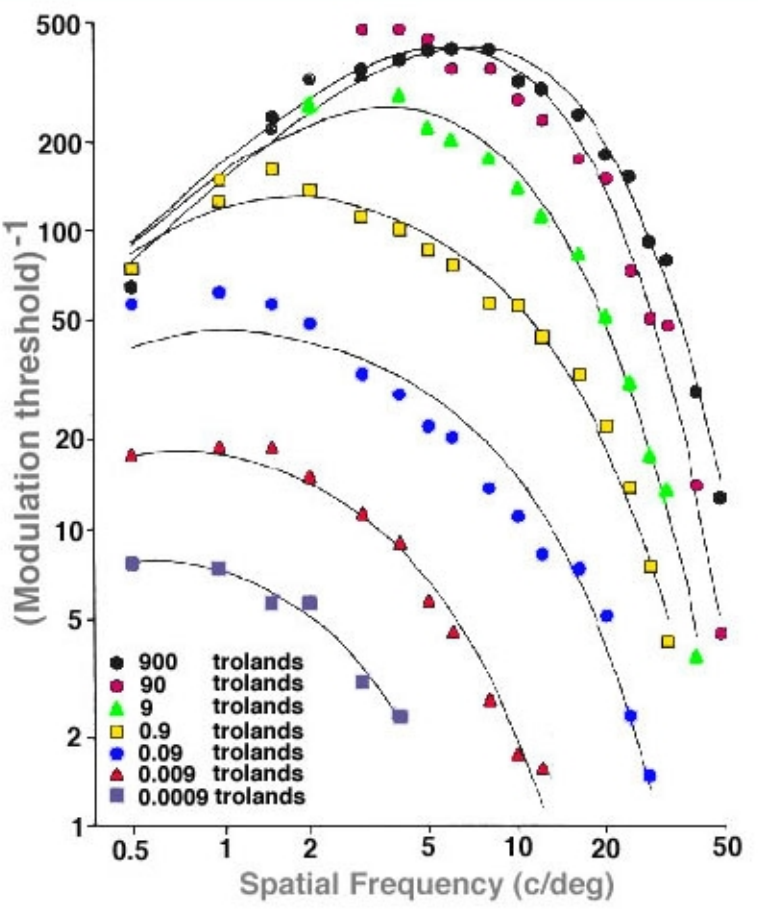

Figure 24. Contrast sensitivity function showing a change in shape from low pass at low luminances and bandpass at high luminances. van Ness' data from Lamming (23).

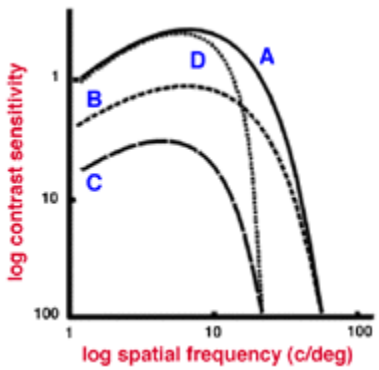

Figure 25. Examples of how the CSF is altered due to refractive error or disease.

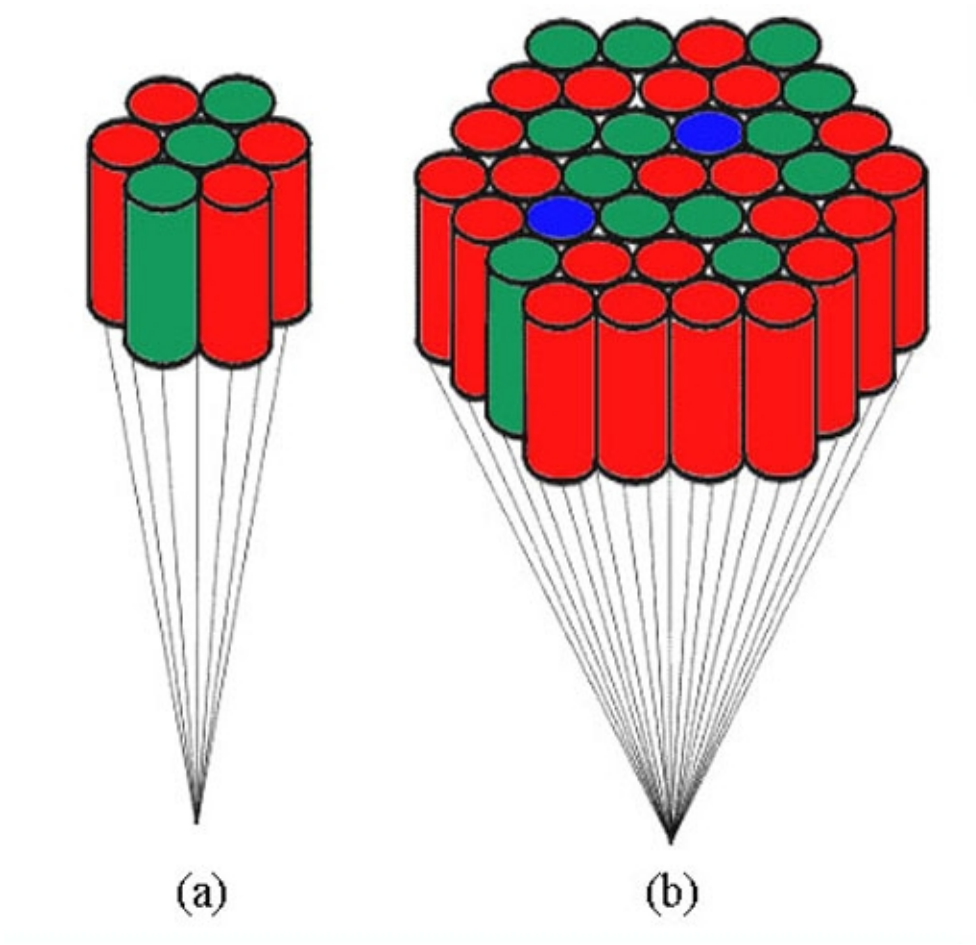

Figure 26. Schematic illustration of the size of receptive fields in the parafoveal region (7° eccentricity) (a) and in the peripheral retina (35° eccentricity) (b).

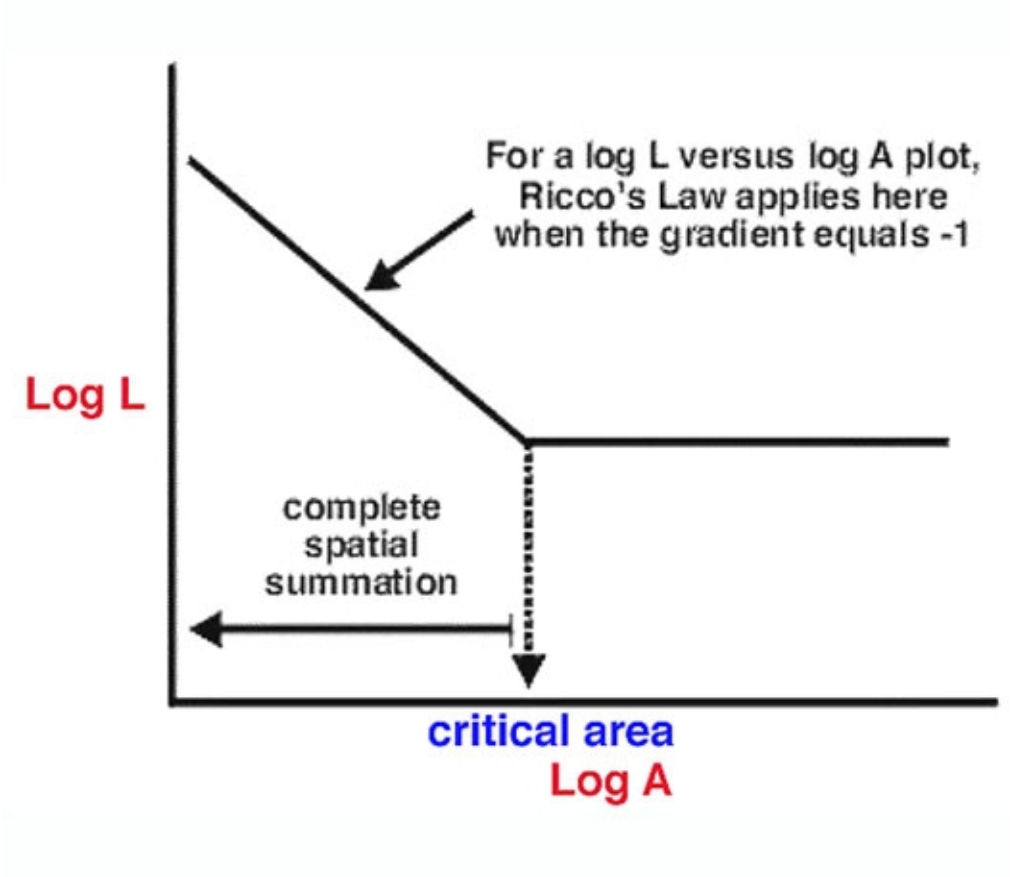

Figure 27. Spatial summation data plotted on a logarithmic scale as log L versus log A.

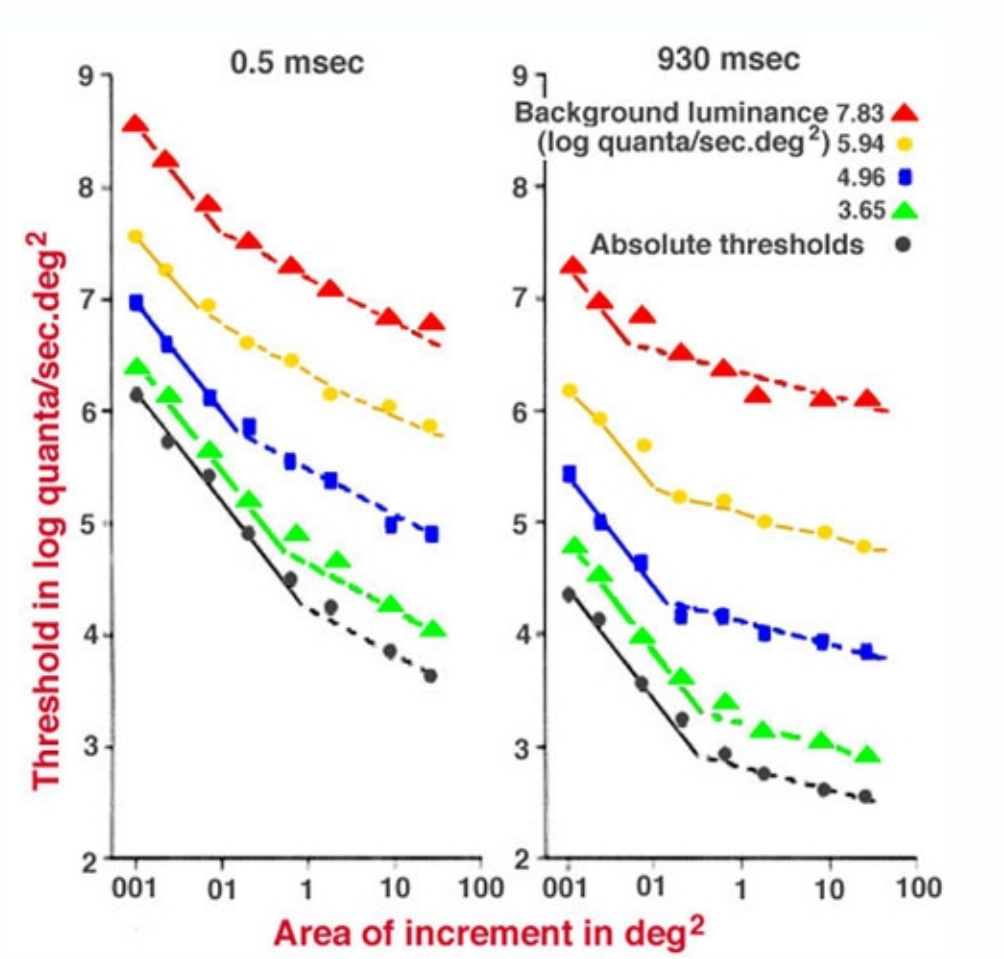

Figure 28. Log luminance (quanta/sec.deg^2 is a another method of expressing illuminance, similar to troland) as a function of area for two different stimulus durations. Ricco's law is represented by the solid line with a gradient of −1. Barlow's data from Lamming (24).

About the Authors

Michael Kalloniatis was born in Athens Greece in 1958. He received his optometry degree and Master's degree from the University of Melbourne. His PhD was awarded from the University of Houston, College of Optometry, for studies investigating colour vision processing in the monkey visual system. Post-doctoral training continued at the University of Texas in Houston with Dr Robert Marc. It was during this period that he developed a keen interest in retinal neurochemistry, but he also maintains an active research laboratory in visual psychophysics focussing on colour vision and visual adaptation. He was a faculty member of the Department of Optometry and Vision Sciences at the University of Melbourne until his recent move to New Zealand. Dr. Kalloniatis is now the Robert G. Leitl Professor of Optometry, Department of Optometry and Vision Science, University of Auckland. e-mail: m.kalloniatis@unsw.edu.au

Charles Luu was born in Can Tho, Vietnam in 1974. He was educated in Melbourne and received his optometry degree from the University of Melbourne in 1996 and proceeded to undertake a clinical residency within the Victorian College of Optometry. During this period, he completed post-graduate training and was awarded the post-graduate diploma in clinical optometry. His areas of expertise include low vision and contact lenses. During his tenure as a staff optometrist, he undertook teaching of optometry students as well as putting together the "Cyclopean Eye", in collaboration with Dr Michael Kalloniatis. The Cyclopean Eye is a Web based interactive unit used in undergraduate teaching of vision science to optometry students. He is currently in private optometric practice as well as a visiting clinician within the Department of Optometry and Vision Science, University of Melbourne.

References

1. Smith G, Atchison DA. The eye and visual optical instrument. New York: Cambridge University Press; 1997.
2. Bailey IL, Lovie JE. New design principles for visual acuity letter charts. Am J Optom Physiol Opt. 1976;53:740–745. PubMed PMID: 998716.
3. Waugh SJ, Levi DM. Spatial alignment across gaps: contributions of orientation and spatial scale. J Opt Soc Am A Opt Image Sci Vis. 1995;12:2305–2317. PubMed PMID: 7500212.
4. Westheimer G. Visual acuity and spatial modulation thresholds. In: Jameson D, Hurvich LM, editor. Handbook of sensory physiology. Visual psychophysics. Vol. 7. Berlin: Springer-Verlag; 1972. pt. 4. p. 170-187.
5. Green DG. Regional varitations in the visual acuity for interference fringes on the retina. J Physiol. 1970;207:351–356. PubMed PMID: 5499023.
6. Helmholtz HV. Handbuch der physiologischen optik. Leipzig: Leopold Voss; 1867.

7. Campbell FW, Green DG. Optical and retinal factors affecting visual resolution. J Physiol. 1965;181:576–593. PubMed PMID: 5880378.
8. Curcio CA, Sloan KR, Kalina RE, Hendrickson AE. Human photoreceptor topography. J Comp Neurol. 1990;292:497–523. PubMed PMID: 2324310.
9. Roorda A, Williams DR. The arrangement of the three cone classes in the living human eye. Nature. 1999;397:520–522. PubMed PMID: 10028967.
10. Atchison DA, Smith G, Efron N. The effect of pupil size on visual acuity in uncorrected and corrected myopia. Am J Optom Physiol Opt. 1979;56:315–323. PubMed PMID: 495689.
11. Hecht S. The relation between visual acuity and illumination. J Gen Physiol. 1928;11:255–281.
12. Graham CH. Vision and visual perception. 1965.
13. Kolb H, Linberg KA, Fisher SK. Neurons of the human retina: a Golgi study. J Comp Neurol. 1992;318:147–187. PubMed PMID: 1374766.
14. Wässle H, Grunert U, Chun MH, Boycott BB. The rod pathway of the macaque monkey retina: identification of AII-amacrine cells with antibodies against calretinin. J Comp Neurol. 1995;361:537–551. PubMed PMID: 8550898.
15. Mills SL, Massey SC. AII amacrine cells limit scotopic acuity in central macaque retina: a confocal analysis of calretinin labeling. J Comp Neurol. 1999;411:19–34. PubMed PMID: 10404105.
16. van Nes FL, Bouman MA, Maarten A. Spatial modulation transfer in the human eye. J Opt Soc Am. 1967;57:401–406.
17. Harwerth RS, Smith EL, Duncan GC, Crawford ML, von Noorden GK. Multiple sensitive periods in the development of the primate visual system. Science. 1986;232:235–238. PubMed PMID: 3952507.
18. Arden GB. The importance of measuring contrast sensitivity in cases of visual disturbance. Br J Ophthalmol. 1978;62:198–209. PubMed PMID: 348230.
19. H. Davson. Davson's physiology of the eye. 5th ed. London: Macmillan Academic and Professional Ltd.; 1990.
20. Shapley R, Enroth-Cugell C. Visual adaptation and retinal gain controls. Prog Retinal Res. 1984;3:263–346.
21. Riggs LA. Visual acuity. In: Graham CH, editor. Vision and visual perception. New York: John Wiley and Sons, Inc.; 1965.
22. Westheimer G. Visual acuity. In: Moses RA, Hart WM, editor. Adler's physiology of the eye. Clinical application. St. Louis (MO): The C.V. Mosby Company; 1987.
23. Lamming D. Contrast sensitivity. In: Cronly-Dillon J, editor. Vision and visual dysfunction. Vol. 5. London: Macmillan Press; 1991.
24. Lamming D. Spatial frequency channels. In: Cronly-Dillon J, editor. Vision and visual dysfunction. Vol. 5. London: Macmillan Press; 1991.

Temporal Resolution

Michael Kalloniatis and Charles Luu.[1]

Created: May 1, 2005; Updated: June 5, 2007.

The eye can function over a large range of luminance levels; it must also be able to handle the different rates of change in luminance. Our eyes are constantly sampling information of images projected onto the retina in a periodic manner. Information is then integrated so objects around us appear to be stable or move smoothly. Because there is a finite amount of time required to collect and process information, there are limitations to the responsiveness of our visual system to rates of change. When intermittent stimuli are presented to the eye, they are perceived as separate if the rate at which they are presented is below a certain value. If the rate of presentation of the intermittent stimuli is slow, it appears to stay on but with changes in intensity, producing the sensation called flicker. Above a certain critical rate, the flicker ceases. This point is called the critical flicker frequency and is influenced by a number of factors. The first factor to be considered is the temporal summation property of the visual system.

Temporal Summation

Temporal Resolution and Temporal Summation

In the spatial domain, detection of two lights in space requires the appropriate detector array (Fig. 1). For us to discriminate the two lines, a response given by detector array C to F is required. All of these detector arrays provide a Yes-No-Yes response and thus allow the discrimination of the two lines.

In the temporal domain, the same principle applies, except now the stimulus is separated in time (Fig. 2). The separation between the two lines is in the temporal domain (two flashes are delivered) after a time interval *t*. The detector array now has different temporal integration times. For example, detector A integrates over time = *t*, whereas detector array B has an integration time of time = 0.5*t*, array C, time = 0.33*t*, and so on. Because of the shorter integration time for detector array C and beyond, such an array will be able to discriminate the two flashes that are separated by an interval of *t*.

To detect a flash of light one after the other, an appropriate integration time is required (Fig. 3). The period of integration is up to 0.1 seconds or 100 ms (for rods) and 10 to 15 ms for cones. The advantage of long integration time is that under limited light level conditions, a threshold will be reached, whereas when light levels are not limiting (cone or photopic vision), a short integration time is preferable to improve temporal resolution.

Temporal integration time is related to temporal summation. Temporal summation refers to the eye's ability to sum the effects of individual quanta of light over time. However, temporal summation only occurs within a certain period of time, called the critical duration or critical period. According to Bloch's law of vision, within this critical duration, the threshold is reached when the total luminous energy is reached. Bloch's law of temporal summation is analogous to Ricco's law of spatial summation. Bloch's law states that total luminous energy is a constant value (k), thus threshold is reached when the product of luminance (L) and stimulus duration (t) equals this constant. In other words, when luminance is halved, a doubling in stimulus duration is required to reach threshold. When luminance is doubled, the threshold can be reached in half the duration. Bloch's law is expressed as:

$$L \cdot t^{n} = k$$

Author Affiliation: 1 Department of Optometry and Vision Sciences University of Melbourne, Australia.

where L is the luminance of the stimulus, t is the duration of the stimulus, k is a constant value, and n describes whether temporal summation is complete ($n = 1$) or partial ($0 < n < 1$). No temporal summation occurs when $n = 0$ (Fig. 4).

Critical duration is shorter for stimulus of high luminance as threshold is reached faster and slower for stimulus of low luminance as a longer period of time is required to sum the quanta to reach threshold. Temporal summation ceases beyond the temporal integration time. Above this value, threshold is dependent only on luminance rather than the product of luminance and duration.

Temporal summation is also affected by other test variables, such as background luminance and the size of the stimulus. Critical duration is longer for brighter background and smaller test stimuli. When temporal summation data areplotted as log$L$ t *versus* log$t$ rather than log$L$ *versus* log$t$ (as in Fig. 4), the slope of zero identifies Bloch's law (Fig. 5).

The above plots show that temporal summation is longer for low light levels, indicating the larger temporal summation characteristics for scotopic vision. As light intensity is increased, e.g., 25,000 trolands, the critical duration is of the order of 20–30 msec. The interrelationship between temporal integration and spatial summation is shown on the right panel, where Bloch's law is measured for different sizes of test stimuli. Decreasing test size results in increased temporal summation, and hence poorer temporal discrimination. We will investigate this phenomenon further when we review flicker discrimination for different sized stimuli in the next section.

Broca-Sulzer Effect

In addition to basic discrimination characteristics of temporal resolution, there are several interesting perceptual phenomena. One of these phenomena is the Broca-Sulzer effect, which describes the apparent transient increase in brightness of a flash of short duration. Subjective flash brightness occurs with flash durations of 50 to 100 milliseconds. This phenomenon is associated with temporal summation and explains the leveling off of brightness to a plateau. When the light is turned on, time is required for temporal summation to reach threshold for light of low luminance. Light of high luminance reaches this threshold very quickly. As flash duration increases, brightness levels off to a plateau as temporal summation begins to breakdown, according to Bloch's law, after the critical duration. The apparent transient peak in brightness is probably attributable to an underlying neural mechanism (Fig. 6).

Critical Flicker Frequency

Critical flicker frequency (CFF) is the transition point of an intermittent light source where the flickering light ceases and appears as a continuous light. There are a multitude of factors that determine our perception of flicker that includes the intensity and size of the test stimulus.

Factors Affecting CFF

The **Ferry-Porter law** states that CFF is proportional to the logarithm of the luminance of flickering stimulus (L). It can be expressed as:

$$CFF = a \log L + b$$

where a and b are constants. With foveal observation, this relationship holds over a wide range (0.5 to 10,000 trolands) (Fig. 7). The above equation implies that when CFF is plotted as a function of log$L$, a straight line will identify the region where the Ferry-Porter law holds. As the intensity of the test stimulus is increased, our perception of flicker also increases. From a practical point of view, if a stimulus is flickering, such as computer monitor, decreasing the intensity level will eliminate the flicker.

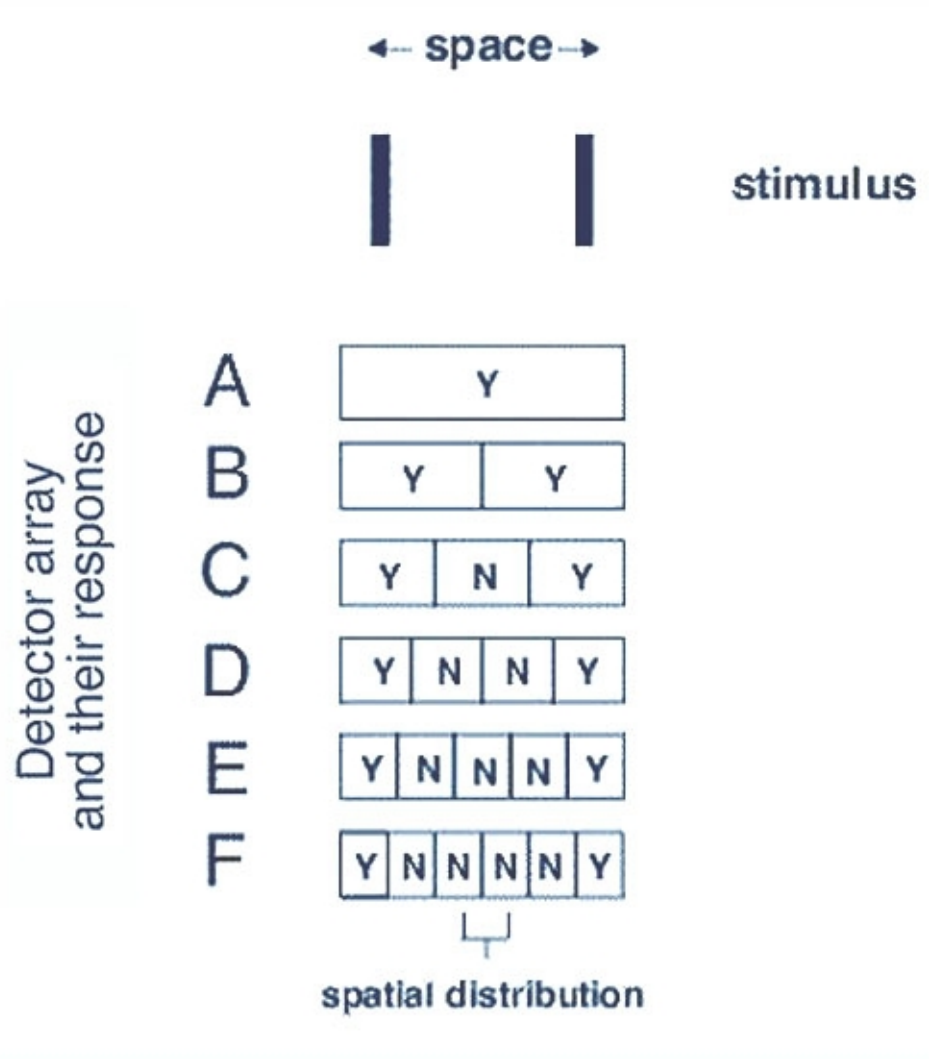

Figure 1. Detector array C and beyond allows the detection of the two lines.

Spectral Composition

Under photopic levels, lights of different wavelengths, when adjusted to match them for brightness, conforms to the Ferry-Porter law and follows the logarithmic function as brightness increases. However, under scotopic levels (rods functioning), the wavelengths fan out (Fig. 8). This is attributable to the different spectral sensitivities of the scotopic system to the photopic system. If plotted as scotopic photons, the bottom part of the curve would collapse into one and appear like the 19° curve in Fig. 10. Note that the temporal resolution to short wavelength test stimuli is different. However, in general terms, the plot below is correct, although the units chosen for the scotopic component (lower branches) give the misconception that temporal resolution is different for the rod system.

An important aspect of cone vision is that when the short-wavelength pathway is isolated (1), the temporal resolution is lower, close to 10–15 Hz, rather than the closer to 60 Hz for the longer wavelength pathways. This general phenomenon is characteristic of the short-wavelength pathway that is known to have larger spatial summation approximately 15' at about one degree eccentricity (the location of high S-cone density), whereas the longer wavelength pathways have a spatial summation of 4' (2). In the temporal domain, at high light levels, the S-cone pathways has a temporal summation time of approximately 100 ms, whereas the longer-wavelength cone pathway has a temporal integration of approximately 50 msec (3).

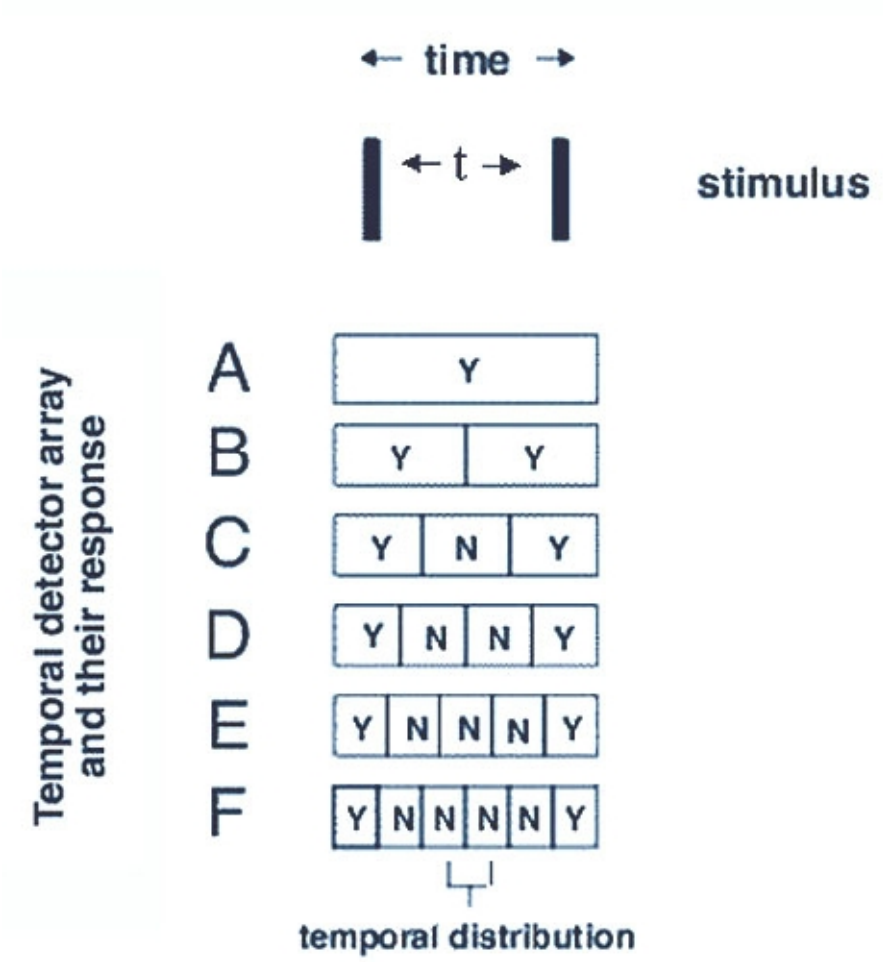

Figure 2. Speed of integration allows the detection of intermittent stimuli. Detector arrangement C and beyond allows discrimination of the stimuli over time.

Retinal Position

Because the CFF is different for rod and cones, the CFF for the test field will depend on the proportion of rods and cones being stimulated. Because the proportion of rod and cones changes with eccentricity, a foveal test stimulus will follow the Ferry-Porter law and show no kink (one branch only) in the curve because only cones are present at the fovea. An extrafoveal test stimulus will show a kink (two branches) in the CFF function because the rods determine the CFF at low retinal illuminances and the cones determining CFF at higher retinal illuminance. Note that the Ferry-Porter law applies over a decreasing range as the eccentricity increases, and that temporal resolution is poorer for eccentric locations (Fig. 9).

The Ferry-Porter law has been further examined for a single cone type, using conditions that eliminate detection of the flickering stimulus by rods. Under these conditions, the law has been found to hold, despite changes in stimulus size or modulation amplitude (4). However, the slope of the Ferry-Porter law changes with eccentricity, becoming steeper with eccentrically presented targets. This latter finding is consistent with previous work, suggesting that there is an increase in the speed of photopic retinal responses in the periphery, once stimuli have been appropriately scaled (5). This increase in speed has been hypothesized to relate to the change in cone photoreceptor outer-segment length that occurs in the periphery (5). Such scaling has not been performed to the classic data sets presented here.

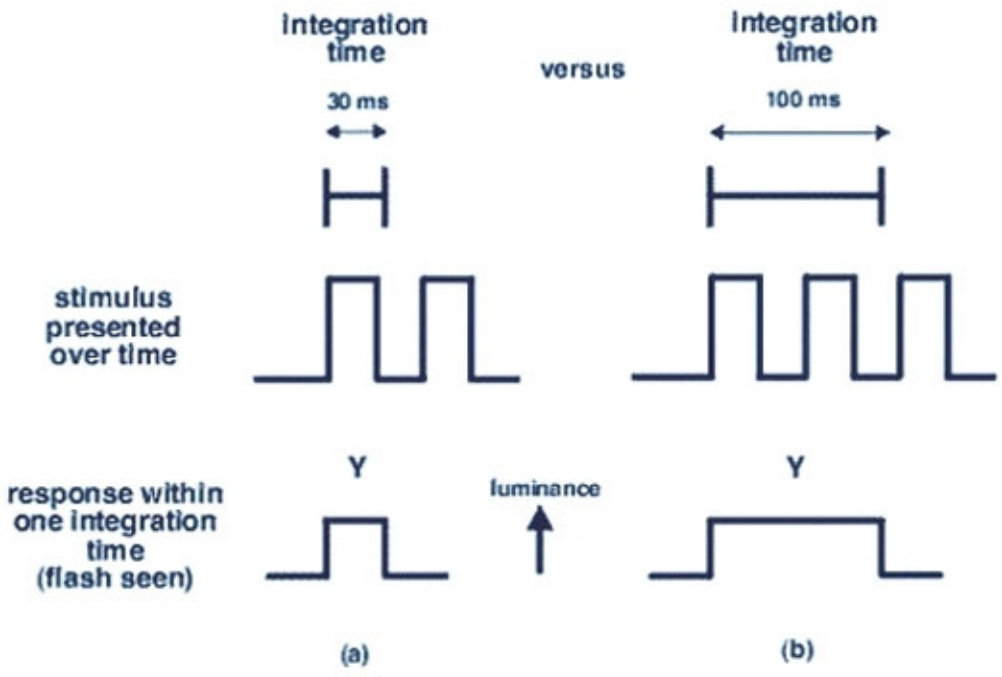

Figure 3. Flashes of light are presented to the eye. (a) With a short integration time, the flashes are detected. (b) No flashes are perceived (that is, the stimulus appeared as one bright flash) with a long integration time.

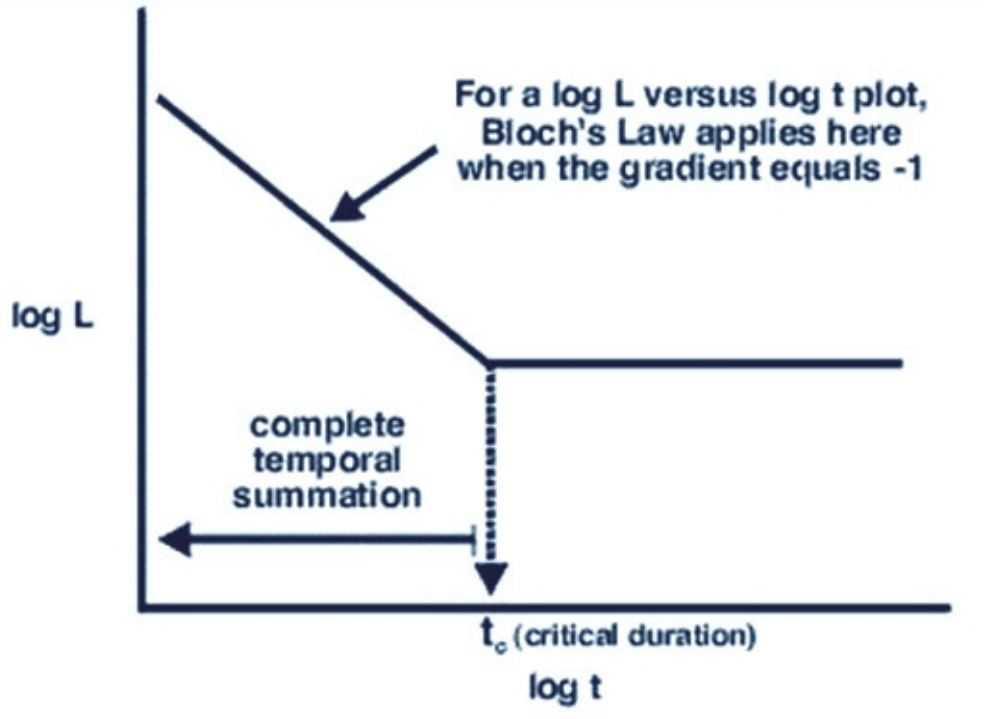

Figure 4. Temporal summation data plotted as log*L versus* log*t*, showing where Bloch's law applies.

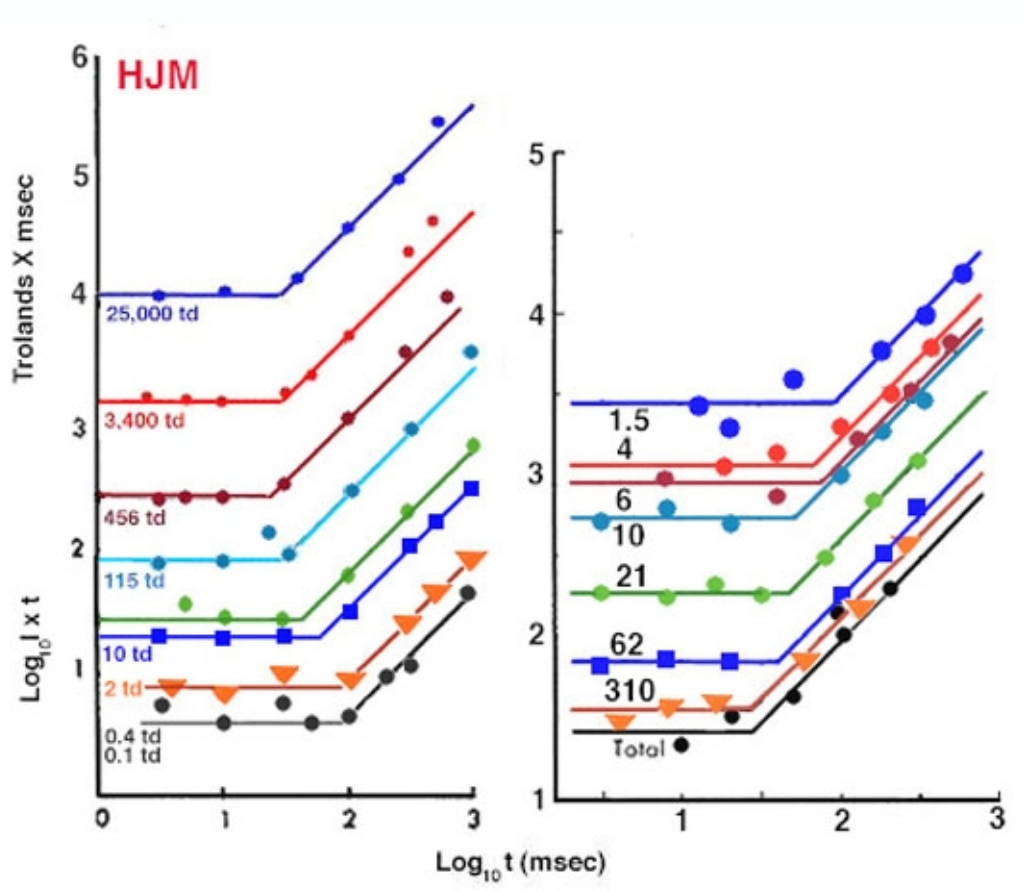

Figure 5. Luminance-duration *versus* time curves. Bloch's law holds when the gradient of the line is zero. Integration time (critical duration) can be determined from above. Beyond critical duration, Bloch's law breaks down (when the gradient is greater than zero). (a) 1° foveal test spot on different backgrounds. (b) Foveal test spots of different diameter (in minutes of arc) and for whole-eye stimulation (total). Kahneman and Norman's data from Hart (8).

Size of Test Field

Because of the different populations of rods and cones in the retina and different spatial summation properties, CFF will be dependent on the area of the retina being stimulated. Instead of varying retinal eccentricity as above, the size of the centrally fixated test field is varied (Fig. 10). As the test field increases, two branches begin to appear. The lower branch represents rod function. The maximum CFF, and hence maximum temporal resolution, is achieved by large test targets that have the shortest integration time noted earlier.

The **Talbot-Plateau law** describes the brightness of an intermittent light source that has a frequency above the CFF. This law states that above CFF, subjectively fused intermittent light and objectively steady light (of equal color and brightness) will have exactly the same luminance. In another words, brightness sensation from the intermittent light source is the same as if the light perceived during the various periods of stimulation had been uniformly distributed over the whole time. The Talbot-Plateau law applies only above the CFF.

The **Brücke-Bartley** (brightness enhancement) effect is a phenomenon related to the Broca-Sulzer effect. When the frequency is gradually lowered below the CFF, the effective brightness of the test field begins to rise. Not only does the brightness reach a value equal to that of the uninterrupted light, but the brightness even transcends it, reaching a maximum when the flash rate is about 8 to 10 Hz.

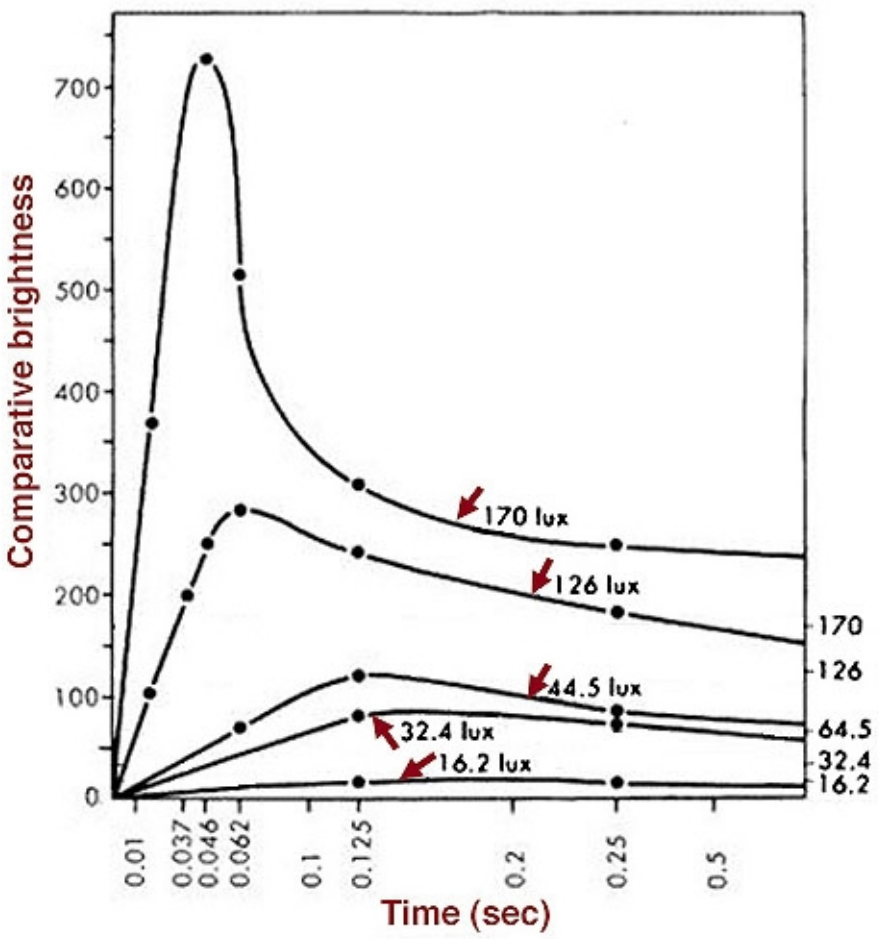

Figure 6. Apparent brightness of flashes with various luminances, as a function of flash duration. Broca and Sulzer data from Hart (8).

Temporal Contrast Sensitivity

In the spatial domain, spatial vision can be characterized by the contrast sensitivity function (CSF). To thoroughly investigate the visual system to flicker, a Temporal Contrast Sensitivity Function (TSF), or a de Lange function, can be plotted (6). A TSF is a plot of how flicker varies with contrast and *vice versa*. Above the curve represents no flicker, whereas flicker can be detected below the curve (Fig. 11). The eye appears to be most sensitive to a frequency of 15 to 20 Hz at high luminances (photopic vision). At photopic light levels, less than 1% contrast is required to detect the stimulus, and the high temporal frequency cut off is close to 60 Hz. At low light levels, the maximum contrast is about 20% and the high temporal frequency cut off is approximately 15 Hz. To detect flicker of high frequencies, maximum contrast is required. Temporal resolution is not as efficient at low luminances (scotopic vision).

Different sensitivity profiles exist for the different components of the visual system (opponent *versus* non-opponent) to discriminate motion. For the luminance system, detection, identification, and direction discrimination provide equivalent thresholds. However, at all eccentricities tested, the chromatic system required approximately 0.3 log units higher contrast levels to signal direction of motion (Fig. 12) (7). Overall, these results imply that both luminance (non-opponent) and chromatic (opponent) visual channels are involved in motion discrimination.

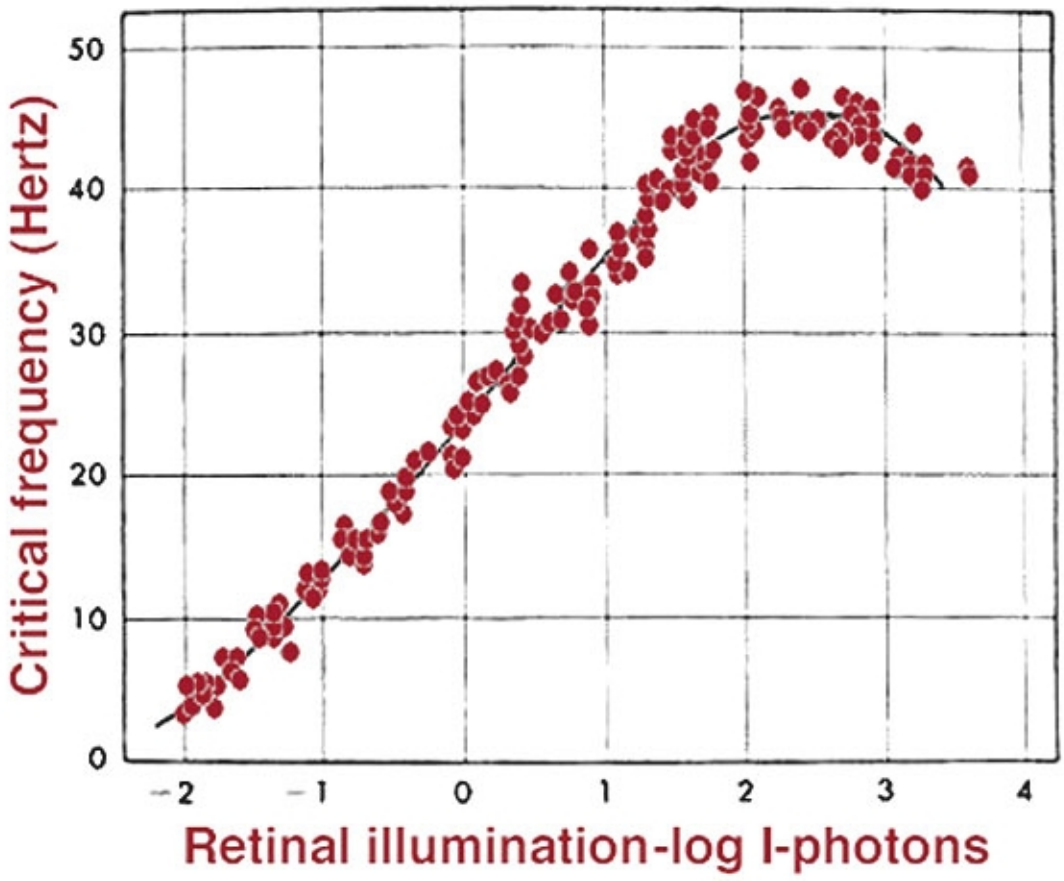

Figure 7. CFF at the fovea over a range of retinal illuminance (photon = troland) of the test field, showing conformity of the Ferry-Porter law over four logarithmic units. Hecht and Verrijp's data from Hart (8).

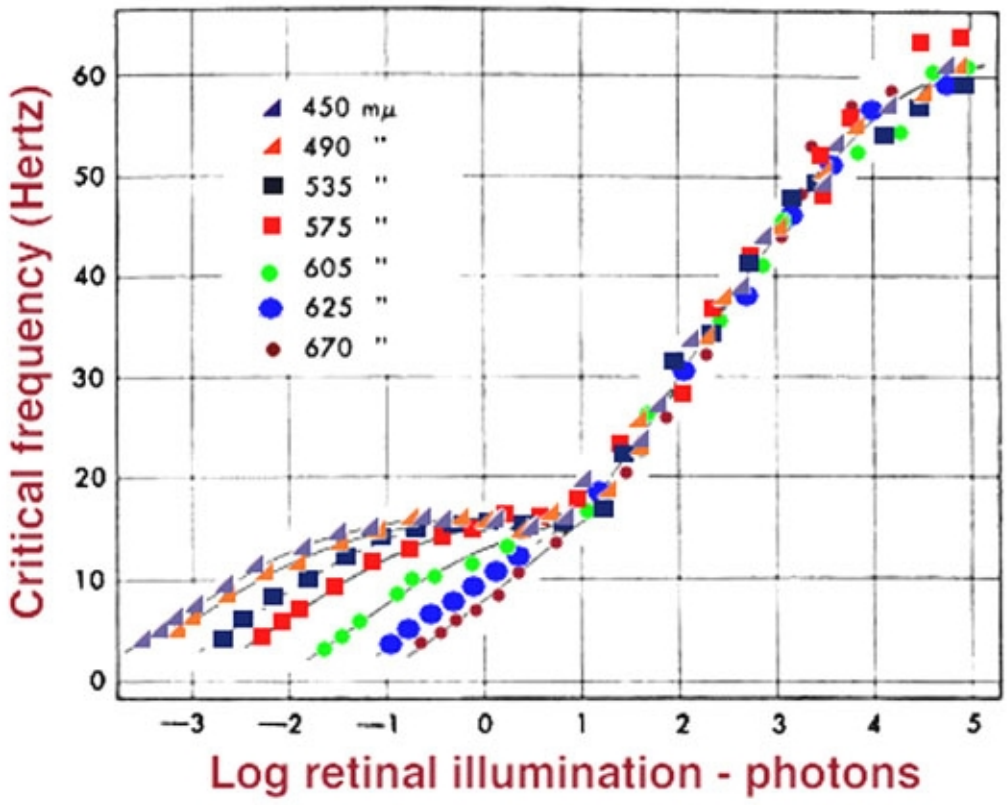

Figure 8. CFF of 19° test field over a range of retinal illuminance (photon = troland) for different monochromatic lights of different wavelengths. Hecht and Shlaer's data from Hart (8).

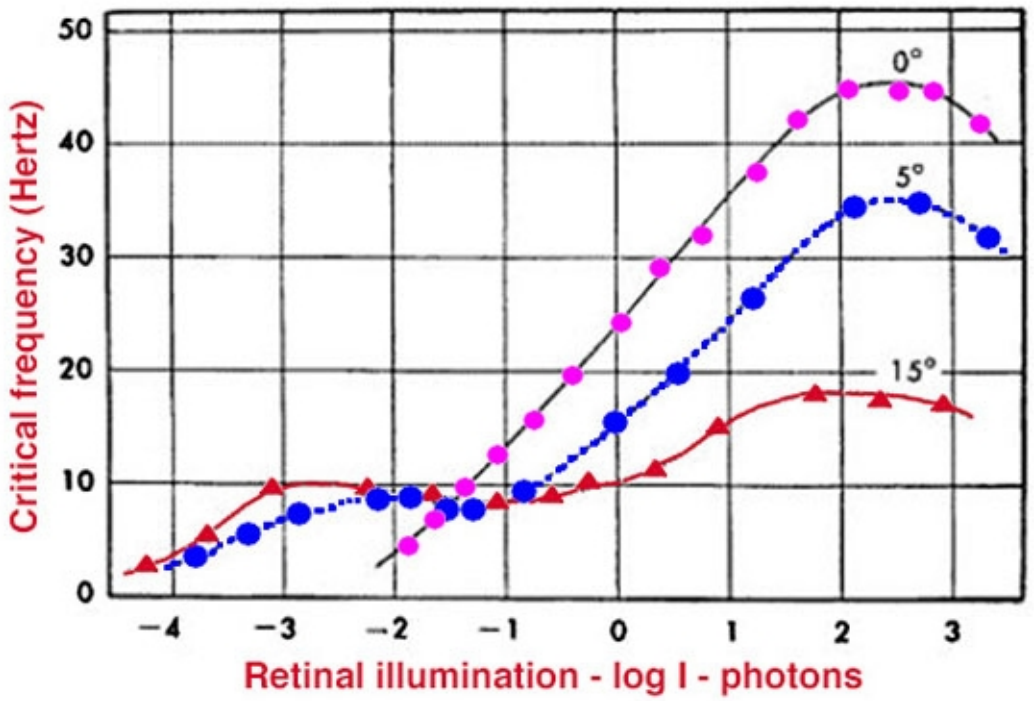

Figure 9. CFF of a 2° white test field over a range of retinal illuminances (photon = troland) measured at the fovea, 5° above the fovea, and 15° above the fovea. Hecht and Verrijp's data from Hart (8).

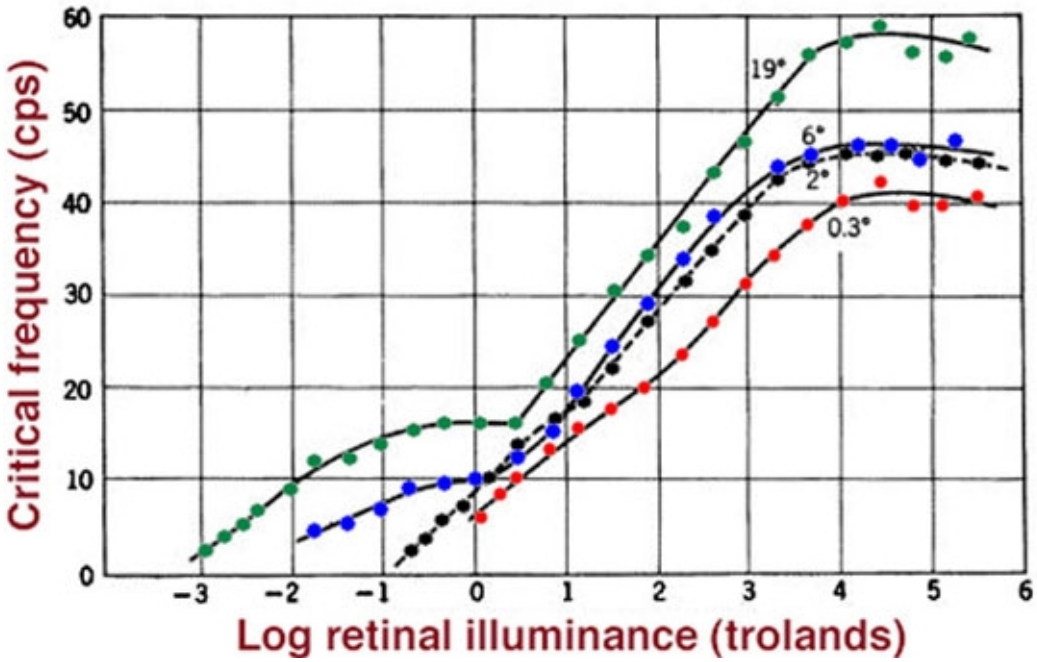

Figure 10. CFF over a range of retinal illuminance (photon = troland) for a centrally fixated test stimulus of different sizes. Hecht and Smith's data from Brown (9).

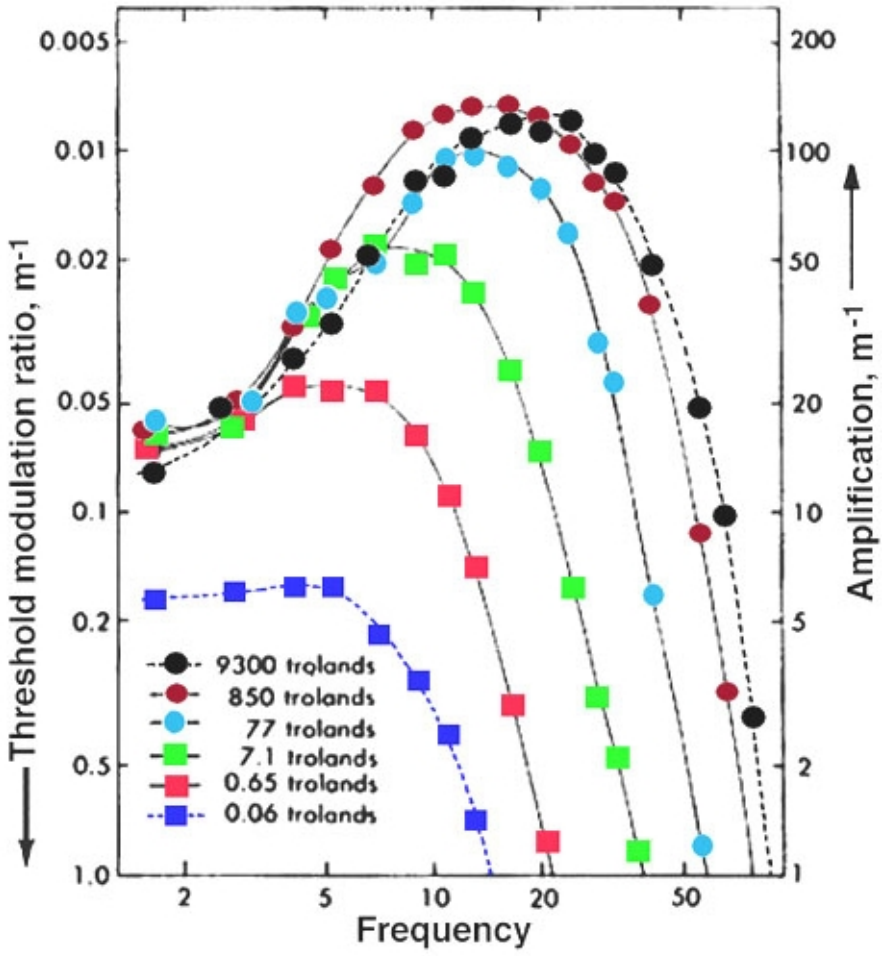

Figure 11. Temporal Contrast Sensitivity Function (TSF) for various adapting fields. Kelly's data from Hart (8).

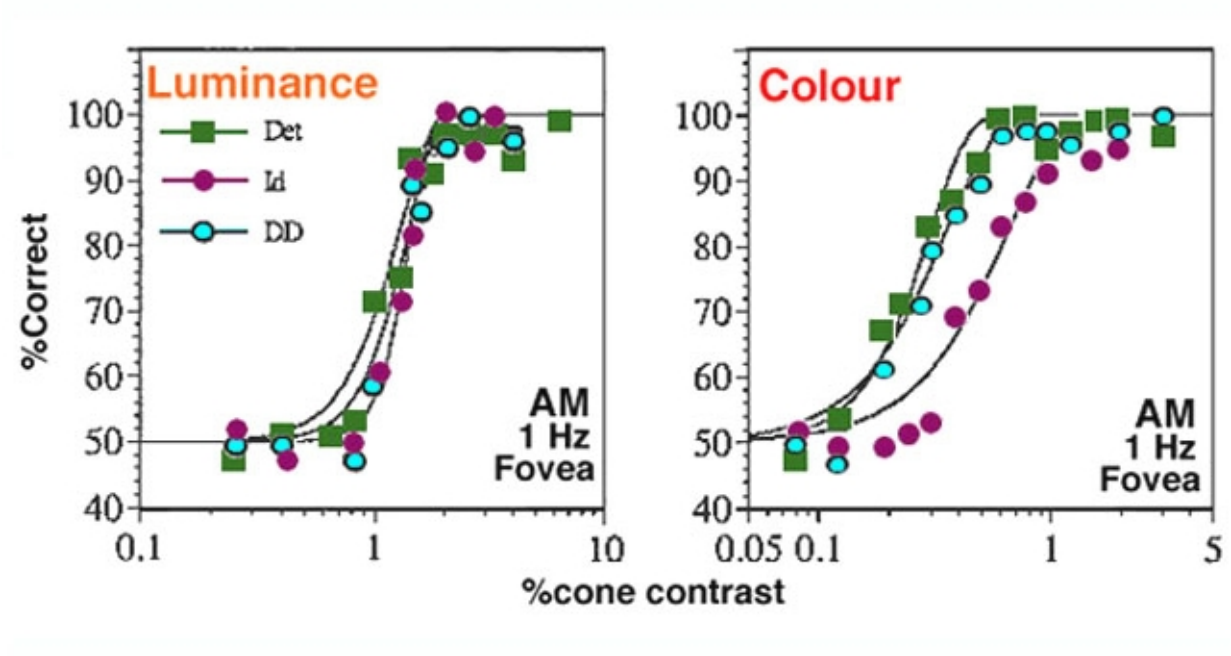

Figure 12. Psychometric functions for detection (squares), identification (filled circles), and direction discrimination (open circles) for 1 Hz stimulus that selected for the luminance channel (left panel) or chromatic channel (right panel). Data modified from Mehta et al. (7).

About the Authors

Michael Kalloniatis was born in Athens Greece in 1958. He received his optometry degree and Master's degree from the University of Melbourne. His PhD was awarded from the University of Houston, College of Optometry, for studies investigating colour vision processing in the monkey visual system. Post-doctoral training continued at the University of Texas in Houston with Dr Robert Marc. It was during this period that he developed a keen interest in retinal neurochemistry, but he also maintains an active research laboratory in visual psychophysics focussing on colour vision and visual adaptation. He was a faculty member of the Department of Optometry and Vision Sciences at the University of Melbourne until his recent move to New Zealand. Dr. Kalloniatis is now the

Robert G. Leitl Professor of Optometry, Department of Optometry and Vision Science, University of Auckland. e-mail: m.kalloniatis@unsw.edu.au

Charles Luu was born in Can Tho, Vietnam in 1974. He was educated in Melbourne and received his optometry degree from the University of Melbourne in 1996 and proceeded to undertake a clinical residency within the Victorian College of Optometry. During this period, he completed post-graduate training and was awarded the post-graduate diploma in clinical optometry. His areas of expertise include low vision and contact lenses. During his tenure as a staff optometrist, he undertook teaching of optometry students as well as putting together the "Cyclopean Eye", in collaboration with Dr Michael Kalloniatis. The Cyclopean Eye is a Web based interactive unit used in undergraduate teaching of vision science to optometry students. He is currently in private optometric practice as well as a visiting clinician within the Department of Optometry and Vision Science, University of Melbourne.

References

1. Kelley DH. Spatio-temporal frequency characteristics of color-vision mechanisms. J Opt Soc Am. 1974;64:983–990. PubMed PMID: 4841935.
2. Brindley GS. The summation areas of human colour-receptive mechanisms at increment threshold. J Physiol. 1954;124:400–408. PubMed PMID: 13175140.
3. Krauskopf J, Mollon JD. The independence of the temporal integration properties of individual chromatic mechanism in the human eye. J Physiol. 1971;219:611–623. PubMed PMID: 5157595.
4. Tyler CW, Hamer RD. Analysis of visual modulation sensitivity. IV. Validity of the Ferry-Porter law. J Opt Soc Am A. 1990;7:743–759. PubMed PMID: 2338596.
5. Tyler CW. Analysis of visual modulation sensitivity. II. Peripheral retina and the role of photoreceptor dimensions. J Opt Soc Am A. 1985;2:393–398. PubMed PMID: 3981280.
6. De Lange DZN H. Research into the dynamic nature of the human fovea–cortex systems with intermittent and modulated light. II. Phase shift in brightness and delay in color perception. J Opt Soc Am. 1958;48:784–789. PubMed PMID: 13588451.
7. Metha AB, Vingrys AJ, Badcock DR. Detection and discrimination of moving stimuli: the effects of color, luminance, and eccentricity. J Opt Soc Am A Opt Image Sci Vis. 1994;11:1697–1709. PubMed PMID: 8046536.
8. Hart WM Jr. The temporal responsiveness of vision. In: Moses RA, Hart WM, editors. Adler's physiology of the eye. Clinical application. St. Louis (MO): The C. V. Mosby Company; 1987.

9. Brown JL. Flicker and intermittent stimulation. In: Graham CH, editor. Vision and visual perception. New York: John Wiley and Sons, Inc., 1965.

Light and Dark Adaptation

Michael Kalloniatis and Charles Luu.[1]

Created: May 1, 2005; Updated: July 9, 2007.

Dark Adaptation

The eye operates over a large range of light levels. The sensitivity of our eye can be measured by determining the absolute intensity threshold, that is, the minimum luminance of a test spot required to produce a visual sensation. This can be measured by placing a subject in a dark room and increasing the luminance of the test spot until the subject reports its presence. Consequently, dark adaptation refers to how the eye recovers its sensitivity in the dark after exposure to bright lights. Aubert (1) in 1865 was the first to estimate the threshold stimulus of the eye in the dark by measuring the electrical current required to render the glow on a platinum wire just visible. He found that the sensitivity had increased 35 times after time in the dark, and he also introduced the term "adaptation".

Dark adaptation forms the basis of the Duplicity Theory, which states that above a certain luminance level (about 0.03 cd/m^2), the cone mechanism is involved in mediating vision: photopic vision. Below this level, the rod mechanism comes into play, providing scotopic (night) vision. The range where two mechanisms are working together is called the mesopic range, as there is not an abrupt transition between the two mechanisms.

The dark adaptation curve shown in Fig. 1 depicts this duplex nature of our visual system. The first curve reflects the cone mechanism. The sensitivity of the rod pathway improves considerably after 5-10 minutes in the dark and is reflected by the second part of the dark adaptation curve. One way to demonstrate that the rod mechanism takes over at low luminance levels is to observe the color of the stimuli. When the rod mechanism takes over, colored test spots appear colorless, as only the cone pathways encode color. This duplex nature of vision will affect the dark adaptation curve in different ways and is discussed below.

To produce a dark adaptation curve, subjects gaze at a pre-adapting light for about 5 minutes, and then the absolute threshold is measured over time (Fig. 1). Pre-adaptation is important for normalization and to ensure that a biphasic curve is obtained.

From the above curve, it can be seen that initially there is a rapid decrease in threshold, then it declines slowly. After 5 to 8 minutes, a second mechanism of vision comes into play, where there is another rapid decrease in threshold, then an even slower decline. The curve asymptotes to a minimum (absolute threshold) at about 10^{-5} cd/m^2 after about 40 minutes in the dark.

Factors Affecting Dark Adaptation

There are four factors that affect dark adaptation, which will be discussed below:

1. intensity and duration of the pre-adapting light
2. size and position of the retina are used in measuring dark adaptation
3. wavelength distribution of the light used
4. rhodopsin regeneration

Intensity and Duration of Pre-adapting Light

Different intensities and duration of the pre-adapting light will affect the dark adaptation curve in a number of areas. With increasing levels of pre-adapting luminances, the cone branch becomes longer while the rod branch

Author Affiliation: 1 Department of Optometry and Vision Sciences University of Melbourne, Australia.

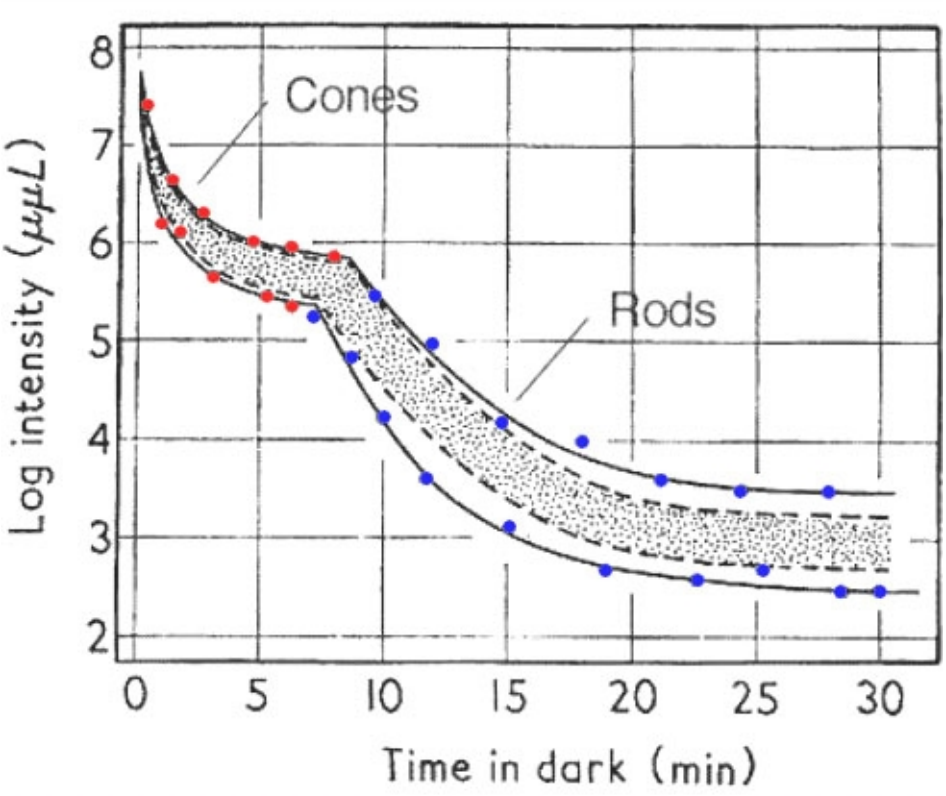

Figure 1. Dark adaptation curve. The shaded area represents 80% of the group of subjects. Hecht and Mandelbaum's data are from Pirenne (9).

becomes more delayed. The absolute threshold also takes longer to reach. At low levels of pre-adapting luminances, rod threshold drops quickly to reach absolute threshold (Fig. 2).

The shorter the duration of the pre-adapting light, the more rapid the decrease in dark adaptation (Fig. 3). For extremely short pre-adaptation periods, a single rod curve is obtained. It is only after long pre-adaptation that a biphasic cone and rod branches are obtained.

Size and Location of the Retina Used

The retinal location used to register the test spot during dark adaptation will affect the dark adaptation curve because of the distribution of the rod and cones in the retina (Fig. 4).

When a small test spot is located at the fovea (eccentricity of 0°), only one branch is seen with a higher threshold compared with the rod branch. When the same size test spot is used in the peripheral retina during dark adaptation, the typical break appears in the curve representing the cone branch and the rod branch (Fig. 5).

A similar principle applies when different sizes of the test spot is used. When a small test spot is used during dark adaptation, a single branch is found because only cones are present at the fovea. When a larger test spot is used during dark adaptation, a rod-cone break would be present because the test spot stimulates both cones and rods. As the test spot becomes even larger, incorporating more rods, the sensitivity of the eye in the dark is even greater (Fig. 6), reflecting the larger spatial summation characteristics of the rod pathway.

Wavelength of the Threshold Light

When stimuli of different wavelengths are used, the dark adaptation curve is affected. In Fig. 7, a rod-cone break is not seen when using light of long wavelengths, such as extreme red. This occurs because of rods and cones

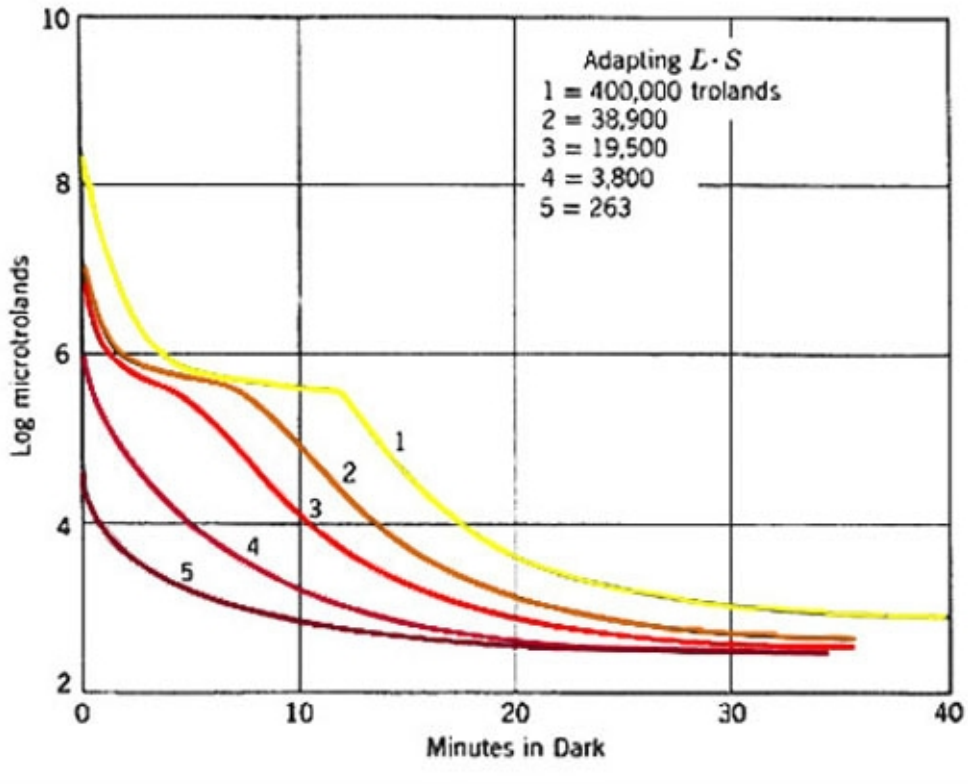

Figure 2. Dark adaptation curves following different levels of pre-adapting luminances. Hecht, Haig and Chase's data are from Bartlett (10).

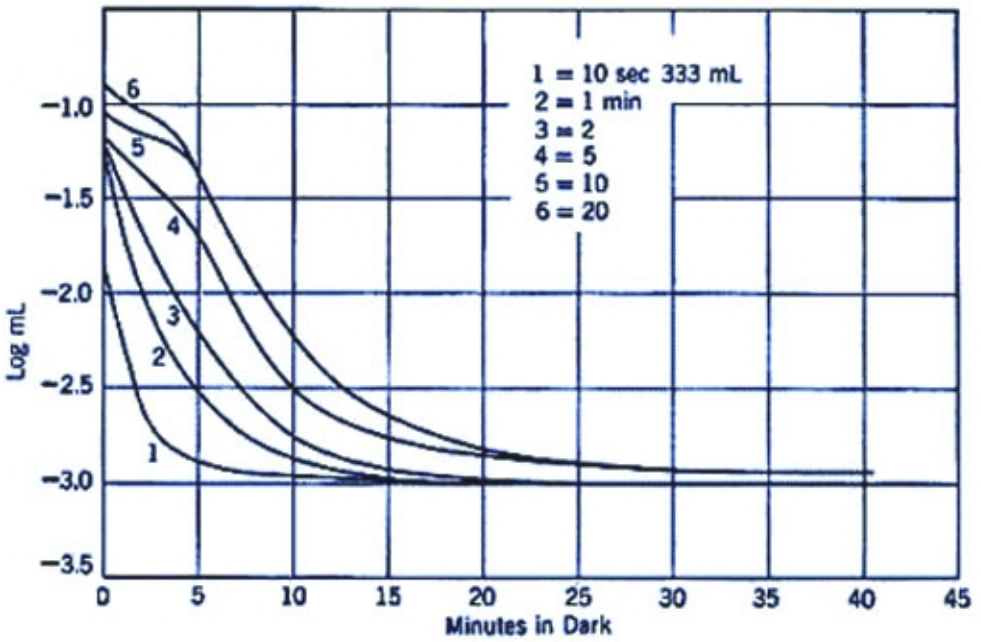

Figure 3. Dark adaptation curves following different durations of a pre-adapting luminance. Wald and Clark's data are from Bartlett (10).

having similar sensitivities to light of long wavelengths (Fig. 8). Fig. 8 depicts the photopic and scotopic spectral sensitivity functions to illustrate the point that the rod and cone sensitivity difference is dependent upon test

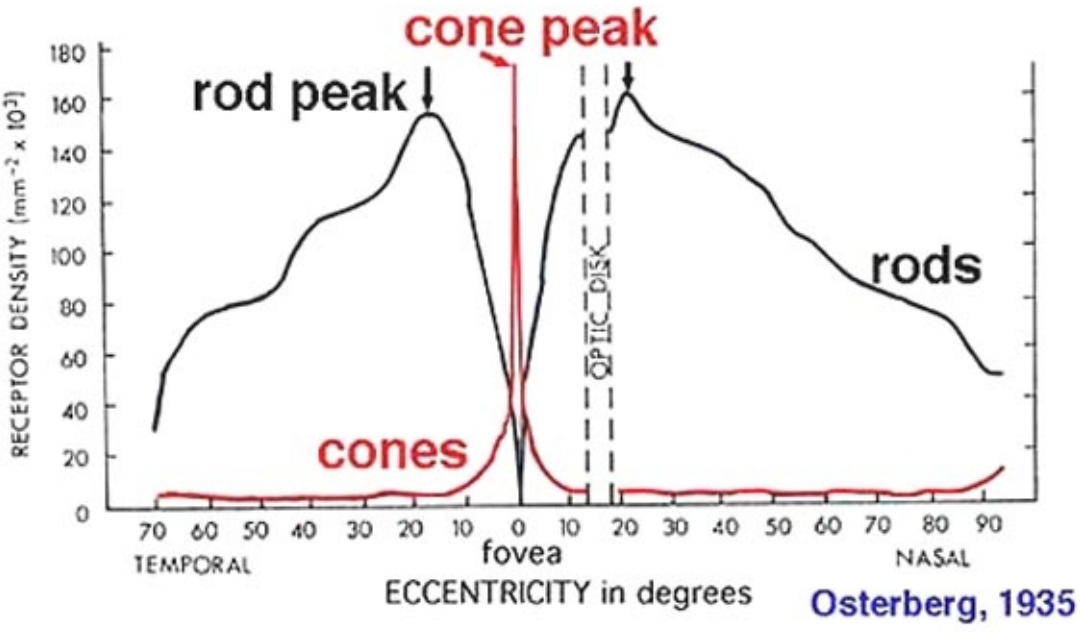

Figure 4. Graph to show rod and cone densities along the horizontal meridian. From Osterberg (11).

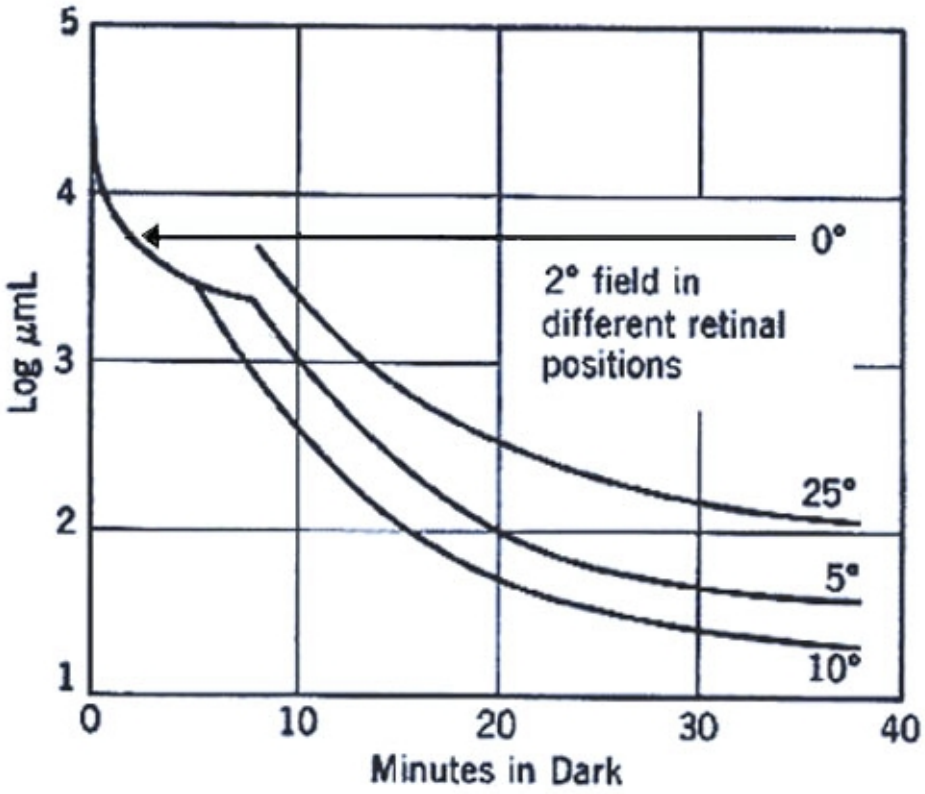

Figure 5. Dark adaptation measured with a 2° test spot at different angular distances from fixation. The subject was pre-adapted for 2 minutes to 300 mL. Hecht, Haig, and Wald's data are from Bartlett (10).

wavelength (although normalization of spatial, temporal, and equivalent adaptation level for the rod and cones is not present in this figure). On the other hand, when light of short wavelength is used, the rod-cone break is most

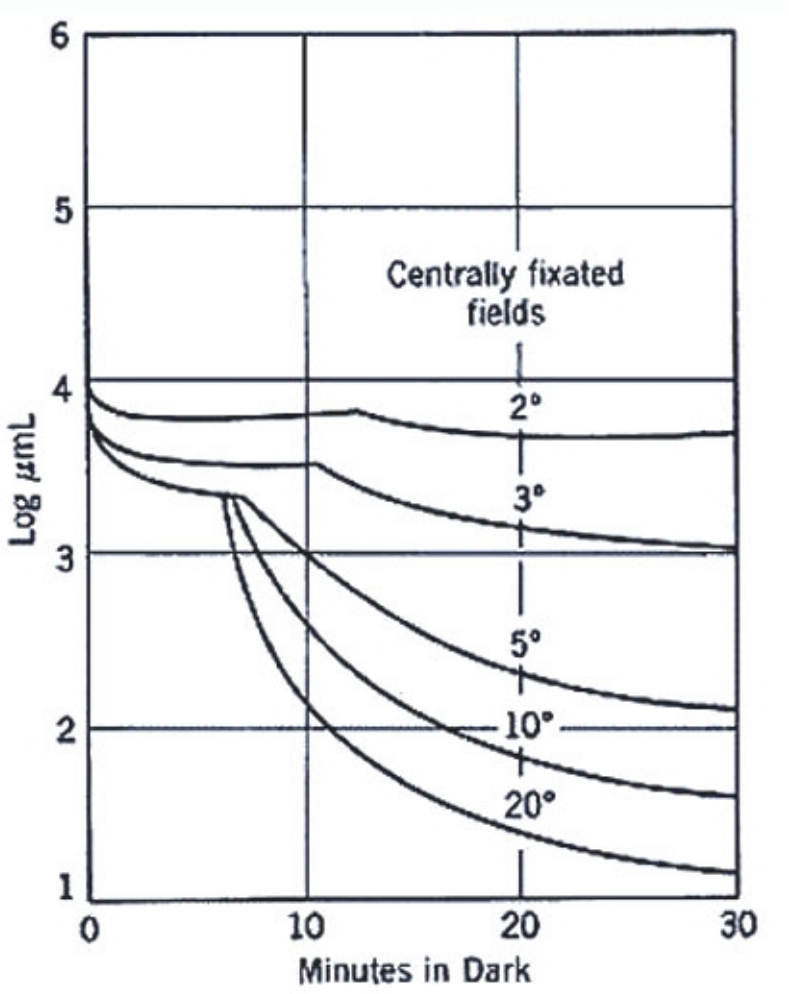

Figure 6. Dark adaptation measured using different size test spots. Hecht, Haig, and Wald's data are from Bartlett (10).

prominent because the rods are much more sensitive than the cones to short wavelengths once the rods have dark adapted.

Rhodopsin Regeneration

Dark adaptation also depends upon photopigment bleaching. Retinal (or reflection) densitometry, which is a procedure based on measuring the light reflected from the fundus of the eye, can be used to determine the amount of photopigment bleached. Using retinal densitometry, it was found that the time course for dark adaptation and rhodopsin regeneration was the same. However, this does not fully explain the large increase in sensitivity with time. Bleaching rhodopsin by 1% raises the threshold by 10 (decreases sensitivity by 10). In Fig. 9, it can be seen that bleaching 50% of rhodopsin in rods raises the threshold by 10 log units, whereas bleaching 50% of cone photopigment raises the threshold by about 1.5 log units. Therefore, rod sensitivity is not fully accounted for at the receptor level and may be explained by further retinal processing. The important thing to note is that bleaching of cone photopigment has a smaller effect on cone thresholds.

Light Adaptation

With dark adaptation, we noticed that there is progressive decrease in threshold (increase in sensitivity) with time in the dark. With light adaptation, the eye has to quickly adapt to the background illumination to be able to

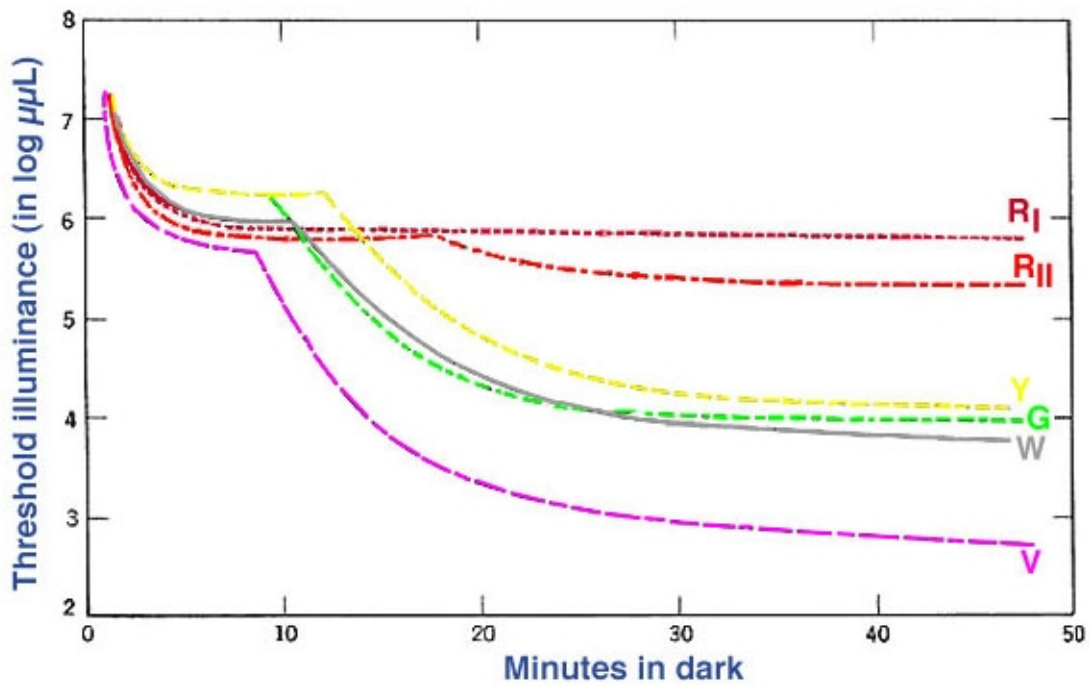

Figure 7. Dark adaptation curve using different test stimuli of different wavelengths. Subjects were pre-adapted to 2,000 mL for 5 minutes. A 3° test stimulus was presented 7° on the nasal retina. The colors were: RI (extreme red), 680 nm; RII (red), 635 nm; Y (yellow), 573 nm; G (green), 520 nm; V (violet), 485 nm; W (white). Chapanis' data are from Bartlett (10).

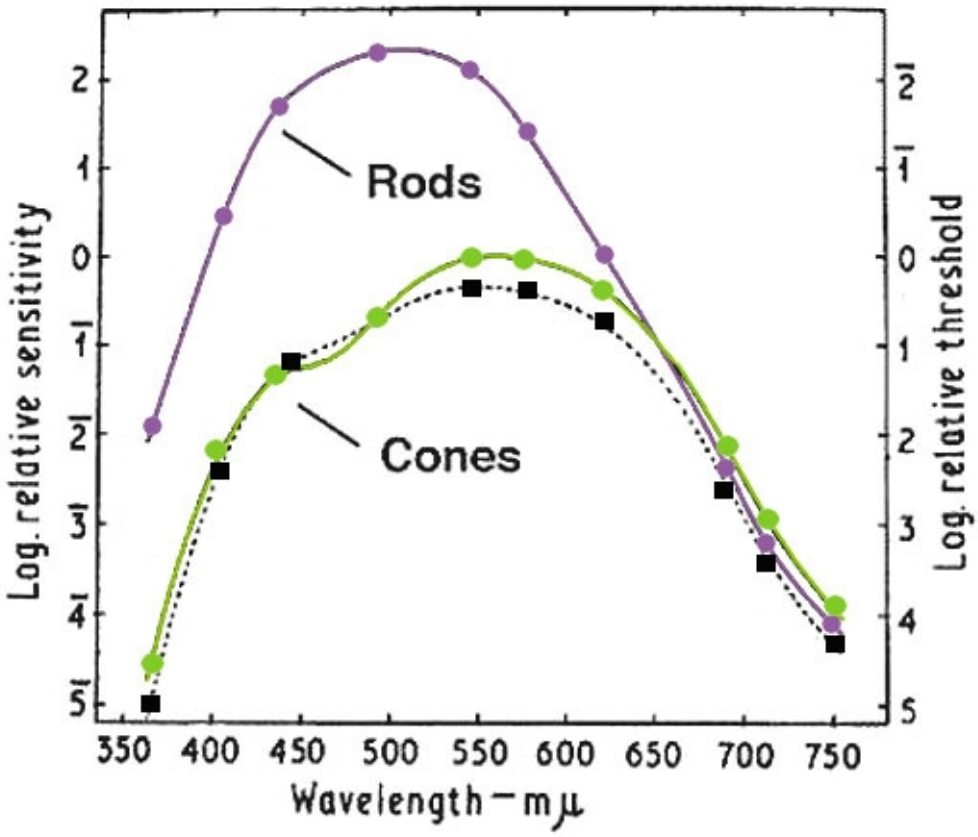

Figure 8. Scotopic (rods) and photopic (cones) spectral sensitivity functions. Wald's data from are from Davson (7).

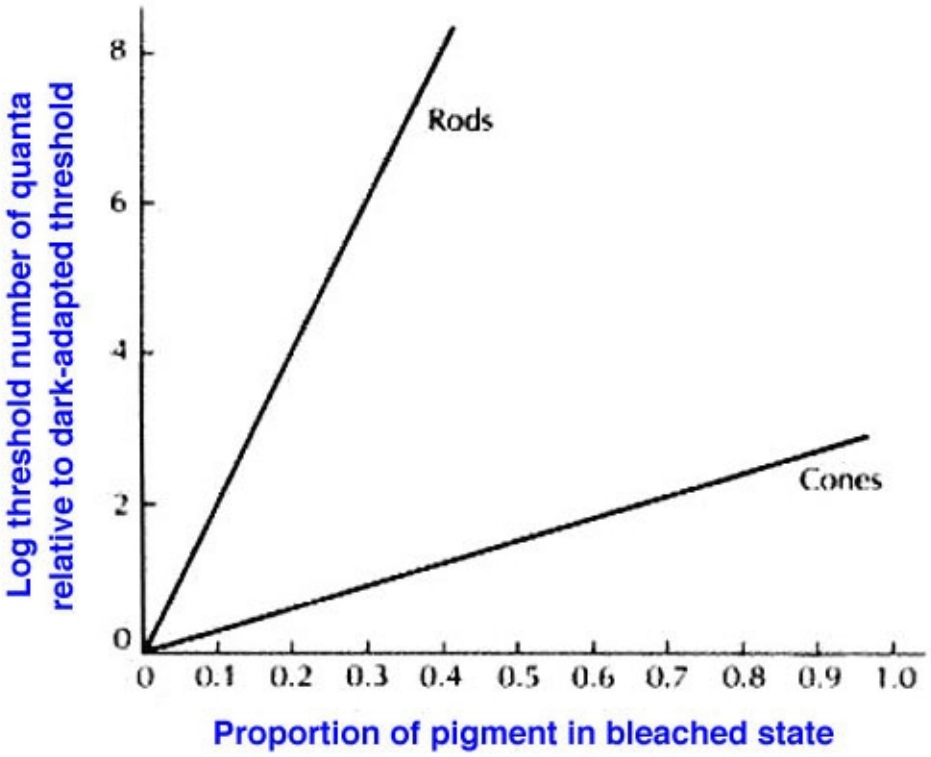

Figure 9. Log relative threshold as a function of the percentage of photopigment bleached. From Cornsweet (6).

distinguish objects in this background. Light adaptation can be explored by determining **increment thresholds**. In an increment threshold experiment, a test stimulus is presented on a background of a certain luminance. The stimulus is increased in luminance until the detection threshold is reached against the background (Fig. 10). Therefore, the independent variable is the luminance of the background, and the dependent variable is the threshold intensity or luminance of the incremental test required for detection. Such an approach is used when visual fields are measured in clinical practice.

The experimental conditions shown in Fig. 10 can be repeated by changing the background field luminance. Depending upon the choice of test and background wavelength, the test size, and retinal eccentricity, a monophasic or biphasic threshold *versus* intensity (tvi) curve is obtained. Fig. 11 illustrates such a curve for parafoveal presentation of a yellow test field on a green background. This stimulus choice leads to two branches. A lower branch belongs to the rod system. As the background light level increases, visual function shifts from the rod system to the cone system. A dual-branched curve reflects the duplex nature of vision, similar to the biphasic response in the dark adaptation curve.

When a single system (e.g., the rod system) is isolated under certain experimental conditions, four sections of the curve are apparent. These experimental conditions involve using a red background to suppress the cone photoreceptors and a green test spot to stimulate the rod photoreceptors (2). The curve in Fig. 12 can also be obtained by performing increment threshold experiments on rod monochromats that lack cone photoreceptors. When the rod system is isolated using the conditions of Aguilar and Stiles (2), four sections are obtained:

1. dark light
2. Square Root Law (de Vries-Rose Law)
3. Weber's Law
4. saturation

The threshold in the **linear portion** of the tvi curve is determined by the dark/light level. As background luminance is increased, the curve remains constant (and equal to the absolute threshold). Sensitivity in this section is limited by neural (internal) noise, the so-called "dark light". The background field is relatively low and does not significantly affect threshold. This neural noise is internal to the retina, and examples of these include thermal isomerisations of photopigment, spontaneous opening of photoreceptor membrane channels, and spontaneous neurotransmitter release.

The second part of the tvi curve is called the **Square Root Law** or (**de Vries-Rose Law**) region. This part of the curve is limited by quantal fluctuation in the background. Rose (3) proposed that the visual threshold would be quantal limited. The visual system is usually compared with a theoretical construct, an **ideal light detector**. An ideal detector can detect and encode each absorbed quantum of light and is limited only by the noise due to quantal fluctuations in the source. To detect the stimulus, the stimulus must be sufficiently exceed the fluctuations of the background (noise).

Because the variability in quanta increases with the number of quanta absorbed, threshold would increase with background luminance. In fact, the increase in threshold should be proportional to the square root of the background luminance, hence, the slope of 0.5 in a log-log plot. For the rod pathway, a slope of 0.6 is often found (4). Barlow (5) explored the conditions that influenced the transition from the Square Root Law to **Weber's Law** (see below). He concluded that for brief, small test spots, increment thresholds rise as the square root of the background over the entire photopic range. Spots of large areas and long durations have slopes close to Weber's Law. Other spatio-temporal configurations result in different proportions of each region.

When plotted using log ΔL versus log L coordinates, the Weber law section ideally has a slope 1. For the rod pathway, a slope 0.8 or less is found, implying that the rod pathway does operate under true Weber conditions. This section of the curve demonstrates an important aspect of our visual system. Our visual system is designed to distinguish objects from its background. In the real world, objects have contrast, which is constant and independent of ambient luminance. Therefore, the principle of Weber's law can be applied to contrast that remains constant regardless of illumination changes. This is called contrast constancy or contrast invariance, with this contrast level defined as Weber's constant. Contrast constancy can be mathematically expressed as $\Delta L / L$ = constant. ΔL is the increment threshold on a background L. The constant is also known as the Weber constant or Weber fraction. The Weber constant for the rod and cone is 0.14 (6) and 0.02 to 0.03 (7), respectively. Within the cone pathways, the S-cone pathway again has different characteristics to those of the longer-wavelength pathway with a Weber constant of around 0.09 (8).

Section 4 of the curve (Fig. 12) shows rod **saturation** at high background luminance. The slope begins to increase rapidly, and the rod system starts to become unable to detect the stimulus. This section of the curve occurs for the cone mechanism under high background light levels.

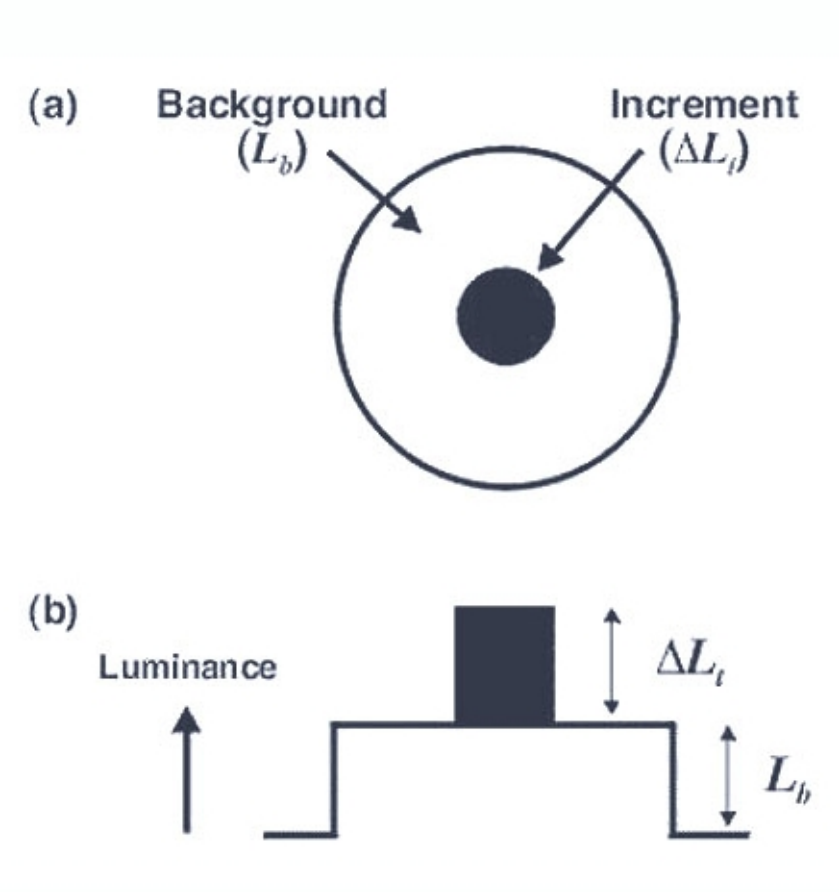

Figure 10. Light adaptation using an increment threshold experiment. a, example of the stimulus used. b, luminance profile of the stimulus.

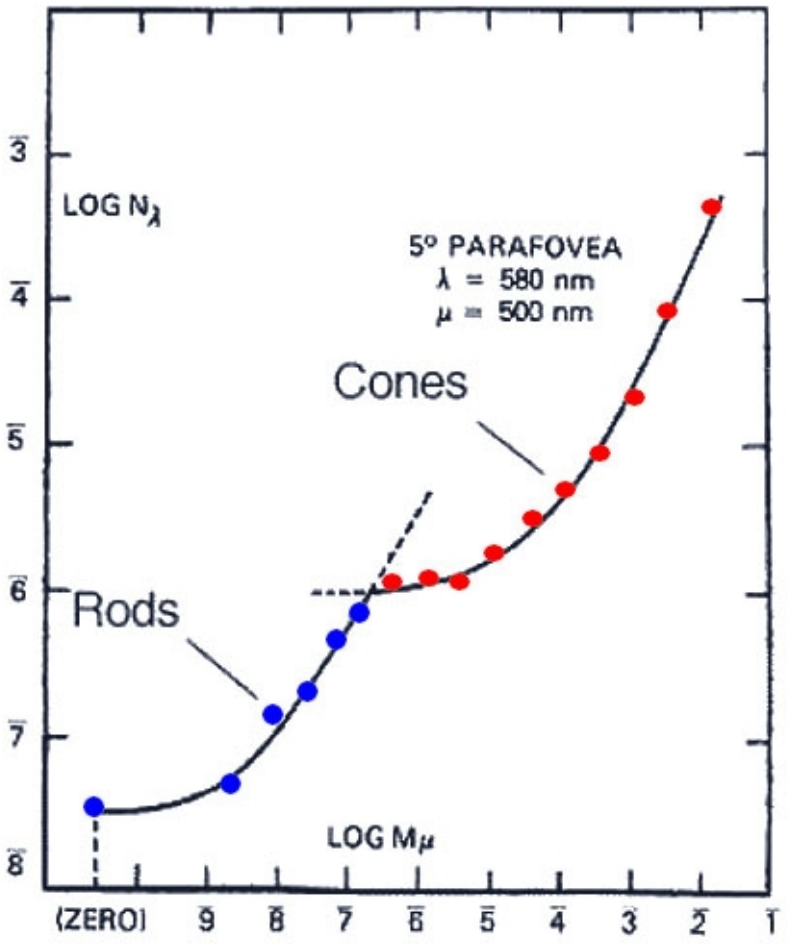

Figure 11. Light adaptation curve plotted as increment threshold *versus* background luminance (or a threshold-*versus*-intensity: tvi curve). The above plot shows increment threshold (Nλ) and background luminance (Mμ). Light of two different wavelengths is used in this case (580 nm for the test and 500 nm for the background). Stiles' data are from Davson (7).

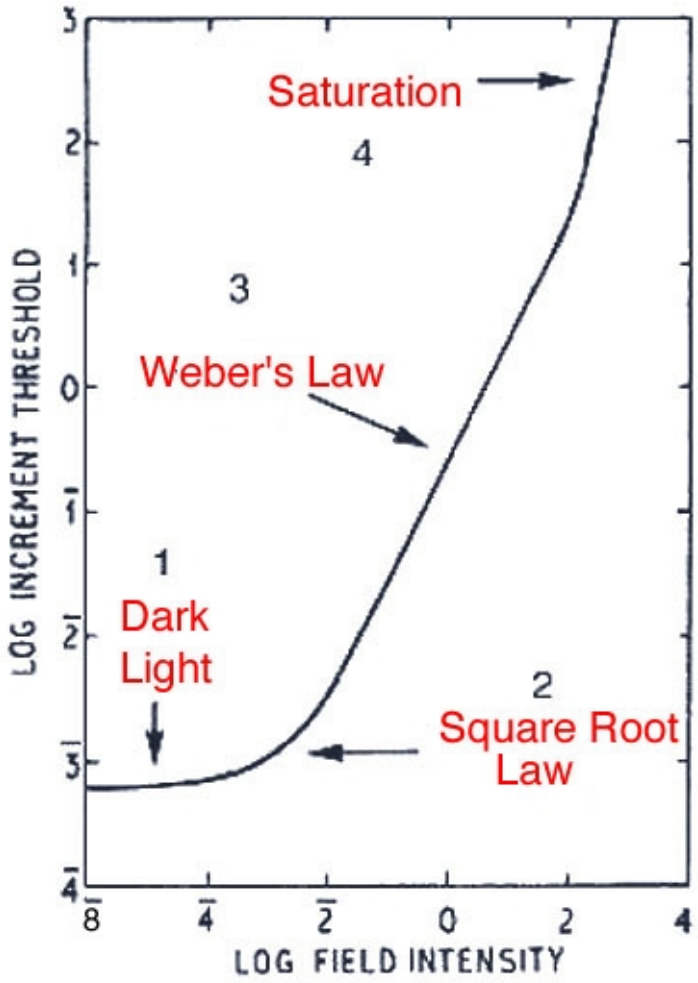

Figure 12. Schematic of the increment threshold curve of the rod system. Aguilar and Stiles' data are from Davson (7).

About the Authors

Michael Kalloniatis was born in Athens Greece in 1958. He received his optometry degree and Master's degree from the University of Melbourne. His PhD was awarded from the University of Houston, College of Optometry, for studies investigating colour vision processing in the monkey visual system. Post-doctoral training continued at the University of Texas in Houston with Dr Robert Marc. It was during this period that he developed a keen interest in retinal neurochemistry, but he also maintains an active research laboratory in visual psychophysics focussing on colour vision and visual adaptation. He was a faculty member of the Department of Optometry and Vision Sciences at the University of Melbourne until his recent move to New Zealand. Dr. Kalloniatis is now the Robert G. Leitl Professor of Optometry, Department of Optometry and Vision Science, University of Auckland. e-mail: m.kalloniatis@unsw.edu.au

Charles Luu was born in Can Tho, Vietnam in 1974. He was educated in Melbourne and received his optometry degree from the University of Melbourne in 1996 and proceeded to undertake a clinical residency within the Victorian College of Optometry. During this period, he completed post-graduate training and was awarded the post-graduate diploma in clinical optometry. His areas of expertise include low vision and contact lenses. During his tenure as a staff optometrist, he undertook teaching of optometry students as well as putting together the "Cyclopean Eye", in collaboration with Dr Michael Kalloniatis. The Cyclopean Eye is a Web based interactive unit used in undergraduate teaching of vision science to optometry students. He is currently in private optometric practice as well as a visiting clinician within the Department of Optometry and Vision Science, University of Melbourne.

References

1. Aubert H. Physiologie der Netzhaut. Breslau: E. Morgenstern; 1865.
2. Aguilar M, Stiles WS. Saturation of the rod mechanism of the reina at high levels of stimulation. Opt Acta (Lond). 1954;1:59–65.
3. Rose A. The sensitivity performance of the human eye on a absolute scale. J Opt Soc Am. 1948;38:196–208.
4. Hallett PE. The variations in visual threshold measurement. J Physiol. 1969;202:403–419. PubMed PMID: 5784294.
5. Barlow HB. Increment thresholds at low intensities considered as signal noise discriminations. J Physiol. 1958;141:337–350. PubMed PMID: 13539843.
6. Cornsweet TN. Visual perception. New York: Academic Press; 1970.
7. H Davson. Physiology of the eye. 5th ed. London: Macmillan Academic and Professional Ltd.; 1990.

8. Stiles WS. Colour vision: the approach through increment threshold sensitivity. Proc Natl Acad Sci U S A. 1959;75:100–114.
9. Pirenne MH. Dark adaptation and night vision. In: Davson H, editor. The eye. Vol 2. London: Academic Press; 1962.
10. Bartlett NR. Dark and light adaptation. In: Graham CH, editor. Vision and visual perception. New York: John Wiley and Sons, Inc.; 1965.
11. Osterberg G. Topography of the layer of rods and cones in the human retina. Acta Ophthalmol Suppl. 1935;6:1–103.

The Perception of Color

Michael Kalloniatis and Charles Luu.[1]

Created: May 1, 2005; Updated: July 9, 2007.

Overview

Color vision processing in the primate visual system is initiated by absorption of light by three different spectral classes of cones. Consequently, color vision is described as being trivariant or trichromatic, and initial psychophysical studies demonstrated that colors could be matched by the use of three different primaries. In 1802, Thomas Young (1) proposed a model that perception of color can be coded by three principal color receptors rather than thousands of color receptors coding for individual colors.

Spectral sensitivity of cones can be determined through several methods. Two of these methods include isolating receptoral responses (2) using calculations from color matching function of normals and dichromats (a dichromat is a subject whose retina has one cone photopigment missing) (3), microspectrometry (4), or reflection densitometry (5, 6). The microspectrometer technique involves isolating a single cone and passing light through it. The change in transmission of different wavelengths can be used to calculate the spectral absorption of the cone or determine the change in electrical response. Reflection densitometry involves directing light in the retina and determining the change in absorption as a function of wavelength. These results are subsequently used to calculate spectral absorption.

Three classes of cones in the human retina have been isolated from the above techniques. These three classes of cones are the short-wavelength-sensitive (S-cones), middle-wavelength-sensitive (M-cones), and long-wavelength-sensitive (L-cones), and all have different but overlapping spectral sensitivities. The spectral sensitivity of S-cones peaks at approximately 440 nm, M-cones peak at 545 nm, and L-cones peak at 565 nm after correction for pre-retinal light loss, although the various measuring techniques result in slightly different maximum sensitivity values (Fig. 1).

Color Matches

The trichromatic nature of color vision will enable almost any color to be matched by a mixture of three colors. This trichromacy of vision is also linear. This means that colorimetric equations have properties of an ordinary equation.

The color matches of quantity C_s of a stimulus S can be expressed as:

$$Cs(S) = C1(l1) + C2(l2) + C3(l3)$$

where *li* are the three primary colors (not necessarily monochromatic spectral colors) and *Ci* are tristimulus values.

Tristimulus values represent the quantities of each of the three primaries necessary to achieve a match for color and luminosity (Fig. 2). They can be expressed in units of luminous flux or radiant flux, or even an arbitrary scale provided that the arbitrary scale conveys the relative proportions of the three quantities.

Author Affiliation: 1 Department of Optometry and Vision Sciences University of Melbourne, Australia.

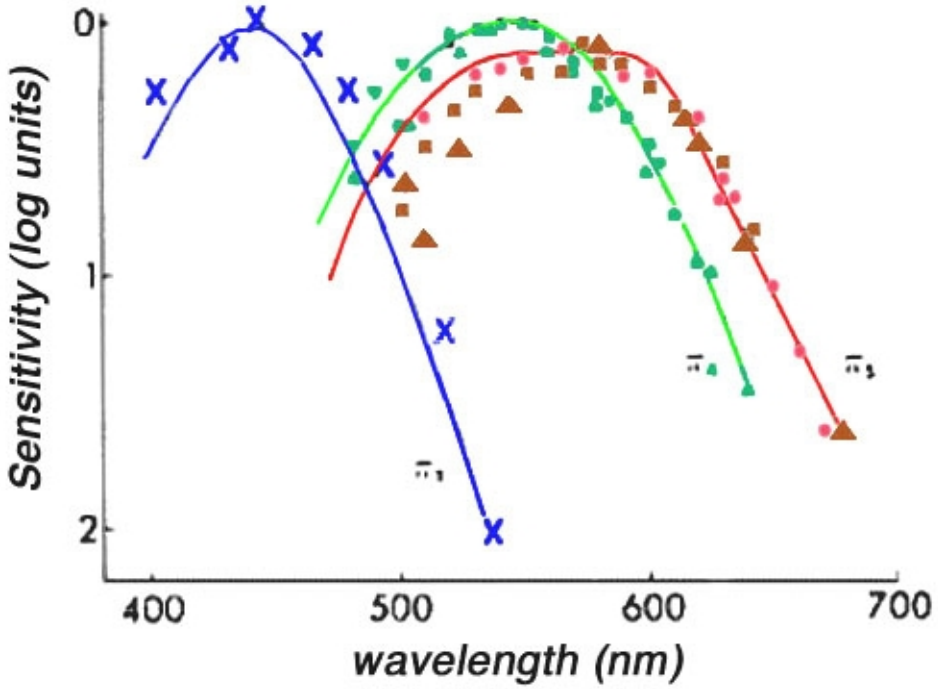

Figure 1. Spectral sensitivity of the S-cone, M-cone, and L-cone. Combined results from various authors using different methods including retinal densitometry from Rushton (▼ and ▿), microspectrometry from Brown and Wald (■ and □) and increment threshold producing artificial monochromasy from Brinley (▵and ▲), and increment threshold measurements from Wald (×). From Moses and Hart (26).

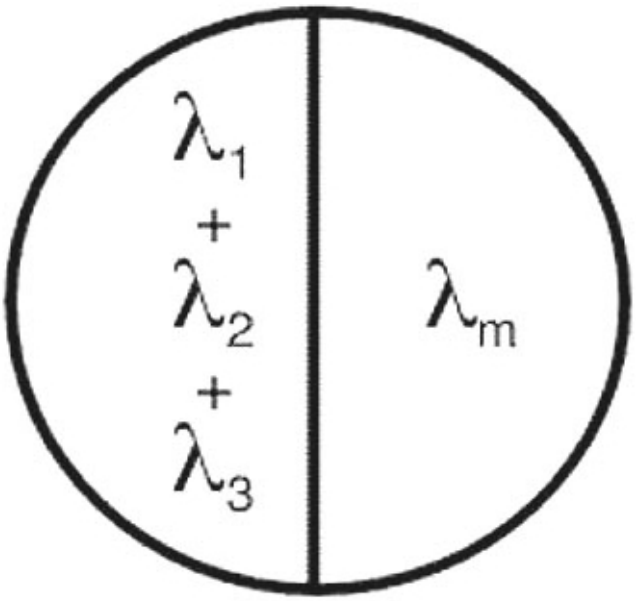

Figure 2. Subjects are asked to adjust three colors on the left-hand side of the bipartite field to match a standard color presented on the right-hand side of the bipartite field.

Additive and Subtractive Color Mixtures

Two or more colors can be added together to produce a new color composed of the mixture of the initial colors used. This can be demonstrated on a white screen with three colors: blue, green, and red. Cyan, magenta, yellow, and white are formed from the mixture of these colors (Fig. 3). One of the requirements in choosing colors to be used in color mixing experiments is that two of them cannot be mixed to produce the third.

Subtractive color mixtures involve the selective absorption of wavelengths. Cyan, magenta, and yellow are subtractive primaries. If white light was shone through a yellow filter, the yellow filter will absorb blue and transmit red and green (which makes yellow). Therefore, yellow can be considered as a -B filter. A magenta filter subtracts or absorbs green (-G filter) from white light, and cyan subtracts or absorbs red (-R filter) from white light (Fig. 4).

Grassmann's Laws provide a quantitative description of color matching data (7). They hold up well within a prescribed set of conditions (with respect to brightness, adaptation of the observer, size of the field, etc). Grassmann's Laws are useful in quantifying color matching data, but as a rule, color matching data are affected by the following:

- macular pigment (xanthophyll) variations in subject's central 4-5 degrees of vision
- chromatic aberrations
- rod intrusion, especially when large fields and low photopic light levels are involved
- failure of Abney's Law of luminance additivity including the Helmholtz-Kohlrausch effect
- Bezold-Brücke hue shift at bright intensities

Color Specification

The Munsell Color System

All colors can be fully specified in terms of their hue, lightness, and saturation. The Munsell system has three dimensions: hue, value, and chroma. These three dimensions correspond to the three perceptual attributes of human color vision.

The three dimensions of the Munsell color system are:

1. Hue: Related to wavelength or dominant wavelength. Hue is denoted by a combination of letters and numbers making up a 100-step scale (Fig. 5). There are 10 letter categories used to denote hue, with each of these further subdivided (by the use of numerals 1 to 10) into 10 subgroups. If the numeral denoting the hue subgroup is 5, then it can be omitted (e.g., 5R is the same hue as R).
2. Value: Specified on a numerical scale from 1 (black) to 10 (white), and this attribute is related to reflectance and luminosity (or lightness).
3. Chroma: The Munsell term corresponding to saturation. It is indicated numerically on a scale of 0 to the various maxima, dependent on the saturation obtainable with available pigments.

For example, a color may have a notation 2GY 6/10. This means it is a green/yellow that is quite close to being a yellow; it has a value of 6 (i.e., almost midway in the black/white scale) and a chroma of 10 (i.e., it is saturated).

The scaling used in the Munsell system is designed to be perceptually uniform. In other words, the color samples are arranged in equal, visual steps. For example, the perceived difference between a chroma of 3 and a chroma of 4 is (nominally) the same as the perceived difference between chroma 4 and 5. This scaling is the same for all three dimensions, although step sizes along different dimensions are *not* comparable (that is, a single step difference in hue does not have the same perceptual difference as a single step in saturation).

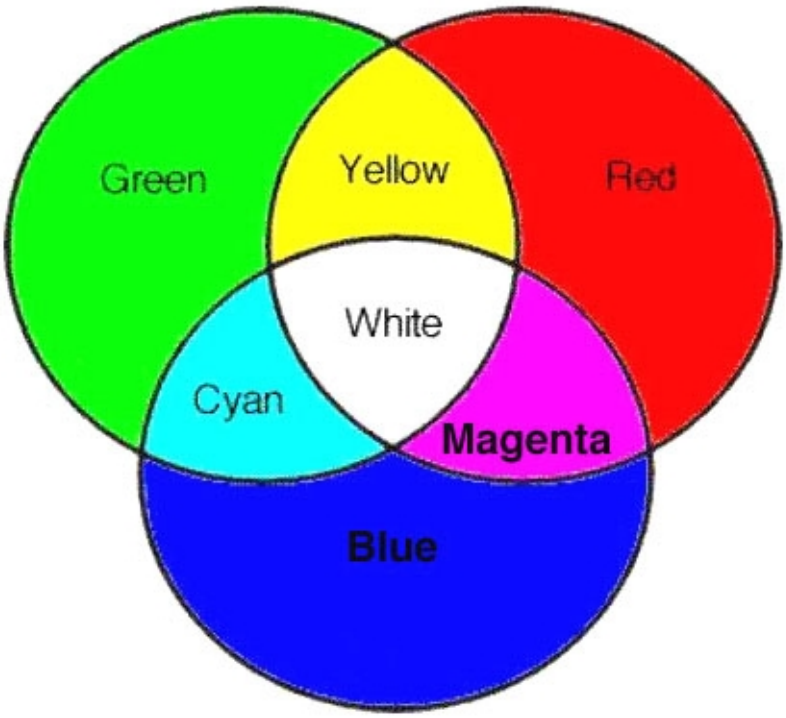

Figure 3. Additive color mixtures of blue, green, and red to produce cyan, magenta, yellow, and white.

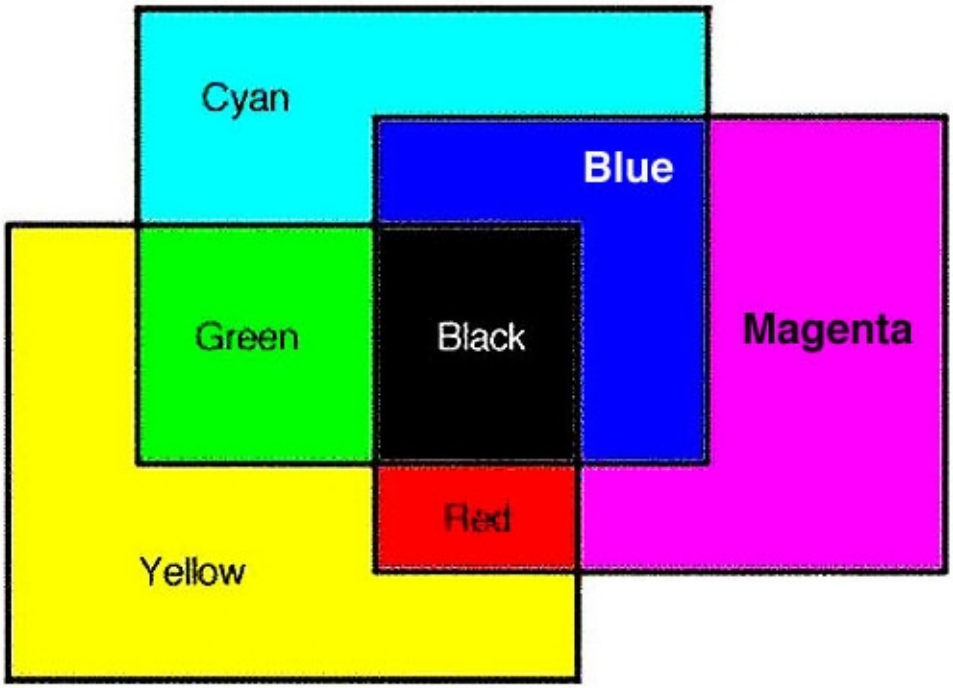

Figure 4. Subtractive color mixtures of cyan, magenta, and yellow to produce blue, green, and red.

A schematic representation of the Munsell system is shown in Fig. 6. The value scale is on the vertical axis, the hue scale is on the perimeter of the cylinder, and chroma is on a radial scale. The Munsell top, shown in Fig. 5, is a more precise representation of this concept.

1931 Commision Internationale d'Elairage (CIE) Chromaticity System

Trichromatic color matches using three colors can be illustrated on Newton's color circle (Fig. 7). Newton's color circle consists of the following components:

- a circle representing the spectral colors (although not shown here, mixtures of blue and red (purple locus) are not spectral colors, and hence, a straight line between R and B is more appropriate)
- a triangle whose vertices represent the three primary colors used to make color matches (R, G, and B)
- the center of the circle representing white (W)

Newton's color circle provides a qualitative description of color matches and can be used to explain why two colors may not be sufficient to make color matches and to also explain the use of "negative" colors. For example, if 500 nm is required to be matched (spectral color located on the circle), blue and green will be required. However, blue and green primaries alone will produce a desaturated 500 nm. Therefore, red must be added to the spectral color to desaturate it and make the match (Fig. 8). When the third primary is added to desaturate the color mixture, negative tristimulus values result (Fig. 5). This can be demonstrated by the following equation:

$$500\ \text{nm}\ (\text{S}) + \text{R} \equiv \text{G} + \text{B}$$

or

$$500\ \text{nm}\ (\text{S}) \equiv \text{G} + \text{B} - \mathbf{R}$$

To deal with the "negative" colors, the CIE devised the XYZ system that uses unreal (imaginary) primaries to describe color space. The 1931 CIE chromaticity system chose three imaginary primaries (reference stimuli) X, Y, and Z, so that all spectral loci lying inside this triangle will be positive. The alychne are locus of colors with no luminosity, and this was chosen to lie along the X to Z on the XYZ chromaticity system. All luminosity is expressed in Y. The reference loci of Y was chosen to just enclose the domain of real colors. Equi-energy white was chosen to have equal chromaticity co-ordinates, that is, 0.33, 0.33 (Fig. 9 and Fig. 10). Chromaticity co-ordinates represents the relative contribution of the three primaries, and the sum of the co-ordinates equals 1.0. Therefore, z can be calculated, by knowing the co-ordinates x and y because $x + y + z = 1$.

Dominant wavelength, complementary wavelength, and excitation purity can be easily located for a sample. The dominant wavelength represents the principle wavelength of the color. The complementary wavelength is the wavelength that produces white when mixed in appropriate portions with the dominant wavelength. Spectral complementaries can be found when a line joined by a line passes through the achromatic point shown as C (Fig. 11). The dominant wavelength of A is given by the spectral wavelength at DA, and the complementary is given by the wavelength at CA (Fig. 11). Point C identifies the location of the white point and B identifies another wavelength that, when mixed at the appropriate proportions, will produce white.

The achromatic point varies, depending upon the standard illuminant that is used (Fig. 12). A shift in the *x* and *y* co-ordinates occurs as color temperature increases. For standard illuminant C, there is no complimentary wavelengths for green (between wavelengths 492 nm to 567 nm). However, white light can be formed with a suitably chosen purple light (Fig. 12).

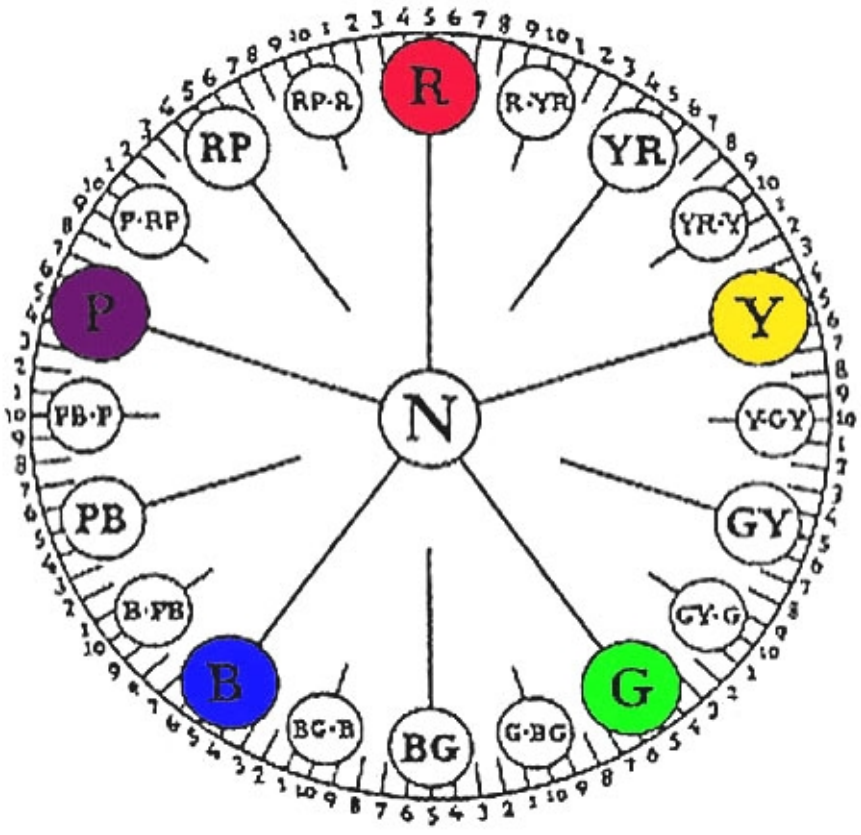

Figure 5. The Munsell top showing the location of the different colors.

Color Discrimination Functions

The three variables in color vision—hue, saturation, and brightness—all depend on wavelength. Color discrimination experiments allow us to know how much change in wavelength is required to detect a difference in hue, saturation, and brightness.

Hue discrimination describes the amount of change in wavelength (l + Δl) that is required to be able detect a change in hue. For blue and red light, a large change in wavelength is required to detect a change in hue, whereas a less than 2-nm change in wavelength is needed for most of the spectrum for a person with normal color vision (Fig. 13).

Saturation discrimination describes the degree of paleness of the color. Saturation is related to colorimetric purity (P), which is also defined as:

$$P = L/(Lw+L)$$

where *L* is the luminance of the spectral color and *Lw* is the luminance of the white that is mixed with the spectral color. The colorimetric purity of a color quantifies the amount of white mixed with the spectral color. If the spectral color is pure (no white added), then the colorimetric purity is 1.

In saturation discrimination experiments, the luminance is kept constant. A bipartate field is used with white (*Lw*) on one side and white mixed with the spectral color on the other side (Lw + ΔL). It can be seen in Fig. 14

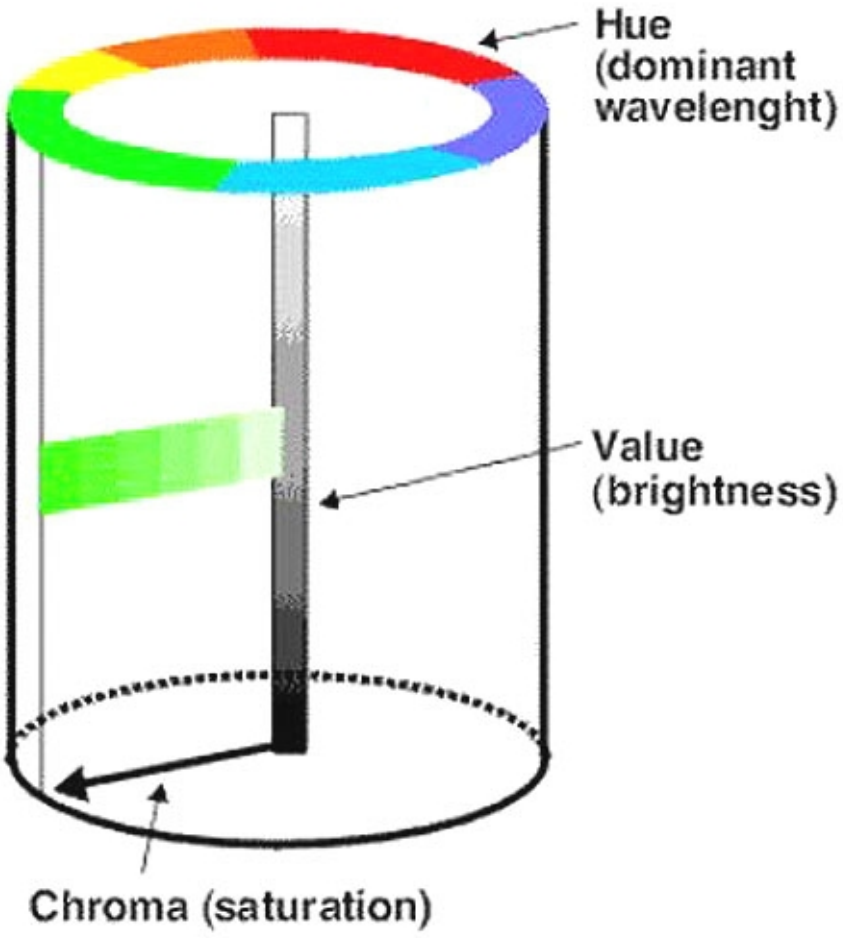

Figure 6. Munsell color system, illustrating hue, value, and chroma.

that more 570-nm color is required to make the white patch appear colored. Therefore, yellow has low saturating power, whereas blue and red have high saturation power.

The V(λ) function closely matches the sensation of brightness and hence is commonly considered to reflect **brightness discrimination**. The wavelength 555 nm is perceived as the brightest in the color spectrum (see the earlier section on the photopic and scotopic luminosity function).

Theories of Color Vision

Any theory of color vision must predict all the perceptual attributes noted earlier. We present here a simplistic view of the trichromatic and color opponent theories. See the Color Vision chapter by Peter Gouras for a discussion on the physiological correlate of color opponency.

The **trichromatic theory** was first proposed by Thomas Young in 1802 (1) and was explored further by Helmholtz (8) in 1866. This theory is primarily based on color mixing experiments and suggests that a combination of three channels explain color discrimination functions.

Evidence for the trichromatic theory includes:

- identification of the spectral sensitivities of two cone pigments by Rushton's retinal densitometry (5)
- identification of three cone pigments by microspectrometry (9)

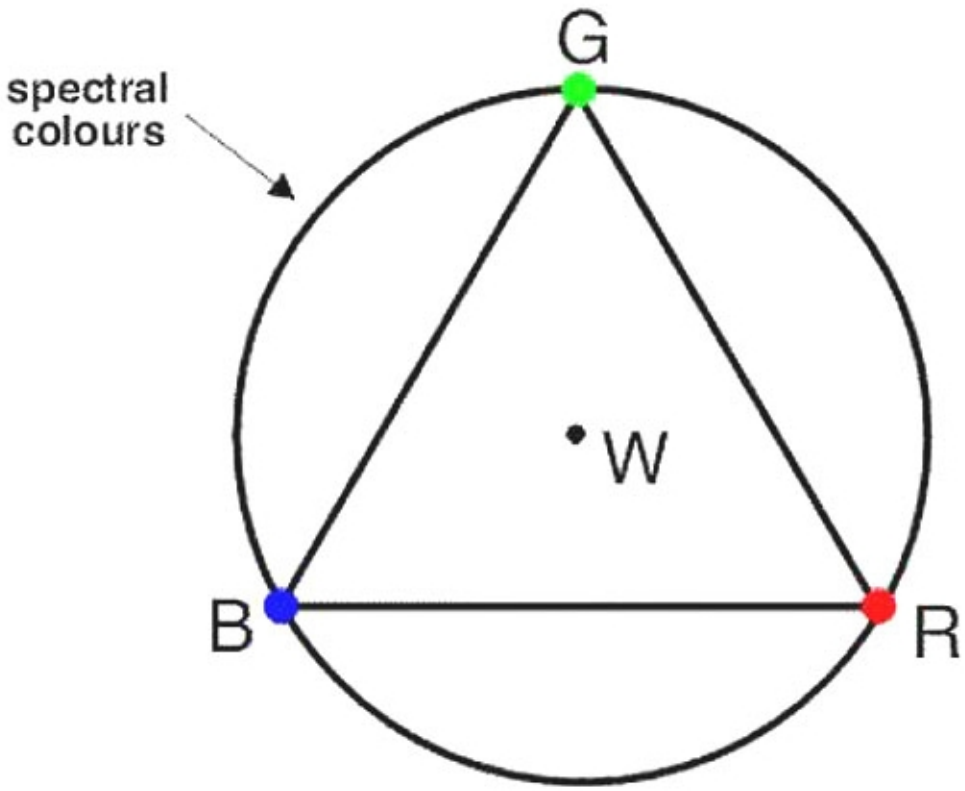

Figure 7. Newton's color circle.

- identification of the genetic code for L, M, and S cones (10, 11)
- color matching functions
- isolating photoreceptors and measuring their physiological responses as a function of wavelength (2)
- Spectral sensitivity measurements (Wald-Marre spectral sensitivity functions and Stiles' π-mechanisms)

However, the trichomatic theory fails to account for the four unique colors—red, green, yellow and blue—and also fails to explain why dichromats can perceive white and yellow. It also fails to fully explain color discrimination functions and opponent color percepts.

The **opponent color theory** was first proposed by Hering (12) in 1872. At the time, this theory rivaled the well-accepted trichromatic theory, which explains the trichromasy of vision and predicts color matches. Hering's opponent color theory suggests that there are three channels, red-green, blue-yellow, and black-white, with each responding in an antagonist way. That is, either red or green is perceived and never greenish-red. Hering, however, never challenged the initial stages of processing expressed by the trichromatic theory. He simply argued that any color vision theory should explain our perception, that is, color opponency as revealed by colored after images.

Hurvich and Jameson (13) provided quantitative data for color opponency. Using hue cancellation paradigms, the psychophysical color opponent channels were isolated. The Vλ function was used for brightness discrimination to describe the perception of blackness and whiteness. Therefore, by adjusting the amount of blue or yellow AND red or green, any sample wavelength can be matched (Fig. 15). Complementary wavelengths can be used to cancel each other for all wavelengths except the four unique hues (blue, green, yellow, and red).

Other evidence supporting the opponent color theory include:

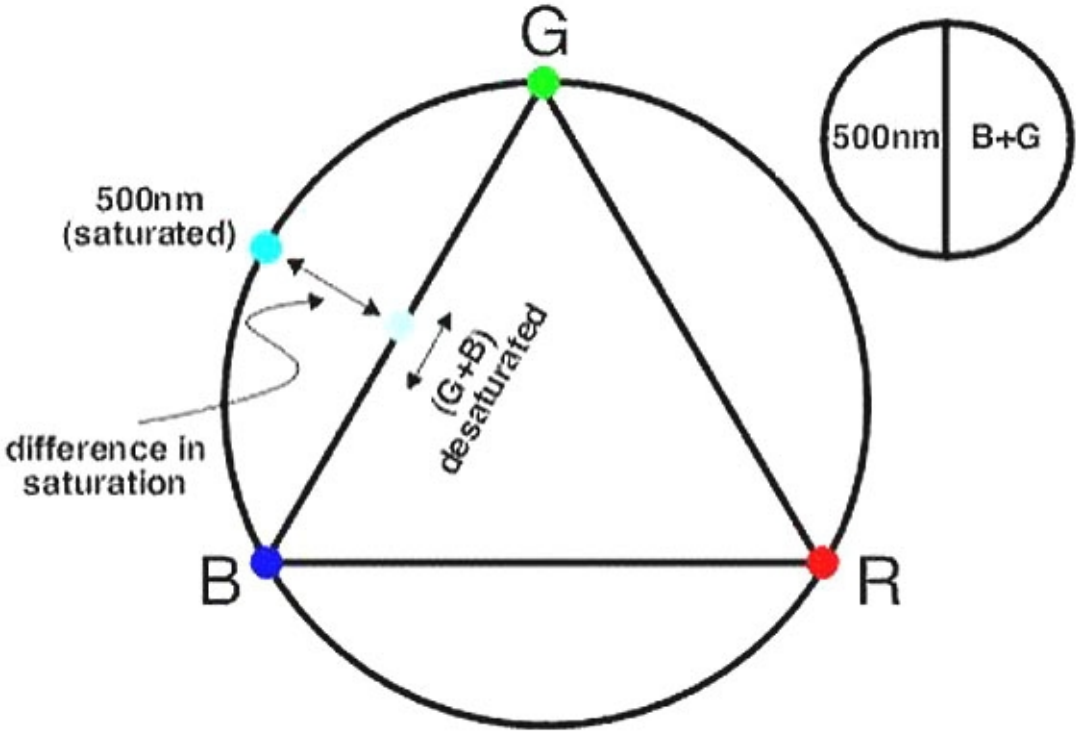

Figure 8. The use of Newton's color circle to illustrate matching a spectral color of 500 nm using the three primaries.

- Electrical recordings of horizontal cells from fish retina show blue-yellow opponent process and red-green opponent (14).
- Electrical recordings from the lateral geniculate nucleus show opponent color processes (15).
- Electrical recordings of ganglion cells from primate retinas show opponent color processes (16-18).

Stage Theory

This has led to the modern model of normal color vision, which incorporates both the trichromatic theory and the opponent color theory into two stages (Fig. 16). The first stage can be considered as the receptor stage, which consists of the three photopigments (blue, green, and red cones). The second is the neural processing stage, where the color opponency occurs. The second stage is at a post-receptoral level and occurs as early as the horizontal cell level.

Color Vision Deficiencies

Color vision deficiencies (CVDs) can be congenital or acquired. Congenital CVD means that the CVD is present at birth and is inherited, whereas acquired CVD occurs secondary to eye disease. Congenital CVD affects ~8% of males and ~0.5% of females.

CVDs are classified into three groups. These are monochromasy, dichromasy, and anomalous trichromasy. People with normal color vision are called trichromats. Monochromats are typically totally color blind and may have one cone pathway in addition to the rod pathway. Dichromats have a cone photopigment missing; therefore, they only have two cone channels. Anomalous trichromats have all three cone photopigments;

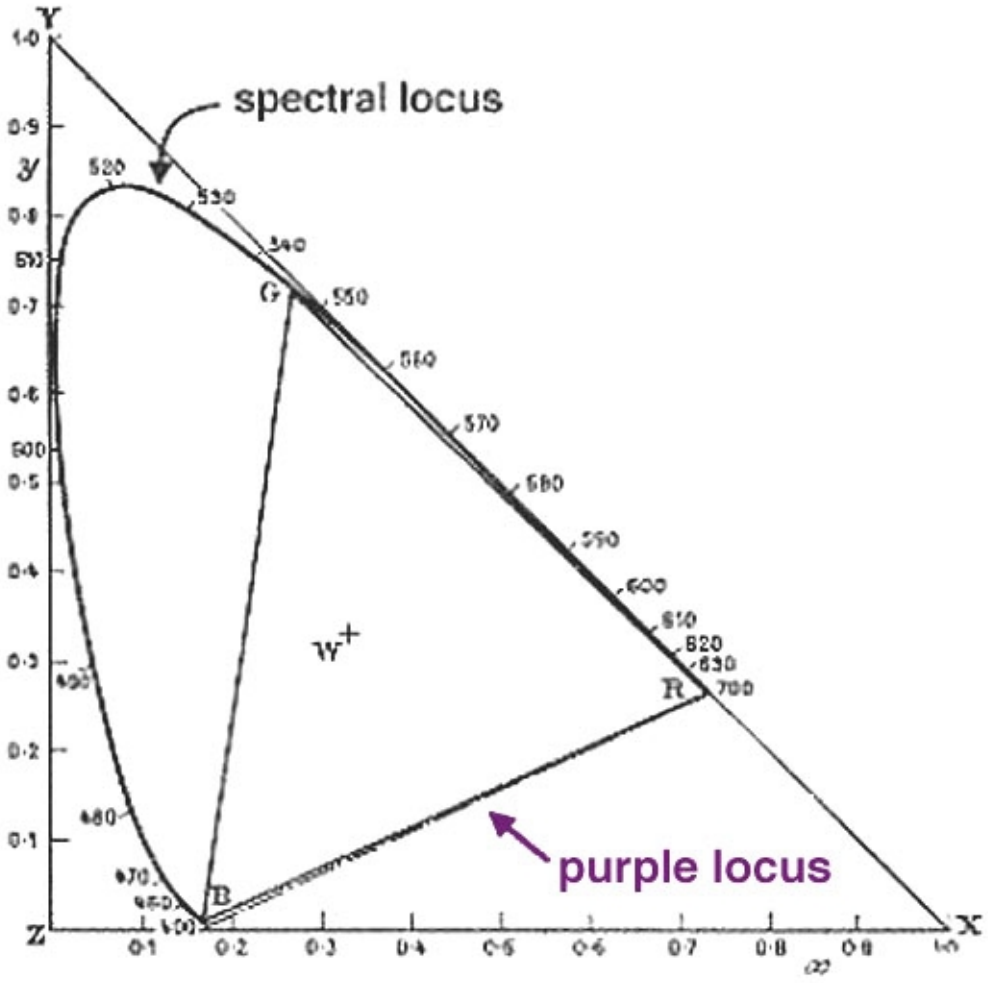

Figure 9. 1931 CIE chromaticity diagram. The triangle represents the three primaries used in the RGB system. From Le Grand (27).

however, one cone photopigment is anomalous, having a shifted peak sensitivity The types and prevalence of CVDs are listed in Table 1.

Dichromasy and anomalous trichromasy can be classified according to the affected cone photopigment. Three terms that are used also used to describe CVD are protan, deutan, and tritan (from the Greek protos, first; deuteros, second; and tritos, third; the order that the CVDs were described). A protan has the longer wavelength cone photopigment missing or anomalous, a deutan has the middle wavelength cone photopigment missing or anomalous, and the tritan has the shorter wavelength cone photopigment missing or anomalous (Fig. 17).

The pattern of inheritance for deutan (red-green) CVD is sex-linked recessive, whereas a tritan CVD has an autosomal dominant inheritance. The genetics of CVDs is particularly important in the clinic because patients are often keen to understand why they are CVD and whether they will pass their CVD to their children. For some time, it was thought that congenital inherited tritanopia did not exist because so few cases had been reported. Also, tritan-like CVDs are associated with disease, making it essential to discriminate between acquired and congenital tritan defects. The existence of congenital inherited tritanopia was originally established by family studies (19-21) and subsequently confirmed by molecular genetics (10, 11).

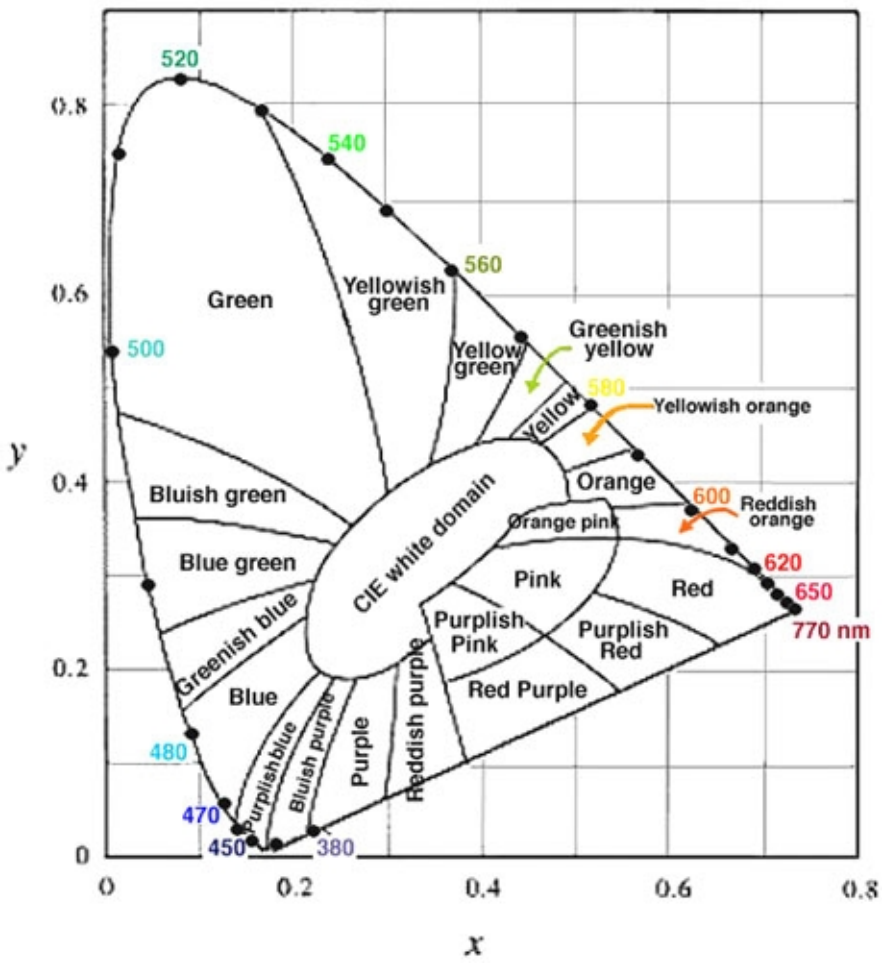

Figure 10. 1931 CIE chromaticity diagram with approximate color representation. From Benjamin (28).

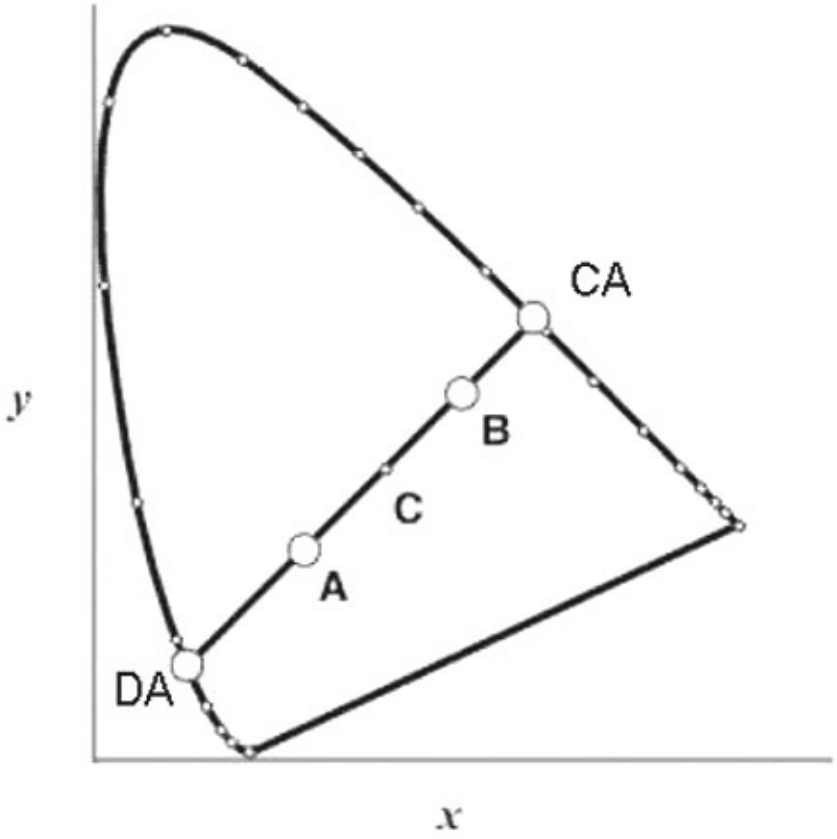

Figure 11. Complementary and dominant spectral wavelengths of color A. Color B is also complementary to color A, because an appropriate mix of the two wavelengths will produce white.

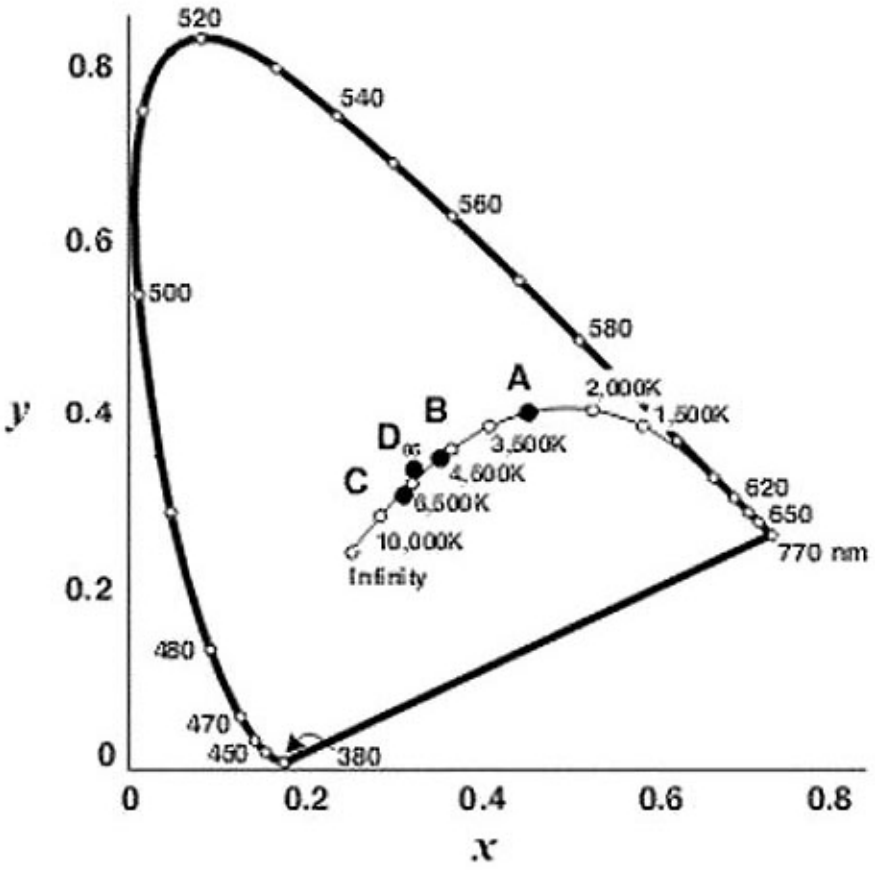

Figure 12. Variation position of the achromatic point according to color temperature. From Benjamin (28).

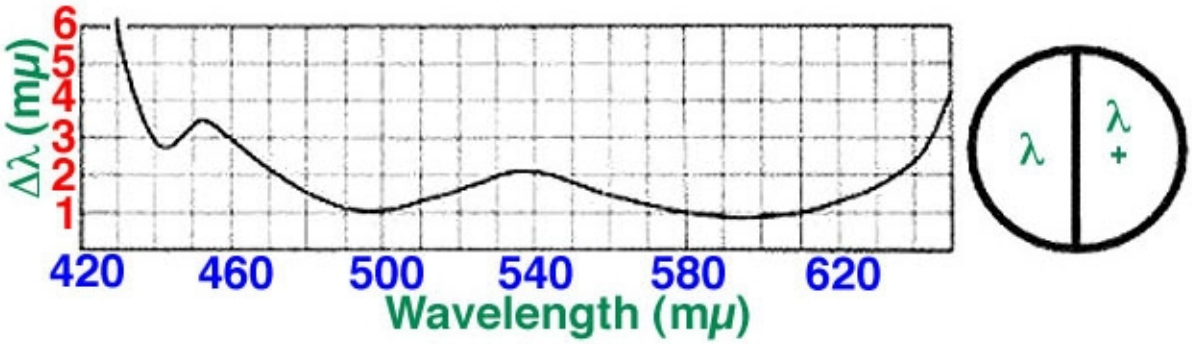

Figure 13. Mean wavelength discrimination curve. From Davson (29). See also Marriott (30).

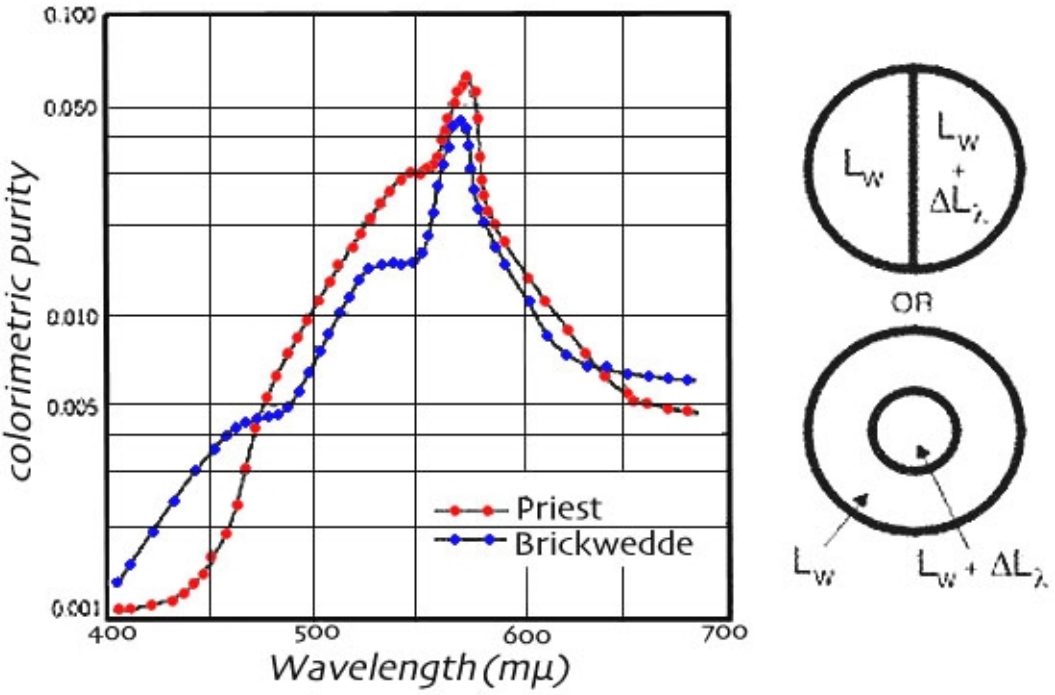

Figure 14. Saturation discrimination of Priest and Brickwide in 1938. From Graham (31).

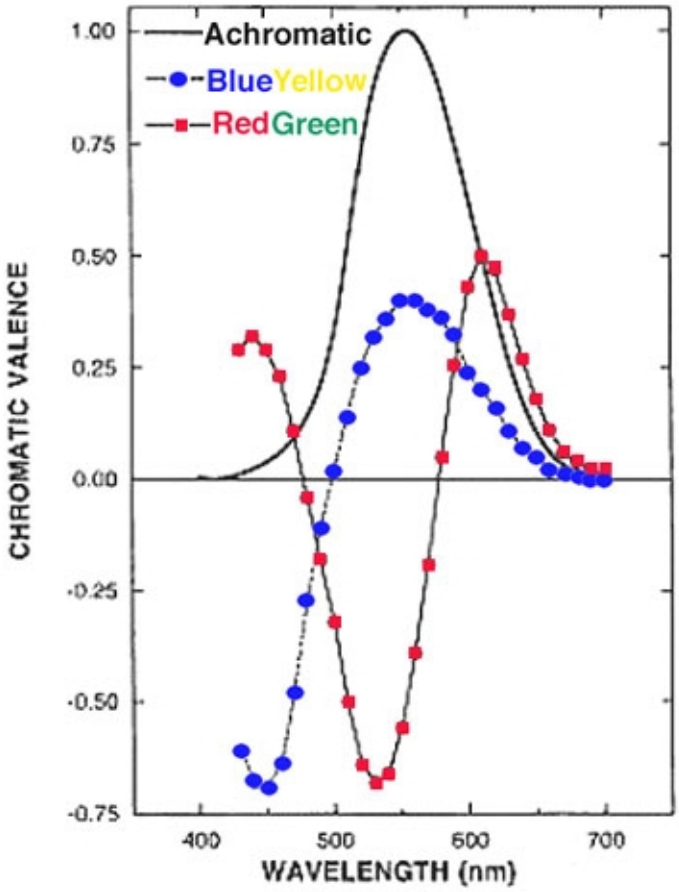

Figure 15. Hurvich and Jameson experiment using blue or yellow AND red or green to match all wavelengths of the visible spectrum (13). From Benjamin (28).

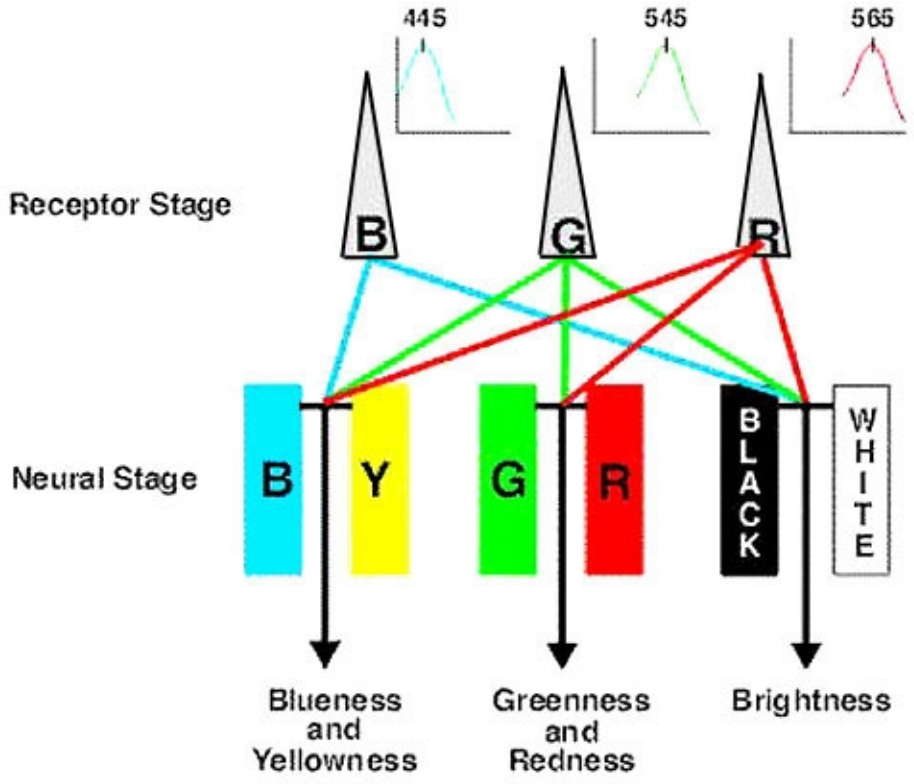

Figure 16. Model for normal human color vision.

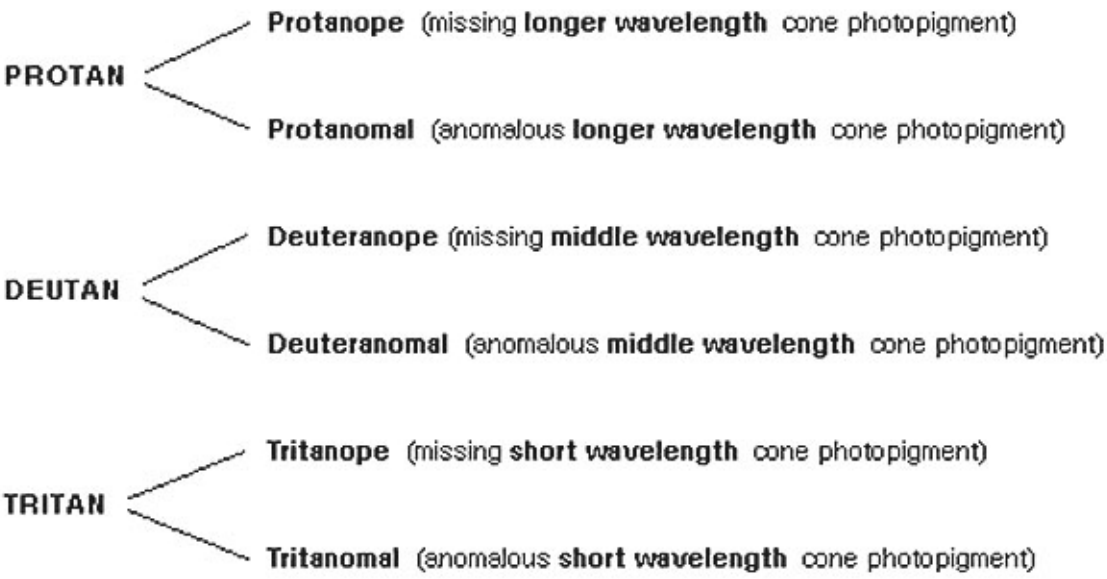

Figure 17. Classification according to the cone photopigment affected.

Table 1. **Prevalence of congenital color deficiencies.**

Types of color vision deficiency	Males	Females
Overall	~8%	~0.5%
Anomalous trichromasy		
Protanomaly	1%	0.01%
Deutanomaly	5%	0.4%
Tritanomaly	Rare	Rare
Dichromasy		
Protanopia	1%	0.01%
Deuteranopia	1.5%	0.01%
Tritanopia*	0.008%	0.008%
Monochromasy		
Rod monochromasy	Rare	Rare
Cone monochromasy	Rare	Rare
Atypical monochromasy	Very rare	Very rare

*Modified after Cole (33), Pease (22), and estimates from Wright (34).

Using the CIE Diagram to Develop Diagnostic Color Vision Tests

Discrimination of color by dichromats is limited due to one photopigment being absent. Therefore, when it comes to color matching, certain colors are confused with another. Confusion lines are lines joining points on the chromaticity diagram that appear the same in color for dichromats. The number of confusion lines also provide information about the amount of change in wavelength (Δl) before another color is discriminated (when the next confusion line is met). All confusion lines converge to a point called the copuntal point (Fig. 18).

Fig. 19 shows the confusion lines for a protanope and a deuteranope. There are 17 confusion lines for a protanope and 27 confusion lines for a deuteranope. Therefore, deuteranopes can discriminate more colors because smaller changes in wavelength (Δl steps) can be discerned. Fig. 20 shows the confusion lines for the tritanope.

Color Vision Tests

Confusion lines form the basis of many color vision tests such as the Farnsworth Panel D-15 and Ishihara Pseudoisochromatic plates. Pseudoisochromatic plate tests are also commonly used in the clinic to screen for color vision deficiency. Colors are carefully chosen based on the confusion lines. The most commonly used pseudoisochromatic plate in the clinic would be the Ishihara Isochromatic plates (for screening red-green color vision deficiency) and the Tritan (F-2) plate.

Pseudoisochromatic plates are designed in four ways:

1. Transformation plates: where a person with normal color vision sees one figure and a CVD person sees another (Fig. 21a).
2. Vanishing plates: where a person with normal color vision sees the figure whereas a CVD person will not (Fig. 21b).

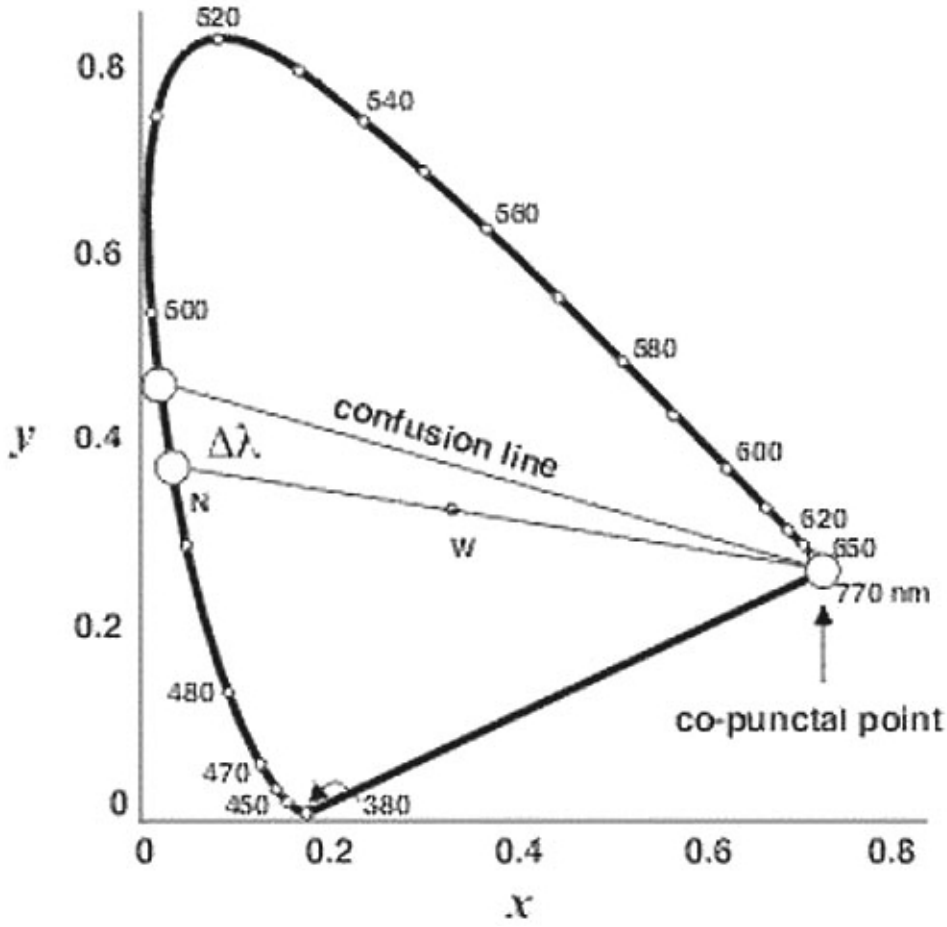

Figure 18. Schematic of two confusion lines showing the copunctal point and Δλ for a protanope.

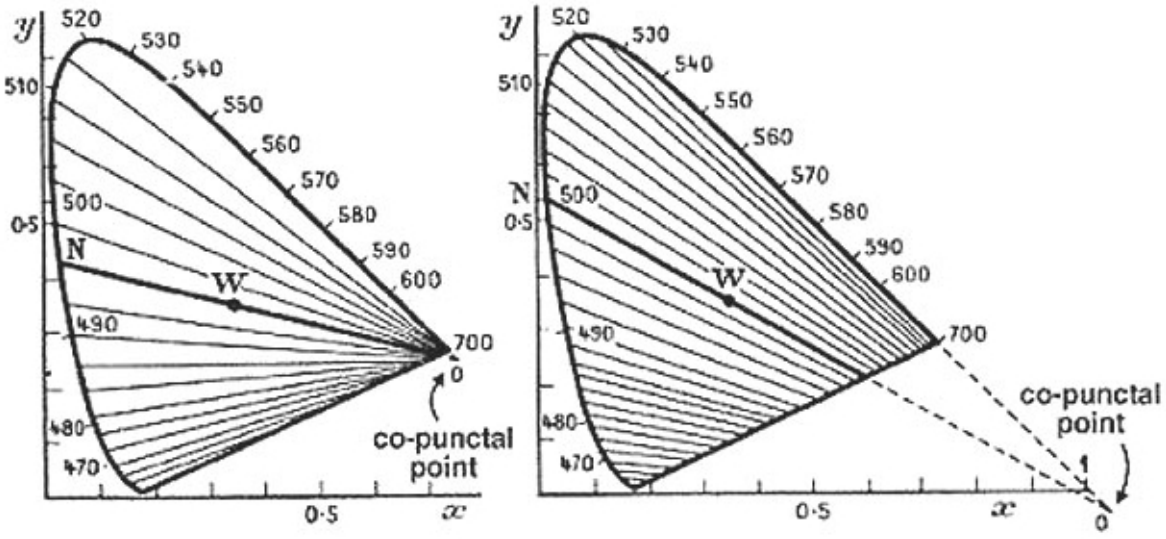

Figure 19. Confusion lines for a protanope (a) and a deuteranope (b). Pitts' data in 1935 from Le Grand (27).

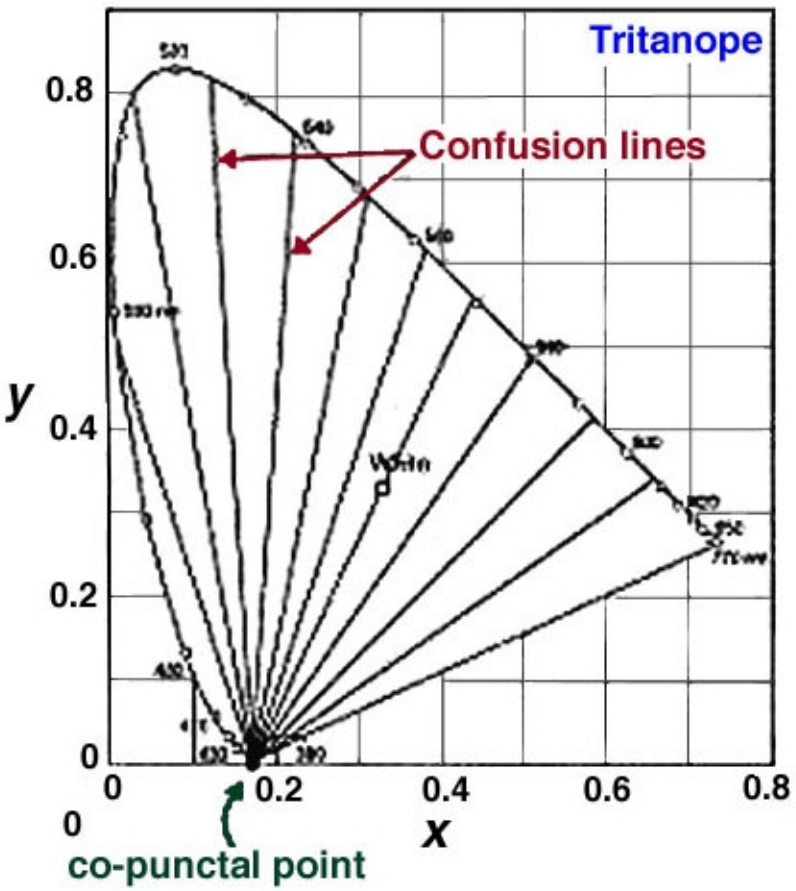

Figure 20. Confusion lines for a tritanope. From Benjamin (28).

3. Hidden-digit plates: where a person with normal color vision does not see a figure whereas a CVD will see the figure (Fig. 22a).
4. Diagnostic plates: designed to be seen by normal subjects and persons with CVDs see one number more easily than another (Fig. 22b).

The Ishihara color vision test is a screening test, and the fail criterion for the Ishihara is typically four or more plates. Further color vision testing will be required to confidently diagnose the type of color vision defect. Another useful screening plate test is the Farnsworth F-2 plate (22). There are many color vision tests available for screening and for diagnosis, of which only a few will be discussed here. The colors of the Panel D-15 are also carefully chosen from the CIE diagram so that they are all isoluminant (that is, have the same value), as seen in Fig. 23.

Patients are asked to arrange 15 colored caps in sequential order based on the similarity from the pilot color cap (Fig. 24). The type of color vision defect can be detected from their arrangement of the caps. These color caps are arranged in a particular fashion because of the confusion of colors that lie on the confusion lines (Fig. 25). The criterion for failure in the Panel D-15 test is two or more major crossings (i.e., greater than a two-cap error). Deutan, protan, and tritan will produce characteristic errors (crossings) according to their confusion lines. Rod monochromats are color blind, and their Vl peaks at about 507 nm. They arrange the D-15 caps according to the scotopic reflectance of the D-15 caps.

Other arrangement color tests include the L'Anthony's Desaturated Panel D-15, saturated H-16, and the Farnsworth 100-Hue Test. The desaturated panel D-15 is particularly useful in the early diagnosis of acquired diseases and mild congenital deficiencies. The sequence of test administration includes screening for CVDs with a pseudo-isochromatic plate test such as the Ishihara and F-2 plate. Failure of either of these tests implies proceeding to the panel D-15. A patient who fails the Panel D-15 is said to be a moderate to severe anomalous dichromat, or a dichromat. A patient who then fails the H-16 is a dichromat or very severe anomalous trichromat, whereas a moderate anomalous trichromat will pass the H-16. A subject who passes the D-15 can proceed to the desaturated D-15, which can pick up the mild anomalous trichomats. The very mild anomalous trichromats who may or may not fail pseudoisochromatic plates can be diagnosed with the Nagel anomaloscope.

The Farnsworth 100-Hue is another arrangement test (Fig. 26). Unlike the tests mentioned above where the colors are specifically chosen to lie close to the confusion lines, the Farnsworth100-Hue is a discrimination test. Fig. 27 shows where the colors of the 100-Hue lie on the chromaticity diagram. The colors are chosen to have the same Munsell value and chroma. Originally, there were 100 hues, but Farnsworth removed 15 to make the series more uniform. Performance on the Farnsworth 100-Hue is rated by calculating the total error score.

Lantern tests have been used since the19th century as a means of assessing color vision, especially for occupational reasons. Lantern tests simulate colored signal lights. They usually present pairs of red, white, and green lights, because these are the signal colors used at sea and in air navigation, and the subject is required to name the colors. There are a great number of different lantern tests that vary quite widely in the level of difficulty they present. The level of difficulty depends on the size of the stimulus and its intensity (see Cole and Vingrys (23, 24) for a review). The lanterns in current use are the Farnsworth lantern, now superseded by the Optec 900, the Holmes Wright Type A and B lanterns, and the Beyne lantern (Fig. 28).

Lantern tests are usually failed by dichromats and anomalous trichromats whose defect is severe enough to cause them to fail the Farnsworth D15 test, but the ability to recognize small colored signal lights can vary quite widely among those with mild anomalous trichromasy. A pass at the D15 test or a small range at the anomaloscope does not necessarily mean that signal light colors can be recognized (25).

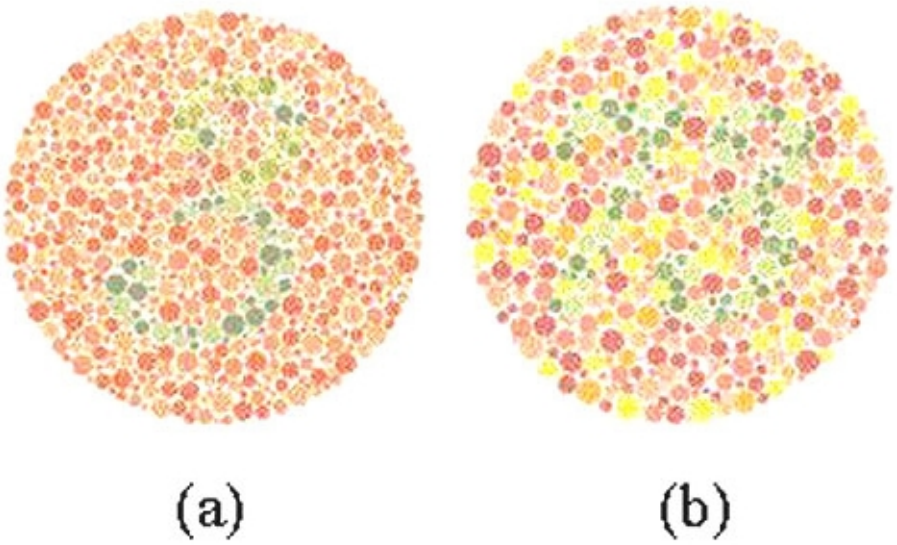

Figure 21. a, the transformation plate of the Ishihara. Normal should see 3, whereas a CVD person should see 5. b, the vanishing plate of the Ishihara. Normal should see 73, whereas a CVD person will not read the figures correctly.

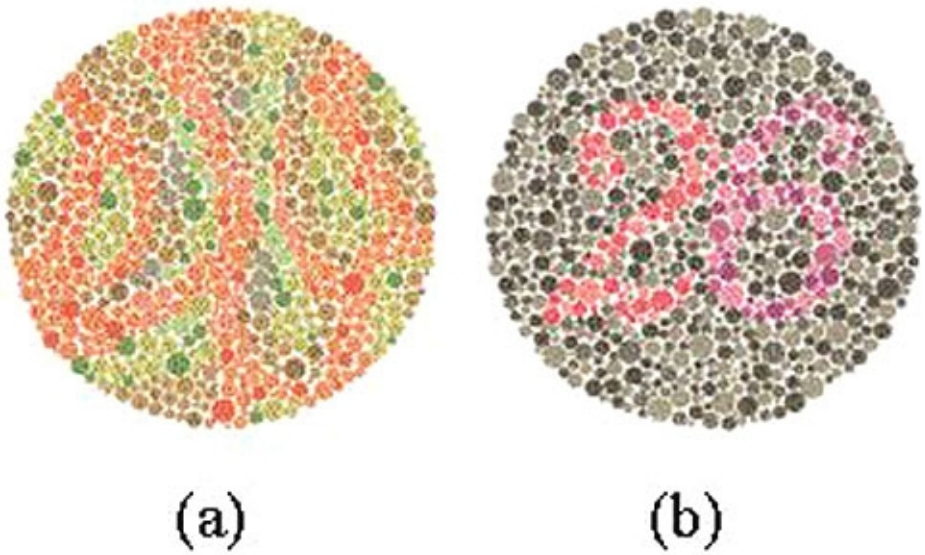

Figure 22. a, the hidden-digit plate of the Ishihara. Normal should not see anything, whereas a CVD person should see 5. b, the diagnostic plate of the Ishihara. Normal should see both the 2 and the 6. Deutan-type CVD should see 2 more easily, whereas a protan-type CVD should see the 6 more easily.

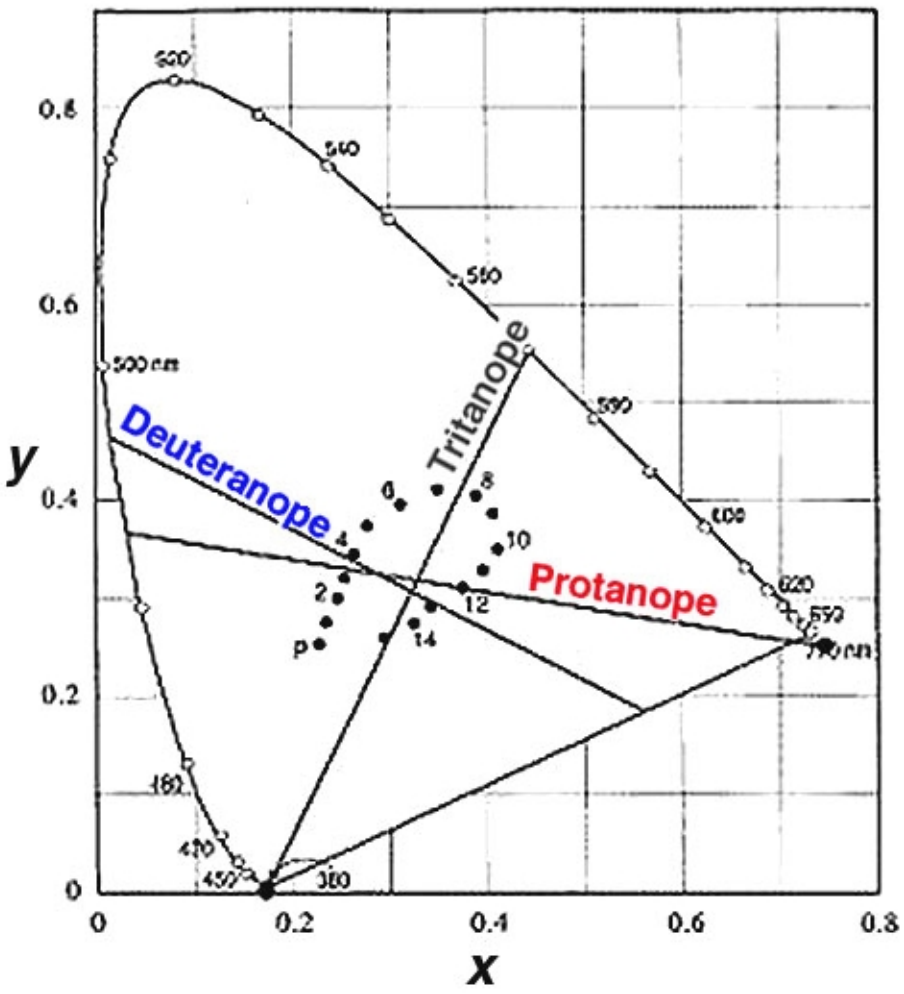

Figure 23. Chromaticity co-ordinates of the colors of the Farnsworth Panel D-15. From Benjamin (28).

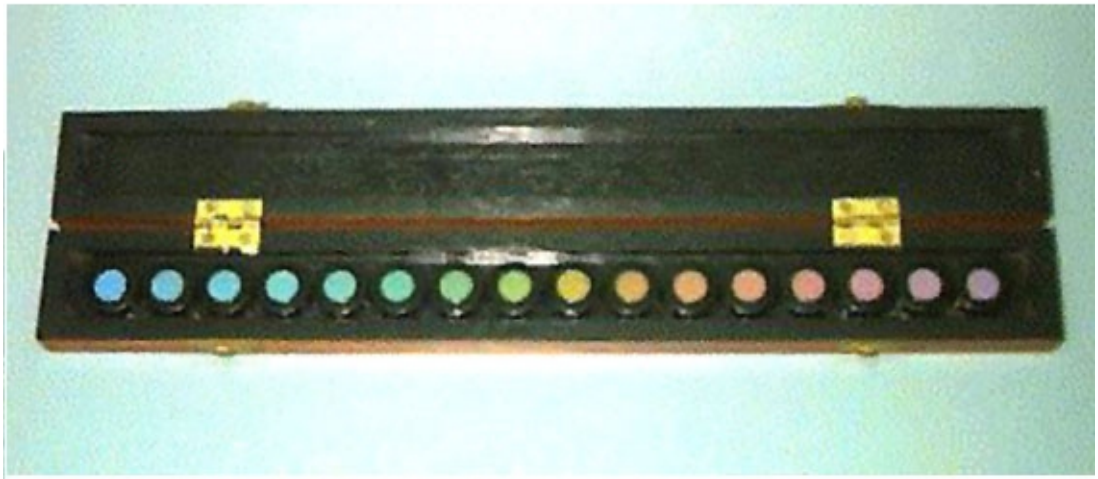

Figure 24. Farnsworth Panel D-15.

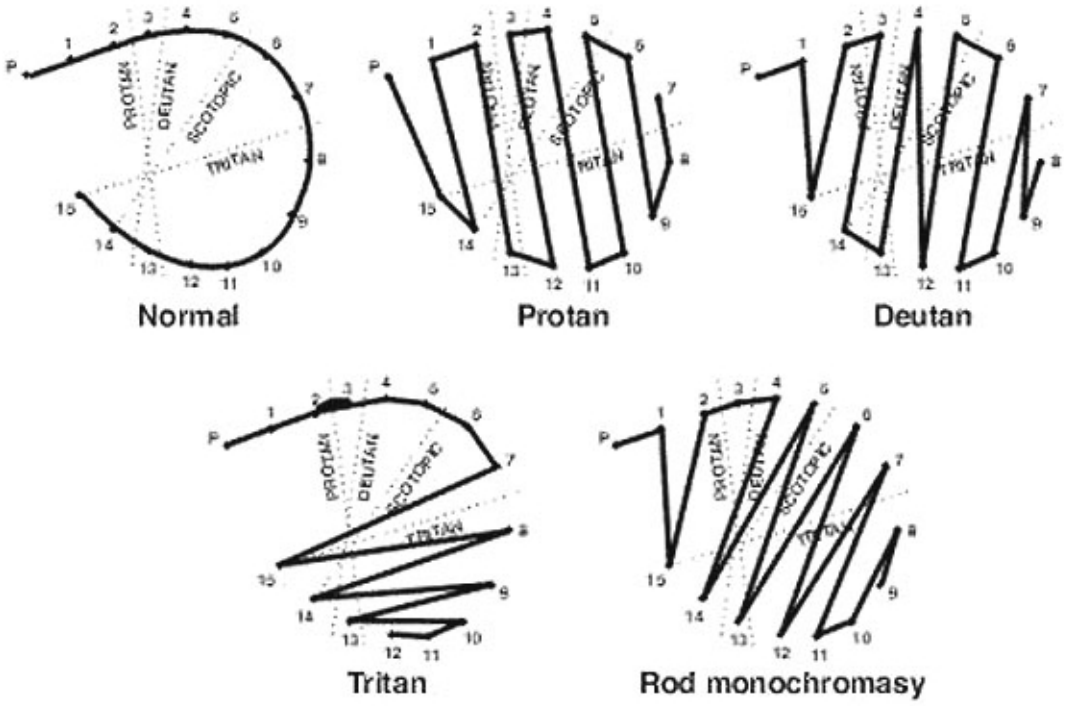

Figure 25. The Farnsworth Panel D-15 results from patients with various CVDs. The rod monochromatic results are idealised to illustrate the scotopic axis along 5-14. As a rule, rod monochromats give variable results, with a tendency of crossing errors to fall along the 5-14 axis.

Figure 26. Farnsworth 100-Hue.

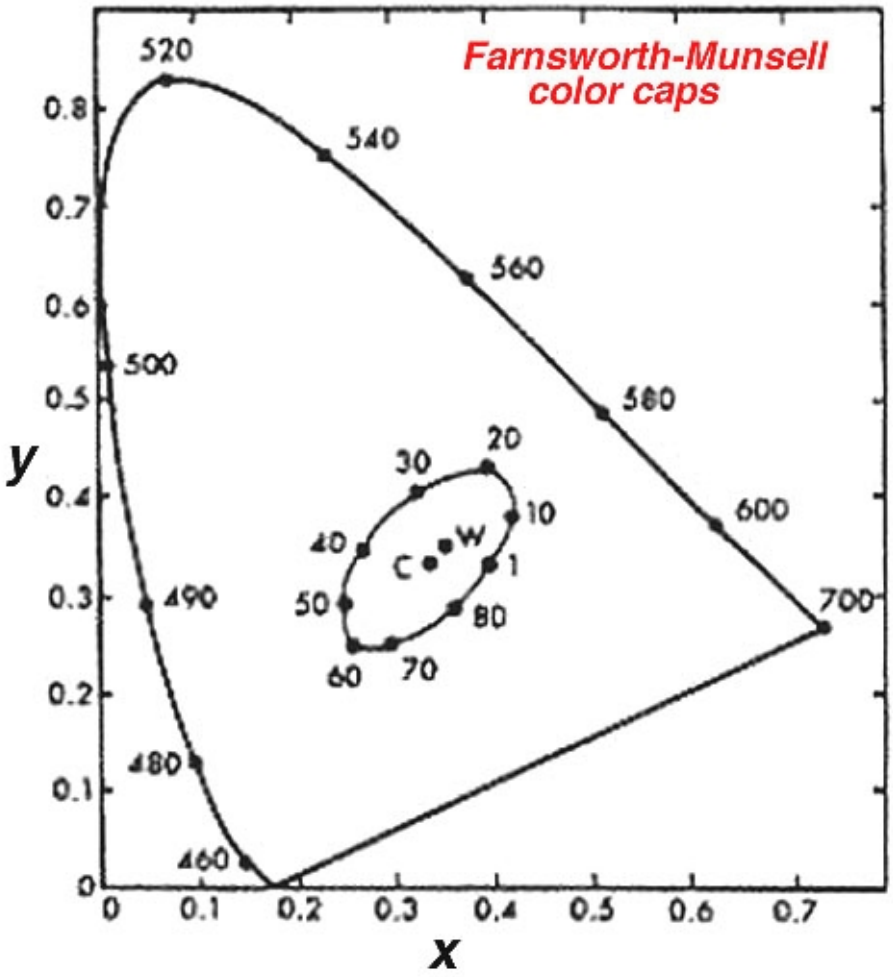

Figure 27. Colors of the 100-Hue on the chromaticity diagram. Point C represents testing conditions using standard illuminant C and point W is the equal energy white. From Hart (32).

Figure 28. The different lanterns used in occupational testing of color vision.

About the Authors

Michael Kalloniatis was born in Athens Greece in 1958. He received his optometry degree and Master's degree from the University of Melbourne. His PhD was awarded from the University of Houston, College of Optometry, for studies investigating colour vision processing in the monkey visual system. Post-doctoral training continued at the University of Texas in Houston with Dr Robert Marc. It was during this period that he developed a keen interest in retinal neurochemistry, but he also maintains an active research laboratory in visual psychophysics focussing on colour vision and visual adaptation. He was a faculty member of the Department of Optometry and Vision Sciences at the University of Melbourne until his recent move to New Zealand. Dr. Kalloniatis is now the Robert G. Leitl Professor of Optometry, Department of Optometry and Vision Science, University of Auckland. e-mail: m.kalloniatis@unsw.edu.au

Charles Luu was born in Can Tho, Vietnam in 1974. He was educated in Melbourne and received his optometry degree from the University of Melbourne in 1996 and proceeded to undertake a clinical residency within the Victorian College of Optometry. During this period, he completed post-graduate training and was awarded the post-graduate diploma in clinical optometry. His areas of expertise include low vision and contact lenses. During

his tenure as a staff optometrist, he undertook teaching of optometry students as well as putting together the "Cyclopean Eye", in collaboration with Dr Michael Kalloniatis. The Cyclopean Eye is a Web based interactive unit used in undergraduate teaching of vision science to optometry students. He is currently in private optometric practice as well as a visiting clinician within the Department of Optometry and Vision Science, University of Melbourne.

References

1. Young T. On the theory of light and colours. Philos Trans R Soc Lond. 1802;92:12–48.
2. Baylor DA, Nunn BS, Schnapf JL. The photocurrent, noise and spectral sensitivity of rods of the monkey Macaca fascicularis. J Physiol. 1984;357:575–607. PubMed PMID: 6512705.
3. Smith VC, Pokorny J. Spectral sensitivity of the foveal cone photopigments between 400 and 500 nm. Vision Res. 1975;15:161–171. PubMed PMID: 1129973.
4. Bowmaker JK, Dartnall HJ. Visual pigments of rods and cones in human retina. J Physiol. 1980;298:501–511. PubMed PMID: 7359434.
5. Rushton WAH. A cone pigment in protanope. J Physiol. 1963;168:345–359. PubMed PMID: 14062681.
6. Rushton WAH. Densitometry of pigments in rods and cones of normal and color defective subjects. Invest Ophthalmol. 1966;5:233–241. PubMed PMID: 5296487.
7. Grassmann HC. Zur theorie der farbenmischung. Ann Phys. 1853;89:69–84.
8. von Helmholtz H. Handbuch der physiologischen Optik. Hamburg: L. Voss; 1866. [English translation in MacAdam DL.(1970). Sources of color science. Cambridge (MA): MIT Press; 1970].
9. Marks WB, Dobelle WH, MacNichol JR. Visual pigments of single primate cones. Science. 1964;143:1181–1183. PubMed PMID: 14108303.
10. Nathans J, Piantanida TP, Eddy RL, Shows TB, Hogness DS. Molecular genetics of inherited variation in human color vision. Science. 1986;232:203–210. PubMed PMID: 3485310.
11. Nathans J, Thomas D, Hogness DS. Molecular genetics of human color vision: genes encoding blue, green, and red pigments. Science. 1986;232:193–202. PubMed PMID: 2937147.
12. Hering KEK. Zur Lehre vom Lichtsinne. Sitzungsberichte der kaiserlichen Akademie der Wissenschaften. Mathematisch–naturwissenschaftliche Classe, Wien, 3. Abtheilung. 1872;66:5–24.
13. Hurvich LM, Jameson D. An opponent-process theory of color vision. Psychol Rev. 1957;64:384–404. PubMed PMID: 13505974.
14. Svaetichin G. Spectral response curves from single cones. Acta Physiol Scand Suppl. 1956;39:17–46. PubMed PMID: 13444020.
15. De Valois RL, Abramov I, Jacobs GH. Analysis of response patterns of LGN cells. J Opt Soc Am. 1966;56:966–977. PubMed PMID: 4959282.
16. De Monasterio FM, Gouras P. Functional properties of ganglion cells of the rhesus monkey retina. J Physiol. 1975;251:167–95. PubMed PMID: 810576.
17. Gouras P. Identification of cone mechanisms in monkey ganglion cells. J Physiol. 1968;199:533–547. PubMed PMID: 4974745.
18. Zrenner E, Gouras P. Characteristics of the blue sensitive cone mechanism in primate retinal ganglion cells. Vision Res. 1981;21:1605–1609. PubMed PMID: 7336593.
19. Cole BL, Henry GH, Nathan J. Phenotypical variations of tritanopia. Vision Res. 1966;6:301–313.
20. Henry GH, Cole BL, Nathan J. The inheritance of congenital tritanopia with the report of an extensive pedigree. Ann Hum Genet. 1964;27:219–231. PubMed PMID: 14128207.
21. Smith DP, Cole BL, Isaacs A. Congenital tritanopia without neuroretinal disease. Invest Ophthal. 1973;12:608–617. PubMed PMID: 4542649.
22. Pease PL. (1998). Color vision (Chapter 9). In: Benjamin WJ, editor. Borish's clinical refraction. Philadelphia: W. B. Saunders Company.
23. Cole BL, Vingrys AJ. A survey and evaluation of lantern tests of color vision. Am J Optom Physiol Opt. 1982;59:346–374. PubMed PMID: 7048937.

24. Cole BL, Vingrys AJ. Who fails lantern tests? Doc Ophthalmol. 1983;55:157–173. PubMed PMID: 6603960.
25. Cole BL, Maddocks JD. Can clinical colour vision tests be used to predict the results of the Farnsworth lantern test? Vision Res. 1998;38:3483–3485. PubMed PMID: 9893869.
26. Moses RA, Hart WM. Adler's physiology of the eye. Clinical application. 8th ed. St. Louis (MO): The C. V. Mosby Company; 1987.
27. Le Grand Y. Light color and vision. 2nd ed. London: Chapman and Hall; 1968.
28. Benjamin WJ, editor. Borish's clinical refraction. Philadelphia: W. B. Saunders Company; 1998.
29. Davson H. The eye. London: Academic Press; 1962;
30. Marriott FHC. Colour vision: colour-matches (Chapter 13). In: Davson H, editor. The eye. Vol 2. London: Academic Press; 1962.
31. Graham CH. Color: data and theories (Chapter 15) and Discriminations that depend on wavelength (Chapter 12). In: Graham CH, editor. Vision and visual perception. New York: John Wiley and Sons, Inc.; 1965.
32. Hart WM. Acquired dyschromatopsias. Surv Ophthalmol. 1987;32:10–31. PubMed PMID: 3310294.
33. Cole BL. The handicap of abnormal colour vision. Aust J Optom. 1972;55:304–310.
34. Wright WD. The characteristics of tritanopia. J Opt Soc Am. 1952;42:509–520. PubMed PMID: 14946611.

The Perception of Space

Michael Kalloniatis and Charles Luu.[1]

Created: May 1, 2005; Updated: June 6, 2007.

Retinal Disparity

When we look at an object with two eyes, we perceive it as singular, like we do other parts of the visual scene stimulating points on our retina that share a common visual direction. These points are termed "retinal corresponding points" and fall on an area called the "horopter". Points outside the horopter fall on slightly different retinal areas and so do not have the identical visual direction and lead to "retinal disparity", the basis of our depth discrimination. This retinal image disparity occurs due to the lateral displacement of the eyes. The region in visual space over which we perceive single vision is known as "Panum's fusional area", with objects in front and behind this area being in physiological diplopia (i.e., double vision). Our visual system suppresses this diplopia, and hence we do not perceive double vision under normal viewing conditions. To understand the discussion on the horopter and Panum's fusional space, the sense of direction will be introduced. Two terms describing direction sense are oculocentric and egocentric visual direction.

Oculocentric Visual Direction

The visual direction of an object can be represented by a line that joins the object and the fovea called the Principal Visual Direction or visual axis. On the basis of the principal visual direction, the direction of all other objects in the subject's visual field is determined. This is the called oculocentric visual direction. Therefore, each point of the retina can be considered to have it own sense of direction. For example, when we look at an object, the object is imaged on the fovea. Other objects imaged above the fovea are seen as "below", and those imaged below the fovea are seen as "above". Visual sense of direction is organized about the fovea. For a given position of the eye, objects having superimposed retinal images will be seen as being in alignment in the visual field, but at a different distance from the eye (Fig. 1).

Egocentric Visual Direction

Egocentric visual direction refers to the direction of an object in space relative to one self, rather than the eyes. Egocentric direction is determined by retinal position, proprioceptive information about the eye, head and body position, and the vestibular apparatus. All this information allows us to determine whether a change in retinal position is due to object movement or due to eye or head movement. In Fig. 2a, a stationary object is imaged on the fovea with the head and the body stationary. When the eye moves, the stationary object is then imaged on a new retinal position. Therefore, oculocentric direction has changed, but the egocentric direction has not changed as the object has remained stationary. In another example, the eye tracks a moving object (Fig. 2b). As the object is imaged on the fovea at all times, the oculocentric direction is the same, but the egocentric direction is changing.

In binocular vision, the idea of corresponding retinal points has been used to describe the principle visual direction. Corresponding retinal points are points stimulated on the retina that give rise to the same visual direction. When objects stimulate non-corresponding points, this gives rise to different visual directions. These retinal points are called disparate points. Therefore, corresponding points have the same principle visual direction, and non-corresponding points have different visual directions (Fig. 3).

As we see the world single and not double, binocular vision can be represented by a single eye, the cyclopean eye. The cyclopean eye is an imaginary eye situated midway between the two eyes (Fig. 4). Disparate points give rise

Author Affiliation: 1 Department of Optometry and Vision Sciences University of Melbourne, Australia.

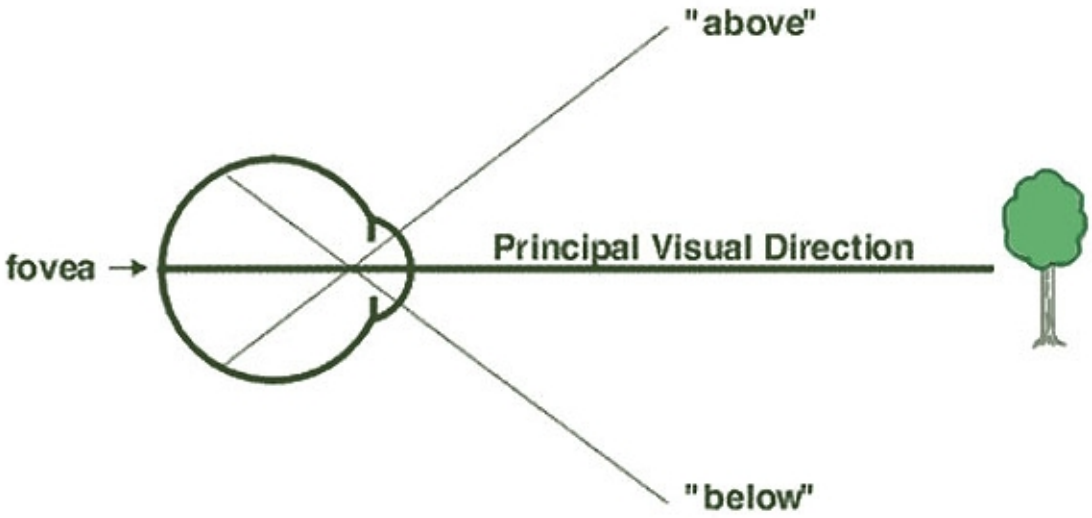

Figure 1. Oculocentric visual direction.

to physiological diplopia (double vision). In Fig. 5, it can be seen that point A stimulates disparate points (non-corresponding retinal points).

Using the cyclopean eye, crossed and uncrossed diplopia can be explored. For an object closer than the fixation point such as point B in Fig. 6a, crossed diplopia occurs as the point B is imaged on the temporal retina of both eyes. This is termed crossed diplopia because the image in the left eye is seen on the right side. For an object located further than the fixation point, the image of the object falls on the nasal retina of both eyes, producing uncrossed diplopia. This is termed uncrossed diplopia because the image in the left eye is seen on the left side (Fig. 6b).

The principle of the cyclopean eye can be applied to patients with strabismus (a turned eye). Patients with strabismus are usually classified according to the direction of the eye turn. Two common types of strabismus are patients with an esotropia, their eye(s) turned in, and patients with exotropia, their eye(s) turned out. Patients with an exotropia will have crossed diplopia, whereas patients with an esotropia will have uncrossed diplopia (Fig. 7).

The Horopter

Our visual world is composed of multiple points, hence the need to develop concepts to deal with the whole visual space. This concept is called the horopter. The horopter is the locus of points in space that stimulates corresponding points, that is, a multitude of points in visual space that lead to single vision.

The Vieth-Muller Circle

The Vieth-Muller circle is a theoretical horopter. All points on this circle should stimulate corresponding points on the retina and lead to single vision, provided that the fixation point lies on the center of the circle and the eyes rotate about its nodal point (instead of their center of rotation). The Vieth-Muller circle assumes there is angular symmetry of the corresponding points (Fig. 8).

Measuring the Horopter

The horopter can be measured through several methods. These methods include:

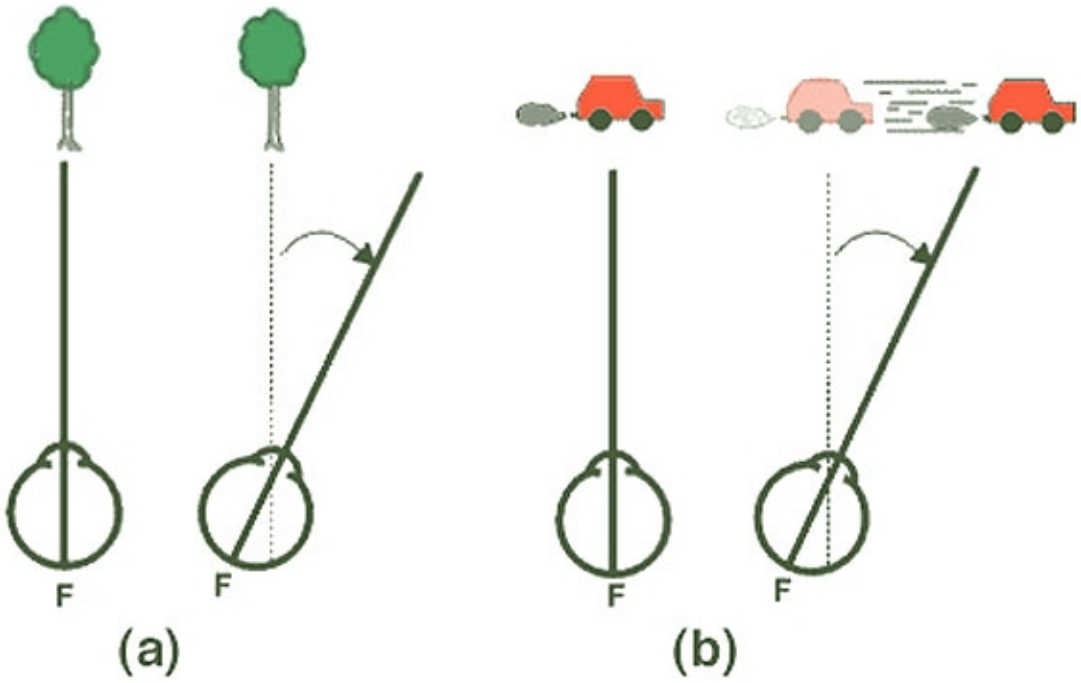

Figure 2. (a) Different oculocentric direction but the same egocentric direction as the object is stationary. (b) Same oculocentric direction but egocentric direction is changing because the object is moving.

- Haplopic method
- Nonius method
- Apparent front-parallel plane (AFPP) method

The Nonius and AFPP methods directly determine the longitudinal horopter, whereas the haplopic method does not. Instead, the haplopic method determines the inner and outer boundaries of single binocular vision, and the horopter is taken as the midline.

Haplopic Method

The haplopic method (method of the region of singular binocular vision) is based on the primary definition of corresponding points; retinal points that correspond give rise to identical visual directions and, as a consequence, single vision. Thus, if diplopia is observed, disparate points are being stimulated. Therefore, the method involves determining the boundaries of single binocular vision (Fig. 9).

Nonius Method

Because corresponding points give rise to identical visual directions, the position of an object that stimulates a pair of corresponding points can be located if each eye sees a different part of the object. If the two parts are seen in the same direction, then the objects are in that position where they stimulate corresponding points. This is the basis of the Nonius method (method of equating visual directions) (Fig. 10).

The Apparent Fronto-Parallel Plane (AFPP) Method

The theory of stereopsis holds that stimulation of disparate points is necessary for the perception of relative depth by stereopsis. If there is no depth difference between an object and the fixation point, then they stimulate corresponding points. Thus, if the subject is asked to arrange a series of objects so that they appear to be in a fronto-parallel plane (i.e., no depth difference between them), then they will lie on the horopter. This is the apparent fronto-parallel plane method (Fig. 11). Note the change in shape of the horopter at different distances.

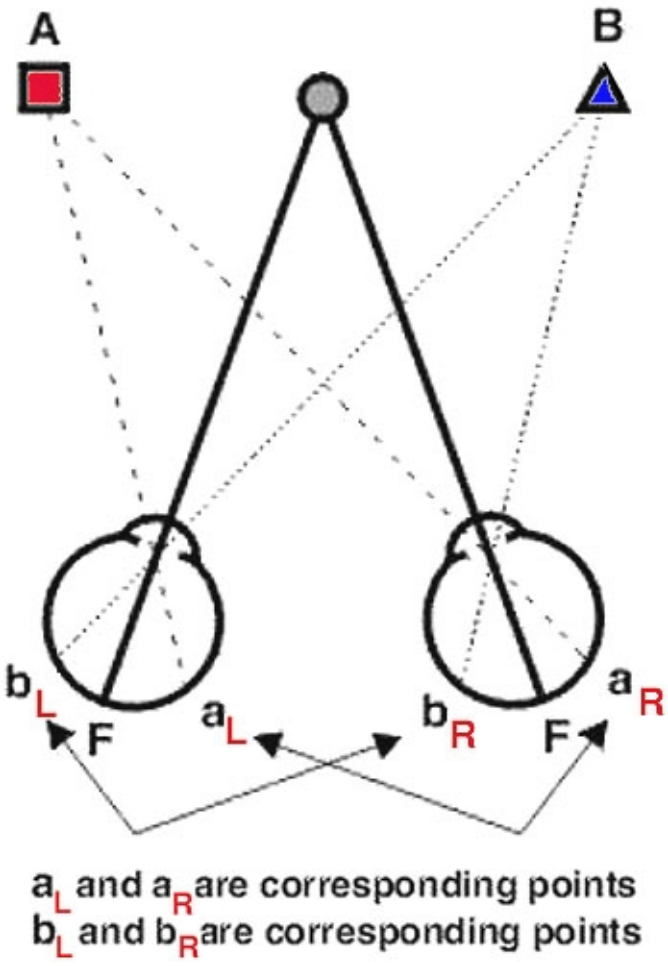

Figure 3. Corresponding points of the two eyes.

Relationship of the Horopter to Panum's Fusional Area

The haplopic method demonstrates the existence of Panum's fusional area. This concept allows for single binocular vision about the point of fixation, even when corresponding retinal points are not being stimulated. An image on the retina of one eye can be fused (and seen as single) with a similar image on the retina of the other eye, although disparity in the retinal image exists. Panum's fusional area is needed for stereopsis; if images do not fall in Panum's area, then diplopia results—and so Panum's fusional area defines the zone of stereovision.

Aniseikonia

Aniseikonia describes a subject's spatial perception when there is a difference in retinal image size of the same object between the two eyes. Anisekonia can be investigated by placing an aniseikonic lens placed in front of one eye (to magnify the retinal image in one eye) while plotting the horopter using the AFPP method. When this is performed, the apparent fronto-parallel plane becomes skewed about the fixation point, with the horopter being nearer on the side of the eye having the increased magnification (Fig. 12). Note that magnification cannot be too large, otherwise, diplopia would result because the two retinal images would fall outside Panum's fusional area. Aniseikonia identifies reshaping of visual space within Panum's fusional area.

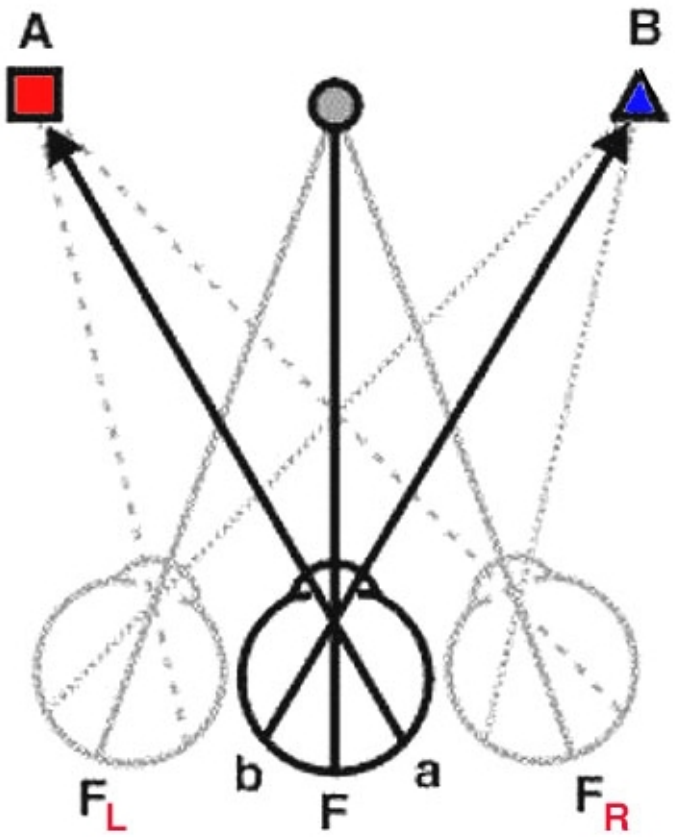

Figure 4. The cyclopean eye is used to determine the direction of point A and point B. Point A stimulating the temporal retina of right eye and the nasal retina of the left eye, that is, stimulates a retinal point to the right of the fovea.

The importance of these plots with the aniseikonic lens is to demonstrate stable corresponding retinal points. As long as the magnification difference between the two eyes is not too large, fusion will be maintained, although spatial distortions will occur. Once the magnification difference exceeds Panum's fusional space, diplopia will result. Aniseikonic symptoms are a common complaint of patients with unequal refractive errors or large astigmatic corrections. The magical 2-week rule applies, i.e., the time taken for sensory adaptation. If symptoms persist, reducing the magnification difference or reducing the correction are two clinical options.

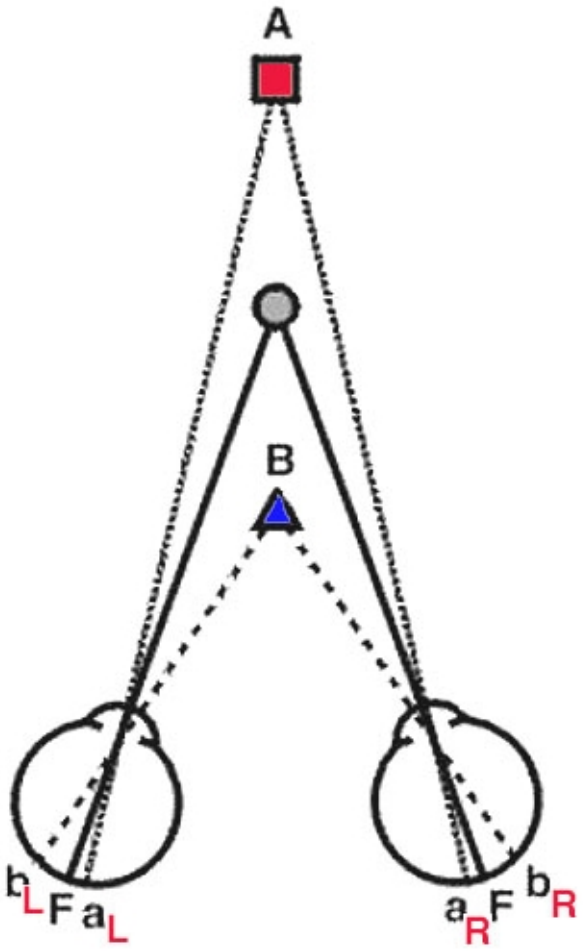

Figure 5. Point A and point B stimulating disparate points. Point A stimulates the nasal retina of both eyes.

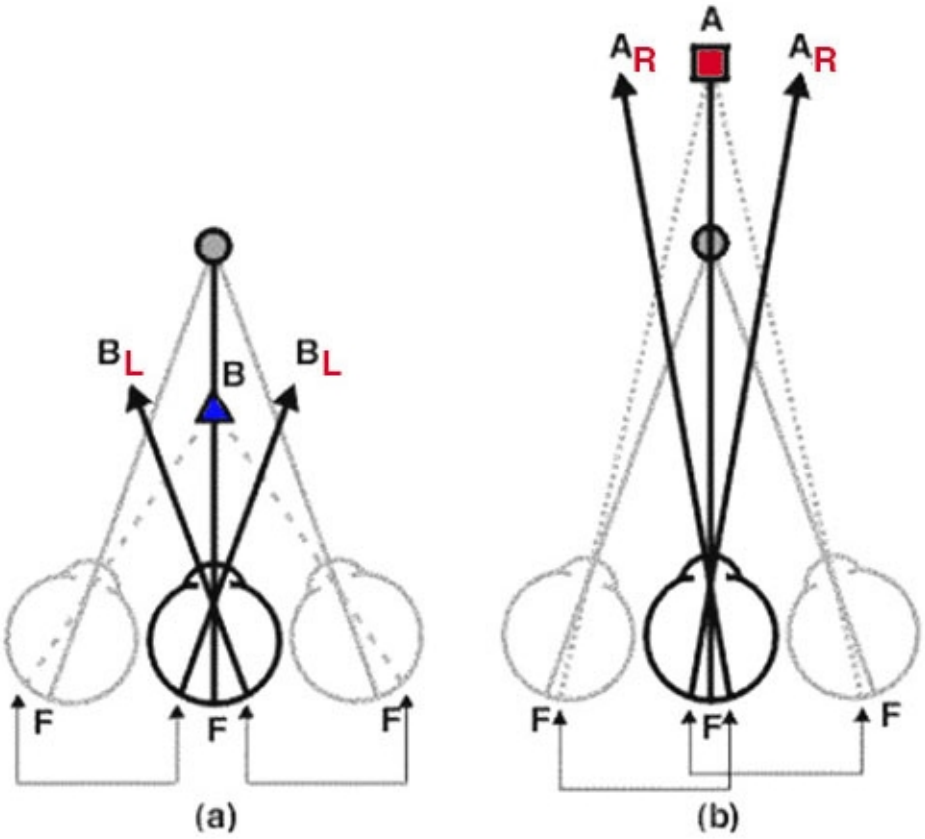

Figure 6. Demonstrating crossed (a) and uncrossed (b) diplopia using the cyclopean eye.

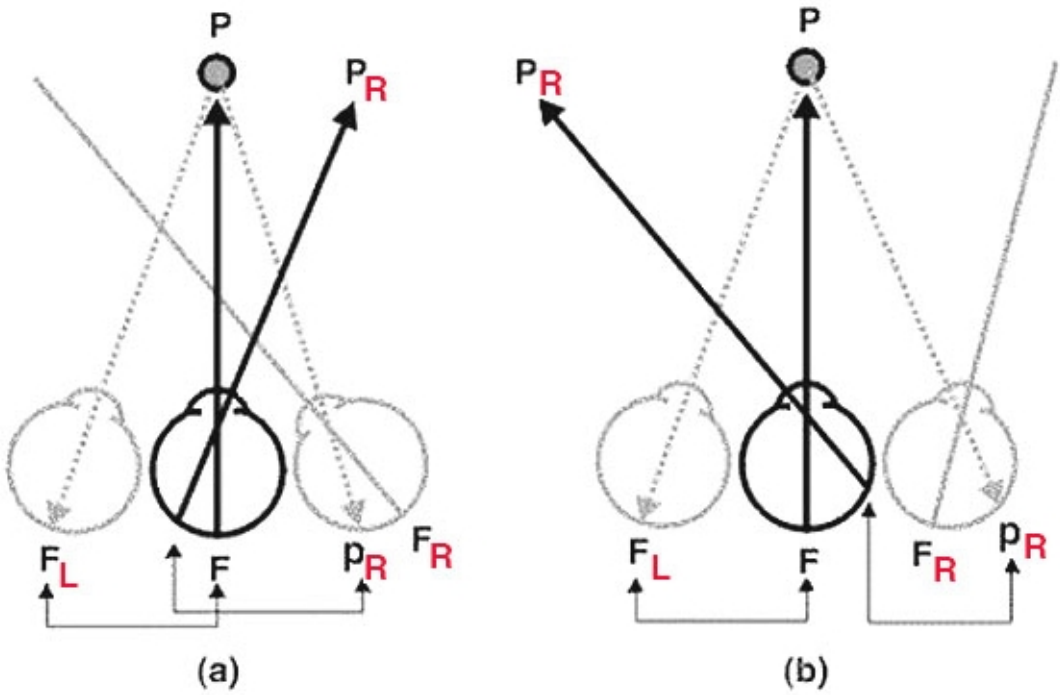

Figure 7. (a) Uncrossed diplopia with an esotropia. (b) Crossed diplopia with an exotropia.

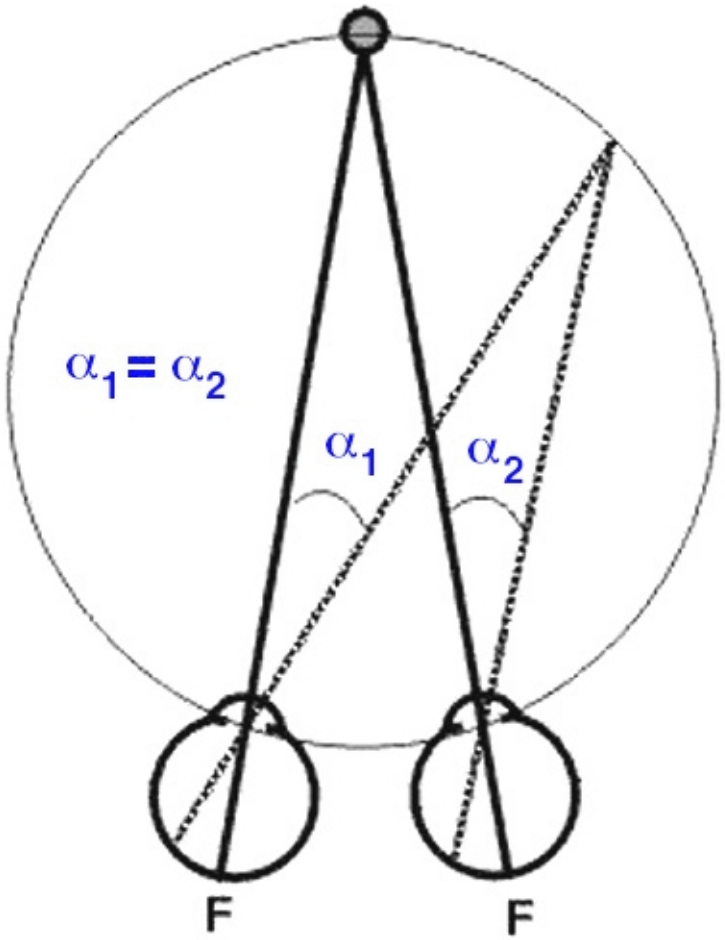

Figure 8. Vieth-Muller circle. The circle represents the theoretical locus of points in space that stimulates corresponding retinal points.

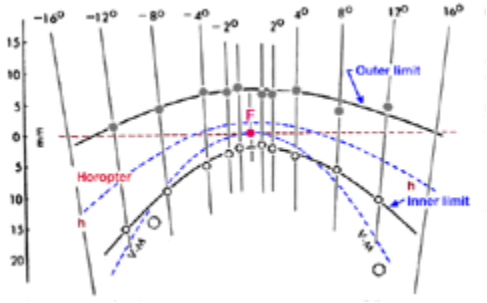

Figure 9. Result of the horopter determined by the haplopic method at a viewing distance of 40 cm. From Moses and Hart (1) and Ogle (2).

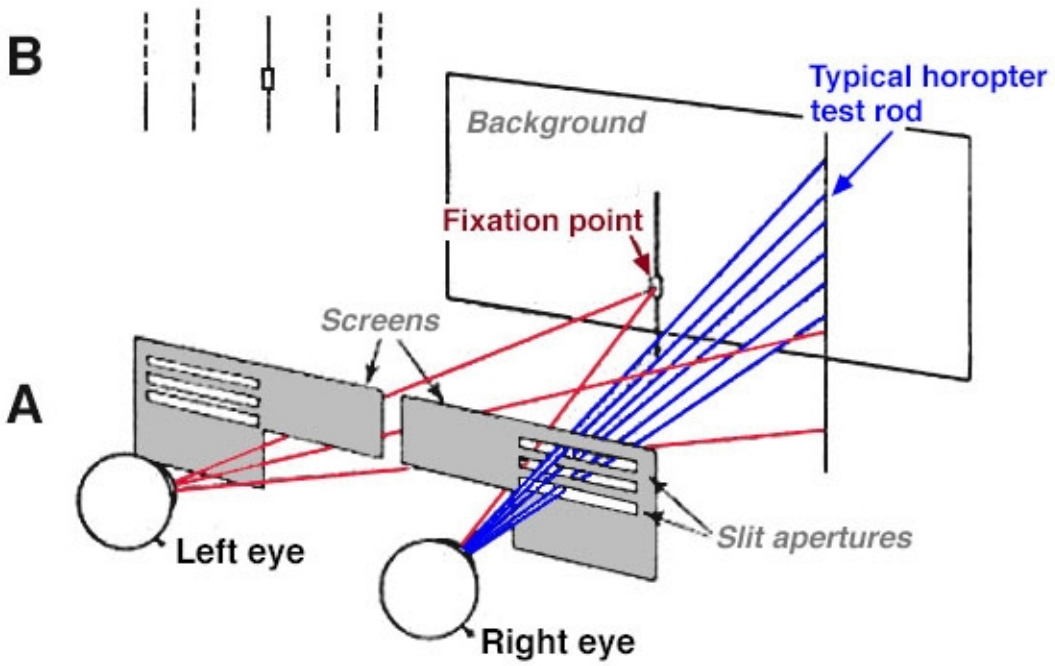

Figure 10. The horopter as determined by the Nonius method. From Moses and Hart (1) and Ogle (2).

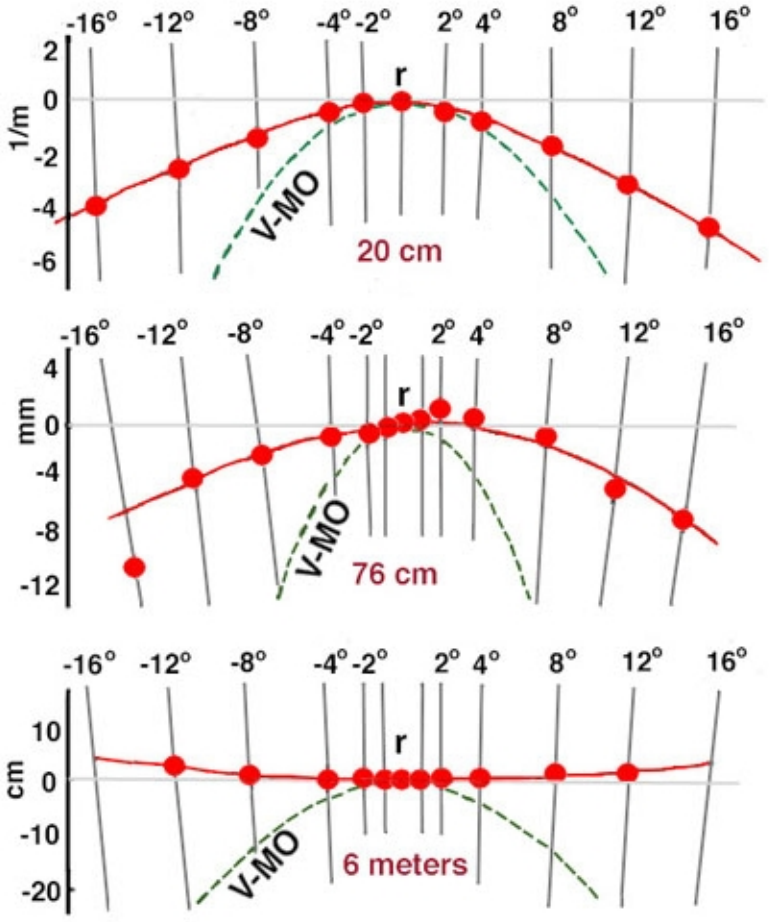

Figure 11. The horopter as determined by the apparent fronto-parallel plane method at different distances (25 cm, 40 cm, and 1 m). From Ogle (2).

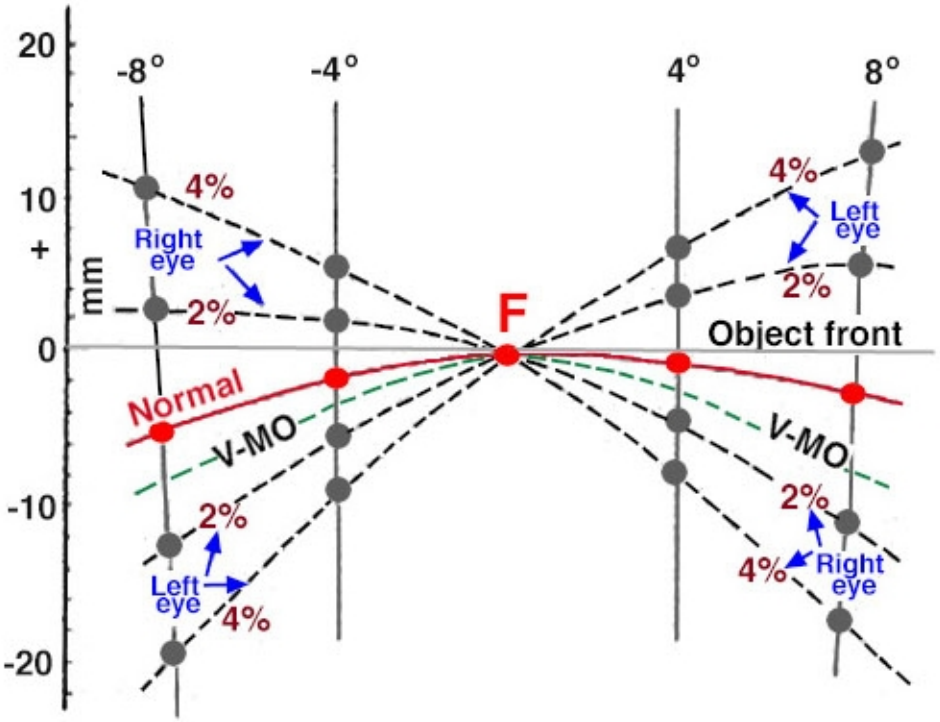

Figure 12. Plot of the horopter at 40 cm using the AFPP method with different magnification (2% and 4% magnification) lenses in front of one eye. From Ogle (2).

About the Authors

Michael Kalloniatis was born in Athens Greece in 1958. He received his optometry degree and Master's degree from the University of Melbourne. His PhD was awarded from the University of Houston, College of Optometry, for studies investigating colour vision processing in the monkey visual system. Post-doctoral training continued at the University of Texas in Houston with Dr Robert Marc. It was during this period that he developed a keen

interest in retinal neurochemistry, but he also maintains an active research laboratory in visual psychophysics focussing on colour vision and visual adaptation. He was a faculty member of the Department of Optometry and Vision Sciences at the University of Melbourne until his recent move to New Zealand. Dr. Kalloniatis is now the Robert G. Leitl Professor of Optometry, Department of Optometry and Vision Science, University of Auckland. e-mail: m.kalloniatis@unsw.edu.au

Charles Luu was born in Can Tho, Vietnam in 1974. He was educated in Melbourne and received his optometry degree from the University of Melbourne in 1996 and proceeded to undertake a clinical residency within the Victorian College of Optometry. During this period, he completed post-graduate training and was awarded the post-graduate diploma in clinical optometry. His areas of expertise include low vision and contact lenses. During his tenure as a staff optometrist, he undertook teaching of optometry students as well as putting together the "Cyclopean Eye", in collaboration with Dr Michael Kalloniatis. The Cyclopean Eye is a Web based interactive unit used in undergraduate teaching of vision science to optometry students. He is currently in private optometric practice as well as a visiting clinician within the Department of Optometry and Vision Science, University of Melbourne.

References

1. Moses RA, Hart WM. Adler's physiology of the eye. Clinical application. 8th ed. St. Louis (MO): The C. V. Mosby Company; 1987.
2. Ogle KN. Researches in binocular vision. London: Saunders; 1950.

The Perception of Depth

Michael Kalloniatis and Charles Luu.[1]

Created: May 1, 2005; Updated: June 6, 2007.

Stereopsis

Stereopsis refers to our ability to appreciate depth, that is, the ability to distinguish the relative distance of objects with an apparent physical displacement between the objects. It is possible to appreciate the relative location of objects using one eye (monocular cues). However, it is the lateral displacement of the eyes that provides two slightly different views of the same object (disparate images) and allows acute stereoscopic depth discrimination.

Monocular Cues

Several strong monocular cues allow relative distance and depth to be judged. These monocular cues include:

- relative size
- interposition
- linear perspective
- aerial perspective
- light and shade
- monocular movement parallax

Relative Size

Retinal image size allow us to judge distance based on our past and present experience and familiarity with similar objects. As the car drives away, the retinal image becomes smaller and smaller. We interpret this as the car getting further and further away. This is referred to as size constancy. A retinal image of a small car is also interpreted as a distant car (Fig. 1).

Interposition

Interposition cues occur when there is overlapping of objects. The overlapped object is considered further away (Fig. 2).

Linear Perspective

When objects of known distance subtend a smaller and smaller angle, it is interpreted as being further away. Parallel lines converge with increasing distance such as roads, railway lines, electric wires, etc. (Fig. 3).

Aerial Perspective

Relative color of objects gives us some clues to their distance. Because of the scattering of blue light in the atmosphere, creating a "wall" of blue light, distance objects appear more blue (Fig. 4). Thus, distant mountains appear blue. Contrast of objects also provide clues to their distance. When the scattering of light blurs the outlines of objects, the object is perceived as distant. Mountains are perceived to be closer when the atmosphere is clear.

Author Affiliation: 1 Department of Optometry and Vision Sciences University of Melbourne, Australia.

Figure 1. Relative size. A retinal image of a small car is considered to be distant.

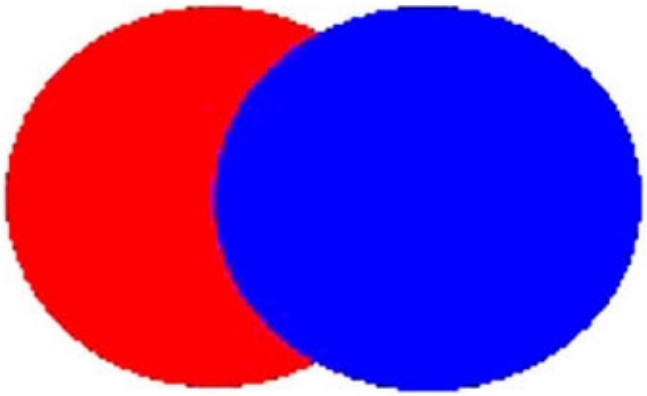

Figure 2. Interposition. The blue circle is reported to be closer because it overlaps the red circle.

Light and Shade

Highlights and shadows can provide information about an object's dimensions and depth (Fig. 5). Because our visual system assumes that the light comes from above, a totally different perception is obtained if the image is viewed upside down.

Monocular Movement Parallax

When our heads move from side to side, objects at different distances move at a different relative velocity. Closer objects move "against" the direction of head movement and farther objects move "with" the direction of head movement.

Figure 3. Linear perspective. Parallel lines, such as railway lines, converge with increasing distance.

Figure 4. Aerial perspective. Mountains in the distance appear more blue.

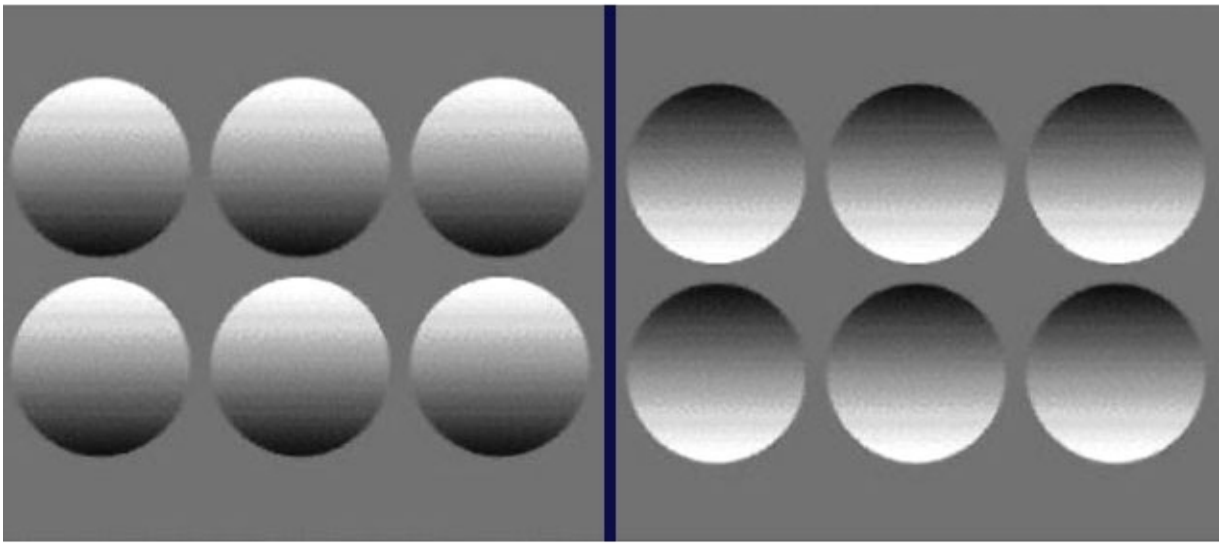

Figure 5. Highlights and shadows provide information about depth.

Binocular Cues

Stereopsis is an important binocular cue to depth perception. Stereopsis cannot occur monocularly and is due to binocular retinal disparity within Panum's fusional space. Stereopsis is the perception of depth produced by binocular retinal disparity. Therefore, two objects stimulate disparate (non-corresponding) retinal points within Panum's fusional area.

Fusion describes the neural process that brings the retinal images in the two eyes to form one single image. Fusion occurs to allow single binocular vision. Fusion takes place when the objects are the same. When the objects are different, suppression, superimposition, or binocular ("retinal") rivalry may occur. Suppression occurs to eliminate one image to prevent confusion. Superimposition results in one image presented on top of the other image. Binocular rivalry describes alternating suppression of the two eyes, resulting in alternating perception of the two images. This usually occurs when lines that are presented to the two eyes differ in orientation, length, or thickness. An example of binocular rivalry occurs when one eye is presented with a horizontal line and the other eye is presented with a vertical line. Binocular rivalry occurs at the intersection of the lines, and some suppression also exists (Fig. 6).

Panum's fusional area is the region of binocular single vision. Outside Panum's fusional area, physiological diplopia occurs. Using the haplopic method of determining the horopter, Panum's area can be determined (Fig. 7).

Retinal Disparity

Retinal disparate points are retinal points that give rise to different principal visual direction and diplopia. However, retinal disparity within Panum's fusional area (zone of single binocular vision) can be fused, resulting in single vision. Retinal disparity is essential for stereoscopic depth perception because stereoscopic depth perception results from fusion of slightly dissimilar images. Because of the lateral displacement of our eyes, slightly dissimilar retinal images result from the different perception of the same object from each eye.

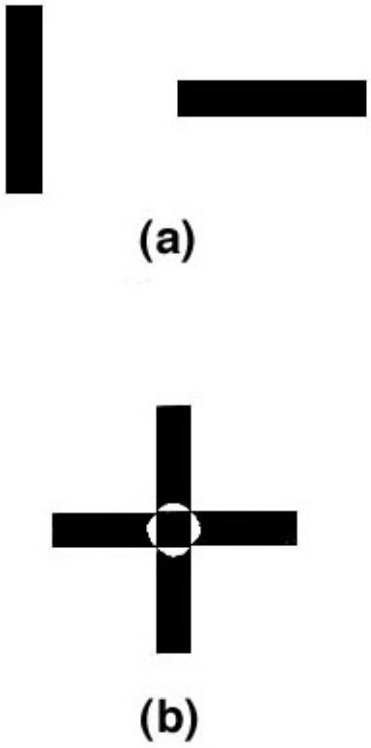

Figure 6. (a) Binocular rivalry can be demonstrated by placing a pen between yourself and the screen. Keep your eye on the tip of the pen, and notice the two bars merge. You may need to slowly move the pen from the screen toward you. (b) Result of (a).

Clinical Tests Used to Measure Stereopsis

There are two groups of clinical tests used to measure stereopsis. These are the contour stereotests and the random-dot stereotest. Random-dot stereograms were first used by Julesz (1) to eliminate monocular cues. As there are no contours, depth perception (stereopsis) can only be appreciated when binocular fusion occurs. Two process of stereopsis are used, and these are local and global stereopsis. Local stereopsis exists to evaluate the two horizontally disparate stimuli. This process is sufficient for contour stereotests. Global stereopsis is required in random-dot stereogram when the evaluation and correlation of corresponding points and disparate points are needed over a large retinal area.

An example of a contour stereotest used in the clinic is the Titmus Fly Stereotest. In the Titmus Fly Stereotest, horizontal disparity is presented via the vectographic technique (2). When tested at 40 cm, the fly has a disparity of 3,600 sec of arc; the disparities of the animals range from 400 to 100 sec of arc, and the disparities of the Wirt rings range from 800 to 40 sec of arc (Fig. 8).

Examples of random-dot stereotests used in the clinic are the Frisby Stereotest, the Randot Stereotest, the Random-dot E Stereotest, and the Lang Stereotest. The Frisby Stereotest (Fig. 9) uses real depth to determine stereoacuity. Three perspex of different thicknesses are used. Four squares of geometric shapes are painted on one side of the perspex. In one of the squares, a circle of these geometric shapes is painted on the other side of the perspex. Both the Randot (Fig. 10) and the Random-dot E uses crossed polarized filters. Disparity is also constructed vectographically. The Randot Stereotest uses modified animals and ring designs with random dot backgrounds to eliminate monocular cues. The Lang Stereotest uses a panographic technique (2) to present

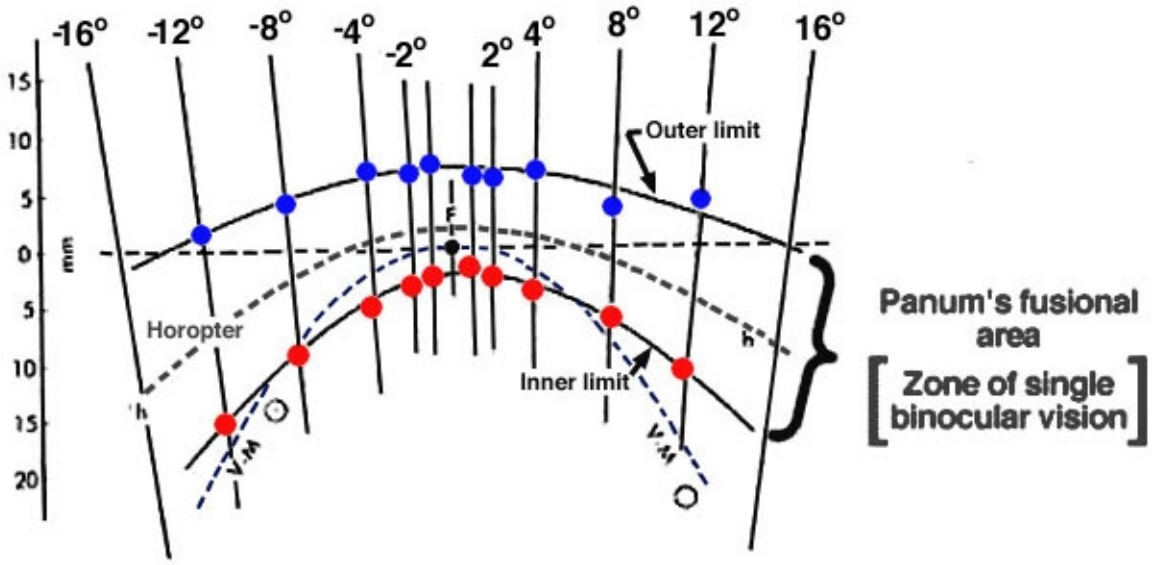

Figure 7. Haplopic method of determining the horopter involves locating the region of single binocular vision at a distance of 40 cm. Panum's fusional area lies between the outer and inner limits of the region of single binocular vision.

disparity; therefore, no filters are required. Patients are required to identify pictures on the Lang Stereotest. The Lang II Stereotest has a monocularly visible shape on it (Fig. 11).

All of the tests provide a measure of stereoacuity by asking the patient to identify the correct target that has stereoscoptic depth (target with disparity). The working distance and interpupillary distance will need to be taken into consideration when calculating stereoacuity. Patients with disturbed binocular vision or different refractive error in one eye will perform poorly on depth discrimination tests.

Acknowledgments

We thank Tim Fricke for providing Figs. 8-11. Further readings on this topic can be found in Ogle (3), Moses and Hart (4), and Schwartz (5).

Figure 8. Titmus Fly Stereotest.

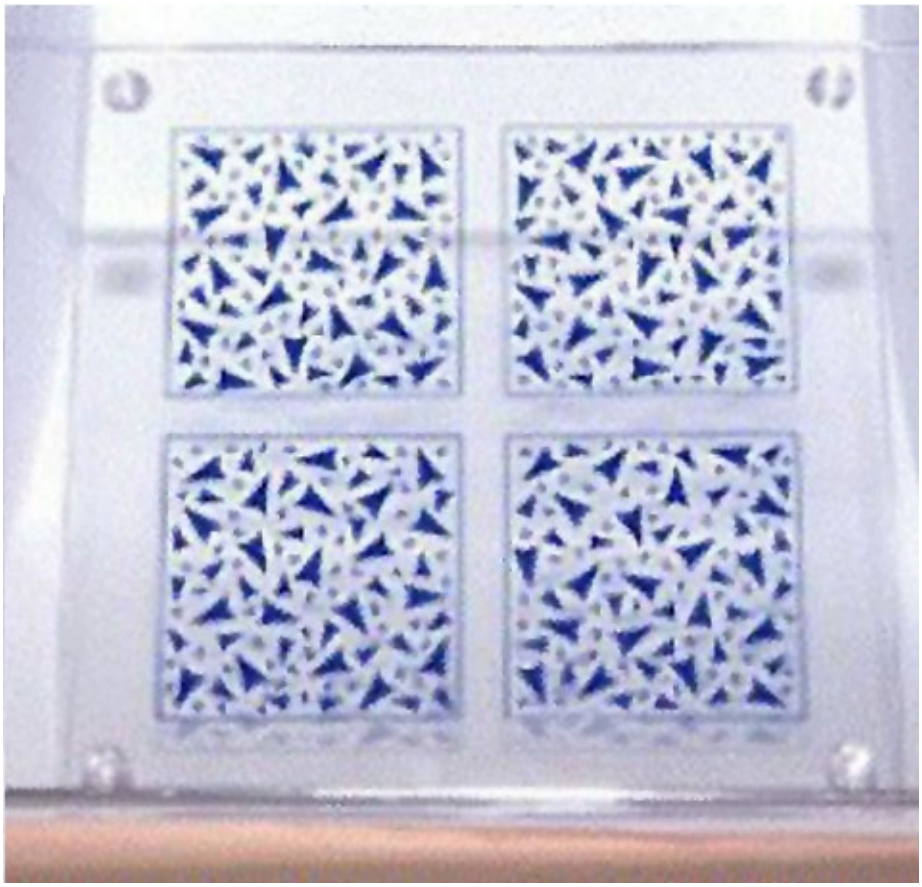

Figure 9. The Frisby Stereotest.

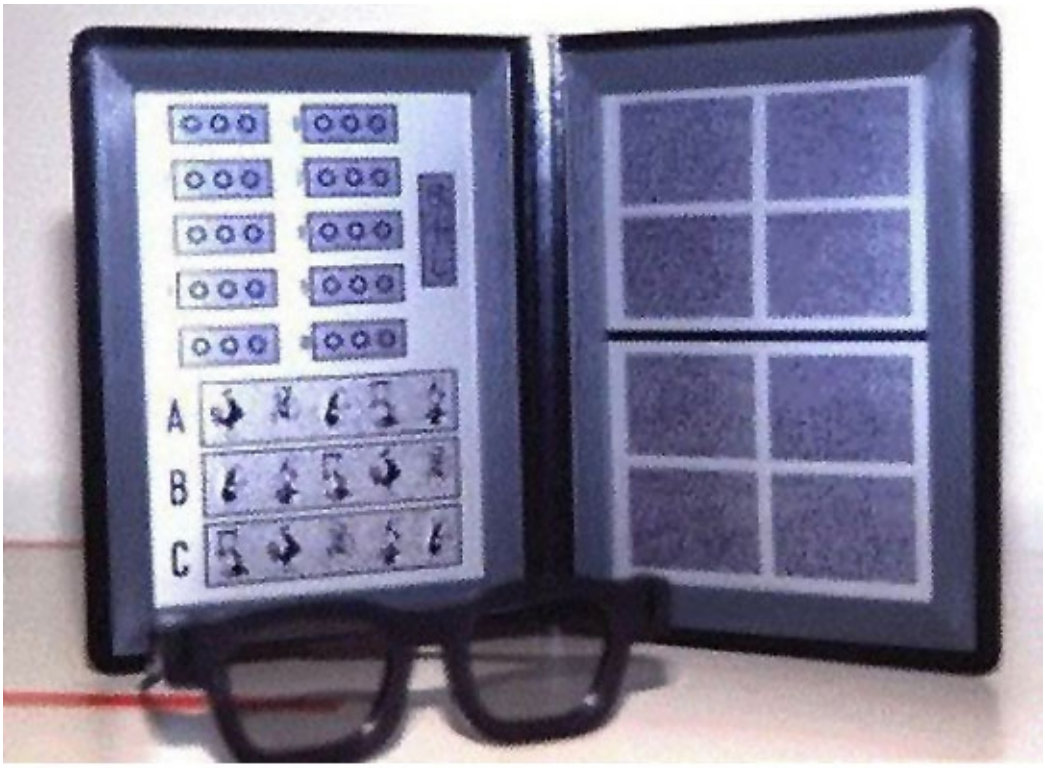

Figure 10. The Randot Stereotest.

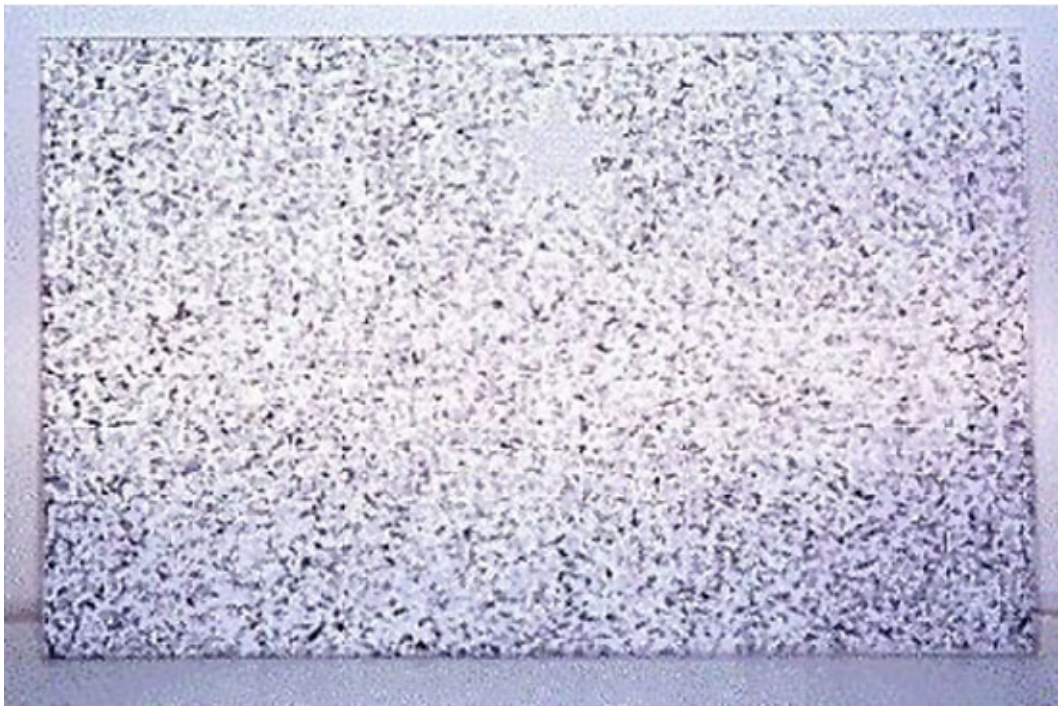

Figure 11. The Lang II.

About the Authors

Michael Kalloniatis was born in Athens Greece in 1958. He received his optometry degree and Master's degree from the University of Melbourne. His PhD was awarded from the University of Houston, College of Optometry, for studies investigating colour vision processing in the monkey visual system. Post-doctoral training continued at the University of Texas in Houston with Dr Robert Marc. It was during this period that he developed a keen interest in retinal neurochemistry, but he also maintains an active research laboratory in visual psychophysics focussing on colour vision and visual adaptation. He was a faculty member of the Department of Optometry and Vision Sciences at the University of Melbourne until his recent move to New Zealand. Dr. Kalloniatis is now the Robert G. Leitl Professor of Optometry, Department of Optometry and Vision Science, University of Auckland. e-mail: m.kalloniatis@unsw.edu.au

Charles Luu was born in Can Tho, Vietnam in 1974. He was educated in Melbourne and received his optometry degree from the University of Melbourne in 1996 and proceeded to undertake a clinical residency within the Victorian College of Optometry. During this period, he completed post-graduate training and was awarded the post-graduate diploma in clinical optometry. His areas of expertise include low vision and contact lenses. During

his tenure as a staff optometrist, he undertook teaching of optometry students as well as putting together the "Cyclopean Eye", in collaboration with Dr Michael Kalloniatis. The Cyclopean Eye is a Web based interactive unit used in undergraduate teaching of vision science to optometry students. He is currently in private optometric practice as well as a visiting clinician within the Department of Optometry and Vision Science, University of Melbourne.

References

1. Julesz B. Binocular depth perception of computer generated patterns. Bell Syst Tech J. 1960;39:1125–1162.
2. Fricke TR, Siderov J. Stereopsis, stereotest and their relation to vision screening and clinical practice. Clin Exp Optom. 1997;80:165–172.
3. Ogle KN. Researches in binocular vision. London: Saunders; 1950.
4. Moses RA, Hart WM. Adler's physiology of the eye. Clinical application. 8th ed. St. Louis (MO): The C. V. Mosby Company; 1987.
5. Schwartz SH. Visual perception. 2nd ed. (CT): Appleton and Lange; 1999.

Brain Visual Areas

The Primary Visual Cortex

Matthew Schmolesky

Created: May 1, 2005; Updated: June 14, 2007.

Introduction

The human visual system can detect and discriminate between an incredibly diverse assortment of stimuli that may be chromatic or achromatic, in motion or not, patterned or unpatterned, two-dimensional or three. Remarkably, the neural end-product of visual stimuli impacting upon the retina is, in one sense, always the same. After the complexities of phototransduction, lateral interactions provided by horizontal and amacrine cells, and integration of signals by ganglion cell dendrites, only the constantly changing stream of action potentials propogating along ganglion cell axons is left to inform our visual perception. These seemingly identical signals must somehow be processed in the subcortex and cortex to create the full range of visual percepts we experience. How this is achieved is a puzzle that currently occupies the professional lives of thousands of researchers, and the basic framework of a solution has only begun to unfold in the last several decades.

To achieve an understanding of cortical and subcortical processing, we can ask two basic questions about the signals leaving the retina:

- What are the discrete anatomical pathways that carry the signal?
- What information do the signals actually carry?

The answers to these questions do not exist. That is, the answers we have thus far are incomplete and, in many cases, conflicting. I point this out first because the reader should be aware that vision research is a burgeoning field, where new articles published every week bring additional details about how the brain copes with its monumental task. To complicate matters, the animals most commonly studied to understand visual processing (monkey, cat, ferret, rat, mouse, hamster, zebrafish, goldfish, etc.) do not conveniently carry small, medium, large, and extra-large copies of the same brain within their craniums. Although evolution has settled upon many visual system designs that are shared by these species, substantial differences also exist. For the purpose of this review, I will focus almost entirely upon the macaque monkey visual system for the reason that it is one of the most understood and best models that we have for human vision to date. I will begin with a historical perspective on visual system research and continue by attempting to answer the two basic questions posed above in relation to the primary visual cortex, or V1.

Historical Perspective

The relationship between vision and the eye must have been correctly understood from the earliest times of human existence. Surpassing this most basic understanding, however, required careful dissection of the eye, optical fibers, and brain structures of animals and/or humans. One view holds that the religious and social doctrines of the Pre-Classical civilizations (e.g., Egyptians, Sumerians, Assyrians, Babylonians, Hindus, Chinese, Indians, etc.) did not permit such dissections. The more primitive herdsman and farmers surrounding the Mediterranean Sea did not have such inhibitions and are believed to have studied basic anatomy, albeit nonsystematically, during sacrificial rituals. These herdsman and farmers evolved a terminology for the anatomical structures that they discovered.

Polyak (1) maintains that this terminology was quickly adopted by the Greeks of 600–400 B.C. when the study of anatomical organization was rigorously pursued. During this time, physicians such as Hippocrates (460–380 B.C.), Alkmaeon (520 B.C.), and Anaxagoras (500 B.C.) carried out dissections of animal and human bodies and brains and held opinions of some accuracy concerning brain function, such as movement, sensation, and thinking.

The height of Greek medical scientific knowledge was reached during the Hellenistic or Alexandrian period from 323 to 212 B.C. The most prolific of medical scientists was the "Prince of Physicians" Galen (129–201 A.D.) of Pergamon (present day Turkey). As noted by Polyak (1), Galen's contributions to the understanding of human anatomy and physiology under normal and pathological conditions were vast and provided a foundation for medicine in the Arab period and, subsequently, the Revival in Europe during the late Middle Ages and Modern Times. Fig. 1 shows the Arab adaptation of Galen[1]s ideas on the pathways of the visual sytem from eyes to forebrain.

Although Galen accurately described much of the visual system gross anatomy, he did not recognize the decussation of fibers at the optic chiasm, nor did he trace the fibers to the dorsal lateral geniculate nucleus (LGNd) of the thalamus (Fig. 1). Instead, he suggested that they were connected to the lateral ventricles (which he named the "thalami"). This belief was consistent with the prevailing view on nerves in general at the time, namely that they were hollow channels carrying various "spirits", such as the visual spirit. Over 1,000 years later, the beliefs of humanist scientists such as Leonardo Da Vinci (who pictorally described the same optic fiber to the lateral ventricle pathway) (Fig. 2) and Des Cartes (who promoted the view of nerves carrying animal spirits) echoed Galen's teachings and demonstrate how little progress had been made in such a long time.

Following the Hellenistic period, the ethics supported during the first several centuries of the Christian Era denied medical practitioners and scientists the right to dissect human corpses. This stricture was expanded in the Dark Ages to include the dissection of animals, and from this point until the 1600s, healers were forced to rely almost entirely upon what little information they could glean from the Classical period (Fig. 3, Fig. 4).

Between 1600 and 1860 A.D., the most basic understanding of central visual system anatomy and function was obtained. The partial decussation of optical fibers at the chiasm was deduced. The projection of these fibers into the LGNd and the optic radiations to the cortex were described. Accidental and experimentally induced cortical lesions were correlated to symptomologies found in the patients and experimental animals, respectively, leading to the notion of localized cortical function. Cortical dissections were carefully performed, and the line of Gennari (the dense, myelinated fiber bundle running through V1 layer 4B, named for its discoverer) in the primary visual cortex was described (Fig. 5).

This striation gave rise to the term "striate cortex" to describe V1. Unstained sections of cortex were examined on slides revealing the six cortical layers to Baillarger. The notion of retinotopic organization in central structures gained wide acceptance.

In the late 1800s and early 1900s, several advances in histological preparation led to a boom in cellular studies of the visual cortex. Better chemical treatments were found for hardening the brain prior to cutting thin slices; gross neuronal and fiber staining dye protocols were developed (e.g., those of Weigert (2) and Nissl (3)); and the Golgi technique for labeling individual cells, complete with their extensive axonal and dendritic arborizations, was established (Fig. 6).

For the first time, researchers could view the intricacies of neuronal morphology and the details of laminar differences. No single researcher contributed more in this regard than Santiago Ramón y Cajal (1852–1934). Ramón y Cajal (4) gave a detailed account of the cellular morphologies throughout the cortex (visual and otherwise) using the Golgi method and his own modified silver staining method. The incredible detail afforded by these techniques allowed Ramón y Cajal to suggest certain neural pathways and circuits and theorize on the functional significance of the cortical constituents. The advent of electron microscopy permitted researchers to describe the details of synaptic connections. The development of "tracer" dyes that are taken up by distal fibers and transported toward the cell body (retrograde tracers) or taken up by the cell/dendrites and transported along the fibers to the distal terminals (anterograde tracers) greatly enhanced the search for feedforward and feedback pathways in the visual system. (Specific transsynaptic degeneration following lesions in nuclei and/or fiber bundles was used previously, but with far less success.)

All of the progress described above is anatomical in nature. What about the function of the visual pathways? How were researchers approaching this issue in the late 1800s and early 1900s? Clinical cases described over the centuries already pointed to the functional specialization of discrete cortical areas. Experimental lesions within the cortex confirmed this notion. Electrical stimulation of the cortex (e.g., Fritsch and Hitzig (5) on dog and monkey motor cortex) provided the *coup de grace* to the doctrine of functional equivalence and established the theory of functional cerebral localization in its place. Surgeons such as Penfield (6) were mechanically stimulating the brains of conscious patients during operations and recording the sensations evoked (Fig. 7). The critical step in obtaining a functional map of the visual system, however, came when researchers moved from electrical stimulation to electrical recording.

Scalp recordings of visual evoked potentials (VEPs) were used to map visually responsive cortical areas and examine retinotopic organization and binocularity in rabbit, cat, and monkey (7-9). Simultaneously, microelectrodes were being used to study single cells/fibers (or small groups) in the retina/optic tract (10, 11) and somatosensory cortex (12, 13). Hubel and Wiesel first applied the single unit recording technique to the visual cortex of cats (14, 15) and monkeys (16-18) with stunning results. With this incredible series of experiments (for which David Hubel (19) and Torston Wiesel later won the Nobel Prize in 1982), the modern era of visual cortex research was ushered in.

With this historical perspective in mind, we should turn our attention to the current understanding of the primary visual cortex and its place in the visual pathways.

Which Anatomical Pathways Carry the Visual Signal?

Basic Anatomy

The macaque primary visual cortex, like that of all mammals studied, resides in the posterior pole of the occipital cortex (Fig. 8). V1 extends rostrally almost to the lunate sulcus and posterolaterally almost to the inferior occipital sulcus; the V1/V2 border is met before either sulci. Much of V1 is found within the calcarine sulci, and the limits of V1 within these folds can be marked by the distinct appearance of V1 layer 4 (Fig. 9).

The anatomy of the primate primary visual cortex has been worked out in great detail. The three basic organizing principles of primate V1 are the: 1) laminar and 2) columnar arrangement of excitatory and inhibitory neurons (an arrangement shared with other neocortical areas) and 3) the regular spacing of anatomical/functional compartments revealed by cytochrome oxidase (CO) labeling.

Several simple facts and rules of thumb can be stated before addressing the details of these anatomical features:

- The six cortical layers introduced by Brodmann (layer 1 most dorsal, layer 6 most ventral) have been subdivided time and again as additional aspects of the neurons and their connections have been revealed.
- Layer 1 is nearly aneuronal, composed predominantly of dendritic and axonal connections. In 1 mm^3 of V1 tissue, one could expect to find approximately 4,700 neurons, 2,900 microglia, 3,400 oligodendrocytes and 49,000 astrocytes (20). Of the neurons present, over 80% are GABAergic (21).
- Approximately 20% of the neurons in layers 2–6 are inhibitory interneurons (GABAergic) that make major contributions to the function of V1 circuits but do not project axons outside of this area.
- Layers 2/3 (the "supergranular" layers) contain many excitatory projection neurons that send axons to extrastriate cortical regions (e.g., V2, V3, V4, MT, etc.).
- Layer 4 (the "granular" layer) is divided into four horizontal sublayers: 4A, 4B, 4Cα, and 4Cβ. Layers 4Cα and 4Cβ are the major recipients of LGNd innervation. The LGNd magnocellular (M) and parvocellular (P) layers project to 4Cα and the 4Cβ, respectively. Thus, the M and P streams remain segregated at this stage (but see qualification below).

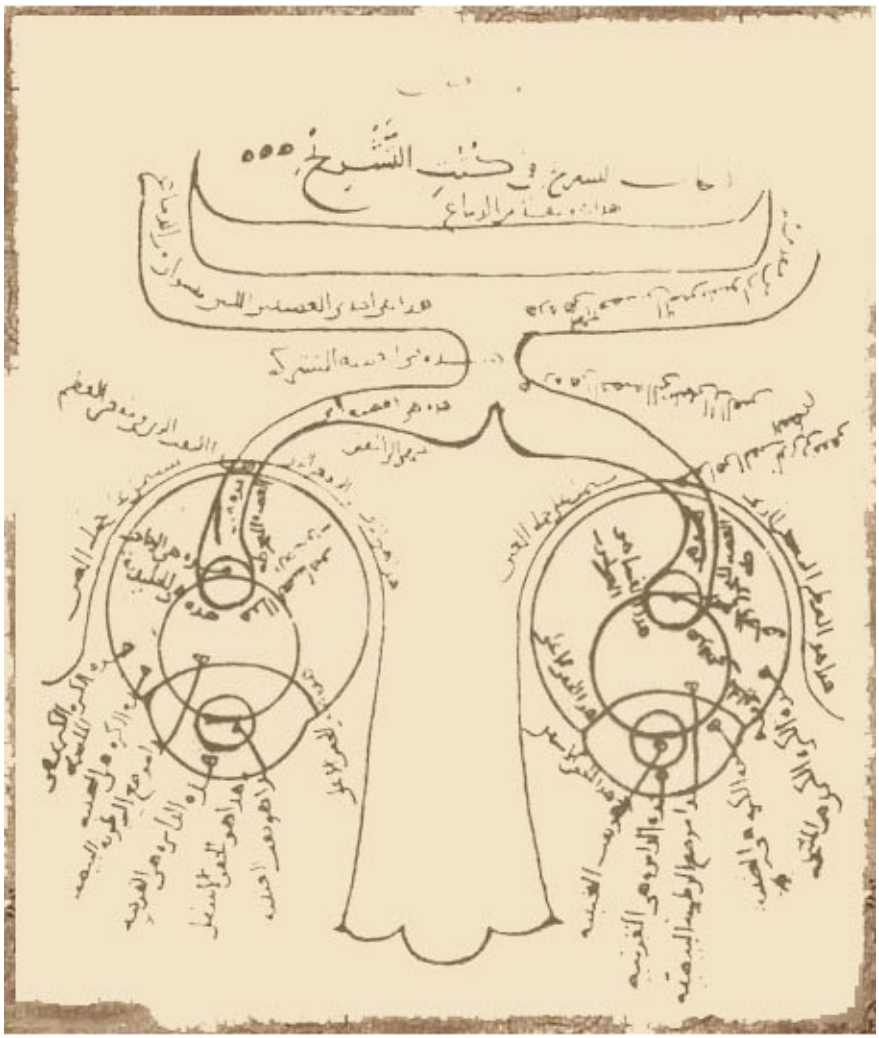

Figure 1. Diagrammatic representation of the visual system from the oldest existing copy of the "Book of Optics" by Ibn Al-Haitham, an Arab physicist written in the 11 century A.D. From Polyak (1).

- Layers 5/6 (the "infragranular" layers) contain many excitatory projection neurons that innervate the LGNd to provide feedback to this relay area.
- Labeling of V1 and V2 for CO content has revealed CO-rich and -poor regions termed "blobs" (or puff, spots, or patches) and "interblobs" in V1 and the thick, thin, and pale stripes in V2. The relevance of these compartments is still a matter of some debate.
- CO blobs do not extend uniformly from the surface of layer 1 to the base of layer 6. Instead, they concentrate in layers 3B, 4B, and 4C (Fig. 10).
- Projections to and from the CO blobs and interblobs are relatively distinct as follows (Fig. 11):
    - Pβ (for primate P or midget ganglion cells) project to the LGNd parvocellular layers (see the chapter on midget pathways of the retina), which project to V1 layer 4C and then project to the interblobs of V1 layers 2/3; and finally these layers project to the pale stripes of the V2 geniculate.
    - The blue-yellow ganglion cells (see the chapters on S-cone pathways and color vision) project to the intercalated layers and S/K (K for "koniocellular") layers of the LGNd, which project to the blobs of V1 layers 2/3, which project to the thin stripes of V2.
    - Pα (M cells or parasol ganglion cells) project to the LGNd magnocellular layers and thence to layer 4C of V1. This layer projects to the blobs of V1 layers 2/3 and also to layer 4B of V1. Layer 4B, in turn, projects to the mediotemporal area (MT) and to the thick stripes of V2.
- Layers 1 and 2 receive feedback inputs from extrastriate cortex.

Figure 2. Drawing by Leonardo DaVinci of the projection of the eyes to the ventricles of the brain. From Polyak (1).

- The neuroglia in the young adult macaque V1 account for 20-35% of all cells (not including pericytes). The neuroglia can be divided into oligodendrocytes (~7-10% of cells), astrocytes (~11-20% of cells), and microglial cells (~1.5-3% of cells) (20, 22).

Neuronal Constituents

There are three basic types of neurons in the primate V1 (Fig. 12):

- spiny pyramidal cells (excitatory)
- spiny stellate cells (excitatory)
- smooth or sparsely spinous interneurons (almost all are GABAergic)

The pyramidal cells, as you might guess, have cell bodies that appear like pyramids, have apical dendrites (that is, extending toward the white matter), and their dendrites are covered with spines. Spiny stellate cells are generally smaller, and their cell bodies more resemble a star shape. They also have spiny dendrites (Fig. 12A). The interneurons have more rounded cell bodies and have little or no spines on their dendrites. Over the years, anatomists have given more or less descriptive appelations to a number of unique subtypes, which are briefly described below.

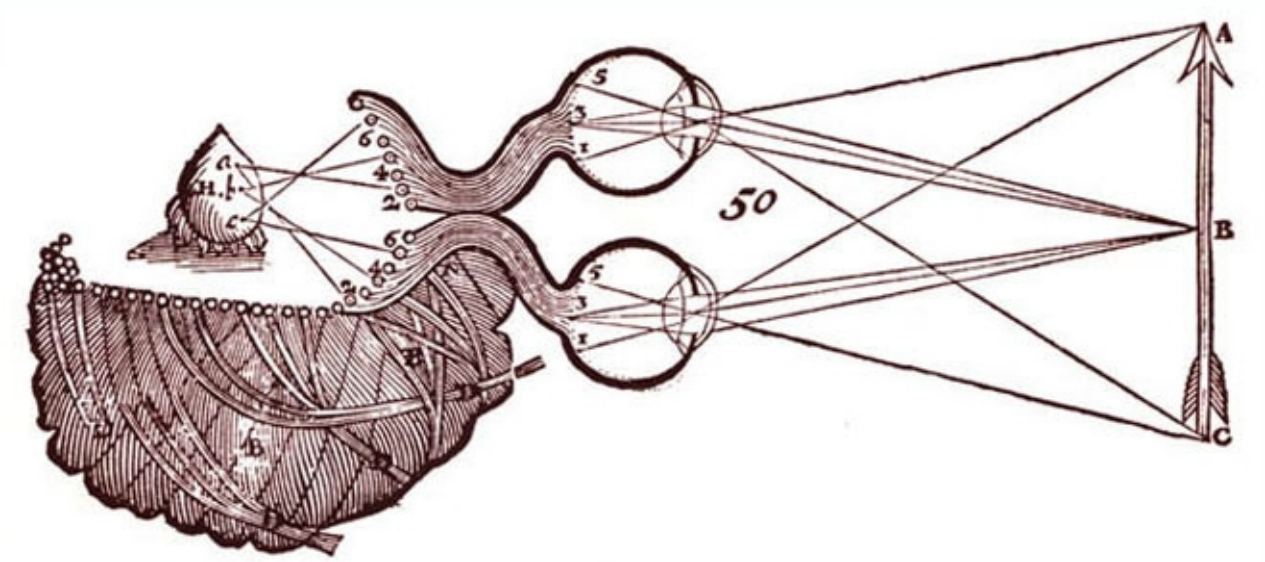

Figure 3. Binocular stereoscopic visual system as imagined by Des Cartes. The two retinal images of the arrow are accurately, point for point, projected upon the surface of the cerebral ventricles and thence to the centrally located pineal gland, H, the supposed "seat of imagination and common sense". From Polyak (1).

- Chandelier cell – inhibitory; axons show characteristic branching into vertical sections resembling candlesticks (Fig. 12E).
- Neurogliaform cells – inhibitory; resembling glial cells but definitively neurons; axon and dendrites branch but remain in the locale of the soma, giving rise to a dense spherical region of fibers (Fig. 12G).
- Double bouquet cell – inhibitory; axon collaterals and bitufted dendrites extend vertically in a tight bundle (Fig. 12C). Antibodies to calbindin specifically mark these cells, and by using this strategy, researchers have found that these cells are regularly spaced in layer 3, thereby forming yet another columnar unit. There are approximately 7 to 15 double bouquet cells per 10,000 μm^2 (23).
- Basket cells (24, 25) – inhibitory; relatively large cell bodies extend myelinated axonal branch laterally for a great distance. The axonal branches terminate on pyramidal cell bodies and dendrites in a manner resembling a basket. Dendrites extend vertically (Fig. 12, D and H).
- Cajal-Retzius cells – inhibitory; Cajal and Retzius found this cell type independently in layer 1 of neonatal animals and humans, respectively. They may or may not exist in the adult.
- Meynert cell – excitatory; large pyramidal cell first described by Meynert; the "outer" Meynert cell bodies are found in 4B and are regularly distributed relative to pyramidal cell cones (22) (see below). These cells project to area MT. The "inner" Meynert cell bodies are regularly spaced at the layer 5/6 border, lying below CO interblobs. These cells are also found in layer 6. These cells typically have asymmetric, lateral dendritic arborizations, are highly direction selective, and are also known to project to area MT.

The cell types described above represent only a few of the more unique varieties. Jennifer Lund and colleagues (26-29) have rigorously studied the presumptive interneurons of the macaque V1 using the Golgi impregnation staining method. On the basis of a range of morphological criteria (the laminar position of somata, axonal arborization, dendritic arborization, pattern and extent of branching), they have described over 40 types of interneurons alone.

Additional low-density interneurons might remain unidentified. The classes that have been described might be further divided based on chemical content and/or physiological response properties (Fig. 12). Alternatively, it should be noted that many of the anatomically distinct types may be physiologically indistinguishable from one another.

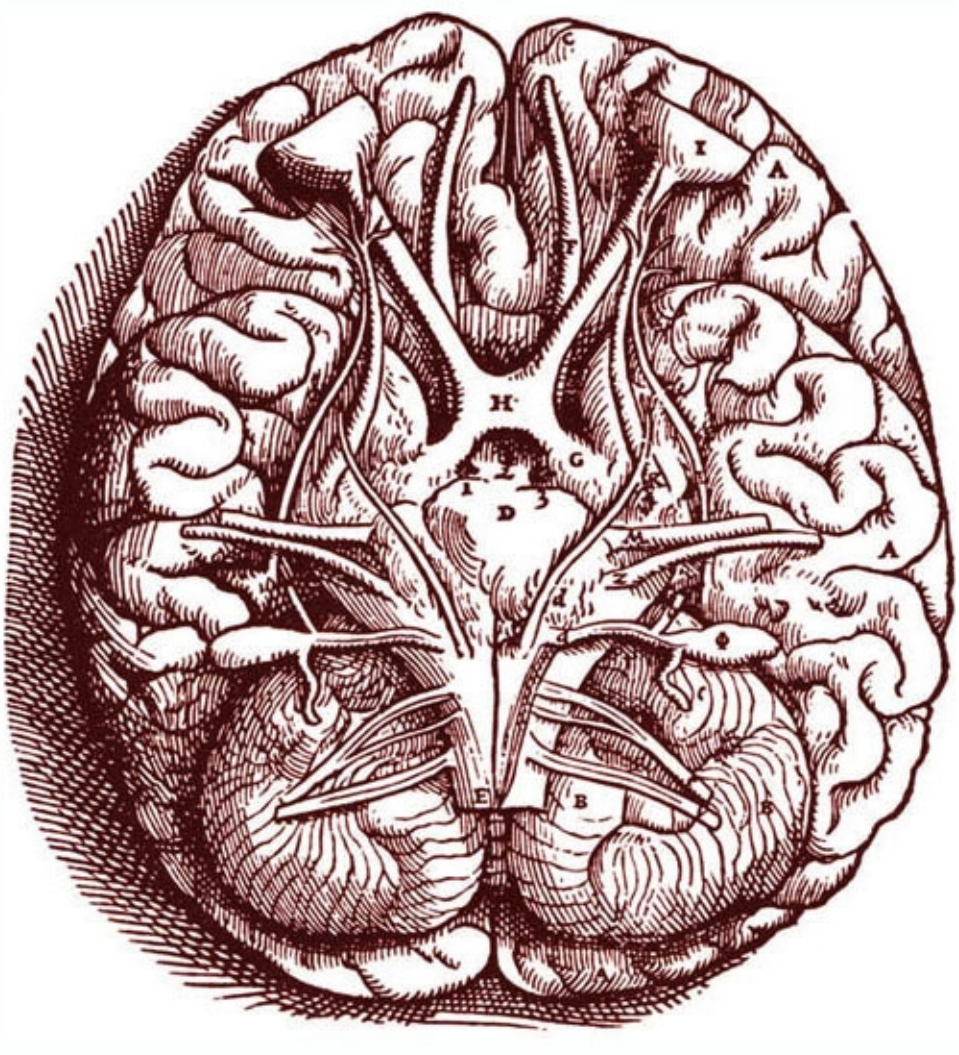

Figure 4. Woodcut from the "Fabrica" (1555) by Vesalius showing the basal aspect of the human brain with the origins of the cranial nerves and the brain stem. From Polyak (1).

The Cortical Layers

Many numbering schemes exist for the neocortical layers in general and the layers of V1 in particular. I have adopted the basic scheme of Brodmann, who defined the cortical layers based on careful histology. I have also adopted the refinements suggested by the work of Lund and colleagues (see below) (Fig. 13).

Layer 1 is composed of a dense network of synapses formed between the apical dendrites of layer 2–5B pyramidal cells (29) and the collected inputs from LGNd K layers (30, 31), the pulvinar, feedback pathways from extrastriate areas, nonspecific thalamic nuclei, and other subcortical regions. Thus, although layer 1 contains few neurons, it is a networking layer that has a direct, concerted affect on the firing properties of pyramidal cells in deeper layers.

The supragranular layers (2, 3A, and 3B) contain many somata and dendrites of pyramidal cells. Layers 2 and 3A receive little thalamic inputs (the K layer projection to V1 blobs is focused mainly in 3B). They do not receive direct inputs from layer 4C, in contrast to layer 3B that receives a massive 4C input. Layers 2 and 3A do contain many axons and dendrites of neurons found in all other cortical layers.

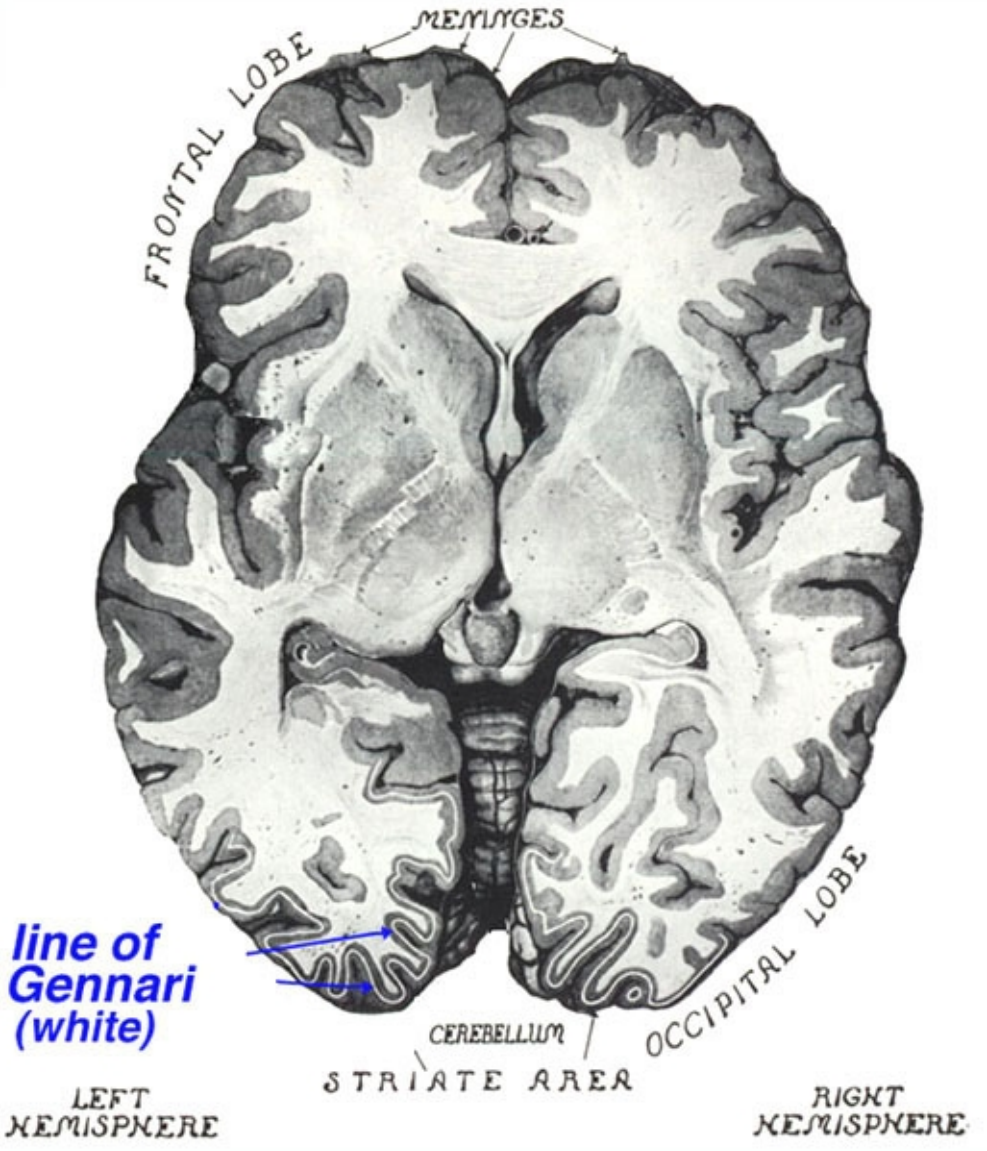

Figure 5. Horizontal section of the brain showing the line of Gennari in the striate cortex. From Polyak (1).

Layer 4A shows up in the Nissl stain as a dark band of small, granule-like cells. This and the lack of pyramidal cells set this layer apart from layer 3B.

Layer 4B is a cell-poor layer that contains a low density arrangement of pyramidal cells—the large outer Meynert cells. This layer receives a strong input from the underlying 4Cα, and the Meynert cells are known to project directly to area MT as well as the superior colliculus (SC) (32). Cells in layer 4B also project to the thick CO stripes of V2, which in turn project to MT. Thus, this layer plays a substantial role in conveying information in the M pathway/dorsal stream.

Layer 4C is distinguished from 4B in part due to the great density of stellate cell packing in this layer. Polyak (1) divided 4C into the α and β divisions, based solely on histology; upper 4C neurons are more dispersed. Differences in geniculate innervation patterns (i.e., the M layers of LGNd to 4Cα and the P layers to 4Cβ) (33, 34), the projection patterns of the 4C cells (35) and physiological properties (36) have overwhelmingly supported this division. Additional evidence has suggested that the upper and lower divisions of 4Cα may be distinct as well (26, 33, 37, 38).

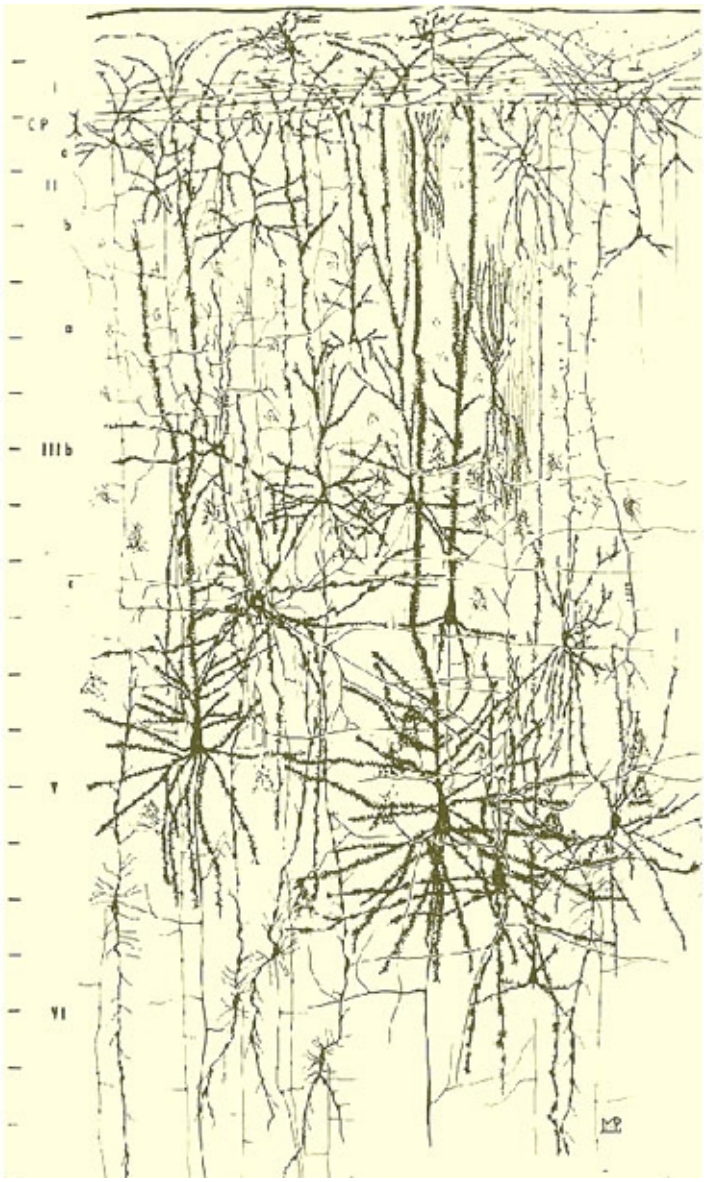

Figure 6. Composite figure of a mosaic of camera lucida drawings showing the morphological features (size, location, and distribution) of the principal neuronal types of the human cortex. From rapid-Golgi preparations. Scale: 100 μm.

4Cβ spiny stellate neurons provide a dense innervation of layers 4A and 3B and sparse innervation in 4C, 5, and maybe 6 (35). No direct projections from 4Cβ to 3A, 4B, or 5B have been found (26). In contrast, as already noted, 4Cα projects heavily to 4B.

Local layer 5A neurons do not project to 4B and only weakly innervate 4Cβ. They innervate all other layers. 5A neurons appear to project primarily to 3B and 1 (26). Pyramidal neurons in 5B send recurrent axons to layer 3A (39). Meynert cells at the 5/6 border and within layer 6 project to both MT and SC (40).

Layer 6: It is known that neurons in layer 6 send recurrent axons into 4Cβ (39). Other neurons (or possibly even the same ones) project axons back to the LGNd (41). Layer 6 also receives a direct input from the LGNd (42), thereby forming a neural loop.

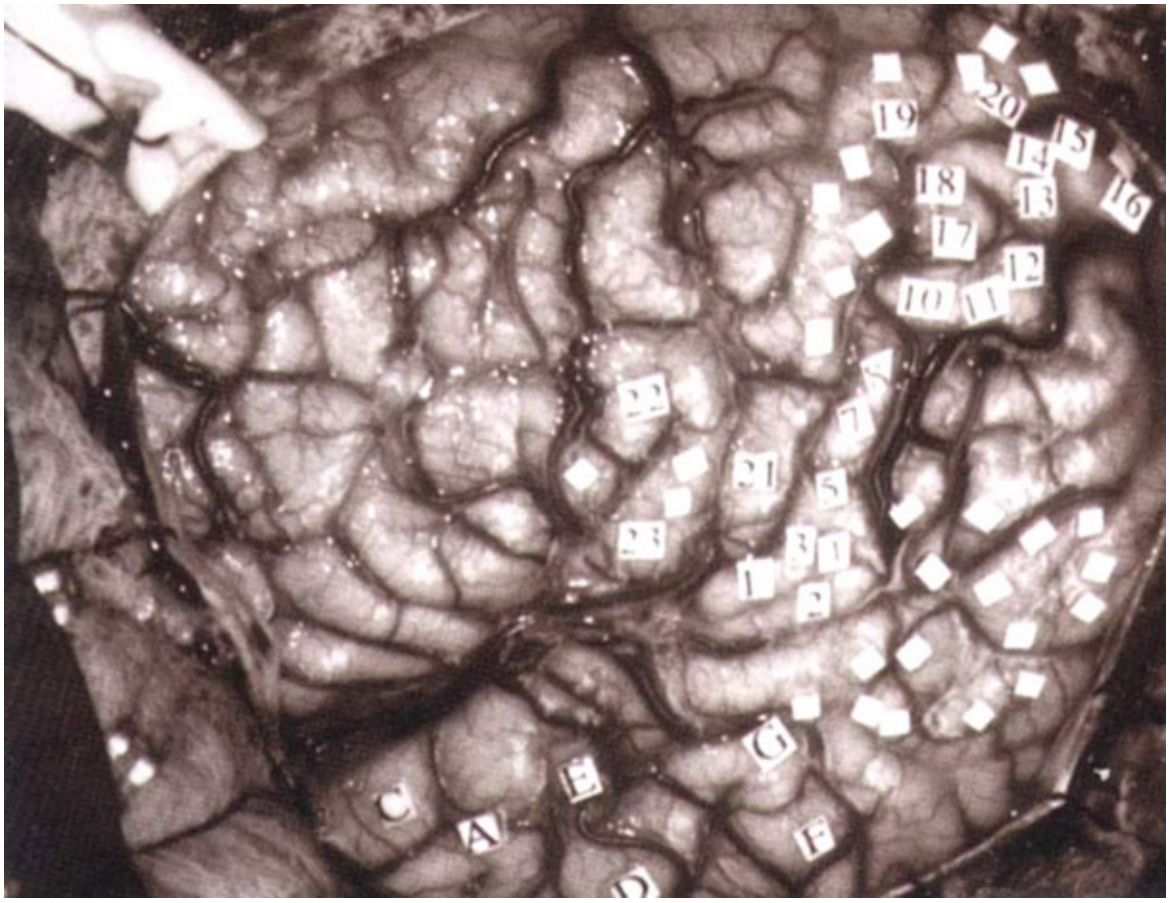

Figure 7. Human brain labeled as to cortical areas during neurosurgery. From Penfield and Boldrey (6).

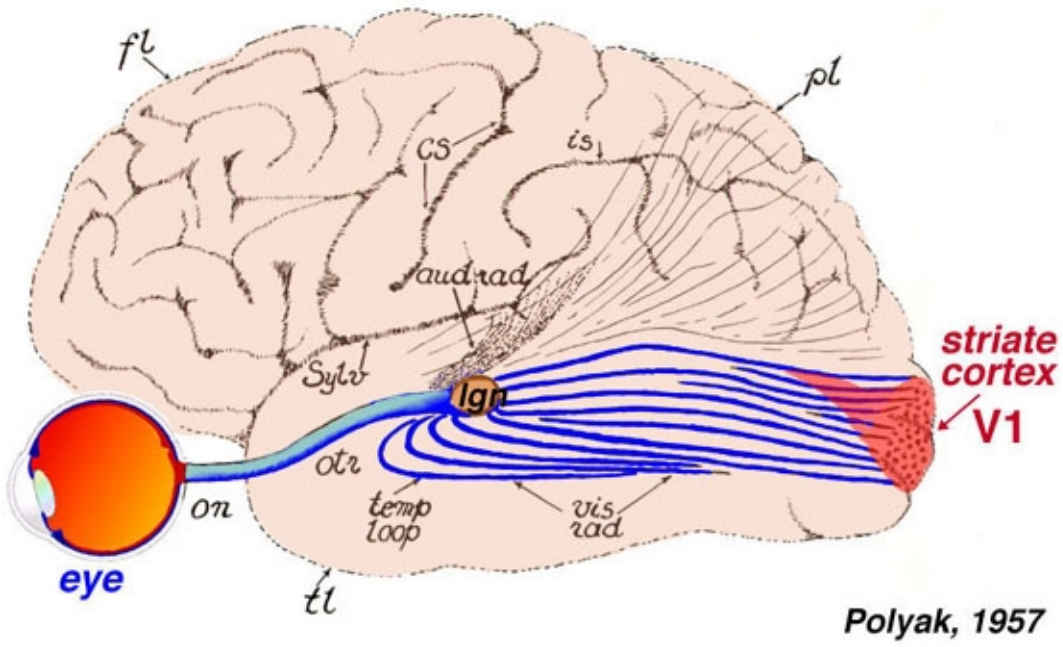

Figure 8. Visual input to the brain goes from eye to LGN and then to primary visual cortex, or area V1, which is located in the posterior of the occipital lobe. Adapted from Polyak (1).

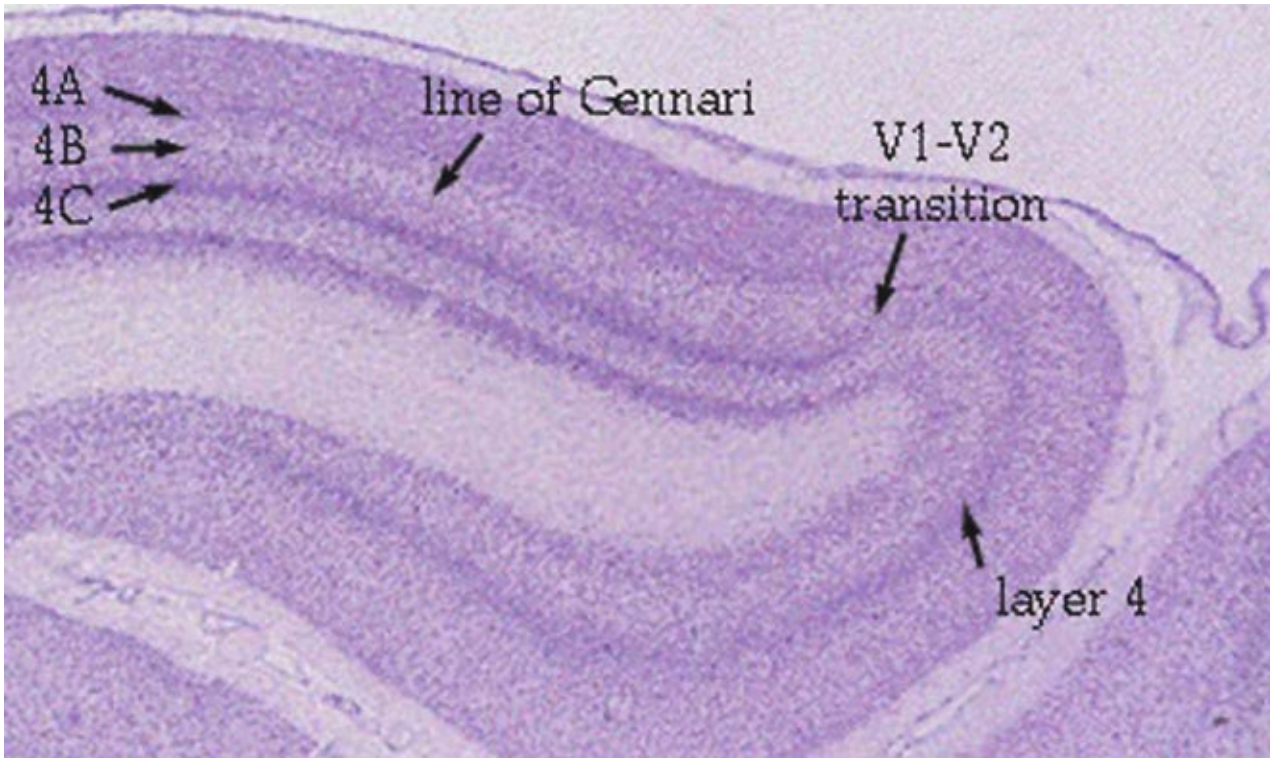

Figure 9. Nissl-stained section to show the border between area 17 (V1) and area 18 (V2).

V1 Cortical Columns

The term "cortical column" refers to the notion that cells arranged vertically from the surface of the cortex to the white matter might compose functional or anatomical units. Thus, a cortical column can be defined on the basis of anatomical features (e.g., stereotyped patterns of pyramidal cell apical dendrite bundles), functional features (e.g., columns of cortical cells, all responding to the same stimulus orientation), or both.

Many types of columns have been proposed including ocular dominance, orientation, spatial frequency, and color columns. The details of these columnar arrangements will be described in later sections dealing with the physiology of V1. However, I will here briefly describe the ocular dominance columns to provide an example of columnar arrangement in the primary visual cortex.

Ocular Dominance Columns

Visual signals from the two eyes remain segregated in the LGNd (Fig. 11) and in the geniculorecipient layers of area V1 (Fig. 14). One can observe this segregation by measuring the electrophysiological responses of the units in layer 4C. As the recording electrode is moved within layer 4C, there is an abrupt shift as to which eye drives the unit. In layer 4C, the shift from one eye to the other takes place over a distance of less than 50 μm. Signals from these bands converge on individual neurons in the superficial layers of the cortex, thereby forming columns dominated by one eye or the other in an alternating fashion (Fig. 15).

Cytochrome Oxidase Labeling

CO is an integral transmembrane protein that is found in the inner mitochondrial membrane. Because it acts to catalyze the generation of adenosine triphosphate (ATP), which is itself an energy molecule used in an enormous range of cellular processes; the amount of CO in a cell or nucleus can be used as an indicator of cellular activity. In 1978, Margaret Wong-Riley discovered that, quite apart from its use as an activity indicator,

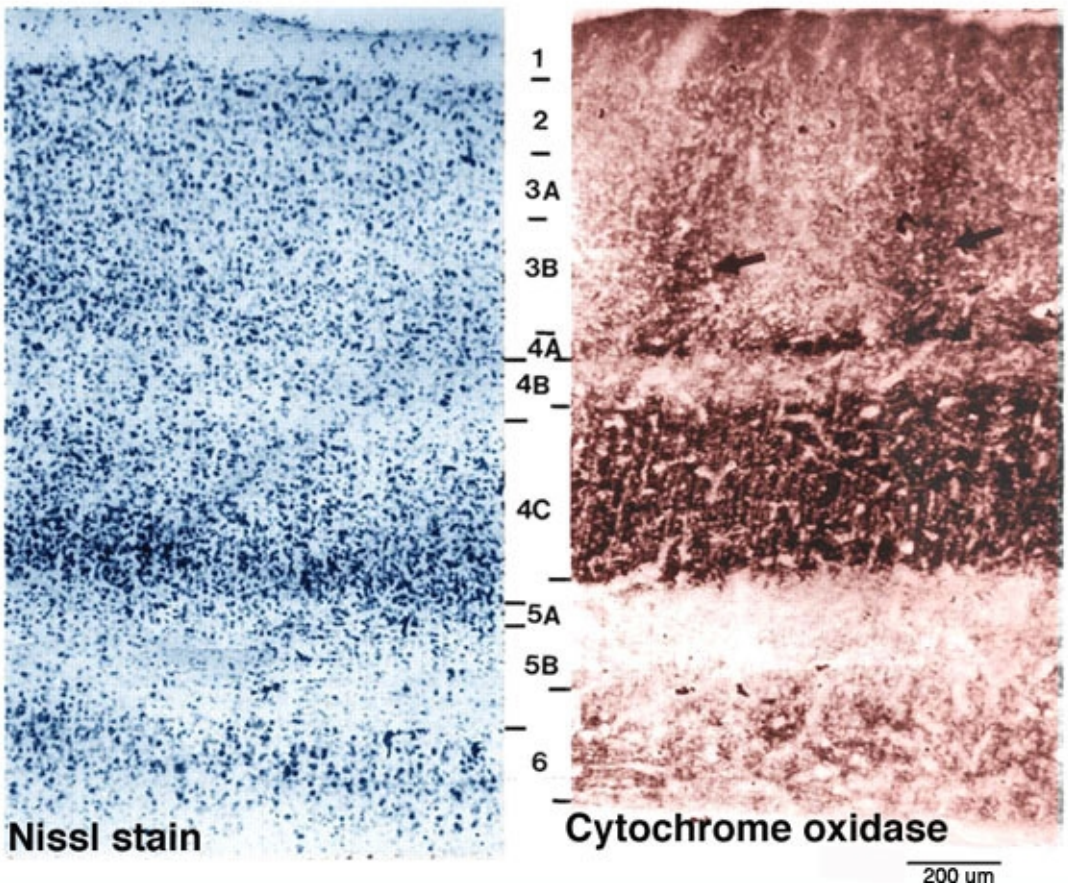

Figure 10. Nissl (left) and cytochrome oxidase (right) labeled cross sections of the visual cortex of a macaque monkey, showing the individual layers.

CO labeling in the primary visual cortex reveals a striking array of CO-rich and -deficient regions (i.e., blobs and interblobs) (Fig. 16).

Presumably, these regions reflect stable differences in energy consumption in two populations of neurons that were previously undistinguished. Assuming this were true, what other differences might exist between blobs and interblobs? It should be noted that dense CO staining does not exist throughout the entire cortical depth. Instead, CO blobs are most visible in layers 3B, 4A, and 4C. Be that as it may, if these dense regions were in fact different from their CO-deficient neighbors in some way, the cells directly above and below rich and poor regions might also show differences in connectivity and functional characteristics, correlating with the cells above and below them.

For instance, blobs in layer 3B have been shown to correspond to specific geniculate innervation in macaques (43, 44). Boyd and Casagrande (45) found recently that V1 cells projecting to MT in bush babies and owl monkeys were more numerous below the CO blobs of layer 3B than below the interblobs. Similar data in macaque monkeys also shows clustering of MT projecting cells in periodical steps through the lateral extent of V1 (46-48) but did not find a correlation between these clusters and the CO (Fig. 17 and Fig. 18).

Feedforward and Feedback Pathways

The signals from the two retinas are communicated to area V1 via the LGN. In the macaque monkey, after the signals are processed in V1 they are communicated via multiple pathways to the 30+ visually responsive, extrastriate cortical areas (Fig. 19).

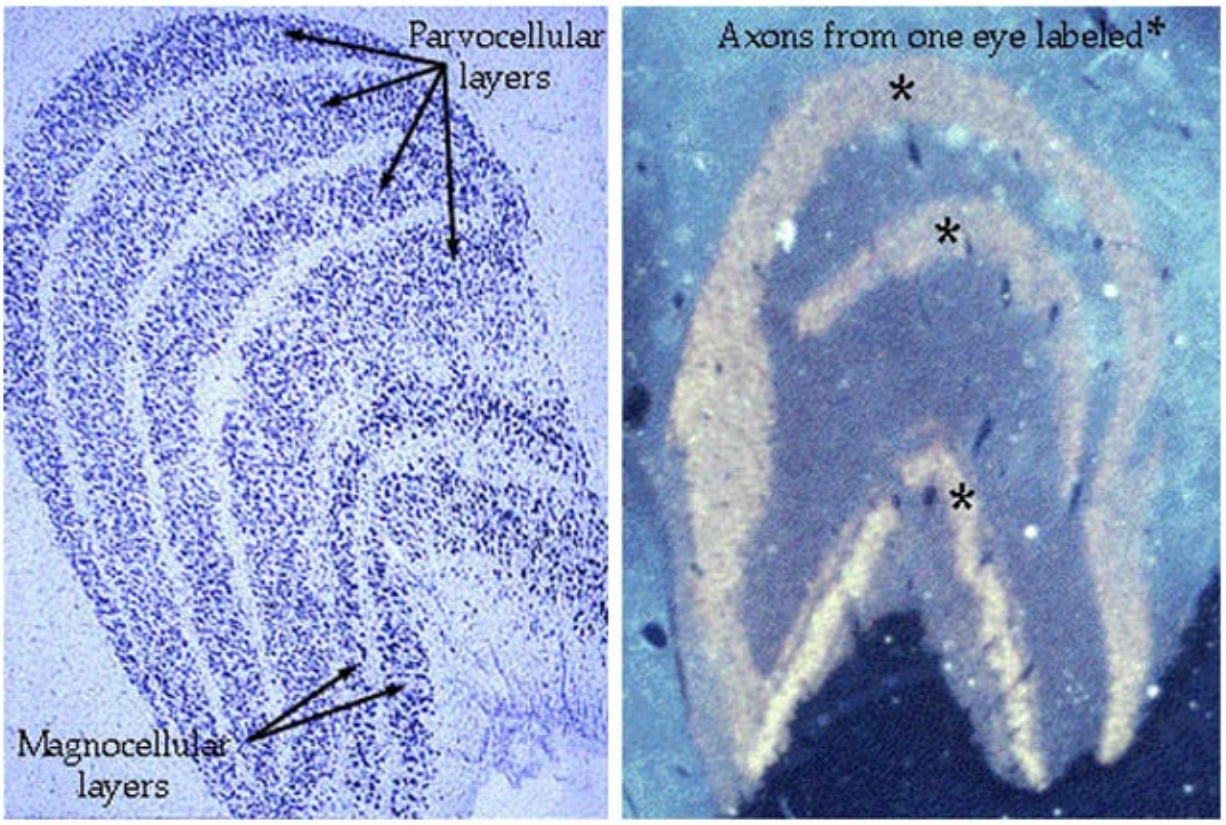

Figure 11. The projections of the small (P cells) and large (M cells) ganglion cells from the two eyes to parvocellular and magnocellular layers of the LGN, respectively.

Anatomical hierarchical models place the visual cortical areas into a multi-level processing model based upon the pattern of feedforward, lateral, and feedback pathways found in each area. In general, feedforward pathways are considered to be those that project from the supragranular layers of one area and terminate in layer 4 of the target area. In contrast, feedback projections are those that arise from the infragranular layers of one area and terminate outside of layer 4 in the target area (49-51).

In the previous sections, I have described the anatomical borders of V1, the cells that exist in this area, the arrangement of those cells in layers, columns, and CO compartments, and I have hinted at the visual pathways that course into and out of V1. It is true that visual information is passed from the retina to the LGNd to V1 to the higher cortical areas and that the higher areas project back to V1 and V1 to the LGNd (there are no efferent projections to the primate retina). However, although this view of visual processing is accurate, it does not capture the wealth of upstream and downstream connections found in V1.

Direct feedforward projections to V1 originate from the pulvinar, LGNd, claustrum, nucleus paracentralis, raphe system, locus coeruleus, and the nucleus basalis of Meynert (31, 33, 43, 52-57).

Direct feedforward projections from V1 extend to V2, V3, V5 or MT, MST, and FEF (41, 46-48, 58-63).

Direct feedback projections to V1 originate from V2, V3, V4, V5 or MT, MST, FEF, LIP, and inferotemporal cortex (47-49, 57, 61, 62, 64, 65).

Direct feedback projections from V1 extend to SC, LGNd, pulvinar, and pons (32, 41, 54, 66, 67).

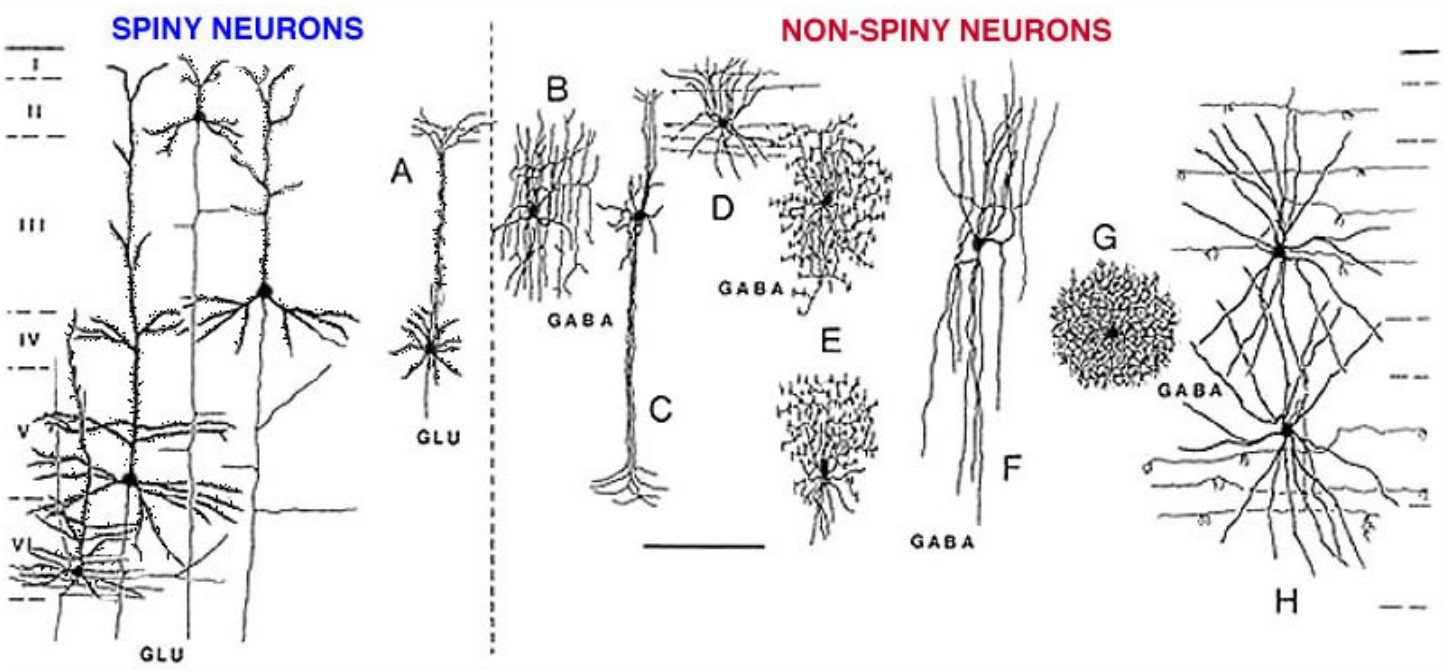

Figure 12. Basic cell types in the monkey cerebral cortex. Left: spiny neurons that include pyramidal cells and stellate cells (A). Spiny neurons use the neurotransmitter glutamate (Glu). Right: smooth cells that use the neurotransmitter GABA. B, cell with local axon arcades; C, double bouquet cell; D and H, basket cells; E, chandelier cells; F, bitufted, usually peptide-containing cell; G, neurogliaform cell.

The connections listed above represent only a subset of the direct and indirect projections that carry signals into and out of the primary visual cortex and do not even begin to describe the extensive lateral connections within V1 itself.

What Information Does the Visual Signal Carry?

We now know the arrangement of neurons, dendrites, and axons in the layers, columns, and CO compartments of V1. We know many of the pathways extending into and out of V1 involving the retina, subcortex, and extrastriate cortex. We can imagine light impinging upon the eye and, from this origin point, a cascade of action potentials streaming from neuron to neuron, area to area— forward, lateral, and back again. In the abstract, we know that it is these signals that are responsible for our vision of the external world. But how do these millions of patterned spikes resolve themselves into an actual percept? A partial answer is to consider that every image can itself be broken down into components (e.g., lines, colors, textures, shades, and motion, etc.) and that visual cortical neurons are specialized to detect only a subset of these components.

Receptive Field Properties

Each cell in the visual cortex has a receptive field (RF), a discrete area in space relative to the fovea where the presentation or removal of a visual stimulus will cause cellular activation. By definition, stimuli presented outside of this receptive field will neither increase nor decrease the ongoing activity of that individual cell. The location and size of a RF can be considered among the most basic of RF properties.

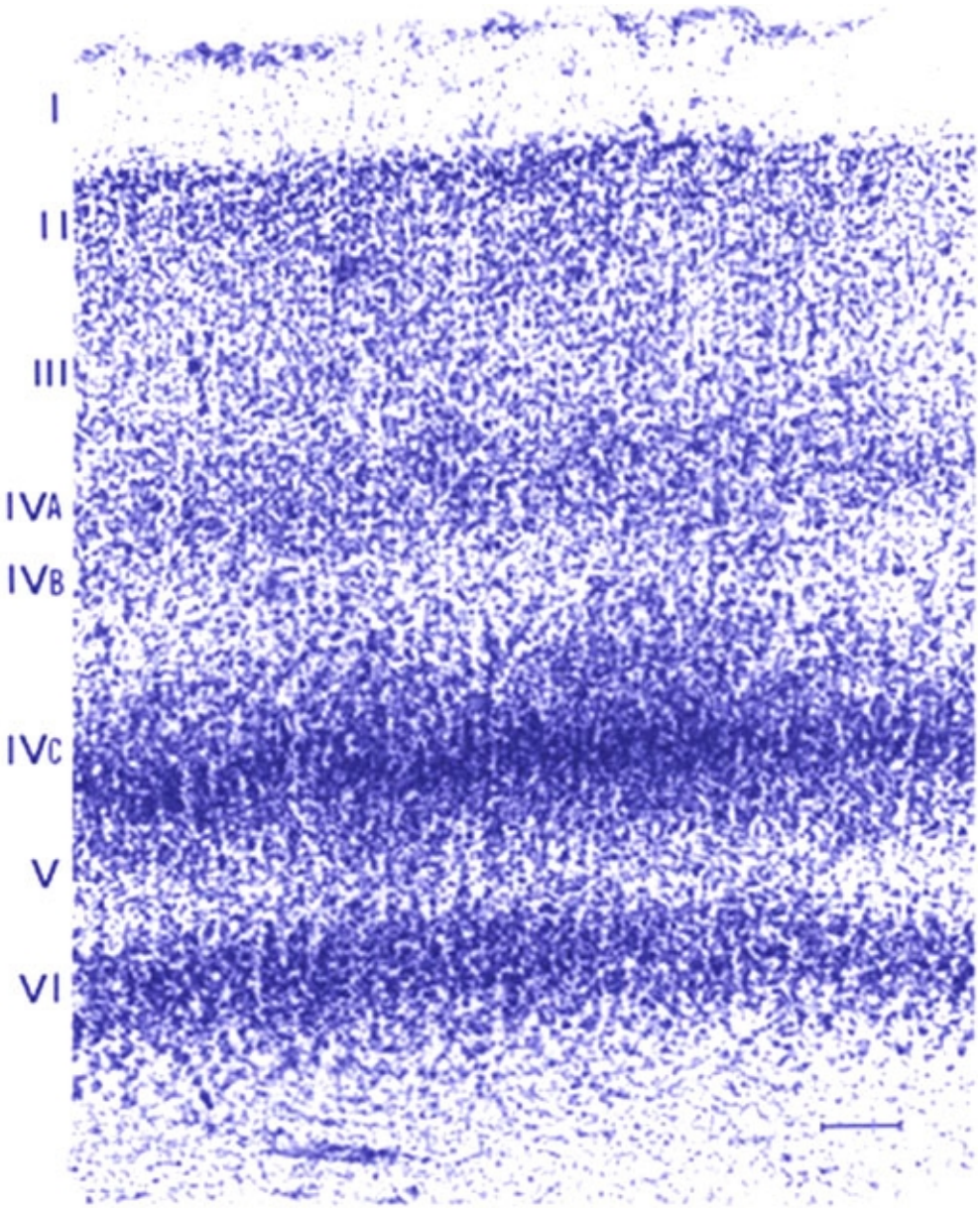

Figure 13. Nissl stain of the visual cortex reveals the different layers quite clearly.

Retinotopic Maps in V1

The spatial position of the ganglion cells within the retina is preserved by the spatial organization of the neurons within the LGN layers. The posterior LGN contains neurons whose RF are near the fovea. Progressing from posterior to anterior, the RF locations become increasingly peripheral in the retina (68). This spatial layout is called retinotopic organization because the topological organization of the RFs in the LGN parallels the organization of the retina.

The signals in area V1 are also retinotopically arranged. From electrophysiology in monkeys, one can measure the location of RFs with an electrode that penetrates tangentially through layer 4C, transversing through the ocular dominance columns. The RF centers of neurons along this path correspond systematically to locations from the fovea to the periphery. This trend is interrupted locally by small, abrupt jumps at the ocular dominance borders. Thus, the striate cortex retains the retinotopic map of the contralateral visual field that is developed in the LGN.

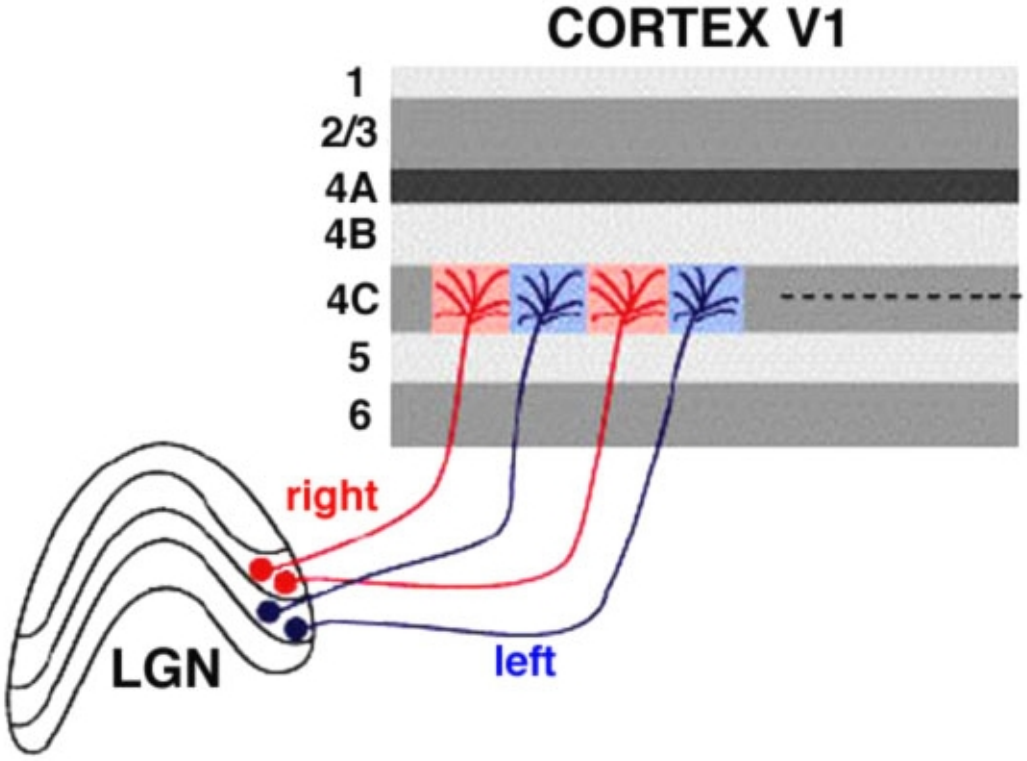

Figure 14. The signals from each eye are segregated into different ocular dominance columns within area V1, layer 4C.

Orientation and Direction Selectivity

V1 is the first site where strong orientation and direction selectivities are observed in the macaque monkey (16). Although the vast majority of V1 cells show some degree of orientation selectivity, only approximately 25-35% of V1 cells are strongly directionally selective (69, 70). The classic method for testing orientation and direction selectivity is to measure the spike rate of a single cell in response to drifting oriented luminance bars and/or drifting luminance spots (see Fig. 21).

The concept of an orientation column can be easily appreciated by examining Fig. 20 and Fig. 21. When an electrode is lowered into V1 at an angle relatively parallel to the cortical layers (Fig. 22), the orientation selectivities of the cells encountered vary systematically, where adjacent cellular regions share approximate orientation preferences.

Such recordings led Hubel and Wiesel to propose models of functional organization like the one shown in Fig. 23.

Recently, the orientation columns of V1 first described by Hubel and Wiesel have also been recast into more complex geometries, such as partial columns ("slabs") and pinwheels, as dictated by the increasing volumes of evidence (71).

Binocularity and Binocular Disparity

Hubel and Wiesel (15) first demonstrated the presence of cells in primate V1 that responded preferentially to visual stimulation in both eyes as opposed to one eye alone. They classified cells using a 7-point scale where:

- 1 – cells excited by the contralateral eye alone.
- 2 – cells with a strong bias for contralateral stimulation.

Figure 15. The ocular dominance columns in area V1 can be visualized by using markers. When the marker is injected into one eye, it is transported via the LGN nucleus to the cortex. The light bands in this tangential section show the places where the marker was located and thus reveal the ocular dominance columns. From Olavarria and Van Essen (94).

- 3 – cells with a weak bias for contralateral stimulation.
- 4 – cells that responded maximally to stimulation in both eyes.
- 5 – cells with a weak bias for ipsilateral stimulation.
- 6 – cells with a strong bias for ipsilateral stimulation.
- 7 – cells excited by the ipsilateral eye alone.

The proportion of monocular cells (points 1, 2, 6, and 7) *versus* binocular cells (points 3, 4, and 5) was found to vary with the layer in which cells were recorded. Cells in the retinogeniculato-recipient layers 4Cα and 4Cβ were found to be exclusively monocular. Anatomical studies have since shown that these cells receive monocular inputs from the LGNd that do not converge from the alternating layers (34, 39).

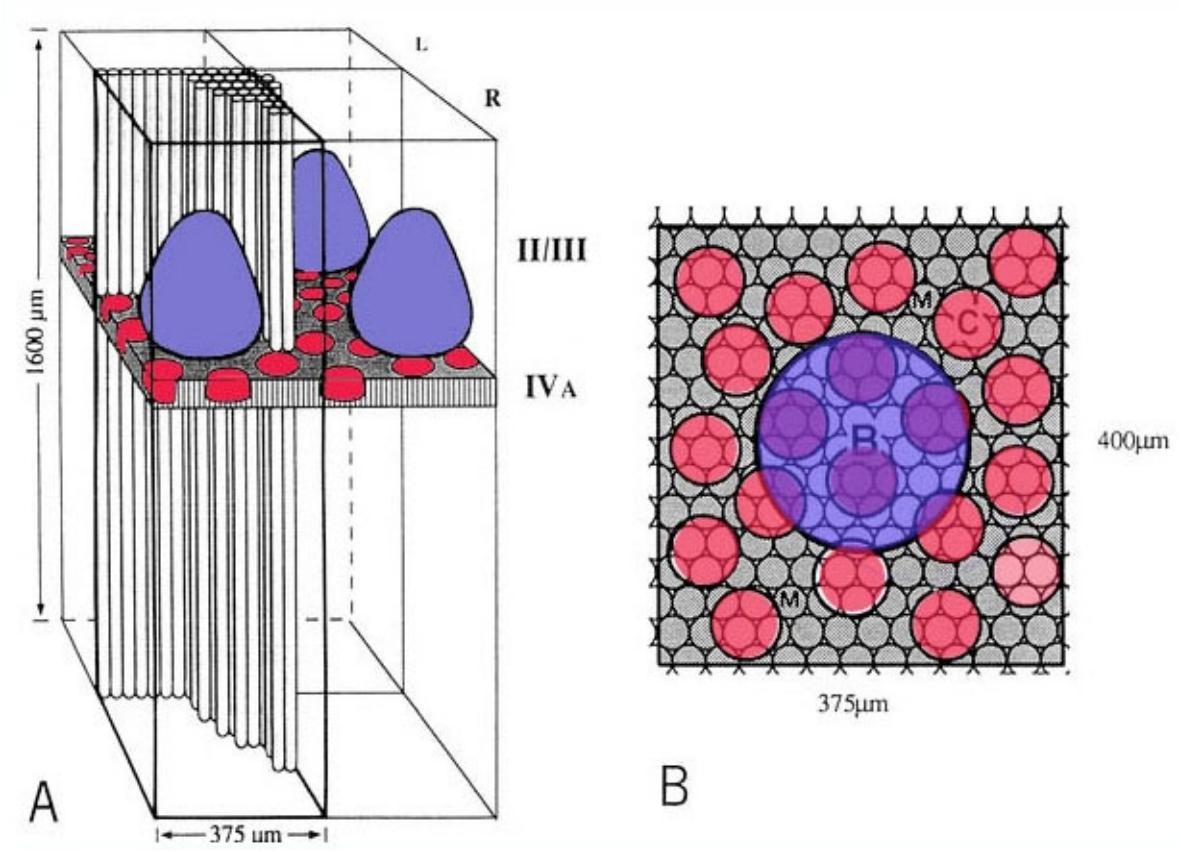

Figure 16. Diagrammatic representation of the relationships between CO "blobs", layer 4 cones, and pyramidal cell modules. A, three-dimensional representation. The "blobs" in layer 2/3I are aligned in single rows along the 400 µm-wide ocular dominance columns (R and L), and they have a center-to-center spacing of 375 µm. Each blob, which is the focus of a blob-centered module, lies above the cones of neurons in layer 4A, and throughout the entire cortex is a matrix of long, thin pyramidal cell modules. B, a diagram of the contents of a blob-centered module as though looking down from the pial surface. The blobs (B) are about 200 µm wide. An average of 20 layer 4A cones (C) would occupy such an area, which would also contain some 180 pyramidal cells modules (M). From Peters and Sethares (22).

What might be the usefulness of binocular cells? When an observer fixates on a visual object, the image of this object is positioned on corresponding regions of the two retinas. At the same time, however, objects in front of and behind the fixation point create images that lie on non-corresponding regions of the two retinas. The degree to which the images are non-corresponding (as measured by difference scores in retinal eccentricity for instance) is defined as binocular disparity. The ability to use binocular disparity to determine the distance of an object from oneself, and its relation to the fixation plane, is called stereopsis.

Hubel and Wiesel first described the presence of neurons in V1 that are sensitive to binocular disparity. That is, some neurons may show maximal firing rates when a stimulus has positive disparity and weak or even inhibited (below baseline) firing rates to 0 disparity stimuli (in the fixation plane) or negative disparity stimuli. These cells would be described as disparity sensitive and negative disparity tuned. If the tuning were reasonably sharp, the cell might be described as negative disparity selective, i.e., it responds soley, not simply preferentially, to negative disparity. We now know the percentage of disparity-sensitive cells and the proportion of positive, negative, and 0-disparity tuned cells. Clearly, there are no disparity tuned cells in layers 4Cα and 4Cβ because binocularity is a prerequisite for disparity sensitivity. As Livingstone (72) noted, it is safe to assume that negative and positive disparity selective cells are involved in stereopsis. Of the 0-disparity tuned cells, all may be involved in stereopsis or, alternatively, perhaps only those with very narrow tuning (i.e., selective ones) contribute to this perceptual ability (73). The work of DeAngelis, Newsome, and Cumming (74, 75) elegantly addresses this issue by

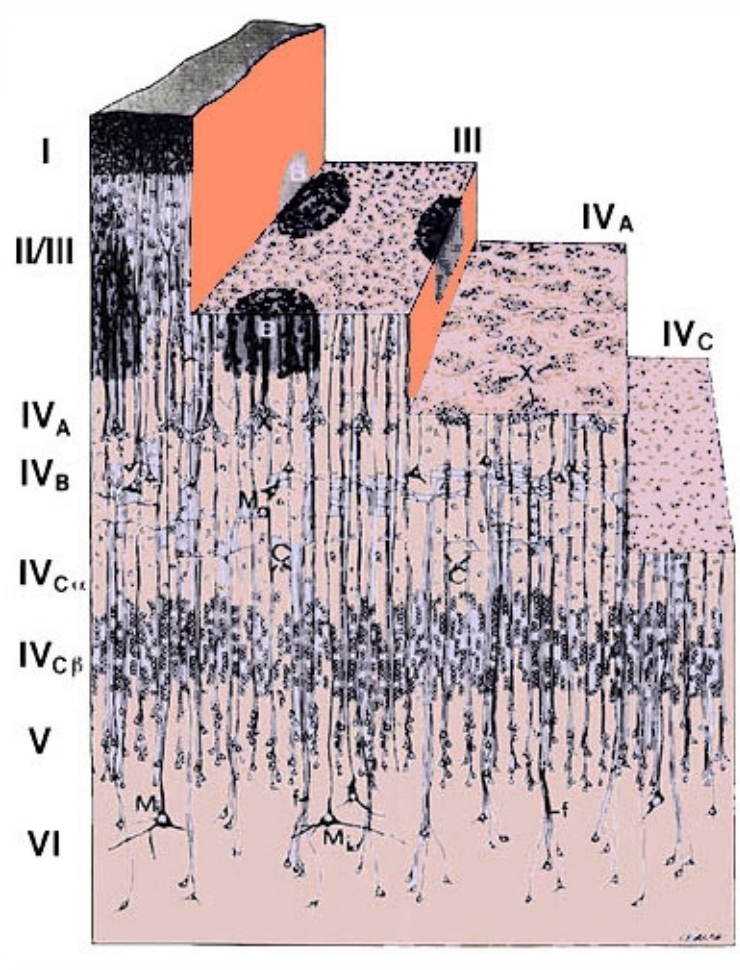

Figure 17. Schematic drawing of the visual cortex to show neurons, layers, columns, and CO blobs.

attempting to alter stereopsis in trained monkeys by microstimulating subregions of disparity-tuned cells in area MT.

Response Timing in the Visual Pathways

Another feature of visually evoked, single-cell response that is currently gaining attention is timing. The order in which visual areas become active and the range of activation times within any given area are important issues. As described above, a prevailing model of primate vision proposes hierarchical stages of visual areas based on anatomical connectivity (49, 50, 76-78). There is no doubt that a single stimulus initiates a characteristic flow of neuronal discharge from the retina to the LGNd to V1 in a hierarchical manner. Unfortunately, the complexity of corticocortical connections and functional differentiation in primate visual streams renders further predictions highly speculative (51).

We could hypothesize, for instance, that the heavily myelinated path from V1 to MT would lead to fast activation of this area. However, would all MT cells be activated in this manner, or would others wait for activation via the more indirect V1 to V2 to MT route? Many studies have reported response onset latencies from a single visual area. Using these data to construct a chart of activation times across the visual system, however, reveals a host of complications (79).

To begin with, the vast majority of studies that report latencies do so for only one or two visual areas. An activation analysis in 10 visual areas, therefore, might involve cross-comparisons between 5 and 10 separate

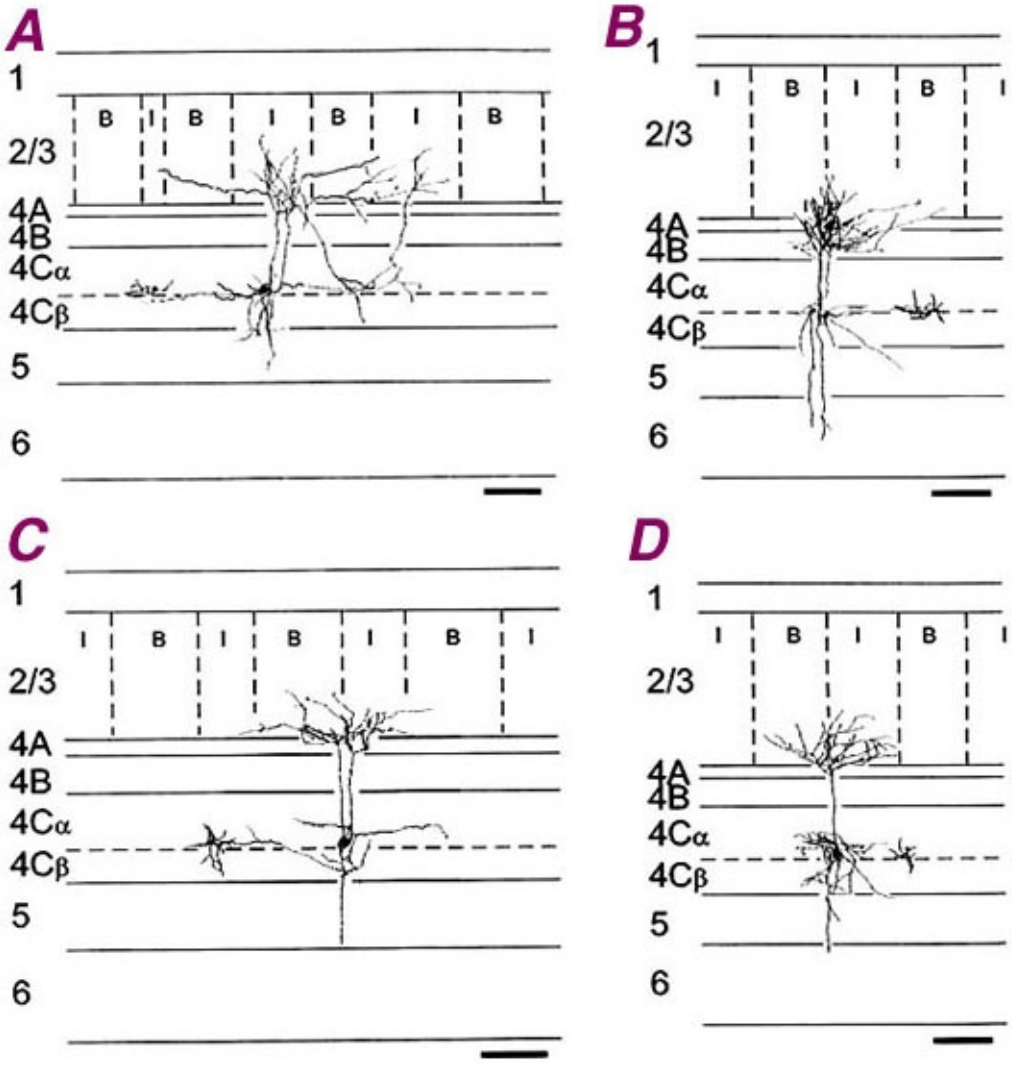

Figure 18. Reconstructions of neurobiotin-injected V1 4C cells that have dendrites confined to layer 4C and dense axonal terminations in interblobs (A, B) or dendrites extending into layer 4C and dense axonal terminations in both blobs and interblobs. From Yabuta and Callaway (37, 38).

studies. In one such comparison, we might conclude that, on average, V1 cells become active long before cells in the frontal eye field area (FEF) (80, 81). In another such comparison, we would be forced to conclude the opposite (82) (for a review, see Nowak and Bullier (79)).

The cause for this seeming discrepancy, and many others like it, is undoubtedly the use of different experimental and data analysis protocols. The visual stimuli used (flashing *versus* moving; spot, bar, grating, or otherwise; low *versus* high luminance or contrast, etc.), animal preparation used (anesthetized or not), and data analysis strategy taken for marking latencies (qualitative or quantitative, etc.) all vary across the existing reports.

Consequently, in a recent study, we sought to remove these confounds by obtaining onset latencies from many primate visual areas using the same experimental and analytical techniques (83). The results demonstrated that the two major functional streams in the primate visual system (the M/dorsal stream involved in motion perception and tracking and the P/ventral stream involved in object recognition and color coding) respond with very different time courses (Fig. 24).

In general, M-stream areas respond rapidly and concurrently, whereas their P-stream counterparts respond slowly and sequentially. Particularly relevant to this review, the LGNd M cells become active 15 to 20 msec faster

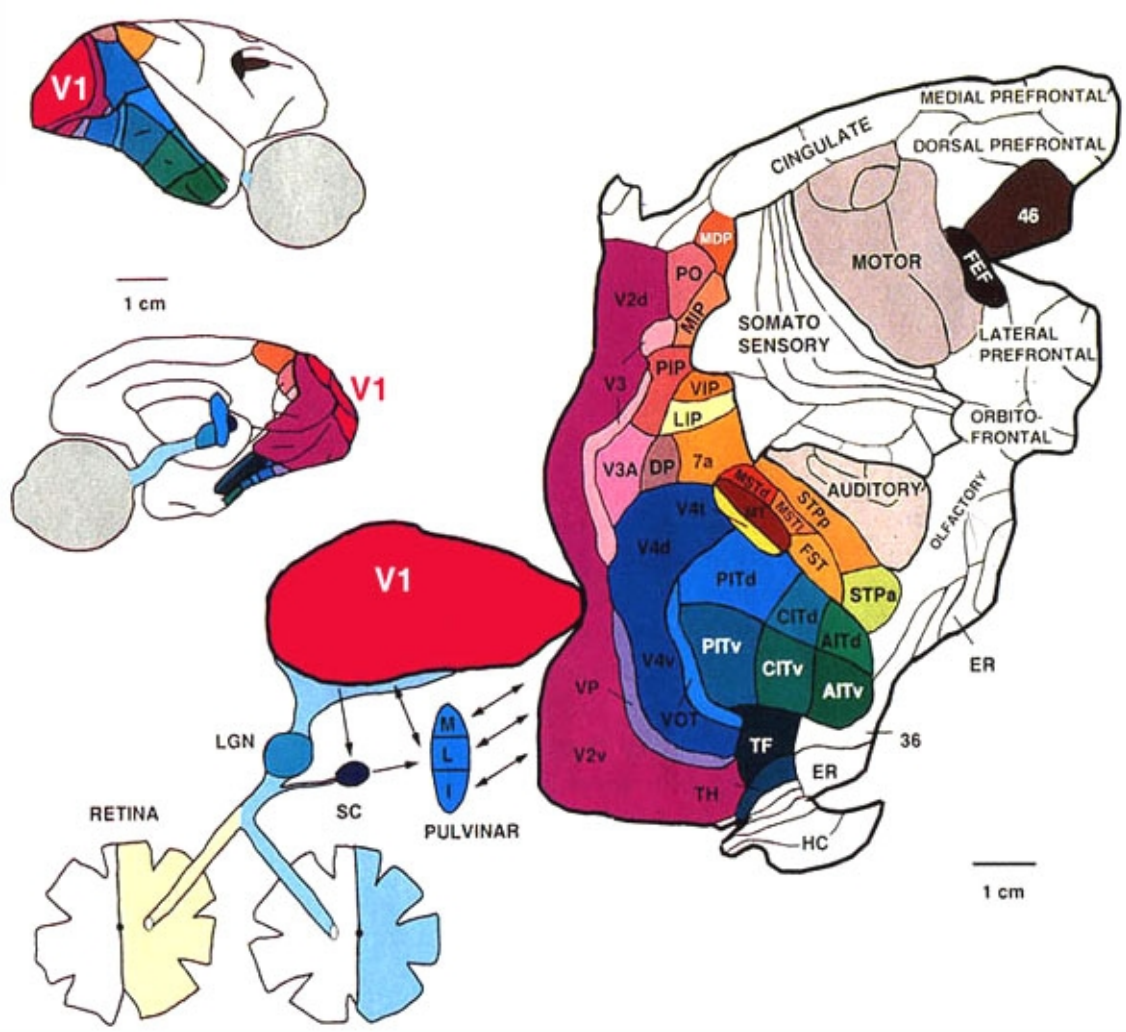

Figure 19. Much of V1 is located in the calcarine sulci, and its relationship to other brain areas is best shown by unfolding the brain and showing it flattened open. The visually responsive areas of the macaque monkey are shown in color. From Van Essen et al. (78).

than do their P-cell counterparts (83, 84), and this temporal separation is maintained in the geniculorecipient layers 4Cα and 4Cβ (80, 82, 83). Thus, a functional separation in response timing exists in the M and P pathways of the subcortex and V1 and appears to be conveyed to the dorsal and ventral streams of the extrastriate cortex.

Illusory Contour Perception

The modern view of visual perception is one of dynamic processes that go beyond the simple replication of visual information provided to the retina. For over 80 years, Gestalt psychologists have argued that the act of perception creates a Gestalt, a figure or form that is not a property of an object observed but represents the organization of sensations by the brain (85). This dynamism is thought to be crucial for the performance of simple, everyday visual tasks, such as the recognition of an object that is partially occluded. Thus, the study of how the brain is capable of filling in the missing pieces is an important topic; one that has most often been carried out through the use of "illusory contours".

Illusory contours (ICs) are defined by their subjective appearance in the absensce of any luminance differences in the image itself. A classic example of an IC is the illusory square, where four sectored discs oriented in an appropriate manner generate the percept of a square. In this instance, it is clear that no true luminance differences exist to form a complete square, and yet a square is perceived (Fig. 25).

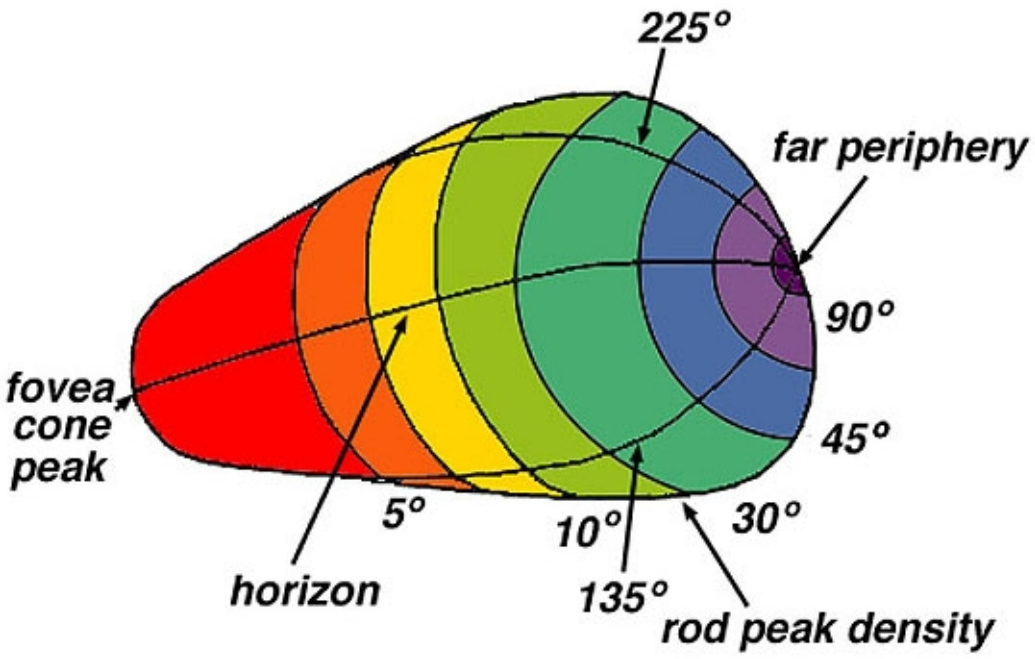

Figure 20. The unfolded striate cortex has a shape like a pear. It would be a quarter sphere if the visual fields were equally represented everywhere, but instead it is greatly distorted by the disproportionate representation of parts near the center of gaze (fovea), a feature termed "cortical magnification". In contrast, the far periphery is greatly underrepresented.

Behavioral tests indicate that cats and monkeys are capable of perceiving such contours (86-88). Recent physiological studies have examined whether single cells in striate and extrastriate cortex respond similarly to conventional luminance contours and those defined by illusions (89-92). In each of these studies, IC-responsive cells were reported. However, these studies provide conflicting evidence about the origin of IC responsivity, arguing for or against the presence of IC-responding cells in V1. The use of alternative ICs in the different studies confuses this issue further.

We sought to approach illusory contour perception from the broader issue of contour perception in general (93). The issue here is how the brain encodes a stimulus boundary (e.g., a square) when the visual cue that defines that boundary (e.g., color, luminance, texture, motion, illusion, etc.) is varied. As Gestalt psychologists would note, the stimulus is very different in each of these cases, but the fundamental percept, the square, remains the same. We asked two fundamental questions. First, are there V1 or V2 cells in cat and monkey capable of responding in a similar fashion to a boundary, regardless of the cue defining it? Alternatives to this include the origin of cue invariance at later stages of visual processing or the separate channeling of cue information via different subpopulations of cells, each responsible for one cue. Second, if such cells exist, are they equally prevalent in V1 and V2? Our results demonstrated that a subpopulation of cells in both regions can respond to a stimulus boundary, such as an oriented bar, in a cue-invariant manner, although this property was rare in V1 while prevalent in V2 (Fig. 26).

One conclusion from this work is that cells in the very first stage of cortical processing are already capable of responding to a single stimulus boundary in a complex manner that allows for object detection, even as the cues defining the object change or are partially occluded (93).

Understanding Vision: A Problem of Reverse Engineering

Our attempt to understand the visual pathways is very much like approaching a machine about which we know nothing but its basic functions. By way of analogy, we all know how to operate a car (more or less) and recognize

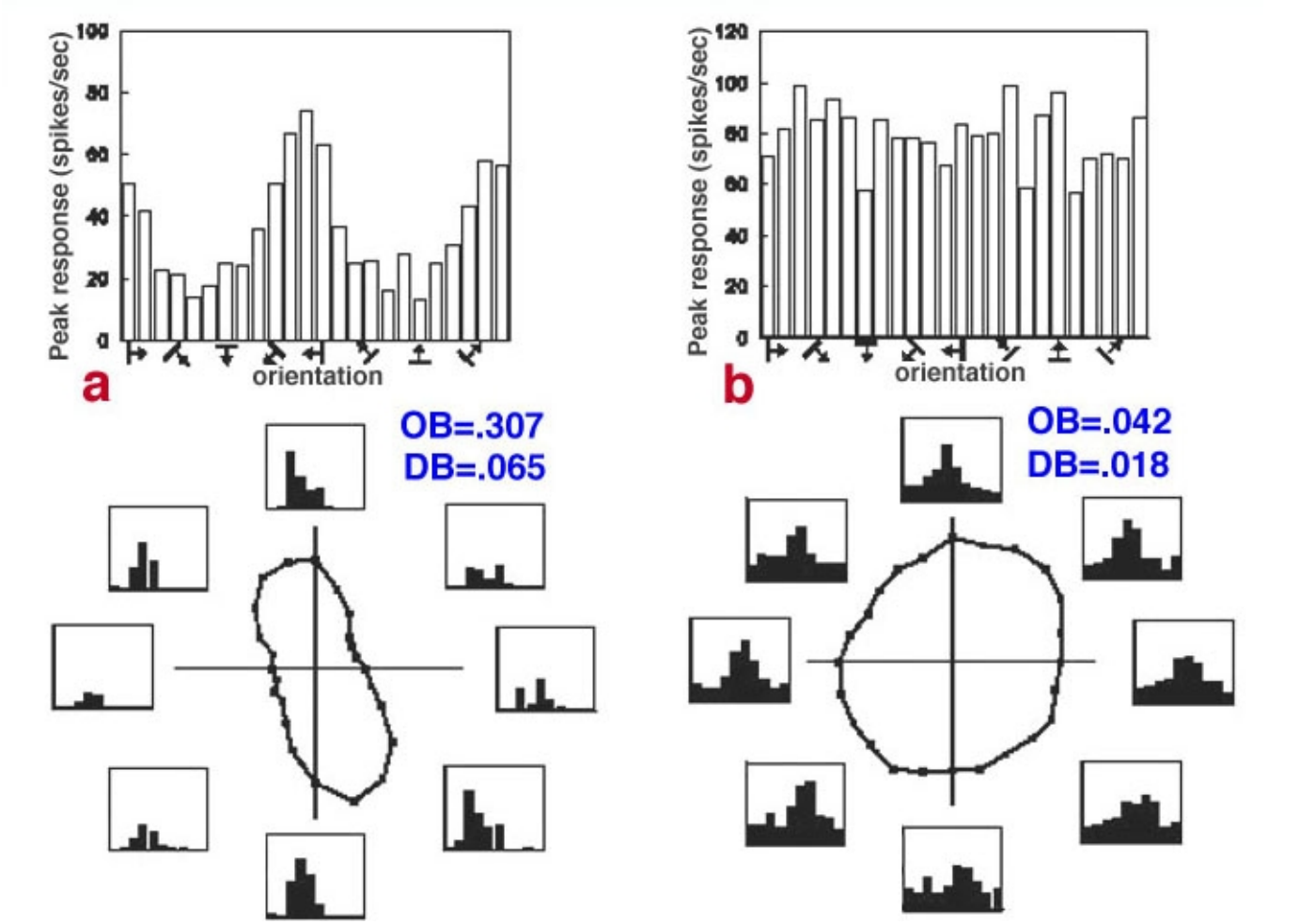

Figure 21. A tuning curve and corresponding polar plot obtained from two macaque V1 cells in response to drifting luminance bars of systematically varied orientation and direction. The responses of one orientation selective cell and one nonselective cell are provided for comparison. Histograms surrounding the polar plots demonstrate the cellular response as a function of time. Orientation bias (OB) and direction bias (DB) are measures of how selective a cell is, where >0.1 is significant and 0.3 is approximately an 8:1 maximum firing rate to minimum firing rate ratio. From Schmolesky et al. (95).

its basic function—to get us from one place to another. Now let us assume that we knew absolutely nothing but this and, for some reason, decided we should learn every detail of the car's inner workings. We might start by trying to figure out the parts of the car devoted to this central function and those that are not. We remove the bumper, horn, AC, and windshields and find that the car still runs splendidly. We remove small parts of the engine, piece by piece until the car no longer starts, analogous to the lesion studies in the brain. Slowly, we begin to understand what parts of the car (brain) are involved in locomotion (vision). In vision research, we are very much at this stage of the game, still wanting to know what each part actually does, when it does it, and how all the individual parts act in concert. It is the hope of many researchers, myself included, that a careful investigation into the structure and function of the visual pathways using chemical, electrophysiological, genetic, and behavioral approaches will culminate in a true understanding of how the brain provides us with this most crucial of sensory capabilities, vision (Fig. 27).

Under Construction

Additional sections dealing with RF properties are under construction: They include: 1) ON/OFF RF subunit composition; 2) transient *versus* sustained responsivity; 3) spatial and temporal frequency; 4) contrast sensitivity; and 5) color selectivity.

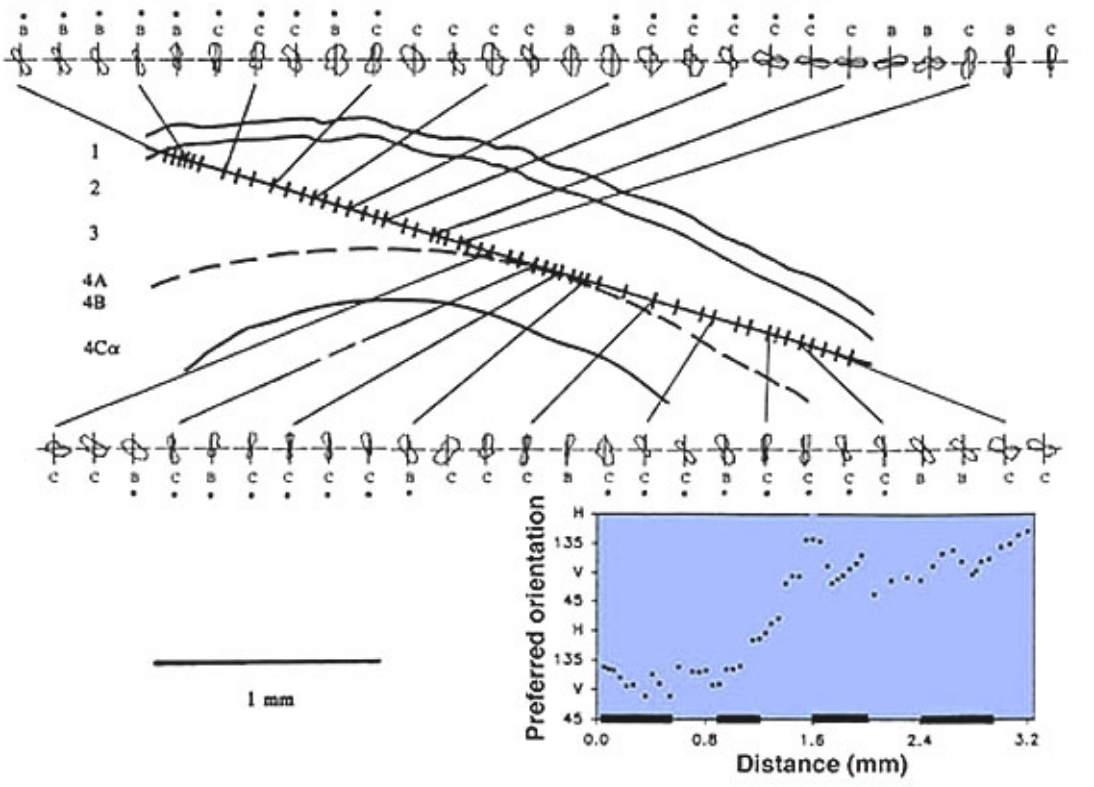

Figure 22. One extensive electrode penetration in macaque V1. The short, near-vertical lines represent recording sites, and polar plots for each site are indicated. This figure shows the preferred orientation of each cell in relation to the cortical layers, CO compartments (a filled circle indicates a blob; lack of this circle indicates an interblob), and color selectivity (C, color selective; B, broadband) in macaque V1. From Leventhal et al. (96).

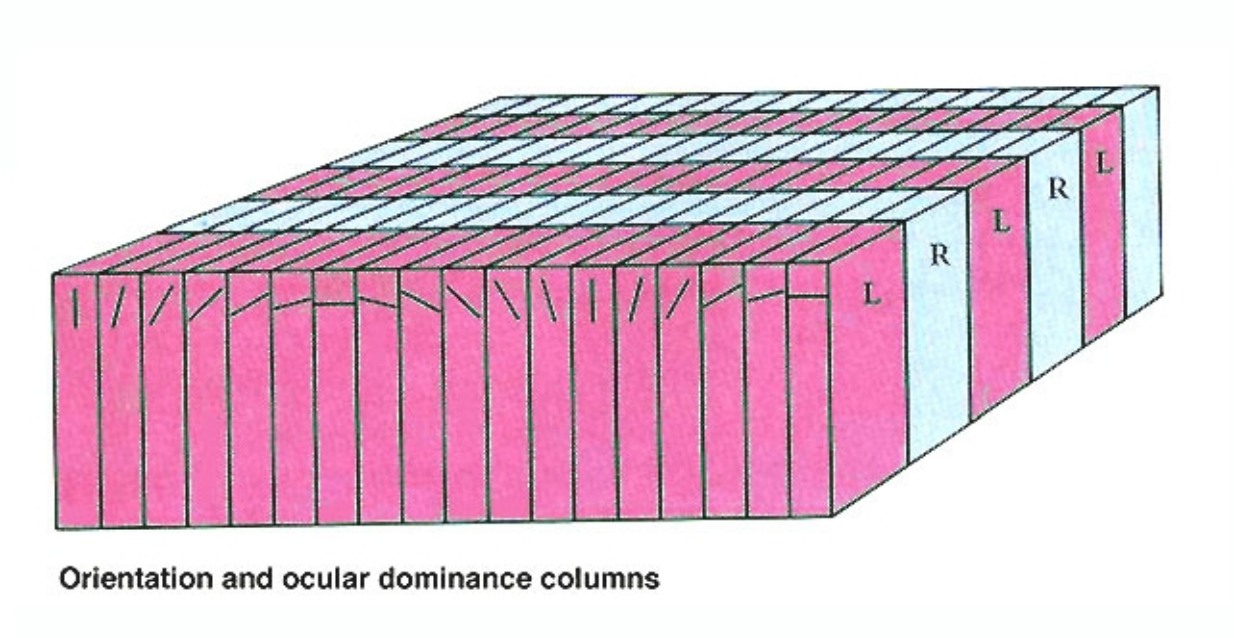

Figure 23. The ice-cube model of the cortex. It illustrates how the cortex is divided, and at the same time, into two kinds of slabs, one set of ocular dominance (left and right) and one set for orientation. The model should not be taken literally: Neither set is as regular as this, and the orientation slabs especially are far from parallel or straight.

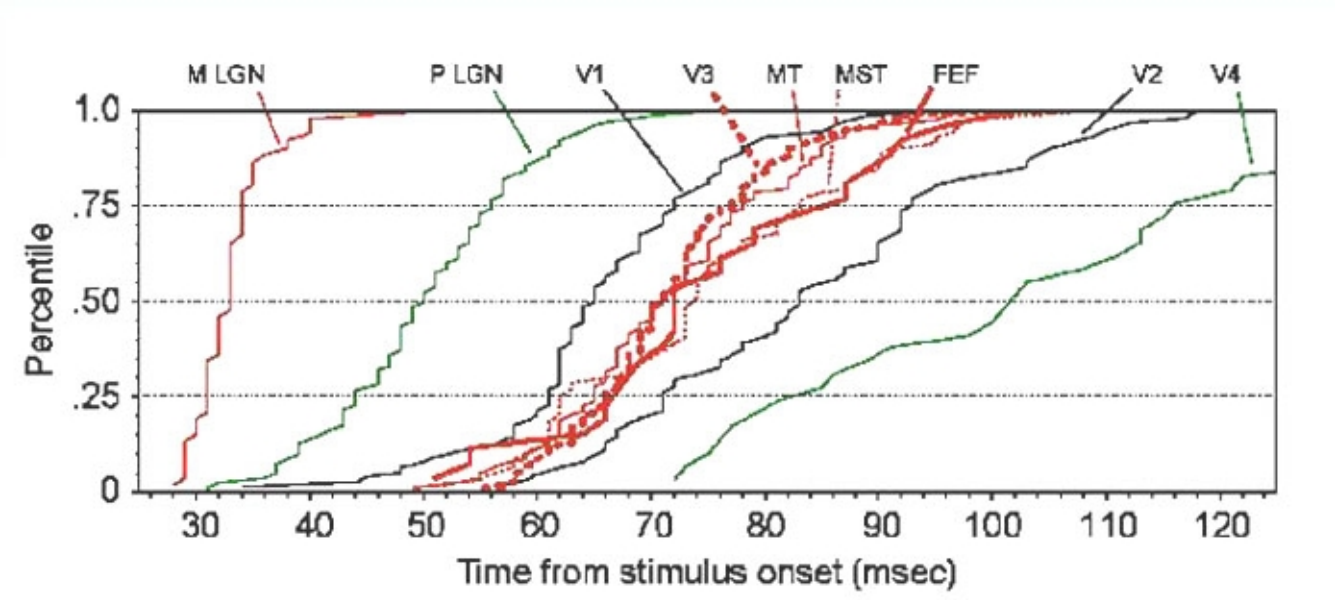

Figure 24. Onset latencies. Cumulative distributions of visually evoked onset response latencies in the LGNd, striate, and extrastriate areas as labeled. The percentiles of cells that have begun to respond are plotted as a function of time from stimulus presentation. The V4 curve is truncated to increase resolution of the other curves: the V4 range extends to 159 ms. From Schmolesky et al. (83).

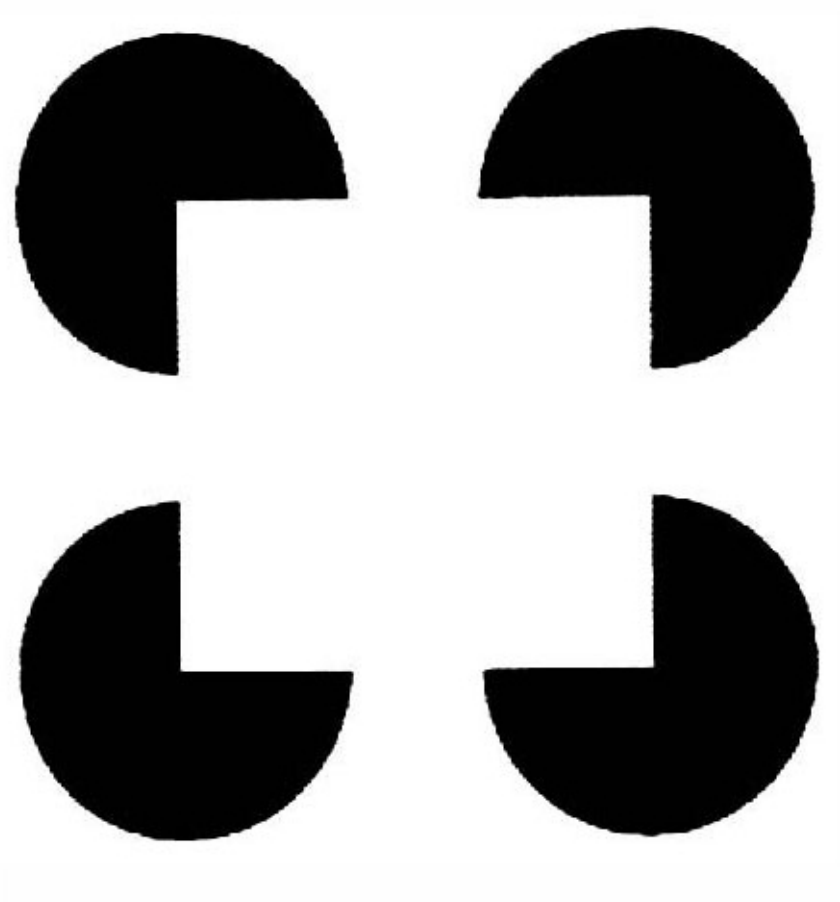

Figure 25. Illusory contours as seen in the illusory square.

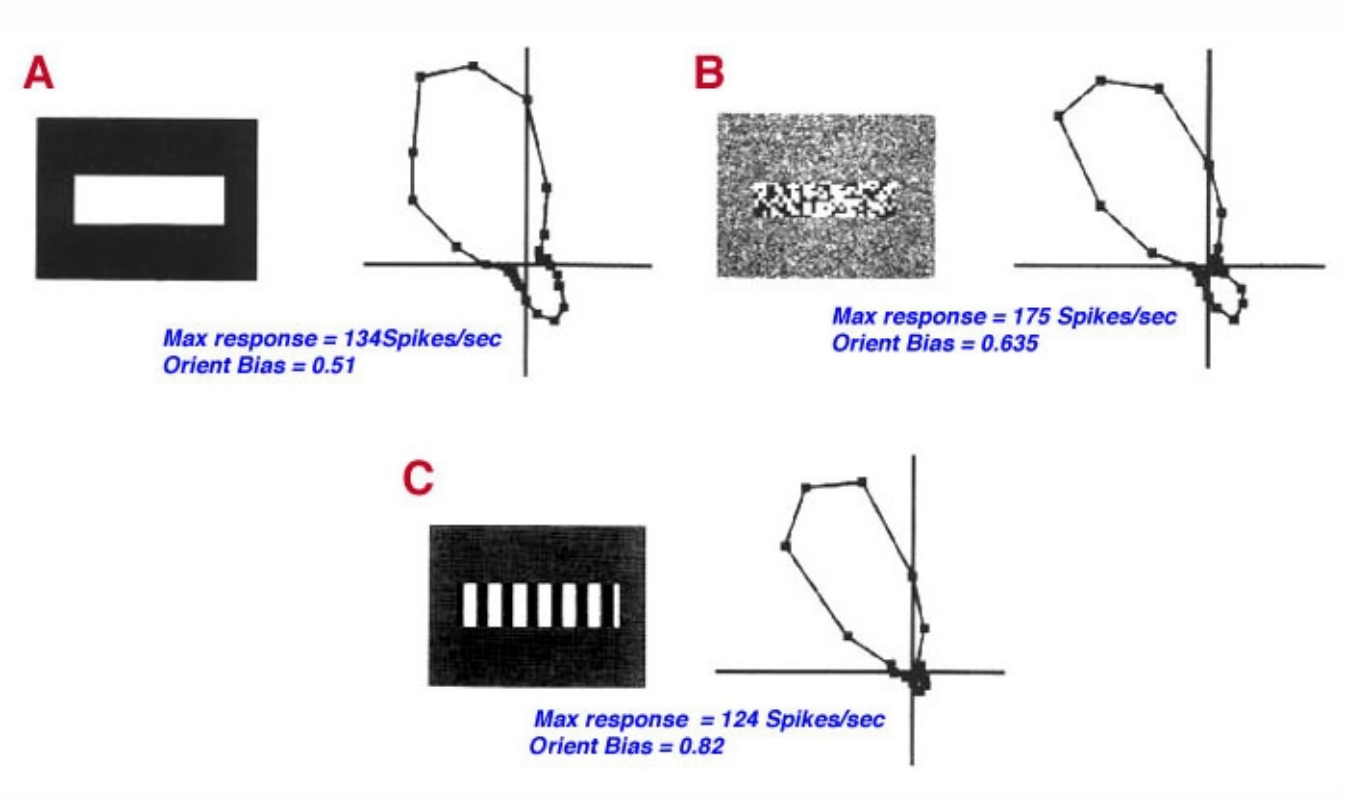

Figure 26. Example of a cue-invariant cell in cat area 18. This cell responds with the same degree of orientation bias and to the same preferred orientation, regardless of whether the bar is defined by simple luminance (top), texture (middle), or isoluminant gratings (bottom). From Leventhal et al. (93).

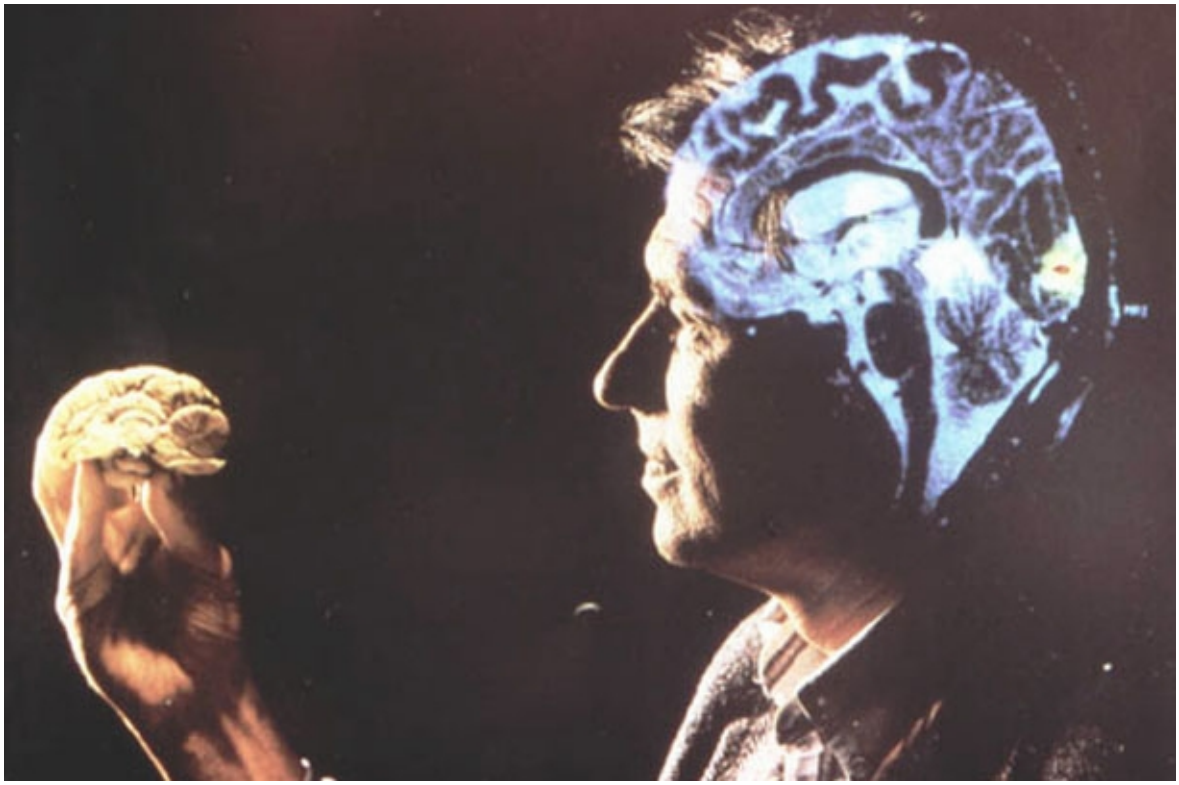

Figure 27. Reverse engineering: the brain studying the brain.

About the Author

Dr. Matthew Schmolesky was born in West Palm Beach, Florida. He received his B.A. in Psychology and Philosophy from Furman University, Greenville, South Carolina in 1993. He received his Masters in Experimental Psychology from Wake Forest University in 1995 and his Ph.D. in Neuroscience from the University of Utah in 2000, respectively. While studying at the University of Utah, he conducted research on the visual pathways in cat and monkey with Dr. Audie Leventhal, looking at aspects of color, orientation, and aging. He recently completed a Grass Fellowship at the Marine Biological Laboratory in Woods Hole, MA. Matt is currently a Research Fellow at Erasmus University Rotterdam in the Netherlands, where he is studying synaptic plasticity in the cerebellum at the cellular and behavioral levels.

References

1. Polyak S. The vertebrate visual system. 1957.
2. Carl Weigert (1845-1904). JAMA. 1964;189:769–770. PubMed PMID: 14174058.
3. Franz Nissl (1860-1919), neuropathologist. JAMA. 1968;205:460–461.
4. Cajal SR. La retine des vertebres. In: Thorpe SA, Glickstein M, translators. The structure of the retina. Springfield (IL): Charles C. Thomas Publisher; 1933.
5. Fritsch G, Hitzig E. Ueber die elektrische Erregbarkeit des Grosshirns. On the electrical excitability of the cerebrum. Archiv fur Anatomie, Physiologie und wissenschaftliche Medizin. 1870;37:300–332.
6. Penfield W, Boldrey E. Somatic motor and sensory representation in the cerebral cortex of man as studied by electrical stimulation. Brain. 1937;60:389–443.
7. Daniel PM, Whitteridge D. The representation of the visual field on the calcarine cortex in baboons and monkeys. J Physiol. 1959;148:33P.
8. Talbot SA, Marshall WH. Physiological studies on neural mechanisms of visual localization and discrimination. Am J Ophthal. 1941;24:1255–1263.
9. Thompson JM, Woolsey CN, Talbot SA. Visual areas I and II of cerebral cortex of rabbit. J Neurophysiol. 1950;13:277–288. PubMed PMID: 15422390.
10. Hartline HK. The response of single optic nerve fibers of the vertebrate eye to the illumination of the retina. Am J Physiol. 1938;121:400–415.
11. Kuffler SW. Discharge patterns and functional organization of mammalian retina. J Neurophysiol. 1953;16:37–68. PubMed PMID: 13035466.
12. Mountcastle VB. Modality and topographic properties of single neurons of cat's somatic sensory cortex. J Neurophysiol. 1957;20:408–434. PubMed PMID: 13439410.

13. Powell TP, Mountcastle VB. Some aspects of the functional organization of the cortex of the postcentral gyrus of the monkey: a correlation of findings obtained in a single unit analysis with cytoarchitecture. Bull Johns Hopkins Hosp. 1959;105:133–162. PubMed PMID: 14434571.
14. Hubel DH, Wiesel TN. Receptive fields of single neurones in the cat's striate cortex. J Physiol. 1959;150:91–104.
15. Hubel DH, Wiesel TN. Receptive fields, binocular interaction and functional architecture in the cat's visual cortex. J Physiol. 1962;160:106–154. PubMed PMID: 14449617.
16. Hubel DH, Wiesel TN. Receptive fields and functional architecture of the monkey striate cortex. J Physiol. 1968;195:215–243. PubMed PMID: 4966457.
17. Hubel DH, Wiesel TN. Sequence regularity and geometry of orientation columns in the monkey striate cortex. J Comp Neurol. 1974;158:267–293. PubMed PMID: 4436456.
18. Hubel DH, Wiesel TN, Stryker MP. Orientation columns in macaque monkey visual cortex demonstrated by the 2-deoxyglucose autoradiographic technique. Nature. 1977;269:328–330. PubMed PMID: 409953.
19. Hubel DH. Exploration of the primary visual cortex, 1955–78. Nature. 1982;299:515–524. PubMed PMID: 6750409.
20. O'Kusky J, Colonnier M. A laminar analysis of the number of neurons, glia, and synapses in the visual cortex (area 17) of adult macaque monkeys. J Comp Neurol. 1982;210:278–290. PubMed PMID: 7142443.
21. Fitzpatrick D, Lund JS, Schmechel DE, Towles AC. Distribution of GABAergic neurons and axon terminals in the macaque striate cortex. J Comp Neurol. 1987;264:73–91. PubMed PMID: 3680625.
22. Peters A, Sethares C. Organization of pyramidal neruons in rhesus monkey primary visual cortex. J Comp Neurol. 1991;306:1–23. PubMed PMID: 1710236.
23. DeFelipe J, Hendry SHC, Hashikawa T, Molinari M, Jones EG. A microcolumnar structure of monkey cerebral cortex revealed by immunocytochemical studies of double bouquet cell axons. Neuroscience. 1990;37:655–673. PubMed PMID: 1701039.
24. DeFelipe J, Hendry SH, Jones EG. A correlative electron microscopic study of basket cells and large GABAergic neurons in the monkey sensory-motor cortex. Neuroscience. 1986;17:991–1009. PubMed PMID: 2423922.
25. Somogyi P, Kisvarday ZF, Martin KA, Whitteridge D. Synaptic connections of morphologically identified and physiologically characterized large basket cells in the striate cortex of cat. Neuroscience. 1983;10:261–294. PubMed PMID: 6633861.
26. Lund JS. Local circuit neurons of macaque moniey striate cortex. I. Neurons of laminae 4C and 5A. J Comp Neurol. 1987;257:60–92. PubMed PMID: 3571519.
27. Lund JS, Hawken MJ, Parker AJ. Local circuit neurons of macaque moniey striate cortex. II. Neurons of laminae 5B and 6. J Comp Neurol. 1988;276:1–29. PubMed PMID: 2461395.
28. Lund JS, Yoshioka T. Local circuit neurons of macaque moniey striate cortex. III. Neurons of laminae 4B, 4A, and 3B. J Comp Neurol. 1991;311:234–258. PubMed PMID: 1721632.
29. Lund JS, Wu CQ. Local circuit neurons of macaque moniey striate cortex. IV. Neurons of laminae 1–3A. J Comp Neurol. 1997;384:109–126. PubMed PMID: 9214543.
30. Fitzpatrick D, Itoh K, Diamond IT. The laminar organization of the lateral geniculate body and the striate cortex in the squirrel monkey (Saimiri sciureus). J Neurosci. 1983;3:673–702. PubMed PMID: 6187901.
31. Lachica EA, Casagrande VA. Direct W-like geniculate projections to the cytochrome-oxidase (CO) blobs in primate visual cortex: axon morphology. J Comp Neurol. 1992;319:141–158. PubMed PMID: 1375606.
32. Fries W, Distel H. Large layer V1 neurons of monkey striate cortex (Meynert cells) project to the superior colliculus. Proc R Soc Lond B Biol Sci. 1983;219:53–59. PubMed PMID: 6137827.
33. Blasdel GG, Lund JS. Termination of afferent axons in macaque striate cortex. J Neurosci. 1983;3:1389–1413. PubMed PMID: 6864254.
34. Hubel DH, Wiesel TN. Laminar and columnar distribution of geniculo-cortical fibers in the macaque monkey. J Comp Neurol. 1972;146:421–450. PubMed PMID: 4117368.
35. Lund JS. Organization of neurons in the visual cortex, area 17, of the monkey (Macaca mulatta). J Comp Neurol. 1973;147:455–496. PubMed PMID: 4122705.

36. Blasdel GG, Fitzpatrick D. Physiological organization of layer 4 in the macaque striate cortex. J Neurosci. 1984;4:880–895. PubMed PMID: 6200586.
37. Yabuta NH, Callaway EM. Functional streams and local connections of layer 4C neurons in primary visual cortex of macaque monkey. J Neurosci. 1998a;18:9489–9499. PubMed PMID: 9801386.
38. Yabuta NH, Callaway EM. Cytochrome-oxidase blobs and intrinsic horizontal connections of layer 2/3 pyramidal neurons in primate V1. Vis Neurosci. 1998b;15:1007–1027. PubMed PMID: 9839966.
39. Lund JS, Boothe RG. Interlaminar connections and pyramidal neuron organization in the visual cortex, area 17, of the macaque monkey. J Comp Neurol. 1975;159:305–334.
40. Fries W, Keizer K, Kuypers HG. Large layer VI cells in macaque striate cortex (Meynert cells) project to both superior colliculus and prestriate visual area V5. Exp Brain Res. 1985;58:613–616. PubMed PMID: 3839191.
41. Lund JS, Lund RD, Hendrickson AE, Bunt AH, Fuchs AF. The origin of efferent pathways from the primary visual cortex, area 17, of the macaque monkey as shown by retrograde transport of horseradish peroxidase. J Comp Neurol. 1975;164:287–303. PubMed PMID: 810501.
42. Hendrickson AE, Wilson JR, Ogren MP. The neuroanatomical organization of pathways between the dorsal lateral geniculate nucleus and visual cortex in Old World and New World primates. J Comp Neurol. 1978;182:123–136. PubMed PMID: 100530.
43. Hendry SH, Yoshioka T. A neurochemically distinct third channel in the macaque dorsal lateral geniculate nucleus. Science. 1994;264:575–577. PubMed PMID: 8160015.
44. Livingstone MS, Hubel DH. Thalamic inputs to cytochrome oxidase-rich regions in monkey visual cortex. Proc Natl Acad Sci U S A. 1982;79:6098–6101. PubMed PMID: 6193514.
45. Boyd JD, Casagrande VA. Relationships between cytochrome oxidase (CO) blobs in primary visual cortex (V1) and the distribution of neurons projecting to the middle temporal area (MT). J Comp Neurol. 1999;409:573–591. PubMed PMID: 10376741.
46. Shipp S, Zeki S. Segregation of pathways leading from area V2 to areas V4 and V5 of macaque monkey visual cortex. Nature. 1985;315:322–325. PubMed PMID: 2987702.
47. Shipp S, Zeki S. The organization of connections between areas V5 and V1 in macaque monkey visual cortex. Eur J Neurosci. 1989;1:309–332. PubMed PMID: 12106142.
48. Shipp S, Zeki S. The organization of connections between areas V5 and V1 in macaque monkey visual cortex. Eur J Neurosci. 1989;1:333–354. PubMed PMID: 12106143.
49. Barone P, Batardiere A, Knoblauch K, Kennedy H. Laminar distribution of neurons in extrastriate areas projecting to visual areas V1 and V4 correlates with the hierarchical rank and indicates the operation of a distance rule. J Neurosci. 2000;20:3263–3281. PubMed PMID: 10777791.
50. Felleman DJ, Van Essen DC. Distributed hierarchical processing in the primate cerebral cortex. Cereb Cortex. 1991;1:1–47. PubMed PMID: 1822724.
51. Hilgetag CC, O'Neill MA, Young MP. Indeterminate organization of the visual system. Science. 1996;271:776–777. PubMed PMID: 8628990.
52. Adams MM, Hof PR, Gattass R, Webster MJ, Ungerleider LG. Visual cortical projections and chemoarchitecture of macaque monkey pulvinar. J Comp Neurol. 2000;419:377–393. PubMed PMID: 10723012.
53. Doty RW. Nongeniculate afferents to striate cortex in macaques. J Comp Neurol. 1983;218:159–173. PubMed PMID: 6886069.
54. Graham J. Some topographical connections of the striate cortex with subcortical structures in Macaca fascicularis. Exp Brain Res. 1982;47:1–14. PubMed PMID: 7117434.
55. Ogren M, Hendrickson A. Pathways between striate cortex and subcortical regions in Macaca mulatta and Saimiri sciureus: evidence for a reciprocal pulvinar connection. Exp Neurol. 1976;53:780–800. PubMed PMID: 826404.
56. Rezak M, Benevento LA. A comparison of the organization of the projections of the dorsal lateral geniculate nucleus, the inferior pulvinar and adjacent lateral pulvinar to primary visual cortex (area 17) in the macaque monkey. Brain Res. 1979;167:19–40. PubMed PMID: 88245.

57. Perkel DJ, Bullier J, Kennedy H. Topography of the afferent connectivity of area 17 in the macaque monkey: a double-labelling study. J Comp Neurol. 1986;253:374–402. PubMed PMID: 3793996.
58. Fitzpatrick D, Usrey WM, Schofield BR, Einstein G. The sublaminar organization of corticogeniculate neurons in layer 6 of macaque striate cortex. Vis Neurosci. 1994;11:307–315. PubMed PMID: 7516176.
59. Livingstone MS, Hubel DH. Connections between layer 4B of area 17 and the thick cytochrome oxidase stripes of area 18 in the squirrel monkey. J Neurosci. 1987;7:3371–3377. PubMed PMID: 2824713.
60. Maunsell JH, Van Essen DC. The connections of the middle temporal visual area (MT) and their relationship to a cortical hierarchy in the macaque monkey. J Neurosci. 1983;3:2563–2586. PubMed PMID: 6655500.
61. Ungerleider LG, Desimone R. Projections to the superior temporal sulcus from the central and peripheral field representations of V1 and V2. J Comp Neurol. 1986a;248:147–163. PubMed PMID: 3722456.
62. Ungerleider LG, Desimone R. Cortical connections of visual area MT in the macaque. J Comp Neurol. 1986b;248:190–222. PubMed PMID: 3722458.
63. Boussaoud D, Ungerleider LG, Desimone R. Pathways for motion analysis: cortical connections of the medial superior temporal and fundus of the superior temporal visual areas in the macaque. J Comp Neurol. 1990;296:462–495. PubMed PMID: 2358548.
64. Rockland KS, Saleem KS, Tanaka K. Divergent feedback connections from areas V4 and TEO in the macaque. Vis Neurosci. 1994;11:579–600. PubMed PMID: 8038130.
65. Suzuki W, Saleem KS, Tanaka K. Divergent backward projections from the anterior part of the inferotemporal cortex (area TE) in the macaque. J Comp Neurol. 2000;422:206–228. PubMed PMID: 10842228.
66. Fries W. Pontine projection from striate and prestriate visual cortex in the macaque monkey: an anterograde study. Vis Neurosci. 1990;4:205–216. PubMed PMID: 2078502.
67. Gutierrez C, Cusick CG. Area V1 in macaque monkeys projects to multiple histochemically defined subdivisions of the inferior pulvinar complex. Brain Res. 1997;765:349–356. PubMed PMID: 9313911.
68. Erwin E, Baker FH, Busen WF, Malpeli JG. Relationship between laminar topology and retinotopy in the rhesus lateral geniculate nucleus: results from a functional atlas. J Comp Neurol. 1999;407:92–102. PubMed PMID: 10213190.
69. De Valois RL, Yund EW, Hepler N. The orientation and direction selectivity of cells in the macaque visual cortex. Vision Res. 1982;22:531–544. PubMed PMID: 7112953.
70. Schiller PH, Finlay BL, Volman SF. Quantitative studies of single-cell properties in monkey striate cortex. I. Spatiotemporal organization of receptive fields. J Neurophysiol. 1976;39:1288–1319. PubMed PMID: 825621.
71. Bonhoeffer T, Grinvald A. Iso-orientation domains in cat visual cortex are arranged in pinwheel-like patterns. Nature. 1991;353:429–431. PubMed PMID: 1896085.
72. Livingstone MS. Mechanisms of direction selectivity in macaque V1. Neuron. 1998;20:509–526. PubMed PMID: 9539125.
73. Ringach DL, Hawken MJ, Shapley R. Dynamics of orientation tuning in macaque primary visual cortex. Nature. 1997;387:281–284. PubMed PMID: 9153392.
74. DeAngelis GC, Cumming BG, Newsome WT. Cortical area MT and the perception of stereoscopic depth. Nature. 1998;394:677–680. PubMed PMID: 9716130.
75. DeAngelis GC, Newsome WT. Organization of disparity-selective neurons in macaque area MT. J Neurosci. 1999;19:1398–1415. PubMed PMID: 9952417.
76. DeYoe EA, Felleman DJ, Van Essen DC, McClendon E. Multiple processing streams in occipitotemporal visual cortex. Nature. 1994;371:151–154. PubMed PMID: 8072543.
77. Van Essen DC, Newsome WT, Maunsell JH, Bixby JL. The projections from striate cortex (V1) to areas V2 and V3 in the macaque monkey: asymmetries, areal boundaries, and patchy connections. J Comp Neurol. 1986;244:451–480. PubMed PMID: 3958238.
78. Essen DC, Van Anderson CH, Felleman DJ. Information processing in the primate visual system: an integrated systems perspective. Science. 1992;255:419–423. PubMed PMID: 1734518.

79. Nowak LG, Bullier J. The timing of information transfer in the visual system. In: Kaas JH, Rockland K, Peters A, editors. Cerebral cortex. New York: Plenum Press; 1998. p. 205–241.
80. Maunsell JH, Gibson JR. Visual response latencies in striate cortex of the macaque monkey. J Neurophysiol. 1992;68:1332–1344. PubMed PMID: 1432087.
81. Thompson KG, Hanes DP, Bichot NP, Schall JD. Perceptual and motor processing stages identified in the activity of macaque frontal eye field neurons during visual search. J Neurophysiol. 1996;76:4040–4055. PubMed PMID: 8985899.
82. Nowak LG, Munk MH, Girard P, Bullier J. Visual latencies in areas V1 and V2 of the macaque monkey. Vis Neurosci. 1995;12:371–384. PubMed PMID: 7786857.
83. Schmolesky MT, Wang YC, Hanes DP, Thompson KG, Leutgeb S, Schall JD, Leventhal AG. Signal timing across the macaque visual system. J Neurophysiol. 1998;79:3272–3278. PubMed PMID: 9636126.
84. Maunsell JH, Ghose GM, Assad JA, McAdams CJ, Boudreau CE, Noerager BD. Visual response latencies of magnocellular and parvocellular LGN neurons in macaque monkeys. Vis Neurosci. 1999;16:1–14. PubMed PMID: 10022474.
85. Kandel ER. Perception of motion, depth, and form. In: Kandel ER, Schwartz JH, Jessel TM, editors. Principles of Neural Science. Norwalk (CT): Appleton & Lange; 1991.
86. Bravo M, Blake R, Morrison S. Cats see subjective contours. Vision Res. 1988;28:861–865. PubMed PMID: 3250081.
87. De Weerd P, Vandenbussche E, De Bruyn B, Orban GA. Illusory contour orientation discrimination in the cat. Behav Brain Res. 1990;39:1–17. PubMed PMID: 2390193.
88. De Weerd P, Desimone R, Ungerleider LG. Cue-dependent deficits in grating orientation discrimination after V4 lesions in macaques. Vis Neurosci. 1996;13:529–538. PubMed PMID: 8782380.
89. Grosof DH, Shapley RM, Hawken MJ. Macaque V1 neurons can signal 'illusory' contours. Nature. 1993;365:550–552. PubMed PMID: 8413610.
90. Peterhans E, von der Heydt R. Mechanisms of contour perception in monkey visual cortex. II. Contours bridging gaps. J Neurosci. 1989;9:1749–1763. PubMed PMID: 2723748.
91. von der Heydt R, Peterhans E, Baumgartner G. Illusory contours and cortical neuron responses. Science. 1984;224:1260–1262. PubMed PMID: 6539501.
92. von der Heydt R, Peterhans E. Mechanisms of contour perception in monkey visual cortex. I. Lines of pattern discontinuity. J Neurosci. 1989;9:1731–1748. PubMed PMID: 2723747.
93. Leventhal AG, Wang Y-C, Schmolesky MT, Zhou Y. Neural correlates of boundary perception. Vis Neurosci. 1998;15:1107–1118. PubMed PMID: 9839975.
94. Olavarria JF, Van Essen DC. The global pattern of cytochrome oxidase stripes in visual area V2 of the macaque monkey. Cereb Cortex. 1997;7:395–404. PubMed PMID: 9261570.
95. Schmolesky MT, Wang Y, Pu M, Leventhal AG. Degradation of stimulus selectivity of visual cortical cells in senescent rhesus monkeys. Nat Neurosci. 2000;3:384–390. PubMed PMID: 10725929.
96. Leventhal AG, Thompson KG, Liu D, Zhou Y, Ault SJ. Concomitant sensitivity to orientation, direction, and color of cells in layers 2, 3, and 4 of monkey striate cortex. J Neurosci. 1995;15:1808–1818. PubMed PMID: 7891136.

Repair and Regeneration of Visual Neurons

Cellular Remodeling in Mammalian Retina Induced by Retinal Detachment

Steven K. Fisher, Geoffrey P. Lewis, Kenneth A. Linberg, Edward Barawid, and Mark R. Verardo

Created: May 1, 2005; Updated: July 3, 2007.

Introduction

What Is Retinal Detachment?

The retina is firmly attached to the apical surface of the retinal pigmented epithelium, or RPE (see earlier retinal anatomy sections). When the retina is separated from its normal position apposed to the RPE surface, it is said to be "detached." This detachment creates a pathological, fluid-filled space between the neural retina and the retinal pigmented epithelium. It also creates a greater distance between the photoreceptors and their sole blood supply, the choroidal circulation.

Clinical Retinal Detachments Occur as Different Types

There are three recognized types of retinal detachment in clinical practice:

1. Rhegmatogenous: the most common type. In this form, the retina experiences a physical tear through the retinal layers, and the torn retina peals away from the retinal pigmented epithelium by the movement of fluid into the space between the two.
2. Tractional: in which some force (usually contracting cells or vitreal "strands") acts on the surface of the retina to pull it away from the retinal pigmented epithelium.
3. Exudative: in which fluid accumulates between the neural retina and the retinal pigmented epithelium, pushing the two apart; the retinal tissue is not torn.

Retinal detachment can cause permanent visual loss or permanent reduction of visual function, especially if the macula is involved, in which case it is considered a medical emergency in the United States. For more information on the types and causes of retinal detachment, see the National Eye Institute's website.

Cellular Remodeling in the Retina

Many specific neural circuits have been identified in the retina (1-4), and only recently has evidence been found that these circuits change (remodel) in an adult mammal, usually in response to injury and disease. Before this, the retina was considered a "hard-wired" part of the central nervous system by most scientists. A change in circuitry may mean a change in vision, so understanding these changes and ways to prevent them or repair them is important.

Some Examples of Retinal Remodeling

The few earlier descriptions of cellular remodeling in vertebrate retina came from studies of fish retinas (5-7), where specific synaptic connections between photoreceptors and second-order neurons structurally changed with the daily lighting cycle. In 1984, Peichl and Bolz (8) described structural remodeling of retinal neurons in mammals in response to severe retinal degeneration induced by a neurotoxin, kainic acid. It was nearly a decade later that reports of cellular remodeling in mammalian retina in response to injury or disease began to appear with some regularity (9-12). Even total photoreceptor cell loss had not been regarded as causing significant changes to the inner retina until that time.

Photoreceptor Cell Death Differs Among Models

Many recent descriptions of structural remodeling in mammalian retina are from studies in humans or rodent species in which massive photoreceptor cell death is induced by light damage or genetic mutations (13). Retinal detachment provides information that complements those data because in most species there is not massive photoreceptor cell death after detachment. Another important distinction is that the earliest and most obvious damage induced by detachment, outer segment degeneration, is reversible by reattaching the retina. Retinal reattachment surgery probably induces its own remodeling of retinal circuits as recovery occurs, but this has been less explored at the present time.

Retinal Detachment and Reattachment as Experimental Systems

Fig. 1 illustrates cell types observed to remodel after detachment, these include: RPE, Muller cells, photoreceptors, rod bipolar cells, horizontal cells, ganglion cells, and astrocytes. It seems likely that remodeling will be identified in other cell types as well.

Outer segment degeneration, photoreceptor cell death, Muller cell hypertrophy, and changes in the RPE apical surface were all recognized as events induced by detachment in early studies (14-16). More recently, studies have demonstrated photoreceptor cell death occurs by apoptosis in both animals and humans. Currently, there is no method for replacing lost photoreceptors. Other events may be reversed by reattachment, often incompletely and usually slowly, over a time course that can vary from days to years.

Why Remodeling Is Difficult to Discover

The huge numbers of neurons and glial cells involved in the retina, the vast range of neuronal cell architectures, the small size of neuronal cell bodies relative to other cells, and the small size of the neuronal processes that intertwine to make up the plexiform layers of the retina make discovery of subtle changes in these cells difficult. Historically, it was the Golgi impregnation method that provided the breakthrough allowing for a detailed description of individual neurons and their morphologic diversity (17). A similar reliable method that would allow us to observe changes in the branching of individual neurons would be ideal for studying remodeling. Unfortunately, the Golgi method is unreliable and quixotic and, therefore, does not provide a method for the systematic study of events such a neuronal remodeling. What will undoubtedly emerge as technology evolves will be the invaluable tools for observing structural remodeling of retinal neurons in living tissue.

Making Use of New Technology to Describe Remodeling Events

Immunocytochemistry and other techniques that allow for the labeling of individual cells or populations of cells, coupled with advances in image technology such as laser scanning and confocal microscopy, have provided us with new and powerful tools for describing remodeling events in the retina in recent years.

Rod photoreceptor, rod bipolar, and horizontal cell remodeling (11) was the first to be studied in detail with this technology. In fact, results with antibody labeling confirmed speculation based on electron microscopy data published in 1983: "In addition to the effects of retinal detachment in the outer retina, we strongly suspect that the inner nuclear layer, IPL, ganglion cell layer and, perhaps, more central areas of the visual system may be affected as well" (15). Remodeling has now been firmly established in the inner retina and leads one to believe more strongly that central changes, for example ganglion cell axonal arborization and synaptic contacts, will be eventually identified as well. Technologies involving other forms of imaging, including the imaging of living cells in retinal wholemounts or tissue slices and techniques such as dye injection into single cells, will undoubtedly contribute greatly to this rapidly growing knowledge base.

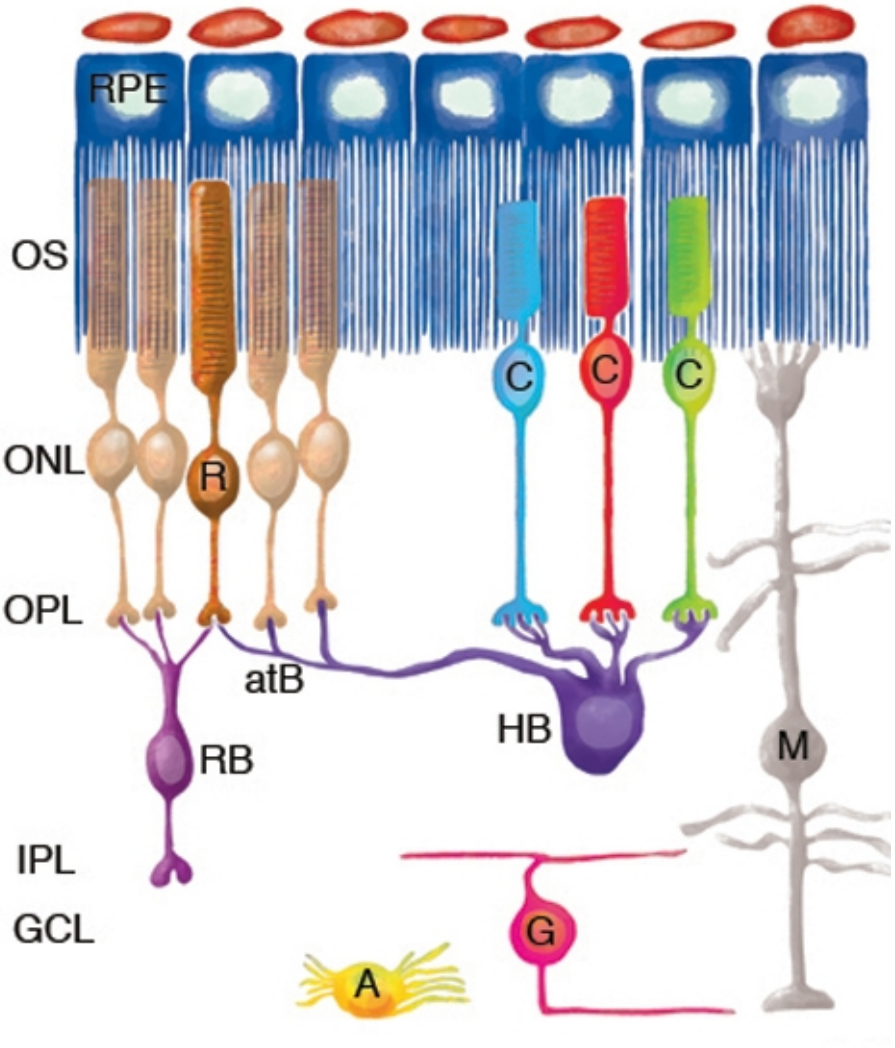

Figure 1. A drawing of the relevant retinal cell types discussed in this review. Blood vessels of the choriocapillaris lie adjacent to the retinal pigmented epithelium (RPE), opposite the retina. A, astrocytes; atB, axon terminal of B-type horizontal cell (HB); C, cone photoreceptors; GCL, ganglion cell layer; M, Muller cells; OS, photoreceptor outer segments; R, rod; RB, rod bipolar cells.

Levels of Remodeling

Remodeling can involve whole populations of cells; for instance, all RPE cells remodel their apical processes (Fig. 2, A-C, asterisk), and all photoreceptors undergo outer segment degeneration after detachment, or it can involve some subset of cells within a population. The apical surface of every RPE cell must remodel in response to both detachment and reattachment as the complex apical processes are transformed into microvilli after detachment and then regenerated after reattachment. Interestingly, the remodeling after reattachment does not appear to be consistent from cell to cell (Fig. 2, D and E). Thus, regeneration of the apical surface is not a perfect recapitulation of development. All Muller cells in the zone of detachment upregulate intermediate filament proteins, and all probably undergo some structural remodeling, but only some show extreme changes where they actually grow out of the retina, creeping into the subretinal space or onto the vitreal surface. Both of these conditions result in serious, sight-threatening, ophthalmic complications. Defining what stimulates this subpopulation to undergo such growth is medically important. Only a subpopulation of ganglion cells appears to

remodel in response to detachment (18), and identifying which types may lead to a better understanding of some of the visual disturbances that occur after successful reattachment surgery.

Retinal Deafferentation

Deafferentation in the central nervous system (CNS) refers to removing the sensory input from some motor pathway. Although there is no "motor" component to the retina's output to the brain, the massive loss of photoreceptors (usually approaching 100%) that occurs in some diseases such as retinitis pigmentosa (or in animal models of this disease) has been described as "deafferentation" (13). Remodeling in these systems and in such conditions as light damage in albino rats has been described as largely in response to this "deafferentation". The changes that we are focused on here are those that occur within hours or days of detachment, because it is these changes that may be successfully manipulated by therapeutic intervention and thus lead to better visual recovery. These are not responses to massive death of photoreceptors, although they may represent responses to the death of individual photoreceptors and therefore partial deafferentation of individual cells or neural circuits. Remodeling is also associated with the recovery phase after retinal reattachment, during a time when photoreceptor cell death does not occur.

Basic Information Relevant to Understanding the Responses to Retinal Detachment

Although the retina is a developmental outgrowth of the brain, it does have several features unique to its specialized functions. Photoreceptors have the highest metabolic rate of any cells in the body, and yet there are no blood vessels among them (their presence presumably would blur the visual image)—they are nourished almost solely by the capillaries of the choroid, which lie on the opposite side of the RPE (Fig. 1) (19). Traditional astrocytes are not scattered throughout the retina as they are in the brain and spinal cord but reside only among the ganglion cells and their axons. The retina has a large population of highly differentiated, polarized radial glia, or Muller cells, that may assume many of the functions of astrocytes in the brain and spinal cord but are, at the same time, distinct from them. Ganglion cell axons in most species are not myelinated until after they enter the optic nerve, and thus, the retina does not have a population of oligodendrocytes, the myelin-producing glial cells. The retina does have a resident population of microglial (scavenger) cells, but these appear to be restricted to the IPLs and outer plexiform layers (OPLs) in the healthy eye.

Animal Models of Detachment and Reattachment

The choice of which species to use has been driven by many issues including: 1) how closely the retina structurally resembles that of humans; 2) knowledge of retinal circuitry, physiology, or biochemistry in the species; 3) the reliability with which controlled detachments and reattachments can be created; and 4) the specific goals of the study.

Different Species React Differently: Finding the Best Model

Different species do react differently to detachment, and not all of these accurately reflect what little we know about the reaction of the human retina. The rabbit retina (with about the same rod/cone ratio as the feline retina) exhibits very rapid and complete degeneration of much of the neural retina (20, 21); thus, it is not a good model for longer-term events. The ground squirrel has a retina dominated by cones (22, 23) and thus is a potential model for the reactivity of the human macula (except that ground squirrel cones do not structurally resemble macular cones). The ground squirrel retina, however, shows a rapid and eventually complete degeneration of the photoreceptor layer but almost no RPE or glial reactivity or neuronal remodeling (24, 25). Unlike the rabbit, it does not show inner retinal degeneration. We have used all of these in various studies, but the species that seems to most closely model what is known about events in human detachments is the common

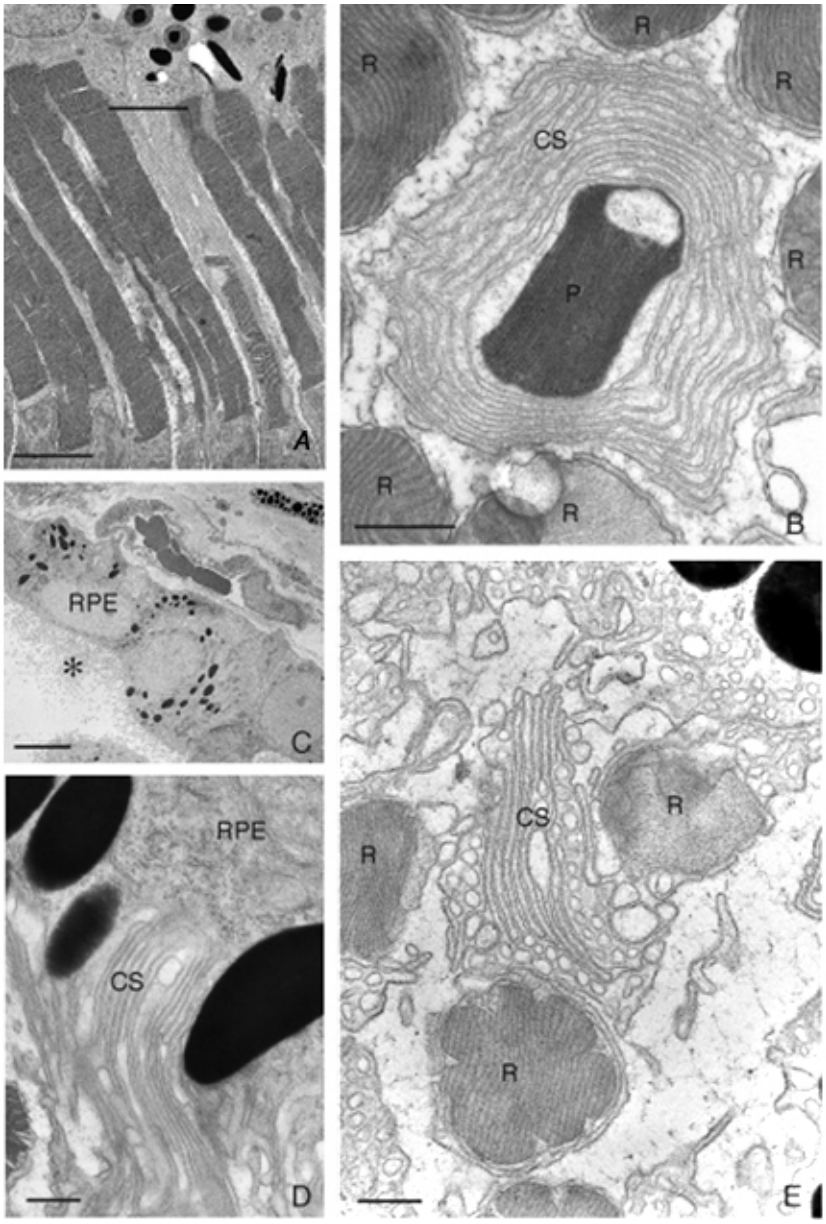

Figure 2. Electron microscopy. A, normal feline retina. Rod outer segments (ROS, R) terminate close to the retinal pigmented epithelium (RPE). Cone outer segments (COS) are shorter and surrounded by an elaborate cone sheath arising from specialized apical processes. From Fisher and Anderson (123). B, a cone sheath (CS) in cross-section (at the location of the line in part A). P, a phagosome shed from the cone. C, the apical surface of the RPE after detachment consists of a fringe of microvilli (*). D and E, the retina detached for 3 days and reattached for 28 days. CS are always structurally different from those in normal retina. (compare to parts A and B). Scale bars: A and C, 2 μm; B, D, and E, 0.5 μm.

domestic cat. The retina of many primate species are foveated, but their use is often prohibitive for a variety of ethical and financial reasons.

Developing New Model Systems

Because of the availability of genetic information and the ability to readily do genetic manipulations, developing a reliable method for producing large, controlled detachments in the mouse eye has become a high priority in recent years (e.g., Nour et al. (26) and Yang et al. (27)). Current data from that model show many of the same reactions found in the feline model, although there may be less Muller cell reactivity. The height of a detachment, that is, the distance separating the detached neural retina from the RPE, is probably an important parameter in

human detachments, and high detachments are harder to produce in mice because of the small size of the eye and the fact that the lens fills much of the vitreous cavity. Reattachments using the same procedures as in humans can be done in larger species; whether they will be possible in a mouse eye remains to be seen. Simply allowing the retina to settle instead of actively reattaching it provides one method, but with less precise control over the time of reattachment. Another promising area is the use of cold-blooded animals (e.g., frogs, fish, and salamanders) in similar experiments because their retinas are relatively easy to maintain in culture, and because many of them have very large photoreceptor cells that are amenable for high-resolution imaging and other types of single-cell analyses. Currently, most work is, however, being done with mammalian species.

The Feline Model

The feline retina, similar to the peripheral human retina, is rod dominated. It is a species with a robust intraretinal circulation (as in all species, it is excluded from the photoreceptors). The cat retina has also been the subject of decades worth of anatomical and physiological studies. The feline eye is large, allowing for easy surgical access, and for the production of defined detachments and simple reattachments using the same procedures as in human patients.

Detachments are created by slowly infusing fluid into the interface between the RPE and neural retina through a tapered glass pipette with a tip diameter of about 100 µm (28). It has been argued (29) that this does not model a rhegmatogenous detachment because there is no large tear (referred to as a "retinal break") through the retinal tissue. However, our observations of tissue from human rhegmatogenous detachments and reattachments tend to validate the feline model as producing the same cellular responses (30).

The Details of Cellular Remodeling after Detachment and Reattachment

Fig. 1 shows the cell types that have been identified to date as undergoing remodeling after detachment and reattachment. We have only preliminary evidence for the structural remodeling of amacrine cells, although this has been described in late-stage human retinitis pigmentosa (10). Little is known about changes in retinal astrocytes except that they proliferate after detachment. Retinal microglia respond robustly to detachment by assuming macrophage-like characteristics (31, 32). They will not be discussed here, although they undoubtedly play an important role in the overall "injury response" of the retinal tissue.

Retinal Pigmented Epithelium

The morphology of the RPE changes stereotypically after detachment in all species studied. In species such as cat, dog, rabbit, and human, there are vast differences between the apical processes that interact with rods and cones (33-36), with the "cone sheath" forming a unique structure consisting of a highly complex, multi-layered array of sheets of apical processes (Fig. 2, A, and B). Regardless of their structure in the normal eye, these apical processes all disappear after detachment and are replaced very quickly, probably within hours, by a fringe of simple microvillus-like processes (37) (Fig. 2, C, asterisk). The RPE has the remarkable ability to re-form these elaborate apical processes after reattachment. In the case of the feline retina, this also means regenerating the highly complex cone sheaths. However, a month after reattachment, these cone sheaths still do not appear "normal". The presence of slightly truncated, often thickened or misaligned, cone sheaths is almost always a clear indicator that the retina was detached at some earlier time (compare the structures labeled "CS" in Fig. 2, A, B, D, and E). The fact that the cone sheaths re-differentiate only in association with cone outer segments indicates some form of signaling mechanism retained in the adult retina that allows for the RPE to know when its apical surface is opposite a cone.

The RPE proliferates in response to detachment, and this can result in a complete remodeling of the geometry of this layer. Newly proliferated RPE cells can migrate into the subretinal space, where they assume complex

geometric arrangements: single cells, long strands, or multiple layers with reversed apical-basal polarity (38). If the basal surface faces the neural retina, photoreceptor outer segment regeneration does not occur after reattachment (39). It is not known if photoreceptor function is compromised when outer segments regenerate in the presence of multiple layers of RPE.

Photoreceptor Deconstruction, Outer Segment Degeneration, and Cell Death

In the feline model, and probably in the human retina, detachment sends all of the photoreceptors, both rods and cones, within the zone of detachment, along a pathway of structural changes that we have termed "deconstruction" (40). The outer and inner segment response appears to be the same in rods and cones, but the synaptic terminal responses differ. In both feline and human retinas, it is clear that many cells survive detachment for very long periods of time. Deconstructive changes may occur as a mechanism to assure the cells' survival under adverse environmental conditions, i.e., a means of saving metabolic energy. It is not clear why in some species (ground squirrel, rabbit) detachment leads to deconstruction and cell death of virtually all photoreceptors, whereas in other species, the majority survive for long periods of time.

After detachment, outer segment material is lost until only a few disks remain, along with the connecting cilium (14). The complex mechanism of disc morphogenesis is not lost in these cells (41) because once reattached, they retain their ability to reconstruct an outer segment even though that reconstruction may not be perfect. Remaining rod photoreceptor outer segments, even if composed of only a few discs (Fig. 3, A-C) are still positive for their respective opsins (Fig. 3 and Fig. 4) (42, 43) as well as other proteins.

Death by Apoptosis

Most photoreceptor cell death after detachment is by apoptosis (programmed cell death). On the basis of our results in the feline retina, there is an early period, around the first 3 days after detachment, when about 20% of the photoreceptors die by apoptosis (44, 45), but retinas detached for 450 days can retain at least 50% of their photoreceptors (15). Observations of human detachments also show that apoptosis is a part of their response to detachment, but as in the feline model, large portions of the photoreceptor population also survive (46). There is no information about the survivability of foveal photoreceptors after detachment. Cell death in the inner retina in response to detachment is very rarely observed in the feline model; although sporadic cell death may be important, it is also difficult to document.

Internal Reorganization of Photoreceptor Inner Segments

After detachment, electron microscopy as well as immunocytochemical labeling for mitochondrial components shows a decrease in the number of mitochondria in the inner segments as well as a much less distinctive compartmentalization of all organelles (14, 15, 40). Maintaining the highly compartmentalized and polarized structure of a photoreceptor must be metabolically costly. Having the cells assume a much simpler organization may assure their survival under environmentally challenging conditions. In the case of detachment, that challenge would include hypoxia and probably hypoglycemia that is created by physically moving the retina away from its choroidal blood supply (19, 28, 40). This hypothesis is supported by studies in which providing increased environmental oxygen lessens photoreceptor deconstruction and cell death after detachment (25, 28, 47).

A Comparison of Rod and Cone Responses

The outer and inner segment of rods and cones undergo similar structural changes, but a prominent response of rods is the withdrawal of their axons (Fig. 5, A and B) and a reconfiguration of the single synaptic invagination with its 3-5 postsynaptic processes (48, 49). This response is not observed in cones.

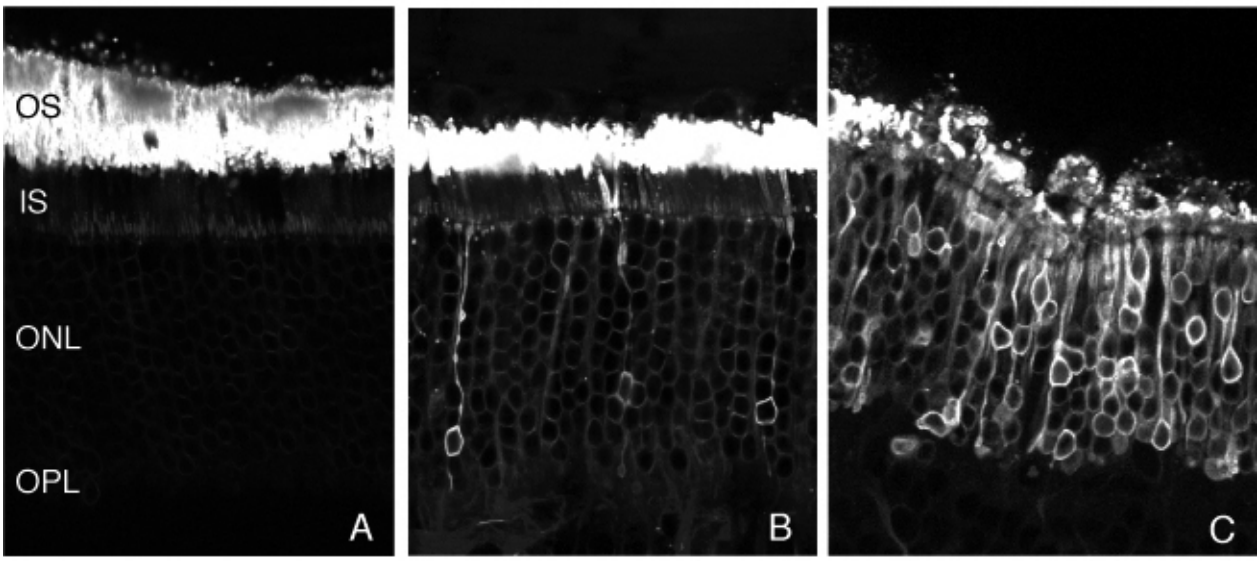

Figure 3. Normal and detached retina labeled with an antibody to rod opsin. A, normal retina. Rod outer segments (OS) are labeled. B, retina detached for 3 days. The OS layer narrows as rod OS degenerate, and the antibody now labels the plasma membrane of rod cells in the ONL. C, retina detached for 28 days. Remaining fragments of rod OS contain rhodopsin.

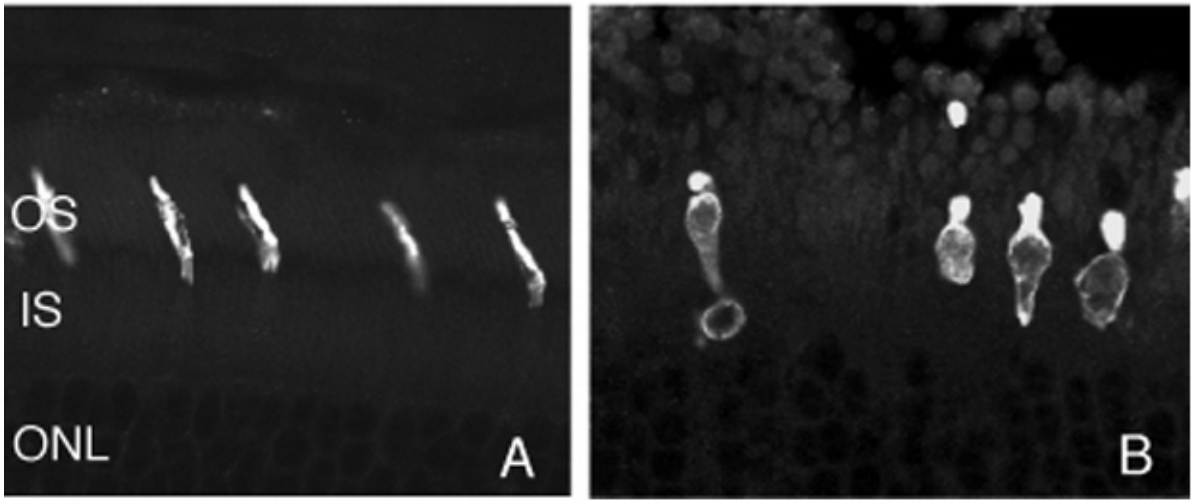

Figure 4. Normal and detached retina labeled with an antibody to medium (M)- and long (L)-wavelength-sensitive cone opsins. A, in normal retina all M-COS are labeled. B, retina detached for 3 days. The M-COS are degenerating, and the antibody labels the plasma membrane of cones in the ONL. After 3-7 days of detachment, there is down-regulation of protein synthesis by these cells and no labeling.

This disruption can be appreciated by immunocytochemical labeling with antibodies to presynaptic vesicle proteins, such as synaptophysin (Fig. 5) or VAMP (synaptobrevin). After detachment, labeled terminals appear near the rod nuclei scattered throughout the outer nuclear layer (ONL) (Fig. 5B). Terminal withdrawal and reorganization begins within a day. The electron micrograph in Fig. 6 shows the highly compact organization of the rod terminals in the OPL in a normal feline retina. After detachment, the deep synaptic invagination in each becomes more shallow (Fig. 7, A and B, arrows) and is eventually lost altogether (Fig. 7, C and D). There are still membrane specializations associated with the "postsynaptic" processes adjacent to the base of the retracted terminals (Fig. 7, B-D). Those terminals that do not retract may also change with a "looser" organization of postsynaptic processes (Fig. 7B).

Withdrawn rod terminals show a sparse population of synaptic vesicles and synaptic ribbons that vary more in size, configuration, and location than expected. Although there are one or two long, arc-shaped synaptic ribbons in normal feline rod spherules (48, 50), the presence of 1-3 shortened ribbons is common in the retracted terminals (Fig. 7, A, C, and D, arrowheads).

Cone pedicles do not withdraw from the OPL. However, the pedicle itself undergoes unpredictable changes in shape. The axons of some become tortuous instead of streaming straight across the ONL from their cell body (Fig. 8, A-C). In all cases, however, these terminals appear to lose the 9-14 synaptic invaginations (48) (Fig. 9, A and B), giving their base a flattened appearance (Fig. 8C) (also see Erickson et al. (15)).

Presynaptic Ribbons Change in Both Rods and Cones

Presynaptic ribbons appear to grow shorter, and some may disappear (Fig. 9, A and B). This ribbon response is dramatic when observed by immunocytochemical labeling using antibodies specific to them (51). Ribbons in rod terminals appear as "clumps" (compare the red synaptic ribbons in Fig. 10, B and C, to those in Fig. 10, D). Within the cone pedicles, the characteristic array of ribbons (Fig. 10, C, arrowheads) is no longer detected in the OPL (Fig. 10D). By electron microscopy, very short ribbons remain within the affected cone terminals, and some post-synaptic processes are still recognizable (Fig. 9).

Following the remodeling of rod terminals has been made relatively simple because of their outlining by displaced rhodopsin. Documenting longer-term changes in cone synapses is complicated by the fact that the expression of proteins in the cones rapidly decreases to levels that are below detection (52, 53), making them difficult to visualize by immunocytochemistry. (Fig. 8, A-D). In Fig. 11, there are long expanses of the retina in which only the rod outer segments (green) are labeled by the anti-PDEg, and there are no labeled cones.

The Population of Cones Is Heterogeneous

The lectin, peanut agglutinin (PNA), labels the extracellular matrix domain (matrix sheath) around cone photoreceptors (54) and can be used to define the total population of cone cells. Fig. 12A is a density map of PNA-labeled cone sheaths in the superior temporal quadrant of a control (normal) feline retina (also see Steinberg et al. (55)).

There are specific antibodies that recognize the different spectral classes of cone photoreceptors (56-58). The feline retina contains mid-wavelength-sensitive (M) and short-wavelength-sensitive (S) cones, and the latter are not distributed evenly over the retinal topography (Fig. 3A). Whereas the total number of cones peaks in the area centralis, the density of S-cones is highest in the inferior retina, but even there, they compose only about 20% of the cone population (52).

The expression of opsin genes reliably defines distinct subpopulations of photoreceptors. The expression of other proteins by these cells is less consistent. An antibody to the calcium binding protein calbindin D labels entire cone cells in many species, including humans and felines. The density of calbindin D-positive cells matches very closely the density of PNA-labeled cone matrix sheathes in the peripheral retina, but there is significant disparity in the area centralis, where the antibody fails to label a majority of cones (Fig. 14A). This phenomenon also occurs in monkey and human retinas, where foveal cones do not label with anti-calbindin D (59-61).

Protein Expression in Cone Photoreceptors after Detachment: Analyzing the Surviving Cone Photoreceptor Array

What follows is a fairly detailed description of changes in the cone population after detachment and reattachment as summarized in Fig. 12 and Fig. 13. For those who want to skip the details: cones appear to be lost from the retina after detachment because they: 1) lose their outer segments; and 2) lose the expression of specific proteins. Using the return of cone proteins as an indicator of cone recovery after reattachment shows

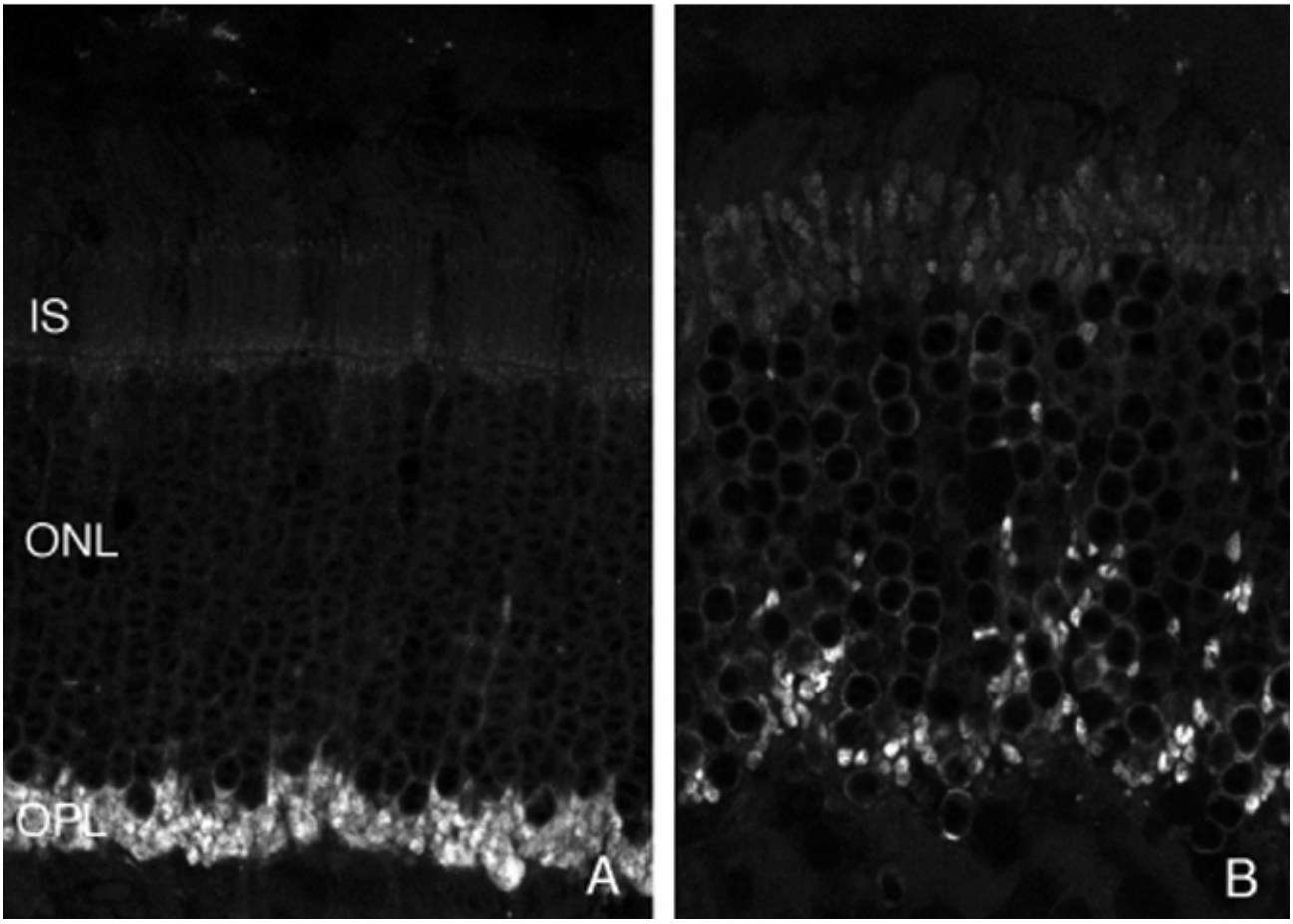

Figure 5. A, normal retina labeled with an antibody to the presynaptic protein, synaptophysin. Labeling is specific to the layer of photoreceptor synaptic terminals in the OPL. B, retina detached for 3 days. The compact OPL is disrupted, and RS retract into the ONL.

that at 28 days after reattachment, the cone mosaic is not the same as in normal retinas. Both types of cones recover, although the recovery of the S-cones may not be as complete as that of the M-cones. The retinal cone mosaic is disturbed by detachment, and inconsistencies in its recovery may account for visual defects after reattachment, especially if the fovea is involved. There is nothing known about the recovery of the cone mosaics within the fovea.

As rod outer segments degenerate, rod opsin labeling begins to increase in the plasma membrane of the cells until the whole cell is outlined (see Fig. 3) (24, 42, 43, 53). Thus, antibodies to rod opsin can be used as markers for the presence of rod cells (and the redistribution of labeling is also a remarkable indicator of stress or injury to them). Although antibodies to the cone opsins begin to show a similar redistribution (Fig. 4) after only 24 h of detachment, many cones fail to label with these antibodies (53). A similar phenomenon occurs in retinas of humans with late-stage genetic degeneration (62).

Thus, markers for cones in the normal retina are not reliable for estimating the cone population that survive detachment (52). Indeed, if the lack of labeled cones after detachment was an accurate reflection of cone survival, then the effects of detachment on the cone population would be devastating (52). Further confounding the use of markers for cones is the fact that the response is not consistent from marker to marker, nor even from one retinal region to another.

In the central region of a control retina, anti-calbindin D labels about 19,700 photoreceptors/mm^2, and the antibody to S-cone opsin about 1,100/mm^2. After 24 h of detachment, these numbers drop to 9,000/mm^2 (46%

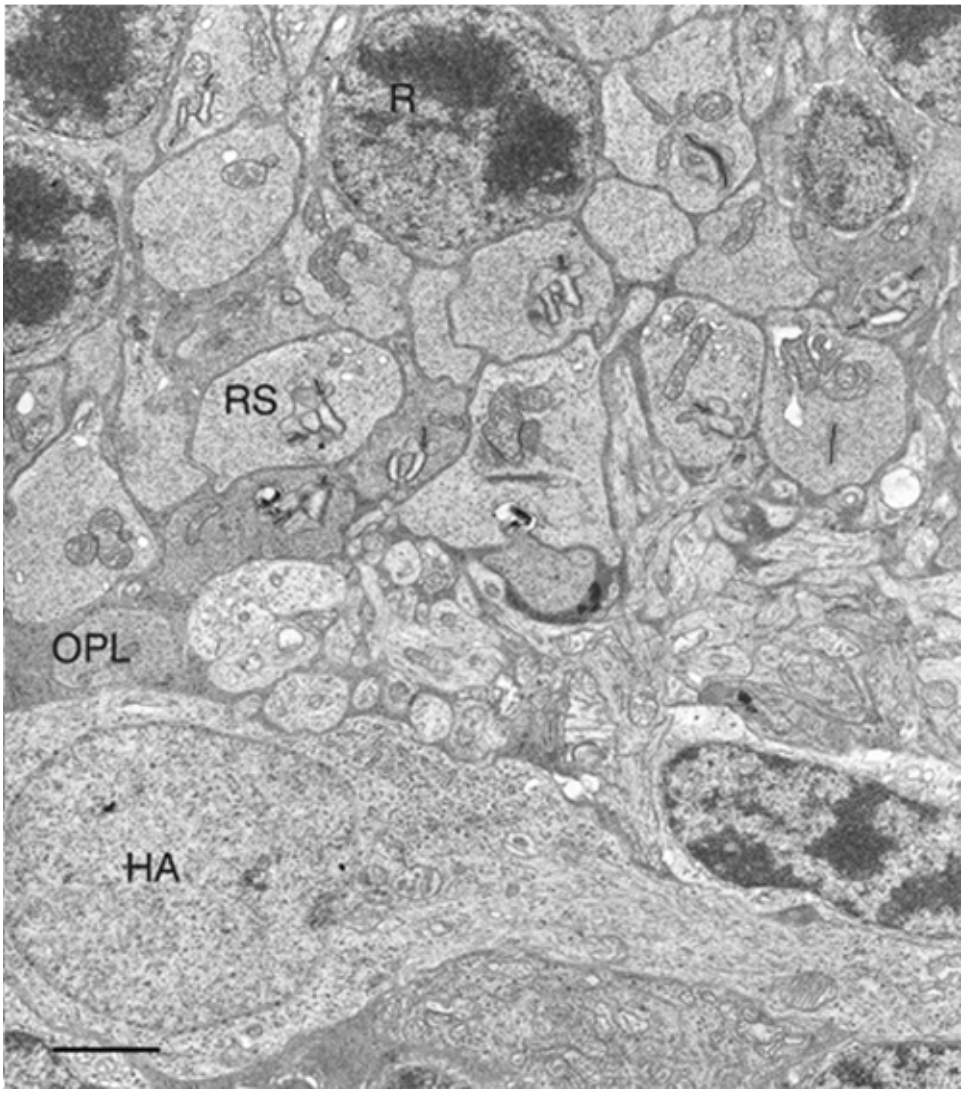

Figure 6. The OPL of normal feline retina. RS lie just distal to the OPL. R, rod nuclei in the ONL. Scale bar, 2 μm.

of control values) and 700/mm^2 (63% of control values), respectively. By 28 days of detachment, there were no cells labeled with the anti-calbindin D, but 200/mm^2 (18% of control values) labeled with the anti-S-opsin (52) (Fig. 13, B, and Fig. 14, B-D). In detached retinas, there are large areas in which no labeling appears at all with the cone markers (see the example for PDEg in Fig. 10 and Fig. 11), as if all of the cones in the region were gone. These dramatic changes are reflected in the density maps for both S-opsin and anti-calbindin D labeling (Fig. 13 and Fig. 14). In the latter, the central area is nearly unrecognizable by 1 day of detachment and completely undefined after 3 days. Similarly, the number of S-cones drops from between 700 and1,100/mm^2 in the control retina to less than 300 in a 3-day detachment. Because of the relatively large bins used to create these maps, they do not show the substantial islands in which there were no labeled cones. The wide variations in numbers of labeled cones gives the retinal wholemounts a "patchiness" that is not observed in control retinas, where the transitions in cone density are smoothly graded.

We approached the question of cone survival in another way: by examining the recovery of cone markers after reattachment (63). We chose 3 days of detachment because there is already a significant drop in the cone population labeled with peanut agglutinin (PNA), anti-cone-opsin, or anti-calbindin D at that time. The superior retina in the right eye of three animals was detached for 3 days and then reattached for 28. The retinas were harvested and labeled with PNA (Fig. 12, PNA = all cones, only the superior temporal quadrant is illustrated)

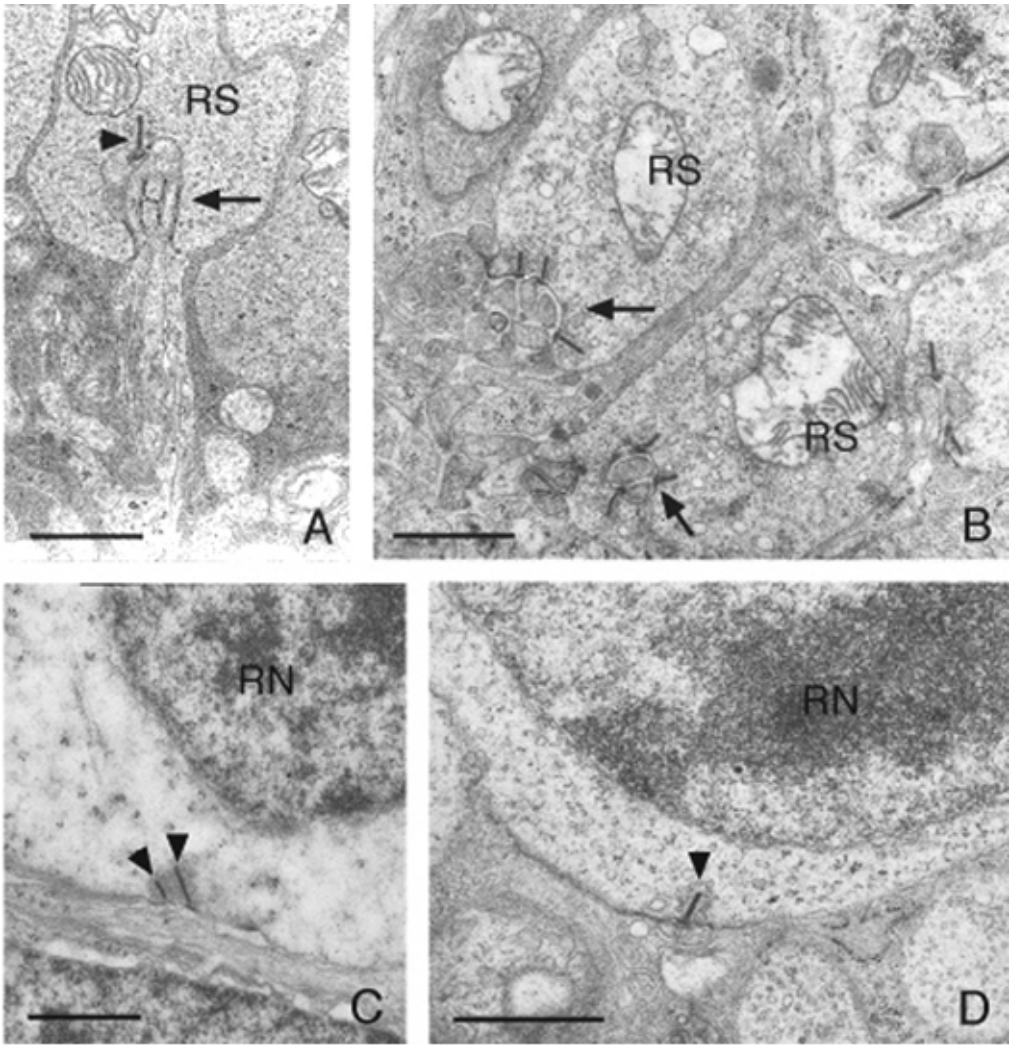

Figure 7. A, normal retina. Organized postsynaptic processes enter the synaptic invagination (arrow) of the RS. Arrowhead, presynaptic ribbon in a RS. B, in a detached retina, the synaptic invaginations (arrows) are flatter, and post-synaptic processes are less organized. Note the three synaptic ribbons at each invagination. C and D, two examples of retracted RS lying in the mid ONL. Short synaptic ribbons (arrowheads) are adjacent to sites without deep synaptic invaginations. RN, rod nucleus. Scale bar, 1 μm.

and the antibody to S-opsin (Fig. 13). Comparisons can be made to the maps for total cones (calbindin D labeling, control and 3 days, Fig. 14, A and C; PNA labeling, control retina, Fig. 12, A) and S-cones (S-cone opsin labeling, control and 3 days, Fig. 13, A and B). There is a recovery of both the PNA and S-cone population after reattachment; indeed, a central-to-peripheral gradient is apparent in the PNA labeling pattern, although the density remains depressed. None of the animals recovered densities greater than 17,000-20,000 cones/mm^2 (Fig. 12, B-D). Similarly, the S-cone population recovers, but recovery is not complete (Fig. 13, C-E). The high density area of S-cones in the far periphery of the superior-temporal quadrant is not recovered at 28 days of reattachment, and in all three animals, recovery in the central retina was in the range of 300-700 cells/mm^2, compared with the 700-1,100 cells/mm^2 observed in the control retina (the detachment did not extend into the yellow/red colored area in the central area of Fig. 13, E).

Because these numbers are generated as counts from small sampling areas and the contour lines on the maps drawn by eye, it is difficult to choose an average value for cone density within the reattached retina, but using estimates of cone density sampled over a fairly broad region, results from two animals with reattachments show a recovery of 40-60% of PNA labeling in the area centralis and approaching 100% recovery in the periphery.

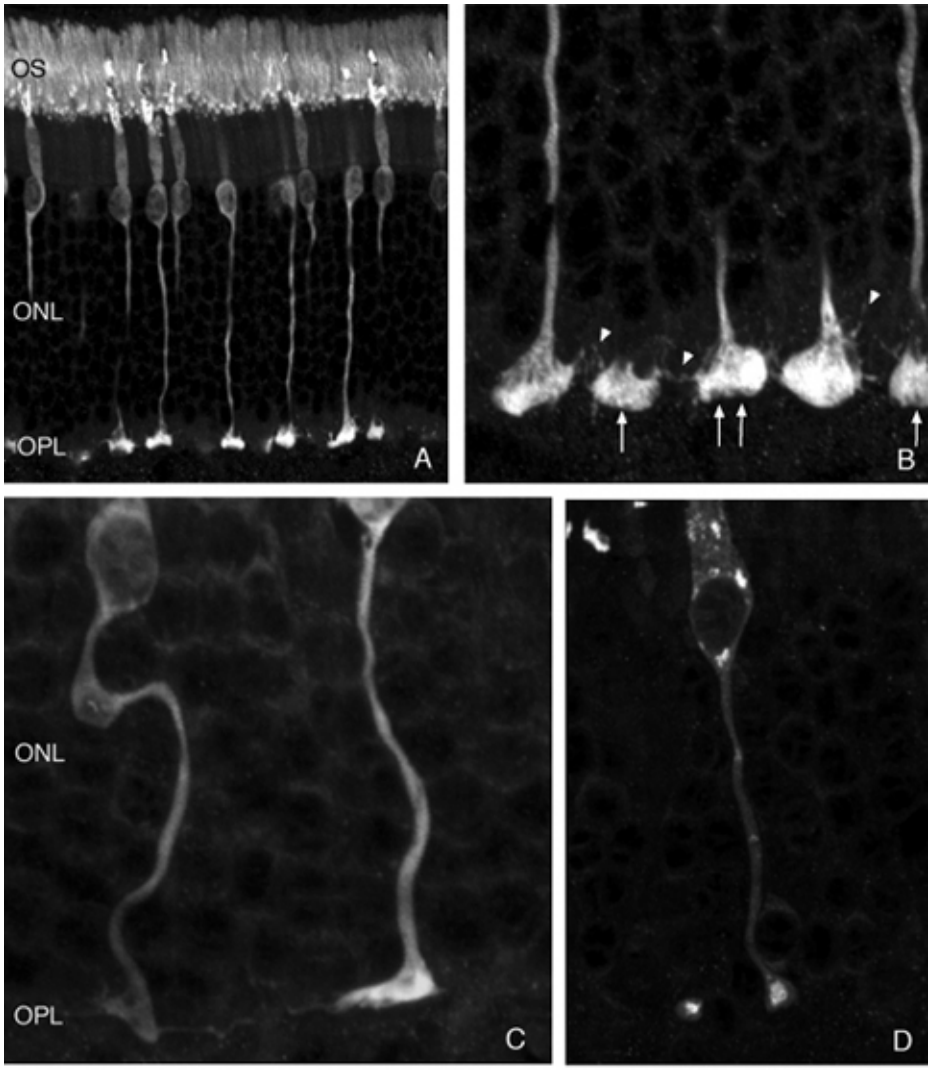

Figure 8. Expression of the g subunit of the photoreceptor-specific phosphodiesterase (PDAg). A, normal retina. The antibody labels both rod and cone outer segments (OS), and cones in their entirety. B, CP labeling in normal retina. Arrowheads, fine telodendria. Multiple synaptic invaginations in single CP are indicated by the arrows. C and D, retina detached for 7 days. Labeled cones are difficult to find and often assume tortuous paths across the ONL.

S-cone recovery seems more variable, ranging between 0 and 40% with no pattern readily discernable across the retina. Whereas PNA-labeled cone matrix sheaths were remarkably evenly distributed across the retina and showed a central to peripheral decline, S-opsin labeling showed large swatches within the reattached retinal map with no visible labeling. These data demonstrate quantitatively that the absence of marker molecules in the detached retinas does not indicate the absence of cone photoreceptors, because cells recovered across the entire retina, in some cases to numbers comparable with those in the control eyes. It is unknown, of course, if there would be more recovery of these proteins over a longer reattachment time.

Structurally, the S-cone outer segments in the 28-day reattached retina are not equivalent to those in the normal eye. They are often only punctate "dots," a fraction of their normal size. The S-cone population has been reported to be more sensitive to damage in human retinas with detachments (64) with all S-cones either lost or showing signs of "irreversible damage" within a few days of detachment. Our data from feline retinas may support the concept that S-cones are more fragile, more susceptible to cell death, and slower to recover than the M-cones; however, it does not support the conclusion that all of the S-cones are irreversibly damaged.

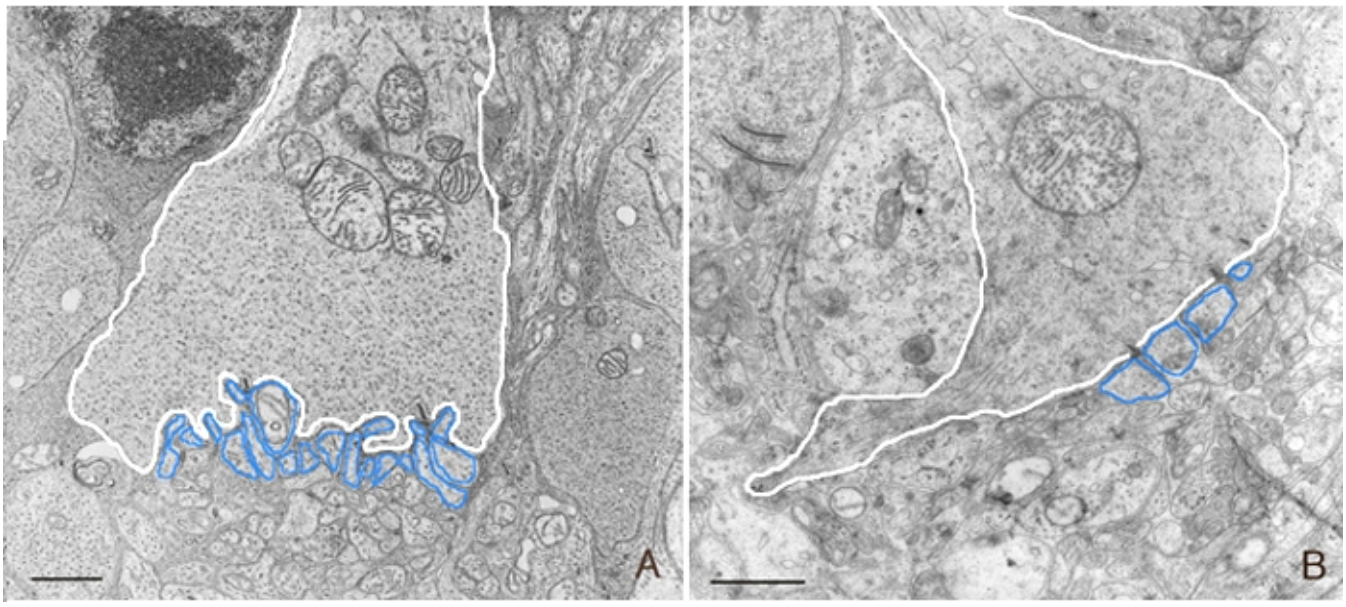

Figure 9. Cone synapses. Electron micrographs of CP (outlined white) in normal (A) and detached (B) retina. Post-synaptic processes outlined with blue. Notice lack of deep invaginations and reduced number of post-synaptic processes after detachment. The population of synaptic vesicles and ribbons appears reduced in CP of the detached retina. Also see Fig. 10. Scale bar, 1 μm.

Combined electrophysiological (ERG) and immunocytochemical studies in the cone-dominant ground squirrel retina did not show any particular difference in recovery of signals from S- and M/L-cones in that species (65).

What may be the most remarkable conclusion from this and other studies is that cones appear to stop expressing specific proteins when the cells are under some type of physiological stress, and then, at least in the case of reattachment, to begin re-expressing these proteins as part of a recovery process. In their studies of human retinal tissue, Nork et al. (64) reported that carbonic anhydrase reactivity became an unreliable marker for M-cones after detachment, indicating that it may join the list of severely down-regulated proteins, and its loss may not be an indicator of irreversible damage.

Whether foveal cones show similar responses is an unanswered question. Peripheral cones are structurally different from foveal cones in the primate retina (33, 66), so their reaction to injury and their capacity for recovery may differ as well.

A differential loss of M/L- and S-cones, or a differential recovery of these cells in humans, may explain some of the color vision deficiencies reported in reattachment patients and could underlie losses in visual acuity when the fovea is involved.

Remodeling of Photoreceptors after Reattachment

The fact that photoreceptor outer segments regrow after reattachment has been recognized since 1968 (67-69). This remarkable ability is mechanistically explained by the fact that photoreceptors constantly add new outer segment material as part of the outer segment renewal process (70). Thus, they are poised to rebuild their outer segment as soon as favorable conditions allow.

Studies of detached retina in fact show that radiolabeled proteins continue to be transported into the truncated outer segments of rods that degenerate after detachment (43), although studies of rod-opsin, peripherin/rds (42) and ROM-1 (G.P. Lewis and S.K. Fisher, unpublished observations) distribution suggest that protein targeting and trafficking is altered when the outer segment degenerates in the rod cells.

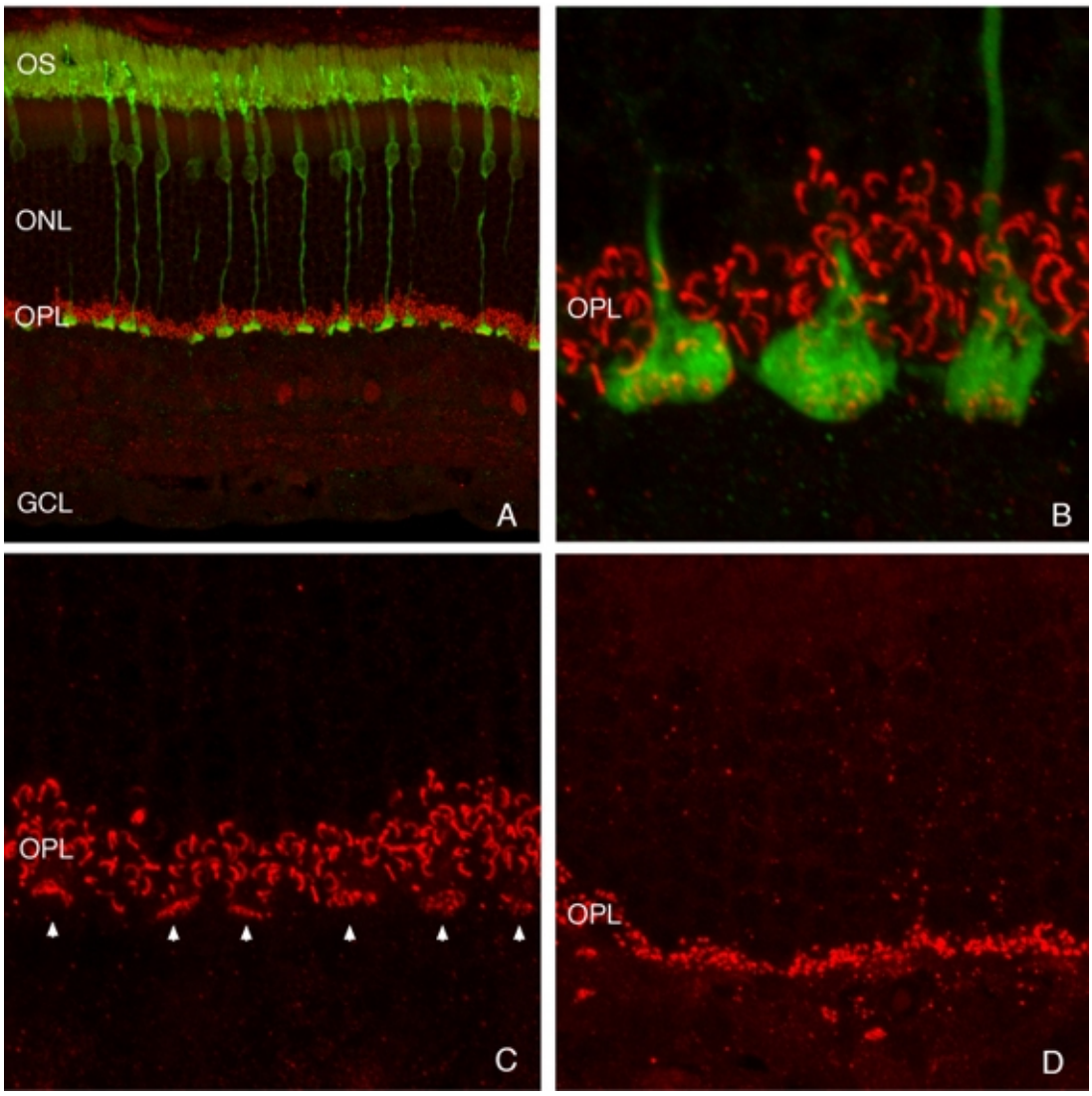

Figure 10. Labeling with anti-PDEg (green; see Fig. 8) and with anti-CtBP2 (red), which labels synaptic ribbons. A, normal retina. The antibody to CtBP2 labels synaptic ribbons in rod and cone synaptic endings (green). B, normal retina. CP contain many ribbons (their yellow color coming from the superposition of the green and red labeling). Note the arcuate shape of the individual rod ribbons. C, normal retina. Organized arrays of ribbons in individual CP (arrowheads). D, retina detached for 3 days, CtBP2 labeling. Note lack of organized arrays of cone ribbons and the smaller "clumped" appearance of ribbons in RS. Labeling in the ONL represents ribbons within retracted RS.

There is some evidence from experimental data that the presence of opsin in the plasma membrane may make photoreceptors more vulnerable to apoptotic cell death (71).

The recovering rods appear structurally more like those in a normal retina than do cones, which are often distorted in shape. Recovering primate cones also show altered outer segment structure when observed by electron microscopy (72). It is now recognized that vision may continue to recover over years in reattachment patients (73, 74), and this may reflect a slow recovery of cone outer segments in the fovea. The recovery of cone vision may be further complicated by the complex optical nature of cones and their alignment with respect to the pupil (see the discussion in Rodieck (75) and also the Stiles-Crawford effect (76)) (reviewed by Enoch (77) and Rodieck (75)), and their structurally specialized interface with the apical RPE.

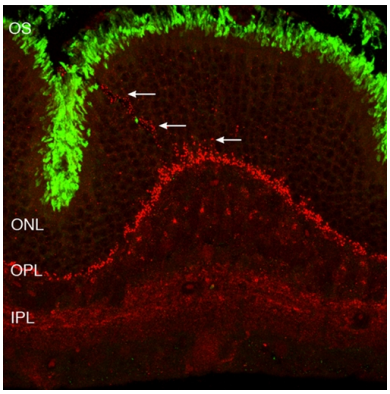

Figure 11. A 7-day detached retina. Demonstrates the prominent reduction in labeling with cone-specific antibodies after detachment. Labeled with the anti-PDEg (green) and CtBP2 (red). Rod outer segments (OS) still label with the antibody to PDEg, but there is a complete lack of cone labeling proximal to the outer segment layer (compare to Fig. 10A). Also notice the large amount of CtBP2 labeling found in the ONL arising from ribbons in retracted RS (arrows).

The Recovery of Photoreceptor Synaptic Terminals

The opposite pole of rod cells must also recover. Some recovery of the withdrawn rod terminals occurs because after 1 month of reattachment, the outer border of the OPL is again composed of a relatively compact layer of rod synaptic terminals. This is in contrast to the highly disrupted layer occurring in the detached retina (Fig. 5, compare B to A). There have been no detailed structural, molecular, or physiological analyses of these regenerated synapses.

Some Rod Axons Overgrow

Because some rods continue to express opsin in their plasma membrane after reattachment, we were able to identify rod axons that extend well beyond the OPL and into the inner retina, terminating at different levels in the INL and IPL (Fig. 15, B-D, arrowheads). The endings of these "overgrown" axons also label with antibodies to the proteins associated generally with synaptic vesicles, synaptophysin and VAMP (not shown), but they do not express the ribbon-specific protein, ribeye.

A population of rods also "overshoot" their synaptic target layer during early retinal development, providing much the same picture as we observed in the reattached retina (78), in human retinas with advanced inherited retinal degeneration (10), and in those with a history of complex detachments and reattachments (30). It is curious that they do not seem to occur in the detached feline retinas, only appearing after reattachment. The ectopic terminals have fine filopodia-like extensions (Fig. 15, C and D, arrowheads). Whether the overgrown axons remain in place or are eventually retracted, or even if the cells bearing them eventually die, is unknown for both development and reattachment.

Remodeling of Cone Terminals after Reattachment

To date, there is little data on the "redifferentiation" or remodeling of the extraordinarily complex synapses of the cone terminals after reattachment. Cone pedicles with synaptic invaginations do reappear in retinas detached for 3 days and reattached for 28. In general, the redifferentiation of photoreceptor synapses, along with profiles for the expression of specific pre- and postsynaptic molecules after reattachment, is unexplored territory, but one that seems critical to fully understanding the events related to visual recovery.

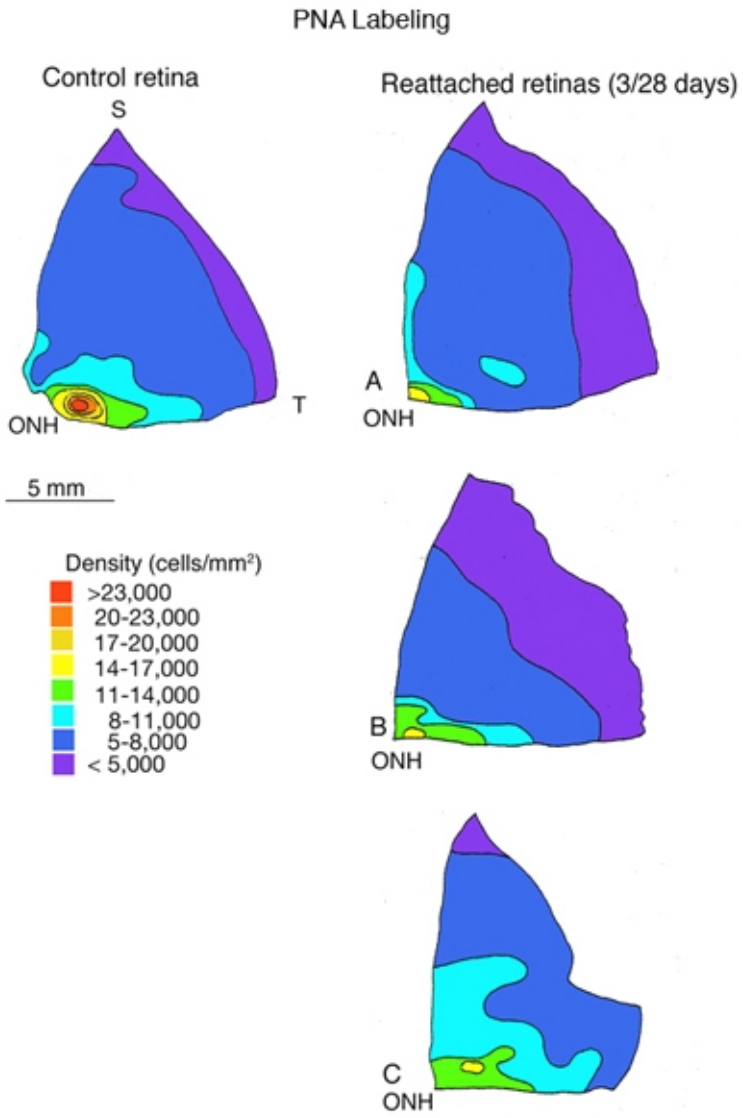

Figure 12. The lectin peanut agglutinin (PNA) binds to extracellular matrix around the cone outer segments (COS; cone matrix sheath) as seen in wholemount retinas. The wholemounts were photographed, and the number of labeled cone sheaths were counted and expressed as isodensity contours. A retinal detachment was created that covered most of the superior (S)-temporal (T) quadrant, and the retina was reattached 3 days later. Reattached tissue was harvested 28 days later. In general, the central to peripheral gradient of cone density is restored in the reattached retina; however, the area of highest cone density, or area centralis, (the red/orange area in the control retina) has not recovered at 28 days and in the 3 experimental eyes (A, B, and C). The density of cone sheaths in the central retina was only about 50% of that in normal retina. ONH, optic nerve head.

Remodeling of Second- and Third-Order Neurons

Rod Bipolar Cells

Rod bipolar cells innervate the rod spherules. Each rod spherule is usually presynaptic to two different rod bipolar cells, and each rod bipolar cell contacts between 16 and 20 rod spherules (79). The rod bipolar dendrites penetrate deeply into the invagination of the rod spherule to terminate opposite one of the two (on average) synaptic ribbons (Fig. 6 and Fig. 7A) (48).

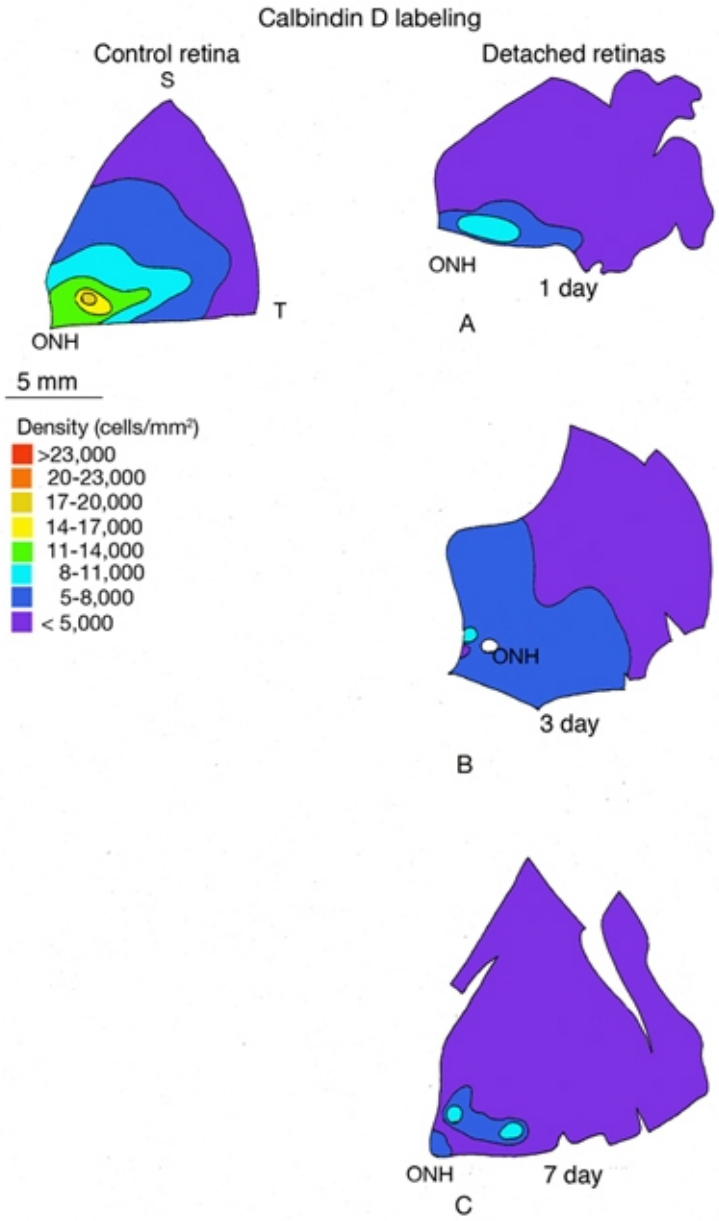

Figure 14. Isodensity contours for cones labeled with an antibody to the calcium binding protein calbindin D in normal (left) and detached (right) feline retinas. In the periphery, this antibody binds to all cone outer segments except in the area centralis, where cones fail to label (see difference between the density of cones in central retina here and in Fig. 12). After detachment (A, B, and C), there is a rapid drop in the number of labeled cones, and there is no central to peripheral gradient.

The general relationship between rod bipolar cells and rod spherules can be observed by confocal imaging using antibodies (80, 81) to label each cell type (Fig. 16A). In the normal feline retina, the compact layer of rod spherules stands out (Fig. 5A and Fig. 16A, green). Rod bipolar dendrites do not extend beyond them into the ONL.

Rod Bipolar Dendrites Remodel as Rod Terminals Withdraw

As the layer of rod terminals becomes disrupted after detachment, there is an emergence of fine, tapered dendritic processes that reach from the rod bipolar cells into the ONL, usually ending adjacent to withdrawn rod synaptic terminals (Fig. 16B, arrowheads). Such remodeled dendritic branches are readily apparent within 3 days of a detachment, and their number increases with detachment time.

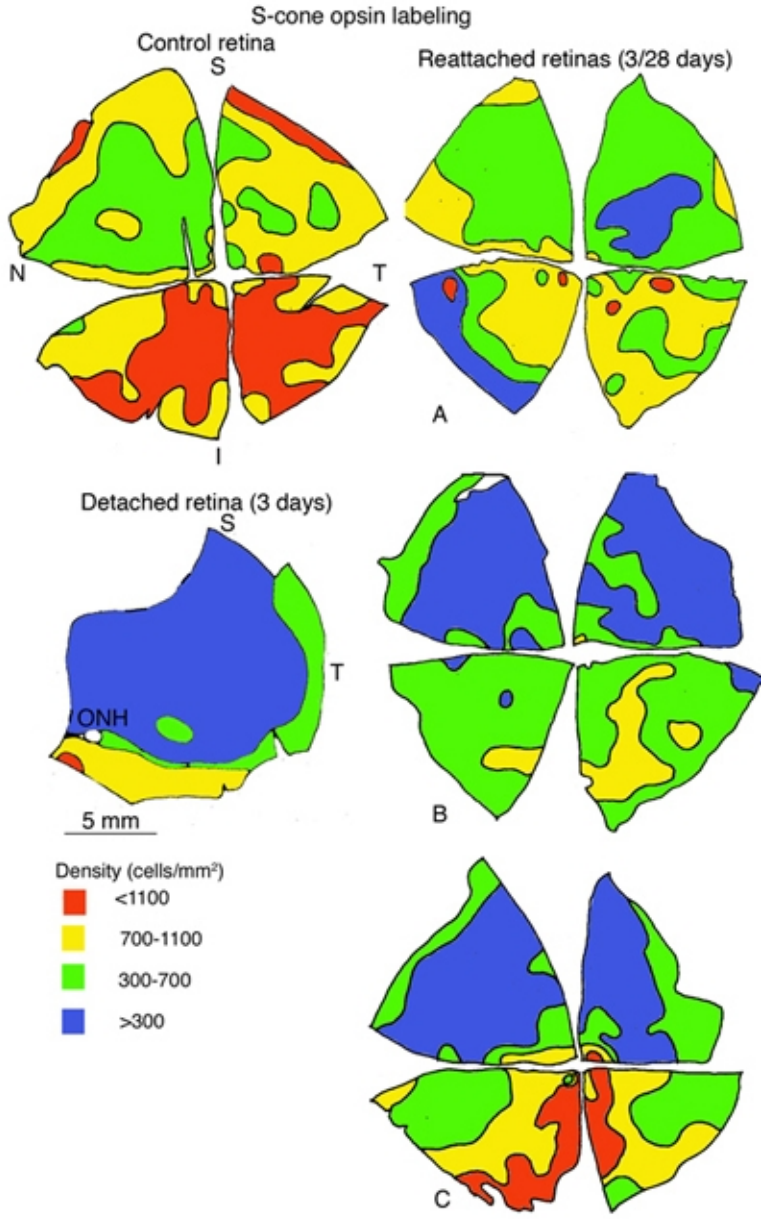

Figure 13. Isodensity contours for short-wavelength sensitive (S)-cones labeled with an antibody to S-cone opsin in normal, detached, and reattached feline retinas. The greatest density of S-cones occurs in the inferior retina in control retina. When the retina is detached for 3 days, S-cones drop dramatically (the yellow and orange areas inferior to the optic nerve head (ONH) were not detached). In the three reattached retinas (A, B, and C), most of the superior retina was detached for 3 days and then reattached for 28. S-cone labeling in the reattached retinas was patchy and of low density by comparison with the normal retina. Many areas showed no S-cone labeling at all.

There probably is also "pruning" of dendritic branches on these cells. In control retinas, the dendrites appear as fine, "wispy" outgrowths extending from the cell body into the OPL (Fig. 16D). In detached retinas, these are not nearly as prominent, leading to the impression that some dendrites have withdrawn while others have grown in length (Fig. 16E). Pruning of dendrites appears to be the major response of bipolar cells in other forms of retinal degeneration (13), but in those cases the response appears late in the diseases.

Horizontal Cells

The feline retina has two morphologically distinct horizontal cells (Fig. 17): one with stout tapering dendrites and no axon (A-type), and the other with somewhat finer, highly branched dendrites and a long thin axon that

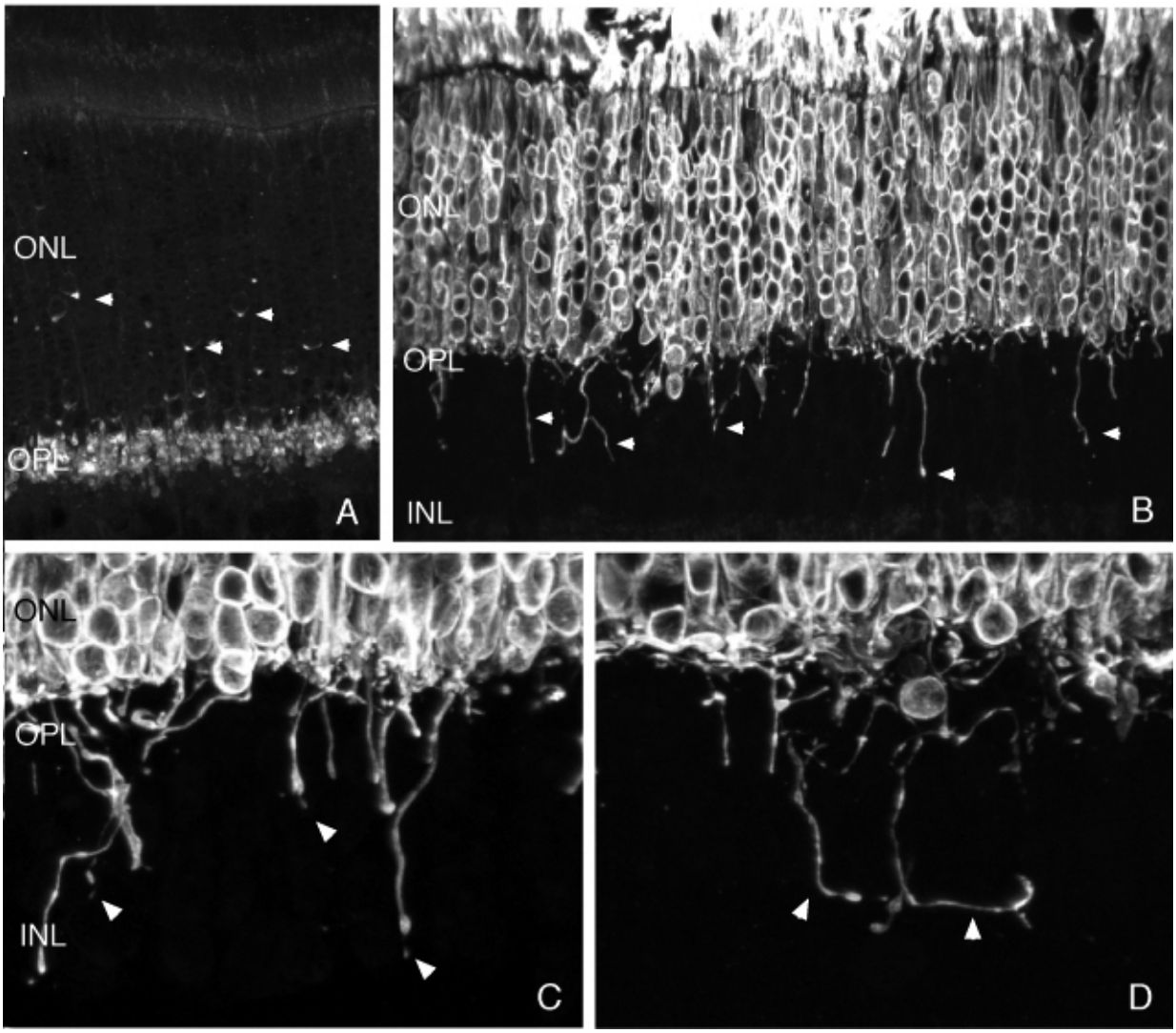

Figure 15. Labeling of RS and rod outer segments (ROS) in retinas detached for 3 days and reattached for 28. A, anti-synaptophysin labeling shows a relative return of organization to the layer of synaptic terminals in the OPL. The number of labeled terminals (arrowheads) in the ONL is dramatically reduced. B-D, anti-rod opsin labeling shows that there is growth of rod axons (arrowheads) into the inner retina after reattachment. Most terminate in a rounded terminal with fine projections. More recent (unpublished) data indicate that these overgrown terminals do not contain synaptic ribbons.

forms an elaborate axon terminal (B-type) (82, 83). Electron microscopy demonstrated that the dendrites of both the A- and B-type cells innervate the cone terminals, whereas only the branches of the axon terminal innervate rod spherules (49). The thin B-cell axon does not communicate electrically with the cell body (84).

Antibody Labeling Signatures Define Horizontal Cell Subtypes

Neurofilaments are plentiful in the A-type cell, and although not completely absent, they are sparse in the B-type cell. This is reflected in the heavy labeling of the A-type cell by antibodies to the 70- and 200-Kd subunits of the neurofilament protein complex. Antibodies to the calcium binding proteins calbindin D and calretinin also label horizontal cells. The use of these three antibodies allowed us to differentiate the two subtypes in feline retina.

We initially observed fairly thick, beaded calbindin D-positive processes in the ONL after detachment (red process, left of Fig. 18A; green processes, Fig. 18C). These outgrowths label with the antibody to neurofilament protein. Indeed, there is a large increase in the intensity of horizontal cell labeling with this antibody after

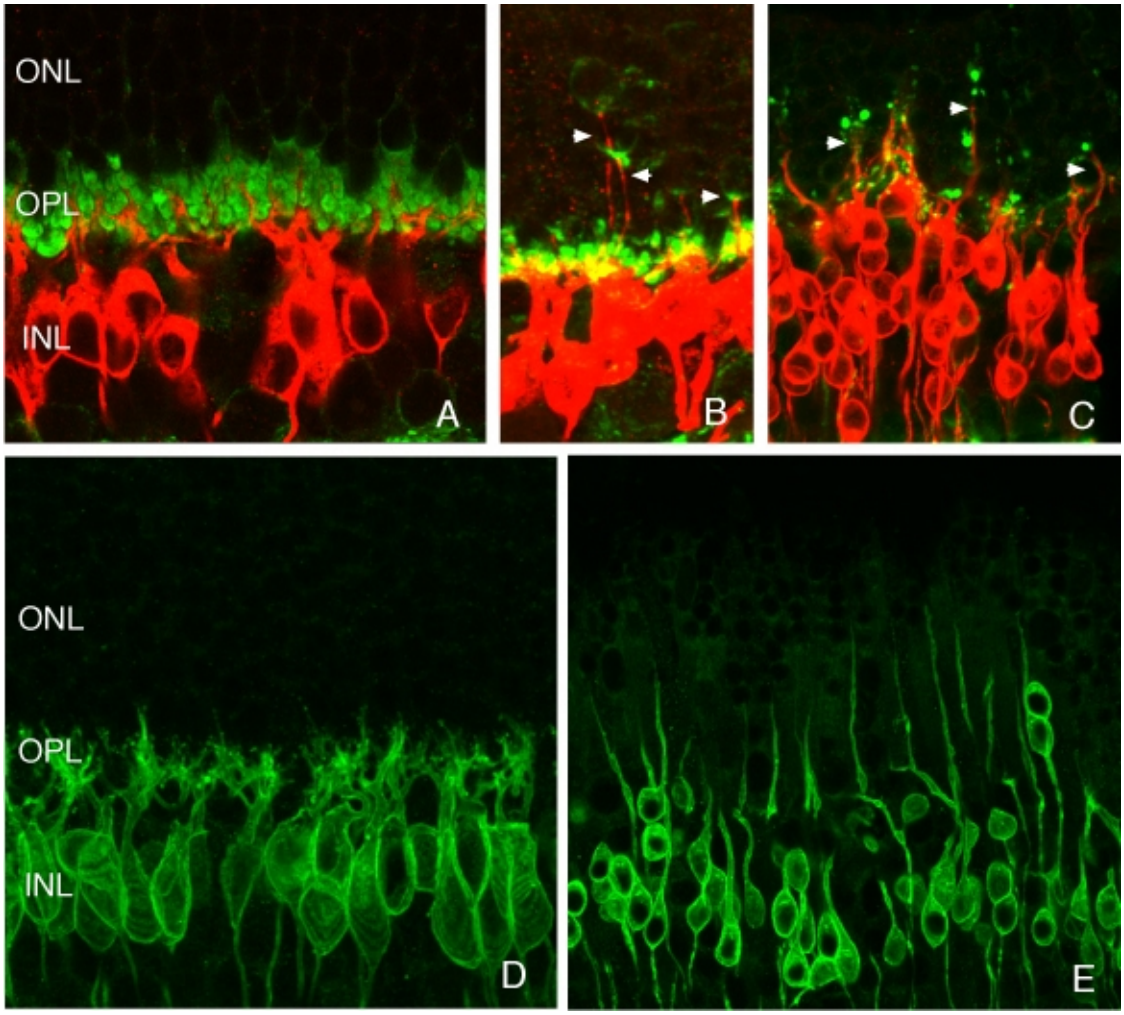

Figure 16. Remodeling of RB cells after detachment. In parts A-C, RB cells are labeled with anti-protein kinase C (PKC, red) and photoreceptor synaptic terminals with anti-synaptophysin (green). In parts D and E, only anti-PKC labeling (green) is shown. A, dendrites of RB cells specifically enter the synaptic invaginations of the rod spherules. B and C, 3 days detached. Many fine RB cell neurites (arrowheads) extend into the ONL, where they terminate adjacent to retracted RS. D, normal retina. RB cell dendrites have a "thin and wispy" appearance. E, 28 days of detachment. The RB dendrites have a thicker appearance as they grow into the ONL. Many of the short, "wispy" processes appear to be missing, perhaps indicative of pruning as well as outgrowth.

detachment (Fig. 19, A and B, red, OPL), most likely indicating an upregulation of protein expression in the remodeled cells (85).

Using any of these three antibodies, we can actually detect two types of horizontal cell outgrowths: those that terminate adjacent to retracted rod spherules (Fig. 18, A and B, arrowheads), i.e., "directed" and those that do not, i.e., "undirected" (examples in Fig. 18A, Fig. 19B, and Fig. 20, D and E). Whether the strikingly dramatic "undirected" outgrowths serve some functional or survival role for the horizontal cells or are merely vestiges of an injury response is unknown. Amazingly, in detachments of 3 days or longer, these outgrowths often extend beyond the outer limiting membrane and into the subretinal space. This always occurs in conjunction with Muller cell processes (Fig. 19, B and C, green). Once in the subretinal space, the horizontal cell outgrowths (Fig. 19D, red) were never observed growing on the exposed photoreceptor cells themselves but always embedded within a meshwork of Muller cell processes (Fig. 19D, green), where they could run for long distances.

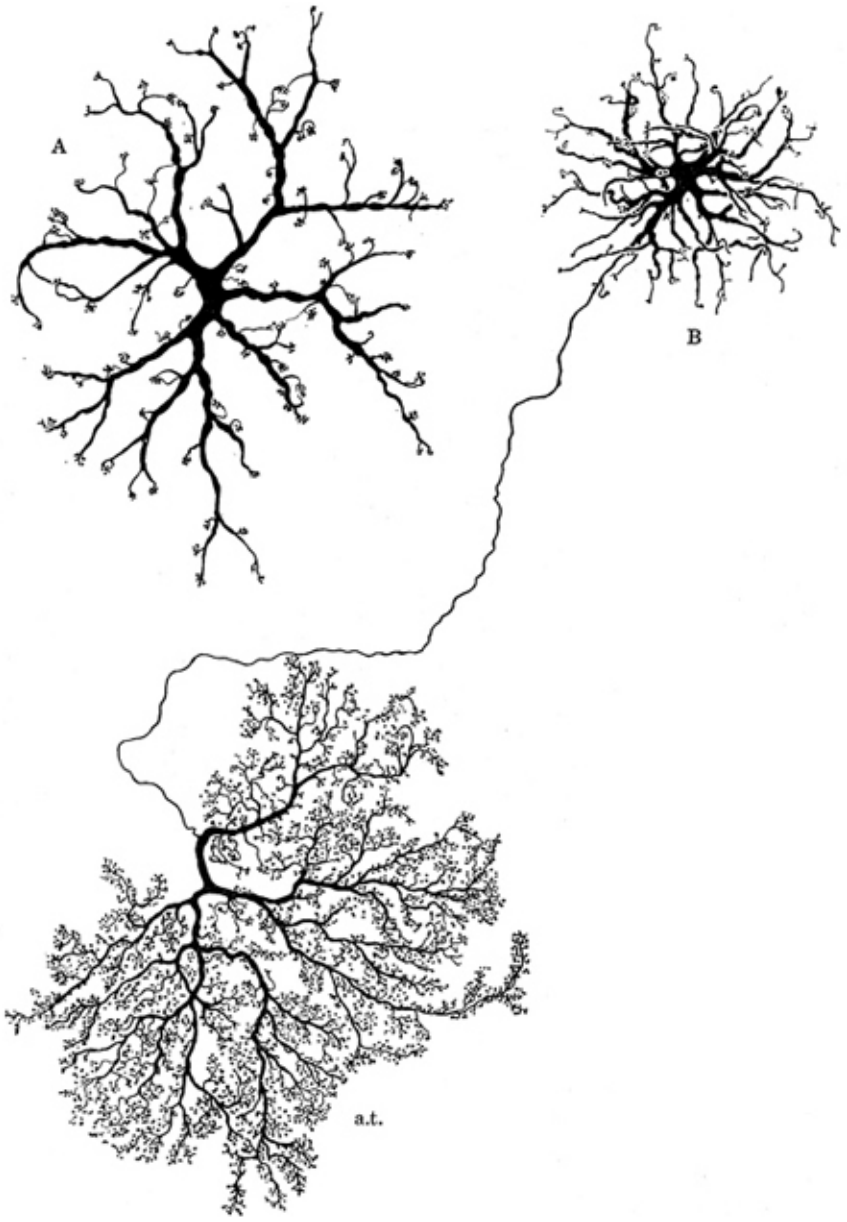

Figure 17. Two types of horizontal cells in the feline retina. A, HA with a dendritic spread of about 250 μm × 250 μm has no axon, and its dendrites contact only cone photoreceptors. B, HB has a smaller dendritic field than HA (about 150 μm × 150 μm) but an elaborately branched axon terminal system (a.t.). The dendrites of HB contacts only cones, whereas the axon terminal contacts only rods. From Fisher and Boycott (83).

Horizontal Cells Extend Both Ascending and Descending Neuritis

Some horizontal cell outgrowths are fairly thick processes descending from the horizontal cells into the inner retina, although these were observed with much less regularity than those ascending into the ONL. The descending processes were also observed by Marc et al. (13, 86) in the detached feline retina and in other forms of retinal degeneration. Indeed, they seem to be the most commonly encountered form of horizontal cell remodeling in cases of extreme photoreceptor loss (13). The "undirected" ascending processes in both sectioned material and wholemounts appear in two structural types: one composed of thin, often beaded cylindrical processes, and the other as flattened, ribbon-like processes. These can both occur singly and in clusters (Fig. 18C). Within the subretinal space, the long extended processes all appear thin, cylindrical, and often beaded (Fig. 19D). But, when thicker, fleshier processes occur there, they usually branch profusely, giving rise to

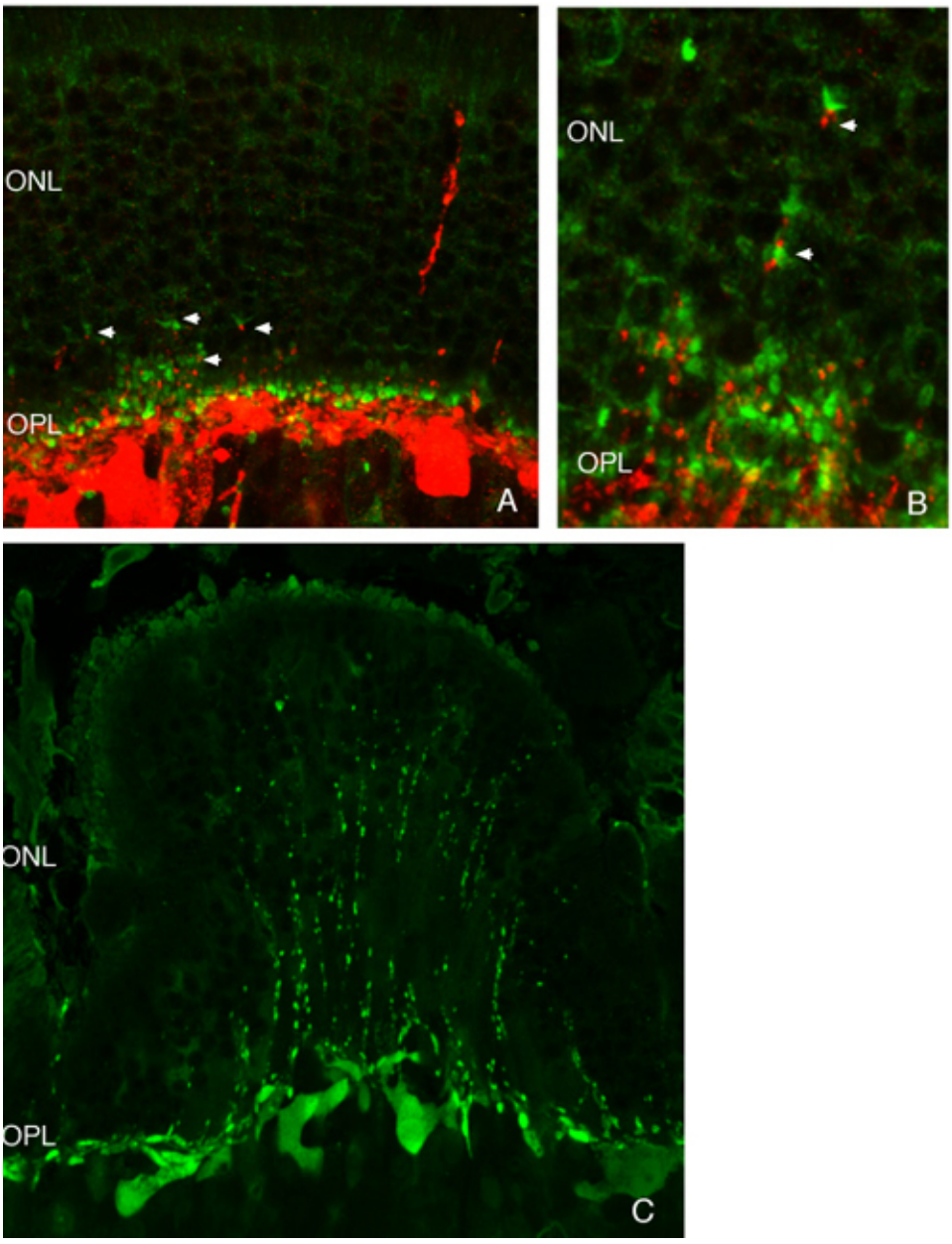

Figure 18. Horizontal cell remodeling after detachment. A and B, horizontal cells (red) are labeled with anti-calbindin D and the synaptic terminals of photoreceptors with anti-synaptophysin (green). Many fine red processes from the horizontal cells extend into the ONL (arrowheads). Many terminate adjacent to withdrawn RS, but some do not, such as the thick process in part A. C, anti-calbindin D labeling. A cluster of fine, beaded horizontal cell outgrowths extending into the ONL after 7 days of detachment.

complex assemblies reminiscent of sparse versions of axon terminals of the B-type cell within the OPL (Fig. 20F).

The Origin of the Horizontal Cell Outgrowths

By labeling with a combination of antibodies to neurofilament protein, calbindin D, and calretinin and assigning the output colors as green, blue, and red, respectively, we determined that the characteristically shaped A-type cells are blue/white in color (i.e., heavily labeled with all three antibodies; HA in Fig. 20, A-C), whereas cells with the appropriate shape and location to be the B-type are red or near-red in color (because of the near lack of labeling with the anti-neurofilament antibody; HB in Fig. 20, B and C). The outgrowths into the ONL, including the long processes that reach the subretinal space, all bear an immunochemical labeling "signature" of the B-type

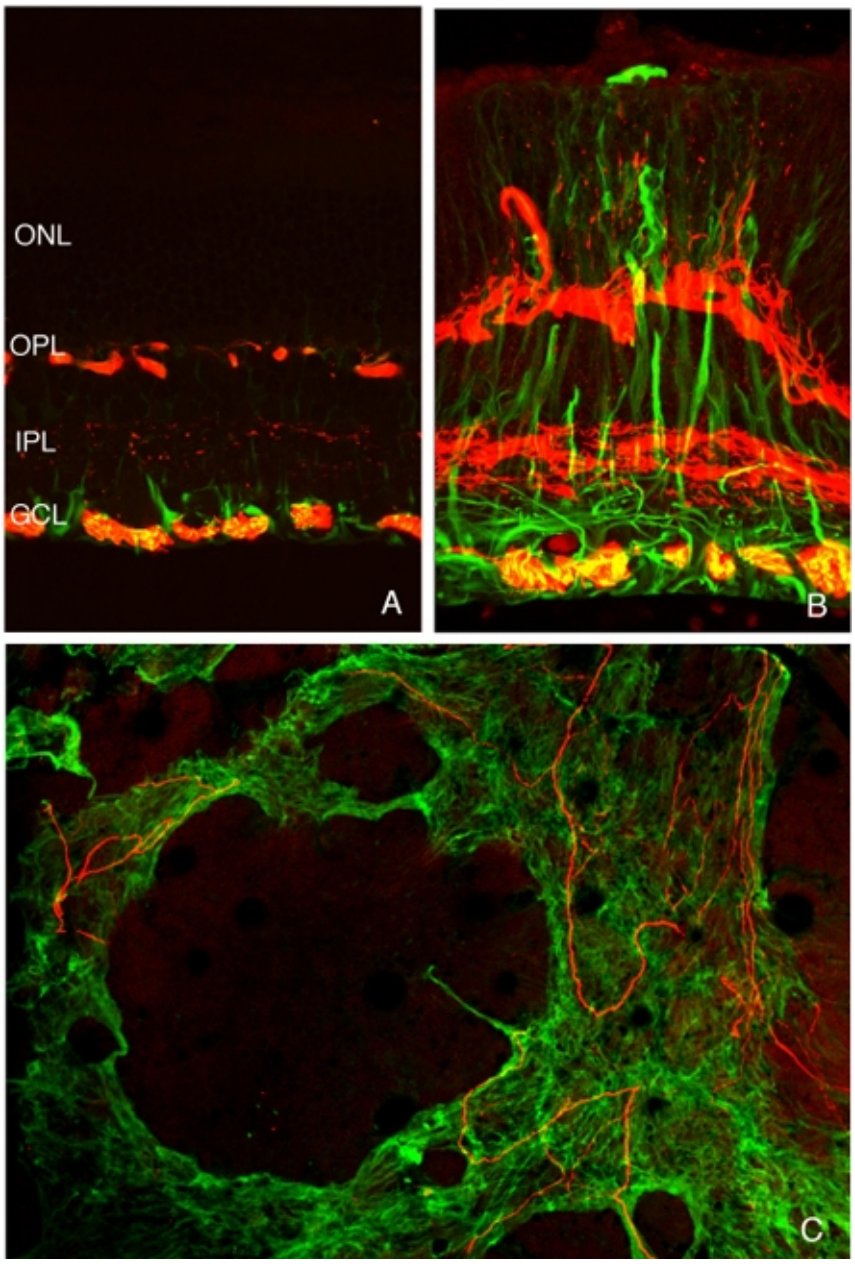

Figure 19. Horizontal cell remodeling after detachment seen by anti-neurofilament protein labeling (red). Anti-GFAP (green) is used to label Muller cells. A, normal retina. Prominent labeling with anti-neurofilament of thick horizontal cell processes in the OPL, probably those of the A-type horizontal cell, of ganglion cell axons in the GCL, and some labeling of fine ganglion cell dendrites in the IPL. B, 7 days of detachment. There is an increase in labeling of the horizontal cells (and ganglion cells), and many horizontal cell neurites extend into the ONL. Strong responsiveness by horizontal cells is accompanied by a high degree of anti-GFAP labeling in Muller cells. C, the subretinal space in a retinal wholemount of detached retina. Long, fine anti-neurofilament labeled outgrowths of horizontal cells (red) occur in the subretinal space, where they are always associated with Muller cell processes (green). (See movie.).

cell (Fig. 20, D-F, arrows). When an outgrowth that gives rise to a branched process in the subretinal space was traced back through the ONL, it was found to arise from a complex plexus with an organization characteristic of the axon terminal and with the B-type cell immunochemical signature (Fig. 20, D and E, arrows). Thus, the evidence points to these processes as arising from the axon terminal of the B-type horizontal cell (see the movie of horizontal cell neurites growing out of a surrounding mass of Muller cells).

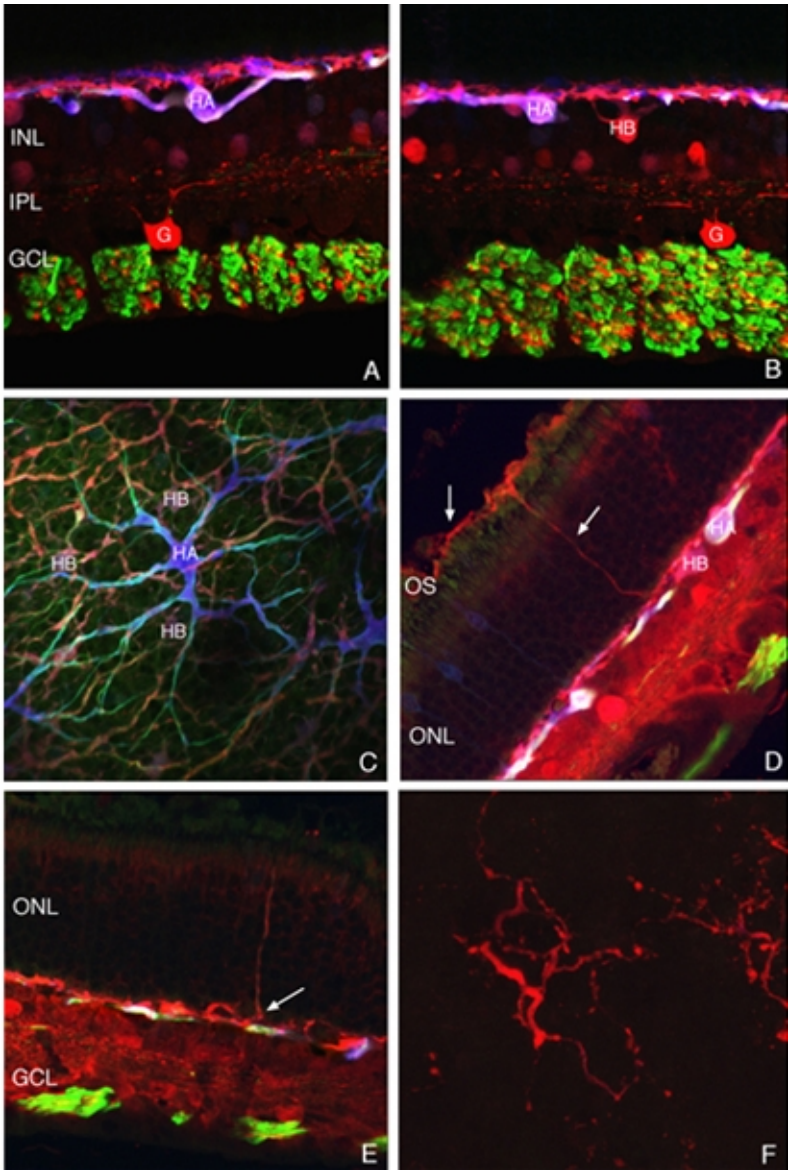

Figure 20. Remodeled horizontal cell processes probably arise from the axon terminal system of HB cells. Labeling is with: anti-calretinin (red), anti-calbindin D (blue), and anti-neurofilament (green). A and B, radial sections, normal retina. HA have a "blue/white" color, stout processes, and a cell body that lies on the outer border of the INL. HB are red, have finer processes emerging from the cell body, and lie lower in the INL. G, calretinin-positive ganglion cells with their cell bodies in the GCL and dendrites extending into the IPL. C, flat-mounted retina. The plane of focus is at the level of the A-type cell bodies (HA) with the smaller, finer B-type cell bodies (HB) lying slightly deeper in the tissue. D, a radial section of retina detached for 28 days. One of the fine horizontal cell outgrowths (red, arrows) extends through the ONL into the subretinal space, where it branches extensively (OS). E, a radial section after 28 days of detachment. A fine HB cell outgrowth (arrow) runs through the ONL. This process arises from a dense plexus on the border of the OPL characteristic of the axon terminal system of these cells. F, an optical section through the subretinal space in a flat-mounted retina detached for 28 days. The three sets of red branching processes in this figure were traced back through the ONL to the OPL to HB axon terminals.

What Drives the Outgrowth of Rod Bipolar and Horizontal Cell Neurites?

Although growth in response to the release (or lack) of some factor from the rods is one possibility, another mechanism is suggested from studies of cultured neurons in which mechanical tension can elicit neurite outgrowth (87). If the rod bipolar cell dendrites and the horizontal cell axon terminal endings remain mechanically connected to retracting rod spherules, tension generated by the retracting rod spherules may

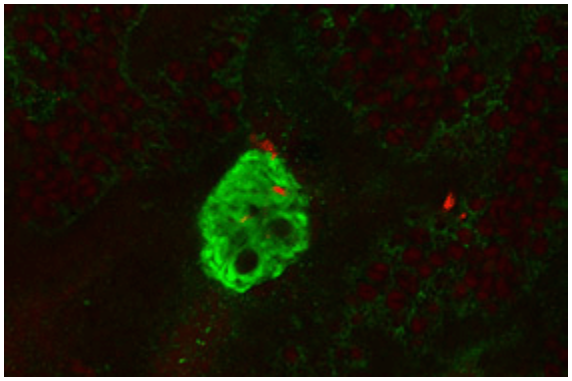

Movie 1. A movie of horizontal cell neurites (red) growing out of a surrounding mass of Muller cell processes (green) in a detached retina.

Download video

initiate a growth response from the post-synaptic neurons. Whether the same mechanism accounts for the generation of directed and undirected outgrowths is unanswered.

Remodeling of Ganglion Cells

A subset of ganglion cell remodels vigorously in response to detachment. Ganglion cells are the retinal neurons farthest removed from the site of the detachment. It is important, however, to remember that ganglion cells are surrounded by Muller cell processes, and the apical end of the Muller cells are in direct physical contact with the actual site of the injury (the subretinal space). Muller cells also react to detachment very quickly (88) and, thus, could easily drive ganglion cell reactivity. Additionally, ganglion cell responsiveness could be dependent on the trans-neuronal changes originating with changes at the rod and cone synapses.

GAP 43 Expression, Neurofilament Protein Expression, and Ganglion Cell Remodeling

Growth associated protein (GAP 43) expression is generally associated with axonal growth cones and synaptogenesis (89-92), and it is generally down-regulated significantly after the developmental period associated with synaptogenesis (89-91, 93-97). Mice in which GAP 43 has been genetically removed show a tangling of axons in the optic nerve (98), whereas mice overexpressing GAP 43 show an enhanced sprouting of axon terminals in both central and peripheral neurons (99).

GAP 43 expression in the retina appears as the ganglion cells migrate into their specific layer and begin the process of axon outgrowth. It remains in adults only as stratified labeling in the IPL (90, 95, 100-102). This is the pattern observed in the adult feline retina (18). Immunoblot analysis also reveals that there is some GAP 43 protein expressed in normal adult feline retina (18).

Immunoblot, immunocytochemical, and real-time PCR data all show a rise in GAP 43 expression beginning 1 day after a retinal detachment and continuing to increase at the last experimental timepoint at 28 days. Immunohistochemistry data reveal a population of ganglion cell bodies that are heavily labeled in the 7-day postdetachment animals (Fig. 21A, red processes) (18). The GAP 43-positive ganglion cells also show a major increase in labeling with the anti-neurofilament protein antibody. In the normal retina, this antibody labels only a few processes in the IPL and ganglion cell axons (Fig. 19A, red, IPL and GCL labeling) (18). After detachment, it heavily labels processes in the IPL and cell bodies in the ganglion cell layer (Fig. 19B and Fig. 21, B and C: red, IPL, GCL labeling). This labeling colocalizes with the increased anti-neurofilament labeling.

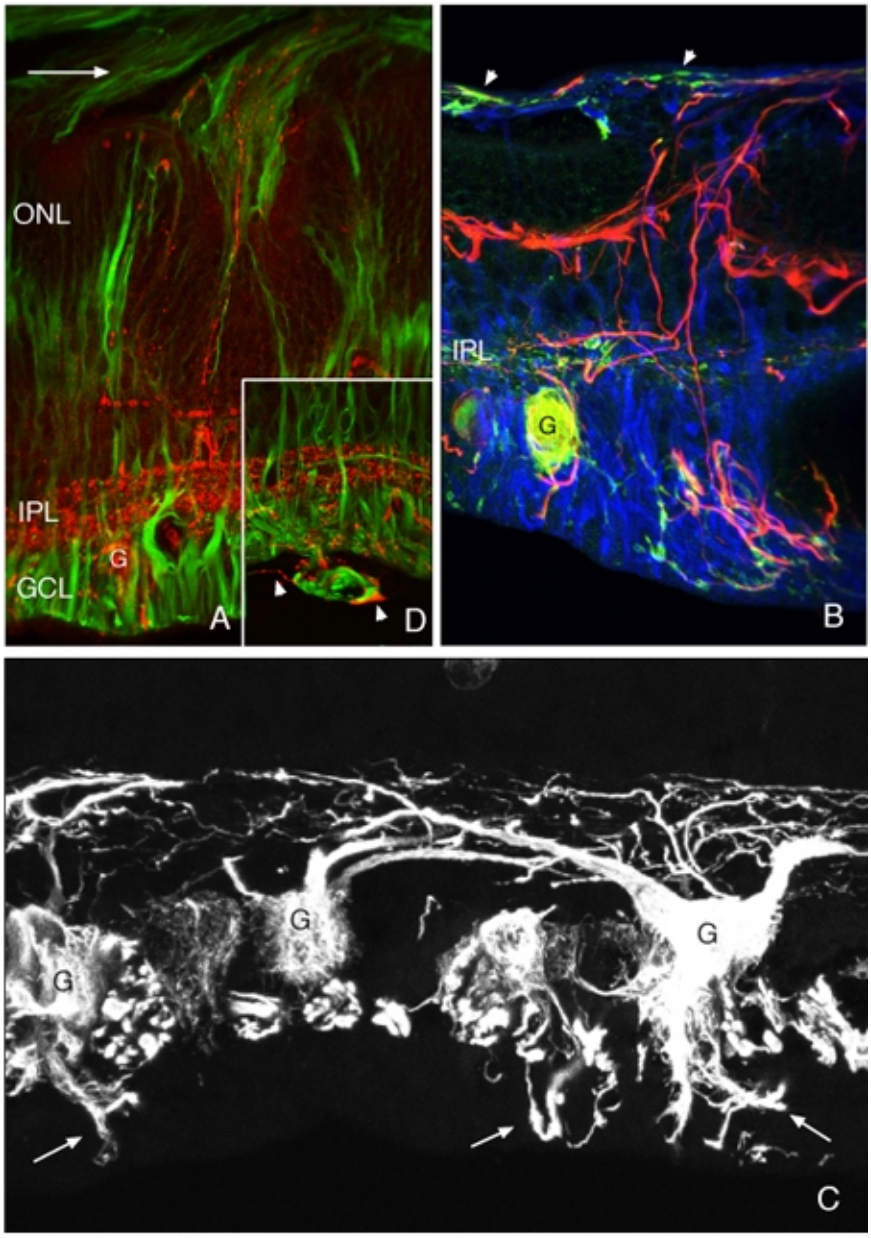

Figure 21. Reactivity of ganglion cells to retinal detachment. A, anti-growth associated protein 43 (GAP 43, red) labels only fine processes in the IPL of normal adult retina. In retina detached for 28 days, anti-GAP 43 labels a subpopulation of cell bodies in the GCL, many processes in the IPL, and some that grow beyond the IPL into the ONL and often into the subretinal space (arrow). GAP 43-positive processes in the outer retina are always closely associated with reactive Muller cell processes (anti-GFAP, green). B, detached (28 days) retina triple-labeled with antibodies to neurofilament protein (red), GAP 43 (green), and GFAP (blue). In detached retina, a subpopulation of ganglion cell bodies label heavily with both the neurofilament and GAP 43 antibodies, giving the yellow color to the cell labeled "G." Red processes represent remodeled process from the horizontal cells. The fine yellow/green processes in the subretinal space (arrowheads) represent outgrowths from remodeled ganglion cells. C, the inner retina after detachment. Anti-neurofilament labeling. Labeling in the normal retina is limited to fine processes in the IPL (Fig. 15A). In the detached retina, large ganglion cells label, along with their processes in the IPL. The labeled ganglion cells have many branched, "spikey" processes growing from their basal surface toward the vitreous (arrows). D, after retinal reattachment, neurites from ganglion cells (arrowheads) can grow into the vitreous in association with Muller cell endfeet (green) and form epiretinal membranes.

Ganglion Cell Morphology after Detachment

After detachment, the GAP 43/neurofilament-positive ganglion cells exhibit an unusual morphology, unlike any reported in the literature for feline (or other mammalian retinas) ganglion cells, with numerous small, spikey processes extending from their cell body toward the nerve fiber layer (Fig. 21C) (18). As detachment duration increases, there is an astonishing increase in GAP 43/neurofilament-positive neurites that extend from the labeled ganglion cells and course completely across the neural retina and into the subretinal space (Fig. 21, B and C, arrows). These processes are generally of a uniform caliber without obvious branching.

Remodeling of Ganglion Cells Is "Extreme"

Thus, the picture that emerges for remodeled ganglion cells is very much like that of the remodeled horizontal cell axon terminals, inasmuch as both produce a large number of "undirected" processes that can grow for long distances through the retina and into the subretinal space. The neurites from ganglion cells also tend to appear adjacent to the processes of reactive Muller cells, either within the retina or in the subretinal space. Interestingly, neuronal processes have been identified in subretinal membranes removed surgically from human eyes (G.P. Lewis and S.K. Fisher, unpublished observations).

Which Ganglion Cell Type(s) Remodels?

Size measurements from retinal wholemounts were used to produce a frequency distribution for the somal area of the GAP 43-labeled ganglion cells. The data show a large peak at 600 μm^2 but also a small population of cells clustering around 3,000 μm^2 (18), suggesting that it is the alpha ganglion cell types (103, 104) that remodel.

Ganglion Cell Remodeling after Reattachment

Retinal reattachment appears to elicit the extensive growth of ganglion cell neurites into the vitreous, where they associate with epiretinal membranes produced by Muller cells (Fig. 21C, arrows; Fig. 21D, arrowheads). Thus, the response in the vitreous is similar to the response in the subretinal space; neurite outgrowths associate with reactive Muller cell processes, but the vitreal growth is initiated only after reattachment, probably because reattachment also initiates the growth of Muller cells into the vitreous cavity (105). Data from pathology specimens of human vitreal membranes also show the presence of anti-neurofilament labeled processes (30).

Glial Cell Remodeling

Muller Cells

Muller cells undergo extensive hypertrophy after detachment. They also show nuclear migration, cell division, and growth into the subretinal space. All of these are obvious by simple histological observation (14, 15, 39, 69).

The Intermediate Filament Cytoskeleton and Remodeling

The structural hypertrophy of these cells correlates with increased expression of intermediate filament proteins, glial fibrillary acidic protein (GFAP), and vimentin (106, 107). Electron microscopy also shows a large increase in the number of intermediate filaments in the cytoplasm of these reactive cells (Fig. 22) (108).

Astrocytes in the brain and spinal cord react similarly, especially with respect to an upregulation of GFAP (14, 109).

The Muller Cell Response Is Distinct and Dramatic

What makes the Muller cell GFAP response so dramatic is the fact that these filamentous proteins are almost exclusively localized to the endfoot region in a normal retina (Fig. 23A, red/yellow labeling) and, in some species

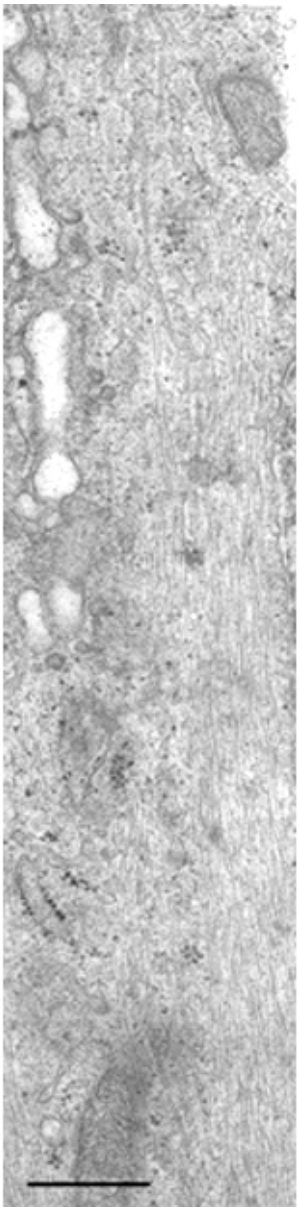

Figure 22. 10-nm-diameter filaments in the cytoplasm of a Muller cell in the outer retina after retinal detachment. These intermediate filaments label with antibodies to both GFAP and vimentin. In the normal retina, they are mainly limited to the endfoot region of these cells. Scale bar, 0.5 μm.

such as rats and mice, barely detectable by current immunocytochemical technology (Fig. 23C) (110-112). On injury, the cytoskeletal remodeling in these cells correlates closely with changes in morphology. Indeed, the correlation is so close that they are generally assumed to be functionally linked events. In support of this argument is the fact that in the ground squirrel retina, Muller cells do not hypertrophy in response to detachment, and their intermediate filament cytoskeleton remains unchanged (24). Following brain injury, astrocytic scar formation is impaired in $vim^{-/-}/GFAP^{-/-}$ mice but not in mice lacking only one of the two intermediate filament genes (113). Whether a similar principle applies to Muller cells remains to be determined.

The Muller Cell Endfoot as the Origin of the Intermediate Filament Response

Within a day of a detachment, intermediate filament proteins within the endfoot become more dense in number, often forming whorl-like or wavy bundles (Fig. 23B, red/yellow labeling) (108). They appear to grow from this

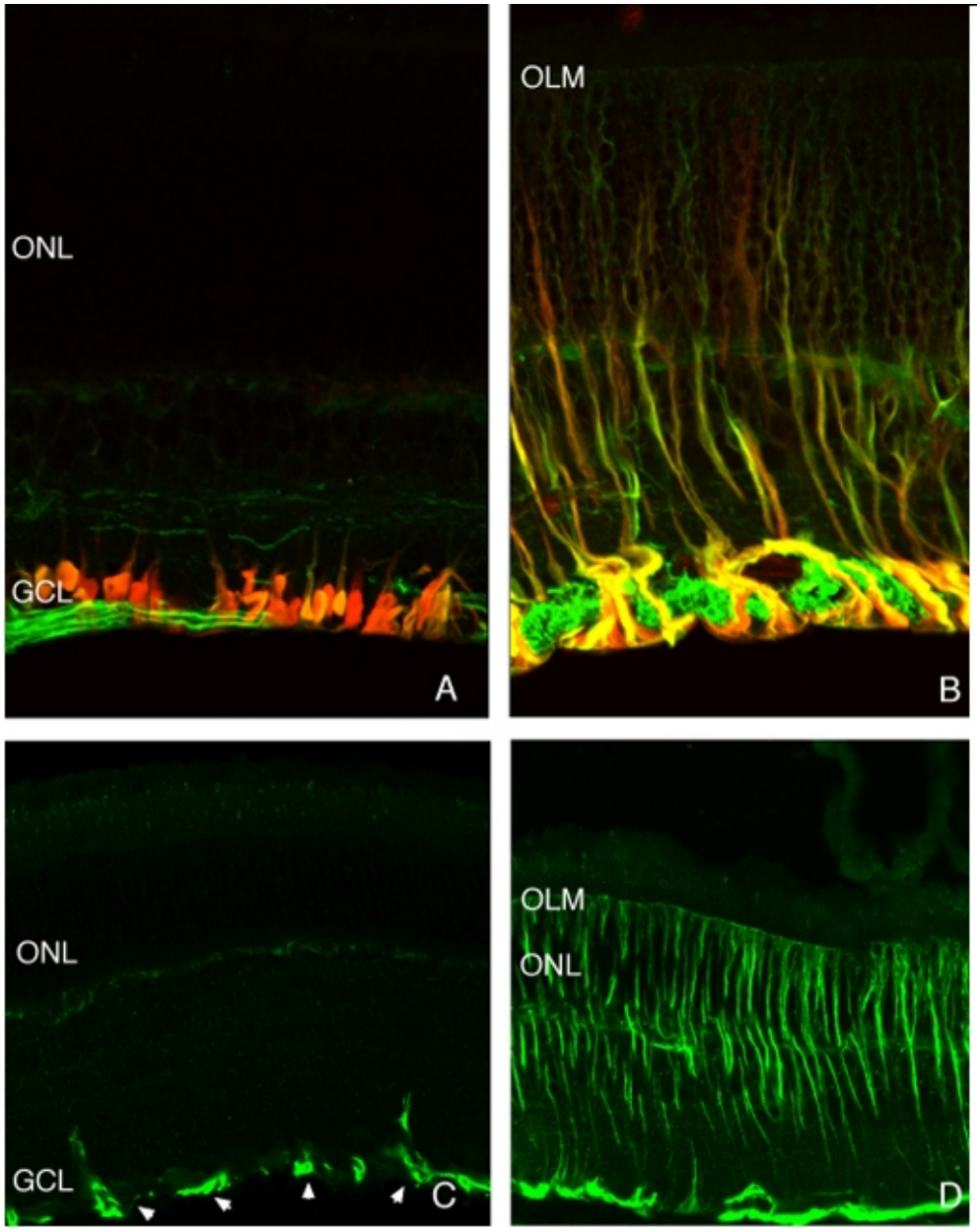

Figure 23. Labeling with antibodies to the intermediate filament proteins GFAP (green) and vimentin (red). A, in the normal retina, they are concentrated in the endfoot region of the Muller cells. Vimentin predominates over GFAP (astrocytes, however, show a preponderance of GFAP). B, after 3 days of detachment, the intermediate filaments expand from the endfoot into the outer retina. There is also a shift toward the yellow and green colors, indicating a greater increase in GFAP than vimentin. C, mouse retina labeled with the antibody to GFAP. In some species such as the mouse, there is no detectable GFAP in Muller cell endfeet, the only labeling occurring in astrocytes (arrowheads). D, when the mouse retina is detached for 7 days, the GFAP reactivity of Muller cells is striking, with labeling extending across the entire neural retina to the outer limiting membrane (OLM).

distal mass, extending both into branches of the endfoot, which increase in size and in number with detachment time, and apically towards the cell body and then into the outer retina (Fig. 23 and Fig. 24) (107, 114).

Subretinal Growth of Muller Cells after Detachment

As intermediate filaments expand into the apical cytoplasm of the activated Muller cells, some of them begin to grow, expanding into the subretinal space where they can elaborate into multilayered clinical "membranes" (Fig. 25, A and B).

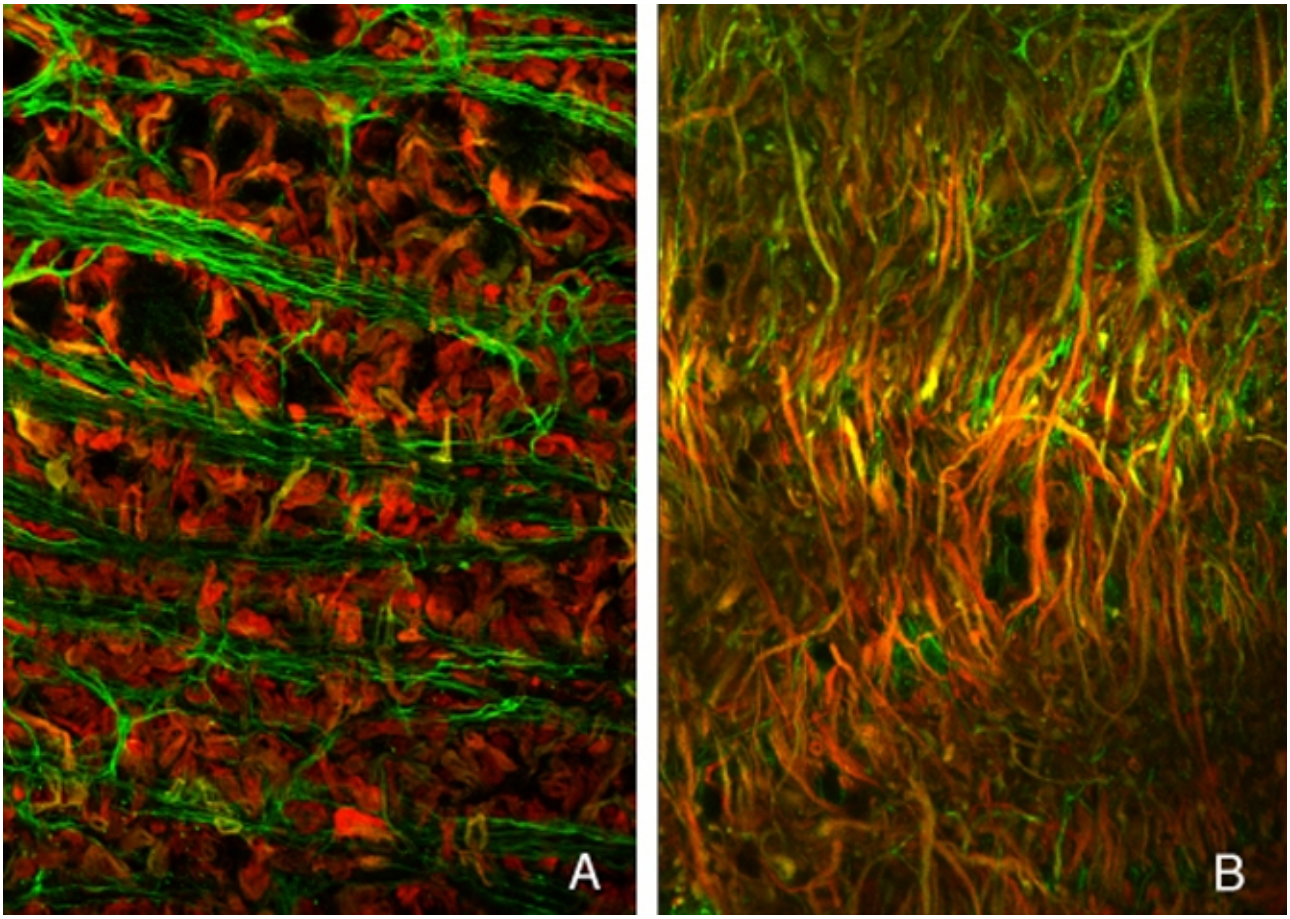

Figure 24. Retinal flat-mounts labeled with antibodies to GFAP (green) and vimentin (red) viewed from the ganglion cell surface to show changes in the Muller cell endfeet after detachment. A, normal retina. The endfeet are "hoof-shaped", and their labeling is dominated by vimentin. The long, thin green processes are from astrocytes. The "holes" represent ganglion cell bodies that are negative for both proteins. B, retina detached for 7 days. The endfeet processes have grown on the retinal surface. Astrocyte processes appear disorganized. Axon bundles are no longer prominent, probably because they are overlaid by the thicker endfeet processes.

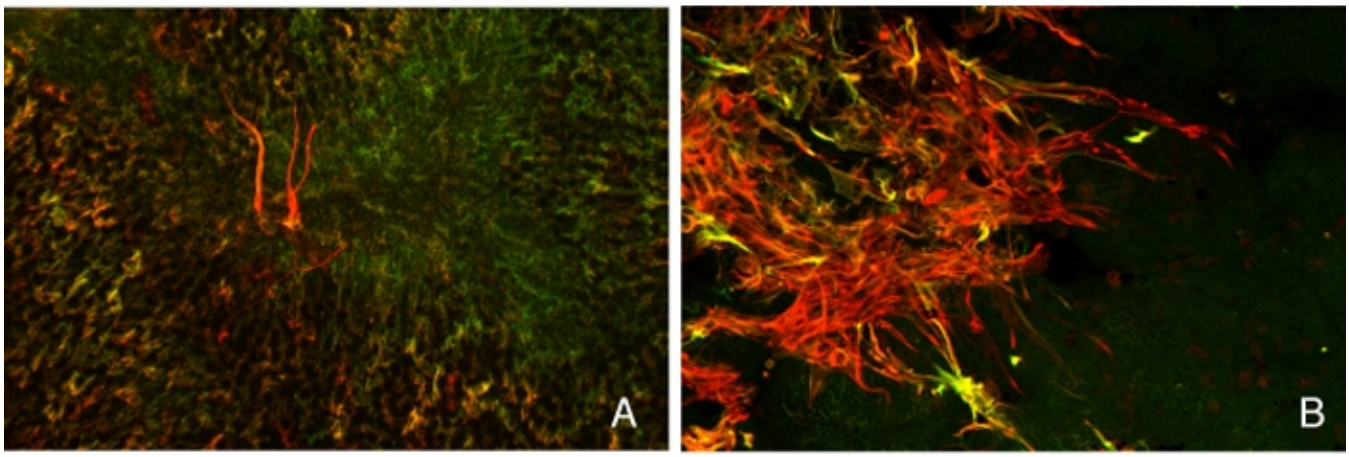

Figure 25. The subretinal space in retinal flat-mounts prepared after detachment and labeled with antibodies to vimentin (red) and GFAP (green). A, retina detached for 3 days. Initial outgrowth of a Muller cell process (red) from the neural retina into the subretinal space. The greenish background represents labeling with anti-GFAP within the neural retina. The processes that grow into the subretinal space show a predominance of vimentin. B, 28 days of detachment. At this time, there is a large "membrane" growing in the subretinal space composed of overlapping Muller cell processes. Vimentin continues to predominate over GFAP.

GFAP and Vimentin: Details of Their Responses in the Muller Cells Subretinal Space

GFAP and vimentin can copolymerize to form intermediate filaments, but we have observed in double-labeling studies that there is a differential expression of the two in feline Muller cells. In the normal retina, vimentin predominates. The endfeet label most heavily with this antibody, and labeling extends farther into the neural retina than it does for GFAP. In the main trunk of the reactive cells, GFAP seems to predominate. As the apical microvilli begin to grow into the subretinal space, vimentin labeling predominates (Fig. 25A, red tapering forked processes). This imbalance in expression continues as the processes expand into the subretinal space (Fig. 25B) (114). The "leading edge" of the growing processes always shows a predominance of anti-vimentin labeling, with GFAP expression becoming increasingly intense at the point of exit from the neural retina. These processes or "membranes" essentially form glial scars in the subretinal space. Their presence does not appear to prevent physical reattachment of the retina, but it does inhibit the regeneration of outer segments (39) (see the movie of Muller cell processes growing out into subretinal space).

Reattachment Stimulates Growth of Muller Cells

Vitreous Space

A novel endfoot response occurs in the feline retina in response to reattachment. In this case, the branched endfoot processes that remained closely adherent to the vitreal surface of the retina begin growing into the vitreous chamber. It is these "branchlets" of the endfoot that expand into the vitreous to form epiretinal membranes. The initial outgrowths appear as fine, flat "ribbons" of cytoplasm extending away from the neural retina into the vitreous cavity (Fig. 26, A and B) (see the movie of Muller cell endfeet growing out into the vitreous).

These delicate, flattened processes have a very different morphology from the fine, tapered, and branched processes that expand into the subretinal space. In these endfoot outgrowths, GFAP expression dominates over that of vimentin (Fig. 26, A and B). Although vimentin expression "leads the way" in the expanding Muller cell processes within the subretinal space, it is GFAP that holds this position in the endfoot processes that grow into the vitreous (Fig. 26, C and D). The growth of these cellular processes into the vitreous can have significant consequences on vision because they can become contractile (115) and cause wrinkling and eventual re-detachment of the neural retina—a serious sight-threatening event if the fovea is involved.

Astrocytes

There is little known about the reactive capacity of these cells in the retina. They proliferate in response to detachment (116, 117), and observations of optic nerve fiber layer in retinal wholemounts show that their regular array and stellate shape are lost as the endfeet of the Muller cells expand on the retinal surface (114).

Retinal Remodeling after Detachment and Reattachment: An Overview

Studies of detached (and reattached) retina have shown us that the mammalian retina has remarkable remodeling capabilities. Fig. 27 shows, in summary form, the remodeling of the neural retina described here.

Rod outer segments and cone outer segments are greatly shortened and separated from the apical surface of the pigmented epithelium. Many RS are withdrawn from the OPL. After reattachment, some rod axons grow into the inner retina (the cell on the left). CP remain in place, although they undergo significant structural remodeling. The dendrites of RB cells grow into the ONL, where they terminate adjacent to withdrawn RS. The axon terminals of HB remodel extensively, with some processes terminating next to withdrawn RS, whereas

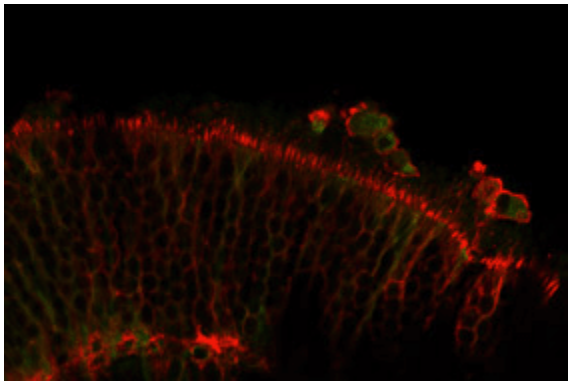

Movie 2. A movie of Muller cell processes (green) growing out into subretinal space in a detached retina.
Download video

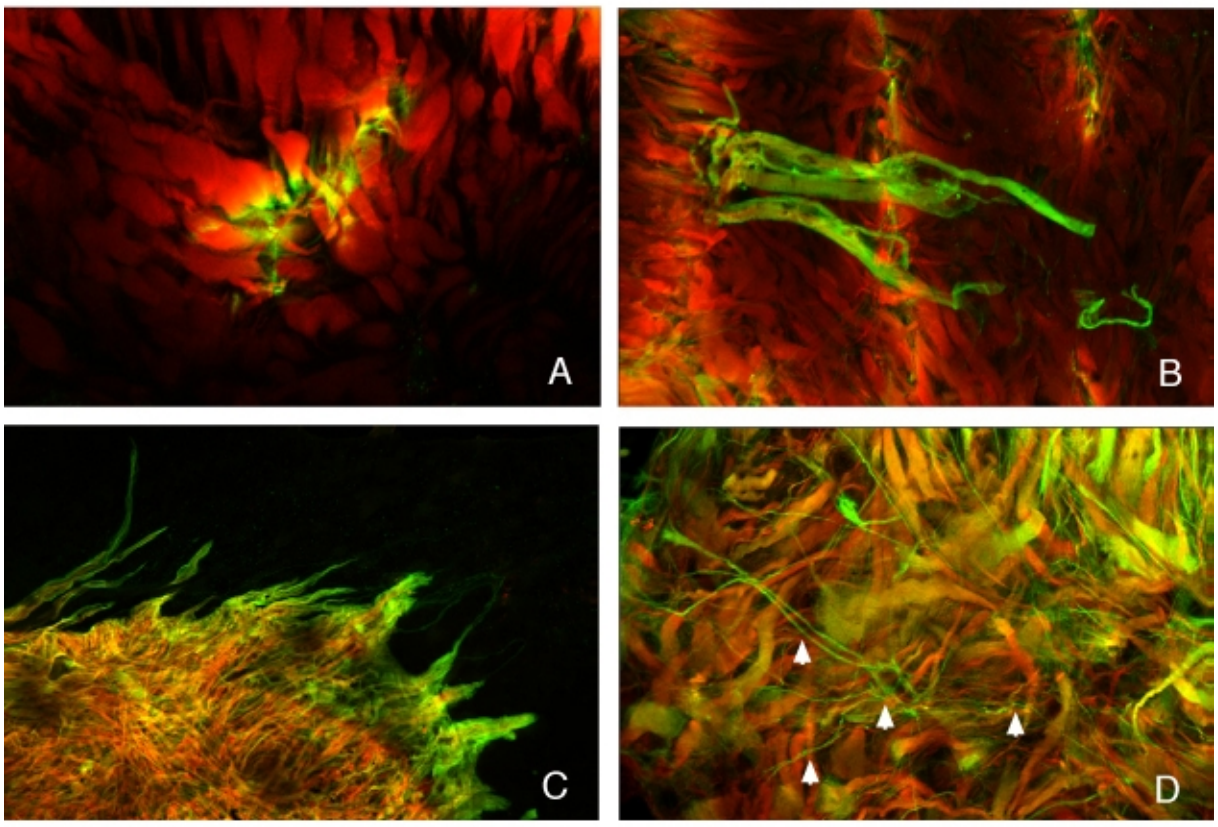

Figure 26. The vitreal surface of retinal flat-mounts prepared after the retinas were detached for 3 days and reattached for 28 days and labeled with antibodies to vimentin (red) and GFAP (green). A, high magnification image of the retinal surface. The Muller cell endfeet are largely club shaped, and the red color indicates a predominance of vimentin. The vitreal edge of some of these endfeet show predominant GFAP (yellow/green color). B, an image showing the outgrowth of ribbon-like extensions of Muller cells' cytoplasm into the vitreous. Within the retina the endfeet are red, indicating a predominance of vimentin, whereas the endfeet outgrowths into the vitreous are green, indicating a shift to GFAP. C, a complex epiretinal "membrane" growing on the vitreal surface. These membranes consist mainly of Muller cell processes in which the "leading" edge of the membrane shows a predominance of GFAP (green). D, a higher magnification image showing the complex structure of the epiretinal membranes with their mixture of Muller cell endfeet and branched cells, presumed to be astrocytes based on their structure and labeling with the antibody to GFAP (arrowheads).

others grow wildly into the outer retina and into the subretinal space adjacent to reactive Muller cells. HB axon terminals can also grow into the inner retina, although this reaction appears less frequently. A subpopulation of

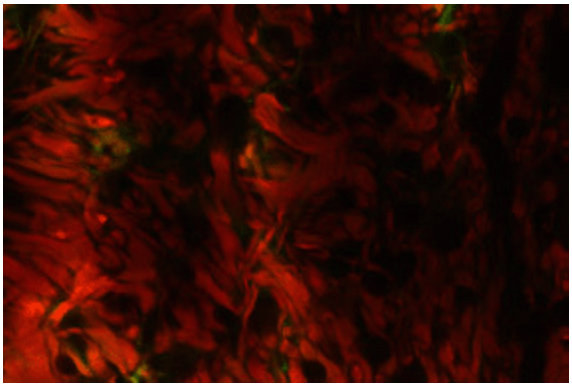

Movie 3. A movie of Muller cell endfeet (green) growing out into the vitreous in a detached retina.
Download video

ganglion cells extend short, spikey neurites from their base after and can also grow processes into the outer retina, where they behave much like the neurites of horizontal cells. In the reattached retinas, ganglion cell processes can also grow into epiretinal membranes formed by Muller cell growth into the vitreous. Muller cells are highly reactive to detachment and grow in the subretinal space to form membranes or glial scars on the exposed photoreceptor OS. After detachment, their endfeet expand but remain within the ILM. After reattachment, their specialized endfeet can grow into the vitreous to form epiretinal membranes as part of the disease, proliferative vitreoretinopathy. Astrocytes proliferate and often appear in epiretinal membranes, but their responses to detachment have not been characterized in detail.

Muller cell changes may occur in response to photoreceptor cell deconstruction and/or cell death or they may arise independently. Although it would seem logical that the remodeling changes in second-order neurons would be signaled from photoreceptor changes and remodeling of third-order neurons signaled by changes in bipolar cells, this has not been proven experimentally.

Future Challenges

Data from the detachment model, as well as from a variety of other studies, now suggests that retinal neurons remain capable of significant structural remodeling in adult mammals. This in turn may provide increased optimism for a variety of therapies for blinding diseases in which photoreceptor degeneration is the primary cause of visual loss. Although preventing photoreceptor cell death is the optimum therapy in these diseases, alternatives to this daunting challenge include technology for replacing photoreceptors, whether it is by way of cellular transplantation (118) or the use of progenitor cells (119-121). This success, however, would be hollow if the second-order neurons did not retain sufficient plasticity to form functional connections with the new photoreceptors. It may seem far-fetched at the present that such connections would form circuitry for functional vision. However, the degree of remodeling we have observed may be an indicator that the inner retina has more of a capacity for remodeling itself than previously imagined. Studies of patients with foveal reattachments—indicating that visual recovery may occur over years, not weeks—could conceivably represent the re-formation of appropriately functional retinal circuits, or even a remodeling of the RPE/photoreceptor interface to properly align the foveal cones. In the case of detachment, preventing both photoreceptor and Muller cell reactivity may also be key to treating the injury and preventing threats to sight through diseases such as subretinal fibrosis and proliferative vitreoretinopathy. Adjuncts to therapy do not seem so distant in these cases, because treatment with something as simple as elevated oxygen concentration appears to help attain these goals in animal models (25, 40, 47, 122).

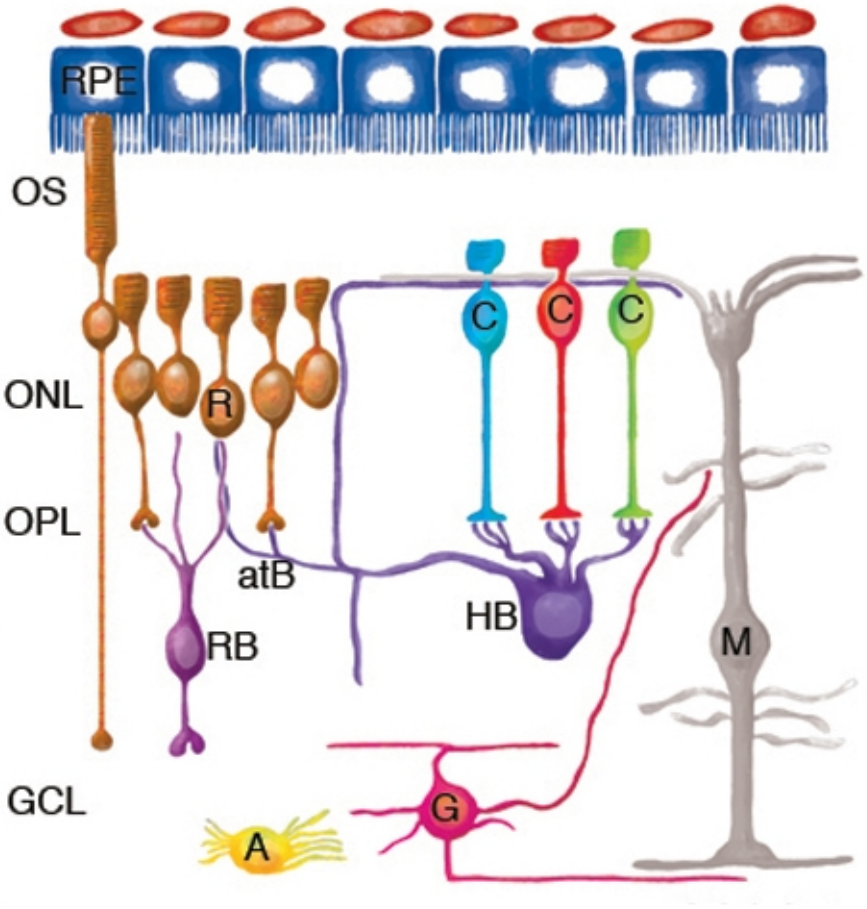

Figure 27. A drawing summarizing the remodeling events in the feline retina as a result of detachment. A, astrocytes; atB, axon terminal of B-type horizontal cell; C, cone; COS, cone outer segments; G, ganglion cells; HB, B-type horizontal cells; M, Muller cells; OPL, outer plexiform layer; ONL, outer nuclear layer; R, rod; ROS, rod outer segments; RB, rob bipolar cells; RPE, retinal pigmented epithelium.

About the Author

Dr. Steven Fisher was born in a small farm village in northern Indiana. He received his B.S. (Experimental Psychology, 1964), M.S. (Physiology, 1966), and Ph.D. (Neurobiology, 1969) degrees from Purdue University. His

mentor for the Ph.D. was (the late) Professor Marcus Jacobson. Steve then did an NIH Postdoctoral Fellowship in 1969 in the laboratory of Dr. John Dowling at the Wilmer Institute. His first academic appointment was in 1971 as an Assistant Professor of Biology at the University of California, Santa Barbara. He remains at UCSB as Professor of Molecular Cellular and Developmental Biology and a member of the Neuroscience Research Institute. He was the founding Director of that Institute. His research interests include the organization of the vertebrate retina, the cell biology of retinal injury regeneration within the retina. Recently, he has moved into the world of bio-image informatics, and he is now part of the Center for BioImage Informatics at UCSB (http://www.bioimage.ucsb.edu/). The NSF-supported Center has as its mission the building of large, distributed, searchable databases of biological tissue and the building of special tools for the analysis of biological images. He has been honored with a Research Career Development Award and a M.E.R.I.T. Award from the National Eye Institute, and in 2002 with the Ludwig Von Sallmann Prize for Vision Research.

References

1. Dowling JE. Organization of vertebrate retinas. Invest Ophthalmol. 1970;9:655–680. PubMed PMID: 4915972.
2. Kolb H, Famiglietti EV. Rod and cone pathways in the retina of the cat. Invest Ophthalmol. 1976;15:935–946.
3. Kolb H, Nelson R, Ahnelt P, Cuenca N. Cellular organization of the vertebrate retina. In: Kolb H, Ripps H, Wu S, editors. Prog. Brain Res. 131. Concepts and challenges in retinal biology. A tribute to John E. Dowling. Amsterdam: Elsevier; 2001. p. 3-26.
4. Linberg K, Cuenca N, Ahnelt P, Fisher S, Kolb H. (2001). Comparative anatomy of major retinal pathways in the eyes of nocturnal and diurnal mammals. In: Kolb H, Ripps H, Wu S, editors. Concepts and challenges in retinal biology. A tribute to John E. Dowling. Prog Brain Res. 131: 27-52.
5. Wagner H-J. Quantitative changes of synaptic ribbons in the cone pedicles of Nannacara: light dependent or governed by a circadian rhythm? In: Ali MA, editor. Vision in fishes: new approaches in research. 1974 NATO Advanced Study Institute. New York: Plenum Press; 1975. p. 679-686.
6. Wagner H-J, Ali MA. Cone synaptic ribbons and retinomotor changes in the brook trout, Salvelinus fontinalis (Salmonidae, Teleostei), under various experimental conditions. Can J Zool. 1977;55:1684–1691. PubMed PMID: 922611.
7. Wagner H-J. Light-dependent plasticity of the morphology of horizontal cell terminals in cone pedicles of fish retinas. J Neurocytol. 1980;9:573–590. PubMed PMID: 7441304.
8. Peichl L, Bolz J. Kainic acid induces sprouting of retinal neurons. Science. 1984;223:503–504. PubMed PMID: 6691162.
9. Chu Y, Humphrey MF, Constable IJ. Horizontal cells of the normal and dystrophic rat retina: a wholemount study using immunolabeling for the 28 kDa calcium binding protein. Exp Eye Res. 1993;57:141–148. PubMed PMID: 8405180.
10. Fariss RN, Li ZY, Milam AH. Abnormalities in rod photoreceptors, amacrine cells, and horizontal cells in humans with retinitis pigmentosa. Am J Ophthalmol. 2000;129:215–223. PubMed PMID: 10682975.
11. Lewis GP, Linberg KA, Fisher SK. Neurite outgrowth from bipolar and horizontal cells following experimental retinal detachment. Invest Ophthalmol Vis Sci. 1998;39:424–434. PubMed PMID: 9478003.
12. Li ZY, Kljavin IJ, Milam AH. Rod photoreceptor neurite sprouting in retinitis pigmentosa. J Neurosci. 1995;15:5429–5438. PubMed PMID: 7643192.
13. Marc RE, Jones BW, Watt CB, Strettoi E. Neural remodeling in retinal degeneration. Prog Retin Eye Res. 2003;22:607–655. PubMed PMID: 12892644.
14. Anderson DH, Stern WH, Fisher SK, Erickson PA, Borgula GA. Retinal detachment in the cat: the pigment epithelial-photoreceptor interface. Invest Ophthalmol Vis Sci. 1983;24:906–926. PubMed PMID: 6862795.
15. Erickson PA, Fisher SK, Anderson DH, Stern WH, Borgula GA. Retinal detachment in the cat: the outer nuclear and outer plexiform layers. Invest Ophthalmol Vis Sci. 1983;24:927–942. PubMed PMID: 6862796.

16. Kroll AJ, Machemer R. Experimental retinal detachment in the owl monkey. III. Electron microscopy of retina and pigment epithelium. Am J Ophthalmol. 1968;66:410–427. PubMed PMID: 4970987.
17. Ramon y Cajal S. La r tine des vert br s. Cellule. 1892;9:119–225.
18. Coblentz FE, Radeke MJ, Lewis GP, Fisher SK. Evidence that ganglion cells react to retinal detachment. Exp Eye Res. 2003;76:333–342. PubMed PMID: 12573662.
19. Linsenmeier RA, Padnick-Silver L. Metabolic dependence of photoreceptors on the choroid in the normal and detached retina. Invest Ophthalmol Vis Sci. 2000;41:3117–3123. PubMed PMID: 10967072.
20. Berglin L, Algvere PV, Seregard S. Photoreceptor decay over time and apoptosis in experimental retinal detachment. Graefes Arch Clin Exp Ophthalmol. 1997;235:306–312. PubMed PMID: 9176679.
21. Faude F, Francke M, Makarov F, Schuck J, Gartner U, Reichelt W, Wiedemann P, Wolburg H, Reichenbach A. Experimental retinal detachment causes widespread and multilayered degeneration in rabbit retina. J Neurocytol. 2001;30:379–390. PubMed PMID: 11951049.
22. Kryger Z, Galli-Resta L, Jacobs GH, Reese BE. The topography of rod and cone photoreceptors in the retina of the ground squirrel. Vis Neurosci. 1998;15:685–691. PubMed PMID: 9682870.
23. Long KO, Fisher SK. The distributions of photoreceptors and ganglion cells in the California ground squirrel Spermophilus beecheyi. J Comp Neurol. 1983;221:329–340. PubMed PMID: 6655087.
24. Linberg KA, Sakai T, Lewis GP, Fisher SK. Experimental retinal detachment in the cone-dominant ground squirrel retina: morphology and basic immunocytochemistry. Vis Neurosci. 2002;19:603–619. PubMed PMID: 12507327.
25. Sakai T, Lewis GP, Linberg KA, Fisher SK. The ability of hyperoxia to limit the effects of experimental detachment in cone dominated retina. Invest Ophthalmol Vis Sci. 2001;42:3264–3273. PubMed PMID: 11726632.
26. Nour M, Quiambao AB, Peterson WM, Al-Ubaidi MR, Naash MI. P2Y2 receptor agonist INS37217 enhances functional recovery after eetachment caused by subretinal injection in normal and rds mice. Invest Ophthalmol Vis Sci. 2003;44:4505–4514. PubMed PMID: 14507899.
27. Yang L, Bula D, Arroyo JG, Chen DF. Preventing retinal detachment-associated photoreceptor cell loss in Bax-deficient mice. Invest Ophthalmol Vis Sci. 2004;45:648–654. PubMed PMID: 14744910.
28. Lewis GP, Linberg KA, Geller SF, Guerin CJ, Fisher SK. Effects of the neurotrophin BDNF in an experimental model of retinal detachment. Invest Ophthalmol Vis Sci. 1999;40:1530–1544. PubMed PMID: 10359336.
29. Aaberg TM. Does hyperoxygenation limit retina degeneration after retinal detachment? Am J Ophthalmol. 1999;128:231. PubMed PMID: 10458181.
30. Sethi CS, Lewis GP, Fisher SK, Leitner WP, Mann DL, Luthert PJ, Charteris DG. Glial remodeling and neural plasticity in human retinal detachment with proliferative vitreoretinopathy. Invest Ophthalmol Vis Sci. 2005;46:329–342. PubMed PMID: 15623793.
31. Lewis GP, Sethi CS, Carter KM, Charteris DG, Fisher SK. Microglial cell activation following retinal detachment: a comparison between species. Mol Vis. 2005. PubMed PMID: 16052164.
32. Thanos S, Moore S, Hong Y. Retinal microglia. Prog Retin Eye Res. 1996;15:331–361.
33. Anderson DH, Fisher SK. The relationship of primate foveal cones to the pigment epithelium. J Ultrastruct Res. 1979;67:23–32. PubMed PMID: 109622.
34. Fisher SK, Steinberg RH. Origin and organization of pigment epithelial apical projections to cones in cat retina. J Comp Neurol. 1982;206:131–145. PubMed PMID: 6806335.
35. Steinberg RH, Wood I. Pigment epithelial cell ensheathment of cone outer segments in the retina of the domestic cat. Proc R Soc Lond Biol. 1974;187:461–478. PubMed PMID: 4155505.
36. Steinberg RH, Wood I, Hogan MJ. Pigment epithelial ensheathment and phagocytosis of extrafoveal cones in human retina. Philos Trans R Soc Lond Biol. 1977;277:459–474. PubMed PMID: 16301.
37. Immel J, Negi A, Marmor MF. Acute changes in RPE apical morphology after retinal detachment in rabbit. An SEM study. Invest Ophthalmol Vis Sci. 1986;27:1770–1776. PubMed PMID: 3793410.

38. Anderson DH, Stern WH, Fisher SK, Erickson PA, Borgula GA. The onset of pigment epithelial proliferation following retinal detachment. Invest Ophthalmol Vis Sci. 1981;21:10–16. PubMed PMID: 7251293.
39. Anderson DH, Gurin CJ, Erickson PA, Stern WH, Fisher SK. Morphological recovery in the reattached retina. Invest Ophthalmol Vis Sci. 1986;27:168–183. PubMed PMID: 3943943.
40. Mervin K, Valter K, Maslim J, Lewis GP, Fisher SK, Stone J. Limiting the death and deconstruction during retinal detachment: the value of oxygen supplementation. Am J Ophthalmol. 1999;128:155–164. PubMed PMID: 10458170.
41. Steinberg RH, Fisher SK, Anderson DH. Disc morphogenesis in vertebrate photoreceptors. J Comp Neurol. 1980;190:501–518. PubMed PMID: 6771304.
42. Fariss RN, Molday RS, Fisher SK, Matsumoto B. Evidence from normal and degenerating photoreceptors that two outer segment integral membrane proteins have separate transport pathways. J Comp Neurol. 1997;387:148–156. PubMed PMID: 9331178.
43. Lewis GP, Erickson PA, Anderson DH, Fisher SK. Opsin distribution and protein incorporation in photoreceptors after experimental retinal detachment. Exp Eye Res. 1991;53:629–640. PubMed PMID: 1835933.
44. Cook B, Lewis GP, Fisher SK, Adler R. Apoptotic photoreceptor degeneration in experimental retinal detachment. Invest Ophthalmol Vis Sci. 1995;36:990–996. PubMed PMID: 7730033.
45. Lewis GP, Sethi CS, Charteris DG, Leitner WP, Linberg KA, Fisher SK. The ability of rapid retinal reattachment to stop or reverse the cellular and molecular events initiated by detachment. Invest Ophthalmol Vis Sci. 2002;43:2412–2420. PubMed PMID: 12091445.
46. Chang CJ, Lai WW, Edward DP, Tso MO. Apoptotic photoreceptor cell death after traumatic retinal detachment in humans. Arch Ophthalmol. 1995;113:880–886. PubMed PMID: 7605279.
47. Lewis GP, Talaga KC, Linberg KA, Avery RL, Fisher SK. The efficacy of delayed oxygen therapy in the treatment of experimental retinal detachment. Am J Ophthalmol. 2004;137:1085–1095. PubMed PMID: 15183794.
48. Boycott BB, Kolb H. The connections between bipolar cells and photoreceptors in the retina of the domestic cat. J Comp Neurol. 1973;148:91–114. PubMed PMID: 4633446.
49. Kolb H. The connections between horizontal cells and photoreceptors in the retina of the cat: electron microscopy of Golgi preparations. J Comp Neurol. 1974;155:1–14. PubMed PMID: 4836060.
50. Migdale K, Herr S, Klug K, Ahmad K, Linberg K, Sterling P, Schein S. Two ribbon synaptic units in rod photoreceptors of macaque, human, and cat. J Comp Neurol. 2003;455:100–112. PubMed PMID: 12454999.
51. Schmitz F, Konigstorfer A, Sudhof TC. RIBEYE, a component of synaptic ribbons: a protein's journey through evolution provides insight into synaptic ribbon function. Neuron. 2000;28:857–872. PubMed PMID: 11163272.
52. Linberg KA, Lewis GP, Shaaw C, Rex TS, Fisher SK. Distribution of S- and M-cones in normal and experimentally detached cat retina. J Comp Neurol. 2001;430:343–356. PubMed PMID: 11169472.
53. Rex TS, Fariss RN, Lewis GP, Linberg KA, Sokal I, Fisher SK. A survey of molecular expression by photoreceptors after experimental retinal detachment. Invest Ophthalmol Vis Sci. 2002;43:1234–1247. PubMed PMID: 11923271.
54. Johnson LV, Hageman GS, Blanks JC. Interphotoreceptor matrix domains ensheath vertebrate cone photoreceptor cells. Invest Ophthalmol Vis Sci. 1986;27:129–135. PubMed PMID: 3080382.
55. Steinberg RH, Reid M, Lacy PL. The distribution of rods and cones in the retina of the cat (Felis domesticus). J Comp Neurol. 1973;148:229–248. PubMed PMID: 4700509.
56. Szel A, Takacs L, Monostori E, Vigh-Teichmann I, Rohlich P. Heterogeneity of chicken photoreceptors as defined by hybridoma supernatants. An immunocytochemical study. Cell Tissue Res. 1985;240:735–741. PubMed PMID: 3893724.
57. Szel A, Diamantstein T, Rohlich P. Identification of the blue-sensitive cones in the mammalian retina by anti-visual pigment antibody. J Comp Neurol. 1988;273:593–602. PubMed PMID: 3209737.

58. Wang Y, Macke JP, Merbs SL, Zack DJ, Klaunberg B, Bennett J, Gearhart J, Nathans J. A locus control regtion adjacent to the human read and green visual pigment genes. Neuron. 1992;9:429–440. PubMed PMID: 1524826.
59. Haley TL, Pochet R, Baizer L, Burton MD, Crabb JW, Parmentier M, Polans AS. Calbindin D-28k immunoreactivity of human cone cells varies with retinal position. Vis Neurosci. 1995;12:301–307. PubMed PMID: 7786851.
60. Pasteels B, Rogers J, Blachier F, Pochet R. Calbindin and calretinin localization in retina from different species. Vis Neurosci. 1990;5:1–16. PubMed PMID: 2125465.
61. Rohrenbeck J, Wassle H, Boycott BB. Horizontal cells in the monkey retina: immunocytochemical staining with antibodies against calcium binding proteins. Eur J Neurosci. 1989;1:407–420. PubMed PMID: 12106128.
62. John SK, Smith JE, Aguirre GD, Milam AH. Loss of cone molecular markers in rhodopsin-mutant human retinas with retinitis pigmentosa. Mol Vis. 2000;6:204–215. PubMed PMID: 11063754.
63. Linberg K.A., Lewis G.P., Barawid E.L., Sakai T., Fisher S.K. A quantitative study of cone matrix sheath and S-cone recovery in reattached retina. Invest Ophthalmol Vis Sci. 2002;43:ARVO E-Abstract 4536.
64. Nork TM, Millecchia LL, Stickland BD, Linberg JV, Chao G. Selective loss of blue cones and rods in human retinal detachment. Arch Ophthalmol. 1995;113:1066–1073. PubMed PMID: 7639660.
65. Jacobs GH, Calderone JB, Sakai T, Lewis GP, Fisher SK.In: Mollon JD, Pokorny J, Knoblauch K, editors. Normal & defective colour vision. Effects of retinal detachment on S and M cone function in an animal model. Oxford (UK): Oxford University Press; 2003. p. 381-388.
66. Anderson DH, Fisher SK, Steinberg RH. Mammalian cones: disc shedding, phagocytosis, and renewal. Invest Ophthalmol Vis Sci. 1978;17:117–133. PubMed PMID: 415019.
67. Kroll AJ, Machemer R. Experimental retinal detachment in the owl monkey. V. Electron microscopy of reattached retina. Am J Ophthalmol. 1969;67:117–130. PubMed PMID: 4973407.
68. Kroll AJ, Machemer R. Experimental retinal detachment and reattachment in the rhesus monkey. Am J Ophthalmol. 1969;68:58–77. PubMed PMID: 4978398.
69. Machemer R. Experimental retinal detachment in the owl monkey. IV. The reattached retina. Am J Ophthalmol. 1968;66:1075–1091. PubMed PMID: 4973290.
70. Young RW. The renewal of photoreceptor cell outer segments. J Cell Biol. 1967;33:61–72. PubMed PMID: 6033942.
71. Zhang N, Townes-Anderson E. Regulation of structural plasticity by different channel types. J Neurosci. 2002;22:7065–7079. PubMed PMID: 12177203.
72. Guerin CJ, Anderson DH, Fariss RN, Fisher SK. Retinal reattachment of the primate macula: photoreceptor recovery after short-term detachment. Invest Ophthalmol Vis Sci. 1989;30:1708–1725. PubMed PMID: 2527212.
73. Liem AT, Keunen JE, van Meel GJ, van Norren D. Serial foveal densitometry and visual function after retinal detachment surgery with macular involvement. Ophthalmology. 1994;101:1945–1952. PubMed PMID: 7997333.
74. Ross WH. Visual recovery after macula-off retinal detachment. Eye. 2002;16:440–446. PubMed PMID: 12101451.
75. Rodieck RW. In: The first steps of seeing. Chapter 4. Sunderland (MA): Sinauer Assoc, Inc.; 1998. p. 70 -87.
76. Stiles WS, Crawford BH. The luminous efficiency of rays entering the eye pupil at different points. Proc R Soc Lond B Biol Sci. 1933;112:428–450.
77. Enoch JJ. Optical properties of ther etinal receptors. J Opt Soc Am. 1963;53:71–85.
78. Johnson PT, Williams RR, Cusato K, Reese BE. Rods and cones project to the inner plexiform layer during development. J Comp Neurol. 1999;414:1–12. PubMed PMID: 10494074.
79. Freed MA, Bsmith RG, Sterling P. Rod bipolar array in the cat retina: pattern of input from rods and GABA-accumulating amacrine cells. J Comp Neurol. 1987;266:445–455. PubMed PMID: 3693619.
80. Negishi K, Kato S, Teranishi T. Dopamine cells and rod bipolar cells contain protein kinase C-like immunoreactivity in some vertebrate retinas. Neurosci Lett. 1988;94:247–252. PubMed PMID: 3205402.

81. Wassle H, Yamashita M, Greferath U, Grunert U, Muller F. The rod bipolar cell of the mammalian retina. Vis Neurosci. 1991;7:99–112. PubMed PMID: 1718403.
82. Dowling JE, Brown JE, Major D. Synapses of horizontal cells in rabbit and cat retinas. Science. 1966;153:1639–1641. PubMed PMID: 5917075.
83. Fisher SK, Boycott BB. Synaptic connexions of the horizontal cells in the outer plexiform layer of the retina of the cat and the rabbit. Proc R Soc Lond B Biol Sci. 1974;186:317–331. PubMed PMID: 4154444.
84. Nelson R, von Lutzow A, Kolb H, Gouras P. Horizontal cells in cat retina with independent dendritic systems. Science. 1975;189:137–139. PubMed PMID: 1138370.
85. Linberg K.A., Lewis G.P., Carter K.M., Fisher S.K. Immunocytochemical evidence that B-type horizontal cell axon terminals remodel in response to retinal detachment in the cat. Invest Ophthalmol Vis Sci. 2004;45:ARVO E-Abstract 4604.
86. Marc RE, Murry RF, Fisher SK, Linberg KA, Lewis GP. Amino acid signatures in the detached cat retina. Invest Ophthalmol Vis Sci. 1998;39:1694–1702. PubMed PMID: 9699559.
87. Lamoureux P, Ruthel G, Buxbaum RE, Heidemann SR. Mechanical tension can specify axonal fate in hippocampal neurons. J Cell Biol. 2002;159:499–508. PubMed PMID: 12417580.
88. Geller SF, Lewis GP, Fisher SK. FGFR1, signaling, and AP-1 expression following retinal detachment: reactive Muller and RPE cells. Invest Ophthalmol Vis Sci. 2001;42:1363–1369. PubMed PMID: 11328752.
89. Benowitz LI, Perrone-Bizzozero NI. The expression of GAP-43 in relation to neuronal growth and plasticity: when, where, how, and why? Prog Brain Res. 1991;89:69–87. PubMed PMID: 1839072.
90. Benowitz LI, Perrone-Bizzozero NI. The relationship of GAP-43 to the development and plasticity of synaptic connections. Ann N Y Acad Sci. 1991;627:58–74. PubMed PMID: 1831963.
91. Skene JH. Axonal growth-associated proteins. Annu Rev Neurosci. 1989;12:127–156. PubMed PMID: 2648946.
92. Strittmatter SM, Vartanian T, Fishman MC. GAP-43 as a plasticity protein in neuronal form and repair. J Neurobiol. 1992;23:507–520. PubMed PMID: 1431834.
93. Benowitz LI, Apostolides PJ, Perrone-Bizzozero N, Finkelstein SP, Zwiers H. Anatomical distribution of the growth-associated protein GAP-43/B-50 in the adult rat brain. J Neurosci. 1988;8:339–352. PubMed PMID: 3339416.
94. Gispen WH, Nielander HB, De Graan PN, Oestreicher AB, Schrama LH, Schotman P. Role of the growth-associated protein B-50/GAP-43 in neuronal plasticity. Mol Neurobiol. 1991;5:61–85. PubMed PMID: 1840422.
95. Kapfhammer JP, Christ F, Schwab ME. The expression of GAP-43 and synaptophysin in the developing rat retina. Brain Res Dev Brain Res. 1994;80:251–260. PubMed PMID: 7955350.
96. Kruger L, Bendotti C, Rivolta R, Samanin R. Distribution of GAP-43 mRNA in the adult rat brain. J Comp Neurol. 1993;333:417–434. PubMed PMID: 8349850.
97. Meberg PJ, Routtenberg A. Selective expression of protein F1/(GAP-43) mRNA in pyramidal but not granule cells of the hippocampus. Neuroscience. 1991;45:721–733. PubMed PMID: 1837850.
98. Strittmatter SM, Fankhauser C, Huang PL, Mashimo H, Fishman MC. Neuronal path finding is abnormal in mice lacking the neuronal growth cone protein GAP-43. Cell. 1995;80:445–452. PubMed PMID: 7859286.
99. Aigner L, Arber S, Kapfhammer JP, Laux T, Schneider C, Botteri F, Brenner HR, Caroni P. Overexpression of the neural growth-associated protein GAP-43 induces nerve sprouting in the adult nervous system of transgenic mice. Cell. 1995;83:269–278. PubMed PMID: 7585944.
100. De la Monte SM, Federoff HJ, Ng SC, Grabczyk E, Fishman MC. GAP-43 gene expression during development: persistence in a distinctive set of neurons in the mature central nervous system. Brain Res Dev Brain Res. 1989;46:161–168. PubMed PMID: 2720952.
101. McIntosh H, Blazynski C. GAP-43-like immunoreactivity in the adult retina of several species. Brain Res. 1991;554:321–324. PubMed PMID: 1834305.
102. Reh TA, Tetzlaff W, Ertlmaier A, Zwiers H. Developmental study of the expression of B50/GAP-43 in rat retina. J Neurobiol. 1993;24:949–958. PubMed PMID: 8228972.

103. Kolb H, Nelson R, Mariani A. Amacrine cells, bipolar cells and ganglion cells of the cat retina: a Golgi study. Vision Res. 1981;21:1081–1114. PubMed PMID: 7314489.
104. Boycott B, Wassle H. Parallel processing in the mammalian retina: the Proctor Lecture. Invest Ophthalmol Vis Sci. 1999;40:1313–1327. PubMed PMID: 10359312.
105. Lewis GP, Sethi CS, Linberg KA, Charteris DG, Fisher SK. Experimental retinal reattachment. A new perspective. Mol Neurobiol. 2003;28:159–175. PubMed PMID: 14576454.
106. Lewis GP, Erickson PA, Guerin CJ, Anderson DH, Fisher SK. Changes in the expression of specific Muller cell proteins during long-term retinal detachment. Exp Eye Res. 1989;49:93–111. PubMed PMID: 2503391.
107. Lewis GP, Matsumoto B, Fisher SK. Changes in the organization of cytoskeletal proteins during retinal degeneration induced by retinal detachment. Invest Ophthalmol Vis Sci. 1995;36:2404–2416. PubMed PMID: 7591630.
108. Erickson PA, Fisher SK, Gurin CJ, Anderson DH, Kaska DD. Glial fibrillary acidic protein increases in Muller cells after retinal detachment. Exp Eye Res. 1987;44:37–48. PubMed PMID: 3549345.
109. Eng LF, DeArmond SJ. 1981.
110. Bignami A, Dahl D. The radial glia of Muller in the rat retina and their response to injury. An immunofluorescence study with antibodies to the glial fibrillary acidic (GFA) protein. Exp Eye Res. 1979;28:63–69. PubMed PMID: 376324.
111. Eisenfeld AJ, Bunt-Milam AH, Sarthy PV. Muller cell expression of glial fibrillary acidic protein after genetic and experimental photoreceptor degeneration in the rat retina. Invest Ophthalmol Vis Sci. 1984;25:1321–1328. PubMed PMID: 6386743.
112. Sarthy V, Ripps H. The retinal Muller cell. In: Blakemore C, editor. Perspectives in vision research. New York: Plenum Press; 2001.
113. Pekny M, Johansson CB, Eliasson C, Stakeberg J, Wallen A, Perlmann T, Lendahl U, Betsholtz C, Berthold C-H, Frisen J. Abnormal reaction to central nervous system injury in mice lacking glial fibrillary acidic protein and vimentin. J Cell Biol. 1999;145:503–514. PubMed PMID: 10225952.
114. Lewis GP, Fisher SK. 2003. Upregulation of GFAP in response to retinal injury: Its potential role in glial remodeling and a comparison to vimentin expression. In: K.W. Jeon, editor. Int. Rev. Cytol. A Survey of Cell Biology. Vol. 230. San Diego (CA): Elsevier Academic Press; 2003. p. 263-290.
115. Ryan SJ. The pathophysiology of proliferative vitreoretinopathy in its mangagement. Am J Ophthalmol. 1985;100:188–193. PubMed PMID: 4014372.
116. Fisher SK, Erickson PA, Lewis GP, Anderson DH. Intraretinal proliferation induced by retinal detachment. Invest Ophthalmol Vis Sci. 1991;32:1739–1748. PubMed PMID: 2032796.
117. Geller SF, Lewis GP, Anderson DH, Fisher SK. Use of the MIB-1 antibody for detecting proliferating cells in the retina. Invest Ophthalmol Vis Sci. 1995;36:737–744. PubMed PMID: 7890504.
118. Aramant RB, Seiler MJ. Progress in retinal sheet transplantation. Prog Retin Eye Res. 2004;23:475–494. PubMed PMID: 15302347.
119. Fischer AJ, Reh TA. Muller glia are a potential source of neural regeneration in the postnatal chicken retina. Nat Neurosci. 2001;4:247–252. PubMed PMID: 11224540.
120. Fischer AJ, Reh TA. Potential of Muller cells to become neurogenic regeneration retinal progenitor cells. Glia. 2003;43:70–76. PubMed PMID: 12761869.
121. Tropepe V, Coles BL, Chiasson BJ, Horsford DJ, Elia AJ, McInnes RR, van der Kooy D. Retinal stem cells in the adult mammalian eye. Science. 2000;287:2032–2036. PubMed PMID: 10720333.
122. Kerns JM, Hinsman EJ. Neuroglial response to sciatic neurectomy. II. Electron microscopy. J Comp Neurol. 1973;151:255–280. PubMed PMID: 4744474.
123. Fisher SK, Anderson DH. Cellular effects of detachment on the neural retina and the retinal pigment epithelium. In: Ryan SJ, Wilkinson CP, editors. Retina, Surgical retina. Vol. 3. 3rd ed. St. Louis (MO): Mosby; 2001.

Regeneration in the Goldfish Visual System

Sam Nona

Created: May 1, 2005; Updated: June 20, 2007.

Overview

The visual system of the goldfish has been the subject of intensive studies for over a quarter of a century. It differs from the visual system of most other vertebrates, including mammals, in that it continues to grow by the addition of new neurons throughout much of the animal's life. This unusual characteristic has presented neuroscientists with an opportunity to examine how the existing visual pathway accommodates the new growth, for example as the axons of the newly born retinal ganglion cells exit the eye to join the older axons in the optic nerve tract—a conduit that carries visual impulses from the retina to the brain. Furthermore, for largely unknown reasons, the visual system of the goldfish is endowed with the capacity for repair if injured, culminating in the recovery of vision. Much research has been undertaken to identify the cellular and molecular components that support this phenomenon, not least because the knowledge gained may be helpful in the quest to understand why a similar injury in mammals—including humans—invariably leads to an irreversible loss of function.

The following commentary is a pictorial journey through the visual system of the common strain of the goldfish, *Carassius auratus*. It highlights, by the use of species-specific immunocytochemical markers and electron microscopy (EM), the system's many unique structural features, which are quite unlike those in other vertebrates, and are thus of interest because of the likelihood that they reflect a patterning better suited for the restoration of its cytoarchitecture after injury.

In this commentary, I first describe the organization of the normal goldfish visual system and point to those features that distinguishe it from the visual system of other vertebrates. This will be the foundation for the main theme of the commentary, in which I describe some of the cellular events that accompany the process of repair in the injured optic nerve of the goldfish.

General Features of the Goldfish Visual System

Like the brain and the spinal cord, the visual system of the vertebrates is a component of the central nervous system (CNS). In the goldfish, the visual system is made up of three distinct compartments (Fig. 1):

- the retina
- the optic nerve
- the tectal target in the brain

The **retina** lines the posterior of the eye. Axons of retinal ganglion cells emerge from the back of the eye, acquire myelin sheath, and become grouped into bundles, thus forming the **optic nerve**. The two optic nerves cross bodily at the midline—a region known as chiasm—where they enter the skull to join the **tectal target in the brain** contralaterally, not ipsilaterally as in most other vertebrates. Thus, axons of retinal ganglion cells represent the only structure that is common to all three compartments, which are, nevertheless, distinguished by different types of astrocytes, or astroglia cells, which form the principal framework, locally adapted to serve the needs of the tissue, as described below.

Astrocytes in the Retina

The Muller cells are the principal glia (Latin: "glue") cells of the teleost retina. They form architectural support structures stretching radially across the thickness of the retina. At the turn of last century, Cajal (1) described the fine structure of Muller cells in several species using Golgi staining, a technique that bathes the tissue in silver

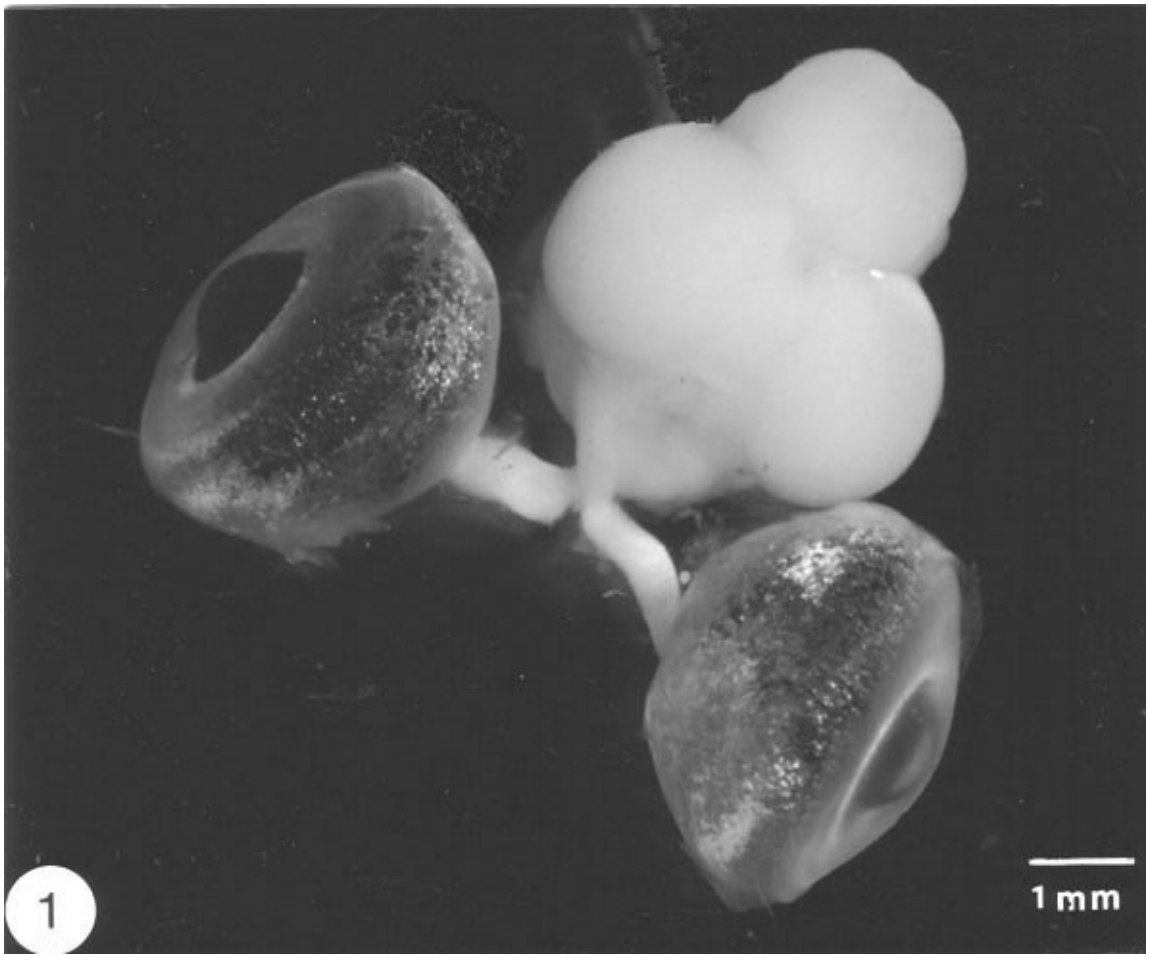

Figure 1. The visual system of the goldfish. Note the complete crossover of the two nerves at the chiasm. (Dissected by Carole Bartlett).

salts to reveal the fine details of individual cells. The Muller cell bodies lie in the inner nuclear layer of the retina and project thick and thin processes in either direction to the outer and inner limiting membranes. Muller cell processes insinuate themselves between cell bodies of neurons in the nuclear and plexiform layers and enwrap neuronal cell bodies (2). Through this extensive system of cell processes, Muller cells are believed to provide metabolic support to the retinal neurons, as well as remove their waste.

The Muller cells are considered to be a type of astrocyte because their processes are filled with intermediate filaments, so-called because their diameter is intermediate between myosin filaments (15 nm) and actin filaments (6 nm), that stain dramatically with antibodies to glial fibrillary acidic protein (GFAP), the subunit protein of the filaments found in astrocytes (reviewed by Traub (3). The GFAP subunit is well conserved across the vertebrate phylum, and in goldfish, as in rat, it has a molecular weight of 51,000, as determined by SDS-polyacrylamide elctrophoresis (4). The antiserum to goldfish GFAP, when applied to sections of goldfish retina, specifically recognizes Muller cells' radial processes, which at the basal end enwrap retinal ganglion cell perikarya and form end-feet at the vitreal surface of the retina, while at the other extremity, they elaborate a network of fine processes that terminate at the photoreceptors (Fig. 2). The Muller cells perikarya and lateral processes, both of which are readily seen by the Golgi method, are not revealed by anti-GFAP, possibly because these structures do not contain GFAP in detectable amounts. Nevertheless, the specificity of the antiserum is nicely demonstrated by the absence of staining elsewhere in the retina. In this context it is interesting that "free" astrocytes, of the type described in the nerve fiber layer of mammalian retina (5), are absent from the teleost retina.

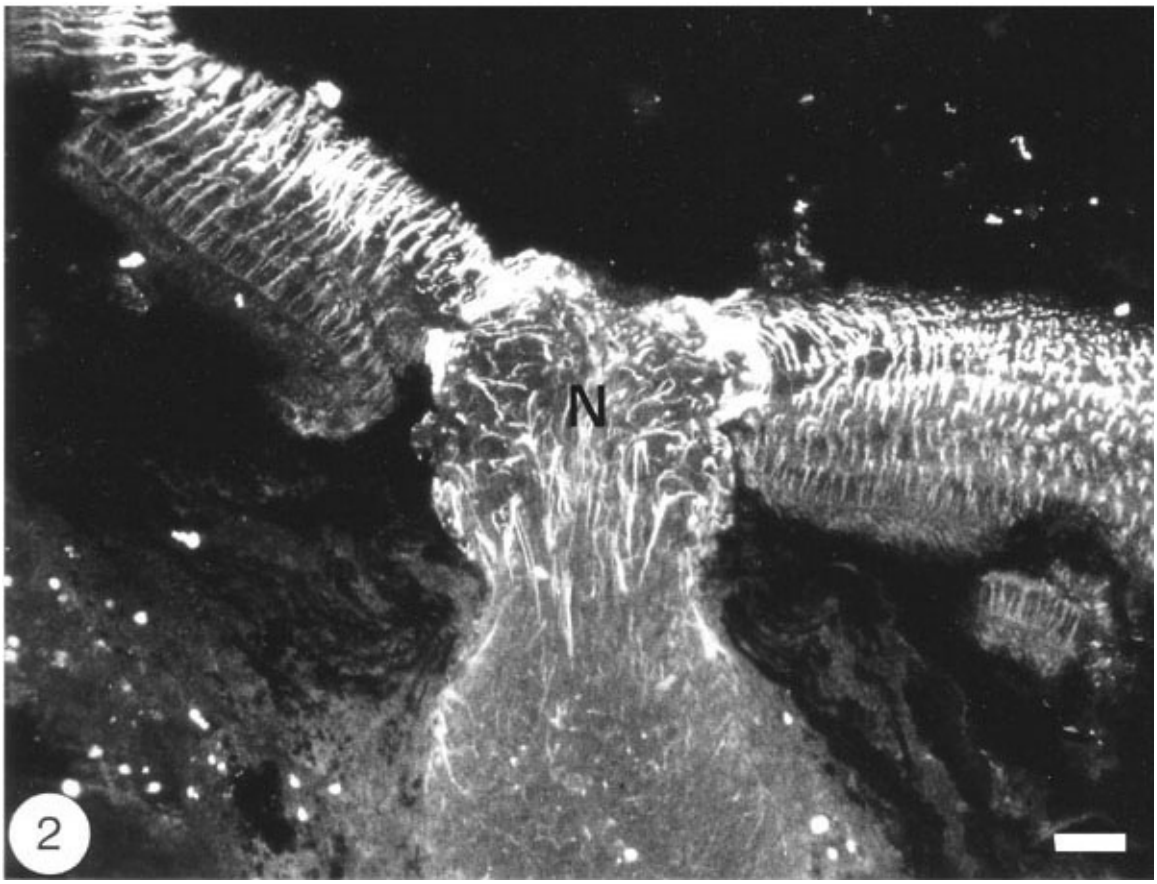

Figure 2. Longitudinal section of goldfish retina and optic nerve head stained for GFAP. Note the radial orientation of Muller cells in the retina and astrocytes in the optic nerve head (N). Bar = 50 μm.

Astrocytes in the Optic Nerve

The structure of the fish optic nerve has been described by several workers using various methodologies (6-8). This author intends to add another dimension to these reports, by describing the pattern of glial cells and optic fibers in the normal goldfish optic nerve as revealed by goldfish-specific antibodies to GFAP and neurofilament protein, respectively. These studies are complemented by ultrastructural studies to provide a detailed picture of the optic nerve structure and, therefore, a template with which to compare the structure of the repaired nerve following injury.

In the goldfish, the optic nerve is cylindrical in shape, measuring 0.5 mm in diameter and 2.5 mm in length (in a 5-cm long fish). The optic nerve is white in appearance because of the lipid-rich myelin sheath that enwraps its fibers (Fig. 1). For the purpose of this discussion, the optic nerve will be divided into two parts: 1) the intraocular optic nerve, and 2) the intraorbital optic nerve, through to the chiasm.

The Intraocular Optic Nerve

The tip of the optic nerve, which lies within the retina, has a conical shape. Axons of retinal ganglion cells converge onto the optic disc to be funneled into the optic nerve head by a resident population of GFAP-positive astrocytes whose radial orientation corresponds to the trajectories of the axons (Fig. 2). This arrangement implies that astrocytes at the optic nerve head direct the axons away from the rest of the retina and into the optic nerve head, perhaps through the expression of a combination of attractant and repellant molecules on their surface (9-11). Astrocytes, additionally, envelop the surface of the optic nerve head in a characteristic fashion

known as glia limitans, thus forming a tube-like structure through which the axons are funneled (Fig. 3). Running through the center of the optic nerve head is the central artery, which is also enwrapped by astrocyte processes. It is thus reasonable to assume that the manner with which the astrocytes envelop the vasculature and the axons signifies some primitive disposition of blood-brain barrier, as well as providing a nutritive service, much like the Muller cells in the retina.

The Intraorbital Optic Nerve

After the optic nerve leaves the retina and passes through the globe's outer layer, the sclera, its tightly packed fibers more than double in size as they enter the orbit. This transition is a landmark, for it signifies that the hitherto naked fiberes have acquired myelin sheath. Thereafter, the glial cells sculpt the optic nerve into an intricate pattern, the fine details of which are beautifully revealed by immunocytochemistry.

An unexpected finding, reported nearly simultaneously by several laboratories, revealed that astrocytes in the normal fish optic nerve do not contain an appreciable amount of GFAP (4), the universal marker for astrocytes (12). Rather, astrocytes of goldfish optic nerve (7, 13) and cichlid optic nerve (8) are composed largely of cytokeratin polypeptides—proteins that are normally found in epithelial tissue. This finding led some workers to propose that the absence of GFAP is a reflection of the immaturity of the tissue and is, therefore, the reason why fish optic nerve has the capacity for robust regeneration (13). However, this suggestion has been mooted by the author and his colleagues, who were the first to demonstrate that the attenuated level of GFAP in the goldfish optic nerve (14) is greatly enhanced following an injury to the visual system (Fig. 4).

Interestingly, the dramatic response of fish optic nerve astrocytes to injury, although in keeping with what is generally observed in all damaged CNS tissue, was to be followed by more dramatic cellular responses in the optic nerve that set this tissue apart from its mammalian counterpart, and offered an explanation for its spontaneous recovery after injury.

The response of the goldfish optic nerve to injury reveals a striking pattern underlying the tissue's framework: it shows that the first one-quarter of the optic nerve is made up of GFAP-positive astrocytes that are organized as a dense, lace-like pattern with no evidence of segmentation into discrete domains, an observation that is reflected in the organization of the fibers that appear closely bundled, with no discernible spaces between them (15). Further along the nerve, however, up to the nerve-tract boundary, myelinated axons are organized into discrete domains, known as fascicles (Fig. 5). In longitudinal profile, the fascicles appear as linear channels or tubes bound by parallel astrocyte processes (glia limitans), and each fascicle is separated from its neighbors by parallel rows of connective tissue septae. The pattern shows greater intricacy in transverse profile, with the astrocytes-bound fascicles being further divided into smaller compartments by fine processes (Fig. 6), a pattern that is also seen with an antibody to goldfish cytokeratin (7).

Ultrastuctural studies of the optic nerve are in complete agreement with these observations (6, 16). They show the optic nerve to be made up of bundles of myelinated axons enclosed by astrocyte processes, thus forming discrete fascicles that are separated from adjacent fascicles by septae, containing collagen, fibroblasts and capillaries. Furthermore, each fascicle is divided into smaller compartments by astrocyte processes that form characteristic desmosomal junctions. The close correspondence between ultrastructural and immunocytochemical findings is depicted in Fig. 6.

EM analyses additionally reveal that the optic nerve contains microglia, which equate to the macrophages normally found in the peripheral nervous system (PNS), and become phagocytic if the tissue is damaged, as well as a unique class of non-phagocytic granular cells that reside normally within the sheath/septae. A full complement of the cells and structures that make up the goldfish optic nerve is given in Fig. 7.

It is instructive to return briefly to the epithelioid characteristics of the fish optic nerve by referencing the cichlid optic nerves, which are formed as ribbons rather than discrete fascicles seen in the goldfish. The tissue pattern in

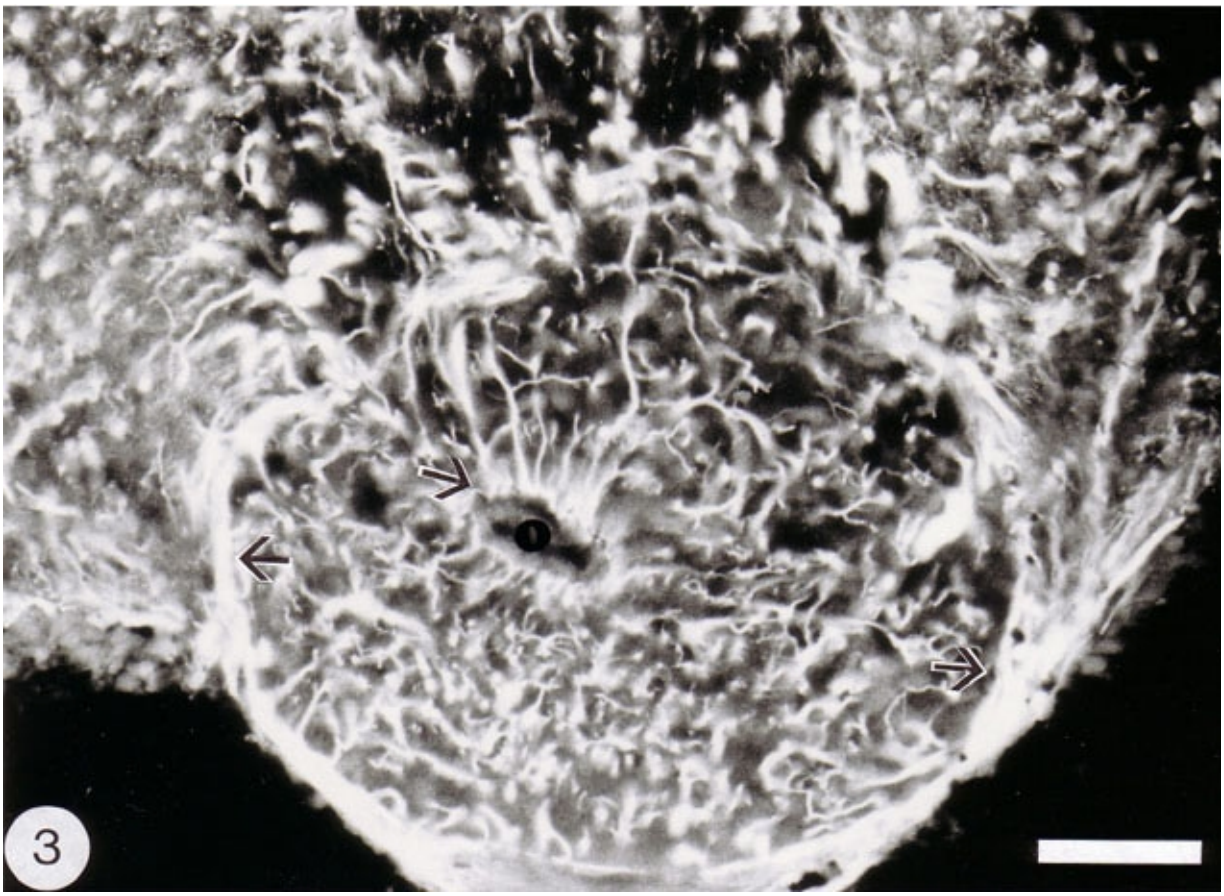

Figure 3. Cross-section of goldfish optic nerve head stained for GFAP. Astrocytes (→) enwrap the nerve head and the central artery (O). Bar = 50 μm.

the cichlid optic nerve appears to be more elaborate, with the longitudinally oriented astrocyte processes being connected at regular spacing by a lace-like network of finer astrocytes processes, laid out as sheets running at right angles to the optic fibers. Scholes and colleagues have proposed that this astrocytic pattern is linked throughout with desmosomal junction, thus providing the fish optic nerve with mechanical resilience needed during rapid eye movement. Astocytes in the cichlid optic nerves have been described as reticular astrocytes because they form a network pattern that complements the wavy pattern of the optic axons, enabling them to accommodate small stretches reversibly in a concertina-like action (17). And, as if to emphasize that eye movement in the fish can only be accommodated by a framework made up of an atypical phenotype (epithelioid) astroglia, both in terms of its organization and protein composition, the domain of the cytokeratin-expressing astrocytes in the optic nerves comes to an abrupt end at the nerve-tract boundary, beyond which, and throughout the brain, astrocytes are typically of radial morphology and express GFAP only (4).

Taken together, the above results demonstrate that astrocytes in the fish optic nerve express both cytokeratins and GFAP intermediate filaments, in contrast to the mammalian optic nerve astrocytes, which express GFAP only. One possible explanation is that astrocytes may have a relict evolutionary status (18). For example, the most primitive of extant vertebrates, the cyclostomes, have astroglia with similar cytology throughout the CNS, showing dense intermediate filaments linked with desmosomes (19). Scholes has suggested that fish optic nerve has retained elements of an ancient glial pattern that became outmoded as the CNS became armored in bone, but still appropriate in the orbit (17).

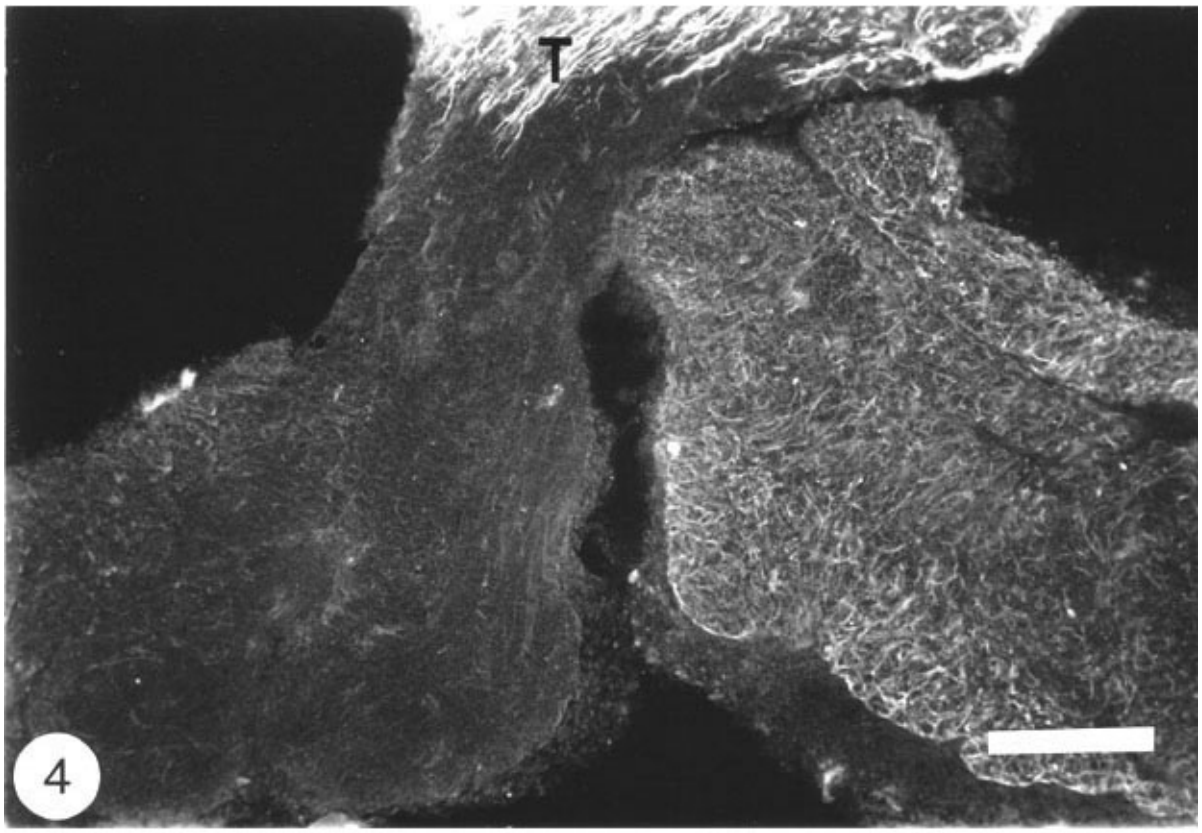

Figure 4. GFAP staining of normal (left) and injured (right) goldfish optic nerves at the chiasm. Astocytes are more prominent in the injured nerve. Astrocytes of the optic tract (T) are normally GFAP+. Bar = 50 µm.

Astrocytes in the Brain

Just beyond the chiasm, at the optic nerve-optic tract boundary, the astrocyte's phenotype changes abruptly in two respects. First, whereas before astrocytes were of reticular morphology, now they have a radial morphology. Second, whereas reticular astrocytes expressed strongly cytokeratin proteins and only faintly GFAP, radial astrocytes show a pronounced expression of GFAP, and there is an absence of cytokeratin expression (4, 7, 20).

Astrocytes in the Optic Tract

Astrocytes in the goldfish optic tract appear to arise from two sources. The radial astrocytes that are seen at the commencement of the tract arise from cells whose perikarya line the optic recess. Evidence for this comes from the staining pattern of two adjacent sections of the optic tract, with anti-GFAP and anti-S-100 protein, respectively. Although the former marker recognizes a profusion of radial processes, the latter additionally highlights a population of brightly stained round cell bodies at the nerve-tract boundary, extending into the optic recess (Fig. 8). The validity of S-100 protein as a marker for astrocytes has been documented for mammalian astrocytes (21, 22).

The second source of astrocytes in the optic tract are the cells that line the walls of the third ventricle, from where one subpopulation of radial astrocytes runs along the dorsal aspect of the tract, parallel to the optic fibers, while a second population of radial astrocytes traverses the tract to terminate as end-feet on its surface. Where the optic tract bifurcates, at the nucleus rotundus, before it joins the optic tectum, radial astrocytes are no longer discernible immunocytochemically (4).

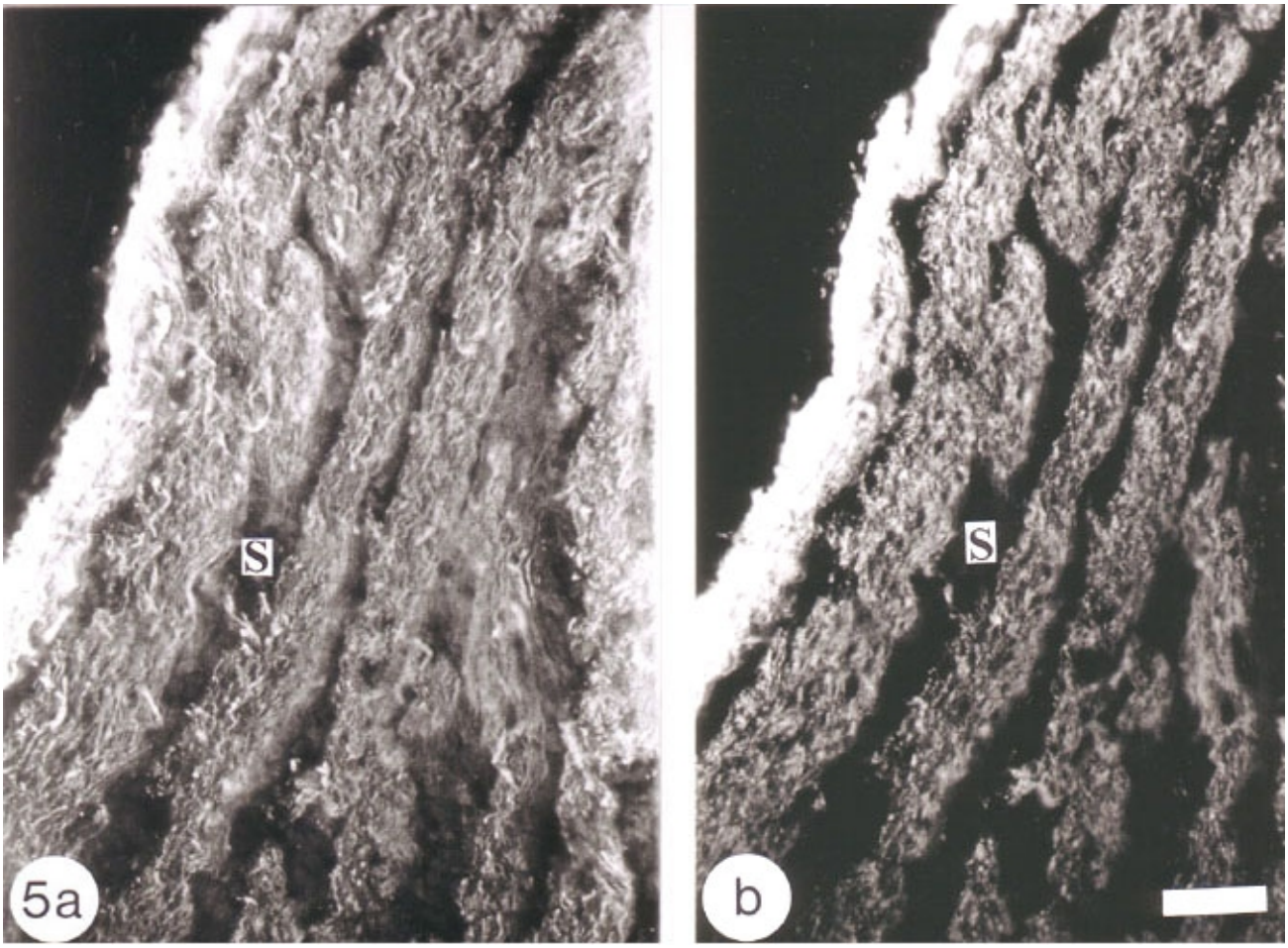

Figure 5. Longitudinal section of goldfish optic nerve stained with neurofilament marker IF145 (a) and myelin marker 6D2 (b). The optic fibers are contained within fascicles, separated by negatively stained septae (S). Bar = 50 μm.

Astrocytes in the Optic Tectum

In the optic tectum of the teleost, there are two distinct populations of GFAP-positive astrocytes. The ependymal region contains an extensive meshwork of astrocyte processes that border on the ventricular margin and extend dorsally toward the neuronal stratum periventricular layer (4). Arising prominently from this region and extending across all of the tectal layers is a well-organized system of radial processes that terminate as end-feet on the pia surface (Fig. 9). There has been much debate as to the source of these two astrocyte populations, with some authorities suggesting that they arise from a common cell body (23). However, studies conducted by the author, using anti-S-100 protein, have revealed two distinct populations of cell bodies: one that is scattered in the ependymal region, and another, one or two cells deep, that is interposed between the ependymal and the stratum periventricular regions. It is from this second population of perikarya that fine radial processes emerge to traverse the tectum (4, 24), a finding that is supported by EM studies (25). A curiosity is that in fish, neither the astrocytes in the brain nor those in the optic nerve conform to the classical description of astrocytes.

What Are Astrocytes?

Strictly speaking, astrocytes are the star shaped GFAP-positive glia cells (Fig. 10) (26) in the adult mammals and birds, which have end-feet on CNS blood vessels (for an excellent review, see Bignami (12). They lack desmosomes, and they appear late in development by proliferation of radial glia, following withdrawal of the pial and ependymal contacts (27). In the fish, on the other hand, GFAP-positive glia cells in the brain (4) and spinal

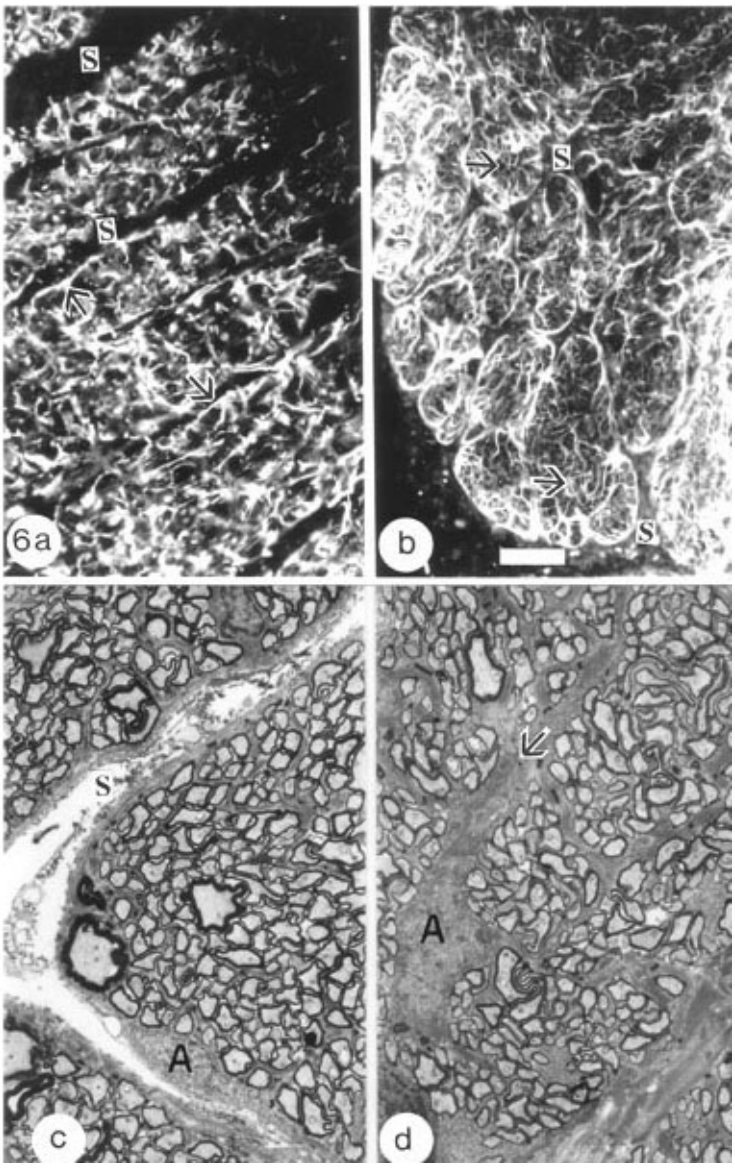

Figure 6. The fascicular pattern of the goldfish optic nerve is defined by the tissue's astrocytes. (a) and (b) show the pattern in longitudinal and transverse profiles, respectively, stained for GFAP. Note the fine details of each fascicle in (b). The pattern is nicely reproduced in EM sections (c) and (d), which correspond to (a) and (b), respectively. (S) septae, (→) astrocyte processes, (A) astrocytes cell body. Bar = 50 μm for (a) and (b). (c) ×3.5K; (d) 8K.

cord (28) retain their radial morphology in the adult. The persistence of radial astrocytes may signify some dependence on cell contact with the ependymal lining of the CNS ventricle. The absence of the ependymal structure from the optic nerve of the fish, therefore, explains nicely why astrocytes here differentiate as a specialized form—the reticular astrocytes (17).

Axon Regeneration in Injured Goldfish Optic Nerve

The literature abounds with studies that confirm an observation made by Ramon y Cajal (29) almost a century ago that, with a few exceptions, severed axons of the neurons in the mammalian CNS are capable only of abortive sprouting that provides little functional recovery. In contrast, neurons in the PNS have a greater capacity for regrowing their damaged axons, and under appropriate conditions, there is a recovery of function. It has not been possible to put forward a direct and simple explanation of this difference in regenerative capacity. Recent studies, however, give credence to Cajal's notion that the fault in CNS regeneration lies with the extrinsic

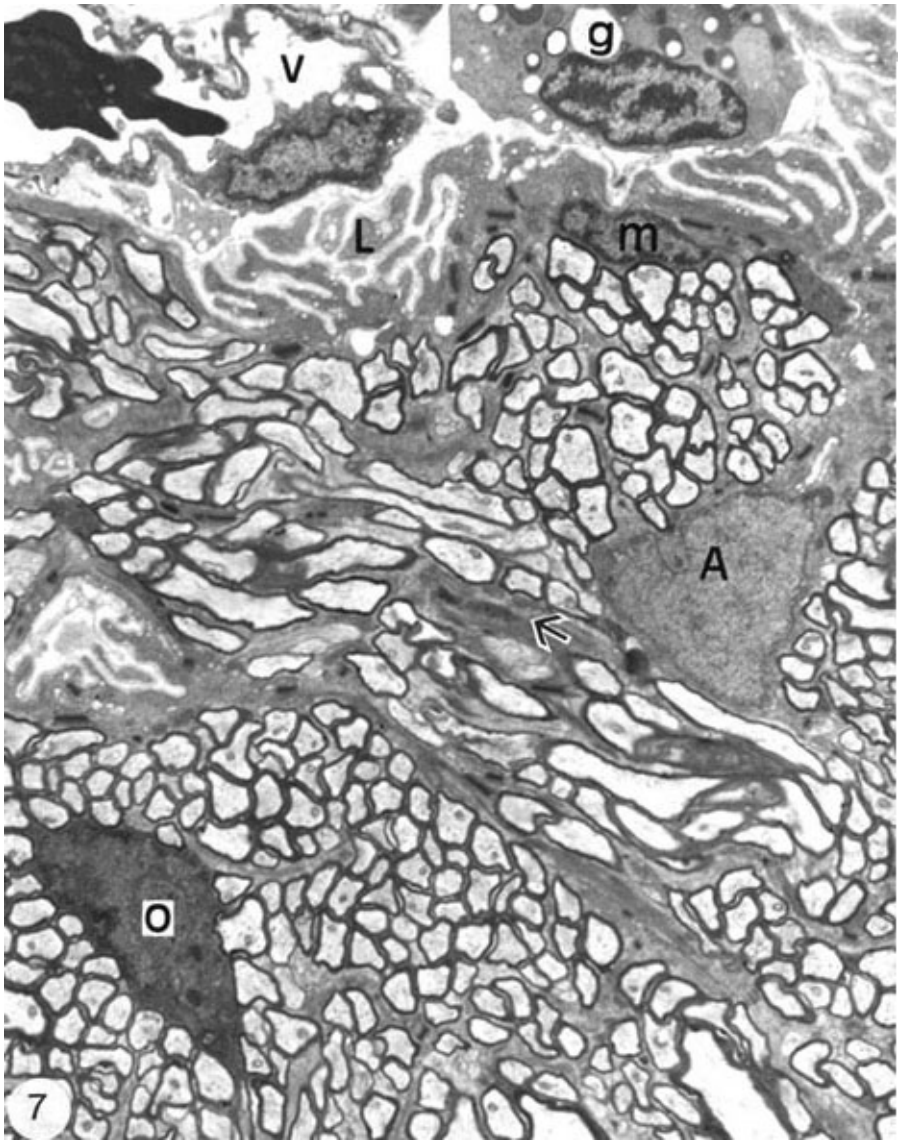

Figure 7. Composition of normal goldfish optic nerve as revealed by EM. Axons are myelinated and appear in transverse and longitudinal profiles due to the sinusoidal pattern of the fibers. Astrocyte processes (→), joined by desmosomes, arrange the fibers into bundles. Astrocytes also form a continuous limiting membrane (L) that excludes the septae contents from the interior of the CNS tissue. (A) astrocyte, (O) oligodensrocyte, (m) microglia, (g) granular macrophage, (v) blood vessel. ×15K.

environment surrounding the neuron. Such explanation clearly does not encompass lower vertebrates, in particular the fish, whose CNS axons are endowed with a remarkable capacity for spontaneous repair after injury, despite having an extrinsic environment that shares many of the features found in mammalian CNS.

Set out below is a brief description of the components that make up the environment of the CNS and PNS in mammals and how their reaction to injury is perceived to impact upon the failure and success of axonal regeneration, respectively. This is followed by a detailed analysis of the events that accompany the repair process in the injured goldfish optic nerve, highlighting the environment of the lesion and distal nerve and how each region adapts over a period of several months to accommodate first axonal regrowth and later myelination. Immunocytochemical and ultrastructural evidence will be presented to show that regeneration in fish optic nerve is accompanied by several events that are common to regeneration in mammalian PNS, and that the CNS environment surrounding the regenerating axons actively supports, rather than inhibits, axonal outgrowth.

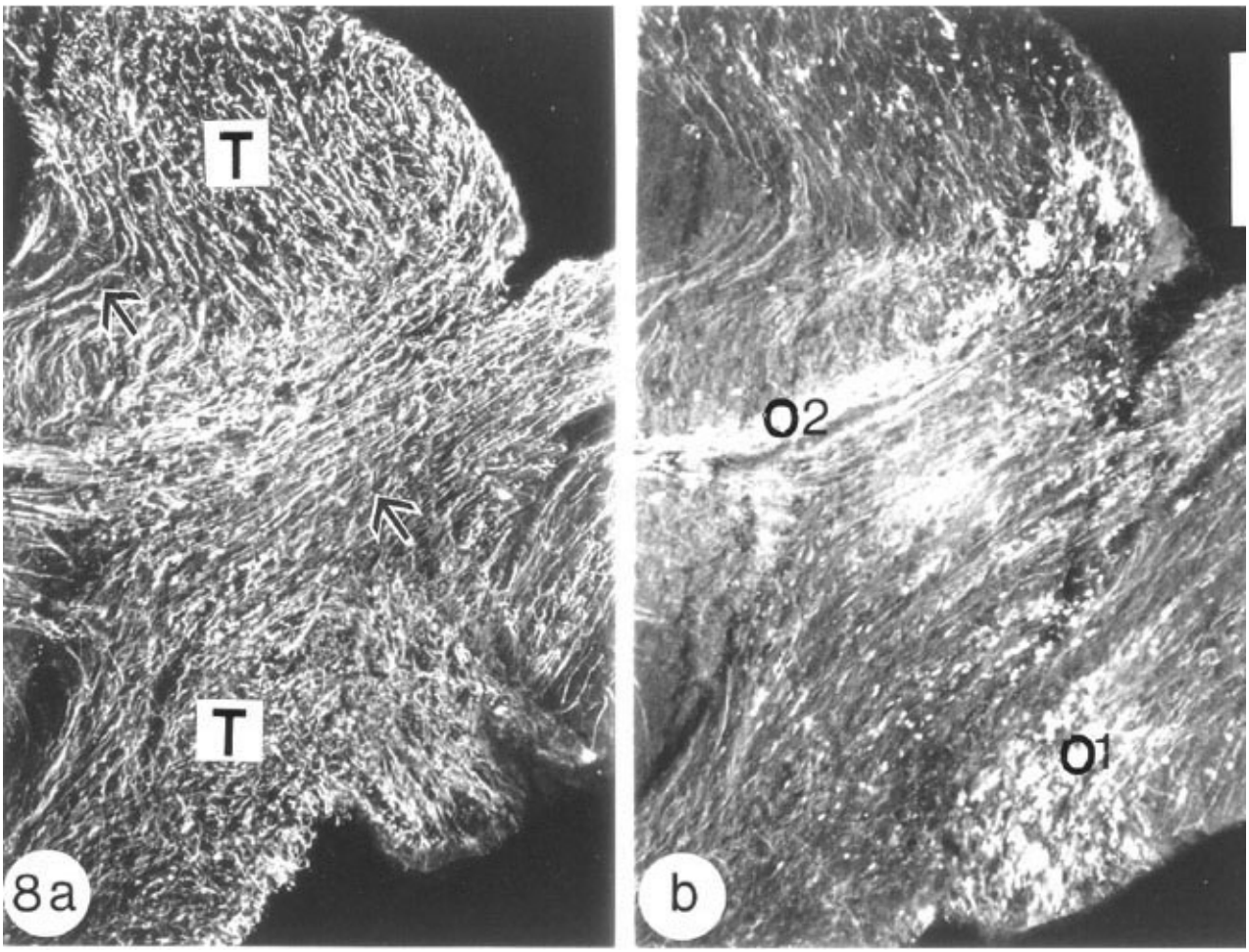

Figure 8. Astrocytes in goldfish optic tracts (T) stained for GFAP (a) and S100 protein (b). Astrocytes have a radial morphology (→) and arise from cells at the optic recess (O1) and the walls of third ventricle (O2). Bar = 100 μm.

Glial Environment of Axons in Mammalian CNS

One of the components of the milieu that surrounds an axon in the CNS is the astrocyte. During embryonic development, astrocytes act in guiding axon growth and neuronal development (30, 31). This capacity appears to be lost in the adult, with the consequence that an injury to the CNS induces tissue damage that creates barriers to regeneration. One of the main barriers is the glial scar, which consists primarily of hypertrophied (enlarged/reactive) astrocytes. Reactive astrocytes are perceived to form a physical wall that wards off any further damage to the tissue. The process leads, however, to the formation of the glial scar, beyond which axons cannot regenerate (32). Recent studies have sought to identify the molecular constituents of the glial scar that may play an additional role in inhibiting axon regeneration. It is recognized that although astrocytes can produce growth-promoting molecules, such as laminin, which aid in attachment and migration of neurons during development, it appears that adult astrocytes also produce a heterogeneous class of molecules known as proteoglycans—proteins to which are attached large sugar residues—whose expression increases in the glial scar, and as a result are thought to act as chemical barriers to axon regeneration in the CNS (33, 34).

A second protagonist in axon regeneration failure in the CNS appears to be myelin-producing oligodendrocytes, an idea first proposed by Berry (35). Studies based on tissue culture assays have shown that oligodendrocytes, and at least two different molecules that are associated with oligodendrocyte myelin, lead to the collapse of the growing axon tip, the growth cone (36). In molecular terms, growth cone arrest is attributed to the unfavorable interaction of growth cone receptors with ligands (myelin proteins) that are bound to oligodendrocyte

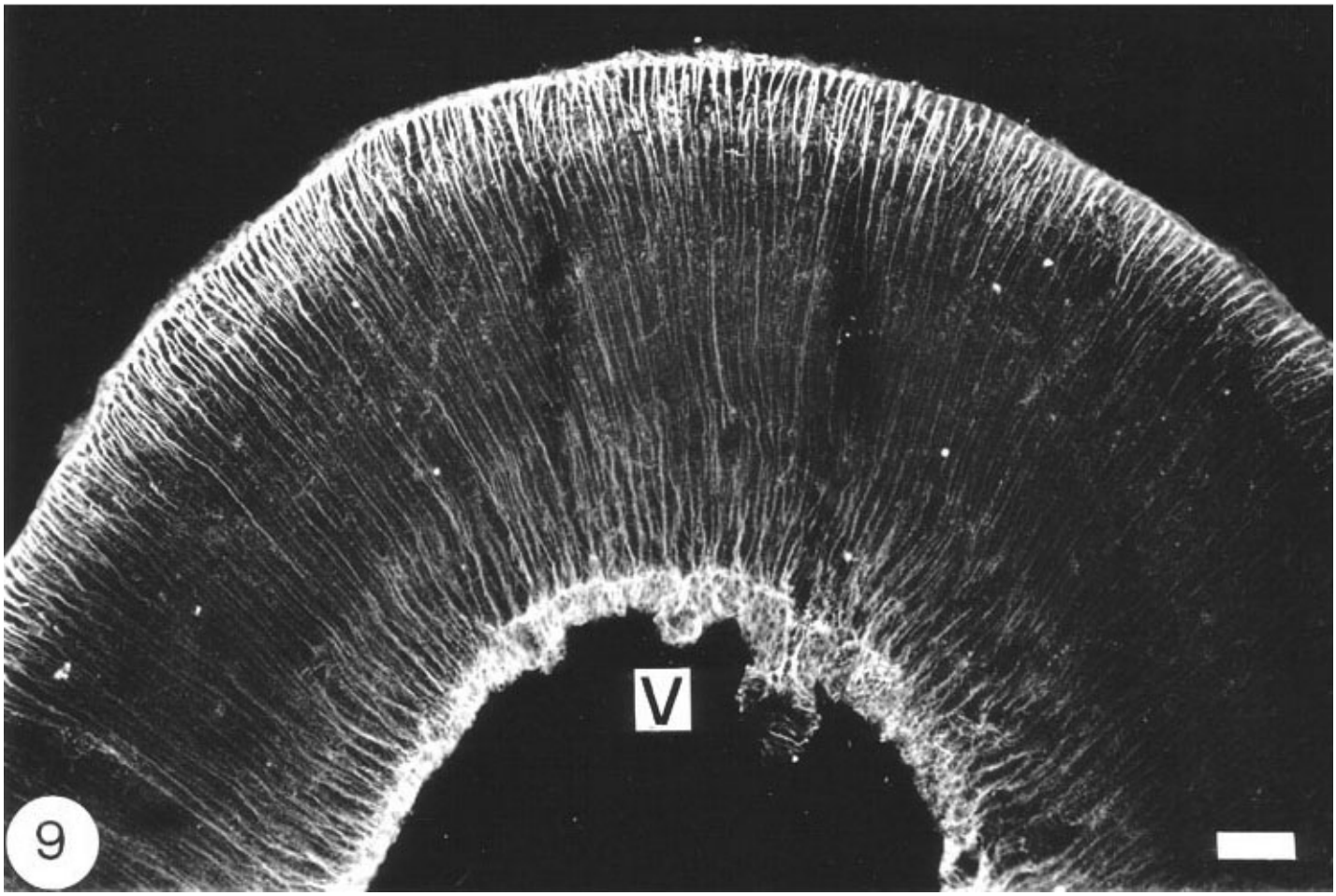

Figure 9. Sagittal section of fish tectum stained for GFAP. Radial astrocytes arising from near the ventricle (V) span the entire width of the tectum, terminating as end feet at the surface. Bar = 100 μm.

membrane, and that neutralization of the proteins promotes regeneration *in vivo* (37). From these and related observations, it is concluded that myelin-associated molecules are one of the principal causes of failure of regeneration of cut axons in the intact adult CNS (reviewed by Filbin (38).

Glial Environment of Axons in Mammalian PNS

The extrinsic environment of the PNS, on the other hand, contains neither astrocytes nor oligodendrocytes. Instead, one cell type, the Schwann cell, performs the dual task of axon guidance and myelination. The Schwann cell also produces basal lamina (cf. laminin in CNS), a protein-rich membrane that surrounds the Schwann cell-axon unit, forming a tubular structure along the entire length of the nerve. A substantial amount of additional matrix, particularly fibrous collagen that imparts tensile strength to the peripheral nerve, is deposited between these tubular structures. The Schwann cell is believed to impart trophic support to the regenerating axon, which extends to its target by adhering to the substrate made up of the matrix molecules, in a recapitulation of the events that take place during development. The cellular and extracellular components are retained during peripheral axon regeneration (reviewed by Martini (39)); their absence from the CNS has long been thought as the reason why this system lacks the regenerative capacity. To this end, a number of laboratories have recently reported that the usually abortive axonal sprouting near the lesion site in the injured rat optic nerve can be mobilized to trigger a limited axonal regeneration if an autologous peripheral nerve containing viable Schwann cells is anastomosed to the cut end of the optic nerve (40-42).

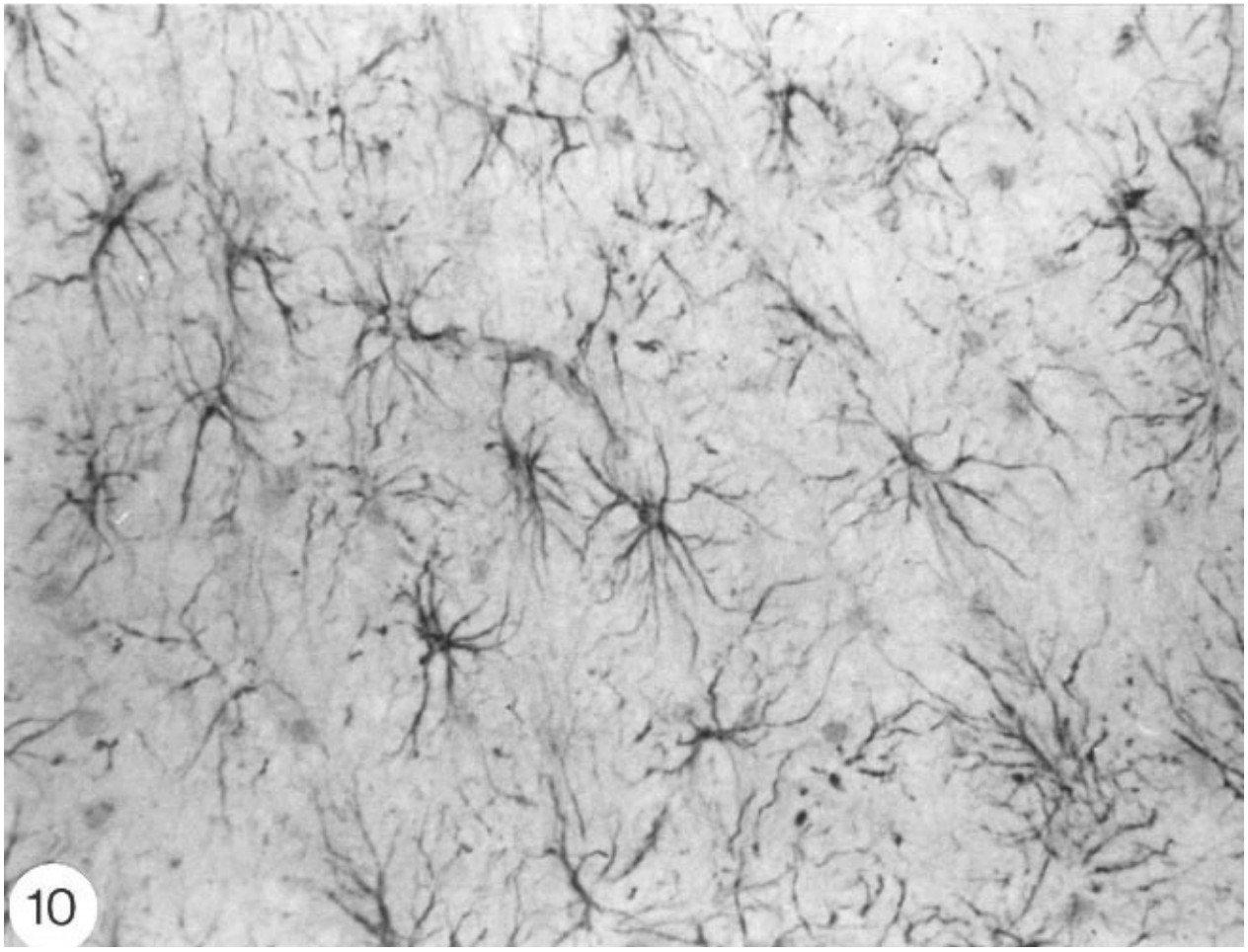

Figure 10. Astrocyte of stellate morphology in rat cerebellum stained with antibody to goldfish GFAP. ×100.

Glial Environment of Axons in Goldfish Optic Nerve

Interestingly, failure of axon regeneration in the CNS is not common to all vertebrates. In lower vertebrates, particularly the fish, axon regeneration in the CNS is the norm, and this is accompanied by the recovery of function. Much research has focused on the visual system of the goldfish in search of a direct explanation as to why it is endowed with the capacity for functional regeneration, especially because it appears that its glial environment is made up of the same agencies, namely astrocytes and oligodendrocytes, which are believed to be responsible for the inhibition of regeneration in adult mammalian CNS.

The Optic Nerve as a Model for Axon Regeneration Studies

The optic nerve has been a popular morphological model for the study of central nerve regeneration. It represents a circumscribed, unidirectional white matter tract, supported by astrocytes and oligodendrocytes, and composed almost entirely of fibers of one origin, namely optic axons arising from the retinal ganglion cells. In the goldfish, injury of the optic nerve induces an anabolic response in the ganglion cells that is the prelude to the regenerative response. The metabolic response, known as chromatolysis, is associated with increased biosynthesis of cytoskeletal proteins (43-45), so-called growth-associated or GAP proteins (46, 47) and lipid products in the cell body. GAPs and lipids are transported by the cytoskeletal proteins to the cut end of the axon, where they are incorporated into the membrane of the growth cone (48). Such a response by retinal ganglion cells to axotomy is crucial if the damaged axons are to traverse the lesion and reach the brain. In the goldfish,

this feat is accomplished through the survival of more than 90% of the axotomized retinal ganglion cells (49). In the frog, retinal ganglion cells also undergo chromatolysis, but only around 50% of retinal ganglion cells survive axotomy and reach the brain; the remainder of the retinal ganglion cells attempt to regenerate, but their axons fail to cross the lesion and consequently die (50). Significantly, in mammals only a minimal number of damaged axons cross the lesion unaided; virtually all of the axotomized retinal ganglion cells undergo atrophy through programmed cell death or apoptosis (51, 52). The programmed cell death is caused by several factors, including absence of chromatolysis, excitotoxicity to glutamate transmitter (53) as well as loss of endogenous and target-derived neurotrophins. Furthermore, a significant number of retinal ganglion cells seem to die because their axons fail to overcome the lesion. The evidence for this comes from studies in which the cut end of rat optic nerve is grafted to a segment of peripheral nerve: axons are able to extend several millimeters beyond the junctional zone, i.e., the lesion, even in the absence of agents that prevent cell death (40, 42).

The above comparative studies, while highlighting the gradation of responses of retinal ganglion cells to axotomy across the vertebrate taxa, also offer a clear indication that survival of axotomized retinal ganglion cells is dependent to an appreciable degree on their axon overcoming a major hurdle—the site of lesion. Rather surprisingly, however, even in regeneration competent systems there has not been a systematic study of the site of lesion, possibly because the region is considered too disorganized for meaningful analyses. We have taken advantage of the recent availability of several specific antibodies (4, 15, 54) to examine the cellular composition of the lesion in the goldfish optic nerve, from shortly after optic nerve crush to several months after injury. Our aim has been to discover if endogenous glial cells, or cells arising from the sheath/septae, reoccupy the lesion shortly after injury, possibly serving as scaffolding for the regenerating axons to traverse the lesion. In the course of the study, it became apparent that instructive changes also take place as the regrowing axons extend beyond the lesion, through the CNS environment of the distal nerve, and these events will also be described. Throughout the study, the term proximal is used to denote that portion of the optic nerve between the eye and the lesion site, and the term distal to denote the nerve between the lesion and the brain.

Events That Follow a Crush to Goldfish Optic Nerve

Immediately after the optic nerve has been crushed, and for at least 4 days thereafter, the lesion appears as a gap between the two nerve stumps, which are held in position by the intact sheath. The tissue-free constriction at the center of the lesion becomes flanked by a region 200 μm wide that is devoid of astrocytes, as noted by the absence of GFAP, B7, and Pax-2 immunoreactivity, and contains only a tiny number of cells, most of which are mitotic (bromodeoxyuridine positive, BrdU+) and appear to be derived from the sheath/septae where similar cells are present. At this stage, myelin disruption is barely noticeable, either in the proximal stump or distally (55). It is important to recognize that a lesion of the type described in this study leads not only to the severance of axons but also to the destruction of local astrocytes. In other words, the continuity of the nerve's fascicular structure is disrupted as a result of crush injury (Fig. 11).

During the following 10 days, there is a large accumulation of mitotic cells in the sheath/septae extending into the core of the lesion (Fig. 12) which, nevertheless, remains devoid of astrocytes, unlike in the proximal and distal stumps (and the retina), where astrocytes express an elevated level of GFAP immunoreactivity compared with that in the uninjured nerve—a response that is indicative of injury to CNS tissue.

The appearance of mitotic cells in the lesion coincides with a strong regrowth of axons (IF145+) from the proximal stump into the lesion, apparently unperturbed by a sea of punctate myelin debris that is scattered throughout the area (Fig. 12). However, by 14 days after injury, debris is no longer present in the lesion, which takes on a translucent appearance, in contrast to the opacity of the two nerve stumps (55, 56).

An important question to address relates to the cellularity of the early lesion and the means by which the regenerating axons traverse the lesion. The cells in the astrocyte-free lesion stain strongly with isolectin IB4 (Fig. 13), which has been used as a general marker for microglia/macrophages in rat (57) and amphibians (58).

However, in the absence of a more specific marker, a careful study was conducted using EM, with the aim of identifying the cells in the lesion. The study revealed unequivocally that the majority of cells in the early lesion are phagocytic macrophages, as distinct from microglia residing in the distal stump, on account of their morphology as well as the substantial amount of myelin debris present within their cytoplasm (Fig. 14).

The phagocytes are first seen at 4 days after injury, peaking 3 days later, coincidental with the appearance of regenerating axons across the lesion. The number of BrdU+ cells also peaks at this time, indicating that the increase in the number of macrophages is attributable to proliferation as well as recruitment, possibly mediated by mitogenic signals from the necrotic tissue. Indeed, macrophages are confined to the lesion where CNS tissue has been destroyed and do not infiltrate the degenerating distal stump, where CNS environment prevails, an observation that has been confirmed by other workers (59). By week 3, the cellularity of the lesion is minimal, phagocytes loaded with myelin debris are noted only in the sheath/septae, and naked axons are the hallmark of the lesion. The cells found among the naked axons have several characteristics that are reminiscent of immature glia cells—a well-structured nucleolus and short cytoplasmic processes that extend into the axons domain (Fig. 15). The cells have since been identified as precursor Schwann cells, as will be shown later.

The early appearance of macrophages at the lesion may be important for the outgrowth of axons in several respects: 1) if myelin debris were inhibitory to axonal outgrowth in the fish optic nerve *in vivo*, as it is *in vitro* (60) (see also Bastmeyer et al. (9)), then macrophages are playing a crucial role by removing inhibitory molecules from the path of regrowing axons; 2) the outgrowth of the axons may be further enhanced by macrophages releasing growth-assisting molecules such as NGF, the expression of which is noted in all of the IB4+ cells in the lesion (Nona, unpublished results). NGF is known to promote regeneration in mammalian PNS (61, 62); 3) macrophages may be aiding axonal extension across the lesion in a more direct manner: clusters of regenerating axons ranging from a few to 100 or more per cluster, often associated with a growth cone, are seen abutting the perimeter of the macrophages, which appear to be acting as a bridging substrate or carpet for the growing axons, in a manner akin to that observed in the lesioned optic nerve of the frog (50). In other words, macrophages in the lesion, in addition to their phagocytic role, also present growth-promoting and physical substrate to assist the axons to overcome the lesion. Significantly, the absence of astrocytes from the lesion means that endogenous glial cells are not acting as bridges for regenerating axons, as noted also by other workers (63-65).

The above results appear to suggest functional parallels between fish optic nerve lesion site and the mammalian PNS, where an injury is characteristically followed by a rapid influx of phagocytic macrophages, as a prelude to successful regeneration (66-68). By contrast, only limited recruitment of macrophages, and by implication debris clearance, is noted in lesioned rat optic nerve (69), a phenomenon that has been attributed to inhibitory factors released by resident glial cells (67). To overcome this imbalance, Schwartz and colleagues have introduced monocytes, previously cultured in the presence of fragments of sciatic nerve, into transected optic nerve of rat, to assess the effect of efficient debris clearance by macrophages on axon regeneration. The study showed that 15 times as many retinal ganglion cell axons regenerated in the treated nerve compared with untreated control nerve, thus confirming the importance of macrophages in axon regeneration (70, 71). In the injured fish optic nerve, in addition to the phagocytic macrophages, the early lesion also contains non-phagocytic granular macrophages, a unique class of cells found in goldfish optic nerve (72, 73). As shown in Fig. 7, these cells normally reside in the sheath/septae; their appearance in the lesion is attributable to the local disruption of the nerve's fascicular pattern and, by implication the astrocytic integrity, and strongly suggests that the phagocytic macrophages too are derived from the sheath/septae (Fig. 14). Interestingly, the status of the early lesion as a tissue with PNS characteristics was placed beyond doubt when Schwann cells took up residence in older lesion (see later).

It is instructive to add that the prompt clearance of debris in injured goldfish CNS is not confined to the optic nerve but also takes place in the optic tract (20) and spinal cord (28). And as is the case in the injured optic

nerve, regenerating axons in the optic tract and spinal cord use phagocytic cells, not astrocytes, as scaffolding to traverse the lesion.

Fish Optic Nerve *versus* Rat Optic Nerve

The apparent ease with which injured axons in fish optic nerve traverse the site of lesion is in stark contrast to the events in injured rat optic nerve, where attempts by the damaged axons to cross the lesion invariably end in failure. As noted earlier, much emphasis has been placed on the role of myelin proteins as one of the principal causes of failure of regeneration of damaged axons in the adult CNS. However, several recent observations favor the contention that inhibition of axon growth by oligodendrocytes/CNS myelin is not the entire answer to the question of why mammalian CNS axons do not regenerate after injury. For example, the myelin inhibitory hypothesis does not explain why axons fail to regenerate through the gray matter, where there is no myelin. Similarly, optic fibers of BW mutant rat, in which both oligodendrocytes and CNS myelin are absent, fail to regenerate in an exclusively astrocytic environment (74). Several authorities have, therefore, reopened the "inhibitory" debate, by asserting that astrocytes rather than oligodendrocytes are the main cause of axon regeneration failure in the CNS (75, 76).

The meticulous studies of axon regeneration in rat optic nerve by Berry and colleagues have highlighted the fact that astrocytes and mesodermal elements (fibroblasts and collagen) become organized into an impenetrable glia limitans of the scar that envelops the proximal and distal stump ends, largely because injured axons appear unable to initiate an early attempt to regrow, generally within 5 days of injury (77). Furthermore, injured optic axons can be made to overcome the glial scar and extend into the environment of myelin debris, if provided with sufficient trophic support. By inserting segments of peripheral nerve containing viable Schwann cells as a source of trophic support into the vitreous and simultaneously crushing the optic nerve, Berry and colleagues have observed that 10% of the injured axons are able to cross the lesion and extend 4 mm into the distal segment (77). It is proposed that peripheral nerve implants secrete trophic factors into the vitreous that are then taken up by the retinal ganglion cells and transported to the axon tip, thus stimulating its rapid growth across the lesion before there is a build up of astroglial scar. Earlier studies, in which peripheral nerve containing viable Schwann cells was grafted to the cut end of rat optic nerve, yielded similar results in terms of retinal ganglion cell survival and axon regrowth beyond the site of anastomoses, that is, into the peripheral nerve (40, 42, 51). These results do not argue against the view that glial scarring may, in some way, curtail axonal outgrowth. They do, however, suggest that the effect of trophic influences derived from viable Schwann cells are capable of nullifying the inhibitory effects on axonal outgrowth exerted by a scar of limited dimension. Put another way, the ability of a cut axon to regrow is dependent on the balance between the intrinsic ability of the axon to regrow and the permissiveness of the environment surrounding it.

In the injured fish optic nerve, the conditions appear to favor retinal ganglion cell survival and vigorous axonal outgrowth in the absence of external manipulations. The clearance of myelin debris is entrusted to phagocytic macrophages whose presence stimulates an early and robust axonal regrowth, which ensures that astrocytes around the stump ends, although markedly hypertrophied and showing an elevated expression of proteoglycans (72), do not become organized into an impenetrable, limiting membrane. On the contrary, both at the edge of the proximal nerve and throughout the degenerating distal nerve, the disrupted fascicular pattern of the optic nerve is gradually restored, as the regenerating axons encounter the awaiting astrocytes, in a recapitulation of events occurring in normal development and growth of the fish optic nerve (cf. Scholes et al. (17)).

Regeneration in Goldfish Optic Nerve Distal to Lesion

By around 10 days after injury, regenerating axons begin to emerge from the lesion proper into the distal nerve to be confronted by an environment dominated by hypertrophied astrocytes, myelin, and axonal debris. The progress of the regenerating axons through this apparently chaotic environment is best followed using EM (55).

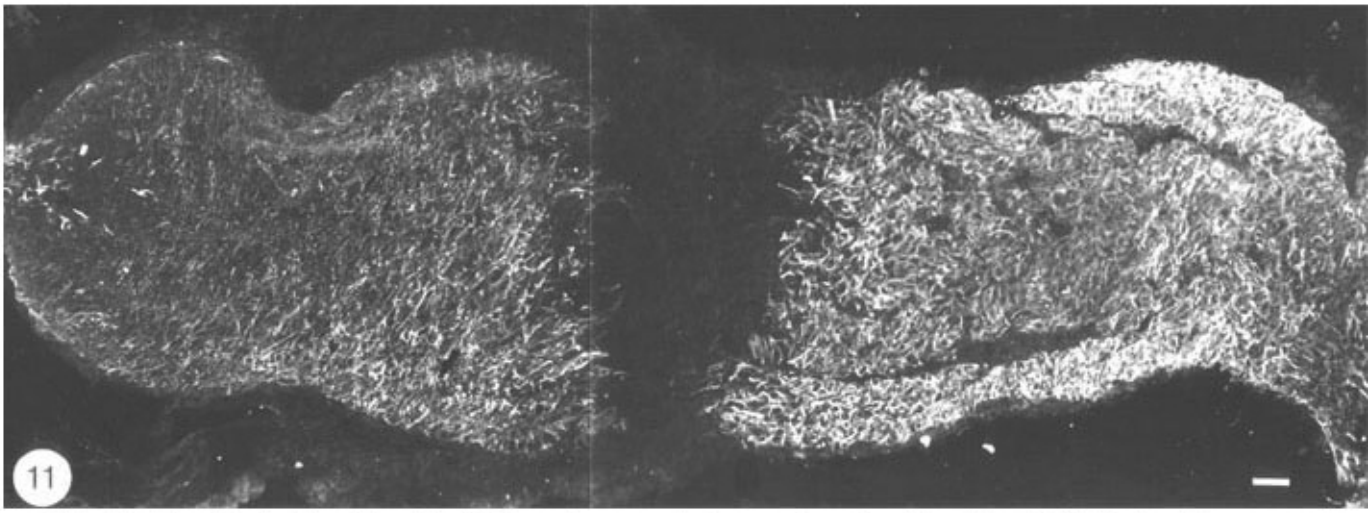

Figure 11. Longitudinal section of goldfish optic nerve 4 days after crushing, stained for GFAP. Astrocytes are nicely revealed along the length of the nerve, except at the site of lesion, where they are destroyed by the crush injury. Bar = 100 μm.

At first, small groups of new axons appear among radial processes of hypertrophied astrocytes where there is also a scatter of myelin debris. Astrocyte processes, connected by desmosomal junctions, form a myriad of irregular loops that enclose the newly arrived axons into loosely organised bundles (Fig. 16).

By 14 days, these have swollen into large bundles of tightly fasciculated axons, surrounded and separated from one another by cordons of lamellar astrocyte processes. Myelin debris, which was haphazardly distributed at earlier times, now is neatly confined to the periphery of these fascicles, alongside and within the astrocytic cordon (Fig. 17a).

Between 14 and 25 days after being crushed, the appearance of the distal edge of the nerve is reminiscent of the proximal edge at an earlier time after crushing: 1) astrocyte radial processes have enwrapped the axon bundles, thus demarcating the new fascicles; and 2) myelin debris is largely confined to the margins of the fascicles alongside the interposing astrocyte processes. More distally, the old fascicular structure is completely lost, and a substantial amount of debris still remains, present mostly within astrocyte processes, with surprisingly little debris seen in microglia, a finding that has been confirmed by other studies (59). The early axons that have reached the chiasm are invariably seen in debris-free areas or enveloped by astrocyte processes.

By around 43 days, little myelin debris remains, and the cytoarchitecture of the regenerated nerve begins to resemble that of the normal nerve, with astrocyte processes dividing the tissue into glial channels/compartments, thus restoring the fascicular pattern of the nerve. The patterning precedes axon remyelination (Fig. 17b)), which is known to be a protracted process, taking several weeks for near completion, and is rarely observed before around 40 days after nerve injury, that is, several weeks after the regenerating axons have crossed the lesion (16, 72, 73). In this study, there was little evidence of remyelination before around 50 days after the crushing injury. By 90 days, however, virtually all of the new axons in the distal nerve were myelinated by oligodendrocytes, much like the normal tissue (Fig. 21b), but in total contrast to remyelination in the lesion (see below).

It is important to emphasize that although there are structural similarities between the peripheral nerve and the optic nerve of the goldfish, in that both nerves consist of a multitude of cylindrical tubules or compartments, the mechanisms of axon regeneration in the two systems are quite different. In the regeneration of the peripheral nerve, growth cones are found exclusively in contact with the inner surface of the basal lamina of the Schwann tube (78). During regeneration of the optic nerve, however, new axons (this study), preceded by their growth cone (79) are only found deep within astrocyte fascicles, among other axons. This suggests that astrocytes, rather than basal lamina, support axonal growth during regeneration, and this pattern forming interaction with the

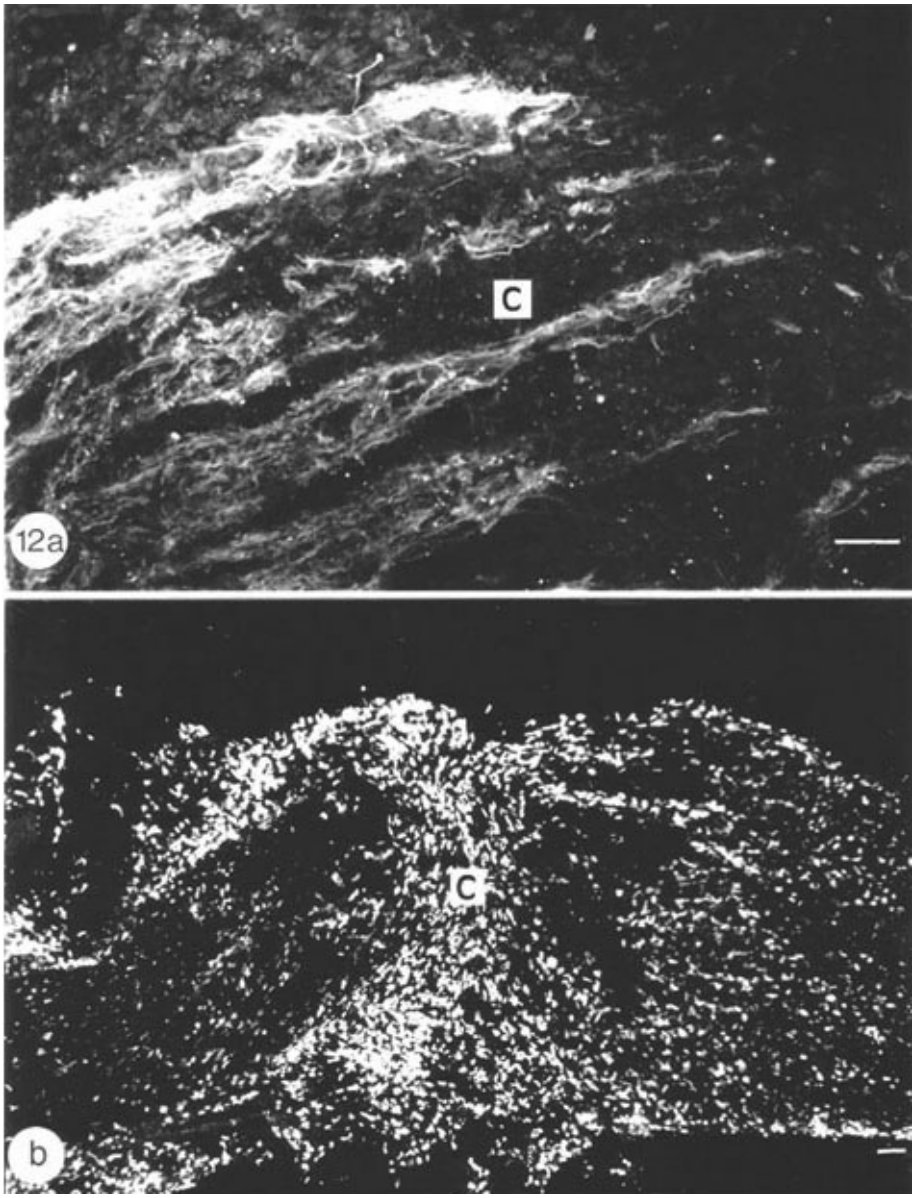

Figure 12. Seven days after the optic nerve crush, regenerating axons (a) extend into the crush site (C), coincidental with the arrival of mitotic cells from the sheath/septae (b). Bar = 40 μm. Compare with Fig. 13.

astrocytes, forming glial channels that exclude the degenerating myelin debris, may greatly facilitate the growth of the many axons that follow (55).

In this study, it is assumed that the pioneering axons emerging into the distal optic nerve will, in all probability, encounter not only astrocytes but also myelin debris. That this mixed environment appears not to disrupt the progress of regenerating axons owes much to the vigorous growth of the growth cone as well as, perhaps, myelin debris characteristics. In the trout, for example, CNS myelin lacks the mammalian protein PLP but contains two proteins, IP1 and IP2, which are immunologically related to PNS myelin protein P0 (80). On this basis, it may be argued that fish myelin proteins have similar properties to myelin proteins found in the PNS, which are known not to inhibit neurite extension *in vitro* (36). However, more recent studies have established that CNS myelin in fish does contain proteins that inhibit axonal extension *in vitro*, much like their mammalian counterparts (60).

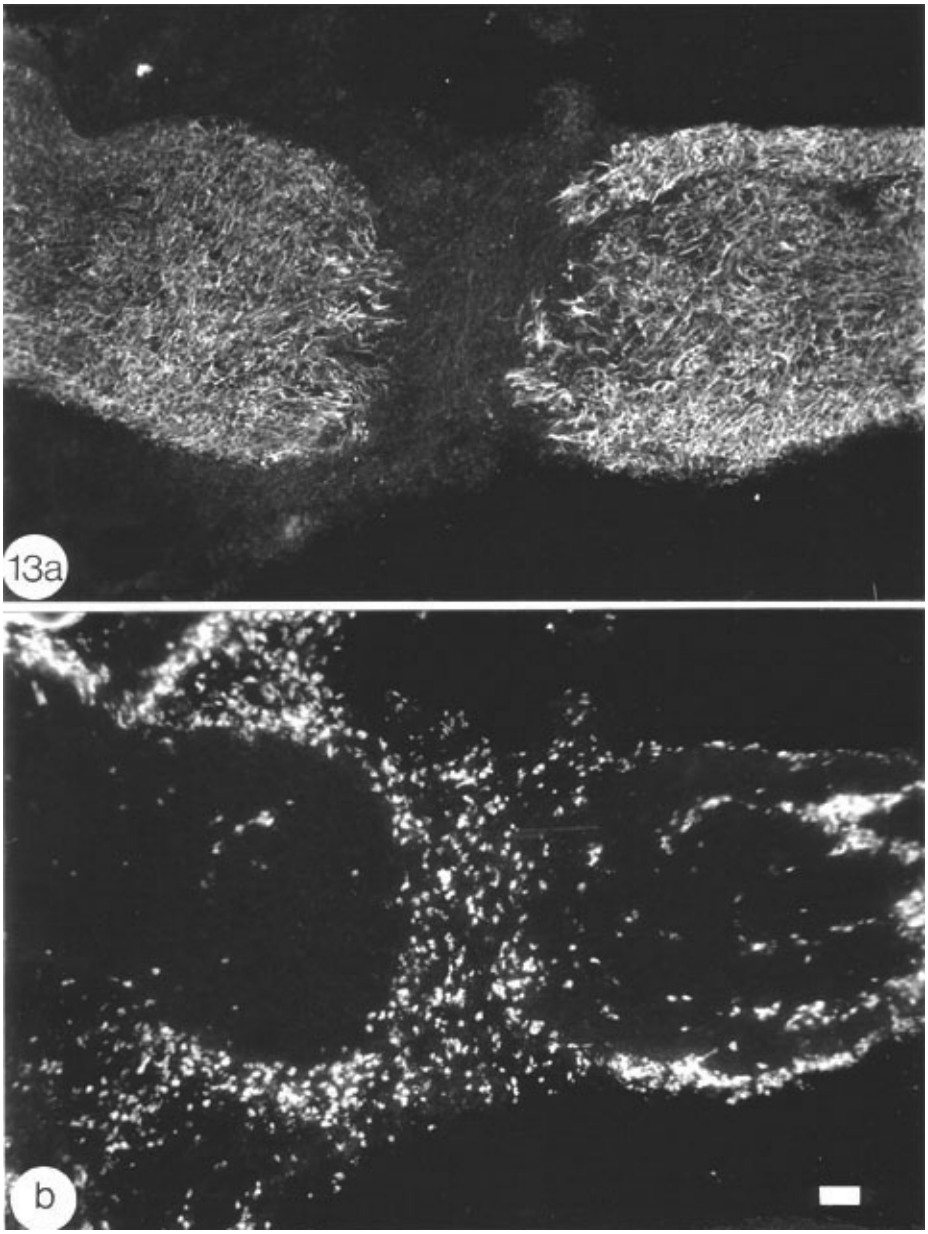

Figure 13. The absence of astrocytes (GFAP–) from the 7-day-old lesion (a) attracts IB4+ monocytes from the sheath (b). Bar = 100 μm.

Myelination of Regenerating Goldfish Optic Nerve Axons in the Lesion by Schwann Cells

Thus far, much emphasis has been placed on the paucity of cells in general, and that of astrocytes in particular, in the lesion. The substantial number of mitotic cells that accumulate in the lesion by day 7, and identified as macrophages, is much attenuated a week later, as the phagocytes quickly clear the debris and then disperse into the sheath/septae (see above). In the following weeks, the rate of division in the lesion is no greater than in the rest of the nerve.

Consistently, however, a second wave composed of large numbers of dividing BrdU+/S100– cells appear in the lesion at around 43 days after nerve injury (16, 56, 81). Over a period of several weeks, the number of dividing cells gradually decreases, to be replaced concomitantly by S100+ cells, whose spindly nuclei and bipolar

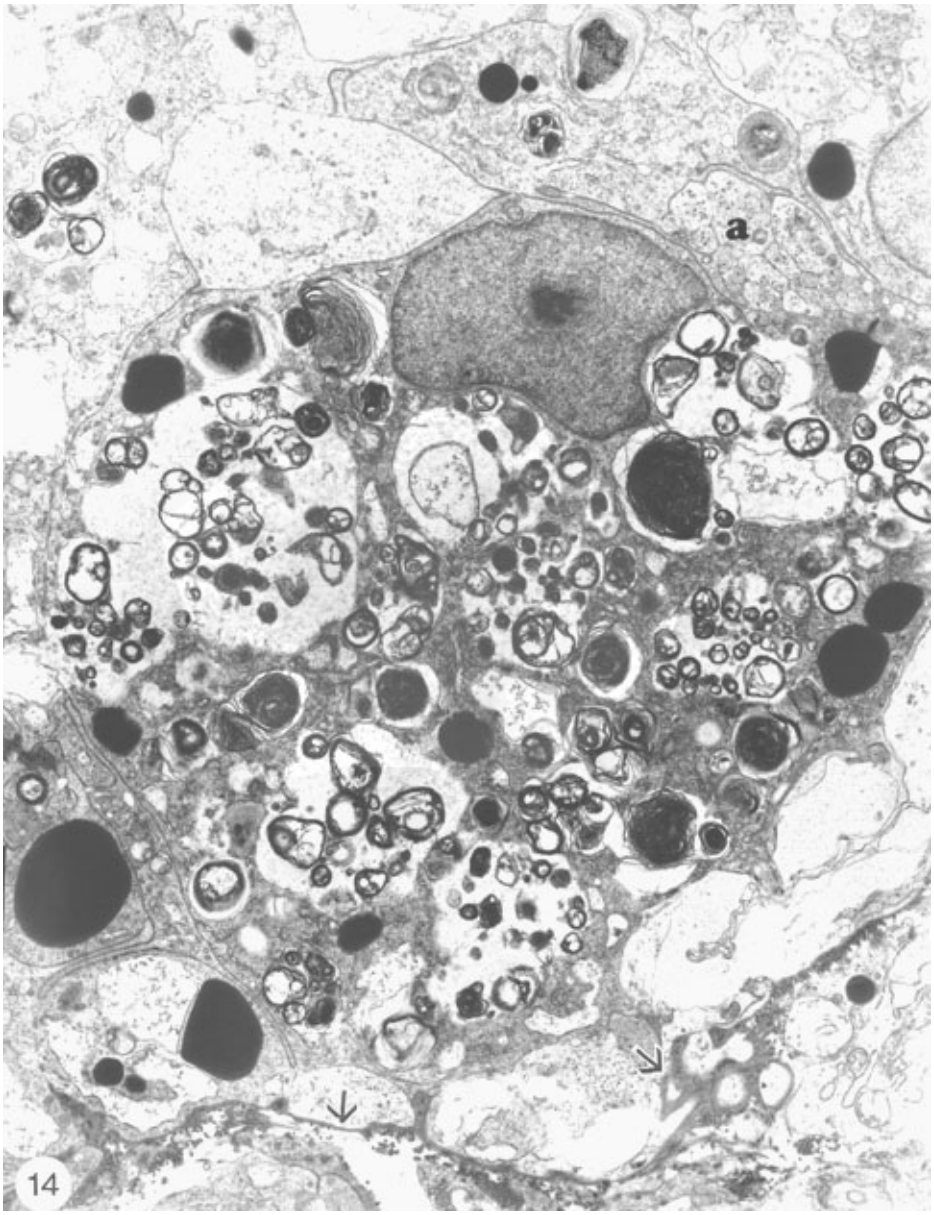

Figure 14. EM of a typical phagocytic macrophage in 7-day-old optic nerve lesion. Whorls of myelin as well as lipid droplets fill the phagocyte's cytoplasm. In the top right corner, a large group of regenerating axons (a) abut the phagocyte's membrane. The phagocyte lies close to a stretch of limiting membrane that is bruised and leaky (→). ×19K.

morphology match precisely that of Schwann cells in the peripheral nerve. By 90 days, BrdU+ cells are virtually absent from the lesion, which, nevertheless, is packed with S100+ cells (Fig. 18).

Antibodies to two fish-derived myelin proteins (central myelin 36K, and peripheral/central myelin 6D2) (82) have proved invaluable in confirming the identity of these previously unreported cells in the optic nerve lesion (16, 81). In sections from 90-day-old optic nerve, 36K antibody fails comprehensively to recognise myelin in the lesion, which is nevertheless flanked by bright central staining in both proximal and distal nerves. 6D2 antibody, on the other hand, recognizes myelin in the lesion and throughout the optic nerve. It is noteworthy that the appearance of S100+ cells coincided with the expression of 6D2 in the lesion, with a striking correspondence between the two labels. That the expression of 6D2 heralds the beginning of axonal remylination is supported by studies that show that the earliest expression of myelin-related antigens in dissociated cell populations of trout CNS coincides with the first appearance of myelinated fibers in defined brain regions (80). Our observations are

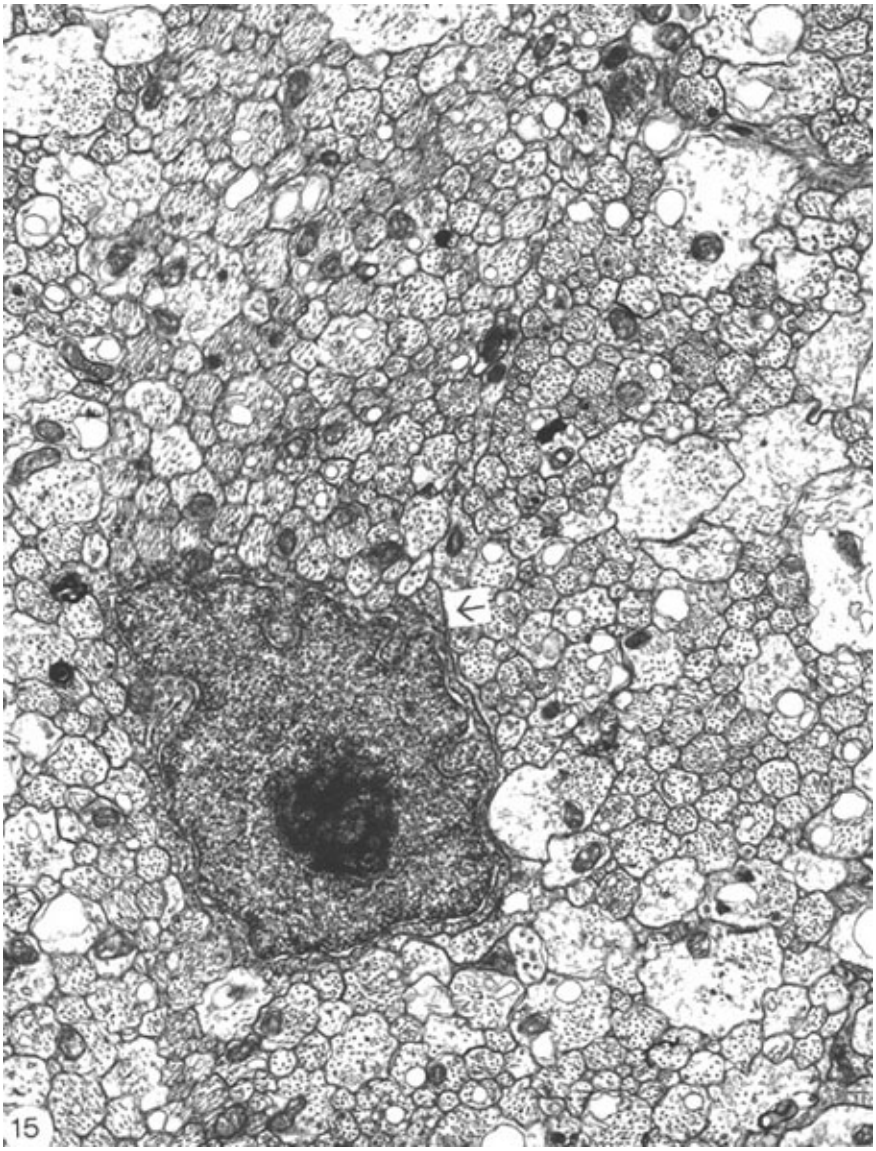

Figure 15. EM of 3-week-old lesion. Regenerating axons make up the bulk of the lesion, save for the presence of the odd cell with a well-structured nucleolus and short cytoplasmic processes (→). ×28K. Compare with Fig. 19.

also in agreement with those from the developing mammalian PNS, in which the expression of S100 marks the transition from precursor to mature Schwann cells and coincides with the commencement of myelination (83).

Further evidence in support of the identity of the cells in the lesion as Schwann cells comes from ultrastructural studies. First, the cells form a 1:1 association with myelinated axons, and each cell:axon unit is enclosed by basal lamina, thus resembling Schwann cells of the PNS. Second, in contrast to the compact arrangement of the tissue in proximal and distal stumps, the lesion contains considerable collagen and extracellular space, characteristic of PNS tissue. Third, the environment in the lesion contains none of the elements, namely astrocytes, that define a CNS environment elsewhere in the nerve (Fig. 21a).

Source of Schwann Cells in Regenerating Goldfish Optic Nerve

Although the appearance of Schwann cells in the lesion has been observed in every injured optic nerve studied by the author and his colleagues, the source of the Schwann cells and their arrival in the lesion have only recently been addressed. In normal CNS tissue, ectopic Schwann cells are rarely seen. They are excluded by astrocyte

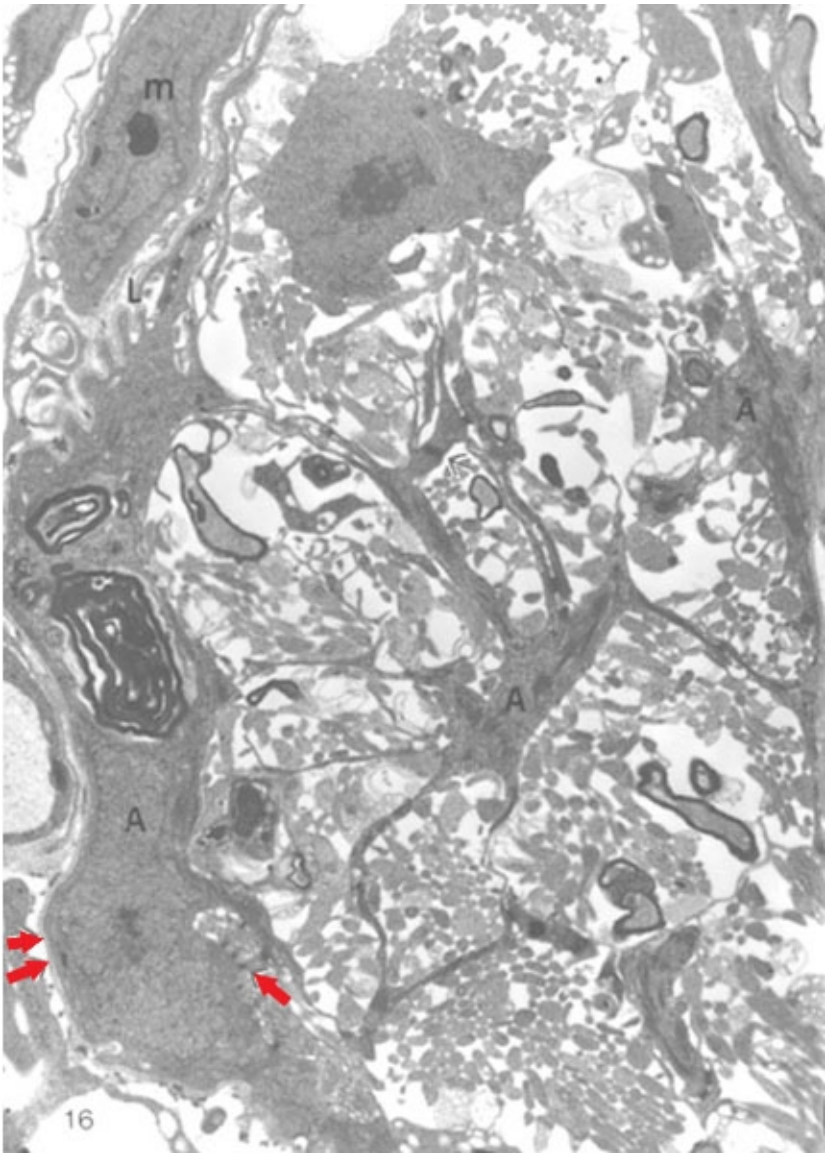

Figure 16. Processes of hypertophied astrocytes (A) at the tip of the distal nerve joined via desmosomes (→) to enclose the regenerating axons emerging from the lesion into discrete bundles. Astrocytes, not microglia (m), contain myelin whorls. Note the intactness (double→) of the limiting membrane (L). ×20K.

processes that are arranged as a glia limitans, forming a boundary between CNS and PNS. It is, therefore, not unreasonable to suggest that in the present study the colonization of the lesion by Schwann cells, much as its earlier colonization by macrophages, is the result of disruption of the astrocytic glia limitans (see Fig. 14). Support for this notion comes from studies of optic nerves that have received two or more adjacent lesions, which show that the larger the area over which astrocytes are destroyed, the greater is the Schwann cell invasion. Such correlation between Schwann cell invasion and the extent of astrocyte destruction has also been described in rat spinal cord following local injection of gliotoxic agents (84, 85).

As stated earlier, a characteristic feature of the goldfish optic nerve is that it is interleaved by connective tissue septae, which are an integral part of the nerve sheath. This arrangement brings a network of mesenchymal cells and capillaries within the outline of the fiber array. This poorly understood mix, elsewhere excluded from the interior of the CNS tissue, could well contain cells of neural crest origin and, in the event of glia limitans disruption, the pattern is well deployed to supply them locally as precursor Schwann cells (see Fig. 15). In this context, it is interesting that ectopic Schwann cells are never observed beyond the nerve-tract boundary, a line

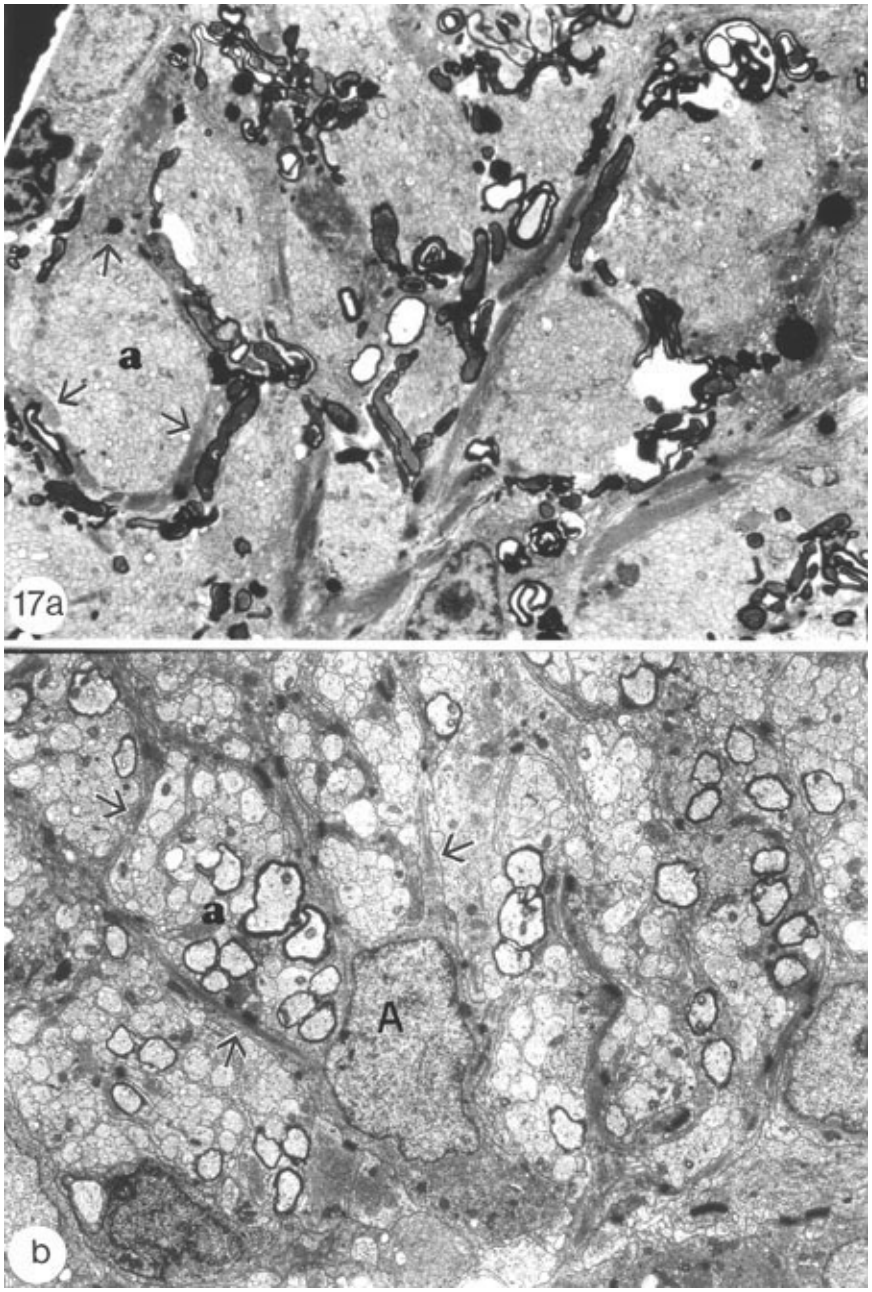

Figure 17. Reconstruction of the CNS envirnment in the distal optic nerve, 14 days (a) and 50 days (b) after the lesion. In (a), bundles of regenerating axons are enclosed by astrocytic cordons (→) that confine myelin debris to the periphery. In (b), the fascicular pattern defined by astrocyte processes (→) is the hallmark of the tissue, and myelination of the regenerated axons is commencing. a, ×5.4K; b, ×13.5K.

that also defines the limit of the reticular astrocytes in the optic nerve (20). We have carried out a detailed ultrastructural study of the lesion site to track down the precursor Schwann cell in the goldfish optic nerve.

Careful studies of the injured optic nerve, ranging from 14 days to 3 months of age, have confirmed that the younger lesions do indeed contain the occasional cell (Fig. 15) having several elongated cytoplasmic sheets that insinuate between the regenerated naked axons, which they enwrap communally (Fig. 19). In this respect, these cells have a striking resemblance to precursor Schwann cells found in the nerve of rat hind leg (see Fig. 1 in Jessen et al. (86). Connective tissue spaces and extracellular matrix are absent from the early lesion, and the tissue here remains compact because of the large number of axons it contains. In older lesions, individual cells

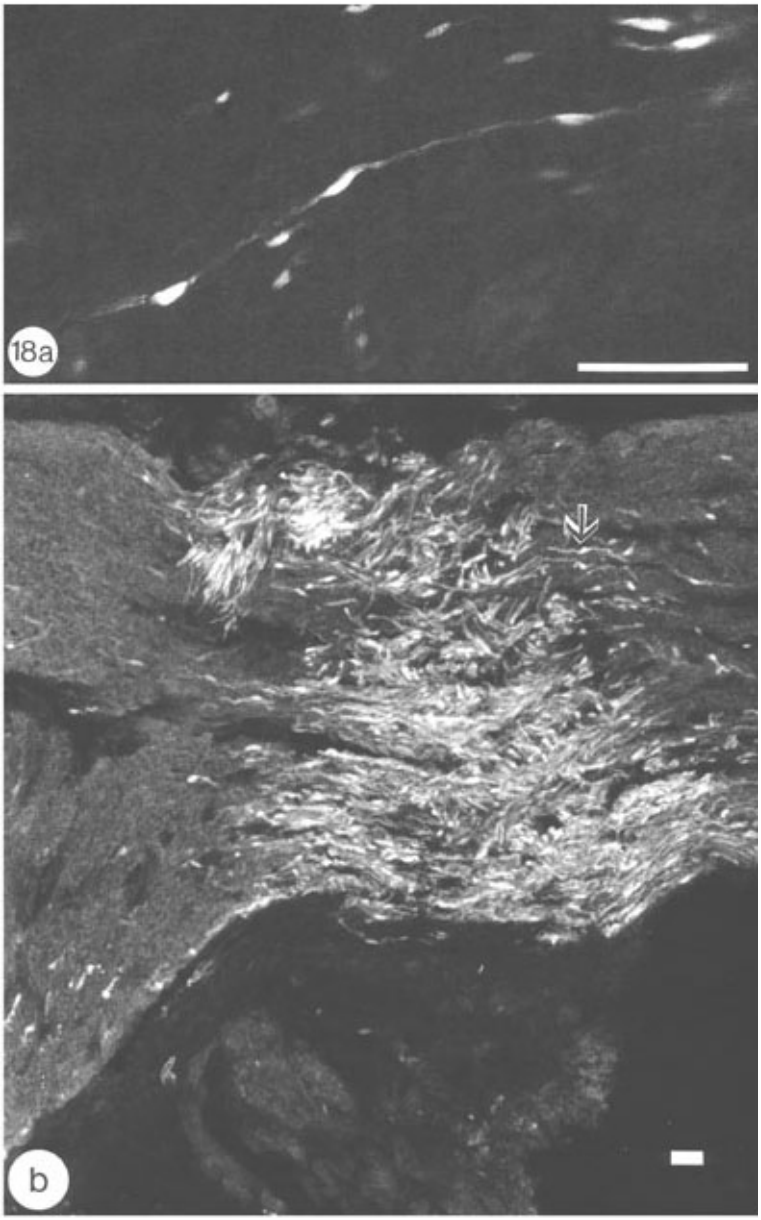

Figure 18. Appearance of Schwann cells at the site of lesion in goldfish optic nerve. Staining for S100 showing that at around 45 days after the injury, several weeks after regenerating axons cross the lesion, cells in a head-to-tail arrangement (a) appear in the lesion. The number of cells increases gradually, so that by 90 days after the injury (b), the lesion is colonized by a solid band of Schwann cells (→). Bar = 40 μm.

are noted in a unitary relationship with an axon, but such encounters are rare prior to around 40 days after lesioning.

Consistently, however, the lesions around 50 days of age begin to take on characteristics that are unmistakably those of peripheral nerve tissue. Axons in a 1:1 association with cells begin to acquire myelin, and these units are invariably surrounded by collagen matrix that form "rivers" through the tissue (Fig. 20).

The delayed differentiation of precursor Schwann cells into myelinating cells corresponds nicely with the late appearance of S100+/6D2+ immunoreactivity in the lesion, which means that both central (discussed earlier) and peripheral myelination commence synchronously. Furthermore, as already described for the distal nerve, myelination in the lesion is also a protracted process. By 90 days, however, myelinating Schwann cells colonize

the lesion (15, 16), building a perfect segment of peripheral nerve tissue intercalated into the regenerated visual pathway (Fig. 21).

Thoughts on Delayed Remyelination in Goldfish Optic Nerve

We interpret the observations relating to myelin formation in the regenerated fish optic nerve as follows. Schwann cells arise from a small number of continually dividing founder cells that colonize the lesion inconspicuously at an early stage, rather than by massive expansion at a late stage in regeneration. To distinguish between the two possibilities, established Schwann cells were challenged with renewed axonal regrowth from a second optic nerve injury, but again they only began to divide immediately before the onset of myelin formation, around 45 days, in synchrony with the peak of Schwann cell division in the new lesion (16). The failure of Schwann cells to respond to axotomy is, therefore, in contrast to the prompt response of injured axons in mammalian PNS, which show division at the first appearance of the regenerating axons (87). The observations in fish optic nerve, therefore, firmly identify a delayed wave of mitogenic signals occurring several weeks after initial axon outgrowth through the lesion.

The ectopic Schwann cells in the fish optic nerve thus conform to a schedule for myelin formation that is characteristic of CNS in general, whereby oligodendrocyte myelination begins late in development at widely different times in different pathways (88). The lengthy period over which myelination is taking place corresponds with the critical period in optic nerve regeneration when the initial disorderly pattern of axon terminals in the tectum is refined into an accurate point-to-point map (89).

Presumably, myelin formation is triggered by target-related changes in individual optic axons that occur at some stage during refinement. During the disorderly process of re-innervating the optic tectum, some axons may be better placed from the outset than others to retract their initial widespread branches into focused retinotopic arbors: these could be the axons that are myelinated first, whereas the less well-placed axons take longer (90). In other words, myelination proceeds on a fiber-to-fiber basis, and each fiber is continually myelinated throughout its length (16). The goldfish visual pathway is well suited to test this hypothesis (Fig. 22).

Conclusions

In this commentary, we have demonstrated the robustness of the fish visual system to manipulations. Severed retinal ganglion cells axons can initiate more than one round of regrowth through a glial environment that shares many of the physical and molecular properties of its counterpart in mammals, but with totally different outcome.

Neither astrocytes nor myelin, both of which are thought to contribute to axon regeneration failure in mammals, impede axonal regeneration in fish optic nerve. On the contrary, astrocytes show much plasticity in response to injury, not by forming a swathe of contiguous impenetrable membrane, but by enwrapping the new axons intimately into bundles and in the process consigning myelin debris to the periphery, where it is phagocytosed, not by microglia, but by astrocytes.

However, none of this would be possible were it not for an early and robust response by the damaged axons, aided by invading macrophages, which clear the site of injury of debris and act as scaffolding for the regrowing axons. The versatility of fish optic fibers to accommodate more than one type of environment is further demonstrated in older lesions, which Schwann cells colonize to form a perfect PNS tissue intercalated within the CNS tissue. Thus, severed fish CNS axons make use of glial cells derived from CNS as well as PNS environments for their repair.

The findings may have implications for axonal regeneration in mammals. It is now recognized that by boosting the rate of phagocytosis in lesioned rat optic nerve, through implantation of reactive macrophages, there is a

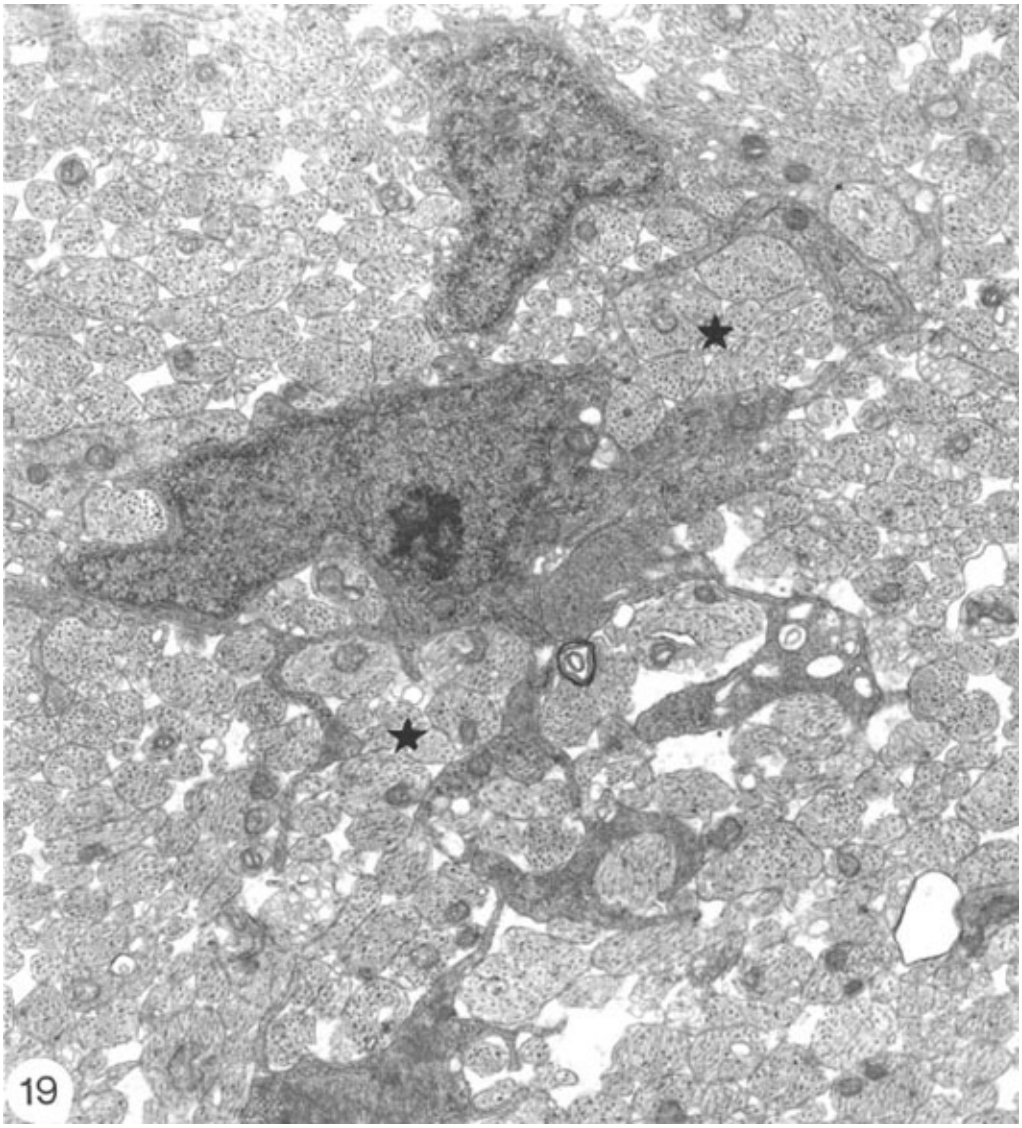

Figure 19. EM of the site of lesion 28 days after optic nerve injury. Precursor Schwann cells extend cytoplasmic processes that engulf the regenerating naked axons unitarily as well as communally. ×19.8K.

substantial increase in the number of regenerating axons beyond the lesion. A similar response in noted through the provision of factors derived from Schwann cells that are supplied either to the retinal ganglion cells or applied as implants to the cut end of the axons. Thus, insights from the fish and other regenerating species can provide strategies to overcome the many obstacles of regrowth in mammals and ultimately lead to successful optic nerve repair in humans.

A major unresolved problem in the regrowth of retinal ganglion cell axons is that the initial axotomy results in the death of 90% of retinal ganglion cells. Clearly, substantially more cells must be rescued if a meaningful retinotopic map is to be formed (91). Evolution has already conducted an experiment along these lines, with results of great interest. The optic nerve of reptilians regenerates efficiently, but for some reason refinement of the tectal map fails to occur: the axon terminals persist indefinitely in a diffused array over the tectal surface and the animal never recovers sight (92).

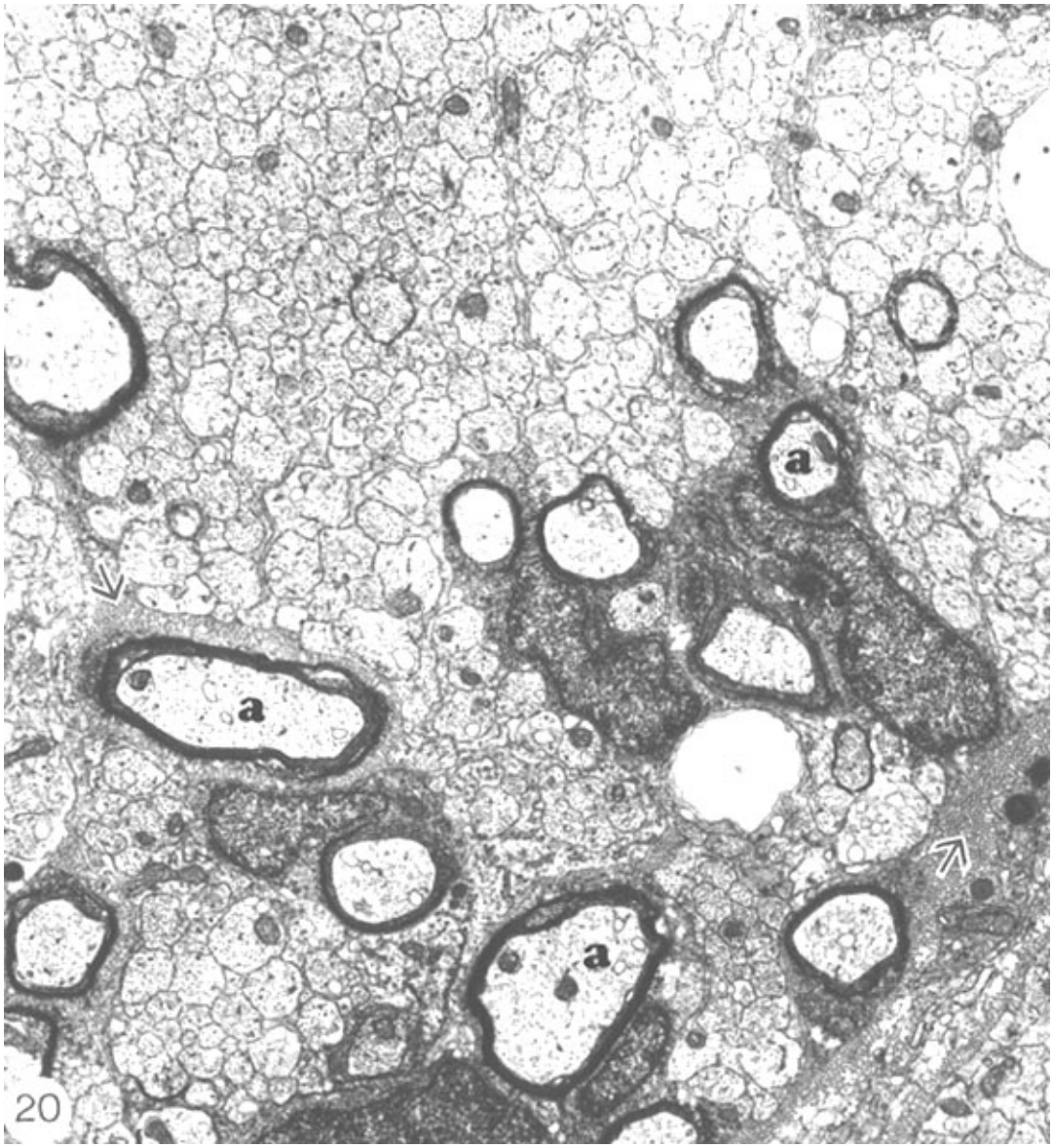

Figure 20. The site of lesion 50 days after optic nerve injury. Commencement of myelination by Schwann cells, some in a 1:1 association with their axon (a). Note the abundance of collagen (→) throughout. ×21.5K.

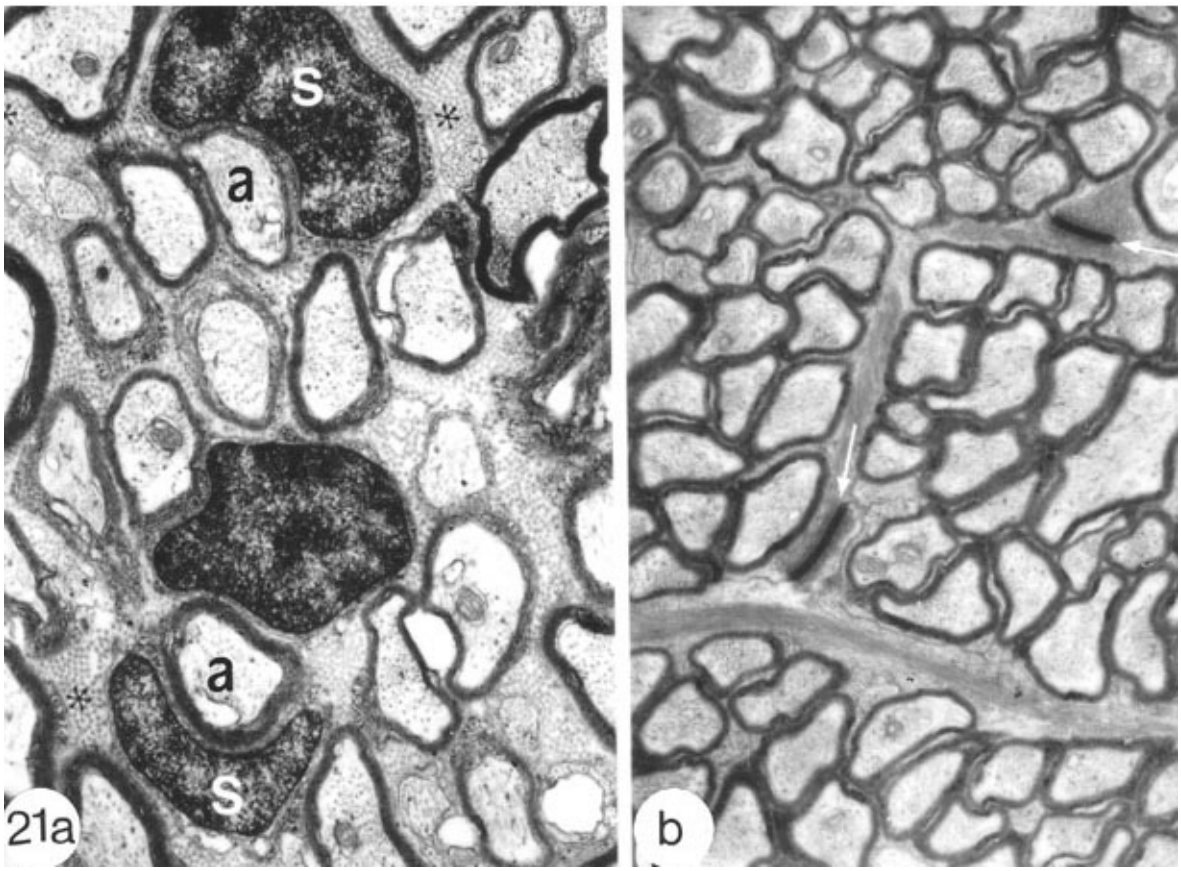

Figure 21. EM of the site of lesion (a) and distal nerve (b) 90 days after goldfish optic nerve crush. In (a), axons are myelinated by Schwann cells (S), and the tissue contains much collagen matrix (*). In (b), myelination is of central type, and astrocytes (→) are prevalent throughout the tissue. ×26K.

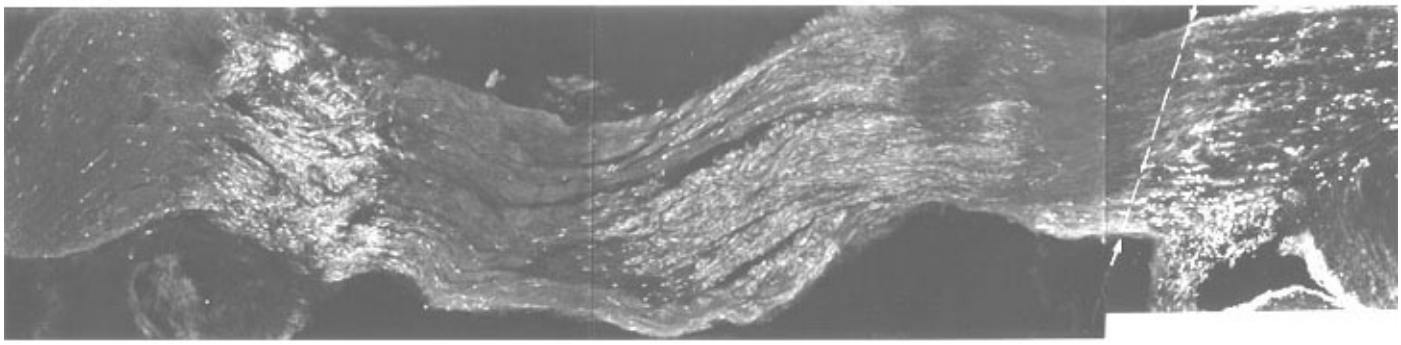

Figure 22. Montage of goldfish optic nerve from just behind the eye (extreme left) to optic tract recess (right), to illustrate the manipulability of the tissue. There are three distinct areas of cells stained for S100. The central area contains Schwann cells that are the result of a lesion 180 days old. To the left is a younger lesion, 90 days old, that is also packed with Schwann cells. On either side of the Schwann cells areas are regions of CNS. Remyelination commences synchronously throughout the nerve. Beyond the dashed line (→) are cell bodies of astrocytes at the optic tract recess.

About the Author

the age of 17, he gained a scholarship to study in England. He graduated with distinction from The Royal Institute of Chemistry in 1968 and went on to complete his PhD in Chemistry under the direction of Professor R.N. Haszeldine, FRS at the University of Manchester in 1971. After an enjoyable period of research in the field of organic fluorine chemistry, he was propelled into neuroscience when he joined Professor John Cronly-Dillon, whose group was studying the process of repair in the visual system of lower vertebrates. Dr. Nona and his colleagues have created a battery of goldfish-specific antibodies, which they have used with great effect to identify several important stages of axon regeneration in the goldfish visual system. He has enjoyed a fruitful collaboration with Dr. John Scholes of UCL, aimed at understanding the behavior of ectopic Schwann cells in CNS environment. Recently, Dr. Nona moved to Sydney and currently holds the position of Visiting Fellow in the School of Optometry and Vision Science at University of New South Wales, Australia.

References

1. Cajal SR. In: Thorpe SA, Glickstein M, translators. (1972).The structure of the retina. Springfield (IL): Thomas; 1989.
2. Reichenbach A, Schneider H, Richter W, Reichelt W, Schaaf P. The course of axons within thte postnatal rabbit retina. J Hirnforsch. 1989;30:505–511. PubMed PMID: 1761741.
3. Traub P. Intermediate filaments. Berlin: Springer-Verlag; 1985.
4. Nona SN, Shehab SAS, Stafford CA, Cronly-Dillon JR. Glial fibrillary acidic protein (GFAP) from goldfish: its localisation in visual pathway. Glia. 1989;2:189–200. PubMed PMID: 2526081.
5. Schnitzer J. Astrocytes in mammalian retina. Prog Retinal Res. 1988;7:209–231.

6. Easter SS, Rusoff AC, Kisk PE. The growth and organisation of the optic nerve and tract in juvenile and adult goldfish. J Neurosci. 1981;1:793–811. PubMed PMID: 7346585.
7. Levine RL. Organisation of astrocytes in the visual pathways of the goldfish: an immunohistochemical study. J Comp Neurol. 1989;285:231–246. PubMed PMID: 2760263.
8. Maggs A, Scholes J. Reticular astrocytes in the fish optic nerve: macroglia with epithelial characteristics form an axially repeated lacework pattern to which nodes of Ranvier are apposed. J Neurosci. 1990;10:1600–1614. PubMed PMID: 2332800.
9. Bastmeyer M, Beckman M, Schwab ME, Stuermer CAO. Growth of regenerating goldfish axons is inhibited by rat oligodendrocytes and CNS myelin, but not by goldfish optic nerve tract oligodendrocyte-like cells and fish CNS myelin. J Neurosci. 1991;11:626–640. PubMed PMID: 2002357.
10. Stuermer CAO, Bastmeyer M. The retinal axons' pathfinding to the optic disk. Prog Neurobiol. 2000;62:197–214. PubMed PMID: 10828383.
11. Dingwell KS, Holt CE, Harris WA. The multiple decisions made by growth cones of RGCs as they navigate from the retina to the tectum in the Xenopus. J Neurobiol. 2000;44:246–259. PubMed PMID: 10934326.
12. Bignami A . Glial cells in the central nervous system. Geneva: FESN-Elsevier; 1991.
13. Fuchs C, Druger RK, Glasgow E, Schechter NJ. Differential expression of keratins in goldfish optic nerve during regeneration. J Comp Neurol. 1994;343:332–340. PubMed PMID: 7517963.
14. Stafford CA, Shehab SAS, Nona SN, Cronly-Dillon JR. Expression of glial fibrillary acidic protein (GFAP) in goldfish optic nerve following injury. Glia. 1990;3:33–42. PubMed PMID: 2138134.
15. Nona SN, Stafford CA, Shehab SAS, Cronly-Dillon JR. A polyclonal antibody to to goldfish neuronal 145kDa intermediate filament protein. Brain Res. 1990;524:133–138. PubMed PMID: 2400924.
16. Nona SN, Thomlinson AM, Bartlett CA, Scholes J. Schwann cells in the regenerating fish optic nerve: evidence that CNS axons not the glia determine when myelin formation begins. J Neurocytol. 2000;29:285–300. PubMed PMID: 11276180.
17. Scholes J, Maggs A, Dowding AJ. Glial axonal pattern formation in the fish optic nerve. In: Nona SN, Cronly-Dillon JR, Ferguson M, Stafford CA, editors. Development and regeneration of the nervous system. London: Chapman-Hall; 1992. p. 109-43.
18. Rungger-Brandle E, Achtstatter T, Franke WW. An epithelial-type cytoskeleton in a glial cell: astrocytes of amphibian optic nerves contain cytokeratin filaments and are connected by desmosomes. J Cell Biol. 1989;109:705–716. PubMed PMID: 2474553.
19. Bertolini B. Ultrastructure of the spinal cord of the lamprey. J Ultrastruct Res. 1964;11:1–24. PubMed PMID: 14202317.
20. Nona SN. Repair by Schwann cells in the regenerating goldfish visual pathway. In: Vernadakis A, Roots B, editors. Neuron-glia interactions during phylogeny. Vol. 2. Totowa (NJ): Humana; 1995. p. 347-65.
21. Ghandour MS, Labourdette G, Vicendon G, Gombos G. A biochemical and immunochemical study of S-100 protein in developing rat cerebellum. Dev Neurosci. 1981;4:98–109. PubMed PMID: 7014178.
22. Ludwin SK, Kosek KC, Eng LE. The topographic organisation of S-100 and GFA proteins in the adult rat brain: and immunohistochemical study using horseradish peroxidase-labelled antibody. J Comp Neurol. 1976;165:197–208. PubMed PMID: 1107363.
23. Kruger L, Maxwell DS. The fine structure of ependymal processes in the teleost optic tectum. Am J Anat. 1966;119:479–497. PubMed PMID: 5972733.
24. Rabe H, Koschorech E, Nona SN, Ritz HJ, Jeserich G. Voltage-gated sodium and potassium channels in radial glial cells of trout optic tectum studied by patch clamp analysis and single cell RT-PCR. Glia. 1999;26:221–232. PubMed PMID: 10340763.
25. Stevenson JA, Yoon MG. Morphology of radial glia, ependymal cells, and periventricular neurons in the optic tectum of goldfish (Carassius auratus). J Comp Neurol. 1982;205:128–138. PubMed PMID: 7076888.
26. Shehab SS, Stafford CA, Nona SN, Cronly-Dillon JR. Anti-goldfish glial fibrillary acidic protein (GFAP) recognises asrtrocytes from rat CNS. Brain Res. 1989;504:343–346. PubMed PMID: 2598035.

27. Schmechel DE, Rakic P. A Golgi study of radial glial cells in developing monkey telencephalon: morphogenesis and transformation into astrocytes. Anat Embryol (Berl). 1979;156:115–132. PubMed PMID: 111580.
28. Nona SN, Stafford CA. Glial repair at the lesion site in regenerating goldfish spinal cord: an immunohistochemical study using species specific antibodies. J Neurosci Res. 1995;42:350–356. PubMed PMID: 8583503.
29. Cajal S. Ramon Y. 1928. In: Degeneration and Regeneration of the Nervous System. (Translated by May, R.M., 1959). New York. Hafner.
30. Hatten MB. Astroglia as scaffold for development of the CNS. Semin Neurosci. 1990;2:455–465.
31. Rakic P. Intrinsic and extrinsic factors influencing the shape of neurons and their assembly into neuronal circuits. In: Seeman P, Brown GM, editors. Frontiers in neurology and neuroscience research. Toronto: University of Toronto Press; 1976. p. 112-32.
32. Reier PJ, Stensaas LJ, Guth L. The astrocyte scar as an impediment to regeneration in central nervous system. In: Kao CC, Bunge RP, Reier PJ, editors. Spinal cord reconstruction. New York: Raven; 1983. p. 163-95.
33. Asher RA, Morgenster DA, Moon LD, Fawcett JW. Chondroitin sulphate proteoglycans: inhibitory components of the glial scar. Prog Brain Res. 2001;132:611–619. PubMed PMID: 11545024.
34. Chierzi S, Fawcett JW. Regeneration in the mammalian optic nerve. Restor Neurol Neurosci. 2001;19:109–118. PubMed PMID: 12082232.
35. Berry M. Post-injury myelin breakdown products inhibit axonal growth: an hypothesis to explain the failure of axonal regeneration in the mammalian central nervous system. Bibliothetica Anat. 1982;23:1–11.
36. Schwab ME, Theonen H. Dissociate neurons regenerate into sciatic but not optic nerve explants in culture irrespective of neurotrophic factors. J Neurosci. 1985;5:2415–2423. PubMed PMID: 4032004.
37. Schnell L, Schwab ME. Axonal regeneration in rat spinal cord produced by antibody against myelin associate neurite growth. Nature. 1990;343:269–272. PubMed PMID: 2300171.
38. Filbin MT. Myelin-associated inhibitors of axonal regeneration in the adult mammalian CNS. Nat Rev Neurosci. 2003;4:703–713. PubMed PMID: 12951563.
39. Martini R. Expression and functional roles of neural cell surface molecules and extracellular matrix components during development and regeneration of peripheral nerves. J Neurocytol. 1994;23:1–28. PubMed PMID: 8176415.
40. Berry M, Hall S, Follows R, Rees L, Gregson N, Sievers J. Response of axons at the site of anastomosis between the optic nerve and cellular or acellular sciatic nerve grafts. J Neurocytol. 1988;17:727–44. PubMed PMID: 3148025.
41. Keirstead SA, Rasminsky M, Fukuda Y, Carter DA, Aguayo AJ, Vidal-Sanz M. Electrophysiologic responses in hamster superior colliculus evoked by regenerating retinal axons. Science. 1989;246:255–257. PubMed PMID: 2799387.
42. Vidal-Sanz M, Bray GM, Villegas-Perez MP, Thanos S, Aguayo AJ. Axonal regeneration and synapse formation in the superior colliculus by retinal ganglion cells in the adult rat. J Neurosci. 1987;7:2894–2909. PubMed PMID: 3625278.
43. Grafstein B, Murray M. Transport of proteins in goldfish optic nerve during regeneration. Exp Neurol. 1969;25:494–508. PubMed PMID: 5362566.
44. Grafstein B, Murray M. Transport of protein in goldfish optic nerve during regeneration. Exp Neurol. 1969;25:494–508. PubMed PMID: 5362566.
45. Quitsche W, Schechter N. Specific optic nerve proteins during regeneration of the goldfish retinotectal pathway. Brain Res. 1983;258:68–78.
46. Benowitz LI, Lewis ER. Increased transport of 44,000-49,000 Dalton acidic proteins during regeneration of the goldfish optic nerve: a two-dimensional gel analysis. J Neurosci. 1983;3:2153–2163. PubMed PMID: 6631474.
47. Perrone-Bizzozero NI, Benowitz LI. Expression of a 48 kilodalton growth associated protein in the goldfish retina. J Neurochem. 1987;48:644–652. PubMed PMID: 3794726.

48. Grafstein B. The retina as a regeneration organ. In: Adler R, Farber D, editors. The retina–a model for cell biology studies. Part II. London: Academic; 1986. p. 273-335.
49. Murray M. A quantitative study of regenerative sprouting by optic axons in goldfish. J Comp Neurol. 1982;209:352–62. PubMed PMID: 7130462.
50. Dunlop SA, Tennant M, Beazley LD. Extent of retinal ganglion cell death in the frog Litoria moorei after optic nerve regeneration induced by lesions of different sizes. J Comp Neurol. 2002;446:276–287. PubMed PMID: 11932943.
51. Berry M, Rees L, Hall S, Yiu P, Sievers J. Optic axons regenerate into sciatic nerve grafts only in the presence of Schwann cells. Brain Res Bull. 1988;20:223–231. PubMed PMID: 3370505.
52. Quigley HA, Nickells RW, Kerrigan LA, Pease ME, Thibault DJ, Zack DJ. Retinal ganglion cell death in experimental glaucoma and after axotomy occurs by apoptosis. Invest Ophthalmol Vis Sci. 1995;36:774–786. PubMed PMID: 7706025.
53. Silveira LC, Russelakis-Carneiro M, Perry VH. The ganglion cell response to optic nerve injury in the cat: differential responses revealed by neurofibrillar staining. J Neurocytol. 1994;23:75–86. PubMed PMID: 8195813.
54. Nona SN, Stafford CA, Shehab SAS, Cronly-Dillon JR. GFAP as a marker for astrocytes in normal and regenerating goldfish visual system. In: Nona SN, Cronly-Dillon JR, Ferguson M, Stafford CA, editors. Developmental and regeneration of the nervous system. London: Chapman-Hall; 1992. p. 97-108.
55. Nona SN, Thomlinson AM, Stafford CA. Temporary colonisation of the site of lesion by macrophages is a prelude to the arrival of regenerating axons in the regenerating goldfish optic nerve. J Neurocytol. 1998;27:791–803. PubMed PMID: 10451426.
56. Nona SN. Invited review: Repair in goldfish central nervous system. Restor Neurol Neurosci. 1998;12:1–11. PubMed PMID: 12671316.
57. Streit WJ, Kreutzberg GW. Lectin binding by resting and reactive microglia. J Neurocytol. 1987;16:249–260. PubMed PMID: 3625239.
58. Naujoks-Manteuffel C, Niemann U. Microglia cells in the brain of Pleurodeles watl (Urodela salamaderia, Salamandridae) after Wallerian degeneration in the primary visual system using Bandeiraea simplicifolia isolectin B4 cytochemistry. Glia. 1994;10:101–113. PubMed PMID: 8168864.
59. Colavincenzo J, Levine RL. Myelin debris clearance during Wallerian degeneration in the goldfish visual system. J Neurosci Res. 2000;59:47–62. PubMed PMID: 10658185.
60. Sivron T, Schwab ME, Schwartz M. Presence of growth inhibitors in fish optic nerve myelin: postinjury changes. J Comp Neurol. 1994;343:237–246. PubMed PMID: 8027441.
61. Brown MC, Perry VH, Lunn ER, Gordon S, Heumann R. Macrophage dependence of peripheral sensory nerve regeneration: possible involvement of nerve growth factor. Neuron. 1991;6:359–370. PubMed PMID: 1848079.
62. Heumann R, Lindholm D, Bandtlow C, Meyer MS, Radekc MJ, Misko TP, Shooter E, Theonen H. Differential regulation of mRNA encoding nerve growth factor and its receptor in sciatic nerve during development, degeneration and regeneration: role of macrophages. Proc Natl Acad Sci U S A. 1987;84:8735–8739. PubMed PMID: 2825206.
63. Blaugrund E, Cohen I, Hani Y, Schwartz M. Axonal regeneration is associated with glial migration: comparison of the injured optic nerves of fish and rats. J Comp Neurol. 1993;330:105–112. PubMed PMID: 8468398.
64. Hirsch S, Cahill MA, Stuermer CAO. Fibroblasts at the transection site of the injured goldfish optic nerve and their potential role during retinal axonal regeneration. J Comp Neurol. 1995;360:599–611. PubMed PMID: 8801252.
65. Levine RL. Gliosis during optic fiber regeneration in the goldfish: an immunohistochemical study. J Comp Neurol. 1991;312:549–560. PubMed PMID: 1761741.
66. Griffin JW, George R, Laboto C, Williams RT, Yan LC, Glass JD. Macrophage reponses and myelin clearance during Wallerian degeneration: relevance to immune-mediated demyelination. J Neuroimmunol. 1992;40:153–166. PubMed PMID: 1430148.

67. Hirschberg DL, Schwartz M. Macrophage recruitment to acutely injured central nervous system is inhibited by a resident factor: a basis for an immune-brain barrier. J Neuroimmunol. 1995;61:89–96. PubMed PMID: 7560018.
68. Perry VH, Brown MC. Role of macrophage in peripheral nerve degeneration and repair. Bioessays. 1992;14:401–416. PubMed PMID: 1323962.
69. Perry VH, Brown MC, Gordon S. The macrophage response to central and peripheral nerve injury. A possible role for macrophages in regeneration. J Exp Med. 1987;165:1218–1223. PubMed PMID: 3559478.
70. Lazarov-Spiegler O, Solomon AS, Zeev-Brann AB, Hirschberg DL, Lavie V, Schwartz M. Transplantation of activated macrophages overcomes central nervous system regrowth failure. FASEB J. 1996;10:1296–1302. PubMed PMID: 8836043.
71. Rapalino O, Lazarov-Spiegler O, Agranov E, Katz A, Hadani M, Schwartz M. Implantation of stimulated homologous macrophages results in partial recovery of paraplegic rats. Nat Med. 1998;4:814–821. PubMed PMID: 9662373.
72. Battisti WP, Wang J, Bozek K, Murray M. Macrophages, microglia and astrocytes are rapidly activated after crush injury of the goldfish optic nerve: a light and electron microscopic analysis. J Comp Neurol. 1995;354:306–320. PubMed PMID: 7540185.
73. Wolburg H. Axonal transport, degeneration, and regeneration in the visual system of the goldfish. Adv Anat Embryol Cell Biol. 1981;67:1–94. PubMed PMID: 6164262.
74. Berry M, Hall S, Rees L, Carlile J, Wyse JPH. Regeneration of axons in the optic nerve of adult Browman-Wyse (BW) mutant rat. J Neurocytol. 1992;21:426–448. PubMed PMID: 1403007.
75. Raisman G. Myelin inhibitors: does no mean go? Nat Rev Neurosci. 2004;5:157–161. PubMed PMID: 14735118.
76. Silver J, Miller JH. Regeneration beyond the glial scar. Nat Rev Neurosci. 2004;5:146–156. PubMed PMID: 14735117.
77. Berry M, Carlile J, Hunter A. Peripheral nerve explants grafted into the vitreous body of the eye promote the regeneration of retinal ganglion cell axons severed in the optic nerve. J Neurocytol. 1996;25:147–170. PubMed PMID: 8699196.
78. Scherer SS, Easter SS. Degenerative and regenerative changes in the trochlear nerve of the goldfish. J Neurocytol. 1984;13:519–565. PubMed PMID: 6481411.
79. Easter SS. Retinal axons and the basal lamina. In: Wolff JR et al., editors. Mesenchymal-epithelial interactions in neural development. Berlin: Springer; 1987. p. 385-96.
80. Jeserich G, Muller A, Jacque C. Developmental expression of myelin proteins by oligodendrocytes in the CNS of trout. Brain Res Dev Brain Res. 1990;51:27–34. PubMed PMID: 1688743.
81. Nona SN, Duncan A, Stafford CA, Maggs A, Jeserich G, Cronly-Dillon JR. Myelination of regenerated axons in goldfish optic nerve by Schwann cells. J Neurocytol. 1992;21:391–401. PubMed PMID: 1403004.
82. Jeserich G, Waehneldt TV. Characterisation of antibodies against major fish CNS myelin proteins: immunoblot analysis immunochemical localisation of 36K and IP2 proteins in trout nerve tissue. J Neurosci Res. 1986;15:147–157. PubMed PMID: 2421005.
83. Jessen KR, Mirsky R. Developmental regulation in the Schwann cell lineage. Adv Exp Med Biol. 1999;468:3–12. PubMed PMID: 10635015.
84. Blakemore WF. Remyelination by Schwann cells of axons demyelinated by intraspinal injections of 6-aminonicotinamide. J Neurocytol. 1975;4:745–757. PubMed PMID: 127832.
85. Blakemore WF. Remyelination of demyelinated spinal cord axons by Schwann cells. In: Kao CL, Bunge RP, Reier JP, editors. Spinal cord reconstruction. New York: Raven; 1983. p. 281-91.
86. Jessen KR, Brennan A, Morgan AL, Mirsky R, Kent A, Hashimoto Y, Gravrilovic J. The Schwann cell precursor and its fate: a study of cell death and differentiation during gliogenesis in rat embryonic nerves. Neuron. 1994;12:509–527. PubMed PMID: 8155318.
87. Pellegrino RG, Spencer PS. Schwann cell mitotis in response to regenerating peripheral axons in vivo. Brain Res. 1985;341:16–25. PubMed PMID: 3929995.

88. Schwab ME, Schnell L. Region specific appearance of myelin constituents in the developing rat spinal cord. J Neurocytol. 1989;18:161–169. PubMed PMID: 2471819.
89. Schmidt JT. Long term potentiation and activity dependent retinotopic sharpening in the regenerating retinotectal projection of the goldfish: common sensitive period and sensitivity to NMDA blockers. J Neurosci. 1990;10:233–246. PubMed PMID: 2153773.
90. Meyer RL, Kageyama GH. Large-scale synaptic errors during map formation by regenerating optic axons in the goldfish. J Comp Neurol. 1999;409:299–312. PubMed PMID: 10379922.
91. Sauve Y, Sawai H, Rasminsky M. Topological specificity in reinnervation of the superior colliculus in regenerated retinal ganglion axons in adult hamsters. J Neurosci. 2001;21:951–960. PubMed PMID: 11157081.
92. Dunlop SA, Tee LBG, Stirling V, Taylor AL, Runham PB, Barber AB, Kutchling G, Roger J, Roberts JD, Harvey AR, Beazley LD. Failure to restore vision after optic nerve regeneration in reptiles: interspecies variation in response to axotomy. J Comp Neurol. 2004;478:292–305. PubMed PMID: 15368531.

Regeneration in the Visual System of Adult Mammals

Yves Sauve and Frederic Gaillard

Created: May 1, 2005; Updated: June 21, 2007.

Introduction

> "...once development was ended, the founts of growth and regeneration of the axons and dendrites dried up irrevocably. In adult centres the nerve paths are something fixed, ended, immutable. Everything may die, nothing may be regenerated. It is for the science of the future to change, if possible, this harsh decree. Inspired with high ideals, it must work to impede or moderate gradual decay of neurons, to overcome the almost invincible rigidity of their connections, and to re-establish normal nerve paths, when disease has severed centres that were intimately associated." (Santiago Ramon y Cajal, 1913-14).

Over 90 years after Ramon y Cajal's farsighted work (1) (Fig. 1), we are still unable to solve the great mystery of regeneration in the adult mammalian central nervous system (CNS). Retinal degeneration leading to loss of photoreceptors and retinal ganglion cells (RGCs) is still largely untreatable, although recent experimental work is beginning to provide possible solutions to these devastating conditions. Other untreatable pathologies leading to loss of sight involve lesions to the CNS visual centers or projection pathways. There are two fundamental experimental approaches presently used to tackle both these problems. One involves reconstructing lost circuitry by replacement with (usually fetal) neuronal tissue, and the other is attempting to slow the rate of the degeneration.

Reconstruction of Primary Visual Pathways

Without any experimental intervention, nerve lesions in the adult CNS of mammals produce only a limited and brief period of abortive sprouting and then to the death of axotomized neurons. In sharp contrast, the peripheral nervous system (PNS) and the immature CNS of mammals, as well as the mature CNS of cold-blooded vertebrates, all display varying levels of successful spontaneous regeneration after injury. The development of experimental repair strategies has relied on lessons learned from these systems. Combined with advances in anatomical tracing and immunohistochemical methods, these strategies have revealed the surprising capacity for regeneration and synapse formation in the adult mammalian CNS. For instance, Dr. Albert Aguayo and colleagues have used an experimental approach (2-4) based on the concept that regeneration in the PNS is dependent on the permissive environment provided by Schwann cells present in the nerve tube. They suggested that the absence of this permissive environment in the mature CNS was the reason for failure of regeneration. Thus, they postulate that damaged neurons from the mature CNS might be able to regenerate axons if placed in close proximity to Schwann cells. In fact, this hypothesis was suggested by Ramon y Cajal (1) over a century ago and was later tested by Tello in 1907 (5) (Fig. 2) in a series of experiments on rabbits. There was a suggestion that retinal axons could regenerate after axotomy if the cut optic nerve end was anastomosed to a sciatic nerve graft (5). The lack of anatomical tracers at that time did not allow us to see whether such regenerating axons were indeed of CNS origin, namely from RGCs. The indisputable proof that some CNS neurons do have this regenerative potential had to wait until specific axonal tracing techniques became available in the late 1970s (6, 7). Further work applied to primary visual pathways showed that if directed into the brain (Fig. 3), regenerating RGC axons were able to re-establish connections in visual centers of the brainstem (4). These connections appeared capable of transmitting visual information (8, 9).

The concept that neural regeneration depends on a permissive environment does not alone explain why most mature mammalian CNS neurons do not regenerate an axon. For instance, in the absence of axonal myelin-associated growth inhibitors such as Nogo, axonal sprouting itself is not improved (10). The role of axonal growth inhibitors in axonal regeneration remains a controversial issue (11). When developing experimental

Figure 1. Santiago Ramon y Cajal at work. From the Cajal Institute (http://www.cajal.csic.es/).

strategies, other factors have to be considered, such as axotomy-induced cell death and secondary degeneration (12), scar formation (13), and factors intrinsic to neurons themselves. We know that most CNS neurons loose their capacity for axonal regeneration at a specific point in early development, even before myelination (14-16).

The abundant and diverse experiments directed at reconstructing visual circuitry (several will be discussed below) have all uncovered a range of difficulties, such as: 1) establishing a permissive interface between sprouting and/or regenerating axons, or between graft and host; 2) providing the optimal conditions for appropriately directed axon outgrowth; 3) achieving sufficient amount of axon outgrowth for proper function; and 4) limiting or controlling the local neural responses to initial injury, such as cell death, which may in itself mitigate against effective recovery. A central point to all such work is that visual function should be used as the yardstick for success (see Generation of Action Potentials in Target Neurons).

Requirements for Recovery of Function following Lesions of CNS Pathways

The recovery of lost function following axonal interruption in any neuronal system depends on the fulfillment of the following prerequisites:

- survival of axotomized neurons and prevention of secondary degeneration
- axonal extension of the neurons surviving axotomy
- guidance of regenerating axons toward their appropriate target(s)
- target innervation and synapse formation onto recipient neurons
- supra-threshold activation in target neurons caused by regenerated afferents
- restoration of ordered functional connections
- preservation of local and downstream circuitry

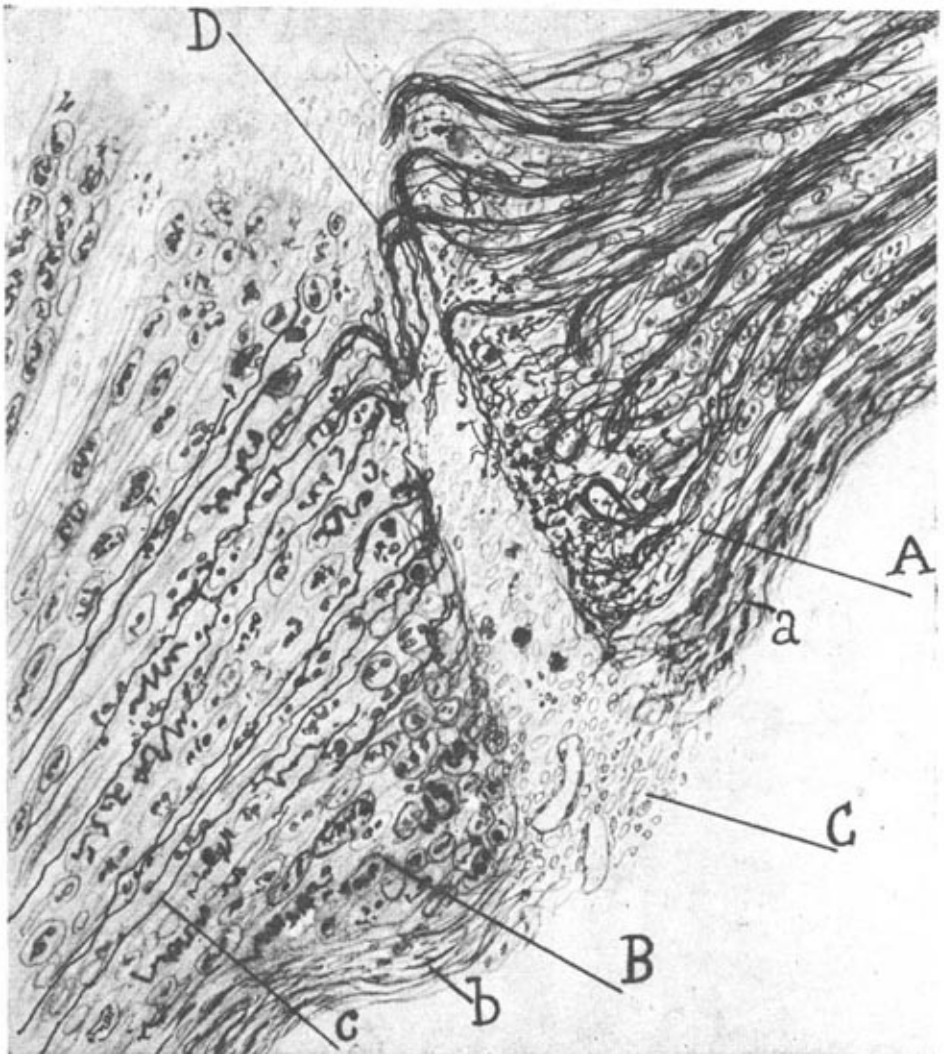

Figure 2. Sciatic nerve graft (B) anastomosed on the optic nerve stump (A) in an adult rabbit. Axons can be seen to cross the anastomosis site (D). A scar has formed at the anastomosis site (C). Letters in lowercase indicate a vein in the optic nerve (a), "neurilema" in the sciatic nerve graft (b), fibers that might correspond to RGC axons regenerated in the sciatic nerve graft (c). Taken from Tello (5).

The retinocollicular pathway is particularly suitable for addressing the above-mentioned points for at least three reasons: 1) RGC axons project to the superior colliculus (SC) through the optic nerve, which can be easily lesioned, replaced, and anatomically traced; 2) because RGCs are excited by light, they can be selectively stimulated in a physiological manner without the use of less selective electrical pulses, which would concomitantly excite other pathways; 3) intact RGC axons arborize preferentially in the superficial layers of the SC, onto which they form a point-to-point representation of the retina (17-19) and which allows comparison of the regenerated pathway with those intact, using either morphological or physiological approaches.

We will review the extent to which these requirements can be achieved by using the example of the interrupted retinocollicular pathway and attempts for reconstruction using PN grafts replacing the optic nerve. In brief, the potential for regeneration of optic axons after being damaged was first indicated by studying hamsters in which the optic nerve was cut and a peripheral nerve graft placed in association with the retinal optic fiber layer (3) (Fig. 3). Optic axons grew into this nerve graft, and studies in cat, in this instance, showed that the major classes characterized, both anatomically and physiologically, contribute to this regenerative growth (20). Subsequent experiments (21) refined the approach and were able to show that up to 10% or so of the normal optic projection was able to regenerate into the nerve graft. If the other end of the nerve graft was placed in an appropriate brain

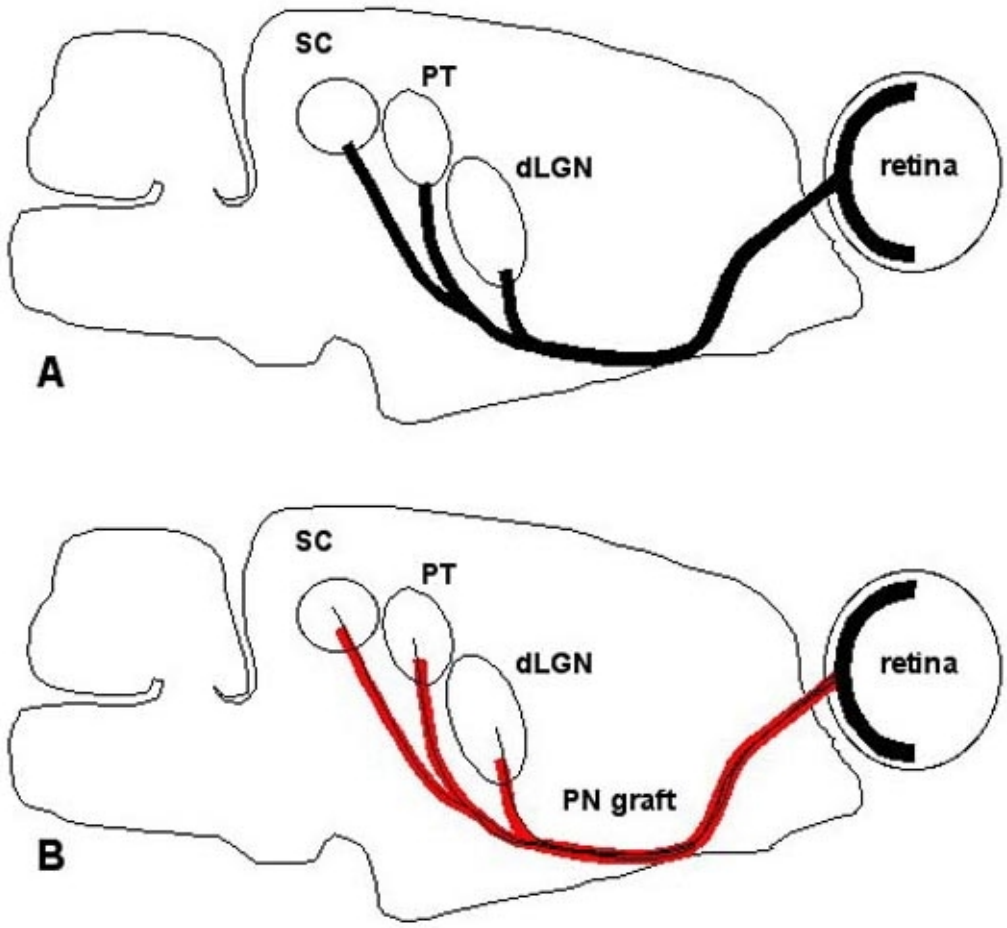

Figure 3. Schematic of peripheral nerve graft bridging the retinofugal pathways. A, normal optic pathway projecting to superior colliculus (SC), pretectum (PT), and dorsal lateral geniculate nucleus (dLGN). B, regeneration of optic axons through a peripheral nerve graft (red) to reach the various visual centers.

region, a proportion of these axons could reach regions normally innervated by them (4, 22). If the central stump was placed in close proximity to a visual center, the axons formed terminal ramifications and synapses within that region (23). If placed at a distance from a visual center, axons were able to grow as much as 6 mm through the brainstem to specific targets of optic input, ignoring in the process other brain regions, including ones that had lost their primary input during the surgical procedure (22). Although an anatomical study of topological representation of the regenerated axons has not been done, physiological experiments (24) have indicated that although the precise map encountered in the normal retinotectal projection was not seen, there was indication of a tendency for the naso-temporal representation of the visual field to be appropriately arrayed along the rostrocaudal SC axis. Whether this would be sufficient for an animal to be able to perform a behavior requiring topographically encoded information, such as head tracking, is not clear. The further possibility that some sort of training regimen might improve the tightness of the map has not been explored either, but this preparation does lend itself to such exploration.

Promoting the Survival of Axotomized RGCs

RGCs Die after Optic Nerve Transection

After a complete intraorbital lesion of the adult mammalian optic nerve, the majority of RGCs are lost within 2 weeks (21, 25-27). Axotomized RGCs start dying after 1 week post-lesion, via programmed cell death. This

process, known as apoptosis, is also responsible for the naturally occurring cell death of RGCs during development. Cells undergoing apoptosis, such as axotomized RGCs, are characterized by the condensation of their nucleus, DNA fragmentation, and the formation of apoptotic bodies (25, 28). The pathways responsible for the apoptotic death of axotomized RGCs involve the activation of caspases types 3, 8, 9, and CPP32-like (29-33), and the p38 mitogen-activated protein kinase p38MAPK (34). The inhibition of either or all of these caspases (30, 32, 35, 36) or of p38MAPK (34) enhances the survival of axotomized RGCs. Furthermore, optic nerve transection leads to the elevation of proapoptotic protein Bax and the decrease of the antiapoptotic proteins Bcl-2 and Bcl-X (37). The overexpression of Bcl-2 in transgenic mice has been shown to protect RGCs for axotomy-induced death (38, 39). Finally, transfection of RGCs with the X-linked inhibitor of apoptosis or with the caspase inhibitor p35 can both protect RGCs from axotomy-induced cell death (40). The conclusion from these findings is that axotomy-induced death of RGCs involves the activation of not only one but several apoptotic pathways. Therefore, strategies aimed at preventing the death of axotomized RGCs would have to target multiple pathways.

Strategies to Prevent the Death of Axotomized RGCs

Most strategies developed to prevent RGC death involve the supply of various trophic factors either exogenously, through cell-based therapy, or via gene transfection (for reviews, see Yip and So (41), Cui et al (42), Weishaupt and Bahr (43), and Koeberle and Bahr (44)). The rationale for supplying neurotrophins to axotomized RGCs is that their death might be related to the loss of retrogradely supplied trophic factors, such as brain-derived neurotrophic factor (BDNF), from their targets in the SC (45-47). Axotomized RGCs can be rescued by experimentally supplying the retina with BDNF, either via intravitreal injections (26, 48-50) or via gene transfection of retinal cells (51). Furthermore, transfection of retinal cells with the high-affinity BDNF receptor TrkB also enhances the survival of axotomized RGCs (52). Axotomized RGCs have also been rescued by the experimental addition of several other neurotrophic factors (some of which having additive effects with each other): neurotrophin NT-4/5 (26, 53); NGF (54); GDNF (55, 56); Neurturin (57); and CNTF (50, 58-60). Several growth factors mediate their action by binding to their specific receptors and activating the mitogen-activated protein kinase (MAPK) and phosphatidylinositide-3-kinase (PI3K) transduction cascade pathways. For details on secondary messengers and factors interfering with these cascades, see reviews by Kaplan and Miller (61), Patapoutian and Reichardt (62), and Koeberle and Bahr (44). In brief, neurotrophic factors may prevent axotomy-induced RGC death by interfering with caspase pathways and by promoting the expression of pro-survival genes.

The neurotrophic factors tested to date for their survival effect on axotomized RGCs all have only short-term effects, suggesting that trophic withdrawal is not the only trigger for the apoptosis of axotomized RGCs. Blockade of axonal transport (63) has minimal effects on the death of RGCs in neonatal rats. Other factors have been identified, among them, the up-regulation of inducible nitric oxide synthase (iNOS) by Muller cells after RGC axotomy (64). Inhibition of NOS has been shown to promote the survival of axotomized RGCs (64), and when done in combination with BDNF, it potentiates the effect of this neurotrophin (48). Modulation of microglial cells and macrophage activity has also been shown to have an effect on the survival of axotomized RGCs (65-67).

Finally, the prevention of axotomy-induced RGC death has been explored using a vaccination approach known as "protective autoimmunity" (for a review, see Schwartz (68)). Dr. Michal Schwartz and colleagues recently demonstrated that T cells specific to self-proteins residing in the site of the CNS insult can be neuroprotective. With the aim of boosting autoimmunity for neuroprotection without risking the induction of an autoimmune disease, Dr. Schwartz's group has developed the use of Cop-1 (an FDA-approved drug for the treatment of multiple sclerosis) as an active vaccination for neuroprotection. This approach is currently under investigation as a potential preventive treatment for glaucoma.

Promoting the Growth of Axotomized RGC Axons

Anastomosis of a PN graft onto the optic nerve stump has been shown to have a survival effect on RGCs (21, 69) as well as acting as an environment permissive to RGC axonal regeneration (3, 4). A maximum of 10% of the total RGC population in rodents (10,000 of 100,000 in rats and hamsters) (Fig. 4a, Fig. 4b, Fig. 4c) can regenerate an axon as far as the distal end of an autologous PN graft, covering a distance of up to 2.5 cm. This allows them to reach areas of the primary visual targets, such as the contralateral superior colliculus. The RGCs that have regenerated an axon along the PN graft appear to survive longer than the RGCs that have failed to do so (21). Whether some RGCs have intrinsic survival or axonal regenerative capacities or whether some RGCs simply randomly succeed to regenerate an axon by chance (for instance, proximity to the PN graft stump before retrograde degeneration beyond the optic disc) remains to be clarified.

The promotion of RGC axonal regeneration seems to involve different mechanisms than the ones promoting their axonal extension: most trophic factors shown to promote RGC survival fail to promote their axonal regeneration. The discovery of new candidate molecules promoting axonal extension comes in part from the observation that lens scratching induces the production of low molecular weight molecules that can promote both RGC survival and axonal regeneration within the intracranially lesioned optic nerve (70). Furthermore, macrophage stimulation, which is associated with the release of similarly acting molecules (71) can also promote RGC axonal extension within the lesioned optic nerve. The neutralization of myelin-associated growth inhibitors can promote RGC axonal regeneration within lesioned optic nerves, but only if RGCs are in an "active growth state", such as stimulated by the small molecules mentioned above (72).

The ability of RGCs to regenerate an axon does not only depend on their environment but also on their intrinsic state. As mentioned in the introduction, most CNS neurons such as RGCs appear to loose their capacity for axonal regeneration during maturation (15, 16). Some recent experimental manipulations have showed that it might be possible to reverse, at least to some extent, this state. Dr Lisa McKerracher and colleagues have shown that inactivation of the small GTPase Rho can promote RGC axonal regeneration after micro-lesions of the optic nerve in adult rats (for a review, see Ellezam et al. (73). Another approach, investigated by Dr. Mary Filbin and colleagues, involves elevating the intracellular level of cyclic AMP in neurons (74) (for a review, see Spencer and Filbin (75)).

Guidance of Regenerating RGC Axons Toward Their Appropriate Target

On the basis of what we know about developmental events, the challenges for regenerating RGC axons to successfully reach their appropriate targets are severe. First, as during development (for a review, see Oster et al. (76)), regenerating axons have to navigate within the retina, find their way to the optic disc, exit it, and finally enter into the optic nerve. After PN grafting (anastomosed on the intraorbitally cut optic nerve stump) combined with intravitreal BDNF (to increase the survival of axotomized RGCs), a minority of RGC axons do successfully regenerate an axon into a peripheral nerve graft. However, many regenerating RGC axons never actually exit the optic disc (77). Several axons from surviving RGCs appear to turn sharply just before the optic disc, growing in the opposite direction, forming numerous collateral branches and loops, with erratic growing patterns (Fig. 5).

A second challenge facing the regenerating RGC axon consists of navigating across the optic chiasma by crossing or not crossing the midline, again depending on the RGC type and/or location in the retina (for a review, see Williams et al. (78)). After which, regenerating RGC axons, again depending on their types, have to extend all the way into their appropriate target(s); some individual RGCs even have to send collaterals to multiple targets, such as both the SC and the dorsolateral geniculate nucleus (dLGN), and even more as shown in Fig. 6.

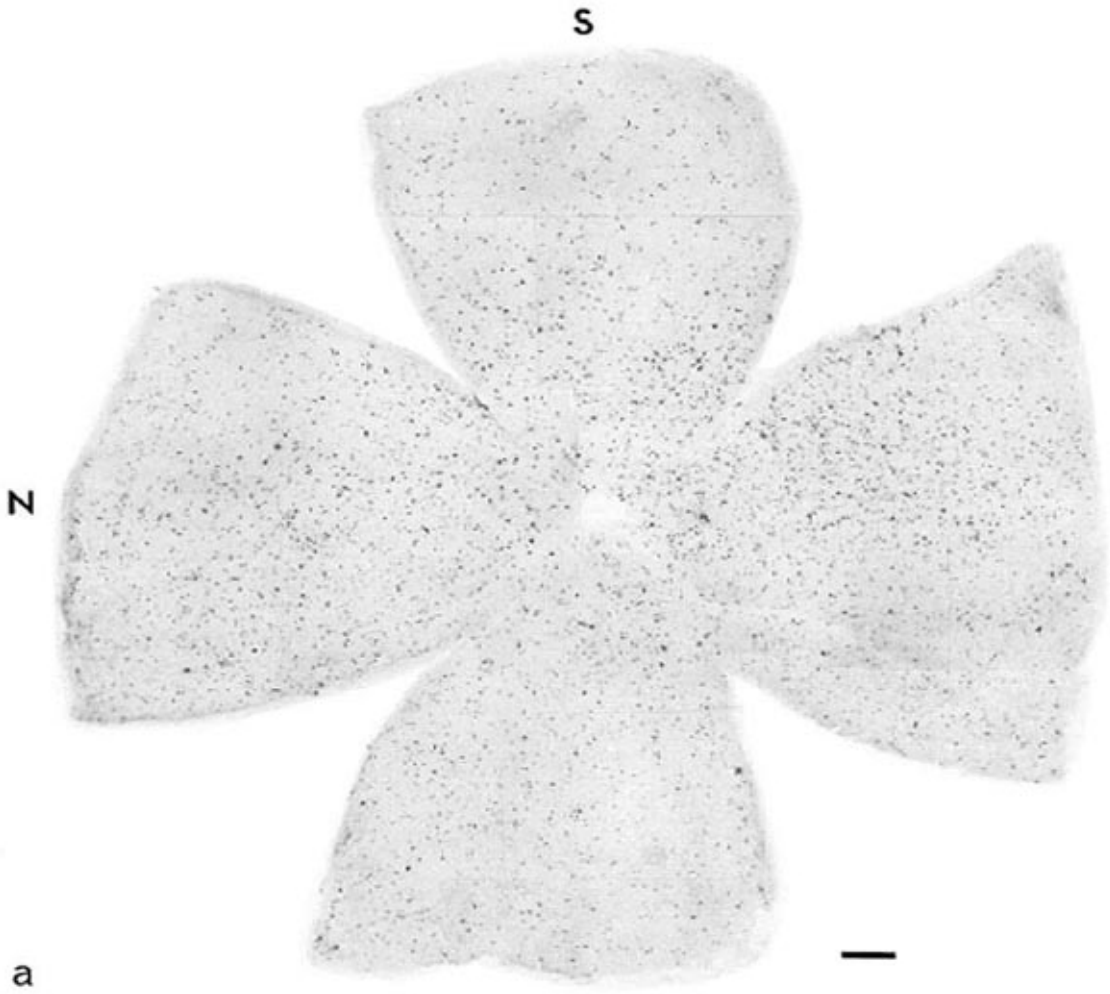

Figure 4a. Demonstration of hamster RGC axonal regeneration in PN grafts. Photomicrographic montage of a flattened retinal whole-mount from an animal with a PN graft attached to the ON. The montages were prepared from 24 overlapping photographs printed at a magnification of ×45. S, superior; N, nasal. Bars, 500 μm. The retina was reacted for peroxidase histochemistry 2 days after application of HRP to the distal end of the graft; this retina contains 12,385 ganglion cells that are retrogradely labeled with the tracer.

By using PN grafts, it has been possible to guide regenerating RGC axons into their appropriate targets such as the SC (4, 8, 9, 22, 24, 79), the dLGN (80), the pretectal nuclei (Fig. 7) (23), or deliberately into inappropriate targets such as the inferior colliculus or cerebellum (81).

However, in some animals following insertion of the distal end of the PN graft into a chosen target, only a minority or even none of the regenerating RGC axons can enter a target (23). In such cases, several RGC axons (anterogradely labeled with a tracer from the eye) are confined to a neuroma-like formation at the interface between the graft and the CNS target (Fig. 8).

The cause of the formation of the neuroma-like endings is unclear. Three main factors have to be considered: 1) glial reactions that might be associated with the lack of axonal penetration into the CNS target; 2) the presence of inhibitory molecules, which may also be responsible for the curtailed growth observed in CNS targets, and that are known to be expressed in the damaged CNS (82) and at the PNS-CNS interface (83-88); and 3) the perturbation, due to graft insertion procedure, of the tri-dimensional structure of the extracellular matrix that might act as "guiding railways" coated with molecules that have growth-inhibitory or -promoting properties such as laminin, vimentin, and chondroitin sulfate proteoglycans (CSPGs).

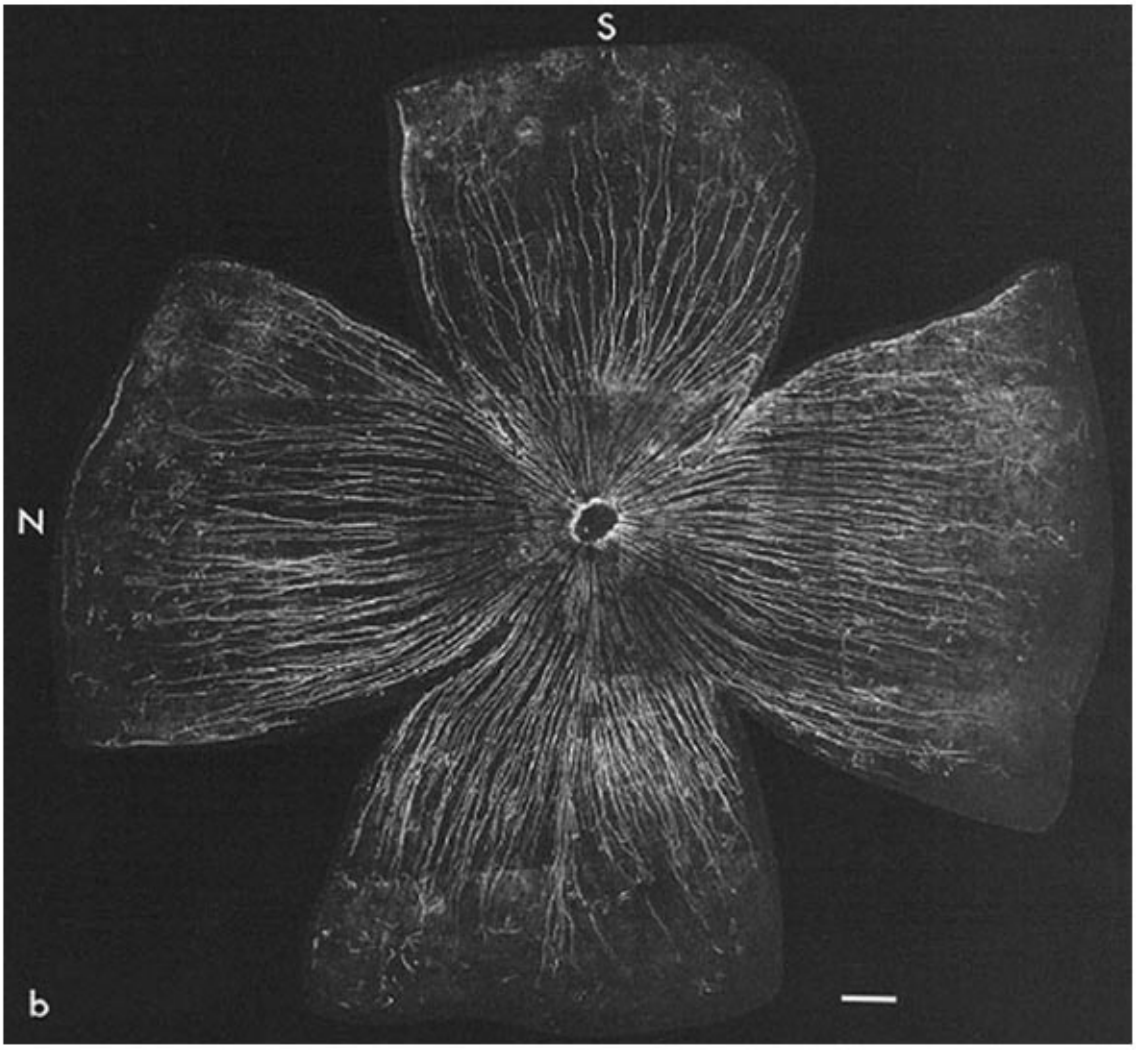

Figure 4b. Same retina as in A, incubated with the monoclonal antibody, RT 97, the immunofluorescent axons of retinal ganglion cells converge toward the central optic disk.

In some instances, PN grafts cannot be directly inserted into appropriate targets because of the small size of the nucleus. In the study of Aviles-Trigueros et al. (23), successful innervation of the olivary pretectal nucleus (OPN) and the nucleus of the optic tract (NOT) was achieved by inserting the distal end of a PN graft into the superficial aspect of the midbrain, between these two nuclei, by carefully avoiding touching them. Under such circumstances, some axons were seen crossing the midline to innervate the contralateral nuclei. This led the investigators to insert the nerves some distance further away from the nuclei. Axons, although coursing for long distances through the brainstem, still showed selectivity for optic target regions (Fig. 9, Fig. 10, Fig. 11). This occurred even though some nuclei within their trajectory were deafferented by the surgery associated with graft insertion.

The specificity of innervation of visual and non-visual targets would appear to be at odds with the observation of Zwimpfer et al. (81) showing innervation of the cerebellum by optic axons regenerating through PN grafts. There is, however, a significant difference in experimental design in that in the study of Aviles-Trigueros et al. (23), the axons have a "choice" of optic or non-optic targets, whereas in the cerebellum study, no choice is available. To complicate the issue, there is evidence that when two of the principal targets of retinofugal axons, the SC and dLGN, are ablated in newborn hamsters and the somatosensory (ventrobasal) or auditory (medial geniculate) thalamic nuclei are partially deafferented, the optic axons form permanent, abnormal connections in the latter

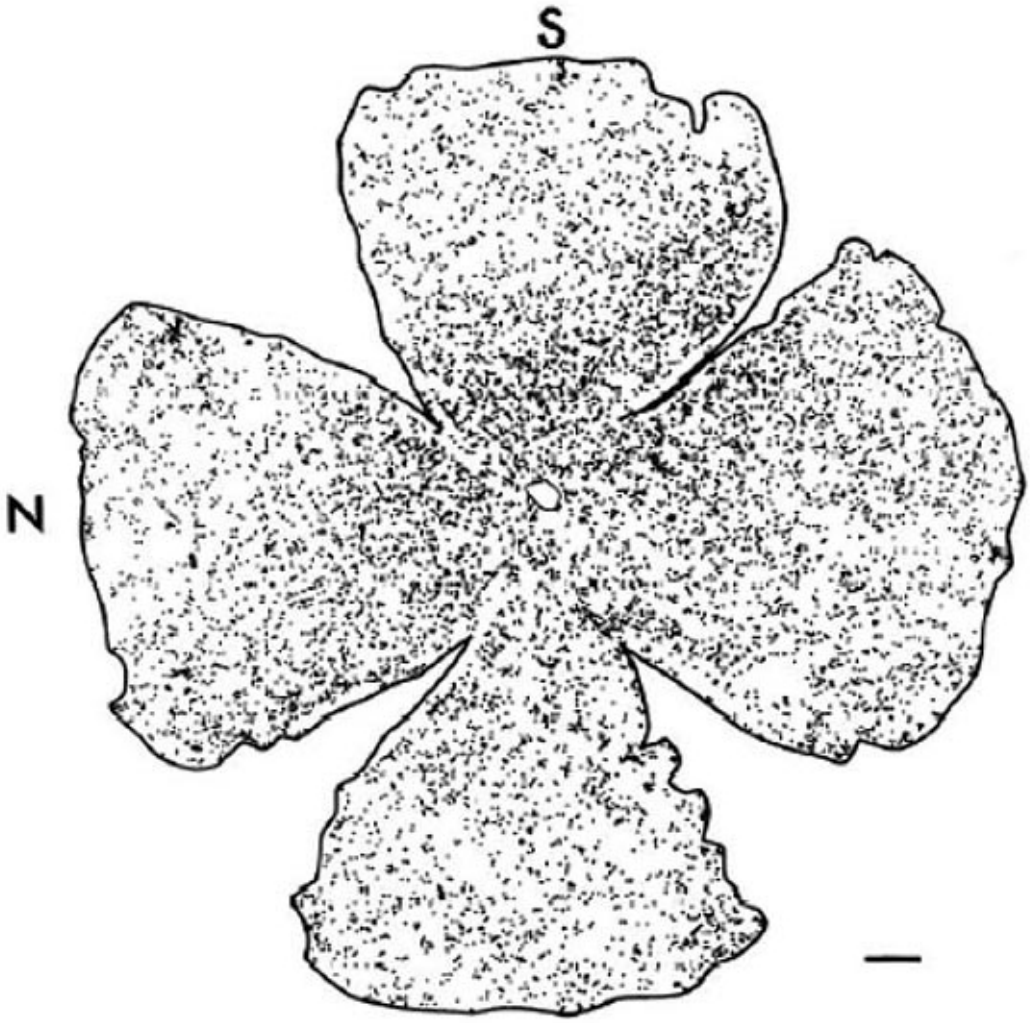

Figure 4c. Diagram, drawn from a photographic montage of a flattened retinal whole-mount from a different retina, indicating the location of 9451 neurons (dots) retrogradely labeled with HRP applied to the unconnected, extracranial end of the graft. The montage was prepared from 24 overlapping photographs printed at a magnification of ×45. S, superior; N, nasal. Bar, 500 μm. From Vidal-Sanz et al. (4).

nuclei (89). The mechanisms responsible for "apparent" preference of appropriate target in studies such as by Aviles-Trigueros et al. (23) are still unclear.

In addition to PN grafting, several studies have reported successful RGC axonal regeneration within the severed optic nerve (70, 73, 90-93). However, it remains unclear as to what is the growth pattern of individual regenerating RGC axons, especially at the level of the optic chiasm, and distally.

Arborization and Synapse Formation by RGC Axons Regenerating into Their CNS Targets

Studies involving PN grafting to bridge the retinofugal pathways have shown that regenerating RGC axons can form distinct arborizations in the target which they reinnervate (4, 23, 94, 95). The study of Aviles-Trigueros et al. (23) suggests that regenerated retinal axons adopt distinctive patterns of terminal arborizations, depending on the target they reinnervate. For instance, while axons entering the OPN show little ramification and swellings reminiscent of the typical retinal innervation of this nucleus, in the NOT axons tend to show more profuse ramifications and arborizations with terminal swellings (Fig. 12 and Fig. 13).

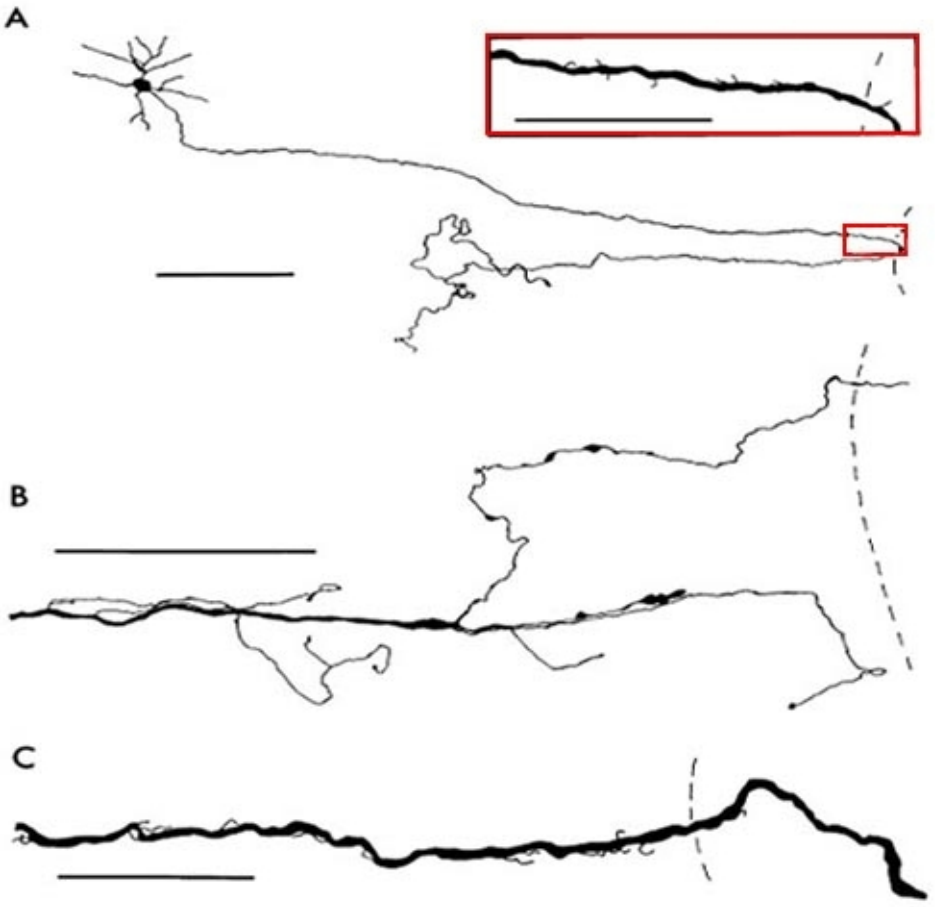

Figure 5. Camera lucida drawings of neurobiotin-labeled RGC axons in flat-mounted retinas 2 weeks after optic nerve (ON) transection alone (A) or with the intravitreal administration of BDNF (B) or NT-3 (C) at the time of transection. The broken lines indicate the edge of the ON head. A, an axon in an untreated retina turns at the edge of the ON head, grows toward the periphery of the retina for 824 μm, and then forms a branch that is 445 μm in length. The main axon then turns toward the ON head and ends as a growth cone. Scale bar, 200 μm. Inset, drawn at higher magnification, the axon shown in A also has numerous small branches near the ON head. Scale bar, 50 μm. B, an axon in a retina treated with 5 μg of BDNF at the time of ON transection has eight branches that range in length from 11 to 363 μm. Scale bar, 100 μm. C, an RGC axon in a retina treated with 5 μg of NT-3 ends over the ON head and has many short branches. Scale bar, 50 μm. From Sawai et al. (77).

These types of terminals are reminiscent of the terminals previously described for such retinorecipient nuclei in another rodent (96). In this context, what is also remarkable, is the similarity of the morphology of the elaborate arborizations found in the superficial layers of the superior colliculus (Fig. 14) with that described in normal animals (96). This indicates further specificity of terminal arborization within the retinorecipient reinnervated target. Thus, it appears that the morphology of the arborization is dictated by the recipient region, more than by the type of retinal fiber arriving to target (80), and that regenerating axons modify their arbors to adapt to the local conditions of the target nucleus.

In 1987, Vidal-Sanz et al. (4) provided experimental evidence that regenerating RGC axons were able to re-establish connections in visual centers of the brainstem (Fig. 15). These connections appear to persist for the life span of the rodent, i.e., up to 2 years of age (97). The type of synaptic contacts formed, the ratios of contacts to terminal perimeter, and the domains of the postsynaptic neurons contacted are similar to those of intact retinofugal pathways (22). Therefore, regenerated RGC axons can establish well-differentiated synapses with neurons in the SC. On the basis of their results, Carter et al. (22) concluded that, "The synaptic differentiation attained by such reformed retinocollicular projections suggests that regenerating CNS axons and their target

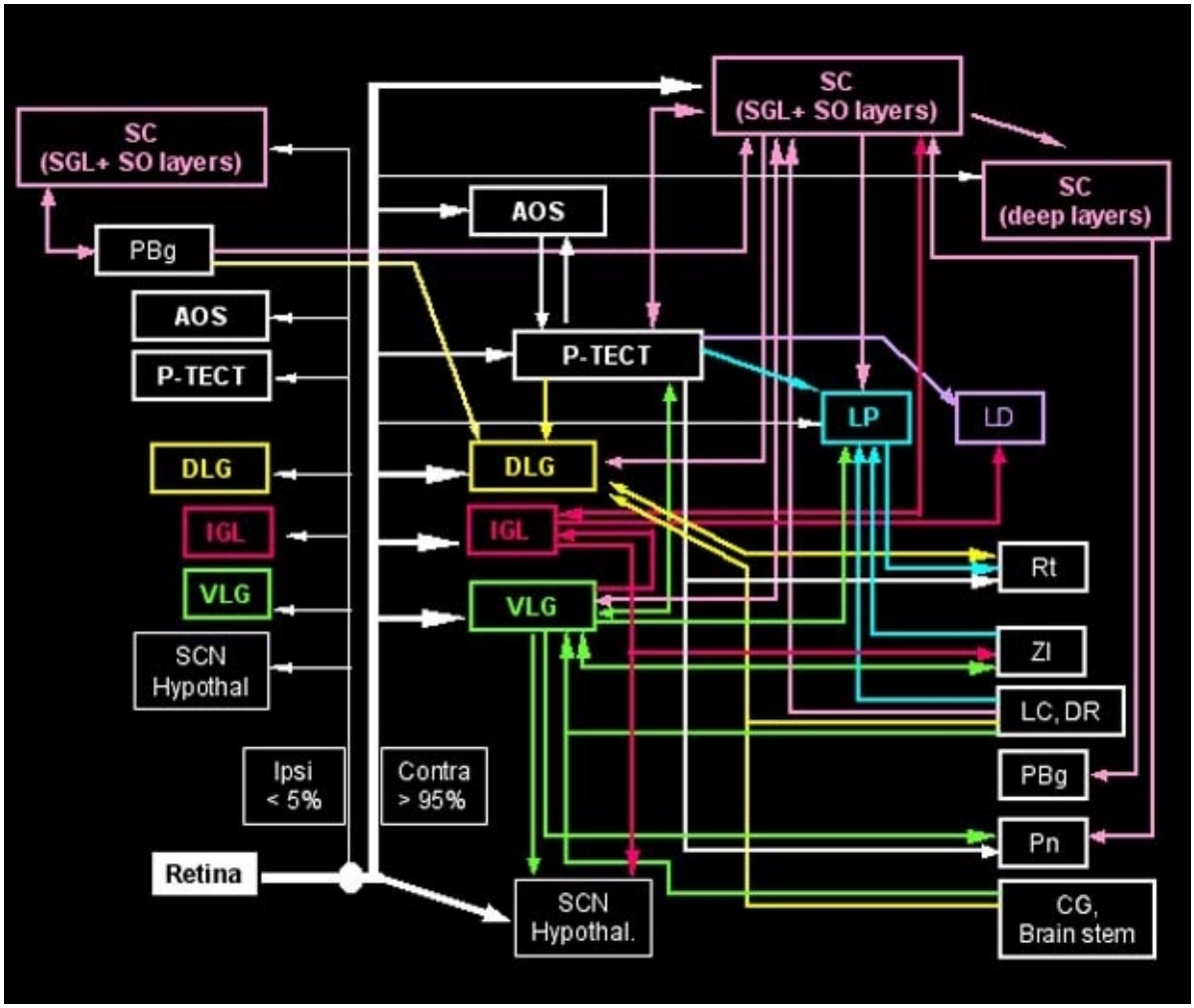

Figure 6. Retinal projections to the primary visual centers (white arrows) and their major links with homolateral secondary subcortical areas. Double arrows indicate reciprocal connectivity. For abbreviations, see later. Cortical connections are given in Fig. 28.

neurons in the adult mammalian brain may retain or reexpress certain molecular determinants of normal connectivity". There are, however, morphological differences between the regenerated and control synapses: 1) larger size of some regenerated terminals; 2) greater mean length of the regenerated synapses; and 3) higher proportion of contacts with dendrites that contain vesicles in regenerated *versus* intact synapses.

Generation of Action Potentials in Target Neurons

Dr. Sue Keirstead and colleagues (8) provided electrophysiological evidence that the synapses, such as the ones described at the electron-microscopic level by Vidal-Sanz et al. (4), could mediate the transynaptic activation of neurons in the superior colliculus of adult mammals. Extracellular recordings in the superior colliculus, 15 to 18 weeks after PN graft insertion into the SC, revealed excitatory and inhibitory postsynaptic responses to visual stimulation of the eye that had received PN anastomosis onto its completely cut optic nerve (Fig. 16). Specific stimulation protocols (involving paired electrical stimulation of the PN graft) were used to verify that postsynaptic activity could be elicited in the reinnervated SC.

Additional studies by Sauve et al. (9), using the same experimental preparation, indicated that each element of a typical bursting response to light (excitatory type of response; Fig. 17) consists of a terminal potential (TP) arising from a regenerated RGC axon terminal arborization, followed by a longer duration focal synaptic potential (FSP) that is selectively blocked by GABA. FSPs are extracellular changes in potential that reflect

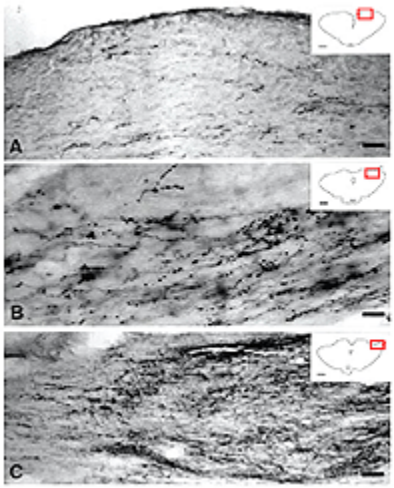

Figure 7. Light micrographs of 40-µm-thick cryostat coronal sections illustrating CTB-labeled retinal axons in the pretectum 16 weeks after grafting a segment of peripheral nerve between the left retina and the lateral side of the left diencephalon. A, CTB-labeled fibers extend through the dorsal aspect of the midbrain toward the midline. These fibers arborize within the NOT and OPN. Scale bar, 50 mm. B, CTB-labeled fibers show numerous varicosities within the NOT. Scale bar, 20 µm. C, PN graft entry zone lateral to the diencephalon. Note the interface between the PN graft and the midbrain and regenerated fibers crossing the interface. Scale bar, 50 µm. Insets in A-C are drawings of the respective section of the midbrain, and the red boxes indicate the region photographed. Scale bar, 1 mm. From Aviles-Trigueros et al. (23).

summation of excitatory postsynaptic potentials (EPSPs) in neurons within the terminal field of the regenerated RGC axon (Fig. 18). In some instances, superimposed on these FSPs are spikes (Fig. 19), which arise after three to four consecutive closely spaced impulses from RGS (as inferred from the TPs).

The results from Sauve et al. (9) indicate that terminal arborizations of individual regenerated RGC axons can synapse with multiple neurons in the SC and that convergence of inputs from regenerated RGC axons is not required for activation of SC neurons in response to light.

Finally, *in vitro* studies by Turner et al. (98) indicate that the deafferentation of the SC, caused by optic nerve cut, and a surgical approach to insert the PN graft into the SC together, lead to ultrastructural changes reflected functionally at the synaptic level in the target structure, even after potential RGC axonal regeneration. Such changes are likely to compromise the ability of the target structure to function normally during information processing. Therefore, although axons regenerating along peripheral nerve grafts can make functional synaptic connections, their efficacy in activating the target structure will probably be compromised by the local changes in synaptic connectivity.

Restoration of Retinotopy

Is Restoration of Retinotopy Needed for Recovery of Function?

Yes it is, for the appropriate execution of visually guided behaviors. We owe the proof to the 1981 Physiology Nobel Prize co-winner Dr. Roger W. Sperry (Fig. 20), who ingeniously took advantage of the spontaneous functional recovery of the retinotectal system in frogs (for a review, see Gaze (99)).

Sperry's impressive demonstration involved sectioning a frog's optic nerve and rotating the eye by 180° (100). After spontaneous regeneration of the retinotectal pathway, the frog's attempt to catch a prey resulted in an attack directed to the diametrically opposed direction (Fig. 21). The frog's behavior gave clues as to how the regenerating RGC axons had reconnected in the tectum. Note: the structure equivalent to SC is named "tectum" in lower vertebrates. Sperry inferred that the regenerating axons had returned to their original position in the

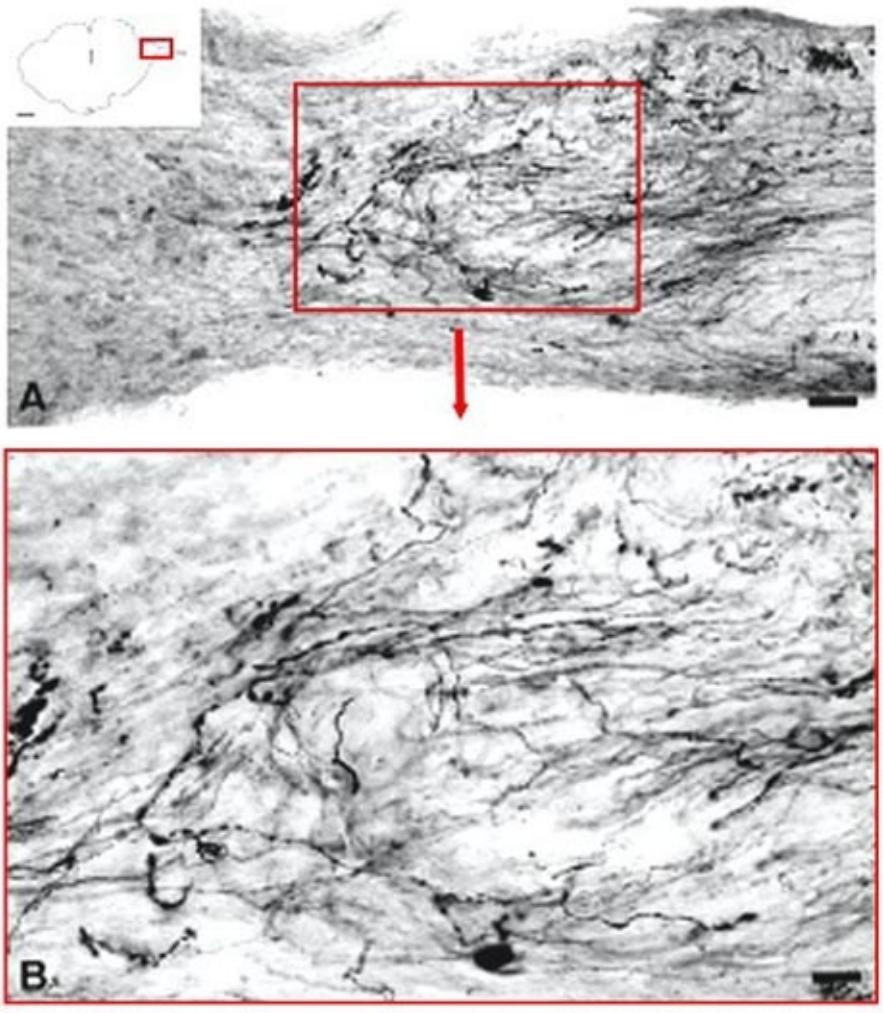

Figure 8. Light micrographs of a 40-µm-thick cryostat coronal section illustrating retinal axons 24 weeks after connecting the left eye and the ipsilateral brainstem with a segment of peripheral nerve and 5 days after intraocular injection of CTB. A, interface between PN graft and diencephalon. Most of the retinal axons do not exit the PN graft and appear within a neuroma-like formation. Scale bar, 47 µm. Inset is a drawing of the section, and the box indicates the region photographed. Scale bar, 1 mm. B, detail from box in A showing CTB-labeled axons that reach the distal end of the PN segment but turn around and do not enter the brainstem. Scale bar, 19 µm. From Aviles-Trigueros et al. (23).

tectum, regardless of the new position they occupied in the rotated eye. This gave experimental support for his chemo-specificity theory (100), which stipulates that "The connections are governed by intrinsic specificity of the advancing fibre tip plus that of the various cellular elements it encounters in its outgrowth" (101).

We can learn about the extent to which retinotopic projections have to be re-established to achieve behavioral recovery by comparing species that have various levels of regeneration of their retinotectal system and examining the level of visually guided behavior they can recover. The capacity for RGC axon regeneration in the vertebrate visual pathway is summarized in the study of Dunlop et al. (102). For instance, there is variability between various species of lizards. Some achieve a stable restoration of retinotectal organization (accompanied by restoration of visually guided behaviors), whereas others (*Ctenophorus ornatus*) fail to maintain a retinotopic ordering of the regenerated projection and lose their capacity to perform visually guided tasks (103). However, training on a visual task has been shown to improve the outcome of optic nerve regeneration in *Ctenophorus ornatus* lizards (104).

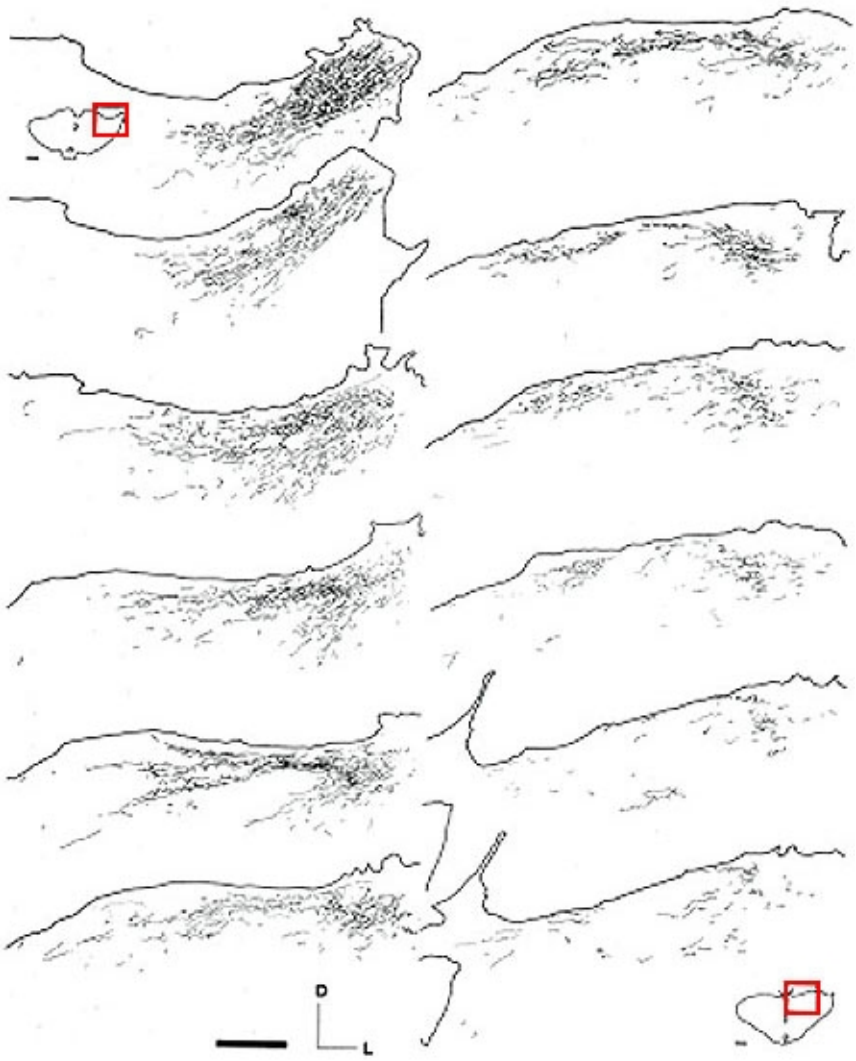

Figure 9. Drawings of alternate 40-µm-thick cryostat coronal sections through the brainstem, from caudal (top left) to rostral (bottom right), of a rat 16 weeks after grafting a peripheral nerve segment between the left retina and the lateral aspect of the left diencephalon. The drawings illustrate the distribution of regenerated retinal fibers orthogradely labeled with CTB injected 5 days earlier into the PN-grafted retina. Note the extensive reinnervation through the pretectum. Scale bar, 0.5 mm. The insets are drawings of the most caudal and rostral sections, respectively. Scale bar, 1 mm. From Aviles-Trigueros et al. (23).

Guidance Cues in the Injured Retinotectal Pathway

The retinotectal system is the model of choice for studying the mechanisms governing the formation of ordered connections in the CNS. In intact mature rodents, axons from RGCs located in the temporal retina project to the rostral (anterior) part of the contralateral SC, whereas axons from RGCs located in the nasal retina project to the caudal (posterior) contralateral SC (17-19). Ventral RGCs project axons medially and dorsal RGCs project axons laterally in the contralateral SC (Fig. 22).

To elucidate the mechanisms involved in axonal guidance, especially with regard to specificity of polarities in the tectum, Dr. Friedrich Bonhoeffer and colleagues developed an *in vitro* assay, known as the "stripe assay" (105, 106). The basis of this assay involves growing retinal explants on stripes made up of tissues alternating from rostral and caudal parts of the tectum. Results using tissues from developing chicks or rodents show that temporal RGC axons avoid stripes made up of caudal tectal tissue, whereas nasal RGC axons grow equally well

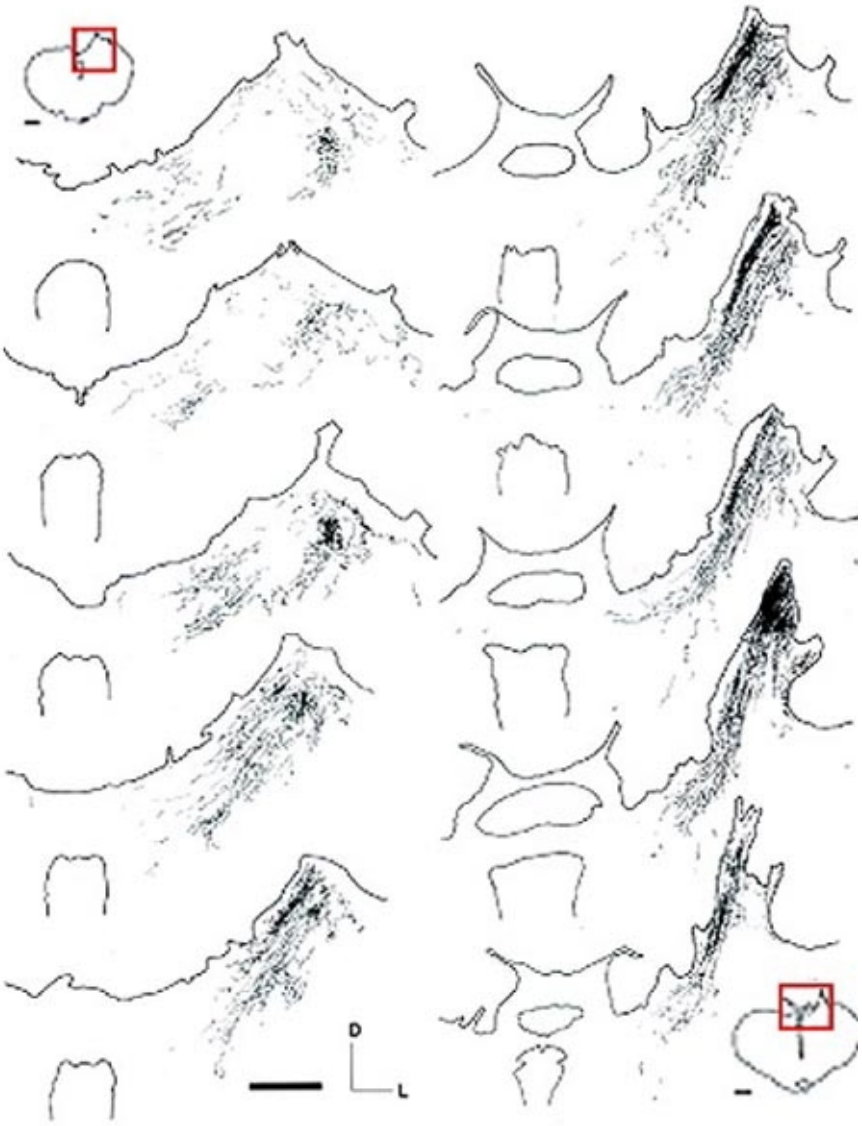

Figure 10. Drawings of consecutive 40-μm-thick cryostat coronal sections through the brainstem, from caudal (top left) to rostral (bottom right), of a rat 46 weeks after grafting a peripheral nerve segment between the left retina and the dorsal aspect of the left midbrain between the OPN and NOT. The drawings illustrate the distribution of regenerated retinal fibers orthogradely labeled with CTB injected 5 days earlier into the PN-grafted retina. Note the segregation of the retinal axons between OPN and NOT from the rostral to the caudal aspect. Scale bar, 0.5 mm. The insets are drawings of the most caudal and rostral sections, respectively. Scale bar, 1 mm. From Aviles-Trigueros et al. (23).

on either rostral or nasal tectal tissue stripes (105-108) or show a preference for nasal stripes providing specific pre-treatments (109). This preference appears to be developmentally regulated in a way that is lost in the mature system. However, Dr. Mathias Bahr and colleagues (110-112) showed that this capacity can be partially restored following optic nerve cut in adult rats. Their results indicate that guidance cues might be re-expressed in the deafferented retinotectal system of adult mammals, and that these cues might retain some level of function.

Several axonal guidance molecules and their respective receptors have been identified. Among them, the best studied compose these four classes: netrins, semaphorins, slits, and ephrins (for a review, see Koeberle and Bahr (44)). In the goldfish, in which spontaneous regeneration occurs, Eph/ephrins are upregulated as gradients at the time that topography is restored during optic nerve regeneration (113). Furthermore, the Eph/ephrin system is

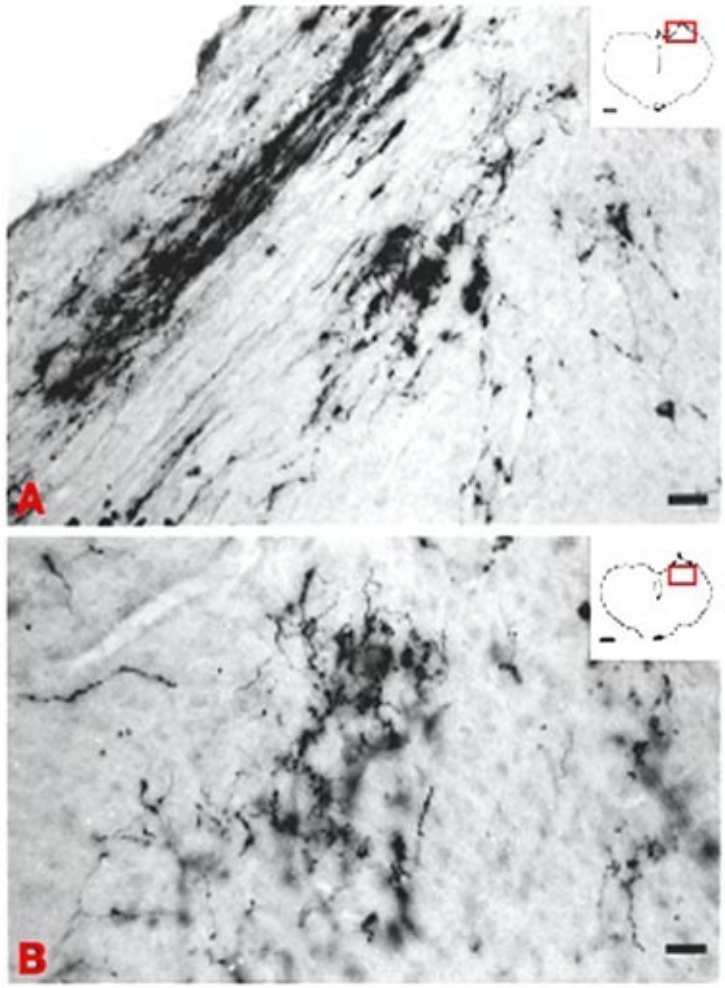

Figure 11. Light micrographs of 40-µm-thick cryostat coronal sections illustrating regenerated retinal fibers in the pretectum 46 weeks after grafting a segment of peripheral nerve between the left retina and the dorsal aspect of the left midbrain between the OPN and NOT and 5 days after intraocular injection of CTB. A, CTB-labeled retinal axons innervate the OPN extensively (toward the top left) and the rostral limit of the NOT (toward the middle and right). Scale bar, 35 µm. B, extensive innervation of the NOT area with numerous varicosities resembling bouton-like endings in a more caudal section. Scale bar, 28 µm. Insets in A and B are drawings of the respective section of the midbrain, and the red boxes indicate the region photographed. Scale bar, 1 mm. From Aviles-Trigueros et al. (23).

required to restore topography because blocking their interactions *in vivo* with fusion proteins results in abnormal topography (114). In rodents, in which spontaneous regeneration does not occur, most of the known guidance molecules have been shown to be modulated after deafferentation. However, although some molecules are up-regulated to levels similar to those achieved in development, some (such as the ephrin receptor EphA5 in the retina and the ephrin-B) are actually down-regulated. Therefore, it remains improbable that these various changes might actually recapitulate developmental events. How experimental manipulations might achieve such recapitulation of developmental events is, for now, a mind-boggling puzzle.

Can RGC axon regenerated through a PN graft resume topological specificity when reinnervating the superior colliculus? See an example from the study of Sauve et al. (24).

The study of Sauve et al. (24) indicates that regenerating mammalian RGC axon terminals do not form a precise retinotopic map (compared with normal intact animals; Fig. 23) when reinnervating the SC (Fig. 24).

However, superimposed on the apparent randomness of distribution of RGC terminals, there appears to be a small but nonetheless statistically significant tendency for these terminals to array themselves appropriately

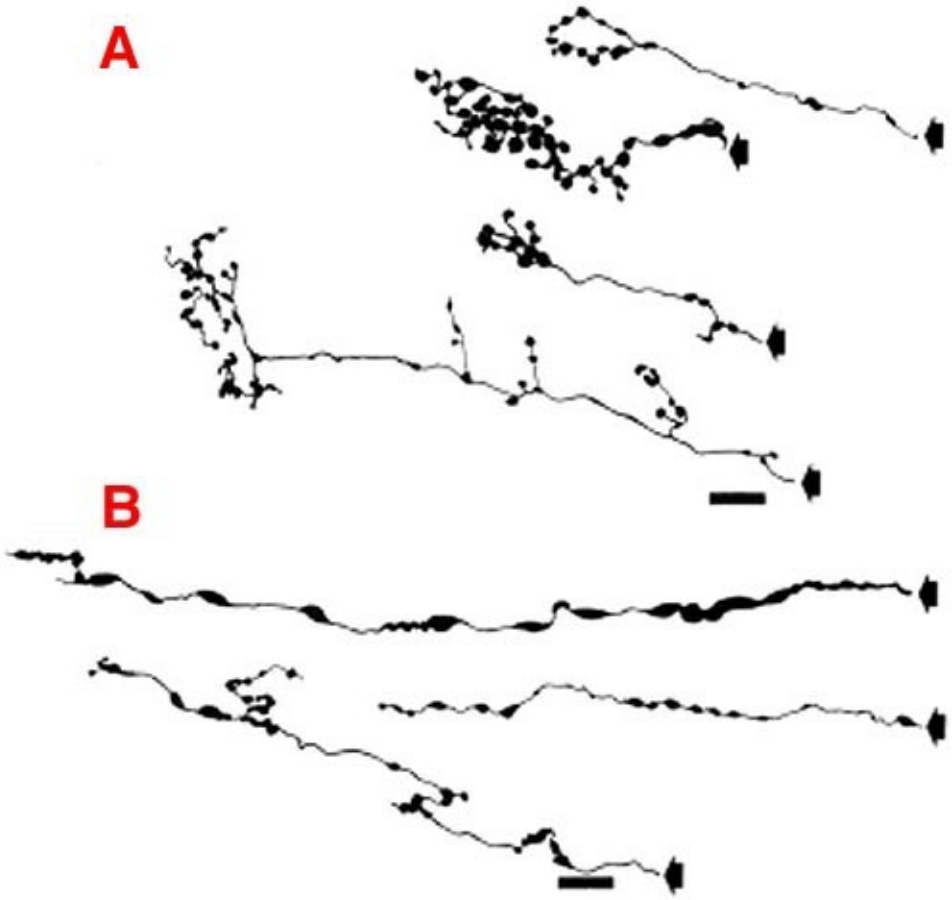

Figure 12. Drawings of retinal fibers 46 weeks after grafting a segment of peripheral nerve between the left retina and the dorsal aspect of the left midbrain between the OPN and NOT and 5 days after intraocular injection of CTB. A, retinal fibers divide into fine branches decorated with numerous medium and small varicosities and terminal swellings, frequently forming rosette-like clusters. These fibers predominate in the NOT area. Scale bar, 9 μm. B, retinal fibers with little branching decorated with large elliptical varicosities along the length of the axon and with terminal swellings of different sizes. These fibers predominate in the OPN area and resemble en passant fibers. Scale bar, 9 μm. The stem axons are indicated by arrows. From Aviles-Trigueros et al. (23).

within the rostrocaudal axis of the SC. Because the PN graft tip was placed at different locations in different animals, the assessment of topography was of necessity a comparison of the relative positions of reinnervating axon terminals for each animal rather than an identification of the absolute position of each terminal. It must also must be emphasized that the method used by Sauve et al. (24) assessed terminal positions but not trajectories of regenerating RGC axons. Nonetheless, these results suggest that factor(s) may be present in the reinnervated SC, as in the newly innervated SC, that can influence the direction of axonal growth and/or the area within which arborization and synapse formation occur.

Topographic ordering of projections during normal development of retinofugal pathways is thought to reflect at least two processes: 1) an initial pathfinding to the approximately correct area directed by spatially specific molecular cues as first suggested by Sperry (115); and 2) a subsequent phase of refinement of the projection due to activity-dependent processes in which near-simultaneous firing of neighboring RGCs (for a review, see Wong (116)) serves mutually to stabilize the connections of their shared target neurons in the LGN or tectum (117-121). Initial pathfinding of RGC axons in the tectum may be very precise, as in frogs and fish (122, 123), or more exuberant and diffuse, as in rodents (166, 167). Computer simulations suggest that a combination of positional cues and activity-dependent mechanisms gives rise to a very precise retinotectal topology in a variety

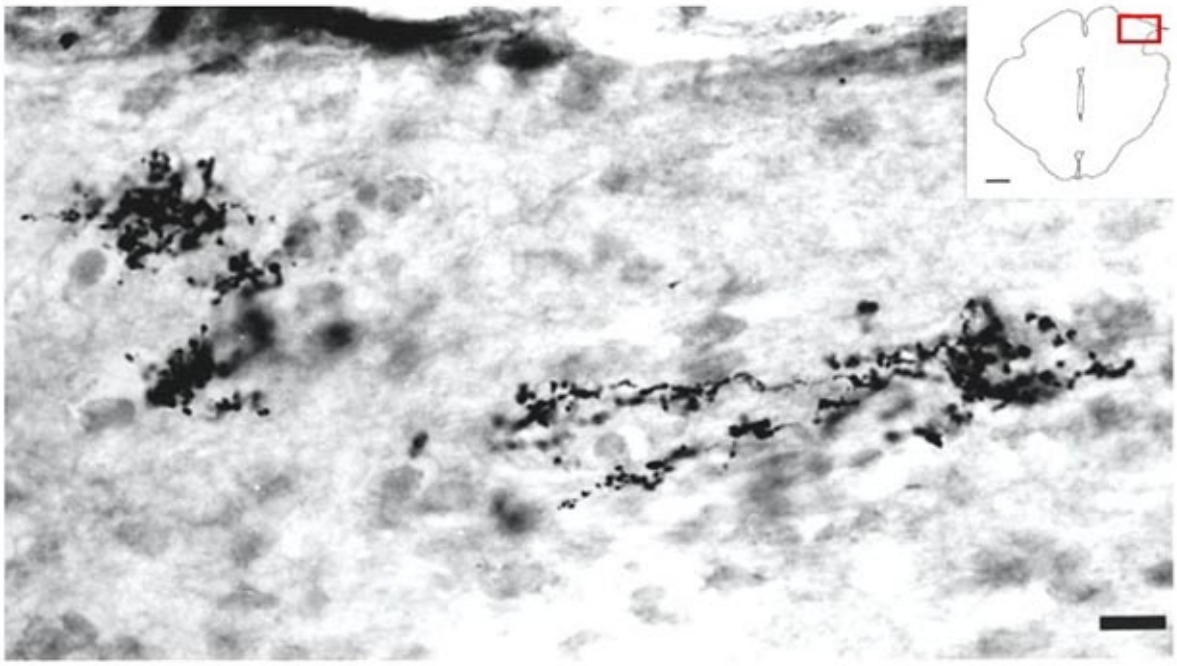

Figure 13. Light micrograph of a 40-µm-thick cryostat coronal section of the midbrain illustrating retinal fibers in the superficial gray 40 weeks after grafting a peripheral nerve segment between the left eye and the lateral aspect of the ipsilateral SC and 5 days after intraocular injection of CTB. Near the site of the PN graft entry, orthogradely labeled axons extend through the superficial layers of the SC forming typical arborizations. Note the high density of varicosities and terminal swellings resembling bouton-like endings on branching fibers. Scale bar, 17 µm. Inset illustrates a drawing of the section and indicates the region photographed. Scale bar, 1 mm. From Aviles-Trigueros et al. (23).

of experimental situations (124, 125), for example even if a molecular gradient is only transiently expressed during the initiation of innervation of the tectum (126).

During regeneration of the retinotectal pathway in frogs and fish, the initial topography is only roughly organized. Functional synapses are formed indiscriminately by regenerating goldfish RGC axons as they enter the tectum. These may be unstable if inappropriately located (127, 128). Projections become refined into a more precise retinotopic map over a period of several weeks by mechanisms that depend upon ongoing activity in neighboring RGC axons (117, 129).

In vitro experiments have shown that molecules with topological specificity with respect to the rostral and caudal tectum or SC are transiently expressed in the neonatal mammalian SC (105). These topologically specific markers disappear after the retinocollicular pathway is laid down but reappear about 2 weeks after denervation of the SC (112). Such positionally specific markers may be more strongly expressed in deafferented SC than in embryonic SC (130). The experimental results of Sauve et al. (24, 131) are consistent with the possibility that a gradient of such positionally specific markers could serve as an influence on the exploration of the SC by regenerating RGC axons (132-134), either by exerting a repulsive or tropic effect on their axonal growth cones (105, 106, 135-138), or by influencing their branching patterns (108). Positionally specific markers could also influence the deployment of regenerating RGC axons within the nerve graft as they approach the SC (139).

The question arises as to why the effects of these factor(s), if present, are so minimally expressed or so difficult to document in the reinnervated mammalian SC. In the reinnervated SC, the extent of exploration by a regenerated RGC axon is 1 mm or less (140). More extensive exploration of the SC is perhaps limited by the presence of factors inhibitory to axonal growth (141-144) that are present in the adult animal as well as by the developmental

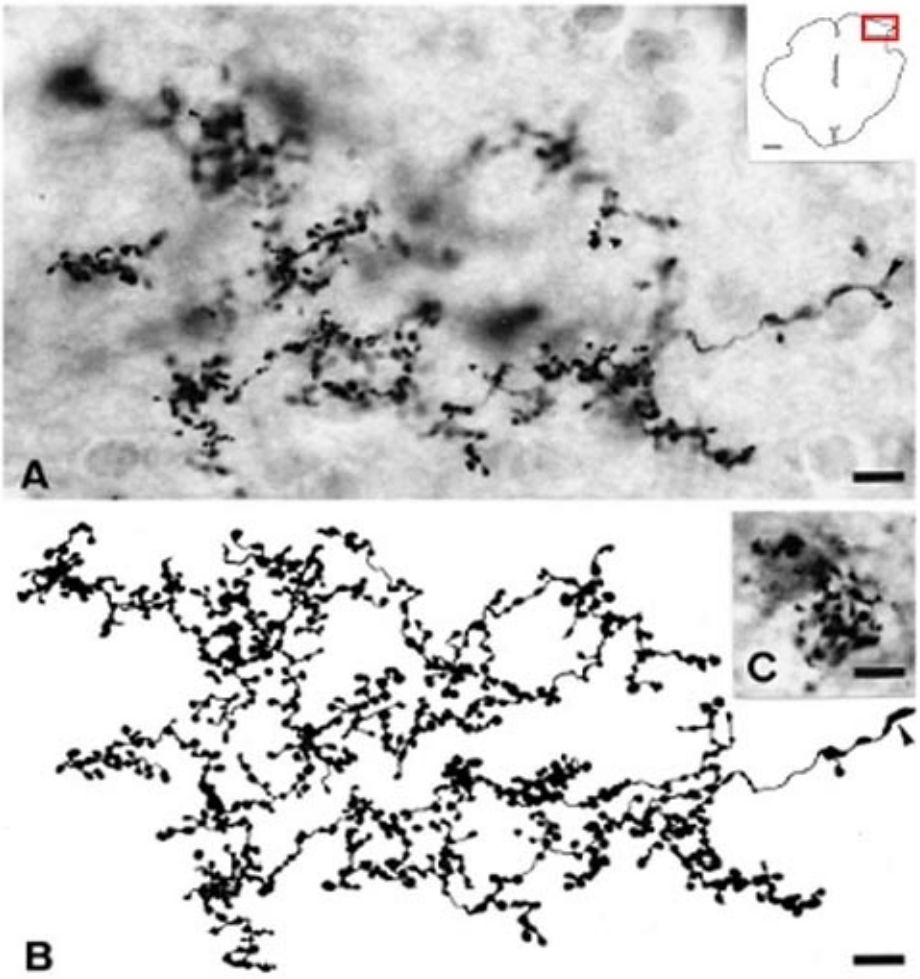

Figure 14. Light micrographs and drawing illustrating regenerated retinal fibers in the stratum griseum superficiale of 40-μm-thick cryostat sections of the midbrain 48 weeks after grafting a segment of PN between the left eye and the lateral side of the ipsilateral SC and 5 days after intraocular injection of CTB. A, single regenerated RGC axon in the SGS of the SC forming many branches that bear multiple varicosities of similar appearance and uniform size. Scale bar, 10 μm. Inset illustrates a drawing of the midbrain section and indicates the region photographed. Scale bar, 1 mm. The stem axon is indicated by an arrowhead. B, high-power reconstruction of the terminal arbor in A. Scale bar, 9 μm. C, close interrelation between terminal cluster of bouton-like endings of regenerated retinal projections and SC neurons. Scale bar, 8 μm. From Aviles-Trigueros et al. (23).

down-regulation of growth permissive molecules (145, 146) and receptors (147, 148). This is in contrast to the situation during normal development, where RGC axons from all portions of the retina initially innervate the entire SC (149, 150). In the PN graft regeneration paradigm, no more than 10% of the normal total number of RGCs usually regenerate their axons across the PN graft, and only a portion of these reinnervate the SC (4). Many axons terminate growth immediately after penetrating the CNS (23). One way to increase sprouting of regenerating RGC axons in the SC could be to provide BDNF and chondroitinase ABC (151). However, even in these conditions, with surviving RGCs widely separated in the retina and their axon terminals widely dispersed within the SC, the influence of activity-dependent mechanisms in shaping the topological pattern of innervation would be expected, *a priori*, to be much more limited than in normal development. Furthermore, with little competition among axons for synaptic sites, it is possible that inappropriately located synapses, once formed, would be much more stable than in the reinnervated frog or goldfish tectum. Such premature formation of synapses could in turn curtail the further exploration of the SC by regenerated RGC axons.

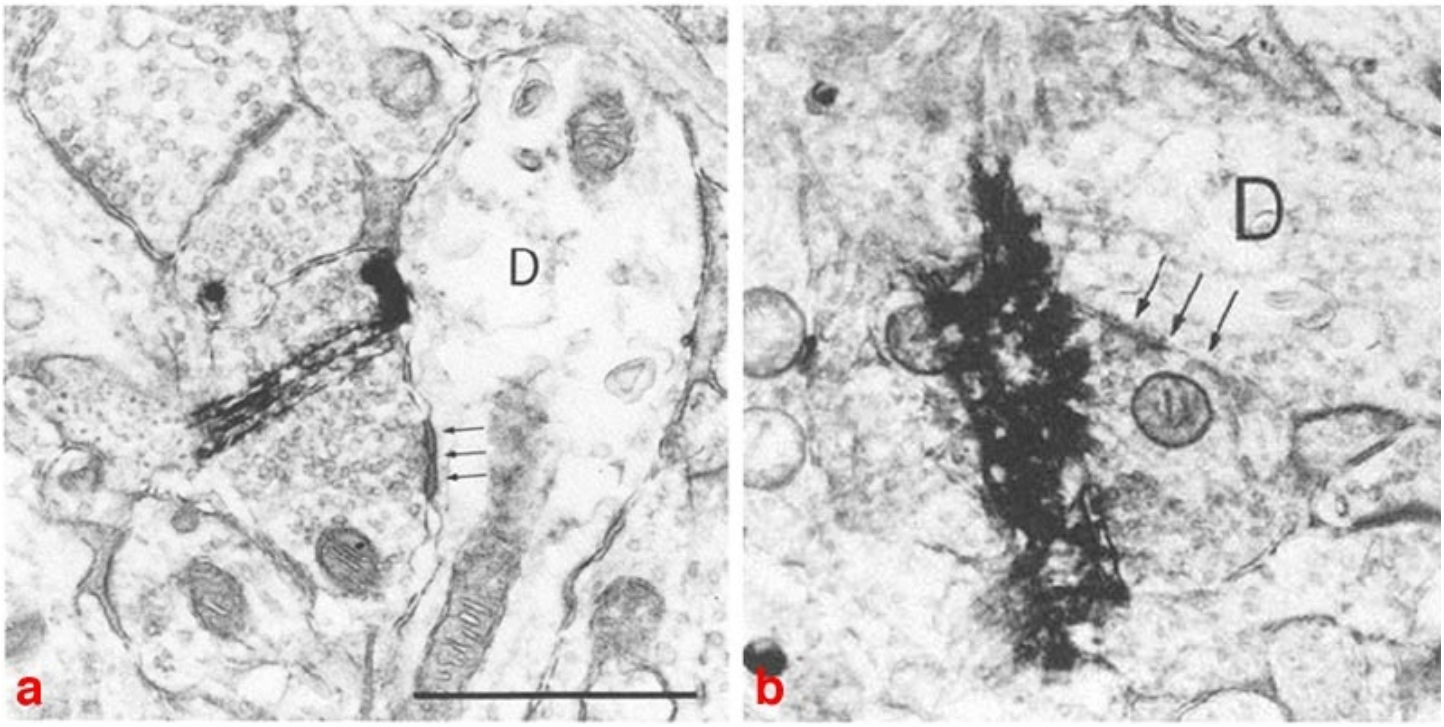

Figure 15. Electron micrographs of presynaptic profiles in the superficial SC (strata zonale and griseum superficiale) lightly labeled with HRP injected in the PN-grafted eyes of group IIb rats. D, dendrites. The presynaptic terminals contain vesicles that are predominantly round or spheroidal. The thickenings of the pre- and postsynaptic membranes at the synaptic contacts are indicated by arrows. a, characteristic DAB-Co-stabilized TMB reaction product (175) is confined to the presynaptic axon terminal. b, as occasionally occurs with this "technique", the reaction product extends beyond the boundary of the terminal. Bars, 1 µm. From Vidal-Sanz et al. (4).

Preservation of Local and Downstream Circuitry

In the study by Turner et al. (98), the local synaptic connectivity in the superficial gray layer of the SC was assessed after RGC axonal regeneration through a PN graft into the rat SC, using *in vitro* brain slice techniques. Repair was achieved between the ipsilateral eye and SC, after bilateral lesion of optic nerves and ablation of ipsilateral occipital cortex.

Impact of Deafferentation

The normal rat superficial gray layer (SGL) of the SC receives the majority (90%) of its excitatory input from the retina (152) (Fig. 25) and the remainder (10%) from the visual cortex (153).

Interconnectivity within the SGL appears to be mediated by local GABAergic interneurons (154, 155). Both the GABAergic processes of local circuit interneurons (152, 156) and the axon terminals of other projections proliferate (157, 158) after optic deafferentation. These new neural processes appear to form additional synapses or to take up positions apposed to the postsynaptic densities left vacant by the degenerating retinal afferents in the SC (152). As a result, the synapse-to-neuron ratio stays the same in the SC (159), although it is not known whether these synaptic contacts are functional. Because the subsequent repair of retinal afferents is also going to alter the balance between excitatory and inhibitory inputs, the connectivity between restored retinal afferents and target neurons is likely to be very different from that in the normal SGL (Fig. 26).

There is as yet no evidence for local excitatory connections in the SGL. Electrophysiological studies are consistent with the anatomical organization, in that retinal input to the SGL is monosynaptic and there is no evidence for local network-related activity, even when inhibition is blocked (160). In addition, contralateral

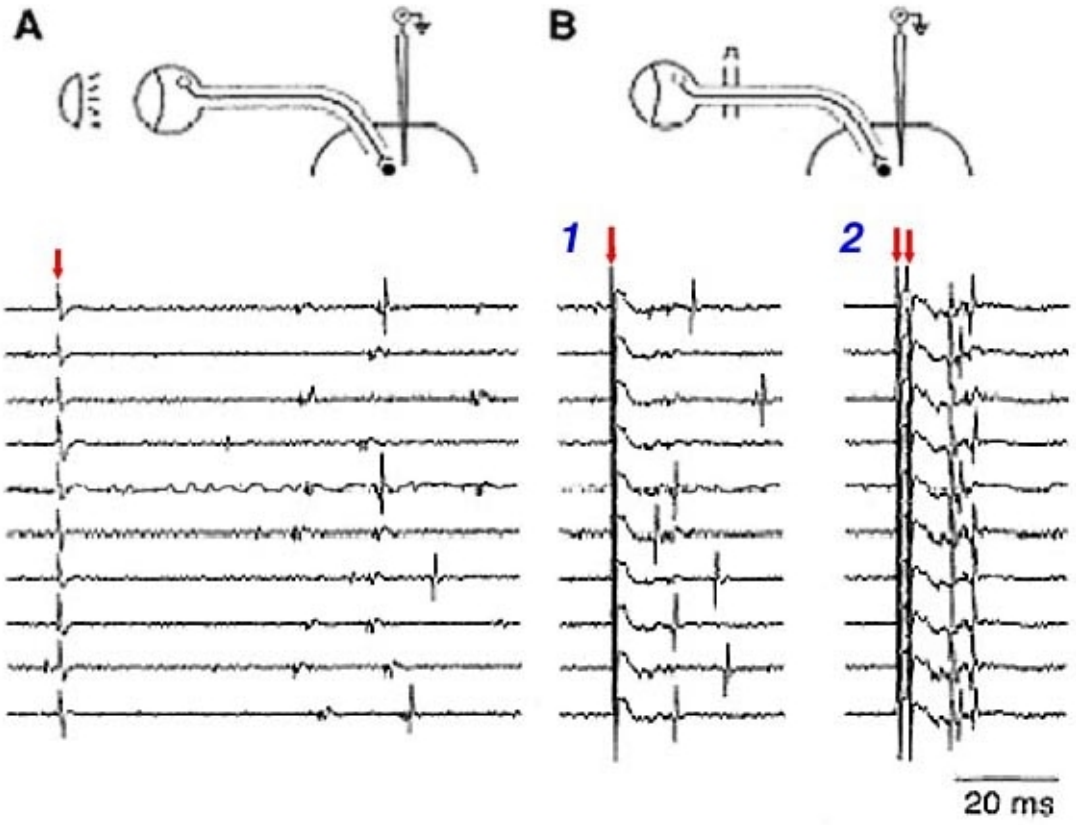

Figure 16. A, 10 successive responses to light flash (at arrow) recorded at a depth of 250 μm in the SC. The large unit responds with a single spike on 4 of 10 iterations. B, the same unit responds erratically with inconsistent latency to (traces 1) single electrical stimuli (arrow) delivered to the graft and responds at a more constant latency, often with multiple spikes, to (traces 2) paired electrical stimuli (arrows) of the same intensity. This pattern of response is inconsistent with that anticipated from an RGC axon and thus identifies this unit as an SC neuron. All recordings were filtered (band pass 500 Hz to 5 KHz) and stored on magnetic tape. From Keirstead et al. (8).

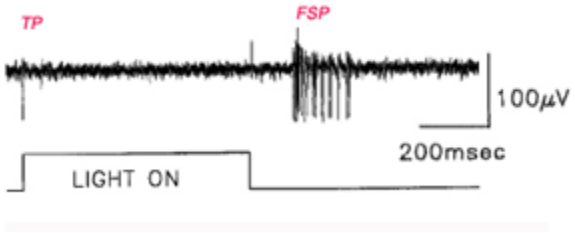

Figure 17. Unitary response to static illumination of a spot 4" in diameter recorded at a depth of 190 μm in a reinnervated SC 37 weeks after graft insertion. Bandpass 100 Hz to 5 kHz. From Sauve et al. (9).

enucleation 14 days before recording is sufficient to result in a complete loss of excitatory inputs to the SGL *in vitro* after intracollicular stimulation (161). However, the study by Turner et al. (98) suggests that this is not always the case: optic tract stimulation 3–9 months after optic nerve transection leads to excitation in the SC, and this is likely attributable to the recruitment of corticocollicular projections, which run close to the optic tract (162). Indeed, anatomical studies have shown that 30–45 days after contralateral enucleation, there is a reactive synaptogenesis of corticocollicular terminals (157). The nature of this responsiveness also suggests that this cortical input recruits local recurrent excitatory connections that have been formed as part of the reactive process to retinal deafferentation.

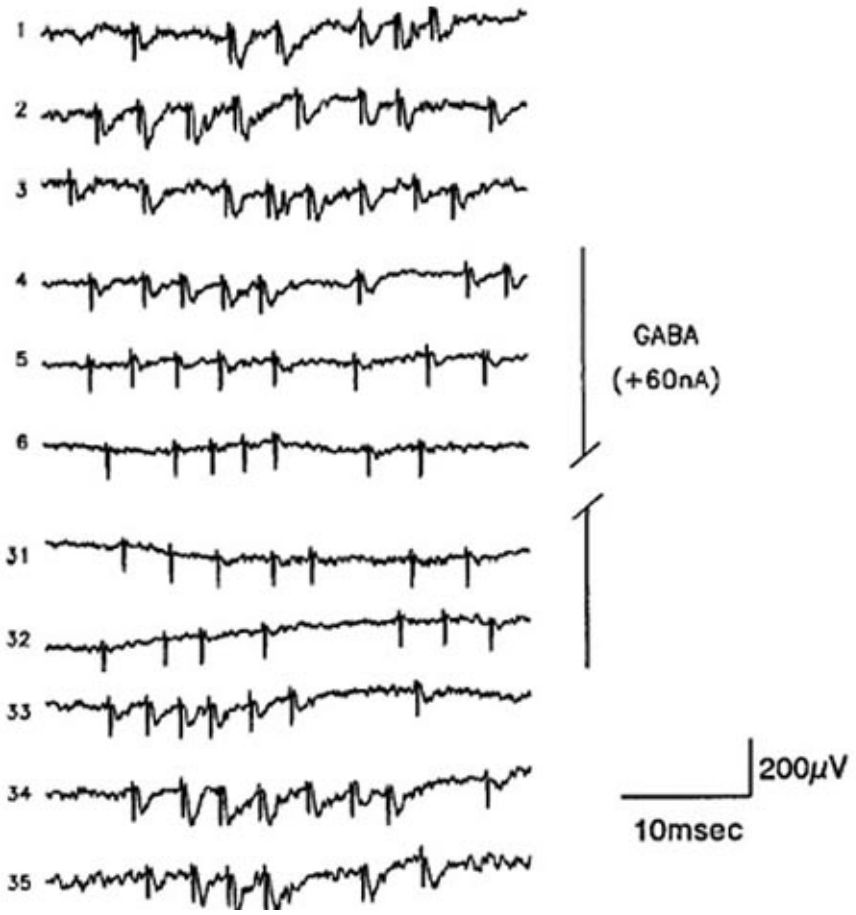

Figure 18. Successive OFF responses to repetitive light stimuli every 3.1 sec from the same unit as in Fig. 1. Traces begin 125 msec after offset of light. Band pass 10 Hz to 5 kHz. After application of GABA between traces 3 and 4, the second component of each unitary response is attenuated (traces 4 and 5) and then disappears on subsequent traces. When GABA application is discontinued after approximately 90 sec, the second component of each unitary response gradually recovers, becoming larger between traces 33 and 34. The gradual attenuation and recovery of the second component indicates that the effect of iontophoretic administration of GABA is not a current effect. Traces 7 to 30, during which GABA was continuously applied, are omitted. From Sauve et al. (9).

Evidence of New Inputs after PN Graft Repair

After combined retinal and cortical deafferentation (as part of the surgery for PN bridging the retinocollicular pathway), all normal excitatory inputs to the SGL are abolished. However, there is evidence from the study by Turner et al. (98) for the presence of both spontaneous and evoked EPSP-like events in SC slices from the PN graft repair preparation. This suggests that excitatory inputs can form new synaptic contacts on neurons within the SGL. These connections are likely to be attributable to reactive sprouting of excitatory neurons, either in the SGL itself or the deeper layers of the SC, such as the intermediate gray layer (IGL). Because both the SGL and IGL contain neurons that have dendrites that extend across the SO, this could provide a substrate on which such reactive synaptogenesis could form a recurrent excitatory network. Certainly, the delay (20–30 ms) in the onset of the network depolarizations after electrical stimulation (reported by Turner et al. (98)) suggests that sprouted excitatory input is polysynaptic, resulting from the recruitment of a relatively remote population of neurons, as may be located in the IGL. Indeed, the structure of the IGL is conducive to bursting activity because IGL neurons form a recurrent collateral network in normal animals and produce long-lasting synaptic responses in the presence of bicuculline (160). The network reorganization in the PN graft preparation (recorded *in vitro* (98)) is not that surprising, in view of the impact of deafferentation in other structures, e.g., cerebral cortex (163) or the dentate gyrus of the hippocampus (164). In both cases, this process leads to sprouting of excitatory axons

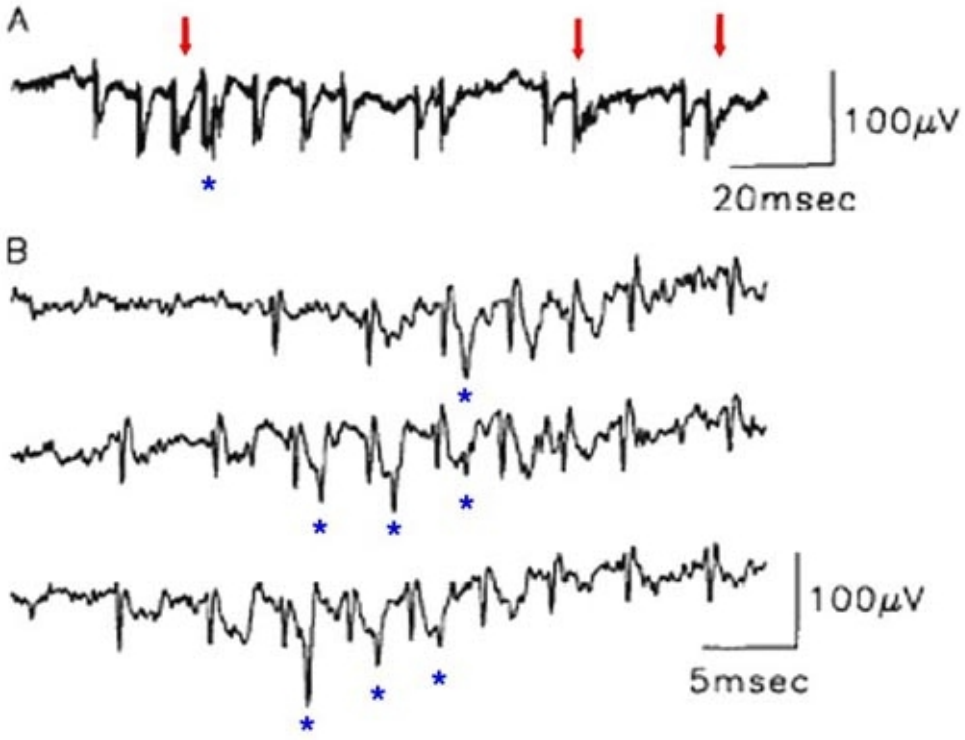

Figure 19. Spike-like activity arising from FSPs in single sweeps in response to static illumination of a spot. Recordings from units from two different animals. A, an OFF response. Depth, 200 μm. Note increase in baseline noise after closely spaced impulses in RGCs (arrows) and spike-like responses that are not TPs (asterisk). B, 3hree ON responses with multiple associated spike-like responses (asterisks) arising from FSPs. Depth, 100 μm. From Sauve et al. (9).

to form new recurrent excitatory connections. One consequence of the reactive events found in most SC slices (from PN graft repair preparation) is that they are likely to obscure efficacy of regenerated RGC axons that had established monosynaptic connections of retinorecipient neurons.

Impact of PN Graft Repair Surgery on the SGL Function: The Future for Repair Strategies

It is clear from the work of Turner et al. (98) that intrinsic changes in response patterns will impact the way the SGL will function during visual stimulation. Keirstead et al. (8) demonstrated that, in comparison with normal controls, restoration of functional retinal inputs into the SC, using the PN-graft method, had delays in the onset of post-synaptic action (165). This delay probably reflects the fact that the underlying synaptic responses involve the recruitment of recurrent excitatory connections. It may also reflect the profound impact that GABAergic inhibition has in controlling this network. The impact of visual deafferentation needs to be assessed throughout the SC to identify the locus/loci of the reactive changes that underlie(s) altered network behavior. In addition, for improvements in the current strategies of pathway repair, there is the need to limit or reverse these deafferentation-induced changes because: 1) this would allow a better assessment of the efficacy of new connections; and 2) it would probably improve system function.

In conclusion, axonal regeneration to a target alone clearly does not guarantee functional recovery. The study by Turner et al. (98) highlights the fact that the functional state of the target area is of fundamental importance for whether normal function can be restored, once axonal reinnervation has been achieved.

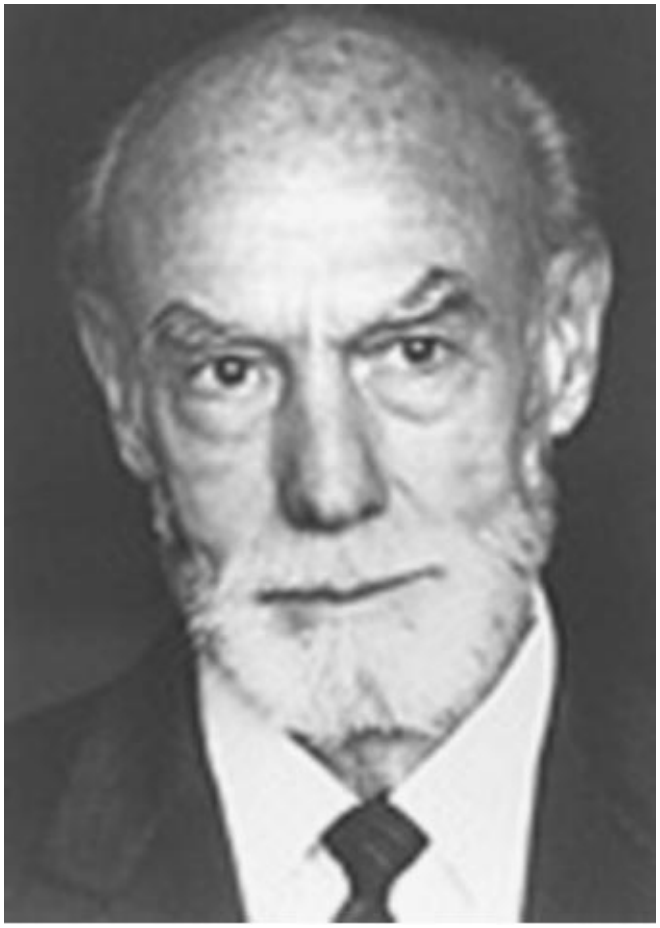

Figure 20. Photograph of Nobelist Roger Sperry.

Evidence for Some Level of Recovery of Function in the PN-bridged Retinofugal Pathways

The question of whether visual functions can be mediated by regenerated axons has been explored by looking at: 1) the pupillary light reflex, a conditioned response; 2) EEG desynchronization; and 3) behavioral arousal. It was found that the regenerated pathway could mediate pupillary constriction to light (166). Additional studies (167) showed that at best, the response amplitude and latency could be within normal range, but one noticeable difference was that although in normals, repetitive stimulation gave repeated responses of similar amplitude, regenerated pathways showed substantially reduced amplitudes with successive stimulation. The conditioned response studied, i.e., escape from a shuttle box in response to a light flash as a predictor of an electric shock, showed that this task could be performed in rats with regenerated optic input (168). Finally, animals were tested to demonstrate whether the regenerated pathways could mediate EEG desynchronization behavior to light (169). This depended on the fact that, under normal conditions, rats show a slow wave sleep pattern. A sensory stimulus, such as a flash of light or auditory signal, desynchronizes this high-amplitude slow wave activity, replacing it with low-amplitude, high-frequency activity. When presented with a light flash, blinded rats do not show this response, but animals with nerve grafts connected into the SC do. Associated with this, the rats also show a range of behavioral arousals.

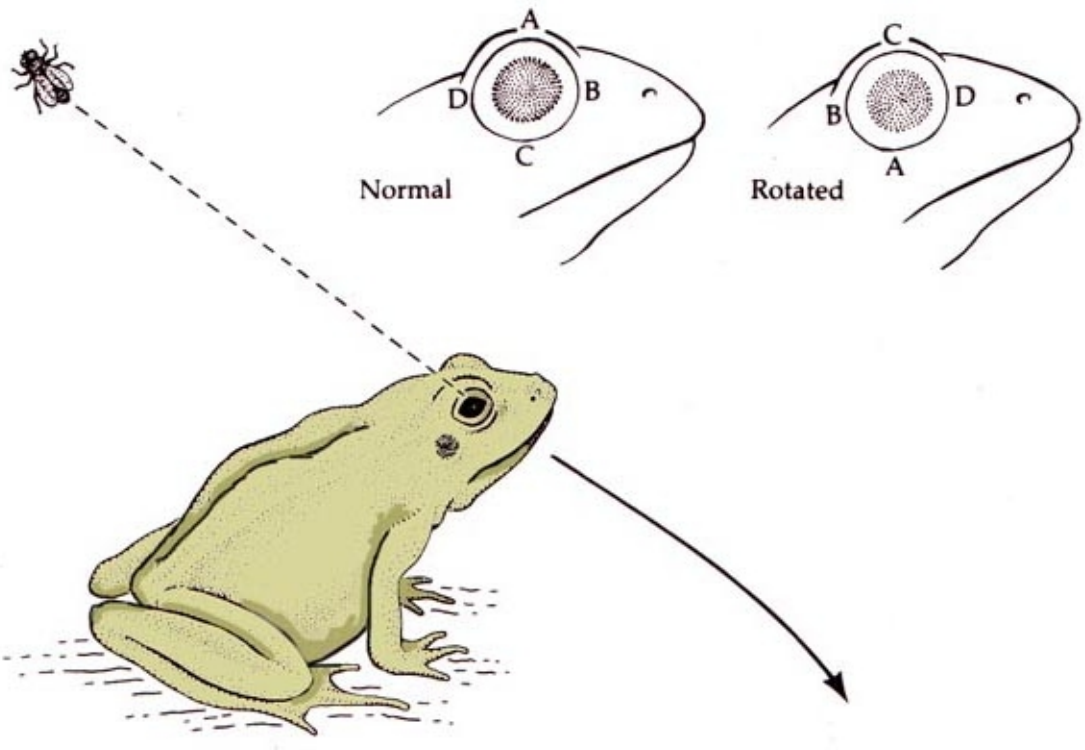

Figure 21. When the eye is rotated 180°, the frog's prey-catching behavior is inverted. After Sperry, 1956.

Visual Function Assessment

Visual function runs at many levels from unconscious responses to perception. These various functions are generally mediated through specific primary visual centers. Unconscious responses include driving circadian rhythms (relayed through the suprachiasmatic nucleus), photophobic responses (not specifically localized to any specific visual center), pupillary light reflex (mediated by the olivary pretectal nucleus), orienting responses (involving the SC), and head tracking to moving stripes (involving the SC also, but requiring cortical input for higher spatial frequencies). Perception requires elaborate decoding and integration of a set of visual signals to achieve a representational image at the level of the cortex.

For some visually driven functions, such as circadian rhythms and photophobia, all that is needed is to recognize a gradient, either temporal or spatial, of light and dark. For the pupillary light reflex, ability to encode the light intensity is also important, because the amount of pupillary constriction depends on brightness. For orienting responses and head tracking, some level of topographic encoding must be present. For perception, a much more elaborate degree of encoding must be achieved. In any attempt to reconstruct the damaged visual system, or indeed to limit its deterioration, the ideal is to recreate or preserve exactly the normal substrates of the various visually driven behaviors. This is rarely possible and indeed may not always be necessary. The CNS can sometimes adapt to an imperfect sensory input and demonstrate a level of adaptation sufficient to achieve a normal response (170-173): even in an intact animal, the system is able to operate over a wide range of luminance and contrast sensitivity (174). It is also apparent, especially in conditions involving re-establishment of connections, that specific visual responses can be modulated by associated events and may be interdependent.

To reconstruct a particular function, therefore, it is necessary for axons to innervate the appropriate brain region, subserving that function. Beyond this, it may also be necessary for a topological representation of the

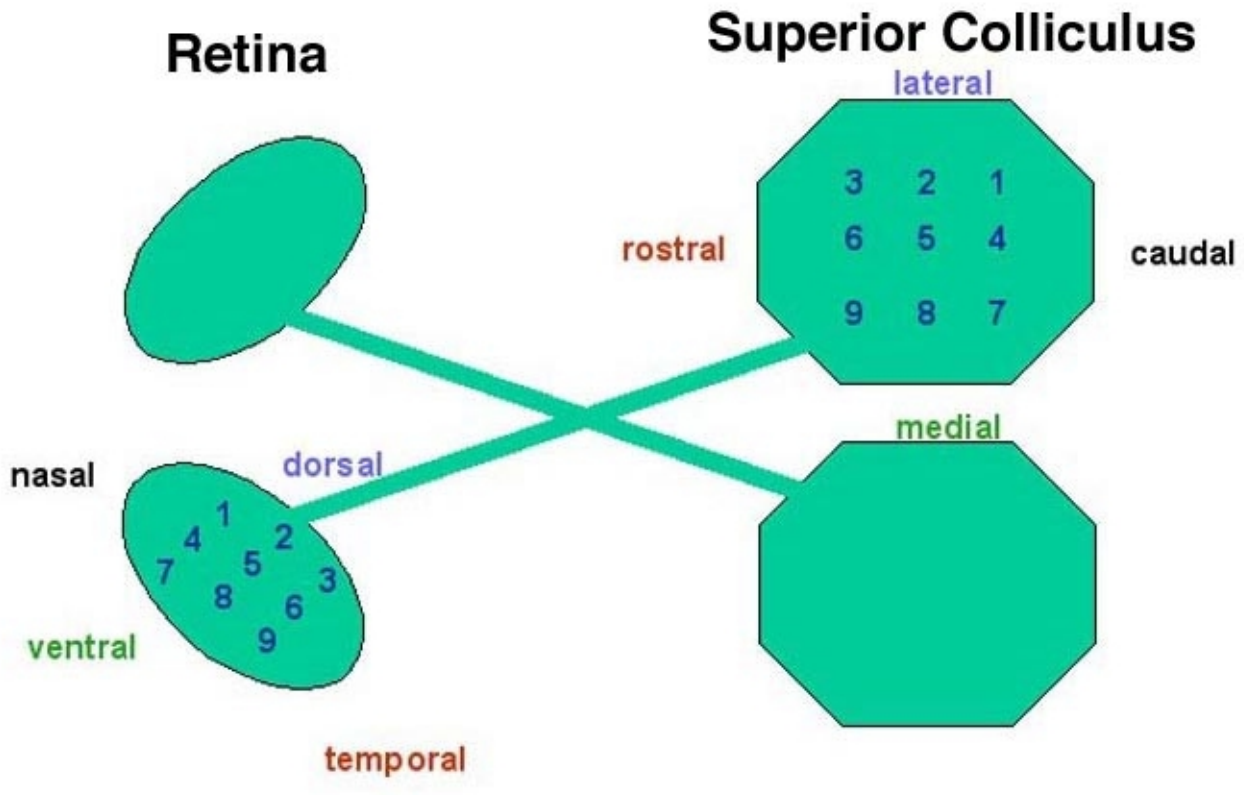

Figure 22. Ventral view schematic of retinotectal projections.

retina to be resumed within the region. Despite the likely neural circuit remodeling in a retinorecipient nucleus previously devoid of visual inputs, information processing within this particular nucleus should be relatively normal, and this becomes particularly important when cortical functions are involved. Finally, the information must have "significance" to the animal so that it can elaborate a suitable response strategy or develop a percept.

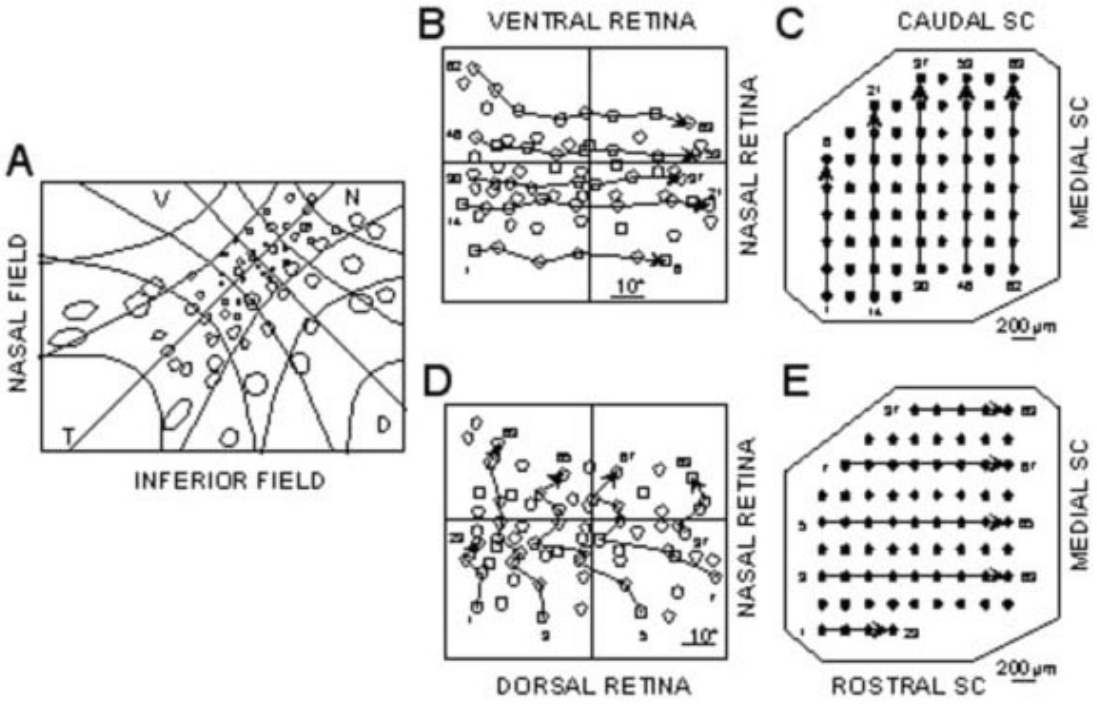

Figure 23. A, multiunit receptive fields were recorded from the left eye of a normal hamster, plotted on a tangent screen 20 cm from the eye, and viewed from the side of the screen opposite to the animal. The nasotemporal axis of the eye, defined by the position of the medial and lateral rectus muscles, is indicated by the line labeled NT. The projection of the optic disk is at the intersection with the orthogonal dorsoventral axis of the eye (line labeled DV). The calibration grids delineate 20°. B and D, the positions of these receptive fields are replotted as the corresponding positions on the retina with angular coordinates represented on a linear scale. C and E, the corresponding recording sites within the contralateral right SC are indicated. The numbers indicate the association of each receptive field with a recording site. Displacements from rostral to caudal of projection sites in the SC (C) are associated with parallel displacements from temporal to nasal of RGC positions in the retina (B), irrespective of the position in the retina or the SC. Displacements from lateral to medial of projection sites in the SC (E) are associated with less parallel displacements of RGC positions from dorsal to ventral in the retina (D). From Sauve et al. (24).

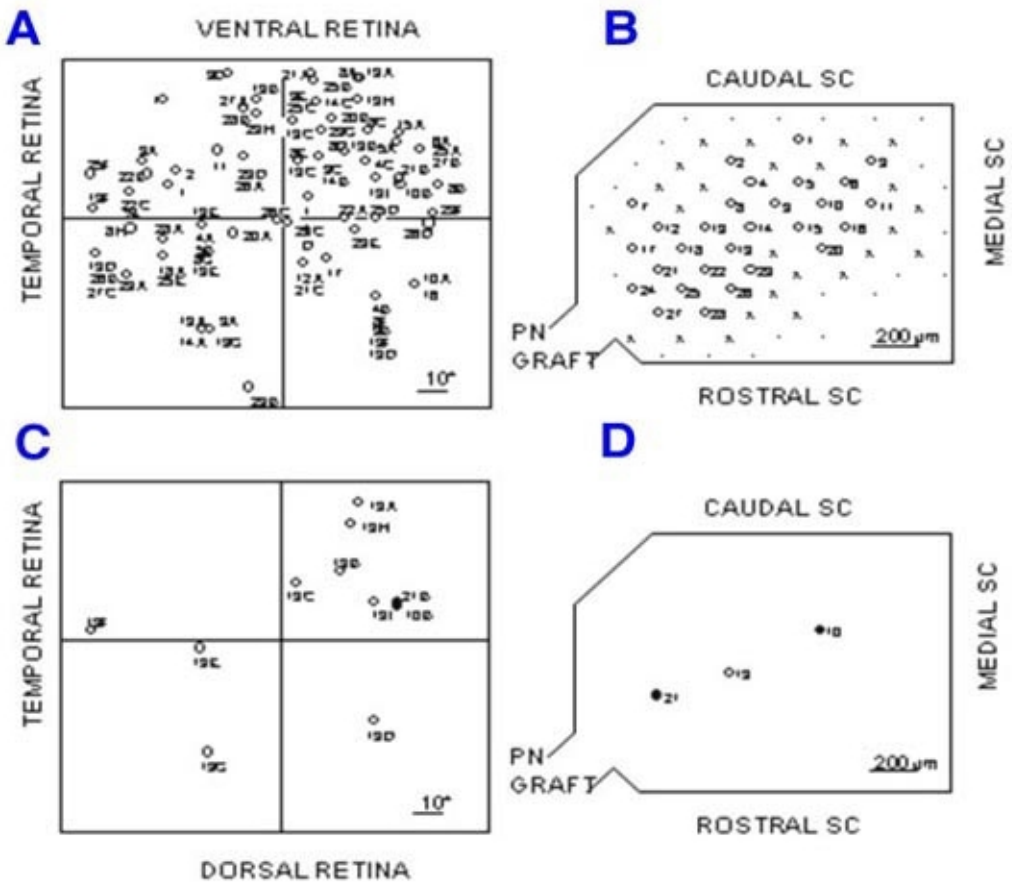

Figure 24. Positions of RGCs in the left retina and the projection sites of their respective axon terminals in the contralateral right SC of a grafted animal. Numbers refer to the recording sites in the SC. Letters indicate multiple receptive fields recorded at a single SC site. A, the positions of RGCs are inferred from the positions of the visual receptive fields as described in Fig. 1. The positions of RGCs are plotted on a linear scale in degrees from the optic disk, located at the intersection of the nasotemporal and ventrodorsal axes. B, in the diagram of the SC, the numbered open circles indicate recording sites at which unitary responses were recorded, crosses indicate sites at which responses to flash were recorded but receptive fields could not be identified, and filled squares are sites at which no visual response could be recorded. C and D, the lower diagrams, extracted from the upper diagrams (A and B), show projection of nine widely separated RGCs to the same recording site (site 19) in the SC (open circles) and projection of two neighboring RGCs to widely separated recording sites (sites 10, 21) in the SC (filled circles). PN, peripheral nerve. From Sauve et al. (24).

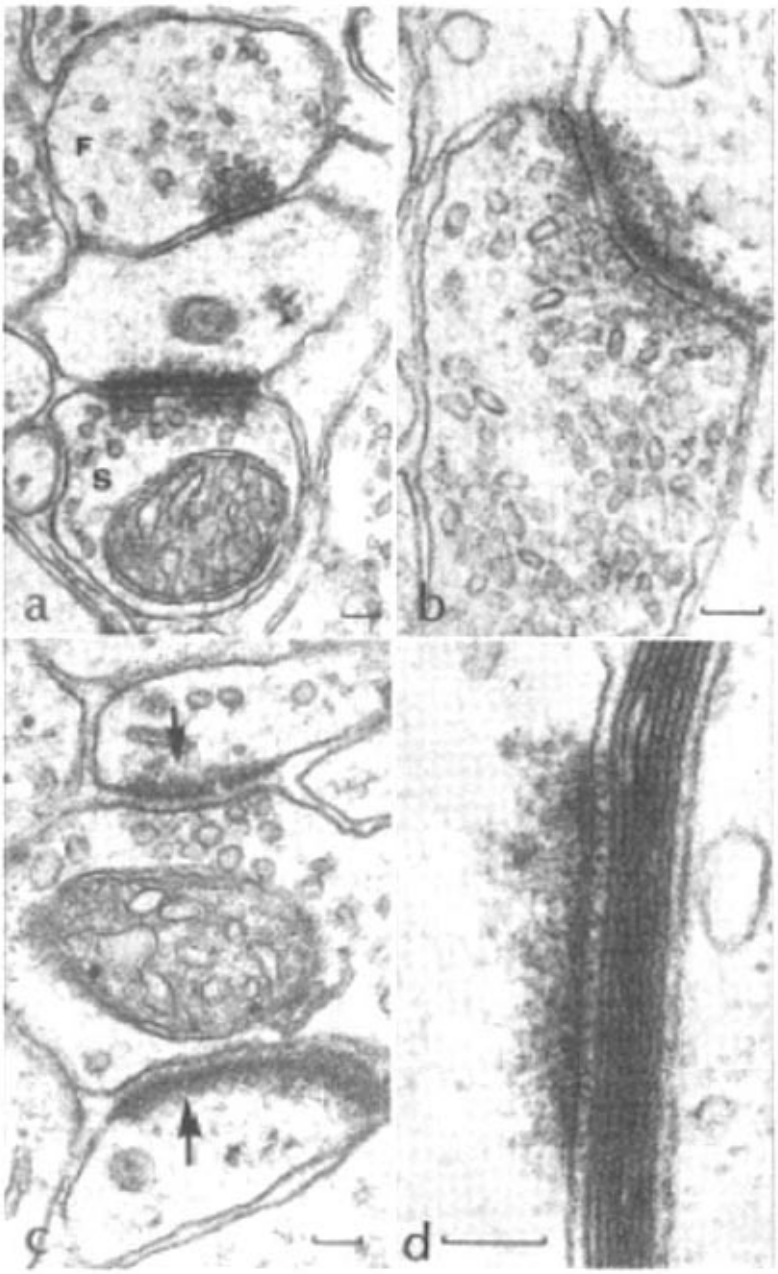

Figure 25. Details of a vesicle and contact morphology in the normal SC of the rat. a, normal S terminal make asymmetric contact (S) and F terminal make symmetric contact (F). b, an F terminal makes symmetric contact. c, an S terminal makes two asymmetric contacts (arrows); only one contact has vesicles aggregated to it. d, myelin lamellae make asymmetric contact. Scale indicates 0.1 μm. From Lund and Lund (152).

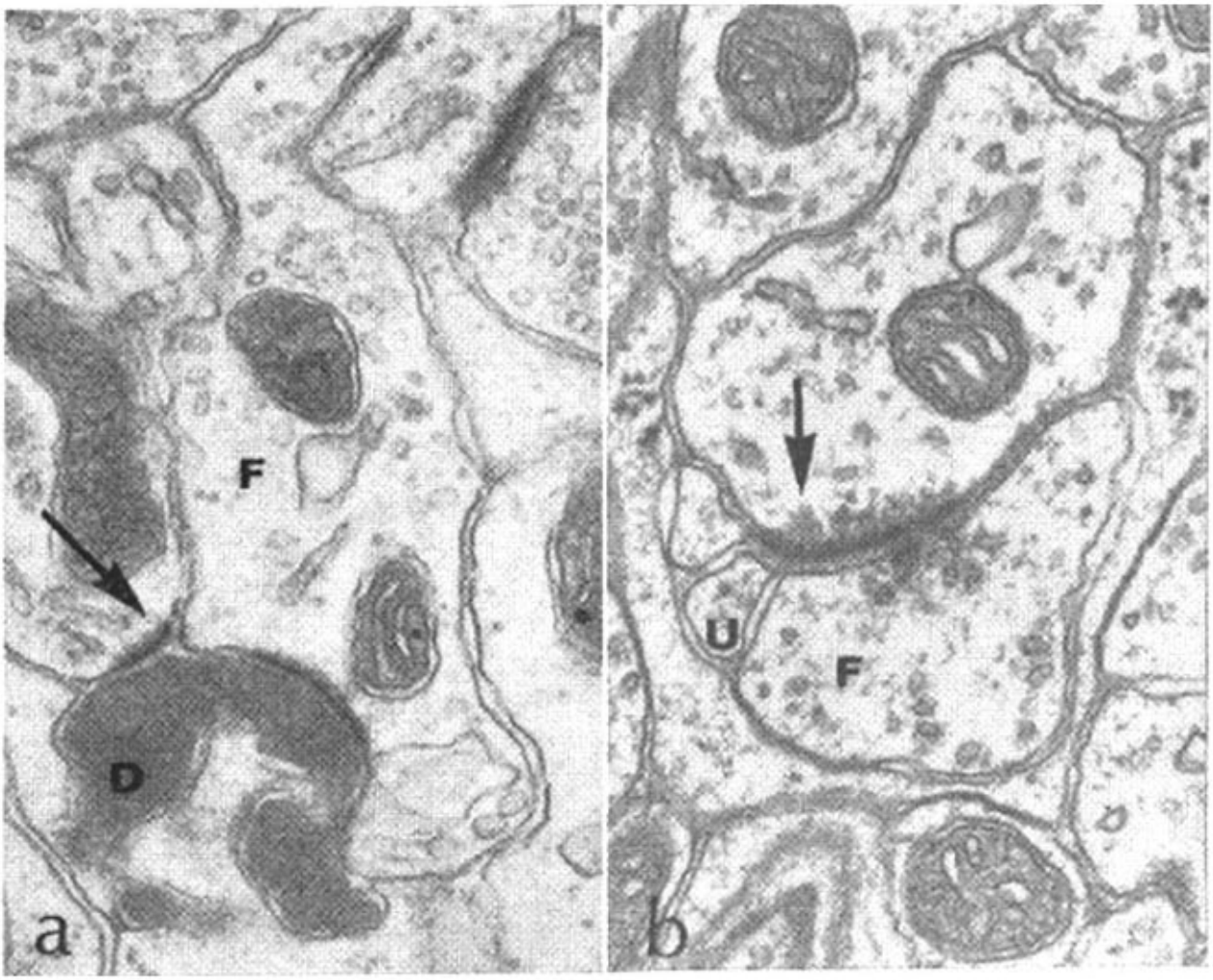

Figure 26. Partial occupation of postsynaptic contacts. a, the contact (arrow) has a degenerate terminal (D) and an F terminal (F) adjacent to it. b, the contact (arrow) is shared by an F terminal (F) and an unidentified profile (U). Magnification ×50,000. From Lund and Lund (152).

About the Authors

Dr. Yves Sauve was born in Montreal, Canada. He attended the University of Montreal where he received his B.Sc. in Biochemistry in 1983 and his M.Sc. in Neuroscience in 1988 with Dr. Thomas Reader, focusing on the neurochemistry of catecholamines and their receptors in the CNS. He then obtained his Ph.D. in Physiology under Dr. Michael Rasminsky at McGill University in 1995, where his research focused on the electrophysiological evaluation of reformed synapses between regenerating RGC axons and neurons in the superior colliculus, using the preparation developed in Dr. Albert Aguayo's group. Dr. Sauve subsequently undertook postdoctoral studies with Dr. Raymond Lund at the Institute of Ophthalmology (University College London), where he developed electrophysiological approaches to evaluate visual responsiveness in rodent models of retinal degeneration. In 2001, he became assistant professor of Ophthalmology and Visual Sciences at the Moran Eye Center (University of Utah), where he is currently evaluating rod and cone function following retinal degeneration, transplant therapies, and regeneration in the adult mammalian visual pathways.

Dr. Frederic Gaillard was born in Tours, France. He attended the University of Poitiers, where he received his B.Sc. (1969) and his M.Sc. (1971) in physiology. He then obtained a Ph.D. (1975) and a Doctorates-Sciences (1984) in neurophysiology. Until recently, most of his studies focused on aspects of binocular information processing in the amphibian visual system, mainly on the functional properties of the crossed isthmo-tectal pathway. He is now examining host-graft relationships in the adult mammalian visual system. Since 1977, Dr. Gaillard has been a senior investigator (Charge de recherches) of the Centre National de la Recherche Scientifique (CNRS) at the Institut de Physiologie et Biologie Cellulaires (UMR 6187), Poitiers, France.

References

1. >Cajal SR. (1913–1914). Estudios Sobre la Degeneraci—n y Regeneraci—n del Sistema Nervioso. Madrid: Moya. Translated into English as Degeneration and Regeneration of the Nervous System (R. M. May, tran. and Ed.). London: Oxford University Press, 1928. Reprinted and edited with additional translations by J. DeFelipe and E. G. Jones (), Cajal's Degeneration and Regeneration of the Nervous System. New York: Oxford University Press;1991
2. Aguayo AJ, Rasminsky M, Bray GM, Carbonetto S, McKerracher L, Villegas-Perez MP, Vidal-Sanz M, Carter DA. Degenerative and regenerative responses of injured neurons in the central nervous system of adult mammals. Philos Trans R Soc Lond B Biol Sci. 1991;331:337–343. PubMed PMID: 1677478.
3. So KF, Aguayo AJ. Lengthy regrowth of cut axons from ganglion cells after peripheral nerve transplantation into the retina of adult rats. Brain Res. 1985;328:349–354. PubMed PMID: 3986532.
4. Vidal-Sanz M, Bray GM, Villegas-Perez MP, Thanos S, Aguayo AJ. Axonal regeneration and synapse formation in the superior colliculus by retinal ganglion cells in the adult rat. J Neurosci. 1987;7:2894–2909. PubMed PMID: 3625278.
5. Tello F. La regeneration dans les voies optiques. Trab Lab Invest Biol Univ Madr. 1907;5:237–248.
6. David S, Aguayo AJ. Axonal elongation into peripheral nervous system "bridges" after central nervous system injury in adult rats. Science. 1981;214:931–933. PubMed PMID: 6171034.
7. Richardson PM, McGuinness UM, Aguayo AJ. Axons from CNS neurons regenerate into PNS grafts. Nature. 1980;284:264–265. PubMed PMID: 7360259.

8. Keirstead SA, Rasminsky M, Fukuda Y, Carter DA, Aguayo AJ, Vidal-Sanz M. Electrophysiologic responses in hamster superior colliculus evoked by regenerating retinal axons. Science. 1989;246:255–257. PubMed PMID: 2799387.
9. Sauve Y, Sawai H, Rasminsky M. Functional synaptic connections made by regenerated retinal ganglion cell axons in the superior colliculus of adult hamsters. J Neurosci. 1995;15:665–675. PubMed PMID: 7823170.
10. Kim JE, Li S, GrandPre T, Qiu D, Strittmatter SM. Axon regeneration in young adult mice lacking Nogo-A/B. Neuron. 2003;38:187–199. PubMed PMID: 12718854.
11. Raisman G. Myelin inhibitors: does NO mean GO? Nat Rev Neurosci. 2004;5:157–161. PubMed PMID: 14735118.
12. Schwartz M. Optic nerve crush: protection and regeneration. Brain Res Bull. 2004;62:467–471. PubMed PMID: 15036559.
13. Rhodes KE, Fawcett JW. Chondroitin sulphate proteoglycans: preventing plasticity or protecting the CNS? J Anat. 2004;204:33–48. PubMed PMID: 14690476.
14. Bouslama-Oueghlani L, Wehrle R, Sotelo C, Dusart I. The developmental loss of the ability of Purkinje cells to regenerate their axons occurs in the absence of myelin: an in vitro model to prevent myelination. J Neurosci. 2003;23:8318–8329. PubMed PMID: 12967994.
15. Chen DF, Jhaveri S, Schneider GE. Intrinsic changes in developing retinal neurons result in regenerative failure of their axons. Proc Natl Acad Sci U S A. 1995;92:7287–7291. PubMed PMID: 7638182.
16. Shewan D, Berry M, Cohen J. Extensive regeneration in vitro by early embryonic neurons on immature and adult CNS tissue. J Neurosci. 1995;15:2057–2062. PubMed PMID: 7891152.
17. Finlay BL, Schneps SE, Wilson KG, Schneider GE. Topography of visual and somatosensory projections to the superior colliculus of the golden hamster. Brain Res. 1978;142:223–235. PubMed PMID: 630383.
18. Siminoff R, Schwassmann HO, Kruger L. An electrophysiological study of the visual projection to the superior colliculus of the rat. J Comp Neurol. 1966;127:435–444. PubMed PMID: 5968989.
19. Tiao YC, Blakemore C. Functional organization in the superior colliculus of the golden hamster. J Comp Neurol. 1976;168:483–503. PubMed PMID: 939819.
20. Fukuda Y, Watanabe M, Sawai H, Miyoshi T. Functional recovery of vision in regenerated optic nerve fibers. Vision Res. 1998;38:1545–1553. PubMed PMID: 9667019.
21. Villegas-Perez MP, Vidal-Sanz M, Bray GM, Aguayo AJ. Influences of peripheral nerve grafts on the survival and regrowth of axotomized retinal ganglion cells in adult rats. J Neurosci. 1988;8:265–280. PubMed PMID: 2448429.
22. Carter DA, Bray GM, Aguayo AJ. Regenerated retinal ganglion cell axons can form well-differentiated synapses in the superior colliculus of adult hamsters. J Neurosci. 1989;9:4042–4050. PubMed PMID: 2479728.
23. Aviles-Trigueros M, Sauve Y, Lund RD, Vidal-Sanz M. Selective innervation of retinorecipient brainstem nuclei by retinal ganglion cell axons regenerating through peripheral nerve grafts in adult rats. J Neurosci. 2000;20:361–374. PubMed PMID: 10627613.
24. Sauve Y, Sawai H, Rasminsky M. Topological specificity in reinnervation of the superior colliculus by regenerated retinal ganglion cell axons in adult hamsters. J Neurosci. 2001;21:951–960. PubMed PMID: 11157081.
25. Berkelaar M, Clarke DB, Wang YC, Bray GM, Aguayo AJ. Axotomy results in delayed death and apoptosis of retinal ganglion cells in adult rats. J Neurosci. 1994;14:4368–4374. PubMed PMID: 8027784.
26. Peinado-Ramon P, Salvador M, Villegas-Perez MP, Vidal-Sanz M. Effects of axotomy and intraocular administration of NT-4, NT-3, and brain-derived neurotrophic factor on the survival of adult rat retinal ganglion cells. A quantitative in vivo study. Invest Ophthalmol Vis Sci. 1996;37:489–500. PubMed PMID: 8595949.
27. Villegas-Perez MP, Vidal-Sanz M, Rasminsky M, Bray GM, Aguayo AJ. Rapid and protracted phases of retinal ganglion cell loss follow axotomy in the optic nerve of adult rats. J Neurobiol. 1993;24:23–36. PubMed PMID: 8419522.

28. Quigley HA, Nickells RW, Kerrigan LA, Pease ME, Thibault DJ, Zack DJ. Retinal ganglion cell death in experimental glaucoma and after axotomy occurs by apoptosis. Invest Ophthalmol Vis Sci. 1995;36:774–786. PubMed PMID: 7706025.
29. Cheung ZH, Chan YM, Siu FK, Yip HK, Wu W, Leung MC, So KF. Regulation of caspase activation in axotomized retinal ganglion cells. Mol Cell Neurosci. 2004;25:383–393. PubMed PMID: 15033167.
30. Kermer P, Klocker N, Labes M, Šhr MB. Inhibition of CPP32-like proteases rescues axotomized retinal ganglion cells from secondary cell death in vivo. J Neurosci. 1998;18:4656–4662. PubMed PMID: 9614240.
31. Kermer P, Klocker N, Labes M, Thomsen S, Srinivasan A, Bahr M. Activation of caspase-3 in axotomized rat retinal ganglion cells in vivo. FEBS Lett. 1999;453:361–364. PubMed PMID: 10405176.
32. Kermer P, Ankerhold R, Klocker N, Krajewski S, Reed JC, Bahr M. Caspase-9: involvement in secondary death of axotomized rat retinal ganglion cells in vivo. Brain Res Mol Brain Res. 2000;85:144–150. PubMed PMID: 11146116.
33. Weishaupt JH, Diem R, Kermer P, Krajewski S, Reed JC, Bahr M. Contribution of caspase-8 to apoptosis of axotomized rat retinal ganglion cells in vivo. Neurobiol Dis. 2003;13:124–135. PubMed PMID: 12828936.
34. Kikuchi M, Tenneti L, Lipton SA. Role of p38 mitogen-activated protein kinase in axotomy-induced apoptosis of rat retinal ganglion cells. J Neurosci. 2000;20:5037–5044. PubMed PMID: 10864961.
35. Chaudhary P, Ahmed F, Quebada P, Sharma SC. Caspase inhibitors block the retinal ganglion cell death following optic nerve transection. Brain Res Mol Brain Res. 1999;67:36–45. PubMed PMID: 10101230.
36. Kermer P, Klocker N, Bahr M. Long-term effect of inhibition of ced 3-like caspases on the survival of axotomized retinal ganglion cells in vivo. Exp Neurol. 1999;158:202–205. PubMed PMID: 10448432.
37. Isenmann S, Wahl C, Krajewski S, Reed JC, Bahr MB. Up-regulation of Bax protein in degenerating retinal ganglion cells precedes apoptotic cell death after optic nerve lesion in the rat. Eur J Neurosci. 1997;9:1763–1772. PubMed PMID: 9283831.
38. Bonfanti L, Strettoi E, Chierzi S, Cenni MC, Liu XH, Martinou J-C, Maffei L, Rabacchi SA. Protection of retinal ganglion cells from natural and axotomy-induced cell death in neonatal transgenic mice overexpressing bcl-2. J Neurosci. 1996;16:4186–4194. PubMed PMID: 8753880.
39. Chierzi S, Cenni MC, Maffei L, Pizzorusso T, Porciatti V, Ratto GM, Strettoi E. Protection of retinal ganglion cells and preservation of function after optic nerve lesion in bcl-2 transgenic mice. Vision Res. 1998;38:1537–1543. PubMed PMID: 9667018.
40. Kugler S, Straten G, Kreppel F, Isenmann S, Liston P, Bahr M. The X-linked inhibitor of apoptosis (XIAP) prevents cell death in axotomized CNS neurons in vivo. Cell Death Differ. 2000;7:815–824. PubMed PMID: 11042676.
41. Yip HK, So KF. Axonal regeneration of retinal ganglion cells: effect of trophic factors. Prog Retin Eye Res. 2000;19:559–575. PubMed PMID: 10925243.
42. Cui Q, So KF, Yip HK. Major biological effects of neurotrophic factors on retinal ganglion cells in mammals. Biol Signals Recept. 1998;7:220–226. PubMed PMID: 9730581.
43. Weishaupt JH, Bahr M. Degeneration of axotomized retinal ganglion cells as a model for neuronal apoptosis in the central nervous system - molecular death and survival pathways. Restor Neurol Neurosci. 2001;19:19–27. PubMed PMID: 12082226.
44. Koeberle PD, Bahr M. Growth and guidance cues for regenerating axons: where have they gone? J Neurobiol. 2004;59:162–180. PubMed PMID: 15007834.
45. Caleo M, Menna E, Chierzi S, Cenni MC, Maffei L. Brain-derived neurotrophic factor is an anterograde survival factor in the rat visual system. Curr Biol. 2000;10:1155–1161. PubMed PMID: 11050383.
46. Quigley HA, McKinnon SJ, Zack DJ, Pease ME, Kerrigan-Baumrind LA, Kerrigan DF, Mitchell RS. Retrograde axonal transport of BDNF in retinal ganglion cells is blocked by acute IOP elevation in rats. Invest Ophthalmol Vis Sci. 2000;41:3460–3466. PubMed PMID: 11006239.
47. Spalding KL, Rush RA, Harvey AR. Target-derived and locally derived neurotrophins support retinal ganglion cell survival in the neonatal rat retina. J Neurobiol. 2004;60:319–327. PubMed PMID: 15281070.

48. Klocker N, Cellerino A, Bahr M. Free radical scavenging and inhibition of nitric oxide synthase potentiates the neurotrophic effects of brain-derived neurotrophic factor on axotomized retinal ganglion cells in vivo. J Neurosci. 1998;18:1038–1046. PubMed PMID: 9437024.
49. Mansour-Robaey S, Clarke DB, Wang YC, Bray GM, Aguayo AJ. Effects of ocular injury and administration of brain-derived neurotrophic factor on survival and regrowth of axotomized retinal ganglion cells. Proc Natl Acad Sci U S A. 1994;91:1632–1636. PubMed PMID: 8127857.
50. Mey J, Thanos S. Intravitreal injections of neurotrophic factors support the survival of axotomized retinal ganglion cells in adult rats in vivo. Brain Res. 1993;602:304–317. PubMed PMID: 8448673.
51. Di Polo A, Aigner LJ, Dunn RJ, Bray GM, Aguayo AJ. Prolonged delivery of brain-derived neurotrophic factor by adenovirus-infected Muller cells temporarily rescues injured retinal ganglion cells. Proc Natl Acad Sci U S A. 1998;95:3978–3983. PubMed PMID: 9520478.
52. Cheng L, Sapieha P, Kittlerova P, Hauswirth WW, Di Polo A. TrkB gene transfer protects retinal ganglion cells from axotomy-induced death in vivo. J Neurosci. 2002;22:3977–3986. PubMed PMID: 12019317.
53. Cohen A, Bray GM, Aguayo AJ. Neurotrophin-4/5 (NT-4/5) increases adult rat retinal ganglion cell survival and neurite outgrowth in vitro. J Neurobiol. 1994;25:953–959. PubMed PMID: 7964706.
54. Carmignoto G, Maffei L, Candeo P, Canella R, Comelli C. Effect of NGF on the survival of rat retinal ganglion cells following optic nerve section. J Neurosci. 1989;9:1263–1272. PubMed PMID: 2467970.
55. Klocker N, Braunling F, Isenmann S, Bahr M. In vivo neurotrophic effects of GDNF on axotomized retinal ganglion cells. Neuroreport. 1997;8:3439–3442. PubMed PMID: 9427303.
56. Koeberle PD, Ball AK. Effects of GDNF on retinal ganglion cell survival following axotomy. Vision Res. 1998;38:1505–1515. PubMed PMID: 9667015.
57. Koeberle PD, Ball AK. Neurturin enhances the survival of axotomized retinal ganglion cells in vivo: combined effects with glial cell line-derived neurotrophic factor and brain-derived neurotrophic factor. Neuroscience. 2002;110:555–567. PubMed PMID: 11906793.
58. Cui Q, Harvey AR. CNTF promotes the regrowth of retinal ganglion cell axons into murine peripheral nerve grafts. Neuroreport. 2000;11:3999–4002. PubMed PMID: 11192617.
59. Watanabe M, Fukuda Y. Survival and axonal regeneration of retinal ganglion cells in adult cats. Prog Retin Eye Res. 2002;21:529–553. PubMed PMID: 12433376.
60. Weise J, Isenmann S, Klocker N, Kugler S, Hirsch S, Gravel C, Bahr M. Adenovirus-mediated expression of ciliary neurotrophic factor (CNTF) rescues axotomized rat retinal ganglion cells but does not support axonal regeneration in vivo. Neurobiol Dis. 2000;7:212–223. PubMed PMID: 10860786.
61. Kaplan DR, Miller FD. Neurotrophin signal transduction in the nervous system. Curr Opin Neurobiol. 2000;10:381–391. PubMed PMID: 10851172.
62. Patapoutian A, Reichardt LF. Trk receptors: mediators of neurotrophin action. Curr Opin Neurobiol. 2001;11:272–280. PubMed PMID: 11399424.
63. Fagiolini M, Caleo M, Strettoi E, Maffei L. Axonal transport blockade in the neonatal rat optic nerve induces limited retinal ganglion cell death. J Neurosci. 1997;17:7045–7052. PubMed PMID: 9278540.
64. Koeberle PD, Ball AK. Nitric oxide synthase inhibition delays axonal degeneration and promotes the survival of axotomized retinal ganglion cells. Exp Neurol. 1999;158:366–381. PubMed PMID: 10415143.
65. Koeberle PD, Gauldie J, Ball AK. Effects of adenoviral-mediated gene transfer of interleukin-10, interleukin-4, and transforming growth factor-beta on the survival of axotomized retinal ganglion cells. Neuroscience. 2004;125:903–920. PubMed PMID: 15120851.
66. Raibon E, Sauve Y, Carter DA, Gaillard F. Microglial changes accompanying the promotion of retinal ganglion cell axonal regeneration into peripheral nerve grafts. J Neurocytol. 2002;31:57–71. PubMed PMID: 12652088.
67. Thanos S, Mey J, Wild M. Treatment of the adult retina with microglia-suppressing factors retards axotomy-induced neuronal degradation and enhances axonal regeneration in vivo and in vitro. J Neurosci. 1993;13:455–466. PubMed PMID: 7678855.
68. Schwartz M. Vaccination for glaucoma: dream or reality? Brain Res Bull. 2004;62:481–484. PubMed PMID: 15036561.

69. Bahr M, Eschweiler GW, Wolburg H. Precrushed sciatic nerve grafts enhance the survival and axonal regrowth of retinal ganglion cells in adult rats. Exp Neurol. 1992;116:13–22. PubMed PMID: 1559562.
70. Leon S, Yin Y, Nguyen J, Irwin N, Benowitz LI. Lens injury stimulates axon regeneration in the mature rat optic nerve. J Neurosci. 2000;20:4615–4626. PubMed PMID: 10844031.
71. Yin Y, Cui Q, Li Y, Irwin N, Fischer D, Harvey AR, Benowitz LI. Macrophage-derived factors stimulate optic nerve regeneration. J Neurosci. 2003;23:2284–2293. PubMed PMID: 12657687.
72. Fischer D, He Z, Benowitz LI. Counteracting the Nogo receptor enhances optic nerve regeneration if retinal ganglion cells are in an active growth state. J Neurosci. 2004;24:1646–1651. PubMed PMID: 14973241.
73. Ellezam B, Dubreuil C, Winton M, Loy L, Dergham P, Selles-Navarro I, McKerracher L. Inactivation of intracellular Rho to stimulate axon growth and regeneration. Prog Brain Res. 2002;137:371–380. PubMed PMID: 12440379.
74. Cai D, Qiu J, Cao Z, McAtee M, Bregman BS, Filbin MT. Neuronal cyclic AMP controls the developmental loss in ability of axons to regenerate. J Neurosci. 2001;21:4731–4739. PubMed PMID: 11425900.
75. Spencer T, Filbin MT. A role for cAMP in regeneration of the adult mammalian CNS. J Anat. 2004;204:49–55. PubMed PMID: 14690477.
76. Oster SF, Deiner M, Birgbauer E, Sretavan DW. Ganglion cell axon pathfinding in the retina and optic nerve. Semin Cell Dev Biol. 2004;15:125–136. PubMed PMID: 15036215.
77. Sawai H, Clarke DB, Kittlerova P, Bray GM, Aguayo AJ. Brain-derived neurotrophic factor and neurotrophin-4/5 stimulate growth of axonal branches from regenerating retinal ganglion cells. J Neurosci. 1996;16:3887–3894. PubMed PMID: 8656282.
78. Williams SE, Mason CA, Herrera E. The optic chiasm as a midline choice point. Curr Opin Neurobiol. 2004;14:51–60. PubMed PMID: 15018938.
79. Thanos S, Mey J. Type-specific stabilization and target-dependent survival of regenerating ganglion cells in the retina of adult rats. J Neurosci. 1995;15:1057–1079. PubMed PMID: 7869083.
80. Carter DA, Jhaveri S. Retino-geniculate axons regenerating in adult hamsters are able to form morphologically distinct terminals. Exp Neurol. 1997;146:315–322. PubMed PMID: 9270040.
81. Zwimpfer TJ, Aguayo AJ, Bray GM. Synapse formation and preferential distribution in the granule cell layer by regenerating retinal ganglion cell axons guided to the cerebellum of adult hamsters. J Neurosci. 1992;12:1144–1159. PubMed PMID: 1556590.
82. Dusart I, Morel MP, Wehrle R, Sotelo C. Late axonal sprouting of injured Purkinje cells and its temporal correlation with permissive changes in the glial scar. J Comp Neurol. 1999;408:399–418. PubMed PMID: 10340514.
83. Bandtlow C, Zachleder T, Schwab ME. Oligodendrocytes arrest neurite growth by contact inhibition. J Neurosci. 1990;10:3837–3848. PubMed PMID: 2269887.
84. Davies SJA, Fitch MT, Memberg SP, Hall AK, Raisman G, Silver J. Regeneration of adult axons in white matter tracts of the central nervous system. Nature. 1997;390:680–684. PubMed PMID: 9414159.
85. Davies SJA, Goucher DR, Doller C, Silver J. Robust regeneration of adult sensory axons in degenerating white matter of the adult rat spinal cord. J Neurosci. 1999;19:5810–5822. PubMed PMID: 10407022.
86. Fawcett JW. Astrocytic and neuronal factors affecting axon regeneration in the damaged central nervous system. Cell Tissue Res. 1997;290:371–377. PubMed PMID: 9321700.
87. Liuzzi FJ, Lasek RJ. Astrocytes block axonal regeneration in mammals by activating the physiological stop pathway. Science. 1987;237:642–645. PubMed PMID: 3603044.
88. Smith GM, Rutishauser U, Silver J, Miller RH. Maturation of astrocytes in vitro alters the extent and molecular basis of neurite outgrowth. Dev Biol. 1990;138:377–390. PubMed PMID: 2318341.
89. Frost DO. Development of anomalous retinal projections to nonvisual thalamic nuclei in Syrian hamsters: a quantitative study. J Comp Neurol. 1986;252:95–105. PubMed PMID: 3793977.
90. Berry M, Carlile J, Hunter A. Peripheral nerve explants grafted into the vitreous body of the eye promote the regeneration of retinal ganglion cell axons severed in the optic nerve. J Neurocytol. 1996;25:147–170. PubMed PMID: 8699196.

91. Eitan S, Solomon A, Lavie V, Yoles E, Hirschberg DL, Belkin M, Schwartz M. Recovery of visual response of injured adult rat optic nerves treated with transglutaminase. Science. 1994;264:1764–1768. PubMed PMID: 7911602.
92. Fischer D, Heiduschka P, Thanos S. Lens-injury-stimulated axonal regeneration throughout the optic pathway of adult rats. Exp Neurol. 2001;172:257–272. PubMed PMID: 11716551.
93. Li Y, Sauve Y, Li D, Lund RD, Raisman G. Transplanted olfactory ensheathing cells promote regeneration of cut adult rat optic nerve axons. J Neurosci. 2003;23:7783–7788. PubMed PMID: 12944507.
94. Carter DA, Aguayo AJ, Bray GM. Retinal ganglion cell terminals in the hamster superior colliculus: an ultrastructural study. J Comp Neurol. 1991;311:97–107. PubMed PMID: 1719046.
95. Carter DA, Bray GM, Aguayo AJ. Regenerated retinal ganglion cell axons form normal numbers of boutons but fail to expand their arbors in the superior colliculus. J Neurocytol. 1998;27:187–196. PubMed PMID: 10640178.
96. Ling C, Schneider GE, Jhaveri S. Target-specific morphology of retinal axon arbors in the adult hamster. Vis Neurosci. 1998;15:559–579. PubMed PMID: 9685208.
97. Vidal-Sanz M, Bray GM, Aguayo AJ. Regenerated synapses persist in the superior colliculus after the regrowth of retinal ganglion cell axons. J Neurocytol. 1991;20:940–952. PubMed PMID: 1809272.
98. Turner JP, Sauve Y, Lund RD, Salt TA. Retinotectal synaptic transmission in vitro after the repair of cut optic nerve with a peripheral nerve graft. Soc Neurosci Abstr. 2001;27
99. Gaze RM. The formation of nerve connections. New York: Academic Press; 1970.
100. Sperry RW. Neural basis of the spontaneous optokinetic response produced by visual inversion. J Comp Physiol Psychol. 1950;43:482–489. PubMed PMID: 14794830.
101. Sperry RW. (1965) Embryogenesis of behavioral nerve nets. In: DeHann RL, Ursprung H, editors. Organogenesis. New York: Holt, Rinehart and Winston. p.161-186.
102. Dunlop SA, Tee LB, Stirling RV, Taylor AL, Runham PB, Barber AB, Kuchling G, Rodger J, Roberts JD, Harvey AR, Beazley LD. Failure to restore vision after optic nerve regeneration in reptiles: interspecies variation in response to axotomy. J Comp Neurol. 2004;478:292–305. PubMed PMID: 15368531.
103. Dunlop SA, Stirling RV, Rodger J, Symonds AC, Bancroft WJ, Tee LB, Beazley LD. Failure to form a stable topographic map during optic nerve regeneration:abnormal activity-dependent mechanisms. Exp Neurol. 2003;184:805–815. PubMed PMID: 14769373.
104. Beazley LD, Rodger J, Chen P, Tee LB, Stirling RV, Taylor AL, Dunlop SA. Training on a visual task improves the outcome of optic nerve regeneration. J Neurotrauma. 2003;20:1263–1270. PubMed PMID: 14651812.
105. Walter J, Henke-Fahle S, Bonhoeffer F. Avoidance of posterior tectal membrane by temporal retinal axons. Development. 1987;101:909–913. PubMed PMID: 3503703.
106. Walter J, Kern-Veitis B, Huf J, Stolze B, Bonhoeffer F. Recognition of position specific properties of tectal cell membranes by retinal axons in vitro. Development. 1987;101:685–696. PubMed PMID: 3503693.
107. Godement P, Bonhoeffer F. Cross-species recognition of tectal cues by retinal fibers in vitro. Development. 1989;106:313–320. PubMed PMID: 2591317.
108. Roskies AL, O'Leary DDM. Control of topographic retinal axon branching by inhibitory membrane-bound molecules. Science. 1994;265:799–803. PubMed PMID: 8047886.
109. von Boxberg Y, Deiss S, Schwarz U. Guidance and topographic stabilization of nasal chick retinal axons on target-derived components in vitro. Neuron. 1993;10:345–357. PubMed PMID: 8461131.
110. Bahr M, Eschweiler GW. Regenerating adult rat retinal axons reconnect with target neurons in-vitro. Neuroreport. 1991;2:581–584. PubMed PMID: 1661620.
111. Bahr M, Eschweiler GW. Formation of functional synapses by regenerating adult rat retinal ganglion cell axons in midbrain target regions in vitro. J Neurobiol. 1993;24:456–473. PubMed PMID: 8515251.
112. Wizenmann A, Thies E, Klostermann S, Bonhoeffer F, Bahr M. Appearance of target-specific guidance information for regenerating axons after CNS lesions. Neuron. 1993;11:975–983. PubMed PMID: 8240818.

113. King CE, Wallace A, Rodger J, Bartlett C, Beazley LD, Dunlop SA. Transient up-regulation of retinal EphA3 and EphA5, but not ephrin-A2, coincides with re-establishment of a topographic map during optic nerve regeneration in goldfish. Exp Neurol. 2003;183:593–599. PubMed PMID: 14552900.
114. Rodger J, Vitale PN, Tee LB, King CE, Bartlett CA, Fall A, Brennan C, O'Shea JE, Dunlop SA, Beazley LD. EphA/ephrin-A interactions during optic nerve regeneration: restoration of topography and regulation of ephrin-A2 expression. Mol Cell Neurosci. 2004;25:56–68. PubMed PMID: 14962740.
115. Sperry RW. Chemoaffinity in the orderly growth of nerve fiber patterns and connections. Proc Natl Acad Sci U S A. 1963;50:703–709. PubMed PMID: 14077501.
116. Wong RO. Retinal waves and visual system development. Annu Rev Neurosci. 1999;22:29–47. PubMed PMID: 10202531.
117. Cline HT. Activity-dependent plasticity in the visual systems of frogs and fish. Trends Neurosci. 1991;14:104–111. PubMed PMID: 1709534.
118. Debski EA, Cline HT. Activity-dependent mapping in the retinotectal projection. Curr Opin Neurobiol. 2002;12:93–99. PubMed PMID: 11861170.
119. Penn AA, Riquelme PA, Feller MB, Shatz CJ. Competition in retinogeniculate patterning driven by spontaneous activity. Science. 1998;279:2108–2112. PubMed PMID: 9516112.
120. Schmidt JT. Activity-driven sharpening of the retinotectal projection: the search for retrograde synaptic signaling pathways. J Neurobiol. 2004;59:114–133. PubMed PMID: 15007831.
121. Shatz CJ. Impulse activity and the patterning of connections during CNS development. Neuron. 1990;5:745–756. PubMed PMID: 2148486.
122. Holt CE, Harris WA. Order in the initial retinotectal map in Xenopus: a new technique for labelling growing nerve fibres. Nature. 1983;301:150–152. PubMed PMID: 6823290.
123. Stuermer CA, Bastmeyer M, Bahr M, Strobel G, Paschke K. Trying to understand axonal regeneration in the CNS of fish. J Neurobiol. 1992;23:537–550. PubMed PMID: 1431836.
124. Fraser SE, Perkel DH. Competitive and positional cues in the patterning of nerve connections. J Neurobiol. 1990;21:51–72. PubMed PMID: 2181067.
125. Honda H. Topographic mapping in the retinotectal projection by means of complementary ligand and receptor gradients: a computer simulation study. J Theor Biol. 1998;192:235–246. PubMed PMID: 9637060.
126. Hua SE, Massone LL, Houk JC. Model of topographic map development guided by a transiently expressed repulsion molecule. Neuroreport. 1993;4:1319–1322. PubMed PMID: 8260613.
127. Matsumoto N, Kometami M, Nagano K. Regenerating retinal fibers of the goldfish make temporary and unspecific but functional synapses before forming the final retinotopic projection. Neuroscience. 1987;22:1103–1110. PubMed PMID: 3683848.
128. Meyer RL, Kageyama GH. Large-scale synaptic errors during map formation by regeneration of optic axons in the goldfish. J Comp Neurol. 1999;409:299–312. PubMed PMID: 10379922.
129. Udin SB, Fawcett JW. Formation of topographic maps. Annu Rev Neurosci. 1988;11:289–327. PubMed PMID: 3284443.
130. Bahr M, Wizenmann A. Retinal ganglion cell axons recognize specific guidance cues present in the deafferented adult rat superior colliculus. J Neurosci. 1996;16:5106–5116. PubMed PMID: 8756440.
131. Sauve Y, Girman SV, Wang S, Lawrence JM, Lund RD. Progressive visual sensitivity loss in the Royal College of Surgeons rat: perimetric study in the superior colliculus. Neuroscience. 2001;103:51–63. PubMed PMID: 11311787.
132. Baier H, Bonhoeffer F. Axon guidance by gradients of a target-derived component. Science. 1992;255:472–475. PubMed PMID: 1734526.
133. Wizenmann A, Bahr M. Growth characteristics of ganglion cell axons in the developing and regenerating retinotectal projection of the rat. Cell Tissue Res. 1997;290:395–403. PubMed PMID: 9321703.
134. Wizenmann A, Bahr M. Growth preferences of adult rat retinal ganglion cell axons in retinotectal cocultures. J Neurobiol. 1998;35:379–387. PubMed PMID: 9624620.
135. von Boxberg Y, Deiss S, Schwarz U. Guidance and topographic stabilization of nasal chick retinal axons on target-derived components in vitro. Neuron. 1993;10:345–357. PubMed PMID: 8461131.

136. Davenport RW, Thies E, Zhou R, Nelson PG. Cellular localization of ephrin-A2, ephrin-A5, and other functional guidance cues underlies retinotopic development across species. J Neurosci. 1998;18:975–986. PubMed PMID: 9437019.
137. Ichijo H, Bonhoeffer F. Differential withdrawal of retinal axons induced by a secreted factor. J Neurosci. 1998;18:5008–5018. PubMed PMID: 9634566.
138. Nakamoto M, Cheng HJ, Friedman GC, McLaughlin T, Hansen MJ, Yoon CH, O'Leary DD, Flanagan JG. Topographically specific effects of ELF-1 on retinal axon guidance in vitro and retinal axon mapping in vivo. Cell. 1996;86:755–766. PubMed PMID: 8797822.
139. Goodhill GJ. Mathematical guidance for axons. Trends Neurosci. 1998;21:226–231. PubMed PMID: 9641531.
140. Carter DA, Bray GM, Aguayo AJ. Long-term growth and remodeling of regenerated retino-collicular connections in adult hamsters. J Neurosci. 1994;14:590–598. PubMed PMID: 7507980.
141. Caroni P, Schwab ME. Antibody against myelin-associated inhibitor of neurite growth neutralizes nonpermissive substrate properties of CNS white matter. Neuron. 1988;1:85–96. PubMed PMID: 3272156.
142. Ghosh A, David S. Neurite growth-inhibitory activity in the adult rat cerebral cortical gray matter. J Neurobiol. 1997;32:671–683. PubMed PMID: 9183745.
143. McKerracher L, David S, Jackson DL, Kottis V, Dunn RJ, Braun PE. Identification of myelin-associated glycoprotein as a major myelin-derived inhibitor of neurite growth. Neuron. 1994;13:805–811. PubMed PMID: 7524558.
144. Smith-Thomas LC, Fok-Seang J, Stevens J, Du J-S, Muir E, Faissner F, Geller HM, Rogers JH, Fawcett JW. An inhibitor of neurite outgrowth produced by astrocytes. J Cell Sci. 1994;107:1687–1695. PubMed PMID: 7962209.
145. McLoon SC, McLoon LK, Palm SL, Furcht LT. Transient expression of laminin in the optic nerve of the developing rat. J Neurosci. 1988;8:1981–1990. PubMed PMID: 3385486.
146. Rager G, Morino P, Schnitzer J, Sonderegger P. Expression of the axonal cell adhesion molecules axonin-1 and Ng-CAM during the development of the chick retinotectal system. J Comp Neurol. 1996;365:594–609. PubMed PMID: 8742305.
147. Cohen J, Burne JF, Winter J, Bartlett P. Retinal ganglion cells lose response to laminin with maturation. Nature. 1986;322:465–467. PubMed PMID: 2874498.
148. de Curtis I, Reichardt LF. Function and spatial distribution in developing chick retina of the laminin receptor alpha 6 beta 1 and its isoforms. Development. 1993;118:377–388. PubMed PMID: 8223267.
149. Simon DK, O'Leary DDM. Responses of retinal axons in vivo and in vitro to position-encoding molecules in the embryonic superior colliculus. Neuron. 1992;9:977–989. PubMed PMID: 1419004.
150. Simon DK, O'Leary DDM. Development of topographic order in the mammalian retino collicular projection. J Neurosci. 1992;12:1212–1232. PubMed PMID: 1313491.
151. Tropea D, Caleo M, Maffei L. Synergistic effects of brain-derived neurotrophic factor and chondroitinase ABC on retinal fiber sprouting after denervation of the superior colliculus in adult rats. J Neurosci. 2003;23:7034–7044. PubMed PMID: 12904464.
152. Lund RD, Lund JS. Synaptic adjustment after deafferentation of the superior colliculus of the rat. Science. 1971;171:804–807. PubMed PMID: 5549304.
153. Harvey AR, Worthington DR. The projection from different visual cortical areas to the rat superior colliculus. J Comp Neurol. 1990;298:281–292. PubMed PMID: 2212104.
154. Mize RR. Immunocytochemical localization of gamma-aminobutyric acid (GABA) in the cat superior colliculus. J Comp Neurol. 1988;276:169–187. PubMed PMID: 3220979.
155. Pinard R, Benfares J, Lanoir J. Electron microscopic study of GABA-immunoreactive neuronal processes in the superficial gray layer of the rat superior colliculus: their relationships with degenerating retinal nerve endings. J Neurocytol. 1991;20:262–276. PubMed PMID: 1646864.
156. Houser CR, Lee M, Vaughn JE. Immunocytochemical localization of glutamic acid decarboxylase in normal and deafferented superior colliculus: evidence for reorganization of gamma-aminobutyric acid synapses. J Neurosci. 1983;3:2030–2042. PubMed PMID: 6619922.

157. Garcia del Cano G, Gerrikagoitia I, Martinez-Millan L. Plastic reaction of the rat visual corticocollicular connection after contralateral retinal deafferentiation at the neonatal or adult stage: axonal growth versus reactive synaptogenesis. J Comp Neurol. 2002;446:166–178. PubMed PMID: 11932934.
158. Gerrikagoitia I, Garcia Del Cano G, Martinez-Millan L. Changes of the cholinergic input to the superior colliculus following enucleation in neonatal and adult rats. Brain Res. 2001;898:61–72. PubMed PMID: 11292449.
159. Smith SA, Bedi KS. Unilateral eye enucleation in adult rats causes neuronal loss in the contralateral superior colliculus. J Anat. 1997;190:481–490. PubMed PMID: 9183672.
160. Isa T, Endo T, Saito Y. The visuo-motor pathway in the local circuit of the rat superior colliculus. J Neurosci. 1998;18:8496–8504. PubMed PMID: 9763492.
161. Miyamoto T, Sakurai T, Okada Y. Masking effect of NMDA receptor antagonists on the formation of long-term potentiation (LTP) in superior colliculus slices from the guinea pig. Brain Res. 1990;518:166–172. PubMed PMID: 1975212.
162. Bourassa J, Deschenes M. Corticothalamic projections from the primary visual cortex in rats: a single fiber study using biocytin as an anterograde tracer. Neuroscience. 1995;66:253–263. PubMed PMID: 7477870.
163. Salin P, Tseng GF, Hoffman S, Parada I, Prince DA. Axonal sprouting in layer V pyramidal neurons of chronically injured cerebral cortex. J Neurosci. 1995;15:8234–8245. PubMed PMID: 8613757.
164. Laurberg S, Zimmer J. Lesion-induced sprouting of hippocampal mossy fiber collaterals to the fascia dentata in developing and adult rats. J Comp Neurol. 1981;200:433–459. PubMed PMID: 7276246.
165. Fortin S, Chabli A, Dumont I, Shumikhina S, Itaya SK, Molotchnikoff S. Maturation of visual receptive field properties in the rat superior colliculus. Brain Res Dev Brain Res. 1999;112:55–64. PubMed PMID: 9974159.
166. Thanos S. Adult retinofugal axons regenerating through peripheral nerve grafts can restore the light-induced pupilloconstriction reflex. Eur J Neurosci. 1992;4:691–699. PubMed PMID: 12106313.
167. Whiteley SJ, Sauve Y, Aviles-Trigueros M, Vidal-Sanz M, Lund RD. Extent and duration of recovered pupillary light reflex following retinal ganglion cell axon regeneration through peripheral nerve grafts directed to the pretectum in adult rats. Exp Neurol. 1998;154:560–572. PubMed PMID: 9878191.
168. Sasaki H, Inoue T, Iso H, Fukuda Y, Hayashi Y. Light-dark discrimination after sciatic nerve transplantation to the sectioned optic nerve in adult hamsters. Vision Res. 1993;33:877–880. PubMed PMID: 8506630.
169. Sasaki H, Coffey P, Villegas-Perez MP, Vidal-Sanz M, Young MJ, Lund RD, Fukuda Y. Light induced EEG desynchronization and behavioral arousal in rats with restored retinocollicular projection by peripheral nerve graft. Neurosci Lett. 1996;218:45–48. PubMed PMID: 8939477.
170. Gilbert CD. Adult cortical dynamics. Physiol Rev. 1998;78:467–485. PubMed PMID: 9562036.
171. Kaas JH, Merzenich MM, Killackey HP. The reorganization of somatosensory cortex following peripheral nerve damage in adult and developing mammals. Annu Rev Neurosci. 1983;6:325–356. PubMed PMID: 6340591.
172. Merzenich MM, Nelson RJ, Stryker MP, Cynader MS, Schoppmann A, Zook JM. Somatosensory cortical map changes following digit amputation in adult monkeys. J Comp Neurol. 1984;224:591–605. PubMed PMID: 6725633.
173. Xerri C, Merzenich MM, Peterson BE, Jenkins W. Plasticity of primary somatosensory cortex paralleling sensorimotor skill recovery from stroke in adult monkeys. J Neurophysiol. 1998;79:2119–2148. PubMed PMID: 9535973.
174. MacEvoy SP, Paradiso MA. Lightness constancy in primary visual cortex. Proc Natl Acad Sci U S A. 2001;98:8827–8831. PubMed PMID: 11447292.
175. Lemann W, Saper CB, Rye DB, Wainer BH. Stabilization of TMB reaction product for electron microscopic retrograde and anterograde fiber tracing. Brain Res Bull. 1985;14:277–281. PubMed PMID: 2581677.

Fetal Tissue Allografts in the Central Visual System of Rodents

Frederic Gaillard and Yves Sauve

Created: May 1, 2005; Updated: June 25, 2007.

Introduction

Injury to the brain areas concerned with vision can cause a variety of disorders ranging from visual field defects to much more complex deficits, such as visual agnosia. It all depends on the location and the extent of the damage. Injury to the occipital striate cortex results in corresponding homonymous visual field defects where typically all visual capacities are lost in the fields. Injury to occipito-temporal structures can affect discrimination, selection, and recognition of visual stimulus dimensions and, at higher stages of processing, of objects, faces, scenes, and letters (for review, see Zihl (1)) (Fig. 1).

Since the 1970s, numerous investigations have focused on trying to restore lost function by replacement of injured brain structures with homologous, allogeneic, embryonic neural tissue. Such approaches have even reached the clinical level as a therapy for the treatment of some neurological disorders such as Parkinson's and Huntington's diseases. With the exception of these specific cases, though, we are not yet ready to go to the clinic. Intracerebral grafting presently remains an experimental model used to address fundamental questions concerning brain development, neuronal plasticity, regeneration, and formation of topographic connections. The latter is a minimal requirement for functional recovery in point-to-point sensory systems such as the visual system (see previous chapter).

Putting fetal brain tissue grafts in the mature central nervous system (CNS) differs from peripheral nerve (PN) grafting in at least the following two ways. First, although a PN graft is used to bridge two brain areas, an intracerebral embryonic tissue graft is meant to restore the function of the damaged area. The fetal grafted tissue must develop its own set of connections with the right structures in the host brain, and these connections must be orderly arranged. Second, although all elements in PN grafting are at the same age, the intracerebral embryonic tissue graft is heterochronic with respect to the host tissue. For a short period after implantation, grafted tissue behaves as an immature piece of brain. Theoretically, this immature status should allow circuitry reconstruction. Donor embryonic cells have a greater potential for axonal outgrowth and regeneration than mature host neurons (2, 3). Thus, they may be better at establishing contacts with host target cells. Furthermore, the fetal graft may produce trophic factors or signaling cues, which are present in the brain only at early developmental stages, and should reactivate neurotropic processes in "dormant" host neuron populations. For instance, embryonic cortical transplants will produce NT-3, which is absent from the cortex past 2 weeks of age (4, 5). In vitro assays (6) have shown that NT-3 has dual effects on layer 2-3 and layer 6 cortical neurons. Fifteen days after implant, cortical grafts will also produce a glial cell line-derived neurotrophic factor (GDNF), a potent survival factor for claustral neurons that project to the occipital cortex (7, 8).

Unfortunately, there is abundant literature suggesting that environmental constraints from the mature host brain alter the restorative capacities of fetal grafts in various ways. First, the mature environment affects both the number of surviving neurons within a graft and the size of the graft itself (9-12). Second, the mature CNS environment is non-permissive for axonal regeneration of host neurons (13-17) (see section 2 from the previous chapter). Third, the mature CNS environment is poorly permissive for receiving outgrowing axons from embryonic allogeneic neurons (18-23).

These above-mentioned results suggest that intracerebral embryonic tissue grafts might only be effective in "diffuse" projection systems, i.e., by exerting a paracrine effect (24-28). In opposition to this, a few investigations have demonstrated that such grafts can restore, at least partially, complex motor behaviors (skilled forelimb reaching for food) that require a precise interaction between neuronal circuits, much more than expected of

paracrine effects (19, 29, 30). However, even in such reports, the donor neurons appear to establish a very limited number of connections with the host.

Pioneer work in the visual system model was done in the mid-1970s by Drs. Raymond Lund and Alan Harvey and colleagues, who transplanted parts of the embryonic CNS to various brain locations in neonatal rats (for a review, see Lund (31)). Most of their studies were focused on CNS development and, therefore, consisted of examining whether such grafts developed near-normal architecture and established extensive connections with appropriate host structures. The outcome of fetal grafts into adult hosts has been studied less extensively, but a limited number of reports suggest that fetal tissues can integrate functionally within the adult host CNS. We will review these investigations that, in contrast to the mainstream opinion, show that tectal and cortical allografts can receive highly ordered inputs and can project to distant visual targets in the adult brain.

The Visual System of Rodents: A Brief Overview

Unless reconstruction of neural circuitries comparable to normal in terms of amount, extension, and topical organization are achieved, we cannot expect complete functional recovery in point-to-point neural systems. The normal structural and functional organization of the visual system of adult rodents has been investigated extensively and now forms a basis for regeneration experiments (for reviews, see Sefton and Dreher (32), Zilles and Wree (33), and Sefton et al (34)). A brief summary of the major findings is given below for comparative purposes.

Retinal Output

In the adult rat, virtually all (>95%) retinal ganglion cells (RGCs) project contralaterally to the superior colliculus (SC) and to the dorsal division of the lateral geniculate nucleus (DLG). In the SC, axons from the retina enter at the level of the stratum opticum (SO) and arborize in the SO and the superficial gray layer (SGL). Dense terminals are also found in lateral posterior nucleus, LP; ventral division of the lateral geniculate nucleus, magnocellular part, VLG; intergeniculate leaflet, IGL; and pretectal nuclei (nucleus of the optic tract, OT; olivary pretectal nucleus, OPT; posterior pretectal nucleus, PPT). Some of these inputs (30-50%) are collateral branches of retinocollicular axons. A small contingent (<5%) of the RGCs contacts the same structures ipsilaterally. Thus, each retinorecipient center receives input from both eyes. Sparse projections are found in the suprachiasmatic nucleus (SCN), the various nuclei of the accessory optic system, the hypothalamus, and the inferior colliculus. A schematic view of these connections is given in Fig. 6 of the previous chapter.

Subcortical Network

The DLG is much more than a relay center for RGC projections to the cortex. In fact, it receives most of its input from structures other than the retina, namely the visual thalamic reticular nucleus (Rt), layer 6 small pyramidal neurons in the occipital cortex (areas 17, 18, 18a; also called, respectively, areas Oc1, Oc2M, Oc2L; or areas V1, V2M, V2L), the SC (SGL layer), some pretectal nuclei (OT, OPT), and the contralateral parabigeminal nucleus (PBg), a homolog of the isthmo-optic nucleus in lower vertebrates. Projections arising from relay cells in the DLG are restricted to Rt (dorsal part) and occipital cortex.

The retinorecipient layers of the SC have reciprocal connections with the VLG, the pretectum, and the ipsilateral PBg nucleus (ventral and dorsal divisions). They receive further afferents from the contralateral PBg and from layer 5 pyramidal neurons in the visual cortex. Major efferents go to the DLG, the LP thalamic nucleus, and to the intermediate (IGL) and deep (DpL) gray layers of the SC, where other sensory systems are represented. The LP nucleus (equivalent of the LP-pulvinar in cats and of the pulvinar in primates) has reciprocal connections with visual (mainly Oc2L, layers 5 and 6) and temporal areas in the ipsilateral cortex. The LP receives additional inputs from the Rt, zona incerta (ZI), and the pretectum (OT). Neurons in the IGL and DpL layers of the SC project to various structures in the pons, brain stem, cervical spinal cord, and hypothalamus.

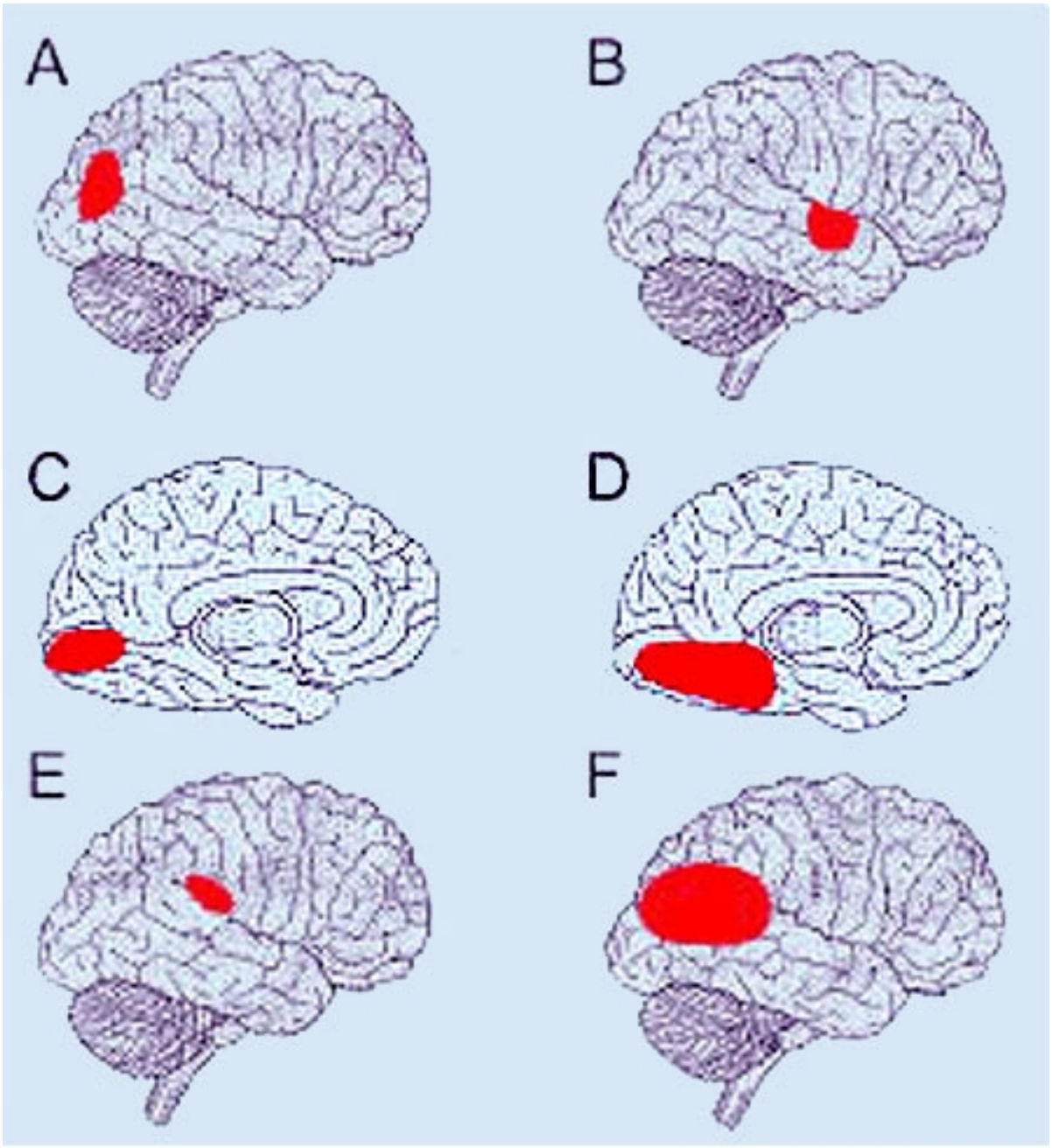

Figure 1. Visual deficits in human and related injured brain regions. A, visual location (lateral occipital gyrus). B, motion blindness (middle temporal gyrus). C, achromatopsia (occipito-temporal gyrus). D, visual agnosia (posterior and medial temporo-occipital cortex). E, visual neglect (inferior parietal lobe). F, Balint-Holmes syndrome (posterior parietal lobe). For more details, see Zihl (1).

The VLG has reciprocal connections with the pretectum (OT, OPT and APT, the anterior pretectal nucleus), SC (SGL and SO layers), and its contralateral homolog. It receives further projection from the occipital cortex (layer 5 neurons) and projects to the ZI, central gray, pons, and the suprachiasmatic nucleus (SCN). Finally, in addition to retinal and collicular inputs, the pretectum receives cortical afferents from the occipital cortex and projects to the LP, to the adjacent lateraldorsal (LD) thalamic nucleus (which has reciprocal connections with the occipital cortex), and to the pons (largely to the reticulotegmental nucleus) (Fig. 2).

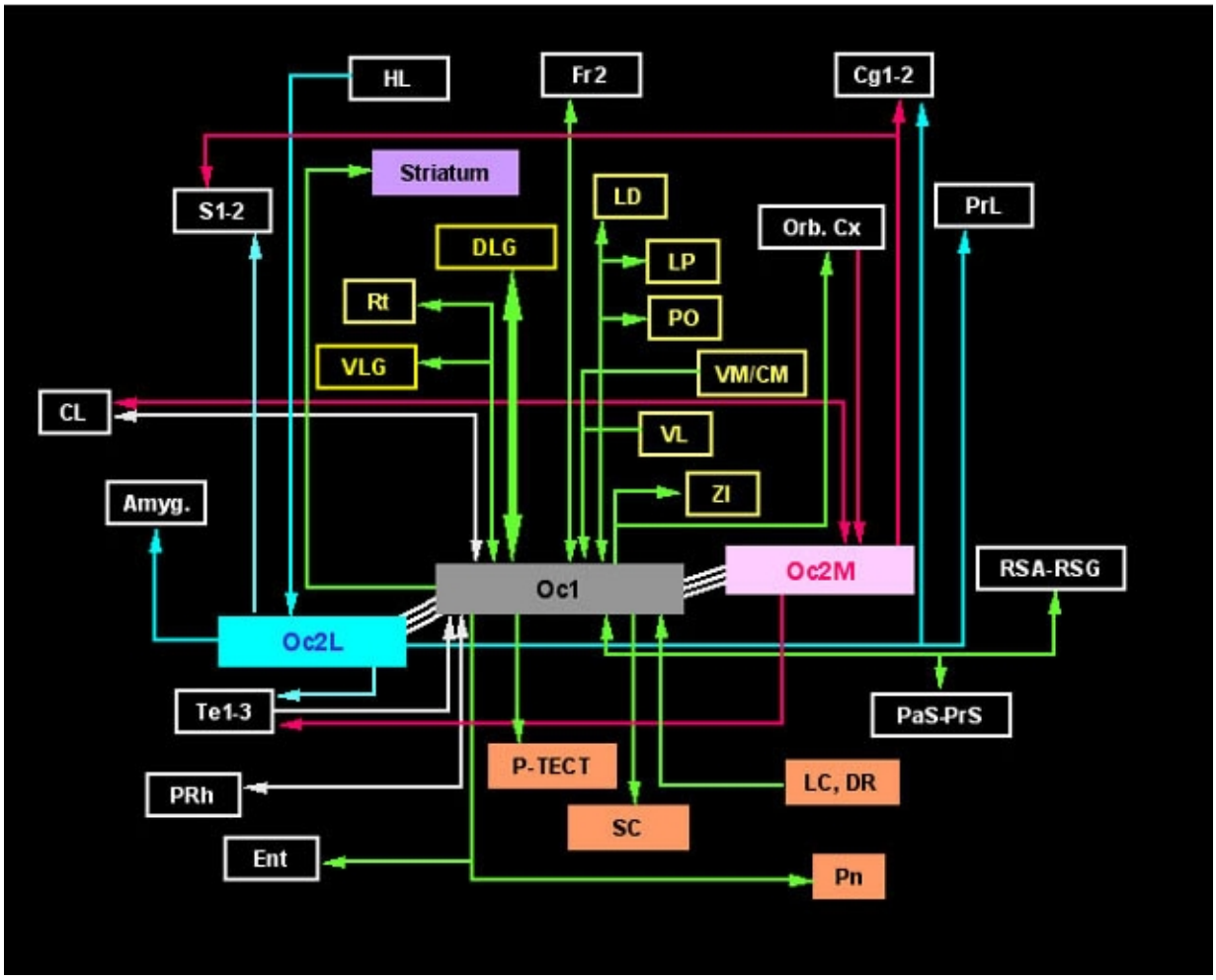

Figure 2. Major ipsilateral connections (designed as arrows) of the visual cortex of rodents. Green-coded connections are valid for all areas. Specific, additional connections for Oc1 (area 17) are white coded; those for Oc2M (area 18) are red coded; and those for Oc2L (area 18a) are blue coded. Reciprocal connections between visual areas are symbolized by large stripes. Abbreviations are given in text.

Cortical Network

Afferents to cortical area Oc1 originate predominantly from the three thalamic relay nuclei: DLG, LP, and LD. Termination sites are localized in layers 4, lower 3, 6, and 1. Other thalamic sources are the posterior complex (Po), ventromedian (VM), centromedian (CM), and the ventrolateral (VL) nuclei. Projections from Po and VM terminate in layer 1; those from CM and VL in layers 1 and 6. Further afferents are provided by frontal (Fr2), temporal (Te1-2), retrosplenial (RSA/RSG), perirhinal (PRh), and adjacent visual areas in the ipsilateral cortex. With respect to this scheme, area Oc2M receives no afferent from Te2 and PRh but an additional input from orbital cortical areas (MO/VO/VLO), whereas area Oc2L receives no afferent from Te1 and PRh but an additional input from the hindlimb region (HL) in the sensorimotor cortex. Afferents from the claustrum (CL) are mostly distributed in the infragranular layers of Oc1 and/or Oc2M areas (35, 36). Oc1-2 areas also receive some callosal inputs from visual areas (layer 2-3 and 5-6 neurons) in the opposite cortex. Callosal terminations extend throughout the cortical depth at the borders of area Oc1 and adjacent extrastriate areas as well as in multiple patches through Oc2M-L areas. Prominent labeling also occurs in the infragranular layers of the temporal cortex. Finally, the visual cortex and subcortical retinorecipient nuclei both receive nonspecific cholinergic, noradrenergic, and serotonergic innervations from various structures in the basal forebrain, from locus coeruleus (LC) and from dorsal raphe nuclei (DR), respectively.

In addition to reciprocal connections, visual cortical areas have widespread ipsilateral projections through the normal adult brain. At the cortical level, efferents from area Oc1 are found into the dorsomedial frontal area Fr2 (layers 1 and 6), the ventrolateral orbital area (VLO), the retrosplenial areas (layers 1 and 6), the perirhinal area (layer 5-6, up to the caudalmost pole of the cortex), and the entorhinal cortex. Additional efferents originating from area Oc2M are observed in the cingulate area Cg1, the parietal areas S1-2 (caudal part; layers 1-3 and 6), the temporal areas Te1-3 (layer 1-3 and 6, mainly), and the claustrum (full extent). Efferents from area Oc2L also target the dorsal half of the prelimbic cortex (PrL area) as well as lateral, basal, and central amygdaloid nuclei (37). Projections from Oc2 areas to Fr2 and Cg1 extend up to the rostralmost pole of the cortex. At the subcortical level, Oc1 and Oc2 areas have dense terminals in hippocampal structures (presubiculum, PrS; and parasubiculum, PaS), striatum (the dorsomedial portion) (38), visual thalamic nuclei (DLG, VLG, LP/LD, Po, Rt), ZI, various pretectal nuclei (P-TECT), SGL and IGL layers of the SC, and pontine nuclei (dorsolateral division) (39). Contralateral projections are confined to Oc1-2 and Te1 areas as well as, but sparsely, to the dorsomedial sector of the striatum and the dorsolateral subdivision of the amygdala.

Visual Field Topography

Retinofugal axons arising in different retinal quadrants maintain their relative positions in the optic nerve, lose this initial order as they progress toward the chiasm, and reform a distinct dorsal-ventral arrangement in the optic tract before reaching primary visual targets, where they terminate in a precise topographic manner (40-43). Retinotopy in visual centers was first seen by Lashley (44, 45) and then abundantly documented by both electrophysiological and anatomical approaches (46-52). Recently, optical imaging techniques have confirmed all previous findings (53, 54). A schematic representation of the visual field topography onto the DLG, SC, and visual cortex is given below (Fig. 3).

At the geniculate level (Fig. 3, A and D), the nasal field (temporal retina) is represented caudally and dorsomedially; the temporal field (nasal retina) occupies most of the rostral part of the nucleus; the lower field (upper retina) is mostly represented in the caudal part of the nucleus, lateroventrally; and the upper field (lower retina) projects mainly to the rostral part of the nucleus, dorsally. The dorsomedial part of the DLG also receives input from the lower temporal quadrant (red sector; Fig. 3B) of the ipsilateral retina. On the contralateral SC (Fig. 3, A and C), the nasal visual field is mapped rostrally; the temporal visual field, caudally; the upper field, medially; and the lower field, laterally. In rats, the representation of the central visual field is not substantially magnified. The ipsilateral retinal contingent projects anteromedially (red sector; Fig. 3B).

At the cortical level (area Oc1/17), the naso-temporal axis of the visual field projects from lateral to medial, the lower field (upper retina) projects rostrally, and the upper field projects caudally. A restricted caudal region of area Oc1 receives input from the ipsilateral retina. The vertical meridian (body axis) is set at the border between area 17 and area 18. Beyond this point, the naso-temporal direction is inverted. Borderline zones in areas 17 and 18 contain binocular neurons. Multiple ordered representations of the visual field are present in the adjacent extrastriate areas (for discussion, see Rosa and Krubitzer (55)).

Standard Strategy for Intracerebral Transplantation: Graft Morphology

Grafts usually consist of blocks or sheets of neural tissue excised from 15-16-day-old (E15-16) embryos, which are put into previously surgically made cavities in the host. Older grafts survive poorly and have reduced size (56, 57). Although not critical for axonal sprouting (see below), delayed implantation has been assumed to enhance cell survival and outgrowth (58-60), probably because endogenous neurotrophic factors can accumulate at the lesion site (61) (Fig. 4).

As in newborns (62, 63), primary connections with the host brain appear 3-4 days after transplantation (64), whereas neovascularization and blood supply require approximately another week to be completed, a delay that

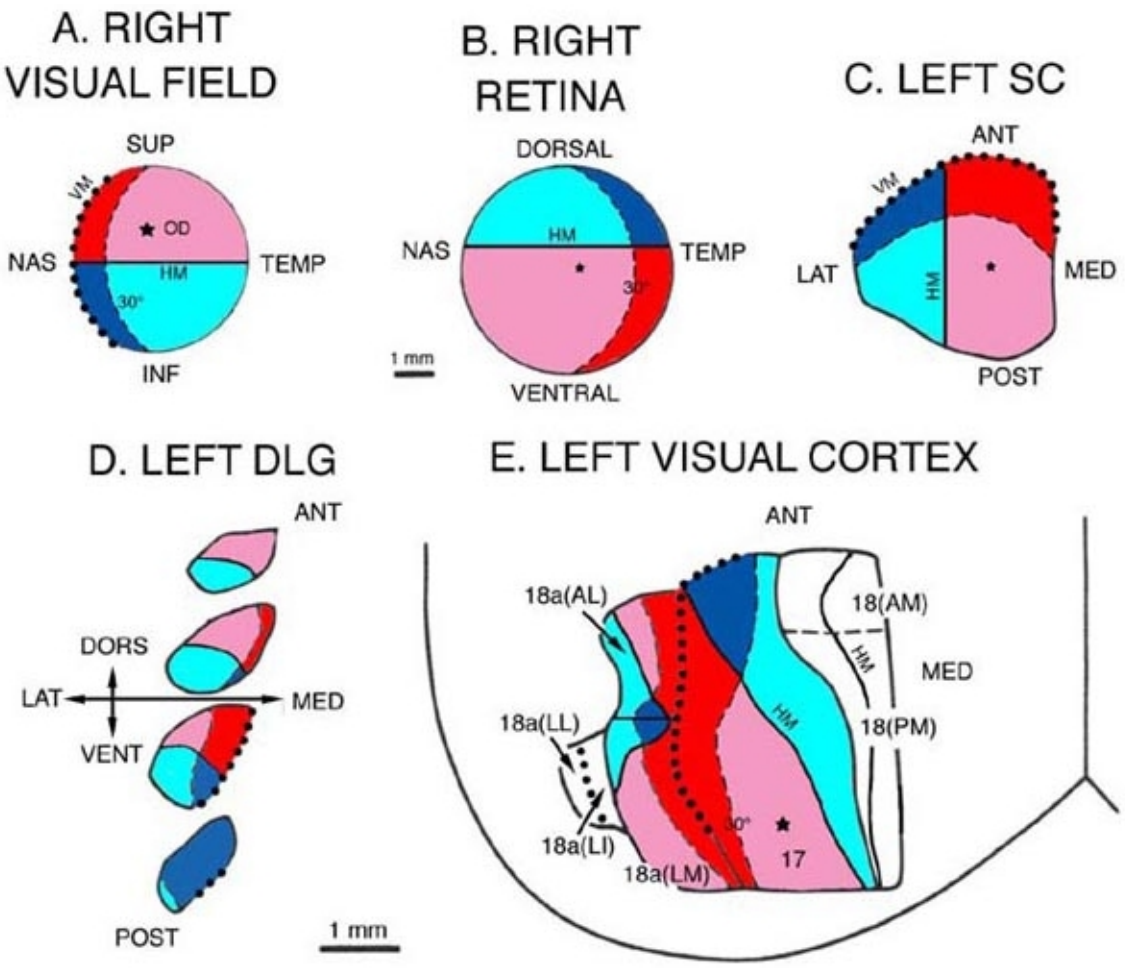

Figure 3. Schematic representation of the right visual field topography onto the DLG, SC, and visual cortex of normal rats. Color code: red, upper nasal field; pink, upper temporal field; deep blue, lower nasal field; sky blue, lower temporal field. Subdivisions of extrastriate areas are from Espinoza and Thomas (47). Visual topography in areas 18 (AM/PM) and 18a (LL/LI) is not shown. AL, anterolateral area; AM, anteromedial area; ANT, anterior; DORS, dorsal; HM, horizontal meridian; INF, inferior; LAT, lateral; LI, laterointermediate area; LL, laterolateral area; LM, lateromedial area; MED, medial; NAS, nasal; OD, optic disk (black stars); PM, posteromedial area; POST, posterior, SUP, superior; TEMP, temporal; VENT, ventral; VM, vertical meridian (dotted line). Adapted from Sefton et al. (34).

may seriously hamper graft cell metabolism (65). Nonetheless, both graft implantation and development in adults can be as successful as in neonate recipients (62, 66, 67). Investigations are usually performed 3-4 months after grafting.

In serial histological sections, all implants look like disorganized cellular masses that are more or less clearly separated from the host tissue by a region of lower cell density or host white matter. Glial scarring at the host-graft interface, although highly variable, is usually minimal (60, 68). At this time point, graft development is achieved. Most neurons in cortical grafts (60-80%) seem mature (expression of Hu/Elav proteins) (66) and look "normal" at the ultrastructural level (69). The remaining neurons have immature characteristics, such as multiple nucleoli or binuclear somas (60, 70) (Fig. 5).

A typical feature of fetal tectal tissue transplants in adult hosts is the presence of dorsally located, myelinated "fiber-free" areas (Fig. 6). In addition, there is a proponderance of cells with small perikarya and short dendrites (67, 71), a relatively high acetylcholinesterase (AChE) activity, a high concentration of alpha-bungarotoxin binding sites, and a low number of neuroglial elements (57, 72-74). Similar characteristics are found in the

retinorecipient layers of the SC in normal rats. In neonate hosts, the "fiber-free" layer over the "fiber-rich" core of the graft (Fig. 6) is penetrated by regenerated retinal afferents (75, 76).

Grafts of blocks of fetal cortex lack the typical layered organization when integrating into the host CNS. Neurons are 60-80% of the normal density and gathered into clusters separated by myelinated bundles (Fig. 7, A-C). They also contain high number of neuroglial and microglial cells (69). Regardless of their origin, cortical grafts typically receive diffuse cholinergic and aminergic input, mostly in their lower part, near the corpus callosum (66, 77-79).

Although roughly similar at a first glance, different cortical grafts show differences in their neuronal phenotypes. On the basis of Golgi-Cox stained material, Aleksandrova and Girman (80) proposed a three-group classification:

- Type I: grafts contain multiple neuron morphologies resembling those in the normal cortex. The small layer 2-3 pyramids have small or medium perikarya (10-16 and 20-26 μm in diameter, respectively) and apical dendrites running for considerable distances along the graft boundary with unpredictable orientations.
- Type II: grafts contain a single class of multipolar neuron with oval or pyriform soma, a short apical dendrite, and several thick processes. Soma sizes are typically large or hypertrophied, ranging between 16 and 50 μm in diameter (Fig. 7D).
- Type III: grafts have intermediate characteristics. In addition to the neuronal phenotypes found in the first group, one-third of the neurons have large somas (30-32 μm in diameter). Interestingly, whereas type I and III graft neurons respond to visual stimuli (see below), type II graft neurons do not, displaying only highly synchronized, burst-like spontaneous discharges (Fig. 10). It remains to be clarified whether unresponsiveness is linked to abnormal neuron morphology or lack of input(s), or both (81).

Neurons within the Transplant Can Be Driven by Host Eye Visual Stimulation

What we learned from the above-mentioned and other histological studies is that fetal tissue blocks grafted in a mature brain will never develop the specific architecture of the normal tissue that they replace. They lack continuity with the host tissue, intrinsic laminar organization, and neuronal arrangement in columns. Structural disorganization, however, does not prevent the formation of synapses able to excite grafted neurons (69, 82-86). Girman and Golovina (87) provided indisputable evidence that both transplanted tectal and cortical neurons can respond to visual stimuli presented to the adult host eye.

Tectal Graft Responsiveness

Girman (71) reported good visual activity in about half of the tectal implants. Spontaneously active at rest, single-units respond to flashing light spots as well as to stationary and manually moved targets (5-16 degrees in diameter) with circular receptive fields (RFs). Best responses are obtained with small (3-5 degrees in diameter) black disks moved on a white background. Some units (29%) are direction selective. Response latencies to flashing spots (Fig. 8) are in the normal range. Tactile and auditory stimuli are ineffectual. No visual response can be recorded in cortical tissue grafts placed at the tectal level.

Cortical Graft Responsiveness

Both field potential (FP) and single-unit recordings have been done in types I and III cortical grafts. FPs in grafts always consist of a negative/positive component. Wave onset and peak have normal latencies (66, 87-89). However, it is interesting to note that none of the FPs undergo polarity reversal with depth, as occus in the

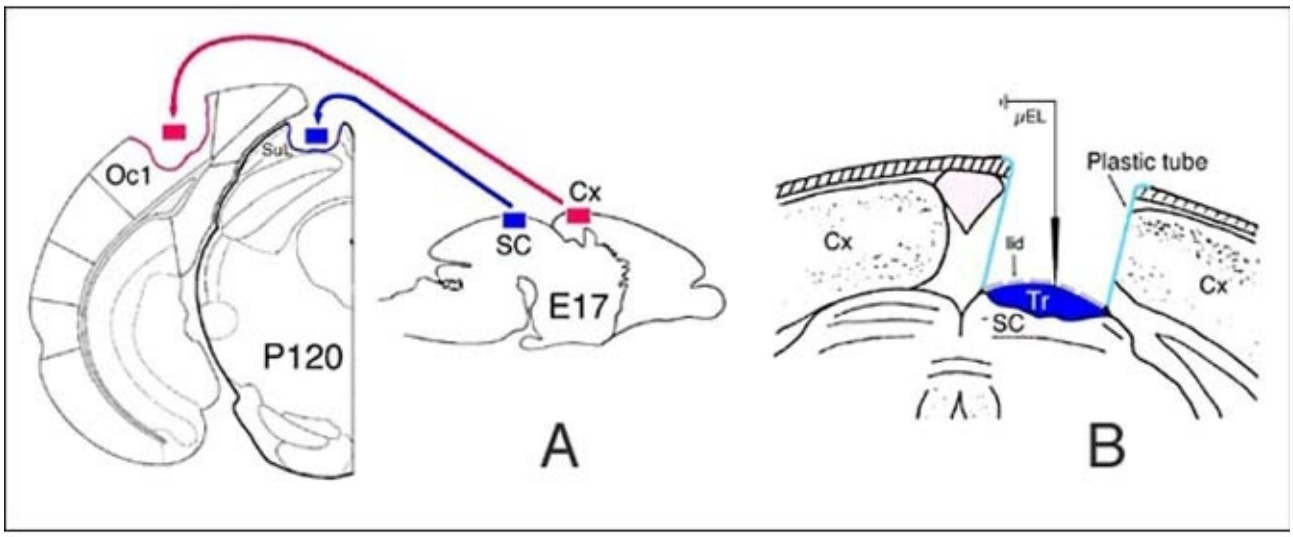

Figure 4. Basic transplantation protocols. A, for current anatomical studies. Blocks of embryonic tissue were implanted in aspirated lesion cavities performed in the host brain 3 days earlier. B, used by Girman (71) for electrophysiological recordings. Grafts are covered by a perforated plastic lid, allowing multiple recording sessions of the same locus. Cx, host cortex; Oc1, rat visual area 17 (174).

normal rat primary visual cortex (90), and peak amplitudes correlate with the density of afferents (Fig. 9 and Fig. 10).

Although recording field potentials is useful for delineating the graft outer limits and the most active zones within the graft for tracer injections, field potentials do not mean that these neurons can actually partake in any visual operation. Girman and Golovina (87), however, showed, at the single-unit level, that many graft neurons did respond to visual stimuli. Approximately 84% of the spontaneously active neurons in type I grafts have well-defined RFs (5-20 degrees in diameter; Fig. 11) and exhibit clear responses for either moving or stationary stimuli. Cells preferring the same stimulus seem to be in clusters. Flashing light spots typically evoke a biphasic excitatory/inhibitory response of 36-62 ms latency, followed by a second excitatory discharge. Movement-sensitive neurons fire weakly, or not at all, to light spots. Most of them show clear direction selectivity and orientation specificity. A few active neurons (16.5%) can be driven by stimulation of either eye, the contralateral stimulation being dominant. Visually driven neurons are less frequently encountered in type III grafts. These neurons have larger RFs (20-30 degrees) and react only to light spots after a long delay (100-250 ms).

Finally, graft neurons also fire in response to electrical stimulation (10-50 µA) of either the host ipsilateral DLG nucleus or the contralateral visual cortex. An important finding, suggestive of some form of topographic organization between the DLG and the cortical graft, is that small displacements (200 µm) of the stimulating electrode from the optimal geniculate site lead to a decrease or a complete loss of response.

Are Responses from the Graft Retinotopically Ordered?

To a degree, they are. The same studies by Girman and Golovina (87) indicate that large (3 mm in diameter), highly responsive cortical grafts contain an ordered representation of the contralateral visual field, at least of its central part, which projects normally onto area 17. First, neurons recorded simultaneously at a given electrode position have roughly the same RF location. Second, there is no change in RF position with depth during a single penetration. Third, ordered changes in the recording positions on the graft surface induce concomitant changes in the RF locations. Fourth, the orientation of the visual field projection onto the graft appears normal relative to the skull landmarks (Fig. 12). A rough retinotopic order is also observed in large, type III grafts. The larger the grafts, the better the visual field projection: small grafts contain only a non-ordered representation of a

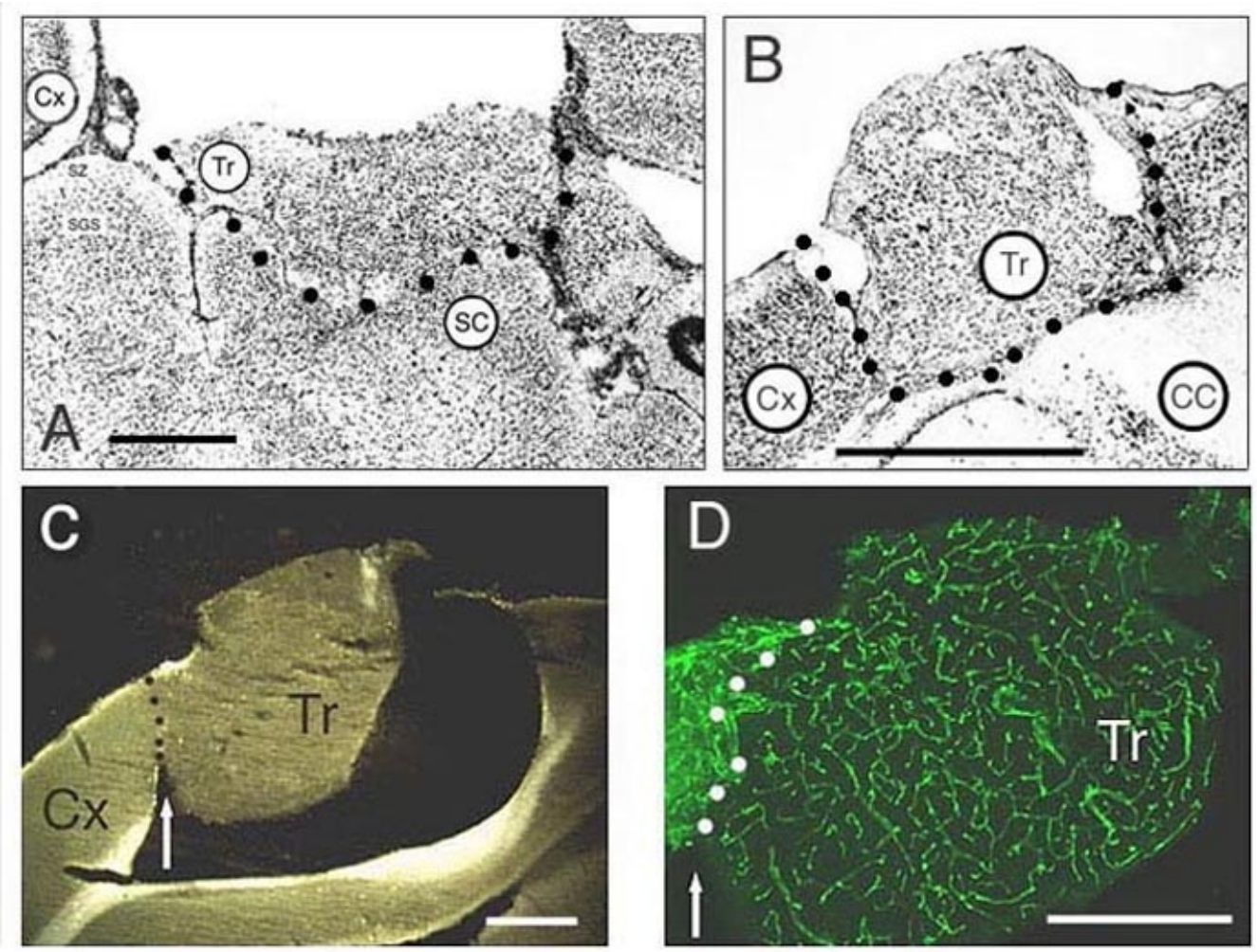

Figure 5. A and B, typical cellular aspect of tectal (from Girman (71)) and occipital (from Domballe et al. (66)) grafts 3 months after grafting. Nissl staining. C and D, graft vascularization as observed in wild-type E15 mouse cortical tissue grafted in an adult mouse expressing the eGFP protein under the control of a β-actin promoter (161). C, low-power view of the graft (which did not filled the lesion cavity). Darkfield microscopy. D, blood flow supply to the graft relies on the formation of new vessels by the host (GFP-positive labeled endothelial cells). Fluorescence microscopy. CC, corpus callosum; Cx, host cortex; SC, superior colliculus; Tr, transplant. Scale bars: A and B, 1 mm; C and D, 400 µm.

restricted part (20-30 degrees wide) of the nasal visual field. Visual map order and neuron properties remain unchanged up to at least 10 months after grafting. This is a logical result in view of the fact that long-term survival (2 years *in situ*) does not significantly affect the basic morphological features of cortical grafts (91).

Do Grafts Receive Extensive Afferents?

By this point, it seems evident that under some highly controlled and replicable experimental conditions, allogeneic fetal tissue grafts implanted at homotopic positions in the visual brain can respond to visual stimulation of the host eye. Some cells from the graft perform rather complex operations of visual driven signals, just like the SC and area 17 in the normal rat (92-95). The graft can resume at least a partial, ordered map of the visual field, a prerequisite for recovery of function. However, topographic visual field representation on a graft is likely to involve many more regenerated host afferents than the few, randomly branching fibers reportedly able to generate light flash responses in the PN graft paradigm (96-98). Direction selectivity, orientation specificity, and binocular activation imply sophisticated synaptic input to graft neurons (99). The next question, then, is

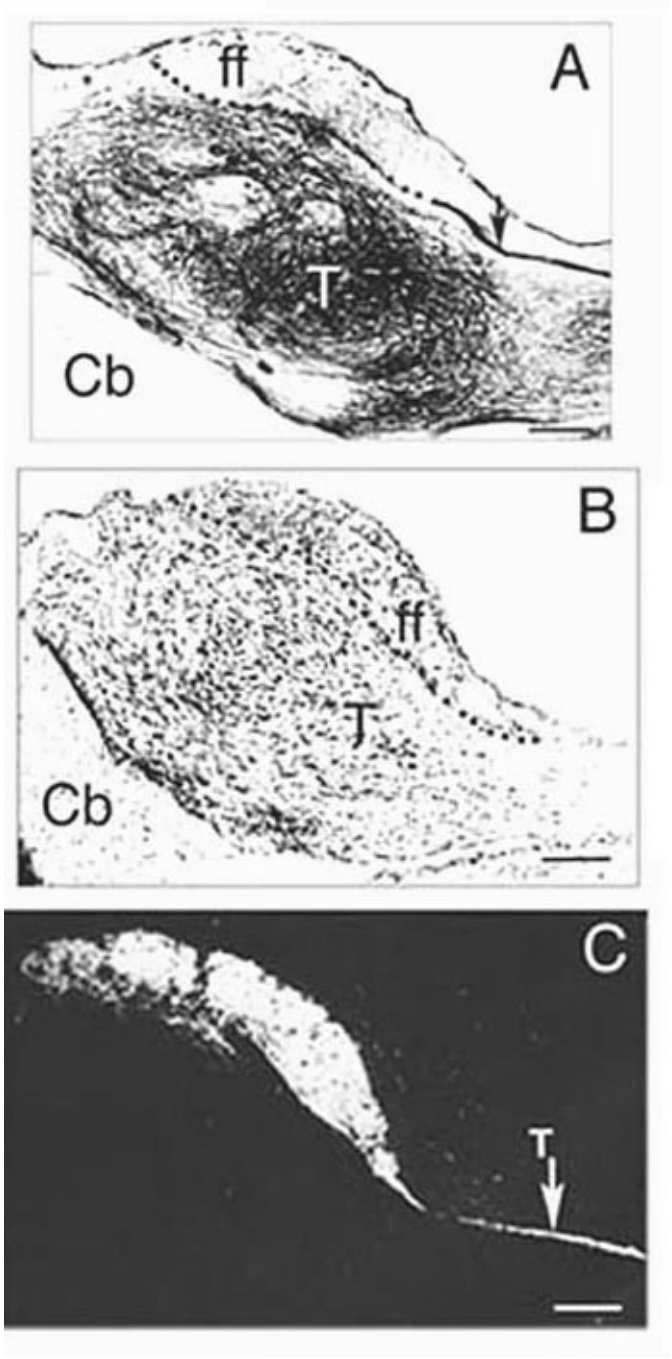

Figure 6. Typical morphological features of embryonic tectal grafts (sheets of tissue) in neonate hosts. A, Holmes neurofibrillar staining. Note the fiber-free (ff) area covering the fiber-rich core of the graft (T). B, Nissl staining. C, widespread retinal input throughout the fiber-free lamina. Autoradiogram after ^{3}[H]-labeled proline injection in the contralateral eye. Arrow points to the afferent retinal tract. Cb, cerebellum. Scale bars, 190 μm. From Lund and Harvey (75).

whether homologous fetal grafts in the adult primary visual cortex receive extensive input from appropriate brain areas.

Tectal Graft Connectivity

The actual substrate of the visual responses recorded in tectal grafts is a puzzling, still unsolved problem. Receptive field properties, latency values, and ordered organization together suggest the presence of direct, widely distributed host retinal input to the grafts. However, the early studies in neonate hosts showed that retinal

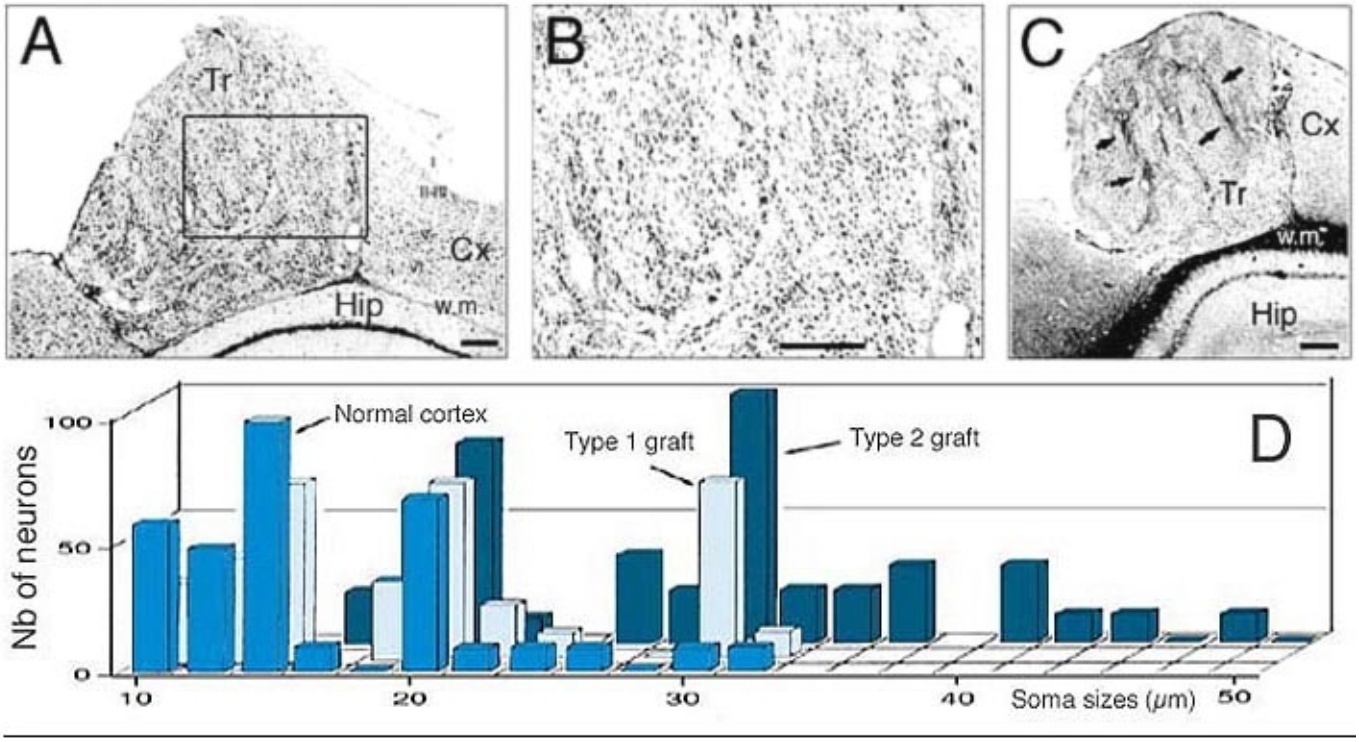

Figure 7. Gross morphology of cortical grafts. A, absence of lamination. Cresyl violet staining. B, typical cell cluster (inset in A). C, intragraft myelin sheets (arrows). Luxol blue staining. D, distribution of the soma sizes in the normal rat cortex, responsive type I grafts and unresponsive type II grafts. Golgi-Cox staining method. Redrawn from Aleksandrova and Girman (80). Cx, host cortex; Hip, hippocamus; Tr, transplant; w.m., white matter. Roman numbers denote cortical layers. Scale bars, 200 μm.

afferents never filled the transplants and were restricted to discrete, fiber-free patches. Within these patches, the density of optic terminals was nearly equivalent to that seen in the stratum griseum superficiale of normal rats. By electron microscopy, these terminals made asymmetric (excitatory) contacts onto small, post-synaptic profiles, many of which were dendritic spines (75). However, in striking contrast with Girman's findings, neither visually (light flash and moving disk) nor electrically (optic nerve stimulation) evoked activity were obtained from these grafts (100, 101). Only a minor fraction of the tested units could be excited orthodromically from the ipsilateral visual cortex, the major source of graft input in these preparations (Fig. 8). The failure to record retinal activity in the latter experiments could be attributable to the low number of electrode tracks.

Tectal tissue grafts implanted in juvenile (P15/P18) and adult hosts with the same technical approach also display discrete "fiber-free" patches dispersed dorsally within the fiber-rich core. However, no definitive projections from the host brain have been identified (67), and retinal innervation to the patches remains a matter of debate (67, 73, 102, 103). In short, there is yet very little anatomical evidence for the visual responsiveness recorded in tectal grafts. As suggested earlier by Golden et al. (100), a possible reason for this discrepancy may be the grafting technique. Although grafts done by Golden et al. (100) consist of partly dissociated cells injected onto the surface of the SC, the transplants done by Girman consist of "solid sheets of embryonic tectal tissue laid in the appropriate dorsoventral orientation over the SC surface devoid of superficial laminae". In neonates, a similar paradigm as used by Girman leads to the formation of a single, densely innervated retinorecipient lamina covering a large part of the graft surface (Fig. 6) (75). Up to now, neither the connectivity nor the neurofibrillar structure of such tectal implants in adult hosts have been studied.

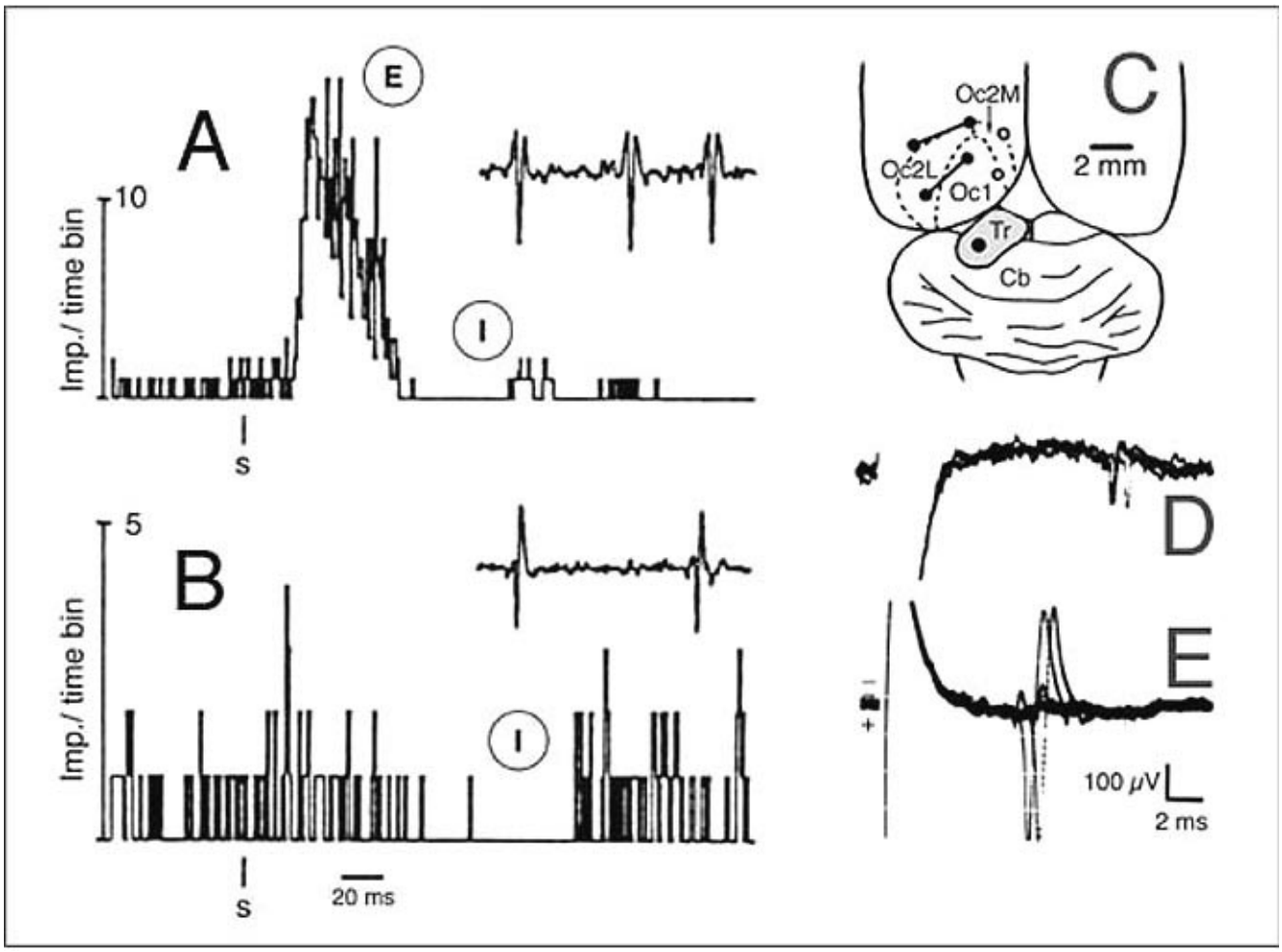

Figure 8. Neuronal discharges in visually responsive (A) and unresponsive (B) tectal grafts in response to light flashes (s). PSTH for 30 presentations. E, excitatory phase; I, inhibitory phase. Time bin: 1 ms. Redrawn from Girman (71). C, stimulating electrodes pairs (solid lines) in the occipital cortex (neonate host) are effective in driving units from the transplant (black dot). B, graft unit response (four sweeps). Note the short latency (Å, 6.7 ms) and the weak amplitude. C, response to the same stimulus but in the host inferior colliculus. Adapted from Harvey et al. (101).

Host Afferents to Cortical Grafts

As the electrophysiological data suggest, there should be a strong relationship between graft responsiveness and the presence of regenerating axons (or collateral sprouts) from ipsilateral DLG neurons. Indeed, retrograde tracers injected in type I grafts label high numbers of DLG neurons (one-third of which projected initially to the lesioned cortical site), whereas similar injections in type II grafts produce no labeling at all (81). Whether direct DLG input alone can account for graft visual responsiveness is, however, very unlikely, because some type I grafts receive only extra-geniculate, and no direct geniculate, inputs.

Major Graft Input Originates in Host Layer 5-6

After retrograde tracer (CTB, cholera toxin, b subunit) injection into types I-III grafts, Gaillard and colleagues (66, 88, 89) saw a diversity of afferents. These afferents (always in very low number; Fig. 17) appear in visual-related brain structures ipsilateral to the graft. The densest labeling (55-90%) is observed in the isocortex, mostly in the occipital areas surrounding the graft (see also Galick et al. (104) and Schultz et al. (78)). Together, neurons in claustrum, periallocortical areas, and various non-visual subcortical nuclei account for some 20% of the graft input. As expected, labeling in dorsal thalamus is highly variable. Although practically absent in one-half of the

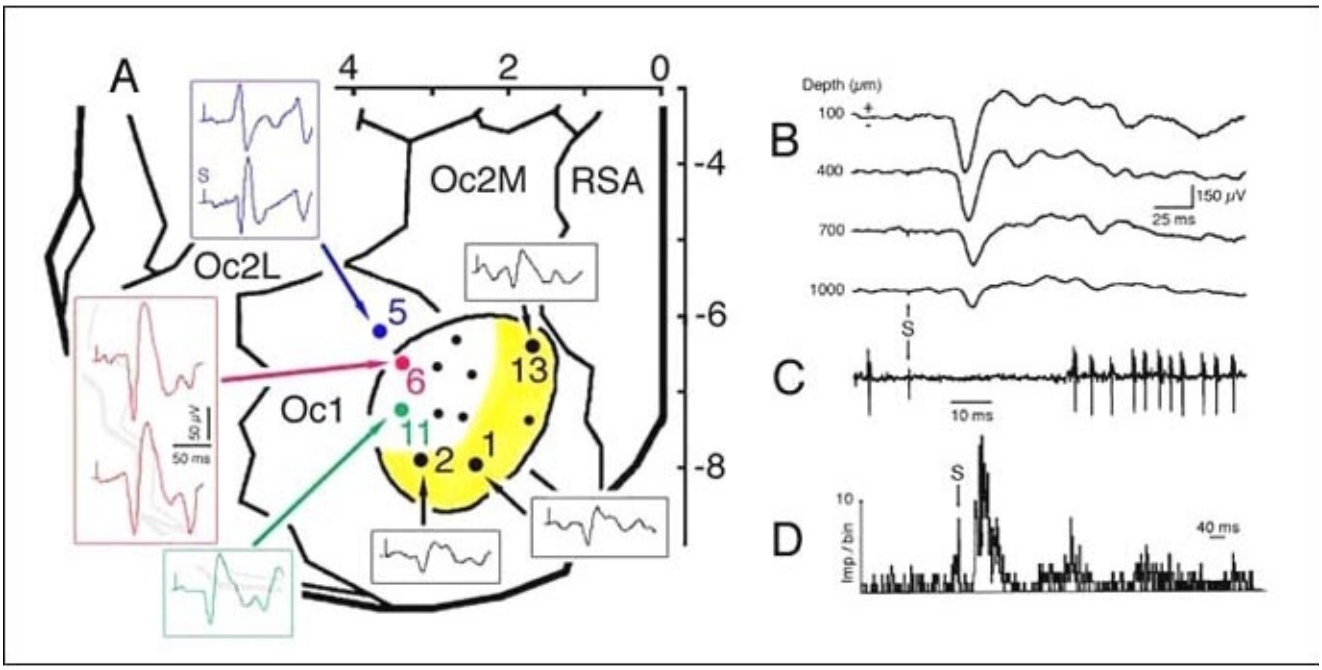

Figure 9. A, field potential mapping in a large occipital tissue graft. Low responses are from the medial yellowish area devoid of thalamic afferents (see Fig. 10). Note the wave reversal with depth (400 *versus* 100 µm) in the adjacent host cortex (point 5), not in graft (point 6). B, depth profile of FPs (average of 20 stimulations; F = 1 Hz) elicited by a flashing light spot placed adequately in the visual field. C, single neuron discharge induced by this flash. D, post-stimulus time histogram (PSTH) for the same neuron (compiled for 20 stimulations; time bin: 2 ms). B-D, redrawn from Girman and Golovina (87).

subjects, it represents 10-30% of all the graft afferents in the other one-half. DLG input never exceeds 10% of the total graft input. Orbital (VO/VLO), motor (Fr2), and brainstem structures (such as the basal nucleus of Meynert, locus coeruleus, and dorsal raphe), all projecting to the normal visual cortex (Fig. 12), are never labeled (33). Labeling in the hemisphere opposite to the graft is always negligible.

Apart from the isocortical area, most labeled neurons (91%) are confined to the infragranular layers (Fig. 13 and Fig. 14), noticeably layer 6 and sublayer 6b, close to the white matter. Layer 6b neurons in normal adult rodents exhibit diverse cell body morphologies (Fig. 14 and Fig. 15) and have widespread terminal arborizations (>3-4 mm) in superficial cortical layers (105). They appear to be remnants of subplate neurons (106-108), which have pivotal functions during early cortical development, for instance in guiding thalamic fibers to their appropriate cortical target area (109-111) and in governing the functional maturation of connections between DLG axons and layer 4 neurons (112). They are also involved in coordinating ocular dominance column formation (113, 114). In the adult cat, subplate (white matter) and pyramidal cells of the normal and inverted types in the infragranular cortical layers support long-range, tangential connections (115).

This Pattern Is Specified by Eye Opening

When performed in neonate hosts, the same experiments always lead to greater density and diversity of graft inputs (89, 116). At the cortical level, for instance, frontal (Fr2; the frontal eye field in primates) and orbital (LO/VLO) areas are moderately but systematically labeled, and the somas of the isocortical afferents distribute about equally between layers 2-3 and 5-6. At the thalamic level, owing to the severe (75%) atrophy of the DLG (117, 118), most inputs originate in the LP/LD complex and the central intralaminar nuclei, an unlabeled cell group in adult hosts (Fig. 16).

We conclude that the age of the recipient appears to affect both the density and the topology of the graft afferents (for similar data with parietal grafts, see Castro et al. (119) and Schultz et al (78).). Additional studies show,

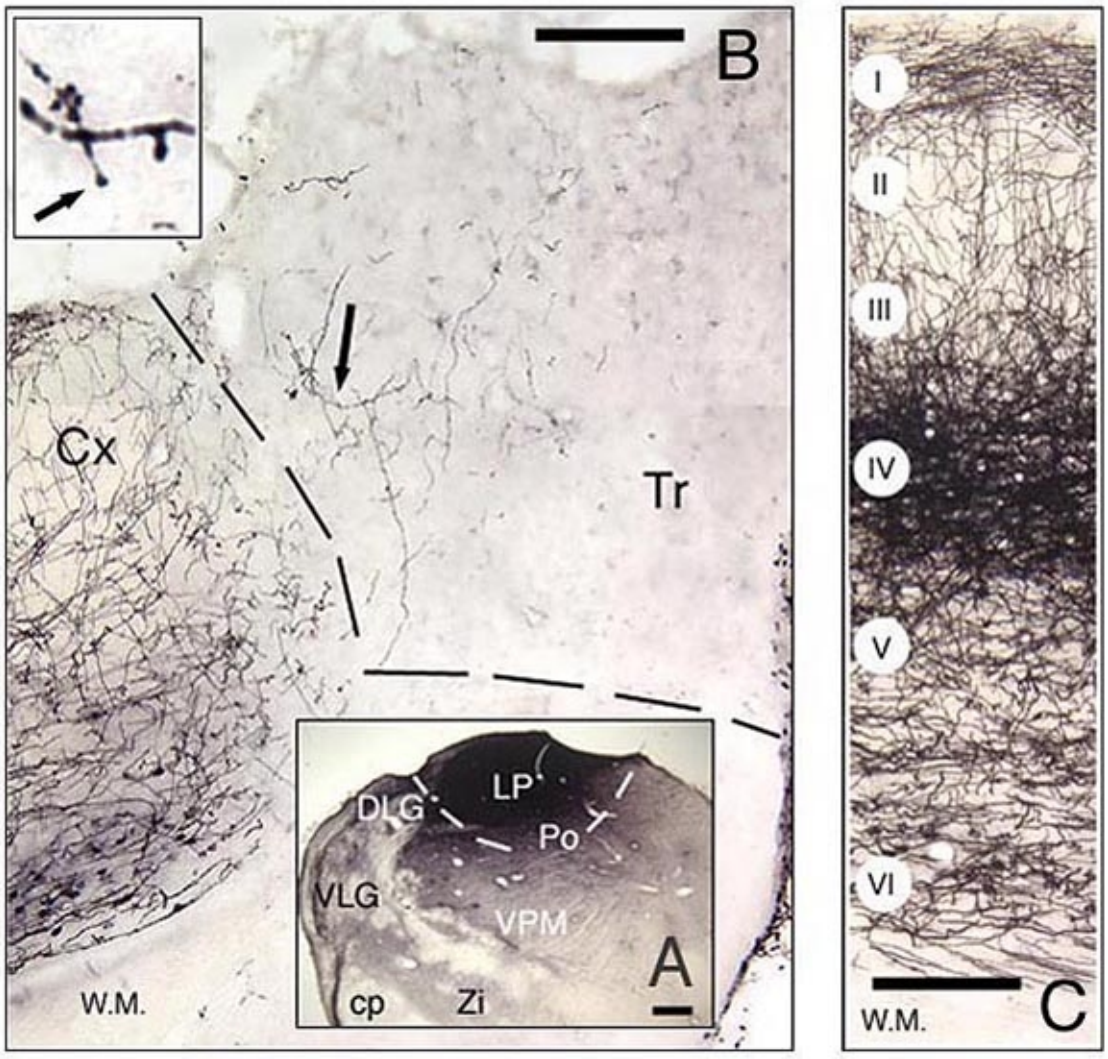

Figure 10. Thalamic input to the preceeding graft (see Fig. 9A) is restricted to the most responsive area. A, biotinylated dextran amine (BDA) injection confined mostly to the LP nucleus (dotted line, lower inset). Strong projections are present in the host cortex either close to the graft (B) or more laterally, in the Oc2L area (C). In contrast, very sparse thalamic fibers innervate the graft (B). The arrow points to a bouton-like terminal structure (see upper inset). cp, cerebral peduncle; Cx, host cortex; DLG, dorsal lateral geniculate nucleus; LP, lateral posterior nucleus; Po, posterior thalamic nucleus; Tr, transplant; VLG, ventral lateral geniculate nucleus; VPM, ventral posteromedian nucleus; w.m., white matter. Roman numbers denote cortical layers. Scale bars, 100 μm.

moreover, that the most dramatic changes in the afferent pattern occur in the second postnatal week, before the onset of the critical period for rat visual cortex (120). Nearly all isocortical inputs to the graft in P15 hosts originate in the infragranular layers, mostly from layer 6, a proportion not significantly different from that found in older recipients (66). This age-related laminar shaping is a two-step process that affects all layers, but the supragranular layers are affected more specifically. It is completed in frontal and temporal areas about 1 week earlier than in the occipital areas surrounding the graft (Fig. 17). The delay is likely related to the cortical ontogenetic program that proceeds radially (121) as well as tangentially through rostrocaudal and lateromedial directions (122, 123).

The Potential of Layer 6 Neurons to Survive Injury and to Drive Grafts

A major outcome of all the above-mentioned studies is that afferent innervation to a cortical graft in adult host originates mostly from a small population of layer 6 neurons located in the immediate graft surround. Cortical layer 6 is a target for thalamic fibers. The layer 6 neurons display all known visual response types (94, 95),

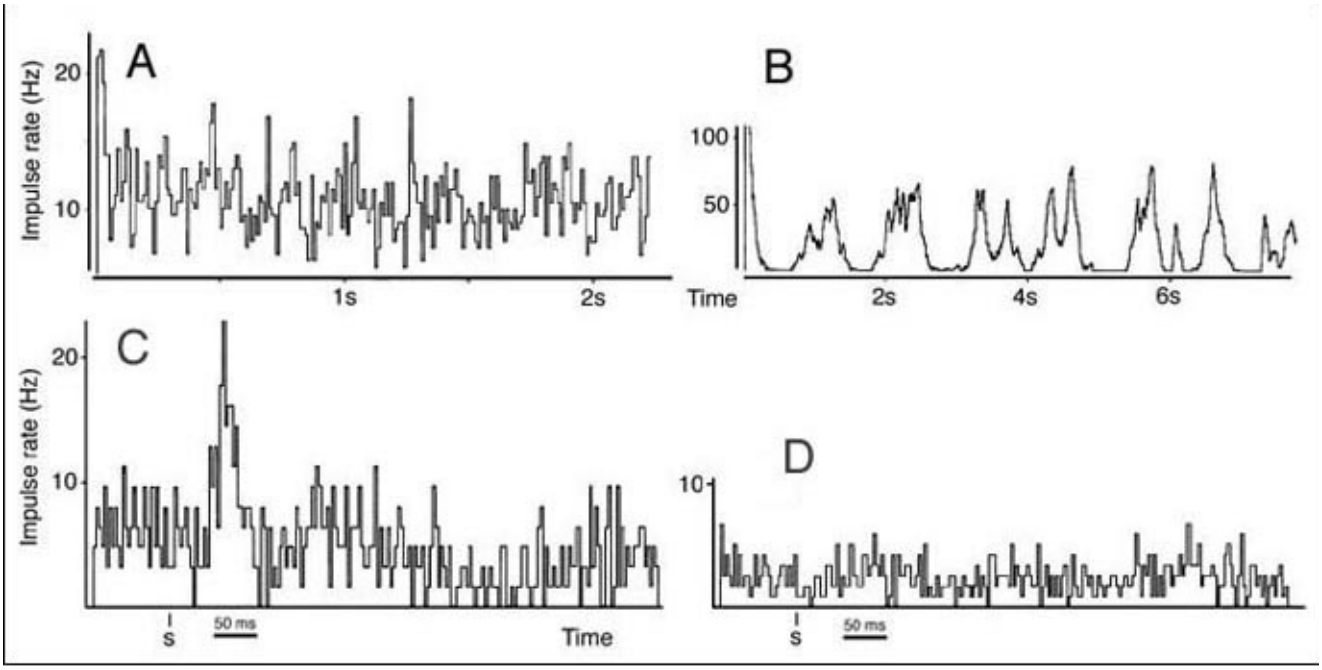

Figure 11. Upper row: autocorrelograms of spontaneous neuronal activity. A, in visually responsive grafts (desynchronized regular pattern). As in the intact visual cortex (94), the spike rate increases with the recording depth. B, in unresponsive grafts (periodic bursting). Time bin: 10 ms. Lower row: evidence that graft neurons have defined receptive fields. C, flashing light spot placed at the center of the most responsive spatial locus for this neuron. D, flashing light spot placed 20° away from the central position. PSTHs for 50 presentations. Recording depth: 100 μm. Time bin: 3 ms. Redrawn from Girman and Golovina (87).

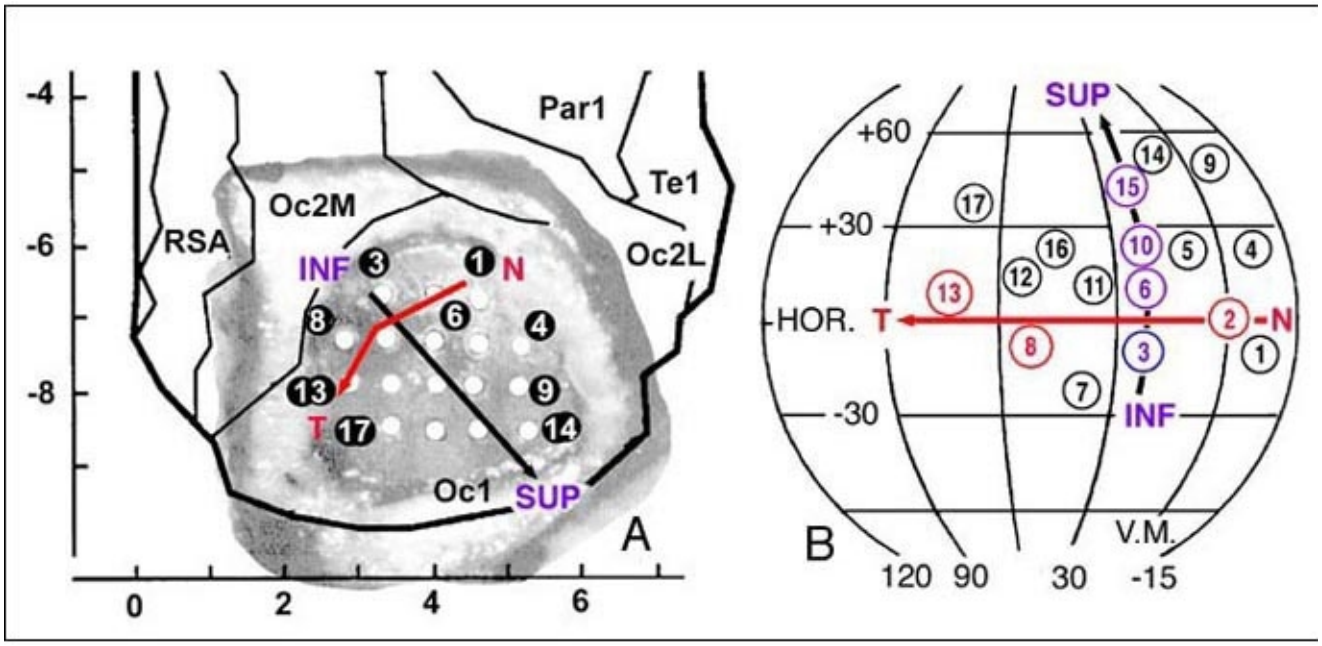

Figure 12. Near-normal visuotopic projections in type I graft placed in the right primary visual area (Oc1/V1) of an adult rat. A, recording loci at graft level (grayish inset). Dorsal view. Graft is centered approximately 8 mm caudal to bregma and 4 mm lateral to the sagital midline. B, map of the related receptive fields in the left eye visual field. Animal is facing the screen. Graft locus 1 projects to the nasal field (N); graft locus 13 projects to the temporal field (T); graft locus 3 projects to the lower field (INF); graft locus 15 projects to the upper field. HOR., horizontal plane. V.M., vertical meridian. Redrawn from Girman and Golovina (87).

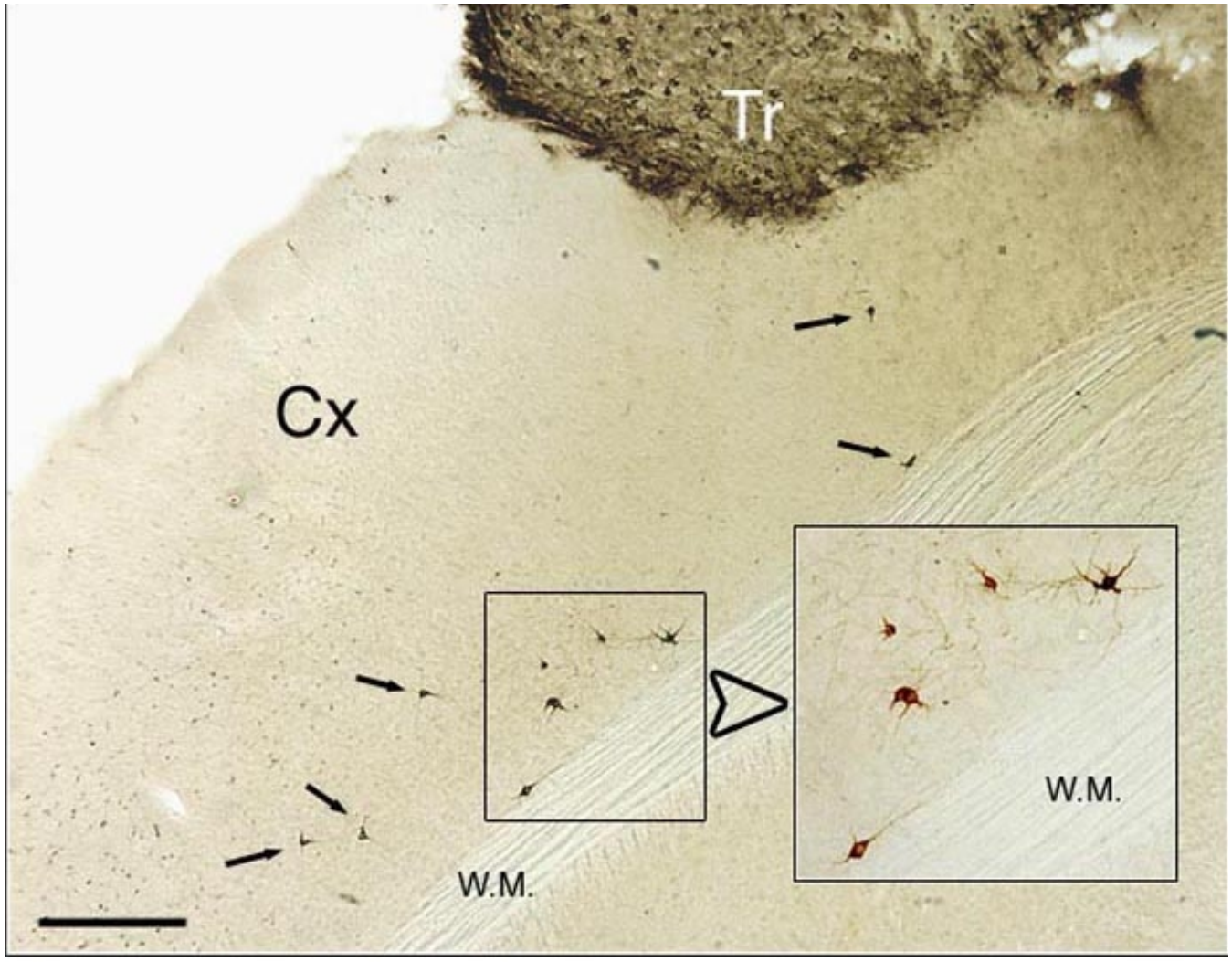

Figure 13. Representative labeling of projection neurons (arrows) in the host cortex (Cx) after injection of a retrograde tracer (CTb; cholera toxin, b-subunit) in a visually responsive graft (Tr). Note their location in layer 6, close to the white matter (w.m.). Non-counterstained, DAB treated material. Scale bar, 200 μm.

regardless of their morphology. Of the four layer 6 cells injected with HRP by Parnavelas et al. (124), one multipolar cell was an "ON-OFF" cell, two pyramidal cells were "complex" cells, and the last fusiform cell type was a "non-oriented" cell. In the absence of direct thalamic input, layer 6 neurons may thus be able to drive visual information to the graft.

Why layer 2-3 neurons do not contact the graft in adults is not understood. Among many possibilities, one would be that these late-generated (E17-E20) corticocortical projection neurons, which have low survival rates during development (125), are very sensitive to lesion-induced retrograde degeneration and/or deleterious changes in their environment (but see Szele et al. (126)). Conversely, these neurons may be able to regenerate axons, but these axons do not penetrate the graft because of negative influences from reactive astroglial elements and/or graft neurons. For instance, *in vitro* assays (6) have shown that endogenous levels of neurotrophin-3 (NT-3) reduce axonal branching and repel layer 2-3 neurons but have opposite effects on layer 6 neurons. For some days after implantation, the graft (which is producing NT-3) may thus be repulsive to layer 2-3 axons but attractive to layer 6/6b neurons, which express NT-3 receptors (127). Regardless of how fascinating these latter observations are, multiple survival and growth-promoting factors produced by the graft and the injured cortex may also allow layer 6 neuron survival and axonal elongation. For instance, neurotrophin-4 (NT-4) is as effective as NT-3 in increasing the length of the dendritic processes of layer 6 pyramidal cells of juvenile ferrets (128).

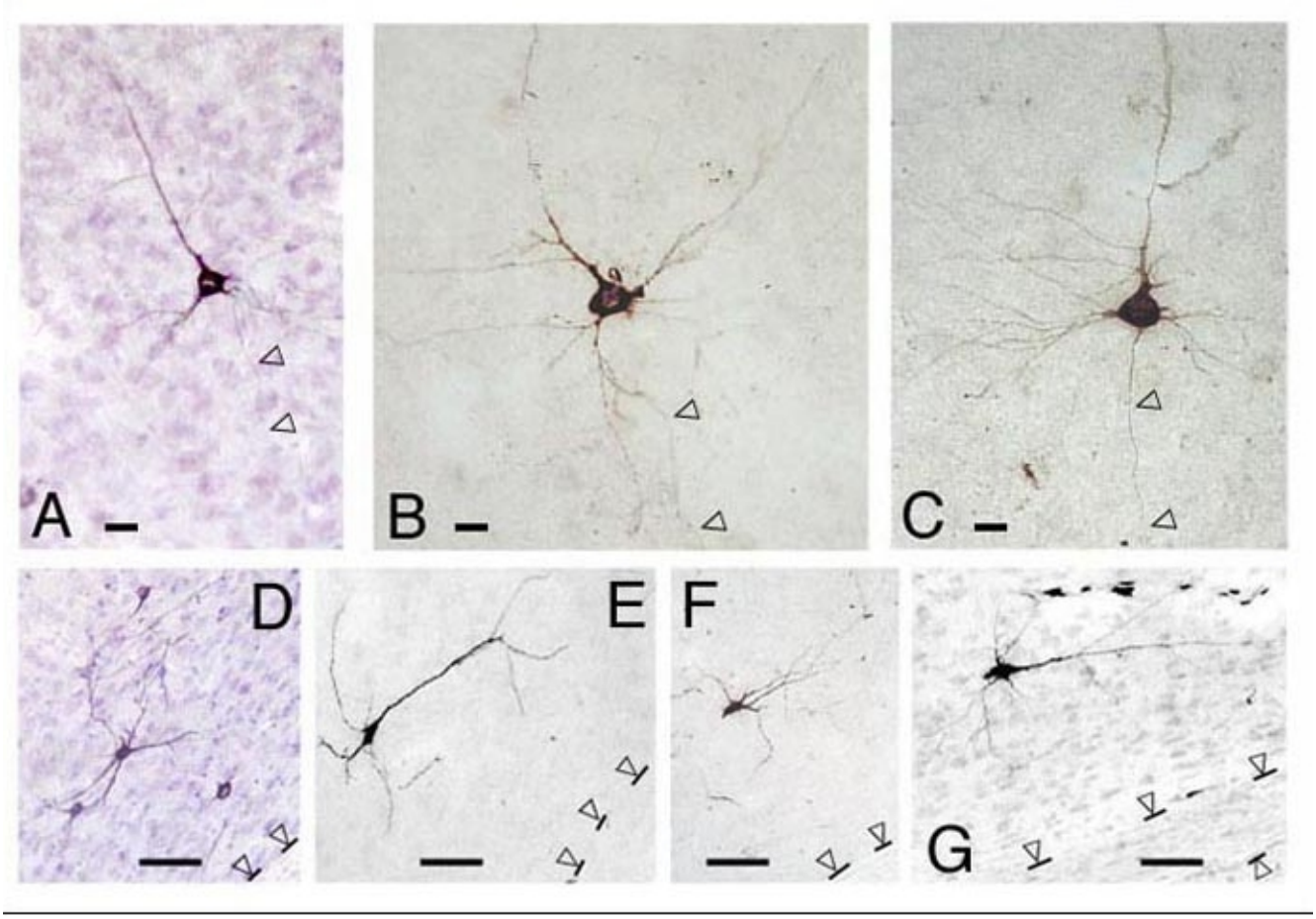

Figure 14. A-C, gallery of retrogradely labeled layer 5 pyramidal cells after CTb injection into three different responsive grafts. Arrowheads indicate axons. All cells are located 400-500 μm from the graft boundary. Scale bars, 13 μm. D-G, gallery of retrogradely labeled cells in layer 6 of visual area Oc2L. These cells are found in the same subject, between 500 and 900 μm from the lateral border of the graft. Arrowheads denote the upper limit of the white matter. Scale bars, 50 mm.

Furthermore, layer 6b neurons have receptors to basic fibroblast growth factor (FGF-2), a critical survival substrate for subplate neurons (129). FGF-2 is suspected to protect adult layer 6b neurons from death after lesions (130) but has no survival effect on 1-week-old, layer 2-3 callosal projection neurons (131). Deciphering why some layer 6 neurons in the adult brain have the potential for elongating their axons and whether these neurons have excitatory phenotypes will be an interesting challenge, especially in the context of these cells consistently labeling regardless of the grafting strategy (78, 132).

Anatomical Support for Topographic Order in Grafts Is Still Lacking

Mapping studies suggest that host afferents are topically organized in large tectal and cortical E15-17 embryonic tissue grafts. These results need anatomical confirmation, however. Beside occasional statements (119), this issue has only been specifically addressed in a single study using neonate recipients. The triple labeling approach by Worthington and Harvey (133) shows that tectal tissue grafts receive non-topographically organized, but nevertheless non-random, rudimentarily ordered cortical inputs. To date, no such investigation has been carried out with adult hosts, likely because one can hardly imagine how the discrete afferent projections reviewed above may form a coherent visual map onto grafts (see section 2.7.3 from the previous chapter). This negative reasoning does not consider: first that map formation may require a specific, highly controlled transplantation procedure (71, 133), including possibly the correct orientation of the graft in the lesion cavity (134, 135); second, that labeled graft afferents may reflect only a negligible proportion of the actual projecting host neurons; and

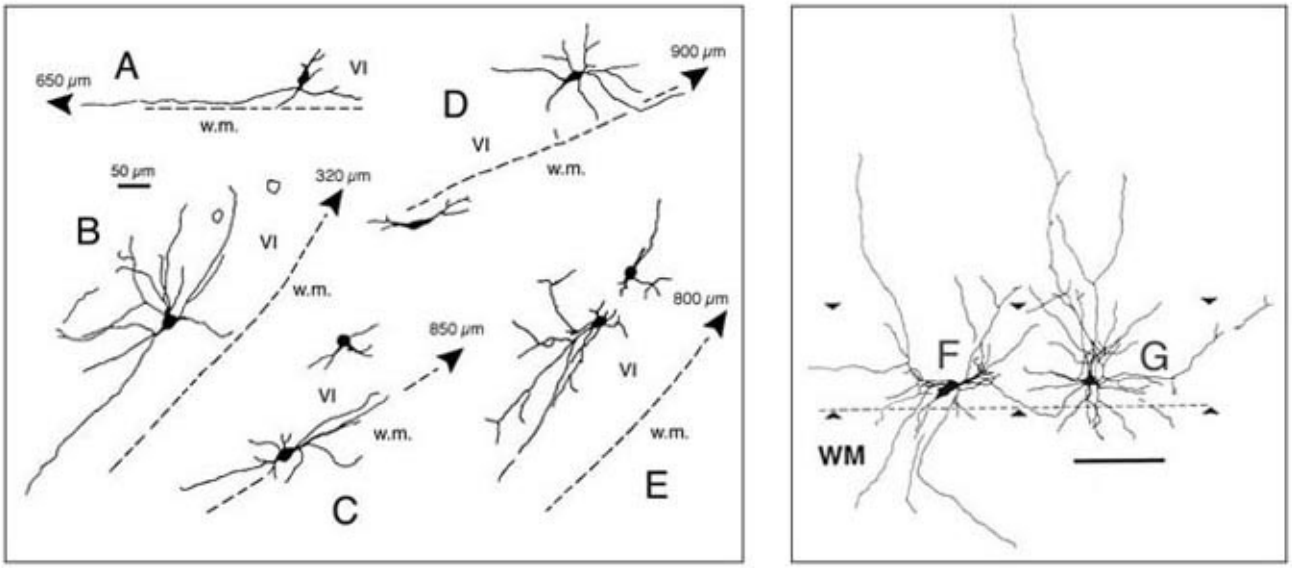

Figure 15. Left panel: camera lucida drawings of retrogradely labeled cells in layer 6b after CTb injection into another responsive graft. Dotted lines denote the upper limit of the white matter (w.m.). Arrowheads indicate the location and the distance of the graft. A, fusiform bipolar cell (Oc1B). B, giant multipolar cell (Oc1B). C, horizontally oriented pyramid-like cell (Oc2L). D, multipolar and flat bipolar cells (Oc2L). E, multipolar cell (Oc2L). Right panel: camera lucida drawings of representative subgriseal neurons filled with intracellular injections of biocytin. Normal adult rodent. F, fusiform neuron. G, triangular neuron. Arrows indicate location of the majority of corticocortical fibers. Scale bar, 100 µm. From Clancy and Cauller (105).

third, that single-unit recordings with carefully engineered microelectrodes (136) may be more powerful than tracer injections to detect small point-to-point shifts in connectivity between restricted brain areas. Meticulous surgical preparation, ingenious recording conditions, and use of self-made, highly specific tungsten in glass electrodes of the Levick's type may together account for Girman's successful recordings (94). In our opinion, unequivocal assessment of topographic host-graft projections requires further studies combining an optimal surgical strategy, a highly sensitive fiber detection process (see below), and a careful electrophysiological approach replicating Girman's approach.

Can Grafts Send Afferents to Host Targets?

In line with numerous results showing low numbers of afferents coming to the transplant, it has been repeatedly assumed that allogeneic embryonic tissue grafts do not send long-range projections to the adult host. Our own attempts using either biotinylated dextran amine (BDA) or the carbocyanine dye DiI (1,1'-didodecyl-3,3,3',3'-tetramethyl-indocarbocyanine perchlorate) as anterograde tracers confirm this assumption. This failure is commonly attributed to growth inhibitory conditions present in the mature brain (14, 137). Possible technical limitations are rarely addressed (138-141). Yet, there are some intriguing morpho-functional observations (84, 85, 142-148), suggesting that blocks of embryonic neurons grafted into the mature brain might not be able to transport exogenously provided tracers beyond the graft-host transition zone. In opposition to this, long axonal trajectories have been clearly detected in some experimental conditions, either after pre-loading dissociated donor cells with dyes (149, 150) or by targeting specific markers expressed by grafted cells (Thy-1.2 allelic system; microtubule-associated protein MAP1x/1B) (151-155). This has been a routine procedure for xenogeneic tissue grafts (for examples, see Lund et al. (156), Li and Raisman (157), Davies et al. (158), Isacson and Deacon (159), and Armstrong et al. (18)). A plausible hypothesis is, then, that all fetal graft neurons, regardless of their origins, are intrinsically capable of elongating processes when placed in a mature brain, but that detection of these processes outside the graft structure requires a non-invasive, anatomical approach. This hypothesis has

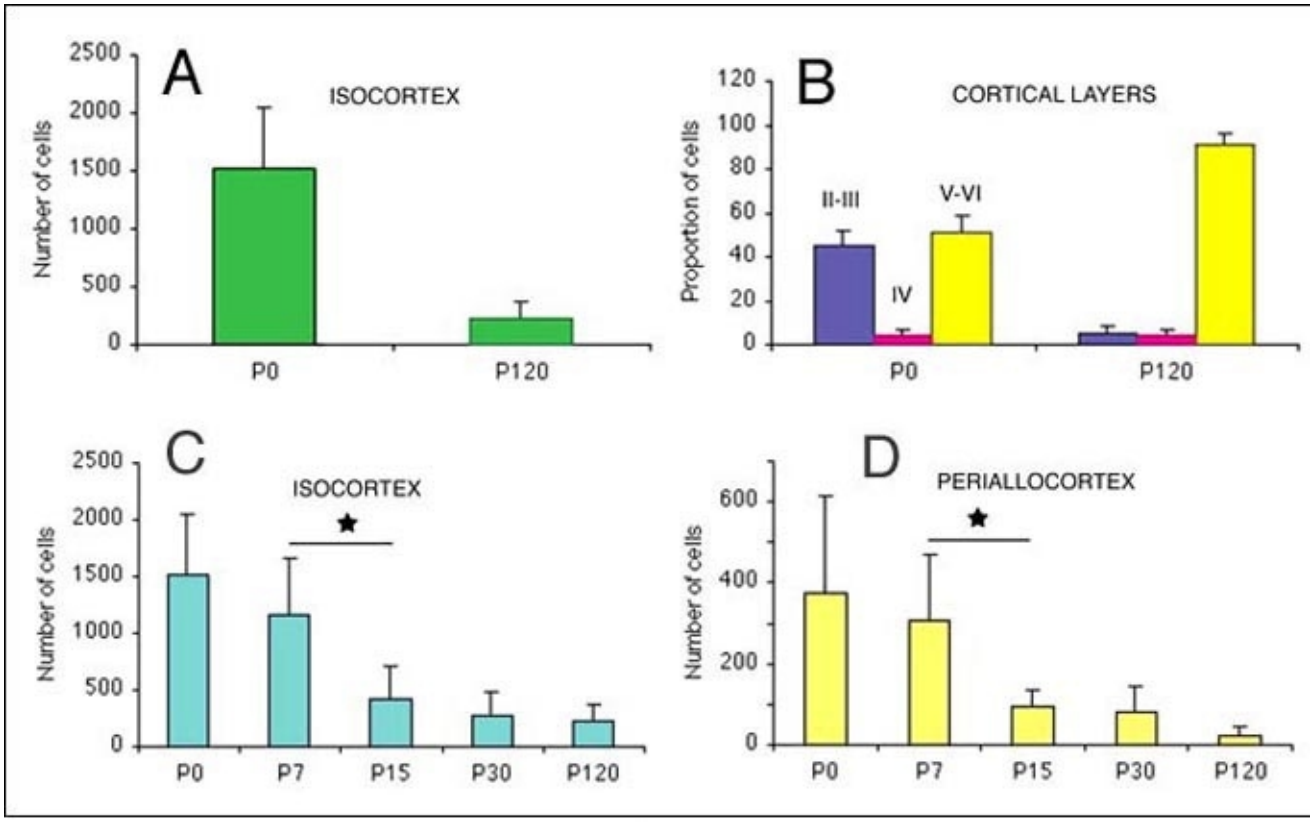

Figure 16. Upper row: quantitative differences (mean ± SD) in graft input between neonates (P0) and adult (P120) recipients. A, raw number of isocortical cells. B, proportions of cells per isocortical layer. Counts performed on half the brain of each subject. Redrawn from Domballe et al. (66). Lower row: decrease in graft afferents (mean ± SD) with the age of the host. A, in the isocortex. B, in the periallocortex (cingulate, perirhinal, and retrosplenial areas). Stars indicate significant differences ($p < 0.05$). Counts performed on half the brain of each subject. Redrawn from Domballe et al. (66).

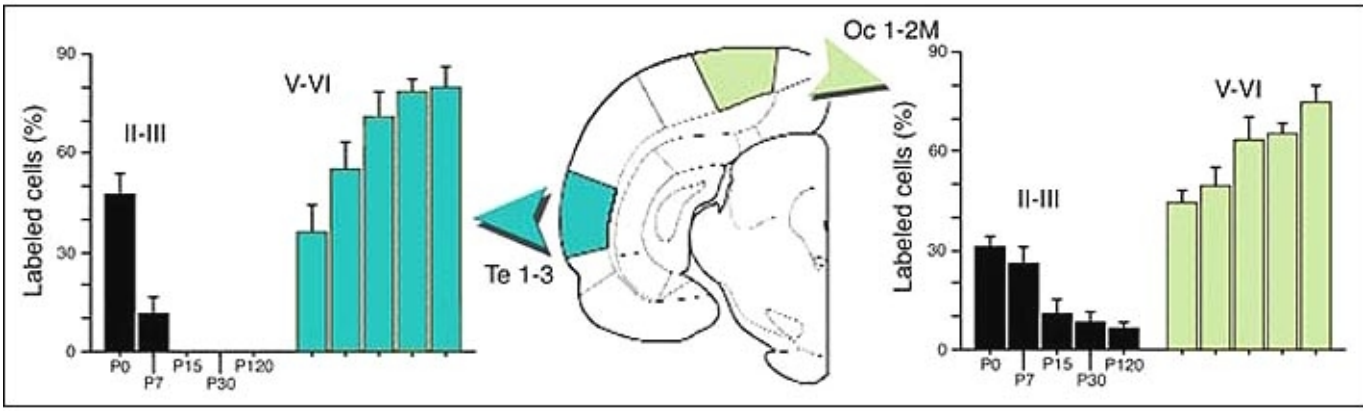

Figure 17. Proportions of labeled cells (mean ± SD) in the temporal (Te1-3) and occipital (Oc1-2M) areas as a function of the age of the host. Note the absence of supragranular input from temporal areas in 2-week-old recipients. Redrawn from Domballe et al. (66).

been verified recently in occipital cortex tissue grafts (160) using transgenic E15 mouse fetuses expressing a GFP protein variant under the control of a chicken beta-actin promoter (161) as donors (Fig. 18 and Fig. 19).

Figure 18. Dr. Okabe's eGFP-expressing neonate mice look "green" all over their body when illuminated with an UV source. See: http://kumikae01.gen-info.osaka-u.ac.jp/tg/tg-ad.cfm.

Embryonic Cortical Tissue Allografts Have Massive Efferents

A major finding of the above study is that despite immediate implantation, nearly all grafts into mature (P60/P90), wild-type mice appear physically well integrated in the host cortex (Fig. 19). Moreover, they show massive outgrowth all along their interface with the cortical parenchyma and send extensive efferents throughout the host ipsilateral pallium, mainly to its cortical mantle (Fig. 20).

Rostrally, graft fibers innervate a large medial sector of the brain including frontal association (FrA), secondary motor (M2), prelimbic (PrL), anterior cingulate (Cg1-2), medial orbital (MO), and infralimbic (IL) areas. Discrete fibers terminate within the orbital areas VO/LO and the claustrum (CL). At the bregma level, efferents distribute from area Cg1 medially to the somatosensory cortex laterally. Labeling extends throughout layers 2-3 and 5-6 in motor (Fr2) and sensorimotor (HL) areas but remains in lamina 6b at the barrel field (BF) level (Fig. 21 and Fig. 22).

At the transplant level and beyond, labeling from the GFP donor tissue fills the host ipsilateral cortex from the retrosplenial granular area to the lateral entorhinal region. Efferents in V2L and Te1-2 areas are especially dense in layers 1-3, 5a, and 6. Further caudally, labeled fibers occupy predominantly the cortical layers 5-6 as well as the PrS/PaS hippocampic regions.

Finally, afferents with terminal-like profiles are systematically present in the dorsomedial sector (as well as along the lateral rim) of the striatum and into the basolateral and central amygdaloid nuclei (Fig. 23). All these structures, including the cortical areas listed above, are normal targets of the rodent visual cortex (see Fig. 2).

Although always disrupted by surgery (Fig. 19 and Fig. 27), the white matter (external capsule and corpus callosum) never appears to provide an attractive substrate for graft efferents. Even at the exit point from the

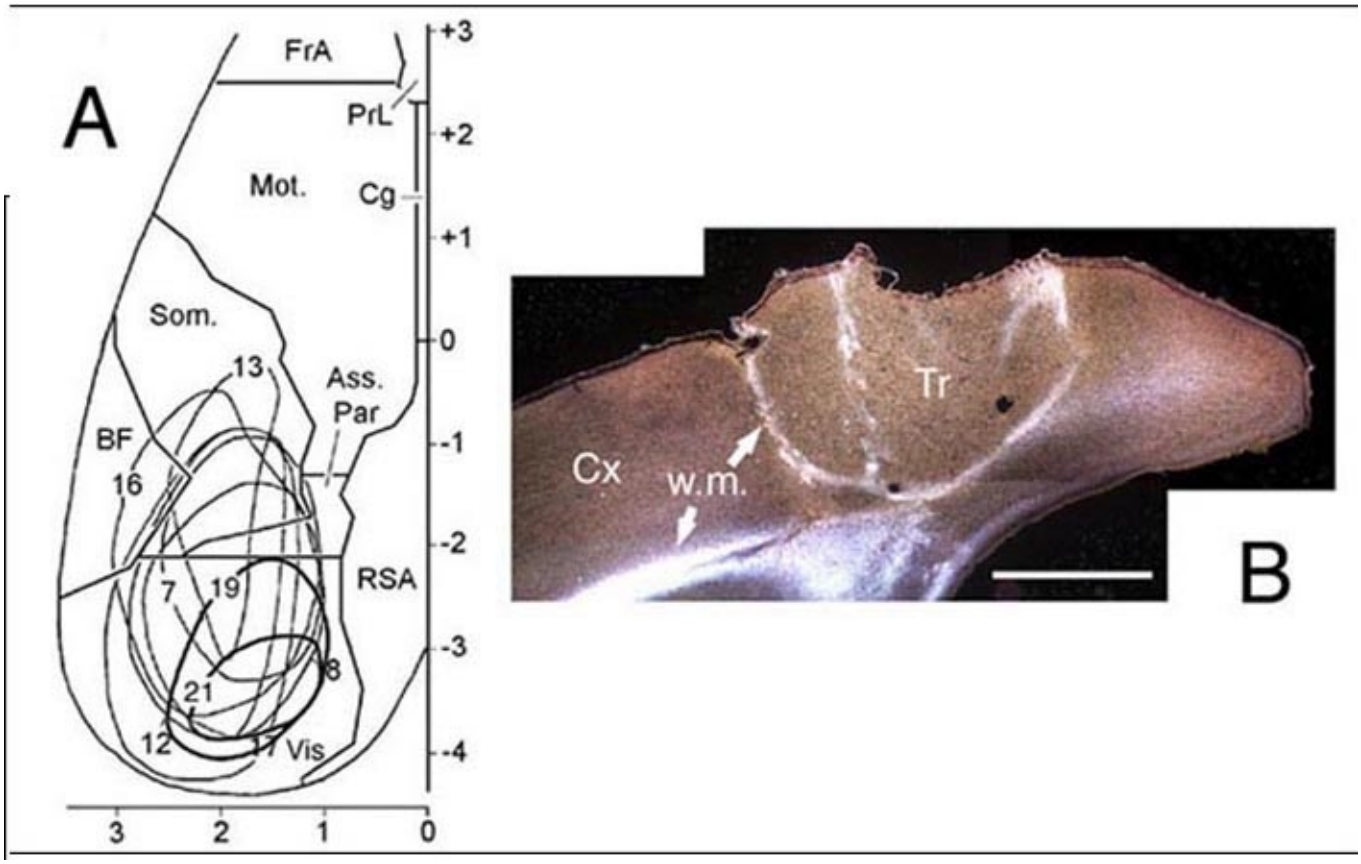

Figure 19. A, location of the eGFP-positive grafts at the cortical surface with respect to bregma (B = 0) after reconstruction from serial brain sections. B, representative implantation (B-3.5). Darkfield microscopy. Note white matter bundles around and within the grafted tissue. Abbreviations are given in text. Scale bar, 500 μm. From Gaillard et al. (163).

graft, outgrowing fibers always appear to prefer elongating through the deep gray matter (layer 6) of the cortex, the major pathway for long distance, intrahemispheric corticocortical axons in rodents (162) (Fig. 24).

Very few fibers can, therefore, extend to subcortical visual targets and the opposite hemisphere. Terminal-like arrangements can nevertheless be detected in the dorsal visual thalamus (Rt, LP/LD, DLG, Po), the pretectum (APT), SC, and even in the lateral division of the pontine nuclei (Pn; Fig. 22), the ultimate target of the rodent visual cortex (39) (Fig. 25 and Fig. 26).

Implications for Future Research

Besides the unequivocal demonstration that developing and regenerating fetal allograft neurons possess a strong capacity for extending axons over considerable distances in the mature host brain parenchyma, the results deserve further comments. First, allowing a delay between tissue sampling and implantation is clearly not necessary for outgrowth. Using a similar surgical protocol, extensive outgrowth can be achieved with cortical frontal and substantia nigra tissue grafts (64, 163). For instance, 11 days after grafting, frontal graft growth cone-like figures end up in the cerebral peduncle. Second, the massive fiber outgrowth taking place along the graft-host parenchyma interface argues against the current suggestion that lesion-induced glial scar formation and local overexpression of repulsive molecules (137) impede neurite growth *in vivo*. Third, most outgrowing axons follow a normal route in the brain parenchyma and terminate in normal target fields, indicating that cues for correct axonal guidance are readily present in the mature brain (159, 164). However, some outgrowing axons spread into inappropriate targets. Fibers and terminal fields have been detected at considerable distances from the graft locus in the acumbens area, olfactory peduncle, tenia tecta, and PBg nucleus, raising again the question

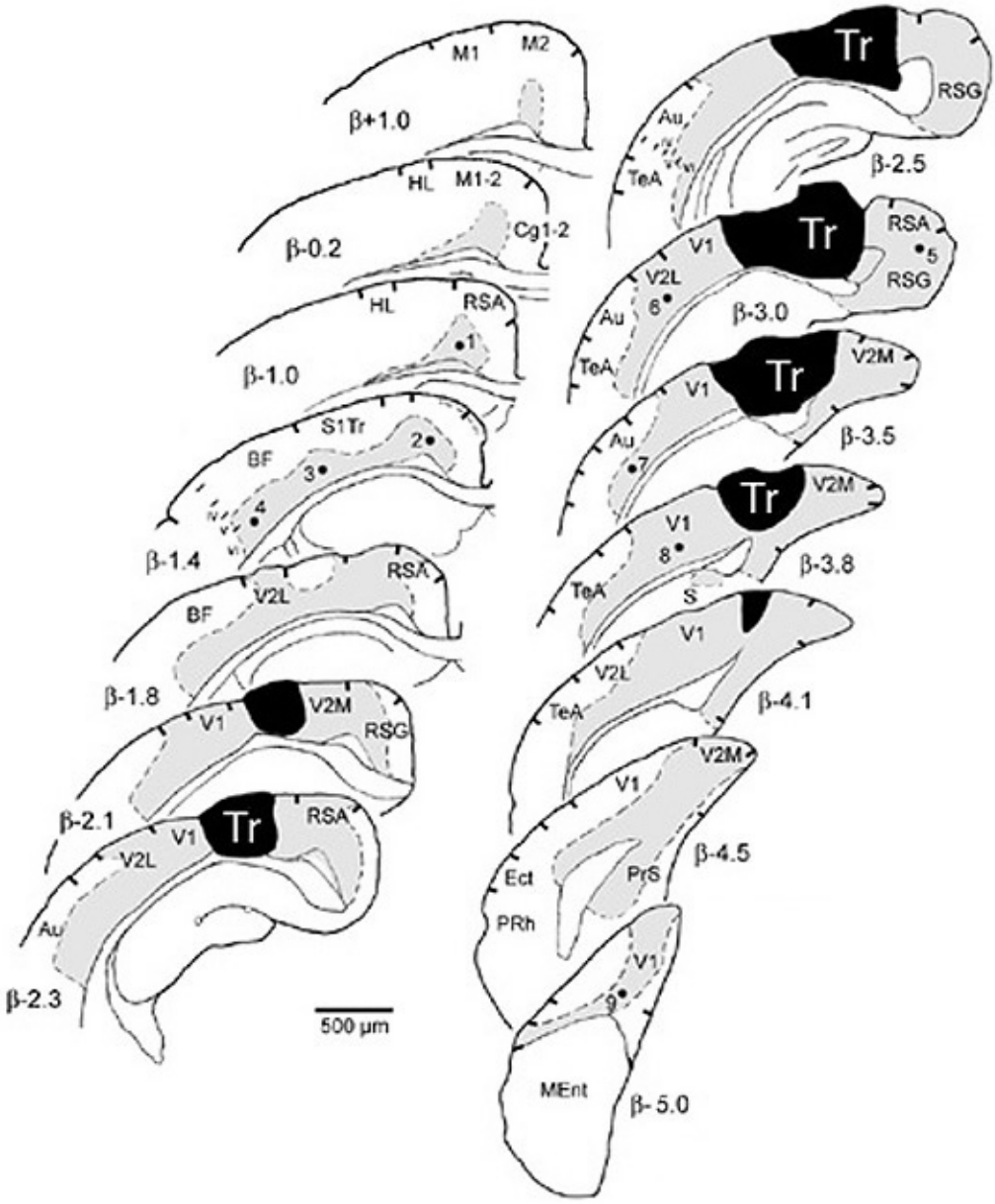

Figure 20. Camera lucida drawings of graft projections into the ipsilateral cortex of the former case as seen at a low magnification power (×4). Brain sections are arranged according to their bregma level. The grayish zone in each section corresponds to the extent of the labeling readily detectable in this condition. Outside this zone, fiber detection requires a higher magnification. Except for local variations in fiber density, present topography is valid for all grafts. From Paxinos and Franklin (175).

of the specificity of innervation (see section 2.4 from the previous chapter). Non-target-directed elongation in the mature brain has already been reported for olfactory bulb neurons transplanted ectopically into the frontal cortex (152). Fourth and finally, adult white matter appears to be an insurmountable obstacle for most developing axons in view that graft fibers grow clearly less through white matter tracts than through infragranular cortical gray layers. In addition, accidental removal of the white matter during surgery allows graft efferents to invade the underlying hippocampic structures (neuropil layers, dentate gyrus, and subiculum).

Neurite growth inhibition by myelin is currently (but not exclusively (165)) explained by interactions between myelin-related inhibitory factors (Nogo-A protein; myelin-associated glycoprotein, MAG; and oligodendrocytes-myelin glycoprotein, OMgp) and a common neuronal Nogo receptor (166-168). Whether such inhibitory

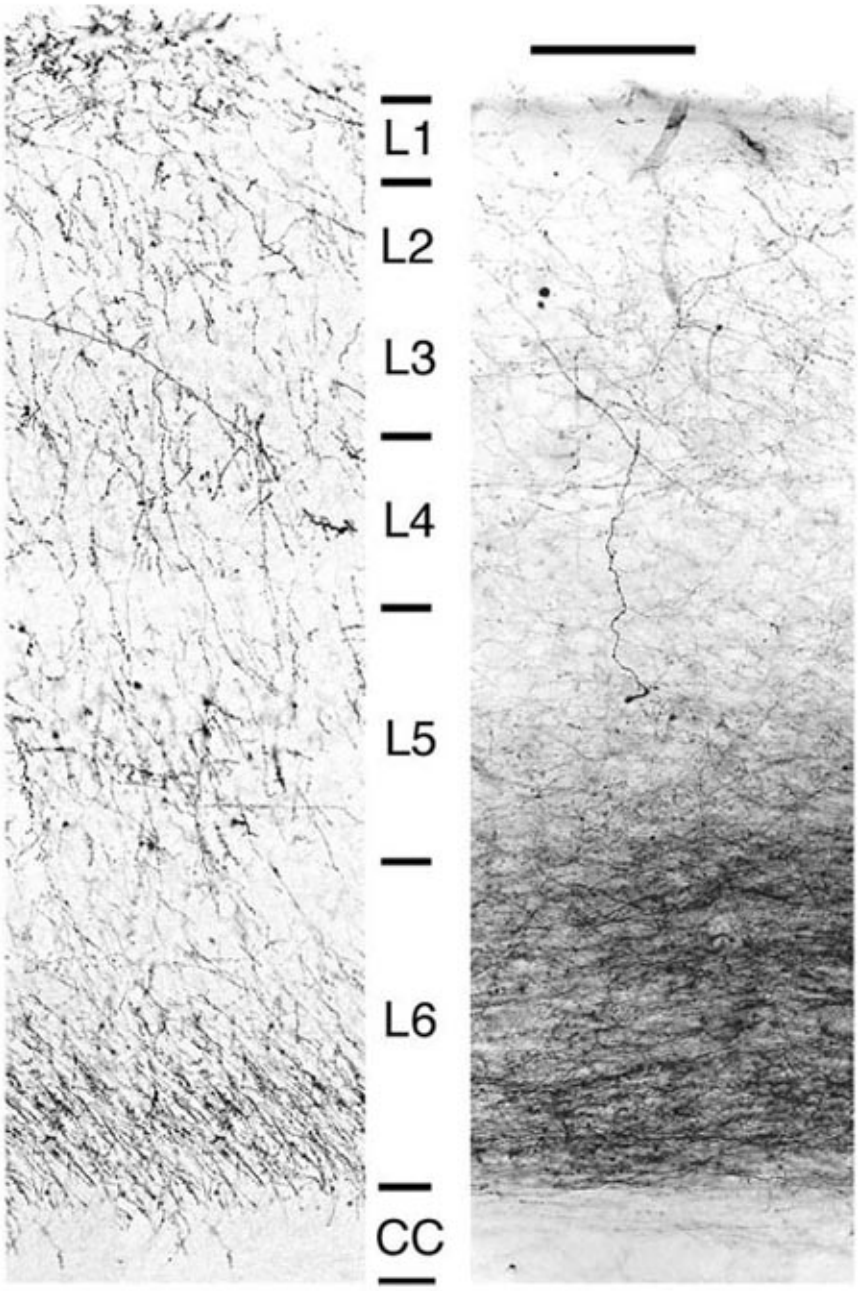

Figure 21. Composite images showing the cortical distribution of graft efferents in HL (left) and V2L (right) areas of two different animals. Note the high density of fibers in layer 6. Inverted contrast from fluorescent material. Corpus callosum (CC) is downward. Scale bar, 100 μm.

interactions make for graft axon repulsion in graft situations is debatable, in part because the neuronal Nogo receptor seems barely detectable in the normal brain, at least until the end of the first postnatal week (169). The implication is that graft axons would be able to navigate for some 2 weeks in white matter tracts before being stopped by inhibitory ligands. This is clearly not what we saw.

Restoration of Visual Behavior

Only a few behavioral studies have investigated whether fetal tectal or occipital grafts can mediate recovery of impaired visual function in adult rats. Results are inconsistent. Stein et al. (170) transplanted frontal and occipital E18-19 tissue blocks into bilateral aspirated occipital cortices and then trained subjects (albino rats) on

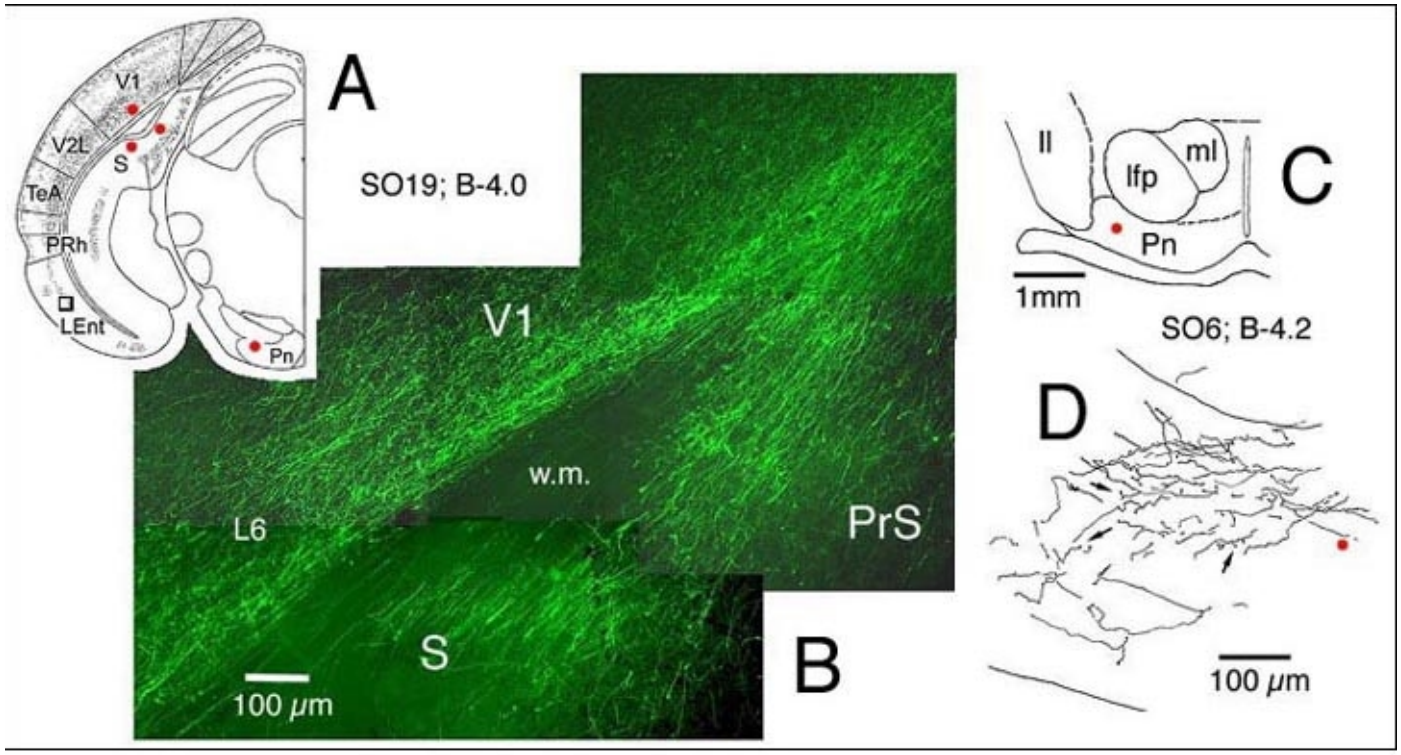

Figure 22. Graft efferents in the caudal brain (4 mm beyond bregma). A, schematic drawing (adapted from Paxinos and Franklin (175)) showing the location of the accompanying pictures (red dots). Gray levels are representative of the fiber density. B, efferents in occipital (V1, layer 6) and hippocampic (S and PrS) regions. Fluorescence microscopy. Note the fiber-free white matter (w.m.). C and D, terminal field in the lateral pontine nucleus (Pn). Camera lucida drawing. Arrows point to bouton-like profiles. Abbreviations are given in text.

both a brightness (neutral-grey levels) and a pattern (oblique stripes) discrimination task. Rats with frontal tissue grafts can learn the brightness task more rapidly and more accurately than animals with lesions alone. Occipital tissue grafts are inefficient. None of the grafted subjects can solve the pattern discrimination problem. In no case can graft efferents be clearly identified following HRP tracing methods. In a later work, Stein and Mufson (171) obtained equally good results in both types of transplants in solving both tasks after pretreatment of the recipients (pigmented rats) with cyclosporin A. How these experimental modifications might affect the performance of rats having occipital tissue grafts is not discussed in this study. The puzzling effect of the frontal grafts is attributed to the release of specific (but unknown) recovery-promoting factors able to spare some residual visual circuits in the host brain. Some studies emphasize, however, that sparing of function is possible only with homotopic grafts (172), and that heterotopic transplants cannot form viable synapses with the host tissue (173). Clearly, the behavioral performance of adult subjects with occipital grafts needs closer examination.

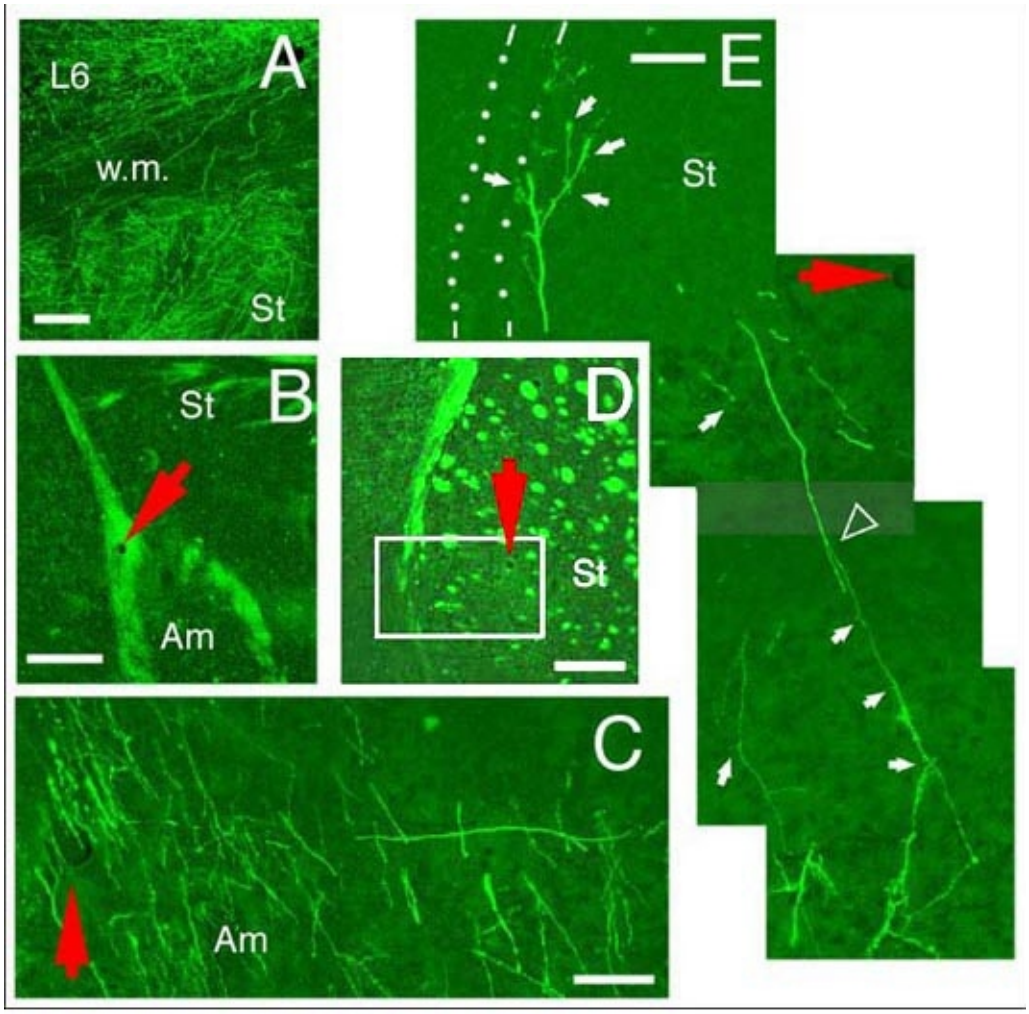

Figure 23. Graft efferents in the striatum and the amygdala. Fluorescence microscopy. A, labeling in the dorsomedial striatum, below area Fr1 (B+1.2). Scale bar, 100 μm. B and C, labeling in the amygdala, laterodorsal nucleus (B+1.0). Scale bars, 150 and 50 μm, respectively. D and E, labeling in the striatum, lateroventral rim (B = 0). Scale bars, 150 and 50 μm, respectively. Red arrows point to blood vessels as landmarks. White arrows indicate terminal-like profiles. Open triangle shows collateral branching. Am, amygdala; St, striatum; w.m., white matter.

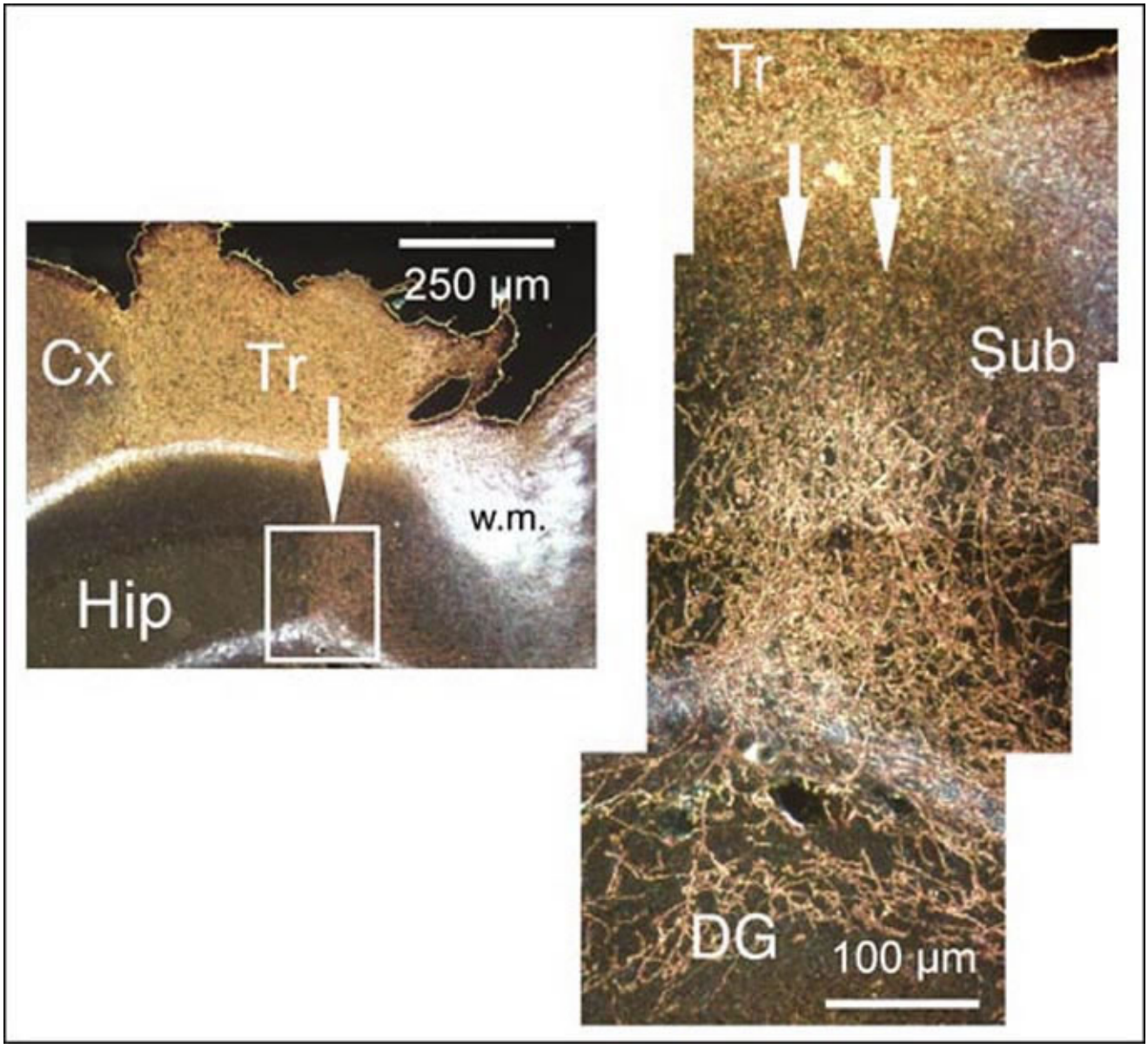

Figure 27. Destruction of the underlying white matter (arrows) allows graft efferents to invade the hippocampus (B-3.6). Darkfield microscopy. Cx, host cortex; DG, dentate gyrus; Hip, hippocampus; Tr, transplant; Sub, subiculum; w.m., white matter.

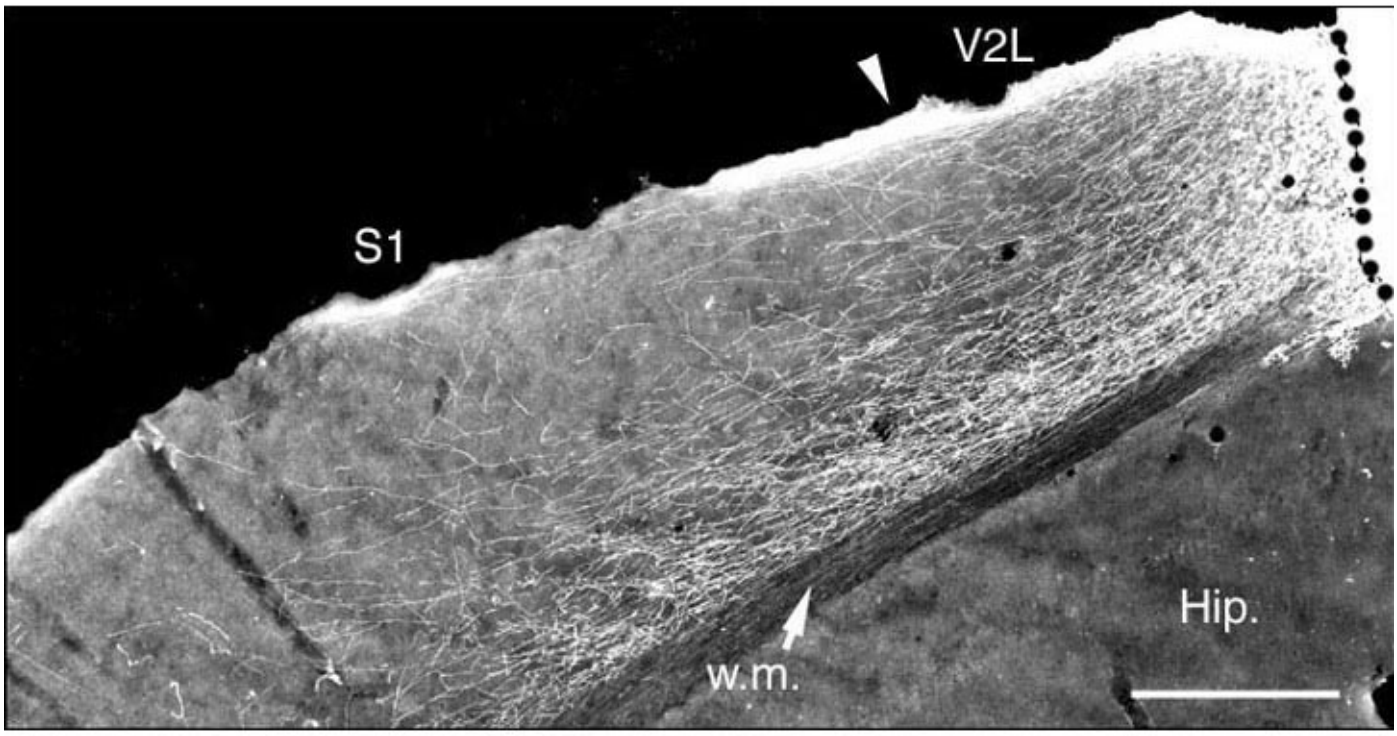

Figure 24. Fiber outgrowth from a small (0.5 mm^2) transplant centered 2 mm caudal to bregma within the lateral parietal association (LptA) area. Outgrowth occurs throughout the graft-cortex junction (V2L area). More laterally (S1 area), fibers display obvious preference for the deep gray *versus* white matter (w.m.). Photographic montage from unstained, DAB-treated material. Hip., hippocampus. Scale bar, 250 μm.

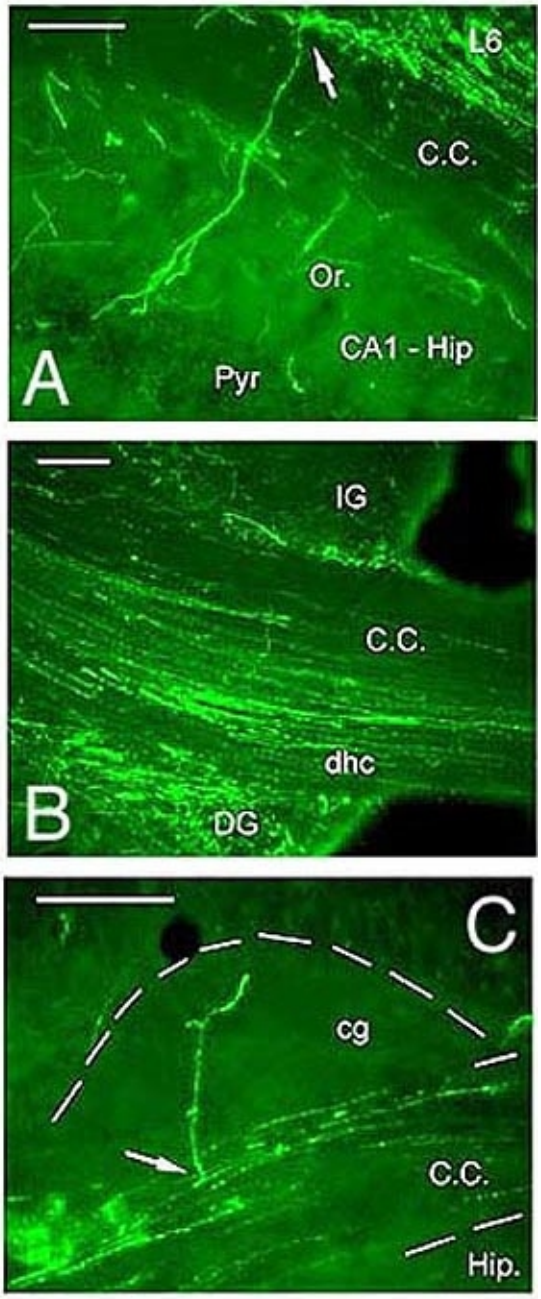

Figure 25. Graft efferents into the corpus callosum (CC). All pictures are taken between the cingulate bundle (cg) and the brain midline. Fluorescence microscopy from Alexa-fluor-treated material. A, callosal fibers are rare at this brain level (B-1.7). Note the fiber coursing vertically from cortical layer 6 to the pyramidal layer (Pyr) of the hippocampic (Hip) CA1 field, a non-visual target. B, just at the rostral pole of the graft (B-2.1), callosal fibers appear much denser. A significant contingent travels into the dorsal hippocampic commissure (dhc). C, contralaterally, very few fibers extend beyong the cingulate bundle (cg). Note the branching pattern to this structure. Or, oriens layer; IG, indusium griseum; DG, dentate gyrus. Scale bars, 100 μm.

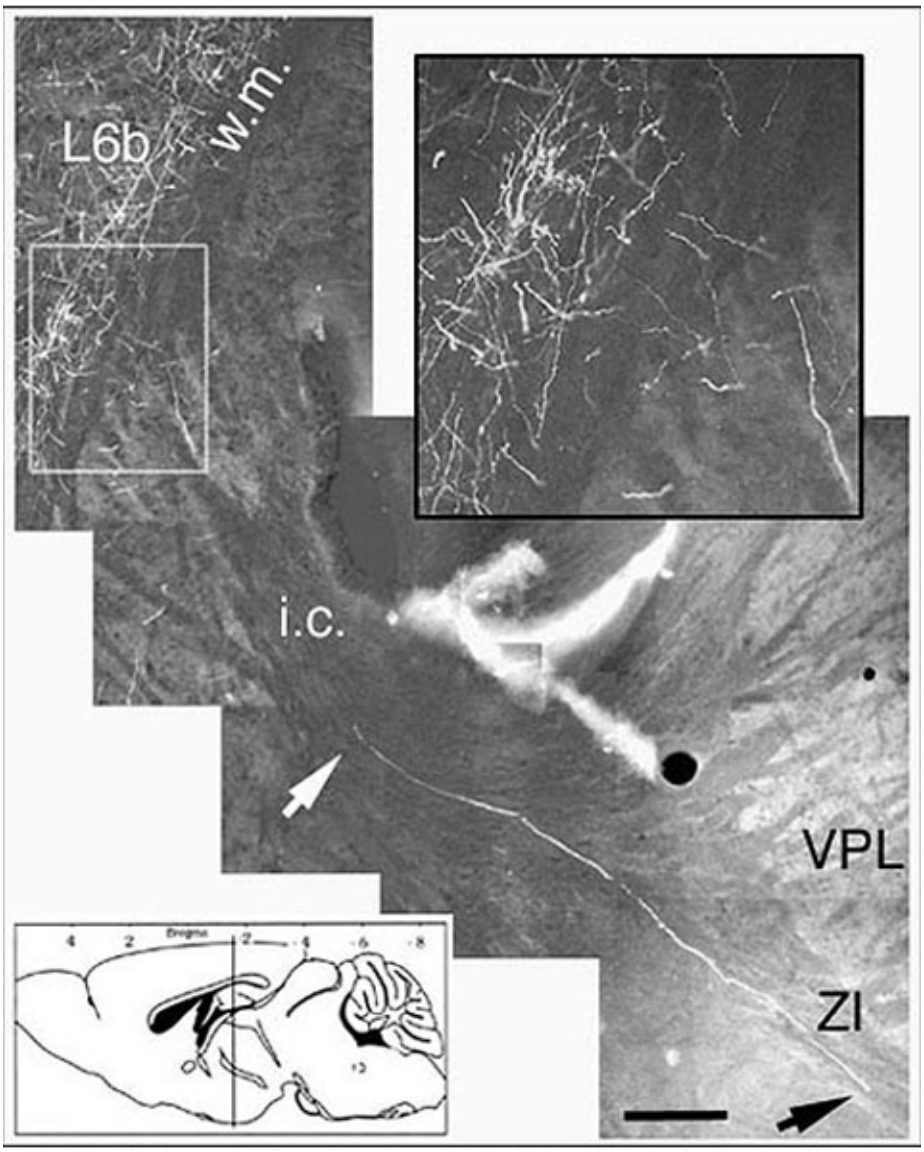

Figure 26. Single graft fiber elongating in the internal capsule to zona incerta, a normal subthalamic target of the occipital cortex. Terminal fields are never seen in this region. Fluorescence microscopy. Scale bar, 150 μm. Upper inset, enlargement of the selected area. Lower inset, location of the section (B-1.6 mm). i.c., internal capsule; VPL, ventral posterolateral nucleus; w.m., white matter; ZI, zona incerta. From Gaillard et al. (163).

About the Authors

University of Poitiers, where he received his B.Sc. (1969) and his M.Sc. (1971) in physiology. He then obtained a Ph.D. (1975) and a Doctorates-Sciences (1984) in neurophysiology. Until recently, most of his studies focused on aspects of binocular information processing in the amphibian visual system, mainly on the functional properties of the crossed isthmo-tectal pathway. He is now examining host-graft relationships in the adult mammalian visual system. Since 1977, Dr. Gaillard has been a senior investigator (Charge de recherches) of the Centre National de la Recherche Scientifique (CNRS) at the Institut de Physiologie et Biologie Cellulaires (UMR 6187), Poitiers, France.

Dr. Yves Sauve was born in Montreal, Canada. He attended the University of Montreal where he received his B.Sc. in Biochemistry in 1983 and his M.Sc. in Neuroscience in 1988 with Dr. Thomas Reader, focusing on the neurochemistry of catecholamines and their receptors in the CNS. He then obtained his Ph.D. in Physiology

under Dr. Michael Rasminsky at McGill University in 1995, where his research focused on the electrophysiological evaluation of reformed synapses between regenerating RGC axons and neurons in the superior colliculus, using the preparation developed in Dr. Albert Aguayo's group. Dr. Sauve subsequently undertook postdoctoral studies with Dr. Raymond Lund at the Institute of Ophthalmology (University College London), where he developed electrophysiological approaches to evaluate visual responsiveness in rodent models of retinal degeneration. In 2001, he became assistant professor of Ophthalmology and Visual Sciences at the Moran Eye Center (University of Utah), where he is currently evaluating rod and cone function following retinal degeneration, transplant therapies, and regeneration in the adult mammalian visual pathways.

References

1. Zihl J. Localised CNS lesions and their effect on visual function. 2000.
2. Chen DF, Jhaveri S, Schneider GE. Intrinsic changes in developing retinal neurons result in regenerative failure of their axons. Proc Natl Acad Sci U S A. 1995;92:7287–7291. PubMed PMID: 7638182.
3. Shewan D, Berry M, Cohen J. Extensive regeneration in vitro by early embryonic neurons on immature and adult CNS tissue. J Neurosci. 1995;15:2057–2062. PubMed PMID: 7891152.
4. Friedman WJ, Black B, Kaplan DR. Distribution of the neurotrophins brain-derived neurotrophic factor, neurotrophin-3 and neurotrophin-4/5 in the postnatal rat brain: an immunocytochemical study. Neuroscience. 1998;84:101–114. PubMed PMID: 9522366.
5. Schoups AA, Elliot RC, Friedman WJ, Black IB. NGF and BDNF are differentially modulated by visual experience in the developing geniculocortical pathway. Brain Res Dev Brain Res. 1995;86:326–334. PubMed PMID: 7656424.
6. Castellani V, Bolz J. Opposing roles for neurotrophin-3 in targeting and collateral formation of distinct sets of developing cortical neurons. Development. 1999;126:3335–3345. PubMed PMID: 10393113.
7. Matsuo A, Nakamura S, Akiguchi I. Immunohistochemical localization of glial cell line-derived neurotrophic factor family receptor alpha-1 in the rat brain: confirmation of expression in various neuronal system. Brain Res. 2000;859:57–71. PubMed PMID: 10720615.
8. Trupp M, Belluardo N, Funosaki H, Ibanez CF. Complementary and overlapping expression of glial cell line-derived neurotrophic factor (GDNF), c-ret proto-oncogene and GDNF receptor alpha indicates multiple mechanisms of trophic actions in the adult rat CNS. J Neurosci. 1997;17:3554–3567. PubMed PMID: 9133379.
9. Collier TJ, Sortwell CE, Daley BF. Diminished viability, growth and behavioral efficacy of fetal dopamine neuron grafts in aging rats with long-term dopamine depletion: an argument for neurotrophic supplementation. J Neurosci. 1999;19:5563–5573. PubMed PMID: 10377363.
10. Crutcher KA. Age-related decrease in sympathetic sprouting is primarily due to decreased target receptivity: implications for understanding brain aging. Neurobiol Aging. 1990;11:175–183. PubMed PMID: 2362650.
11. Gage FH, Bjorklund A, Steveni U, Dunnett SB. Intracerebral grafting of neuronal cell suspensions. VII. Survival and growth of implants of nigral and septal suspensions in intact brains of aged rats. Acta Physiol Scand Suppl. 1983;522:67–75. PubMed PMID: 6586057.
12. Hallas BH, Das GD, Das KG. Transplantation of brain tissue in the brain of rat. II. Growth characteristics of neocortical transplants in hosts of different ages. Am J Anat. 1980;158:147–159. PubMed PMID: 7416052.
13. Caroni P, Schwab ME. Two membrane protein fractions from rat central myelin with inhibitory properties for neurite growth and fibroblast spreading. J Cell Biol. 1988;106:1281–1288. PubMed PMID: 3360853.
14. Schwab ME. Molecules inhibiting neurite growth: a minireview. Neurochem Res. 1996;21:755–761. PubMed PMID: 8873079.
15. Schwab ME. Nogo and axon regeneration. Curr Opin Neurobiol. 2004;14:118–124. PubMed PMID: 15018947.

16. Schwab ME, Caroni P. Rat CNS myelin and a subtype of oligodendrocytes in culture represent a non-permissive substrate for neurite growth and fibroblast spreading. J Neurosci. 1988;8:2381–2393. PubMed PMID: 3074158.
17. Spencer T, Domeniconi M, Cao Z, Filbin MT. New roles for old proteins in adult CNS axonal regeneration. Curr Opin Neurobiol. 2003;13:133–139. PubMed PMID: 12593992.
18. Armstrong RJE, Hurelbrink CB, Tyers P, Ratcliffe EL, Richards A, Dunnett SB, Rosser AE, Barker RA. The potential for circuit reconstruction by expanded neural precursor cells explored through porcine xenografts in a rat model of Parkinson's disease. Exp Neurol. 2002;175:98–111. PubMed PMID: 12009763.
19. Cicirata F, Serapide MF, Nicotra G, Raffaele R. Homotopic transplant of fetal cortex to lesioned motor cortex of adult rats. A comportamental and anatomical study. Arch Ital Biol. 1992;130:101–111. PubMed PMID: 1632721.
20. Grabowski M, Johansson BB, Brudin P. Neocortical grafts in the infarcted brain of adult rats: few or no efferent fibers grow from transplant to host. Exp Neurol. 1995;134:273–276. PubMed PMID: 7556547.
21. Sofroniew MV, Dunnett SB, Isacson O. Remodelling of intrinsic and afferent systems in neocortex with cortical transplants. Prog Brain Res. 1990;82:313–320. PubMed PMID: 2290944.
22. Sorensen JC, Grabowski M, Zimmer J, Johansson BB. Fetal neocortical tissue blocks implanted in brain infarcts of adult rats interconnect with the host brain. Exp Neurol. 1996;138:227–235. PubMed PMID: 8620921.
23. Walker PD, McAllister JP. Minimal connectivity between neostriatal transplants and the host brain. Brain Res. 1987;425:34–44. PubMed PMID: 3427424.
24. Bjorklund A. Neural transplantation. An experimental tool with clinical possibilities. Trends Neurosci. 1991;14:319–322. PubMed PMID: 1721733.
25. Dunnett SB. Repair of the damaged brain. The Alfred Meyer memorial lecture 1998. Neuropathol Appl Neurobiol. 1999;25:351–362. PubMed PMID: 10564524.
26. Gage FH, Fisher LJ. Intracerebral grafting: a tool for the neurobiologist. Neuron. 1991;6:1–12. PubMed PMID: 1986771.
27. Lescaudron L, Stein DG. Functional recovery following transplants of embryonic brain tissue in rats with lesion of visual, frontal and motor cortex: problems and prospects for future research. Neuropsychologia. 1990;28:585–599. PubMed PMID: 2203995.
28. Stein DG, Glasier MM. Some practical and theoretical issues concerning fetal brain tissue grafts as therapy for brain dysfunctions. Behav Brain Sci. 1995;18:36–45.
29. Plumet J, Ebrahimi-Gaillard A, Guitet J, Roger M. Partial recovery of skilled forelimb reaching after transplantation of fetal cortical tissue in adult rats with motor cortex lesion. Anatomical and functional aspects. Restor Neurol Neurosci. 1993;6:9–27.
30. Riolobos AS, Heredia M, de la Fuente JA, Criado JM, Yajeya J, Campos J, Santacana M. Functional recovery of skilled forelimb use in rats obliged to use the impaired limb after grafting of the frontal cortex lesion with homotopic fetal cortex. Neurobiol Learn Mem. 2001;75:274–291. PubMed PMID: 11300734.
31. Lund RD. Development and plasticity of the brain: an introduction. New York: Oxford University Press; 1978.
32. Sefton AJ, Dreher B. Visual system. In: G. Paxinos, editor. The rat nervous system 2nd ed. Sydney: Academic Press; 1995. p. 833-898.
33. Zilles K, Wree A. Cortex: areal and laminar structure. In: Paxinos G, editor. The rat nervous system. 2nd ed., Academic Press, Sydney; 1995. p. 649-685.
34. Sefton AJ, Dreher B, Harvey AR. Visual system. In: G. Paxinos, editor.The rat nervous system. A handbook for neuroscientists. 3rd ed. Sydney: Academic Press; 2004. p. 1083-1165.
35. Carey RG, Neal TL. The rat claustrum: afferent and efferent connections with visual cortex. Brain Res. 1985;329:185–193. PubMed PMID: 3978440.
36. Shameem N, Sanderson K, Dreher B. Claustral afferents to the rat's visual cortex. Neurosci Lett. 1984;49:247–252. PubMed PMID: 6493606.

37. McDonald AJ, Mascagni F. Cortico-cortical and cortico-amygdaloid projections of the rat occipital cortex: a Phaseolus vulgaris leucoagglutinin study. Neuroscience. 1996;71:37–54. PubMed PMID: 8834391.
38. Serizawa M, McHaffie JG, Hoshino K, Norita M. Corticostriatal and corticotectal projections from visual cortical areas 17, 18 and 18a in the pigmented rat. Arch Histol Cytol. 1994;57:493–507. PubMed PMID: 7537509.
39. Wiesendanger R, Wiesendanger M. The corticopontine system in the rat. II. The projection pattern. J Comp Neurol. 1982;208:227–238. PubMed PMID: 7119159.
40. Baker GE, Jeffrey G. Distribution of uncrossed axons along the course of the optic nerve and chiasm of rodents. J Comp Neurol. 1989;289:455–461. PubMed PMID: 2808779.
41. Chan SO, Chung KY. Changes in axon arrangement in the retinofugal pathway of mouse embryos: confocal microscopy study using single- and double-dye label. J Comp Neurol. 1999;406:251–262. PubMed PMID: 10096609.
42. Chan SO, Guillery RW. Changes in fiber order in the optic nerve and tract of rat embryos. J Comp Neurol. 1994;344:20–32. PubMed PMID: 8063954.
43. Simon DK, O'Leary DD. Relationship of retinotopic ordering of axons in the optic pathway to the formation of visual maps in central targets. J Comp Neurol. 1991;307:393–404. PubMed PMID: 1856329.
44. Lashley KS. The mechanisms of vision. VII. The projection of the retina upon the primary optic centers in the rat. J Comp Neurol. 1934;59:341–373.
45. Lashley KS. The mechanisms of vision. VIII. The projection of the retina upon the cerebral cortex of the rat. J Comp Neurol. 1934;60:57–79.
46. Drager UC. Receptive fields of single cells and topography in mouse visual cortex. J Comp Neurol. 1975;160:269–290. PubMed PMID: 1112925.
47. Espinoza SG, Thomas HC. Retinotopic organization of striate and extrastriate visual cortex in the hooded rat. Brain Res. 1983;272:137–144. PubMed PMID: 6616189.
48. Lund RD, Lund JS, Wise RP. The organization of the retinal projection to the dorsal lateral geniculate nucleus in pigmented and albino rats. J Comp Neurol. 1974;158:383–403. PubMed PMID: 4448860.
49. Montero VM, Brugge JF, Beitel RE. Relation of the visual field to the lateral geniculate body of the albino rat. J Neurophysiol. 1968;31:221–236. PubMed PMID: 5687382.
50. Olavarria J, Montero VM. Relation of callosal and strite-extrastriate cortical connections in the rat: morphological definition of extrastriate visual areas. Exp Brain Res. 1984;54:240–252. PubMed PMID: 6723844.
51. Siminoff R, Schwassmann HO, Kruger L. An electrophysiological study of the visual projection to the superior colliculus of the rat. J Comp Neurol. 1966;127:435–444. PubMed PMID: 5968989.
52. Wagor E, Mangini NJ, Pearlman AL. Retinotopic organization of striate and extrastriate visual cortex in the mouse. J Comp Neurol. 1980;193:187–202. PubMed PMID: 6776164.
53. Hubener M. Mouse visual cortex. Curr Opin Neurobiol. 2003;13:413–420. PubMed PMID: 12965287.
54. Schuett S, Bonhoeffer T, Hubener M. Mapping retinotopic structure in mouse visual cortex with optical imaging. J Neurosci. 2002;22:6549–6559. PubMed PMID: 12151534.
55. Rosa MGP, Krubitzer LA. The evolution of visual cortex: where is V2? Trends Neurosci. 1999;22:242–248. PubMed PMID: 10354599.
56. Jaeger CB, Lund RD. Transplantation of embryonic occipital cortex to the brain of newborn rats. An autoradiographic study of transplant histogenesis. Exp Brain Res. 1980;40:265–272. PubMed PMID: 7428881.
57. Majda BT, Harvey AR. Tectal tissue grafted to the midbrain of newborn rats: effect of donor age on survival, growth and connectivity of transplants. J Neural Transplant. 1989;1:95–103. PubMed PMID: 2485121.
58. Bjorklund A, Stenevi U. Reconstruction of the nigrostriatal dopamine pathway by intracerebral nigral transplants. Brain Res. 1979;177:555–560. PubMed PMID: 574053.

59. Grabowski M, Johansson BB, Brudin P. Survival of fetal neocortical grafts implanted in brain infarcts of adult rats: the influence of postlesion time and age of donor tissue. Exp Neurol. 1994;127:126–136. PubMed PMID: 8200430.
60. Sprick U. Morphology of embryonic hippocampus transplants and generation of long-distance extrinsic graft fiber connections to the lateral septum and the entorhinal cortex in mature rat brain. Restor Neurol Neurosci. 1991;3:23–34.
61. Nieto-Sampedro M, Lewis ER, Cotman CW, Manthorpe M, Skaper SD, Barbin G, Longo FM, Varon S. Brain injury causes a time-dependent increase in neuronotrophic activity at the lesion site. Science. 1982;217:860–861. PubMed PMID: 7100931.
62. Harvey AR, Lund RD. Transplantation of tectal tissue in rats. IV. Maturation of transplants and development of host retinal projection. Brain Res. 1984;314:27–37. PubMed PMID: 6697254.
63. Kurotani T, Yamamoto N, Toyama K. Development of neural connections between visual cortex and transplanted lateral geniculate nucleus in rats. Brain Res Dev Brain Res. 1993;71:151–168. PubMed PMID: 8491038.
64. Roger M., Gaillard A. Upon transplantation, embryonic cortex neurons extend axons over long distance within the damaged adult brain. FENS Abstr. 2004;2:A147.14.
65. Rosenstein JM. Why do neural transplants survive? An examination of some metabolic and pathophysiological considerations in neural transplantation. Exp Neurol. 1995a;133:1–6. PubMed PMID: 7601258.
66. Domballe L, Gaillard F, Gaillard A. Axonal regrowth of layer II-III projecting cortical neurons in rats fails beyond eye opening. Exp Neurol. 2003;180:110–122. PubMed PMID: 12684025.
67. McLoon SC, Lund RD. Development of fetal retina, tectum and cortex transplanted to the superior colliculus of adult rats. J Comp Neurol. 1983;217:376–389. PubMed PMID: 6886059.
68. Bjorklund A, Stenevi U. Intracerebral neural implants: neuronal replacement and reconstruction of damaged circuitries. Annu Rev Neurosci. 1984;7:279–308. PubMed PMID: 6370080.
69. Albert EN, Das GD. Neocortical transplants in the rat brain: an ultrastructural study. Experientia. 1984;40:294–298. PubMed PMID: 6698191.
70. Alexandrova MA, Polezhaev LV. Transplantation of various regions of embryonic brain tissue into the brain of adult rats. J Hirnforsch. 1984;25:89–98. PubMed PMID: 6725942.
71. Girman SV. Retinal afferents innervate functionally tectal but not neocortical grafts placed in lesioned superior colliculus of adult rats. Brain Res. 1993;607:167–176. PubMed PMID: 8481793.
72. Harvey AR, MacDonald AM. The development of acetylcholinesterase activity in normal and transplanted superior colliculus in rats. J Comp Neurol. 1985;240:117–127. PubMed PMID: 4056106.
73. Harvey AR, Gan SK, Pauken JM. Fetal tectal or cortical tissue transplanted into brachial lesion cavities in rats: influence on the regrowth of host retinal axons. J Comp Neurol. 1987;263:126–136. PubMed PMID: 3667968.
74. Tan MML, Harvey AR. The development and distribution of alpha-bungarotoxin binding sites in rat tectal transplants. Brain Res Dev Brain Res. 1987;36:293–298.
75. Lund RD, Harvey AR. Transplantation of tectal tissue in rats. I. Organization of transplants and pattern of distribution of host afferents within them. J Comp Neurol. 1981;201:191–209. PubMed PMID: 7287926.
76. Lund RD, Hauschka SD. Transplanted neural tissue develops connections with host rat brain. Science. 1976;193:582–584. PubMed PMID: 959815.
77. Leong SF, Leung TKC, Leong SK. The expression of proteins and activities of metabolic enzymes in transplanted brain tissue. Brain Res. 1991;560:50–54. PubMed PMID: 1760746.
78. Schulz MK, Hogan TP, Castro AJ. Connectivity of fetal neocortical block transplants in the excitotoxically ablated cortex of adult rats. Exp Brain Res. 1993;96:480–486. PubMed PMID: 7507863.
79. Schulz MK, McNulty JA, Hogan TP, Zimmer J, Castro AJ. Biochemical and anatomical analysis of cholinergic, noradrenergic and serotonergic innervation of fetal neocortical transplants placed in excitotoxin-induced neocortical lesions of adult rats. Restor Neurol Neurosci. 1995;7:127–136.

80. Aleksandrova MA, Girman SV. Correlation between the morphological and electrophysiological characteristics of neocortical transplants placed in the visual cortex of adult rats. Dokl Akad Nauk. 1995;340:705–708. PubMed PMID: 7735095.
81. Girman SV. Neocortical grafts receive functional afferents from the same neurons of the thalamus which have innervated the visual cortex replaced by the graft in adult rats. Neuroscience. 1994;60:989–997. PubMed PMID: 7523990.
82. Bragin AG, Bohne A, Vinogradova OS. Transplants of the embryonal rat somatosensory neocortex in the barrel field of the adult rat: responses of the grafted neurons to sensory stimulation. Neuroscience. 1988;25:751–758. PubMed PMID: 3405428.
83. Bragin AG, Bohne A, Vinogradova OS. Responses to electrical stimulation of the recipient's brain in rat somatosensory cortical neurons transplanted into the area of vibrissa representation in the neocortex. Neurosci Behav Physiol. 1989;19:449–456. PubMed PMID: 2615956.
84. Lubke J, Wood MJA, Clarke DJ. Morphological assessment of grafted rat and mouse cortical neurons: a light and electron microscopic study. J Comp Neurol. 1994;341:78–94. PubMed PMID: 8006225.
85. Walsh JP, Zhou FC, Hull CD, Fisher RS, Levine MS, Buchwald NA. Physiological and morphological characterization of striatal neurons transplanted into the striatum of adult rats. Synapse. 1988;2:37–44. PubMed PMID: 3420529.
86. Wilson CJ, Xu ZC, Emson PC, Feler C. Anatomical and physiological properties of the cortical and thalamic innervations of neostriatal tissue grafts. Prog Brain Res. 1990;82:417–426. PubMed PMID: 2290955.
87. Girman SV, Golovina IL. Electrophysiological properties of embryonic neocortex transplants replacing the primary visual cortex of adult rats. Brain Res. 1990;523:78–86. PubMed PMID: 2207692.
88. Gaillard F, Girman SV, Gaillard A. Afferents to visually responsive grafts of embryonic occipital neocortex tissue implanted into V1 (Oc1) cortical area of adult rats. Restor Neurol Neurosci. 1998;12:13–25. PubMed PMID: 12671317.
89. Gaillard F, Letang J, Frappe I, Gaillard A. Laminar distribution of isocortical neurons projecting to occipital grafts in neonate and adult rats. Exp Neurol. 2000;162:225–233. PubMed PMID: 10716903.
90. Montero VM. Evoked responses in the rat's visual cortex to contralateral, ipsilateral and restricted photic stimulation. Brain Res. 1973;53:192–196. PubMed PMID: 4572482.
91. Russell MJ, Vijayan VK, Gibbs RB, Geddes JW, Jacobson CH, Cotman CW. Long-term survival of neural transplants to senescence in rats. Exp Neurol. 1990;108:105–108. PubMed PMID: 2335191.
92. Burne RA, Parnavelas JG, Lin CS. Response properties of neurons in the visual cortex of the rat. Exp Brain Res. 1984;53:374–383. PubMed PMID: 6200352.
93. Fukuda Y, Iwama K. Visual receptive-field properties of single cells in the rat superior colliculus. Jpn J Physiol. 1978;28:385–400. PubMed PMID: 713186.
94. Girman SV, Sauve Y, Lund RD. Receptive field properties of single neurons in rat primary visual cortex. J Neurophysiol. 1999;82:301–311. PubMed PMID: 10400959.
95. Wiesenfeld Z, Kornel EE. Receptive fields of single cells in the visual cortex of the hooded rat. Brain Res. 1975;94:401–412. PubMed PMID: 1156851.
96. Keirstead SA, Rasminsky M, Fukuda Y, Carter DA, Aguayo AJ, Vidal-Sanz M. Electrophysiologic responses in hamster superior colliculus evoked by regenerating retinal axons. Science. 1989;246:255–257. PubMed PMID: 2799387.
97. Sauve Y, Sawai H, Rasminsky M. Functional synaptic connections made by regenerated retinal ganglion cell axons in the superior colliculus of adult hamsters. J Neurosci. 1995;15:665–675. PubMed PMID: 7823170.
98. Thanos S, Naskar T, Heiduschka P. Regenerating ganglion cells axons in the adult rat establish retinofugal topography and restore visual function. Exp Brain Res. 1997;114:483–491. PubMed PMID: 9187284.
99. Hubel DH, Wiesel TN. Receptive fields, binocular interaction and functional architecture in the cat's visual cortex. J Physiol. 1962;160:106–154. PubMed PMID: 14449617.

100. Golden GT, Reyes PF, Fariello RG. Morphological and functional studies of rat tectal transplants. Brain Res Bull. 1989;22:461–468. PubMed PMID: 2468404.
101. Harvey AR, Golden GT, Lund RD. Transplantation of tectal tissue in rats. III. Functional innervation of transplants by host afferents. Exp Brain Res. 1982;47:437–445. PubMed PMID: 6290252.
102. Harvey AR. Transplantation of fetal tectum into young rats. Neurosci Lett Suppl. 1984;15:S35.
103. Harvey AR, Tan MML. Spontaneous regeneration of adult rat retinal ganglion cell axon in vivo. Neuroreport. 1992;3:239–242. PubMed PMID: 1515575.
104. Galik J, Macias-Gonzalez R, Valouskova V, Bures J. Integration of neocortical embryonal grafts with the neocortex of host rats examined by Leao's spreading cortical depression. Exp Neurol. 1991;112:321–327. PubMed PMID: 2029932.
105. Clancy B, Cauller LJ. Widespread projections from subgriseal neurons (layer VII) to layer I in adult rat cortex. J Comp Neurol. 1999;407:275–286. PubMed PMID: 10213095.
106. Marin-Padilla M. Dual origin of the mammalian neocortex and evolution of the cortical plate. Anat Embryol (Berl). 1978;152:109–126. PubMed PMID: 637312.
107. Reep RL, Goodwin GS. Layer VII of rodent cerebral cortex. Neurosci Lett. 1988;90:15–20. PubMed PMID: 3412636.
108. Valverde F, Facal-Valverde MV, Santacana M, Heredia M. Development and differentiation of early generated cells of sublayer VIb in the somatosensory cortex of the rat: a correlated Golgi and autoradiographic study. J Comp Neurol. 1989;290:118–140. PubMed PMID: 2480368.
109. Bayer SA, Altman J. Development of layer I and the subplate in the rat cortex. Exp Neurol. 1990;107:48–62. PubMed PMID: 2295319.
110. Chun JJ, Shatz CJ. A fibronectin-like molecule is present in the developing cat cerebral cortex and is correlated with subplate neurons. J Cell Biol. 1988;106:857–872. PubMed PMID: 3346327.
111. Ghosh A, Antonini A, McConnell SK, Shatz CJ. Requirement for subplate neurons in the formation of thalamocortical connections. Nature. 1990;347:179–181. PubMed PMID: 2395469.
112. Kanold PO, Kara P, Reid RC, Shatz CJ. Role of subplate neurons in functional maturation of visual cortical columns. Science. 2003;301:521–525. PubMed PMID: 12881571.
113. Grossberg S, Seitz A. Laminar development of receptive fields, maps and columns in visual cortex: the coordinating role of the subplate. Cereb Cortex. 2003;13:852–863. PubMed PMID: 12853372.
114. Lein ES, Finney EM, McQuillen PS, Shatz CJ. Subplate neuron ablation alters neurotrophin expression and ocular dominance column formation. Proc Natl Acad Sci U S A. 1999;96:13491–13495. PubMed PMID: 10557348.
115. Galuske RAW, Singer W. The origin and topography of long-range intrinsic projections in cat visual cortex: a developmental study. Cereb Cortex. 1996;6:417–430. PubMed PMID: 8670668.
116. Chang FL, Steedman JG, Lund RD. Embryonic cerebral cortex placed in the occipital region of newborn rats makes connections with the host brain. Brain Res. 1984;315:164–166. PubMed PMID: 6722577.
117. Cunningham TJ, Huddelston C, Murray M. Modification of neuron numbers in the visual system of the rat. J Comp Neurol. 1979;184:423–434. PubMed PMID: 762291.
118. Frappe I, Roger M, Gaillard A. Transplantation of fetal frontal cortex grafted into the occipital cortex of newborn rats receive a substantial thalamic input from nuclei normally projecting to the frontal cortex. Neuroscience. 1999;89:409–421. PubMed PMID: 10077323.
119. Castro AJ, Sorensen JC, Tonder N, Bold L, Zimmer J. Fetal neocortical transplants grafted into cortical lesion cavities made in newborn rats receive multiple host afferents. A retrograde fluorescent tracer analysis. Restor Neurol Neurosci. 1989;1:13–23.
120. Fagiolini M, Pizzorusso T, Berardi N, Domenici L, Maffei L. Functional postnatal development of the rat primary visual cortex and the role of visual experience: dark rearing and monocular deprivation. Vision Res. 1994;34:709–720. PubMed PMID: 8160387.
121. Rakic P. Neurons in the rhesus monkey visual cortex: systematic relation between time of origin and eventual disposition. Science. 1974;183:425–427. PubMed PMID: 4203022.

122. Ignacio MP, Kimm EJ, Kageyama H, Robertson RT. Postnatal migration of neurons and formation of laminae in rat cerebral cortex. Anat Embryol (Berl). 1995;191:89–100. PubMed PMID: 7726396.
123. Luskin MB, Shatz CJ. Neurogenesis of the cat's primary visual cortex. J Comp Neurol. 1985;242:611–651. PubMed PMID: 4086673.
124. Parnavelas JG, Burne RA, Lin CS. Distribution and morphology of functionally identified neurons in the visual cortex of the rat. Brain Res. 1983;261:21–29. PubMed PMID: 6301626.
125. Miller MW. Relationship of the time of origin and death of neurons in the rat somatosensory cortex: barrel versus septal cortex and projection versus local circuit neurons. J Comp Neurol. 1995;355:6–14. PubMed PMID: 7636014.
126. Szele FG, Alexander C, Chesselet MT. Expression of molecules associated with neuronal plasticity after aspiration and thermocoagulatory lesions of the cerebral cortex in adult rats. J Neurosci. 1995;15:4429–4448. PubMed PMID: 7790918.
127. Ringstedt T, Lagercrantz H, Persson H. Expression of members of the trk family in the developing postnatal rat brain. Brain Res Dev Brain Res. 1993;72:119–131. PubMed PMID: 8453762.
128. McAllister AK, Lo DC, Katz LC. Neurotrophins regulate dendritic growth in developing visual cortex. Neuron. 1995;15:791–803. PubMed PMID: 7576629.
129. Cooke S, Grant G, McLauchlan C, Beau Lotto R, Price DJ. Basic fibroblast growth factor promotes subplate cell survival in explant cultures of embryonic mouse cortex. Neurosci Lett. 1999;271:143–146. PubMed PMID: 10507689.
130. Gomez-Pinilla F, Cotman CW. Transient lesion-induced increase of basic fibroblast growth factor and its receptor in layer VIb (subplate cells) of the adult rat cerebral cortex. Neuroscience. 1992;49:771–780. PubMed PMID: 1436480.
131. Catapano LA, Arnold MW, Perez FA, Macklis JD. Specific neurotrophic factors support the survival of cortical projection neurons at distinct stages of development. J Neurosci. 2001;21:8863–8872. PubMed PMID: 11698598.
132. Barbe MF, Levitt P. Age-dependent specification of the corticocortical connections of cerebral grafts. J Neurosci. 1995;15:1819–1834. PubMed PMID: 7891137.
133. Worthington DR, Harvey AR. Organization of visual cortical projections to fetal tectal transplants in rats: a study using multiple retrograde tracers. Brain Res. 1990;536:153–162. PubMed PMID: 2085743.
134. Andres FL, van der Loos H. Removal and reimplantation of the parietal cortex of the neonatal mouse: consequences for the barrelfield. Brain Res. 1985;352:115–121. PubMed PMID: 4005613.
135. Kawaguchi S, Iwashita Y, Murata M. Neural repairing of the point-to-point projections in the mammalian nervous system. Biomed Res. 1994;15 Suppl. 1 127–134.
136. Levick WR. Another tungsten microelectrode. Med Biol Eng. 1972;10:510–515. PubMed PMID: 4627562.
137. Fournier AE, Strittmatter SM. Repulsive factors and axon regeneration in the CNS. Curr Opin Neurobiol. 2001;11:89–94. PubMed PMID: 11179877.
138. Nelms JL, LeSauter J, Silver R, Lehman MN. Biotinylated dextran amine as a marker for fetal hypothalamic homografts and their efferents. Exp Neurol. 2002;174:72–80. PubMed PMID: 11869035.
139. Senatorov VV, Nyakas C, Fulop Z. Visualization of outgrowing axons of grafted neurons by anterograde labelling with Phaseolus vulgaris leucoagglutinin in the motor cortex of the rat. Restor Neurol Neurosci. 1993;5:337–345.
140. Vercelli A, Repici M, Garbossa D, Grimaldi A. Recent techniques for tracing pathways in the central nervous system of developing and adult mammals. Brain Res Bull. 2000;51:11–28. PubMed PMID: 10654576.
141. Wu CC, Russel RM, Nguyen RT, Karten HJ. Tracing developing pathways in the brain: a comparison of carbocyanine dyes and cholera toxin B subunit. Neuroscience. 2003;117:831–845. PubMed PMID: 12654336.
142. Rosenstein JM. Developmental expression of neuron-specific enolase immunoreactivity and cytochrome oxidase activity in neocortical transplants. Exp Neurol. 1993;124:208–218. PubMed PMID: 8287924.

143. Rosenstein JM. Diminished expression of microtubule-associated protein (MAP-2) and ?-tubulin as a putative marker for ischemic injury in neocortical transplants. Cell Transplant. 1995b;4:83–91. PubMed PMID: 7728337.
144. Rutherford A, Garcia-Munoz M, Dunnett SB, Arbuthnott GW. Electrophysiological demonstration of host cortical inputs to striatal grafts. Neurosci Lett. 1987;83:275–281. PubMed PMID: 3441309.
145. Triarhou LC, Brundin P, Doucet G, Norton J, Bjorklund A, Ghetti B. Intrastriatal implants of mesencephalic cell suspensions in weaver mutant mice: ultrastructural relationships of dopaminergic dendrites and axons issued from the graft. Exp Brain Res. 1990;79:3–17. PubMed PMID: 1968850.
146. Woodhams PL, Calvert R, Dunnett SB. Monoclonal antibody G10 against microtubule-associated protein 1x distinguishes between growing and regenerating axons. Neuroscience. 1989;28:49–59. PubMed PMID: 2761695.
147. Xu ZC, Wilson CJ, Emson PC. Synaptic potentials evoked in spiny neurons in rat neostriatal grafts by cortical and thalamic stimulation. J Neurophysiol. 1991;65:477–493. PubMed PMID: 1711104.
148. Xu ZC, Wilson CJ, Emson PC. Morphology of intracellularly stained spiny neurons in rat striatal grafts. Neuroscience. 1992;48:95–110. PubMed PMID: 1584428.
149. Hernit-Grant CS, Macklis JD. Embryonic neurons transplanted to regions of targeted photolytic cell death in adult mouse somatosensory cortex re-form specific callosal projections. Exp Neurol. 1996;139:131–142. PubMed PMID: 8635560.
150. Stoppinni L, Helm GA, Stringer JL, Lothman EW, Benett JP. In vitro and vivo transplantation of fetal rat brain cells following incubation with various anatomic tracing substances. J Neurosci Methods. 1989;27:121–132. PubMed PMID: 2709881.
151. Brook GA, Woodhams PL, Shah B, Raisman G. Monoclonal antibody G10 which recognizes microtubule-associated protein 1x identifies growing axons of neurons microtransplanted into adult rat hippocampus. Neurosci Lett. 1993;163:148–150. PubMed PMID: 7508587.
152. Fujii M. Non-specific characteristics of intracerebral fiber elongation from the olfactory bulb transplanted into the young adult host neocortex or hippocampal formation, demonstrated immunochemically by the mouse Thy-1 allelic system. Neurosci Res. 1991;9:285–291. PubMed PMID: 1674127.
153. Fujii M. Transplant-to-host neuron migration and neurite projection from homotopically transplanted olfactory bulb as demonstrated by mouse allelic Thy-1 form. Exp Neurol. 1994;128:97–102. PubMed PMID: 8070527.
154. Zhou CF, Raisman G, Morris RJ. Specific patterns of fiber outgrowth from transplants to host mice hippocampi, shown immunohistochemically by the use of allelic forms of Thy-1. Neuroscience. 1985;16:819–833. PubMed PMID: 2419790.
155. Zhou CF, Li Y, Raisman G. Embryonic entorhinal transplants project selectively to the denervated entorhinal zone of adult mouse hippocampi as demonstrated by the use of Thy-1 allelic immunohistochemistry. Effect of timing of transplantation in relation to deafferentation. Neuroscience. 1989;32:349–362. PubMed PMID: 2573861.
156. Lund RD, Chang FLF, Hankin M, Lagenaur CF. Use of a species-specific antibody for demonstrating mouse neurons transplanted to rat brains. Neurosci Lett. 1985;61:221–226. PubMed PMID: 3909001.
157. Li Y, Raisman G. Long axon growth from embryonic neurons transplanted into myelinated tracts of the adult rat spinal cord. Brain Res. 1993;629:115–129. PubMed PMID: 8287266.
158. Davies SJA, Field PM, Raisman G. Long interfascicular axon growth from embryonic neurons transplanted into adult myelinated tracts. J Neurosci. 1994;14:1596–1612. PubMed PMID: 8126557.
159. Isacson O, Deacon TW. Specific axon guidance factors persist in the adult brain as demonstrated by pig neuroblasts transplanted to the rat. Neuroscience. 1996;75:827–837. PubMed PMID: 8951876.
160. Gaillard A., Roger M., Senee A., Jaber M. Intranigral transplantation of embryonic mesencephalic cells in an animal model of Parkinson's disease restores dopaminergic innervation to the striatum. FENS Abstr. 2004;2:A214.5.
161. Okabe M, Ikawa M, Kominami K, Nakanishi T, Nishimune Y. "Green mice" as a source of ubiquitous green cells. FEBS Lett. 1997;407:313–319. PubMed PMID: 9175875.

162. Vandevelde IL, Duckworth E, Reep RL. Layer VII and the gray matter trajectories of corticocortical axons in rats. Anat Embryol (Berl). 1996;194:581–593. PubMed PMID: 8957534.
163. Gaillard F, Domballe L, Gaillard A. Fetal cortical allografts project massively through the adult cortex. Neuroscience. 2004;126:631–637. PubMed PMID: 15183512.
164. Isacson O, Deacon TW. Neural transplantation studies reveal the brain's capacity for continuous reconstruction. Trends Neurosci. 1997;20:477–482. PubMed PMID: 9347616.
165. Raisman G. Myelin inhibitors: does NO means GO? Nat Rev Neurosci. 2004;5:157–161. PubMed PMID: 14735118.
166. Filbin MT. Myelin-associated inhibitors of axonal regeneration in the mammalian CNS. Nat Rev Neurosci. 2004;4:1–11.
167. Fournier AE, Grandpre T, Strittmatter SM. Identification of a receptor mediating Nogo-66 inhibition of axonal regeneration. Nature. 2001;409:341–346. PubMed PMID: 11201742.
168. McGee AW, Strittmatter SM. The Nogo-66 receptor: focusing myelin inhibition of axon regeneration. Trends Neurosci. 2003;26:193–198. PubMed PMID: 12689770.
169. Wang X, Chun SJ, Treolar H, Vartanian T, Greer CA, Strittmatter SM. Localization of Nogo-66 receptor proteins at sites of axon myelin and synaptic contact. J Neurosci. 2002;22:5505–5515. PubMed PMID: 12097502.
170. Stein DG, Labbe R, Attela MJ, Rakowsky HA. Fetal brain tissue transplants reduce visual deficits in adult rats with bilateral lesions of the occipital cortex. Behav Neural Biol. 1985;44:266–277. PubMed PMID: 4062780.
171. Stein DG, Mufson EJ. Morphological and behavioral characteristics of embryonic brain tissue transplants in adult, brain-damaged subjects. Ann NY Acad Sci. 1987;495:444–464. PubMed PMID: 3037969.
172. Barth TM, Stanfield BB. Homotopic, but not heterotopic, fetal cortical transplants can result in functional sparing following neonatal damage to the frontal cortex in rats. Cereb Cortex. 1994;4:271–278. PubMed PMID: 8075532.
173. Zhou W, Raisman G, Zhou C. Transplanted embryonic entorhinal neurons make functional synapses in adult host hippocampus. Brain Res. 1998;788:202–206. PubMed PMID: 9555013.
174. Paxinos G, Watson C. The rat brain in stereotaxic coordinates. Sydney: Academic Press; 1986.
175. Paxinos G, Franklin KBJ. The mouse brain in stereotaxic coordinates. 2nd ed. San Diego: Academic Press; 1997.

Electrophysiology

The Study of Light-Evoked Field Potentials

Visually Evoked Potentials

Donnell Creel, PhD[1]

Created: March 1, 2012.

Introduction

The terms visually evoked potential (VEP), visually evoked response (VER) and visually evoked cortical potential (VECP) are equivalent. They refer to electrical potentials, initiated by brief visual stimuli, which are recorded from the scalp overlying visual cortex. VEP waveforms are extracted from the electro-encephalogram (EEG) by signal averaging. VEPs are used primarily to measure the functional integrity of the visual pathways from retina via the optic nerves to the visual cortex of the brain. VEPs better quantify functional integrity of the optic pathways than scanning techniques such as magnetic resonance imaging (MRI).

Any abnormality that affects the visual pathways or visual cortex in the brain can affect the VEP. Examples are cortical blindness due to meningitis or anoxia, optic neuritis as a consequence of demyelination, optic atrophy, stroke, and compression of the optic pathways by tumors, amblyopia, and neurofibromatosis. In general, myelin plaques common in multiple sclerosis slow the speed of VEP wave peaks. Compression of the optic pathways such as from hydrocephalus or a tumor also reduces amplitude of wave peaks.

This review covers a brief history of visual evoked potentials, the most commonly used stimuli to initiate visual evoked potentials, the methods of recording, the sources of visual potentials, the effects of maturation and acuity, and sample patients.

History

VEPs initiated by strobe flash were noticed in the early years of clinical encephalography (EEG) in the 1930s. A VEP can often be seen in the background EEG recorded from the occipital scalp following a flash of light (Fig. 1). Evoked potentials, whether auditory, visual or somatosensory, are extracted from the EEG by a simple program. This technique of extracting a signal from random noise is one of the oldest applications of computer technology. This process is similar to programs used to extract radar signals from jamming nearly 70 years ago. Adding the electrical activity for set time periods is called "signal averaging". Dawson first demonstrated a signal-averaging device in 1951 and signal-averaging computers have been available since the early 1960s. The computer programs save a defined time period of EEG activity following a visual stimulus, which is repeated over and over adding the signals together. The random EEG activity averages away, leaving the visually evoked potential. Depending on the signal to noise ratio, an evoked potential can be seen forming following only a few stimuli such as flashes of light.

Electrode locations on the scalp

Visually evoked potentials elicited by flash stimuli can be recorded from many scalp locations in humans. Visual stimuli stimulate both primary visual cortices and secondary areas. Clinical VEPs are usually recorded from occipital scalp overlying the calcarine fissure. This is the closest location to primary visual cortex (Brodmann's area 17). A common system for placing electrodes is the "10-20 International System" which is based on measurements of head size (1). The mid-occipital electrode location (0Z) is on the midline. The distance above the inion calculated as 10% of the distance between the inion and nasion, which is 3-4 cm in most adults (Fig. 2). (The inion is the most prominent projection of the occipital bone at the posterioinferior (lower rear) part of the skull. The nasion is the intersection of the frontal bone and two nasal bones of the human skull.) Lateral occipital

Author Affiliation: 1 Moran Eye Center, University of Utah; Email: Donnell.creel@hsc.utah.edu.

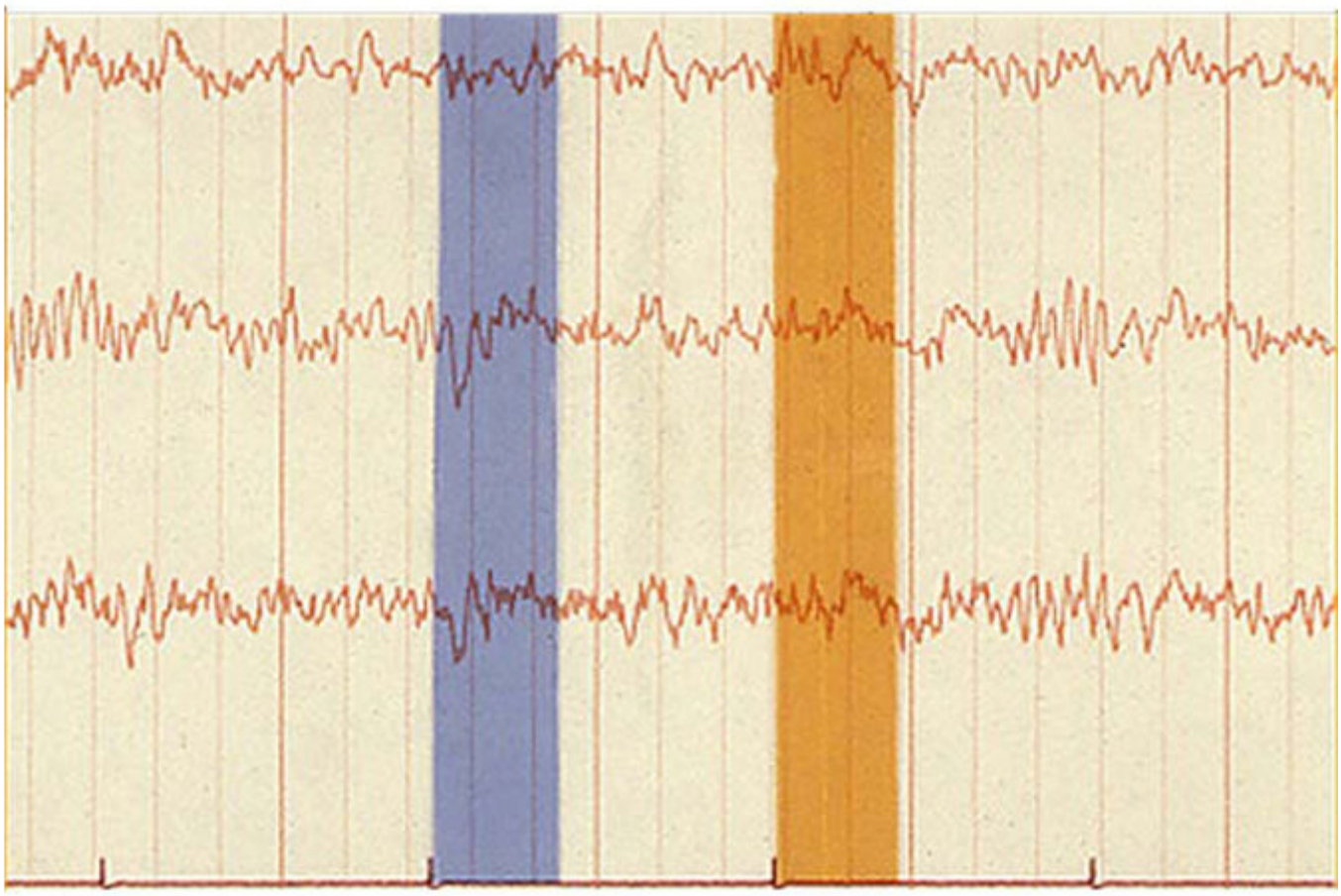

Figure 1. EEG tracings showing the time periods following flash presentations (blue and yellow areas) that are typically the waveforms of the VEP.

electrodes (01, 02) are a similar distance off the midline. Another set of locations is the "Queen Square system" in which the mid-occipital electrode is placed 5 cm above the inion) on the midline and 5 cm lateral from that location for lateral occipital electrodes (2). The Queen Square locations, further off the midline, are better able to lateralize anomalies such as when using hemi-field stimulation. Some laboratories, and unique applications, have other preferred scalp locations.

Many laboratories record from an array of locations placed horizontally across occipital scalp in an attempt to lateralize pathology. Other laboratories use only a single positive midline recording electrode at OZ with one earlobe as negative location and the other earlobe as ground location. A second montage is necessary for recording multifocal visually evoked potentials (mfVEPs). A common mfVEP montage is to place two electrodes on the midline one just below the inion and another 3 centimeters above the inion; and laterally place electrodes 3-4 centimeters off the midline several centimeters above the inion.

Sources of visual evoked potentials

Most of primary visual cortex in humans is located in fissures, not on the cortical surface of the occipital pole. At most, only about the central 10 degrees of visual field are located on the surface of the occipital pole. Furthermore, the area located on the surface of the occipital pole is quite variable, even between hemispheres of the same individual. Because most electrical potentials are generated in sulci (deep cortical fissures) simultaneously at multiple locations, and because of the vertical cancellation that occurs between upper and lower fields, lateralization of pathology is difficult. Potentials occurring at different cortical locations in vertical

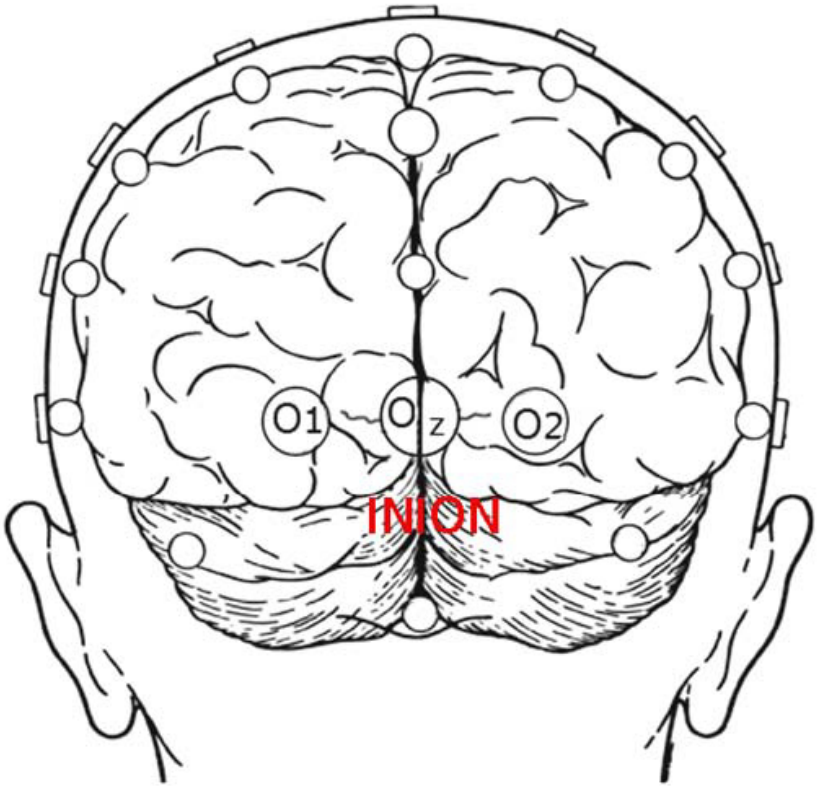

Figure 2: Occipital scalp electrode locations using the 10-20 International System. The INION is the scull location at the position shown. The nasion is on the face between the eyes.

and horizontal planes that vary between hemispheres produce paradoxical lateralization and obscures source localization.

The series of MRIs in Figure 3 demonstrate locations of significantly higher blood flow in occipital visual areas while the subject views a video monitor. The monitor subtends a 30-degree field displaying a 100% contrast, checkerboard pattern, flashing at 4 Hz. Note the lack of high levels of activity on the surface of the occipital pole and the interhemispheric variation (Fig. 3).

The neural generators of the waves of the visual evoked potential (VEP) (see Fig. 5) are not clearly defined. Research with multichannel scalp recordings, visual MRI activity and dipole modeling, supports the interpretation that the visual cortex is the source of the early components of the VEP (N1, N70) prior to P1 ("P100") (3). The early phase of the P1 component with a peak around 95-110 msec, is likely generated in dorsal extrastriate cortex of the middle occipital gyrus. The later negative component N2 (N150) is generated from several areas including a deep source in the parietal lobe (4).

As depicted in the functional visual MRIs in Figure 3, brain activity varies considerably in the occipital area. A number of dipole fields are generated resulting in a complicated interaction (5). These multiple sites of generators interact at different levels in the visual areas making source localization difficult when making individual clinical decisions. Because of individual idiosyncrasies in occipital anatomy and visual projections, one cannot make the assumptions about sources that one can using electroretinograms (ERGs), (see basic and clinical chapters on ERGs in webvision) or auditory brainstem responses.

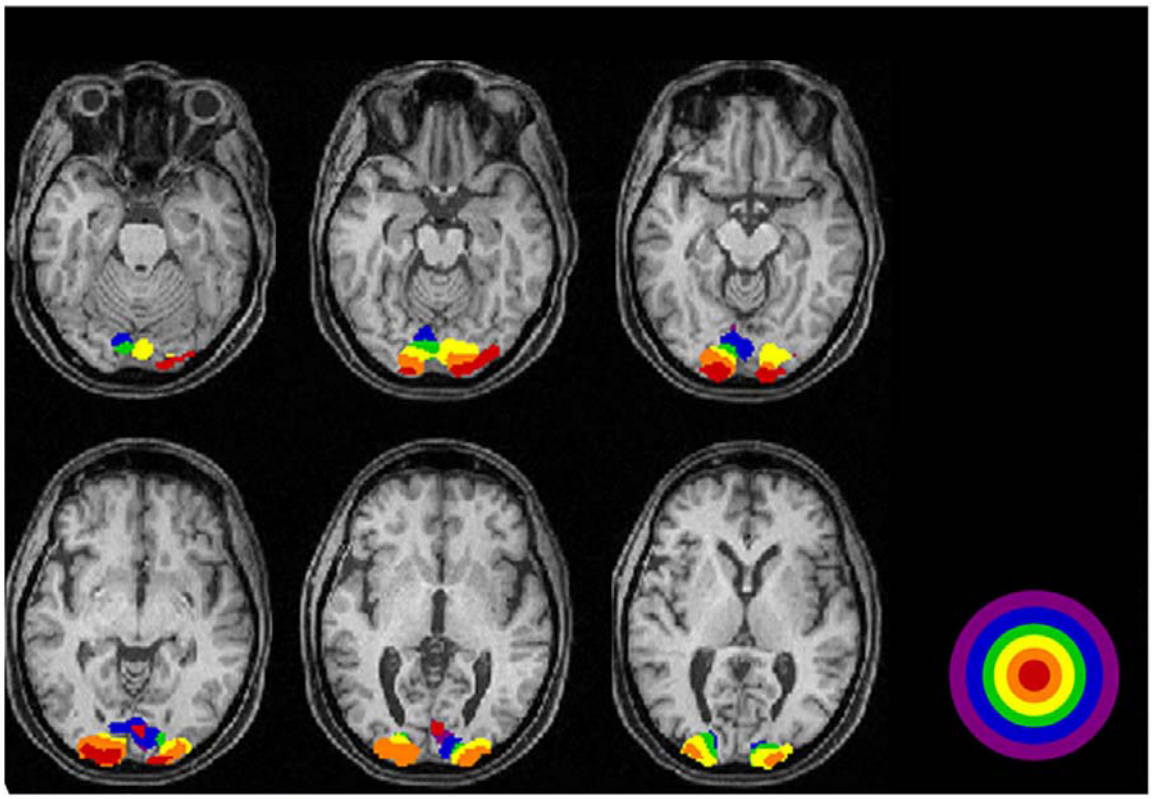

Figure 3: Functional MRI sections of the occipital visual areas showing maximal blood flow (activity) during visual pattern stimulation. Maximum is red, minimum is blue to purple. These functional MRIs were provided by Jeffrey Anderson, University of Utah.

VEP Recording methods

When applying electrodes, and cleaning scalp locations for electrodes one must remember the computer adage "garbage in, garbage out". Scalp locations need to be cleaned to produce low electrode impedance. One must be precise about recording with low impedance and choosing electrode locations.

A reference electrode is usually placed on the earlobe, on the midline on top of the head or on the forehead. A ground electrode can be placed at any location, mastoid, scalp or earlobe. The time period analyzed is usually between 200 and 500 milliseconds following onset of each visual stimulus. When testing young infants, analysis time should be 300 msec or longer because components of the VEPs may have long peak latencies during early maturation. Most children and adults may be tested using an analysis time of 250 msec or less. The most common amplifier bandpass frequency limits are 1 Hz and 100 Hz. Amplifier sensitivity settings vary with +/- 10 μV common for older children through adults and +/- 20 to 50 μV for infants and younger children. Sometimes the sensitivity setting must be changed to accommodate larger EEG voltage in all age groups. See the ISCEV (International Society for Clinical Electrophysiology of Vision) standard for clinical VEPs for variety of recommended test protocols (6). Commonly used visual stimuli are strobe flash, flashing light-emitting diodes (LEDs), transient and steady state pattern reversal and pattern onset/offset.

The most common stimulus used is a checkerboard pattern, which reverses every half-second (Fig. 4). Pattern reversal is a preferred stimulus because there is more inter-subject VEP reliability than with flash or pattern onset stimuli. Several laboratories developed pattern reversal visual stimuli in the 1970s including A. M. Halliday at Queen Square in London and Lorrin A. Riggs at Brown University. Originally Halliday back-projected a checkerboard pattern onto a translucent screen with two projectors that each projected reversed checkerboard

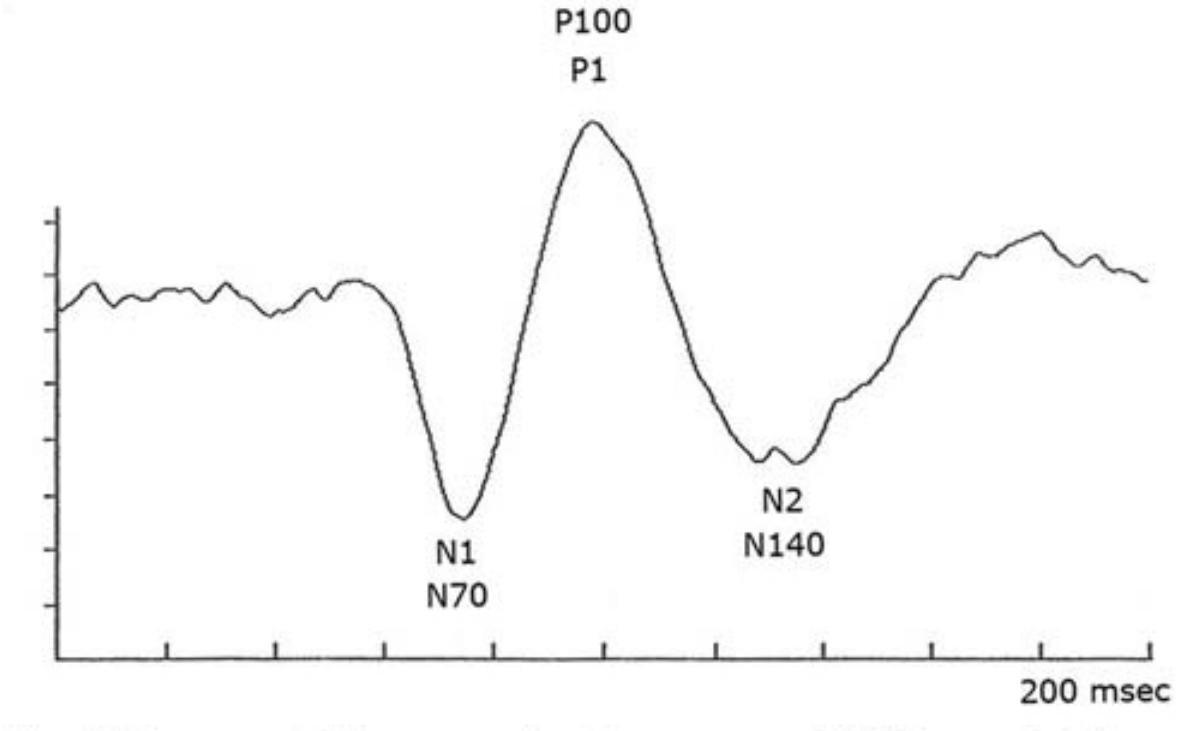

Figure 5: Representative normal pattern reversal VEP recorded from mid-occipital scalp using 50' checkerboard pattern.

images. Camera shutters on each projector controlled the display of each checkerboard reversing at a rate 2 per second. Riggs originally projected alternating vertical stripes using a reversing mirror system. Commercially produced visual evoked potential systems simulating these pattern reversals now use video monitors.

Using cathode ray tube monitors (CRT) nearly everyone with close to normal visual function produces a similar evoked potential using pattern reversal stimuli. There is a prominent negative component at peak latency of about 70 msec (N1, Fig. 5), a larger amplitude positive component at about 100 msec (P1, Fig. 5) and a more variable negative component at about 140 msec (N2, Fig. 5). The major component of the VEP is the large positive wave peaking at about 100 milliseconds (Fig. 5). This "P100" or P1 in the jargon of evoked potentials, is very reliable between individuals and stable from about age 5 years to 60 years. The mean peak latency of the "PI00" only slows about one millisecond per decade from 5 years old until 60 years old.

Video monitors that produce brighter, faster changing patterns such as liquid crystal displays (LCD) evoke faster VEPs than cathode ray tube video monitors. The "P100" or P1 component is much faster using liquid crystal displays (LCD) evoking P1 peak latency times of less than 90 milliseconds. Variation in stimulus parameters is a good reason for each laboratory to have their own normative data even if the manufacturer provides such data.

The size of each check in the pattern and size of the visual field affects the VEP. Most laboratories initially screen patients using a video display with field subtending 10-40 degrees of arc and fairly large individual check size of about 1 degree of arc. A large check size is used because most clinical laboratories are recording from patients who lack good visual acuity. The largest amplitude, fastest peak latency VEP is recorded using the smallest check size the subject can see sharply. A person with 20/20 (6/6) or better vision will produce the largest amplitude, fastest VEP components using a small check size (a visual field comprised of checks only 5-6 mm viewed at 1 meter). Each check would measure about 15-20' of arc. A person with poor visual acuity would produce the largest amplitude, fastest components with a larger check size subtending a degree or more (such as a 20 mm

check or larger viewed at 1 meter distance). This is the basis for one being able to estimate acuity by testing a subject with several check sizes. The "P100" (P1) component is sensitive to defocusing and can, therefore, be measured following stimulation with different check sizes to estimate refractive error. For most clinical screening, a single check size of about 1 degree of arc, or a little smaller, such as about 50' of arc, is sufficient. One need not use larger checks for children. Once a child is mature enough to attend and maintain fixation their visual systems are mature enough to use the same size stimuli as adults.

The VEP waveform, amplitudes and peak latencies depend upon the parameters of the stimulus. Steady state VEPs are those recorded using stimulation rates of 3 or more per second. Transient VEPs are recorded using rates of less than 3 per second. Transient pattern VEPs have components that can be followed during maturation, pathological conditions and changes of acuity. Flash-evoked and pattern onset VEPs are reliable in form within the individual but vary considerably between patients. The checkerboard pattern can also be made to appear (onset) and disappear (offset). In many individuals the pattern onset VEP is opposite in polarity compared to flash and pattern reversal VEPs. The pattern onset VEP usually includes a positive component at about 80 msec and a large negative component at about 110 msec. Another advantage of the pattern reversal VEP is that it has a smaller standard deviation for the P1 component (about 6 msec). The P110 component of the flash VEP and the N110 component of the pattern onset VER have standard deviations of about 10 msec.

Maturation of VEPs with age

By age three years, children can usually co-operate fully allowing use of the same recording parameters as adults. The problem is not that a child's visual system is developed insufficiently. It is. The problem for children less than 3 years of age is one of maintaining fixation. Below approximately age three, in examinations under anesthesia, trauma cases, and other causes of very poor vision, flash stimuli generated by strobe or LED flash may be required. Retinal development, cortical cell density, myelination and visual acuity are close enough to that of an adult by age 5 years, that children by this age produce adult VEP waveforms. There are changes that take place into adolescence, but these have subtle effects on the VEP.

Thus, the most dramatic changes are in the first several years after birth (7). What will mature into the "P1" component of the flash VEP can be recorded in the full term infant within 5 weeks of age with a peak latency of less than 200 msec. VEPs change rapidly in form and complexity in the first six months. As the infant matures this late "P1" appears earlier and earlier so that by about age 4-5 years, peak latency shortens to about 100 msec using pattern reversal stimuli, and about 110 msec using flash stimuli. Peak latency times remain at this point for most of one's adult life with no statistically significant change until after age 55 years.

Components of the VEP change gradually after age 55 displaying attenuation in amplitude and slowing of the P1 component (Fig. 6). Thus, the two periods in life that vary most in VEP physiology are the first few years during early maturation and during aging after age 60 years. Aging adults late in life vary even more than developing children. Figure 6 shows a sample scattergram of P1 peak latencies across age.

The amplitude of the mature P1 component of flash and pattern VEPs is greatest at about age 7-8 years. The brain reaches 90% of adult size as early as age 6 years. Preadolescence is the period when the brain is largest relative to skull, scalp and muscle thickness. As children enter adolescence and mature these tissues thicken attenuating the brain's signal as recorded from the overlying scalp. The amplitude and speed of VEPs remains stable until about age 28 years at which time amplitudes begin to attenuate (8).

The VEP recorded from mid-occipital scalp is about 90% weighted in that it reflects the function of the central 10 degrees of the visual field. Ten degrees is about the maximum visual field that is on the occipital cortical surface. Whatever method is used, it is important for a laboratory to replicate testing of each subject and to gather normative data. Each subject should be placed the same distance from the visual stimuli, and room lighting should be the same.

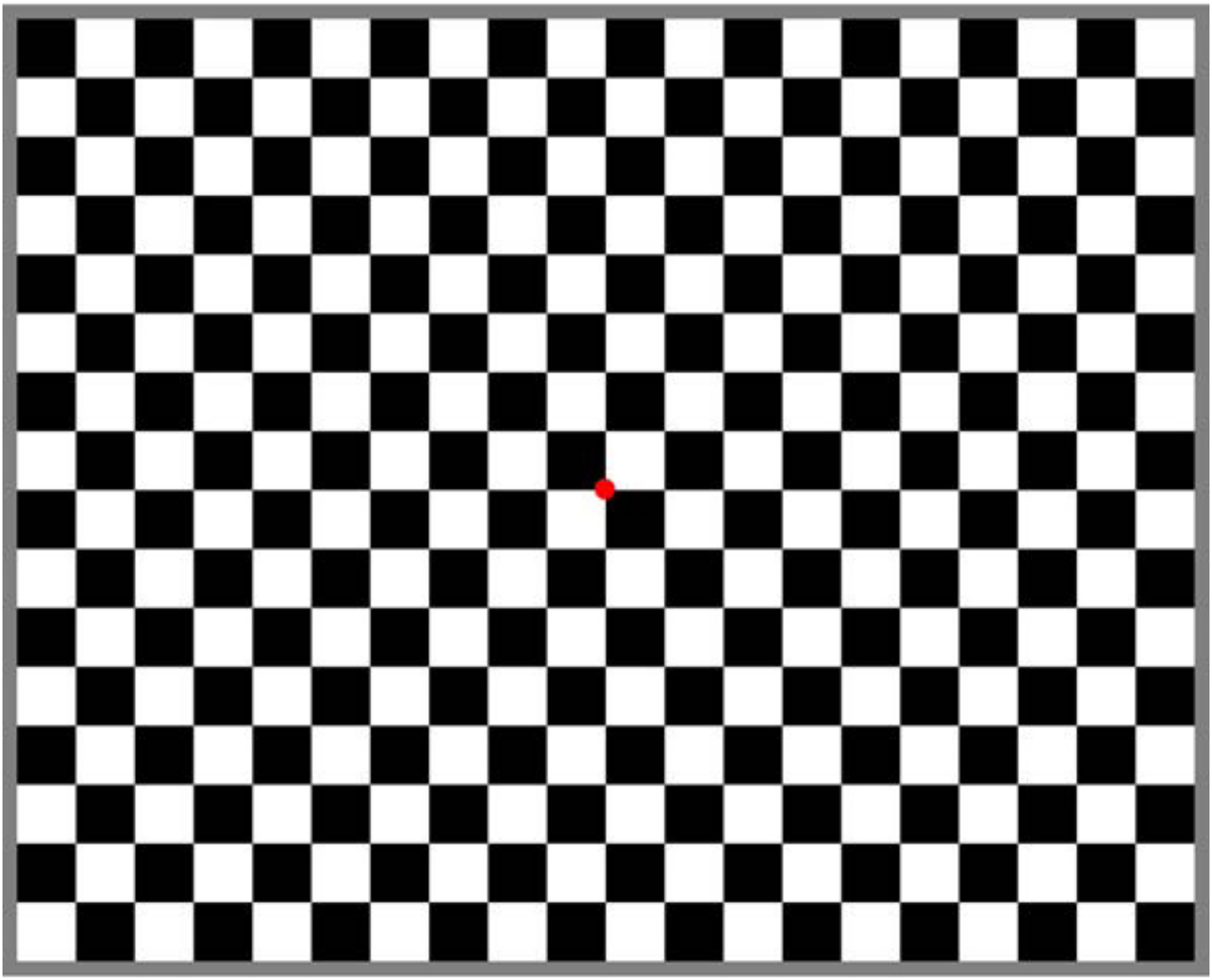

Figure 4: Checkerboard pattern with red fixation point.

VEPs quantify visual system function. Abnormal VEPs can be symptomatic of dysfunction, but are not diagnostic of it until carefully considered within the context of the patient's clinical picture. When recording VEPs the diagnostic yield is dependent upon appropriate selection of visual stimuli.

If the history and ophthalmic examination of a patient raises the possibility of dysfunctional retina, optic nerves, tracts or cortices, the VEP may yield diagnostically useful information. A common clinical referral is patients where the question is whether their visual problems are due to retinal or central visual dysfunction. Recording both an electroretinogram (ERG) and VEP will usually answer this question.

VEP testing under anesthesia (E.U.A.)

Examinations under anesthesia (E.U.A.) can be conducted recording both VEPs and ERGs. Anesthesia is used for various reasons ranging from 'the patient is unexamineable while alert' to, more often, that some of the examination procedures are uncomfortable or painful (such as biopsies). Unfortunately, anesthesia affects the

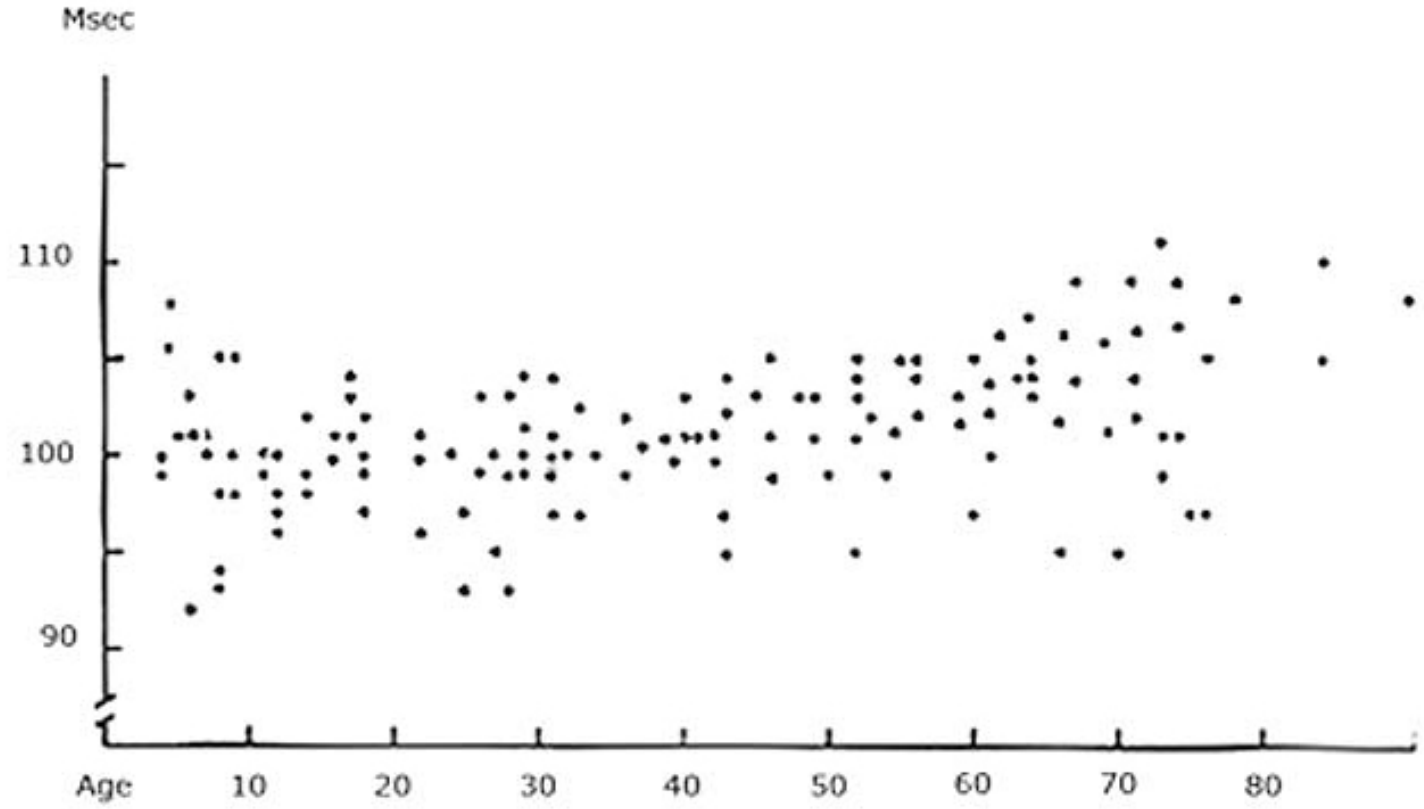

Figure 6: Scattergram of pattern reversal VEP "P100" component peak latencies recorded from normal individuals ages 5-90 years of age.

VEP, varying with type and depth of anesthesia. Most surgical deep anesthetics obliterate the cortical activity necessary to produce the VEP. Yet auditory brainstem responses (ABRs) and somatosensory evoked potentials (SEPs) can still be recorded. Most VEP computers display the EEG. If the EEG is flat you will not record VEPs.

Anesthesiologists start with fairly deep anesthesia while putting in lines. I usually ask the anesthesiologist: "When the patient is stable will you please lighten the anesthesia as much as you are comfortable with." Ask permission before touching the patient. This is especially important if you wish to raise the head to place the occipital electrode. Raising the head may crimp the tracheal tube.

If recording both ERGs and VEPs under anesthesia, record the ERG first because it is more resistant to anesthesia. In the minutes it takes for the ERG recording, the patient's anesthetic depth lightens further. Rarely must one wait more minutes for the patient to lighten.

The influence of refractive error

If pattern stimuli are to be used, it is important that a patient be tested with refractive error corrected. Refractive errors will affect the interpretation of the VEP results. For example, adults with LASIK correction so that one eye is for distance vision, the other for near, will affect VEP amplitudes and peak latencies. Select the most powerful stimulus that the visual acuity and cooperation of the patient will allow. If the corrected visual acuity of the patient is approximately 20/200 (6/60) or better, and the patient does not have nystagmus, the stimulus of first choice would be pattern reversal starting with about a 50' check. If the resulting VEP appears well formed, and if measuring acuity is an issue, next use a smaller check size in the range of about 15-20' of arc. When testing for

refractive errors such as estimating acuity, smaller check sizes (e.g., 15') and lower contrast (<50%) are recommended. In the normal infant 20/20 (6/6) vision is present by about 9 months of age. Check sizes subtending 10-20' of arc are the best stimuli for testing foveal vision. Checks of 40-50' are superior in evaluating parafoveal function, therefore using more than one check size increases diagnostic yield. If the resulting VEP using the 50' check is poorly formed, retest using a larger check size or use a pattern onset stimulus. Pattern reversal stimuli are the best choice in cooperative patients with good visual acuity, particularly when testing for possible effects of optic neuritis, hydrocephalus, ventriculitis, cortical hematomas, optic atrophy, neurofibromatosis or compression of the optic pathways.

If the corrected acuity of the patient is approximately 20/200 to 20/400 (6/60-6/120) and/or the patient has nystagmus, the preferred stimulus would be pattern onset. Pattern onset or "pattern flash" stimuli produce a more robust VEP than does pattern reversal. Pattern reversal stimuli usually exacerbate nystagmus interfering with the ability of the eye to maintain foveal fixation. Pattern onset stimuli can also be the most productive stimulus in conditions such as monitoring amblyopia, in patients with poor acuity, possible hemispheric asymmetry or a defect in geniculo-striate projections. Pattern onset usually produces a more robust VEP initiated from the central 30 degrees of retina (9).

If the patient's acuity is approximately 20/400 (6/120) or worse, or the patient is uncooperative, unconscious, sedated or anesthetized, the stimulus of choice is strobe or LED flash. Flash stimuli are useful in infants who will not maintain fixation on a pattern. The resulting VEP will usually detect significant optic atrophy and other abnormalities of the central visual pathways. In many cases of cortical blindness the flash VEP will be abnormal, although sometimes it is normal. The VEP is often prognostic in delayed maturation of the visual system (usually the infant with delayed maturation has a normal flash VEP). Permanently cortically blind infants usually have abnormal VEPs. Flash stimuli produced by LEDs can be useful in some patients. LED arrays are available inside goggles and on discs about 50 mm in diameter. These are more effective than a strobe lamp for monocular stimulation, and useful in the operating room when monitoring VEPs during surgery or E.U.A.

For initial screening of most patients the electrode montage of choice is a single recording electrode placed on the midline overlying the central pole of the occipital cortex, which lies approximately 3-4 cm above the inion. The VEP recorded from this location exaggerates the contribution of the macular portion of the retina due to the fact that only the macula is projected onto the occipital pole. This recording site is referred to an electrode placed on the earlobe or on the midline of the upper forehead or head. There is no significant difference in the VEPs obtained using most reference points although technically the earlobe is the more electronically neutral site than scalp locations. As mentioned earlier, correct lateralization of pathology by using recording electrodes off the midline overlying occipital cortex, is difficult using the VEP. Information obtained from computed tomography (CT) and MRI scans better localize such pathology.

Examples of VEP recordings in different retina-brain pathologies

There are hundreds of syndromes and visual anomalies that can affect VEPs. A limited sampling is presented but in the same format as in Figure 7 for all the following case figures. The N1 wave is called N75, The P1 wave is called P100 and the N2 wave is called N145, in all our data (VEP normal averages under our testing conditions).

Multiple Sclerosis

The visually evoked potentials in Figure 7 were recorded from a patient with early signs of multiple sclerosis including optic neuritis. As is usual in these cases, initially one nerve (right eye measurements, top traces, Fig. 7) yields normal evoked potentials (98 msec close to the P100 norm. Scale is 25 msecs between vertical ticks). The left nerve, affected with retrobulbar optic neuritis shows a delayed P100 component (Fig. 7, left eye measurements P100 is 110 msecs, lower traces). Since the standard deviation for the peak latency of P1 is usually about 6 milliseconds, a P1 peak of 110 milliseconds is considered abnormal. Patients with MS usually develop

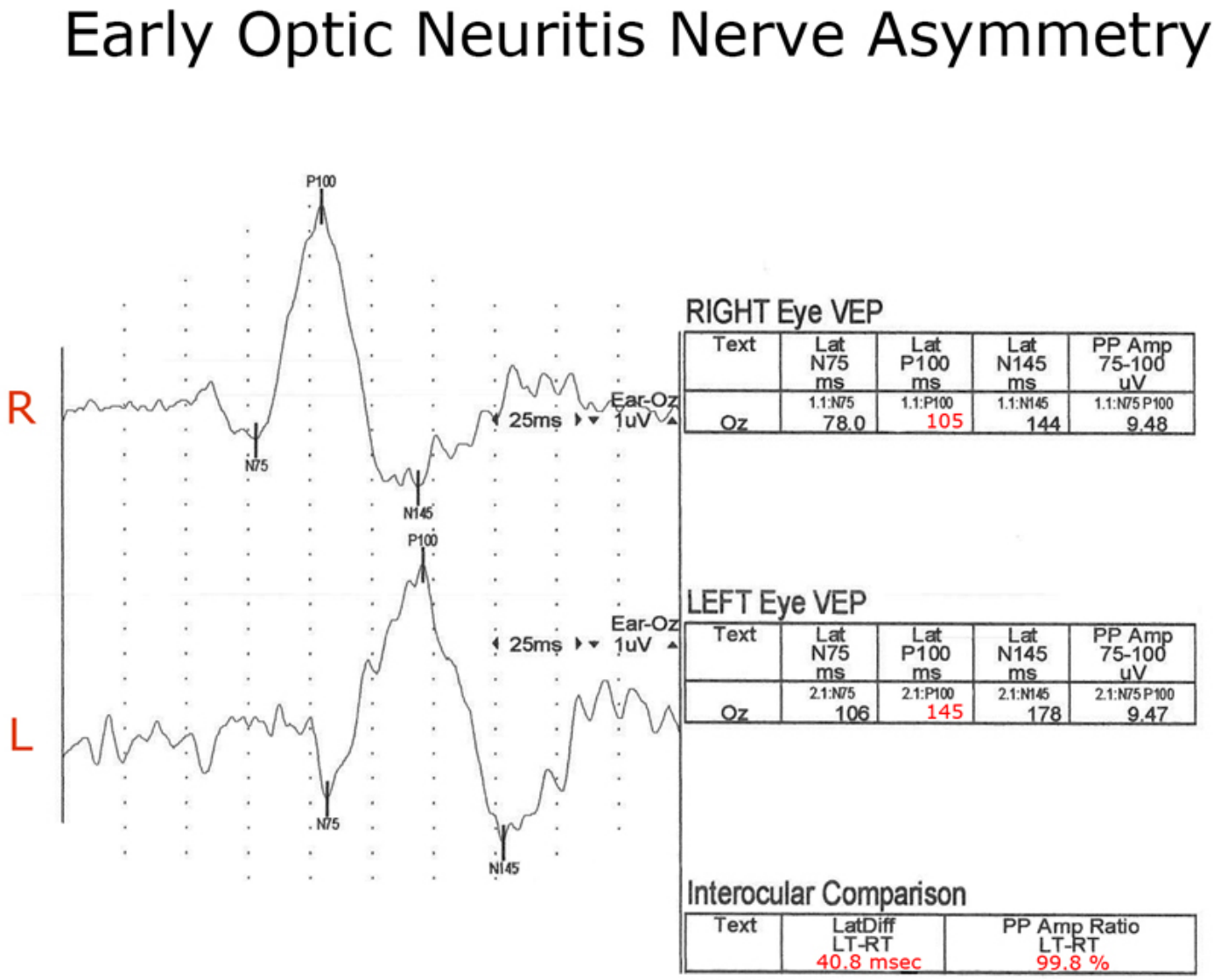

Figure 7: Pattern reversal VEPs recorded from adult female with early unilateral optic neuritis. N75, P100 and N145 waves are labeled. VEP traces of Right and Left eye stimulation are displayed. The vertical tick marks are in 1uV intervals. The RIGHT eye peak latencies are normal range. The LEFT eye peak latencies are significantly slow. The Interocular differences are shown in the lowest box.

optic neuritis later in the other nerve (Fig. 8). Over the years the VEPs in patients with MS become progressively slower eventually attenuating in amplitude as demyelination increases (Fig. 9).

Trauma

Another application of VEPs is to quantify visual system function following trauma. It is not unusual that compression of optic pathways immediately after severe trauma results in no recordable VEPs. However, VEPs may be recordable days later when inflammation subsides. Figures 10, 11 and 12 show the sequence of recovery in an infant with head trauma producing compression of the optic nerves and the occipital brain area.

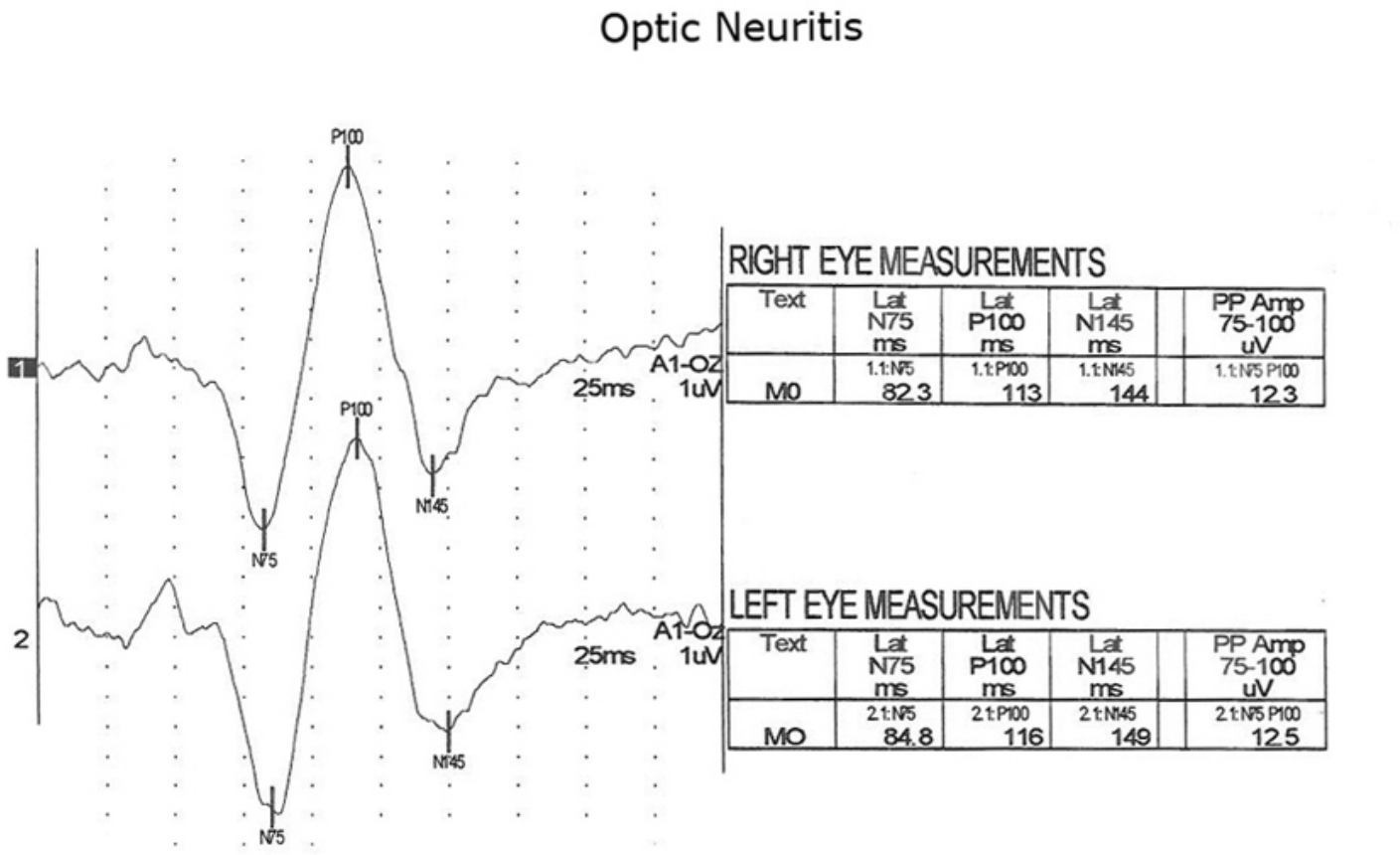

Figure 8: Pattern reversal VEPs recorded from a 37 year old with bilateral optic neuritis showing slowing of components.

Tumors

Children with neurofibromatosis type 1 (NF1) are vulnerable to development of optic nerve gliomas. The VEP can be a more sensitive and cost effective test to follow the progress of nerve pathology than MRI tests alone. Essentially all children with NF1 show slowing of VEPs by school age (Fig. 13).

As is true for any space-occupying tumor or other compression such as hydrocephalus affecting visual pathways, the VEP is useful to quantify compression of pathways. The next three figures (14, 15 and 16) show progression of development of bilateral optic nerve gliomas in a child with NF1.

Recovery of function

VEPs are also useful in following recovery of most optic pathway dysfunction. The next two figures (17 and 18) show flash VEPs recorded prior to and 2 weeks following removal of a large orbital mass from a 3 year old.

Figure 19 shows the VEPs of another type of tumor in a child - a unilateral neuroblastoma.

VEPs can be useful in quantifying and following the progression of optic nerve hypoplasia, optic atrophy or pale nerve. Figure 20 is an ocular fundus photo of a child with a pale optic nerve. Figure 21 displays flash VEPs recorded from the 9-year old child with pale optic nerves (Fig. 20). The VEPS are both attenuated in amplitude and have prolonged component peak latencies.

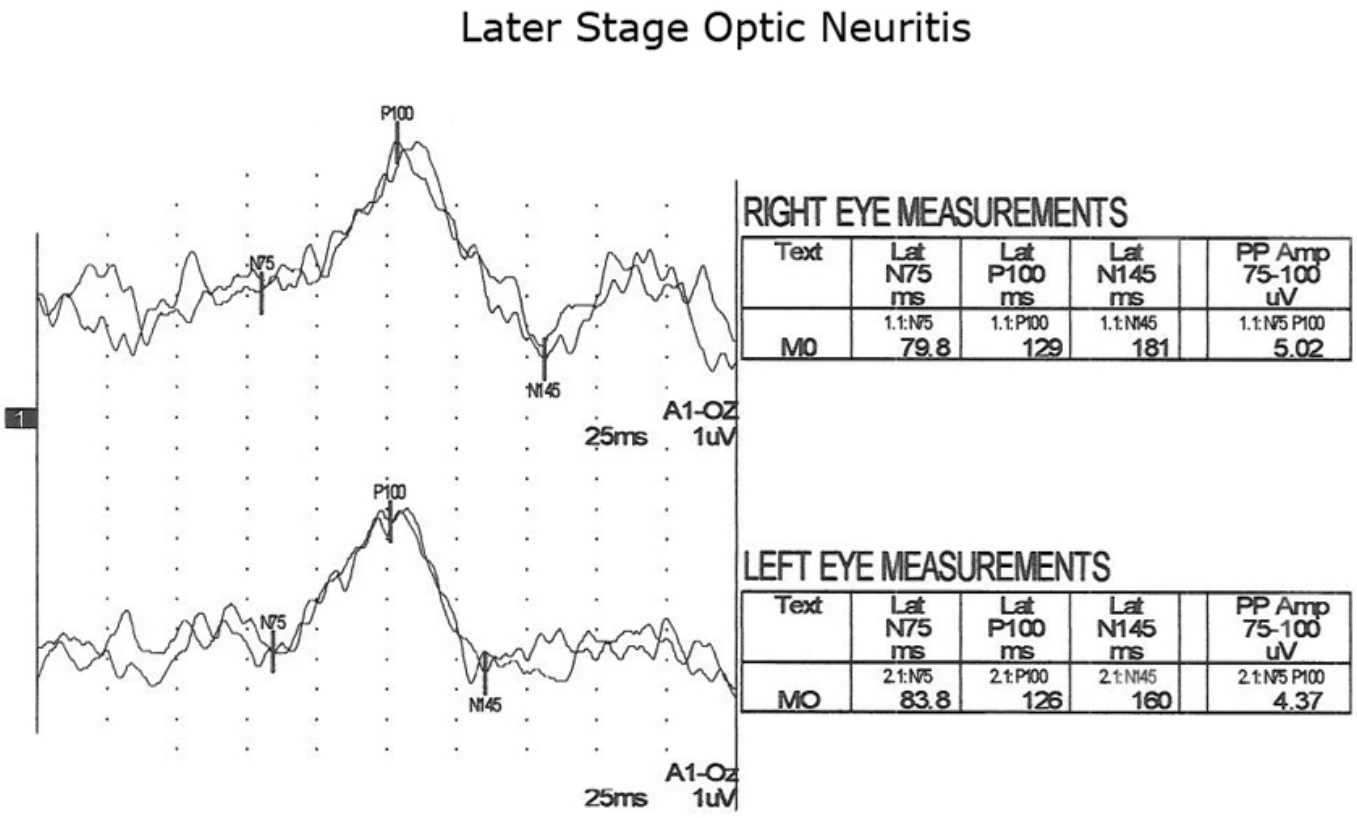

Figure 9: Pattern reversal VEPs of the MS patient years after initial onset of optic neuritis showing progressively slower P100s.

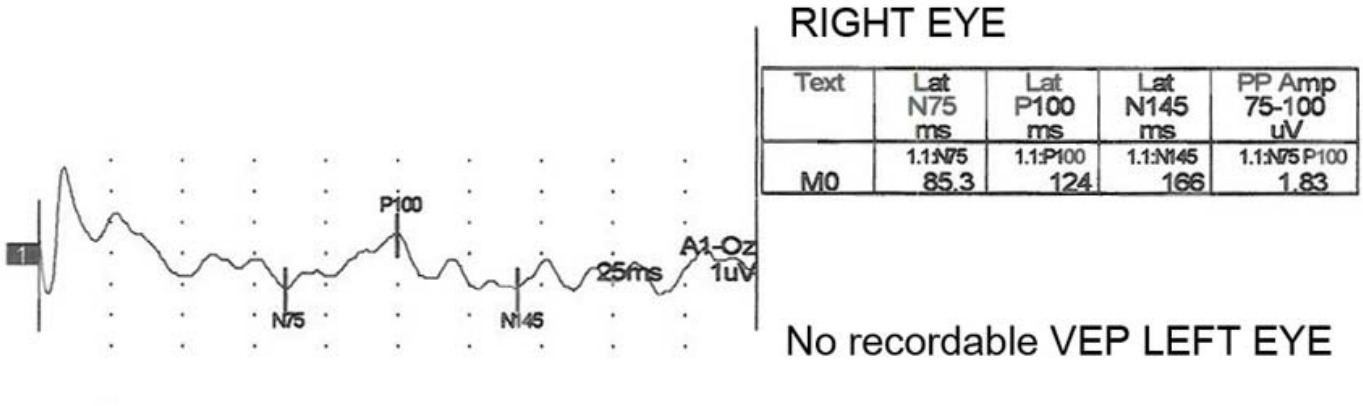

Figure 10: Flash VEPs recorded soon after occipital trauma in a 2 year old showing a small VEP amplitude in the right eye and no VEP in the left eye.

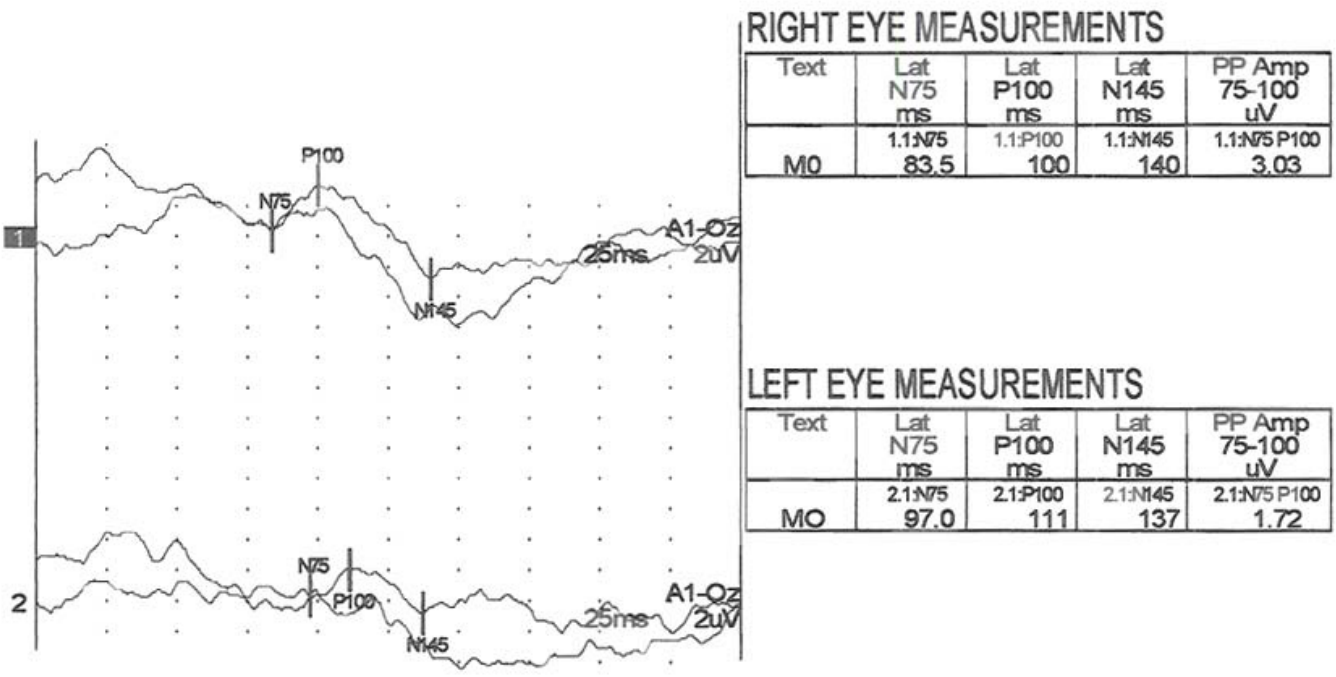

Figure 11: Flash VEPs recorded from the 2 year old, one month after occipital trauma showing some recovery of the optic nerve pathways.

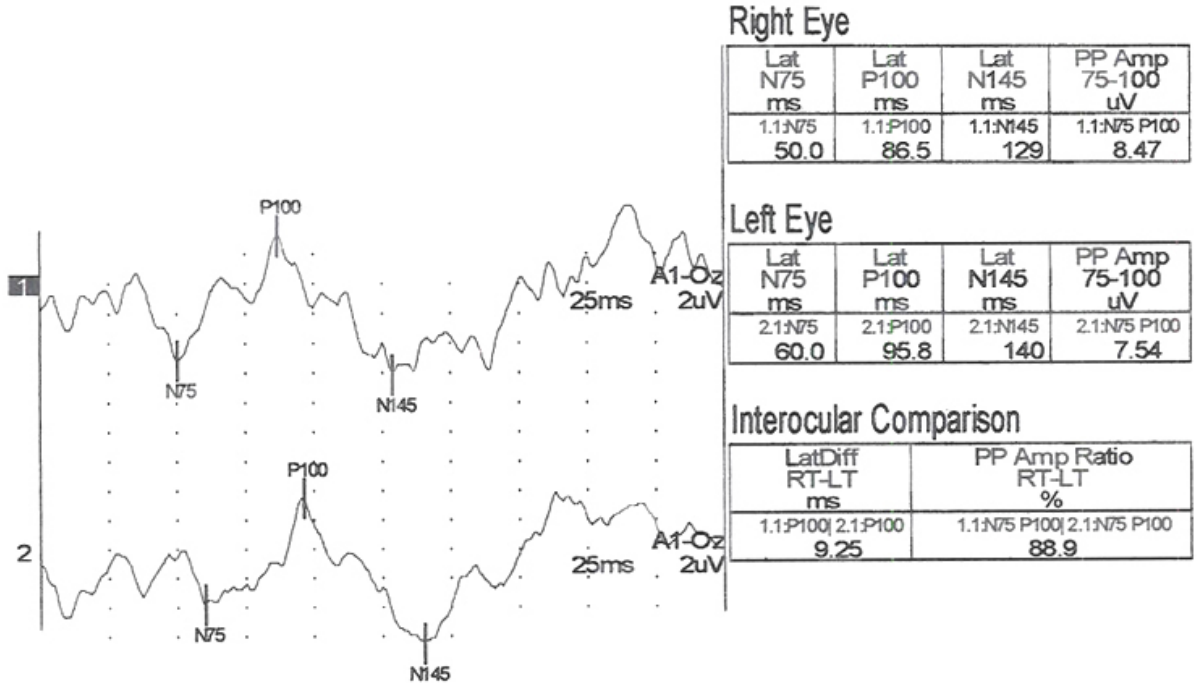

Figure 12: Flash VEPs recorded from the 2 year old, two months after occipital trauma showing further recovery.

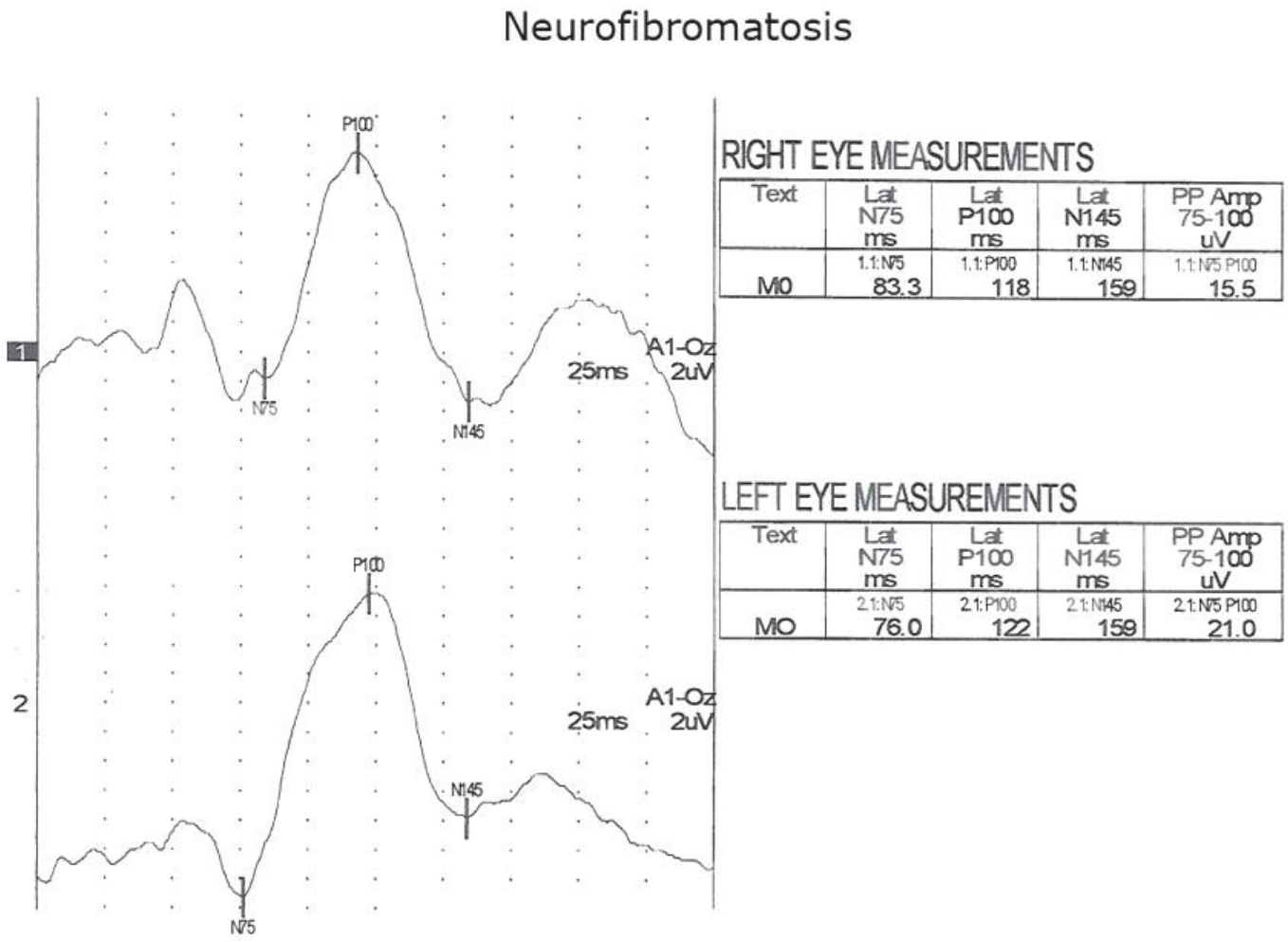

Figure 13: Pattern reversal VEPs recorded from a 5 year old with neurofibromatosis type 1 (NF1) showing slowing of VEP components in both optic nerves.

Optic Nerve Toxicity

Some medications can be toxic to optic nerve function. Figure 22 displays pattern reversal VEPs in an adult with Ethambutol optic nerve toxicity. Again there are delayed peak latencies.

There are several medications that can be toxic to the optic nerves including Amiodarone an antiarrhythmic medication used to treat ventricular tachycardia or ventricular fibrillation. In some patients Amiodarone is associated with ischemic optic neuropathy. The VEPs of these patients show prolonged peak latencies.

A partial list of toxins and medications associated with optic neuropathy includes carbon monoxide, ethylene glycol, and methanol. The antimicrobials Ethambutol, Isoniazid and Linezolid, are drugs that have indirect effect on the optic nerve. Sildenafil (Viagra) and Infliximab can also affect optic nerve function. VEPs also provide information about visual cortical function. VEPs, recorded from patients suffering from birth anoxia or near-death drowning, will quantify the degree of occipital cortex dysfunction. In general recordable VEPs are a positive prognostic sign.

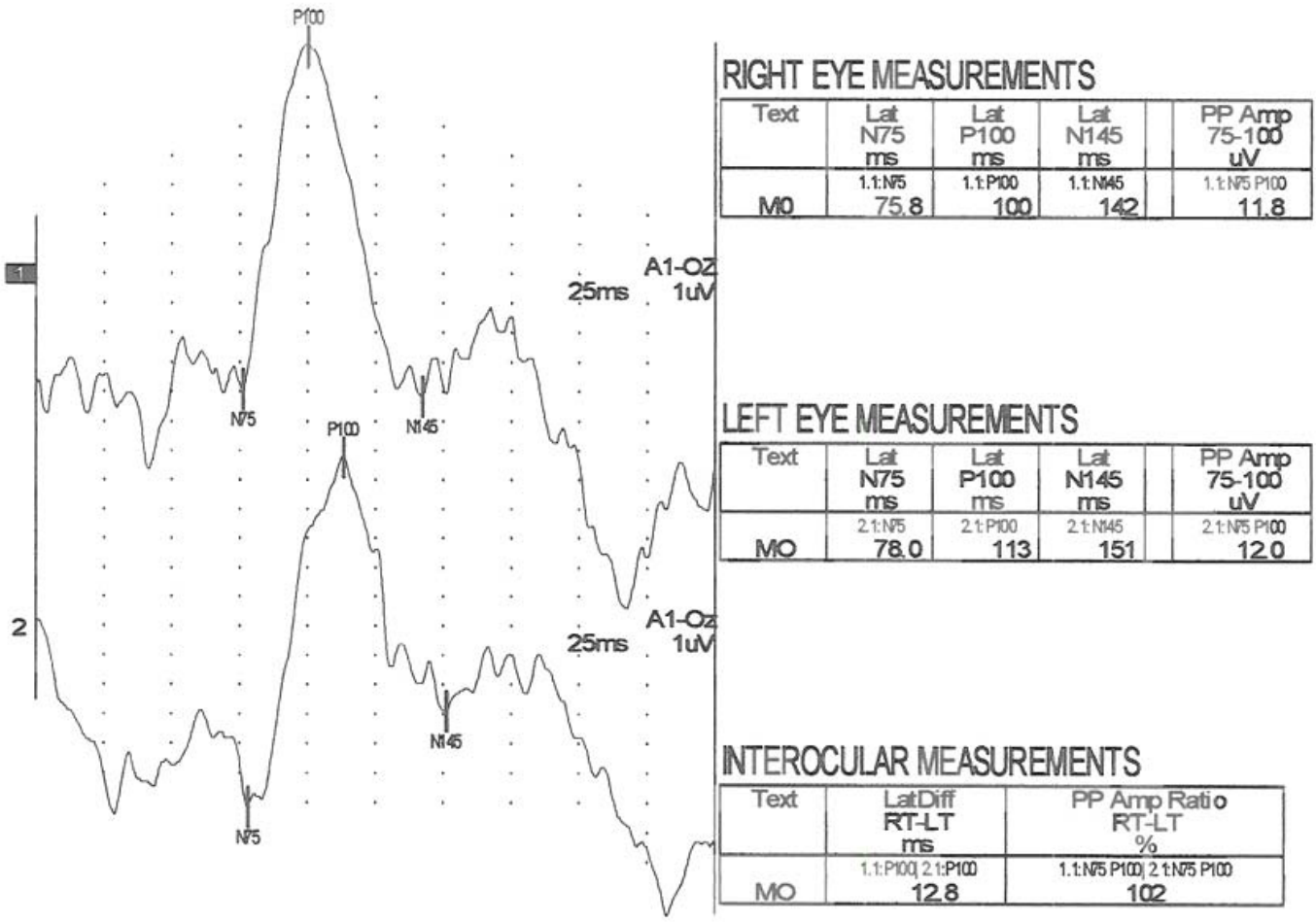

Figure 14: Initial pattern reversal VEPs recorded from an 8 year old with NF1 showing slowing of the left nerve but good amplitude.

Infections

Similar to dysfunction in the visual pathways, any pathology affecting visual cortices can be quantified using VEPs. Figure 23 shows pattern reversal VEPs in an adult with meningeal tuberculosis. Here slow VEP peak latencies are also seen (Fig. 23).

Multifocal VEPs

An important development in VEPs is the multifocal VEP (mfVEP). Erich Sutter adapted the mathematical sequences called binary m-sequences creating a program that can extract hundreds of VEPs from occipital scalp. This program allows assessment of VEP activity in over 100 "channels" of each optic pathway (10).

Traditional VEPs evaluate the optic nerves and central pathways as a whole. Often small or localized optic pathway dysfunction is not detected. Using multifocal VEP analysis one may isolate smaller dysfunctional areas using hundreds of stimulations presented in the same amount of time it would take to record a single whole nerve VEP with conventional methods (11). Multifocal VEPs best evaluate asymmetry of visual function caused by optic nerve dysfunction. Pathology can sometimes be detected that may be missed with a traditional single VEP.

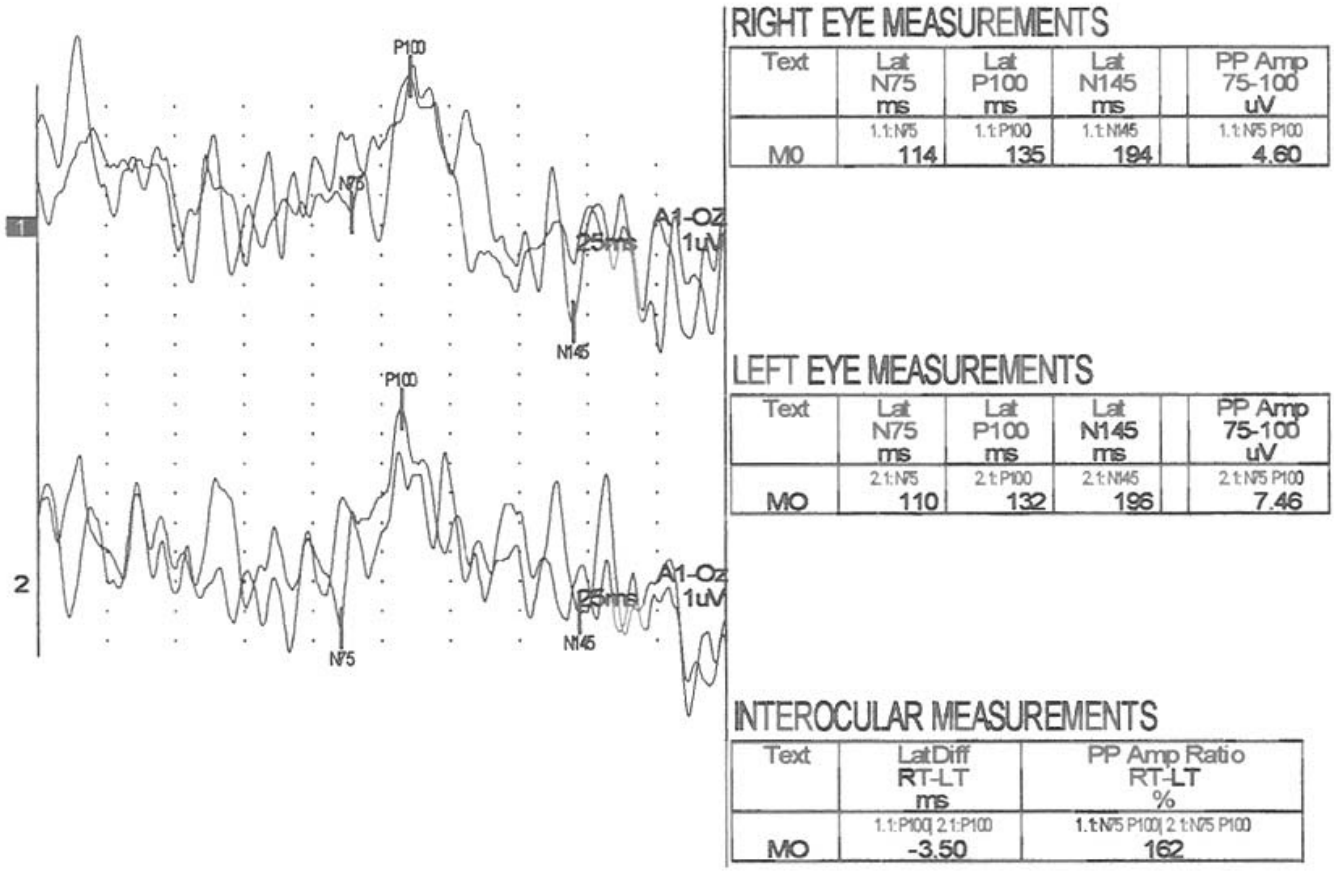

Figure 15: Pattern reversal VEPs of the same patient as Fig. 14 at age 11 showing prolongation of VEPs and amplitude attenuation.

Whereas stimulus patterns for multifocal electroretinograms (mfERGs) are an array of flickering patterns, multifocal visually evoked potentials (mfVEPs) are better elicited with reversing checkerboard patterns (10).

Four occipital scalp electrodes are required to record mfVEPs. A common mfVEP montage is to first place two electrodes on the midline. One just below the inion and another 3-4 centimeters above the inion; and laterally place electrodes 4 centimeters off the midline several centimeters above inion. The ground lead can be anywhere on the body. See Hood et al. (12) for suggested International Standard for recording mfERGs.

The stimulus for multifocal electroretinograms is a focal pattern stimulation m-sequence modulated flicker (See chapter on The Electroretinogram: Clinical Applications by Donnell Creel). The common stimulus for multifocal visually evoked potentials (mfVEPs) is a dartboard pattern with each sector a contrast reversing check pattern (Fig. 24).

Multifocal visually evoked potentials from a normal subject are shown in Figure 25. Red traces are from right eye stimulation. Blue traces are from left eye stimulation.

Sample patients tested with mfVEPs

A common application of mfVEPs is recording these potentials from patients with optic neuritis. Usually optic neuritis appears first in one optic nerve. Figure 26 displays the VEPs of a patient with unilateral optic neuritis

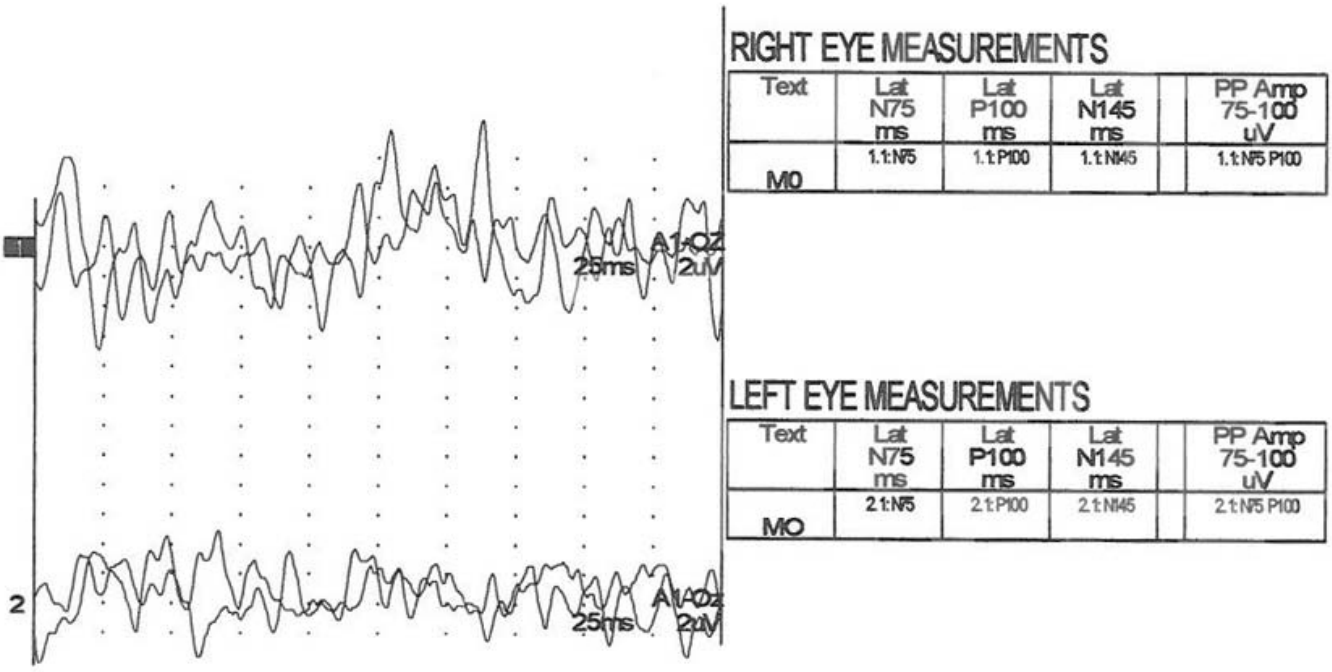

Figure 16: Pattern reversal VEPs of the same patient as Figs. 14 and 15 at age 12 showing obliteration of VEPs due to the growth of the gliomas.

during the acute phase affecting the right optic nerve. During the acute phase most of the responses in the central 30 degrees were abnormal. Many responses in the central 5 degrees were nearly extinguished.

This same patient tested 2 months later shows significant recovery in the amplitudes of the responses, but slower peak latencies persist due to demyelination (Fig. 27).

An example of another optic nerve disorder is a patient with optic nerve damage due to glaucoma. The mfVEPs of a patient with unilateral glaucoma are shown in Figure 28.

Summary

Visually evoked potentials are useful to quantify nerve dysfunction from retina to visual cortex. VEP recordings are done by a number of methods to evaluate visual pathway function (13, 14). Choices of which VEP stimuli and protocol to apply need to be made based on the patient's symptoms, history and other information available. Abnormalities seen in VEPs are symptomatic, but not diagnostic. VEP abnormalities do not specify etiology. For example, retinal disease alone will drastically alter VEPs. Interpretation of VEPs must be considered within the context of the patient's clinical appearance and information available from other tests and examinations.

About the Author

Dr. Donnell Creel's biography and photograph are seen in the chapter entitled "The Electroretinogram: Clinical Applications" in Webvision

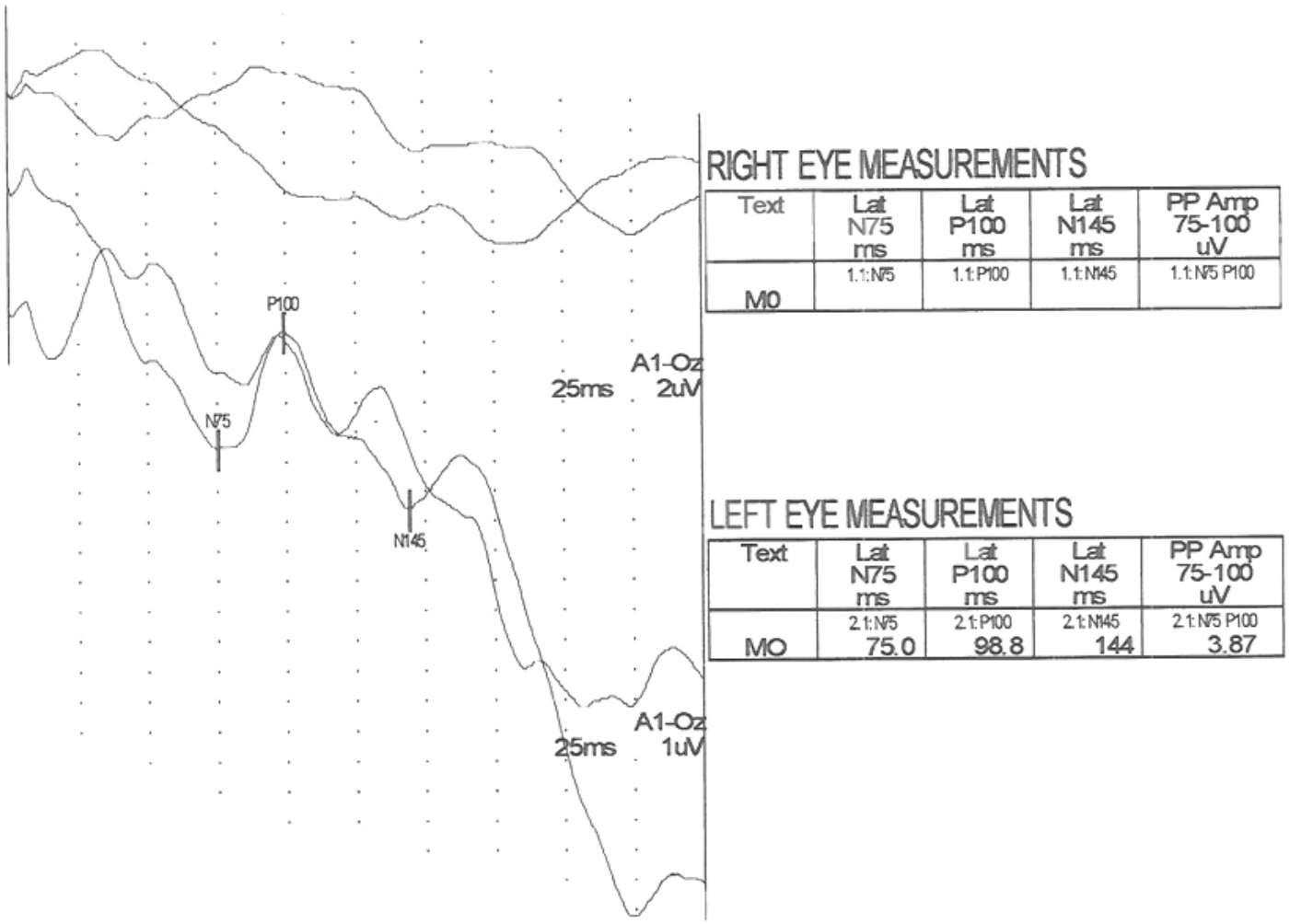

Figure 17: Flash VEPs recorded from a 3 year old prior to removal of an orbital mass, showing no recordable VEP in the right eye.

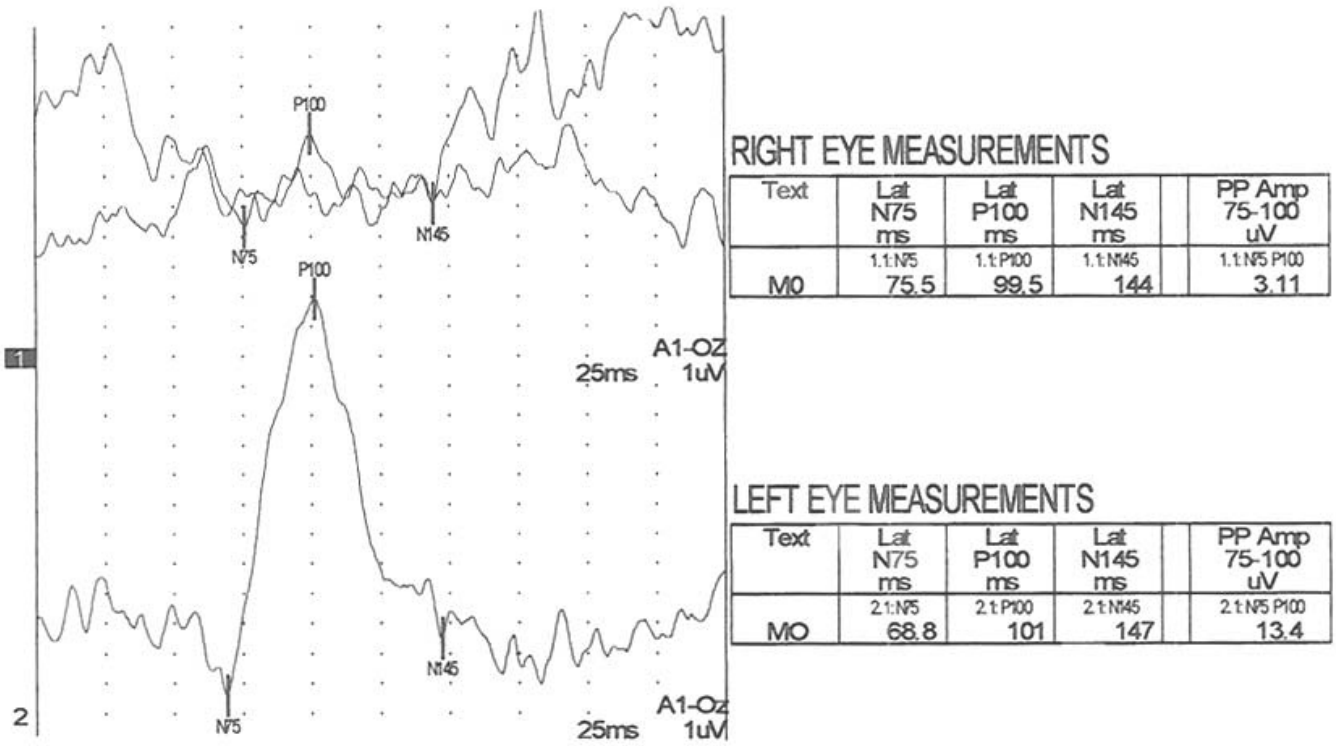

Figure 18: Flash VEPs from the same patient as Fig. 17, recorded 2 weeks after removal of the orbital mass. The VEP shows recovery of the right nerve and improvement of the left nerve function.

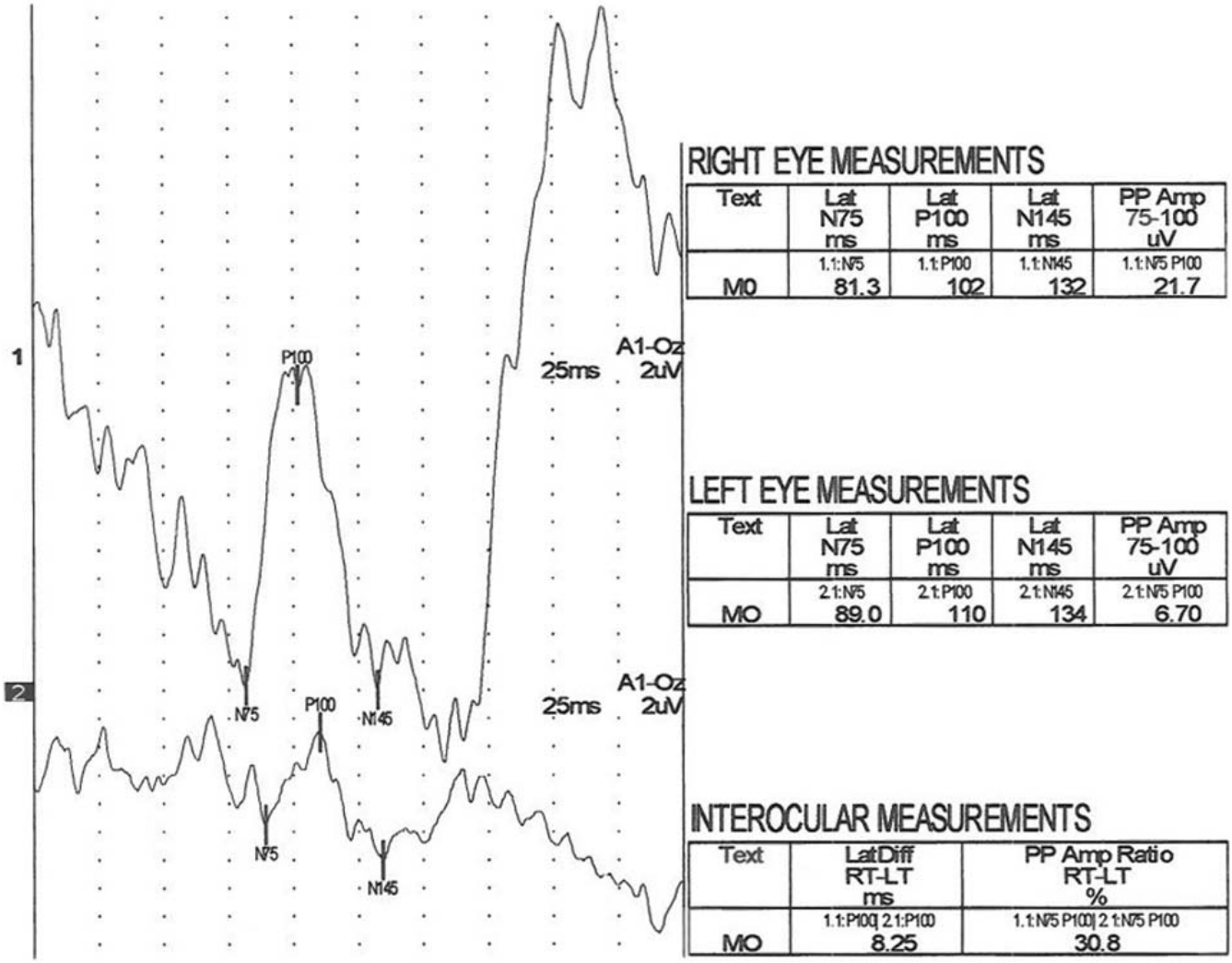

Figure 19: Flash VEPs from a 2 year old with a left nerve neuroblastoma, showing prolonged times and amplitude attenuation of the left nerve.

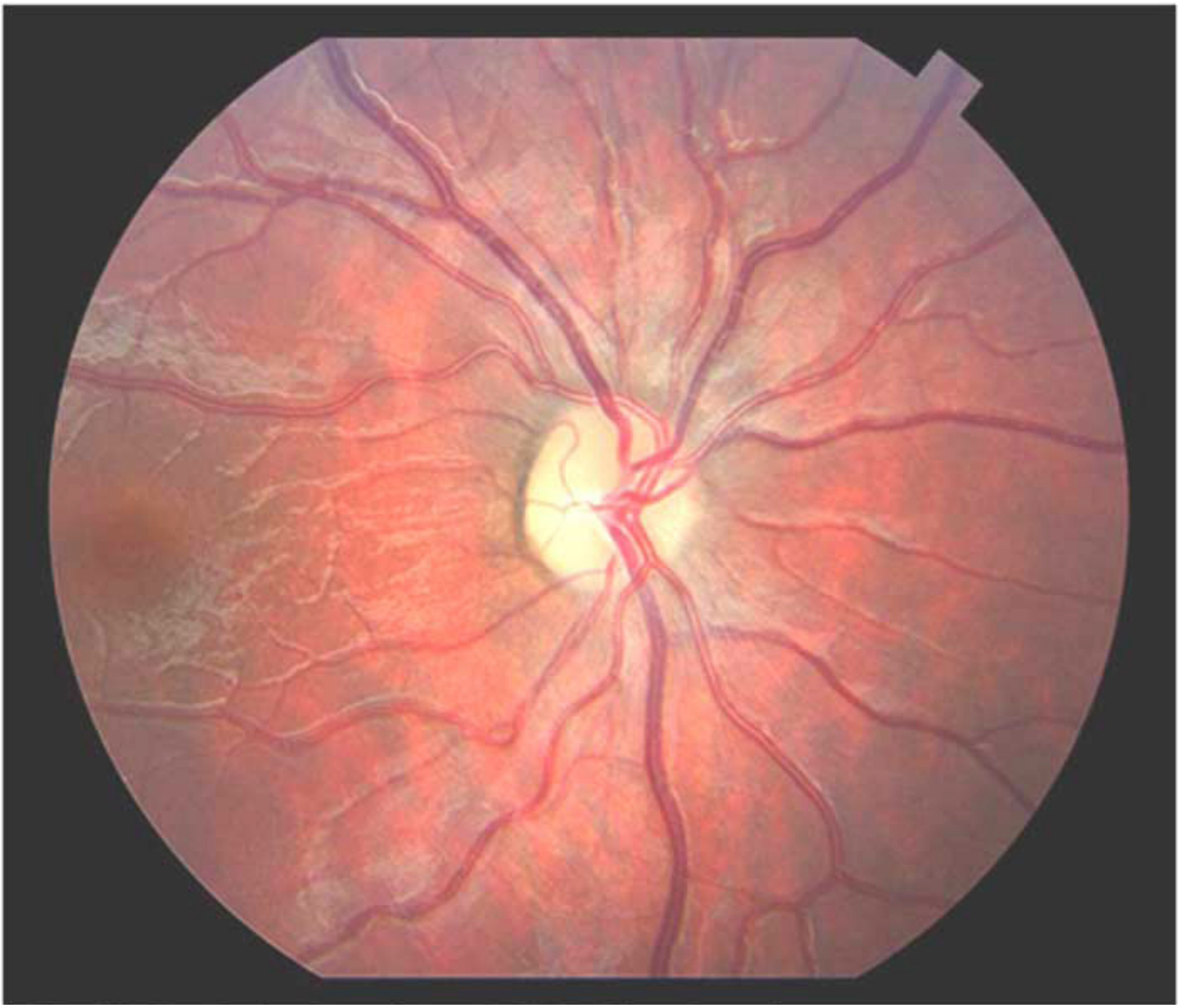

Figure 20: Ocular fundus photo of a child with a pale optic nerve head.

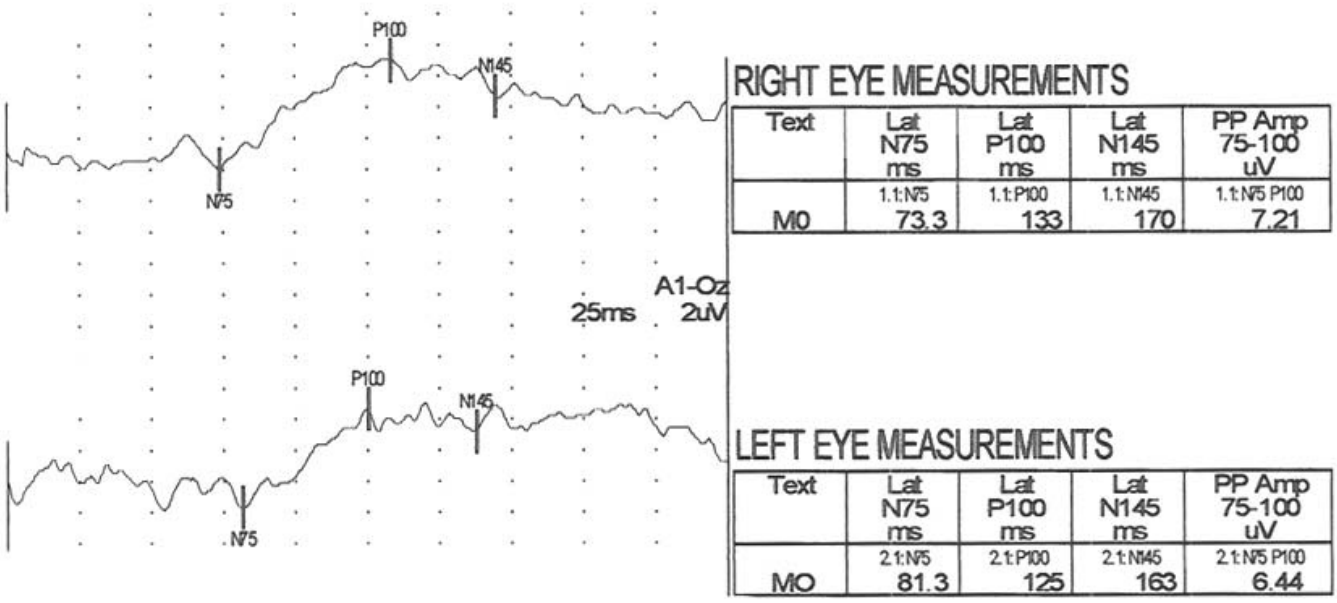

Figure 21: VEPS of a child with pale optic nerve heads showing reduced amplitudes and slow P100s.

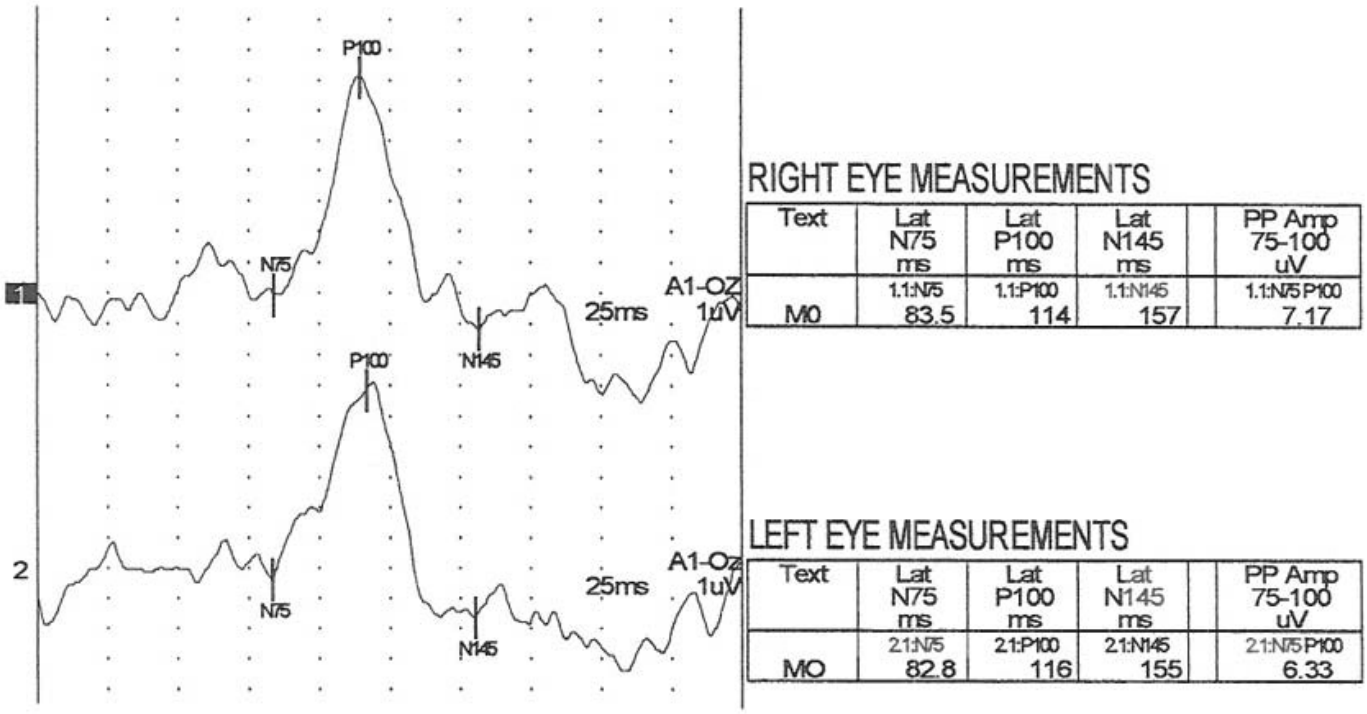

Figure 22: Pattern reversal VEPs recorded from an adult with optic nerve Ethambutol toxicity, showing slow P100 peak latencies.

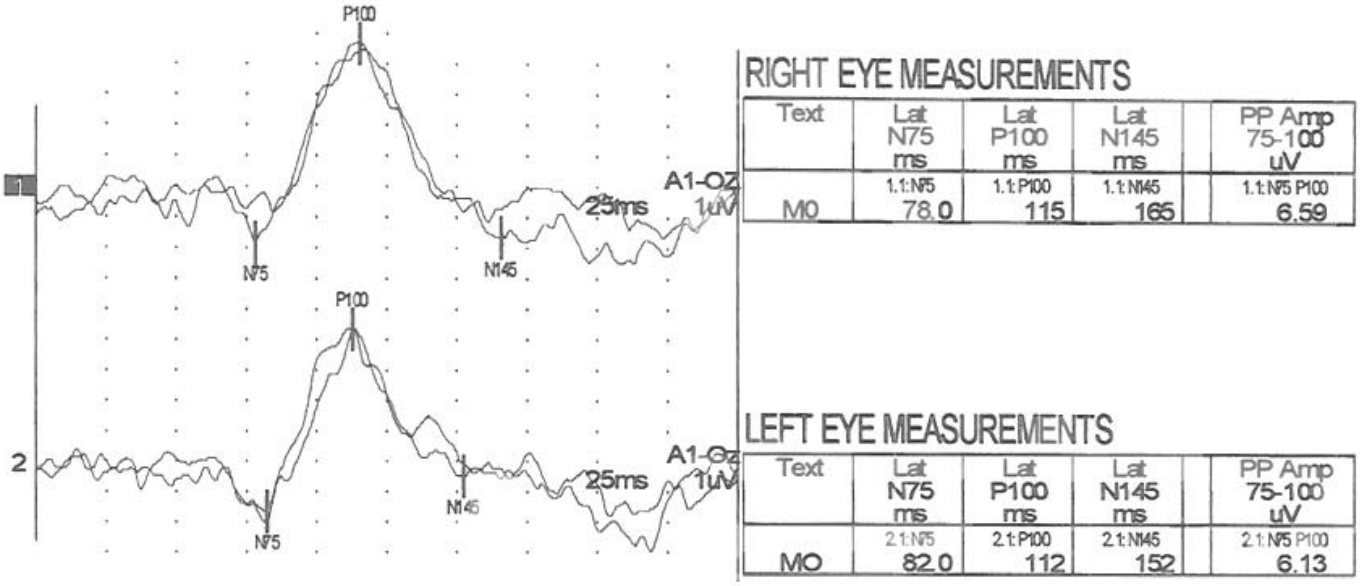

Figure 23: Pattern reversal VEPs recorded from an adult with meningeal tuberculosis, showing slow P100 peak latencies.

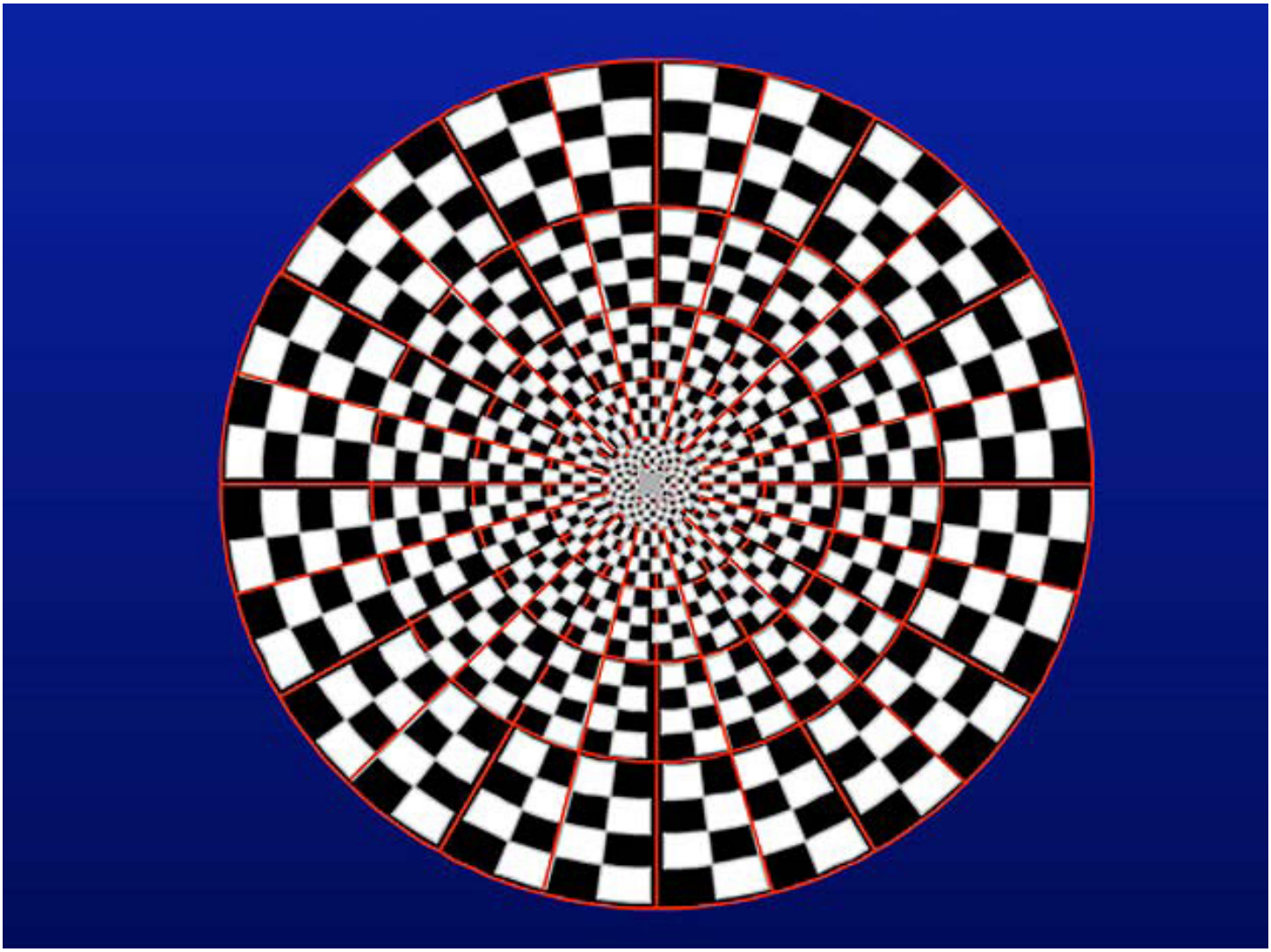

Figure 24: Sample dartboard pattern stimulus used to record multifocal VEPs.

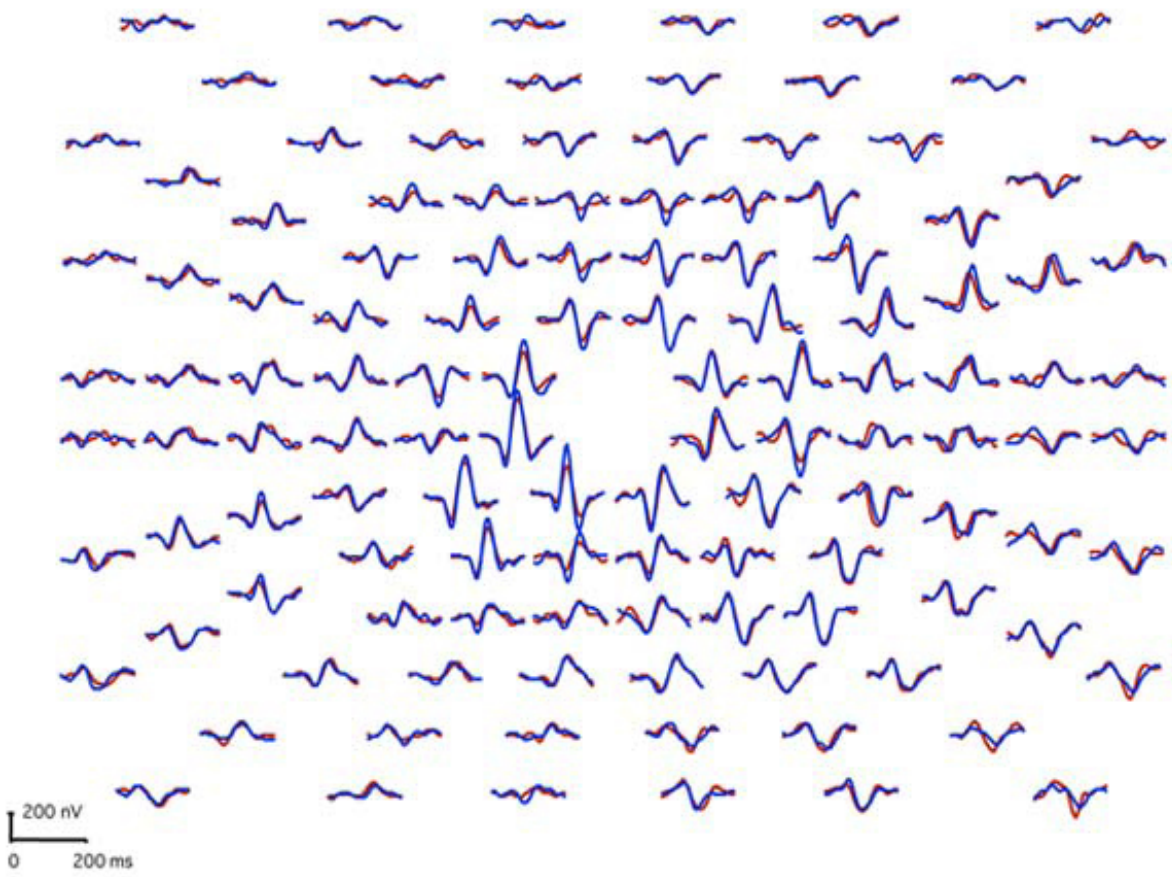

Figure 25: Multifocal VEPs recorded stimulating each eye in a normal adult. Right (2) traces. Left eye (blue) traces.

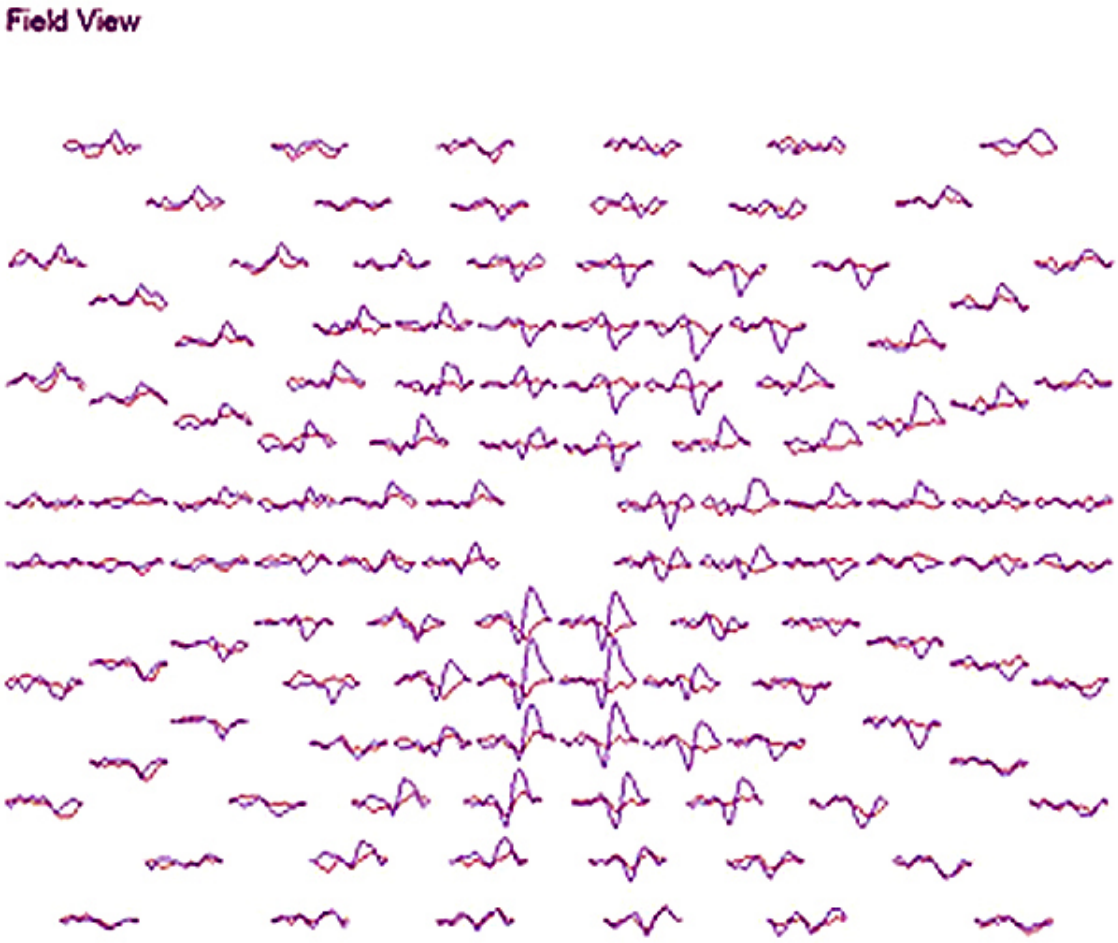

Figure 26: Multifocal VEPs showing the right optic nerve (2)versus the left nerve (blue) during the acute phase of optic neuritis.

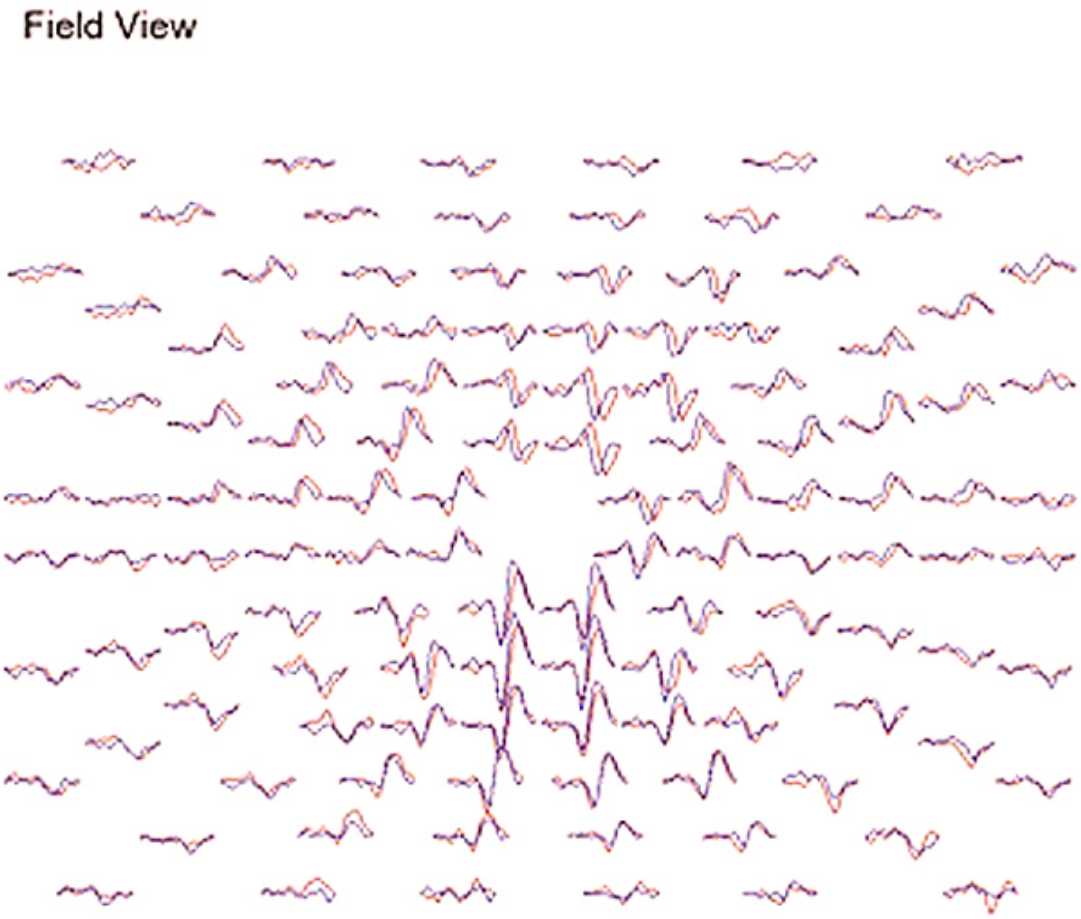

Figure 27: Multifocal VEPs of the same patient showing significant recovery in amplitudes mfVEPs 2 months after the acute phase of optic neuritis. There are persistent delays in peak latencies in the right nerve recordings(2).

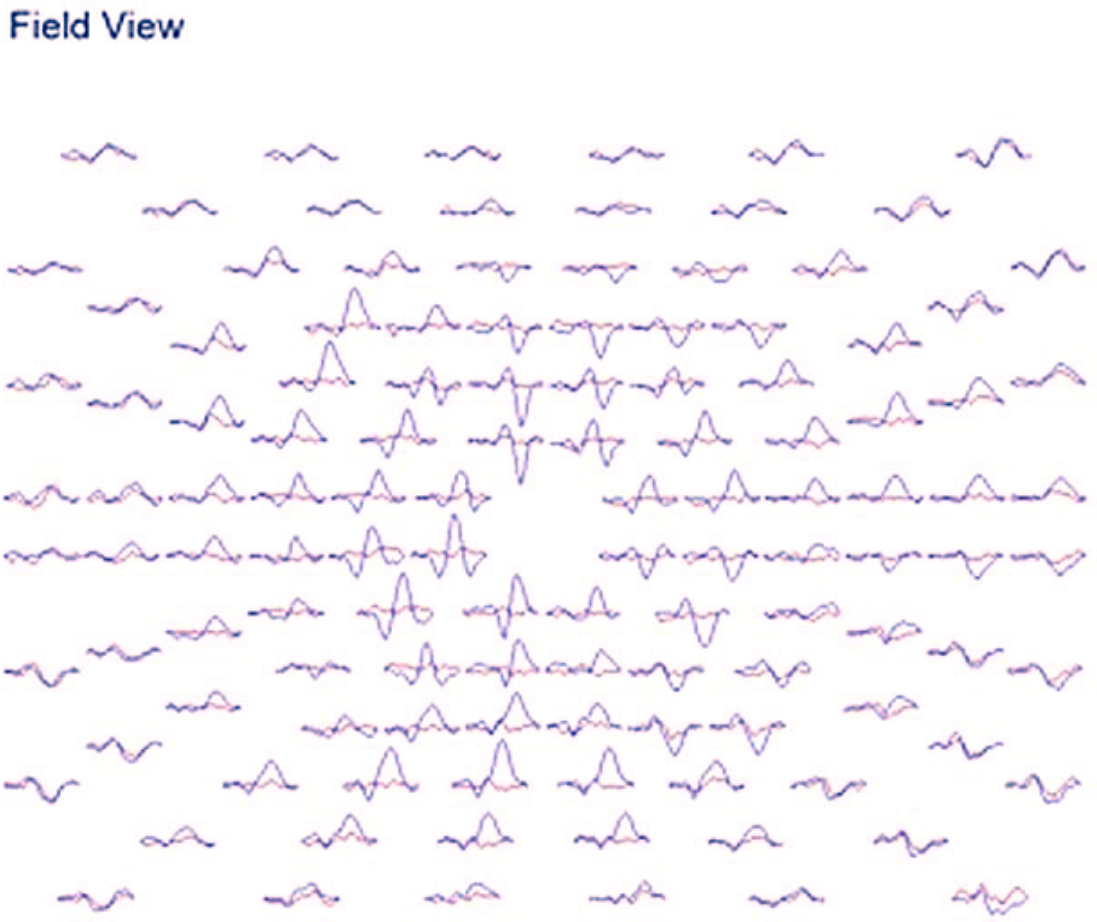

Figure 28: Multifocal VEPs recorded from a patient with unilateral (right) glaucoma.

References

1. Jasper H.H. Report of Committee on Methods of Clinical Examination in Electroencephalography. Electroenceph. Clin. Neurophysiol. 1958;10:370–375.
2. Blumhardt L.D., et al. The asymmetrical visual evoked potential to pattern reversal in one half field and its significance for the analysis of visual field effects. Br. J. Ophthalmol. 1977;61:454–61. PubMed PMID: 889758.
3. Slotnick S.D., et al. Using multi-stimulus VEP source localization to obtain a retinotopic map of human primary visual cortex. Clin Neurophysiol. 1999;110(10):1793–1800. PubMed PMID: 10574294.
4. Di Russo F., et al. Cortical sources of the early components of the visual evoked potential. Hum Brain Map. 2002;15(2):95–111. PubMed PMID: 11835601.
5. Towle V.L., et al,. Locating vep equivalent dipoles in magnetic resonance images. 1995. 80: p. 105-116.
6. Odom J.V., et al. ISCEV standard for clinical visual evoked potentials (2009 update). Doc Ophthalmol. 2010;120:111–119. PubMed PMID: 19826847.
7. Fulton A., R.M. Hansen, and A. Moskowitz. Assessment of vision in infants and young children. In: Celesia GC, ed. Handbook of Clinical Neurophysiology: Disorders of Visual Processing. New York, NY: Elsevier Science Inc; 2005.
8. Emmerson-Hanover R., et al. Pattern reversal evoked potentials: Gender differences and age related changes in amplitude and latency. Electroenceph Clin Neurophysiol. 1999;92:93–101. PubMed PMID: 7511515.

9. Hoffmann, M.B., S. Straube and M. Bach. Pattern-onset stimulation boosts central multifocal VEP responses. Journal of Vision, 2003. B(6): p. 432-439.
10. Sutter, E.E., Noninvasive Testing Methods: Multifocal Electrophysiology. In: Darlene A. Dartt, editor. Encyclopedia of the Eye, Vol 3. Oxford: Academic Press, 2010: p. 142-160 (2010).
11. Klistorner A.I., et al. Multifocal Topographic Visual Evoked Potential: Improving Objective Detection of Local Visual Field Defects. Invest Ophthal Vis Sci. 1998;39(6):937–50. PubMed PMID: 9579473.
12. Hood D.C., et al. A.M. ISCEV guidelines for clinical multifocal electroretinography. Doc Ophthalmol. 2008;116:1–11. PubMed PMID: 17972125.
13. Regan, D. Human brain electrophysiology. New York: Elsevier, 1989.
14. Regan D. Some Early Uses of Evoked Brain Responses in Studies of the Human Visual System. (Eds. V. Lamme and D. Regan), Vision Research, 47, 2008. 6, V-VII.

The Electroretinogram: ERG

Ido Perlman

Created: May 1, 2001; Updated: June 27, 2007.

Historical View

As early as 1865, Holmgren found that a light stimulus could cause a change in the electrical potential of the amphibian eye. Shortly afterwards, similar findings were reported by Dewar from Scotland. He showed that light illumination through the pupil, which had previously been covered, caused a slight movement of a galvanometer, suggestive of a positive electrical change in the cornea relative to the back of the eye (1). This light-induced electrical activity of the eye was called the electroretinogram. Now, the electroretinogram response is commonly abbreviated to the ERG.

Gotch (2) was the first to report that the response of the eye to a light flash consisted of two waves; first the cornea became negative and then a positive wave of larger amplitude appeared. Later, Einthoven and Jolly (3) separated the ERG response into three waves. The first wave to appear immediately after turning on a light stimulus was negative on the cornea. It was followed by a positive wave and a final slower wave that was also positive. Einthoven and Jolly (3) suggested that the light stimulus triggered a chain of reactions leading to the formation of products A, B, and C, and that every electrical wave indicated a change in a "relevant" product. These authors' work was the foundation for the form of analysis of the ERG used to the present day. The waves are called a-, b- and c-waves. An additional corneal-positive wave, that is more rarely recorded at the termination of the light flash, is called the d-wave.

Fig. 1 shows ERG responses from different species. These responses are to bright light stimuli applied in the dark-adapted state. The ERG of the turtle eye (Fig. 1A) as elicited by a long (900-ms) step of light, shows an a-wave and b-wave complex separated from the d-wave, which is generated at stimulus offset. A bright light stimulus of 40 sec duration is used to record the ERG of the bullfrog in Fig. 1B (4). The a-wave and b-wave are followed by the slow, corneal-positive c-wave. After termination of the stimulus, a d-wave develops. The ERG responses of the rabbit (Fig. 1C) and the human (Fig. 1D) are elicited by fast bright flashes (50 or 100 ms in duration), and therefore, only the a-wave and b-wave are seen. In the human response (Fig. 1D), fast oscillations can also be seen on the ascending limb of the b-wave. These ERGs in the different species clearly differ in amplitude and pattern. Some of this variability is due to species differences, particularly the relative densities of rods and cones, whereas technical factors, such as duration and intensity of photostimulation and method of recording, also affect the waveform. Nevertheless, ERG responses of turtle, bullfrog, rabbit, and human (Fig. 1), in addition to those recorded from other vertebrate species, are characterized by the basic features of a negative a-wave followed by a positive b-wave.

In 1911, Piper published his analysis of the ERG. He divided the ERG into three components: I, II, and III (1). Unlike Einthoven and Jolly, who suggested that the waves reflected transient chemical processes, Piper suggested that all the ERG components lasted for the duration of the light stimulus. According to Piper, the first two waves, I and II, were characterized by different latencies and temporal properties so that the interaction between them resulted in the formation of the a- and b-waves. Wave III was equivalent to the c-wave. Although Piper's analysis was very speculative and based only on a few facts, this interpretation together with that of Einthoven and Jolly's has set the basis for the idea that the ERG is the result of a few components. In 1933, Ragnar Granit published a more detailed study of the components of the cat ERG as illustrated in Fig. 2a and Fig. 2b (5). He recorded the ERG from the anesthetized cat using corneal electrodes and observed the gradual removal of the different components as the level of anesthesia was deepened. Granit termed the different components in sequence of their disappearance: P-I, P-II, and P-III. The P-I component is a slow, cornea-positive wave. P-II is also a corneal-positive wave that rises relatively fast to a peak amplitude and then recovers to an intermediate potential while the light stimulus is still on. The last component, P-III, which was the most resistant to the level of anesthesia, is

a cornea-negative wave that develops faster than the other two and remains as a negative potential for as long as the light stimulus is on. The component analysis of Granit has been modified slightly over the years but remains the basis for our understanding of the ERG. For his work on the ERG, Ragnar Granit won the Nobel Prize for Physiology and Medicine in 1967.

The Electrical Basis of ERG Recordings

ERG responses are recorded with an active extracellular electrode positioned either on the cornea, in the vitreous, or at different levels inside the retina. An extracellular recording of electrical activity of living tissue is rendered possible when electrical currents spread along an extracellular matrix with electrical resistance. An example of extracellular electrical current in the vertebrate retina is the "dark" current spreading from the inner segments to the outer segments of the photoreceptors (see the chapter on photoreceptors).

In the vertebrate retina, the photoreceptors are arranged in parallel, and therefore, their "dark" currents are in parallel and sum up, giving rise to a strong radial extracellular current flowing away from the inner nuclear layer toward the pigment epithelium. Similarly, extracellular currents from all retinal cell types will sum up only if they are directed radially. In contrast, lateral currents will cancel each other because the retinal lateral arrangement is completely symmetrical. Therefore, when a homogeneous light stimulation is directed at the whole retina, only radial extracellular currents are formed. We assume that a light stimulus elicits extracellular electrical currents that flow from sources to sinks. These currents will flow through different pathways, including local and remote ones. We can divide these currents into two principal pathways, the local one (A) and the remote one (B), as shown schematically in Fig. 3a. The current in pathway A flows through a local route remaining entirely within the retina, whereas the current flowing through pathway B leaves the retina through the vitreous and anterior ocular tissue and returns to the retina through the sclera, the choroid, and the pigment epithelium layer. The light-induced current flowing through pathway B can be recorded in a noninvasive manner, with extraocular electrodes, as illustrated in Fig. 3a.

According to Ohm's law in electricity, when an electrical current flows through a resistor, a gradient of electrical potential is formed that equals the product of multiplying the magnitude of the current by that of the resistance. By applying this law, we can derive the relationships between the currents, IA and IB (Fig. 3a), the resistances of the ocular tissues, and the measurements of potential differences. Fig. 3b shows an equivalent electrical circuit of the eye (6). A light stimulus elicits an extracellular current (source I) that divides into two pathways; one flowing through the retina (local pathway, IA in Fig. 3a) and the other through extra-retinal and extra-ocular tissues (remote pathway, IB in Fig. 3a). Each tissue (e.g., retina, vitreous, sclera, choroid, and pigment epithelium) is represented in Fig. 3b by an electrical resistor. According to Ohms' law, the potential difference between two points is independent of the pathway through which the current is flowing. Therefore, the voltage difference between points A and B can be calculated for the local or remote pathways.

$$I_A R_1 = I_B (R_2 + R_3 + R_4 + R_5 + R_6) \text{ (Equation 1)}$$

Since the sum of the resistances on the right side of the equation ($R_2 + R_3 + R_4 + R_5 + R_6$) is larger than R_1, the current I_A in the local pathway must be greater than current I_B.

When using two electrodes to record light-induced electrical activity of the retina, the largest light-induced potential change will be monitored if the measurement is done between points A and B, which are on the two sides of the cells producing the electrical response. However, when the electroretinogram is recorded from humans or from laboratory animals during chronic experiment, the electrodes cannot be inserted into the retina. The alternative is to record from extraocular sites by placing both active and reference electrodes outside the eye. If these electrodes are placed at the loci designated in Fig. 3b as C and D, the voltage gradient between them is given by

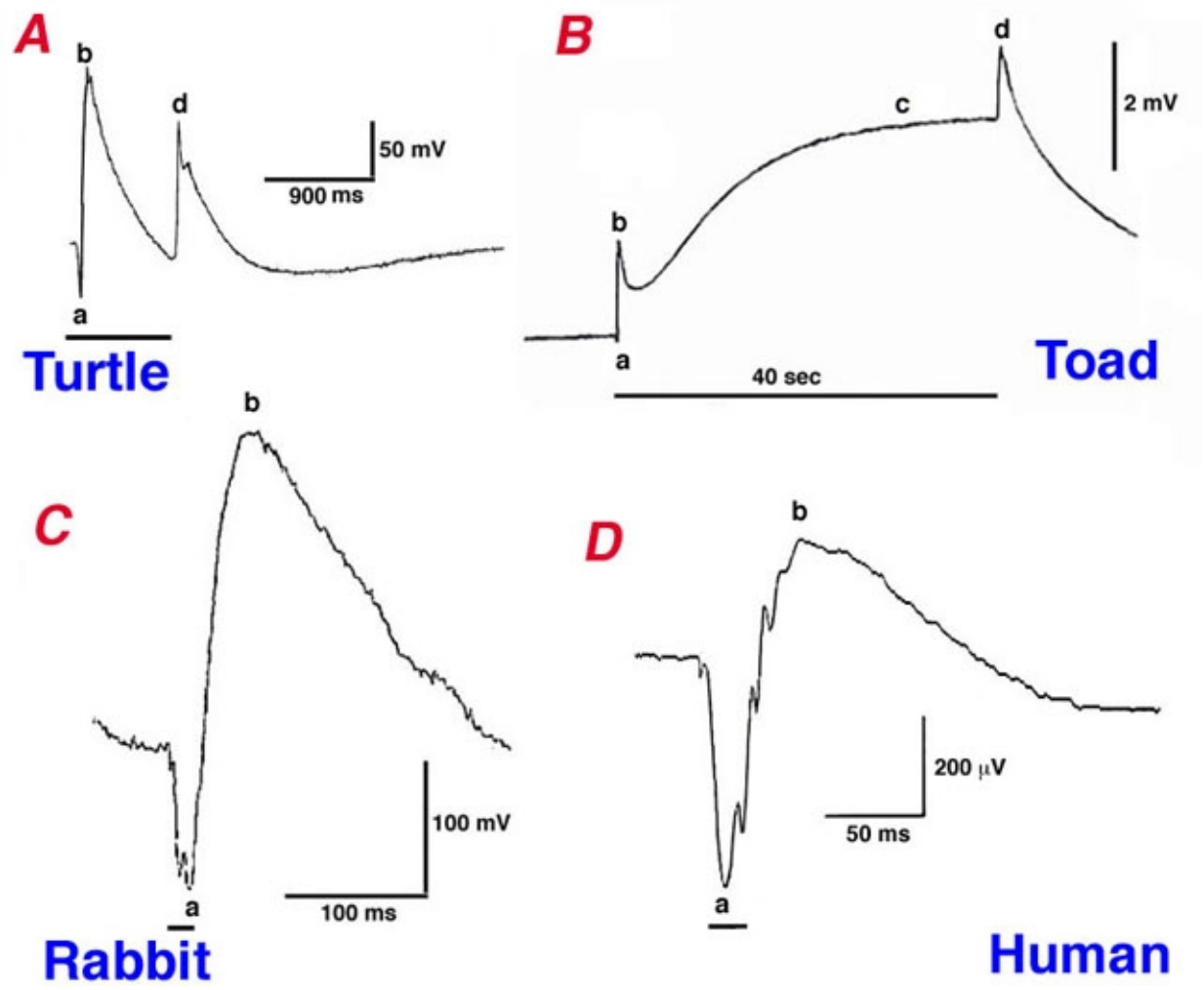

Figure 1. A, ERG response of turtle *Pseudemys scripta elegans* elicited by a 900-ms light stimulus to separate the a-wave and b-wave from the d-wave. B, the ERG of the bullfrog elicited by a long (40-sec) light stimulus to show the c-wave in addition to the a-, b-, and d-waves (4). C, the ERG response of a rabbit to a flash (20 μs) flash of white light. D, the ERG response from a human as typically recorded in the clinic. Note the fast oscillations on the ascending limb of the b-wave. Calibration bars are denoted separately for each ERG response.

$$V_C - V_D = I_B * R_4 \text{ (Equation 2)}$$

or

$$V_C - V_D = I_A R_1 - I_B(R_2 + R_3 + R_5 + R_6) \text{ (Equation 3)}$$

This is the ERG: the light-induced potential change that is related to light-induced electrical activity within the retina. In general, when retinal function deteriorates, the light-induced electrical activity in the retina reduces. The currents I_A and I_B will be smaller and the ERG will be smaller, too, thus indicating retinal pathology.

However, we have to remember that the magnitude of the different resistances, and more so, the relationships between them, can also affect the ERG that is measured with extraocular electrodes. The division of the current originating from the light-induced retinal activity into the local and remote pathways depends upon the relative resistances of the two pathways. From Equation 1, we can derive the following relationship:

Figure 2a. Ragnar Granit, winner of the Nobel Prize for Physiology and Medicine in 1954.

$$I_A/I_B = (R_2 + R_3 + R_4 + R_5 + R_6)/ R_1 \text{ (Equation 4)}$$

Any change in one of the resistances will cause a change in the magnitude of the current in the extraocular pathway (I_B) and the ERG ($V_C - V_D$) can change irrespective of retinal function. Therefore, knowledge of the different resistances and understanding the factors that affect them is needed for proper use of the ERG for clinical and/or research purposes.

The pigment epithelium layer (R-membrane) offers the highest resistance to electrical current along the ocular tissues (7-10) as denoted by a large resistor R6 in Fig. 3b. Therefore, any change in the magnitude of this resistor will affect the distribution of currents between the retinal pathway (I_A) and the remote pathway (I_B). This change will be reflected in the ERG responses that are measured with extraocular electrodes. Such changes in the distribution of resistances may account for species differences in the magnitude of the ERG responses and for intrasubject differences within a given species. The importance of the resistances of the ocular tissues has been recognized by Arden and Brown (11). They replaced the vitreous humor of cats with heavy oil to abolish current flow from the retina to distant sites and thereby ensured large potential recordings of local ERG from the retinal

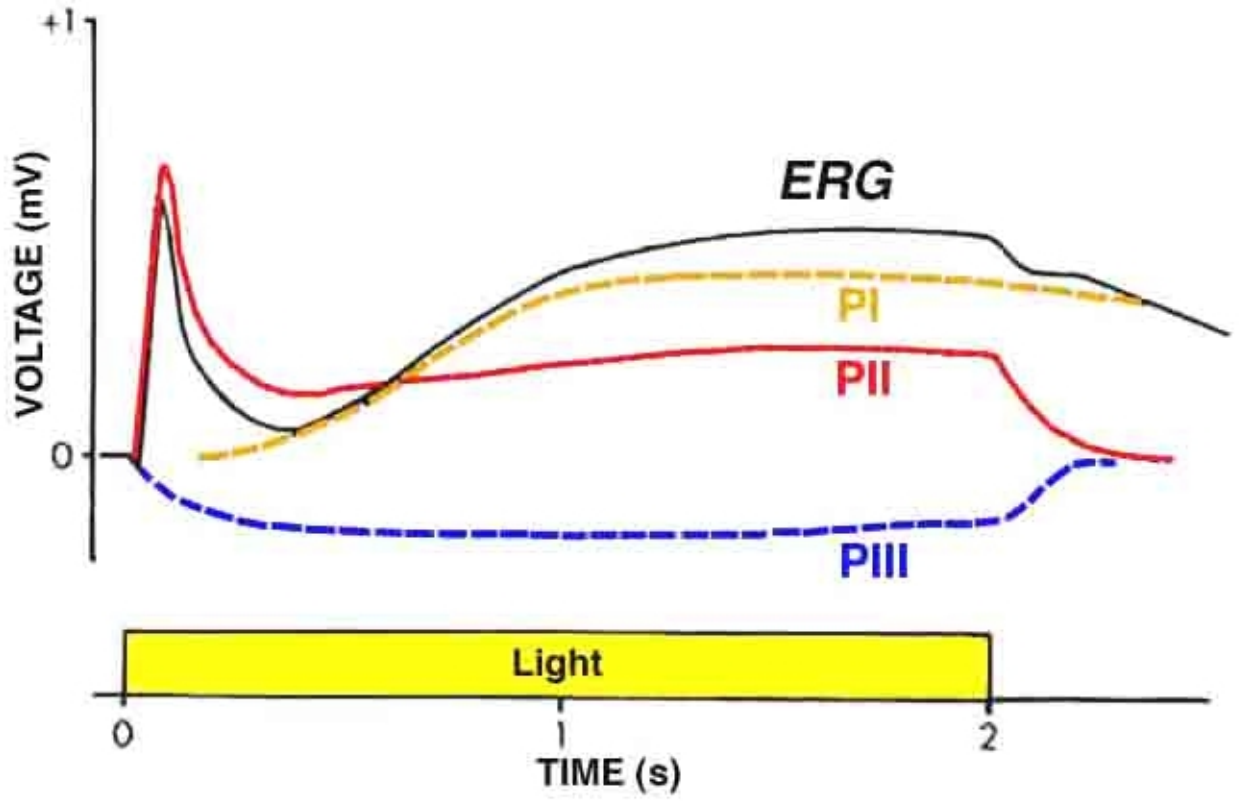

Figure 2b. The ERG of a cat in response to a 2-sec light stimulus. The components, P-I, P-II, and P-III, have been isolated by deepening the state of anesthesia (5).

surface. In the clinical environment, it is well documented that the ERG can be reduced significantly in patients with giant retinal tears who have undergone vitrectomy surgery and injection of silicon oil into the vitreous. Since silicon oil does not conduct electric currents, the resistance of the vitreous increases by several folds causing the current I_B to be so reduced that the ERG becomes very small in amplitude (12-14).

The Origin of the Major ERG Waves

Granit (5) divided the cat's ERG into three components; P-I, P-II and P-III (Fig. 2a and Fig. 2b). From his analysis, we know that the negative a-wave is the leading edge of the negative P-III component; the positive b-wave reflects the summation of P-II and P-III, whereas the slow c-wave is the summation of P-I and P-III. However, the cellular origin of the different components needs to be understood. Basically, two types of approaches, physiological and pharmacological, have been used to dissect out these cellular origins. The physiological experiments are based on the assumption that the generators of specific ERG components are located in specific retinal layers, and therefore, when these are passed by the intra-retinal microelectrode, the polarity of the specific ERG waves will reverse. These current source-density analyses have indeed revealed the anatomical location within the retina of the different ERG components. The pharmacological approaches to ERG analyses are based on retinal physiology and biophysics. In these experiments, specific agonists and antagonists of cellular mechanisms are applied and their effects on the ERG then analyzed.

In the following section, the sources of the a-, b-, and c-waves will be discussed, not according to the order of their timing in the ERG response but according to the retinal level at which they are generated, starting from the most distal layer, the pigment epithelium.

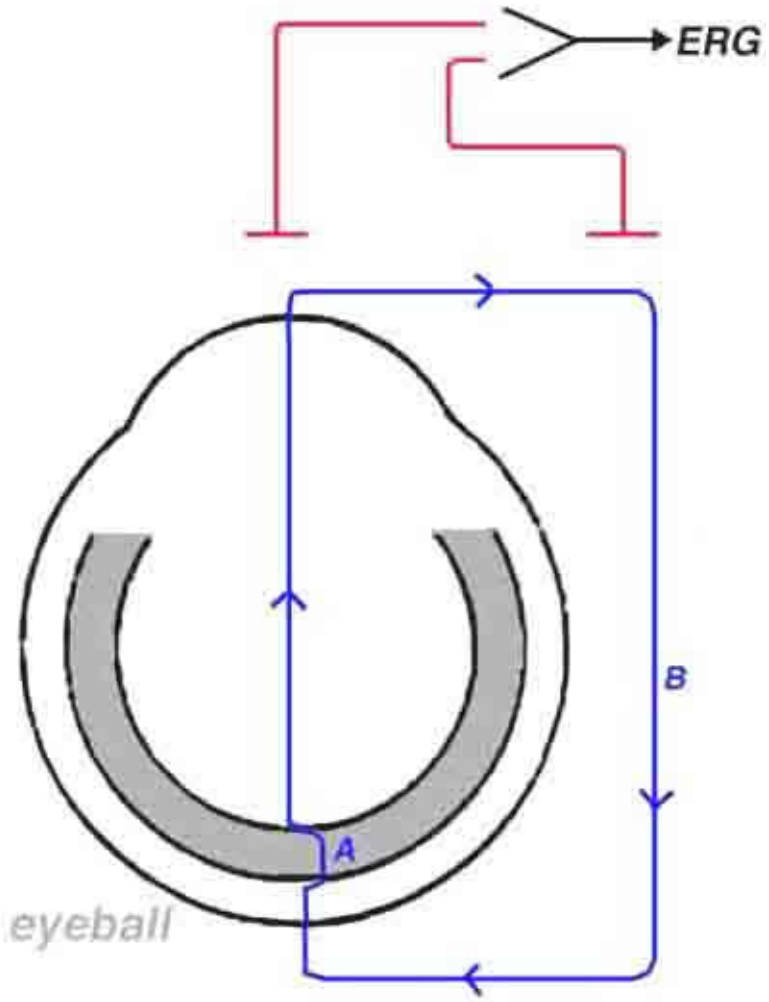

Figure 3a. A schematic representation of the extracellular currents that are formed after light stimulation. Pathway A represents local currents within the retina, whereas pathway B shows the currents leaving the retina through the vitreous and the cornea and returning to the retina through the choroid and the pigment epithelium. ERG recording in human is done along the B path.

The c-Wave

The c-wave, which corresponds to the P-I component of Granit (Fig. 2a and Fig. 2b), is now known to originate in the pigment epithelium. The first indication of this was reported by Noell (15). He showed that systemic injection of sodium azide elicited an electrical potential from the retina similar to the ERG c-wave. The azide-induced potential was not influenced by iodoacetic acid, which is known to destroy photoreceptors, or by cutting the optic nerve, which causes degeneration of the ganglion cells. This interpretation of the c-wave origin was proven directly when intracellular recordings were made from pigment epithelial cells. The potential changes that were recorded from these cells in response to light stimuli were identical in shape and temporal properties to the ERG c-wave (16). Furthermore, when the retina was separated from the pigment epithelium, the ERG response contained normal a- and b-waves, but the c-wave disappeared. Fig. 4 shows ERG recording from the skate eyecup that consists of a-wave, b-wave, and c-wave (upper trace). When the retina is separated from the sclera and pigment epithelium, the ERG response contains only the a- and b-waves. Furthermore, aspartate, by blocking transmission from photoreceptors to bipolar cells, completely removes the b-wave (Fig. 4) (17).

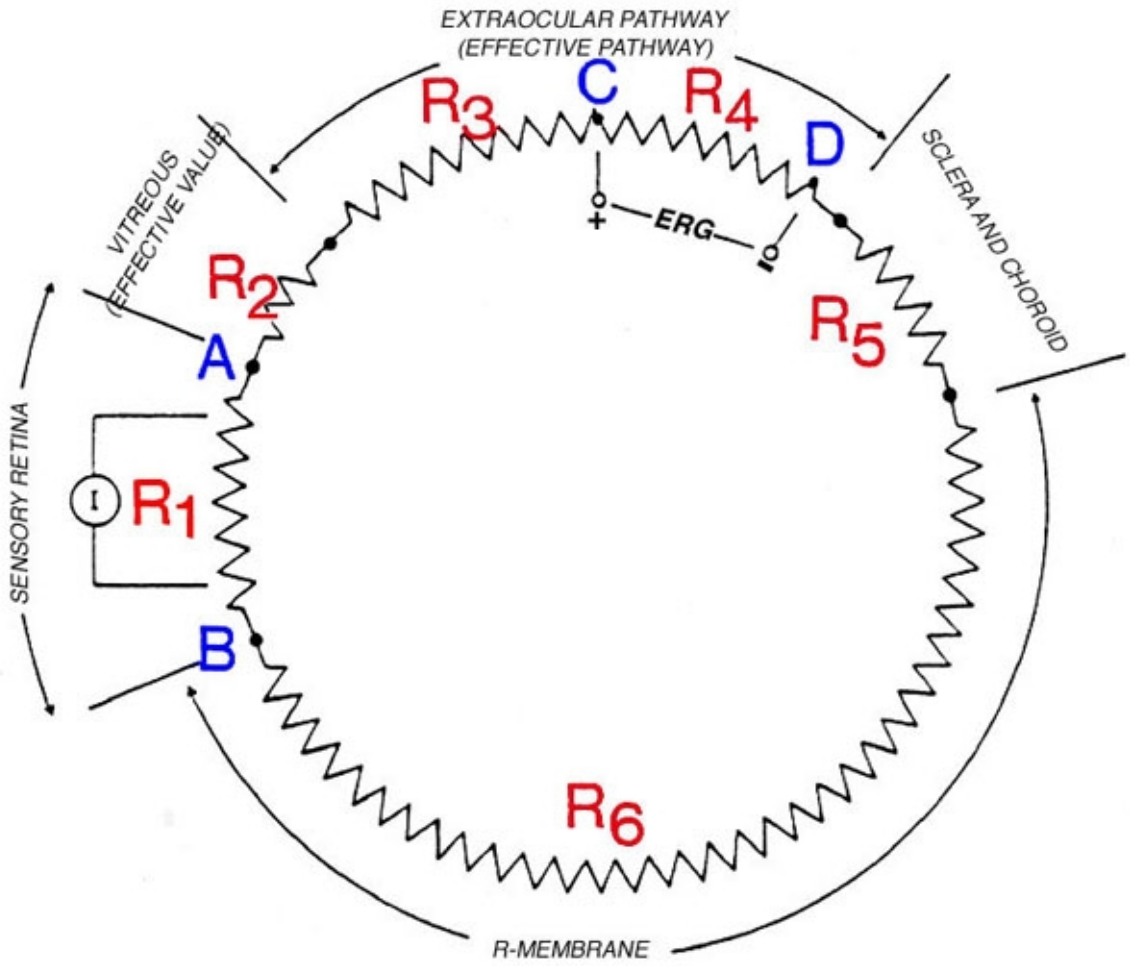

Figure 3b. An electrical scheme of the resistances through which currents IA and IB (Fig. 3a) flow when the retina is stimulated with light. The current source I represents the electrical current that is generated in the retina in response to a light stimulus. Pathway A is the local intra-retinal route of current flow, and pathway B is the remote route going from the retina and through the vitreous, lens, cornea, extraocular tissues, and back to the retina through the sclera, choroid, and pigment epithelium.

The exact mechanisms whereby the pigment epithelial cells generate the c-wave were revealed only when potassium-sensitive microelectrodes were developed. The pigment epithelium cells are functionally asymmetrical cells with their basal membrane (toward the choroid) less permeable to potassium ions than the apical membrane (retinal side). This asymmetry causes a constant potential difference between the retina and the choroid with the retinal side positive relative to the choroidal side. This is also called "the standing potential of the eye". The standing potential is very sensitive to the extracellular concentration of potassium ions. Any change in concentration of potassium ions at one side will be expressed in a change in the whole trans-epithelial potential. Measurements with potassium-sensitive microelectrode in the photoreceptor layer shows a light-induced decrease in the extracellular concentration of potassium ions, due to light-induced electrical activity in the photoreceptors. The reduction in the extracellular concentration of potassium ions near the apical membrane of the pigment epithelial cells is expressed as an increase in the trans-epithelial potential with the retinal side becoming more positive relative to the choroidal side. This is the ERG c-wave when recorded with a corneal electrode (4, 18). Fig. 5 shows simultaneous recordings of the ERG and the potassium retinogram (KRG) in the frog retina. To simplify the comparison, the KRG responses are inverted; thus, a positive deflection in this figure means a reduction in the extracellular concentration of potassium ions. The intensity series (Fig. 5A) indicates that the temporal properties of the KRG match closely with those of the ERG c-wave. The intensity-response

curves show excellent correlation between peak amplitude of the c-wave and peak reduction in potassium concentration (Fig. 5B).

Although the c-wave originates from the pigment epithelium, it depends upon the integrity of the photoreceptors, because light absorption in the photoreceptors triggers the chain of events leading to the decrease in extracellular concentration of potassium ions. Therefore, the ERG c-wave can be used to assess the functional integrity of the photoreceptors, the pigment epithelial cells, and the interactions between them.

The a-Wave

The ERG a-wave is the leading part of Granit's P-III component. It has now been shown that P-III can be divided into two components: a fast P-III and a slow P-III (19, 20). The most important information on the origin of these waves was obtained from ERG recordings with intra-retinal microelectrodes (21-25). These studies suggested the photoreceptor layer as the origin of the fast P-III wave. Differential recording in the rat retina using two microelectrodes revealed that the a-wave resulted from extracellular radial current. This is the "light" current and basically reflects the reduction in the "dark" currents because of light absorption in the photoreceptor outer segments and closure of cGMP-gated cationic channels (see the chapter on photoreceptors) (26, 27).

A pharmacological approach to the study of the origin of the ERG a-wave became possible when the identity of the neurotransmitter released from the photoreceptors became known. Because L-glutamate is the neurotransmitter of the photoreceptors, exposing the retina to agonists or antagonists of L-glutamate can effectively block synaptic transmission from the photoreceptors and isolate the contribution of the photoreceptors to the ERG. This can be achieved by exposing the isolated skate retina to L-aspartate, an excitatory, acidic amino acid (Fig. 4, lower trace). Fig. 6 shows ERG responses from dark-adapted rabbits that were recorded 3 hours after intravitreal injection of L-glutamate or 2-amino-phosphonobutyric acid (APB) into one eye and saline into the fellow control eye (A and B, respectively). Both drugs effectively isolated the P-III component of the ERG in the experimental eye, compared with the control eye. These and numerous other studies indicate that the P-III component of the ERG, or more specifically the fast P-III, reflects light-induced activity of the photoreceptors. This component of the ERG is also referred to as "the receptor component".

The slow component of the P-III cannot be identified in a regular ERG response because of the large-amplitude, positive P-I wave. However, by separating the retina from the pigment epithelium, P-I can be eliminated; and by exposing the retina to drugs, such as aspartic acid, which blocks synaptic transmission from the photoreceptors to the neurons in the inner nuclear layer, the P-III component can be isolated and studied (28). Measurements of the extracellular concentration of potassium ions and of the isolated P-III component of the ERG at different retinal depths reveal the involvement of retinal glial (Müller) cells in the generation of the slow P-III. The Müller cells are highly permeable to potassium ions. Therefore, the reduction in the extracellular concentration of potassium ions in the photoreceptor layer, due to light absorption in the photoreceptors, elicits changes in the trans-membrane potential of the Müller cells and is expressed as the slow P-III component of the ERG.

The b-Wave

The ERG b-wave has been the subject of extensive research by many groups because it is the major component of the human ERG recording as used in clinical and experimental analysis of retinal function. The data in Fig. 4 and Fig. 6 clearly indicate that the b-wave originates in retinal cells that are post-synaptic to the photoreceptors. Blocking synaptic transmission from the photoreceptors to second-order retinal neurons by saturating the post-synaptic receptors with L-aspartate (Fig. 4) or L-glutamate (Fig. 6A) eliminates the ERG b-wave and isolates the P-III component. In fact, any procedure that blocks synaptic transmission from the photoreceptors, such as superfusion with cobalt ions or with high magnesium, low calcium solutions, will eliminate the ERG b-wave (20, 29, 30). The b-wave is also eliminated when the blood flow through the central retinal artery is blocked either

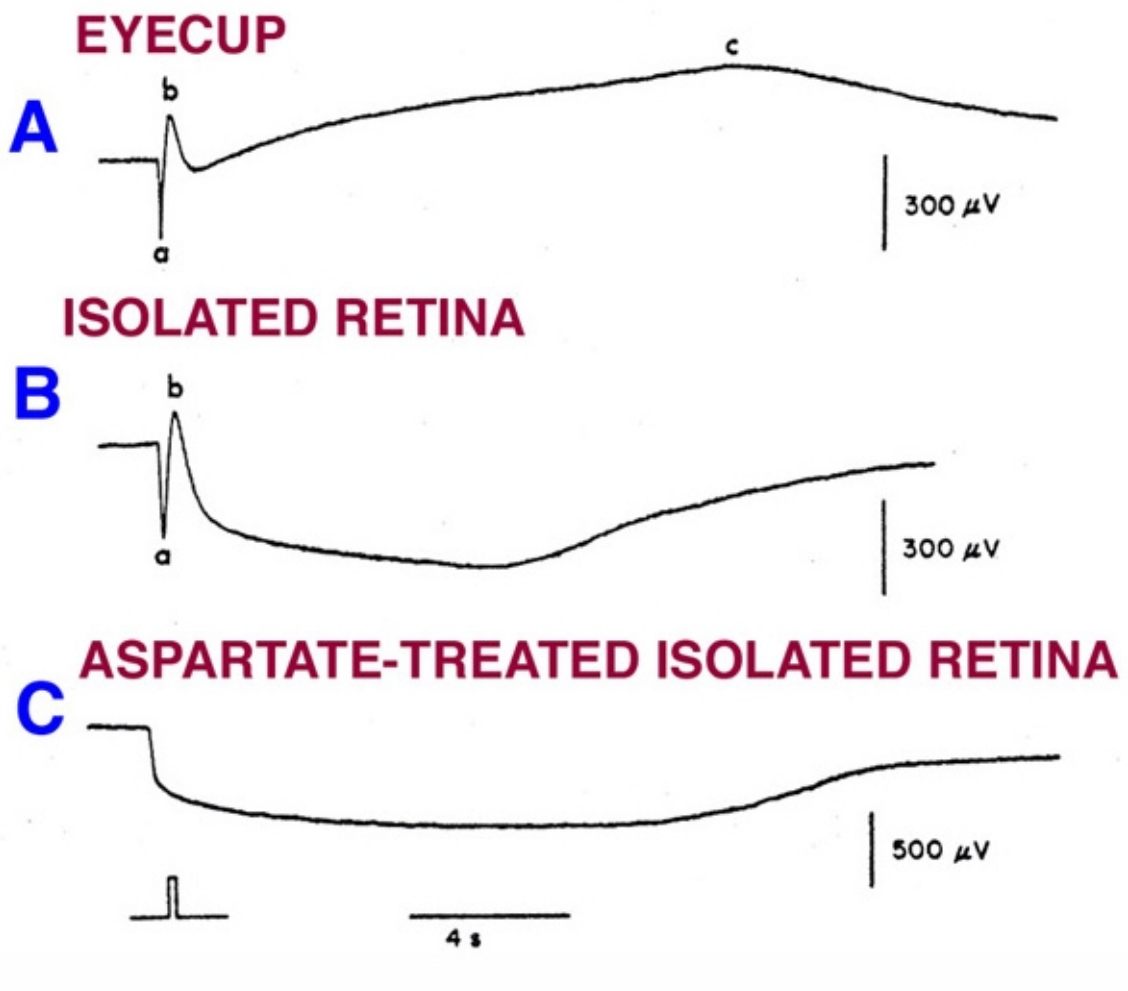

Figure 4. ERGs recording from the skate. The recording was done from the whole eyecup (upper trace), following the separation of the retina from the pigment epithelium (middle trace) and after exposing the retina to aspartic acid (lower trace) (17).

intentionally in laboratory animals (15, 31) or in human patients (32). Because the neural retina is supplied by the retinal vasculature and the photoreceptors by the choroidal plexus, this experimental manipulation, or pathological cases, effectively eliminate light-induced electrical activity in the neural retina from the photoreceptors.

Applying sink-source analysis to electrophysiological recordings of the intra-retinal ERG responses at different retinal depths further reveals the location of the b-wave (P-II) generators. Faber (33) was the first to calculate the extracellular currents that underlie the ERG b-wave of the rabbit eye. He reported that a sink for the b-wave was in the distal part of the retina, most probably in the outer plexiform layer, whereas the source was distributed proximally and distally to the sink. The only retinal elements that have a spatial distribution similar to the b-wave sources and sinks are the Müller glial cells. Indeed, intracellular recording from Müller cells in the Nectars retina supported Faber's ideas (34). The slow depolarizing response of Müller cells to a light stimulus followed a temporal pattern, similar to that of the ERG b-wave recorded from the same retina. Furthermore, the amplitude-stimulus intensity relationship was similar for the Müller cell photo responses and the ERG b-wave. On the basis of these observations, Miller and Dowling (34) suggested that depolarization of the Müller cell membrane in the distal retina resulted in extracellular currents that were expressed as the b-wave. A change in the extracellular concentration of ions that permeate through the Müller cells' membrane may cause a change in membrane potential. The most effective are potassium ions (35).

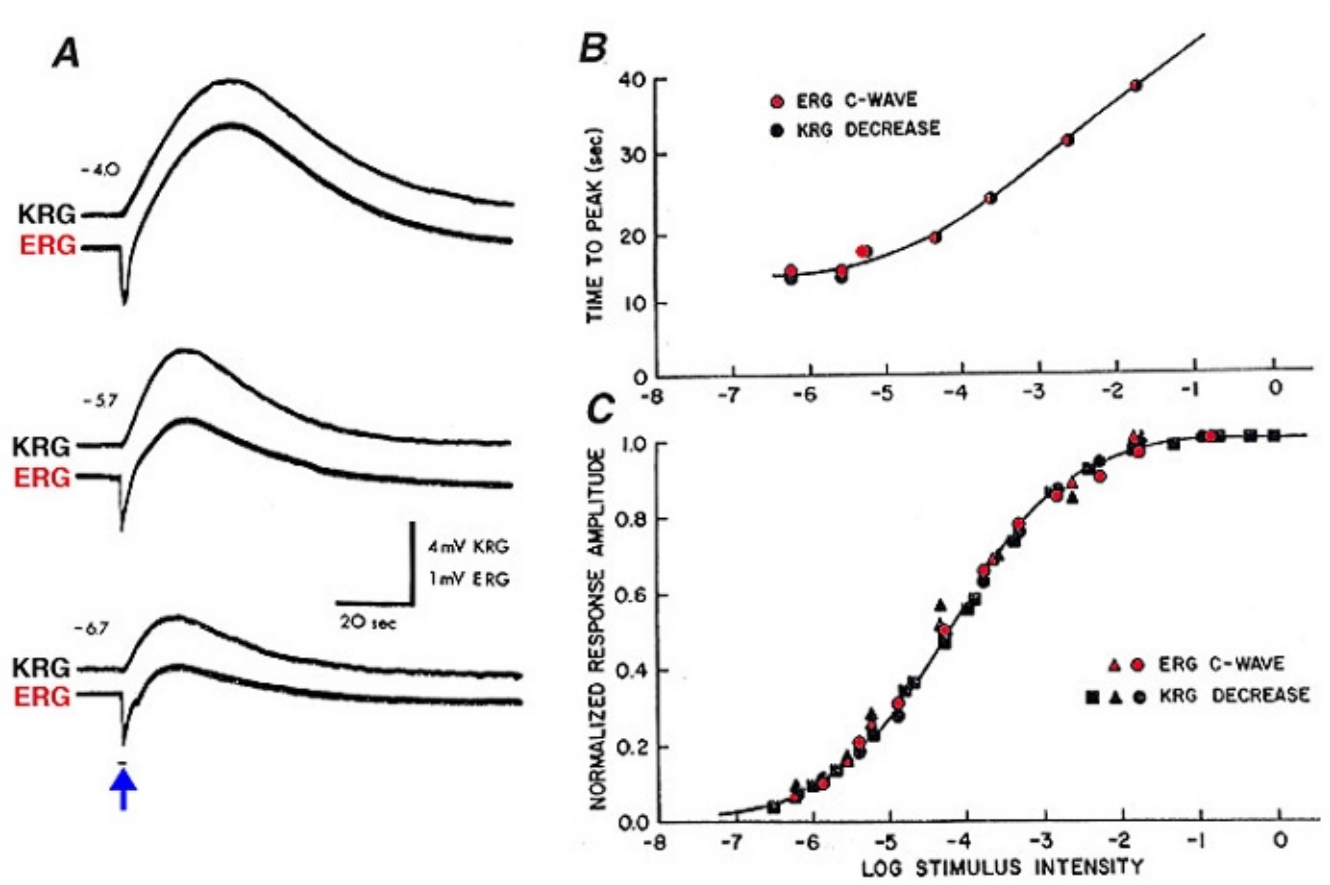

Figure 5. A, simultaneous recordings with double-barrel microelectrode of the ERG and the changes in the KRG from the distal retina of the frog. The KRG responses were inverted in polarity to compare with the ERG c-wave. Three different intensities of the light stimulus were applied. B, comparing time-to-peak (upper panel) and peak amplitude (lower panel) of the ERG c-wave and the KRG (18).

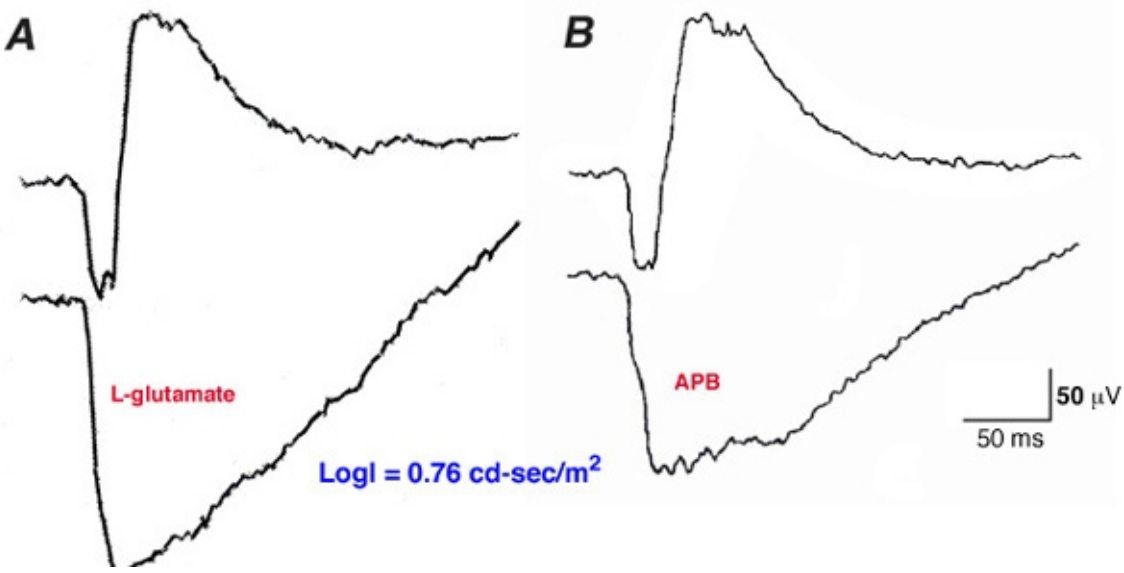

Figure 6. Elimination of the ERG b-wave (P-II) in rabbits by intravitreal injection of L-glutamate (A) or 2-amino-phosphonobutyric acid (APB) (B). The experimental drug was injected into the right eye (lower trace) and saline into the left eye (upper trace) as a control. In both experiments, the drugs successfully eliminated P-II, thus revealing the entire time course of the P-III component.

The idea that the b-wave results from changes in the membrane potential of the Müller cells due to light-induced changes of extracellular potassium concentration underlies the basis for the "Müller-cell hypothesis". Since first proposed, this idea has been tested by many investigators using intracellular recordings from Müller cells, measurements of extracellular concentrations of potassium, and recording of the ERG at different retinal depths. Studies were done in mudpuppy (36, 37), frog (38-40), fish (41, 42), rabbit (43, 44), cat (11, 23, 24), and monkey (45, 46). These and other studies reported a light-induced increase in extracellular potassium in the outer and inner plexiform layers. This increase was thought most likely attributable to leakage from depolarizing retinal neurons. It was assumed that the origin of potassium increases in the outer plexiform layer was bipolar cells, most specifically ON-center bipolar cells that were depolarized by light (47). In the inner plexiform layer, the increase in extracellular potassium resulted from light-induced activity of amacrine and ganglion cells (47, 48). The change in potassium alters the membrane potential of Müller cells, generating electrical currents in these two regions of the Müller cell and exiting through its distal and proximal ends (49). Depth recordings of extracellular concentration of potassium and of local field potentials are shown in Fig. 7a (36). The reduction of $[K^+]_o$ in the photoreceptor layer and the increase in the outer and inner plexiform layers are clearly seen. Current source-density analysis of data like these (Fig. 7a) led to the current pathways shown in Fig. 7b (40).

More evidence concerning the source of the ERG b-wave was gained with specific agonists and antagonists to glutamate receptors. Exposing the vertebrate retina to 2-amino-4-phosphonobutyric acid (APB), a specific agonist of glutamate metabotropic receptors, eliminates the ERG b-wave (50) as shown in Fig. 6B. Because APB-sensitive metabotropic glutamate receptors are found only in ON-center bipolar cells (51), this finding constitutes a clear indication of the involvement of these bipolar cells in the generation of the b-wave. Further support came from experiments in which the effects of 6,7-dinitroquinoxaline-2,3-dione (DNQX) upon the ERG were tested. This drug is a specific antagonist to AMPA/KA type glutamate receptors and enhances the b-wave, probably by removing current sources that oppose those forming the b-wave. In primates, Sieving and coauthors (52) proposed that the b-wave of the photopic ERG response is mainly contributed by the ON-center bipolar cells but is opposed by OFF-center bipolar cells. This leads to a "push-pull model" of these cell types (52). More recent detailed sink-source analyses (44), pharmacological dissection of the ERG (53), and experiments with mGluR6 knockout mice (54) (mGluR6 is the specific receptor for photoreceptor to ON-bipolar transmission in the retina; see the chapter on bipolar cells) points directly to the ON-center bipolar cells as generating the ERG b-wave without the Müller cells.

Experiments with injection of barium ions into the vitreous of rabbits did not eliminate the ERG b-wave. Under certain conditions, barium ions even caused augmentation of the b-wave as shown in Fig. 8 (55). Because barium ions block almost completely the potassium permeability of Müller cells (56-58), the dose used was expected to abolish the ERG b-wave if the Müller cell hypothesis for the b-wave generation was correct. This was not the case as shown by the ERG response in Fig. 8. The effects of barium chloride solution injected into the vitreous of one eye, while saline was injected into the vitreous of the other eye, were tested. The ERGs of the experimental eye that was being injected with barium chloride are augmented compared to those of the control eye. This observation opposes the Müller cells hypothesis for the ERG b-wave and thus supports the ON-center bipolar cell hypothesis.

Even more recent studies have searched for inner retina contributions to the ERG b-wave. Using tetrodotoxin (TTX) to block action potentials in third-order retinal neurons (amacrine and ganglion cells) and specific antagonists to GABA and glycine receptors, it was concluded that third-order neurons contributed to the amplitude and kinetics of the ERG b-wave (59). Because the a-wave is the sum of P-III and P-II, the a-wave is also affected by TTX application. In Fig. 9A, bright flash ERG responses from the rabbit are shown in control conditions and after intravitreal injection of bicuculline and strychnine to block, respectively, $GABA_A$ and glycine receptors, and after addition of TTX. The basic waveform of the ERG (a-wave b-wave complex) was not changed by these drugs; however, after bicuculline and strychnine, the b-wave was augmented, indicating removal of inhibitory contributions. After TTX, the b-wave was slightly reduced but was mainly delayed,

indicating the removal of a fast component. Averages (± s.d.) of the effects of the above drugs in five rabbits are shown in Fig. 9B. The data indicate that the amplitude of the b-wave is significantly increased by the mixture of bicuculline + strychnine, whereas TTX significantly delays the time-to-peak. The above conclusions are supported by another study on the retina-eyecup preparation of the tiger salamander, showing that drugs disrupting the activity of third-order neurons cause enhancement of the b-wave (60). The b-wave is also found to be affected by drugs that modulate $GABA_C$-type receptors, indicating that negative feedback from amacrine cells onto bipolar cells can shape the photoresponses of the bipolar cells and thus the amplitude and kinetics of the ERG b-wave (61). $GABA_A$ and $GABA_C$ pathways are also found to affect the ERG b-wave of the rat retina (62). Bicuculline, the antagonist for $GABA_A$-type receptors, augments the b-wave, whereas 3-aminopropylphosphono acid (3-APMPA), the antagonist for $GABA_C$-type receptors, reduces it.

Additional Minor Components of the ERG

In addition to the three major waves (a, b, and c), other components can be identified in the ERG, depending upon the experimental recording conditions. Some of these serve for evaluation of human retinal function in the clinic, whereas others are mainly used for research purposes.

The Early Receptor Potential (ERP)

This component of the light-induced activity of the eye was first revealed when a very bright light flash was used to stimulate the monkey eye (22, 63), the rat eye (64), or the human eye (65). This electrical response appears immediately after stimulus on set and has a biphasic pattern as shown in Fig. 10. The ERP in humans ends within 1.5 ms and is followed by the a-wave. Depth recordings of the ERP with microelectrodes and intracellular recordings led to the conclusion that the ERP originated in the photoreceptors (66, 67). The amplitude of the ERP depends directly upon stimulus intensity and the concentration of visual pigment in the outer segments of the photoreceptors. Therefore, the ERP is believed to reflect dipole changes in the visual pigment molecules because of conformational changes that are elicited by photon absorption. The ERP has been used in research to follow non-invasively the concentration of the visual pigment during light adaptation and in the dark after an exposure to bright light that causes substantial pigment bleaching (68). In humans, ERP recording have been done only occasionally to estimate rhodopsin density in patients suffering from retinitis pigmentosa, a disease of the photoreceptors (69, 70). Furthermore, it was shown that carriers of X-linked retinitis pigmentosa, who had no visual defects, could be identified by their reduced ERP recordings (70).

The Oscillatory Potential (OP)

When a bright light stimulus is used to elicit the ERG in humans or in animals, low-amplitude oscillating waves can be identified on the rising phase of the b-wave. These wavelets are much faster than the complex of the a- and b-waves. Their frequency is in the range of 100-150 Hz, and they are best isolated by using a band-pass filter on the ERG wave to eliminate the slow, large amplitude a- and b-waves. An example is shown in Fig. 11 (71). The small-amplitude, fast wavelets can be seen in the ERG response (Fig. 11a), but they cannot be measured. When an appropriate digital filter is applied and the amplification increased, the oscillatory potentials are isolated (Fig. 11b). A Fast Fourier Transform (FFT) can be applied to derive the power spectrum (Fig. 11c) and quantitative assessment of the amplitude and frequency of these potentials.

Depth recordings reveal that the OPs attain maximum amplitude when the microelectrode is in the inner retina (21). Because the amplitude-stimulus intensity of the OPs differs significantly from that of the b-wave, it is thought that these waves are generated in the inner plexiform layer (72, 73). The exact cellular origin of OPs is not yet known for certain. Pharmacological studies and depth recordings lead us to believe they reflect extracellular electrical currents generated by negative feedback pathways between amacrine cells, ganglion cells, and bipolar cells (73-75).

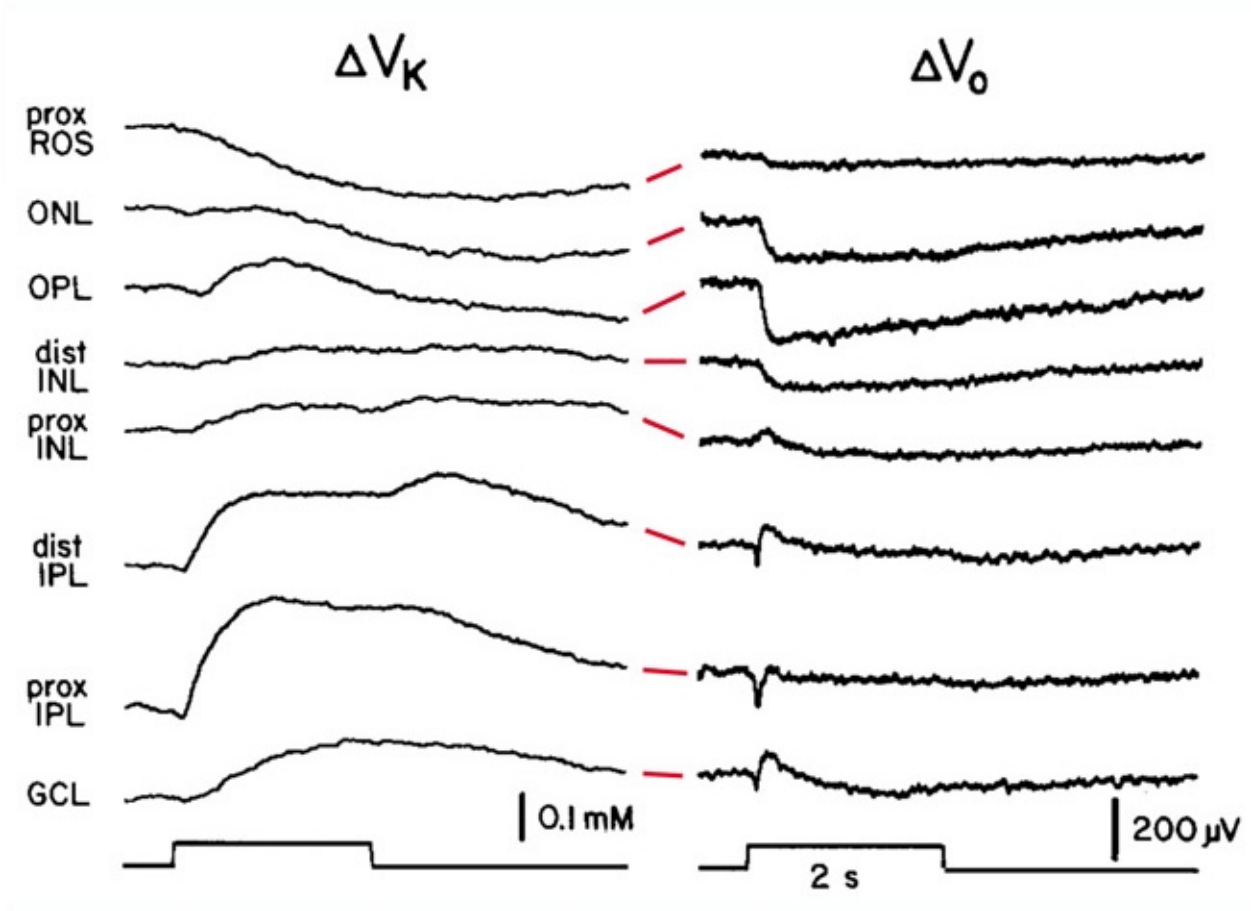

Figure 7a. The Muller cell hypothesis of the ERG b-wave. Depth profile of light-induced changes in the extracellular concentration of potassium ions (ΔVK) and of local field potential (ΔV0) (36).

OPs are very sensitive to ischemia in localized retinal areas. Therefore, in situations where the a- and b-waves remain normal in waveform and amplitude, OP recording scans indicate mild retinal ischemia in the inner retina (76). This occurs in diabetic retinopathy. Thus, OP recordings have sometimes been used as an indicator of background diabetic retinopathy (71, 77-79).

The d-Wave

The d-wave is seen only when the ON and OFF phases of the ERG response are separated in time, by using light stimuli of relatively long duration (>100 ms). Current source-density analysis shows its source to be the OFF-center bipolar cells (80, 81). Pharmacological studies in amphibian retinas (50, 82, 83) and in primates (52), using selective blockers for ON bipolar cell glutamate metabotropic receptors and OFF bipolar cell AMPA/KA type receptors, have shown that the d-wave of the ERG depends entirely on AMPA/KA type synaptic transmission, i.e., between photoreceptors and OFF-center bipolar cells (Fig. 12).

In Fig. 12, responses were recorded with a microelectrode in the distal retina, and therefore, the polarities of the waves are opposite to that obtained with the active recording in the proximal retina or vitreous or cornea. The a-wave is positive, the b-wave negative, and the d-wave negative. After exposure to DNQX, a specific antagonist for AMAP/KA-type glutamate receptors, the a-wave is reduced, the b-wave enhanced, and the d-wave reverses in polarity (Fig. 12b). The enhancement of the b-wave reflects the removal of opposing contribution from third-order retinal neurons (59, 60). The reduction in the amplitude of the a-wave does not reflect a direct action of DNQX but rather the enhancement of P-II that usually opposes P-III. The reversal in polarity of the d-wave

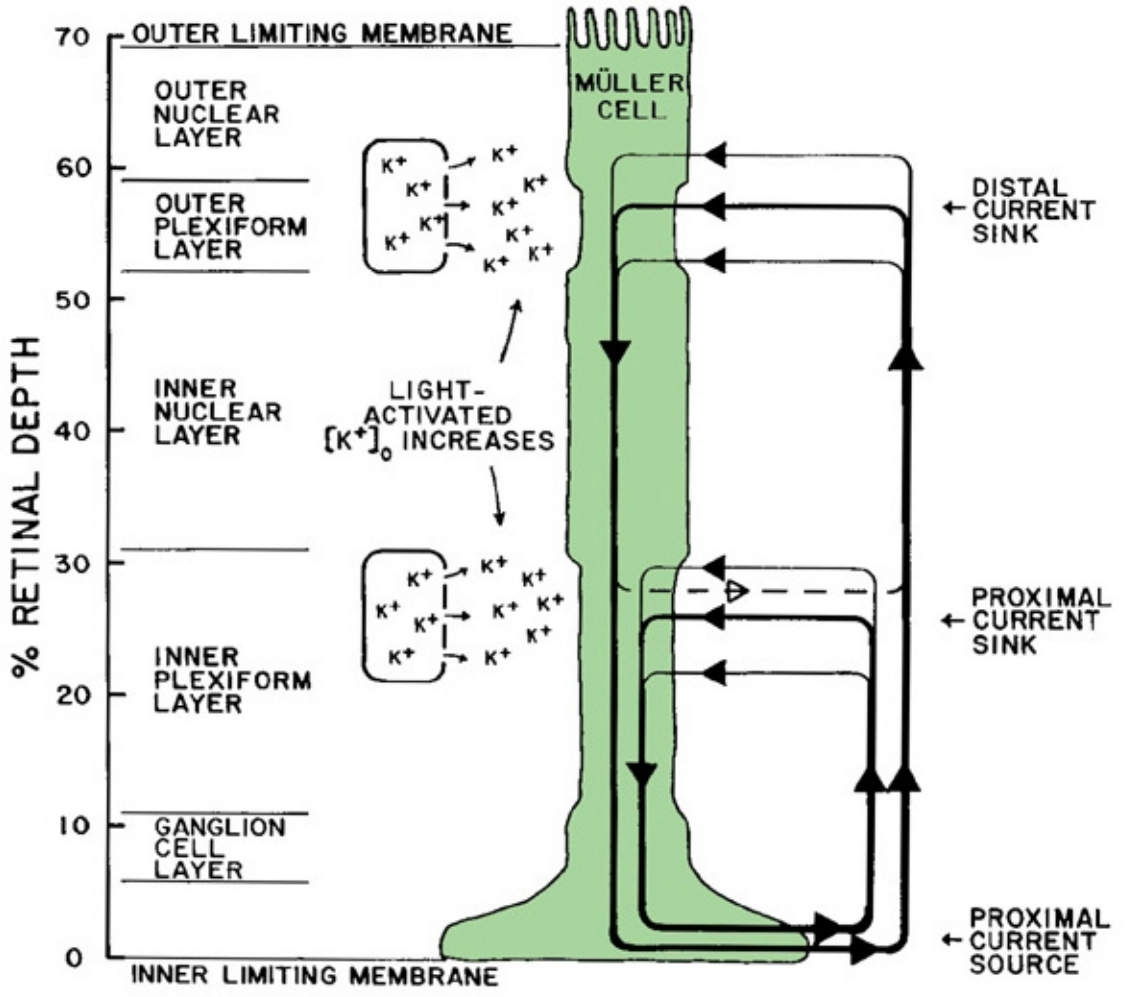

Figure 7b. The pathways of the extracellular currents that have been suggested to underlie the generation of the ERG b-wave. The two sinks (OPL and IPL) reflect the increase in extracellular potassium ions attributable to light-induced electrical activity. The vitreous serves as a large current source due to the high potassium conductance of the end feet of the Muller cells (40).

reflects its origin in OFF-center bipolar cells. Third-order retinal neurons may also contribute to the ERG d-wave (60).

The d-wave can be recorded only with prolonged light stimuli. With light stimuli of shorter durations, the d-wave tends to combine with the b-wave. This phenomenon led early studies of patients with congenital stationary night blindness (CSNB) or with melanoma-associated retinopathy (MAR) to conclude that the cone system was functioning normally and only the rod system was affected. The use of light stimuli of long duration revealed that the ON pathway in both rod system and cone system was affected, and only the OFF pathway of the cone system exhibited normal function (see the chapter on bipolar cells) (84, 85).

Scotopic Threshold Response (STR)

When very dim light stimuli (below the P-II threshold) are applied in the dark-adapted state, a slow corneal negative potential is recorded from toad (86), cat (11, 87), sheep (88), monkey (89), and humans (90, 91). This potential was called the scotopic threshold response (STR) to indicate that it was recorded with light stimuli near rod threshold. Simultaneous recording of field potentials and potassium concentrations with double-barreled electrodes, at different retinal depths of the dark-adapted cat retina, indicates that the STR originates from light-induced changes in the extracellular concentration of potassium ions in the proximal retina (affecting the

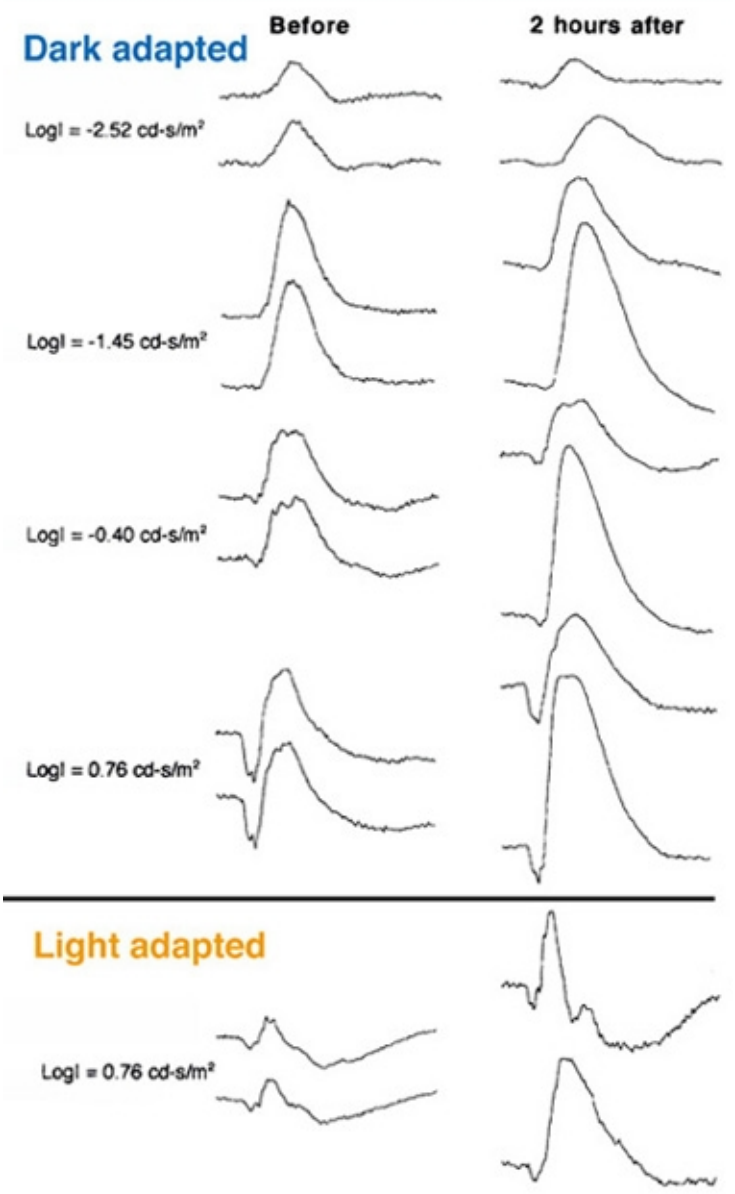

Figure 8. The effects of barium ions on the ERG responses of the rabbit. Saline solution containing barium chloride was injected into the vitreous of the right eye and saline into the vitreous of the left eye (lower and upper traces, respectively). The ERG responses after 2 hours were augmented in the eye injected with barium ions (55).

membrane potential of Müller cells) (87, 92). Barium ions that block potassium conductance of the Müller cells, but not light-induced increase in extracellular potassium concentration, also eliminate the STR as shown in Fig. 13 (92).

Because the STR is a corneal negative component that is sometimes followed by a positive component, it resembles the ERG a-wave/b-wave complex and can be misinterpreted. In a detailed study in cat and monkey, it was found that the STR could be eliminated by aspartate while the a-wave that was elicited by bright light stimuli was spared, supporting the post-receptoral origin of the STR (89). Fig. 14 compares amplitude-intensity (A) and latency- intensity (B) data for cat STR and a-wave in normal conditions and after intravitreal injection of L-aspartate (89). The STR responses were recorded with light stimuli that were dimmer by more than 3 log units. L-Aspartate eliminated the STR but did not affect the a-wave.

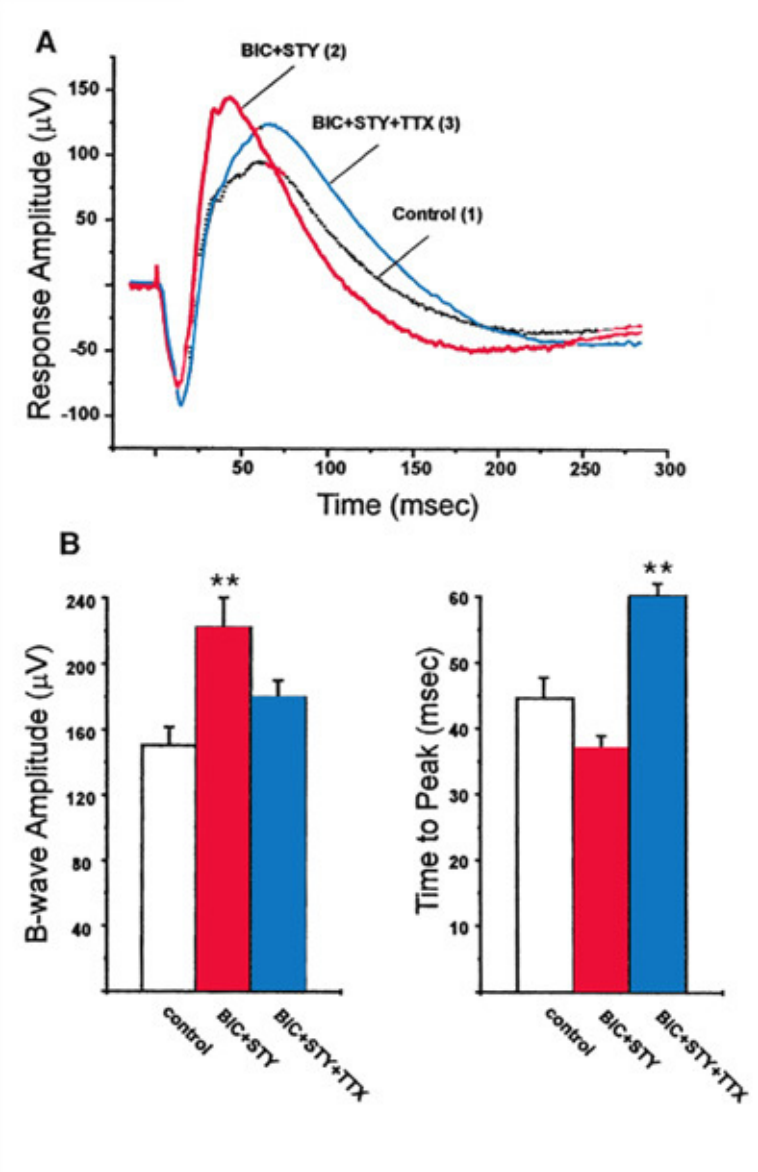

Figure 9. A, the effects of a mixture of bicuculline + strychnine on the ERG, response of one rabbit (trace 2). Then, TTX was added to the mixture to block spiking activity (trace 3). The drugs were injected into the vitreous of the rabbit eye. B, average effects of the different drugs on the b-wave amplitude (left) and time-to-peak (right). Significant difference at the $p<0.01$ level is denoted by two asterisks (59).

The M-Wave

The M-wave was first described in cold-blooded vertebrates as a negative-going potential change at stimulus onset and offset (48). The M-wave has also been described in the light-adapted retina of the cat (93, 94). It was proposed to represent changes in membrane potential of Müller cells due to light-induced increases in the extracellular potassium in the proximal retina (37, 48). This suggestion was later supported by experiments in which barium ions, used to block the potassium conductance of Müller cells, eliminated the M-wave (95).

We can learn more about the M-wave from simultaneous recordings of field potentials and potassium concentrations at different retinal depths under changing light stimulation and by modulating the activity of the ON- and OFF-channels by specific drugs. Fig. 15 compares the M-wave to potassium changes for different spot sizes of light. The M-wave is composed of ON and OFF waves that decrease in amplitude as the stimulus diameter is increased. The light-induced potassium increases are of similar waveform; transient increases occur

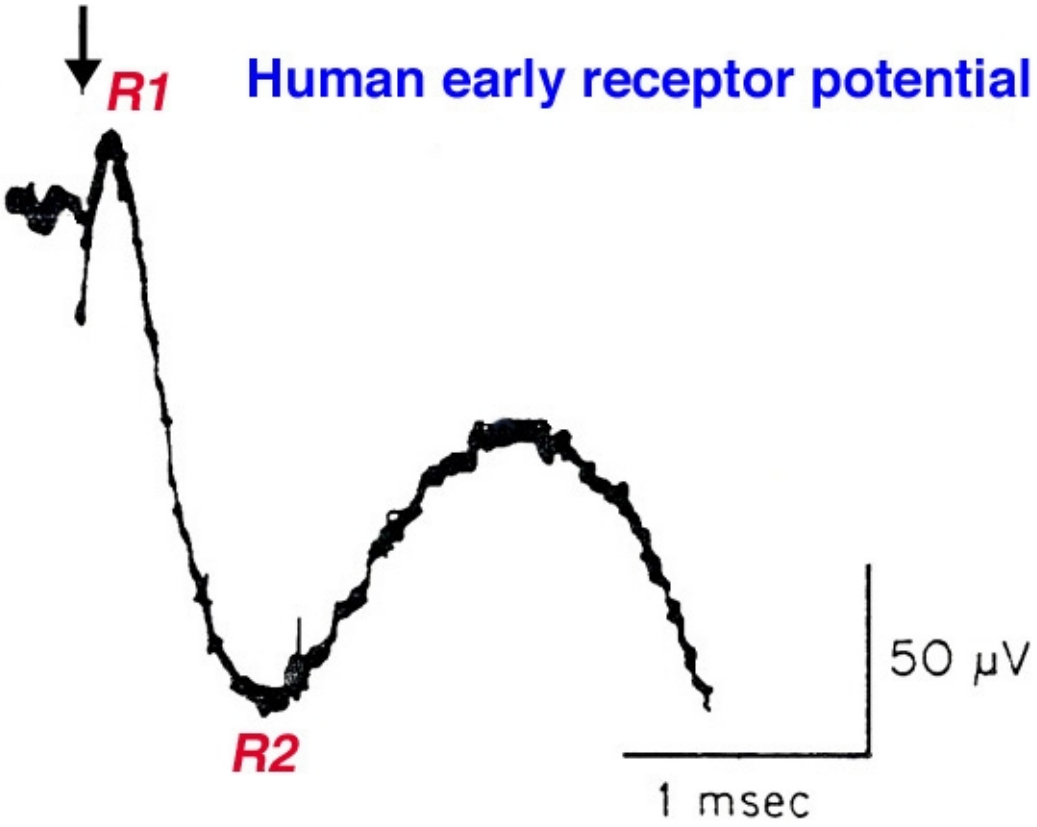

Figure 10. A typical early receptor potential (ERP) of the human eye that was elicited by a very bright light flash (arrow). Two waves are identified, the positive R1 followed by the negative R2 (65).

at stimulus onset and offset. The relationship to the diameter of the stimulating light is similar. These experiments support the hypothesis that the M-wave, in the light-adapted cat retina, is attributable to changes in extracellular potassium concentration in the proximal retina and to activity in both ON and OFF channels (93). Adding barium ions to block potassium conductance of the Müller cells does not completely eliminate the M-wave. A small, sustained depolarizing component is seen at light onset plus a negative OFF component. Evidently, direct neuronal contributions cause the M-waves, and the major contribution is to the OFF wave (93).

The ERG results discussed here and in the previous section indicate similarities between the STR and the M-wave. Both are negative-going field potentials that reflect the effects of light-induced potassium changes upon the Müller cells in the proximal retina. The difference between these field potentials arises from their photoreceptor basis. Whereas the STR reflects rod-mediated vision, the M-wave is dominated by the cone system. Therefore, the former is a slow potential at stimulus onset recorded in the dark-adapted retina, whereas the latter contains ON and OFF components and is recorded in light-adapted conditions (compare Fig. 13 and Fig. 15). Furthermore, the STR seems to be solely dependent upon potassium-Müller cell interactions, whereas the M-wave reflects also direct contributions from neuronal activity, particularly to its OFF component.

Summary of the ERG Components

The ERG is an electrical response of the eye and is made up of several components. In the previous sections, the major and minor components of the ERG were described, and their cellular origins were discussed. Researchers and clinicians who are interested in objective assessment of retinal function need to become familiar with the

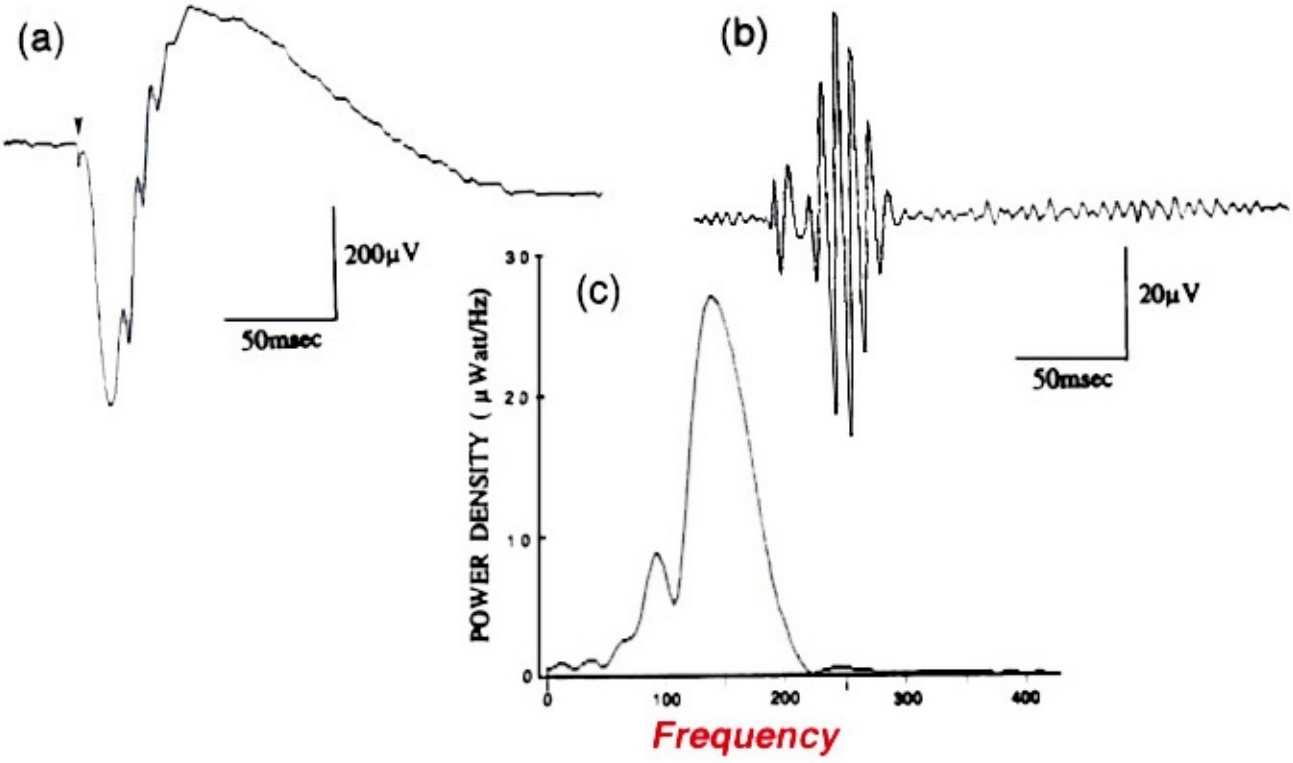

Figure 11. Isolating the oscillatory potentials from the bright flash ERG response of the human eye (a) by applying a digital filter (b). An FFT procedure was applied to the isolated oscillatory potential to obtain the power spectrum (c) (71).

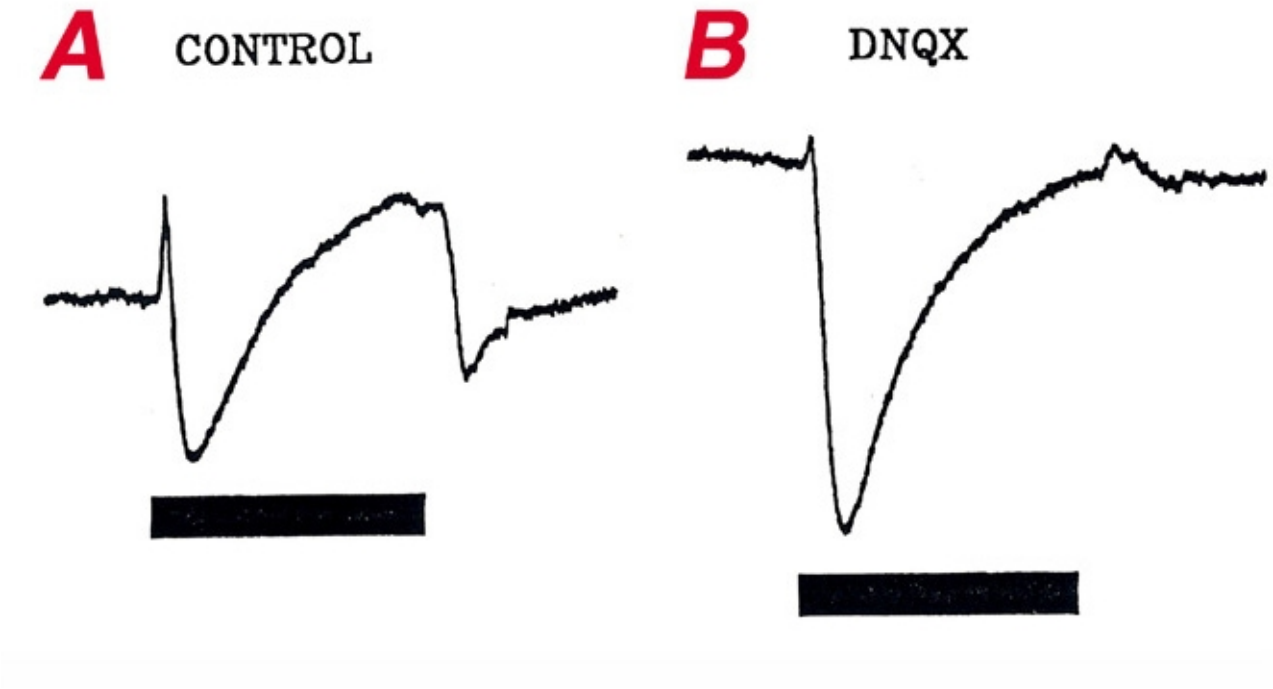

Figure 12. The effects of DNQX, a specific antagonist of AMPA/KA-type glutamate receptors, upon the ERG response of the tiger salamander. The polarity of the waves is reversed; the a-wave is positive, the b-wave negative, and the d-wave negative (50).

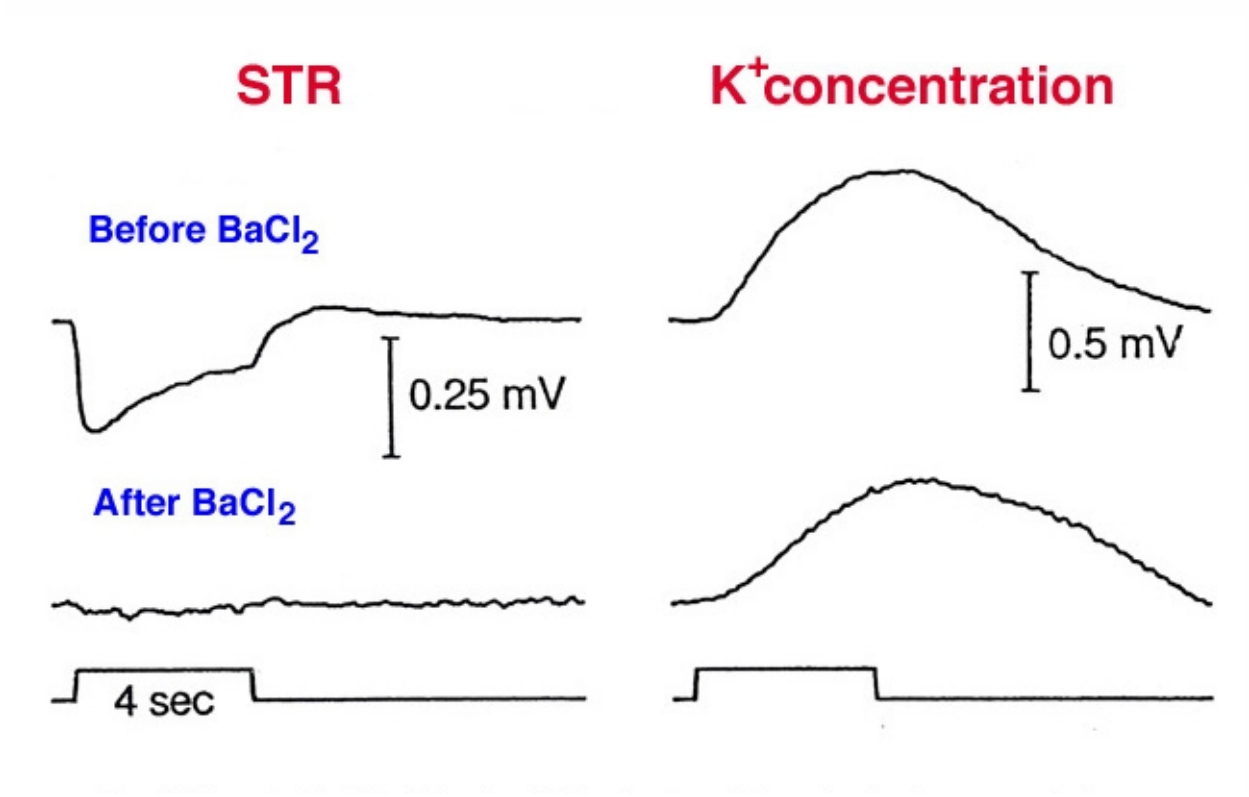

Figure 13. The effects of $BaCl_2$ on the STR and extracellular potassium ion concentration recorded from the proximal retina of the dark-adapted cat. Barium ions eliminate the STR but have no effect on the light-induced increase in extracellular potassium concentration in the proximal retina (92).

ERG waves. With proper analysis, the functional integrity of different retinal structures can be dissected out, and we are able to understand information processing mechanisms and/or the sites of retinal disorders.

The ERG originates from extracellular currents that are generated in response to a light stimulus. In the ophthalmic clinic, the most common recording of ERG responses contains the negative a-wave and the positive b-wave. Light absorbance by the visual pigment molecules in the outer segments of the photoreceptors reduces the "dark" current and, therefore, can be viewed as eliciting a "light" current. This current is expressed as a negative wave when recorded from the vitreous or the cornea and constitutes the fast P-III (the receptor potential). The a-wave of the electroretinogram is the leading edge of the fast P-III and, therefore, reflects the functional integrity of the photoreceptors. However, the amplitude of the a-wave also depends upon the development of the positive Granit's P-II component. Early development of P-II will result in a subnormal a-wave, whereas a slow P-II will be expressed in a supernormal a-wave. Any analysis that allows separation of P-III from the overall ERG response will provide valuable information about the photoreceptors.

The exact source of the ERG b-wave is still under dispute. The major contribution comes from light-induced activity in ON-center bipolar cells. The extracellular currents that generate the b-wave either originate directly in these cells or reflect potassium-induced changes in the membrane potential of the Müller cells enveloping them. Regardless of the exact mechanism, the b-wave is telling us about light-induced electrical activity in retinal cells post-synaptic to the photoreceptors. The b-wave is also affected by OFF-center bipolar cells and by light-induced activity in third-order retinal neurons (amacrine and ganglion cells). This contribution can be isolated in the laboratory by using specific drugs, but in the clinical environment, the ERG b-wave of patients reflects all contributions summed together. In the future, more sophisticated analytical approaches may allow separation of the different contributions and allow identity of more exact sites of retinal diseases.

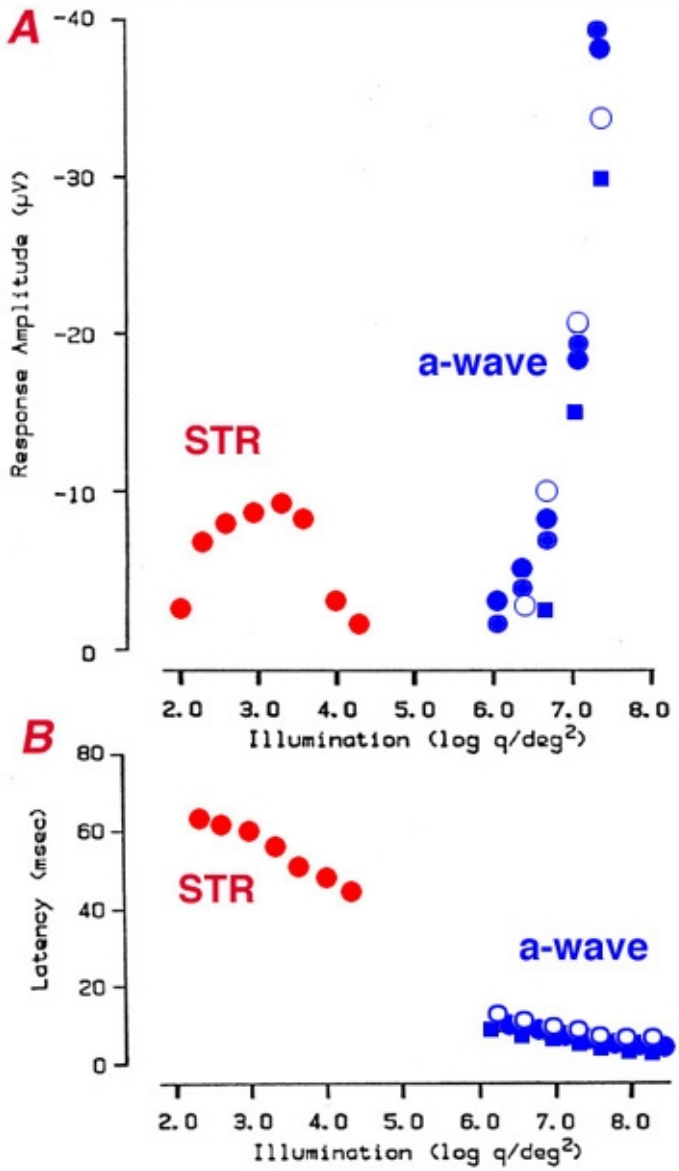

Figure 14. Amplitude-intensity (A) and latency-intensity (B) for the STR and a-wave that were recorded in the dark-adapted cat. Measurements obtained before and after intravitreal injection of L-aspartate are compared (open circles and filled symbols, respectively) (89).

Under special conditions of ERG recordings, the c-wave can be observed in patients. As has been discussed above, the c-wave reflects light-induced decrease in the extracellular concentration of potassium ions in the photoreceptor layer due to light-induced activity in the photoreceptors. The c-wave itself is a manifestation of the change in the trans-epithelial potential. Therefore, the c-wave can be used to assess the functional integrity of the pigment epithelial cells, the photoreceptors, and the interactions between the two.

Among the minor components of the ERG, only the oscillatory potentials and the d-wave are used for clinical assessment of retinal function. The OPs are often used to assess the balance between retinal metabolic needs and retinal vascular supply, because in many retinal vascular disorders, they are the first to be affected (75, 76). The d-wave is used only when the cone ON- and OFF-channels need to be separated to identify defects specific to ON-channels (84, 85).

The other components of the ERG—the early receptor potential (ERP), scotopic threshold response (STR), and M-wave—are more difficult to isolate in the routine clinical setup and are measured only for research purposes.

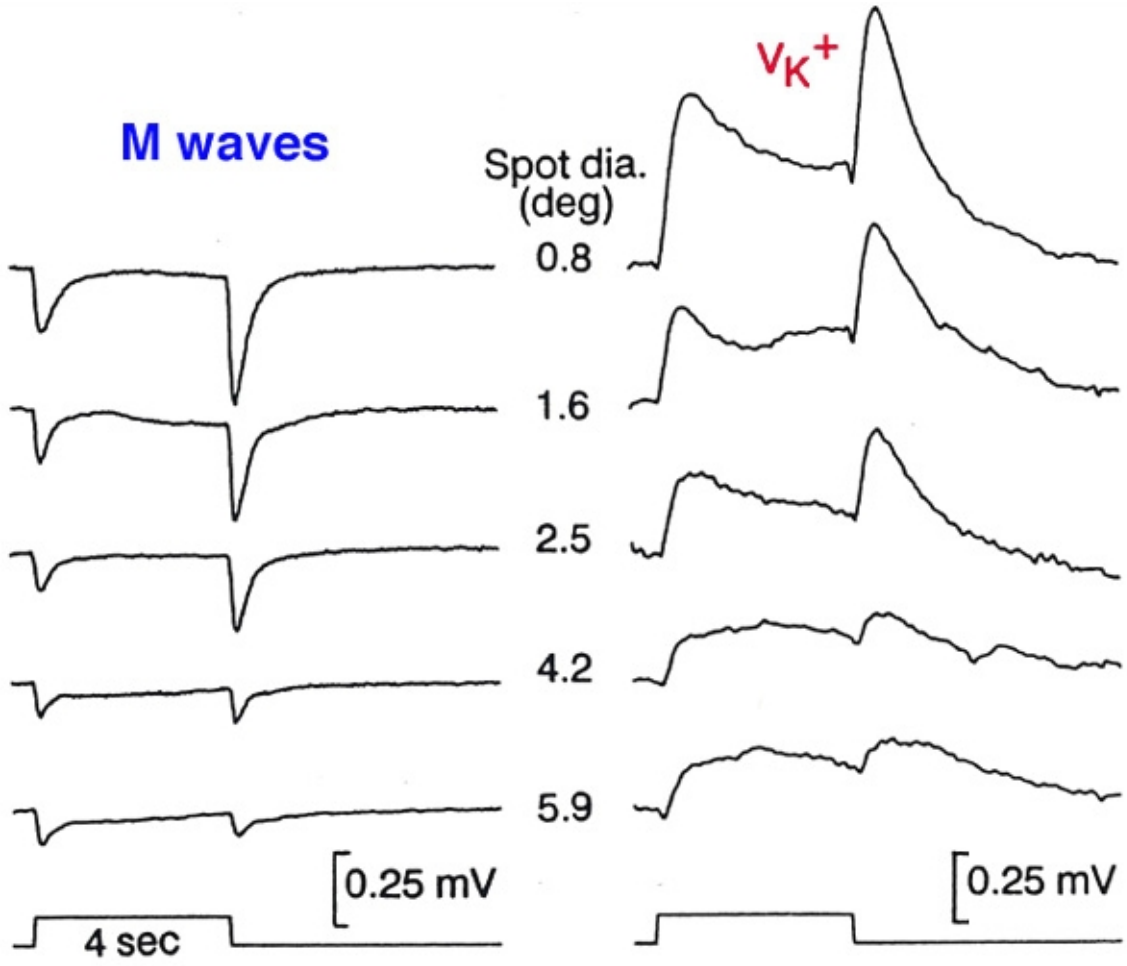

Figure 15. The effects of changing the diameter of the stimulating light upon the M-wave (left column) and the extracellular potassium concentration (right column). The field potential and the potassium concentration were recorded simultaneously with a double-barreled electrode from the proximal retina of the dark-adapted cat (93).

Factors Affecting the ERG

To use the ERG in the most efficient way for retinal research and for electrodiagnosis of retinal function, the parameters that affect the ERG response need to be known.

State of Adaptation

The visual system in vertebrates can be roughly divided into two subsystems, the rod system (night vision) and the cone system (day vision). Both systems operate independently with very few interactions between them. The most sensitive system under particular conditions is the one that determines vision. In some species, the rod system dominates (e.g., skates, rats), whereas in others, the cone system is the dominant one (e.g., some fresh water turtles, ground squirrels). However, in most species including humans, both systems are found. These are duplex retinas. Rod-mediated vision is very sensitive to dim light stimuli in the dark-adapted state; while under background illumination, it saturates and does not respond to light increment or decrement (96). In contrast, the cone system is not as sensitive but is characterized by the ability to adapt to bright lights—processes that allow vision to adapt to background illumination over a wide range of intensities. To separate cone function from rod function, we can modulate the state of adaptation as shown in Fig. 16. When a given light stimulus is applied under background illumination that saturates the rod system, the ERG reflects activity in the cone system. The

ERG under these conditions is of small amplitude but of very fast kinetics—time to peak is about 30-32 ms (Fig. 16, left). In contrast, if the same light stimulus is applied after the subject is kept in darkness for about 30 min, the ERG is of considerably larger amplitude (about 4 folds) and is characterized by slow temporal properties—time to peak of the b-wave is about 60 ms (Fig. 16, right). This ERG response is a mixed rod-cone response (the cone system is operational, too) but mainly reflects the activity in the rod system because the cone system contribution is considerably smaller.

Light Intensity

In Fig. 17, dark-adapted ERG responses of one volunteer are shown to light stimuli of different intensities covering a range of about 5 log units. With a dim light stimulus, the ERG is a slow positive wave of small amplitude. This is the b-wave. As the stimulus intensity is increased, the ERG b-wave increases in amplitude and becomes faster in kinetics. With yet brighter stimuli, a negative wave (the a-wave) precedes the positive b-wave. With further increase in the flash intensity, both the a-wave and the b-wave increase in amplitude and become faster. With the brightest flash used here, fast wavelets (oscillatory potentials) are seen on the rising phase of the b-wave.

It is clear from Fig. 17 that the ERG responses of humans and of other vertebrate species depend upon the intensity of the light stimulus used. Therefore, it is crucial for a research laboratory as well as a clinical set-up to control the light intensity of the ERG system and to verify that technical factors will not contaminate the data and, therefore, the conclusions. The size of the pupil is the major determinant of light intensity to the retina. A 3-fold change in pupil diameter means a 9-fold change in light intensity reaching the retina (almost 1 log unit). Opaque optical media should also be considered. Mature cataract or vitreal hemorrhage will absorb some of the impinging light and will, therefore, reduce the light intensity reaching the retina. These latter factors usually absorb about 50% of the light, thereby reducing light intensity by 0.3 log units.

Color of Light Stimulus

Fig. 18 shows the spectral sensitivity curves of cone-mediated vision and of rod-mediated vision in human observers. The rod curve peaks at the blue-green region of the visible spectrum (around 500 nm). The spectral sensitivity curve of cone-mediated vision is the sum of all three spectral types of cone: long-wavelength sensitive (red), medium wavelength-sensitive (green), and short wavelength-sensitive (blue), and, in net, has peak sensitivity in the orange range of the visible spectrum (around 560 nm). Throughout most of the visible spectrum (less than 620 nm), the rod system is more sensitive than the cone system by as much as 3 log units (a factor of 1000). For wavelengths longer than 620 nm, the sensitivity of both systems is similar, and cone vision may even exhibit a slightly higher sensitivity than rod vision.

Therefore, light stimuli of different spectral content can elicit ERG responses that are dominated by one or the other systems as shown in Fig. 19. These ERG responses were recorded in a volunteer in the dark-adapted state using dim blue or bright red light stimuli. The blue stimulus elicits a slow positive ERG of the more sensitive rod system (A). The red light stimulus produces an ERG response composed of two parts: a fast wave peaking around 30 ms, and a slow wave peaking at 100 ms (B). This ERG is a combination of rod and cone contributions, with the cone-mediated response being of fast kinetics and the rod-mediated response of slow time-to-peak. The fast cone-mediated ERG is sometimes referred to as the x-wave (97, 98). The two light stimuli were balanced to produce equal rod excitation as evidenced by the equality in the slow ERG component (Fig. 19C). With this procedure, cone-mediated function can be isolated from the large-amplitude rod ERG and allows analysis of the cone *versus* rod system in the dark-adapted state.

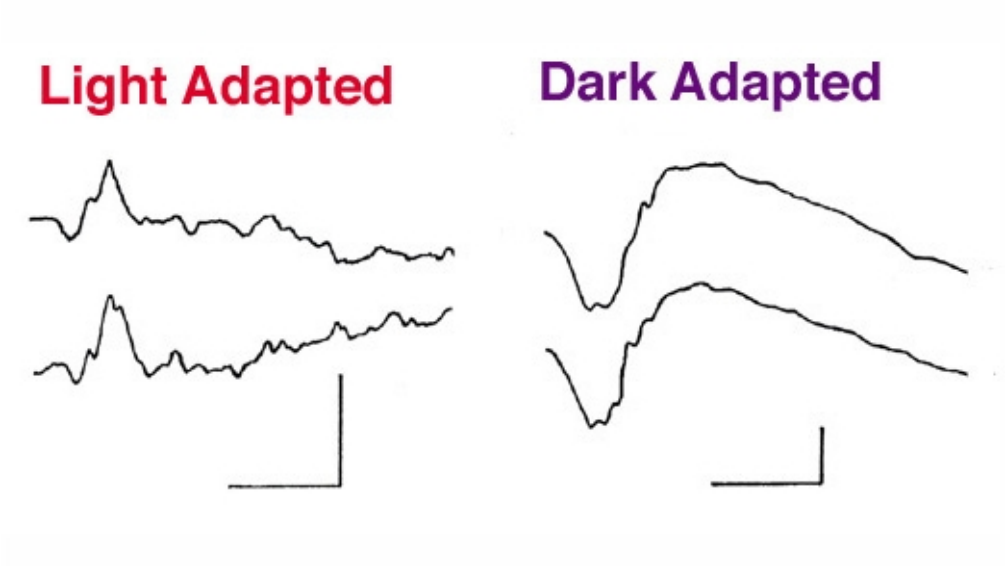

Figure 16. The ERG responses of a volunteer that were elicited with the same light stimulus during continuous background illumination (A) and after 30 min in the dark (B). Note the different temporal properties and amplitudes of the two responses.

Frequency of Photostimulation

Another experimental approach to separate rod-mediated vision from cone-mediated vision is based upon the differences in temporal properties between these two visual systems. Measurements of critical fusion frequency (CFF), the maximal frequency of stimulation that can be perceived as flickering, show low CFF in dim illumination that rises with stimulus intensity until a plateau phase of about 15 Hz is reached. Under cone vision conditions, high-intensity stimuli can be perceived as flickering at frequencies of 30 and even 50 Hz (99). However, when special care is taken to selectively desensitize the cones and thus reveal the rod function under bright illumination, flicker fusion frequencies are achieved at 28 Hz (99).

In ERG recording, CFF is determined by the frequency of photic stimulation that just elicits flickering electrical signal. The relationship between the ERG-determined CFF and stimulus intensity shows a discontinuity that marks the transition from rod vision to cone vision. The highest CFF for rod vision is about 15 Hz, whereas the cones can follow flickering stimulations up to 50 Hz (100). Recent, more careful ERG recordings reveal that rod-mediated electrical activity can follow flickering frequencies higher than 15 HZ, reaching as high as 28 Hz (101). It has been argued, based on recent findings on the rod system in mammals and primates, that rod signals can be transmitted via two pathways. The first one involves the rod bipolar cells. This is the slow pathway that can follow flickering stimuli up to 15 Hz. The second pathway involves rod-to-cone gap junctions that transmit rod-mediated signals via the cone bipolar cells that can follow flickering stimuli up to 28 Hz (101).

To reveal the fast flicker of the rod signals, special care is needed for recording conditions. Under regular recording conditions of the ophthalmic clinic, it can be accepted that rod-mediated electrical signals can follow flickering stimuli up to 15 Hz. Therefore, it is customary to apply bright light stimuli at a frequency of 30 Hz to isolate the cone system from the rod system. The responsiveness of the cone system and its ability to follow fast flickering stimuli depend upon the level of ambient illumination as shown in Fig. 20 (102). In this figure, ERG recording was performed from one subject using 31.3 Hz flicker of constant intensity while changing the level of ambient illumination. The responses are of larger amplitude and are characterized by faster rise times as the irradiance of the adapting field is raised. This observation is consistent with the notion that the cone system is suppressed in the dark-adapted state and that light adaptation removes this inhibitory action. However, by using scotopically matched backgrounds, one can see that mechanisms intrinsic to the cone system itself are also involved (102).

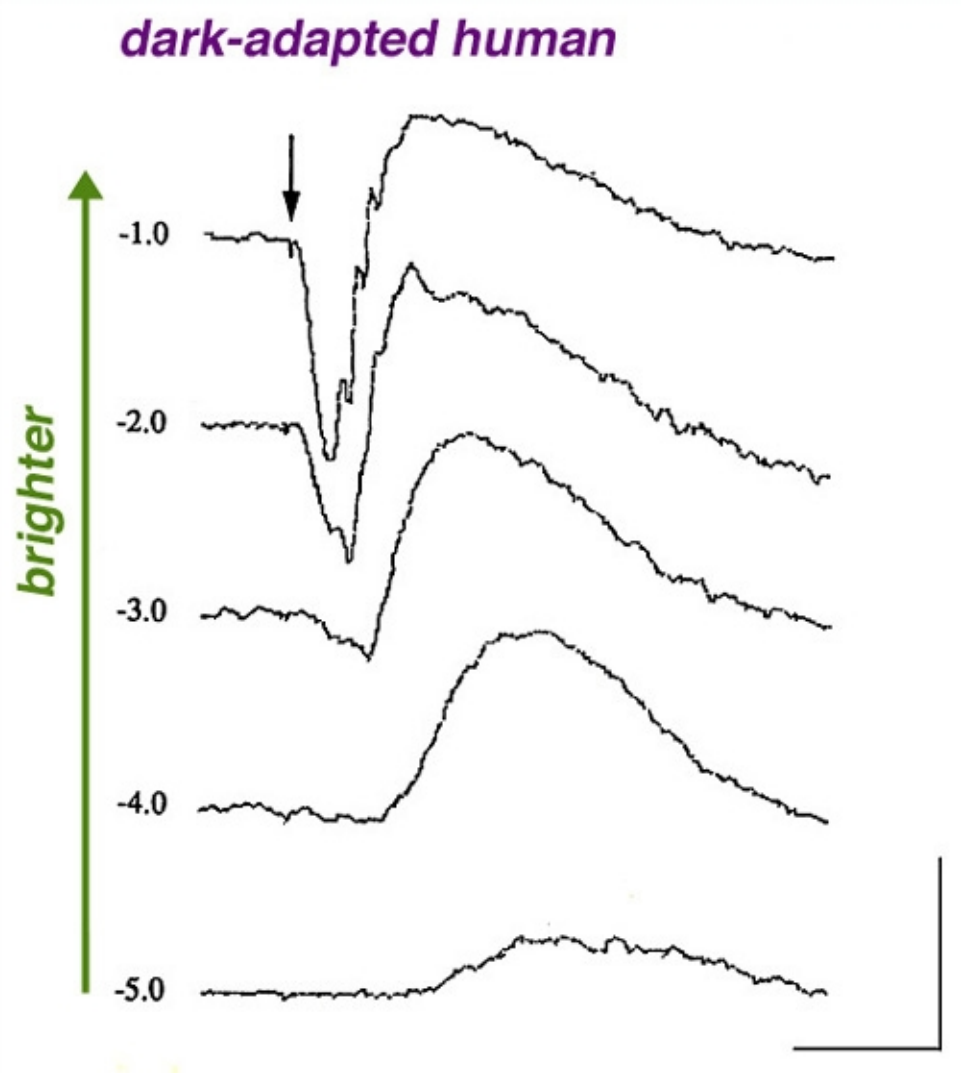

Figure 17. ERG responses that were recorded from one subject with corneal electrode in the dark-adapted state. Several intensities were used covering a range of 4 log units.

Analysis of the ERG

Over the years, since the first recording of the ERG responses and with greater understanding of retinal function at the cellular and molecular levels, more advanced analytical approaches have been developed. In this section, the more classical means of analysis and some of the recent approaches to clinical ERG analysis will be discussed.

Amplitude and Implicit Time Measurements

The most common ERG response from a human, which is elicited with a full-field (Ganzfeld) flash of light, contains the a-wave and the b-wave as shown in Fig. 21. The amplitude of the a-wave is measured from a baseline that is monitored before the light stimulus, to the trough of the negative wave. Because the b-wave reflects the sum of the negative P-III component and the positive P-II component, its amplitude is measured from the trough of the a-wave to the peak of the b-wave. The temporal properties of the ERG response are usually defined by the time-to-peak (implicit time) of the b-wave and are measured from stimulus onset to the peak of the b-wave (L_b in Fig. 21). In some laboratories, the time-to-peak of the a-wave is also measured (L_a in

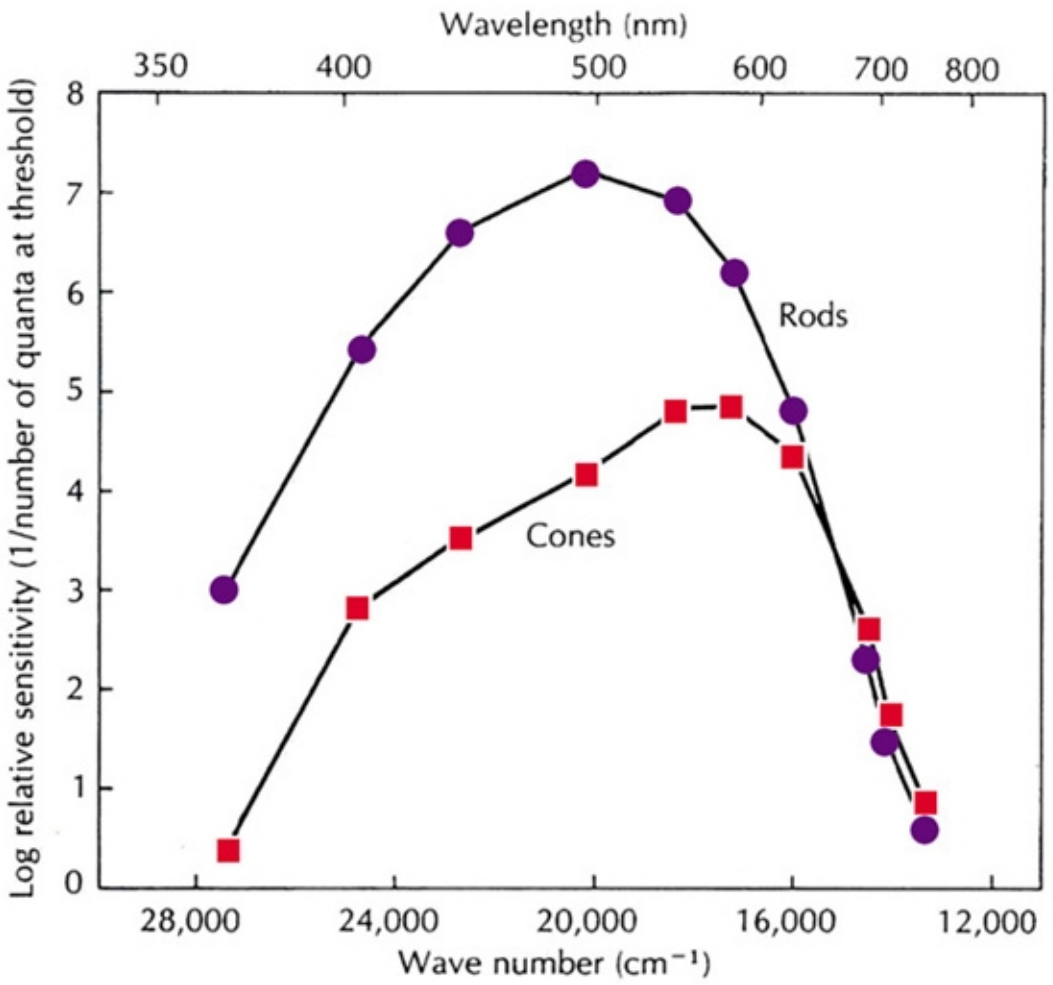

Figure 18. Spectral sensitivity of rod vision (purple circles) and cone vision (red squares).

Fig. 21). These ERG parameters change with the intensity of the light stimulus (Fig. 17) and with the state of adaptation (Fig. 16), as we have seen earlier.

Fig. 22 shows the dependency of the ERG amplitudes and temporal properties upon stimulus intensity (A and B, respectively). These curves were constructed from ERG measurements in 20 volunteers with no visual defects and were conducted in the dark-adapted state. Data represent average (± s.d.) of the amplitude and time-to-peak of the a-wave and the b-wave. For dim light stimuli, the ERG consists of only the b-wave (Fig. 22A). As stimulus intensity is increased, the b-wave increases in amplitude until a plateau is reached at intensities brighter by about 2 log units than that needed to elicit the smallest recordable b-wave. At these intensities, the a-wave becomes evident. With further increases in intensity, both a- and b-waves grow in amplitude. The effect of stimulus intensity upon the kinetics of the ERG response is clearly seen in the dependency of the a- and b-wave time-to-peaks upon stimulus intensity (Fig. 22B). The brighter the flash stimulus, the faster the ERG response and the shorter the time-to-peaks of both waves are. This type of analysis can give valuable information about retinal function in a clinical set-up where all conditions of measurements are maintained at a constant.

The relationship between amplitude and intensity of the ERG waves can be described by the following hyperbolic function (103, 104).

$$V/V_{max} = I/(I + \sigma) \text{ (Equation 1)}$$

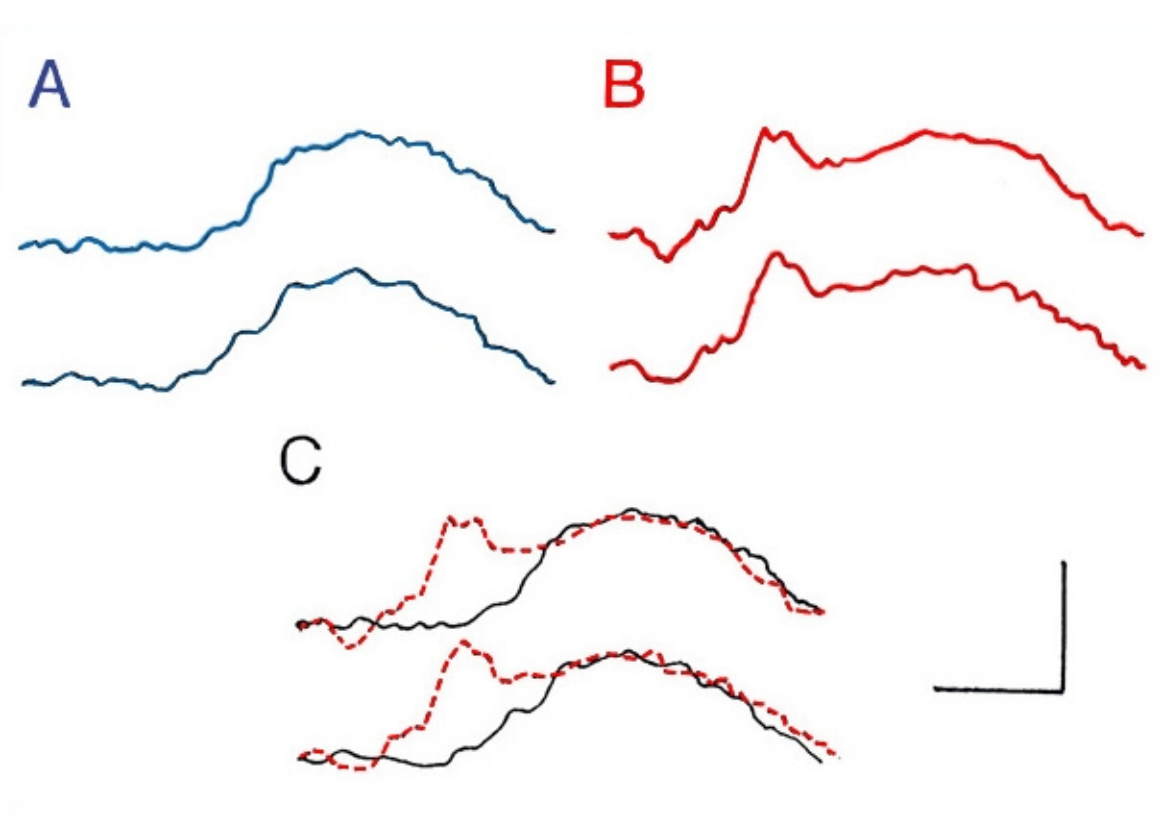

Figure 19. The effects of color on the dark-adapted ERG response of human. Dim blue (A) and bright red (B) light stimuli were used to elicit the ERG responses. These light stimuli were matched for rod-mediated vision, as can be appreciated from the comparison in part C. The slow, positive wave in both responses represents rod function and, therefore, exhibits a good match. The early, positive wave is sometimes referred to as the x-wave and represents cone function.

In this equation, V and V_{max} are the amplitudes that are measured with light stimulus of intensity I and with super-saturating stimulus, respectively. The parameter σ is the semi-saturation constant and is the stimulus intensity needed to elicit a response of half-maximal amplitude. This parameter also describes the location of the intensity-response curve along the intensity axis. When very dim light stimuli are used ($I < \sigma$), Eq. 1 can be reduced to:

$$V/V_{max} = I/\sigma \text{ (Equation 2)}$$

Namely, the amplitude V is linearly related to the light intensity I with a slope of V_{max}/σ. Thus, the semi-saturation constant is also used as a measure of sensitivity.

The values V_{max} and σ have been calculated for normal subjects under different conditions to study retinal mechanisms during adaptation or development (103, 105-107). In patients, these parameters provide quantitative assessment of retinal function during the progress of retinal diseases and the success of treatment (108, 109). Furthermore, these parameters indicate the nature of the disease: progressive or static; affecting the entire retina or only patches; and the site of the disorder (106, 108, 110, 111).

Ratio of b-Wave to a-Wave

ERG analysis that is based only upon amplitude measurements may lead to erroneous conclusions if the pupil is not maximally dilated. Furthermore, exchange of information between laboratories that use different recording conditions has always been problematical. One way to circumvent this difficulty is to compare a series of ERG

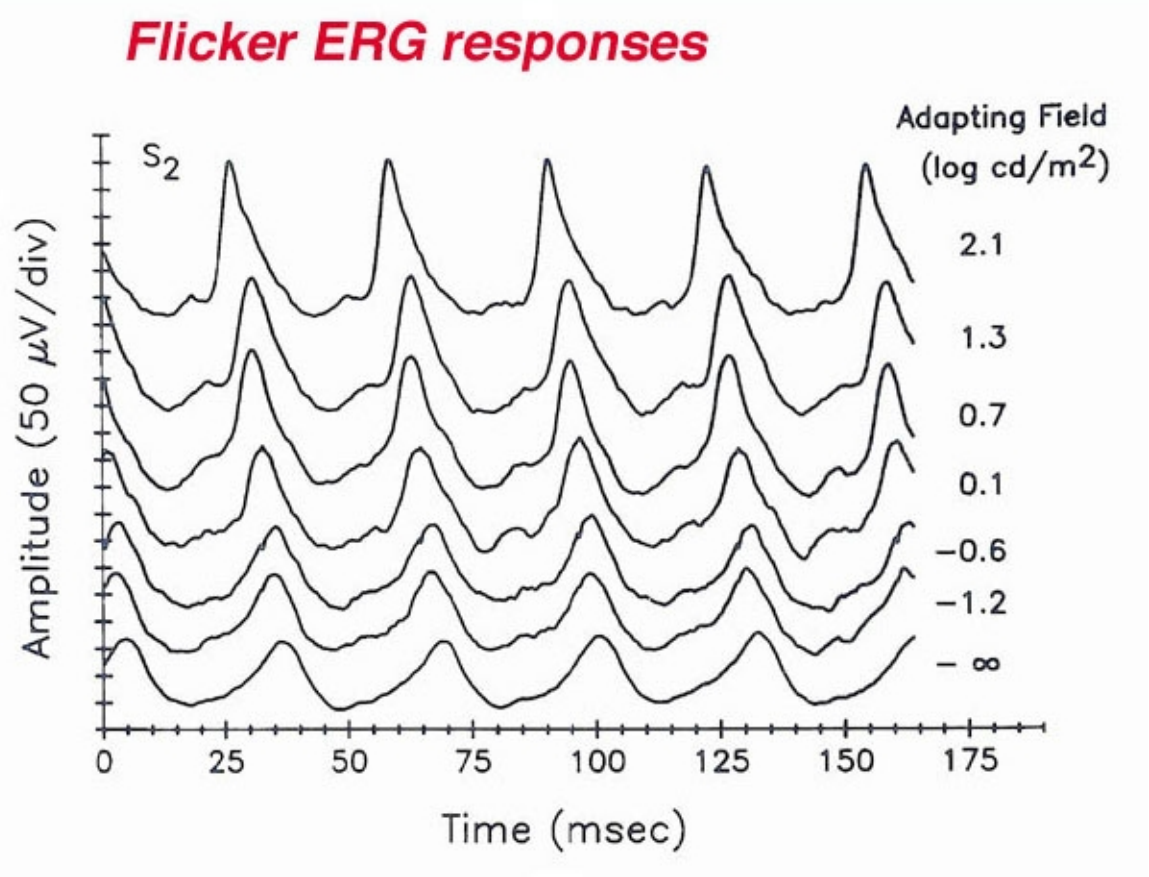

Figure 20. Flicker ERG responses to stimulation at 31.1 Hz with a stimulus intensity of 0.8 log cd-s/m2. The lowest trace was obtained in the dark-adapted state. Other traces were recorded after 30 min adaptation to white background of intensity denoted on the right (102).

responses for the relationship between the a-wave and the b-wave (112). This analysis is based upon our understanding of retinal physiology and the origin of the ERG waves. If the a-wave reflects activity in the photoreceptors and the b-wave originates from post-synaptic neurons, than normal signal transmission in the distal retina will be expressed in a normal relationship between the b-wave and the a-wave. Such analysis can also be used to compare ERG data between laboratories as shown in Fig. 23. The figure was constructed from ERG data of 20 volunteers with normal vision who were tested in the dark-adapted state with light stimuli of different intensities. The relationship between the b- and a-waves was derived for each subject, and the normal mean (continuous line) and range (± s.d., dashed lines) are shown in the figure. ERG data from two other laboratories that use different corneal electrodes and different light sources are shown (red dots, blue triangles). The data points from these laboratories fall within our normal range, indicating normal retinal function.

This type of analysis can also help in understanding the site of disorder. Any disorder that is localized to the photoreceptors and does not involve more proximal sites will be expressed in abnormal a-wave amplitude but normal b-wave:a-wave ratio. In contrast, a defect in signal transmission in the outer plexiform layer will show abnormal b-wave:a-wave ratio, but the amplitudes of the ERG waves may even increase. This is illustrated in Fig. 24 for two cases. In this figure, the b-wave:a-wave ratio is plotted in a different manner. The a-wave is used as the independent variable and is used together with the normal b-wave:a-wave ratio (of Fig. 23) to derive the expected b-wave. Then, the ratio of the measured b-wave:expected b-wave tells us about signal transmission in the OPL. In Fig. 24, the mean (± s.d) of the b-wave ratios for 20 volunteers with normal vision is plotted as a function of the a-wave amplitude. The data from normal subjects that were recorded in another two laboratories (red and blue symbols) fall well within the normal range of my laboratory. The b-wave ratios of a patient with

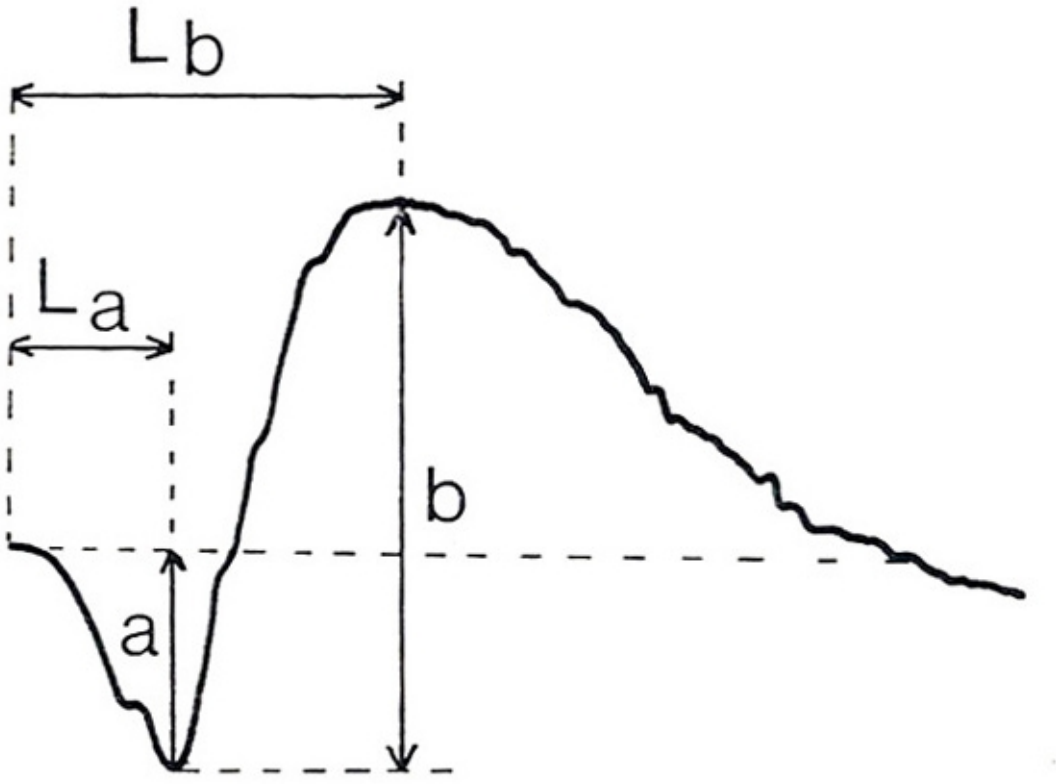

Figure 21. The ERG parameters that are customarily measured in the ophthalmic clinic for electrodiagnosis. The size of the a-wave is measured from the baseline to the trough of the wave. The size of the b-wave is measured from the trough of the a-wave to the peak of the b-wave. The time-to-peak for both waves (La and Lb) is determined from stimulus onset to the trough or peak of the waves.

high myopia and of a patient suffering from congenital stationary night blindness (CSNB) are compared with the normal range. The patient with high myopia is characterized by subnormal ERG responses because of the reduced function of the photoreceptors. However, the b-wave ratio is normal, indicating normal signal transmission. The CSNB patient is characterized by subnormal b-wave ratio, in agreement with the known defect in synaptic transmission from rods to bipolar cells.

Reconstruction of P-III

For over 50 years, since the analysis by Granit (5) of the ERG components, the a-wave has been used to assess the functional integrity of the photoreceptors. Extracellular recordings of the photoreceptors currents (113) and the introduction of the suction electrode technique to record the photocurrents from individual photoreceptors (114) allows creation of a mathematical model to fit to the ERG a-wave. This describes the entire contribution of the photoreceptors to the ERG- the P-III component (115, 116). The model is based upon the two-component model of the light-induced currents of mammalian rods (114, 117, 118) and is given by the following equation:

$$P_3(i, t) = \{1 - \exp[-iS(t- t_d)^2]\}R_{mP3} \quad \text{(Equation 3)}$$

In this equation, P_3, the amplitude of Granit's P-III component, is a function of flash energy i and time of measurement t after light onset. S is a sensitivity parameter, R_{mP3}, is the maximum amplitude of P-III, and t_d is a delay.

To derive the relationship between P_3 and time for the entire ERG range, very bright flashes that saturate the photoreceptors (i.e., shut down the "dark" current completely) are needed (Fig. 25A). As can be seen in these

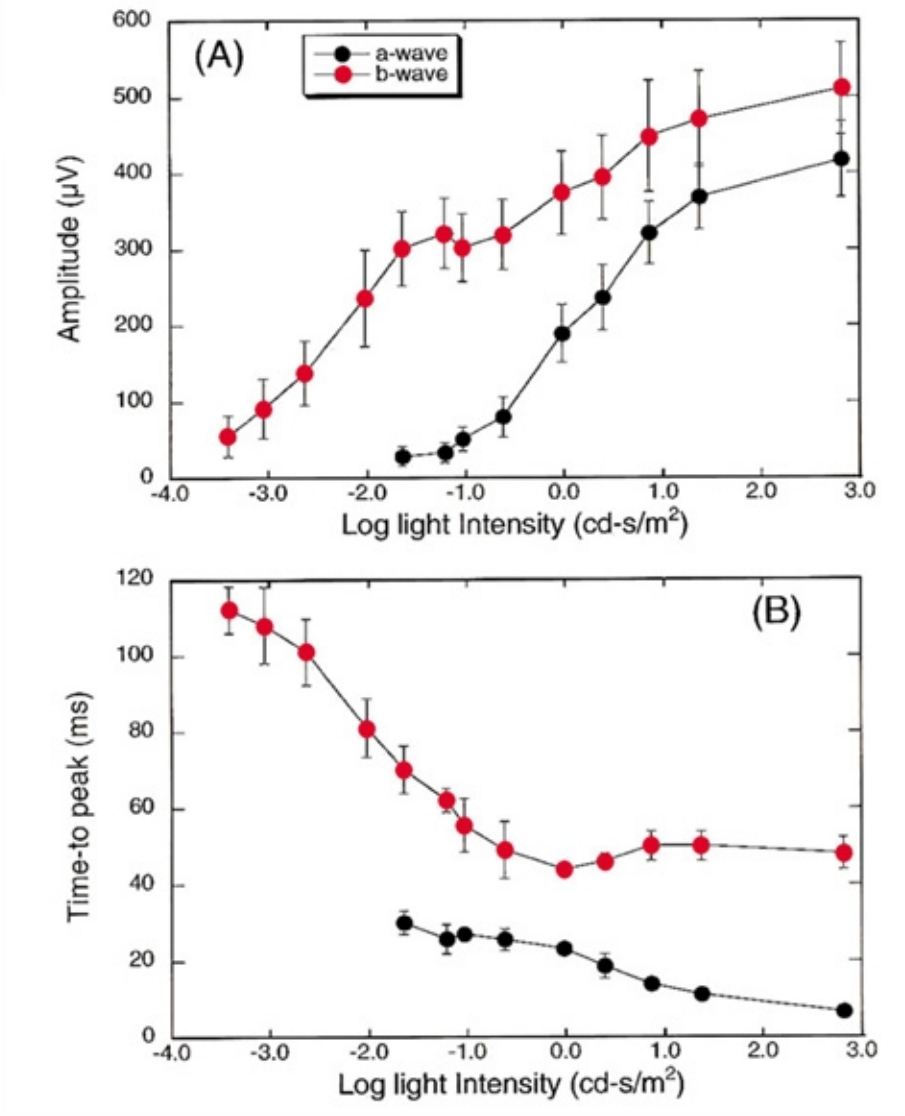

Figure 22. The ERG parameters for a normal range (N = 20) as determined in the dark-adapted state. The dependencies of amplitudes (A) and of time-to-peaks (B) of the a-wave and the b-wave upon log stimulus intensity are shown.

ERG records, the a-wave saturates for the two brightest light stimuli. Time of analysis is limited to the period before b-wave intrusion, as shown by the two dashed vertical lines (Fig. 25A). Application of Eq. 3 to these ERG data is shown in Fig. 25B. The data points are the amplitude measurements of the ERG responses, and the continuous curves are the fitted model. The fit of the theoretical curves to the actual data is quite good for the first 25 ms of the ERG responses. Longer intervals cannot be compared because the positive P-II component starts to develop and to affect the ERG recordings.

The bright-flash ERG response predominantly reflects rod function with a small contribution of the cone photoreceptors. To derive the isolated rod P-III wave and allow analysis of rod function alone, a procedure for a rod-isolating technique has been suggested (115). ERG responses are also elicited by long-wavelength light stimuli (>605 nm). These responses reflect mainly cone contribution and can be subtracted from the responses to white light stimuli and thus isolate the rod ERG responses.

A model, similar to that suggested for the rod P-III, has also been suggested for the cone P-III (116, 119). However, to construct the cone P-III from the a-wave of the bright flash photopic ERG response, a low-pass, exponential filter needs to be added, after the phototransduction process (116). This filter represents membrane

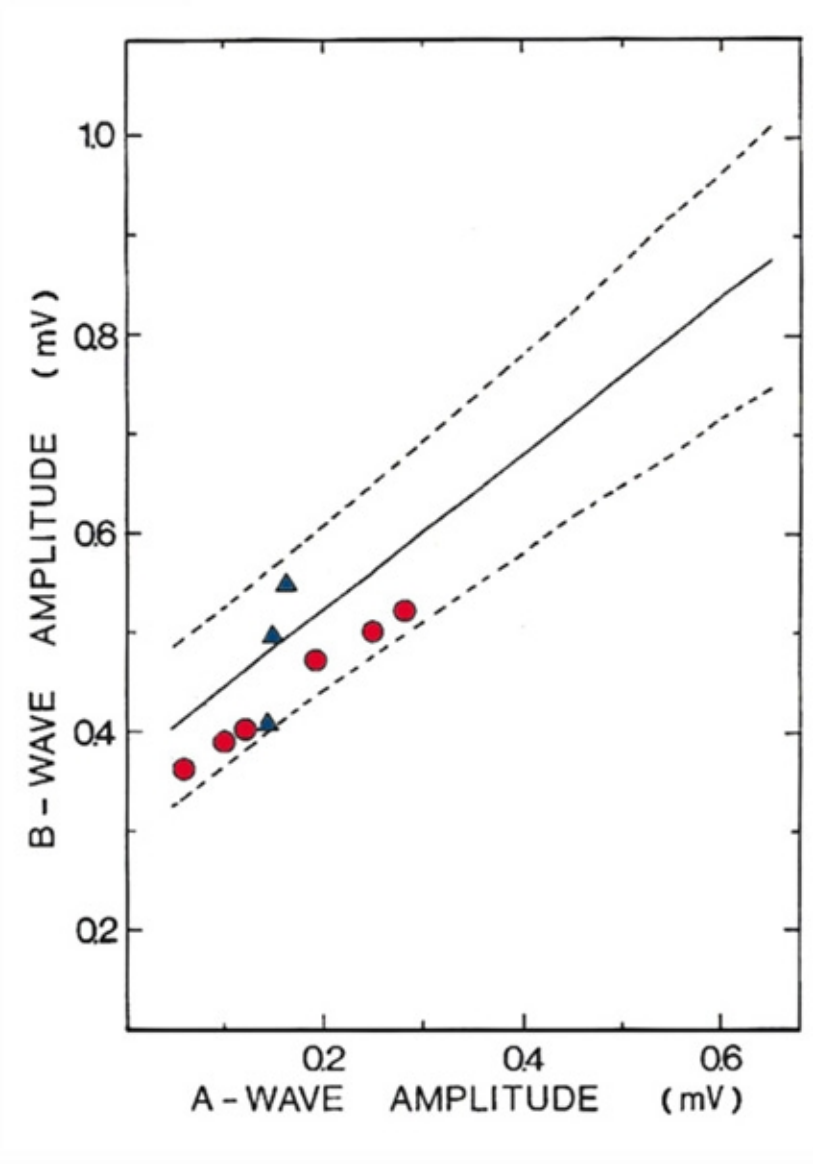

Figure 23. The relationship between the a-wave amplitude and the b-wave amplitude for 20 subjects with normal vision. The average (continuous line) and the range (dashed lines) are given. The data points (red circles and blue triangles) represent data from normal subjects recorded in two different laboratories (112).

capacitance that determines the rate at which the photocurrent is translated into membrane potential. With the rods, the membrane capacitance is relatively small and, therefore, the development of membrane potential follows quite accurately the development of photocurrent. This is not true for the cone photoreceptors, probably because of the in-foldings of the plasma membrane that make the outer segment discs and contribute to membrane capacitance. The importance of adding this low-pass filter to fit the phototransduction model to the cone a-wave is illustrated in Fig. 26. The ERG responses were elicited by a series of red light stimuli of moderate to bright intensities that were applied during background illumination. When the rod model (Eq. 3) was fitted to the cone a-wave (Fig. 26A), a substantial discrepancy between the theoretical curves and measured ones was seen (dashed and continuous curves, respectively). However, when a low-pass filter with t = 1.8 ms was added, a good fit was obtained between the theoretical and measured responses (Fig. 26B, dashed and continuous traces, respectively).

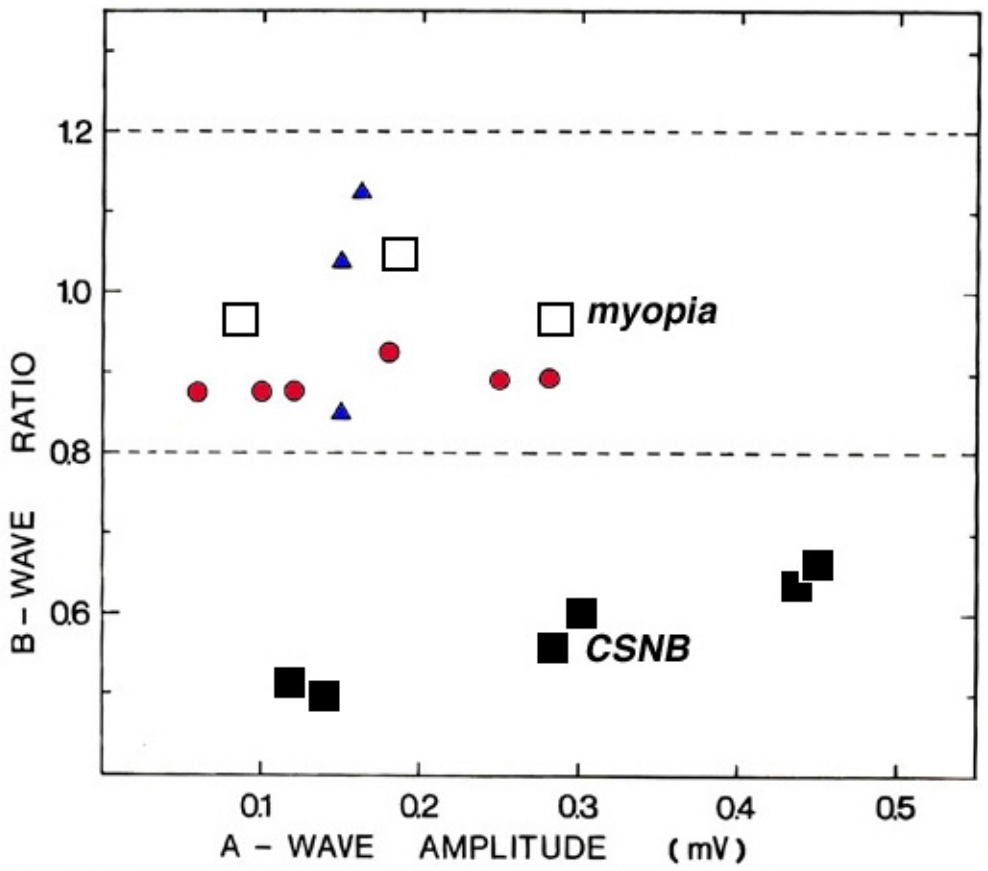

Figure 24. The b-wave ratio was computed from Fig. 23 as follows. For a given a-wave, there is an expected b-wave if synaptic transmission is normal and the b-wave generators function properly. The b-wave ratio is the ratio of the measured b-wave relative to the expected b-wave. The continuous and dashed lines represent the average ± s.d. of 20 subjects with normal vision. The colored symbols represent normal ERG data from two other laboratories. The myopic patient (open squares) exhibits reduced a-wave, but the b-wave ratio is normal, indicating normal synaptic transmission and normal functioning of the second-order neurons (ON-center bipolar cells). The patient with congential stationary night blindness (CSNB) exhibits reduced b-wave ratio, indicating abnormal signal transmission in the rod pathway (black squares) (112).

The model discussed above, or an extension of it using bright light stimuli to elicit ERG responses (120), can be used to analyze biophysical mechanisms of the phototransduction process. These can be used for research purposes to study non-invasively and in a chronic manner, photoreceptor function in primates (121), or to analyze the disorder locus in patients with retinal diseases (122, 123). By fitting rod a-waves to the phototransduction model (Eq. 3), it is possible to isolate disorders that affect the sensitivity of the rods from disorders that affect their maximum response. A more simple approach is to record the ERG to bright white flash and compare the patient ERG to the normal range. A disease that leads to a reduction in the maximum response (R_{mP3}) will show as a smaller maximum a-wave in the ERG that can be scaled up to fit the normal one. In contrast, a disorder that affects the sensitivity (S) will cause a smaller or even normal amplitude a-wave, but when scaled to the normal one, a delay in its development will be seen (123). An example is shown in Fig. 27. The thick continuous traces show the range of a-waves that were recorded from 10 volunteers with normal vision in the dark-adapted state using a white light stimulus of 664 cd-s/m^2. The colored traces are the actual ERG responses of a patient who was diagnosed with enhanced short-wavelength cone syndrome (enhanced SWS cones). His dark-adapted a-wave is smaller in amplitude than that of the normal range and when scaled up exhibits considerably slower kinetics. Thus, the dark-adapted a-wave of this patient is characterized by smaller maximum response and reduced sensitivity. This patient also complained of difficulty at night and had an abnormal dark-adaptation curve with only cone adaptation and no rod function (124).

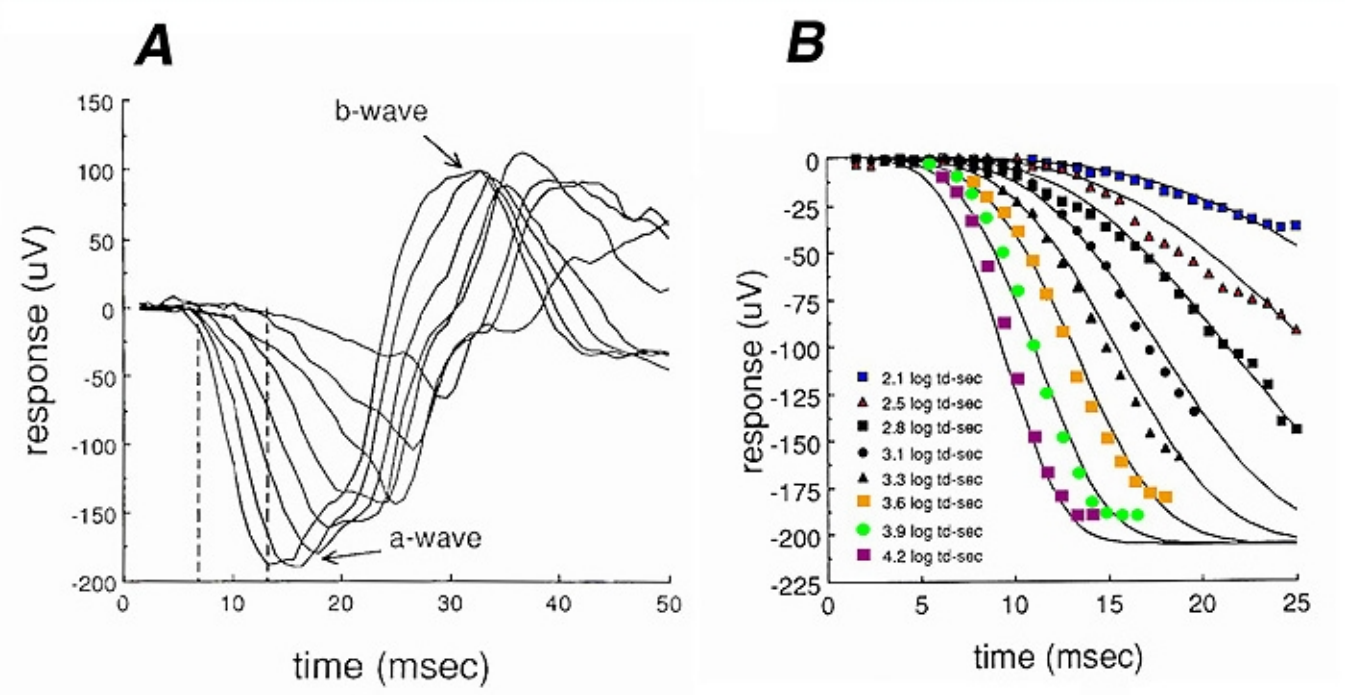

Figure 25. A, the ERG responses of one subject in the dark-adapted state by bright short-wavelength light stimuli. These are rod responses that were obtained by computer subtraction of the cone contribution as described in the text. The vertical dashed lines represent the time frame used to derive the theoretical rod P-III component. B, the data points (different symbols describe different intensities) represent the first 25 ms of the records in A. The continuous traces were obtained by fitting the phototransduction model (Eq. 3) to the data points (115).

Reconstruction of P-II

Granit's P-II component is generated in the neural retina mainly by ON-center bipolar cells with minor contributions from OFF-center bipolar cells and third-order neurons. Accurate measurement of the P-II amplitude can supply valuable information to the clinician on the functional integrity of the retina. However, the b-wave of the ERG is the sum of the positive P-II and the negative P-III. Therefore, changes in the b-wave can reflect changes in either of these components. The best estimate of the b-wave is by measuring it from the trough of the a-wave to the peak of the b-wave; however, this method will always underestimate the amplitude of P-II. Furthermore, the temporal properties of P-II are of value to the clinician. However, the time-to-peak of the ERG b-wave is not the time-to peak of the isolated P-II component but rather depends upon the summation of P-II and P-III (104).

Because the ERG P-III component can be reconstructed from bright flash ERG responses using the phototransduction model (Eq. 3), P-II can be estimated for any stimulus intensity by subtracting the estimated P-III from the measured ERG (Fig. 28) (104). Dark-adapted ERG responses of a normal subject were elicited by a standard series of light stimuli (Fig. 28A). The dashed traces are the theoretical rod responses that were derived from bright flash responses as described above. By subtracting the rod responses from the measured ERG responses, the P-II components can be isolated (Fig. 28B). From this set of data, the actual amplitude and time-to-peak of the ERG P-II component can be obtained and used to understand retinal changes (125).

Paired-Flash Analysis of the Rod Response

A test flash of fixed intensity induces a rod response that reflects the degree to which the "dark" current is reduced, and the time course of closure, followed by opening, of the cGMP-gated channels. This rod response underlies the receptor component (P-III) of the ERG. It is normally masked throughout most of its period by the

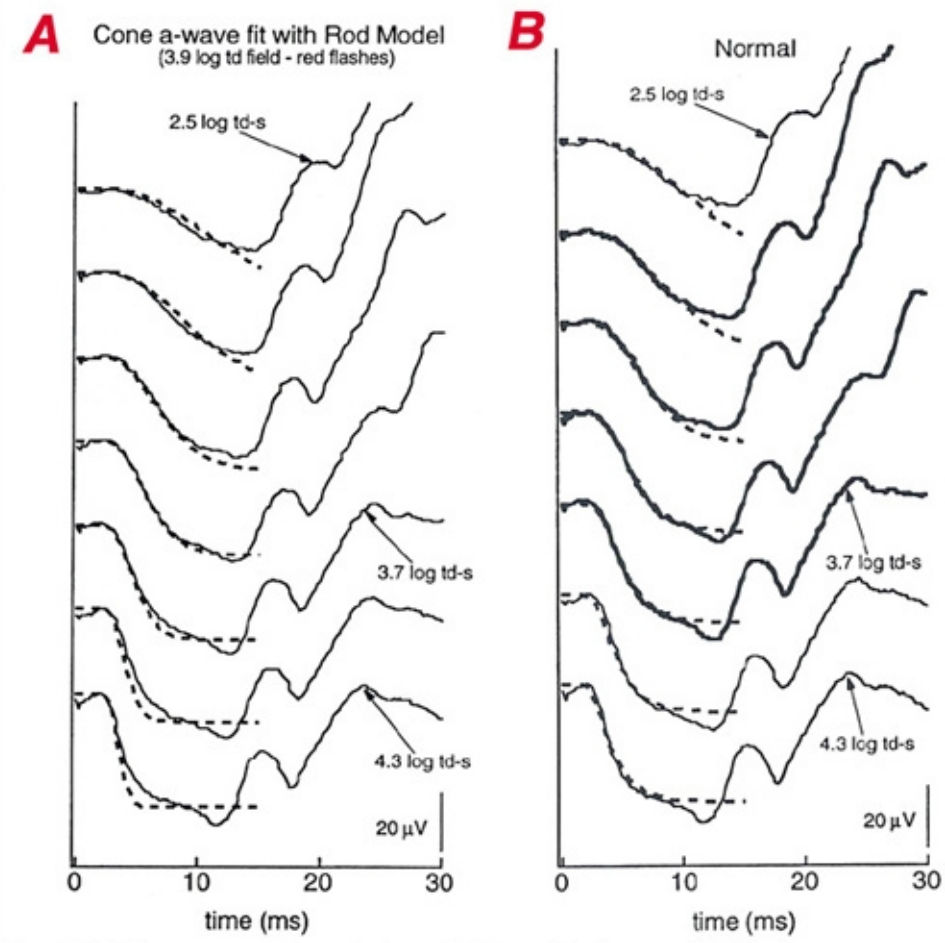

Figure 26. Fitting cone a-waves to the phototransduction model. A, cone a-waves that were elicited in the light-adapted state using long-wavelength light stimuli of different intensities. The rod model (Eq. 3) could be used to fit the a-waves that were recorded in response to light stimuli of moderate intensities (upper four traces) but failed with bright stimuli. The theoretical traces (dashed) are faster than the measured responses (continuous). B, adding a low-pass filter after the phototransduction process to the theoretical equation to account for the large membrane capacitance (long time constant) of the cones improved the fitting of the cone a-wave (continuous traces) to the phototransduction model (dashed traces) (116).

large, positive b-wave. The paired-flash technique has been developed to reconstruct the P-III component (126, 127). The concept of the paired-flash approach is that a super-bright flash delivered after a test flash will completely shut down the remaining "dark" current, and therefore, the amplitude of the a-wave, which is elicited by the probe flash, can be used as a measure of the prevailing rod "dark" current at that time. Thus, two stimuli are applied at variable time intervals. A test flash of fixed intensity (I test) that is given at t = 0 and a bright probe flash (I probe) that is expected to shut down the "dark" current and is delivered at a variable time interval, t probe, after the test flash. For long time intervals, the a-wave of the probe flash will be large and constant, because the rods have recovered from the effects of the test flash, and the probe flash induces an a-wave of saturating amplitude. However, with short inter-flash intervals, the probe flash can only shutdown the "dark" current that exists at that time, and therefore, the amplitude of the a-wave will be smaller. Such an experiment is illustrated in Fig. 29. The a-waves elicited by probe flashes at different time intervals after the test flash are shown in Fig. 29A. The shorter the inter-flash interval, the smaller the a-wave that is elicited by the probe flash. These a-waves are corrected for cone contributions in Fig. 29B. Fig. 29C illustrates the construction of the rod response underlying the test flash. The a-waves elicited by the probe flashes are arranged according to their inter-flash interval so that all of their peaks reach the same level—the level where all of the "dark" current is shut off. Connecting the baselines of the probe a-waves gives the time course of the rod response of the test flash.

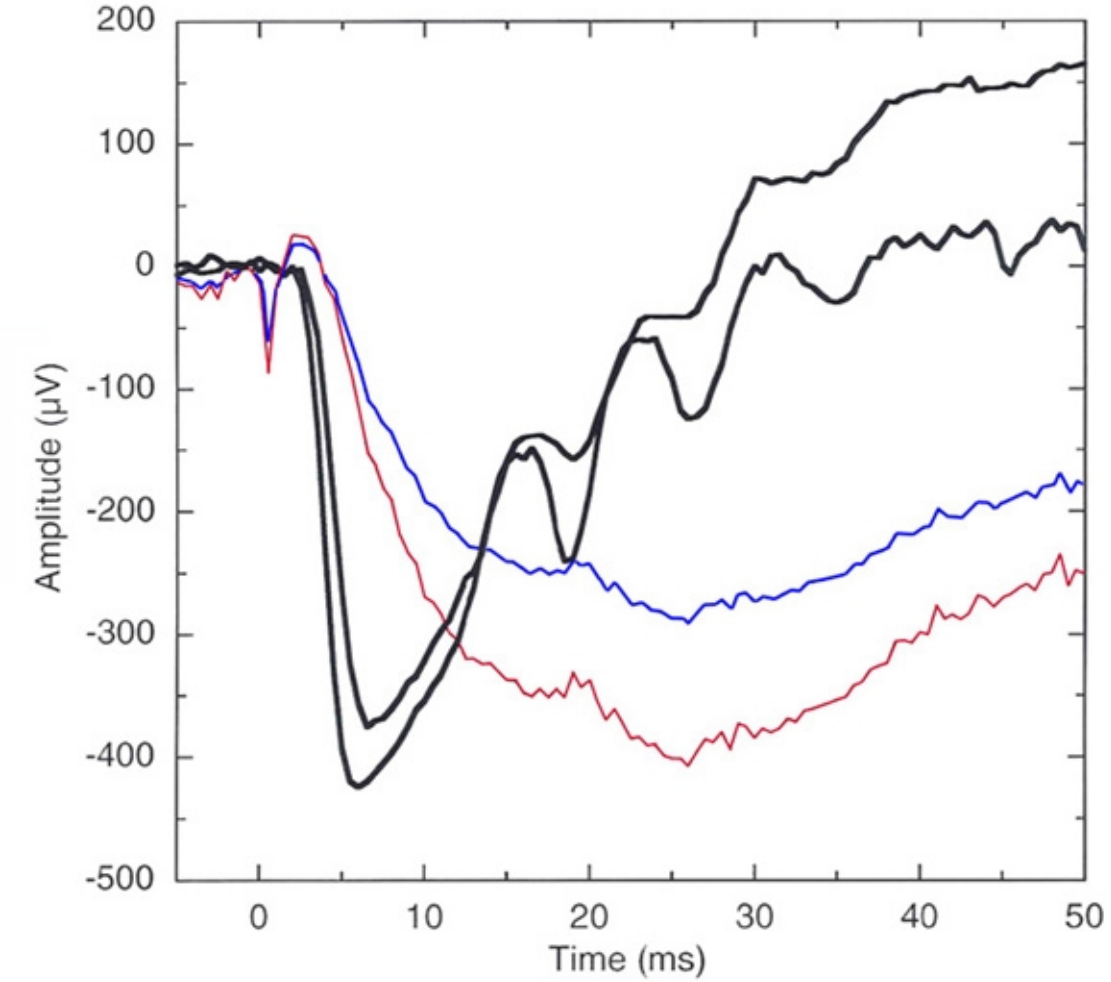

Figure 27. Analyzing the rod phototransduction in a patient with enhanced SWS cone syndrome. The range of bright flash, dark-adapted ERG a-wave of 10 normal subjects is given by the thick continuous traces. The patient's maximum ERG a-wave is smaller in amplitude and slower in kinetics after normalizing the a-wave to the normal range.

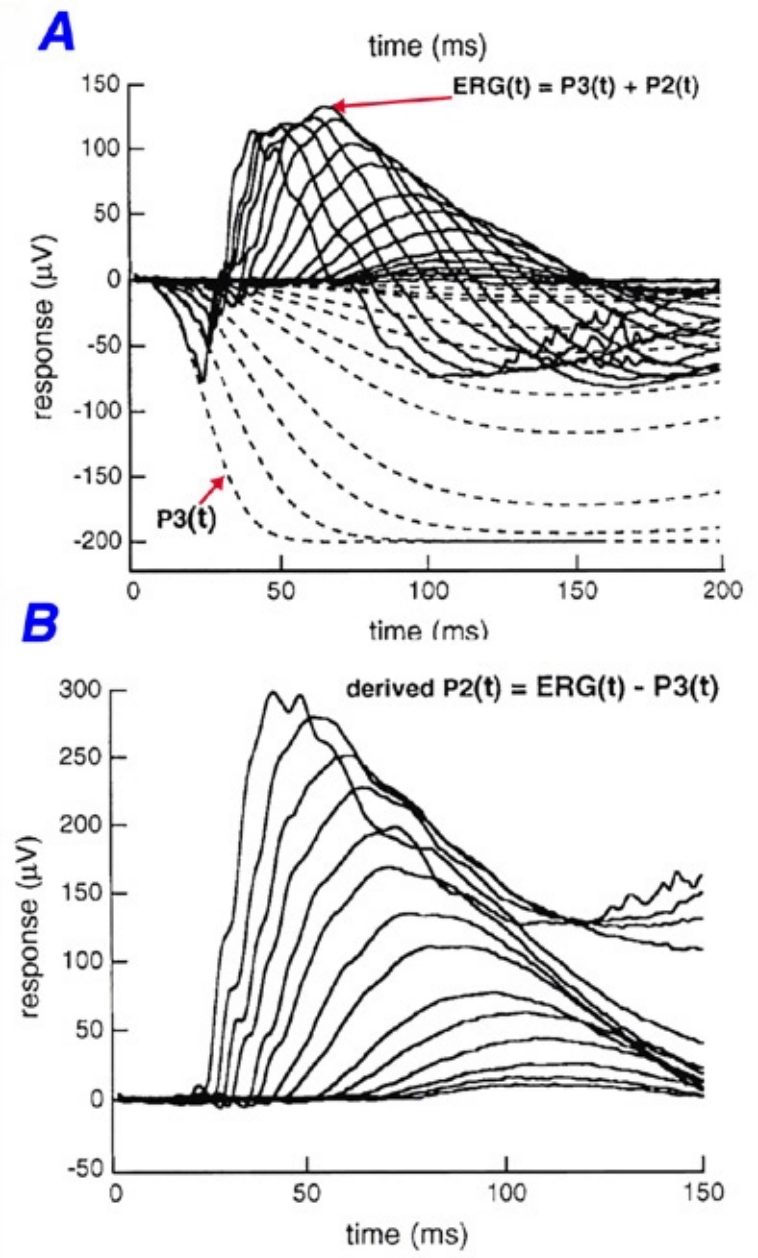

Figure 28. Reconstructing the P-II component of the human ERG response. A, the ERG responses that were elicited in the dark-adapted state using light stimuli of different intensities. The dashed traces are the reconstructed P-III component of each ERG response according to the method described in the text (Eq. 3). B, reconstructed P-II components of the ERG responses of part A by subtracting the reconstructed P-III from the measured ERG (128).

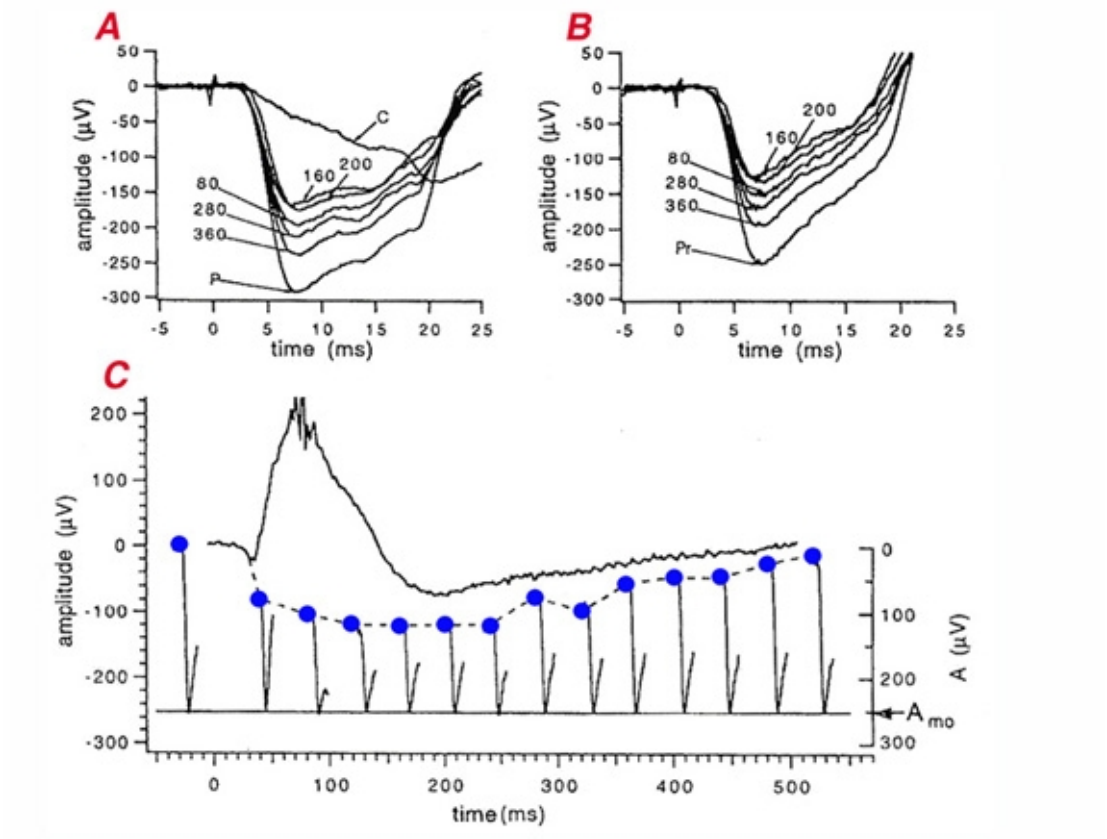

Figure 29. The paired-flash technique to reconstruct the rod response from the ERG response. A test flash of fixed intensity was followed at different time intervals by a probe flash of super-saturating intensity. A, the a-wave part of the ERG responses that were elicited by the probe flash at different time intervals after the test flash. The trace marked P is the effect of the probe flash alone. The trace marked C is a photopically matched long-wavelength probe flash. B, the responses in A were corrected for cone contribution. C, reconstruction of the rod response underlying the ERG response to the test flash (continuous trace). The responses to the different probe flashes were arranged such that they all reached the same low level (Amo), denoting the shutdown of the "dark" current. The trace connecting the baselines of the probe a-waves (dashed trace) is the rod response of the test ERG response (127).

About the Author

Dr. Ido Perlman was born in Haifa, Israel. He received his B.S. from the Technion-Israel, Institute of Technology, Haifa, in Chemistry in 1970 and his Ph.D. in Physiology from the University of Michigan, Ann Arbor, in 1976 under the mentorship of Dr. Matthew Alpern. Dr. Perlman then pursued postdoctoral studies with Dr. Richard Normann at the National Institutes of Health, on aspects of information processing in the turtle retina. He returned to Israel and became a professor of physiology at the Rappaport Faculty of Medicine, Technion-Israel in Haifa, Israel. His research interests have continued to be information processing in the vertebrate retina with a particular interest in horizontal cell physiology. Ido has always run an advanced, scientifically based, clinical ERG service for patients with visual disorders in northern Israel and has made major contributions to the field of clinical ERG work.

References

1. Armington JC. The electroretinogram. New York: Academic Press; 1974.
2. Gotch F. The time relations of the photoelectric changes on the eyeball of the frog. J Physiol. 1903;29:388–416. PubMed PMID: 16992679.
3. Einthoven W, Jolly WA. The form and magnitude of the electrical response of the eye to stimulation by light at various intensities. Q J Exp Physiol. 1908;1:373–416.
4. Oakley B. Potassium and the photoreceptor-dependent pigment epithelium hyperpolarization. J Gen Physiol. 1977;70:405–425. PubMed PMID: 303279.
5. Granit R. The components of the retinal action potential in mammals and their relation to the discharge in the optic nerve. J Physiol. 1933;77:207–239. PubMed PMID: 16994385.
6. Rodieck RW. The vertebrate retina: principles of structure and function. San Francisco: W.H. Freeman; 1973.
7. Brindley GS. The passive electrical properties of the frog's retina, choroid and sclera for radial fields and currents. J Physiol. 1956;134:339–352. PubMed PMID: 13398915.
8. Brindley GS, Hamasaki DI. The properties and nature of the R membrane of the frog's eye. J Physiol. 1963;167:599–606. PubMed PMID: 14015497.
9. Byzov AL. Localization of the R-membrane in the frogeye by means of an electrode marking method. Vision Res. 1968;8:697–700. PubMed PMID: 5729912.
10. Ogden TE, Ito H. Avian retina. II. An evaluation of retinal electrical anisotropy. J Neurophysiol. 1971;34:367–373. PubMed PMID: 5560038.
11. Arden GB, Brown KT. Some properties of components of the cat electroretinogram revealed by local recordings under oil. J Physiol. 1965;176:429–461. PubMed PMID: 14288517.
12. Doslak MJ. A theoretical study of the effect of silicone oil on the electroretinogram. Invest Ophthalmol Vis Sci. 1988;29:1881–1884. PubMed PMID: 3192378.
13. Doslak MJ, Plonsey R, Thomas CW. The effects of variations of the conducting media in homogeneities on the electroretinogram. IEEE Trans Biomed Eng. 1980;27:88–94. PubMed PMID: 7353900.
14. Foerster MH, Esser J, Laqua H. Silicone oil and its influence on electrophysiologic findings. Am J Ophthalmol. 1985;99:201–206. PubMed PMID: 3970125.
15. Noell WK. The origin of the electroretinogram. Am J Ophthalmol. 1954;38:78–90. PubMed PMID: 13180621.
16. Steinberg RH, Schmidt R, Brown KT. Intracellular responses to light from cat pigment epithelium: origin of the electroretinogram c-wave. Nature. 1970;227:728–730. PubMed PMID: 5432076.
17. Pepperberg DR, Brown PK, Lurie M, Dowling JE. Visual pigment and photoreceptor sensitivity in the isolated skate retina. J Gen Physiol. 1978;71:369–396. PubMed PMID: 660156.
18. Oakley B, Green DG. Correlation of light-induced changes in retinal extracellular potassium concentration with c-wave of the electroretinogram. J Neurophysiol. 1976;39:1117–1133. PubMed PMID: 1086346.
19. Murakami M, Kaneko A. Sub components of P3 in cold-blooded vertebrate retinae. Nature. 1966;210:103–104. PubMed PMID: 5956338.

20. Sillman AJ, Ito H, Tomita T. Studies on the mass receptor potential of the isolated frog retina. I. General properties of the response. Vision Res. 1969a;9:1435–1442. PubMed PMID: 5367433.
21. Brown KT. The electroretinogram: its components and their origin. Vision Res. 1968;8:633–677. PubMed PMID: 4978009.
22. Brown KT, Murakami M. A new receptor potential of the monkey retina with no detectable latency. Nature. 1964a;201:626–628. PubMed PMID: 14160664.
23. Brown KT, Wiesel TN. Analysis of the intra retinal electroretinogram in the intact cat eye. J Physiol. 1961a;158:229–256. PubMed PMID: 13873686.
24. Brown KT, Wiesel TN. Localization of origins of electroretinogram components by intra retinal recording in the intact cat eye. J Physiol. 1961b;158:257–280. PubMed PMID: 13873687.
25. Tomita T. Studies on the intraretinal action potential. I. Relation between the localization of micropipette in the retina and the shape of the intraretinal action potential. Jpn J Physiol. 1950;1:110–117.
26. Penn RD, Hagins WA. Signal transmission along retinal rods and the origin of the electroretinographic a-wave. Nature. 1969;223:201–205. PubMed PMID: 4307228.
27. Sillman AJ, Ito H, Tomita T. Studies on the mass receptor potential of the isolated frog retina. II. On the basis of the ionic mechanism. Vision Res. 1969b;9:1443–1451. PubMed PMID: 5367434.
28. Witkovsky P, Dudek EF, Ripps H. Slow P-III component of the carp electroretinogram. J Gen Physiol. 1975;65:119–134. PubMed PMID: 1117278.
29. Furukawa T, Hanawa I. Effects of some common cations on electroretinogram of the toad. Jpn J Physiol. 1955;5:289–300. PubMed PMID: 13306415.
30. Pepperberg DR, Masland RH. Retina-induced sensitization of light-adapted rabbit retina. Brain Res. 1978;151:194–200. PubMed PMID: 209858.
31. Brown KT, Watanabe K. Isolation and identification of a receptor potential from the pure cone fovea of the monkey retina. Nature. 1962;193:958–960. PubMed PMID: 13873685.
32. Nilsson SEG. Human retinal vascular obstructions. A quantitative correlation of angiographic and electroretinographic findings. Acta Ophthalmol (Copenh). 1971;49:111–133. PubMed PMID: 5108391.
33. Faber DS. Analysis of the slow trans-retinal potentials in response to light. Buffalo (NY): State University of New York; 1969.
34. Miller RF, Dowling JE. Intracellular responses of the Müller (glial) cells of the mudpuppy retina: their relation to the b-wave of the electroretinogram. J Neurophysiol. 1970;33:323–341. PubMed PMID: 5439340.
35. Miller RF. Role of K^+ in generation of b-wave of electroretinogram. J Neurophysiol. 1973;36:28–35. PubMed PMID: 4540959.
36. Karwoski CJ, Newman EA, Shimazaki H, Proenza LM. Light-evoked increases in extracellular K^+ in the plexiform layers of amphibian retinas. J Gen Physiol. 1985;86:189–213. PubMed PMID: 3876405.
37. Karwoski CJ, Proenza LM. Neurons, potasium and glia in proximal retina of Necturus. J Gen Physiol. 1980;75:141–162. PubMed PMID: 6246191.
38. Newman EA. Current source-density analysis of the b-wave of frog retina. J Neurophysiol. 1980;43:1355–1366. PubMed PMID: 6246222.
39. Newman EA, Odette LL. Model of electroretinogram b-wave generation: a test of the K^+ hypothesis. J Neurophysiol. 1984;51:164–182. PubMed PMID: 6319623.
40. Newman EA. Current source-density analysis of the b-wave of frog retina. J Neurophysiol. 1980;43:1355–1366. PubMed PMID: 6246222.
41. Kline RP, Ripps H, Dowling JE. Generation of b-wave currents in the skate retina. Proc Natl Acad Sci U S A. 1978;75:5727–5731. PubMed PMID: 281719.
42. Kline RP, Ripps H, Dowling JE. Light-induced potassium fluxes in the skate retina. Neuroscience. 1985;14:225–235. PubMed PMID: 3974879.
43. Dick E, Miller RF, Bloomfield S. Extracellular K^+ activity changes related to electroretinogram components. II. Rabbit (E-type) retinas. J Gen Physiol. 1985;85:911–931. PubMed PMID: 2410539.

44. Karwoski CJ, Xu X. Current source-density analysis of light-evoked field potentials in rabbit retina. Vis Neurosci. 1999;16:369–377. PubMed PMID: 10367970.
45. Heynen H, van Norren D. Origin of the electroretinogram in the intact macaque eye. I. Principal compound analysis. Vision Res. 1985a;25:697–707. PubMed PMID: 4024470.
46. Heynen H, van Norren D. Origin of the electroretinogram in the intact macaque eye. II. Current source-density analysis. Vision Res. 1985b;25:709–715. PubMed PMID: 4024471.
47. Dick E, Miller RF. Extracellular K^+ activity changes related to electroretinogram components. I. Amphibian (I-type) retinas. J Gen Physiol. 1985;85:885–909. PubMed PMID: 3926945.
48. Karowski CJ, Proenza LM. Relationship between Müller cell responses, a local transretinal potential and potassium flux. J Neurophysiol. 1977;40:244–259. PubMed PMID: 845622.
49. Ripps H, Witkovsky P. Neuron-glia interaction in the brain and retina. In: Osborne N, Chader G, editors. Progress in retinal research. Vol. 4. Pergamon Press; 1985. p. 181–219.
50. Gurevich L, Slaughter MM. Comparison of the waveforms of the ON bipolar neuron and the b-wave of the electroretinogram. Vision Res. 1993;33:2431–2435. PubMed PMID: 8249322.
51. Slaughter MM, Miller RF. 2-Amino-4-phosphonobutyric acid: a new pharmachological tool for retinal research. Science. 1981;211:182–185. PubMed PMID: 6255566.
52. Sieving PA, Murayama K, Naarendorp F. Push-pull model of the primate photopic electroretinogram: a role for hyperpolarizing neurons in shaping the b-wave. Vis Neurosci. 1994;11:519–532. PubMed PMID: 8038126.
53. Green DG, Kapousta-Bruneau NV. A dissection of the electroretinogram from the isolated rat retina with microelectrode and drugs. Vis Neurosci. 1999;16:727–741. PubMed PMID: 10431921.
54. Masu M, Iwakabe H, Tagawa Y, Miyoshi T, Yamashita M, Fukuda Y, Sasaki H, Hiroi K, Nakamura Y, Shigemoto R, Takada M, Nakamura K, Nakao K, Katsuki M, Nakanishi S. Specific deficit of the ON response in visual transmission by targeted disruption of the mGluR6 gene. Cell. 1995;80:757–765. PubMed PMID: 7889569.
55. Lei B, Perlman I. The contribution of voltage- and time-dependent poassium conductances to the electroretinogram in rabbits. Vis Neurosci. 1999;16:743–754. PubMed PMID: 10431922.
56. Linn DM, Solessio E, Perlman I, Lasater EM. The role of potassium conductance in the generation of light responses in Müller cells of the turtle retina. Vis Neurosci. 1998;15:449–458. PubMed PMID: 9685198.
57. Newman EA. Potassium conductance block by barium in amphibian Müller cells. Brain Res. 1989;498:308–314. PubMed PMID: 2790485.
58. Reichelt W, Pannicke T. Voltage-dependent K^+ currents in guinea pig Müller (glial) cells show different sensitivities to blockade by Ba^{2+}. Neurosci Lett. 1993;155:15–18. PubMed PMID: 8361658.
59. Dong CJ, Hare WA. Contribution to the kinetics and amplitude of the electroretinogram b-wave by third-order retinal neurons in the rabbit retina. Vision Res. 2000;40:579–589. PubMed PMID: 10824262.
60. Awatramani G, Wang J, Slaughter MM. Amacrine and ganglion cell contributions to the electroretinogram in amphibian retina. Vis Neurosci. 2001;18:147–156. PubMed PMID: 11347812.
61. Dong CJ, Hare WA. $GABA_C$ feedback pathway modulates the amplitude and kinetics of ERG b-wave in a mammalian retina in vivo. Vision Res. 2002;42:1081–1087. PubMed PMID: 11997047.
62. Kapousta-Bruneau NV. Opposite effects of $GABA_A$ and $GABA_C$ receptor antagonists on the b-wave of ERG recorded from the isolated rat retina. Vision Res. 2000;40:1653–1665. PubMed PMID: 10814754.
63. Brown KT, Murakami M. Biphasic form of the early receptor potential of the monkey retina. Nature. 1964b;204:739–740. PubMed PMID: 14235663.
64. Cone RA. Early receptor potential of the vertebrate retina. Nature. 1964;204:736–739. PubMed PMID: 14235662.
65. Yonemura D, Kawasaki K. The early receptor potential in the human electroretinogram. Jpn J Physiol. 1967;17:235–244. PubMed PMID: 5299089.
66. Brown KT, Watanabe K, Murakami M. The early and late receptor potential of monkey cones and rods. Cold Spring Harb Symp Quant Biol. 1965;30:457–482. PubMed PMID: 4956619.

67. Murakami M, Pak WL. Intracellularly recorded early receptor potential of the vertebrate photoreceptors. Vision Res. 1970;10:965–975. PubMed PMID: 5492796.
68. Hodgkin AL, O'Bryan P. Internal recordings of the early receptor potential in turtle retina. J Physiol. 1977;267:737–766. PubMed PMID: 874877.
69. Berson EL, Goldstein EB. The early receptor potential in dominantly inherited retinitis pigmentosa. Arch Ophthalmol. 1970a;83:412–420. PubMed PMID: 5437901.
70. Berson EL, Goldstein EB. The early receptor potential in sex-linked retinitis pigmentosa. Invest Ophthalmol. 1970b;9:58–63. PubMed PMID: 5411252.
71. Asi H, Perlman I. Relationships between the electroretinogram a-wave, b-wave and oscillatory potentials and their application to clinical diagnosis. Doc Ophthalmol. 1992;79:125–139. PubMed PMID: 1591967.
72. Ogden TE. The oscillatory waves of the primate electroretinogram. Vision Res. 1973;13:1059–1074. PubMed PMID: 4197416.
73. Wachtmeister L, Dowling JE. The oscillatory potentials of the mudpuppy retina. Invest Ophthalmol Vis Sci. 1978;17:1176–1188. PubMed PMID: 721390.
74. Heynen H, Wachtmeister L, van Norren D. Origin of the oscillatory potentials in the primate retina. Vision Res. 1985;25:1365–1373. PubMed PMID: 4090272.
75. Yonemura D, Kawasaki K. New approaches to ophthalmic electrodiagnosis by retinal oscillatory potential, drug-induced responses from retinal pigment epithelium and cone potential. Doc Ophthalmol. 1979;48:163–222. PubMed PMID: 119621.
76. Speros P, Price J. Oscillatory potentials: history, techniques and potential use in the evaluation of disturbances of retinal circulation. Surv Ophthalmol. 1981;25:237–252. PubMed PMID: 7010647.
77. Bresnick GH, Palta M. Oscillatory potential amplitude. Relation to severity of diabetic retinopathy. Arch Ophthalmol. 1987;105:929–933. PubMed PMID: 3606452.
78. Frost-Larsen K, Larsen HW, Simonsen SE. Oscillatory potential and nyctometry in insulin-dependent diabetics. Acta Ophthalmol (Copenh). 1980;58:879–888. PubMed PMID: 7036647.
79. Simonsen SE. The value of the oscillatory potential in selecting juvenile diabetics at risks of developing proliferative diabetic retinopathy. Acta Ophthalmol (Copenh). 1980;58:865–877. PubMed PMID: 7331773.
80. Xu X, Karwoski CJ. Current source density analysis of retinal field potentials. II Pharmacological analysis of the b-wave and M-wave. J Neurophysiol. 1994;72:96–105. PubMed PMID: 7965036.
81. Xu X, Karwoski CJ. Current source density analysis of the electroretinographic d-wave of frog retina. J Neurophysiol. 1995;73:2459–2469. PubMed PMID: 7666152.
82. Stockton RA, Slaughter MM. B-wave of the electroretinogram. A reflection of ON bipolar cell activity. J Gen Physiol. 1989;93:101–122. PubMed PMID: 2915211.
83. Szikra T, Witkovsky P. Contributions of AMPA- and kainate-sensitive receptors to the photopic electroretinogram of Xenopus retina. Vis Neurosci. 2001;18:187–196. PubMed PMID: 11417793.
84. Alexander KR, Fishman GA, Peachey NS, Marchese AL, Tso MOM. 'ON' response defect in paraneoplastic night blindness with cutaneous maliganant melanoma. Invest Ophthalmol Vis Sci. 1992;33:477–483. PubMed PMID: 1544774.
85. Miyake Y, Yagasaki K, Horiguchi M, Kawase Y. On- and off-responses in photopic electroretinogram in complete and incomplete types of congenital stationary night blindness. Jpn J Ophthalmol. 1987;31:81–87. PubMed PMID: 3498069.
86. Gouras P. Electrical activity of toad retina. Am J Ophthalmol. 1958;46:59–72. PubMed PMID: 13571359.
87. Sieving PA, Frishman LJ, Steinberg RH. Scotopic threshold response of proximal retina in cat. J Neurophysiol. 1986a;56:1049–1061. PubMed PMID: 3783228.
88. Knave B, Moller A, Persson HE. A component analysis of the electroretinogram. Vision Res. 1972;12:1669–1684. PubMed PMID: 5078789.
89. Wakabayashi K, Gieser J, Sieving P. Aspartate separation of the scotopic threshold response(STR) from the photoreceptor a-wave of the cat and monkey ERG. Invest Ophthalmol Vis Sci. 1988;29:1615–1622. PubMed PMID: 3182196.

90. Finkelstein D, Gouras P, Hoff M. Human electroretinogram near the absolute threshold of vision. Invest Ophthalmol. 1968;7:214–218. PubMed PMID: 5641569.
91. Sieving PA, Nino C. Scotopic threshold response (STR) of the human electroretinogram. Invest Ophthalmol Vis Sci. 1988;29:1608–1614. PubMed PMID: 3182195.
92. Frishman LJ, Steinberg RH. Light-evoked changes in $[K^+]_o$ in proximal portion of dark-adapted cat retina. J Neurophysiol. 1989b;61:1233–1243. PubMed PMID: 2746323.
93. Frishman LJ, Yamamoto F, Bogucka I, Steinberg RN. Light-evoked changes in $[K^+]_o$ in proximal portion of light-adapted retina. J Neurophysiol. 1992;67:1201–1212. PubMed PMID: 1317916.
94. Sieving PA, Frishman LJ, Steinberg RH. M-wave of proximal retina in cat. J Neurophysiol. 1986b;56:1039–1048. PubMed PMID: 3783227.
95. Karwoski CJ, Lu H-K, Newman EA. Spatial buffering of light-evoked potassium increases by Müller (glia) cells. Science. 1989;244:578–580. PubMed PMID: 2785716.
96. Hood DC, Finkelstein MA. Sensitivity to light. In: Boff KR, Kaufman L, Thomas JP, editors. Handbook of perception and human performance. Vol 1: Sensory processes and perception. New York: John Wiley and Sons; 1986. p. 1–66.
97. Berson EL, Howard J. Temporal aspects of the electroretinogram in sector retinitis pigmentosa. Arch Ophthalmol. 1971;86:653–665. PubMed PMID: 5128159.
98. Bornschein H, Goodman G, Gunkel RD. Temporal aspects of the human electroretinogram; a study of the implicit time-amplitude relationship of the b-wave. AMA Arch Ophthalmol. 1957;57:386–392. PubMed PMID: 13410222.
99. Conner JD, MacLeod DI. Rod photoreceptors detect rapid flicker. Science. 1977;195:698–699. PubMed PMID: 841308.
100. Dodt E. Cone electroretinography by flicker. Nature. 1951;168:738. PubMed PMID: 14882334.
101. Stockman A, Sharpe LT, Rüther K, Nordby K. Two signals in the human rod visual system: a model based on electrophysiological data. Vis Neurosci. 1995;12:951–970. PubMed PMID: 8924418.
102. Peachey NS, Alexander KR, Derlacki DJ, Fishman GA. Light adaptation, rods, and the human cone flicker ERG. Vis Neurosci. 1992;8:145–150. PubMed PMID: 1558826.
103. Fulton AB, Rushton WAH. The human rod ERG: correlation with psychophysical responses in light and dark adaptation. Vision Res. 1978;18:793–800. PubMed PMID: 676087.
104. Hood DC, Birch DG. A computational model of the amplitude and implicit time of the b-wave of the human ERG. Vis Neurosci. 1992;8:107–126. PubMed PMID: 1558823.
105. Fulton AB, Hansen RM. Background adaptation in human infants: analysis of b-wave responses. Doc Ophthalmol. 1982;31:191–197.
106. Fulton AB, Hansen RM. Scotopic stimulus/response relations of the b-wave of the electroretinogram. Doc Ophthalmol. 1988;68:293–304. PubMed PMID: 3402318.
107. Peachey NS, Alexander KR, Fishman GA. The luminance-response function of the dark-adapted human electroretinogram. Vision Res. 1989;29:263–270. PubMed PMID: 2788958.
108. Arden GB, Carter RM, Hogg CR, Powell DJ, Ernst WJK, Clover GM, Lyness AL, Quinlan MP. A modified ERG technique and the results obtained for X-linked retinitis pigmentosa. Br J Ophthalmol. 1983;67:419–430. PubMed PMID: 6860609.
109. Massof RW, Wu L, Finkelstein D, Perry C, Starr SJ, Johnson MA. Properties of electroretinographic intensity-response functions in retinitis pigmentosa. Doc Ophthalmol. 1984;57:279–296. PubMed PMID: 6468246.
110. Hood DC. The ERG and sites and mechanisms of retinal disease, adaptation, and development. In: Advances in photoreception. Washington (DC): National Academy Press; 1990. p. 41–58.
111. Johnson MA, Hood DC. A theoretical interpretation of ERG abnormalities in central retinal vein occlusion. Opt Soc Am Tech Dig. 1988;3:84–87.
112. Perlman I. Relationship between the amplitudes of the b wave and the a wave as a useful index for evaluating the electroretinogram. Br J Ophthalmol. 1983;67:443–448. PubMed PMID: 6602626.

113. Penn RD, Hagins WA. Kinetics of the photocurrent of retinal rods. Biophys J. 1972;12:1073–1094. PubMed PMID: 5044581.
114. Baylor DA, Nunn BJ, Schnapf JL. The photocurrent, noise and spectral sensitivity of rods of monkey Macaca fascicularis. J Physiol. 1984;357:575–607. PubMed PMID: 6512705.
115. Hood DC, Birch DG. Aquantitative measure of the electrical activity of human rod photoreceptors using electroretinography. Vis Neurosci. 1990;5:379–387. PubMed PMID: 2265151.
116. Hood DC, Birch DG. Phototransduction in human cones measured using the a-wave of the ERG. Vision Res. 1995;35:2801–2810. PubMed PMID: 8533321.
117. Lamb TD, Pugh EN. A quantitative account of the activation steps involved in phototransduction in amphibian photoreceptors. J Physiol. 1992;449:719–758. PubMed PMID: 1326052.
118. Pugh EN, Lamb TD. Amplification and kinetics of the activation steps in phototransduction. Biochim Biophys Acta. 1993;1141:111–149. PubMed PMID: 8382952.
119. Hood DC, Birch DG. Human cone receptor activity: the leading edge of the a-wave and models of receptors activity. Vis Neurosci. 1993;10:857–871. PubMed PMID: 8217936.
120. Cideciyan AV, Jacobson SG. An alternative photo transduction model for human rod and cone ERG a-wave: normal parameters and variation with age. Vision Res. 1996;36:2609–2621. PubMed PMID: 8917821.
121. Jamison JA, Bush RA, Lei B, Sieving P. Characterization of the rod photoresponse isolated from the dark-adapted primate ERG. Vis Neurosci. 2001;18:445–455. PubMed PMID: 11497421.
122. Hood DC, Birch DG. Rod phototransduction in retinitis pigmentosa: estimation of parameters derived from the rod a-wave. Invest Ophthalmol Vis Sci. 1994a;35:2948–2961. PubMed PMID: 8206712.
123. Hood DC, Birch DG. Assessing abnormal rod photoreceptor activity with the a-wave of the electroretinogram: applications and methods. Doc Ophthalmol. 1996-1997;92:253–267. PubMed PMID: 9476593.
124. Perlman I, Leibu R, Barth J. Night blindness: a new type with abnormal properties of the electroretinogram. Clin Vis Sci. 1993;8:159–169.
125. Hood DC, Shady S, Birch DG. Understanding changes in the b-wave of the ERG caused by heterogenous receptor damage. Invest Ophthalmol Vis Sci. 1994b;35:2477–2488. PubMed PMID: 8163337.
126. Hetling JR, Pepperberg DR. Sensitivity and kinetics of mouse rod flash responses determined in vivo from paired-flash electroretinograms. J Physiol. 1999;516:593–609. PubMed PMID: 10087356.
127. Pepperberg DR, Birch DG, Hood DC. Photoresponses of human rods in vivo derived from paired-flash electroretinograms. Vis Neurosci. 1997;14:73–82. PubMed PMID: 9057270.
128. Hood DC, Birch DG. beta wave of the scotopic (rod) electroretinogram as a measure of the activity of human on-bipolar cells. J Opt Soc Am A Opt Image Sci Vis. 1996;13:623–633. PubMed PMID: 8627419.

Clinical Electrophysiology

Donnell J. Creel

Created: May 1, 2005; Updated: July 2, 2007.

Introduction

Electrophysiological testing of patients with retinal disease began in clinical departments in the late 1940s. Under the influence of the great Swedish pioneers, Holmgren (1) and Granit (2), the electroretinogram was being dissected into component parts, and early intraretinal electrode studies were beginning to tell which cells or cell layers gave rise to the various components. A detailed discussion of the electroretinogram, or ERG as it is commonly abbreviated, is found in the accompanying chapter by Ido Perlman. A little after the introduction of the ERG as a test of the state of the patient's retina, another diagnostic test called the electrooculogram (EOG) was introduced to the clinic (3). The EOG had advantages over the ERG in that electrodes did not touch the surface of the eye. The changes in the standing potential across the eyeball were recorded by skin electrodes during simple eye movements and after exposure to periods of light and dark. Over the years, ERG recording techniques have become progressively more sophisticated, even in the clinical setting. With the advent of perimetry and pattern ERG techniques, more precise mapping of lesioned areas of the retina is now possible. The most recent advance in ERG technology is the multifocal pattern ERG, analysed and mapped by computer averaging techniques. It allows a detailed assessment of the state of the macular area.

Where the previous chapter (The Electroretinogram: ERG) presents the basic science behind the waveforms and components of the massed ERG response, in this chapter the intention is to show purely the clinical use of the various electrophysiological tests. The chapter is based on experience in the ERG clinic of the Moran Eye Center.

The Electroretinogram (ERG)

The global or full-field electroretinogram (ERG) is a mass electrical response of the retina to photic stimulation. The ERG is a test used worldwide to assess the status of the retina in eye diseases in human patients and in laboratory animals used as models of retinal disease.

The basic method of recording the electrical response, known as the global or full-field ERG, is by stimulating the eye with a bright light source, such as a flash produced by a strobe lamp. The intense flash of light elicits a biphasic waveform recordable at the cornea similar to that illustrated in Fig. 1. The two components that are most often measured are the a- and b-waves. The a-wave is the first large negative component, followed by the b-wave, which is corneal positive and usually larger in amplitude.

Two principal measures of the ERG waveform are taken: 1) the amplitude (a) from the baseline to the negative trough of the a-wave, and the amplitude of the b-wave measured from the trough of the a-wave to the following peak of the b-wave; and 2) the time (t) from flash onset to the trough of the a-wave and the time (t) from flash onset to the peak of the b-wave (Fig. 2). These times, reflecting peak latency, are referred to as "implicit times" in the jargon of electroretinography.

The a-wave, sometimes called the "late receptor potential," reflects the general physiological health of the photoreceptors in the outer retina. In contrast, the b-wave reflects the health of the inner layers of the retina, including the ON bipolar cells and the Muller cells (4). Two other waveforms that are sometimes recorded in the clinic (see the previous chapter) are the c-wave originating in the pigment epithelium (5) and the d-wave indicating activity of the OFF bipolar cells (Fig. 3a). Later, we shall discuss some wavelets that occur on the rising phase of the b-wave known as oscillitatory potentials (OPs). OPs are thought to reflect activity in amacrine cells.

The ERG of a normal full-term infant looks similar to a mature ERG. The ERG attains peak amplitude in adolescence and slowly declines in amplitude throughout life (6). After age 55-60 years, the amplitude of the ERG declines even more. Implicit times slow gradually from adolescence through old age as well. Below are two figures illustrating how the b-wave attenuates in amplitude with age and slows in its implicit time (Fig. 3a and Fig. 3b). There is considerable variation among individuals, but the linear regression line in each figure indicates the trend of aging affects on the ERG.

ERG Recording Electrodes

The ERG can be recorded several ways. The pupil is usually dilated. There are a number of corneal ERG electrodes that are in common use. Some are speculum structures (Fig. 4) that hold the eye open and have a contact lens with a wire ring that "floats" on the cornea supported by a small spring (7). Some versions use carbon, wire, or gold foil to record electrical activity. There are also cotton-wick electrodes (Fig. 4) (8).

There are yet other simpler ERG recording devices (Fig. 5) using gold Mylar tape that can be inserted between the lower lid and sclera/cornea. Most electrodes are monopolar, i.e., are referred to another electrode site most commonly on the forehead. Some are bipolar with the reference electrodes built into a metal surface on a speculum.

Each of these electrodes records large voltage responses directly from the cornea, and each has advantages and disadvantages. We use Burian speculum electrodes when possible. Sizes are available down to a size that fits in the eye of most full-term babies. When the eye is too small for speculum recording electrodes, we use the ERG Jet type most of the time. When the eye is very small, such as in some microphthalmic eyes or cases of trauma to tissue surrounding the eye, we use a carbon-wick or gold Mylar tape.

The ERG can also be recorded using skin electrodes placed just above and below the eye, or below the eye and next to the lateral canthus. Because skin electrodes are not in direct contact with the cornea, there is significant attenuation in amplitude of the ERG, so a number of individual responses to flash stimulation must be averaged by computer. Pictured in Fig. 6 is a comparison of bright white flash ERGs recorded from the same person using three types of recording devices and an averaged ERG from skin electrodes.

If electrodes are to be reused, they must be sterilized with a solution that neutralizes prion-transmitted diseases such as Creutzfeldt-Jakob disease (CJD). We use household bleach, e.g., Chlorox (active ingredient, sodium hypochlorite), diluted to a 10% solution with distilled water. The electrodes need only be submerged in this solution for 1 minute. Do not leave electrodes in this solution more than a few minutes.

Light Stimulation for ERGs

There are also several methods of stimulating the eye. Some laboratories use a strobe lamp that is mobile and can be easily placed in front of a person whether sitting or reclining (Fig. 7). The mobility of a strobe lamp or an array of LEDs is a necessity in some situations, such as at the hospital bedside or in the operating room.

For patients over 5 years of age, most laboratories use a Ganzfeld (globe) with a chin rest and fixation points (Fig. 8). The Ganzfeld allows the best control of background illumination and stimulus flash intensity. Either strobe lamp or Ganzfeld methods of flash presentation can be used to record the ERG after a single flash or to average responses to several flashes with the aid of a computer. Clinical decisions can be made from ERGs generated by either methodology.

Testing Infants for ERGs

Infants up to about 2 years of age can usually be tested without sedation by the parent holding them bundled in a blanket. It is difficult to get a child less than 5 years of age to allow a contact lens or speculum recording

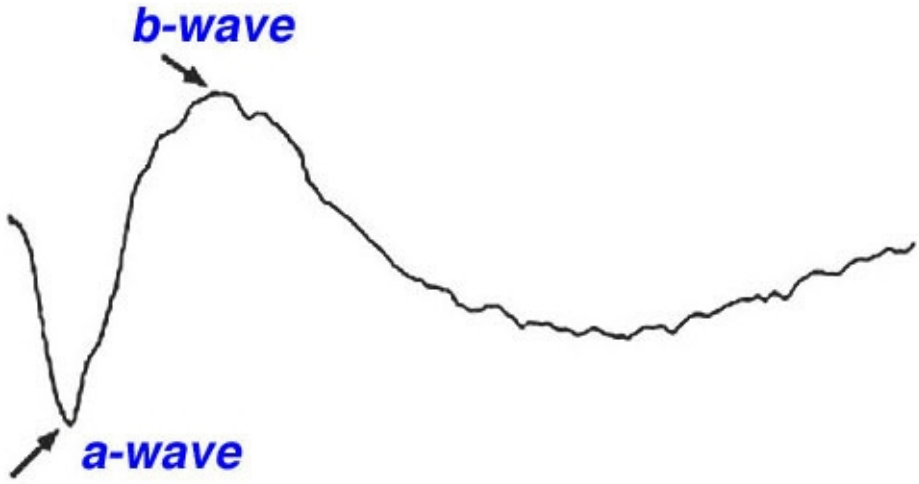

Figure 1. The biphasic waveform of the typical normal patient.

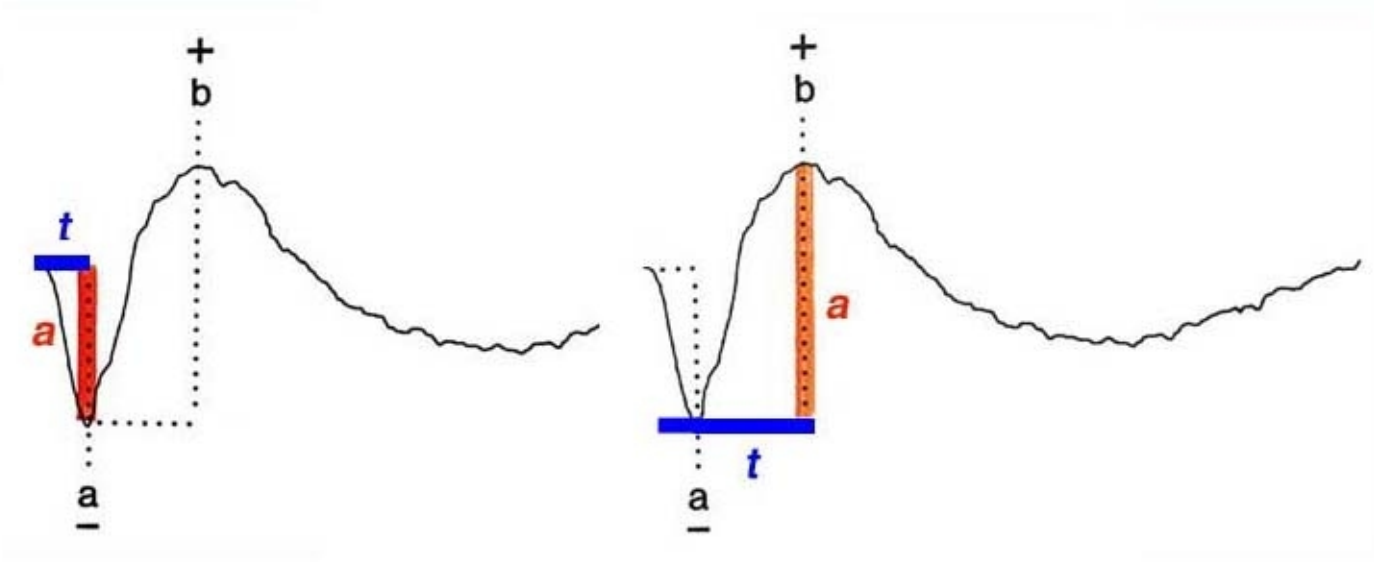

Figure 2. Amplitude and implicit time measurements of the ERG waveform.

electrode in the eye, so skin or scleral electrodes can be used, with their limitations. Alternatively, the child is sedated or anesthetized. Many clinics use chloral hydrate or the 3-in-1 "cardiac cocktail" to sedate pediatric patients. Chloral hydrate has several limitations, including that dose restrictions limit the use to patients weighing less than about 15 kg.

Both of these sedatives have little effect on the ERG. ERG testing is also sometimes performed as part of a more extensive exam under anesthesia (EUA). Few laboratories have Ganzfeld stimulators that can be tilted and placed over the face of a sedated patient, and it is difficult to use such equipment in the operating room. Thus, flash stimuli with sedated patients are usually delivered with a strobe lamp (Fig. 7). In an ERG laboratory, the sedated patient can be dark adapted, and a more or less normal series of stimuli can be used, although the length

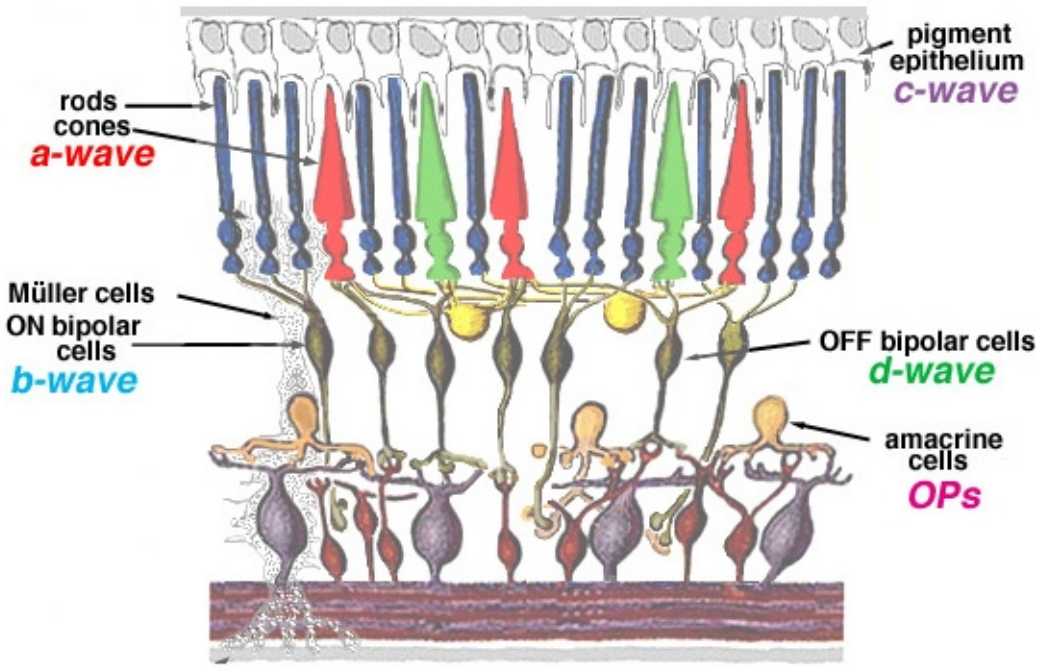

Figure 3a. Schematic of the retina to show where the major components of the ERG originate.

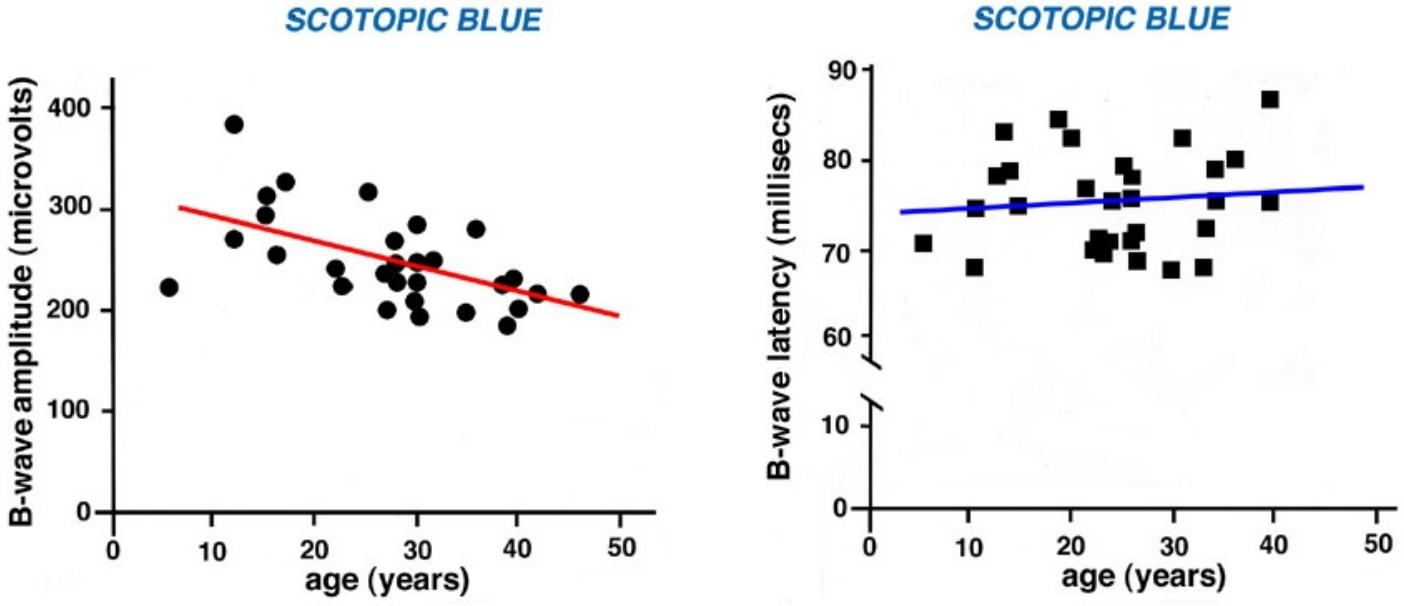

Figure 3b. Scatter plot of b-wave amplitudes and latencies with age with regression lines to show the aging effects.

of effect of the sedative usually necessitates that the method be abbreviated to just three or four stimuli. Dark adaptation, even for a few minutes, followed by single flashes of white or blue will assess scotopic ERG function. Photopic single flashes and 30 Hz flicker can be used to evaluate cone function.

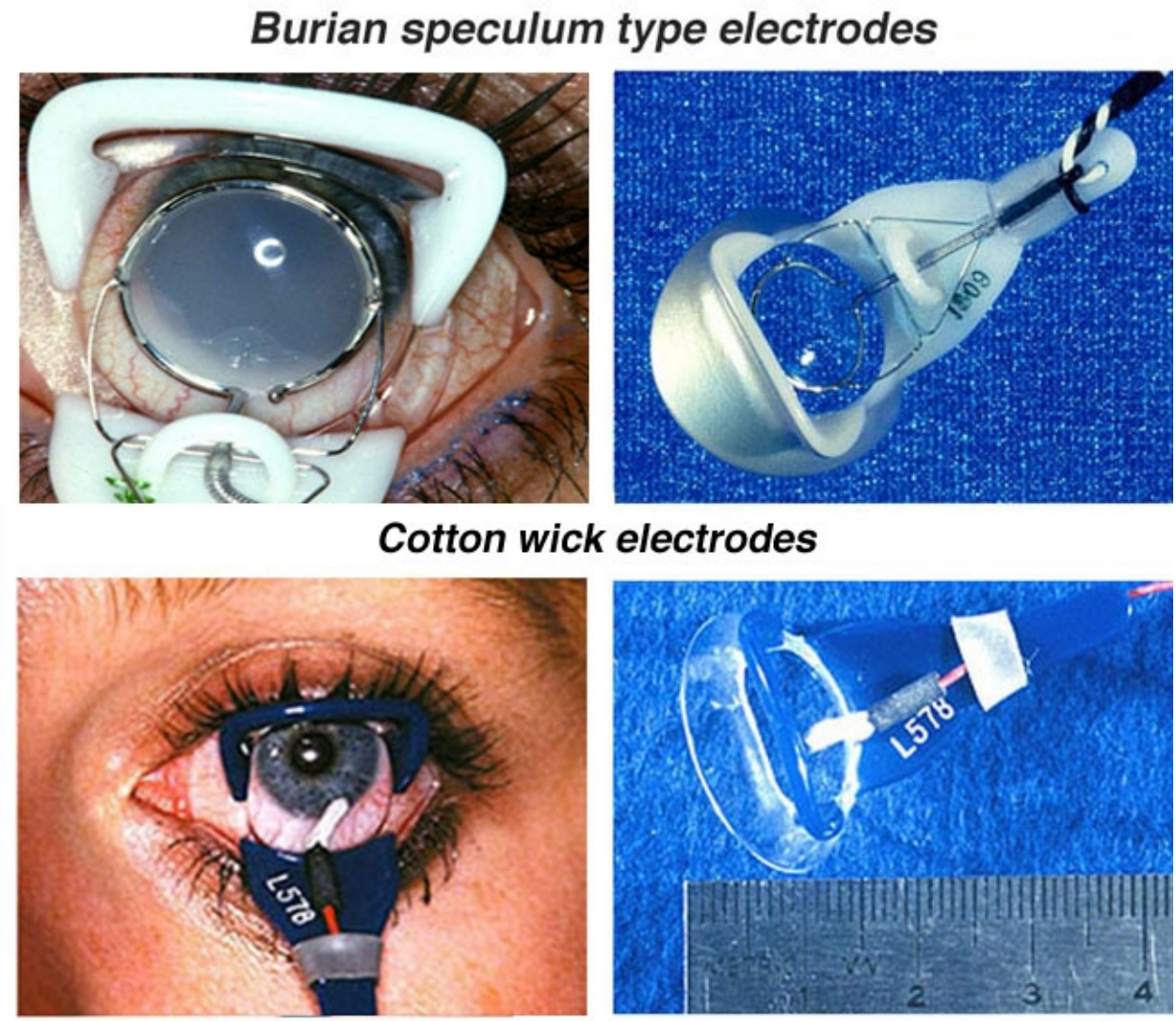

Figure 4. Speculum or Burian-type electrodes used to record the human ERG.

It is usually not possible to completely darken the operating room, so abbreviated testing is accomplished under mesopic and photopic light conditions. Anesthesia affects the ERG, varying with type and depth of anesthesia. Some anesthetics can attenuate b-wave amplitude as much as 50%. Light levels of anesthesia have little affect, and most anesthetics do not usually affect a-waves or implicit times.

Separating Rod and Cone ERGs

Most disorders of the retina are detected by an attenuation of amplitude. Implicit times, of both a- and b-waves, are also affected in some conditions. Implicit times and amplitudes vary, depending upon whether the eye is dark adapted, and brightness and color of the light stimulus. These parameters allow separation of rod and cone activity in any duplex retina.

Rods and cones differ in number, peak color sensitivity, threshold, and recovery. There are about 120 million rods in each retina, and about 6-7 million cones (see the Facts and Figures chapter). Because of sheer numbers, the ERG following a white flash is dominated by the mass response of the rods. By manipulating adaptation level and background illumination, flash intensity, color of the flash, and rate of stimulation, rod and cone activity can be significantly isolated.

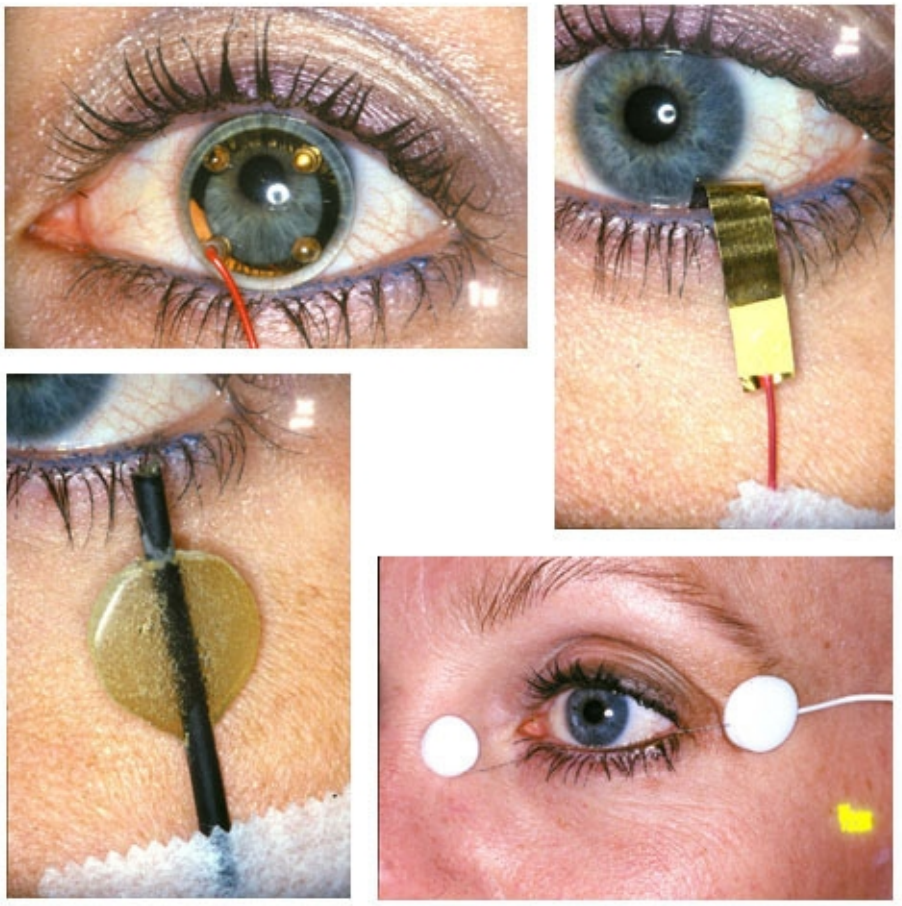

Figure 5. Other simple types of electrodes used to record the human ERG.

Using Color Stimuli

Peak wavelength sensitivity for rods is around 510 nm, and the peak sensitivity of cones as a group is about 560 nm (tennis ball yellow). By using color filters such as the Kodak Blue and Red Wratten series shown in Fig. 9a, you can essentially isolate rod and cone ERGs using dim flash stimuli into photopic (cone) and scotopic (rod) signals as illustrated in Fig. 9b. Dim red analyses both rod and cone function by identifying b_x and b-wave. Rods are about three log units more sensitive than cones. However, cones recover faster than rods.

Using different rates (flicker) of stimulus presentation also allows rod and cone contributions to the ERG to be separated. Even under ideal conditions, rods cannot follow a flickering light up to 20 per second, whereas cones can easily follow a 30-Hz flicker, which is the rate routinely used to test if a retina has good cone physiology (Fig. 9c).

ERG Recording Methods

There are many ways of recording ERGs from patients (9, 10). I recommend reviewing ISCEV standards before recording ERGs (11). Most procedures give similar results but vary mainly in sequence. Some laboratories record the light-adapted state first, and others dark-adapt first. Some laboratories use only white flashes, and others included colored flashes. Many laboratories use a scotopic intensity series as well. Supplemental analysis, such as Perlman's (12) relationship between the ratio of a- and b-wave amplitudes, can be extracted from this intensity series. If only bright white flash stimuli are used, subtle abnormalities will be missed.

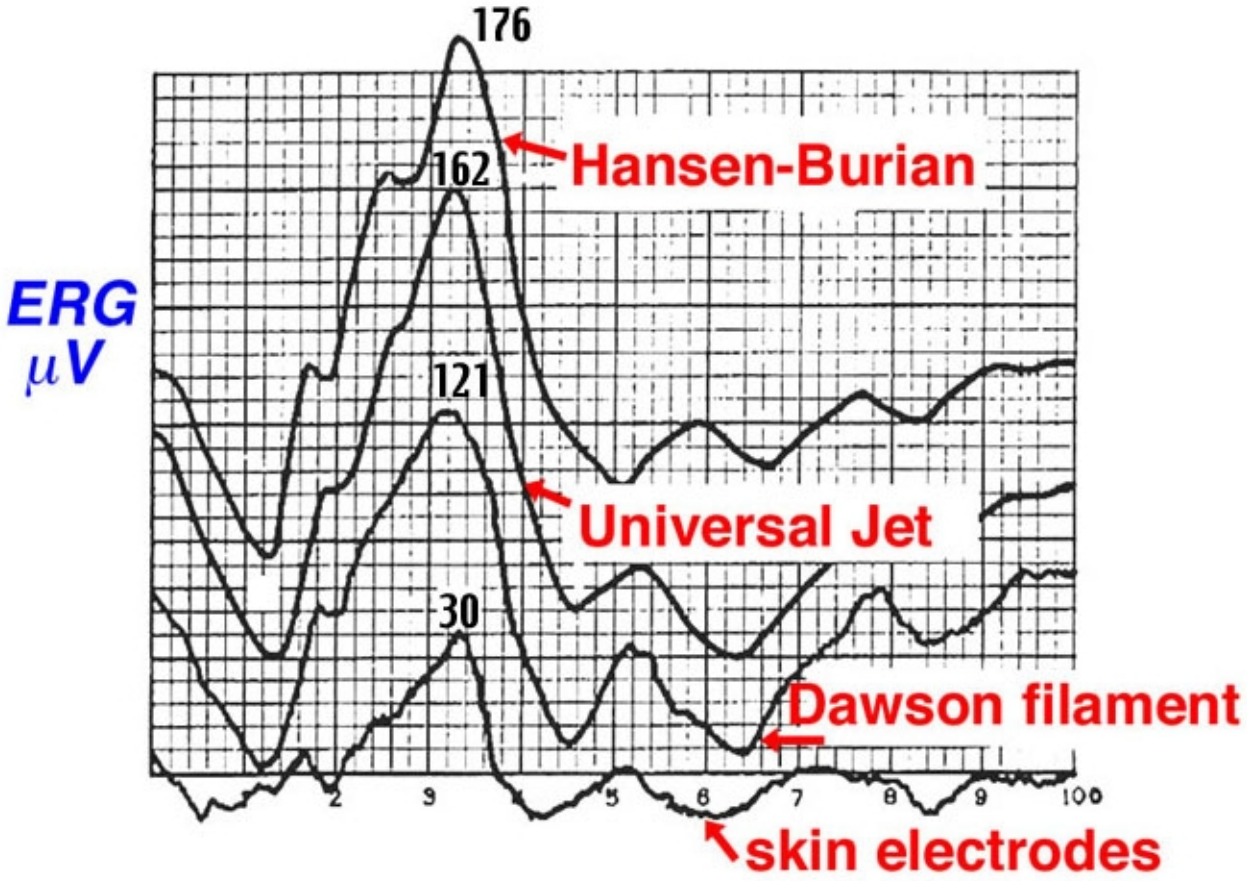

Figure 6. Typical ERGs as recorded with different electrodes.

The method we use in our clinic is:

1. Dark adapt patient for a set time of 30 minutes.
2. Attach electrodes using dim red illumination. We use an indirect headlamp with several Wratten 26 red filters so that a mobile dark room "safe" light is simulated.
3. Record ERG using single, scotopically balanced, dim blue and red flashes and bright white flashes, as illustrated in the sample ERGs of Fig. 9b. Some laboratories average several responses.
4. Turn on moderately high background illumination of about 10 ftL for about 10 minutes and record ERGs using 30-Hz flicker and bright white flashes (Fig. 9c). Responses recorded using moderately high background illumination accentuate the cone system by bleaching the rods, and only cones can recover fast enough between flashes to accurately follow a flickering 30-Hz light.

Recording Scotopic ERGs

Thirty minutes or more in the dark produces a state of 98% or more dark adaptation in most individuals. The use of two or more log unit filters to reduce flash intensity and dim blue filters limits the ERG to reflecting rods only. "Scotopically balanced" blue and red filters (Fig. 9b) mean that deep blue and red filters with transmission spectra that do not overlap are matched through trial and error addition of neutral density filters until the ERGs produce b-wave amplitudes of the same size. The purpose of this is to establish a standard so that differences between rod and cone physiology can be more easily detected. We do this routinely for all patients tested in our clinic. The scotopic dim blue ERG is the most sensitive, not only to rod disorders but also to systemic metabolic aberrations and retinal toxicity.

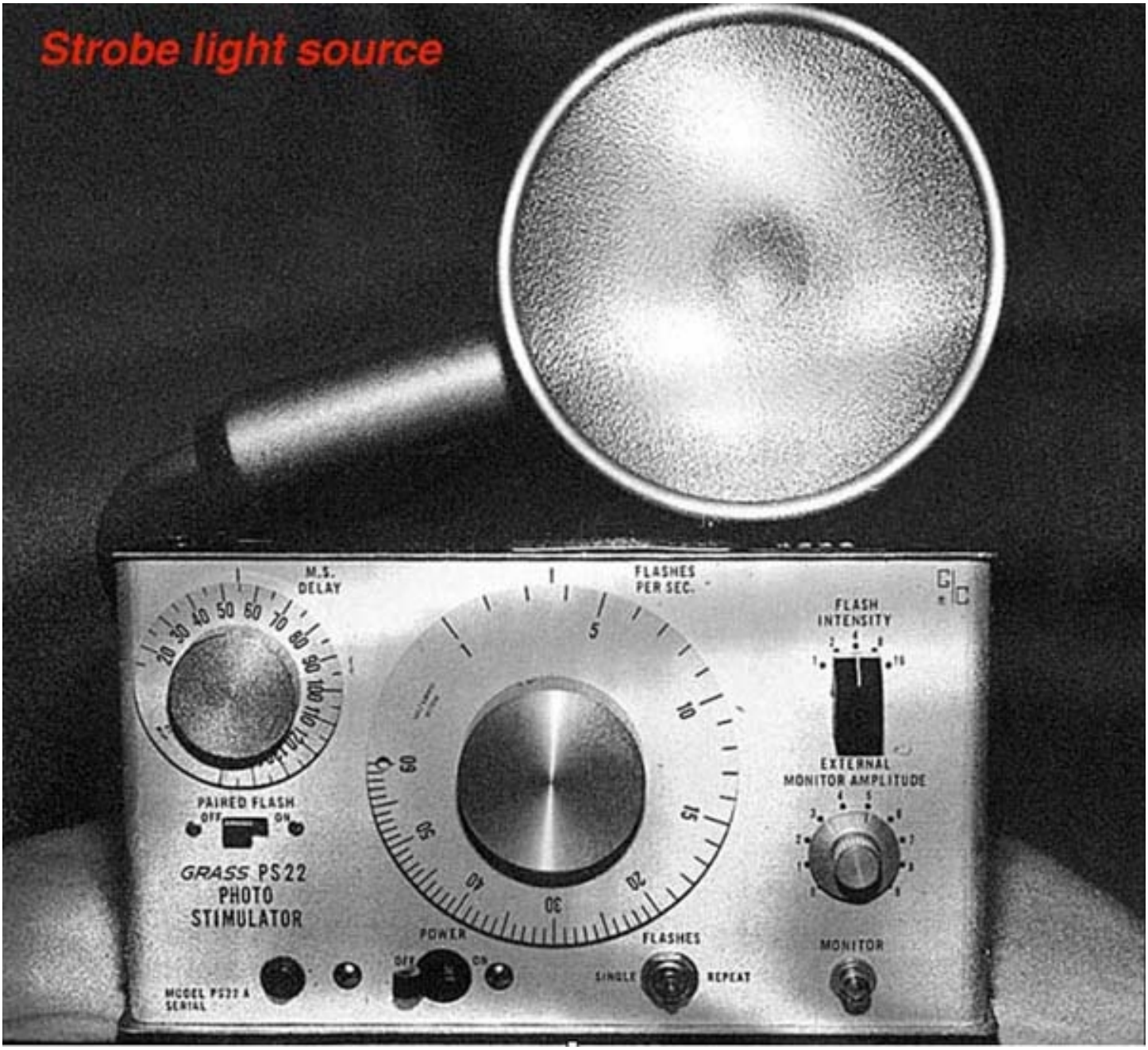

Figure 7. Portable strobe light source.

Oscillatory Potentials (OPs)

Some laboratories also include recording oscillatory potentials (OPs). OPs seen on the ascending limb of most b-waves, in both scotopic and photopic bright flash ERG recordings, were first described by Cobb and Morton (13). By raising the low bandpass from the usual <1 Hz up to around 100 Hz, the slower a- and b-wave components are filtered out, leaving a burst of cone OPs following a bright white flash between about 15 and 40 msec (Fig. 10). Scotopic rod OPs produced by dim blue flash appear later between about 25 and 55 msec. OPs are thought to reflect activity initiated by amacrine cells in the inner retina (14).

This brings up an interesting clinical anecdote that also indicates the vulnerability of the ERGs to changes in retinal chemistry. For over 50 years, the irrigating solution of choice when removing enlarged prostate glands

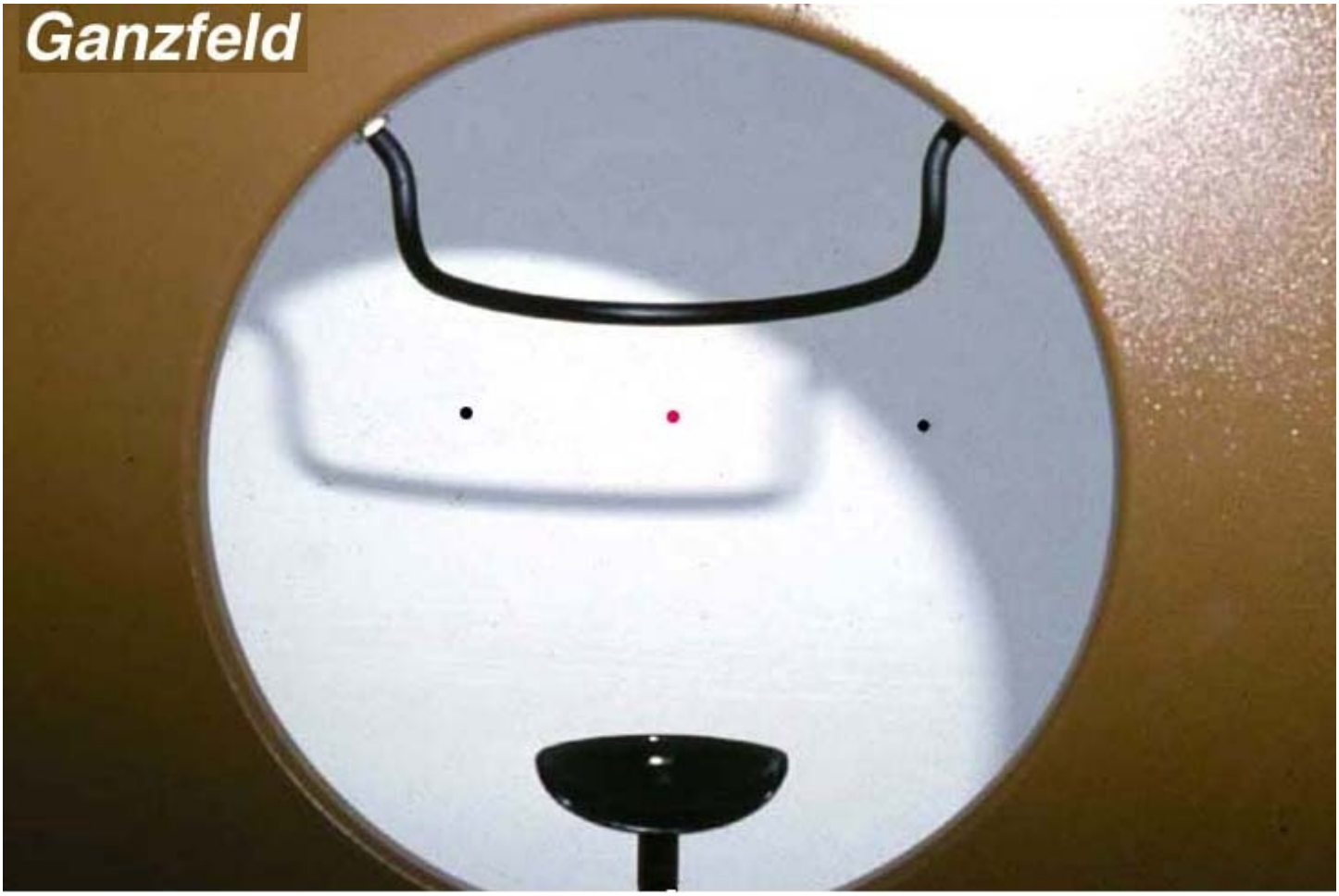

Figure 8. The Ganzfeld stimulation globe.

has been glycine. When the procedure takes a long time or the surgeon cuts deeply into the venous beds surrounding the prostate gland, an awake patient under spinal block anesthesia has said, "Why did you turn the lights off?" This can create considerable consternation among personnel in a brightly illuminated operating room. Glycine is an inhibitory transmitter in the retina, particularly associated with amacrine cells. When the glycine reaches retinal circulation, it short circuits the amacrine cell pathways in the retina and turns off the source of OPs (15). OPs specifically disappear from the ascending limb of the b-wave. OPs and vision return to the patient over several hours as the glycine is metabolized (Fig. 11).

OPs are significantly attenuated in various retinal degenerations, among them are the following:

- Retinitis pigmentosa
- Central serous retinopathy
- CSNB type 2
- Birdshot choroidopathy
- Retinoschisis
- Carriers of X-linked CSNB
- Diabetic retinopathy
- Hypertensive retinopathy
- CRVO and CRAO
- Takayasu's (pulseless) disease

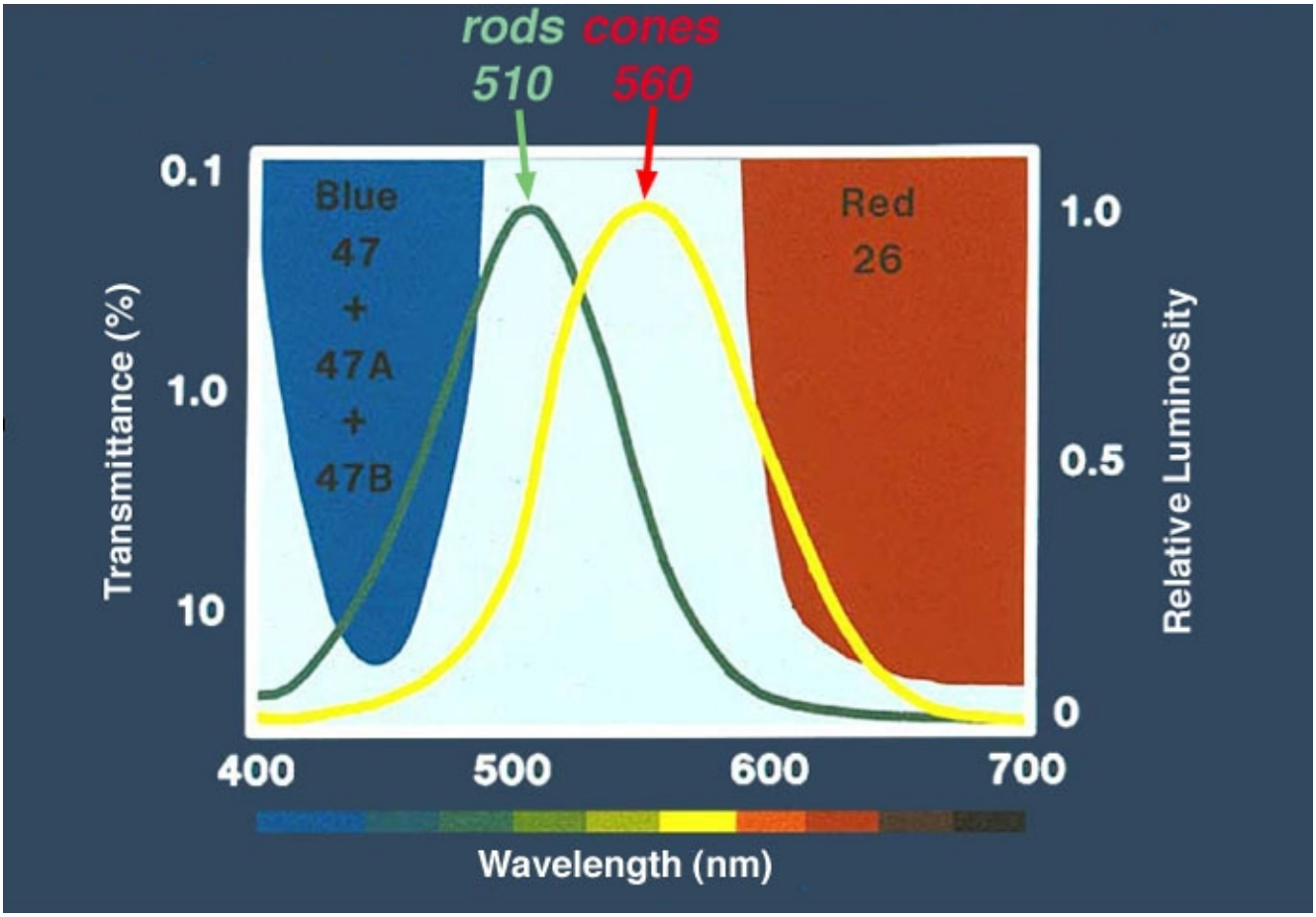

Figure 9a. Filter conditions used to isolate rod and cone components of the ERG using dim scotopic flashes.

ERGs in Retinitis pigmentosa-like Diseases

In all forms of retinal pathology, there is considerable variability. There are no absolute rules. Genetic variation in penetrance and expression, in combination with individual differences, affects retinal electrophysiology.

ERGs recorded from a representative normal subject (Fig. 12a) and from a patient with retinitis pigmentosa (RP) (Fig. 12b) using the above methodology are illustrated in Fig. 13. The scotopic blue and red ERG traces are 200 msec, and the other traces are 100 msec. The vertical calibration is 100 microvolts. The low bandpass limit was 0.1 Hz, and the upper bandpass limit was 1 KHz. When dim stimuli are used, such as an intensity series starting with low intensity white or dim scotopic red and blue flashes, it is important that the low bandpass be less than 1 Hz. The slow b-wave initiated by dim stimuli will be attenuated if a low bandpass is not used.

The first two responses are scotopically matched blue and red ERGs. The blue flash was dim enough that no a-wave can be discerned in a normal patient, leaving only the rod-dominated slower b-wave. The red flash is bright enough that oscillations can be observed just after the a-wave. Bright white flash in the dark produces the largest amplitude ERG. The 30-Hz flicker illustrates the response of the rapidly recovering cones, and the photopic response is representative of a normal response, with the more sensitive rods bleached by background illumination. Oscillatory potentials on the ascending b-wave are seen in responses to moderately high intensity white flashes and in response to red, yellow, and green flashes (Fig. 13).

This particular case of RP was selected because the individual was tested early in the onset of RP, as a young adult when she still had remnants of a cone ERG. As in most cases of RP, the rods are affected most severely, as

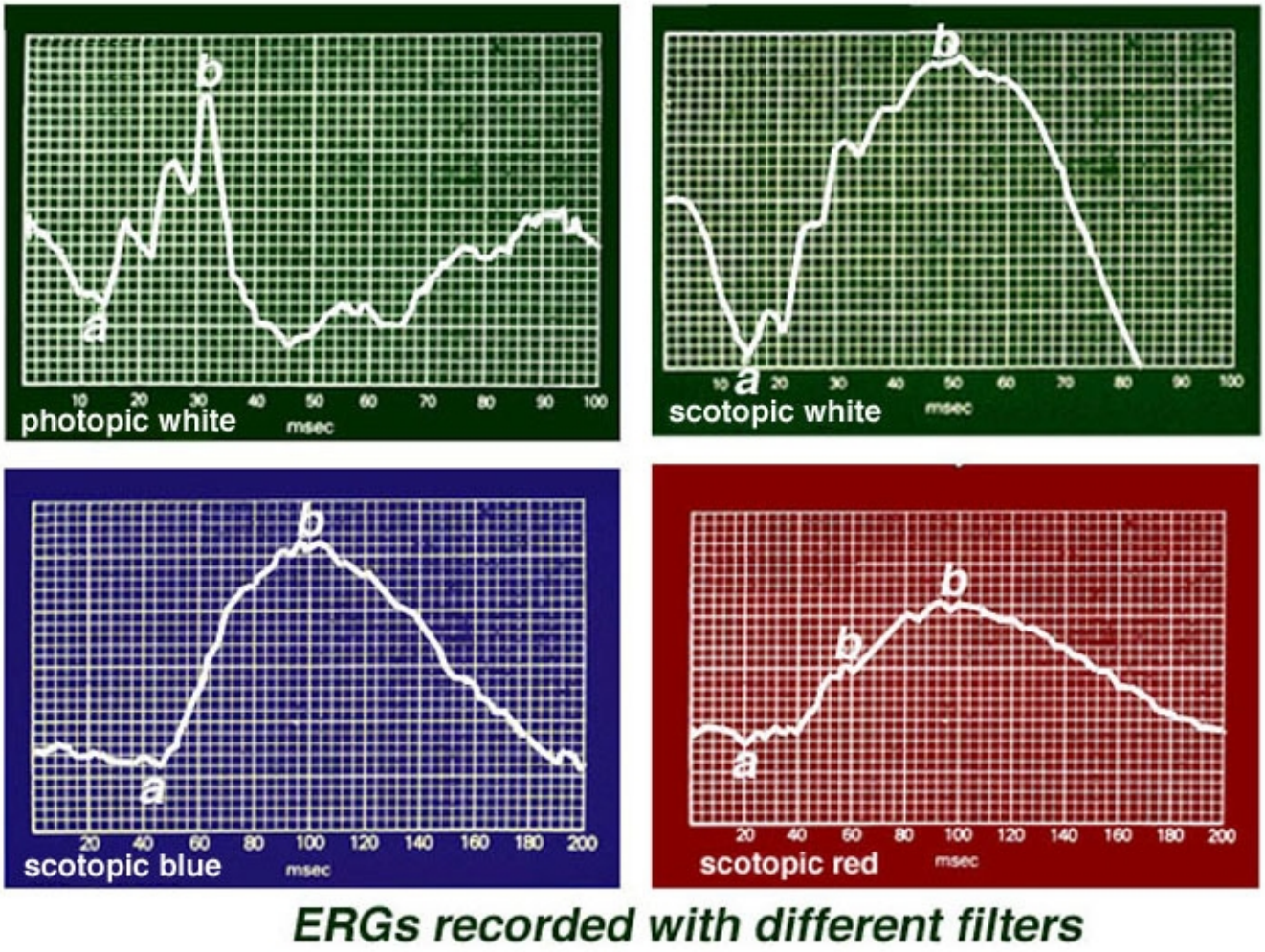

Figure 9b. Typical testing parameters used in our ERG recording set up.

evidenced by the extinguished response to the blue flash. Although it may take some imagination, some of those "squiggles" in the first half of the response to red flashes are remnants of photopic cone physiology. There are also remnants of cone physiology in the responses to bright white flash in the dark, 30-Hz flicker, and photopic white flash. In many individuals with RP, the electrophysiological progression is more severe with all ERGs extinguished, similar in appearance to the response to scotopic dim blue flash. Both scotopic and photopic b-wave peak implicit times are usually prolonged. Almost always, it is impossible to record OPs.

Early in the clinical onset of RP, with the exception of severe expressions such as Leber's congenital amaurosis or X-linked RP (Fig. 14), there are recordable ERGs, at least to bright photopic stimuli. Some individuals with dominantly inherited RP maintain recordable ERGs throughout most of their lives. I have tested over 100 members of one extended family with dominantly inherited RP. Some of the affected members showed no ERG changes until their mid-teens. Expression of RP in all forms of inheritance varies considerably, even between siblings. Female carriers of the X-linked form can show fundus changes and somewhat abnormal ERGs.

Atypical cases of RP are common. There are occasional cases of RP without the usual pigment changes in the fundus (retinitis pigmentosa sine pigmento). Often these cases represent early stages of the disease. Sector RP usually results in a subnormal ERG proportional to the area of retina involved. Paravenous RP (Fig. 15) is associated with a poor ERG most of the time, but again, similar to sector RP, the ERG may be attenuated proportional to the extent of retinal involvement.

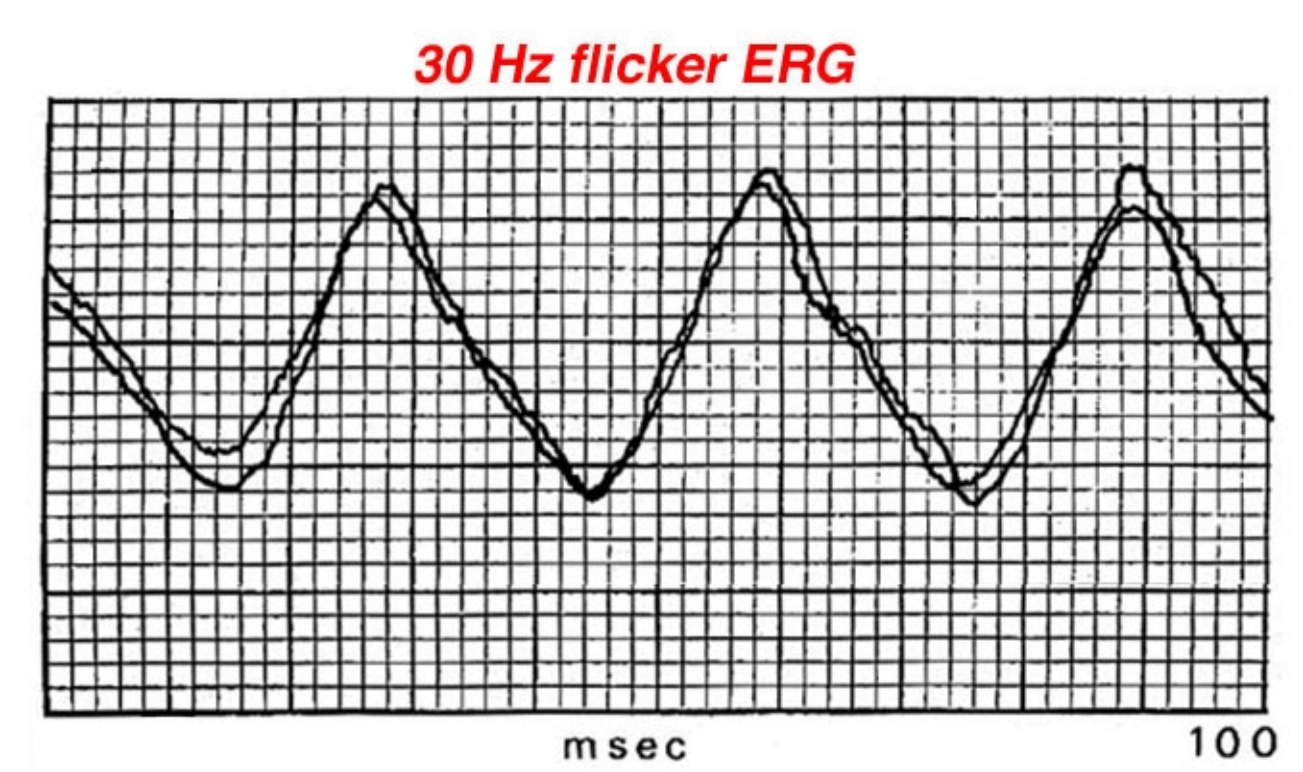

Figure 9c. Typical 30-Hz flicker ERG recorded in our clinic.

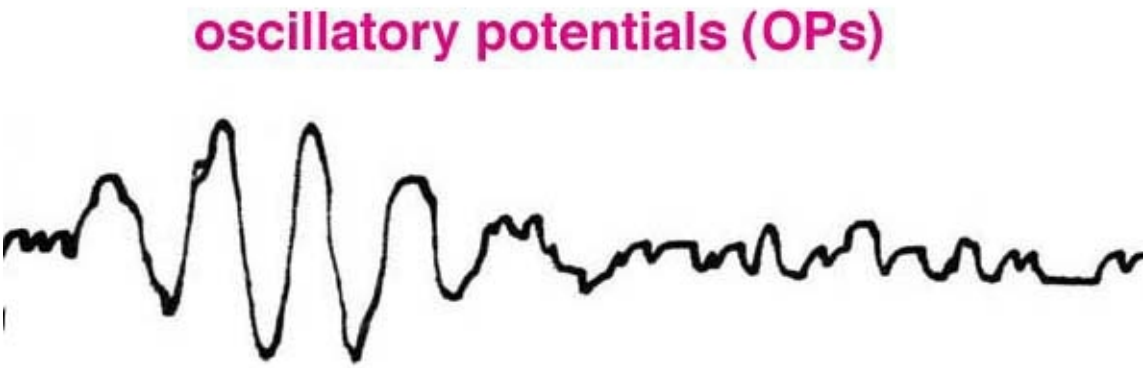

Figure 10. Oscillatory potentials.

RP is seen as a component of a number of syndromes with variability in expression. A common syndrome is Usher's. Usher's syndrome is congenital deafness plus RP. Usher's syndrome may comprise over 20% of RP cases not associated with other syndromes (16).

Myotonic dystrophy (MD) can show ocular changes similar to RP (Fig. 16). Even without fundus changes, the ERG in MD patients is usually moderately affected like that seen in early dominantly inherited RP (17). It is interesting to note that minimally affected individuals without neurological symptoms usually have significant attenuation of their dim flash scotopic ERG b-wave amplitudes. Thus, the ERG can be used to identify the minimally affected parent with MD (Fig. 16, the mother) in cases where neither parent of a child with MD exhibits neurological symptoms.

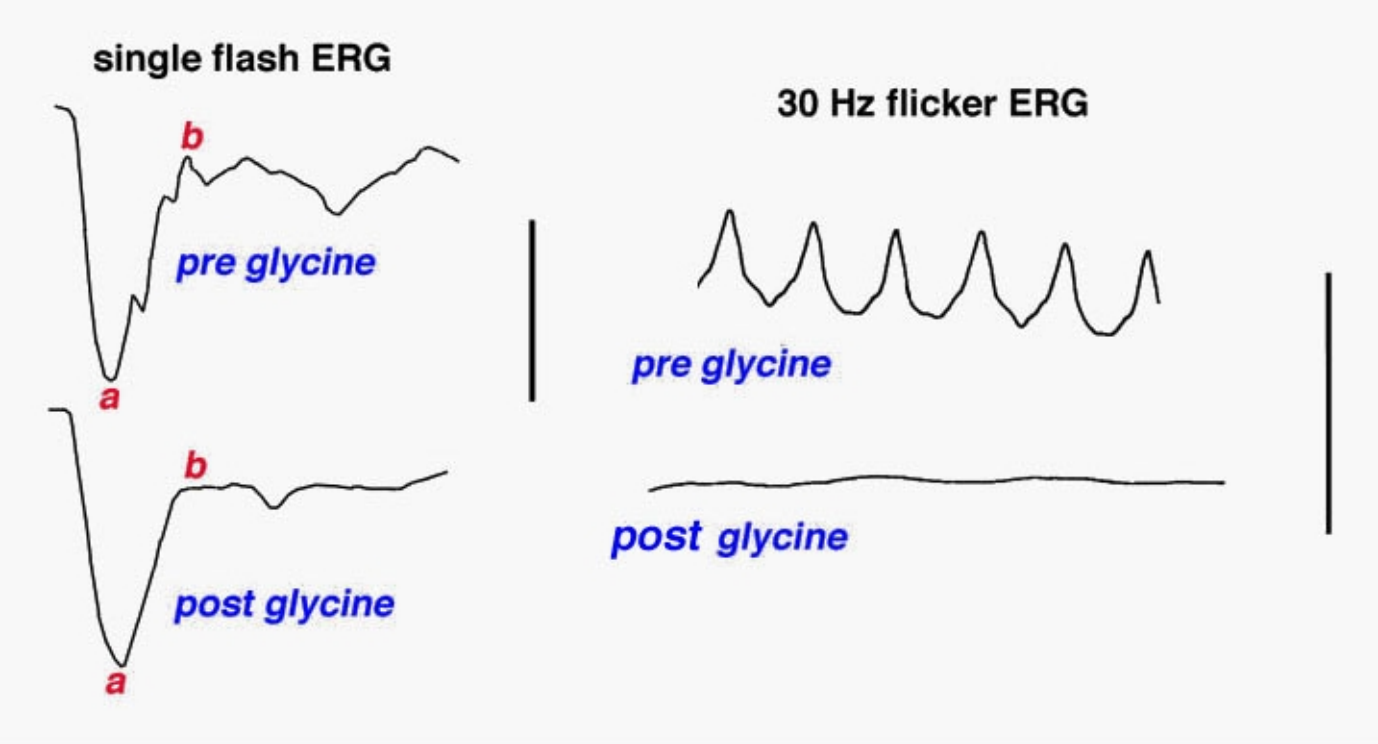

Figure 11. Patient with glycine overload.

There are a number of central nervous system syndromes with RP-like ocular involvement. Prominent among these are the mucopolysaccharidoses, such as the Hurler, Scheie, and Hunter syndromes, which often have abnormal ERGs early in the disease. Another group is the neuronal ceroid lipofuscinoses, such as Batten's disease, which have abnormal ERGs, usually attenuated b-waves.

There are syndromes that may include RP. The following list summarizes many of these syndromes:

- Alagille syndrome: ERG normal or subnormal
- Albers-Schonberg syndrome (osteopetrosis): ERG often abnormal
- Alport's syndrome: ERG normal or subnormal
- Alstrom's syndrome: ERG abnormal
- Ataxia with isolated vitamin E deficiency (AVED) and RP: ERG abnormal
- Bassen-Kornzweig syndrome (a-beta-lipoproteinemia): ERG abnormal
- Cockayne's syndrome: ERG often abnormal
- Cystinosis: ERG abnormal in older children
- Flynn-Ard syndrome: ERG sometimes abnormal
- Friedreich's ataxia: ERG sometimes abnormal
- Hallervorden-Spatz syndrome: ERG often abnormal
- Infantile phytanic acid storage disease: ERG usually abnormal
- Jeune's syndrome: ERG usually abnormal
- Joubert's syndrome: ERG abnormal
- Kearn's-Sayres syndrome: ERG some abnormal
- Laurence-Moon-Bardet-Biedl syndrome: ERG usually abnormal
- Methylmalonic aciduria with homocystinuria: ERG some abnormal
- Mucopolysaccharidoses (Hurler, Scheie, Hunter): ERG often has b-wave attenuation
- Myotonic dystrophy: ERG abnormal, dim scotopic ERGs

- Neuronal ceroid lipofuscinosis: (Haltia-Sanavouri, Jansky-Bielschowsky, Batten's): ERG often has b-wave attenuation
- Neuropathy ataxia and retinitis pigmentosa (NARP): ERG abnormal
- Refsum's disease: ERG often abnormal
- Saldino-Merzbacher syndrome: ERG usually abnormal
- Senior-Loken syndrome: ERG usually abnormal
- Spinocerebellar atrophy Type 7 (SPA7): ERG abnormal
- Usher's syndrome: ERG abnormal
- Zellweger's syndrome: ERG usually abnormal

In the differential diagnosis of RP, there are a number of disorders in which the ERG can be used to distinguish the correct diagnosis. Pigment in the retina is prominent in many infectious diseases and may not solely be an indication of RP. Syphilis, particularly the congenital form, can mimic the fundus appearance of RP (Fig. 17), but the ERG is usually normal or only slightly subnormal.

Rubella and viral infections, such as mumps, measles, and herpes, can produce pigment changes in the retina (Fig. 18). These ERGs are usually normal.

Stationary Rod Dystrophies

Congenital stationary night blindness (CSNB) is found in several forms. Although rare, CSNB is more often seen in the form with a normal-appearing retina and may be inherited in any fashion. Within this form are two types. Type 1 has an abnormal dim scotopic ERGs, but the bright-flash ERG maintains OPs on the ascending limb of the b-wave. Type 2 (Fig. 19) has a very abnormal, dim scotopic ERG, and the bright-flash scotopic ERG has a large a-wave and no b-wave (Fig. 20). OPs are also missing.

CSNB with retinal lesions is quite rare. Oguchi's disease is CSNB with an unusual golden-to-rust coloration of the fundus that is reversed with long dark adaptation. This is called Mizuo's sign and requires 2-3 hours of dark adaptation. The ERG resembles CSNB type 2 with no b-wave, although cases have been reported that the ERG returns to normal after hours of dark adaptation. Another rare form of night blindness is stationary albipunctate degeneration, also referred to as fundus albipunctata. This disorder includes stationary night blindness with white dots scattered throughout the fundus. The ERG b-wave is attenuated but returns to normal after long dark adaptation. A third form is Kandori's syndrome, characterized by large, irregular, hyperfluorescent flecks in the peripheral and central retina. In nyctalopia, the ERG is similarly affected as in stationary albipunctate degeneration.

Other retinal atrophies

The bright flash ERG b-wave is selectively attenuated in:

- Juvenile retinoschisis
- Coat's disease
- Central retinal vein occlusion and central retinal artery occlusion
- Myotonic dystrophy
- Congenital stationary night blindness type 2
- Oguchi's disease
- Lipopigment storage diseases (Batten's disease)

Choroideremia represents an X-linked, diffuse atrophy of the choroid and pigment epithelium. In its mature form, the fundus appearance is white to yellow-white with some small islands of choroid (Fig. 21). Carriers are asymptomatic except for more subtle peripheral fundus abnormalities (Fig. 22). ERGs are usually abnormal.

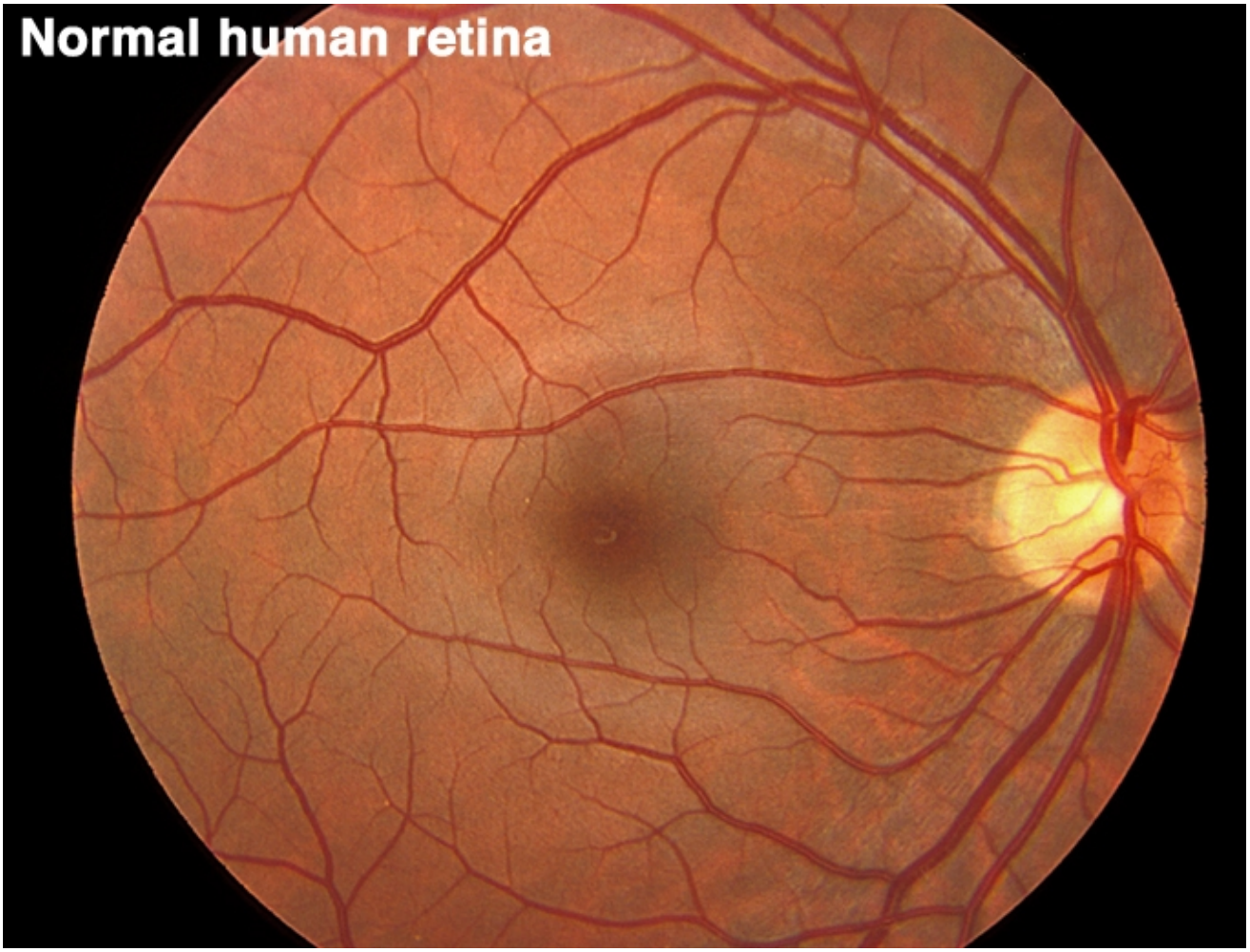

Figure 12a. Fundus photo of a normal human retina.

Gyrate atrophy (Fig. 23) is a recessively inherited atrophy of the pigment epithelium and choroid caused by a deficient mitochondrial enzyme ornithine aminotransferase (OAT).

Gyrate atrophy is less extensive than choroideremia, and the fundus usually shows scalloped borders to degenerative areas (Fig. 23). ERGs are abnormal and progressly deteriorate according to the extent of degeneration of retinal pigment.

X-linked juvenile retinoschisis is a splitting or schisis in the central retina with a characteristic fundus appearance (Fig. 24). These patients have poor acuity. The ERG has a specific abnormality showing a normal a-wave but no b-wave. It is a negative ERG (Fig. 24). The picture is similar to that recorded in central retinal artery occlusion and congenital stationary night blindness type 2.

Patients with Creutzfeldt-Jakob disease (CJD) can also show selective loss of the b-wave (18), even in early stages. We have followed several patients with CJD that have shown unusual ERG waveforms (Fig. 24, a). Similar in appearance to the ERGs of retinoschisis, the b-wave is greatly attenuated (Fig. 24, a). In later stages, the a-wave and OPs are also affected. This pattern is seen in very few disorders, principally X-linked retinoschisis and congenital stationary night blindness type 2.

Except for some retinal dystrophies such severe RP or Leber's congenital amaurosis, most retinal disorders produce reduced, "graded" amplitude attenuation of the ERG, as we have seen in the above cases. However, a few disorders result in a completely extinguished ERG. They include the following:

Figure 12b. Fundus photo of a patient with retinitis pigmentosa.

- Leber's congenital amaurosis
- Severe retinitis pigmentosa
- Retinal aplasia
- Total detachment of retina
- Ophthalmic artery occlusion

Leber's congenital amaurosis unfortunately presents with significant visual loss in the first year after birth. The fundus usually has a salt and pepper appearance. The ERGs are usually unrecordable.

The ERG in Cone Dystrophies

In contrast to RP, the ERGs of a patient with a cone dystrophy exhibit good rod b-waves that are just slower. However, the early "cone" portion (b_x) of the scotopic red flash ERG is missing. The scotopic bright-white ERG is fairly normal in appearance but with slow implicit times. The 30-Hz flicker and photopic white ERGs dependent upon cones are very poor. Cone dystrophies are inherited in all forms and include poor color vision and poor acuity. The most common fundus findings are a "bullseye" appearance or diffuse pigmentation in the macular area (Fig. 25). Many patients have nystagmus and photophobia. Cone-rod dystrophy appears to involve only cones early in the disease, but the ERGs usually show attenuated rod physiology after a while (Fig. 26).

Other dystrophies are the flecked retina disorders, such as fundus flavimaculatus (Fig. 27) and Stargardt's disease. The retinas display an abnormal accumulation of lipofuscin. The ERG in these disorders is normal except in very late stages, where it may become slightly subnormal.

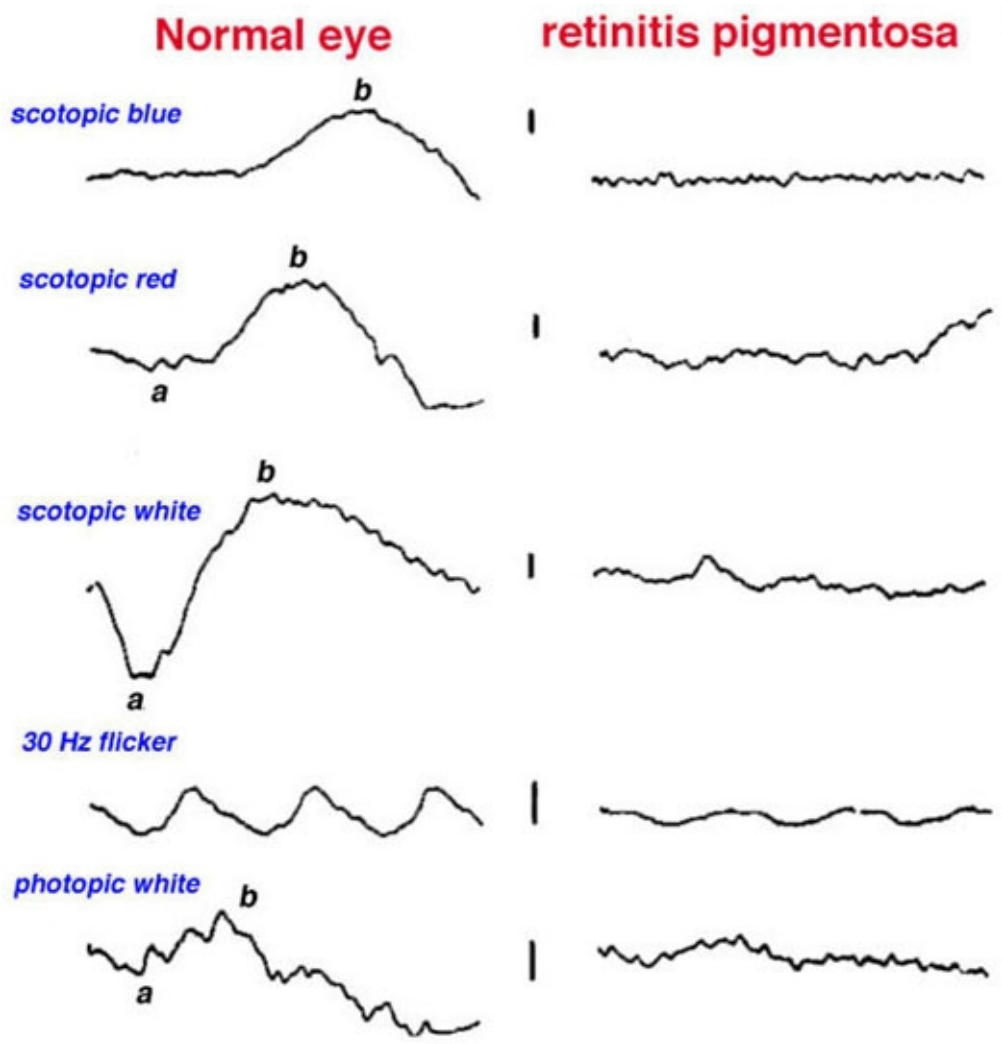

Figure 13. ERG recordings in a normal patient and one with retinitis pigmentosa.

ERGs in Retinal Vascular Disease

Vascular occlusions, such as central retinal artery thrombosis, produce a characteristic avascular appearance to select areas of the fundus (Fig. 28a) and an ERG with no b-wave (Fig. 28b). Ophthalmic artery occlusions usually result in unrecordable ERGs.

Foreign Bodies and Trauma

The ERG is useful to assess cases of retinal foreign bodies and trauma to estimate the extent of retinal dysfunction. Foreign bodies affect retinal function, depending on the extent of tearing of the retina, and the location and composition of the object. A small piece of stainless steel or plastic outside the macula may have a minor effect on the retina. However, a piece of copper or iron (Fig. 29) would likely have deleterious affects within a few weeks (Fig. 30a and Fig. 30b). In general, if b-wave amplitudes are reduced 50% or greater compared with the fellow eye, it is unlikely that the retinal physiology will recover unless the foreign body is removed.

The ERG can be used to estimate the extent of functional retina in cases of retinal detachment. An interesting case is shown in Fig. 31a and Fig. 31b. The patient had a small retinal detachment of the macular area in one eye (Fig. 31a, arrows point to circle of detachment). With the new techniques of optical coherence tomography

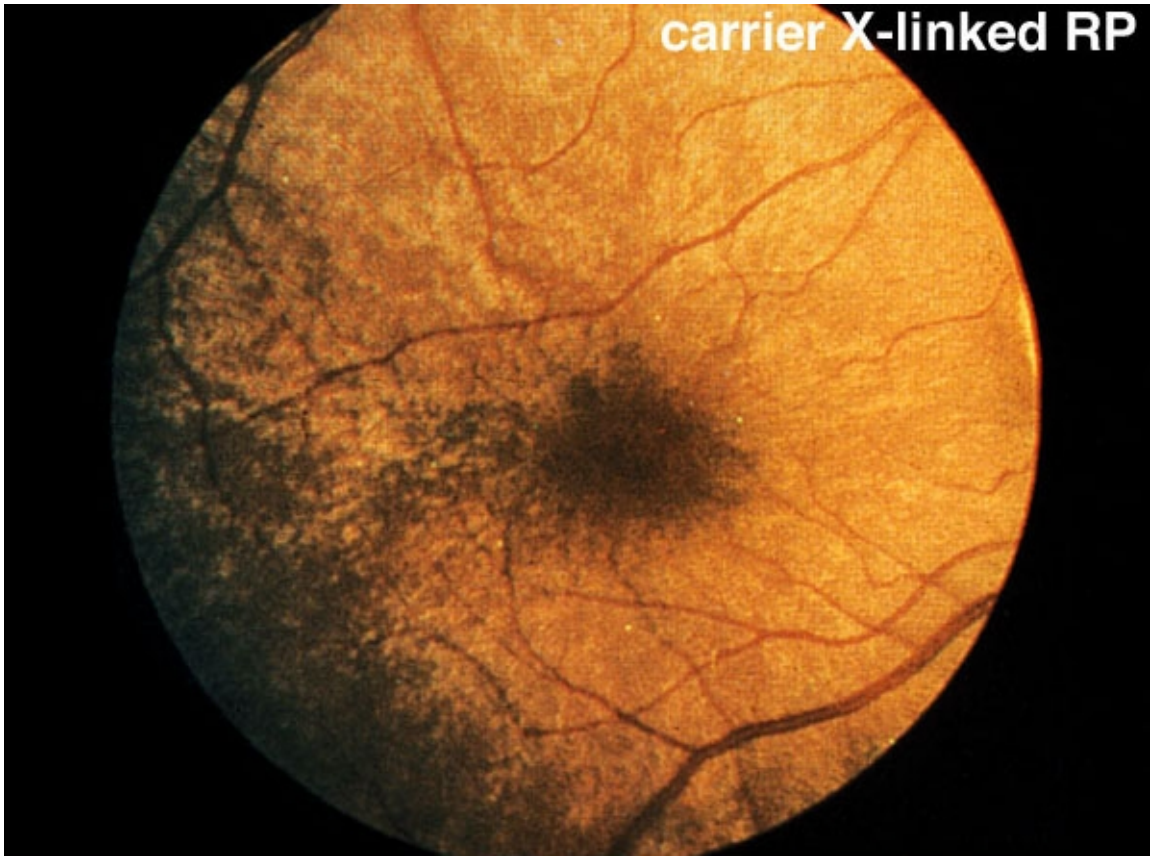

Figure 14. Fundus photo of patient with carrier X-linked retinitis pigmentosa.

(OCT), which gives an optical image like a vertical section plane, the detached portion of the retina in the foveal and macular area can be clearly seen, in comparison with the normal attached macular area in the fellow eye. In general, ERG b-wave amplitudes correspond to the amount of attached healthy retina, although the detached retina may function for some time.

Drug Toxicities

A number of drugs given in high doses or for long periods of time can produce retinal degeneration with pigmentary changes. Traditional culprits are thioridazine (Mellaril), chlorpromazine (Thorazine), and the antimalarial chloroquine. These are drugs usually taken at high dosages for many years and can end up damaging the retina and producing a retinopathy. Chloroquine retinopathy shows as a characteristic "bullseye" appearance of the macula (Fig. 32). The ERGs become abnormal in these cases (Fig. 33).

Hydroxychloroquine (Plaquenil) is usually less disruptive to the retina than chloroquine, but ERG changes can still occur. Other drugs can end up being accidentally toxic to the retina. Cisplatinum, used to treat brain tumors, sometimes reaches ophthalmic vascularization (Fig. 34) and causes a reduction in ERG waveform in the affected eye (OD in this case) (Fig. 35).

An interesting case was seen in our clinic, where an intranasal steroid injection affected the retina of the patient's right eye (OD) only. The fundus photo shows a cherry red spot in the macula (Fig. 36). The ERG response was diminished in size, particularly following dim scotopic flashes (Fig. 37).

Talc retinopathy is also seen occasionally (Fig. 38). Again, the global ERG is attenuated in such cases (Fig. 39).

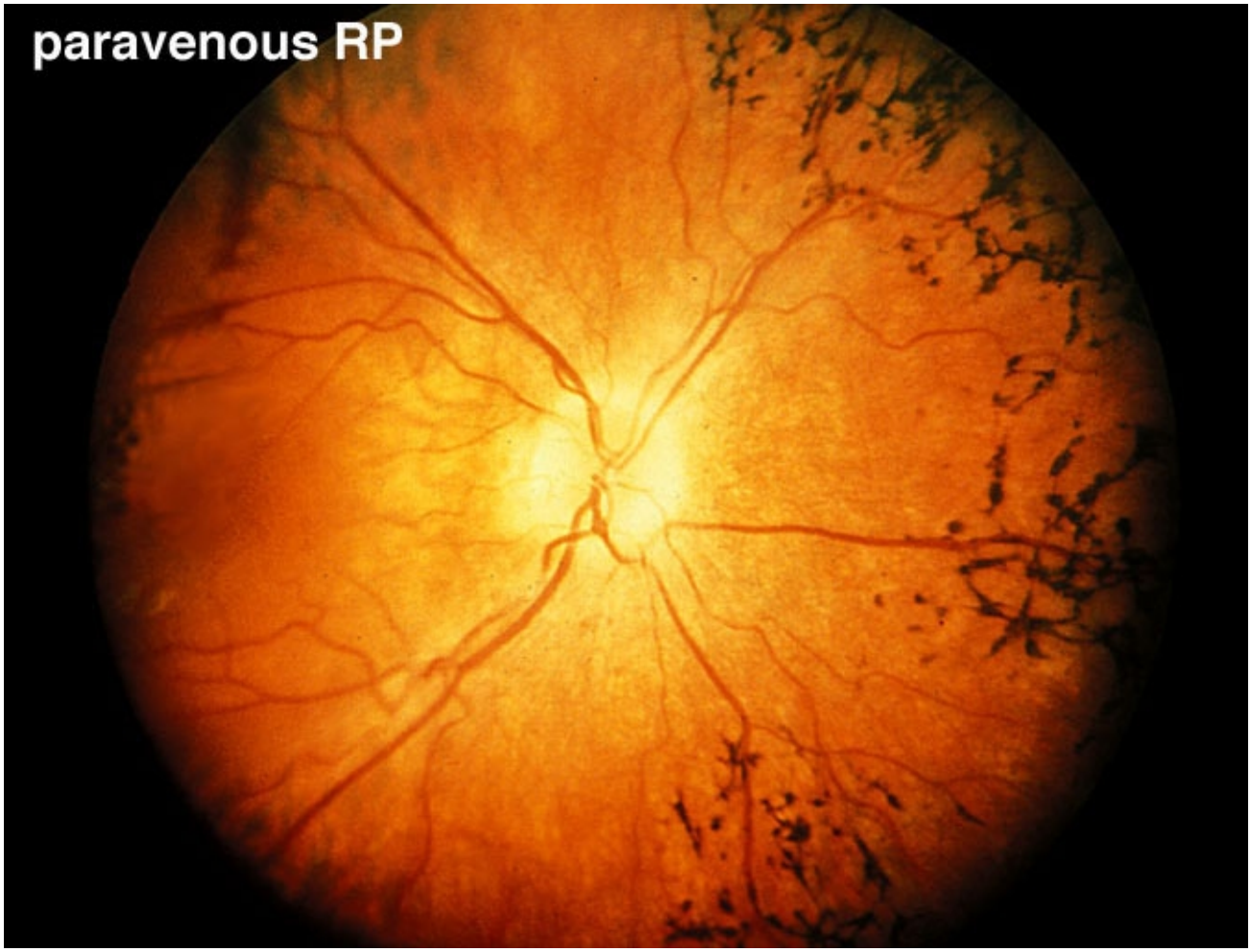

Figure 15. Fundus photo of a patient with paravenous retinitis pigmentosa.

Systemic Disorders and the ERG

Systemic metabolic disorders are reflected in retinal physiology. Liver and kidney disease and drugs that affect those organ systems, usually reduce ERG b-wave amplitudes, particularly in scotopic dim flash ERGs. For example, deferoxamine, an iron-chelating drug used to reduce iron overload, can be toxic to the retina. This is reflected in reduced a- and b-waves of the ERG (Fig. 40).

The Multifocal ERG (mfERG)

A limitation of the traditional global or full-field ERG is that the recording is a massed potential from the whole retina. Unless 20% or more of the retina is affected with a diseased state, the ERGs are usually normal. In other words, a legally blind person with macular degeneration, enlarged blind spot, or other central scotomas will have normal global ERGs.

The most important development in the ERG field in recent years is the multifocal ERG (mfERG) recording system (19). This system allows assessment of ERG activity in small areas of retinal dysfunction. With this method, one can record mfERGs from hundreds of small retinal areas (100 μm) simultaneously in less than 10 minutes per eye (20). A bipolar Burian speculum contact is usually used to record ERGs from the cornea from a dilated eye. Scotomas of only a couple of millimeters in diameter can be mapped, and the extent of retinal dysfunction can be quantified very accurately.

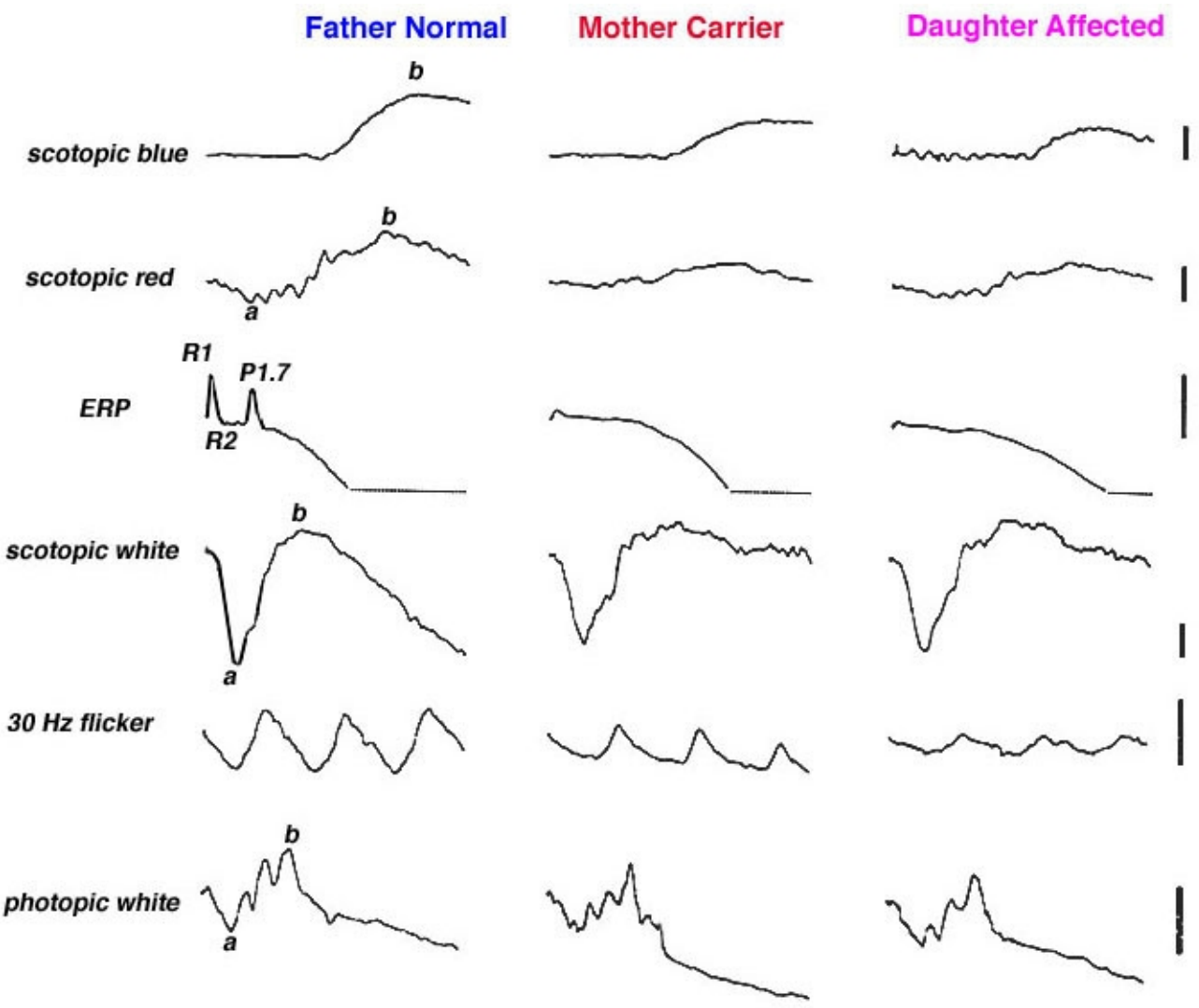

Figure 16. ERG of a family with a child with myotonic dystrophy.

Below are the mfERGs of a patient tested at the Moran Eye Center (Fig. 41b and Fig. 42). The patient is an elderly woman with macular degeneration. The fundus photograph of another patient with age-related macular degeneration (AMD) is seen in Fig. 41a. In Fig. 41b are 103 multifocal ERGs from approximately the central 50 degrees of retinal field. In Fig. 42 are the b-wave voltages from these 103 locations transformed into a 3-D color plot. The lower far right (Fig. 42) shows a plot of a normal patient for comparison. The top color transformation is the difference between the patient's multifocal ERGs and a normal group, which points out the worst areas of retinal function. Colors reflect standard deviations (S.D.) from average ERG amplitudes. These plots can be rotated from 3-D to 2-D so that they resemble visual field plots.

One of the best uses of mfERGs is for distinguishing between retinal and central etiology of visual problems in patients with no apparent abnormalities in the ocular fundus. These types of patients can include MEWDS (Multiple Evanescent White Dot Syndrome) and AZOOR (acute zonal occult outer retinopathy). Figure 43 is example of 17-year-old male diagnosed with AZOOR associated with a viral prodrome. The mfERGs are clearly showing the retinal abnormalities coincident with the visual field losses (Fig. 43). In contrast, the only visible fundus abnormalities were small, easily overlooked pinpoint hyperfluorescent lesions in Indocyanine Green Chorioangiography (ICG).

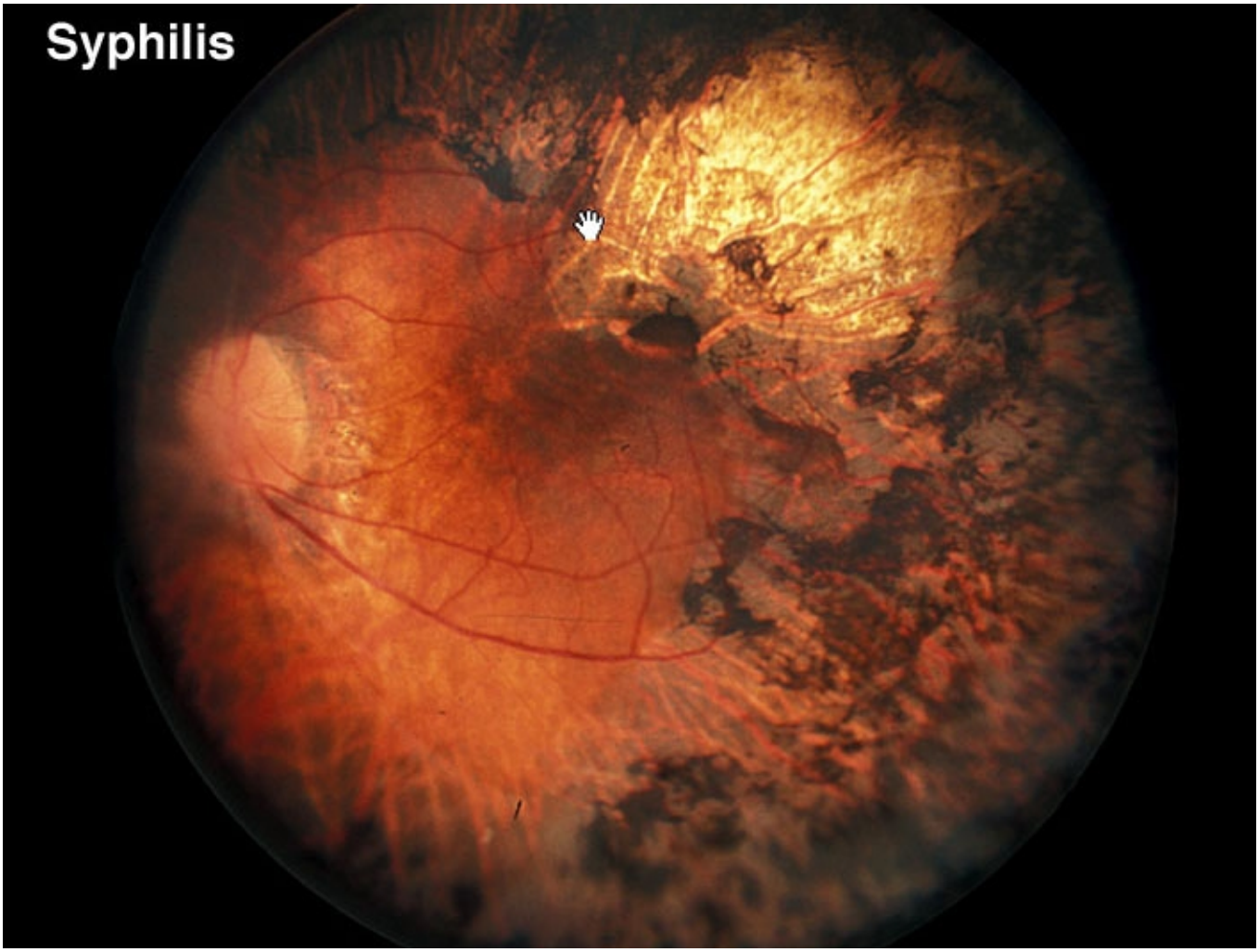

Figure 17. Fundus photo of patient with syphilis.

The mfERG method is a very reliable test and really helps in following the progression of a macular (or other limited retinal area) disorders.

The Electrooculogram (EOG)

The electrooculogram (EOG) measures the potential that exists between the cornea and Bruch's membrane at the back of the eye. The potential produces a dipole field with the cornea approximately 5 millivolts positive compared with the back of the eye, in a normally illuminated room. Although the origin of the EOG is the pigment epithelium of the retina, the light rise of the potential requires both a normal pigment epithelium and normal mid-retinal function. Elwin Marg named the electrooculogram in 1951 (21), and Geoffrey Arden (3) developed the first clinical application. With the cornea constantly positive, movement of the eye produces a shift of this electrical potential. By attaching skin electrodes on both sides of an an eye (Fig. 44), the potential can be measured by having the subject move his or her eyes horizontally a set distance (Fig. 45). The eyes are usually dilated. Skin electrodes are attached near the lateral and medial canthus of each eye (Fig. 44). A ground electrode is attached usually to either the forehead or earlobe. It is helpful, but not necessary, that the patient have a chin rest to reduce head movement. Either inside a Ganzfeld, or on a screen in front of the patient, small red fixation lights are place 30 degrees apart (Fig. 46). The distance the lights are separated is not critical for routine testing. Any set distance subtending from 20 to 40 degrees of visual angle is satisfactory.

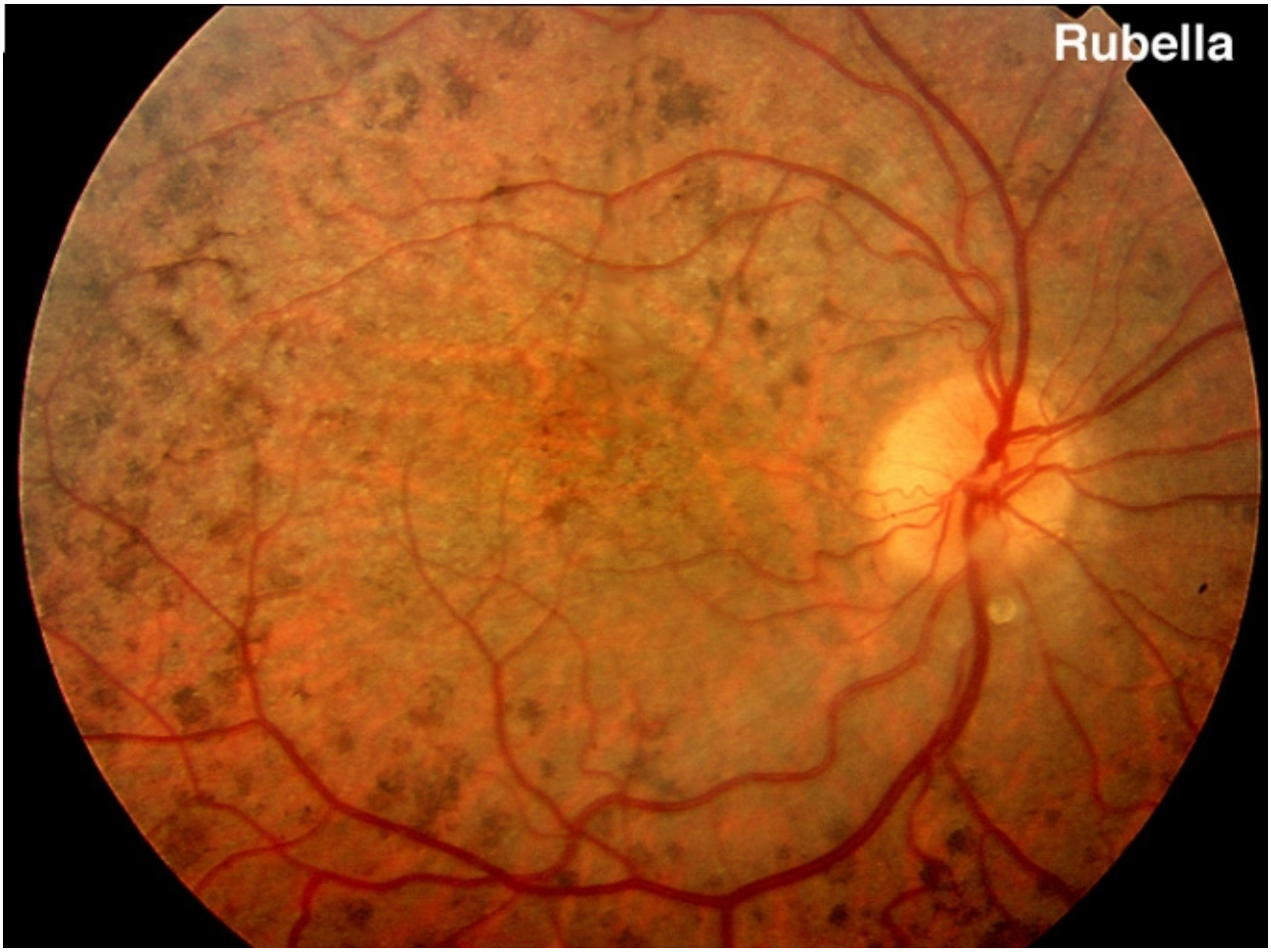

Figure 18. Fundus photo of patient with rubella.

The patient should be light adapted such as in an well-illuminated room, and their eyes dilated. After the electrodes are attached, the procedure is explained and the patient is asked to practice several times while baseline data are recorded. The procedure is simply that the patient keeps his or her head still while moving the eyes back and forth, alternating between the two red lights. The movement of the eyes produces a voltage swing of approximately 5 millivolts between the electrodes on each side of the eye, which is charted on graph paper or stored in the memory of a computer. In Fig. 47 are 10-sec periods of eye movement back and forth between two red LED lights placed 30 degrees apart inside a Ganzfeld.

After training the patient in the eye movements, the lights are turned off. About every minute, a sample of eye movement is taken as the patient is asked to look back and forth between the two lights (Fig. 47). Some laboratories have the patients move their eyes the entire testing period. After 15 minutes, the lights are turned on, and the patient is again asked about once a minute to move his or her eyes back and forth for about 10 sec. The top of Fig. 48 shows segments of eye movement that have been cut from 10-sec samples from a normal person. The chart (Fig. 48) graphs the change in voltage in the eye through 15 minutes of dark adaptation and 15 minutes of bright light. Typically, the voltage becomes a little smaller in the dark, reaching its lowest potential after about 8-12 minutes, the so-called "dark trough." When the lights are turned on, the potentials rise, and the light rise reaches its peak in about 10 minutes. When the size of the "light peak" is compared with the "dark trough", the relative size should be about 2:1 or greater (Fig. 48). A light:dark ratio of less than about 1.7 is considered abnormal. Fig. 49 shows an abnormal response recorded from a patient with Best's disease.

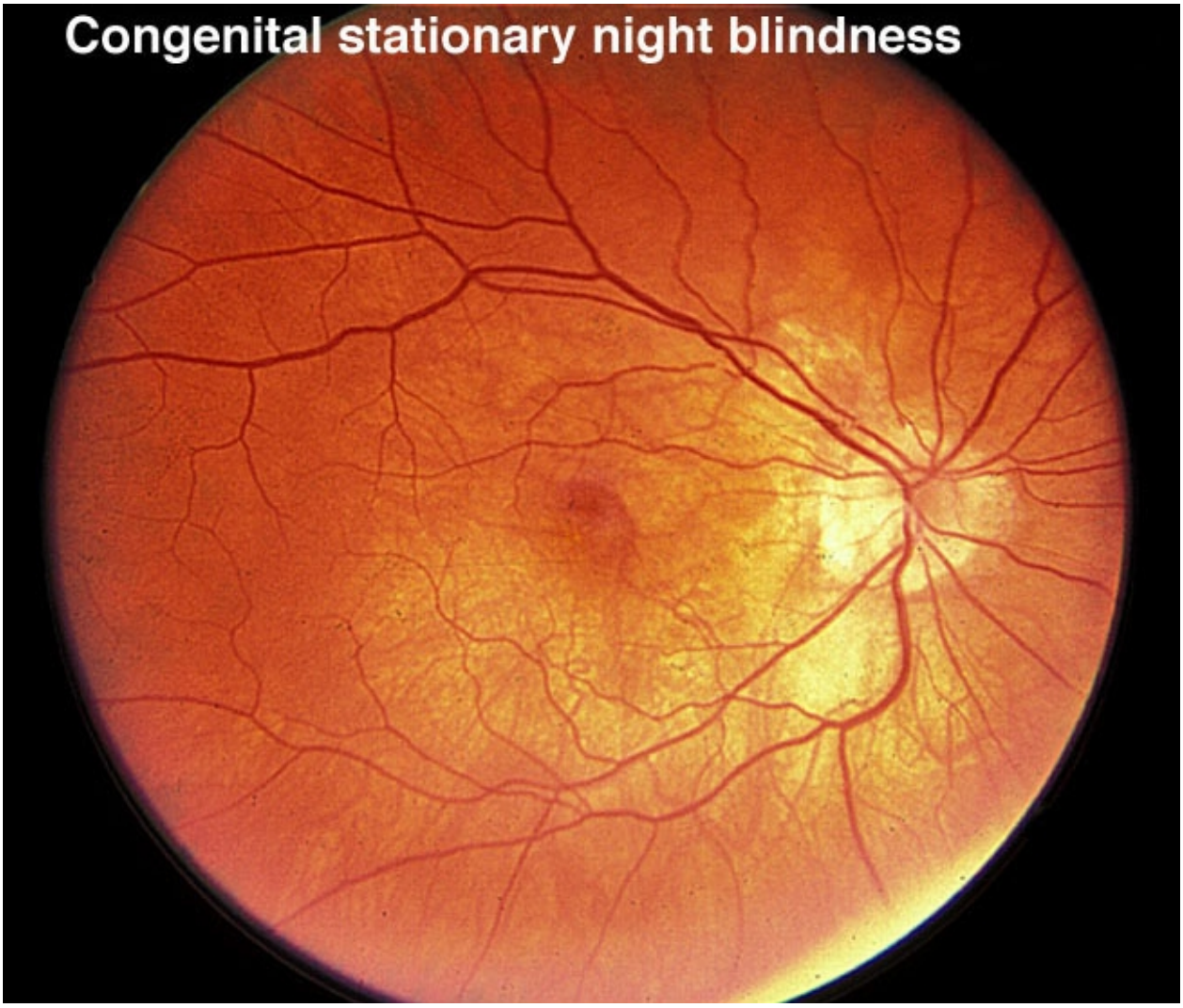

Figure 19. Fundus photo of patient with CSNB type 2.

The EOG is redundant with the ERG in most retinal disorders. Retinal diseases producing an abnormal EOG will usually have an abnormal ERG, which is the better test for analysis of scotopic and photopic measures. The most common use of the EOG is to confirm Best's disease. Best's vitelliform macular dystrophy and variants of this disease are usually identified by the appearance of a retinal lesion resembling an egg yolk early in the disease (Fig. 50). In vitelliform macular dystrophy (Fig. 51), the ERG will be normal but the EOG will be abnormal.

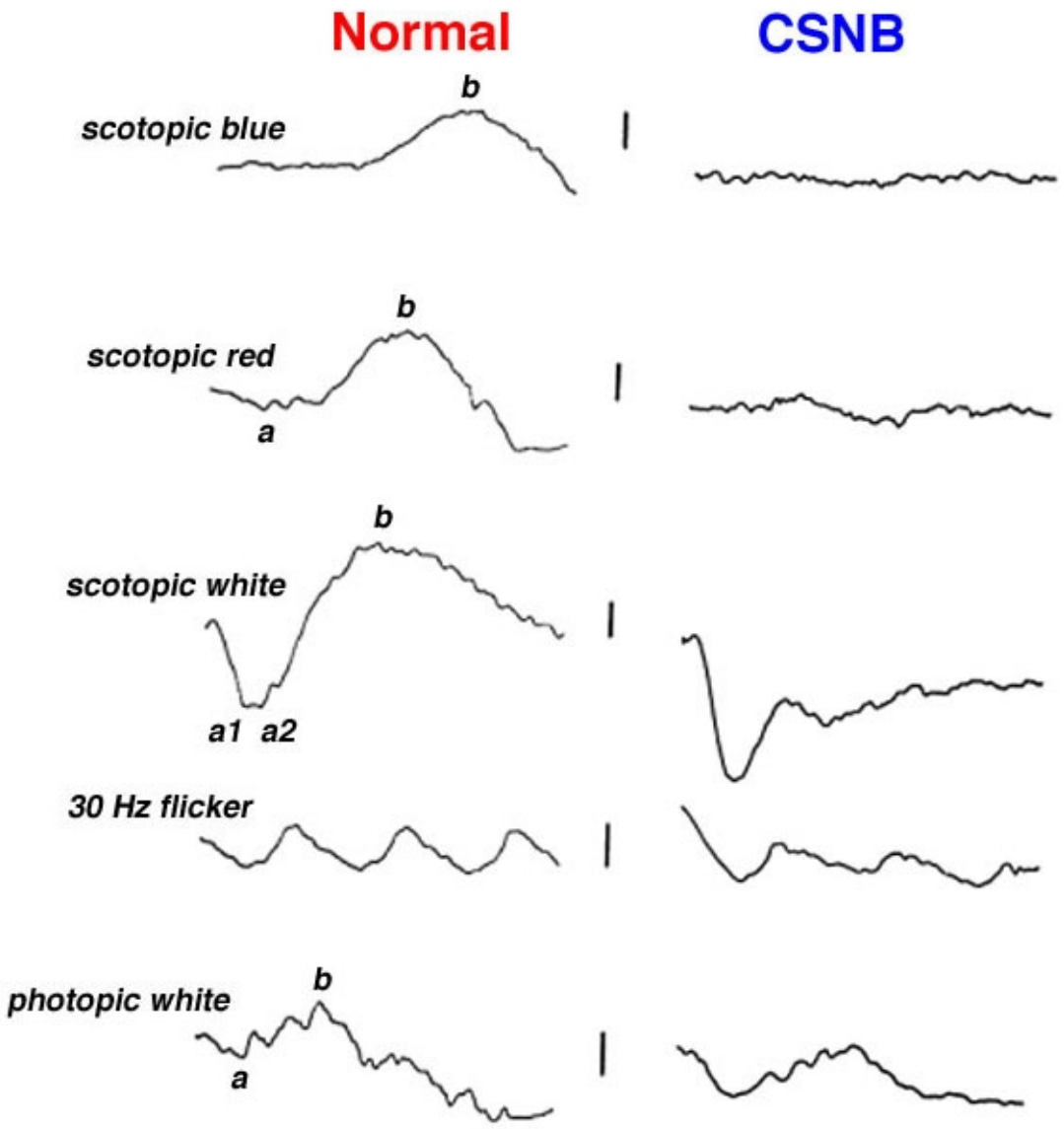

Figure 20. ERGs in a patient with CSNB type 2.

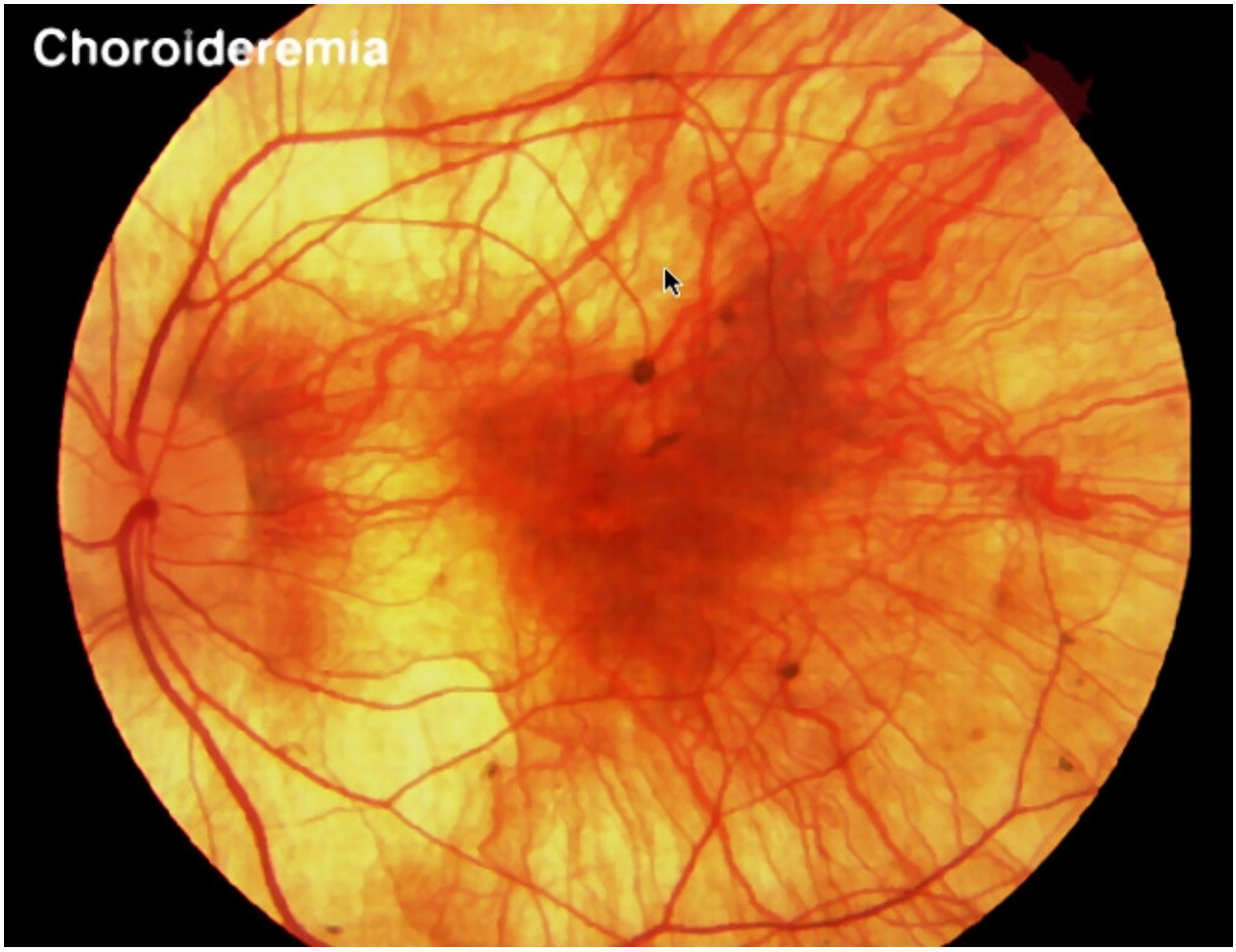

Figure 21. Fundus photo of patient with choroideremia.

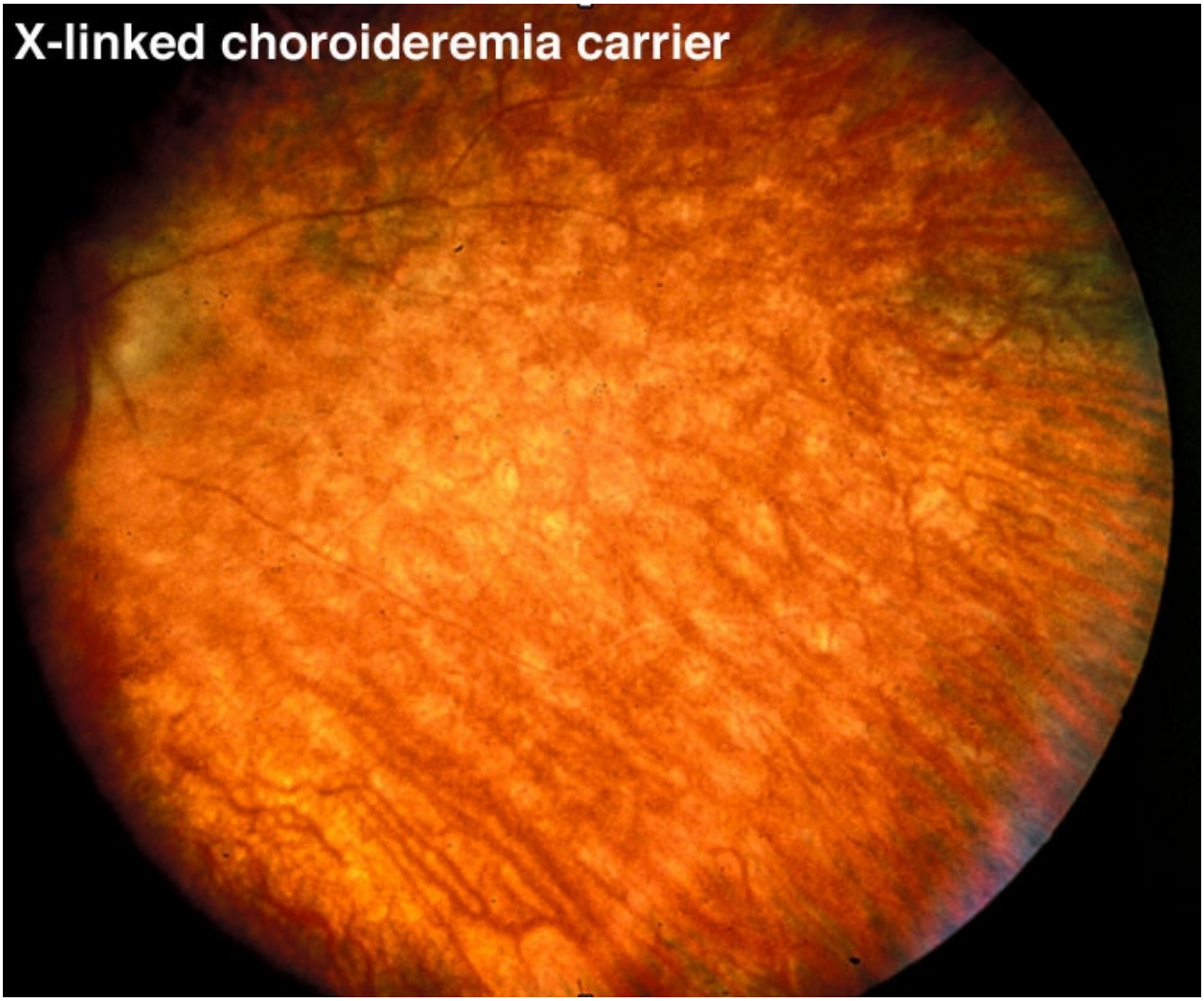

Figure 22. Fundus photo of a patient with X-linked choroideremia carrier.

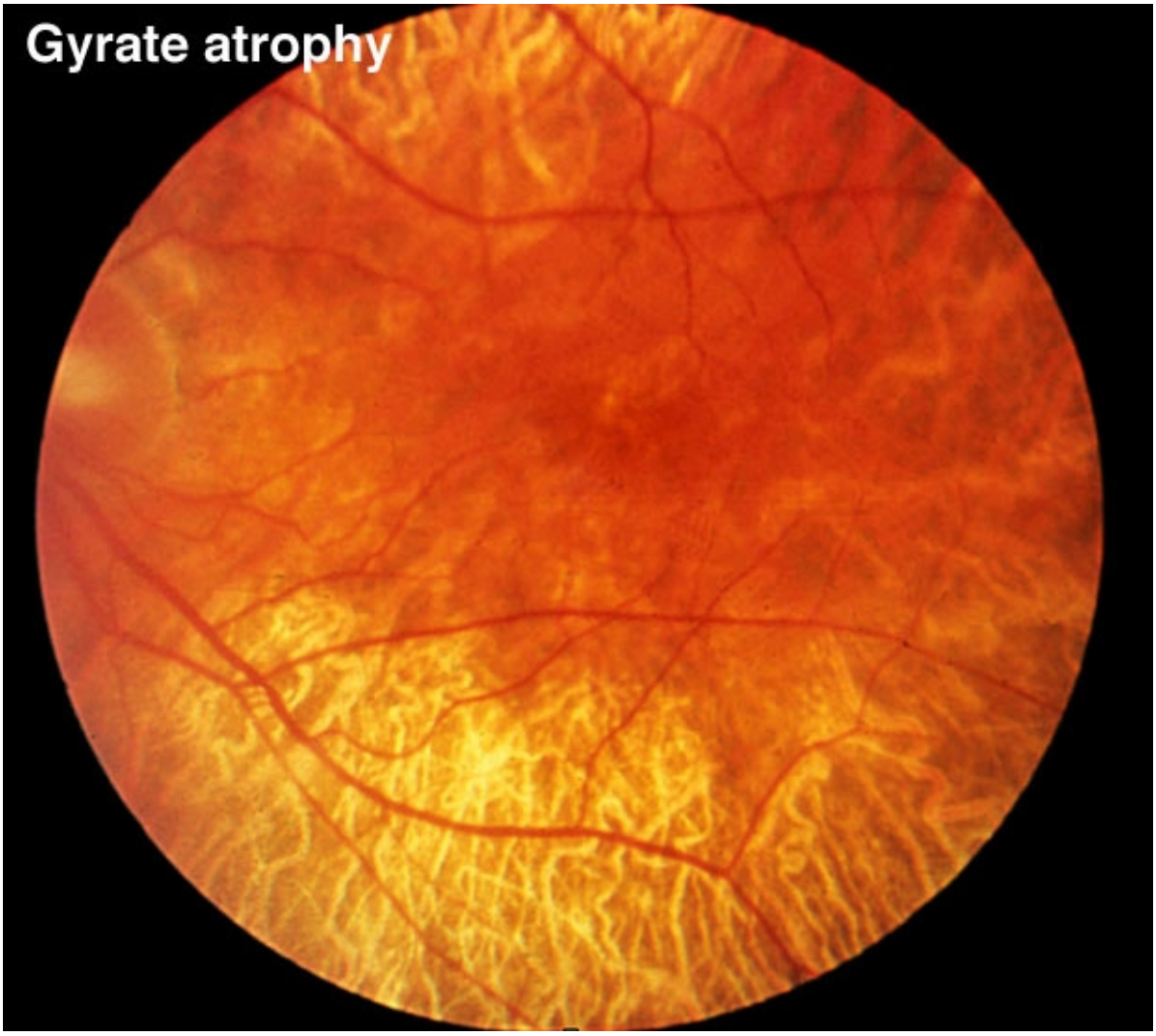

Figure 23. Fundus photo of a patient with gyrate atrophy.

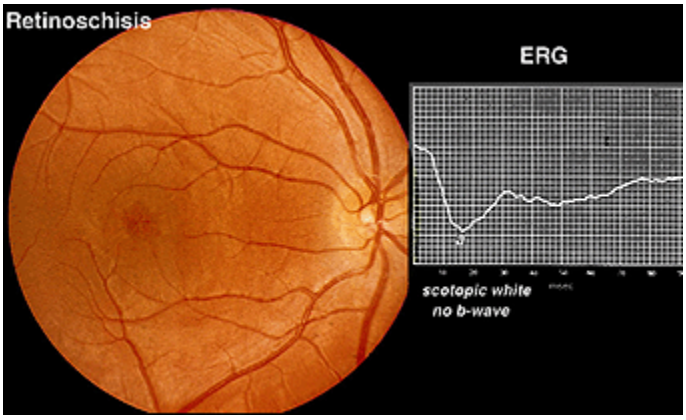

Figure 24. Fundus photo and bright-flash ERG of patient with retinoschisis.

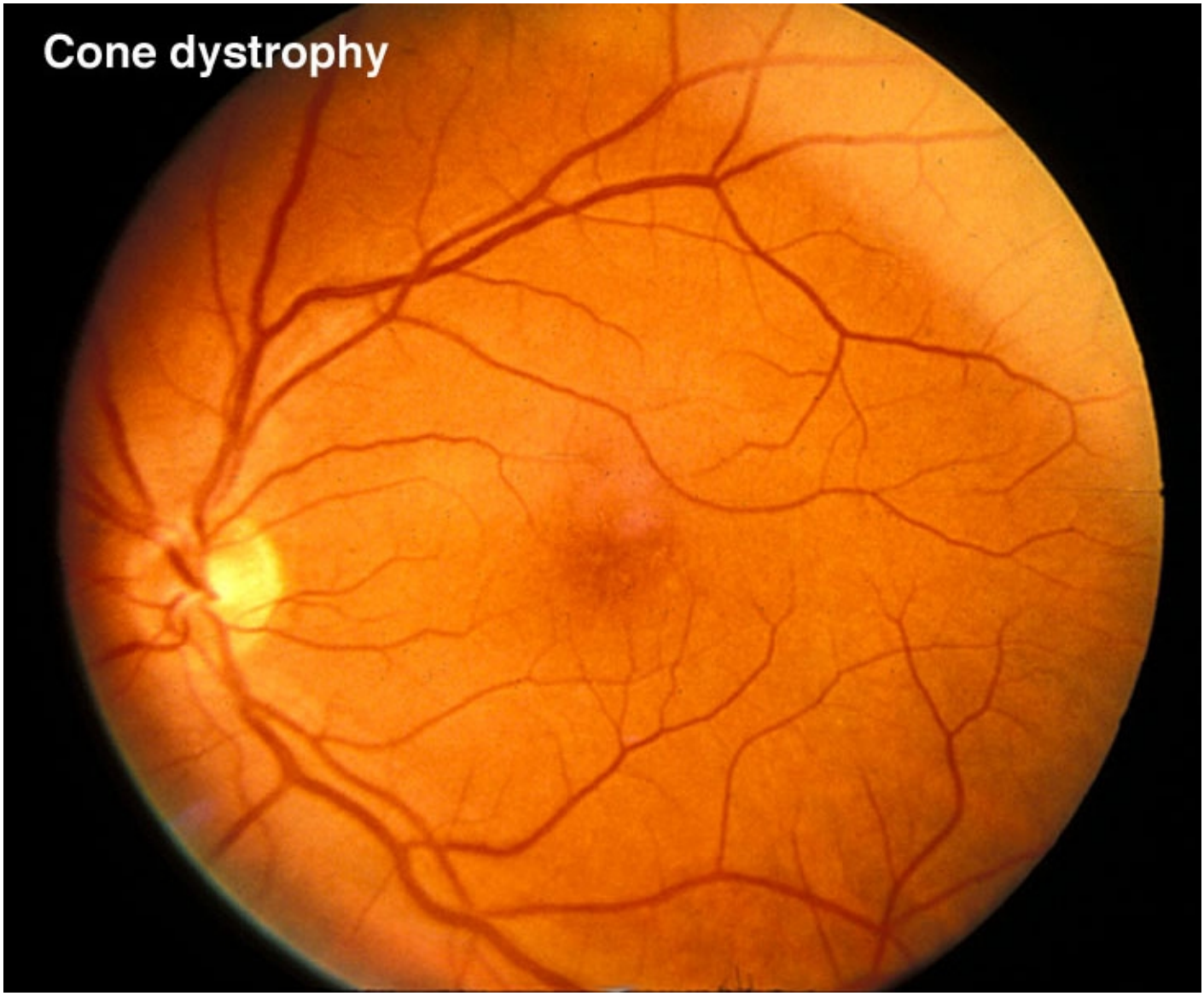

Figure 25. Fundus photo of patient with cone dystrophy.

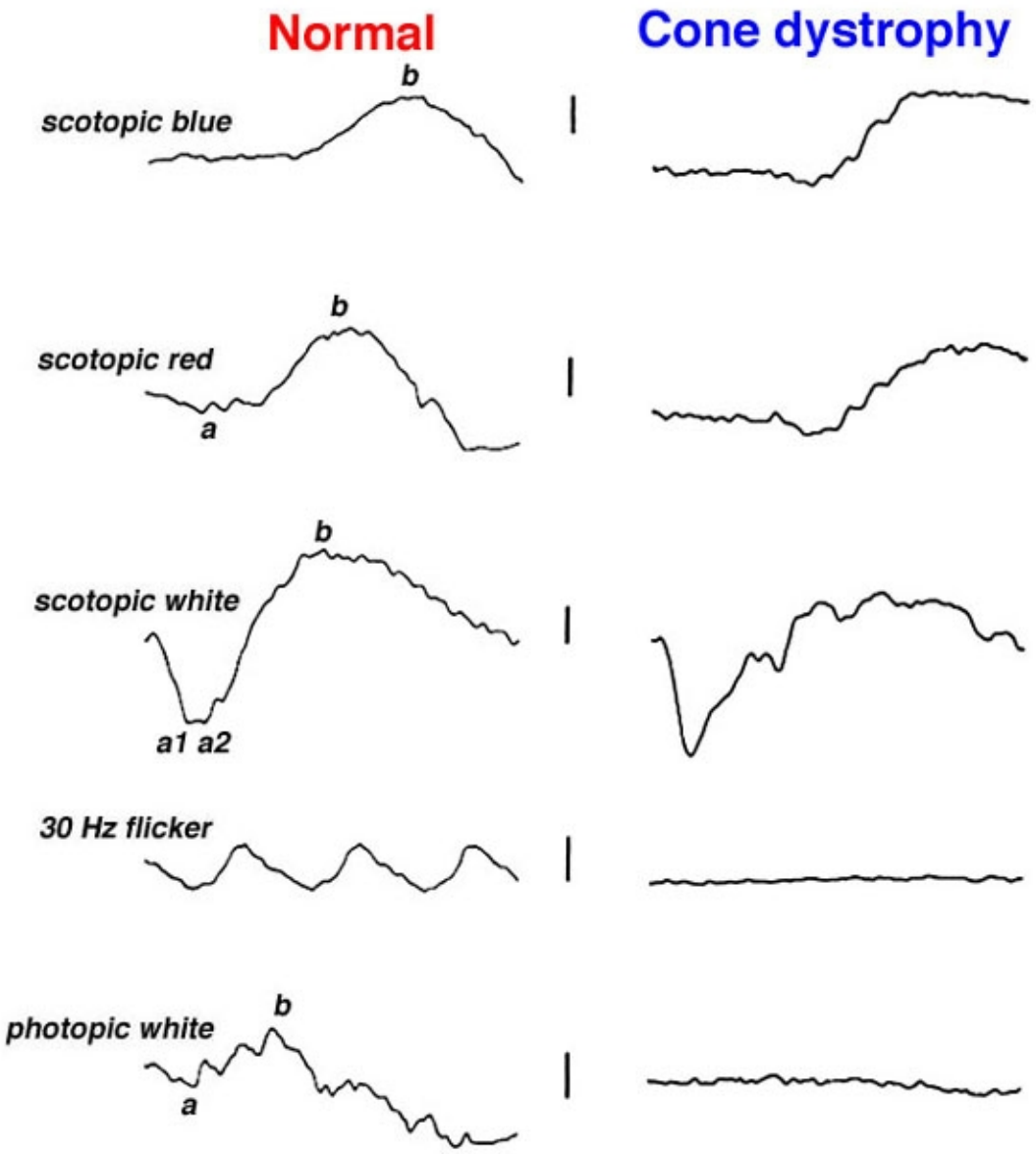

Figure 26. ERGs in a patient with cone dystrophy.

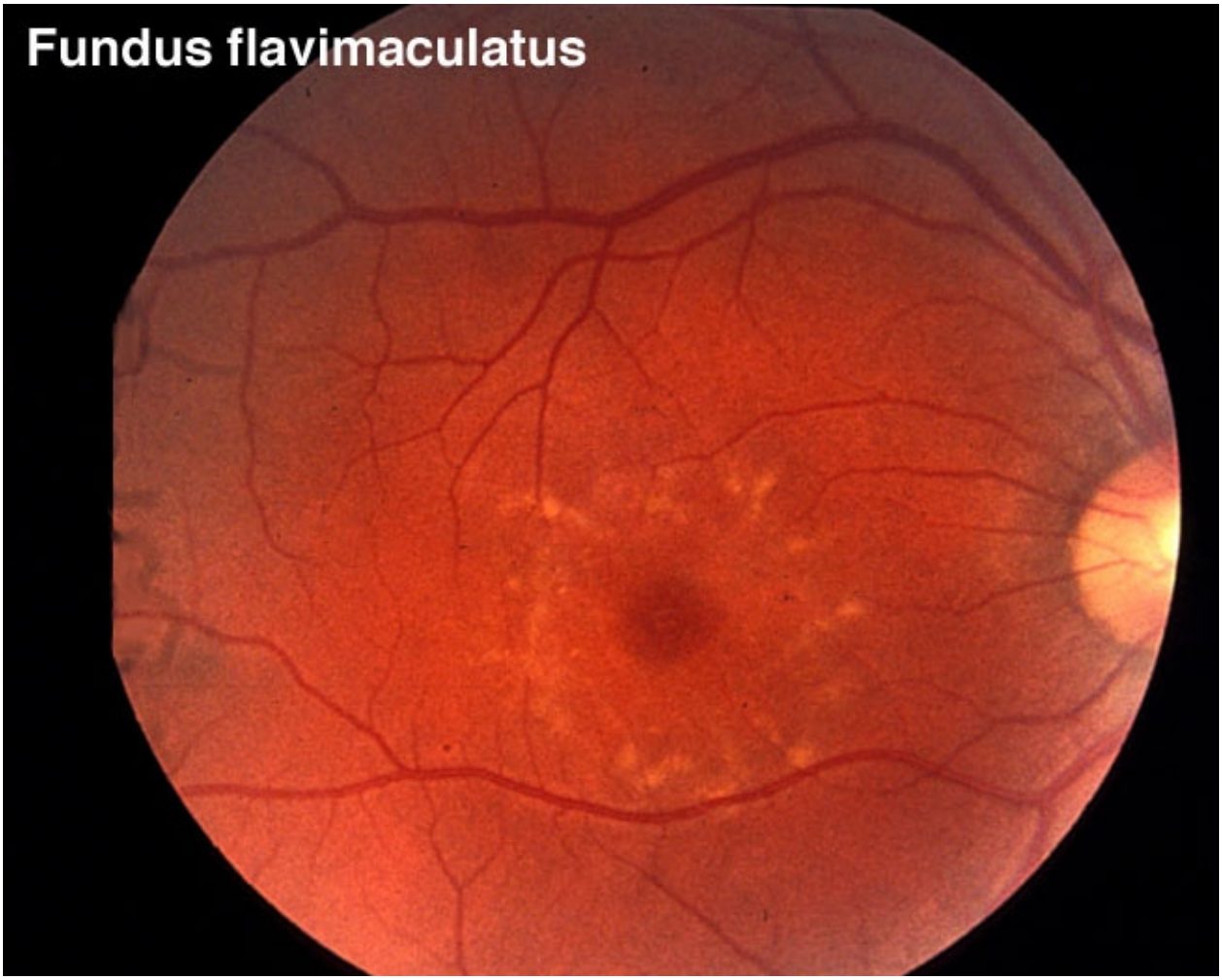

Figure 27. Fundus photo of patient with fundus flavimaculatus.

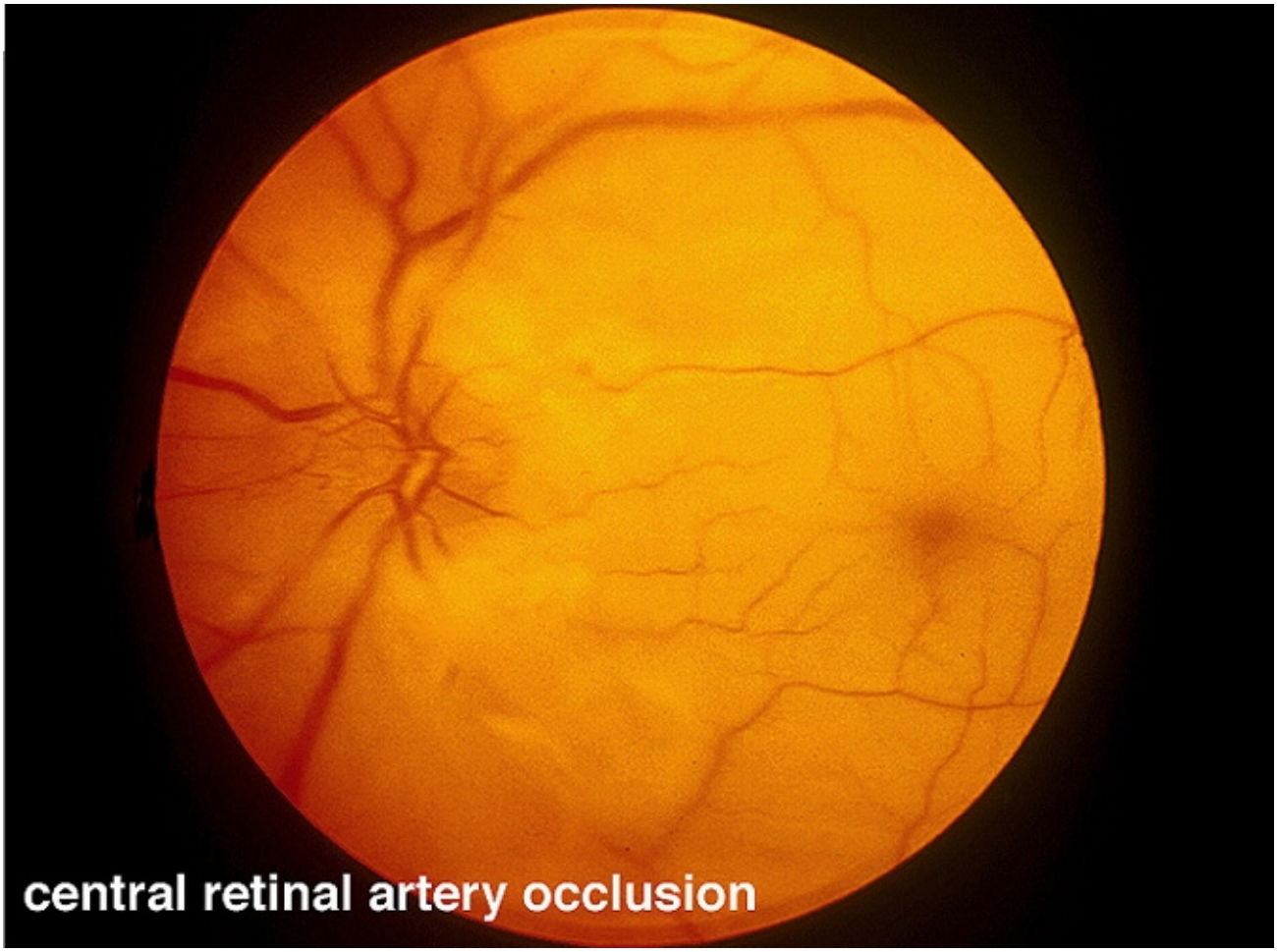

Figure 28a. Fundus photo of patient with central retinal artery occlusion.

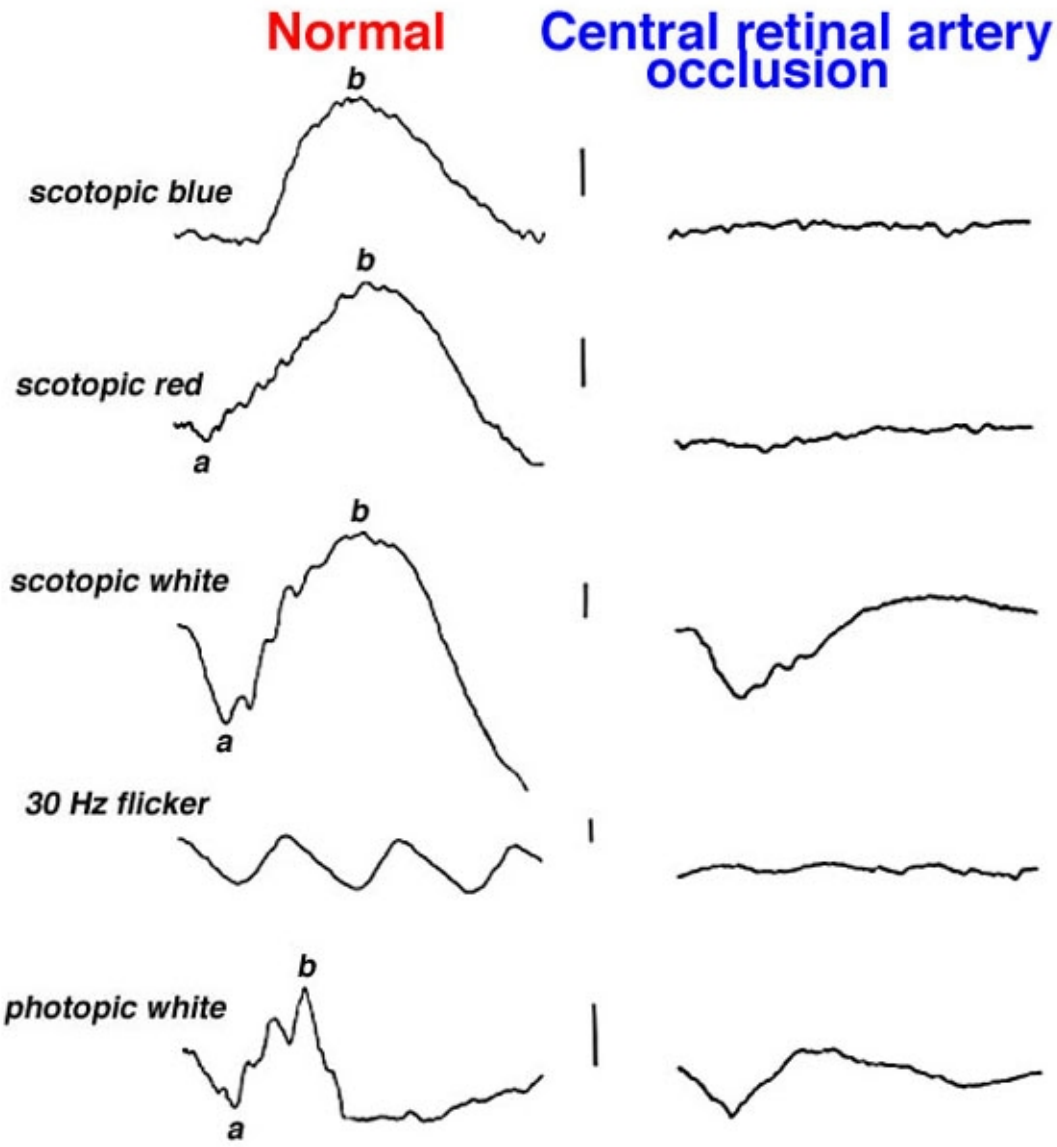

Figure 28b. ERGs in a patient with central retinal artery occlusion.

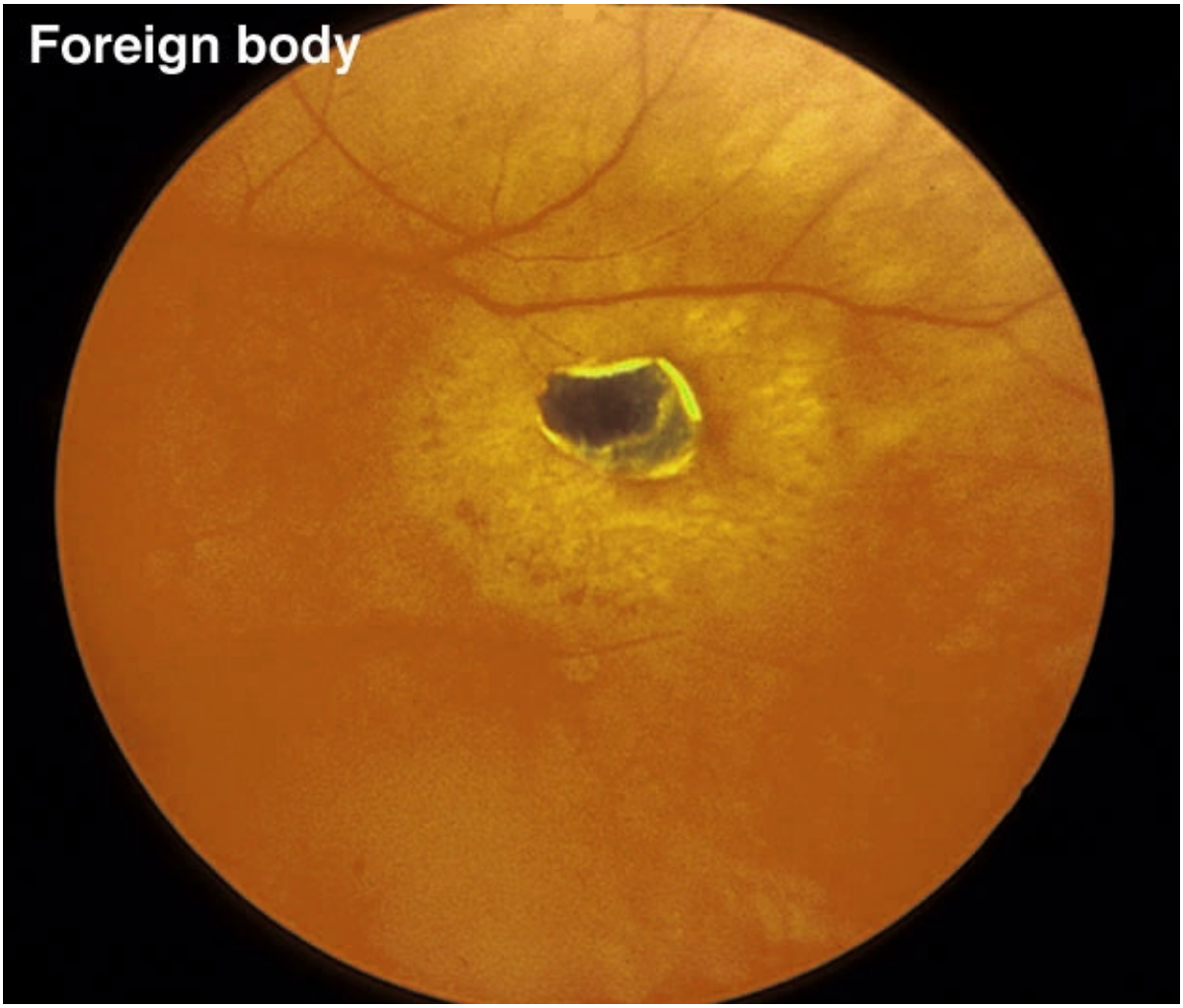

Figure 29. Fundus photo of a patient with a hole in the retina caused by a metallic foreign body.

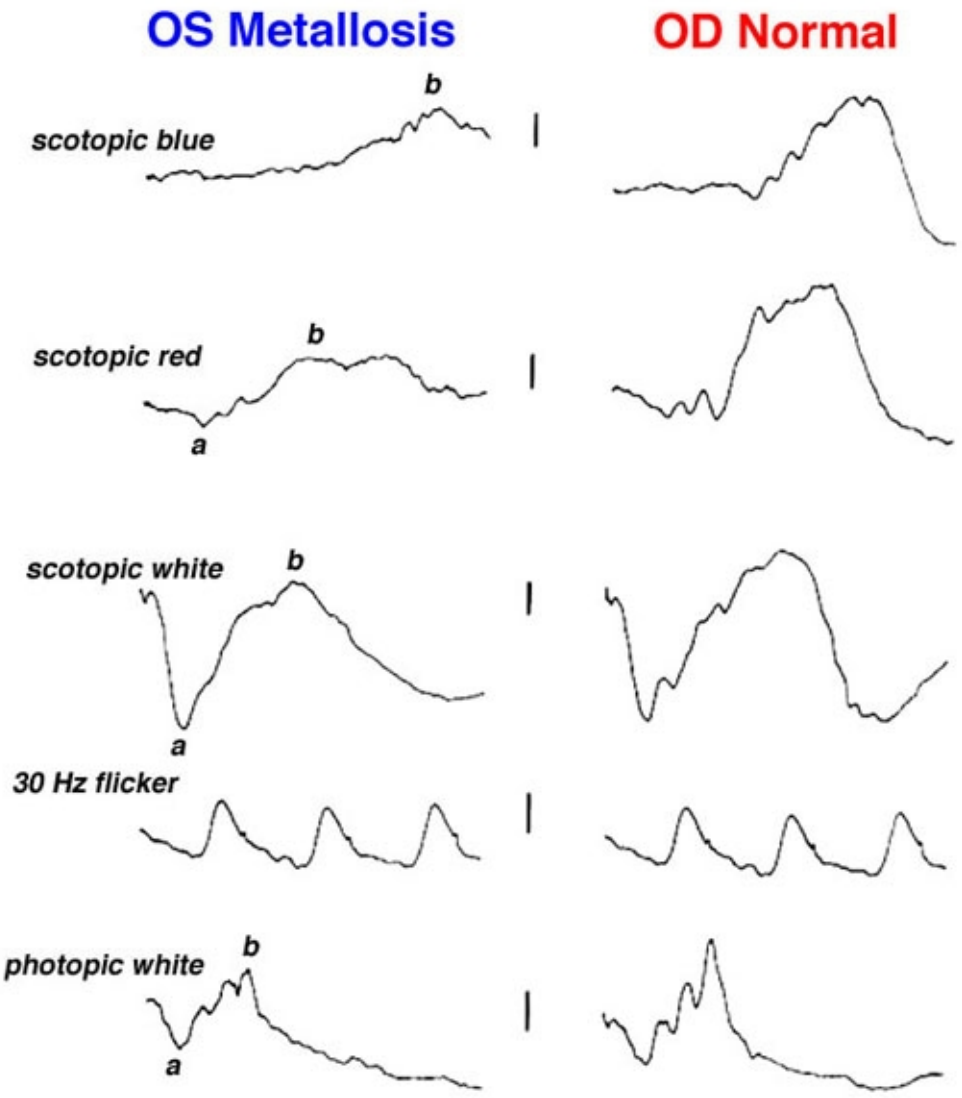

Figure 30a. The effect of the foreign body on the ERG waveform.

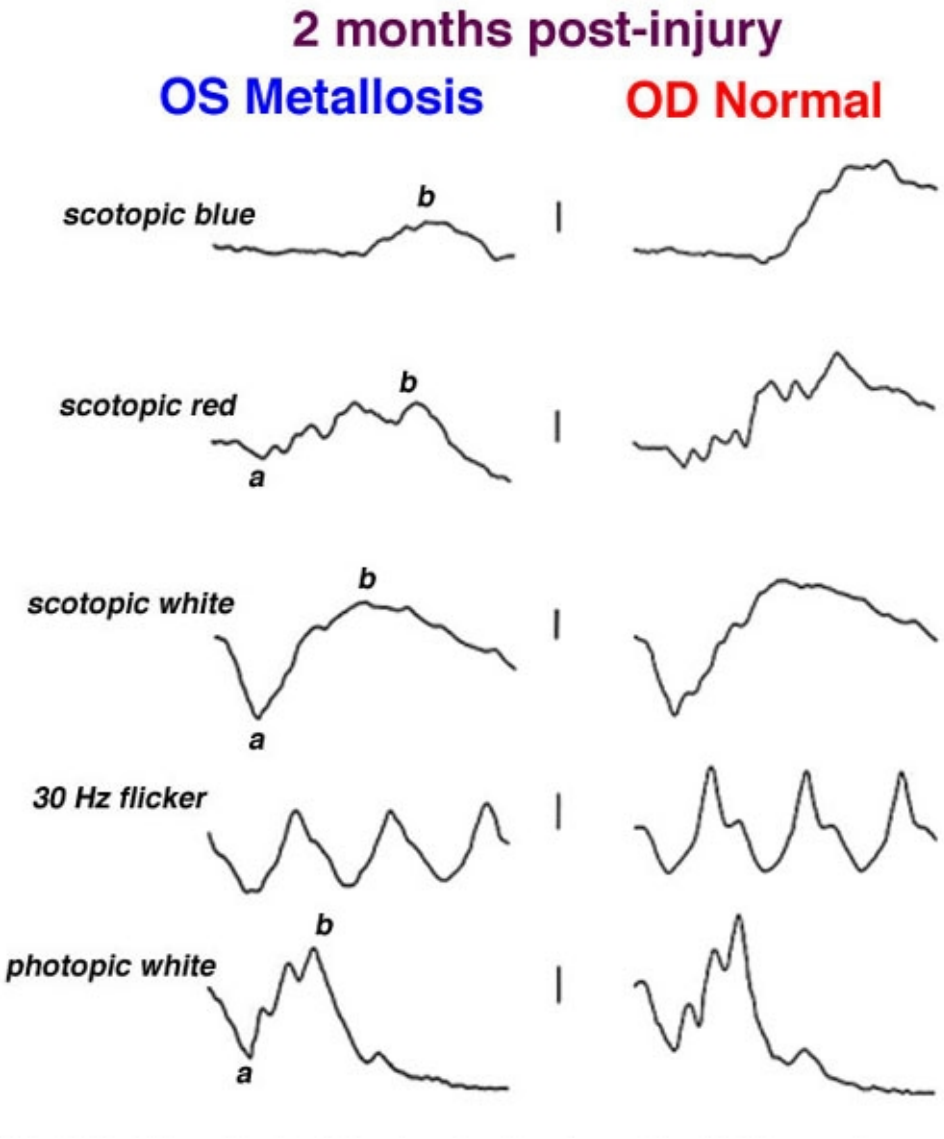

Figure 30b. The effect of the foreign body on the ERG waveform some weeks later.

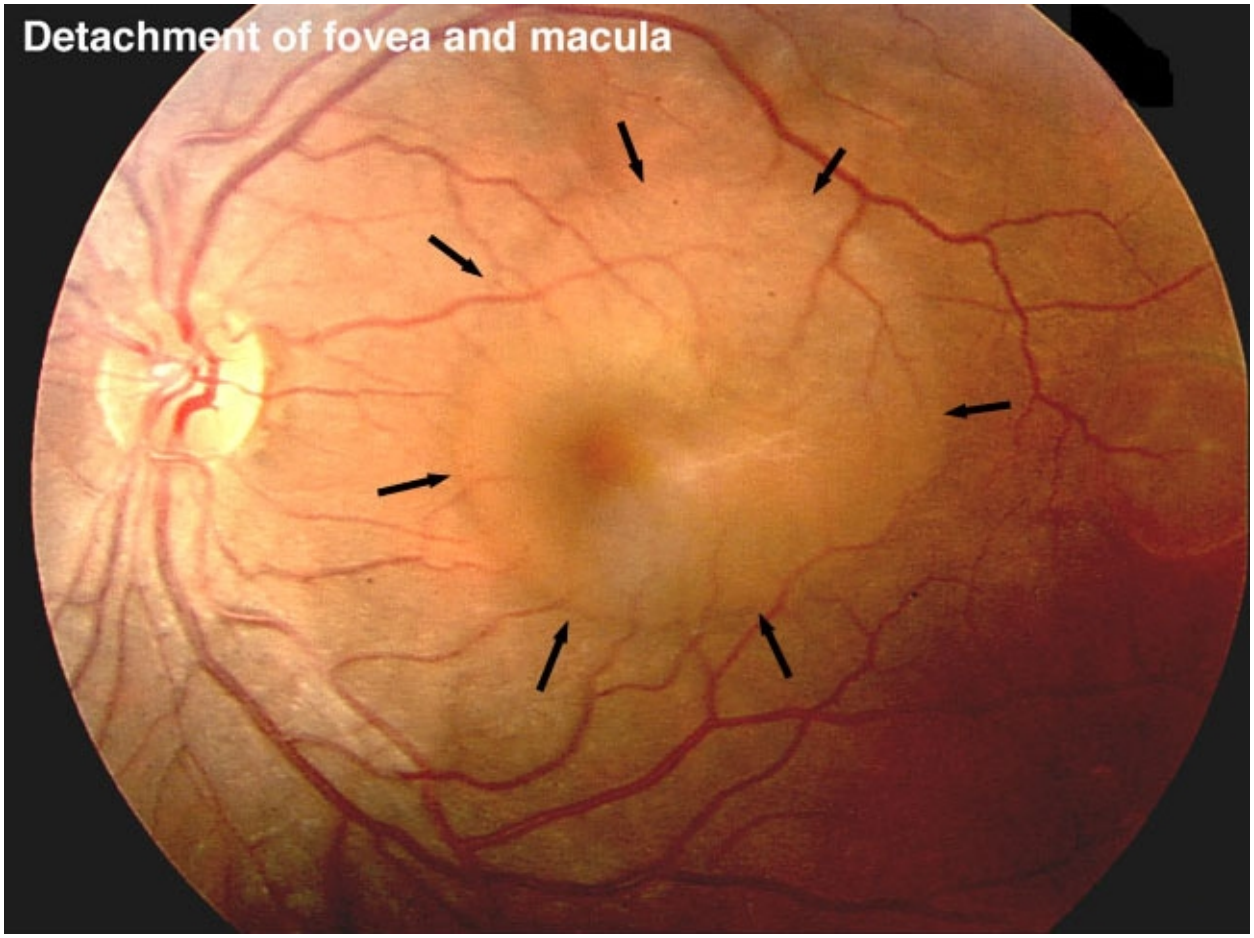

Figure 31a. Fundus photo of a patient with a retinal detachment at the fovea and macula in one eye.

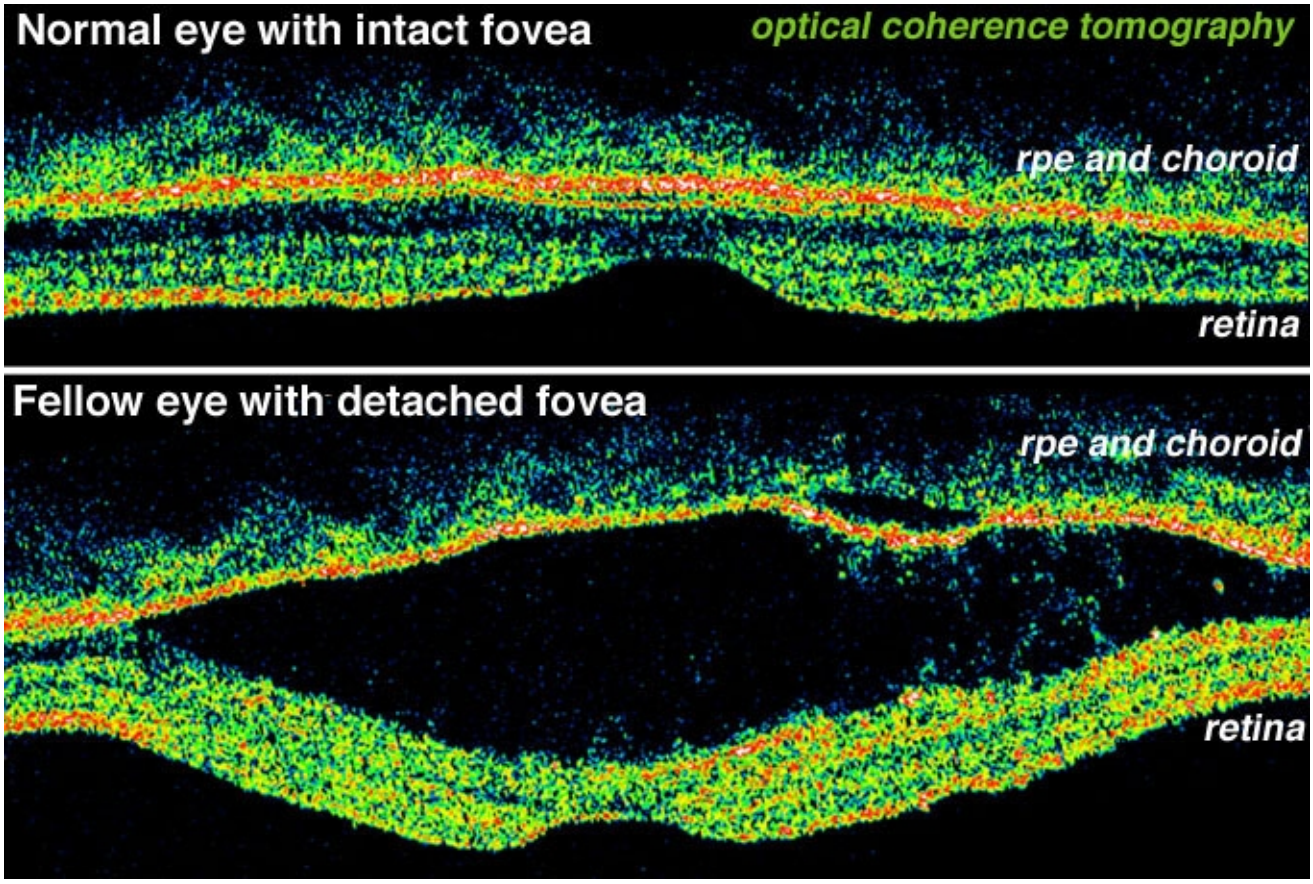

Figure 31b. Optical coherence tomography (OCT) images of the patient's normal macula and of the retina in the other eye with the macular detachment.

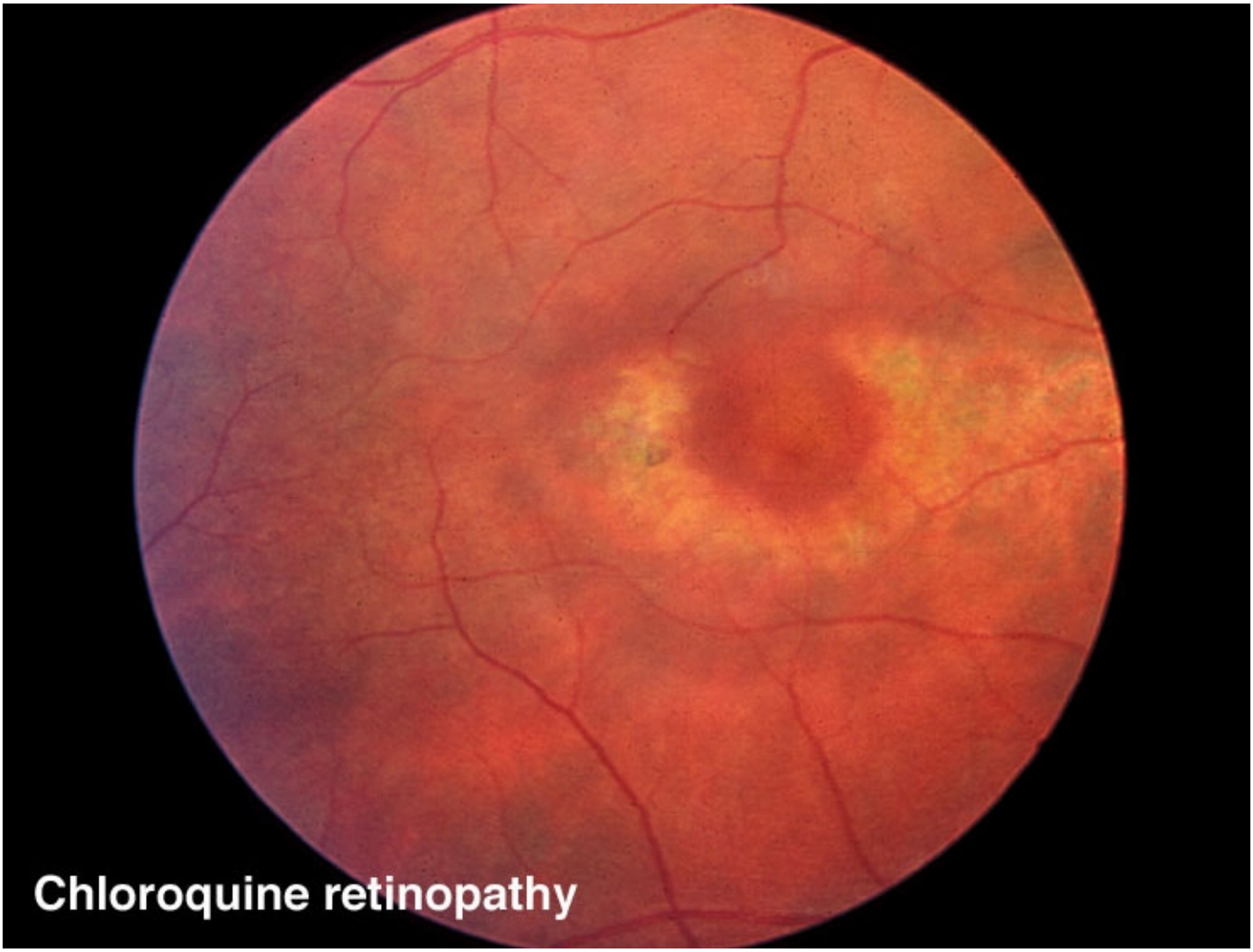

Figure 32. Fundus photo of patient with chloroquine retinopathy.

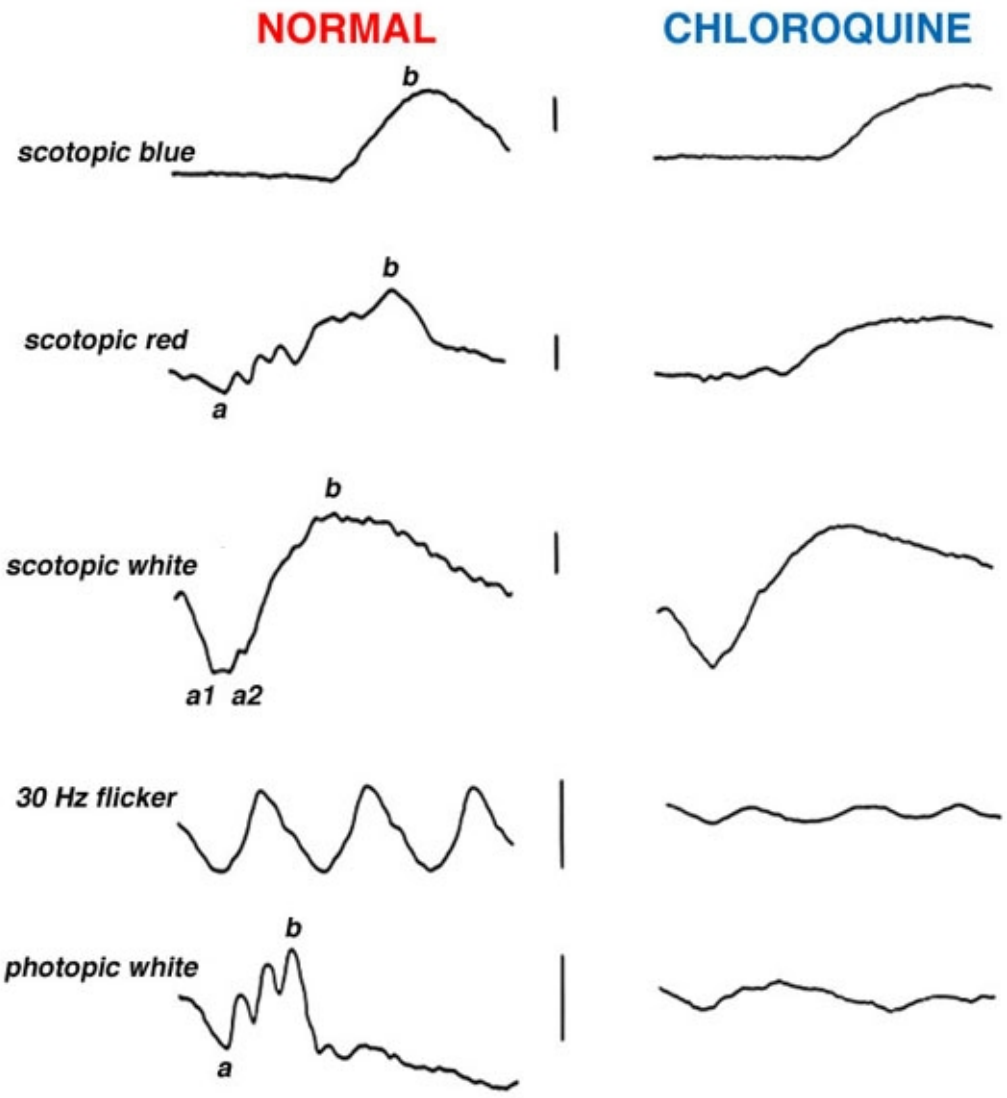

Figure 33. ERGs in a patient with chloroquine retinopathy.

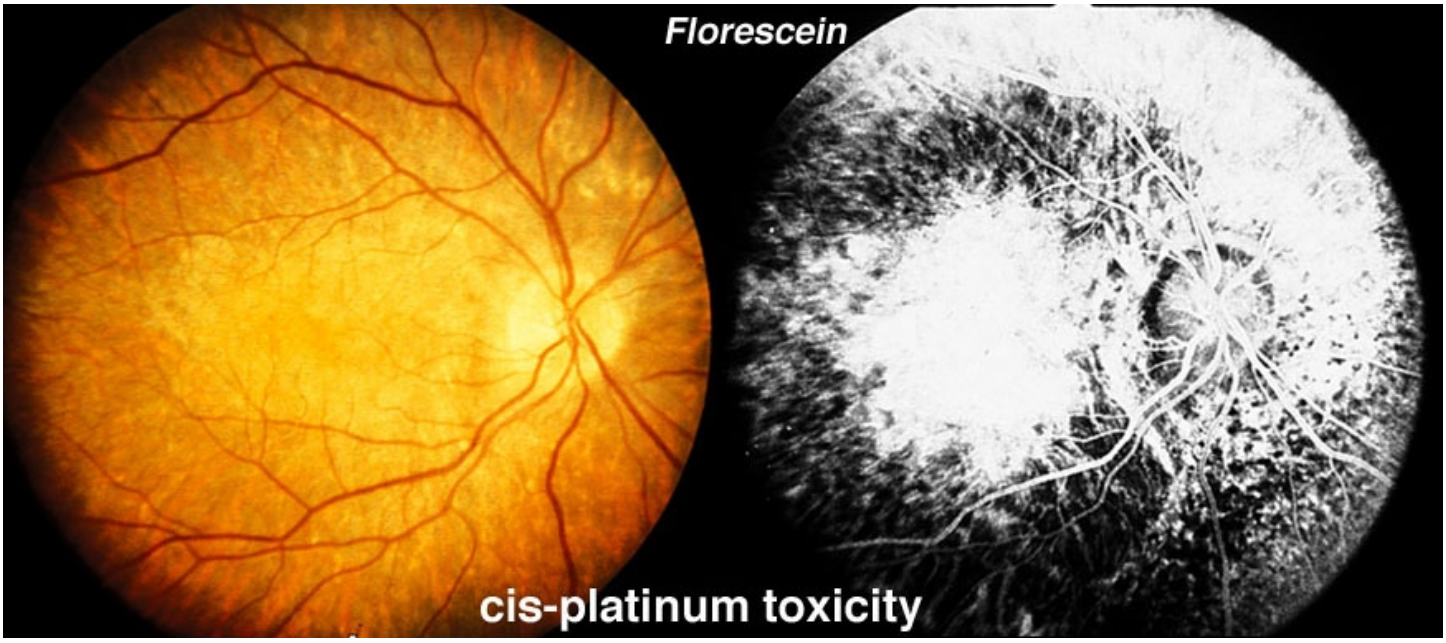

Figure 34. Fundus photo of patient with OD cisplatinum toxicity.

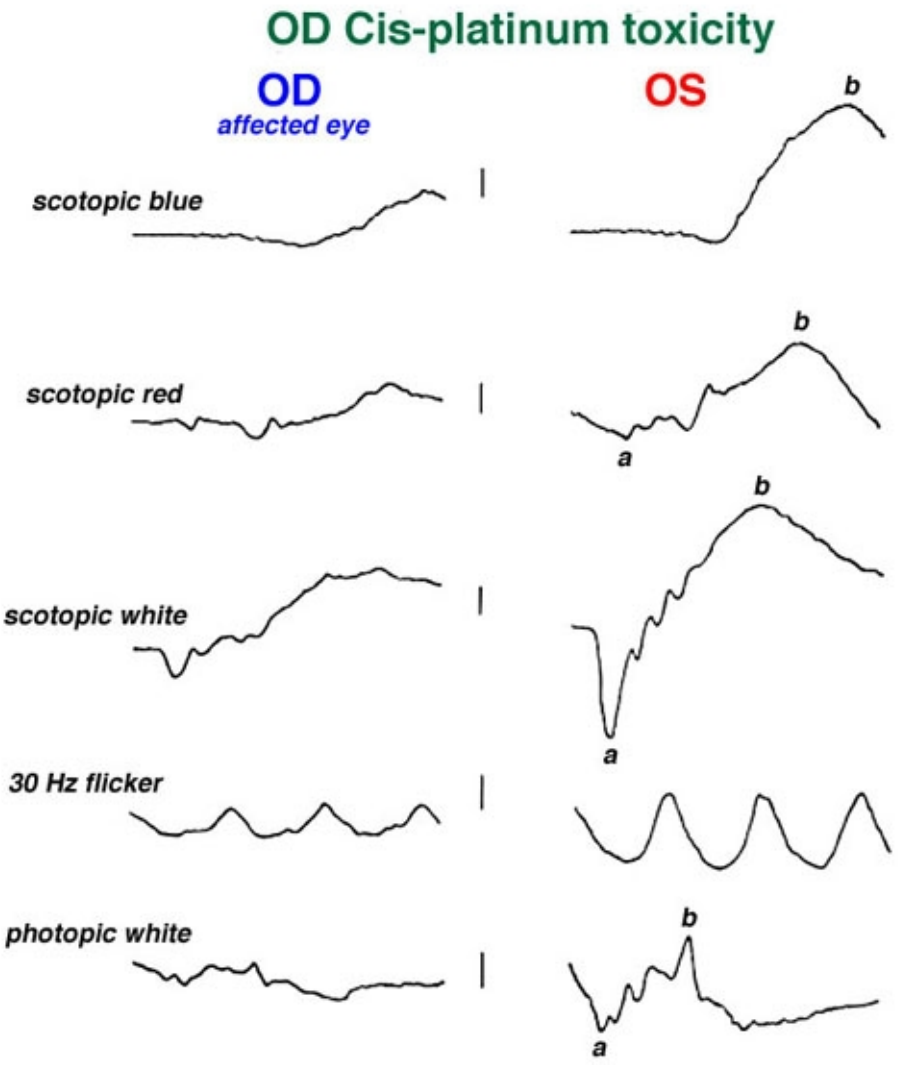

Figure 35. ERGs in a patient with OD cisplatinum toxicity.

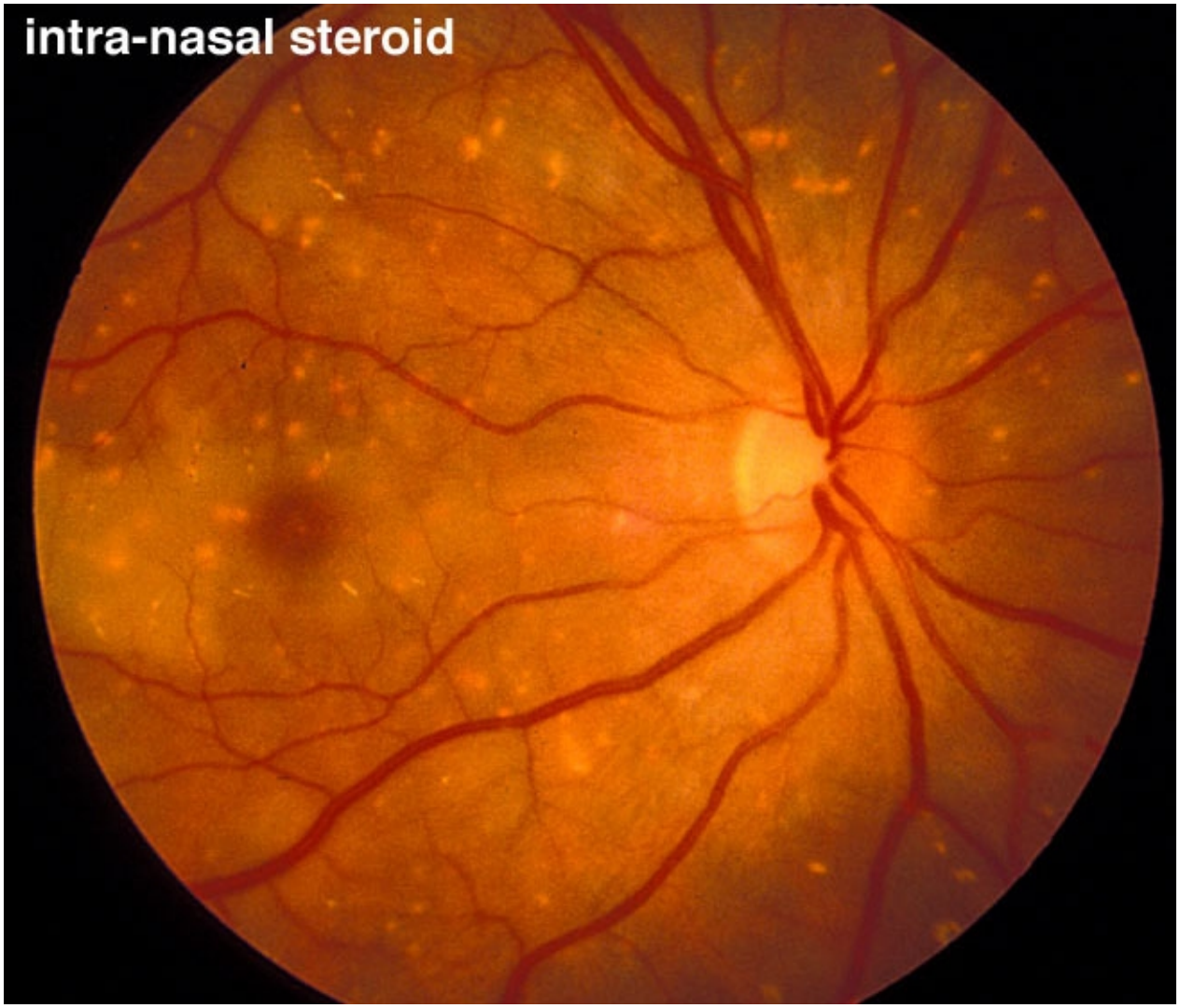

Figure 36. Fundus photo of patient with steroid retinopathy.

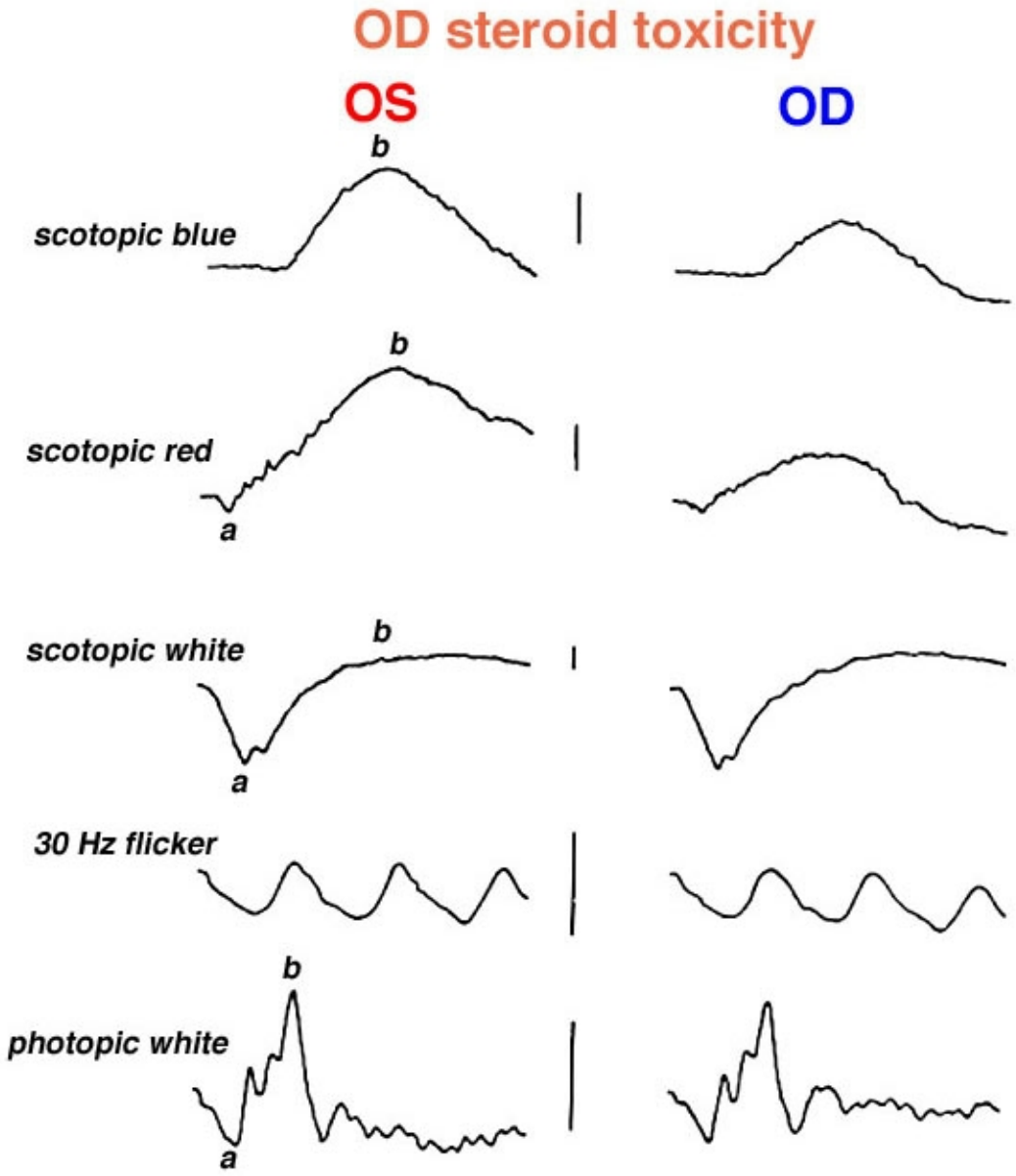

Figure 37. ERGs in a patient with steroid retinopathy.

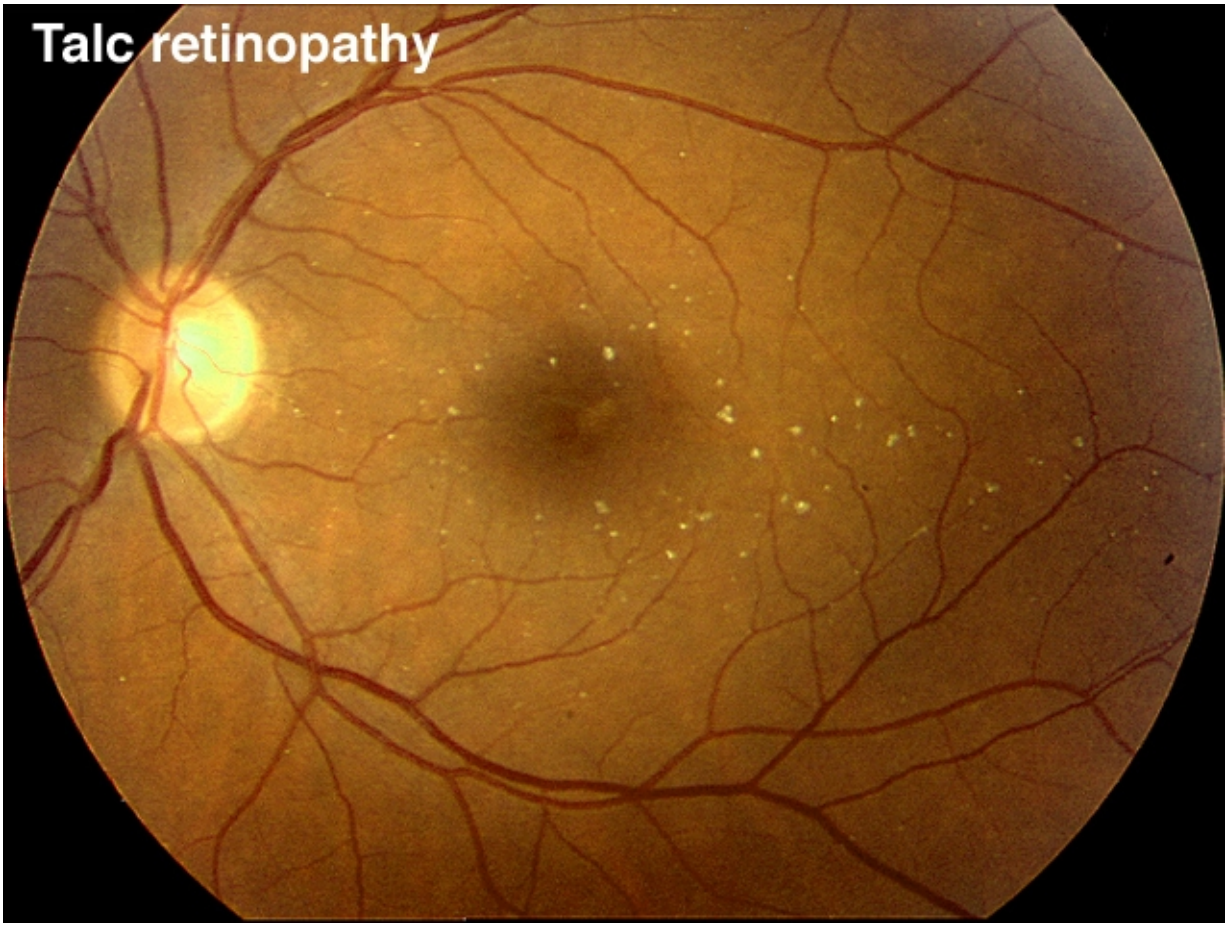

Figure 38. Fundus photo of patient with talc retinopathy.

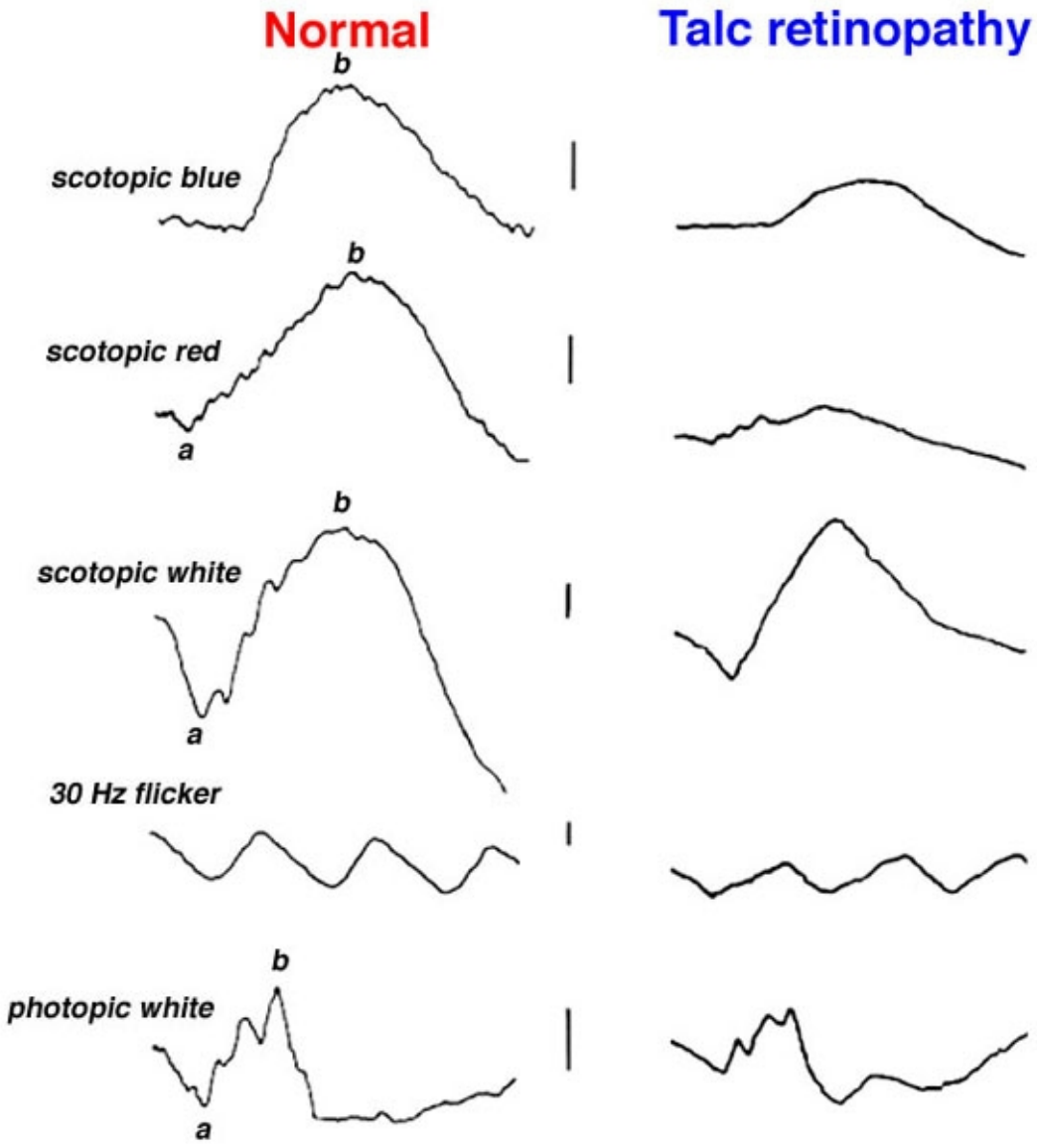

Figure 39. ERGs in a patient with talc retinopathy.

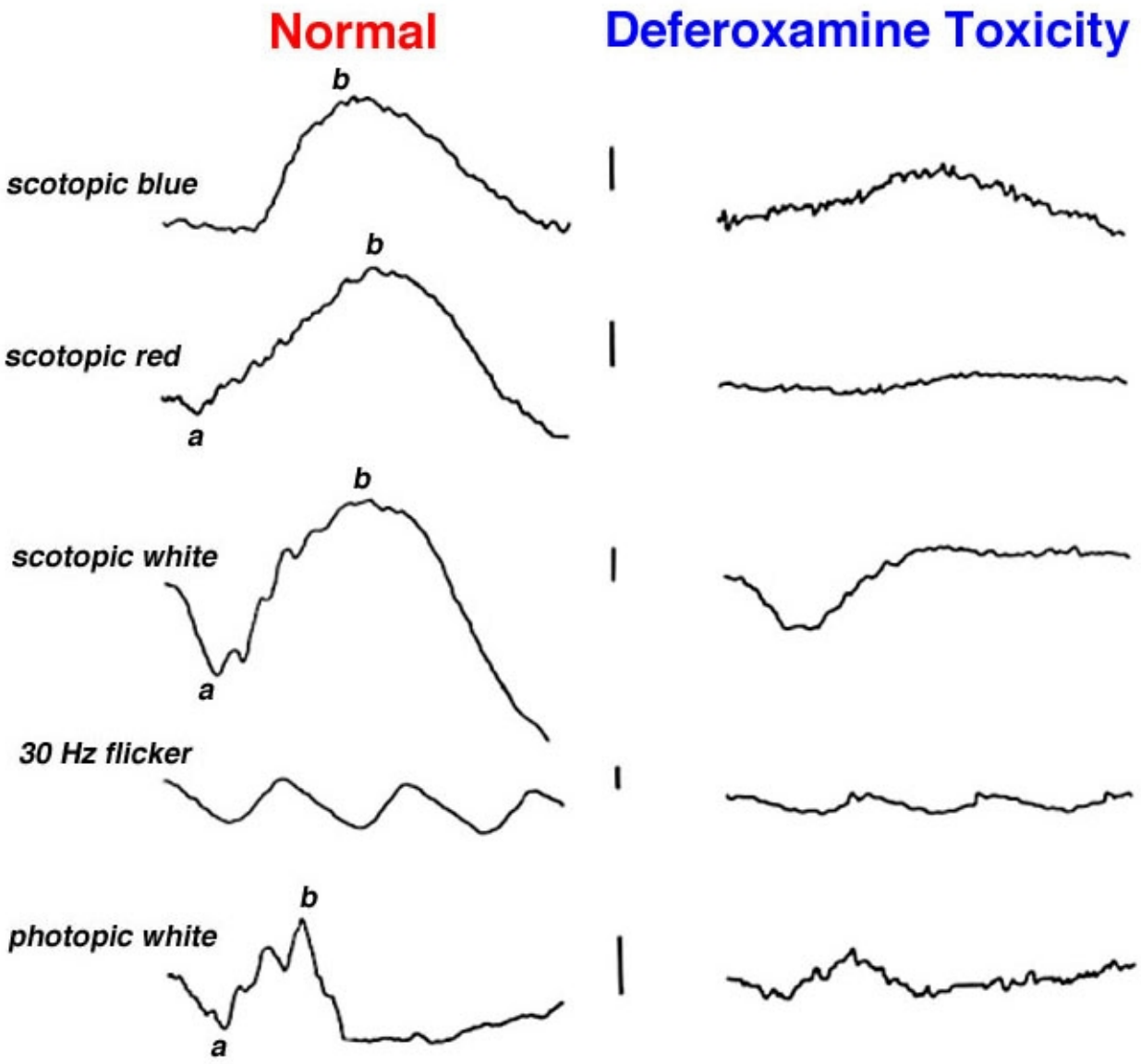

Figure 40. Deferoxamine toxicity effects on the ERG.

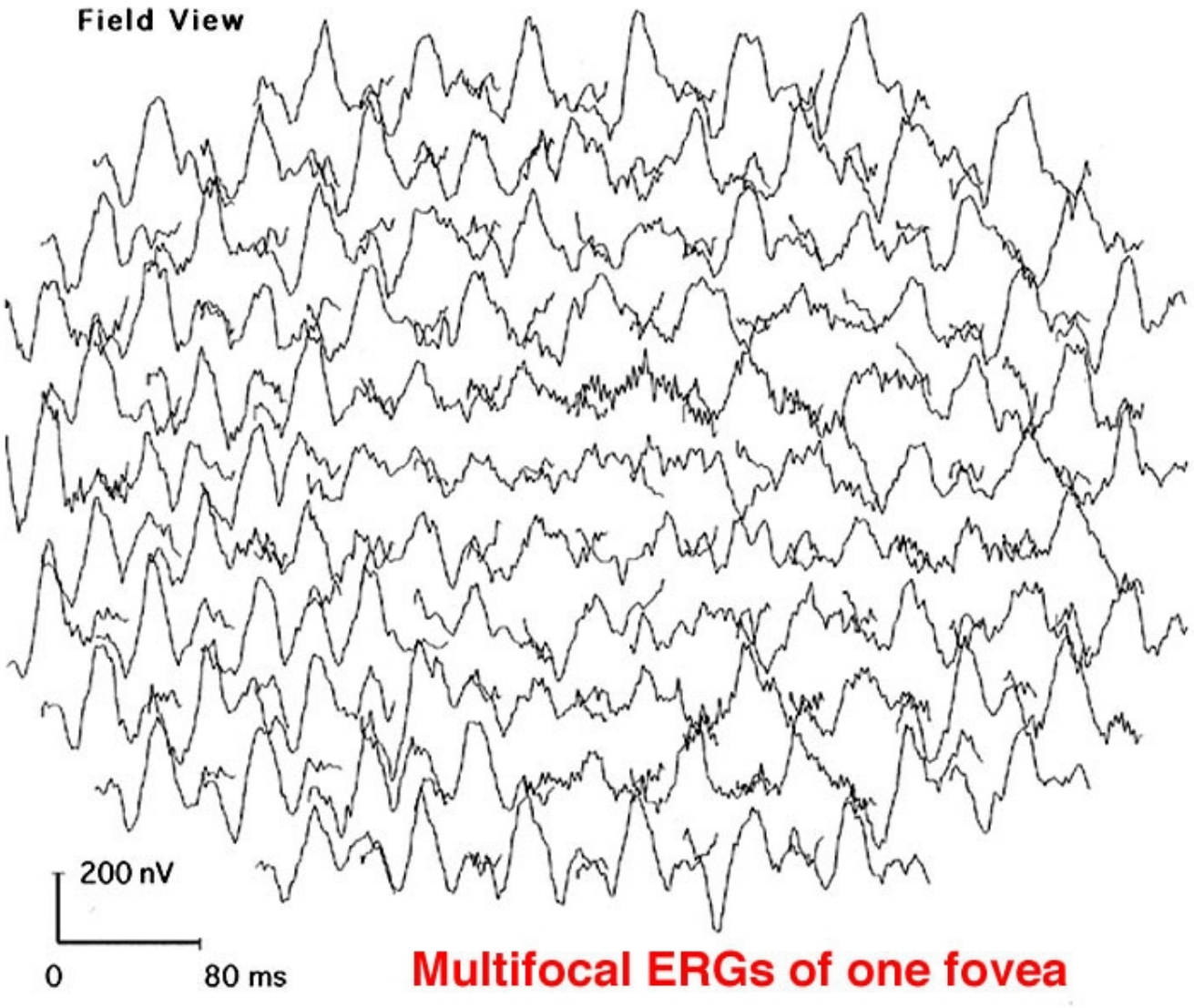

Figure 41b. Multifocal ERG recordings in a patient with age-related macular degeneration (AMD).

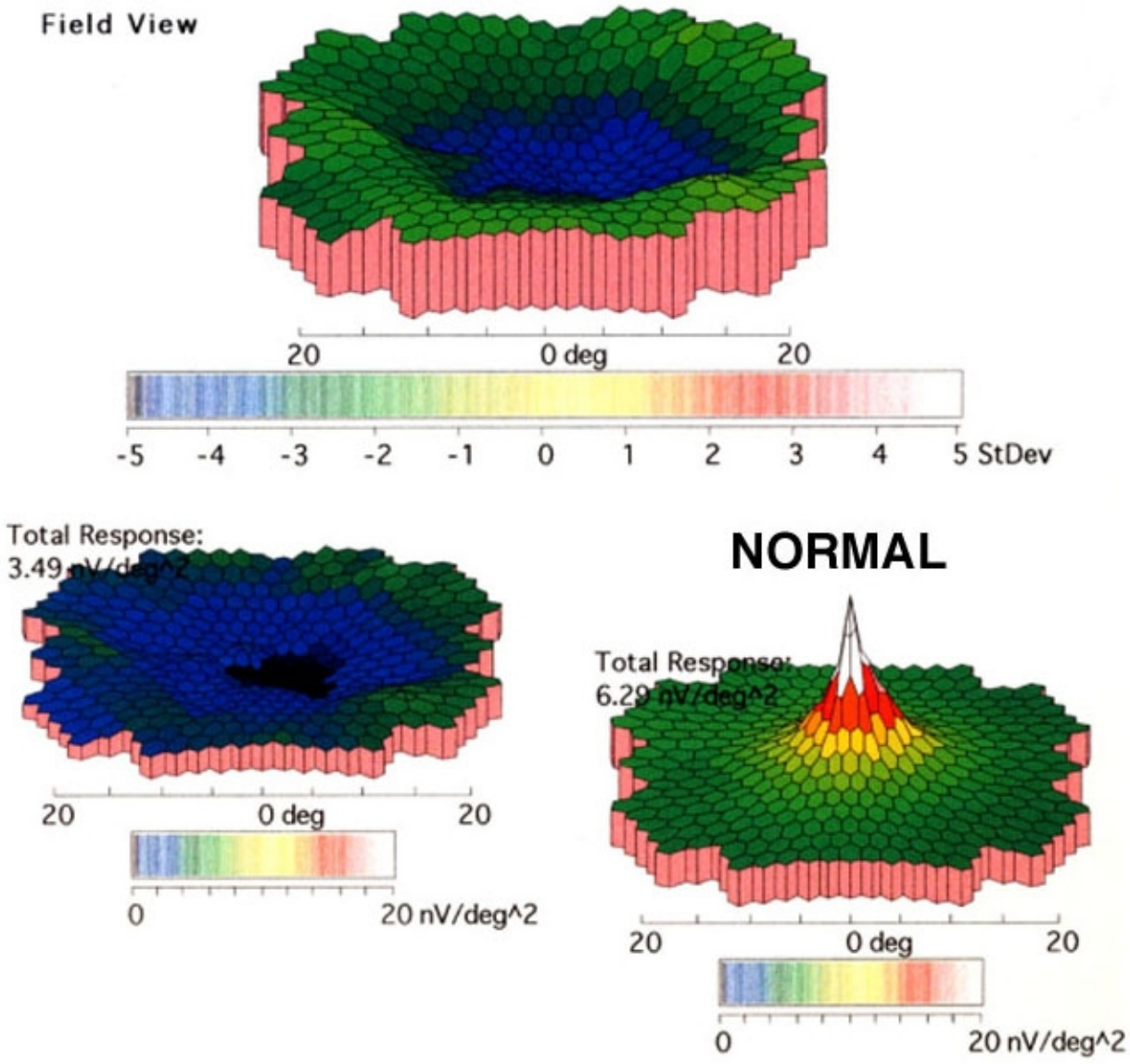

Figure 42. Multifocal ERG recordings transformed into 3-D maps of the macular area in a patient with AMD compared with a normal patient.

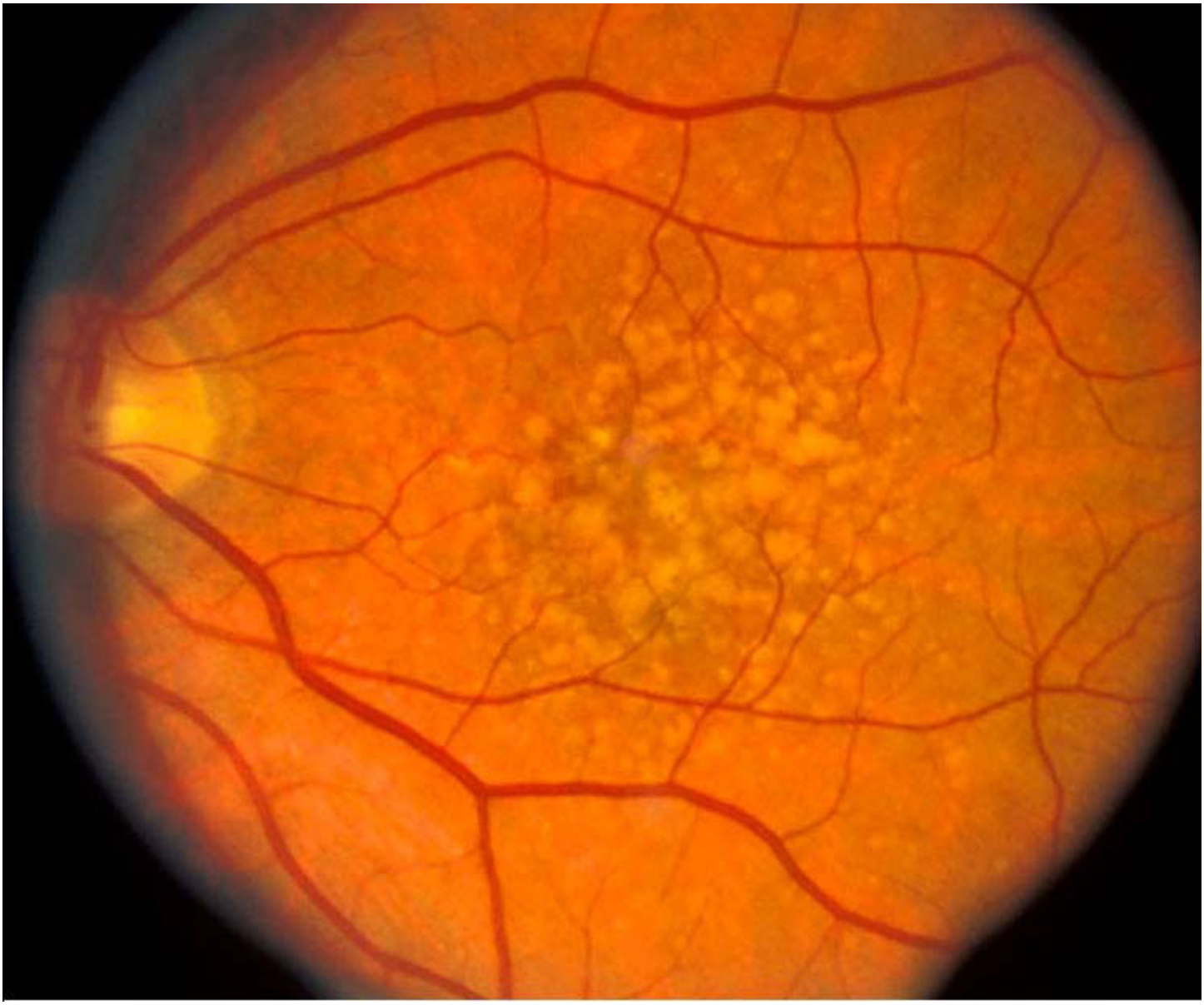

Figure 41a. Fundus photograph of a patient with age-related macular degeneration.

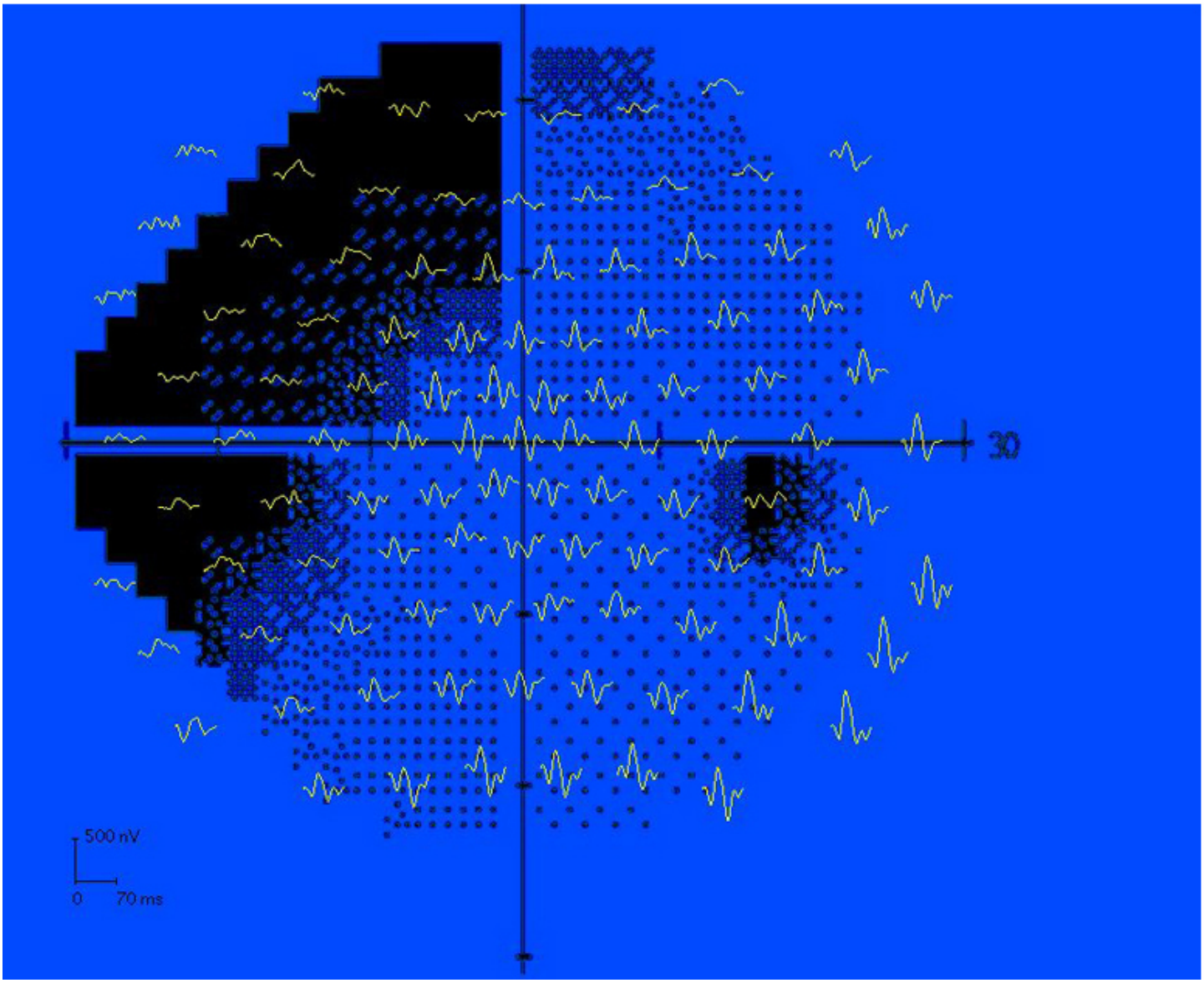

Figure 43. Multifocal ERGs (yellow) superimposed on Humphrey 24-2 visual field plot of the right eye in a patient with acute zonal accult outer retina. mfERG abnormalities match the visual field loss very well.

Figure 44. Placement of the electrodes for recording an EOG.

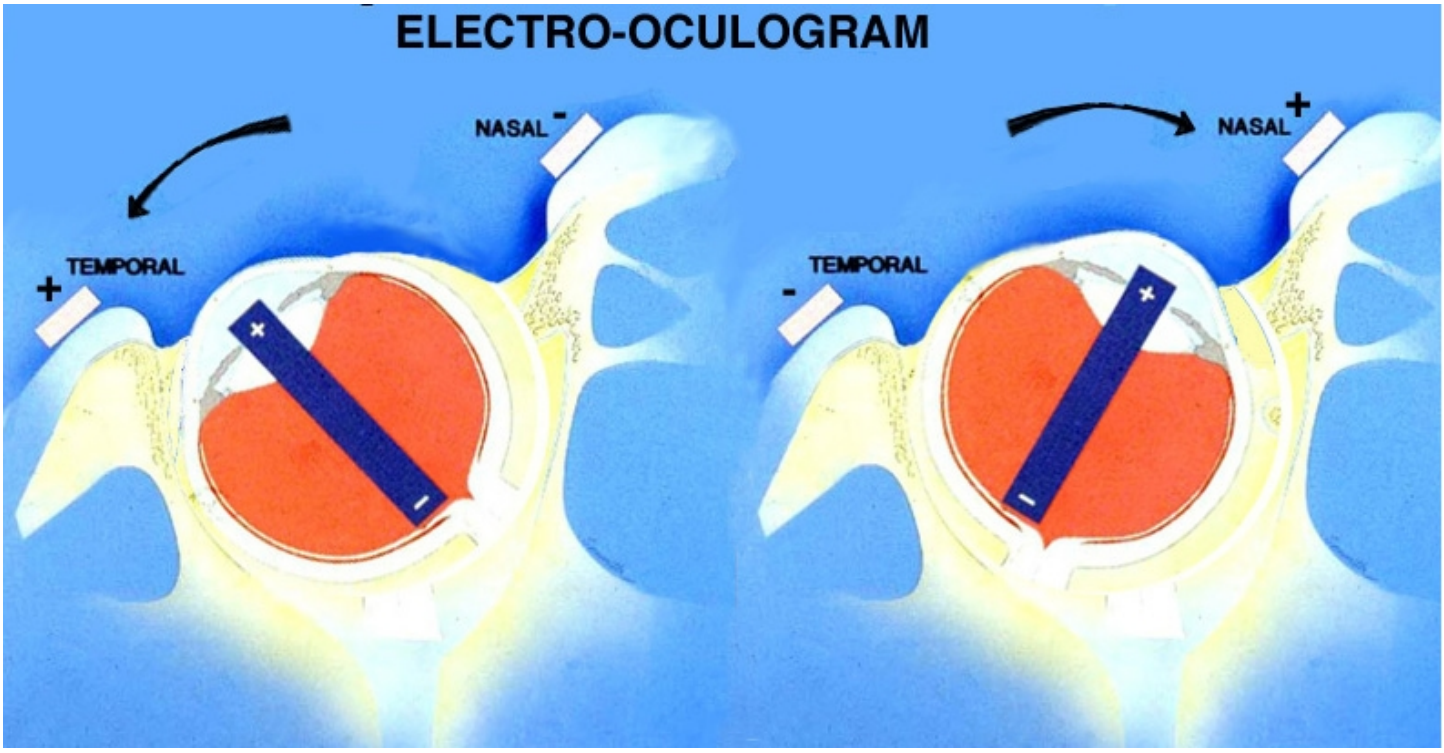

Figure 45. How the EOG potential is measured as the eyes turn toward and away from the skin electrodes.

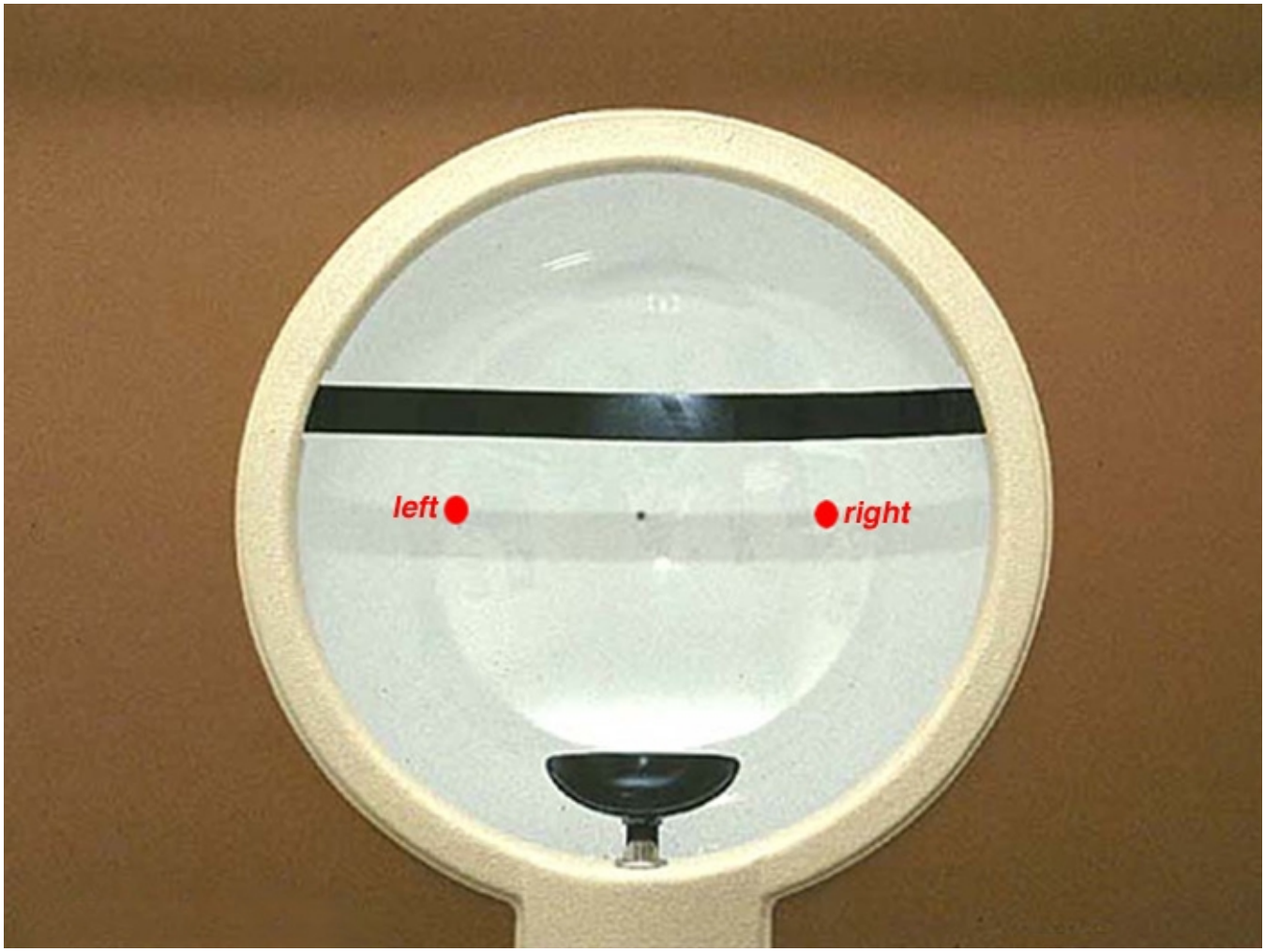

Figure 46. Ganzfeld used for stimulating the EOG waveform.

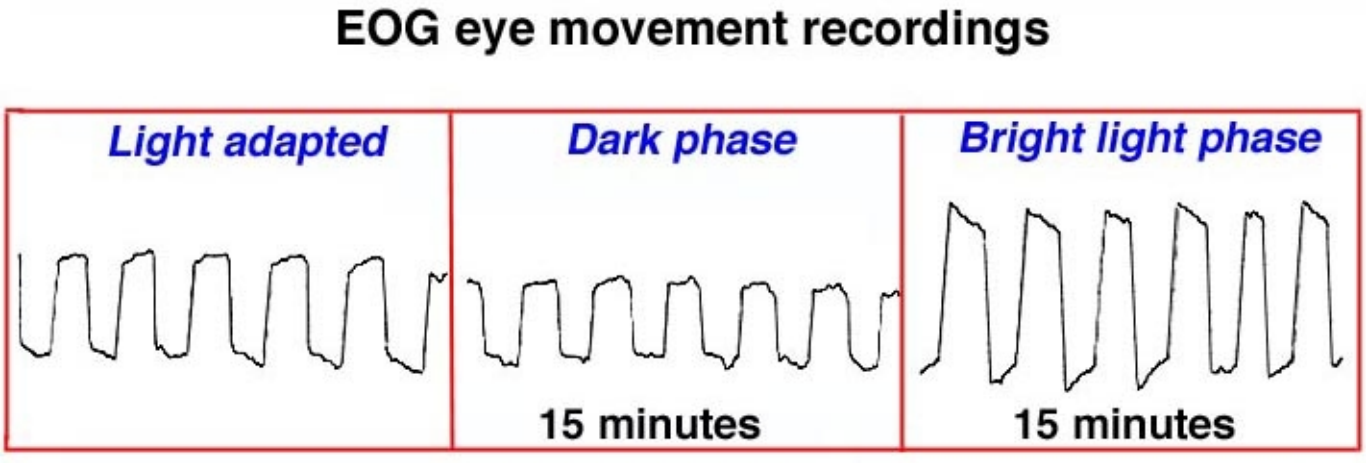

Figure 47. Light-adapted pre-EOG, dark adaptation phase and light-rise phase.

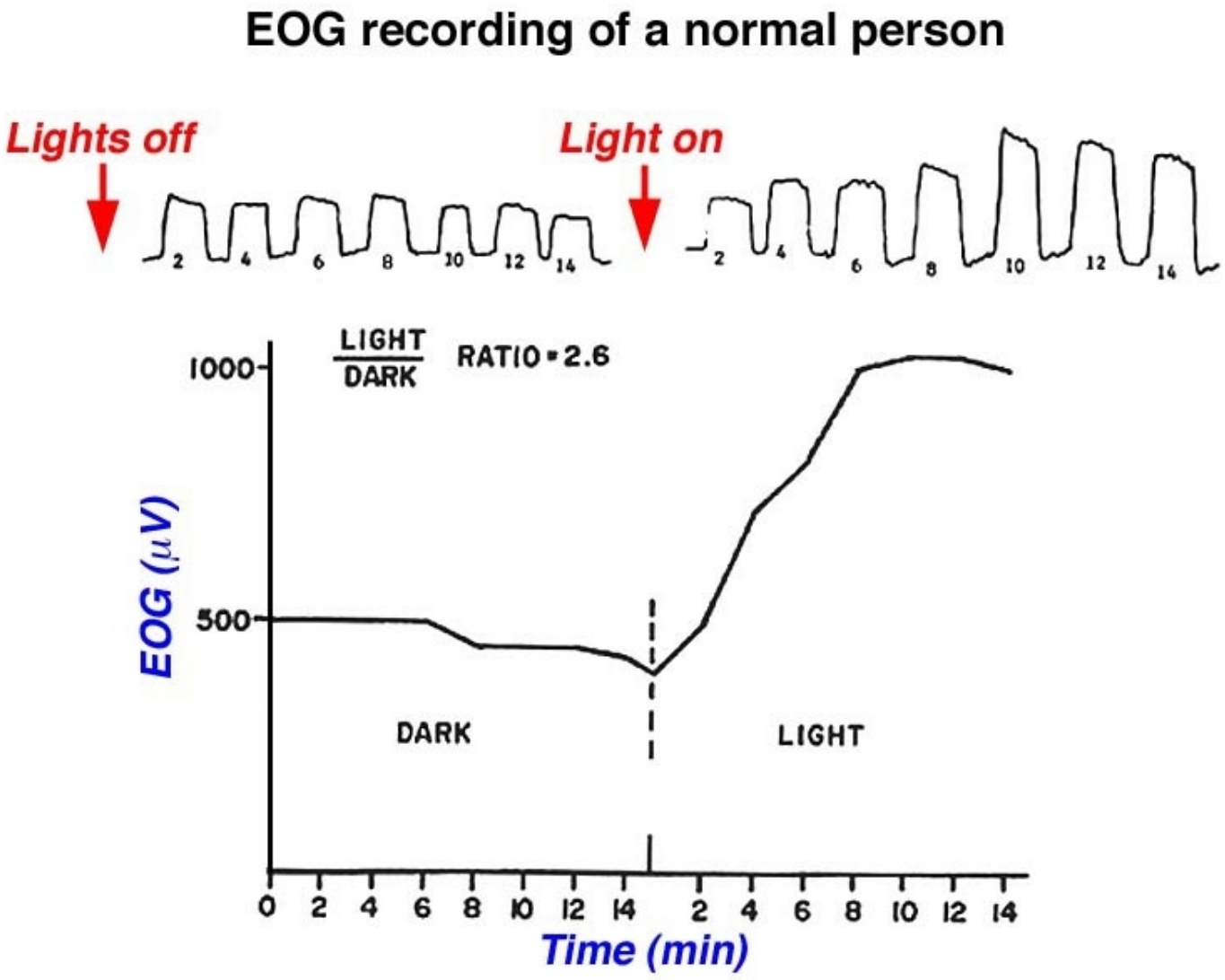

Figure 48. Normal EOG recording.

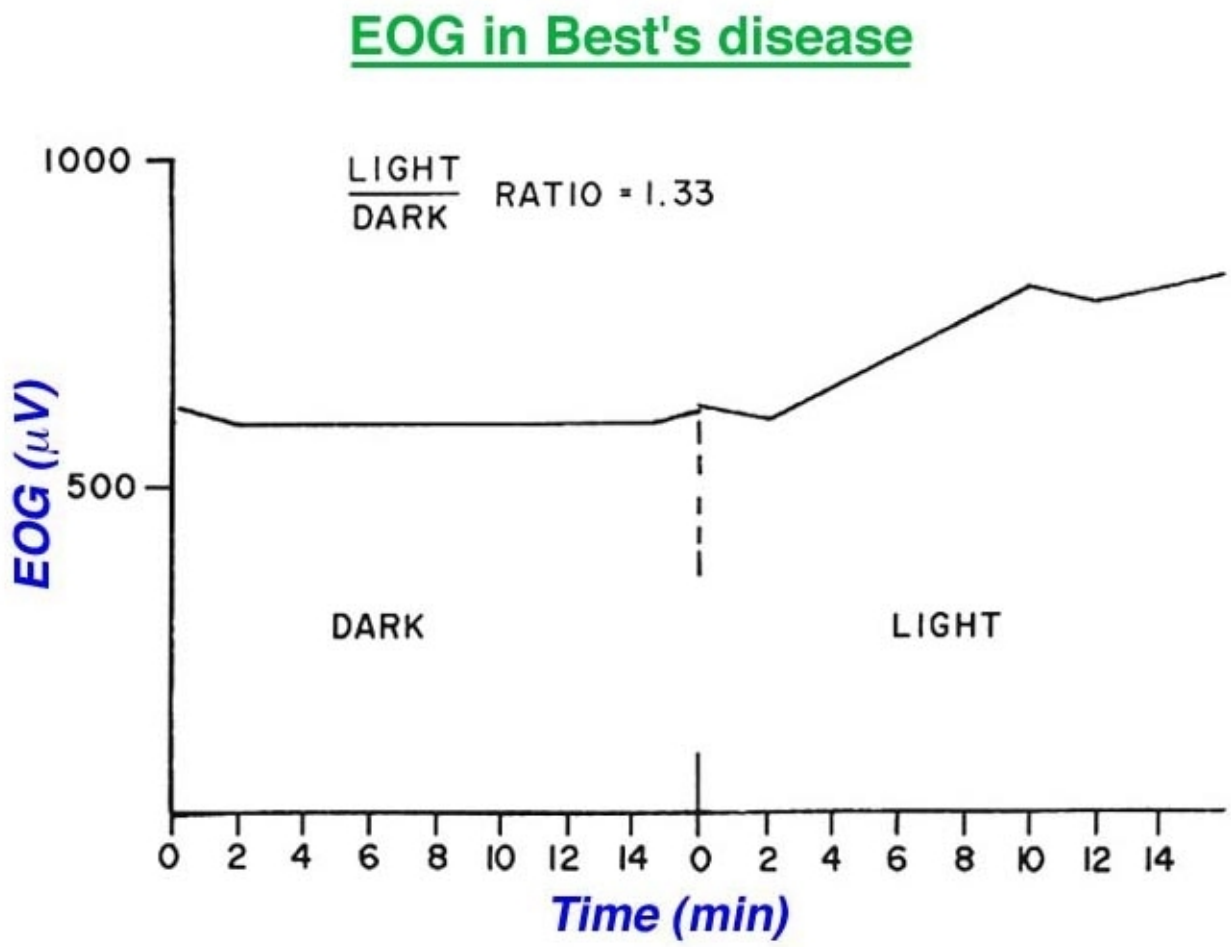

Figure 49. EOG from a patient with Best's disease.

Figure 50. Fundus photo in Best's disease.

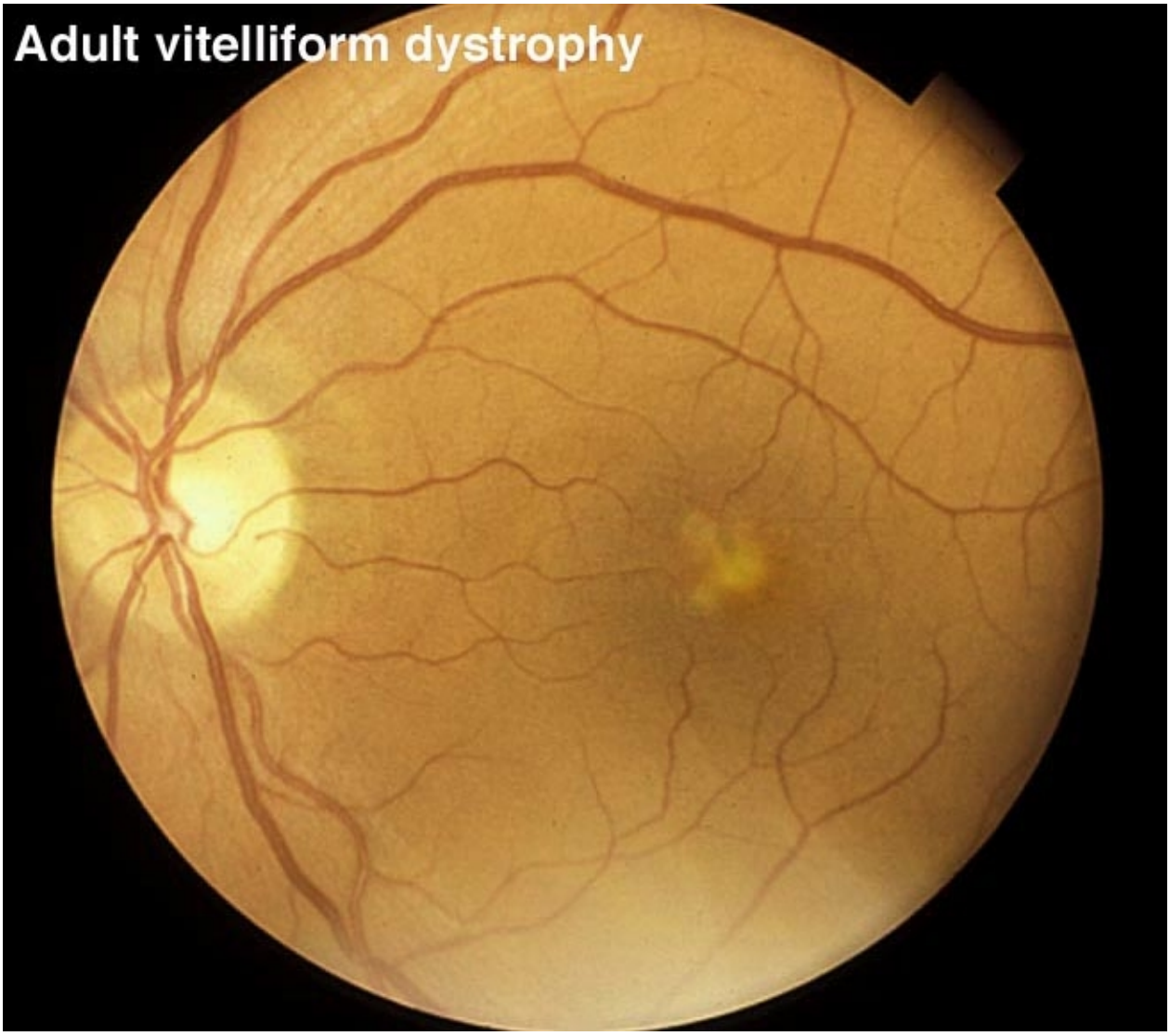

Figure 51. Fundus in adult viteliform dystrophy.

About the Author

Dr. Donnell Creel was born in Kansas City, Missouri. He attended the University of Hawaii and received his B.A and M.A. from the University of Missouri at Kansas City. His Ph.D. was in Neuropsychology from the University of Utah in 1969. Don's doctoral thesis and post-doctoral research centered on abnormal decussation of retinal ganglion cell fibers at the optic chiasm in albino mammals. In the early 1970s, he created a visual evoked potential test that detects this misrouting in human albinos. Later research demonstrated that melanin pigment in the inner ear is necessary for normal auditory function and that lack of pigment in albinos has consequences affecting normal cell development in the brainstem. Don has been in the Department of Ophthalmology, University of Utah Medical Center since 1980, and Director of Clinical Electrophysiology at the Moran Eye Center since its inception in 1993. Clinical research interests center around the application of visual and auditory evoked potentials and electroretinography.

References

1. Holmgren F. Metod att objektivera effektenav ljusintryck pa retina. Upsala lakaref Forhandl. 1865;1:177–191.
2. Granit R. The components of the retinal action potential in mammals and their relation to the discharge in the optic nerve. J Physiol. 1933;77:207–239. PubMed PMID: 16994385.
3. Arden GB, Barrada A, Kelsy JH. New clinical test of retinal function based on the standing potential of the eye. Br J Ophthalmol. 1962;46:449–467.
4. Miller RF, Dowling JE. Intracellular responses of the Muller (glial) cells of mudpuppy retina: their relation to the b-wave of the electroretinogram. J Neurophysiol. 1970;33:323–341. PubMed PMID: 5439340.
5. Marmor MF, Hock PA. A practical method for c-wave recording in man. Doc Ophthalmol Proc Ser. 1982;31:67–72.
6. Weleber RG. The effect of age on human cone and rod ganzfeld electroretinograms. Invest Ophthalmol Vis Sci. 1981;20:392–399. PubMed PMID: 7203883.
7. Lawwill T, Burian HM. A modification of the Burian-Allen contact-lens electrode for human electroretinography. Am J Ophthalmol. 1966;61:1506–1509. PubMed PMID: 5938319.
8. Sieving PA, Fishman GA, Maggiano J. Corneal wick electrode for recording bright flash electroretinograms and early receptor potential. Arch Ophthalmol. 1978;96:899–900. PubMed PMID: 655931.
9. Fishman GA, Birch DG, Holder GE, Brigell MG. Electrophysiologic testing in disorders of the retina, optic nerve, and visual pathway. 2nd ed. American Academy of Ophthalmology; 2001;

10. Marmor MF, Zrenner E. Standard for clinical electro-oculography. Arch Ophthalmol. 1993;111:601–604. PubMed PMID: 8489436.
11. Marmor MF, Zrenner E. Standard for clinical electroretinography (1999 update). Doc Ophthalmol. 1998;97:143–156. PubMed PMID: 10765968.
12. Perlman I. Relationship between the amplitudes of the b wave and the a wave as a useful index for evaluating the electroretinogram. Br J Ophthalmol. 1983;67:443–448. PubMed PMID: 6602626.
13. Cobb WA, Morton HB. A new component of the human electroretinogram. J Physiol. 1954;123:36P–37P.
14. Wachtmeister L, Dowling JE. The oscillatory potentials of the mudpuppy retina. Invest Ophthalmol Vis Sci. 1978;17:1176–1188. PubMed PMID: 721390.
15. Creel DJ, Wang JM, Wong KC. Transient blindness associated with transurethral resection of the prostate. Arch Ophthalmol. 1987;105:1537–1539. PubMed PMID: 3675286.
16. Boughman JA, Fishman GA. A genetic analysis of retinitis pigmentosa. Br J Ophthalmol. 1983;67:449–454. PubMed PMID: 6860611.
17. Creel DJ, Crandall AS, Ziter FA. Identification of minimal expression of myotonic dystrophy using electroretinography. Electroencephalogr Clin Neurophysiol. 1985;61:229–235. PubMed PMID: 2411500.
18. Katz BJ, Warner JEA, Digre KB, Creel DJ. Selective loss of the electroretinogram b-wave in a patient with Creutzfeldt-Jakob disease. J Neuroophthalmol. 2000;20:116–118. PubMed PMID: 10870926.
19. Bearse MA, Sutter EE. Imaging localized retinal dysfunction with the multifocal electroretinogram. J Opt Soc Am A Opt Image Sci Vis. 1996;13:634–641. PubMed PMID: 8627420.
20. Marmor MF, Hood DC, Keating D, Kondo M, Seeliger MW, Miyake Y. Guidelines for basic multifocal electroretinography (mfERG). Doc Ophthalmol. 2003;106:105–115. PubMed PMID: 12678274.
21. Marg E. Development of electro-oculography; standing potential of the eye in registration of eye movement. AMA Arch Ophthalmol. 1951;45:169–185. PubMed PMID: 14799014.

Visual and Auditory Anomalies Associated with Albinism

Donnell J. Creel, PhD[1]

Created: June 18, 2015.

1. Introduction

One of the evolutionary characteristics of the mammalian visual system is the increase of binocular overlap of vision as eyes progress from being located on side of the head such as the guinea pig to the frontal position in Haplorrhine primates. Concomitantly as the proportion of temporal retina increases the number of uncrossed optic neurons at the optic chiasm expands from as little as 1% in guinea pigs to approximately 45% in primates including human beings (1, 2). Figure 1 illustrates the approximate distribution of crossed and uncrossed retinal ganglion cells (RGCs) in the visual pathways of normally pigmented human beings.

C. L. Sheridan (3) compared the interocular visual pathways in "split brain" ocularly pigmented (hooded) rats and albino rats. Sheridan concluded “Perhaps the paucity of uncrossed fibers that characterized rodents in general is even further reduced in the albino". That year Lund (4) verified Sheridan's hypothesis anatomically. Lund stated albino rats display no organized uncrossed optic fibers. Lund agreed with previous estimates that pigmented rats possess up to 10% uncrossed optic fibers. Figure 2 is a diagram of crossed and uncrossed optic projections in wild-type rodents.

Mammals with few uncrossed retinal ganglion cell fibers (RGCs) such as rodents and lagomorphs do not exhibit the laminated dorsal lateral geniculate nucleus (dLGN) seen in carnivores and primates including human beings. Carnivores and Haplorrhine primate dLGN contain up to six monocular layers with point-to-point representation of visual space organized in columns through these layers. The 90%+ crossed RGCs at the optic chiasm in rodents and lagomorphs fill the contralateral dLGN, with only a pocket of the ipsilateral dLGN devoted to the fewer uncrossed fibers. Figure 3 illustrates RGC fiber terminations in horizontal sections through the dLGN comparing black and albino rats. The fewer uncrossed fibers in albino rodents are also projected to the dLGN in a fragmented fashion as opposed to a close organization in pigmented rodents.

2. Visual learning studies

A retrospective review of visual learning experiments, which isolated uncrossed optic pathways in rats, published 1924 to 1966 indicated that ocularly pigmented rats can learn visual discriminations using uncrossed optic fibers, whereas albino rats cannot (5-9). This correlation was not noticed until 1965. These studies were all designed similar to depicted in Figure 4 of rat visual pathways. A combination of limiting visual input to one eye with ablation of visual cortex restricted visual information in rats to either crossed 90-95% of RGCs or 5-10% of uncrossed RGCs. Studies reported pigmented rats can learn visual pattern discriminations using uncrossed pathways. The uncrossed terminations in albino rats are minimal. Albino rats do not learn visual pattern discriminations when limited to uncrossed visual pathways.

3. Siamese cats

For several years the anatomical anomaly of few uncrossed RGCs at the optic chiasm in albinos appeared to be limited to rats and rabbits (10). Guillery (11) described aberrant retinogeniculate organization in Siamese cats, but the connection to albinism was not recognized.

Author Affiliation: 1 Department of Ophthalmology, University of Utah Medical Center.; Email: Donnell.creel@hsc.utah.edu.

Corresponding author.

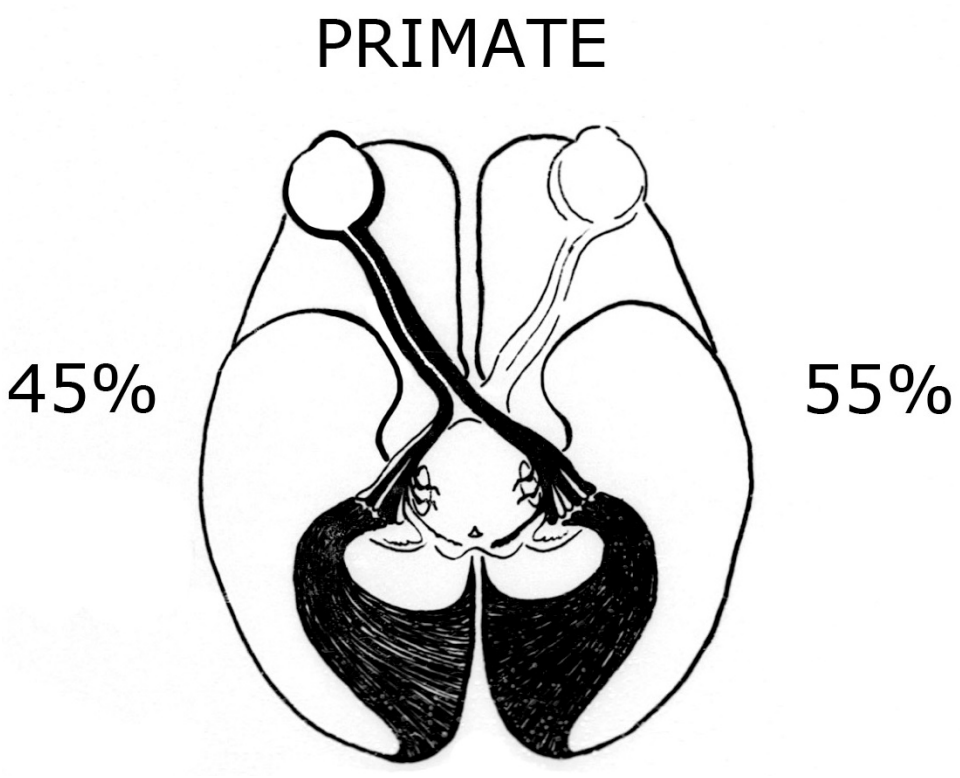

Figure 1. Schematic of approximate distribution of crossed and uncrossed retinal ganglion cells at the optic chiasm in primates including humans.

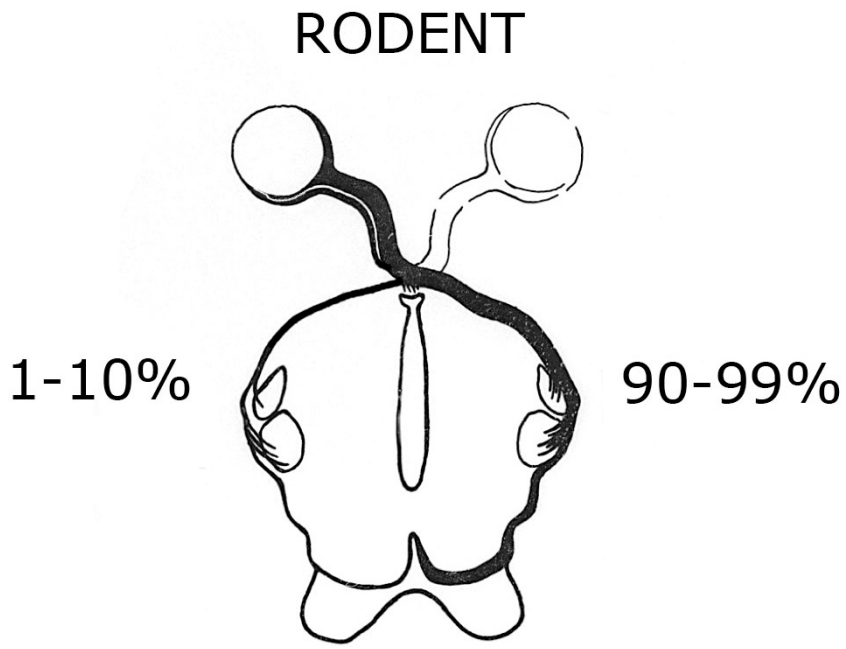

Figure 2. Schematic of range of crossed and uncrossed retinal ganglion cell fibers at optic chiasm in rodents.

The first link between Siamese cats and albinism, and suggestion that reduced uncrossed optic fibers likely is a "highly general trans-species phenomenon in albinic mammals" was in 1971 (12, 13). Siamese cats possess a tyrosinase-locus mutation that is a temperature sensitive pigmentation defect, i.e. pigment forms only on the cold parts of the body similar to Himalayan mice, rats and rabbits. This mutation is sometimes referred to as the

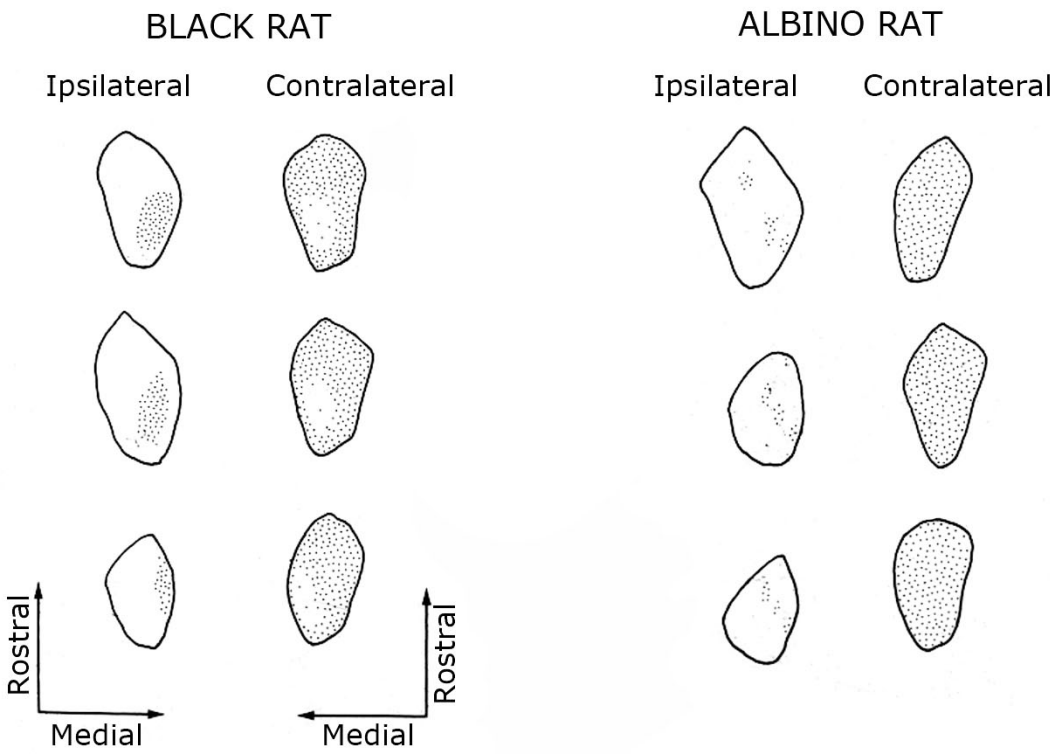

Figure 3. The distribution of pericellular optic fiber degeneration in the dorsal lateral geniculate nucleus (dLGN) of BLACK and ALBINO rats in serial horizontal section at three levels of dLGN.

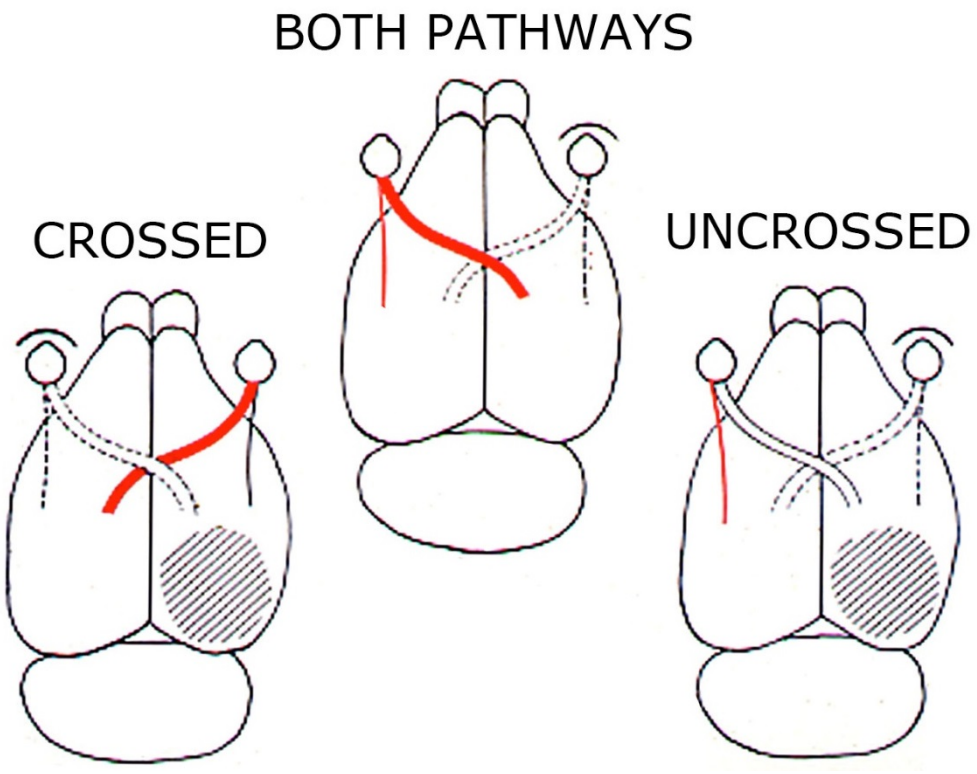

Figure 4. Illustration depicting functioning optic pathways combining occlusion and visual striate cortex ablation (cross hatched areas).

Siamese - Himalayan temperature effect. Cortical mapping of visual projection areas in normally pigmented and Siamese cats demonstrated significant differences in their uncrossed optic pathways. Figure 5 depicts monocular visual evoked potentials recorded from a Siamese cat's cortical visual area showing preponderance of contralateral innervation.

These cat studies discovered that a single recording site over each visual cortical projection area could reflect differences between pigmented and albino cats (Figure 6). This observation was the basis for testing human albinos using scalp-recorded visually evoked potentials (14).

4. Albino animal studies

Many animal studies in the 1970s reported that all albino mammals with oculocutaneous, or only ocular albinism, demonstrate reduced uncrossed optic projections (15-17). A review with figures characterizing types of visual organization in the Siamese cat is R. W. Guillery's 1974 publication in Scientific American (18). One human albino brain (19, 20) and an albino monkey brain were studied verifying similar anomalies in albino primates (21, 22). Defects identified in albino mammals encompass a decreased number of photoreceptors, foveal/area centralis hypoplasia, misrouting of the temporal retinal ganglion cell axons across the chiasm, variation of central RGC terminations, vascular intrusion into area centralis, anomalous cortical organization, and fewer cones and RGCs in macular area (23-27).

The organization of the visual system varies considerably among mammals. Haplorrhine primates display well-defined foveae, foveal avascular zone, and large numbers of uncrossed optic fibers, whereas rodents and even carnivores exhibit only a central fixation area in the retina. In the domestic cat there is a trend towards an avascular zone with only capillary vessels found in the area centralis. Mammals vary not only in numbers of optic nerve fibers that decussate but further in embryonic development and proportion of optic projections terminating in various levels of the optic system from suprachiasmatic nuclei, to midbrain, to geniculate nuclei, to cortex.

An animal model manifesting dramatic effects of misrouting is the albino cat. Figure 7 is a photograph of a litter of albino cats homologous to Type 1 tyrosinase-locus oculocutaneous human albinism (OCA1) with no ability to make pigment. All these cats had observable nystagmus and many strabismus. Figure 8 pictures the optic chiasm of an OCA1 albino cat showing almost all RGCs cross at the chiasm.

Figure 9 depicts the geniculate nuclei of a Type 1 albino cat compared to a normally pigmented cat. The dLGN of albino cats containing only one small pocket of ipsilateral projections is almost as primitive as a rodent dLGN. Four patterns of geniculocortical organization are described in albino mammals (18, 22, 28-30). All forms likely exist in human albinos. Abnormal proportions of ipsilateral and contralateral RGCs continue to mid-brain nuclei probably providing the basis for atypical optokinetic nystagmus in albino mammals.

Few of the rare forms albinism have been investigated anatomically in carnivores or primates. One rare form that has is the Chediak-Higashi syndrome (CHS), which occurs in mammals including human beings and cats. Decreased oculocutaneous pigmentation, enlarged cytoplasmic granules, increased susceptibility to infections, and hemorrhagic tendencies characterize CHS. Ocular anomalies include pale irides and albinotic fundi. Cats with CHS exhibit photophobia and prolonged post-rotatory nystagmus. Figure 10 depicts littermate cats of a Blue Smoke Persian strain. The hypopigmented cat on the left is affected with CHS. Visual projections of CHS cats misroute at the optic chiasm fragmenting layer A1 of the dLGN into several islands (Figure 11), similar to the disruption of A1 outlined in the Siamese cat (31). Visual and auditory anomalies resembling those in albinos were described in human beings with CHS using evoked potentials (32).

Phylogenetically older connections are less abnormal in albino mammals. Retinohypothalamic projections predate vertebrates, existing in early chordates that possess retinal pigment matching vertebrates (33). Melanopsin-sensitive retinal ganglion cells are completely crossed or bilaterally projecting to suprachiasmatic

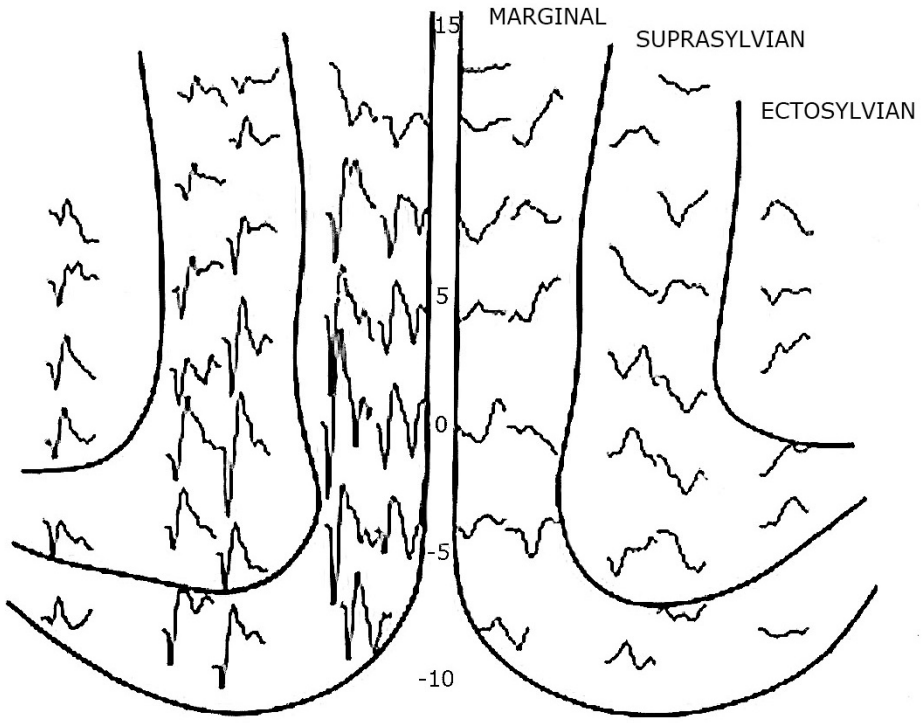

Figure 5. Map of dorsal surface of Siamese cat visual cortex chowing monocular visual evoked potentials via crossed (left) and uncrossed (right) optic projections. From Creel, 1971 (12).

nuclei, and not affected (34, 35). The phylogenetically older bilateral projections to suprachiasmatic nuclei in albino cat (Figure 8) appear to be unaffected (36). The crossed/uncrossed ratio of approximately 1.4:1 of retinal ganglion fibers to the suprachiasmatic nuclei in albino cats corresponds to the ratio reported for normally pigmented cats (37).The later-evolving vertebrate rod-cone-RPE-ganglion cell system is vulnerable to alteration in albino mammals whereas the phylogenetically older melanopsin pathway is generally not.

5. Genetic mechanisms

Sprinkled through publications since the 1970s are suggestions that genetic effects are paramount. Sanderson et al. (38) and Sanderson (15) in the mink and rabbit, and Creel & Giolli (16, 39) in guinea pigs and rats early addressed genetic factors modifying expression of anomalies in ocularly hypopigmented models. In the cat model there are indications of genetic control including reports of heterozygote effects in pigmented cats (29, 40). Carriers of the genes for human albinism do not show detectable visual anomalies (41). Up to 90% of obligate carriers of X-linked ocular albinism exhibit pigmentary mosaicism in their ocular fundus, a lyonization effect, but with no further visual anomalies yet discovered (42).

Many candidate agents, including signaling and transcription factors have been suggested that plausibly control targeting of retinal ganglion cells coursing through the chiasm and other visual features associated with albinism. Likely many of these conclusions are correct within the model studied, but not a general solution within mammals. Each species appear to vary. For example, significant differences between mouse and human embryogenesis specific to chiasm formation are described (43). These differences include that the nodal point of neurogenesis in the human/primate retina is the fovea, while in rodents it is the optic nerve head. In rodents uncrossed cells are born early for their retinal location. This is not the case in primates. Consequently temporal patterning of axon arrival at the optic chiasm and their course through the chiasm are different between man and mouse. In addition there are no absolutes. The expression of these genetically determined traits has a statistical probability of occurrence (16).

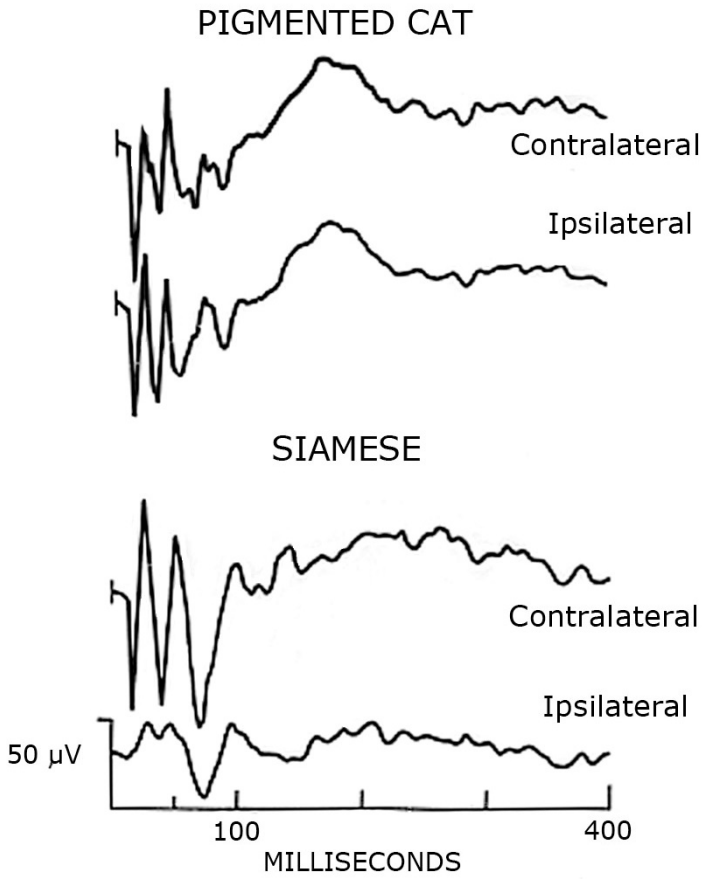

Figure 6. Visually evoked potentials recorded by single dural electrode from normally pigmented and Siamese cat showing dramatic difference in proportion of ipsilateral optic projections. From Creel, 1971 (13).

Figure 7. Litter of Type 1 oculocutaneous albino kittens. All displayed nystagmus and some strabismus.

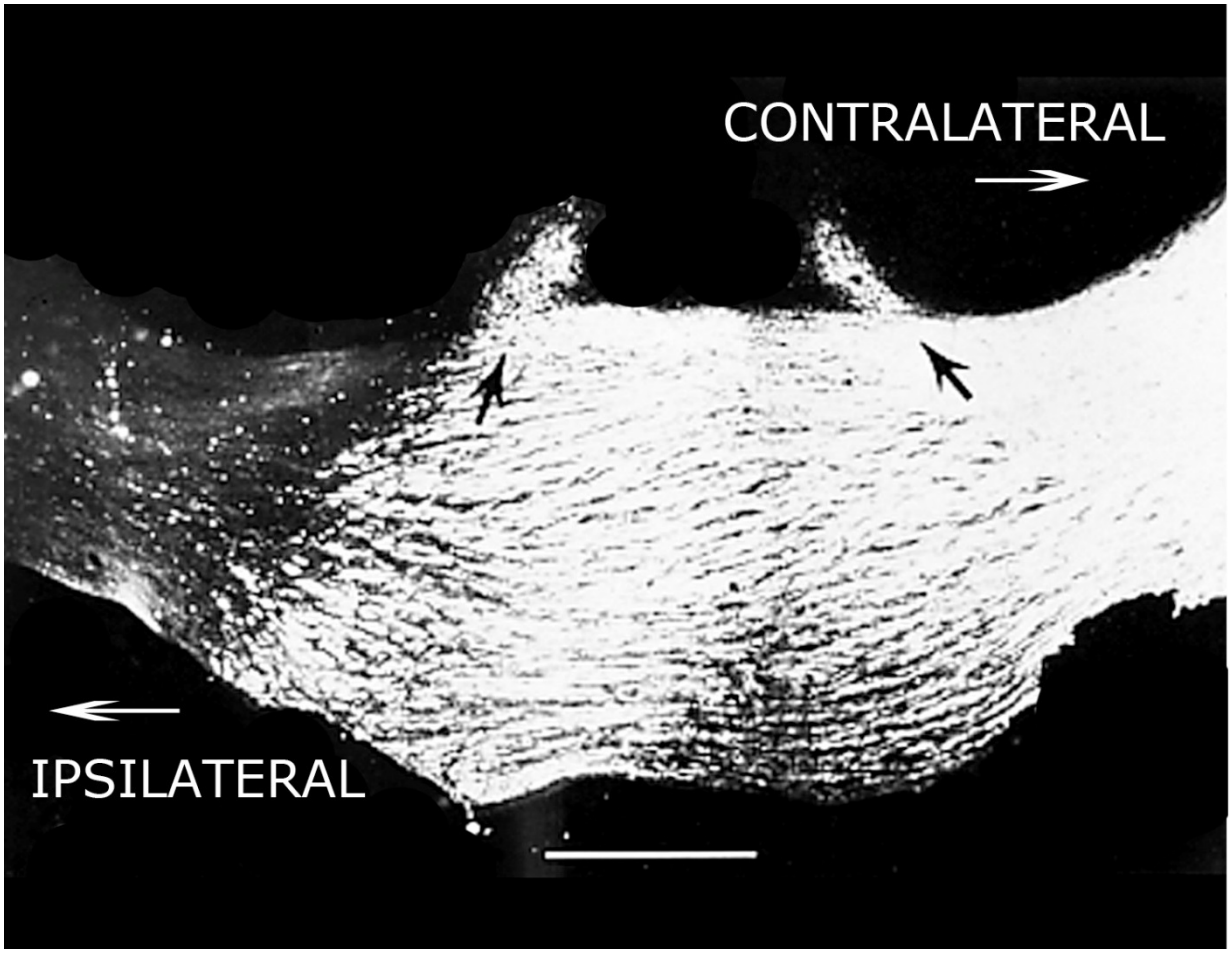

Figure 8. Dark-field autoradiograph of coronal section through the optic chiasm of a Type 1 albino cat after injection of tritiated leucine into right eye showing difference between contralateral and ipsilateral RGC projections. Almost all RGCs cross at the optic chiasm. Arrows point to projections to suprachiasmatic nuclei. Scale bar 1 mm. From Creel et al, 1982 (211).

Variation can also be seen in the drift of retinal evolution even in Haplorrhine primates. Old World and New World monkeys evolved different retinal color vision receptors (44) and different cortical visual organization (45). Another example of variability concerning pigment chemistry is that human tyrosinase-related sequence locus on chromosome 11pll.2 is described in gorilla, but not chimpanzee (46). Even minor differences in pigment metabolism alter metabolic proteins, which possibly could initiate a cascade of effects on visual embryogenesis.

Due to millions of years of divergent evolution the micro mechanisms of axon guidance underlying optic neuron decussation and target fate are likely idiosyncratic for each species. Pax2, Pax6, SOX2 appear to be necessary for ocular development. Only the most fundamental, ancient, conserved loci such as SOX, ROBO 3 and 4, homeobox (VSX2), Sonic hedgehog (Shh) and PAX2/PAX 6 interaction are likely perpetual and contributing to guidance and angiogenesis decisions in most mammals (47-51). The conservation of some genes spans hundreds of millions of years. SOX21, active in developing retina and inner ear, occupies the same human loci (13q31-32) as DCT (L-dopachrome tautomerase), active in melanogenesis and tyrosine metabolism, has maintained 90-100% identity across species for hundreds of millions of years of divergent evolution (52, 53). Worth noting is mutations of ROBO 3 and 4 are associated with non-decussation of the pyramidal motor pathways (54). ROBO 3 and 4 may affect visual pathway decussation by interacting with tyrosinase loci on the same arm of chromosome 11q. Tyrosinase loci 11q13-22 are millions of base pairs from loci 11q23-24.2, but possibly communicate by interacting with noncoding RNA target sites close in three-dimensional space such as by

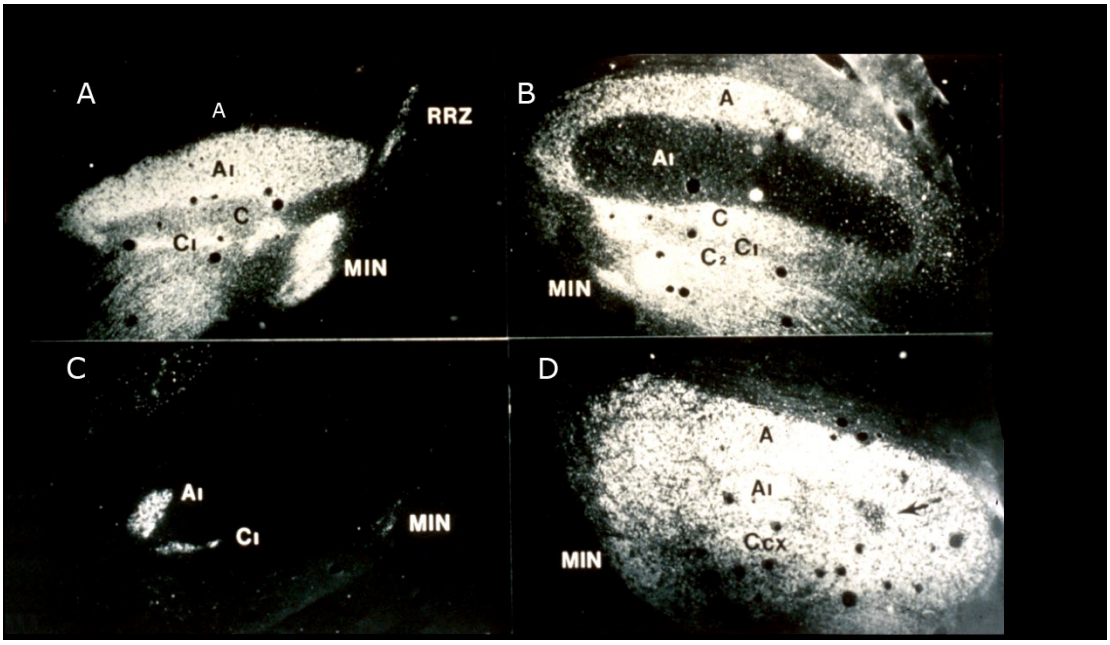

Figure 9. Dark-field autoradiographs of coronal sections through the ipsilateral (A) and contralateral (B) dLGN of a pigmented cat and the ipsilateral (C) and contralateral (D) dLGN of a Type 1 albino cat. The arrow in (D) points to small ipsilateral A1 input. From Creel et al, 1982 (211).

Figure 10. Photograph of 2 littermate Blue Smoke Persian cats. The cat on the left is affected with Chediak-Kigashi syndrome.

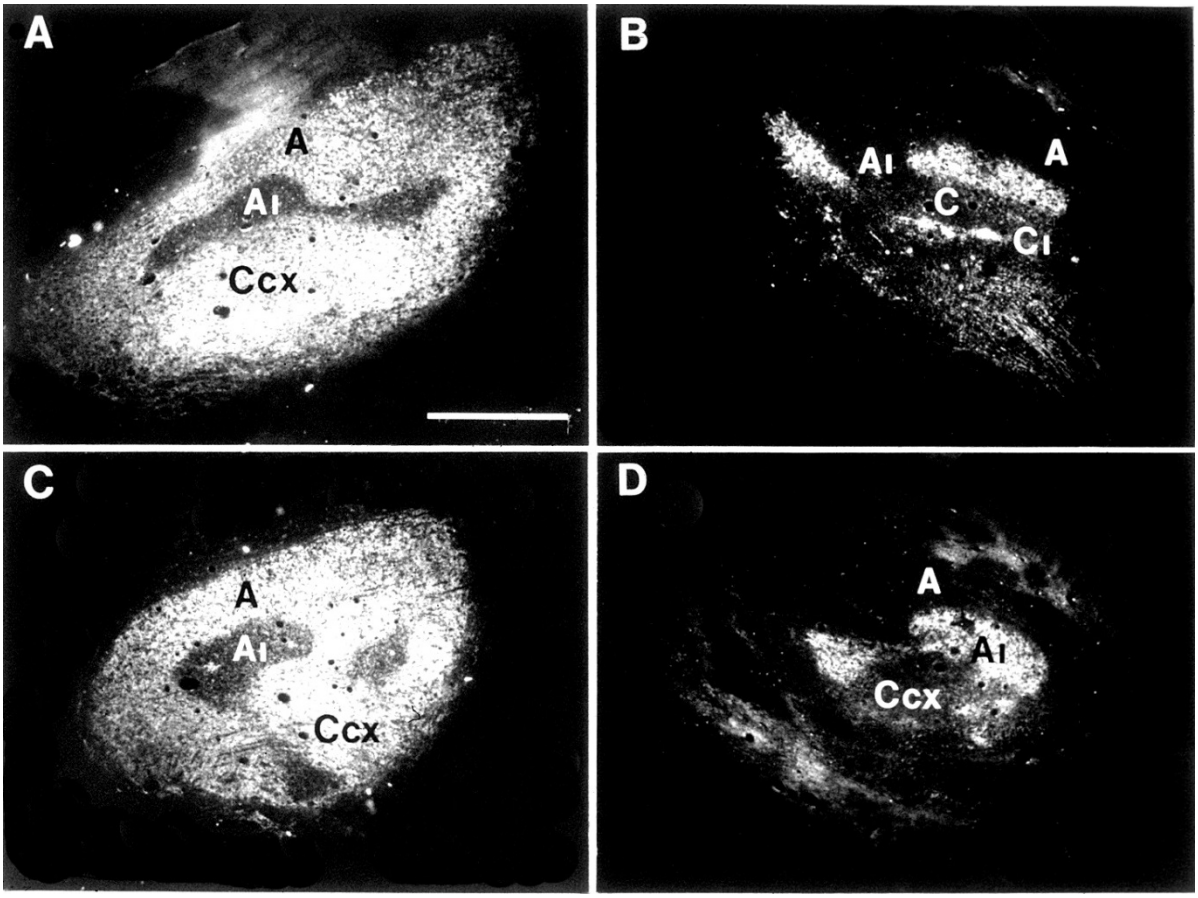

Figure 11. Dark-field autoradiographs of sections through the dLGN of a cat with Chediak-Higashi syndrome (HS). Contralateral (A) and ipsilateral (B) sections about two-thirds through the dLGN, and contralateral (C) and ipsilateral (D) sections about one-third through the dLGN are shown. These sections show fragmented laminae A1 and nearly complete filling of laminae C. From Creel et al., 1982 (31).

chromosomal looping rather than linear sequence such as suggested for the X chromosome (55, 56). Chromosome 11q possibly contains a domain coordinating tyrosine metabolism and coding for decussation (57).

More intra-genome communication is probably taking place than currently credited. In addition to control of visual embryogenesis by protein coding, embryogenesis is plausibly affected by contributions from noncoding DNA or conserved noncoding portions of the genome. Noncoding DNA sequences are located near or within developmental gene loci that likely contribute to modulation or expression, and provide communication to bridge the gap between loci (52, 53, 58). Species-specific differences appear to originate more in noncoding space (59). Species likely evolve unique noncoding sequences contributing to variation in embryogenesis between species, and presumably are responsible for singular features in human CNS development (60).

The chromosomal proximity of tyrosinase loci and ROBO 3 and 4 is not replicated in most mammalian genomes, but primate vision is the most complicated of mammals, and interactive gene control likely is more centralized in human beings. In other mammals loci on different chromosomes plausibly communicate to coordinate their expression (61). The "ROBO code" is likely a code of gene expression not an environmental interaction during embryogenesis (62).

6. Melanin pigment

Melanin pigment is a phylogenetically and genetically consistent metabolic vertebrate pathway dating back to at least the evolution of early chordates. The presence of melanin pigment is as fundamental as any characteristic of vertebrates. During mammalian embryonic development melanin pigment is pervasive as is its interaction with neural crest cell migration, along with ocular and auditory system development. Additionally the chemical pathways of melanin pigment, brain catecholamines, liver, thyroid and adrenal gland metabolism maintain a delicate balance anchored by tyrosine metabolism (63). Even in phenotypically pigment-less cavefish that mutated to not express pigment the ability to produce pigment is preserved in neural crest derived melanoblasts (64).

Melanin's role in visual function can be traced back to the hydra and jellyfish 600 million years ago (65). Melanin pigment's roles in the eye are different than other parts of the body. Melanin pigment is conspicuously present and melanocytes are most active early in vertebrate embryogenesis. Ocular melanocytes are relatively dormant after embryogenesis and unlike extra-ocular melanocytes do not secrete melanin. The genetic basis of pigment cell development and differentiation is conserved from teleosts to mammals. The melanin pigment chemical pathway initiated with tyrosine is expressed similarly from drosophila to primates. The common ancestor of drosophila and primate eye was likely an organism similar to a rag worm 500 million years ago (66). The molecular sequence leading to eye formation in the fly is recapitulated in the developing human eye (67, 68). In general, phylogeny is recapitulated in the embryonic development of the visual system.

7. Human albinos

The features associated with hypopigmented retinae vary between species and individuals. Readily observable in most human albinos is anomalous foveal development and lack of vascular sparing of central foveal area of retina (24, 69). Less obvious is the predominance of crossed optic fibers at the optic chiasm quantified by visually evoked potential, functional magnetic resonance imaging (fMRI) (27), cortical thickening (26) and aforementioned anatomical studies. Retinal ganglion cells (RGCs) in pigmented retinae that originate from the nasal side of fovea cross at the optic chiasm. RGCs originating temporal side of fovea in pigmented human beings do not cross at the optic chiasm. Figure 12 is a schematic approximation of differences between the optic chiasm of ocularly pigmented and albino human beings.

In mammalian hypopigmented retinae optic nerve ganglion cells that originate from retinae nasal side of fovea, and nearly all RGC neurons originating from up to 15 degrees in temporal retina also cross at the optic chiasm (Figure 12). The proportion is not known in human beings and likely varies considerably. In many albino animals essentially all optic neurons from nasal and temporal retina cross at the optic chiasm. In Figure 12 the 80% crossed and 15 degree shift of vertical meridian in human albinos was estimated based on animal anatomical studies and multifocal visually evoked potential studies (29, 41).

The routing of RGCs through the chiasm of human and other Haplorrhine primates is organized similar to schematic Figure 13 in that uncrossed RGCs originate and remain lateral at the chiasm (70), whereas in rodents and carnivores the nasal and temporal RGCs mix within the chiasm before routing ipsilateral or contralateral (2, 71). In marsupials, insectivores and primates the RGCs projecting to either hemisphere remain largely segregated with uncrossed fibers located laterally in the chiasm. In rodents and carnivores RGCs mix in the caudal nerve.

Figure 14 depicts comparison of optical coherence tomography (OCT) through the foveal area of an ocularly pigmented human being (A) and a human albino's (B) foveal areas. In (A) note the foveal depression and that the nerve fiber layer, i.e. red layer on top, is not present across the foveal area. In most human albino retinae the nerve fiber layer (B) continues over the potential foveal area. Figure 15 pictures OCTs of four albinos examined at the Moran Eye Center. To view more human albino OCTs see Gargiulo et al. (72) and McAllister et al. (69).

Foveal under development and considerable variability among albino foveae is likely due to amount of ocular pigment and genetic background (73). Albino human beings manifest a reduction in cone density in the central retina of infants (74) and adults (25). Multifocal ERG studies provide evidence of arrested postnatal development of foveae in albino infants (75). Primates are the only mammals with foveae, but in almost all mammals with albinism the central retina is underdeveloped (76, 77).

An exception is the albino squirrel (78). Squirrel retinae contain a very large cone population. Rods are disrupted in albino development probably because they develop slightly later in retinal development and that cell cycle events get out of control when rod production is taking place. Cell cycle control is relatively normal early in retinal development when cones are being generated.

Retinal vascularization in human pigmented retinae spares the foveal area, whereas in albino human retinae small vessels and capillaries intrude into foveal area. Figure 16 compares the central vascular organization in ocularly pigmented and albino human retinae. Retinae of ocularly pigmented human beings exhibit an avascular zone surrounding the fovea, albinos do not. There are likely many modifying factors such as extent of hypopigmentation specific to the loci tempering phenotypic expression.

The neural retina and retinal pigment epithelium (RPE) demonstrate an intimate embryonic relationship to the extent that each can differentiate into the other (79). An interaction exists between melanin pigment in the RPE and the development of the fovea and choriocapillaris, the blood supply to the retina, and RGC axon guidance (80). The RPE-derived vascular endothelial growth factor (VEGF) is essential for choriocapillaris development (81, 82). Additionally, pigment epithelium derived factor (PEDF) was isolated in the developing fovea suggesting axon guidance genes presumably accompany early mechanisms determining vascular patterning in macular area (83). The PEDF has a major function in development of the foveal avascular area (84).

8. Scalp-recorded VEPs in human beings

In 1974 using scalp-recorded visually evoked potentials (VEPs) four genetic forms of human oculocutaneous albinism exhibited electrophysiological evidence of reduced uncrossed optic fibers (14). Similar results were published for human ocular albinos (85) and replicated in early studies by Taylor (86) and Coleman et al. (87). Reviews of research in this area: Guillery (88), Hoffman et al. (41), Neveu & Jeffery (2) and Bridge et al. (26).

The best visual stimulus to use recording VEPs from most albinos is a pattern onset/offset with individual checks subtending about 1 degree of arc. For individuals with very poor vision and infants, flash stimuli are preferred. In some albinos comparing evoked potentials using the International 10-20 System locations O1 and O2 (89) demonstrate the misrouting. In most albinos more lateral locations along the same plane about halfway to T5 and T6 (H3 and H4), marked in Figure 17 as blue area, better demonstrate misrouting. An early finding was that with monocular stimulation the “difference” potential comparing 10-20 International System scalp locations O1-O2, or H3-H4 across the midline is an efficient way to exhibit chiasmic misrouting in albinos (90). The worst stimulus is pattern reversal, which exacerbates nystagmus in albinos blurring the image.

To detect misrouting at the chiasm a minimum of two recording sites is required, one positive electrode and one negative location in each hemisphere about 3 cm above the inion in an adult and 4 cm or more off the midline. This bipolar montage records a "difference" potential, requiring no additional reference electrode. The ground electrode can be attached anywhere on the person. In ocularly pigmented human beings innervation of visual cortex from nasal and temporal retinae is comparable so the "difference" potential recorded between hemispheres would be similar in form whether stimulating the left or right eye (Figure 18). In contrast, most central visual field retinal ganglion fibers (RGCs) cross to the contralateral hemisphere in albinos so the "difference" potential recorded between occipital hemispheres will change polarity across the occipital area when VEPs following monocular stimulation are compared (Figure 19).

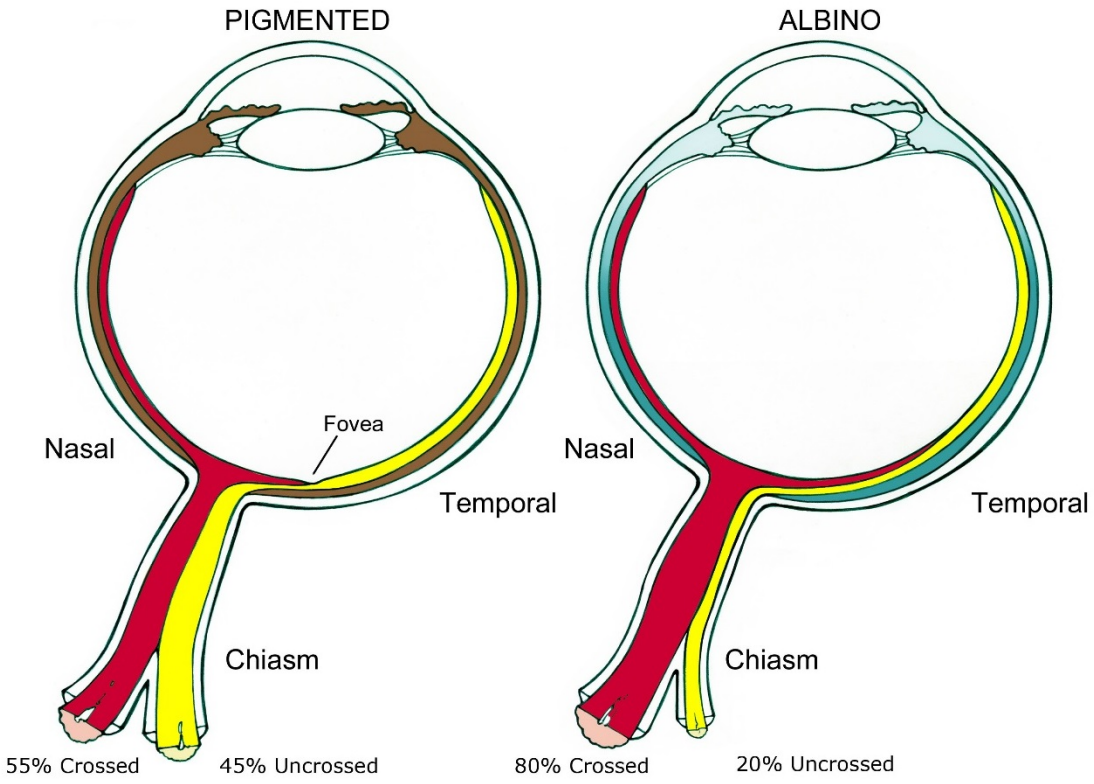

Figure 12. Schematic of approximate distribution of crossed and uncrossed RGCs at the optic chiasm in albino human beings.

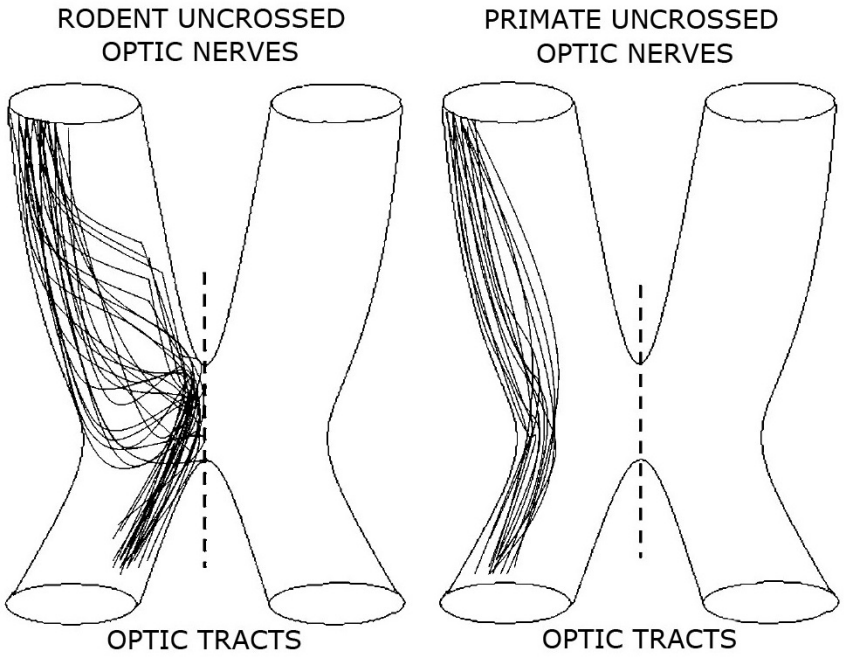

Figure 13. Schematic drawings of two forms of RGC axon projection through the optic chiasm to the ipsilateral optic tract. Ipsilateral RGCs of the rodent mix with RGCs from the other eye. Primate and marsupial RGCs maintain a lateral course through the chiasm. From Neveu and Jeffery, 2007 (2).

An important addition to VEP methodology was the development of multifocal visually evoked potential (mfVEP) technology by Erich Sutter (91). The first publication of mfVEPs in human albinos was by Michael

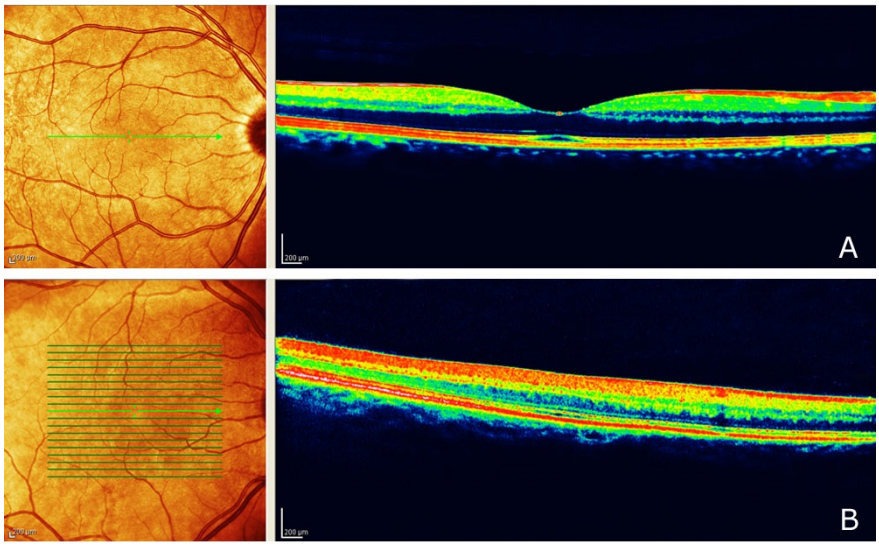

Figure 14. Ocular coherence tomography (OCT) through the fovea of a normally pigmented (A) and albino (B) human being. Note the absence of foveal pit and the nerve fiber layer (red) coursing over foveal area in albino compared to pigmented (A) nerve fiber layer (red) ending before fovea.

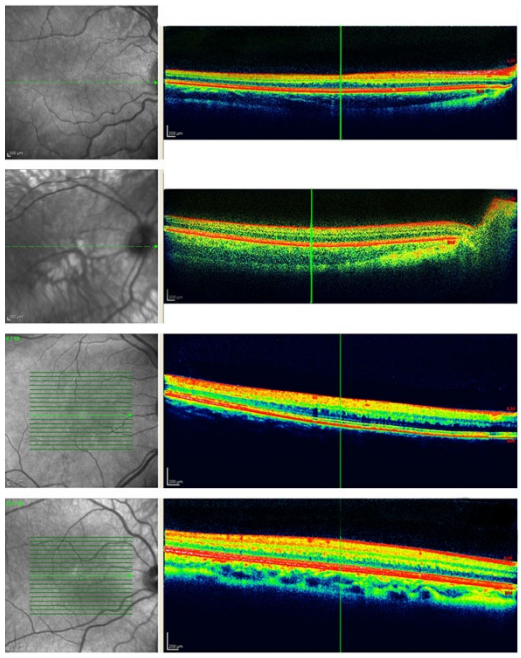

Figure 15. Ocular coherence tomography (OCT) of four albinos showing lack of foveal pit and top nerve fiber layer (red) coursing over foveal area.

Hoffmann and colleagues (41). This group has continued to publish advances in dissecting the human albino visual system using mfVEPs and fMRI studies (26, 92-95).

VEPs are of profound value in detecting the misrouting of the optic nerves in human albinism and revealed that an on average a central ±8 degree wide vertical strip in the central is affected by the resulting representation abnormality (96). The extent of the misrouting varies, depending on pigmentation deficit, between 2 and 15 degrees. This indicates that RGCs originating up to 15 degrees into temporal retina erroneously cross at the optic chiasm. The most important addition of mfVEPs is allowing for a spatially resolved characterization of VEP responses. This approach can be combined with the misrouting VEP paradigm (90, 97) to yield visual field

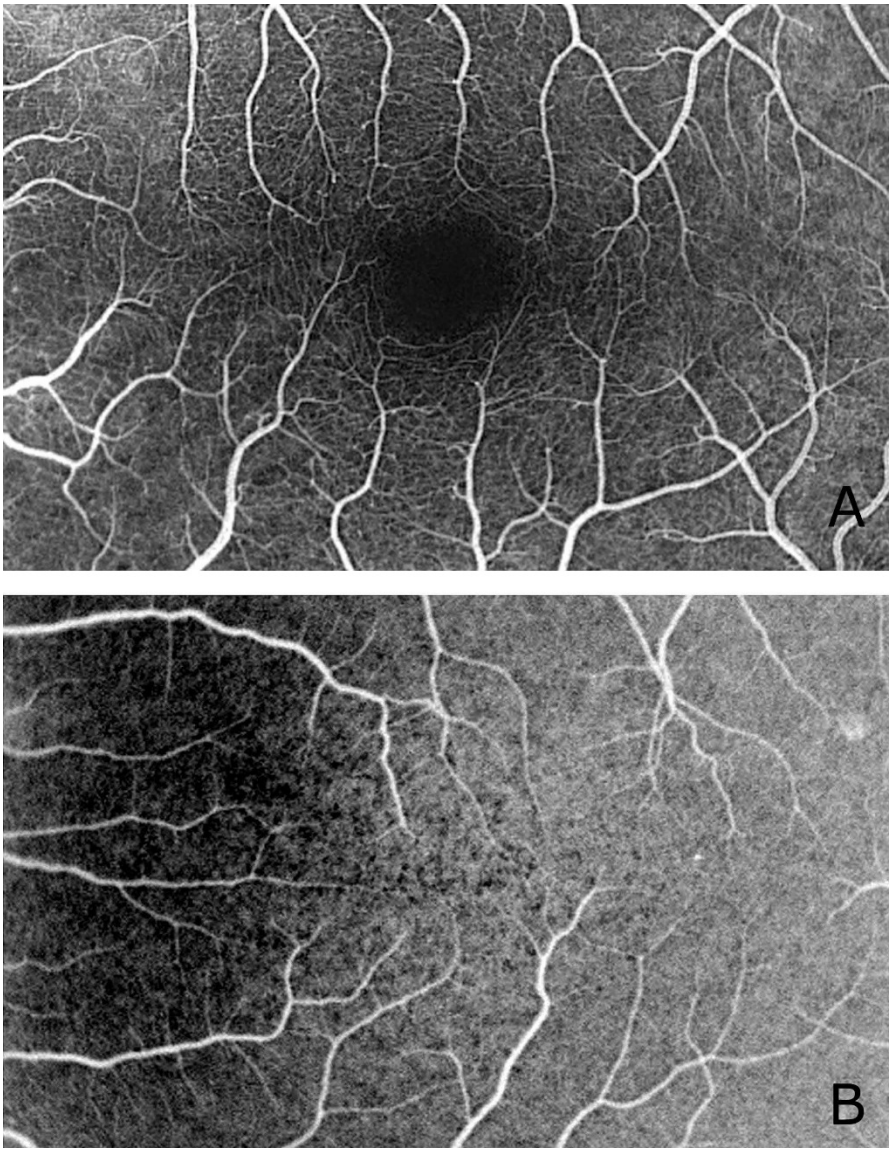

Figure 16. Angiogram of choriocapillaris of normally pigmented human ocular fundus (A) showing vascular sparing of the foveal area, compared to negative of red-free photograph of human albino ocular fundus (B) showing vascular intrusion into foveal area.

topography of the abnormal visual field representations typical for albinism as pioneered by Michael Hoffmann et al. (41). Figure 20 is a print of mfVEPs recorded from a Type 1 oculocutaneous albino (OCA1). This person has nystagmus and exotropia, but exceptional acuity for a Type 1 oculocutaneous albino. His acuity meets requirements of visual acuity required for a driver's license. The central visual field stimulated for these mfVEPs extended over 35 degrees horizontally and 30 degrees vertically, similar to the perceptual field of a Humphrey 24-2 visual field perimeter test. Potentials that reverse in polarity indicate temporal retinal field areas projecting RGCs that cross the optic chiasm. MfVEPs require reasonably stable fixation (41, 96, 98), but they are a useful extension of the classical misrouting VEP paradigm as they permit the detection of locally confined, i.e. only small misrepresentations. Their prime use is to explore the specificity of misrouting for albinism. MfVEP studies confirmed the absence of evidence of misrouting in carriers of OA (41).

While fMRI was used to validate the misrouting VEP (27, 92), it further assists in uncovering the organization of the human visual cortex in albinism, and higher cortical function (30, 99). These studies indicate that the unrepresentative visual input to each hemisphere is propagated to higher processing stages (95) and is made available for perceptual (94, 100) and visuo-motor integration (101). Further, structural

MRI investigations underscore that the anatomy of the visual cortex in human albinism appears to be affected more strongly by the foveal hypoplasia than by the misrouting of the optic nerves (26, 102).

Maturation and aging of the visual system produce measurable changes reflected in visually evoked potentials. Neveu et al. (103) described dramatic differences in a population of albino human beings ranging from 8 months to 60 years. Visual acuity usually improves until adolescence due to physiological maturation, dampening of nystagmus, finding a favorable head position, and learning how to manage poor acuity, including perceptual cues (104-106).

Acuity is significantly diminished in most human albinos averaging from 20/80 to 20/200 with a wide range of 20/40 to 20/400. Nystagmus, usually horizontal, pendular or jerky in character is almost always present. A high incidence of strabismus is also seen in albinism including both horizontal and vertical misalignment (86, 107).

Contributing to differences in optic tract development are possible differences in axon sizes and myelination in the albino mammal's optic tract (108). When RGC axons go to the wrong side of the brain they may not myelinate properly. Myelination changes with age add weight to Neveu et al.'s (103) finding of age-related changes in VEP development.

9. Visual perception

Studies demonstrate that albino human beings do not fuse binocular stimuli (104, 109, 110). Few binocular cells are located in areas 17, 18 and 19 in Siamese cats and cats with complete albinism, disturbing the underlying anatomical connections for stereovision (111-113). Some individuals with albinism manifest coarse binocular fusion with some stereovision (114). In addition, while areas 17/18 of the Siamese cat do not contain binocular cells, the postero-medial lateral suprasylvian area (PMLS) includes binocular cells (115). The superior colliculus (SC) also possesses binocular cells (116). The corpus callosum possibly is an anatomical connection enabling some binocular vision (117-120). Stereovision may be accomplished through these cortico-cortical connections. Although stereovision is dramatically affected in albinos, spatial perception remains (94).

Adjustments improving perception appear to be made at each level as the anomalous visual information in albino visual pathways progress towards the cortex. In the albino cat the disaster at the level of the dLGN where only 46% of cells responded normally improves to 84% in cortical area 17, and to 70% of cells in cortical area 18 (121). The competence of the albino visual system improves greatly at the cortical level of cats and human beings (100) resulting in near-normal visual perceptual abilities within the limits of an individual's acuity.

In general the level of pigmentation of an albino correlates negatively with severity of expression of visual anomalies (73) (122). It is likely that the more pigment present in the retina, the more normally routed RGC fibers.

10. Genetic classifications of forms of human albinism

Current classification of forms of albinism is based on genetic locus. Figure 21 is a photograph of an individual with Type 1 oculocutaneous albinism. Chromosomal location has been identified for twenty forms of human albinism on twelve different chromosomes: oculocutaneous albinism (*OCA1-7)*, ocular albinism (*OA1*), nine forms of Hermansky Pudlak syndrome (*HPS1-9*), Chediak Higashi syndrome (*CHS*) and Griscelli syndrome (*GS*) (123, 124). An additional syndromic form of albinism to be added is the rare Vici syndrome (*VICIS*) (125-127). Phenotypic expression varies considerably within genetic forms of albinism, and even between siblings (128, 129). Many genes modify expression of albinism (130). For tyrosinase enzymes alone more than 100 mutations are involved in coding (see Albinism Database (http://www.ifpcs.org/albinism/index.html).

Visual abnormalities reported in albinism do not include disorders of hypopigmentation due to embryonic migration defects of neurons and pigment cells from the neural crest such as in Waardenburg syndrome and

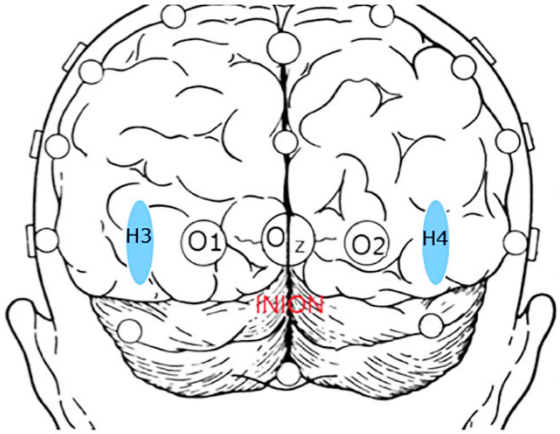

Figure 17. Schematic of occipital area indicating 10-20 International System scalp electrode locations highlighting locations H3 and H4.

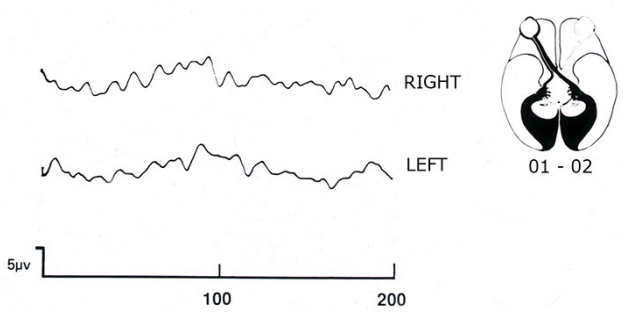

Figure 18. Pattern onset/offset visually evoked potentials recorded across occipital scalp in normally pigmented human being showing little difference between monocular RIGHT and LEFT visual stimulation. From Creel et al, 1990 (212).

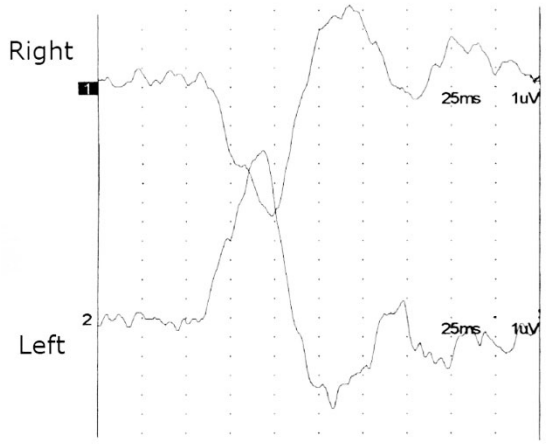

Figure 19. Pattern onset/offset visually evoked potentials recorded across occipital scalp from an albino showing the significant difference between Right and Left monocular simulation.

deaf white cat (*W* gene), vitiligo or piebald spotting, nor other forms of hypopigmentation such as phenylketonuria. These conditions do not exhibit the visual anomalies.

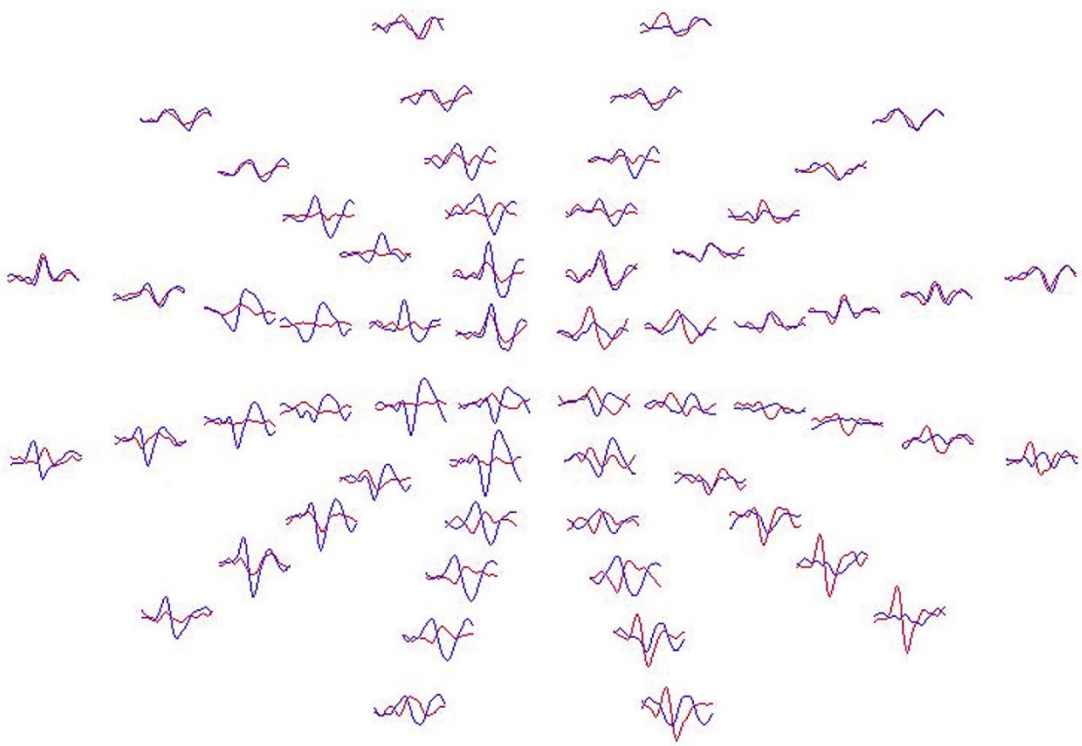

Figure 20. Multifocal visually evoked potentials recorded from a Type 1 human albino reflecting the central 35 degrees of visual field. Potentials that reverse in polarity indicate locations in temporal retina that retinal ganglion cells (RGCs) cross at the optic chiasm.

11. Exceptions to direct association with albinism

Recently a novel gene mutation on human chromosome 16 was described that is associated with foveal hypoplasia, optic-nerve-decussation defects, and anterior segment dysgenesis (FHONDA) in the absence of pigment deficits (131, 132). Current research addresses whether in this condition optic nerve misrouting is initiated by a mechanism that is independent of the one that is associated with the pigment deficit in albinism. While enhanced crossing of the optic nerves at the optic chiasm was previously viewed to be specific for albinism or related only to ocular pigment deficits there may be exceptions. FHONDA may be an important exception. A possible site of common determination of visual abnormalities in FHONDA and albinism could be the similar influences affecting optic anomalies in both such as genetic control by Sonic hedgehog (Shh), VSX2, PAX 2 and PAX 6.

There are reports of optic misrouting in human non-albinos such as some with Kartagener syndrome (133), and selected hypopigmented patients with Prader-Willi syndrome (134), with microdeletion at tyrosinase locus 15q11-13 superimposed on the most prominent albino sequence. The Kartagener syndrome loci, 15q24-25, are on same arm of chromosome 15q as the most prominent human albino sequence. Few individuals with the Kartagener syndrome show optic misrouting (135). Other exceptions are some individuals with congenital stationary night blindness (CSNB) reported to express optic misrouting (136, 137). Genetic loci for forms of CSNB range from chromosome Xp11 to Xp22 (138). These mutations are located on the same arm of X chromosome located Xp22. Some of these exceptions are possibly due to interaction with albino loci or a common feature to both of dysregulation within these sequences. Communication may be enhanced by noncoding DNA bridging the gap between nearby loci.

Figure 21. Type 1 oculocutaneous albino (OCA1).

12. Underlying mechanisms

Many studies were published pursuing a causal relationship between retinal pigmentation and determination of neuronal routing at the optic chiasm. No mechanism has been described that can be generalized across species and genetic loci. Prominent theories include the role of tyrosinase or its precursor DOPA as critical in the synthesis of melanin such as reporting addition of DOPA to albino eyes in vitro normalizes patterns of cell production (139). Ocular albinism (OA1) associated with a mutation of the GPR143 (G-protein-coupled receptor) gene on the X chromosome (Xp22.3) provides evidence of another possible function of DOPA. The GPR143 gene regulates melanin biosynthesis (140). The OA1 GPCR protein encoded by GPR143 gene was found to be a selective DOPA receptor, where both Dopamine and DOPA compete to bind at its site (141). DOPA function in the melanin pathway may also play a role in the downstream effects that affect the developing retina (142).

Other factors influencing ganglion cell targeting at the optic chiasm include, in different species, growth cone action, molecules, and regulatory genes including laminin, NCAM, L1 and cadherins (143). Evidence that Netrin-1 (144), Slit ligand molecules that are expressed at the optic pathway and their associated axon guidance receptors from the Roundabout (Robo) family (145), Sema5A (146), Sonic Hedgehog (Shh) (147), transcription factor 2 (Zic-2) regulated by Islet 2 in mice (148, 149), and EphrinB2 (EphB2) (150) are also suggested as impacting cell fate. The transcription factor visual system homeobox 2 (VSX2) probably also affects the retinal anomalies (151, 152). Many signals likely vary between species.

13. Vision and hearing

Vision and hearing have an ancient history of evolving in parallel traced back to the PaxB gene, which functions as a single gene controlling eye and hearing (mechanoreceptors) genesis in box jellyfish predating the later-appearing separate Pax 2 and Pax 6 genes (153). The continuity of SOX 21 was mentioned earlier (53). There are evolutionary connections between eyes and mechanoreceptors of the inner ear to the extent that during evolution, "sensory cells can shift their sensory modalities" (154).

There is a history of both functional integration and anomalous syndromes involving the visual and auditory systems such as Usher's Syndrome, which includes retinitis pigmentosa and congenital deafness. In spite of their differences in embryogenesis further similarities were recently described in retinal and inner ear hair cell physiology. The same Usher protein functions in retinal rod physiology and inner ear hair cell physiology (155, 156) and ribbon synapses are similar in structure and function in both photoreceptors and hair cells (157). Further metabolic roles of melanin in the inner ear, and the similarities of retinal and inner ear physiology are yet to be elucidated. Melanin pigment is located in the stria vascularis of the inner ear (158, 159). Figure 22 depicts a decalcified cochlea of pigmented guinea pig (A) displaying a band of melanin pigment (P) in the stria vascularis, and a section through a pigmented guinea pig cochlea (B) showing melanin pigment. Figure 23 is an enlargement of an area in a different guinea pig similar to that boxed in Figure 22B illustrating detail of pigment deposition. Melanocytes are adjacent to and wrap around capillaries in the stria vascularis.

In most mammals auditory cues mainly tell vision where to look (160, 161). Within each species spatial vision and auditory localization evolve in a coordinated manner. Analogous evolutionary and functional relationships exist in vision and audition. The second level termination of visual neurons is cortical including synapses with binocular cells, the substrate for binocular, stereo, and spatial vision. The second level neuron terminations in the auditory system are in the superior olivary complex where binaural cells receive input from each ear giving similar spatial information. The auditory space map in the brainstem is strongly related to the cortical visual space map (162). Visual and auditory spaces are connected to the extent that in human beings fMRIs depict more recruitment of visual cortex than auditory cortex when blind individuals perform auditory echo localization (163).

Albino mammals are not hearing impaired, per se. The auditory and visual deficits in albino mammals are connected in that similar anomalies are present in processing the highest-level integration of spatial localization.

Auditory anomalies are reported in albino mammals. The absence of melanin pigment in the inner ear of albinos is associated with susceptibility to noise damage (164, 165). In human beings and animal models prolonged sensitivity to noise measured as a longer temporary threshold shift (TTS) following exposure to loud sounds is documented (166-168). Cell size and dendritic length in the medial superior olivary nucleus is reduced in albinos (167, 169). Functionally the reduced cell size in brainstem olivary nuclei was associated with reduced binaural cell responses in medial superior olive of albino cats (170). One study demonstrated reduced ipsilateral projections from the cochlear nuclei in hypopigmented ferrets (171).

The auditory brainstem response (ABR) is an auditory version of a visually evoked potential except the generators measured end at the level of the superior colliculus. Auditory brainstem responses are recorded by placing a positive electrode on top of the head at 10-20 International System position Cz. A negative pole electrode is placed on ipsilateral earlobe or mastoid. Often the contralateral earlobe or mastoid is used for ground location. Click stimuli at one or more intensity approximately 70 dB above hearing level threshold (HL) are presented to one ear at click rates of 10 or more per second. Potentials appearing in the first 10 milliseconds evoked by about 2,000 clicks are averaged. Audiologists record a more complicated sequence using several click intensities, tones bursts, and bone conduction testing to evaluate hearing.

A feature of the ABR is that in addition to anomalies in the auditory brainstem pathways, alterations in adjacent brainstem structures such as cranial nerve nuclei IV to VII are often detected. The ABR is of use locating etiology of ocular and facial movement disorders such as Duane's retraction syndrome, Marcus-Gunn ptosis, blepharospasm, facial cranial nerve palsies, and is a common site of demyelination in patients with multiple sclerosis. Another feature of the ABR is the first five peaks, I – V, are associated with the level of the brainstem generating each component.

A sample human ABR is depicted with generators labeled in Figure 24. ABRs of most mammals contain 5 or more components in the first 6 milliseconds following click stimuli. ABRs of some rodents include a double component III due to separate medial and lateral olivary nuclei generators. A variant in some human ABRs is coalesced components IV and V into one wave. In albino human beings and animal models component III of ABRs are attenuated. These are generated in region of the medial superior olivary nuclei reflecting the reduced neuronal size and dendritic length in albino mammals (32, 167, 169, 172). Figure 25 illustrates sample abnormal ABRs in a Type 1 oculocutaneous human albino with components III – IV attenuated in amplitude.

14. Eye Movement: Albinism, Dissociated Vertical Deviation, Latent Nystagmus

Adjacent to the brainstem auditory centers are the nuclei integrating sensory input including the superior colliculus and other nuclei involved in eye alignment and fixation. Abnormal proportions of ipsilateral RGCs in albino mammals include reduced RGCs to mid-brain nuclei that contribute to strabismus, nystagmus, and atypical optokinetic nystagmus in albino mammals. In albino guinea pigs, rabbits and ferrets there are no ipsilateral optic projections to the ventral lateral geniculate nucleus (LGNv), superior colliculus (SC), pretectum, nucleus of the optic tract (NOT) or accessory optic system (AOS) (173-175).

In the normally pigmented cat about 50% of RGCs project via the LGN to the ipsilateral cortex. 24% of RGCs originating in temporal retina project to the ipsilateral superior colliculus (176), and about 15% of RGCs project to the ipsilateral pretectum (177). The albino cat has very few ipsilateral projections to the pretectum and almost no ipsilateral projections to superior colliculus (31). All albino cats have nystagmus and many have strabismus.

Several types of aberrant optokinetic nystagmus (OKN) are described in human albinos (178-180). The nuclei responsible for the OKN are the terminal nuclei of the accessory optic system: the dorsal terminal nucleus (DTN), lateral terminal nucleus (LTN), medial terminal nucleus (MTN) and the Nucleus of the Optic Tract (NOT). Figure 26 depicts the rat and rabbit accessory optic system showing the connections of the medial terminal nucleus (MTN) (181). Figure 27 illustrates the accessory optic system (AOS) projections from the lateral terminal nucleus (LTN) of a primate, the Marmoset.

Albinism in mammals is associated with most RGCs crossing in the optic chiasm. Few RGCs project to the ipsilateral side ultimately projecting to the cortex and brainstem. The optic chiasm plays a pivotal role in human binocularity. Hemidecussation in the optic chiasm dictates the nasal retinal ganglion cells to cross to the other side of the brain, and temporal retinal ganglion cells to stay on the same side of the brain. Retinotopy directs ganglion cells, one nasal and one temporal from each eye, to pair up at the cortex. In this way each pair finally drives one binocular cell in the visual cortex. Besides hemidecussation in the optic chiasm, the corpus callosum and commissural connections in the brainstem are essential building blocks of mammalian binocularity. Identical binocular retinotopic loci on both sides of the cortex are connected through the corpus callosum. These connections facilitate fusion of the eyes, and the right and left visual hemifield (182, 183). Albinism, characterized by a substantial reduction in ipsilateral projections of RGCs in the optic chiasm, and poor binocularity, results in less coordination and loss of association between the eyes, and infantile strabismus occurs. Dissociated Vertical Deviation (DVD) and Latent Nystagmus (LN), both occurring in infantile

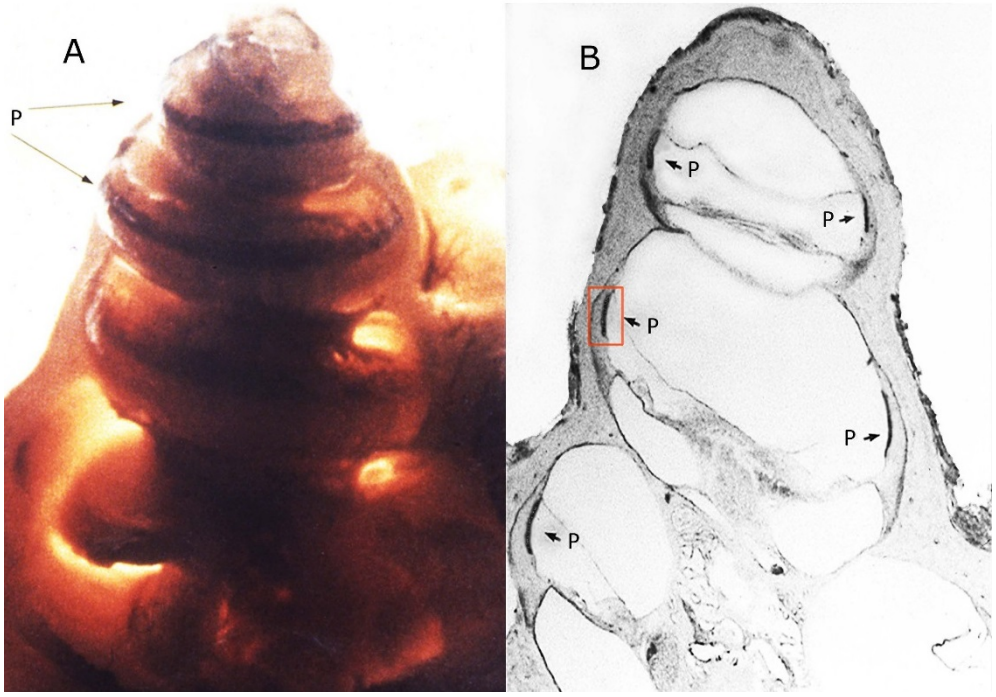

Figure 22. Decalcified guinea pig cochlea (A) and sagittal section (B) through a guinea pig cochlea show deposition of melanin pigment (P) in stria vascularis Red boxed area enlarged in Figure 23.

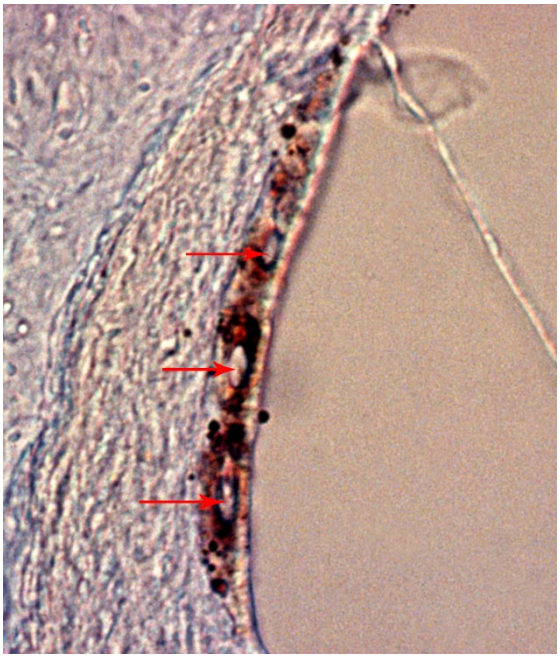

Figure 23. Red-boxed area in Figure 22 enlarged showing melanin deposition adjacent to capillaries indicated by red arrows. From Conlee et al., 1989 (158).

strabismus, are characterized by binocular motor dissociation. The co-occurrence of both DVD and LN in albinos suggests a common dissociative origin (182).

There are several theories rooted in the argument that older evolutionary connections dominate during the first several months of human infancy before cortical pathways have matured. Michael C. Brodsky and colleagues propose atavistic reflexes of the accessory optic system generate the dissociated eye movements associated with

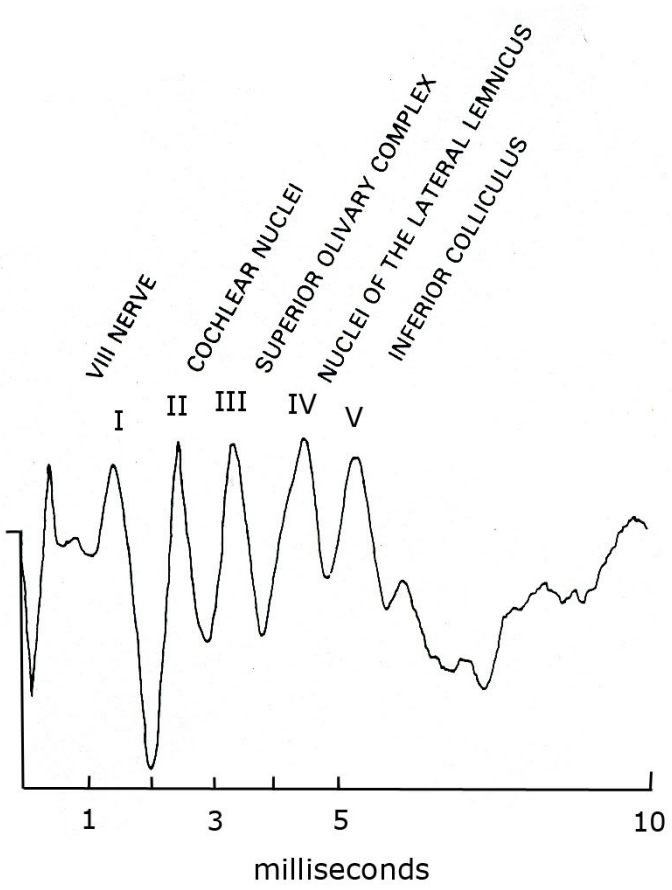

Figure 24. Auditory brainstem response (ABR) recorded from pigmented human being at click intensity of 70 dB HL and rate of 11.9 per second.

infantile strabismus (184-187). They argue that when foveal vision develops slowly in early infancy, the phylogenetically older optokinetic system prominent in lateral-eyed vertebrates that is expressed in first 2 months of infancy continues to be expressed. Monocular, subcortical, nasotemporal optokinetic asymmetry normal in lateral-eyed vertebrates is suppressed in human beings with cortical binocular vision. They suggest cases of possible infantile nystagmus may be due to genetically determined maturational delay in development of cortical binocular vision allowing phylogenetically older pathways to dominate; "[hypothesizing] that the oculomotor disturbances of infantile strabismus correspond to subcortical binocular visual reflexes that are operative in lateral-eyed animals."; and that the vestibulocerebellum actively contributes to generating infantile nystagmus (184).

Marcel ten Tusscher also proposes a fall back to older evolutionary connections including the corpus callosum, lateral geniculate nucleus, lack of normal binocularity at the cortex, and subsequent loss of binocular input to the subcortical centers including the superior colliculus (182, 188-191).

The evolution of the eye and the brain provides a possible explanation for both the anomalous eye movements in albino mammals, and the dissociation of infantile esotropia and its motor characteristics. In the course of evolution, the eyes moved from a lateral to a frontal position. In 300 million years, modern mammals, birds and reptiles evolved from a common ancestor, the captorhinidea (192, 193). Consequently, the monocular visual fields progressed forward on the head to overlap resulting in a binocular visual field. In lateral-eyed animals, the retinae project to the contralateral visual cortices only. These projections are also found in binocular mammals and birds with binocular visual fields. In binocular mammals there are also uncrossed projections from the

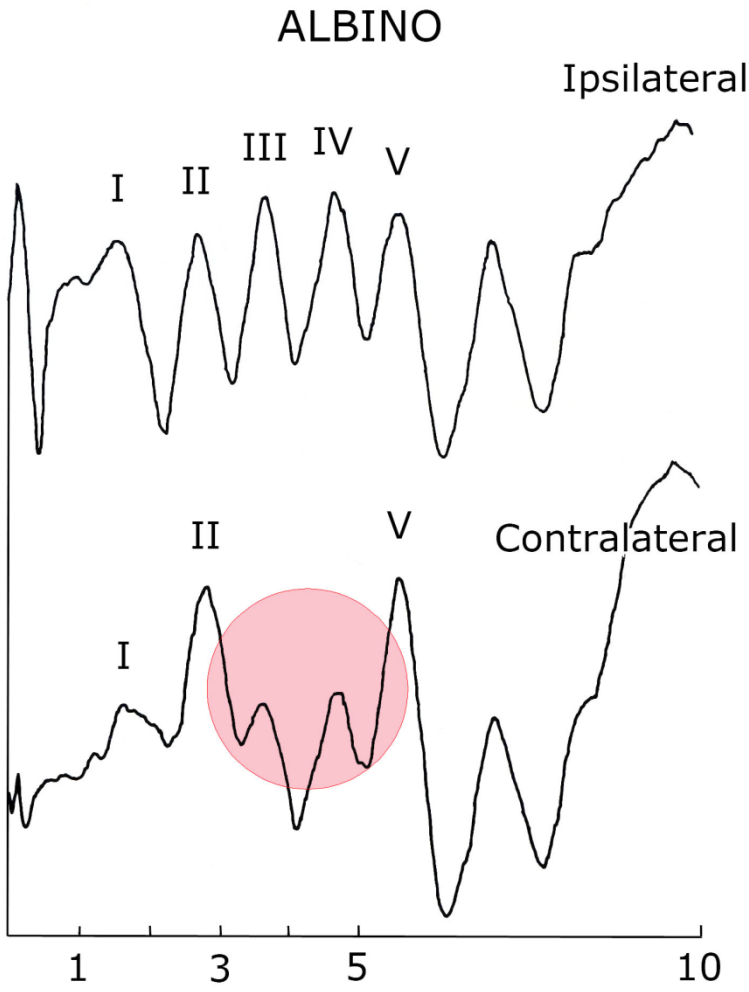

Figure 25. Auditory brainstem response (ABR) recorded from a Type 1 oculocutaneous human albino (OCA1) showing attenuated component III in contralateral ABR. From Creel et al., 1980 (172).

temporal retinae to the visual cortex. Partial chiasmal decussation and the corpus callosum provide the necessary connections for binocular vision to develop (194). Disruption of normal binocular development causes a loss of binocularity in the primary visual cortex and adjacent areas. Outside the primary visual cortex, the contralateral eye dominates while the temporal retinal signal appears to lose influence.

Complete motor dissociation between the eyes often results from sensory dissociation between the eyes. In human achiasma, where all retinal nerve fibers project to the ipsilateral cortex, saccades are executed monocularly. Dissociation with monocular saccades also occurs in animals with lateral eyes, e.g. reptiles. Retinal ganglion cells in these species show 100% crossing in the optic chiasm.

Eye movements in animals with laterally-located eyes are intended to stabilize the visual environment. The vestibular ocular reflex compensates for body movements and the optokinetic reflex compensates for optic flow. Motion sensitive neurons in the retina project to the contralateral brainstem, i.e. the terminal nuclei of the accessory optic system (Figure 27) that comprise the afferents of the optokinetic reflex. The nucleus of the optic tract (NOT) is one of these nuclei. The right NOT senses horizontal movement to the right, and the left NOT senses movement to the left. The major target of the optic tract in lateral-eyed animals, however, is the superior colliculus that is responsible for directing gaze movements and sensory integration. Similar neuroanatomical pathways and eye movements also exist in human beings. Human beings, in addition, demonstrate saccades,

pursuit and vergence, all of which are initiated by the visual cortex, not the brainstem. The retinal ganglion cells partially decussating in the optic chiasm are one of the evolutionary solutions for combining information from frontal eyes, enabling a correlated binocular signal in the visual cortex. The binocular human cortex ties the temporal retina of one eye together with the nasal retina of the fellow eye. Binocular visual experience overrules the brainstem through an ipsilateral signal directly from the retina, but even more so, via the visual cortex. The optokinetic reflex interacts with the pursuit system, while the superior colliculus (SC) interacts with the saccade and vergence systems (182).

Newborn children have smooth nasally directed monocular pursuit and impaired temporal-directed pursuit (195). At birth, the eye is controlled by the contralateral nucleus of the optic tract (NOT) (196). The right nucleus of the optic tract senses movement to the right, the left nucleus to the left. The newer pathways (ipsilateral from retina to nucleus of the optic tract (NOT), and the more abundant cortical projection to the NOT are activated through binocular visual experience. When the primary visual cortex does not receive realistic binocular input from both eyes the crossed older pathway dominates. The corticotectal pathway is dominated by the contralateral pathways (196, 197). Van Rijn et al. (198) showed that the same mechanism responsible for LN might be true for DVD (Figure 28). DVD combines vertical vergence with binocular torsional version. The elevating eye shows excyclotorsion while the fixating eye shows incyclotorsion. Van Rijn et al. (198) measured eye movements in DVD and showed that these movements are similar to the eye movements in disparity-induced vertical vergence. They suggested that, like LN that likely results from dissociation in the optokinetic /pursuit pathways, DVD might result from dissociation in the vergence pathways (190, 198). In LN the optokinetic pathway is driven by the signal that originates in the crossed retinal ganglion cells due to sensory dissociation, and less so the uncrossed cortical influence on the NOT in the brainstem. DVD likely is a supranuclear cortical problem of the pathways responsible for vergence originating in the crossed retinal ganglion cells due to sensory dissociation and less binocular cortical influence on the brainstem level (190).

DVD appears as a result of inhibition of the uncrossed temporal retinal signal. Beyond the primary visual cortex and the reciprocal connection of the callosum, a biased cortical activation leads to corticotectal stimulation dominated by the nasal retina. Figure 28 depicts the neuroanatomical summary of the pathways involved in DVD projection from nasal retina of the contralateral eye that dominate the superior colliculi in infantile strabismus. With occlusion of the left eye, the nasal bias in ocular dominance in the visual cortex in a patient with infantile strabismus gives rise to dominance of the left visual cortex and the left corticotectal pathway. The left superior colliculus (SC) projects to the left interstitial nucleus of Cajal (INC) and the right omnipause (OPN) neurons that results in elevation of the left eye and counterclockwise cycloversion. The pathway from the superior colliculi (SC) to the interstitial nuclei of Cajal (INC) links the two dimensional cortex and superior colliculus to the three dimensional brainstem. A monocular vertical signal leads to torsional vergence, DVD.

Partial decussation in the optic chiasm appears to be only one of the components important for binocularity. In rodents, e.g. the rat, with 95% crossing in the optic chiasm binocularity of the visual cortex depends on the combination of a signal from the contralateral eye through the geniculate pathway, and a signal from the ipsilateral eye to the contralateral geniculate and back through the corpus callosum. But even in cats that have substantial hemidecussation at the optic chiasm, transection of all crossing retinal ganglion cell axons in the optic chiasm appears not to affect most kinds of disparity (183). In mammals without partial decussation in the optic chiasm and without a corpus callosum, like marsupials, e.g., the wallaby, binocularity is still demonstrated in brainstem neurons (199). Binocularity appears to depend on commissural connections between both superior colliculi and between the nuclei of the optic tract. So, mammalian binocularity includes information provided by 1) partial decussation in the optic chiasm, 2) the corpus callosum and 3) commissural connections in the brainstem (182).

A high percentage of both infantile exotropia (67%) and esotropia (49%) patients were found to have a coexisting ocular or systemic abnormality (200). Agenesis of the corpus callosum underlines the importance of

the corpus callosum for normal binocular fusion. Strabismus is found in 46% of patients with partial agenesis of the corpus callosum (201). Moreover, hemispherectomy early in life often causes strabismus (202). Hemidecussation in the optic chiasm allows retinotopic matching between the nasal and the temporal retina. In albinism, many RGCs originating in temporal retina project to the contralateral LGN then to contralateral visual cortex. The border between crossed and uncrossed ganglion cell fibers in most human albinos appears to vary from point of fixation to 6–14 degrees into the temporal retina. Besides prominent misrouting in the chiasm, as in albinism, or agenesis of the corpus callosum, more subtle misrouting may cause a mismatch between temporal and nasal signals or between the direct thalamic and the indirect corpus callosum signal. Also the vertical meridian of one retina may not coincide with the overlapping zone of the other eye. In a primate study, the retinal vertical meridian in one of three monkeys was found not to coincide with the fovea (203).

Both esotropia induced by prisms or surgery in the sensitive postnatal period, and infantile esotropia change the binocular response of neurons in the primary visual cortex dramatically. After early surgically induced strabismus, neurons in the primary visual cortex, area 17, of kittens were found to be responsive to one eye only. An approximately equal representation of both eyes was found in both hemispheres. These results have often been confirmed, although a small bias of the non-operated eye in the ocular dominance columns sometimes occurred. Also most cortical neurons distal to area 17, the extrastriate cortex, could exclusively be triggered by one eye. An equal representation of both eyes is not found in the extrastriate cortex. The large majority of neurons in, for example, area 18, respond to the contralateral eye exclusively. In contrast to this huge contralateral dominance, only a slight dominance of the non-operated eye was found. In electrophysiological studies cortical neurons representing the temporal retina were found to be unresponsive to a stimulus from the squinting eye. In the early postnatal period, crossing nasal retinal afferents were found to be far less vulnerable than temporal uncrossed retinal afferents (204).

Crossed retinal dominance beyond the primary visual cortex appears to explain Dissociated Vertical Deviation and Latent Nystagmus, however, the cause of DVD is often explained differently. In a 2014 overview of a symposium on dissociated vertical divergence (DVD), Christoff et al. (185) discussed two popular theories on the origin of DVD: a hypothesis that suggests that DVD results from damping of latent nystagmus (LN), and another theory that postulates an atavistic origin: a righting reflex in fish.

Ten Tusscher argues the co-occurrence of both DVD and LN in infantile strabismus may well suggest a common dissociative origin, or perhaps one of these phenomena may be the result of the other. It is postulated to be the latter because damping of latent nystagmus occurs after the start of vertical divergence in DVD. However, DVD is more frequent than latent nystagmus. Moreover, DVD is a unique binocular cyclovertical eye movement. It is suggested to occur in order to suppress a horizontal eye movement and only if this movement is latent. Why does it not occur in manifest latent nystagmus and why not in congenital nystagmus? ten Tusscher argues the righting reflex observed in fish as the origin of DVD is less likely (190, 191). They argue the righting reflex is a postural reflex, not an ocular one and is orchestrated by the torus longitudinalis and the valvula cerebelli, and that both of these have no analogue in the human brain. Moreover, during a righting reflex the eye that is illuminated most, will move downward and the other upward. In DVD, however, blinding an eye by light will cause an upward movement of the blinded eye (the Bielschowsky phenomenon). Also, in contrast with the righting reflex, DVD is influenced by blur and by fixation. DVD combines vertical vergence with binocular torsional version. The elevating eye shows excyclotorsion while the fixating eye shows incyclotorsion. Early research measured eye movements in DVD. DVD characteristics appeared similar to the eye movements in disparity-induced vertical vergence (198).

Albinism is an example that sensory dissociation may be the result of a change in chiasmal decussation. Dissociated Vertical Deviation (DVD) and Latent Nystagmus (LN), are characterized by binocular motor dissociation with a common dissociative origin. Brain pathology may cause sensory dissociation, which may subsequently lead to motor dissociation. The binocular link between the cortex and the brainstem nuclei like the

NOT and the superior colliculus, is a key element in the origin of motor dissociation in infantile strabismus. In primates with infantile strabismus, the visual cortex beyond V1 is dominated by the crossed retinal signal. The equilibrium between the crossed and the uncrossed signal is not established. The brainstem is deprived of normal binocular input. This causes the NOT and superior colliculus to be driven mostly by the contralateral eye (Figure 28). If an eye is connected mostly to the contralateral NOT it will be more sensitive to motion directed towards the nose. This asymmetry causes latent nystagmus during monocular viewing. Fixation, saccades and vergence rely on the information from visual cortex to the superior colliculus. Loss of uncrossed retinal signal to the superior colliculus causes the upward movement of the eye. Cortical deactivation of this system causes Bell's phenomenon and the upward movement of the eyes during the early stages of general anesthesia that is related to the loss of cortical influence. The two dimensional cortex and superior colliculus are connected to a three dimensional brainstem. Vertical eye movements are associated with torsional movements by way of a pathway from the superior colliculus to the contralateral interstitial nucleus of Cajal (191, 205). If the contralateral eye dominates the cortical information to the superior colliculus, vertical vergence and torsional version (DVD) result.

If all features of infantile strabismus can be explained with a general principle based on proven changes in primate neuroanatomy, ten Tusscher suggests Occam's razor applies; and there is no reason to explain one of its features with a body reflex with characteristics different from DVD originating from the fish brain that phylogenetically bears little relationship to the primate brain, or assume it arises to facilitate viewing during occlusion of one eye. It follows that sensory dissociation beyond V1, most likely due to active suppression by the older evolutionary crossed pathway (crossed retinal dominance) leads to the eye movement dissociation that is typically seen in the infantile strabismus syndrome.

15. Creel theory

The Creel theory proposes that the lack of melanin pigment initiates atavistic expression of visual and auditory embryogenesis. In albino mammals' embryogenesis vision and hearing take an analogous step back. Visual anomalies in albino mammals, including human beings, represent a developmental field defect that occurs as a normal developmental state in closely related species (206). As pointed out by Meckel (207), primary malformations, in this case complete optic decussation, are not aberrant. Complete decussation of retinal ganglion cells at the optic chiasm is a conventional ancestral state in non-mammalian vertebrates, and reduced non-decussated optic fibers are the norm in ancestral mammals.

In an embryonic environment, neural stem cells, lacking positive signals to progress, transition into more primitive neural precursor cells (208). Melanin pigment in the nascent retina, or likely genetic coding for melanin pigment, is the positive inductive signal launching normal retinal development and retinal ganglion cell targeting. When retinal melanin is reduced, retinal embryogenesis defaults to the conserved genetic package existing when the species first evolved with a cascade of consequences.

The vertebrate genome includes coding of genetic past. Charles Darwin (209) popularized atavism as the term for reappearance of ancestral characteristics in future generations. Most atavistic expression is probably not random, but due to an error in early embryonic environment triggering expression of genes conserved across evolution. Actuating atavistic optic misrouting likely includes several possible events.

Mammals retain the evolutionary base instruction package for complete crossing of the retinal ganglion cells in ancestral vertebrates, and little genetic information re area centralis development, foveal, or vascular sparing of the foveal area. As each mammalian species or subspecies branched off and went their own way the genetic control of visual and auditory system development evolved to fit the environment of the species, revising embryogenesis that existed at the time the species became independent.

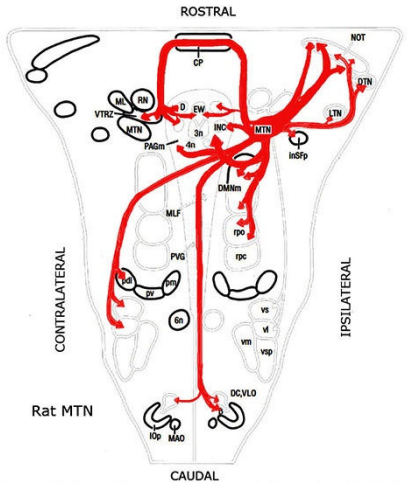

Figure 26. The efferent projections in the rat and rabbit of the medial terminal nucleus (MTN) are depicted. The plane of this figure is horizontal. Arrows depict projections of the MTN. (Re-labeled with permission from Giolli et al., 2006 (181).

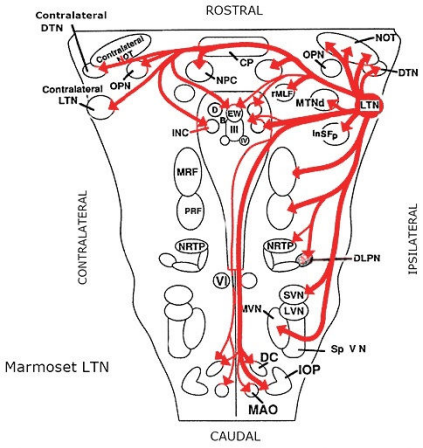

Figure 27. Diagram of the projections from the lateral terminal nucleus (LTN) in the marmoset. The illustration depicts a horizontal plane. (Re-labeled with permission from Giolli et al., 2006 (181).

The essence of this theory is that retinal melanin pigment is so fundamental to retinal, vascular, and early retinal ganglion cell targeting that insufficient retinal melanin triggers a switch resulting in the conventional genetic instructions not to be completed. Mammals with nondecussating retinal ganglion cells are genetically unstable. In albinos genetic instruction defaults to the simpler, more entrenched, platform. An atavistic expression of the conserved, more stable, genetic platform skewed toward complete crossing of retinal ganglion cells at the chiasm, and commensurate visual and auditory anomalies, develops consistent with genetics of each species' evolutionary origin.

A genome is not comprised of independently functioning loci on chromosomes, but an interactive compilation of coded instructions that reacts to alterations in the genome. The inductive signals for entirely crossed optic fibers are conserved in mammals. The atavistic fallback to this morphology is an easy misstep because of the phylogenetically recent development of the temporal retina, vascular sparing in macula, and foveal development in primates. As suggested by Gehring (210) regarding early evolution of eyes, morphogenetic pathways are progressively being modified by intercalation of novel genes. Phylogenetically late genetic addendums to conserved instructions are vulnerable to not being expressed if genetic cues, such as sufficient retinal melanin

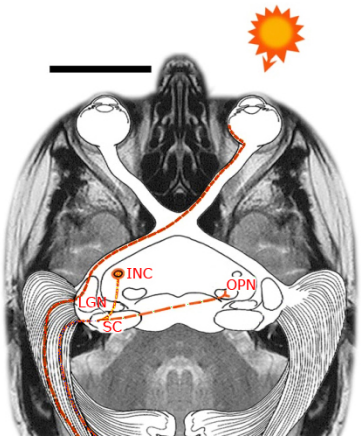

Figure 28. Neuroanatomical summary of the pathways involved in dissociated vertical deviation (DVD). (Redrawn with permission from ten Tusscher, 2014 (182).

pigmentation, are not present to support variation from highly conserved coding. Coding for reduced pigment in the retina also possibly disrupts silencing of ancestral genes, which dictate complete decussation of optic neurons and more primitive vascular and retinal development.

About the Authors

Dr. Donnell Creel's biography and photograph are seen in the chapter entitled "The Electroretinogram: Clinical Applications" in Webvision

References

1. Polyak, S.L., The vertebrate visual system; its origin, structure, and function and its manifestations in disease with an analysis of its role in the life of animals and in the origin of man, preceded by a historical review of investigations of the eye, and of the visual pathways and centers of the brain. 1957, Chicago: University of Chicago Press. xviii, 1390 p.
2. Neveu M.M., Jeffery G. Chiasm formation in man is fundamentally different from that in the mouse. Eye (Lond). 2007;21(10):1264–70. PubMed PMID: 17914429.
3. Sheridan C.L. Interocular Transfer of Brightness and Pattern Discriminations in Normal and Corpus Callosum-Sectioned Rats. J Comp Physiol Psychol. 1965;59:292–4. PubMed PMID: 14288359.
4. Lund R.D. Uncrossed Visual Pathways of Hooded and Albino Rats. Science. 1965;149(3691):1506–7. PubMed PMID: 17791642.
5. Lashley K. Studies of cerebral function in learning: V. The retention of motor habits after destruction of the so-called motor areas in primates. Archives of Neurology & Psychiatry. 1924;12(3):249–276.
6. Chang M. Neural mechanism of monocular vision: I. Disturbance of monocular pattern discrimination in the albino rat after destruction of the cerebral visual area. Chin. J. Psychol. 1936;1:10.
7. Muntz W., Sutherland N. The role of crossed and uncrossed optic nerve fibers in the visual discrimination of shape by rats. Journal of Comparative Neurology. 1964;122(1):69–77.
8. Sheridan C.L. Interocular transfer of brightness and pattern discriminations in normal and corpus callosum-sectioned rats. Journal of comparative and physiological psychology. 1965;59(2):292. PubMed PMID: 14288359.
9. Creel D.J., Sheridan C.L. Monocular acquisition and interocular transfer in albino rats with unilateral striate ablations. Psychonomic Science. 1966;6(3):89–90.
10. Giolli R.A., Guthrie M.D. The primary optic projections in the rabbit. An experimental degeneration study. Journal of Comparative Neurology. 1969;136(1):99–125. PubMed PMID: 5795899.

11. Güillery R. A quantitative study of synaptic interconnections in the dorsal lateral geniculate nucleus of the cat. Zeitschrift für Zellforschung und mikroskopische Anatomie. 1969;96(1):39–48. PubMed PMID: 5772028.
12. Creel D.J. Differences of ipsilateral and contralateral visually evoked responses in the cat: strains compared. J Comp Physiol Psychol. 1971;77(1):161–5. PubMed PMID: 5120681.
13. Creel D.J. Visual system anomaly associated with albinism in the cat. Nature. 1971;231(5303):465–6. PubMed PMID: 4931610.
14. CREEL. D., C.J. WITKOP, and R.A. KING, Asymmetric visually evoked potentials in human albinos: evidence for visual system anomalies. Investigative Ophthalmology & Visual Science. 1974;13(6):430–440.
15. Sanderson K. Retinogeniculate projections in the rabbits of the albino allelomorphic series. Journal of Comparative Neurology. 1975;159(1):15–27. PubMed PMID: 1109379.
16. Creel D., Giolli R.A. Retinogeniculate projections in albino and ocularly hypopigmented rats. Journal of Comparative Neurology. 1976;166(4):445–455. PubMed PMID: 1270616.
17. Guillery R., Oberdorfer M., Murphy E. Abnormal retino-geniculate and geniculo-cortical pathways in several genetically distinct color phases of the mink (Mustela vison). Journal of Comparative Neurology. 1979;185(4):623–655. PubMed PMID: 447875.
18. Guillery R. Visual pathways in albinos. Scientific American. 1974. PubMed PMID: 4822986.
19. Guillery R., Okoro A.N., Witkop C.J. Abnormal visual pathways in the brain of a human albino. Brain research. 1975;96(2):373–377. PubMed PMID: 1175020.
20. Hickey T., Guillery R. Variability of laminar patterns in the human lateral geniculate nucleus. Journal of Comparative Neurology. 1979;183(2):221–246. PubMed PMID: 762256.
21. Gross K., Hickey T. Abnormal laminar patterns in the lateral geniculate nucleus of an albino monkey. Brain research. 1980;190(1):231–237. PubMed PMID: 6769535.
22. Guillery R., et al. Abnormal central visual pathways in the brain of an albino green monkey (Cercopithecus aethiops). Journal of Comparative Neurology. 1984;226(2):165–183. PubMed PMID: 6330179.
23. Elschnig A. Zur anatomie des menschlichen albinoauges. Graefe's Archive for Clinical and Experimental Ophthalmology. 1913;84(3):401–419.
24. Fulton A.B., Albert D.M., Craft J.L. Human albinism: light and electron microscopy study. Archives of ophthalmology. 1978;96(2):305–310. PubMed PMID: 629678.
25. Wilson H.R., et al. Albino spatial vision as an instance of arrested visual development. Vision research. 1988;28(9):979–990. PubMed PMID: 3254652.
26. Bridge H., et al. Changes in brain morphology in albinism reflect reduced visual acuity. Cortex. 2014;56:64–72. PubMed PMID: 23039995.
27. Mcketton L., Kelly K.R., Schneider K.A. Abnormal lateral geniculate nucleus and optic chiasm in human albinism. Journal of Comparative Neurology. 2014;522(11):2680–2687. PubMed PMID: 24639208.
28. Hubel D., Wiesel T. Aberrant visual projections in the Siamese cat. The Journal of physiology. 1971;218(1):33–62. PubMed PMID: 5130620.
29. Leventhal A.G., Vitek D.J., Creel D.J. Abnormal visual pathways in normally pigmented cats that are heterozygous for albinism. Science. 1985;229(4720):1395–1397. PubMed PMID: 3929383.
30. Hoffmann M.B., et al. Organization of the visual cortex in human albinism. The Journal of neuroscience. 2003;23(26):8921–8930. PubMed PMID: 14523094.
31. Creel D., et al. Abnormal retinal projections in cats with the Chediak-Higashi syndrome. Invest Ophthalmol Vis Sci. 1982;23(6):798–801. PubMed PMID: 7141822.
32. Creel D., Conlee J.W., Parks T.N. Auditory brainstem anomalies in albino cats. I. Evoked potential studies. Brain research. 1983;260(1):1–9. PubMed PMID: 6824946.
33. Vopalensky P., et al. Molecular analysis of the amphioxus frontal eye unravels the evolutionary origin of the retina and pigment cells of the vertebrate eye. Proc Natl Acad Sci U S A. 2012;109(38):15383–8. PubMed PMID: 22949670.
34. Lucas R., et al. Diminished pupillary light reflex at high irradiances in melanopsin-knockout mice. Science. 2003;299(5604):245–247. PubMed PMID: 12522249.

35. Hattar S., et al. Central projections of melanopsin-expressing retinal ganglion cells in the mouse. Journal of Comparative Neurology. 2006;497(3):326–349. PubMed PMID: 16736474.
36. Creel D., Hendrickson A.E., Leventhal A.G. Retinal projections in tyrosinase-negative albino cats. The Journal of Neuroscience. 1982;2(7):907–911. PubMed PMID: 6808091.
37. Hendrickson A.E., Wagoner N., Cowan W.M. An autoradiographic and electron microscopic study of retino-hypothalamic connections. Z Zellforsch Mikrosk Anat. 1972;135(1):1–26. PubMed PMID: 4629413.
38. Sanderson K., Guillery R., Shackelford R. Congenitally abnormal visual pathways in mink (Mustela vison) with reduced retinal pigment. Journal of Comparative Neurology. 1974;154(3):225–248. PubMed PMID: 4826094.
39. Creel D.J., Giolli R.A. Retinogeniculostriate projections in guinea pigs: albino and pigmented strains compared. Experimental neurology. 1972;36(3):411–425. PubMed PMID: 5071805.
40. Ault S.J., et al. Abnormal ipsilateral visual field representation in areas 17 and 18 of hypopigmented cats. Journal of Comparative Neurology. 1995;354(2):181–192. PubMed PMID: 7782497.
41. Hoffmann M.B., et al. Assessment of cortical visual field representations with multifocal VEPs in control subjects, patients with albinism, and female carriers of ocular albinism. Investigative ophthalmology & visual science. 2006;47(7):3195–3201. PubMed PMID: 16799067.
42. Summers C.G. Albinism: classification, clinical characteristics, and recent findings. Optometry & Vision Science. 2009;86(6):659–662. PubMed PMID: 19390472.
43. Neveu M.M., et al. Early midline interactions are important in mouse optic chiasm formation but are not critical in man: a significant distinction between man and mouse. European Journal of Neuroscience. 2006;23(11):3034–3042. PubMed PMID: 16819992.
44. Dulai K.S., et al. The evolution of trichromatic color vision by opsin gene duplication in New World and Old World primates. Genome Research. 1999;9(7):629–638. PubMed PMID: 10413401.
45. Hendrickson A., Wilson J., Ogren M. The neuroanatomical organization of pathways between the dorsal lateral geniculate nucleus and visual cortex in Old World and New World primates. The Journal of comparative neurology. 1978;182(1):123–136. PubMed PMID: 100530.
46. Oetting W., et al. Evolution of the tyrosinase related gene (TYRL) in primates. Pigment cell research. 1993;6(3):171–177. PubMed PMID: 8234203.
47. Azuma N. Nippon Ganka Gakkai Zasshi. 2000;104(12):960–985. [Molecular cell biology on morphogenesis of the fovea and evolution of the central vision]. PubMed PMID: 11193946.
48. Arendt D. Evolution of eyes and photoreceptor cell types. Int J Dev Biol. 2003;47(7-8):563–71. PubMed PMID: 14756332.
49. Kozmik Z. Pax genes in eye development and evolution. Current opinion in genetics & development. 2005;15(4):430–438. PubMed PMID: 15950457.
50. Kozmik Z. The role of Pax genes in eye evolution. Brain research bulletin. 2008;75(2):335–339. PubMed PMID: 18331895.
51. Herbert S.P., Stainier D.Y. Molecular control of endothelial cell behaviour during blood vessel morphogenesis. Nature reviews Molecular cell biology. 2011;12(9):551–564. PubMed PMID: 21860391.
52. Woolfe A., et al. Highly conserved non-coding sequences are associated with vertebrate development. PLoS biology. 2004;3(1):e7. PubMed PMID: 15630479.
53. Woolfe A., et al. Highly conserved non-coding sequences are associated with vertebrate development. PLoS Biol. 2005;3(1):e7. PubMed PMID: 15630479.
54. Jen J.C., et al. Mutations in a human ROBO gene disrupt hindbrain axon pathway crossing and morphogenesis. Science. 2004;304(5676):1509–1513. PubMed PMID: 15105459.
55. Dimond A., Fraser P. Long Noncoding RNAs Xist in Three Dimensions. Science. 2013;341(6147):720–721. PubMed PMID: 23950517.
56. Engreitz J.M., et al. The Xist lncRNA exploits three-dimensional genome architecture to spread across the X chromosome. Science. 2013;341(6147):1237973. PubMed PMID: 23828888.
57. Dixon J.R., et al. Topological domains in mammalian genomes identified by analysis of chromatin interactions. Nature. 2012;485(7398):376–380. PubMed PMID: 22495300.

58. Woolfe A., Elgar G. Organization of conserved elements near key developmental regulators in vertebrate genomes. Advances in genetics. 2008;61:307–338. PubMed PMID: 18282512.
59. Lee K.A. Molecular recognition by the EWS transcriptional activation domain. Adv Exp Med Biol. 2012;725:106–25. PubMed PMID: 22399321.
60. Prabhakar S., et al. Accelerated evolution of conserved noncoding sequences in humans. Science. 2006;314(5800):786–786. PubMed PMID: 17082449.
61. Kioussis D. Gene regulation: kissing chromosomes. Nature. 2005;435(7042):579–580. PubMed PMID: 15931207.
62. Spitzweck B., Brankatschk M., Dickson B.J. Distinct protein domains and expression patterns confer divergent axon guidance functions for Drosophila Robo receptors. Cell. 2010;140(3):409–420. PubMed PMID: 20144763.
63. Creel D. Inappropriate use of albino animals as models in research. Pharmacology Biochemistry and Behavior. 1980;12(6):969–977. PubMed PMID: 7403210.
64. McCauley D.W., Hixon E., Jeffery W.R. Evolution of pigment cell regression in the cavefish Astyanax: a late step in melanogenesis. Evolution & development. 2004;6(4):209–218. PubMed PMID: 15230961.
65. Plachetzki D.C., Fong C.R., Oakley T.H. Cnidocyte discharge is regulated by light and opsin-mediated phototransduction. BMC biology. 2012;10(1):17. PubMed PMID: 22390726.
66. Arendt D., et al. Ciliary photoreceptors with a vertebrate-type opsin in an invertebrate brain. Science. 2004;306(5697):869–871. PubMed PMID: 15514158.
67. Hanson, I.M. Mammalian homologues of the Drosophila eye specification genes. in Seminars in cell & developmental biology. 2001: Elsevier.
68. Kumar J.P., Moses K. EGF receptor and Notch signaling act upstream of Eyeless/Pax6 to control eye specification. Cell. 2001;104(5):687–697. PubMed PMID: 11257223.
69. McAllister J.T., et al. Arrested development: high-resolution imaging of foveal morphology in albinism. Vision research. 2010;50(8):810–817. PubMed PMID: 20149815.
70. HOYT. W.F. and O. LUIS, The primate chiasm: details of visual fiber organization studied by silver impregnation techniques. Archives of ophthalmology. 1963;70(1):69–85. PubMed PMID: 13955217.
71. Jeffery G., Levitt J.B., Cooper H. Segregated hemispheric pathways through the optic chiasm distinguish primates from rodents. Neuroscience. 2008;157(3):637–643. PubMed PMID: 18854206.
72. Gargiulo A., et al. Molecular and clinical characterization of albinism in a large cohort of Italian patients. Investigative ophthalmology & visual science. 2011;52(3):1281–1289. PubMed PMID: 20861488.
73. Dorey S., et al. The clinical features of albinism and their correlation with visual evoked potentials. British journal of ophthalmology. 2003;87(6):767–772. PubMed PMID: 12770978.
74. Yuodelis C., Hendrickson A. A qualitative and quantitative analysis of the human fovea during development. Vision research. 1986;26(6):847–855. PubMed PMID: 3750868.
75. Kelly J.P., Weiss A.H. Topographical retinal function in oculocutaneous albinism. American journal of ophthalmology. 2006;141(6):1156–1158. PubMed PMID: 16765699.
76. Hendrickson A., et al. Development of the neural retina and its vasculature in the marmoset Callithrix jacchus. Journal of Comparative Neurology. 2006;497(2):270–286. PubMed PMID: 16705674.
77. Jeffery G. The albino retina: an abnormality that provides insight into normal retinal development. Trends in neurosciences. 1997;20(4):165–169. PubMed PMID: 9106357.
78. Esteve J.V., Jeffery G. Reduced retinal deficits in an albino mammal with a cone rich retina: a study of the ganglion cell layer at the area centralis of pigmented and albino grey squirrels. Vision research. 1998;38(6):937–940. PubMed PMID: 9624442.
79. Fuhrmann S. Eye morphogenesis and patterning of the optic vesicle. Current topics in developmental biology. 2010;93:61. PubMed PMID: 20959163.
80. Le Y.Z., et al. Temporal requirement of RPE-derived VEGF in the development of choroidal vasculature. Journal of neurochemistry. 2010;112(6):1584–1592. PubMed PMID: 20067573.

81. Marneros A.G., et al. Vascular endothelial growth factor expression in the retinal pigment epithelium is essential for choriocapillaris development and visual function. The American journal of pathology. 2005;167(5):1451–1459. PubMed PMID: 16251428.
82. Zhu, M., et al., Presence of RPE-produced VEGF in a timely manner is critical to choroidal vascular development, in Retinal Degenerative Diseases. 2012, Springer. p. 299-304.
83. Kozulin P., et al. Differential expression of anti-angiogenic factors and guidance genes in the developing macula. Molecular vision. 2009;15:45. PubMed PMID: 19145251.
84. Kozulin P., et al. The cellular expression of antiangiogenic factors in fetal primate macula. Investigative ophthalmology & visual science. 2010;51(8):4298–4306. PubMed PMID: 20357200.
85. Creel D., O'Donnell F., Witkop C. Visual system anomalies in human ocular albinos. Science. 1978;201(4359):931–933. PubMed PMID: 684419.
86. Taylor W. Edridge-Green Lecture, 1978. Visual disabilities of oculocutaneous albinism and their alleviation. Transactions of the ophthalmological societies of the United Kingdom. 1977;98(4):423–445. PubMed PMID: 115122.
87. Coleman J., et al. Abnormal visual pathways in human albinos studied with visually evoked potentials. Experimental neurology. 1979;65(3):667–679. PubMed PMID: 467566.
88. Guillery R. Why do albinos and other hypopigmented mutants lack normal binocular vision, and what else is abnormal in their central visual pathways? Eye. 1996;10(2):217–221. PubMed PMID: 8776451.
89. JASPER. H.H., The ten twenty electrode system of the international federation. Electroencephalography and clinical neurophysiology. 1958;10:371–375.
90. Creel D., Spekreijse H., Reits D. Evoked potentials in albinos: efficacy of pattern stimuli in detecting misrouted optic fibers. Electroencephalography and clinical neurophysiology. 1981;52(6):595–603. PubMed PMID: 6172258.
91. Sutter, E., Noninvasive testing methods: multifocal electrophysiology. Encyclopedia of the Eye, 2010. 3: p. 142-160.
92. von dem Hagen E.A., Hoffmann M.B., Morland A.B. Identifying human albinism: a comparison of VEP and fMRI. Investigative ophthalmology & visual science. 2008;49(1):238–249. PubMed PMID: 18172098.
93. Hoffmann M.B., et al. Plasticity and stability of the visual system in human achiasma. Neuron. 2012;75(3):393–401. PubMed PMID: 22884323.
94. Klemen, J., M.B. Hoffmann, and C.D. Chambers, Cortical plasticity in the face of congenitally altered input into V1. cortex, 2012. 48(10): p. 1362-1365.
95. Kaule F.R., et al. Impact of chiasma opticum malformations on the organization of the human ventral visual cortex. Human brain mapping. 2014;35(10):5093–5105. PubMed PMID: 24771411.
96. Hoffmann M.B., et al. Misrouting of the optic nerves in albinism: estimation of the extent with visual evoked potentials. Investigative ophthalmology & visual science. 2005;46(10):3892–3898. PubMed PMID: 16186379.
97. Apkarian P., et al. A decisive electrophysiological test for human albinism. Electroencephalography and clinical neurophysiology. 1983;55(5):513–531. PubMed PMID: 6187545.
98. Zhang B., et al. Effects of fixation instability on multifocal VEP (mfVEP) responses in amblyopes. Journal of vision. 2008;8(3):16. PubMed PMID: 18484822.
99. Morland A.B., et al. Abnormal retinotopic representations in human visual cortex revealed by fMRI. Acta psychologica. 2001;107(1):229–247. PubMed PMID: 11388137.
100. Hoffmann M.B., Seufert P.S., Schmidtborn L.C. Perceptual relevance of abnormal visual field representations: static visual field perimetry in human albinism. British journal of ophthalmology. 2007;91(4):509–513. PubMed PMID: 17372340.
101. Wolynski B., et al. Self-organisation in the human visual system—Visuo-motor processing with congenitally abnormal V1 input. Neuropsychologia. 2010;48(13):3834–3845. PubMed PMID: 20863844.
102. Hagen E.A., et al. Retinal abnormalities in human albinism translate into a reduction of grey matter in the occipital cortex. European Journal of Neuroscience. 2005;22(10):2475–2480. PubMed PMID: 16307590.

103. Neveu M.M., et al. Age-related changes in the dynamics of human albino visual pathways. European Journal of Neuroscience. 2003;18(7):1939–1949. PubMed PMID: 14622226.
104. Kinnear P., Jay B., Witkop C. Albinism. Survey of ophthalmology. 1985;30(2):75–101. PubMed PMID: 3934778.
105. Weiss A.H., Kelly J.P. Acuity development in infantile nystagmus. Investigative ophthalmology & visual science. 2007;48(9):4093–4099. PubMed PMID: 17724192.
106. Dijkstal J.M., et al. Change in visual acuity in albinism in the early school years. Journal of Pediatric Ophthalmology Strabismus. 2011.:1–6. PubMed PMID: 21732575.
107. Summers C.G. Vision in albinism. Transactions of the American Ophthalmological Society. 1996;94:1095. PubMed PMID: 8981720.
108. Guibal C., Baker G.E. Abnormal axons in the albino optic tract. Investigative ophthalmology & visual science. 2009;50(12):5516–5521. PubMed PMID: 19628745.
109. St John R., Timney B. Sensitivity deficits consistent with aberrant crossed visual pathways in human albinos. Investigative ophthalmology & visual science. 1981;21(6):873–877. PubMed PMID: 7309439.
110. Witkop C.J. Jr, et al. Optic and otic neurologic abnormalities in oculocutaneous and ocular albinism. Birth Defects Orig Artic Ser. 1982;18(6):299–318. PubMed PMID: 6756499.
111. Distefano M., et al. Lack of binocular activation of cells in area 19 of the Siamese cat. Brain research. 1984;303(2):391–395. PubMed PMID: 6744031.
112. Leventhal A.G., Creel D.J. Retinal projections and functional architecture of cortical areas 17 and 18 in the tyrosinase-negative albino cat. The Journal of neuroscience. 1985;5(3):795–807. PubMed PMID: 2983049.
113. Kalberlah C., Distler C., Hoffmann K.-P. Sensitivity to relative disparity in early visual cortex of pigmented and albino ferrets. Experimental brain research. 2009;192(3):379–389. PubMed PMID: 18726091.
114. Lee K.A., King R.A., Summers C.G. Stereopsis in patients with albinism: clinical correlates. Journal of American Association for Pediatric Ophthalmology and Strabismus. 2001;5(2):98–104. PubMed PMID: 11304818.
115. Bacon B.A., et al. Spatial disparity sensitivity in area PMLS of the Siamese cat. Brain research. 2001;906(1):149–156. PubMed PMID: 11430872.
116. Antonini A., et al. Differences in binocular interactions between cortical areas 17 and 18 and superior colliculus of Siamese cats. Journal of Comparative Neurology. 1981;200(4):597–611. PubMed PMID: 7263961.
117. Berlucchi G., Gazzaniga M., Rizzolatti G. Microelectrode analysis of transfer of visual information by the corpus callosum. Archives italiennes de biologie. 1967;105(4):583–596. PubMed PMID: 5585725.
118. Shatz C.J. Anatomy of interhemispheric connections in the visual system of Boston Siamese and ordinary cats. Journal of Comparative Neurology. 1977;173(3):497–518. PubMed PMID: 856894.
119. Marzi C., et al. Callosum-dependent binocular interactions in the lateral suprasylvian area of Siamese cats which lack binocular neurons in areas 17 and 18. Brain research. 1980;197(1):230–235. PubMed PMID: 7397556.
120. Zeki S., Fries W. A function of the corpus callosum in the Siamese cat. Proceedings of the Royal Society of London. Series B. Biological Sciences. 1980;207(1167):249–258. PubMed PMID: 6102767.
121. Schmolesky M.T., et al. Abnormal retinotopic organization of the dorsal lateral geniculate nucleus of the tyrosinase-negative albino cat. Journal of Comparative Neurology. 2000;427(2):209–219. PubMed PMID: 11054689.
122. Schmitz B., et al. Configuration of the optic chiasm in humans with albinism as revealed by magnetic resonance imaging. Investigative ophthalmology & visual science. 2003;44(1):16–21. PubMed PMID: 12506050.
123. Westbroek W., et al. Cellular defects in Chediak-Higashi syndrome correlate with the molecular genotype and clinical phenotype. The Journal of investigative dermatology. 2007;127(11):2674. PubMed PMID: 17554367.
124. Montoliu L., et al. Increasing the complexity: new genes and new types of albinism. Pigment cell & melanoma research. 2014;27(1):11–18. PubMed PMID: 24066960.

125. Vici C.D., et al. Agenesis of the corpus callosum, combined immunodeficiency, bilateral cataract, and hypopigmentation in two brothers. American journal of medical genetics. 1988;29(1):1–8. PubMed PMID: 3344762.
126. Cullup T., et al. Recessive mutations in EPG5 cause Vici syndrome, a multisystem disorder with defective autophagy. Nature genetics. 2013;45(1):83–87. PubMed PMID: 23222957.
127. Filloux F.M., et al. Ophthalmologic features of vici syndrome. Journal of pediatric ophthalmology and strabismus. 2014;51(4):214–220. PubMed PMID: 24779424.
128. Summers C.G., et al. Variable expression of vision in sibs with albinism. American journal of medical genetics. 1991;40(3):327–331. PubMed PMID: 1951438.
129. Cheong P., King R., Bateman J. Oculocutaneous albinism: variable expressivity of nystagmus in a sibship. Journal of pediatric ophthalmology and strabismus. 1991;29(3):185–188. PubMed PMID: 1432506.
130. Oetting W.S., et al. Oculocutaneous albinism type 1: the last 100 years. Pigment cell research. 2003;16(3):307–311. PubMed PMID: 12753405.
131. Poulter J.A., et al. Recessive mutations in SLC38A8 cause foveal hypoplasia and optic nerve misrouting without albinism. The American Journal of Human Genetics. 2013;93(6):1143–1150. PubMed PMID: 24290379.
132. Al-Araimi M., et al. A new recessively inherited disorder composed of foveal hypoplasia, optic nerve decussation defects and anterior segment dysgenesis maps to chromosome 16q23. 3-24.1. Molecular vision. 2013;19:2165. PubMed PMID: 24194637.
133. van Genderen M.M., et al. Chiasmal misrouting and foveal hypoplasia without albinism. British journal of ophthalmology. 2006;90(9):1098–1102. PubMed PMID: 16707527.
134. Creel D.J., et al. Abnormalities of the central visual pathways in Prader–Willi syndrome associated with hypopigmentation. New England Journal of Medicine. 1986;314(25):1606–1609. PubMed PMID: 3713758.
135. Hoffmann M.B., et al. Optic nerve projections in patients with primary ciliary dyskinesia. Investigative ophthalmology & visual science. 2011;52(7):4617–4625. PubMed PMID: 21508109.
136. Tremblay F., et al. Visual evoked potentials with crossed asymmetry in incomplete congenital stationary night blindness. Investigative ophthalmology & visual science. 1996;37(9):1783–1792. PubMed PMID: 8759345.
137. Ung, T., et al., Is optic nerve fibre mis-routing a feature of congenital stationary night blindness? Documenta ophthalmologica, 2005. 111(3): p. 169-178.
138. Gal A., et al. Gene of X-chromosomal congenital stationary night blindness is closely linked to DXS7 on Xp. Human genetics. 1989;81(4):315–318. PubMed PMID: 2564836.
139. Ilia M., Jeffery G. Retinal mitosis is regulated by dopa, a melanin precursor that may influence the time at which cells exit the cell cycle: analysis of patterns of cell production in pigmented and albino retinae. Journal of Comparative Neurology. 1999;405(3):394–405. PubMed PMID: 10076934.
140. Giordano F., Simoes S., Raposo G. The ocular albinism type 1 (OA1) GPCR is ubiquitinated and its traffic requires endosomal sorting complex responsible for transport (ESCRT) function. Proceedings of the National Academy of Sciences. 2011;108(29):11906–11911. PubMed PMID: 21730137.
141. Roffler-Tarlov S., et al. L-Dopa and the albino riddle: content of L-Dopa in the developing retina of pigmented and albino mice. PloS one. 2013;8(3):e57184. PubMed PMID: 23526936.
142. Lopez V.M., et al. L-DOPA is an endogenous ligand for OA1. PLoS biology. 2008;6(9):e236. PubMed PMID: 18828673.
143. Jeffery G., Erskine L. Variations in the architecture and development of the vertebrate optic chiasm. Progress in retinal and eye research. 2005;24(6):721–753. PubMed PMID: 16027026.
144. Deiner M.S., et al. Netrin-1 and DCC mediate axon guidance locally at the optic disc: loss of function leads to optic nerve hypoplasia. Neuron. 1997;19(3):575–589. PubMed PMID: 9331350.
145. Plump A.S., et al. Slit1 and Slit2 cooperate to prevent premature midline crossing of retinal axons in the mouse visual system. Neuron. 2002;33(2):219–232. PubMed PMID: 11804570.
146. Oster S.F., et al. Invariant Sema5A inhibition serves an ensheathing function during optic nerve development. Development. 2003;130(4):775–784. PubMed PMID: 12506007.

147. Trousse F., et al. Control of retinal ganglion cell axon growth: a new role for Sonic hedgehog. Development. 2001;128(20):3927–3936. PubMed PMID: 11641217.
148. Petros T.J., Rebsam A., Mason C.A. Retinal axon growth at the optic chiasm: to cross or not to cross. Annu. Rev. Neurosci. 2008;31:295–315. PubMed PMID: 18558857.
149. Rebsam A., Bhansali P., Mason C.A. Eye-specific projections of retinogeniculate axons are altered in albino mice. The Journal of Neuroscience. 2012;32(14):4821–4826. PubMed PMID: 22492037.
150. Williams S.E., et al. Ephrin-B2 and EphB1 mediate retinal axon divergence at the optic chiasm. Neuron. 2003;39(6):919–935. PubMed PMID: 12971893.
151. Zou C., Levine E.M. Vsx2 controls eye organogenesis and retinal progenitor identity via homeodomain and non-homeodomain residues required for high affinity DNA binding. PLoS genetics. 2012;8(9):e1002924. PubMed PMID: 23028343.
152. Phillips M.J., et al. Modeling Human Retinal Development with Patient-Specific Induced Pluripotent Stem Cells Reveals Multiple Roles for Visual System Homeobox 2. Stem Cells. 2014;32(6):1480–1492. PubMed PMID: 24532057.
153. Piatigorsky J., Kozmik Z. Cubozoan jellyfish: an Evo/Devo model for eyes and other sensory systems. Int J Dev Biol. 2004;48(8-9):719–729. PubMed PMID: 15558464.
154. Fritzsch B., Piatigorsky J. Ancestry of photic and mechanic sensation? Science. 2005;308(5725):1113–1114.
155. Yang, J., Usher syndrome: genes, proteins, models, molecular mechanisms, and therapies. 2012: INTECH Open Access Publisher.
156. Cosgrove D., Zallocchi M. Usher protein functions in hair cells and photoreceptors. The international journal of biochemistry & cell biology. 2014;46:80–89. PubMed PMID: 24239741.
157. Nouvian R., et al. Structure and function of the hair cell ribbon synapse. The Journal of membrane biology. 2006;209(2-3):153–165. PubMed PMID: 16773499.
158. Conlee J.W., et al. Comparative anatomy of melanin pigment in the stria vascularis. Evidence for a distinction between melanocytes and intermediate cells in the cat. Acta Otolaryngol. 1989;107(1-2):48–58. PubMed PMID: 2929316.
159. Conlee J.W., et al. Pigment-dependent differences in the stria vascularis of albino and pigmented guinea pigs and rats. Hearing research. 1994;72(1):108–124. PubMed PMID: 8150728.
160. Heffner R.S., Heffner H.E. Visual factors in sound localization in mammals. Journal of Comparative Neurology. 1992;317(3):219–232. PubMed PMID: 1577997.
161. Feng W., et al. Sounds activate visual cortex and improve visual discrimination. J Neurosci. 2014;34(29):9817–24. PubMed PMID: 25031419.
162. Grothe B., Pecka M., McAlpine D. Mechanisms of sound localization in mammals. Physiological Reviews. 2010;90(3):983–1012. PubMed PMID: 20664077.
163. Thaler L., Arnott S.R., Goodale M.A. Neural correlates of natural human echolocation in early and late blind echolocation experts. PLoS One. 2011;6(5):e20162. PubMed PMID: 21633496.
164. Gottesberge A. Physiology and pathophysiology of inner ear melanin. Pigment Cell Research. 1988;1(4):238–249. PubMed PMID: 3070525.
165. Murillo-Cuesta S., et al. Melanin precursors prevent premature age-related and noise-induced hearing loss in albino mice. Pigment cell & melanoma research. 2010;23(1):72–83. PubMed PMID: 19843244.
166. Garber S.R., et al. Auditory system abnormalities in human albinos. Ear Hear. 1982;3(4):207–10. PubMed PMID: 7117717.
167. Conlee J.W., et al. Differential susceptibility to noise-induced permanent threshold shift between albino and pigmented guinea pigs. Hearing research. 1986;23(1):81–91. PubMed PMID: 3733554.
168. Barrenäs M.-L., Lindgren F. The influence of inner ear melanin on susceptibility to TTS in humans. Scandinavian audiology. 1990;19(2):97–102. PubMed PMID: 2371541.
169. Conlee J.W., et al. Auditory brainstem anomalies in albino cats: II. Neuronal atrophy in the superior olive. Journal of Comparative Neurology. 1984;225(1):141–148. PubMed PMID: 6725637.
170. Yin T., Carney L., Joris P. Interaural time sensitivity in the inferior colliculus of the albino cat. Journal of Comparative Neurology. 1990;295(3):438–448. PubMed PMID: 2351762.

171. Moore D.R., Kowalchuk N.E. Auditory brainstem of the ferret: effects of unilateral cochlear lesions on cochlear nucleus volume and projections to the inferior colliculus. Journal of Comparative Neurology. 1988;272(4):503–515. PubMed PMID: 2843582.
172. Creel D., et al. Auditory brainstem anomalies in human albinos. Science. 1980;209(4462):1253–5. PubMed PMID: 7403883.
173. Giolli R.A., Creel D.J. The primary optic projections in pigmented and albino guinea pigs: an experimental degeneration study. Brain Res. 1973;55(1):25–39. PubMed PMID: 4123355.
174. Gayer N.S., Horsburgh G.M., Dreher B. Developmental changes in the pattern of retinal projections in pigmented and albino rabbits. Brain Res Dev Brain Res. 1989;50(1):33–54. PubMed PMID: 2582607.
175. Zhang H.Y., Hoffmann K.P. Retinal projections to the pretectum, accessory optic system and superior colliculus in pigmented and albino ferrets. Eur J Neurosci. 1993;5(5):486–500. PubMed PMID: 8261124.
176. Wassle H., Illing R.B. The retinal projection to the superior colliculus in the cat: a quantitative study with HRP. J Comp Neurol. 1980;190(2):333–56. PubMed PMID: 7381061.
177. Koontz M.A., Rodieck R.W., Farmer S.G. The retinal projection to the cat pretectum. J Comp Neurol. 1985;236(1):42–59. PubMed PMID: 4056090.
178. Collewijn H., Apkarian P., Spekreijse H. The oculomotor behaviour of human albinos. Brain. 1985;108(1):1–28. PubMed PMID: 3978393.
179. Collewijn H., Winterson B.J., Dubois M.F. Optokinetic eye movements in albino rabbits: inversion in anterior visual field. Science. 1978;199(4335):1351–1353. PubMed PMID: 628845.
180. Huber-Reggi S.P., et al. Severity of infantile nystagmus syndrome-like ocular motor phenotype is linked to the extent of the underlying optic nerve projection defect in zebrafish belladonna mutant. J Neurosci. 2012;32(50):18079–86. PubMed PMID: 23238723.
181. Giolli R.A., Blanks R.H., Lui F. The accessory optic system: basic organization with an update on connectivity, neurochemistry, and function. Prog Brain Res. 2006;151:407–40. PubMed PMID: 16221596.
182. ten Tusscher M.P. Does dominance of crossing retinal ganglion cells make the eyes cross? The temporal retina in the origin of infantile esotropia–a neuroanatomical and evolutionary analysis. Acta ophthalmologica. 2014;92(6):e419–e423. PubMed PMID: 25259397.
183. Pietrasanta M., Restani L., Caleo M. The corpus callosum and the visual cortex: plasticity is a game for two. Neural Plast. 2012;2012:838672. PubMed PMID: 22792494.
184. Brodsky M.C., Dell'Osso L.F. A unifying neurologic mechanism for infantile nystagmus. JAMA Ophthalmol. 2014;132(6):761–8. PubMed PMID: 24525626.
185. Christoff A., et al. DVD--a conceptual, clinical, and surgical overview. J AAPOS. 2014;18(4):378–84. PubMed PMID: 25173903.
186. Brodsky M.C. The accessory optic system: the fugitive visual control system in infantile strabismus. Arch Ophthalmol. 2012;130(8):1055–8. PubMed PMID: 22893078.
187. Brodsky M.C. An expanded view of infantile esotropia: bottoms up! Arch Ophthalmol. 2012;130(9):1199–202. PubMed PMID: 22965598.
188. ten Tusscher M.P. A neural model for cyclovertical eye movements and their disorders. Strabismus. 2011;19(4):162–165. PubMed PMID: 22107122.
189. ten Tusscher M.P. Dissociated deviation in the infantile strabismus syndrome. Strabismus. 2012;20(1):33–34.
190. ten Tusscher M.P., van Rijn R.J. A hypothetical mechanism for DVD: unbalanced cortical input to subcortical pathways. Strabismus. 2010;18(3):98–103. PubMed PMID: 20843186.
191. ten Tusscher M.P., van Rijn R.J. There is nothing fishy about the cerebral cortex. Strabismus. 2011;19(2):69–70.
192. Carroll, R.L., Vertebrate paleontology and evolution. 1988.
193. Husband, S. and T. Shimizu. Evolution of the avian visual system. . Avian visual cognition 2001 [cited 2001.
194. Aboitiz F., et al. Fiber composition of the human corpus callosum. Brain Res. 1992;598(1-2):143–53. PubMed PMID: 1486477.

195. Atkinson, J., Development of optokinetic nystagmus in the human infant and monkey infant: an analogue to development in kittens, in Developmental neurobiology of vision. 1979, Springer. p. 277-287.
196. Hoffmann K.P., Distler C., Ilg U. Callosal and superior temporal sulcus contributions to receptive field properties in the macaque monkey's nucleus of the optic tract and dorsal terminal nucleus of the accessory optic tract. J Comp Neurol. 1992;321(1):150–62. PubMed PMID: 1377205.
197. Mustari M.J., Ono S., Vitorello K.C. How disturbed visual processing early in life leads to disorders of gaze-holding and smooth pursuit. Prog Brain Res. 2008;171:487–95. PubMed PMID: 18718344.
198. Van Rijn L.J., Simonsz H.J., Tusscher M.P. Dissociated vertical deviation and eye torsion: Relation to disparity-induced vertical vergence. Strabismus. 1997;5(1):13–20. PubMed PMID: 21314389.
199. Ibbotson M.R., Marotte L.R., Mark R.F. Investigations into the source of binocular input to the nucleus of the optic tract in an Australian marsupial, the wallaby Macropus eugenii. Experimental brain research. 2002;147(1):80–88. PubMed PMID: 12373372.
200. Berman N., Murphy E.H. The critical period for alteration in cortical binocularity resulting from divergent and convergent strabismus. Brain Res. 1981;254(2):181–202. PubMed PMID: 7272776.
201. Goyal R., Watts P., Hourihan M. Ocular findings in pediatric patients with partial agenesis of corpus callosum. J Pediatr Ophthalmol Strabismus. 2010;47(4):236–41. PubMed PMID: 19791713.
202. Koenraads Y., et al. Visual function and compensatory mechanisms for hemianopia after hemispherectomy in children. Epilepsia. 2014;55(6):909–17. PubMed PMID: 24754334.
203. Fukuda Y., et al. Nasotemporal overlap of crossed and uncrossed retinal ganglion cell projections in the Japanese monkey (Macaca fuscata). J Neurosci. 1989;9(7):2353–73. PubMed PMID: 2545836.
204. Bisti S., Carmignoto G. Monocular deprivation in kittens differently affects crossed and uncrossed visual pathways. Vision Res. 1986;26(6):875–84. PubMed PMID: 3750870.
205. Klier E.M., Wang H., Crawford J.D. Interstitial nucleus of cajal encodes three-dimensional head orientations in Fick-like coordinates. J Neurophysiol. 2007;97(1):604–17. PubMed PMID: 17079347.
206. Opitz J.M. 2011 William Allan Award: Development and Evolution. Am J Hum Genet. 2012;90(3):392–404. PubMed PMID: 22405084.
207. Meckel, J., Handbuch der Pathologischen Anatomie. 1812: Halle:Kummer.
208. Smukler S.R., et al. Embryonic stem cells assume a primitive neural stem cell fate in the absence of extrinsic influences. The Journal of cell biology. 2006;172(1):79–90. PubMed PMID: 16390999.
209. Charles, D., The variation of animals and plants under domestication, Volume 2. 1868: John Murray.
210. Gehring W.J. New perspectives on eye development and the evolution of eyes and photoreceptors. Journal of Heredity. 2005;96(3):171–184. PubMed PMID: 15653558.
211. Creel D., Hendrickson A.E., Leventhal A.G. Retinal projections in tyrosinase-negative albino cats. J Neurosci. 1982;2(7):907–11. PubMed PMID: 6808091.
212. Creel D.J., Summers C.G., King R.A. Visual anomalies associated with albinism. Ophthalmic Paediatr Genet. 1990;11(3):193–200. PubMed PMID: 2280977.

Diseases of the Eye and Retina

Retinal Degeneration, Remodeling and Plasticity

Bryan William Jones, Ph. D.,[1,*] Robert E. Marc, Ph. D.,[2,†] and Rebecca L. Pfeiffer, B.A./B.S.[3,‡]

Created: October 28, 2016.

1. Introduction

Retinal degeneration and remodeling encompasses a group of pathologies at the molecular, cellular and tissue levels that are initiated by inherited retinal diseases like retinitis pigmentosa (RP), genetic and environmental diseases like age-related macular degeneration (AMD) and other insults to the eye/retina including trauma and retinal detachment. These retinal changes and apparent plasticity result in neuronal rewiring and reprogramming events that include alterations in gene expression, de novo neuritogenesis as well as formation of novel synapses, creating corruptive circuitry in bipolar cells through alterations in the dendritic tree and supernumerary axonal growth. In addition, neuronal migration occurs throughout the vertical axis of the retina along Müller cell columns showing altered metabolic signals, and retinal pigment epithelium (RPE) invades the retina forming the pigmented bone spicules that have been classic clinical observations of RP diseases.

Retinal photoreceptors drive signal processing networks in the neural retina comprising bipolar, horizontal, amacrine and ganglion cells. It has been historically thought that retinal degenerative diseases such as RP affect the sensory retina, leaving the neural retina relatively unscathed. This is incorrect as the resulting loss of rod and cone input to the neural retina constitutes deafferentation and remodeling at the cellular and molecular level becomes unavoidable (1-22) .

Retinal degenerative diseases have a number of potential initiating events that result from naturally occurring disease processes (23), trauma like retinal detachment (24, 25) or any of the forms of retinitis pigmentosa (5, 23, 26, 27), but regardless of cause, if photoreceptors are lost, particularly cones, a sequence of progressive events is initiated that induces negative plastic remodeling of the neural retina (9-11, 14, 15, 21, 22, 28, 29). Essentially every disease process that results in photoreceptor loss triggers retinal remodeling as the final common pathway culminating with cell death and topological restructuring of the retina. The progression of retinal remodeling is like the negative plasticity that occurs in CNS pathologies like trauma and epilepsy and constitutes substantial impediments to rescue strategies of all types.

2. Phases of retinal remodeling.

Retinal remodeling occurs in phases: In *Phase 1*, photoreceptor stress initiates early remodeling & reprogramming events. In *Phase 2*, microglia, Müller glia and RPE cells become involved. Outer nuclear layer (ONL) thinning/ablation occurs and cell stress pathways are engaged, while Müller cells begin sealing the retina off from the choroid. In *Phase 3*, de novo neurite formation, rewiring and neuronal death start a process that continues to progress with neuronal translocation and massive topological restructuring of the retina. We will

Author Affiliations: 1 Department of Ophthalmology and Visual Sciences, University of Utah School of Medicine, Salt Lake City, UT 84132; Email: bryan.jones@m.cc.utah.edu. 2 Department of Ophthalmology and Visual Sciences, University of Utah School of Medicine, Salt Lake City, UT 84132; Email: robert.marc@hsc.utah.edu. 3 Graduate Program, Interdepartmental Program in Neuroscience, University of Utah School of Medicine, Salt Lake City, UT 84132; Email: R.Pfeiffer@utah.edu.

Corresponding author.

* See 'About the authors'

† See 'About the authors'

‡ See 'About the authors'

show in this chapter that all retinal degenerative diseases examined to date including natural, crafted and induced models demonstrate remodeling to some extent and the severity of the negative plasticity depends upon coherency of insult and whether cones survive. Additionally, the early retinal remodeling is often clinically occult and occurs prior to any notable clinical fundoscopic imaging.

3. Age-related macular degeneration (AMD).

In contrast to normal retina (Figure 1), AMD presents with another set of clinical findings including fundoscopic drusen or yellow spots as well as areas of chorioretinal atrophy seen in dry AMD also called geographic atrophy (GA) (Figure 2). The disease is progressive, as seen in Video 1.

Histological presentations of AMD show drusen development in dry AMD that appears to induce photoreceptor cell stress and loss (30). Wet AMD is another disease process entirely that results in death of photoreceptors due to blood vessel development and leakage of blood and serum into the neural retina. This sub retinal blood can also result in RPE detachment that can have its own retinal degenerative mechanisms as well as direct retinal death.

Clinically, patients with dry AMD will often complain of difficulty seeing at night or in dark environments, and of needing brighter lights to work with. They report problems with decreases in color saturation and increases in blurriness of printed words or images in the central part of their vision. Vision deficits progress until there are distortions in the central visual field and ultimately blindness as the degenerative process progresses.

While most of the discussion in this chapter will focus on Retinitis Pigmentosa (RP), it should be noted that the terminal phases of retinal remodeling discussed above and the plasticity and remodeling that will be elaborated on below also occur in AMD, particularly dry forms of AMD (30).

4. Retinitis pigmentosa (RP)

RP is a progressive, genetic, neuro-degenerative disease that typically begins in the periphery and progresses to the center of the retina. There are many different forms of RP with a variety of initiating etiologies including defects in the retinal pigment epithelium, defects in rhodopsin processing and trafficking, defects in rhodopsin stacking, defects in the cilia and many others. RP comes in 3 main categories that include rod-degenerative, mixed rod/cone degenerative and debris-associated forms like mertk defects, and models like the light damage models in albino mice/rats. Regardless of the initial insult, the outcome is the same: photoreceptors undergo stress and subsequent cell death, which effectively deafferents the neural retina, resulting in neural remodeling events that alter the topologies and circuitry of the neural retina.

The clinical sequelae depend upon the broad category of RP involved. Initially, the rod/cone dystrophies manifest with complaints about night blindness beginning in the teenage years or early 20's. Changes in the electroretinogram (ERG) can often be observed prior to fundoscopic findings, most notably in the X-linked form of RP as rods begin to undergo stress and cell death. This reveals a fundamental finding: Photoreceptor function is altered or impaired prior to photoreceptor cell death and gross alterations in the histology become evident. Glutamate channel permeation studies with 1-amino-4-guanidobutane or agmatine (AGB) in early degenerate retina also support this finding by documenting alterations in subpopulations of bipolar cells and glutamate channel expression before loss of bipolar cell populations (22, 31).

By the time the classic fundoscopic image (Figure 3) appears, retinal degeneration is advanced, many cell populations have been dramatically altered or lost, and Müller cells have become hypertrophic, acting as highways for neuronal translocation as well as pigment translocations into the inner retina from the RPE (22, 31).

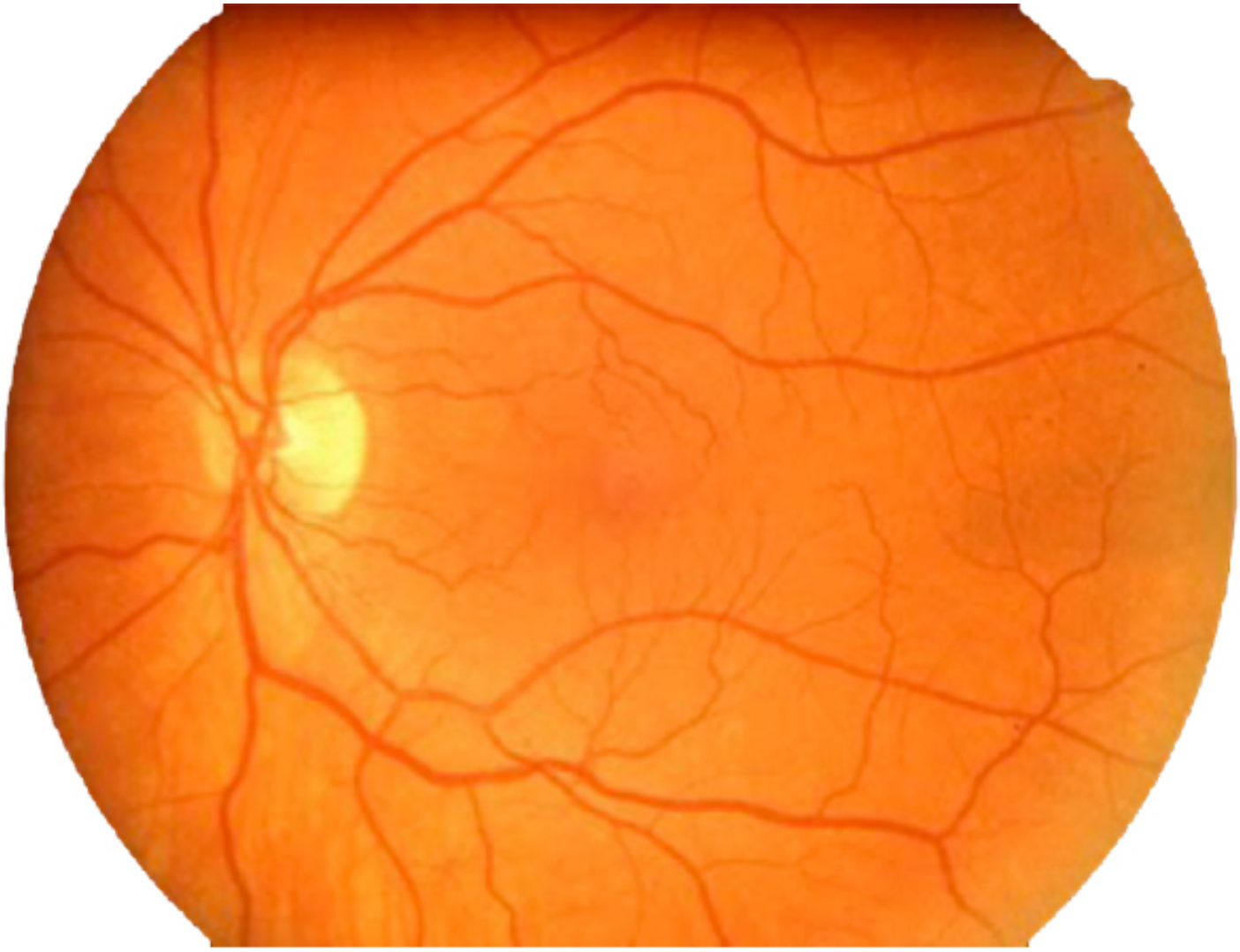

Figure 1. Normal funduscopic examination of a human eye. The clinical picture of retinal degeneration varies depending upon the insult. Above is a standard funduscopic image showing the optic cup, optic disc, fovea, macula, arteries and veins. We see normal color, pigment and vascular distribution.

Pigmented bone spicules in retinitis pigmentosa are accumulations of pigment granules from the RPE that have been coalesced into ribbons and clumps and pulled down into the neural retina. Figure 4 is a backlit and magnified image of a globe and intact retina that is focus stacked to illustrate the structure of pigmented bone spicules in an intact globe.

When you consider how the pigmented bone spicules form, the status of other classes of cells in the retina becomes a question. This is particularly true in advanced cases of RP that are being proposed for bionic and biological interventions that we'll discuss at the end of this chapter. (See also the Webvision section on Visual Prosthesis). Visual science has been examining the histology of retinal degenerative diseases for some time and there have been lots of descriptions made, yet somehow important features have gone missing or were briefly discussed, then forgotten. In 2010 Jaissle et. al. (32) looked at how pigmented bone spicules form in the rhodopsin knockout mouse model rho-/- and concluded that RPE pigment granules migrate along blood vessels. However, we now know that Müller cells act as conduits of migration that are seen not only in the rho-/-, but in many other models as well.

Considering Figure 4 and the obvious changes to retinal topology that are demonstrated in late stage RP, the condition of individual cell classes in the retina as well as their connectivities comes into question. If you do an

Figure 2. Funduscopic image of classic drusen seen in AMD in human eye. AMD presents with another set of clinical findings including funduscopic drusen or yellow spots as well as areas of chorioretinal atrophy seen in dry AMD also called geographic atrophy (GA).

Video 1. An animation of the progression of age-related macular degeneration (AMD), also called Geographic Atrophy (GA), over 6 years.

Download video

accounting of the types of cells that make up a retina, you find upwards of ~82-84 classes of cells that might each be affected in different ways in degenerate retina. Nominally, we have 1 transport epithelium class, the RPE cell, 3 photoreceptor cell classes composed of 2 cone photoreceptor classes and 1 rod photoreceptor class, 2 glial cell classes: Müller cells and Astrocytes, 2 horizontal cell classes (1 horizontal cell class in the mouse eye in Figure 5), 2 vascular cell classes, 35 amacrine or association cell classes, 10 bipolar cell classes, 1 immune cell class and 18-20 ganglion cell classes (19).

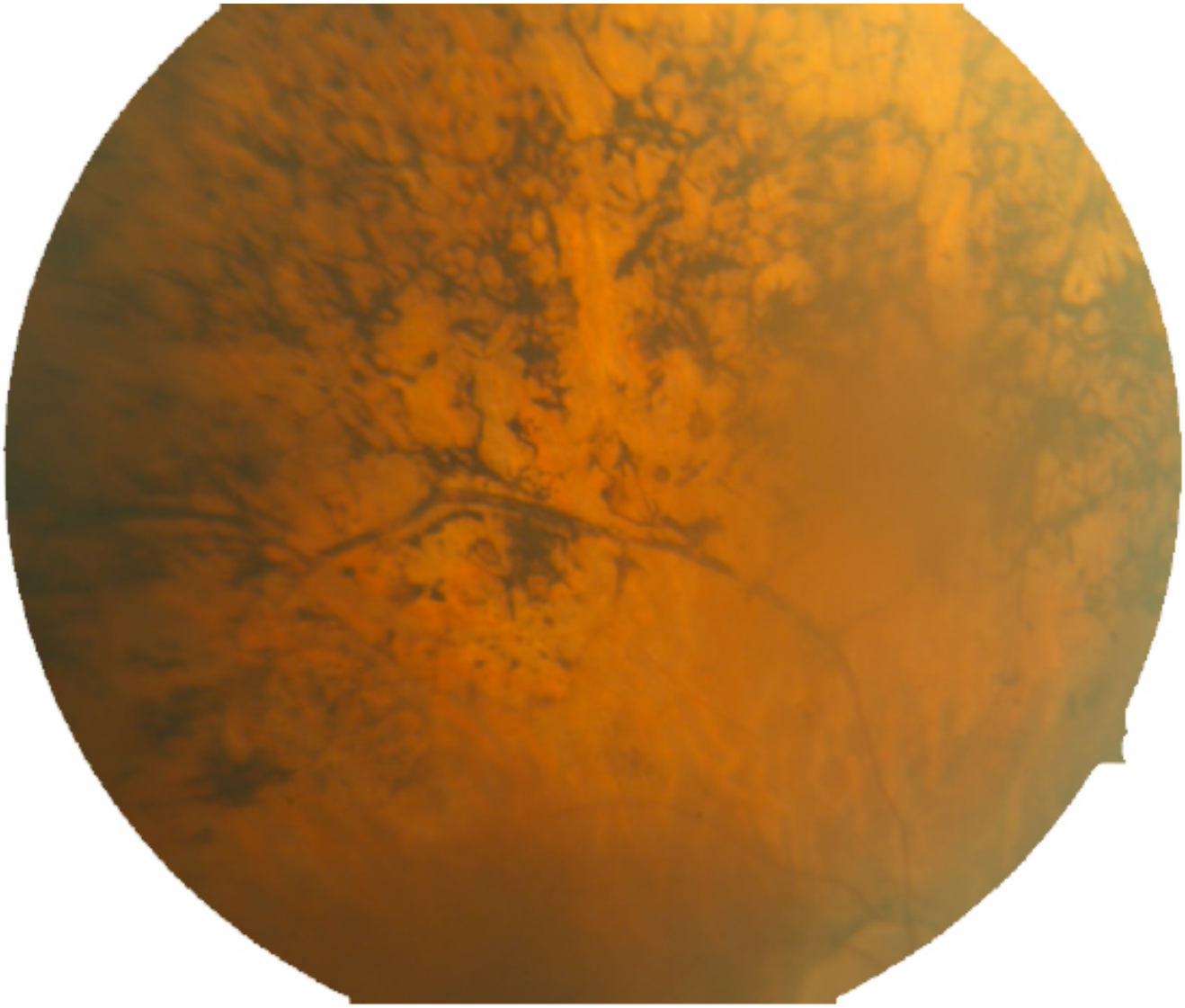

Figure 3. Funduscopic image of advanced RP seen in a human eye.

5. Historical histological methods.

Traditional histological preparations like toluidine blue in Figure 5 and Figure 6 are the common currency in much of the literature and they give us the ability to easily discriminate layers and count the numbers or layers of photoreceptor cell bodies, which has been a traditional measure of the level of integrity of the retina. These measures give us morphometric descriptors and provide some metric for degree of degeneration.

It turns out that this type of histology while incredibly informative, got us, the vision community, into a bit of trouble over the past few years. Examining Figure 6 seems to demonstrate a thinner outer nuclear layer that has been described as partial thickness, but the rest of the retina, at least here, looks OK, leading many to make assumptions on the level of intactness of the neural retina. When discussions of retinal rescue arose, along with subsequent strategies designed to intervene and cure blindness, they were based upon this assumed level of knowledge about retinal integrity, to rescue vision.

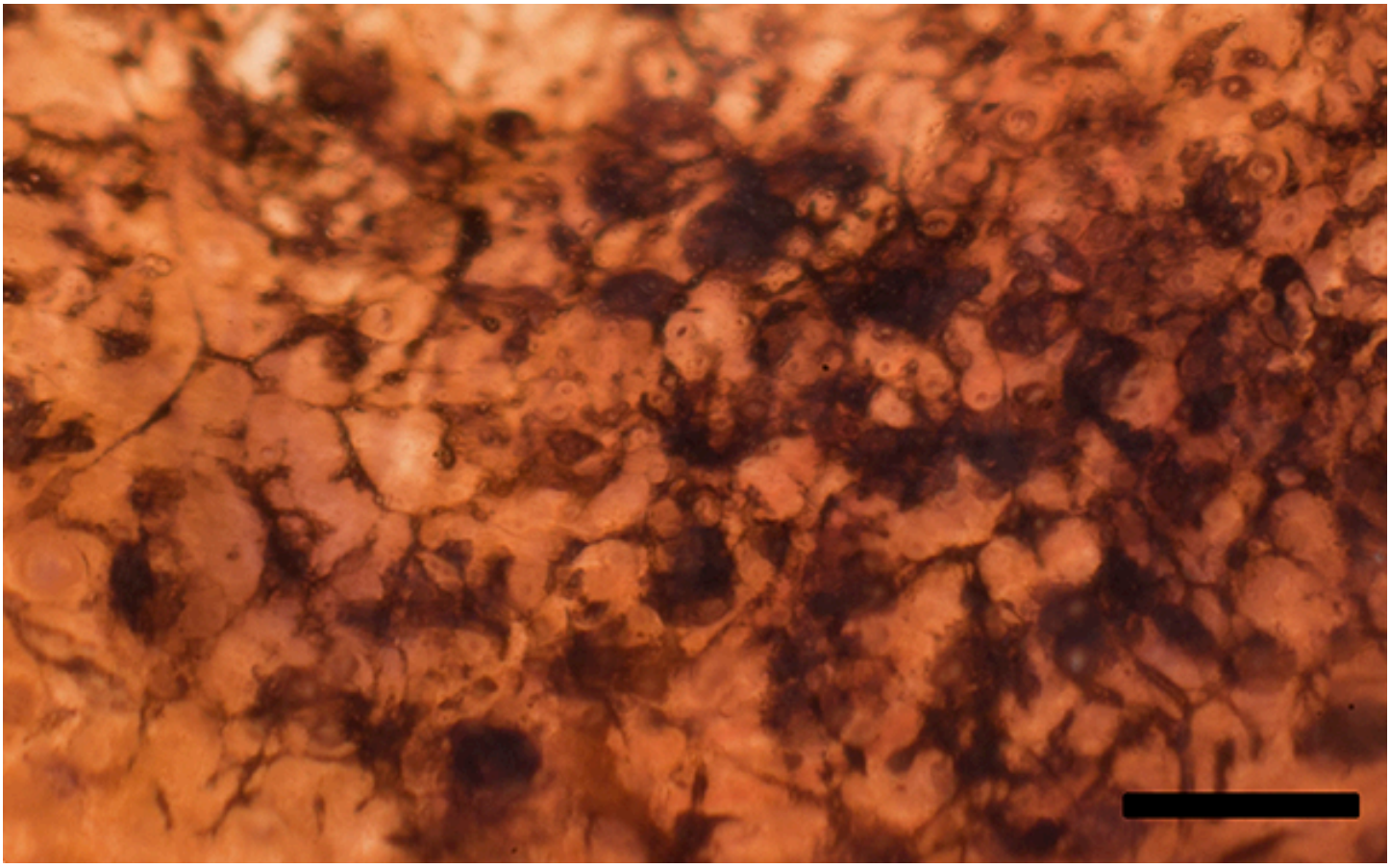

Figure 4. Retina from a human patient with advanced RP. The illustration shows pigmented bone spicules or accumulations of RPE pigment granules that derive from translocations of Müller cells, which alter the topology of the neural retina and cause the accumulation of pigment along clumps, lines and grooves in the vertical axis of the neural retina. Scale bar = 200 µm.

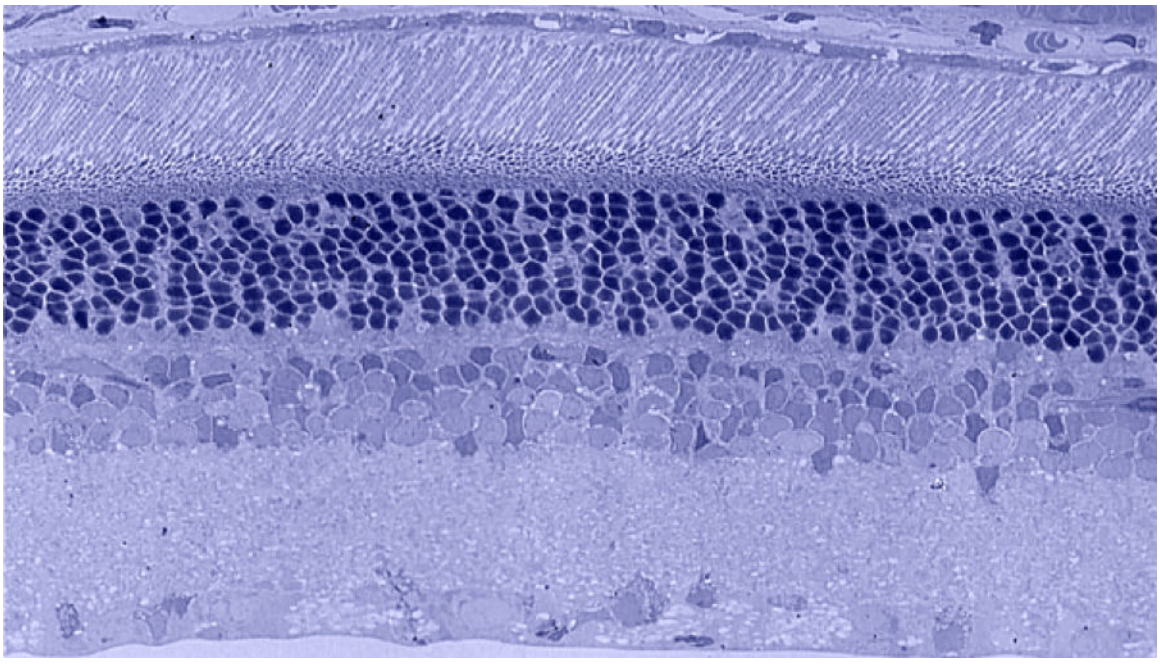

Figure 5. Toluidine blue stain of wild type mouse retina. The photoreceptor layer is at top with the ganglion cell layer on bottom.

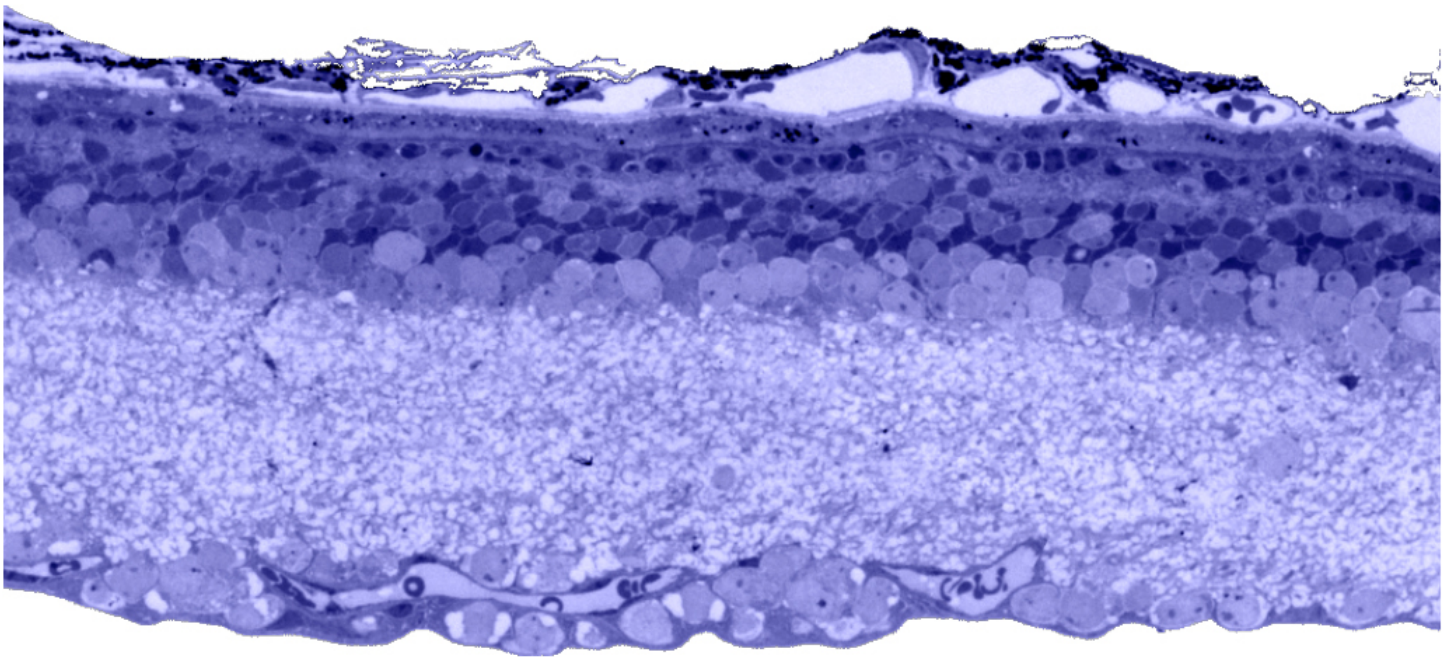

Figure 6. Toluidine blue stain of light damage albino mouse retina. The (now decimated) photoreceptor layer is at top with the ganglion cell layer at bottom.

6. Plasticity in the retina.

Of course, the retina is neural tissue, and plasticity in the central nervous system (CNS) or retina is not a new concept. We have also known for quite some time that the developing retina is highly plastic. This knowledge goes back to 1933 with Ramon Y Cajal in his elegant illustrations of Golgi stains from developing retina, shown in Figure 7. (33).

Another classic example of retinal plasticity in development was illustrated by Hinds and Hinds in 1978 (34) (Figure 8) with an elegant serial section study that showed amacrine cell neurite development from embryonic day 13 to 17. Hinds and Hinds also explored autoradiographic studies on the origin of cells prior to E15. Interestingly, Hinds and Hinds also confirmed the Cajal observations of bipolar shaped amacrine cells in the developing outer ventricular layer 45 years prior.

Over the last 40 years many studies of retinal development have shown how the different retinal cell types develop and go through various morphologies and migrations through the retina to finally reach their mature retinal positions and involvements in neural circuits. The interactions of cells with others and establishment of synaptic circuitry often with pharmacological as well as light and pattern stimulation leads to a mature retina. See chapters in Webvision by Ning Tian, Rachel Wong and Marla Feller concerning these developmental stages in retinal organization. These studies have shown conclusively that the developing retina is very plastic. However, it was assumed that the adult retina remained hard-wired, once established.

Some clues that this is not so came from studies in non-mammalian species. Fish are known to add rod photoreceptors and some secondary retinal interneurons in the retina throughout life (35-37). Moreover, amphibians can regenerate a complete retina and even connections between retina and brain when the eye is damaged (38). A subtler instance of plasticity in the sub-mammalian retina was shown, again in the fish, as a response to just the daily light and dark cycle. There are retinomotor movements of the retinal pigment epithelium in light and dark in fish retina for instance (39). Additionally, there is evidence of neural plasticity in the photoreceptor synapses with horizontal cells with the coming and going of spinules according to light conditions in the adult retina (see chapter on horizontal cells in Webvision). Furthermore, the bipolar synapses

in the inner plexiform layer show synaptic apparatus i.e. synaptic ribbons, appearing and disappearing with light and dark adaptation (Figure 9) (40).

But fish possess a more sophisticated retina than the mammalian because so much visual information processing goes on the retina as compared the mammal, where the equivalent visual processing takes place in the brain (Dowling's original concept of simple mammalian retinas versus non mammalian complex retinas, (41)). So, the question of plasticity in the adult normal mammalian retina had not been established until recently.

However, in 1984, Peichl and Bolz (42) exposed retinas to kainic acid to induce structural remodeling (Figure 10) which they described as dose-dependent morphological changes in horizontal cells of adult mammalian retinas (cats and rabbits). Of course, they found that high concentrations of kainic acid killed the cells, but when exposed to sublethal doses, horizontal cells contracted their dendritic fields and sent sprouting processes into the inner retina. Their conclusions were, quote: "It appears that kainic acid can induce neuronal growth as well as degeneration and that the potential for morphological plasticity is still present in neurons of the adult mammalian retina". So, under certain experimental conditions, it appeared that some retinal neurons could remodel and plasticity was suggested for the first time in species other than fish.

We now know from studies of retinal degenerations that adult mammalian retinas can undergo substantial plastic and aberrant reorganization in response to damage. The rest of this chapter illustrates plasticity in the retina under traumatic and degenerative retinal disease.

7. The plasticity and remodeling that occurs in retinitis pigmentosa like diseases in mammalian retinas.

It has been already mentioned that classical histological examination of human retinas with retinitis pigmentosa (RP) or rodent models with this type of degeneration were being done in the 1960-70s, and gave the impression that, apart from photoreceptors degenerating (Figure 6), the remaining neural retina was normal. It took electron microscopy to show that there were changes other than photoreceptor degeneration that were also occurring in the neuropil of the inner retina.

In 1967 and later in 1974, there were ultrastructural studies in the literature on RP that documented an autosomal dominant form of the disease (43, 44). Papers by Szamier, Berson et al (45, 46) followed later. These papers all concentrated on the pigment epithelium and state of the rods and cones in the diseased retinas simply because that is all that seemed to be recognizable as retinal elements by electron microscopy at the time. The rod photoreceptors in all these examples were degenerating or totally absent. The cones of the fovea were best preserved (Figure 11, a) but outside the fovea, cones were reduced to inner segment stubs (Figure 11 b). Higher magnification of the foveal cones showed they had disorganized outer segment discs (Figure 11, c and d), but presumably these cones were functional because the patient had corrected vision of 20/25 in the same eye examined by EM (Figure 11) (43). The foveal inner retina was not examined in this RP retina and inner retina in the parafoveal area was an indistinguishable tissue of vacuoles and debris (Figure 11b).

Kolb and Gouras (43) were also able to look at the bone spicules in this human RP retina (Figure 12). This electron micrograph shows that cells comprising the pigment clump are of the same type as the cells of the peripheral pigment epithelium. This observation pointed out that RPE cells had migrated into the neural retina, thus forming the characteristic bone spicules of advanced retinitis pigmentosa seen in fundus photography (Figure 4). This early finding could now be interpreted as plasticity and remodeling of retina in response to degenerating retinal integrity.

It was not until almost two decades later that another paper came out that examined aberrant plasticity in retinal tissues. The 1993 paper from Chu, Humphrey and Constable (47) showed that the RCS rat demonstrated retinal remodeling (though they called it disorganization) of horizontal cell processes in the degenerate retina (Figure

Figure 7. Ramón y Cajal's illustration of developing retina from 1933 (33).

13). Interestingly, they also noted that the "disorganization" was not uniform across the retina with the most "disorganized" horizontal cells in the posterior pole where all outer nuclear layers had been lost. These horizontal cells also showed marked morphological aberrations with "swelling" or hypertrophy.

In 1995, Li, Kljavin and Milam (1) reported that rhodopsin positive neurites extended from the photoreceptor layer down into the inner retina and ganglion cell layer in 15 human RP samples (Figure 14). This was the very

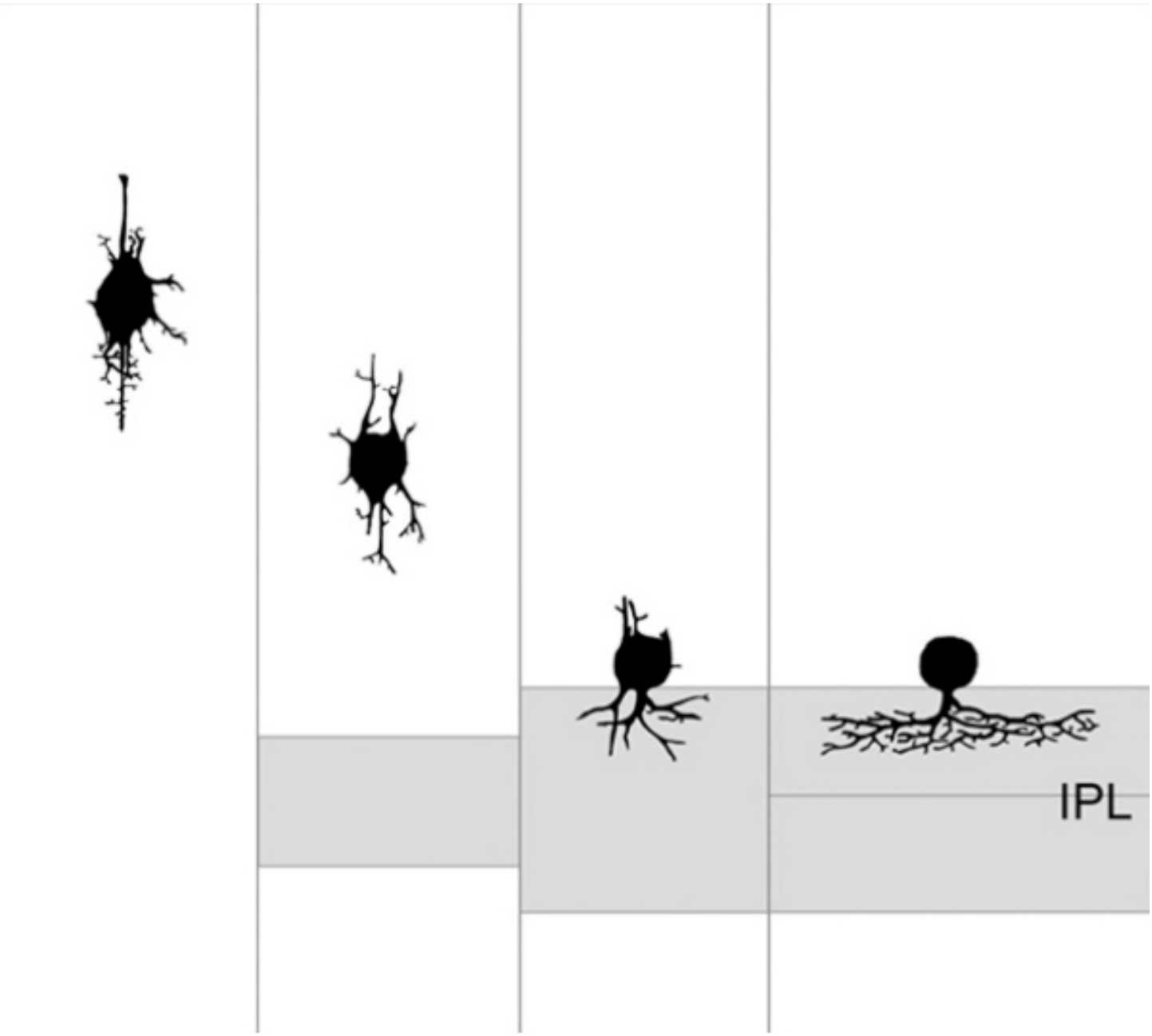

Figure 8. Proposed sequence of amacrine cell neurite development from serial EM studies from Hinds and Hinds, 1978 (34).

first paper that showed neurites sprouting from photoreceptor cells and demonstrated conclusively that rhodopsin delocalized into the membrane of the photoreceptor cell, apparently after mis-trafficking. The authors mention in the paper that "the rod neurites in the human RP retinas resemble the long, branched processes formed by rods cultured on Müller cells or on purified N-CAM". It turned out that they were more correct than they imagined as we will see later, Müller cells form the conduits or scaffolding for cellular migration in the degenerate retina. The Li et al paper (1) was also seminal in that the authors were thinking about potential implications for therapies in this manuscript and suggested that these changes to the "retinal microenvironment may impede function integration of transplanted photoreceptors", ringing the warning bell for the biological transplant community that largely went ignored for a number of years.

Three years later, in 1998, Lewis, Linberg and Fisher (25) explored horizontal and rod bipolar cells in experimental retinal detachment (Figure 15). They conclusively demonstrated aberrant sprouting of fine

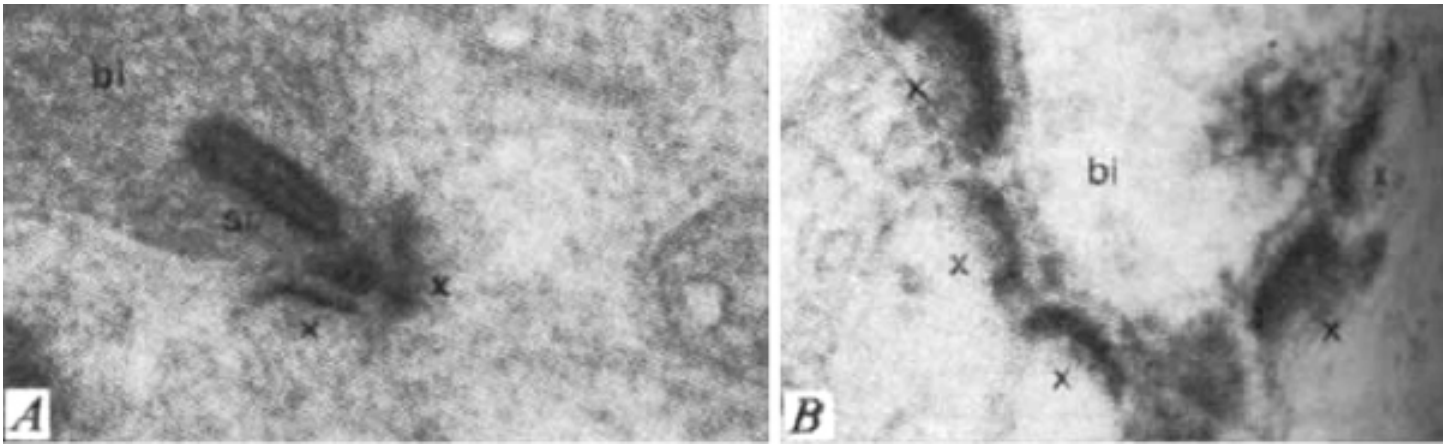

Figure 9. Bipolar terminals (bi) in the inner plexiform layer of the Nannacara (cyclid fish) retina. A. In the light-adapted animal, a bipolar-cell ribbon synapse with two postsynaptic elements, either ganglion or amacrine cell processes (x). Note the pentalaminate structure of the synaptic ribbon (s.r.). B. In the dark-adapted fish, a bipolar terminal flanked by five synaptic processes (x). It does not contain any ribbons. Os-EPTA; magnification x 48,000. From Wagner, 1973 (40).

dendritic processes from rod bipolar cells projecting into the outer nuclear layer (ONL) in response to retinal detachment in the feline retina. They also noted horizontal cell processes growing into the ONL and concluded that processes from horizontal and rod bipolar cells "lengthen after retinal detachment, perhaps in response to a withdrawal of their presynaptic targets, the photoreceptor synaptic terminals. The important thing with respect to interventions for blinding diseases is that these authors also invoked the implications of sprouting inner retinal neurons for therapies like retinal photoreceptor transplant. This work is documented extensively in another chapter here on Webvision, Cellular Remodeling in Mammalian Retina Induced by Retinal Detachment.

Two years later in 2000, Fariss, Li and Milam (4) examined rod photoreceptors, amacrine cells and horizontal cells in human RP retinas and demonstrated aberrant sprouting in those cell classes, particularly in GABA positive amacrine cells and calbindin positive horizontal cells (Figure 16). They also noted that rod neurites that projected into the inner retina, and at least contacted the somas of GABA positive amacrine cells, though no mention of synaptic connectivity was noted. This study continued the previous work, and included GABAergic amacrine cells into those neurons in the retina that contribute to the rewiring phenomenon that was starting to emerge. Also of note in this paper, the authors note that these changes may form the basis for some of the psychophysical abnormalities noted by patients (phosphenes and visual hallucinations) as well as form the basis for progressive visual function decline in patients with RP and again reiterated from the 1995 paper (1) that these alterations may complicate vision rescue strategies.

Also in 2000, Strettoi and Pignatelli (6) showed in the rd mouse (48), an animal model of RP, bipolar and horizontal cells undergoing "morphological modifications accompanying photoreceptor loss" (Figure 17). The authors concluded that these modifications were dependent upon photoreceptor loss and again raised the specter of potential impact on retinal rescue models.

The year 2000 was also the year our research lab came into the retinal degenerative community with some reticence. Robert Marc had published 5 years previously, the first paper using Computational Molecular Phenotyping (CMP) (49) and we were busy using these technologies to explore mammalian and non-mammalian retinas. CMP is a fusion of 3 techniques including anti-hapten IgG libraries, tissue array fabrication and computational pattern recognition. CMP allows for simultaneous quantitative probing of multiple immunolabels (3-20 or more) with hapten-specific IgG probes, with subcellular resolution in all cells. The technique profiles the metabolic state of every cell in a tissue. Figure 18 is a typical 3-space reconstruction of molecular data in human retinal tissue that uses red (r), green (g) and blue (b) color space to visually present differential labeling of small-molecule concentrations in tissues. In Figure 18, we can see taurine, glycine and

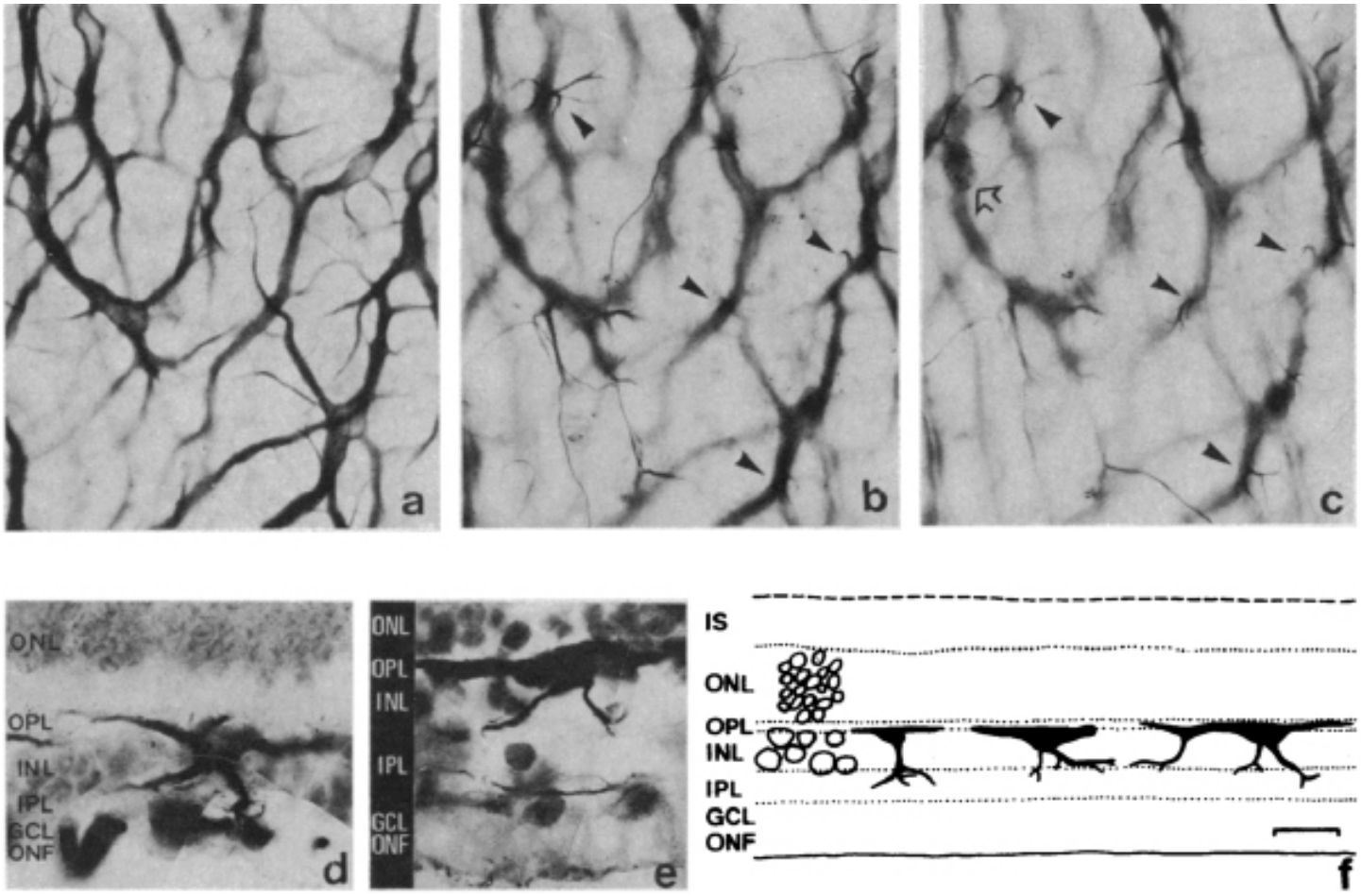

Figure 10. Sprouting A-type horizontal cells. (a to c) Micrographs of a field near the visual streak of a rabbit retina treated with 100 nM of KA. (a) Focal plane at the horizontal cell plexus (OPL and INL boundary); somata and dendrites in focus. (b) Focus at the INL, showing sprouts (some indicated by arrowheads) that branch off main horizontal cell dendrites and enter the INL. (c) Focal plane at the boundary of the IPL and ganglion cell layer (GCL), where the sprouts end in short fine branches (some indicated by arrowheads). The open arrow points to a ganglion cell. All horizontal cells in this field showed sprouting. (d and e) Sprouting horizontal cells in 35-µm vertical sections. Each horizontal cell shows two inward sprouts in addition to its normal OPL dendrites. The relative thickness of the layers in cat (d) and rabbit (e) retina differs. The ganglion cell layer and optic nerve fiber (ONF) layer are thin and disorganized due to KA- induced degeneration. (f) Schematic of vertical section of cat retina, showing sprouting horizontal cells. The OPL dendrites are incomplete where they leave the section. IS, photoreceptor inner segments. Scale bars: 20 µm (a to c and f) and 10 µm (d and e). From Peichel and Bolz, 1974 (42).

glutathione represented, revealing the vascular choroid in blue at top, the RPE in pink, photoreceptor cell classes in orange, ON-cone bipolar cells with low concentrations of glycine in light green, due to coupling with AII and other glycinergic amacrine cells, and their fine processes extending down into the IPL in bright green.

We were interested in, and intensely focused on, the normal circuitry of the retina and decidedly uninterested in pathology, but two events conspired to bring us into the field. The first event was a generous gift by Ann Milam of some human RP tissues to examine. At this point, we knew relatively little about retinal remodeling and were largely unaware of these few studies mentioned above. That said, upon processing the tissues that Dr. Milam had sent us, the following image is the first thing we saw.

This first image that came out of that initial analysis is shown in Figure 19. We were unprepared for what it revealed to us. In fact, it is fair to say that since we had no context to understand what we were seeing, we were completely flummoxed as the topology looked nothing like retina. In this image with the small molecular mapping as in Figure 18, you can see that the entire topology of the retina is altered. What should have been

photoreceptors up at the top was now a Müller cell seal. Müller cells are in dark red. Glycinergic amacrine cells in bright green are jumbled and altered in their lamination and appearance. Isolated RPE cells are seen with punctate light green labeling throughout the retina and unknown glutathione rich cells are colored blue. Despite some curiosity, we did not know what to do with these tissues and set them aside returning to what we knew, the normal vertebrate retina.

The second event that brought us into the study of retinal degenerative diseases was a colleague, Jeanne Frederick who came by the lab with aged samples of GHL, mutant rhodopsin, mice (adRP mimic) that she and Wolfgang Baehr had created (27), asking if I might be interested in the retinas of "some old, blind mice". The tissues Dr. Frederick was offering were osmicated and in blocks ready to be sectioned for transmission electron microscopy (TEM) and examined. CMP is compatible with TEM analysis, so we decided to see what aged mouse retina from a degenerate model looked like and we were stunned to see that these GHL mouse retinas looked precisely like the tissues from the human RP retinas that Ann Milam had sent and exhibited the same progressive degeneration as human RP retinas (Video 20).

The problem with this was that there were more than a few papers that stated definitively that the neural retina was refractory to photoreceptor loss. To explore this conflict, we set out over the next couple of years to track as many retinal degenerative examples as we could find using both naturally occurring models and engineered models including the S334ter rat, P23H rat, RCS rat, rd1 mouse, the GHL mouse, TG9N mouse, nr, or, chx10, pcd, rd2, rho-/-, rdcl, hrhoG, GC1&2 DKO, rhoDCTA mouse models as well as the P347L rabbit and the P23H pig. We also examined induced models like the light damage models and oxidative stress models. Colleagues from all over the planet were more than gracious in assisting us and some like Matt LaVail went above and beyond by contributing dozens of samples collected over the previous 30 years of work. The fundamental truth that came out was that everywhere we looked in retinal degeneration, despite what was in much of the retinal transplant and vision rescue literature, we saw retinal remodeling from the molecular to the histologic scales.

The stunning thing was how little work was in the literature at this time. For example, when we reviewed the literature in 2003, there were fewer than 30 papers in retinal degeneration that mentioned anything about inner retina neurons.

The remarkable thing about the community being misinformed about the state of the retina is that the histology in advanced forms of the disease, is dramatically altered from the normal appearance of the retina. One of the explanations might be that rodent models rarely get older than a year of age and for many investigators, once the photoreceptors were degenerated, they did not bother waiting longer for the more dramatic changes to ensue. That said, while aged rodent models of retinal disease are uncommon, there have been plenty of opportunities to study advanced human disease. Our explorations of advanced human RP have revealed dramatic alterations in the glial substrate as well as shown new structures termed microneuromas that form from neuritic sprouting from all neuronal cell classes in the retina (Figure 21).

It is also important to note that retinal remodeling and plasticity are not exclusive to RP and RP-like disorders. In addition to human RP and animal models of RP, we've examined human AMD tissues and found extensive evidence of remodeling and retinal plasticity involving bipolar cells and Müller glia stress responses (22). Figure 22 is from a patient with an early geographic atrophy diagnosis. Notably, there are a couple other papers in the literature documenting remodeling in AMD (8, 50).

An induced model, light induced retinal degeneration (LIRD) in albino mice/rats, represents a coherent stress insult to photoreceptors that results in massive loss of photoreceptors followed by subsequent retinal remodeling and reprogramming (29). Again, overall anatomical structure of the neural retina, particularly the inner nuclear layer, inner plexiform layer and ganglion cell layer seems normal or close to normal. However early in LIRD, key synaptic markers in inner retina demonstrate rapid inner retina responses to photoreceptor stress that lead to functional reprogramming of neuronal responses. This reprogramming is a result of AMPA GluR2 subunits

largely associated with inner retinal processing, exhibiting rapid changes in protein level. GluR expression in LIRD changes over 60 days post light damage, with low conductance AMPA receptor GluR2 subunits increasing 65% while high conductance KA receptor GluR5 subunits decrease 50%. AMPA receptor GluR1 subunits show no significant change in expression (51). Later in LIRD, there are massive changes and neuronal "escape" from the neural retina where bipolar and amacrine cells are observed leaving through breaks in Bruch's membrane, into the choroidal space (Figure 23).

Another non-RP model of retinal plasticity we have explored is the DBA/2J mouse model of glaucoma. Cuenca (52) demonstrated remodeling events in the ON-rod bipolar cells and horizontal cells in an increased pressure intraocular model in adult albino Swiss mice. Work in our lab in collaboration with Monica Vetter and Alejandra Bosco demonstrated remodeling events of GABAergic amacrine cell processes (Figure 24), which shows that negative retinal plasticity is not limited to photoreceptor deafferentations.

8. The TgP347L rabbit and P23H porcine models of retinitis pigmentosa

In addition to the mouse models, there are two viable large eye models of RP currently available. One, the P23H pig (53) shown in Figure 25 contains a Pro23His (P23H) rhodopsin (RHO) mutation that is the most common form of autosomal dominant RP (adRP) observed in humans. Porcine P23H models of RP show progressive loss of photoreceptors and loss of ERG b-wave (53). These porcine models demonstrate aberrant Müller cell signatures seen in human (Figure 22) and other models of retinal degeneration (Figure 30). Progressive loss of photoreceptors followed by loss of visual percepts, as measured by ERG (53), is just like the human rodent and rabbit (22). Porcine tissues also exhibit neuritic sprouting in both the GABAergic and glycinergic amacrine cell populations prior to retinal photoreceptor degeneration, suggesting that there are stressors in the system that induce downstream responses in the inner neural retina.

The P347L TG rabbit was generated by Mineo Kondo and Hiroko Terasaki as a large eye model of autosomal dominant RP (54). The rabbit expresses a rhodopsin proline 347 to leucine transgene (Figure 26). Drs. Kondo and Terasaki approached us that same year to evaluate this model and compare it to models of RP as well as human RP. This work was published in 2011 documenting the progression of retinal degeneration and subsequent remodeling of the sensory and neural retina (21). We have analyzed degeneration, remodeling and reprogramming at the molecular, physiological, and the histological levels and have shown that disease progression in the TgP347L rabbit closely tracks human cone-sparing RP, including the cone-associated preservation of bipolar cell signaling, and the triggering of glutamate channel reprogramming.

The TgP347L rabbit as well as the P23H pig model are attractive as models of retinal disease for many reasons. This model is a large eye model and there is a substantial existing knowledge base in ophthalmology including retinal anatomy and circuitry. Some advantages of the TgP347L rabbit is the relatively fast disease progression combined with a manageable and affordable approach making the TgP347L rabbit an excellent model for gene therapy, cell biological intervention, progenitor cell transplantation, surgical interventions, and bionic prosthetic studies.

Because of the similarity of the TgP347L rabbit to human adRP, most of the remodeling specific discussion that follows will derive from data from that model system.

Retinal degeneration in the mammalian retina occurs in phases. *Phase 1* is typified by photoreceptor stress, which is the beginning of early remodeling & clinically occult reprogramming events at the cellular and molecular levels. *Phase 2* of retinal remodeling involves the microglia, Müller glia and RPE cells, as the Müller glia begin to exhibit signs of cell stress and reactivity to the degenerating retina. Müller cells also begin to hypertrophy and grow up between photoreceptor cells to initiate the Müller cell seal. Cell death in the ONL begins to occur in *Phase 2* as well. *Phase 3* is where we begin to see neuritic sprouting from all neural cell classes

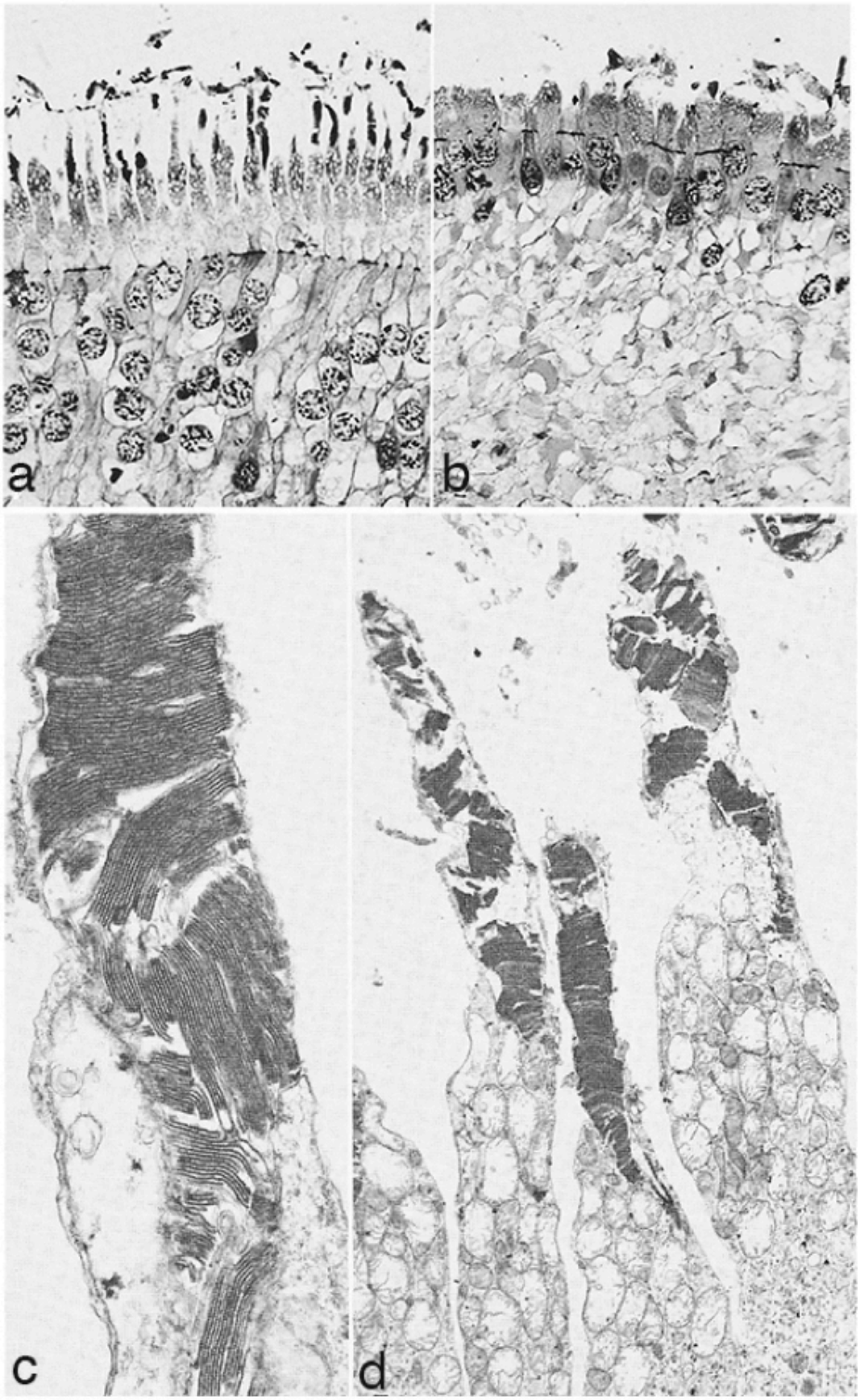

Figure 11. Light (a, b) and Electron micrographs (c, d) of cone photoreceptors in the foveal region of retina of a patient with autosomal dominant retinitis pigmentosa. The inner segments are normal in length but wider than normal for the fovea. The outer segments have broken disorganized discs often at unusual angles to each other. From Kolb and Gouras, 1974 (43).

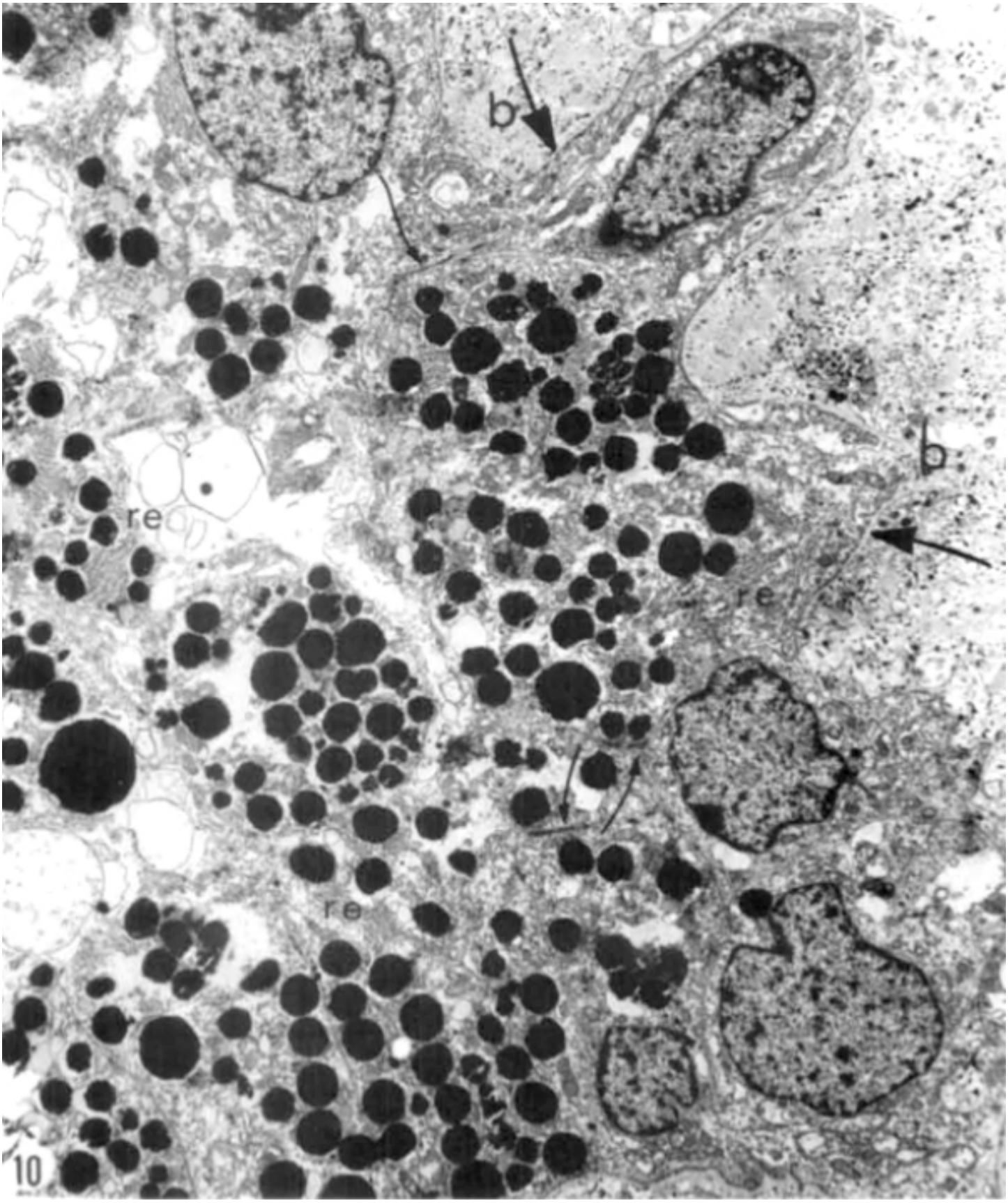

Figure 12. Electron micrograph of a portion of bone corpuscular pigmentation. The cells comprising the pigment clump appear to be of the same type as the cells of the peripheral pigment epithelium. The surface is folded due to the projecting cells, each of which has basement membrane material (b, thick arrows). Each cell contains melanin granules and rough endoplasmic reticulum (r.e.) and is joined to neighboring cells by zonulae adherens and gap junctions (thin arrows). From Kolb and Gouras, 1974 (43).

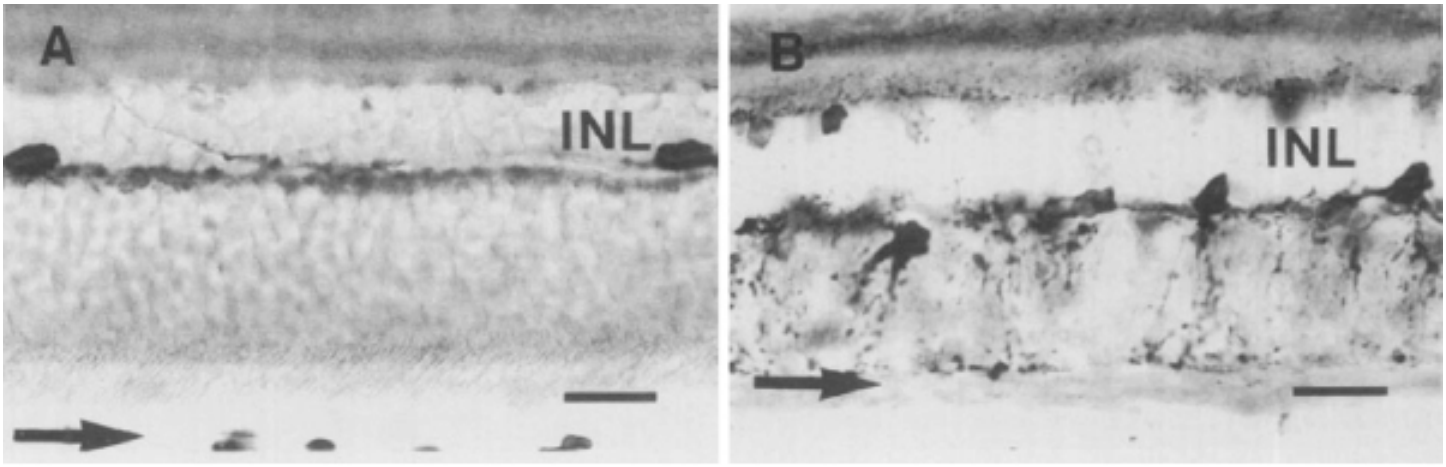

Figure 13. Sprouting of horizontal cell dendrites in RCS rat retinas. Fifty-micrometer-thick cross-sections from RCS-rdy+ (A) and RCS (B) rat retinas oriented with the ganglion cell layer uppermost (the ganglion cell layer is not visible). INL = inner nuclear layer. Arrows indicate the pigment epithelium. A. In RCS-rdy+ retinas a monoclonal antibody against the 28kD calcium-binding protein (28-kDa CaBP) labelled horizontal cell processes were confined to the narrow plexus of the OPL and the cell somas were confined to the outer INL. Bar = 25μm. B. In the RCS rat retinas the 28-kDa CaBP labelled horizontal cell processes extended throughout the outer nuclear layer and debris zone, and were tortuous and swollen. Some of the somas were displaced from the INL, as is evident in the cell on the far left in this micrograph. Bar = 25μm. From Chu, Humphrey and Constable, 1992 (47).

resulting in new neuronal circuits. Neuronal cell death also begins to occur in the bipolar, horizontal and amacrine cell populations. The end stage of retinal remodeling is a neural retina bereft of cells and unable to provide coherent visual pathways to higher centers for processing.

Progression of retinal degeneration and remodeling in the Tg P347L rabbit closely tracks the sequelae of events seen in human RP, though it appears to happen at an accelerated rate, progressing to total photoreceptor loss at 1yr of age. At 12-16 weeks in the TgP347L rabbit, *Phase 1* of retinal remodeling has begun early in the retinal degenerative process, before photoreceptors have degenerated. The photoreceptor structure appears largely intact except for some disorganization in the outer segments of photoreceptors. Some portions of outer segments break off and appear to remain in the subretinal space, rather than being phagocytosed by the RPE (Figure 27). The most compelling feature of this region is the large numbers of small, vesicular rod photoreceptor outer segments that break off and appear as a rhodopsin "froth" in the subretinal RPE/photoreceptor interface space. We speculate that this "froth" increases oxidative cell stress in RPE and photoreceptor cells.

By 40 weeks in the Tg P347L rabbit, some opsin expression can still be found in cones, however, it is delocalized, much as described in Li et. al in 1995 (1). While photoreceptors can still be found in abundance, the rhodopsin delocalization into the membrane surrounding the cell body suggests substantial photoreceptor cell stress (22).

Figure 28 shows glutamine immunoreactivity in *Phase 1-2* in the Tg P347L rabbit retina at 4 months, where the glutamine signal begins to demonstrate alterations between Müller cells. Glutamine is present in most retinal neurons, but most notably in Müller cells. It is also found at high concentrations in the RPE cells, but at 4 months, glutamine levels in isolated Müller cells are revealing multiple metabolic states, a result never observed in normal retina (21).

Further into *Phase 2* at 10 months in the Tg P347L rabbit retina, glutamine synthetase (GS) levels also show quantifiably different levels of expression (Figure 29). GS mediates the recycling of glutamate, GABA and ammonia to form glutamine, and becomes dramatically unregulated in some Müller glia, explaining the mosaicked levels of glutamine observed in Figure 28, but also revealing specifically that nitrate reduction and amino acid degradation pathways are being altered in the degenerate retina (21).

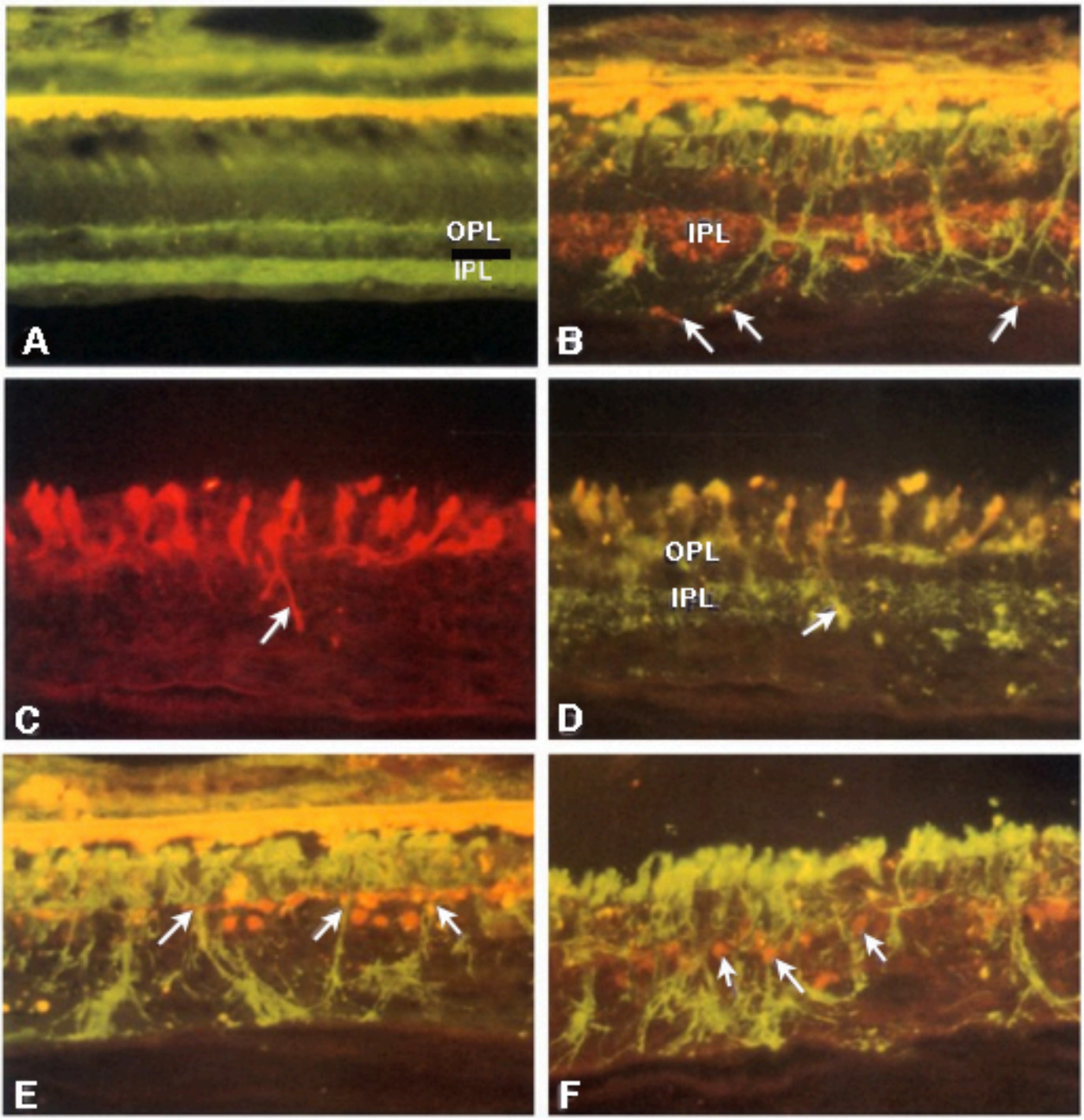

Figure 14. Normal and retinitis pigmentosa (RP) human retinas after immunofluorescence labeling. A. Distribution of SV2 synaptic vesicle protein in the inner (IPL) and outer (OPL) plexiform layers of a normal retina. The yellow band corresponds to autofluorescent lipofuscin in the retinal pigment epithelium. B. Double labeling for SV2 (rhodamine, red) and rhodopsin (FITC, green) in an RP retina. The anti-SV2 labels the OPL and IPL, plus bulb-shaped varicosities (arrows) on the rhodopsin-positive rod neurites. C. Cones in the peripheral region of an RP retina labeled for cone transducin alpha, which fills the cone cytoplasm. Some cone axons (arrow,) are abnormally long and branched, extending into the inner plexiform layer (see D). D. Section in C is double labeled for cone transducin alpha (rhodamine) and synaptophysin (FITC) in both the IPL and the OPL. The cones are labeled with both antibodies, and the cone axon (arrow) extends into the IPL. E. Double labeling for calbindin (rhodamine) and rhodopsin (FITC) in an RP retina. The rhodopsin-positive rod neurites pass through the band of calbindin-positive horizontal cell processes (arrows). Five amacrine cells are also labeled with anti-calbindin. F. Double labeling of L-7 protein (rhodamine) and rhodopsin (FITC) in the peripheral region of an RP retina. The rhodopsin-positive rod neurites course between and past the labeled rod bipolar cells (arrows) and reach the inner limiting membrane. Magnification, 280X. From Li, et. al. 1995 (1).

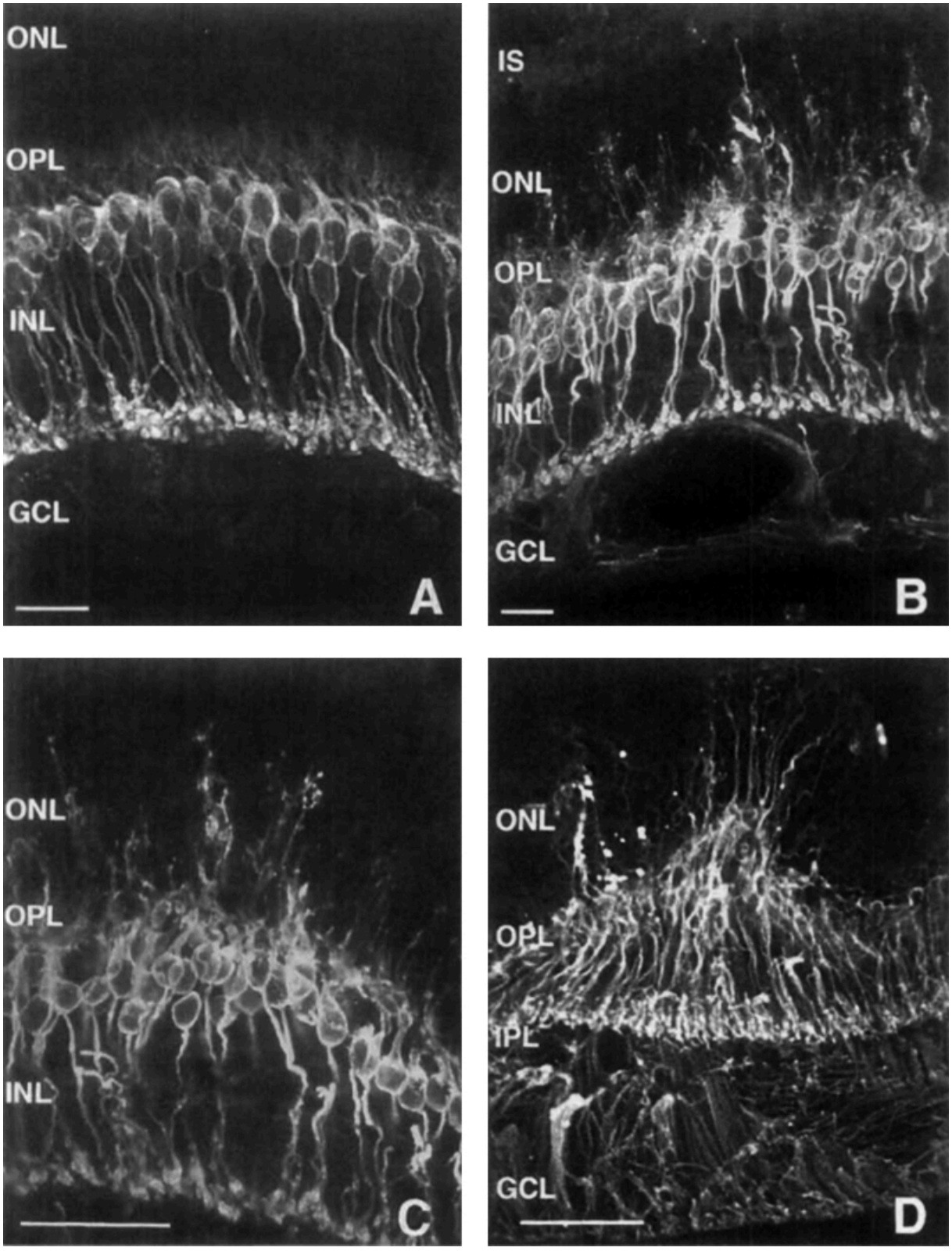

Figure 15. Anti-protein kinase C labeling of normal (A) and detached (B, C, D) retinal sections from cat. A. Normal retina. Labeling occurs only in the rod bipolar cells, including the fine dendritic processes in the outer plexiform layer (OPL), the cell bodies in the inner nuclear layer (INL), the axon, and the axon terminal. B. 1-day retinal detachment. Labeling is present in bipolar cell processes extending into the outer nuclear layer (ONL). Faint labeling also begins to appear in other cell types in the ganglion cell layer (GCL). C. 1-day retinal detachment. Higher magnification of the bipolar cell labeling in the ONL in a different area than shown in C. D. 28-day retinal detachment. Low magnification showing labeled bipolar cell processes extending into the ONL. The fainter signal in the inner retina is from other cell types, including Muller cell and astrocyte processes, and does not extend past the inner plexiform layer (IPL). A, C, and D are projections of nine images; B, is a projection of 13 images. Bars, 20 μm. From Lewis, Linberg and Fisher, 1998 (25).

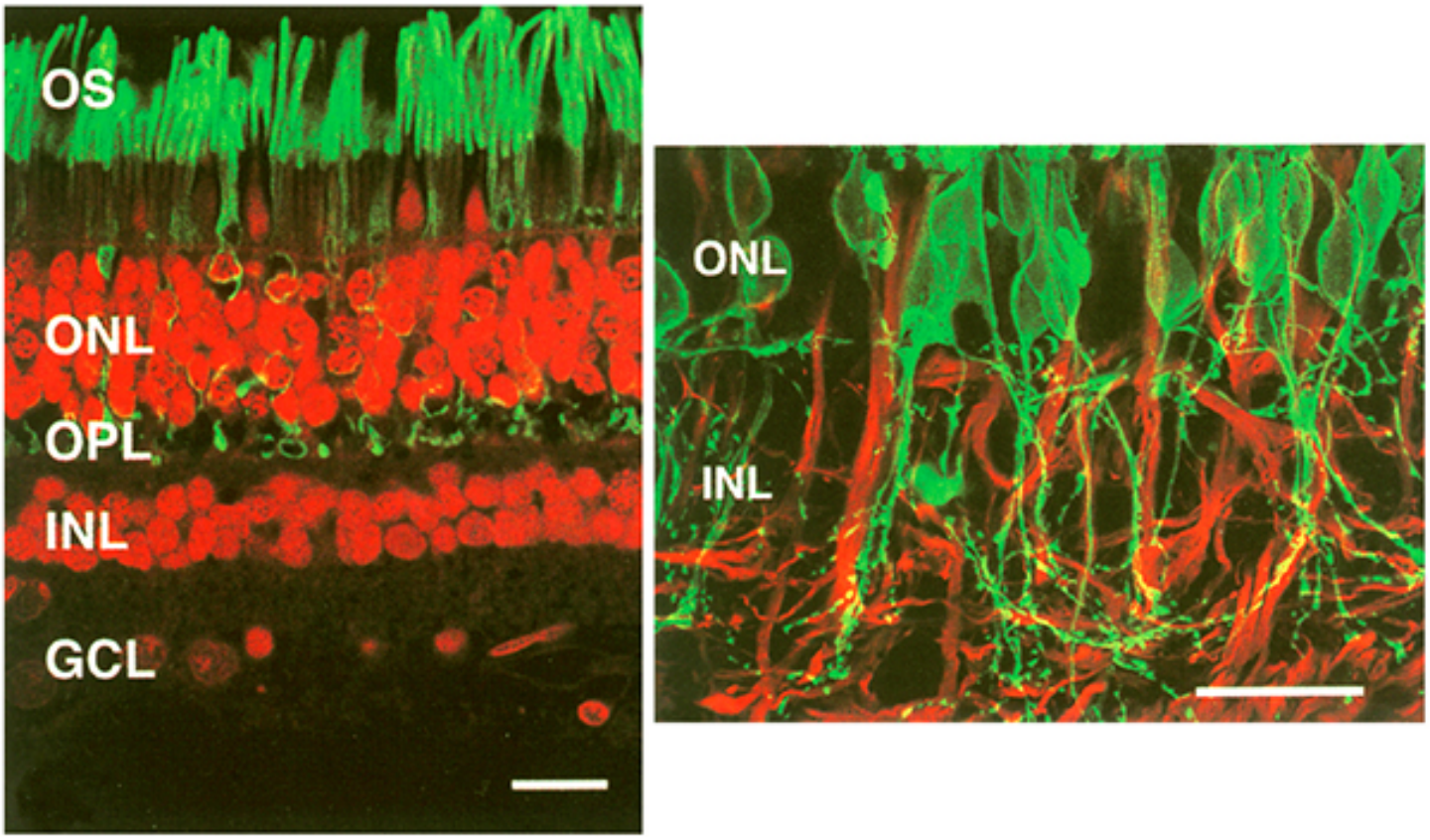

Figure 16. Immunolabeling of rod photoreceptors with anti-opsin (green) in normal human and in retinitis pigmentosa retinas. Nuclei in the outer nuclear layer (ONL), inner nuclear layer (INL), and ganglion cell layer (GCL) are stained red with propidium iodide. Scale bar = 20 µm. (Left image) Normal retina (UW-0802-95). Opsin immunolabeling (green) is strongest in the outer segments (OS) and weak in the plasma membranes of rod somata in the outer nuclear layer and synapses in the outer plexiform layer. (Right image) Retinitis pigmentosa retina (FFB 340). Localization of opsin (green) in rods in the outer nuclear layer (ONL) and glial fibrillary acid protein (red) in reactive Müller cells (red). The rod neurites are closely associated with the surfaces of the glial fibrillary acidic protein–positive Müller cells. INL = inner nuclear layer. Scale bar = 25 µm. Figure from Fariss, Li and Milam, 2000 (4).

CMP visualization in the 10 month old TG P347L rabbit retina in *Phase 2-3* with τQE :: rgb (τ-taurine, red; Q-glutamine, green; E-glutamate, blue) visualization (Figure 30) allows retinal pigmented epithelium and Müller cells to be observed independent from all other cell classes. In this visualization, L-glutamate labeling in combination with taurine demonstrates 3 surviving cones protruding above the Müller cell seal (pink cells). Additionally, the mosaicism in the Müller cell signatures is evident demonstrating the pathological heterogeneity of small molecular signals. In this region of retina, the Müller cell seal is essentially complete, isolating the neural retina from the RPE and choroid and the retina is bereft of any photoreceptors save the 3 isolated cone photoreceptors in this region (21).

Phase 3 is typified by extensive, de novo neurite formation, new synapse formation and neuronal death. In the Tg P347L rabbit, the retina is fully involved in *Phase 3* remodeling by 10 months. Maximal projection confocal images of protein kinase C immunoreactivity (PKC), rhodopsin 1D4 immunoreactivity (Rho 1D4), and a nuclear stain (DAPI) as red, green and blue respectively, demonstrate not only the reduced rhodopsin immunoreactivity associated with degenerate rod photoreceptors, but also bipolar cell axons that have become multipolar cells, projecting along the top border of the IPL (Figure 31). These processes extend outside of the normal lamination of the bipolar cell population, coursing across the IPL, forming swellings also suggestive of synaptic connections and implying new retinal connectivities (21). These bipolar cells also are downregulating iGluR and mGluR6 expression, results observed previously in rodent and human retinal degenerative diseases (31).

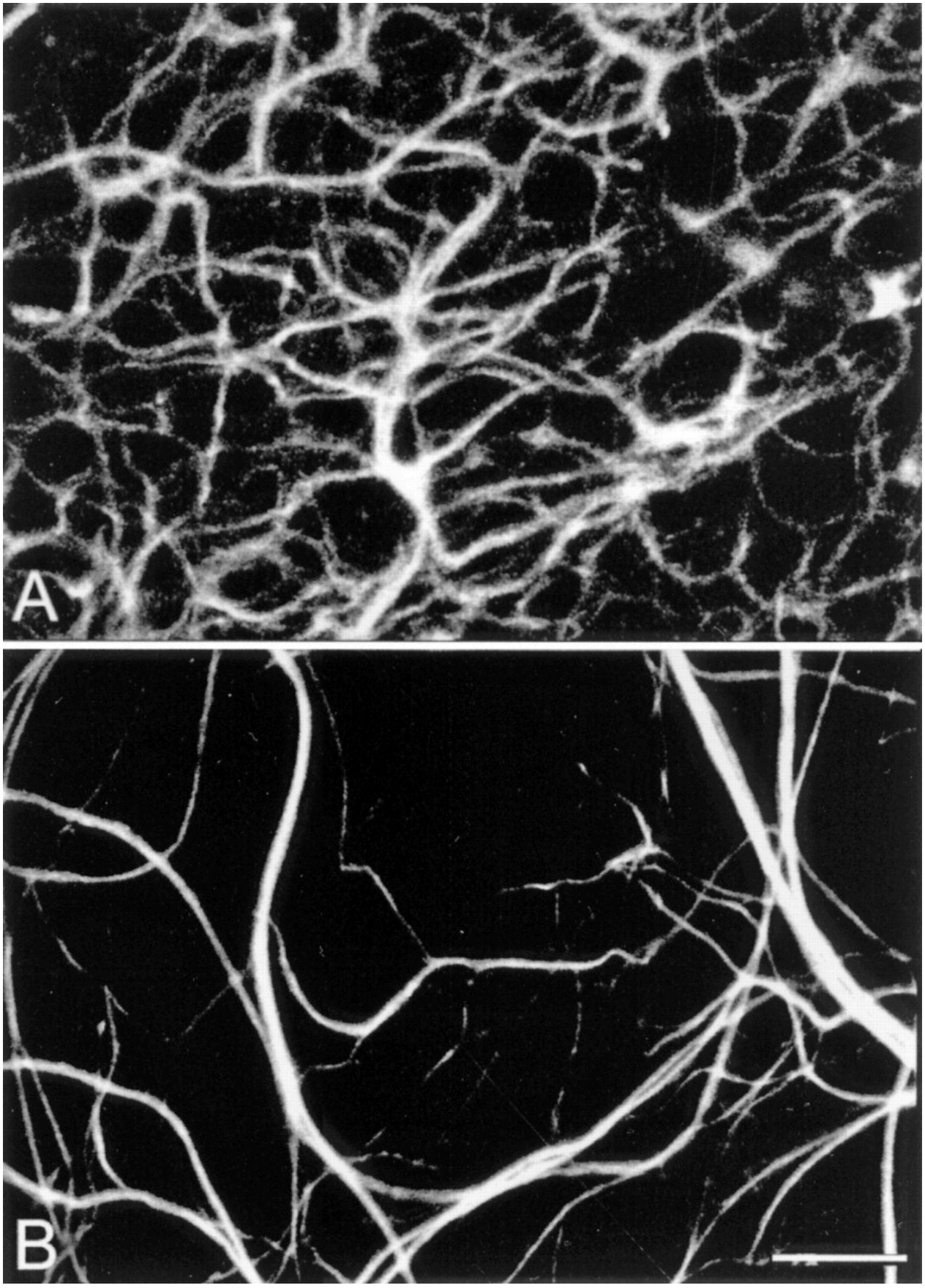

Figure 17. Whole-mount staining of horizontal cells with neurofilament antibodies. Compare the tight network made by horizontal cell axonal endings in the OPL of wt mouse retinas (A) to the loose arrangements of hypertrophic process in the rd mouse (B). From Strettoi and Pignatelli, 2000 (6).

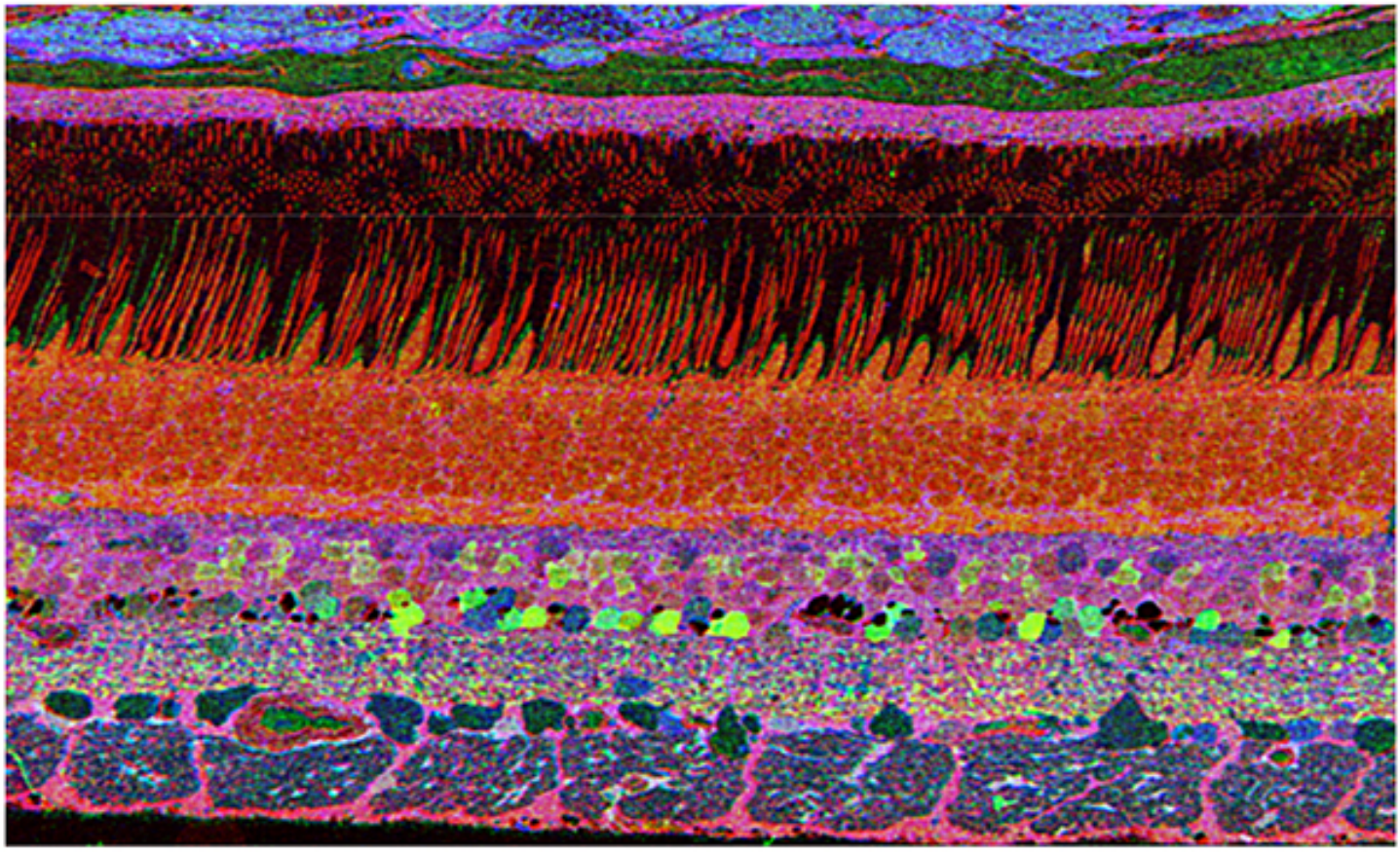

Figure 18. Human retina with taurine, glycine and glutathione assigned to red, green and blue color channels respectively, revealing varied cell classes.

In another region of Tg P347L rabbit retina at 10 months, *Phase 3* remodeling can also be documented through persistent neurite formation of horizontal cells. In Figure 32, a maximal projection confocal image shows immunohistochemistry of PKC, calbindin (a calcium binding protein) and DAPI as red, green and blue respectively, demonstrating calbindin labeling in horizontal cells. Horizontal cell processes are seen projecting down into the IPL in an aberrant fashion (21). Calbindin has been used extensively before to examine alterations in the horizontal cell populations (4) and these results correlate nicely with those observed in the human retina.

Examining neuritic sprouting from amacrine cells in the Tg P347L rabbit in *Phase 3* at 10 months shows new GABAergic and glycinergic neurite formation. Figure 33 is a γGE :: rgb image, visualizing photoreceptor cells, bipolar cells, GABA+(γ) and glycine+(G) amacrine cells, and glutamate+ (E) ganglion cell superclasses. Overall the lamination of the IPL appears normal, but this belies excitatory and inhibitory cell populations in these retinas that are creating new neurites, seen here as fine filamentous magenta signals running underneath the Müller cell seal seen in Figure 30, and above most remaining bipolar cell populations (21).

Figure 34 shows GABA labeling in *Phase 3* of remodeling in the Tg P347L rabbit retina at 10 months, revealing GABAergic amacrine cell sprouting. Again, the overall lamination of the IPL revealed by GABA immunoreactivity appears normal despite early GABAergic sprouting events, including persistent neurite formation, new synapse formation and neuronal death (21). This is still early in *Phase 3*, prior to large scale topographic reorganization which occurs as Müller cells continue hypertrophic responses and additional numbers of cells from each cell class undergo cell death.

Sprouting from amacrine, bipolar, horizontal and ganglion cell populations can continue to elaborate, forming large tangles of GABAergic, glycinergic and glutamatergic processes into microneuromas, or tufts of neuropil

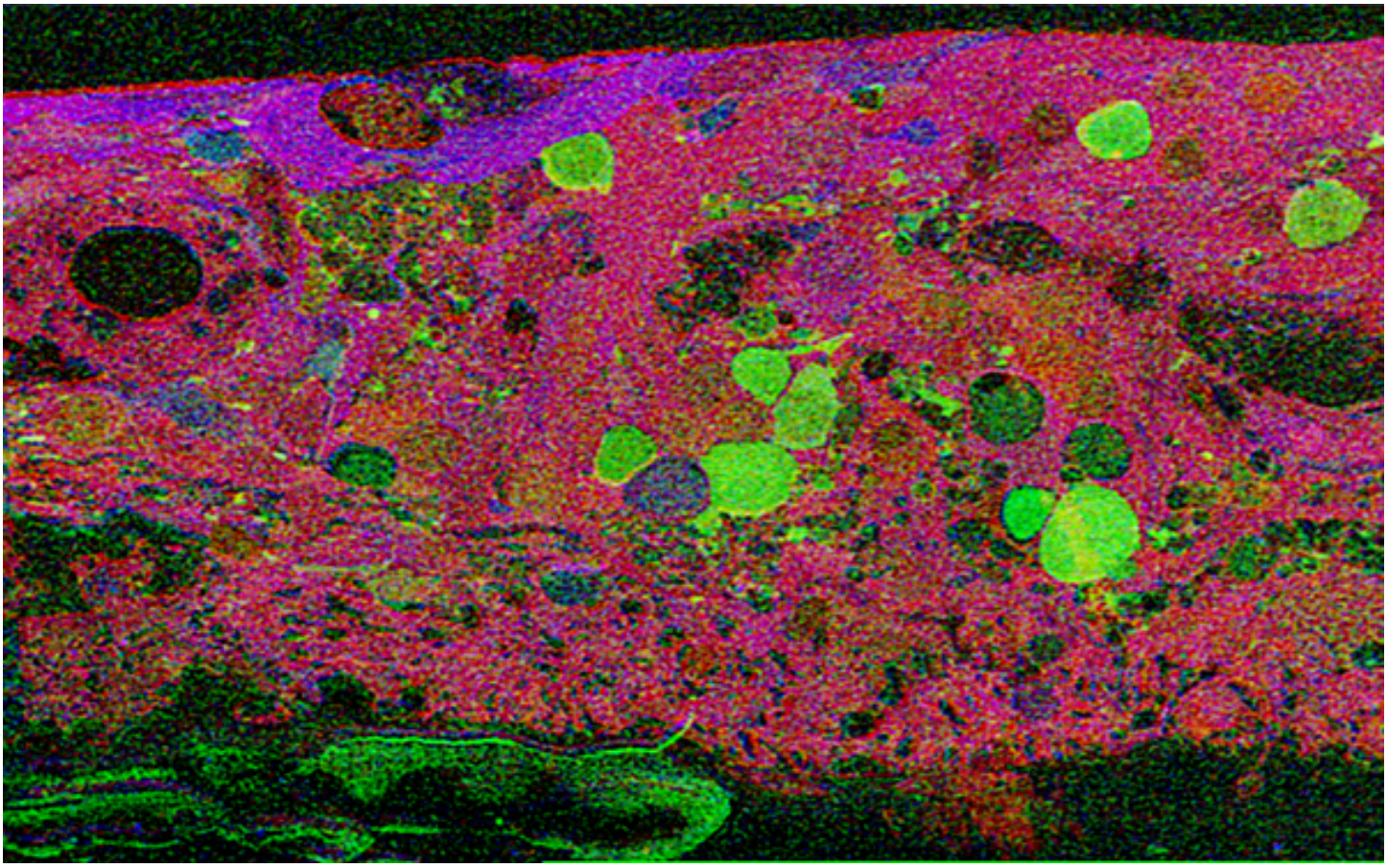

Figure 19. Late stage molecular imaging of human retina from a patient with RP with taurine, glycine, glutathione mapped to red, green and blue color channels respectively.

Video 20. An image of a GHL mouse retina with taurine, glutamine and glutamate mapped to red, green and blue color channels respectively. A video showing a digital morphing animation of retinal degeneration, spanning 700 + days in the life of a GHL Tg mouse retina is linked to the image.

Download video

formed de novo, post retinal maturation and development. These microneuromas break traditional rules of plexiform lamination and can be seen in Figure 35 in the hrhoG mouse, erupting out of the IPL and coursing up to the top of the retina underneath the RPE.

By late stage in *Phase 3*, persistent neurite formation, new synapse formation and neuronal death continue with all cell classes participating. As cell classes continue to sprout processes from bipolar, amacrine, horizontal and ganglion cells, many processes begin to co-fasiculate and run together in microneuroma structures, complete with synaptic connectivity. Figure 36 is a collection of neuritic processes moving from one location to another within an area of Müller cell seal. Microneuromas are not silent structures as they contain both ribbon and conventional synapses with a number of synaptic arrangements including, but not exclusively, amacrine > amacrine, bipolar > amacrine, and amacrine > bipolar, and bipolar > bipolar (9).

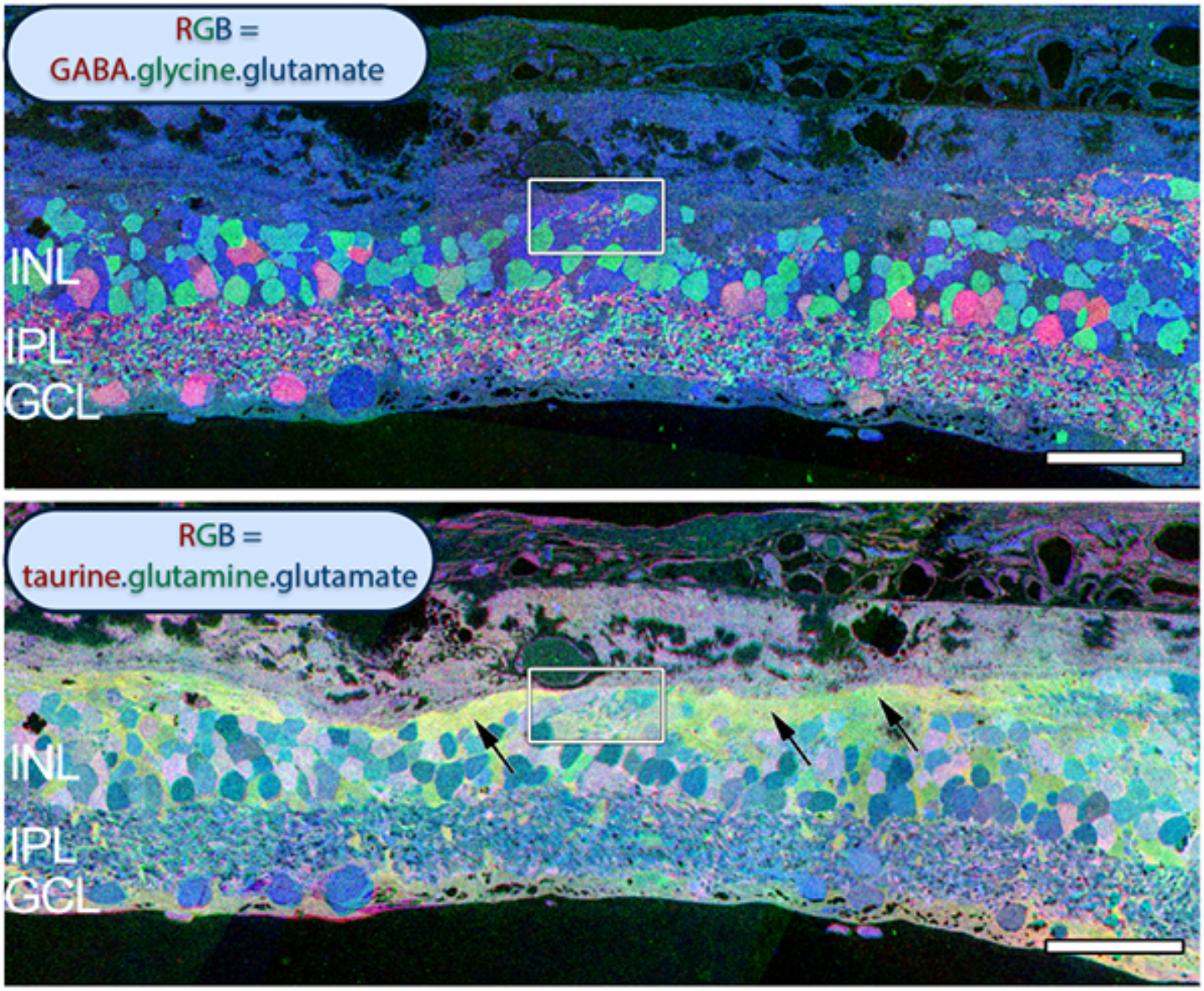

Figure 21. Human retina from a patient with advance autosomal dominant RP. GABA, glycine, glutamate (red, green, blue) mapping in the top panel reveals novel tufts of neuropil, termed microneuromas (box) with amacrine cells abutting Bruch's membrane and the choroid. The bottom panel shows taurine, glutamine, glycine (red, green, blue) mapping of the same region demonstrating Müller cell revision and Müller cell seal formation (arrows) walling off the neural retina. Scale bar = 90µm.

9. The earliest changes in the retina occur before obvious histological changes occur.

In models of RP where rods and cones die simultaneously, bipolar cells lose dendrites and all iGluR/mGluR responsivity. From *Phase 0-1*, rod bipolar cells down-regulate GluR expression in the dendrites. In *Phase 1-2*, rod and cone photoreceptor stress and subsequent cell death happen, while dendritic modules are lost. In *Phase 3*, wider retinal remodeling ensues, resulting in sprouting and formation of new axonal modules. In models of RP where cones outlive rods, some bipolar cell dendrites switch targets. In normal rod bipolar cell architecture, dendrites from rod bipolar cells bypass cone pedicles. In *Phase 0-1*, as in rod/cone dystrophies, rod bipolar cells down regulate GluR expression in the dendrites. In *Phase 1-2* with rod stress and death, dendritic modules are lost. In late *Phase2/Phase 3*, some rod bipolar cells form sprouts that contact cone pedicles, making peripheral

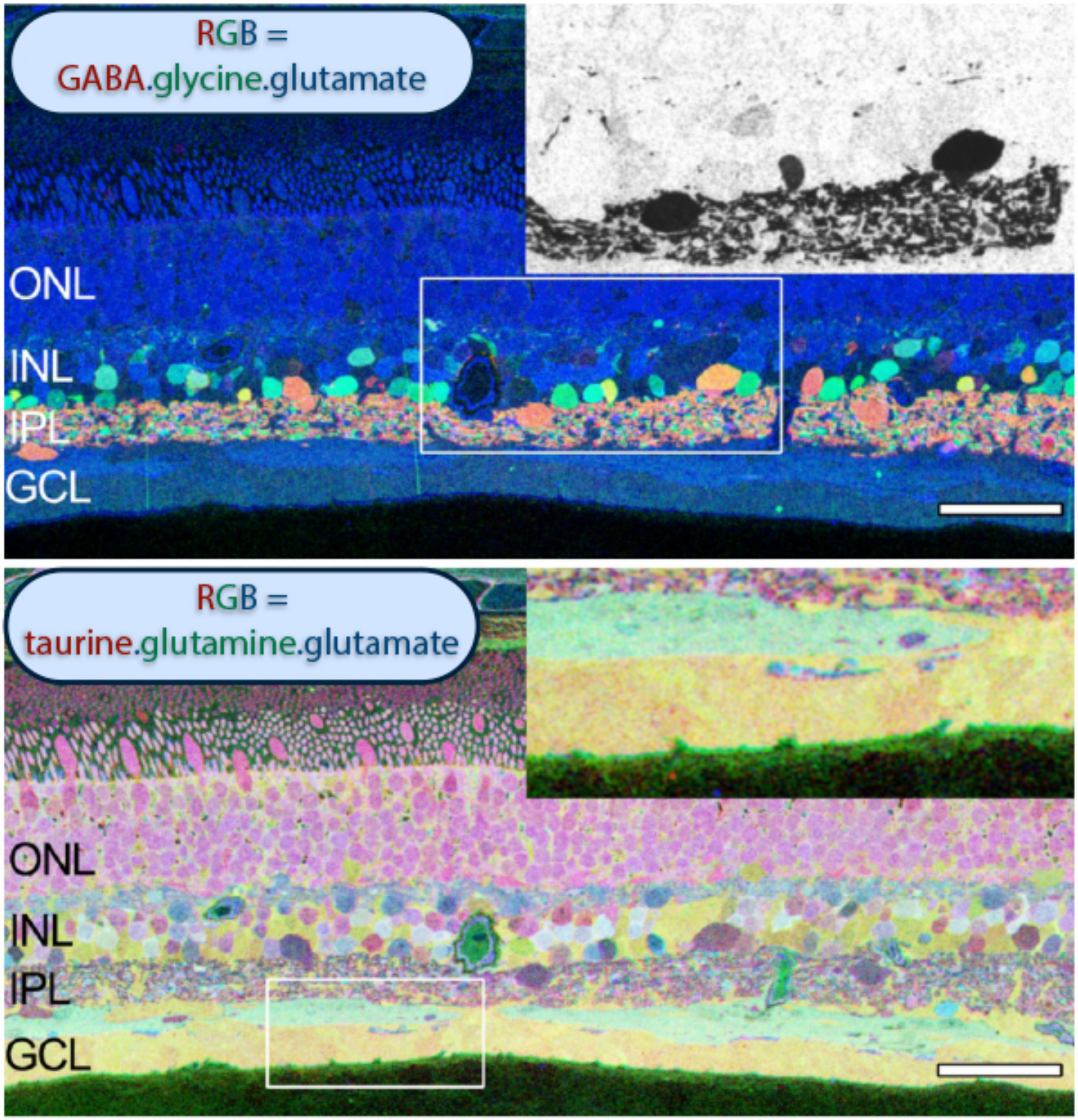

Figure 22. Early-stage human geographic atrophy/AMD. The top panel shows GABA, glycine, glutamate (red, green, blue) mapping in early stage human geographic atrophy/AMD tissue demonstrating processes arising from both glycinergic and GABAergic amacrine cells (GABAergic processes extending into the outer plexiform layer in inset). These processes are the beginnings of microneuroma formation. The bottom panel shows taurine, glutamine, glutamate (red, green, blue) mapping that demonstrates alterations in Müller cell signatures, notably an increase in the amount of taurine in subsets of Müller cells indicative of Müller cell stress (inset). Scale bar = 90μm.

contacts on cone pedicles. Video 37 and Figure 38 summarize the degenerative phases that a retina with RP type degeneration goes through, as described above. In human RP, it is clear that the peripheral retina goes into

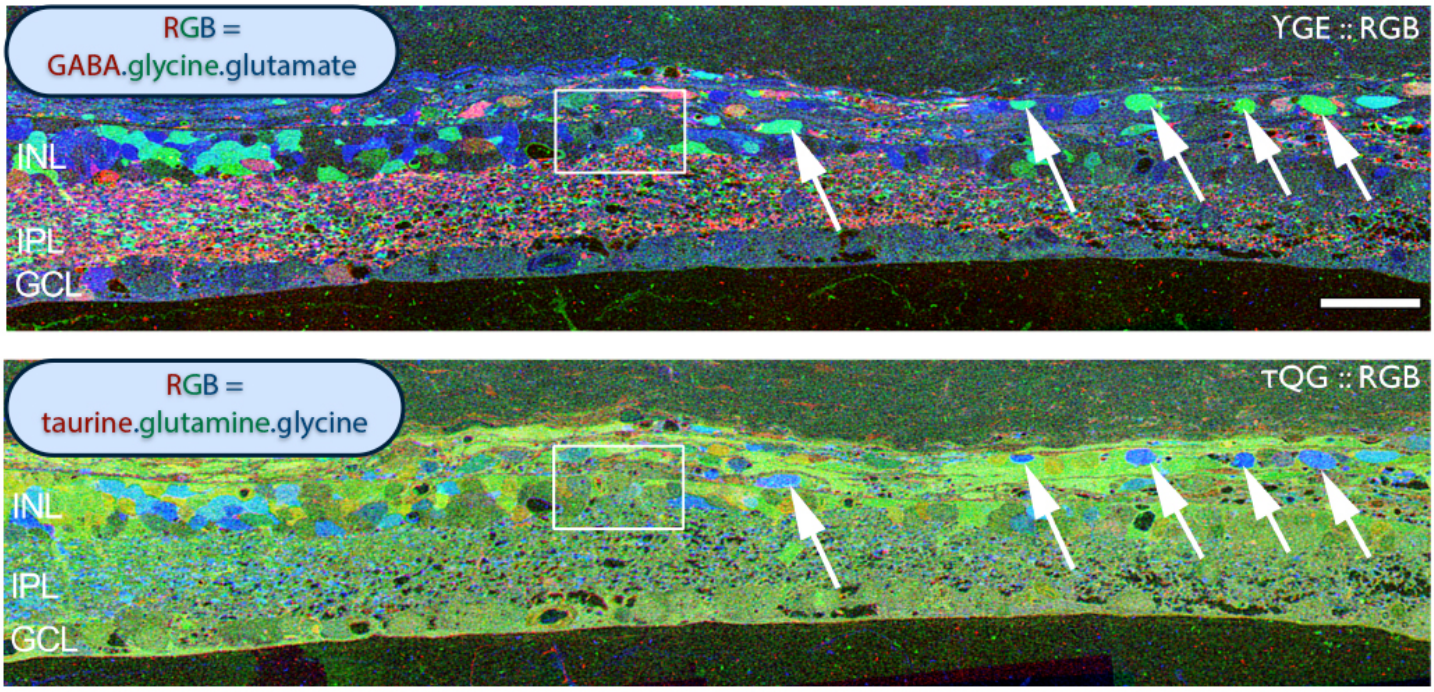

Figure 23. Neural emigration in a rat light damage model of retinal degeneration. Top panel. γGE::RGB: GABA, glycine, glutamate mapped as red, green, blue, demonstrates both GABAergic and glycinergic amacrine cells in addition to bipolar cells escaping the neural retina into the choroid (arrows). Bottom panel. τQG::RGB: taurine, glutamine, glycine mapped as red, green, blue, demonstrates Müller glia with glycinergic amacrine cells embedded among them, passing outside of the retina through a break (box) in Bruch's membrane. Scale bar = 90μm.

Phases 1-3 long before the central retina and fovea does. The RP patient eyes that have been looked at with good anatomical techniques have *Phase 3* retina in the periphery and phase 1 in the fovea (4, 43, 45, 46, 55).

10. Conclusion

Fundamentally, in every instance of retinal disease and every model of retinal degeneration examined to date, the survival of cones appears to at least delay the gross onset of *Phase 3* remodeling. This can be seen in local patches of retina where cones persist with preserved bipolar cell dendritic structures. Even when cones are severely compromised and lack outer segments, visual pigment expression and are altered in morphology, as long as cones are present, the retina appears to maintain its state in *Phase 2*. This may suggest the involvement of integrins, or demonstrate that mere connectivity through the established circuit is enough to maintain Ca^{++} signaling and gene expression profiles. At the very least, it provides evidence that prolonging cone survival is a substantial advantage to maintaining vision or making subsequent vision rescues, such as survival factors, stem or progenitor cell transplantation, fetal retinal sheet transplantation, and gene therapies, more successful.

As we move forward into genetic models with various treatments designed to delay or recover vision loss, we need to consider the potential shown by plasticity in the retina. Retinal remodeling in *Phase 1* and *Phase 2* might for instance, be reversible and may in fact respond to the right therapeutic interventions. However, by the time the retina enters *Phase 3*, with its alterations to wiring and neuritogenesis, cell migration and cell death, it is likely too late. The problem with gene therapies for rods and cones is that they depend upon photoreceptor survival. If we can prolong cone survival, this might point the way to a "cure". However, as we noted above, photoreceptor involvement in retinal degenerative disease begins long before the photoreceptors die. This begins to define "windows of opportunity" where gene therapies might succeed, and suggests that combination gene therapy with survival factor administration might be a reasonable approach to prolong photoreceptor survival through delivery of neurotrophins.

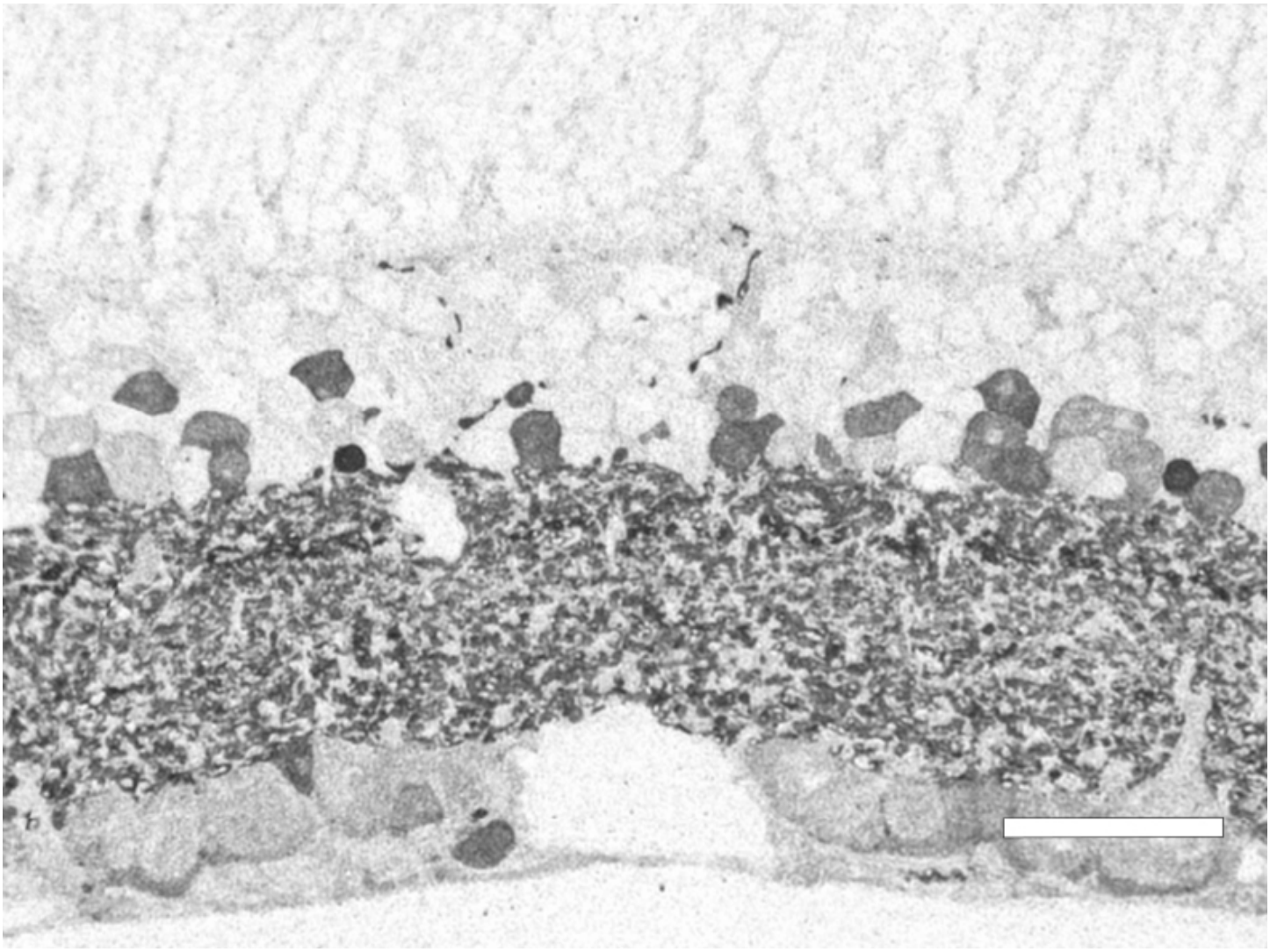

Figure 24. Retina from a 23-month-old male DBA/2J mouse labeled for GABA. The staining demonstrates aberrant GABAergic amacrine cell remodeling with new neurites projecting upwards into the outer plexiform layer. Scale bar = 30μm.

About the authors

Bryan William Jones, Ph.D., is Associate Research Professor at the John A. Moran Eye Center at the University of Utah. His work involves disorders of retinal degeneration and how those diseases affect the intrinsic retinal circuitry including the implications for rescue of vision via gene therapy, and retinal bionic or biological implants. Other research efforts involve exploring metabolomics for application in understanding physiology and medicine and for drug development.

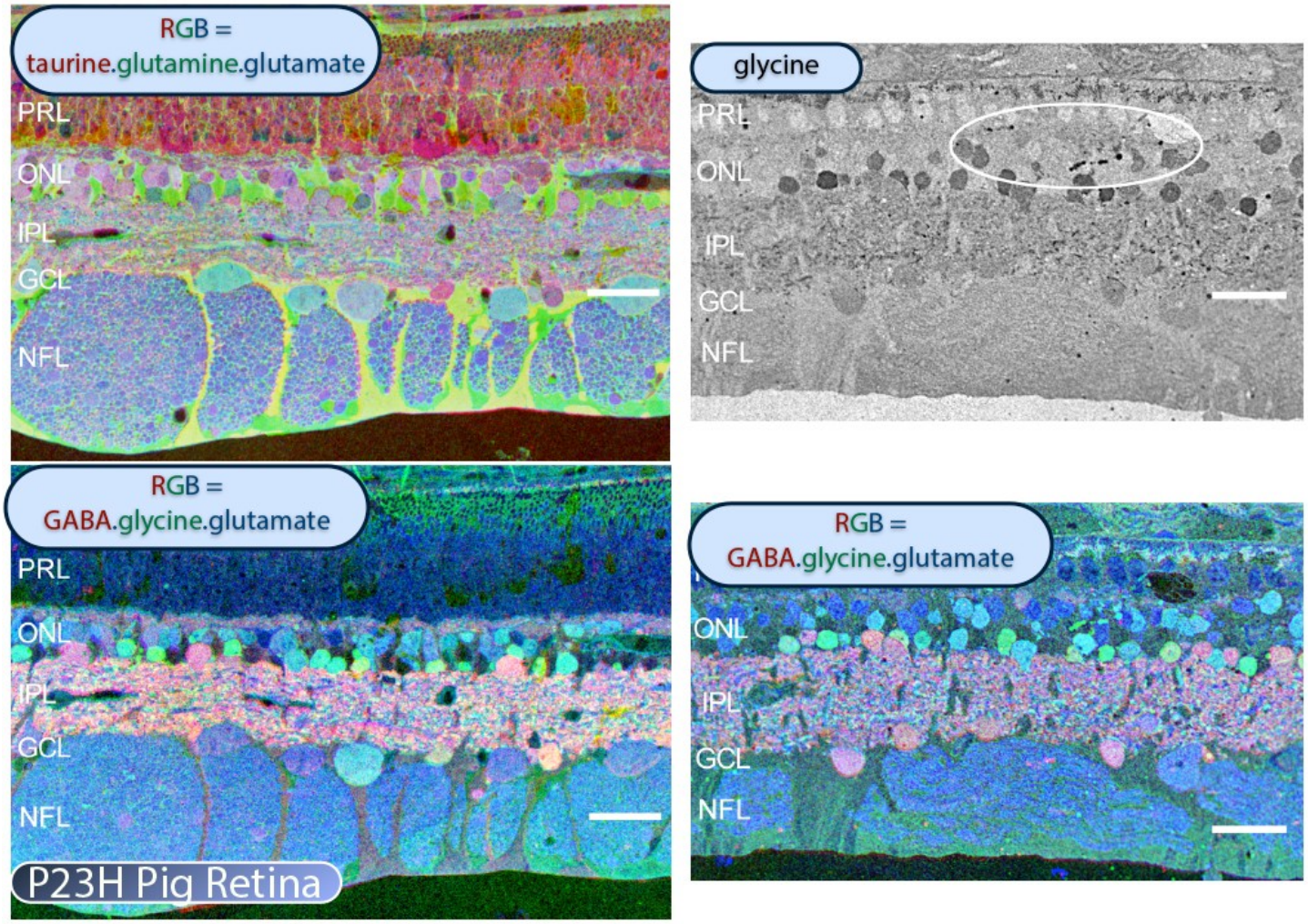

Figure 25. Early stage porcine P23H model of retinal degeneration. Top left, Taurine, glutamine, glutamate (red, green, blue) showing reduced photoreceptor outer segment length and early stages of Müller cell stress and alteration of molecular signatures (green/yellow). Bottom left) GABA, glycine, glutamate (red, green, blue) of same region showing normal appearing OPL, IPL and neuronal signatures. Top right, glycine immunohistochemistry demonstrating early retinal remodeling/sprouting in the glycinergic amacrine cell populations. Bottom right) GABA, glycine, glutamate (red, green, blue) mapping demonstrates dramatically truncated photoreceptor outer and inner photoreceptor segments with the glycine signal shown in the glycine image at top right, in the green channel demonstrating remodeling events. Scale bar = 30μm.

Robert E. Marc, Ph.D., is Distinguished Emeritus Professor of Ophthalmology at the John A. Moran Eye Center at the University of Utah. Professor Marc taught for 37 years at the graduate level, graduated 9 PhDs, and supervised 10 post-doctoral fellows. Robert is currently the co-owner of Stray Arrow Ranch, and CEO

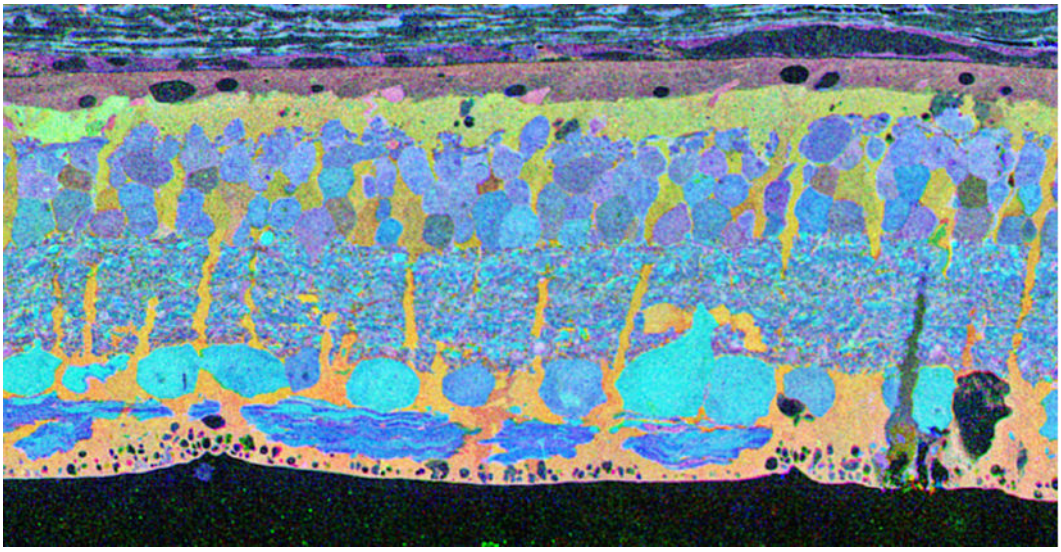

Figure 30. τQE :: rgb (taurine, glutamine, glutamate as red, green, blue) visualization in the 10 month Tg P347L rabbit retina. The Müller cell seal in this region is almost complete. Four to five remnant cone photoreceptors are evident in this image as light pink structures embedded in the Müller cell seal.

Figure 26. The founder TgP347L rabbit seen with low light illumination. The TgP347L rabbit precisely mimics autosomal dominant RP in the human including the photoreceptor degeneration, bipolar cell, horizontal cell, amacrine and ganglion cell involvement. Glial cell involvement is also appropriately represented with Müller cell seal formation. The second large eye model and our favorite animal model for autosomal dominant RP is the TgP347L rabbit.

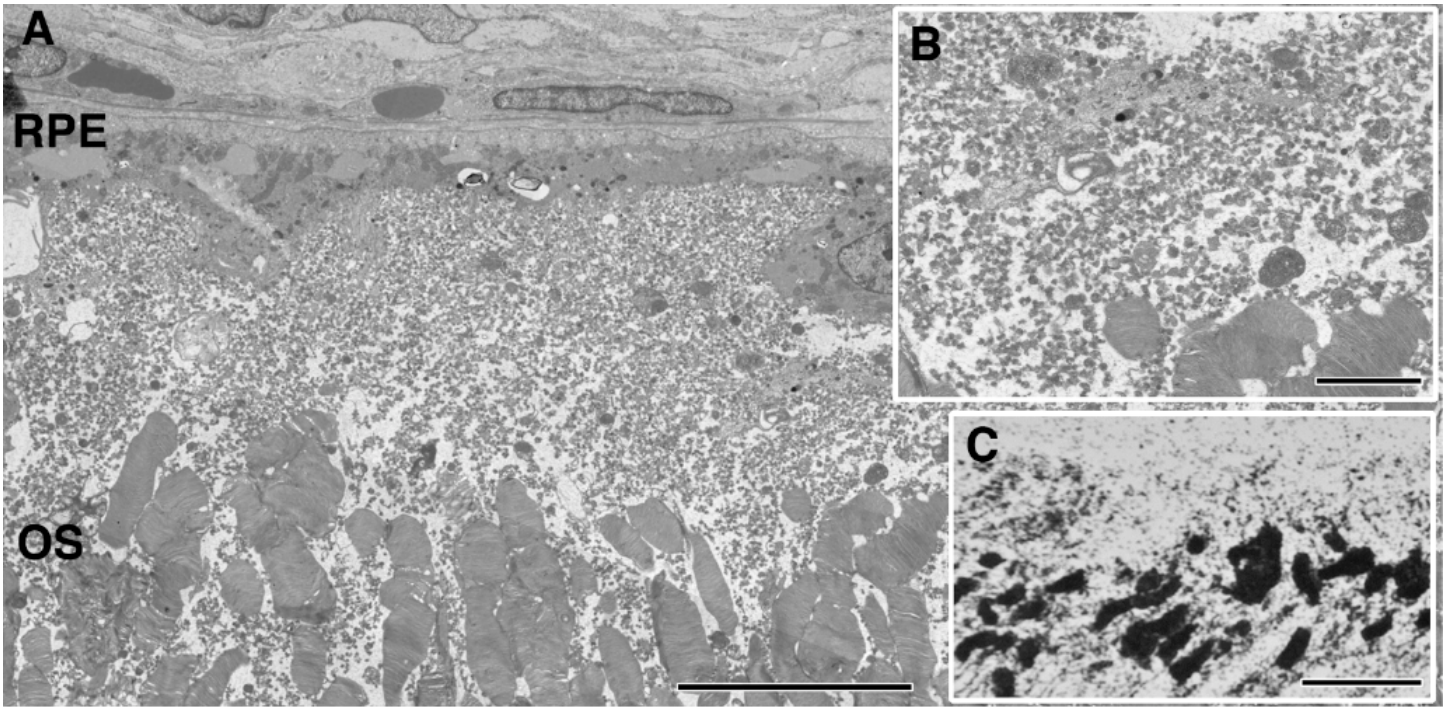

Figure 27. TEM of the photoreceptor/RPE interface in a 16-week old TgP347L rabbit. A) Debris found in the subretinal space composed of vesicles from 40-300nm in size. Scale bar = 10μM. B) Inset is a higher magnification view of the debris around outer segments. Scalebar = 2μM. C) All vesicles are immunoreactive for rod opsin. Scale bar = 10μm.

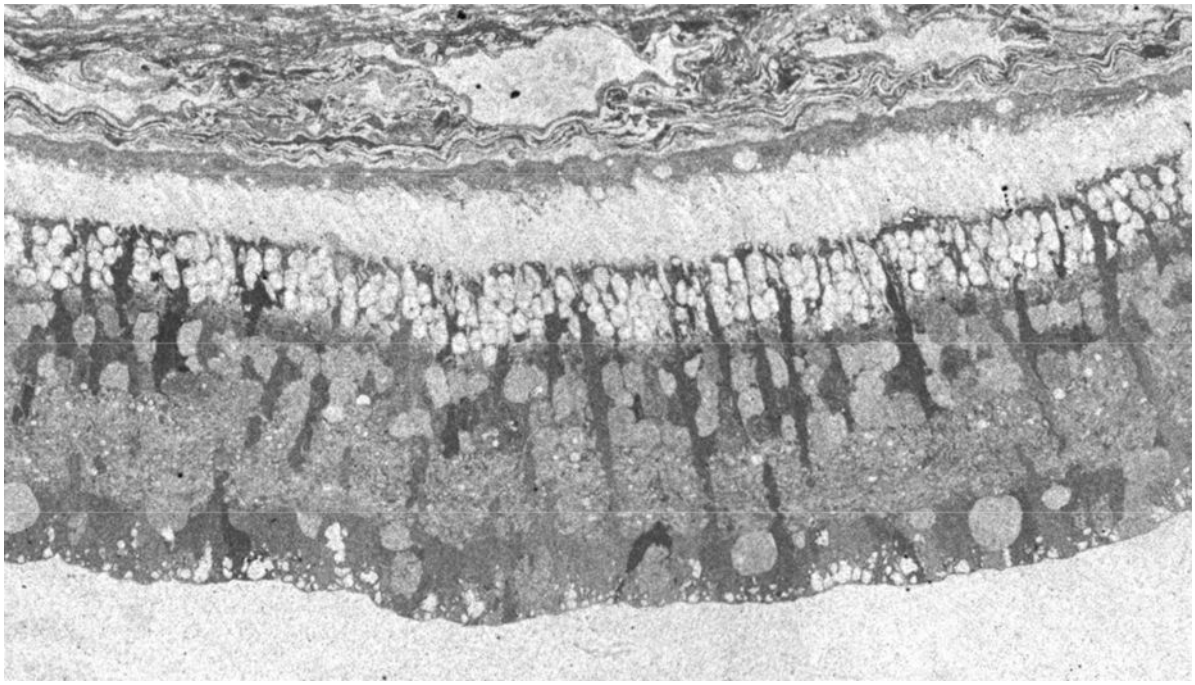

Figure 28. A 4-month-old Tg P347L rabbit retina showing varying glutamine signals in the Müller cells.

of Signature Immunologics. He is credited with the creation of Computational Molecular Phenotyping, developing channel mapping and visualization technologies as well as building the first comprehensive connectome with the resolution and features required to identify neurons and map connectivities.

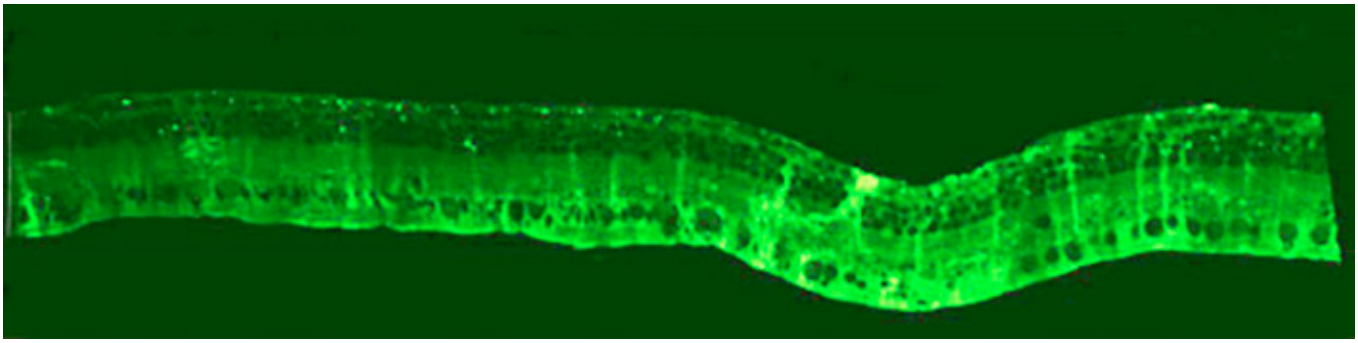

Figure 29. A panoramic image composed of 6 panels of a 10-month-old Tg P347L rabbit retina showing mosaicked glutamine synthetase expression.

Rebecca L. Pfeiffer, BA/BS, is a Graduate Student of the Interdepartmental Program in Neuroscience in the Marc Lab at the John A. Moran Eye Center at the University of Utah. Her research focus is on understanding the progression of retinal disease. This is being evaluated using a combined metabolomics and connectomics approach to evaluate the multiple stages of retinal remodeling and its impact on both neurons and surrounding glia.

Acknowledgements

Our thanks to Mineo Kondo and Hiroko Terasaki for making this work possible:

Mineo Kondo, M.D., Ph.D., Professor of Ophthalmology, Mei University Graduate School of Medicine, Tsu, Japan and is responsible along with Hiroko Terasaki for the generation of the P347L rabbit. Mineo's work focuses on using the electroretinogram for the diagnosis of various retinal diseases as well as exploring animal models of human retinal and optic nerve diseases.

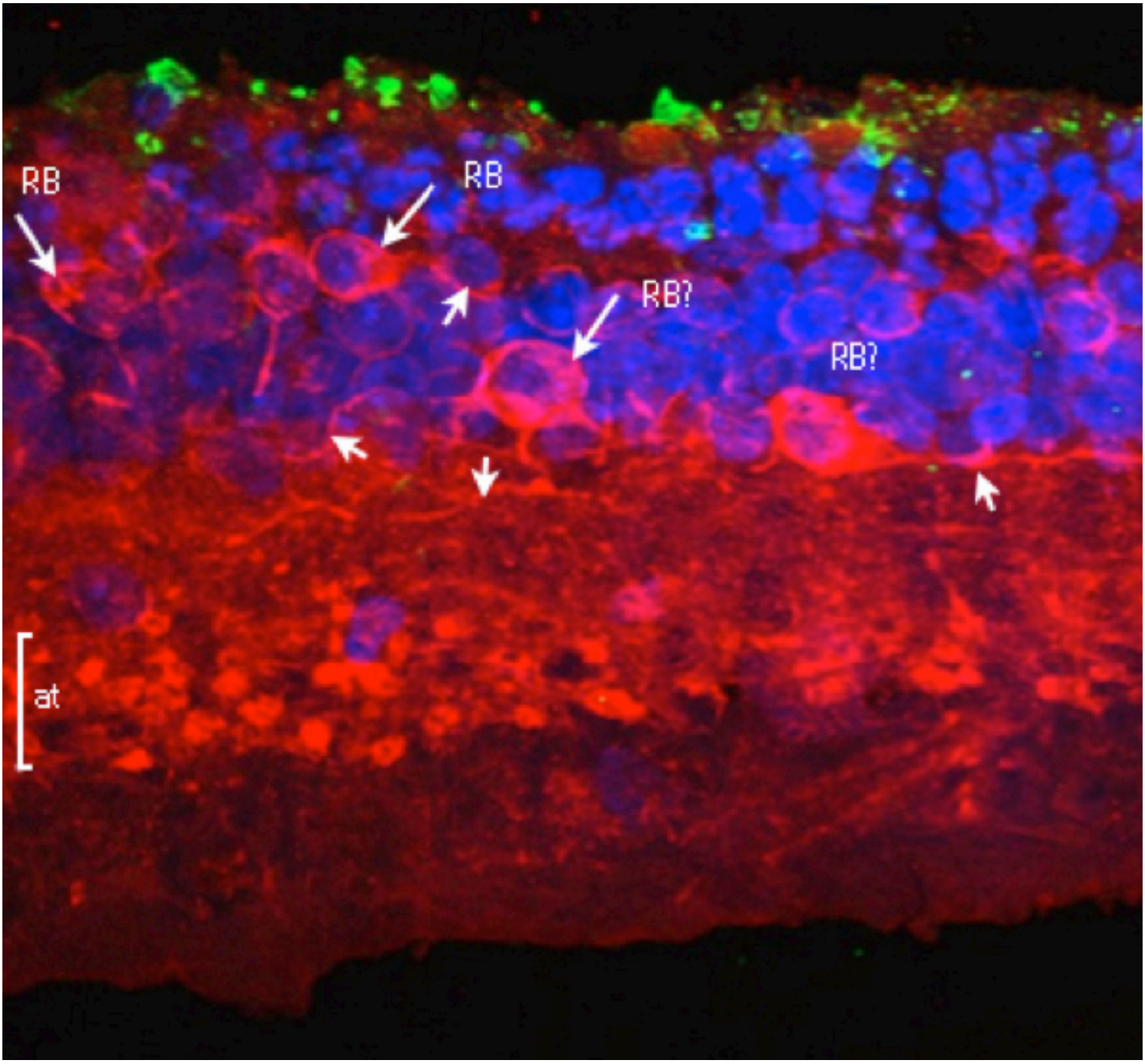

Figure 31. Maximal projection image of PKC (red), Rho 1D4 (green), and DAPI (blue) in the Tg P347L rabbit retina. Figure demonstrates reduced rhodopsin immunoreactivity (green spots in ONL) and some rod bipolar cells (red) with aberrant dendrites and axons (small arrows) compared with normal rod bipolar axon terminals in the lower IPL (white bracket , at).

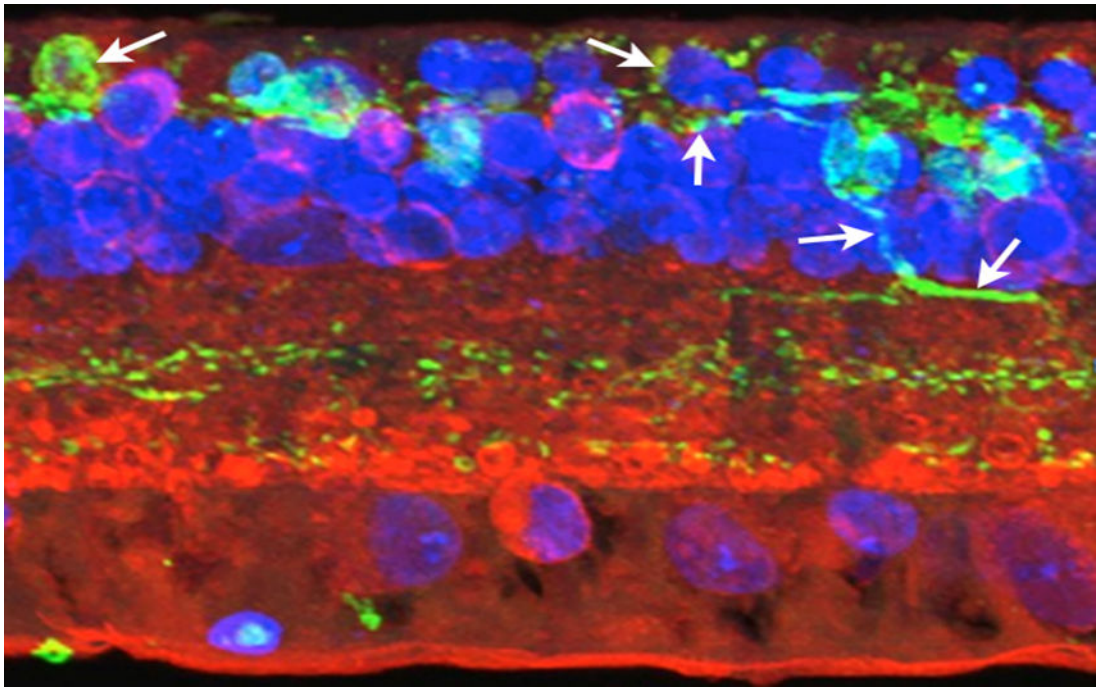

Figure 32. Maximal projection image of PKC (red), calbindin (green), and DAPI (blue) in the Tg P347L rabbit retina. Figure demonstrates calbindin labeling in horizontal cell abnormalities. Horizontal cell processes can be seen projecting into the IPL and ramifying therein.

Hiroko Terasaki, M.D., Ph.D., is Professor and Chairman of Ophthalmology at Nagoya University Hospital. Hiroko is responsible, along with Mineo Kondo for producing the P347L rabbit model of retinal degenerative disease. Professor Terasaki received her medical and ophthalmological training at the Medical School of Nagoya University under the tutorship of emeritus Professors Hiroshi Ichikawa, Shinobu Awaya, and Yozo Miyake. She was also trained at the Schepens Eye Research Institute in Boston, MA under the guidance of Professor Tatsuo Hirose.

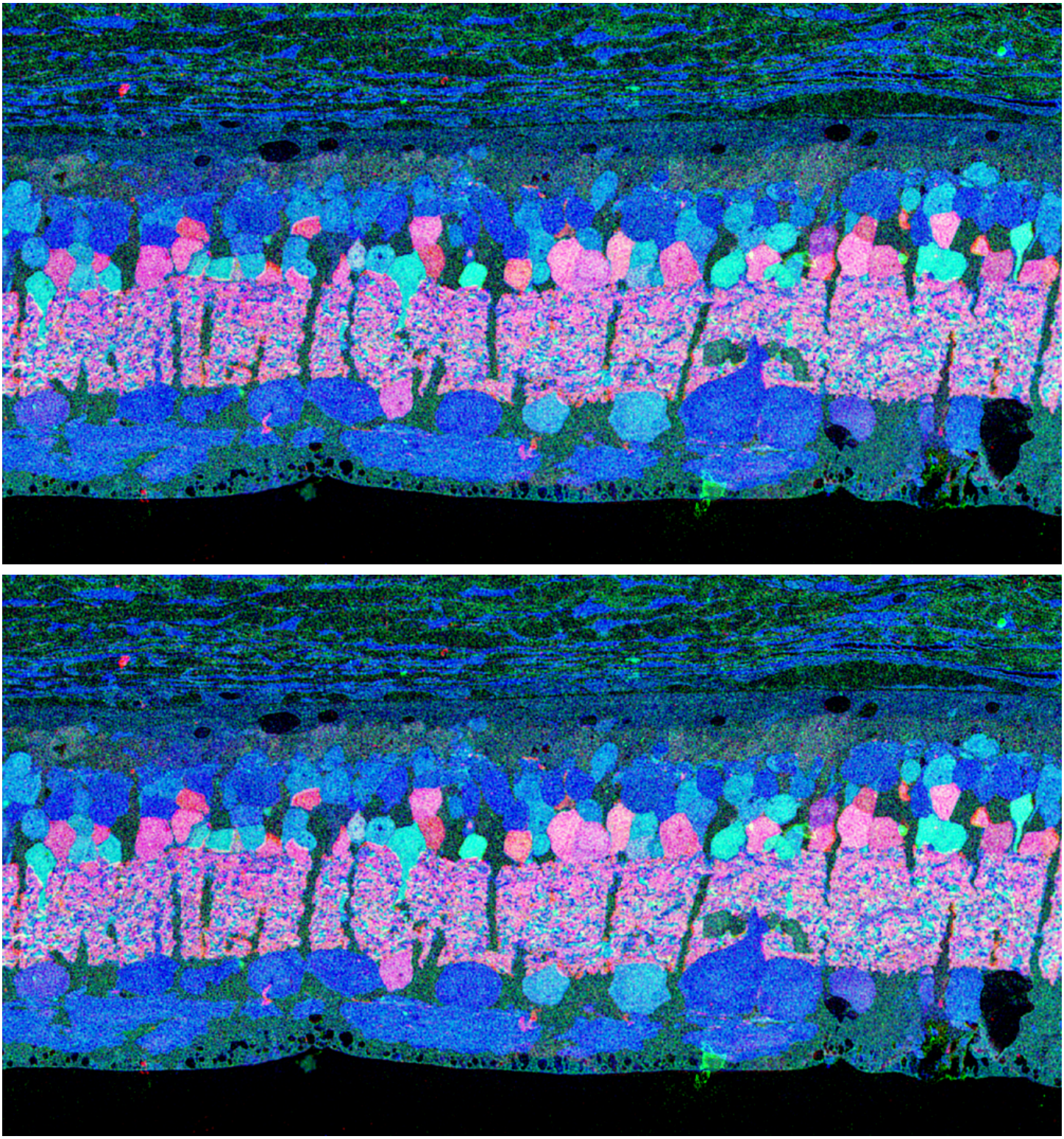

Figure 33. γGE :: rgb (tyrosine, glycine, glutamate as red, green, blue) visualization of the rabbit Tg P347L retina demonstrating photoreceptor, bipolar cell, GABA, and glycine amacrine cells and ganglion cell superclasses. Sprouting of both GABAergic and glycinergic amacrine cell processes can be visualized in the red and green channels with processes from both cell superclasses appearing outside their normal lamination.

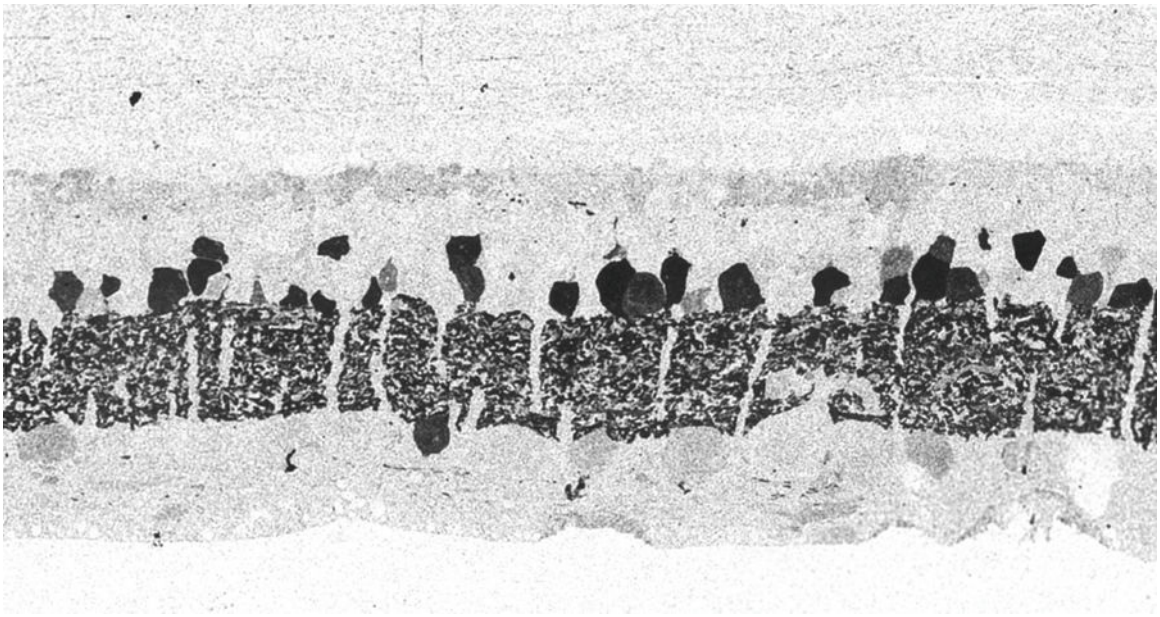

Figure 34. GABA channel from Figure 33 showing increased expression of GABA in the Müller cells and anomalous neurites from GABAergic amacrine cells running beneath the Müller cell seal.

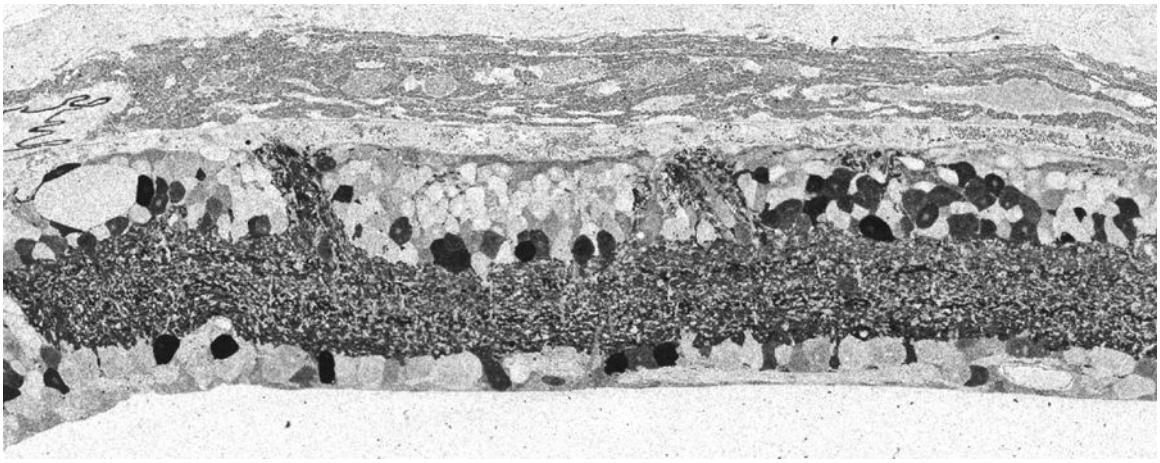

Figure 35. GABA channel showing elaboration of microneuroma formation in an 10.5 month old hrhoG mouse.

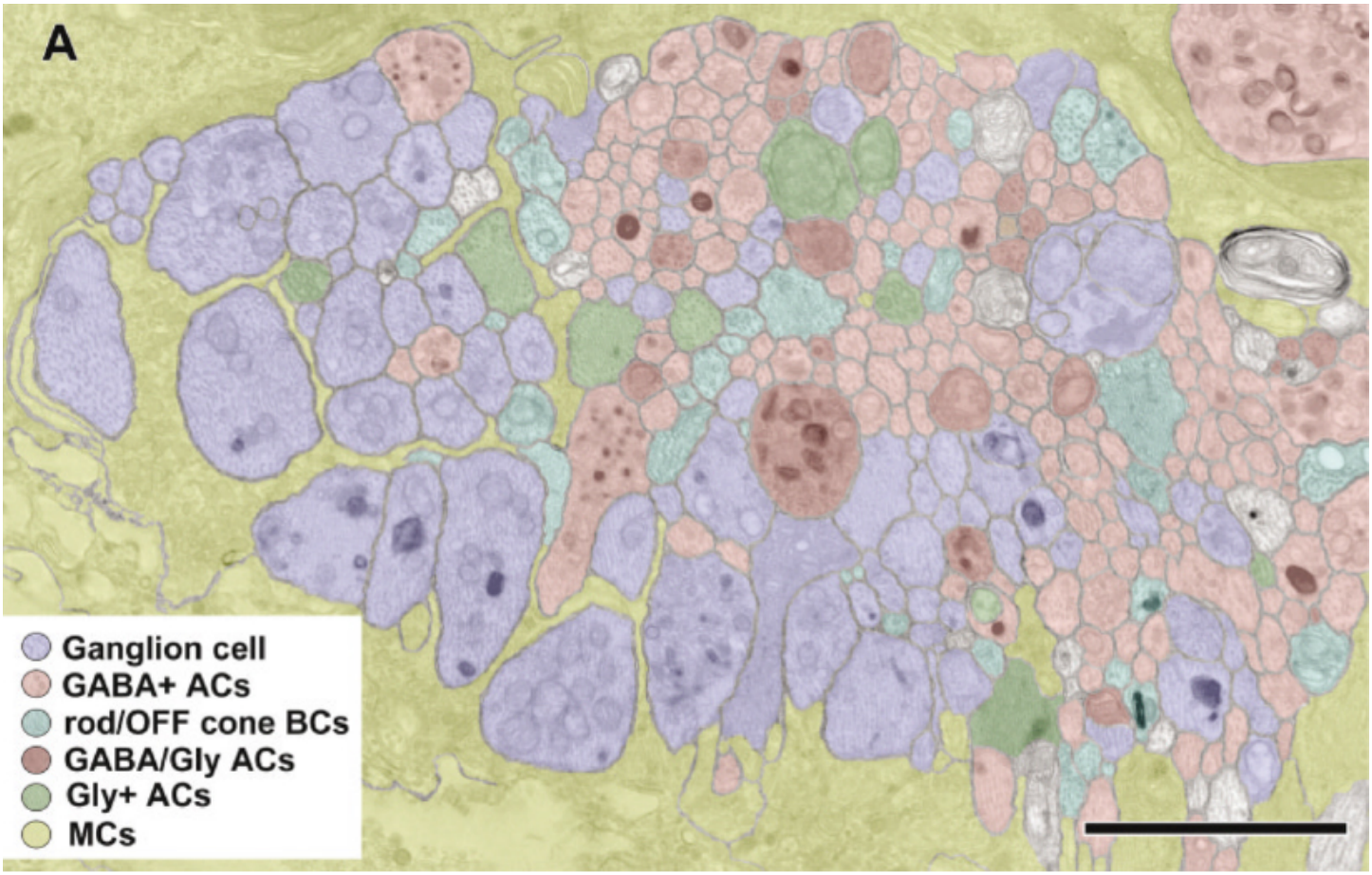

Figure 36. A microneuroma fascicle approximately 2 μm away from the distal margin of the neural retina underneath the Müller cell seal in an RCS rat retina. Six classes of neurons are color-coded according to their CMP signatures: ganglion cells (blue; high glutamate, low taurine); GABAergic amacrine cells (light red; high GABA); glycinergic amacrine cells (olive; high glycine); a mixed glycine+ and GABA+ class (dark red); bipolar cells (cyan, high glutamate, high taurine); Müller cells (yellow, high taurine, high glutamine). Unclassified elements are not colored.

Video 37. An animation of bipolar cell remodeling where rod photoreceptors die, followed later by cone photoreceptors.

Download video

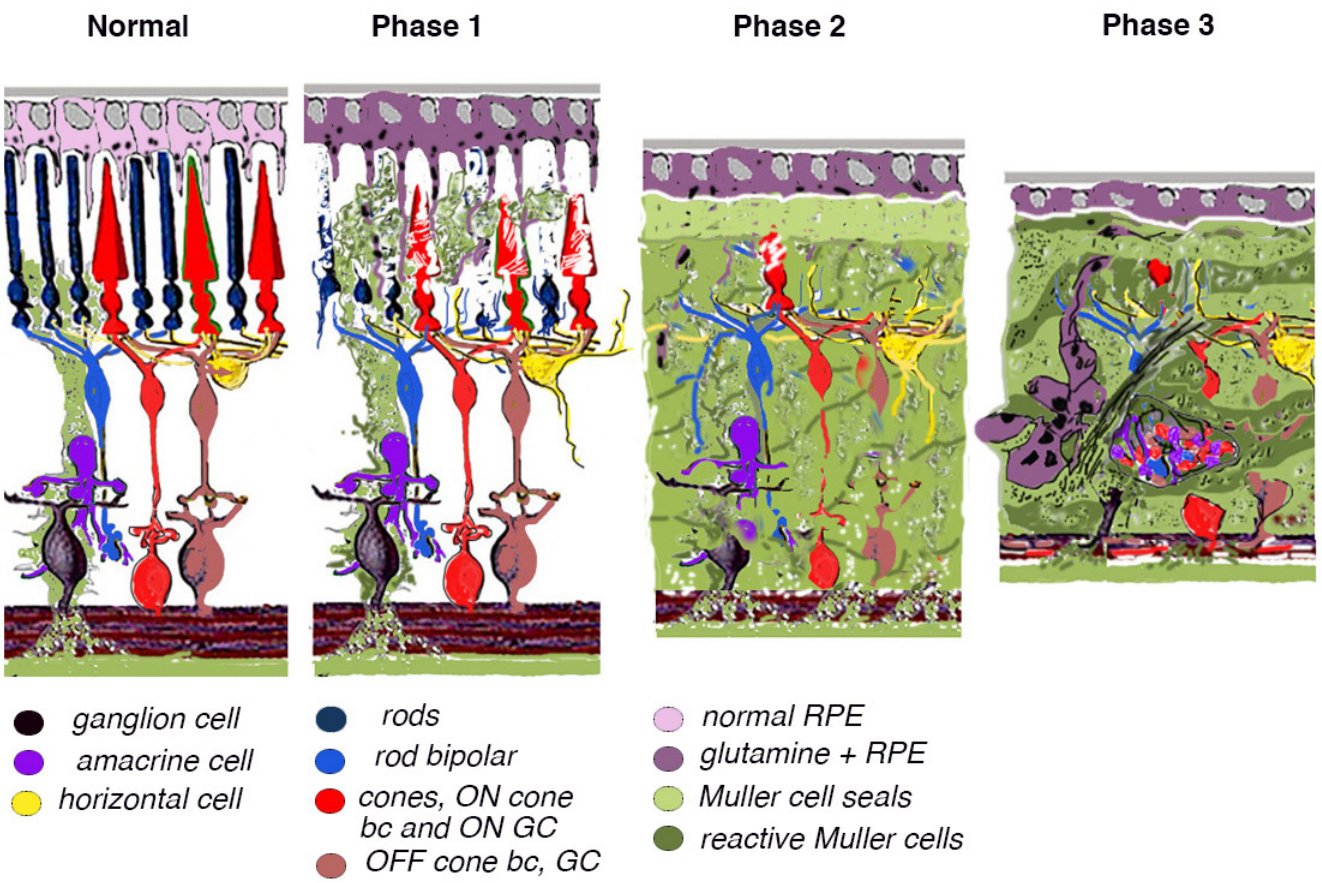

Figure 38. Summary figure of the normal organization of the retina (left) and the subsequent Phase *1*, *Phase 2*, and *Phase 3* (left to right) that happen as the retina goes through degeneration, plasticity and remodeling as a result of the disease of retinitis pigmentosa in humans and animal models. Figure courtesy of Helga Kolb.

References

1. Li Z., Kljavin I., Milam A. Rod photoreceptor neurite sprouting in retinitis pigmentosa. The Journal of neuroscience. 1995;15(8):5429–5438. PubMed PMID: 7643192.
2. De Raad S., Szczesny P., Munz K., Reme C. Light damage in the rat retina: glial fibrillary acidic protein accumulates in Müller cells in correlation with photoreceptor damage. Ophthalmic research. 1996;28(2):99–107. PubMed PMID: 8792360.
3. Fletcher E.L., Kalloniatis M. Neurochemical architecture of the normal and degenerating rat retina. Journal of Comparative Neurology. 1996;376(3):343–360. PubMed PMID: 8956104.
4. Fariss R.N., Li Z.-Y., Milam A.H. Abnormalities in rod photoreceptors, amacrine cells, and horizontal cells in human retinas with retinitis pigmentosa. American journal of ophthalmology. 2000;129(2):215–223. PubMed PMID: 10682975.
5. Machida S., Kondo M., Jamison J.A., Khan N.W., Kononen L.T., Sugawara T., Bush R.A., Sieving P.A. P23H rhodopsin transgenic rat: correlation of retinal function with histopathology. Investigative ophthalmology & visual science. 2000;41(10):3200–3209. PubMed PMID: 10967084.
6. Strettoi E., Pignatelli V. Modifications of retinal neurons in a mouse model of retinitis pigmentosa. Proceedings of the National Academy of Sciences. 2000;97(20):11020–11025. PubMed PMID: 10995468.

7. Strettoi E., Porciatti V., Falsini B., Pignatelli V., Rossi C. Morphological and functional abnormalities in the inner retina of the rd/rd mouse. The Journal of neuroscience. 2002;22(13):5492–5504. PubMed PMID: 12097501.
8. Sullivan R., Penfold P., Pow D.V. Neuronal migration and glial remodeling in degenerating retinas of aged rats and in nonneovascular AMD. Investigative ophthalmology & visual science. 2003;44(2):856–865. PubMed PMID: 12556422.
9. Jones B.W., Watt C.B., Frederick J.M., Baehr W., Chen C.K., Levine E.M., Milam A.H., Lavail M.M., Marc R.E. Retinal remodeling triggered by photoreceptor degenerations. Journal of comparative neurology. 2003;464(1):1–16. PubMed PMID: 12866125.
10. Marc R.E., Jones B.W. Retinal remodeling in inherited photoreceptor degenerations. Molecular neurobiology. 2003;28(2):139–147. PubMed PMID: 14576452.
11. Marc R.E., Jones B.W., Watt C.B., Strettoi E. Neural remodeling in retinal degeneration. Progress in retinal and eye research. 2003;22(5):607–655. PubMed PMID: 12892644.
12. Cuenca N., Pinilla I., Sauvé Y., Lu B., Wang S., Lund R.D. Regressive and reactive changes in the connectivity patterns of rod and cone pathways of P23H transgenic rat retina. Neuroscience. 2004;127(2):301–317. PubMed PMID: 15262321.
13. Cuenca N., Pinilla I., Sauvé Y., Lund R. Early changes in synaptic connectivity following progressive photoreceptor degeneration in RCS rats. European journal of neuroscience. 2005;22(5):1057–1072. PubMed PMID: 16176347.
14. Jones B.W., Marc R.E. Retinal remodeling during retinal degeneration. Experimental eye research. 2005;81(2):123–137. PubMed PMID: 15916760.
15. Jones, B.W., R.E. Marc, C.B. Watt, D.K. Vaughan, and D.T. Organisciak, *Neural plasticity revealed by light-induced photoreceptor lesions*, in *Retinal Degenerative Diseases*. 2006, Springer. p. 405-410.
16. Pu M., Xu L., Zhang H. Visual response properties of retinal ganglion cells in the royal college of surgeons dystrophic rat. Investigative ophthalmology & visual science. 2006;47(8):3579–3585. PubMed PMID: 16877432.
17. Aleman T.S., Cideciyan A.V., Sumaroka A., Schwartz S.B., Roman A.J., Windsor E.A., Steinberg J.D., Branham K., Othman M., Swaroop A. Inner retinal abnormalities in X-linked retinitis pigmentosa with RPGR mutations. Investigative ophthalmology & visual science. 2007;48(10):4759–4765. PubMed PMID: 17898302.
18. Specht D., Tom Dieck S., Ammermüller J., Regus-Leidig H., Gundelfinger E.D., Brandstätter J.H. Structural and functional remodeling in the retina of a mouse with a photoreceptor synaptopathy: plasticity in the rod and degeneration in the cone system. European journal of neuroscience. 2007;26(9):2506–2515. PubMed PMID: 17970721.
19. Marc, R.E., *Functional neuroanatomy of the retina.* Albert and Jakobiec's Principles and Practice of Ophthalmology. 3rd ed: Elsevier. 2008:1565-1592.
20. Stasheff S.F. Emergence of sustained spontaneous hyperactivity and temporary preservation of OFF responses in ganglion cells of the retinal degeneration (rd1) mouse. Journal of neurophysiology. 2008;99(3):1408–1421. PubMed PMID: 18216234.
21. Jones B.W., Kondo M., Terasaki H., Watt C.B., Rapp K., Anderson J., Lin Y., Shaw M.V., Yang J.H., Marc R.E. Retinal remodeling in the Tg P347L rabbit, a large-eye model of retinal degeneration. Journal of comparative neurology. 2011;519(14):2713–2733. PubMed PMID: 21681749.
22. Jones B., Kondo M., Terasaki H., Lin Y., McCall M., Marc R.E. Retinal remodeling. Japanese journal of ophthalmology. 2012;56(4):289–306. PubMed PMID: 22644448.
23. Baehr W., Frederick J.M. Naturally occurring animal models with outer retina phenotypes. Vision research. 2009;49(22):2636–2652. PubMed PMID: 19375447.
24. Chang C.-J., Lai W.W., Edward D.P., Tso M.O. Apoptotic photoreceptor cell death after traumatic retinal detachment in humans. Archives of ophthalmology. 1995;113(7):880–886. PubMed PMID: 7605279.

25. Lewis G.P., Linberg K.A., Fisher S.K. Neurite outgrowth from bipolar and horizontal cells after experimental retinal detachment. Investigative ophthalmology & visual science. 1998;39(2):424–434. PubMed PMID: 9478003.
26. Humphries M.M., Rancourt D., Farrar G.J., Kenna P., Hazel M., Bush R.A., Sieving P.A., Sheils D.M., McNally N., Creighton P. Retinopathy induced in mice by targeted disruption of the rhodopsin gene. Nature genetics. 1997;15(2):216–219. PubMed PMID: 9020854.
27. Frederick J.M., Krasnoperova N.V., Hoffmann K., Church–Kopish J., Rüther K., Howes K., Lem J., Baehr W. Mutant rhodopsin transgene expression on a null background. Investigative ophthalmology & visual science. 2001;42(3):826–833. PubMed PMID: 11222546.
28. Jones B.W., Watt C.B., Marc R.E. Retinal remodelling. Clin Exp Optom. 2005;88(5):282–91. PubMed PMID: 16255687.
29. Marc R.E., Jones B., Watt C., Vazquez-Chona F., Vaughan D., Organisciak D. Extreme retinal remodeling triggered by light damage: implications for age related macular degeneration. Molecular vision. 2008;14:782. PubMed PMID: 18483561.
30. Jones B., Pfeiffer R., Ferrell W., Watt C., Marmor M., Marc R. Retinal remodeling in human retinitis pigmentosa. Experimental eye research. 2016;150:149–165. PubMed PMID: 27020758.
31. Marc R.E., Jones B.W., Anderson J.R., Kinard K., Marshak D.W., Wilson J.H., Wensel T., Lucas R.J. Neural reprogramming in retinal degeneration. Investigative ophthalmology & visual science. 2007;48(7):3364–3371. PubMed PMID: 17591910.
32. Jaissle G.B., May C.A., van de Pavert S.A., Wenzel A., Claes-May E., Gießl A., Szurman P., Wolfrum U., Wijnholds J., Fisher M. Bone spicule pigment formation in retinitis pigmentosa: insights from a mouse model. Graefe's archive for clinical and experimental ophthalmology. 2010;248(8):1063–1070. PubMed PMID: 20012642.
33. Cajal, S.R., *The structure of the retina*. 1972, Translated by S.A. Thorpe and M. Glickstein Springfield IL: Charles C. Thomas Publisher.
34. Hinds J.W., Hinds P.L. Early development of amacrine cells in the mouse retina: an electron microscopic, serial section analysis. Journal of comparative neurology. 1978;179(2):277–300. PubMed PMID: 641219.
35. Lenkowski J.R., Raymond P.A. Müller glia: Stem cells for generation and regeneration of retinal neurons in teleost fish. Progress in retinal and eye research. 2014;40:94–123. PubMed PMID: 24412518.
36. Raymond, P.A., *Retinal regeneration in teleost fish.* Regeneration of vertebrate sensory receptor cells. 1991:171-191.
37. Fadool J.M. Rod genesis in the teleost retina as a model of neural stem cells. Experimental neurology. 2003;184(1):14–9. PubMed PMID: 14637072.
38. Jacobson, M., *Developmental Neurobiology*. 1970, New York: Holt, Rinehart and Winston Inc., .
39. Menger G.J., Koke J.R., Cahill G.M. Diurnal and circadian retinomotor movements in zebrafish. Visual neuroscience. 2005;22(02):203–209. PubMed PMID: 15935112.
40. Wagner H.-J. Darkness-induced reduction of the number of synaptic ribbons in fish retina. Nature. 1973;246(150):53–55. PubMed PMID: 4519029.
41. Dowling J.E. Organization of Vertebrate Retinas, The Jonas M. Friedenwald Memorial Lecture. Investigative ophthalmology & visual science. 1970;9(9):655–680.
42. Peichl L., Bolz J. Kainic acid induces sprouting of retinal neurons. Science. 1984;223(4635):503–504. PubMed PMID: 6691162.
43. Kolb H., Gouras P. Original Articles: Electron Microscopic Observations of Human Retinitis Pigmentosa, Dominantly Inherited. Investigative ophthalmology & visual science. 1974;13(7):487–498.
44. Mizuno K., Nishida S. Electron microscopic studies of human retinitis pigmentosa: Part 1. Two cases of advanced retinitis pigmentosa. American journal of ophthalmology. 1967;63(4):791–803. PubMed PMID: 6022249.
45. Szamier R.B., Berson E.L. Retinal ultrastructure in advanced retinitis pigmentosa. Investigative ophthalmology & visual science. 1977;16(10):947–962. PubMed PMID: 908648.

46. Szamier R.B., Berson E.L., Klein R., Meyers S. Sex-linked retinitis pigmentosa: ultrastructure of photoreceptors and pigment epithelium. Investigative ophthalmology & visual science. 1979;18(2):145–160. PubMed PMID: 761969.
47. Chu Y., Humphrey M.F., Constable I.J. Horizontal cells of the normal and dystrophic rat retina: a wholemount study using immunolabelling for the 28-kDa calcium-binding protein. Experimental eye research. 1993;57(2):141–148. PubMed PMID: 8405180.
48. Bowes C., Li T., Danciger M., Baxter L.C., Applebury M.L., Farber D.B. Retinal degeneration in the rd mouse is caused by a defect in the β subunit of rod cGMP-phosphodiesterase. Nature. 1990;347(6294):677. PubMed PMID: 1977087.
49. Marc R.E., Murry R., Basinger S. Pattern recognition of amino acid signatures in retinal neurons. The Journal of neuroscience. 1995;15(7):5106–5129. PubMed PMID: 7623139.
50. Sullivan R.K., WoldeMussie E., Pow D.V. Dendritic and synaptic plasticity of neurons in the human age-related macular degeneration retina. Investigative ophthalmology & visual science. 2007;48(6):2782–2791. PubMed PMID: 17525213.
51. Lin Y., Jones B.W., Liu A., Vazquéz-Chona F.R., Lauritzen J.S., Ferrell W.D., Marc R.E. Rapid glutamate receptor 2 trafficking during retinal degeneration. Molecular neurodegeneration. 2012;7(1):1. PubMed PMID: 22325330.
52. Cuenca N., Pinilla I., Fernández-Sánchez L., Salinas-Navarro M., Alarcón-Martínez L., Avilés-Trigueros M., de la Villa P., de Imperial J.M., Villegas-Pérez M.P., Vidal-Sanz M. Changes in the inner and outer retinal layers after acute increase of the intraocular pressure in adult albino Swiss mice. Experimental eye research. 2010;91(2):273–285. PubMed PMID: 20650699.
53. Ross J.W., de Castro J.P.F., Zhao J., Samuel M., Walters E., Rios C., Bray-Ward P., Jones B.W., Marc R.E., Wang W. Generation of an inbred miniature pig model of retinitis pigmentosa. Investigative ophthalmology & visual science. 2012;53(1):501–507. PubMed PMID: 22247487.
54. Kondo M., Sakai T., Komeima K., Kurimoto Y., Ueno S., Nishizawa Y., Usukura J., Fujikado T., Tano Y., Terasaki H. Generation of a transgenic rabbit model of retinal degeneration. Investigative ophthalmology & visual science. 2009;50(3):1371–1377. PubMed PMID: 19074802.
55. Bonilha V.L., Rayborn M.E., Li Y., Grossman G.H., Berson E.L., Hollyfield J.G. Histopathology and functional correlations in a patient with a mutation in RPE65, the gene for retinol isomerase. Investigative ophthalmology & visual science. 2011;52(11):8381–8392. PubMed PMID: 21931134.

Age-Related Macular Degeneration (AMD)

Gregory S. Hageman, Karen Gehrs, Lincoln V. Johnson, and Don Anderson

Created: January 1, 2008.

Introduction

Age-related macular degeneration (AMD), the leading cause of worldwide blindness in the elderly, is a bilateral ocular condition that affects the central area of retina known as the macula. The macula lutea, which derives its name from the deposition of yellow xanthophyll pigments (see chapter on simple anatomy), is located temporal to the optic disc and is bounded by the temporal superior and inferior vascular arcades (Fig. 1). Although the macula comprises only four percent of retinal area, it is responsible for the majority of useful photopic vision. The fovea lies at the center of the macula (Fig. 1, asterisk) and is approximately 2mm in diameter. The fovea is particularly well seen in vertical section view using ocular coherence tomography techniques in living eyes (Fig. 2). The fovea contains the highest density of cone photoreceptor cells and is the only region of the retina where 20/20 vision is attainable. The macula accounts for almost 10% of the entire visual field. Thus, lesions developing in this region can have a major impact on visual function.

AMD has a tremendous impact on the physical and mental health of the geriatric population and their families. Prior to 1990, AMD of all forms was often referred to as "senile macular degeneration" or SMD, a reflection of the fact that the vision loss associated with AMD manifests late in life when most affected individuals are looking forward to enjoying retirement activities and maintaining independence. Instead, millions with AMD suffer bilateral central vision loss such that they can no longer drive, read a newspaper, prepare meals, or enjoy recreational activities. For many patients, the visual impairment associated with AMD means a loss of independence, depression, increased financial concerns and the need to adapt to vision loss at a time when they are likely suffering from other debilitating conditions (1-5).

The cost to society is only now being appreciated. A recent analysis of AMD in Australia predicts that the disease costs $2.6 billion per year (6). This is projected to grow to $6.5 billion by 2025, a total cost of $59 billion over the next 20 years. A treatment that reduced the progression by only 10% would save Australia $5.7 billion over that same period of time. Similar analyses for the United States are lacking, but given the demographics and higher cost of medical care in the US, the costs would be projected to as much as twenty-fold higher.

Clinically, AMD is classified into the nonexudative "dry" or atrophic form and the exudative "wet" or neovascular form. More severe vision loss is typically associated with the "wet" form that occurs in about 15% of all patients with AMD but up to 20% of legal blindness from AMD is due to the "dry" form (7).

Clinical Aspects of AMD

Clinical Presentation of AMD

Although autopsy studies have documented histological and ultrastructural changes associated with AMD in the retina, retinal pigment epithelium (RPE), choriorcapillaris and choroid in middle age, the disease typically does not manifest clinically before age 55 (10). AMD is generally thought to progress along a continuum from atrophic or "dry" AMD (Figs. 3 and 4) to neovascular "wet" AMD with approximately 10% - 15% of all AMD patients eventually developing the wet form. Occasionally patients with no prior signs of dry AMD present with exudative changes as the first manifestation of the condition. The typical clinical sign of "dry" AMD is pigment disruption and drusen (small yellowish deposits in Figs. 3maculardegen.F4maculardegen.F5-6) in the retina. Drusen may be small "hard" (small with discrete margins) or "soft" (larger with indistinct edges) (Figs. 3-maculardegen.F4maculardegen.F56). They lie between the RPE and an adjacent basement membrane complex known as Bruch's membrane (BM) (See later Figs. 13-maculardegen.F14maculardegen.F1516). Geographic

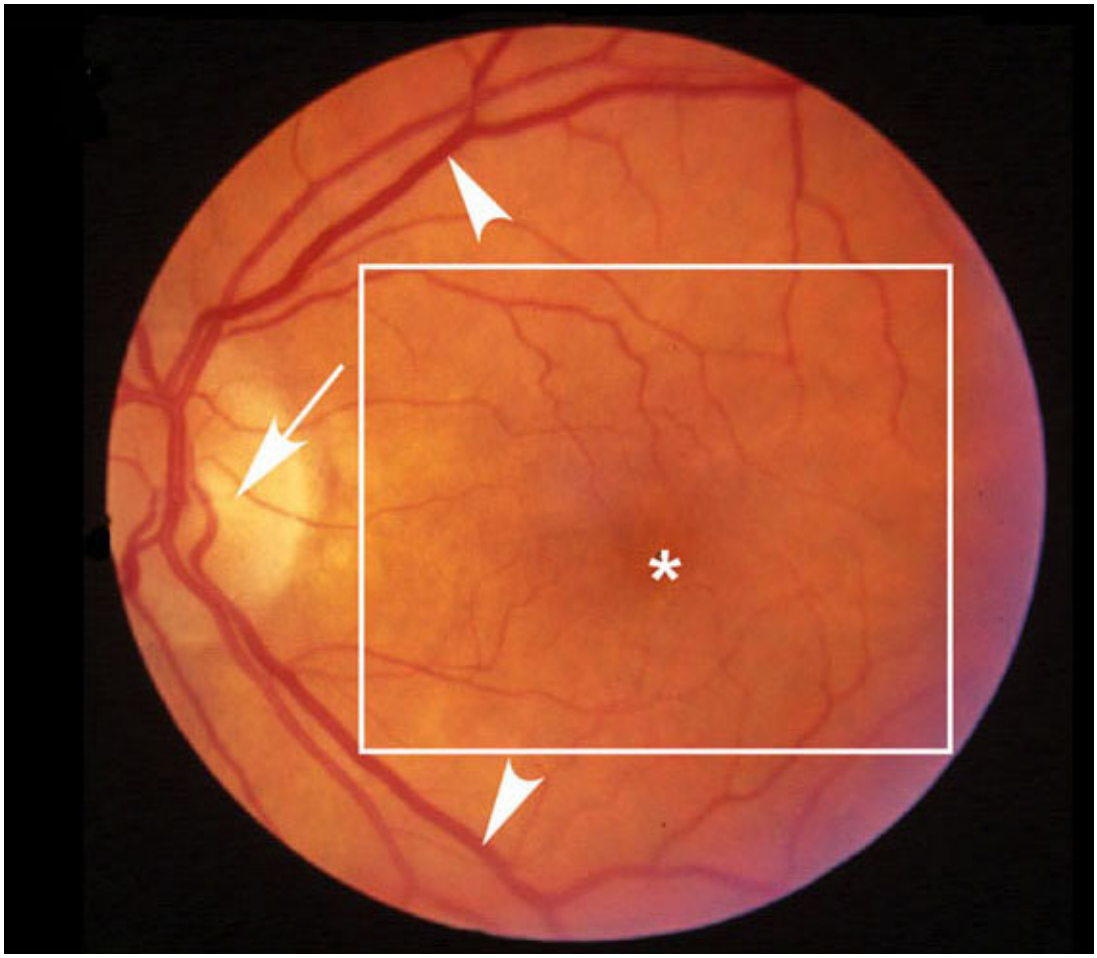

Figure 1. Normal macula of an elderly patient. The asterisk represents the location of the fovea, which lies directly in the visual axis. The macula (boxed area), which is adapted for high acuity vision, is located temporal to the optic nerve (arrow). It is approximately 6mm in diameter and centered on the fovea. The vascular arcades are indicated by arrowheads.

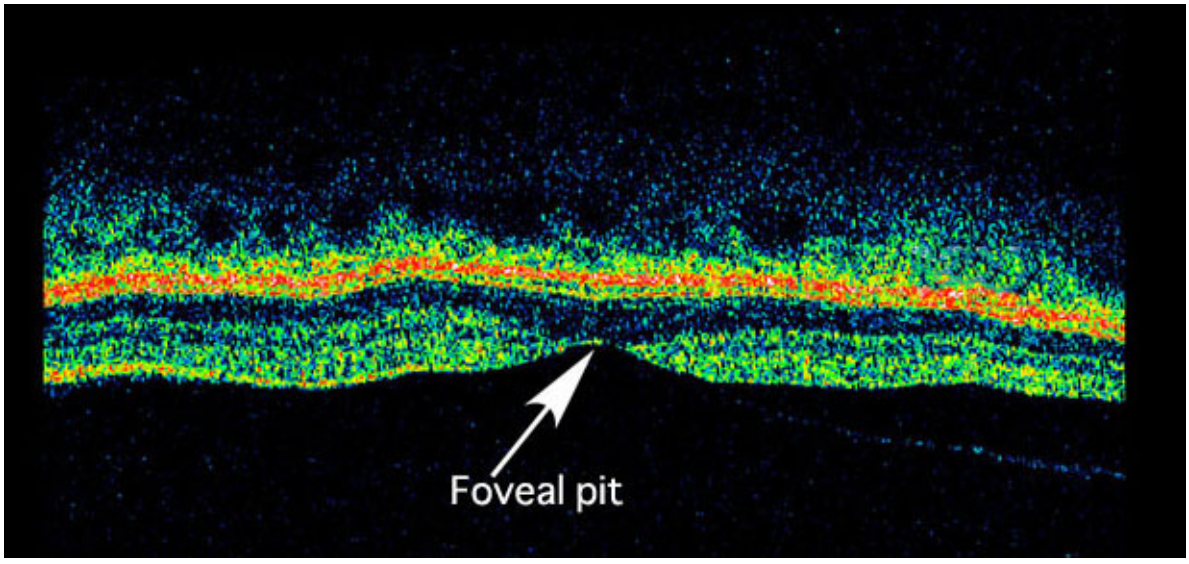

Figure 2. Ocular coherence tomogram (OCT) of a normal macula. The central area of depression (arrow) represents the fovea, corresponding to the asterisk in Figure 1. Ret, retina.

atrophy (GA) and RPE changes are also observed in dry AMD (Fig. 7). Several classification schemes have been developed that subdivide dry AMD into categories based on the number and size of drusen, amount of GA, and degree of pigmentary changes in the macula (25-28).

Angiography using sodium fluorescein dye is commonly performed when signs of AMD are observed and and particularly when exudative changes are suspected.

The natural history of dry AMD is progressive, with gradual loss of visual function that may span over many years time. Many patients with dry AMD are asymptomatic and unaware of the disease. In 10-15% percent of patients with dry AMD the deterioration is more rapid and extensive and they suffer significant vision loss due to geographic atrophy.

In approximately 10-15% of patients the condition progresses to the "wet" or neovascular form. Left untreated, the natural history of wet AMD advances further to a cicatrical stage referred to as a disciform scar. This process usually takes place over several months and typically results in a 4-8 mm diameter fibrotic scar underlying the macula accompanied by a central scotoma with severe central vision loss in one eye (Fig. 11). Patients with neovascular AMD in one eye have a 4 - 12% per year cumulative risk of developing neovascular AMD in the fellow eye. Thus, the risk of bilateral loss of central vision is high in those with the neovascular form of the disease (30).

The designation of exudative or "wet" AMD implies that fluid, exudates and/or blood are present in the extracellular space between the neural retina and the RPE (i.e. the subretinal space) and/or, as in the case of RPE detachments, between the RPE and Bruch's membrane (i.e. the sub-RPE space).

The neovascular tissue associated with exudative AMD is most commonly referred to as choroidal neovascularization (CNV) because it originates from the normal choriorcapillaris and extends through a dehiscence in Bruch's membrane into the subretinal or sub-RPE space. Sometimes multiple soft drusen become confluent and create large pigment epithelial detachments (PED's), which represent an elevation of the retinal pigment epithelium under the retina (Fig.10). Neovascularization associated with PEDs can be difficult to visualize clinically or image using fluorescein angiography; therefore, it is difficult to treat (29).

The following figures show pictures of different patients' retinas with advanced cases of AMD of the wet form. Fig. 8 shows a color fundus picture (a) and an early (b) and late fluorescein angiogram (c) from an individual with a classic choroidal neovascularization (CNV). Subretinal blood and fluid (arrowhead depicts edge) is clearly visible within the macular region in (a). The blood vessels have a lacey appearance (asterisk) in the early angiogram. Marked leakage of fluorescein (asterisk), with indistinct edges of hyperfluorescence (white area) is clearly visible in the late angiogram.

Fig. 9 shows a similar set of fundus pictures from an individual with occult choroidal neovascularization. A single, small punctate region of hemorrhage (arrow) and a ring of exudates (arrowhead depicts edge) appear more pronounced than typically occur in classic CNV. This patients had a minimal hyperfluorescence in the early phase of the angiogram, in contrast to that observed in the early stage of classic CNV. Speckled macular hyperfluorescence is visible in the late stage angiogram (Fig. 9c).

In the case shown in Fig. 10, the individual had a macular pigment epithelial detachment (PED). A multilobulated, hyperfluorescent lesion with sharply demarcated borders (arrow) is clearly visible in the late stage angiogram of Fig. 10a, arrow. The OCT shown in Fig. 10b, contrasts with a normal OCT of the fovea (Fig. 2) by being a blister-like elevation of the retina and retinal pigment epithelial layer off Bruch's membrane and the choroid.

The end stage of such lesions of the macula as shown in the three previous patients is illustrated by the last patient (Fig. 11). The color fundus photograph shows that the patient has end stage (cicatricial) exudative AMD.

A large disciform scar (arrowhead) covers the whole macular region. Such a patient would be almost totally blind in that eye.

Pathology of AMD

Overview

Until quite recently, the majority of research on AMD and the development of therapeutics for the disease has focused upon late-stage neovascular events. No clear-cut sequence for the initiation and progression of AMD has been identified that would allow it to be monitored and treated in its earliest stages. Moreover, the pathologic correlates of the different clinical phenotypes of AMD remain poorly understood, and there is a paucity of animal models that accurately mimic the characteristic features of the disease. Nevertheless, recent discoveries are beginning to provide a much clearer picture of the relevant cellular events, genetic factors, and biochemical processes that are associated with early AMD. This new information should hasten significantly the development of clinically effective diagnostics and therapeutics for the treatment of this devastating condition.

Morphological Correlates of Early AMD

From a histopathologic standpoint, the earliest detectable changes associated with AMD occur at the interface between the macular retina and the underlying layer of connective tissue and blood vessels known as the choroid (66-70). At this location lie the outer segments of rod and cone photoreceptors, the retinal pigment epithelial (RPE) cells, a stratified basement membrane complex termed Bruch's membrane (BM), and the choroidal capillary bed or choriocapillaris (Figs. 12, 13, BV of choroid).

The initial clinical diagnosis of early AMD is based on seeing drusen - the hallmark indicators of disease - and/or pigmentary changes in the macula. Drusen look like yellow-white spots in the retina (Figs. 3-maculardegen.F4maculardegen.F5maculardegen.F67). They are extracellular deposits located between the retinal pigment epithelial (RPE) basal lamina and the inner collagenous layer of the elastin-containing Bruch's membrane as illustrated in the schematic of Fig. 13 (71); The normal retinal choroidal interface is shown in comparison to the drusen bearing abnormal interface. Fig. 14 shows an actual histological section of retina where drusen are seen between the choroid and Bruch's membrane.

Bruch's membrane consists of an elastin core flanked on both sides by a collagenous layer and a basal lamina (see Fig. 13) (76-79). It is widely believed that the barrier properties of the RPE and Bruch's membrane limit cellular migration, especially the invasion of neovascular tissue from the choroid into the subretinal space. Our understanding of the molecular composition of Bruch's membrane, the molecular traffic that occurs across it, and the homeostatic mechanisms that maintain it, during normal aging as well as in AMD, is still rudimentary (80).

Links between AMD and structural abnormalities in Bruch's membrane have been documented in numerous histopathologic studies. Classically, these Bruch's membrane defects have been described as fragmentation or fracturing in association with calcification (81-85). Additional age-related changes in Bruch's membrane are typified by; a) Progressive thickening of the two collagenous layers; b) Modification and degeneration of collagen and elastin; c) Increased levels of advanced glycation end products, noncollagenous proteins and lipids; and d) Accumulation of several types of sub-RPE deposits (Fig. 13) (86-95). It has also been suggested that the age-related abnormalities in Bruch's membrane eventually lead to photoreceptor degeneration as a result of increased hydrophobicity, reduced permeability, and impaired nutrient exchange between the choroid and the RPE. Functionally, such changes result in an exponential reduction in the hydraulic conductivity of Bruch's membrane as a function of age (96-99). Much less is known about changes in Bruch's membrane hydraulic conductivity in individuals with AMD.

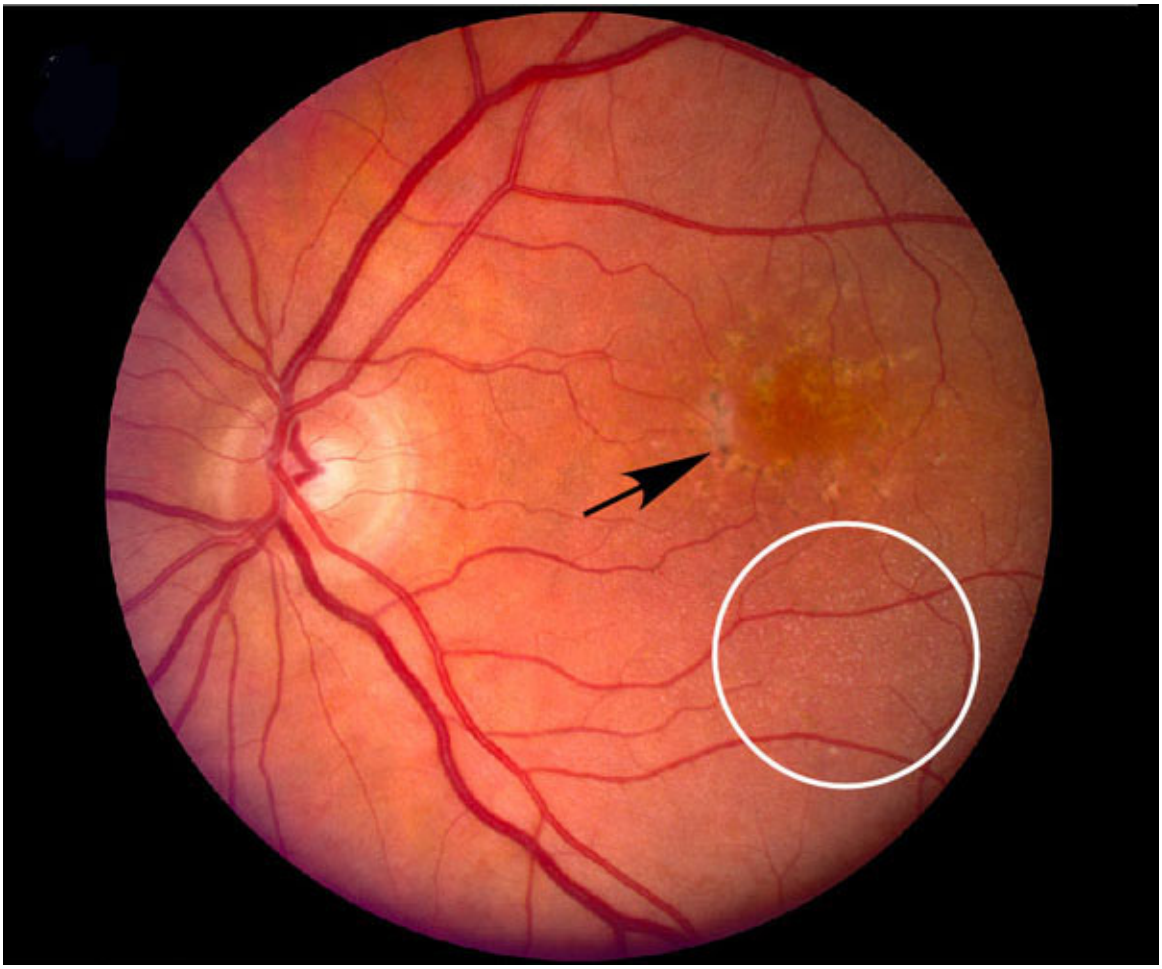

Figure 3. Color fundus photograph derived from an individual with early, dry AMD. RPE pigment disruption is present in the macula (arrow) and numerous small (< 63 microns in diameter) hard drusen are present inferior to this region (oval).

It has been proposed that topographic variations in Bruch's membrane may render the macula more susceptible to the ingrowth of new blood vessels from the choroidal vasculature that characterizes neovascular AMD. Morphometric data indicate that the elastic lamina of Bruch's membrane in the macula is 3-6 fold thinner and 2-5 fold less dense relative to that in the mid-periphery in individuals of all ages (100). Elastin fiber destruction in the macula could also play a key role in the initiation of neovascular events because elastin degradation peptides are highly angiogenic and possess macrophage recruiting activity (101).

In addition to drusen, basal laminar deposits (BLamD) and basal linear deposits (BLinD) accumulate within the extracellular environment of the RPE-choroid interface (Figs. 13, 15-maculardegen.F1617). These are identified based upon their morphological appearance and location. Both types of deposits have been proposed by various investigators to be involved in the pathogenesis of AMD (103). Neutral lipid (including esterified cholesterol) and apolipoproteins B and E are abundant in these basal deposits and in drusen in the eyes of aged donors and donors with a documented history of AMD (88, 94, 104-107).

Basal laminar deposits (BLamD) that accumulate between the RPE basal plasma membrane and its basal lamina (Figs.13, 15-maculardegen.F1617) do not appear to be specific to or 'diagnostic' for AMD. However, there is a strong relationship between macular BLamD and exudative AMD, disciform scarring, and visual loss (74, 84, 108-115). BLamD-like deposits are also seen in other macular disorders with a clinical appearance similar to what is observed in AMD. These include Sorsby's fundus dystrophy, Late Onset Retinal Degeneration (LORD), adult foveomacular pigment epithelial dystrophy and Malattia leventinese (116). The molecular composition and

Figure 4. Color fundus photograph from an individual with dry AMD. Numerous small and intermediate-sized drusen are visible in the macular region (oval).

origin of BLamD has not yet been identified (117-119), but its morphological similarity to long-spacing collagen is striking. Electron microscopy has revealed that its banding pattern matches that of type VI collagen (120).

Electron microscopy shows the changes that occur at the choroids RPB interface in AMD at a more detailed level. Figures 18 and 19 indicate a normal retinal choroidal interface (Fig. 18) compared with an abnormal AMD-like situation where there are drusen forming at this interface (Fig. 19).

BlinD lies between the RPE basal lamina and the elastic layer of Bruch's membrane (Fig. 20). The principal component of BLinD is a distinct form of membranous debris, thought to be comprised primarily of lipoprotein particles containing neutral lipids, including esterified cholesterol. It is likely that BLinD is derived from local ocular sources (e.g. RPE cells) (121). BLinD were initially described by Sarks and colleagues (122) as lipid-like vesicles with varying diameters.

It is believed that the pigmentary changes often observed in the macula of AMD eyes are attributable to degenerative changes in the highly melanized RPE cells (Fig. 20). This notion has gained wide acceptance because most of the early clinical signs and histopathological changes have been localized to this cell layer (123-126). It has long been recognized that the RPE is essential for the transport of ions, nutrients, and metabolites from the circulation to the neural retina and vice versa (127). If the RPE interface to the Bruch's membrane is broken down, amongst other things, blood vessels from the choroids can grow into this space (Fig. 21).

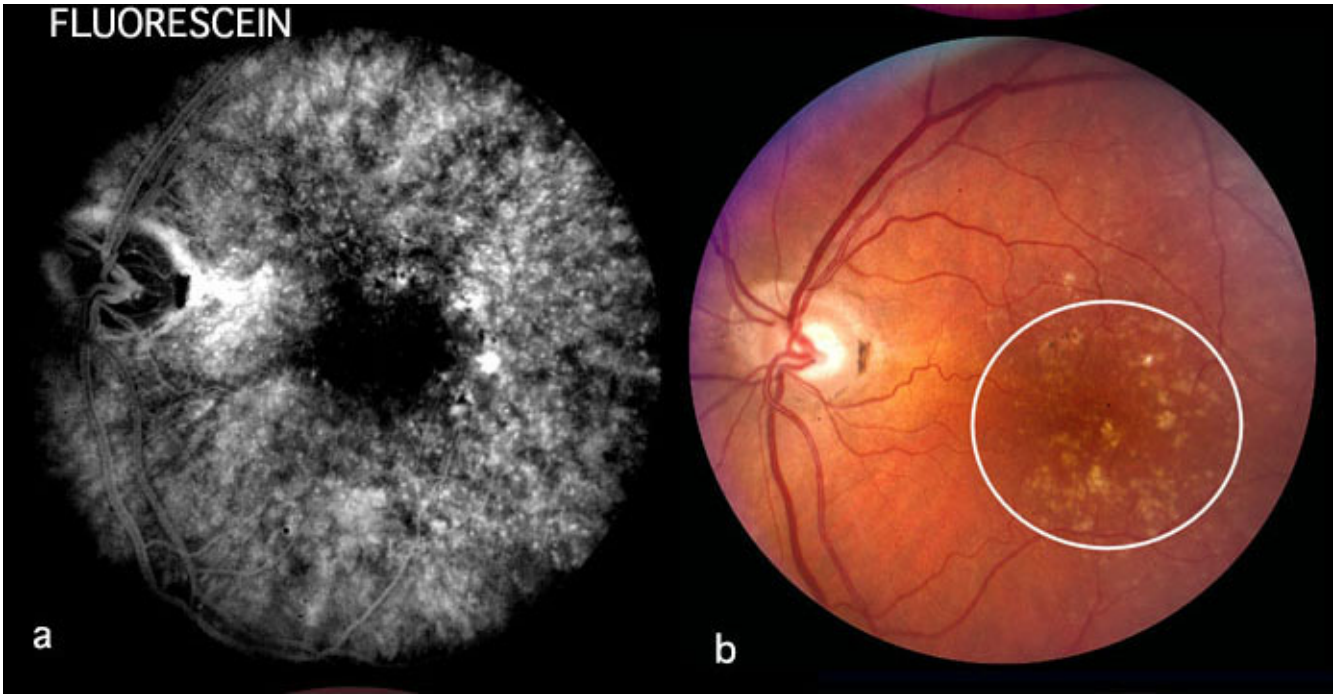

Figure 5. Corresponding fluorescein angiogram (a) and color fundus photograph (b) images from an individual with dry AMD. Although larger and confluent drusen are visible in the color image (circle), the number and extent of drusen distribution is appreciated even more clearly in the angiogram. The hyperfluorescent drusen observed in the angiogram are of uniform size and often referred to as cuticular drusen.

A viable RPE is also essential for normal photoreceptor cell metabolism and functioning of the visual cycle. Therefore, it is not surprising that RPE degeneration is accompanied by concomitant photoreceptor degeneration. RPE dysfunction in the macula, whether caused by local environmental insults and/or genetic defect(s), would have a profound impact on the overlying photoreceptors and, therefore, on central vision. However, the nature of the insult(s) that causes RPE dysfunction has yet to be ascertained, although a variety of hypotheses have been advanced over the years including genetic factors, ischemia, oxidative stress, phagocytic overload, cigarette smoke, lipofuscin toxicity and, most recently, microbial infection (128-134).

The choriocapillaris has also been suspected to play a role in the etiology of AMD. The density and diameters of the choriocapillaris capillaries decreases with age, and this decrease is even greater in patients with AMD. The overall loss appears most marked in regions of geographic atrophy (135, 136).

Physiology of early AMD

There is substantial evidence of photoreceptor involvement in early AMD, particularly in those patients with soft or large drusen in the macula (137-145). Contrast sensitivity, the rate of recovery after photostress, the amplitude and latency of the foveal electroretinogram (ERG) response, and dark adaptation are all affected adversely in early AMD patients, including those with normal visual acuity (140, 146-151). Fig. 22 shows the multifocal ERG responses from the macular area of a patient with AMD (see chapter on the clinical ERG, multifocal ERG). The responses of the fovea are reduced in amplitude. In the 3-D map (Fig. 23) it can be seen that the foveal area is flat, suggesting no cone activity, compared with the characteristic peak of responses in the normal retina.

It has been shown that photoreceptor cells in areas impacted by drusen exhibit morphologic and biochemical signs of degeneration, including decreased expression of synapse-associated proteins and increased expression of stress-response molecules. There are also drusen-associated reductions in photoreceptor cell densities, thus suggesting that degenerative changes in photoreceptors ultimately lead to cell death (152, 153).

Figure 6. Color fundus photograph from an individual with dry AMD, depicting the presence of numerous large (>125 micron diameter), calcified drusen deposited primarily within the peri- and parafoveal regions. Smaller drusen are present in the foveal region (asterisk).

Inflammation and AMD

Recent studies of the molecular composition of drusen have implicated local inflammation as a key element in the pathogenesis of AMD (154-160). Drusen contain numerous proteins related to the process of inflammation or its aftermath (106, 161-164). In particular, many of these proteins are associated with the complement cascade and its regulation. Some of the proteinaceous components in drusen and the sub-RPE space are activated complement components and fragments associated with assembly of the membrane attack complex (MAC) (162, 165-168). Other drusen components including vitronectin (161), clusterin, complement receptor 1 (CR1), and membrane cofactor protein (MCP-1) (164) are known complement regulatory proteins. Still others include known activators of the complement cascade such as cholesterol (169), C-reactive protein (155), and the amyloidogenic peptide amyloid b (153, 170). Metallic zinc, an amyloid b binding molecule, is also a drusen constituent (171). This compositional profile forms the basis for the conclusion that drusen are a manifestation of chronic, local inflammation at the level of Bruch's membrane.

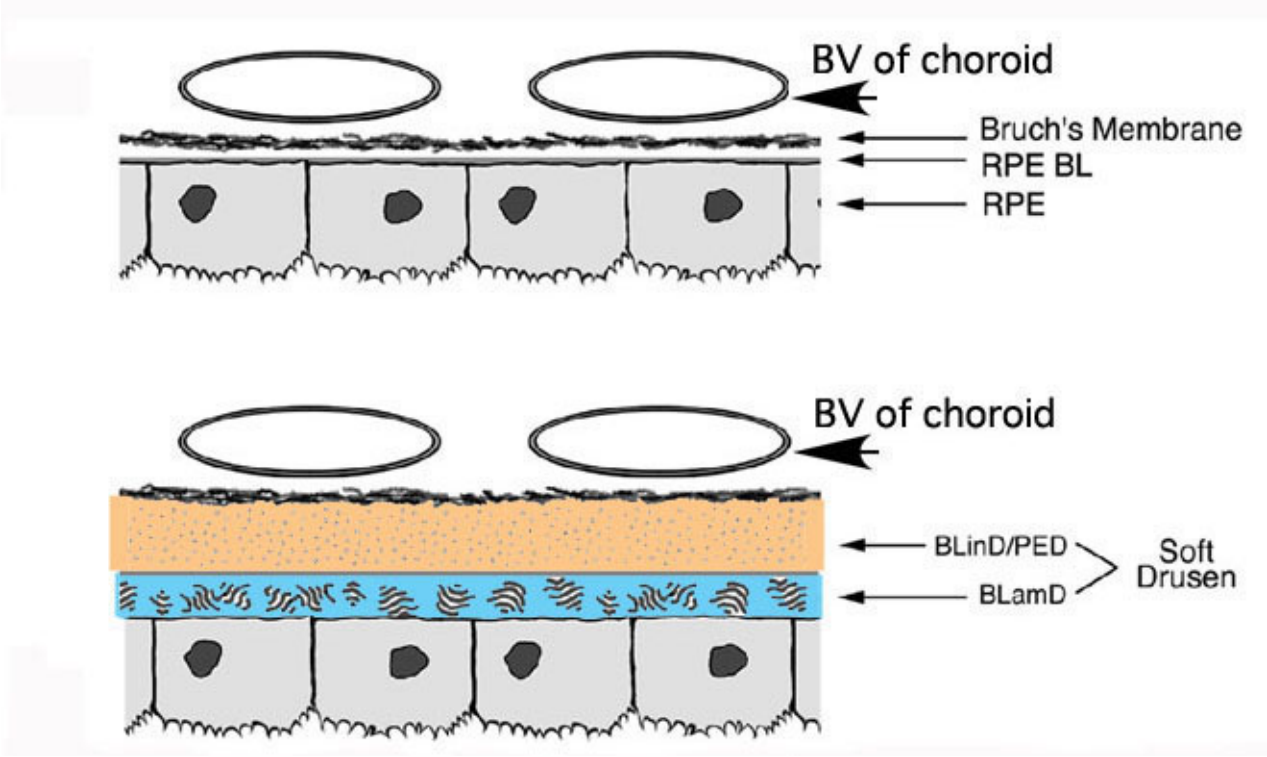

Figure 13. Schematic images depicting the choroid-RPE-retina interface in a normal retina and an AMD interface. The choriocapillaris-RPE interface in unaffected (top) and affected (bottom). The majority of early AMD-associated extracellular lesions - including drusen, basal laminar deposit (BLamD), and basal linear deposits (BLinD) - form along this interface.

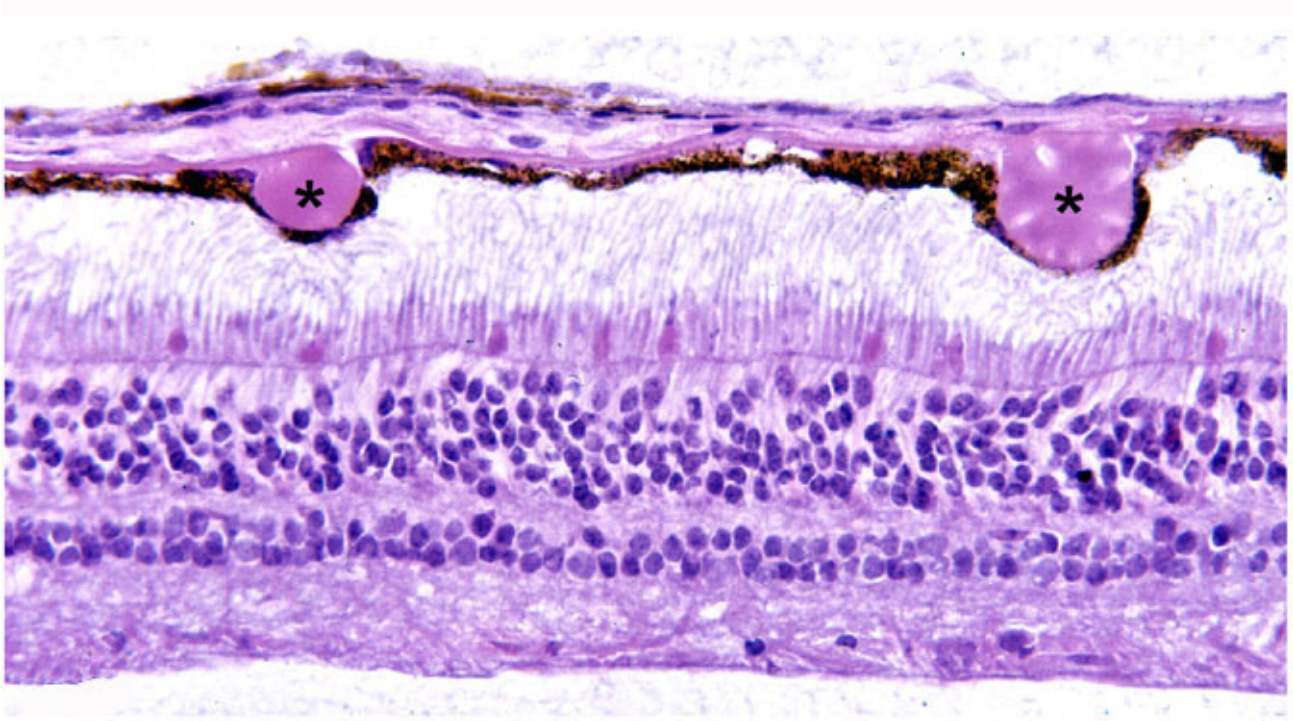

Figure 14. Histological section shows drusen (asterisks) forming between the RPE and Bruch's membrane in an early AMD case.

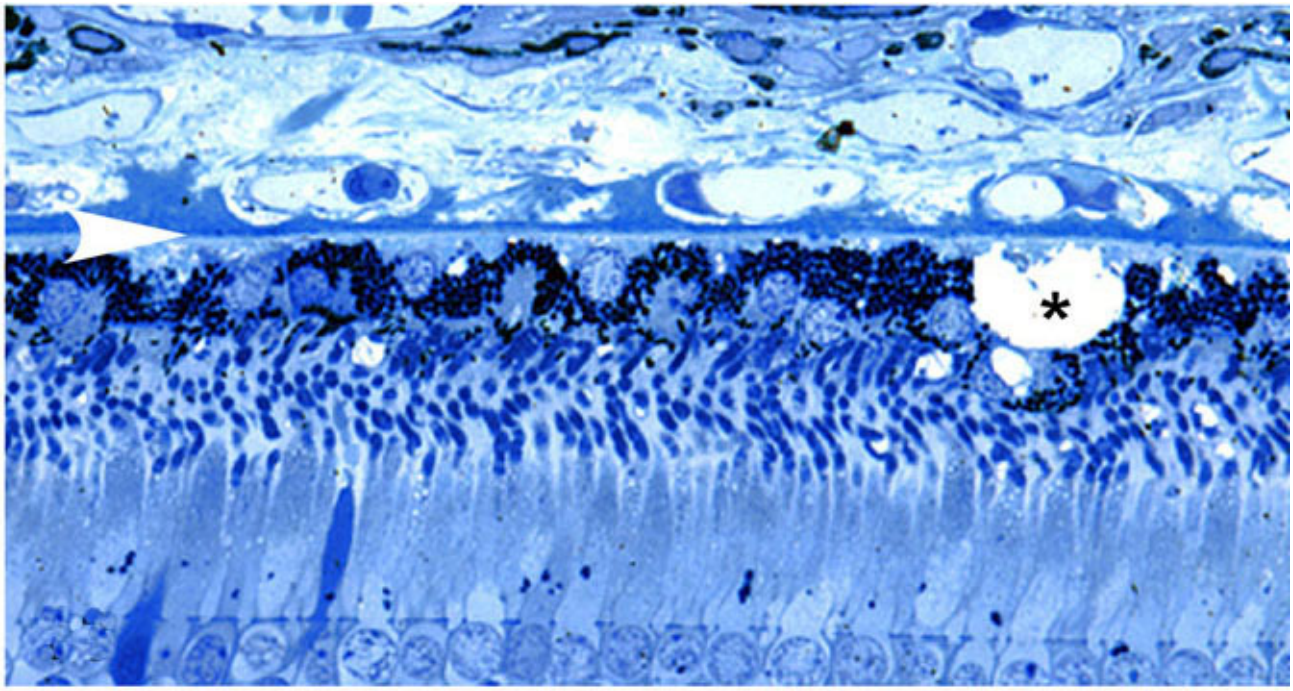

Figure 15. Drusen (asterisks), form between the RPE and Bruch's membrane.

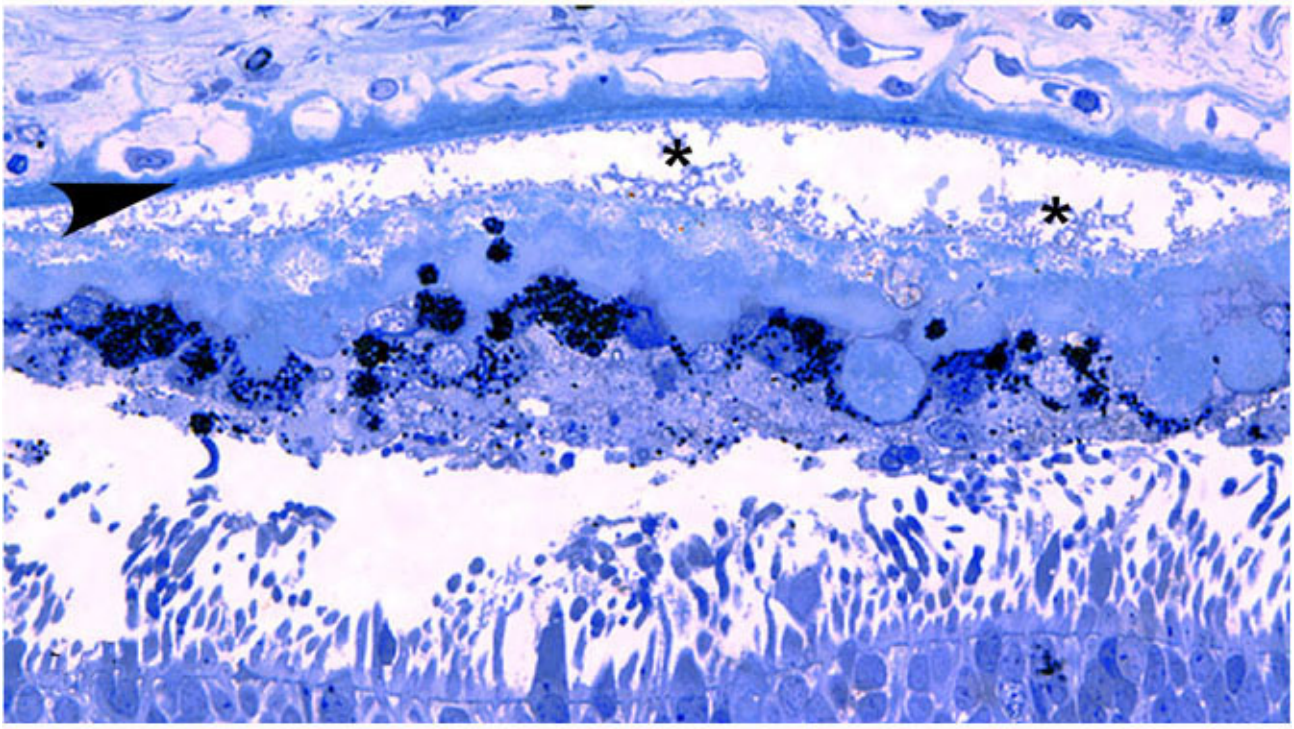

Figure 16. Extensive accumulation of BLamD (asterisks) is also commom between the RPE and Bruch's membrane.

The Complement System and AMD

Three complement pathways can be distinguished by the "triggers" that activate them. 1) antigen-antibody binding triggers the "classical pathway". 2) carbohydrate residues bound to invading pathogens trigger the "lectin

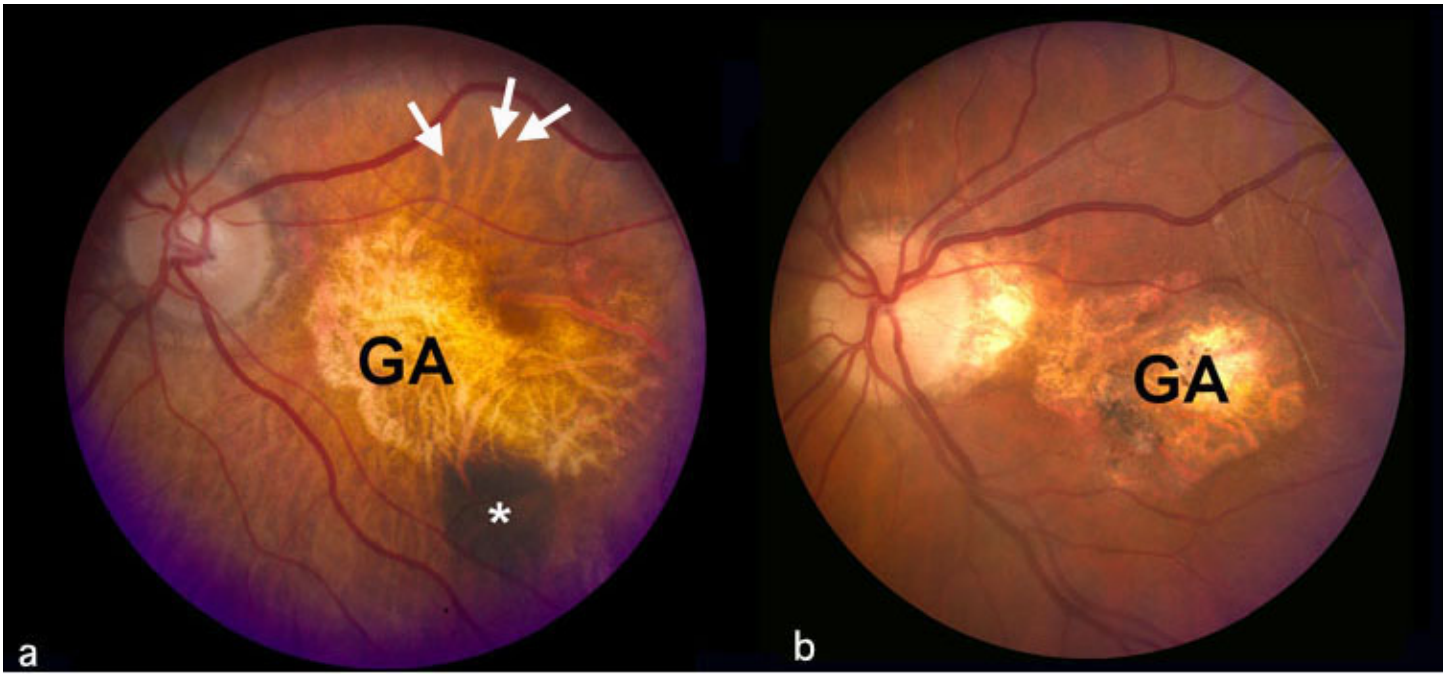

Figure 7. Color fundus photograph from two patients (a and b) with macular geographic atrophy (GA). The margins of the regions of RPE atrophy are clearly delineated (arrowheads). Choroidal blood vessels (arrows) are more easily visualized in these regions of atrophy because of the loss and/or absence of the RPE pigment. A choroidal nevus (asterisk) is indicated in eye a. These eyes would be expected to have poor central vision due to the extensive atrophy.

pathway. 3) A low level of spontaneous activation known as "tickover" characterizes the "alternative pathway". This continuous background level of activation is amplified rapidly by ubiquitous components present on the surfaces of many bacteria, viruses, as well as constituents present in cigarette smoke.

Complement Factor H, the Complement Alternative Pathway and AMD

Factor H is the main soluble inhibitor of the "alternative pathway" and, like most complement components, the liver is responsible for 80-90% of Factor H protein synthesis (190-192). We now know that variants in the gene encoding Factor H play a central role in one's susceptibility to AMD (see below). All of the available data are consistent with the conclusion that uncontrolled activation of the alternative pathway of complement at the level of Bruch's membrane is a key element in the process of drusen formation and a major contributing factor to the pathogenesis of AMD.

Although the liver is responsible for most circulating Factor H, the eye is also capable of producing it, in addition to other complement components. Not surprisingly, Factor H protein is also a molecular constituent of drusen (193). It co-localizes with its ligand C3b (a complement pathway component) in substructural spherules within drusen that contain amyloid b, further implicating these structures as candidate complement activators (170, 194). Factor H and the MAC co-distribute in drusen and at the interface between the RPE and choroid. Finally, Factor H and C5b-9 (MAC) immunolabeling are more intense in the macula compared to tissues from more peripheral areas in the same eye (Hageman and Mullins, unpublished).

We have advanced a working model of AMD pathobiology based upon our studies (155, 195) and the work of others (157, 196). In this model, RPE atrophy and the subsequent deposition of cellular debris in the sub-RPE space is construed as a local pro-inflammatory "seeding" event, leading to activation of the innate immune system at the RPE-choroid interface. Complement attack, in turn, induces significant bystander damage to macular cells and tissues, thus rendering them susceptible to additional RPE atrophy, photoreceptor

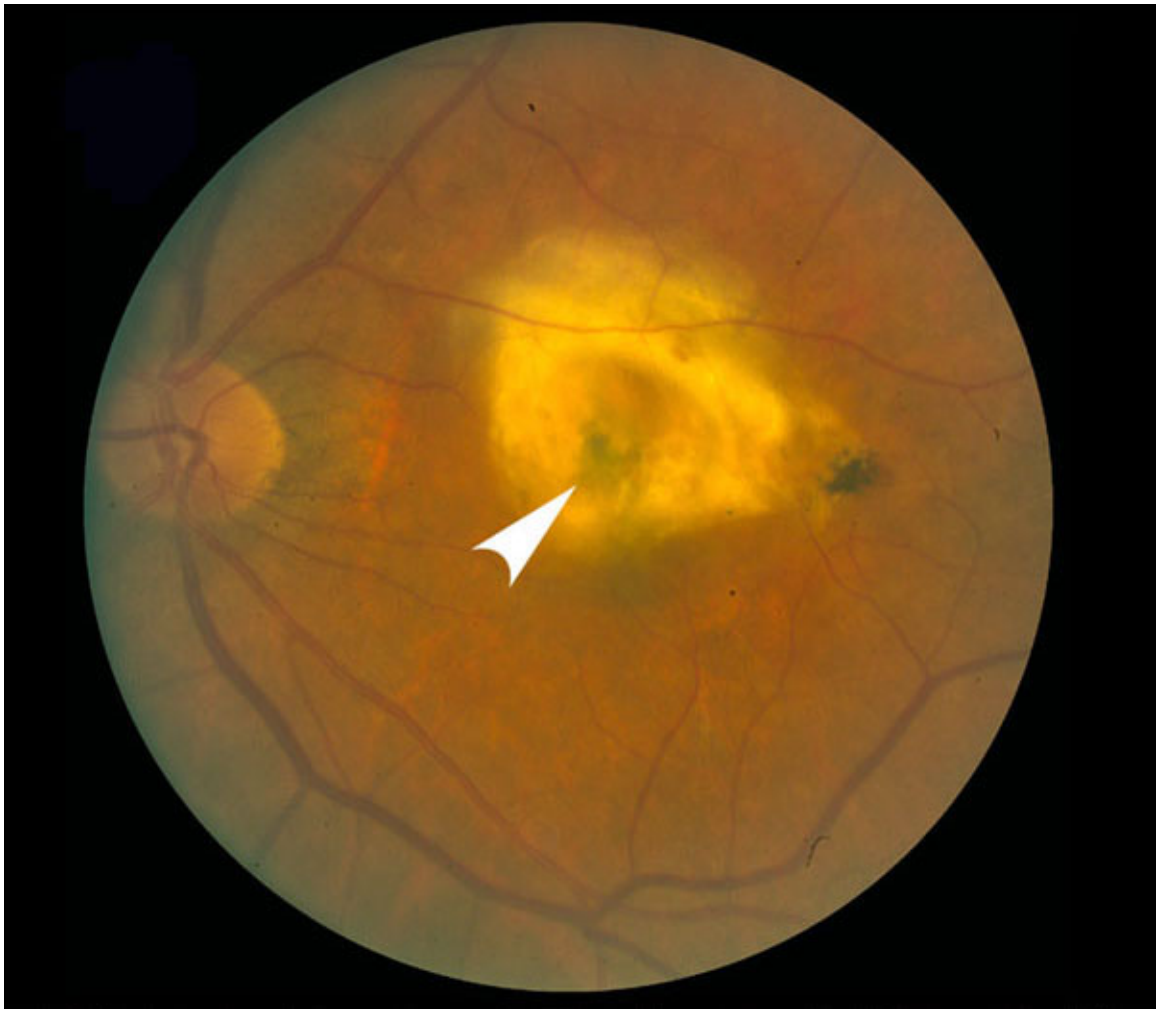

Figure 11. Color fundus photograph from an individual with end stage (cicatricial) exudative AMD. A large disciform scar (arrowhead) covering the macular region is distinctly visible.

degeneration, and CNV.(The reader, who is interested, can see diagrams showing the way the complement cascade works, in a paper by Ricklin and Lambris, 2007) (247).

Molecular genetics of AMD

Overview

AMD is often regarded as a group of complex, late onset diseases caused by the convergence of multiple risk factors (197, 198). Family history is a consistent risk factor according to most epidemiological studies of AMD conducted to date. Familial aggregation studies have shown that a genetic contribution is identified in up to 25% of AMD cases (199). Twin studies also support a genetic basis for the disease, with the concordance of clinical features (drusen and pigmentary changes) for both early and late onset disease being approximately twice as high in monozygotic (identical) twins compared to dizygotic (non-identical) twins (200, 201).

Genome-wide linkage analyses of extended families with AMD have identified a number of chromosomal loci that are linked to AMD (202-210). The most consistent occurs at chromosome 1q31 (211). Between 15-40% of multiplex AMD families segregate with a disease gene in the 1q31 region (205). Further analysis of this region reveals an allelic variant in exon 104 of the fibulin-6 gene (FBLN-6) in members of one AMD family, as well as in some sporadic AMD cases (212). A number of other candidate genes have also been linked to AMD. However,

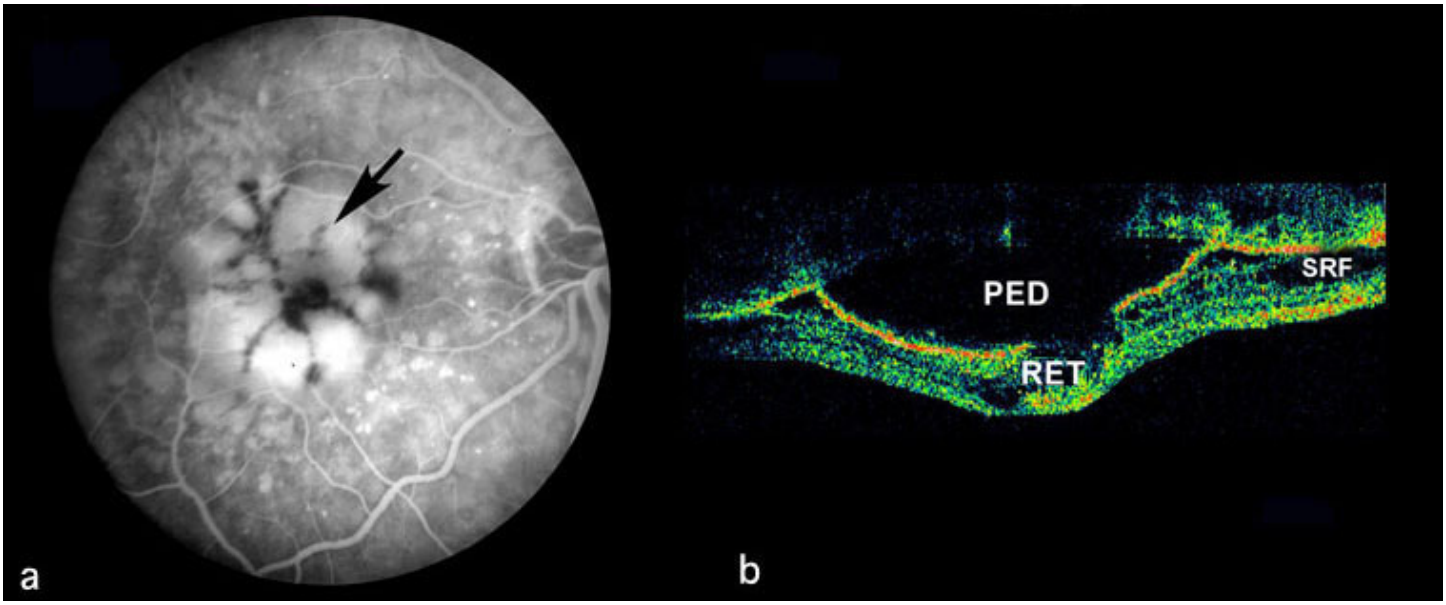

Figure 10. Corresponding angiographic (a) and OCT images (b) from an individual with a macular pigment epithelial detachment (PED). A multilobulated, hyperfluorescent lesion with sharply demarcated borders (arrow) is clearly visible in a 16. The blister-like elevation of the retina and retinal pigment epithelial layer, which correlates with the PED shown a, is appreciated in the OCT view (b). SRF, subretinal fluid; RET, retina.

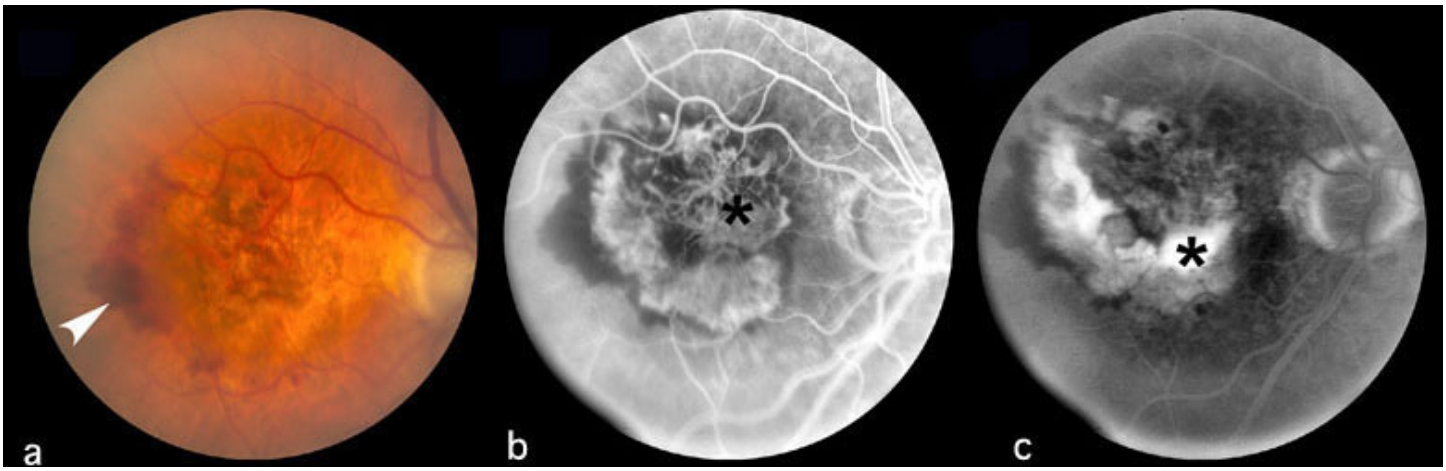

Figure 8. Color fundus photograph (a), early fluorescein angiogram (b) and late fluorescein angiogram (c). Arrowhead depicts edge of macular lesion. Note the lacey appearance of vessels (asterisk) in the early angiogram.

most of these results have not yet been replicated in subsequent studies. These genes include ELOVL4 (213), VEGF, VLDLR, and LRP6 (214), FIBLN5 (215) and TLR-4 (216).

In contrast, the e4 allele of the apolipoprotein E (APOE) gene has consistently been shown to be protective for AMD (217-219), whereas the e2 allele appears to influence progression and to result in an earlier age of onset (219). ABCA4 confers increased risk for AMD too (220).

In early 2005, four groups reported independently that common variants [single nucleotide polymorphisms (SNPs)] in the gene encoding complement Factor H (CFH) confer major susceptibility to, or protection from, AMD (193, 221-223). Individuals who possess a single copy of the risk-conferring CFH haplotype have 2-4 fold higher lifetime risk of developing AMD, and those with two copies possess a 5-7 fold higher lifetime risk. Haplotype analysis showed that a SNP in the CFH gene can account for up to 50% of AMD cases in the human

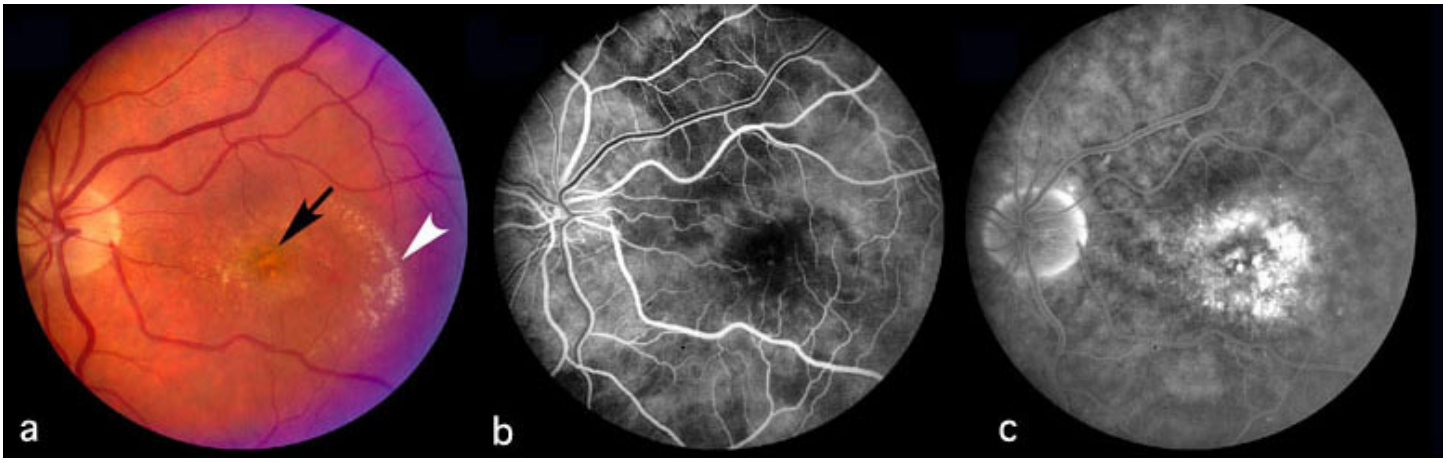

Figure 9. Color fundus photograph (a), early fluorescein angiogram (b) and late fluorescein angiogram (c) from an individual with occult choroidal neovascularization. A single, small punctate region of hemorrhage (asterisk) and a ring of exudates (arrowhead depicts edge) occur.

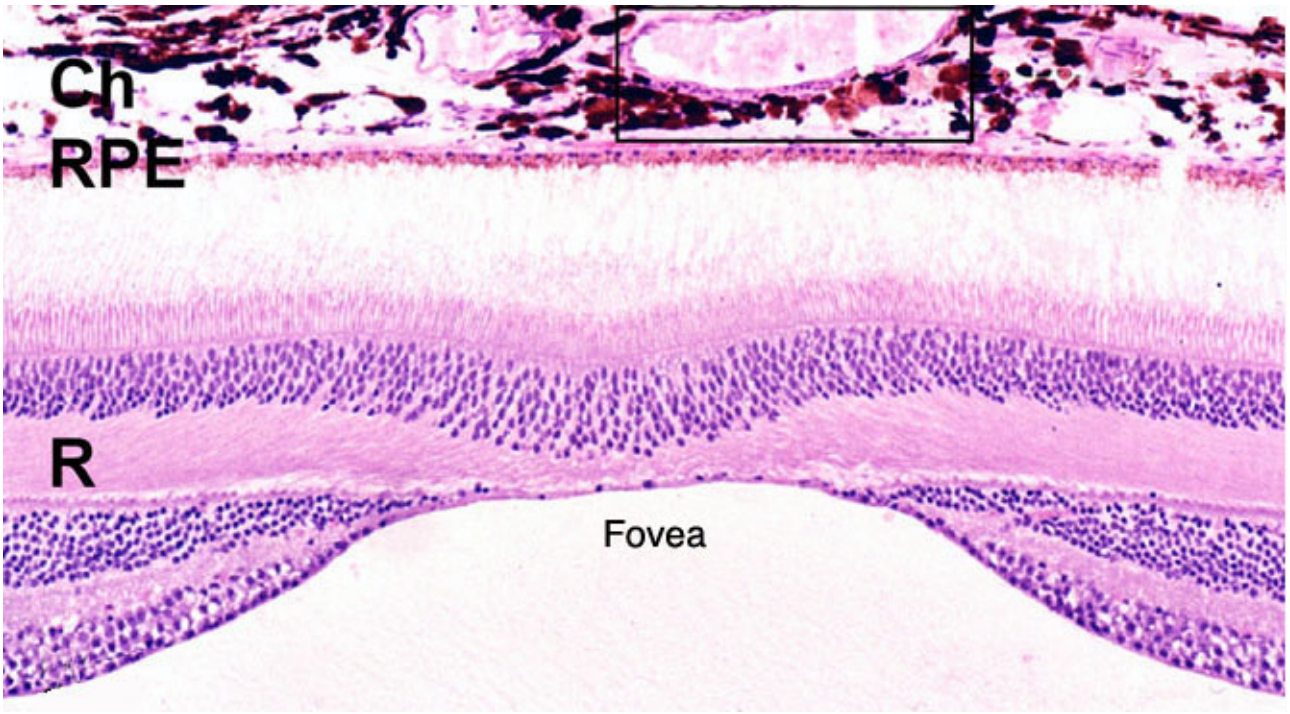

Figure. 12. Light microscopic image depicting the choroid-RPE-retina interface. A section shows the normal anatomical relationships of the macular choroid (CH) with blood vessels (BV), retinal pigment epithelium (RPE) and neural retina (R); the section passes directly through the fovea.

population, a number approaching 50,000,000 worldwide. Follow-up reports have since confirmed these findings in additional cohorts in the United States (213, 224), Iceland (225), the United Kingdom (226), and France (227). Interestingly, the major CFH risk haplotype in the Japanese population appears to be different than that reported in other populations, although the protective haplotype is the same (228).

In early 2006, a study showed that allelic variants in two other complement-related genes, Factor B (BF) and complement component C2, were linked to AMD (229). These are paralogous genes located 500bp apart on chromosome 6p21, and both reside in the major histocompatibility complex (MHC) class III region. BF is a component of the alternative pathway of complement, whereas C2 is a component of the classical pathway. Both

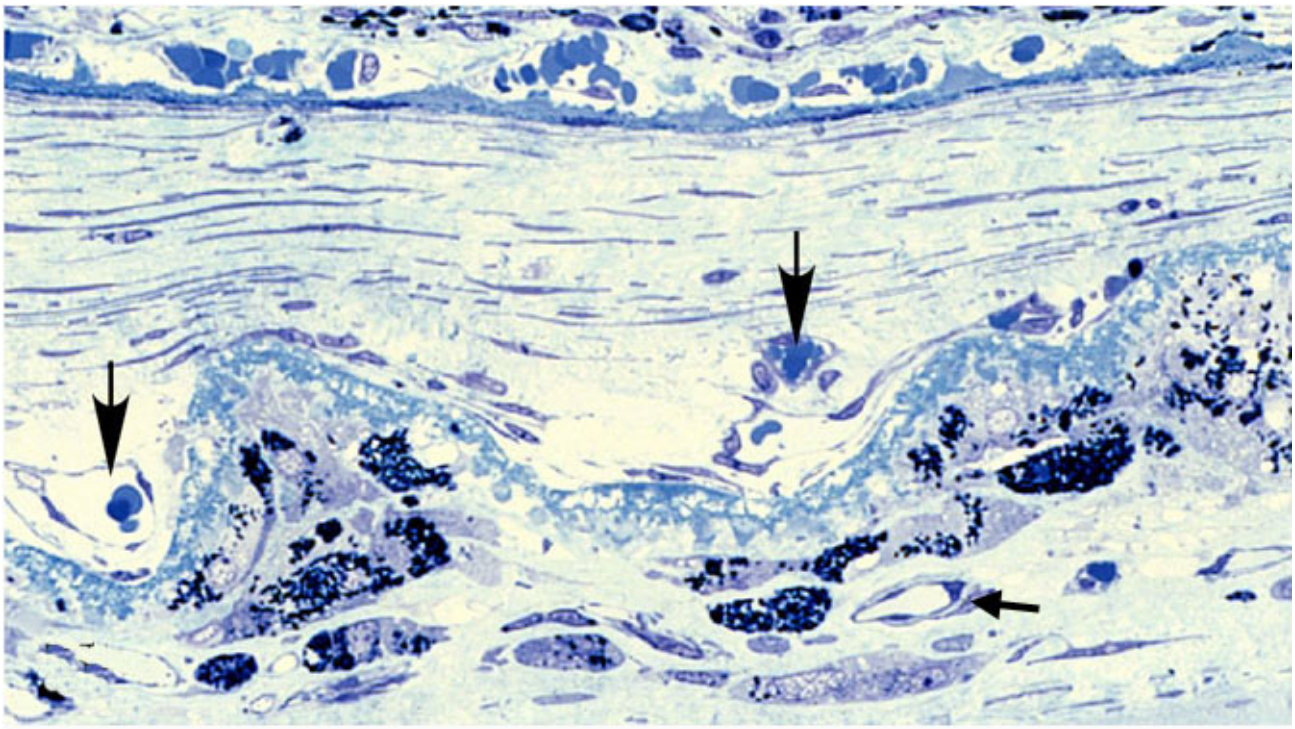

Figure 17. Light microscopic image depicting the choroid-RPE-retina interface. New choroidal blood vessels are located in both the sub-RPE and subretinal spaces (arrows).

variants together can account for nearly 74% of the risk of developing AMD. The protective haplotype for each of the three genes was completely absent in nearly 75% of all AMD cases; whereas 56% of controls possessed at least one copy of a protective CFH or BF haplotype. Approximately 60% of the risk in AMD cases, and 65% of the protection in controls, can be assigned to the CFH gene locus alone.

In addition to the 1q31 locus, a region on chromosome 10q26 has been identified in several recent studies of AMD (211) on a scale similar to that of the CFH Tyr402His variant. PLEKHA1 (pleckstrin homology domain-containing, family A, member 1) and a predicted LOC387715 gene were identified as the relevant candidate genes at that locus (231). A subsequent study concluded that SNP rs10490924 in LOC387715 was the most likely AMD-susceptibility allele (232). A third study identified a coding change in the LOC387715 gene as the significant allele that results in a non-synonymous substitution of alanine to serine at position 69 of the hypothetical protein. In addition, a significant statistical relationship between the LOC387715 variant and a history of cigarette smoking has been found (233). Thus far, there is no published evidence for expression of the LOC387715 gene product at either the RNA or protein levels; nor is there any indication of its likely functional properties.

Therapy for AMD

The molecular pathogenesis of AMD has only recently begun to be elucidated. So, it is not surprising that the therapeutic approaches for AMD have been of only limited benefit to most patients. Therapeutic interventions have focused almost exclusively upon the exudative "wet" form that comprises approximately 10% of the AMD patient population because it is the most debilitating and rapidly progressive form of the disease. Until recently, such therapies have resulted in a benefit to less than 50% of patients with "wet" AMD, and therefore less than 5% of all AMD patients. Developing therapeutics to delay onset or progression of "dry" AMD or the conversion from "dry" to "wet" AMD, have proven even more difficult. This due to the long study duration and large numbers of participants needed to achieve meaningful statistical results.

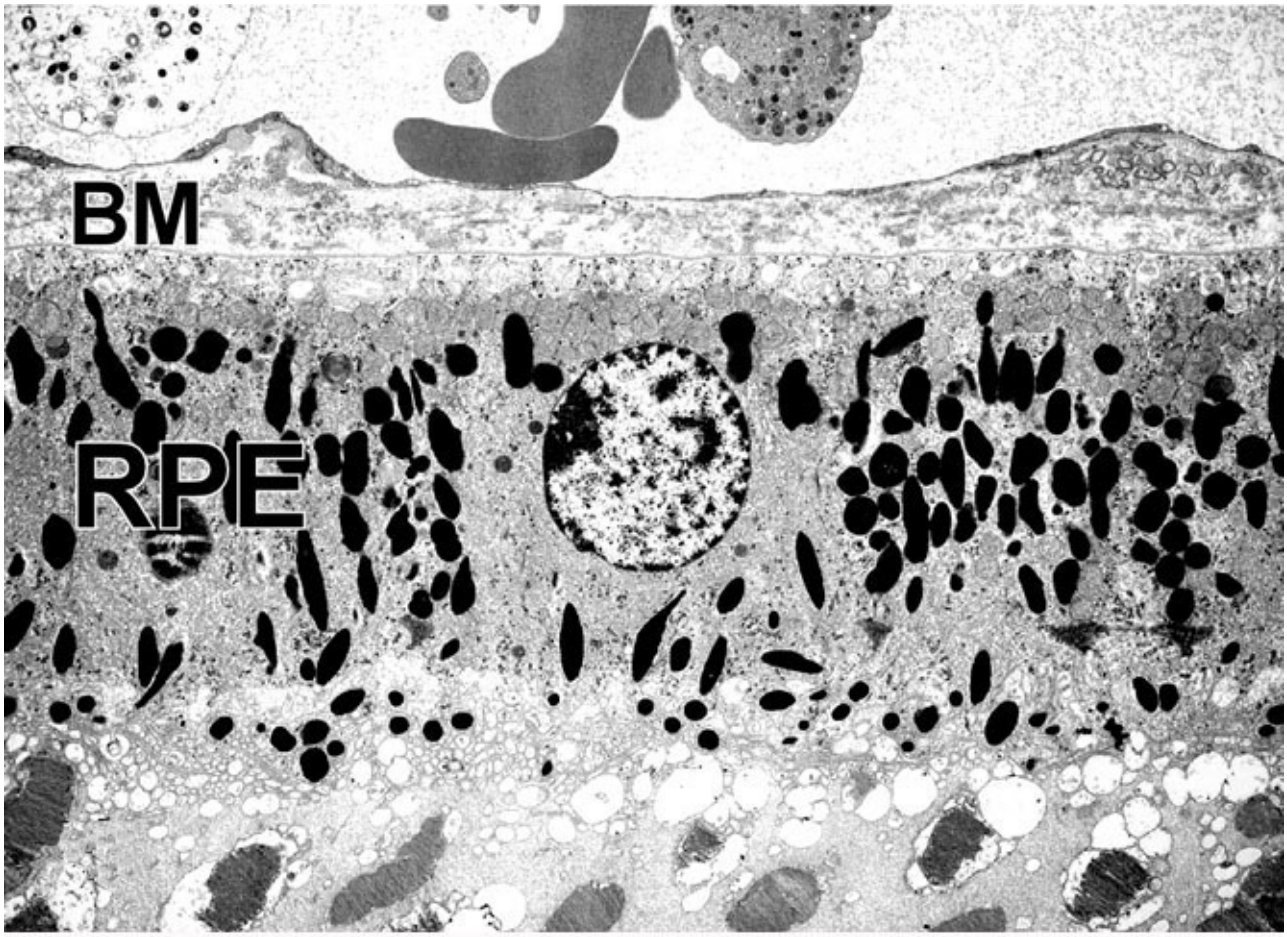

Figure 18. Transmission electron micrograph of the RPE-choroid interface in a normal human donor eye.

Over the last 30 years epidemiological studies have repeatedly identified four risk factors for AMD: age, cigarette smoking, increased body mass index, and inheritance (10, 31, 32). These same studies have produced conflicting information regarding the roles of dietary antioxidant supplementation and fat intake. In 1992 the Age-related Eye Disease Study (AREDS) group began enrolling subjects in a prospective, multicenter, randomized, controlled study (33). Patients enrolled in the AREDS had either mild, moderate, or severe dry AMD in both eyes, or exudative AMD in one eye only. The study tried to determine whether antioxidant therapy prevented vision loss, slowed the progression of dry AMD, or prevented conversion from dry to wet AMD. The results of 6.3 years of follow-up in the AREDS study were published in 2001 (33). The study results demonstrated that daily antioxidant therapy in the form of 15 mg beta carotene, 500 mg vitamin C, 50 mg vitamin E, 80 mg zinc (as zinc oxide), and 2mg copper (as cupric oxide) daily was superior to a placebo in delaying progression of advanced dry AMD, and in slowing conversion from dry to wet AMD. Specifically, the odds ratio of progression to advanced AMD was decreased to 0.72 in the group who took the above combination of antioxidants as compared to placebo. No benefit of antioxidant supplementation was demonstrated in the milder forms of AMD. However, because the early stages of AMD often persist for many years, it is quite possible that the study design was not long enough to demonstrate a benefit to patients with milder stages of AMD.

Another therapeutic intervention is laser therapy for eyes with drusen. Three prospective trials, the Choroidal Neovascularization Prevention Trial (CNVPT), Complications of AMD Prevention Trial (CAPT) and Prophylactic Treatment of Age-Related Macular Degeneration Trial (PTAMD) evaluated the efficacy and safety of light macular grid laser in reducing the risk of developing CNV in eyes with drusen. The CNVPT and CAPT used argon laser and the PTAMD used an 810 nm diode laser (34-36). In both the CNVPT and PTAMD studies,

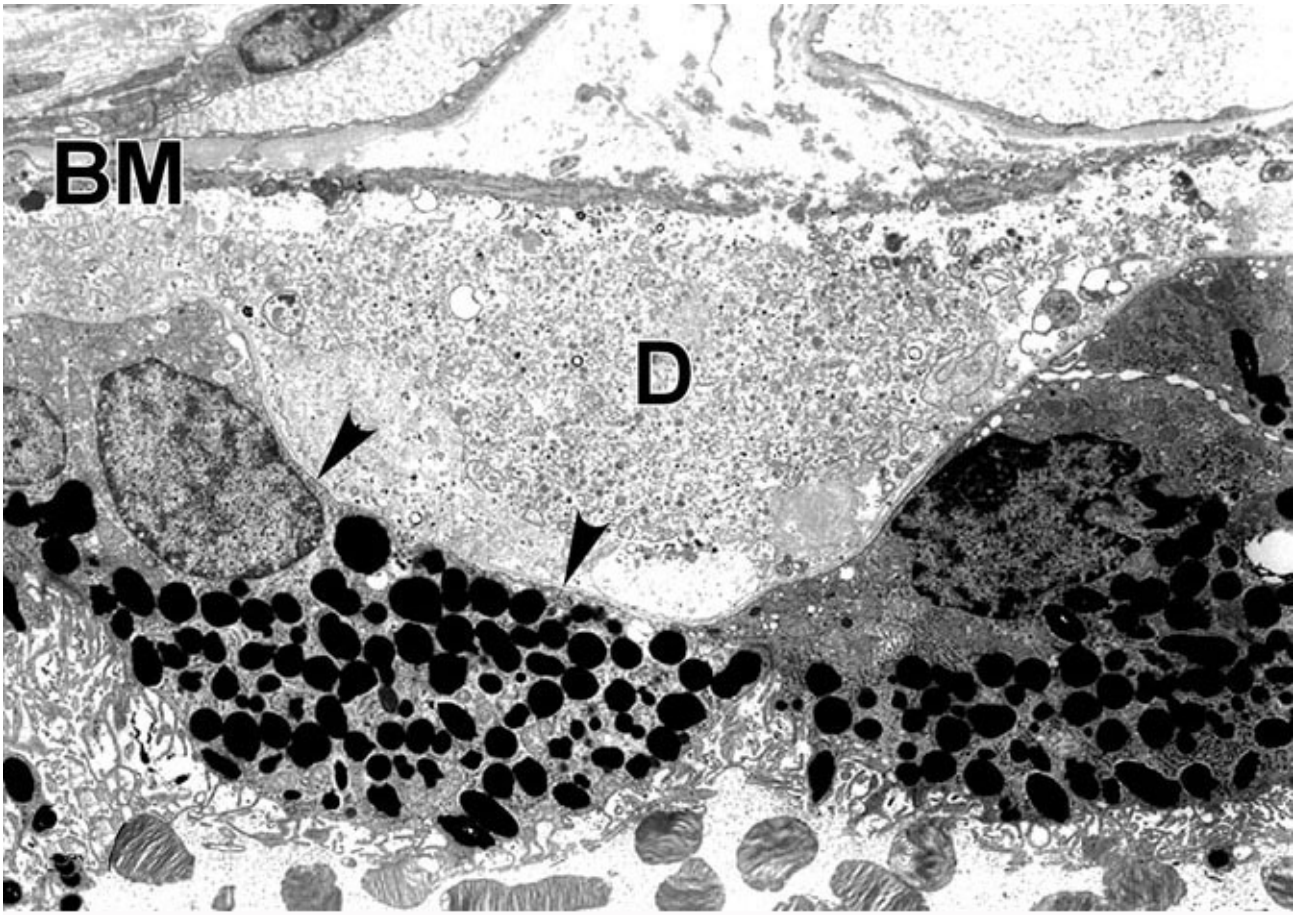

Figure 19. Transmission eectron micrograph of a donor eye with AMD. A single drusen (D) is shown to be located between the RPE basal lamina (arrowheads) and Bruch's membrane (BM).

grid laser treatment increased the risk of CNV. Therefore grid laser of eyes with drusen is not recommended if the fellow eye has CNV (36, 37). Recent results of the PTAMD bilateral drusen study reported no decrease in CNV development but a four-letter gain in visual acuity in treated versus control eyes after three years of follow-up (38). The larger CAPT study of treatment of one eye in the setting of bilateral drusen is ongoing but near completion of five years of follow-up. Until the results of the CAPT study are known, prophylactic laser of eyes with bilateral drusen is not a recommended therapy.

Therapy for exudative AMD has evolved from thermal laser photocoagulation in the early to mid 1980's, to photodynamic therapy for CNV beginning in 2000 and, most recently to inhibition of vascular growth factors. The three year results of the Macular Photocoagulation Studies (MPS) for AMD was published in 1986. It demonstrated a benefit for "extrafoveal" CNV located between 200 and 3,000 microns from the fovea (Fig. 24). Subsequent MPS studies for juxtafoveal (1 - 200 microns from the fovea) CNV and subfoveal CNV respectively, demonstrated a benefit for laser treatment versus no treatment (Fig. 24) (39-41).

However, visual loss was common even in those eyes with successful obliteration of CNV (42). Additionally, the closer the CNV was to the fovea, the poorer the visual outcome and the higher the rate of recurrence even in those who initially responded to treatment (43). In 1993, Freund and coworkers demonstrated that only 13% of new patients with exudative AMD (or approximately 1.3% of all AMD patients) met criteria for thermal laser treatment based on the MPS (Fig. 25) (44).

In the late 1980's to mid-1990's there was significant interest in vitreoretinal surgical approaches to exudative AMD. Vitrectomy surgery with evacuation of subretinal blood and neovascular membranes reported variable

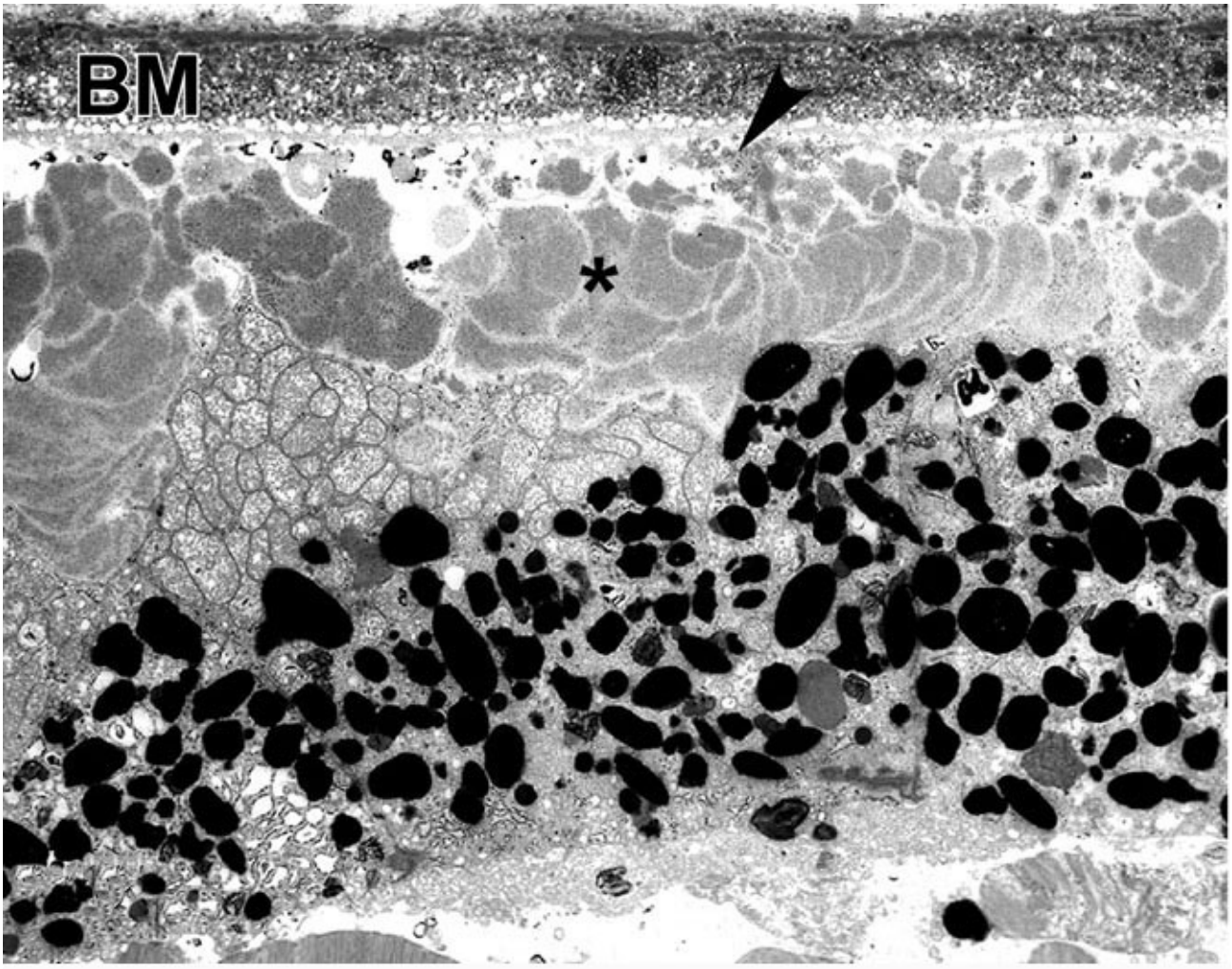

Figure 20. Electron micrograph shows BLamD (asterisk) accumulates between the basal surface of the RPE and its basal lamina (arrow), whereas BLinD is located within the innermost aspect of Bruch's membrane, in a case of AMD.

success rates. Trial designs were nonstandard, results were conflicting, and long-term follow-up in these pilot trials was lacking. Given the potential morbidity and expense of major eye surgery, the National Eye Institute sponsored the prospective, randomized, controlled Submacular Surgery Trials (SST). The results of the trial demonstrated that surgery did not increase the chance of stable or improved vision, and it prevented severe vision loss only in those eyes with large subretinal hemorrhages. Submacular surgery was also associated with some risk of rhegmatogenous retinal detachment. Given these results, and the advent of less-invasive therapy with anti VEGF agents (described below) submacular surgery is no longer recommended for exudative AMD except, perhaps, in select cases with large submacular hemorrhage (45, 46).

Other surgical approaches, which have been investigated in small pilot trials, are macular translocation (Machemer and Steinhorst, 47), and limited macular translocation developed later by deJuan (48). The former technique involves creation of a total retinal detachment, while the latter is limited to a partial retinal detachment. Both techniques involve displacement of the macular retina from an area of CNV to a location where the retinal pigment epithelium is thought to be healthier. While pilot trials have suggested a benefit from these therapies for a small subset of patients, the emergence of less invasive and more broadly applicable pharmacological therapies for exudative AMD have resulted in much less frequent application of macular translocation in recent years (Figs. 26-maculardegen.F2728).

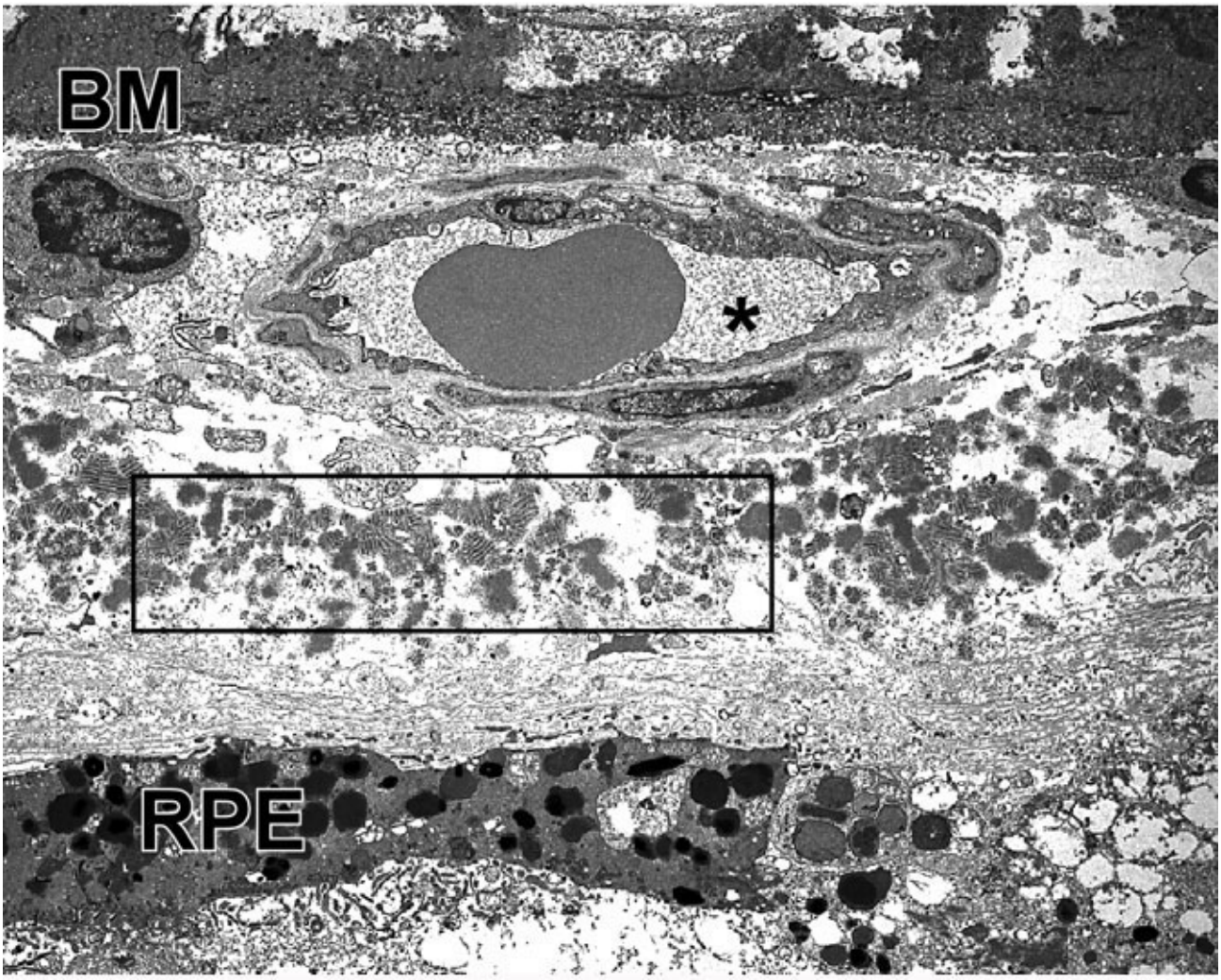

Figure 21. Electron micrograph shows a patent choroidal neovessel (asterisk), lying between BM and a layer of BLamD (rectangle) in a case of advanced AMD. RPE, retinal pigment epithelium; BM, Bruch's membrane.

In 2000, photodynamic therapy with Visudyne (tm) (verteporfin), a light-activated compound, was approved by the FDA for exudative AMD with predominately (>50%) classic, subfoveal CNV that was no larger than 5600 microns in diameter. FDA approval was based on the results of the Treatment of Age-Related Macular Degeneration with Photodynamic Therapy Investigation (TAP) study. In the TAP study, subfoveal CNV was divided into subgroups based on initial visual acuity, lesion size, and fluorescein leakage characteristics: enrolled subjects were randomized to Visudyne(tm) or placebo (49). Photodynamic therapy (PDT) involves intravenous administration of the photoactivatable compound, Visudyne (tm) followed 15 minutes later by irradiation of the CNV with a low energy, non-thermal laser. Activated Visudyne(tm) generates singlet oxygen that damages the CNV endothelium resulting in thrombosis (50). In the TAP study an average of 3.5 treatments spaced at three month intervals were required to ablate the CNV, so the process is a lengthy one. Visual results, though better than with any prior treatment, were less than optimal with only 67% of treated patients with predominately classic CNV losing fewer than three lines of visual acuity (as compared to 39% of placebo treated eyes). At 1 year, 16% of Visudyne treated patients gained one or more line of vision, and 15% of treated patients lost more than six lines of visual acuity. Over the course of the next several years, subgroup analysis of data from the TAP studies as well as additional trials with Visudyne(tm) treatment for lesions other than predominately classic CNV led to its application for other lesion types. However, the visual results for lesions that were predominantly occult CNV were less favorable than those with predominately classic CNV (51, 52).

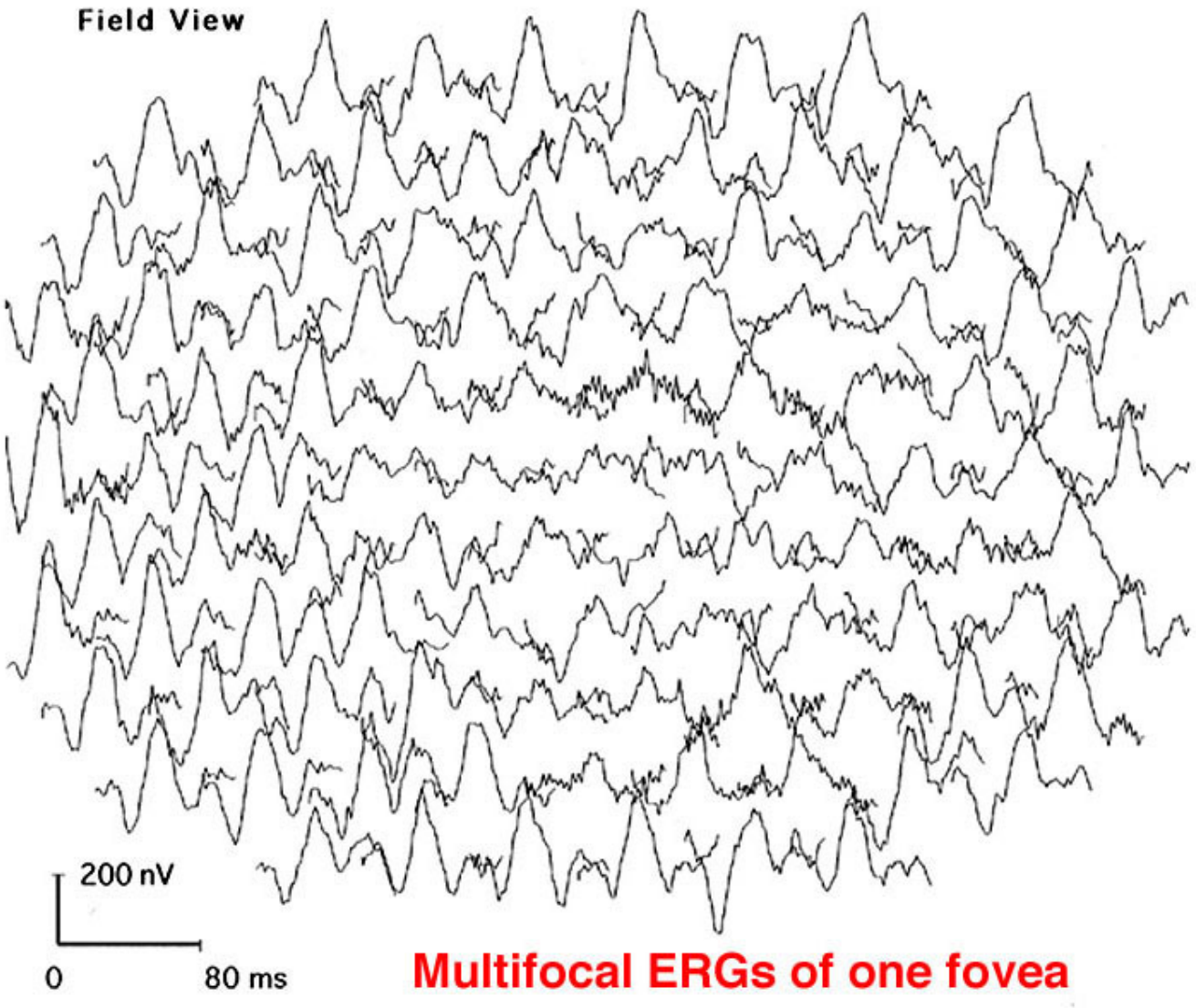

Figure 22. Multifocal ERG recordings in a patient with age related macular degeneration (AMD). Note the central resposes where the fovea is located are much reduced in amplitude.

Figs. 29-maculardegen.F30maculardegen.F3132 demonstrate a favorable response to PDT with Visudyne as seen in our clinic.

As noted above, however, not all eyes fare well with PDT therapy. Below is a photograph of an eye that did not demonstrate a significant benefit from PDT treatment with Visudyne (Fig. 33).

Other ablative treatments for CNV include transpupillary thermotherapy (TTT) and radiation therapy. TTT utilizes low energy diode laser (810 nm) applied to the CNV slowly over one minute. Small pilot trials of TTT for occult CNV initially showed promise but a randomized, prospective clinical trial (TTT4 CNV) demonstrated no significant benefit. Similarly, low dose radiation therapy for AMD was investigated in multiple small pilot trials with conflicting results (53-55). Although no definitive prospective clinical trial of radiation therapy for AMD has ever been conducted, the concept has become less popular in recent years, especially in light of the interest in pharmacological therapies for AMD.

The current era of therapy for exudative AMD utilizes administration of anti-neovascular agents periocularly or intraocularly. Studies implicating various cellular growth factors, including vascular endothelial growth factor

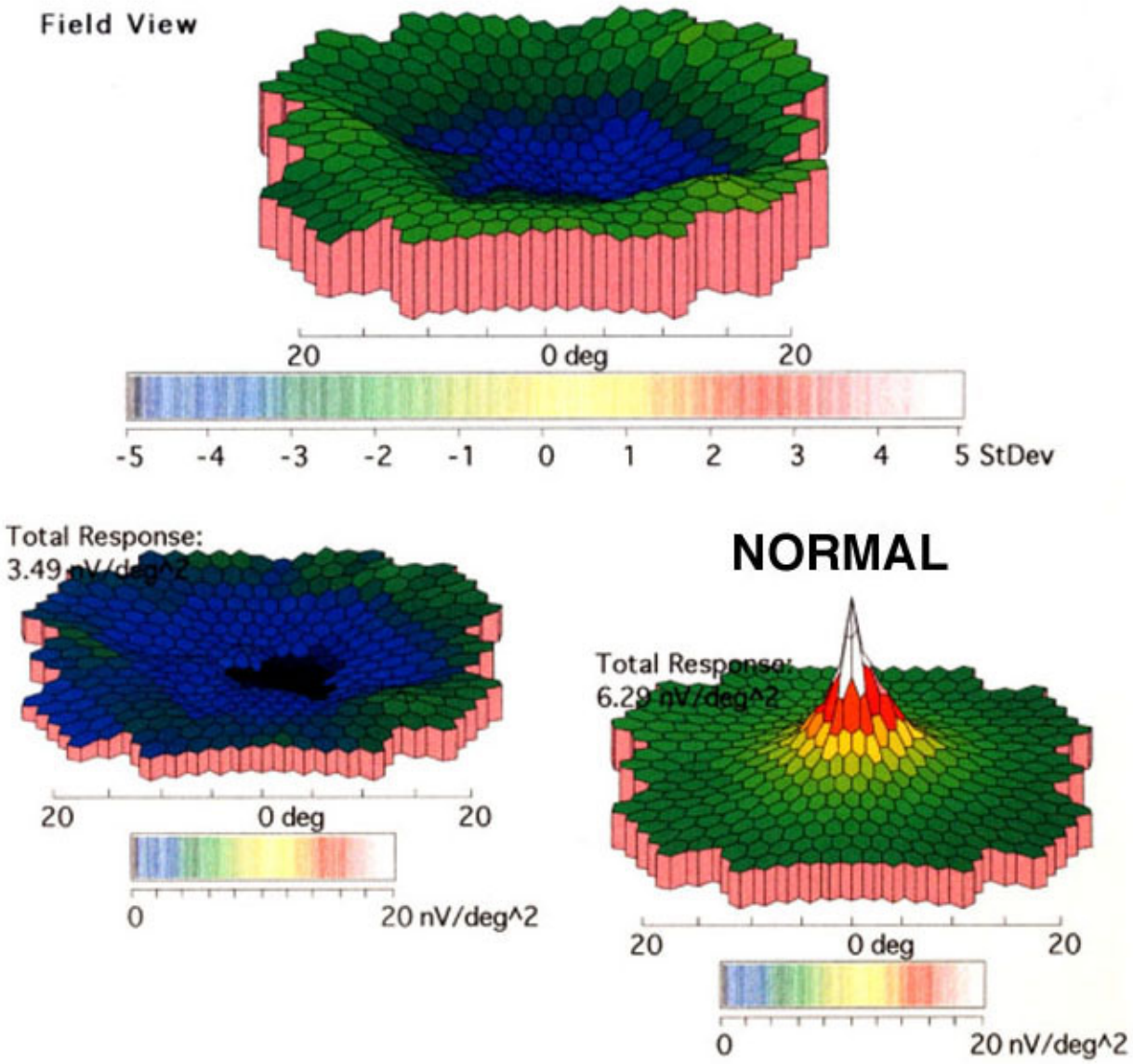

Figure 23. Multifocal ERG recordings transformed into 3-D maps of the macular area in a patient with AMD compared to a normal patient. The AMD patient has no responses in the fovea.

(VEGF) in a variety of ocular neovascular processes has led to the development of VEGF inhibitors, VEGF antibodies and other "broad-spectrum" antiangiogenic molecules that inhibit pro-angiogenic cytokines. In 2004, Macugen(tm) (Pegantanib Sodium) was the first of the VEGF inhibitors to be approved by the FDA for exudative AMD. Macugen is an aptamer which binds to the A isoform of VEGF-165 at its heparin binding site and prevents VEGF-165 from binding to its receptor on endothelial cells. Macugen is administered by intravitreal injection (i.e. injected into the vitreous cavity of the eye) every 6 weeks for up to a two-year course of therapy. Based on the Macugen (tm) study results of 1186 patients after one-year, 70% of subjects treated with 0.3 mg pegaptanib, 70% lost fewer than 3 lines of vision compared to 55% of controls. The risk of severe vision loss (> 6 lines of vision) was reduced from 22% in controls to 10% in treated subjects (56).

Another VEGF inhibitor undergoing clinical trials is ranibizumab or Lucentis(tm). Lucentis(tm) is derived from the Fab fragment of an antibody to isoform A of VEGF. The fragment blocks VEGF binding to its receptor on endothelial cells, thus inhibiting its biological activity. The ANCHOR trial was presented recently (57). The data demonstrated not only a preservation of vision in nearly 95% of patients treated with Lucentis(tm)

(ranibizumab) at year one but, for the first time, an improvement in vision in 30-38% of patients with exudative AMD. Another recently published trial comparing Lucentis alone to PDT alone demonstrated superior visual results with Lucentis. (ref: Anchor Trial). Lucentis(tm) was FDA approved for the treatment of exudative AMD in June 2006. Although the initial trials with Lucentis utilized monthly intravitreal injection with the drug, more recent studies indicate that some patients my respond favorably to a treatment regimen utilizing fewer than 24 injections over a 2 year period (Fung et al., 2007) (248). Currently, studies are underway to determine factors which might influence frequency and duration of treatment with Lucentis.

Avastin(tm) (beclumizabab), a VEGF antibody derived from the same parent antibody as Lucentis(tm), is approved by the FDA to treat colon cancer and is gaining popularity as an "off-label" intravitreal therapy for AMD. It is important to note that Avastin(tm) has not yet undergone the toxicity studies and controlled trials that are required by the FDA for ocular application (58, 59). Other anti-angiogenic therapies currently under study include anecortave acetate (Retane, an antiangiogenic steroid (60, 61)), squalene and triamcinolone (which carries a significant risk of causing cataract and steroid-induced glaucoma). Additional studies are underway to investigate the potential for a combination of Anti-VEGF therapy with Visudyne(tm) photodynamic therapy utilizing light doses lower than those applied in the TAP an VIP studies with Visudyne (62, 63, 249).

Figures 34 and 35 show results of pre (Fig. 34, Fig. 35) and post anti-VEGF treatment (Fig. 36).

As a result of the anti-VEGF treatment much improvement can be seen in the macular area along with good visual restoration. The OCT scans (Fig. 36) show filling in of the disrupted cell types in the retina (the holes of Fig 36a get occupied by cells) and glial cells react to restore damaged retina (Fig. 36b and Fig. 36c, green upward streaks).

One concern with all anti-angiogenic agents is their potential for systemic inhibition of VEGF that may produce cardiovascular or cerebrovascular complications, or inhibit wound healing. The immediate and long-term systemic effects of these drugs, especially those prescribed "off-label", are largely unknown and difficult to determine in an elderly population already prone to vascular events. Additional drawbacks to the intravitreally administered therapeutics include patient discomfort, intraocular infection (endophthalmitis), retinal tear or detachment, and lens damage in phakic patients (64). The incidence of endophthalmitis in published trials with Macugen and Lucentis were 0.16%/injection and 1.3% - 1.4% of patients respectively and the incidence of retinal tears and/or detachment in these studies were 0.08%/injection and 0% - 0.4% respectively. (see Macugen and Lucentis trials refs below) Risk of lens damage in phakic patients treated with intravitreal anti-VEGF therapy can be minimized by visualization of the needle tip with the indirect ophthalmoscope during injection and by proper patient preparation (anesthetic, education, and reassurance) during the injection process to minimize the risk of sudden patient movement. Some patients do quite well with topical anesthetic alone while others require subconjunctival anesthetic injection (249-251).

Recent discoveries of the role that inflammation plays in AMD pathogenesis (see above) has led to an interest in investigating the anti-inflammatory effects of statins on AMD. Several clinical population-based studies of the effects of statins on AMD development and progression have yielded conflicting results (65). Thus, more studies in this area will be required to assess efficacy.

In the near future, therapy for exudative AMD will likely involve multiple anti-neovascular agents, possibly coupled with less frequent application of photodynamic therapy, in order to maximize the beneficial effects of each and minimize the frequency of adverse side effects. Further on the horizon are anti-angiogenic agents in longer acting forms that require less frequent administration. The ultimate therapy for AMD, however, will lie in preclinical identification of those who are genetically "at risk" for the disease, coupled with preventative strategies that are designed to minimize or compensate for one's genetic predisposition.

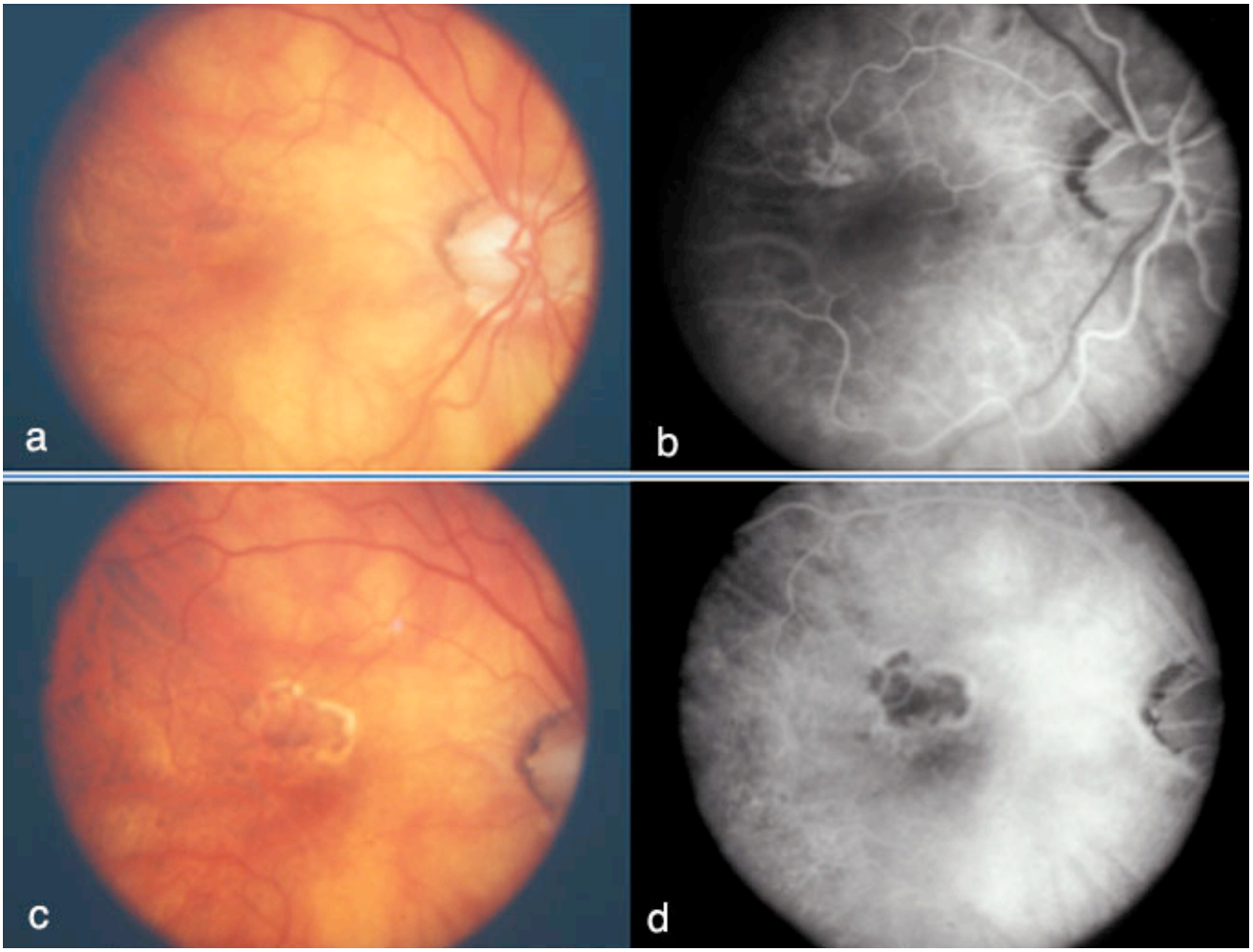

Figure 24. a) New extrafoveal CNVM. b) angiogram of extrafoveal CNVM (photos from KMG files). c) Laser scar after MPS-style laser for extrafoveal CNVM. d) Angiogram of laser scar after MPS- style laser for extrafoveal CNVM (photos from KMG files).

Conclusion

Complement Factor H is the first gene identified in multiple independent studies that confers a significant risk for the development of AMD. This finding, together with the subsequent identification of AMD-associated variants in the related complement genes BF and C2, provide compelling evidence that the innate immune system and, more specifically, uncontrolled regulation of the alternative pathway of complement, plays a central role in the pathobiology of AMD. At this point, the most likely scenario is that exposure to infection or some other triggering event in genetically susceptible individuals, coupled with impaired complement regulatory function leads to the sustained activation of complement cascade, drusen formation and, eventually, development of AMD.

The emergence of this new paradigm of AMD pathogenesis sets the stage for the rapid development of early diagnostics, novel bioassays, and new animal models that faithfully mimic aspects of the disease process. Furthermore, the way is now paved for development of novel therapeutic interventions aimed at modulating the alternative pathway of complement in "at risk" individuals prior to the onset of choroidal neovascularization or geographic atrophy.

Now that the genetic basis for a major proportion of AMD cases has been elucidated, what additional scientific progress may be anticipated, and what will be the significance of these new findings for the diagnosis and

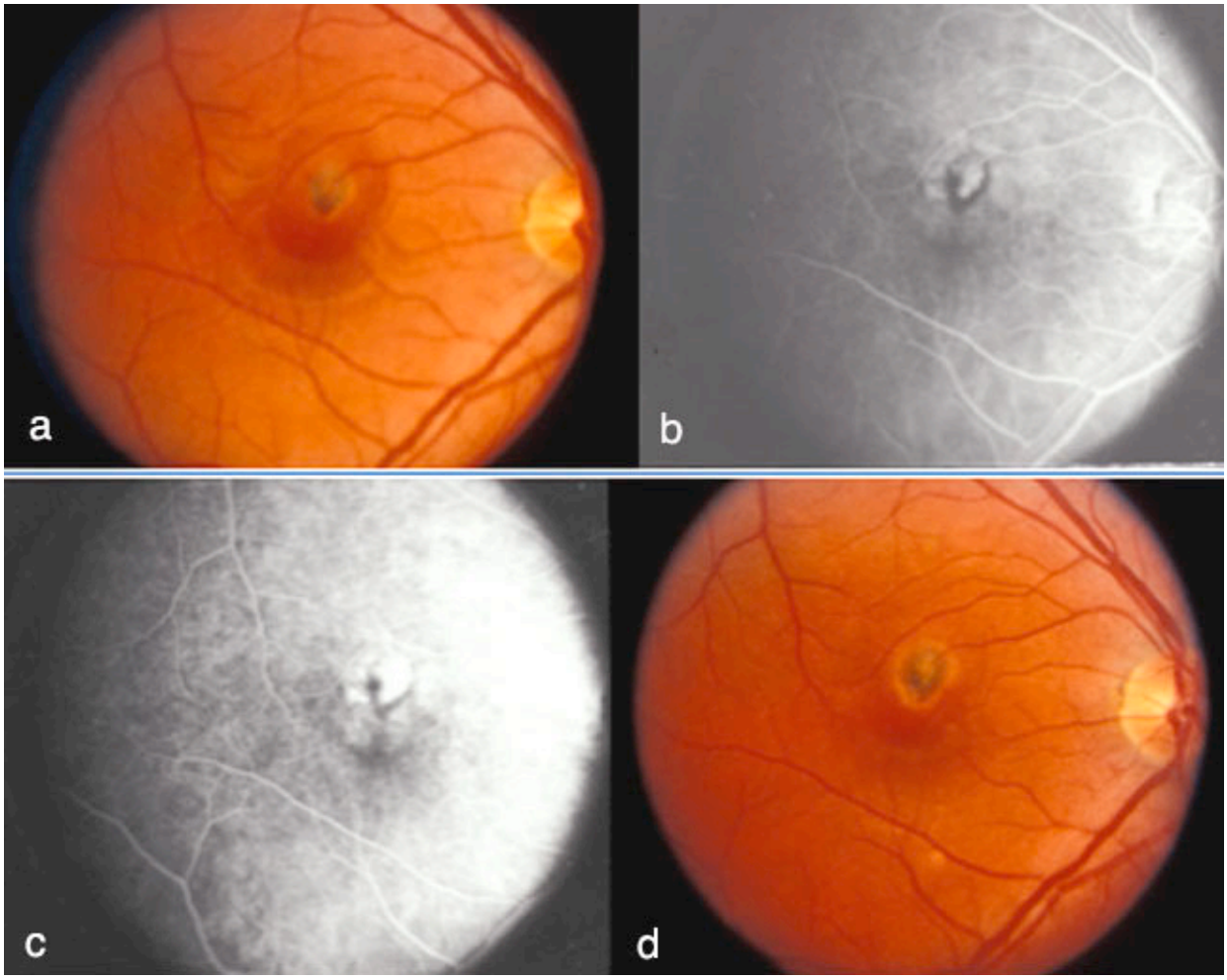

Figure 25. a) Subretinal hemorrhage and CNMV. b) Fluorescein angiogram demonstrates juxtafoveal CNVM in the transit phase. c) Fluorescein angiogram demonstrates late leakage from juxtafoveal CNVM. d) Dry laser scar 1 month after MPS style laser for juxtafoveal CNVM (photos from KMG files).

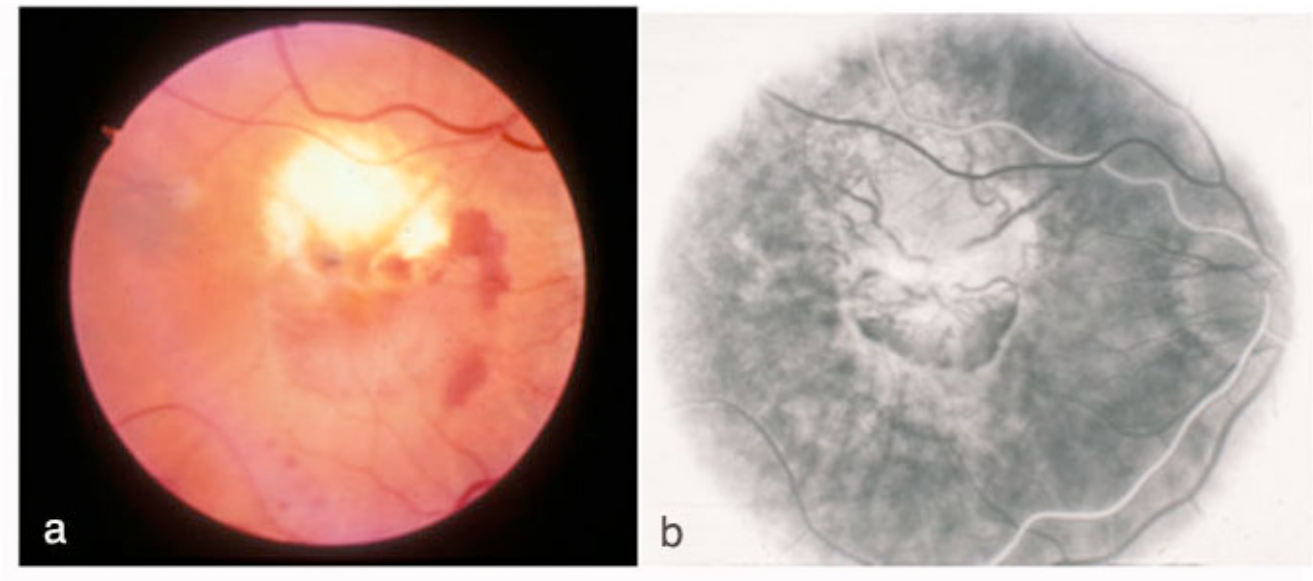

Figure 26. a) pre-operative color photo of subfoveal CNVM just inferior to prior laser scar. b) preoperative angiogram demonstrating a large, classic subfoveal CNVM (photos from KMG files).

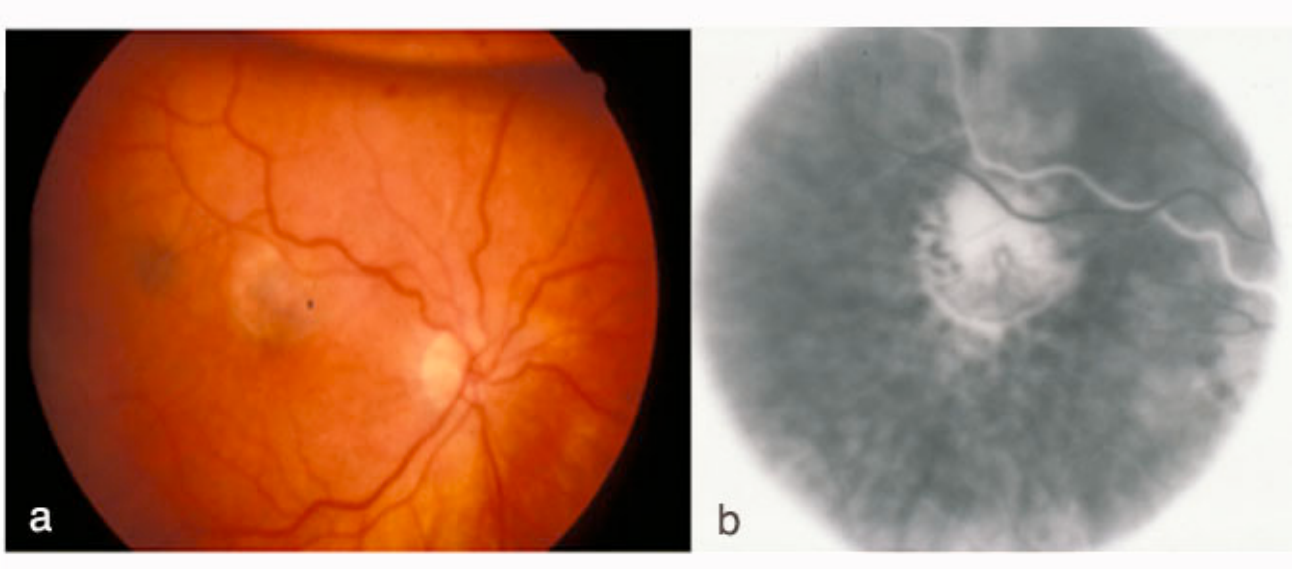

Figure 27. a) 4 day post-operative appearance after limited macular translocation (note air-bubble still present in the eye and superotemporal arcade has been displaced more superiorly than preoperatively). b) 4 day post-operative angiogram demonstrating previously subfoveal CNVM has been displaced superior to the fovea. (photos from KMG files).

Figure 28. Color photo 4 months after macular translocation and subsequent laser of CNVM. Vision improved from 20/80 preoperatively to 20/40. Unfortunately the CNVM recurred subfoveally with a chorioretinal anastamosis by 9 months post-operatively (photo from KMG files).

Figure 29. Color photo of subfoveal CNVM adjacent to an area of geographic atrophy .

treatment of AMD? In the near term, a more comprehensive understanding of the genetic basis of AMD should rapidly emerge. It will not be surprising, for example, if genetic polymorphisms in additional complement components, complement regulators and, possibly, immune system effectors and inflammatory mediators are implicated in AMD. Secondly, it may be anticipated that the gene variants linked to AMD also contribute to other prevalent age-related diseases where chronic, local inflammatory processes are involved. For example, a significant statistical relationship between the CFH Tyr402His "risk" variant and the incidence of myocardial infarction has recently been reported (243, 245, 246). Based upon this new genetic information, it will be possible to devise genetic screening tests that will identify those individuals who are most at risk of developing AMD later in life. This will enable clinicians to monitor susceptible individuals from an early age, and to develop and test new preventive treatments in the early stages of the disease. Finally, the development of new diagnostic and pharmacological approaches will be hastened by the identification of the alternative pathway of complement as a prime therapeutic target. As our understanding of the pathogenesis of AMD continues to improve, so does the prospects for new diagnostic and therapeutic approaches. Hopefully, we will eventually eradicate AMD and dramatically improve the quality of life in our older generation.

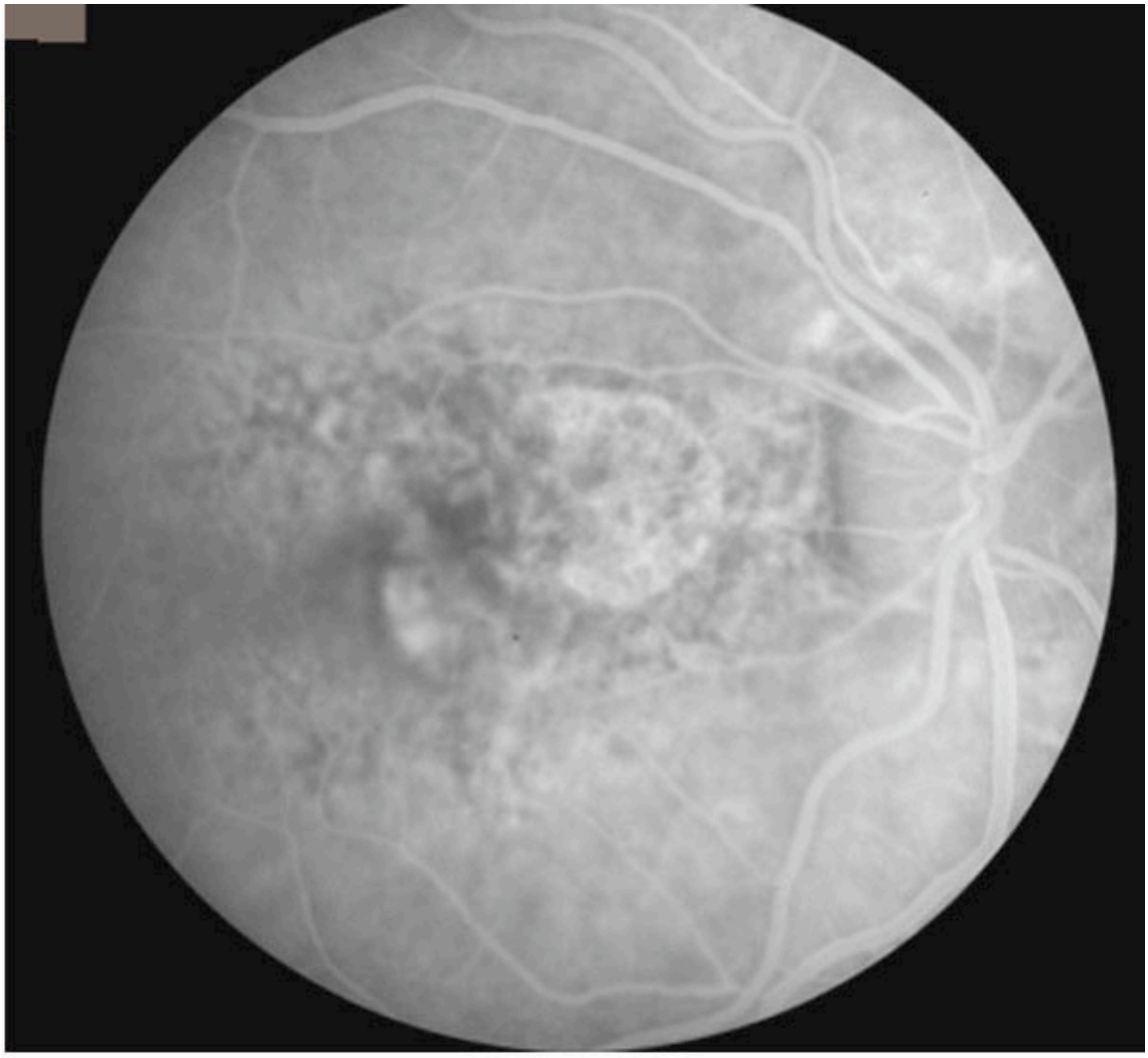

Figure 30. Angiogram demonstrating predominately classic subfoveal CNVM adjacent to an area of geographic atrophy.

The Author

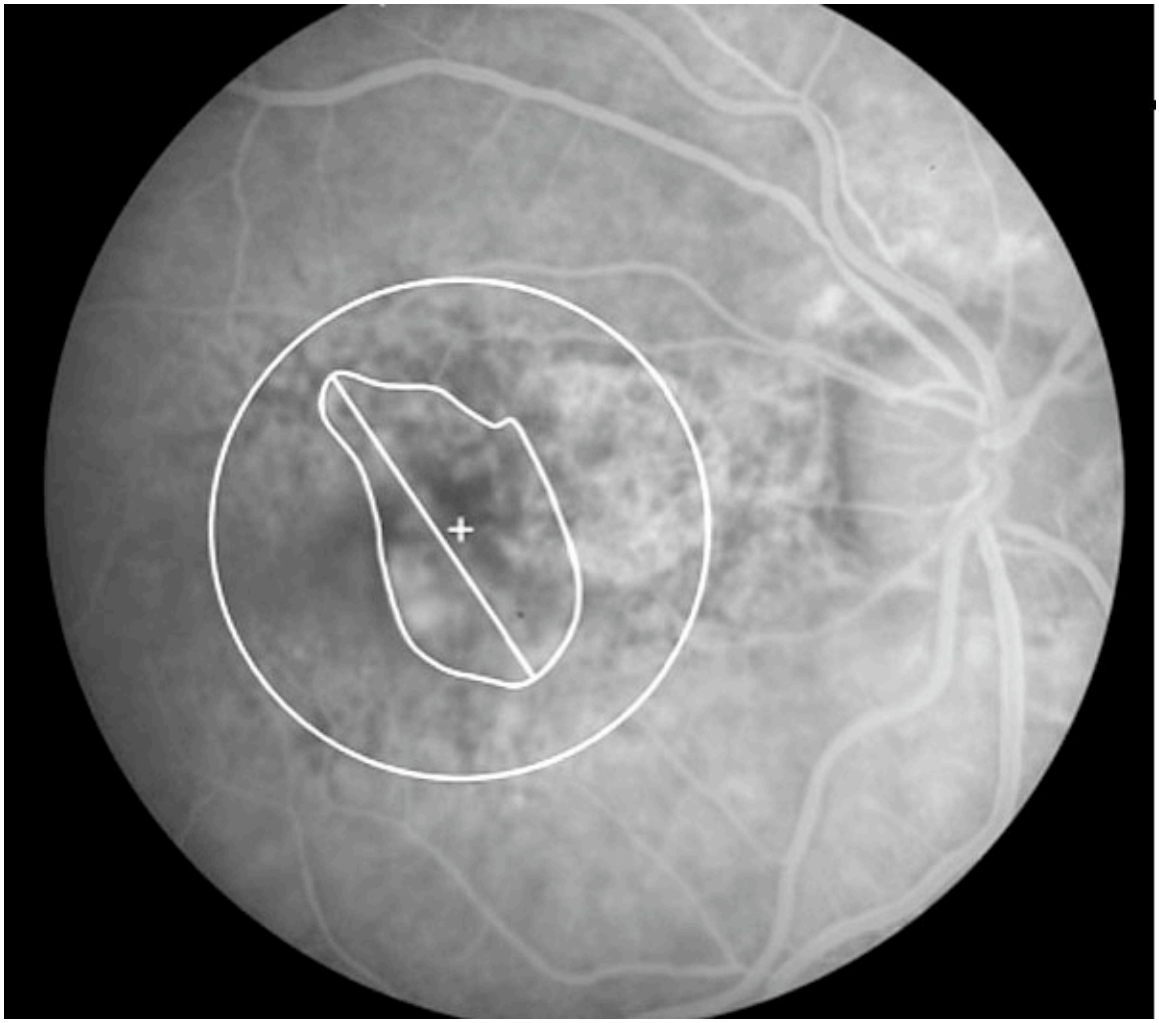

Figure 31. Late phase angiogram of predominately classic subfoveal CNVM with superimposed greatest linear diameter (GLD) and PDT treatment guide.

Gregory S. Hageman, Ph.D., is a John A. Moran Presidential Professor of Ophthalmology and Visual Sciences, and Director of the Moran Center for Translational Medicine at the University of Utah. He is a graduate of the University of Southern California, where he conducted both his undergraduate and graduate studies in biology and marine biology. Most of his previous research career was at the Iowa Carver College of Medicine and his primary research interests have always been assessment of pathways involved in the etiology of age-related macular degeneration (AMD). Dr. Hageman is an active member of various professional and honorary organizations including the Macula Society and has also served on a number of national and international advisory boards, service panels and review committee. Moreover, he serves or has served as an advisor to Genentech, Alcon, Pfizer, OccuLogix, Novartis, Tanox and American Home Products. Dr. Hageman is an author or co-author of more than 100 refereed and invited publications, as well as multiple issued patents and pending patent applications. He was recently invited to present his research findings to Congress. He received the Trustee Award from Foundation Fighting Blindness, the Roger Johnson Prize for Macular Degeneration.

Figure 32. Post-PDT treatment for subfoveal CNVM without evidence of recurrence or significant and retention of good vision at 3 months after the last PDT treatment.

Figure 33. Example of an eye which developed disciform scarring after PDT (photo from KMG files).

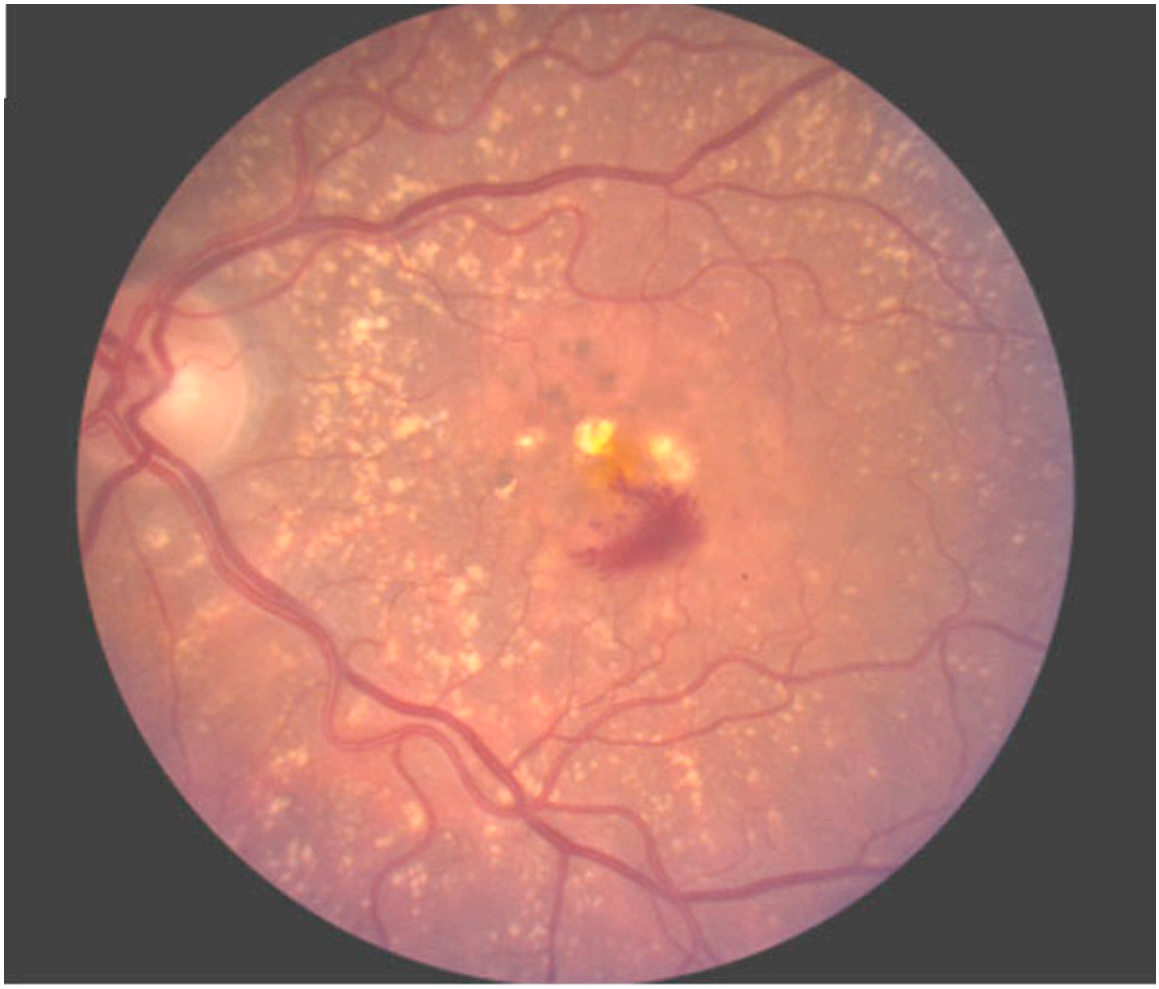

Figure 34. Color photo of subfoveal CNVM and hemorrhage due to AMD (photo from KMG files).

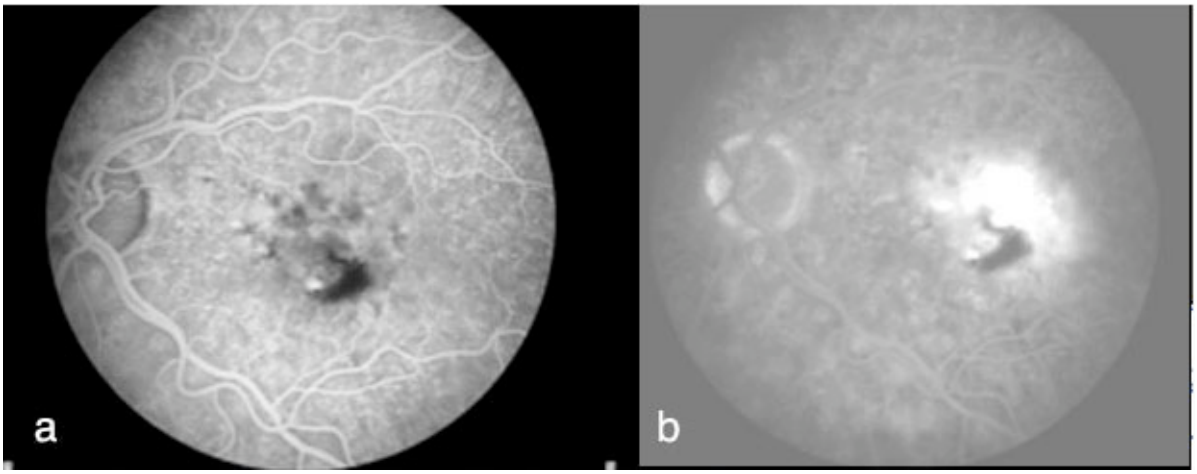

Figure 35. Above: Early and late phase angiogram of subfoveal, predominately occult CNVM due to AMD (photo from KMG files).

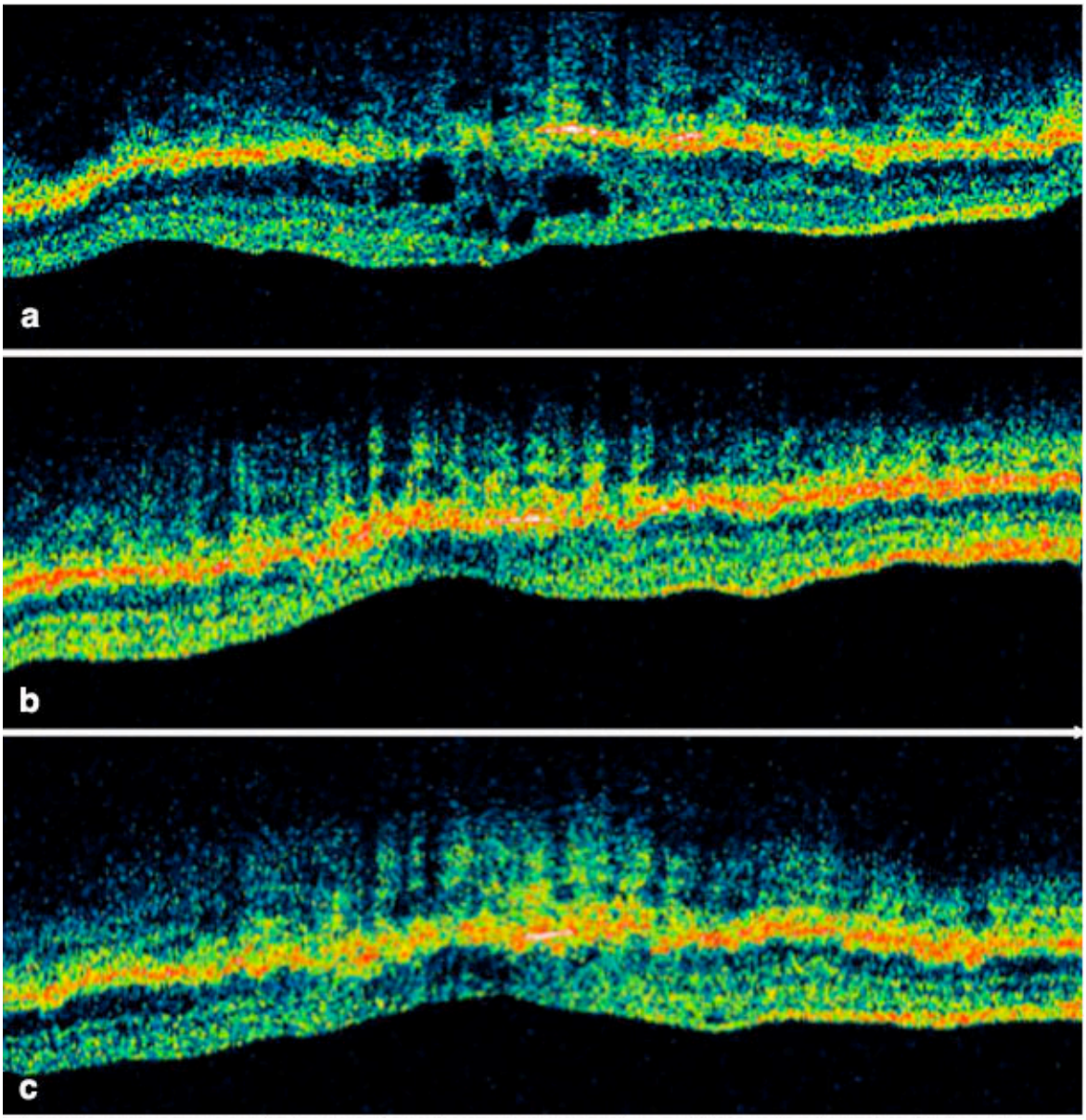

Figure 36. a) Horizontal OCT scan throught the foveal region of subfoveal CNV seen in the photos above before anti-VEGF therapy. b) Horizontal OCT scan throught the fovea after multiple injections with anti-VEGF therapy (both bevicizumab and ranibizumab). c) : Horizontal OCT scan through the fovea 6 months after the last anti-VEGF therapy injection without recurrence of subretinal or intraretinal fluid and visual acuity maintained at the 20/25 level.

References

1. Uhlmann RF, Larson EB, Koepsell TD, Rees TS, Duckert LG. Visual impairment and cognitive dysfunction in Alzheimer's disease. J Gen Intern Med. 1991;6(2):126–32. PubMed. PubMed PMID: 2023019.
2. Lin MY, Gutierrez PR, Stone KL, Yaffe K, Ensrud KE, Fink HA, et al. Vision impairment and combined vision and hearing impairment predict cognitive and functional decline in older women. J Am Geriatr Soc. 2004;52(12):1996–2002. PubMed. PubMed PMID: 15571533.
3. Rovner BW, Casten RJ, Tasman WS. Effect of depression on vision function in age-related macular degeneration. Arch Ophthalmol. 2002;120(8):1041–4. PubMed. PubMed PMID: 12149057.
4. Abyad A. In-office screening for age-related hearing and vision loss. Geriatrics. 1997 Jun;52(6):45-6, 51-4, 7.

5. Berman K, Brodaty H. Psychosocial effects of age-related macular degeneration. Int Psychogeriatr. 2006.:1–14. PubMed PMID: 16466594.
6. Taylor H, Guymer R, Keeffe J. The Impact of Age-Related Macular Degeneration. In: Limited AEP, editor. Melbourne: University of Melbourne; 2006. p. 1-72.
7. Sunness JS. The natural history of geographic atrophy, the advanced atrophic form of age-related macular degeneration. Mol Vis. 1999;5:25PubMed.
8. Magnitude and causes of visual impairment. 2004
9. Resnikoff S, Pascolini D, Etya'ale D, Kocur I, Pararajasegaram R, Pokharel GP, et al. Global data on visual impairment in the year 2002. Bull World Health Organ. 2004;82(11):844–51. PubMed. PubMed PMID: 15640920.
10. Klein R, Peto T, Bird A, Vannewkirk MR. The epidemiology of age-related macular degeneration. Am J Ophthalmol. 2004;137(3):486–95. PubMed. PubMed PMID: 15013873.
11. Smith W, Assink J, Klein R, Mitchell P, Klaver C, Klein B, et al. Risk factors for age-related macular degeneration: Pooled findings from three continents. Ophthalmology. 2001;108:697–704. PubMed. PubMed PMID: 11297486.
12. Mitchell P, Smith W, Attebo K, Wang J. Prevalence of age-related maculopathy in Australia. The Blue Mountains Eye Study. Ophthalmology. 1995;102:1450–60. PubMed. PubMed PMID: 9097791.
13. VanNewkirk M, Nanjan M, Wang J, Mitchell P, Taylor H, McCarty C. The prevalence of age-related maculopathy: the visual impairment project. Ophthalmology. 2000;107:1593–600. PubMed. PubMed PMID: 10919916.
14. Wolfs RC, Borger PH, Ramrattan RS, Klaver CC, Hulsman CA, Hofman A, et al. Changing views on open-angle glaucoma: definitions and prevalences--The Rotterdam Study. Invest Ophthalmol Vis Sci. 2000;41(11):3309–21. PubMed. PubMed PMID: 11006219.
15. Mitchell P, Wang JJ, Foran S, Smith W. Five-year incidence of age-related maculopathy lesions: the Blue Mountains Eye Study. Ophthalmology. 2002;109(6):1092–7. PubMed. PubMed PMID: 12045049.
16. Friedman DS, O'Colmain BJ, Munoz B, Tomany SC, McCarty C, de Jong PT, et al. Prevalence of age-related macular degeneration in the United States. Arch Ophthalmol. 2004;122(4):564–72. PubMed. PubMed PMID: 15078675.
17. Taylor HR, Keeffe JE, Vu HT, Wang JJ, Rochtchina E, Pezzullo ML, et al. Vision loss in Australia. Med J Aust. 2005;182(11):565–8. PubMed. PubMed PMID: 15938683.
18. Jonasson F, Arnarsson A, Peto T, Sasaki H, Sasaki K, Bird AC. 5-year incidence of age-related maculopathy in the Reykjavik Eye Study. Ophthalmology. 2005;112(1):132–8. PubMed. PubMed PMID: 15629833.
19. Andersen N. Age-related macular degeneration among the Inuit in Greenland. Int J Circumpolar Health. 2004;63 Suppl 2:320–3. PubMed. PubMed PMID: 15736677.
20. Vingerling JR, Dielemans I, Hofman A, Grobbee DE, Hijmering M, Kramer CF, et al. The prevalence of age-related maculopathy in the Rotterdam Study. Ophthalmology. 1995;102(2):205–10. PubMed. PubMed PMID: 7862408.
21. Krishnaiah S, Das T, Nirmalan PK, Nutheti R, Shamanna BR, Rao GN, et al. Risk factors for age-related macular degeneration: findings from the Andhra Pradesh eye disease study in South India. Invest Ophthalmol Vis Sci. 2005;46(12):4442–9. PubMed. PubMed PMID: 16303932.
22. Munoz B, Klein R, Rodriguez J, Snyder R, West SK. Prevalence of age-related macular degeneration in a population-based sample of Hispanic people in Arizona: Proyecto VER. Arch Ophthalmol. 2005;123(11):1575–80. PubMed. PubMed PMID: 16286621.
23. Leske MC, Wu SY, Hennis A, Nemesure B, Yang L, Hyman L, et al. Nine-year incidence of age-related macular degeneration in the Barbados Eye Studies. Ophthalmology. 2006;113(1):29–35. PubMed. PubMed PMID: 16290049.
24. Wong TY, Loon SC, Saw SM. The epidemiology of age related eye diseases in Asia. Br J Ophthalmol. 2006;90(4):506–11. PubMed. PubMed PMID: 16547337.
25. Klein R, Davis MD, Magli YL, Segal P, Klein BE, Hubbard L. The Wisconsin age-related maculopathy grading system. Ophthalmology. 1991;98(7):1128–34. PubMed. PubMed PMID: 1843453.

26. The Age-Related Eye Disease Study (AREDS). design implications. AREDS report no. 1. Control Clin Trials. 1999;20(6):573–600. PubMed. PubMed PMID: 10588299.
27. Davis MD, Gangnon RE, Lee LY, Hubbard LD, Klein BE, Klein R, et al. The Age-Related Eye Disease Study severity scale for age-related macular degeneration: AREDS Report No. 17. Arch Ophthalmol. 2005;123(11):1484–98. PubMed. PubMed PMID: 16286610.
28. Ferris FL, Davis MD, Clemons TE, Lee LY, Chew EY, Lindblad AS, et al. A simplified severity scale for age-related macular degeneration: AREDS Report No. 18. Arch Ophthalmol. 2005;123(11):1570–4. PubMed. PubMed PMID: 16286620.
29. Wray S, Kuwabara T, Sanderson P. Menkes' kinky hair disease: a light and electron microscopic study of the eye. Investigative Ophthalmology. 1976;15:128–38. PubMed. PubMed PMID: 1245386.
30. Abugreen S, Muldrew KA, Stevenson MR, VanLeeuwen R, DeJong PT, Chakravarthy U. CNV subtype in first eyes predicts severity of ARM in fellow eyes. Br J Ophthalmol. 2003;87(3):307–11. PubMed. PubMed PMID: 12598444.
31. Clemons TE, Milton RC, Klein R, Seddon JM, Ferris FL. Risk factors for the incidence of Advanced Age-Related Macular Degeneration in the Age-Related Eye Disease Study (AREDS) AREDS report no. 19. Ophthalmology. 2005;112(4):533–9. PubMed. PubMed PMID: 15808240.
32. Thornton J, Edwards R, Mitchell P, Harrison RA, Buchan I, Kelly SP. Smoking and age-related macular degeneration: a review of association. Eye. 2005;19(9):935–44. PubMed. PubMed PMID: 16151432.
33. A randomized, placebo-controlled, clinical trial of high-dose supplementation with vitamins C and E, beta carotene, and zinc for age-related macular degeneration and vision loss: AREDS report no. 8. Arch Ophthalmol. 2001;119(10):1417–36. PubMed. PubMed PMID: 11594942.
34. Choroidal neovascularization in the Choroidal Neovascularization Prevention Trial. The Choroidal Neovascularization Prevention Trial Research Group. Ophthalmology. 1998;105(8):1364–72. PubMed. PubMed PMID: 9709744.
35. The Complications of Age-Related Macular Degeneration Prevention Trial (CAPT): rationale, design and methodology. Clin Trials. 2004;1(1):91–107. PubMed. PubMed PMID: 16281465.
36. Friberg TR, Musch DC, Lim JI, Morse L, Freeman W, Sinclair S. Prophylactic treatment of age-related macular degeneration report number 1: 810-nanometer laser to eyes with drusen. Unilaterally eligible patients. Ophthalmology. 2006 Apr;113(4):622 e1.
37. Prenner JL, Rosenblatt BJ, Tolentino MJ, Ying GS, Javornik NB, Maguire MG, et al. Risk factors for choroidal neovascularization and vision loss in the fellow eye study of CNVPT. Retina. 2003;23(3):307–14. PubMed. PubMed PMID: 12824829.
38. Friberg T. The Prophylactic Treatment of AMD Multi-Centered Trial (PTAMD): Results From the Bilateral Study Arm. 2006
39. Argon laser photocoagulation for neovascular maculopathy. Three-year results from randomized clinical trials. Macular Photocoagulation Study Group. Arch Ophthalmol. 1986;104(5):694–701. PubMed. PubMed PMID: 2423061.
40. Krypton laser photocoagulation for neovascular lesions of age-related macular degeneration. Results of a randomized clinical trial. Macular Photocoagulation Study Group. Arch Ophthalmol. 1990;108(6):816–24. PubMed. PubMed PMID: 1693496.
41. Laser photocoagulation of subfoveal neovascular lesions in age-related macular degeneration. Results of a randomized clinical trial. Macular Photocoagulation Study Group. Arch Ophthalmol. 1991;109(9):1220–31. PubMed. PubMed PMID: 1718250.
42. Han DP, Folk JC, Bratton AR. Visual loss after successful photocoagulation of choroidal neovascularization. Ophthalmology. 1988;95(10):1380–4. PubMed. PubMed PMID: 2465519.
43. Persistent and recurrent neovascularization after krypton laser photocoagulation for neovascular lesions of age-related macular degeneration. Macular Photocoagulation Study Group. Arch Ophthalmol. 1990;108(6):825–31. PubMed. PubMed PMID: 1693497.
44. Freund KB, Yannuzzi LA, Sorenson JA. Age-related macular degeneration and choroidal neovascularization. Am J Ophthalmol. 1993;115(6):786–91. PubMed. PubMed PMID: 7685148.

45. Bressler NM, Bressler SB, Childs AL, Haller JA, Hawkins BS, Lewis H, et al. Surgery for hemorrhagic choroidal neovascular lesions of age-related macular degeneration: ophthalmic findings: SST report no. 13. Ophthalmology. 2004;111(11):1993–2006. PubMed. PubMed PMID: 15522364.
46. Hawkins BS, Bressler NM, Miskala PH, Bressler SB, Holekamp NM, Marsh MJ, et al. Surgery for subfoveal choroidal neovascularization in age-related macular degeneration: ophthalmic findings: SST report no. 11. Ophthalmology. 2004;111(11):1967–80. PubMed. PubMed PMID: 15522362.
47. Machemer R, Steinhorst UH. Retinal separation, retinotomy, and macular relocation: II. A surgical approach for age-related macular degeneration? Graefes Arch Clin Exp Ophthalmol. 1993;231(11):635–41. PubMed. PubMed PMID: 8258397.
48. de Juan E Jr, Loewenstein A, Bressler NM, Alexander J. Translocation of the retina for management of subfoveal choroidal neovascularization II: a preliminary report in humans. Am J Ophthalmol. 1998;125(5):635–46. PubMed. PubMed PMID: 9625547.
49. Photodynamic therapy of subfoveal choroidal neovascularization in age-related macular degeneration with verteporfin: one-year results of 2 randomized clinical trials--TAP report. Treatment of age-related macular degeneration with photodynamic therapy (TAP) Study Group. Arch Ophthalmol. 1999;117(10):1329–45. PubMed. PubMed PMID: 10532441.
50. Schmidt-Erfurth U, Hasan T. Mechanisms of action of photodynamic therapy with verteporfin for the treatment of age-related macular degeneration. Surv Ophthalmol. 2000;45(3):195–214. PubMed. PubMed PMID: 11094244.
51. Verteporfin therapy of subfoveal choroidal neovascularization in age-related macular degeneration: two-year results of a randomized clinical trial including lesions with occult with no classic choroidal neovascularization--verteporfin in photodynamic therapy report 2. Am J Ophthalmol. 2001;131(5):541–60. PubMed. PubMed PMID: 11336929.
52. Bressler NM, Arnold J, Benchaboune M, Blumenkranz MS, Fish GE, Gragoudas ES, et al. Verteporfin therapy of subfoveal choroidal neovascularization in patients with age-related macular degeneration: additional information regarding baseline lesion composition's impact on vision outcomes-TAP report No. 3. Arch Ophthalmol. 2002;120(11):1443–54. PubMed. PubMed PMID: 12427056.
53. Stevenson MR, Hart PM, Chakravarthy U, Mackenzie G, Bird AC, Owens SL, et al. Visual functioning and quality of life in the SubFoveal Radiotherapy Study (SFRADS): SFRADS report 2. Br J Ophthalmol. 2005;89(8):1045–51. PubMed. PubMed PMID: 16024863.
54. Goverdhan SV, Gibbs FA, Lotery AJ. Radiotherapy for age-related macular degeneration: no more pilot studies please. Eye. 2005;19(11):1137–41. PubMed. PubMed PMID: 15543181.
55. Marcus DM, Peskin E, Maguire M, Weissgold D, Alexander J, Fine S, et al. The age-related macular degeneration radiotherapy trial (AMDRT): one year results from a pilot study. Am J Ophthalmol. 2004;138(5):818–28. PubMed. PubMed PMID: 15531318.
56. Gragoudas ES, Adamis AP, Cunningham ET, Feinsod M, Guyer DR. Pegaptanib for neovascular age-related macular degeneration. N Engl J Med. 2004;351(27):2805–16. PubMed. PubMed PMID: 15625332.
57. Heir J, Shapiro H, Singh A. Randomized, Controlled Phase III Study of Ranibizumab (Lucentis) for Minimally Classic or Occult Neovascular Age-Related Macular Degeneration: Two-Year Efficacy Results of the MARINA Study. 2006
58. Rosenfeld PJ, Moshfeghi AA, Puliafito CA. Optical coherence tomography findings after an intravitreal injection of bevacizumab (avastin) for neovascular age-related macular degeneration. Ophthalmic Surg Lasers Imaging. 2005;36(4):331–5. PubMed. PubMed PMID: 16156152.
59. Avery RL, Pieramici DJ, Rabena MD, Castellarin AA, Nasir MA, Giust MJ. Intravitreal bevacizumab (Avastin) for neovascular age-related macular degeneration. Ophthalmology. 2006 Mar;113(3):363-72 e5.
60. Vinores SA. Anecortave (Alcon Laboratories). IDrugs. 2005;8(4):327–34. PubMed. PubMed PMID: 15800808.
61. D'Amico DJ, Goldberg MF, Hudson H, Jerdan JA, Krueger DS, Luna SP, et al. Anecortave acetate as monotherapy for treatment of subfoveal neovascularization in age-related macular degeneration: twelve-month clinical outcomes. Ophthalmology. 2003 Dec;110(12):2372-83; discussin 84-5.

62. Spaide RF, Sorenson J, Maranan L. Photodynamic therapy with verteporfin combined with intravitreal injection of triamcinolone acetonide for choroidal neovascularization. Ophthalmology. 2005;112(2):301–4. PubMed. PubMed PMID: 15691567.
63. Quiram PA, Gonzales CR, Schwartz SD. Severe steroid-induced glaucoma following intravitreal injection of triamcinolone acetonide. Am J Ophthalmol. 2006;141(3):580–2. PubMed. PubMed PMID: 16490518.
64. Jonas JB, Kreissig I, Spandau UH, Harder B. Infectious and noninfectious endophthalmitis after intravitreal high-dosage triamcinolone acetonide. Am J Ophthalmol. 2006;141(3):579–80. PubMed. PubMed PMID: 16490517.
65. Guymer RH, Chiu AW, Lim L, Baird PN. HMG CoA reductase inhibitors (statins): do they have a role in age-related macular degeneration? Surv Ophthalmol. 2005;50(2):194–206. PubMed. PubMed PMID: 15749309.
66. Sarks S, Arnold J, Killingsworth M, Sarks J. Early drusen formation in the normal and aging eye and their relation to age-related maculopathy: a clinicopathological study. British Journal of Ophthalmology. 1999;83:358–68. PubMed. PubMed PMID: 10365048.
67. McConnell V, Silvestri G. Age-related macular degeneration. Ulster Med J. 2005;74(2):82–92. PubMed. PubMed PMID: 16235759.
68. Provis JM, Penfold PL, Cornish EE, Sandercoe TM, Madigan MC. Anatomy and development of the macula: specialisation and the vulnerability to macular degeneration. Clin Exp Optom. 2005;88(5):269–81. PubMed. PubMed PMID: 16255686.
69. Donoso LA, Kim D, Frost A, Callahan A, Hageman G. The role of inflammation in the pathogenesis of age-related macular degeneration. Surv Ophthalmol. 2006;51(2):137–52. PubMed. PubMed PMID: 16500214.
70. Arnold J, Sarks S. Age related macular degeneration. Clin Evid. 2004;(11):819–34. PubMed. PubMed PMID: 15652038.
71. Hageman G, Mullins R.. Molecular composition of drusen as related to substructural phenotype. Molecular Vision. 1999;5:28PubMed.
72. Sarraf D, Gin T, Yu F, Brannon A, Owens SL, Bird AC. Long-term drusen study. Retina. 1999;19(6):513–9. PubMed. PubMed PMID: 10606451.
73. Klein R, Klein B, Jensen S, Meuer S. The five-year incidence and progression of age-related maculopathy: the Beaver Dam Eye Study. Ophthalmology. 1997;104:7–21. PubMed. PubMed PMID: 9022098.
74. Spraul C, Grossniklaus H. Characteristics of drusen and Bruch's membrane in postmortem eyes with age-related macular degeneration. Archives of Ophthalmology. 1997;115:267–73. PubMed. PubMed PMID: 9046265.
75. Sarks JP, Sarks SH, Killingsworth MC. Evolution of soft drusen in age-related macular degeneration. Eye. 1994;8(Pt 3)(3):269-83.
76. Guymer R, Bird A. Bruch's membrane, drusen, and age-related macular degeneration. In: Marmor M, Wolfensberger T, editors. The Retinal Pigment Epithelium. New York: Oxford University Press; 1998. p. 693-705.
77. Zarbin MA. Current concepts in the pathogenesis of age-related macular degeneration. Arch Ophthalmol. 2004;122(4):598–614. PubMed. PubMed PMID: 15078679.
78. Sivaprasad S, Bailey TA, Chong VN. Bruch's membrane and the vascular intima: is there a common basis for age-related changes and disease? Clin Experiment Ophthalmol. 2005;33(5):518–23. PubMed. PubMed PMID: 16181282.
79. Marshall J, Hussain A, Starita C, Moore D, Patmore A. The Retinal Pigment Epithelium. New York: Oxford University Press; 1998
80. Guymer R, Luthert P, Bird A. Changes in Bruch's membrane and related structures with age. Progress in Retinal & Eye Research. 1999;18(1):59–90. PubMed PMID: 9920499.
81. Hogan M, Alvarado J. Studies on the human macula. Aging changes in Bruch's membrane. Archives of Ophthalmology. 1967;77:410–20. PubMed. PubMed PMID: 6019564.
82. Sarks SH. Ageing and degeneration in the macular region: a clinico-pathological study. British Journal of Ophthalmology. 1976;60(5):324–41. PubMed. PubMed PMID: 952802.

83. Green WR, McDonnell PJ, Yeo JH. Pathologic features of senile macular degeneration. Ophthalmology. 1985;92(5):615–27. PubMed. PubMed PMID: 2409504.
84. Feeney-Burns L, Ellersieck M. Age-related changes in the ultrastructure of Bruch's membrane. American Journal of Ophthalmology. 1985;100:686–97. PubMed. PubMed PMID: 4061550.
85. Grindle C, Marshall J. Ageing changes in Bruch's membrane and their functional implications. Trans Ophthal Soc UK. 1978;98:172–5. PubMed. PubMed PMID: 285503.
86. Pauleikhoff D, Sheraidah G, Marshall J, Bird A, Wessing A. Biochemical and histochemical analysis of age related lipid deposits in Bruch's membrane. Ophthalmologe. 1994;91(6):730–4. PubMed. PubMed PMID: 7849423.
87. Handa JT, Verzijl N, Matsunaga H, Aotaki-Keen A, Lutty GA, te Koppele JM, et al. Increase in the advanced glycation end product pentosidine in Bruch's membrane with age. Investigative Ophthalmology and Visual Science. 1999;40(3):775–9. PubMed. PubMed PMID: 10067983.
88. Curcio C, Millican C, Bailey T, Kruth H. Accumulation of cholesterol with age in human Bruch's membrane. Investigative Ophthalmology & Visual Science. 2001;42:265–74. PubMed. PubMed PMID: 11133878.
89. Kamei M, Hollyfield J. TIMP-3 in Bruch's membrane: changes during aging and in age-related macular degeneration. Invest Ophthalmol Vis Sci. 1999;40:2367–75. PubMed. PubMed PMID: 10476804.
90. Newsome D, Huh W, Green W. Bruch's membrane age-related changes vary by region. Current Eye Research. 1987;6:1211–21. PubMed. PubMed PMID: 3677781.
91. Ishibashi T, Murata T, Hangai M, Nagai R, Horiuchi S, Lopez P, et al. Advanced glycation end products in age-related macular degeneration. Arch Ophthalmol. 1998;116:1629–32. PubMed. PubMed PMID: 9869793.
92. Hewitt A, Nakazawa K, Newsome D. Analysis of newly synthesized Bruch's membrane proteoglycans. Investigative Ophthalmology and Visual Science. 1989;30:478–86. PubMed. PubMed PMID: 2925318.
93. Karwatowski W, Jeffries T, Duance V, Albon J, Bailey A, Easty D. Preparation of Bruch's membrane and analysis of the age-related changes in the structural collagens. Br J Ophthalmol. 1995;79(10):944–52. PubMed. PubMed PMID: 7488585.
94. Haimovici R, Gantz DL, Rumelt S, Freddo TF, Small DM. The lipid composition of drusen, Bruch's membrane, and sclera by hot stage polarizing light microscopy. Invest Ophthalmol Vis Sci. 2001;42(7):1592–9. PubMed. PubMed PMID: 11381066.
95. Li CM, Chung BH, Presley JB, Malek G, Zhang X, Dashti N, et al. Lipoprotein-like particles and cholesteryl esters in human Bruch's membrane: initial characterization. Invest Ophthalmol Vis Sci. 2005;46(7):2576–86. PubMed. PubMed PMID: 15980251.
96. Starita C, Hussain A, Pagliarini S, Marshall J. Hydrodynamics of ageing Bruch's membrane: implications for macular disease. Experimental Eye Research. 1996;62:565–72. PubMed. PubMed PMID: 8759524.
97. Moore D, Clover G. The effect of age on the macromolecuar permeability of human Bruch's membrane. Invest Ophthalmol Vis Sci. 2001;42:2970–5. PubMed. PubMed PMID: 11687544.
98. Hussain A, Rowe L, Marshall J. Age-related alterations in the diffusional transport of amino acids across the human Bruch's-choroid complex. Journal of the Optical Society of America. 2002;19:166–72. PubMed. PubMed PMID: 11778720.
99. Moore D, Hussain A, Marshall J. Age-related variation in the hydraulic conductivity of Bruch's membrane. Invest Ophthalmol Vis Sci. 1995;36:1290–7. PubMed. PubMed PMID: 7775106.
100. Chong NH, Keonin J, Luthert PJ, Frennesson CI, Weingeist DM, Wolf RL, et al. Decreased thickness and integrity of the macular elastic layer of Bruch's membrane correspond to the distribution of lesions associated with age-related macular degeneration. Am J Pathol. 2005;166(1):241–51. PubMed. PubMed PMID: 15632016.
101. Nackman G, Karkowski F, Halpern V, Gaetz H, Tilson M. Elastin degradation products induce adventitial angiogenesis in the Anidjar/Dobrin rat aneurysm model. Surgery. 1997;122:39–44. PubMed. PubMed PMID: 9225913.

103. Marshall J, Hussain A, Starita C, Moore D, Patmore A. Aging and Bruch's membrane. In: Marmor M, Wolfensberger T, editors. The Retinal Pigment Epithelium. New York: Oxford University Press; 1998. p. 669-92.
104. Holz F, Sheraiadah G, Pauleikhoff D, Marshall J, Bird A. Analysis of lipid deposits extracted from human macular and peripheral Bruch's membrane. Archives of Ophthalmology. 1994;112:402–6. PubMed. PubMed PMID: 8129668.
105. Pauleikhoff D, Harper C, Marshall J, Bird A. Aging changes in Bruch's membrane. Ophthalmology. 1990;97:171–8. PubMed. PubMed PMID: 1691475.
106. Anderson D, Ozaki S, Nealon M, Neitz J, Mullins R, Hageman G, et al. Local cellular sources of apolipoprotein E in the human retina and retinal pigmented epithelium: Implications for the process of drusen formation. American J Ophthalmol. 2001;131:767–81. PubMed PMID: 11384575.
107. Farkas T, Sylvester V, Archer D, Altona M. The histochemistry of drusen. American Journal of Ophthalmology. 1971;71:1206–15. PubMed. PubMed PMID: 4253686.
108. Green W, Enger C. Age-related macular degeneration histopathologic studies. Ophthalmology. 1993;100:1519–35. PubMed. PubMed PMID: 7692366.
109. Kliffen M, van der Schaft TL, Mooy CM, de Jong PT. Morphologic changes in age-related maculopathy. Microscopy Research & Technique. 1997;36(2):106–22. PubMed PMID: 9015257.
110. Feher J, Valu L. Albrecht Von Graefes Arch Klin Exp Ophthalmol. 1967;173(2):162–7. PubMed. PubMed PMID: 4172029.
111. Green WR, Enger C. Age-related macular degeneration histopathologic studies. The 1992 Lorenz E. Zimmerman Lecture. Ophthalmology. 1993;100(10):1519–35. PubMed. PubMed PMID: 7692366.
112. Loffler KU, Lee WR. Basal linear deposit in the human macula. Graefes Arch Clin Exp Ophthalmol. 1986;224(6):493–501. PubMed. PubMed PMID: 3792844.
113. van der Schaft TL, de Bruijn WC, Mooy CM, Ketelaars DA, de Jong PT. Is basal laminar deposit unique for age-related macular degeneration? Archives of Ophthalmology. 1991;109(3):420–5. PubMed. PubMed PMID: 2003806.
114. van der Schaft T, Mooy C, de Bruijn W, Oron F, Mulder P, de Jong P. Histological features of age-related macular degeneration. A statistical analysis. Ophthalmology. 1992;99:278–86. PubMed. PubMed PMID: 1553220.
115. Spraul CW, Lang GE, Grossniklaus HE. Morphometric analysis of the choroid, Bruch's membrane, and retinal pigment epithelium in eyes with age-related macular degeneration. Invest Ophthalmol Vis Sci. 1996;37(13):2724–35. PubMed. PubMed PMID: 8977488.
116. Milam AH, Curcio CA, Cideciyan AV, Saxena S, John SK, Kruth HS, et al. Dominant late-onset retinal degeneration with regional variation of sub-retinal pigment epithelium deposits, retinal function, and photoreceptor degeneration. Ophthalmology. 2000;107(12):2256–66. PubMed. PubMed PMID: 11097607.
117. Kliffen M, Mooy CM, Luider TM, Huijmans JG, Kerkvliet S, de Jong PT. Identification of glycosaminoglycans in age-related macular deposits. Archives of Ophthalmology. 1996;114(8):1009–14. PubMed. PubMed PMID: 8694708.
118. Kliffen M, Mooy CM, Luider TM, de Jong PT. Analysis of carbohydrate structures in basal laminar deposit in aging human maculae. Investigative Ophthalmology and Visual Science. 1994;35(7):2901–5. PubMed. PubMed PMID: 8206707.
119. van der Schaft T, Mooy C, de Bruijn W, Bosman F, de Jong P. Immunohistochemical light and electron microscopy of basal laminar deposit. Graefe's Archives for Clinical and Experimental Ophthalmology. 1994;232:40–6. PubMed PMID: 8119600.
120. Knupp C, Amin S, Munro P, Luthert P, Squire J. Collagen VI assemblies in age-related macular degeneration. J Struct Biol. 2002;139:181–9. PubMed. PubMed PMID: 12457848.
121. Curcio CA, Presley JB, Millican CL, Medeiros NE. Basal deposits and drusen in eyes with age-related maculopathy: evidence for solid lipid particles. Exp Eye Res. 2005;80(6):761–75. PubMed. PubMed PMID: 15939032.

122. Sarks S, Van Driel D, Maxwell L, Killingsworth M. Softening of drusen and subretinal neovascularization. Transactions of the Ophthalmological Society of the United Kingdom. 1980;100:414–22. PubMed PMID: 6171074.
123. Okubo A, Rosa R, Bunce C, Alexander R, Fan J, Bird A, et al. Relationship of age changes in retinal pigment epithelium and Bruch's membrane. IOVS. 1999;40:443–9. PubMed PMID: 9950604.
124. Hogan M. Role of the retinal pigment epithelium in macular disease. Transactions of the American Academy of Ophthalmology and Otolaryngology. 1972;76:64–80. PubMed PMID: 5024602.
125. Bird A. Pathophysiology of AMD. In: Hampton G, PT N, editors. Age-related macular degeneration: principles and practice. New York: Raven Press; 1992. p. chap. 3.
126. Dorey C, Wu G, Ebenstein D. Cell loss in the aging retina: Relationship to lipofuscin accumulation and macular degeneration. IOVS. 1989;30:1691–9. PubMed PMID: 2759786.
127. Bird AC. Bruch's membrane change with age. Br J Ophthalmol. 1992;76(3):166–8. PubMed. PubMed PMID: 1540562.
128. Katz ML, Robison WG. Age-related changes in the retinal pigment epithelium of pigmented rats. Exp Eye Res. 1984;38(2):137–51. PubMed. PubMed PMID: 6714331.
129. Feeney-Burns L, Hilderbrand E, Eldridge S. Aging human RPE: morphometric analysis of macular, equatorial and peripheral cells. IOVS. 1984;25:195–200. PubMed PMID: 6698741.
130. Wing G, Blanchard G, Weiter J. Topography and age relationship of lipofuscin concentration in the RPE. IOVS. 1978;7:601–7.
131. Rozanowska M, Jarvis-Evans J, Korytowski W, Boulton ME, Burke JM, Sarna T. Blue light-induced reactivity of retinal age pigment. In vitro generation of oxygen-reactive species. J Biol Chem. 1995;270(32):18825–30. PubMed. PubMed PMID: 7642534.
132. Holz F, Bellman C, Staudt S, Schutt F, Volcker H. Fundus autofluorescence and development of geographic atrophy in age-related macular degeneration. Invest Ophthalmol Vis Sci. 2001;42:1051–6. PubMed. PubMed PMID: 11274085.
133. Katz ML. Potential role of retinal pigment epithelial lipofuscin accumulation in age-related macular degeneration. Arch Gerontol Geriatr. 2002;34(3):359–70. PubMed. PubMed PMID: 14764336.
134. Sparrow JR, Boulton M. RPE lipofuscin and its role in retinal pathobiology. Exp Eye Res. 2005;80(5):595–606. PubMed. PubMed PMID: 15862166.
135. Ramrattan R, van der Schaft T, Mooy C, de Bruijn W, Mulder P, de Jong P. Morphometric analysis of Bruch's membrane, the choriocapillaris, and the choroid in aging. Investigative Ophthalmology & Visual Science. 1994;35:2857–64. PubMed. PubMed PMID: 8188481.
136. McLeod DS, Taomoto M, Otsuji T, Green WR, Sunness JS, Lutty GA. Quantifying changes in RPE and choroidal vasculature in eyes with age-related macular degeneration. Invest Ophthalmol Vis Sci. 2002;43(6):1986–93. PubMed. PubMed PMID: 12037009.
137. Midena E, Segato T, Blarzino MC, Degli Angeli C. Macular drusen and the sensitivity of the central visual field. Documenta Ophthalmologica. 1994;88(2):179–85. PubMed. PubMed PMID: 7781486.
138. Curcio C, Medeiros N, Millican C. Photoreceptor loss in age-related macular degeneration. Investigative Ophthalmology & Visual Science. 1996;37:1236–49. PubMed. PubMed PMID: 8641827.
139. Jackson GR, Owsley C. Visual dysfunction, neurodegenerative diseases, and aging. Neurol Clin. 2003;21(3):709–28. PubMed. PubMed PMID: 13677819.
140. Li J, Tso MO, Lam TT. Reduced amplitude and delayed latency in foveal response of multifocal electroretinogram in early age related macular degeneration. Br J Ophthalmol. 2001;85(3):287–90. PubMed. PubMed PMID: 11222332.
141. Owsley C, Jackson GR, Cideciyan AV, Huang Y, Fine SL, Ho AC, et al. Psychophysical evidence for rod vulnerability in age-related macular degeneration. Invest Ophthalmol Vis Sci. 2000;41(1):267–73. PubMed. PubMed PMID: 10634630.
142. Jackson GR, Owsley C, Curcio CA. Photoreceptor degeneration and dysfunction in aging and age-related maculopathy. Ageing Res Rev. 2002;1(3):381–96. PubMed. PubMed PMID: 12067593.

143. Owsley C, Jackson GR, White M, Feist R, Edwards D. Delays in rod-mediated dark adaptation in early age-related maculopathy. Ophthalmology. 2001;108(7):1196–202. PubMed. PubMed PMID: 11425675.
144. Jackson GR, McGwin G, Phillips JM, Klein R, Owsley C. Impact of aging and age-related maculopathy on activation of the a-wave of the rod-mediated electroretinogram. Invest Ophthalmol Vis Sci. 2004;45(9):3271–8. PubMed. PubMed PMID: 15326151.
145. Owsley C, McGwin G, Jackson GR, Heimburger DC, Piyathilake CJ, Klein R, et al. Effect of short-term, high-dose retinol on dark adaptation in aging and early age-related maculopathy. Invest Ophthalmol Vis Sci. 2006;47(4):1310–8. PubMed. PubMed PMID: 16565362.
146. Stangos N, Voutas S, Topouzis F, Karampatakis V. Contrast sensitivity evaluation in eyes predisposed to age-related macular degeneration and presenting normal visual acuity. Ophthalmologica. 1995;209:194–8. PubMed. PubMed PMID: 8545092.
147. Sunness J, Massof R, Johnson M, Bressler N, Bressler S, Fine S. Diminished foveal sensitivity may predict the development of advanced age-related macular degeneration. Ophthalmology. 1989;96:375–81. PubMed. PubMed PMID: 2710529.
148. Kleiner RC, Enger C, Alexander MF, Fine SL. Contrast sensitivity in age-related macular degeneration. Arch Ophthalmol. 1988;106(1):55–7. PubMed. PubMed PMID: 3337707.
149. Sandberg MA, Gaudio AR. Slow photostress recovery and disease severity in age-related macular degeneration. Retina. 1995;15(5):407–12. PubMed. PubMed PMID: 8594633.
150. Eisner A, Klein ML, Zilis JD, Watkins MD. Visual function and the subsequent development of exudative age-related macular degeneration. Invest Ophthalmol Vis Sci. 1992;33(11):3091–102. PubMed. PubMed PMID: 1399412.
151. Eisner A, Stoumbos VD, Klein ML, Fleming SA. Relations between fundus appearance and function. Eyes whose fellow eye has exudative age-related macular degeneration. Invest Ophthalmol Vis Sci. 1991;32(1):8–20. PubMed. PubMed PMID: 1987108.
152. Johnson PT, Brown MN, Pulliam BC, Anderson DH, Johnson LV. Synaptic pathology, altered gene expression, and degeneration in photoreceptors impacted by drusen. Invest Ophthalmol Vis Sci. 2005;46(12):4788–95. PubMed. PubMed PMID: 16303980.
153. Johnson PT, Lewis GP, Talaga KC, Brown MN, Kappel PJ, Fisher SK, et al. Drusen-associated degeneration in the retina. Invest Ophthalmol Vis Sci. 2003;44(10):4481–8. PubMed. PubMed PMID: 14507896.
154. Hageman GS, Luthert PJ, Victor Chong NH, Johnson LV, Anderson DH, Mullins RF. An integrated hypothesis that considers drusen as biomarkers of immune- mediated processes at the rpe-bruch's membrane interface in aging and age-related macular degeneration. Prog Retin Eye Res. 2001;20(6):705–32. PubMed. PubMed PMID: 11587915.
155. Anderson D, Mullins R, Hageman G. LV J. A role for local inflammation in the formation of drusen in the aging eye. Am J Ophthalmol. 2002;134:411–31. PubMed. PubMed PMID: 12208254.
156. Killingsworth M, Sarks J, Sarks S. Macrophages related to Bruch's membrane in age-related macular degeneration. Eye. 1990;4:613–21. PubMed. PubMed PMID: 2226993.
157. Penfold PL, Madigan MC, Gillies MC, Provis JM. Immunological and Aetiological Aspects of Macular Degeneration. Progress in Retinal Research. London: Elsevier Science Ltd; 2001. p. 385-414.
158. Heriot W, Henkind P, Bellhorn R, Burns M. Choroidal neovascularization can digest Bruch's membrane. A prior break is not essential. Ophthalmology. 1984;91(12):1603–8. PubMed. PubMed PMID: 6084226.
159. Penfold P, Killingsworth M, Sarks S. An ultrastructural study of the role of leucocytes and fibroblasts in the breakdown of Bruch's membrane. Australian Journal of Ophthalmology. 1984;12:23–31. PubMed. PubMed PMID: 6732655.
160. Dastgheib K, Green W. Granulomatous reaction to Bruch's membrane in age-related macular degeneration. Archives of Ophthalmology. 1994;112:813–8. PubMed. PubMed PMID: 7516148.
161. Hageman G, Mullins R, Russell S, Johnson L, Anderson D. Vitronectin is a constituent of ocular drusen and the vitronectin gene is expressed in human retinal pigmented epithelial cells. FASEB Journal. 1999;13(3):477–84. PubMed. PubMed PMID: 10064614.

162. Mullins RF, Russell SR, Anderson DH, Hageman GS. Drusen associated with aging and age-related macular degeneration contain proteins common to extracellular deposits associated with atherosclerosis, elastosis, amyloidosis, and dense deposit disease. Faseb J. 2000;14(7):835–46. PubMed. PubMed PMID: 10783137.
163. Johnson L, Ozaki S, Staples M, Erickson P, Anderson D. A potential role for immune complex pathogenesis in drusen formation. Exp Eye Res. 2000;70:441–9. PubMed. PubMed PMID: 10865992.
164. Johnson L, Leitner W, Staples M, Anderson D. Complement activation and inflammatory processes in drusen formation and age related macular degeneration. Exp Eye Res. 2001;73:887–96. PubMed. PubMed PMID: 11846519.
165. Mullins RF, Johnson LV, Anderson DH, Hageman GS. Characterization of drusen-associated glycoconjugates. Ophthalmology. 1997;104(2):288–94. PubMed. PubMed PMID: 9052634.
166. Russell SR, Mullins RF, Schneider BL, Hageman GS. Location, substructure, and composition of basal laminar drusen compared with drusen associated with aging and age-related macular degeneration. Am J Ophthalmol. 2000;129(2):205–14. PubMed. PubMed PMID: 10682974.
167. Mullins RF, Aptsiauri N, Hageman GS. Structure and composition of drusen associated with glomerulonephritis: implications for the role of complement activation in drusen biogenesis. Eye. 2001;15(Pt 3):390–5. PubMed. PubMed PMID: 11450763.
168. Johnson LV, Leitner WP, Rivest AJ, Staples MK, Radeke MJ, Anderson DH. The Alzheimer's A beta -peptide is deposited at sites of complement activation in pathologic deposits associated with aging and age-related macular degeneration. Proc Natl Acad Sci U S A. 2002;99(18):11830–5. PubMed. PubMed PMID: 12189211.
169. Malek G, Li CM, Guidry C, Medeiros NE, Curcio CA. Apolipoprotein B in cholesterol-containing drusen and basal deposits of human eyes with age-related maculopathy. Am J Pathol. 2003;162(2):413–25. PubMed. PubMed PMID: 12547700.
170. Anderson D, Talaga K, Rivest A, Barron E, Hageman G, Johnson L. Characterization of beta amyloid assemblies in drusen: the deposits associated with aging and age-related macular degeneration. Exp Eye Res. 2004;78:243–56. PubMed. PubMed PMID: 14729357.
171. Peto T, Lengyel I, Frederickson C, Vankuijk F. Zinc in Drusen. ARVO Abstract. 2005 May 3, 2005
190. Rodriguez de Cordoba S, Esparza-Gordillo J, Goicoechea de Jorge E, Lopez-Trascasa M, Sanchez-Corral P. The human complement factor H: functional roles, genetic variations and disease associations. Mol Immunol. 2004;41(4):355–67. PubMed. PubMed PMID: 15163532.
191. Pangburn MK, Pangburn KL, Koistinen V, Meri S, Sharma AK. Molecular mechanisms of target recognition in an innate immune system: interactions among factor H, C3b, and target in the alternative pathway of human complement. J Immunol. 2000;164(9):4742–51. PubMed. PubMed PMID: 10779780.
192. Zipfel PF. Complement factor H: physiology and pathophysiology. Semin Thromb Hemost. 2001;27(3):191–9. PubMed. PubMed PMID: 11446652.
193. Hageman GS, Anderson DH, Johnson LV, Hancox LS, Taiber AJ, Hardisty LI, et al. A common haplotype in the complement regulatory gene factor H (HF1/CFH) predisposes individuals to age-related macular degeneration. Proc Natl Acad Sci U S A. 2005;102(20):7227–32. PubMed. PubMed PMID: 15870199.
194. Johnson LV, Talaga KC, Rivest AJ, Staples MK, Radeke MJ, Barron E, et al. Characterization of Beta Amyloid-Containing Vesicles within Drusen. ARVO Abstract. 2003
195. Hageman G, Luthert P, Chong N, Johnson L, Anderson D, Mullins R. An integrated hypothesis that considers drusen as biomarkers of immune-mediated processes at the RPE-Bruch's membrane interface in aging and age-related macular degeneration. Prog Retin Eye Res. 2001;20:705–32. PubMed. PubMed PMID: 11587915.
196. Miller DM, Espinosa-Heidmann DG, Legra J, Dubovy SR, Suner IJ, Sedmak DD, et al. The association of prior cytomegalovirus infection with neovascular age-related macular degeneration. Am J Ophthalmol. 2004;138(3):323–8. PubMed. PubMed PMID: 15364212.
197. Klein M, Mauldin W, Stoumbos V. Heredity and age-related macular degeneration. Observations in monozygotic twins. Archives of Ophthalmology. 1994;112(7):932–7. PubMed. PubMed PMID: 8031273.

198. Heiba I, Elston R, Klein B, Klein R. Sibling correlations and segregation analysis of age-related maculopathy: the Beaver Dam Eye Study. Genetic Epidemiology. 1994;11:51–67. PubMed. PubMed PMID: 8013888.
199. Seddon J, Ajani U, Mitchell B. Familial aggregation of age-related maculopathy. American Journal of Ophthalmology. 1997;123:199–206. PubMed. PubMed PMID: 9186125.
200. Meyers SM, Greene T, Gutman FA. A twin study of age-related macular degeneration. Am J Ophthalmol. 1995;120(6):757–66. PubMed. PubMed PMID: 8540549.
201. Hammond CJ, Webster AR, Snieder H, Bird AC, Gilbert CE, Spector TD. Genetic influence on early age-related maculopathy: a twin study. Ophthalmology. 2002;109(4):730–6. PubMed. PubMed PMID: 11927430.
202. Abecasis GR, Yashar BM, Zhao Y, Ghiasvand NM, Zareparsi S, Branham KE, et al. Age-related macular degeneration: a high-resolution genome scan for susceptibility loci in a population enriched for late-stage disease. Am J Hum Genet. 2004;74(3):482–94. PubMed. PubMed PMID: 14968411.
203. Iyengar SK, Song D, Klein BE, Klein R, Schick JH, Humphrey J, et al. Dissection of genomewide-scan data in extended families reveals a major locus and oligogenic susceptibility for age-related macular degeneration. Am J Hum Genet. 2004;74(1):20–39. PubMed. PubMed PMID: 14691731.
204. Klein ML, Schultz DW, Edwards A, Matise TC, Rust K, Berselli CB, et al. Age-related macular degeneration. Clinical features in a large family and linkage to chromosome 1q. Archives of Ophthalmology. 1998;116(8):1082–8. PubMed. PubMed PMID: 9715689.
205. Majewski J, Schultz DW, Weleber RG, Schain MB, Edwards AO, Matise TC, et al. Age-related macular degeneration--a genome scan in extended families. Am J Hum Genet. 2003;73(3):540–50. PubMed. PubMed PMID: 12900797.
206. Schick JH, Iyengar SK, Klein BE, Klein R, Reading K, Liptak R, et al. A whole-genome screen of a quantitative trait of age-related maculopathy in sibships from the Beaver Dam Eye Study. Am J Hum Genet. 2003;72(6):1412–24. PubMed. PubMed PMID: 12717633.
207. Seddon JM, Santangelo SL, Book K, Chong S, Cote J. A genomewide scan for age-related macular degeneration provides evidence for linkage to several chromosomal regions. Am J Hum Genet. 2003;73(4):780–90. PubMed. PubMed PMID: 12945014.
208. Weeks DE, Conley YP, Mah TS, Paul TO, Morse L, Ngo-Chang J, et al. A full genome scan for age-related maculopathy. Hum Mol Genet. 2000;9(9):1329–49. PubMed. PubMed PMID: 10814715.
209. Weeks DE, Conley YP, Tsai HJ, Mah TS, Rosenfeld PJ, Paul TO, et al. Age-related maculopathy: an expanded genome-wide scan with evidence of susceptibility loci within the 1q31 and 17q25 regions. Am J Ophthalmol. 2001;132(5):682–92. PubMed. PubMed PMID: 11704029.
210. Weeks DE, Conley YP, Tsai HJ, Mah TS, Schmidt S, Postel EA, et al. Age-Related Maculopathy: A Genomewide Scan with Continued Evidence of Susceptibility Loci within the 1q31, 10q26, and 17q25 Regions. Am J Hum Genet. 2004;75(2) PubMed PMID: 15168325.
211. Fisher SA, Abecasis GR, Yashar BM, Zareparsi S, Swaroop A, Iyengar SK, et al. Meta-analysis of genome scans of age-related macular degeneration. Hum Mol Genet. 2005;14(15):2257–64. PubMed. PubMed PMID: 15987700.
212. Schultz D, Klein M, Humpert A, Luzier C, Persun V, Schain M, et al. Analysis of the ARMD1 locus: Evidence that a mutation in HEMICENTIN-1 is associated with age-related macular degeneration in a large family. Hum Mol Genet. 2003. PubMed PMID: 14570714.
213. Conley YP, Thalamuthu A, Jakobsdottir J, Weeks DE, Mah T, Ferrell RE, et al. Candidate gene analysis suggests a role for fatty acid biosynthesis and regulation of the complement system in the etiology of age-related maculopathy. Hum Mol Genet. 2005;14(14):1991–2002. PubMed. PubMed PMID: 15930014.
214. Haines JL, Schnetz-Boutaud N, Schmidt S, Scott WK, Agarwal A, Postel EA, et al. Functional candidate genes in age-related macular degeneration: significant association with VEGF, VLDLR, and LRP6. Invest Ophthalmol Vis Sci. 2006;47(1):329–35. PubMed. PubMed PMID: 16384981.

215. Stone EM, Braun TA, Russell SR, Kuehn MH, Lotery AJ, Moore PA, et al. Missense variations in the fibulin 5 gene and age-related macular degeneration. N Engl J Med. 2004;351(4):346–53. PubMed. PubMed PMID: 15269314.
216. Zareparsi S, Buraczynska M, Branham KE, Shah S, Eng D, Li M, et al. Toll-like receptor 4 variant D299G is associated with susceptibility to age-related macular degeneration. Hum Mol Genet. 2005;14(11):1449–55. PubMed. PubMed PMID: 15829498.
217. Souied EH, Benlian P, Amouyel P, Feingold J, Lagarde JP, Munnich A, et al. The epsilon4 allele of the apolipoprotein E gene as a potential protective factor for exudative age-related macular degeneration. American Journal of Ophthalmology. 1998;125(3):353–9. PubMed. PubMed PMID: 9512153.
218. Klaver CC, Kliffen M, van Duijn CM, Hofman A, Cruts M, Grobbee DE, et al. Genetic association of apolipoprotein E with age-related macular degeneration. American Journal of Human Genetics. 1998;63(1):200–6. PubMed. PubMed PMID: 9634502.
219. Baird PN, Guida E, Chu DT, Vu HT, Guymer RH. The epsilon2 and epsilon4 alleles of the apolipoprotein gene are associated with age-related macular degeneration. Invest Ophthalmol Vis Sci. 2004;45(5):1311–5. PubMed. PubMed PMID: 15111582.
220. Allikmets R, Shroyer N, Singh N, Seddon J, Lewis R, Bernstein P, et al. Mutation of the Stargardt disease gene (ABCR) in age-related macular degeneration. Science. 1997;277:1805–7. PubMed. PubMed PMID: 9295268.
221. Klein RJ, Zeiss C, Chew EY, Tsai JY, Sackler RS, Haynes C, et al. Complement factor H polymorphism in age-related macular degeneration. Science. 2005;308(5720):385–9. PubMed. PubMed PMID: 15761122.
222. Edwards AO, Ritter R, Abel KJ, Manning A, Panhuysen C, Farrer LA. Complement factor H polymorphism and age-related macular degeneration. Science. 2005;308(5720):421–4. PubMed. PubMed PMID: 15761121.
223. Haines JL, Hauser MA, Schmidt S, Scott WK, Olson LM, Gallins P, et al. Complement factor H variant increases the risk of age-related macular degeneration. Science. 2005;308(5720):419–21. PubMed. PubMed PMID: 15761120.
224. Zareparsi S, Branham KE, Li M, Shah S, Klein RJ, Ott J, et al. Strong association of the Y402H variant in complement factor H at 1q32 with susceptibility to age-related macular degeneration. Am J Hum Genet. 2005;77(1):149–53. PubMed. PubMed PMID: 15895326.
225. Magnusson KP, Duan S, Sigurdsson H, Petursson H, Yang Z, Zhao Y, et al. CFH Y402H confers similar risk of soft drusen and both forms of advanced AMD. PLoS Med. 2006;3(1):e5PubMed.
226. Sepp T, Khan JC, Thurlby DA, Shahid H, Clayton DG, Moore AT, et al. Complement factor H variant Y402H is a major risk determinant for geographic atrophy and choroidal neovascularization in smokers and nonsmokers. Invest Ophthalmol Vis Sci. 2006;47(2):536–40. PubMed. PubMed PMID: 16431947.
227. Souied EH, Leveziel N, Richard F, Dragon-Durey MA, Coscas G, Soubrane G, et al. Y402H complement factor H polymorphism associated with exudative age-related macular degeneration in the French population. Mol Vis. 2005;11:1135–40. PubMed. PubMed PMID: 16379025.
228. Okamoto H, Umeda S, Obazawa M, Minami M, Noda T, Mizota A, et al. Complement factor H polymorphisms in Japanese population with age-related macular degeneration. Mol Vis. 2006;12:156–8. PubMed. PubMed PMID: 16541016.
229. Gold B, Merriam JE, Zernant J, Hancox LS, Taiber AJ, Gehrs K, et al. Variation in factor B (BF) and complement component 2 (C2) genes is associated with age-related macular degeneration. Nat Genet. 2006;38(4):458–62. PubMed. PubMed PMID: 16518403.
230. Lokki ML, Koskimies SA. Allelic differences in hemolytic activity and protein concentration of BF molecules are found in association with particular HLA haplotypes. Immunogenetics. 1991;34(4):242–6. PubMed. PubMed PMID: 1916952.
231. Jakobsdottir J, Conley YP, Weeks DE, Mah TS, Ferrell RE, Gorin MB. Susceptibility genes for age-related maculopathy on chromosome 10q26. Am J Hum Genet. 2005;77(3):389–407. PubMed. PubMed PMID: 16080115.

232. Rivera A, Fisher SA, Fritsche LG, Keilhauer CN, Lichtner P, Meitinger T, et al. Hypothetical LOC387715 is a second major susceptibility gene for age-related macular degeneration, contributing independently of complement factor H to disease risk. Hum Mol Genet. 2005;14(21):3227–36. PubMed. PubMed PMID: 16174643.
233. Schmidt S, Hauser MA, Scott WK, Postel EA, Agarwal A, Gallins P, et al. Cigarette smoking strongly modifies the association of LOC387715 and age-related macular degeneration. Am J Hum Genet. 2006;78(5):852–64. PubMed. PubMed PMID: 16642439.
234. Saunders RE, Goodship TH, Zipfel PF, Perkins SJ. An interactive web database of factor H-associated hemolytic uremic syndrome mutations: insights into the structural consequences of disease-associated mutations. Hum Mutat. 2006;27(1):21–30. PubMed. PubMed PMID: 16281287.
235. Heinen S, Sanchez-Corral P, Jackson MS, Strain L, Goodship JA, Kemp EJ, et al. De novo gene conversion in the RCA gene cluster (1q32) causes mutations in complement factor H associated with atypical hemolytic uremic syndrome. Hum Mutat. 2006;27(3):292–3. PubMed. PubMed PMID: 16470555.
236. Warwicker P, Goodship TH, Donne RL, Pirson Y, Nicholls A, Ward RM, et al. Genetic studies into inherited and sporadic hemolytic uremic syndrome. Kidney Int. 1998;53(4):836–44. PubMed. PubMed PMID: 9551389.
237. Esparza-Gordillo J, Goicoechea de Jorge E, Buil A, Carreras Berges L, Lopez-Trascasa M, Sanchez-Corral P, et al. Predisposition to atypical hemolytic uremic syndrome involves the concurrence of different susceptibility alleles in the regulators of complement activation gene cluster in 1q32. Hum Mol Genet. 2005;14(5):703–12. PubMed. PubMed PMID: 15661753.
238. Caprioli J, Castelletti F, Bucchioni S, Bettinaglio P, Bresin E, Pianetti G, et al. Complement factor H mutations and gene polymorphisms in haemolytic uraemic syndrome: the C-257T, the A2089G and the G2881T polymorphisms are strongly associated with the disease. Hum Mol Genet. 2003;12(24):3385–95. PubMed. PubMed PMID: 14583443.
239. Caprioli J, Noris M, Brioschi S, Pianetti G, Castelletti F, Bettinaglio P, et al. Genetics of HUS: the impact of MCP, CFH and IF mutations on clinical presentation, response to treatment, and outcome. Blood. 2006 Apr 18. PubMed PMID: 16621965.
240. Atkinson JP, Liszewski MK, Richards A, Kavanagh D, Moulton EA. Hemolytic uremic syndrome: an example of insufficient complement regulation on self-tissue. Ann N Y Acad Sci. 2005;1056:144–52. PubMed. PubMed PMID: 16387683.
241. Abrera-Abeleda MA, Nishimura C, Smith JL, Sethi S, McRae JL, Murphy BF, et al. Variations in the Complement Regulatory Genes Factor H (CFH) and Factor H Related 5 (CFHR5) are Associated with Membranoproliferative Glomerulonephritis Type II (Dense Deposit Disease). J Med Genet. 2005 Nov 18. PubMed PMID: 16299065.
242. Appel GB, Cook HT, Hageman G, Jennette JC, Kashgarian M, Kirschfink M, et al. Membranoproliferative glomerulonephritis type II (dense deposit disease): an update. J Am Soc Nephrol. 2005;16(5):1392–403. PubMed. PubMed PMID: 15800116.
243. Robman L, Mahdi O, McCarty C, Dimitrov P, Tikellis G, McNeil J, et al. Exposure to Chlamydia pneumoniae infection and progression of age-related macular degeneration. Am J Epidemiol. 2005;161(11):1013–9. PubMed. PubMed PMID: 15901621.
244. Erkkila H, Raitta C, Niemi K. Ocular findings in four siblings with pseudoxanthoma elasticum. Acta Ophthalmol (Copenh). 1983;61:589–99. PubMed. PubMed PMID: 6637420.
245. Zee RY, Diehl KA, Ridker PM. Complement factor H Y402H gene polymorphism, C-reactive protein, and risk of incident myocardial infarction, ischaemic stroke, and venous thromboembolism: A nested case-control study. Atherosclerosis. 2005 Oct 13. PubMed PMID: 16229850.
246. Zee RY, Diehl KA, Ridker PM. Complement factor H Y402H gene polymorphism, C-reactive protein, and risk of incident myocardial infarction, ischaemic stroke, and venous thromboembolism: A nested case-control study. Atherosclerosis. 2006;187(2):332–5. PubMed. PubMed PMID: 16229850.
247. Fung AE, Lalwani GA, Rosenfeld PJ, Dubovy SR, Michels S, Feur WJ, Puliafito CA, Davis JL, Flynn HW, Esquiabro M. An optical coherence tomography-guided, variable dosing regimen with intravitreal

ranibizumab (Lucentis) for neovascular, age-related macular degeberation. Am J Ophthalmol. 2007;143(4):566–83. PubMed. PubMed PMID: 17386270.

248. Kaiser PK. Verteporfin photodynamic therapy and anti-angiogenic drugs: potential for combination therapy in exudative age-related macular degeneraion. Curr med res Opin. 2007;23(3):477–87. PubMed. PubMed PMID: 17355729.
249. VEGF Inhibition Study in Ocular Neovascularization (V.I.S.I.O.N.) Clinical Trial Group. D'Amico DJ, Masonson HN, Patel M, Adamis AP, Cunningham ET Jr, Guyer DR, Katz B. Pegaptanib sodium for neovascular age-related macular degeneration: two-year safety results of the two prospective, multicenter, controlled clinical trials. Ophthalmology. 2006 Jun;113(6):992–1001.e6. Epub 2006 Apr 27. PubMed PMID: 16647134.
250. Brown DM, Kaiser PK, Michels M, Soubrane G, Heier JS, Kim RY, Sy JP, Schneider S; ANCHOR Study Group. Ranibizumab versus verteporfin for neovascular age-related macular degeneration. N Engl J Med. 2006;355(14):1432–44. PubMed. PubMed PMID: 17021319.
251. Rosenfeld PJ, Brown DM, Heier JS, Boyer DS, Kaiser PK, Chung CY, Kim RY; MARINA Study Group. Ranibizumab for neovascular age-related macular degeneration. N Engl J Med. 2006;355(14):1419–3. PubMed. PubMed PMID: 17021318.

Diabetic retinopathy and a novel treatment based on the biophysics of rod photoreceptors and dark adaptation

Geoffrey B. Arden, MD, PhD[1,*] and David J. Ramsey, MD, PhD[2,†]

Created: July 14, 2015.

1. Introduction

There is a *pandemic* of diabetes. More than 350 million people are affected world-wide. In the UK more than 4.2 million people (6.3% of the population) are estimated to be living with diabetes, many without even knowing it (1). In the USA 29.1 million (9.3% of the population) have diabetes (2). Most individuals have type-2 diabetes, the onset of which is nearly universally attributed to the adoption of a "western diet", rich in calories from refined carbohydrates and saturated fat. But type 1 diabetes is also increasing. Furthermore, type 2 diabetes now appears at much earlier ages, even in children, and increasing numbers of people with type-2 are insulin dependent (3). Individuals are not only developing diabetes at earlier ages, but also living longer. There are now various ways of controlling diabetes, but sadly these are not as successful in treating the *complications* of diabetes that are related to the heart, major blood vessels, peripheral nerves, kidneys and the eye (4). With an estimated 150,000 people in the UK developing diabetes each year, the prevalence of very long standing diabetes is growing even more rapidly than the prevalence of diabetes itself. This sets up a 'perfect storm' for the complications of diabetes which develop after long periods.

2. Classification of diabetes

Diabetes literally means "a passer through; a siphon," so named because of the immoderate discharge of urine containing glucose which is a cardinal feature of the disease. The word comes to English by way of the Latin (diabetes) from the Ancient Greek (διαβήτης [diabêtês]). The earliest meaning of the noun "diabetes" was "compass" (5th cent. B.C.); it was not used in the sense of "siphon" (a passer through) until the 2nd or 1st cent. BC. Its first attestation as the name of a disease is in the 2nd century A.D. by Aretaeus, a Cappadocian (Greek) physician and medical writer (Figure 1), and by his contemporary Galen.

Aretæus of Cappadocia, writing in the 2nd century A.D., is the earliest physician whose account of this disease is extant: "Diabetes is a wonderful affection, not very frequent among men, being a melting down of the flesh and limbs into urine." (5)

The first occurrence in English may be in a 1425 translation into Middle English (*non vidi*) of Chauliac's seminal work on surgery, *Chirurgia magna*, which was finished in 1363. In seven volumes, the treatise covers anatomy, bloodletting, cauterization, drugs, anesthetics, wounds, fractures, ulcers, special diseases, and antidotes. The earliest attestation of "diabetes" in a primary English work comes from circa 1541, R. Copland's *Formularie of Helpes of Woundes & Sores in Guy de Chauliac's "Questyonary Cyrurgyens"* "Yiijv, Auycen Graunteth in diabete the water of the clere mylke of a shepe.", closely followed by an even clearer reference to the disease in Dean William Turner's book *Natures Bathes (1562)*: "It is good for the flixe to the chamber pot called of the beste Physicianes Diabetes, that is when a man maketh water oft and much."

Author Affiliations: 1 Moorfields Eye Hospital, London; Email: geoffreyarden@aol.com. 2 Lahey Clinic, Burlington MA; Email: ramsey@post.harvard.edu.

* About the Authors

† About the Authors

Diabetes can further be broadly divided into two classes of disorders, diabetes mellitus and diabetes insipidus. Both share in common the production of copious quantities of urine, as well as an associated risk of dehydration and electrolyte imbalances; however, the two diseases originate from very different sources. When the term "diabetes" is used without qualification, it almost always refers to diabetes mellitus. Diabetes mellitus is a group of severe metabolic disorders marked by high levels of blood glucose resulting from defects in the production of insulin, resistance to that action of insulin, or a combination both. Greek physicians used to diagnose the condition by tasting the urine to detect saccharine matter. In 1675, the English epidemiologist Thomas Willis (1621–1675) rediscovered this phenomenon and appended the term "mellitus," meaning "honey-sweet," to the name diabetes (6). To some extent this diagnostic practice continued into the 20th century among physicians who were taught to use literally *all* of their senses in the art (and science) of diagnosis. Diabetes insipidus is a relatively rare disorder and glucose does not ordinarily spill into the urine of patients, hence the term "insipidus," Latin for "tasteless," appended to the name (6).

3. Types of diabetes mellitus

There are two main forms of diabetes mellitus: type 1 and type 2. In years gone by, these were sometimes referred to as 'Juvenile' versus 'Adult' or 'Insulin dependent' versus 'non-insulin dependent', but some type 1 cases develop in older age, and many type 2 cases are treated with insulin. Hyperglycemia is the hallmark of both forms of the disease, the result of a failure in insulin signaling. In type 1, diabetes results from diminished secretions of insulin because of a nearly complete loss of β cells of the islets of Langerhans due to autoimmune attack. In type 2 disease a number of defects conspire to reduce the effective secretion of insulin and its activity at its receptors in various tissues. Gestational diabetes mellitus (GDM) has been retained as a separate diagnosis category (7), and a new category called "other specific types" created to cover the growing number of cases where specific genetic defects, surgery, drugs, or other cause of hyperglycemia have been identified (8).

Type 1 diabetes

Type 1 diabetes results from the near complete loss of insulin secretion from the pancreas. Its onset is usually acute and associated with increased output of urine, associated thirst, tiredness and weight loss (the 'four T's' of toilet, thirst, tiredness, and thinner). For an unknown reason, autoantibodies are produced that destroy the insulin-producing β cells of the pancreatic islets. The loss of β cells may begin years before diabetes is detected, and in some cases children with type 1 disease have a short remission of symptoms during the early stages of the disorder; in rare instances a complete remission may even occur (9). There is a strong genetic risk for the disease associated with the major histocompatibility complex (MHC) genes, especially certain human leukocyte antigens (HLA) alleles, but genes outside of the MHC have also been associated with increased risk of the disease (10, 11). The mechanism by which heredity makes the β cells more susceptible to autoimmune attack remains obscure.

Type 1 diabetes only accounts for five to ten per cent of all diabetic patients, but is the most common form of diabetes in children and adolescents. The prevalence is approximately one out of every 500 children and adolescents in the United States (12, 13), having risen more than thirty per cent within the last decade. The mean age of onset of type 1 diabetes is approximately 9 years of age and has been reported to occur at a slightly earlier age in girls (8.7±3.8 years) than in boys (9.1±4.1 years) (14). Recently, the incidence of type 1 disease is increasing in many populations (by as much as three to four per cent a year), a fact that cannot be explained by genetics alone (10). Although epidemiological studies have failed to identify a specific causal entity (15), space-time clustering of cases suggests that an infectious etiology is possible (16). In certain instances, a virus, again most likely by initiating the development of autoantibodies, may also induce type 1 diabetes.

Figure 1: Aretæus of Cappadocia. Illustration depicting "Aretæus of Cappadocia," modified after a lithograph from Johannes Sambucus (1531-1584), *Icones Veterum aliquot ac Recentium Medicorum Philosophorumque* (Images of Some Ancient and Recent Physicians and Philosophers), 1901.

Type 2 diabetes

Type 2 diabetes is by far the more prevalent from of the disease, accounting for roughly ninety to ninety-five per cent of diabetic patients in the United States (17). The onset of type 2 diabetes is usually in adulthood and occurs decades after elements of the 'metabolic syndrome' appear. Type 2 diabetes usually has an insidious onset, and patients are for the most part unaware of the onset until they suffer from acute side effects of extreme hyperglycemia, or another illness which leads to its discovery (for example, repeated infections). Diabetes UK has estimated that up to 25% of patients who consult their general practitioners for other reasons may have undetected type 2 diabetes, and recommend that all patients have tests for glycosylated hemoglobin levels (Hb1Ac).

The hallmark of type 2 diabetes is insulin resistance, accompanied by variable defects in insulin secretion. In type 2 disease, insulin is usually present, but its activity is insufficient to meet the metabolic needs of the body. Initially, the β cells of the pancreas may be able to augment their secretion of insulin when faced with insulin

resistance, but over time β cell output fails. This may result from either increasing insulin resistance, β cell exhaustion (degeneration), or both. Insufficient insulin activity causes patients to become "glucose intolerant", i.e. experience abnormally elevated blood glucose levels following carbohydrate loads. Whereas nearly all patients with type 1 diabetes are aware that they have the disease because of the effects of severe insulin deficiency, roughly 6.2 million people in the United States with the type 2 disease are currently unaware that they have diabetes (3, 17). Often the onsets of symptoms are so gradual, or the effects of diabetes so mild or intermittent, that people with diabetes fail to recognize that they have a disorder of blood glucose regulation. However, if left untreated the consequences of diabetes are devastating. Together, these metabolic defects take their toll on the body, lead to a series of complications, and patients often succumb to an early death (15,18).

4. The effect of diabetes on the eye

Here we specifically concentrate on the damage that occurs at the level of the light-sensitive retina at the back of the eye. Already 240,000 people in the UK with diabetes have diabetic retinopathy. Visual impairment may occur from bleeding in the eye, often with accompanying abnormal proliferating blood vessels, retinal detachment from associated scar tissue, or even more commonly the leakage of fluid from damaged capillaries in the central part of the retina. This is called diabetic macular edema (DME). In the USA, DME is the leading cause of blindness in people of working age (3). In the UK although the prevalence is similar, there has been a recent increase in the incidence of hereditary retinal degeneration, so DME is now the second most common cause of registered blindness in the working age group (4).

5. Detection and screening

Once diabetes has damaged the retina, vision is often permanently lost. For this reason all efforts are being made to detect diabetic retinopathy (DR) as early as possible by taking photographs of the back of the eye (Figure 2) each year in every person who had diabetes. In the UK, for example, over 3 million people are examined in this way each year, and over 100,000 of these are referred to the eye departments of NHS Trusts, which are struggling to cope with these large numbers of patients. National eye screening programs using fundus photography and reading centers have been set up in many health care centers throughout the world.

Clinically, DR is divided into nonproliferative and proliferative disease, the latter of which is marked by evidence of new vessel formation. Non-proliferative diabetic retinopathy (NPDR) can further be divided into mild, moderate and severe, "pre-proliferative" diabetic retinopathy. The term "background retinopathy" is no longer used.

As patients with sight-threatening retinopathy may not have symptoms, life-long evaluation for retinopathy by annual screening is a valuable and necessary strategy. Pediatric patients with type 1 diabetes generally do not need to have a screening exam for retinopathy before age 9, or within 3 to 5 years of diagnosis, but should have them yearly thereafter (19). This is because DR generally does not start to develop until approximately five years after the onset of diabetes and is unusual before puberty; on average, only half of patients with type 1 diabetes develop retinopathy by eight to ten years after the onset of disease (20, 21). By contrast, because patients with type 2 disease may have had diabetes for ten or fifteen years prior to their diagnosis (22), it is essential that they are screened at baseline and yearly thereafter (23-25). Recent data from the Liverpool eye study suggest that a longer interval after an initial exam may be appropriate for type 2 patients. Type 2 patients without clinically detectible retinopathy at baseline remained free of sight-threatening DR for an average of 5.4 years (26). The complications develop insidiously often going unnoticed by patients until there is a sudden and dramatic loss of visual acuity caused for example by preretinal hemorrhages from new vessels or loss of central vision from retinal swelling. The fundus photographs (Figure 2) show small circular "dark lesions", which are microaneurysms or "dot and blot" hemorrhages, or lighter exudates. Swelling of the macular retina is also detectable (for more details see (27)). Microaneurysms are thought to be due in part to loss of pericytes (27). In

the resulting capillary dilatation, blood flow is sluggish and localised clotting may occur. In the end stages of this process the whole capillary is often obliterated. This can be seen histologically as 'ghost vessels' and on fluorescein angiography of the retinal circulation localized areas appear where the inner retinal capillary blood supply is lost. Dark-adapted thresholds are elevated early in diabetes (26, 28-31) and selective loss of blue–yellow colour contrast sensitivity occurs early in the disease (32-34). Clinical screening by slit lamp biomicroscopy and indirect ophthalmoscopy, complimented by fundus photography, and often optical coherence tomography (OCT) is necessary to monitor the disease in individuals. More recently, the advent of wide field and now ultra-wide field angiography have the potential to aid in the diagnosis and management of retinopathy (35, 36) but have not yet been incorporated into any screening programme.

In animals, results similar to those in man can be seen, but there are species differences. Rodents develop microaneurysms (37) but these changes are much less pronounced than in man (38) and proliferative retinopathy is not seen or the later hemorrhagic changes seen in man. These do appear in longer-lived species such as dogs. Swelling of the retina can be seen in mouse, but it is not clear how closely related this is to human DME.

The different stages of the disease are seen in the following series of retinal photographs. The progress of DR is most clearly seen in fluorescein angiographs where the damage to the retinal vessels and arterioles are more obvious than in the fundus photos. These studies also highlight regions of capillary dropout and other microvascular abnormalities.

6. Clinical grading of diabetic retinopathy and stage of disease

Nonproliferative retinopathy

In man the earliest stages of the disease, loss of retinal capillary pericytes, contributes to mechanical changes in the retinal blood vessels, altering their patency and permeability (39). These changes consist of microaneurysms (i.e. focal dilations) of retinal capillaries located in the inner nuclear layer that can be appreciated by the direct ophthalmoscope as tiny red dots about the size of a pinhead in the retina. (Isolated microaneurysms also appear in a number of other retinal diseases, including glaucoma, hypertensive retinopathy, and venous occlusal diseases like central retinal vein obstruction). These vascular changes often progress to yield hemorrhages within the retina. Hemorrhages in early DR usually appear as either "dot/blot" or "flame" hemorrhages, however, severe retinal bleeding can occur. Dot hemorrhages (tiny) and blot hemorrhages (larger) are the result of the rupture of weakened capillaries (i.e. aneurysms) within the neural retina. Flame hemorrhages are the result of the same underlying process, but occur in the superficial layers of the retina causing the blood to track along nerve fiber bundles. Hard exudates, appreciable as yellow-white spots in the peripheral retina or sometimes in a pattern of streaks around the macula, also tend to increase in number. These precipitates consist of lipoproteins and other proteins that have been extravasated from leaky retinal blood vessels as a result of the failure of the blood retinal barrier (40). Finally, microretinal infarcts often occur in the nerve fiber layer of the retina to give rise to patches of dead retinal tissue with vague borders known as "cotton wool" spots—transient findings that are no longer considered as predictive of high risk disease as many of the other vascular features discussed below.

The patient in Figure 3 has mild non-proliferative diabetic retinopathy (NDPR) and the fundus photograph at first blush looks almost normal. The changes clinically apparent are microaneurysms, some red spots of hemorrhage, and hard yellow exudates, and on close inspection early signs of ischemia. The damage to the retina in DR is most clearly seen in the angiographs where the damage to the retinal vessels and arterioles are more obvious than in the fundus photos. The fluorescein angiogram (right) shows the hemorrhages as dark spots. This photograph was taken as the dye began to fill the vessels, and a few bright spots indicate the presence of microaneurysms. In later frames of the angiogram (not shown) these cause leakage, which is one of the mechanisms by which retinal swelling is known to occur.

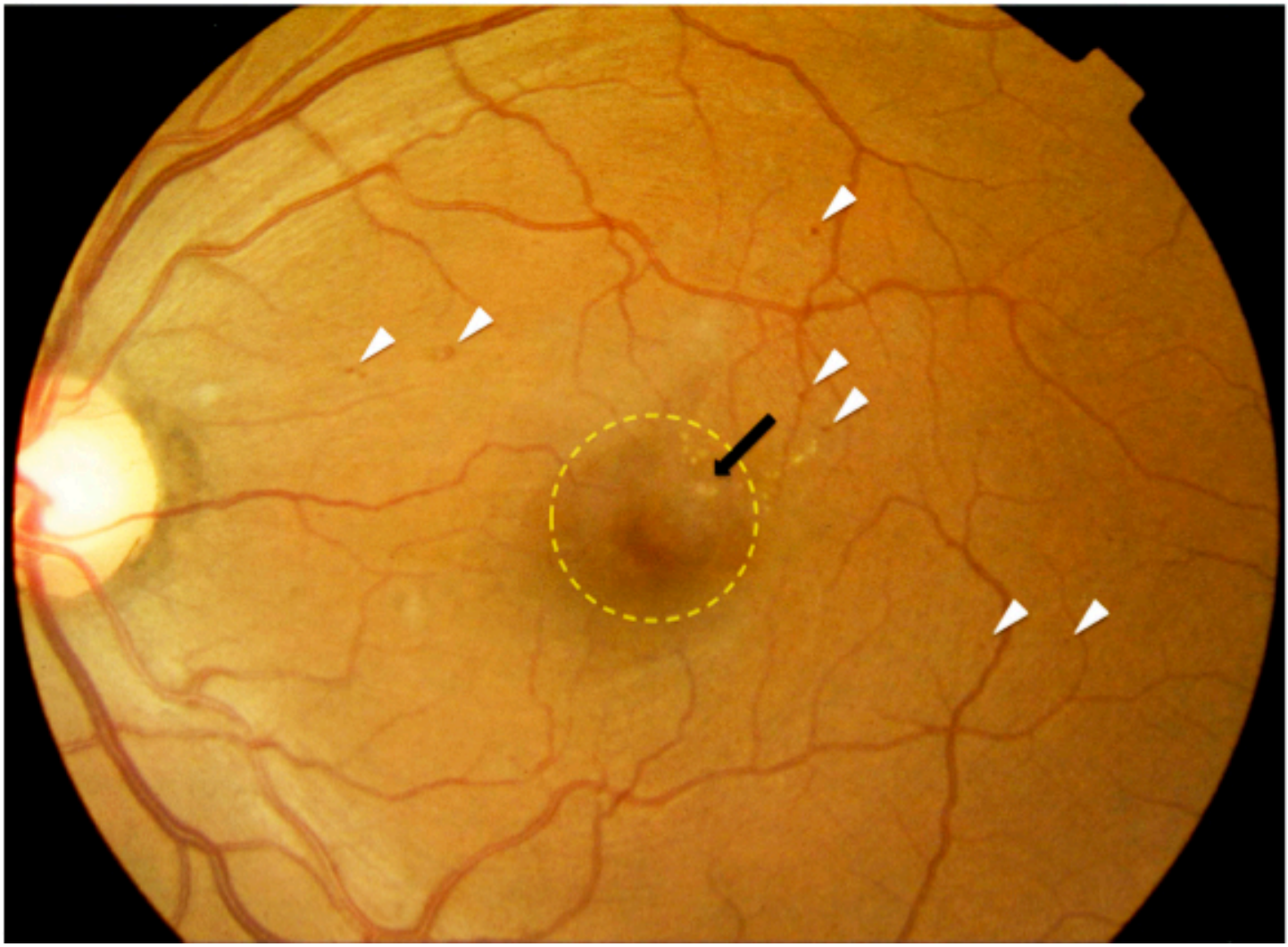

Figure 2: Fundus photograph of a person with mild (early) nonproliferative diabetic retinopathy with centre-involving diabetic macular edema (DME) in the left eye. The white arrow-heads highlight typical examples of small red "dot" (microaneurysms) and "blot" (hemorrhages). The black arrow points to retinal exudates several of which are within 500 microns of the centre of the fovea. The yellow circle delineates an area of central thickening of the retina (edema).

Pre-Proliferative diabetic retinopathy

Pre-proliferative retinopathy (PPDR) consists of a series of signs in the retinal vasculature that heralds the worsening retinal ischemia that can ultimately lead to formation of new vessels. Progression to the pre-proliferative stage of diabetic retinopathy is marked by 1: a rapid increase in the size and confluence of hemorrhages, 2: the appearance of >5 cotton-wool spots (ischemic nerve fiber layer infarcts), 3: venous dilation and beading (focal variation in the caliber of retina veins in response to ischemia), and 4: arterial abnormalities and remodeling of existing retinal capillary beds (causing intraretinal microvascular abnormalities that do *not* leak fluorescein). Of these clinical signs, venous beading is considered the most significant predictor of progression to proliferative diabetic retinopathy (PDR), whereas cotton-wool spots are the least significant (because they are so transient, lasting often only a few days to a couple of weeks). About half of eyes with these retinal characteristics progress to PDR within 12 to 24 months, indicating a strong need for careful monitoring at this stage. Unfortunately, no preventative or restorative treatment exists for PPDR, although anti-VEGF agents have shown some promise in clinical trials in patients with concurrent DME (41).

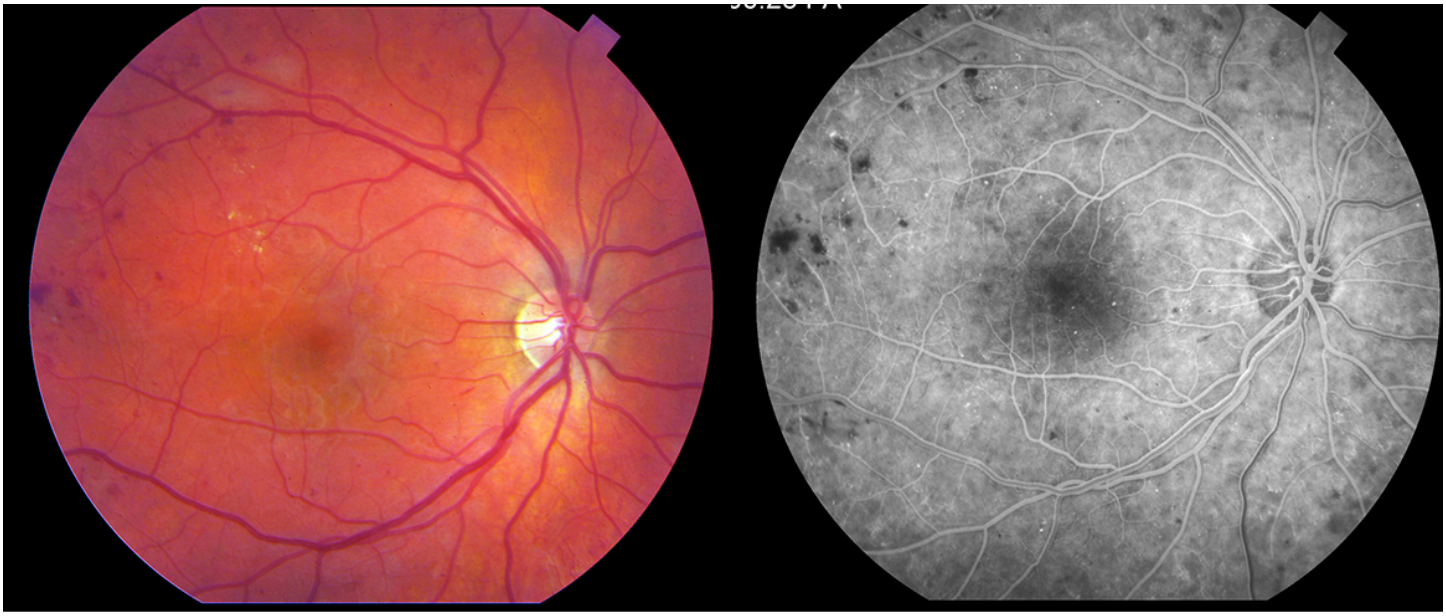

Figure 3: Fundus photograph and angiogram of patient with mild non-proliferative diabetic retinopathy (NDPR).

Proliferative retinopathy

The hallmark of proliferative diabetic retinopathy (PDR) is neovascularization of the retina at the edges of zones of capillary non-perfusion, most often near the optic disc or within three disc diameters of major retinal vessels (42). The new blood vessels that form around the optic nerve head are referred to as "new vessel disc" (NVD) and other vessels are clinically termed "new vessels elsewhere" (NVE). In some respects, the formation of new vessel can be viewed as an attempt by the retina to revascularize areas of capillary non-perfusion; however, this process does not occur in an orderly fashion and is largely unsuccessful at restoring any lost function. These new vessels penetrate the internal limiting membrane and form a dense capillary plexus between the inner surfaces of the retina or penetrate into the vitreous humor to grow along the outer surface of the vitreous body (46). The new vessels are also highly delicate and markedly permeable and may cause vision loss by intravitreal or pre-retinal (beneath the internal limiting membrane) hemorrhage. Early signs of changes in vasculature permeability can often be demonstrated by fluorescein angiography (FANG). In the late stages of the disease, these new vessels may regress, leaving only lattices of avascular fibrous tissue adhering to the retina and the posterior hyaloid membrane (42, 44). Fibroglial tissue may lead to mechanical deformation of the macula by putting traction on the retina as the vitreous body contracts, either with age or secondary to retinal ischemia (39). Retinal detachment may also occur, in some cases remaining stable for years, but other eyes rapidly progress to involve the macula and the rest of the retina, resulting in blindness if not rapidly reversed (42).

Historically, the incidence of proliferative diabetic retinopathy had been as high as 40-50% in some populations after 20-25 years of diabetes; however, the figure is now more commonly ten to fifteen per cent, nearly a four-fold decline due largely to tight glucose control that is the hallmark of modern diabetes care (43-45). However, the absolute number of new cases of blindness has not been decreasing as rapidly because of the ever expanding numbers of patients with diabetes and the earlier age of onset.

The patient whose imaging results are shown in Figure 4 illustrates many of the features of advanced PDR. There are blot and dot hemorrhages, flame hemorrhages (within the nerve fiber layer), cotton wool spots (infarcts in the nerve fiber layer), and neovascularization elsewhere (NVE) and of the disc (NVD). Inferiorly, there is a boat-shaped hemorrhage (in the lower portion of the image) that occurred some time ago. This eye has high risk features and requires treatment. The angiogram (Figure 4, right), taken at a later stage with dye filling both

arteries and the veins, demonstrates leakage from the areas of NVE and NVD, as well as many more microaneurysms. Dye has leaked from the capillaries into the extracellular compartment so there is a background glow. However in some areas the capillaries have been obliterated and these areas of ischemia appear dark in appearance and are essentially dead. There is also enlargement of the foveal avascular zone (FAZ) in the central macula, which may limit central vision due to damage to the fine capillary network that services this essential region. There is also significant ischemia in the periphery (not shown).

Figure 5 is from a patient with legal blindness from end stage diabetic retinopathy. This particular case is taken from a patient with type 1 diabetes who ran away from home at an early age. Living on the streets made it difficult if not impossible to handle her disease appropriately for many years. By the time she got treatment, in this case pan retinal laser photocoagulation (PRP) (seen as the scattered bright white spots in the color photography that act as window defects in the fluorescein due to the loss of pigment epithelium and overlying retina) the treatment was too late to arrest the progressive ischemic retinopathy. Ischemic maculopathy has developed, along with a central scar. Many of the larger retinal arteries and even some of the veins are no longer perfused, appearing as white ischemic vessels that remain unperfused on the FAZ. The optic disc is pale and yet new vessels emanate from the disc associated leakage seen in the FAZ. The patient unfortunately died from other complications from her diabetes in her late 20s. The progression of directly observable retinopathy often provides insight to the other complications of diabetes.

Diabetic macular edema

One of the most serious complications of diabetic retinopathy is diabetic macular edema (DME). Most of the early manifestations of diabetic retinopathy involve the peripheral retina, where changes in retinal function may be silent because of the ability of the CNS to ignore defects that develop in the peripheral visual field (46). However, as DR progresses, retinal vascular changes increase not only in number and severity, and tend to spread to the central retina where they can involve the macula, the region of the retina that underlies high acuity vision (Figure 6).

Anatomically, diabetic macular edema is the thickening of the center of the macula, i.e. fovea, due to the accumulation of fluid and plasma proteins as a result of leaky capillaries and a failure of the blood retinal barrier. Although the fovea is avascular, diabetes-induced damage to the fine capillary network that supports the function of this highly specialized region of the retina can lead to DME as the blood retinal barrier fails (40). Swelling that distorts the contour of the fovea (Figure 6), the neuroanatomical specialization at the center of the macula, can lead to a precipitous decline in visual acuity. DME usually presents as a progressive, painless loss of central vision. Patients usually report a decline in visual acuity that may develop suddenly or have a more gradual onset. DME requiring treatment may be present even when visual acuity is not yet significantly reduced (45, 46). The incidence of DME in the Wisconsin Epidemiologic Study of Diabetic Retinopathy (46-49) and the Early Treatment Diabetic Retinopathy Study (ETDRS) demonstrated that 6.4% of patients with DM develop permanent severe vision loss due to DME (44, 48-52). DME that occurs in the foveal center, if left untreated, can lead to permanent blindness (47-49). Extensive capillary closure, i.e. ischemic maculopathy, or scarring may also lead to vision loss (52). The development of optical coherence tomography (Figure 6), which uses timing or frequency differences in light reflected by different layers of the retina to examine the cross-section of the retina in real-time, has advanced our ability to diagnose and follow DME (53). Whereas “clinically significant” DME was originally based on biomicroscopic finding of macular thickening in ETDRS, many cases of DME where there are mild increases in retinal thickening sufficient to impact vision may be missed without that aid of an OCT scan (Figure 6) (54).

The standardised fundus photographs taken by screening centers (see Figure 2) have been used in attempts to grade the severity of a patient’s disease: The individual’s result is compared to a number of standardised views, by trained, registered observers whose estimates must agree. Either 2 or 7 standard areas of the retina are viewed and graded. This sort of quantitation has led to the Airlie House and the modified Airlie house grading (56, 57),

Figure 4: Fundus photograph and accompanying fluorescein angiogram in the early to mid-phase in a patient with more advanced (high risk) proliferative retinopathy.

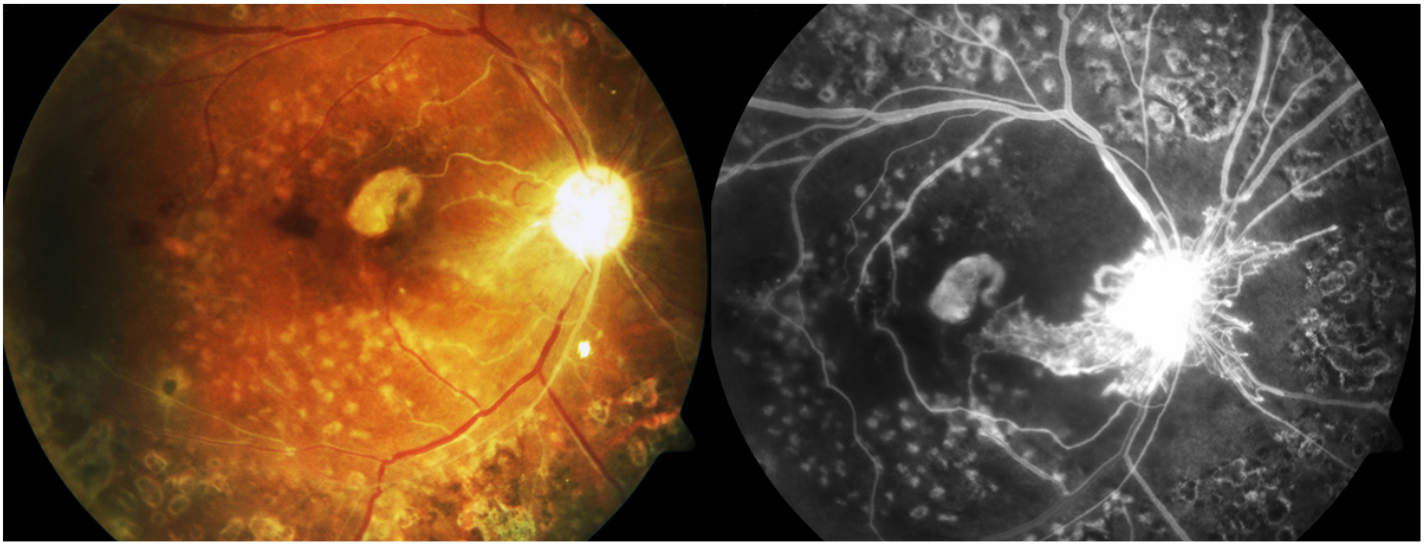

Figure 5: Advanced proliferative diabetic retinopathy with associated ischemic maculopathy. Note the laser scars form panretinal laser photocoagulation, including areas of focal grid laser treatment within the macula. The extensive capillary dropout represents end-stage diabetic retinopathy. Although additional laser may arrest the proliferative changes, very little vision remains secondary to the obliteration of the inner retinal vasculature.

which has proven value for research. The latest form of the grading appears in (27). The clinical usefulness of the classification has recently been questioned in view of the introduction of newer techniques like the OCT (55).

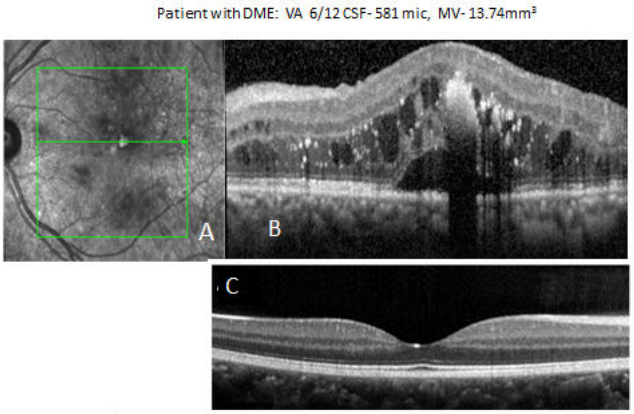

Figure 6: (A) Infrared image showing the location of the ocular coherence tomography (OCT) scan over laid on an infrared image of the fundus. The green box shows the border of the scans with the green arrow indicating the location of the scan shown in cross section in part B. (B) Cross sectional view through the fovea of a diabetic patient with severe clinically significant macular edema (CSME). The OCT can measure retinal thickness and volume can be extrapolated from a series of scans. Note the intraretinal cystoid fluid and highly reflective signals indicative of hemorrhages and/or exudates within the retina. (C) A representative OCT scan through the fovea of a normal eye (43).

7. Treatment of diabetic retinopathy

Laser panretinal photocoagulation (PRP)

Panretinal (scatter) laser photocoagulation (PRP) is effective in treating proliferative retinopathy, reducing the risk of severe visual loss by 50% (43). Figure 7 shows the end results of such treatment. The image is a collage of different areas of retina, photographed with the same equipment as the previous figures. Care is taken to avoid PRP in the central region or macula, as this would damage the central vision, although focal laser applications are sometimes used within macula to treat areas of leakage.

The white areas in Figure 7 are full thickness scars, in which the retina is dead. At first it was thought that the laser treatment prevented injurious substances leaking from those parts of the retina affected by diabetes (56, 57), but in fact, the burns can be placed anywhere in the peripheral retina and the treatment is successful in arresting progression of the disease as long as a sufficient area of the retina is treated. But the outcome is far from perfect. The treatment is often given after loss of visual acuity has already occurred, and it does not act to restore vision. Indeed after 5 years, slight further deterioration of acuity is the rule, although vision is conserved in patients who receive treatment compared to those who forgo PRP (58-60). Furthermore, the destruction of the peripheral retina has as an unavoidable side effect, loss of peripheral vision: and patients often complain of decreased night vision and reduced colour vision. Furthermore, the retinal nerve fiber layer in eyes that have been treated with PPR are thinner with abnormal cupping, but should not be mistaken for glaucomatous optic neuropathy (61).

2) Focal laser

The ETDRS demonstrated a 50% reduction in moderate visual loss (≥ 15 letters) in eyes with mild to moderate nonproliferative diabetic retinopathy and “clinically significant” DME (62). While a small percentage of eyes treated with laser photocoagulation had improvement in visual acuity, most did not and with time lesions often developed into focal areas of chorioretinal atrophy or scarring.

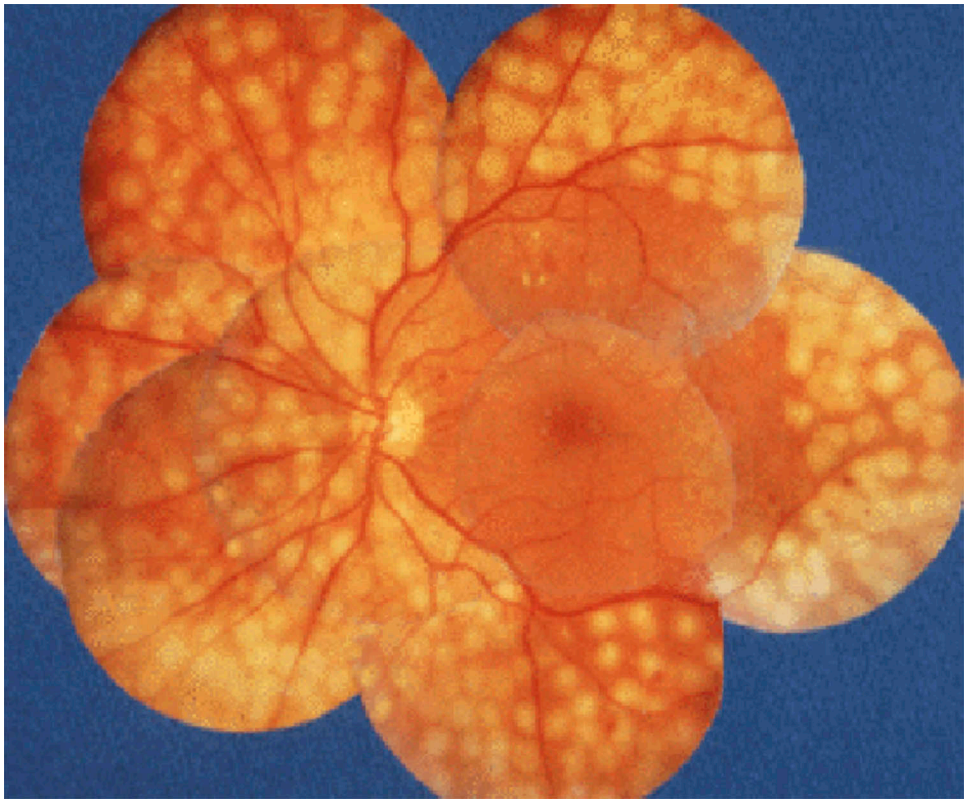

Figure 7: A montage of 7 fundus photographs from a patient who had undergone pan-retinal photocoagulation (PRP) some years previously. The optic nerve head is at the centre, and the blood vessels can be seen radiating from it. The white spots are scars left from the laser burns. Initially 400 μm across, they have enlarged with time. In these areas there is no retinal function.

The superiority of intravitreal treatment with anti-VEGF agents, specifically ranibizumab monotherapy over focal laser alone has been noted for DME (63). In the treatment of DME, laser photocoagulation may still be used as an additional, or "rescue", treatment. For example, in the case of the RISE and RIDE trials (identical, double-masked, sham-controlled, multicenter Phase III trials evaluating the impact of monthly ranibizumab injections on DME) laser was applied if it was found that central foveal thickness was >250 μm or if there was a 50-μm worsening from the prior month.

Recently, the development of subthreshold photocoagulation promises to greatly reduce the risk of structural and functional retinal damage from laser treatment, while retaining the therapeutic efficacy of conventional laser treatment (55, 56, 60 64, 65). The development of the diode laser with micropulsed emission with a longer wavelength in the near-infrared (810 nm) greatly reduces the thermal diffusion to the neurosensory retina and allows focal treatment without a visible burn endpoint (61). Although no retinal damage is detectable at the time of treatment, changes from the laser treatment, i.e. scarring, still develops albeit in a smaller proportion of patients compared to conventional green laser photocoagulation (64, 65, 66).

3) Intravitreal injection of medications

The situation has been transformed over the last decade with the introduction of intravitreal agents that target vascular endothelial growth factor (VEGF), one of the key cytokines whose abnormal expression has been strongly associated with the progression of diabetic eye disease. This discovery arose from an appreciation that angiogenesis of the retina of new-born animals was related to the development of local hypoxia in the retina driving the production of VEGF (67, 68). Soon after, increased VEGF expression was recognised in animal models of diabetes (69-71), as well as in samples of vitreous taken from patients operated upon for the complication of proliferative diabetic retinopathy (72). While awaiting FDA approval for ranibizumab

(Lucentis), a humanized small antibody fragment (Fab) with a high binding affinity for human VEGF, was specifically designed for intraocular use (73, 74). With a smaller size compared to its parent molecule bevacizumab (Avastin) (75, 76), ophthalmologists began treating neovascular AMD with off-label bevacizumab (76). This has since become a widely adopted as a lower-cost alternative to ranibizumab. A new drug, aflibercept (Eylea), which targets all VEGF isoforms and PEGF, has been recently approved for the treatment of DME (77, 78). Ongoing studies indicate that these and related compounds may actually slow the progression of diabetic retinopathy (79). Furthermore, they are highly effective therapies for DME, often resulting in an increase in visual acuity, although some patients do not respond and other have such extensive damage that vision is permanently lost (80-85). Unfortunately, the effects are also too often short lived and the effects of diabetes progressive, necessitating repeat injections of these very costly medications (86). Delivery methods for sustained release of anti-VEGF therapy are under development (87). DME may also be treated with intravitreal glucocorticoids, particularly triamcinolone acetonide, dexamethasone, and fluocinolone acetonide.

Beginning in the late 1990s, intraocular injection of triamcinolone acetonide was proposed as an adjunctive treatment of DME and numerous clinical trials for DME followed (88). In addition, in certain cases of DME that have proved refractory to anti-VEGF treatment, steroids may provide some benefit (89, 90). In addition, sustained release devices are available and approved from some ophthalmic indications, including diabetic macular edema (91). Although these medications can be effective, the risks associated with intravitreal administration of steroid medications, especially cataract formation and ocular hypertension or glaucoma, need to be taken into account.

So the list of available treatments is short, and the results and access to treatment are not particularly inspiring. But the important message of this paper is that it is almost certain that an entirely new method of treatment, which is not only non-invasive and without side effects, but is also so inexpensive, and simple you can 'do it yourself' has been discovered. Below the rationale and the supporting evidence is given.

8. Pathogenesis of diabetic retinopathy

Pathological features of diabetes can broadly be divided into acute metabolic problems and long-term complications stemming from hyperglycemia-induced dysfunction, broadly divided between those that affect the macrovasculature versus the microvasculature. The general metabolic problems associated with diabetes are largely due to: (1) decrease in the proper utilization of glucose, leading to high blood glucose levels that result in an osmotic diuresis as glucose spills into the urine; (2) abnormalities in lipid metabolism, leading to the deposition of cholesterol in arterial walls and atherosclerosis; and (3) increased ketone production, with the associated risks of diabetic ketoacidosis when insulin signaling is severely depressed for long periods of time.

The most pronounced and often-cited effect of diabetes is a chronic rise in blood glucose levels. However, it is very unlikely that elevated blood glucose plays a singular causative role in the development of diabetic complications; many other cellular metabolic parameters are no less seriously altered by a lack of insulin signaling.

9. Biochemistry of diabetic retinopathy

Investigations of hyperglycemia on cellular metabolism have demonstrated that cells and tissues cultured in added glucose, or animal models made hyperglycemic by the injection of streptozotocin, experience both active and passive damage to their biochemical machinery. Increased concentration of available glucose triggers abnormalities in a range of metabolic pathways that collectively leads to "oxidative stress" as the concentration of a group of energetic radicals increases (92-94). Another line of enquiry relates to the formation of advanced glycosylated end-products (AGEs), which are modifications of proteins or lipids that become non-enzymatically glycosylated when exposed to aldose sugars and oxidative stress (95, 96). The formation of AGEs degrade the function of cellular enzymes of metabolism, as well as those that serve antioxidant functions, further

contributing to oxidative stress. AGEs also contribute directly to the generation of reactive oxygen species (ROS) as a result of activating cellular mechanisms designed to rid the cell of damaged macromolecules.

Oxidative Stress

Oxidative stress occurs when the concentration of a group of energetic radicals increases (92-94). These are known collectively as ROS. ROS may include singlet or triplet oxygen, but the major contributor is the superoxide anion $O_2^{\bullet -}$. In addition, in the presence of nitric oxide (NO), the oxygen radicals can react to form nitroso-compounds, but although these have slightly differing properties, and engage in different chemical reactions to the superoxide (97) this is ignored in the treatment that follows. Active species have short lifetimes and the superoxide ion rapidly transmutes into hydrogen peroxide (H_2O_2). The lifetimes of all these molecules depend very greatly on the local reducing environment. In cells they are surrounded by compounds and enzymes that quench them very effectively so that a sustained rise in the concentration of ROS requires either an overproduction or a reduction in the rate of their destruction. This is the case with diabetes where the production of ROS increases simultaneously with a decrease in the ability of endogenous quenchers.

Mitochondria produce ROS

Of the ways in which ROS can be produced, the mitochondria are the most important (97, 98). ROS are produced by the normal operation of mitochondria producing ATP from oxygen and trioses derived from glucose (99-103) as part of the process of oxidative phosphorylation (Figure 8). In many types of cell increased blood sugar levels in diabetes lead to increased intracellular glucose, which enters via membrane glucose transporters (104, 105). Increased glucose concentrations drive mitochondrial oxidative phosphorylation, limited by the availability of oxygen, to produce ROS (92 99-103). Figure 8 diagrams the processes occurring in the mitochondrion. Because of the short half-life of ROS, it is common to measure their activity indirectly using reporter dyes, molecules that are chemically altered by oxidation (106, 107).

It is now possible to introduce fluorescent proteins into the mitochondrial genome and observe the process of ROS production in real time. Confocal microscopy of reporter proteins transfected into cells has demonstrated that ROS are produced in localised places on the mitochondria, where electrons leak from the electron transfer chain (ETC) in brief pulses (107). About 5% of the oxygen is diverted into this pathway and modern techniques have shown that they are emitted as discontinuous flashes (146).

The plasma membrane produces ROS

Another method of production of ROS is situated in the cell membrane and involves the enzyme NADPH oxidase (109) (Figure 9). Its activity is controlled by a complex regulatory system that involves the G protein Rac (109, 110). In resting cells, a membrane-embedded heterodimer of two polypeptides (p22phox and gp91phox)—which also contains two heme groups and copper as well as a flavine adenine dinucleotide (FAD) group—enables the transfer of electrons from cytosolic NADPH across the membrane to molecular oxygen without NADPH oxidase activity. It is believed that the charge compensation occurs when gp91phox polypeptide also acts as a proton pump. Upon stimulation, a number of polypeptides (p47phox, p67phox, and p40phox) translocate to the inner face of the plasma membrane to form a fully active enzyme complex that contains NADPH oxidase activity. The central polypeptide gp91phox also acts as a Ca^{2+} or H^+ channel, and the ROS produced appear to regulate signaling pathways (109, 110).

Targets of oxidative stress

Most ROS are formed in a highly reducing environment inside cells, and must pass through cell membranes into the extracellular environment (which also contains quenchers) before they can diffuse to other cells. Oxidative stress makes membranes more permeable (111, 112), and reduces the quencher concentrations. But initially, in the early stage of diabetes, ROS are unlikely to travel more than a few microns, lasting for very short periods,

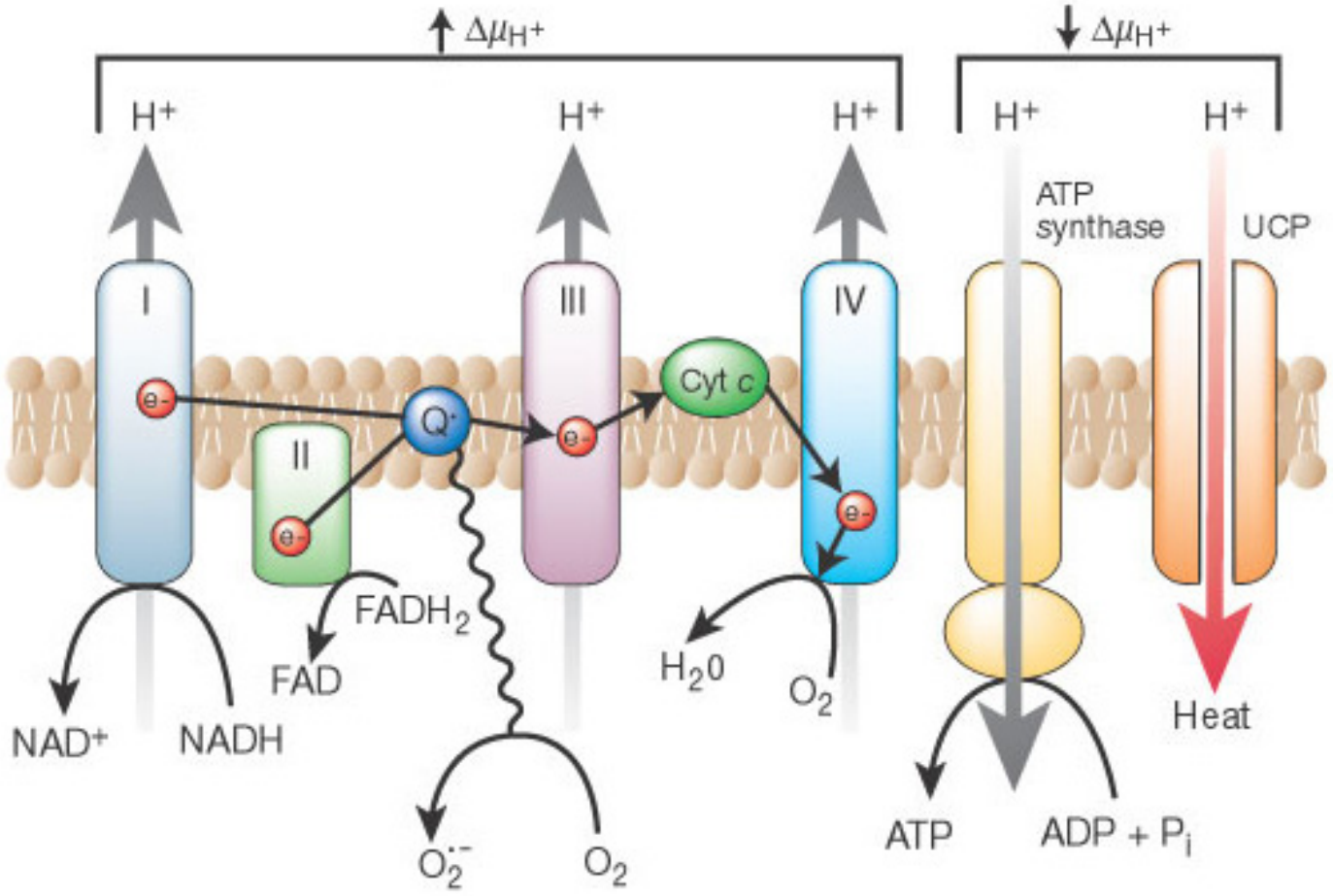

Figure 8: Diagram of the mitochondrial membrane showing the electron transfer chain (on the left) which results in the production of the superoxide anion, and a hydrogen ion gradient ($\Delta\mu H^+$) which when collapsed (on the right) produces ATP. From (102).

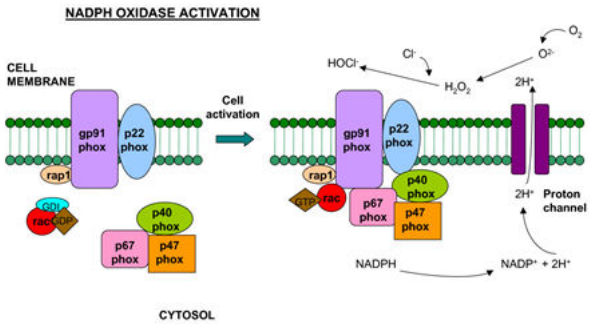

Figure 9: Production of superoxide ($O_2^{\bullet -}$) and hydrogen peroxide (H_2O_2) in the cell membrane. The 2 polypeptides gp91phox and p22phox together form flavocytochrome b_{558}, which is membrane-bound (upper diagram). When activated, the other polypeptides indicated in the diagram, which are usually free in the cytoplasm, bind to it and allow electrons to be transferred across the cell membrane (lower diagram). From (110). Image from (267). There are a number of different activating stimuli, including light. The difference spectrum, the change in absorbance from reduced to unreduced form as a function of wavelength, peaks at 640 nm (268).

before being captured and quenched, and therefore the earliest damaged in diabetic retinopathy occurs because of changes initiated intracellularly (113). Morphological evidence of intracellular oxidative stress is the swollen and disrupted cristae of mitochondria (114). Evidence of oxidative stress can be seen in many of the layers of the retina, for example the inner nerve fiber layer and ganglion cell layers, and this recently has been correlated with changes in the OCT (115). Localised oxidative stress in rodent retinal capillaries appears to develop rather late. Most of the ROS production however is in the photoreceptor layer (116). Although photoreceptor cells are major contributors to diabetes-induced oxidative stress and local inflammation, the functional disturbance to the phototransduction process is minimal, limited to the recovery rate after intense bleaching, and the responses to threshold stimulation (117-121).

Caveats to the oxidative stress theory

Despite this evidence, the precise mechanism by which hyperglycemia leads to the increased concentration of ROS is uncertain. In humans, there is no simple relationship between hyperglycemia and the development of retinopathy (122-124) (except for the very highest levels of hyperglycemia), so the determining factor may be when hyperglycemia reduces the capacity of antioxidant defences (125, 126). Experiments on tissues in raised glucose are usually confined to comparing the results in 5mM with 25 or 30mM glucose. In one case (studies implicating increased glucosamine with oxidative stress) (127), the threshold appears to be about 12mM. This corresponds to the highest levels of hyperglycemia found in normally functioning patients (122-124). At the glucose levels utilized in most biochemical investigations in excess of this level, patients would soon be severely ketotic or comatose with hyperosmolar non-ketotic decompensation syndrome, a condition that carries a mortality of 40% (128). It is therefore difficult to be sure that the 'downstream' abnormalities demonstrated in laboratory experimentation in "high" glucose have key roles to play in the development of retinal lesions, which develop in patients with relatively better controlled hyperglycemia. Rodents made diabetic with streptozotocin have body weights, which are up to 40% less than age-matched "controls", and results obtained under these conditions are possibly not directly applicable to clinical situations either. In fact, oscillating levels of elevated blood glucose levels appear to be more damaging than persistently elevated levels (129). Hyperglycemia can only have a direct effect if it results in higher intra-cellular glucose. While glucose can penetrate some cell membranes, in most it is ferried by glucose transporters (130), and either the number of portals increases or each turns over faster. It is of interest that in human retinal endothelial cells grown in monoculture, glucose transport does not increase under conditions of excess glucose, intracellular hyperglycemia does not occur, and the cells in culture do not show signs of oxidative stress (130, 131). This leads to the conclusion that the damage to capillaries by ROS (which are fundamental to the development of diabetic retinopathy) is due to a paracrine mechanism, i.e. they are secondary to some less direct effects caused by hyperglycemia.

Polyol pathways

Excess glucose not consumed by the tricarboxylic cycle may also be shunted to glycolytic pathways or enter the polyol (sorbitol) (133, 136) and hexosamine pathways leading to a build of up of metabolites that damages cellular function. Protein Kinase C (PKC) has also been found to be elevated in hyperglycemia. Increased glycolysis leads to the synthesis of diacylglycerol (DAG) which is a key activator of PKC. PKC in turn increases endothelial permeability, the production of VEGF, and leucostasis as well as endothelial cell proliferation (134, 135). Sorbital build up has been found in many cells (including retinal pericytes from diabetic animals). The reaction involves oxidation of glucose by NADPH, and this can cause a reduction of glutathione, one of the reducing agents that remove ROS (132), and increased accumulation of sorbitol is also thought to cause osmotic damage (133). Activation of these metabolic pathways leads to microvascular dysfunction, neuronal apoptosis, glial reactivity and inflammation (137, 138) (Figure 10).

Mitochondria also respond to hypoxia. The first effect is to reduce the formation and release of ROS (139, 140): However mitochondria and other cell-surface mechanisms, also initiate signaling cascades that increase ROS

(141-143, 144-152). The effect of alteration of the ROS output is however uncertain because change in pO_2 can also increase the output of quenchers, (148) at the same time as ROS are increased.

Advanced glycosylation end products

Hyperglycemia also results in the formation of complex molecules known as advanced glycosylation end products (AGEs) that affect the development of oxidative stress in several different ways (148) (Figure 11).

AGES contribute to the thickened basal membranes found in diabetes, which hinder diffusion of oxygen and nutrients both from blood to extracellular fluid and also within tissues. In additions, there are smaller molecule AGEs which interact with a receptor named RAGE, found on Müller and other cells, which, when satisfied, contribute directly to oxidative stress by directly affecting the NADPH oxidase system (149). RAGE also causes apoptopic cell death of retinal neurones by a mechanism involving the overproduction of nitric oxide (150). AGEs also directly affect retinal blood vessels causing leakage which is associated with increased VEGF and VEGF mRNA expression (95, 96, 150). The immediate effect of hypoxia is to reduce the production of ROS, as would be expected as the metabolism of the mitochondria slows (150). But part of the mechanism of production of ROS, the NAD/NADH ratio is changed by AGEs, producing "pseudo hypoxia", and this change increases oxidative stress (109, 144, 147).

The search for treatments

Many of the pathways involved in producing oxidative stress-induced cell death have been investigated by using selected animal models in which the activity of a particular pathway is increased. If the same experiments are carried out in animals in which quenchers are also increased, oxidative stress is reduced or may not appear (152, 153). If the stimulus driving oxidative stress is removed (e.g. hyperglycemia reduced) biochemical changes may not be restored to normal. It has been shown that ROS and reactive nitrogen species (RNS) activate a spectrum of transcription factors, including nuclear factor kappa B (NFκB), AP-1, p53, Ets transcriptional factor (Ets-1), hypoxia-inducible factor-1α (HIF-1α), and Nrf2. (154, 155) and following reversal of hyperglycemia to normoglycemia the transcription and regulation of proteins remains affected for months. This has been described as 'molecular memory' and due to changes in the nucleus. Damage to mitochondrial DNA also occurs(151, 155), and variations in mitochondrial DNA are associated with different probabilities of development of severe diabetic retinopathy (156) related, at least in part, to the expression levels of particular proteins. Amongst these is the expression of Vascular Endothelial Growth Factor (VEGF), interleukin 2 and transforming growth factor (TGF). All this experimental work has provided a number of blocking agents which can reduce the production of oxidative stress in laboratory conditions (157-171), but almost all have had inconclusive results in subsequent clinical trials (171-176). This has been explained (155) by the hypothesis that so many biochemical pathways contribute to and result from oxidative stress that blocking one is relatively ineffectual (108, 177).

Cytokines

The relatively spectacular improvement seen clinically with anti-VEGF drugs emphasises the importance of this cytokine as a final common pathway of damage to the retina and its vasculature. In turn the damage caused by excess VEGF prompts the production of abnormal concentrations of other related growth factors. Another observation quite unexplained, is the finding that in dogs, after 5 years of hyperglycemia, pericyte loss and capillary dropout occurs in retinal capillaries but not in brain (178): there appears to be a specific *retinal* cause for diabetic retinopathy, although the two tissues have the same neuroectodermal origin.

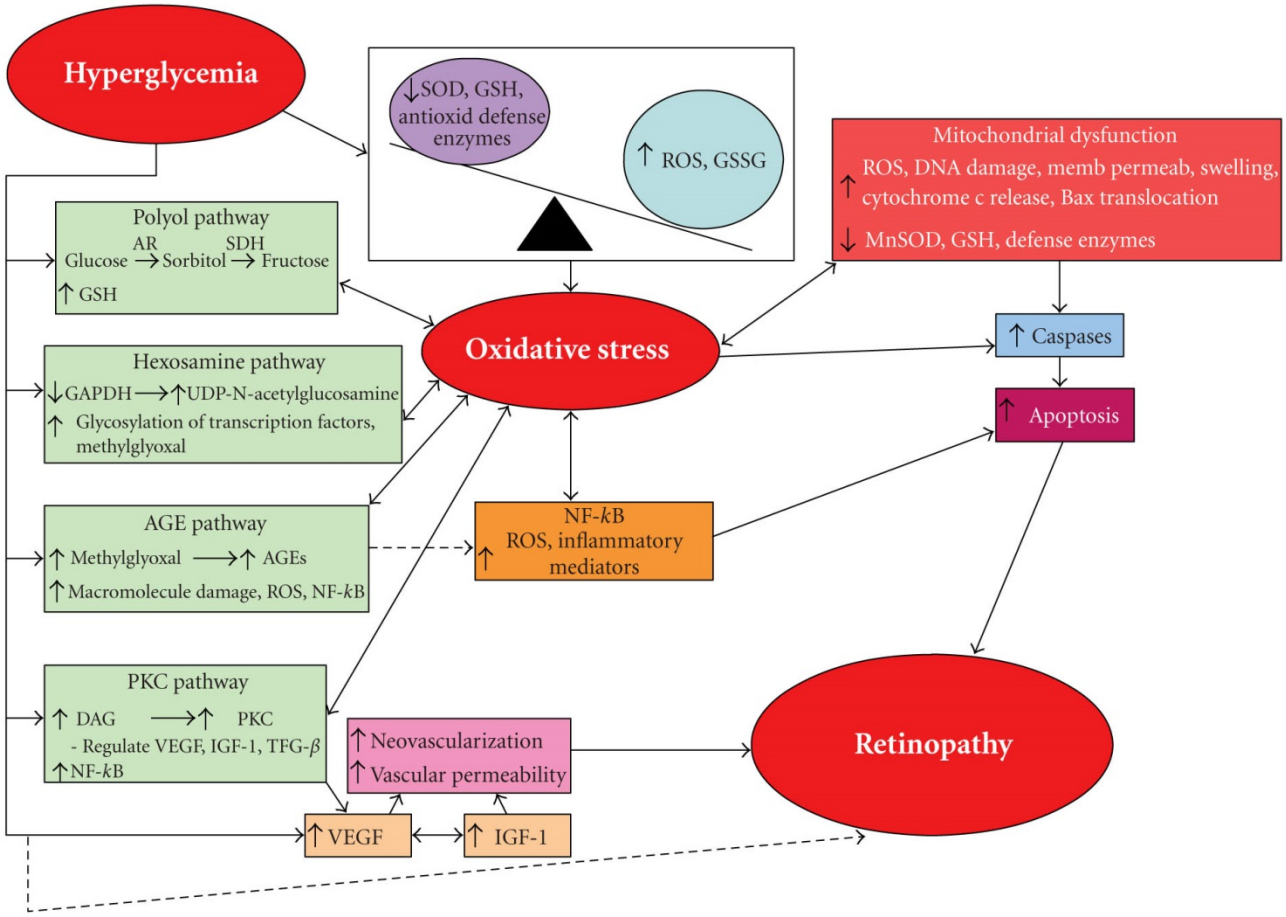

Figure 10: Summary of mechanisms by which oxidative stress in diabetes causes retinopathy. Four distinct glucose metabolic pathways are activated by hyperglycemia: Diacylglycerol (DAG)–protein kinase C (PKC) (137), advanced glycation end-products/receptor for advanced glycation end-products (AGE/RAGE), Polyol (sorbitol), and Hexosamine pathways.

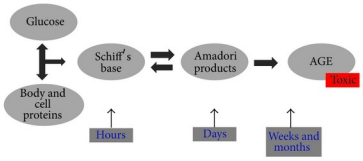

Figure 11. Mechanism of production of advanced glycation end-products (AGEs). From (136).

10. Neuronal abnormalities in early diabetes

In addition to the biochemical changes discussed above, which may cause the clinical vasculopathy, it has been known for many years that retinal neuronal damage occurs early in the condition (179). The examination of human post-mortem material (180) showed loss of tissue and excess TUNEL staining characteristic of apoptosis (181, 182). Thinning of the retina in living diabetic patients has been described (183). However the damage is selective: Ganglion cells and short wavelength cone receptors are preferentially damaged (184). Experiments on streptozotocin-induced diabetes in rodents (185) have led to similar claims. Thus more apopotosis has been claimed by some (186, 187), but has been reported absent by others (188). An example of damage to astrocytes and disappearance of connexin-43 normally seen in association with astrocytes is shown in Figure 12 (187).

Electrophysiological testing (189-191) both in man and rodents indicates inner retinal functions are disturbed much more than outer retinal function (31, 191). In psychophysical testing, losses in tritan colour vision, originally thought to be due to scattering changes, have been shown to be neural, to occur very early, and to be ameliorated by oxygen inhalation (192). Similar aberrations are seen with other psychophysical measures (189, 193-196).

There is some doubt about whether the neural changes precede the onset of the vasculopathy (197-198). Most biochemical experiments are studies after >4 week period of diabetes (216). Hypoxia and inner retinal neural changes have been reported at 2 weeks and the earliest vascular changes (leakage of fluid from retinal capillaries) can only be seen after 4 weeks. The early neuronal changes (187, 197, 198, 200) also occur in the absence of changes in the ERG which are dependent on the outer retina (201) (and see below). So it is possible that vascular and neuronal changes in the rodent retina are produced by different mechanisms, just as may be the case in man.

In superfused retinal slices, patch clamp recordings have demonstrated changes in glutamate release and activity in the rod pathway. These changes in spontaneous excitatory postsynaptic currents (spEPSCs) are an indicator of retinal neuronal activity and are controlled by hyper-glycemia. Thus excess activity in spEPSCs can be seen in the rod bipolar terminals recorded in slices from the retinas of rats made diabetic with streptozotocin (202). The activity returns to normal when the superfusing saline contains less glucose. The rod bipolar cell has a metabotropic glutamate receptor at its synapses with rod photoreceptors, and becomes depolarised on light stimulation. It releases glutamate at its axonal synapses with AII and A17 amacrine cells (see chapter in **Webvision** on Rod pathways through the retina). The glutamate release is increased in diabetics and returns to normal if the superfusing fluid does not contain extra glucose. The glutamate affects the α-amino-3-hydroxy-5-methyl-4-isoxazolepropionic acid receptor (AMPAR) receptor in A17 cells. This, by affecting $[Ca^{2+}]_{in}$, reduces the inhibitory GABAc receptor activity at the rod bipolar cell and A17 synapse, and, in turn, still further increases the glutamate output by the rod bipolar cell (Figure 13) (202) (see chapter in **Webvision** on GABAc in the retina).

Thus not only does there appear to be a specific *retinal* cause for diabetic retinopathy (178), but also this cause is linked to hypoxia and metabolic overload, both in neuronal and vascular retinal elements. This was the trigger for the new hypothesis discussed below.

11. A new hypothesis based on rod photoreceptor biophysics

Hypoxia, driven by dark adaptation, accelerates the development of diabetic retinopathy (189, 203-205). There are several reasons why this occurs: Rod photoreceptors in the outer retina are ***maximally*** depolarized in the dark and continuously release large amounts of their neurotransmitter glutamate and this increases energy utilization and oxygen consumption (206-208) (Figure 14).

In darkness rods consume more oxygen than any other cell in the body (208-210) because the water and ions entering the rod outer segment need to be pumped out by pumps localized near the large mitochondria of the inner segment (Figure 14) (this pumping has similarities to a fireboat squirting out extreme amounts of water, Figure 15). Even though the choroidal blood supply is very profuse, the partial pressure of oxygen at the level of the inner segments of the photoreceptors is near zero in darkness compared with the 30 mm Hg common in most tissues. In animal experiments, the partial pressure of oxygen rises suddenly and briefly when the retina is stimulated by a flash of light (211). With normal oxygen concentrations, the rods receive sufficient oxygen, but if oxygen is reduced somehow, the rod sensitivity falls. This occurs with only a modest reduction of oxygen corresponding to a reduction in air pressure that occurs at an elevation of about 4000 ft. Thus, in commercial jet aircraft, which are pressurised to around 7000 ft., healthy normal observers have slightly reduced rod sensitivity and some individuals, particularly those with heart or lung disease, may experience symptoms of dimmed vision, fatigue, nausea, headaches, loss of consciousness, and (on extended flights) even pulmonary edema or death from altitude sickness (212). Consequently, if in retinal disease the availability of oxygen is reduced due to

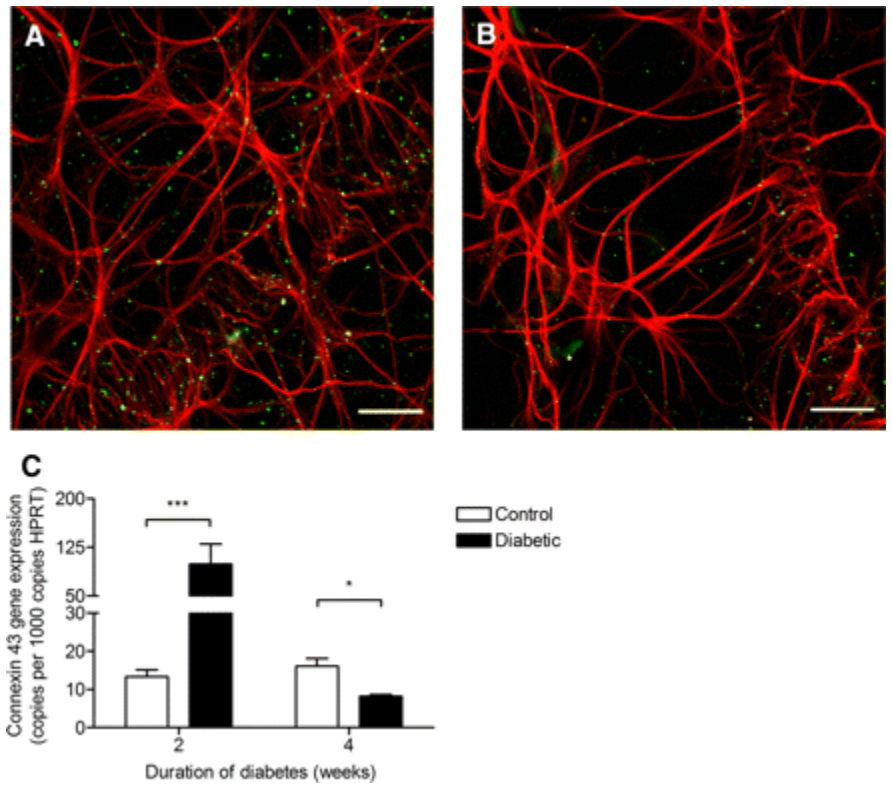

Figure 12: Changes in connexin-43 gene expression during early in diabetes. Control (A) and diabetic (B) rat retinas were immunolabeled with an antibody to connexin-43 (green) and the expression colocalized to astrocytes (GFAP, red). C) Connexin-43 gene expression was also quantified after 2 and 4 weeks diabetes using qPCR and the data are expressed relative to the housekeeping gene, HPRT. Connexin-43 gene expression is upregulated after only 2 weeks of diabetes, whereas its expression is decreased after 4 weeks. Data are expressed as mean ± SEM, ***P< 0.001, *P < 0.05, n > 9. Scale bar: 50 μm. Note the early and non-sustained expression of connexion in astroyctes, which contrasts with the more delayed and progressive changes in vascularity. From (187).

decreased function of the retinal circulation, or the relative demand for oxygen increases due to metabolic stress, there will be an imbalance which will lead to hypoxia in not only the outer retina (which is avascular) but also in the inner part, which is supplied primarily, but not completely, by the retinal arterial circulation. These processes are diagrammed in Figure 16.

Increased blood sugar levels in diabetics will lead to increased glucose transport through cell membranes in many cell types (but not apparently in rods due to their high affinity glucose transporters) (130, 131). On entering the tricarboxylic cycle, the excess sugars will lead to an increased demand for oxygen. This also results in the formation of advanced glycosylation end products (AGEs), which are modifications of proteins or lipids that become non-enzymatically glycosylated when exposed to aldose sugars and oxidative stress (213-215). Recent experimental evidence shows that rod photoreceptor cells are major contributors to diabetes-induced oxidative stress by producing reactive oxygen species and local inflammation in the retina (216).

These changes accumulate with time affecting both intracellular and extracellular function and by engaging the receptor for advanced glycation end products (RAGE). Activation of RAGE by AGEs causes upregulation of the transcription factor nuclear factor κ β (NFκβ) and its target genes. In Müller cells this promotes the expression of glial fibrillary acidic protein (GFAP) which is seen very early in diabetes, and the secretion of the cytokine, VEGF. As already alluded to above, VEGF causes changes to small vessels and makes them leaky (VEGF was initially identified as a vascular permeability factor [VPF] (217). Other AGEs contribute to the increase in basal membrane thickness which occurs in many tissues, including the capillaries of the retinal circulation (218-222). All these factors reduce oxygen transport into the retina. Additional biochemical alterations are known to occur in the diabetic retina, but once hypoxia is established, it will cause a cascade of effects that drive the production

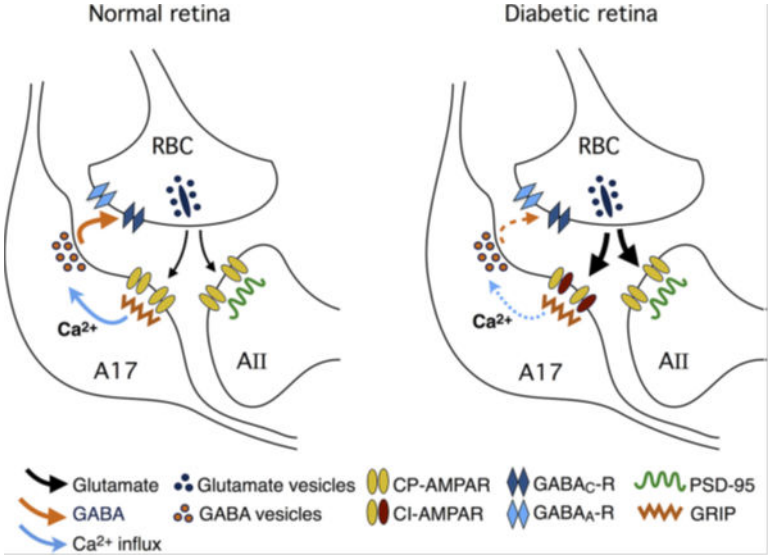

Figure 13: The rod bipolar- to-A17-amacrine feed-forward and feed-back interactions are affected by hyperglycemia. The rod bipolar cell (RBC) has postsynaptic metabotropic glutamate receptors, activated by rod signals. Its presynaptic surface is in a dyad into which the RBC releases glutamate. A17 amacrines and AII amacrines complete the dyad. Glutamate mobilizes calcium in the A17 and as a result, the amacrine releases GABA, an inhibitory feedback transmitter to the rod bipolar. This inhibition is weakened in high glucose, and consequently RBC output increases, as does AII output. (AII is the narrow field amacrine which connects to cone bipolar axons and ganglion cells). From (202). Of note, the sensitivity of the inhibitory GABAc receptor activity is increased in diabetic RBCs (269), most likely through its effect on the efficacy of gene transcription (201,270).

of VEGF (Figure 16) leading to further changes associated with diabetic retinopathy: and these changes in turn will exacerbate any underlying hypoxia.

Since a major cause of retinal hypoxia is the demand of the rods during periods of dark adaptation, reducing rod dark current should ameliorate diabetic changes. However, many other biochemical changes seen in diabetic retina have been connected to the overproduction of reactive oxygen species. (223). If these pathways are more important than the rod oxygen demand, increasing the retinal oxygen tension could either have little effect, or might even accelerate the progression of diabetic retinopathy. However, pan-retinal laser photocoagulation, the mainstay of treatment for proliferative diabetic retinopathy, has been shown to restore local oxygen levels to normal within weeks of its application (224). It is thought to work mainly by destroying large numbers of rods in the peripheral retina thereby increasing the oxygen supply to the remaining tissue (225). Furthermore, vascular responsiveness to oxygen inhalation also improves following photocoagulation (226-228).

12. Evidence for a new treatment based on the hypothesis that retinal hypoxia can be reduced by keeping rods light adapted at night

The success of panretinal photocoagulation is mainly because the treatment destroys rod photoreceptors, thereby reducing oxygen demand of the outer retina, particularly under dark adapted conditions. The remaining rods benefit, but even more importantly, there is improved ability of oxygen to reach the inner retina from the choroid because of the reduction in the number of rod photoreceptors with their oxygen-absorbing mitochondria. This may change the balance in the supply of oxygen to the inner retina, which already has a compromised retinal circulation.

The use of anti-VEGF drugs is now the most common initial treatment for diabetic eye disease, and hypoxia is the major determinant of VEGF production, but this is almost a circular argument. Direct measurement of

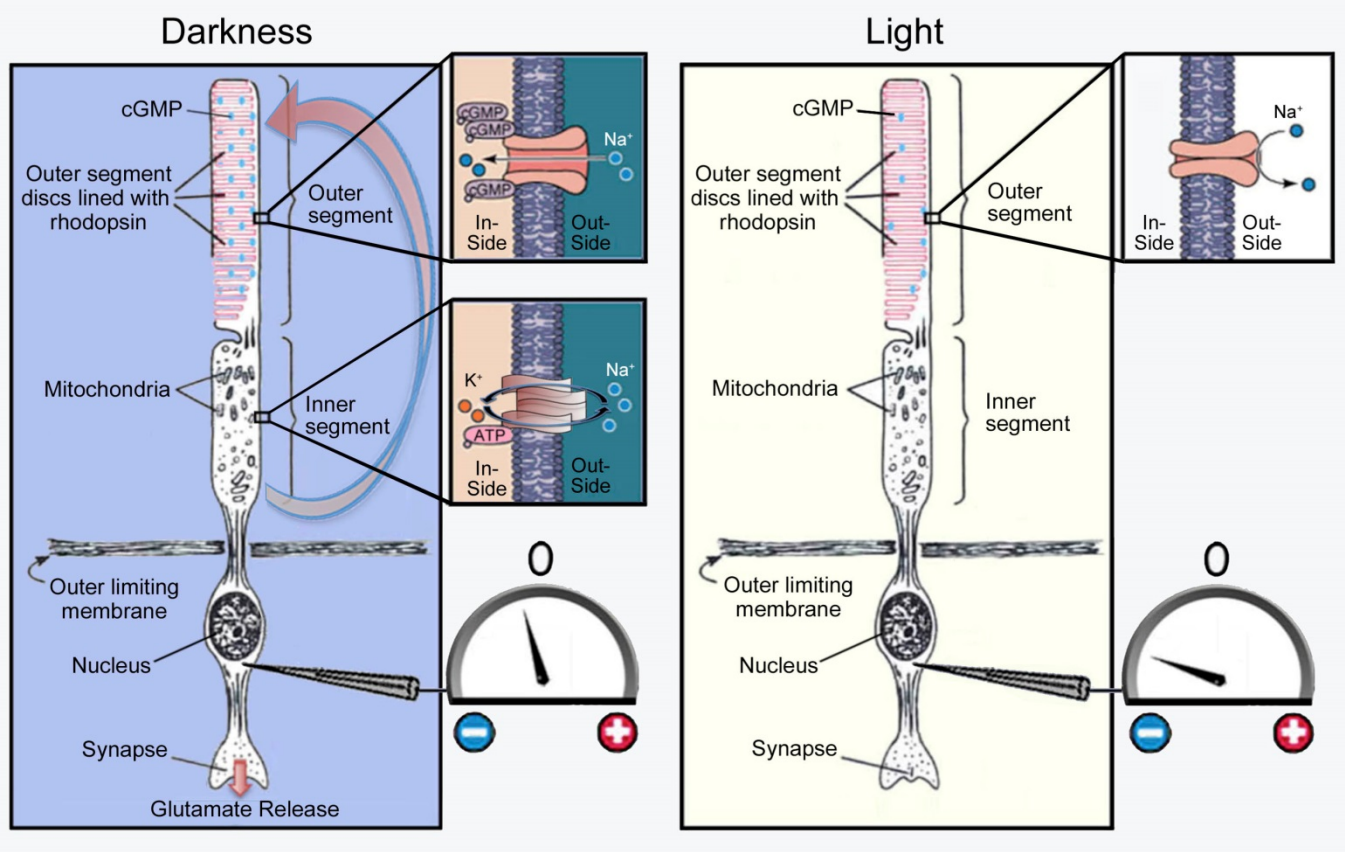

Figure 14: Mechanism of rod excitation. In darkness, non–specific cation channels in the outer segment membrane are open (as indicated by the left upper inset), and there is a net inward gradient of ions and water. This depolarizes the rod, as indicated in the diagram by the voltmeter recording from the nuclear region. In light, the ion channels close (upper inset right) and the rod repolarizes (hyperpolarizes). The water and ions entering the rod outer segment are pumped out by pumps localized in proximity to the large mitochondria of the inner segment. This causes a longitudinal current to flow from the inner to outer limb of the cell as indicated by the red arrow in darkness. In light this stops. The electrochemical changes that occur in response to an incremental change in light can also be measured electrophysiologically by the flash electroretinogram (ERG), recorded as a negative potential at the cornea known as the a-wave (not shown). Modified from (208).

oxygen tension in diabetic cat retina shows that the inner retina is more hypoxic than that of normal felines even in regions where there is no capillary dropout evident (229, 230) (Figure 17). The partial pressure of oxygen falls rapidly from the arterial level when the electrode moves from the RPE into the outer retina, and in darkness reaches a level of zero in the region of the rod inner limb mitochondria (229, 230). This rate of decline is the maximum theoretically possible if the choroid is an infinite source of oxygen, and the mitochondria, an infinite sink. As the electrode tip moves into the inner vascularized retina (see Figure 17A, top left tracing) the partial pressure increases again. Calculation shows that the rod mitochondria must also be absorbing oxygen from the retinal vessels. In light the oxygen tension is higher for all retinal locations, but especially at the level of the rod inner limbs, where it increases by about 30 mm Hg. (not illustrated). This shows how rapid the rate of respiration is, and how quickly it is affected by the processes of transduction. In addition in diabetic cat retina, even in regions in which there is no capillary dropout, the inner retinal oxygen tension is lower than in normal retina (Figure 17). There are also species differences in the oxygen tension profiles. In the miniature pig (224) and macaque (232), although the profiles resemble those shown in Figure 17A (from the cat (211)), the pO_2 at the level of the inner limbs does not fall to zero but about 5 mmHg. Nevertheless the outer retinal oxygen consumption greatly exceeds the inner retinal oxygen consumption. In guinea pigs (232) and rabbits (232, 235) animals with poorly developed retinal vessels, more of the inner retina's oxygen supply is provided by the choroid, but the same general relationships may be seen, and oxygen consumption and hypoxia of the outer

Figure 15: Allowing for the difference in volume, the rod in darkness pumps 10 times more than water from a fireboat! This produces heat, and demands a great deal of energy in the form of ATP, primarily produced by oxidative phosphorylation by the large mitochondria of the inner segment of the photoreceptor (of course the rod does not pump under pressure, like the fireboat!).

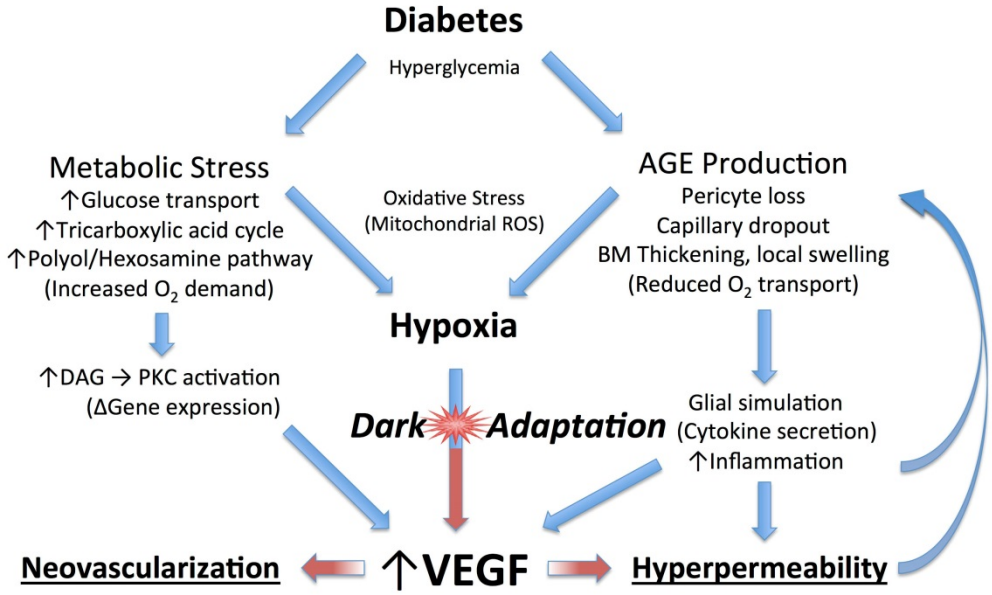

Figure 16: Diagram of how diabetes leads to vascular changes in the inner retina.

retina increases as the photoreceptors develop and their outer limbs lengthen. In the species studied in dark adaptation, diabetic animals have an inner retinal hypoxia more evident than in controls (224, 234). However, in the rat retina, the retinal profiles are different especially in the RCS rat (232), with the minimal pO_2 being found in the inner not the outer retina. Nevertheless the difference in oxygen consumption when in light or darkness is greatest in the outer retina, and corresponds to photoreceptor usage. This is supported by the change in profiles in the developing retina, and the change in profile when photoreceptor degenerations develop (233-235). So, in

rat (199), direct measurements of intraretinal pO_2 using oxygen microelectrodes have not shown hypoxia or change in diabetes. However, this last observation is difficult to reconcile with the other data measured in larger eyes, which are similar to human eye size (195, 235, 236) and to indirect evidences of rod-associated retinal hypoxia (237-239).

Human beings have many inherited diseases that selectively destroy rods, producing retinal dystrophies - Retinitis Pigmentosa is the most common of these conditions. Rod loss in many cases is slow, and diabetes can occur independently in conjunction with the slow loss of photoreceptors. However, in such patients, diabetic retinopathy-type changes rarely happen (Table 1) (240).

Another line of evidence comes from patients with maternally inherited diabetes and deafness (MIDD). These patients have mutation of mitochondrial DNA at position 3243 which manifests in a number of ways and can cause a type of retinal degeneration. This may or may not occur together with diabetes. If the retinal degeneration occurs together with the diabetes, the incidence of microaneurysms is less than if the diabetes occurs alone (241-243).

In some individuals, the efficiency of hypoxia in increasing VEGF and VEGF *RNA* levels is much reduced and can be seen by incubating white blood cells under normoxic and hypoxic conditions. Among this group, retinopathy does not appear in individuals who also have diabetes (243). In addition, breathing oxygen improves several visual functions in patients with diabetic retinopathy and DME (192, 193, 196, 189, 244, 245).

Finally, patients with diabetes who have sleep apnea, (defined as more than 5 periods, called *dips*, when oxyhemoglobin saturation falls below 90%), have more rapid development of diabetic eye complications than those who do not have sleep apnea. The increased risk is reduced in patients with sleep apnea who are treated with positive pressure ventilation (246-250). There are several recent reviews that include a more detailed discussion of the hypothesis that rod photoreceptor dark adaptation causes hypoxia and consequent damage to the retina in diabetic retinopathy (251, 252).

Given all the above evidence that hypoxia in the inner retina in diabetic patients causes the vascular damage of diabetic retinopathy, and evidence that rods are responsible for most of the oxygen consumption during their active metabolic time in darkness, it seems reasonable to suggest that curbing the rod activity at night would be beneficial. A simple treatment for impending diabetic retinopathy might be to prevent rod activity during darkness by the application of constant nocturnal light. This is the basis for the new treatment paradigm described below.

We have carried out clinical trials, in which patients wear "light masks" which provide retinal illumination through the closed eyelids during sleep. Sufficient light penetrates the lid to partially light adapt the rods. The light sources were either chemo-luminescent (glow-patches) or light-emitting diodes (LEDs). The green or blue-green light was used to selectively stimulate rods (95% of all photoreceptors are rods) rather than cones, because the sensations aroused by rod stimulation are less intrusive and tend to fade to insignificance as patients adapt to a low background luminance. In order to reduce inter-personal differences, the subjects wore masks which illuminated only one eye, with the other, in darkness being used as a control (253).

The results of a 6 month Phase I trial showed that no adverse reactions were encountered and patients accepted the idea of wearing a mask during sleep. However, unusual for a Phase 1 trial, the therapy caused a significant improvement in the 10 trial eyes relative to their controls. Figure 18 shows the results in one patient.

Fundus photographs such as shown in Figure 18 were examined under high magnification and the total areas of microaneurysms measured. The improvement in the condition (decrease in areas of affected central retina) was significant. A similar result was obtained when changes in tritan – blue-yellow - colour vision (known to be damaged early in diabetic retinopathy) was assessed (253) (not shown).

In a Phase II trial of 42 patients with non-center-involving DME, a similar benefit was shown. A high proportion of the treated eyes improved, while this did not occur in untreated eyes (Table 2). Much of this occurred during the first 3 months. Furthermore, whereas four of the patients recruited to the trial dropped out because the unilluminated fellow eyes received laser or intravitreal bevacizumab for DME during the study, none of the illuminated eyes required such treatment.

Ocular coherence tomography showed that cysts characteristic of DME disappeared, and significant reduction in thickness occurred (Figure 19) (254). The results of these changes in OCT measurements are shown in Table 3. The patients in this trial had very early DME, and in many patients the swelling did not involve the area within 300 μm of the fovea. Hence if there is a reduction observed in local swelling in one retinal region, might swelling simply be occurring in another region? In order to evaluate this, measurements were made in the Early Treatment Diabetic Retinopathy (ETDRS) zones, and the region with maximal swelling was compared to its opposite "mirror" zone. It can be seen that decrease in thickness occurs only in treated eyes (Figure 20). A small but significant improvement in visual acuity and contrast sensitivity also occurred among the light adapted eyes in this trial (table 4). It should be noted, that almost all the patients recruited were at an early stage of diabetic retinopathy with DME and had good visual acuity at baseline so a larger average increase in acuity would not be expected.

Such studies provide a "Proof of Principle" that retinal hypoxia in darkness must be an important driving force for diabetic retinopathy. However, further work is required to establish the role that 'light-at-night' may play in the treatment or prevention of the various complications of diabetic eye disease. Furthermore, we do not know how 'light at night' interacts with the other treatments for the condition. For this Phase III and IV clinical trials are required. This presents a difficulty, because for new pharmaceuticals, such trials are largely funded directly by the drug companies, while there is no such equivalent for medical devices. Small commercial companies have manufactured masks which can be used in such trials, and apparently in one trial carried out in the Department of Ophthalmology, Vinohrady, Prague, Czech Republic, produced encouraging results. These results have not been published in detail yet. Further trials are starting in London (255) Cardiff (UK) (256) and Boston (USA). There is a considerable need for this research because the cost of the present day "gold standard" treatment of repeated injections is becoming unsustainable (257). (Figure 21 refers of age related macular degeneration, but for diabetes the same economic criteria will apply).

Anti-VEGF drugs are expensive: Avastin costs about 1/40th of the price of Lucentis, but the cost of treatment by the two is not so different, in part because of the associated cost of administration (Figure 21). But only in the first world are incomes high enough for a significant proportion of the population with vision threatening diabetic eye disease to access treatment (257) and even then many individuals with vision threatened by complications from diabetes are not accessing available eye care (258). Worldwide there is not only a shortage of funding for available treatments, but a severe shortage of personnel trained to diagnose the condition and manage it appropriately (259). By contrast, the requirements of light-based treatment to interrupt nocturnal dark adaptation, for example through the use of a light masks, are relatively inexpensive, and so safe and easy to use that it could be made available with only basic instruction. This treatment may not replace medical intervention, but promises to complement or reduce the need for traditional therapies, thereby bringing down the cost of caring for patients with diabetic eye disease. We propose that more research and development be done so that light masks (or a similar device) may be manufactured on a scale that will reduce the cost to a level reaching the masses with diabetic eye disease.

It is possible that the evidence presented above concerning preventing dark adaptation in the diabetic retina, may also apply to other retinal conditions in which anti-VEGF drugs have been shown to be beneficial: Retinal diseases such as "wet" age related macular degeneration (257-265) (see chapter on age related macular degeneration (AMD) in **Webvision**) and retinopathy of prematurity (266) .

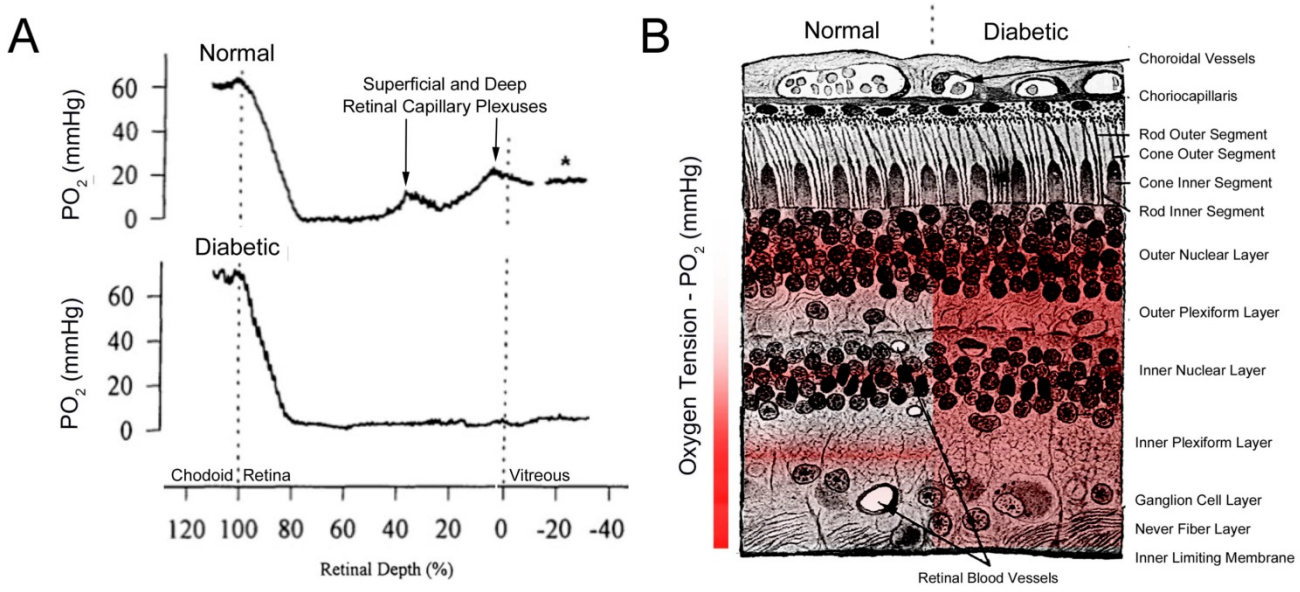

Figure 17: Retinal Oxygen Tension in Normal and Diabetic Cat. (A) Measurements (averaged) of oxygen partial pressure in retina, using O2 microelectrodes. The high tension in the choroid indicates blood with arterial saturation. A: upper part in normal animals, the rapid decrease as the electrode is withdrawn (proceeding from left to the right) is followed by an increase as the electrode passes through the deep and superficial capillary plexuses until the vitreous is reached (see * on trace). In the diabetic eye, (lower part) oxygen partial pressure is markedly lower in the inner retina. Modified after (230). (B) Cross section of the human retina with the gradient of oxygen partial pressure overlaid in red. The relative oxygen tensions are indicated by the depth of red shading, much reduced in diabetes. The left hand side of the retina illustrates the conditions present in the normal dark adapted retina (corresponding to the top trace in part A). There are regions in the outer retina and inner retina where oxygen tensions drop to very low levels (red shading). The right hand side illustrates what happens to oxygen tension in the diabetic state (corresponding to the bottom trace in part A). Modified after (231).

Acknowledgements

The authors thank Carol Spencer (Lahey Hospital Library) for research support. Figures 3, 4 and 5 were kindly provided by the ocular photography department of the Moran Eye Center. Neither of the authors have any direct financial interest in any devices used in the clinical work described.

Classification of diabetes	Type 1	Type 2
Number of replies validated by doctor	25	30
Mean age (SD)	60.8 (16.8)	65.5 (15.3)
Mean age at diagnosis	35	34
Mean duration of diabetes	19	14
Interval between onset of night blindness and diabetes (years)	7.2 (n=10)	19.5 (n=24)
# of cases of diabetic retinopathy	0	0
# of cases of other major diabetic complications (non-ocular)	5 (n=11)	8 (n=18)

Table 1: Incidence of diabetic retinopathy in patients with both diabetes and rod degenerations (retinitis pigmentosa): None of the patients (discovered by a web-based search of patient-societies with surveys validated by attending ophthalmologists) has the characteristic changes, though many had severe vascular and other disease in other organs attributable to diabetes, adapted from (240).

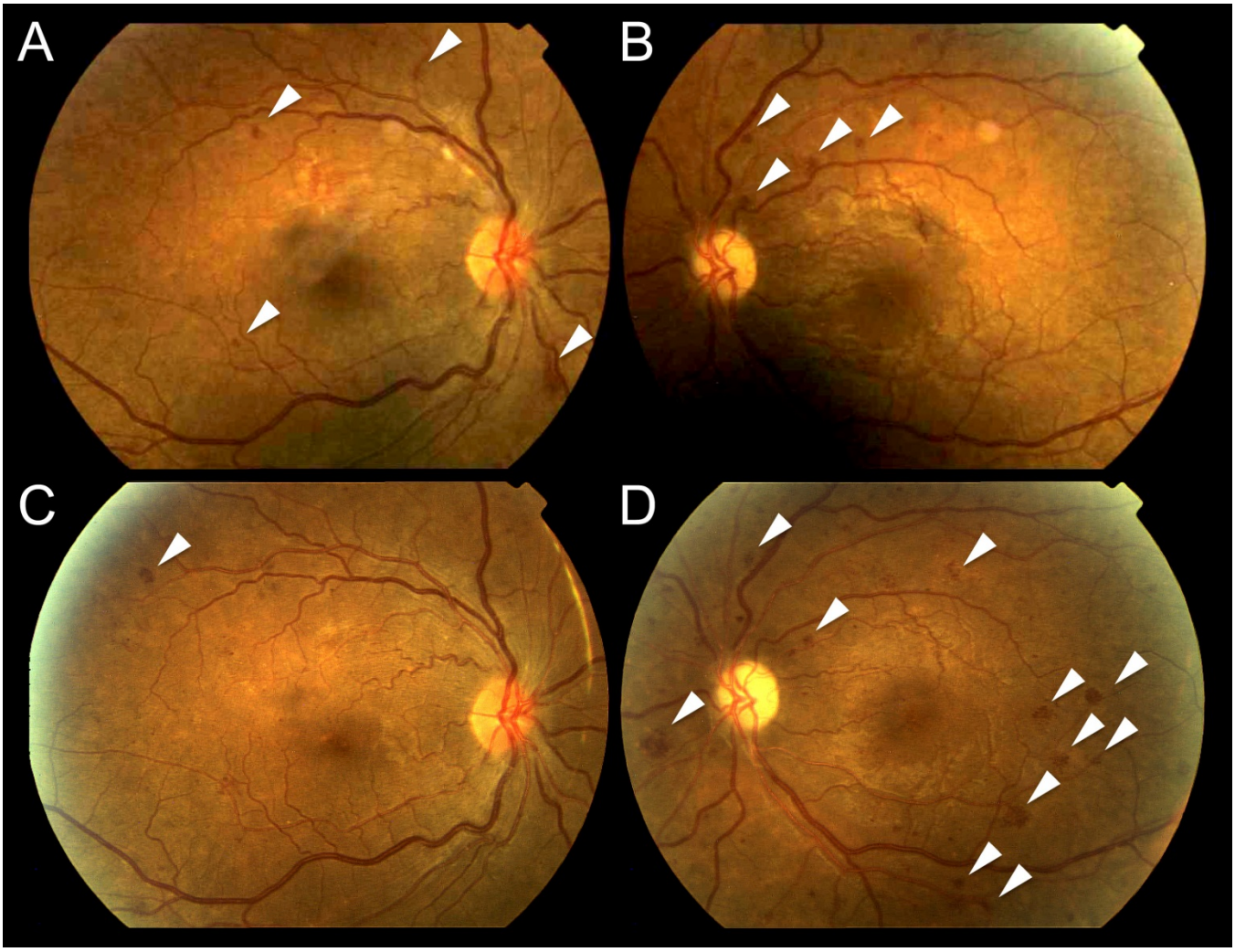

Figure 18: Representative fundus photographs from a patient with diabetic retinopathy. The upper row shows fundus photographs at baseline in the right (A) and left (B) eyes. The lower row shows the same patient following three months of light at night treatment of the right eye (C) with the left eye serving as a control (D). Note that in C the areas of hemorrhage (white arrows) have faded compared to A, consistent with an improvement in the clinical stage of retinopathy. In fact, in many light treated patients no new lesions developed. In contrast, the control eye (B and D) demonstrates many new and worsening hemorrhages at 3 months.

OCT macular fluid extent at 3 MONTHS

	Trial Eye	Control Eye	*P* value* (chi-squared)
Number improved	17	3	
Number unchanged	6	17	0.0003
Number worse	3	6	

Table 2: Change in DME at 3 months. Initial clinical results looking at change in macular thickness in a Phase II trial demonstrated that a majority of eyes treated with light at night improved, while untreated eyes in the fellow patient more often stayed the same or even worsened over the course of the trial (254).

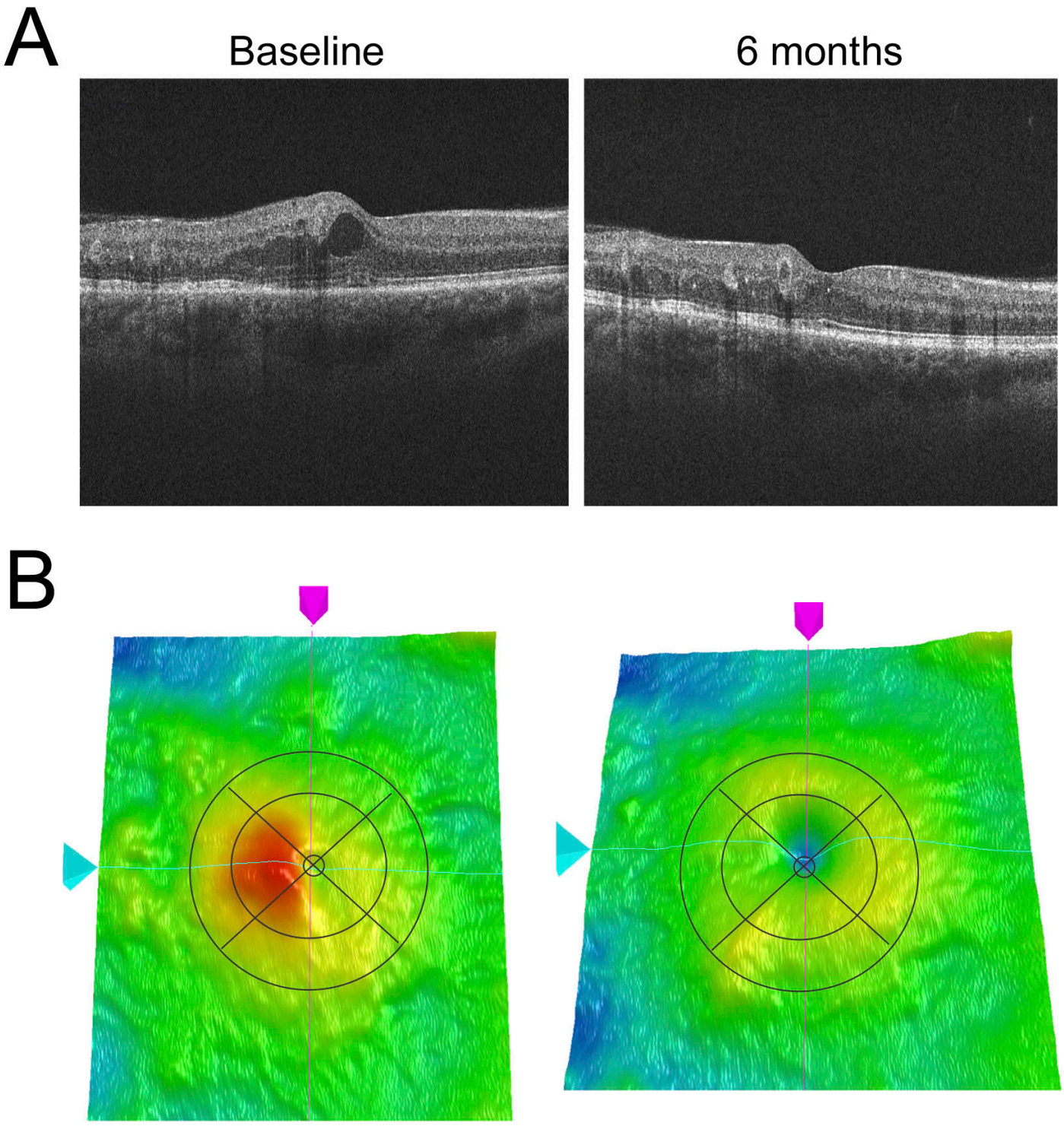

Figure 19: Illustrative OCT results on an eye before and after light treatment. (A) Cross- sectional views of the retina showing swelling and cyst at baseline, which has largely vanished at 6 months. (B) The False colour 3-dimensional OCT images from the same examinations. The overlay represents the ETDRS zones. The central small disc is zone 1 and contains the foveal pit. The area of maximal swelling (red) is in this case zone 2. The remaining zones of the inner ring, going clockwise are zones 3, 4 and 5, and the outer ring comprises zones 6, 7, 8, 9. The red-false colour in zone 2 indicates an abnormality. In the clinical trial the thickness of the maximally affected zone was compared to the relatively unaffected "mirror zone" 4 – or in other instances, if zone 3 was maximally affected, it was compared to zone 5. In this way it could be shown that the edema was reduced and had not merely moved to a different retinal locus (254).

OCT measures of retinal thickness

[change in trial eye] -[change in fellow eye] (μm)

Zone	mean	SE	95% CI	p =
Central	-11	1.92	-14.7...-.6.9	0.026
maximal	-13	2.26	-17.5....-7.2.	0.052
mirror	2.4	2.41	-2.5..... .7.3	0.144

Table 3: Summary of changes in OCT measures. The zones are illustrated by the overlays of the OCT images in Figure 19 (254).

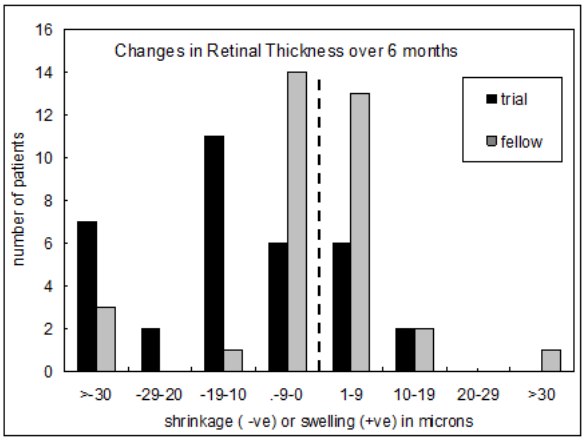

Figure 20: Changes in retinal thickness associated with light adaptation in the Phase II trial (254).

Test	Trial Eyes – numbers of letters read: Initial Values Mean SD	Trial Eyes – numbers of letters read: Final Values Mean SD	Fellow Eyes- numbers of letters read: Initial Values Mean SD	Fellow Eyes- numbers of letters read: Final Values Mean SD	Change and 95% CI after 6 months
Visual Acuity (ETDRS charts)	78.04 7.80 range 85-60	80.18 5.32 range 85-60	76.52 8.10 range 86-67	74.59 8.52 range 87-47	4.21 2.64-5.78
Constrast sensitivity (Pelli – Robson)	31.71 5.39 Range 38-20	33.14 4.57 Range 41-20	30.16 4.71 range 36-23	30.50 4.95 range 36-20	2.00 1.25- 2.75

Table 4: Summary of results of visual acuity and contrast sensitivity testing in study and fellow eyes in a Phase II trial of light adaptation (254).

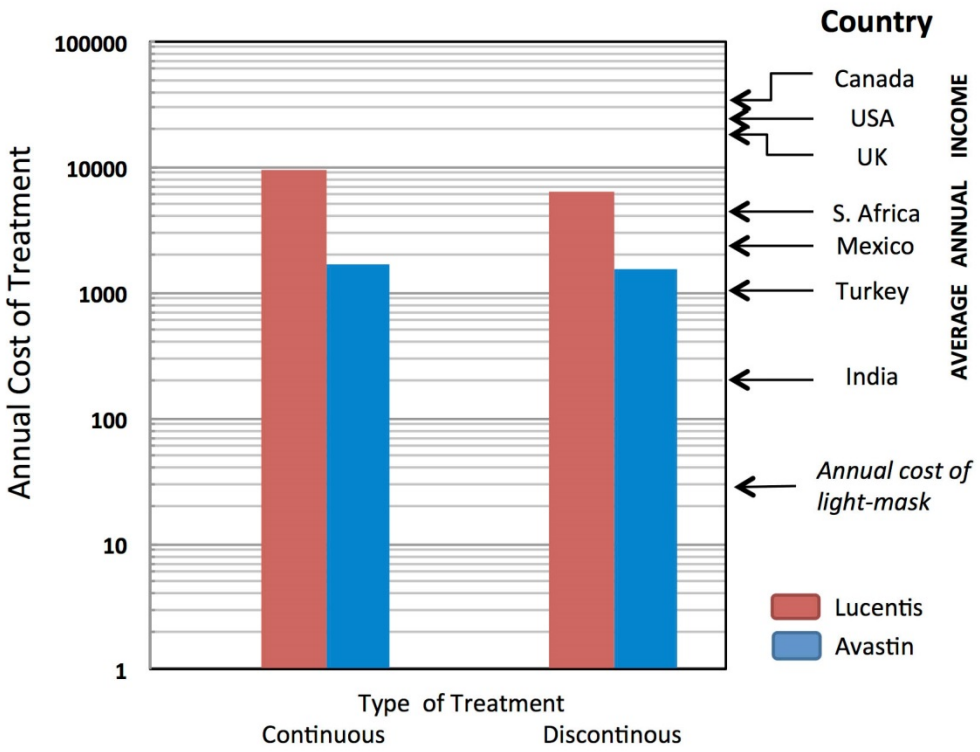

Figure 21: Health economics results of treatment of neovascular age related macular degeneration (AMD). Relative costs (£) of treatment by ranibizumab (Lucentis) and bevacizumab (Avastin) used at fixed intervals (continuous) or when required (discontinuous). Note the logarithmic ordinate. Lucentis is 40 times more costly to purchase than Avastin, but the difference in the total cost of treatment is much less. At the right, the median incomes in a number of different countries are indicated. Note only in the most affluent countries is the use of these drugs even possible for most of the population at risk. The cost estimate shown in this figure would be similar for DME. From (257).

About the Authors

Geoffrey Arden graduated in 1951 from University College London (UCL) and joined the MRC Vision Research Unit in the newly formed Institute of Ophthalmology. He obtained a Ph.D. in photochemistry under HJA Dartnall, and returned to UCL to complete a medical degree. After studying neurophysiological techniques with Ragnar Granit in Stockholm and KT Brown in San Francisco, he returned to the Institute of Ophthalmology. In the absence of any equipment except an ECG he devised the electro-oculogram (EOG) as a clinical test and

developed the first clinical electrophysiological department in the UK. He was appointed Professor, Honorary Consultant at Moorfields Eye Hospital and Director of the Electrodiagnostic department in 1968. He pioneered the use of cortical evoked potentials and the pattern ERG and devised clinical techniques for the measurement of achromatic and colour-contrast sensitivity. In an emeritus capacity he continues projects with investigators from Europe and the US and has turned his attention to the causes and treatment of diabetic retinopathy. He served a term as Chief Editor of the journal Vision Research.

Dr. David J. Ramsey received his M.D. and Ph.D. degrees from the University of Illinois at Chicago in 2008. He completed his residency in Ophthalmology at the Wilmer Eye Institute of the Johns Hopkins School of Medicine in 2012 followed by a combined medical/surgery fellowship in vitreoretinal diseases at the Massachusetts Eye and Ear Infirmary in 2014. Dr. Ramsey is currently a senior staff physician at the Lahey Clinic and sees patients in Burlington, MA. He also sees patients and performs surgery in Peabody, MA. His research focuses on the prevention of dark adaptation in patients with diabetes as a means to ameliorate diabetic changes in the retina. Future clinical trials will seek to determine whether this noninvasive, environmental intervention can limit the progression of diabetic retinopathy to PDR and/or reduce levels of sight-impairing macular edema.

References

1. Health Topics, Noncommunicable Diseases, Diabetes. Regional Office for Europe, World Health Organization. At Available at: http://www.euro.who.int/en/health-topics/noncommunicable-diseases/diabetes
2. National Diabetes Statistics Report, 2014. National Center for Chronic Disease Prevention and Health Promotion, Centers for Disease Control and Prevention. At: Available at: http://www.cdc.gov/diabetes/pubs/statsreport14/national-diabetes-report-web.pdf
3. Facts About Diabetic Retinopathy. National Eye Institute. At Available at: http://www.nei.nih.gov/health/diabetic/retinopathy.asp
4. Liew G1. Michaelides M, Bunce C. A comparison of the causes of blindness certifications in England and Wales in working age adults (16-64 years), 1999-2000 with 2009-2010. BMJ Open. 2014;4:e004015. PubMed PMID: 24525390.
5. Adams, F in Adams, F ed (1856): The extant works of Aretaeus the Cappadocian, p. 338. London: The Sydenham Soclety.
6. Allen FM. Current judgments on metabolic control and complications in diabetes. N Engl J Med. 1953;248:133–136. At . PubMed PMID: 13013504.
7. Ramsey DJ, Sunness JS. "Pregnancy and the Mother's Eye." In Tasman W., Jaeger E.A., eds., Duane's Clinical Ophthalmology, Vol. 5, Chapter 32, 2013.

8. Vaxillaire M, Froguel P. Monogenic diabetes in the young, pharmacogenetics and relevance to multifactorial forms of type 2 diabetes. Endocr Rev. 2008; **29:** 254-64. doi: 10.1210.
9. Abdul-Rasoul M, Habib H, Al-Khouly M. 'The honeymoon phase' in children with type 1 diabetes mellitus: frequency, duration, and influential factors. Pediatr Diabetes. 2006; **7:** 101-7.
10. Daneman D., Type I. Diabetes. Lancet. 2006;9513:847–858. PubMed PMID: 16530579.
11. Kelly MA, Mijovic CH, Barnett AH Genetics of type 1 diabetes. Best Pract Res Clin Endocrinol Metab. 2001; **15:** 279-91.
12. Dabelea D, Mayer-Davis EJ, Saydah S, Imperatore G, Linder B, Divers J, Bell R, Badaru A, Talton JW, Crume T, Liese AD, Merchant AT, Lawrence JM, Reynolds K, Dolan L, Liu LL, Hamman RF; SEARCH for Diabetes in Youth Study. JAMA. 2014;311:1778–86. PubMed PMID: 24794371.
13. Dabelea D, Ma Y, Knowler WC, Marcovina S, Saudek CD, Arakaki R, White NH, Kahn SE, Orchard TJ, Goldberg R, Palmer J, Hamman RF; Diabetes Prevention Program Research Group. Diabetes autoantibodies do not predict progression to diabetes in adults. Diabet Med. 2014;31:1064–8. PubMed PMID: 24646311.
14. Taplin CE, Craig ME, Lloyd M, Taylor C, Crock P, Silink M, Howard NJ. The rising incidence of childhood type 1 diabetes in New South Wales, 1990-2002. Med J Aust. 2005; **183:** 243-6.
15. Hyöty H, Hiltunen M, Knip M, Laakkonen M, Vähäsalo P, Karjalainen J, Koskela P, Roivainen M, Leinikki P, Hovi T, et al. A. prospective study of the role of coxsackie B and other enterovirus infections in the pathogenesis of IDDM. Childhood Diabetes in Finland (DiMe) Study Group. Diabetes. 1995;44:652–7. PubMed PMID: 7789630.
16. Zhao M, Pan SS. Discussion of correlative factors and risk in patients with diabetic erectile dysfunction. Zhonghua Nan Ke Xue. 2002;8:395–7. Chinese. PubMed PMID: 12593008.
17. Centers for Disease Control and Prevention. National diabetes fact sheet: national estimates and general information on diabetes and prediabetes in the United States, 2011. Atlanta, GA: U.S. Department of Health and Human Services, Centers for disease control and prevention 2011.
18. Leung MY, Pollack LM, Colditz GA, Chang SH. Life years lost and lifetime health care expenditures associated with diabetes in the U.S., National Health Interview Survey, 1997-2000. Diabetes Care. 2015; **38**: 460-8. doi: 10.233.
19. Lueder GT, Silverstein J; American Academy of Pediatrics Section on Ophthalmology and Section on Endocrinology. Screening for retinopathy in the pediatric patient with type 1 diabetes mellitus. Pediatrics. 2005; **116:** 270-3.
20. Verougstraete C, Toussaint D, De Schepper J, Haentjens M, Dorchy H. First microangiographic abnormalities in childhood diabetes--types of lesions. Graefes Arch Clin Exp Ophthalmol. 1991; **229:** 24-32.
21. Younis N, Broadbent DM, Harding SP, Vora JP. Incidence of sight-threatening retinopathy in Type 1 diabetes in a systematic screening programme. Diabet Med. 2003; **20:** 758-65.
22. Eastman RC, Javitt JC, Herman WH, Dasbach EJ, Zbrozek AS, Dong F, Manninen D, Garfield SA, Copley-Merriman C, Maier W, Eastman JF, Kotsanos J, Cowie CC, Harris M. Diabetes Care. 1997;20:725–34. PubMed PMID: 9135934.
23. Malone JI, Morrison AD, Pavan PR, Cuthbertson DD; Diabetic Control and Complications Trial. Diabetes Care. 2001;24:522–6. PubMed PMID: 11289479.
24. Klein R, Meuer SM, Moss SE, Klein BE. Arch Ophthalmol. 1995;113:1386–91. PubMed PMID: 7487599.
25. [No authors listed] Epidemiology of Diabetes Interventions and Complications (EDIC). Design, implementation, and preliminary results of a long-term follow-up of the Diabetes Control and Complications Trial cohort. Diabetes Care. 1999; **22:** 99-111.
26. Younis N, Broadbent DM, Vora JP, Harding SP; Liverpool Diabetic Eye Study. Lancet. 2003;361(9353):195–200. PubMed PMID: 12547541.
27. Joussen AM Gardner TW Kirchoff B and Ryan SJ (eds) Retinal Vascular disease. Springer. 2007; p. 778.
28. Henson DB, North RV. Dark adaptation in diabetes mellitus. Br J Ophthalmol. 1979; **63:** 539-41.

29. Schulze DP, Freese R, Sauerwald R. Nyktometric examinations on eye function in diabetic retinopathyKlin Monbl Augenheilkd. 1976; **169:** 369-72.
30. Abraham FA[1], Haimovitz J, Berezin M. The photopic and scotopic visual thresholds in diabetics without diabetic retinopathy. Metab Pediatr Syst Ophthalmol. 1988; **11:** 76-7.
31. Greenstein VC, Thomas SR, Blaustein H, Koenig K, Carr RE. Optom Vis Sci. 1993;70:18–23. PubMed PMID: 8430004.
32. Birch J, Dain SJ. An averaging method for the interpretation of the Farnsworth-Munsell 100-Hue Test--II. Colour vision defects acquired in diabetic retinopathy. Ophthalmic Physiol Opt. 1987; **7:** 281-91.
33. Arden G, Gündüz K, Perry S. Color vision testing with a computer graphics system: preliminary results Doc Ophthalmol. 1988; **69:** 167-74.
34. Fong DS, Barton FB, Bresnick GH. Impaired color vision associated with diabetic retinopathy: Early Treatment Diabetic Retinopathy Study Report No. 15. Am J Ophthalmol. 1999; **128:** 612-7.
35. Rasmussen ML, Broe R, Feydkjaer-Olson U, Olsen BS, Mortensen HB, Peto T, Grauslund J. Comparison between Early Treatment Diabetic Retinopathy Study 7-field retinal photos and non-mydriatic, mydriatic and mydriatic steered widefield scanning laser ophthalmoscopy for assessment of diabetic retinopathy. J Diabetes Complications. 2015;29:99–104. PubMed PMID: 25240716.
36. Silva PS, Cavallerano JD, Sun JK, Soliman AZ, Aiello LM, Aiello LP. Peripheral lesions identified by mydriatic ultrawide field imaging: distribution and potential impact on diabetic retinopathy severity. Ophthalmology. 2013;120:2587–95. PubMed PMID: 23778092.
37. Papachristodoulou D, Heath H, Kang SS. The development of retinopathy in sucrose - sucrose-fed and streptozotocin-diabetic rats. Diabetologia. 1976;12:367–74. PubMed PMID: 134921.
38. Kern TS, Engerman RL. Comparison of retinal lesions in alloxan- diabetic rats and galactose-fed rats. Curr Eye Res. 1994; **13:** 863-7.
39. Lutty GA. Effects of diabetes on the eye. Invest Ophthalmol Vis Sci. 2013;54:13–12979. PubMed PMID: 24335073.
40. Wu M, Chen Y, Wilson K, Chirindel A, Ihnat MA, Yu Y, Boulton ME, Szweda LI, Ma JX, Lyons TJ. Intraretinal leakage and oxidation of LDL in diabetic retinopathy. Invest Ophthalmol Vis Sci. 2008;49:2679–85. PubMed PMID: 18362112.
41. Osaadon P, Fagan XJ, Lifshitz T, Levy J. A review of anti-VEGF agents for proliferative diabetic retinopathy. Eye (Lond). 2014;28:510–20. PubMed PMID: 24525867.
42. Albert and Jakobiec, 1994 Albert & Jakobiec's Principles & Practice of Ophthalmology: 4-Volume Set and Website R Twerk &Co.
43. Techniques for scatter and local photocoagulation treatment of diabetic retinopathy: Early Treatment Diabetic Retinopathy Study Report no. 3. The Early Treatment Diabetic Retinopathy Study Research Group. Int Ophthalmol Clin. 1987;27:254–64. [No authors listed]. PubMed PMID: 3692707.
44. ETDRS report no. 19. Early Treatment Diabetic Retinopathy Study Research Group. Arch Ophthalmol. 1995;113:1144–55. PubMed PMID: 7661748.
45. Nordwall M, Bojestig M, Arnqvist HJ, Ludvigsson J; Linköping Diabetes Complications Study. Declining incidence of severe retinopathy and persisting decrease of nephropathy in an unselected population of Type 1 diabetes-the Linköping Diabetes Complications Study. Diabetologia. 2004;47:1266–72. Epub 2004 Jul 2. PubMed PMID: 15235773.
46. Focal photocoagulation treatment of diabetic macular edema. Relationship of treatment effect to fluorescein angiographic and other retinal characteristics at baseline: ETDRS report no. 19. Early Treatment Diabetic Retinopathy Study Research Group. Arch Ophthalmol. 1995;113:1144–55. [No authors listed]. PubMed PMID: 7661748.
47. Blumenkranz MS. Optimal current and future treatments for diabetic macular oedema. Eye (Lond). 2010;24:428–34. PubMed PMID: 20075969.
48. Klein R, Klein BE, Moss SE, Davis MD, DeMets DL. The Wisconsin epidemiologic study of diabetic retinopathy. III. Prevalence and risk of diabetic retinopathy when age at diagnosis is 30 or more years. Arch Ophthalmol. 1984;102:527–32. PubMed PMID: 6367725.

49. Klein, et al. 1995 Klein R., Klein B.E.K., Moss S.E. The Wisconsin epidemiologic study of diabetic retinopathy. XV. The long term incidence of macular edema. Ophthalmology. 1995;102:7–16. PubMed PMID: 7831044.
50. Photocoagulation for diabetic macular edema. Early Treatment Diabetic Retinopathy Study report number 1. Early Treatment Diabetic Retinopathy Study research group. Arch Ophthalmol. 1985;103:1796–806. [No authors listed]. PubMed PMID: 2866759.
51. Fluorescein angiographic risk factors for progression of diabetic retinopathy. ETDRS report number 13. Early Treatment Diabetic Retinopathy Study Research Group. Ophthalmology. 1991;98 Suppl:834–40. [No authors listed]. PubMed PMID: 2062516.
52. Bresnick GH, De Venecia G, Myers FL, Harris JA, Davis MD. Retinal ischemia in diabetic retinopathy. Arch Ophthalmol. 1975;93:1300–10. PubMed PMID: 1200895.
53. Panozzo G, Gusson E, Parolini B, Mercanti A. Role of OCT in the diagnosis and follow up of diabetic macular edema. Semin Ophthalmol. 2003;18:74–81. PubMed PMID: 14566626.
54. Brown JC, Solomon SD, Bressler SB, Schachat AP, DiBernardo C, Bressler NM. Detection of diabetic foveal edema: contact lens biomicroscopy compared with optical coherence tomography. Arch Ophthalmol. 2004;122:330–5. PubMed PMID: 15006844.
55. Wu L, Fernandez-Loaiza P, Sauma J, Hernandez-Bogantes E, Masis M. Classification of diabetic retinopathy and diabetic macular edema. World J Diabetes. 2013;4:290–294. PubMed PMID: 24379919.
56. Diabetic retinopathy study. Report Number 6. Design, methods, and baseline results. Report Number 7. A modification of the Airlie House classification of diabetic retinopathy. Prepared by the Diabetic Retinopathy. Invest Ophthalmol Vis Sci. 1981;21(1 Pt 2):1–226. PubMed PMID: 7195893.
57. Early Treatment Diabetic Retinopathy Study Research Group. Grading diabetic retinopathy from stereoscopic color fundus photographs--an extension of the modified Airlie House classification. ETDRS report number 10. Ophthalmology. 1991;98(5 Suppl):786–806. PubMed PMID: 2062513.
58. Haut J, Rousselie F, Guyot C, Pinon F, Dureuil J, Baltazis S. Treatment of diabetic retinopathy by centripetal pan-retinal photocoagulation with the argon laser Arch Ophtalmol Rev Gen Ophtalmol. 1975; **35:** 951-60.
59. Coscas G, Chaine G. Treatment of diabetic retinopathy with laser photocoagulation. Diabetes Metab. 1979; **5:** 247-59.
60. Jyothi S, Sivaprasad S. Eye (Lond). 2011;25:851–8. PubMed PMID: 21587271.
61. Lim MC, Tanimoto SA, Furlani BA, Lum B, Pinto LM, Eliason D, Prata TS, Brandt JD, Morse LS, Park SS, Melo LA Jr. Effect of diabetic retinopathy and panretinal photocoagulation on retinal nerve fiber layer and optic nerve appearance. Arch Ophthalmol. 2009;127:857–62. PubMed PMID: 19597104.
62. [No authors listed] Photocoagulation for diabetic macular edema. Early Treatment Diabetic Retinopathy Study report number 1. Early Treatment Diabetic Retinopathy Study research group. Arch Ophthalmol. 1985; **103:** 1796-806.
63. Nguyen QD, Brown DM, Marcus DM, Boyer DS, Patel S, Feiner L, Gibson A, Sy J, Rundle AC, Hopkins JJ, Rubio RG, Ehrlich JS; RISE and RIDE Research Group. Ranibizumab for diabetic macular edema: results from 2 phase III randomized trials: RISE and RIDE. Ophthalmology. 2012;119:789–801. PubMed PMID: 22330964.
64. Sivaprasad S, Elagouz M, McHugh D, Shona O, Dorin G. Micropulsed diode laser therapy: evolution and clinical applications. Surv Ophthalmol. 2010;55:16–30. PubMed PMID: 20850854.
65. Friberg TR, Karatza EC. The treatment of macular disease using a micropulsed and continuous wave 810-nm diode laser. Ophthalmology. 1997;104:2030–8. PubMed PMID: 9400762.
66. Figueira J1. Khan J, Nunes S, Sivaprasad S, Rosa A, de Abreu JF, Cunha-Vaz JG, Chong NV. Prospective randomised controlled trial comparing sub-threshold micropulse diode laser photocoagulation and conventional green laser for clinically significant diabetic macular oedema. Br J Ophthalmol. 2009;93:1341–4. PubMed PMID: 19054831.

67. Stone J1. Itin A, Alon T, Pe'er J, Gnessin H, Chan-Ling T, Keshet E. Development of retinal vasculature is mediated by hypoxia-induced vascular endothelial growth factor (VEGF) expression by neuroglia. J Neurosci. 1995;15:4738–47. PubMed PMID: 7623107.
68. Provis JM1. Leech J, Diaz CM, Penfold PL, Stone J, Keshet E . Development of the human retinal vasculature: cellular relations and VEGF expression. Exp Eye Res. 1997;65:555–68. PubMed PMID: 9464188.
69. Murata T1. Ishibashi T, Khalil A, Hata Y, Yoshikawa H, Inomata H.Vascular endothelial growth factor plays a role in hyperpermeability of diabetic retinal vessels. Ophthalmic Res. 1995;27:48–52. PubMed PMID: 7596559.
70. Murata T1. Nakagawa K, Khalil A, Ishibashi T, Inomata H, Sueishi K. The relation between expression of vascular endothelial growth factor and breakdown of the blood-retinal barrier in diabetic rat retinas. Lab Invest. 1996;74:819–25. PubMed PMID: 8606491.
71. Campochiaro PA, Wykoff CC, Shapiro H, Rubio RG, Ehrlich JS. Neutralization of vascular endothelial growth factor slows progression of retinal nonperfusion in patients with diabetic macular edema. Ophthalmology. 2014;121:1783–9. PubMed PMID: 24768239.
72. Aiello LP, Avery RL, Arrigg PG, Keyt BA, Jampel HD, Shah ST, Pasquale LR, Thieme H, Iwamoto MA, Park JE, et al. Vascular endothelial growth factor in ocular fluid of patients with diabetic retinopathy and other retinal disorders. N Engl J Med. 1994;331:1480–7. PubMed PMID: 7526212.
73. Rosenfeld PJ, Schwartz SD, Blumenkranz MS, Miller JW, Haller JA, Reimann JD, Greene WL, Shams N. Maximum tolerated dose of a humanized anti-vascular endothelial growth factor antibody fragment for treating neovascular age-related macular degeneration. Ophthalmology. 2005;112:1048–53. PubMed PMID: 15885778.
74. Andreoli C. M., Miller J. W. Anti-vascular endothelial growth factor therapy for ocular neovascular disease. Current opinion in ophthalmology. 2007;18:502–508. PubMed PMID: 18163003.
75. Chen HX1. Gore-Langton RE, Cheson BD. Clinical trials referral resource: Current clinical trials of the anti-VEGF monoclonal antibody bevacizumab. Oncology (Williston Park). 2001;15:1017. PubMed PMID: 11548974.
76. Rosenfeld P. J., Moshfeghi A. A., Puliafito C. A. Optical coherence tomography findings after an intravitreal injection of bevacizumab (avastin) for neovascular age-related macular degeneration. Ophthalmic surgery, lasers & imaging. 2005;36:331–335. PubMed PMID: 16156152.
77. Nicholson B. P., Schachat A. P. A review of clinical trials of anti-VEGF agents for diabetic retinopathy. V. Graefe's Arch. Clin exper. Ophthalmol. 2010;248:915–930. PubMed PMID: 20174816.
78. Stefanini FR, Badaro E, Falabella P, Koss M, Farah ME and Maia M. Anti-VEGF for the management of Diabetic Macular Edema . J. Immunolog Res 2014 article ID 632307.
79. Intravitreal ranibizumab and bevacizumab: a review of risk. Semin Ophthalmol. 2007;22:201–4. PubMed PMID: 17763246.
80. Azanza Perea JR, García Layana A. Ranibizumab versus bevacizumab. Pharmacological considerations. Arch Soc Esp Oftalmol. 2012;87 Suppl 1:3-9.
81. Mitchell P, Bandello F, Schmidt-Erfurth U, Lang GE, Massin P, Schlingemann RO, Sutter F, Simader C, Burian G, Gerstner O, Weichselberger A; RESTORE study group. The RESTORE study: ranibizumab monotherapy or combined with laser versus laser monotherapy for diabetic macular edema. Ophthalmology. 2011;118:615–25. PubMed PMID: 21459215.
82. Salam A, DaCosta J, Sivaprasad S. Anti-vascular endothelial growth factor agents for diabetic maculopathy. Br J Ophthalmol. 2010;94:821–826. PubMed PMID: 19556214.
83. Elman MJ, Aiello LP, Beck RW, Bressler N M, Bressler SB, Edwards AR; Diabetic Retinopathy Clinical Research Network et al. Randomized trial evaluating ranibizumab plus prompt or deferred laser or triamcinolone plus prompt laser for diabetic macular oedema. Ophthalmology. 2010;117:1064–1077. PubMed PMID: 20427088.

84. Michaelides M, Kaines A, Hamilton RD. A prospective randomized trial of intravitreal bevacizumab or laser therapy in the management of diabetic macular oedema (BOLT study) 12-month data: report 2. Ophthalmology. 2010;117:1078–1086. Fraser-Bell S Rajen am R, Quhi U et al. PubMed PMID: 20416952.
85. Azza El-Remessy M. A l i Behzadian A, Abou-Mohamed G, Franklin T, Caldwell RW, Caldwell RB. Experimental diabetes causes breakdown of the blood-retina barrier by a mechanism involving tyrosine nitration and increases in expression of vascular endothelial growth factor and urokinase plasminogen activator receptor. Am J Pathol. 2003;162:1995–2004. PubMed PMID: 12759255.
86. Stein JD1. Newman-Casey PA, Kim DD, Nwanyanwu KH, Johnson MW, Hutton DW. Cost-effectiveness of various interventions for newly diagnosed diabetic macular edema. Ophthalmology. 2013;120:1835–42. PubMed PMID: 23642372.
87. El Sanharawi M, Kowalczuk L, Touchard E, Omri S, de Kozak Y, Behar-Cohen F. Protein delivery for retinal diseases: from basic considerations to clinical applications. Prog Retin Eye Res. 2010;29:443–65. PubMed PMID: 20398784.
88. Silva PS, Sun JK, Aiello LP. Role of steroids in the management of diabetic macular edema and proliferative diabetic retinopathy. Semin Ophthalmol. 2009;24:93–9. PubMed PMID: 19373693.
89. Jeon S, Lee WK. Effect of intravitreal triamcinolone in diabetic macular edema unresponsive to intravitreal bevacizumab. Retina. 2014;341:606–11. PubMed PMID: 24553409.
90. Thomas BJ, Shienbaum G, Boyer DS, Flynn HW Jr. Evolving strategies in the management of diabetic macular edema: clinical trials and current management. Can J Ophthalmol. 2013;48:22–30. PubMed PMID: 23419295.
91. Yilmaz T, Cordero-Coma M, Lavaque AJ, Gallagher MJ, Padula WV. Triamcinolone and intraocular sustained-release delivery systems in diabetic retinopathy. Curr Pharm Biotechnol. 2011;12:337–46. PubMed PMID: 20939800.
92. Kanwar M, Chan PS, Kern TS, Kowluru RA. Oxidative damage in the retinal mitochondria of diabetic mice: possible protection by superoxide dismutase. Invest Ophthalmol Vis Sci. 2007;48:3805–11. PubMed PMID: 17652755.
93. Kowluru RA, Atasi L, Ho YS. Role of mitochondrial superoxide dismutase in the development of diabetic retinopathy. Invest Ophthalmol Vis Sci. 2006;47:1594–9. PubMed PMID: 16565397.
94. Kowluru RA, Kowluru V, Xiong Y, Ho YS. Overexpression of mitochondrial superoxide dismutase in mice protects the retina from diabetes-induced oxidative stress. Free Radic Biol Med. 2006;15(41):1191–6. PubMed PMID: 17015165.
95. Kobayashi T, Oku H, Komori A, Okuno T, Kojima S, Obayashi H, Sugiyama T, Hasegawa G, Fukui M, Nakamura N, Ikeda T. Advanced glycation end products induce death of retinal neurons via activation of nitric oxide synthase. Exp Eye Res. 2005;81:647–654. PubMed PMID: 15975578.
96. Stitt AW, Bhaduri T, McMullen CB, Gardiner TA, Archer DB. Advanced glycation end products induce blood-retinal barrier dysfunction in normoglycemic rats. Mol Cell Biol Res Commun. 2000;3:380–8. PubMed PMID: 11032761.
97. Pryor WA. OXY-RADICALS AND RELATED SPECIES: Their Formation, Lifetimes, and Reactions Ann. Rev. Physiol. 1986;48:657–67. PubMed PMID: 3010829.
98. Grivenkova VG, Vinogradov AD. Generation of superoxide by the mitochondrial Complex I. Biochem Biophys Acta. 2006;1757:553–61. PubMed PMID: 16678117.
99. Baines JW. Role of Oxidative Stress in Development of Complications in Diabetes. Diabetes. 1991;40:405–12. PubMed PMID: 2010041.
100. Wu Y, Tang L, Chen B. Oxidative stress: implications for the development of diabetic retinopathy and antioxidant therapeutic perspectives. Oxid Med Cell Longev. 2014;2014:752387. Article ID. PubMed PMID: 25180070.
101. Cave AC, Brewer AC, Narayanapanicker A, Ray R, Grieve DJ, Walker S, et al. NADPH oxidases in cardiovascular health and disease. Antioxid Redox Signal. 2006;8:691–72. PubMed PMID: 16771662.
102. Brownlee M. Biochemistry and molecular Cell Biology of diabetic complications. Nature. 2001;414:813–820. PubMed PMID: 11742414.

103. Lee MY, Griendling KK. Redox signaling, vascular function, and hypertension. Antioxid Redox Signal. 2008;10:1045–10598. PubMed PMID: 18321201.
104. Gupte SA, Wolin MS. Oxidant and redox signaling in vascular oxygen sensing: implications for systemic and pulmonary hypertension. Antioxid Redox Signal. 2008;10:1137–1152. PubMed PMID: 18315496.
105. Kaiser N, Sasson S, Feener EP, et al. Differential regulation of glucose transport and transporters by glucose in vascular endothelial and smooth muscle cells. Diabetes. 1993;42:80–89. PubMed PMID: 7678404.
106. Souza HP, Liu X, Samouilov A, Kuppusamy P, Laurindo FR, Zweier JL. Quantitation of superoxide generation and substrate utilization by vascular NAD(P)H oxidase. Am J Physiol Heart Circ Physiol. 2002;282:H466–74. PubMed PMID: 11788393.
107. Wang W, Fang H, Groom L, Cheng A, Zhang W, Liu J, Wang X, Li K, Han P, Zheng M, Yin J, Mattson MP, Kao JP, Lakatta EG, Sheu SS, Ouyang K, Chen J, Dirksen RT, Cheng H. Superoxide flashes in single mitochondria. Cell. 2008;134:279–290. PubMed PMID: 18662543.
108. Brownlee M. Biochemistry and molecular Cell Biology of diabetic complications. Nature. 2001;414:813–820. PubMed PMID: 11742414.
109. Hancock JT. R. Desikan R, Neill SJ. Role of Reactive Oxygen Species in Cell Signaling Pathways. Biochemical and Biomedical Aspects of Oxidative Modification. Biochemical Society Transactions. 2001;29:345–350. PubMed PMID: 11356180.
110. Bokoch GM, Diebold BA. Current molecular models for NADPH oxidase regulation by Rac GTPase. Blood. 2002; **100:** 2692-6.
111. Yang W, Block ER. Effect of hypoxia and reoxygenation on the formation and release of reactive oxygen species by porcine pulmonary artery endothelial cells. J Cell Physiol. 1995;164:414–23. PubMed PMID: 7622587.
112. Cervellati F1. Cervellati C, Romani A, Cremonini E, Sticozzi C, Belmonte G, Pessina F, Valacchi G. Hypoxia induces cell damage via oxidative stress in retinal epithelial cells. Free Radic Res. 2014;48:303–12. PubMed PMID: 24286355.
113. Ng CF, Schafer FQ, Buettner GR, Rodgers VG. The rate of cellular hydrogen peroxide removal shows dependency on GSH: mathematical insight into in vivo H2O2 and GPx concentrations. Free Radic Res. 2007;41:201–11. PubMed PMID: 17886026.
114. Madsen-Bouterse SA. Zhong Q Mohamed G Ho Y-S and Kowluru RA . Oxidative damage of mitochondrial DNA in diabetes and its protection by manganese superoxide dismutase. Free Radic Res. 2010;44:313–321. PubMed PMID: 20088710.
115. Kern TS. Interrelationships between the Retinal Neuroglia and Vasculature in Diabetes. Diabetes Metab J. 2014;38:163–70. PubMed PMID: 25003068.
116. Du Y, Veenstra A, Palczewski K, Kern TS. Photoreceptor cells are major contributors to diabetes-induced oxidative stress and local inflammation in the retina. Proc Natl Acad Sci USA. 2013;110:16586–91. PubMed PMID: 24067647.
117. Kurtenbach A, Mayser HM, Jagle H, Fritsche A, Zrenner E. Hyperoxia, hyperglycaemia and photoreceptor sensitivity in normal and diabetic subjects. Vis. Neurosci. 2006;23:651–661. PubMed PMID: 16962009.
118. Tzekov R., Arden G. B. The electroretinogram in diabetic retinopathy. Surv Ophthalmol. 1999;44:53–60. PubMed PMID: 10466588.
119. Holfort SK1. Jackson GR, Larsen M. Dark adaptation during transient hyperglycemia in type 2 diabetes. Exp Eye Res. 2010;91:710–4. PubMed PMID: 20732318.
120. McFarland RA, Forbes WH. The effects of variations in the concentration of oxygen and of glucose on dark adaptation. J Gen Physiol. 1940;24:69–98. PubMed PMID: 19873200.
121. Holopigian K, Greenstein VC, Seiple W, Hood DC, Carr RE. Evidence for Photoreceptor Changes in Patients With Diabetic Retinopathy. Invest Ophthalmol Vis Sci. 1997;38:2355–2365. PubMed PMID: 9344359.
122. Wong TY, Liew G, Tapp RJ, Schmidt MI, Wang JJ, Mitchell P, Klein R, Klein BE, Zimmet P, Shaw J. Relation between fasting glucose and retinopathy for diagnosis of diabetes: three population-based cross-sectional. Lancet. 2008;371:736–43. PubMed PMID: 18313502.

123. Kundu D, Mandal T, Nandi M, Osta M, Bandyopadhyay U, Ray D. Oxidative stress in diabetic patients with retinopathy. Ann Afr Med. 2014;13:41–6. PubMed PMID: 24521578.
124. Tapp RJ, Zimmet PZ, Harper CA, de Courten MP, McCarty DJ, Balkau B, Taylor HR, Welborn TA, Shaw JE; Aus Diab Study Group. Diagnostic thresholds for diabetes: the association of retinopathy and albuminuria with glycaemia. Diabetes Res Clin Pract. 2006;73:315–21. PubMed PMID: 16644057.
125. Zhong Q, Kowluru RA. Diabetic retinopathy and damage to mitochondrial structure and transport machinery. Invest Ophthalmol Vis Sci. 2011;52:8739–46. PubMed PMID: 22003103.
126. Kanwar M, Chan PS, Kern TS, Kowluru RA. Oxidative damage in the retinal mitochondria of diabetic mice: possible protection by superoxide dismutase. Invest Ophthalmol Vis Sci. 2007;48:3805–11. PubMed PMID: 17652755.
127. Kolm-Litty V, Sauer U, Nerlich A. Lehmann and Schleicher ED . High Glucose induced Transforming Growth Factor β1 Production is mediated by the hexosamine Pathway in porcine Glomerular Mesangial cells. J Clin Invest. 1998;101:160–9. PubMed PMID: 9421478.
128. Small M, Alzaid A, MacCuish AC. Diabetic hyperosmolar non-ketotic decompensation. J Med. 1988;66:251–7. PubMed PMID: 3059389.
129. Ceriello A, Esposito K, Piconi L, et al. Oscillating glucose is more deleterious to endothelial function and oxidative stress than mean glucose in normal and type 2 diabetic patients. Diabetes. 2008;57:1349–54. PubMed PMID: 18299315.
130. Busik JV, Olson LK, Grant MB, Henry DN. Glucose-induced activation of glucose uptake in cells from the inner and outer blood–retinal barrier. Invest Ophthalmol Vis Sci. 2002;43:2356–63. PubMed PMID: 12091438.
131. Busik JV, Mohr S, Grant MB., Busik JV, Mohr S, Grant MB. Hyperglycemia-induced reactive oxygen species toxicity to endothelial cells is dependent on paracrine mediators. Diabetes. 2008;57:1952–65. PubMed PMID: 18420487.
132. Kador PF, Akagi Y, Terubayashi H, Wyman M, Kinoshita JH. Prevention of pericyte ghost formation in retinal capillaries of galactose-fed dogs by aldose reductase inhibitors. Archives of Ophthalmology. 1988;106:1099–1102. PubMed PMID: 3401138.
133. Gabbay KH. The sorbitol pathway and the complications of diabetes. The New England Journal of Medicine. 1973;288:831–836. PubMed PMID: 4266466.
134. Koya D, King GL. Protein kinase C activation and the development of diabetic complications. Diabetes. 1998;47:859–866. PubMed PMID: 9604860.
135. Aiello LP, Bursell SE, Clermont A, et al. Vascular endothelial growth factor-induced retinal permeability is mediated by protein kinase C in vivo and suppressed by an orally effective β-isoform-selective inhibitor. Diabetes. 1997;46:1473. PubMed PMID: 9287049.
136. Tarr JM, Kaul K, Chopra M, Kohner EM, Chibber R. Pathophysiology of diabetic retinopathy. ISRN Ophthalmol. 2013;2013:343560. PubMed PMID: 24563789.
137. Kowluru RA, Chan PS. Oxidative stress and diabetic retinopathy. Exp Diabetes Res. 2007;2007:43603. PubMed PMID: 17641741.
138. Zhang X, Zeng H, Sheian B, Wang N, Gillies MC. Diabetic macular edema: new concepts in patho-physiology and treatment. Cell & Bioscience. 2014;4:27–41. PubMed PMID: 24955234.
139. Yang W, Block ER. Effect of hypoxia and reoxygenation on the formation and release of reactive oxygen species by porcine pulmonary artery endothelial cells. J Cell Physiol. 1995;164:414–23. PubMed PMID: 7622587.
140. Bernardini A, Brockmeier U, Metzen E, Berchner-Pfannschmidt U, Harde E, Acker-Palmer A, Papkovsky D, Acker H, Fandrey J. Type I cell ROS kinetics under hypoxia in the intact mouse carotid body ex vivo: a FRET based study. Am J Physiol Cell Physiol. 2015;308(1):C61–C67. PubMed PMID: 25318107.
141. Eshaq RS, Wright WS, Harris NR. Oxygen delivery, consumption, and conversion to reactive oxygen species in experimental models of diabetic retinopathy. Redox Biol. 2014;2:661–6. PubMed PMID: 24936440.

142. Chandel NS, Schumacker PT. Cellular oxygen sensing by mitochondria: old questions, new insight. J Appl Physiol. 1985;2000(88):1880–9. PubMed PMID: 10797153.
143. Chandel NS1. McClintock DS, Feliciano CE, Wood TM, Melendez JA, Rodriguez AM, Schumacker PT. Reactive oxygen species generated at mitochondrial complex III stabilize hypoxia-inducible factor-1alpha during hypoxia: a mechanism of O2 sensing. J Biol Chem. 2000;275:25130–8. PubMed PMID: 10833514.
144. Strasser A, Stanimirovic D, Kawai N, McCarron RM, Spatz M. Hypoxia modulates free radical formation in brain microvascular endothelium. Acta Neurochir Suppl. 1997;70:8–11. PubMed PMID: 9416263.
145. Zuo L, Shiah A, Roberts WJ, Chien MT, Wagner PD, Hogan MC. Low PO_2 conditions induce reactive oxygen species formation during contractions in single skeletal muscle fibers. Am J Physiol Regul Integr Comp Physiol. 2013;304:R1009–16. PubMed PMID: 23576612.
146. Hernansanz-Agustín P, Izquierdo-Álvarez A, Sánchez-Gómez FJ, Ramos E, Villa-Piña T, Lamas S, Bogdanova A, Martínez-Ruiz A. Acute hypoxia produces a superoxide burst in cells. Free Radic Biol Med. 2014;71:146–56. PubMed PMID: 24637263.
147. Gao L, Mann GE. Vascular NAD(P)H oxidase activation in diabetes: a double-edged sword in redox signalling. Cardiovasc Res. 2009;82:9–20. PubMed PMID: 19179352.
148. Jakus V, Rietbock N. Advanced Glycation End-Products and the Progress of Diabetic Vascular Complications. Physiol. Res. 2004;53:131–142. PubMed PMID: 15046548.
149. Baynes J W., Thorpe S R. Role of oxidative stress in diabetic complications: a new perspective on an old paradigm. Diabetes. 1999;48:1–9. PubMed PMID: 9892215.
150. Yamada H1. Yamada E, Hackett SF, Ozaki H, Okamoto N, Campochiaro PA. Hyperoxia causes decreased expression of vascular endothelial growth factor and endothelial cell apoptosis in adult retina. J Cell Physiol. 1999;179:149–56. PubMed PMID: 10199554.
151. Kanwar M, Chan PS, Kern TS, Kowluru RA. Oxidative damage in the retinal mitochondria of diabetic mice: possible protection by superoxide dismutase. Invest Ophthalmol Vis Sci. 2007;48:3805–11. PubMed PMID: 17652755.
152. Kowluru RA, Atasi L, Ho YS. Role of mitochondrial superoxide dismutase in the development of diabetic retinopathy. Invest Ophthalmol Vis Sci. 2006;47:1594–9. PubMed PMID: 16565397.
153. Kowluru RA, Kowluru V, Xiong Y, Ho YS. Overexpression of mitochondrial superoxide dismutase in mice protects the retina from diabetes-induced oxidative stress. Free Radic Biol Med. 2006;41:1191–6. PubMed PMID: 17015165.
154. Ishii T, Itoh K, Takahashi S, Sato H, Yanagawa T, Katoh Y, et al. Transcription factor Nrf2 coordinately regulates a group of oxidative stress-inducible genes in macrophages. J Biol Chem. 2000;275:16023–16029. PubMed PMID: 10821856.
155. Mishra M, Kowluru RA. Retinal mitochondrial DNA mismatch repair in the development of diabetic retinopathy, and its continued progression after termination of hyperglycemia. Invest. Ophthalmol. Vis. Sci. 2014;55:6960–7. PubMed PMID: 25249609.
156. Estopinal CB, Chocron IM, Parks MB, Wade EA, Roberson RM, Burgess LG. Brantley. M Jr and Samuels DC. Mitochondrial haplogroups are associated with severity of diabetic retinopathy. Invest Ophthalmol Vis Sci. 2014;55:5589–95. PubMed PMID: 25118268.
157. Kowluru RA, Kowluru V, Xiong Y, Ho YS. Overexpression of mitochondrial superoxide dismutase in mice protects the retina from diabetes-induced oxidative stress. Free Radic Biol Med. 2006;41:1191–6. PubMed PMID: 17015165.
158. Li J, Wang JJ, Yu Q, Chen K, Mahadev K, Zhang SX. Inhibition of reactive oxygen species by Lovastatin downregulates vascular endothelial growth factor expression and ameliorates blood-retinal barrier breakdown in db/db mice: role of NADPH oxidase 4. Diabetes. 2010;59:1528–38. PubMed PMID: 20332345.
159. Satofuka S1. Ichihara A, Nagai N, Noda K, Ozawa Y, Fukamizu A, Tsubota K, Itoh H, Oike Y, Ishida S. (Pro)renin receptor-mediated signal transduction and tissue renin-angiotensin system contribute to diabetes-induced retinal inflammation. Diabetes. 2009;58:1625–33. PubMed PMID: 19389828.

160. Silva KC1. Rosales MA, Biswas SK, Lopes de Faria JB, Lopes de Faria JM. Diabetic retinal neurodegeneration is associated with mitochondrial oxidative stress and is improved by an angiotensin receptor blocker in a model combining hypertension and diabetes. Diabetes. 2009;58:1382–90. PubMed PMID: 19289456.
161. Drel VR1, Xu W, Zhang J, Kador PF, Ali TK, Shin J, Julius U, Slusher B, El-Remessy AB, Obrosova IG. Poly(ADP-ribose)polymerase inhibition counteracts cataract formation and early retinal changes in streptozotocin-diabetic rats. Invest Ophthalmol Vis Sci. 2009; **50:** 1778-90.4.
162. Fukumoto M1. Takai S, Ishizaki E, Sugiyama T, Oku H, Jin D, Sakaguchi M, Sakonjo H, Ikeda T, Miyazaki M. Involvement of angiotensin II-dependent vascular endothelial growth factor gene expression via NADPH oxidase in the retina in a type 2 diabetic rat model. Curr Eye Res. 2008;33:885–91. PubMed PMID: 18853323.
163. Zheng L, Szabó C, Kern TS. Poly(ADP-ribose) polymerase is involved in the development of diabetic retinopathy via regulation of nuclear factor-kappaB. Diabetes. 2004;53:2960–7. PubMed PMID: 15504977.
164. Inoguchi T1. Li P, Umeda F, Yu HY, Kakimoto M, Imamura M, Aoki T, Etoh T, Hashimoto T, Naruse M, Sano H, Utsumi H, Nawata H. High glucose level and free fatty acid stimulate reactive oxygen species production through protein kinase C--dependent activation of NAD(P)H oxidase in cultured vascular cells. Diabetes. 2000;49:1939–45. PubMed PMID: 11078463.
165. Kern TS1. Tang J, Mizutani M, Kowluru RA, Nagaraj RH, Romeo G, Podesta F, Lorenzi M. Response of capillary cell death to aminoguanidine predicts the development of retinopathy: comparison of diabetes and galactosemia. Invest Ophthalmol Vis Sci. 2000;41:3972–8. PubMed PMID: 11053301.
166. Nishikawa T1. Edelstein D, Du XL, Yamagishi S, Matsumura T, Kaneda Y, Yorek MA, Beebe D, Oates PJ, Hammes HP, Giardino I, Brownlee M. Normalizing mitochondrial superoxide production blocks three pathways of hyperglycaemic damage. Nature. 2000;404:787–790. PubMed PMID: 10783895.
167. Ganz MB1. Seftel A. Glucose-induced changes in protein kinase C and nitric oxide are prevented by vitamin E. Am J Physiol Endocrinol Metab. 2000;278:E146–52. PubMed PMID: 10644549.
168. Mohammad G, Siddiquei MM, Abu El-Asrar AM. Poly (ADP-ribose) polymerase mediates diabetes-induced retinal neuropathy. Mediators Inflamm. 2013;2013:510451. Article ID. PubMed PMID: 24347828.
169. Zhu Y, Zhang XL, Zhu BF, Ding YN. Effect of antioxidant N-acetylcysteine on diabetic retinopathy and expression of VEGF and ICAM-1 from retinal blood vessels of diabetic rats. Mol Biol Rep. 2012;39:3727–35. PubMed PMID: 21952821.
170. Kowluru RA, Santos JM, Zhong Q. Sirt1, A Negative Regulator of Matrix Metalloproteinase-9 in Diabetic Retinopathy. Invest. Ophthalmol. Vis. Sci. 2014;55:5653–60. PubMed PMID: 24894401.
171. Bolton WK, Cattran DC, Williams ME, Adler SG, Appel GB, Cartwright K, Foiles PG, Freedman BI, Raskin P, Ratner RE, Spinowitz BS, Whittier FC, Wuerth JP. ACTION I Investigator Group. Randomized trial of an inhibitor of formation of advanced glycation end products in diabetic nephropathy. Am J Nephrol. 2004;24:32–40. PubMed PMID: 14685005.
172. Keech AC1. Mitchell P, Summanen PA, O'Day J, Davis TM, Moffitt MS, Taskinen MR, Simes RJ, Tse D, Williamson E, Merrifield A, Laatikainen LT, d'Emden MC, Crimet DC,O'Connell RL, Colman PG; FIELD study investigators. Effect of fenofibrate on the need for laser treatment for diabetic retinopathy (FIELD study): a randomised controlled trial. Lancet. 2007;370(9600):1687–97. PubMed PMID: 17988728.
173. Gerss J, Hammes HP, Kampik A, Ulbig MW; RETIPON Study Group. Alpha-lipoic acid for the prevention of diabetic macular edema. Ophthalmologica. 2011;226:127–37. PubMed PMID: 21811051.
174. PKC-DRS2 Group1, Aiello LP, Davis MD, Girach A, Kles KA, Milton RC, Sheetz MJ, Vignati L, Zhi XE. Effect of ruboxistaurin on visual loss in patients with diabetic retinopathy. Ophthalmology. 2006;113:2221–30. PubMed PMID: 16989901.
175. Sheetz MJ, Aiello LP, Davis MD, Danis R, Bek T, Cunha-Vaz J, Shahri N, Berg PH. MBDL and MBCU Study Groups. The effect of the oral PKC β inhibitor ruboxistaurin on vision loss in two phase 3 studies. Invest Ophthalmol Vis Sci. 2013;54:1750–7. PubMed PMID: 23404115.

176. Ellis EA1. Guberski DL, Somogyi-Mann M, Grant MB. Increased H_2O_2, vascular endothelial growth factor and receptors in the retina of the BBZ/Wor diabetic rat. Free Radic Biol Med. 2000;28:91–101. PubMed PMID: 10656295.
177. Brownlee M. The pathobiology of diabetic complications: a unifying mechanism. Diabetes. 2005;54:1615–25. PubMed PMID: 15919781.
177. Droge W. Free radicals and the physiological control of cell function. Physiol Rev. 2002;83:47–95. PubMed PMID: 11773609.
178. Kern TS, Engerman RL. Capillary lesions develop in retina rather than cerebral cortex in diabetes and experimental galactosemia. Arch Ophthalmol. 1996;114:306–10. PubMed PMID: 8600891.
179. Kern TS, Barber AJ. Retinal ganglion cells in diabetes. J Physiol. 2008;586:4401–8. PubMed PMID: 18565995.
180. Wolter JR. Diabetic Retinopathy. Amer J. Ophthalmol. 1961;51:1123–41. PubMed PMID: 13786453.
181. Kerrigan LA, Zack DJ, Quigley HA, Smith SD, Pease ME. TUNEL-positive ganglion cells in human primary open-angle glaucoma. Arch Ophthalmol. 1997;115:1031–5. PubMed PMID: 9258226.
182. Barber AJ, Lieth E, Khin SA, Antonetti DA, Buchanan AG, Gardner TW. Neural apoptosis in the retina during experimental and human diabetes. Early onset and effect of insulin. J Clin Invest. 1998;102:783–91. PubMed PMID: 9710447.
183. Takahashi H, Goto T, Shoji T, Tanito M, Park M. Chihara. Diabetes-associated retinal nerve fiber damage evaluated with scanning laser polarimetry. Amer J Ophthalmol. 2006;142:88–94. PubMed PMID: 16815255.
184. Cho NC, Poulsen GL, Ver Hoeve JN, Nork TM. Selective loss of S-cones in diabetic retinopathy. Arch Ophthalmol. 2000;118:1393–400. PubMed PMID: 11030822.
185. Martin PM, Roon P, Van Ells TK, Ganapathy V, Smith SB. Death of retinal neurons in streptozotocin-induced diabetic mice. Invest Ophthalmol Vis Sci. 2004;45:3330–6. PubMed PMID: 15326158.
186. Énzsöly A, Szabó A, Kántor O, Dávid C, Szalay P, Szabó K, Szél Á, Németh J, Lukáts Á. Pathologic alterations of the outer retina in streptozotocin-induced diabetes. Invest Ophthalmol Vis Sci. 2014;55:3686–99. PubMed PMID: 24845643.
187. Ly A, Yee P, Vessey KA, Phipps JA, Jobling AI, Fletcher EL. Early Inner Retinal Astrocyte Dysfunction during Diabetes and Development of Hypoxia, Retinal Stress, and Neuronal Functional Loss. Invest Ophthalmol Vis Sci. 2011;52:9316–9326. PubMed PMID: 22110070.
188. Hombrebueno JR, Chen M, Penalva RG, Xu H1.Loss of synaptic connectivity, particularly in second order neurons is a key feature of diabetic retinal neuropathy in the Ins2Akita mouse. PLoS One. 2014; **9:** e97970. doi: 10.1371.
189. Drasdo N, Chiti Z, Owens DR, North RV. Effect of darkness on inner retinal hypoxia in diabetes. Lancet. 2002;359(9325):2251–2253. PubMed PMID: 12103292.
190. Fortune B, Schneck ME, Adams AJ. Multifocal electroretinogram delays reveal local retinal dysfunction in early diabetic retinopathy. Invest Ophthalmol Vis Sci. 1999;40:2638–51. PubMed PMID: 10509661.
191. Ng JS, Bearse MA Jr, Schneck ME, et al. Local diabetic retinopathy prediction by multifocal ERG delays over 3 years. Invest Ophthalmol Vis Sci. 2008;49:1622–8. PubMed PMID: 18385083.
192. Dean FM, Arden GB, Dornhorst A. Partial reversal of protan and tritan colour defects with inhaled oxygen in insulin dependent diabetic subjects. Br J Ophthalmol. 1997;81:27–30. PubMed PMID: 9135404.
193. Kurtenbach A, Mayser HM, Jägle H, Fritsche A, Zrenner E. Hyperoxia, hyperglycemia, and photoreceptor sensitivity in normal and diabetic subjects. Vis Neurosci. 2006;23:651–61. PubMed PMID: 16962009.
194. Wong R, Khan J, Adewoyin T, Sivaprasad S, Arden GB, Chong V. The ChromaTest, a digital color contrast sensitivity analyzer, for diabetic maculopathy: a pilot study. BMC Ophthalmol. 2008;8:15. PubMed PMID: 18706104.
195. Cringle SJ, Yu DY, Alder V, Su EN. Light and choroidal PO2 modulation of intraretinal oxygen levels in an avascular retina. Invest Ophthalmol Vis Sci. 1999; **40:** 2307-13.
196. Harris A, Danis RP, Evans S, et al. Hyperoxia improves contrast sensitivity in early diabetic retinopathy. Br J Ophthalmol. 1996;80:209–13. PubMed PMID: 8703857.

197. Van Dijk HW, Kok PH, Garvin M, et al. Selective loss of inner retinal layer thickness in type 1 diabetic patients with minimal diabetic retinopathy. Invest Ophthalmol Vis Sci. 2009;50:3404–9. PubMed PMID: 19151397.
198. Van Eeden PE, Tee LB, Lukehurst S, et al. Early vascular and neuronal changes in a VEGF transgenic mouse model of retinal neovascularization. Invest Ophthalmol Vis Sci. 2006;47:4638–45. PubMed PMID: 17003462.
199. Lau JC, Linsenmeier RA. Increased intraretinal PO_2 in short-term diabetic rats. Diabetes. 2014;63(12):4338–4342. PubMed PMID: 25028524.
200. Puro DG. Diabetes-induced dysfunction of retinal Müller cells. Trans Am Ophthalmol Soc. 2002;100:339–52. PubMed PMID: 12545700.
201. Ramsey DJ, Ripps H, Qian H. An electrophysiological study of retinal function in the diabetic female rat. Invest Ophthalmol Vis Sci. 2006;47:5116–24. PubMed PMID: 17065533.
202. Castilho A, Ambrosio A, Hartveit E, Veruki M. Disruption of a neural microcircuit in the rod pathway of the Mammalian Retina by Diabetes mellitus. J Neurosci. 2015;35:5422–5433. PubMed PMID: 25834065.
203. Arden GB, Wolf JE, Collier J, Wolff C, Rosenberg M. Dark adaptation is impaired in diabetic before photopic loss can be seen. Can hypoxia contribute to diabetic retinopathy? In: Hollyfield JG (ed). Retinal Degenerative Diseases and Experimental Therapy. Plenum Press: New York, 1999, pp 305-325.
204. Arden GB, Sidman RL, Arap W, Schlingemann RO. Spare the rod and spoil the eye. Br J Ophthalmol. 2005;89:764–9. PubMed PMID: 15923516.
205. Arden GB, Wolf JE, Tsang Y. Does dark adaptation exacerbate diabetic retinopathy? Evidence and a linking hypothesis. Vision Res. 1998;38:1723–9. PubMed PMID: 9747505.
206. Hagins WA, Penn RD, Yoshikami S. Dark current and photocurrent in retinal rods. Biophys J. 1970;10:380–412. PubMed PMID: 5439318.
207. Hodgkin AL, McNaughton PA, Nunn BJ, Yau KW. Effect of ions on retinal rods from Bufo marinus. J Physiol. 1984;350:649–680. PubMed PMID: 6205141.
208. Neuroscience, 2nd edition Ed: Dale Purves, George J Augustine, David Fitzpatrick, et al. Sinauer Associates; 2001. In Chapter 11. Vision: The Eye: Phototransduction
209. Warburg O. Uber die Klassifizierung tierischer Gewebe nach ihrem Stoffwechsel. Biochem Z. 1927;184:484–488.
210. Warburg O, Posener K, Negelein E . Uber den Stoffwechsel der Carcinomzelle Biochemedische Zeitschrift 1924; **152:** 309-43.
211. Linsenmeier RA. The effect of light and darkness on oxygen distribution and consumption in the cat retina. J Gen Physiol. 1986;88:521–542. PubMed PMID: 3783124.
212. Daniele S, Daniele C. Aggravation of laser-treated diabetic cystoid macular edema after prolonged flight: a case report. Aviat Space Environ Med. 1995;66:440–2. PubMed PMID: 7619038.
213. Khalifah RG, Bayners JW, Hudson BG, Amadorin S. Novel post-Amadori inhibition of advanced glycation reactions. Biochem Biophys Res Commum. 1999;257:251–8.
214. Goldin A, Beckman JA, Schmidt AM, Creager MA. Advanced glycation end products: sparking the development of diabetic vascular injury. Circulation. 2006;114:597–605. PubMed PMID: 16894049.
215. Chen M, Curtis TM, Stitt AW. Advanced glycation end products and diabetic retinopathy. Curr Med Chem. 2013;20:3234–40. PubMed PMID: 23745547.
216. Du Y, Veenstra A, Palczewski K, Kern TS. Photoreceptor cells are major contributors to diabetes-induced oxidative stress and local inflammation in the retina. PNAS. 2013;110:16586–16591. PubMed PMID: 24067647.
217. Senger DR, Galli SJ, Dvorak AM, Perruzzi CA, Harvey VS, Dvorak HF. Tumor cells secrete a vascular permeability factor that promotes accumulation of ascites fluid. Science. 1983;219:983–985. PubMed PMID: 6823562.
218. Klaassen I, Van Noorden CJ, Schlingemann RO. Molecular basis of the inner blood-retinal barrier and its breakdown in diabetic macular edema and other pathological conditions. Prog Retin Eye Res. 2013;34:19–48. PubMed PMID: 23416119.

219. Mohammad G, Siddiquei MM, Othman A, Al-Shabrawey M, Abu El-Asrar AM. High-mobility group box-1 protein activates inflammatory signaling pathway components and disrupts retinal vascular-barrier in the diabetic retina. Exp Eye Res. 2013;107:101–9. PubMed PMID: 23261684.
220. Milne R, Brownstein S. Advanced glycation end products and diabetic retinopathy. Amino Acids. 2013;44:1397–407. PubMed PMID: 21909978.
221. Zong H, Ward M, Stitt AW. AGEs, RAGE, and diabetic retinopathy. Curr Diab Rep. 2011;11:244–52. PubMed PMID: 21590515.
222. Stitt AW. AGEs and diabetic retinopathy. Invest Ophthalmol Vis Sci. 2010;51:4867–74. PubMed PMID: 20876889.
223. Madsen-Bouterse SA, Kowluru RA. Oxidative stress and diabetic retinopathy: pathophysiological mechanisms and treatment perspectives. Rev Endocr Metab Disord. 2008;9:315–327. PubMed PMID: 18654858.
224. Pournaras CJ, Riva CE, Tsacopoulos M, Strommer K. Diffusion of O2 in the retina of anesthetized miniature pigs in normoxia and hyperoxia. Exp Eye Res. 1989;49:347–60. PubMed PMID: 2792232.
225. Frank RN. Visual fields and electroretinography following extensive photocoagulation. Arch Ophthalmol. 1975;93:591–8. PubMed PMID: 1171677.
226. Grunwald JE, Riva CE, Brucker AJ, Sinclair SH, Petrig BL. Altered retinal vascular response to 100% oxygen breathing in diabetes mellitus. Ophthalmology. 1984;91:1447–52. PubMed PMID: 6084214.
227. Feke GT, Buzney SM, Ogasawara H, Fujio N, Goger DG, Spack NP, Gabbay KH. Retinal circulatory abnormalities in type 1 diabetes. Invest Ophthalmol Vis Sci. 1994;35:2968–75. PubMed PMID: 8206714.
228. Bursell SE, Clermont AC, Kinsley BT, Simonson DC, Aiello LM, Wolpert HA. Retinal blood flow changes in patients with insulin-dependent diabetes mellitus and no diabetic retinopathy. Invest Ophthalmol Vis Sci. 1996;37:886–97. PubMed PMID: 8603873.
229. Ahmed J, Hatchell DL, et al. Retinal hypoxia in long-term diabetic cats. Invest Ophthalmol Vis Sci. 1998;39:1647–1657. PubMed PMID: 9699554.
230. Linsenmeier RA, Braun RD, McRipley MA, Padnick LB, Ahmed J, Hatchell DL, McLeod DS, Lutty GA. Retinal hypoxia in long-term diabetic cats. Invest Ophthalmol Vis Sci. 1998;39:1647–57. PubMed PMID: 9699554.
231. Minot, CS. The Problem of Age, Growth and Death. The Popular Science Monthly.
232. Yu DY, Cringle SJ. Oxygen distribution and consumption within the retina in vascularised and avascular retinas and in animal models of retinal disease. Prog Ret. Eye Res. 2001;20:175–208. PubMed PMID: 11173251.
233. Yu DY, Cringle SJ, Alder VA, Su EN. Intraretinal oxygen distribution in rats as a function of systemic blood pressure. Am J Physiol. 1994;267:H2498–507. PubMed PMID: 7810746.
234. Yu DY, Cringle SJ. Outer retinal anoxia during dark adaptation is not a general property of mammalian retinas. Comp Biochem Physiol. 2002;A132:47–52. PubMed PMID: 12062190.
235. Yu DY, Cringle SJ. Oxygen distribution and consumption within the retina in vascularised and avascular retinas and in animal models of retinal disease. Prog Retin Eye Res. 2001;20:175–208. PubMed PMID: 11173251.
236. Birol G, Wang S, Budzynski E, Wangsa-Wirawan ND, Linsenmeier RA. Oxygen distribution and consumption in the macaque retina. Am J Physiol Heart Circ Physiol. 2007; 293: H1696-704.
237. Tofts PS, Porchia A, Jin Y, Roberts R, Berkowitz BA. Toward clinical application of manganese-enhanced MRI of retinal function. Brain Res Bull. 2010;81:333–8. PubMed PMID: 19524028.
238. de Gooyer TE, Stevenson KA, Humphries P, Simpson DA, Curtis TM, Gardiner TA, Stitt AW. Rod photoreceptor loss in Rho-/- mice reduces retinal hypoxia and hypoxia-regulated gene expression. Invest Ophthalmol Vis Sci. 2006;47:5553–60. PubMed PMID: 17122148.
239. de Gooyer TE1. Stevenson KA, Humphries P, Simpson DA, Gardiner TA, Stitt AW. Retinopathy is reduced during experimental diabetes in a mouse model of outer retinal degeneration. Invest Ophthalmol Vis Sci. 2006;47:5561–8. PubMed PMID: 17122149.

240. Arden GB. The absence of diabetic retinopathy in patients with retinitis pigmentosa: implications for pathophysiology and possible treatment. Brit J Ophthalmol. 2001;85:366–370. PubMed PMID: 11222350.
241. Smith PR, Bain SC, Good PA, et al. Pigmentary retinal dystrophy and the syndrome of maternally inherited diabetes and deafness caused by the mitochondrial DNA 3243 tRNA(Leu) A to G mutation. Ophthalmology. 1999;106:1101–1108. PubMed PMID: 10366077.
242. Holmes-Walker DJ, Mitchell P, Boyages SC. Does mitochondrial genome mutation in subjects with maternally inherited diabetes and deafness decrease severity of diabetic retinopathy? Diabet Med. 1998;15:946–952. PubMed PMID: 9827849.
243. Marsh S, Nakhoul FM, Skorecki K, Rubin A, Miller BP, Leibu R, Levy NS, Levy AP. Hypoxic induction of vascular endothelial growth factor is markedly decreased in diabetic individuals who do not develop retinopathy. Diabetes Care. 2000;23:1375–1380. PubMed PMID: 10977036.
244. Harris A, Arend O, Danis RP, Evans S, Wolf S, Martin BJ. Hyperoxia improves contrast sensitivity in early diabetic retinopathy. Br J Ophthalmol. 1996;80:209–213. PubMed PMID: 8703857.
245. Nguyen QD, Shah SM, Van Anden E, Sung JU, Vitale S, Campochiaro PA. Supplemental oxygen improves diabetic macular oedema: a pilot study. Invest Ophthalmol Vis Sci. 2004;45:617–624. PubMed PMID: 14744906.
246. Shiba T, Sato Y, Takahashi M. Relationship between proliferative diabetic retinopathy and sleep-disordered breathing. Nippon Ganka Gakkai Zasshi. 2007;111:899–904. PubMed PMID: 18051820.
247. Shiba T, Sato Y, Takahashi M. Relationship between diabetic retinopathy and sleep-disordered breathing. Am J Ophthalmol. 2008;147:1017–1021. PubMed PMID: 19268888.
248. West SD, Groves DC, Lipinski HJ, et al. The prevalence of retinopathy in men with Type 2 diabetes and obstructive sleep apnoea. Diabet Med. 2010;27:423–430. PubMed PMID: 20536514.
249. Kosseifi S, Bailey B, Price R, Roy TM, Byrd RP Jr, Peiris AN. The association between obstructive sleep apnea syndrome and microvascular complications in well-controlled diabetic patients. Mil Med. 2010;175:913–916. PubMed PMID: 21121505.
250. Mason RH, West SD, Kiire CA, et al. High prevalence of sleep disordered breathing in patients with diabetic macular edema. Retina. 2012;32:1791–8. PubMed PMID: 22714043.
251. Arden GB, Sivaprasad S. Hypoxia and oxidative stress in the causation of diabetic retinopathy. Curr Diabetes Rev. 2011;7:291–304. PubMed PMID: 21916837.
252. Arden GB, Sivaprasad S. The pathogenesis of early retinal changes of diabetic retinopathy. Doc Ophthalmol. 2012;124:15–26. PubMed PMID: 22302291.
253. Arden GB, Gŭndŭz MK, Kurtenbach A, Volker M, Zrenner E, Gŭndŭz SB, et al. Preliminary trial to determine whether prevention of dark adaptation affects the course of early diabetic retinopathy. Eye. 2010;24:1149–1155. PubMed PMID: 20139913.
254. Arden GB, Jyothi S, Hogg CH, Lee YL, Sivaprasad S. Regression of early diabetic macular oedema is associated with prevention of dark adaptation. Eye. 2011;25:1546–1554. PubMed PMID: 22020171.
255. Sivaprasad S, Arden G, Prevost AT, Crosby-Nwaobi R, Holmes H, Kelly J, Murphy C, Rubin G, Vasconcelos J, Hykin P. A multicentre phase III randomised controlled single-masked clinical trial evaluating the clinical efficacy and safety of light-masks at preventing dark-adaptation in the treatment of early diabetic macular oedema (CLEOPATRA): study protocol for a randomised controlled trial. Trials. 2014 Nov 22;15:458. PubMed PMID: 25417120.
256. McKeague C, Margrain TH, Baliey C, Binns AM. Low-level night-time therapy for age-related macular degeneration (Alight): study protocol for a randomised controlled trial. Trials. 2014;15:246. PubMed PMID: 24965385.
257. Chakravaty U, Harding SP. Ranibizumab versus bevacizumab to treat neovascular AMD one-year findings from the IVAN randomized trial. Ophthalmology. 2012;119:1399–411. Rogers et al. PubMed PMID: 22578446.
258. Rosenfeld PJ, Rich RM, Lalwani GA. Ranibizumab: Phase III clinical trial results. Ophthalmol Clin North Am. 2006;19:361–72. PubMed PMID: 16935211.

259. Chen L, Magliano DJ, Zimmet PZ. The worldwide epidemiology of type 2 diabetes mellitus--present and future perspectives. Nat Rev Endocrinol. 2011;8:228–36. PubMed PMID: 22064493.
260. Bressler NM, Varma R, Doan QV, Gleeson M, Danese M, Bower JK, Selvin E, Dolan C, Fine J, Colman S, Turpcu A. Underuse of the health care system by persons with diabetes mellitus and diabetic macular edema in the United States. JAMA Ophthalmol. 2014;132:168–73. PubMed PMID: 24357541.
261. Rosenfeld PJ, Rich RM, Lalwani GA. Ranibizumab: Phase III clinical trial results. Ophthalmol Clin North Am. 2006;19:361–72. PubMed PMID: 16935211.
262. Bloch SB, Larsen M. Treatment of wet age-related macular degeneration with vascular endothelial growth factor. A survey of a Cochrane review. Ugeskr Laeger. 2009;16(171):3435–7. PubMed PMID: 19925729.
263. Mitchell P. Cytokines in neovascular age-related macular degeneration: fundamentals of targeted combination therapy. Br J Ophthalmol. 2011;95:1631–7. PubMed PMID: 21546514.
264. Stewart MW. The expanding role of vascular endothelial growth factor inhibitors in ophthalmology. Mayo Clin Proc. 2012; 87): 77-88.
265. Wolf A, Kampik A. Efficacy of treatment with ranibizumab in patients with wet age-related macular degeneration in routine clinical care: data from the COMPASS health services research. Graefes Arch Clin Exp Ophthalmol. 2014;252:647–55. PubMed PMID: 24424409.
266. Micieli JA, Surkont M, Smith AF. A systematic Analysis of the Off-Label Use of Bevacizumab for Severe Retinopathy of Prematurity. Am J Ophthalmol. 2009;148:536–43. PubMed PMID: 19660736.
267. Assari T Chronic Granulomatous Disease; fundamental stages in our understanding of CGD. *Medical Immunology* e. 2006;5:4–31.
268. Kita K, Konishi K, Anraku Y. Terminal oxidases of Escherichia coli aerobic respiratory chain. II. Purification and properties of cytochrome b558-d complex from cells grown with limited oxygen and evidence of branched electron-carrying systems. J. Biol Chem. 1984;259:3375–3381. PubMed PMID: 6321507.
269.
270. Ramsey DJ, Ripps H, Qian H. Streptozotocin-induced diabetes modulates GABA receptor activity of rat retinal neurons. Exp Eye Res. 2007;85:413–22. Epub 2007 Jun 19. PubMed PMID: 17662714.

The Science Behind Myopia

Brittany J. Carr, Ph.D.[1,*] and William K. Stell, M.D., Ph.D.[2,†]

Created: November 7, 2017.

Introduction

Myopia (near-sightedness) is the most common refractive vision disorder in children. It is characterized by blurring of objects viewed at a distance, and is commonly the result of abnormal elongation of the eyeball – which causes the refractive image formed by the cornea and the lens to fall in front of the photoreceptors of the retina (Figure 1).

The underlying biological cause of myopia is unknown, and there is no widely accepted means of prevention or cure. The optical error of myopia can be corrected only by using spectacle or contact lenses or corneal surgery. If left untreated, moderate myopia is one of the leading causes of visual impairment worldwide. The greater the degree of myopia, the greater the risk of complications such as macular degeneration, retinal detachment, cataracts, and glaucoma (1); the risk is especially great when the negative refractive error is more negative than -6.00 D (diopters), a condition called 'high myopia'. The prevalence of myopia varies greatly, depending on ethnicity, geographical location, and socioeconomic status, but is rising rapidly in most populations studied (2) (Figure 2). Myopia is a centuries-old problem, and although we have made great progress in scientific investigation of its underlying cause, we have been unsuccessful in preventing it from becoming named by the World Health Organization as an ever-increasing global health concern (3).

Clinical aspects & health care burden

There are two clinical designations for myopia: pathological degenerative myopia, and spontaneous-onset or school age myopia. Pathological myopia is characterized by rapid, extreme axial elongation of the globe, leading to a high refractive error (typically far more negative than -6.00D). This extreme stretching puts stress on the ocular structures (retina, choroid, and sclera), which can then result in degenerative changes in the eye (Figure 3), and irreversible vision loss. Fortunately, pathological myopia is relatively rare, affecting 0.9-3.1% of the population (4).

The most common form of myopia is school-age myopia; this is the form that will be discussed in this chapter, and it will be called simply "myopia" from this point on. It progresses slowly, and usually stabilizes by the age of 20. The retina looks normal. Recently, is has been projected that 2.5 billion people (1/3 of the world's population) will have some degree of myopia by 2030 (2).

Genes may play a role in development of myopia

Myopia prevalence varies greatly in different ethnic and geographical populations (1). Recent studies of American preschool children (aged 6–72 months) revealed a prevalence of 1.2% in non-Hispanic whites, 3.7% in Hispanics, 3.98% in Asians, and 6.6% in African Americans (5, 6). Among older children, the difference between Asian and Caucasian populations is obvious; a study of Australian adolescents reported prevalence of 42.7% in

Author Affiliations: 1 Center for Macular Research, University of British Columbia; Email: bcarr@ucalgary.ca. 2 Cell Biology and Anatomy, Cumming School of Medicine, University of Calgary; Email: wstell@ucalgary.ca.

Corresponding author.

* About the authors

† About the authors

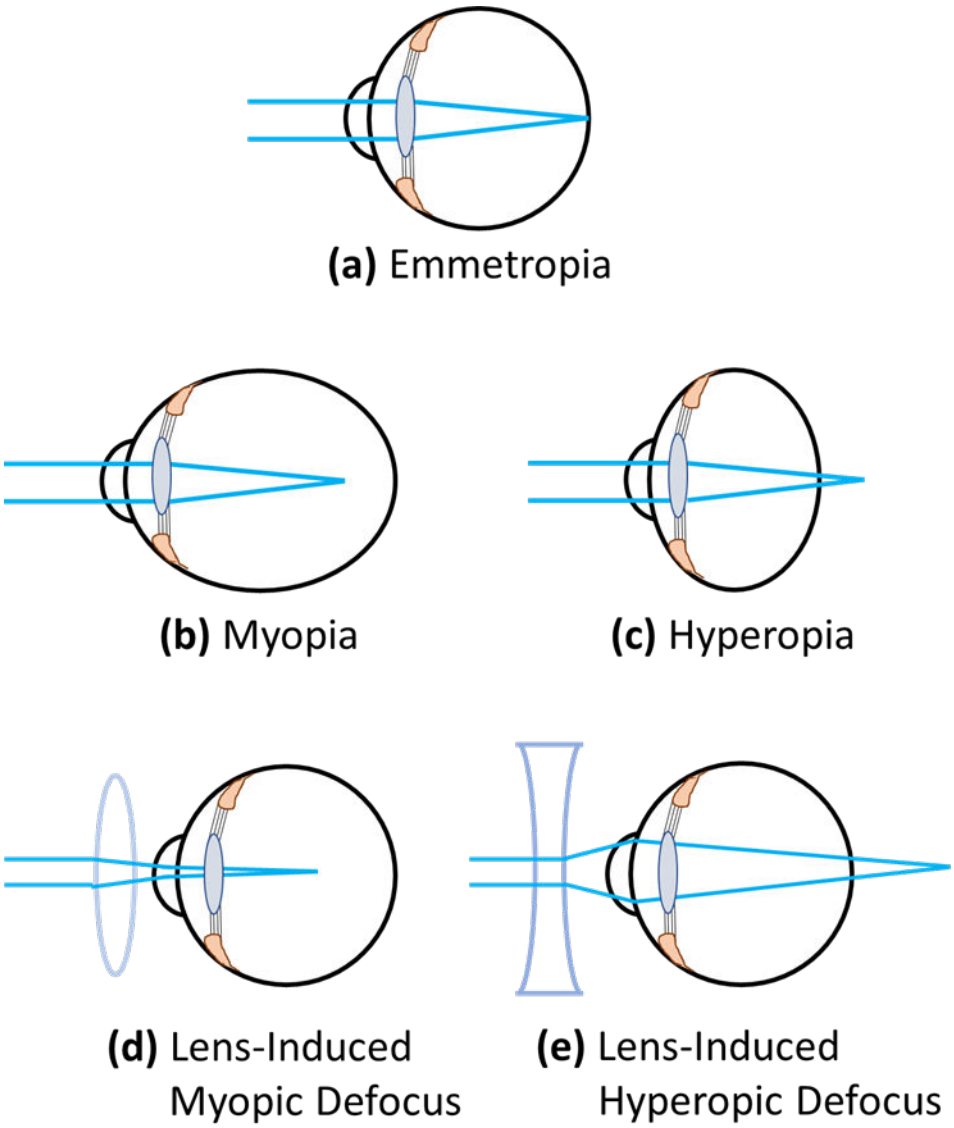

Figure 1. Exaggerated representation of simple refractive errors caused by abnormal eye growth. Emmetropia (normal vision) is the state of refraction in which light is focussed perfectly on retinal rod and cone photoreceptors (**a**). Myopia (near- or short-sightedness) occurs when the axial length of the eye is too long, and light is focussed in front of the photoreceptors (**b**). Hyperopia (far-sightedness) occurs when the axial length of the eye is too short, and light is focussed behind the photoreceptors (**c**). Refractive error can be modified using lenses: In an emmetropic eye, positive lenses impose myopic defocus (**d**), and negative lenses impose hyperopic defocus (**e**).

12 yr old and 59.1% in 17 yr old children of East Asian ethnicity, compared to 8.3% in 12 yr old and 17.7% in 17 yr old children of European Caucasian descent (7).

There have been attempts to identify genes that may be important in myopia development. "Genome-wide association studies" (GWAS), which examine genetic variations between individuals to determine whether certain variants are associated with a specific trait (in this case myopia), have identified correlations between variations in certain genes and an increased risk of myopia. The recently published Consortium for Refractive Error And Myopia (CREAM) study is the largest international genome-wide meta-analysis on myopia and refractive error ever conducted. It is based on data from 32 studies encompassing Europe, the United States, Australia and Asia (8). Twenty-four genomic variations were associated with up to a 10x increase in risk of myopia. These genetic variations are involved in many apparently unrelated ocular functions, instead of a single underlying system or structure. Thus, the CREAM study provided significant evidence that the risk of

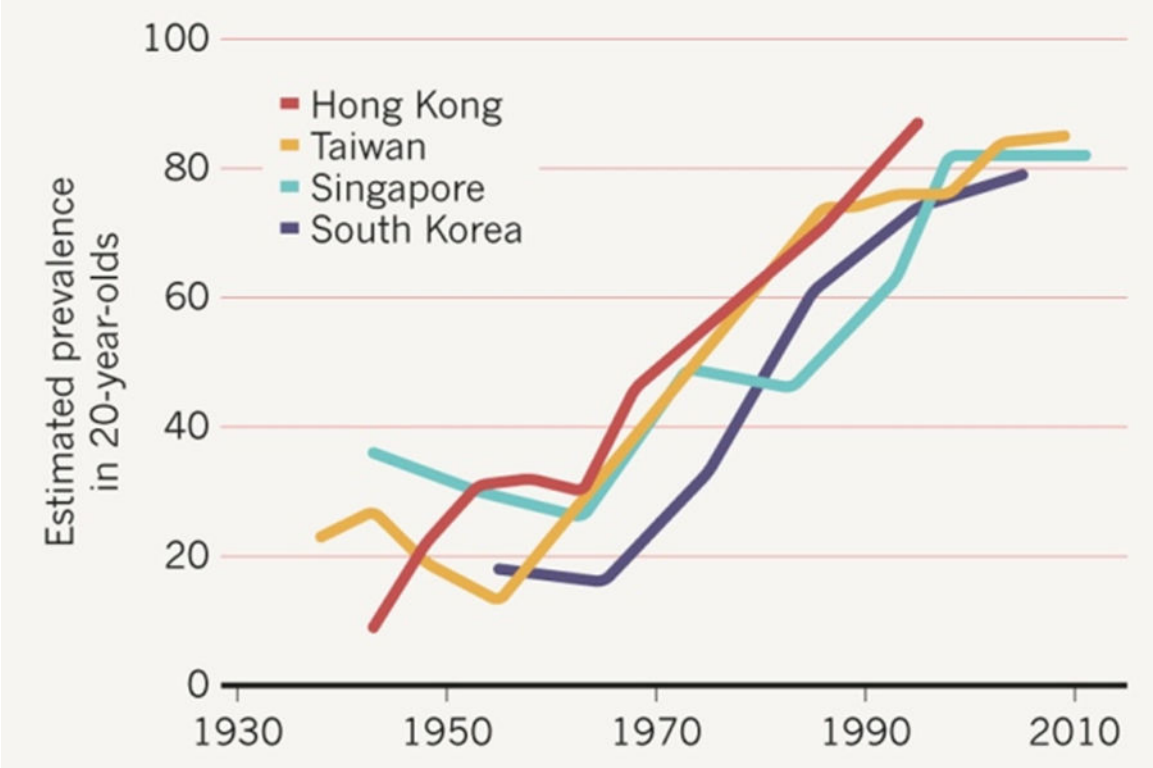

Figure 2. Myopia prevalence has been increasing steadily since the 1950's, especially in Southeast Asian countries. Reproduced with permission from Dolgin, E. (2015) (2). Figure source: Ian Morgan, Australian National University.

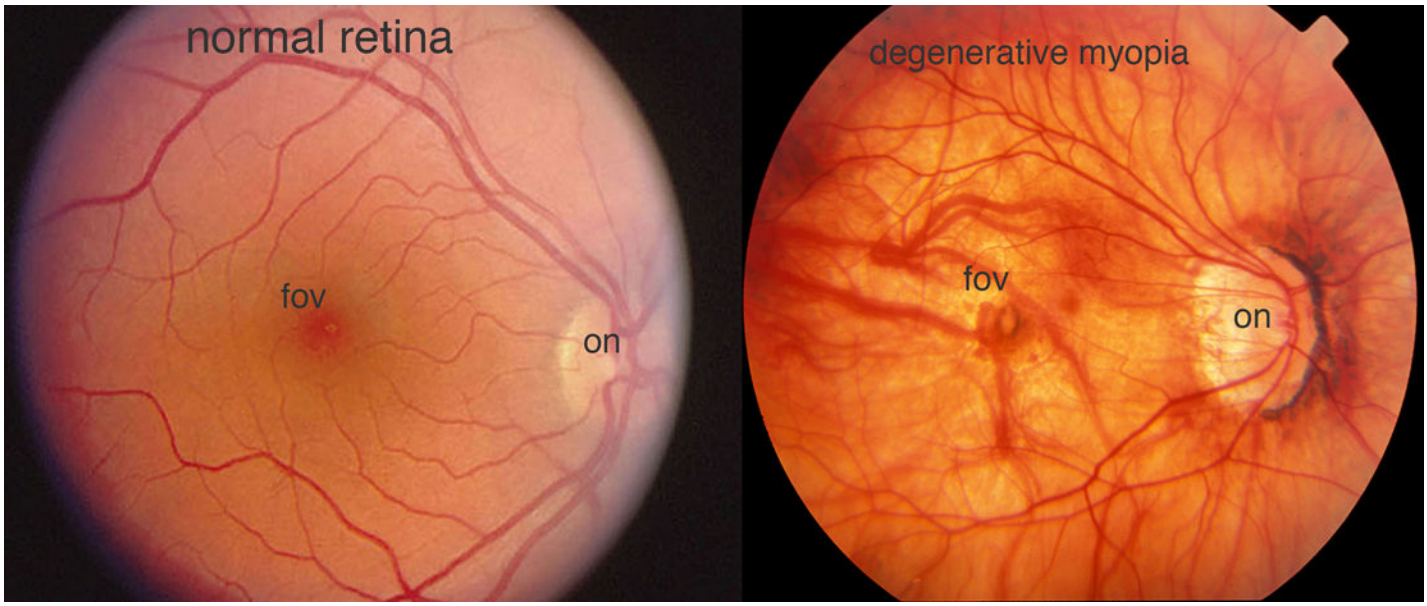

Figure 3. A fundus photograph of the retina of a person with degenerative myopia (right) is compared with that of a normal person's retina (left). The myope's retina is stretched and thinned, with thin blood vessels, a distorted optic nerve head (on), some folds in the thin retina, and pigmentation at the fovea (fov). Fundus photos provided by James Gilman and the Moran Eye Center ophthalmic photography department.

developing myopia may be affected by many unrelated genetic abnormalities, instead of a single underlying cause (Figure 4).

Twin studies and parental myopia studies have also been conducted to try to assess the role of genetics in development of myopia (9). Twin studies have reported that the correlation of prevalence of myopia was significantly higher in identical twins than fraternal twins (9-11). Age, and the methods used to gather and analyze the data, are important, however, as myopia correlations determined by such studies can range from r = 0.11 (low correlation) to r = 0.94 (high correlation) (10). There is strong evidence to suggest that increased risk of myopia is highly correlated with the number of myopic parents (12-16), and that this risk is independent of environmental factors (13, 15). One problem with twin and familial studies, however, is that few of them bothered to control for environmental factors that would be likely be shared among family members – for example, the likelihood that identical twins engage in the same activities in a much higher frequency than fraternal twins or non-twin siblings.

It is reasonable to assume that genes play a part in myopia risk, but they alone cannot account for the rapid changes in myopia prevalence that are being observed all over the world, nor for the dramatic differences in myopia prevalence within the same ethnic populations – in urban vs. rural environments, for example (2, 17). Thus, the underlying cause of spontaneous-onset myopia is most likely to be a combination of genes and environmental triggers. Most of the identified risk factors for myopia are correlated with environmental influences, such as an increased socioeconomic status, residing in an urban environment, higher education and IQ, increased time spent performing near work, and increased time spent indoors (1, 18). These risk factors are based on observations of human populations over many decades, but they do not provide a mechanistic explanation as to why they are associated with an increased risk of myopia.

To understand the roles of environmental risk factors for the cause of myopia (which are difficult to study in human subjects under stringently controlled conditions), scientists have turned to animal models. The results have demonstrated clearly that, while genetics may determine myopia susceptibility (e.g.: age of onset, rate of progression, ultimate refractive error), environmental factors are powerful modifiers of eye growth, and they may override genetic predispositions. For a comprehensive review on the biological basis and mechanisms of the eye's self-regulation of growth see, "Homeostasis of eye growth and the question of myopia", by Wallman & Winawer (19).

Animal models of myopia: What we see controls how the eye grows

The first reported case of myopia in experimental animals was observed serendipitously in non-human primates, during investigations into the cortical effects of monocular visual deprivation in young macaques. In these animals, sewing the eyelids shut for many months resulted in high levels of myopia (20); the longer the period of visual deprivation, the greater the resultant refractive error (21). The establishment of this "form-deprivation" model of myopia in primates led to parallel studies of experimentally-induced myopia in young tree shrews (22) and chickens (23). Instead of sewing the eyelids shut, scientists now use frosted plastic goggles to induce deprivation myopia, or lenses with a strong negative power to cause "lens-induced myopia" (24) (Figure 5). Today, the most commonly-used myopia model animals are chicks and guinea pigs, but tree shrews, non-human primates, and mice are also studied (25).

That we can experimentally-induce myopia in young, rapidly growing animals tells us that the visual environment plays an important role in regulation of eye growth. Applying goggles over the eye works even when the optic nerve has been cut, which tells us that the eye alone – or more specifically, a specialized sensorineural tissue in the eye called the retina – can discriminate whether the image is well focussed or not, and act locally to mediate optically-induced changes in eye growth (19, 26, 27). Affixing a frosted goggle or negative lens over the eye causes excessive axial elongation of the eye, and myopia, but affixing a positive lens over the eye causes inhibition of axial elongation, and far-sightedness (hyperopia) (Figure 6). The complementary effects of positive and negative defocus reveal that the eye – most probably the retina itself – can discriminate between

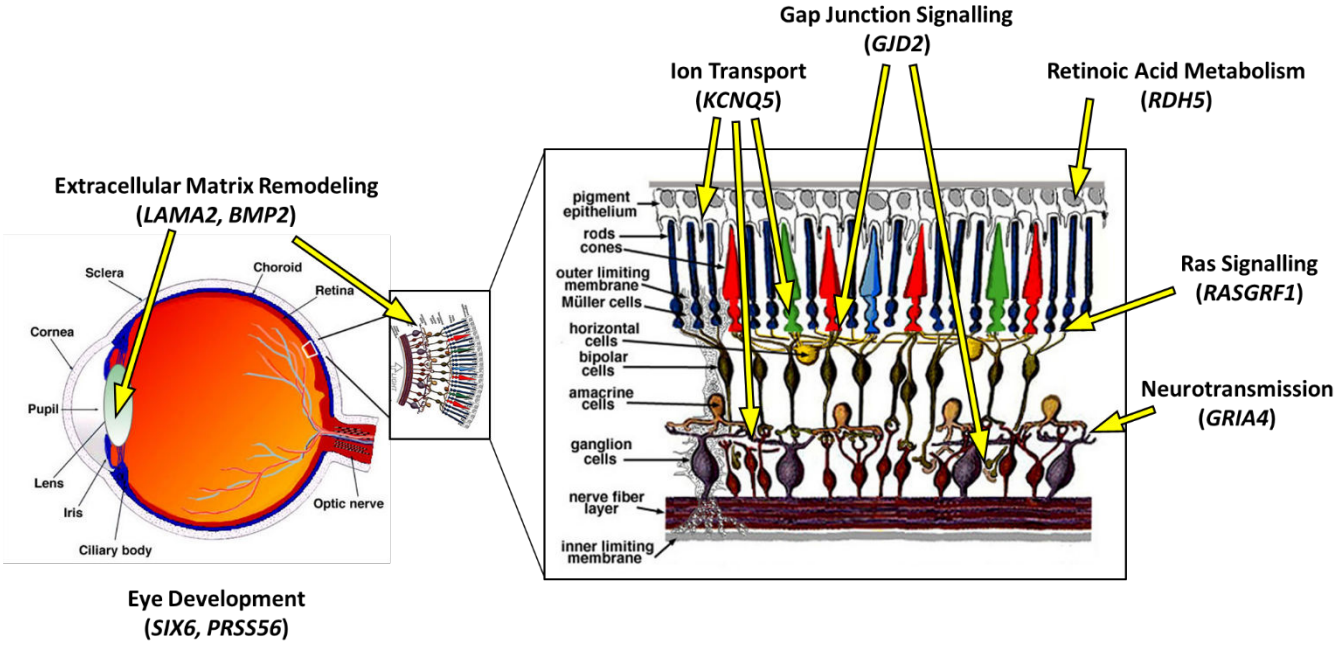

Figure 4. Localization and functions of a few genes identified by the CREAM study (8) in the eye and retinal tissues. Some of the genes identified are functionally involved in processes that facilitate communication between cells in the retina (*KCNQ5, GJD2, RASGFR1, GRIA4*) or control the ability of photoreceptors to respond to light (*RDH5*). Some others are involved in pre-natal eye growth and development (*LAMA2, BMP2, SIX6, PRSS56*).

positive and negative defocus, as well as between unfocussed blur (form-deprivation) and blur due to negative lens treatment, even though the static images produced by the two different treatments appear very similar (Figure 5, b vs. c). We do not know whether eye growth is controlled by two different signals, one "start" and one "stop", operating in push-pull fashion (like turning the steering of an automobile to left or right) – or by a single signal that increases elongation ("grow" or "on") or decreases it ("stop" or "off") (like increasing or decreasing pressure on the accelerator pedal of an automobile). We also do not know the identities of these hypothetical "start" or "stop" growth signals, but a number of signalling substances have been identified that are very strong candidates for "eye growth regulators" (discussed in greater detail below).

Myopia-inducing stimuli require prolonged exposures (days-weeks) for a significant effect. In the chick, however, it takes only ≥2 hrs per day of unobstructed viewing of a richly textured visual environment to completely block the development of form-deprivation myopia (28), and positive-lens wear for only 2 min, four times per day, is enough to block lens-induced myopia (29). In addition, the eye can "recover" from experimentally induced myopia and return to an emmetropic refractive state, if the animal (or human) is young enough. Once an organism has reached adulthood, however, there is no known way to decrease the size of the globe, without surgical intervention.

Inhibiting accommodation does not prevent myopia

Perhaps you are familiar with the old wives' tale, "Don't sit too close to the TV, or you'll ruin your eyes!". This is likely because the most common and longstanding hypothesis about the cause of myopia development was that excessive near work results in accommodative fatigue, which then causes myopia. Accommodative fatigue occurs when the ciliary muscle weakens due to overexertion – as arm or leg muscles would – in response to an entire day of heavy lifting. Weakening of the ciliary muscle would result in loss of the focussing power of the lens, leading to hyperopic defocus when objects are viewed up close (Figure 7). As discussed previously in the

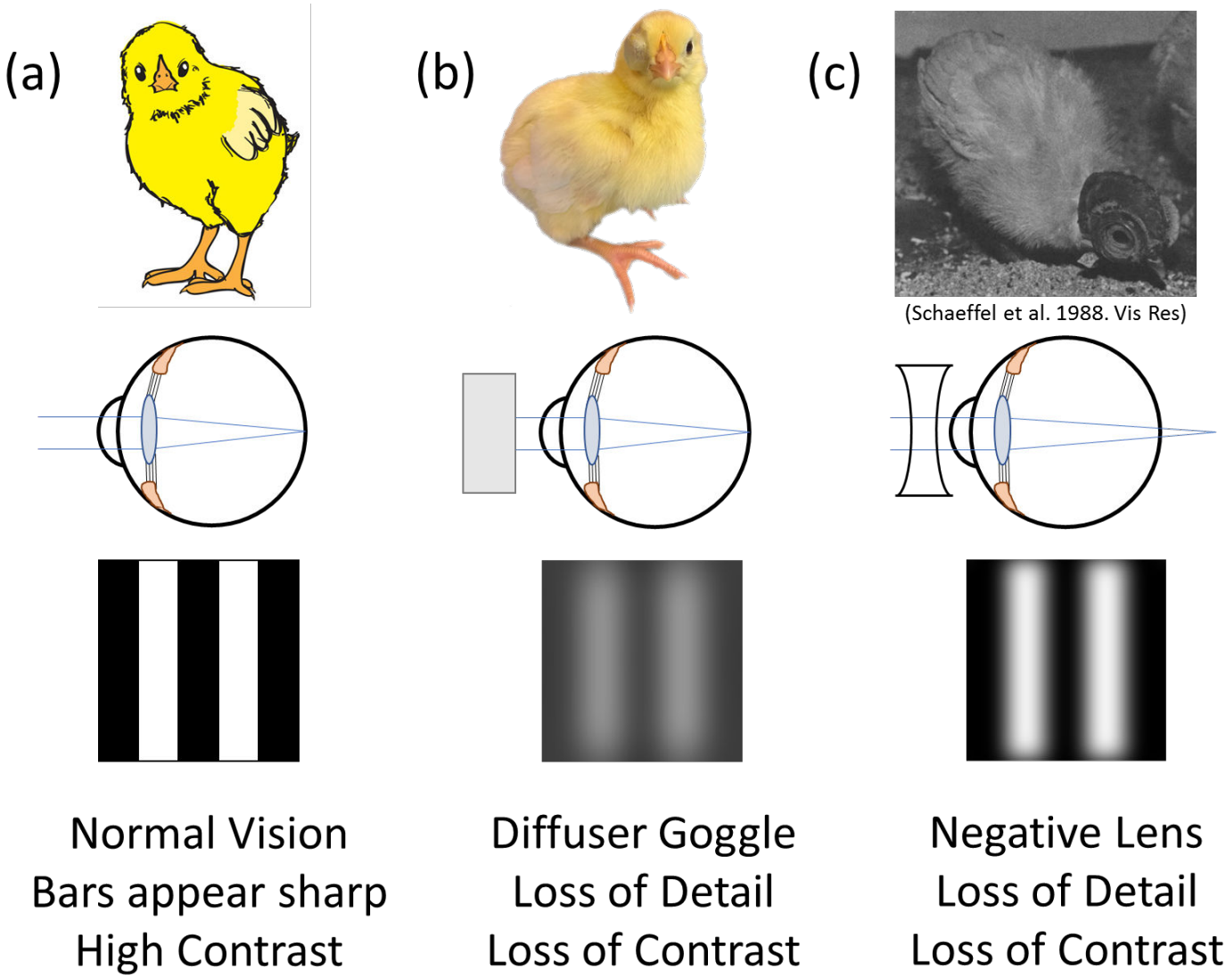

Figure 5. The effects of goggles on the initially focused image of a square-wave grating. When no goggle is applied, the grating image appears as sharply defined black and white lines (**a**). Myopia can be induced by manipulating retinal images optically, in animal models such as the chick, by application of a frosted diffuser goggle (**b**) or a negative-powered lens (**c**). Both treatments reduce spatial contrast of the image (difference between white and black), especially at higher spatial frequencies (the sharpness of the line borders).

section about animal models of myopia, hyperopic defocus (pushing the plane of focus behind the photoreceptors) can be a stimulus for eye growth.

To investigate whether reducing the need for accommodation in children would be preventative against myopia, scientists have utilized progressive-addition lenses (PALs). In principle, the use of PALs should allow accommodation (contraction of the ciliary muscle) to relax, while keeping a blur-free image on the retina (30) (Figure 8).

"The Correction Of Myopia Evaluation Trial" (COMET) was the largest and most significant human clinical trial ever conducted to test whether relaxation of accommodation through the use of PALs could help to inhibit the progression of myopia in children. It was a multicenter, randomized, double-masked, controlled clinical trial that took place over a period of three years (n = 469 children). At the end of the study, a statistically significant 3-year mean difference was found in children who wore PALs versus single vision lenses (SVL) (refractive error progression: PAL: −1.28 ± 0.06 D *vs.* SVL: −1.48 ± 0.06 D, p = 0.004; axial length elongation: PAL: 0.64 ± 0.02

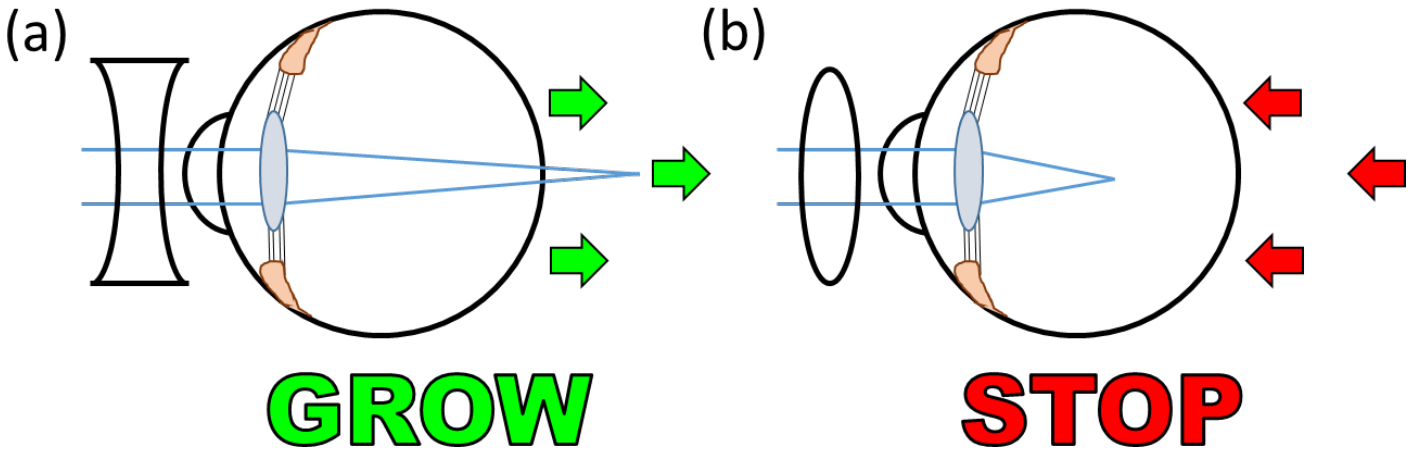

Figure 6. Affixing a negative (concave or diverging) lens over the eye pushes the focal plane of the visual image behind the retina, inducing an increase in axial elongation and a more myopic refraction (**a**). Conversely, affixing a positive (convex or converging) lens over the eye pushes the focal plane of the visual image in front of the retina, inducing a decrease in axial elongation and a more hyperopic refraction (**b**).

mm *vs.* SVL: 0.75 ± 0.02 mm, p = 0.0002). These data supported the hypothesis that changes in accommodation can affect myopia progression. Unfortunately, this effect was too small to be considered clinically significant, although one subset of children – those who had high accommodative lag – seemed to benefit significantly from PAL wear (Figure 9). Subsequent studies have confirmed these findings (31), reporting a statistically significant, but small, reduction in myopia progression in children wearing PALs versus SVLs; these effects were not dependent on accommodative lag, as high-lag children had similar results as others. The accumulation of experimental evidence from animal models and further human trials, however, does not support a significant role of accommodation in myopia development (32). It remains possible that most PAL-wearers in the COMET study did not use the lenses properly, but tolerated the blur that resulted from accommodative fatigue and continued near-work without adjusting viewing angle for better focus.

A second hypothesis is that accelerated eye growth can occur because of over-correction of myopic refractive error (similar to lens-induced myopia). To test this hypothesis, children were under-corrected by +0.5 to +0.75 D. This trial therapy was largely unsuccessful; myopia progressed more rapidly in under-corrected children than in fully-corrected controls (33, 34). Interestingly, a recently published study (35) reported that myopia and axial elongation progressed more rapidly in fully under-corrected than in fully corrected myopic children. This held true even when controls were applied for other risk variables, such as baseline refractive error and axial length, number of myopic parents, age at myopia onset, and time spent doing near work and outdoors (35). Thus, there is still no consensus on whether under-correction may be an effective anti-myopia therapy.

Intense outdoor light protects against myopia

In recent years, spending time outdoors has been reported to reduce the risk of developing myopia, and this effect does not seem to be dependent on the amount of physical activity (7, 36). We do not yet know the mechanisms through which outdoor light might protect against myopia, but some ideas are that it might (a) stimulate intensity- or wavelength-dependent anti-myopia systems in the retina, (b) cause sustained pupillary constriction via the melanopsin system – thus improving retinal image quality by reducing longitudinal aberrations, (c) increase the production of vitamin D in the skin, (d) increase the average viewing distance of objects outdoors compared to indoors, thereby reducing accommodative fatigue, or (e) increase the activation of spatiotemporal image-response mechanisms in the retina, which inhibit myopia development. For a recent review on the roles each of these factors may play in myopia, please refer to "The role of luminance and

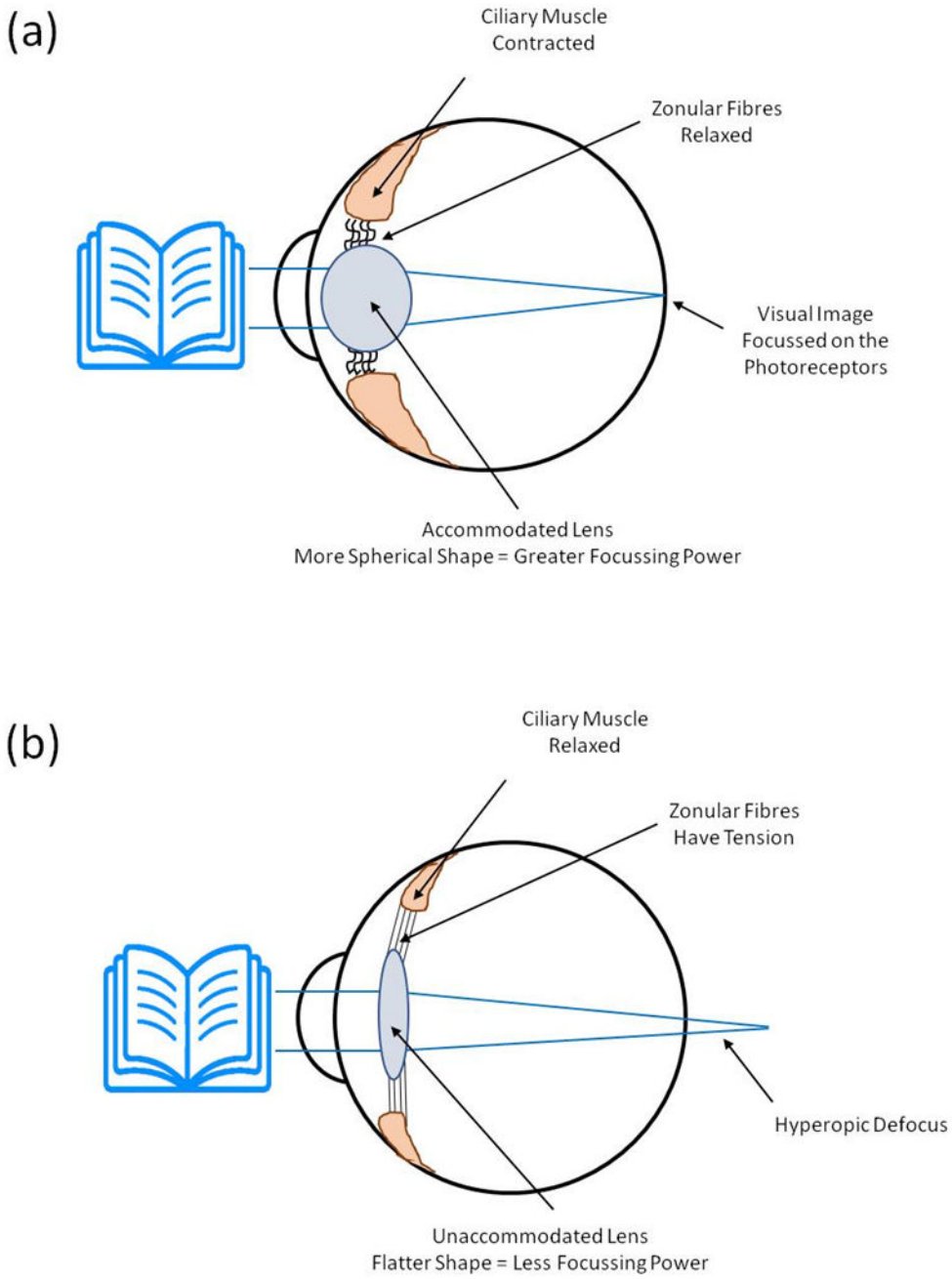

Figure 7. The effect of ciliary muscle contraction or relaxation on the focussing power of the lens. When the ciliary muscle is contracted, the lens becomes more spherical – and has increased focussing power – due to a lessening of tension on the zonular fibres (**a**). When the ciliary muscles relax, these fibres become taut – pulling the lens out into a flatter shape, which has less focussing power (**b**). Accommodative fatigue, the decrease in focussing power while continuing near-work, results in hyperopic defocus, which, in principle, might act as a stimulus for eye growth.

chromatic cues in emmetropization" by Frances Rucker (37). For more information about the melanopsin system, refer to the Webvision chapter "Melanopsin-expressing, Intrinsically Photosensitive Retinal Ganglion Cells (ipRGCs)" by Dustin M. Graham and Kwoon Y. Wong.

High-intensity illumination

When Rose et al. studied the effects of time spent outdoors on the development of myopia in Australian children, they found that children who spent more time outdoors had lower associated myopic refractive errors

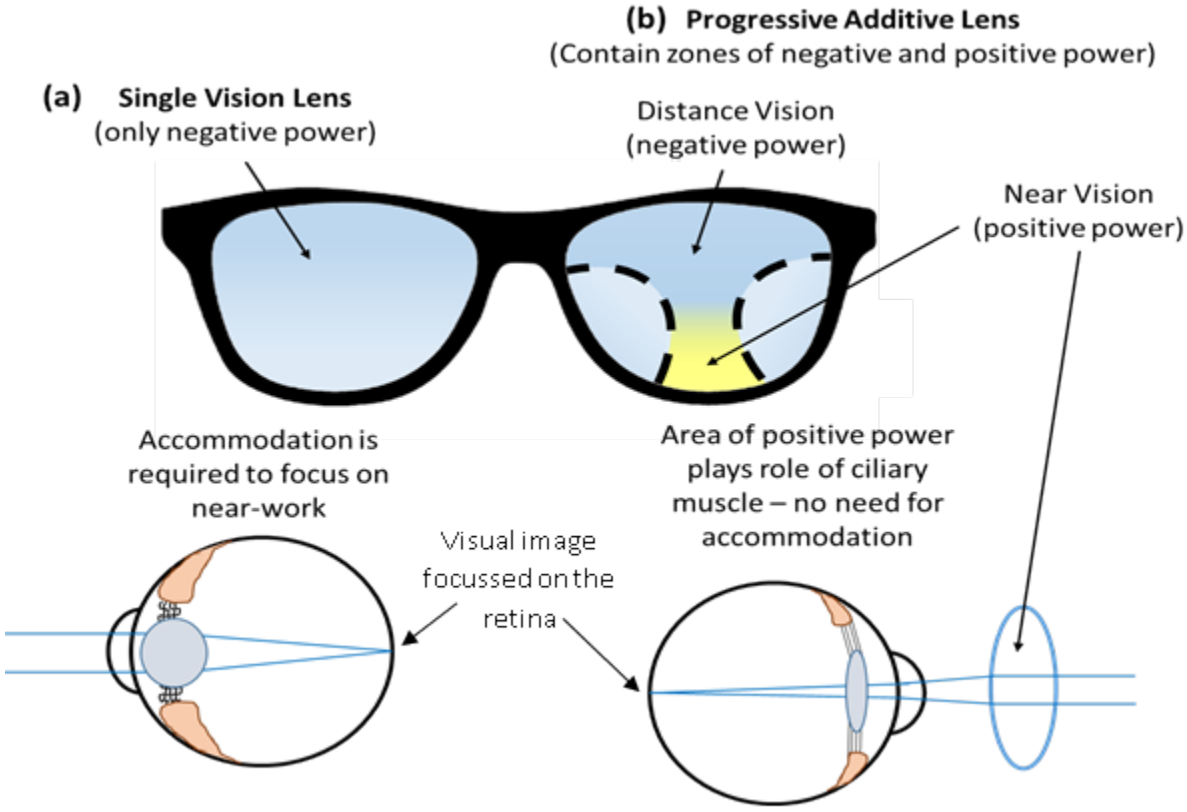

Figure 8. The two types of lenses used in the COMET study. Single vision lenses (a), which have only one power across their entire area, are the most common for correction of myopia. Progressive addition lenses (b) have multiple lens powers distributed across specific areas of the lens. This allows the wearer to focus at a distance (by looking through the top of the lens) or near (by looking through the bottom of the lens). In theory, the positive power in the bottom of the lens should have allowed children wearing PALs to perform near-work without the risk of accommodative fatigue.

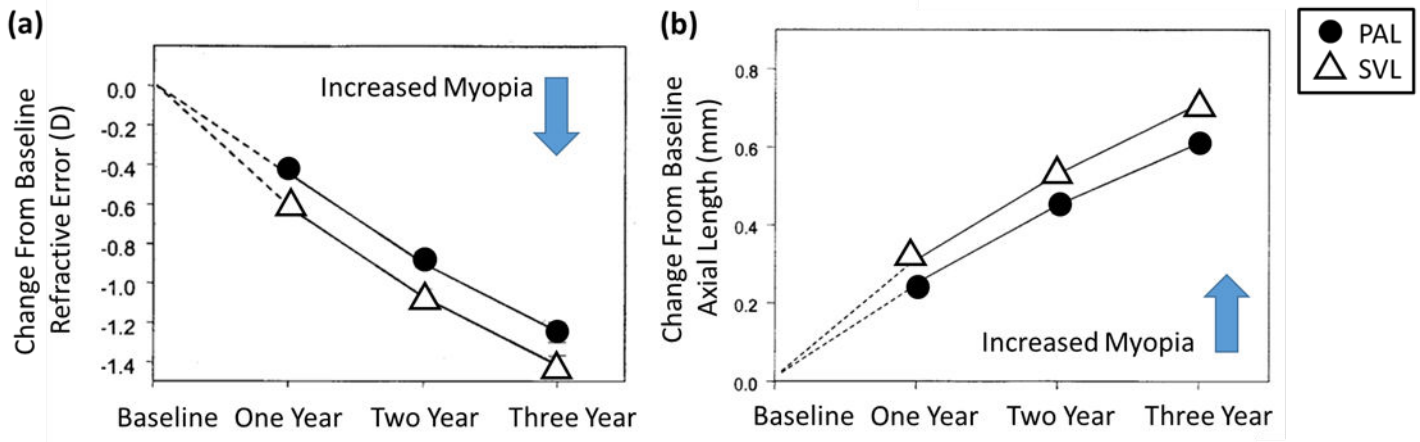

Figure 9. Example data from the COMET studies. A small, but clinically insignificant anti-myopia effect was gained by children wearing the progressive additive lenses (PAL; black circles) as evidenced by slightly less negative refractive error (**a**) and slightly decreased axial length (**b**) compared to children wearing single vision lenses (SVL; open triangles). Reproduced and modified from Gwiazda, J. *et al.* (2003) (30).

than children who spent most of their time indoors, even after adjusting for near-work, parental myopia, and ethnicity (38). Exercise versus leisure did not affect associated levels of myopia (Figure 10).

Therefore, it was proposed that the higher mean illuminance (light intensity) outdoors – which can be as much as 100,000 lux in Sydney AU, compared to typical indoor values of 350-500 lux – was responsible for the protective effect of outdoor activity against myopia progression. Human pilot studies to test this hypothesis have been successful in inhibiting myopia, in a small cohort of Chinese schoolchildren (39) and in a larger cohort of Australian schoolchildren (36). High-intensity light is also protective against experimentally-induced myopia in monkeys (40, 41) and chicks (42, 43). The mechanism through which intense light may prevent myopia is unknown, but we can use animal models to investigate the signalling molecules that may be involved. There are substantial links to the up-regulation of neuromodulators such as dopamine (44) and nitric oxide (45). These neurotransmitters are strongly correlated with myopia-inhibition on their own (46, 47), and they may also work together in the same myopia-inhibiting pathway (48).

Wavelength

During emmetropization, the eye needs some sort of visual cue to determine the direction of blur (29), and chromatic aberrations have been suggested as a possible cue (37). The most common chromatic aberration is longitudinal chromatic aberration (LCA), in which different wavelengths of light are focussed at different distances along the same axis (Figure 11).

In humans, the fovea is most densely populated with medium- and long-wavelength-sensitive cones. One idea is that the eye should be guided to grow to a size at which middle wavelengths in the visible spectrum (yellow-green, 550-570nm) will be the most sharply focussed, with the highest contrast, to attain the highest possible spatial acuity. If this were the case, the in-focus image of an eye that is too small will be blue-shifted, with high contrast at short-wavelengths (450-470 nm), whereas the in-focus image of an eye that is too large will be red-shifted with high contrast at long-wavelengths (610-630 nm) (Figure 12).

The results of research on the effects of LCA on emmetropization in the eye show that it is sufficient to detect the direction of retinal blur (49), but it does not seem to be necessary for emmetropization (49-51). Despite this, many studies have demonstrated clearly that the chromaticity (spectral composition) of light can be an important modulator of eye growth, although its effects do not seem to be the same in all animal models. In chickens raised *without* goggles or lenses, short-wavelength (blue) light retards eye growth, whereas long-wavelength (red) light promotes it; white light (which contains all spectral wavelengths) has no effect (52). In chicks wearing monocular diffusers, long-wavelength illumination (achieved using filters) is myopia-promoting, while short-wavelength illumination is myopia-inhibiting (Ghodsi & Stell (53), and Nguyen & Stell unpublished studies; Figure 13). Form-deprivation myopia in guinea pigs also responds to narrow-band long- or short-wavelength exposure in the same way as chicks (54-56). In contrast, long-wavelength light is growth-inhibiting and short-wavelength light is growth-promoting in rhesus monkey (57) and tree shrew (58). Thus, further investigations are needed to explore the effects of light spectrum on myopia development and to identify the underlying retinal mechanisms, in various animal models.

Retinal circuitry and ocular pathways of myopia

Emmetropization is an active-feedback process, guided by visual cues. It aims to match the axial length and resting focal power of the eye in such a way that images of objects viewed at any distance, can be focussed onto the retinal photoreceptors without accommodation (59).

Past studies indicate that the retina is the primary source of signals that regulate eye growth (19), while pathways involving transmission between retina and brain, via the optic nerve, may play roles in focal refinement of the visual image (60).

The retina is a highly specialized neural tissue that lies at the back of the eye (Figure 14), and although evidence suggests that the retina is the source of ocular growth-regulating signals (19), we do not know the specific cell

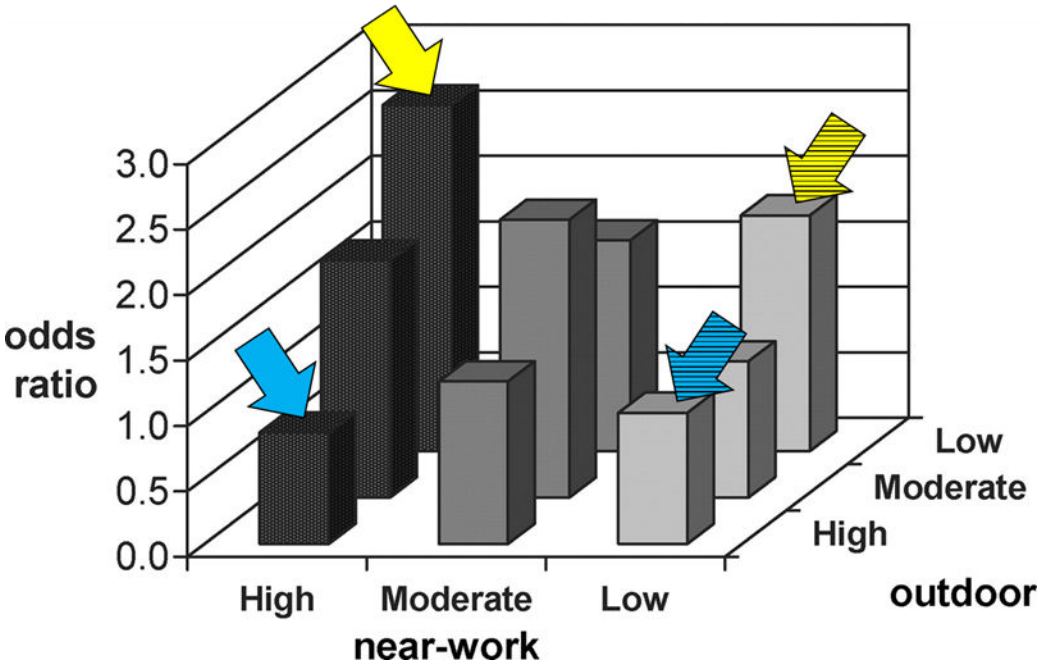

Figure 10. Multivariable-adjusted odds ratios (adjusted for gender, ethnicity, parental myopia, parental employment, and education) for myopia development by reported average daily hours spent on near-work versus outdoor activities in 12-year-olds. Activities were divided into columns of high, moderate, and low levels. The group with high levels of outdoor activity and low levels of near work (striped blue arrow) is the reference group. The blue arrow denotes the group with high levels of near work and high levels of outdoors activity. Yellow and yellow-striped arrows denote high near work and low outdoors activity, and low near work and low outdoors activity, respectively. Reproduced and modified from Rose, K. A. et al. (2008) (38).

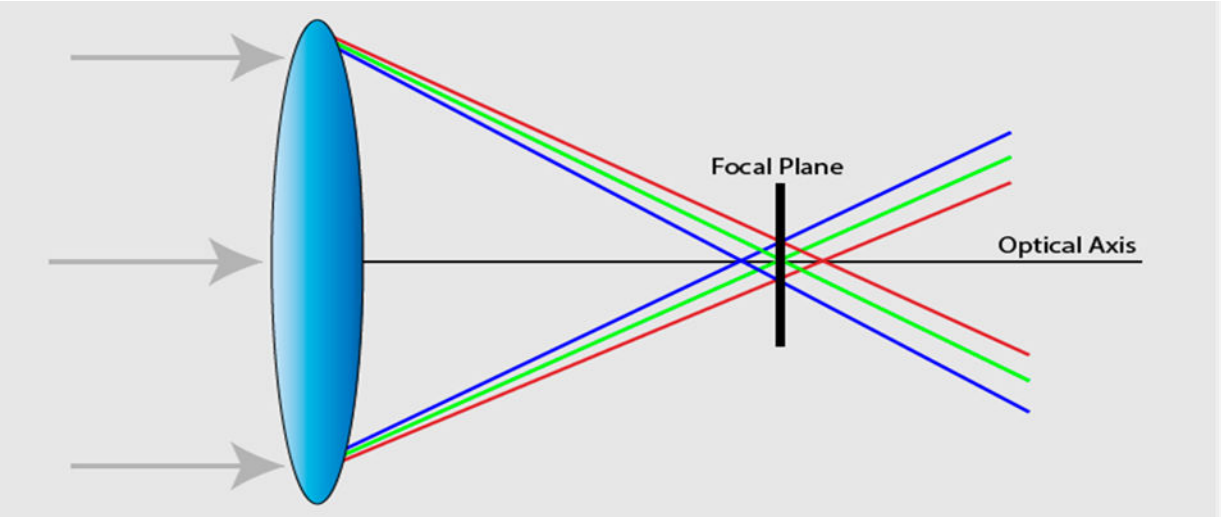

Figure 11. Longitudinal chromatic aberration is due to wavelength-dependent differences in refraction of light by the same lens. Light of shorter wavelengths, which appears violet to blue-green, is refracted more strongly than light of longer wavelength, such as that which appears yellow-green or red, and consequently is focused closer to the lens. From Photography Element .

types involved in emmetropization. There is no evidence for the direct involvement of horizontal cells, but destruction of photoreceptors (PRs) and/or amacrine cells (ACs) in the chick retina has been associated with increased axial growth of the eye (61, 62). Given the broad-spectrum action of toxins on retinal neurons, the relative roles of PRs and ACs in myopia-control in these types of studies are not well-defined, and molecular tools which would disrupt function of retinal cell types more specifically than toxins are not as widely-

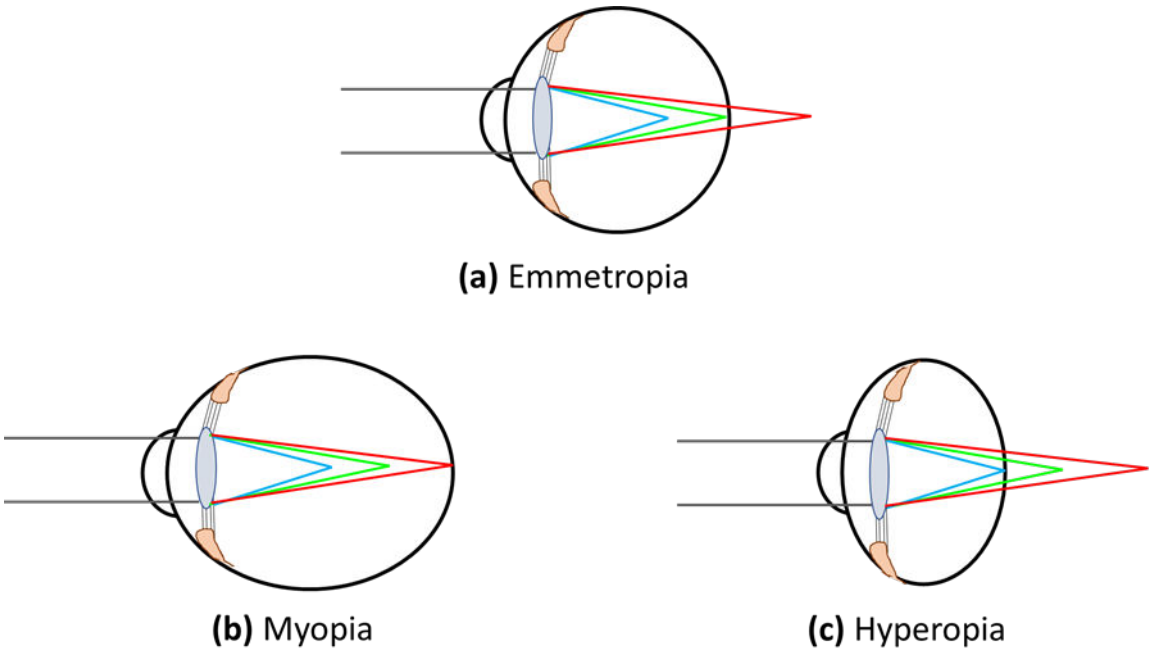

Figure 12. One hypothesis about the effect of LCA on defocus and contrast. In an emmetropic eye (a), the green region of the spectrum (middle-wavelengths) would be the most in-focus and have the highest contrast. If the eye is too short (b), the blue region of the spectrum (short-wavelengths) will be the most in-focus and have the highest contrast. If the eye is too long (c), the red region spectrum (long-wavelengths) will be most in-focus and have the highest contrast.

researched or available in chicks, the most common myopia model organism. Animals in which molecular tools are currently available – such as mice – are less suitable for studies of eye growth because their eyes are extremely small. This makes it very difficult to measure accurately any changes in axial growth or refractive error. This drawback of the chick model may change with a new genome-editing technology called CRISPR (63, 64), which is an exciting development that could be applied to the myopia-research field. Delivery of gene-silencing agents constructed from older technologies to cells in the retina of hatched chicks presents challenges that we have still not overcome (65).

That is not to say that myopia experiments in mice have not been performed. Genetic "knockout" mice models – in which their genome has been edited to "remove" certain retinal cell types or visual processing mechanisms by causing mutations – were used to determine the contributions of rods, cones, and retinal ON-pathways (some bipolar cells) to emmetropization (66). Eyes of mice with mutations causing severe degeneration of rods and cones (*rd1*$^{-/-}$ & *rd10*$^{-/-}$) were more susceptible to form-deprivation myopia than those of their wild-type (unmanipulated) counterparts (67) (Figure 15), while the eyes of rod-specific knockout *Gnat1*$^{-/-}$ mice, which exhibit little retinal damage, were unresponsive to form-deprivation (68). Eyes of mice with a mutation in nyctalopin (*Nyx*$^{nob/nob}$) – a protein important in ON-bipolar cell signalling – exhibited an increased susceptibility to form-deprivation myopia (69).

This led the authors to conclude that perhaps rod-mediated signalling in the retina is more important for emmetropization than cone-mediated signalling. This revolutionary concept is supported further by the fact that rod photoreceptors signal primarily through ON-bipolar cells, which likely mediate the effects of the injected glutamate analog, L-APB, on eye growth in chicks (70). Furthermore, rods vastly outnumber cones in most mammalian retinas, including those of mice and humans; and vision with high spatial resolution, which is not mediated by rods, is not necessarily required for the retina to successfully detect blur (19, 71). It is possible that the transgenic ablation of rod-ON-BCs could have damaged the inner-retinal circuitry that produces myopia-

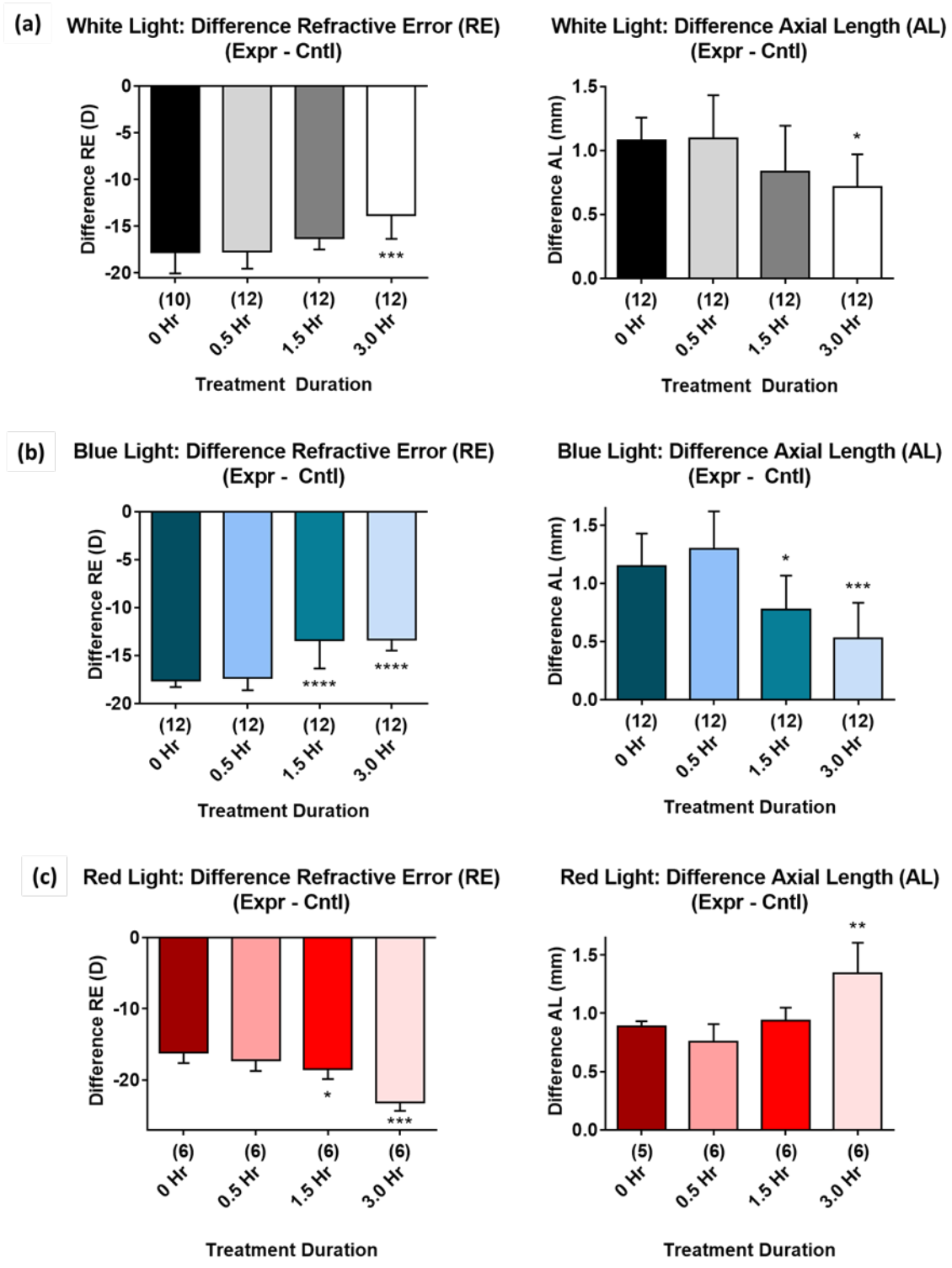

Figure 13. The effects of 10,000 lux white light (**a**), blue-filtered 10,000 lux light (**b**), and red-filtered 10,000 lux light (**c**) on form-deprivation myopia in chicks. Significance in relation to control group; ****p<0.0001, ***p<0.001, **p<0.01, **p<0.05. Reproduced from Nguyen & Stell, unpublished studies.

STOP signals, and the ability of mice with intact rods, but no cones, to develop FDM has not yet been investigated. Thus, we would hope to see further evidence in support of this hypothesis.

Ganglion cells, and therefore cortical visual pathways, do not seem to contribute significantly to homeostatic eye growth, even though ganglion cell axons make up the optic nerve. Disconnection of the optic nerve – either by

surgery or toxins – has little effect on emmetropization and/or compensation to induced defocus (72-75), and eyes will still respond to deprivation myopia (26). Retinal efferent (centrifugal) fibres also run through the optic nerve, in birds and other animals. Unilateral lesioning of this system, while leaving retinal ganglion cell axons intact, results in hyperopia in the eye contralateral to the disrupted fibre tract. By 21 days after surgery, however, the eyes return to an emmetropic state (76) – suggesting, perhaps, that the initial hyperopic shift was due to short-term release of neuroactive substance(s) such as NO from the retinal axon terminals of the damaged cells, or retrograde signalling within the retina by axotomized RGCs. There is a precedent for a process such as this in the induction of rod-precursor proliferation in goldfish, which can be elicited by sectioning of the optic nerve and ablation of olfactory bulb/tract – the source of efferent fibres in fish (77). Many studies do not report intra-ocular effects of treatment, even though direct retino-retinal connections have been shown to exist in rats and mice (78, 79).

Amacrine cells are the visual processing powerhouses of the retina, and the most likely source of retina-derived eye growth-regulating molecules (19). There are as many as 30 different confirmed subtypes of amacrine cells, and it is likely that more remain to be discovered (80, 81). The majority of amacrine cells provide inhibitory feedback to bipolar cells via GABA- and glycine-mediated signalling; but they can also contact and provide feedback to other amacrine cells and ganglion cells (81, 82), as well as release neuromodulatory substances that modify properties such as excitability, gain, synaptic transmission, and cell-cell coupling of many retinal neurons and circuits, through non-synaptic mechanisms. They are responsible for higher-level processes in the retina such as detecting environmental changes in movement (83), contrast, and blur (84). For more information on amacrine cell function, see the Webvision chapter "Roles of Amacrine Cells" by Helga Kolb.

Many studies have shown that various signalling molecules found in amacrine cells can affect myopia onset and inhibition (47, 50, 85-88), such as dopamine (47), nitric oxide (46), and neuropeptides (VIP, glucagon, somatostatin, and neurotensin) (80). Destruction of subpopulations of amacrine cells by toxins has significant effects on normal eye growth and induction of form-deprivation myopia (61, 62, 89-91). The functions of most amacrine cells identified remain to be discovered, but the contribution of specific amacrine cell-derived signalling molecules to emmetropization and myopia inhibition will be discussed in more detail below. Most likely, signalling molecules originating from the retina do not control eye growth directly; instead, they are assumed to act via a signalling cascade that relays eye growth-regulating signals through the RPE and choroid, which may then release different signalling molecules that directly affect scleral growth (19) (Figure 16).

Muscarinic acetylcholine receptors, dopamine, and nitric oxide are strongly implicated in regulation of eye growth

Muscarinic acetylcholine receptors (mAChRs)

Muscarinic receptors in the eye mediate contraction of the pupillary constrictor muscle, as well as the ciliary muscle, which controls accommodation. As discussed previously, it was long thought that myopia inhibition could be achieved by blockade of accommodative fatigue. However, the failure of clinical trials such as COMET (discussed above), plus experimental evidence from animal models, does not support the hypothesis that mAChR antagonists (blockers) inhibit myopia via paralysis of the ciliary muscle alone (32). For example chicks can develop experimentally-induced myopia and/or respond to treatment with drugs such as atropine or pirenzepine – which block muscarinic receptors (92, 93) – even though their ciliary muscles are controlled by nicotinic receptors, which atropine and pirenzepine do not target. Pirenzepine inhibits the progression of myopia in humans (32) and a wide range of animal species (25) including monkey (94, 95), tree shrew (96, 97), and chick (92, 98-100), even though it has little effect on iris and ciliary musculature (95, 100-103). Finally, lesioning of the ciliary nerve does not impair development of either form-deprivation or lens-induced myopia; chicks with damaged ciliary nerves develop similar amounts of myopia as intact controls (104).

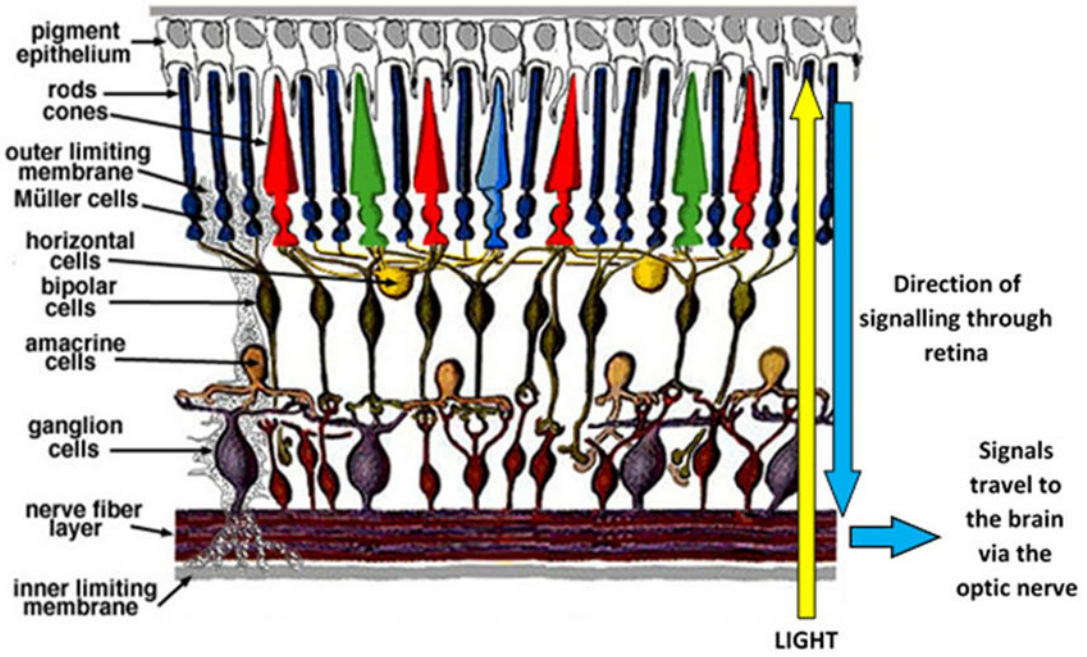

Figure 14. Light (yellow arrow) must first travel through the retina before interacting with the rod and cone photoreceptors (PRs). PRs signal their responses via synapses to bipolar cells (BCs) and hence to ganglion cells (RGCs) – thin blue arrow. Axons from the RGCs make up the nerve fibre layer, and relay retinal signals to the brain –horizontal blue arrow. Horizontal cells (HCs) and amacrine cells (ACs) help to fine-tune signals – between the PRs and BCs, and between the BCs and RGCs, respectively.

These data have largely ruled out accommodative activity or the ciliary muscle as an important eye-growth-regulator; thus, we have turned to the retina, choroid, or sclera as possible target sites for myopia-inhibition by mAChR antagonists. Muscarinic receptors are present in the retina, RPE, choroid, and sclera (105). Fischer et al. localized chick mAChR orthologues (cM_2, cM_3, cM_4) in chick eye tissues and showed that immunoreactive sites are present in the inner retina (cholinergic amacrine cells and ganglion cells), retinal pigment epithelium (RPE), and choroid, as well as the ciliary body (106). Expression patterns in the tree shrew (107), and rabbit (108) are similar to those reported for the chick (Figure 17). However, even though there is evidence for mAChRs in the ocular tissues, it remains uncertain exactly which ocular tissues, cells, or receptors mediate the anti-myopia effects of mAChR antagonists. The theorized mechanism of action of myopia-inhibition by these drugs is heavily dependent on the *assumption* that they block signalling through mAChRs, but this has never been proven conclusively.

In fact, substantial evidence argues for a non-retinal or non-muscarinic mode of action (109). For example, only some muscarinic antagonists inhibit myopia in humans (110-114) and animals (96, 98, 115), while the vast majority have no effect (98); high concentrations of these drugs are required for a significant effect. Protein and mRNA expression studies utilizing radioligand binding and real-time PCR techniques have found no change in receptor density or receptor gene expression for any mAChR subtypes in the retina or choroid of chick (116) or tree shrew (107), even when there is significant myopia development. This is strange, as it would be expected that significant changes in eye growth should cause changes in the expression of target receptors. Interestingly, the full population of amacrine cells that make the neurotransmitter required for action by mAChRs (acetylcholine) do not seem to be required for emmetropization, development of experimentally-induced myopia, or atropine-mediated suppression of form-deprivation myopia (117). This is again very strange, because 'orthosteric' mAChR antagonists such as atropine should have no action by themselves; they simply block access

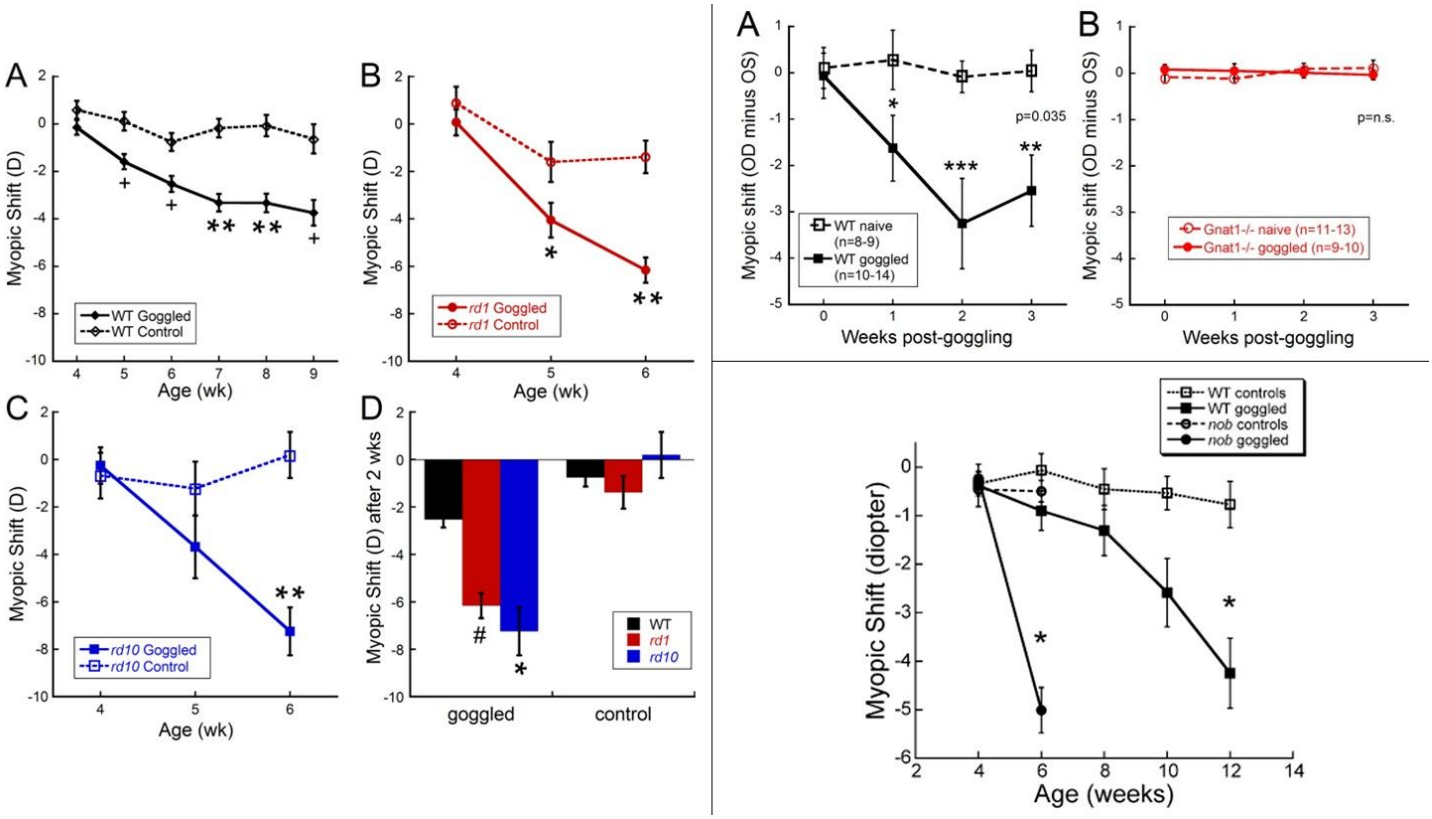

Figure 15. Results from studies utilizing mutant mice. Mice with mutations that cause degeneration of rods and cones($rd1^{-/-}$ & $rd10^{-/-}$) are more susceptible to form-deprivation myopia (FDM) than mice with no mutations (**panel A**). This is also the case for mice with mutations in signalling pathways that involved ON-bipolar cells ($nob^{-/-}$) (**panel B**). Mice with mutations that affect rods, but not cones ($Gnat1^{-/-}$), are not susceptible to FDM (**panel B**). Figures reproduced from: Park et al. (2013) (67); Park et al. (2014) (68) and Pardue et al. (2008) (69).

of the signalling neurotransmitter to the target receptor. Thus, if myopia inhibition by atropine is mediated by mAChRs, atropine should not inhibit myopia if the source of acetylcholine has been destroyed.

These data support a few possible theories: The first is that the cells responsible for myopia inhibition by mAChR antagonists are not in the retina, but instead in the RPE, choroid, or sclera. When muscarinic antagonists are administered by injection into whole, intact eyes, this is a possibility. For a drug to have a significant effect on a system, it must be present in a certain concentration at the receptor for binding and activation to occur. The inverse of this effective concentration is called 'potency'. Atropine is a very potent drug; thus, it requires an extremely low concentration to block mAChR signalling (1-10 nM). If it were working at a target far away from the intravitreal injection site (i.e., the choroid or sclera), the requirement for a large concentration of drug could be justified because it is possible that only a small amount of atropine might reach its target, through loss by diffusion through the vitreous, and/or blockade by the RPE and blood-retinal barrier. If the target tissues (retina, choroid, sclera) are isolated, however, the requirement for large concentrations of drug should be eliminated, because these barriers have been removed. One study examining the effects of mAChR agonists (stimulators) and antagonists on eye cups consisting of the RPE/choroid/sclera (*in vitro*; retina removed) demonstrated that stimulation of mAChRs by carbachol, oxotremorine, arecadinine, and pilocarpine resulted in choroidal thinning, and that pirenzepine caused choroidal thickening; atropine was not tested, and oxyphenonium had no effect (118). Another study on the effects of atropine on isolated scleral cells found that it can slow proliferation, which would be expected if atropine inhibited myopia by directly affecting scleral growth. Unfortunately, however, because the concentrations of drugs used in these isolated tissues were very high (0.6-5 mM), neither study conclusively indicates a non-retinal origin for mAChR-control of eye growth control.

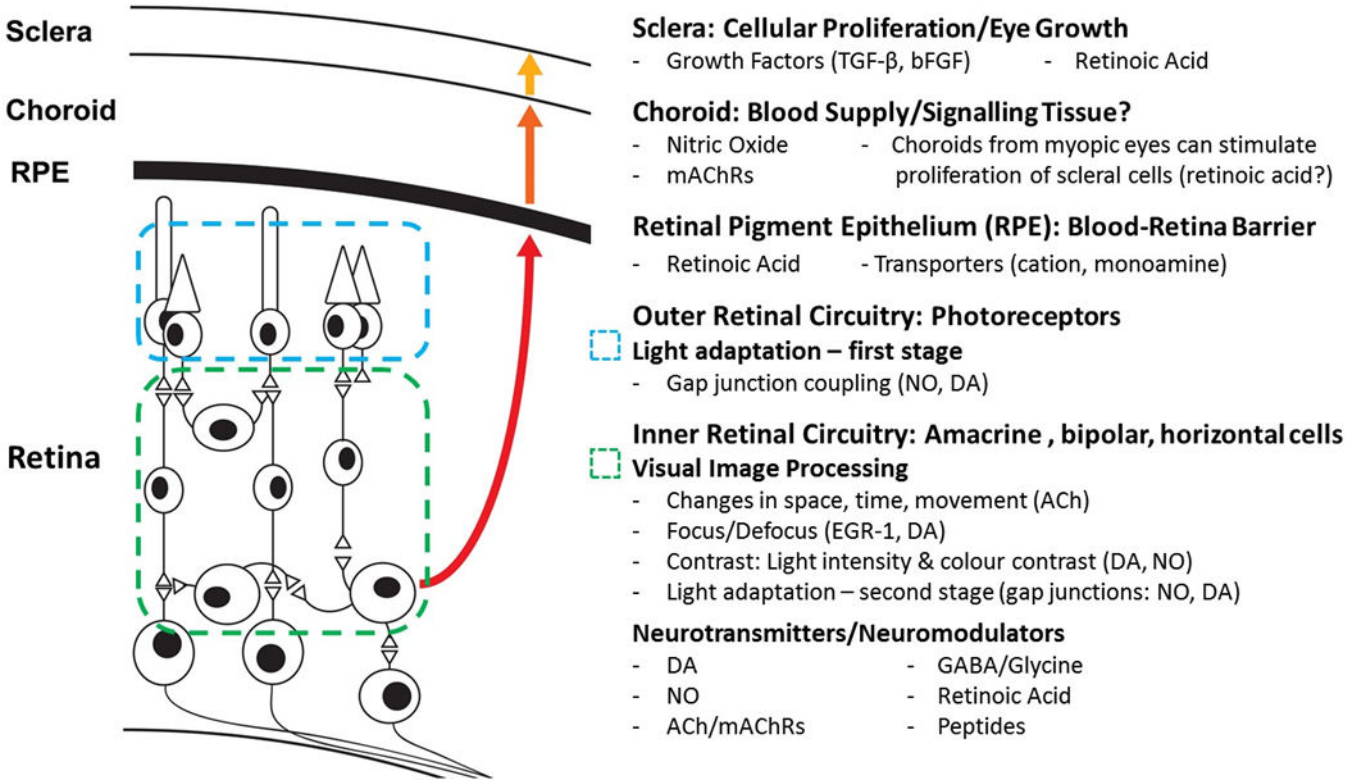

Figure 16. It is not likely that signals from the retina will control scleral growth directly. Instead, retina-derived chemical messengers probably activate signalling cascades that create a chain reaction of signalling, which moves through the RPE, choroid and sclera (arrows). For example, dopamine and/or nitric oxide signalling in the retina can cause changes in light adaptation, which might then result in the release of retinoic acid from the choroid. Choroidal retinoic acid release could then result in inhibition of scleral proliferation, and inhibition of myopia. Although all the molecules listed in the diagram have been shown to affect eye growth, the places where they may act are still theoretical, and have not yet been proven conclusively. ***Abbreviations:*** **TGF-β**, transforming growth factor beta; **bFGF**, basic fibroblast growth factor; **mAChRs**, muscarinic acetylcholine receptors; **NO**, nitric oxide; **DA**, dopamine; **EGR-1**, early growth response protein 1 (also known as **ZENK**); **ACh**, acetylcholine; **GABA**, gamma-aminobutyric acid.

A second possibility is that high concentrations of mAChR antagonists are required for myopia inhibition because these drugs are not acting at mAChRs, but instead at some other, unknown receptor. All drugs are "dirty", or promiscuous, meaning they can, and will, bind to unintended receptors; the risk of this "off-target" or "non-specific" binding increases as the concentration of drug increases. In the case of myopia-inhibition, extremely high concentrations – up to *one-million* times greater than those required for binding (1 mM used vs. 1 nM required; see above) – are used routinely. Thus, it's no great stretch of the imagination to speculate that when drugs are used at concentrations such as these, they will act in ways we cannot accurately predict. To determine whether "off-target" binding of mAChR antagonists is possible, we conducted *in vitro* experiments using isolated human mAChR M_4 receptor (M_4), chicken mAChR M_4 receptor (cM_4), and human $alpha_{2A}$-adrenoceptor (hADRA2A). Our hypothesis was that myopia-inhibiting mAChR antagonists would bind to hADRA2A – an "off-target" receptor – when applied at high concentrations. We found that myopia-inhibiting mAChR antagonists bind to hADRA2A when applied at concentrations similar to those expected to be present when these drugs are used to treat myopia in the chick model (0.001-1 mM) (98), while mAChR antagonists that do not inhibit myopia did not bind to this receptor with any significant activity, or at all. Interestingly, the correlations between the ability of mAChR antagonists to bind to M_4/cM_4 receptors and their reported ability to inhibit myopia in chick (98) were very poor, whereas correlations between mAChR antagonist binding at hADRA2A and myopia inhibition in chick were significantly better (Figure 18).

Of additional importance were our findings regarding the experimental anti-myopia ligand, MT3, a polypeptide isolated from venom of the green mamba snake. Recently, it has been reported that MT3 inhibits myopia in

chicks at concentrations significantly lower than those required for atropine (2.5-10 μM vs. 1-100 mM, respectively) (119, 120), and MT3 is known to be selective for mammalian mAChR M_4 over all other mAChR subtypes (121). Thus, the authors of these studies claimed that because MT3 inhibits myopia at a much lower concentration than atropine, mAChR M_4 must be the "myopia-controlling" receptor. However, in our studies, we found that MT3 is the *least* potent antagonist of all tested at the chicken (cM_4) receptor – 56x less potent than at human M_4 (Figure 19). This disconnect between MT3-potency at cM_4 and its rank as the most potent anti-myopia ligand in the chick – and the fact that MT3 binds with high potency, not only to mAChR M_4, but also to alpha$_{1A}$-, alpha$_{1D}$-, and alpha$_{2A}$-adrenoceptors (122, 123) – casts further doubt on the theory that M_4/cM_4 are the target receptors that mediate inhibition of myopia by muscarinic antagonists.

These data are preliminary, however, and should be interpreted with caution. They do not prove a role for alpha$_{2A}$-adrenoceptors in control of eye growth. Rather, they disprove M_4/cM_4 as a likely target, and offer alpha$_{2A}$-adrenoceptors as one possible alternative out of many – including other subtypes of mAChRs, such as M_1/cM_2. There is some evidence for a role of alpha-adrenoceptors and their neurotransmitters, norepinephrine (NE) and epinephrine (E), in the eye. NE and E are the primary neurotransmitters in the sympathetic nervous system, from which the superior cervical ganglion originates. This ganglion projects to the eye and controls processes such as pupil dilation via the iris dilator papillae, reduction of ocular blood flow via vasoconstriction, and regulation of intraocular pressure via control of aqueous humor outflow (124). A few studies have localized alpha-adrenoceptors in these ocular tissues, which is not surprising, but these receptors also seem to be present in the retina (125, 126). One hypothesized role of alpha$_2$-adrenoceptors in the retina is that they might be involved in regulation of dopamine synthesis (127-129). There is strong evidence that dopamine is a very important molecule in myopia-inhibition and regulation of eye growth (see below). Confirming these studies, and expanding upon them, may help to refine whether there is alpha$_2$-adrenoceptor-mediated signaling in the retina, whether it can affect retinal dopamine regulation, and possibly identify cell types that might be involved. Confoundingly, although there is evidence for the presence of alpha$_2$-adrenoceptors and the enzyme phenylethanolamine N-methyltransferase (PMNT) – which converts NE into E – in the retina, there is no significant evidence that either NE or E act as a retinal neurotransmitter (129). For now, the function and activating transmitters of the alpha-adrenoceptors in the retina remains largely unknown. Significant further investigation will be required to determine whether these receptors are a worthy target for anti-myopia therapies.

Dopamine

Dopamine is perhaps one of the most-studied neurotransmitters in regards to regulation of eye growth. For an in-depth review of the studies investigating the effects of dopamine and dopaminergic systems on myopia, please see "An updated view on the role of dopamine in myopia" by Feldkaemper and Schaeffel (47) and "Dopamine signaling and myopia development: What are the key challenges" by Zhou et al (130).

Dopamine is a catecholamine neurotransmitter/neuromodulator that acts as a light-adaptive signalling molecule in the retina (131). It is synthesized in and released from tyrosine hydroxylase-containing amacrine cells. Intravitreal injection of dopamine agonists is strongly correlated with inhibition of eye growth (24, 47, 50, 132-139) (Figure 20), while injection of dopamine antagonists before unrestricted vision prevents myopia rescue (140).

In addition to a direct role of dopamine agonism on inhibition of myopia in chicks, retinal dopamine levels and subsequent effects on myopia are sensitive to modulation by other drugs. Myopia-prevention by the cholinomimetic agent diisopropylfluorophosphate (141), mamba toxin-3 in chick (142), and mamba toxin-7 (MT7) in tree shrew (143), can be blocked by dopamine antagonism. Interestingly, intravitreal injection of atropine or *in vitro* application of atropine to the chick retina causes increased levels of dopamine metabolite DOPAC and retinal dopamine release (137), and like atropine (46), myopia-inhibition by dopamine is blocked by simultaneous injection of nitric oxide synthase inhibitors (48, 144). Interestingly, the effects of dopamine

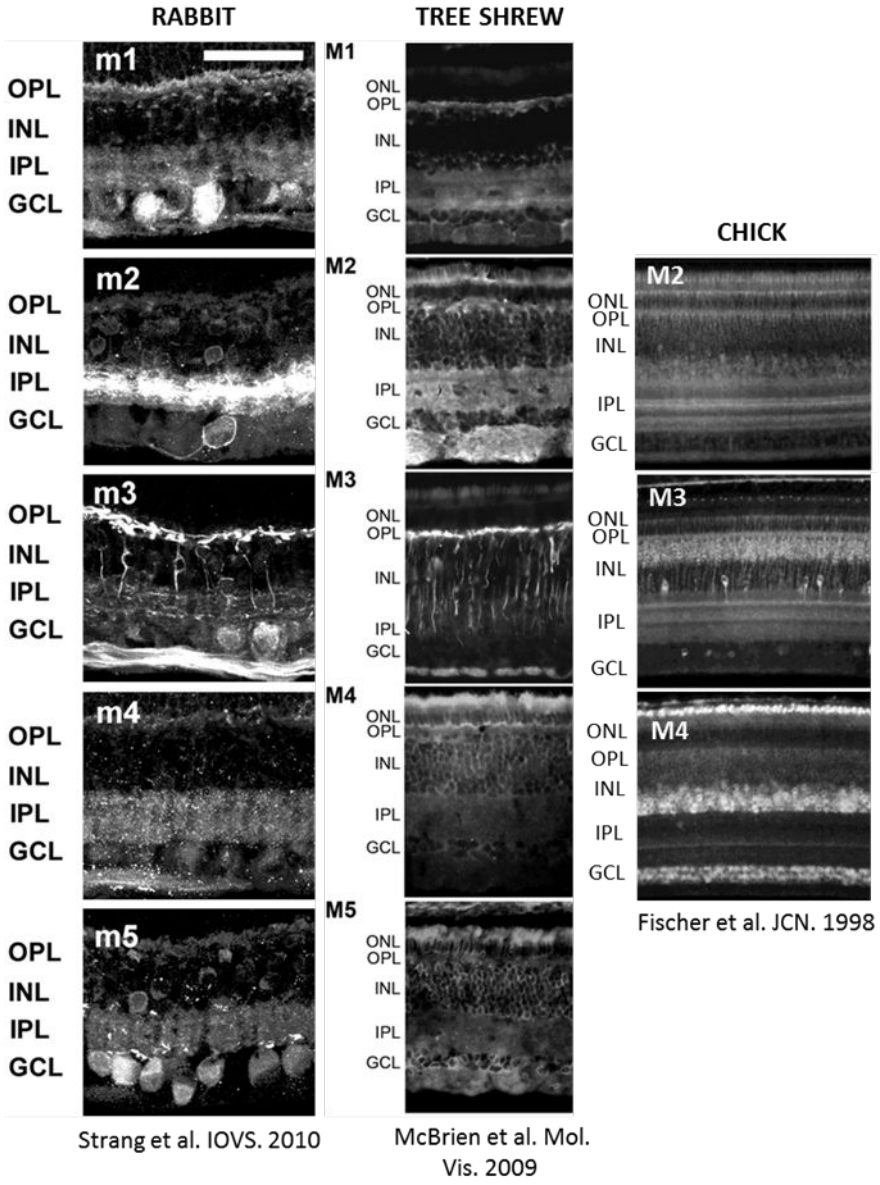

Figure 17. Reported expression patterns of retinal mAChRs in rabbit (left), tree shrew (middle), and chick (right). Chicks do not have an M1-type mAChR subtype (209). Modified and reproduced with permission from Strang et al. (2010) (108); McBrien et al. (2009) (107) and Fischer et al. (1998) (106).

agonists and muscarinic antagonists are not additive (138). This led the authors to suggest that acetylcholine and dopamine may act at different points of a common pathway to prevent myopia; further investigation into this hypothesis has not been undertaken.

Nitric Oxide

Nitric oxide (NO) is a small-molecule gas that can act as a non-conventional neurotransmitter and neuromodulator in the retina. It is difficult to image NO directly, because it is volatile and chemically unstable. Consequently, past studies utilized histochemical activity of the enzyme NADPH-diaphorase (145) and antibody-labelling of NO-synthesizing enzymes (nitric oxide synthase, NOS) to determine the localization of NO action in tissues. NADPH-diaphorase activity and immunoreactive neuronal NOS (nNOS, NOS-1) are found in subpopulations of all major cell types in the chick retina and choroid, and at least 15 types of identified retinal neurons (146, 147). Direct imaging of NO has been accomplished by means of an indicator molecule that

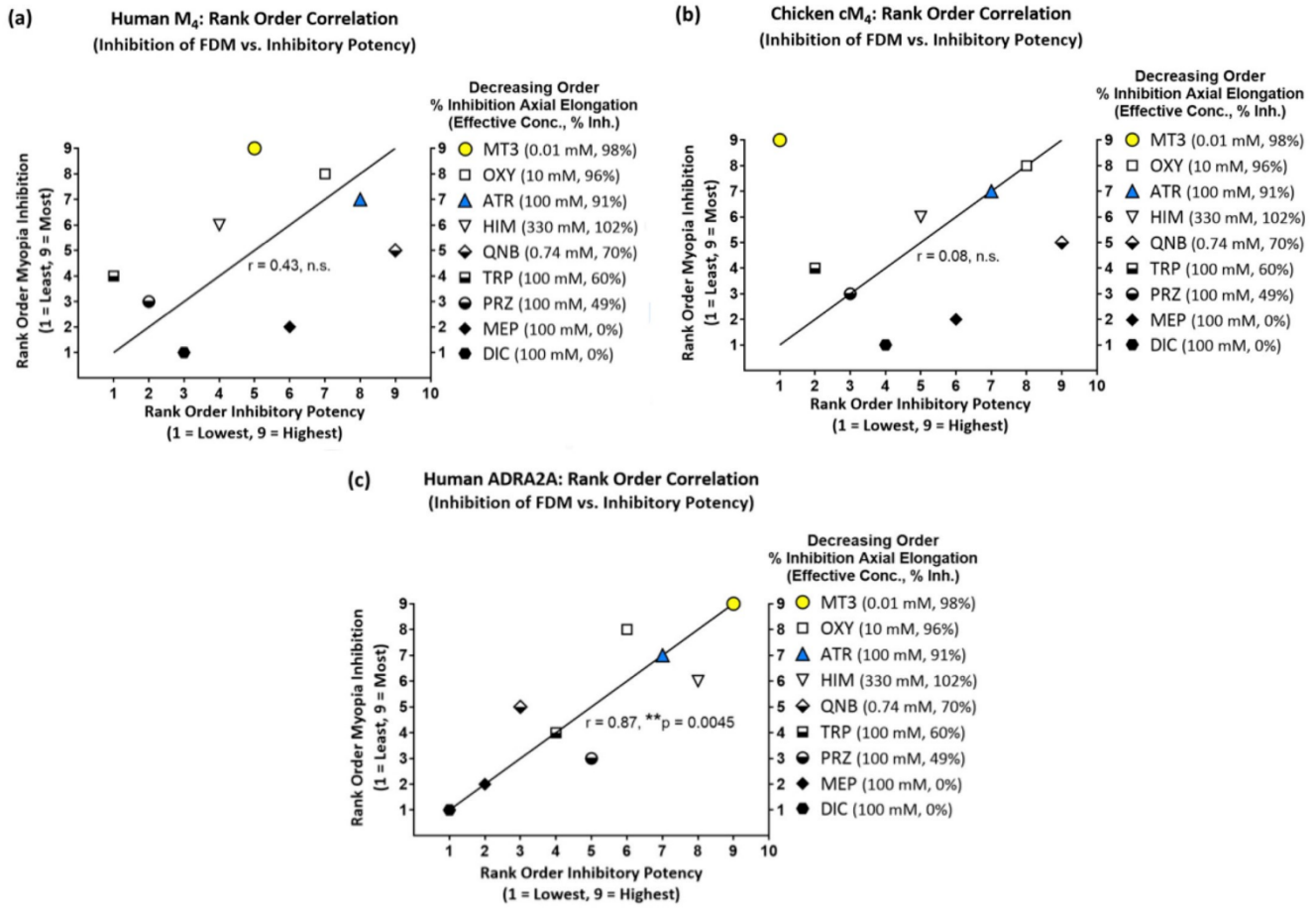

Figure 18. Rank-order correlations of inhibitory potency of mAChR antagonists at M_4, cM_4, and hADRA2A, and reported ability to inhibit FDM in chicks. Statistics: Spearman's Ranked Correlation (non-parametric). ***Abbreviations*: MT3:** mamba toxin-3; **OXY:** oxyphenonium; **ATR:** atropine; **HIM:** himbacine; **QNB:** 3-Quinuclidinyl benzilate; **TRP:** tropicamide; **PRZ:** pirenzepine; **MEP:** mepenzolate; **DIC:** dicyclomine; **n.s.**: not significant. Open/coloured symbols: full myopia inhibition; partially-filled symbols: partial myopia inhibition; closed symbols: no myopia inhibition; according to previously-published research (98, 115, 119). Reproduced from Carr BJ. (2017). PhD Thesis. University of Calgary (210).

fluoresces after reacting with NO (148), which has been used to refine further the localization of various NOS isoforms, and where NO may act in the retina (149, 150).

The investigation of the role of NO as a regulator of eye growth is still in its early stages, but preliminary results are promising. Non-specific inhibitors of NO synthesis, L-NAME (151) and L-NMMA (152), cause transient thinning of the choroid – a change correlated with myopiagenesis. Blockade of NO synthesis with L-NAME abolishes the rescue effect of unoccluded vision (153), and experiments in mice have verified that pharmacological blockade of NO synthesis increases myopia susceptibility (154); this further implicates NO as a possible "stop" signal for eye growth. Finally, intravitreal injection of drugs that cause increased levels of NO in chick retina and RPE, dose-dependently inhibited the development of form-deprivation myopia (Figure 21).

The mechanism of NO-mediated prevention of myopia remains to be elucidated. Increased retinal NO acts as a signal for light-adaptation (155-158), and retinal NO synthesis is increased under intense illumination (45). NO donors in dark-adapted chicks mimic the adaptational effects of increased illumination (159), while NOS inhibitors mimic the effects of decreased illumination in light-adapted chicks (160). Thus, increased NO may be a possible mechanism by which high-intensity environmental illumination protects against myopia. In addition, NO inhibits cell-cell coupling via gap junctions in the retina (161), and uncoupling of gap junctions containing

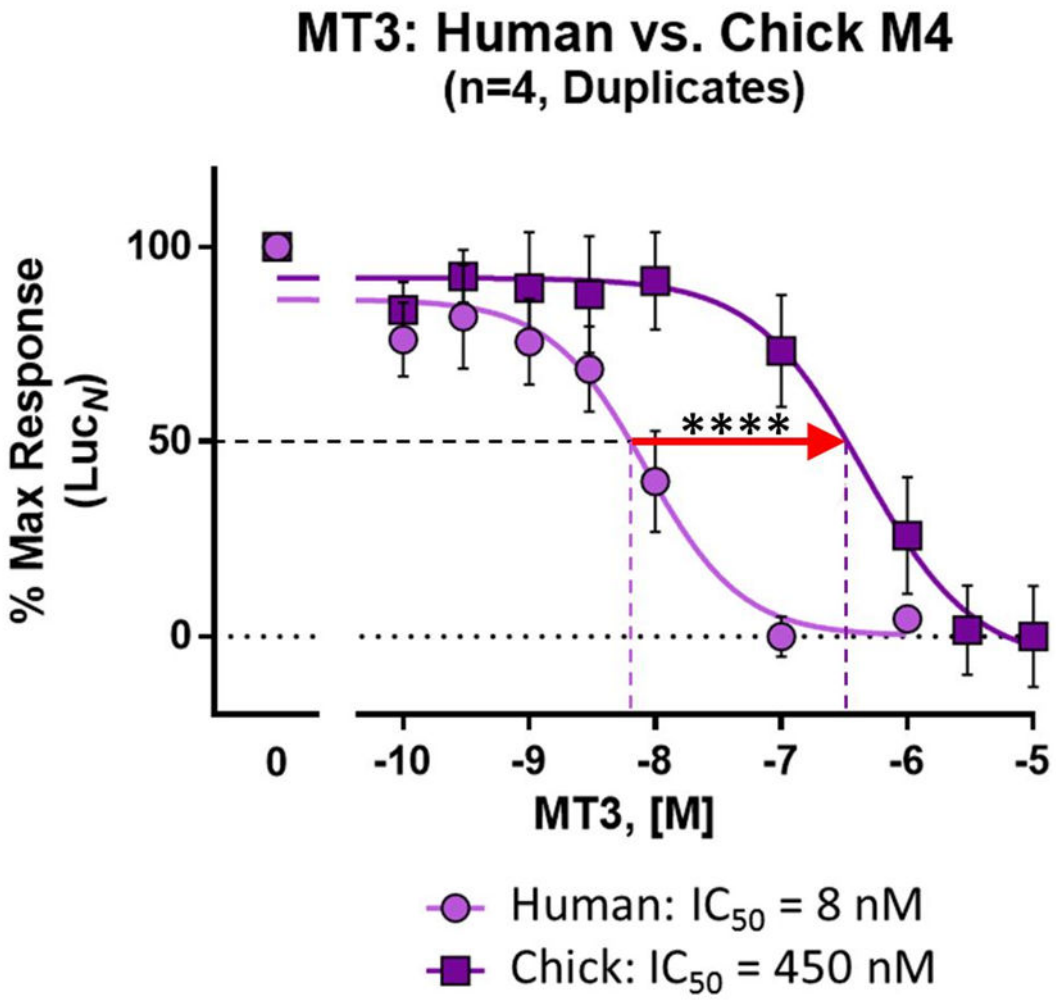

Figure 19. Inhibition curves for MT3 at the human (M_4) and chicken (cM_4) muscarinic receptors. MT3 is 56x less potent at cM_4 than M_4 at the 50% effective inhibitory dose (dotted lines, IC_{50}), effectively becoming a low-potency ligand at the chicken receptor; ****p<0.0001, unpaired t-test, two-tailed. Reproduced from Carr BJ. (2017). PhD Thesis. University of Calgary (210).

connexin-35/36 (Cx35 in chicks) – which sharpens spatial tuning of retinal function – has also been implicated in myopia-inhibition (162) (and unpublished results of Teves et al (163)).

Although we do not know the receptors through which atropine may act, we do know that myopia-prevention by atropine is also dependent on induction of nitric oxide (NO). Simultaneous injection of atropine with nitric oxide synthase inhibitors – which blocks the ability of cells to make NO – completely abolishes all protective effects of atropine in chicks (46) (Figure 22).

Many other molecules can affect eye growth

Adenosine receptors and 7-methylzanthine (7-MX)

7-MX is a caffeine derivative, which has some affinity to adenosine receptors. Recent clinical trials of 7-MX have provided evidence that it may be useful in combatting axial myopia (164). Children with a fast base-line rate of myopia progression, fed daily tablets containing 400mg 7-MX for >2 years, experienced slowing of axial elongation and myopia progression compared to placebo controls. This myopia-inhibiting effect halted as soon

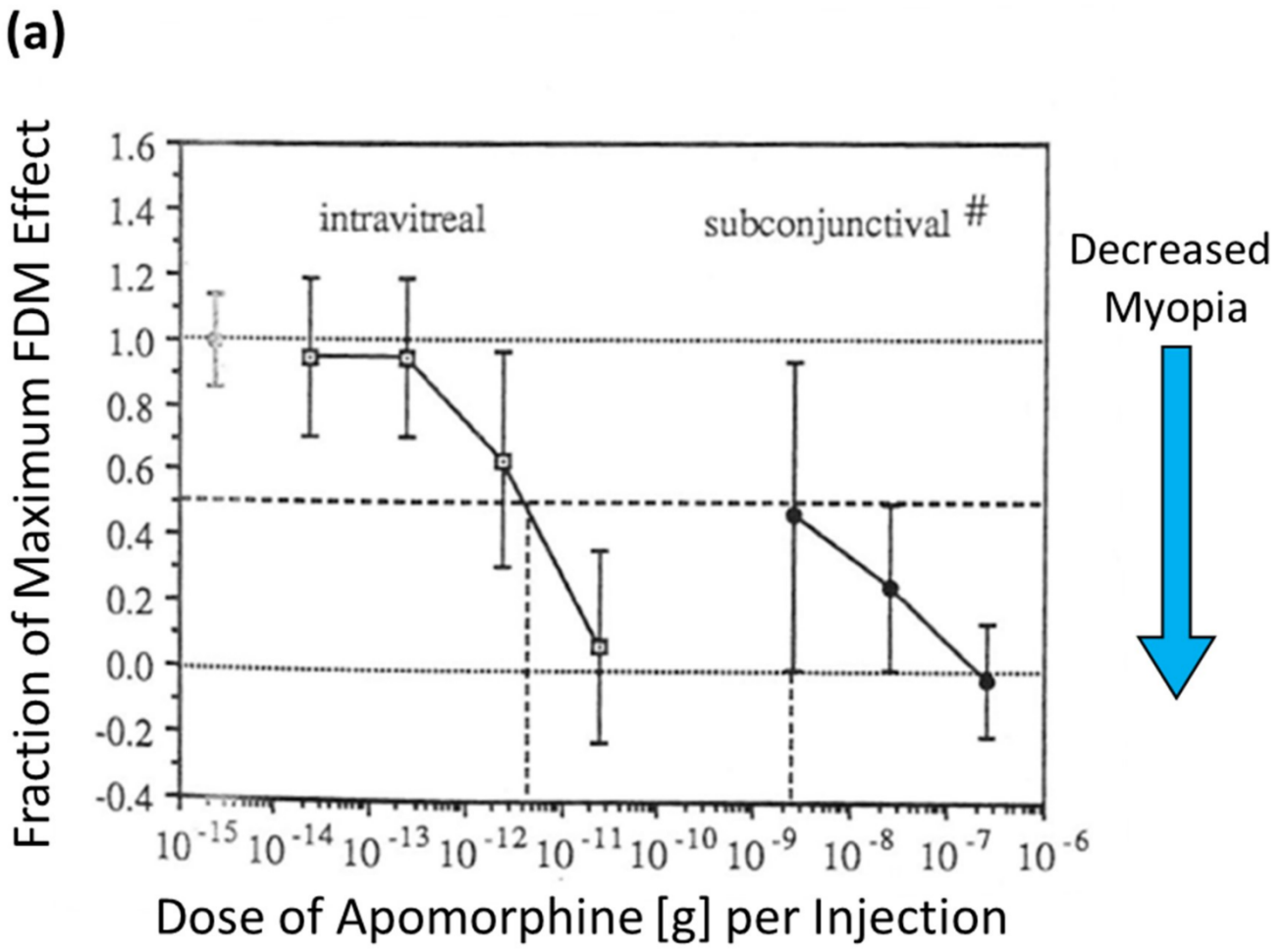

Figure 20. The non-specific dopamine-receptor agonist (activator), apomorphine, inhibits form-deprivation myopia in the chick when injected via intravitreal and subconjunctival routes. Reproduced and modified with permission from Rohrer, B., Spira, A. W. & Stell, W. K. (1993) (132).

as 7-MX treatment was discontinued. The mechanism through which 7-MX may prevent myopia is currently unknown, but there are two working hypotheses: (i) that it causes stiffening of the sclera, which prevents axial elongation (165, 166); or (ii) that it blocks adenosine receptors in the retina and/or ciliary muscle, and consequently causes changes in acetylcholine and dopamine neurotransmitter release (164).

Alpha$_2$-Adrenoceptors

Recent studies have shown that alpha$_2$-adrenoceptor agonists can inhibit form-deprivation myopia in the chick (167). Intravitreal injection of high concentration clonidine (200 nmoles) or guanfacine (20-200 nmoles) significantly inhibited changes in refractive error and axial elongation (Figure 23). These studies are appealing, because the alpha$_2$-adrenoceptor agonist brimonidine is already approved for use in humans, as a glaucoma treatment (168). Thus, it would be much easier to translate these findings into a clinical trial than it would for experimental ligands such as mamba toxin-3. These data are very preliminary, but could yield new pharmaceutical targets for anti-myopia therapies lacking the negative side-effects of atropine treatment.

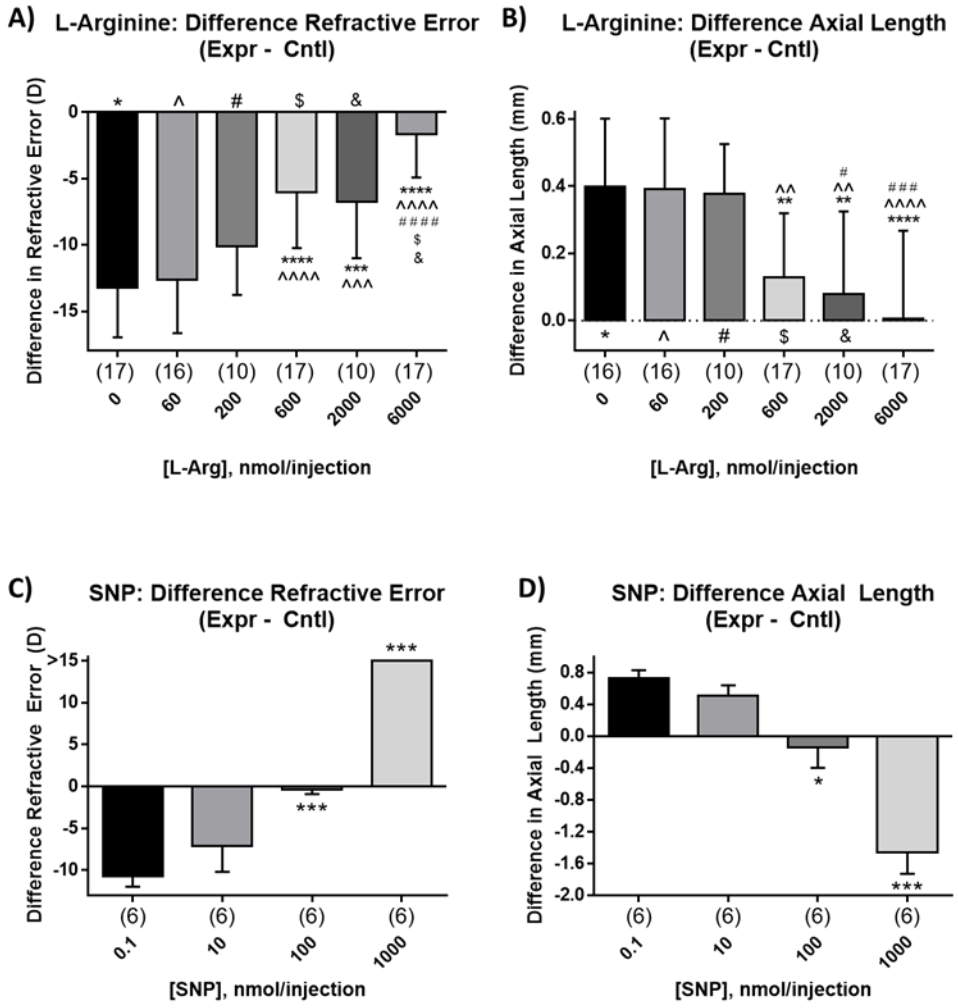

Figure 21. The effects of exogenous nitric oxide (NO), delivered intravitreally as NOS-substrate (L-Arginine; L-Arg) or NO-donor (sodium nitroprusside; SNP), on form-deprivation myopia in chicks, expressed as the mean difference between values in the goggled/drug-injected eye (gradations of gray fill) and in the contralateral open/vehicle-injected eye (solid black fill). L-Arg (**A,B**) and SNP (**C,D**) dose-dependently inhibited the development of myopic refractive error (**A,C**) and axial length (**B,D**) in goggled chick eyes. Doses represent the number of moles of drug injected, per injection, 3 times at 48-hr intervals. The refractions and sizes of control eyes were not affected by drugs delivered to the goggled eyes. Statistics: *p < 0.05, **p < 0.01, ***p < 0.001; One-Way ANOVA + Tukey's post-hoc (L-Arg) or Kruskal-Wallis + Dunn's post-hoc (SNP); n = 6. Reproduced with permission from Carr, B.J. and Stell, W. K. (2016) (46).

Gamma-aminobutyric Acid (GABA)

Gamma (γ)-aminobutyric acid (GABA) is the primary mediator of inhibitory synaptic transmission in the central nervous system (CNS). For more detailed reviews of the localization and function of the GABA in the retina, please see previous Webvision chapters, "Neurotransmitters in the Retina" by Helga Kolb, and "$GABA_C$ Receptors in the Vertebrate Retina" by Haohua Qian.

There is significant evidence that GABA receptors are involved in the regulation of eye growth. Daily intravitreal injections of a wide variety of GABA receptor antagonists into form-deprived eyes resulted in reduction of eye growth (mostly in the equatorial dimension) (169). One of the most effective anti-myopia GABAergic drugs is the $GABA_{AOr/C}$ antagonist (1,2,5,6-Tetrahydropyridin-4-yl)methylphosphinic acid (TPMPA), which has been shown to significantly inhibit goggle-induced myopic refractive error, vitreal chamber depth, and equatorial diameter in the chick (169) and guinea pig (170, 171). Novel $GABA_{AOr/C}$ drugs *cis*- and *trans*-3-ACPBPA also

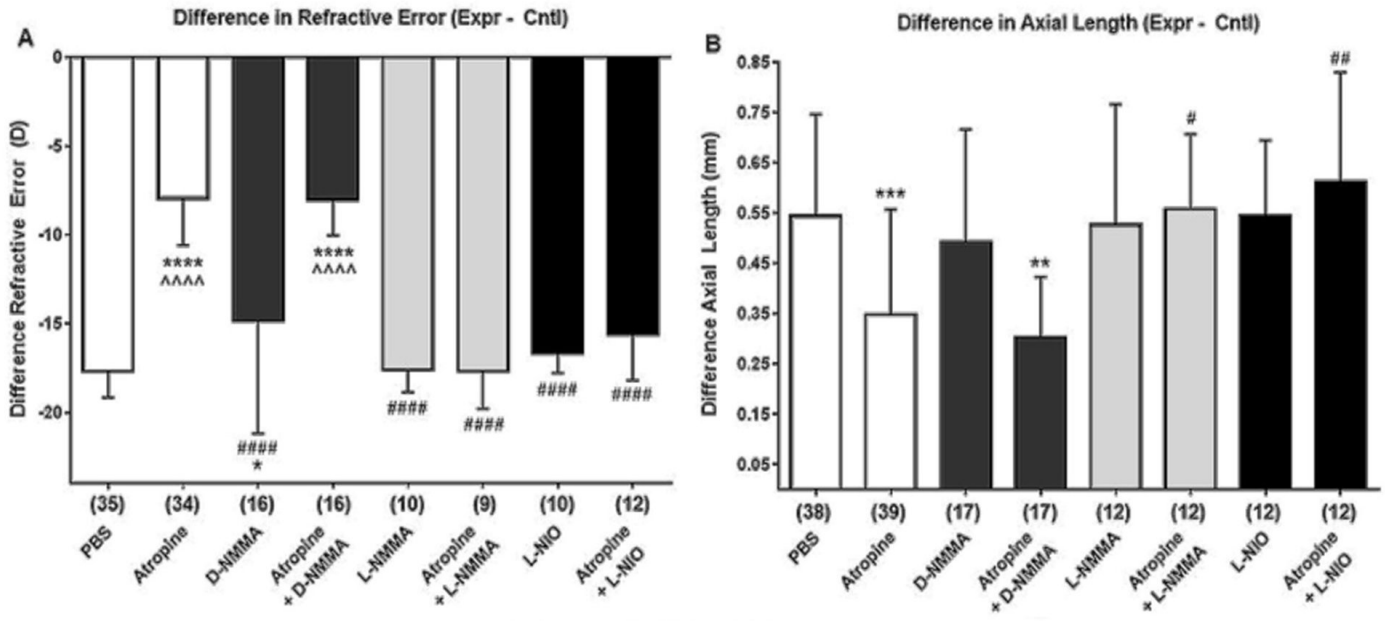

Figure 22. The effects of atropine (240 nmoles), NOS inhibitors (6 nmoles; L-NIO, L-NMMA), D-NMMA (6 nmoles), and the combination of atropine + NOS inhibitors (L-NIO, L-NMMA), or atropine + D-NMMA on refractive error (**A**) and axial length (**B**); doses represent the number of moles of drug injected, per injection, 3 times at 48-hr intervals. ***Abbreviations***: **L-NIO**: N^G-(1-Iminoethyl)-L-ornithine; **L-NMMA**: L-N^G-monomethyl arginine; **D-NMMA**: D-N^G-monomethyl arginine. ***Symbols***: asterisk (*): comparison to effect of PBS-treatment; pound (#): comparison to effect of atropine-treatment; caret (^): comparison to effect of D-NMMA-treatment. ***Statistics***: ●●●● $p < 0.0001$, ●●● $p < 0.001$, ●● $p < 0.01$, ● $p < 0.05$; One-Way ANOVA + Tukey's post-hoc. Data are represented as the means of the differences in values for the experimental eye minus those for the control eye, ± SD; sample sizes (n) are denoted in brackets below each column. Reproduced with permission from Carr BJ & Stell WK. (2016) (46).

inhibit lens-induced myopia in chicks, the cis form being much more potent (172). How $GABA_{AOr/C}$ antagonists may inhibit myopia is not known, and GABA can be expected to play a role in practically every visual processing mechanism in the retina; but there is some evidence of interaction with retinal dopaminergic systems, in the particular (173), as well as possible effects on scleral glycosaminoglycans (174).

Growth Factors: TGF-β and bFGF

Transforming growth factor-beta (TGF-β) and basic fibroblast growth factor (bFGF) seem to operate in a push-pull manner to regulate scleral growth during experimentally-induced myopia. Intravitreal injection of bFGF in chicks is protective against myopia, and co-administration of TGF-β with bFGF blocks this effect (175). In the guinea pig, Chen et al. confirmed that bFGF prevents experimentally-induced myopia. They also reported that bFGF protein expression was decreased, while TGF-β expression was increased, in scleral tissues of eyes that had undergone light induced myopia for extended periods of time (15-30 days) (176). The mechanism of bFGF-mediated myopia inhibition has not been elucidated. Attempts were made to link bFGF with the dopaminergic system, because bFGF protein content is upregulated during light and it is co-localized with tyrosine-hydroxylase – the cell marker for dopaminergic amacrine cells (175). However, other studies revealed that the two pathways are likely not related (50).

Peptide Hormones: Glucagon and Insulin

Glucagon is a pancreatic peptide hormone whose best-known role in mammals is to raise the concentration of glucose in the blood; insulin, another pancreatic peptide hormone, plays the opposite role – to lower blood sugar levels. However, many (perhaps all) gut peptides and their receptors are also expressed by neurons in the central and peripheral nervous systems, where they presumably play neuromodulatory roles. Glucagon-positive cells in

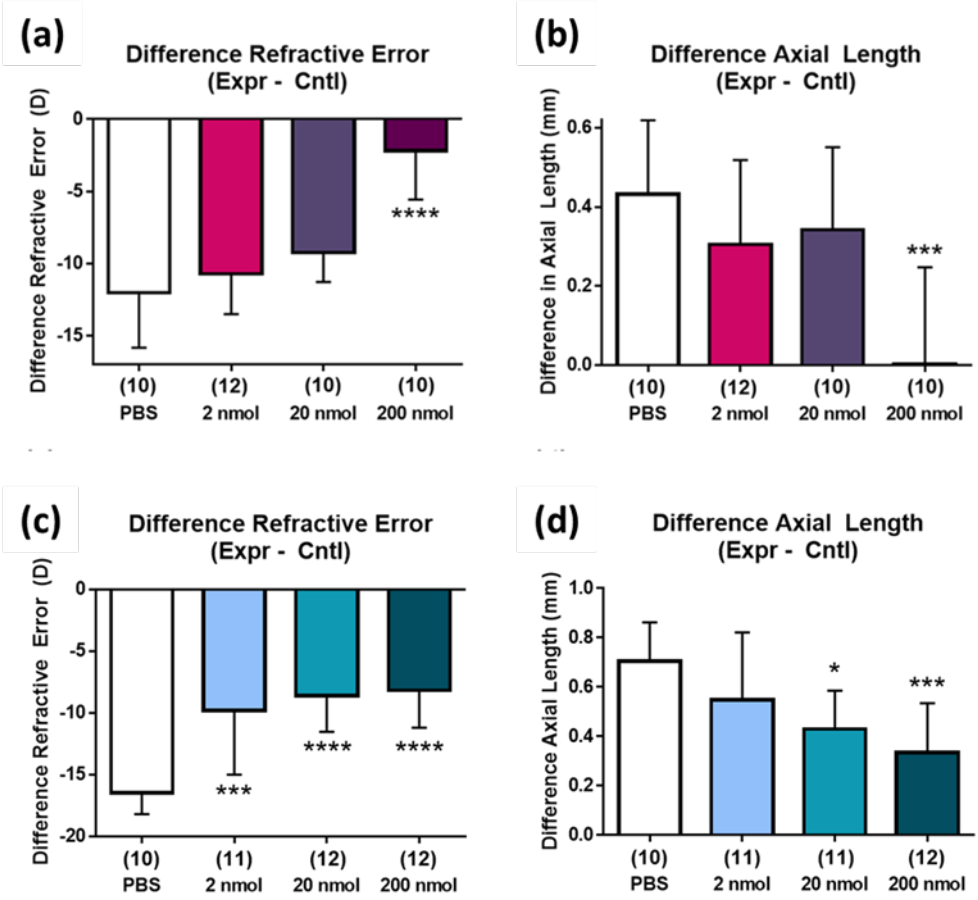

Figure 23. Effects of intravitreal injection of clonidine (top) and guanfacine (bottom) on FDM in chicks. 200 nmoles clonidine, and 20 and 200 nmoles guanfacine, significantly inhibited the induced difference in refractive error (a,c) and axial length (b,d), compared to PBS-controls. There was no significant effect of 2 or 20 nmoles clonidine-treatment or 2 nmoles guanfacine-treatment on difference in axial length. ***Statistics***: $^{****}p < 0.0001$, $^{***}p < 0.001$, $^{*}p < 0.05$; One-Way ANOVA + Tukey's post-hoc. Data are represented as the means of the difference in values for the experimental eye minus those for the control eye, ± SD; sample sizes (n) are denoted in brackets below each column. Reproduced from Carr BJ. (2017). PhD Thesis. University of Calgary (210) and Carr BJ & Stell WK. (210, 211).

the retina consist of a subset of amacrine cells in the inner retina of birds and reptiles, about 40% of which are also GABAergic (177, 178). The activity of glucagon amacrine cells in the chick retina changes dramatically in response to defocus, as revealed by changes in these cells' content of an activity-inducible transcription factor, early growth response protein 1 (EGR-1 or ZENK). Positive-lens defocus, or removal of the diffuser after inducing form-deprivation myopia, causes stronger and more widespread labeling of EGR-1, whereas negative-lens defocus or form-deprivation results in little or no labeling (179). The activity-dependent induction of Egr-1 is best interpreted as an indicator of cell depolarization, and therefore is an indicator of increased transmitter release. Egr-1 is likely to upregulate the transcription of genes whose products are important in functional compensation for prolonged increases in cell activity, rather than directly to affect downstream actions of the activated cell such as those involved in myopia-inhibition.

In the chick, injection of a glucagon agonist into form-deprived eyes inhibits myopia development (180), and injection of a glucagon antagonist blocks myopia recovery from clear vision (181). Intravitreal injection of insulin has the opposite effect, acting as a powerful myopiagenic agent (182). Glucagon inhibits the development of myopia in chicks, even after most amacrine cells have been ablated by neurotoxins, suggesting that (in chicks at least) glucagon amacrine cells could be the final or near-final output of "stop" signals acting on the RPE (183).

The relevance of these interesting findings in the chick model to the control of refractive development in mammalian eyes remains uncertain. A comparable role of glucagon in the retina of mammals remains elusive. To date, glucagon has not been identified or localized in any mammalian retina; and although many other members of the glucagon polypeptide family are present, their expression is not changed upon treatment of the eyes with form-deprivation stimuli. However, other kinds of amacrine cells, which have been labelled by similar focus- and defocus-dependent induction of Egr-1 in macaque monkey (184, 185) and tree shrew (186) are plausible candidates for playing similar roles in the control of eye growth.

Retinoic Acid

Retinoic acid (RA) is a member of the retinoid family of compounds, which also includes Vitamin A. Retinoic acid stands out among other candidate regulators in the control of eye growth, because its levels are bi-directionally modulated in response to opposing defocus stimuli (187). In the chick, retinal and choroidal RA levels and mRNA expression of its synthesizing enzyme, aldehyde dehydrogenase-2 (AHD2), are predictably changed in response to defocus stimuli; increasing in response to negative defocus and decreasing in response to positive defocus (187-189). Treatment of form-deprived chicks with a blocker of RA synthesis, disulfiram, caused myopia inhibition, but this effect was not carried over in response to lens-induced myopia (189). RA might act as a regulator of eye growth by inducing changes in scleral extracellular matrix (74) or modulating cell-cell coupling (74, 190, 191).

Choroidal changes correspond to changes in eye growth

Although the origin of homeostatic growth-regulating signals is most likely the retina, experimental and therapeutic treatments may affect any target within other ocular tissues – the retinal pigment epithelium (RPE), choroid, and/or sclera most likely. It is unlikely that a single kind of molecule is responsible for transmission of growth-regulating signals, because of difficulties in crossing the occluding junctions of the RPE (a major component of the blood-retina-barrier), and drug loss due to protein binding and dilution of the drug during *en route* transport into cells. More likely, a cascade of molecules may relay signals from retina-to-RPE, RPE-to-choroid, and then choroid-to-sclera (Figure 16).

Interestingly, the choroid responds to induced defocus in a compensatory fashion (192) – thickening in response to myopic defocus (positive lenses, removal of myopia-inducing goggles) and myopia-inhibiting treatments (118, 151-153, 193), and thinning in response to diffusers or hyperopic defocus (negative lenses) (Figure 24). Whether the directional changes in the choroid are responsible for scleral changes in eye growth – or just an initial compensatory step/by-product of other mechanisms that are themselves the primary regulators – remains to be determined, although the authors of a recent study have reported that changes in choroidal thickness are not predictive of changes in eye growth in eyes with experimentally-induced myopia (194). Nevertheless, it may be assumed that the choroid should play some role in the regulation of ocular refraction and/or the cause(s) and prevention of myopia (195), and that it may be the source of growth-regulating signals that act on the sclera (196).

Human therapies and recommendations for myopia prevention

Pharmaceutical Interventions: Atropine

Although many neurotransmitter/neuromodulator agonists and antagonists have been investigated for their ability to control eye growth, very few laboratory discoveries have been translated into clinical therapies. The most widely used pharmaceutical agent, atropine, was championed almost 40 years ago by Bedrossian (197) and subsequently became the subject of numerous clinical trials and scientific scrutiny. In 2006, Chua et al. published the results of the Atropine in the Treatment Of Myopia (ATOM) study (111). This was a two-year,

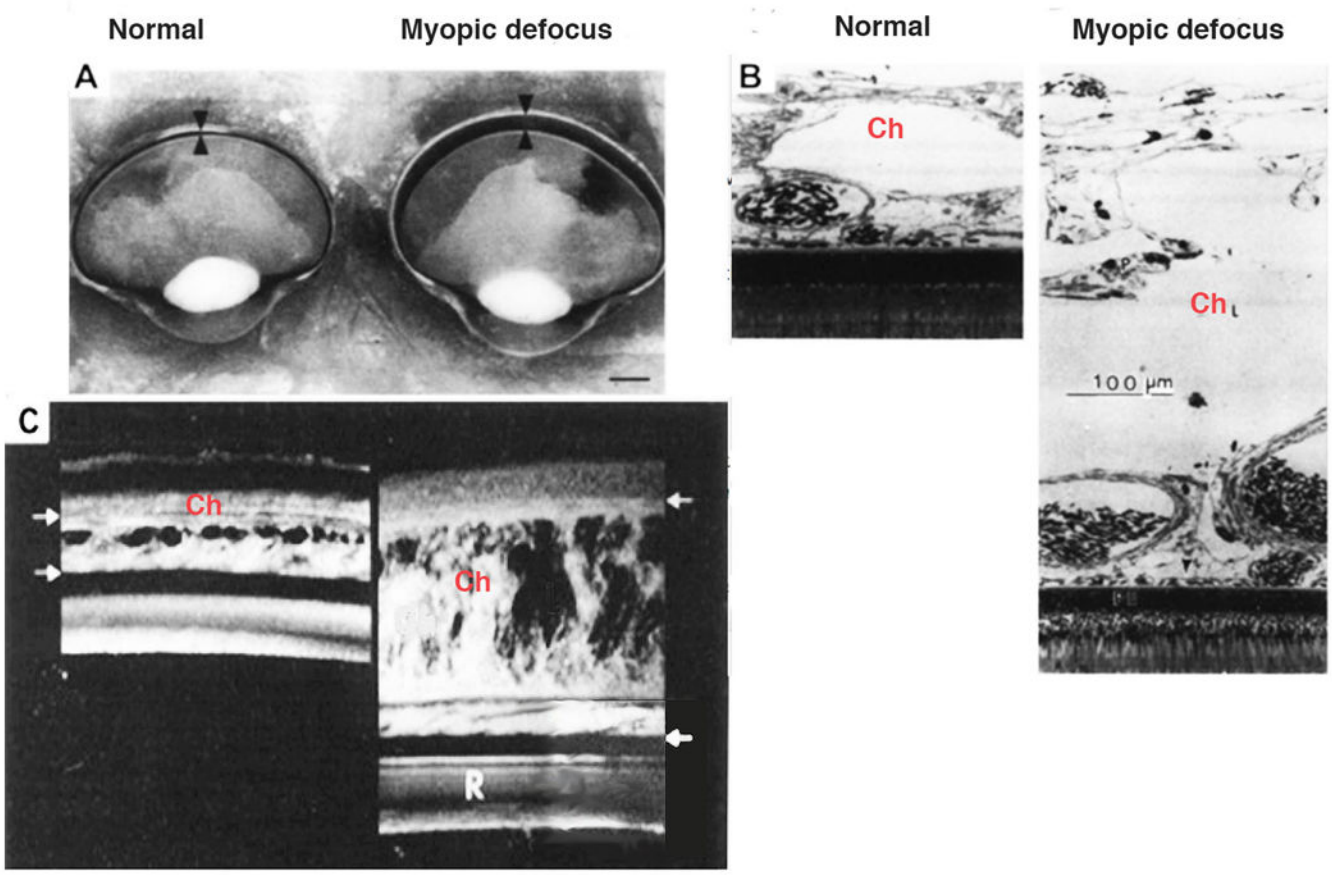

Figure 24. Choroidal modulation of refractive state. (**A**) Unfixed hemisected chick eyes. One eye is a normal control while the other has received myopic defocus. Arrowheads delimit choroidal thickness. (**B**) Plastic-embedded sections of the back of the eyes. Ch (red): choroid; R: retina. (**C**) One-mm-thick section of the posterior eye wall. Ch: choroid, delimited by arrows show the relative thickness of the choroid in normal and myopic defocus eyes. Reproduced with permission from Wallman et al., (1995) (192).

comprehensive, randomized, placebo-controlled, double-blind trial of 346 Asian children to determine the effectiveness and safety of daily 1% atropine eye drops for the prevention of myopia progression. ATOM was significant in that it was one of the first clinical trials with double-blind and placebo-controlled groups, which provided a much more objective measurement of the effects of atropine for human myopia. The outcomes revealed that atropine significantly reduced the mean progression of myopic refractive error: 84% of placebo-treated children experienced myopic progression of -0.5 D or more, while only 34% of atropine-treated children experienced the same (Figure 25). No serious adverse effects were reported, but the common side-effects – photophobia, glare, allergic reaction, and headaches caused by blurred vision – caused some children to drop out. In addition, a subset of children experienced a "rebound effect", in which myopia returned and progressed much more rapidly after atropine-treatment had ceased (198). Chia et al. (110) repeated the ATOM study (ATOM2), using lower concentrations of atropine (0.5%, 0.1%, and 0.01%) for two years, and found that the drug retained most of its efficacy at these lower concentrations. Minimal side effects were reported, but many children continued to suffer from blurred vision, conjunctivitis, and eyelid dermatitis at the higher concentrations. The "rebound effect" was also still present in the higher-concentration treatment groups (0.5% and 0.1%) (199).

In an attempt to address the rebound effect, the study was repeated, but with a different treatment schedule (200). Children were treated with 0.5%, 0.1%, or 0.01% atropine for two years, and then treatment was

discontinued for one year to see whether rebound would occur. Treatment was restarted only in children who experienced myopic progression of -0.50 diopters or more in at least one eye, and then continued for another two years. It was found that there was an inverse dose-related increase in myopia by the end of phase 2 (period with no treatment – 'wash-out') caused by rebound, resulting in the greatest effect of the 0.01% treatment group. Children requiring a second round of atropine-treatment were 24%, 59%, and 68% for the 0.01%, 0.1%, and 0.5% groups, respectively. Results from the second round of treatment confirmed that the most effective concentration of atropine was 0.01%; children treated with 0.01% atropine had the least rebound during the wash-out period, but still experienced significant inhibition of myopia-progression during treatment (Figure 26). Side-effects for the 0.01%-treatment group were mild – only minimal pupillary dilation, minimal loss of accommodation, and no significant loss of near-vision – compared with those at the higher concentrations.

Corneal-Reshaping Lenses: Orthokeratology

Orthokeratology (Ortho-K, Overnight Vision Correction, Corneal Refractive Therapy) uses gas-permeable contact lenses, worn at night and removed during the day, to temporarily reduce refractive errors. The lenses reshape the cornea while the user is sleeping, are removed in the morning, and refractive correction is maintained well throughout the day. Not only does Ortho-K correct myopia without drugs or surgery, but clinical trials of Ortho-K have demonstrated a strong correlation between Orth-K treatment and inhibition of myopia progression (201). The Longitudinal Orthokeratology Research in Children (LORIC) study, in Hong Kong, was a non-randomized two-year pilot study that investigated the ability of overnight Ortho-K lens wear (i) to correct myopic vision, and (ii) to slow the progression of myopia (n=35) (202). Positive results from this small pilot study led to the first larger-scale, single-masked, randomized clinical trial named the Retardation Of Myopia In Orthokeratology (ROMIO) study (203), in which 78 children (37 Ortho-K, 41 controls) took part for two years. The children wearing Ortho-K lenses experienced significantly slower axial elongation during the study than those wearing single-vision lenses, and at the end of the treatment period had significantly shorter eyes (Figure 27). Some children (5) did drop out of the study for ocular health reasons related to lens-wear, but their vision was not permanently affected once Ortho-K treatment was stopped. The mechanism by which orthokeratology inhibited myopia progression remains unclear, but studies have suggested that Ortho-K lenses may induce relative peripheral myopia, as well as increases in spherical aberration and amplitude of accommodation (204). However, alternative mechanisms – such as neurally mediated reflex control of ocular elongation or corneal curvature – have not yet been ruled out.

Alternative Strategies: High Environmental Illuminance

Human trials investigating the effects of high-intensity outdoor light on myopia prevention have so far been very promising (36, 38, 39) (Figure 10). Sending children outdoors is by far the least invasive treatment-option currently available. In countries where the intensity of outdoor light is generally lower, because of air pollution or short duration of natural daylight – such as Canada or Scandinavia in the winter, or Beijing year-around – sunlight therapy could be supplemented in the form of SAD lights (approved and used for Seasonal Affective Disorder), which have an output of ~2,000-10,000 lux and are sold to combat depressive symptoms brought on by seasonal affective disorder. This alternative will become even more attractive, when the spectral region responsible for myopia-prevention in primates has been identified.

Where do we go from here?

The world is experiencing a "myopia boom" (2), and viable treatment options are becoming more crucial than ever before. Atropine is considered to be the best pharmaceutical treatment we have. It is the only one currently available, and is rather widely accepted and used, despite remaining off-label for the purpose of treating myopia. Advocates of atropine use would claim that the occurrence of unwanted side-effects and its unknown mechanism of action are not serious enough drawbacks to warrant discontinuation of therapy. Unlike atropine,

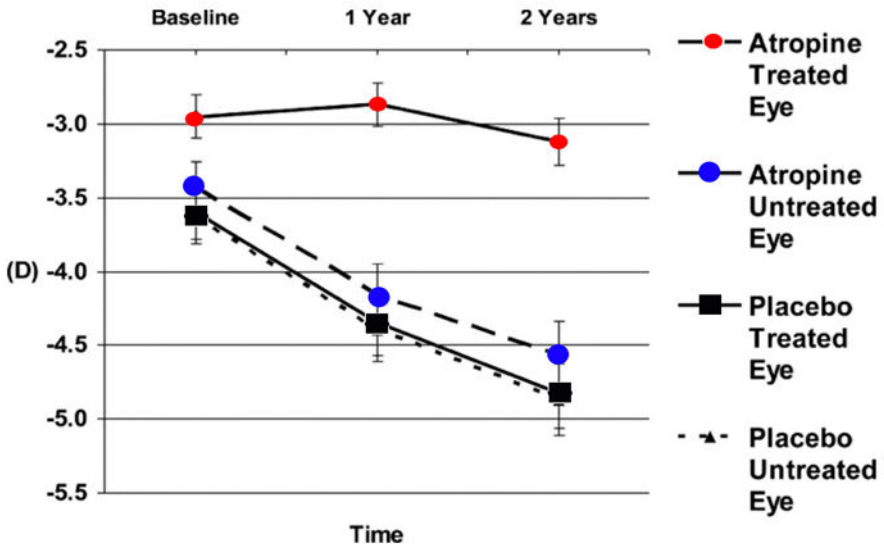

Figure 25. The effect of 1% atropine and placebo on the progression of myopic refractive error in children over the course of two years. Reproduced from Chua, W. H. et al. (2006) (111).

single-vision lenses do not prevent continued myopia progression, which can lead to blindness-inducing vision problems later in life; and overall, topical atropine-treatment in children has been proven to be effective and quite safe. Parents should be aware of the most common side effects: possible photophobia due to pupil dilation, impairment of near-vision due to paralysis of the ciliary muscle, allergic reactions, and rebound after cessation of treatment. It should also be noted, that not all children will respond to atropine-treatment (205).

It is imperative to determine the mechanism through which atropine inhibits myopia, because a better agent might be found, ideally, an agent as effective topically as atropine, but completely lacking the unacceptable side-effects of even 0.01% atropine eye-drops – mild photophobia, blur, and allergies. There is evidence that mAChRs may not be the receptors that mediate myopia-inhibition (109), and learning the true targets could effectively eliminate atropine's three most common side-effects. Lowering the required concentrations or treatment frequency could mitigate the allergic reactions caused by daily atropine use, and using a non-mAChR-specific drug would eliminate both photophobia and loss of accommodation, which are mediated by known target receptors of atropine (mAChRs).

Retrospective reviews have been performed to determine the safety and efficacy of Ortho-K lens-wear; however, although gas-permeable Ortho-K lenses have been determined to be quite safe (201, 206), caution is still advised. Long-term use of these lenses may be required, which can increase the risk of microbial keratitis, and discontinuation of use has resulted in a rebound effect similar to that seen in pharmacological treatments of myopia (198, 199, 204). Recently, a study was performed that combined the anti-myopia effects of atropine (0.01%) and Ortho-K. The authors reported that combining the two therapies resulted in a significantly greater effect than Ortho-K treatment alone (207). Long-term studies on the safety and efficacy of cornea-reshaping lenses are vital; whether overall eye health can be maintained while using lenses that change eye shape by applying a significant amount of physical pressure to corneal cells for many hours every day remains to be determined.

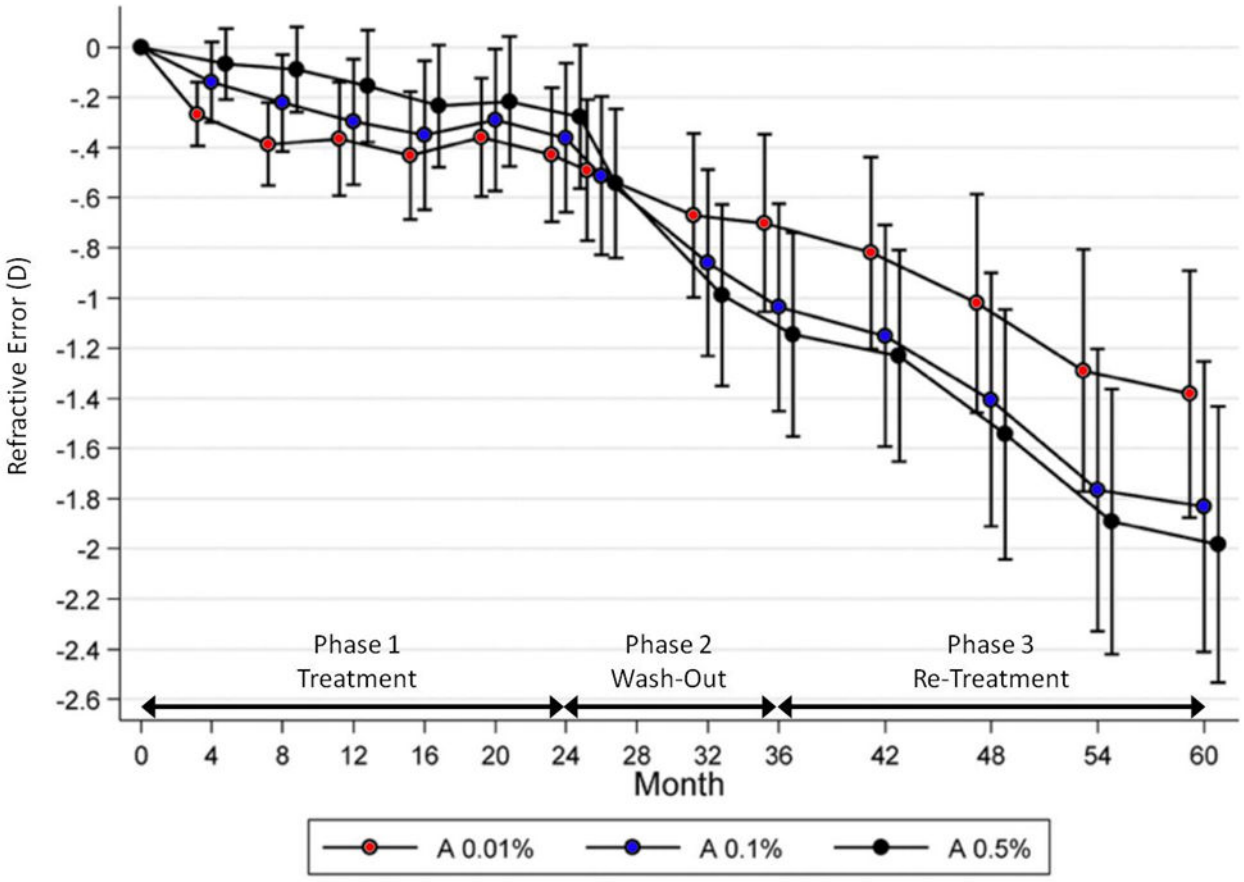

Figure 26. Mean change in refractive error over time within different treatment groups (atropine 0.01%, 0.1%, and 0.5%). Error bars represent 1 standard deviation. Reproduced from Chia, A., Lu, Q. S. & Tan, D. (2016) (200).

Outdoor-light therapy may offer the ideal treatment for myopia. Not only does encouraging children to play outside combat other major health concerns – such as childhood obesity, juvenile diabetes, and depression – but also, light therapy presents little to no serious health concerns or side-effects compared to those of other available myopia-treatments. Exposure to potentially-harmful UV radiation can be avoided by wearing UVA/UVB-blocking sunglasses and sunscreen. Alternative light sources such as commercially available SAD lights do not contain UV-radiation, and have been shown to be nearly equally effective in myopia-prevention in animal models. This approach seems to be particularly promising, if further testing of non-human primates, followed by clinical trials, confirms that long (rather than short) wavelengths of visible light are the ones that can protect humans against myopia, as blue-light can be potentially harmful to the retina (208).

Although we have made significant progress in determining possible treatments for myopia, much still needs to be done before we understand fully the homeostatic mechanisms responsible for regulation of eye growth. New discoveries about the way visual feedback regulates eye size may lead to new treatment options for myopia, and further our understanding of a fundamental mechanism of human eye development and emmetropization, a poorly understood, but highly important function of visual processing in the retina.

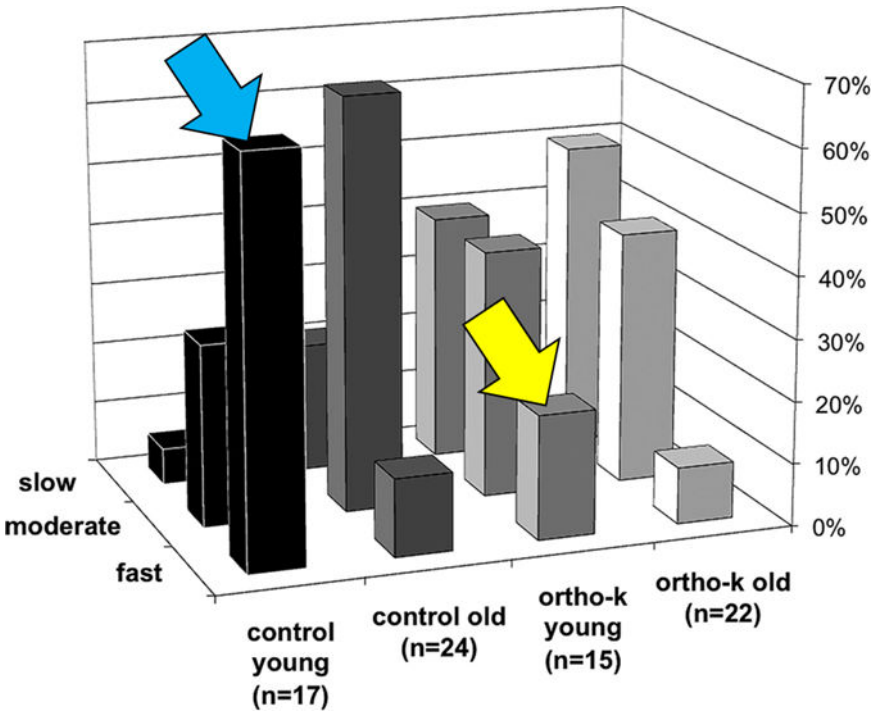

Figure 27. Percentages of subjects demonstrating slow (0.18 mm/y), moderate (>0.18 and ≤0.36 mm/y), and fast (>0.36 mm/y) myopia-progression in younger (6–8 years old) and older (9–10 years old) children, in the Ortho-K and control groups. The blue arrow indicates the percentage of young myopes that experienced rapid myopia-progression without Ortho-K treatment (65%), while the yellow arrow indicates the percentage of young myopes that experienced rapid myopia progression with Ortho-K treatment (20%). Reproduced and modified from Cho, P. & Cheung, S. W. (2012) (203).

About the authors

Brittany Carr graduated with Honours from the Bachelor of Health Sciences program at the University of Calgary in 2011, and earned her PhD in Neuroscience at the Cumming School of Medicine at the University of Calgary, Alberta, Canada, in April 2017. Mentored by Dr. William K. Stell and Dr. Morley D. Hollenberg, her doctorate research was concerned with investigating the signalling mechanisms involved in atropine-mediated inhibition of myopia. By investigating the pharmacological behavior of atropine and other myopia-inhibiting muscarinic acetylcholine receptor (mAChR) antagonists, she successfully demonstrated that myopia inhibition by atropine may not be controlled by mAChRs, but instead some other unknown target receptor(s) or pathway(s), possibly involving alpha$_{2A}$-adrenoceptors. She is currently a postdoctoral fellow, studying retinal degeneration at the University of British Columbia Centre for Macular Research (Vancouver, BC, Canada).

Bill Stell has been Professor of Cell Biology and Anatomy in the Cumming School of Medicine, University of Calgary, since 1980. He graduated from Swarthmore College with High Honors in Zoology in 1961, and received his Ph.D. in Anatomy in 1966 and M.D. in 1967, both from the University of Chicago. Subsequently he was at the NINDS, NIH, in the laboratories of Drs. Thomas G. Smith, Jr., K.C. Richardson, Henry G. Wagner, and M.G.F. Fuortes. In 1972 he joined the faculty of the Jules Stein Eye Institute, UCLA for 8 years, and finally found a home in Neuroscience at the University of Calgary, Alberta. Originally known for pioneering studies in EM of Golgi-impregnated neurons in fish retina, more recently Bill became interested in the retinal origins of myopia. Since then, he – with outstanding PhD. Students such as Dr. Carr – has made many and varied contributions to understanding the role(s) of the retina in causing and preventing myopia.

References

1. Foster P.J., Jiang Y. Epidemiology of myopia. Eye (Lond). 2014;28(2):202–8. PubMed PMID: 24406412.
2. Dolgin E. The myopia boom. Nature. 2015;519(7543):276–8. PubMed PMID: 25788077.
3. The Impact of Myopia and High Myopia. World Health Organization. 2015.
4. Wong T.Y., Ferreira A., Hughes R., Carter G., Mitchell P. Epidemiology and disease burden of pathologic myopia and myopic choroidal neovascularization: an evidence-based systematic review. Am J Ophthalmol. 2014;157(1):9–25.e12. PubMed PMID: 24099276.
5. Prevalence of myopia and hyperopia in 6- to 72-month-old african american and Hispanic children: the multi-ethnic pediatric eye disease study. Ophthalmology. 2010;117(1):140–147.e3. PubMed PMID: 19926137.
6. Wen G., Tarczy-Hornoch K., McKean-Cowdin R., Cotter S.A., Borchert M., Lin J., Kim J., Varma R. Prevalence of myopia, hyperopia, and astigmatism in non-Hispanic white and Asian children: multi-ethnic pediatric eye disease study. Ophthalmology. 2013;120(10):2109–16. PubMed PMID: 23953098.
7. French A.N., Ashby R.S., Morgan I.G., Rose K.A. Time outdoors and the prevention of myopia. Exp Eye Res. 2013;114:58–68. PubMed PMID: 23644222.
8. Verhoeven V.J., Hysi P.G., Wojciechowski R., Fan Q., Guggenheim J.A., Hohn R., MacGregor S., Hewitt A.W., Nag A., Cheng C.Y., Yonova-Doing E., Zhou X., Ikram M.K., Buitendijk G.H., McMahon G., Kemp J.P., Pourcain B.S., Simpson C.L., Makela K.M., Lehtimaki T., Kahonen M., Paterson A.D., Hosseini S.M., Wong H.S., Xu L., Jonas J.B., Parssinen O., Wedenoja J., Yip S.P., Ho D.W., Pang C.P., Chen L.J., Burdon K.P., Craig J.E., Klein B.E., Klein R., Haller T., Metspalu A., Khor C.C., Tai E.S., Aung T., Vithana E., Tay W.T., Barathi V.A., Chen P., Li R., Liao J., Zheng Y., Ong R.T., Doring A., Evans D.M., Timpson N.J., Verkerk A.J., Meitinger T., Raitakari O., Hawthorne F., Spector T.D., Karssen L.C., Pirastu M., Murgia F., Ang W., Mishra A., Montgomery G.W., Pennell C.E., Cumberland P.M., Cotlarciuc I., Mitchell P., Wang J.J., Schache M., Janmahasatian S., Igo R.P. Jr, Lass J.H., Chew E., Iyengar S.K., Gorgels T.G., Rudan I., Hayward C., Wright A.F., Polasek O., Vatavuk Z., Wilson J.F., Fleck B., Zeller T., Mirshahi A., Muller C., Uitterlinden A.G., Rivadeneira F., Vingerling J.R., Hofman A., Oostra B.A., Amin N., Bergen A.A., Teo Y.Y., Rahi J.S., Vitart V., Williams C., Baird P.N., Wong T.Y., Oexle K., Pfeiffer N., Mackey D.A., Young T.L., van Duijn C.M., Saw S.M., Bailey-Wilson J.E., Stambolian D., Klaver C.C., Hammond C.J. Genome-wide meta-analyses of multiancestry cohorts identify multiple new susceptibility loci for refractive error and myopia. Nat Genet. 2013;45(3):314–8. PubMed PMID: 23396134.

9. Dirani M., Chamberlain M., Garoufalis P., Chen C., Guymer R.H., Baird P.N. Refractive errors in twin studies. Twin Res Hum Genet. 2006;9(4):566–72. PubMed PMID: 16899164.
10. Ding X., Wang D., Huang Q., Zhang J., Chang J., He M. Distribution and heritability of peripheral eye length in Chinese children and adolescents: the Guangzhou Twin Eye Study. Invest Ophthalmol Vis Sci. 2013;54(2):1048–53. PubMed PMID: 23329669.
11. Kim M.H., Zhao D., Kim W., Lim D.H., Song Y.M., Guallar E., Cho J., Sung J., Chung E.S., Chung T.Y. Heritability of myopia and ocular biometrics in Koreans: the healthy twin study. Invest Ophthalmol Vis Sci. 2013;54(5):3644–9. PubMed PMID: 23620424.
12. Guo, L., J. Yang, J. Mai, X. Du, Y. Guo, P. Li, Y. Yue, D. Tang, C. Lu, and W.H. Zhang, *Prevalence and associated factors of myopia among primary and middle school-aged students: a school-based study in Guangzhou.* Eye (Lond). 2016.
13. Ip J.M., Huynh S.C., Robaei D., Rose K.A., Morgan I.G., Smith W., Kifley A., Mitchell P. Ethnic differences in the impact of parental myopia: findings from a population-based study of 12-year-old Australian children. Invest Ophthalmol Vis Sci. 2007;48(6):2520–8. PubMed PMID: 17525179.
14. Lam D.S., Fan D.S., Lam R.F., Rao S.K., Chong K.S., Lau J.T., Lai R.Y., Cheung E.Y. The effect of parental history of myopia on children's eye size and growth: results of a longitudinal study. Invest Ophthalmol Vis Sci. 2008;49(3):873–6. PubMed PMID: 18326705.
15. Mutti D.O., Mitchell G.L., Moeschberger M.L., Jones L.A., Zadnik K. Parental myopia, near work, school achievement, and children's refractive error. Invest Ophthalmol Vis Sci. 2002;43(12):3633–40. PubMed PMID: 12454029.
16. Xiang F., He M., Morgan I.G. The impact of parental myopia on myopia in Chinese children: population-based evidence. Optom Vis Sci. 2012;89(10):1487–96. PubMed PMID: 22922777.
17. Rose K.A., Morgan I.G., Smith W., Mitchell P. High heritability of myopia does not preclude rapid changes in prevalence. Clin Experiment Ophthalmol. 2002;30(3):168–72. PubMed PMID: 12010207.
18. Ramessur R., Williams K.M., Hammond C.J. Risk factors for myopia in a discordant monozygotic twin study. Ophthalmic Physiol Opt. 2015;35(6):643–51. PubMed PMID: 26376775.
19. Wallman J., Winawer J. Homeostasis of eye growth and the question of myopia. Neuron. 2004;43(4):447–68. PubMed PMID: 15312645.
20. Hubel D.H., Wiesel T.N., LeVay S. Functional architecture of area 17 in normal and monocularly deprived macaque monkeys. Cold Spring Harb Symp Quant Biol. 1976;40:581–9. PubMed PMID: 820507.
21. Wiesel T.N., Raviola E. Myopia and eye enlargement after neonatal lid fusion in monkeys. Nature. 1977;266(5597):66–8. PubMed PMID: 402582.
22. Norton T.T., Casagrande V.A., Sherman S.M. Loss of Y-cells in the lateral geniculate nucleus of monocularly deprived tree shrews. Science. 1977;197(4305):784–6. PubMed PMID: 887922.
23. Wallman J., Turkel J., Trachtman J. Extreme myopia produced by modest change in early visual experience. Science. 1978;201(4362):1249–51. PubMed PMID: 694514.
24. Schaeffel F., Bartmann M., Hagel G., Zrenner E. Studies on the role of the retinal dopamine/melatonin system in experimental refractive errors in chickens. Vision Res. 1995;35(9):1247–64. PubMed PMID: 7610585.
25. Schaeffel F., Feldkaemper M. Animal models in myopia research. Clin Exp Optom. 2015;98(6):507–17. PubMed PMID: 26769177.
26. Troilo D., Gottlieb M.D., Wallman J. Visual deprivation causes myopia in chicks with optic nerve section. Curr Eye Res. 1987;6(8):993–9. PubMed PMID: 3665562.
27. Wallman J., Gottlieb M.D., Rajaram V., Fugate-Wentzek L.A. Local retinal regions control local eye growth and myopia. Science. 1987;237(4810):73–7. PubMed PMID: 3603011.
28. Napper G.A., Brennan N.A., Barrington M., Squires M.A., Vessey G.A., Vingrys A.J. The duration of normal visual exposure necessary to prevent form deprivation myopia in chicks. Vision Res. 1995;35(9):1337–44. PubMed PMID: 7610595.
29. Zhu X., Winawer J.A., Wallman J. Potency of myopic defocus in spectacle lens compensation. Invest Ophthalmol Vis Sci. 2003;44(7):2818–27. PubMed PMID: 12824218.

30. Gwiazda J., Hyman L., Hussein M., Everett D., Norton T.T., Kurtz D., Leske M.C., Manny R., Marsh-Tootle W., Scheiman M. A randomized clinical trial of progressive addition lenses versus single vision lenses on the progression of myopia in children. Invest Ophthalmol Vis Sci. 2003;44(4):1492–500. PubMed PMID: 12657584.
31. Berntsen D.A., Sinnott L.T., Mutti D.O., Zadnik K. A randomized trial using progressive addition lenses to evaluate theories of myopia progression in children with a high lag of accommodation. Invest Ophthalmol Vis Sci. 2012;53(2):640–9. PubMed PMID: 22205604.
32. Galvis V., Tello A., Parra M.M., Merayo-Lloves J., Larrea J., Julian Rodriguez C., Camacho P.A. Topical Atropine in the Control of Myopia. Med Hypothesis Discov Innov Ophthalmol. 2016;5(3):78–88. PubMed PMID: 28293653.
33. Adler D., Millodot M. The possible effect of undercorrection on myopic progression in children. Clin Exp Optom. 2006;89(5):315–21. PubMed PMID: 16907670.
34. Chung K., Mohidin N., O'Leary D.J. Undercorrection of myopia enhances rather than inhibits myopia progression. Vision Res. 2002;42(22):2555–9. PubMed PMID: 12445849.
35. Sun Y.Y., Li S.M., Li S.Y., Kang M.T., Liu L.R., Meng B., Zhang F.J., Millodot M., Wang N. Effect of uncorrection versus full correction on myopia progression in 12-year-old children. Graefes Arch Clin Exp Ophthalmol. 2017;255(1):189–195. PubMed PMID: 27796670.
36. Read S.A., Collins M.J., Vincent S.J. Light Exposure and Eye Growth in Childhood. Invest Ophthalmol Vis Sci. 2015;56(11):6779–87. PubMed PMID: 26567790.
37. Rucker F.J. The role of luminance and chromatic cues in emmetropisation. Ophthalmic Physiol Opt. 2013;33(3):196–214. PubMed PMID: 23662955.
38. Rose K.A., Morgan I.G., Ip J., Kifley A., Huynh S., Smith W., Mitchell P. Outdoor activity reduces the prevalence of myopia in children. Ophthalmology. 2008;115(8):1279–85. PubMed PMID: 18294691.
39. He M., Xiang F., Zeng Y., Mai J., Chen Q., Zhang J., Smith W., Rose K., Morgan I.G. Effect of Time Spent Outdoors at School on the Development of Myopia Among Children in China: A Randomized Clinical Trial. Jama. 2015;314(11):1142–8. PubMed PMID: 26372583.
40. Smith E.L. 3rd, Hung L.F., Arumugam B., Huang J. Negative lens-induced myopia in infant monkeys: effects of high ambient lighting. Invest Ophthalmol Vis Sci. 2013;54(4):2959–69. PubMed PMID: 23557736.
41. Smith E.L. 3rd, Hung L.F., Huang J. Protective effects of high ambient lighting on the development of form-deprivation myopia in rhesus monkeys. Invest Ophthalmol Vis Sci. 2012;53(1):421–8. PubMed PMID: 22169102.
42. Ashby R., Ohlendorf A., Schaeffel F. The effect of ambient illuminance on the development of deprivation myopia in chicks. Invest Ophthalmol Vis Sci. 2009;50(11):5348–54. PubMed PMID: 19516016.
43. Ashby R.S., Schaeffel F. The effect of bright light on lens compensation in chicks. Invest Ophthalmol Vis Sci. 2010;51(10):5247–53. PubMed PMID: 20445123.
44. Ashby R. Animal Studies and the Mechanism of Myopia-Protection by Light? Optom Vis Sci. 2016;93(9):1052–4. PubMed PMID: 27560692.
45. Hoshi H., Sato M., Oguri M., Ohtsuka T. In vivo nitric oxide concentration in the vitreous of rat eye. Neurosci Lett. 2003;347(3):187–90. PubMed PMID: 12875917.
46. Carr B.J., Stell W.K. Nitric Oxide (NO) Mediates the Inhibition of Form-Deprivation Myopia by Atropine in Chicks. Scientific Reports. 2016;6(1):9. PubMed PMID: 28442706.
47. Feldkaemper M., Schaeffel F. An updated view on the role of dopamine in myopia. Exp Eye Res. 2013;114:106–19. PubMed PMID: 23434455.
48. Nickla D.L., Lee L., Totonelly K. Nitric oxide synthase inhibitors prevent the growth-inhibiting effects of quinpirole. Optom Vis Sci. 2013;90(11):1167–75. PubMed PMID: 24061155.
49. Rucker F.J., Wallman J. Cone signals for spectacle-lens compensation: differential responses to short and long wavelengths. Vision Res. 2008;48(19):1980–91. PubMed PMID: 18585403.
50. Rohrer B., Iuvone P.M., Stell W.K. Stimulation of dopaminergic amacrine cells by stroboscopic illumination or fibroblast growth factor (bFGF, FGF-2) injections: possible roles in prevention of form-deprivation myopia in the chick. Brain Res. 1995;686(2):169–81. PubMed PMID: 7583283.

51. Wildsoet C.F., Howland H.C., Falconer S., Dick K. Chromatic aberration and accommodation: their role in emmetropization in the chick. Vision Res. 1993;33(12):1593–603. PubMed PMID: 8236848.
52. Foulds W.S., Barathi V.A., Luu C.D. Progressive myopia or hyperopia can be induced in chicks and reversed by manipulation of the chromaticity of ambient light. Invest Ophthalmol Vis Sci. 2013;54(13):8004–12. PubMed PMID: 24222304.
53. Ghodsi, L. and W.K. Stell. *Blue SAD light protects against form deprivation myopia in chickens, by local signaling within the retina*. in *15th International Myopia Conference (IMC 2015)*. 2015. Wenzhou, China: Eye and Vision 2016.
54. Jiang L., Zhang S., Schaeffel F., Xiong S., Zheng Y., Zhou X., Lu F., Qu J. Interactions of chromatic and lens-induced defocus during visual control of eye growth in guinea pigs (Cavia porcellus). Vision Res. 2014;94:24–32. PubMed PMID: 24216006.
55. Long Q., Chen D., Chu R. Illumination with monochromatic long-wavelength light promotes myopic shift and ocular elongation in newborn pigmented guinea pigs. Cutan Ocul Toxicol. 2009;28(4):176–80. PubMed PMID: 19888887.
56. Qian Y.F., Liu R., Dai J.H., Chen M.J., Zhou X.T., Chu R.Y. Transfer from blue light or green light to white light partially reverses changes in ocular refraction and anatomy of developing guinea pigs. J Vis. 2013;13(11) PubMed PMID: 24071588.
57. Smith E.L. 3rd, Hung L.F., Arumugam B., Holden B.A., Neitz M., Neitz J. Effects of Long-Wavelength Lighting on Refractive Development in Infant Rhesus Monkeys. Invest Ophthalmol Vis Sci. 2015;56(11):6490–500. PubMed PMID: 26447984.
58. Gawne T.J., Siegwart J.T., Ward A.H., Norton T.T. The wavelength composition and temporal modulation of ambient lighting strongly affect refractive development in young tree shrews. Experimental eye research. 2017;155:75–84. PubMed PMID: 27979713.
59. Charman W.N. Keeping the world in focus: how might this be achieved? Optom Vis Sci. 2011;88(3):373–6. PubMed PMID: 21270674.
60. Morgan I.G., Ashby R.S., Nickla D.L. Form deprivation and lens-induced myopia: are they different? Ophthalmic Physiol Opt. 2013;33(3):355–61. PubMed PMID: 23662966.
61. Ehrlich D., Sattayasai J., Zappia J., Barrington M. Effects of selective neurotoxins on eye growth in the young chick. Ciba Found Symp. 1990;155:63–84discussion 84-8. PubMed PMID: 2088682.
62. Fischer A.J., Morgan I.G., Stell W.K. Colchicine causes excessive ocular growth and myopia in chicks. Vision Res. 1999;39(4):685–97. PubMed PMID: 10341956.
63. Oishi I., Yoshii K., Miyahara D., Kagami H., Tagami T. Targeted mutagenesis in chicken using CRISPR/Cas9 system. Sci Rep. 2016;6:23980. PubMed PMID: 27050479.
64. Sanjana N.E., Shalem O., Zhang F. Improved vectors and genome-wide libraries for CRISPR screening. Nat Methods. 2014;11(8):783–4. PubMed PMID: 25075903.
65. Waldner D., Visser F., Stell W.K. An Avian Adeno-Associated Viral Vector for Visualization of Post-Natal Chick Retinal Circuitry. Investigative Ophthalmology & Visual Science. 2017;58(8):5905–5905.
66. Chakraborty R., Pardue M.T. Molecular and Biochemical Aspects of the Retina on Refraction. Prog Mol Biol Transl Sci. 2015;134:249–67. PubMed PMID: 26310159.
67. Park H., Tan C.C., Faulkner A., Jabbar S.B., Schmid G., Abey J., Iuvone P.M., Pardue M.T. Retinal degeneration increases susceptibility to myopia in mice. Mol Vis. 2013;19:2068–79. PubMed PMID: 24146540.
68. Park H., Jabbar S.B., Tan C.C., Sidhu C.S., Abey J., Aseem F., Schmid G., Iuvone P.M., Pardue M.T. Visually-driven ocular growth in mice requires functional rod photoreceptors. Invest Ophthalmol Vis Sci. 2014;55(10):6272–9. PubMed PMID: 25183765.
69. Pardue M.T., Faulkner A.E., Fernandes A., Yin H., Schaeffel F., Williams R.W., Pozdeyev N., Iuvone P.M. High susceptibility to experimental myopia in a mouse model with a retinal on pathway defect. Invest Ophthalmol Vis Sci. 2008;49(2):706–12. PubMed PMID: 18235018.
70. Fujikado T., Hosohata J., Omoto T. ERG of form deprivation myopia and drug induced ametropia in chicks. Curr Eye Res. 1996;15(1):79–86. PubMed PMID: 8631207.

71. Ritchey E.R., Zelinka C., Tang J., Liu J., Code K.A., Petersen-Jones S., Fischer A.J. Vision-guided ocular growth in a mutant chicken model with diminished visual acuity. Exp Eye Res. 2012;102:59–69. PubMed PMID: 22824538.
72. McBrien N.A., Moghaddam H.O., Cottriall C.L., Leech E.M., Cornell L.M. The effects of blockade of retinal cell action potentials on ocular growth, emmetropization and form deprivation myopia in young chicks. Vision Res. 1995;35(9):1141–52. PubMed PMID: 7610575.
73. Norton T.T., Essinger J.A., McBrien N.A. Lid-suture myopia in tree shrews with retinal ganglion cell blockade. Vis Neurosci. 1994;11(1):143–53. PubMed PMID: 8011577.
74. Troilo D., Nickla D.L., Mertz J.R., Summers Rada J.A. Change in the synthesis rates of ocular retinoic acid and scleral glycosaminoglycan during experimentally altered eye growth in marmosets. Invest Ophthalmol Vis Sci. 2006;47(5):1768–77. PubMed PMID: 16638980.
75. Wildsoet C., Wallman J. Choroidal and scleral mechanisms of compensation for spectacle lenses in chicks. Vision Res. 1995;35(9):1175–94. PubMed PMID: 7610579.
76. Dillingham C.M., Guggenheim J.A., Erichsen J.T. Disruption of the centrifugal visual system inhibits early eye growth in chicks. Invest Ophthalmol Vis Sci. 2013;54(5):3632–43. PubMed PMID: 23599339.
77. Owusu-Yaw V., Kyle A.L., Stell W.K. Effects of lesions of the optic nerve, optic tectum and nervus terminalis on rod precursor proliferation in the goldfish retina. Brain Res. 1992;576(2):220–30. PubMed PMID: 1515918.
78. Avellaneda-Chevrier V.K., Wang X., Hooper M.L., Chauhan B.C. The retino–retinal projection: Tracing retinal ganglion cells projecting to the contralateral retina. Neuroscience Letters. 2015;591:105–109. PubMed PMID: 25700948.
79. Nadal-Nicolas F.M., Valiente-Soriano F.J., Salinas-Navarro M., Jimenez-Lopez M., Vidal-Sanz M., Agudo-Barriuso M. Retino-retinal projection in juvenile and young adult rats and mice. Exp Eye Res. 2015;134:47–52. PubMed PMID: 25797477.
80. Kolb, H., *Roles of Amacrine Cells.* Webvision: The Organization of the Retina and Visual System. 2012: (Online) Available at: http://webvision.med.utah.edu.
81. Masland R.H. Cell populations of the retina: the Proctor lecture. Invest Ophthalmol Vis Sci. 2011;52(7):4581–91. PubMed PMID: 21712414.
82. Masland R.H. The neuronal organization of the retina. Neuron. 2012;76(2):266–80. PubMed PMID: 23083731.
83. Famiglietti E.V. Dendritic co-stratification of ON and ON-OFF directionally selective ganglion cells with starburst amacrine cells in rabbit retina. J Comp Neurol. 1992;324(3):322–35. PubMed PMID: 1383291.
84. Gollisch T., Meister M. Eye smarter than scientists believed: neural computations in circuits of the retina. Neuron. 2010;65(2):150–64. PubMed PMID: 20152123.
85. Bitzer M., Kovacs B., Feldkaemper M., Schaeffel F. Effects of muscarinic antagonists on ZENK expression in the chicken retina. Exp Eye Res. 2006;82(3):379–88. PubMed PMID: 16143326.
86. Feldkaemper M.P., Schaeffel F. Evidence for a potential role of glucagon during eye growth regulation in chicks. Vis Neurosci. 2002;19(6):755–66. PubMed PMID: 12688670.
87. Ganesan P., Wildsoet C.F. Pharmaceutical intervention for myopia control. Expert Rev Ophthalmol. 2010;5(6):759–787. PubMed PMID: 21258611.
88. Lan W., Yang Z., Feldkaemper M., Schaeffel F. Changes in dopamine and ZENK during suppression of myopia in chicks by intense illuminance. Exp Eye Res. 2015;145:118–124. PubMed PMID: 26657138.
89. Bitzer M., Schaeffel F. Effects of quisqualic acid on retinal ZENK expression induced by imposed defocus in the chick eye. Optom Vis Sci. 2004;81(2):127–36. PubMed PMID: 15127932.
90. Li X.X., Schaeffel F., Kohler K., Zrenner E. Dose-dependent effects of 6-hydroxy dopamine on deprivation myopia, electroretinograms, and dopaminergic amacrine cells in chickens. Vis Neurosci. 1992;9(5):483–92. PubMed PMID: 1360257.
91. Wildsoet C.F., Pettigrew J.D. Kainic acid-induced eye enlargement in chickens: differential effects on anterior and posterior segments. Invest Ophthalmol Vis Sci. 1988;29(2):311–9. PubMed PMID: 3338888.

92. Leech E.M., Cottriall C.L., McBrien N.A. Pirenzepine prevents form deprivation myopia in a dose dependent manner. Ophthalmic Physiol Opt. 1995;15(5):351–6. PubMed PMID: 8524553.
93. McBrien N.A., Moghaddam H.O., Reeder A.P. Atropine reduces experimental myopia and eye enlargement via a nonaccommodative mechanism. Invest Ophthalmol Vis Sci. 1993;34(1):205–15. PubMed PMID: 8425826.
94. Raviola E., Wiesel T.N. An animal model of myopia. N Engl J Med. 1985;312(25):1609–15. PubMed PMID: 4000200.
95. Tigges M., Iuvone P.M., Fernandes A., Sugrue M.F., Mallorga P.J., Laties A.M., Stone R.A. Effects of muscarinic cholinergic receptor antagonists on postnatal eye growth of rhesus monkeys. Optom Vis Sci. 1999;76(6):397–407. PubMed PMID: 10416935.
96. Arumugam B., McBrien N.A. Muscarinic antagonist control of myopia: evidence for M4 and M1 receptor-based pathways in the inhibition of experimentally-induced axial myopia in the tree shrew. Invest Ophthalmol Vis Sci. 2012;53(9):5827–37. PubMed PMID: 22836762.
97. Mckanna, J.A. and V.A. Casagrande, Atropine Affects Lid-Suture Myopia Development, in Third International Conference on Myopia Copenhagen, August 24–27, 1980, H.C. Fledelius, P.H. Alsbirk, and E. Goldschmidt, Editors. 1981, Springer Netherlands: Dordrecht. p. 187-192.
98. Luft W.A., Ming Y., Stell W.K. Variable effects of previously untested muscarinic receptor antagonists on experimental myopia. Invest Ophthalmol Vis Sci. 2003;44(3):1330–8. PubMed PMID: 12601066.
99. Metlapally S., McBrien N.A. The effect of pirenzepine on positive- and negative-lens-induced refractive error and ocular growth in chicks. Invest Ophthalmol Vis Sci. 2010;51(11):5438–44. PubMed PMID: 20539000.
100. Stone, R.A., T. Lin, and A.M. Laties, Muscarinic antagonist effects on experimental chick myopia, Volume 52, in Exp Eye Res. 1991: England. p. 755-8.
101. Bartlett J.D., Niemann K., Houde B., Allred T., Edmondson M.J., Crockett R.S. A tolerability study of pirenzepine ophthalmic gel in myopic children. J Ocul Pharmacol Ther. 2003;19(3):271–9. PubMed PMID: 12828845.
102. Cottriall C.L., McBrien N.A. The M1 muscarinic antagonist pirenzepine reduces myopia and eye enlargement in the tree shrew. Invest Ophthalmol Vis Sci. 1996;37(7):1368–79. PubMed PMID: 8641840.
103. Cottriall C.L., McBrien N.A., Annies R., Leech E.M. Prevention of form-deprivation myopia with pirenzepine: a study of drug delivery and distribution. Ophthalmic Physiol Opt. 1999;19(4):327–35. PubMed PMID: 10645389.
104. Wildsoet C. Neural pathways subserving negative lens-induced emmetropization in chicks--insights from selective lesions of the optic nerve and ciliary nerve. Curr Eye Res. 2003;27(6):371–85. PubMed PMID: 14704921.
105. Barathi V.A., Weon S.R., Beuerman R.W. Expression of muscarinic receptors in human and mouse sclera and their role in the regulation of scleral fibroblasts proliferation. Mol Vis. 2009;15:1277–93. PubMed PMID: 19578554.
106. Fischer A.J., McKinnon L.A., Nathanson N.M., Stell W.K. Identification and localization of muscarinic acetylcholine receptors in the ocular tissues of the chick. J Comp Neurol. 1998;392(3):273–84. PubMed PMID: 9511918.
107. McBrien N.A., Jobling A.I., Truong H.T., Cottriall C.L., Gentle A. Expression of muscarinic receptor subtypes in tree shrew ocular tissues and their regulation during the development of myopia. Mol Vis. 2009;15:464–75. PubMed PMID: 19262686.
108. Strang C.E., Renna J.M., Amthor F.R., Keyser K.T. Muscarinic acetylcholine receptor localization and activation effects on ganglion response properties. Invest Ophthalmol Vis Sci. 2010;51(5):2778–89. PubMed PMID: 20042645.
109. McBrien N.A., Stell W.K., Carr B. How does atropine exert its anti-myopia effects? Ophthalmic Physiol Opt. 2013;33(3):373–8. PubMed PMID: 23662969.

110. Chia A., Chua W.H., Cheung Y.B., Wong W.L., Lingham A., Fong A., Tan D. Atropine for the treatment of childhood myopia: safety and efficacy of 0.5%, 0.1%, and 0.01% doses (Atropine for the Treatment of Myopia 2). Ophthalmology. 2012;119(2):347–54. PubMed PMID: 21963266.
111. Chua W.H., Balakrishnan V., Chan Y.H., Tong L., Ling Y., Quah B.L., Tan D. Atropine for the treatment of childhood myopia. Ophthalmology. 2006;113(12):2285–91. PubMed PMID: 16996612.
112. Iribarren R. Tropicamide and myopia progression. Ophthalmology. 2008;115(6):1103–4. PubMed PMID: 18519078.
113. Siatkowski R.M., Cotter S., Miller J.M., Scher C.A., Crockett R.S., Novack G.D. Safety and efficacy of 2% pirenzepine ophthalmic gel in children with myopia: a 1-year, multicenter, double-masked, placebo-controlled parallel study. Arch Ophthalmol. 2004;122(11):1667–74. PubMed PMID: 15534128.
114. Siatkowski R.M., Cotter S.A., Crockett R.S., Miller J.M., Novack G.D., Zadnik K. Two-year multicenter, randomized, double-masked, placebo-controlled, parallel safety and efficacy study of 2% pirenzepine ophthalmic gel in children with myopia. J aapos. 2008;12(4):332–9. PubMed PMID: 18359651.
115. Cottriall C.L., Truong H.T., McBrien N.A. Inhibition of myopia development in chicks using himbacine: a role for M(4) receptors? Neuroreport. 2001;12(11):2453–6. PubMed PMID: 11496128.
116. Vessey K.A., Cottriall C.L., McBrien N.A. Muscarinic receptor protein expression in the ocular tissues of the chick during normal and myopic eye development. Brain Res Dev Brain Res. 2002;135(1-2):79–86. PubMed PMID: 11978396.
117. Fischer A.J., Miethke P., Morgan I.G., Stell W.K. Cholinergic amacrine cells are not required for the progression and atropine-mediated suppression of form-deprivation myopia. Brain Res. 1998;794(1):48–60. PubMed PMID: 9630509.
118. Nickla D.L., Zhu X., Wallman J. Effects of muscarinic agents on chick choroids in intact eyes and eyecups: evidence for a muscarinic mechanism in choroidal thinning. Ophthalmic Physiol Opt. 2013;33(3):245–56. PubMed PMID: 23662958.
119. McBrien N.A., Arumugam B., Gentle A., Chow A., Sahebjada S. The M4 muscarinic antagonist MT-3 inhibits myopia in chick: evidence for site of action. Ophthalmic Physiol Opt. 2011;31(5):529–39. PubMed PMID: 21539592.
120. Nickla D.L., Yusupova Y., Totonelly K. The Muscarinic Antagonist MT3 Distinguishes Between Form Deprivation- and Negative Lens-Induced Myopia in Chicks. Curr Eye Res. 2015;40(9):962–7. PubMed PMID: 25310574.
121. Potter L.T. Snake toxins that bind specifically to individual subtypes of muscarinic receptors. Life Sci. 2001;68(22-23):2541–7. PubMed PMID: 11392624.
122. Blanchet G., Collet G., Mourier G., Gilles N., Fruchart-Gaillard C., Marcon E., Servent D. Polypharmacology profiles and phylogenetic analysis of three-finger toxins from mamba venom: case of aminergic toxins. Biochimie. 2014;103:109–17. PubMed PMID: 24793485.
123. Nareoja K., Kukkonen J.P., Rondinelli S., Toivola D.M., Meriluoto J., Nasman J. Adrenoceptor activity of muscarinic toxins identified from mamba venoms. Br J Pharmacol. 2011;164(2b):538–50. PubMed PMID: 21557730.
124. McDougal D.H., Gamlin P.D. Autonomic control of the eye. Compr Physiol. 2015;5(1):439–73. PubMed PMID: 25589275.
125. Woldemussie E., Wijono M., Pow D. Localization of alpha 2 receptors in ocular tissues. Vis Neurosci. 2007;24(5):745–56. PubMed PMID: 17986363.
126. Ruuskanen J.O., Peitsaro N., Kaslin J.V., Panula P., Scheinin M. Expression and function of alpha-adrenoceptors in zebrafish: drug effects, mRNA and receptor distributions. J Neurochem. 2005;94(6):1559–69. PubMed PMID: 16000146.
127. Iuvone P.M., Rauch A.L. Alpha 2-adrenergic receptors influence tyrosine hydroxylase activity in retinal dopamine neurons. Life Sci. 1983;33(24):2455–63. PubMed PMID: 6139733.
128. Iuvone P.M. Regulation of retinal dopamine biosynthesis and tyrosine hydroxylase activity by light. Fed Proc. 1984;43(12):2709–13. PubMed PMID: 6147273.

129. Nguyen-Legros J., Martin-Martinelli E., Simon A., Denoroy L., Vigny A. Co-localization of tyrosine hydroxylase and phenylethanolamine-N-methyltransferase immunoreactivity in the rat retina: a re-examination using double labeling on semi-thin sections. Exp Eye Res. 1986;43(4):575–84. PubMed PMID: 2878821.
130. Zhou X., Pardue M.T., Iuvone P.M., Qu J. Dopamine signaling and myopia development: What are the key challenges. Prog Retin Eye Res. 2017. PubMed PMID: 28602573.
131. DeVries S.H., Schwartz E.A. Modulation of an electrical synapse between solitary pairs of catfish horizontal cells by dopamine and second messengers. J Physiol. 1989;414:351–75. PubMed PMID: 2558170.
132. Rohrer B., Spira A.W., Stell W.K. Apomorphine blocks form-deprivation myopia in chickens by a dopamine D2-receptor mechanism acting in retina or pigmented epithelium. Vis Neurosci. 1993;10(3):447–53. PubMed PMID: 8494798.
133. Seko Y., Tanaka Y., Tokoro T. Apomorphine inhibits the growth-stimulating effect of retinal pigment epithelium on scleral cells in vitro. Cell Biochem Funct. 1997;15(3):191–6. PubMed PMID: 9377797.
134. Weiss S., Schaeffel F. Diurnal growth rhythms in the chicken eye: relation to myopia development and retinal dopamine levels. J Comp Physiol A. 1993;172(3):263–70. PubMed PMID: 8510054.
135. Nickla D.L., Totonelly K. Dopamine antagonists and brief vision distinguish lens-induced- and form-deprivation-induced myopia. Exp Eye Res. 2011;93(5):782–5. PubMed PMID: 21872586.
136. Iuvone P.M., Tigges M., Stone R.A., Lambert S., Laties A.M. Effects of apomorphine, a dopamine receptor agonist, on ocular refraction and axial elongation in a primate model of myopia. Invest Ophthalmol Vis Sci. 1991;32(5):1674–7. PubMed PMID: 2016144.
137. Schwahn H.N., Kaymak H., Schaeffel F. Effects of atropine on refractive development, dopamine release, and slow retinal potentials in the chick. Vis Neurosci. 2000;17(2):165–76. PubMed PMID: 10824671.
138. Schmid K.L., Wildsoet C.F. Inhibitory effects of apomorphine and atropine and their combination on myopia in chicks. Optom Vis Sci. 2004;81(2):137–47. PubMed PMID: 15127933.
139. Stone R.A., Lin T., Laties A.M., Iuvone P.M. Retinal dopamine and form-deprivation myopia. Proc Natl Acad Sci U S A. 1989;86(2):704–6. PubMed PMID: 2911600.
140. McCarthy C.S., Megaw P., Devadas M., Morgan I.G. Dopaminergic agents affect the ability of brief periods of normal vision to prevent form-deprivation myopia. Exp Eye Res. 2007;84(1):100–7. PubMed PMID: 17094962.
141. Cottriall C.L., Brew J., Vessey K.A., McBrien N.A. Diisopropylfluorophosphate alters retinal neurotransmitter levels and reduces experimentally-induced myopia. Naunyn Schmiedebergs Arch Pharmacol. 2001;364(4):372–82. PubMed PMID: 11683525.
142. Arumugam B., McBrien N. The D2 Antagonist Spiperone Prevents Muscarinic Antagonist Control of Experimentally-Induced Myopia in Chick. IOVS. ARVO E-Abstract. 2010;51:1195.
143. Arumugam B., McBrien N. Spiperone Prevents M1 Muscarinic Antagonist Inhibition of Myopia in Tree shrew. IOVS. ARVO E-Abstract. 2012;53:3431.
144. Moinul P., Cheng E., Stell W.K. Nitric Oxide Prevents Form-Deprivation Myopia in Chicks Without Requiring a Dopamine D2-Receptor Relay. IOVS. ARVO E-Abstract. 2012;53:3434.
145. Elphick M.R. Localization of nitric oxide synthase using NADPH diaphorase histochemistry. Methods Mol Biol. 1997;72:153–8. PubMed PMID: 9249743.
146. Fischer A.J., Stell W.K. Nitric oxide synthase-containing cells in the retina, pigmented epithelium, choroid, and sclera of the chick eye. J Comp Neurol. 1999;405(1):1–14. PubMed PMID: 10022192.
147. Wilson M., Nacsa N., Hart N.S., Weller C., Vaney D.I. Regional distribution of nitrergic neurons in the inner retina of the chicken. Vis Neurosci. 2011;28(3):205–20. PubMed PMID: 21554774.
148. Eldred W.D., Blute T.A. Imaging of nitric oxide in the retina. Vision Res. 2005;45(28):3469–86. PubMed PMID: 16171845.
149. Tekmen-Clark M., Gleason E. Nitric oxide production and the expression of two nitric oxide synthases in the avian retina. Vis Neurosci. 2013;30(3):91–103. PubMed PMID: 23721886.
150. Blom J., Giove T., Deshpande M., Eldred W.D. Characterization of nitric oxide signaling pathways in the mouse retina. J Comp Neurol. 2012;520(18):4204–17. PubMed PMID: 22592770.

151. Nickla D.L., Wildsoet C.F. The effect of the nonspecific nitric oxide synthase inhibitor NG-nitro-L-arginine methyl ester on the choroidal compensatory response to myopic defocus in chickens. Optom Vis Sci. 2004;81(2):111–8. PubMed PMID: 15127930.
152. Nickla D.L., Damyanova P., Lytle G. Inhibiting the neuronal isoform of nitric oxide synthase has similar effects on the compensatory choroidal and axial responses to myopic defocus in chicks as does the non-specific inhibitor L-NAME. Exp Eye Res. 2009;88(6):1092–9. PubMed PMID: 19450449.
153. Nickla D.L., Wilken E., Lytle G., Yom S., Mertz J. Inhibiting the transient choroidal thickening response using the nitric oxide synthase inhibitor l-NAME prevents the ameliorative effects of visual experience on ocular growth in two different visual paradigms. Exp Eye Res. 2006;83(2):456–64. PubMed PMID: 16635488.
154. Chakraborty R., Bergen M.A., Landis E., Lee D.C., Iuvone M., Pardue M. Pharmacological inhibition of nitric oxide increases myopia susceptibility in mice. IOVS. ARVO E-Abstract. 2016;57:4742.
155. Noll G.N., Billek M., Pietruck C., Schmidt K.F. Inhibition of nitric oxide synthase alters light responses and dark voltage of amphibian photoreceptors. Neuropharmacology. 1994;33(11):1407–12. PubMed PMID: 7532822.
156. Sato M., Ohtsuka T., Stell W.K. Endogenous nitric oxide enhances the light-response of cones during light-adaptation in the rat retina. Vision Res. 2011;51(1):131–7. PubMed PMID: 20951158.
157. Shiells R., Falk G. Retinal on-bipolar cells contain a nitric oxide-sensitive guanylate cyclase. Neuroreport. 1992;3(10):845–8. PubMed PMID: 1358250.
158. Tsuyama Y., Noll G.N., Schmidt K.F. L-arginine and nicotinamide adenine dinucleotide phosphate alter dark voltage and accelerate light response recovery in isolated retinal rods of the frog (Rana temporaria). Neurosci Lett. 1993;149(1):95–8. PubMed PMID: 8469390.
159. Wellard J.W., Morgan I.G. Nitric oxide donors mimic the effects of light on photoreceptor melatonin synthesis. Aust N Z J Ophthalmol. 1996;24(2 Suppl):61–3. PubMed PMID: 8811248.
160. Shi, Q., Mechanisms of Adaptation to Mean Light Intensity in the Chick Retina, in Neuroscience. 2014, University of Calgary: University of Calgary.
161. Bloomfield S.A., Volgyi B. The diverse functional roles and regulation of neuronal gap junctions in the retina. Nat Rev Neurosci. 2009;10(7):495–506. PubMed PMID: 19491906.
162. Teves M., Shi H., Eng D., Stell W.K. The role of cell-cell coupling in myopia development and light adaptation. IOVS. ARVO E-Abstract. 2014;55:3036.
163. Teves, M., N. Odermatt, S. Q, B.J. Carr, D. Eng, and W.K. Stell. Retinal gap junctions containing Connexin-35/36: Roles in visual regulation of eye growth and prevention of myopia. in 15th International Myopia Conference 2015 (IMC 2015). 2015. Wenzhou, China.
164. Trier K., Munk Ribel-Madsen S., Cui D., Brogger Christensen S. Systemic 7-methylxanthine in retarding axial eye growth and myopia progression: a 36-month pilot study. J Ocul Biol Dis Infor. 2008;1(2-4):85–93. PubMed PMID: 20072638.
165. Cui D., Trier K., Zeng J., Wu K., Yu M., Hu J., Chen X., Ge J. Effects of 7-methylxanthine on the sclera in form deprivation myopia in guinea pigs. Acta Ophthalmol. 2011;89(4):328–34. PubMed PMID: 19860777.
166. Nie H.H., Huo L.J., Yang X., Gao Z.Y., Zeng J.W., Trier K., Cui D.M. Effects of 7-methylxanthine on form-deprivation myopia in pigmented rabbits. Int J Ophthalmol. 2012;5(2):133–7. PubMed PMID: 22762036.
167. Carr B.J., Stell W.K. Alpha$_2$-Adrenergic Agonists Inhibit Form-Deprivation Myopia (FDM) in the ChickAlpha2-Adrenergic Agonists Inhibit Form-Deprivation Myopia (FDM) in the Chick. IOVS. ARVO E-Abstract. 2016;57:4738.
168. Cantor L.B. Brimonidine in the treatment of glaucoma and ocular hypertension. Ther Clin Risk Manag. 2006;2(4):337–46. PubMed PMID: 18360646.
169. Stone R.A., Liu J., Sugimoto R., Capehart C., Zhu X., Pendrak K. GABA, experimental myopia, and ocular growth in chick. Invest Ophthalmol Vis Sci. 2003;44(9):3933–46. PubMed PMID: 12939312.
170. Cheng Z.Y., Wang X.P., Schmid K.L., Han X.G. Inhibition of form-deprivation myopia by a GABAAOr receptor antagonist, (1,2,5,6-tetrahydropyridin-4-yl) methylphosphinic acid (TPMPA), in guinea pigs. Graefes Arch Clin Exp Ophthalmol. 2014;252(12):1939–46. PubMed PMID: 25120102.

171. Cheng, Z.Y., X.P. Wang, K.L. Schmid, Y.F. Han, X.G. Han, H.W. Tang, and X. Tang, *GABAB receptor antagonist CGP46381 inhibits form-deprivation myopia development in guinea pigs.* Biomed Res Int. 2015; 2015:207312.
172. Chebib M., Hinton T., Schmid K.L., Brinkworth D., Qian H., Matos S., Kim H.L., Abdel-Halim H., Kumar R.J., Johnston G.A., Hanrahan J.R. Novel, potent, and selective GABAC antagonists inhibit myopia development and facilitate learning and memory. J Pharmacol Exp Ther. 2009;328(2):448–57. PubMed PMID: 18984654.
173. Schmid K.L., Strasberg G., Rayner C.L., Hartfield P.J. The effects and interactions of GABAergic and dopaminergic agents in the prevention of form deprivation myopia by brief periods of normal vision. Exp Eye Res. 2013;110:88–95. PubMed PMID: 23474145.
174. Christian P.G., Harkin D.G., Schmid K.L. GABAergic agents modify the response of chick scleral fibroblasts to myopic and hyperopic eye cup tissues. Curr Eye Res. 2014;39(2):172–87. PubMed PMID: 24073754.
175. Rohrer B., Tao J., Stell W.K. Basic fibroblast growth factor, its high- and low-affinity receptors, and their relationship to form-deprivation myopia in the chick. Neuroscience. 1997;79(3):775–87. PubMed PMID: 9219941.
176. Chen B.Y., Wang C.Y., Chen W.Y., Ma J.X. Altered TGF-beta2 and bFGF expression in scleral desmocytes from an experimentally-induced myopia guinea pig model. Graefes Arch Clin Exp Ophthalmol. 2013;251(4):1133–44. PubMed PMID: 23381656.
177. Zhang D., Eldred W.D. Colocalization of enkephalin-, glucagon-, and corticotropin-releasing factor-like immunoreactivity in GABAergic amacrine cells in turtle retina. Brain Res. 1992;596(1-2):46–57. PubMed PMID: 1468002.
178. Fischer A.J., Skorupa D., Schonberg D.L., Walton N.A. Characterization of glucagon-expressing neurons in the chicken retina. J Comp Neurol. 2006;496(4):479–94. PubMed PMID: 16572462.
179. Ashby R., Kozulin P., Megaw P.L., Morgan I.G. Alterations in ZENK and glucagon RNA transcript expression during increased ocular growth in chickens. Mol Vis. 2010;16:639–49. PubMed PMID: 20405027.
180. Vessey K.A., Lencses K.A., Rushforth D.A., Hruby V.J., Stell W.K. Glucagon receptor agonists and antagonists affect the growth of the chick eye: a role for glucagonergic regulation of emmetropization? Invest Ophthalmol Vis Sci. 2005;46(11):3922–31. PubMed PMID: 16249465.
181. Stell W.K., Lencses K.A., Ahm J.M., Hruby V.J. Glucagon synthesizing amacrine cells mediate choroidal compensation for plus-defocus in the chick eye.European Journal of Neuroscience. 2000;12:487. *(abstract)* .
182. Feldkaemper M.P., Neacsu I., Schaeffel F. Insulin acts as a powerful stimulator of axial myopia in chicks. Invest Ophthalmol Vis Sci. 2009;50(1):13–23. PubMed PMID: 18599564.
183. Beloukhina N., Vessey K., Stell W. Glucagon prevents myopia via distal retina or RPE. Investigative Ophthalmology & Visual Science. 2005;46(13):3337–3337.
184. Zhong, X., J. Ge, S.E.L. 3rd, and W.K. Stell, *Selective activation of a subpopulation of GABAergic amacrine cells by focused and defocused images in Macaque retina (abstract).* European Retina Meeting, Frankfurt, Germany. 2007.
185. Zhong X., Ge J., Smith E.L. 3rd, Stell W.K. Image defocus modulates activity of bipolar and amacrine cells in macaque retina. Invest Ophthalmol Vis Sci. 2004;45(7):2065–74. PubMed PMID: 15223778.
186. Stell W., Tao J., Karkhanis A., Siegwart J. Jr, Norton T. Amacrine cells responsive to optical conditions regulating eye growth in the tree shrew, Tupaia glis belangeri. Investigative Ophthalmology & Visual Science. 2004;45(13):1159–1159.
187. Seko Y., Shimizu M., Tokoro T. Retinoic acid increases in the retina of the chick with form deprivation myopia. Ophthalmic Res. 1998;30(6):361–7. PubMed PMID: 9731117.
188. Seko Y., Shimokawa H., Tokoro T. In vivo and in vitro association of retinoic acid with form-deprivation myopia in the chick. Exp Eye Res. 1996;63(4):443–52. PubMed PMID: 8944551.
189. Bitzer M., Feldkaemper M., Schaeffel F. Visually induced changes in components of the retinoic acid system in fundal layers of the chick. Exp Eye Res. 2000;70(1):97–106. PubMed PMID: 10644425.

190. Weiler R., Pottek M., He S., Vaney D.I. Modulation of coupling between retinal horizontal cells by retinoic acid and endogenous dopamine. Brain Res Brain Res Rev. 2000;32(1):121–9. PubMed PMID: 10751661.
191. Zhang D.Q., McMahon D.G. Direct gating by retinoic acid of retinal electrical synapses. Proc Natl Acad Sci U S A. 2000;97(26):14754–9. PubMed PMID: 11114157.
192. Wallman J., Wildsoet C., Xu A., Gottlieb M.D., Nickla D.L., Marran L., Krebs W., Christensen A.M. Moving the retina: choroidal modulation of refractive state. Vision Res. 1995;35(1):37–50. PubMed PMID: 7839608.
193. Nickla D.L., Totonelly K., Dhillon B. Dopaminergic agonists that result in ocular growth inhibition also elicit transient increases in choroidal thickness in chicks. Exp Eye Res. 2010;91(5):715–20. PubMed PMID: 20801115.
194. Nickla D.L., Totonelly K. Choroidal thickness predicts ocular growth in normal chicks but not in eyes with experimentally altered growth. Clin Exp Optom. 2015;98(6):564–70. PubMed PMID: 26769180.
195. Nickla D.L., Wallman J. The multifunctional choroid. Prog Retin Eye Res. 2010;29(2):144–68. PubMed PMID: 20044062.
196. Summers J.A. The choroid as a sclera growth regulator. Exp Eye Res. 2013;114:120–7. PubMed PMID: 23528534.
197. Bedrossian R.H. The effect of atropine on myopia. Ophthalmology. 1979;86(5):713–9. PubMed PMID: 545205.
198. Tong L., Huang X.L., Koh A.L., Zhang X., Tan D.T., Chua W.H. Atropine for the treatment of childhood myopia: effect on myopia progression after cessation of atropine. Ophthalmology. 2009;116(3):572–9. PubMed PMID: 19167081.
199. Chia A., Chua W.H., Wen L., Fong A., Goon Y.Y., Tan D. Atropine for the treatment of childhood myopia: changes after stopping atropine 0.01%, 0.1% and 0.5%. Am J Ophthalmol. 2014;157(2):451–457.e1. PubMed PMID: 24315293.
200. Chia A., Lu Q.S., Tan D. Five-Year Clinical Trial on Atropine for the Treatment of Myopia 2: Myopia Control with Atropine 0.01% Eyedrops. Ophthalmology. 2016;123(2):391–9. PubMed PMID: 26271839.
201. Xie P., Guo X. Chinese Experiences on Orthokeratology. Eye Contact Lens. 2016;42(1):43–7. PubMed PMID: 26704137.
202. Cho P., Cheung S.W., Edwards M. The longitudinal orthokeratology research in children (LORIC) in Hong Kong: a pilot study on refractive changes and myopic control. Curr Eye Res. 2005;30(1):71–80. PubMed PMID: 15875367.
203. Cho P., Cheung S.W. Retardation of myopia in Orthokeratology (ROMIO) study: a 2-year randomized clinical trial. Invest Ophthalmol Vis Sci. 2012;53(11):7077–85. PubMed PMID: 22969068.
204. Gifford P., Gifford K.L. The Future of Myopia Control Contact Lenses. Optom Vis Sci. 2016;93(4):336–43. PubMed PMID: 26636396.
205. Loh K.L., Lu Q., Tan D., Chia A. Risk factors for progressive myopia in the atropine therapy for myopia study. Am J Ophthalmol. 2015;159(5):945–9. PubMed PMID: 25640408.
206. Liu Y.M., Xie P. The Safety of Orthokeratology--A Systematic Review. Eye Contact Lens. 2016;42(1):35–42. PubMed PMID: 26704136.
207. Kinoshita N., Konno Y., Hamada N., Kakehashi A. *Suppressive effect of combined treatment of orthokeratology and 0.01% atropine instillation on axial length elongation in childhood myopia.* IOVS. ARVO E-Abstract. 2017;57:2386.
208. Tosini G., Ferguson I., Tsubota K. Effects of blue light on the circadian system and eye physiology. Mol Vis. 2016;22:61–72. PubMed PMID: 26900325.
209. Tietje K.M., Nathanson N.M. Embryonic chick heart expresses multiple muscarinic acetylcholine receptor subtypes. Isolation and characterization of a gene encoding a novel m2 muscarinic acetylcholine receptor with high affinity for pirenzepine. J Biol Chem. 1991;266(26):17382–7. PubMed PMID: 1840593.
210. Carr, B.J., *Molecular Targets of Atropine- and Mamba Toxin 3-Mediated Inhibition of Form-Deprivation Myopia in the Chick: A Case of Mistaken Receptor Identity?*, in *Neuroscience*. 2017, University of Calgary: Calgary. p. 185.

211. Carr B.J., Stell W.K. *Alpha2-Adrenergic Agonists Inhibit Form-Deprivation Myopia (FDM) in the Chick.* IOVS. ARVO E-Abstract. 2016;57:4738.

Crystalline Lens and Cataract

Joah F. Aliancy, MD[1,*] and Nick Mamalis, MD[1,†]

Created: August 15, 2017.

Introduction

The lens of the eye is a biconvex, relatively acellular, optically transparent intraocular structure that with the cornea serves to transmit light to the retina with minimal light scattering (Figure 1a). Early anatomists viewed the lens as the location of meaningful visualization. We now know that this is the function of the retina, with the lens serving as a conduit of light transmission and focus to the retina. The lens can change shape with the aid of the ciliary muscles, thereby changing the focal distance to the retina and bringing the image into sharp focus on the retina. This adjustment of the lens is known as accommodation (similar to the focusing of a photographic camera via movement of its lenses). The lens is flatter on its anterior side than on its posterior side. (Figure 1b).

Development of the lens

The mature lens originates from surface ectoderm and develops through a highly organized process correlated with the neuroectoderm germ cell layer. Early in embryogenesis the diencephalon, neuroectoderm derived tissue, forms two outpouchings called the optic vesicles. The optic vesicles induce formation of the immature lenticular cells when they come in contact with surface ectoderm. The immature lenticular cells thicken to form the lens placode. Concurrently, the optic vesicles invaginate causing an indentation on the lens placode called the lens pit (Figure 2a).

At this point, the lens vesicle is made up of a single layer of cells enveloped within an outer basement membrane. This basement membrane will eventually form the lens capsule. While encased in the basement membrane, the cells in the posterior pole of the lens vesicle extend anteriorly to form the primary lens fibers (Figure 2b).

The anterior cells become the lens epithelial cells, while the primary lens fibers collectively form the embryonic nucleus. Subsequently, secondary lens fibers begin to elongate from the lens epithelial cells to form the fetal nucleus during the gestation period and continue to grow multiple layers. As the secondary lens fibers elongate from the equator, they form Y-shaped sutures by meeting anteriorly and posteriorly during fetal growth. The secondary lens fibers eventually grow to form the adult nucleus with new layers of lens fibers forming the lenticular cortex. During lenticular development, the hyaloid artery delivers nutrition and growth factors through the tunica vasculosa lentis, a vascular structure that envelopes the lens nucleus. However, this structure undergoes involution prior to birth to resemble the avascular lens seen in the adult. A firm understanding of the embryology and development of the lens will provide great insight into the pathology associated with cataract formation.

Figure 3 shows a stained section of the adult human lens with anterior part of the lens in the top section and the posterior part in the lower section.

The lens is composed of 4 structures: capsule, epithelium, cortex and nucleus (Figure 3). The capsule is the basement membrane with type VI collagen elaborated by the epithelium layer, and stains positively with Periodic

Author Affiliation: 1 John A. Moran Eye Center, University of Utah School of Medicine, Salt Lake City; Email: joah.aliancy@utah.edu; Email: nick.mamalis@hsc.utah.edu.

Corresponding author.

* About the authors

† About the authors

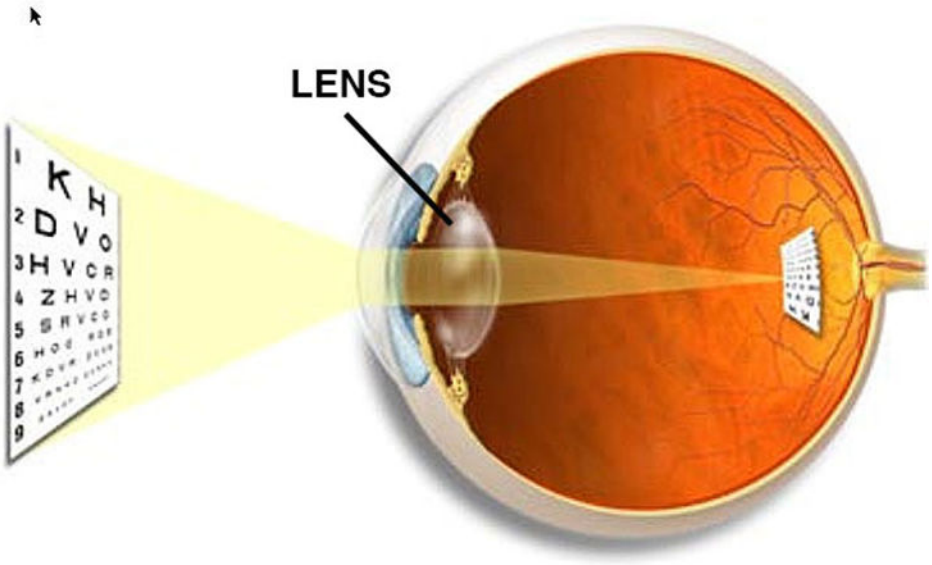

Figure 1a. A human eyeball cut in half to show the lens and the passage of light through it from the object ahead to the focus on the retina.

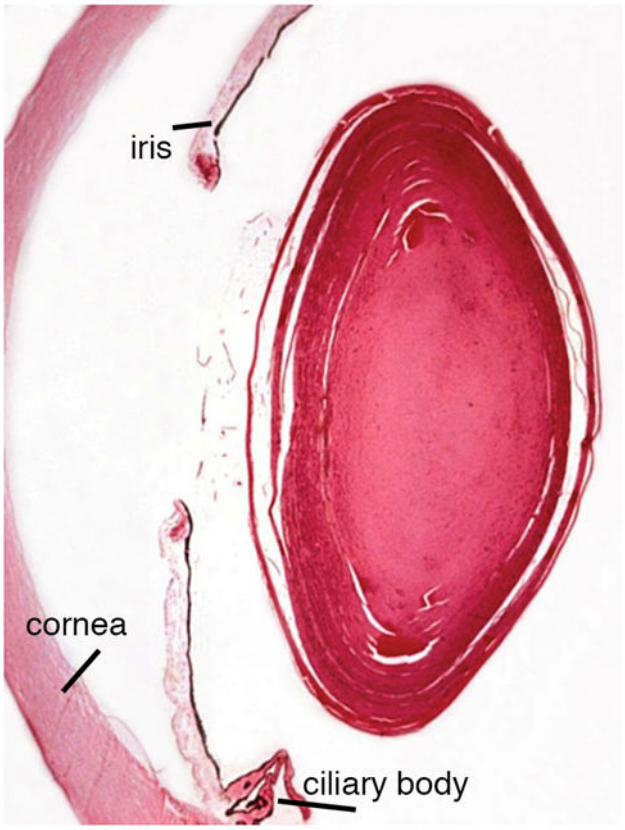

Figure 1b. Histological section of normal crystalline lens (H&E stain, X2). The sectioned iris is shown (**iris**) but the **ciliary body** is mostly out of the plane of the section. Notice the lens is flatter anteriorally, facing the cornea (**cornea**).

acid-Schiff (PAS) stain. It is optically clear and acellular. The lens is held in place by zonular fibers, otherwise known as the zonules of Zinn (Figure 4). These elastic fibers originate from the nonpigmented epithelium layer of the ciliary body and articulate with the outer layer of the capsule, the capsular lamellar layer. There is a reduction of zonular tension with contraction of the ciliary muscle leading to a more spherical shape allowing focus on more proximal objects. This process is called accommodation.

The lens epithelium has mitotically active cells that undergo further differentiation via an elongation process, increase in intracellular protein and loss of organelles. These cells are arranged in one layer across the posterior aspect of the anterior capsule. The equatorial bow region of the lens is where lens epithelial cells elongate to form lens fiber cells (Figure 5). Terminal differentiation of the epithelium eventually leads to the fiber layers of both the cortex and nucleus, with older fibers being located more centrally.

While the nucleus is denser, histologically, there is no distinction between the cortex and nucleus (Figure 5). The only appreciable difference is age, with older layers located more centrally. Interestingly, as the cortex and nucleus layers grow, the overall diopter strength of the lens increases owing to the increased diameter and curvature of the lens. The lack of organelles within the nucleus and cortex serves to provide an optically clear media for light transmission. The adult lens is almost three times the mass of its corresponding neonatal version, 90 mg to 250 mg.

In the adult, the lens lacks vascularity or innervation thus the metabolic demands of the lens are met by a constant flow of aqueous humor that serves as a conduit for both removal of waste and the delivery of nutrients.

Cataract formation and types of cataracts

Congenital cataracts

Congenital cataracts are lenticular opacities that cause significant light scattering at birth or are noted shortly after (Figure 6). An estimated 200,000 children worldwide are blind as a result of congenital cataracts, with an incidence of 40,000 in developing countries (1, 2). In regards to laterality, the prevalence appears to be the same for unilateral vs. bilateral (2). Surgical intervention for both unilateral and bilateral cataract is paramount to prevent long term deprivation amblyopia or visual loss (3, 4). Amblyopia is defined as a dysfunction in visual processing, characterized by poor visual acuity in one or both eyes and abnormal binocular depth perception (5). While both unilateral and bilateral cataracts are critical to detect, the long term severity of bilateral visual deprivation appears to be less than its unilateral counterpart (6).

Nuclear cataracts

A common cause of visual impairment in older adults is age-related cataract, which is subcategorized as nuclear, cortical or subcapsular in type. Cumulative incidence of nuclear, cortical and posterior cortical are 29.7%, 22.9% and 8.4% respectively (7, 8). Nuclear cataract is the most common age-related problem (Figure 7, Figure 8).

With age, nuclear fibers become more compacted and cause increased light scattering. As a result, sclerotic lens nuclei decrease in transparency and result in visual aberrations and annoying glare at night. Clinically, the sclerotic nuclear lens changes in color, from a clear transparent material to yellow or orange, eventually even to brown (brunescent) if left to mature (Figure 9). Histologically, nuclear sclerotic lenses are characterized by a dense homogenous material.

Aging causes the lenticular material to increase in overall size and become more amorphous. As the lens fibers continue to age, the nucleus becomes more compact and less pliable decreasing the ability of the lens to effectively accommodate. The increased coloration is due to protein aggregation in the nuclear lens, decreasing its transparency and leading to various symptoms including visual impairment, decrease in contrast sensitivity, dull color perception and a myopic shift.

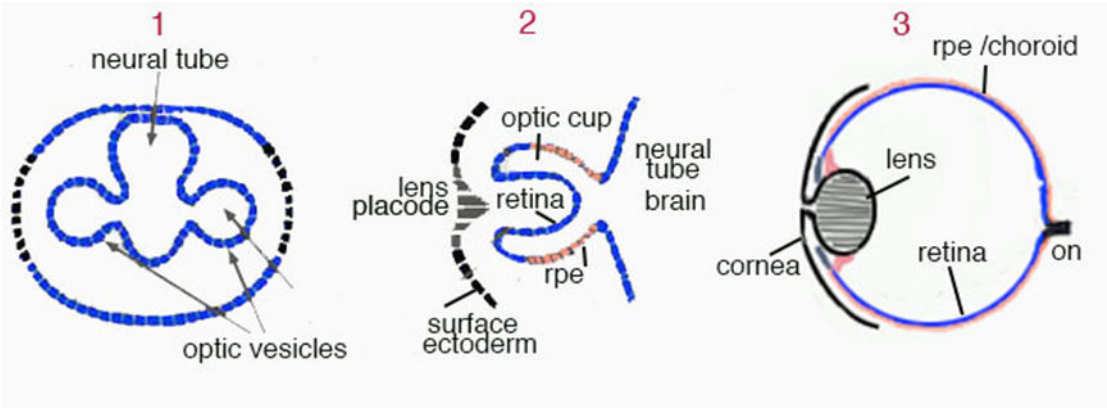

Figure 2a. A cartoon to show the development of the eye from the embryonic neural tube. 1. **Optic vesicles** form from the **neural tube**. 2. The **optic cup** forms by invagination, as the **retina** folds back upon the pigment epithelium. The developing optic cup induces the **lens placode** to be formed from the **surface ectoderm**. 3. Finally, the **lens** is pinched off and settles in place with the developing iris and ciliary body in the front of the eyeball. **rpe**; retinal pigment epithelium, **on**, optic nerve.

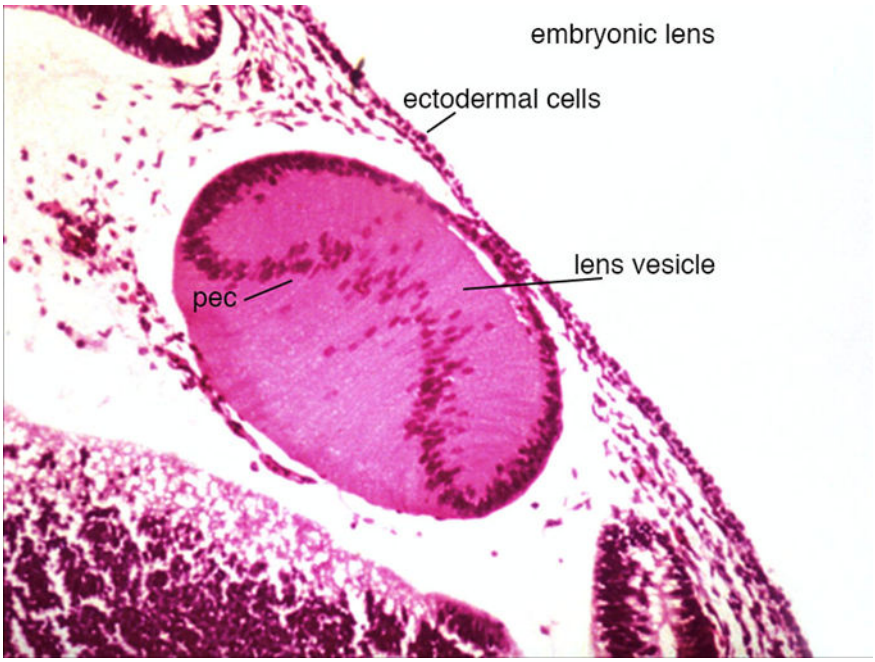

Figure 2b. **Embryonic lens**. **Lens vesicle** posterior epithelial cells (**pec**) elongate to form the primary lens fibers (H&E stain, X10).

As the cataract continues to mature, the cortical material begins to liquefy and the nucleus increases in opacity. A hyper-mature cataract is the final stage of the aging process. The liquefied cortex is resorbed, and the dense nucleus sinks within the capsular bag. If left untreated, proteinaceous material can leak across the capsular lining and cause trabecular meshwork (TM) obstruction leading to a phacolytic glaucomatous reaction. This inflammatory reaction is mediated by macrophages that respond to the leakage of lenticular protein and contribute to the TM obstruction. Changes within the lens nucleus do not occur independent of the other lenticular structure, instead, cortical subcapsular cataracts may and typically do occur simultaneously. However, nuclear sclerotic cataract is by far the most common age-related lenticular opacity.

Figure 10 shows a photograph of a patient's eye with dense mature cataract that has both nuclear and cortical (see below) components. Obviously, the patient was "blind" in this eye, and this cataract needed to be removed to restore sight to the eye.

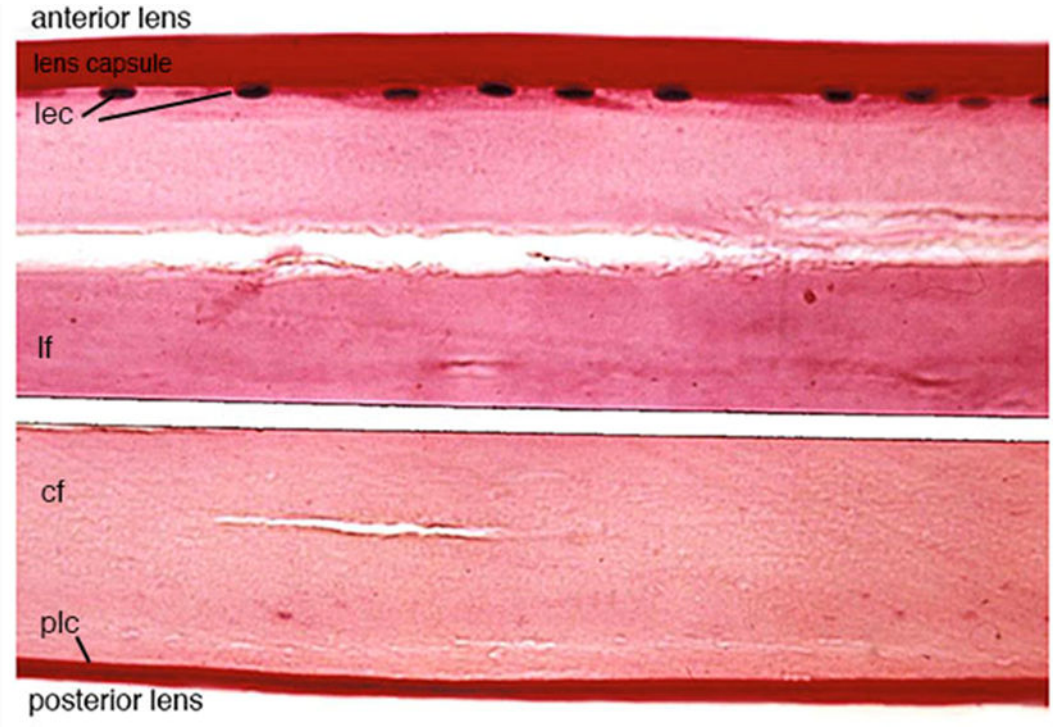

Figure 3. Layers of the lens. Upper section is through the anterior **lens capsule** showing lens epithelial cells, **lec**, and lens fibers, **lf**. Lower section is of the posterior lens capsule, **plc** and cortical fibers (**cf**). (H&E stain, X40).

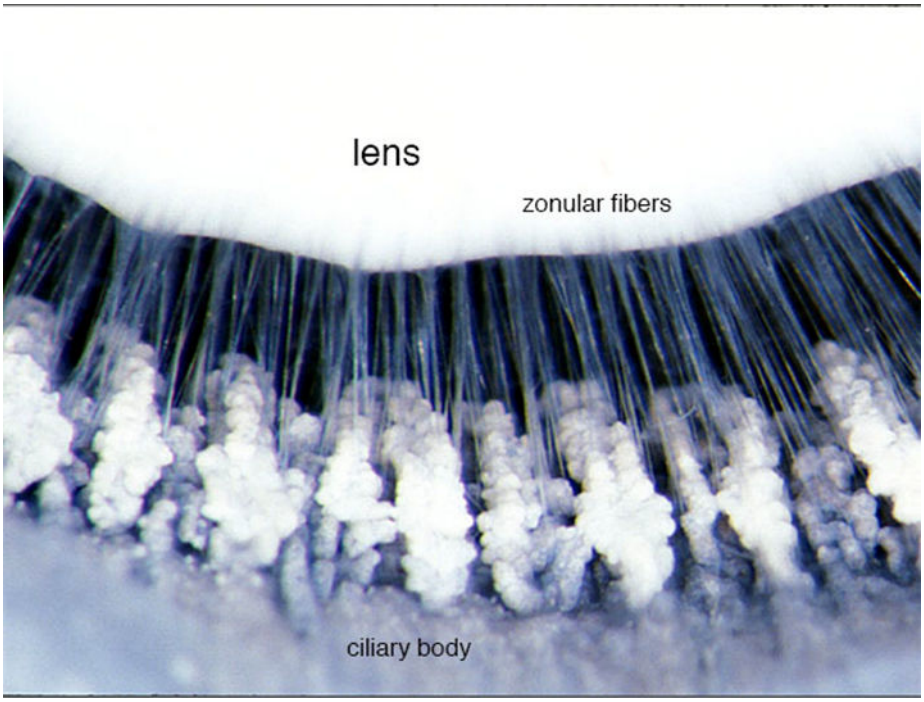

Figure 4. Scanning electron micrograph of **zonular fibers**. The fibers originate from the nonpigmented epithelium layer of the **ciliary body** and insert into the lens capsule.

Figure 5. Lens bow region. Lens epithelial cells (**ec**) originating from the equatorial region elongate to form new **lens fibers** (H&E stain, X10).

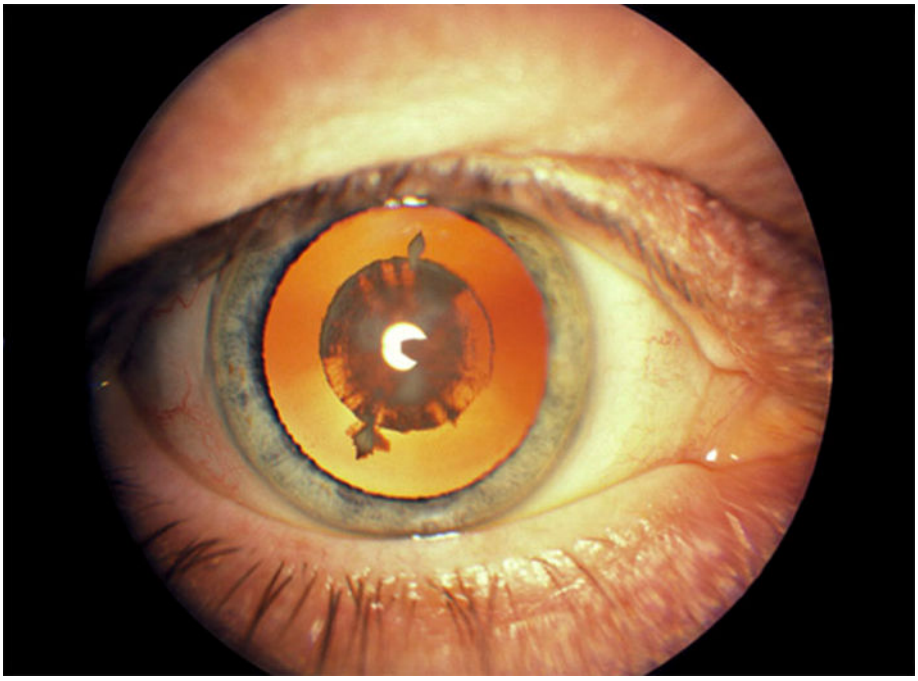

Figure 6. Clinical photograph of an eye with a dilated pupil to show a congenital cataract in the original fetal lens nucleus.

Cortical cataracts

As in nuclear sclerotic lens changes, aging can cause similar degenerative changes in the lens cortex. The opacities formed within the lens cortex are quite unique. Sharp clear fluid clefts, resembling opaque spokes

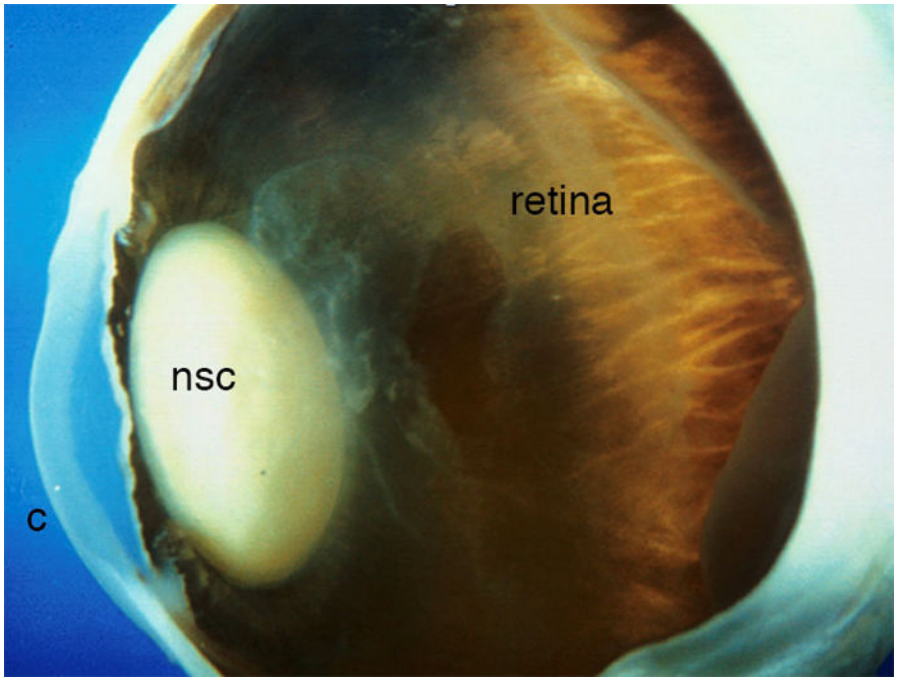

Figure 7. Sagittal section of part of the eyeball to show a mature nuclear sclerotic cataract, **nsc**; retina (**retina**); cornea, (**c**).

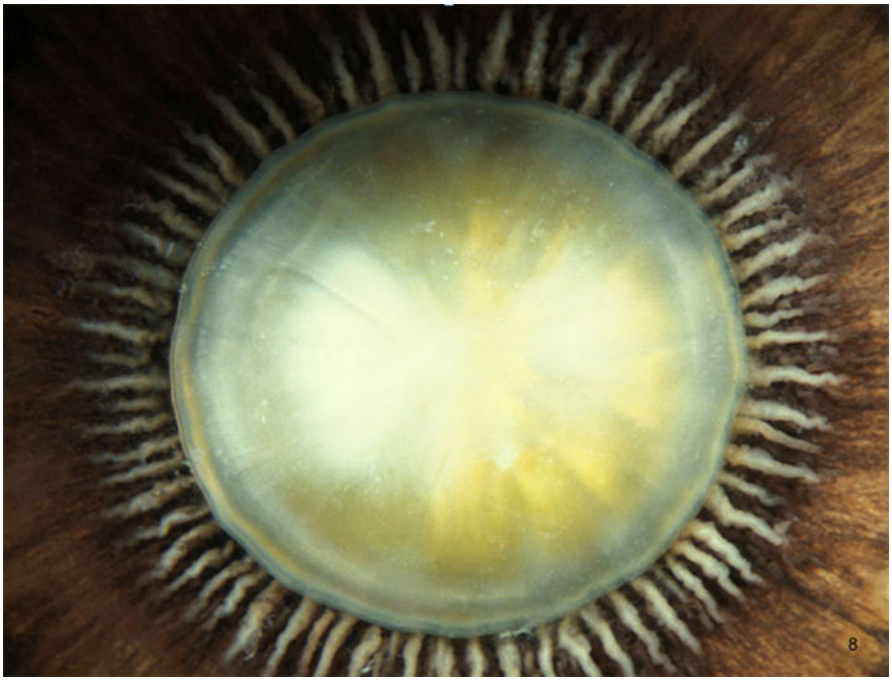

Figure 8. Posterior view of a nuclear sclerotic cataract using the Miyake-Apple technique of removing the back part of the eyeball.

within the lens cortex, are seen. Figure 11 and Figure 12 show the typical appearance of cortical cataract shown from the front (Figure 11) and the back (Figure 12).

Histologically, cortical cataracts are characterized by an accumulation of pink staining eosinophilic fluid between cortical fibers (Figure 13). This fluid accumulation causes shifts between lenticular cells leading to displacement and degeneration of bordering cells. The shift accounts for the spokes seen clinically (Figure 11, Figure 12). Globules of proteinaceous material, called Morgagnian globules, may be released from the

Figure 9. Isolated brunescent cataract. Nuclear sclerotic cataract has a deep brown color with age.

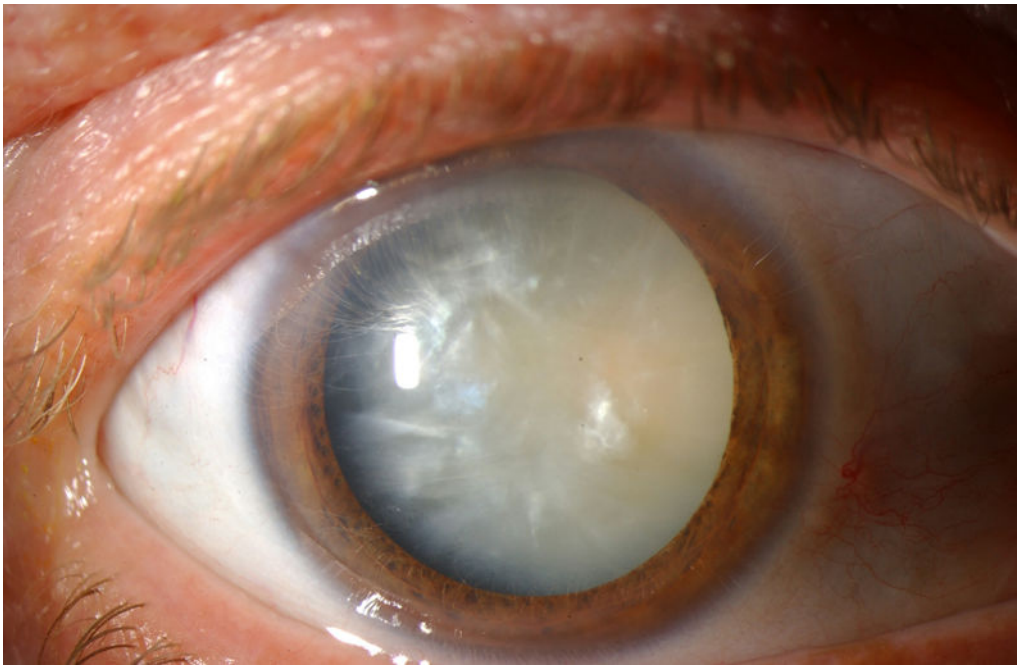

Figure 10. Photograph of a patient's right eye with a dense mature cataract. Courtesy of James Gilmore, Photography department at the Moran Eye Center.

degeneration of the cortical lens cells (Figure 14). As the cortical cataract continues to mature, the entire cortical region can be replaced by these globules and thus becomes a mature Morgagnian cataract (Figure 15).

Another characteristic appearance of the cortical cataract is a Christmas tree cataract. This occurs when crystals form within the deep cortex. These crystals are typically composed of cholesterol, lipids, calcium or other compounds. Interestingly, Christmas tree cataracts do not typically cause significant visual impairment.

While a cortical cataract can occur independently of a nuclear sclerotic cataract, biomechanical changes within the lens nucleus can actually induce cataractous changes in the lens cortex. The ability to effectively accommodate decreases with age, in general. The altered biomechanics between the sclerotic nucleus and cortex creates residual sheer stress and results in parallel micro-ridges at the area of lamellar separation. This process helps to explain the histologic patterns seen in cortical cataracts.

Posterior subcapsular cataract

Posterior subcapsular cataracts (PSC) develop due to the posterior migration of lens epithelial cells in response to external stimulus. Although most cases are spontaneous, PSC also can develop secondarily to metabolic causes, such as diabetes, inflammation, uveitis, or from long-term topical or systemic corticosteroid use. PSC tend to occur in younger patients and progress more quickly than the other cataract subtypes. The opacity is located at the posterior pole of the lens on the anterior surface of the posterior capsule (Figure 16, Figure 17).

An ultrastructural study involving 13 eyes with PSC showed the changes that took place as lens epithelial cells migrated from the equator of the lens to the PSC region. The study concluded that there was a mitotic change as cells migrated towards the posterior pole. The equatorial region cells resembled normal lens epithelial cells but the cells near the PSC showed increased mitotic activity. The authors suggested that the cells were responding to some type of noxious stimuli at the posterior pole. The resultant activity caused the cells to mature into lens fibers or enlarge into bladder-like cells called Wedl cells and the formation of PSC (Figure 18). The migrating cells probably contribute to cataract formation by secreting extracellular materials, cytolysis, cell dissolution, and possibly release of lysosomal enzymes (9).

Anterior subcapsular cataract

Anterior subcapsular cataracts (ASC) develop because of the degeneration of anterior lens epithelial cells. They can develop secondary to trauma, medical treatment iatrogenic causes, or spontaneously. The area of damage causes a migration of lens epithelial cells into the area and subsequent transformation of the cells into myofibroblasts in a process known as fibrous metaplasia. This results in an opacity on the anterior surface of the lens beneath the anterior capsule.

In one of the first studies on ASC, 5 lenses with ASC were examined by light and electron microscopy and confirmed the ability of the lens epithelium to undergo transformation to a fibrous plaque. The lens epithelial cells lost their normal cuboidal shape and elongated into a more spindle-shaped cell (Figure 19: a, b, c). These cells were found frequently to be in contact with one another, resulting in the fibrous plaque known as ASC. This process can be broken down into two phases: a proliferative and a degenerative phase. The proliferative phase was most evident near the periphery of the plaque, showing numerous spindle-shaped cells and mitotically active cells. It is followed by a degenerative phase, which results in an almost structure-less hyaline mass with fewer spindle-shaped cells (10).

Although the cause of ASC is varied, an association between ASC and the formation of synechiae after trauma or inflammation has been hypothesized. The synechiae would form between the posterior iris and anterior lens capsule, resulting in a stagnation of aqueous humor and accumulation of toxic metabolites that could produce a toxic effect on anterior lens epithelium (10).

Traumatic cataract

Direct injury to the head or eye can cause significant mechanical disruption and lead to cataract formation. A Vossius ring can occur if the insult caused the posterior iris pigment epithelium to imprint on the lens capsule. The pigment deposition may abate and resolve completely with time. Severe blunt injury can cause stellate lenticular opacities in the cortex and capsule. Such insult can lead to lens epithelium dysfunction, resulting in a significant edematous response to the superficial cortical lens. Vacuole pockets can then become trapped

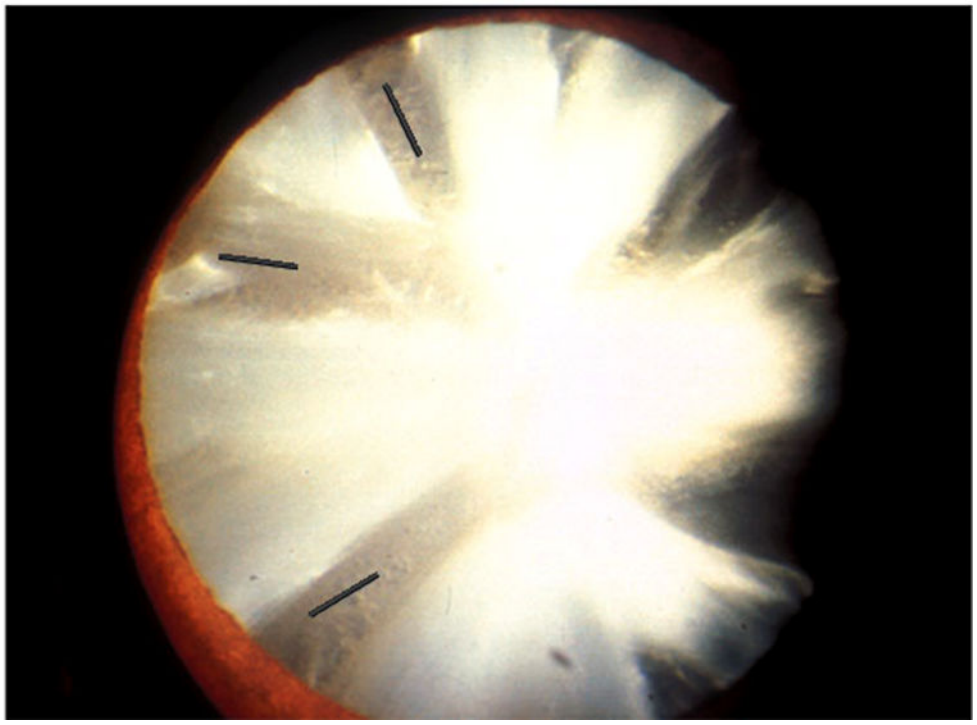

Figure 11. Clinical photograph of a cortical cataract with prominent cortical fluid clefts (black lines).

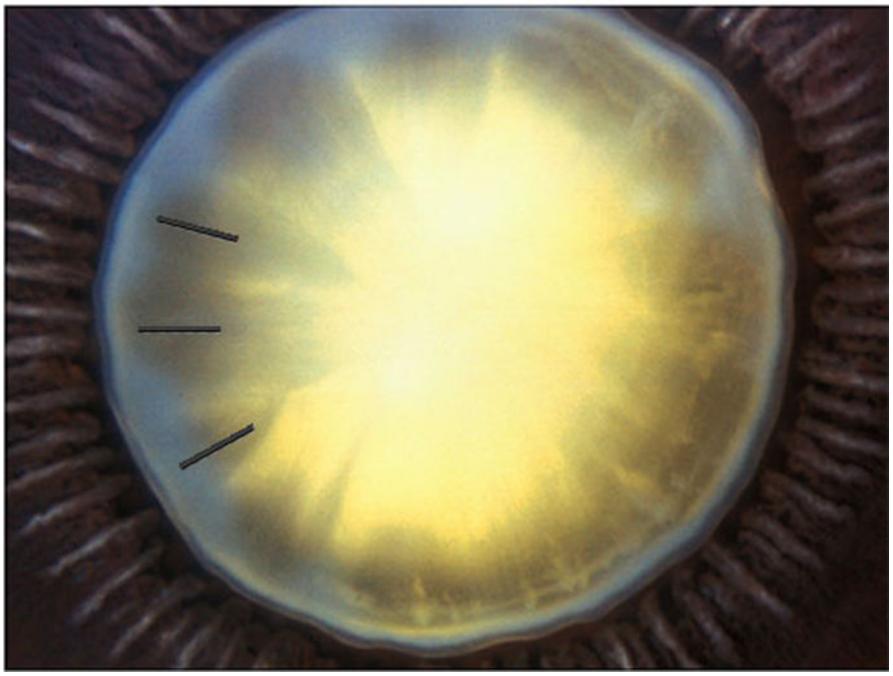

Figure 12. Posterior view of a cortical cataract using the Miyake-Apple technique to display the lens. The fluid clefts are obvious (black lines).

permanently within the lamellar zone, becoming integrated within the lenticular fibers while new layers are elaborated over the lesion. Alternatively, blunt trauma can also cause cataract formation within all the lenticular layers, leading to a diffuse fibrous metaplasia (Figure 20). Other forms of trauma that can lead to cataract formation include exposure to radiation, infrared, extreme heat and electrical injury.

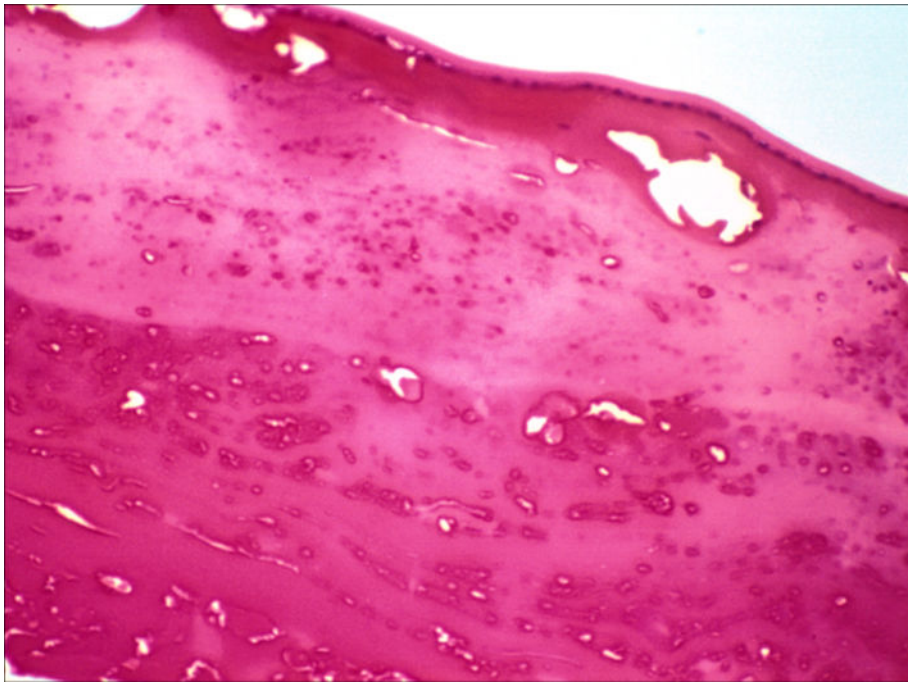

Figure 13. Cortical cataract. Histology of early liquified cortical changes displaying accumulation of eosinophilic fluid (pink background) between the lenticular fibers. (H&E stain, X10).

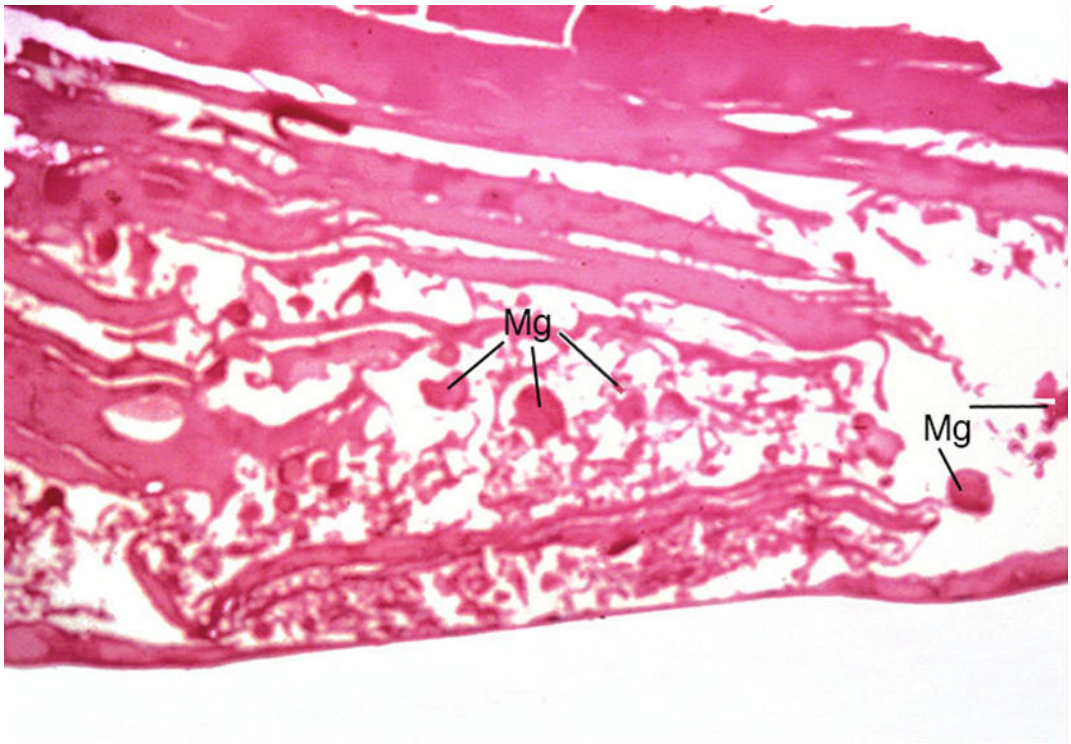

Figure 14. Histology of advanced cortical cataract displaying extensive protein breakdown forming Morgagnian globules (**Mg**, arrows). (H&E stain, X10).

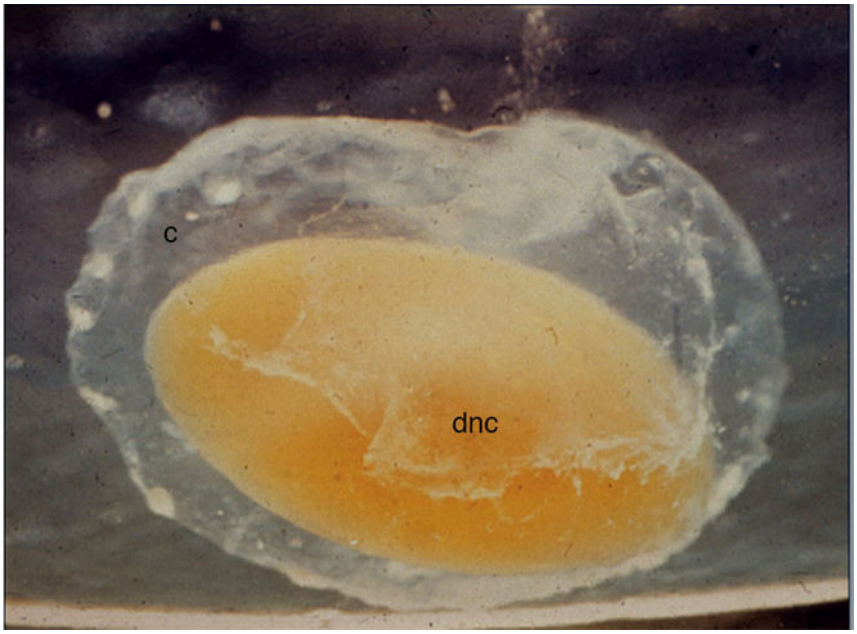

Figure 15. Morgagnian cataract. A hypermature cataract with a liquified cortex (**c**) and a dense nuclear cataract (**dnc**).

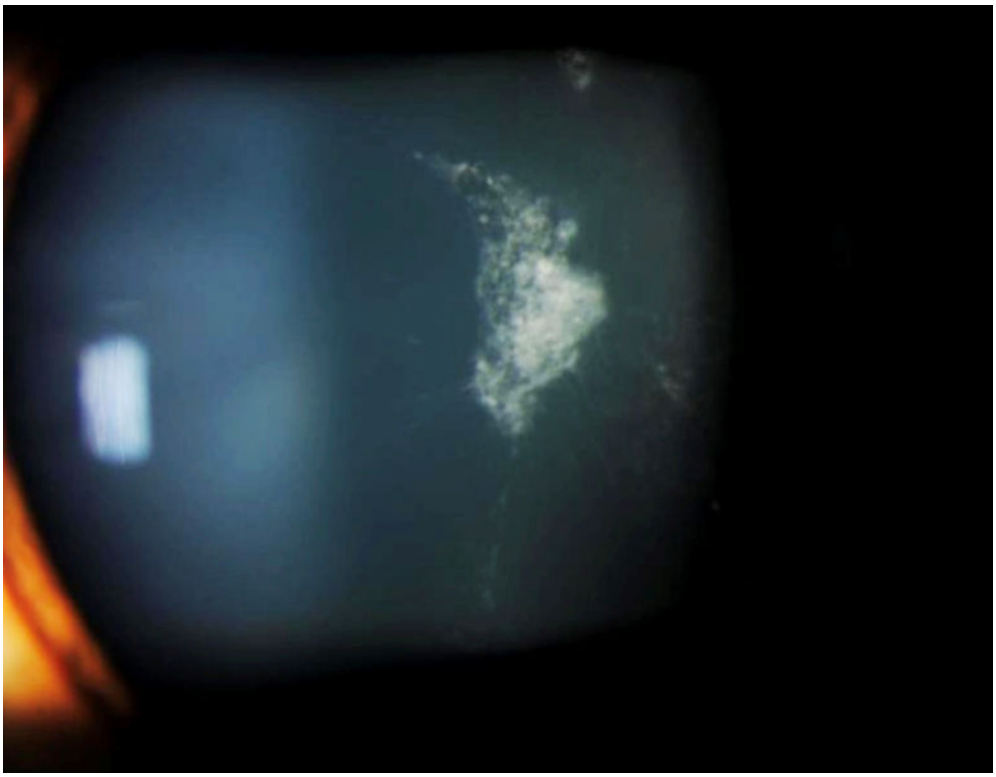

Figure 16. Slit lamp clinical photograph of a focal opacified area (white granular appearance) of posterior subcapsular cataract.

Drug-induced cataract

Several pharmacological agents have been shown to cause cataract formation. Long term corticosteroid therapy and anabolic steroid use are among the most common agents associated with cataract formation, particularly posterior subcapsular cataract (11). The incidence and severity of PSC is directly related to the dose and duration of use (12). Interestingly, steroid therapy has become a frequent treatment option in the management of

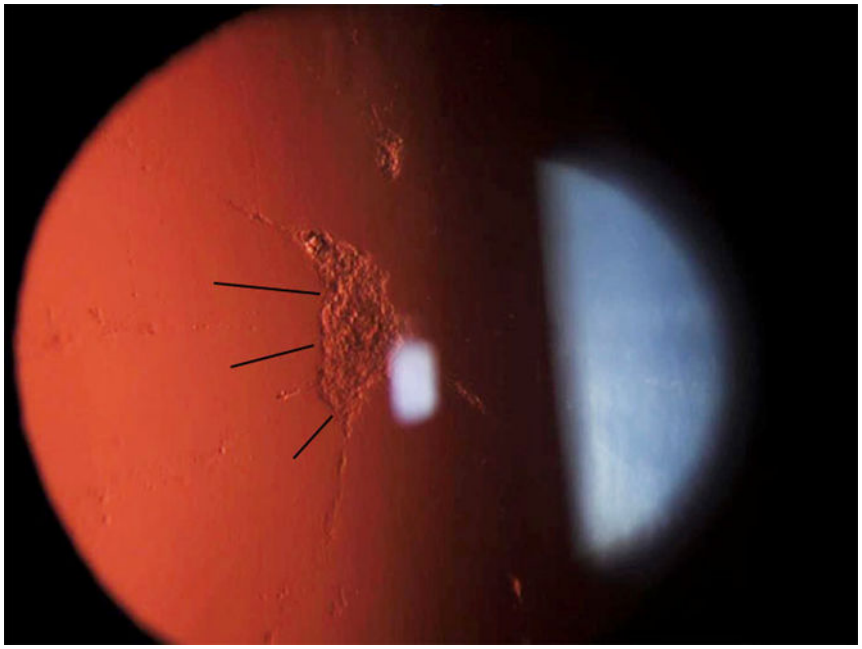

Figure 17. Retroillumination clinical photograph of a focal granular area (arrows) of a posterior subcapsular cataract.

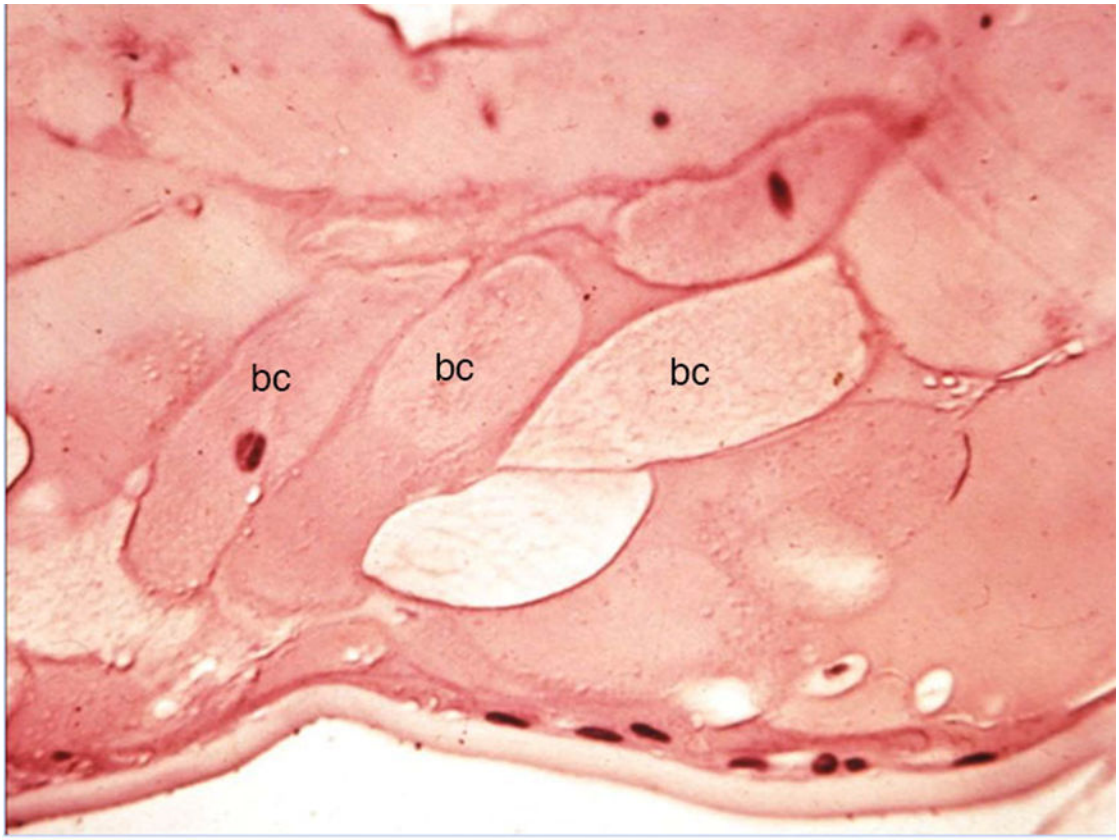

Figure 18. Bladder cells (**bc**) or Wedl cells. Swollen lens epithelial cells that have migrated posteriorally to the posterior capsule in a subcapsular cataract (H&E stain, X20).

retinal pathologies, and in turn increases the rates of cataract formation. There does not appear to be any distinction between PSC induced by steroid use or a pure age-related PSC (13). Phenothiazine is another

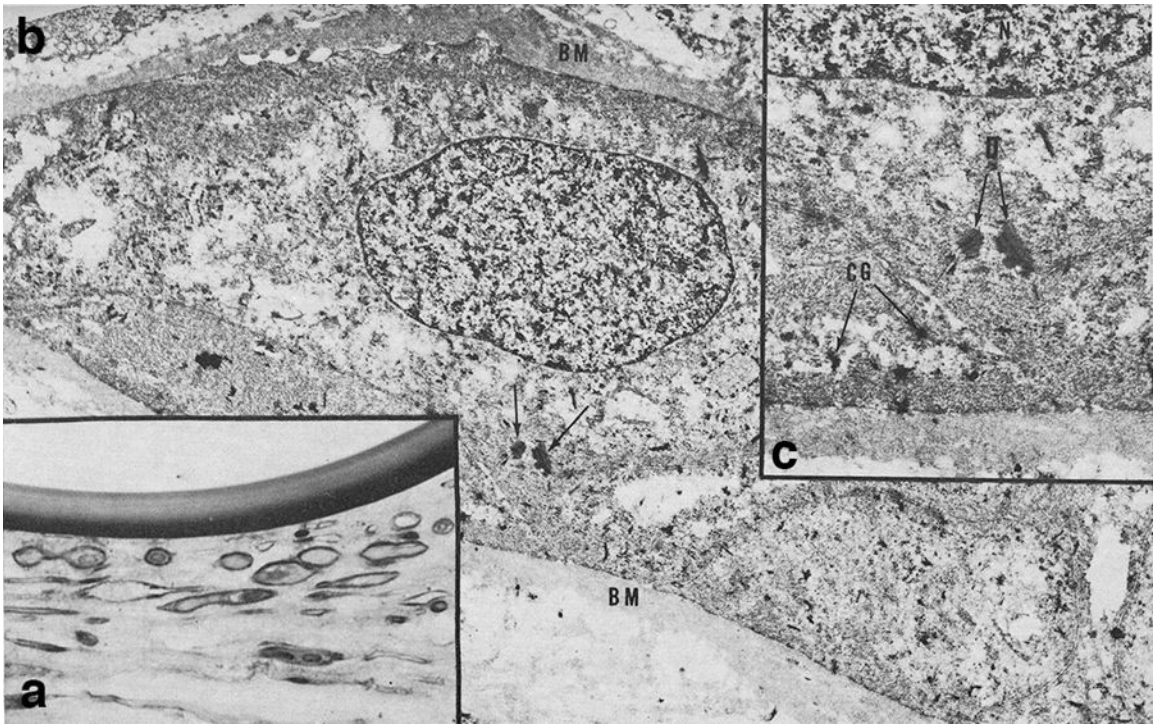

Figure 19. Electron micrographs of the anterior lens epithelial cells in anterior subcapsular cataract. a) Low magnification view of the anterior epithelial cells lying in basement membrane. X440. b) Higher magnification of spindle-shaped epithelial cells that will form myofibroblasts. **BM**, basement membrane. X12,000. c) Even higher magnification of the arrowed desmosomal inclusions, **D**, and calcified granules, **CG**, in b), which are precursors to fibrosis. X27,500. From Font, R. and Brownstein, S. 1974 (10).

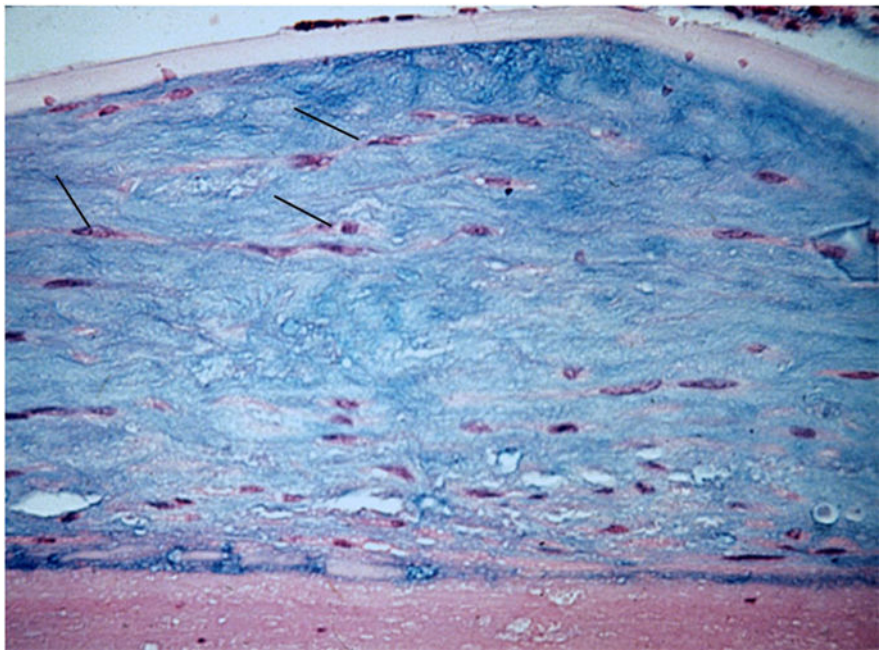

Figure 20. Traumatic cataract. Extensive anterior fibrous metaplasia (arrows) displaying prominent collagen staining (blue) in a traumatic cataract (Trichrome stain, X20).

therapeutic agent that can cause lenticular opacities. Psychotropic agents, particularly phenothiazine, induce deposition of pigmented material into the anterior lens epithelium in a very distinct axial configuration (14). Other pharmaceutical agents known to cause lenticular cataracts include miotics, and amiodarone (15).

Other causes of cataract

While age-related changes remain the leading factor for cataract formation, specifically senile cataract, other contributory factors include smoking, systemic disease, excessive exposure to sunlight and the aforementioned pharmacological agents (16-19). Many systemic diseases can cause cataracts, such as, diabetes mellitus, hypocalcemia, myotonic dystrophy and Wilson's disease (19-21); In diabetic patients, cortical and PSCs appear to occur earlier, particularly among patients with poor glycemic control. Hypocalcemia-induced cataracts usually initiate as small white dot opacities that can coalesce into larger flakes.

Smoking, sun exposure and systemic disease management are modifiable risk factors, so taking measures to change these factors can delay the onset and progression of cataract formation. Phytonutrients, such as xanthophyll carotenoids, lutein and zeaxanthin may play a potential role in limiting or neutralizing light induced oxidative changes within the lens (22). Currently, there are several ongoing studies evaluating other possible protective agents. Although there is no definitive measure to prevent cataract formation, cataract surgery remains an extremely safe and highly successful intervention.

Cataract surgery

Surgery for cataracts has undergone extensive evolution. Ancient knowledge viewed the cataratous eye as an imbalance of humors that needed displacement to recover vision. Using a needle, the surgeon would proceed to displace the abnormal humor until the crystalline lens dislocated. Modern cataract surgery has undergone significant changes and is now characterized by several steps: corneal incision, continuous curvilinear capsulorrhexis (CCC), hydrodissection, phacoemulsification, cortical aspiration, and intraocular lens (IOL) implantation.

Earlier surgical interventions to remove the entire cataractous lens required a 12-mm incision with subsequent suture closure. However, a small 2.4 to 2.8 mm wide clear corneal incision is enough to facilitate entry of the phaco handpiece while remaining sutureless for closure. The CCC technique was developed by Gimbel and Neuhann in the 1980s and truly revolutionized the phacoemulsification technique (23). CCC involves creating a tear in the anterior capsule then continuing the tear in a circular continuous fashion while minimizing shear forces exerted on the zonular fibers. After creation of the CCC, phacoemulsification is used to fragment and emulsify both the cortical and nuclear material. Originally pioneered by Kelman in 1967, phacoemulsification remains a vital part of cataract surgery (24, 25). The CCC opening is large enough to allow implantation of the entire optic and haptics of an intraocular lens (IOL) within the remnant lens capsular bag. The prior use of non-foldable polymethylmethacrylate lenses required a relatively large clear corneal incision for implantation. However, the development of the foldable silicone and acrylic IOLs allowed insertion through a small incision mostly less than 4.0 mm in length. Innovation is constantly improving these steps of cataract surgery, from novel IOLs with unique design to minimize the corneal incision, to use of the femtosecond laser to create an automated corneal incision, CCC and to fragment the nucleus prior to aspiration (26, 27).

Details of the types of intraocular lenses, that are presently being used in cataract surgery, are presented in the following chapter in Webvision by Jason Nguyen, and Liliana Werner.

About the authors

Joah F. Aliancy, MD, originally from Haiti, received his undergraduate degree from the University of South Florida in Chemistry with honors distinction and his medical degree from Florida State University. Presently he is an ocular pathology research fellow at the John A. Moran Eye Center. In a year, Dr. Aliancy will attend the Harkness Eye Institute at Columbia University for his Ophthalmology residency training. His research interests

include novel intraocular lens technology, mechanisms to decrease capsular lens opacification, toxic anterior segment syndrome and nitric oxide as a treatment modality in glaucomatous disease. He has been honored with induction into both Alpha Omega Alpha and Gold Humanism Honor societies and recipient of the National Medical Association Rabb-Venable Award. Dr. Aliancy can be contacted at joah.aliancy@utah.edu.

Nick Mamalis is a Professor of Ophthalmology at the John A. Moran Eye Center of the University of Utah in Salt Lake City. He received his BA in Biochemistry from Harvard University and his MD from the University of Utah, School of Medicine. After a fellowship in Ophthalmic Pathology at the University of Utah he completed his residency in Ophthalmology at Loyola University Medical Center. He is currently the Director of Ophthalmic Pathology as well as the co-Director of the Intermountain Ocular Research Center at the University of Utah. He is the Editor of the *Journal of Cataract and Refractive Surgery* as well as a member of the Cataract Clinical Committee and the Executive Committee of the American Society of Cataract and Refractive Surgery (ASCRS). Dr. Mamalis is a former President of the Utah Ophthalmology Society. He was given the American Academy of Ophthalmology Honor Award in 1994, Senior Achievement Award in 2005, and a Life Achievement Honor in 2015. He was the recipient of the Brinkhorst Medal of Honor in 2013 by the ASCRS. He is known nationally and internationally, has published over 200 peer review journal articles and has written multiple textbooks and textbook chapters. Dr. Mamalis can be contacted at nick.mamalis@hsc.utah.edu.

References

1. Foster A., Gilbert C., Rahi J. Epidemiology of cataract in childhood: a global perspective. Journal of Cataract & Refractive Surgery. 1997;23:601–604. PubMed PMID: 9278811.
2. Sheeladevi S., Lawrenson J., Fielder A., Suttle C. Global prevalence of childhood cataract: a systematic review. Eye. 2016. PubMed PMID: 27518543.
3. Birch E.E., Cheng C., Stager D.R., Weakley D.R. The critical period for surgical treatment of dense congenital bilateral cataracts. Journal of American Association for Pediatric Ophthalmology and Strabismus. 2009;13(1):67–71. PubMed PMID: 19084444.
4. Birch E.E., Stager D.R. The critical period for surgical treatment of dense congenital unilateral cataract. Investigative Ophthalmology & Visual Science. 1996;37(8):1532–1538. PubMed PMID: 8675395.
5. Holmes J.M., Clarke M.P. Amblyopia. The Lancet. 2006;367(9519):1343–1351. PubMed PMID: 16631913.
6. Birch E.E., Stager D., Leffler J., Weakley D. Early treatment of congenital unilateral cataract minimizes unequal competition. Investigative Ophthalmology & Visual Science. 1998;39(9):1560–1566. PubMed PMID: 9699545.
7. Klein B.E., Klein R., Lee K.E., Gangnon R.E. Incidence of age-related cataract over a 15-year interval: the Beaver Dam Eye Study. Ophthalmology. 2008;115(3):477–482. PubMed PMID: 18171585.

8. Seddon J., Fong D., West S.K., Valmadrid C.T. Epidemiology of risk factors for age-related cataract. Survey of Ophthalmology. 1995;39(4):323–334. PubMed PMID: 7725232.
9. Streeten B.W., Eshaghian J. Human posterior subcapsular cataract: a gross and flat preparation study. Archives of Ophthalmology. 1978;96(9):1653–1658. PubMed PMID: 687210.
10. Font R.L., Brownstein S. A light and electron microscopic study of anterior subcapsular cataracts. American Journal of Ophthalmology. 1974;78(6):972–984. PubMed PMID: 4140696.
11. Urban R.C., Cotlier E. Corticosteroid-induced cataracts. Survey of Ophthalmology. 1986;31(2):102–110. PubMed PMID: 3541262.
12. McGraw B.F., Rollins C.L. Topical-Corticosteroid-Induced Cataracts. Drug Intelligence & Clinical Pharmacy. 1979;13(9):537–538.
13. Havre D.C. Cataracts in children on long-term corticosteroid therapy. Archives of Ophthalmology. 1965;73(6):818–821. PubMed PMID: 14302515.
14. Isaac N.E., Walker A.M., Jick H., Gorman M. Exposure to phenothiazine drugs and risk of cataract. Archives of Ophthalmology. 1991;109(2):256–260. PubMed PMID: 1671548.
15. Abraham S., Teller J. Influence of various miotics on cataract formation. The British Journal of Ophthalmology. 1969;53(12):833. PubMed PMID: 5386373.
16. West S., Munoz B., Emmett E.A., Taylor H.R. Cigarette smoking and risk of nuclear cataracts. Archives of Ophthalmology. 1989;107(8):1166–1169. PubMed PMID: 2757547.
17. Christen W.G., Manson J.E., Seddon J.M., Glynn R.J., Buring J.E., Rosner B., Hennekens C.H. A prospective study of cigarette smoking and risk of cataract in men. Jama. 1992;268(8):989–993. PubMed PMID: 1501324.
18. Hankinson S.E., Willett W.C., Colditz G.A., Seddon J.M., Rosner B., Speizer F.E., Stampfer M.J. A prospective study of cigarette smoking and risk of cataract surgery in women. Jama. 1992;268(8):994–998. PubMed PMID: 1501325.
19. Delcourt C., Carrière I., Ponton-Sanchez A., Lacroux A., Covacho M.-J., Papoz L. Light exposure and the risk of cortical, nuclear, and posterior subcapsular cataracts: the Pathologies Oculaires Liees a l'Age (POLA) study. Archives of Ophthalmology. 2000;118(3):385–392. PubMed PMID: 10721962.
20. Khurana, A., *Diseases of the lens*, in *Comprehensive Ophthalmology*. 2015, JP Medical Ltd: London. p. 179-218.
21. Gupta V.B., Rajagopala M., Ravishankar B. Etiopathogenesis of cataract: an appraisal. Indian Journal of Ophthalmology. 2014;62(2):103. PubMed PMID: 24618482.
22. Liu X.-H., Yu R.-B., Liu R., Hao Z.-X., Han C.-C., Zhu Z.-H., Ma L. Association between lutein and zeaxanthin status and the risk of cataract: a meta-analysis. Nutrients. 2014;6(1):452–465. PubMed PMID: 24451312.
23. Gimbel H.V., Neuhann T. Continuous curvilinear capsulorhexis. Journal of Cataract & Refractive Surgery. 1991;17(1):110–111. PubMed PMID: 2005552.
24. Kelman C.D. Phacoemulsification in the anterior chamber. Ophthalmology. 1979;86(11):1980–1982. PubMed PMID: 552621.
25. Kelman C.D. The history and development of phacoemulsification. International Ophthalmology Clinics. 1994;34(2):1–12. PubMed PMID: 8071012.
26. Nagy Z., Takacs A., Filkorn T., Sarayba M. Initial clinical evaluation of an intraocular femtosecond laser in cataract surgery. Journal of Refractive Surgery. 2009;25(12) PubMed PMID: 20000286.
27. Roberts T.V., Lawless M., Bali S.J., Hodge C., Sutton G. Surgical outcomes and safety of femtosecond laser cataract surgery: a prospective study of 1500 consecutive cases. Ophthalmology. 2013;120(2):227–233. PubMed PMID: 23218822.

Intraocular Lenses for Cataract Surgery

Jason Nguyen, MD[1,*] and Liliama Werner, MD, PhD[1,†]

Created: August 5, 2017.

Introduction

The crystalline lens contributes approximately +15 to +20 diopters (D) to the refractive power of the human eye in its non-accommodative state. A further 43 diopters is provided by the cornea (see chapter “Facts and Figures” in webvision). So, when cataracts occur (almost inevitably in the ageing eye) the cataractous lens must be removed to restore a clear image passage through to the retina. After removal of an opacified crystalline lens in cataract surgery, the refractive power of a normal clear lens needs to be restored (1) In modern cataract surgery, a central opening of approximately 5.5 mm is made to the anterior capsule of the crystalline lens (capsulorhexis) and the opacified contents within the capsular bag are then removed by phacoemulsification and irrigation/aspiration. An artificial intraocular lens (IOL) is then placed within the intact capsular bag. However, if an IOL is not implanted inside the eye, the refractive power of the removed cataractous crystalline lens can still be restored by contact lenses or spectacles (2). And that is what happened in the old days. The offending cataractous lens was removed and the patient was given a pair of thick spectacles. An eye with a natural crystalline lens is called a phakic eye and without a natural crystalline lens but with an IOL is called a pseudophakic eye.

During World War II, Sir Harold Ridley, an ophthalmologist in London, saw Royal Air Force casualties with eye injuries, and observed that when splinters of acrylic plastic from aircraft cockpit canopies became lodged in their eyes, this did not trigger inflammatory rejection as did glass splinters. This led him to propose the use of artificial lenses made of Perspex (polymethyl methacrylate - PMMA), to treat cataracts. On 29 November 1949 at St Thomas' Hospital, Ridley achieved the first implant of an IOL, although it was not until 8 February 1950 that he left an IOL permanently in place in an eye (2).

Cataract surgery with IOL implantation has now become the most prevalent eye operation in the United States with more than 3 million procedures performed in 2006 alone (3). For patients with dense cataracts this surgery has become a “miracle” restoring clear sight again. A variety of new artificial IOL designs, manufactured from different biomaterials, are continuously being made available to cataract surgeons nowadays. In this chapter, we provide an overview of the characteristics of IOLs used in cataract surgery (Video 1, Video 2), as well as possible complications associated with their use.

IOL materials

IOL materials can be broken down into four general types. The initial breakdown can distinguish between groups of lenses made of acrylic or silicone material. When describing acrylic lenses, composed of acrylic acid, they can be further broken down into non-foldable or foldable types, referring to their flexibility. The non-foldable lenses are made up of Polymethyl methacrylate (PMMA) material. Within the foldable lenses, they can be further broken up into hydrophobic acrylic or hydrophilic acrylic materials. Silicone lenses are the last group of materials, and all silicone lenses are foldable. The utility of flexible, foldable materials is that the lenses can

Author Affiliation: 1 Moran Eye Center, University of Utah School of Medicine, Salt Lake City; Email: jvwin04@gmail.com; Email: liliana.werner@hsc.utah.edu.

Corresponding author.

* About the authors

† About the authors

Video 1: Cataract surgical procedures from the anterior or surgeon's view of the anterior segment of the human eye.

Download video

Video 2: Cataract surgical procedures from the posterior view of the anterior segment of the human eye.

Download video

then be inserted (with forceps) or injected (with injector systems) into the eye via small incisions, generally 3.0 mm wide or less (4-7).

Polymethyl methacrylate (PMMA) lenses were the first lenses to be used in the human eye (in 1949). They were rigid and required a large incision to be placed in the eye. As cataract surgery technology has advanced, they are now the least used IOL material in developed countries (5).

The decrease in usage of PMMA lenses was primarily attributed to the advent of small incision cataract surgery techniques utilizing ultrasound phacoemulsification, and the increase in popularity of the foldable acrylic lenses. Foldable acrylic lenses can either be composed of hydrophobic acrylic or hydrophilic acrylic material. Generally, hydrophobic acrylic lenses absorb very little water (<1%). On the other hand, hydrophilic acrylic lenses absorb significantly higher amounts (18-38%). Each currently available foldable acrylic lens design is manufactured from a different copolymer acrylic, resulting in a different refractive index, glass transition temperature (the polymer is flexible above this temperature and rigid below), water content, mechanical properties, etc. The flexibility and high water-content allows for certain hydrophilic acrylic lenses to be inserted through very small incisions, approximately 1.8 mm, in microincision cataract surgery (4).

Silicone lenses were the first foldable IOLs available on the market. They are composed of a polyorganosilone backbone and have refractive indexes (e.g., 1.46) that are usually lower than those of acrylic lenses (e.g., 1.55). As a result, they are thicker lenses than their acrylic counterparts (4,7).

Ultraviolet (UV)-absorbing compounds (chromophores) are another important element of the IOL optic component. They protect the retina from UV radiation in the 300-400 nm range, a feature normally provided by the normal crystalline lens. Yellow hydrophobic acrylic IOLs containing a blue light-filtering chromophore (different from the standard chromophore for protection against UV radiation) are also available on the market (Figure 1). The addition of a covalently bonded yellow dye results in an IOL with an UV/visible light transmittance curve that mimics the protection provided by the normal crystalline lens in adult humans. There is indirect evidence showing that this may result in a reduction of the risk for development and progression of macular degeneration. But this remains a controversial issue (4).

IOL designs

In modern cataract surgery, an IOL is ideally fixated within the capsular bag. If the capsular bag is not intact at the end of surgery, an IOL can still be fixated at other sites. However, the design of the lens has to be adapted for implantation in each different site of fixation. IOL designs can be categorized in different ways. According to the fixation site, IOLs may be implanted in the anterior or posterior chamber of the eye. Anterior chamber lenses can be placed in the anterior chamber angle or fixated to the iris. Posterior chamber lenses can be fixated within the capsular bag or the ciliary sulcus (Figure 2) (5).

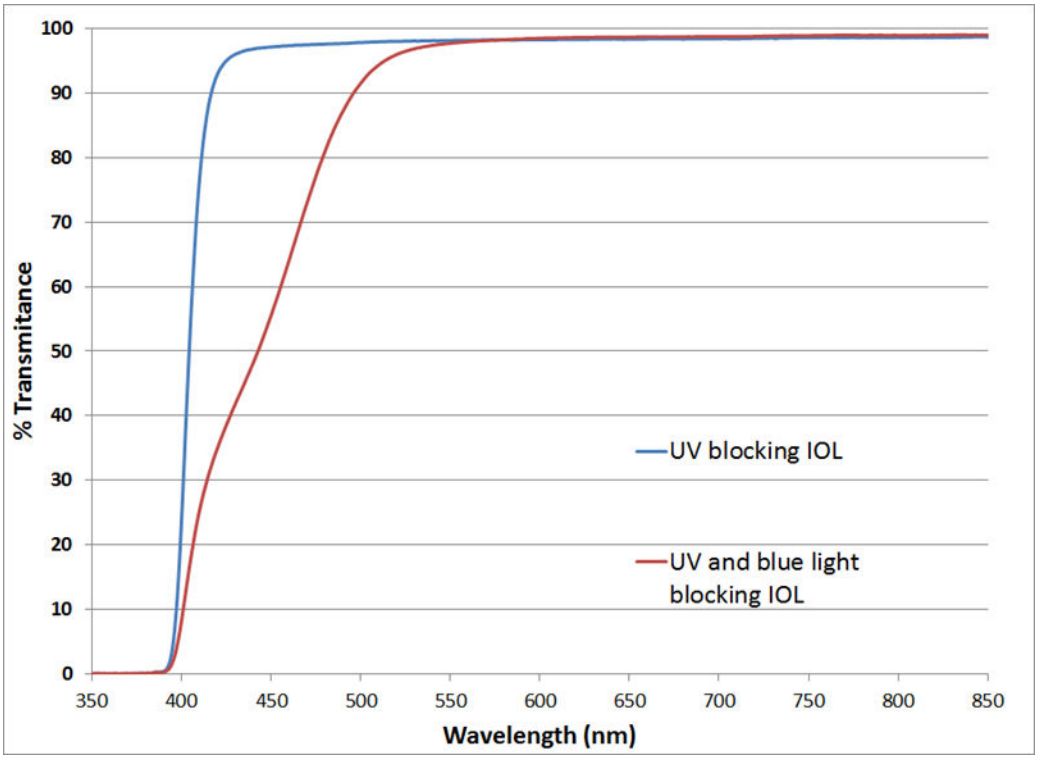

Figure 1: Light transmittance curves of a UV blocking IOL and a UV blocking IOL with a blue chromophore added. The curves demonstrate the difference in light transmittance between the two lenses. The addition of the blue-light filtering chromophore (red line) shifts the curve to the right, providing additional protection similar to that of a normal crystalline lens.

IOLs can also be described as single-piece (the entire lens is manufactured from the same material) or multi-piece (generally described as 3-piece lenses, the optic lens from one source and the loops manufactured from a different material). Anterior chamber lenses placed in the angle that are currently available on the market are based on the Kelman Multiflex design (Figure 3). These are single-piece lenses made of PMMA with open loops. The overall diameter of these lenses generally ranges between 12 and 14 mm. The size is chosen according to the anterior chamber diameter of the eye receiving the implant. There is an angulation between the optic component and the loops that makes the optic more anteriorly located.

Anterior chamber lenses fixated to the iris are generally based on the iris-claw design (Figure 4). These lenses are also single-piece lenses made of PMMA, with an overall diameter of approximately 8.5 mm. The fixation of the lens to the iris stroma is obtained through small claws situated on both sides of the optic component (Figure 4, arrows) (5).

Posterior chamber lenses designed for fixation within the lens capsular bag come in a large variety of designs (Figure 5). They can be single-piece or multi-piece lenses. Single-piece lenses may be open loop designs or overall plate lenses. Overall plate lenses can incorporate a number of different fixation elements, generally represented by small open or closed loops (otherwise known as haptics). Different materials may be used for the manufacture of the haptic component of three-piece lenses, including PMMA, polypropylene (Prolene), polyimide (Elastimide) and poly(vinylidene) fluoride (PVDF) (5,8). Fixation of flexible-looped IOLs is achieved by exerting centripetal pressure on the surrounding ocular tissues. During IOL insertion, the loops are bent centrally and re-expand as the forces exerted on the loops are released. The two factors that contribute to the ability of IOL loops to maintain their original symmetrical configuration are loop rigidity, the resistance of the haptic to external forces that act to bend the loops centrally, and loop memory, the ability of the loops to re-expand laterally to their original size and configuration. Ideally, IOL loops should have enough flexibility to allow easy insertion and accommodation to the circular shape of the eye. Furthermore, they should prevent

damage to supporting structures during insertion and in the postoperative period. They should also have appropriate rigidity to resist external forces, such as capsular bag contraction from capsular fibrosis (8).

There must be some angle between the optic component and the loops of 3-piece lenses manufactured for implantation in the posterior chamber of the eye (capsular bag or ciliary sulcus (Figure 2), to make the optic component more posteriorly located. If the capsular bag is not intact at the end of the surgery, a posterior chamber lens may be fixated in the ciliary sulcus, in front of the anterior lens capsule if there is enough capsular support present. Clinical evidence suggests that IOLs fixated in the sulcus should have a smooth rounded anterior optic edge and thin haptics (Figure 6, A). This will minimize their interaction with the posterior iris surface and prevent complications such as pigmentary dispersion syndrome (9,10). The diameter of ciliary sulcus fixated lenses must be sufficiently large to prevent IOL displacement from the center (at least 13 mm). If the residual capsular support is insufficient, a posterior chamber lens can still be fixated in the ciliary sulcus by suturing the IOL loops to the sclera. There are also techniques to suture the loops of these lenses to the iris.

Biocompatibility

Biocompatibility is one of the most important prerequisites of an IOL. It is important to note that IOLs are progressively being used at earlier stages of life. As a result, it is vital that they can stay in the intraocular environment and remain transparent without complications for many years.

The term uveal biocompatibility is generally used to describe the inflammatory response of the eye towards the artificial IOL (foreign-body reaction) (11-13). Cataract surgery with implantation of an IOL results in a breakdown of the blood-aqueous barrier, causing a release of proteins and cells into the anterior chamber. Protein adsorption on the surface of the IOL is the first phenomenon observed and it influences the subsequent cell interaction between the interface material and tissue. The complement system is activated by the alternative pathway, which results in the attraction of polymorphonuclear leukocytes and monocytes. These cells are the beginning of the macrophages and giant cells that constitute a foreign-body reaction against the IOL (Figure 7). Inflammatory cell deposits are a normal occurrence on the lens surface for up to 1 year after surgery. This consists of two distinct processes: a response with small round and fibroblast-like cells, which peaks by 1 month, and a later giant cell response, which peaks at 3 months. Giant cells then degenerate and detach from the IOL surface, leaving only an acellular proteinaceous membrane usually surrounding the IOL, which isolates it from the surrounding ocular tissues (11-13).

One of us (Liliana Werner) reviewed several published studies that analyzed postoperative flare values and found that there were no clinically relevant differences between different biomaterials. She further went on to note that there was variation in the intensity and duration of each cellular inflammatory response (small cells or giant cells) amongst different biomaterials. However, the cellular reaction was low grade and therefore clinically insignificant (4).

Capsular biocompatibility

When discussing capsular biocompatibility, the relationship of an IOL with remaining lens epithelial cells (LECs) within the capsular bag after cataract surgery (11), it is important to understand the epithelium of the normal crystalline lens. This consists of a sheet of anterior epithelial cells ("A" cells) that are in continuity with the cells of the equatorial lens bow ("E" cells) (see Chapter on "Lens and Cataract" in Webvision, by Alliancy and Mamalis). The two cell types differ in function, growth patterns, and pathologic processes. E cells are germinal cells that undergo mitosis and form new lens fibers, whereas A cells do not. When disturbed by pathologic processes (or surgery), A cells do not have the tendency to migrate whereas E cells tend to migrate posteriorly toward the posterior lens capsule. A-cells tend to transform into fibrous-like tissue (fibrous metaplasia). In contrast, E cells typically enlarge into bladder-like cells referred to as Elschnig pearls (see accompanying chapter). These cells' differences become particularly important when examining different forms of

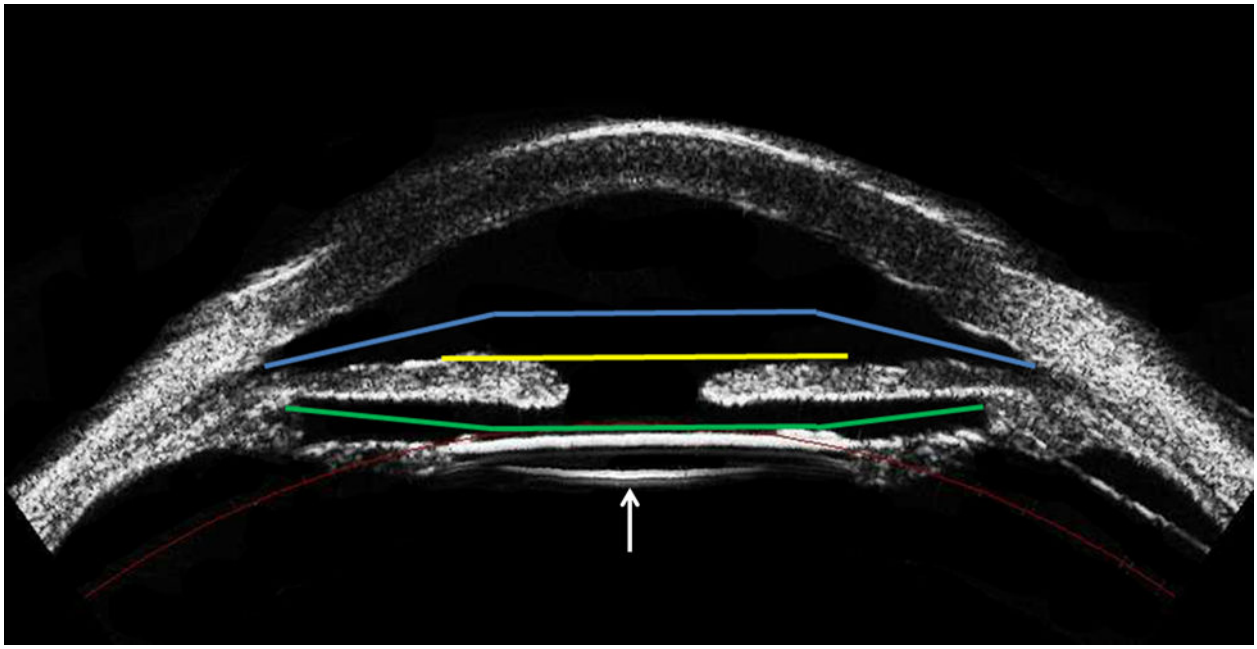

Figure 2: High-frequency ultrasound scan of the anterior segment of a human eye containing an IOL fixated within the capsular bag (arrow). The colored lines indicate the other sites where an IOL can be fixated in the anterior and posterior chambers. Blue: Anterior chamber angle. Yellow: Iris. Green: Ciliary sulcus.

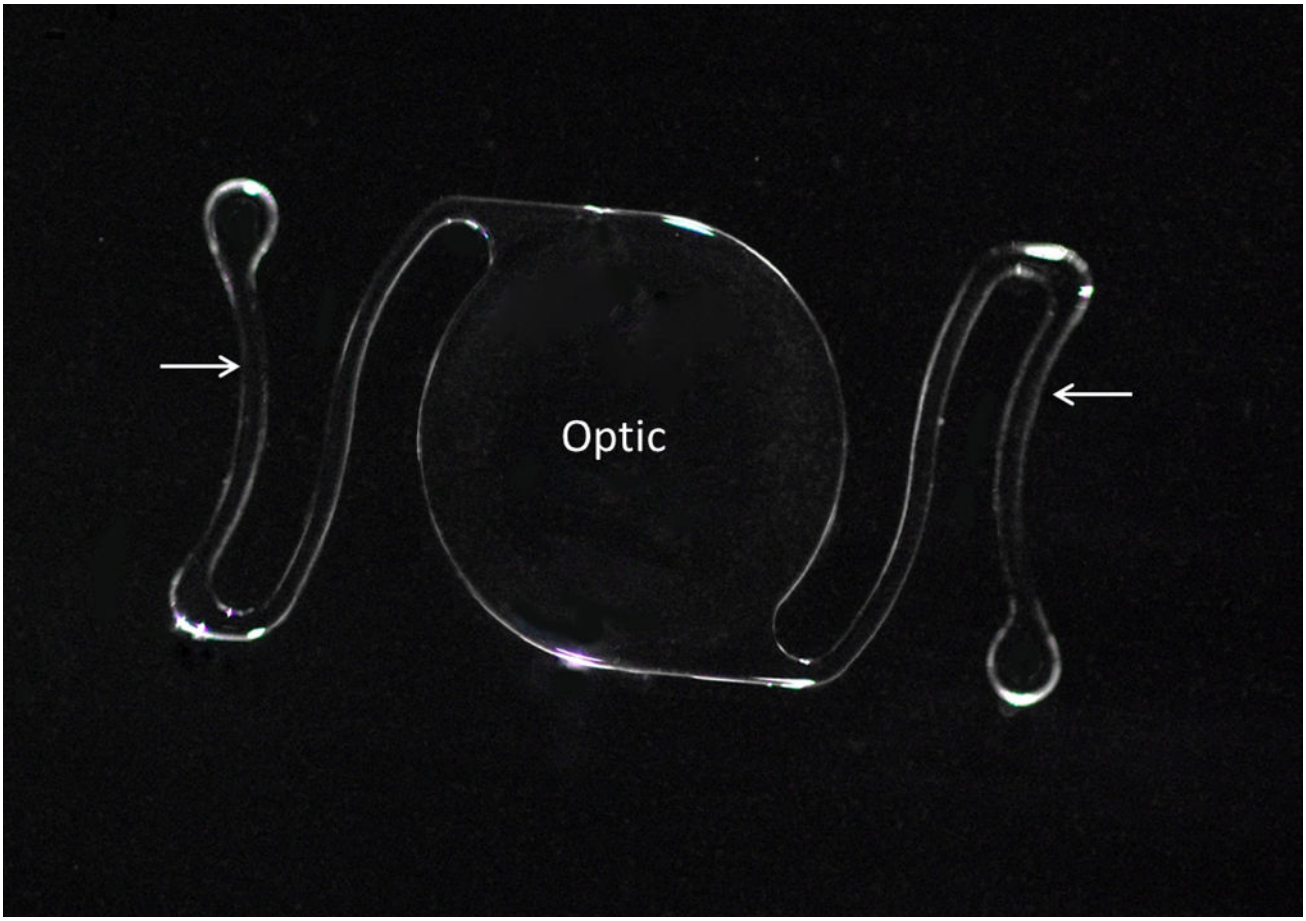

Figure 3: Gross photograph showing the overall design of a Kellman Multiflex PMMA IOL. The arrows show the loops of the lens.

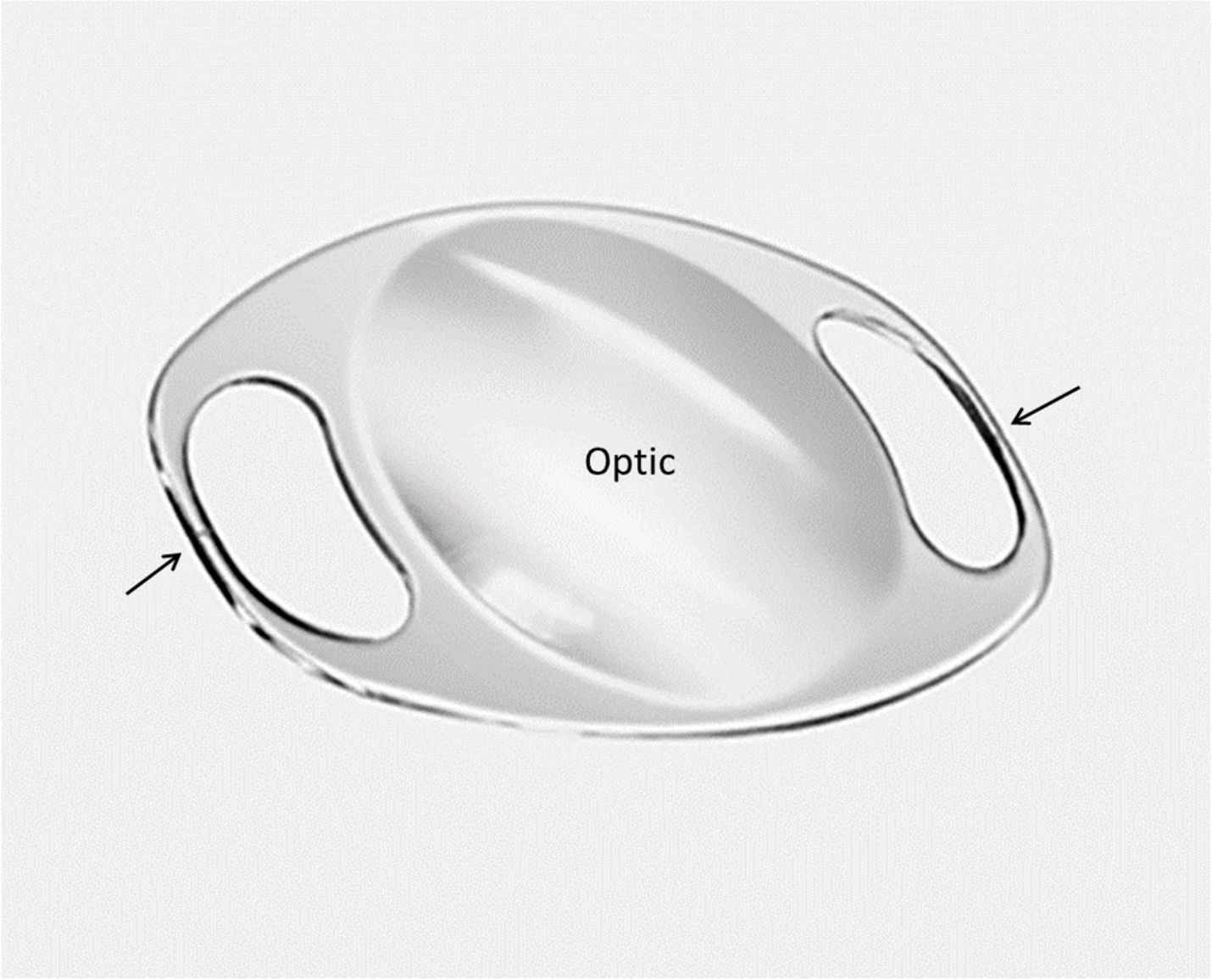

Figure 4: Schematic drawing showing the overall design of an iris-claw IOL. The arrows show the claws for iris fixation.

postoperative opacification of the capsular bag, such as anterior capsule opacification and posterior capsule opacification (14).

Anterior capsule opacification (ACO) occurs as a result of the anterior surface of an IOL optic coming in contact with the posterior aspect of the residual anterior lens capsule (Figure 8). This causes the A cells of the lens to undergo fibrous metaplasia and results in capsule opacification (15-16). ACO is essentially a fibrotic reaction. This is of concern due to the development of the new accommodating IOLs, which are usually designed to move within the capsular bag during accommodation. The resulting fibrosis may restrict these movements.

Contraction of fibrotic tissue may also cause capsulorhexis phimosis (which is the decrease in diameter of the capsulorhexis opening to less than 3 mm), which may lead to the IOL being thrown off center and possibly even deformation of IOLs that are very thin and flexible (Figure 9) (17-19). ACO may be prevented by surgical polishing of the inner surface of the anterior capsule during surgery that results in the removal of residual A cells. Also, ACO can be prevented by implantation of an IOL that does not maintain a large area of contact with the inner surface of the anterior capsule (20).

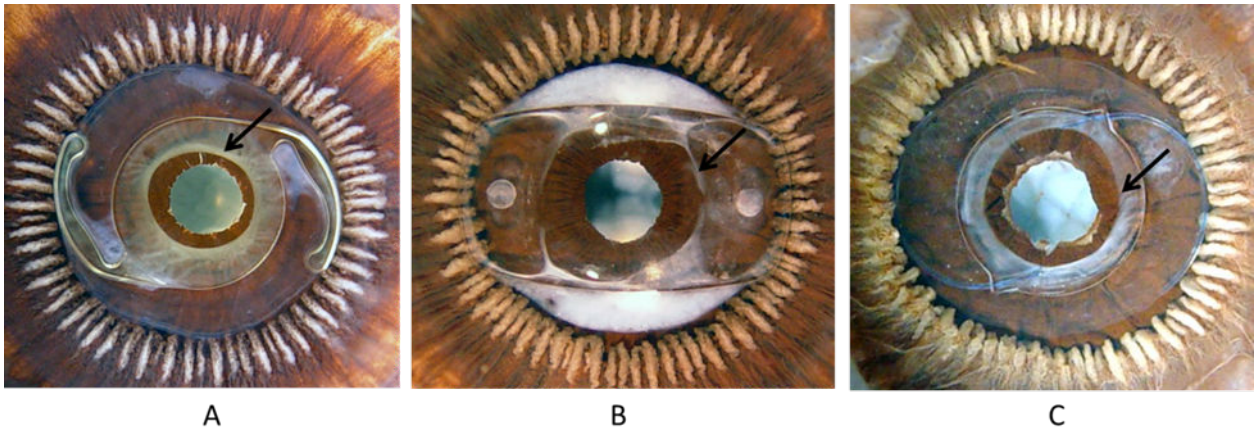

Figure 5: Gross photographs taken from the posterior or Miyake-Apple view of the anterior segment of pseudophakic human eyes obtained postmortem, showing different designs of posterior chamber IOLs. The arrows show the capsulorhexis opening in all eyes. A) Single-piece hydrophobic acrylic IOL. The loops and optic are made of the same material. B) Plate haptic silicone IOL. C) Multi-piece silicone IOL, with PMMA loops.

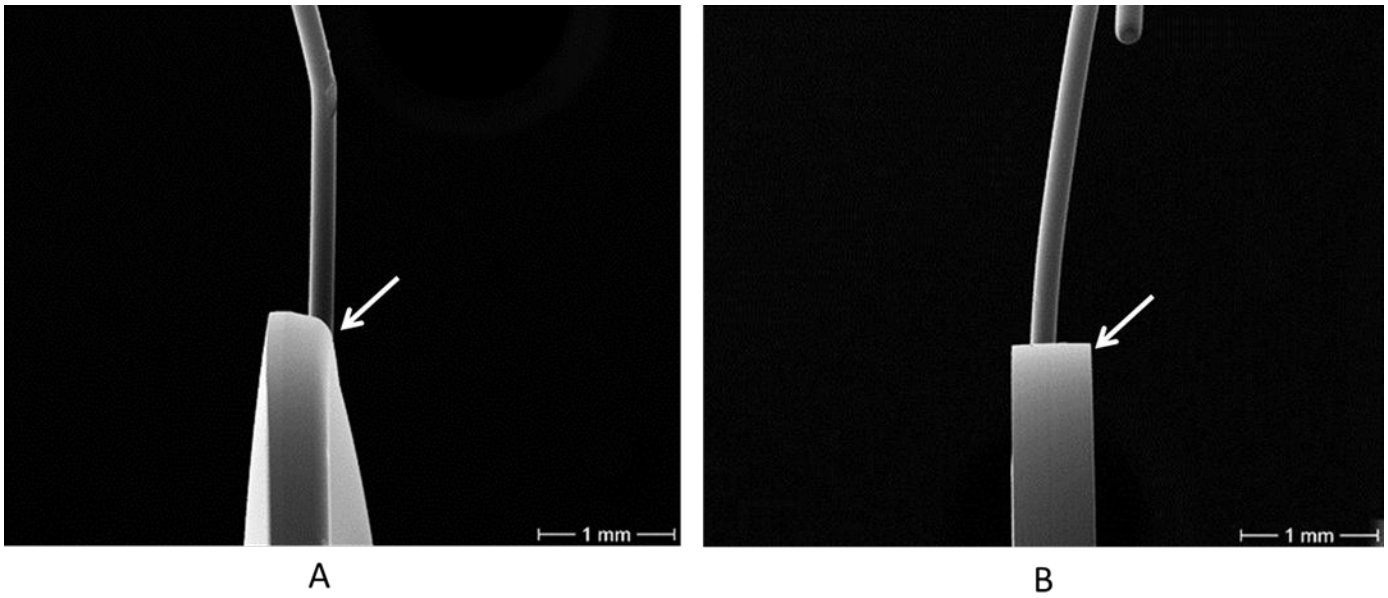

Figure 6: Scanning electron photomicrographs of two types of 3-piece hydrophobic acrylic IOLs. The arrows show the anterior optic edge of the lenses. A) Round edge. B) Square edge.

Whereas ACO is more of an effect of the residual A cells, posterior capsule opacification (PCO) has fibrotic and regeneratory or "pearl" components (21-24). PCO is the most common postoperative complication of cataract surgery, occurring at a rate of between 3-50% in the first five postoperative years. It occurs because of residual LECs that remain within the capsular bag following the removal of the crystalline lens during cataract surgery. These cells can proliferate and migrate across the posterior capsule where they may cause wrinkling and complete opacification of this structure. As a result, the patient will describe distortion, decrease of vision, and glare. The LECs have higher proliferative capacity in younger patients; therefore, the incidence of PCO formation is higher (21-24).

Regeneratory PCO is attributed more to the action of residual E Cells (24). These cells are responsible for formation of a Soemmering's ring, defined as a doughnut-shaped lesion composed of retained/regenerated

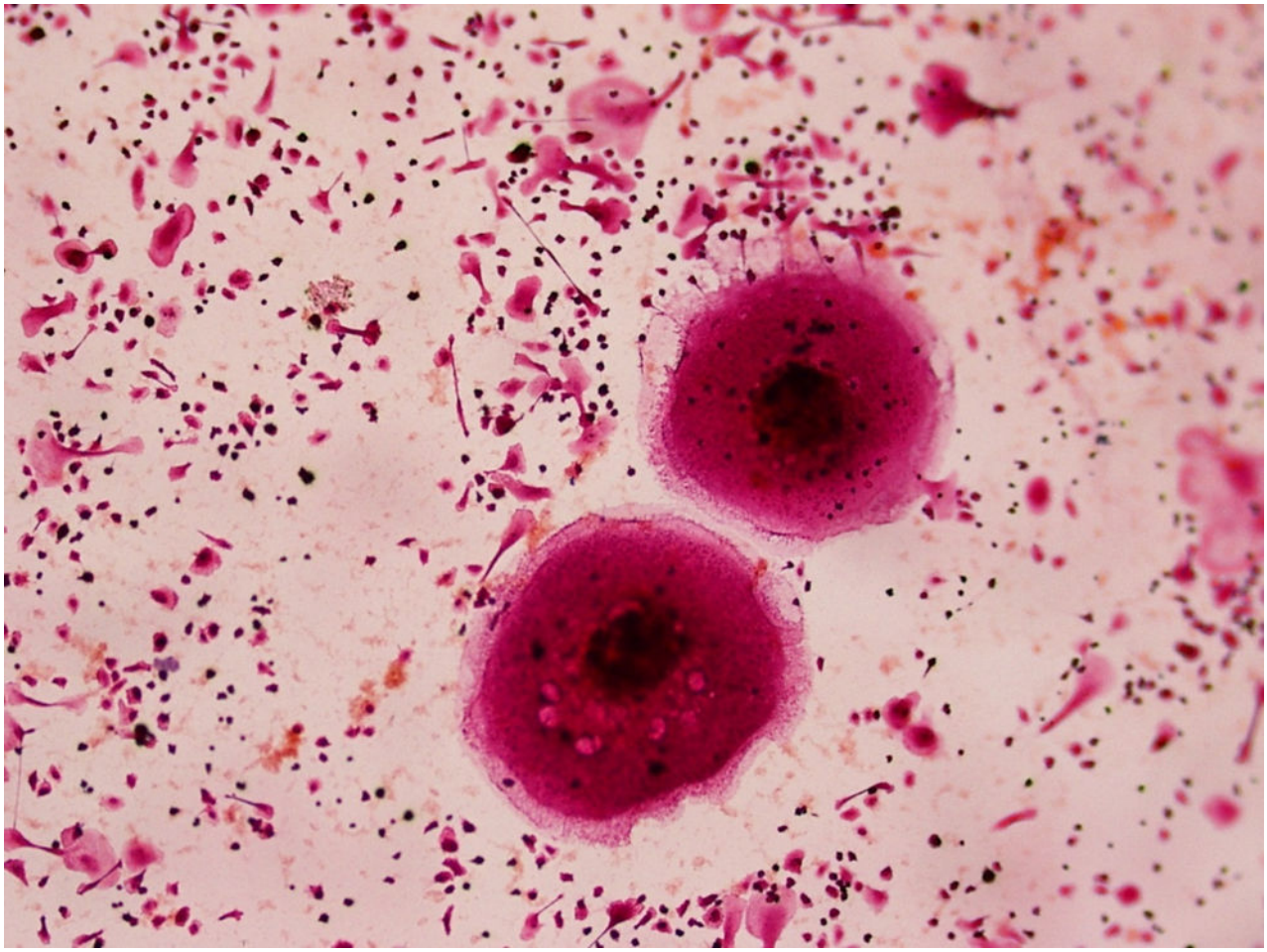

Figure 7: Light photomicrograph of an explanted IOL after implant cytology stain. Cell deposits composed of 2 giant cells, multiple fibroblastic-like small cells, and macrophages can be observed on the surface of the lens.

cortex and cells that may form following any disruption of the anterior lens capsule. For practical purposes, it is useful to consider this lesion as the basic precursor of classic PCO, especially the "pearl" form (Figure 10) (23).

The treatment of PCO is typically neodymium:YAG (Nd:YAG) laser posterior capsulotomy (Figure 11). This is a simple procedure in most cases, but it is not without risks. Complications include IOL damage, IOL subluxation or dislocation, retinal detachment, or secondary glaucoma. Therefore, prevention of this complication is important, not only because of the risks associated with its treatment, but also because of the costs involved in the procedure (14, 23).

While basic research on the effective mechanism for PCO eradication evolves, the practical surgeon can already apply some principles to prevent it. Studies in our laboratory and clinical studies at other centers resulted in the definition of three surgery-related factors that help in the prevention of PCO: 1) Hydrodissection-enhanced cortical clean-up, 2) In-the-bag IOL fixation, and 3) Performance of a capsulorhexis slightly smaller than the diameter of the IOL optic (for a shrink-wrap effect of the IOL by the capsule). The same studies helped in the definition of three IOL-related factors for PCO prevention: 1) Use of a biocompatible IOL to reduce cellular proliferation, 2) Enhancement of the contact between the IOL optic and the posterior capsule, and 3) An IOL with a square, truncated posterior optic edge. The last two IOL factors enhance the barrier effect of the IOL optic against material coming from the Soemmering's ring, a precursor for PCO (Figure 12) (14, 23, 25-30).

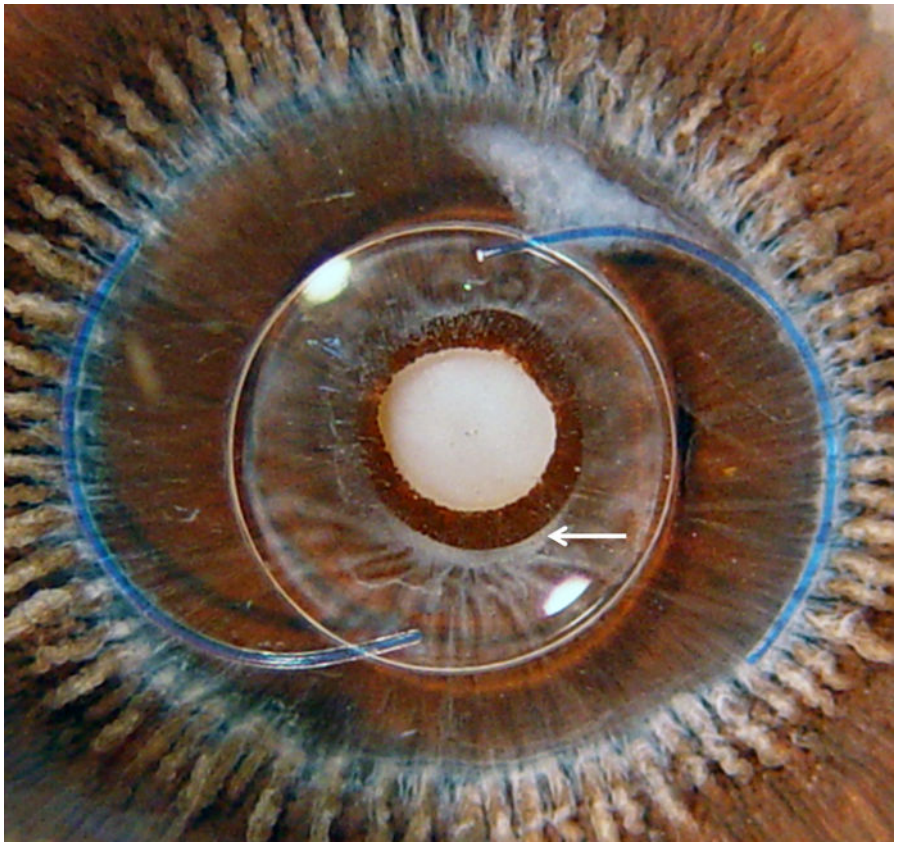

Figure 8: Gross photograph taken from the posterior or Miyake-Apple view of the anterior segment of a pseudophakic human eye obtained postmortem, containing a 3-piece silicone lens. The anterior capsule is opacified where it keeps contact with the IOL surface. The arrow indicates the phimosis of the capsulorhexis opening (the opening is less than 3 mm in diameter) that can take place due to contraction of fibrotic tissue.

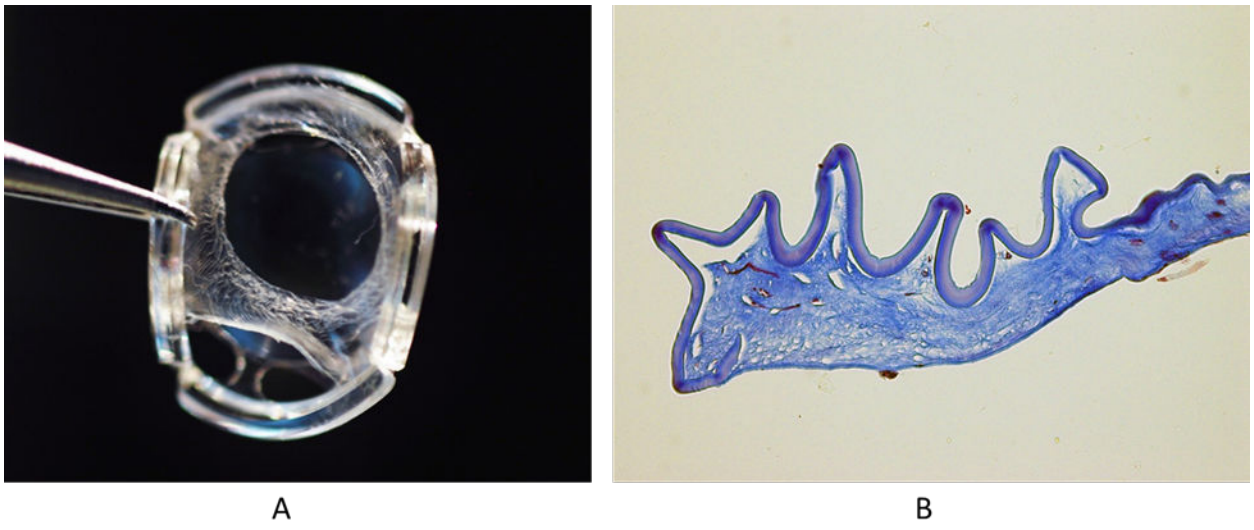

Figure 9: A) Gross photograph of an IOL that was explanted within the capsular bag. The IOL is deformed/flexed due to extreme contraction of the capsular bag. B) Light photomicrograph of a histopathological section cut through the same specimen, showing the fibrotic tissue attached to the inner surface of the anterior capsule. Contraction of the tissue led to significant folds in the anterior capsule.

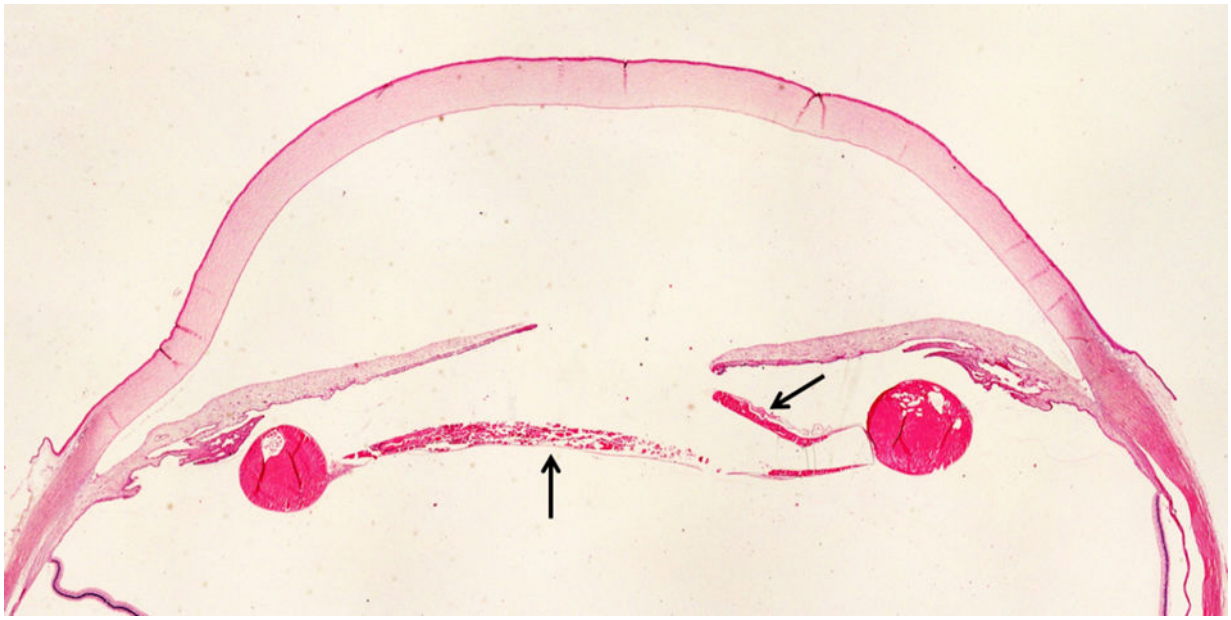

Figure 10: Light photomicrograph of a histopathological section cut through a rabbit eye that had been implanted with an IOL. Soemmering's ring formation (red spherical structures) can be seen on both sides of the section. The arrows indicate the anterior and posterior capsules, which are opacified due to proliferative material growing on their inner surface.

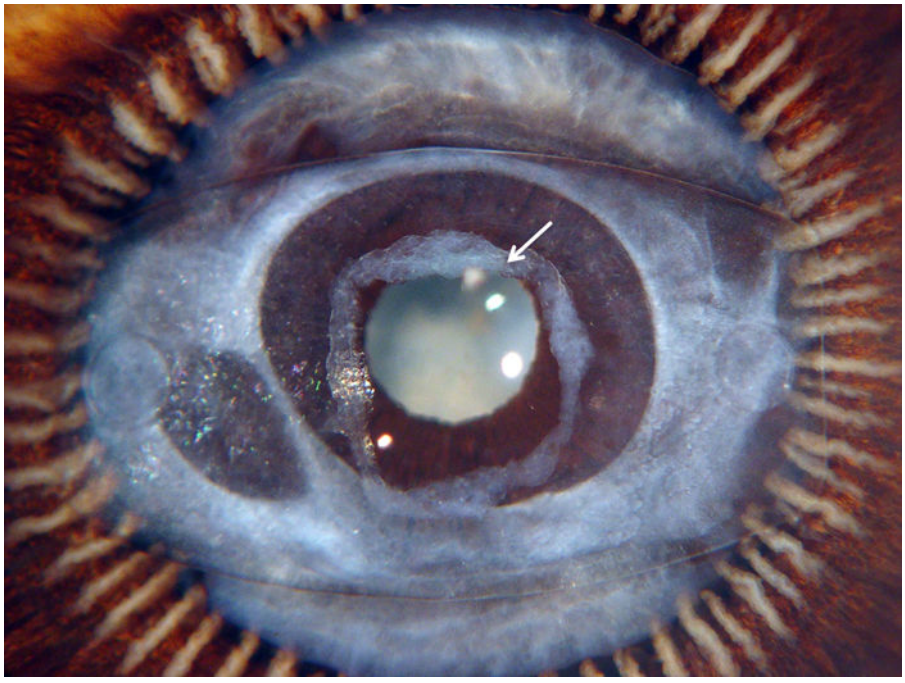

Figure 11: Gross photograph taken from the posterior or Miyake-Apple view of the anterior segment of a pseudophakic human eye obtained postmortem, containing a silicone plate lens. The eye exhibits anterior and posterior capsule opacification. The arrow indicates the opening of the Nd:YAG laser posterior capsulotomy, which was performed to treat PCO.

Causes of IOL opacification

Postoperative opacification of the IOL optic is a rare complication, but it can ultimately lead to the necessity of explantation and exchange of the IOL because of decreased visual function (31). Postoperative calcification may be observed with some hydrophilic acrylic lenses. Additionally, silicone lenses can also suffer from calcification

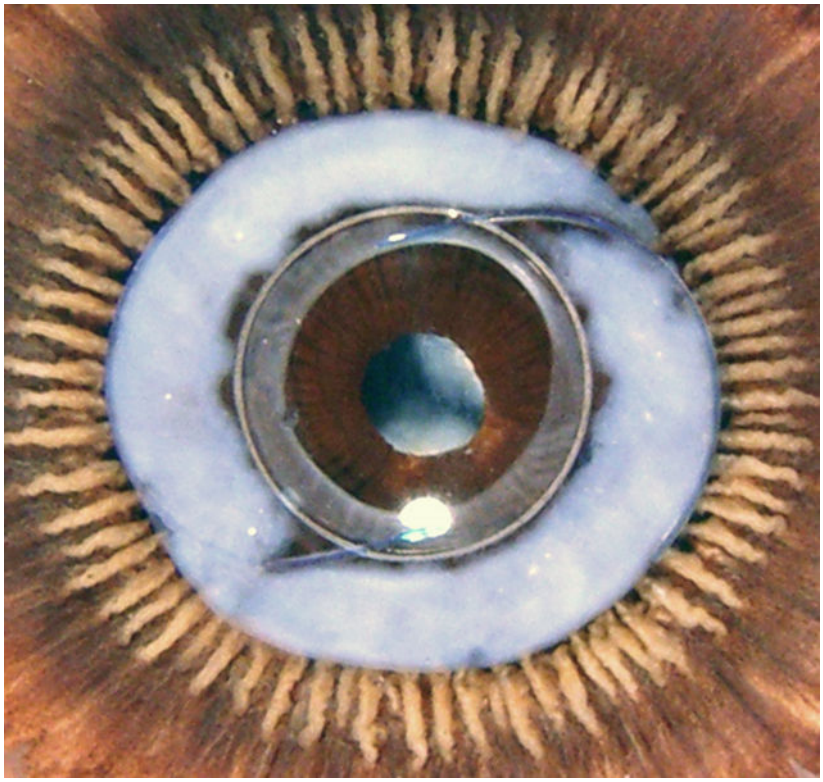

Figure 12: Gross photograph taken from the posterior or Miyake-Apple view of the anterior segment of a pseudophakic human eye obtained postmortem, containing a 3-piece silicone lens. A prominent Soemmering's ring formation can be observed. The square edge of the IOL optic caused a barrier effect, preventing PCO formation. The anterior capsule is opacified where it keeps contact with the IOL surface (ACO).

in certain conditions (history of asteroid hyalosis, which is a condition where there are many calcium deposits floating in the vitreous). Some PMMA lenses may exhibit a specific form of degeneration called snowflake degeneration (32).

Calcification of hydrophilic acrylic lenses appears to be caused by many problems. Factors related to IOL manufacturing, IOL packaging, surgical techniques and adjuvants, and the patient's metabolic condition are possible causes. As the exact combination of factors and sequence of events ultimately leading to calcification of the lenses is still unsure, continuous research on this complication is ongoing (32,33). The majority of the studies on calcified hydrophilic acrylic lenses describe explantation during the second postoperative year or earlier. In some cases the deposits causing the opacification are found on the optical surface or subsurface of the lenses (Figure 13, A, B) (34,35). However, in other cases they are predominantly found within the optic substance (Figure 13, C) (36,37).

In cases of calcification of silicone lenses in eyes with asteroid hyalosis, studies demonstrated deposits only on the posterior optic surface of the lenses (Figure 13, D). The deposits can be partially removed with Nd:YAG laser, but there is a re-accumulation after the procedure because the asteroid bodies are rich in calcium/phosphate. Asteroid hyalosis is a degenerative condition in which hydroxyapatite (calcium/phosphate) bodies form in the vitreous of the eye. The opacification formed on the silicone IOLs is unique because this type of calcification had not been reported in patients without asteroid hyalosis (38-41).

Snowflake degeneration is a slowly progressive opacification that has been observed in three-piece PMMA lenses implanted between the early 1980s and the mid-1990s. They were generally manufactured by a technique called injection molding. Snowflake degeneration is the result of PMMA degradation caused by long-term UV light exposure, not calcium deposition. The degree of optic opacification on the majority of the PMMA lenses

requiring explantation may take 10-20 years to develop. The intraoptic spherical lesions (resembling snowflakes) observed in these cases are thought to correspond to sites of degenerated PMMA material. The lesions are clustered around the center of the optic as opposed to the periphery, which could be protected from UV exposure by the iris (Figure 14) (42-46).

Conclusion

In summary, cataract surgery is the most prevalent operation in the United States, and likely worldwide, resulting in implantation of large numbers of artificial IOLs every year. A variety of new IOL designs, manufactured from different biomaterials, are continuously being made available to cataract surgeons to replace the refractive power of the removed opacified crystalline lens. The biomaterials used in IOL manufacture are basically divided into acrylic (rigid and foldable) and silicone (foldable). Posterior capsule opacification PCO remains the most common postoperative complication of cataract surgery. Its incidence has decreased over the past few decades as the understanding of its pathogenesis has become available. Advances in surgical technique, IOL design, and materials have all contributed to the gradual decline in PCO incidence. Although relatively rare, explantation of an IOL may be required due to problems related to postoperative opacification of the IOL, among others. With the increasing number of new lenses in the market every year, constant vigilance regarding overall IOL biocompatibility is warranted and ongoing in our laboratory.

About the authors

Liliana Werner, MD, PhD is a Tenured Professor of Ophthalmology and Visual Sciences, and Co-Director of the Intermountain Ocular Research Center, at the John A. Moran Eye Center, University of Utah. She has an MD/Ophthalmology degree from Brazil, and a PhD degree (Biomaterials) from France (Université Paris V, René Descartes). Dr. Werner's research is centered on the interaction between ocular tissues and different intraocular lens designs, materials and surface modifications. These include intraocular lenses implanted after cataract surgery, and also phakic lenses for refractive surgery and ophthalmic implantable devices in general. She has authored more than 300 peer-reviewed publications and book chapters on the subject, co-edited 3 books, and received numerous awards in international meetings for scientific presentations, videos and posters. She has also been a guest speaker in different international meetings in at least 20 countries, and is a consultant for different companies manufacturing IOLs and other ocular biodevices. Liliana can be reached at liliana.werner@hsc.utah.edu

Figure 13: Gross photographs of IOLs that were explanted because of postoperative calcification. A) Calcification on the surface of a hydrophilic acrylic IOL. B) High magnification view showing the calcified deposits on the surface of a hydrophilic acrylic IOL. C) Calcification within the substance of a hydrophilic acrylic IOL. D) Calcification on the posterior surface of a silicone IOL.

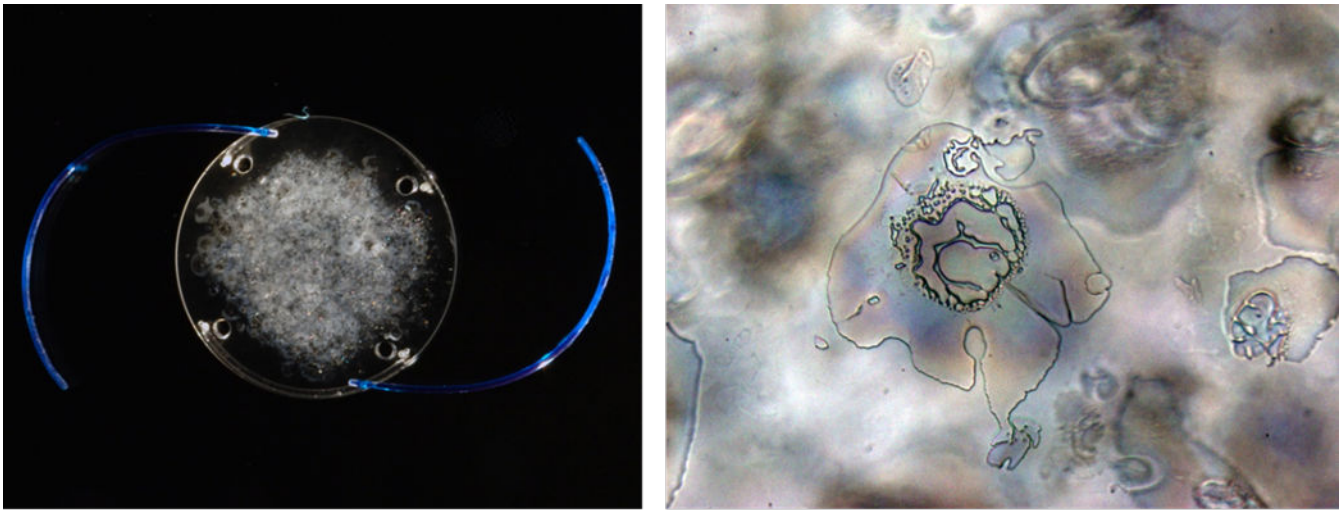

Figure 14: Opacification of PMMA IOLs by snowflake degeneration. A) Gross photograph of an explanted PMMA lens showing opacification of the central/paracentral part of the optic. B) Light microscopic view of the "snowflake" lesions.

Jason Nguyen, MD is an Ocular Pathology and Research Fellow at the Intermountain Ocular Research Center, Moran Eye Center, University of Utah. He graduated with a MD degree from the University of Oklahoma College of Medicine and will be starting his Ophthalmology residency at West Virginia University in July 2018. Jason can be reached at jvwin04@gmail.com.

References

1. Normal Crystalline Lens. American Academy of Ophthalmology, ONE Network. Available at: http://www.aao.org/bcscsnippetdetail.aspx?id=f38d473f-c836-4fe6-8555-20d34ce19816
2. Buratto L, Werner L, Zanini M, Apple DJ, Editors. Phacoemulsification: Principles and Techniques (Second Edition). Slack Inc., Thorofare, NJ, USA, 2003.
3. Rush SW, Gerald AE, Smith JC, Rush JA, Rush RB. Prospective analysis of outcomes and economic factors of same-day bilateral cataract surgery in the United States. J Cataract Refract Surg. 2015;41:732–739. PubMed PMID: 25754380.
4. Werner L. Biocompatibility of intraocular lens materials. Curr Opin Ophthalmol. 2008;19(1):41–49. PubMed PMID: 18090897.
5. Werner L. Lentes Intraoculares: Materiais e Desenhos. In: Ambrósio Jr. R, Crema A, eds. Tratado Brasileiro de Catarata e Cirurgia Refrativa. Grupo Editorial Nacional, Rio de Janeiro, RJ, Brazil, 2014; chapter 47, pp. 265-271.
6. Ness PJ, Werner L, Maddula S, Davis D, Zaugg B, Stringham J, Burrow M, Yeh O. Pathology of 219 human cadaver eyes with 1-piece or 3-piece hydrophobic acrylic intraocular lenses: capsular bag opacification and sites of square-edged barrier breach. J Cataract Refract Surg. 2011;37:923–930. PubMed PMID: 21419595.
7. Maddula S, Werner L, Ness PJ, Davis D, Zaugg B, Stringham J, Burrow M, Yeh O. Pathology of 157 human cadaver eyes with round-edged or modern square-edged silicone intraocular lenses: analyses of capsule bag opacification. J Cataract Refract Surg. 2011;37:740–748. PubMed PMID: 21420600.
8. Izak AM, Werner L, Apple DJ, Macky TA, Trivedi RH, Pandey SK. Loop memory of different haptic materials used in the manufacture of posterior chamber intraocular lenses. J Cataract Refract Surg. 2002;28:1229–1235. PubMed PMID: 12106733.
9. Kirk KR, Werner L, Jaber R, Strenk S, Strenk L, Mamalis N. Pathologic assessment of complications with asymmetric or sulcus fixation of square-edged hydrophobic acrylic intraocular lenses. Ophthalmology. 2012;119:907–913. PubMed PMID: 22424575.
10. Ollerton A, Werner L, Strenk S, Strenk L, Leishman L, Bodnar Z, Kirk KR, Michelson J, Mamalis N. Pathologic comparison of asymmetric or sulcus fixation of 3-piece intraocular lenses with square versus round anterior optic edges. Ophthalmology. 2013;120:1580–1587. PubMed PMID: 23597794.
11. Amon M. Biocompatibility of intraocular lenses. J Cataract Refract Surg. 2001;27:178–179. (letter). PubMed PMID: 11292059.

12. Obstbaum SA. The Binkhorst Medal Lecture. Biologic relationship between poly(methyl methacrylate) intraocular lenses and uveal tissue. J Cataract Refract Surg. 1992.:219–231. PubMed PMID: 1593427.
13. Hollick EJ, Spalton DJ, Ursell PG, Pande MV. Biocompatibility of poly(methyl methacrylate), silicone, and AcrySof intraocular lenses: randomized comparison of the cellular reaction on the anterior lens surface. J Cataract Refract Surg. 1998;24:361–366. PubMed PMID: 9559472.
14. Apple DJ, Werner L. Complications of cataract and refractive surgery: A clinicopathological documentation. Trans Am Ophthalmol Soc. 2001;99:95–109. PubMed PMID: 11797325.
15. Werner L, Pandey SK, Escobar-Gomez M, et al. Anterior capsule opacification: A histopathological study comparing different IOL styles. Ophthalmology. 2000;107:463–471. PubMed PMID: 10711882.
16. Werner L, Pandey SK, Apple DJ, et al. Anterior capsule opacification: correlation of pathological findings with clinical sequelae. Ophthalmology. 2001;108:1675–1681. PubMed PMID: 11535472.
17. Zaugg B, Werner L, Neuhann T, Burrow M, Davis D, Mamalis N, Tetz M. Clinicopathologic correlation of capsulorhexis phimosis with anterior flexing of single-piece hydrophilic acrylic intraocular lens haptics. J Cataract Refract Surg. 2010;36:1605–1609. PubMed PMID: 20692577.
18. Epstein RH, Liu ET, Werner L, Kohnen T, Kaproth OK, Mamalis N. Capsulorhexis phimosis with anterior flexing of an accommodating IOL: Case report and histopathological analyses. J Cataract Refract Surg. 2014;40:148–152. PubMed PMID: 24355727.
19. Kramer GD, Werner L, Neuhann T, Tetz M, Mamalis N. Anterior haptic flexing and in-the-bag subluxation of an accommodating intraocular lens due to excessive capsular bag contraction. J Cataract Refract Surg. 2015;41(9):2010–2013. PubMed PMID: 26471049.
20. Kramer GD, Werner L, Mamalis N. Prevention of postoperative capsular bag opacification using intraocular lenses and endocapsular devices maintaining an open or expanded capsular bag. J Cataract Refract Surg. 2016;42:469–484. PubMed PMID: 27063529.
21. Apple DJ, Solomon KD, Tetz MR, et al. Posterior capsular opacification. Major review. Surv Ophthalmol. 1992;37:73–116. PubMed PMID: 1455302.
22. Saika S, Werner L, Lovicu FJ, Editors. Lens Epithelium and Posterior Capsular Opacification. Springer Japan, Tokyo, Japan, 2014.
23. Werner L. The Lens, Secondary Cataract (Chapter 5.16). In: Yanoff M, Ducker JS, eds. Ophthalmology (Fourth Edition). Philadelphia, PA: Elsevier Saunders, 2013.
24. Georgopoulos M, Findl O, Menapace R, Buehl W, Wirtitsch M, Rainer G. Influence of intraocular lens material on regeneratory posterior capsule opacification after neodymium:YAG laser capsulotomy. J Cataract Refract Surg. 2003;29(8):1560–1565. PubMed PMID: 12954306.
25. Nishi O, Yamamoto N, Nishi K, Nishi Y. Contact inhibition of migrating lens epithelial cells at the capsular bend created by a sharp-edged intraocular lens after cataract surgery. J Cataract Refract Surg. 2007;33:1065–1070. PubMed PMID: 17531703.
26. Nishi O, Nishi K, Sakanishi K. Inhibition of migrating lens epithelial cells at the capsular bend created by the rectangular optic edge of a posterior chamber intraocular lens. Ophthalmic Surg Lasers. 1998;29:587–594. PubMed PMID: 9674010.
27. Boyce JF, Bhermi GS, Spalton DJ, El-Osta AR. Mathematical modeling of the forces between an intraocular lens and the capsule. J Cataract Refract Surg. 2002;28:1853–1859. PubMed PMID: 12388041.
28. Werner L, Müller M, Tetz M. Evaluating and defining the sharpness of intraocular lenses. Microedge structure of commercially available square-edged hydrophobic lenses. J Cataract Refract Surg. 2008;34:310–317. PubMed PMID: 18242459.
29. Werner L, Tetz M, Feldmann I, Bücker M. Evaluating and defining the sharpness of intraocular lenses: microedge structure of commercially available square-edged hydrophilic intraocular lenses. J Cataract Refract Surg. 2009;35:556–566. PubMed PMID: 19251151.
30. Werner L, Mamalis N, Pandey SK, et al. Posterior capsule opacification in rabbit eyes implanted with hydrophilic acrylic intraocular lenses with enhanced square edge. J Cataract Refract Surg. 2004;30:2403–2409. PubMed PMID: 15519096.

31. Mamalis N, Brubaker J, Davis D, Espandar L, Werner L. Complications of foldable intraocular lenses requiring explantation or secondary intervention--2007 survey update. J Cataract Refract Surg. 2008;34:1584–1591. PubMed PMID: 18721724.
32. Werner L. Causes of intraocular lens opacification or discoloration. J Cataract Refract Surg. 2007;33:713–726. PubMed PMID: 17397749.
33. Barra D, Werner L, Costa JLP, Morris C, Ribeiro T, Ventura BV, Dornelles F. Light scattering and light transmittance in a series of calcified single-piece hydrophilic acrylic intraocular lenses of the same design. J Cataract Refract Surg. 2014;40:121–128. PubMed PMID: 24269137.
34. Werner L, Apple DJ, Escobar-Gomez M, Öhrström A, Crayford BB, Bianchi R, Pandey SK. Postoperative deposition of calcium on the surfaces of a hydrogel intraocular lens. Ophthalmology. 2000;107:2179–2185. PubMed PMID: 11097592.
35. Neuhann IM, Werner L, Izak AM, Pandey SK, Kleinmann G, Mamalis N, Neuhann TF, Apple DJ. Late postoperative opacification of a hydrophilic acrylic (hydrogel) intraocular lens: A clinicopathological analysis of 106 explants. Ophthalmology. 2004;111:2094–2101. PubMed PMID: 15522377.
36. Werner L, Apple DJ, Kaskaloglu M, Pandey SK. Dense opacification of the optical component of a hydrophilic acrylic intraocular lens: a clinicopathological analysis of 9 explanted lenses. J Cataract Refract Surg. 2001;27:1485–1492. PubMed PMID: 11566535.
37. Werner L, Hunter B, Stevens S, Chew JJL, Mamalis N. Role of silicon contamination on calcification of hydrophilic acrylic intraocular lenses. Am J Ophthalmol. 2006;141:35–43. PubMed PMID: 16386974.
38. Foot L, Werner L, Gills JP, Shoemaker DW, Phillips PS, Mamalis N, Olson RJ, Apple DJ. Surface calcification of silicone plate intraocular lenses in patients with asteroid hyalosis. Am J Ophthalmol. 2004;137:979–987. PubMed PMID: 15183780.
39. Werner L, Kollarits CR, Mamalis N, Olson RJ. Surface calcification of a three-piece silicone intraocular lens in a patient with asteroid hyalosis: A clinicopathologic case report. Ophthalmology. 2005;112:447–452. PubMed PMID: 15745772.
40. Stringham J, Werner L, Monson B, Theodosis R, Mamalis N. Calcification of different designs of silicone intraocular lenses in eyes with asteroid hyalosis. Ophthalmology. 2010;117:1486–1492. PubMed PMID: 20537395.
41. Espandar L, Mukherjee N, Werner L, Mamalis N, Kim T. Diagnosis and management of opacified silicone intraocular lenses in patients with asteroid hyalosis. J Cataract Refract Surg. 2015;41:222–225. PubMed PMID: 25532646.
42. Apple DJ, Peng Q, Arthur SN, Werner L, Merritt JH, Vargas LG, Hoddinott DS, Escobar-Gomez M, Schmidbauer JM. Snowflake degeneration of polymethyl methacrylate posterior chamber intraocular lens optic material: a newly described clinical condition caused by unexpected late opacification of polymethyl methacrylate. Ophthalmology. 2002;109:1666–1675. PubMed PMID: 12208715.
43. Dahle N, Werner L, Fry L, Mamalis N. Localized, central optic snowflake degeneration of a PMMA intraocular lens: Clinical report with pathological correlation. Arch Ophthalmol. 2006;124:1350–1353. PubMed PMID: 16966636.
44. Michelson J, Werner L, Ollerton A, Leishman L, Bodnar Z. Light scattering and light transmittance in intraocular lenses explanted because of optic opacification. J Cataract Refract Surg. 2012;38:1476–1485. PubMed PMID: 22814055.
45. Werner L, Michelson J, Ollerton A, Leishman L, Bodnar Z. Anterior segment optical coherence tomography in the assessment of postoperative intraocular lens optic changes. J Cataract Refract Surg. 2012;38:1077–1085. PubMed PMID: 22624909.
46. Werner L, Stover JC, Schwiegerling J, Das KK. Effects of intraocular lens opacification on light scatter, stray light, and overall optical quality/performance. Invest Ophthalmol Vis Sci. 2016;57(7):3239–3247. PubMed PMID: 27315539.

What is glaucoma?

David Križaj, Ph.D.[1,2,3,4,*]

Created: May 30, 2019.

Abstract

Glaucoma, a leading cause of blindness in the world, can be challenging to diagnose because symptoms often appear at late stage of the disease, and challenging to treat because of the irreversible loss of retinal neurons. The term encompasses a heterogenous group of diseases that are characterized by altered biomechanics of anterior and posterior eye. These diseases tend to manifest as stiffening of the trabecular meshwork and increased production/reduced drainage of aqueous humor, together with retinal inflammation associated with activated microglia, Müller cells and astrocytes, and degeneration of retinal ganglion cells. In general, the phenotype is caused by a conjunction of risk factors such as age, family history, ethnic origin, high myopia, vascular disease and intraocular pressure (IOP). Current treatments are limited to lowering and stabilizing IOP, indicating that glaucoma is principally a disease of ocular mechanotransduction. Although the events that lead from IOP elevations to ganglion cell damage are not well defined, a body of recent work has pointed at mechanotransducing TRPV4, piezo and TREK-1 channels and immune mechanisms as key pressure targets in trabecular meshwork, ciliary body, retinal ganglion, endothelial cells and glia. Data indicate that dysfunctions of mechanotransduction mechanisms within the ganglion cell soma-dendrite, Müller cells and microglia may precede axonal degeneration, cupping of the optic nerve head and visual field damage which over the years have represented the golden standard of glaucoma diagnosis. Collectively, these recent studies predict the development of new therapies and diagnostic strategies to be contingent upon systematic delineation of molecular mechanisms that sense and transduce pressure in the eye. Thus, neuroprotection, a currently elusive goal, may be achieved via parallel suppression of pressure sensing in the anterior eye, retinal neurons, blood vessels and glia in order to achieve normalization of neuron-glia-blood vessel interactions, and the attendant reduction in immune activation.

Introduction

Glaucoma, a group of optic neuropathies characterized by progressive degeneration of retinal ganglion cells (RGCs), represents the leading cause of irreversible blindness in the developed world. Typical symptoms include gradual loss of peripheral (side) vision that is followed by progressive loss of central vision. If left untreated, glaucoma can progress to complete blindness. Because the damage to the eye is slow and painless, only half of the carriers are aware of the disease and irreparable harm often takes place long before diagnosis. Glaucoma is generally identified by abnormal regulation of intraocular pressure (IOP) and/or pathological mechanosensitivity of ocular cells but the relationship between mechanical forces and the disease remains enigmatic and a matter of considerable academic, clinical and economic interest. The proportion of blindness attributable to glaucoma varies considerably from the lowest values in South Asia to high prevalence in sub-Saharan Africa (1). By 2020, the disease is expected to affect >76 million people, with an estimated 3 million afflicted in the United States alone. There is currently no cure because retinal neurons that die do not regenerate, however, progression of the disease may be slowed with drugs that lower intraocular pressure (IOP). The

Author Affiliations: 1 Department of Ophthalmology & Visual Sciences, Moran Eye Institute; Email: david.krizaj@hsc.utah.edu. 2 Interdepartmental Program in Neuroscience; Email: david.krizaj@hsc.utah.edu. 3 Department of Bioengineering; Email: david.krizaj@hsc.utah.edu. 4 Department of Neurobiology & Anatomy, University of Utah, Salt Lake City, UT; Email: david.krizaj@hsc.utah.edu.

Corresponding author.

* About the authors

economic burden (medical costs, assistance programs in the U.S. estimated at ~$3 billion/year) doubles when considering indirect costs associated with productivity loss, physical consequences (increase in hip fractures; increase in family care) and decreased quality of life. Given that early detection of glaucoma, initiation and adherence to treatment strongly correlate with socioeconomic status (2), there is much room for improvement in providing care.

First descriptions of glaucoma-like eye disease conditions are from ancient Greece. Aristotle and Hippocrates (~500 BC) used the term *glaukos* (γλαυκός) to describe a late-stage condition characterized by the gray-green-blue hue of the pupil (3). In a remarkable approximation of close angle glaucoma, Galen (c.129-199 AD) linked this glaucous hue to deficient levels of aqueous humor, a shallow anterior chamber and/or anteriorly prominent lens. The "Book of Hippocratic Treatment" by Al-Tabari, a 10th century Arab physician, may have provided some of the first references to intraocular pressure yet medieval Europe continued to categorize glaucoma as an incurable green (*viriditas*) cataract ("waterfall") and "excessive hardness" of the lens (4). Confusion ensued when removal of the opaque lens turned out to improve vision but the link to IOP was resurrected in the mid- 19th century by Franciscus Cornelius Donders (Dutch) who developed the first tonometer. Albrecht von Graefe (German) and Antoine-Pierre Demours (French) linked the disease to the iridocorneal dysfunction however glaucoma was defined and canonized by William Mackenzie (Scottish) in his "Practical Treatise of the Diseases of the Eye" (1853) (5). The medieval designation of glaucoma as "green cataract" continues to persist in some languages (such as Slovenian).

A distinctive feature of glaucoma is the obligatory association between biological processes that take place in two distinct locations within the eyeball (Figure 1). A pressure gradient in the **anterior eye** contributes - through mechanisms that are still unclear – to optic neuropathy in the **posterior eye** (retina). To adapt to increased mechanical forces, trabecular meshwork cells in the anterior eye, retinal ganglion cells and glia undergo structural and functional changes known as glaucomatous remodeling. This process involves includes many mechanisms at nanoscale (gene expression), mesoscale (changes in enzymes, ion channels, cytoskeletal proteins, receptors and secreted molecules) to macroscale (neuropathy) levels with the final common consequence of the lost retinal output to the brain (Figure 1).

Among the broad range of risk factors that influence the likelihood of developing glaucoma are age, ethnic origin, family history, corneal thickness, low blood pressure, cerebrospinal fluid pressure, intraocular pressure and vascular dysregulation. The multiplicity of these stressors, some of which are IOP-independent, underlies the differences in the rate of glaucomatous progression and response to treatment across individual patients.

It is important to note that criteria for diagnosing glaucoma cannot yet identify molecular and physiological markers of the disease and that the **lack of a structure-function framework that unifies the bewildering constellation of glaucoma risk factors and phenotypes represents a significant unmet need in both the diagnosis and treatment of glaucoma**. The widely used textbook definition of glaucoma as "*an optic neuropathy defined by 'cupping' of the optic nerve head*" is an antiquated description of a late stage condition at which early warnings stages of IOP- induced changes in retinal neuronal excitability, synaptic remodeling, neuroinflammation and altered light responsiveness have already taken place. It also fails to bring insight into the ongoing debate whether glaucoma is one disease with a continuum across phenotypes or a group of diseases with distinct genetic origin and signaling mechanisms. This review presents a bird's eye overview of some of the current topics of controversy and/or areas where knowledge is currently lacking. It reflects the author's personal views and also regrets that the large majority of the relevant studies could not be cited directly (although many are referenced in the secondary literature).

Diagnosis of glaucoma

The current clinical diagnosis of glaucoma is based on the measurements of IOP, visual function and retinal structure. Stereoscopic "slit lamp" ophthalmoscopy and optical coherence tomography (OCT) check for the

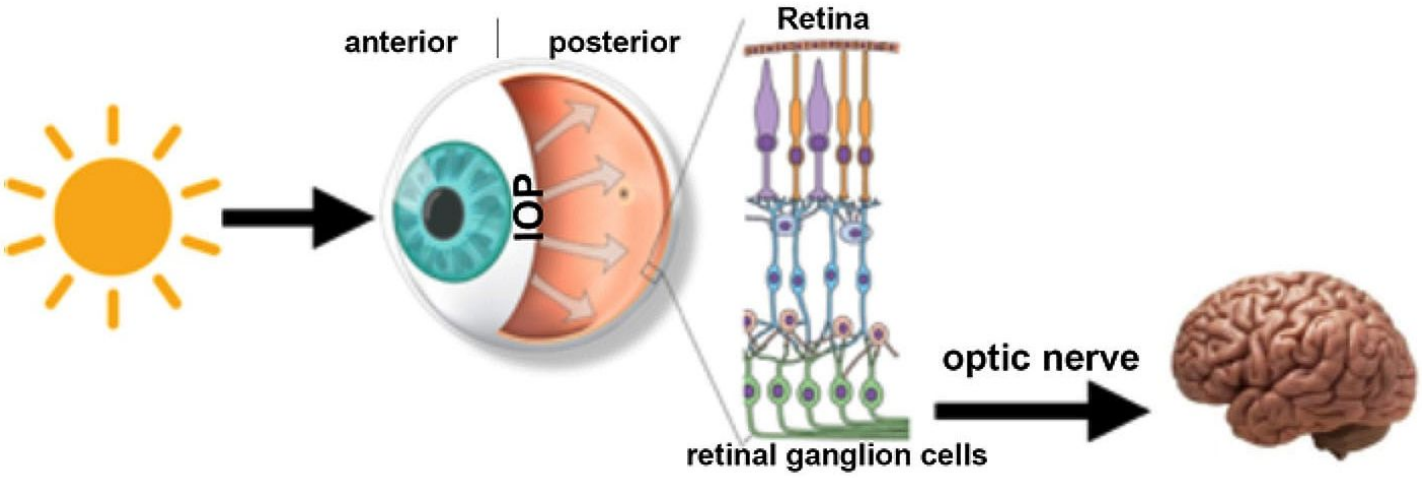

Figure 1. IOP generated in front of the eye (anterior) compromises the function of retinal ganglion cells (green, RGC) located in the back of the eye (posterior). RGC axons traveling through the optic nerve represent the sole output through with the eye communicates the visual signal to the visual areas of the brain. Axonal loss in glaucoma therefore impairs vision and may lead to blindness.

"cupping" (concavity) of the optic nerve head and degeneration of the retinal nerve fiber layer (composed of RGC axons); perimetry documents the functional damage in vision by testing for arcuate scotoma (regional loss of peripheral vision), and tonometry is used to measure IOP (6, 7). Patients at risk for the primary angle-closure type of disease (see below) are additionally examined with gonioscopy, which bounces light into the eye using a specialized lens. An example of the ophthalmoscopic examination of the interior surface ("fundus") of the eye is shown in Figure 2 and Figure 3. An "excavated" or "cupped" optic nerve head in Figure 2 is associated with reduced vascularization of the foveal region whereas Figure 3 shows a typical late-stage example, with magnified views of the optic nerve head of a normal patients retina (left) and the same view of a patient's retina with severe glaucoma (right).

In the glaucomatous eye the optic nerve head appears larger because the neuroretinal rim is narrower and the center is cupped. In fundus photos of advanced glaucoma, degeneration of ganglion cell axons can be seen by the appearance of remaining axons in so called "wedge-shapes" that differ from the picture of healthy ganglion cell axons radiating in superior and inferior arches to the optic nerve head (Figure 4).

In general, functional loss can be detected once >30% of RGCs have died, although patients and animals may not notice that their vision is compromised until much later. Figure 5 shows that RGCs are the main neuronal cell type lost in a non-human primate retina with induced glaucoma. Macaque retinas with induced glaucoma (8) show substantial loss of RGCs following chronic IOP elevation (Figure 5A) but show visual sensitivity that is compromised only after the monkeys lost ~50% of their RGCs (Figure 5B).

Patients with glaucoma often describe experiencing colored "haloes" that may reflect corneal epithelial edema and transient compression of the ONH. Many anecdotal cases link strong emotional trauma to acute manifestation of the disease however the relationship between the emotional/anxiety states and glaucoma remains to be systematically evaluated. In contrast to the wealth of studies in non-human primates, there have been relatively few histological investigations of glaucomatous human retinas. One example is shown in a 2003 study by Pavlidis and colleagues (Figure 6) (9). Like the macaque (Figure 5), few ganglion cells remained in the human retina with advanced glaucoma. The rare ganglion cells that were stained are atrophied, with few dendritic branches and loss of bushiness (Figure 6, panel K), shrunken cell bodies and notably beaded axons running in the nerve fiber layer (Figure 6, panels B,C,E, F and H, I) compared with normal midget ganglion cells (Figure 6. panels A, D, G and J). Larger cell types such as parasol ganglion cells were similarly affected in the advanced glaucomatous retina (9). For ganglion cell types in human retina see "Primate ganglion cells" in

Morphology and circuitry of ganglion cells section in Webvision. For rodent **models**, see later in this chapter and review by Nickells et al. (2012) (10).

Types of glaucoma

"Primary" glaucomas show optic neuropathy in the presence or absence of elevated IOP (i.e., the cause of the disease is not known) whereas "secondary" glaucomas are defined by known pathological mechanisms that elevate IOP above normal. Both types of disease have in common dysfunction of the anterior eye, symptoms (RGC loss and optic neuropathy) and treatment (IOP lowering). Diagnosis continues to be a problem, as all too often glaucoma is identified after many RGCs (green cells in Figure 1) had been irretrievably lost. The most common forms of glaucoma do not show Mendelian inheritance, yet genetic and racial background is clearly important as ethnic groups show striking differences in the prevalence of types of glaucoma. For example, primary open-angle glaucoma (POAG) is widespread in Africa (4.2%) whereas primary angle closure glaucoma (PACG) is more common in Asia (1.1%). With respect to the population sizes, however, Asians still account for the majority (~53%) of worldwide POAG cases (2, 11). In general, gene mutations with large biological effects (i.e., optic neuropathy) are rare whereas gene variants associated with smaller effects are common (12) (see below). Treatment for all forms of glaucoma is limited to pharmacological lowering of IOP (the sole treatable risk factor) and, in rare cases, anterior eye surgery and laser photo/thermocoagulation but there are no treatments for neuronal degeneration (reviewed in (13-15)).

Primary open-angle glaucoma (POAG)

POAG is the most common form of glaucoma that accounts for >80% of cases in the Western hemisphere. The 'angle' refers to the iridocorneal cleft between the iris and the cornea which is "open" in normal eye and POAG (Figure 7A & Figure 7B) and offers access to aqueous humor flowing into the trabecular meshwork and Schlemm's canal. Clinically, POAG is diagnosed by the open angle, IOP > 21 mm Hg and loss of visual field associated with the degeneration of ganglion cell axons ("optic neuropathy") (16). While relatively uncommon under the age 50, POAG strikes nearly 8% of Americans over 80; it is about five times more common among African Americans than Caucasians, with earlier onset and faster time-course of progression in individuals with African heritage (17). On the other hand, people with European ancestry are more vulnerable compared to Africans or Asians when assessing the odds ratio of POAG per decade (18). The prevalence seems to be higher in men. In most cases of POAG, the disease may progress to total blindness without the patients experiencing any pain or discomfort, which however may occur when the rate of tension is very high, and IOP exceeds ~50 mm Hg.

A key, heritable OAG risk factor is IOP, which varies between ~7 and >20 mm Hg. Every 1 mm Hg increase in baseline elevates the risk of developing the disease by 10-14% over any 5 – 9 -year period (19). Untreated eyes with IOP in the range of 21 – 25 mm Hg show ~14.4 years to progress from early to late stage of POAG but the lag period is shortened to ~2.9 years at IOP >30 mm Hg. Individuals with myopia are at risk for both elevated IOP and POAG, possibly due to weaker connective tissue support (18). It is important to note that the disease is unpredictable as there is a substantial fraction of patients with elevated IOP who show no signs of axonal degeneration, visual field defects and vision loss.

POAG has a clear genetic foundation, with heritability amongst twins ~0.95, and siblings of affected individuals having nearly an eight-fold increase risk of developing the disease. In contrast to macular degeneration (AMD), in which genome-wide studies (GWAS) identified ~60% of responsible genes, known POAG sequences comprise less than 10% of known cases. These include ~50 gene loci, with mutations in three Mendelian genes - myocilin (MYOC), optineurin (OPTN) and TANK binding kinase (TBK1) accounting for ~5% of POAG cases with little influence from other genes or environmental factors (12, 20). MYOC is a secreted calcium-binding protein with no known function, and is expressed in TM cells, retinal pigment epithelium and astrocytes. Mice and humans

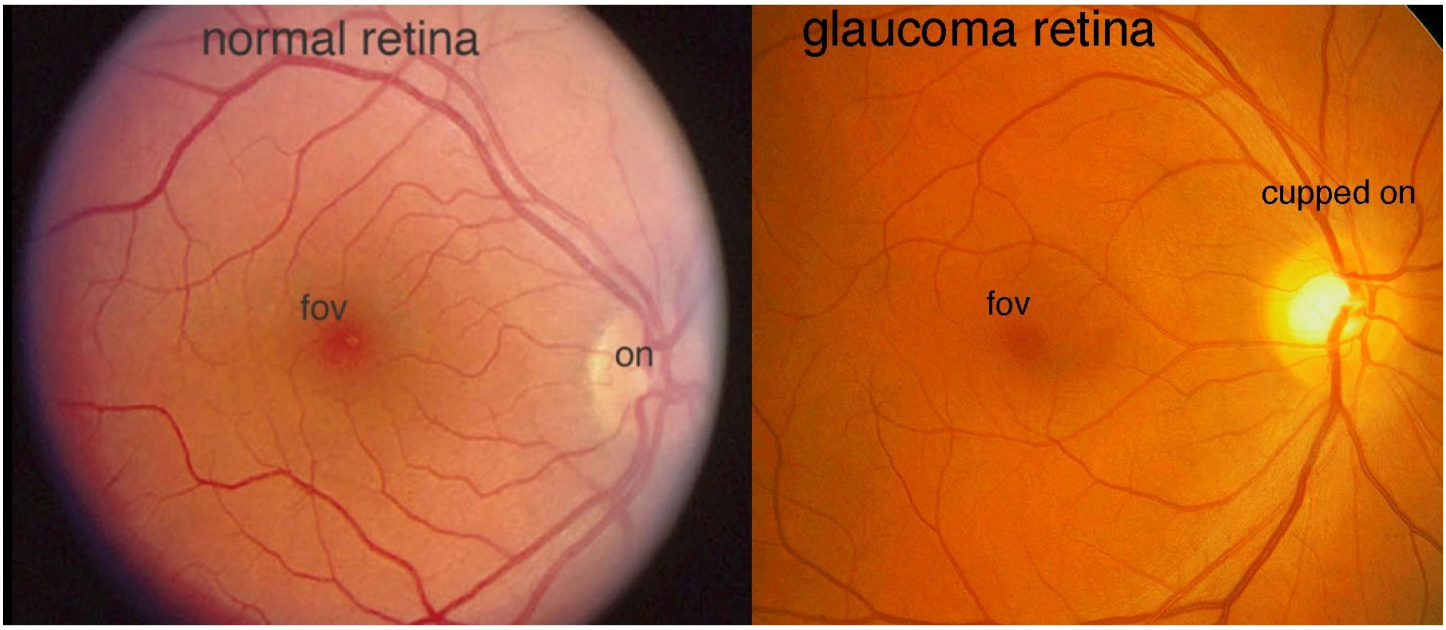

Figure 2. An ophthalmoscopic view of the retina (right) of a patient who has glaucoma, in comparison to a normal retina (left). The characteristic picture is of a cupped optic nerve head (on) and poor vascular supply towards the fovea (fov). Courtesy of James Gilman, Ophthalmology photography, Moran Eye Center.

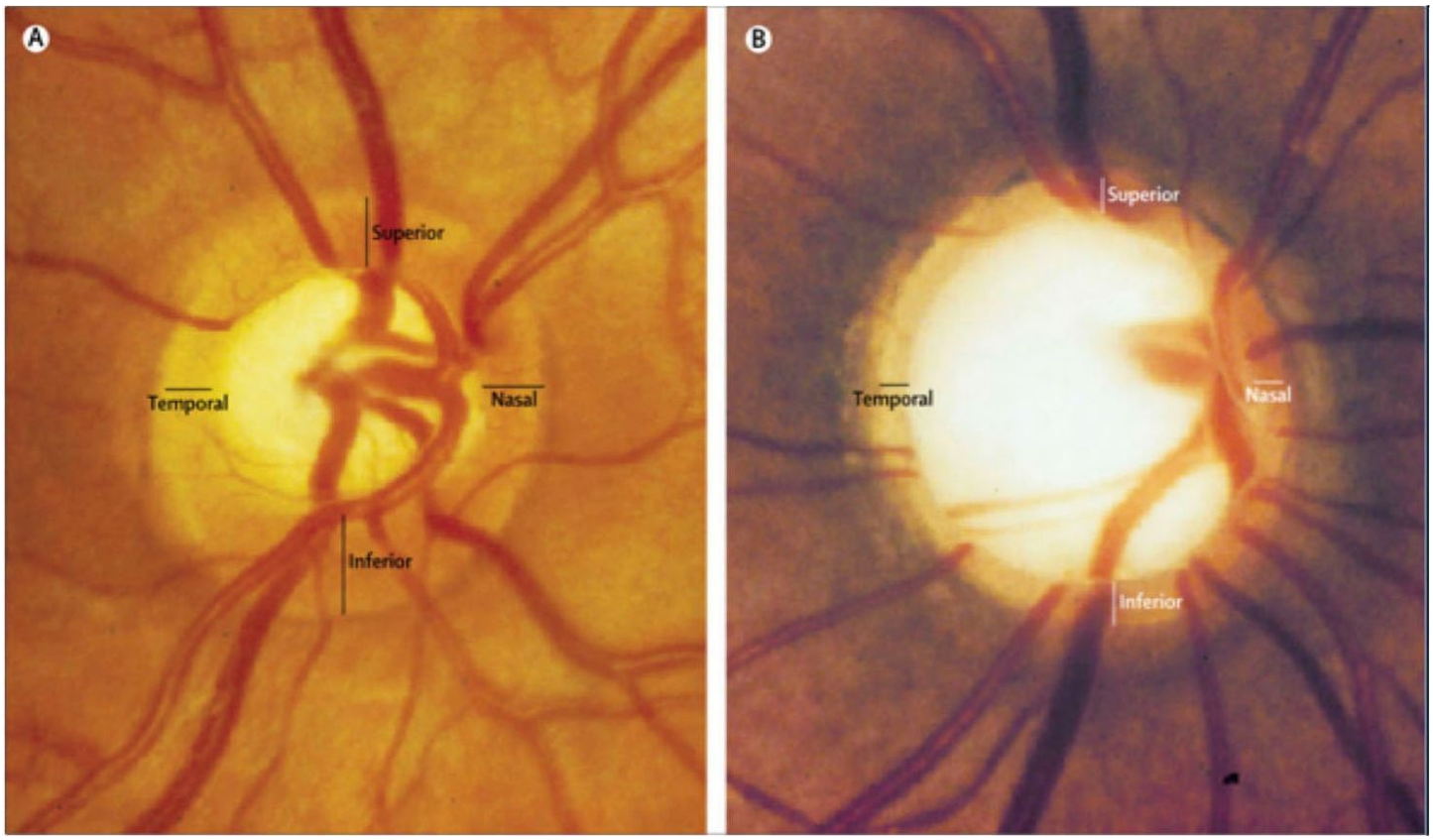

Figure 3. Ophthalmic photographs of healthy (A) and a glaucoma patient optic disks (B). The optic disk is the optic nerve head. (A) The optic disk is a normal shape, with a normally sized neuroretinal rim (superior, inferior, nasal and temporal). In (B) the neuroretinal rim is thinner, and the optic disk is larger, with a deep cup.

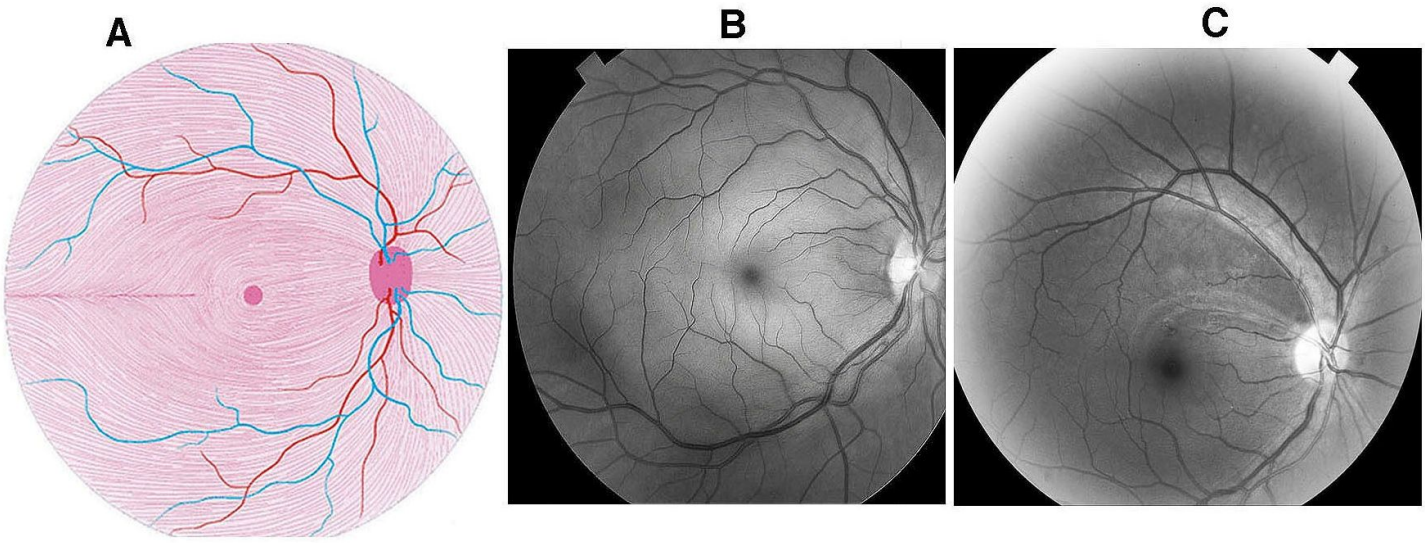

Figure 4. The course of ganglion cell axons towards the optic nerve head. (A) Schematic of normal nerve fiber layer axons (137). (B) Retinal fundus photograph of a normal retina where the nerve fiber layer appears as an even, white area composed of fibers sweeping towards the optic nerve head. The nerve fibers are particularly obvious in this patient due to a central retinal artery occlusion. (C) In advanced glaucoma the fiber layer (white streaks) is defective and appears to have a wedge shape. This indicates drop out of ganglion cell axons. (B) and (C) courtesy of James Gilman, Photography Department, Moran Eye Center.

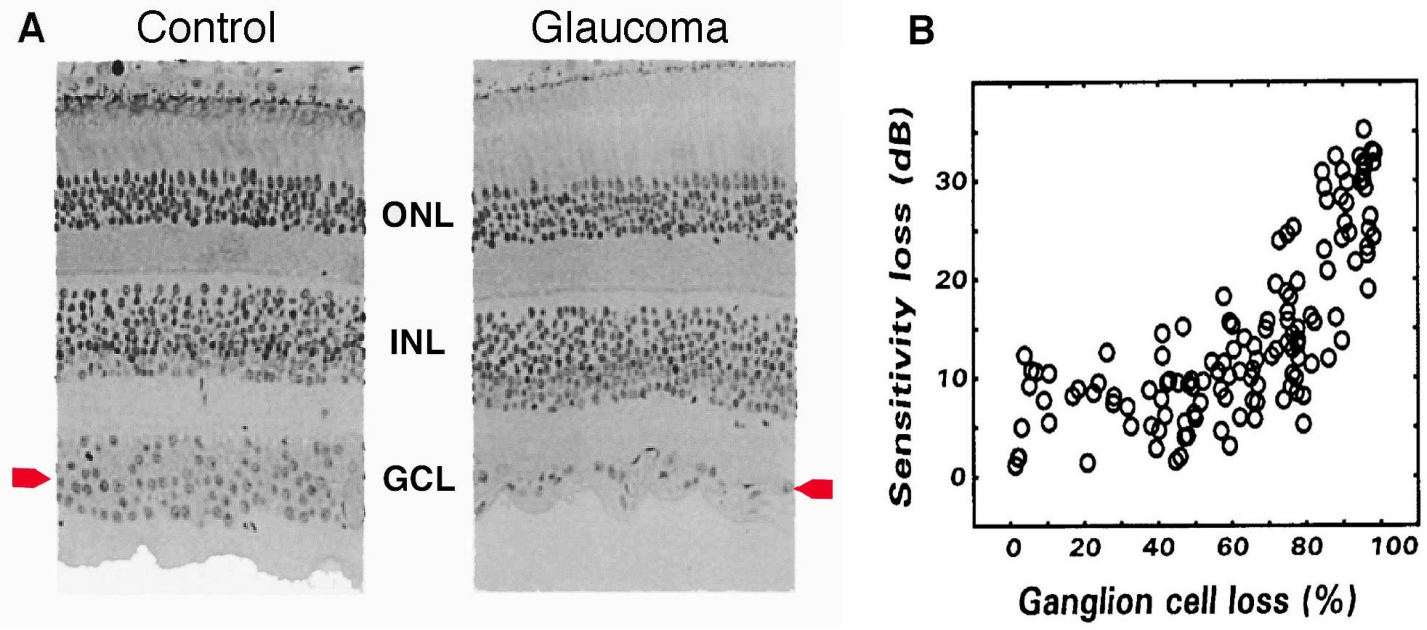

Figure 5. Retinal morphology in the primate (macaque) model of experimental glaucoma. (A) IOP elevation selectively compromises the survival of retinal ganglion cells (RGCs, arrowheads). (B) Vision loss takes place when a significant proportion (~50%) of RGCs are lost.

that lack or overexpress MYOC have normal aqueous drainage and do not develop high IOP whereas mice expressing the human Tyr437His mutation in the olfactomedin domain develop elevated IOP and optic nerve damage that mirrors human glaucoma (21). Carriers of MYOC mutations develop glaucoma in ~90% of cases, presumably due to deranged protein-protein interactions, intracellular accumulation of misfolded proteins and ER/endosomal stress (12). OPTN encodes a scaffold protein that has at least 23 binding partners, 8 protein

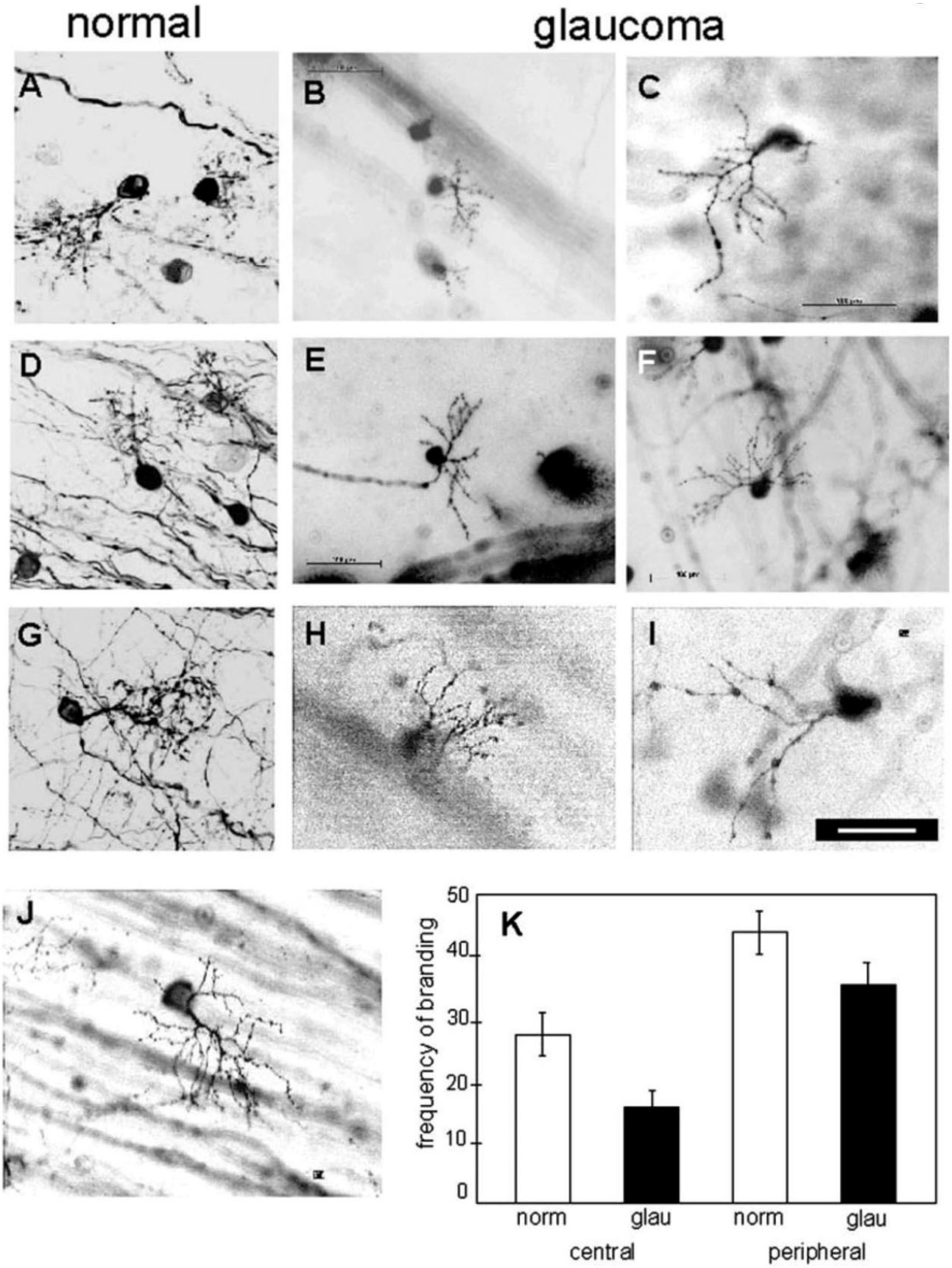

Figure 6. (A, D, G, J) Normal midget ganglion cells stained at increasing eccentricity from the fovea. Carbo-cyanine dye (DiI) staining. (B, C, E, F, H, I) Midget ganglion cells stained by DiI in the glaucomatous retina at similar distances from the fovea as the normal cells. Note the absence of surrounding stained cells and stained ganglion cell axons in comparison to the normal retinas. Also, there is distinct atrophy of the dendritic branching compared to normal midgets as shown in the histogram (K). From Pavilidis et al, 2003 (9).

binding sites and likely roles in multiple signaling pathways, including autophagy and vesicle trafficking in TM cells and RGCs (22).

A widely shared view of POAG is that of a multifactorial disease in which multiple genes, protein and lipid signaling pathways are dysregulated, but may also be influenced by environmental stressors and epigenetic mechanisms. The molecular "interactomes" that underpin pressure-sensitive and insensitive aspects of POAG remain to be fully characterized with potential clues from recent genome-wide association study (GWAS) analyses of adult-onset POAG loci including genes that encode cholesterol-binding caveolin proteins CAV1/2, ABCA1 (ATP-binding cassette transporter 1), TGFBR3 (transforming growth factor beta receptor 3), FOXC1 (forkhead box C1), ELOVL5 (elongation of long chain fatty acids family member 5), ATOH7 (atonal homolog 7), CYP1B1 (a cytochrome P450 enzyme) and ATXN2 (ataxin isoform 2) proteins. On their own, these proteins may be harmless – and/or independent of IOP - but may accumulate risk when combined with pathological mechanotransduction. IOP-independent [e.g., SIX6 (a transcription factor) and CDKN2AS (a non-coding RNA)] genes (12) could compound pressure-mediated injury. Some GWAS loci may be ethnicity-specific: lipid rafts - macromolecular complexes that regulate cell mechanotransduction - have been linked to POAG in European cohorts (23) via mutations in CAV1 and CAV2. Accordingly, cholesterol-lowering drugs (e.g., statins) may decrease the risk of contracting POAG in these populations (24). In addition to changes in gene composition, glaucoma risk may also be associated with copy number variations (base deletions/duplications) (25).

Pressure-dependent dysregulation of signaling mechanisms in anterior eye is reflected in aqueous humor composition, which shows altered levels of a striking number of signaling molecules that include adenosine, nitric oxide, ATP, endothelin-1 (ET-1), lipids (endocannabinoids, prostaglandins, cholesterol), transforming growth factor (TGFβ), CTGF (connective tissue growth factor), angiotensin II and cochlin. ET-1 and TGFβ2 modulate the deposition of ECM molecules within the trabecular pathway, which in turn might affect aqueous outflow (26). Another protein of interest is CYP1B1, a member of the cytochrome P450 enzyme consortium that metabolizes fatty acid molecules downstream from arachidonic acid. CYP1B1 mutations were associated with glaucoma in children and young adults (2), with the protein expressed in glaucoma-relevant ocular tissues such as the trabecular meshwork, retina and the ciliary body where it could affect the cells' sensitivity to mechanical stressors (27). The calcium-permeable TRPM3 channel (expressed in the ciliary body and lens) represents a combined risk factor for high-tension glaucoma and cataracts (28). Other important signaling mechanisms involve Rho and MAP kinases which modulate the expression of proteolytic enzymes, proinflammatory cytokines, autophagy and contractility (29, 30).

Normal-tension glaucoma (NTG)

NTG is seen in ~30% of POAG patients in which degenerating RGCs show the typical hourglass pattern of axonal loss and visual field defects at "normal" IOP (31), i.e., levels that are consistently lower than 21 mm Hg. Risk factors including female gender, race (more common in Japanese than Caucasians), vascular dysregulation and low blood pressure (32). Two NTG genes (OPTN and TBK1) with prevalence of 1-2% are shared with POAG and encode proteins associated with autophagy (an intracellular protein degradation mechanism) (33). Axonal injury in NTG could be augmented by the pressure gradient caused by abnormally low cerebrospinal fluid pressure across the optic nerve head (32). IOP-lowering regimens improve the prognosis in some patients: after 6 years, ~55% of patients treated with IOP-lowering medications showed stable vision as opposed to ~40% of untreated patients (31, 34). Given that pathological responses NTG patients appear to involve innocuous mechanical stressors, these patients could possess gain-of-function mutations that increase their sensitivity to IOP. Similar hypersensitivity (hyperalgesia) to mechanical stressors is a well-known property of neuropathic pain mechanisms that involves altered function of mechanosensitive ion channels in the peripheral nervous system (35).

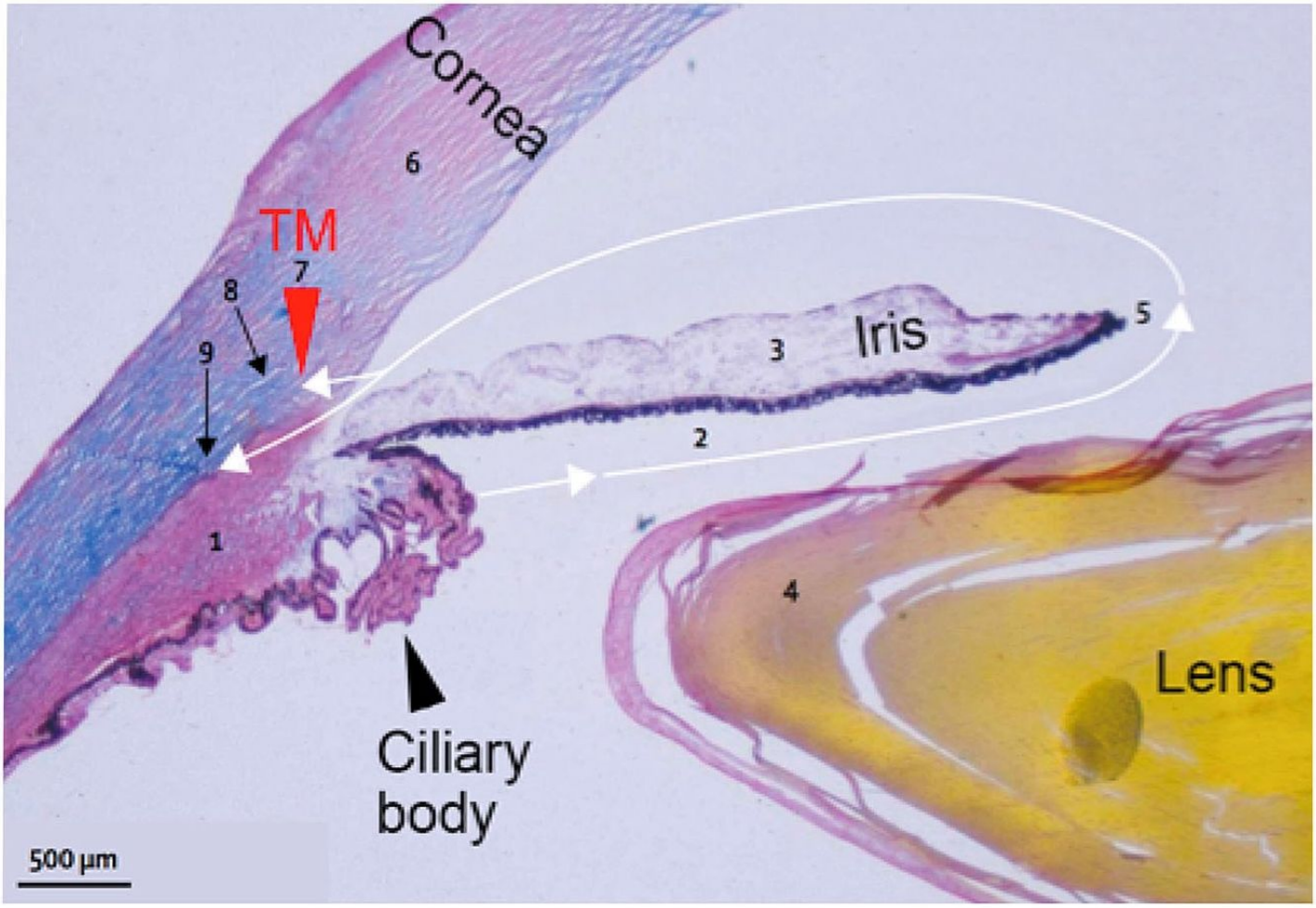

Figure 7A. The anterior chamber contains the ciliary body **1**, the site of aqueous humor production. The aqueous humor percolates around the lens **4** and the iris **3** to drain (white lines **2**) from the posterior chamber into the anterior chamber through the pupil **5**. The anterior chamber angle is located between the peripheral cornea **6** and the peripheral iris, and it contains the trabecular meshwork (TM **7** red arrow) and Schlemm's canal **8**. The aqueous humor leaves the eye through the trabecular meshwork and Schlemm's canal, and through the uveo-scleral outflow pathway in the ciliary muscle **9**. Modified from Jonas et al, 2017 (13).

Primary angle-closure glaucoma (PACG)

Angle-closure glaucoma, common in East Asian populations and rare in Caucasians, is responsible for a disproportionate number of patients with severe vision loss. The pathology is caused by disorders of iris, lens and retrolenticular structures which impede drainage of aqueous humor by narrowing the angle between the iris and the cornea (Figure 7B). It is more likely in women and persons with extreme hyperopia (farsightedness). In about a third of PACG patients, an abrupt increase in IOP (often above 30 mm Hg) triggers acute symptoms (severe pain and nausea, conjunctival hyperemia, corneal edema and vomiting) that require immediate medical intervention (12). The disease is highly heritable with gene association studies implicating genes that encode polymorphisms in extracellular matrix (ECM) molecules (e.g., MMP, HSP70, NOS3) or ocular development (the Frizzled related MFRP protein, hepatocyte growth factor HGF). Additional candidates identified by GWAS studies include collagen XI (COL11A1), pleckstrin homology domain proteins (PLEKHA7, PLEKHC1; required for the stabilization of adherens junctions), protein glycosylation (DPM2), acetylcholine biosynthesis (CHAT), ST18 (suppression of tumorigenicity 18) and transcriptional regulation (GLIS3) (36). Unsurprisingly, many of these risk genes encode processes associated with cell adhesion, ECM homeostasis and mechanotransduction (focal adhesion, cell junctions, collagen).

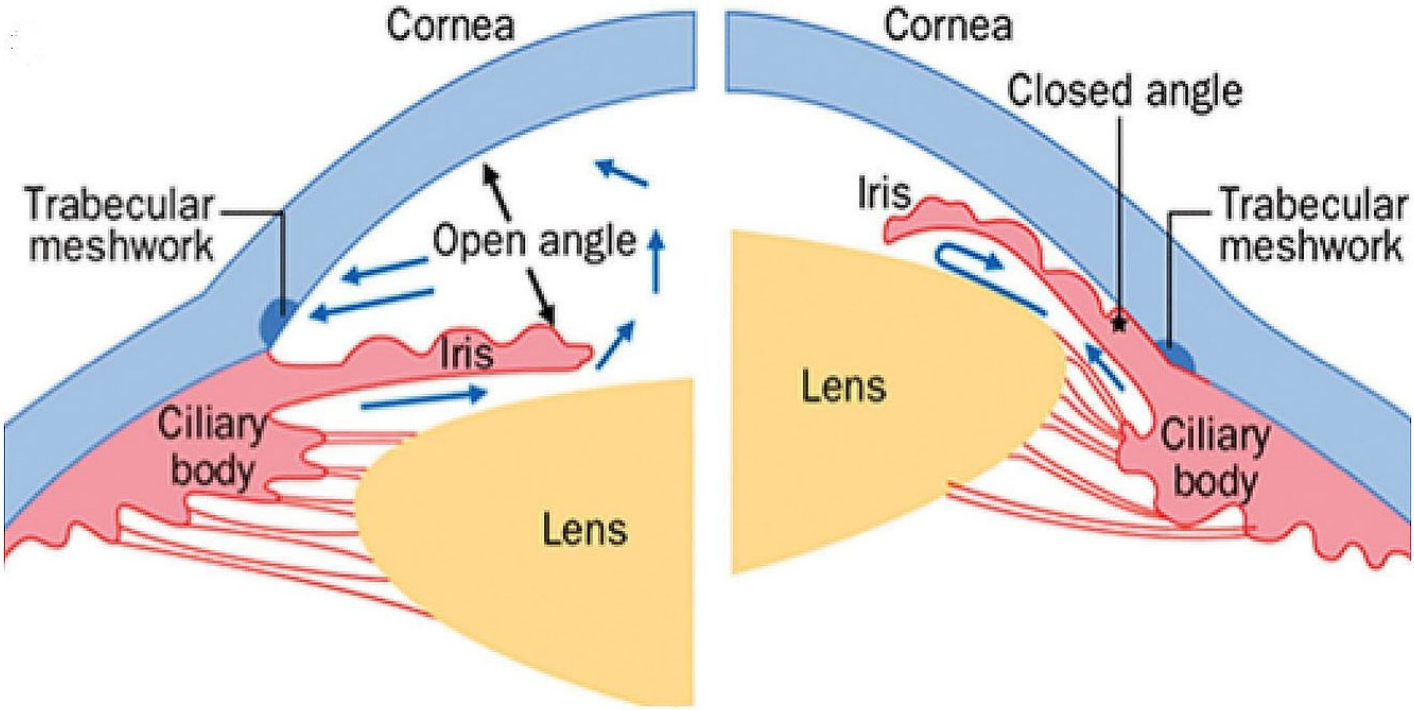

Figure 7B. A schematic diagram of the anterior eye in open angle (left) and closed angel (right) glaucoma, showing how the displacement of the lens and the iris obstructs the fluid outflow across the Trabecular meshwork (TM) in the case of closed angle glaucoma. From Wiggs and Pasquale, 2017 (12).

After an acute PACG there may be a period of normal tension, taking the eye multiple days or week to recover from the shock and start producing aqueous fluid at a normal rate that elevates IOP to levels that conform to the extent of angle closure (12).

Secondary glaucomas

Secondary glaucomas reflect pathological mechanisms that elevate IOP above the normal range due to pathological production and/or reduced drainage of aqueous flow. Variants include pseudoexfoliative glaucoma, neovascular glaucoma, pigmentary glaucoma and steroid-induced glaucoma. ***Pseudoexfoliative glaucoma*** occurs when clumps of protein accumulate in the anterior chamber and clog the outflow through the trabecular meshwork. It has higher incidence in Scandinavian populations, shares risk factors with Parkinson's disease and Alzheimer's diseases and was associated with mutations in the lysyl-oxidase-like 1 (LOXL1) gene, and mutations in loci encoding CACNA1A, TMEM136, SEMA6A and other genes. ***Neovascular glaucoma:*** proliferation of blood vessels in the iridocorneal angle ("iris tufts") results in leakage of fibrous material which closes the angle. Is associated with retinal ischemia. Risk factors include diabetes. ***Steroid-induced glaucoma*** occurs in patients who take steroid medications to suppress macular edema, corneal transplant rejection, immune hyper-reactivity and injury-related inflammations. The resulting structural changes in the trabecular meshwork (including the induction of MYOC) increase its resistance to aqueous humor outflow and elevate IOP. Untreated, this induces POAG in 40% of patients ('steroid responders') (37). **Pigmentary glaucoma** typically originates from the "pigment dispersion syndrome" caused by the atrophy of the pigmented epithelial cells in the iris. Dispersal of melanin into the trabecular meshwork impedes aqueous outflow and elevates IOP. The DBA/2J mouse strain, which develops a similar phenotype of chronic glaucoma, has mutations in the *Gpnmb* gene (encoding a lysosomal-related glycosylated protein) and the *Tyrp1* gene (encoding a melanosomal protein with possible enzymatic and structural functions) (38, 39) . **Other types of glaucoma** are associated with cataract formation, certain eye tumors, uveitis (ocular inflammation), myopia and early onset (juvenile glaucomas).

Aging and glaucoma

Aging and cellular senescence represent a central risk factor for progression of glaucoma. We lose 10,000 ganglion cells (0.3 – 0.6%) and 0.58% of TM cells per year – by the age 80, a healthy individual with normal IOP loses about 30% of their RGCs (8). The loss of ganglion cells in aged individuals correlates with the general decline in cognitive, motor and other functions in aged people and bears many similarities to glaucoma, including dendritic remodeling, reduced axonal transport in the optic nerve (which halves during the lifetime of a rodent), decreased quality control mechanisms in ganglion and trabecular cells, and lower recovery rates following injury. 97.6% of patients over 40 have a median age of glaucoma diagnosis of 64 years, with the prevalence rising steeply from 0.2% - 2.7% in individuals aged 50 – 59 years to 1.6% - 12.8% after age of 80 years (40).

While age is a strong predictor of POAG we *don't know what critical stress is communicated to RGCs in older eyes to make them less resistant to elevated IOP*. One possible contributing factor may be the increased stiffness of ocular structures ("ocular rigidity") which may augment trabecular contractility (which elevates IOP) and increase the susceptibility of ganglion cells and glia to pressure-mediated stress. Older individuals may also have deficient ocular metabolism that is accompanied by age-dependent oxidative stress, mitochondrial dysfunction (41) and loss of neuroprotective mechanisms (42).

Intraocular pressure generation in the eye

It is important to note that **IOP reflects the balance between production and outflow of aqueous humor** (Figure 7A & Figure 7B). Details of aqueous humor regulation are discussed in reviews by Accott et al. (2014) (43) and Braunger al. (2015) (26) but it is important to note that this transparent, nutritious fluid is continually generated by the ciliary body (~2.4 µl/min at daytime in healthy adults; black arrowhead in Figure 7A) to feed the nonvascularized lens. Aqueous fluid is drained (white arrows) through the trabecular meshwork (TM; red arrowhead, #8 in Figure 7A). In primates, TM supports ~80-90% of aqueous outflow and thus represents the principal bottleneck for fluid outflow whereas the auxiliary 'uveoscleral' outflow pathway in the ciliary muscle (#1 in Figure 6A) supports the rest. Aqueous fluid outflow is ~50% lower at night compared with daytime, with consequent increased risk for developing acute pressure-induced eye damage during sleep (44). Both abnormal production of aqueous fluid or its deficient drainage through the TM and the Schlemm's canal (a pipe composed of endothelial-like cells that feeds the fluid collected from TM into the venous system) can lead to glaucoma.

IOP-dependence contributes a significant proportion of glaucoma cases. Any level of IOP can contribute to pathology but the risk for contracting glaucoma increases exponentially when chronic IOP exceeds 20 mm Hg (Figure 8). The magnitude and duration of IOP correlate with disease severity, with larger IOP elevations precipitating both disease onset and speed of progression (AGIS 2000). Similarly, the longer the duration of ocular hypertension, the higher the likelihood of developing optic neuropathy (31). Importantly, many individuals with elevated IOP do not develop glaucoma and up to 50% of patients with glaucoma ("normal tension" patients) may not have statistically elevated IOP (45). These patients probably express protective factors that counterbalance morbidity factors that drive neurodegeneration whereas "normal tension glaucoma" patients probably express gain-of-function transducer mechanisms that make them super-sensitive to mechanical stress.

Increased intraocular pressure as a risk factor in glaucoma

The vertebrate eye is a highly dynamic environment where IOP provides the hydrostatic pressure that is necessary for maintaining the shape, growth and optical properties of ocular tissues. Together with old age, increased intraocular pressure (IOP) represents the most important risk factor for the onset and progression of glaucoma (Figure 8). IOP-dependence contributes ~30 – 70% of glaucoma cases (46). The average IOP in

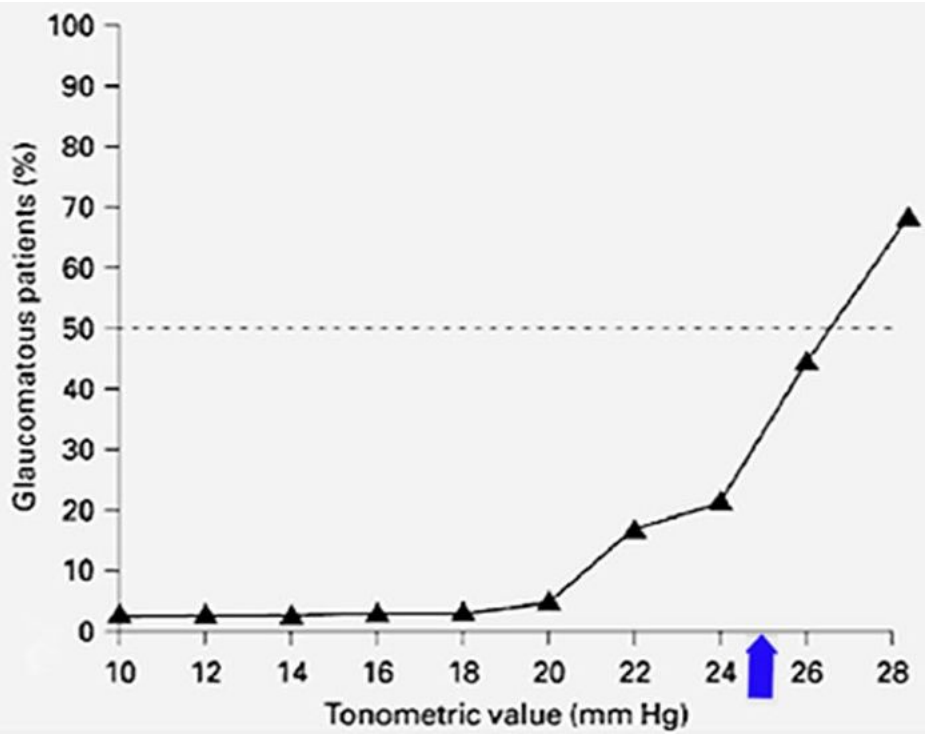

Figure 8. The relationship between IOP, tonometric value (mm Hg) and the diagnosis of glaucoma. Prevalence of 50% of patients is at 27 mm Hg. From Bonomi et al., 2001 (138).

newborn rodents and primates that ranges between 6 – 8 mm Hg, increases to 7 – 15 mm Hg in adults. IOP amplitudes tend to be slightly higher in the right eye than the left but the lifetime variability in IOP amplitude for individual eyes is minuscule (<2 mm Hg) (31). In contrast to the average IOP amplitudes which remain stable across lifetime, IOP is complex in the time-domain, showing pulsatility, circadian periodicity and oscillations (~3 mm Hg at ~1 Hz) (47). Blinking, eye scratching, sneezing, lens accommodation, arterial blood pressure and eye movements all transiently elevate IOP (by up to 200 mm Hg). The amplitude and rhythm of IOP fluctuations are regulated by *Cry1*/*Cry2* clock genes and local release of melatonin, which peaks at night and is more pronounced in glaucoma patients (48). IOP and risk for developing glaucoma may be increased by body position (eg, yoga inversion practices), weight lifting and swimming goggles whereas moderate physical exercise and diet rich in ω3/ω6 polyunsaturated fatty acids can decrease IOP by ~4 - 5 mm Hg. A confounding factor, however, is given the wide assortment of risk factors and glaucoma-associated signaling mechanisms there are no clear IOP threshold values that allow us to consistently identify the patients at risk for optic neuropathy.

Currently accepted treatments of glaucoma are largely limited to IOP lowering, a strategy that usually stops disease progression if pressure can be decreased by ~30–50%. Anti-glaucoma medications target aqueous fluid production in the ciliary body and/or the secondary (uveoscleral) outflow pathway. Because IOP lowering may also reduce the progression of vision loss in patients with 'normal' IOP (8-15 mm Hg) levels (17), glaucoma can be viewed as a **disease that involves increased susceptibility of the eye to mechanical stress at any IOP level**. Unfortunately, the most commonly used IOP lowering agent latanoprost (a prostaglandin $F_{2\alpha}$ analog) does not lower IOP more than 20% in a significant fraction (25-50%) of patients whereas up to 6% of POAG patients are unresponsive or do not tolerate any IOP medications (31, 45). Some treatments that showed efficacy in experimental paradigms, such as cannabinoids targeting the CB1 receptor (49), angiotensin II receptor blockers, melatonin receptor 3, adenosine receptor 1 agonists, TRPV4 channel, TREK-1 channel and endothelin receptor-1 blockers have yet to complete clinical trials. No medications were capable of targeting the main (trabecular) outflow mechanism until 2017, when several Rho kinase (ROCK) inhibitors (e.g., ripasudil) were approved for topical treatment of POAG. Unfortunately, the disagreeable side effects (e.g., hyperemia) may limit

their usefulness to many patients. Developing drugs that target the trabecular outflow component without side effects should therefore be a priority.

Details of the Trabecular Meshwork (TM)

TM cells play a central role in IOP regulation through their control of fluid outflow into the canal of Schlemm (Figure 7A). The cells form three adjacent strata (uveal, corneoscleral and juxtacanalicular) that differ in terms of their gene expression patterns and relative contribution to phagocytosis, fluid filtration, stiffness and resistance to fluid flow (50) but are difficult to pigeonhole from ontogenetic, morphological or functional standpoints: (i) Similar to macrophages, they express histocompatibility and other immune markers, and show phagocyte-like scavenger activity; (ii) Similar to glia, they play important volume regulatory functions and participate in the release of inflammatory cytokines (such as IL-1α and TNFα); (iii) Similar to endothelia, they form a barrier with antithrombotic and antigen-presenting functions; (iv) Similar to fibroblasts, they release extracellular matrix and contribute to contractility yet (v) They express smooth muscle actin (αSMA), a protein typical of smooth muscle cells. Pressure-evoked TM contractions mediated through actomyosin are thought to elevate IOP by increasing the resistance of the outflow pathway to fluid flow (30). **The chronic increase in outflow resistance underlies a positive feedback between elevated IOP, stiffening of the cytoskeleton and increased contractility.** In other words, **cytoskeletal and ECM remodeling underpin both cytological and functional hallmarks of hypertensive glaucoma**. Similar positive feedbacks between mechanical stretch and pathology have been described in other tissues, including lung and heart where cell sensing of small changes in tissue stiffness drives severe, fibrotic remodeling.

At the subcellular level, an increase in pressure induces an upregulation of actin stress fibers, adhesion molecules and remodeling of the extracellular matrix (ECM) in TM cells (Figure 9C & D), together with up/downregulation of hundreds of genes associated with cell adhesion, metabolism, ion transport, inflammation and cell cycle (29). Although not every step of this dynamic response is understood, recent studies showed that mechanical stress induces increases in intracellular calcium concentration $[Ca^{2+}]_i$ of both TM cells (Figure 9A) and ciliary body cells that regulate aqueous fluid outflow and inflow, respectively (51). Calcium in turn regulates almost every aspect of cell physiology, including modulation of contractility, stiffness and increased levels of the cytokine TGF-β, activation of Mitogen-Activated Protein (MAP) kinases, release of metalloproteinases (MMPs) and deposition of ECM molecules such as fibronectin and versican (Figure 9D). The effect of pressure on $[Ca^{2+}]_i$ and cytoskeletal remodeling that is seen in vitro and in vivo models of trabecular outflow and IOP regulation has been broken experimentally by inhibiting stretch-activated TRPV4 channels (Figure 9B), which triggers an immediate IOP lowering (51).

Chronic increases in IOP trigger up- and downregulation of thousands of trabecular and retinal genes, many of which encode signaling pathways associated with glial activation, upregulation of complement genes, endothelial dysfunction and RGC degeneration in animals and humans. A useful online resource that showcases the complexity of these pathways is the Glaucoma Discovery Platform from Jackson Laboratories (http://glaucomadb.jax.org/glaucoma).

Details of retinal ganglion cells (RGCs)

Mammals have >45 classes of RGCs - projection neurons with unique inputs, functional properties and axonal projections to the brain (*G,* red cell in Figure 10). *In vitro* and *in vivo* studies in animal models (mainly non-human primates and mice) have established the disproportionate vulnerability of RGCs to many types of mechanical stress - including IOP, compression, tensile stretch and prolonged swelling (35, 52, 53). The spatial pattern of pressure-induced injury of RGCs correlates with the location of their axons within the ONH whereas other classes retinal neurons tend to be (at least initially) spared from IOP-induced injury (Figure 5) (8, 54). The molecular and cellular changes induced by IOP (altered transcription, organelle function, calcium signaling, neurotransmitter uptake, synaptic organization and cellular architecture) in turn compromise the cells' function

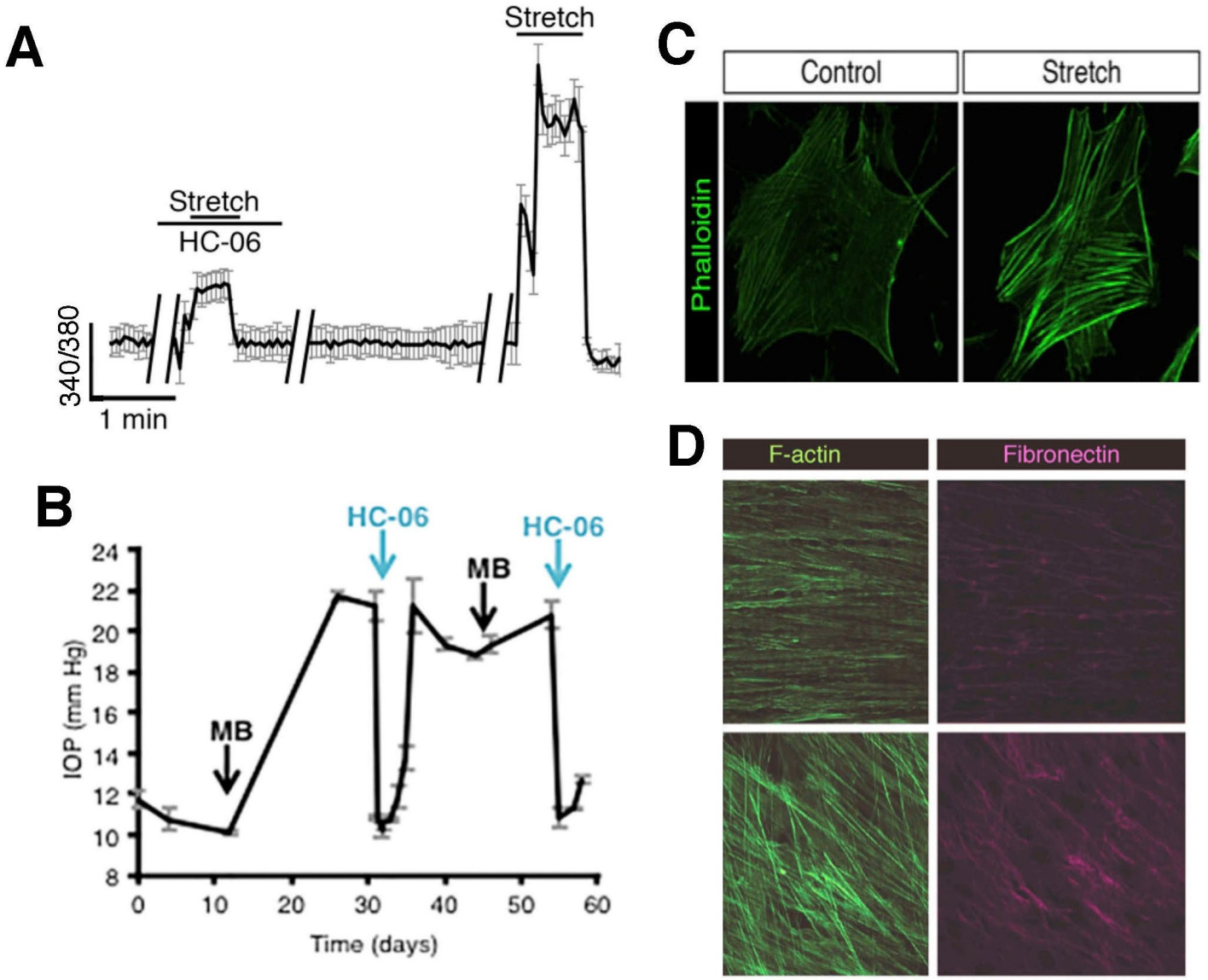

Figure 9. TRPV4 drives mechanically induced calcium signaling, cytoskeletal and ECM remodeling in human TM cells. (A) Substrate stretch (substrate deformation, 6%) elevates $[Ca^{2+}]_i$ in TM cells, an effect that is suppressed by a selective TRPV4 antagonist. (B) Injection of a TRPV4 antagonist into a mouse eye with experimentally elevated IOP results in dramatic IOP lowering. (C) Stretch drives the upregulation of ventral actin stress fibers. (D) *In vitro* model of trabecular outflow using bioengineered 3D nanoscaffolds populated with TM cells. Pressure upregulates actin stress fibers and increases release of fibronectin. This effect is antagonized by TRPV4 blockers (not shown). Adapted from Ryskamp et al (2016) (51).

that is manifested in their light response, synaptic output and survival. **Figuring out *why* and *how* IOP preferentially targets RGCs currently represents a central challenge in glaucoma research.**

Although 'glaucoma' is a late-stage designation of the injured retina, RGCs are remarkably sensitive to acute changes in pressure which result in immediate changes in excitability, loss of spatiotemporal contrast sensitivity and reduced visual acuity (55, 56). Functional dysfunction correlates with the retraction, thinning and reduced complexity of RGC dendrites, loss of synapses and changes in axonal transport (54, 57-60) (Figure 11). Pressure-induced changes in cell firing and dendritic injury are compounded by the obstruction of (anterograde/retrograde) transport of neurotrophic factors and organelles (61) which, if it persists, can contribute to gross structural remodeling at the optic nerve head. Macroscopic remodeling of the ONH tends to be observed months (rodents) or years (primates) after the onset of ocular hypertension, time lags when it tends to be too

late for neuroprotective intervention. Recent studies instead suggest that IOP-induced alterations in dendritic architecture and glial activation (see below) represent better early markers of glaucoma than transport loss. The importance of nonaxonal pressure targets was accentuated in a landmark study by Morgan's group, which demonstrated that *pressure-induced dendritic retraction and RGC loss occur in the presence of intact axons* (62). The studies of early pressure sensitivity and nonaxonal targets (55, 56) thus emphasize the need for early neuroprotective treatment that targets preservation of dendritic morphology and maintenance of synaptic connectivity within the retina.

There are disagreements regarding the onset of pressure-evoked optic nerve damage and pressure sensitivity of RGC subtypes. An early primate study reported RGCs with large perikarya to be disproportionally sensitive to pressure (63) but these results were not reproduced in primates (64) or rodents, where RGC damage appears to be topographic but not subclass-specific (65). IOP-induced RGC loss was not restricted to specific locations in the retina (55) and there seems to be little correlation between perikaryal size and neurodegeneration (58).

To better understand the disease it would be very helpful to know whether particular classes and subtypes of RGCs are disproportionately sensitive or resistant to mechanical stress. Some electrophysiological recordings combined with analysis of reporter-tagged RGCs point at OFF RGCs as more sensitive to elevated IOP from their ON counterparts (55, 58) but another study, employing similar approaches, reached an opposite conclusion (66). Similarly, Ou et al. (54) found IOP-induced dendritic remodeling to be more extensive in OFF cells yet other studies show no apparent differences in pressure-induced dendritic pruning across functional subtypes (67). It is possible these disparities were caused by different ways of inducing ocular hypertension. In any case, it is very possible that early RGC pressure damage in glaucoma reflects molecular/functional, rather than anatomical, parameters (68). For example, susceptibility of OFF-type cells may reflect different responses from local vasculature or glia, and/or altered availability of trophic factors (58). Intrinsically photosensitive RGCs (ipRGCs) tend to resist IOP elevations (69) (see chapter in Webvision on melanopsin expressing ganglion cells), perhaps due to diminished numbers of pressure transducing molecules (70).

John's compartmental model (39) transcends such either/or dichotomies by providing a heuristic framework for the early effects of elevated IOP. The model has profoundly advanced the conceptual disease paradigm by positing that RGCs degeneration in glaucoma involves parallel effects of pressure on molecularly distinct local self-destruct programs in dendrites, somata and axons. A plausible multi-compartmental regulator of pressure-induced damage could be the calcium ion, which drives the remodeling of dendrites, somata and axons through Ca^{2+}-dependent proteases, caspases, MAP kinases, ER stress, autophagy and apoptotic cascades (71-73) (see below). Abnormal autophagy and endoplasmic reticulum (ER) damage, which compromise RGC viability due to intracellular accumulation of misfolded proteins, loss of calcium homeostasis and deficient protein trafficking (73) represent additional early features of pressure-related RGC stress, whereas axonal constriction constitutes both a possible early insult and potential coup de grâce that instigates apoptosis. Consistent with the compartmentalization model, local axonal damage can be ameliorated by reducing oxidative damage, targeting the dual leucine zipper kinase (DLK) enzyme and potentially with exercise. Accordingly, preclinical experimental strategies that aim to increase RGC survival in glaucoma can be separated into approaches that (i) facilitate expression of endogenous protective mechanisms, (ii) supply RGCs with exogenous neurotrophic factors, (iii) target pressure-sensing mechanisms, (iv) prevent downstream remodeling (v) slow down cell death by targeting the final common apoptotic pathway and/or (vi) use pharmacological agents with wide-spread or unclear neuroprotective mechanisms of action. Adult ganglion cells in mammals show little or no regenerative response after pressure injury however their survival can be extended for short periods of time with recombinant and virally expressed delivery of neurotrophic factors (e.g., BDNF, CNTF, NT-4, FGF-2, neurturin) which partially protect RGCs in animal models of glaucoma (59, 74). Degrees of protection have been observed following treatments with Rho kinase inhibitors, endothelin ET-2 inhibitors, erythropoietin, resveratrol, NMDA receptor antagonists, NO donors, antioxidants, α_2-adrenergic agonists (brimonidine), cannabinoids (e.g., Δ^9-THC) and β-adrenergic blockers. Memantine, an antagonist of NMDA receptors, has shielded rodent and non-

human primate ganglion cells from glaucoma (75) but was ineffective in human trials. Enigmatically, exposure to long-wavelength red light (850 – 1100 nm) was reported to be protective (76), and visual (neuronal) activity was proposed to facilitate regeneration of injured RGC axons (77). The multiplicity and variability of protective effects suggests that many therapeutic strategies may have been targeting secondary molecular mechanisms that are downstream from the actual RGC mechanotransducers.

Optic nerve head (ONH)

Degeneration ("cupping" or "excavation") of the ONH is the current diagnostic marker that separates glaucoma from other RGC diseases (e.g., nonarteritic anterior optic neuropathy (NAION), traumatic optic neuropathy, optic neuritis and multiple sclerosis). Cupping correlates with the manifestation of "arcuate scotoma" (loss of sensitivity) in visual testing (perimetry) and correlates with axonal loss observed in imaging studies. Because topology of RGC loss and defects in the visual field (radial in humans, sectorial in rodents) correlate with the position of axons within the ONH (10, 38), the ONH is widely seen to be important in determining the extent of final axonal damage that drives neurodegeneration.

The ONH contains unmyelinated (early) and myelinated (late) parts of RGC axons together with their extracellular matrix ECM/glial scaffolds and the capillary blood supply (Figures 12 & 13) (reviewed in (10, 38)). The biomechanics of this region are affected by the stiffness and thickness of the sclera that surrounds it and by glial deposition of ECM molecules (78). The "papilla" where the optic nerve enters the retina (Figure 12) represents the weakest part of the sclera as the axons (~1.2 million in humans) make a 90^{o} turn to enter the optic nerve through ~200-400 pores of varying sizes that are part of the structure called the *lamina cribrosa*. 12% of axons must squeeze through these collagenous pores. Axons from the peripheral retina pass in the peripheral part of the lamina whereas those from the central retina pass through its center but axons from the same retinal eccentricity may pass at different levels within the optic nerve.

The primate lamina cribrosa is a specialized region of ~10 interconnected ECM beams composed of collagen I, III, IV and elastin. These beams are lined with astrocytes, microglia, fibroblasts and an extensively branched vascular supply all of which may interact. Small ECM-cell adhesions may persist for tens of seconds whereas linkages between focal adhesions, intracellular actin cytoskeleton and ECM proteins (fibronectin, tenascin, collagens, etc.) can form on the scales of minutes-to-hours (78). Mechanical strains experienced at the ONH at normal IOPs (~15 mm Hg) range between 5 and 6% whereas IOP elevations to 50 mm Hg may increase them to 8 – 10% (79). Typically, 5-10% cellular stretch is sufficient to substantially affect calcium levels, cytoskeletal organization and tissue physiology across tissues and organs. Biomechanical modeling and 3D reconstruction studies points at the viscoelasticity of ONH structures as a determinant of the dynamic ONH response to changes in IOP. Cribrosal ECM plates in particular are seen as the weakest contact point for mechanical strain/compression (80). Increases in pressure stiffen the ONH yet it is not clear whether a stiffer lamina is better at countering mechanical stress. A useful analogy may be the hypertrophic (fibrotic, stiffer) heart which allows stronger pumping against high back-pressure, but is ultimately detrimental for cardiovascular health.

It must be pointed out that our understanding of the types of strain that affect RGC axons remains incomplete due to the anisotropy of the ONH and the likelihood that subregions with different geometry experience different tensions in response to the same IOP stimulus (78). The size of the pressure differential between IOP and the optic nerve is unknown and it remains unclear that it is affected by cerebrospinal fluid pressure, whether and how stretch of scleral tissues contributes to RGC injury, whether certain RGC classes (which?) are selectively sensitive/resistant to IOP, why retinal glia are so sensitive to elevated IOP, what (if any) is the role of ischemic compression at moderate IOP elevations and which signaling pathways mediate the acute vs. chronic effects of ocular hypertension. These pathways might be linked via IOP-dependent obstruction of anterograde and retrograde transport of pro-survival growth factors (BDNF, NT-3/4, NGF, CNTF), changes in immune gene expression, local chemotaxis, cell-ECM interactions and mitochondria (81, 82). It is possible if not likely that

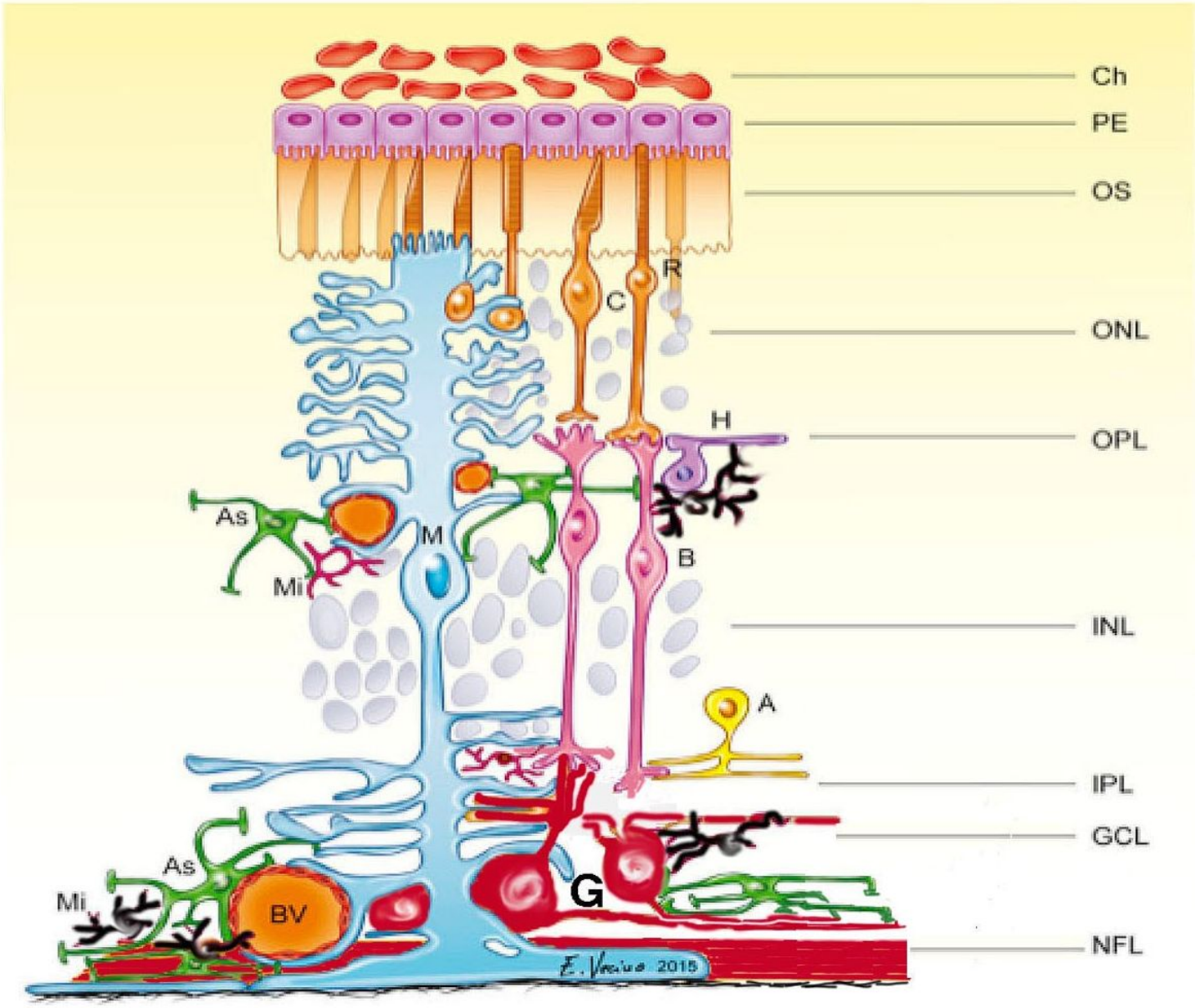

Figure 10. Schematic drawing of the glia and their relationship to neurons, retinal pigment epithelium and blood vessels in a prototypical vascularized mammalian retina. Amacrine cells (A), astrocytes in green (AS), bipolar cells (B), cones (C), ganglion cells (G), horizontal cells (H), Müller cells in blue (M), microglia in black (Mi), rods (R), optic nerve (ON), nerve fiber layer (NFL), ganglion cell layer (GCL), inner plexiform layer (IPL), inner nuclear layer (INL), outer plexiform layer (OPL), outer nuclear layer (ONL), outer segment layer (OS), pigment epithelium (PE), choroid (Ch). Note the proximity of blood vessels (BV), astroglia, Müller glial endfeet, and neuronal processes. From Vecino et al. (2016) (139). Drawing modified by Helga Kolb. (2018).

pressure affects these manifold processes via mechanotransducer mechanisms (such as mechanosensitive TRPV4 and TREK-1 channels and integrins; see below), which mediate the responses to scleral stretch, ONH compression, tension & shear. Activation of these mechanotransducers in different cell types (RGCs, glia, vasculature) may determine the relative balance of axonal vs. nonaxonal injury and the importance of neuroinflammation between individuals (and species) with glaucoma.

Many of the studies that implicate axonal involvement in glaucoma have been conducted in optic nerve crush models that are not directly relevant to pressure-induced axonal injury. Studies in animal models of primary open angle (microbead-induced) and secondary closed angle (DBA/2J) glaucoma clearly show that pressure

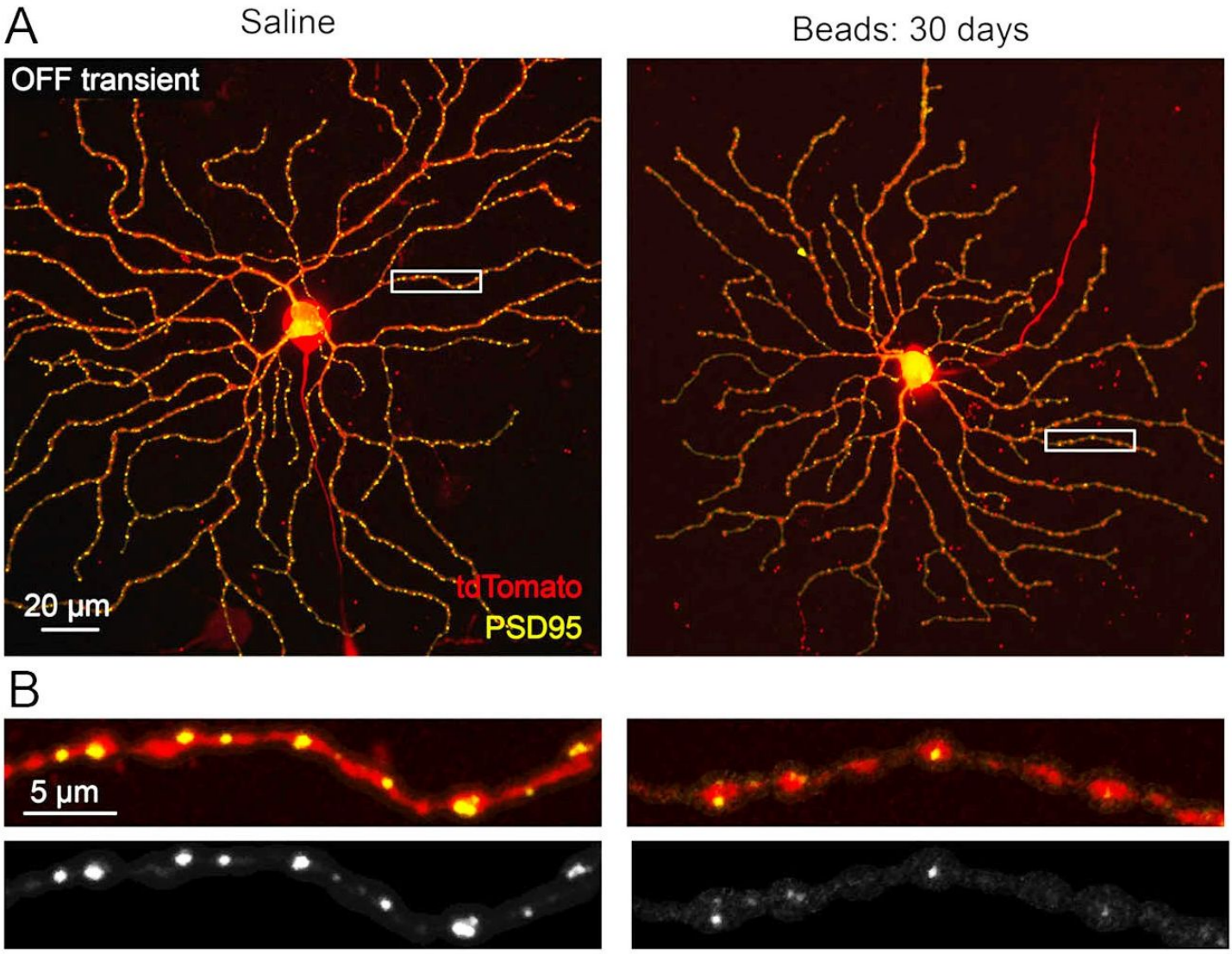

Figure 11. The effect of high intraocular pressure on certain ganglion cells in the mouse model of glaucoma (made glaucomatous by injection of microbeads into the anterior chamber of the eye). (A) immunocytochemical staining of biolistically labeled OFF sustained retinal ganglion cells in microbead injected and in control (saline injected) retinas. The glaucomatous ganglion cell is less robust in dendritic branching and exhibits less synaptic sites (yellow staining spots) than the control ganglion cell. (B) The dendrites are stained by tdTomato, and their synaptic sites by PSD95-CFP. Synaptic sites are more numerous on the control ganglion cell dendrites, but fewer and weakly stained in the bead-injected (high IOP model) retina. From Della Santini et al., 2013 (55).

elevations compromise axonal transport (61) but its importance for neurodegeneration remains to be established given that long-lasting reductions in transport don't impact RGC survival in axonal diseases such as papilledema. Moreover, many types of RGC tolerate loss of transported survival-promoting factors, whereas the lack of sustained RGC survival in retinas supplemented with neurotrophic factors argues against the obligatory consequences of their loss in animals with blocked axonal transport. Furthermore, changes in axonal transport in DBA/2J mice (9-12 months) tend to occur much later (83) than dendritic remodeling (1-3 weeks; (55)), glial reactivity (3-6 months) and defective signaling of the optic nerve (~6 months) (72, 84, 85) . The observation that anterograde transport is compromised before retrograde transport (83) argues against a key role for ONH constriction predicted in most biomechanical models. Instead, recent studies suggest a key role for nonaxonal mechanisms that include physiological deficits in RGC activity (55, 83) and inflammatory signaling (35, 81).

Another important argument against the obligatory role of the lamina cribrosa in glaucoma is supplied by evolution. Laminar ECM plates are well developed in pigs, cats, guinea pigs, tree shrews and dogs but are absent in rodents. In rats and mice, structural and metabolic support to passing RGC axons (~50,000 in mice) is provided by a "glial lamina" composed of astrocytes that form tubes around the axonal bundles (38, 86) (Figure 13). Because these animals still develop glaucoma in response to elevated IOP, neither ECM plates nor the lamina cribrosa are likely to be necessary for pressure-induced axonal loss.

IOP causes neuropathy in the brain

Glaucomatous damage is not restricted to the eye but includes the entire visual pathway from the retina to the brain. IOP increases cause spatial vision loss (87) together with decreases in the size, number and metabolic activity levels in P-, K-and M-layers of the lateral geniculate nucleus (LGN), and cells in magnocellular layers apparently more susceptible to damage compared to parvocellular cells. Furthermore, changes can manifest in layer 4C of the primary visual cortex (88). Hence, regenerative strategies in glaucoma will have to ensure axonal survival and regrowth, perhaps through stimulation of the retinorecipient afferents (89). This will require attention to glaucoma-related changes to RGC axon terminals within the midbrain and retinotopic specificity of ganglion cell projections (61).

Glaucoma effects on the Sclera and Cornea

Sclera is a dense (400-1000 μm thick) connective-like tissue mainly composed of collagen and elastin fiber and populated with ECM-producing fibroblasts. It extends from the cornea to the optic nerve and provides mechanical support of the retina and an insertion for extraocular muscles. It contacts the lamina cribrosa within the "peripapillary" region (Figure 12A) that is expanded by, and thus resists, IOP. The sclera may therefore be considered biomechanically active system that experiences tension due to IOP and muscular contractions imposed by accommodation/convergence that in turn may be transmitted from the sclera to the adjacent lamina cribrosa, optic nerve and the vasculature that feeds the ONH (78, 80). We know that mechanical stress regulates the composition, growth and size of the eye (90) in part through activity of scleral MMP-2/TIMP2 enzymes (91). Similar to ONH and TM tissues, sclera becomes stiffer and thinner with age and in glaucoma, which may compromise its ability to bear IOP-induced stress and protect the more compliant retina and axons.

Increased risk for IOP-dependent vision loss has been correlated with thinner central corneal thickness and viscoelastic damping ("corneal hysteresis") (40). This might suggest that glaucoma involves changes in molecular mechanotransduction and biomechanical properties across all tissues in the eye. Subjective vision loss in glaucoma often results from corneal edema caused by a rapid rise in IOP. Unfortunately, little is known about how corneal epithelial/endothelial cells sense pressure and tensile stretch (40).

Neuroinflammation in glaucoma: the crucial functions of glial cells

Pressure-dependent activation of retinal glia is a central if sometimes underappreciated feature of glaucoma. In healthy retinas, **Müller cells** (Figure 10, M, blue cells) provide essential metabolic, osmotic support and maintain the excitatory-inhibitory balance through removal of extracellular glutamate. **Astrocytes** (Figure 10, As, green) maintain the ONH structure, support axons, and maintain the blood-retina barrier. **Microglia** (Figure 10, Mi, black) regulate proper synapse formation, phagocytosis and immune signaling, whereas **oligodendrocytes** (not shown in Figure 10) myelinate RGC axons from the lamina to midbrain in the optic nerve.

Glaucomatous glial cells exhibit response patterns that mirror the responsiveness of their brain counterparts to neuronal damage from physical trauma, pathological swelling and neurodegenerative disease. IOP elevations evoke profound changes in retinal glial gene expression, gliotransmitter release, and compromise their roles in

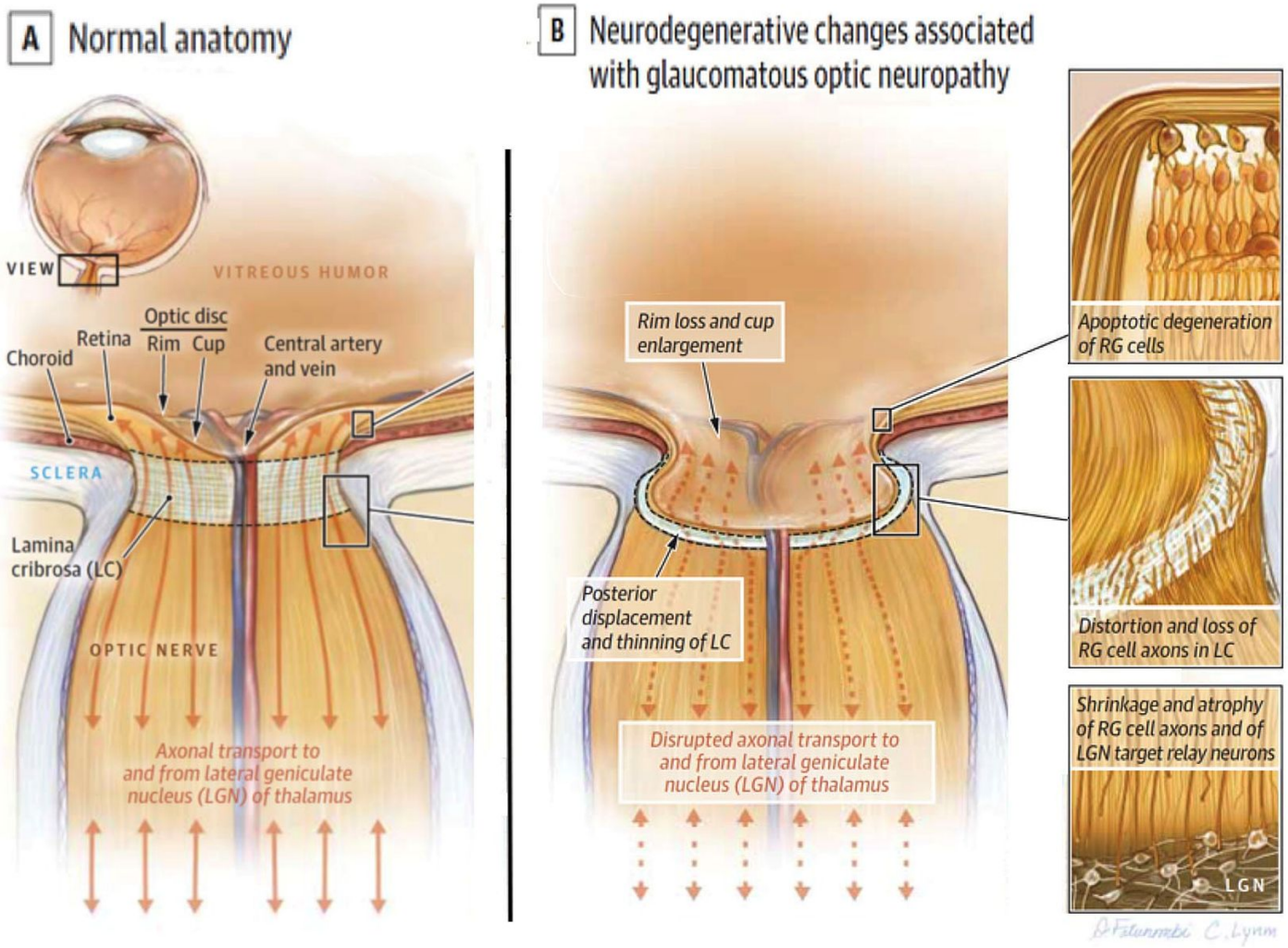

Figure 12. (A) The optic nerve head (optic disk) is composed of neural, vascular, and connective tissues. (A) The convergence of axons of retinal ganglion cells (RG) at the optic disc creates the neuroretinal rim that surrounds the cup, a central shallow depression in the optic disc. RG axons exit the eye through the lamina cribrosa (LC), forming the optic nerve, and travel to relay nuclei for vision within the midbrain (including the LGN). (B) Optic neuropathy in glaucoma involves damage and remodeling of the optic disc and LC that lead to vision loss. Note the displaced and thinned LC that is associated with axonal loss and contributes to the excavation of the cup. Strain placed on the LC causes molecular and functional changes in astrocytes and microglia, remodeling of the extracellular matrix and impairing of local microcirculation. Adapted from Weinreb et al (2014).

nitric oxide, cytokine, chemokine, immune-like molecule (e.g., complement, CX3CL1, TNFα, IL-1β) and reactive oxygen species (ROS) signaling (35, 85). Short and mild increases in IOP may induce reactive activation of Müller cells, astrocytes and microglia prior to significant RGC/axonal damage. One prominent example is glial-dependent changes in cytoskeletal, ECM proteins and structural proteins (the glial acidic fibrillary protein GFAP, vimentin, collagens, laminin and tenascin) and downregulation of proteoglycans (92). Ocular hypertension also underlies metabolomic remodeling in the retinal glia, with includes downregulation of glial glutamate uptake and biosynthesis of glutamine that could impact neuronal excitability and function. A less understood aspect to the yang of pressure-induced proinflammatory glial signaling is the yin of trophic protection from glial release of protective neurotrophic CNTF and/or BDNF factors, and JAK/STAT3 signaling.

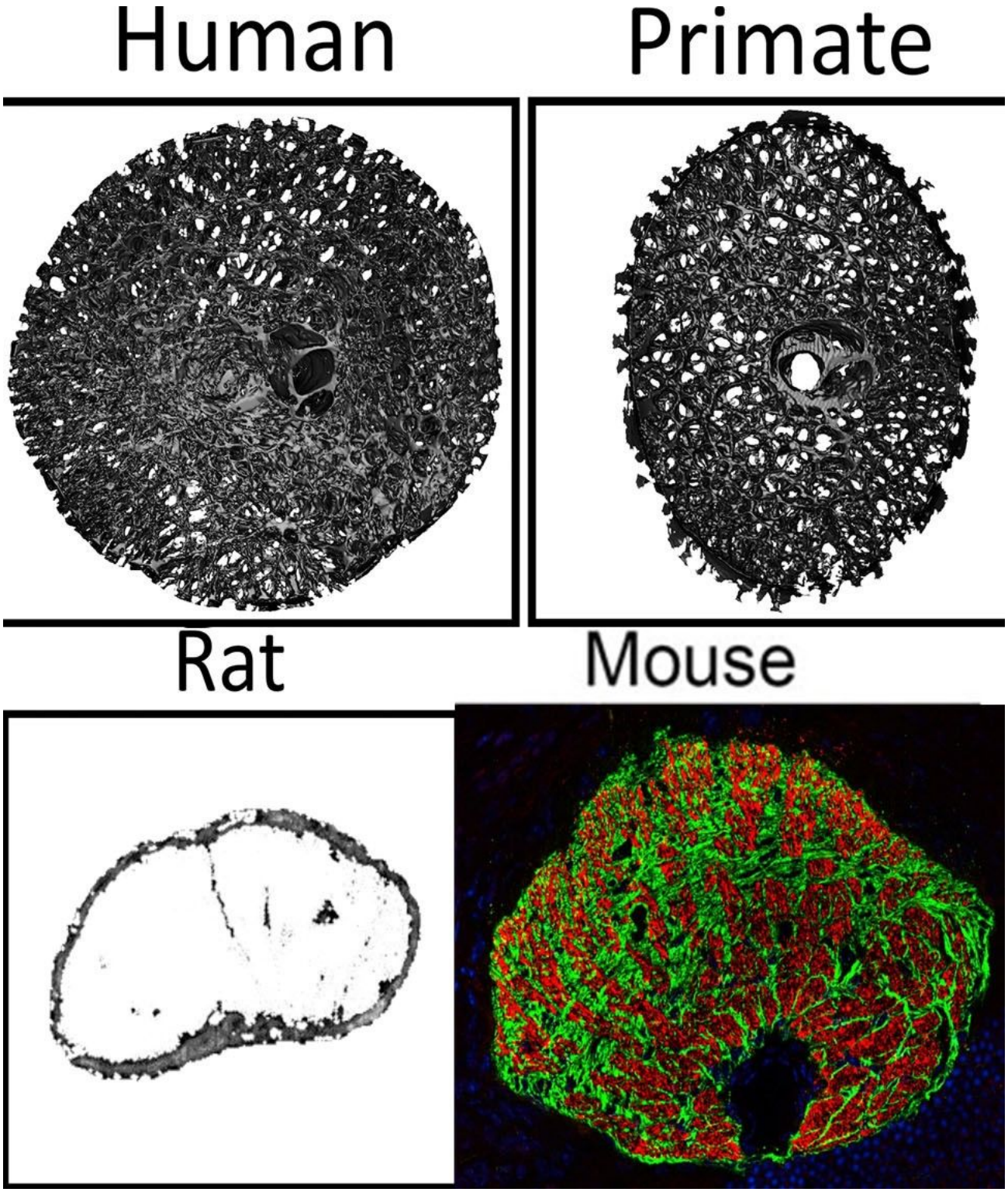

Figure 13. Collagenous lamina are obvious in human and primate, but minimal in rats After Samuels et al., 2018 (140). The lamina in the mouse shows astrocytes (green) between the axons (red). The ophthalmic artery is the hole in all images. From Rudolf Fuchshofer, in Tamm and Ethier, 2017(141).

Astrocytes in the optic nerve head and in glaucoma

Astrocytes are less abundant in the retina than in the brain but still comprise ~50% of cells in the primate ONH. Their retinal functions include maintenance of vascular tone, ECM production and structural support (93).

Astrocytes regulate neuronal activity and neurovascular coupling via ATP, prostaglandin, angiotensin, adenosine and EET (epoxyeicosatrienoic acid) release. Moreover, as the dominant producers of the ECM, astrocytes contribute to the mechanical compliance of the lamina cribrosa and its remodeling in glaucoma. The mammalian retina contains astrocytes with distinct molecular and anatomical signatures. Type I GFAP-positive astrocytes, located in the prelaminar and unmyelinated regions of the human ONH (green in Figures 10 & 14, red in Figure 15A), cover ECM beams and cribrosal pores, ensheath axonal bundles, surround blood vessels and mediate transfer of metabolites between axons and capillaries (green in Figures 10 & 14). Another subtype, the $GFAP^-$negative and α-SMA (smooth muscle actin)- negative Type 2 astrocytes dominate the myelinated postlaminar region of the ONH (94) where they coexist with a subset of recently discovered $GFAP^-$ $\alpha\text{-}SMA^+$ "lamina cribrosa cells" that may weaken the ONH through dysfunctional synthesis of collagens, elastin and fibronectin (95). In rodents, astrocytes are classified using morphological rather than molecular criteria into protoplasmic and fibrous subtypes (92). As in mammals, rodent astrocytes tile the retina to regulate neurovascular function (Figure 10, Figure15B panel E) and send out fine processes that ensheath and compartmentalize axonal bundles. In contrast to the ONH, rodent astrocytes also provide structural support within the "glial lamina" (Figure 13). However, in animals with avascular retinas (such as rabbits), astrocytes are absent from areas that lack blood vessels,

Neighboring astrocytes are coupled through homomeric (e.g., Cx 43) and heterotypic gap junctions that redistribute calcium ions and metabolites across the glial network but also regulate neuronal function via release of neuroactive compounds (96, 97). The cells are a major source of fibronectin, but also upregulate many ECM proteins in response to mechanical stressors (pressure, stretch) under both *in vivo* and *in vitro* conditions (e.g., tenascin, laminin, collagens, elastin and thrombospondin) (e.g., Figure 14) together with genes associated with cell motility and migration (gelsolin, LIMBP1, periplakin) and downregulation of integrin genes (92, 98).

Mechanical stressors dramatically alter the gene expression, morphology and function of retinal astrocytes and push the cells into a reactive state called *astrogliosis* that manifests as the inflammation and fibrosis of the lamina, and correlates with weakened ONH architecture, compromised blood supply and axonal loss (86, 98, 99). Astrocytes in the glaucomatous ONH exhibit thickened processes, calcium-dependent hypertrophy and proliferation (86, 99). The list of genes/proteins associated with IOP-induced astrogliosis comprises hundreds of genes that encode cell cycle proteins, mitogen-activated protein kinases (MAPKs), bone morphogenetic proteins (BMPs), endothelin receptors (ET_A and ET_B), matrix metalloproteinases (MMPs), JAK/STAT3 transcription, cytoskeletal proteins (GFAP, vimentin, collagens, laminin and tenascin), cell adhesion components, signal transduction molecules (NF-kB, STAT5, MCP-1, glypicans), immune/complement systems (C1q, cytokines such as IL-6, LIF), periostin, phagocytosis-related gene *Mac-2,* and/or NF-κB-dependent assembly of the astroglial inflammasome (81, 100, 101). The cytokine TGF-β2 released from retinal astroglia suppresses MMP-dependent ECM degradation while promoting the expression of collagens, elastin and fibronectin (92) that may result in a stiffer lamina and ONH damage. Another hallmark of pressure-activated astrocytes is the migratory response that allows them to crawl out of laminar cribriform plates (102).

While we don't understand how elevated IOP induces astrogliosis, physiological studies show a direct link between mechanical stress and astroglial $[Ca^{2+}]_i$ (97). Physical forces induce transmembrane currents across retinal astrocyte membranes (103), trigger propagation of calcium waves between astrocytes and Müller glia and stimulate release of proinflammatory mediators. Retinal astroglial mechanotransduction is therefore best viewed within the context of feedback loops with adjacent microglia, Müller cells, microvasculature and RGCs (104).

Microglia and monocytes in glaucoma

Glaucoma involves both adaptive and innate immune mechanisms, with retinal microglia - which constitute the innate immune system - as one of the earliest sentinels of mechanical stress. In healthy retinas, microglial processes (*Mi*; black in Figure 10) engage in dynamic surveillance of the local milieu and shaping of local

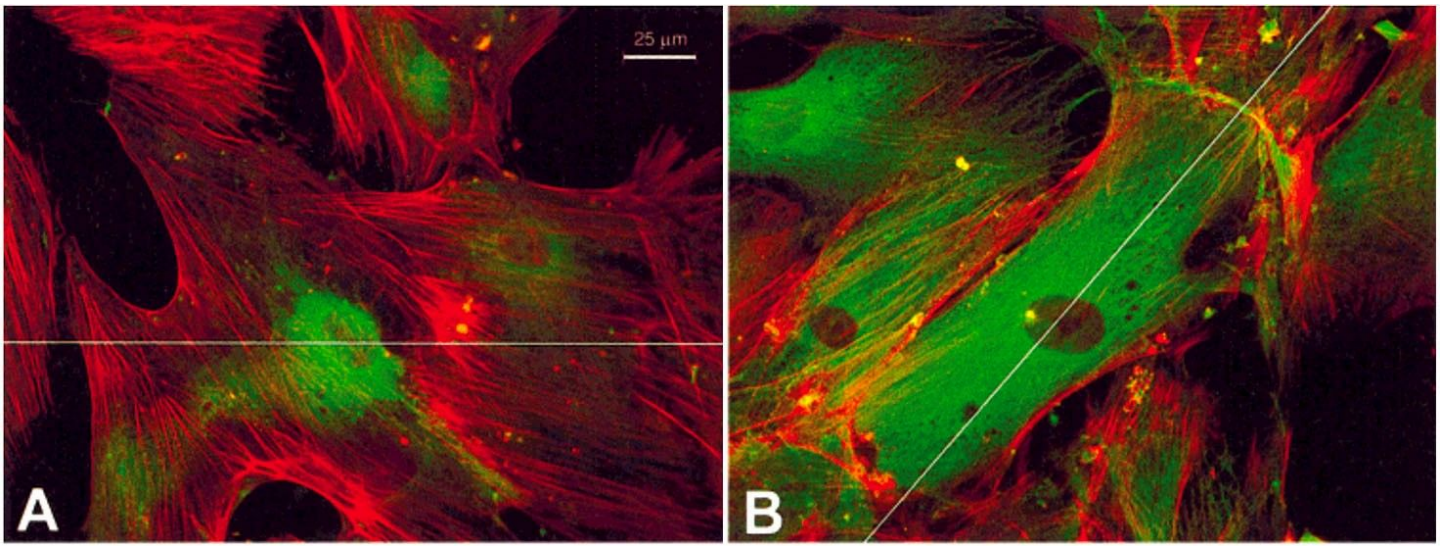

Figure 14. Cultured Type B astrocytes from explanted human lamina cribrosa. (A) Control astrocytes immunostained with tropoelastin (green) and phalloidin (for F-actin, red). (B) Astrocytes exposed to 10 cm H_2O pressure have increased intracellular tropoelastin (green) and displacement of the F-actin filaments (phalloidin, red) to the periphery of the cells. From Hernandez et al., 2000 (98).

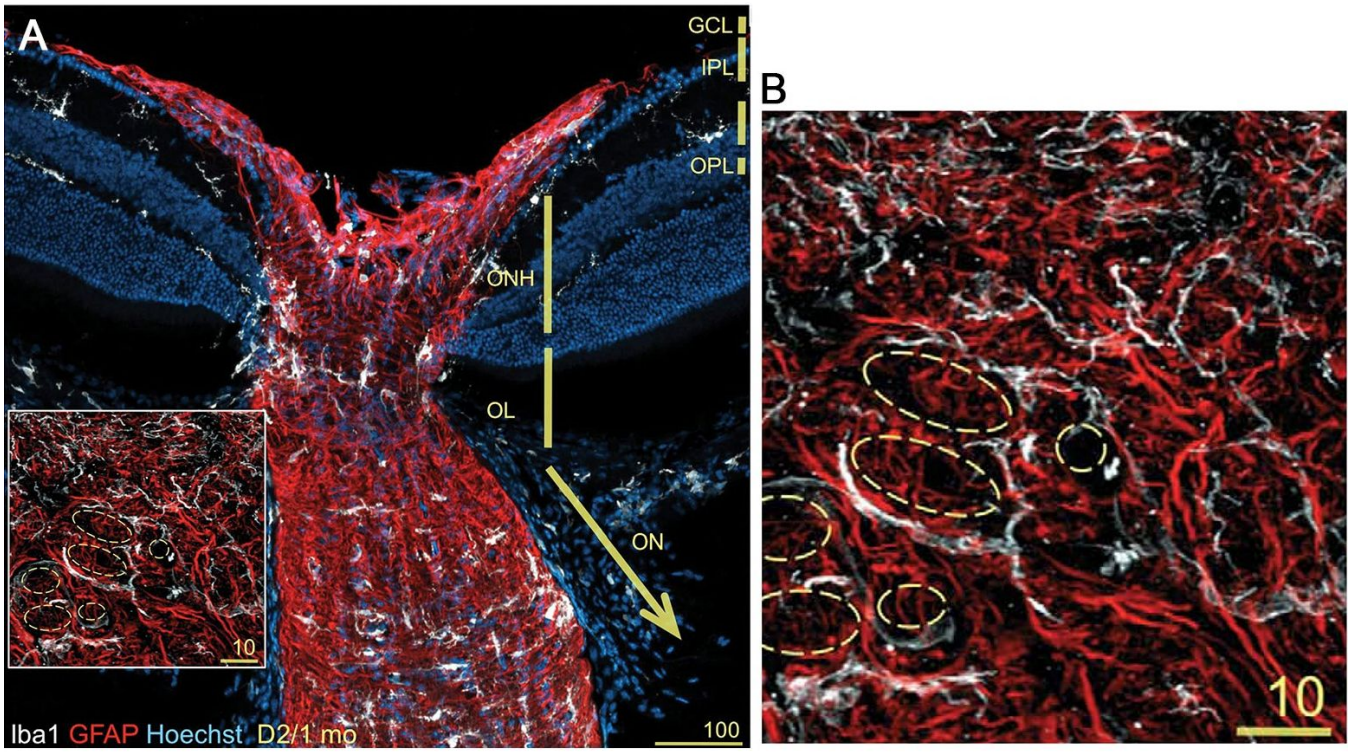

Figure 15A. (A) The mouse optic nerve head (ONH) labels for microglia (Iba1, white) and astroglia (GFP, red) and cell bodies (blue). ONH astrocytes maintain the laminar structure associated with microglia and ganglion cell axons. (B) Higher magnification of the optic lamina with microglial lining and astrocytic tunnels containing GC axons. From Bosco et al., 2011 (84).

synaptic contacts but this activity is dramatically altered in the proinflammatory phenotype associated with glaucomatous microglia. These cells can be characterized by proliferation, process retraction and upregulation of complement, toll-like receptor (TLR2-4), TNFR1α & β receptors, nitric oxide synthase, heat-shock proteins (HSP27, HSP60, HSP72), chemokine (IL-8) and cytokine (IL-1β, IL-6, CCL2, TNFα) signaling as well as the

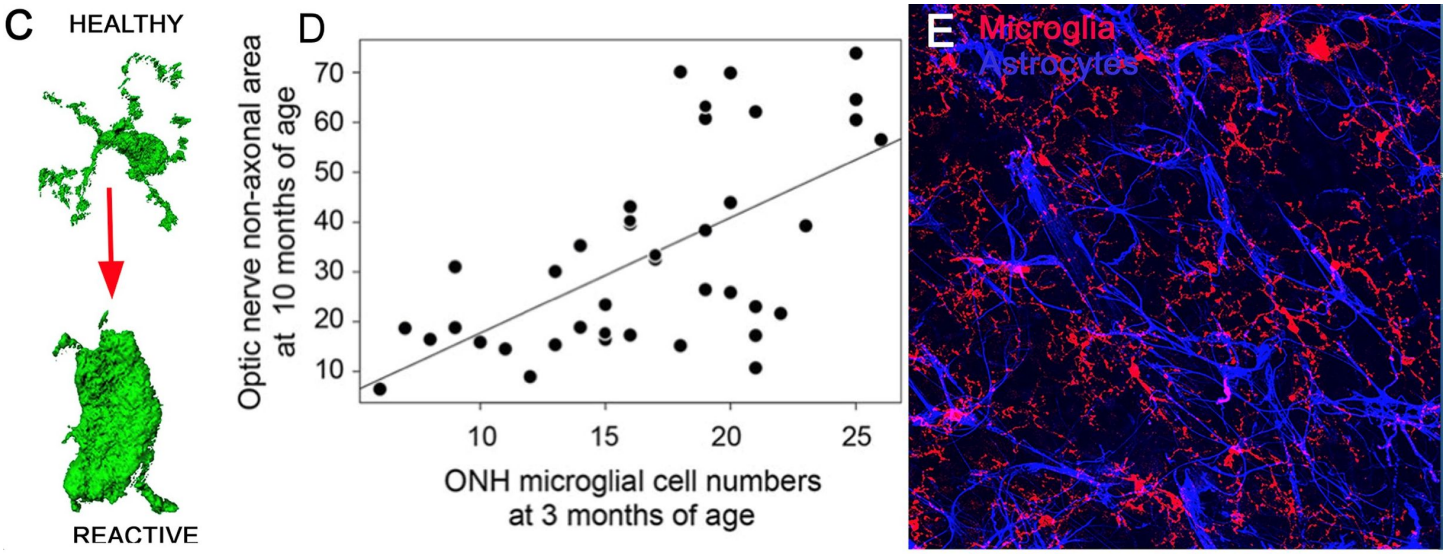

Figure 15B. (C) Typical examples of resting, ramified microglial cell (top) and reactive, amoeboid cell (bottom). (D) The number of microglia in the ONH at the early stage of glaucoma correlates with the later axonal loss. (E) Early glaucoma (mouse). Microglia were labeled with the CD11b (red), astrocytes with GFAP (blue). The cells show signs of hypertrophy (thickened processes and enlarged somata). Images from Jonn Lieff (142) (C), Bosco et al. (2015) (109) (D), and F. Vazquez and D. Krizaj, unpublished data (E).

suppression of anti-inflammatory TGFβ signaling (35, 105). Release of metalloproteinases (MMP-1-3) may alter and destabilize the ECM early in the disease. An important recent study from the Vetter laboratory recently demonstrated a key role for microglia in selecting the surviving RGCs during development (106). Within the ONH, microglial activation is first detected in the areas of early axonal damage (Figure 15A, Figure 15B), potentially in response to loss of fractalkine (CX3CL1) inputs from RGCs (107) and altered cross-talk with Müller glia (108). Both minocycline, a small-molecule inhibitor of microglial activation, and bosentan, an inhibitor of microglial endothelin (ET1/2) receptors, increased ganglion cell survival in the DBA/2J mouse glaucoma model (81, 109).

Another important feature of immune activation in the glaucomatous retina is the permeability loss of the blood-retina barrier, which allows the invasion of activated monocytes and dendritic cells from systemic circulation (81, 105). Glaucoma has been linked to microglial changes in the classical and alternative complement pathways, with the 'alternative' C1q complex (38) presumably promoting activation of the 'classical' C3 convertase that instigates synaptic pruning and somatic phagocytosis. Another important player are the cytokines IL-1β and TNFα, which promote RGC apoptosis in the glaucomatous retina (105). IOP elevation in one eye triggers microglial activation in both eyes, providing evidence that the involvement of immune mechanisms in glaucoma involves the spread of diffusible systemic factors. Consistent with this, activated microglia form clusters around blood vessels in hypertensive eyes (110) and dendritic and synaptic architecture in rodent glaucoma can be protected not only by inhibiting the C1q protein or deleting its gene, but also by blocking pressure-induced immigration of macrophages/monocytes (60, 81). In addition, microglia may respond to mechanically released chemokines such as the monocyte chemoattractant protein (MCP-1) from Müller glia (111) and fractalkine (CX3CL1) from ganglion cells (107).

Müller cells

Müller cells (*M*; blue in Figure 10) are radial glia that extend from the outer to the innermost retina. They ensheath every neuron and regulate virtually every aspect of retinal function, from energy metabolism to volume regulation, blood flow, uptake and recycling of neurotransmitters and immune signaling (112). Their membrane properties are dominated by potassium channel Kir 4.1-dependent inward rectification, which

drowns the contributions from other ion channels. Müller endfeet contribute to the neurogliovascular unit that maintains the blood-retina barrier (Figure 16, control) and also secrete the basement membrane forming the inner limiting membrane through which the retina interacts with IOP. Endfeet strongly express stretch-activated TRPV4 channels and are therefore very sensitive to tensile stretch, poking and changes in volume (27, 113).

Müller glia are amongst the first retinal cells to respond to elevated IOP (85). Acute and chronic IOP elevations push them into a reactive state (reactive gliosis) that is typically visualized by immunolabeling the retina for the intermediate filament GFAP (Figure 16; chronic and acute glaucoma). Mice lacking GFAP may be more sensitive to mechanical injury (114), perhaps because these cytoskeletal elements resist mechanical stress. In the reactive mode, Müller cells are likely to modulate vascular permeability and neuronal survival via the release of nitric oxide, TNFα/IL-1β/NF-κB/mTOR signaling and release of the cytokine MCP-1 (35, 111). Among other aspects of Müller signaling affected by pressure are the downregulation of glutamine synthesis/glutamate uptake, upregulation of cytoskeletal proteins, and changes in expression of aquaporin AQP4 (water) channels, calcium channels (ryanodine receptors), complement proteins (C1q) and advanced glycation end products (RAGE) (72, 115, 116).

Endothelial cells, pericytes and local blood supply

Blood supply to the ONH originates in the ophthalmic artery which branches into the central retinal artery, perfusing the nerve fiber layer (Figure 10) and two posterior ciliary arteries. Venous blood drains into the central vein that travels in the optic nerve (Figure 12). Large IOP increases induce ischemia, which compromises the diffusion of glucose, oxygen and lactate through capillary compression, however, even small (3-5 mm Hg) elevations in IOP may result in hypoxia, accumulation of reactive oxygen species and hypoxia-induced factors (e.g., HIF-1α and HIF-2α), downregulation of astroglial glutathione content and induction of the autophagosome (117).

Research challenge for the future

The importance of calcium

The past decades have seen intense efforts to determine the final common mechanism(s) in glaucomatous retinal injury. With respect to RGCs, these mechanisms include ER stress, activation of proapoptotic cascades and dysregulation of calcium homeostasis within axonal and nonaxonal compartments (35, 39). Calcium, a 2nd messenger, plays critical functions in cellular physiology and pathology across the body and it is not surprising that virtually every cell type associated with glaucoma, and every stage of the disease, appear to involve Ca^{2+} dysregulation. The sources and pathways associated with pathological Ca^{2+} homeostasis in glaucoma may include ion channels within the plasma membrane and calcium release from intracellular compartments such as the endoplasmic reticulum (ER), mitochondria and lysosomes. It is not inconceivable that such changes in $[Ca^{2+}]_i$ promote TM contractility, drive inflammatory activation of retinal glia and facilitate the susceptibility of RGCs to secondary insults.

Experiments *in vitro* have demonstrated that mechanical stress triggers $[Ca^{2+}]_i$ elevations in retinal ganglion cells, microvascular endothelial cells, nonpigmented cells of the ciliary body, glia and the trabecular meshwork (51, 113, 118-120) whereas Ca^{2+} removal from the external medium or calcium chelation block stretch- and swelling-induced Ca^{2+} influx and stretch-induced remodeling of the cytoskeleton. There is evidence that $[Ca^{2+}]_i$ increases in glaucomatous RGCs occur in dendrites and somata (121), which might account for the increased ER stress and Ca^{2+}-dependent signals (immediate early genes (c-fos, JNK2/3, CREB), proteases, caspases and MAP kinases) in glaucomatous RGCs. Another Ca^{2+}-dependent mechanism involves constitutive activation of calpains, Ca^{2+}-dependent enzymes that promote caspase activation and protein degradation. Inhibition of calpains was protective in models of rodent ganglion cell injury, presumably through the Ca^{2+}-activated

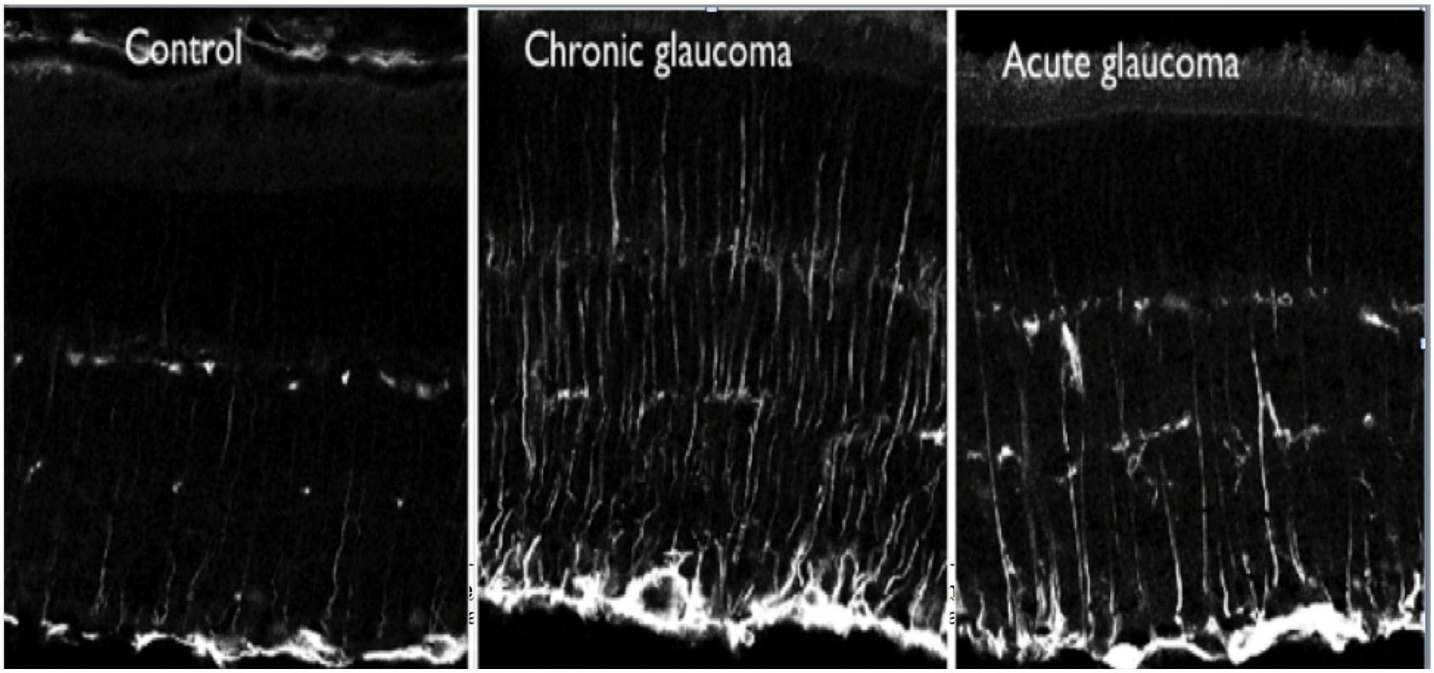

Figure 16. Reactive Müller gliosis in chronic (DBA/2J) and acute (microbead) mouse models of glaucoma. IOP elevations are associated with pressure-dependent upregulation of GFAP (glial fibrillary acid protein) in endfeet and radial processes (Krizaj laboratory, unpublished data).

phosphatase calcineurin (71). It is also possible, however, that the calcineurin-calpain pathway may contribute to axonal regeneration (122).

The findings described above suggest that targeting pressure-induced calcium influx might help alleviate retinal pathology. Such protective effects were seen under non-physiological conditions (optic nerve transection/crush), with the blockade of voltage- and glutamate-dependent calcium influx conferring largely protective effects on RGC survival and axonal degeneration. We hypothesize that blocking calcium-permeable channels that are sensitive to pressure or its biomechanical corollaries (such as tensile stretch) might result in even more significant injury amelioration in hypertensive eyes.

Importance of mechanotransduction

A crucial requirement without which glaucoma in animals and humans cannot be understood, is to define the molecular links between ocular pressure sensing, aqueous humor dynamics and neurodegeneration. To achieve this, we need a better understanding of actual sites of mechanical impact within the eye and identification of mechanical stressors (tensile strain, shear flow, compression etc.) that are sensed by cells in both the anterior and the posterior eye. Studies in animal models of glaucoma and in isolated cells show that most glaucoma-relevant cell types (trabecular meshwork cells, retinal glia and RGCs) respond to pressure with fast onset electrical and calcium signals (~milliseconds to ~seconds), whereas sustained exposure to mechanical stressors tends to evoke phenotypes that are characteristic of glaucomatous injury. In addition to characterizing the pressure transducer molecules, it will also be important to determine how ocular cells ignore steady-state IOP, and how they respond to and compensate for transient IOP fluctuations triggered by blinking, coughing, eye rubbing, circadian periodicity, swelling, ocular trauma, and exercise (e.g., swimming goggles, yoga practice). To identify the molecular mechanisms, we can now build on the vast trove of information available from investigations of cellular mechanosensing.

Mechanobiology is an emerging field that combines biology and bioengineering to study how physical forces and changes in mechanical properties of cells contribute to cell development, differentiation, proliferation and disease. Its common theme is that every cell converts mechanical inputs into electrical or biochemical signals by using specialized proteins that govern the mechanical stability and mechanical signal transmission at virtually every level of organization, from the nanoscale to macroscale (123, 124). These mechanotransduction machines impose regulatory constraints at the level of cell-cell and tissue-tissue networks but some cells are better at mechanotransduction than others, and therefore more sensitive to mechanical forces and dysregulated in disease. Often cited examples of mechanotransduction gone awry are hearing and balance diseases caused by mutations in mechanosensitive proteins, but there are many other examples of bone, cartilage, lung, bladder, immune system, heart and eye diseases caused by increased pressure and stretch (125). Glaucoma and myopia, for example, can be considered as mechanotransduction diseases that reflect the dysfunctional response of cells in the eye to specific types of local mechanical stress.

Many protein families respond to mechanical forces with conformational changes. Mechanosensitive proteins include focal adhesion proteins, cell-cell adhesion, integrin and ECM proteins, receptor tyrosine kinases, G-protein-coupled receptors, cytoskeletal proteins and, importantly, ion channels that are activated by minute changes in membrane curvature and stretch in the absence of chemical ligands (124-126). These m*echanosensitive channels* evolved for sensing submicrometer displacements of the plasma membrane but show huge differences in primary structure, ion selectivity, conductance and pharmacology (Figure. 17). They have been classified into Na^+-permeable (ENaC/degenerins), K^+-permeable (TREK, TRAAK) and nonselective cation (TRP and piezo) channel families, which show isoform-specific mechanical thresholds, time courses, adaptation to sustained stimulation as well as differences in how they tether to the cytoskeleton and respond to posttranslational modulation.

Conceptually, mechanochannels function as bandpass filters that can transmit specific amplitudes and types of mechanical stress (i.e., compression, tension, swelling, shear flow etc.) that range from gentle touch, pressure, texture, vibration, sound, shear flow to physical trauma and pain. Recent studies show that glaucoma-relevant tissues in the eye (TM, ciliary body, neurons, glia, cornea, endothelial cells) express multiple types of mechanosensitive TRP, piezo and tandem pore K^+ channels (27, 127-129). Pharmacological suppression and genetic ablation of these channels ameliorate the inflammatory and degenerative retinal phenotypes associated with ocular hypertension (119), suggesting possible roles in glaucoma.

Figure 17 illustrates the basic topology of vanilloid TRP (TRPV) and TREK (TWIK-1 related K+) mechanotransducers. TRPV4, a member of the vanilloid TRP family mediates influx of Na^+ and Ca^{2+} ions in response to a wide variety of mechanical and chemical stimuli (130, 131) that include pressure, stretch, swelling, poking and body temperature (34 - 37^{o}C). It is expressed in ~60-70% of mouse RGCs, 100% of Müller cells (Figure 18A) and the majority of trabecular and corneal epithelial cells (70, 113, 132), with some RGCs sharing TRPV4 expression with the cognate TRPV1 channel (Figure 18B) (70, 128). Interestingly, the channel appears to be absent from neuronal classes that are less sensitive to glaucoma (photoreceptors, bipolar, amacrine cells; Figure 10) and mice lacking TRPV4 show no deficits in outer retinal function (Figure 18C). TRPV4 channels are often integrated into cells' cytoskeleton network through ankyrin repeats in the N-terminus (Figure 17A) and are linked to ECM networks through α2 integrin molecules and focal adhesions. They are sensitive to pressure (129), drive stretch-induced cytoskeletal remodeling and may contribute to the loss of tensile homeostasis during chronic IOP elevations (51).

Many ocular manifestations of glaucoma (IOP changes, calcium overloads, reactive gliosis, cytokine release, microvascular dysfunction, actin upregulation, fibronectin secretion and RGC apoptosis) can be mimicked pharmacologically by stimulating TRPV4 channels in RGCs, glial, endothelial, ciliary body and trabecular meshwork cells (27, 111, 127, 133). TRPV4-induced phenotypes include RGC degeneration (133), reactive gliosis (27), glial swelling (113) and increased permeability of the blood-retina barrier (127, 134) whereas mice

lacking the TRPV4 gene seem to be protected from some types of mechanical and nociceptive stress (130) and do not appear to develop glaucoma (51). Cholesterol and polyunsaturated fatty acids - potential risk factors in glaucoma - also modulate TRPV4 activation (135).

How is mechanical homeostasis in the healthy eye maintained in counterpoint to TRP and piezo channel activation? A possible mechanotransducer candidate that opposes excessive TRPV4 activation might be the K^+-permeable TREK-1 channel. TREK-1 is eerily sensitive to stimuli that gate TRPV4 (membrane stretch, swelling, body temperature, and arachidonic acid) and is often co-expressed with TRPV4 (O. Yarishkin, F. Vazquez-Chona and D.K., unpublished observations). Mice lacking TRPV4 channels are less sensitive to mechanical stress (131) whereas mice with ablated TREK/TRAAK channels are hypersensitive to mechanical forces and local pH changes (136). According to this model, the tensile homeostasis of at least some ocular tissues might be maintained by concomitant activation of TRPV4/piezo vs. TREK-1 (and its cognate TRAAK) channels.

Summary and Conclusion

Glaucoma is a leading cause of irreversible blindness worldwide. There are multiple forms of the disease, but all involve dysfunctional signaling in the anterior eye that is linked to optic neuropathy. There is no cure and at present there is no way to regain sight that had been lost. This is a problem, because glaucoma is often asymptomatic until very late stages and many people with the disease do not realize they have the disease until it is too late for effective treatment. It is therefore important that patients with risk factors (i.e., elderly individuals with family history and/or African ancestry) are screened at regular intervals. After diagnosis, treatment will be lifelong but requires vigorous compliance with the treatment regimen (IOP-lowering eye drops).

What is glaucoma? The clearest answer is that we still don't know, as pathology can reflect a multifactorial pathology and/or a collection of diseases with a similar final common pathology. Interestingly, mechanotransduction in aged individuals and those with glaucoma appear to be compromised across all tissues of the eye (cornea, sclera, TM, retina), suggesting broad dysfunctions in the cells' ability to generate and process mechanical forces. Most forms of glaucoma appear to be hereditary, but it is likely that in order for the pathology to manifest, mutations/alterations in multiple proteins and/or lipids are required and identification of causal genes and mutations will immensely advance the diagnosis and treatment. For now, only 5-10% of cases have been linked to specific genes.

IOP lowering - currently the main treatment - begin with eye drops, with refractory or advanced cases relegated to laser procedures and incisional surgeries. At this time, anti-glaucoma agents largely target a secondary pathway that mediates a minuscule fraction of fluid outflow and there is much scope for improvement, especially in targeting trabecular outflow. Another priority is to protect retinal neurons and glia from pressure, which necessitates the elucidation of molecular/cellular mechanisms that sense and transduce mechanical stress. Specifically, improved treatment requires research scientists, clinicians and biomedical engineers to (i) Determine the quantitative relationships between risk factors, genetic susceptibility and molecular mechanisms that underlie cellular interactions in the front and the back of the eye, (ii) Develop standardized tests to define where the optic neuropathy in a particular patient falls in the spectrum between 'normal' aging and glaucoma, (iii) Develop novel technologies (such as optical coherence tomography) for early diagnosis (iv) Improve the efficacy of pharmacological agents that target TM while eliminating side effects and (v) Protect the pressure sensitive targets within the trabecular meshwork, retinal ganglion cells and glia. This requires investment into neuroprotective treatments, which has been discouraged by disagreements among scientists about RGC mechanotransduction mechanisms, the prohibitive expense of clinical trials, and recent pricey failures of putative neuroprotection drugs.

A main goal for future treatments must be to lower IOP together with the protection from pressure-dependent inflammation and neurodegeneration, an approach that may include direct targeting of the pressure sensing proteins themselves. Unfortunately, at this moment there seems to be - despite decades of intense research - no

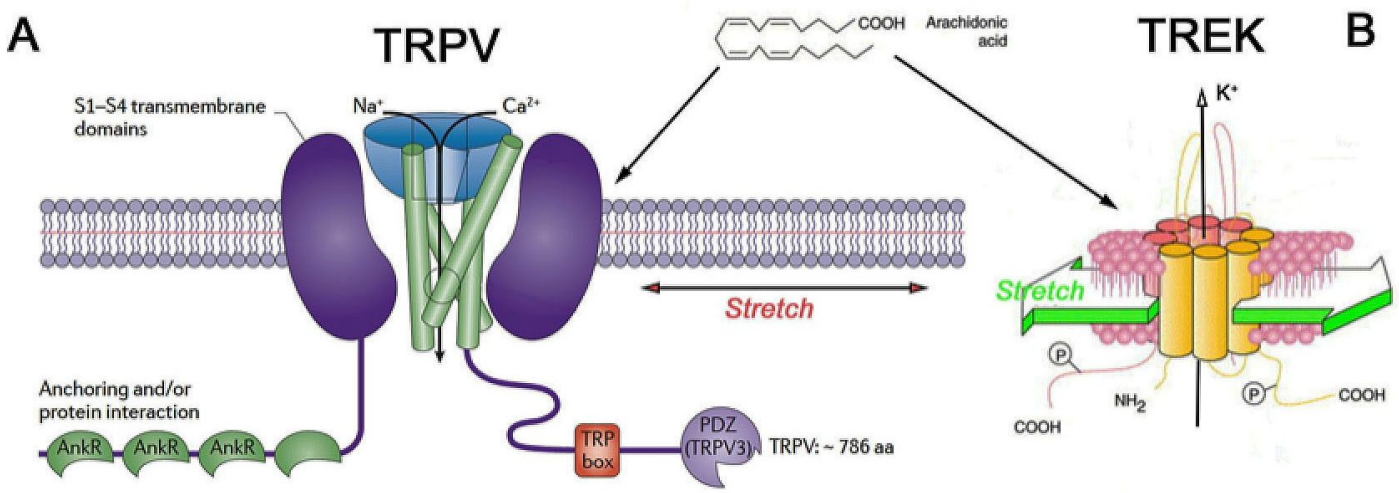

Figure 17. Schematic representation of mechanosensitive vanilloid TRP (TRPV) and tandem-pore TREK/TRAAK channels. (A) TRPV channels include amino terminal ankyrin repeats (AnkR), the TRP box which is thought to be involved in channel gating, and a PDZ/PSD95 domain that may regulate cytoskeletal interactions. (B) TREK and TRAAK channels are formed by two loop-forming (P) subunit tetramer domains which dimerize to form the functional channel. Adapted from Moran et al., 2011 (143) and Patel and Honoré, 2001 (144).

consensus regarding the early retinal targets of IOP (dendrites? somata? axons? glia? blood vessels? ONH?). It is becoming obvious, for example, that glia are amongst the earliest responders to elevated pressure and that neurodegeneration can continue long after IOP is stabilized. Therefore, any attempts at neuroprotection must take into account IOP-independent vascular, glial and scleral mechanisms. Very possibly, prevention of glaucoma will improve with better understanding of molecular, circadian, caloric restriction and exercise parameters that are increasingly viewed as relevant to ocular health. Another innovative front will definitely be on the technology side, as patients are equipped with real-time telemetric devices, noninvasive ONH measurements become routine, and diagnoses are provided by deep learning (artificial intelligence) algorithms (46). We live in exciting times that, having unveiled the key likely components and patterns of visual damage in glaucoma and old age, can only lead to glorious future where mechanotransduction mechanisms in individuals at risk for disease onset are understood, targeted and used for early diagnosis.

Acknowledgements

Supported by the National Institutes of Health, The Willard L. Eccles Foundation, Glaucoma Research Foundation, University of Utah Technology Acceleration Grant and an Unrestricted Grant from Research to Prevent Blindness to the Department of Ophthalmology at the University of Utah. The author thanks the past and present members of his laboratory for outstanding work over the past decade, Andrea Blitzer, M.D. for help with initial literature review and Drs. Ralph Nelson (NIH) and Helga Kolb (University of Utah) for helpful comments.

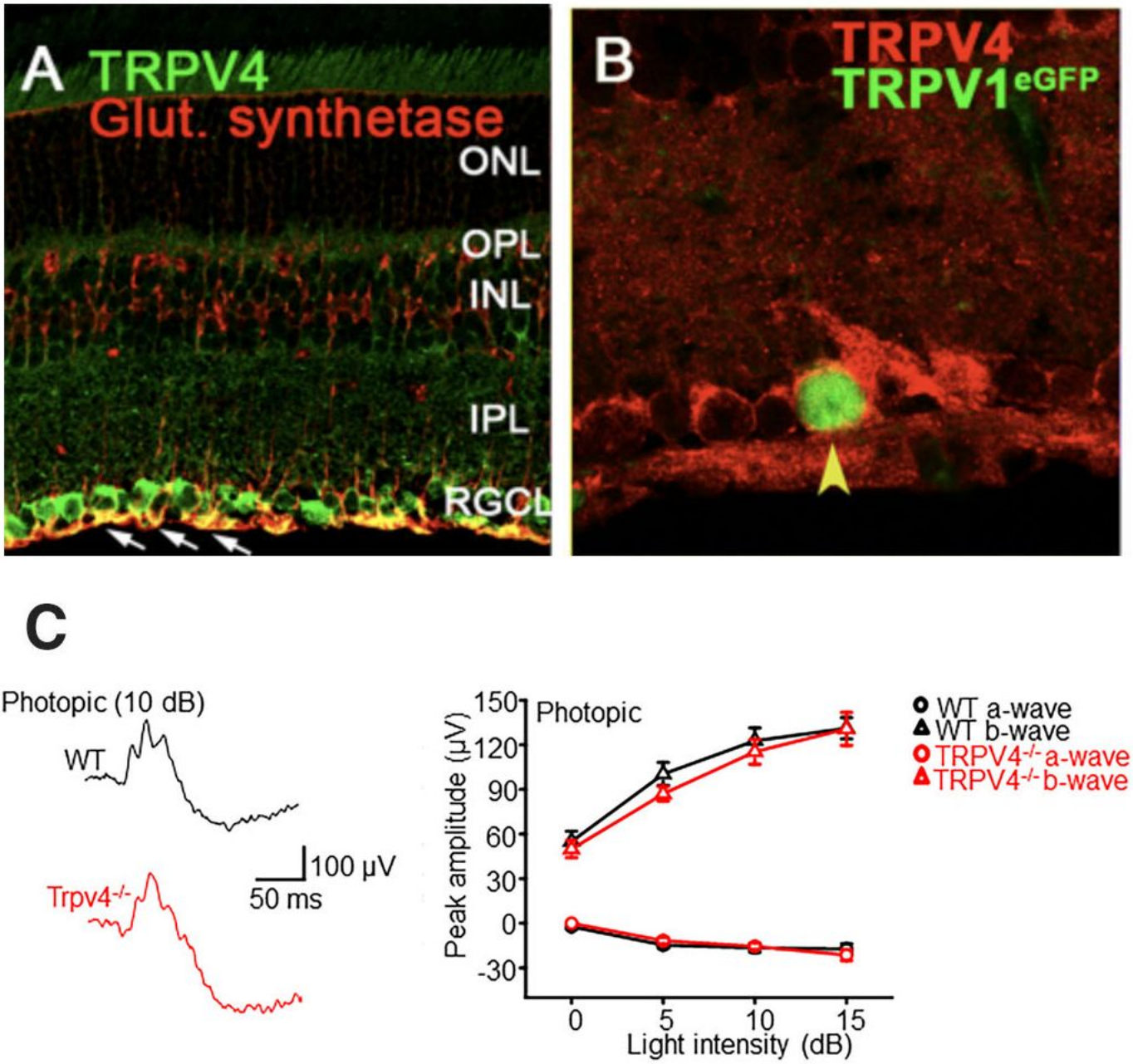

Figure 18. TRPV4 expression in the mouse retina. (A) TRPV4 (green) is expressed in retinal ganglion cells and in the endfeet of Müller glia that were labeled with the anti-glutamine synthetase antibody (red). The endfeet are marked by arrows. After Ryskamp et al., 2014 (27). (B) Detail of the inner retina showing TRPV4 localization (red) to the majority of retinal ganglion cells, whereas the cognate TRPV1 channel (green) is localized to a small subset. After Lakk et al., 2018 (70). (C) Genetic ablation of TRPV4 channels has no effect on the function of the inner retina, as indicated by the field potentials that measure photoreceptor and bipolar function. After Yarishkin et al., 2018 (145).

About the author

David Krizaj received his B.A. at the University of Ljubljana (Slovenia), Ph.D. in Physiology & Biophysics at New York University and completed postdoctoral studies in Retinal Neurobiology at University of California San Francisco. He took a position at the Moran Eye Center at the University of Utah School of Medicine where he holds the John Frederick Carter Endowed Professorship in Ophthalmology. Dr. Krizaj's interests include intracellular signaling pathways with a focus on calcium homeostasis, synaptic transmission and mechanotransduction, and the last 5 years his lab has been actively engaged in studying the roles of mechanosensitive TRP, tandem-pore and piezo channels in the regulation of intraocular pressure. Another main thrust is to define the molecular mechanisms of pressure sensitivity of trabecular meshwork cells, retinal neurons and glia, and how its dysregulation contributes to diabetic retinopathy and glaucoma. Dr. Krizaj can be contacted at david.krizaj@hsc.utah.edu.

References

1. Flaxman S.R., Bourne R.R., Resnikoff S., Ackland P., Braithwaite T., Cicinelli M.V., Das A., Jonas J.B., Keeffe J., Kempen J.H. Global causes of blindness and distance vision impairment 1990–2020: a systematic review and meta-analysis. The Lancet Global Health. 2017;5(12):e1221–e1234. PubMed PMID: 29032195.
2. Ko Y.-C., Hwang D.-K., Chen W.-T., Lee C.-C., Liu C.J. Impact of socioeconomic status on the diagnosis of primary open-angle glaucoma and primary angle closure glaucoma: a nationwide population-based study in Taiwan. PloS one. 2016;11(2):e0149698. PubMed PMID: 26905307.
3. Tsatsos M., Broadway D. Controversies in the history of glaucoma: is it all a load of old Greek? British Journal of Ophthalmology. 2007;91(11):1561–1562. PubMed PMID: 17947272.
4. Leffler, C.T., S.G. Schwartz, F.M. Giliberti, M.T. Young, and D. Bermudez, *What was glaucoma called before the 20th century?* Ophthalmology and eye diseases. 2015; 7:OED. S32004.
5. Mackenzie, W., A. Hewson, and T.W. Jones, *A Practical Treatise on the Diseases of the Eye*. 1855: Blanchard and Lea.
6. Hood D.C. Improving our understanding, and detection, of glaucomatous damage: an approach based upon optical coherence tomography (OCT). Progress in retinal and eye research. 2017;57:46–75. PubMed PMID: 28012881.
7. Smith C., Vianna J., Chauhan B. Assessing retinal ganglion cell damage. Eye. 2017;31(2):209. PubMed PMID: 28085141.
8. Harwerth R.S., Crawford M., Frishman L.J., Viswanathan S., Smith E.L. III, Carter-Dawson L. Visual field defects and neural losses from experimental glaucoma. Progress in retinal and eye research. 2002;21(1):91–125. PubMed PMID: 11906813.

9. Pavlidis M., Stupp T., Naskar R., Cengiz C., Thanos S. Retinal ganglion cells resistant to advanced glaucoma: a postmortem study of human retinas with the carbocyanine dye DiI. Investigative ophthalmology & visual science. 2003;44(12):5196–5205. PubMed PMID: 14638717.
10. Nickells R.W., Howell G.R., Soto I., John S.W. Under pressure: cellular and molecular responses during glaucoma, a common neurodegeneration with axonopathy. Annual review of neuroscience. 2012;35:153–179. PubMed PMID: 22524788.
11. Libby R.T., Gould D.B., Anderson M.G., John S.W. Complex genetics of glaucoma susceptibility. Annual review of genomics and human genetics. 2005.:6. PubMed PMID: 16124852.
12. Wiggs J.L., Pasquale L.R. Genetics of glaucoma. Human molecular genetics. 2017;26(R1):R21–R27. PubMed PMID: 28505344.
13. Jonas J.B., Aung T., Bourne R.R., Bron A.M., Ritch R., Panda-Jonas S. Glaucoma. Lancet. 2017;390(10108):2183–2193. PubMed PMID: 28577860.
14. Quigley H.A. Understanding glaucomatous optic neuropathy: the synergy between clinical observation and investigation. Annual review of vision science. 2016;2:235–254. PubMed PMID: 28532352.
15. Weinreb R.N., Aung T., Medeiros F.A. The pathophysiology and treatment of glaucoma: a review. Jama. 2014;311(18):1901–1911. PubMed PMID: 24825645.
16. Allingham, R.R., K.F. Damji, and M.B. Shields, *Shields textbook of glaucoma*. 6th ed. 2011, Philadelphia: Wolters Kluwer Health/Lippincott Williams & Wilkins. xiv, 610 p.
17. Jonas J.B., Weber P., Nagaoka N., Ohno-Matsui K. Glaucoma in high myopia and parapapillary delta zone. PLoS One. 2017;12(4):e0175120. PubMed PMID: 28380081.
18. Tham Y.-C., Aung T., Fan Q., Saw S.-M., Siantar R.G., Wong T.Y., Cheng C.-Y. Joint effects of intraocular pressure and myopia on risk of primary open-angle glaucoma: the singapore epidemiology of eye diseases study. Scientific reports. 2016;6:19320. PubMed PMID: 26758554.
19. Armaly M. The genetic determination of ocular pressure in the normal eye. Archives of Ophthalmology. 1967;78(2):187–192. PubMed PMID: 4952595.
20. Khor C.C., Do T., Jia H., Nakano M., George R., Abu-Amero K., Duvesh R., Chen L.J., Li Z., Nongpiur M.E. Genome-wide association study identifies five new susceptibility loci for primary angle closure glaucoma. Nature genetics. 2016;48(5):556. PubMed PMID: 27064256.
21. Zode G.S., Bugge K.E., Mohan K., Grozdanic S.D., Peters J.C., Koehn D.R., Anderson M.G., Kardon R.H., Stone E.M., Sheffield V.C. Topical ocular sodium 4-phenylbutyrate rescues glaucoma in a myocilin mouse model of primary open-angle glaucoma. Investigative ophthalmology & visual science. 2012;53(3):1557–1565. PubMed PMID: 22328638.
22. Minegishi Y., Nakayama M., Iejima D., Kawase K., Iwata T. Significance of optineurin mutations in glaucoma and other diseases. Progress in retinal and eye research. 2016;55:149–181. PubMed PMID: 27693724.
23. Thorleifsson G., Walters G.B., Hewitt A.W., Masson G., Helgason A., DeWan A., Sigurdsson A., Jonasdottir A., Gudjonsson S.A., Magnusson K.P. Common variants near CAV1 and CAV2 are associated with primary open-angle glaucoma. Nature genetics. 2010;42(10):906. PubMed PMID: 20835238.
24. McGwin G., McNeal S., Owsley C., Girkin C., Epstein D., Lee P.P. Statins and Other Cholesterol-Lowering Medications and the Presenceof Glaucoma. Archives of ophthalmology. 2004;122(6):822–826. PubMed PMID: 15197056.
25. Davis L.K., Meyer K.J., Schindler E.I., Beck J.S., Rudd D.S., Grundstad A.J., Scheetz T.E., Braun T.A., Fingert J.H., Alward W.L. Copy number variations and primary open-angle glaucoma. Investigative ophthalmology & visual science. 2011;52(10):7122–7133. PubMed PMID: 21310917.
26. Braunger B.M., Fuchshofer R., Tamm E.R. The aqueous humor outflow pathways in glaucoma: A unifying concept of disease mechanisms and causative treatment. European Journal of Pharmaceutics and Biopharmaceutics. 2015;95:173–181. PubMed PMID: 25957840.
27. Ryskamp D.A., Jo A.O., Frye A.M., Vazquez-Chona F., MacAulay N., Thoreson W.B., Križaj D. Swelling and eicosanoid metabolites differentially gate TRPV4 channels in retinal neurons and glia. Journal of Neuroscience. 2014;34(47):15689–15700. PubMed PMID: 25411497.

28. Bennett T.M., Mackay D.S., Siegfried C.J., Shiels A. Mutation of the melastatin-related cation channel, TRPM3, underlies inherited cataract and glaucoma. PloS one. 2014;9(8):e104000. PubMed PMID: 25090642.
29. Liton P.B., Gonzalez P., Epstein D.L. The role of proteolytic cellular systems in trabecular meshwork homeostasis. Experimental eye research. 2009;88(4):724–728. PubMed PMID: 19046967.
30. Rao P.V., Pattabiraman P.P., Kopczynski C. Role of the Rho GTPase/Rho kinase signaling pathway in pathogenesis and treatment of glaucoma: Bench to bedside research. Experimental eye research. 2017;158:23–32. PubMed PMID: 27593914.
31. Leske M.C., Heijl A., Hussein M., Bengtsson B., Hyman L., Komaroff E. Factors for glaucoma progression and the effect of treatment: the early manifest glaucoma trial. Archives of ophthalmology. 2003;121(1):48–56. PubMed PMID: 12523884.
32. Mozaffarieh M., Flammer J. New insights in the pathogenesis and treatment of normal tension glaucoma. Current Opinion in Pharmacology. 2013;13(1):43–49. PubMed PMID: 23092679.
33. Fingert J.H., Miller K., Hedberg-Buenz A., Roos B.R., Lewis C.J., Mullins R.F., Anderson M.G. Transgenic TBK1 mice have features of normal tension glaucoma. Human molecular genetics. 2016;26(1):124–132. PubMed PMID: 28025332.
34. Kamal D., Hitchings R. Normal tension glaucoma—a practical approach. British journal of ophthalmology. 1998;82(7):835–840. PubMed PMID: 9924383.
35. Križaj D., Ryskamp D.A., Tian N., Tezel G., Mitchell C.H., Slepak V.Z., Shestopalov V.I. From mechanosensitivity to inflammatory responses: new players in the pathology of glaucoma. Current eye research. 2014;39(2):105–119. PubMed PMID: 24144321.
36. Vithana E.N., Khor C.C., Qiao C., Nongpiur M.E., George R., Chen L.J., Do T., Abu-Amero K., Huang C.K., Low S., Tajudin L.A., Perera S.A., Cheng C.Y., Xu L., Jia H., Ho C.L., Sim K.S., Wu R.Y., Tham C.C.Y., Chew P.T.K., Su D.H., Oen F.T., Sarangapani S., Soumittra N., Osman E.A., Wong H.T., Tang G., Fan S., Meng H., Huong D.T.L., Wang H., Feng B., Baskaran M., Shantha B., Ramprasad V.L., Kumaramanickavel G., Iyengar S.K., How A.C., Lee K.Y., Sivakumaran T.A., Yong V.H.K., Ting S.M.L., Li Y., Wang Y.X., Tay W.T., Sim X., Lavanya R., Cornes B.K., Zheng Y.F., Wong T.T., Loon S.C., Yong V.K.Y., Waseem N., Yaakub A., Chia K.S., Allingham R.R., Hauser M.A., Lam D.S.C., Hibberd M.L., Bhattacharya S.S., Zhang M., Teo Y.Y., Tan D.T., Jonas J.B., Tai E.S., Saw S.M., Hon D.N., Al-Obeidan S.A., Liu J., Chau T.N.B., Simmons C.P., Bei J.X., Zeng Y.X., Foster P.J., Vijaya L., Wong T.Y., Pang C.P., Wang N., Aung T. Genome-wide association analyses identify three new susceptibility loci for primary angle closure glaucoma. Nat Genet. 2012;44(10):1142–1146. PubMed PMID: 22922875.
37. Clark A.F., Wordinger R.J. The role of steroids in outflow resistance. Experimental eye research. 2009;88(4):752–759. PubMed PMID: 18977348.
38. Howell G.R., Libby R.T., Jakobs T.C., Smith R.S., Phalan F.C., Barter J.W., Barbay J.M., Marchant J.K., Mahesh N., Porciatti V. Axons of retinal ganglion cells are insulted in the optic nerve early in DBA/2J glaucoma. J Cell Biol. 2007;179(7):1523–1537. PubMed PMID: 18158332.
39. Whitmore A.V., Libby R.T., John S.W. Glaucoma: thinking in new ways—a role for autonomous axonal self-destruction and other compartmentalised processes? Progress in retinal and eye research. 2005;24(6):639–662. PubMed PMID: 15953750.
40. Liu B., McNally S., Kilpatrick J.I., Jarvis S.P., O'Brien C.J. Aging and ocular tissue stiffness in glaucoma. Survey of ophthalmology. 2018;63(1):56–74. PubMed PMID: 28666629.
41. Izzotti A., Longobardi M., Cartiglia C., Sacca S.C. Mitochondrial damage in the trabecular meshwork occurs only in primary open-angle glaucoma and in pseudoexfoliative glaucoma. PLoS One. 2011;6(1):e14567. PubMed PMID: 21283745.
42. Levkovitch-Verbin H., Vander S., Makarovsky D., Lavinsky F. Increase in retinal ganglion cells' susceptibility to elevated intraocular pressure and impairment of their endogenous neuroprotective mechanism by age. Molecular vision. 2013;19:2011. PubMed PMID: 24146536.

43. Acott T.S., Kelley M.J., Keller K.E., Vranka J.A., Abu-Hassan D.W., Li X., Aga M., Bradley J.M. Intraocular pressure homeostasis: maintaining balance in a high-pressure environment. Journal of Ocular Pharmacology and Therapeutics. 2014;30(2-3):94–101. PubMed PMID: 24401029.
44. Liu J.H., Zhang X., Kripke D.F., Weinreb R.N. Twenty-four-hour intraocular pressure pattern associated with early glaucomatous changes. Investigative ophthalmology & visual science. 2003;44(4):1586–1590. PubMed PMID: 12657596.
45. Heijl A., Leske M.C., Bengtsson B., Hyman L., Bengtsson B., Hussein M. Reduction of intraocular pressure and glaucoma progression: results from the Early Manifest Glaucoma Trial. Archives of ophthalmology. 2002;120(10):1268–1279. PubMed PMID: 12365904.
46. Crooks K.R., Allingham R.R., Qin X., Liu Y., Gibson J.R., Santiago-Turla C., Larocque-Abramson K.R., Del Bono E., Challa P., Herndon L.W. Genome-wide linkage scan for primary open angle glaucoma: influences of ancestry and age at diagnosis. PloS one. 2011;6(7):e21967. PubMed PMID: 21765929.
47. Downs J.C. IOP telemetry in the nonhuman primate. Exp Eye Res. 2015;141:91–8. PubMed PMID: 26216571.
48. Agnifili, L., D. Pieragostino, A. Mastropasqua, V. Fasanella, L. Brescia, G.M. Tosi, P. Sacchetta, and L. Mastropasqua, *Molecular biomarkers in primary open-angle glaucoma: from noninvasive to invasive*, Volume 221, in *Progress in brain research*. 2015, Elsevier. p. 1-32.
49. Cairns, E.A., W.H. Baldridge, and M.E. Kelly, *The endocannabinoid system as a therapeutic target in glaucoma.* Neural Plasticity. 2016; 2016.
50. Stamer W.D., Clark A.F. The many faces of the trabecular meshwork cell. Experimental eye research. 2017;158:112–123. PubMed PMID: 27443500.
51. Ryskamp D.A., Frye A.M., Phuong T.T., Yarishkin O., Jo A.O., Xu Y., Lakk M., Iuso A., Redmon S.N., Ambati B. TRPV4 regulates calcium homeostasis, cytoskeletal remodeling, conventional outflow and intraocular pressure in the mammalian eye. Scientific reports. 2016;6:30583. PubMed PMID: 27510430.
52. Grüsser O.-J., Grüsser-Cornehls U., Kusel R., Przybyszewski A. Responses of retinal ganglion cells to eyeball deformation: a neurophysiological basis for "pressure phosphenes". Vision research. 1989;29(2):181–194. PubMed PMID: 2800346.
53. Kong Y.X., Crowston J.G., Vingrys A.J., Trounce I.A., Bui B.V. Functional changes in the retina during and after acute intraocular pressure elevation in mice. Investigative ophthalmology & visual science. 2009;50(12):5732–5740. PubMed PMID: 19643960.
54. Ou Y., Jo R.E., Ullian E.M., Wong R.O., Della Santina L. Selective vulnerability of specific retinal ganglion cell types and synapses after transient ocular hypertension. Journal of Neuroscience. 2016;36(35):9240–9252. PubMed PMID: 27581463.
55. Della Santina L., Inman D.M., Lupien C.B., Horner P.J., Wong R.O. Differential progression of structural and functional alterations in distinct retinal ganglion cell types in a mouse model of glaucoma. Journal of Neuroscience. 2013;33(44):17444–17457. PubMed PMID: 24174678.
56. Kong L., Fry M., Al-Samarraie M., Gilbert C., Steinkuller P.G. An update on progress and the changing epidemiology of causes of childhood blindness worldwide. Journal of American Association for Pediatric Ophthalmology and Strabismus. 2012;16(6):501–507. PubMed PMID: 23237744.
57. Calkins D.J. Critical pathogenic events underlying progression of neurodegeneration in glaucoma. Progress in retinal and eye research. 2012;31(6):702–719. PubMed PMID: 22871543.
58. El-Danaf R.N., Huberman A.D. Characteristic patterns of dendritic remodeling in early-stage glaucoma: evidence from genetically identified retinal ganglion cell types. Journal of Neuroscience. 2015;35(6):2329–2343. PubMed PMID: 25673829.
59. Feng L., Chen H., Yi J., Troy J.B., Zhang H.F., Liu X. Long-term protection of retinal ganglion cells and visual function by brain-derived neurotrophic factor in mice with ocular hypertension. Investigative ophthalmology & visual science. 2016;57(8):3793–3802. PubMed PMID: 27421068.
60. Williams P.A., Tribble J.R., Pepper K.W., Cross S.D., Morgan B.P., Morgan J.E., John S.W., Howell G.R. Inhibition of the classical pathway of the complement cascade prevents early dendritic and synaptic degeneration in glaucoma. Molecular neurodegeneration. 2016;11(1):26. PubMed PMID: 27048300.

61. Calkins D.J., Pekny M., Cooper M.L., Benowitz L., Calkins D., Cooper M., Crowston J., Huberman A., Johnson E., Lu R. The challenge of regenerative therapies for the optic nerve in glaucoma. Experimental eye research. 2017;157:28–33. PubMed PMID: 28153739.
62. Beirowski B., Babetto E., Coleman M.P., Martin K.R. The WldS gene delays axonal but not somatic degeneration in a rat glaucoma model. European Journal of Neuroscience. 2008;28(6):1166–1179. PubMed PMID: 18783366.
63. Quigley H.A., Sanchez R.M., Dunkelberger G.R., L'Hernault N.L., Baginski T.A. Chronic glaucoma selectively damages large optic nerve fibers. Investigative Ophthalmology & Visual Science. 1987;28(6):913–920. PubMed PMID: 3583630.
64. Morgan J.E. Selective cell death in glaucoma: does it really occur? The British journal of ophthalmology. 1994;78(11):875. PubMed PMID: 7848987.
65. Jakobs T.C., Libby R.T., Ben Y., John S.W., Masland R.H. Retinal ganglion cell degeneration is topological but not cell type specific in DBA/2J mice. J Cell Biol. 2005;171(2):313–325. PubMed PMID: 16247030.
66. Feng L., Zhao Y., Yoshida M., Chen H., Yang J.F., Kim T.S., Cang J., Troy J.B., Liu X. Sustained ocular hypertension induces dendritic degeneration of mouse retinal ganglion cells that depends on cell type and location. Investigative ophthalmology & visual science. 2013;54(2):1106–1117. PubMed PMID: 23322576.
67. Risner M.L., Pasini S., Cooper M.L., Lambert W.S., Calkins D.J. Axogenic mechanism enhances retinal ganglion cell excitability during early progression in glaucoma. Proceedings of the National Academy of Sciences. 2018;115(10):E2393–E2402. PubMed PMID: 29463759.
68. Križaj, D., *Polymodal sensory integration in retinal ganglion cells*, in *Retinal Degenerative Diseases*. 2016, Springer. p. 693-698.
69. de Sevilla Müller L.P., Sargoy A., Rodriguez A.R., Brecha N.C. Melanopsin ganglion cells are the most resistant retinal ganglion cell type to axonal injury in the rat retina. PLoS One. 2014;9(3):e93274. PubMed PMID: 24671191.
70. Lakk M., Young D., Baumann J.M., Jo A.O., Hu H., Križaj D. Polymodal TRPV1 and TRPV4 sensors colocalize but do not functionally interact in a subpopulation of mouse retinal ganglion cells. Frontiers in cellular neuroscience. 2018.:12. PubMed PMID: 30386208.
71. Huang W., Fileta J.B., Dobberfuhl A., Filippopolous T., Guo Y., Kwon G., Grosskreutz C.L. Calcineurin cleavage is triggered by elevated intraocular pressure, and calcineurin inhibition blocks retinal ganglion cell death in experimental glaucoma. Proceedings of the National Academy of Sciences. 2005;102(34):12242–12247. PubMed PMID: 16103353.
72. Huang W., Xing W., Ryskamp D.A., Punzo C., Križaj D. Localization and phenotype-specific expression of ryanodine calcium release channels in C57BL6 and DBA/2J mouse strains. Experimental eye research. 2011;93(5):700–709. PubMed PMID: 21933672.
73. Kroeger H., Chiang W.C., Felden J., Nguyen A., Lin J.H. ER stress and unfolded protein response in ocular health and disease. The FEBS journal. 2019;286(2):399–412. PubMed PMID: 29802807.
74. Guymer C., Wood J.P., Chidlow G., Casson R.J. Neuroprotection in glaucoma: recent advances and clinical translation. Clinical & experimental ophthalmology. 2019;47(1):88–105. PubMed PMID: 29900639.
75. Hare W.A., WoldeMussie E., Weinreb R.N., Ton H., Ruiz G., Wijono M., Feldmann B., Zangwill L., Wheeler L. Efficacy and safety of memantine treatment for reduction of changes associated with experimental glaucoma in monkey, II: Structural measures. Investigative ophthalmology & visual science. 2004;45(8):2640–2651. PubMed PMID: 15277487.
76. Rutar M., Natoli R., Albarracin R., Valter K., Provis J. 670-nm light treatment reduces complement propagation following retinal degeneration. J Neuroinflammation. 2012;9:257. PubMed PMID: 23181358.
77. Lim J.-H.A., Stafford B.K., Nguyen P.L., Lien B.V., Wang C., Zukor K., He Z., Huberman A.D. Neural activity promotes long-distance, target-specific regeneration of adult retinal axons. Nature neuroscience. 2016;19(8):1073. PubMed PMID: 27399843.
78. Yang H., Reynaud J., Lockwood H., Williams G., Hardin C., Reyes L., Stowell C., Gardiner S.K., Burgoyne C.F. The connective tissue phenotype of glaucomatous cupping in the monkey eye-clinical and research implications. Progress in retinal and eye research. 2017;59:1–52. PubMed PMID: 28300644.

79. Eilaghi A., Flanagan J.G., Simmons C.A., Ethier C.R. Effects of scleral stiffness properties on optic nerve head biomechanics. Annals of biomedical engineering. 2010;38(4):1586–1592. PubMed PMID: 20039133.
80. Burgoyne C.F., Downs J.C. Premise and prediction–how optic nerve head biomechanics underlies the susceptibility and clinical behavior of the aged optic nerve head. Journal of glaucoma. 2008;17(4):318. PubMed PMID: 18552618.
81. Howell G.R., Soto I., Zhu X., Ryan M., Macalinao D.G., Sousa G.L., Caddle L.B., MacNicoll K.H., Barbay J.M., Porciatti V. Radiation treatment inhibits monocyte entry into the optic nerve head and prevents neuronal damage in a mouse model of glaucoma. The Journal of clinical investigation. 2012;122(4):1246–1261. PubMed PMID: 22426214.
82. Osborne N.N., Núñez-Álvarez C., Joglar B., del Olmo-Aguado S. Glaucoma: focus on mitochondria in relation to pathogenesis and neuroprotection. European journal of pharmacology. 2016;787:127–133. PubMed PMID: 27090928.
83. Dengler-Crish C.M., Smith M.A., Inman D.M., Wilson G.N., Young J.W., Crish S.D. Anterograde transport blockade precedes deficits in retrograde transport in the visual projection of the DBA/2J mouse model of glaucoma. Frontiers in neuroscience. 2014;8:290. PubMed PMID: 25278826.
84. Bosco A., Steele M.R., Vetter M.L. Early microglia activation in a mouse model of chronic glaucoma. Journal of Comparative Neurology. 2011;519(4):599–620. PubMed PMID: 21246546.
85. Inman D.M., Horner P.J. Reactive nonproliferative gliosis predominates in a chronic mouse model of glaucoma. Glia. 2007;55(9):942–953. PubMed PMID: 17457855.
86. Sun D., Lye-Barthel M., Masland R.H., Jakobs T.C. The morphology and spatial arrangement of astrocytes in the optic nerve head of the mouse. Journal of Comparative Neurology. 2009;516(1):1–19. PubMed PMID: 19562764.
87. Ly T., Gupta N., Weinreb R.N., Kaufman P.L., Yücel Y.H. Dendrite plasticity in the lateral geniculate nucleus in primate glaucoma. Vision research. 2011;51(2):243–250. PubMed PMID: 20692280.
88. Gupta N., Greenberg G., De Tilly L.N., Gray B., Polemidiotis M., Yücel Y.H. Atrophy of the lateral geniculate nucleus in human glaucoma detected by magnetic resonance imaging. British Journal of Ophthalmology. 2009;93(1):56–60. PubMed PMID: 18697810.
89. Geeraerts E., Claes M., Dekeyster E., Salinas-Navarro M., De Groef L., Van den Haute C., Scheyltjens I., Baekelandt V., Arckens L., Moons L. Optogenetic stimulation of the superior colliculus confers retinal neuroprotection in a mouse glaucoma model. Journal of Neuroscience. 2019;39(12):2313–2325. PubMed PMID: 30655352.
90. Coulombre, A.J., *Cytology of the developing eye*, Volume 11, in *International review of cytology*. 1961, Elsevier. p. 161-194.
91. Shelton L., Troilo D., Lerner M.R., Gusev Y., Brackett D.J., Rada J.S. Microarray analysis of choroid/RPE gene expression in marmoset eyes undergoing changes in ocular growth and refraction. Molecular vision. 2008;14:1465. PubMed PMID: 18698376.
92. Schneider M., Fuchshofer R. The role of astrocytes in optic nerve head fibrosis in glaucoma. Experimental eye research. 2016;142:49–55. PubMed PMID: 26321510.
93. Tamm E., Ethier C. Lasker/IRRF Initiative on Astrocytes and Glaucomatous Neurodegeneration Participants. Biological aspects of axonal damage in glaucoma: a brief review. Exp Eye Res. 2017;157:5–12. PubMed PMID: 28223179.
94. Jakobs T.C. Differential gene expression in glaucoma. Cold Spring Harbor perspectives in medicine. 2014;4(7):a020636. PubMed PMID: 24985133.
95. Tovar-Vidales T., Wordinger R.J., Clark A.F. Identification and localization of lamina cribrosa cells in the human optic nerve head. Experimental eye research. 2016;147:94–97. PubMed PMID: 27167365.
96. Mansour H., McColm J.R., Cole L., Weible M. II, Korlimbinis A., Chan-Ling T. Connexin 30 expression and frequency of connexin heterogeneity in astrocyte gap junction plaques increase with age in the rat retina. PloS one. 2013;8(3):e57038. PubMed PMID: 23516399.

97. Newman, E.A., *Glial cell regulation of neuronal activity and blood flow in the retina by release of gliotransmitters.* Philosophical Transactions of the Royal Society B: Biological Sciences. 2015; 370(1672):20140195.
98. Hernandez M.R. The optic nerve head in glaucoma: role of astrocytes in tissue remodeling. Progress in retinal and eye research. 2000;19(3):297–321. PubMed PMID: 10749379.
99. Lye-Barthel M., Sun D., Jakobs T.C. Morphology of astrocytes in a glaucomatous optic nerve. Investigative ophthalmology & visual science. 2013;54(2):909–917. PubMed PMID: 23322566.
100. Dvoriantchikova G., Ivanov D. Tumor necrosis factor-alpha mediates activation of NF-κB and JNK signaling cascades in retinal ganglion cells and astrocytes in opposite ways. European Journal of Neuroscience. 2014;40(8):3171–3178. PubMed PMID: 25160799.
101. Johnson E.C., Jia L., Cepurna W.O., Doser T.A., Morrison J.C. Global changes in optic nerve head gene expression after exposure to elevated intraocular pressure in a rat glaucoma model. Investigative ophthalmology & visual science. 2007;48(7):3161–3177. PubMed PMID: 17591886.
102. Tezel G., Hernandez M.R., Wax M.B. In vitro evaluation of reactive astrocyte migration, a component of tissue remodeling in glaucomatous optic nerve head. Glia. 2001;34(3):178–189. PubMed PMID: 11329180.
103. Redmon S., Yarishkin O., Lakk M., Krizaj D. Retinal glial cells respond differently to the activation of the mechanosensitive channel TRPV4. Investigative Ophthalmology & Visual Science. 2018;59(9):3939–3939.
104. Chong R.S., Martin K.R. Glial cell interactions and glaucoma. Current opinion in ophthalmology. 2015;26(2):73. PubMed PMID: 25490529.
105. Wax M.B., Tezel G. Immunoregulation of retinal ganglion cell fate in glaucoma. Experimental Eye Research. 2009;88(4):825–830. PubMed PMID: 19233171.
106. Anderson S.R., Zhang J., Steele M.R., Romero C.O., Kautzman A.G., Schafer D.P., Vetter M.L. Complement targets newborn retinal ganglion cells for phagocytic elimination by microglia. Journal of Neuroscience. 2019;39(11):2025–2040. PubMed PMID: 30647151.
107. Breen K.T., Anderson S.R., Steele M.R., Calkins D.J., Bosco A., Vetter M.L. Loss of fractalkine signaling exacerbates axon transport dysfunction in a chronic model of glaucoma. Frontiers in neuroscience. 2016;10:526. PubMed PMID: 27932942.
108. Wang M., Wang X., Zhao L., Ma W., Rodriguez I.R., Fariss R.N., Wong W.T. Macroglia-microglia interactions via TSPO signaling regulates microglial activation in the mouse retina. Journal of Neuroscience. 2014;34(10):3793–3806. PubMed PMID: 24599476.
109. Bosco A., Romero C.O., Breen K.T., Chagovetz A.A., Steele M.R., Ambati B.K., Vetter M.L. Neurodegeneration severity can be predicted from early microglia alterations monitored in vivo in a mouse model of chronic glaucoma. Disease models & mechanisms. 2015;8(5):443–455. PubMed PMID: 25755083.
110. Karlstetter M., Scholz R., Rutar M., Wong W.T., Provis J.M., Langmann T. Retinal microglia: just bystander or target for therapy? Progress in retinal and eye research. 2015;45:30–57. PubMed PMID: 25476242.
111. Matsumoto H., Sugio S., Seghers F., Krizaj D., Akiyama H., Ishizaki Y., Gailly P., Shibasaki K. Retinal detachment-induced Müller glial cell swelling activates TRPV4 ion channels and triggers photoreceptor death at body temperature. Journal of Neuroscience. 2018;38(41):8745–8758. PubMed PMID: 30143574.
112. Reichenbach, A. and A. Bringmann, *Müller cells in the healthy and diseased retina*. Springer Science & Business Media. 2010, New York: Springer Verlag.
113. Jo A.O., Ryskamp D.A., Phuong T.T., Verkman A.S., Yarishkin O., MacAulay N., Križaj D. TRPV4 and AQP4 channels synergistically regulate cell volume and calcium homeostasis in retinal Müller glia. Journal of Neuroscience. 2015;35(39):13525–13537. PubMed PMID: 26424896.
114. Nawashiro H., Messing A., Azzam N., Brenner M. Mice lacking GFAP are hypersensitive to traumatic cerebrospinal injury. Neuroreport. 1998;9(8):1691–1696. PubMed PMID: 9665584.
115. Morrison J.C., Guo W.O.C.Y., Johnson E.C. Pathophysiology of human glaucomatous optic nerve damage: insights from rodent models of glaucoma. Experimental eye research. 2011;93(2):156–164. PubMed PMID: 20708000.

116. Vargas J.L.C., Osswald I.K., Unsain N., Aurousseau M.R., Barker P.A., Bowie D., Di Polo A. Soluble tumor necrosis factor alpha promotes retinal ganglion cell death in glaucoma via calcium-permeable AMPA receptor activation. Journal of Neuroscience. 2015;35(35):12088–12102. PubMed PMID: 26338321.
117. Jassim A.H., Inman D.M. Evidence of Hypoxic Glial Cells in a Model of Ocular Hypertension. Investigative Ophthalmology & Visual Science. 2019;60(1):1–15. PubMed PMID: 30601926.
118. Jo A.O., Lakk M., Frye A.M., Phuong T.T., Redmon S.N., Roberts R., Berkowitz B.A., Yarishkin O., Križaj D. Differential volume regulation and calcium signaling in two ciliary body cell types is subserved by TRPV4 channels. Proceedings of the National Academy of Sciences. 2016;113(14):3885–3890. PubMed PMID: 27006502.
119. Križaj, D., *No cell is an island: trabecular meshwork ion channels as sensors of the ambient milieu*, Volume 3, in *Glaucoma Research and Clinical Advances* J.R. Samples and P.A. Knepper, Editors. 2019, Kugler Publications Amsterdam.
120. Lindqvist N., Liu Q., Zajadacz J., Franze K., Reichenbach A. Retinal glial (Müller) cells: sensing and responding to tissue stretch. Investigative ophthalmology & visual science. 2010;51(3):1683–1690. PubMed PMID: 19892866.
121. Niittykoski M., Kalesnykas G., Larsson K.P., Kaarniranta K., Åkerman K.E., Uusitalo H. Altered calcium signaling in an experimental model of glaucoma. Investigative ophthalmology & visual science. 2010;51(12):6387–6393. PubMed PMID: 20592232.
122. Ribas V.T., Koch J.C., Michel U., Bähr M., Lingor P. Attenuation of axonal degeneration by calcium channel inhibitors improves retinal ganglion cell survival and regeneration after optic nerve crush. Molecular neurobiology. 2017;54(1):72–86. PubMed PMID: 26732591.
123. Ingber D.E. Tensegrity: the architectural basis of cellular mechanotransduction. Annual review of physiology. 1997;59(1):575–599. PubMed PMID: 9074778.
124. Ranade S.S., Syeda R., Patapoutian A. Mechanically activated ion channels. Neuron. 2015;87(6):1162–1179. PubMed PMID: 26402601.
125. Jaalouk D.E., Lammerding J. Mechanotransduction gone awry. Nature reviews Molecular cell biology. 2009;10(1):63. PubMed PMID: 19197333.
126. Cox, C.D., N. Bavi, and B. Martinac, *Origin of the force: the force-from-lipids principle applied to piezo channels*, Volume 79, in *Current topics in membranes*. 2017, Elsevier. p. 59-96.
127. Phuong T.T., Redmon S.N., Yarishkin O., Winter J.M., Li D.Y., Križaj D. Calcium influx through TRPV4 channels modulates the adherens contacts between retinal microvascular endothelial cells. The Journal of physiology. 2017;595(22):6869–6885. PubMed PMID: 28949006.
128. Sappington R.M., Sidorova T., Ward N.J., Chakravarthy R., Ho K.W., Calkins D.J. Activation of transient receptor potential vanilloid-1 (TRPV1) influences how retinal ganglion cell neurons respond to pressure-related stress. Channels. 2015;9(2):102–113. PubMed PMID: 25713995.
129. Yarishkin O., Phuong T.T., Bretz C.A., Olsen K.W., Baumann J.M., Lakk M., Crandall A., Heurteaux C., Hartnett M.E., Križaj D. TREK-1 channels regulate pressure sensitivity and calcium signaling in trabecular meshwork cells. The Journal of general physiology. 2018;150(12):1660–1675. PubMed PMID: 30446509.
130. Redmon, S., N., K. Shibasaki, and D. Križaj, *Transient receptor potential cation channel subfamily V member 4*, in *Encyclopedia of Signaling Molecules, 2nd Edition*, S. Choi, Editor. 2017, Springer Press.
131. White J.P., Cibelli M., Urban L., Nilius B., McGeown J.G., Nagy I. TRPV4: molecular conductor of a diverse orchestra. Physiological reviews. 2016;96(3):911–973. PubMed PMID: 27252279.
132. Lapajne L., Lakk M., Gubeljak L., Yarishkin O., Hawlina M., Križaj D. Corneal mechanotransduction drives TRPV4-dependent release of the transmitter ATP. Investigative ophthalmology & visual science. 2019.:60. Suppl. .
133. Ryskamp D.A., Witkovsky P., Barabas P., Huang W., Koehler C., Akimov N.P., Lee S.H., Chauhan S., Xing W., Rentería R.C. The polymodal ion channel transient receptor potential vanilloid 4 modulates calcium flux, spiking rate, and apoptosis of mouse retinal ganglion cells. Journal of Neuroscience. 2011;31(19):7089–7101. PubMed PMID: 21562271.

134. Arredondo D.Z., Noguez R.I., Bautista A.C., Vázquez O.R., Bernardini M., Fiorio A.P., Gkika D., Prevarskaya N., Lopez-Casillas F., Liedtke W. Dual contribution of TRPV4 antagonism in the regulatory effect of vasoinhibins on blood-retinal barrier permeability: diabetic milieu makes a difference. Scientific reports. 2017;7(1):13094–13094. PubMed PMID: 29026201.
135. Lakk M., Yarishkin O., Baumann J.M., Iuso A., Križaj D. Cholesterol regulates polymodal sensory transduction in Müller glia. Glia. 2017;65(12):2038–2050. PubMed PMID: 28856727.
136. Alloui A., Zimmermann K., Mamet J., Duprat F., Noel J., Chemin J., Guy N., Blondeau N., Voilley N., Rubat-Coudert C. TREK-1, a K+ channel involved in polymodal pain perception. The EMBO journal. 2006;25(11):2368–2376. PubMed PMID: 16675954.
137. Harrington, D. and M. Drake, *The visual fields: text and atlas of clinical perimetry. 6th*. 1990, Mosby: Philadelphia. p. 52-60.
138. Bonomi L., Marchini G., Marraffa M., Morbio R. The relationship between intraocular pressure and glaucoma in a defined population. Ophthalmologica. 2001;215(1):34–38. PubMed PMID: 11125267.
139. Vecino E., Rodriguez F.D., Ruzafa N., Pereiro X., Sharma S.C. Glia–neuron interactions in the mammalian retina. Progress in retinal and eye research. 2016;51:1–40. PubMed PMID: 26113209.
140. Samuels B.C., Siegwart J.T., Zhan W., Hethcox L., Chimento M., Whitley R., Downs J.C., Girkin C.A. A Novel Tree Shrew (Tupaia belangeri) Model of Glaucoma. Investigative ophthalmology & visual science. 2018;59(7):3136–3143. PubMed PMID: 30025140.
141. Tamm E.R., Ethier C.R., Dowling J.E., Downs C., Ellisman M.H., Fisher S., Fortune B., Fruttiger M., Jakobs T., Lewis G. Biological aspects of axonal damage in glaucoma: a brief review. Experimental eye research. 2017;157:5–12. PubMed PMID: 28223179.
142. Lieff, J. *Searching for the Mind*. 2013; Available from: http://jonlieffmd.com/blog/are-microglia-the-most-intelligent-brain-cells.
143. Moran M.M., McAlexander M.A., Bíró T., Szallasi A. Transient receptor potential channels as therapeutic targets. Nature reviews Drug discovery. 2011;10(8):601. PubMed PMID: 21804597.
144. Patel A.J., Honoré E. Properties and modulation of mammalian 2P domain K+ channels. Trends in neurosciences. 2001;24(6):339–346. PubMed PMID: 11356506.
145. Yarishkin, O., T.T. Phuong, M. Lakk, and D. Križaj, *TRPV4 does not regulate the distal retinal light response*, in *Retinal Degenerative Diseases*. 2018, Springer. p. 553-560.

Visual Prosthesis

Introduction to Visual Prostheses

Eduardo Fernandez, M.D.[1,*] and Richard Normann, Ph.D.[2,†]

Created: March 9, 2016.

"The best and most beautiful things in the world cannot be seen or even touched – they must be felt with the heart." Helen Keller.

1. Introduction

Loss of vision affects millions of people worldwide and poses extraordinary challenges to individuals in a society that relies heavily on sight. Although in recent years the techniques of molecular genetics have led to a rapid identification of a great number of genes involved in visual diseases (see https://sph.uth.edu/Retnet/sum-dis.htm for an update of genes and loci causing retinal diseases), the nervous system once damaged is capable of little functional regeneration and currently there is no effective treatment for many patients who are visually handicapped as a result of degeneration or damage to: 1) the retina, 2) the optic nerve, or 3) the visual parts of the brain.

While pharmacological interventions provide therapeutic solutions to many physiological problems, a pharmacological approach to the mechanisms of blindness has not been discovered. Furthermore, there remains the pervasive question as to how these molecular approaches will actually restore functional vision after it is completely lost in a given individual. Therefore, there are compelling reasons to pursue the development of sophisticated microelectronic prostheses as a viable rehabilitative and therapeutic options to substitute, and ultimately, restore limited, but useful sight. Such assistive devices have already allowed thousands of deaf patients to hear sounds and acquire language abilities and the same hope exists in the field of visual neurorehabilitation.

Essentially all visual prosthesis efforts share a common principle of providing focal electrical stimulation to intact visual structures (including the retina, optic nerve, lateral geniculate nucleus (LGN) and occipital visual cortex), evoking the sensation of discrete points of light called phosphenes. Figure 1 shows the possible perception of phosphenes generated by stimulating simultaneously 3 electrodes arranged as a triangle.

It is expected that the neural plasticity of the visual system can contribute to an ever-improving correlation between the physical world and evoked phosphenes. Figure 2 shows an example. Immediately after implantation, the evoked phosphenes are likely to induce a poor perception of an object (the letter "E" in this example). However, appropriate learning and rehabilitation strategies will contribute to provide concordant perceptions.

2. The History of Neural Stimulation

Electrical phenomena and some of the effects of electricity upon man were known in ancient times, but it was not until the eighteenth century that a connection was made between electricity and the neural system. In 1791 Luigi Galvani, an Italian physician (Figure 3), observed that dissimilar metals, attached to a frog's leg and connected together can induce the frog's skeletal muscles to contract (1).

Author Affiliations: 1 Department of Histology and Anatomy, University of Miguel Hernández and Biomedical Neuroengineering Research Unit, CIBER-BBN, Spain; Email: e.fernandez@umh.es. 2 Departments of Bioengineering and Ophthalmology, University of Utah; Email: normann@utah.edu.

Corresponding author.

* See 'About the authors'

† See 'About the authors'

Figure 1. Example of patterned phosphenes.

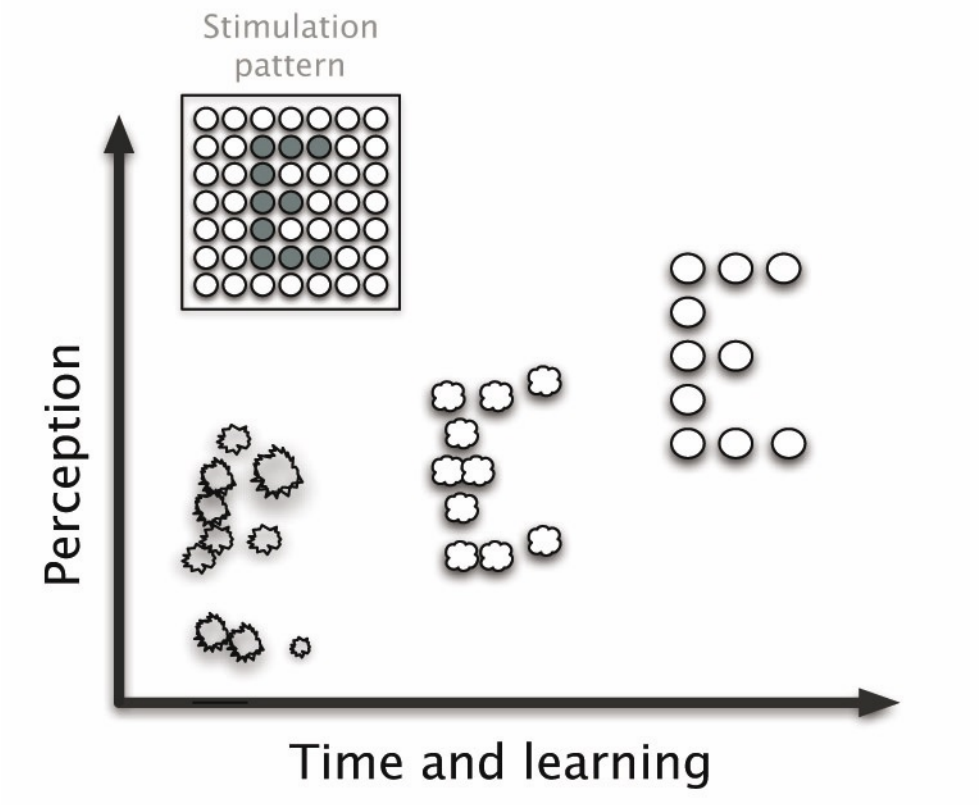

Figure 2. Evoked perceptions of phosphines with time.

These observations lead to the conclusion that nerves and muscles could produce electricity and utilize it to produce function. Subsequent studies led to a further understanding of the nerve impulse and synaptic transmission and to the development of new therapies based on the application of electrical fields.

The first and most successful example of a neural stimulation device is the cardiac pacemaker that has become a standard therapeutic approach to improve cardiac function in millions of patients. Technology partially achieved during the development of the pacemaker has been used successfully for rehabilitation of sensory and/or motor functions in patients with neurological diseases. Thus deep brain stimulators have been implanted successfully in patients for pain management and for control of motor disorders such as Parkinson's disease (2-4), and cochlear implants are being used for restoring auditory function (5-9). Moreover advances in artificial limbs and brain-machine interfaces are now providing hope of increased mobility and independence for amputees and paralyzed patients (10-14), and there is preliminary data showing that electrophysiological methods can be used to extract neural information about the volitional intent of the subjects to move their distal musculature and then translate these signals into models that are able to control external devices (10, 14-20). As more and more patients have benefited from this approach, the interest in neural interfaces and visual prostheses has grown significantly.

In terms of restoring lost sensory function, cochlear implant research has arguably been the most successful, and has been translated into a viable therapeutic option for many profoundly deaf patients (3, 21-23). Simply explained, a wire electrode bundle is surgically inserted into the inner ear thus serving as an electronic replacement for damaged hair cells. A microphone and speech processor picks up and decodes sounds from the environment and the coded signals drive, in turn, the electrodes that stimulate the nerve fibers of the cochlea, and create the sensation of hearing (Figure 4). In conjunction with intense rehabilitation programs that are tailored to the individual, deaf individuals can learn to comprehend and in some cases, even acquire speech. The same hope exists in the field of visual prostheses.

This field is still in its infancy but is experiencing great interest in both academic and commercial sectors. The possibility of merging different technologies and focusing them on a common target is allowing us to develop new systems, devices and interfaces to the nervous system with greater complexity than could have been imagined only a few decades ago. Further, our understanding of the function and dysfunction of the nervous system has improved to the point that, in many cases, researchers have suggested plausible interventional routes whereby neuroprosthetic systems can be expected to be efficacious.

3. The Case for Artificial Vision.

The possibility to restore visual perceptions in blind individuals has a long history in biomedical engineering. A German neurosurgeon, Forester, was the first to expose the human occipital pole under local anesthesia and to electrically stimulate it. In 1929 he noted that electrical stimulation induced the perception of points of light, called phosphenes and usually described as 'stars in the sky', 'clouds' and 'pinwheels', that were dependent on where the stimulation probe was placed. These findings together with the studies of Wilder Penfield and co-workers during the course of neurosurgical interventions for the treatment of epilepsy (24, 25) established the physiological basis for the present efforts to develop a visual prosthesis for the blind.

Subsequent experiments by the group of Giles Brindley in England (26-28), William Dobelle at the University of Utah (29-32), Pollen (33) and others (34) showed that simultaneous stimulation via arrays of electrodes placed on the surface of the brain allowed blind volunteers to recognize simple patterns, including letters and Braille characters.

The results of these studies supported the premise that patterned electrical stimulation of the visual cortex can evoke patterned percepts. However, these early efforts did not culminate in the restoration of a useful visual sense. Problems with this early work were associated mainly with the large surface electrodes that were used to evoke phosphenes. Such large surface area electrodes required relatively high electrical currents to evoke phosphenes and when multiple electrodes were stimulated, these large currents could interact in a non-linear fashion, evoking phosphenes with unpredictable spatial properties. Furthermore, they also found that a visual prosthesis based on relatively large surface electrodes implanted subdurally would have limited usefulness because of occasional elicitation of pain due to meningeal or scalp stimulation, and also the risk of inducing

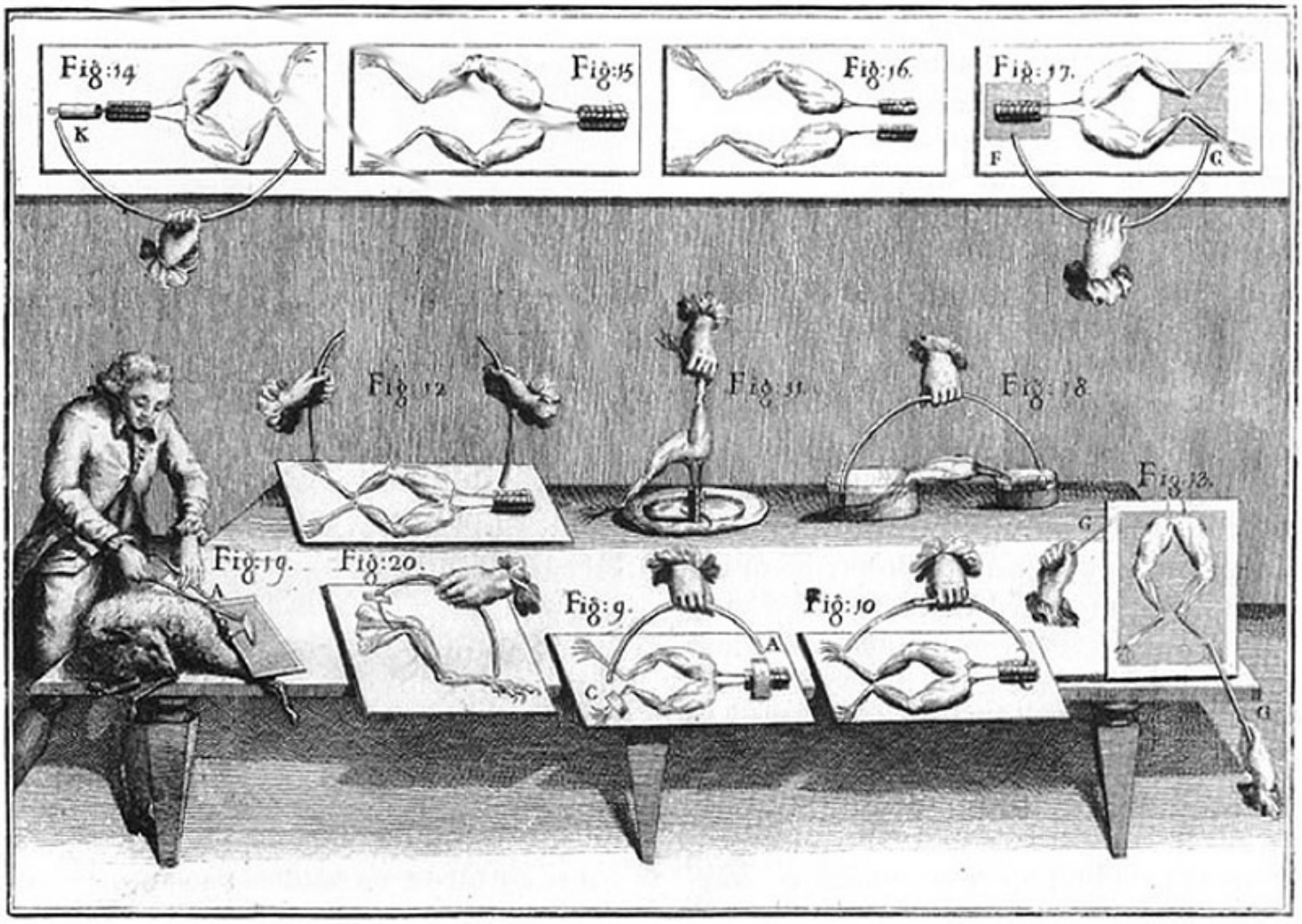

Figure 3. Woodblock engraving of some of Galvani's experiments on animal electricity (from Galvani, 1791).

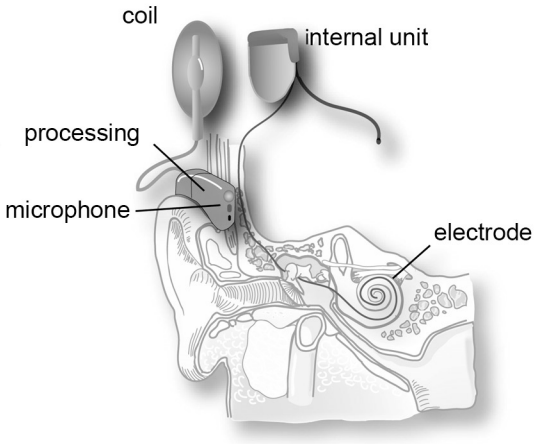

Figure 4. Cochlear implant.

epileptic seizures. This body of work suggests that relatively large surface electrodes may not be a tenable approach to stimulation of the visual cortex, and led a number of investigators to develop a visual prosthesis that

could be implanted directly into the retina, the brain or other parts of the visual pathways. One of the pioneers in this field was Tassicker, an Australian researcher who in 1956 was the first to patent a method of implanting a light-sensitive selenium cell in a blind person's retina (Figure 5) to transiently restore the patient's ability to perceive the sensation of light (35, 36).

4. Visual Pathways: From Real Vision to Visual Neuroprostheses

The concept of artificially producing a visual sense in blind individuals is founded on our present understanding of the structure of the mammalian visual system, its processing elements, and the relationship between electrical stimulation of any part of the visual pathways and the resulting visual sensations (37).

Our entire experience of the external visual world derives from the concerted activity of a restricted number of retinal ganglion cells. These retinal ganglion cells have to send their action potentials through the "bottleneck" optic nerve to the brain (Figure 6).

The retina is essentially a piece of brain whose 150 million photoreceptors get direct stimulation from the outside world's lights and images. Visual input to the retina consists of a stream of photons, which can be unequivocally quantified in space and time. The retina performs spatial, temporal, and chromatic processing of visual information and converts it into a compact "digital" format composed of neural impulses (38). In addition, starting at the retinal level, vision is an active process and eye movements are essential for information processing (39, 40). Thus our entire experience of the external visual world derives from the concerted activity of a restricted number of retinal ganglion cells, which have to send their information, via the one million optic nerve fibers, to higher visual centers. The representation has to be unequivocal and fast (within a few hundreds of milliseconds), in order to ensure object recognition for any single stimulus presentation (41-43). Therefore, the question of how the information about the external world is compressed in the retina, and how this compressed representation is encoded in spike trains is an important challenge for the success of any visual prosthesis.

The next processing center is the lateral geniculate nucleus (LGN), which begins to integrate information from both eyes into a binocular representation of visual space (Figure 7). Once retinal signals arrive within the LGN, they are in a position to be influenced by a wide variety of other inputs as well as the complex feedforward and feedback circuits to and from higher visual centers. These inputs include not only visual information, but also nonvisual information that comes from cortical areas, superior colliculus, pretectum, parabigeminal nucleus, reticular nucleus and other brain stem pathways (44). The number of synapses provided by these non-retinal inputs greatly outnumbers the number of inputs coming from the retina, but their function is not fully understood.

The LGN neurons mainly project to the primary visual cortex (also known as the striate cortex or V1), which was the first cortical area clearly identified in the human brain by Gennari in 1782 (45). Area V1 (Figure 7) is located at the back of the head, in the occipital lobe, and from here the information is distributed to a number of higher cortical centers for further processing (46). The main point, as stated by Hubel and Wiesel, is that the primary visual cortex is in no sense the end of the visual path (47, 48). It is just one stage, probably an early one in terms of the degree of abstraction of the visual information processing (47, 49-51).

Retinal ganglion cells are not themselves homogeneous, but form several parallel and physiologically-distinct pathways from retina to brain (Figure 8). While ON and OFF pathways are well known in vertebrate retinas (52), primate retina makes a further subdivision into magnocellular and parvocellular pathways, or M and P pathways. These are named after the diameters of cell bodies within sublayers of the primate lateral geniculate nucleus, where ganglion-cell axons project. P-cells are color cells, M-cells are low-contrast-sensitive, non-color cells (53).

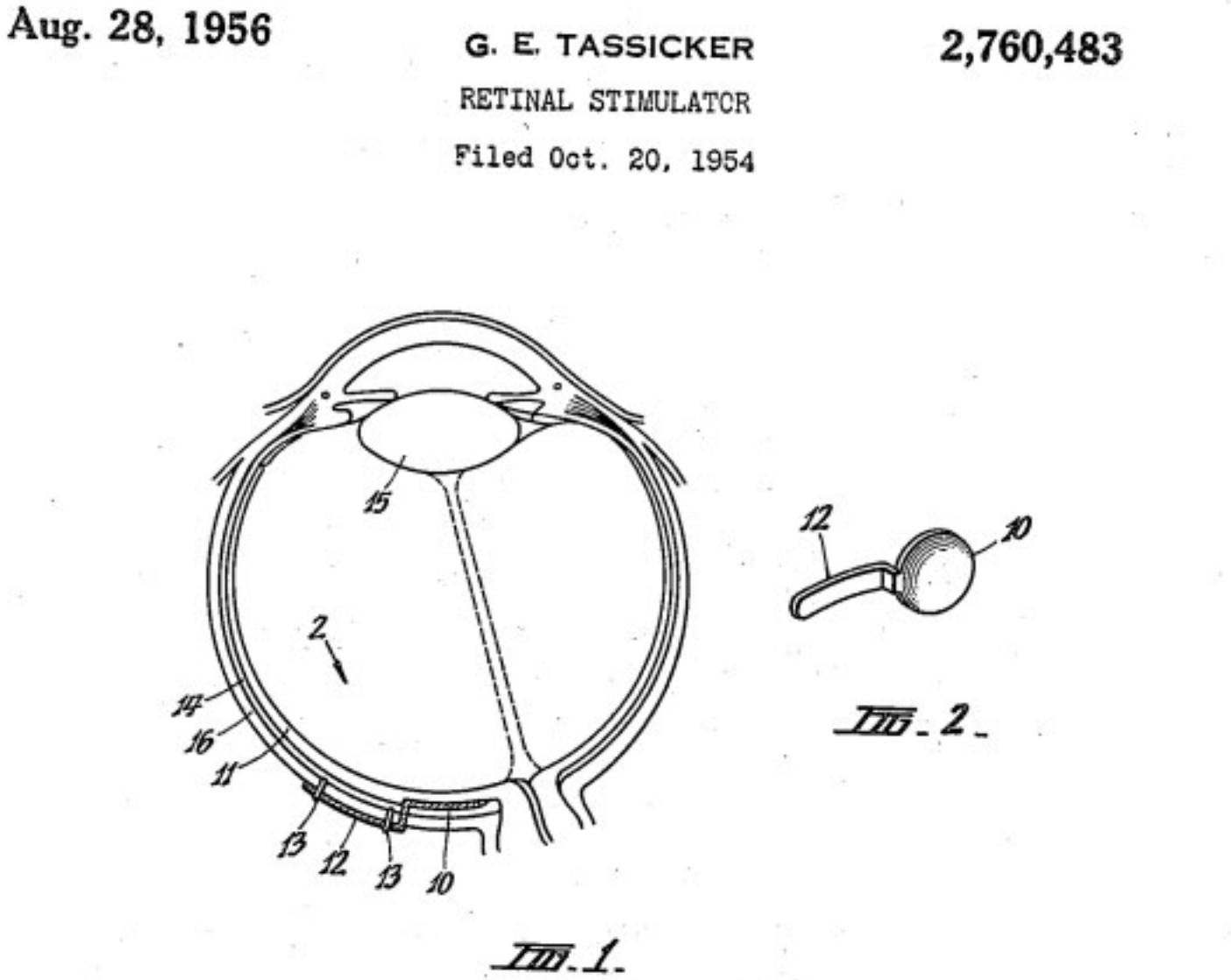

Figure 5. Retinal stimulator comprising a disc which is dished to conform to the curvature of the retina and which is adapted to be inserted surgically into the eye.

Blindness results from an interruption in the normal flow of signals along the visual pathways; a visual prosthesis has to excite the neurons of the pathway at some point after the damage site (54, 55) . The only requirement is that the device should contact still functioning neural elements.

5. Current Approaches to a Visual Prosthesis

Figure 9 shows the main approaches for the design of a visual neuroprosthesis. Since retinal diseases frequently reduce visual acuity and result in non-curable blindness, several groups worldwide are working on the development of different prostheses designed to interact with the remaining healthy retina (36, 56-59), optic nerve (60, 61) and LGN (62-64). However, the output neurons of the eye, the ganglion cells, often degenerate in many retinal blindnesses (65-69), and therefore a retinal, optic nerve or LGN prosthesis would not always be helpful. This extensive degeneration usually spares the neurons in the higher visual regions of the brain, which suggest the enormous potential of a cortical prosthesis designed to stimulate cortical neurons (54, 70-72). Due to

Figure 6. Cross-section of the human retina. Photoreceptors are at the top and ganglion cells at the bottom. Light enters the retina from the bottom and travels through the thickness of the retina to stimulate the photoreceptors at the top in this view. (Drawing courtesy of Helga Kolb).

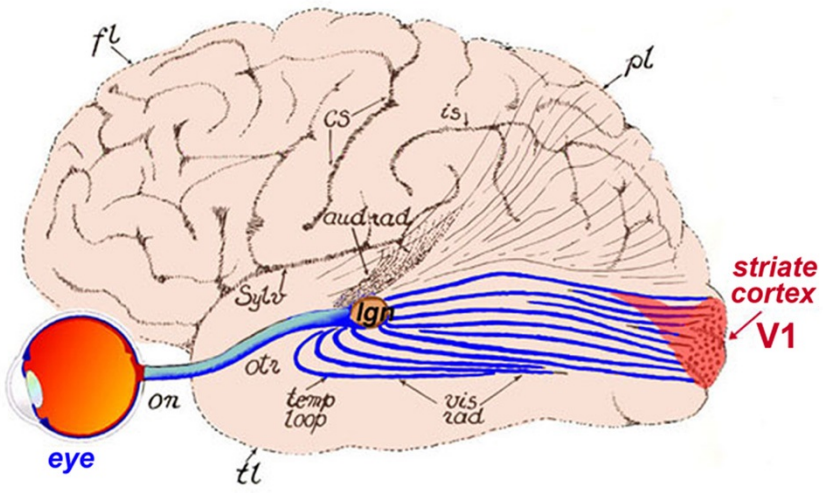

Figure 7. Human visual pathway.

complexity of the interconnectivity and the receptive field characteristics, visual areas beyond V1 have not been proposed as sites for vision prostheses.

Retinal Stimulation

Retinal prostheses are being developed to apply electrical stimulation to the retina in order to restore vision in patients with age-related macular degeneration and retinitis pigmentosa. More than five groups are already pursuing human clinical trials of various retinal prostheses (73-76).

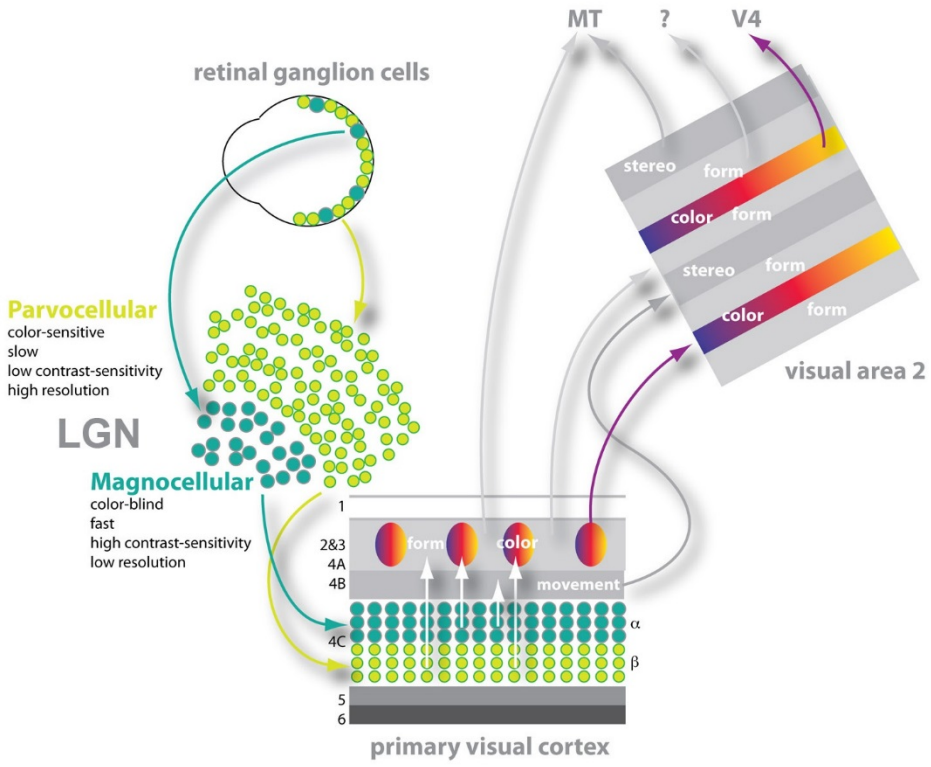

Figure 8. Functional segregation of the visual system, presenting the projection of large retinal ganglion cells to the magnocellular layer of the LGN and further to layer 4Ca of the primary visual cortex. (Image courtesy of Markus Bongard.)

There are significant advantages to the retinal approach as it is less invasive and the implants are lower in the visual pathways, which means that they are closer to the photoreceptors and have more opportunities for natural processing of the visual information. Further, the retinal approach has the advantage that no camera is required to encode the visual world: the optics of the eye provide this function. However there are also some problems related to encapsulation of the device, fixation of the implants, power dissipation and the production of sufficient currents (71, 77). Furthermore for a retinal visual prosthesis to work, there must be a population of functional retinal ganglion cells, and therefore these systems are not capable of treating very advanced retinal degenerations (78, 79).

Currently there are mainly two kinds of retinal implants under development: subretinal and epiretinal. Furthermore some groups are studying the efficacy of the suprachoroidal-transretinal stimulation to generate focal excitation in retinal ganglion cells (80-85). The latest experimental photostimulation approach involves re-engineering retinal ganglion cells or bipolar cells to become light sensitive by incorporation of artificial opsins (86-90). This novel approach is based on laboratory studies in fish or mouse and are nowhere near ready for human application.

Subretinal Implants

As some of the neural retina, with the exception of the photoreceptors layer, is preserved in both age-related macular degeneration and retinitis pigmentosa a reasonable approach to the restoration of vision under these pathologies is the replication of the function of the photoreceptors (36, 74-76, 91). One of the main advantages of this location is that the remaining retinal cells in the outer plexiform layer (vertically running bipolar cells and horizontally oriented horizontal cells) may be utilized to stimulate the amacrine and ganglion cells directly.

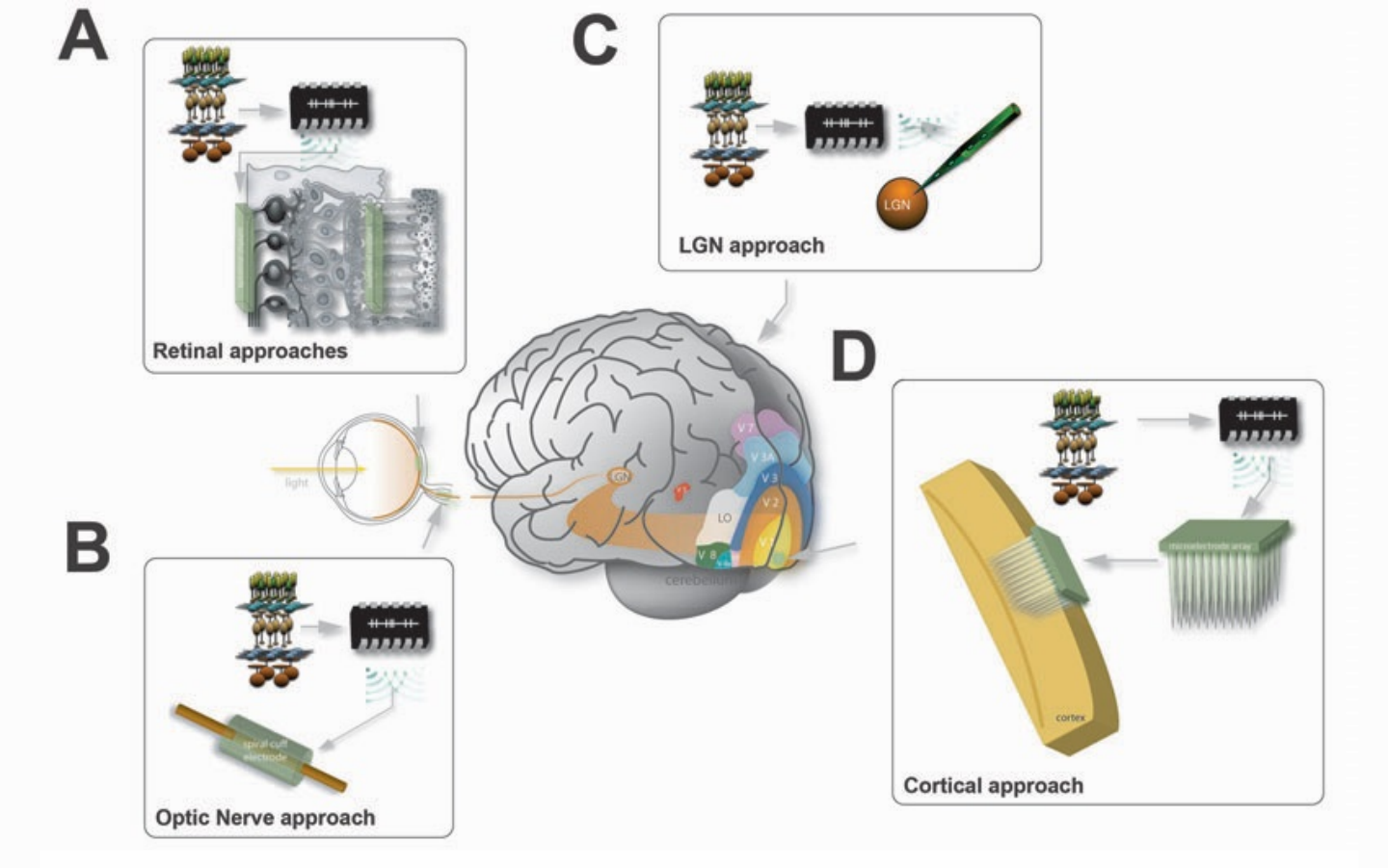

Figure 9. Main approaches for the design of a visual neuroprosthesis.

In a general sense all research groups that have focused on the subretinal approach have proposed a similar method. Thousands of light-sensitive microphotodiodes equipped with microelectrodes are assembled on a very thin plate and placed in the subretinal space. The subretinal device or microphotodiode array (MPDA) is implanted between the pigment epithelial layer and the outer layer of the retina, which contains the photoreceptors. Light falling on the retina generates graded currents in the MPDA that stimulate the dendrites of the bipolar cells in the outer plexiform layer to induce a visual sensation.

The schema is tantalizingly simple. Furthermore, the photodiodes can be tailored to provide either positive or negative current in response to illumination, with the intention of mimicking the function of ON and OFF bipolar cells. However, the success of this approach depends upon three assumptions. First, the bipolar cells of the dysfunctional retina should persist and function in a somewhat physiologically normal manner. Second, the MPDA must generate enough current under normal illumination levels to stimulate the remnant bipolar cells. Third, the electrodes can be placed in close enough proximity to the bipolar cells. Encouraging progress has been reported in each of these areas.

Epiretinal Implants

As an alternative approach to stimulate the retina, other research groups have proposed placing the stimulating electrodes in close proximity to the retinal ganglion cells. This approach attempts to stimulate the remaining retinal neurons of patients who are blind from end-stage photoreceptor diseases and relies on significant numbers or retinal ganglion cells surviving in pathologies such as age-related macular degeneration and retinitis pigmentosa (92, 93).

Both the epiretinal and subretinal approaches imply the use of implanted multielectrode arrays (MEAs) and transcutaneous telemetry to transfer data and power to the implanted MEAs. To date, a number of experiments performed in sighted and blind human subjects have demonstrated the potential for epiretinal electrical stimulation to provide patterned visual perception. One such device, the Argus II epiretinal implant developed by Second Sight (Sylmar, California, USA) has already obtained regulatory approval for marketing in Europe and the United States and has shown improved reading and motion detection in several patients (73, 94, 95). There are, however, issues relevant to the epiretinal approach that need to be solved. The epiretinal devices have to be firmly affixed in place in order to efficiently stimulate the retina and provide a consistent visual perception. Other issues of concern are power dissipation, cross-talk between electrodes, and the long-term viability of the tissues under the implant.

LGN Stimulation

The lateral geniculate nucleus (LGN) is the primary processing center for visual information, meaning that the neural signals encoding visual information have not yet been extensively processed. The LGN receives information directly from the retinal ganglion cells and projects mainly to the primary visual cortex. The LGN holds promise as a target for electrical stimulation for artificial visual percepts since it has been demonstrated that LGN microstimulation in monkeys produces predictable visual percepts (62-64). Therefore, a visual prosthesis based on LGN stimulation could be helpful to restore sight to those who have become blind because of trauma to the eye, or diseases such as glaucoma, macular degeneration, or retinitis pigmentosa.

One possible disadvantage of this approach is the limited number of electrodes that can be inserted in the LGN and hence the limited visual resolution capable with this approach. Moreover, the neurons in the LGN are too close together to be stimulated individually, which would be important in trying to reproduce natural vision. Furthermore, most of the projections to the LGN are from primary visual cortex making it difficult to create complex visual percepts.

Intracortical Stimulation

If primary visual cortex neurons can be stimulated with visual information in a format somewhat similar to the way they were stimulated before the onset of blindness, a blind individual could use this stimulation to extract information about the physical world around him/her (54, 55, 71, 72). Thus in more recent years an intracortical approach with penetrating microelectrodes has been introduced. Penetrating electrodes can activate populations of neurons with greater spatial specificity and lower levels of stimulation than is possible with larger electrodes on the surface of the brain as in the original Brindley and Dobelle experiments. The Utah Electrode Array (96) is an example of such a penetrating microelectrode array that could be used to stimulate many neurons in the visual cortex (Figure 10). The active regions of the electrodes in this electrode array are coated with iridium oxide to facilitate the transfer of charge flowing in the conducting silicon from which the array is made, and the size of these active regions is on the order of 50 µm. Such small electrodes abut small populations of cortical neurons, and electrical currents on the order of 10-30 µA can excite these neurons (this is three orders of magnitude smaller than the currents required with large surface electrodes). The electrodes are 1.5 mm in length and when implanted in visual cortex they reach down to layer 4, the layer of the cortex that receives normal input from the retina (Figure 10). In order to restore useful vision, visual cortex would have to be tiled with from 5-10 UEAs (97).

In 1966, Schmidt et al. (70) described the implantation of 38 floating microelectrodes within the right visual cortex of a 42-year-old woman who had been blind over 22 years. 34 of the microelectrodes were able to elicit phosphenes for a period of 4 months, and most of the microelectrodes had stimulation thresholds below 25 mA. Unfortunately, these microelectrodes were not well suited for long-term application. Thus, due to the breakage of lead wires early in the experiment, only limited tests could be done to evaluate recognition of simple patterns of stimulation. Nevertheless, taken as a whole the results suggested that passing electrical currents through an array

of electrodes inserted into an appropriate location in the visual pathway, is able to produce the perception of phosphenes, and that these phosphenes could be appropriate for restoring some limited but useful sense of vision to the profoundly blind. This intracortical approach requires penetrating electrodes with exposed tips located in layer 4 and with sizes that are of the same order of magnitude as the neurons that are intended to be stimulated.

This approach would be the most viable treatment for complete blindness caused by glaucoma, optic atrophy or diseases of the central visual pathways, such as brain injuries or stroke. Several groups worldwide are presently working on it (55, 71, 72, 98-100).

6. Engineering a Visual Neuroprosthesis

Regardless of the differences in the approaches, all vision prosthesis (with the exception of subretinal prostheses and the photostimulation approach) share a common set of components (37) which are illustrated in Figure 9. One or two cameras provide image acquisition. These visual signals are then processed by a bio-inspired retina-like encoder in order to transform the visual world in front of a blind individual into electrical signals. This first stage performs a multichannel spatio-temporal filtering, to extract and enhance the most relevant features of the scene and also to re-encode this information into a neuromorphic stream of electrode addresses (101). The second stage serializes the information and transmits it through a radio-frequency link to the implanted device. This telemetric transmission provides a wireless transfer of power and data to the internal system. The implanted electronics package must decode the signals, identify the target electrodes and generate the stimulation signals applied using multiple microelectrodes.

Most of the devices include a bio-inspired visual information block (artificial retina) to extract and enhance the most relevant features of the visual scene. A coding block that translates the retina-like output into pulses modulated with different cadences and temporal lags and whose projection onto the electrode matrix must be fully configurable. A radio frequency block provides a wireless transfer of power and data to the implanted electronics package which must decode the signals, identify the target electrodes and conform the voltage shape (D/A converter) of the final waveforms to be applied to the electrodes located near the target neurons (see Figure 11).

These transformations must take into account many issues that are normally performed by the retina. For example, sampling across the retina is not uniform and therefore retinotopic gradients and magnification factors have to be introduced to match image representation. On the other hand, it is clear that several streams of information are processed in parallel from any retinal point by several dozens of interneuronal subtypes before contrast, brightness, orientation movement and color are finally coded as modulation of ganglion cell action potential series (102). While chromatic information is not of utmost priority, a differential characterization will nevertheless be required when designing “achromatic” processing modules for basic representation of image components. The goal of developing such a bio-inspired retinal encoder is not to simply record a high resolution image, but to transmit visual information in a meaningful way to the appropriate site(s) in the retina, optic nerve, LGN or brain.

Although it is not the purpose of this chapter to present a detailed study of the problem of coding/decoding of retinal images by ensembles of retinal ganglion cells, increasing evidence suggests that the retina and the brain utilize distributed codes that can only be analyzed by simultaneously recording activity of multiple neurons (103-106). Far from a simple transducer of light into electrical neural impulses, the retina performs a locally-computed spatio-temporal contrast enhancement function, and a very efficient compression of visual information. These tasks are essential to provide a high adaptation capability to very different lighting conditions, high noise immunity, and to efficiently communicate the visual information by means of a limited number of optic nerve fibers. Thus, our entire experience of the external visual world derives from the concerted activity of a limited number of ganglion cells in the retinal output layer. They have to represent all the features of

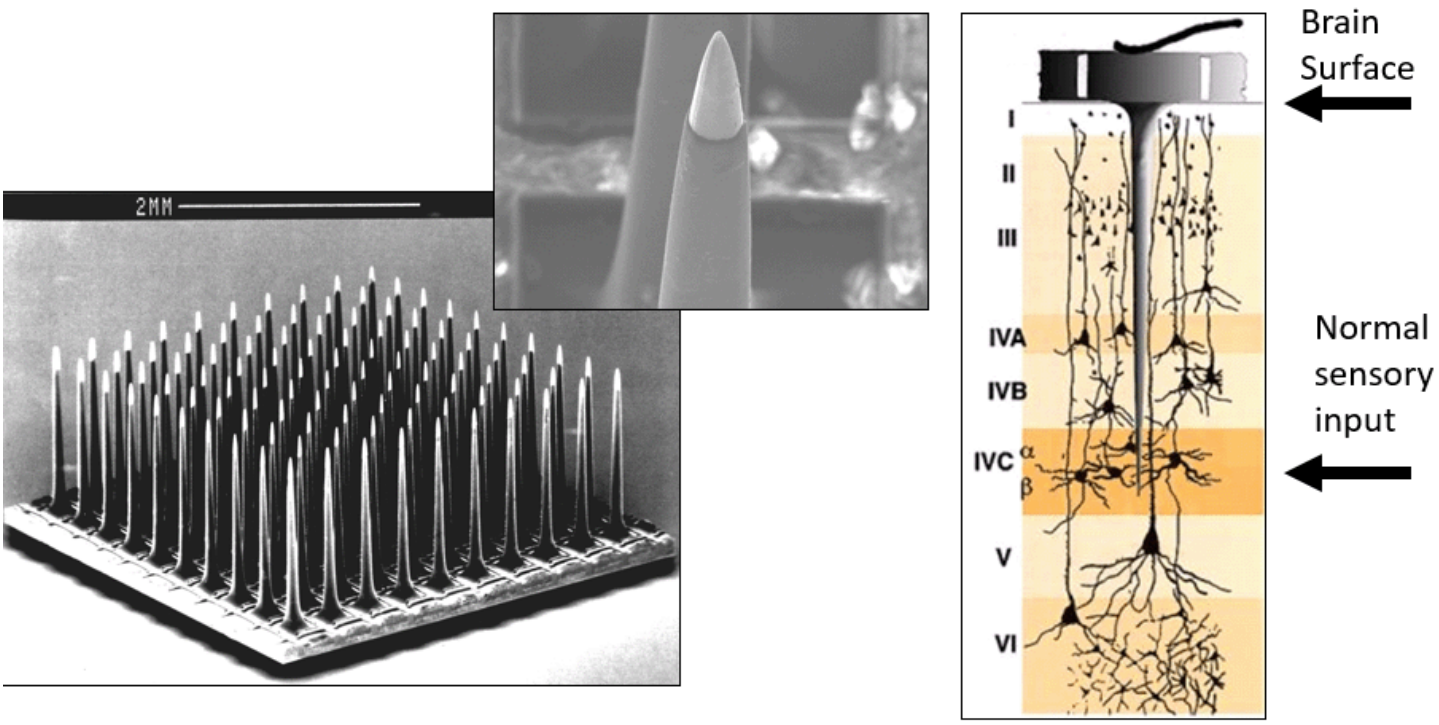

Figure 10. The Utah Electrode Array contains 100, 1.5 mm long penetrating microelectrodes that reach down to layer 4, the region of normal cortical input from the retina.

objects in the visual world, namely their color, intensity, shape, movement, and the changes in these features in time. This representation has to be unequivocal and fast (within a few hundreds of milliseconds) in order to ensure object recognition for any single stimulus presentation.

The development of a bio-inspired visual encoder poses therefore an information processing challenge without parallel in neuroscience, computer science or communication technologies. Consequently, several research programs are developing complex retina encoders for visual implants (107, 108).

Figure 12 summarizes the basic architecture of a typical bio-inspired retinal model. It is based on information about the photoreceptor distribution within the human/primate retina and on electrophysiological recordings from populations of retinal ganglion cells. Through a set of parametrized filters and functions, that simulate the complex operations of the neural retina, a portable model is obtained that can be easily translated into a hardware description for automatic synthesis using the appropriate tools.

The input images are captured by a photosensor array (preferably a logarithmic response camera that has a similar response to the human visual system and can reduce saturation in high contrast visual scenes). These visual signals are processed by a set of separate spatial and temporal filters that enhance specific features of the captured visual information. The model can take into account the irregular distribution of photoreceptors within the human retina: a high density of pixels and smaller receptive field sizes in central areas; lower density and bigger receptive fields in peripheral areas. A gain factor can be specified for every individual channel as well as a global gain. The next stage reduces the information to the resolution of the electrode matrix, with the option of defining specific receptive field shapes and sizes. Finally, a mapping and neuromorphic coding (into output charge-balanced pulses that can be sent to each electrode) is carried out and feeds the radio frequency link that goes to the microelectrode array. Thus the continuously varying input video stream is converted into neuromorphic pulse-coded signals through a circuit that emulates the function of retinal neurons (Figure 13) (55, 108).

The implementation of the model in digital hardware provides a flexible design, achieving a high performance with response times several orders of magnitude lower than that of biological systems. The present version of the whole system is able to work properly up to 40 MHz (55, 71, 101). This means that 40,000 electrodes could be stimulated with an inter-spike temporal resolution equal to or lower than 1msec. The use of reconfigurable circuitry (FPGA) permits one to adjust or even change the spiking model easily (101, 108). Furthermore, this technology can be used for psychophysical experimentation in order to determine the best image processing strategy, and to get insights into the optimal number of electrodes, grey levels and grid size (109, 110).

Finally the output of the bio-inspired retina has to be transmitted to a remote stimulating device that electrically connects with the implanted microelectrode array (Figure 6). Ideally this should be done telemetrically (i.e. without the need of attached wires) to reduce the risk of infections and an opto-coupling stage should be incorporate to protect the patient against electrical risks. Furthermore, for a durable system, the materials used in the implanted system must be biocompatible, and electrical-charge displacements must be within margins of capacitive work, never in an irreversible-faradaic working zone (111).

Several factors should be taken into account, especially safety, size and power consumptions. Thus, this stimulating device should be able to operate in real-time for a high number of electrodes, have low power requirements and be flexible enough to generate different waveforms and adapt to different stimuli and image processing conditions. Basically it should be able to solve the problem of transmitting data and power to multiple microelectrodes having, simultaneously, the possibility of remote control and sensing of microelectrode status. It implies a compromise between the power level requirements of the stimulation circuits and the signal bandwidth requirements (101, 112).

7. Safe and Effective Stimulation of Visual Pathways through Multiple Micro Electrodes

Any visual neuroprosthetic system must be implanted into the retina, optic nerve, LGN or visual cortex and remain fully functional for periods that may eventually extend to many decades. Therefore, these devices must be highly biocompatible and be able to resist the attack of biological fluids, proteases, macrophages or any products of metabolism. Furthermore, it is necessary to take into account the possible damage of neural tissues by continual charge injection and the most effective means of stimulating the visual pathways. On the other hand, although there are no major safety concerns stemming from the pilot studies carried out to date, the risks of the surgical procedures involved are not negligible. All these considerations place unique constraints on the architecture, material, and surgical techniques used in the implementation of visual prostheses interfaces (55, 71, 113-117).

An important problem reported with all available microelectrodes to date, is long-term viability and biocompatibility. Recent studies of the response of neural tissue to stab wound have shown that there are acute and chronic inflammatory reactions which affect both the neural tissue and the surface of the microelectrodes (118-125). These reactions often result in damage to neurons and microelectrodes and lead to the proliferation of a glial scar around the implanted probes which prevents neurons being recorded or stimulated (126-128). The reasons for the inflammatory response lie in molecular and cellular reactions at foreign surfaces (120, 129). These responses can be controlled and one of the big challenges in this field is to create new, more biocompatible surfaces. The solution may involve coating the electrodes with bio-active molecules that are slowly released into the surrounding neural tissue (117).

8. Selection of Suitable Subjects for a Visual Prosthesis

The selection of a specific person for a visual implant is not straightforward. There are no strict standardized criteria for accepting or rejecting a candidate, nor for the best rehabilitation procedure for every type of

Fig 11. Functional blocks of a visual neuroprostheses

Figure 11. Functional blocks of a visual neuroprosthesis.

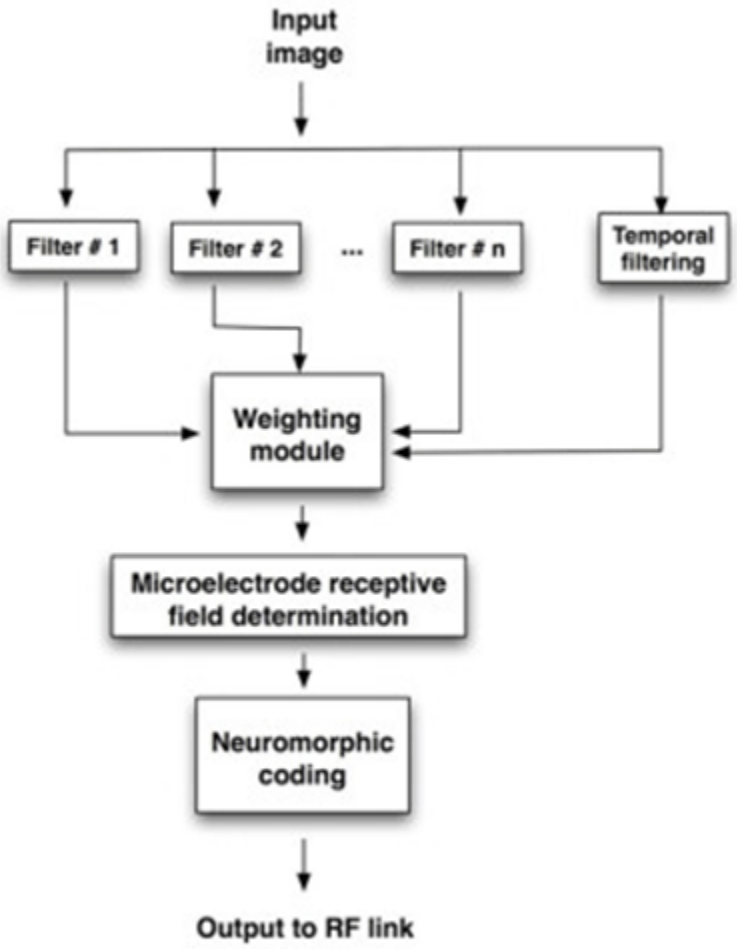

Fig 12. Schematic organization of a bioinspired retina model

Figure 12. Schematic organization of a bio-inspired retina model.

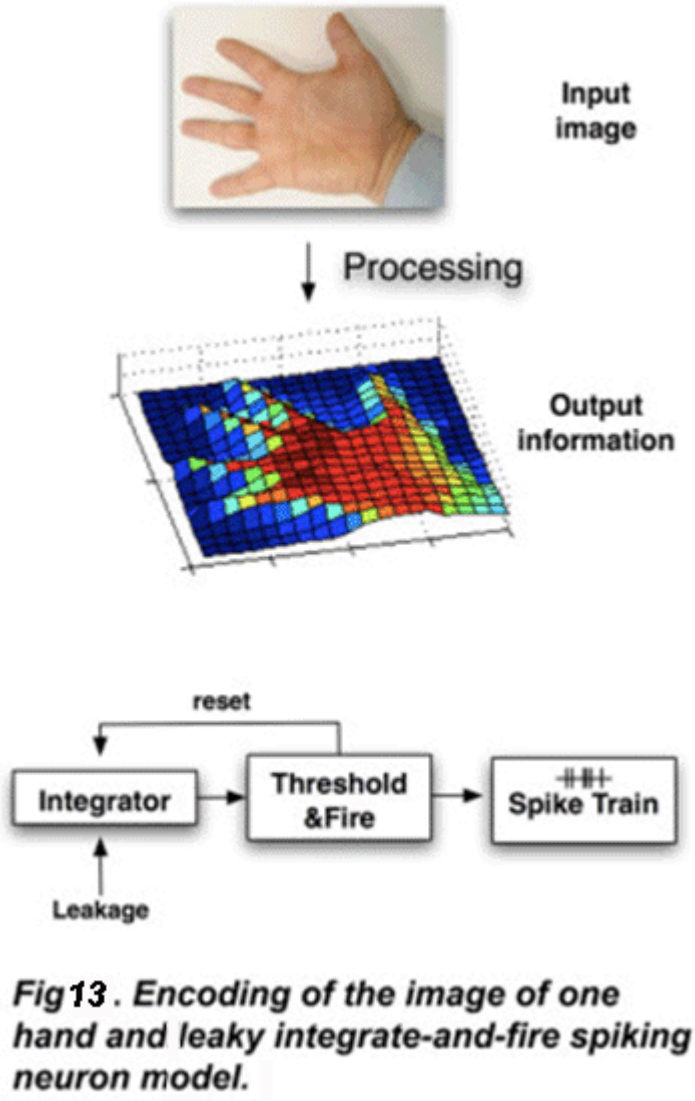

Figure 13. Encoding of the image of one hand and a leaky integrate-and-fire spiking neuron model.

blindness. Generally, a choice should be made between different approaches and/or rehabilitation procedures depending on availability, efficacy or rejection of invasive methods (78, 130, 131). But a pre-surgical protocol and improved methods for predicting success with a visual neuroprosthesis need to be developed (55, 110, 132).

In general, it is considered crucial, at least in these preliminary stages, that the subject should have no residual vision and have had no significant benefit from a conventional visual aid. However, these seemingly straightforward criteria do not always work well in practice and there are different definitions of "residual vision" and "significant benefit from a visual aid". Needs and wishes of individual subjects are also significant variables for implant candidacy. This issue is further complicated because it is not possible to predict success with a visual implant in a specific person. Clearly, our knowledge regarding visual system anatomy and function may allow for crude bio-inspired models and strategies of stimulation. However, what has not been discussed is how the type, onset, duration and temporal profile of an individual's visual loss may have repercussions on the success of the device. To decide what time is the most suitable for intervention is a difficult double-faced ethical decision (130).

Recognizing these limitations, it is generally acknowledged that previous visual experience is necessary for the patient to interpret and recognize the visual patterns that are generated. In this context, it has been presumed that if blindness occurs after the age of ten years of age (i.e. after the critical period), visual pathways should have developed normally and thus remain excitable (78, 130).

Improved networking among research groups would clearly help in developing a common body of standardized test and standardized selection criteria (110). According to Merabet et al (132) the criteria for potential users of a visual neuroprosthesis should include:

- Visual function criteria and pre- and post-implantation testing. Indications in favor of a cortical visual implant could include profound and bilateral visual loss, but more objective and quantitative criteria should be developed. These studies need to incorporate a more quantifiable means of estimating risk and benefit for a given candidate.
- Electrophysiological criteria. Measurement of electroretinogram (ERG) as well as visual evoked potentials (VEP) should be a basic component in candidate selection. Improved methods for predicting success with a visual implant need to be developed. These methods could include a test using data from transcranial magnetic stimulation of visual pathways and new imaging techniques such as functional magnetic resonance (fMRI).
- Medical, anatomical and surgical criteria. The ideal candidate should be a healthy adult. The medical history should include the onset and evolution of the blindness, physical examination, and laboratory tests to include or exclude candidates and to assist the implant team in planning a total program, including post-implant training.
- Evaluation of the risks and limitations associated with the surgery and every specific approach. These are usually small for persons in good general health but increase with age and other pathological conditions.
- Quantitative evaluation of the subjects' needs and performance using standardized psychophysical and behavioral methods.
- Psychological testing to discard psychiatric disorders and other possible mental status that could affect the success of the visual prosthesis.

There are other important issues that should be taken into account and case studies of surgical sight restoration following long-term visual deprivation provide relevant insights (133, 134). For example, following ocular surgical procedures aimed at regaining some degree of functional vision, patients, blinded for many years, experience profound difficulty in various visual tasks, particularly those requiring the identification and recognition of objects. Interestingly, if patients are allowed to explore the same object through touch, they can recognize it immediately as to register their newly acquired visual percepts with their existing senses. These findings demonstrate that even when vision reaches the brain physiologically, visual perception remains nonetheless impaired. Thus, the simple restoration of a lost sensory input may not itself suffice in reconstituting the sense it normally provides. Active visual rehabilitation may be necessary to maximize the adaptation and get the most from these devices. Moreover some form of spatial remapping between the bio-inspired encoder and the stimulation pattern delivered to the array of electrodes implanted in the visual cortex is highly recommended (55, 104, 107, 112, 135). As a result, the right learning, remapping and rehabilitation strategies could potentially help to modulate the plasticity of the brain and contribute to ever-improving performance and more concordant perceptions.

9. Conclusions and Future Perspectives

The field of visual prosthetics is rapidly emerging and requires extraordinary diverse, lengthy and intimate collaborations among basic scientists, engineers and clinicians. Significant challenges to the development of a successful visual prosthesis include limitations to the number of electrodes, biocompatibility, encapsulation, electrode degradation, power interference, signal and imaging processing, interference with residual vision,

functional evaluation and training. Despite all these issues several research groups are developing sophisticated microelectronic devices designed to stimulate viable neuronal tissue in the hopes of generating functional vision artificially.

To date, at least 23 different devices are under development, several groups are pursuing human clinical trials either with acute or chronic implantation of neurostimulating devices and increasing numbers are expected within the next years (136). Thus this type of technology is clearly expanding and ophthalmology has emerged as one of the more interesting areas of research in the neurostimulation field. However, even the most advanced of these experimental devices has only been able to provide evidence that such an approach is feasible. What remains to be conclusively demonstrated is whether or not the visual percepts produced by implanted microelectronic devices can create meaningful visual perceptions that can be translated into functional gains such as the recognition, localization and grasping of objects or skillful navigation in an unfamiliar environment.

The greater impediments to future progress in visual neuroprosthesis approaches are not only the technical, engineering and surgical issues that remain to be solved, but also the development and implementation of strategies designed to interface with the visually deprived brain specifically tailored for an individual patient's own needs. This would particularly involve an improved patient selection and a "custom-tailoring" of visual prosthetic devices to the subject. A key issue in this context that has often been utterly underrated is the role of neural plasticity. Thus, these strategies should take into consideration not only standardized methods and employ current clinical and technological expertise, but also consider newly emerging developmental and neurophysiological evidence. For example, there is considerable evidence that adaptive and compensatory changes occur within the brain following the loss of sight (7, 55, 137-141). These studies have shown that in some patients the occipital parts of the brain that sighted subjects use to process visual information are transformed and utilized to process tactile and auditory stimuli. This plastic change in the brain probably allows blind subjects to extract greater information from touch and hearing, thus improving quality of life and enhancing the integration of the blind in the social and working environment of a sighted society. The modulation and understanding of these neuroplastic processes is crucial for the success of any visual neuroprosthesis and can therefore provide the neuroscientific foundation for improved rehabilitation and teaching strategies for the blind.

Hopefully the advances in medicine, ophthalmology and genetics will be able to devise new ways of preventing diseases of the retina and visual pathways or in transplanting neurons that have been lost. However genetic science and treatment will not help in injuries due to trauma and probably will not eliminate all the visual impairments due to ageing. Therefore, progress in vision prosthesis technologies is regarded as a necessity for the future. We hope that progress in medical technologies, material science and bioengineering, together with the increase of intelligence in these visual neuroprosthetic devices will improve the quality of life of people that are affected by visual impairments, and encourage further development of custom-tailored devices for restoring functional sight in the blind.

About the authors

Dr. Eduardo Fernandez was born in Elda (Spain) in 1962. He received an M.D. degree from the University of Alicante (Spain) in 1986 and a Ph. D. degree in Neurosciences with honors in 1990. His collaboration with Dr. Helga Kolb and Dr. Richard Normann, began with a stay from 1990 to 1991 under a postdoctoral fellowship of the Spanish Government (FPI program). He is currently Director of the Department of Histology and Anatomy of the University Miguel Hernández (Spain) and Director of the Biomedical Neuroengineering Research Unit of the Biomedical Research Networking Center on Bioengineering, Biomaterials and Nanomedicine (CIBER-BBN, Spain). His main interest is to develop innovative interfaces with the human nervous system and to develop a two-way direct communication with neurons and ensembles of neurons, which could enhance the life of the disabled. He is also working on the development of new therapeutic approaches for retinal degenerative diseases in order to preserve eyesight and slow disease progression. In recent years he has been working in close collaboration with Dr. Normann on the development of a cortical visual neuroprosthesis that will be able to provide a limited but useful sense of vision to profoundly blind people.

Richard A. Normann received BS, MS and Ph.D. degrees from the University of California, Berkeley, CA, USA. His original interests were in retinal physiology elucidating photoreceptor adaptation and horizontal cell function. After a 6-year stint in the Neurophysiology lab at the National Institute of Neurological Disorders and Stroke (NINDS), National Institutes of Health, Bethesda MD, USA, he moved to the University of Utah, Department of Bioengineering. His research interests changed from intracellular recordings in retina to a neuro-engineering bent. Dr. Normann invented the Utah Electrode Array originally for use as a cortical neuroprosthesis for the blind. Since then his research has spearheaded the use of the UEA in sensory and motor physiology, and as an interface to the central and peripheral nervous systems. He is presently a Distinguished Professor (emeritus) in the Departments of Bioengineering and Ophthalmology, University of Utah.

References

1. Galvani, L. and G. Aldini, De Viribus Electricitatis In Motu Musculari Comentarius Cum Joannis Aldini Dissertatione Et Notis; Accesserunt Epistolae ad animalis electricitatis theoriam pertinentes. 1792: Apud Societatem Typographicam.
2. Hunter T.B., Yoshino M.T., Dzioba R.B., Light R.A., Berger W.G. Medical Devices of the Head, Neck, and Spine 1. Radiographics. 2004;24(1):257–285. PubMed PMID: 14730051.
3. Peña C., Bowsher K., Samuels-Reid J. FDA-approved neurologic devices intended for use in infants, children, and adolescents. Neurology. 2004;63(7):1163–1167. PubMed PMID: 15477532.
4. Stieglitz T., Schuettler M., Koch K. Neural Prostheses in Clinical Applications–Trends from Precision Mechanics towards Biomedical Microsystems in Neurological Rehabilitation/Neuroprothesen in der klinischen Anwendung–Trends von der Feinwerktechnik zu biomedizinischen Mikrosystemen in der

neurologischen Rehabilitation. Biomedizinische Technik/Biomedical Engineering. 2004;49(4):72–77. PubMed PMID: 15171585.
5. Brors D., Bodmer D. New aspects of inner ear research. Hospital medicine. 2004;65(7):392–395. PubMed PMID: 15287341.
6. Chatelin V., Kim E.J., Driscoll C., Larky J., Polite C., Price L., Lalwani A.K. Cochlear implant outcomes in the elderly. Otology & Neurotology. 2004;25(3):298–301. PubMed PMID: 15129109.
7. Cohen L.G., Celnik P., Pascual-Leone A., Corwell B., Faiz L., Dambrosia J., Honda M., Sadato N., Gerloff C., Catalá M.D. Functional relevance of cross-modal plasticity in blind humans. Nature. 1997;389(6647):180–183. PubMed PMID: 9296495.
8. Balkany T.J., Hodges A., Buchman C.A., Luxford W., Pillsbury C., Roland P., Shallop J., Backous D., Franz D., Graham J. Cochlear implant soft failures consensus development conference statement. Cochlear Implants International. 2005;6(3):105–122. PubMed PMID: 18792329.
9. Chang P. Implantable hearing devices: beyond hearing aids. Australian family physician. 2005;34(3):157. PubMed PMID: 15799665.
10. Donoghue J.P. Connecting cortex to machines: recent advances in brain interfaces. Nature neuroscience. 2002;5:1085–1088. PubMed PMID: 12403992.
11. Nicolelis M.A. Brain–machine interfaces to restore motor function and probe neural circuits. Nature Reviews Neuroscience. 2003;4(5):417–422. PubMed PMID: 12728268.
12. Donoghue J.P., Nurmikko A., Friehs G., Black M. Development of neuromotor prostheses for humans. Supplements to Clinical Neurophysiology. 2004;57:592–606. PubMed PMID: 16106661.
13. Carmena J.M., Lebedev M.A., Henriquez C.S., Nicolelis M.A. Stable ensemble performance with single-neuron variability during reaching movements in primates. The Journal of neuroscience. 2005;25(46):10712–10716. PubMed PMID: 16291944.
14. Hochberg L.R., Serruya M.D., Friehs G.M., Mukand J.A., Saleh M., Caplan A.H., Branner A., Chen D., Penn R.D., Donoghue J.P. Neuronal ensemble control of prosthetic devices by a human with tetraplegia. Nature. 2006;442(7099):164–171. PubMed PMID: 16838014.
15. Barbeau H., McCrea D.A., O'Donovan M.J., Rossignol S., Grill W.M., Lemay M.A. Tapping into spinal circuits to restore motor function. Brain Research Reviews. 1999;30(1):27–51. PubMed PMID: 10407124.
16. Nicolelis M.A., Chapin J.K. Controlling robots with the mind. SCIENTIFIC AMERICAN-AMERICAN EDITION. 2002;287(4):46–55. PubMed PMID: 12271524.
17. Serruya M.D., Hatsopoulos N.G., Paninski L., Fellows M.R., Donoghue J.P. Brain-machine interface: Instant neural control of a movement signal. Nature. 2002;416(6877):141–142. PubMed PMID: 11894084.
18. Paninski L., Fellows M.R., Hatsopoulos N.G., Donoghue J.P. Spatiotemporal tuning of motor cortical neurons for hand position and velocity. Journal of neurophysiology. 2004;91(1):515–532. PubMed PMID: 13679402.
19. Patil P.G., Carmena J.M., Nicolelis M.A., Turner D.A. Ensemble recordings of human subcortical neurons as a source of motor control signals for a brain-machine interface. Neurosurgery. 2004;55(1):27–38. PubMed PMID: 15214971.
20. Sanchez J.C., Carmena J.M., Lebedev M.A., Nicolelis M.A., Harris J.G., Principe J.C. Ascertaining the importance of neurons to develop better brain-machine interfaces. IEEE Transactions on Biomedical Engineering. 2004;51(6):943–953. PubMed PMID: 15188862.
21. Loeb G.E. Cochlear prosthetics. Annual review of neuroscience. 1990;13(1):357–371. PubMed PMID: 2183680.
22. McDermott H.J. Music perception with cochlear implants: a review. Trends in amplification. 2004;8(2):49–82. PubMed PMID: 15497033.
23. Bouccara, D., P. Avan, I. Mosnier, A. Bozorg Grayeli, E. Ferrary, and O. Sterkers, Réhabilitation auditive. M/S Revues: Dossier technique. 2005.
24. Penfield, W. and T. Rasmussen, The cerebral cortex of man; a clinical study of localization of function. 1950.
25. Penfield, W. and H. Jasper, Epilepsy and the functional anatomy of the human brain. 1954.

26. Brindley G.S., Lewin W. The sensations produced by electrical stimulation of the visual cortex. The Journal of physiology. 1968;196(2):479. PubMed PMID: 4871047.
27. Brindley G., Donaldson P., Falconer M., Rushton D. The extent of the region of occipital cortex that when stimulated gives phosphenes fixed in the visual field. The Journal of physiology. 1972;225(2):57P–58P. PubMed PMID: 5074414.
28. Brindley G. Effects of electrical stimulation of the visual cortex. Human neurobiology. 1982;1(4):281. PubMed PMID: 7185798.
29. Dobelle W., Mladejovsky M. Phosphenes produced by electrical stimulation of human occipital cortex, and their application to the development of a prosthesis for the blind. The Journal of physiology. 1974;243(2):553. PubMed PMID: 4449074.
30. Dobelle W.H., Mladejovsky M., Girvin J. Artificial vision for the blind: electrical stimulation of visual cortex offers hope for a functional prosthesis. Science. 1974;183(4123):440–444. PubMed PMID: 4808973.
31. Dobelle W.H., Mladejovsky M.G., Evans J.R. Braille'reading by a blind volunteer by visual cortex stimulation. Nature. 1976;259:111–112. PubMed PMID: 1246346.
32. Dobelle W.H. Artificial vision for the blind by connecting a television camera to the visual cortex. ASAIO journal. 2000;46(1):3–9. PubMed PMID: 10667705.
33. Pollen, D., Some perceptual effects of electrical stimulation of the visual cortex in man. The nervous system. 1975; 2:519-528.
34. Bak M., Girvin J., Hambrecht F., Kufta C., Loeb G., Schmidt E. Visual sensations produced by intracortical microstimulation of the human occipital cortex. Medical and Biological Engineering and Computing. 1990;28(3):257–259. PubMed PMID: 2377008.
35. Tassicker G. Preliminary report on a retinal stimulator. The British journal of physiological optics. 1956;13(2):102–105. PubMed PMID: 13315967.
36. Zrenner E. Will retinal implants restore vision? Science. 2002;295(5557):1022–1025. PubMed PMID: 11834821.
37. Maynard E.M. Visual prostheses. Annual review of biomedical engineering. 2001;3(1):145–168. PubMed PMID: 11447060.
38. Webvision: The Organization of the Retina and Visual System. In: H. Kolb, F. Fernandez, and R. Nelson editors. [Internet]. Salt Lake City (UT): University of Utah Health Sciences Center; 1995-, Available from: http://www.ncbi.nlm.nih.gov/books/NBK11530/.
39. Wilke S.D., Thiel A., Eurich C.W., Greschner M., Bongard M. J. AmmermuÈller, and H. Schwegler, Population coding of motion patterns in the early visual system. Journal of Comparative Physiology A. 2001;187(7):549–558.
40. Greschner M., Bongard M., Rujan P., Ammermüller J. Retinal ganglion cell synchronization by fixational eye movements improves feature estimation. Nature neuroscience. 2002;5(4):341–347. PubMed PMID: 11914721.
41. Bialek W., Rieke F., De Ruyter Van Steveninck R.R., Warland D. Reading a neural code. Science. 1991;252(5014):1854–1857. PubMed PMID: 2063199.
42. van Steveninck R.R.d.R., Lewen G.D., Strong S.P., Koberle R., Bialek W. Reproducibility and variability in neural spike trains. Science. 1997;275(5307):1805–1808. PubMed PMID: 9065407.
43. Smirnakis S.M., Berry M.J., Warland D.K., Bialek W., Meister M. Adaptation of retinal processing to image contrast and spatial scale. Nature. 1997;386(6620):69–73. PubMed PMID: 9052781.
44. Sherman, S.M. and R.W. Guillery, Exploring the thalamus. 2001: Elsevier.
45. Gross, C.G., From Imhotep to Hubel and Wiesel, in Extrastriate Cortex in Primates. 1997, Springer. p. 1-58.
46. Grill-Spector K., Malach R. The human visual cortex. Annu. Rev. Neurosci. 2004;27:649–677. PubMed PMID: 15217346.
47. Hubel, D. Functional architecture of macaque monkey visual cortex (Ferrier Lecture). in Proc. R. Soc. Lond. B. 1977: Citeseer.
48. Hubel, D. and T. Wiesel, Brain mechanism of vision The Perceptual World ed I Rock. 1990, New York: Freeman.

49. Dougherty R.F., Koch V.M., Brewer A.A., Fischer B., Modersitzki J., Wandell B.A. Visual field representations and locations of visual areas V1/2/3 in human visual cortex. Journal of Vision. 2003;3(10):1–1. PubMed PMID: 14640882.
50. Wandell B.A., Wade A.R. Functional imaging of the visual pathways. Neurologic clinics. 2003;21(2):417–443. PubMed PMID: 12916486.
51. Schmolesky, M., The primary visual cortex. 2007.
52. Nelson, R. Visual responses of Ganglion cells. In: H. Kolb, E. Fernandez, and R. Nelson editors. Webvision: The Organization of the Retina and Visual System [Internet]. Salt Lake City (UT): University of Utah Health Sciences Center; 2007, Available from: https://www.ncbi.nlm.nih.gov/books/NBK11550/.
53. Kaplan E., Shapley R.M. The primate retina contains two types of ganglion cells, with high and low contrast sensitivity. Proceedings of the National Academy of Sciences. 1986;83(8):2755–2757. PubMed PMID: 3458235.
54. Normann R.A., Maynard E.M., Guillory K.S., Warren D.J. Cortical implants for the blind. IEEE Spectrum. 1996;33(5):54–59.
55. Fernandez E., Pelayo F., Romero S., Bongard M., Marin C., Alfaro A., Merabet L. Development of a cortical visual neuroprosthesis for the blind: the relevance of neuroplasticity. Journal of Neural Engineering. 2005;2(4):R1. PubMed PMID: 16317227.
56. Eckmiller R. Learning retina implants with epiretinal contacts. Ophthalmic research. 1997;29(5):281–289. PubMed PMID: 9323719.
57. Walter P., Szurman P., Vobig M., Berk H. H.C. LUDTKE-HANDJERY, H. Richter, C. Mittermayer, K. Heimann, and B. Sellhaus, Successful long-term implantation of electrically inactive epiretinal microelectrode arrays in rabbits. Retina. 1999;19(6):546–552. PubMed PMID: 10606457.
58. Humayun M.S., Weiland J.D., Fujii G.Y., Greenberg R., Williamson R., Little J., Mech B., Cimmarusti V., Van Boemel G., Dagnelie G. Visual perception in a blind subject with a chronic microelectronic retinal prosthesis. Vision research. 2003;43(24):2573–2581. PubMed PMID: 13129543.
59. Rizzo J.F., Wyatt J., Loewenstein J., Kelly S., Shire D. Perceptual efficacy of electrical stimulation of human retina with a microelectrode array during short-term surgical trials. Investigative ophthalmology & visual science. 2003;44(12):5362–5369. PubMed PMID: 14638739.
60. Delbeke J., Pins D., Michaux G., Wanet-Defalque M.-C., Parrini S., Veraart C. Electrical stimulation of anterior visual pathways in retinitis pigmentosa. Investigative ophthalmology & visual science. 2001;42(1):291–297. PubMed PMID: 11133881.
61. Veraart C., Wanet-Defalque M.C., Gérard B., Vanlierde A., Delbeke J. Pattern recognition with the optic nerve visual prosthesis. Artificial Organs. 2003;27(11):996–1004. PubMed PMID: 14616518.
62. Pezaris J.S., Reid R.C. Demonstration of artificial visual percepts generated through thalamic microstimulation. Proceedings of the National Academy of Sciences. 2007;104(18):7670–7675. PubMed PMID: 17452646.
63. Pezaris J.S., Eskandar E.N. Getting signals into the brain: visual prosthetics through thalamic microstimulation. Neurosurgical focus. 2009;27(1):E6. PubMed PMID: 19569894.
64. Jeffries A.M., Killian N.J., Pezaris J.S. Mapping the primate lateral geniculate nucleus: a review of experiments and methods. Journal of Physiology-Paris. 2014;108(1):3–10. PubMed PMID: 24270042.
65. Jones B.W., Watt C.B., Frederick J.M., Baehr W., Chen C.K., Levine E.M., Milam A.H., Lavail M.M., Marc R.E. Retinal remodeling triggered by photoreceptor degenerations. Journal of Comparative Neurology. 2003;464(1):1–16. PubMed PMID: 12866125.
66. Marc R.E., Jones B.W. Retinal remodeling in inherited photoreceptor degenerations. Molecular neurobiology. 2003;28(2):139–147. PubMed PMID: 14576452.
67. Jones B.W., Marc R.E. Retinal remodeling during retinal degeneration. Experimental eye research. 2005;81(2):123–137. PubMed PMID: 15916760.
68. Jones B., Kondo M., Terasaki H., Lin Y., McCall M., Marc R.E. Retinal remodeling. Japanese journal of ophthalmology. 2012;56(4):289–306. PubMed PMID: 22644448.

69. Marc R., Pfeiffer R., Jones B. Retinal prosthetics, optogenetics, and chemical photoswitches. ACS chemical neuroscience. 2014;5(10):895–901. PubMed PMID: 25089879.
70. Schmidt E., Bak M., Hambrecht F., Kufta C., O'rourke D., Vallabhanath P. Feasibility of a visual prosthesis for the blind based on intracortical micro stimulation of the visual cortex. Brain. 1996;119(2):507–522. PubMed PMID: 8800945.
71. Normann R.A., Greger B.A., House P., Romero S.F., Pelayo F., Fernandez E. Toward the development of a cortically based visual neuroprosthesis. Journal of neural engineering. 2009;6(3):035001. PubMed PMID: 19458403.
72. Fernández, E., B. Greger, P.A. House, I. Aranda, C. Botella, J. Albisua, C. Soto-Sánchez, A. Alfaro, and R.A. Normann, Acute human brain responses to intracortical microelectrode arrays: challenges and future prospects. The chronic challenge-new vistas on long-term multisite contacts to the central nervous system. 2015:10.
73. Dorn J.D., Ahuja A.K., Caspi A., da Cruz L., Dagnelie G., Sahel J.-A., Greenberg R.J., McMahon M.J., Group A.I.S. The detection of motion by blind subjects with the epiretinal 60-electrode (Argus II) retinal prosthesis. JAMA ophthalmology. 2013;131(2):183–189. PubMed PMID: 23544203.
74. Zrenner, E., Fighting blindness with microelectronics. Science Translational Medicine. 2013; 5(210):210ps16-210ps16.
75. Kitiratschky V.B., Stingl K., Wilhelm B., Peters T., Besch D., Sachs H., Gekeler F., Bartz-Schmidt K.U., Zrenner E. Safety evaluation of "retina implant alpha IMS"—a prospective clinical trial. Graefe's Archive for Clinical and Experimental Ophthalmology. 2015;253(3):381–387. PubMed PMID: 25219982.
76. Stingl K., Bartz-Schmidt K.U., Besch D., Chee C.K., Cottriall C.L., Gekeler F., Groppe M., Jackson T.L., MacLaren R.E., Koitschev A. Subretinal visual implant alpha IMS–clinical trial interim report. Vision research. 2015;111:149–160. PubMed PMID: 25812924.
77. Normann R.A. Technology insight: future neuroprosthetic therapies for disorders of the nervous system. Nature Clinical Practice Neurology. 2007;3(8):444–452. PubMed PMID: 17671522.
78. Dagnelie G. Visual prosthetics 2006: assessment and expectations. Expert review of medical devices. 2006;3(3):315–325. PubMed PMID: 16681453.
79. Dowling J. Current and future prospects for optoelectronic retinal prostheses. Eye. 2009;23(10):1999–2005. PubMed PMID: 19098703.
80. Nakauchi K., Fujikado T., Kanda H., Kusaka S., Ozawa M., Sakaguchi H., Ikuno Y., Kamei M., Tano Y. Threshold suprachoroidal–transretinal stimulation current resulting in retinal damage in rabbits. Journal of neural engineering. 2007;4(1):S50. PubMed PMID: 17325416.
81. Nishida K., Kamei M., Kondo M., Sakaguchi H., Suzuki M., Fujikado T., Tano Y. Efficacy of suprachoroidal–transretinal stimulation in a rabbit model of retinal degeneration. Investigative ophthalmology & visual science. 2010;51(4):2263–2268. PubMed PMID: 19933186.
82. Nayagam D.A., Williams R.A., Allen P.J., Shivdasani M.N., Luu C.D., Salinas-LaRosa C.M., Finch S., Ayton L.N., Saunders A.L., McPhedran M. Chronic electrical stimulation with a suprachoroidal retinal prosthesis: a preclinical safety and efficacy study. PloS one. 2014;9(5):e97182. PubMed PMID: 24853376.
83. Schmid E.W., Fink W., Wilke R. Operational challenges of retinal prostheses. Medical engineering & physics. 2014;36(12):1644–1655. PubMed PMID: 25443535.
84. Shivdasani M.N., Sinclair N.C., Dimitrov P.N., Varsamidis M., Ayton L.N., Luu C.D., Perera T., McDermott H.J., Blamey P.J. Factors Affecting Perceptual Thresholds in a Suprachoroidal Retinal ProsthesisFactors Affecting Retinal Prosthesis Thresholds. Investigative ophthalmology & visual science. 2014;55(10):6467–6481. PubMed PMID: 25205858.
85. Yan Y., Sui X., Liu W., Lu Y., Cao P., Ma Z., Chen Y., Chai X., Li L. Spatial characteristics of evoked potentials elicited by a MEMS microelectrode array for suprachoroidal-transretinal stimulation in a rabbit. Graefe's Archive for Clinical and Experimental Ophthalmology. 2015;253(9):1515–1528. PubMed PMID: 25981117.

86. Degenaar P., Grossman N., Memon M.A., Burrone J., Dawson M., Drakakis E., Neil M., Nikolic K. Optobionic vision—a new genetically enhanced light on retinal prosthesis. Journal of neural engineering. 2009;6(3):035007. PubMed PMID: 19458396.
87. Busskamp V., Picaud S., Sahel J., Roska B. Optogenetic therapy for retinitis pigmentosa. Gene therapy. 2012;19(2):169–175. PubMed PMID: 21993174.
88. Roska B., Busskamp V., Sahel J., Picaud S. Biologie aujourd'hui. 2012;207(2):109–121. [Retinitis pigmentosa: eye sight restoration by optogenetic therapy]. PubMed PMID: 24103341.
89. Sahel J.-A., Roska B. Gene therapy for blindness. Annual review of neuroscience. 2013;36:467–488. PubMed PMID: 23724995.
90. Trenholm S., Roska B. Cell-type-specific electric stimulation for vision restoration. Neuron. 2014;83(1):1–2. PubMed PMID: 24991948.
91. Rizzo J.F., Wyatt J., Humayun M., de Juan E., Liu W., Chow A., Eckmiller R., Zrenner E., Yagi T., Abrams G. Retinal prosthesis. Ophthalmology. 2001;108(1):13–14. PubMed PMID: 11150256.
92. Stone J.L., Barlow W.E., Humayun M.S., de Juan E., Milam A.H. Morphometric analysis of macular photoreceptors and ganglion cells in retinas with retinitis pigmentosa. Archives of Ophthalmology. 1992;110(11):1634–1639. PubMed PMID: 1444925.
93. Santos A., Humayun M.S., de Juan E., Greenburg R.J., Marsh M.J., Klock I.B., Milam A.H. Preservation of the inner retina in retinitis pigmentosa: a morphometric analysis. Archives of Ophthalmology. 1997;115(4):511–515. PubMed PMID: 9109761.
94. Humayun M.S., Dorn J.D., da Cruz L., Dagnelie G., Sahel J.-A., Stanga P.E., Cideciyan A.V., Duncan J.L., Eliott D., Filley E. Interim results from the international trial of Second Sight's visual prosthesis. Ophthalmology. 2012;119(4):779–788. PubMed PMID: 22244176.
95. Stronks H.C., Dagnelie G. The functional performance of the Argus II retinal prosthesis. Expert review of medical devices. 2014;11(1):23–30. PubMed PMID: 24308734.
96. Campbell P.K., Jones K.E., Huber R.J., Horch K.W., Normann R.A. A silicon-based, three-dimensional neural interface: manufacturing processes for an intracortical electrode array. IEEE Trans. Biomed. Eng. 1991;38(8):758–68. PubMed PMID: 1937509.
97. Cha K., Horch K.W., Normann R.A. Mobility performance with a pixelized vision system. Vision Res. 1992;32(7):1367–72. PubMed PMID: 1455709.
98. Bradley D.C., Troyk P.R., Berg J.A., Bak M., Cogan S., Erickson R., Kufta C., Mascaro M., McCreery D., Schmidt E.M. Visuotopic mapping through a multichannel stimulating implant in primate V1. Journal of neurophysiology. 2005;93(3):1659–1670. PubMed PMID: 15342724.
99. Kane S.R., Cogan S.F., Ehrlich J., Plante T.D., McCreery D.B., Troyk P.R. Electrical performance of penetrating microelectrodes chronically implanted in cat cortex. IEEE Transactions on Biomedical Engineering. 2013;60(8):2153–2160. PubMed PMID: 23475329.
100. Lewis P.M., Ackland H.M., Lowery A.J., Rosenfeld J.V. Restoration of vision in blind individuals using bionic devices: a review with a focus on cortical visual prostheses. Brain research. 2015;1595:51–73. PubMed PMID: 25446438.
101. Pelayo F.J., Romero S., Morillas C.A., Martínez A., Ros E., Fernández E. Translating image sequences into spike patterns for cortical neuro-stimulation. Neurocomputing. 2004;58:885–892.
102. Kolb H., Nelson R., Ahnelt P., Cuenca N. Cellular organization of the vertebrate retina. Progress in brain research. 2001;131:3–26. PubMed PMID: 11420950.
103. Fernandez E., Ferrandez J.-M., Ammermüller J., Normann R.A. Population coding in spike trains of simultaneously recorded retinal ganglion cells. Brain research. 2000;887(1):222–229. PubMed PMID: 11134610.
104. Normann R.A., Warren D.J., Ammermuller J., Fernandez E., Guillory S. High-resolution spatio-temporal mapping of visual pathways using multi-electrode arrays. Vision research. 2001;41(10):1261–1275. PubMed PMID: 11322971.
105. Warren D., Fernandez E., Normann R. High-resolution two-dimensional spatial mapping of cat striate cortex using a 100-microelectrode array. Neuroscience. 2001;105(1):19–31. PubMed PMID: 11483297.

106. Schnitzer M.J., Meister M. Multineuronal firing patterns in the signal from eye to brain. Neuron. 2003;37(3):499–511. PubMed PMID: 12575956.
107. Eckmiller R., Neumann D., Baruth O. Tunable retina encoders for retina implants: why and how. Journal of Neural Engineering. 2005;2(1):S91. PubMed PMID: 15876659.
108. Morillas C., Romero S., Martínez A., Pelayo F., Reyneri L., Bongard M., Fernández E. A neuroengineering suite of computational tools for visual prostheses. Neurocomputing. 2007;70(16):2817–2827.
109. Dagnelie G., Keane P., Narla V., Yang L., Weiland J., Humayun M. Real and virtual mobility performance in simulated prosthetic vision. Journal of neural engineering. 2007;4(1):S92. PubMed PMID: 17325421.
110. Dagnelie G. Psychophysical evaluation for visual prosthesis. Annu. Rev. Biomed. Eng. 2008;10:339–368. PubMed PMID: 18429703.
111. Cogan S.F., Troyk P.R., Ehrlich J., Gasbarro C.M., Plante T.D. The influence of electrolyte composition on the in vitro charge-injection limits of activated iridium oxide (AIROF) stimulation electrodes. Journal of neural engineering. 2007;4(2):79. PubMed PMID: 17409482.
112. Romero, S.F., C.A. Morillas, F.J. Pelayo, and E. Fernández. Computer-Controlled Neurostimulation for a Visual Implant. in BIODEVICES (1). 2008.
113. Branner A., Stein R.B., Fernandez E., Aoyagi Y., Normann R.A. Long-term stimulation and recording with a penetrating microelectrode array in cat sciatic nerve. IEEE transactions on biomedical engineering. 2004;51(1):146–157. PubMed PMID: 14723504.
114. Chader G.J., Weiland J., Humayun M.S. Artificial vision: needs, functioning, and testing of a retinal electronic prosthesis. Progress in brain research. 2009;175:317–332. PubMed PMID: 19660665.
115. Cogan S.F., Ehrlich J., Plante T.D., Smirnov A., Shire D.B., Gingerich M., Rizzo J.F. Sputtered iridium oxide films for neural stimulation electrodes. Journal of Biomedical Materials Research Part B: Applied Biomaterials. 2009;89(2):353–361. PubMed PMID: 18837458.
116. Shire D.B., Kelly S.K., Chen J., Doyle P., Gingerich M.D., Cogan S.F., Drohan W.A., Mendoza O., Theogarajan L., Wyatt J.L. Development and implantation of a minimally invasive wireless subretinal neurostimulator. IEEE Transactions on Biomedical Engineering. 2009;56(10):2502–2511. PubMed PMID: 19403357.
117. Marin C., Fernández E. Biocompatibility of intracortical microelectrodes: current status and future prospects. Frontiers in neuroengineering. 2010;3:8. PubMed PMID: 20577634.
118. Hoogerwerf A.C., Wise K.D. A three-dimensional microelectrode array for chronic neural recording. IEEE Transactions on Biomedical Engineering. 1994;41(12):1136–1146. PubMed PMID: 7851915.
119. Woodford B.J., Carter R.R., McCreery D., Bullara L.A., Agnew W.F. Histopathologic and physiologic effects of chronic implantation of microelectrodes in sacral spinal cord of the cat. Journal of Neuropathology & Experimental Neurology. 1996;55(9):982–991. PubMed PMID: 8800094.
120. Heiduschka P., Thanos S. Implantable bioelectronic interfaces for lost nerve functions. Progress in neurobiology. 1998;55(5):433–461. PubMed PMID: 9670213.
121. Agnew B.J., Duman J.G., Watson C.L., Coling D.E., Forte J.G. Cytological transformations associated with parietal cell stimulation: critical steps in the activation cascade. Journal of Cell Science. 1999;112(16):2639–2646. PubMed PMID: 10413672.
122. Liu X., McCreery D.B., Carter R.R., Bullara L.A., Yuen T.G., Agnew W.F. Stability of the interface between neural tissue and chronically implanted intracortical microelectrodes. IEEE transactions on rehabilitation engineering. 1999;7(3):315–326. PubMed PMID: 10498377.
123. Majji A.B., Humayun M.S., Weiland J.D., Suzuki S., D'Anna S.A., de Juan E. Long-term histological and electrophysiological results of an inactive epiretinal electrode array implantation in dogs. Investigative ophthalmology & visual science. 1999;40(9):2073–2081. PubMed PMID: 10440263.
124. Turner J., Shain W., Szarowski D., Andersen M., Martins S., Isaacson M., Craighead H. Cerebral astrocyte response to micromachined silicon implants. Experimental neurology. 1999;156(1):33–49. PubMed PMID: 10192775.

125. McCreery D.B., Agnew W.F., Bullara L.A. The effects of prolonged intracortical microstimulation on the excitability of pyramidal tract neurons in the cat. Annals of biomedical engineering. 2002;30(1):107–119. PubMed PMID: 11874134.
126. Polikov V.S., Tresco P.A., Reichert W.M. Response of brain tissue to chronically implanted neural electrodes. Journal of neuroscience methods. 2005;148(1):1–18. PubMed PMID: 16198003.
127. Seymour J.P., Kipke D.R. Neural probe design for reduced tissue encapsulation in CNS. Biomaterials. 2007;28(25):3594–3607. PubMed PMID: 17517431.
128. McConnell G.C., Rees H.D., Levey A.I., Gutekunst C.-A., Gross R.E., Bellamkonda R.V. Implanted neural electrodes cause chronic, local inflammation that is correlated with local neurodegeneration. Journal of neural engineering. 2009;6(5):056003. PubMed PMID: 19700815.
129. Edell D.J., Toi V., McNeil V.M., Clark L. Factors influencing the biocompatibility of insertable silicon microshafts in cerebral cortex. IEEE Transactions on Biomedical Engineering. 1992;39(6):635–643. PubMed PMID: 1601445.
130. Veraart C., Duret F., Brelén M., Oozeer M., Delbeke J. Vision rehabilitation in the case of blindness. Expert review of medical devices. 2004;1(1):139–153. PubMed PMID: 16293017.
131. Dowling J. Artificial human vision. Expert Review of Medical Devices. 2005;2(1):73–85. PubMed PMID: 16293031.
132. Merabet L.B., Rizzo J.F. III, Pascual-Leone A., Fernandez E. 'Who is the ideal candidate?': decisions and issues relating to visual neuroprosthesis development, patient testing and neuroplasticity. Journal of neural engineering. 2007;4(1):S130. PubMed PMID: 17325411.
133. Fine I., Wade A.R., Brewer A.A., May M.G., Goodman D.F., Boynton G.M., Wandell B.A., MacLeod D.I. Long-term deprivation affects visual perception and cortex. Nature neuroscience. 2003;6(9):915–916. PubMed PMID: 12937420.
134. Gregory R.L. Seeing after blindness. Nature neuroscience. 2003;6(9):909–910. PubMed PMID: 12939616.
135. Fernandez, E., A. Alfaro, J. Tormos, R. Climent, M. Martınez, H. Vilanova, V. Walsh, and A. Pascual-Leone, Mapping of the human visual cortex using image-guided transcranial magnetic stimulation. Brain research protocols. 2002; 10(2):115-124.
136. Lachman, M. Eye disorders are focus of novel neurostimulation technologies. In: editors. Medtech insight [Internet]. London: Informa PLC; 2014, Available from: https://medtech.pharmamedtechbi.com/MT035735/Eye-Disorders-Are-Focus-Of-Novel-Neurostimulation-Technologies.
137. Pascual-Leone, A., R. Hamilton, J. Tormos, J. Keenan, and M. Catala, Neuroplasticity in the adjustment to blindness, in Neuronal plasticity: Building a bridge from the laboratory to the clinic. 1999, Springer. p. 93-108.
138. Bavelier D., Neville H.J. Cross-modal plasticity: where and how? Nature Reviews Neuroscience. 2002;3(6):443–452. PubMed PMID: 12042879.
139. Merabet L.B., Rizzo J.F., Amedi A., Somers D.C., Pascual-Leone A. What blindness can tell us about seeing again: merging neuroplasticity and neuroprostheses. Nature Reviews Neuroscience. 2005;6(1):71–77. PubMed PMID: 15611728.
140. Ptito M., Kupers R. Cross-modal plasticity in early blindness. Journal of integrative neuroscience. 2005;4(04):479–488. PubMed PMID: 16385642.
141. Bernabeu A., Alfaro A., García M., Fernández E. Proton magnetic resonance spectroscopy (1 H-MRS) reveals the presence of elevated myo-inositol in the occipital cortex of blind subjects. Neuroimage. 2009;47(4):1172–1176. PubMed PMID: 19426816.

Retinal Prostheses

Ethan D. Cohen, Ph.D.[1,*]

Created: March 19, 2018.

Abstract

Retina prostheses try to reactivate the residual circuitry in a blind patient's retina to produce a synthetic form of usable vision. Using an array of stimulus electrodes or light-sensitive proteins, the neurons in the degenerate retinal network are activated to elicit a series of light percepts termed "phosphenes". If the patient's phosphenes act as independent spatial percepts in their visual field, a crude type of form vision may be achieved. This form vision could improve a visually impaired patient's ability to orient to landmarks in foreign visual environments, avoid obstacles, and improve social interactions. While most retinal prostheses in the current clinical trials rely on stimulation by electrical pulses from electrode arrays to locally excite the patient's retinal neurons, several research groups are also trying more biologically compatible stimulation methods termed "optogenetics" which deploy viruses to transduce light-activated stimulator protein genes into select groups of retinal neurons which when expressed modulate their neural activity. Each technology presents different challenges and benefits for biological integration into the blind patient's degenerate retina. Coupling and replacing the lost retinal neurons in the central fovea remains a challenge for both electronic and optogenetic combination therapies. There are many common issues involved in the real-world assessment of patient visual benefit from these novel medical technologies. Given the heterogeneity of RP as a disease, the availability of multiple therapies may be useful for patients, each offering different advantages for their type of retinal degeneration and its degree of progression.

Introduction

Retina prostheses try to reactivate the residual circuitry in a blind patient's retina to produce a synthetic form of usable vision (Figure 1). Using an array of stimulus electrodes or light-sensitive proteins, the neurons in the degenerate retinal network are activated to elicit a series of light percepts termed "phosphenes" (Figure 2). If the patient's phosphenes act as independent spatial percepts in the patient's visual field, a crude type of form vision may be achieved.

This form vision could improve a visually impaired patient's ability to orient to landmarks in foreign visual environments, avoid obstacles, and improve social interactions. All prosthetic designs to date rely on the same general image encoding strategy to produce vision. The lost photoreceptor mosaic is replaced with an artificial array of silicon photosensors located in a pair of glasses or a photodiode chip (Figure 3). Photoreceptor adaptation is replaced by an electronic automatic gain control. To simulate the antagonistic center-surround contrast enhancement of the ganglion cell receptive field by horizontal and amacrine cells, a video processor chip scales and edge enhances the viewed image. Neural encoder circuitry then transforms the down-sampled image into a limited set of discrete stimulation levels suitable for activating the retinal network (i.e., modulating spike frequencies for ganglion cells or graded potentials for inner retinal neurons) within its usable dynamic response range. Finally, the stimulator uses this level information to alter the firing patterns of retinal ganglion cells whose action potentials propagate up the optic nerve to generate phosphene patterns in the visual areas of the brain. While most retinal prostheses in the current clinical trials rely on stimulators producing electrical pulses from electrode arrays to locally excite the patient's retinal neurons, several research groups are also trying more

Author Affiliation: 1 Division of Biomedical Physics, Office of Science and Engineering Labs, Center for Devices and Radiological Health, White Oak Federal Research Center. Silver Spring, MD, 20993; Email: Ethan.cohen@fda.hhs.gov.

Corresponding author.

* About the author

biologically compatible stimulation methods termed "optogenetics" which deploy patches of light-activated stimulator proteins expressed in groups of retinal neurons to selectively modulate their neural activity. To be effective, a retinal prosthesis must not only improve visual acuity on eye charts, but also improve visual performance in real-world uncontrolled lighting environment tasks, such as finding doors, navigating streets, socializing, and other activities of daily living. Patient performance test guidelines for these prosthetic devices are currently being formalized by the HOVER consortium to allow better device outcome comparisons (3). For descriptions of earlier retinal prostheses see reviews (4-6).

The retinal prosthetic patient

A patient group commonly involved in visual prosthetic clinical trials has a severe form of a retinal degeneration termed "retinitis pigmentosa" (RP). With time, the patient's peripheral rod and then cone vision is gradually lost resulting in a narrow central visual field some 3–10° in diameter. Upon funduscopic examination, pigmented lesions with the appearance of 'spicules' begin to appear in their peripheral retinae due to RPE cell migration into the retina. Disease progression in RP is highly variable, however a smaller cohort of patients progress to what is termed "late-stage RP", characterized by nearly complete degeneration of both rod and cone photoreceptors resulting in bare or no light perception (10-12). Currently, patients from this late-stage RP group are the main retinal prosthesis users.

RP is a genetically heterogeneous group of diseases, which include rod-cone dystrophies, Usher's syndrome, and Leber's congenital amaurosis. The number of mutations involved in RP is very large, and a significant number of patients may clinically present with unknown genetic variants (13). The types of RP inheritance can be autosomal dominant, X-linked, recessive, and simplex, from roughly 100 different gene families (RetNet, 3/2017). This heterogeneity presents a severe challenge to personalized gene therapies such as autologous stem cell transplants, CRISPR-Cas9 gene excision technology, or the recently approved biallelic RPE65 retinal dystrophy gene therapy which may require timely defect identification and selective treatment of each affected individual. Studies of gene therapy in dog models of some RP subtypes suggest an early genetic intervention is desirable, as the retinal degeneration may continue even after the gene therapy is delivered (14). In contrast, retinal prosthetic (electronic and optogenetics) therapies are not disease gene mutation dependent, which could potentially benefit a larger prosthetic patient cohort.

The end stage retina in RP patients also shows significant remodeling and reorganization of the anatomical organization, receptors, and function in the retinal network (See Marc et al Webvision entry for more details) (15, 16), which presents a challenge for prosthetic therapies replacing lost photoreceptors and foveal cones (17-19). Bipolar cell dendrites retract their processes from the synaptic endings of dying central photoreceptors (5, 16, 19-22). Bipolar and amacrine cells in the inner nuclear layer often survive by making abnormal synaptic contacts. RP patients experience on average a 30% decline in their number of retinal ganglion cells, whose axons are critical for sending phosphene-evoked spikes to the brain through the optic nerve (23). Since all retinal prostheses rely on the presence of functioning retinal ganglion cells, prosthetic candidates are often evaluated for ganglion cell function using a corneal stimulation electrode to induce electrically-evoked phosphenes termed the "electrically-evoked response" (EER) (24-26). Currently, there are two main classes of retinal prostheses: electrical and optogenetic.

Table I.

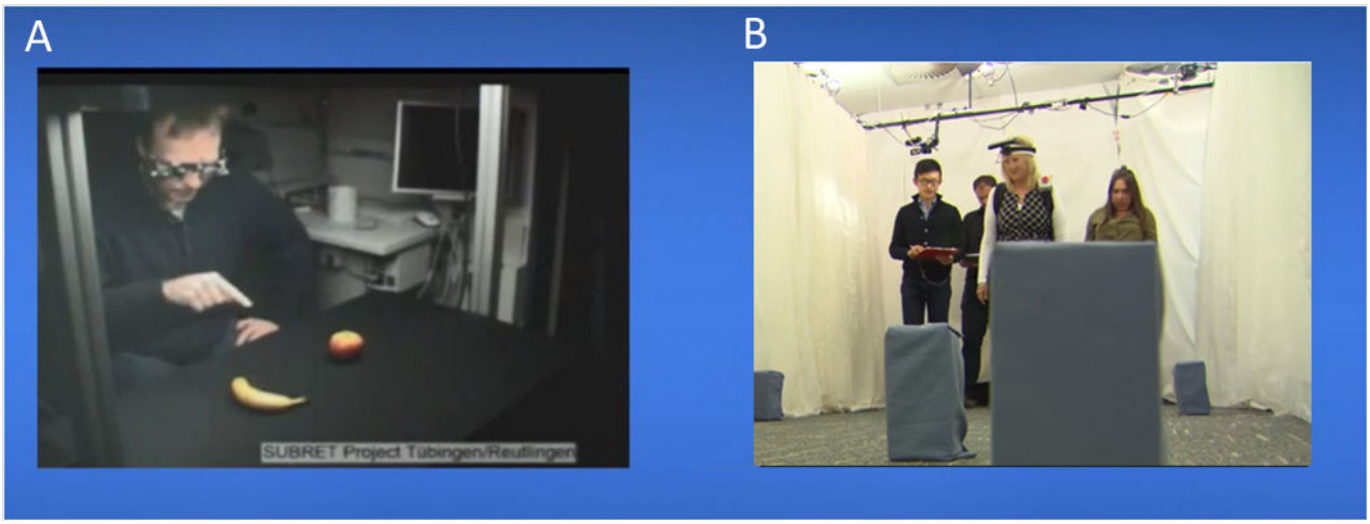

Figure 1. Patients testing retinal prosthetic implants in human clinical trials. A. Subretinal implant patient using the Alpha IMS in a common object identification task. (Retinal Implant AG, retrieved from https://www.youtube.com/watch?v=WSdmWbItsvU). B. Suprachoroidal Australian retinal implant patient negotiating an obstacle avoidance course (Bionic Vision Australia, retrieved from https://www.youtube.com/watch?v=6EmleCs0KGY).

Figure 2. Early examples of electrical phosphenes images resulting from gross stimulation of the eye. Drawings of self-induced phosphenes reported by Purkinje (1823), (1) resulting from direct current stimulation across the eye between conductors in his mouth and forehead (Subfigures 15,16 inside Fig. 3.2). Similar electrical phosphenes evoked by transient current stimulation of the conjunctiva were also self-reported by Volta (1800) (2).

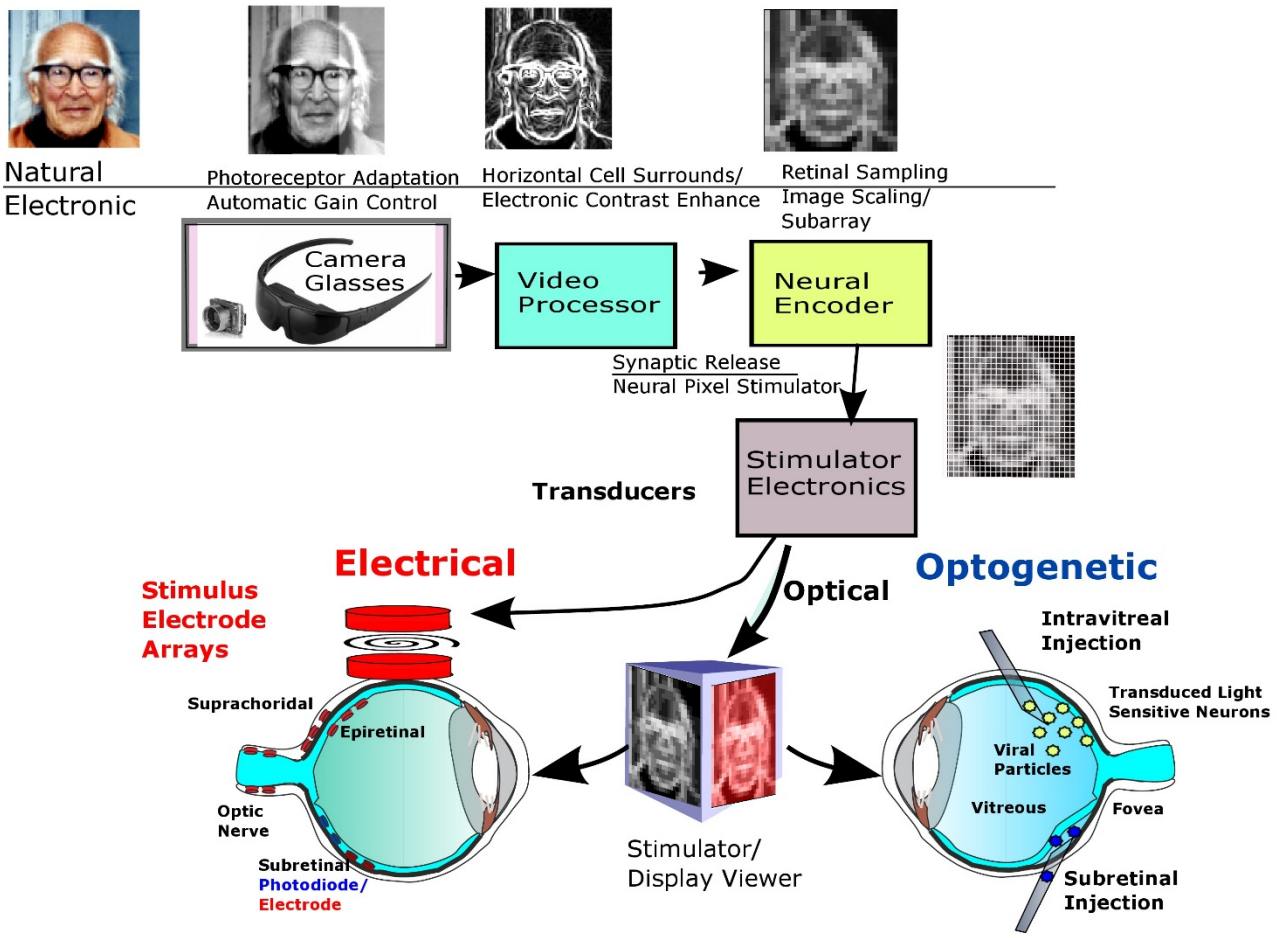

Figure 3. Retinal prosthetic image encoding and stimulation schemes. The image boxes show the natural retinal mechanism and its prosthetic replacement. An example is shown of the conversion of a 250 x 250 pixel color image of a face for retinal stimulation using contrast enhancement methods. The camera-sampled color image is converted to a 256 grayscale b/w image, edge-detected with a Sobel algorithm (8), descaled to a 125 x 125 pixel image, reduced to a 25x25 pixel stimulus pattern with 10 brightness levels similar to the abilities of Argus II patients,~6-10 levels (9), and sent to stimulate the retinal neurons using either external pulses of electrical current (via photodiode or electromagnetic coupling), or pulses of light on a display, activating exogenously expressed photosensitive ion channels in transduced neurons (optogenetics). Image of George Wald (Nobel Prize for discovering the mechanism of rod and cone phototransduction, 1967) kindly provided by Elijah Wald.

Table I: Retinal Implants using electrical stimulation. Devices tested in human clinical trials are shown in bold. See also http://www.eye-tuebingen.de/zrenner/retimplantlist/, and http://www.io.mei.titech.ac.jp/research/retina/index.html

Retinal Implants using Electrical Stimulation Researcher/Company	Therapy Technology	Target	Mode of Stimulation	Status	Location
Rizzo Boston VA/ Bionic Eye Technologies- Boston Retinal Prosthesis	Subretinal Electrode Array	Outer retinal neurons	Electrical, IrOx 256 256 electrodes	Preclinical	Boston, MA, US
Humayun UCLA/ Second Sight Med. Prod. -Argus II	**Epiretinal electrode Array**	**Ganglion cells**	**Electrical Pulses 60 Pt electrodes 6x10 array.**	**FDA US HUD 2013, CE mark EU.**	**Sylmar, CA, US**
Milstain/ Nano Retina	Epiretinal Nanoelectrodes Photodiode power.	Ganglion cells	Electrical Pulses Micro electrode array.	Preclinical	Herzliya, IS

Table I continued from previous page.

Retinal Implants using Electrical Stimulation Researcher/Company	Therapy Technology	Target	Mode of Stimulation	Status	Location
Ren/C-Sight: Chinese Project for Sight	Optic nerve electrode array (64)	Optic Nerve axons	Electrical Pulses Penetrating electrode array.	Preclinical	Beijing, CN
Palanker/Pixium Vision Prima VRS (Mac. Degen. indication)	**Subretinal photodiode stimulator electrode chips.**	**Outer Retinal neurons**	**Electrical pulses, Multi-photodiode powered, IrOx electrode array.**	**Clinical Trial France 11/2017, US 1/2018.**	**Stanford Univ, CA US, Paris, FR.**
Hornig/Pixium Vision IRIS II	**Epiretinal electrode Array**	**Retinal ganglion cells**	**Electrical pulses, 150 Pt electrode array.**	**Clinical Trial in 10 patients (EU)**	**Paris, FR**
Shepherd & Suaning/ Bionic Vision Australia/ Bionic Vision Technologies	**Suprachoroidal space electrode array.**	**Outer Retinal neurons**	**Electrical pulses 44 Pt disc electrodes, Pt**	**Clinical trial of electrode cable in2014 and implant in 2018 in 3 patients**	**Melbourne, Univ. of NSW, AU**
Burkitt, /Bionic Vision Australia/ High Acuity Dev. NSW, Melbourne	Epiretinal electrode array.	Retinal Ganglion cells	Electrical pulses 256 Disc Electrodes	Preclinical	Univ. Melbourne, NSW, AU
Fujikado / Japan Visual Prosthesis Project/Nidek Co.	**Suprachoroidal space**	**Outer Retinal neurons**	**49 bullet-shaped Pt electrodes, 7x7 array (STS)**	**Clinical trial of implant prototype in 3 patients**	**Osaka Univ.- Gamagori, JP**
Kim /Seoul National University .	liquid crystal polymer subretinal array implant.	Outer Retinal neurons	Electrical Pulses 3D-electrodes	Preclinical	Seoul, Korea, KR
Zrenner/Retinal Implant AG Alpha AMS	**Adapting subretinal photodiode stimulator pixel microchip implant**	**Outer Retina**	**Electrical Pulses Subretinal array 1600 30um round IrOx electrodes.**	**CE Mark, EU, 2016. Feasibility trial, US 2017**	**Tübingen, GE**
Fan /Iridium Medical Technologies	Subretinal photosensor electrode prosthesis chip	Outer Retinal neurons	Electrical Pulses 4000 pixel/electrodes	Preclinical	Hsin-Chu Univ, Taiwan,TW
NanoVision	Subretinal Prosthesis.	Outer Retinal Neurons	Silicon Nanowire Electrodes	Unknown	San Diego, US
iBionics	Epiretinal prosthesis	Ganglion cells	1K Nitrogen-doped diamond electrodes	Preclinical	Ottowa, CA, Melbourne, AU

Retinal prostheses using electrical stimulation

A large group of retinal prostheses elicit vision in blind patients by using electrical current pulses to depolarize and activate neurons in the retinal network. Retinal implants using electrical stimulation are classified according to the location of their stimulating electrodes in the eye. The prosthesis electrodes can be placed at the inner retinal surface or inner limiting membrane (ILM) (epiretinal), or in the subretinal space (subretinal), or in the sclera behind the choroidal vasculature (termed “suprachoroidal or episcleral”), or on/in the optic nerve (optic nerve) (Figure 3). Each implant electrode location has different advantages and disadvantages for stimulating the retinal circuitry (Figure 4).

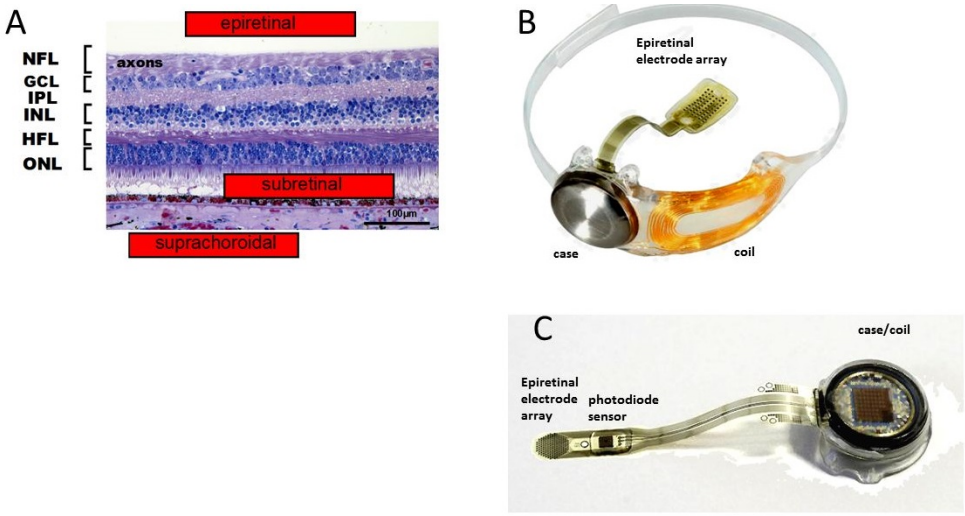

Figure 4. Locations of electrically-stimulating prosthetic electrode array, and examples of epiretinal prostheses. A: Section of the human parafoveal retina showing the main stimulus electrode locations and the retinal layers: from(5) (with permission from IOP Publishing). Nerve fiber layer (NFL) axons, Ganglion cell layer (GCL), inner plexiform layer (IPL), inner nuclear layer (INL), Henle fiber layer of synaptic extensions from foveal cones, and outer plexiform layer (HFL), Outer nuclear layer (ONL), and pigment epithelium (PE). B, C: Examples of epiretinal types of retinal prostheses. B: Argus II retinal prosthesis (US FDA 2013). C: IRIS 2 retinal prosthesis. Images courtesy of Second Sight Medical Products, Pixium Vision, with permissions.

Epiretinal Electrode Prostheses

Epiretinal prostheses electrodes are placed on the inner limiting membrane of the retina, to locally stimulate the underlying retinal ganglion cells and inner retinal neurons. Through an incision in the ora serrata, the surgeon implants a flexible stimulus electrode array close to the ILM surface, where it is held in place with one or more retinal tacks. The array is connected by a cable to the stimulator case and coil, which is sutured on the outside of the globe, and held in place by scleral bands. Telemetry coils mounted on the arm of the patient's camera glasses deliver wireless power and data signals to the implant coil. A pocket visual processor/battery unit allows user-selectable viewing modes. The first epiretinal prosthesis in a clinical trial, the Argus I used a modified cochlear implant stimulator and had a 4 x 4 array of 250-500µm diameter platinum (Pt) epiretinal electrodes (27). For visual scale of electrode size at the retina, 1 degree visual angle is about 280µm on the retina. This is the visual field size of the nail of the index finger held at arm's length (28). Other early epiretinal prosthesis designs clinically tested included the Epi-Ret (29) and the IMI retinal implant (30). The "Argus II Retinal Prosthesis System" is currently the only retinal prosthesis legally marketed in the U.S. It was approved by the U.S. Food and Drug Administration (FDA) in 2013 as a humanitarian use device, and was CE marked (EU) in 2011.

The Argus II uses a 6x10 array of 200µm diameter Pt disc electrodes placed against the inner retinal surface (diagonal visual field of ~20°) (Figure 2, B) (31,32). Most Argus II subjects (~70%), can follow a white line on a black floor, and ~55% were able to find a black door on white wall (HDE FDA report, 2013), while a few (10%) are able to slowly read large white letters on black backgrounds (33).

A newer epiretinal prosthesis, the IRIS II sends event-based camera encoded images of visual scenes to a hexagonal array of 150 stimulus electrodes and in 2017 was implanted in 10 patients in EU clinical trials (Figure 3, C). To avoid the data bottleneck of sending each electrode stimulus level as a radiofrequency (RF) signal through a magnetic coil, the IRIS II uses an IR LED mounted on the patient's glasses to transmit the stimulation signal directly through the patient's lens to a photodiode sensor decoder mounted on the intraocular cable of the implant's stimulus electrode array.

Performance of epiretinal electrode prostheses

The advantage of epiretinal prostheses is that they are minimally invasive to the retina, do not occlude the retinal vasculature, and are easily monitored through the patient's lens using a funduscope or optical coherence tomography (OCT). In animal models, short current pulses (0.1-0.5msec) tend to activate action potentials directly at the ganglion cell. Longer duration pulses may produce delayed spikes due to synaptic transmission from activated bipolar or amacrine cells (35-37). Epiretinal electrode stimulation excites both ON- and OFF-center ganglion cells non-selectively. For Argus II users, phosphene thresholds to biphasic 0.45msec pulses averaged 206.5μA (93nC) (32). Argus I subjects reported phosphene percepts from single stimulated electrodes as elliptical blobs (~4 x 10°), or thin (1°) arcs some 7-15° in length (38, 39), and Argus II subjects have reported similar shaped percepts (40). Phosphene brightness perception of Argus II subjects is limited to some 6-10 stimulus current steps (9). The Argus II's camera glasses are fixed to the patient's head but the electrode array is fixed on the retina in the eye. However, the brain maps the phosphenes induced by epiretinal stimulation electrodes based on the patient's eye gaze position, so if the eyes move so do the phosphenes. Argus II subjects also report a perceptual fading of stimulated phosphenes due to a Troxler-like effect, in some cases in under 0.5 sec, so they often use head scans to study an object of interest (41).

For epiretinal prostheses, close conformation of the stimulus electrode array to the inner retinal surface is necessary to provide uniformly focused stimulation across the electrode array. While stimulus array electrodes near the retinal tack region lie directly against the retina, the proximity of stimulus electrodes of Argus II patients averaged 179.6μm from the retinal surface (32). Incomplete contact could be caused by residual vitreal cortex fibers, posterior hyaloid/epiretinal membranes, patient/gender differences in the retinal curvature, and a lack of conformation to the curved fovea. The closest structures to epiretinal stimulus electrodes are often arcuate nerve fiber bundles under the inner limiting membrane from the axons of peripheral retinal ganglion cells, which course around the fovea, and converge on the optic nerve head (20, 42, 43). The thickness of the perifoveal nerve fiber layer bundles average 80 -120μm (44), and the nerve fiber layer near the macula averages 33.9μm (45). Using submillisecond stimulus pulses, subjects often report seeing arc-like phosphene percepts to electrode stimulation (39, 40, 46, 47). Recent stimulation strategies using long sinusoidal current pulses 10-20msec in duration may reduce this nerve fiber activation which could improve spatial percepts by individual electrodes (47-48).

Subretinal electrode prostheses

Subretinal prostheses place electrode arrays in the subretinal space between the pigment epithelium and the degenerate photoreceptor layer (Figure 5). This places the stimulus electrodes in close proximity to activate the remaining bipolar and amacrine cells of the blind patient, which theoretically could excite the remaining retinal circuitry in a more natural fashion than epiretinal prostheses. Early subretinal devices tested included an ambient light powered 5,000 microphotodiode-stimulator chip, which performed poorly in US clinical trials (51). However, actively-powered photodiode-based subretinal stimulator chips have been more successful in clinical trials with some patients able to read large letters (5-10°) (52-53). A second generation 40 × 40 stimulus electrode/photodiode array (1600 electrodes) termed the Alpha AMS was CE marked in the EU in 2016 with improved durability (53-55). This polyimide-encapsulated combination photodiode and stimulation electrode based chip (3.2 x 4mm, 70 m thick) allows subjects to use natural eye scanning with a synthetic visual field of ~13^{o} to analyze objects. Active power to the AMS chip is provided by a cable from a coil-powered case sutured onto the skull, similar to a cochlear implant. Patients with functional implants had grating acuities which ranged from 0.1 - 3.33 cycles/degree (55). Several other subretinal stimulation implants are in active development by US/EU groups. Recently, the light-powered photodiode stimulation electrode chip concept has been revived by the Palanker group, using a chip whose pixels contain multiple photodiodes in series with a central-stimulus electrode. When actively illuminated, each pixel generates enough voltage to excite the retinal network, which altered ganglion cell firing in animal models (50). Termed the "PRIMA" implant, a camera/view-screen

stimulator goggle generates IR light pulse "images" to power the implant chip array in the blind retina. A clinical trial for the PRIMA is currently started in the EU (11/2017). Other subretinal implant designs include a 256-electrode array by the Rizzo group with a more conventional globe-mounted titanium case/coil and camera glasses (56).

Performance of subretinal electrode prostheses

The advantage of subretinal prostheses is that their electrodes stimulate the remaining neurons of the outer retina such as the bipolar cells. This could provide a more coordinated visual circuitry activation in blind patients, which would propagate through the retinal network. In many subretinal designs, the photosensors are also located directly over the stimulation electrodes. An intraretinal mount allows blind subjects to use natural eye movements to scan objects of interest, and helps prevent the perceptual fading reported for static retinal stimulation (57). However, subretinal chips may also partially block oxygen diffusion from the choriocapillary bed, and some Alpha IMS implant patients exhibit mild leakage of the retinal vessels when studied with fluorescein angiography (58, 59). Subretinal implantation devices need a thin package to fit in the subretinal space, and a durable near-hermetic encapsulation of the implant electronics.

Suprachoroidal electrodes

Suprachoroidal (or episcleral) prostheses place their stimulus electrodes in a scleral pocket directly behind the choroidal blood vessels (Figure 5, C). A suprachoroidal electrode array of 49 bullet shaped stimulus electrodes (0.5-mm diameter) was implanted behind the temporal retina in three subjects in Japan (Fujikado) (49). The array was connected to a multiplexing stimulator case (similar in form to a cochlear implant) which was surgically attached to the patient's temporal bone, and controlled by a camera/processor. Using biphasic pulses (0.5msec duration), large phosphenes extending ≥10 degrees visual angle were reported (60). A second suprachoroidal design developed by the Bionic Vision Australia Consortium used a smaller array of 20 Pt electrodes (400-600um diameter), which was implanted in the temporal suprachoroidal space near the fovea in 3 RP subjects. The cable ended in a percutaneous connector for interfacing with an external camera and stimulator (61). Using either anodic or cathodic first biphasic pulses, 2 subjects reported phosphene shapes with average diameters of 8.4 and 9.0 degrees of visual angle, respectively (62).

The advantages of suprachoroidal prostheses are that minimal surgery is needed for electrode array implantation which causes less risk of retinal detachment, and there is reduced risk of infection, as the vitreal cavity of the eye is never entered. While suprachoroidal electrodes are located behind the retinal pigment epithelium/choroidal vessels, which can spread the stimulus pulse currents at the retina, subjects can perceive simple phosphene shapes, suggesting these devices may have clinical utility for regaining peripheral vision commonly lost in most RP patients. However, strong electrical phosphene stimuli can occasionally evoke a tingling sensation in the trigeminal choroidal nerve (60).

Optic nerve prostheses

Historically, a few groups have investigated stimulating the optic nerve, largely with surface electrodes (63), however each electrode appears to activate large numbers of axons, resulting in multiple phosphene percepts in the patient's visual field. The optic nerve innervates the visual thalamus, or lateral geniculate nucleus, which in turn innervates the occipital lobe of the visual cortex. These are also targets for visual prosthesis, particularly relevant to blindness resulting from ganglion-cell loss, or optic nerve injury. These prostheses are reviewed in the companion Webvision chapter "Introduction to Visual Prosthesis' by Eduardo Fernandez and Richard Normann.

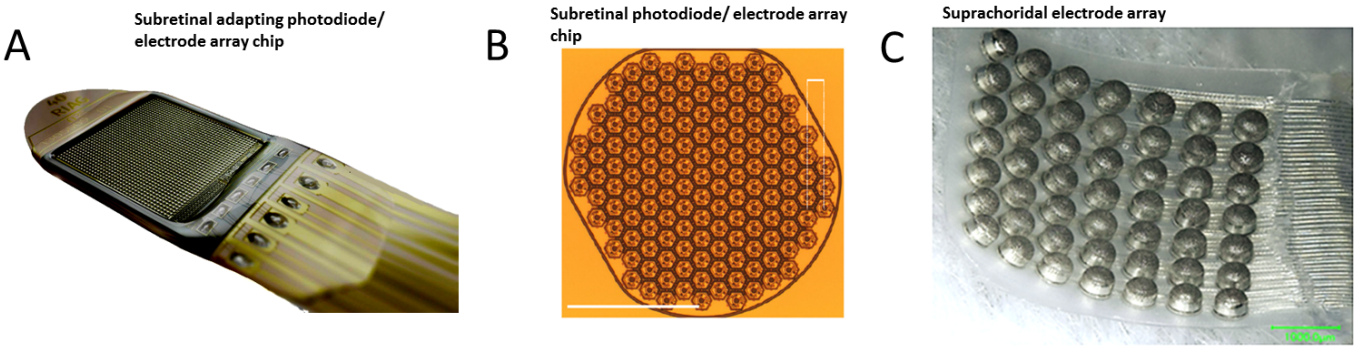

Figure 5. Examples of electrically stimulating suprachoroidal and subretinal prosthetic stimulation electrode arrays. (A, B): Subretinal, and (C) suprachoroidal types of arrays. A: Alpha AMS photodiode/ stimulation electrode chip array and power cable, B: Prima multi-photodiode/stimulator array chip implant prototype. C. Suprachoriodal stimulation electrode array (49). IOVS, with permission. Scale bar 500μm. A, C: Implant case/coil not shown. Images courtesy of, A: Retinal Implant AG, B: ref (50) Nature Pub. group with permissions, and C: ref (49) Invest. Opthalm. & Vis. Sci. (with permission).

Neurotransmitter-releasing retinal prostheses

The amino acid glutamate is the major excitatory neurotransmitter used in synaptic transmission from photoreceptor- to-bipolar-cell, and bipolar-to-ganglion-cell synapses. In theory, glutamate released onto bipolar cells would depolarize OFF-bipolar cells, while simultaneously hyperpolarizing ON-bipolar cells (OBCs). Conceivably, if a glutamate-releasing prosthesis could be placed at the level of the missing photoreceptor endings in RP patients, communication with the remaining bipolar cell dendrites could propagate the visual signal to ganglion cells. Several glutamate-releasing prosthetic designs have recently been proposed; one using optical waveguide uncaging of neurotransmitter near retinal neurons (65), and another using microfluidic neurotransmitter release through miniature orifices (66,67). The Pepperberg group has proposed stimulation using tethered neurotransmitters (68). However, it is unclear how these devices can attract the dendrites of retinal neurons, and replenish released neurotransmitter.

Retinal prostheses using optogenetic stimulation

Optogenetics is a newer prosthetic stimulation technology that relies on viral expression (transduction) of light-sensitive ion channels in blind retinal neurons, enabling subsequent excitation of these neurons by light. This molecular technology has the potential to improve cellular targeting, increase spatial resolution and provide better coupling of the light stimulus to cellular excitation. Optogenetics originates from an 1865 observation by Ferdinand Cohn (69) that certain unicellular algae exhibit phototropism to blue but not red light. Mast in 1916 localized this algal light behavior to an orange eye spot (70) (Figure 6). Suction electrode recordings by Sineshchekov (71, 72) showed that light rapidly activated a current (submsec latency) in the algal membrane, with faster kinetics than rhodopsin. Hegemann and Nagel's group expressed these algal membrane proteins in Xenopus oocytes and found one that acted as a direct light-activated mixed cation channel (73), which they

termed “Channelrhodopsin 2” (ChR 2). Boyden and Diesseroth expressed the ChR2 protein in mammalian neurons and found they could evoke action potentials by single pulses of blue light (74).

Given the large number of genetic mutations involved in RP, a disease-independent gene therapy such as optogenetics could benefit many blind patients. Currently, a variety of optogenetic protein stimulation technologies are currently being evaluated for modulating neurons including light-activated ion channels, ion pumps (ex. bacteriorhodopsin, halorhodopsin), and G-protein-coupled receptors (ex. melanopsin, rhodopsin). Optogenetic proteins all incorporate a vitamin A /retinal analog in the binding pocket of their protein side chains (either all-trans 14-retinal or 13- retinal) (75). Other light-activated proteins also under investigation include: N-ethyl maleimide modified glutamate channels (LiGluR) (76), adenyl/guanyl cyclases (77), phosphodiesterases (78), and IR light-gated G-proteins (ex. snake TrpA1, often termed thermogenetics) (79). However, it is not currently clear whether these mechanisms have the fast kinetics and higher quantal sensitivity needed for activating the retinal network.

All optogenetic proteins currently in development express the optoprotein solely in the neuronal membrane, which severely reduces the quantal catch in comparison to retinal photoreceptors. For example, a foveal cone photoreceptor contains 1000-1200 photopsin-filled membrane infoldings which amplifies quantal catch some 1000X (80, 81), and a similar number of rhodopsin-filled discs are found in rods (82). Therefore, an intense light source is often required to supply the high irradiances ($>10^{15\text{-}17}$quanta/cm^2/sec) needed to adequately activate ChRs in the membrane to depolarize the retinal ganglion cells to action potential threshold (83-85). Because these irradiance levels are rarely encountered in the office environment, most optogenetic prostheses are thought to be combination product technologies that rely on cameras and artificial light sources (i.e. projector glasses) for delivering high flux retinal activation, light adaptation, and scene contrast enhancement (Figure 2). Research is also progressing on the optical stimulus encoder paradigms for delivery of effective light stimuli for the ChR therapy to activate natural retinal network function (Yan and Nirenberg) (86).

Light-activated depolarizing channels for optogenetic therapies

ChR2 was first virally transduced into blind rd1 mouse and rat inner retinal neurons by Bi et al. in 2006 (83). They used an adeno-associated virus (AAV) vector construct coupled to a powerful nonselective promoter to express the ChR2 GFP tag construct (Figure 7). Injected into the vitreous humor, the AAV2 construct transduced many mouse and rat retinal ganglion cells and some inner retinal neurons. Blue light stimuli caused transduced retinal ganglion cells to depolarize and fire action potentials, which could be monitored as visual evoked potentials (VEPs). Currently, an early feasibility clinical trial of a ChR2 therapy has started in the US as of (8/2015), where it has been recently reported (11/17/2017) that some patients can sense the location of windows in rooms (87). Red-shifted ChRs termed "ReaChR" or "Chrimsons" are also being explored in primate and human retinas for blindness indications, also using a non-selective CAG promoter (88). A 2017 EU clinical trial for retinitis pigmentosa patients used the optogenetic combination product “ChrimsonR” ChR and biomimetic “Visual Interface Stimulating Glasses” (NCT03326336 Clinicaltrials.gov).

Like ChR2, OBCs normally produce a sustained depolarization to center light stimulation. In rodents. OBCs can be genetically targeted using the Grm6 promoter (89). Lagali et al. in 2008 used in-vivo electroporation to transfect OBCs with a ChR2 lentiviral gene construct in the eyes of rd1 blind mouse neonates (84). The transfected mice had a measurable optomotor response to moving gratings of up to 0.26 c/degree. Bipolar cell response thresholds as measured by ganglion-cell firing to blue light stimulation were ~3x10^{15} quanta/cm^2/sec. Doroudchi et al in 2011, used AAV Grm6 ChR2 constructs to transduce OBCs in a series of blind mouse lines (rd1, rd10, rd16) (85). They showed that ChR2 expression was stable for up to one year, and found ganglion cell firing thresholds to blue light ~4×10^{16} quanta/cm^2/sec. Transduced blind mice were able to discriminate escape platforms illuminated with blue light in a Morris water maze test (90).

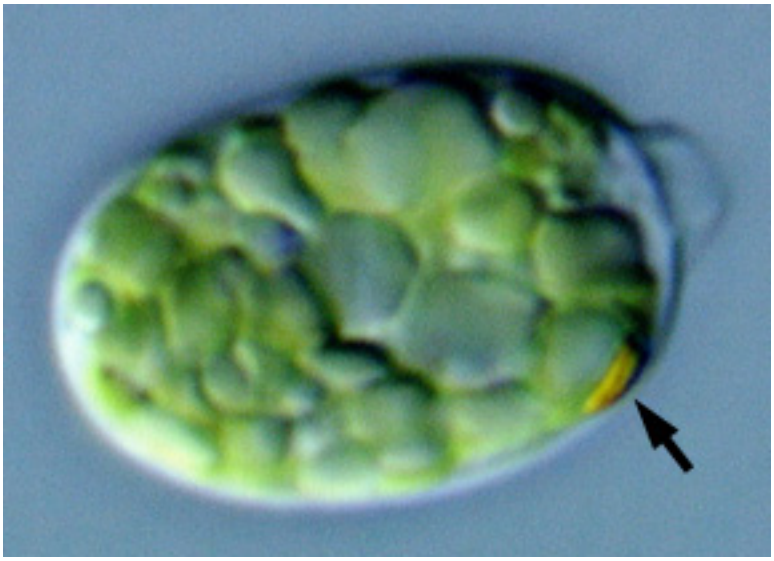

Figure 6. Location of the eyespot opsin pigment (arrow) which induces photaxis in the quadraflagellate freshwater algae Carteria. The flagellar attachment can be seen on the right. From the Connecticut College algae taxonomic database (maintained by P. A. Siver). http://fmp.conncoll.edu/Silicasecchidisk/Pics/Other%20Algae/Green_jpegs/Carteria_Key96.jpg

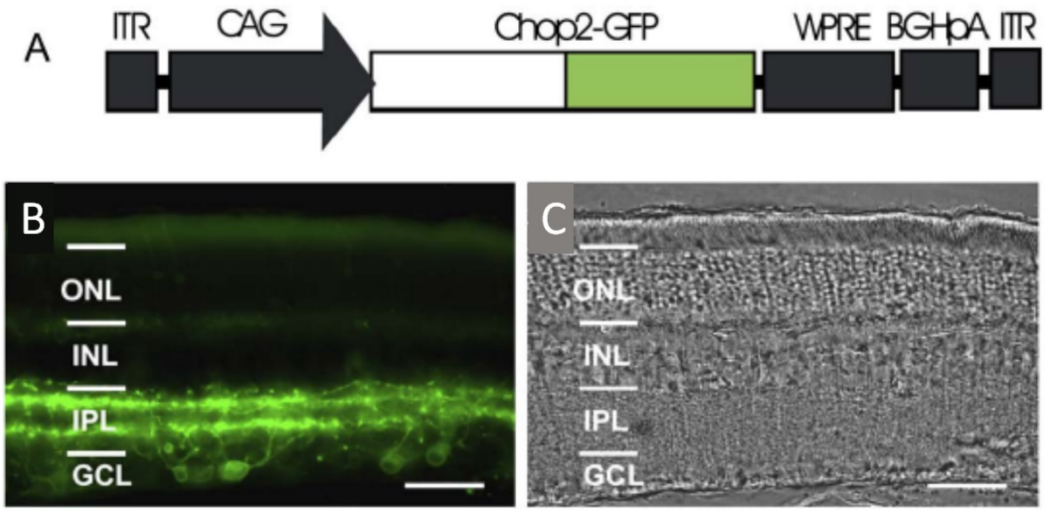

Figure 7. Optogenetic transduction of retinal neurons by ChR2. A: AAV Promoter construct used to transduce retinal neurons using a cytomegalovirus beta actin (CAG) promoter, and a green fluorescent protein tag (GFP). Transduction pattern of the channelrhodopsin II construct in the rat retina. B: AAV CHr2 is transduced largely in inner retinal neurons including ganglion cells. C: Histology of same retina., Ganglion cell layer (GCL), inner plexiform layer (IPL), inner nuclear layer (INL), outer nuclear layer (ONL). Bi et al., 2006 (83) (Cell Press/Elsevier with permissions).

Light-activated hyperpolarizing channels for optogenetic therapies

Optogenetic hyperpolarizing mechansims are also useful for mimicking the light response of photoreceptors and OFF-center bipolar cells, which normally hyperpolarize to light. Several pumps and channels that produce hyperpolarization have been discovered: 1. Halorhodopsin, a yellow-light activated chloride pump hyperpolarizes cells; 2. Light-activation of proton pumps such as Chief or bacteriorhodopsin cause acid-sensing ion channels to open and hyperpolarize cells (91-93); 3. A family of true light-gated chloride channels has recently been discovered, with increased light sensitivity and a green shifted activation spectrum (GtACR1) (94); and 4. The chloride ChR, IC++ has been developed (95). The Pan group transduced inner retinal neurons in rd1

blind mice with a viral combination construct of halorhodopsin and ChR2 for a dual blue light excitatory and yellow light inhibitory ion channel control of these neurons (96).

Degenerate cones have been known to survive in some blind mouse strains. Because halorhodopsin activation hyperpolarizes neurons, similar to the light-evoked hyperpolarizations of photoreceptors, a second application for halorhodopsin was to restore the light response of degenerate cone photoreceptors. (See also Marc et al chapter in Webvision). Busskamp et al, in 2010 used a halorhodopsin EYFP construct and cone-specific promoters to transduce expression in two strains of blind mice (97). Yellow-light stimuli caused the transduced cones to hyperpolarize and synaptically activate the retinal network. Both ON- and OFF-center retinal-ganglion-cell light responses could be recorded in halorhodopsin-transduced cone retinas at thresholds of 10^{14}quanta/cm^2/sec. Improvements in cone-specific promoter transduction for primate and human foveal cones have recently been reported (98).

Light-activated G-protein gated mechanisms for optogenetic therapies

The use of G-protein gated opsins for retinal prostheses, such as rod rhodopsin or melanopsin, employ energetically favorable biochemical amplification mechanisms which significantly increase light sensitivity compared to direct light-gated ion channel ChR counterparts. Early work by Kim et al in 2005 showed light activation of G-protein chimaeras of rhodopsin could be coupled to adrenergic receptors (99), while Qiu et al. in 2005 showed transfection of melanopsin caused light to depolarize kidney cells in culture (100). The first retinal application by Lin et al. 2008 used an AAV cytomegalovirus (CMV) promotor-melanopsin construct to transduce retinal ganglion cells in rd1 blind mice (101). The transduced blind mice were now able to detect light in a 2-channel water maze test.

Currently the ON-center bipolar cell (OBC) is an active target area for optogenetic, G-protein-gated, blindness therapies, due to the abundance of ON-center parafoveal rod and foveal cone bipolar cells, and the dependence of the ON-response on G-protein activation of TrpM1 cation channels (102). Recently, several groups found that transduction of melanopsin (G_q G-protein) or rhodopsin (G_t G-protein) in OBCs could promiscuously activate the mGluR6 metabotropic receptor (G_q) G-protein. This foreign mechanism in the OBCs reverses the closure of the normally open TrpM1 excitatory channels to light, and causes the TrpM1 channel in the OBC to have a light-response which operates in reverse from normal. Van Wyk et al, in 2015, used an AAV-Grm6 melanopsin-mGluR6 chimera construct termed “Opto-mGluR6” to activate the TrpM1-gated excitatory ion channels in OBCs in Rd1 blind mice (103). In Opto-mGluR6 Rd1 blind mice, light thresholds for ganglion cell activation were ~1000X lower than in their Rd1 ChR2 transduced littermates, and both light-ON- and OFF- retinal network responses appeared (Figure 8). A similar increase in light sensitivity in Rd1 blind mice was found using an AAV2-Grm6 rhodopsin construct by Gaub et al in 2015, and by Cehajic-Kapetanovic et al in 2015, who showed a behavioral increase in running distance when presented with a swooping owl movie (104-105).

Performance of the optogenetic therapies

Optogenetic stimulation therapies have the advantage over electrical stimulation of being able to deliver photosensitive stimulation at near cellular resolution to a large retinal area, and to better spatially couple to the blind patient’s neurons in a retinal prosthesis. However, the injection of viral capsids into the central retinae of primates has revealed some unforeseen issues with the transduction of retinal neurons, particularly in the fovea, which is critically used for normal vision in humans. Foveal bipolar and ganglion cell bodies are displaced ~2° from cone photoreceptor inputs in the center (5, 21). In the blind patient, viral transduction of ChRs into these surrounding bipolar and ganglion cell bodies when activated by light may elicit phosphenes that seem to originate from their central cones.

Finally, the primate retina has a series of membrane barriers that currently impede viral transduction, particularly to intravitreal injection of viral construct, which is the preferred method in patients with advanced

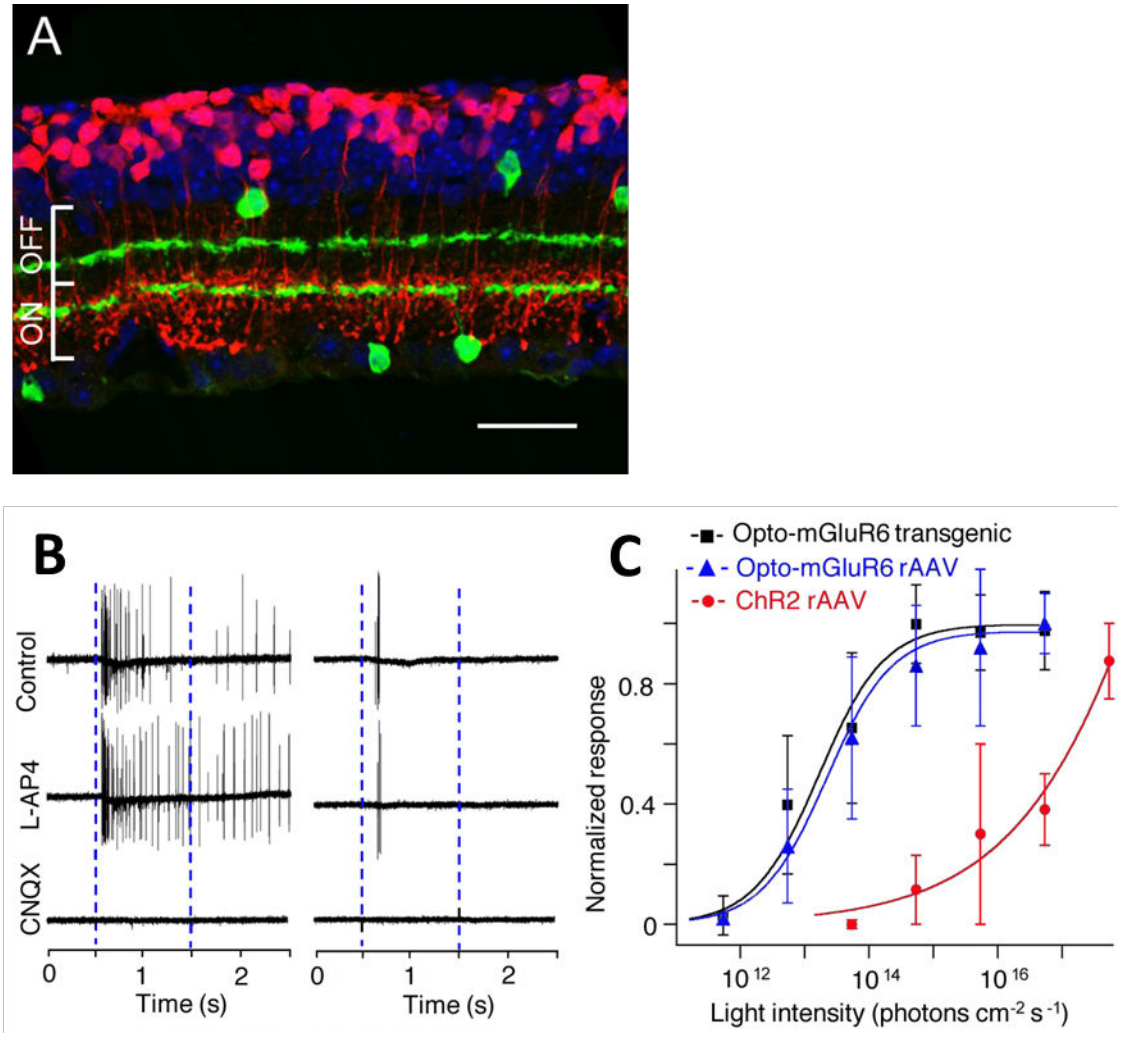

Figure 8. Transduction pattern and light sensitivity of a melanopsin chimaera AAV construct targeted to ON-bipolar cells in a blind mouse model. A: Opto- Grm6 AAV transduction pattern for rod bipolar cells in an rd1 mouse retina. Anti-choline acetyltransferase in green, anti-melanopsin in red, DAPI nuclear stain, blue. (Scale bar 20μm) B: Light stimulation causes melanopsin-mediated firing increases in an extracellularly recorded ganglion cell that is not blocked by APB (blue bars denote light onset/offset). C: Comparison of light-evoked ganglion cell firing thresholds of blind mice transduced with melanopsin chimaeras vs. ChR2. AAV melanopsin, (blue), melanopsin transgenic, (black), ChR2 (red). The G-protein gated opsin constructs are significantly more sensitive to light. From ref (103) with permission from PLOS.

RP. Transduction of some AAV capsid constructs may be reduced in efficacy in primates when compared to mouse models (106,107). There may also be a modest host immune response to the viral capsid and or fluorescent protein tags, (108, 109). The ILM/Müller glia end feet play a complex role in viral transduction, first by preventing diffusion of AAV viral proteins into the retina, but also by providing binding sites for viral attachment for retinal entry. In primates, the ILM appears to be thinnest near the perifovea and in the retinal periphery (110). The ILM is a basement membrane composed of several extracellular matrix proteins (laminin, agrin, perlecan, nidogen, collagen), nucleases and several heparin sulfate proteoglycans (111,112).

Yin et al in 2011 and 2014, and Ivanova et al in 2010, both intravitreally injected AAV2-gene-GFP constructs with actin-based promoters in primate eyes and found that viral transduction of ganglion cell bodies was largely limited to a thin ring-like zone centered 2 degrees around the fovea where the ILM was thinnest, and also to a few isolated spots in peripheral retina (Figure 9) (21, 106, 113, 114). A similar ring-shaped foveal transduction pattern has also been reported with intravitreal injected constructs targeting bipolar cells in primates (107). To reduce the ILM AAV diffusion barriers seen in old world primates eyes, injections of vitreolytic enzymes,

vitrectomies, with or without inner limiting membrane peels have been proposed (113, 115,116); however, these treatments may also reduce AAV construct attachment. This has caused others to advocate limited subretinal injections (<100μL) of AAV constructs (117, 118); however, these injections these may not be suitable for RP patients with advanced retinal disease (106). However even effective optogenetic transduction of the parafoveal retina could provide significant visual benefit in severely blind patients.

Gene expression patterns in a degenerate RP retina may differ from normal, resulting in ineffective AAV therapies. RP patients experience long periods of gradual visual loss that may take many years, unlike most blind rodent models. (See Webvision chapter on retinal degeneration). Although RP has traditionally been represented as a disease that causes loss of photoreceptors, these retinal degenerations also induce retinal remodeling and synaptic reorganization of many inner retinal neurons (119, 120). Inactive gene DNA may be methylated (121-123), which in the degenerate retina may produce gene inactivation/degradation in cells; reducing AAV promoter transduction efficiency, or cause off-target cellular gene expression (103, 124). This is particularly true of AAV therapies for OBCs, where in cultured human retinal explants, transduction by an 4XGrm6 promoter construct was not OBC specific (124). More specific OBC promoters may be required for transducing human retina (107). How these promoter expression patterns change in OBCs in degenerate human RP patients is currently unknown, and may only be revealed by clinical trials.

Table II.

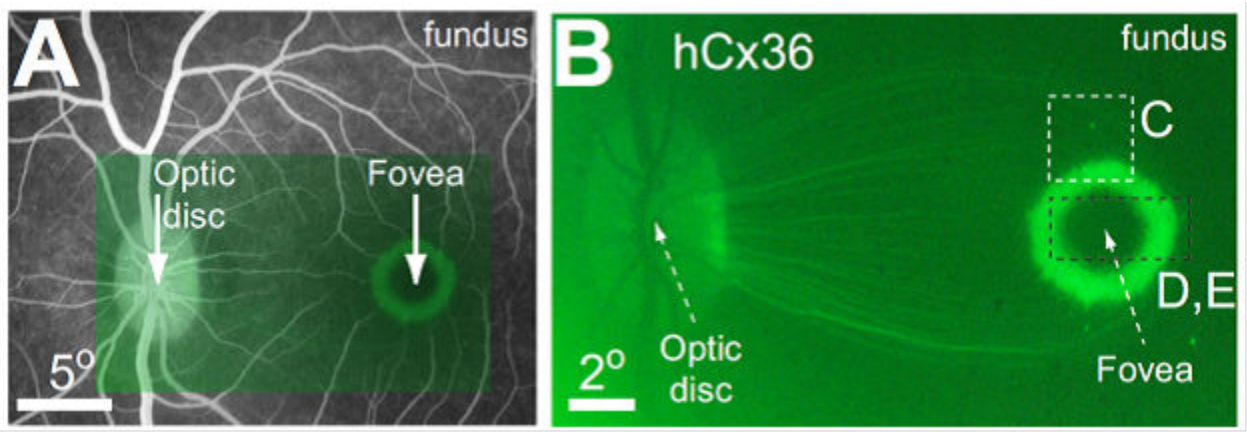

Figure 9. Viral transduction pattern by an intravitreal injection of an AAV capsid in the primate eye. A. Fluorescein angiogram showing retinal location of fluorescent image in B. Transduction of the AAV2/2 hCx –GFP labeled construct occurs in inner retinal neurons especially the ganglion cells. A ring-shaped transduction pattern is observed as the perifoveal inner limiting membrane (ILM) is thin, allowing better capsid entry (Connexin 36 (hCx) from Yin et al. 2011 IOVS) (113) (with permission).

Table II: Retinal Implants using optogenetic combination therapies. Products tested in human clinical trials are shown in bold.

Optogenetic Stimulating Retinal Implants Researcher/Company	Therapy	Target	Mode of Action	Status	Location
Pan, Wayne State Univ./ RetroSense Therapeutics/Allergan, MI	Channelrhodpsin2 RST-001	Nonspecific, Inner retinal neurons	Blue light-gated ChR ion channel	Phase I US Clinical Trial 4 patients 2015	Ann Arbor, MI, Dallas, TX, US
Birge, Lambda Vision	Bacteriorhodopsin	Residual Outer retinal neurons	Depolarization via Light-activated proton pump	Research	Farmington, CT, US
Horsager /Eos Neuroscience	Channelrhodopsin2	On-center rod/cone bipolar cells.	Blue light-gated ion channel	Unknown	Los Angeles, CA, US
Roska, Meissner Inst. Zurich/GenSight Biologics, Paris	GS030-DP ChrimsonR and –MD stimulator glasses	Nonspecific promoter, inner retinal neurons	Red light-gated ChR ion channel	Clinical Trial 2018	Paris, France
Nirenberg, Cornell Univ. Med. School, Hauswirth/AGTC & Bionic Sight	Optogenetics + Neural Encoder and stimulator glasses	Channelrhodopsin Retinal ganglion cells	Light-gated ion channel +Light stimulator for natural retinal fct.	Preclinical	New York, NY, Alachua, FL US
Kubota, Acucela Inc, Kubota Pharmaceutical Group	human rhodopsin (hRho)	ON-center bipolar cells	Light-activated G-protein therapy	Unknown	Seattle WA US/ Tokyo, Japan
Optogenetic Research					
Flannery, /UC Berkeley	Rhodopsin	Bipolar Cells	Light-evoked G-protein chimaera	Research	Berkeley CA, US
Deganaar/ Newcastle Univ.	Camera/LED-based glasses	Optogenetically transduced retinal neurons	Light Stimulator Encoder	Research	Newcastle Univ., UK

Retinal prosthetic stimulation safety

Patients using retinal prostheses in daily life expose their retinal tissue to chronic stimulation conditions. There are limits to the amount of electrical current and light that can be safely tolerated by the retinal tissue. A variety of methods have been developed to assess the retina under stimulation electrodes and to study retinal function by using funduscopes, fluorescence, optically transparent stimulus electrodes and/or optical coherence tomography (125-127). Excessive electrical stimulation can cause electroporation of retinal neurons and glia cells. Overstimulation near the epiretinal surface can cause swelling of the Müller cell end feet lining the ILM, and ganglion cell death (Video 10, Figure 10) (125). However, chronic electrical stimulation damage limits (Hrs.) for the retina are less well defined, may be location specific, and sensitive to tissue proximity (126-129).

For prostheses using light stimulation to excite retinal neurons, standards exist to limit the retinal exposure of normally sighted patients to excessive UV and blue light. RP patients often complain of being sensitive to excess light and glare, while the retinae of RP animal models are very sensitive to light injury by long funduscopic illumination (130). Many earlier ChR-based optogenetic therapies rely on high retinal fluxes of short wavelength light by the camera-projector glasses to provide adequate ChR channel activation of the transduced retinal neurons. However, newer ChRs and G-protein opsins have been developed with sensitivities shifted to longer wavelengths and with higher light sensitivity (Figure 8, C).

Light can damage the retinal layers both thermally and photochemically. Standards for safe levels of illumination of healthy retina at different wavelengths were based on primate eye exposure data by Ham (131, 132), and earlier studies by Noell in rats (133). These studies and others have been adapted into a series of international standards (ANSI Z80.36, ISO15004, ISO 60825 , Rp27.1) among others for ophthalmic devices. Most of these light safety studies relied on photoreceptor-induced light injury as the damage endpoint (134,135). It is currently unresolved how much light can be safely tolerated by the remaining retinal neurons in end-stage RP animal models and patients, with their degenerate photoreceptors and pigment epithelium cells.

Conclusions

There are exciting new developments in retinal prosthetic therapies that use electrical and optogenetic stimulation that have the potential to provide better form vision and improve the quality of life for the severely visually impaired. Each technology presents different challenges and benefits for biological integration into the blind patient's degenerate retina. Coupling and replacing the lost retinal neurons in the central fovea remains a challenge for both electronic and optogenetic combination therapies. There are many common issues involved in the real-world assessment of patient visual benefit from these novel medical technologies. Given the heterogeneity of RP as a disease, the availability of multiple therapies may be useful for patients, each offering different advantages for their type of retinal degeneration and its degree of progression.

Disclaimer

The opinions and/or conclusions expressed herein are solely those of the author and in no way imply a policy or position of the Food and Drug Administration. The mention of commercial products, their sources, or their use in connection with material reported herein is not to be construed as either an actual or implied endorsement of such products by the Department of Health and Human Services.

Acknowledgments

We thank Bruce Drum, Sunder Rajan, and Ksenia Blinova for critical manuscript comments.

Video 10. Example of the use of optical coherence tomography (OCT) to image retinal damage under optically transparent stimulation electrodes in real time. OCT time lapse movie of a 5-minute period of retinal overstimulation (50Hz 749μC/cm2/ph) using a saline-filled transparent epiretinal electrode.

Download video

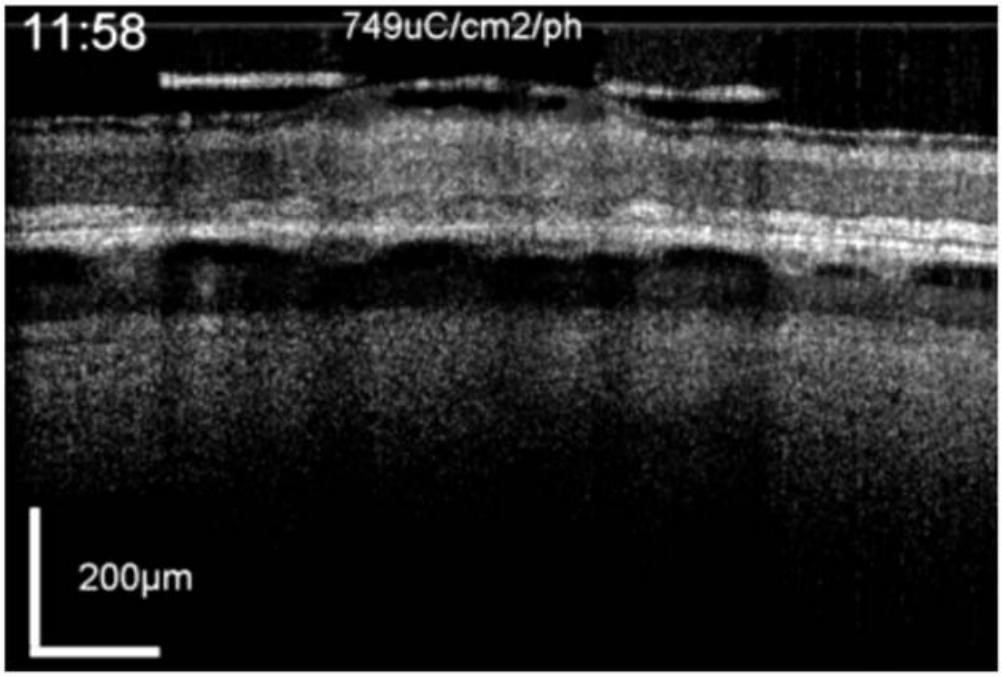

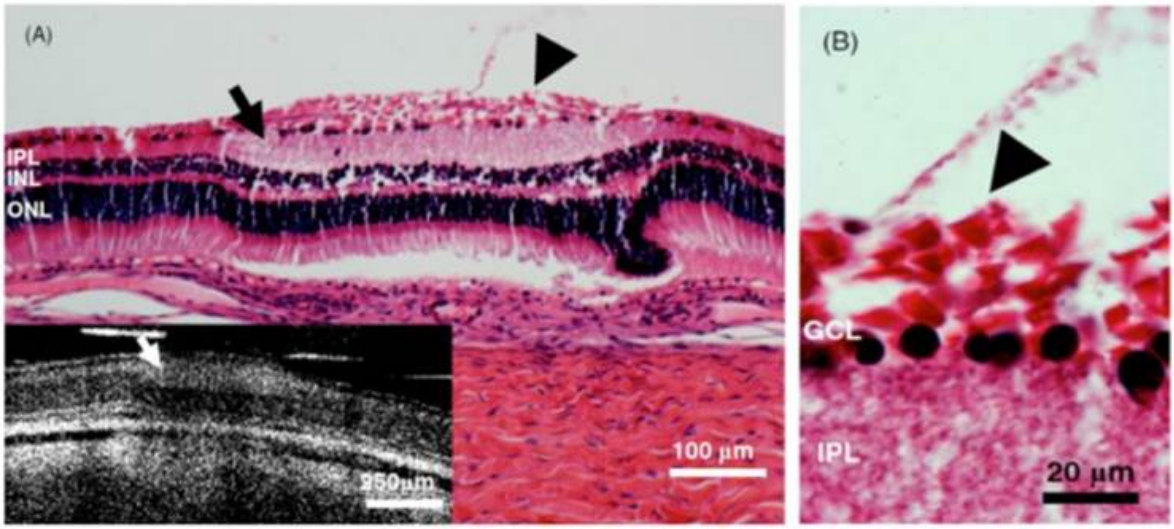

Figure 10. Example of the use of optical coherence tomography (OCT) to image retinal damage under optically transparent stimulation electrodes in real time. Above. OCT time lapse movie of a 5 min period of retinal overstimulation (50Hz 749μC/cm^2/ph) using a saline-filled transparent epirtinal electrode (Video 10). A. Histological analysis under the stimulated zone post imaging shows a localized swelling of the ILM (arrowhead), IPL (arrow), and retinal detachment. B. Detail of swelling of the ILM Muller cell end feet (arrowhead) and pyknotic ganglion cells. From ref (125), with permission from IOP Publishing.

About the author

Dr. Cohen received his Ph.D. in the retina lab of Dr. Peter Sterling at the University of Pennsylvania in 1987. After postdoctoral training in physiology at the University of Minnesota with Dr. Robert Miller, and at the UCLA Jules Stein Eye Institute with Dr. Gordon Fain, he joined the faculty of the Department. of Ophthalmology at Yale University Medical School as a retinal neurophysiologist in 1992. In 2000, he was a visiting professor in the Department of Molecular and Cellular Biology at Harvard University with John Dowling. Since 2003, he is a research scientist at the Office of Science and Engineering Labs at the Center for Devices and Radiological Health at FDA. His research interests include devising new methods to evaluate the safety and effectiveness of visual neurostimulation devices and improving the detection of neurotoxic drugs.

References

1. Purkinje, J., *Beobachtungen und Versuche zur Physiologie der Sinne, Volume 1*. Vol. 1. 1823, Prague: Calve.
2. Volta A. On the Electricity Excited by the Mere Contact of Conducting Substances of Different Kinds. Philosophical Transactions of the Royal Society of London. 1800;90:403–431.
3. Rizzo J.F. III, Ayton L.N. Psychophysical testing of visual prosthetic devices: a call to establish a multi-national joint task force. Journal of neural engineering. 2014;11(2):020301. PubMed PMID: 24556526.
4. Margalit E., et al. Retinal prosthesis for the blind. Survey of ophthalmology. 2002;47(4):335–356. PubMed PMID: 12161210.
5. Cohen E.D. Prosthetic interfaces with the visual system: biological issues. Journal of neural engineering. 2007;4(2):R14. PubMed PMID: 17409473.
6. Winter J.O., Cogan S.F., Rizzo J.F. Retinal prostheses: current challenges and future outlook. Journal of Biomaterials Science, Polymer Edition. 2007;18(8):1031–1055. PubMed PMID: 17705997.
7. Weiland J.D., Cho A.K., Humayun M.S. Retinal prostheses: current clinical results and future needs. Ophthalmology. 2011;118(11):2227–2237. PubMed PMID: 22047893.
8. Sobel, I., *Camera models and machine perception*. 1970, Stanford Univ Calif Dept of Computer Science.
9. Greenwald S.H., et al. Brightness as a function of current amplitude in human retinal electrical stimulation. Investigative ophthalmology & visual science. 2009;50(11):5017–5025. PubMed PMID: 19608533.
10. Grover S., Fishman G.A., Brown J. Patterns of visual field progression in patients with retinitis pigmentosa. Ophthalmology. 1998;105(6):1069–1075. PubMed PMID: 9627658.
11. Fishman G.A. Retinitis pigmentosa: visual loss. Archives of Ophthalmology. 1978;96(7):1185–1188. PubMed PMID: 307377.
12. Berson E.L., et al. Disease progression in patients with dominant retinitis pigmentosa and rhodopsin mutations. Investigative Ophthalmology & Visual Science. 2002;43(9):3027–3036. PubMed PMID: 12202526.
13. Daiger S., Sullivan L., Bowne S. Genes and mutations causing retinitis pigmentosa. Clinical genetics. 2013;84(2):132–141. PubMed PMID: 23701314.

14. Cideciyan A.V., et al. Human retinal gene therapy for Leber congenital amaurosis shows advancing retinal degeneration despite enduring visual improvement. Proc Natl Acad Sci U S A. 2013;110(6):E517–25. PubMed PMID: 23341635.
15. Stasheff S.F. Emergence of sustained spontaneous hyperactivity and temporary preservation of OFF responses in ganglion cells of the retinal degeneration (rd1) mouse. Journal of neurophysiology. 2008. PubMed PMID: 18216234.
16. Strettoi E., Pignatelli V. Modifications of retinal neurons in a mouse model of retinitis pigmentosa. Proceedings of the National Academy of Sciences. 2000;97(20):11020–11025. PubMed PMID: 10995468.
17. Marc R.E., Jones B.W. Retinal remodeling in inherited photoreceptor degenerations. Molecular neurobiology. 2003;28(2):139–147. PubMed PMID: 14576452.
18. Jones B.W., et al. Retinal remodeling triggered by photoreceptor degenerations. Journal of Comparative Neurology. 2003;464(1):1–16. PubMed PMID: 12866125.
19. Jones B., et al. Retinal remodeling in human retinitis pigmentosa. Experimental eye research. 2016;150:149–165. PubMed PMID: 27020758.
20. Sjöstrand J., et al. Morphometric study of the displacement of retinal ganglion cells subserving cones within the human fovea. Graefe's archive for clinical and experimental ophthalmology. 1999;237(12):1014–1023. PubMed PMID: 10654171.
21. Yin L., et al. Imaging light responses of foveal ganglion cells in the living macaque eye. J Neurosci. 2014;34(19):6596–605. PubMed PMID: 24806684.
22. Yang J., et al. Destructive Changes in the Neuronal Structure of the FVB/N Mouse Retina. PLoS One. 2015;10(6):e0129719. PubMed PMID: 26091175.
23. Santos A., et al. Preservation of the inner retina in retinitis pigmentosa: a morphometric analysis. Archives of Ophthalmology. 1997;115(4):511–515. PubMed PMID: 9109761.
24. Potts A.M., Inoue J. The electrically evoked response (EER) of the visual system II. Effect of adaptation and retinitis pigmentosa. Investigative Ophthalmology & Visual Science. 1969;8(6):605–612. PubMed PMID: 5359577.
25. Yanai D., et al. The value of preoperative tests in the selection of blind patients for a permanent microelectronic implant. Transactions of the American Ophthalmological Society. 2003;101:223. PubMed PMID: 14971581.
26. Naycheva L., et al. Phosphene Thresholds Elicited by Transcorneal Electrical Stimulation in Healthy Subjects and Patients with Retinal DiseasesEPTs Elicited by Transcorneal Electrical Stimulation. Investigative ophthalmology & visual science. 2012;53(12):7440–7448. PubMed PMID: 23049087.
27. Humayun M.S., et al. Visual perception in a blind subject with a chronic microelectronic retinal prosthesis. Vision research. 2003;43(24):2573–2581. PubMed PMID: 13129543.
28. O'Shea R.P. Thumb's rule tested: visual angle of thumb's width is about 2 deg. Perception. 1991;20(3):415–8. PubMed PMID: 1762884.
29. Roessler G., et al. Implantation and explantation of a wireless epiretinal retina implant device: observations during the EPIRET3 prospective clinical trial. Investigative ophthalmology & visual science. 2009;50(6):3003–3008. PubMed PMID: 19420330.
30. Keserü M., et al. Acute electrical stimulation of the human retina with an epiretinal electrode array. Acta ophthalmologica. 2012;90(1) PubMed PMID: 22067614.
31. Humayun M.S., et al. Interim results from the international trial of Second Sight's visual prosthesis. Ophthalmology. 2012;119(4):779–88. PubMed PMID: 22244176.
32. Ahuja A., et al. Factors affecting perceptual threshold in Argus II retinal prosthesis subjects. Translational vision science & technology. 2013;2(4):1–1. PubMed PMID: 24049718.
33. Da Cruz, L., et al., *The Argus II epiretinal prosthesis system allows letter and word reading and long-term function in patients with profound vision loss.* British Journal of Ophthalmology, 2013: p. bjophthalmol-2012-301525.
34. Jensen R.J., Ziv O.R., Rizzo J.F. Responses of rabbit retinal ganglion cells to electrical stimulation with an epiretinal electrode. Journal of neural engineering. 2005;2(1):S16. PubMed PMID: 15876650.

35. Jensen R.J., Ziv O.R., Rizzo J.F. Thresholds for activation of rabbit retinal ganglion cells with relatively large, extracellular microelectrodes. Investigative ophthalmology & visual science. 2005;46(4):1486–1496. PubMed PMID: 15790920.
36. Margalit E., Thoreson W.B. Inner retinal mechanisms engaged by retinal electrical stimulation. Investigative ophthalmology & visual science. 2006;47(6):2606–2612. PubMed PMID: 16723477.
37. Fried S.I., Hsueh H.-A., Werblin F.S. A method for generating precise temporal patterns of retinal spiking using prosthetic stimulation. Journal of neurophysiology. 2006;95(2):970–978. PubMed PMID: 16236780.
38. Nanduri D., et al. Frequency and amplitude modulation have different effects on the percepts elicited by retinal stimulation. Investigative Ophthalmology & Visual Science. 2012;53(1):205–214. PubMed PMID: 22110084.
39. Nanduri, D., et al. *Retinal prosthesis phosphene shape analysis*. in *Engineering in Medicine and Biology Society,* 2008. *EMBS 2008. 30th Annual International Conference of the IEEE*. 2008. IEEE.
40. Luo Y.H., et al. Long-term repeatability and reproducibility of phosphene characteristics in chronically implanted Argus II retinal prosthesis subjects. American journal of ophthalmology. 2016;170:100–109. PubMed PMID: 27491695.
41. Fornos A.P., et al. Temporal properties of visual perception on electrical stimulation of the retina. Investigative ophthalmology & visual science. 2012;53(6):2720–2731. PubMed PMID: 22447863.
42. Vrabec F. The temporal raphe of the human retina. American journal of ophthalmology. 1966;62(5):926–938. PubMed PMID: 4162879.
43. FitzGibbon T., Taylor S. Mean retinal ganglion cell axon diameter varies with location in the human retina. Japanese journal of ophthalmology. 2012;56(6):631–637. PubMed PMID: 23011679.
44. Paunescu L.A., et al. Reproducibility of nerve fiber thickness, macular thickness, and optic nerve head measurements using StratusOCT. Investigative ophthalmology & visual science. 2004;45(6):1716–1724. PubMed PMID: 15161831.
45. Tan O., et al. Mapping of macular substructures with optical coherence tomography for glaucoma diagnosis. Ophthalmology. 2008;115(6):949–56. PubMed PMID: 17981334.
46. Fine I., Boynton G.M. Pulse trains to percepts: the challenge of creating a perceptually intelligible world with sight recovery technologies. Phil. Trans. R. Soc. B. 1677;2015(370):20140208. PubMed PMID: 26240423.
47. Weitz, A.C., et al., *Improving the spatial resolution of epiretinal implants by increasing stimulus pulse duration.* Science translational medicine, 2015. **7**(318): p. 318ra203-318ra203.
48. Freeman D.K., et al. Selective activation of neuronal targets with sinusoidal electric stimulation. Journal of neurophysiology. 2010;104(5):2778–2791. PubMed PMID: 20810683.
49. Fujikado T., et al. One-Year Outcome of 49-Channel Suprachoroidal–Transretinal Stimulation Prosthesis in Patients With Advanced Retinitis Pigmentosa. Investigative ophthalmology & visual science. 2016;57(14):6147–6157. PubMed PMID: 27835711.
50. Lorach H., et al. Photovoltaic restoration of sight with high visual acuity. Nature medicine. 2015;21(5):476–482. PubMed PMID: 25915832.
51. Chow A.Y., et al. The artificial silicon retina microchip for the treatment of vision loss from retinitis pigmentosa. Archives of ophthalmology. 2004;122(4):460–469. PubMed PMID: 15078662.
52. Zrenner E., et al. Subretinal electronic chips allow blind patients to read letters and combine them to words. Proc Biol Sci. 1711;2011(278):1489–97. PubMed PMID: 21047851.
53. Stingl, K., et al. *Artificial vision with wirelessly powered subretinal electronic implant alpha-IMS*. in *Proc. R. Soc. B*. 2013. The Royal Society.
54. Stingl K., et al. Interim Results of a Multicenter Trial with the New Electronic Subretinal Implant Alpha AMS in 15 Patients Blind from Inherited Retinal Degenerations. Frontiers in neuroscience. 2017;11:445. PubMed PMID: 28878616.
55. Edwards T.L., et al. Assessment of the Electronic Retinal Implant Alpha AMS in Restoring Vision to Blind Patients with End-Stage Retinitis Pigmentosa. Ophthalmology. 2017. PubMed PMID: 29110946.

56. Kelly, S.K., et al. *Developments on the Boston 256-channel retinal implant*. in *2013 IEEE International Conference on Multimedia and Expo Workshops (ICMEW)*. 2013.
57. Wilke R., et al. Spatial resolution and perception of patterns mediated by a subretinal 16-electrode array in patients blinded by hereditary retinal dystrophies. Invest Ophthalmol Vis Sci. 2011;52(8):5995–6003. PubMed PMID: 21693599.
58. Kitiratschky V.B., et al. Safety evaluation of "retina implant alpha IMS"—a prospective clinical trial. Graefe's Archive for Clinical and Experimental Ophthalmology. 2015;253(3):381–387. PubMed PMID: 25219982.
59. Linsenmeier R.A., Zhang H.F. Retinal oxygen: from animals to humans. Progress in retinal and eye research. 2017. PubMed PMID: 28109737.
60. Fujikado T., et al. Testing of semichronically implanted retinal prosthesis by suprachoroidal-transretinal stimulation in patients with retinitis pigmentosa. Investigative ophthalmology & visual science. 2011;52(7):4726–4733. PubMed PMID: 21436271.
61. Ayton L.N., et al. First-in-human trial of a novel suprachoroidal retinal prosthesis. PLoS One. 2014;9(12):e115239. PubMed PMID: 25521292.
62. Sinclair N.C., et al. The appearance of phosphenes elicited using a suprachoroidal retinal prosthesis. Investigative ophthalmology & visual science. 2016;57(11):4948–4961. PubMed PMID: 27654422.
63. Delbeke J., Oozeer M., Veraart C. Position, size and luminosity of phosphenes generated by direct optic nerve stimulation. Vision research. 2003;43(9):1091–1102. PubMed PMID: 12676250.
64. Sui X., et al. Mechanical analysis and fabrication of a penetrating silicon microprobe as an artificial optic nerve visual prosthesis. Int J Artif Organs. 2012;35(1):34–44. PubMed PMID: 22328332.
65. Safadi M., et al. Development of a microfluidic drug delivery neural stimulating device for vision. Investigative Ophthalmology & Visual Science. 2003;44(13):5082–5082. PubMed PMID: 14638701.
66. Peterman M.C., et al. Localized chemical release from an artificial synapse chip. Proceedings of the National Academy of Sciences of the United States of America. 2004;101(27):9951–9954. PubMed PMID: 15218102.
67. Inayat S., et al. Chemical stimulation of rat retinal neurons: feasibility of an epiretinal neurotransmitter-based prosthesis. Journal of neural engineering. 2014;12(1):016010. PubMed PMID: 25504758.
68. Vu T.Q., et al. Activation of membrane receptors by a neurotransmitter conjugate designed for surface attachment. Biomaterials. 2005;26(14):1895–1903. PubMed PMID: 15576163.
69. Cohn F. Über die Gesetze der Bewegung der microscopischen Pflanzen und Thiere unter Einfluß des Lichtes. Jb. Schles. Ges. Vaterl. Kultur. 1865;42:35–37.
70. Mast S.O. The process of orientation in the colonial organism, Gonium pectorale, and a study of the structure and function of the eye-spot. Journal of Experimental Zoology Part A: Ecological Genetics and Physiology. 1916;20(1):1–17.
71. Litvin F.F., Sineshchekov O.A., Sineshchekov V.A. Photoreceptor electric potential in the phototaxis of the alga Haematococcus pluvialis. Nature. 1978;271(5644):476–8. PubMed PMID: 628427.
72. Sineshchekov O.A., Litvin F.F., Keszthelyi L. Two components of photoreceptor potential in phototaxis of the flagellated green alga Haematococcus pluvialis. Biophysical journal. 1990;57(1):33–39. PubMed PMID: 19431753.
73. Nagel G., et al. Channelrhodopsin-2, a directly light-gated cation-selective membrane channel. Proceedings of the National Academy of Sciences. 2003;100(24):13940–13945. PubMed PMID: 14615590.
74. Boyden E.S., et al. Millisecond-timescale, genetically targeted optical control of neural activity. Nature neuroscience. 2005;8(9):1263–1268. PubMed PMID: 16116447.
75. Bruun S., et al. Light-Dark Adaptation of Channelrhodopsin Involves Photoconversion between the all-trans and 13-cis Retinal Isomers. Biochemistry. 2015;54(35):5389–400. PubMed PMID: 26237332.
76. Szobota S., et al. Remote control of neuronal activity with a light-gated glutamate receptor. Neuron. 2007;54(4):535–545. PubMed PMID: 17521567.
77. Schröder-Lang S., et al. Fast manipulation of cellular cAMP level by light in vivo. Nature methods. 2007;4(1):39–42. PubMed PMID: 17128267.

78. Gasser C., et al. Engineering of a red-light–activated human cAMP/cGMP-specific phosphodiesterase. Proceedings of the National Academy of Sciences. 2014;111(24):8803–8808. PubMed PMID: 24889611.
79. Ermakova Y.G., et al. Thermogenetic neurostimulation with single-cell resolution. Nat Commun. 2017;8:15362. PubMed PMID: 28530239.
80. Dowling J.E. Foveal receptors of the monkey retina: fine structure. Science. 1965;147(3653):57–59. PubMed PMID: 14224526.
81. Hogan, M.J., J.A. Alvarado, and J. Weddell, *Ciliary body and posterior chamber.* Histology of the human eye: an atlas and textbook. Philadelphia: Saunders, 1971.
82. Cohen A.I. New details of the ultrastructure of the outer segments and ciliary connectives of the rods of human and macaque retinas. The Anatomical Record. 1965;152(1):63–79. PubMed PMID: 14316821.
83. Bi A., et al. Ectopic expression of a microbial-type rhodopsin restores visual responses in mice with photoreceptor degeneration. Neuron. 2006;50(1):23–33. PubMed PMID: 16600853.
84. Lagali P.S., et al. Light-activated channels targeted to ON bipolar cells restore visual function in retinal degeneration. Nature neuroscience. 2008;11(6):667–675. PubMed PMID: 18432197.
85. Doroudchi M.M., et al. Virally delivered channelrhodopsin-2 safely and effectively restores visual function in multiple mouse models of blindness. Molecular Therapy. 2011;19(7):1220–1229. PubMed PMID: 21505421.
86. Yan B., Nirenberg S. An Embedded Real-time Processing Platform for Optogenetic Neuroprosthetic Applications. IEEE Trans Neural Syst Rehabil Eng. 2017. PubMed PMID: 29035219.
87. Williams, S., *Optogenetic therapies move closer to clinical use.* in *The Scientist*. 2017, The Scientist: New York.
88. Sengupta A., et al. Red-shifted channelrhodopsin stimulation restores light responses in blind mice, macaque retina, and human retina. EMBO molecular medicine. 2016;8(11):1248–1264. PubMed PMID: 27679671.
89. Kim D.S., Matsuda T., Cepko C.L. A core paired-type and POU homeodomain-containing transcription factor program drives retinal bipolar cell gene expression. Journal of Neuroscience. 2008;28(31):7748–7764. PubMed PMID: 18667607.
90. Morris R. Developments of a water-maze procedure for studying spatial learning in the rat. J Neurosci Methods. 1984;11(1):47–60. PubMed PMID: 6471907.
91. Chow B.Y., et al. High-performance genetically targetable optical neural silencing by light-driven proton pumps. Nature. 2010;463(7277):98–102. PubMed PMID: 20054397.
92. Wagner N.L., et al. Directed evolution of bacteriorhodopsin for applications in bioelectronics. Journal of The Royal Society Interface. 2013;10(84):20130197. PubMed PMID: 23676894.
93. Greco J.A., et al. Stimulation of Retinal Ganglion Cells Using an Ion-Mediated, Protein-Based Retinal Implant. Investigative Ophthalmology & Visual Science. 2017;58(8):4184–4184.
94. Govorunova E.G., et al. Natural light-gated anion channels: A family of microbial rhodopsins for advanced optogenetics. Science. 2015;349(6248):647–650. PubMed PMID: 26113638.
95. Berndt A., et al. Structural foundations of optogenetics: Determinants of channelrhodopsin ion selectivity. Proceedings of the National Academy of Sciences. 2016;113(4):822–829. PubMed PMID: 26699459.
96. Zhang Y., et al. Ectopic expression of multiple microbial rhodopsins restores ON and OFF light responses in retinas with photoreceptor degeneration. Journal of Neuroscience. 2009;29(29):9186–9196. PubMed PMID: 19625509.
97. Busskamp V., et al. Genetic reactivation of cone photoreceptors restores visual responses in retinitis pigmentosa. Science. 2010;329(5990):413–417. PubMed PMID: 20576849.
98. Khabou, H., et al., *Noninvasive gene delivery to foveal cones for vision restoration.* JCI Insight, 2018. **3**(2).
99. Kim J.-M., et al. Light-driven activation of β2-adrenergic receptor signaling by a chimeric rhodopsin containing the β2-adrenergic receptor cytoplasmic loops. Biochemistry. 2005;44(7):2284–2292. PubMed PMID: 15709741.
100. Qiu X., et al. Induction of photosensitivity by heterologous expression of melanopsin. Nature. 2005;433(7027):745–749. PubMed PMID: 15674243.

101. Lin B., et al. Restoration of visual function in retinal degeneration mice by ectopic expression of melanopsin. Proc Natl Acad Sci U S A. 2008;105(41):16009–14. PubMed PMID: 18836071.
102. Koike C., et al. TRPM1 is a component of the retinal ON bipolar cell transduction channel in the mGluR6 cascade. Proceedings of the National Academy of Sciences. 2010;107(1):332–337. PubMed PMID: 19966281.
103. van Wyk M., et al. Restoring the ON switch in blind retinas: opto-mGluR6, a next-generation, cell-tailored optogenetic tool. PLoS biology. 2015;13(5):e1002143. PubMed PMID: 25950461.
104. Gaub B.M., et al. Optogenetic vision restoration using rhodopsin for enhanced sensitivity. Molecular Therapy. 2015;23(10):1562–1571. PubMed PMID: 26137852.
105. Cehajic-Kapetanovic J., et al. Restoration of vision with ectopic expression of human rod opsin. Current Biology. 2015;25(16):2111–2122. PubMed PMID: 26234216.
106. Dalkara, D., et al., *In vivo–directed evolution of a new adeno-associated virus for therapeutic outer retinal gene delivery from the vitreous.* Science translational medicine, 2013. **5**(189): p. 189ra76-189ra76.
107. Lu Q., et al. AAV-mediated transduction and targeting of retinal bipolar cells with improved mGluR6 promoters in rodents and primates. Gene therapy. 2016;23(8):680–689. PubMed PMID: 27115727.
108. Hadaczek P., et al. Transduction of nonhuman primate brain with adeno-associated virus serotype 1: vector trafficking and immune response. Human gene therapy. 2009;20(3):225–237. PubMed PMID: 19292604.
109. Okada H., et al. Robust long-term transduction of common marmoset neuromuscular tissue with rAAV1 and rAAV9. Molecular Therapy—Nucleic Acids. 2013;2(5):e95. PubMed PMID: 23715217.
110. Matsumoto B., Blanks J., Ryan S. Topographic variations in the rabbit and primate internal limiting membrane. Investigative ophthalmology & visual science. 1984;25(1):71–82. PubMed PMID: 6199321.
111. Halfter W., et al. Embryonic synthesis of the inner limiting membrane and vitreous body. Invest Ophthalmol Vis Sci. 2005;46(6):2202–9. PubMed PMID: 15914642.
112. Vacca, O., et al., *Using adeno-associated virus as a tool to study retinal barriers in disease.* Journal of visualized experiments: JoVE, 2015(98).
113. Yin L., et al. Intravitreal injection of AAV2 transduces macaque inner retina. Investigative ophthalmology & visual science. 2011;52(5):2775–2783. PubMed PMID: 21310920.
114. Ivanova E., et al. Evaluation of AAV-mediated expression of Chop2-GFP in the marmoset retina. Investigative ophthalmology & visual science. 2010;51(10):5288–5296. PubMed PMID: 20484599.
115. Tshilenge K.-T., et al. Vitrectomy Before Intravitreal Injection of AAV2/2 Vector Promotes Efficient Transduction of Retinal Ganglion Cells in Dogs and Nonhuman Primates. Human gene therapy methods. 2016;27(3):122–134. PubMed PMID: 27229628.
116. Takahashi K., et al. Improved intravitreal AAV-mediated inner retinal gene transduction after surgical internal limiting membrane peeling in cynomolgus monkeys. Molecular Therapy. 2017;25(1):296–302. PubMed PMID: 28129123.
117. De Silva S.R., et al. Long-term restoration of visual function in end-stage retinal degeneration using subretinal human melanopsin gene therapy. Proceedings of the National Academy of Sciences. 2017;114(42):11211–11216. PubMed PMID: 28973921.
118. Xue K., et al. Technique of retinal gene therapy: delivery of viral vector into the subretinal space. Eye (Lond). 2017;31(9):1308–1316. PubMed PMID: 28820183.
119. Calame M., et al. Retinal degeneration progression changes lentiviral vector cell targeting in the retina. PloS one. 2011;6(8):e23782. PubMed PMID: 21901134.
120. Pignatelli V., Cepko C.L., Strettoi E. Inner retinal abnormalities in a mouse model of Leber's congenital amaurosis. Journal of Comparative Neurology. 2004;469(3):351–359. PubMed PMID: 14730587.
121. Farinelli P., et al. DNA methylation and differential gene regulation in photoreceptor cell death. Cell death & disease. 2014;5(12):e1558. PubMed PMID: 25476906.
122. Arango-Gonzalez B., et al. Identification of a common non-apoptotic cell death mechanism in hereditary retinal degeneration. PLoS One. 2014;9(11):e112142. PubMed PMID: 25392995.
123. Wahlin K.J., et al. Epigenetics and cell death: DNA hypermethylation in programmed retinal cell death. PloS one. 2013;8(11):e79140. PubMed PMID: 24244436.

124. van Wyk M., et al. Present Molecular Limitations of ON-Bipolar Cell Targeted Gene Therapy. Front Neurosci. 2017;11:161. PubMed PMID: 28424574.
125. Cohen E., et al. Optical coherence tomography imaging of retinal damage in real time under a stimulus electrode. Journal of neural engineering. 2011;8(5):056017. PubMed PMID: 21934187.
126. Butterwick A., et al. Tissue damage by pulsed electrical stimulation. IEEE Trans Biomed Eng. 2007;54(12):2261–7. PubMed PMID: 18075042.
127. Cohen E.D. Effects of high-level pulse train stimulation on retinal function. J Neural Eng. 2009;6(3):035005. PubMed PMID: 19458404.
128. Nayagam D.A.X., et al. Chronic electrical stimulation with a suprachoroidal retinal prosthesis: a preclinical safety and efficacy study. PloS one. 2014;9(5):e97182. PubMed PMID: 24853376.
129. McCreery D.B., et al. Charge density and charge per phase as cofactors in neural injury induced by electrical stimulation. IEEE Transactions on Biomedical Engineering. 1990;37(10):996–1001. PubMed PMID: 2249872.
130. De Vera Mudry M.C., et al. Blinded by the light: retinal phototoxicity in the context of safety studies. Toxicologic pathology. 2013;41(6):813–825. PubMed PMID: 23271306.
131. Ham W.T., Mueller H.A., Sliney D.H. Retinal sensitivity to damage from short wavelength light. Nature. 1976;260(5547):153–155. PubMed PMID: 815821.
132. Ham W.T., et al. Sensitivity of the retina to radiation damage as a function of wavelength. Photochemistry and Photobiology. 1979;29(4):735–743. PubMed PMID: 109869.
133. Noell W.K., et al. Retinal damage by light in rats. Investigative Ophthalmology & Visual Science. 1966;5(5):450–473. PubMed PMID: 5929286.
134. Wenzel A., et al. The Rpe65 Leu450Met variation increases retinal resistance against light-induced degeneration by slowing rhodopsin regeneration. Journal of Neuroscience. 2001;21(1):53–58. PubMed PMID: 11150319.
135. Wenzel A., et al. Molecular mechanisms of light-induced photoreceptor apoptosis and neuroprotection for retinal degeneration. Progress in retinal and eye research. 2005;24(2):275–306. PubMed PMID: 15610977.

Facts and Figures Concerning the Human Retina

Facts and Figures Concerning the Human Retina

Helga Kolb

Created: May 1, 2005; Updated: July 5, 2007.

Size of the Retina

- 32 mm from ora to ora along the horizontal meridian (1) (Kolb, unpublished measurements).
- The area of the human retina is 1,094 square mm (Bernstein, personal communication), calculated from the expectations that the average dimension of the human eye is 22 mm from anterior to posterior poles, and that 72% of the inside of the globe is retina (2). See also Penkhus (3).

Size of Optic Nerve Head or Disc

- 1.86 × 1.75 mm (Fig. 1)

Degrees and Distance in Micometers

- One degree of visual angle is equal to 288 µm on the retina without correction for shrinkage (4).

Foveal Position

- 11.8° or or 3.4 mm temporal to the optic disk edge

Cross Diameter of the Macula

- 3 mm of intense pigmentation, surrounded by a 1-mm-wide zone of less pigmentation (5).

Cross Diameter of the Central Fovea from Foveal Rim to Foveal Rim

- 1.5 mm (5)
- 1.2-1.5 mm (Ahnelt and Kolb, unpublished data) (Fig. 2a and Fig. 2b)

Cross Diameter of Central Rod-free Area

- 400-600 µm (5)
- 750 µm (6)
- 570 µm (7)
- 250 µm (8)

Vertical Thickness of the Fovea from Inner Limiting Membrane (ILM) to ELM

- in the foveal pit, 150 µm (7)
- foveal rim, 400 µm

Central Region of Fovea Where There Are No Cone Pedicles

- 250 µm (7)
- 200 µm (6)

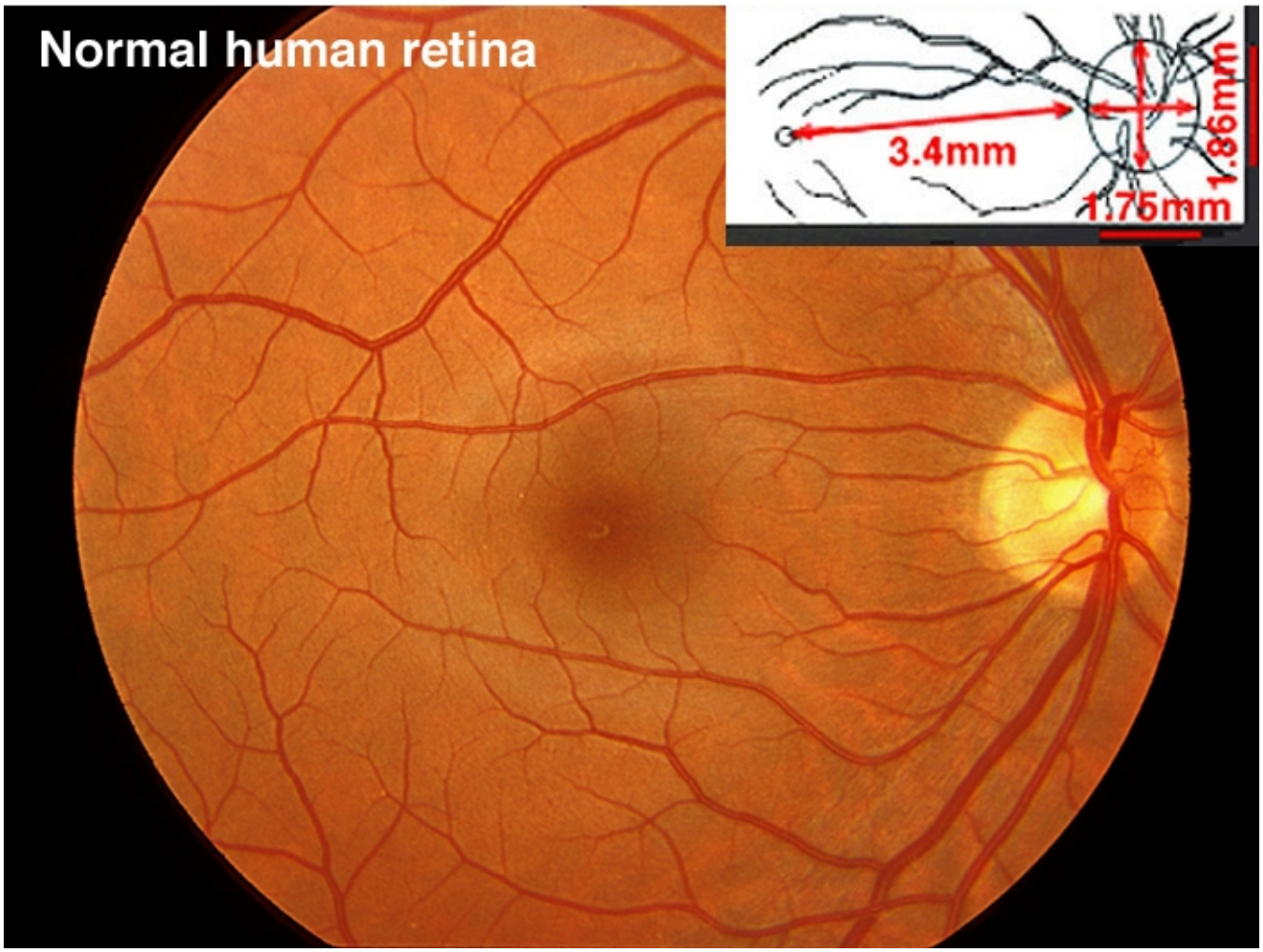

Figure 1. Topography and dimensions of optic nerve and fovea.

- 300 µm (9)

Length of Foveal Axons (Henle Fibers)

- 150-300 µm (9)

Vertical Thickness of the Retina in Different Areas

The vertical extent of the retina across the horizontal meridian at different eccentricities is shown in Fig. 3. This is taken from data given by Sigelman and Ozanics (20). The small black numbers are the originals from Sigelman and Ozanics which were measured in typical histological preparations where there is a great deal of shrinkage. The figures in red are those recently measured by Ahnelt (personal communication) in well fixed EM quality material where there is little or no shrinkage. Hence the latter numbers are larger. The numbers are in mm.

Age When Fovea Is Fully Developed

- not before 4 years of age (6)

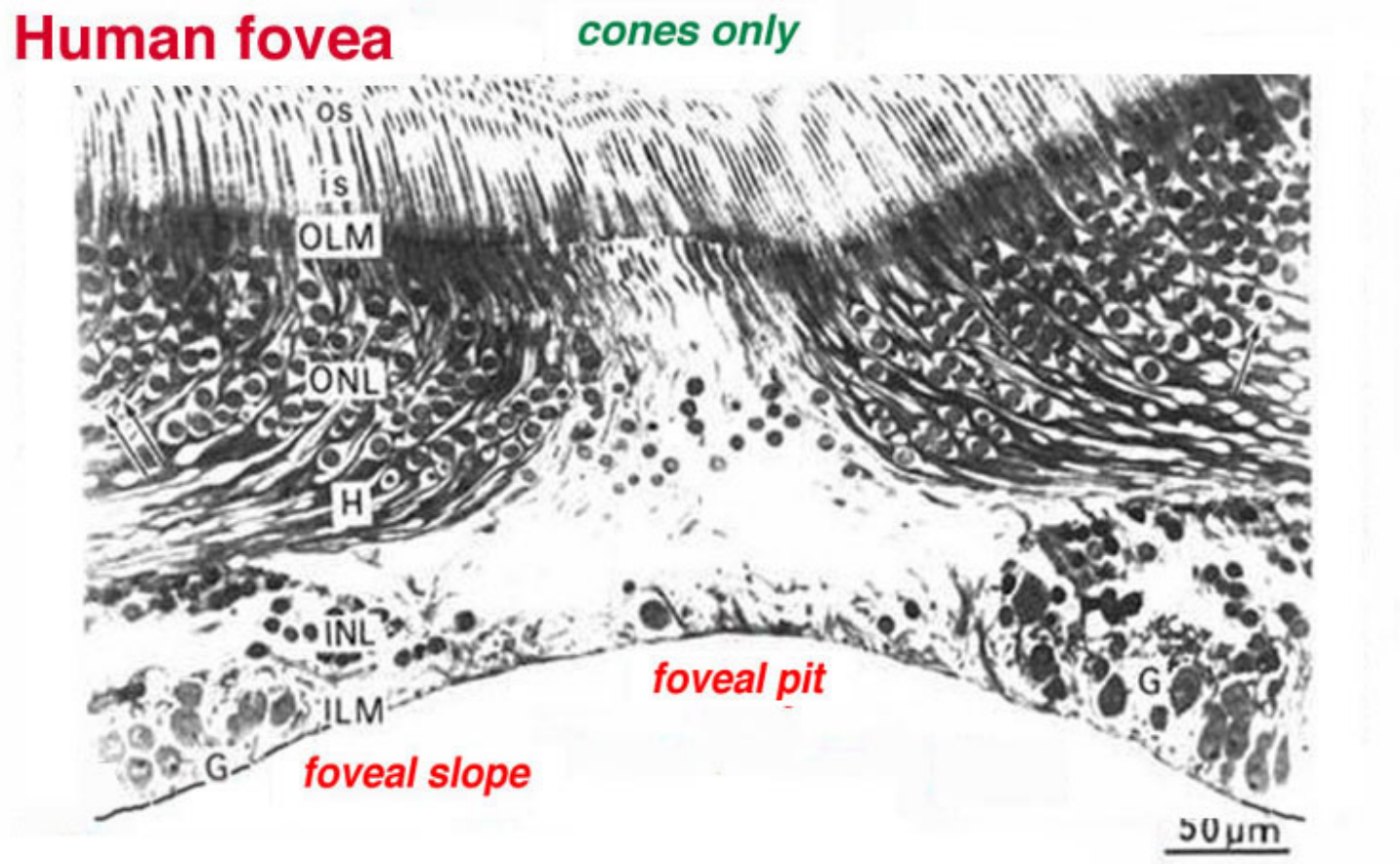

Figure 2a. Vertical section of the human fovea. os, outer segments; is, inner segments; OLM, outer limiting membrane; ONL, outer nuclear layer; H, Henle fibers; INL, inner nuclear layer; ILM, inner limiting membrane; G, ganglion cells. From Yamada (7).

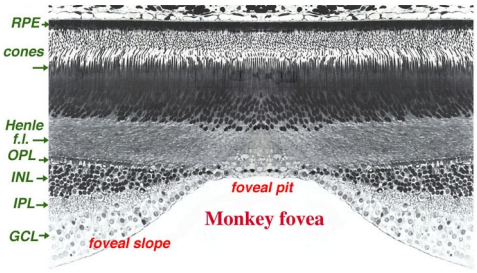

Figure 2b. Vertical section of the monkey fovea. From Hagerman and Johnson (19).

Highest Density of Cones at Center of the Fovea (50 × 50 µm)

- 147,000/mm^2 (10)
- 178,000-238,000/mm^2 (8)
- 96,900-281,000/mm^2; mean, 161,900/mm^2 (11) (Fig. 4)

Total Number of Cones in Fovea

- approximately 200,000. 17,500 cones/degree^2. Rod-free area is 1°; thus, there are 17,500 cones in the central rod-free fovea.

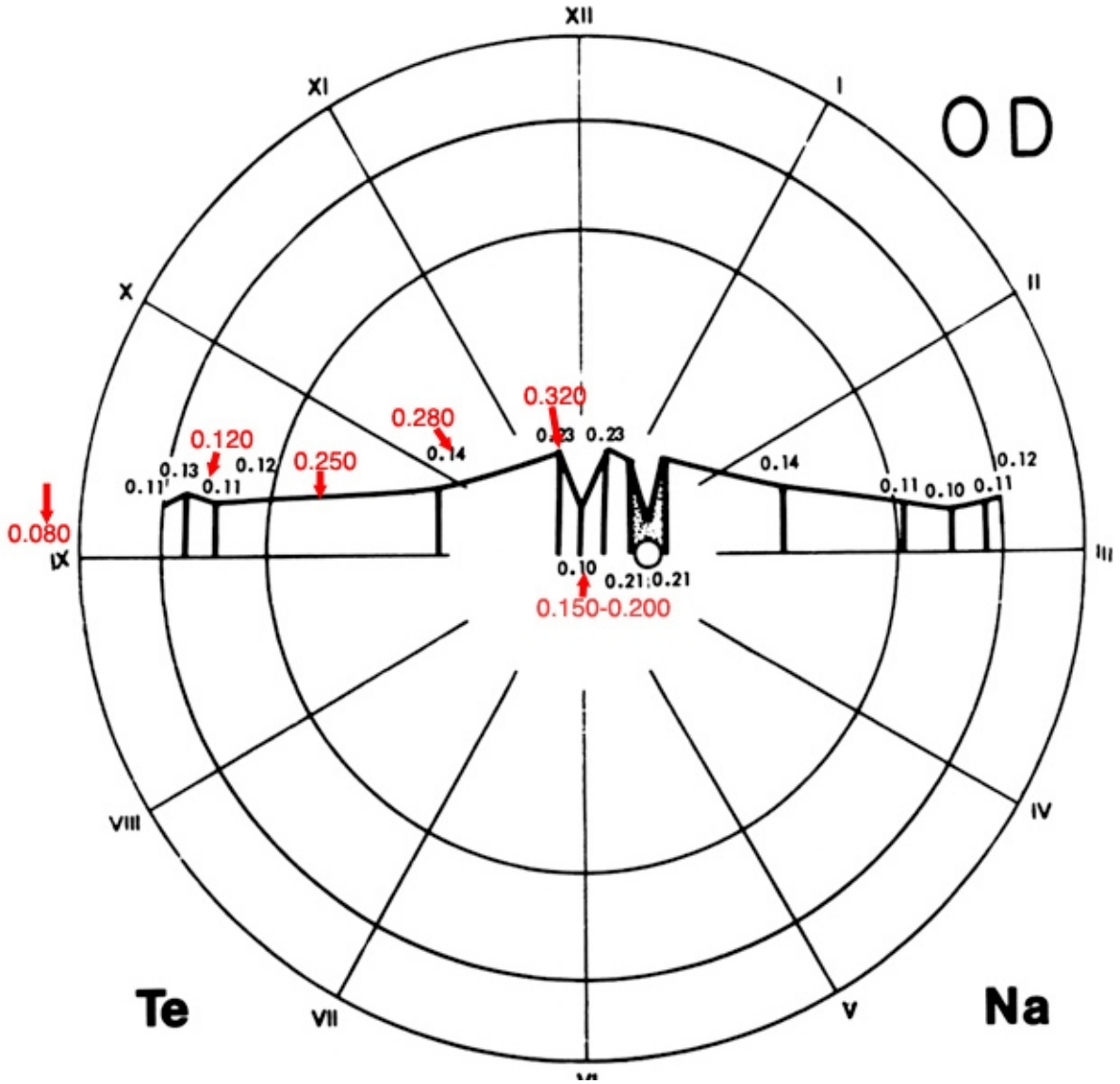

Figure 3. The retinal thickness shows greatest variations in the center. The retina is thinnest at the foveal floor (0.10, 0.150-0.200 mm) and thickest (0.23, 0.320 mm) at the foveal rim. Beyond the fovea the retina rapidly thins until the equator. At the ora serrata the retina is thinnest of all (0.080 mm).

Total Number of Cones in the Retina

- 6,400,000 (10)

Total Number of Rods in the Retina

- 110,000,000 to 125,000,000 (10)

Rod Distribution

- Rods peak in density 18° or 5 mm out from the center of the fovea, in a ring around the fovea at 160,000 rods/mm^2
- No rods in central 200 μm
- Average 80-100,000 rods/mm^2.

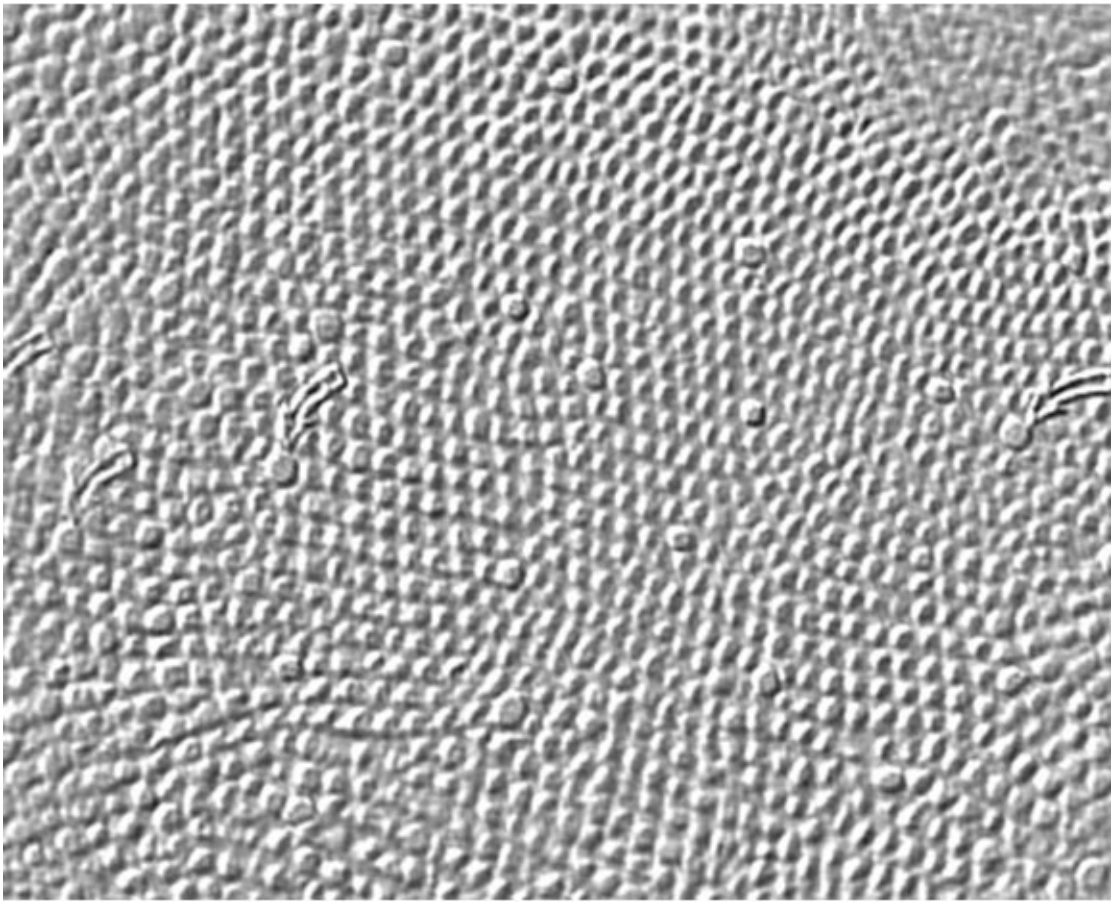

Figure 4. Tangential section through the human fovea. Larger cones (arrows) are blue cones.

- Rod acuity peak is at 5.2° or 1.5 mm from foveal center, where there are 100,000 rods/mm^2 (12) (Fig. 5)

Number of Axons in the Optic Nerve

- 564,776-1,140,030 (13)
- 800,000-1,000,000 (5)
- 1,200,000 (14, 15)

Number of Cones to Ganglion Cells in the Fovea

- 1 cone to 2 ganglion cells out to about 2.2° (16)

Number of Cones/Retinal Pigment Epithelial Cell (RPE)

- 30 cones/RPE in fovea (17)

Number of Rods/Retinal Epithelial Cell (RPE)

- in periphery, 22 rods/RPE cell
- in rod, peak (4-5 mm from foveal center), 28 rods/RPE cell (17)

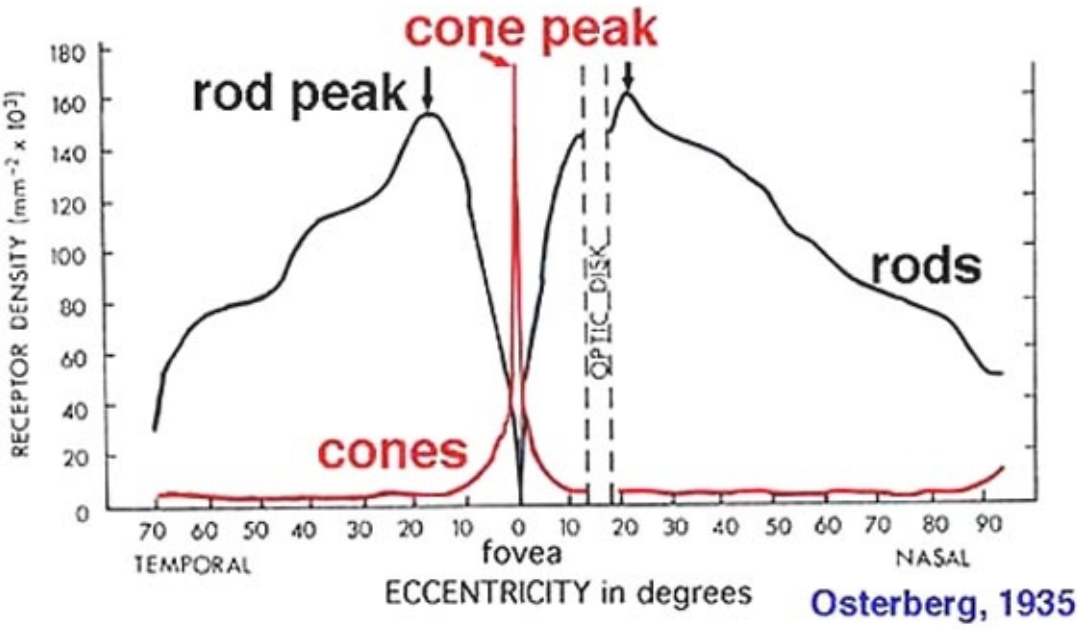

Figure 5. Graph to show rod and cone densities along the horizontal meridian.

Number of Neural and Glial Types in the Retina

The retina consists of many millions of cell types packed together in a tightly knit network spread over the surface of the back of the eye fundus as a thin film of tissue only 1/2 millimeter thick. The retina is like a three-layered cake with three layers containing cell bodies of neurons and two filling layers where synapses between the neurons occur. There are two basic kinds of photoreceptors—rods and cones. The cones are further subdivided into two types (long- and short-wavelength sensitive) in the majority of mammals, i.e., most mammals, which are dichromats and have divariant color vision. In primates, a third wavelength-sensitive cone has developed closely related to the long-wavelength cone type but a little more sensitive in the middle wavelength (i.e., green cone). Thus, primates including humans are trichromats and have trivariant color vision. Many reptiles, birds, and fish have four or even five types of cone, each sensitive to a slightly different peak wavelength.

The second-order neurons, postsynaptic to the photorecepors in the first synaptic (filling layer) (outer plexiform layer), are bipolar cells and horizontal cells. There are nine types of bipolar cell and two to four types of horizontal cell in species from mammals to fish. The third-order neurons are amacrine cells and ganglion cells that synapse in the inner synaptic filling layer (inner plexiform layer). There are two types of interplexiform cells stretching between both plexiform layers, in most vertebrate retinas. There are approximately 22 types of amacrine cell and 20 types of ganglion cell in the typical mammalian retina. There may be 30 or more amacrine cell types in fish and reptilian retinas and 22 or so ganglion cell types. The increased number of third-order neurons is attributable to the greater information processing taking place in the non-mammalian retinas than in mammalian retinas.

All vertebrate retinas also contain large numbers of glial cells. The radial Muller cells stretch from outer to inner limiting membranes and surround and isolate all neural cell types from each other except at synapses. Microglia arise in times of injury and are blood-borne cell types. Astrocytes surround ganglion cell axons and inner retinal blood vessels.

Fig. 6 shows a drawing of the human retina close to the fovea, where all of the cell types that have been studied in detail are depicted in their intricate and marvellous network.

Useful Units in Vision Science

From Wandell (18):

- Radiometric units represent a physical measurement, e.g., radiance is measured in watts sr^{-1} m^{-2}.
- Calorimetric units adjust radiometric units for visual wavelength sensitivity, e.g., luminance is measured in candela per square meter, cd/m^2.
- Lux are units of illumination. Thus, a light intensity of 1 candela produces an illumination of 1 lux at 1 meter.
  - Scotopic luminance units are proportional to the number of photons absorbed by rod photoreceptors to give a criterion psychophysical result.
  - Photopic luminance units are proportional to a weighted sum of the photons absorbed by L- and M-cones to give a criterion psychophysical result.
- Typical ambient luminance levels (cd/m^2):
  - Starlight: 0.001
  - Moonlight: 0.1
  - Indoor lighting: 100
  - Sunlight: 10.000
  - Maximum intensity of common CRT monitors: 100
- One Troland (Td) of retinal illumination is produced when an eye with a pupil size of 1 mm^2 looks at a surface whose luminance is 1 cd/m^2.
- Lens focal length: f (meters); lens power= 1/f (diopters).

Image Formation

From Wandell (18):

- The eyes are 6 cm apart and halfway down the head.
- Visual angle of common objects (degrees, deg)
  - The sun or moon = 0.5 deg
  - Thumbnail (at arm's length) = 1.5 deg
  - Fist (at arm's length) = 8-10 deg
- Visual field (measured from central fixation)
  - Monocular: 160 deg (w) × 175 deg (h)
  - Binocular: 200 deg (w) × 135 deg (h)
  - Region of binocular overlap: 120 deg (w) × 135 deg (h)
- Range of pupil diameters: 1-8 mm
- Refractive indices
  - Air: 1.000
  - Glass: 1.520
  - Water: 1.333
  - Cornea: 1.376
- Optical power (diopters)
  - Cornea: 43
  - Lens (relaxed): 20
  - Whole eye: 60
  - Change in power due to accomodation: 8

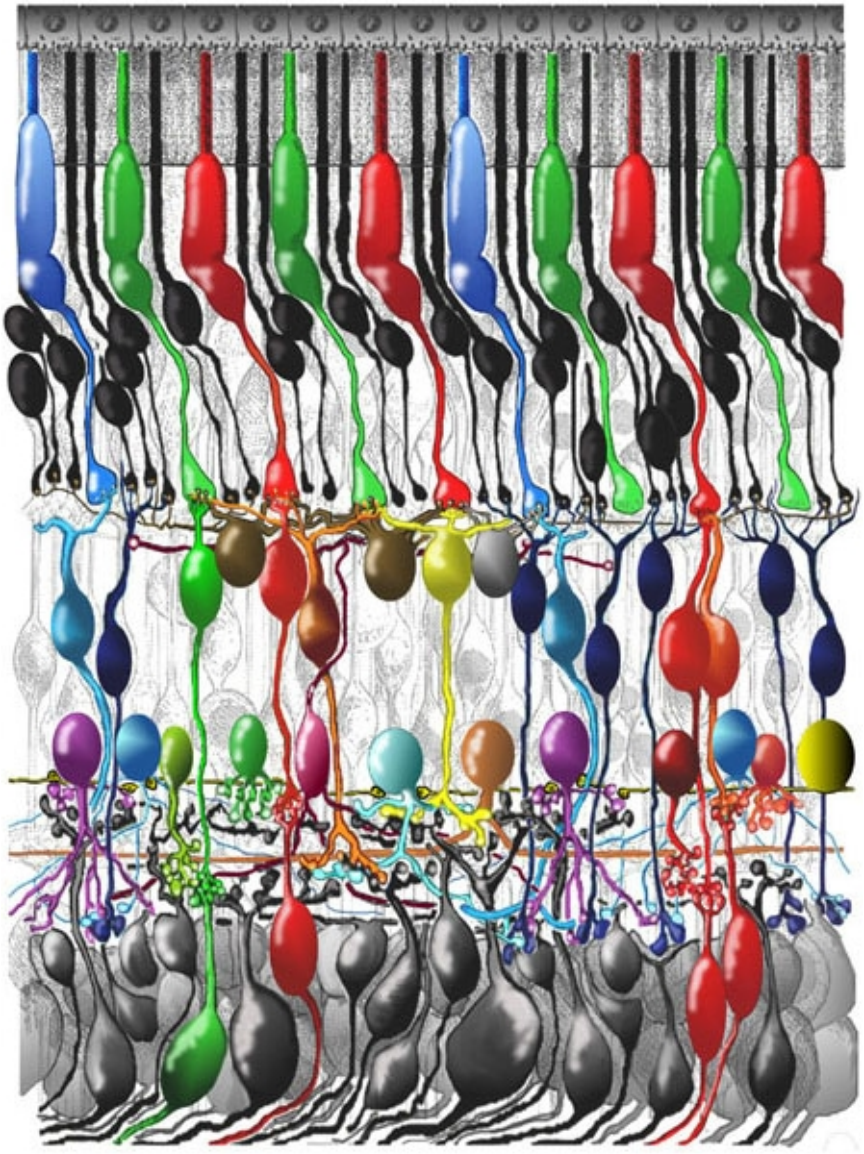

Figure 6. Drawing of a vertical section through the human retina to show the organization of the different neurons and glial cells constituting it.

- Axial chromatic aberration over the visible spectrum: 2 diopters
- Visible spectrum: 370-730 nanometers (nm)
- Peak wavelength sensitivity
  - Scotopic: 507 nm
  - Photopic: 555 nm
- Spectral equilibrium hues
  - Blue: 475 nm
  - Green: 500 nm
  - Yellow: 575 nm
  - No spectral equilibrium: red

References

1. Van Buren JM. The retinal ganglion cell layer. Springfield (IL): Charles C. Thomas; 1963.

2. Michels RG, Wilkinson CP, Rice TA. Retinal detachment. The C.V. Mosby Company; 1990. p. 17.
3. Penkhus J. The ora serrata and its anatomical variations. M.S. Thesis. University of California, Los Angeles; 1965.
4. Drasdo N, Fowler CW. Non-linear projection of the retinal image in a wide-angle schematic eye. Br J Ophthalmol. 1974;58:709–714. PubMed PMID: 4433482.
5. Polyak SL. The retina. Chicago: University of Chicago Press; 1941.
6. Hendrickson AE, Youdelis C. The morphological development of the human fovea. Ophthalmology. 1984;91:603–612. PubMed PMID: 6462623.
7. Yamada E. Some structural features of the fovea central is in the human retina. Arch Ophthalmol. 1969;82:151–159. PubMed PMID: 4183671.
8. Ahnelt PK, Kolb H, Pflug R. Identification of a subtype of cone photoreceptor, likely to be blue sensitive, in the human retina. J Comp Neurol. 1987;255:18–34. PubMed PMID: 2434534.
9. Ahnelt PK, Pflug R. Telodendrial contacts between foveolar cone pedicles in the human retina. Experientia. 1986;42:298–300. PubMed PMID: 3956685.
10. Osterberg G. Topography of the layer of rods and cones in the human retina. Acta Ophthalmol Suppl. 1935;6:1–103.
11. Curcio CA, Sloan KR, Packer O, Hendrickson AE, Kalina RE. Distribution of cones in human and monkey retina: individual variability and radial asymmetry. Science. 1987;236:579–582. PubMed PMID: 3576186.
12. Mariani AP, Kolb H, Nelson R. Dopamine-containing amacrine cells of rhesus monkey retina parallel rods in spatial distribution. Brain Res. 1984;322:1–7. PubMed PMID: 6518360.
13. Bruesch SR, Arey LB. The number of myelinated and unmyelinated fibres in the optic nerve of vertebrates. J Comp Neurol. 1942;77:631.
14. Balazsi AG, Rootman J, Drance SM, Schulzer M, Douglas GR. The effect of age on the nerve fiber population of the human optic nerve. Am J Ophthalmol. 1984;97:760–766. PubMed PMID: 6731540.
15. Quigley HA, Addicks EM, Green WR. Optic nerve damage inhuman glaucoma. III. Quantitative correlation of nerve fibre loss and visual defect in glaucoma ischemic neuropathy and toxic neuropathy. Arch Ophthalmol. 1982;100:135. PubMed PMID: 7055464.
16. Schein SJ. Anatomy of macaque fovea and spatial densities of neurons in foveal representation. J Comp Neurol. 1988;269:479–505. PubMed PMID: 3372725.
17. Rapaport DH, Rakic P, Yasamura D, LaVail MM. Genesis of the retinal pigment epithelium in the macaque monkey. J Comp Neurol. 1995;363:359–376. PubMed PMID: 8847405.
18. Wandell BA. Foundations of vision. Sunderland (MA): Sinauer Associates, Inc; 1965.
19. Hagerman GS, Johnson LV. The photoreceptor-retinal pigmented epithelial interface. In: Heckenlively JR, Arden GB, editors. Principles and practice of clinical electrophysiology of vision. St. Louis: Mosby Year Book; 1991.
20. Sigelman J, Ozanics V. In: Jokobiec FA, editor. Ocular anatomy, embryology and teratology. Philadelphia: Harper and Rowe; 1982.